The biosynthesis of antibiotic F-244 in *Fusarium* sp. ATCC 20788: origin of the carbon, hydrogen, and oxygen atoms

Endang Saepudin and Paul Harrison

Abstract: Biosynthetic incorporation experiments were performed with carbon-13 labelled precursors including sodium [1-^{13}C]-, [2-^{13}C], and [1,2-$^{13}C_2$]-acetate as well as [*methyl*-^{13}C]methionine into antibiotic F-244 (**1**) in growing cultures of *Fusarium* sp. ATCC 20788. After conversion to the methyl ester **2**, analysis by NMR showed that the carbon skeleton of **1** derives from seven intact acetate units; the remaining four carbons are from methionine. Hence, the pathway is similar to that reported for **1** in *Scopulariopsis*. The biogenesis of the hydrogen atoms in **1** was also investigated. Incorporation of sodium [1-^{13}C,$^{18}O_2$]acetate gives **2**, which exhibits ^{18}O-induced isotope shifts at C-1 and C-3. The labelling pattern is consistent with formation of the β-lactone ring by nucleophilic attack of a C-3 hydroxyl group in the nascent polyketide precursor onto the C-1 carbonyl.

Key words: biosynthesis, polyketide, F-244, β-lactone, *Fusarium*.

Résumé : On a effectué des expériences d'incorporation biosynthétiques de précurseurs marqués au carbone-13, y compris des [1^{13}C]-, [2-^{13}C]- et [1,2-$^{13}C_2$]-acétates de sodium ainsi que de la [*méthyl*-^{13}C]méthionine, dans l'antibiotique F-244 (**1**) en effectuant des cultures du *Fusarium* sp. ATCC 20788. Après sa conversion en ester méthylique **2**, un analyse par RMN montre que le squelette carboné du produit **1** dérive de sept unités acétates intactes; les quatre autres unités proviennent de la méthionine. Le chemin réactionnel est donc semblable à celui rapporté pour la synthèse de **1** dans le *Scopulariopsis*. On a aussi examiné la biogenèse des atomes d'hydrogène du composé **1**. L'incorporation du [1-^{13}C, $^{18}O_2$]acétate de sodium fournit du composé **2** qui présente des déplacements isotopiques induits par le ^{18}O pour les C-1 et C-3. Le patron de marquage est en accord avec la formation d'un cycle β-lactone par une attaque nucléophile du groupe hydroxyle en C-3 du précurseur polycétide naissant sur le groupe carbonyle en C-1.

Mots clés : biosynthèse, polycétide, F-244, β-lactone, *Fusarium*.

[Traduit par la rédaction]

Introduction

The β-lactone antibiotic **1** (Fig. 1) was first obtained from *Cephalosporium* sp. ACC 1233 as 1233A (1), and later from *Fusarium* species as L-659,699 (2) and from *Scopulariopsis* species as F-244 (2*a*, 3). Interest in this compound stems from its potent inhibitory effect on the growth of microorganisms (3*a*) as well as plants (4); both in vitro (2, 3*b*, 5) and in vivo (2*b*, 3*b*, 5*b*, 6) experiments have shown the compound to be a specific and potent inhibitor of 3-hydroxy-3-methylglutaryl-CoA synthase. A variety of analogues have been investigated (7), and several elegant syntheses have been reported (8).

Recently, Omura and co-workers investigated the biosynthesis of 1233A in *Scopulariopsis* sp. F-244 (9). The results of incorporation experiments with sodium [1-^{13}C]-, [2-^{13}C]-, and [1,2-$^{13}C_2$]-acetate as well as [*methyl*-^{13}C]methionine showed

Fig. 1. Structure (1) and biosynthetic labelling pattern (9) for F-244 (**1**).

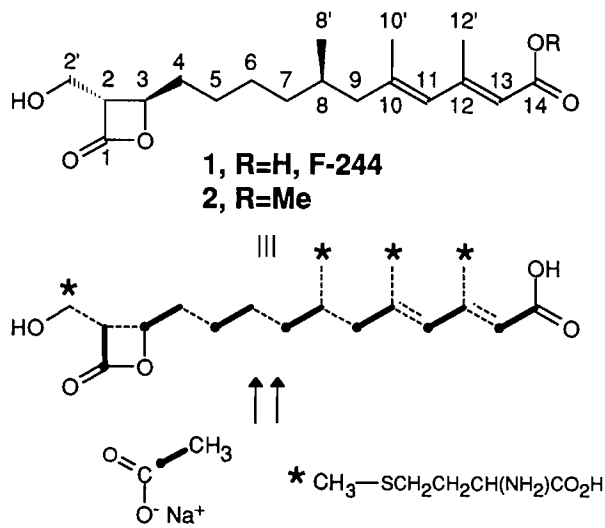

that **1** is a typical heptaketide derived from "head-to-tail" coupling of seven acetate units; the remaining four carbons were efficiently labelled by methionine (Fig. 1). Our interest in

Received August 10, 1994.

E. Saepudin and P. Harrison.[1] Department of Chemistry, McMaster University, 1280 Main Street West, Hamilton, ON L8S 4M1, Canada.

[1] Author to whom correspondence may be addressed: Telephone: (905) 525-9140, ext. 27290. FAX: (905) 522-2509. E-mail: PHARRISO@MCMAIL.CIS.MCMASTER.CA

Can. J. Chem. Downloaded from www.nrcresearchpress.com by 65.111.164.53 on 09/08/12
For personal use only.

Table 1. Carbon-13 and proton chemical shifts for F-244 methyl ester (**2**), and isotopic incorporations.

			% Incorporation[a] from			$J(^{13}C–^{13}C)$
$\delta^{13}C$	$\delta^{1}H$	Assignment	[1-^{13}C]acetate	[2-^{13}C]acetate	[methyl-^{13}C]methionine	from [1,2-$^{13}C_2$]acetate (Hz)
167.5	—	14	[b]	3.2	[b]	76
117.0	5.69	13	1.4	[b]	[b]	76
154.5	—	12	[b]	2.6	[b]	53
129.5	5.73	11	1.4	[b]	[b]	53
141.1	—	10	[b]	3.2	[b]	42
48.9	2.08	9a	1.4	[b]	[b]	42
	1.85	9b				
30.9	1.66	8	[b]	4.1	[b]	35
36.6	1.34	7a	1.5	[b]	[b]	35
	1.13	7b				
26.6	1.41	6a	[b]	4.6	[b]	35
	1.34	6b				
25.2	1.42	5a	1.4	[b]	[b]	35
	1.42	5b				
34.0	1.92	4a	[b]	4.5	[b]	39
	1.78	4b				
74.9	4.59	3	1.4	[b]	[b]	39
58.6	3.41	2	[b]	4.5	[b]	41
169.7	—	1	1.2	[b]	[b]	41
19.6	2.23	12′	[b]	[b]	20	[c]
18.4	1.79	10′	[b]	[b]	25	[c]
19.4	0.84	8′	[b]	[b]	33	[c]
58.0	4.06	2′a	[b]	[b]	24	[c]
	3.88	2′b				
50.8[d]	3.70	OCH_3	0	0	0	[c]

[a]Incorporations expressed after subtraction of the peak height for unlabelled 2.
[b]All values are 0 ± 0.2.
[c]No coupling observed.
[d]Unlabelled internal standard.

Can. J. Chem. Downloaded from www.nrcresearchpress.com by 65.111.164.53 on 09/08/12
For personal use only.

polyketide biosynthesis (10) has prompted a study of the biosynthesis of F-244 in *Fusarium* species. Herein we report that there is a similar biosynthetic origin for the carbon atoms of **1** in both microorganisms. Further, we describe the results of labelling experiments designed to elucidate the origin of the hydrogen and oxygen atoms of F-244.

Results

Fusarium sp. ATCC 20788 was grown in a liquid culture medium that was a modification of that reported in the patent literature (11). Extraction and chromatography gave crude F-244, which was treated with diazomethane and further purified to give methyl ester **2** (1*b*). Extensive multidimensional NMR analysis of **2** afforded unambiguous assignments for all of the carbon atoms (Table 1). The results show that the chemical shifts for the carbon-13 resonances in **2** match closely the shifts in **1** that were reported by Omura and co-workers (9), as well as the results of Mori and co-workers (12), with the exception of the expected difference in chemical shift of C-14 due to methylation.

Addition of sodium [1-^{13}C]acetate (**3***a*) to the growing *Fusarium* cultures under the literature conditions (11) gave **2** with very low incorporations. After some experimentation, it was found that reduction of the corn content of the medium enabled incorporations of ca. 5% to be obtained, without diminishing the yield of F-244. The extent of labelling at each position was determined by comparing peak heights for the labelled and unlabelled **2**, after each peak height was standardized relative to the height of the signal from the ester methyl group. For **3***a*, label was only observed at C-1, C-3, C-5, C-7, C-9, C-11, and C-13, while sodium [2-^{13}C]acetate (**3***b*) gave **2**, which was labelled at the complementary positions C-2, C-4, C-6, C-8, C-10, C-12, and C-14 (Table 1). Incorporation of sodium [1,2-$^{13}C_2$]acetate (**3***c*) gave **2**, which exhibited all of the expected one-bond $^{13}C–^{13}C$ couplings, while addition of L-[*methyl*-^{13}C]methionine (**4***a*) to the cultures gave large incorporations at the remaining four carbon atoms, C-2′, C-8′, C-10′, and C-12′.

Incorporation experiments using sodium [1-^{13}C,$^{2}H_3$]acetate (**3***d*) gave **2** that was enriched with carbon-13 at each of the sites that had been labelled by **3***a*; however, none of the signals exhibited a β-deuterium isotope shift (10; for a detailed discussion of these aspects, see ref. 13), nor was any deuterium detected by ^{2}H NMR. In contrast, addition of [*methyl*-^{13}C,$^{2}H_3$]methionine (**4***b*) to the cultures gave F-244, the deuterium NMR spectrum of which exhibited three doublets corresponding in chemical shift to the three methyl groups of F-

Fig. 2. Expansions of signals due to (a) C-1; and (b) C-3 in the carbon-13 NMR spectrum of **2** derived from incorporation of sodium [1-^{13}C,$^{18}O_2$]acetate; the isotopically shifted signals are apparent.

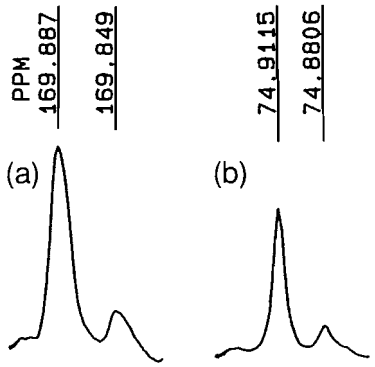

244, as well as signals at shifts equivalent to those for the two diastereotopic protons, H-2′α and H-2′β.

Addition of sodium [1-^{13}C,$^{18}O_2$]acetate (**3***e*) to cultures of the *Fusarium* species gave **2**; the ^{13}C NMR spectrum exhibited enrichments at all of the positions derived from C-1 of acetate. High-resolution carbon-13 NMR showed that, although some molecules of the sample were enriched at C-1 and C-3 with carbon-13 that did not carry ^{18}O substitution, other molecules exhibited isotopically shifted signals (10, 13, 14) induced by the presence of oxygen-18 at both these sites (Fig. 2). At C-1, a single isotopically shifted signal was observed; the magnitude of the shift (Δδ 0.037 ppm) is consistent with that expected for a C=O double bond (i.e., ^{18}O=^{13}C-^{16}O) (15). There was no apparent signal due to the presence of carbon-13 at C-1 attached to either oxygen-18 within the ring (i.e., ^{16}O=^{13}C-^{18}O), or to two oxygen-18 atoms (i.e., ^{18}O=^{13}C-^{18}O). At C-3, a single isotopically shifted signal was observed (Δδ 0.031 ppm). No detectable induced isotope shift was observed at either C-14 or C-2′.

Discussion

Our investigation of F-244 biosynthesis in *Fusarium* sp. ATCC 20788 first required that the origin of the carbon atoms be firmly established, since the results of Omura's study in *Scopulariopsis* (9) cannot be taken *de facto* to apply to the current organism. The results from the carbon-13 labelled acetates **3***a–c* clearly establish that F-244 is derived in *Fusarium* sp ATCC 20788 from "head-to-tail" coupling of seven intact acetate units in a sequence typical of the polyketide secondary metabolites (Fig. 1). Further, the arrangement of units is identical to that observed in *Scopulariopsis*, indicating strong similarities in the biosynthesis of **1** in the two organisms. The carbons of the methyl groups of F-244, as well as C-2′, derive from methionine in both organisms, rather than through incorporation of propionate into the growing polyketide chain. These results enable prediction of the di- and oligo-ketides that are expected to be nascent intermediates in the growth of the carbon chain on the polyketide synthase. Incorporation experiments with advanced intermediates corresponding to the growing chain are currently in progress.

With the biogenesis of the carbon atoms established, the biosynthetic origin of the hydrogen atoms of F-244 was next investigated. The fact that incorporation of carbon-13, but not deuterium, was observed when sodium [1-^{13}C,$^{2}H_3$]acetate (**3***d*)

Fig. 3. Possible mechanisms for in vivo lactone formation.

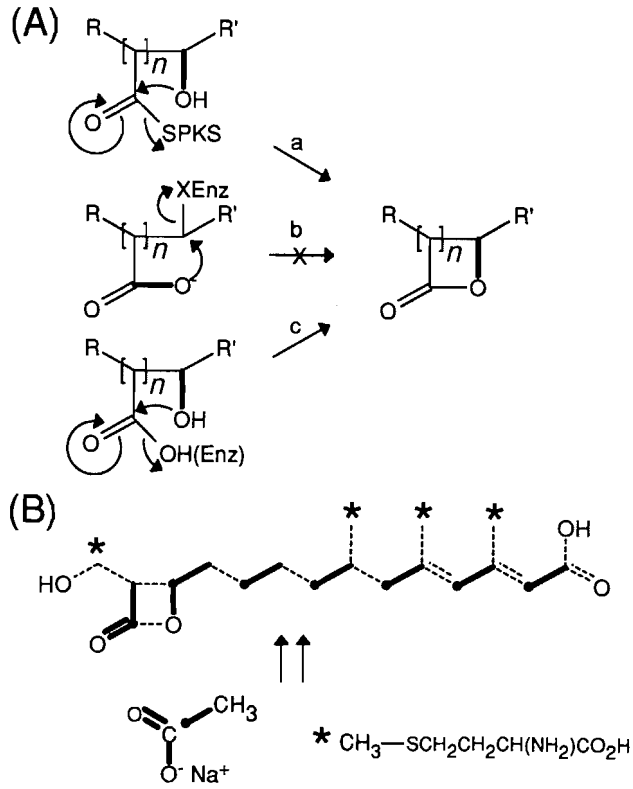

was administered to the cells strongly suggests that "washout" of deuterium occurred during the biosynthetic process, as is common in polyketide biosynthetic studies (13). Deuterium was retained from methionine, however, as expected; all of the deuterium at each site was coupled to carbon-13, demonstrating intact incorporation of the ^{13}C—^{2}H bonds. This observation is consistent with Omura's (9) description of incorporation of tritium from L-[^{3}H]methionine into F-244.

We next embarked on experiments to determine the biosynthetic source of the oxygen atoms of **1**, using the oxygen-18 induced isotope shift method developed by Vederas and Nakashima (13, 14), in order to address questions about the mechanism of formation of the β-lactone moiety. Although this technique has been used, inter alia, to demonstrate that a variety of five-membered or larger lactone rings are formed with retention of the alkyl carbon–oxygen bond (10, 13) (Fig. 3*A*, pathways a or c but not b), there are no reported applications to the biosynthesis of β-lactones. Due to the ring strain inherent in the latter, it was unclear whether ring formation could occur on the polyketide synthase (path a), or whether a separate enzyme was required to effect the lactonization in F-244.

The results of incorporation of **3***e* show partial exchange of oxygen-16 for oxygen-18 at C-1 and C-3 of F-244 during the biosynthesis, a process that is not uncommon in polyketide biosynthesis (13). However, the observation of a small but significant isotopically shifted signal at C-3 indicates that the C-3—O single bond remains intact throughout the biosynthetic process from acetate (Fig. 3*b*). The magnitude of the shift (0.031 ppm) is large compared to many C—O single bonds (15), perhaps as a result of the ring strain inherent in the β-lactone moiety. Similarly, the C-1=O double bond is

Can. J. Chem. Downloaded from www.nrcresearchpress.com by 65.111.164.53 on 09/08/12
For personal use only.

derived intact from acetate. Failure to observe isotope shifts at C-14 or C-2′ is consistent with the oxygen atoms at these sites being derived from oxygen gas in a late-stage oxidation, as would be predicted (10).

The results are consistent with formation of the β-lactone ring by attack of the hydroxyl group at C-3 of the nascent polyketide onto C-1 (Fig. 3*a*, path a or c), but not with nucleophilic attack by a C-1 carboxylate onto C-3 (path b). Perhaps the most likely pathway (a) involves the formation of the β-lactone ring by direct displacement of the acyl intermediate while still attached to the polyketide synthase (PKS), thereby releasing the cyclized product. In contrast to paths b and c, path a does not require a unique β-lactone cyclizing enzyme.

Conclusion

The biosynthesis of F-244 in *Fusarium* sp. ATCC 20788 proceeds by the normal polyketide pathway, with seven acetate units condensing in a "head-to-tail" fashion. A labelling experiment with sodium [1-^{13}C,$^{18}O_2$]acetate shows that the β-lactone ring is formed with retention of the C-3—O bond, suggesting nucleophilic attack of a hydroxyl group at C-3 of the putative precursor, probably still attached to the polyketide synthase, onto an activated carboxylic acid derivative at C-1. Further aspects of the biosynthetic pathway to **1** will be described in due course.

Experimental

General

Fusarium sp. ATCC 20788 was obtained from American Type Culture Collection. Corn meal and tomato paste were Primo brand. Water was from a Barnstead Nano-pure purification system. Isotopically labelled precursors were purchased from MSD Isotopes. Flash column chromatography was performed according to the method of Still et al. (16) on Merck Type 60 silica gel, 230–420 mesh. Carbon-13 NMR spectra were recorded on a Bruker AM-500 NMR spectrometer.

Growth of *Fusarium* sp. ATCC 20788

Cultures of *Fusarium* sp. ATCC 20788 were grown in petri dishes at 26°C for 5 days on potato dextrose agar (200 g potato, 20 g agar, and 20 g dextrose in 1 L water). The resulting spores were transferred in sterile water to liquid growth medium (0.5 g corn meal, 4 g tomato paste, 1 g oat flour, 1 g dextrose, and 100 mL water in a 500-mL Erlenmeyer flask), which had been sterilized at 121°C for 20 min. The flask was incubated in a rotary shaker – incubator at 28°C and 212 rpm for 3 days. Aliquots (3 mL) of the resulting culture were used to inoculate 24 500-mL Erlenmeyer flasks containing production medium, which was composed of corn meal (4 g), trace element solution (25 mL of 0.1 g/L $MgSO_4 \cdot 7H_2O$ plus 0.1 g/L sodium tartrate plus 0.01 g/L $FeSO_4 \cdot 7H_2O$ plus 0.01 g/L $ZnSO_4 \cdot 7H_2O$), and water (175 mL). The flasks were incubated in the rotary shaker – incubator at 25°C and 212 rpm for 10 days.

Addition of labelled precursors

Labelled precursors (total 1 g per 24 flasks) were added as sterilized solutions in water (25 mL) by injection into the production medium over the period from 3 to 9 days after inoculation.

Extraction of F-244 (1), and isolation of methyl ester 2

The cultures were centrifuged. The supernatant was saturated with NaCl, and extracted with CH_2Cl_2 (4 × 400 mL). The pellet was stirred with MeOH:EtOAc (5:95, 300-mL portions until clear) and the extracts combined with those from the supernatant. The extracts were concentrated on the rotary evaporator to give 3.5 g crude material. Flash chromatography (EtOAc:hexane:AcOH, 30–70:70–30:0.5, stepped by 10% increments) gave fractions containing F-244 (**1**), which were combined and concentrated. To the residue was added diazomethane (slight excess, precautions as normal for diazomethane); excess diazomethane was removed by purging with nitrogen, and the resulting solution concentrated. Flash column chromatography (EtOAc:hexane, 30–70:70–30, stepped by 10% increments) afforded fractions containing virtually pure **2**, which were combined. Repetition of the chromatographic separation gave pure **2** (50 mg).

Acknowledgments

This work was financially supported by the Natural Sciences and Engineering Research Council of Canada and by McMaster University.

References

1. (*a*) D.C. Aldridge, D. Giles, and W.B. Turner. J. Chem. Soc. D, 639 (1970); (*b*) J. Chem. Soc. C, 3888 (1971).
2. (*a*) S. Omura, H. Tomoda, H. Kumagai, M.D. Greenspan, J.B. Yudkovitz, J.S. Chen, A.W. Alberts, I. Martin, S. Mochales, R.L. Monaghan, J.C. Chabala, R.E. Schwartz, and A.A. Patchett. J. Antibiot. **40**, 1356 (1987); (*b*) M.D. Greenspan, J.B. Yudkovitz, C.Y.L. Lo, J.S. Chen, A.W. Alberts, V.M. Hunt, M.N. Chang, S.S. Yang, K.L. Thompson, Y.C.P. Chiang, J.C. Chabala, R.L. Monaghan, and R.L. Schwartz. Proc. Natl. Acad. Sci. U.S.A. **84**, 7488 (1987).
3. (*a*) H. Tomoda, H. Kumagai, Y. Takahashi, Y. Tanaka, Y. Iwai, and S. Omura. J. Antibiot. **41**, 247 (1988); (*b*) H. Tomoda, H. Kumagai, H. Tanaka, and S. Omura. Biochim. Biophys. Acta, **922**, 351 (1987).
4. J.M. Jacyno, H.G. Cutler, R.G. Roberts, and R.M. Waters. Agric. Biol. Chem. **55**, 3129 (1991).
5. (*a*) H. Tomoda, H. Kumagai, H. Tanaka, and S. Omura. J. Antibiot. **46**, 872 (1993); (*b*) R.J. Mayer, P. Louis-Flamberg, J.D. Elliott, M. Fisher, and J. Leber. Biochem. Biophys. Res. Commun. **169**, 610 (1990); (*c*) M.D. Greenspan, H.G. Bull, J.B. Yudkovitz, D.P. Hanf, and A.W. Alberts. Biochem. J. **289**, 889 (1993).
6. H. Nagashima, H. Kumagai, H. Tomoda, and S. Omura. Life Sci. **52**, 1595 (1993); H. Kumagai, H. Tomoda, and S. Omura. J. Antibiot. **43**, 397 (1990).
7. (*a*) T. Sunazuka, K. Tsuzuki, H. Kumagai, H. Tomoda, H. Tanaka, H. Nagashima, H. Hashizume, and S. Omura. J. Antibiot. **45**, 1139 (1992); (*b*) K.L. Thompson, M.N. Chang, Y.C.P. Chiang, S.S. Yang, J.C. Chabala, B.H. Arison, M.D. Greenspan, D.P. Hanf, and J. Yudkovitz. Tetrahedron Lett. **32**, 3337 (1991).
8. (*a*) S. Wattanasin, H.D. Do, N. Bhongle, and F.G. Kathawala. J. Org. Chem. **58**, 1610 (1993); (*b*) P.M. Wovkulich, K. Shankaran, J. Kiegiel, and M.R. Uskokovic. J.

Can. J. Chem. Downloaded from www.nrcresearchpress.com by 65.111.164.53 on 09/08/12
For personal use only.

Org. Chem. **58**, 832 (1993); (*c*) K. Mori and Y. Takahashi. Liebigs Ann. Chem. 1057 (1991); (*d*) Y.C.P. Chiang, S.S. Yang, J.V. Heck, J.C. Chabala, and M.N. Chang. J. Org. Chem. **54**, 5708 (1989).
9. H. Kumagai, H. Tomoda, and S. Omura. J. Antibiot. **45**, 563 (1992).
10. (*a*) R.B. Herbert. *In* The biosynthesis of secondary metabolites. 2nd ed. Chapman and Hall, New York. 1989; (*b*) J. Mann. *In* Secondary metabolism. 2nd ed. Clarendon Press, Oxford. 1987. Chap. 2; (*c*) D. O'Hagan. Nat. Prod. Rep. **10**, 593 (1993); (*d*) D. O'Hagan. Nat. Prod. Rep. **9**, 447 (1992); (*e*) J.A. Robinson. Philos. Trans. R. Soc. London, B: **332**, 107 (1991).
11. J.C. Chabala, M.N. Chang, D.W. Graham, S.S. Yang, Y.C.P. Chiang, and N.N. Girotra. Eur. Pat. Appl. no. 285 254 (1988); Chem. Abstr. **110**, 128659d (1989).
12. K. Koseki, Y. Takahashi, K. Shimazaki, T. Ebata, T. Chuman, and K. Mori. Biosci. Biotech. Biochem. **56**, 1728 (1992).
13. J.C. Vederas. Nat. Prod. Rep. **4**, 277 (1987).
14. J.C. Vederas and T.T. Nakashima. J. Chem. Soc. Chem. Commun. 183 (1980).
15. P.E. Hansen. Annu. Rep. NMR Spectrosc. **15**, 107 (1983).
16. W.C. Still, M. Kahn, and A. Mitra. J. Org. Chem. **43**, 2923 (1978).

Can. J. Chem. Downloaded from www.nrcresearchpress.com by 65.111.164.53 on 09/08/12
For personal use only.

Gold-acetylide chemistry: the structure of the complex $[Au_2(\mu\text{-dppm})(C{\equiv}C{-}CMe_3)_2]$

Nicholas C. Payne, Ravindranath Ramachandran, and Richard J. Puddephatt

Can. J. Chem. Downloaded from www.nrcresearchpress.com by 65.111.164.53 on 09/08/12
For personal use only.

Abstract: The complex $[Au_2(\mu\text{-dppm})(C{\equiv}Ct\text{-Bu})_2]$, **1**, dppm = $Ph_2PCH_2PPh_2$, is formed by reaction of [AuC≡C*t*-Bu] with dppm. Compound **1**, as an acetone solvate, crystallizes in the monoclinic space group $P2_1/c$ with cell dimensions $a = 14.047(1)$, $b = 16.124(1)$, $c = 17.140(3)$ Å, $\beta = 103.17(2)°$ and four formula units per cell. The crystal and molecular structures of this salt were solved by X-ray diffraction techniques using 2634 counter data with $I > 2\sigma(I)$. Refinement of 278 variables by full-matrix least squares converged at an agreement factor $R = 0.023$. Thermolysis of complex **1** in refluxing toluene led to intermolecular elimination of *t*-BuC≡CH, by combination of a *t*-BuC≡C ligand of one molecule of **1** with a proton from the CH_2P_2 group of a second, and formation of the stable tetragold(I) complex $[Au_4(\mu_3\text{-}Ph_2PCHPPh_2)(\mu\text{-dppm})(C{\equiv}Ct\text{-Bu})_3]$, **2**, which was characterized by its spectroscopic properties.

Key words: acetylide complexes, gold complexes, X-ray crystallography, nmr spectroscopy, bis(diphenylphosphino)methane.

Résumé : La réaction du [AuC≡C*t*Bu] avec le dppm (dppm = $Ph_2PCH_2PPh_2$) fournit le complexe $[Au_2(\mu\text{-dppm})(C{\equiv}Ct\text{Bu})_2]$, **1**. Les cristaux du composé **1**, sous la forme de solvate d'acétone, sont monocliniques, groupe d'espace $P2_1/c$, avec $a = 14{,}047(1)$, $b = 16{,}124(1)$ et $c = 17{,}140(3)$ Å, $\beta = 103{,}17(2)°$ et quatre unités de formule par motif. On a résolu les structures cristallines et moléculaires de ce sel par des techniques de diffraction des rayons X utilisant 2634 données avec $I > 2\sigma(I)$. L'affinement de 278 par la méthode des moindres carrés a conduit à une convergence avec $R = 0{,}023$. La thermolyse du complexe **1** dans le toluène au reflux conduit à une élimination intermoléculaire du *t*-BuC≡CH par la combinaison d'un coordinat *t*-BuC≡C d'une molécule de **1** avec un proton provenant d'un groupe CH_2P_2 d'une seconde et la formation d'un complexe stable tétraor(I) $[Au_4(\mu_3\text{-}Ph_2PCHPPH_2)(\mu\text{-dppm})(C{=}Ct\text{Bu})_3]$, **2**, qui a été caractérisé par ses propriétés spectroscopies.

Mots clés : complexes d'acétylures, complexe d'or, cristallographie par rayons X, spectroscopie rmn, bis(diphénylphosphino)méthane.

[Traduit par la rédaction]

Introduction

The ligands $R_2PCH_2PR_2$ (R = alkyl, aryl, alkoxy, or aryloxy) are often used as bridging ligands and have played an important role in the development of the organometallic chemistry of bimetallic and cluster complexes (1). These ligands can be deprotonated to give the $[R_2PCHPR_2]^-$ or even the $[R_2PCPR_2]^{-2}$ ligand, which can then coordinate to metal centres in several different ways. Thus the $[R_2PCHPR_2]^{-2}$ ligand can act as a monodentate C-donor, **A** (2), a bidentate chelate P, P donor, **B** (3–5); a bidentate bridging ligand with P,P or P,C donors, **C** or **D** (6–8), or as a tridentate P,C,P donor, **E** (9, 10), **F** (11), or **G** (12). The deprotonation of the methylene group of the diphosphine usually occurs in the presence of a base (7) or on pyrolysis of a cluster complex (9, 10). In other cases, the groups attached to the metal centre are basic enough to deprotonate the diphosphine and an example from gold chemistry is shown in reaction [1] (10–14).

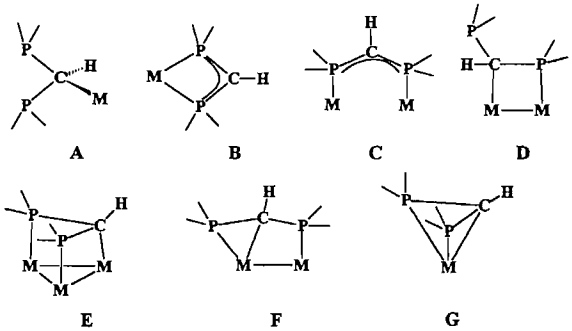

It was shown earlier that the ligand $(MeO)_2\text{-}PCH_2P(OMe)_2$ is easily deprotonated in its complexes with AuC≡C*t*-Bu by intra- or intermolecular elimination of *t*-BuC≡CH, ultimately giving, on decomposition in chloroform solution, the remarkable cage complex $[Au_8Cl_2\{\mu_3\text{-}(MeO)_2PCHP(OMe)_2\}_2\{\mu\text{-}(MeO)_2PCP(OMe)_2\}_2]$ (15). It

Received August 23, 1994.

N.C. Payne, R. Ramachandran, and R.J. Puddephatt. Department of Chemistry, University of Western Ontario, London, ON N6A 5B7, Canada.

Can. J. Chem. Downloaded from www.nrcresearchpress.com by 65.111.164.53 on 09/08/12
For personal use only.

[1] 2 $AuCl(CH_2PPh_3)$ + 2 dppm

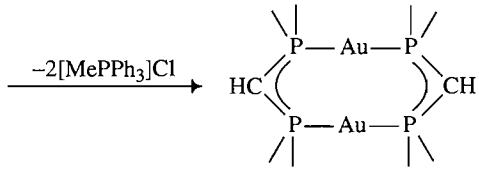

was concluded that the easy deprotonation of the dmopm ligand was aided by the electronegative substituents on phosphorus, which increase the acidity of the CH_2P_2 protons. As a result, the simple binuclear gold(I) acetylide derivative $[Au_2(C{\equiv}Ct\text{-}Bu)_2\{\mu\text{-}(MeO)_2PCH_2P(OMe)_2\}]$ was thermally unstable and could not be crystallized (15). In order to investigate further the nature of binuclear alkynylgold(I) complexes and to study the primary steps in the proposed alkyne elimination reactions, it was decided to study the analogous reactions with $Ph_2PCH_2PPh_2$ (dppm) in place of the $(MeO)_2PCH_2P(OMe)_2$ (dmopm) ligand. It was reasoned that the less electronegative phenyl substituents on the dppm ligand would lead to lower acidity of the methylene protons and hence slower alkyne elimination. The results of this study are reported below.

Experimental

Synthesis of $[Au_2(\mu\text{-dppm})_2(C{\equiv}Ct\text{-}Bu)_2]$, 1

To a suspension of [AuC≡C*t*-Bu] (16) (0.650 g, 2.33 mmol) in acetone (10 mL) was added a solution of dppm (0.453 g, 1.18 mmol) in acetone (10 mL). The yellow suspension dissolved, giving a reddish-yellow solution. After 1 h stirring, the solution was concentrated and layered with *n*-pentane. After 3 h a white crystalline solid precipitated, which was filtered, washed with cold acetone and dried under vacuum. Yield: 77%. Anal. calcd. for $C_{37}H_{40}Au_2P_2$: C 47.2, H 4.3; found: C 47.0, H 4.6. ^{1}H nmr ($CDCl_3$): δ = 2.09 [s, 18H, *t*-Bu]; 4.35 [t, ^2J(PH) = 10 Hz, 2H, P_2CH_2]; 8.0–8.6 [m, 20H, Ph]. ^{31}P nmr ($CDCl_3$) δ = 26.7 (s, dppm). Solvated single crystals of a quality suitable for diffraction experiments were grown by diffusing pentane into an acetone solution at 5°C.

Synthesis of $[Au_4(\mu_3\text{-}Ph_2PCHPPh_2)(\mu\text{-dppm})(C{\equiv}Ct\text{-}Bu)_3]$, 2

A solution of $[Au_2(\mu\text{-dppm})(C{\equiv}Ct\text{-}Bu)_2]$, **1**, (0.100 g, 0.11 mmol) in toluene (10 mL) was heated under reflux under an atmosphere of N_2 for 24 h. The initially colourless solution turned yellow. The solvent was removed under vacuum and the yellow residue was dissolved in acetone and layered with pentane. The pale yellow crystals of the product which separated were filtered, washed with pentane, and dried under vacuum. Yield: 55%. Anal. calcd. for $C_{68}H_{70}Au_4P_4$: C 45.4, 3.9; found: C 45.7, H 4.0. ^{1}H nmr ($CDCl_3$): δ = 1.22, 1.26, 1.41 [s, each 9H, *t*-Bu]; 3.30 [t, 2H, $^2J(PH^a)$ = 11 Hz, P_2CH^a]; 4.48 [dt, 1H, $^2J(P^cH^b)$ = 12.5 Hz, $^2J(P^bH^b)$ = 7 Hz, P_2CH^bAu]; 6.75–8.60 [m, 40H, Ph]. ^{31}P nmr ($CDCl_3$): δ = 28.9 [d, $^2J(P^aP^b)$ = 73 Hz, 1P, P^a]; 32.9 [dt, $^2J(P^aP^b)$ = 73 Hz, $^3J(P^bP^c)$ = 15 Hz, 1P, P^b]; 31.2 [d, $^3J(P^bP^c)$ = 15 Hz, 2P, P^c].

X-ray crystallography

Crystals of $[Au_2(\mu\text{-dppm})\{C{\equiv}C{-}CMe_3\}_2].0.5(CH_3)_2CO$ are colourless, transparent prisms. Precession and Weissenberg photographs established the space group (17) and preliminary cell dimensions. The crystal density was measured by the neutral buoyancy method in a mixture of pentane and 1,2-dibromoethane. Data collection of two symmetry equivalents was carried out on an Enraf-Nonius CAD4F diffractometer (28) in ω–2θ scan mode at variable scan speeds within a maximum time per datum of 60 s. Background estimates were made at 25% scan extensions on each side. Standard reflections were monitored every 180 min of X-ray exposure time. Lorentz, polarization, and background corrections were applied using the Enraf-Nonius S.D.P. programs (19) running on a P.D.P. 11/23+ computer. A Gaussian absorption correction (20) was applied to the 7108 data, which were then averaged to yield 3 560 unique data for structure solution and refinement. *R* factors (on F^2) for averaging all data were 0.061 and 0.024 before and after the correction, respectively. Crystal and experimental data are summarized in Table 1.

The structure was solved from Patterson and difference Fourier syntheses, and preliminary refinement was by full-matrix least-squares techniques on *F* (19). In the final cycles, SHELXL93 was used (21). The Au, P, and non-ring C atoms were assigned anisotropic thermal parameters. The phenyl ring carbon atoms were restrained to C_2 geometry with C—C = 1.392 Å and allotted isotropic thermal parameters. All hydrogen atoms were located successfully by difference Fourier methods, placed in calculated positions (C—H = 0.95 Å), and included in the structure factor calculations. The acetone solvate was disordered over a centre of symmetry (Wyckoff b), but refined satisfactorily. A secondary extinction correction was applied to the data. An analysis of variance suggested that the weighting scheme was appropriate. Refinement on F^2 converged at agreement factors R_1 = 0.0427 and R_2 = 0.0632 for 278 variables and 3393 data.

Selected experimental details of the X-ray determination are given in Table 1. Final positional parameters are given in Table 2, while anisotropic thermal parameters, hydrogen atom parameters, and structure amplitudes are available as supplementary material.[1]

Results and discussion

Synthesis and spectroscopic characterization of $[Au_2(\mu\text{-dppm})(C{\equiv}Ct\text{-}Bu)_2]$, 1

Complex **1** was synthesized by reaction of [AuC≡C*t*-Bu], which is probably a tetramer, with the ligand dppm in a 2:1 molar ratio (reaction [2]).

[2] 2 AuC*Ct*-Bu + dppm

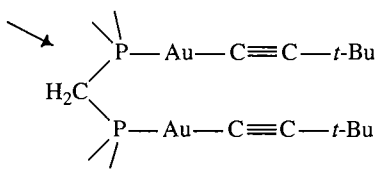

[1] Copies of supplementary material: anisotropic thermal parameters (Table S1), hydrogen atom parameters (Table S2), and bond distances and angles (Table S3) may be purchased from: The Depository of Unpublished Data, Document Delivery, CISTI, National Research Council Canada, Ottawa, Canada K1A 0S2.

Tables S2 and S3 have also been deposited with the Cambridge Crystallographic Data Centre and are available on request from The Director, Cambridge Crystallographic Data Centre, University Chemical Laboratory, 12 Union Road, Cambridge, CB2 1EZ, U.K.

Can. J. Chem. Downloaded from www.nrcresearchpress.com by 65.111.164.53 on 09/08/12
For personal use only.

Table 1. Crystal data and refinement details for $[Au_2dppm\{—C{\equiv}CC(CH_3)_3\}\text{-}0.5\{C_3H_6O\}]$, **1**.

Formula	$C_{38.5}H_{43}Au_2O_{0.50}P_2$
fw	969.60
Crystal system	Monoclinic
Space group	$P2_1/c$
T, K	296(2)
λ(Mo Kα), Å	0.71073
a, Å	14.047(1)
b, Å	16.124(1)
c, Å	17.140(3)
β, deg	103.17(2)
V, Å^3	3779.8(8)
Z	4
ρ(obsvd), Mg m^{-3}	1.724(2)
ρ(calcd), Mg m^{-3}	1.704
μ, mm^{-1}	7.864
Transmission factors	0.395 to 0.162
F(000), e	1864
Crystal size, mm	0.15 × 0.29 × 0.28
Crystal faces	6; {100} and {011}
θ range, deg	1.5–20.0
Index ranges	$-13 \le h \le 13$, $-15 \le k \le 15$, $0 \le l \le 14$
Number of reflections collected	7108
Number of independent reflections	3393
Number of data, [$I > 2\sigma(I)$]	2634
Number of restraints	164
Number of parameters	278
Goodness-of-fit on F^2	1.116
Final R_1, R_2[a]	0.0233, 0.0512
Final R_1, R_2 (all data)	0.0427, 0.0632
Extinction coefficient	0.00036(3)
Difference peak, hole, e Å^{-3}	0.489, −0.398

[a] $R_1 = \Sigma\{||F_o| - |F_c||\}/\Sigma|F_o|$; $R_2 = [\{\Sigma w(|F_o^2| - |F_c^2|)^2\}/\Sigma w(F_o^2)^2]^{0.5}$.

The product $[Au_2(\mu\text{-dppm})(C{\equiv}Ct\text{-}Bu)_2]$ is a colourless, air-stable solid, which was initially characterized by its ^1H and ^{31}P nmr spectra and by elemental analysis. The ^1H nmr spectrum of **1** contained a triplet resonance at δ = 4.35, with $^2J(PH)$ = 10 Hz, due to the methylene protons of the dppm ligand, and the ^{31}P nmr spectrum contained a singlet at δ = 26.7. These data suggest a symmetrical structure for **1**, which was confirmed by X-ray crystallography.

Crystal and molecular structure of complex 1

The crystal structure consists of well-separated complex and acetone solvent molecules. The closest dimer:solvent approach is H(28B)...H(34) at $(-x, 1 - y, -z)$ 2.82, and the shortest dimer:dimer distance is H(33)...H(18A) at $(x - 1, \frac{1}{2} - y, z - 1)$ 2.57 Å.

Selected interatomic distances and angles are given in Table 3; the remainder have been deposited as Table S3. Molecule **1** contains two gold(I) centres bridged by a dppm ligand. Each Au(I) centre is approximately linearly coordinated to a phosphorus atom and a *t*-butyl acetylide group. The molecule is U-shaped, with the two Au—C≡C*t*-Bu units aligned in close proximity with an intramolecular Au...Au distance of 3.331(1) Å. The isoelectronic complexes

Fig. 1. A view of the structure of complex **1**. Thermal ellipsoids are drawn at the 50% probability level.

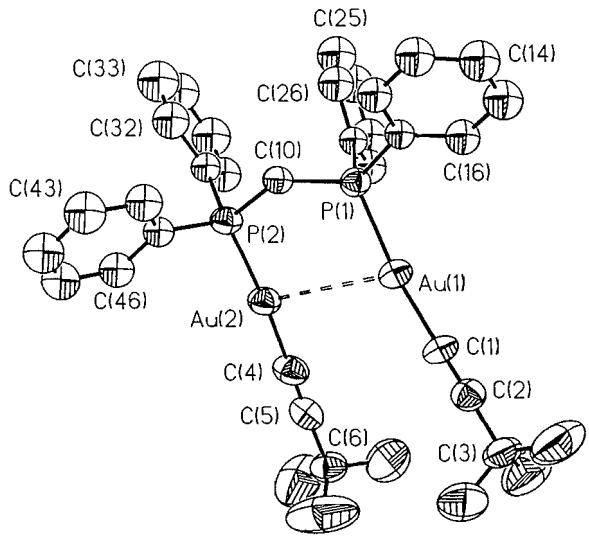

$PP(AuCl)_2$ (PP = bidentate phosphine ligand) possess a similar structure in which the Au—Cl "arms" are parallel. For

Can. J. Chem. Downloaded from www.nrcresearchpress.com by 65.111.164.53 on 09/08/12
For personal use only.

Table 2. Selected atomic positional ($\times 10^4$) and thermal ($\times 10^3$) parameters for **1**.

Atom[a]	x	y	z	U_{eq}[b](Å^2)
Au(1)	397(1)	1385(1)	927(1)	52(1)
Au(2)	825(1)	2480(1)	−606(1)	58(1)
P(1)	−1076(2)	1234(1)	64(1)	45(1)
P(2)	−433(2)	1822(1)	−1441(1)	49(1)
C(1)	1647(6)	1303(5)	1766(6)	53(2)
C(2)	2380(7)	1165(5)	2263(6)	58(3)
C(3)	3284(7)	965(7)	2848(6)	73(3)
C(7)	3112(9)	253(8)	3356(8)	130(5)
C(8)	3581(10)	1704(8)	3415(8)	133(5)
C(9)	4082(9)	790(12)	2449(9)	188(9)
C(4)	1966(7)	3062(6)	74(6)	67(3)
C(5)	2698(7)	3339(6)	485(6)	62(3)
C(6)	3610(7)	3638(6)	1030(7)	67(3)
C(17)	3875(11)	4469(9)	756(8)	163(7)
C(18)	4423(10)	3046(10)	1033(11)	187(8)
C(19)	3466(9)	3739(9)	1863(8)	132(5)
C(10)	−998(6)	994(5)	−965(4)	43(2)
C(11)	−1711(5)	357(4)	369(4)	42(2)
C(12)	−2158(6)	−259(5)	−142(5)	56(2)
C(13)	−2607(6)	−927(5)	143(5)	67(3)
C(14)	−2590(7)	−975(6)	937(5)	76(3)
C(15)	−2173(7)	−366(6)	1454(6)	74(3)
C(16)	−1701(6)	295(5)	1174(5)	60(3)
C(21)	−1946(5)	2075(5)	−13(5)	44(2)
C(22)	−1667(7)	2807(5)	380(5)	68(3)
C(23)	−2339(7)	3456(6)	345(6)	86(3)
C(24)	−3268(7)	3343(6)	−80(6)	88(3)
C(25)	−3560(7)	2629(6)	−490(6)	86(3)
C(26)	−2888(6)	1985(5)	−450(5)	68(3)
C(31)	−1443(6)	2502(5)	−1882(5)	49(2)
C(32)	−2164(7)	2256(6)	−2523(5)	74(3)
C(33)	−2955(8)	2793(6)	−2839(6)	98(4)
C(34)	−2979(7)	3549(6)	−2504(6)	92(3)
C(35)	−2267(7)	3810(6)	−1886(6)	93(4)
C(36)	−1485(7)	3286(5)	−1582(5)	70(3)
C(41)	−113(6)	1326(5)	−2291(5)	47(2)
C(42)	−446(6)	561(5)	−2581(5)	65(3)
C(43)	−186(7)	223(6)	−3256(6)	81(3)
C(44)	404(7)	678(6)	−3632(6)	78(3)
C(45)	745(7)	1432(6)	−3349(6)	74(3)
C(46)	485(6)	1769(5)	−2685(5)	64(3)
O	5122(18)	4466(19)	3985(15)	182(11)
C(27)	5064(18)	4793(22)	4602(19)	105(9)
C(28)	4692(10)	5640(9)	4597(10)	153(6)

[a]Carbon atoms in phenyl residues are numbered C(*rp*), where *p* is the position, ranging from 1 to 6, and *r* is the residue number.

[b]$U_{eq} = \frac{1}{3}\Sigma_i\Sigma_j U_{ij} a_i^* a_j^* \boldsymbol{a}_i \cdot \boldsymbol{a}_j$.

the complex where PP = $(Ph_2P)_2CH_2$, which possesses crystallographic 2-fold symmetry, Au...Au is 3.351 Å and for PP = *cis*-$Ph_2PCHCHPPh_2$ it is 3.05 Å (22, 23). The *cis*-geometry observed leads to some steric repulsion between the *t*-BuC≡C— groups in that the angles P(1)—Au(1)—C(1) = 169.0(3)° and P(2)—Au(2)—C(7) = 176.6(3)° are distorted from the ideal value of 180° (24). Short Au..Au contacts in otherwise linear gold(I) complexes are common and, although longer than conventional bonds, are believed to result from a weak relativistic bonding force (22–30). The methylene carbon atom of the diphosphine ligand is situated above the $Au_2P_2C_2$ plane. Two of the four phenyl rings of, the dppm ligand lie perpendicular to, and two in the plane of the dimer, Fig. 1. Phenyl ring 2 (i.e., atoms C(21) to C(26) inclusive) is situated roughly parallel to, and about 3.5 Å from phenyl ring 3. The angles at the acetylenic carbon atoms C(1), C(2), C(4), and C(5) range from 173.1(8)° to 177.5(10)° as expected. The Au—C distances are 2.005(9) and 1.990(10) Å, values which are slightly longer than those seen in other complexes containing Au—C(acetylenic) bonds (24) (1.935(19) Å in [C_3H_7-NH_2Au—C≡CPh] (25) and 1.993 Å in [Ph_3PAu—C≡C-(C_6F_5)] (26)). The Au—P distances are indistinguishable with a mean of 2.267(2) Å which is normal for gold–phosphine complexes (16, 24).

Synthesis and characterization of [$Au_4(\mu_3$-$Ph_2PCHPPh_2)$-(μ-dppm)(C≡C*t*-Bu)$_3$], 2

When a solution of **1** in toluene was heated under reflux, a yellow solution was obtained, from which the pale yellow product [$Au_4(\mu_3$-$Ph_2PCHPPh_2)$(μ-dppm)(C≡C*t*-Bu)$_3$], **2**, was precipitated by adding *n*-pentane (reaction [3]).

[3] $2[Au_2(\mu\text{-dppm})(CCt\text{-Bu})_2]$

$$\xrightarrow{-t\text{-BuCCH}} [Au_4(\mu\text{-dppm})(\mu_3\text{-}Ph_2PCHPPh_2)(CCt\text{-Bu})_3]$$

Single crystals of the product **2** suitable for an X-ray structure determination could not be obtained but the structure of **2** could be determined with confidence by elemental analysis, and from the informative ^{1}H and ^{31}P nmr spectra. The nmr labelling scheme is shown in structure **2**.

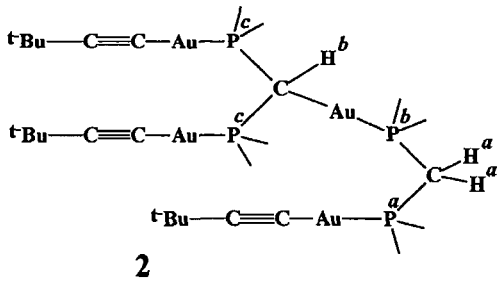

2

The ^{31}P nmr spectrum of **2** contained three resonances, all in the region expected for bridging dppm-type ligands (Fig. 2). The signal due to P^a appeared as a doublet centered at δ = 28.9 with $^2J(P^aP^b)$ = 73 Hz. The resonance due to P^b (δ = 32.9) appeared as a doublet of triplets due to coupling to both P^a [$^2J(P^aP^b)$ = 73 Hz] and the two equivalent phosphorus atoms, P^c [$^3J(P^bP^c)$ = 15 Hz]. The signal due to P^c (δ = 32.2) appeared as a doublet with $^3J(P^bP^c)$ = 15 Hz and this peak was twice as intense as those due to P^a and P^b. The ^{1}H nmr spectrum of **2** contained a triplet resonance at δ = 3.30, with ^2J(PH) = 11 Hz, for the P_2CH^a2 protons of the dppm ligand and a resonance at δ = 4.48 due to the P_2CH^b proton of the $Ph_2PCHPPh_2$ ligand. The latter resonance appeared as a doublet of triplets due to the couplings $^3J(P^bH^b)$ = 7 Hz and

Can. J. Chem. Downloaded from www.nrcresearchpress.com by 65.111.164.53 on 09/08/12
For personal use only.

Table 3. Selected bond lengths (Å) and angles (deg) for **1**.[a]

Atoms	Distance	Atoms	Distance
Au(1)—C(1)	2.005(9)	Au(1)—P(1)	2.266(2)
Au(1)—Au(2)	3.3307(9)	Au(2)—C(4)	1.990(10)
Au(2)—P(2)	2.268(2)	P(1)—C(21)	1.810(8)
P(1)—C(11)	1.813(7)	P(1)—C(10)	1.833(8)
P(2)—C(41)	1.807(8)	P(2)—C(31)	1.816(8)
P(2)—C(10)	1.836(8)	C(1)—C(2)	1.197(11)
C(2)—C(3)	1.464(13)	C(3)—C(9)	1.47(2)
C(3)—C(7)	1.493(14)	C(3)—C(8)	1.53(2)
C(4)—C(5)	1.192(12)	C(5)—C(6)	1.483(14)
C(6)—C(18)	1.488(14)	C(6)—C(19)	1.50(2)
C(6)—C(17)	1.495(14)	O—C(27)	1.20(3)
C(27)—C(28)	1.46(3)	C(27)—C(28) #1	1.51(3)

Atoms	Angle	Atoms	Angle
C(1)—Au(1)—P(1)	169.0(3)	C(4)—Au(2)—P(2)	176.6(3)
C(21)—P(1)—C(11)	103.7(3)	C(21)—P(1)—C(10)	106.0(4)
C(11)—P(1)—C(10)	104.7(3)	C(21)—P(1)—Au(1)	117.9(3)
C(11)—P(1)—Au(1)	109.3(3)	C(10)—P(1)—Au(1)	113.9(3)
C(41)—P(2)—C(31)	104.2(4)	C(41)—P(2)—C(10)	104.4(4)
C(31)—P(2)—C(10)	104.4(4)	C(41)—P(2)—Au(2)	114.5(3)
C(31)—P(2)—Au(2)	113.7(3)	C(10)—P(2)—Au(2)	114.3(3)
C(2)—C(1)—Au(1)	173.1(8)	C(1)—C(2)—C(3)	177.5(10)
C(2)—C(3)—C(9)	111.0(9)	C(2)—C(3)—C(7)	109.8(8)
C(9)—C(3)—C(7)	111.5(11)	C(2)—C(3)—C(8)	109.3(9)
C(9)—C(3)—C(8)	108.5(11)	C(7)—C(3)—C(8)	106.6(10)
C(5)—C(4)—Au(2)	173.5(9)	C(4)—C(5)—C(6)	176.5(11)
C(5)—C(6)—C(18)	110.2(9)	C(5)—C(6)—C(19)	110.6(9)
C(18)—C(6)—C(19)	109.7(11)	C(5)—C(6)—C(17)	109.6(9)
C(18)—C(6)—C(17)	109.2(11)	C(19)—C(6)—C(17)	107.5(10)
P(1)—C(10)—P(2)	113.6(4)	O—C(27)—C(28)	120(3)
O—C(27)—C(28) #1	124(3)	C(28)—C(27)—C(28) #1	116(3)

[a]Symmetry transformations used to generate equivalent atoms: #1 $-x + 1, -y + 1, -z + 1$.

$^2J(P^cP^b)$ = 15 Hz, respectively. Three well-resolved singlet resonances of equal intensity due to the three non-equivalent *t*-BuC≡C groups appeared at δ = 1.22, 1.26, and 1.44. Structure **2** should give two such resonances in a 2:1 ratio, and the resonances at δ = 1.22 and 1.26 may represent the "equivalent" *t*-Bu groups. Thus, the ^1H and ^{31}P nmr spectral data and analytical data together support the proposed structure **2**.

Complex **2** is a novel tetranuclear organogold(I) complex. Each gold(I) centre has the usual linear stereochemistry and each has AuPC coordination. Three of the gold(I) atoms form their Au—C bonds with alkynyl ligands while the fourth binds to the methine carbon of the $Ph_2PCHPPh_2$ ligand. It follows that the formation of **2** from two molar equivalents of **1** occurs by intermolecular elimination of *t*-BuC≡CH. This is likely to be analogous to the first step in the more extensive alkyne elimination reactions leading to formation of the cage complex $[Au_8Cl_2\{\mu_3\text{-}(MeO)_2PCHP(OMe)_2\}_2\{\mu_4\text{-}(MeO)_2PCP(OMe)_2\}_2]$ from $[Au_2(C{\equiv}Ct\text{-}Bu)_2\{\mu\text{-}(MeO)_2PCH_2P(OMe)_2\}]$ (15).

Conclusions

The formation of the U-shaped complex $[Au_2(\mu\text{-}dppm)(C{\equiv}Ct\text{-}Bu)_2]$, **1**, is a simple reaction but the structure strongly suggests the presence of a weak intramolecular Au..Au bond. Thus the structure contains a relatively short Au..Au distance and the "eclipsed" conformation clearly leads to steric interactions between the *t*-butyl substituents. It is interesting that the analogous reaction of [AuC≡CPh] with dppm does not yield the expected complex $[Au_2(\mu\text{-}dppm)(C{\equiv}CPh)_2]$, analogous to **1**, but instead gives the ionic $[Au_3(\mu\text{-}dppm)_2(CCPh)_2][Au(C{\equiv}CPh)_2]$, which also contains short Au..Au distances (27) while the ligand $i\text{-}Pr_2PC_6H_4\text{-}C_6H_4Pi\text{-}Pr_2$ does react with [AuC≡CPh] to give the simple complex $[Au_2(\mu\text{-}i\text{-}Pr_2PC_6H_4C_6H_4Pi\text{-}Pr_2)(C{\equiv}CPh)_2]$ (28). Clearly the preferred product depends on both the nature of the bidentate ligand and the group R in the precursor [AuC≡CR].

The conditions required for formation of **2** from **1** indicate that replacement of the more electronegative substituents R = MeO by less electronegative substituents R = Ph in the ligands $R_2PCH_2PR_2$ does indeed lead to reduced acidity of the P_2CH_2 protons in the alkynylgold(I) complexes. Firstly, the complex $[Au_2(C{\equiv}Ct\text{-}Bu)_2\{\mu\text{-}R_2PCH_2PR_2\}]$ is much more stable towards elimination of *t*-BuC≡CH when R = Ph than when R = MeO, and so complex **1** is sufficiently stable to permit the

Fig. 2. The ^{31}P nmr spectrum (121.5 MHz) of complex **2**.

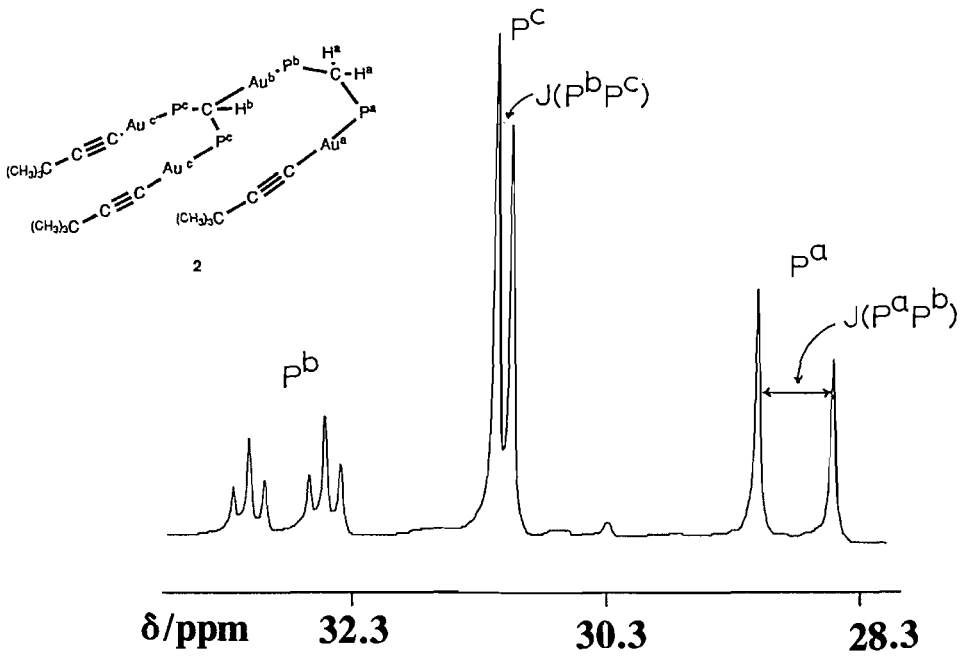

2

easy growth of single crystals for X-ray structure determination. Secondly, the alkyne elimination requires forcing conditions when R = Ph and, even in refluxing toluene, only one *t*-BuC≡CH elimination step occurs whereas, when R = MeO, further eliminations occur (15).

Acknowledgement

We thank the Natural Sciences and Engineering Research Council of Canada for financial support.

1. B. Chaudret, B. Delavaux, and R. Poilblanc. Coord. Chem. Rev. **86**, 191 (1988).
2. R.J. Puddephatt. Chem. Soc. Rev. **99** (1983).
3. J. Browning, G.W. Bushnell, and K.R. Dixon. J. Organomet. Chem. **198**, C11 (1980).
4. H. Schmidbaur and J.R. Mandl. Angew. Chem. Int. Ed. Engl. **16**, 640 (1977); J.M. Basset, J.R. Mandl, and H. Schmidbaur. Chem. Ber. **113**, 1145 (1980).
5. M. Gomez, G. Muller, J. Sales, and X. Solans. J. Chem. Soc. Dalton Trans. 221 (1993); J.J.J. Li and P.R. Sharp. Inorg. Chem. **33**, 183 (1994).
6. H.H. Karsch. Chem. Ber. **117**, 783 (1984).
7. M.P. Brown, A. Yavari, Lj. Manojlovic-Muir, and K.W. Muir. J. Organomet. Chem. **256**, C19 (1983).
8. C.E. Briant, K.P. Hall, and D.P.P. Mingos. J. Organomet. Chem. **229**, C5 (1982).
9. Lj. Manojlovic-Muir, D.A. Brandes, and R.J. Puddephatt. J. Organomet. Chem. **332**, 201 (1987).
10. S.R. Hodge, B.F.G. Johnson, J. Lewis, and P.R. Raithby. J. Chem. Soc. Dalton Trans. 931 (1987); R. Uson, A. Laguna, M. Laguna, M.C. Gimeno, P.G. Jones, C. Fittschen, and G.M. Sheldrick. J. Chem. Soc. Chem. Commun. 509 (1986); E.J. Fernandez, M.C. Gimeno, P.G. Jones, A. Laguna, M. Laguna, and J.M.L. de Luzuriaga. J. Chem. Soc. Dalton Trans. 3365 (1992).
11. G.M. Dawkins, M. Green, J.C. Jeffrey, C. Sambale, and F.G.A. Stone. J. Chem. Soc. Dalton Trans. 499 (1983).
12. S.K. Hao, J.I. Song, H. Aghabozorg, and S. Gambarotta. J. Chem. Soc. Chem. Commun. 157 (1994).
13. A. Camus, N. Marisch, G. Nardin, and L. Randaccio. J. Organomet. Chem. **60**, C39 (1973).
14. E.M. Meyer, S. Gambarotta, C. Floriani, A.C. Villa, and C. Guastini. Ortganometallics, **8**, 1067 (1989).
15. N.C. Payne, R. Ramachandran, I. Treurnicht, and R.J. Puddephatt. Organometallics, **9**, 880 (1990).
16. N.C. Payne, R.J. Puddephatt, R. Ramachandran, and I. Treurnicht. Can. J. Chem. **66**, 3176 (1988).
17. International tables for X-ray crystallography. (*a*) Volume A. D. Reidel Publishing Co., Boston. 1983; (*b*) Volume IV. Kynoch Press, Birmingham, England, 1974.
18. Enraf-Nonius CAD4F Users Manual, Ver. 5; Enraf-Nonius: Delft, The Netherlands. 1982.
19. Enraf-Nonius structure determination package. SDP-PLUS, Ver. 3.0. 1985.
20. P. Coppens et al. Acta Crystallogr. **18**, 1035 (1965).
21. SHELXL-93. G.M. Sheldrick. J. Appl. Crystallogr. In press.
22. H. Schmidbaur, A. Wohlleben, F. Wagner, O. Orama, and G. Huttner. Chem. Ber. **110**, 1748 (1977).
23. P.G. Jones. Acta Crystallogr. **B36**, 2775 (1980).
24. P.G. Jones. Gold Bull. **14**, 102 (1981); **14**, 159 (1981).
25. P.W.R. Corfield and H.M.M. Shearer. Acta Crystallogr. **23**, 156 (1967).
26. M.I. Bruce, E. Horn, J.G. Matisons, and M.R. Shaw. Aust. J. Chem. **37**, 1163 (1984).
27. C.-M. Che, H.-K. Yip, W.-C. Lo, and S.-M. Peng. Polyhedron, **13**, 887 (1994).
28. G. Jia, R.J. Puddephatt, J.D. Scott, and J.J. Vittal. Organometallics, **12**, 3305 (1993).
29. K. Angermaier, E. Zeller, and H. Schmidbaur. J. Organomet. Chem. **472**, 371 (1994).
30. R.J. Puddephatt. Comprehensive coordination chemistry. Vol. 5. *Edited by* G. Wilkinson. Pergamon Press, Oxford. 1987. p. 899.

Can. J. Chem. Downloaded from www.nrcresearchpress.com by 65.111.164.53 on 09/08/12
For personal use only.

Complexation of glucose by α- and β-cyclodextrins

Warren Hirsch, Tamas Muller, Richard Pizer, and P.J. Ricatto

Abstract: The concentration of glucose in aqueous solutions was monitored, using a blood glucose meter, as small weighed cyclodextrin portions were added. Equilibrium constants for the formation of inclusion complexes were calculated. A binding constant determined by this method has been verified by a technique involving competition of the guest with methyl orange indicator dye. ΔH^0 values for the reactions were estimated using calorimetry. These values along with ΔG^0 provided estimates of the standard entropies. The values calculated compare favorably with those from a previously determined empirical equation. The possibility of hydrogen bond formation is suggested by the large negative enthalpies as well as by molecular mechanics calculations.

Key words: α-, β-cyclodextrin, glucose, binding constants.

Résumé : Utilisant un glucomètre pour le sang, on a mesuré la concentration du glucose dans des solutions aqueuses alors qu'on y ajoutait des portions mesurées de cyclodextrine. On a calculé les constantes d'équilibre pour la formation de complexes d'inclusion. Faisant appel à une technique impliquant une compétition de l'hôte pour l'indicateur coloré méthylorange, on a vérifié une constante de fixation déterminée par cette méthode. On a évalué les ΔH^0 des ces réactions en utilisant la calorimétrie. Ces valeurs utilisées de concert avec des ΔG^0 ont fourni des évaluations des entropies standard. Les valeurs calculées se comparent avantageusement avec celles obtenues sur la base d'une équation empirique déterminée antérieurement. La possibilité de formation de liaison hydrogène est suggérée par les fortes enthalpies négatives ainsi que par des calculs de mécanique moléculaire.

Mots clés : α-, β-cyclodextrine, glucose, constantes de fixation.

[Traduit par la rédaction]

Introduction

Cyclohexaamylose and cycloheptaamylose, also known as α- and β-cyclodextrin, respectively, have been the subject of much intensive research (1, 2). The above cyclodextrins are structured roughly in "doughnut" shapes that are composed of six or seven glucose units. Seen from the side, the molecules are probably better described as "lampshade" shaped since the top and bottom openings are unequal. An important reason for the interest in cyclodextrins is their ability to form inclusion complexes with molecules and anions in aqueous solution (1–4). These complexes serve as a model for the study of enzymes (5), and are also being proposed for increased drug bioavailability (6) and for the removal of harmful substances from the body (7).

The relatively large interior of cyclodextrins allows suitably sized molecules or anions to get trapped within the cavity, with conformational changes perhaps aiding the process (3, 4, 8). Possible binding forces within these inclusion complexes may involve hydrophobic, van der Waals, hydrogen bonding, or dipole interactions (1, 2, 9).

Received July 21, 1994.

W. Hirsch,[1] T. Muller, R. Pizer, and P.J. Ricatto. Department of Chemistry, Brooklyn College of the City University of New York, Brooklyn, NY 11210, U.S.A.

[1] Author to whom correspondence may be addressed. Telephone: (718) 951-5743.

In the present work the complexation of the simple sugar, D-glucose, by α- and β-cyclodextrin has been studied in aqueous solutions. There is an apparent scarcity of data on the inclusion of this type of guest. Free glucose concentrations were monitored at different initial concentrations of cyclodextrin and glucose using a blood glucose meter that had been calibrated for aqueous solutions, and association constants were calculated.

Experimental section

To measure glucose concentrations in aqueous solutions, a Glucometer3 blood glucose meter and Glucofilm test strips were obtained. These are products of Miles Laboratories Inc. These items are ordinarily used to monitor glucose concentrations in whole blood. The test strip is a firm plastic strip with a reagent test pad for determining the concentration of glucose in whole blood. The test strips are specific to glucose and their reaction is based on the glucose oxidase method using dry reagent technology. The reaction utilizes the enzymes glucose oxidase and peroxidase. The glucose oxidase catalyzes the oxidation of glucose in blood in the presence of oxygen in the atmosphere, producing gluconic acid and hydrogen peroxide. In the presence of the peroxidase, the hydrogen peroxide oxidizes tetramethylbenzidine (in the reduced form), turning the test pad blue with an intensity proportional to the glucose concentration. The glucose meter then evaluates the color change using spectrophotometry, providing a digital output of glucose concentration in units of mg/dL. The test provides a quantita-

Can. J. Chem. Downloaded from www.nrcresearchpress.com by 65.111.164.53 on 09/08/12
For personal use only.

Table 1. Equilibrium constants and thermodynamic data for the formation of glucose complexes with α- and β-cyclodextrins

	K_{CyG} Glucose meter method (L mol^{-1})	K_{CyG} Indicator method (L mol^{-1})	ΔG^0 (Eq. [5]) (kcal mol^{-1})	ΔH^0 (Eq. [4]) (kcal mol^{-1})	ΔS^0 (Eq. [4]) (cal mol^{-1} K^{-1})	ΔH^0 Calorimetry (kcal mol^{-1})
α-Cy	450 ± 170	380 ± 40	−3.6 ± 0.2	−9.9 ± 0.7	−21 ± 2	−11 ± 4
β-Cy	420 ± 120	—	−3.6 ± 0.15	−9.8 ± 0.6	−21 ± 1	−15 ± 5

tive measurement of glucose in whole blood from 20 to 500 mg/dL (1.1–27.7 mmol/L).[2]

Anhydrous reagent grade D-glucose, obtained from Aldrich Inc., was used without further purification. Five standard glucose solutions were prepared. The concentrations used were in the range 1–5 mmol/L. It was determined that ambient temperature changes did not affect the glucose meter reading. The pH of the solutions was adjusted to 7.4 by addition of a few drops of dilute aqueous reagent grade NaOH in order to simulate blood pH. Although cyclodextrins are known to include OH^- ions, there is no significant reduction in free cyclodextrin concentrations at such low OH^- levels (9). To account for other differences between whole blood and the aqueous glucose solutions (ionic strength, viscosity, etc.) a linear calibration plot was prepared for the instrument. Using the calibration plot, the free glucose concentrations in unknown solutions could be determined from reading the glucose meter.

The α- and β-cyclodextrin, obtained from Aldrich Inc., were used as received. Information on the water content was obtained from the manufacturer in order to correct solution concentrations. As a control, it was determined that the Glucofilm test strips do not react with α- or β-cyclodextrin.

Cyclohexaamylose or cycloheptaamylose was added to standard glucose solutions in weighed portions as free glucose concentrations were monitored with the glucose meter. The free glucose concentrations became progressively lower with increasing additions. At least three strips were used for each cyclodextrin addition to ensure reproducibility. All measurements were performed at 25 ± 2°C. From the measured data, association constants were calculated for each set of initial concentrations of the reactants.

As a test of the preceding technique, an independent method of determining the association constants of α-cyclodextrin was employed. It is well known that α-cyclodextrin has the ability to complex and decolorize the red, acidic form of methyl orange (3). The addition of colorless competing guests to the decolorized solution will tend to release free indicator species, and hence to restore the color. In the present work, the competition at pH 1.5 was monitored by visible spectrophotometry at 515 nm with the temperature equal to 25 ± 2°C. The complete details of the method used, including the mathematical treatment of the data, may be found elsewhere (7). The association constant calculated for the α-cyclodextrin–glucose system obtained from the indicator competition method compared favorably with that obtained from the glucose meter method.

[2] Literature from Miles Inc.

Fig. 1. α-Cyclodextrin–glucose complex.

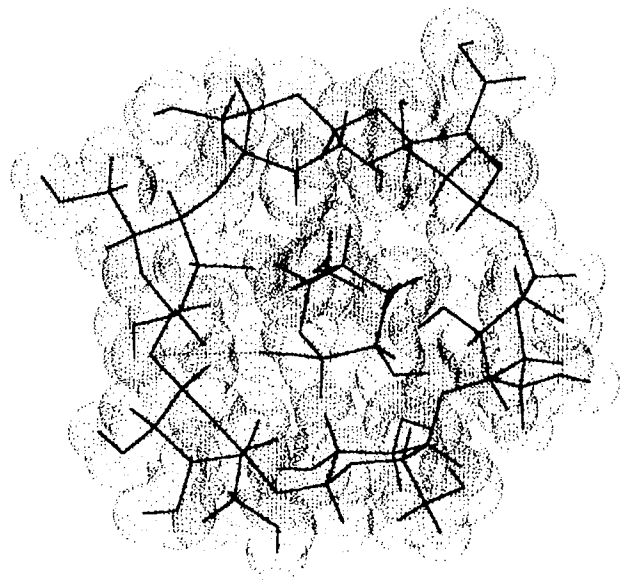

Benchtop calorimetry measurements involved the measurement of the solution enthalpies of glucose in water, cyclodextrin in water, and both of the preceding solids in water together using a calorimetric thermometer accurate to 0.01°C. In the last case, excess glucose was used to ensure complete reaction. At least three separate trials were performed in the determination of each enthalpy. The enthalpy of formation of the cyclodextrin–glucose complex could then be calculated.

Results

The inclusion of the glucose guest in the cyclodextrin cavity may be represented as follows:

[1] $Cy + G \rightleftarrows CyG$

with $K_{CyG} = [CyG]/[Cy]\,[G]$.

Also, we have the mass conservation expressions:

[2] $F_G = [G] + [CyG]$

[3] $F_{Cy} = [Cy] + [CyG]$

where F_G and F_{Cy} represent the total molar concentrations of guest and cyclodextrin species, respectively. Since F_G and F_{Cy} are known and [G] can be determined from the glucose

Can. J. Chem. Downloaded from www.nrcresearchpress.com by 65.111.164.53 on 09/08/12
For personal use only.

Fig. 2. β-Cyclodextrin–glucose complex.

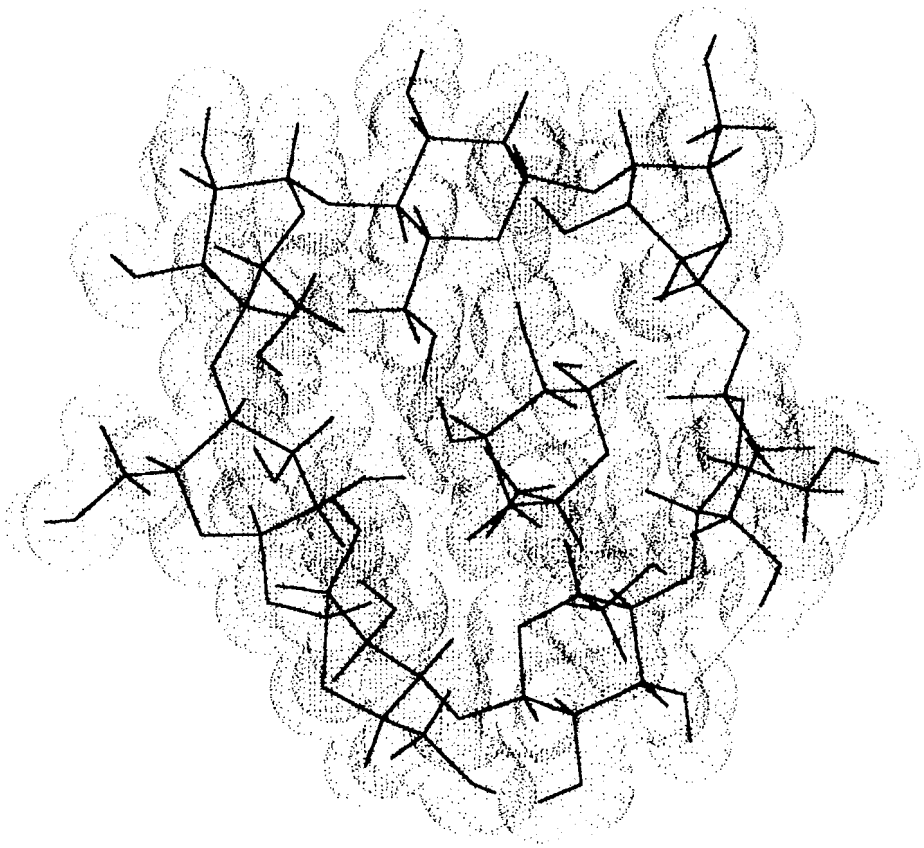

Can. J. Chem. Downloaded from www.nrcresearchpress.com by 65.111.164.53 on 09/08/12
For personal use only.

meter, the concentrations of all species can be found, and the formation constant K_{CyG} can be calculated.

Association constants for inclusion of glucose by cyclohexaamylose and cycloheptaamylose at a temperature of 25 ± 2°C are listed in Table 1 along with the value obtained for the cyclohexaamylose using the indicator competition method at the same temperature.

Discussion

The model equations in the results section assume a 1:1 molecular ratio of glucose to cyclodextrin in each complex. This assumption seems warranted, considering the constancy of the calculated equilibrium constants between the runs, which employed different values for F_{Cy} and F_G. The association constants of α-cyclodextrin obtained by the glucose meter and methyl orange method were in good agreement within experimental error, confirming the accuracy of the glucose meter technique. The binding constants for α- and β-cyclodextrin were indistinguishable within experimental error. Apparently, the "tightness-of-fit" effect is not very important in complexation of glucose by these cyclodextrins.

Molecular mechanics calculations were performed utilizing the graphical interface program HyperChem to set up MM^+ calculations. MM^+ is an "all-atom" force field method that is an extension (providing additional force constants) of the MM2 method of Allinger (10). The calculations further support the 1:1 reaction stoichiometry. Figures 1 and 2 show the fit of glucose within the α- and β-cyclodextrin cavities.

Gelb et al. (11) determined the standard enthalpies and entropies for the complexation of 28 different guests with α-cyclodextrin, by utilizing the temperature dependencies of the formation constants. For these guests, which were quite diverse in nature (anions, aliphatics, aromatic carboxylic acids, and other small organic molecules such as alcohols), the following empirical relationship was determined from a linear least- squares plot of ΔH^0 vs. ΔS^0:

$$[4] \quad \Delta H^0 = (410 \pm 15)\,\Delta S^0 - (1.2 \pm 0.2) \times 10^3$$

where the units for ΔH^0 are kcal mol^{-1} and those of ΔS^0 are cal mol^{-1} K^{-1}. However, there are relatively few data dealing with sugar molecules as guests in cyclodextrin inclusion complexes (12, 13).[3] Assuming that eq. [4] holds true for glucose and can be used to estimate the thermodynamic values for β-cylclodextrin complexes as well as those for α, since

$$[5] \quad \Delta G^0 = -RT \ln K = \Delta H^0 - T\Delta S^0$$

one can calculate the standard enthalpies and entropies using the equilibrium constants obtained by the glucose meter method and eqs. [4] and [5]. These data are listed in Table 1.

[3] Both refs. 12 and 13 report the binding of ribose to β-cyclodextrin, but with different equilibrium constants. Reference 12 reports that cyclohexanol binds strongly to β-cyclodextrin and, in fact, the reported binding constant and our value for the the glucose binding constant are quite similar. Reference 12 also reports little binding of glucose by β-cyclodextrin, a result that is not consistent with our findings.

To confirm the accuracies of the above thermodynamic data, some experiments in benchtop solution calorimetry were performed to estimate the enthalpies of formation of the cyclodextrin–glucose complexes. The results are listed in Table 1. The enthalpies obtained by this method compare favorably with those obtained from eq. [4]. The large negative ΔH^0 in conjunction with little or no tightness-of-fit effect suggests that the intermolecular forces are strong and short range. Therefore, one suspects that hydrogen bonds augment the dipole forces postulated by Gelb et al. (11). These researchers explain the fact that their standard entropy changes are consistently quite negative by conformational changes in the ring. This idea has also been advanced by others (8), and probably occurs with the glucose guest. In fact, the molecular mechanics calculations utilizing the program HYPERCHEM in the MM^+ mode creates models that show hydrogen bonds binding the glucose guests. Intramolecular hydrogen bonds causing conformational changes in the case of the β-cyclodextrin ring are also indicated (Figs. 1 and 2).

References

1. M.L. Bender and M. Komiyama. Cyclodextrin chemistry. Springer-Verlag, New York. 1978.
2. W. Saenger. Angew. Chem. Int. Ed. Engl. **19**, 344 (1980).
3. J. Szejtli. Cyclodextrins and their inclusion compounds. Akadmiai Kiado, Budapest. 1982.
4. M.L. Bender. Cyclodextrins as enzyme models. *In* Proceedings of The First International Symposium on Solution Behavior, Theoretical and Practical Aspects. Vol. 2. *Edited by* K.J.L. Mittal and E.J. Fendler. Plenum Press, New York. 1982.
5. I. Tabushi. Acc. Chem. Res. **15**, 66 (1982).
6. K. Uekama, Y. Horiuchi, M. Kikuchi, F. Harayama, T. Ijitsu, and M. Ueno. J. Inclusion Phenom. **6**, 166 (1988).
7. W. Hirsch, C.K. Choy, K.W. Ng, and V. Fried. Anal. Lett. **22**, 2861 (1989).
8. R.P. Rohrbach, L.J. Rodriguez, and E.M. Eyring. J. Phys. Chem. **81**, 944 (1976).
9. R.I. Gelb, L.M. Schwartz, B. Carelino, H.S. Fuhrman, R. Johnson, and D.A. Laufer. J. Am. Chem. Soc. **103**, 1750 (1981).
10. N.L. Allinger. J. Am. Chem. Soc. **99**, 8127 (1977).
11. R.I. Gelb, L.M. Scwartz, M. Radeos, and D. A. Laufer. J. Phys. Chem. **87**, 3349 (1983).
12. Y. Aoyama, Y. Nagai, J. Otsuki, K. Kobayashi, and H. Toi. Angew. Chem. Int. Ed. Engl. **31**, 746 (1992).
13. A.V. Eliseev and H. Schneider. J. Am. Chem. Soc. **116**, 6081 (1994).

Can. J. Chem. Downloaded from www.nrcresearchpress.com by 65.111.164.53 on 09/08/12
For personal use only.

Investigation of the effect of ring size on the product distribution for the Schiff base reaction of 2-acetylcycloalkanones with diamino alkanes

Raul G. Enriquez, Juan M. Fernandez-G., Ismael Leon, William F. Reynolds, Ji-Ping Yang, and Margaret Yu

Abstract: The Schiff base condensation reaction of 1,2-diaminoethane with a series of 2-acetylcycloalkanones (from cyclopentanone to cyclooctanone) has been investigated and the products characterized by two-dimensional nuclear magnetic resonance. The site of attack of the amino groups, i.e., ring ketone or acetyl ketone, is determined primarily by ring size. 2-Acetylcyclohexanone yields two products in ca. 9:1 ratio, the major product where the two amino groups attack at the ring ketones of two different cyclohexanone molecules, and the minor product where one amino group attacks one ring carbonyl of one cyclohexanone while the second amino group attacks the acetyl group of another. 2-Acetylcyclopentanone yields all three possible products with the major product involving attack at the acetyl groups of two different cyclopentanones. The corresponding reactions for 2-acetylcycloheptanone and 2-acetylcyclooctanone each give a single product corresponding to attack at the acetyl groups of two different cycloalkanones. Similar product distributions are observed for the reactions of the different 2-acetylcycloalkanones with 1,4-diaminobutane.

Key words: Schiff base reactions, diketones, 2D NMR.

Résumé : On a étudié la réaction de condensation conduisant à des bases de Schiff et impliquant le 1,2-diaminoéthane et une série de 2-acétylcycloalcanones (allant de la cyclopentanone à la cyclooctanone) et on a caractérisé les produits par la résonance magnétique nucléaire bidimensionnelle. Le site d'attaque des groupes, à savoir la cétone cyclique ou le groupe acétyle, est principalement déterminé par la grandeur du cycle. La 2-acétylcyclohexanone fournit deux produits, dans un rapport de 9 : 1; le produit principal correspond à un attaque des deux groupes amino sur les cétones cycliques de deux cyclohexanones différentes alors que le produit mineur correspond à l'attaque d'un groupe amino sur le groupe carbonyle d'une cyclohexanone alors que l'autre groupe amino attaque le groupe acétyle d'une autre molécule. L'acétylcyclopentanone fournit les trois produits possibles; le produit majeur est celui qui implique une attaque des groupes acétyles de deux cyclopentanones différentes. Les réactions correspondantes avec la 2-acétylcycloheptanone et la 2-acétylcyclooctanone ne fournissent chacune qu'un seul produit correspondant à l'attaque des groupes acétyles de deux cycloalcanones différentes. On a observé des distributions semblables de produits pour les réactions de diverses 2-acétylcycloalcanones avec le 1,4-diaminobutane.

Mots clés : réactions de bases de Schiff, dicétones, RMN 2D.

[Traduit par la rédaction]

Introduction

In 1973, Moss and Robinson reported the results of a series of reactions involving the Schiff base condensation of either 2-acetylcyclopentanone or 2-acetylcyclohexanone with one of 1,2-diaminoethane, 1,3-diaminopropane, or 1,4-diaminobutane (1). In all cases they concluded that the product had structure **1** = CH_3), i.e., the result of attack at the side-chain ketone.

This is consistent with other studies, which indicated that polyamines condense very readily at the acetyl group in diketones and triketones (2). Similar products were reported for the corresponding diones with R = CH_2CH_3. However, for the diones with R = $CH(CH_3)_2$, it was concluded that the products had structure **2**. The switch from **1** to **2** for R = $CH(CH_3)_2$ was attributed to greater steric hindrance of the side-chain ketone in that case (1). The main evidence for the proposed structures was provided by mass spectral fragmentation patterns.

Very recently, we repeated the reaction of 2-acetylcyclohexanone with 1,2-diaminoethane in order to synthesize tetradentate chelate ligands for transition metal complexes (3).

Received August 3, 1994.

R.G. Enriquez[1] **and J.M. Fernandez-G.** Instituto de Quimica, Universidad Nacional Autonoma de Mexico, Circuito Exterior, Ciudad Universitaria, Coyoacan 04510, Mexico, D.F.
I. Leon. Facultad de Ciencias, Universitad Autonoma del Estado de Morelos, Av. Universidad 1001, Colonia Champila, Cuernavaca, Morelos, Mexico.
W.F. Reynolds,[1] **J.-P. Yang , and M. Yu.** Department of Chemistry, University of Toronto, Toronto, ON M5S 1A1, Canada.
[1] Authors to whom correspondence may be addressed.

Can. J. Chem. Downloaded from www.nrcresearchpress.com by 65.111.164.53 on 09/08/12
For personal use only.

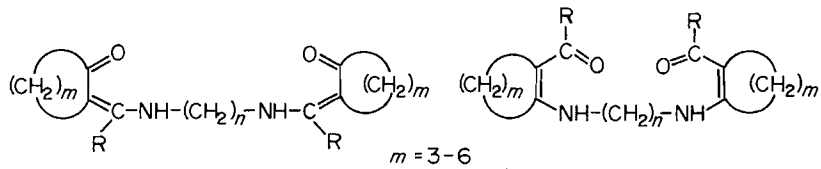

1 2

An X-ray crystal structure determination and a two-dimensional solution nmr investigation of the free ligand and a crystal structure determination of its complex with Cu(II) provided unambiguous evidence that the ligand structure had **2** rather than the previously reported structure **1** (3). Consequently, we decided to carry out a systematic investigation of the reactions of a series of 2-acetylcycloalkanones (with $n = 3$, 4, 5, and 6) with 1,2-diaminoethane in order to determine the structures of the condensation products and the factors determining the preference for structure **1** or **2**. Results of this investigation are reported below. They demonstrate that ring size is the single most important factor in determining the site of attack. Similar product distributions are obtained when 1,2-diaminoethane is replaced by 1,4-diaminobutane, indicating that the length of the bridging group does not affect the course of the reaction.

Results and discussion

We initially repeated the reaction of 2-acetylcyclohexanone with 1,2-diaminoethane and redetermined the ^1H and ^{13}C spectra of the resultant product. Close inspection of these spectra indicated the presence of a second, minor component with peaks ca. 10% as intense as those of the major component. The spectra of the major component were identical to those previously reported. However, while a number of the ^{13}C peaks of the minor component were very similar to those in the major component, some of the peaks had very different chemical shifts. Most noteworthy was the presence of a methyl signal at δ 14.2 (with a corresponding ^1H singlet at δ 1.92) compared to a methyl signal at δ 27.6 ($\delta_H = 2.08$) in the major component. Consequently, a series of two-dimensional spectra (COSY (4), HETCOR (5), and FLOCK (6)) were carried out to obtain further structural information. The FLOCK spectrum was particularly informative since the CH_3 singlet for the major component (δ 2.0) showed cross peaks with carbons at δ 195 and δ 101 (as expected for structure **2**) while the CH_3 singlet at δ 1.92 showed cross peaks with carbons at δ 161 and δ 101, i.e., more consistent with structure **1**. However, in view of the relatively large number of minor component peaks, we suspected that the actual structure of this component was the asymmetric structure **3**.

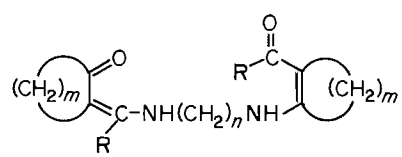

3

To confirm this, the reaction mixture was separated by high-performance liquid chromatography (hplc). A series of 2D experiments (COSY, NOESY (7), HMQC (8), and HMBC (9)) on the separated components allowed us to both confirm that the major component had structure **2** and that the minor component had structure **3** and to fully assign the ^1H and ^{13}C spectra of the two compounds. HMQC and HMBC were used in place of HETCOR and FLOCK because of the limited amount of some of the pure isomers that was available. These data are reported in Table 1.

The corresponding reaction of 2-acetylcyclopentanone with 1,2-diaminoethane proved to be even more complex, since the ^1H and ^{13}C spectra indicated the presence of at least three products. In this case the ^{13}C spectra showed a strong methyl peak at δ 15.65, and three weaker methyl peaks (of roughly equal intensity) at δ 15.61, δ 27.90, and δ 27.94. This suggested the presence of all three possible products **1**, **2**, and **3** with the relative amounts being 70% **1**, 20% **3**, and 10% **2**, i.e., **1** was the favored product in this case. Once again, chromatographic separation into the three components, followed by a series of 2D nmr experiments identical to those listed in the previous paragraph, allowed unambiguous confirmation of the proposed structures and full ^1H and ^{13}C spectral assignments. NOESY cross peaks between methyl (H-7 or H-7′) protons and H-3 or H-3′ protons were particularly helpful in distinguishing C-3 from C-5. Assignments are given in Table 2.

By contrast, the reactions of 2-acetylcycloheptanone and 2-acetylcyclooctanone with 1,2-diaminoethane each gave only one product. In each case this product had structure **1**, as confirmed by 2D nmr. Spectral assignments for the two compounds are listed in Table 3.

Comparison of the results of the reactions of different 2-acetylcycloalkanones with 1,2-diaminoethane clearly demonstrates that the site of Schiff base condensation is primarily determined by ring size. The six-membered ring shows a moderately strong preference for structure **2**, the five-membered ring has a slightly weaker preference for structure **1**, while the seven- and eight-membered rings both show a strong preference for structure **1**. While the relative stabilities of **1** and **2** for the different ring size undoubtedly reflect some complex blend of steric and electronic interactions, this could be regarded as another example of the Dieckmann–Kon rule (10, 11), i.e., the tendency of six-membered rings to prefer endocyclic double bonds rather than exocyclic double bonds (12). Recent work has shown that this tendency is particularly strong for six-membered rings when it involves a choice between an endocyclic double bond (as in **2**) and two adjacent exocyclic double bonds (as in **1**) (13). Structure **1** can also exist as the OH tautomer with an endocyclic double bond (3). However, selective decoupling of the NH protons for the minor product (**3**) of this reaction of 2-acetylcyclohexanone showed that each NH proton was coupled to a CH_2 group, ruling out the OH tautomer for either end of this unsymmetric molecule. Thus, while six-membered ring compounds may prefer to avoid exocyclic double bonds, the preference for the

Can. J. Chem. Downloaded from www.nrcresearchpress.com by 65.111.164.53 on 09/08/12
For personal use only.

Table 1. Assigned ^{1}H and ^{13}C chemical shifts for the products of the reaction of 2-acetylcyclohexanone with 1,2-diaminoethane.

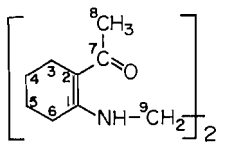

2

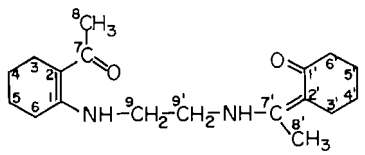

3

Structure **2**			Structure **3**					
Carbon[a]	δ_C	δ_H	Carbon[a]	δ_C	δ_H	Carbon[a]	δ_C	δ_H
1	161.25	—	1	161.15	—	1′	194.68	—
2	101.01	—	2	101.04[c]	—	2′	101.11[c]	—
3	26.16[b]	2.31	3	26.14[b]	2.31	3′	26.47	2.31
4	21.86	1.61	4	21.88	1.60	4′	24.07	1.67
5	23.01	1.59	5	23.01	1.60	5′	22.78	1.67
6	26.19[b]	2.31	6	26.22[b]	2.31	6′	37.97	2.31
7	196.55	—	7	196.63	—	7′	163.81	—
8	27.65	2.08	8	27.63	2.08	8′	14.20	1.92
9	42.67	3.37	9	42.58	3.42	9′	43.73	3.45
NH	—	11.54	NH	—	11.54	NH′	—	12.67

[a]Carbon numbering illustrated above.
[b,c]Pairs of carbons with same superscript letter may be interchanged.

Table 2. The ^{1}H and ^{13}C chemical shifts for the three products of the reaction of 2-acetylcyclopentanone with 1,2-diaminoethane.

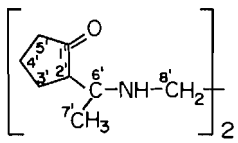

1

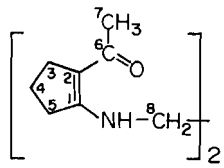

2

Structure **1**[a]			Structure **2**[a]			Structure **3**[b]					
Carbon	δ_C	δ_H	Carbon	δ_C	δ_H	Carbon	δ_C	δ_H	Carbon	δ_C	δ_H
1′	202.34	—	1	166.41	—	1	166.31	—	1′	202.30	—
2′	103.32	—	2	105.48	—	2	105.48	—	2′	103.32	—
3′	27.85	2.50	3	30.13	2.57	3	30.13	2.58	3′	27.86	2.51
4′	20.35	1.80	4	21.41	1.82	4	21.38	1.83	4′	20.36	1.83
5′	39.15	2.30	5	31.53	2.52	5	31.53	2.54	5′	39.11	2.32
6′	157.94	—	6	193.99	—	6	193.99	—	6′	158.14	—
7′	15.74	1.90	7	27.98	2.03	7	27.99	2.03	7′	15.72	1.90
8′	43.54	3.40	8	45.88	3.35	8	45.88	3.37	8′	43.79	3.39
NH′	—	10.38	NH	—	9.50	NH	—	9.51	NH′	—	10.38

[a]Numbering for structures **1** and **2** provided above.
[b]Numbering for the two halves of **3** correspond to those for **1** and **2**.

NH tautomer over the OH tautomer must have an even greater effect in this case.

Our previous investigation showed that mass spectral fragmentation patterns do not provide a reliable criterion for structure elucidation in this family of compounds (3). The ^{13}C chemical shift of the methyl group does appear to provide an unambiguous criterion, due to the large chemical shift differences in the two forms (δ 14–16 for **1**, δ 27–28 for **2**). In cases

Can. J. Chem. Downloaded from www.nrcresearchpress.com by 65.111.164.53 on 09/08/12
For personal use only.

Table 3. The ^{1}H and ^{13}C chemical shifts for the products of reactions of 2-acetylcycloheptanone and 2-acetylcyclooctanone with 1,2-diaminoethane.

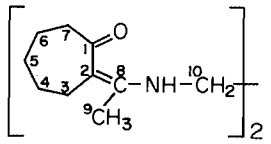

A

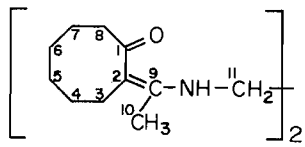

B

Cycloheptanone product (**A**)			Cyclooctanone Product (**B**)		
Carbon[a]	δ_C	δ_H	Carbon[b]	δ_C	δ_H
1	201.20	—	1	199.77	—
2	105.94	—	2	103.18	—
3	27.92	2.35	3	26.35	2.44
4	29.65	1.52	4	30.90	1.45
5	31.39	1.70	5	25.74	1.43
6	25.19	1.64	6	26.91	1,52
7	43.96	2.53	7	29.28	1.71
8	160.78	—	8	40.65	2.52
9	14.57	1.96	9	162.25	—
10	43.84	3.45	10	14.56	1.98
NH	—	11.90	11	43.70	3.74
			NH	—	12.53

[a]Carbon numbering as shown in (**A**) above.
[b]Carbon numbering as shown in (**B**) above.

Table 4. The ^{13}C and ^{1}H chemical shifts for products of reaction of 2-acetylcyclohexane with 1,4-diaminobutane.

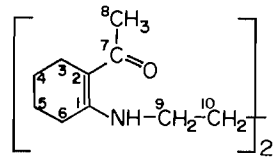

2

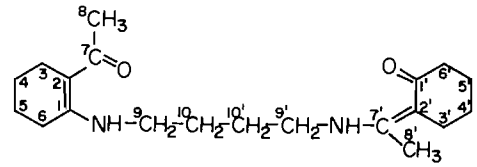

3

Structure **2**			Structure **3**					
Carbon[a]	δ_C	δ_H	Carbon[a]	δ_C	δ_H	Carbon	δ_C	δ_H
1	161.62	—	1	161.64	—	1′	193.96	—
2	100.24	—	2	100.29	—	2′	100.33	—
3	26.11	2.32	3	26.10	2.32	3′	26.41	2.33
4	21.90	1.64	4	21.89	1.62	4′	24.13	1.68
5	23.08	1.62	5	23.08	1.60	5′	22.68	1.71
6	26.37	2.34	6	26.37	2.33	6′	37.89	2.31
7	195.83	—	7	195.87	—	7′	164.06	—
8	27.53	2.07	8	27.52	2.07	8′	14.40	1.93
9	41.73	3.23	9	41.68	3.23	9′	42.92	3.31
10	27.43	1.69	10	27.44	1.71	10′	27.35	1.72
NH	—	11.56	NH	—	11.56	NH	—	12.69

[a]Carbon numbering illustrated above.

where both structures are formed, the NH chemical shift also appears to be consistently larger for **1** than for **2**. However, the variation of this chemical shift with ring size is even greater, presumably reflecting the variation of intramolecular hydrogen bond strength with ring size. It appears that this hydrogen bond is considerably weaker in the five-membered ring compounds than in the other cases, as well as in structure **2** relative to **1**. From these data, it does not appear that the strength of the

Can. J. Chem. Downloaded from www.nrcresearchpress.com by 65.111.164.53 on 09/08/12
For personal use only.

Table 5. The ^{13}C and ^{1}H chemical shifts for products of reaction of 2-acetylcyclopentanone with 1,4-diaminobutane.

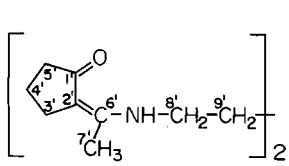

1

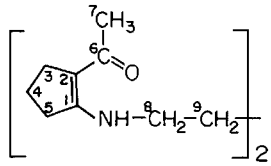

2

1[a]			2[a]			3					
Carbon	δ_C	δ_H	Carbon	δ_C	δ_H	Carbon	δ_C	δ_H	Carbon	δ_C	δ_H
1′	201.67	—	1	166.55	—	1	166.58	—	1′	201.66	—
2′	102.47	—	2	104.66	—	2	104.67	—	2′	102.48	—
3′	27.87	2.52	3	30.05	2.59	3	30.03	2.58	3′	27.87	2.52
4′	20.36	1.84	4	21.35	1.86	4	21.34	1.85	4′	20.36	1.82
5′	39.11	2.32	5	31.54	2.55	5	32.53	2.54	5′	39.10	2.33
6′	153.41	—	6	193.37	—	6	193.38	—	6′	153.44	—
7′	15.83	1.93	7	27.92	2.03	7	27.91	2.03	7′	15.84	1.93
8′	42.53	3.27	8	44.39	3.23	8	44.36	3.23	8′	42.55	3.26
9′	27.64	1.07	9	28.00	1.62	9	28.00	1.65	9′	27.61	1.65
NH′	—	10.42	NH	—	9.49	NH	—	9.51	NH	—	10.42

[a]Numbering for structures **1** and **2** provided above.
[b]Numbering for the two halves of **3** correspond to those for **1** and **2**.

Table 6. The ^{13}C and ^{1}H chemical shifts for products of reactions of 2-acetylcycloheptanone and 2-acetylcyclooctanone with 1,4-diaminobutane.

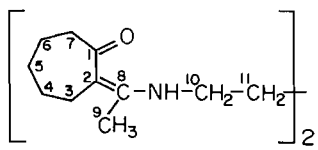

A

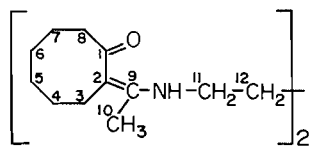

B

Cycloheptanone product (**A**)[a]			Cyclooctanone Product (**B**)[b]		
Carbon	δ_C	δ_H	Carbon	δ_C	δ_H
1	200.56	—	1	198.96	—
2	105.28	—	2	102.67	—
3	27.91	2.36	3	26.40	2.45
4	29.75	1.52	4	31.05	1.45
5	31.54	1.70	5	25.80	1.43
6	25.24	1.65	6	27.01	1.52
7	44.03	2.53	7	29.28	1.70
8	161.10	—	8	40.66	2.52
9	14.87	1.98	9	162.46	—
10	43.05	3.29	10	14.78	2.00
11	27.52	1.72	11	42.99	3.30
NH	—	11.92	12	27.40	1.72
			NH	—	12.52

[a]Carbon numbering shown in **A** above.
[b]Carbon numbering shown in **B** above.

intramolecular hydrogen bond is a major factor in determining the preference for **2** over **1** in the case of the 2-acetylcyclohexanone reactions.

To determine whether the length of the -HN-$(CH_2)_n$-NH- bridge had any effect on the preferred site of attack, the series of reactions were repeated using 1,4-diaminobutane in place

Can. J. Chem. Downloaded from www.nrcresearchpress.com by 65.111.164.53 on 09/08/12
For personal use only.

Can. J. Chem. Downloaded from www.nrcresearchpress.com by 65.111.164.53 on 09/08/12
For personal use only.

of 1,2-diaminoethane. In each reaction, the product distribution was essentially the same as observed for the diaminoethane reactions. Thus the length of the bridging group appears to have little effect on the site of attack in the Schiff base reaction. Product mixtures were again separated chromatographically, with ^{1}H and ^{13}C spectral assignments for the different compounds listed in Tables 4–6.

One unexpected bonus from this investigation is that it has provided a series of tetradentate ligands, which have subtle differences in structure. An investigation is planned to determine how these differences affect the structures and stabilities of four-coordinate transition metal complexes involving these ligands.

Experimental

Melting points were determined in a Fisher–Johns melting point apparatus and are uncorrected; infrared spectra (KBr disks) were recorded on a Perkin–Elmer model 203-B spectrometer; mass spectra were obtained using a Hewlett–Packard instrument model 5985, at 70 eV ionizing potential, nmr spectra on a Varian XL-400 or Unity-500 spectrometer. Initial experiments on isomeric mixtures used ca. 30 mg of sample in $CDCl_3$. Experiments on individual isomers used 2–10 mg of sample in $CDCl_3$. Toluene, 2-acetylcyclopentanone, 2-acetylcyclohexanone, cyclooctylamine, cycloheptylamine, morpholine, acetyl chloride, 1,4-dioxane, 1,2-diaminoethane, and 1,4 diaminobutane were from Aldrich and were used without further purification. 2-Acetylcycloheptanone and 2-acetylcyclooctanone were obtained by the method described by Stork et al. (14).

General synthetic procedure

To a stirred solution of 10 mmol of the β-diketone in toluene (300 mL) was added a solution of 5 mmol of 1,4-diaminobutane or 1,2-diaminoethane in absolute ethanol (10 mL). The solution was heated under reflux with a Dean–Stark trap. The solvent collected for the first time in the column of the trap was discarded and then the mixture was refluxed for 3.5 h. Afterwards, the remaining solvent was distilled off, yielding an oily product. This was separated by chromatography on a silica gel column using a 95:5 mixture of methylene chloride and methanol. The crude product purity was then checked by nmr. If only a single product was noted, the crude product was recrystallized from dichloromethane. In cases where two or more products were observed, hplc was used to further separate and purify the mixture of products.

High-performance liquid chromatography purification

The hplc purification was carried out on a 250 × 10 mm column of Maxsil C_{18} using as eluent a 70:30 CH_3OH:H_2O mixture in isocratic mode, 2 mL/min flux at 30°C. A uv detector set at 280 nm was used. After a sufficient amount of each component was detected, the samples were evaporated under vacuum and used directly for spectroscopic measurements.

Product characterization

The structure of the major product (**2**) of the reaction of 2-acetylcyclohexanone with 1,2-diaminoethane has previously been characterized by X-ray crystallography and 2-dimensional nmr (3).

No analytical data were obtained for individual isomers owing to the limited availability of purified samples. However, all individual products were characterized by the combination of one- and two-dimensional nmr experiments described in the text. High-resolution mass spectrometry was also used to confirm the empirical formulae for the different isomeric mixtures: cyclopentanone/diaminoethane product, calcd. ($C_{16}H_{24}N_2O_2$): 276.1838; found: 276.1830; cyclopentanone/diaminobutane product, calcd. ($C_{18}H_{28}N_2O_2$): 304.2152; found: 304.2150; cyclohexanone/diamonoethane product, calcd. ($C_{18}H_{28}N_2O_2$): 304.2152; found: 304.2144; cyclohexanone/diaminobutane product, calcd. ($C_{20}H_{32}N_2O_2$): 332.2466; found: 332.2449: cycloheptanone/diaminoethane product, calcd. ($C_{20}H_{32}N_2O_2$): 332.2466; found: 332.2457; cycloheptanone/diaminobutane product, calcd. ($C_{22}H_{36}N_2O_2$): 360.2779; found: 360.2776; cyclooctanone/diaminoethane product, calcd. ($C_{22}H_{36}N_2O_2$): 360.2779; found: 360.2780; cyclooctanone/diaminobutane product, calcd. ($C_{24}H_{40}N_2O_2$): 388.3092; found: 388.3082. Mass spectral fragmentation patterns were obtained for some of the individual isomers but, as noted previously (3), these were extremely complex and of little value for structure elucidation.

Acknowledgments

Financial support from CoNaCyT (R.G.E.) and the Natural Sciences and Engineering Research Council of Canada (W.F.R.) is gratefully acknowledged.

References

1. R.C. Moss and F.P. Robinson. Can. J. Chem. **51**, 505 (1973).
2. P. Zanello, S. Tambarini, P.A. Vigato, and G.A. Mazzochin. Coord. Chem. Rev. **77**, 165 (1987).
3. J.M. Fernandez-G., R.G. Enriquez, A. Tobon-Cervantes, M.I. Bernal-Uruchurtu, R. Villena-I., W.F. Reynolds, and J.-P. Yang. Can. J. Chem. **71**, 358 (1993).
4. A. Bax and R. Freeman. J. Magn. Reson. **44**, 542 (1981).
5. A. Bax and G.A. Morris. J. Magn. Reson. **42**, 501 (1981).
6. W.F. Reynolds, S. McLean, M. Perpick-Dumont, and R.G. Enriquez. Magn. Reson. Chem. **27**, 161 (1989).
7. J. Jeener, B.H. Meier, P. Bachmann, and R.R. Ernst. J. Chem. Phys. **71**, 4546 (1979).
8. A. Bax and S. Subramanian. J. Magn. Reson. **67**, 565 (1986).
9. A. Bax and M.F. Summers. J. Am. Chem. Soc. **108**, 2093 (1986).
10. W. Dieckmann. Ber. Dtsch. Chem. Ges. **55**, 2470 (1922).
11. G.A.R. Kon and E.A. Speight. J. Chem. Soc. 2727 (1926).
12. H.C. Brown, J.H. Brewster, and H. Shechter. J. Am. Chem. Soc. **76**, 467 (1954).
13. S. Katayama, T. Watonabe, and M. Yamauchi. Chem. Pharm. Bull. **41**, 439 (1993).
14. G. Stork, A. Brizzolara, H. Landesman, J. Szmuskovicz, and R. Terrel. J. Org. Chem. **85**, 207 (1963).

Étude théorique de la complexation des cations Pb^{2+} et Hg^{2+} par le D-talose

Marc Palma et Yves Louis Pascal

Résumé : Le comportement des conformères du D-talopyranose et du D-talofuranose en présence des cations Pb^{2+} et Hg^{2+} a été simulé, en phase gazeuse et en présence de quelques molécules d'eau, par la méthode AM1. L'analyse conformationnelle du D-talose libre a été réalisée par une méthode de Monte Carlo (logiciel BATCHMIN). Des minima de plus basse énergie ont été identifiés et les différentes orientations des groupements hydroxyle donnés. L'équilibre de distribution des anomères en phase gazeuse est différent de celui obtenu expérimentalement en solution aqueuse. Ce phénomène peut s'expliquer par la prépondérance des liaisons hydrogène intramoléculaires dans le cas de la molécule isolée et des liaisons hydrogène intermoléculaires en milieu aqueux. En présence du cation, l'analyse a été faite par la méthode AM1 pour chacune des conformations du ligand pur. En phase gazeuse, les prédictions d'Angyal ne sont pas respectées. L'énergie la plus basse est représentée par une forme flexible de l'anomère β du talopyranose et certains complexes sont tetra ou pentacoordinés. Pour les furanoses, l'anomère α qui possède sur le cycle, une séquence de trois OH consécutifs en positions *cis-cis-cis*, est le moins stable. Les complexes des carbohydrates en solution aqueuse avec les cations métalliques sont nombreux avec Pb^{2+} alors qu'on n'en connait pas avec Hg^{2+}. Les calculs montrent que, pour les espèces isolées, ce serait l'inverse qui devrait se produire. La moins grande stabilité dans l'eau des complexes mercuriques par rapport à ceux du plomb pourrait s'interpréter par : (1) un effet entropique d'hydratation plus défavorable; (2) une différence d'entropie de translation moins favorable. Une réponse plus complète ne peut être fournie que par l'étude dynamique du système dans l'eau par une méthode de Monte Carlo.

Mots clés : complexation des cations divalents, conformères du D-talopyranose et D-talofuranose.

Abstract: Molecular modeling of interactions between D-talopyranose and D-talofuranose conformers and Pb^{2+} and Hg^{2+} cations was done in the gaseous state using the AM1 method, both with "naked" species and with some water molecules added. A complete conformational analysis of the free D-talose molecule was carried out using a Monte Carlo method (BATCHMIN program). Lower minima were identified, and the different orientations of the hydroxyl groups given. The calculated equilibrium distribution of anomers in the gaseous phase differs from that obtained experimentally in aqueous solution. This could be related to the predominance of intramolecular hydrogen bonding for the isolated molecule and intermolecular hydrogen bonding in aqueous media. In the presence of a cation, the analysis was carried out using the AM1 method for every conformation of the ligand. In the gaseous phase, Angyal's predictions are not respected. The lowest energy is represented by a flexible β-pyranosic form and some complexes are tetra or pentacoordinated. For the furanosic species, the αF forms bearing a *cis-cis-cis* sequence of hydroxyl groups are the less stable. Amongst the complexes of carbohydrates with metal cations in aqueous solutions, Pb^{2+} forms complexes and Hg^{2+} does not. The calculations show that, for the isolated complexes, the reverse should be true. The lesser stability in water of Hg^{2+} complexes with respect to Pb^{2+} could be interpreted in terms of (1) a more unfavourable entropic hydration effect; (2) a less favourable difference of translational entropy. A complete answer requires the dynamical study of the system in water by a Monte Carlo method.

Key words: complexes with divalent cations, D-talopyranose and D-talofuranose conformers.

Introduction

En solution aqueuse certaines conformations d'hexoses paraissent favorables à la complexation des cations divalents (1–6). Des mesures de spectroscopie RMN (7–10) et les travaux d'Angyal en particulier, ont montré que le cation doit être, dans ce cas, lié à trois atomes d'oxygène de groupes hydroxyle consécutifs du cycle situés en positions *ax-eq-ax* pour les formes pyranosiques, et en positions *cis-cis-cis* pour les formes furanosiques. Dans cet article, nous avons essayé de voir si des méthodes de modélisation moléculaire, largement utilisées dans le domaine des carbohydrates (11), permettaient de retrouver et d'expliquer ce mode de complexation dans le cas des conformations les plus stables, et s'il n'existe pas d'autres types de liaisons possibles. Une analyse conformationnelle a été d'abord effectuée sur le ligand seul, puis sur un modèle simulant le cation et le ligand isolés dans le vide. Nous avons examiné ensuite, sur une forme particulière, comment varient la géométrie du système et la nature des liaisons, quand une ou plusieurs molécules du solvant sont ajoutées au voisinage du site d'interaction. Enfin, nous avons

Reçu le 23 décembre 1993. Révision reçue le 16 septembre 1994.

M. Palma.[1] Laboratoire de chimie physique des solutions, Université Blaise Pascal, 63177 Aubière Cedex, France.
Y.L. Pascal. Laboratoire de chimie organique structurale, Université Blaise Pascal, 63177 Aubière Cedex, France.

1. Auteur à qui adresser toute correspondance.

Can. J. Chem. Downloaded from www.nrcresearchpress.com by 65.111.164.53 on 09/08/12
For personal use only.

Can. J. Chem. Downloaded from www.nrcresearchpress.com by 65.111.164.53 on 09/08/12
For personal use only.

essayé de montrer pourquoi la complexation par les hexoses de certains cations divalents, comme Hg^{2+} par exemple, n'a jamais été observée (7).

Parmi les isomères du glucose, le D-talose nous a paru intéressant, car la forme chaise $^4C_1$ de l'α-D-talopyranose possède sur le cycle une séquence de trois OH consécutifs en positions *ax-eq-ax* (fig. 1*a*) et devrait, de ce fait, complexer les cations (1). Au contraire, la forme chaise opposée $^1C_4$, ne possédant pas cette séquence, ne devrait pas donner de complexation significative. Le β-D-talopyranose réalise la séquence dans ses deux formes chaises. Quant aux formes furanosiques, seul le β-D-talofuranose possède à l'intérieur du cycle trois OH consécutifs en positions *cis-cis-cis* (fig. 1*b*). Une étude expérimentale en solution aqueuse effectuée au laboratoire, a montré que ce ligand complexait le cation Ca^{2+} (7). Le choix des cations a été imposé par les paramètres disponibles des logiciels de calcul utilisés. De ce fait, nous avons choisi Pb^{2+} qui apparait expérimentalement très complexé, et Hg^{2+} qui ne l'est pas (7).

Méthodes d'analyse conformationnelle

Afin de permettre la comparaison de propriétés entre les différents isomères, nous avons utilisé une numérotation commune dérivée de la forme ouverte du talose, avec les numéros 1–6 pour les atomes de carbone de la chaîne principale et les liaisons C_1—O_7, C_2—O_8, C_3—O_9, C_4—O_{10}, C_5—O_{11} et C_6—O_{12}.

La description des conformations des cycles pyranosiques et furanosiques est donnée par les paramètres de gauchissement de Cremer et Pople (12) qui permettent d'expliciter les distances z_j des sommets d'un cycle par rapport au plan moyen défini par $\Sigma z_j = 0$. Pour un cycle à cinq côtés, ces écarts sont reliés aux paramètres q (écart maximum des z_j) et φ (angle de phase) par la formule

$$z_j = (2/5)^{1/2} q \cos [\varphi + 4\pi(j - 1)/5]$$

φ vaut respectivement 36 et 36p + 18 degrés (p étant un nombre entier quel conque) pour les conformations enveloppes et croisées. Pour un cycle à six côtés, ces écarts dépendent de trois paramètres par la formule

$$z_j = 3^{-1/2} q(\sin \theta \cos [\varphi + 4\pi(j - 1)/3] + (-1)^{j-1} 6^{-1/2} \cos \theta)$$

q est l'écart maximum des sommets au plan moyen, θ prend les valeurs 0° et 180° pour les formes chaises, et 90° pour les formes flexibles, et l'angle de phase φ vaut respectivement $2p \times 30$ et $(2p + 1) \times 30$ degrés pour les conformations bateau et croisées.

Il faut en plus décrire l'orientation de la chaîne exocyclique et celle des différents groupes OH. Pour les anomères du talopyranose, on peut repérer en projection de Newman la position de C_6—O_{12} par rapport aux liaisons C_5—O_{11}, C_5—C_4 et C_5—H en utilisant les notations habituelles G pour une disposition gauche et T pour trans; mais comme il doit y avoir deux dispositions gauches et une trans, il suffit de considérer seulement deux dièdres, ceux de C_6—O_{12} avec C_5—O_{11} et avec C_5—C_4 (13). Comme certaines conformations apparaissent un peu distordues par rapport aux formes décalées, nous avons utilisé la notation G pour un dièdre compris (en valeur absolue) entre 30° et 80°, T entre 150° et 180°, P entre 80° et 150° et C entre 0° et 30°. De la même façon, nous avons décrit ensuite les positions des liaisons O—H avec les notations précédentes (mais en minuscules g, t, p, c) par les dièdres classés dans l'ordre suivant : H-O_{12}-C_6-C_5, H-O_{12}-C_6-H, H-O_7-C_1-O_{11}, H-O_7-C_1-C_2, H-O_8-C_2-C_1, H-O_8-C_2-C_3, H-O_9-C_3-C_2, H-O_9-C_3-C_4, H-O_{10}-C_4-C_3, H-O_{10}-C_4-C_5.

Pour les anomères du talofuranose, les orientations dans la chaîne -CHOH-CH_2OH ont été décrites dans l'ordre par les dièdres O_{11}-C_5-C_4-O_{10}, O_{11}-C_5-C_4-C_3, C_6-C_5-C_4-O_{10}, C_6-C_5-C_4-C_3, O_{12}-C_6-C_5-O_{11}, O_{12}-C_6-C_5-C_4 (symboles majuscules). Pour les OH ont été utilisés les dièdres H-O_{12}-C_6-C_5, H-O_{12}-C_6-H, H-O_{11}-C_5-C_4, H-O_{11}-C_5-C_6, H-O_7-C_1-O_{10}, H-O_7-C_1-C_2, H-O_8-C_2-C_1, H-O_8-C_2-C_3, H-O_9-C_3-C_2, H-O_9-C_3-C_4 (symboles minuscules).

Une première exploration de la surface d'énergie potentielle de la molécule d'hexose a été effectuée par la méthode MM2,[2] par rotation simultanée autour de deux dièdres endocycliques dans le cas du cycle pyranosique ou d'un seul dans le cas du cycle furanosique. Pour les formes α et β du D-talopyranose (notées respectivement αP et βP) nous avons optimisé les géométries en faisant varier l'angle dièdre 3-4-5-11 du cycle par pas de cinq degrés, de 0° à 60° et, pour chacune de ses valeurs, avec le même incrément et les mêmes limites, l'angle dièdre 11-1-2-3. Les courbes de niveau correspondantes ont permis de localiser correctement les minima. Pour chacune des deux formes du D-talofuranose, nous avons fait varier le dièdre 1-2-3-4 de −45° à +45° de 5 en 5 degrés.

Les conformations finales que l'on obtient correspondent à des minima locaux de la surface d'energie potentielle, pouvant servir de géométries initiales pour des calculs ultérieurs, mais pas forcément au minimum global en ce qui concerne l'orientation des substituants, en particulier des groupes OH. Elles dépendent en fait de la conformation initiale. Comme le nombre de degrés de liberté pour les molécules que nous avons étudiées est trop grand pour réaliser une analyse conformationnelle systématique, nous avons utilisé un échantillonnage de Monte Carlo sur 10 000 configurations générées chaque fois en partant de la moins fréquente et dans une fenêtre d'énergie stérique de 3 kcal mol^{-1}, au moyen du programme BATCHMIN de MACROMODEL (14) avec le champ de force MM2, les liaisons hydrogène étant simulées par des fonctions de Lennard–Jones 10–12. Qu'on parte d'une conformation initiale pyranosique $^1C_4$ ou $^4C_1$, cette méthode conduit uniquement à des conformations $^4C_1$ et à des conformations flexibles (bateaux et croisées) si on n'impose pas de contraintes sur les variations des dièdres endocycliques. Afin d'obtenir les conformations $^1C_4$, il a fallu imposer des variations des dièdres endocycliques limitées à ±55° à partir de αP^1C_4 et de βP^1C_4. Il en résulte 239 conformations αP^4C_1 (6,96–9,97 kcal mol^{-1}, 169,6° ≤ θ ≤ 176,3°) et 349 conformations βP^4C_1 (5,56–8,53 kcal mol^{-1}, 172,9° ≤ θ ≤ 179,5°, 46 flexibles αP(flex) (10,95–13,88 kcal mol^{-1}, 87,3° ≤ θ ≤ 92,4°), 79 chaises véritablement αP^1C_4 (11,81–13,94 kcal mol^{-1}, 2,8° ≤ θ ≤ 11,7°), 53 flexibles βP(flex) (10,82–13,81 kcal mol^{-1}, 88,4° ≤ θ ≤ 95,4°) et 25 chaises βP^1C_4 (13,00–13,83 kcal mol^{-1}, 4,7° ≤ θ ≤ 12,9°).

2. Programme MM2 (85), QCPE n° 501, Department of Chemistry, Indiana University, Bloomington, IN 47408, U.S.A.

Fig. 1*a*. Conformères du D-talopyranose.

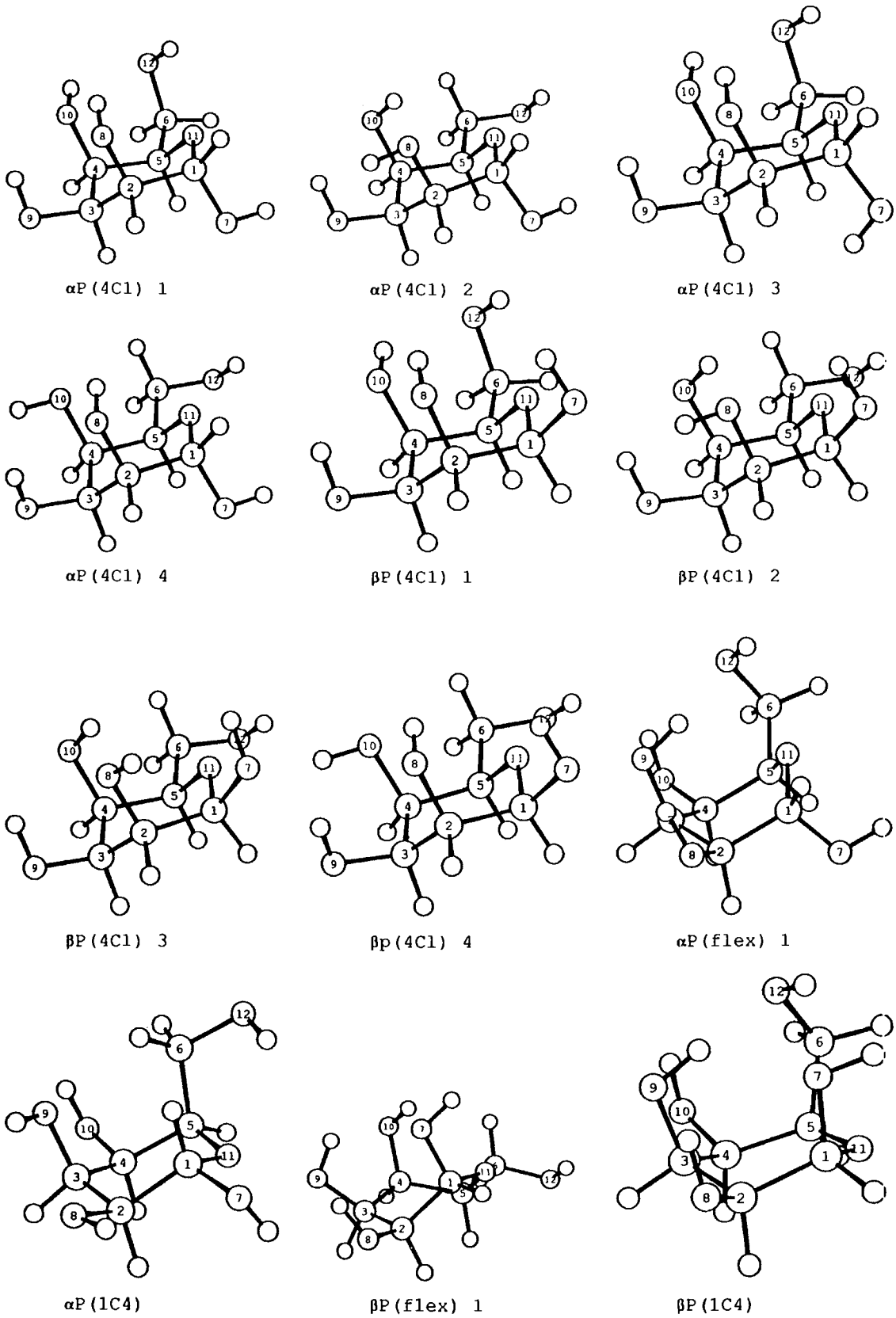

Can. J. Chem. Downloaded from www.nrcresearchpress.com by 65.111.164.53 on 09/08/12
For personal use only.

Fig. 1*b*. Conformères du D-talofuranose.

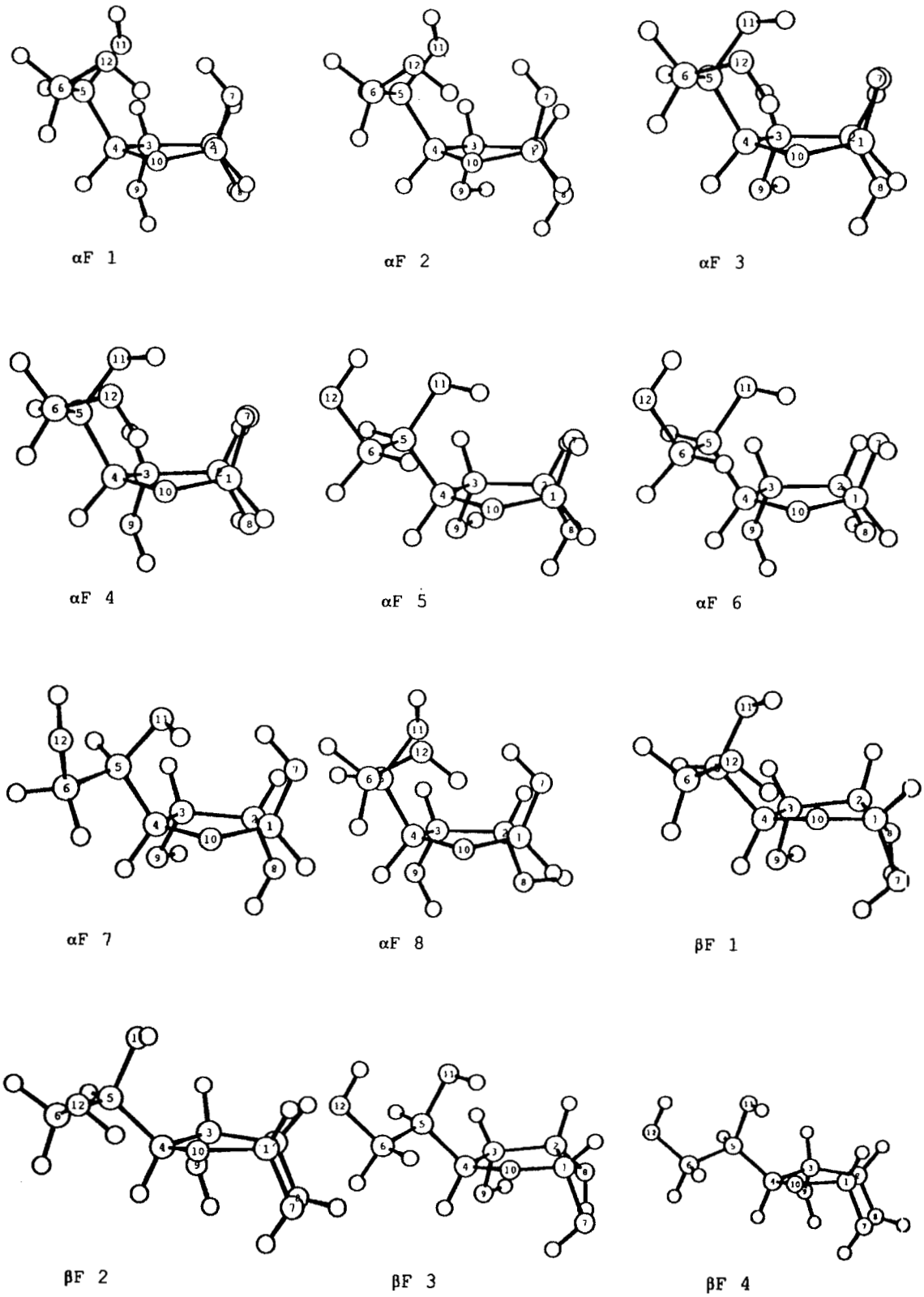

Can. J. Chem. Downloaded from www.nrcresearchpress.com by 65.111.164.53 on 09/08/12
For personal use only.

Can. J. Chem. Downloaded from www.nrcresearchpress.com by 65.111.164.53 on 09/08/12
For personal use only.

Les conformations furanosiques sont encore plus nombreuses à cause de la flexibilité du cycle et des possibilités d'orientation des hydroxyles et de la chaîne latérale -CHOH-CH_2OH et les écarts à la planéité (décrits par le paramètre q de Cremer) assez homogène : 807 conformations αF (10,53–13,53 kcal mol^{-1}, $0{,}308 \leq q \leq 0{,}390$) et 1051 βF (10,45–13,45 kcal mol^{-1}, $0{,}306 \leq q \leq 0{,}410$).

En phase gazeuse, la méthode de Monte Carlo, avec le champs de force MM2, prévoit donc un ordre de stabilité $\beta P^4C_1 > \alpha P^4C_1$ avec des traces des autres configurations.

Les conformations stables ainsi trouvées ont été réoptimisées complètement par la méthode AM1 (15). Beaucoup ont fusionné et d'autres sont sorties de la fenêtre de 3 kcal mol^{-1} (enthalpie de formation) relative à la plus basse dans chaque série. On a ainsi obtenu 15 conformations αP^4C_1 (ΔH_f compris entre −305,76 et −302,62 kcal mol^{-1}, $163{,}2° \leq \theta \leq 178{,}5°$); 16 conformations βP^4C_1 (−304,93 – −301,79 kcal mol^{-1}, $170{,}8° \leq \theta \leq 179{,}4°$); 12 conformations flexibles αP(flex) (−304,23 – −300,24 kcal mol^{-1}, $87{,}7° \leq \theta \leq 97{,}6°$) et 8 chaises αP^1C_4 (−301,58–300,06 kcal mol^{-1}, $4{,}7° \leq \theta \leq 20{,}6°$); 14 conformations flexibles βP(flex), (−304,21 – −301,11 kcal mol^{-1}, $87{,}0° \leq \theta \leq 97{,}5°$) et 11 chaises (−303,87 – −301,09 kcal mol^{-1}, $0{,}7° \leq \theta \leq 19{,}69°$); 13 conformations αF (−306,19 – −303,03 kcal mol^{-1}, $0{,}097 \leq q \leq 0{,}166$) et 20 βF (−304,76 – −301,53 kcal mol^{-1}, $0{,}092 \leq q \leq 0{,}286$). Les cycles furanosiques apparaissent légèrement plus applatis qu'avec le programme BATCHMIN (qui traite moins bien les liaisons hydrogène). Ensuite nous avons mis les conformères les plus stables en présence des cations et nous avons cherché pour chaque configuration de l'ose le complexe d'énergie la plus basse. Enfin, pour une des formes αP^4C_1 les plus stables, nous avons ajouté, une par une, six molécules d'eau près du site d'interaction cation–talose.

Resultats

Stéréisomères du D-talose

Les caractéristiques géométriques des formes cycliques les plus stables du D-talose (en phase gazeuse) sont consignées dans les tableaux 1*a*–1*c*. Les conformations semblent stabilisées chacune par un grand nombre d'interactions du type liaison hydrogène comme l'indiquent les distances entre atomes H et O de groupes hydroxyles voisins inférieures à la somme des rayons de van der Waals atomiques, mais avec des géométries défavorables en ce qui concerne les angles O—H...O. Les chélations les plus typiques (avec la distance H...O ≤ 2,5 Å et l'angle O—H...O > 110°) sont données dans les tableaux 2*a*–2*c*. Il n'apparait pas de relation nette entre le nombre de ces chélations typiques et les stabilités relatives des différents conformères.

Les populations de Boltzmann globales calculées (en phase gazeuse) pour les différentes structures cycliques du D-talose obtenues par la méthode AM1 sont respectivement de 16,69%, 1,13%, 0,03%, pour αPC_1 αP (flex), αP^1C_4; 6,02%, 1,44%, 0,85% pour βP^4C_1, βP (flex), βP^1C_4; 66,83% et 7,01% pour αF et βF. La précision des calculs ne permet pas le calcul exact des populations conformationnelles, mais permet de prévoir correctement qu'il y a mélange des stéréoisomères, avec des populations du même ordre de grandeur; les effets de solvant et les différences d'entropie liées aux rotations des groupes OH dans les positions axiales et équatoriales et aux flexibilités des cycles, n'ont pas été pris en compte pour les calculs des équilibres conformationnels.

L'anomère αP se présente majoritairement sous une forme chaise stable $^4C_1$ et de façon minoritaire sous des formes flexibles bateau et croisée; la forme chaise $^1C_4$ parait négligeable. De même l'anomère βP est surtout représenté par la chaise $^4C_1$ et quelques formes croisées et chaise $^1C_4$. Les formes flexibles sont plus gauchies que les chaises (valeurs plus élevées du paramètre q de Cremer). αF se présente comme un mélange de formes croisées et enveloppes assez aplaties, et βF plutôt comme un ensemble de formes enveloppes aussi plates. Les dessins correspondants aux conformères les plus stables de chaque série sont représentés sur les figures 1*a* et 1*b*.

Complexes cation–D-talose

L'étude a été réalisée avec les cations Pb^{2+} et Hg^{2+} (de numéro 25), sur l'ensemble des diastéréoisomères du D-talose décrits dans les tableaux 1*a*–1*c*. Pour chaque série, nous n'avons décrit dans les tableaux 3 et 4 que les complexes des cations dans une fenêtre énergétique de 3 kcal mol^{-1} au-dessus du plus stable. Pour les série $^1C_4$, les cations ont parfois induit la transformation de la chaise en forme flexible : les complexes correspondants ont alors été comptabilisés avec ceux de la même structure.

Cas de Pb^{2+}

Afin de déterminer le site privilégié de fixation de Pb^{2+} par exemple sur l'α-D-talopyranose (αP^4C_1), nous avons effectué différentes optimisations par AM1 en faisant varier la distance d entre Pb^{2+} et O_8 de 2 à 3,6 Å par incréments de 0,2 Å. Le tracé des courbes ΔH_f^0 et des indices de liaison Pb—O_8, Pb—O_9 et Pb—O_{10} en fonction de d, montrent que la distance optimale est obtenue pour $d \approx 2{,}3$ Å, ce qui correspond bien à la distance Pb—O observée dans les complexes cristallins de Pb(II) (16). À partir d'un complexe tricoordiné, nous avons ensuite fait varier une des autres distances Pb—O (ne correspondant pas à une liaison) par pas de 0,5 Å jusqu'à une distance de 2,3 Å afin de chercher d'autres types de coordination conduisant à des complexes stables. Nous avons opéré de même pour les autres isomères du talopyranose et du talofuranose décrits dans les tableaux 1*a*–1*c*. Les résultats obtenus figurent dans le tableau 3. Les complexes les plus stables sont visualisés dans les figures 2*a* et 2*b*. La considération des distances interatomiques Pb—O_i ainsi que des indices de liaison et l'examen des figures 2 montrent que Pb^{2+} se fixe toujours sur trois atomes d'oxygène, sauf pour les conformations les plus stables de αF pour lesquelles Pb^{2+} est tétetracoordiné. Les interactions de type liaison hydrogène sont très peu nombreuses et sont données dans le tableau 4. Pour les complexes stables, il en reste en général une seule, plus forte que celle signalée dans la forme correspondante de l'ose, parfois accompagnée d'une autre plus faible.

Pour les talopyranoses : il existe une séquence *ax-eq-ax* de trois groupes hydroxyle du cycle consécutifs pour αP^4C_1, βP^4C_1 et βP^1C_4. Effectivement, les coordinations avec le cation utilisent ces orientations pour les plus stables, mais pas uniquement (voir $\beta P^4C_1Pb^{2+}$). Pour αP^1C_4 (qui correspond aussi au complexe le moins stable), cette séquence n'existe pas et l'hydroxyle du groupe -CH_2OH est impliqué ainsi que deux hydroxyles du cycle. En ce qui concerne les formes flex-

Tableau 1*a*. Caractéristiques AM1 des isomères du D-talopyranose $^4C_1$.

	ΔH_f^0 (kcal/mol)	Orientation[a]	Paramètres de Cramer			Populations[b] (%)
			q	θ	φ	
αP^4C_1 1	−305,76	CG.gt.gt.gg.tg	0,535	170,1	19,2	10,77
2	−304,67	GT.gg.gt.tg.pg.gg	0,526	165,1	33,0	1,73
3	−304,41	GG.gt.gg.gg.gg.gg	0,532	170,7	14,9	1,11
4	−304,21	GT.gg.gt.gg.gg.gt	0,522	176,8	1,0	0,80
5	−303,82	GT.gg.gt.gg.gg.pc	0,548	164,2	36,6	0,41
6	−303,80	GT.gg.gt.gg.gg.tg	0,531	172,0	17,2	0,40
7	−303,76	GT.gg.gt.gt.gg.gg	0,530	168,8	24,8	0,37
8	−303,63	PC.gt.gt.tg.gg.gg	0,520	166,3	32,7	0,30
9	−303,32	GG.gg.gt.tg.pg.gg	0,529	163,2	33,5	0,18
10	−303,27	TG.gt.gt.gg.gp.gt	0,515	178,5	310,2	0,16
11	−303,25	GG.gg.gt.gg.gg.pc	0,546	164,6	35,2	0,16
12	−302,86	TG.gt.gt.gt.gg.gg	0,519	172,0	18,4	0,08
13	−302,81	GG.gt.gt.tg.pg.pg	0,514	170,8	17,5	0,08
14	−302,80	GP.gg.gt.gg.gp.gt	0,525	175,9	18,5	0,07
15	−302,62	GG.gg.gt.gt.gg.gg	0,533	167,7	24,2	0,05
βP^4C_1 1	−304,93	GG.gt.gg.gg.gg.tg	0,566	176,6	100,6	2,68
2	−304,48	GT.gg.gg.tg.pg.gg	0,556	173,5	66,7	1,25
3	−303,88	GT.gg.gp.gt.gg.gg	0,545	172,6	45,7	0,45
4	−303,75	GT.gg.gg.gg.gp.gt	0,556	173,5	170,7	0,36
5	−303,62	GT.gg.cp.gt.gg.gg	0,551	176,4	43,7	0,29
6	−303,36	TG.gt.gg.tg.pg.gg	0,549	175,2	86,0	0,19
7	−303,22	GT.gg.gg.gg.gg.tg	0,562	176,3	140,9	0,15
8	−303,01	TG.gt.cp.gt.gg.gg	0,543	179,4	109,9	0,11
9	−303,01	TG.gt.cp.gt.gg.gg	0,538	176,7	59,4	0,11
10	−302,84	GG.gt.gg.tg.pg.pg	0,546	178,8	149,7	0,08
11	−302,80	GT.gg.gg.gg.gg.pc	0,575	171,3	78,4	0,07
12	−302,80	TG.gt.gg.gg.gp.gt	0,553	170,8	178,6	0,07
13	−302,72	GG.gg.cp.gt.gg.gg	0,546	173,4	36,5	0,07
14	−302,69	GG.gg.gg.tg.pg.gg	0,557	173,8	62,2	0,06
15	−302,53	TG.gg.gg.gg.gg.tg	0,556	174,6	175,5	0,05
16	−301,79	GP.gg.gg.gg.gp.gt	0,560	173,0	169,6	0,01
17	−301,50	TG.gt.gg.gg.gg.pg	0,564	170,9	121,1	0,01
18	−301,49	GG.gt.gt.gt.gg.gg	0,540	176,1	240,4	0,01

[a]Dispositions de la chaîne exocyclique et des groupes OH décrites dans l'ordre pour C_6-O_{12} (dièdres O_{12}-C_6-C_5-O_{11}, O_{12}-C_6-C_5-C_4) (lettres majuscules), H-O_{12} (H-O_{12}-C_6-C_5, H-O_{12}-C_6-H), H-O_7 (H-O_7-C_1-O_{11}, H-O_7-C_1-C_2), H-O_8 (H-O_8-C_2-C_1, H-O_8-C_2-C_3), H-O_9 (H-O_9-C_3-C_2, H-O_9-C_3-C_4) et H-O_{10} (H-O_{10}-C_4-C_3, H-O_{10}-C_4-C_5).

[b]Les pourcentages ont été calculés selon une distribution de Boltzmann des populations en phase gazeuse de tous les isomères, en utilisant les ΔH_f^0, sans tenir compte des effets entropiques.

ibles, les coordinations peuvent aussi utiliser O_{18} comme le montre la figure 2*a*.

Pour les talofuranoses : la forme βF est la seule à posséder sur le cycle trois OH consécutifs en positions *cis-cis-cis*, et le cation est lié à ces trois groupes (tableau 3). Pourtant les complexes correspondants sont beaucoup moins stables que ceux de αF qui n'a pas cette séquence favorable et pour laquelle le cation est lié à l'oxygène de l'hétérocycle, à un hydroxyle du cycle et à un hydroxyle (voire deux pour αFPb 1 et 2) du groupe -CHOH-CH_2OH exocyclique (figure 2*b*).

Cas de Hg^{2+}

Les différentes formes de complexes figurant dans le tableau 3 ont été recaluculées par AM1, en remplaçant Pb par Hg. Nous avons cherché par la méthode décrite plus haut d'autres types de coordination plus stables. Les résultats obtenus sont consignés dans le tableau 5. On peut observer une coordination différente de celle des complexes du plomb. Elle est égale à 4 (voire 5) pour les formes les plus stables, et 3 pour les moins stables. Les liaisons hydrogène intramoléculaires peu nombreuses sont données tableau 6. Pour les talopyranoses : les prédictions d'Angyal concernant la séquence *ax-eq-ax* ne sont pas vérifiées pour αP^4C_1 et βP^4C_1. La configuration la plus stable est la forme flexible βP (flex) Hg^{2+} qui est pentacoordinée.

Mêmes conclusions pour les talofuranoses où la forme βF est encore de très loin la moins stable donc inexistante vis-à-vis de αF qui est tétracoordinée.

Addition de molécules d'eau sur le complexe

Afin d'avoir des renseignements sur les phénomènes primaires de solvatation en milieu aqueux, nous avons ajouté une à une jusqu'à six molécules d'eau sur un complexe de αP^4C_1

Can. J. Chem. Downloaded from www.nrcresearchpress.com by 65.111.164.53 on 09/08/12
For personal use only.

Tableau 1*b*. Caractéristiques AM1 des isomères du D-talopyranose $^1C_4$ et flexibles.

		ΔH_f^0 (kcal/mol)	Orientation[a]	Paramètres de Cramer q	θ	φ	Populations[b] (%)
αP(flex)	1	−304,23	GG.gt.gt.pg.gg.gg	0,695	87,7	120,1	0,823
	2	−303,19	TG.gt.gt.gg.gg.gp	0,710	89,2	111,8	0,140
	3	−303,08	GT.gg.gt.pg.gg.gg	0,707	88,9	112,6	0,117
	4	−302,12	GG.gt.gt.gg.tg.pg	0,680	94,1	87,9	0,023
	5	−301,60	GG.pc.gt.gg.gg.gp	0,713	89,5	108,2	0,010
	6	−301,53	GT.gg.gg.gg.gg.gg	0,709	88,3	107,8	0,009
	7	−300,88	GG.gt.gg.gg.tg.pg	0,698	91,5	79,1	0,003
	8	−300,86	GG.gg.gt.gg.tg.gg	0,697	97,6	76,7	0,003
	9	−300,56	GG.gt.gg.gg.gg.tg	0,741	96,2	334,4	0,002
	10	−300,33	GT.gg.gt.gt.gt.gg	0,711	90,1	82,7	0,001
	11	−300,32	PT.gt.gt.gg.tg.gg	0,713	90,4	79,7	0,001
	12	−300,24	TG.gt.gt.gt.gt.gg	0,691	97,4	80,9	0,001
αP$^1C_4$	1	−301.58	GT.gg.gp.gt.gt.gg	0,537	6,7	27,0	0,009
	2	−301,48	PP.gt.gp.gt.gt.gp	0,539	9,1	10,3	0,008
	3	−301,17	TG.gg.gp.gt.gt.gg	0,543	4,7	23,6	0,005
	4	−300,74	CP.gt.gp.gt.gt.gg	0,540	6,3	351,6	0,002
	5	−300,49	CP.gt.gg.gg.gg.gp	0,516	9,3	82,0	0,001
	6	−300,41	GG.gg.gp.gt.gt.gg	0,524	12,2	2,6	0,001
	7	−300,13	PG.pg.gg.gg.gg.cp	0,534	20,6	357,1	0,001
	8	−300,06	PC.gt.gp.gt.gt.gg	0,528	13,7	20,3	0,001
βP(flex)	1	−304,21	GT.gg.gt.gg.gg.gg	0,721	91,5	42,3	0,799
	2	−303,37	GG.gg.gt.gg.gg.pg	0,716	90,9	41,2	0,192
	3	−303,02	GG.gt.gp.gg.gg.tg	0,717	91,3	41,4	0,107
	4	−302,86	GG.gt.gt.gg.pg.pg	0,703	88,5	38,4	0,080
	5	−302,82	GT.gg.cp.gg.gg.gt	0,710	88,0	41,5	0,076
	6	−302,81	GG.gt.gg.gg.tg.pg	0,698	89,3	74,5	0,075
	7	−302,33	GT.gg.gt.gg.gg.gt	0,674	88,0	53,4	0,033
	8	−302,23	GG.gt.gt.gg.tg.tg	0,714	90,1	43,4	0,028
	9	−301,90	GT.gg.gp.gp.gt.gt	0,637	97,5	28,4	0,016
	10	−301,69	TG.gt.gt.gg.gg.gt	0,657	87,0	59,2	0,011
	11	−301,65	GG.gg.gt.gg.gt.gp	0,626	90,3	348,8	0,011
	12	−301,33	CG.gg.gg.gg.tg.gg	0,714	92,0	65,5	0,006
	13	−301,19	GT.gg.gg.gp.gt.gg	0,709	89,6	75,1	0,005
	14	−301,11	GP.gg.cp.gg.gg.gt	0,712	88,1	41,3	0,004
βP$^1C_4$	1	−303,86	GG.gt.gt.gg.gg.gg	0,439	18,3	73,8	0,442
	2	−303,35	GG.pg.cp.gg.gp.cp	0,477	6,6	108,6	0,186
	3	−302,78	PC.gt.gt.gg.tg.gg	0,467	15,4	75,7	0,071
	4	−302,51	GT.gg.pg.gg.tg.tg	0,455	0,7	108,2	0,045
	5	−302,40	GG.pt.tg.pc.gg.gg	0,488	6,5	93,0	0,038
	6	−302,15	GG.tg.cp.gg.gg.gp	0,449	17,0	66,0	0,025
	7	−301,99	GG.tg.cp.gg.gg.gp	0,454	19,7	61,1	0,019
	8	−301,55	PC.pt.pg.gg.tg.gg	0,492	8,4	110,5	0,009
	9	−301,41	PG.gt.gt.gg.gt.gg	0,426	4,6	294,6	0,007
	10	−301,13	GT.tg.gt.gg.gp.gp	0,487	5,5	58,8	0,004
	11	−301,09	GG.gg.gg.cp.gt.gp	0,450	11,5	104,9	0,004

[a,b]Mêmes légendes que pour le tableau 1*a*.

avec Pb^{2+} et Hg^{2+}. Les atomes d'oxygène des molécules d'eau sont successivement nomérotés 26, 29, 32, 35, 38 et 41. Chaque système a été optimisé par AM1 (cf résultats tableau 7). La disposition de la chaîne exocyclique semble inchangée, et les liaisons hydrogène sont données tableau 8.

Discussion

Analyse conformationnelle du D-talose

L'équilibre de distribution des anomères calculé est le suivant : αP = 18%, βP = 8%, αF = 67% et βF = 7%. En solu-

Can. J. Chem. Downloaded from www.nrcresearchpress.com by 65.111.164.53 on 09/08/12
For personal use only.

Tableau 1*c*. Caractéristiques AM1 des isomères du D-talopyranose.

	ΔH_f^0 (kcal/mol)	Orientation[a]	Paramètres de Cramer		Populations[b] (%)
			q	θ	
αF 1	−306,19	GG.GT.GP.gt.pc.gg.tg.gg	0,161	138,4	22,69
2	−306,10	GG.GT.GP.gt.pc.gg.gg.gt	0,166	154,8	19,43
3	−305,42	GG.GT.GG.gt.gg.gt.gg.gt	0,155	147,2	6,13
4	−305,35	GG.GT.GG.gt.gg.gt.tg.gg	0,159	130,9	5,43
5	−305,14	GG.GT.GT.gt.gg.gt.gg.gt	0,098	157,0	3,82
6	−305,05	GG.GT.GT.gt.gg.gt.tg.gg	0,097	133,8	3,29
7	−305,02	GP.PT.CP.gg.gg.gg.gg.gt	0,132	176,0	3,16
8	−304,50	GG.GT.GP.gt.pc.gg.gt.gg	0,153	151,4	1,31
9	−304,03	GG.GT.GT.gg.pc.gg.gg.gt	0,137	164,7	0,59
10	−303,39	GT.TG.GT.gt.gt.gt.gg.gt	0,128	153,8	0,20
11	−303,22	GG.GT.GT.tg.tg.gg.tg.gg	0,137	139,1	0,15
12	−303,13	GG.GT.GT.tg.tg.gg.gg.gt	0,140	158,2	0,13
13	−303,03	GG.GT.GP.gt.pc.gg.gt.gt	0,154	119,1	0,11
βF 1	−304,76	GG.GT.GG.gt.gg.gg.gp.gt	0,161	8,8	2,03
2	−304,65	GG.GT.GG.gt.gg.gg.gt.gg	0,132	250,5	1,67
3	−304,24	GG.GT.GT.gt.gg.gp.gp.gt	0,153	4,5	0,84
4	−304,12	GG.GT.GT.gt.gg.gg.gt.gg	0,149	255,4	0,69
5	−303,64	GG.GT.CP.gg.gg.gp.gp.gt	0,144	2,9	0,30
6	−303,53	GT.TG.GT.gt.gt.cp.gp.gt	0,136	17,5	0,25
7	−303,53	GG.GT.CP.gg.gg.gg.gt.gg	0,142	253,7	0,25
8	−303,41	GT.TG.GT.gt.gt.gp.gg.gt	0,106	337,4	0,21
9	−303,32	GT.TG.GT.gt.gt.gg.gt.gg	0,130	249,6	0,18
10	−303,30	GT.TG.GT.gt.gt.gt.gg.gg	0,286	39,1	0,17
11	−302,99	GT.TG.GG.gg.gt.gg.gt.gg	0,162	257,9	0,10
12	−302,95	GT.TG.GG.gg.gt.gp.gp.gt	0,151	28,0	0,10
13	−302,78	GT.TG.GT.gt.gt.gg.tg.gg	0,092	181,4	0,07
14	−302,75	GT.TG.GT.gt.gt.gp.cp.cp	0,156	279,3	0,07
15	−302,61	GT.TG.TG.gg.gt.gg.gt.gg	0,142	253,4	0,05
16	−302,04	GT.TG.GG.gg.gt.gg.gg.tg	0,257	33,5	0,02
17	−301,88	GG.GT.GG.gt.gg.gg.tg.tg	0,182	264,7	0,02
18	−301,84	GT.TG.GG.gt.gg.gp.cp.cp	0,212	281,8	0,02
19	−301,82	GT.TG.GG.gg.gt.gg.tg.tg	0,198	261,1	0,01
20	−301,53	GT.TG.GT.gt.gt.gg.gg.tp	0,258	34,0	0,01

[a]Les orientations dans la chaîne CHOH-CH_2OH ont été décrites dans l'ordre par les dièdres O_{11}-C_5-C_4-O_{10}, O_{11}-C_5-C_4-C_3, C_6-C_5-C_4-O_{10}, C_6-C_5-C_4-C_3, O_{12}-C_6-C_5-O_{11}, O_{12}-C_6-C_5-C_4 (lettres majuscules) et celles des OH par les dièdres H-O_{12}-C_6-C_5, H-O_{12}-C_6-H, H-O_{11}-C_5-C_4, H-O_{11}-C_5-C_6, H-O_7-C_1-O_{10}, H-O_7-C_1-C_2, H-O_8-C_2-C_1, H-O_8-C_2-C_3, H-O_9-C_3-C_2, H-O_9-C_3-C_4 (lettres minuscules).

[b]Même légende que pour le tableau 1*a*.

tion aqueuse, les résultats de la RMN donnent : αP = 29%, βP = 20%, αF = 20% et βF = 11% (17). Cette différence est vraisemblablement due à la prédominance des liaisons hydrogène intramoléculaires dans le cas du ligand isolé, et aux liaisons hydrogène intermoléculaires en milieu aqueux. On peut également observer que dans le cas des pyranosiques, les formes αP^4C_1 sont avantagées par rapport aux βP^4C_1, alors que les formes βP^1C_4 sont avantagées par rapport aux αP^1C_4. De même pour les furanosiques, les formes α sont prévues plus stables que les formes β. Ce résultat est en accord avec l'effet anomère (11, 12) qui stabilise en phase gazeuse la conformation pour laquelle le OH anomère est axial. Les orientations privilégiées des groupements exocycliques par rapport aux liaisons C_5—O_{11} et C_5—O_4 pour les formes pyranosiques sont dans l'ordre GG et GT; pour les furanosiques, par rapport aux liaisons C_5—O_{10} et C_5—O_4 : GG, GT, GP et GG, GT, GG. Il n'y a pas de règle générale pour les positions des liaisons OH du cycle.

Complexes cations–D-talose

Dans le cas des formes pyranosiques de plus basse énergie, l'orientation de la chaîne exocyclique est en général inchangée par rapport au ligand isolé. L'orientation GG reste prédominante à l'exception de $\beta P^1C_4Pb^{2+}$ orienté PG. Les orientations des OH du cycle quant à elles sont en général modifiées car les liaisons hydrogène intramoléculaires deviennent négligeables devant la forte liaison de coordination avec le cation. À l'inverse, les formes furanosiques ne conservent pas l'orientation de la chaîne exocyclique plus longue donc plus apte à se déformer pour participer à la liaison de coordination. On peut

Can. J. Chem. Downloaded from www.nrcresearchpress.com by 65.111.164.53 on 09/08/12
For personal use only.

Fig. 2*a*. Complexes des conformères du D-talopyranose avec Pb^{2+} (l'ion Pb^{2+} est hachuré).

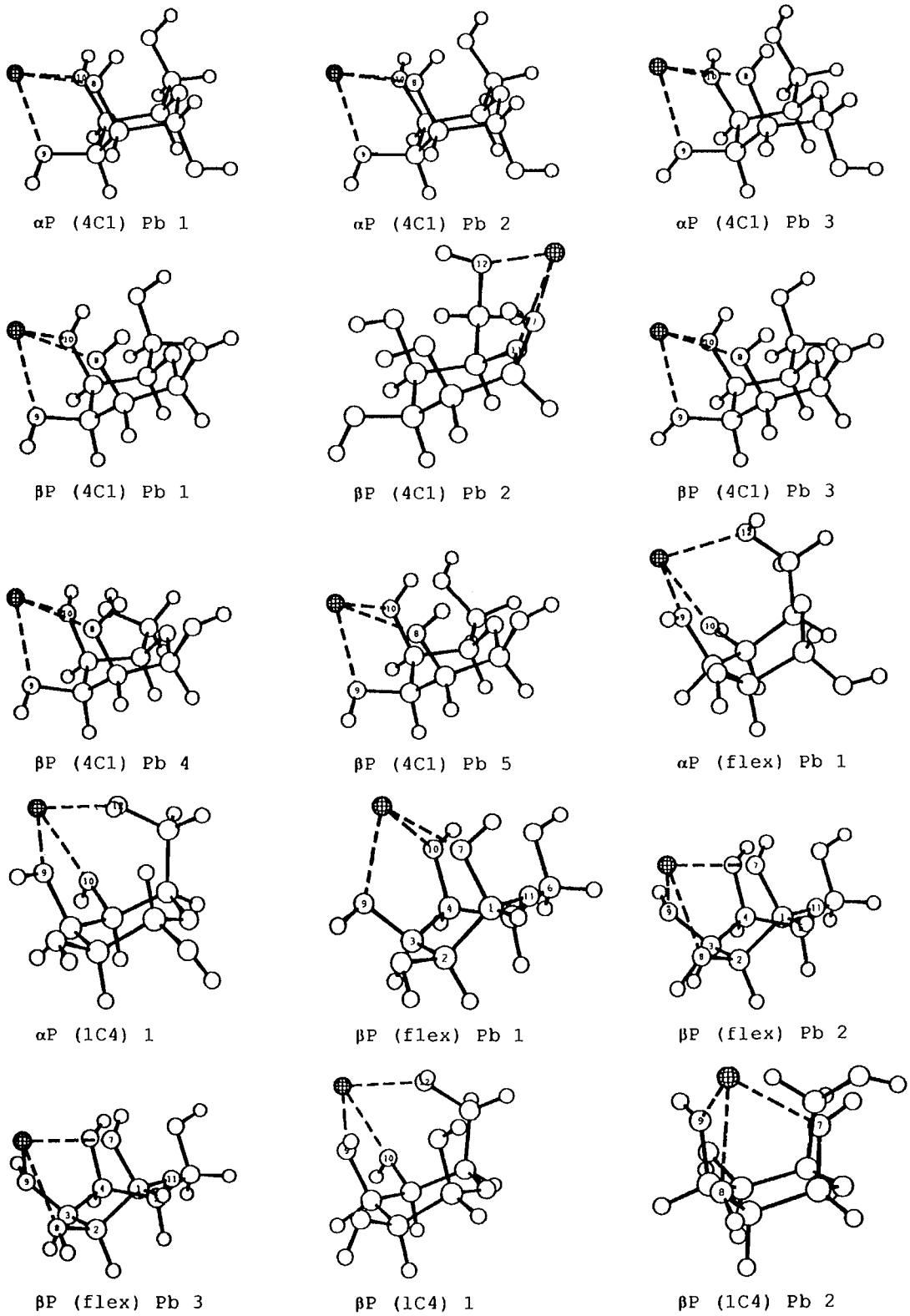

Can. J. Chem. Downloaded from www.nrcresearchpress.com by 65.111.164.53 on 09/08/12
For personal use only.

Can. J. Chem. Downloaded from www.nrcresearchpress.com by 65.111.164.53 on 09/08/12
For personal use only.

Tableau 2*a*. Chélations des isomères du D-talopyraonse $^4C_1$.

		a	*b*	*r*	θ[a]	*a*	*b*	*r*	θ[a]	*a*	*b*	*r*	θ[a]
αP$^4C_1$	1	8	10	2,120	127,6	10	12	2,106	125,5				
	2	10	8	2,290	120,2	9	10	2,234	113,6				
	3	8	10	2,120	125,9	10	12	2,104	126,4				
	4		10	2,192	123,7	9	8	2,230	113,9				
	5	8	10	2,268	130,7	10	11	2,370	110,3				
	6	8	10	2,138	126,1								
	7	10	8	2,202	121,2								
	8	10	8	2,287	121,5	12	10	2,284	123,1	9	10	2,237	113,7
	9	12	10	2,122	124,4	10	8	2,306	118,9	9	10	2,240	113,2
	10	8	10	2,223	123,4	12	10	2,253	121,4	9	8	2,230	114,1
	11	8	10	2,265	129,5								
	12	10	8	2,198	122,7	12	10	2,323	123,0				
	13	9	11	2,203	114,1								
	14	8	10	2,200	122,9	12	10	2,176	131,9	9	8	2,221	114,1
	15	12	10	2,108	123,5	10	8	2,201	119,8				
βP$^4C_1$	1	8	10	2,102	128,5	10	12	2,106	125,3				
	2	10	8	2,229	120,1	9	10	2,216	13,8				
	3	10	8	2,192	122,7								
	4	8	10	2,194	124,5	9	8	2,246	113,9				
	5	10	8	2,150	124,0								
	6	10	8	2,231	121,7	12	10	2,323	122,1	9	10	2,216	113,9
	7	8	10	2,132	126,4								
	8	10	8	2,154	125,5	12	10	2,330	122,2				
	9	10	8	2,185	124,7	12	10	2,332	122,3				
	10	9	10	2,184	114,2								
	11	8	20	2,237	132,0								
	12	8	10	2,238	124,0	12	10	2,260	120,5				
	13	10	8	2,173	122,0	12	10	2,104	120,7				
	14	9	10	2,220	113,4	10	8	2,235	117,6	12	10	2,117	116,9
	15	8	10	2,146	126,9	10	12	2,309	123,6				
	16	8	10	2,208	122,9	12	10	2,154	130,9				
	17	10	8	2,242	114,0								

[a]Chélation O_a—H...O_b : *r* = distance H...O_b en Å; θ = angle (O—H...O) en degrés.

Fig. 2*b*. Complexes des conformères du D-talufuranose avec Pb^{2+} (les ions Pb^{2+} sont hachurés).

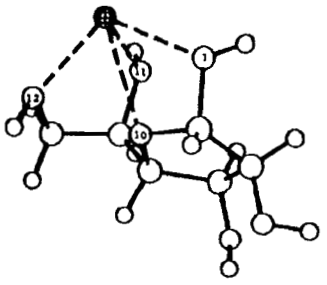

αF Pb 1

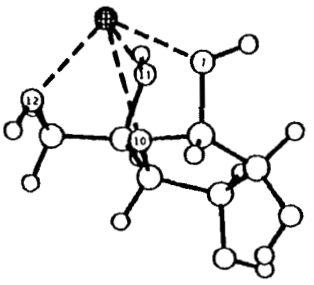

αF Pb 2

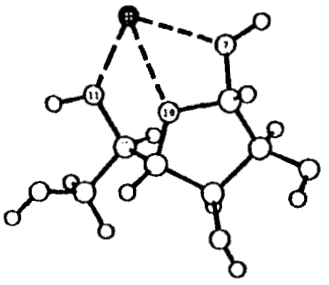

αF Pb 3

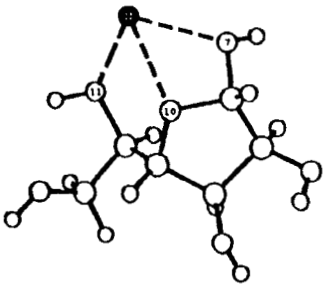

αF Pb 4

Can. J. Chem. Downloaded from www.nrcresearchpress.com by 65.111.164.53 on 09/08/12
For personal use only.

Tableau 2*b*. Chélations des isomères du D-talopyranose $^1C_4$ et formes flexibles.

		a	*b*	*r*	θ[a]	*a*	*b*	*r*	θ[a]	*a*	*b*	*r*	θ[a]
αP(flex)	1	8	9	2,247	112,2	9	11	2,267	120,0	9	12	2,410	137,0
		10	22	2,320	117,4								
	2	8	9	2,299	111,0	9	11	2,217	122,5	10	9	2,254	111,1
	3	9	11	2,217	122,5	8	9	2,292	111,2	10	9	2,276	110,1
	4	10	12	2,190	121,1								
	5	8	9	2,300	110,8	9	11	2,228	112,7	10	9	2,211	121,9
	6	8	9	2,326	110,5	9	11	2,227	122,2				
	7	10	12	2,210	119,7								
	9	8	10	2,192	124,5	10	12	2,162	119,6				
	10	12	10	2,232	123,0								
αP^1C_4	2	10	9	2,213	110,9	12	10	2,273	127,8				
	5	9	12	2,198	158,9	10	9	2,308	112,6				
	6	9	8	2,220	110,2	12	9	2,062	133,1				
	7	9	12	2,069	132,5	12	9	2,144	114,5				
	8	10	12	2,120	124,8	12	9	2,090	113,8				
βP(flex)	1	9	7	2,359	117,4	10	7	2,139	116,8	10	7	2,139	133,3
	2	9	7	2,346	117,4	10	7	2,141	130,4	12	10	2,132	112,7
	3	7	10	2,100	137,8	9	7	2,476	120,8	10	12	2,108	122,9
	4	9	7	2,347	115,2	10	7	2,227	119,1	10	12	2,387	110,7
	5	7	10	2,230	121,8	9	7	2,152	132,0				
	6	7	9	2,161	123,9	10	12	2,206	120,5				
	7	9	7	2,108	129,1								
	8	7	9	2,307	121,0	7	10	2,191	141,4	10	12	2,086	133,1
	9	7	10	2,080	140,9	8	7	2,219	112,3				
	10	9	7	2,104	128,2	12	10	2,260	120,2				
	11	7	12	2,138	121,3	10	7	2,110	117,8	12	10	2,080	122,2
	12	7	9	2,193	121,7								
	13	7	9	2,215	118,1	8	7	2,200	113,4				
	14	7	10	2,291	114,2	9	7	2,130	132,0	12	10	2,137	133,0
βP^1C_4	1	9	7	2,209	125,6	9	12	2,132	135,5	10	12	2,406	117,8
		12	7	2,128	127,3								
	2	7	9	2,199	132,1	8	7	2,275	112,4	12	7	2,311	130,0
	3	9	7	2,057	137,8	9	12	2,209	114,8	10	9	2,193	115,2
	4	12	7	2,130	135,5								
	5	7	9	2,139	135,2	12	7	2,255	131,1				
	6	8	9	2,195	114,8	9	7	2,217	123,0	9	12	2,082	144,0
		10	12	2,454	119,0	12	7	2,083	120,3				
	7	9	7	2,103	130,5	9	12	2,115	130,2	10	9	2,226	110,2
		10	12	2,426	113,6								
	8	7	9	2,126	136,3	10	12	2,072	132,8				
	9	10	12	2,158	125,9	12	7	2,145	134,9				
	10	7	9	2,415	119,0	7	12	2,015	152,0	8	7	2,178	115,2
		12	9	2,100	116,6								

[a]Chélation O_a—H...O_b : *r* = distance H...O_b en Å; θ = angle (O—H...O) en degrés.

remarquer pour les formes αF, qui sont les plus stables, que deux sites de coordination sont constitués par les atomes d'oxygène 11 et 12 de la chaîne exocyclique, portant ainsi la coordination totale à 4. Cette dernière est plus stable que la coordination 3 sur les sites hydroxyles consécutifs du cycle en position *cis-cis-cis*.

Un résultat important de cette étude est que, en milieu isolé, l'association du D-talose avec Hg^{2+} est beaucoup plus forte que celle avec Pb^{2+}. On peut constater en effet que dans les complexes isolés le mercure est plus fortement lié aux atomes d'oxygène du ligand que le plomb, aussi bien en ce qui concerne les énergies de liaison que le nombre de coordinations : tétracoordinances nombreuses, voire pentacoordinance avec Hg; coordinance 3 et une seule conformation de plus basse énergie tétracoordinée avec Pb. Calculons, par exemple, dans le cas des formes αP^4C_1 de plus basse énergie, les enthalpies des réactions de complexation suivantes :

Fig. 3*a*. Complexes des conformères du D-talopyranose avec Hg^{2+} (l'ion Hg^{2+} est hachuré).

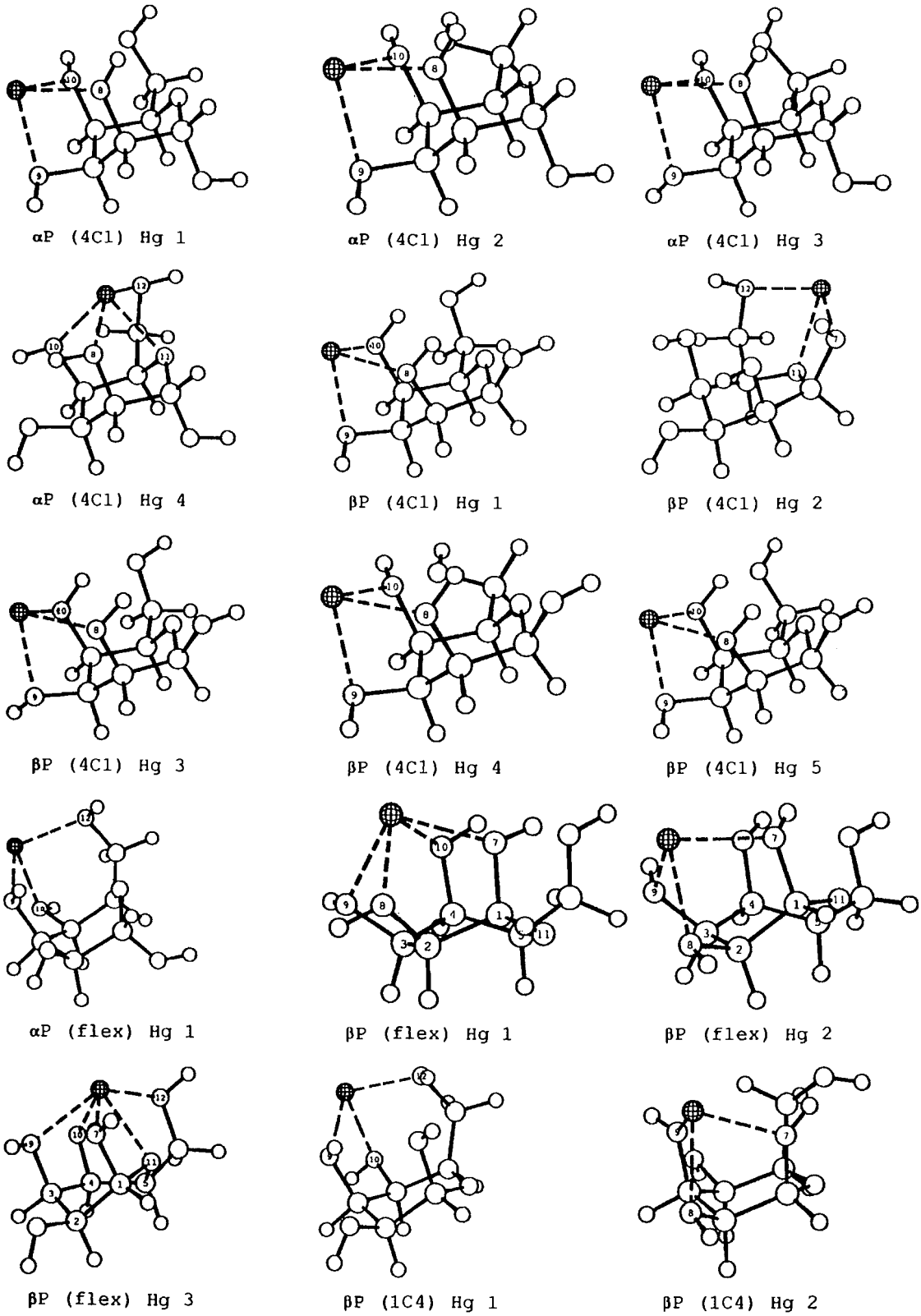

Can. J. Chem. Downloaded from www.nrcresearchpress.com by 65.111.164.53 on 09/08/12
For personal use only.

Tableau 2*c*. Chélations des isomères du D-talofuranose.

		a	*b*	*r*	θ[a]	*a*	*b*	*r*	θ[a]	*a*	*b*	*r*	θ[a]
αF	1	7	11	2,170	147,2	12	10	2,211	125,6				
	2	7	11	2,165	147,8	12	7	2,441	133,1	12	10	2,208	125,8
	3	11	7	2,224	134,2	12	10	2,106	122,2				
	4	11	7	2,212	134,2	12	10	2,107	122,7				
	5	11	7	2,184	149,0								
	6	11	7	2,184	149,0								
	7	7	11	2,174	132,1								
	8	7	11	2,159	148,9	12	10	2,204	126,3				
	9	7	11	2,146	150,1	11	12	2,231	114,3				
	12	7	11	2,143	150,1	11	12	2,260	110,1				
	13	7	11	2,182	146,9	12	10	2,202	126,2				
βF	1	8	7	2,200	110,3	11	12	2,260	110,6	12	10	2,178	124,7
	2	12	10	2,184	125,3								
	3	8	7	2,186	110,7								
	5	8	7	2,175	111,0								
	6	8	7	2,164	111,6								
	10	9	7	2,405	127,5								
	12	11	10	2,195	110,6	8	7	2,168	111,6				
	14	8	7	2,089	111,1	9	8	2,136	111,6				
	15	12	9	2,252	145,8								
	16	11	10	2,232	110,2								
	17	11	12	2,255	110,4	12	10	2,162	124,3				
	18	12	9	2,224	142,3	8	7	2,086	111,6	9	8	2,102	115,2
	19	9	12	2,249	149,0								

[a]Chélation O_a—H...O_b : *r* = distance H...O_b en Å; θ = angle (O—H...O) en degrés.

Fig. 3*b*. Complexes des conformères du D-talofuranose avec Hg^{2+} (les ions Hg^{2+} sont hachurés).

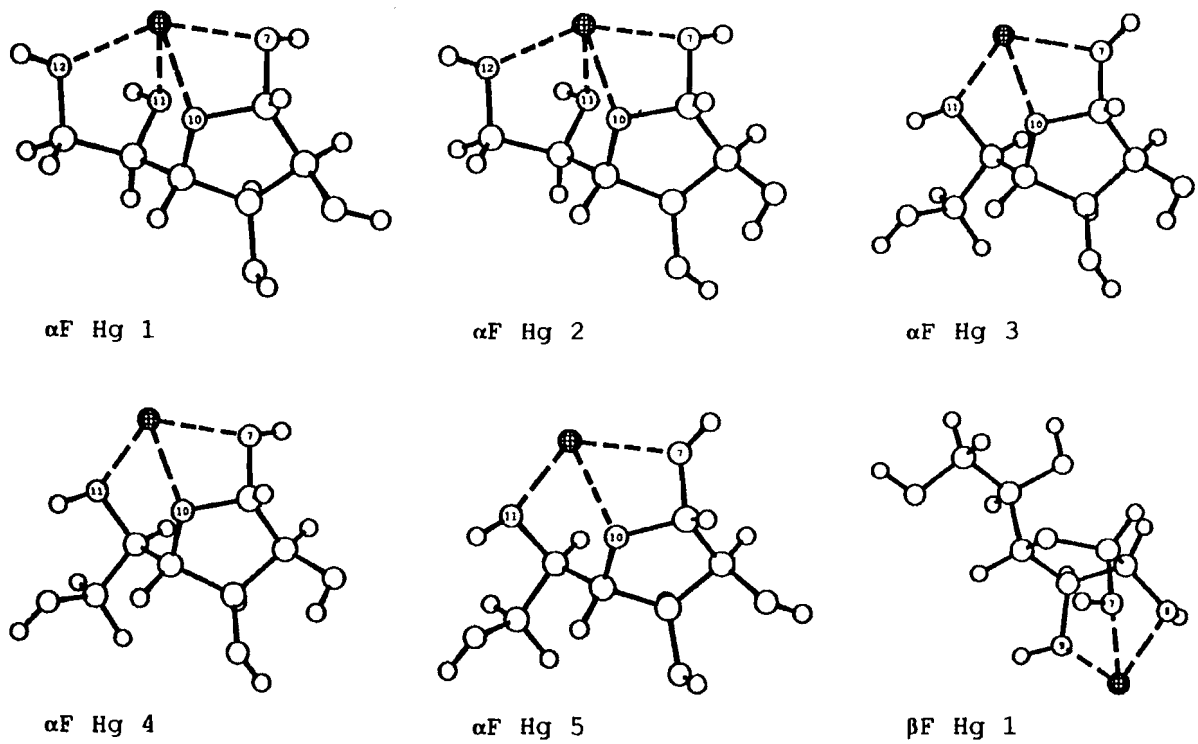

Can. J. Chem. Downloaded from www.nrcresearchpress.com by 65.111.164.53 on 09/08/12
For personal use only.

Can. J. Chem. Downloaded from www.nrcresearchpress.com by 65.111.164.53 on 09/08/12
For personal use only.

Tableau 3. Caractéristiques AM1 des complexes de Pb^{2+} avec les isomères du D-talose.

		ΔH_f^0 (kcal/mol)	Orientation[a]	Paramètres de Cramer			O coordinés à Pb^{2+}
				q	θ	φ	
αP^4C_1 Pb^{2+}	1	138,05	GG.pp.pt.cp.pt.tg	0,582	178,4	196,4	O_8, O_9, O_{10}
	2	138,13	GG.tp.pt.cp.pt.tg	0,581	176,9	206,6	O_8, O_9, O_{10}
	3	138,38	GG.tp.pt.cp.tp.tg	0,582	178,4	196,4	O_8, O_9. O_{10}
βP^4C_1 Pb^{2+}	1	138.14	GG.p.gt.gt.gt.tp	0,544	167,9	67,1	O_8, O_9, O_{10}
	2	138,22	GP.pg.pc.tg.pp.gt	0,461	151,6	336,9	O_7, O_{11}, O_{12}
	3	138,41	GG.pp.gt.gt.tg.pc	0,544	170,8	80,6	O_8, O_9, O_{10}
	4	138,42	PC.tg.gt.ct.gt.tg	0,546	168,1	65,7	O_8, O_9, O_{10}
	5	138,49	PG.tg.gt.gt.gt.pc	0,562	164,3	56,5	O_8, O_9, O_{10}
$\alpha P(flex)Pb^{2+}$	1	139,54	GG.gt.pt.pp.gt.tp	0,661	93,4	130,2	O_9, O_{10}, O_{12}
αP^1C_4 Pb^{2+}	1	147,34	PG.gt.gp.gt.gt.pp	0,493	10,8	332,5	O_9, O_{10}, O_{12}
	2	147,53	TP.pc.gp.gt.gt.tg	0,494	9,0	260,0	O_9, O_{10}, O_{12}
	3	147,73	PG.pp.gp.gt.gt.pp	0,497	21,1	347,9	O_9, O_{10}, O_{12}
$\beta P(flex)Pb^{2+}$	1	137,60	GG.tg.gt.pp.gt.tg	0,694	91,5	40,7	O_7, O_9, O_{10}
	2	138,57	GG.tg.cp.tg.tg.tg	0,695	93,3	40,5	O_7, O_8, O_9
	3	139,98	GG.tg.cp.pt.tg.tg	0,704	93,4	42,8	O_7, O_8, O_9
βP^1C_4 Pb^{2+}	1	137,76	PG.pt.pp.pp.cp.pp	0,469	12,1	43,5	O_9, O_{10}, O_{12}
	2	140,33	CP.pt.ct.pt.tg.pp	0,430	16,0	112,6	O_7, O_8, O_9
αF Pb^{2+}	1	138,90	GG.GT.GG.pp.tg.pc.pp	0,156	246,4		O_7, O_{10}, O_{11}, O_{12}
	2	139,22	GG.GT.GG.pp.tp.pc.gg.pt	0,037	139,2		O_7, O_{10}, O_{11}, O_{12}
	3	140,68	CP.TP.GG.tg.pc.tp.pg.pp	0,160	140,7		O_7, O_{10}, O_{11}
	4	141,08	CP.PP.GG.tg.pc.pc.gg.pp	0,152	141,1		O_7, O_{10}, O_{11}
	5	141,34	CP.PP.GG.tg.pc.tp.tp.gg	0,058	141,3		O_7, O_{10}, O_{11}
	6	141,82	CP.PP.GG.tg.tg.tp.pg.pp	0,153	141,8		O_7, O_{10}, O_{11}
βF Pb^{2+}	1	145,11	GG.GT.TG.tp.tg.gt.tp.tg	0,295	56,6		O_7, O_8, O_9
	2	146,38	GT.TG.PC.tg.pt.gt.tp.tg	0,252	13,5		O_7, O_8, O_9
	3	146,41	GP.TP.TG.gp.gg.gt.pt.tp	0,274	53,8		O_7, O_8, O_9
	4	146,82	GT.TG.PC.pc.pt.gt.pt.tg	0,244	20,3		O_7, O_8, O_9
	5	147,06	GT.TG.PC.tg.pt.gt.pt.tg	0,244	20,9		O_7, O_8, O_9

[a]Même légende que pour le tableau 1a pour les formes pyranosiques et le tableau 1*c* pour les furanosiques.

Tableau 4. Chélations des complexes de Pb^{2+} avec les isomères du D-talose.

		a	b	r	θ[a]	a	b	r	θ[a]
αP^4C_1 Pb^{2+}	1	10	12	1,956	125,8	8	11	2,370	109,6
	2	10	12	1,942	120,9	8	11	2,370	109,6
	3	10	12	1,937	123,3	8	11	2,328	110,5
βP^4C_1 Pb^{2+}	1	10	12	1,931	141,7	8	7	2,073	112,4
	2	12	10	2,133	115,2	7	8	2,023	108,4
	3	10	12	1,935	143,1	8	7	2,091	110,8
	4	10	12	1,951	124,6	8	7	2,059	113,7
	5	10	12	1,946	122,6	8	7	2,067	111,6
$\alpha P(flex)$ Pb^{2+}	1	9	8	2,065	110,3				
αP^1C_4 Pb^{2+}	1	9	8	2,106	106,7				
	2	9	8	2,110	107,3				
	3	9	8	2,052	111,9				
$\beta P(flex)$ Pb^{2+}	1	10	12	1,951	122,1				
	2	10	12	2,022	115,7	7	10	2,168	112,2
	3	10	12	2,020	116,1	7	10	2,180	113,9

Tableau 4. (*concluded*)

		a	*b*	*r*	θ[a]	*a*	*b*	*r*	θ[a]
βP^1C_4 Pb^{2+}	1	9	7	2,196	115,0	12	7	2,009	126,3
	2	7	12	1,947	132,2				
αF Pb^{2+}	3	11	12	2,102	112,4				
	4	11	12	2,103	112,2				
	5	11	12	2,105	112,3				
	6	11	12	2,082	112,7				
βF Pb^{2+}	2	9	12	2,274	120,5				
	4	9	12	2,296	121,5				
	5	9	12	2,323	118,9				

[a]Chélation O_a—H...O_b : *r* = distance H...O_b en Å; θ = angle (O—H...O) en degrés.

Tableau 5. Caractéristiques AM1 des complexes de Hg^{2+} avec les isomères du D-talose.

		ΔH_f^0 (kcal/mol)	Orientation[a]	Paramètres de Cramer			O coordinés à Hg^{2+}
				q	θ	φ	
αP^4C_1 Pb^{2+}	1	194,33	GG.pp.pt.cp.gt.tg	0,593	178,3	311,1	O_8, O_9, O_{10}
	2	194,00	PC.tg.pt.cp.gt.tg	0,590	178,7	278,5	O_8, O_9, O_{10}
	3	195,21	PG.tp.pt.cp.tg.tg	0,594	177,1	234,9	O_8, O_9, O_{10}
	4	176,32	CP.pp.pt.tg.pp.gt	0,551	169,8	180,2	O_8, O_{10}, O_{11}, O_{12}
βP^4C_1 Hg^{2+}	1	195,38	GG.pp.gt.cp.gt.pc	0,552	167,4	64,1	O_8, O_9, O_{10}
	2	186,55	GG.gg.pc.tg.pp.gt	0,460	137,8	333,4	O_7, O_{11}, O_{12}
	3	195,74	GG.pp.gt.cp.tg.pc	0,552	[1]171,5	85,5	O_8, O_9, O_{10}
	4	195,66	PC.tg.gt.cp.gt.tg	0,553	172,01	51,6	O_8, O_9, O_{10}
	5	195,62	GG.tp.gt.cp.gt.pc	0,563	165,2	57,6	O_8, O_9, O_{10}
αP(flex)Hg^{2+}	1	193,27	GG.gt.pt.pp.cp.tg	0,688	93,4	127,4	O_9, O_{10}, O_{12}
αP^1C_4 Hg^{2+}	1	203,47	PG.gt.gp.gt.gt.pp	0,501	7,7	9,4	O_9, O_{10}, O_{12}
	2	201,76	TG.pc.gp.gt.gt.tg	0,512	3,5	246,6	O_9, O_{10}, O_{12}
	3	201,87	GG.tp.gp.gt.ct.gt	0,486	21,9	346,5	O_9, O_{10}, O_{12}
	4	199,74	GT.tg.pc.tg.gg.pt	0,746	81,9	351,5	O_7, O_{11}, O_{12}
βP(flex)Hg^{2+}	1	181,28	GG.tg.cp.tg.tg.tg	0,598	91,8	2,5	O_7, O_8, O_9, O_{10}
	2	195,96	GG.tg.cp.gt.pc.tg	0,697	94,6	38,7	O_7, O_8, O_9
	3	173,39	GG.pp.pp.pp.gt.tg	0,707	84,5	74,4	O_7, O_9, O_{10}, O_{11}, O_{12}
βP^1C_4 Hg^{2+}	1	191,79	GG.gt.pp.pp.cp.gt	0,462	18,4	53,9	O_9, O_{10}, O_{12}
	2	198,42	CP.pt.cp.gt.tg.pp	0,448	21,0	115,3	O_7, O_8, O_9
αF Hg^{2+}	1	173,45	GG.GT.CP.tp.tg.pc.pp.pg	0,121	229,1		O_7, O_{10}, O_{11}, O_{12}
	2	173,55	GG.GT.CP.tp.tg.pc.pg.pt	0,008	156,1		O_7, O_{10}, O_{11}, O_{12}
	3	188,97	CT.TP.GG.tg.gg.pp.pg.pp	0,111	75,7		O_7, O_{10}, O_{11}
	4	189,46	CP.PP.GG.tg.gg.pc.gg.pp	0,102	76,7		O_7, O_8, O_{11}
	5	189,42	CP.PP.GG.tg.gg.pp.tp.gg	0,029	131,0		O_7, O_{10}, O_{11}
	6	204,42	CP.PP.GT.tg.tg.tp.pg.pp	0,153	68,4		O_7, O_{10}, O_{11}
βF Hg^{2+}	1	201,93	GG.GT.TG.tp.tg.gt.tg.tg	0,278	61,4		O_7, O_8, O_9
	2	202,80	GT.TG.PC.tg.pt.gt.tg.tg	0,232	5,5		O_7, O_8, O_9
	3	202,69	GT.TP.TG.tp.gg.gt.gt.pp	0,250	62,6		O_7, O_8, O_9
	4	203,44	GT.TG.PC.pc.pt.gt.gt.tg	0,210	15,3		O_7, O_8, O_9
	5	203,62	GT.TG.PC.tg.pt.gt.gt.tg	0,211	14,2,5		O_7, O_8, O_9

[a]Même légende que pour le tableau 1*a* pour les formes pyranosiques et le tableau 1*c* pour les furanosiques.

Can. J. Chem. Downloaded from www.nrcresearchpress.com by 65.111.164.53 on 09/08/12
For personal use only.

Can. J. Chem. Downloaded from www.nrcresearchpress.com by 65.111.164.53 on 09/08/12
For personal use only.

Tableau 6. Chélations des complexes de Hg^{2+} avec les isomères du D-talose.

		a	*b*	*r*	θ[a]	*a*	*b*	*r*	θ[a]
αP^4C_1 Hg^{2+}	1	10	12	1,964	117,7	8	11	2,422	109,5
	2	10	12	1,972	118,5	8	11	2,413	109,5
	3	10	12	1,946	116,5	8	11	2,342	110,7
	4	10	9	2,154	107,8				
βP^4C_1 Hg^{2+}	1	10	12	1,952	136,2	8	7	2,061	113,5
	2	12	10	2,103	119,0	7	8	2,002	111,0
	3	10	12	1,942	139,0	8	7	2,071	112,9
	4	10	12	1,980	118,26	8	7	2,091	110,5
	5	10	12	1,963	120,8	8	7	2,050	113,7
αP(flex) Hg^{2+}	1	9	8	2,067	110,5				
αP^1C_4 Hg^{2+}	3	9	8	2,034	113,6	8			
βP(flex) Hg^{2+}	1	10	12	1,978	129,1	7	12	139,2	2,151
	2	10	12	2,018	117,2	7	10	2,140	114,6
	3	9	8	2,315	109,3			0	
βP^1C_4 Hg^{2+}	1	9	7	2,182	116,9	12	7	2,005	130,7
	2	7	12	1,931	144,7				
αF Hg^{2+}	3	8	9	2,138	108,1	11	12	2,145	109,8
	4	11	12	2,136	110,6				
	5	11	12	2,153	109,4				
	6	11	12	2,082	112,7	8	9	2,147	108,6
βF Hg^{2+}	2	9	12	2,173	121,1				
	4	9	12	2,165	125,3				
	5	9	12	2,187	121,1				

[a]Chélation O_a—H...O_b : *r* = distance H...O_b en Å; θ = angle (O—H...O) en degrés.

Tableau 7. Caractéristiques AM1 des complexes de Pb^{2+} et Hg^{2+} avec l'isomère αP^4C_1 du D-talose et quelques molécules d'eau.

	ΔH_f^0 (kcal/mol)	Orientation[a]	Paramètres de Cremer			O coordinés au cation
			q	θ	φ	
$(\alpha P^4C_1Pb, 3H_2O)^{2+}$	−96,11	GG.gg.gt.gt.gt.pc	0,509	168,8	124,0	8, 9, 26, 29
$(\alpha P^4C_1Pb, 4H_2O)^{2+}$	−165,32	GG.tp.gt.gt.gt.pg	0,508	162,8	98,2	8, 9, 26, 29, 32
$(\alpha P^4C_1Pb, 5H_2O)^{2+}$	−237,80	GP.pg.gt.pp.gt.tg	0,622	107,6	86,8	8, 9, 26, 29, 32
$(\alpha P^4C_1Pb, 6H_2O)^{2+}$	−305,32	GP.pg.gt.pp.gt.tg	0,690	96,7	90,8	8, 9, 26, 29, 32
$(\alpha P^4C_1Hg, 3H_2O)^{2+}$	−85,40	GG.pt.gt.cp.gt.tg	0,585	177,6	321,1	8, 9, 10, 26, 29, 32
$(\alpha P^4C_1Hg, 4H_2O)^{2+}$	−158,96	GG.pt.gt.cp.gt.tg	0,585	177,3	325,1	8, 9, 10, 26, 29, 32
$(\alpha P^4C_1Hg, 5H_2O)^{2+}$	−236,28	GG.pt.gt.cp.gt.pc	0,571	178,7	122,5	8, 9, 10, 26, 29, 32, 38
$(\alpha P^4C_1Hg, 6H_2O)^{2+}$	−304,68	GG.pt.gt.cp.gt.pc	0,575	177,6	146,3	8, 9, 10, 26, 29, 32, 38

[a]Même légende que pour le tableau 1*a*. Les conformations initiales de $\alpha P^4C_1Pb^{2+}$ et $\alpha P^4C_1Hg^{2+}$ sont celles de plus basse énergie.

Tableau 8. Chélations des complexes de Pb^{2+} et Hg^{2+} avec l'isomère du D-talose et quelques molécules d'eau.

	a	*b*	*r*	θ[a]	*a*	*b*	*r*	θ[a]
$\alpha P^4C_1Pb, 3H_2O)^{2+}$	10	12	2,060	129,90				
$\alpha P^4C_1Pb, 4H_2O)^{2+}$	10	12	2,186	102,18				
$\alpha P^4C_1Pb, 5H_2O)^{2+}$	10	12	2,392	115,15				
$\alpha P^4C_1Pb, 6H_2O)^{2+}$	10	12	2,170	118,35	9	8	2,215	103,67
$\alpha P^4C_1Hg, 3H_2O)^{2+}$	10	12	2,006	124,67				
$\alpha P^4C_1Hg, 4H_2O)^{2+}$	10	12	2,010	124,55				
$\alpha P^4C_1Hg, 5H_2O)^{2+}$	10	12	2,012	140,96	8	11	2,453	108,57
$\alpha P^4C_1Hg, 6H_2O)^{2+}$	10	12	2,014	141,37	8	11	2,433	108,95

[a]Chélation O_a—H...O_b : *r* = distance H...O_b en Å; θ = angle (O—H...O) en degrés.

Fig. 4. $\alpha P^4C_1Pb^{2+}$ et $\alpha P^4C_1Hg^{2+}$ hydratés (les cations sont hachurés).

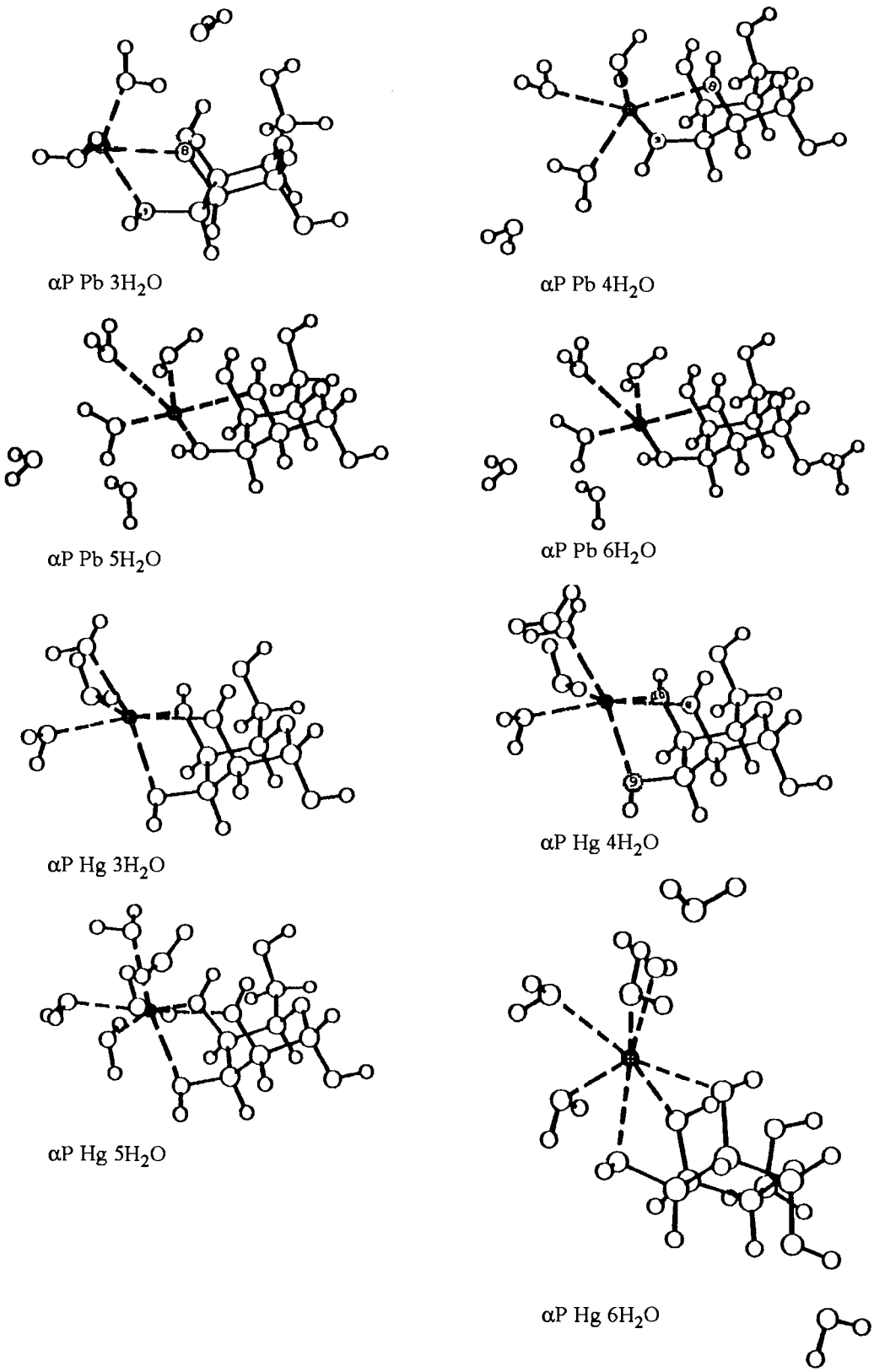

Can. J. Chem. Downloaded from www.nrcresearchpress.com by 65.111.164.53 on 09/08/12
For personal use only.

Can. J. Chem. Downloaded from www.nrcresearchpress.com by 65.111.164.53 on 09/08/12
For personal use only.

[1] $\alpha P + Pb^{2+} = (\alpha PPb)^{2+}$

[2] $\alpha P + Hg^{2+} = (\alpha PHg)^{2+}$

Les valeurs des enthalpies de formation des différents réactifs sont données dans les tableaux ou dans la littérature en ce qui concerne les cations (17). Avec $\Delta H_f(Pb^{2+}) = 514$ kcal mol^{-1} et $\Delta H_f(Hg^{2+}) = 668$ kcal mol^{-1}, on trouve $\Delta H_1 = -70{,}2$ kcal mol^{-1} et $\Delta H_2 = -185{,}9$ kcal mol^{-1}. La différence de l'ordre de 115 kcal mol^{-1} est tellement grande que la contribution entropique à la stabilité des complexes, négligée dans ce calcul, ne semble pas être en mesure d'inverser le phénomène, tout du moins à basse température. Les calculs effectués sur les autres formes donnent des résultats du même ordre de grandeur, étant donné la différence importante d'enthalpies de formation des cations.

En milieu aqueux on a pu mettre en évidence de nombreux complexes hexoses–Pb^{2+}, mais jamais de complexes hexoses–Hg^{2+} (7). Notre étude montre qu'en phase gazeuse c'est l'inverse qui devrait se produire. On sait que dans les associations hexoses–cations, la constante d'association est controlée par les modifications de l'hydratation des espèces, lorsque les molécules d'eau solvatant le cation sont remplacées par les groupes hydroxyle des formes complexées de l'hexose (5). Dans cette optique, il est préférable d'examiner les résultats du système lié à quelques molécules d'eau.

Systèmes (complexes, *n* H_2O)

On note un processus d'hydratation nettement différent pour chacun des deux complexes. L'addition jusqu'à deux molécules d'eau sur l'ion Pb^{2+} ne modifie pas son mode de liaison tricoordiné avec le ligand. Cependant, au bout de la troisième addition, on observe la rupture d'une liaison avec le ligand. Si on poursuit encore l'addition, trois molécules d'eau restent liées au plomb et les nouvelles s'éloignent du site pour former des liaisons hydrogène avec des atomes du ligand situés à proximité ou des molécules d'eau déja liées. Ce résultat montre que, dans ce cas, le mode de liaison serait plus conforme aux conclusions de Reeves (19) qui énonce que la formation d'un tel complexe requiert la présence de deux groupements hydroxyle proches : un équatorial et un axial (ou deux équatoriaux) sur deux atomes de carbone adjacents au cycle.

En ce qui concerne αPHg, les quatre liaisons initiales avec le ligand restent inchangées jusqu'à la troisième addition ou la coordinance baisse à trois et les molécules d'eau sont toutes liées au mercure. À partir de la quatrième addition, et au dela, il en accepte quatre. Ceci indique là encore, un mode de liaison plus intense pour le complexe mercurique, comme le confirment des liaisons métal–oxygène plus courtes et des indices de liaison plus grands que pour les complexes du plomb.

Nous avons effectué le calcul AM1 concernant le système formé par le ligand αP^4C_1 et six molécules d'eau; l'enthalpie de formation correspondante est $\Delta H_f^0 = -709{,}81$ kcal mol^{-1}. Si on calcule les enthalpies de complexation des réactions suivantes :

[3] $(\alpha P, 6H_2O) + Pb^{2+} = (\alpha PPb, 6H_2O)^{2+}$

[4] $(\alpha P, 6H_2O) + Hg^{2+} = (\alpha PHg, 6H_2O)^{2+}$

la difference $\Delta H_4 - \Delta H_3 = 144$ kcal mol^{-1}. Cela veut dire que dans le système à six molécules d'eau, la complexation est encore plus favorable pour le mercure que pour le plomb. Des mesures effectuées au laboratoire sur des complexes hexoses–Ca^{2+} ont montré que les constantes d'association, qui sont faibles lorsque le phénomène de complexation existe, résultent d'une large compensation entre une enthalpie favorable et une entropie défavorable due essentiellement à l'hydratation. On pourrait expliquer l'inversion du phénomène en milieu aqueux par un effet entropique d'hydratation beaucoup plus défavorable pour αPHg que pour αPPb. La corrélation entre les enthalpies et entropies d'association mise en évidence expérimentalement (5) nous suggère que l'effet enthalpique, beaucoup plus favorable pour le mercure, entrainerait un effet promoteur sur les molécules d'eau de la couche de première hydratation. Cela augmenterait la structure globale du solvant par effets coopératifs, et en conséquence l'effet entropique de solvatation défavorable à l'association. On peut remarquer un comportement semblable si l'on considère les grandeurs thermodynamiques d'association du cation Ca^{2+} avec respectivement le D(+)talose, le D(−) ribose, et le D(+) allose. Les données expérimentales (5) sont pour les réactions d'association en solution aqueuse à dilution infinie et à 298,15 K :

	ΔH^θ (kJ Mol^{-1})	$T\Delta S^\theta$ (kJ mol^{-1})	ΔG^θ (kJ mol^{-1})
D(+) talose	−18,6	−17,7	−0,9
D(−) ribose	−16,6	−14,9	−1,7
D(+) allose	−15,9	−13,0	−2,9

ce qui montre que pour un cation divalent donné, plus l'effet enthalpique est favorable, plus l'effet entropique est défavorable. De plus en milieu aqueux le processus de complexation peut être envisagé en deux étapes :

(1) une deshydratation partielle du cation

$$Pb(H_2O)_6^{2+} \rightarrow Pb(H_2O)_3^{2+} + 3\ H_2O$$

$$Hg(H_2O)_6^{2+} \rightarrow Hg(H_2O)_4^{2+} + 2\ H_2O$$

(2) complexation par le ligand

$$\alpha P + Pb(H_2O)_3^{2+} \rightarrow [\alpha PPb(H_2O)_3]^{2+}$$

$$\alpha P + Hg(H_2O)_4^{2+} \rightarrow [\alpha PHg(H_2O)_4]^{2+}$$

ce qui donne le bilan

[5] $Pb(H_2O)_6^{2+} + \alpha P \rightarrow [\alpha PPb(H_2O)_3]^{2+} + 3\ H_2O$

[6] $Hg(H_2O)_6^{2+} + \alpha P \rightarrow [\alpha PHg(H_2O)_4]^{2+} + 2\ H_2O$

Les équations [5] et [6] mettent en évidence une autre contribution entropique beaucoup moins favorable pour les complexes du mercure (passage de 2 espèces libres à 3 au lieu de 2 à 4 pour ceux du plomb).

Dans le cas général, cette addition de molécules d'eau sur le site de complexation ne permet pas d'apporter de conclusions définitives quant à l'hydratation du ligand ou du complexe car le modèle ignore l'environnement dynamique du solvant, sa structure et l'effet entropique global exact. Aussi, dans un article ultérieur, nous présenterons une exploration plus systéma-

tique de l'espace des phases en examinant les différentes formes étudées ici en simulant également l'environnement aqueux par la dynamique moléculaire ou la méthode de Monte Carlo. Ces méthodes, qui présentent l'inconvénient de ne pas bien prendre en compte les effets stéréoelectroniques et les liaisons hydrogène, permettent malgré tout une meilleure simulation des espèces en solution. Un calcul de l'enthalpie libre d'hydratation permettrait de confirmer notre hypothèse et répondre à d'autres questions très importantes. Pourquoi, par exemple, les formes βFPb^{2+} dont les enthalpies de formation sont beaucoup plus élevées que celles des αFPb^{2+} sont les seules à avoir été mises en évidence par la RMN (8, 9)?

Méthodes de calcul

Le programme MM2 $(85)^2$ a permis l'exploration initiale de la surface d'énergie potentielle. L'option AM1 (15) implantée dans le programme MOPAC[3] a été utilisée. Toutes les géométries ont été complètement optimisées par les procédures BFGS suivie de EF. L'indice de liaison entre deux atomes A et B est celui donné par MOPAC[3] et défini par

$$P_{AB} = \sum_{\lambda}^{\epsilon A} \sum_{\sigma}^{\epsilon A} \sigma P_{\lambda\sigma}{}^2 \quad \text{avec} \quad P_{\lambda\sigma} = 2 \sum_{i}^{OCC} C_{i\lambda} C_{i\sigma}$$

où $C_{i\lambda}$ est le coefficient LCAO pour l'orbitale atomique dans l'orbitale moléculaire occupée Φ_i. À cause de la somme des carrés des $P_{\lambda\sigma}$, des contributions antiliantes (négatives) entre atomes sont remplacées par des valeurs positives, ce qui peut augmenter des indices de liaison apparents. Des données complémentaires (coordonnées, orbitales moléculaires, grandeurs thermodynamiques) sont disponibles auprès des auteurs.

Remerciements

Les calculs ont été effectués sur l'ordinateur Vax 6410 du centre de calcul de l'Université Blaise Pascal, les stations de travail DEC α400 et α300 du Département de Chimie.

Nous remercions Monsieur le Professeur J.P. Morel pour les discussions fructueuses que nous avons eues avec lui.

3. Programme MOPAC v6.0, QCPE n° 455, Department of Chemistry, Indiana University, Bloomington, IN 47408, U.S.A.

Bibliographie

1. S.J. Angyal. Carbohydrates in solution. Adv. Chem. Ser. **117**, ACS, Washington, D.C. 1973.
2. S.J. Angyal. Chem. Soc. Rev. **9**, 415 (1980).
3. F. Franks, J.R. Hall, D.E. Irish et K. Norris. Carbohydr. Res. **157**, 53 (1986).
4. J.P. Morel, C. Lhermet et N. Morel-Desrosiers. Can. J. Chem. **64**, 996 (1986); J. Chem. Soc. Faraday Trans. 1, **84**, 2567 (1988).
5. N. Morel-Desrosiers et J.P. Morel. J. Chem. Soc. Faraday Trans. 1, **85**, 3461 (1989).
6. F. Franks, D.S. Reid et A. Sugget. J. Solution Chem. **2**, 99 (1973).
7. S.J. Angyal. Aust. J. Chem. **25**, 1957 (1972).
8. M.C.R. Symons, J.A. Benbow et H. Pelmore. J. Chem. Soc. Faraday Trans. 1, **78**, 3671 (1982).
9. M.C.R. Symons, J.A. Benbow et H. Pelmore. J. Chem. Soc. Faraday Trans. 1, **80**, 1999 (1984).
10. R.E. Lenkinski et J. Reuben. J. Am. Chem. Soc. **11**, 98 (1976).
11. A.D. French, R.S. Rowland et N.L. Allinger. *Dans* Computer modeling of carbohydrate molecules. ACS Symp. Ser. **430** (1990).
12. D. Cremer et J.A. Pople. J. Am. Chem. Soc. **97**, 1354 (1975); **97**, 1358 (1975).
13. P.L. Polavarapu et C.S. Ewig. J. Comput. Chem. **13**, 1255 (1992).
14. W.C. Still. Programme MACROMODEL v4. 0, Department of Chemistry, Columbia University, New York.
15. M.J.S. Dewar, E.G. Zoebish, E.F. Healy et J.J.P. Stewart. J. Am. Chem. Soc. **107**, 3902 (1985).
16. N.N. Greenwood et A. Earnshaw. Chemistry of the elements. Pergamon Press, Oxford.
17. S.J. Angyal. Angew. Chem. Int. Ed. Engl. **8**, 157 (1969).
18. Handbook of chemistry and physics. 64e éd. CRC Press, Boca Raton, Fla. 1983.
19. R.E. Reeves. J. Am. Chem. Soc. **71**, 215 (1949).

Can. J. Chem. Downloaded from www.nrcresearchpress.com by 65.111.164.53 on 09/08/12
For personal use only.

Characterization of the capsular antigen of *Streptococcus pneumoniae* serotype 35B[1]

Linda M. Beynon, James C. Richards, Malcolm B. Perry, and Peter J. Kniskern

Can. J. Chem. Downloaded from www.nrcresearchpress.com by 65.111.164.53 on 09/08/12
For personal use only.

Abstract: The specific capsular antigen of *Streptococcus pneumoniae* serotype 35B was shown by a combination of 2D NMR methods and mass spectrometric and classical carbohydrate chemical techniques to be a high molecular weight polymer containing D-galactose, D-glucose, 2-acetamido-2-deoxy-D-galactose, and ribitol (2:1:1:1). The pentasaccharide repeating unit is polymerized through phosphate diester linkages to give the structure,

Seventy percent of the β-D-Gal_f residues glycosidically linked to the ribitol units carry an *O*-acetyl substituent.

Key words: *Streptococcus pneumoniae*, capsular antigen, polysaccharide structure.

Résumé : Faisant appel à des méthodes de RMN bidimensionnelles, de spectrométrie de masse et de techniques chimiques classiques de hydrates de carbone, on a montré que l'antigène capsulaire spécifique du *Streptococcus pneumoniae*, sérotype 35B, est un polymère de masse moléculaire élevée contenant du D-galactose, du D-glucose, du 2-acétamido-2-désoxy-D-galactose et du ribitol (2 : 1 : 1 : 1). Le motif pentasaccharidique est polymérisé par des liaisons diesters de phosphate de structure

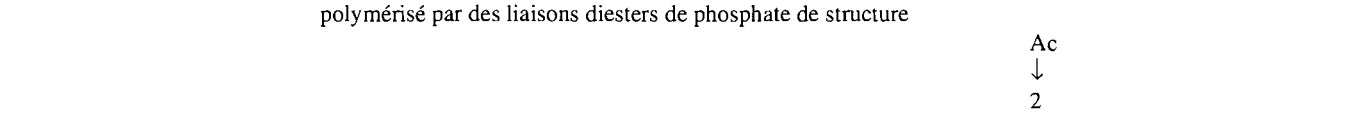

Soixante-dix pour cent des résidus β-D-Gal_f, qui ont un lien glycosidique avec des unités de ribitol, portent un substituant *O*-acétyle.

Mots clés : *Streptococcus pneumoniae*, antigène capsulaire, structure du polysaccharide.

[Traduit par la rédaction]

Introduction

Streptococcus pneumoniae persists as a cause of pneumonia, meningitis, and otitis media despite the availability of antibiotic therapy and capsular polysaccharide vaccines. The composition of the current 23-valent polysaccharide vaccine is based on the serotypes responsible for approximately 90% of infections in the U.S.A. (1). However, the serology of disease isolates varies over time and with the geographical area. Studies on Asian populations have shown that a large proportion of pneumococcal types found in Asia, such as 15A, 23A, 24F, 27, and 34, are not present in the pneumococcal vaccines; furthermore, isolates consisting of the serogroup 35 have been identified in Japan, Taiwan, and China (2). Thus, it may be necessary to develop supplementary vaccines to include some additional types of pneumococcal polysaccharide antigens for use in Asian countries.

Within the group 35 of *S. pneumoniae* four serotypes (35F, 35A, 35B, and 35C) have been recognized and, by the use of factor sera, seven factors (20b, 29b, 34b, 35a, 35b, 35c, and 42a) have been determined (3) although the structural basis for the factors is as yet unknown. *Streptococcus pneumoniae* serotype 35B shows a strong heterologous cross-reaction with antiserum raised against serotype 29 (3). To demonstrate the molecular basis for this observed serological cross-reactivity

Received May 18, 1994.

L.M. Beynon, J.C. Richards, and M.B. Perry.[2] Institute for Biological Sciences, National Research Council of Canada, Ottawa, ON K1A 0R6, Canada.
P.J. Kniskern. Merck Research Laboratories, West Point, PA 19486, U.S.A.

[1] NRCC No. 37419.
[2] Author to whom correspondence may be addressed. Telephone: (613) 990-0837, Fax: (613) 941-1327.

Can. J. Chem. Downloaded from www.nrcresearchpress.com by 65.111.164.53 on 09/08/12
For personal use only.

Fig. 1. The ^{1}H NMR spectra (2.90–5.40 ppm) of the *S. pneumoniae* serotype 35B native capsular polysaccharide (*a*), *O*-deacetylated capsular polysaccharide (*b*), the pentasaccharide repeating unit **1** (*c*). Insert in Fig. 1*a*: the high-field region 2.00–2.25 ppm showing the singlets for the methyl protons of the *N*- (2.05 ppm) and the *O*-acetyl (2.15 ppm) substituents.

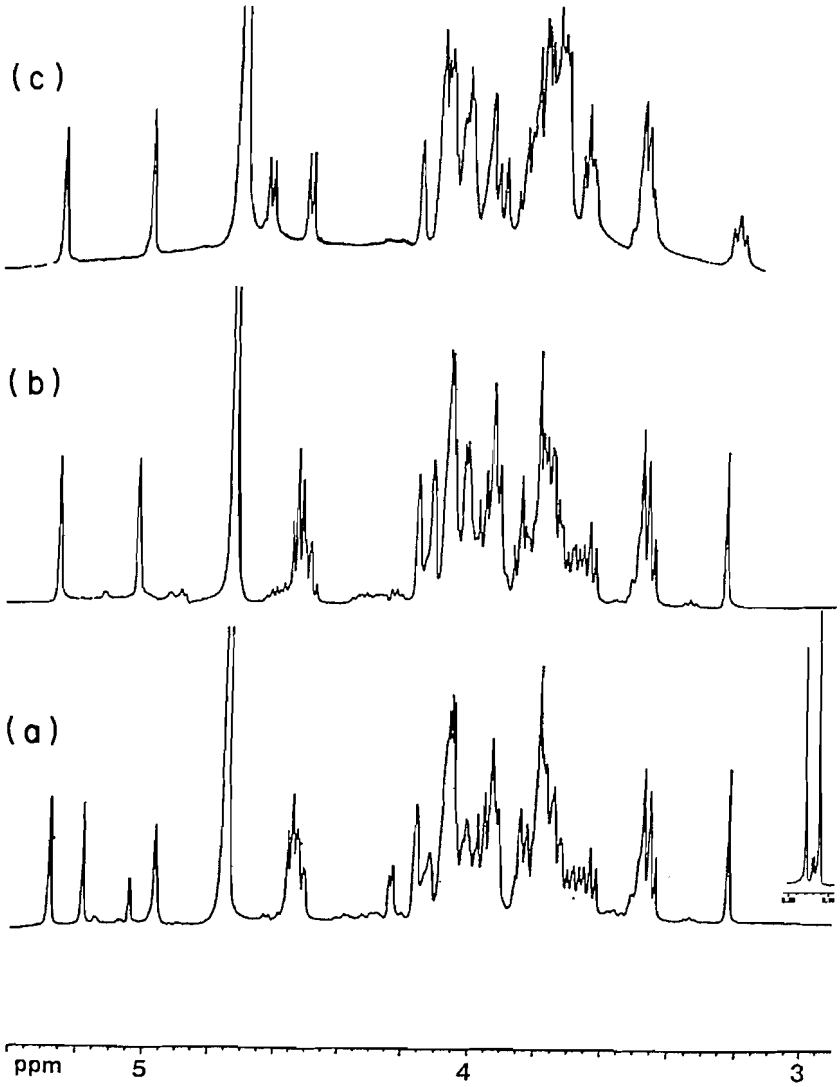

we now report the results of the structural analysis of serotype 35B capsular polysaccharide.

Results and discussion

Type-specific polysaccharide was isolated from the spent growth medium of *S. pneumoniae* serotype 35B cells. The polysaccharide eluted as the void volume fraction on a Sephadex G-50 gel filtration system, indicating it to be a high molecular weight polymer. This material was further purified by DEAE–Sephacel ion-exchange chromatography where it eluted as a homogeneous fraction in a sodium chloride gradient. The polysaccharide obtained was homogeneous across the fraction for neutral glycoses, aminodeoxyglycoses, and phosphate and had $[\alpha]_D$ −34.7 (*c* 0.7, water). Anal. found: C 35.0, H 6.3, N 1.4, ash 7.9%. The phosphate content was determined colorimetrically to be 8.0%.

Complete acid hydrolysis of the 35B polysaccharide and GLC–MS of the derived alditol acetates gave D-Gal, D-Glc, D-GalN, and ribitol in the molar ratios 1.8:1.0:0.4:0.4. A fifth product was tentatively identified as anhydroribitol on the basis of the GLC–EI-MS spectrum. The absolute configurations of the residues were established by GLC of their trimethylsilylated *R*-(+)-methylbenzylamine derivatives (4).

The low-field region of the ^{1}H NMR spectrum of the native polysaccharide contained four signals at 5.28, 5.18, 5.04, and 4.97 ppm (relative intensities, 1.0:0.7:0.3:0.7) (Fig. 1*a*, Table 1). *O*-Deacylation of the native polysaccharide resulted in the disappearance of the signals at 5.18 and 4.97 ppm (Fig. 1*b*, Table 1) and an increase in the relative intensity of the signal at 5.04 ppm to 1.0. The region of the spectrum between 4.50 and 4.60 ppm contained three doublets at 4.55 ($J_{1,2}$ 7.8 Hz), 4.54 ($J_{1,2}$ 7.8 Hz), and 4.52 ($J_{4,5} \leq 1.0$, $^3J_{H,P}$ 8.0 Hz), and the high-field region contained two singlets at 2.05 and 2.15

Table 1. ^{1}H NMR chemical shift data[a,b] for the capsular antigen of *Streptococcus pneumonia* 35B and its degradation products.

	Sugar residue								
	c		**a**		**d**	**b**	**e**		
	→4-β-D-Gal$_p$NAc-(1→6)-β-D-Glc$_f$-(1→3)-β-D-Glc$_p$-(1→6)-β-D-Gal$_f$-(1→1)-ribitol-(5-PO$_4$→								
Compound/residue	H-1 ($J_{1,2}$)	H-1′ ($J_{1',2}$) ($J_{1',1}$)	H-2 ($J_{2,3}$)	H-3 ($J_{3,4}$)	H-4 ($J_{4,5}$)	H-5	H-5′ ($J_{4,5'}$) ($J_{5,5'}$)	H-6 ($J_{5,6'}$)	H-6′ ($J_{5,6'}$) ($J_{6',6}$)
Native polysaccharide									
a	5.28		4.17	4.08	4.06	3.92		3.69	4.06
b (*O*-acetylated)	5.18		4.97	4.23	4.08	3.92		3.69	4.06
b	5.04		4.12	4.08					
c	4.55		3.97	3.83	4.52	3.65		3.94	3.98
d	4.54		3.46	3.64	3.46	3.50		3.93	3.75
e	3.84	3.74	4.03	3.78	3.94	4.14	4.06		
O-Deacylated polysaccharide									
a	5.28 (~1–2)		4.17 (5.01)	4.08	4.07	3.94		4.07	3.71
b	5.04 (~1–2)		4.13 (2.7)	4.09 (5.4)	4.03 (4.5)	3.94		4.07	3.71
c	4.56 (8.4)		3.97 (10.4)	3.84 (4.0)	4.52 (1.7) (8.8)[c]	3.78		3.80	3.80
d	4.55 (7.8)		3.47 (9.1)	3.64 (9.1)	3.48 (9.1)	3.49		3.93 (<1.0)	3.76 (5.4) (12.5)
e	3.86 (6.0)	3.74 (4.2) (12.6)	4.02 (5.6)	3.78 (7.2)	3.93 (3.6)	4.14 (9.1)[c]	4.07 (6.7) (11.8)		
Alkaline degradation product **1**									
a	5.28 (1.6)		4.15	4.07	4.01	3.99		4.08	3.74
b	5.01 (1.6)		4.09	4.07	4.10	4.03		4.04	3.74
c	4.66 (8.5)		3.18	3.83	3.94	3.73		3.78	3.74
d	4.51 (7.8)		3.44	3.63	3.44	3.47		3.89	3.71
e	3.84	3.73	3.94	3.71	3.79	3.78	3.64		
Aqueous HF degradation product 3									
b (*O*-acetylated)	5.18		4.96	4.25	4.09	4.04		4.08	3.78
d	4.51		3.34	3.50	3.40	3.47		3.93	3.74
e	3.85	3.74	3.98	3.73	3.83	3.82	3.67		

[a]Measured at 27°C using internal acetone as a reference (δ 2.225 ppm).
[b]Coupling constants measured in Hz are shown in parentheses.
[c]$^3J_{H,P}$ measured in Hz.

(1.0:0.7) for the methyl groups of an *N*- and an *O*-acetyl substituent, respectively. These results were consistent with 70% of the repeating units of the polysaccharide being substituted with an *O*-acetyl function.

The ^{13}C NMR spectrum of the *O*-deacetylated polysaccharide had four signals for anomeric carbons at 108.6, 107.6, 102.9, and 102.4 ppm (Table 2). Resonances appearing at 53.0, 175.2, and 22.7 ppm were attributed to the C-2, C=O, and CH_3, respectively, of the D-Gal$_p$NAc residues.

Methylation analysis of the polysaccharide (Table 3, col-

Can. J. Chem. Downloaded from www.nrcresearchpress.com by 65.111.164.53 on 09/08/12
For personal use only.

Can. J. Chem. Downloaded from www.nrcresearchpress.com by 65.111.164.53 on 09/08/12
For personal use only.

Table 2. ^{13}C NMR chemical shift data for the capsular antigen of *Streptococcus pneumoniae* 35B and its degradation products.[a]

Compound/residue	C-1	C-2	C-3	C-4	C-5	C-6
Native polysaccharide						
a	108.4	81.4	76.4	84.0	71.3	71.6
b ((*O*-Acetylated)	105.3	83.4	75.5	83.4	71.3	71.6
b	107.4	81.3	—	—	—	—
c	102.9	52.9	70.8	73.0	74.9	61.0
d	103.0	73.6	82.6	68.5	76.0	61.1
e	68.3	70.3	71.7	69.5	67.2	
O-Deacetylated polysaccharide						
a	108.6	81.9	77.4	83.8	71.6	71.8
b	107.6	81.5	77.0	83.5	71.1	71.8
c	102.4	53.0	70.7	73.5[b]	75.2	61.3
d	102.9	73.9	82.9	68.5	76.4	61.3
e	68.1	70.3	72.1	69.7	67.5[c]	
Alkaline degradation product **1**						
a	108.9	82.0	77.5	83.9	70.3	72.1
b	108.0	81.6	77.4	83.6	70.1	71.9
c	100.9	54.1	70.5	68.4	76.2	61.6
d	103.3	74.9	82.7	68.8	76.5	61.4
e	68.8	70.9	72.9	72.9	63.2	
HF Degradation product **3**						
b	105.5	83.9	75.8	84.0	69.5	71.2
d	103.0	73.4	75.9	69.8	76.0	60.9
e	68.3	70.4	72.2	72.2	62.7	

[a]Measured at 27° with acetone as an internal reference (δ 31.07 ppm).
[b]$^2J_{C,P}$ 5.9 Hz.
[c]Broad.

Table 3. Methylation analyses data for *S. pneumonia* serotype 35B capsular polysaccharide and degradation products

Methylated sugars[a] (as alditol acetates)	Molar ratios[b]				
	T_{MG}[c]	I	II	III	IV
2,3,4,5-Rib	0.4	0.2	0.3		1.0
1,2,3,4,5-Gal	0.7			0.9	
2,3,4,6 Glc	1.0			1.0	3.0
2,4,6-Glc	1.4	1.0	1.0		
2,3,5-Gal	1.6	0.9	1.0		1.0
2,3,4,6-GalNAc	2.6		0.7	0.8	

[a]2,3,4,6-Glc represents 1,5-di-*O*-acetyl-2,3,4,6-tetra-*O*-methyl-D-glucitol, etc.
[b]I, native polysaccharide; II, dephosphorylated product **1**, III, HF solvolysis product **2**; IV, HF solvolysis product **3**. Values not corrected for differences in detector response factors.
[c]Retention times relative to that of 1,5-di-*O*-acetyl-2,3,4,6-tetra-*O*-methyl-D-glucitol.

umn I) showed the polysaccharide contained *O*-3 substituted D-Glc_p, *O*-6 substituted D-Gal_f, and ribitol residues substituted at *O*-1. The absence of D-Gal_pN residues suggested that these residues were substituted by phosphate.

The structure of the polysaccharide antigen was determined from analysis of the fully assigned ^1H and ^{13}C NMR spectra of the native and *O*-deacetylated polysaccharides and derived oligosaccharides. These assignments were accomplished via a combination of homo- and heteronuclear chemical shift correlation techniques. The COSY spectrum of the *O*-deacetylated polysaccharide contained resonances for four anomeric protons, which were labelled **a**, **b**, **c**, **d** in order of decreasing chemical shift. The resonances corresponding to the β-D-Glc_p residue (**d**) were well resolved and the corresponding subspectrum was readily identified on the basis of the observed proton coupling constants (Table 1). The relatively deshielded values of H-3**d** (3.64 ppm) and C-3**d** (82.9 ppm) compared with those of published data (5) indicated the β-D-Glc_p residue to be substituted at the *O*-3 position. Direct correlation of the resonance for H-2**c** (3.97 ppm) to the corresponding C-2**c** (53.0 ppm) resonance permitted **c** to be identified as the D-Gal_pN residue characterized by chemical analysis. The low-field position (73.5 ppm) and the heteronuclear coupling ($^2J_{C,P}$ 5.9 Hz) observed for the resonance of C-4**c** indicated substitution by phosphate of the D-Gal_pNAc residue at this position.

Identification of the subspectra corresponding to the two β-D-Gal_f residues **a** and **b** was more difficult in part, due to strong coupling between H-3**a** and H-4**a** that precluded measurement of the vicinal coupling constants for residue **a**. The assignment of the ^1H resonances of residues **a**, **b**, and **e** was achieved partially via the corresponding ^{13}C resonances in the

Can. J. Chem. Downloaded from www.nrcresearchpress.com by 65.111.164.53 on 09/08/12
For personal use only.

Scheme 1. The structures of the oligosaccharides obtained on degradation of the capsular polysaccharide of *S. pneumoniae* serotype 35B.

1

β-D-Gal$_p$NAc-(1→6)-β-D-Gal$_f$-(1→3)-β-D-Glc$_p$-(1→6)-β-D-Gal$_f$-(1→1)-ribitol

(i) 1 M NaOH/NaBH$_4$, 4 h, 100°C
(ii) Alkaline phosphatase

Ac
↓
2

→4)-β-D-Gal$_p$NAc-(1→6)-β-D-Gal$_f$-(1→3)-β-D-Glc$_p$-(1→6)-β-D-Gal$_f$-(1→1)-ribitol-(5→PO$_4$→

48% aqueous HF, 8 h, 0°C

2B
β-D-Gal$_p$NAc-(1→6)-D-Gal

2A
β-D-Glc$_p$-(1→6)-D-Gal

3
β-D-Glc$_p$-(1→6)-β-D-Gal$_f$-(1→1)-ribitol

Fig. 2. Fragment ions obtained by FAB-MS, in the negative ion mode, of the pentasaccharide repeating unit **1** of *S. pneumoniae* serotype 35B capsular polysaccharide.

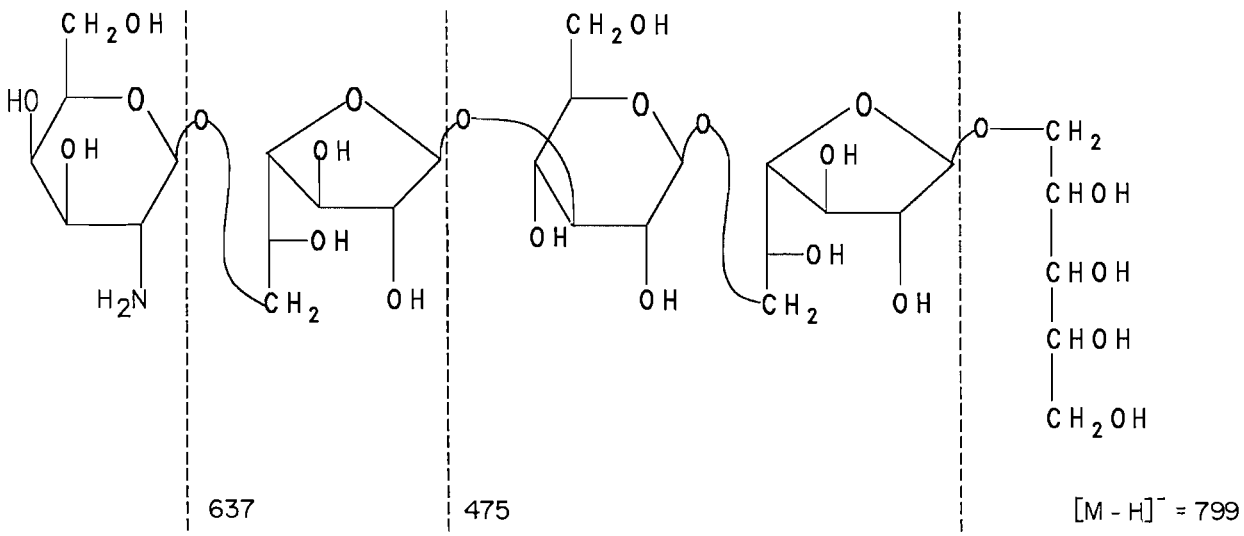

^{1}H–^{13}C chemical shift correlation spectrum with reference to published data (5, 6). Comparison of the chemical shifts for H-2**b** (4.13 ppm) and C-2**b** (81.5 ppm) of the *O*-deacetylated polysaccharide with those for H-2**b** (4.97 ppm) and C-2**b** (83.4 ppm) of the native polysaccharide indicated C-2 to be the site of *O*-acetyl substitution. The downfield shift of the resonances for C-1**e** (68.1 ppm) and C-5**e** (67.5 ppm) in comparison to those of unsubstituted ribitol (C-1 and C-5, 61.8 ppm) suggested that the ribitol residue is linked through both C-1 and C-5 positions. Since only a single phosphate group was indicated by ^{31}P NMR spectroscopy (1.41 ppm) it is probable, from the evidence presented so far, that the repeating unit contains the phosphate diester fragment,

→1)-ribitol-(5→PO$_4$→4)-β-D-Gal$_p$NAc-(1→

Depolymerization of the O-polysaccharide

The polysaccharide was heated in 1 M NaOH containing a trace amount of NaBH$_4$ and subsequently treated with alkaline phosphatase to remove residual phosphate. Fractionation of the sample on a Bio-gel P2 column gave a pentasaccharide **1** (K_{av} 0.38) (Scheme 1), which had $[\alpha]_D$ −42.6 (*c* 2.3, water) and which showed a single discrete spot (R_f 0.09) on analysis

Fig. 3. Fragment ions obtained on GLC–CI-MS analysis of oligosaccharide **3**.

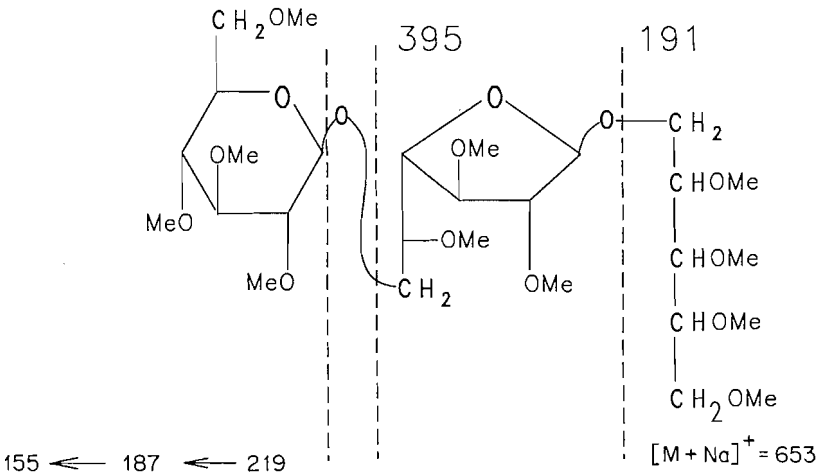

by TLC. FAB-MS of underivatized **1**, in the negative ion mode, gave a $[M - H]^-$ ion at *m/z* 799 and diagnostic fragment ions at *m/z* 637 and 475 (see Fig. 2). Methylation analysis of **1** gave 2,3,4,5-tetra-*O*-methylribitol, 2,4,6-tri-*O*-methylglucitol, 2,3,5-tri-*O*-methylgalactitol, and 2-deoxy-3,4,6-tri-*O*-methy-2-(*N*-methylamino)-galactitol (Table 3, column II).

The ^1H NMR of spectrum of **1** contained four signals in the region for anomeric protons at 5.28 ($J_{1,2}$ 1.6 Hz), 5.01 ($J_{1,2}$ 1.6 Hz), 4.66 ($J_{1,2}$ 8.5 Hz), and 4.51 ppm ($J_{1,2}$ 7.8 Hz) (Fig. 1*c*). A DEPT experiment showed four resonances for anomeric carbons at 108.9, 108.0, 103.3, and 100.9 ppm and five signals for CH_2 at 72.1, 71.9, 69.0, 63.2, 61.6, and 61.0 ppm. The ^1H and ^{13}C NMR spectra were fully assigned using COSY and ^1H–^{13}C chemical shift correlated spectroscopy (Tables 1 and 2). The resonances for H-4**c** (3.94 ppm), C-4**c** (68.4 ppm) and H-5**e**/5′**e** (3.78/3.64 ppm) and C-5**e** (63.2 ppm) were shifted upfield in comparison to those of the native and *O*-deacetylated polysaccharides (Tables 1 and 2) confirming substitution at these positions in these polymers. The sequence of the residues in **1** was determined from a three-bond {HMBC} ^1H–^{13}C chemical shift correlation experiment. The resonances for C-1**a** (108.9 ppm) and C-1**b** (108.0 ppm) showed cross-peaks at H-3**d** (3.63 ppm) and H-1**e**/1′**e** (3.84/3.73 ppm), respectively. The resonance for C-1**c** (100.9 ppm) showed cross-peaks at H-6**a** (3.74 ppm) and H-6′**a** (4.08 ppm), and that of C-1**d** at H-6**b** (3.74 ppm) and H-6′**b** (4.04 ppm). In addition, C-1**c** showed a strong cross-peak at H-2**c** (3.18 ppm), and C-1**d** at H-2**d**/4**d** (3.44 ppm).

Taken together these results allow the structure of **1** to be assigned as,

$$\begin{array}{l} \quad\quad\quad\

35B (7, 8). It differs in the replacement of the β-D-Glc_p residue in the 35B polysaccharide by a β-D-Gal_p residue and also in the lack of *O*-acetyl substituents (8).

$$[\rightarrow 4)\text{-}\beta\text{-D-}Gal_pNAc\text{-}(1\rightarrow 6)\text{-}\beta\text{-D-}Gal_f\text{-}(1\rightarrow 3)\text{-}\beta\text{-D-}Gal_p\text{-}(1\rightarrow 6)\text{-}\beta\text{-D-}Gal_f\text{-}(1\rightarrow 1)\text{-ribitol-}(5\rightarrow PO_4\rightarrow]_n$$

The serological cross-reactivity between *S. pneumoniae* serotypes 35B and 29 is probably related to a structure contained in the common tetrasaccharide component that includes the phosphate diester linkage. The ribitol unit of the *S. pneumoniae* serotype 29 capsular polymer was assigned the D configuration on biosynthetic grounds (7). The absolute stereochemistry of the ribitol residue in the 35B polymer will be determined using the methodology developed by Beynon and Richards (9) for the assignment of the configuration of the glycerol residue in polymers joined by →1)-glycerol-(3→phosphodiester linkages.

Experimental

Isolation of the capsular polysaccharide

Serotype 35B capsular polymer was isolated by ethanol precipitation (50–55% final concentration) from the growth media followed by digestion with DNase, RNase, and trypsin and subsequent fractional precipitation with 2-propanol and serological probing (10) of the fractions. The polysaccharide eluted in the void volume fraction on a Sephadex G-50 column and was further purified by ion exchange chromatography on DEAE–Sephacel as described previously (11).

Analytical methods

Quantitative colorimetric methods used were (*i*) phenol–sulphuric for neutral glycoses (12), (*ii*) the method of Chen et al. for phosphate (13), and (*iii*) the modified Elson-Morgan for aminoglycoses (14).

Analytical GLC–MS was done with a Hewlett–Packard 5985B system and an OV-17 fused silica column (Quadrex Corp.) using an ionization potential of 70 eV (EI) or with ammonia as the reagent gas (CI). The following programs were employed: A (for alditol acetates), 180°C for 2 min, then 4°C/min to 240°C; B (for partially methylated alditol acetates and trimethylsilylated R-(+)-methylbenzylamine derivatives), 180°C for 2 min then 2°C/min to 240°C; C (for methylated oligosaccharides), 210°C for 1 min, then 10°C/min to 290°C.

For analysis of constituent sugars, samples (1 mg) of polysaccharide were hydrolyzed with 4 M trifluoroacetic acid for 1 h at 125°C, and the excess acid was removed by evaporation under a stream of nitrogen gas. Glycoses were determined by GLC–MS of their derived alditol acetates (15).

Methylations were carried out using the method of Ciucanu and Kerek (16). Briefly, to samples (1–2 mg), dissolved in dry DMSO was added powdered NaOH (20–30 mg), followed by iodomethane (0.2 mL), and the mixture stirred for 10 min (15). The products were isolated by partition between dichloromethane and water and the methylated oligosaccharides were analyzed directly by FAB-MS and (or) GLC–CI- and GLC–EI-MS. The methylated products were subsequently hydrolyzed as above, and the methylated glycoses converted to their alditol acetates and analyzed by GLC–EI-MS.

FAB-MS analyses were carried out in the positive and negative ion mode using a JEOL AX505-H mass spectrometer. An accelerating voltage of 3 kV and a mass resolution of 1500 were employed. A Xe atom beam of 5 kV was used to sputter and ionize the sample.

TLC was performed on silica gel (Merck) with 6:3:1 (v/v) *n*-propanol – concentrated NH_3 – water.

NMR spectroscopy

All measurements were made on solutions in D_2O, at 27°C, using a Bruker AMX-500 spectrometer.

Proton spectra, recorded at 500 MHz, were obtained using a spectral width of 1.8 kHz and a 90° pulse. Chemical shifts are expressed relative to internal acetone (δ_H, 2.225 ppm).

Broad-band decoupled ^{13}C NMR spectra were obtained at 125 MHz with a spectral width of 33 KHz and a 90° pulse employing WALTZ decoupling (17). DEPT spectra (18) were obtained with broadband decoupling, a 135° pulse, and a 3.3-ms delay between pulses. Chemical shifts are expressed relative to internal acetone (δ_C, 31.07 ppm).

Phosphorus-31 spectra were recorded at 202 MHz by employing a 90° pulse and a spectral width of 10 KHz. Chemical shifts are referenced to that of an external sample of aqueous 25% phosphoric acid (δ_P 0.0 ppm).

Two dimensional homonuclear chemical shift correlated (COSY) experiments were carried out as previously described (19). The heteronuclear ^{13}C–^1H chemical shift correlations were measured in the ^1H-detected mode via multiple quantum coherence ($^1H\{^{13}C\}$HMQC) with a Bruker 5-mm inverse broadband probe using reverse electronics as previously described (20). The 2D heteronuclear multiple bond correlated ^1H–$^{13}C(^1H\{^{13}C\}$HMBC) experiment on **1** was carried out using the pulse sequence described by Bax and Summer (21).

Depolymerization of the O-polysaccharide

Polysaccharide (30 mg), in 1 M NaOH (6 mL) containing a trace amount of $NaBH_4$, was heated at 100°C for 4 h. The cooled solution was neutralized with glacial CH_3COOH and concentrated via rotary evaporation under reduced pressure. The product was fractionated on a column of Bio-gel P2 and the glycose-positive fractions were pooled and lyophilized. The product (9 mg), dissolved in 0.05 M ammonium carbonate buffer, was mixed with alkaline phosphatase (0.4 mg, Sigma Chemical Co.) dissolved in the same buffer (0.3 mL) and the pH of the solution was adjusted to 10. The mixture was left to react at 37°C for 30 h and was subsequently fractionated on a column of Bio-Gel P2 to give pentasaccharide **1** (K_{av} 0.38).

Polysaccharide (40 mg) was treated with 48% HF at 0°C for 8 h. The reaction was quenched with a mixture of dichloromethane, Dry Ice, and calcium carbonate. Following low-speed centrifugation to remove insoluble material the product was fractionated by Bio-gel P2 chromatography to give oligosaccharides **2** (K_{av} 0.75) and **3** (K_{av} 0.67).

Acknowledgments

We thank Mr. F. Cooper for the expert GLC–MS and FAB analyses.

Can. J. Chem. Downloaded from www.nrcresearchpress.com by 65.111.164.53 on 09/08/12
For personal use only.

References

1. C.J. Lee, S.D. Banks, and J.P. Li. Crit. Rev. Microbiol. **18**, 89 (1991).
2. C.J. Lee. Mol. Immunol. **24**, 1005 (1987).
3. E. Lund and J. Henrichsen. Methods Microbiol. **12**, 241 (1978).
4. R. Oshima, J. Kumanotani, and C. Watanabe. J. Chromatogr. **259**, 159 (1983).
5. J.H. Bradbury and G.A. Jenkins. Carbohydr. Res. **126**, 125 (1984).
6. K. Boch and C. Pedersen. Adv. Carbohydr. Chem. Biochem. **41**, 27 (1983).
7. E.V. Rao, M.J. Watson, J.G. Buchanan, and J. Baddiley. Biochem. J. **111**, 547 (1969).
8. L. Kenne and B. Lindberg. Carbohydr. Res. **184**, 288 (1988).
9. L. M. Beynon and J. C. Richards. Carbohydr. Res. **252**, 263 (1994).
10. V. Daoust, D.J. Carlo, J.Y. Zeltner, and M.B. Perry. Infect. Immun. **32**, 1028 (1981).
11. E. Altman, J.-R. Brisson, and M.B. Perry. Biochem. Cell Biol. **65**, 49 (1987).
12. M. Dubois, K.A. Gilles, J.K. Hamilton, P.A. Rebers, and F. Smith. Anal. Chem. **28**, 350 (1956).
13. P.S. Chen, T.Y. Toribara, and H. Warner. Anal. Chem. **28**, 1756 (1956).
14. R. Gatt and E.R. Berman. Anal. Biochem. **15**, 167 (1965).
15. S.W. Gunner, J.K.N. Jones, and M.B. Perry. Can. J. Chem. **39**, 1892 (1961).
16. I. Ciucanu and F. Kerek. Carbohydr. Res. **131**, 209 (1984).
17. A.J. Shaka, J. Keeler, F. Frenkiel, and R.J. Freeman. J. Magn. Reson. **52**, 335 (1983).
18. D.M. Doddrell, D.T. Pegg, and M.R. Bendall. J. Magn. Reson. **48**, 323 (1982).
19. L.M. Beynon, J.C. Richards, and M.B. Perry. Carbohydr. Res. **209**, 211 (1991).
20. L.M. Beynon, J.C. Richards, and M.B. Perry. Can. J. Chem. **70**, 218 (1992).
21. A. Bax and M.F. Summer. J. Am. Chem. Soc. **108**, 2093 (1986).

Can. J. Chem. Downloaded from www.nrcresearchpress.com by 65.111.164.53 on 09/08/12
For personal use only.

Oxygen transfer reactions. 3. The oxidation of sulfides by sodium perruthenate

Donald G. Lee and Huifa Gai

Abstract: The transfer of oxygen from transition metal oxidants to sulfur ($MO_4^- + R_2S \rightarrow MO_3^- + R_2SO$) has been studied using the oxidation of alkylthio or arylthioacetic acids ($RSCH_2CO_2H$) by perruthenate as models. These reactions exhibit a first-order dependence on the concentrations of both the oxidant and the reductant, and are directly proportional to the basicity of the medium. The Hammet ρ value is negative ($\rho = -0.66$), a better correlation being obtained when σ, rather than σ^+, substituent constants are used. The entropies of activation for the reactions are large and negative, indicating that the transition state is highly structured. A reaction mechanism involving an activating expansion of the ruthenium coordination shell through incorporation of a hydroxide ion is proposed. Oxygen transfer is then initiated by reaction of a nonbonding pair of sulfur electrons with either a vacant ruthenium *d*-orbital or a Ru=O π*-orbital.

Key words: perruthenate, sulfides, oxygen transfer, oxidation.

Résumé : Utilisant l'oxydation des acides alkylthio- et arylthioacétiques ($RSCH_2CO_2H$) par le perruthénate comme modèles, on a étudié le transfert d'oxygène des métaux de transition oxydants au soufre ($MO_4^- + R_2S \rightarrow MO_3^- + R_2SO$). Ces réactions présentent une corrélation du premier ordre avec les concentrations à la fois de l'oxydant et du réducteur et leurs vitesses sont directement proportionnelles avec la basicité du milieu. La valeur ρ de Hammett est négative ($\rho = -0{,}66$) et on obtient une meilleure corrélation lorsqu'on utilise des constantes de substituants σ plutôt que σ^+. Les entropies d'activation des réactions sont importantes et négatives; ceci indique que l'état de transition est fortement structuré. On propose un mécanisme de réaction impliquant une expansion activante de la couche de coordination du ruthénium par l'incorporation d'un ion hydroxyde. Le transfert d'oxygène est souvent initié par une réaction d'une paire non liée d'électrons du soufre avec soit une orbitale *d* du ruthénium, soit une orbitale π* du Ru=O.

Mots clés : perruthénate, sulfures, transfert d'oxygène, oxydation.

[Traduit par la rédaction]

Introduction

Oxygen transfers, a subset of a larger group of reactions generally referred to as oxidations, are necessary steps in the synthesis of a number of commercially important organic compounds (1) as well as being involved in certain essential biochemical processes (2). A better understanding of these reactions could, consequently, have implications for both commerce and health.

Although biochemical oxygen transfer agents are usually porphyrin-complexed metals such as those found in hemoglobin (3, 4), while the oxidants used in organic syntheses are often high-valent transition metal oxides, oxyanions (5), or complexes (6), all contain metal-oxo functional groups that are believed to be essential participants in transfer reactions; i.e., $L_nMO + R_2S \rightarrow L_nM + R_2SO$. Metals most widely used for these purposes are titanium (7, 8), vanadium (9), chromium (10), manganese (11), iron (12), molybdenum (13), ruthenium (14), and osmium (15). Most prominent among the latter are ruthenium oxo compounds that can exist as RuO_4 (14), RuO_4^- (16–21), RuO_4^{2-} (21–23), RuO_2 (24), or as complexes in oxidation states 2 (25), 3 (26), 4 (26–29), 5 (26, 28, 30), and 6 (26, 27, 28, 31, 32).

In this paper we wish to describe results that have been obtained from a study of one oxygen transfer reaction: the conversion of alkyl and arylthioacetates ($RSCH_2CO_2^-$) into the corresponding sulfoxides by treatment with perruthenate ion in aqueous base (eq. [1]). The reaction has been monitored using stopped-flow spectrophotometry to determine the rate law as well as substituent and temperature effects.

$$\text{[1]}\quad ArSCH_2CO_2^- + 2RuO_4^- + 2OH^- \longrightarrow ArSOCH_2CO_2^- + 2RuO_4^{2-} + H_2O$$

Experimental section

Materials

All reagents were of analytical grade. Water was purified by double distillation, the second time from alkaline permanganate.

Substituted acetic acids ($RSCH_2CO_2H$) were used as substrates to ensure good solubility in aqueous alkaline solutions. (Methylthio)acetic acid was obtained commercially (Fluka) in analytically pure form and used without further purification. (Phenylthio)acetic acid was also obtained commercially (Fluka) and recrystallized from carbon tetrachloride before

Received June 28, 1994.

D.G. Lee[1] and H. Gai. Department of Chemistry, University of Regina, Regina, SK S4S 0A2, Canada.

[1] Author to whom correspondence may be addressed. Telephone: (306) 585-4146. Fax: (306) 585-4894.

Can. J. Chem. Downloaded from www.nrcresearchpress.com by 65.111.164.53 on 09/08/12
For personal use only.

Can. J. Chem. Downloaded from www.nrcresearchpress.com by 65.111.164.53 on 09/08/12
For personal use only.

Fig. 1. Sequential scans obtained during the oxidation of (phenylthio)acetic acid (0.01 M) by perruthenate (2×10^{-4} M) in 0.3 M NaOH, at 0.2 s intervals.

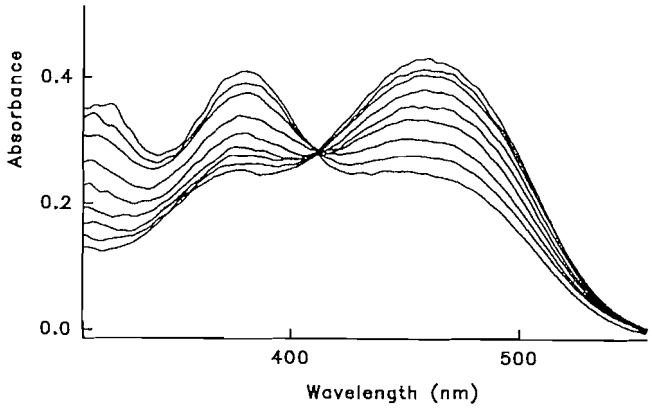

use, mp 63.0–63.5°C (lit. (33) mp 63.5°C). Substituted (phenylthio)acetic acids were synthesized by reaction of substituted thiophenols with bromoacetic acid as previously described (34).

Sodium perruthenate solutions were prepared by distillation of ruthenium tetroxide on a stream of nitrogen into 0.3 M NaOH at 0°C (21). After standing at 5°C overnight, the solutions exhibited an absorption spectrum identical to that previously reported for sodium perruthenate (35).

Kinetic method

The rates of reaction were measured using a Tracor Northern TN-1710A diode array stopped-flow spectrophotometer. Stock solutions of 0.010 M reductant and approximately 6×10^{-4} M perruthenate were placed in thermostated syringes and, after 30 min, equal amounts were forced through the mixing chamber and into the cuvette where the absorbance was monitored from 300 nm to 600 nm as in Fig. 1, the final spectrum being due to ruthenate(VI) (35). Good pseudo-first-order plots were obtained (Fig. 2) using absorbance data at 385 nm (ϵ = 2275).

Products

The products obtained from the oxidation of (phenylthio)acetic acid were identified, from an analysis of the proton NMR spectrum, as the corresponding sulfoxide and sulfone. Potassium perruthenate (1.00 g, 4.9 mmol) was added slowly with stirring (over a 10 min period) to a solution of (phenylthio)acetic acid (0.80 g, 4.8 mmol) in 60 mL of 0.5 M NaOH and, after stirring for an additional 30 min, the solution was filtered. The filtrate was acidified with concentrated HCl and extracted with 5×50 mL CH_2Cl_2. Evaporation of the solvent gave a residue (0.83 g) that was soluble in $CDCl_3$. The proton NMR spectrum of this product exhibited a singlet at 5.3 ppm (solvent, 8.3%), a singlet at 11.1 ppm (1 H, carboxylic acid), and a multiplet at 7.1–7.9 ppm (5 H, aromatic). The region from 3.6 to 4.1 ppm contained three distinct peaks, a singlet at 4.1 ppm, a pair of doublets at 3.7–4.0 ppm, and another singlet at 3.6 ppm. These three peaks were attributed (by comparison with authentic spectra) to the methylene hydrogens at the sulfone, the sulfoxide, and the sulfide, respectively. From the integrals it was then possible to calculate approximate yields of 44% sulfoxide, 36% sulfone, and 11% starting material. When this experiment was repeated using less potassium perruthenate (0.50 g, 2.5 mmol) the yields were 23% sulfoxide, 7% sulfone, and 38% starting material.

Fig. 2. Typical pseudo-first-order rate plot for the oxidation of (methylthio)acetic acid (5.0×10^{-3} M) by perruthenate (3.3×10^{-4} M) in 0.3 M NaOH. Slope = -5.46 s^{-1}. $r = 0.999$.

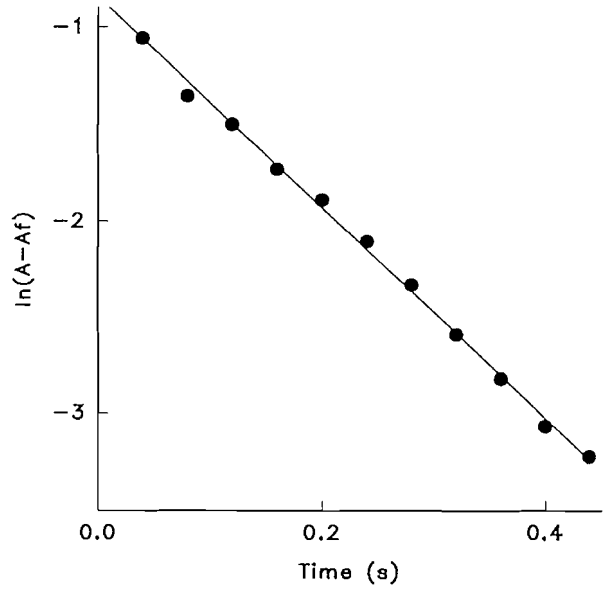

These results suggest that the sulfone is likely formed from the oxidation of the sulfoxide. Under kinetic conditions, where the reductant is held in substantial excess of the oxidant, it is reasonable to assume that very little sulfone would be formed and that the reaction stoichiometry would be given by eq. [1].

Results

The isosbestic point observed at 415 nm (Fig. 1) indicates that no long-lived intermediates are formed during the reaction. Linearity of plots of $\ln(A - A_f)$ vs. time (Fig. 2) indicate that the reaction is first order with respect to perruthenate while plots of log k_1 vs. log[substrate] as in Fig. 3 confirm that the reaction is also first order in reductant. In addition, the reaction exhibited a first-order dependence on the basicity of the solution as indicated in Fig. 4. The rate law for the reaction is therefore given by eq. 2.

[2] $\text{Rate} = -\text{d}[RuO_4^-]/\text{d}t = k_3[RuO_4^-][\text{Reductant}]a_{OH^-}$

Rate constants under various conditions have been collected in Table 1.

Analysis of the rate constants obtained for the oxidation of (arylthio)acetic acids indicated a good correlation ($r = 0.98$) with Hammett σ values (Fig. 5). A less acceptable correlation ($r = 0.88$) was observed when σ^+ values were used.

The activation parameters for the reaction, $\Delta H^{\ddagger}$ and $\Delta S^{\ddagger}$, were determined under conditions of constant basicity. The resulting Eyring plot (36) gives $\Delta H^{\ddagger}$ = 2.7 kcal/mol and $\Delta S^{\ddagger} = -49$ eu for the oxidation of (phenylthio)acetic in 0.3 M NaOH (Fig. 6). A similar plot for the oxidation of (methylthio)acetic acid, also linear (r = 0.993), gave $\Delta H^{\ddagger}$ = 2.8 kcal/mol and $\Delta S^{\ddagger} = -35$ eu in 0.4 M NaOH.

Can. J. Chem. Downloaded from www.nrcresearchpress.com by 65.111.164.53 on 09/08/12
For personal use only.

Fig. 3. Plot for determining the order of the reaction with respect to reductant. Slope = 0.95. $r = 0.993$. [NaOH] = 0.3 M.

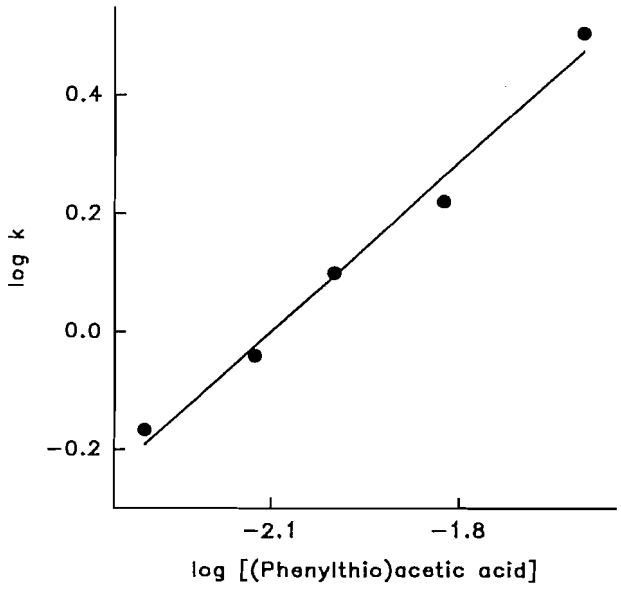

Discussion

Oxygen transfers from metal-oxo's to sulfur (16), phosphorus (32), or nitrogen (37), atoms occur without accompanying bond cleavage in the organic substrate (e.g., $L_nMO + R_2S \rightarrow L_nM + R_2SO$), thereby providing an opportunity to study the mechanisms free from complications encountered with reactions such as allylic oxidations (38) or epoxidations (39) (eqs. [3] and [4]), which require C—H or C—C bond cleavage as well as oxygen transfer.

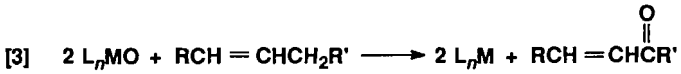

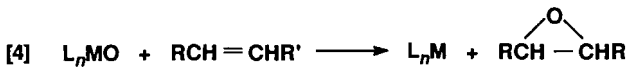

Despite the superficial simplicity of oxygen transfers to atoms such as sulfur or phosphorus, there is currently no definitive general mechanism for these processes. Various possibilities considered in the literature include: (*i*) a reaction initiated by a single electron transfer (40), (*ii*) a one-step oxygen transfer (41), (*iii*) a mechanism initiated by ligand formation using a nonbonding pair of sulfur electrons and an empty *d*-orbital of the metal (34), and (*iv*) a reaction initiated by the interaction of nonbonding sulfur electrons with the π^* orbital of the M=O bond (13). It is therefore of interest to determine which of these four possible mechanisms are most consistent with the results described above.

A negative Hammett ρ value ($\rho = -0.66$, Fig. 5) is consistent with the development of an electron-deficient sulfur in the transition state as required for a single electron transfer mechanism (eq. [5]). However, a reaction resulting in the formation of a radical cation ($ArS\overset{+}{R}$) would be expected to correlate better with σ^+ values than with σ values, as observed for this reaction. The very unfavorable activation entropy $\Delta S^{\neq} =$ −49 eu) is also consistent with a more highly organized transition state than would be expected for a single electron transfer (42).

Fig. 4. Plot illustrating the effect of basicity on the magnitude of the pseudo-first-order rate constants for the oxidation of (phenylthio)acetic acid (1.0×10^{-2} M) by perruthenate (3.4×10^{-4} M). Slope = 1.02, $r = 0.986$. H_- values reported by Rochester (47) were used.

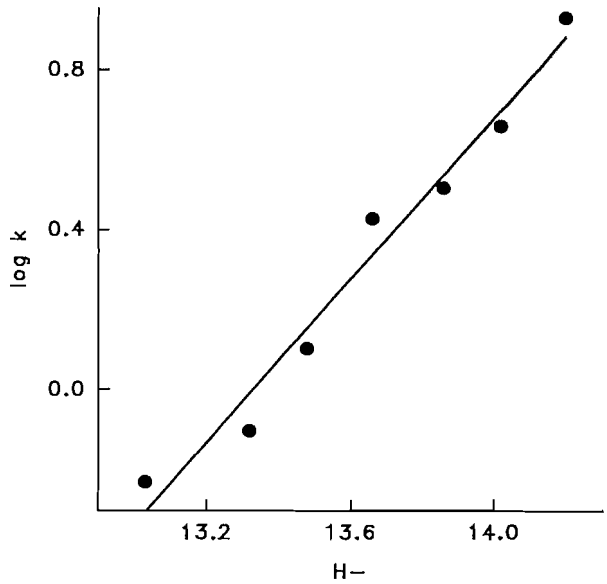

The second possibility, an attack of oxygen by sulfur (eq. [6]) satisfactorily accounts for several features of the reaction including the negative Hammett ρ value and the unfavorable entropy of activation. Such a reaction, however, requires a nucleophilic attack by sulfur on an electron-rich oxygen. On the basis of electrostatic considerations, a nucleophilic attack is more likely to occur at the metal, resulting in the formation of sulfide ligand on ruthenium (eq. [7]).

The observation that the second-order rate constants are directly proportional to the basicity of the solution (Fig. 4) sug-

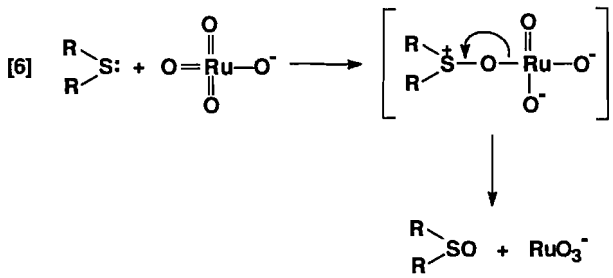

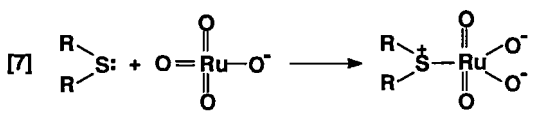

Can. J. Chem. Downloaded from www.nrcresearchpress.com by 65.111.164.53 on 09/08/12
For personal use only.

Table 1. Rate constants for the oxidation of (phenylthio)acetic acid and (methylthio)acetic acid by perruthenate.

Reductant (conc.)	$[RuO_4^-]$ (M)	$[OH^-]$ (M)	k_1 (s^{-1})[a]	k_2 (M^{-1} s^{-1})[b]
(Phenylthio)acetic acid (0.0100 M)	3.3×10^{-4}	0.300	1.26	126
(Phenylthio)acetic acid (0.0250 M)	3.3×10^{-4}	0.300	3.21	128
(Phenylthio)acetic acid (0.0100 M)	3.4×10^{-4}	0.700	3.19	319
(Phenylthio)acetic acid (0.0100 M)	3.4×10^{-4}	1.50	8.44	844
(Methylthio)acetic acid (0.00500 M)	3.4×10^{-4}	0.300	5.28	1.06×10^3
(Methylthio)acetic acid (0.00500 M)	3.4×10^{-4}	1.50	31.0	6.19×10^3

[a]Pseudo-first-order rate constant obtained at 25.0 ± 0.1°C. Each constant is the average of three or more experiments with a standard deviation of ±5% or less.
[b]$k_2 = k_1/[\text{reductant}]$.

gests that the rate-limiting step is preceded by an equilibrium involving the reaction of one of the reactants with a hydroxide ion. A similar observation for the oxidation of alcohols by permanganate (43) has been understood in terms of a proton transfer resulting in the formation of an alkoxide ion (eq. [8]) that would be more easily oxidized than the unionized alcohol. However, deprotonation of (phenylthio)acetate (eq. [9]) would result in the formation of a carbanion with considerable double-bond character between carbon and sulfur (eq. [10]) (44). Oxidation would then be expected to give cleavage products (eq. [11]) rather than sulfoxides and sulfones as observed.

[8] $ROH + OH^- \rightleftharpoons RO^- + H_2O$

[9] $ArSCH_2CO_2^- + OH^- \overset{K}{\rightleftharpoons} ArS\dot{C}HCO_2^- + H_2O$

[10] $ArS-\dot{C}HCO_2^- \longleftrightarrow Ar\dot{S}=CHCO_2^-$

[11] $Ar\dot{S}=CHCO_2^- \xrightarrow[k'_2]{RuO_4^-} ArSO_3^- + OCHCO_2^-$

Furthermore, because the pK_a values for sulfides are so large (estimated by Bordwell (45) to be about 40–45 in DMSO), the concentrations of carbanions in these solutions would be too small to permit the reaction to proceed at a measureable rate; i.e., it can be shown that the required magnitude of the rate constant for eq. [11], k'_2, would need to be greater than those for diffusion-controlled reactions. The observed rate constant, k_{obs}, for a reaction sequence consisting of the equilibrium in eq. [9] followed by reaction [11] would be $k_{obs} = K_a k'_2[OH^-]/K_w$. Therefore, the required value for the rate constant, k'_2, of reaction [11] would be $k'_2 = k_{obs}K_w/K_a[OH^-] = (1.06 \times 10^3\ M^{-1}\ s^{-1} \times 10^{-14}\ M^2)/(10^{-40}\ M \times 0.3\ M) = 3.5 \times 10^{29}\ M^{-1}\ s^{-1}$. Since this value is about 20 orders of magnitude greater than the second-order rate constants for diffusion-controlled reactions (46), it can be concluded that the carbanion is not an intermediate in this reaction.

Fig. 5. Hammett plot for the oxidation of substituted (phenylthio)-acetic acids by perruthenate in 0.30 M NaOH. Slope = −0.66. r = 0.992. T = 25°C.

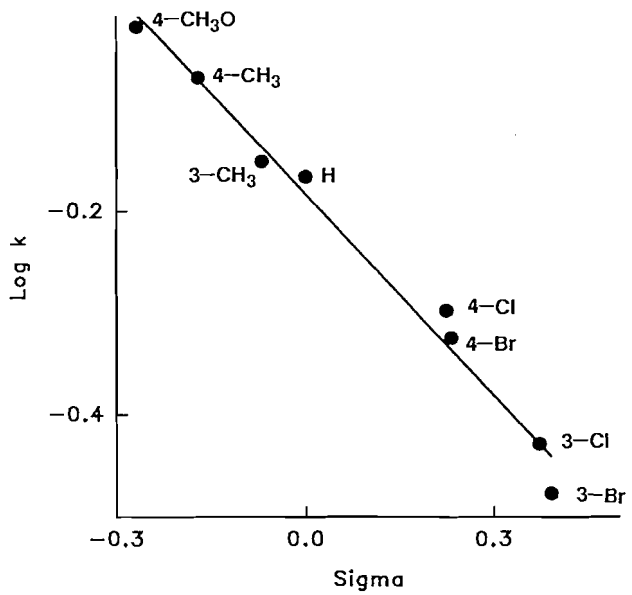

Alternatively, reaction of hydroxide with the oxidant would increase the coordination number of ruthenium from four to five (or six if a molecule of solvent is also incorporated) as in eq. [12]. Replacement of the solvent with a molecule of reduc-

[12] 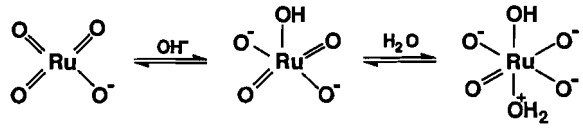

tant would initiate a reaction that could lead to formation of sulfoxide as indicated in Scheme 1. The intermediate, **3**, in this scheme is structurally similar to the one proposed by Dovleto-

Can. J. Chem. Downloaded from www.nrcresearchpress.com by 65.111.164.53 on 09/08/12
For personal use only.

Fig. 6. Eyring plot for the oxidation of (phenylthio)acetic acid (0.010 M) by perruthenate (3.5×10^{-4} M) in 0.30 M NaOH. Slope = -1.38×10^3 K. Intercept = −0.957. $r = 0.998$.

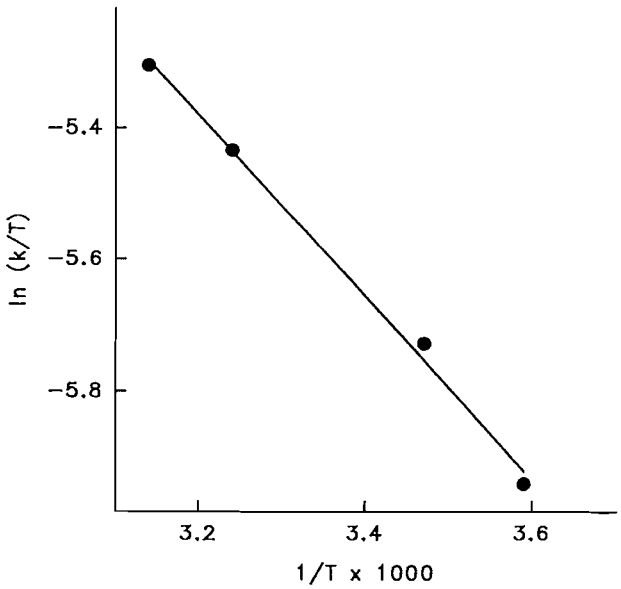

glou and Meyer (32) for the oxidation of phosphines by dioxo complexes of ruthenium(VI).

Activation of the oxidant in this way (by expansion of its coordination shell with incorporation of a basic ligand) is reminiscent of osmium tetroxide oxidations in which it is known that the presence of pyridine (48) or other basic ligands (49) greatly accelerates the rate of reaction.

A negative Hammet ρ value (ρ = −0.66, Fig. 5) is also consistent with the development of an electron-deficient transition state (which would likely resemble **2** and be located somewhere along the reaction coordinate between **1** and **3** in Scheme 1). The highly organized transition state in this scheme is also consistent with the large negative entropy of activation noted above.

Scheme 1. A possible mechanism for the transfer of oxygen from perruthenate to a sulfide.

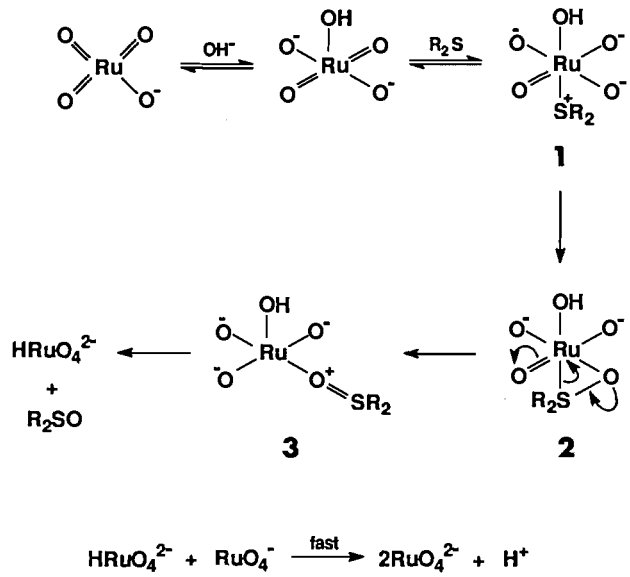

Holm (13) has proposed that the oxidation of triphenylphosphine by molybdenum(VI) is initiated by an interaction of the nonbonding electrons with the π* orbital of the metal–oxo bond. Such a mechanism (eq. [13]) for the reaction of sulfides

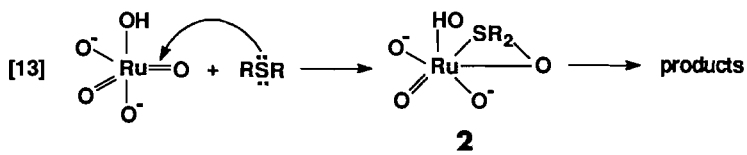

with perruthenate would result in the formation of an intermediate identical to **2** in Scheme 1 and it is therefore impossible, on the basis of the evidence currently available, to distinguish between these two possibilities.

Conclusion

The data obtained from a study of the kinetics of the oxidation of sulfides by perruthenate in basic aqueous solutions are consistent with a mechanism in which oxygen transfer is preceded by an activating expansion of the ruthenium coordination shell through incorporation of an hydroxide ion. Reaction of a nonbonding pair of sulfur electrons with either a vacant ruthenium *d*-orbital or with the Ru=O π*-orbital then initiates oxygen transfer as depicted in Scheme 1. Such a mechanism is consistent with the observed base catalysis, the negative Hammett ρ value, and the unfavorable entropy of activation. Other possible mechanisms such as a single electron transfer or an attack by sulfur on oxygen accommodate the data less well.

Acknowledgement

The financial assistance of the Natural Sciences and Engineering Research Council of Canada is gratefully acknowledged.

References

1. M. Hudlicky. ACS Monogr. **186**, (1990); M.B. Smith. Organic synthesis. McGraw–Hill, New York. 1994. Chap. 3.
2. L.A. Moran, K.G. Scrimgeour, H.R. Horton, R.S. Ochs, and J.D. Rawn. Biochemistry. 2nd ed. 1994. Chap. 5.
3. R.E. Dickerson and I. Geis. Hemoglobin: structure, function, evolution and pathology. Benjamin/Cummings, Menlo Park, Calif. 1983; C. Ho, W.A. Eaton, J.P. Collman, Q.H. Gibson, J.S. Leigh, E. Margoliash, K. Moffat, and W.R. Scheidt. Hemoglobin and oxygen binding. Elsevier Biomedical, New York. 1980; A.B.P. Lever and H.B Gray. Iron porphyrins. Parts 1 and 2. Addison-Wesley, London. 1983.

Can. J. Chem. Downloaded from www.nrcresearchpress.com by 65.111.164.53 on 09/08/12
For personal use only.

4. D.E. Robertson, R.S. Farid, C.C. Moser, J.L. Urbauer, S.E. Mulholland, R. Pidikiti, J.D. Lear, A.J. Wand, W.F. DeGrado, and P.L. Dutton. Nature, **368**, 425 (1994); C.T. Choma, J.D. Lear, M.J. Nelson, P.L. Dutton, D.E. Robertson, and W.F. DeGrado. J. Am. Chem. Soc. **116**, 856 (1994); S. Ozawa, Y. Watanabe, S. Nakashima, T. Kitagawa, and I. Morishima. J. Am. Chem. Soc. **116**, 634 (1994).
5. W.A. Nugent and J.M. Mayer. Metal–ligand multiple bonds. Wiley–Interscience, New York. 1988; R.H. Holm. Chem. Rev. **87**, 1401 (1987).
6. T.J. McMurry and J.T. Groves. *In* Cytochrome P-450. *Edited by* P.R. Ortiz de Montellano. Plenum, New York. 1986. Chap. 1; S. David, B.R. James, D. Dolphin, T.G. Traylor, and M.A. Lopez. J. Am. Chem. Soc. **116**, 6 (1994); G.B. Ray, X-Y. Li, J.A. Ibers, J.L. Sessler, and T.G. Spiro. J. Am. Chem. Soc. **116**, 162 (1994); R.D. Arasasingham, G-X. He, and T.C. Bruice. J. Am. Chem. Soc. **115**, 7985 (1993); C.L. Hill. *In* Activation and functionalization of alkanes. *Edited by* C.L. Hill. Wiley, New York. 1989. Chap. 8; M. Lausmann, I. Zimmer, J. Lex, H. Lueken, K. Wieghardt, and E. Vogel. Angew. Chem. Int. Ed. Engl. **33**, 736 (1994).
7. R.A. Johnson and K.B. Sharpless. *In* Comprehensive organic synthesis. Vol. 7. *Edited by* B.M. Trost. Pergamon, New York. 1991. p. 399; M.G. Finn and K.B. Sharpless. *In* Asymmetric synthesis. Vol. 5. *Edited by* J.D. Morrison. Academic Press, Orlando, Fla. 1985. p. 247.
8. W. Adam and M.J. Richter. Acc. Chem. Res. **27**, 57 (1994).
9. F. Freeman. *In* Organic syntheses by oxidation with metal compounds. *Edited by* W.J. Mijs and C.R.H.I. de Jonge. Plenum, New York. 1986. Chap. 1.
10. S.V. Ley and A. Madin. *In* Comprehensive organic synthesis. Vol. 7. *Edited by* B.M. Trost. Plenum, New York. 1991. p. 251; F. Freeman. *In* Organic syntheses by oxidation with metal compounds. *Edited by* W.J. Mijs and C.R.H.I. de Jonge. Plenum, New York. 1986. Chap. 2; K.G. Wiberg. *In* Oxidation in organic chemistry, Part A. *Edited by* K.B. Wiberg. Academic Press, New York. 1965. Chap. 2.
11. D. Arndt. Manganese compounds as oxidizing agents in organic chemistry. Open Court, La Salle, Ill. 1981; A.J. Fatiadi. Synthesis, 85 (1987); *In* Organic syntheses by oxidation with metal compounds. *Edited by* W.J. Mijs and C.R.H.I. de Jonge. Plenum, New York. 1986. Chap. 3; D.G. Lee. *In* Oxidation in organic chemistry, Part D. *Edited by* W.S. Trahanovsky. Academic Press, New York. 1982. Chap. 2; R. Stewart. *In* Oxidation in organic chemistry, Part A. *Edited by* K.G. Wiberg. Academic Press, New York. 1965. Chap. 1; S. Chang, N.H. Lee, and E.N. Jacobsen. J. Org. Chem. **58**, 6939 (1993), and references therein.
12. D.H.R. Barton and D. Doller. Acc. Chem. Res. **25**, 504 (1992); H-C. Tung, C. Kang, and D.T. Sawyer. J. Am. Chem. Soc. **114**, 3445 (1992); D.H.R. Barton, S.D. Beviere, W. Chavasiri, E. Csuhai, D. Doller, and W-G. Liu. J. Am. Chem. Soc. **114**, 2147 (1992); D.H.R. Barton, E. Csuhai, and N. Ozbalik. Tetrahedron, **46**, 3743 (1990); D.H.R. Barton and N. Ozbalik. *In* Activation and functionalization of alkanes. *Edited by* C.L. Hill. Wiley, New York. 1989. Chap. 9; D.G. Lee and H. Gai. Can. J. Chem. **71**, 1394 (1993); F. Cui and D. Dolphin. Can. J. Chem. **70**, 2314 (1992).
13. R.H. Holm. Coord. Chem. Rev. **100**, 183 (1990).
14. J.L. Courtney. *In* Organic syntheses by oxidation with metal compounds. *Edited by* W.J. Mijs and C.R.H.I. de Jonge. Plenum, New York. 1986. Chap. 8; D.G. Lee and M. van de Engh. Oxidation in organic chemistry, Part B. *Edited by* W.S. Trahanovsky. Academic Press, New York. 1973.
15. H.S. Singh. *In* Organic syntheses by oxidation with metal compounds. *Edited by* W.J. Mijs and C.R.H.I. de Jonge. Plenum, New York. 1986. Chap. 12; A.H. Haines. *In* Comprehensive organic synthesis. *Edited by* B.M. Trost. Pergamon, New York. 1991. p. 437; I. Henderson, K.B. Sharpless, and C-H. Wong. J. Am. Chem. Soc. **116**, 558 (1994).
16. K.R. Guertin and A.S. Kende. Tetrahedron Lett. **34**, 5369 (1993).
17. A.J. Bailey, W.P. Griffith, S.I. Mostafa, and P.A. Sherwood. Inorg. Chem. **32**, 268 (1993).
18. G. Green, W.P. Griffith, D.M. Hollinshead, S.V. Ley, and M. Schroder. J. Chem. Soc. Perkin Trans. 1, 681 (1984).
19. W.P. Griffith. Chem. Soc. Rev. **21**, 179 (1992).
20. W.P. Griffith and S.V. Ley. Aldrichimica Acta, **23**, 13 (1990).
21. D.G. Lee and L.N. Congson. Can. J. Chem. **68**, 1774 (1990); D.G. Lee and S. Helliwell. Can. J. Chem. **62**, 1085 (1984); D.G. Lee, V.S. Chang, and S. Helliwell. J. Org. Chem. **41**, 3644 (1976).
22. T-C. Lau and C-K. Mak. J. Chem. Soc. Chem. Commun. 766 (1993).
23. M. Schroder and W.P. Griffith. J. Chem. Soc. Chem. Commun. 58 (1979).
24. M. Matsumoto and N. Watanabe. J. Org. Chem. **49**, 3435 (1984).
25. M. Bressan and A. Morvillo. *In* New developments in selective oxidation. *Edited by* G. Centi and F. Trifiro. Elsevier, Amsterdam. 1990. p. 119; T-C. Lau, C-M. Che, W-O. Lee, and C-K. Poon. J. Chem. Soc. Chem. Commun. 1406 (1988).
26. W.P. Griffith. Chem. Soc. Rev. **21**, 179 (1992); B.R. James. *In* Dioxygen activation and homogeneous catalytic oxidation. *Edited by* L.I. Simandi. Elsevier, Amsterdam. 1991. p. 195; C-M. Che and V.W-W. Yam. Adv. Inorg. Chem. **39**, 233 (1992).
27. G.A. Neyhart, N. Grover, S.R. Smith, W.A. Kalsbeck, T.A. Fairley, M. Cory, and H.H. Thorp. J. Am. Chem. Soc. **115**, 4423 (1993); M.E. Marmion, R.A. Leising, and K.J. Takeuchi. J. Coord. Chem. **19**, 1 (1988); L. Roecker and T.J. Meyer. J. Am. Chem. Soc. **109**, 746 (1987); M.S. Thompson, W.F. De Giovani, B.A. Moyer, and T.J. Meyer. J. Org. Chem. **49**, 4972 (1984); M.S. Thompson and T.J. Meyer. J. Am. Chem. Soc. **104**, 4106, 5070 (1982).
28. C-M. Che, W-T. Tang, W-O. Lee, W-T. Wong, and T-F. Lai. J. Chem. Soc. Dalton Trans. 2011 (1989).
29. C-M. Che, T-F. Lai, and K-Y. Wong. Inorg. Chem. **26**, 2289 (1987); C-M. Che, C. Ho, and T-C. Lau. J. Chem.

Soc. Dalton Trans. 1259 (1991); C-M. Che, V.W-W. Yam, and T.C.W. Mak. J. Am. Chem. Soc. **112**, 2284 (1990).
30. S-I. Murahashi, T. Naota, and N. Hirai. J. Org. Chem. **58**, 7318 (1993).
31. A.S. Goldstein, R.H. Beer, and R.S. Drago. J. Am. Chem. Soc. **116**, 2424 (1994); Y. Tokita, K. Yamaguchi, Y. Watanabe, and I. Morishima. Inorg. Chem. **32**, 329 (1993); C-M. Che, W-T. Tang, W-O. Lee, K-Y. Wong, and T-C. Lau. J. Chem. Soc. Dalton Trans. 1551 (1992); C-M. Che, W-T. Tang, K-Y. Wong, and C-K. Li. J. Chem. Soc. Dalton Trans. 3277 (1991); J.T. Groves and R. Quinn. J. Am. Chem. Soc. **107**, 5790 (1985).
32. A. Dovletoglou and T.J. Meyer. J. Am. Chem. Soc. **116**, 215 (1994).
33. D.J. Pasto, D. McMillan, and T. Murphy. J. Org. Chem. **30**, 2688 (1965).
34. D.G. Lee and T. Chen. J. Org. Chem. **56**, 5346 (1991).
35. R.E. Connick and C.R. Hurley. J. Am. Chem. Soc. **74**, 5012 (1952).
36. H. Maskill. The physical basis of organic chemistry. Oxford University Press, London. 1985. p. 247.
37. R.D. Bach, M-D. Su, J.L. Andres, and H.B. Schlegel. J. Am. Chem. Soc. **115**, 8763 (1993).
38. P.C. Bulman Page and T.J. McCarthy. *In* Comprehensive organic synthesis. *Edited by* B.M. Trost. Pergamon, New York. 1991. p. 83.
39. A.S. Rao. *In* Comprehensive organic synthesis. *Edited by* B.M. Trost. Pergamon, New York. 1991. p. 357.
40. L.I. Simandi. Catalytic activation of dioxygen by metal complexes. Kluwer, London. 1992. Chap. 12; J.K. Kochi. *In* Comprehensive organic synthesis. Vol. 7. *Edited by* B.M. Trost. Pergamon, New York. 1991. p. 849; D.P. Riley, M.R. Smith, and P.E. Correa. J. Am. Chem. Soc. **110**, 177 (1988); J.P. Dinnocenzo and T.E. Banach. J. Am. Chem. Soc. **108**, 6063 (1986).
41. K.K. Banerji. Tetrahedron, **44**, 2969 (1988).
42. R.G. Wilkins. Kinetics and mechanism of reactions of transition metal complexes. 2nd ed. VCH, Weinheim. 1991. p. 260; H. Taube. Electron transfer reactions of complex ions in solution. Academic Press, New York. 1970. p. 60.
43. R. Stewart. *In* Oxidation in organic chemistry, Part A. *Edited by* K.B. Wiberg. Academic Press, New York. 1965. pp. 48–49.
44. E. Block. Reactions of organosulfur compounds. Academic Press, New York. 1978. p. 45.
45. F.G. Bordwell. Acc. Chem. Res. **21**, 456 (1988).
46. S. Benson. The foundations of chemical kinetics. McGraw–Hill, Toronto. 1960. p. 503.
47. C.H. Rochester. Acidity functions. Academic Press, New York. 1970. p. 237.
48. R.L. Clark and E.J. Behrman. Inorg. Chem. **14**, 1425 (1975).
49. H.C. Kolb, P.G. Andersson, and K.B. Sharpless. J. Am. Chem. Soc. **116**, 1278 (1994).

Can. J. Chem. Downloaded from www.nrcresearchpress.com by 65.111.164.53 on 09/08/12
For personal use only.

Dehydrobromination of 1,1-diaryl-1,2-dibromoalkanes catalyzed by iron and iron bromides. An ion-pair-mediated reaction?

Angela R. Suárez, Alejandra G. Suárez, Sandra E. Martín, and María R. Mazzieri

Abstract: The participation of ion-paired Lewis acid/Lewis base in the dehydrohalogenations of 1,2-dibromo-1,1-diarylalkanes catalyzed by Fe^0 and by Fe(II) and Fe(III) bromides was investigated. The reactivities of the catalyst employed were correlated with their chemical *hardness*. The influence of *para* substituents on the phenyl rings of the substrates and the results obtained in Lewis-acid-catalyzed and thermal dehydrobromination of the same compounds were compared. The experimental results could not be explained in terms of a Lewis-acid-catalyzed dehydrobromination.

Key words: dehydrohalogenation, bromoalkanes, Lewis acid catalysts, ion-pair mechanism.

Résumé : On a étudié la participation d'acide de Lewis/base de Lewis en paires d'ions dans les déshydrohalogénations des 1,2-dibromo-1,1-diarylalcanes, catalysées par le Fe^0 et les bromures de Fe(II) et Fe(III). On a établi une corrélation entre les réactivités des catalyseurs utilisés et leur dureté chimique. On a comparé l'influence des substituants en *para* sur les noyaux phényles des substrats et les résultats obtenus lors de réactions catalysées par des acides de Lewis et ceux obtenus avec les mêmes composés lors de réactions de déshydrobromation. On ne peut pas expliquer les résultats expérimentaux en fonction d'une déshydrobromation catalysée par un acide de Lewis.

Mots clés : déshydrobromation, bromoalkanes, catalyseurs d'acide de Lewis, mécanisme des paires d'ions.

[Traduit par la rédaction]

Introduction

1,2-Dibromo-1,1-diphenylethane, **1***a*, yields 2-bromo-1,1-diphenylethene, **2***a*, in the presence of catalytic amounts of some transition and transition-like metals and their bromides. Solutions of **1***a* in nonpolar solvents were heated in contact with the solid catalysts (1, 2). The reaction is represented by eq. [1].

[1] $$\underset{\mathbf{1}a}{(C_6H_5)_2\text{-}CBr - CH_2Br} + MBr_n \rightarrow \underset{\mathbf{2}a}{(C_6H_5)_2C{=}CHBr} + Hbr$$

M = Al, Fe, and Ru; n = 0–3.

We report here the results of research into the possible participation of an ion-pair-initiated mechanism in these reactions, as had been proposed for metal-ion-catalyzed dehydrohalogenation of haloalkanes in the gas phase (3–6).

The mechanism of elimination reactions from gaseous substrates over solid polar catalysts has been studied by Noller et al. (3, 4). Dehydrochlorination of chloroalkanes with lithium and sodium halides has been interpreted on the basis of the Lewis acidity of the cations and coordination chemistry concepts. An E1 or an E1-like mechanism was proposed for these reactions (3). On this account, it is quite reasonable to expect that a similar ion-pair-mediated mechanism may be involved in hydrogen bromide elimination from **1***a* catalyzed by alkali metal halides.

Comparison of the results obtained with alkali metal catalysts and those of dehydrobrominations carried out with transition metal catalysts could provide decisive evidence on the mechanism operative in the latter reactions. With this purpose, dehydrobromination of **1***a* in carbon tetrachloride solution was carried out with solid NaBr and LiCl as catalysts.

We previously reported evidence of a cationic mechanism in the dehydrohalogenation of 1,1-diaryl-1,2-dihaloalkanes catalyzed by silica gel (7). The same types of compounds were employed in the present work to evaluated the effect of *para* substituents in the phenyl rings on hydrogen bromide elimination catalyzed by powdered Fe^0, anhydrous Fe(III) bromide, and silica gel. Thermal dehydrobrominations of the same compounds were performed for comparison. The substrates employed in this study were 1,1-diphenyl-1,2-dibromoethane, **1***a*; 1,1-bis(4-chlorophenyl)-1,2-dibromoethane, **1***b*; 1,1-bis(4-methylphenyl)-1,2-dibromoethane, **1***c*; 1,1-diphenyl-1,2-dibromopropane, **1***d*; 1,1-bis(4-chlorophenyl)-1,2-dibromopro-

Received June 7, 1994.

A. R. Suárez,[1] A.G. Suárez, S.E. Martín, and M.R. Mazzieri. Departamento de Química Orgánica, Facultad de Ciencias Quimicas, Universidad Nacional de Córdoba, Suc. 16, C.C. 61, (5016) Córdoba, Argentina.

[1] Author to whom correspondence may be addressed. Telephone numbers: [54]-51-60-2512 and 60-8529. FAX: [54]-51-69-4724. E-Mail: <suarez@uncbqo.edu.ar>

Can. J. Chem. Downloaded from www.nrcresearchpress.com by 65.111.164.53 on 09/08/12
For personal use only.

Can. J. Chem. Downloaded from www.nrcresearchpress.com by 65.111.164.53 on 09/08/12
For personal use only.

Table 1. Reactions of 1,2-dibromo-1,1-diphenylethane, **1***a*, with Fe^0, $FeBr_2$, and $FeBr_3$ as catalysts, in CCl_4, at 76°C.[a]

Catalyst	Time (min)	Molar fractions		
		1*a*	**2***a*	1-(**1***a* + **2***a*)
N.C.	30	0.89	0.11	0.00
Fe^0	5	0.22	0.73	0.05
Fe^0	10	0.09	0.81	0.10
Fe^0	15	0.00	1.00	0.00
$FeBr_2$	5	0.18	0.80	0.02
$FeBr_2$	10	0.04	0.86	0.10
$FeBr_2$	15	0.00	1.00	0.00
$FeBr_3$	5	0.18	0.79	0.03
$FeBr_3$	10	0.06	0.83	0.11
$FeBr_3$	15	0.00	1.00	0.00

[a]Average of at least eight reactions. N.C. = thermal reaction performed without catalyst.

Table 2. Reactions of 1,2-dibromo-1,1-diphenylethane, **1***a*, with Fe^0, $FeBr_2$, and $FeBr_3$ as catalysts, in CCl_4, at 50°C.[a]

Catalyst	Time (min)	Molar fractions		
		1*a*	**2***a*	1-(**1***a* + **2***a*)
Fe^0	60	0.52	0.43	0.05
Fe^0	120	0.32	0.58	0.10
Fe^0	180	0.14	0.74	0.12
Fe^0	210	0.08	0.83	0.07
Fe^0	240	0.00	Variable	**2***a* + **3** + **4**[b]
$FeBr_2$	60	0.58	0.39	0.03
$FeBr_2$	120	0.30	0.63	0.07
$FeBr_2$	180	0.15	0.74	0.11
$FeBr_2$	210	0.05	0.84	0.11
$FeBr_2$	240	0.00	Variable	**2***a* + **3** + **4**[b]
$FeBr_3$	60	0.56	0.40	0.04
$FeBr_3$	120	0.37	0.56	0.07
$FeBr_3$	180	0.18	0.69	0.13
$FeBr_3$	210	0.08	0.81	0.11
$FeBr_3$	240	0.00	Variable	**2***a* + **3** + **4**[b]

[a]Average of at least eight reactions.
[b]The **3** + **4** molar fractions measured by ^1H NMR reached as high as 5% of the reaction mixture.

pane, **1***e*; and 1,1-bis(4-methylphenyl)-1,2-dibromopropane, **1***f*.

Results

The results obtained from the dehydrobromination of **1***a* in carbon tetrachloride solutions of different iron-containing catalysts, i.e., Fe^0, Fe(II) bromide, and Fe(III) bromide, at 76°C and at 50°C, are listed in Tables 1 and 2.

The reaction mixtures were evaluated by ^1H NMR spectra. The ^1H NMR spectra of the mixtures of uncompleted reactions showed a deficit of nonaromatic protons, that is, the sum of the molar fraction of methylenic protons from substrate **1***a* and vinylic proton from product **2***a* was lower than 1. Normal proton integration resulted at the end of the reactions and only **2***a* was detected by ^1H NMR. In previous reports, the "undetected" protons in the NMR spectra measured at room temperature were tentatively assigned to the dynamically interchanged protons of organometallic intermediates (1, 2).

The reactions carried out at 50°C, Table 2, secondary products appeared at the end of the reactions. They were identified as 1,1,4,4-tetraphenylbutadiene, **3**, and 1-bromomethyl-1,2,2-triphenylindane, **4**, as described in the experimental section. The total **3** + **4** molar fraction amounted to as much as 5% of the reaction mixture. These products were performed with any of the three iron catalysts. Despite careful searching in the ^1H

Table 3. Reactions of 1,2-dibromo-1,1-diphenylethane, **1***a*, with alkali halide catalysts, in CCl_4, at 76°C.

Catalyst	Time (min)	Molar fractions		
		1*a*	**2***a*	1-(**1***a* + **2***a*)
N.C.	90	0.78	0.22	0.00
N.C.	180	0.55	0.45	0.00
NaBr[a]	90	0.80	0.20	0.00
NaBr[a]	180	0.62	0.38	0.00
NaBr[b]	140	0.00	1.00	0.00
LiCl[a]	90	0.70	0.30	0.00
LiCl[a]	180	0.36	0.64	0.00
LiCl[b]	110	0.00	1.00	0.00

The reported values are the average of three reactions. N.C. = thermal reactions performed without catalyst.
[a]Substrate: catalyst ratio, 10:1.
[b]Substrate: catalyst ratio 1:1.

Table 4. Dehydrobromination of $(4\text{-Z-}C_6H_4)_2CBr\text{-}CH_2Br$, **1***b*, *c*, to $(4\text{-Z-}C_6H_4)_2C{=}CHBr$, **2***b*, *c*, with Fe^0, $FeBr_3$ and without catalyst, in CCl_4, at 76°C.[a]

Z	Substrate	Catalyst	Time (min)	Product	Molar fraction
Cl	**1***b*	Fe^0	5	**2***b*	N.D.
		Fe^0	10	**2***b*	0.18
		Fe^0	45	**2***b*	0.88
		$FeBr_3$	5	**2***b*	0.17
		$FeBr_3$	10	**2***b*	0.65
		$FeBr_3$	20	**2***b*	0.89
		N.C.	90	**2***b*	N.D.
CH_3	**1***c*	N.C.	5	**2***c*	0.69
		N.C.	10	**2***c*	0.78
		22	10	**2***c*	1.00
		Fe^0	5	**2***c*	0.68
		Fe^0	10	**2***c*	0.82
		Fe^0	22	**2***c*	0.94
		$FeBr_3$	5	**2***c*	0.67
		$FeBr_3$	22	**2***c*	0.97

[a]Average of at least eight reactions. N.C. = thermal reactions performed without catalyst. N.D. = nondetected.

Table 5. Dehydrobrominations of (4-Z-$C_6H_4)_2$CBr-$CBrCH_3$, **1***d–f* to (4-$ZC_6H_4)_2C{=}CBrCH_3$, **2***d–f*, with $FeBr_3$,[a] with silica gel,[b] and without catalyst,[c] in CCl_4, at 76°C.

Z	Substrate	Catalyst	Time (min)	Product	Molar fraction
H	**1***d*	$FeBr_3$	5	**2***d*	1.00
		N.C.	35	**2***d*	0.14
		Silica gel	35	**2***d*	0.98
Cl	**1***e*	$FeBr_3$	60	**2***e*	0.68
		$FeBr_3$	90	**2***e*	0.91
		N.C.	90	**2***e*	0.05
		N.C.	720	**2***e*	0.25
		Silica gel	410	**2***e*	0.96
CH_3	**1***f*	$FeBr_3$	5	**2***f*	0.74
		$FeBr_3$	7	**2***f*	0.90
		N.C.	5	**2***f*	0.68
		N.C.	7	**2***f*	0.82
		Silica gel	3	**2***f*	0.87
		Silica gel	5	**2***f*	1.00

[a]Average of at least eight reactions.
[b]Average of at least five reactions.
[c]Average of three reactions. N.C. = thermal reactions performed without catalyst.

NMR spectra of the reactions carried out at 76°C and in earlier samples of reactions at 50°C, the signals corresponding to **3** and **4** could not be detected. To explore a possible origin for these compounds, 2-bromo-1,1-diphenylethane, **2***a*, was refluxed at 50°C for 4 h with 10 mol% of Fe(III) bromide but the signals corresponding to **3** and **4** were absent in the ^1H NMR spectra of the reaction mixtures. According to these results, **3** and **4** were probably formed by reaction of **2***a* with some unidentified reaction intermediate.

At the end of the reactions, the remaining solids arising from the catalysts were analyzed by UV–visible spectroscopy. The results demonstrated that whichever initial catalyst was employed, these solids consisted of Fe(III) bromide (8), indicating that Fe^0 and Fe(II) had been oxidized to Fe(III) by reaction with the hydrogen bromide eliminated from **1***a*.

Results with alkali metal salts are shown in Table 3. The substrate **1***a* dehydrobrominated to **2***a* with NaBr and LiCl in a substrate:catalyst ratio of 1:1. With a 10:1 ratio, a small catalytic effect was detected with LiCl whereas reactions with NaBr behaved similarly to those performed without catalyst.

To investigate the influence of the substituents placed in the phenyl rings on the presumed development of a positive charge in the benzylic carbon, reactions of 1,1-bis(4-chlorophenyl)-1,2-dibromoethane, **1***b*, and 1,1-bis(4-methylphenyl)-1,2-dibromoethane, **1***c*, with Fe^0 and Fe(III) bromide were also studied at 76°C. By comparing the results summarized in Tables 1 and 4, it is evident that **1***b* dehydrobrominations were slower than those of **1***a*. In turn, dehydrohalogenation of **1***c* was very similar either in the presence or in the absence of catalysts.

Dehydrobrominations of **1***d–f* catalyzed by anhydrous Fe(II) bromide showed the same tendency. The *para*-chloro derivative, **1***e*, and the *para*-methyl derivative, **1***f*, were both less reactive than the unsubstituted compound, **1***d*. The order of reactivity was **1***d* > **1***f* ⩾ **1***e*. Conversely, in reactions accomplished by heating solutions of **1***d–f* without catalyst and in silica-gel-catalyzed reactions, the order of reactivity was **1***f* > **1***d* ⩾ **1***e*. These results are listed in Table 5.

Discussion

Considering the chemical *hardness* of both alkali cations, Li^+ and Na^+, and the high ionic degree of their halides, it is expected that active Lewis acid sites should remain on the solid surface of the alkali halides used in this work. Noller and Kladnig proposed that every cation of the surface may be an active Lewis Acid site (3).

The easily polarizable bromine atom in the benzylic position of **1***a* could react at those sites to form an ion pair. Allison and co-workers also suggested the development of a positive charge during halogen atom elimination from alkyl halides in gas-phase reactions catalyzed by bare alkali ions. This initial ion–dipole interaction should be followed by hydrogen halide elimination and formation of a π-complex between the alkali metal and the olefinic product (5, 6).

As shown in Table 3, solid alkali metal halides catalyzed the dehydrobromination of **1***a* to **2***a* when a substrate:catalyst ratio of 1:1 was employed. The reactions carried out with NaBr in a substrate:catalyst ratio of 10:1 behaved similarly to the thermal decomposition of **1***a*, whereas a small catalytic effect was noticed with a 10:1 substrate:LiCl ratio.

A similar ion–dipole complex has been considered as the most probable intermediate in gas-phase reactions of naked transition M^+ metal ions with several alkyl derivatives (5, 6, 9). This Lewis-acid-induced charge-separation mechanism is similar to that proposed by Yoon and Kochi for reactions of halocyclohexanes with anhydrous Fe(III) halides in nonpolar solvents (8).

If this mechanism were operative in the catalytic dehydrobromination reported in this work (Tables 1, 2, and 4) and in previous reports (1, 2), the reactions represented in Scheme 1 should take place:

Scheme 1

$$\underset{\text{RCBrH}}{\overset{|}{\text{Ar}_2\text{C}}} - \text{Br} + \text{MBr}_n \rightarrow \underset{\text{RCBrrH}}{\overset{|}{\text{Ar}_2\text{C}^+}}\ \text{MBr}_{n+1}^-$$

1*a* **5**

$$\mathbf{5} \rightarrow \mathbf{2}a + \text{HBr} + \text{MBr}_n$$

Species **5** in Scheme 1 represents the ion pair formed by the benzylic carbocation and a tetrabromometalate anion. The most likely reaction for the ion pair **5** under our experimental conditions is the abstraction of the β-hydrogen as a proton by the anion to form product **2***a*. Formation of **5** induced by Lewis acid/Lewis base interaction should be the rate-controlling step in an E1-like mechanism.

We have listed below, I, the order of reactivity of the metal catalysts employed in this study and in work previously reported (1, 2). In II are reproduced the chemical hardness values of metal ions and neutral metals given by Pearson (10):

I: $FeBr_3 = FeBr_2 = Fe^0 > RuBr_3 > Ru^0 = AlBr_3 > Al^0 \gg LiCl > NaBr$

II: $Al^{3+} > Li^+ Na+ \gg Fe^{3+} > Ru^{3+} > Fe^{2+} \gg Fe^0 > Ru^0 > Al^0$

Can. J. Chem. Downloaded from www.nrcresearchpress.com by 65.111.164.53 on 09/08/12
For personal use only.

Can. J. Chem. Downloaded from www.nrcresearchpress.com by 65.111.164.53 on 09/08/12
For personal use only.

Evidently, there is no correlation between the order of activity and the Lewis acidity of the catalyst used in our work.

The second series of experiments carried out, to investigate the possible involvement of a Lewis-acid-induced charge-separation mechanism, were those with *para*-phenyl-substituted substrates. Fe(III) bromide was used as catalyst in these reactions because Fe(III) is a hard Lewis acid (10) that should facilitate the formation of the benzylic carbocations in ion pairs like **5**, as shown in Scheme 1. For comparison, reactions catalyzed by Fe^0, a soft Lewis acid (10), and reactions without catalyst were also carried out.

The 4-chlorine substituent in **1***b* and **1***e* and the 4-methyl substituent in **1***c* and **1***f* must produce an opposite effect on the formation of a benzylic carbocation according to the Hammett σ^+ values (11). The results listed in Table 4 demonstrate that both compounds, **1***b* and **1***c*, were less reactive than **1***a*. Moreover, thermal reactions of **1***c*, carried out without catalyst, showed a similar behaviour to reactions observed in the presence of Fe^0 and Fe(III) bromide. It is evident that the contribution of the transition-metal-catalyzed dehydrobromination of **1***c* was negligible. These results do not support the formation of a benzylic carbocation intermediate induced by Lewis acids.

The results of dehydrobromination of compounds **1***d–f* with Fe(III) bromide (Table 5) provide clearer data. In reactions with Fe(III) bromide, the 4-methyl derivative, **1***f*, and the 4-chloro derivative, **1***e*, were both less reactive than the unsubstituted substrate, **1***d*. On the other hand, the activating effect of the 4-methyl group in **1***f* was opposite to the effect of the 4-chlorine atom in **1***e* in the thermal as well as in silica-gel-catalyzed HBr eliminations. This latter behaviour could be explained by a carbenium ion mechanism (7).

Conclusion

Comparison of the activity and Lewis acidity of the catalysts, and the effect of substituents placed on the phenyl rings of the substrates, strongly suggests that, with the exception of the alkali halides, an ion-pair-mediated mechanism cannot be the main route to dehydrobromination of 1,1-diaryl-1,2-dibromoalkanes catalyzed by the metals and metal halides used in our work.

The previously reported spectroscopic evidence indicates that some organometallic intermediates are more probably involved in these reactions (1, 2).

Experimental section

The ^{1}H NMR spectra were obtained using a T-60 Varian spectrometer with TMS as internal standard and CCl_4 as solvent, or a Bruker 200 FT spectrometer with CCl_4 as solvent and a capillary tube containing acetone-d_6 fixed into the NMR tube for locking purposes and as standard references. Electron absorption spectra were recorded in a Shimadzu 260 spectrophotometer. Mass spectra were measured on a Finnigan 3300 spectrometer. IR spectroscopy was carried out using a Nicolet 5 SXC FT-IR spectrometer. Reactions were carried out in a Lauda Ultra-Thermostat provided with an electronic relay, temperature accuracy ±1°C. Melting points were reported without correction.

Materials

Solvents were purified by the usual procedures (12). Carbon tetrachloride used as solvent in the reactions was further dried and maintained over 4A molecular sieves. Fe^0 (Merck, 2–7 μm particle diameter) was washed with ether and vacuum dried before use. Metal halides were the following: anhydrous Fe(II) and Fe(III) bromides supplied by Strem Chemicals Co, NaBr AR from Mallinckrodt, and LiCl was Carlo Erba RP. Silica gel employed as catalyst was Kieselgel 60 from Merck, activated at 110°C for 1 h before use.

Carbon tetrachloride and dichloromethane were Merck Uvasol and bromine was Merck P.A., less than 1×10^{-4}% in heavy metals. Silica gel for column chromatography was Kieselgel Merck 60, and for flash chromatography a Kieselgel Merck 60 H was employed. In both cases they were activated for 1 h at 110°C.

Diphenylethane (Fluka) was flash chromatographed on silica gel with *n*-hexane before use. The 1,1-bis(4-chlorophenyl)-ethane, 1,1-bis(4-methylphenyl)ethane, 1,1-diphenylpropene, 1,1-bis(4-chlorophenyl)propene, 1,1-bis(4-methylphenyl)propene, and 1,1-diphenylethanol were synthesized, purified, and identified by known methods.

The 1,2-dibromides were prepared by addition of a CCl_4 solution of bromine to a solution of the olefins in the same solvent at temperatures from −12°C to −30°C. The dibromides: 1,2-dibromo-1,1-diphenylethane (**1***a*), 1,1-bis(4-chlorophenyl)-1,2-dibromoethane (**1***b*), 1,2-dibromo-1,1-diphenylpropane (**1***d*), and 1,1-bis(4-chlorophenyl)-1,2-dibromopropane (**1***e*) were isolated and purified by different procedures. Physical constants agree with those reported in the literature.

Unstable dibromides 1,1-bis(4-methylphenyl)-1,2-dibromoethane (**1***c*) and 1,1-bis(4-methyl)-1,2-dibromopropane (**1***f*) were not isolated. Addition of the bromine solution to the olefine was checked by ^{1}H NMR and UV spectroscopy. Once the bromine addition was complete, the solutions were used without isolation of these reagents.

General procedure for dehydrobromination reactions

The reaction equipment consisted of a Pyrex tube attached to a condenser and with a water trap on the top. The equipment was dried at 120°C before use and allowed to reach room temperature in a desiccator. The presence of air was not avoided, but the reaction tube was covered with aluminum foil since dibromides of **1** are light sensitive. Because the anhydrous catalysts are decomposed by moisture, they were placed in a preweighed reaction tube in a glovebag under dry atmosphere. The closed tube was weighed again and then a solution of the substrate in carbon tetrachloride was added to the solid. The substrate:catalyst ratio was 10:1 with the exception of some reactions with alkali halides as catalysts that were carried out with a 1:1 substrate:catalyst ratio. The total amount of dibromide employed was about 1 mmol in 2 mL of solvent. The reaction tube with the reagents was then immersed in a bath at the desired temperature. The reaction mixtures were filtered at the appropriate times and checked by ^{1}H NMR.

Yields obtained with the transition metal catalysts were seldom duplicated exactly in the same reaction time. For this reason, two series of six simultaneous reactions were carried out. We considered that a result was valid if at least 8 out of 12 values gave product yields with differences lower than 6% of the total dehydrobromination yield. Yields with higher differences were not taken into account in calculating the reported average values. As thermal reactions and those catalyzed by

alkali halides rendered reproducible results, they were carried out in triplicate.

Electron absorption spectra of the remnant solid arising from the iron catalysts Fe^0, and Fe(II) and Fe(III) bromides were carried out in dichloromethane solutions. The recorded spectra corresponded to that of Fe(III) bromide (8).

Dehydrobrominations of 1a with iron catalysts at 50°C
In reactions of **1***a* catalyzed by Fe^0, and Fe(II) and Fe(III) bromides at 50°C, after 240 min signals appeared in the ^1H NMR spectra that did not correspond to either **1***a* or **2***a*. These signals were identical in reactions with the three iron catalysts. In the ^1H NMR spectra of reactions carried out at 76°C and in earlier examples of reactions at 50°C, these signals were not detected. For this reason, the lack of nonaromatic protons in reactions performed at 50°C was not reported after 240 min of reaction, and the molar fraction of **2***a* was variable.

A number of reaction mixtures were collected and their components isolated by column chromatography on silica gel with *n*-hexane:benzene 80:20 as eluents. After several chromatographic separations two compounds were isolated and their ^1H NMR spectra corresponded to the unknown compounds detected in the reaction mixtures. They were identified as 1,1,4,4-tetraphenylbutadiene, **3**, and an indane derivative, **4**.

1,1,4,4-Tetraphenylbutadiene, 3: Recrystallized from *n*-hexane, mp 192.5–193°C (lit. (13) mp 204–205°C (acetone–ethanol). The ^1H NMR, electron absorption, IR, and mass spectra agree with literature data. Mass spectra overlapped with those of the NBS Library.

1-Bromomethyl-1,2,2-triphenylindane, 4: Recrystallized from *n*-hexane, mp 145–147°C. IR (KBr): typical bands of aliphatic methylene groups, phenyl rings and C–Br stretching bands were observed. UV (*n*-heptane): bands corresponding to transitions of the phenyl rings were observed. ^1H NMR (CCl_4): 3.48–3.61 (dd, 2H, AB system), 3.87 (s, 2H), 7.01–7.39 (m, 19H) ppm. MS (20 eV) *m/z*(%): 442(1), 440(2), 438(1), 358(43), 345(37), 253(96), 255(100), 203(53), 167(55), 91(23).

From the proton NMR and mass spectra and by comparison with the results of Patai et al. (14), we propose the structure **4** for this compound.

Dehydrobrominations catalyzed by silica gel
The experimental arrangement was as described in the General Procedure and was as previously reported (7). Solutions containing 1 mmol of the substrates **1***d–f* were refluxed in contact with 20 mg of silica gel. At the appropriate time, the colourless reaction mixtures were filtered and the silica gel was washed with CCl_4. The filtrate and the washings were combined to evaluate the composition of the reaction mixtures by ^1H NMR, rendering very reproducible yields.

Acknowledgements

We thank the Consejo Nacional de Investigaciones Científicas y Técnicas de la República Argentina (CONICET) and the Consejo de Investigaciones Científicas y Tecnológicas de la Provincia de Córdoba, Argentina (CONICOR), for financial support. A.G.S. and S.E.M. thank CONICET for fellowships.

References

1. A.R. Suárez, M.R. Mazzieri, and A.G. Suárez. J. Am. Chem. Soc. **111**, 763 (1989).
2. A.R. Suárez, A.G. Suárez, and M.R. Mazzieri. Organometallics, **11**, 718 (1992).
3. H. Noller and W. Kladnig. Catal. Rev.-Sci. Eng. **13**, (1976).
4. H. Noller, P. Andrew and M. Hunger. Angew. Chem. Int. Ed. Engl. **10**, 172 (1971).
5. J. Allison and D.P. Ridge. J. Am. Chem. Soc. **101**, 4998 (1979).
6. M.L. Larrivee and J. Allison. J. Am. Chem. Soc. **112**, 7134 (1990).
7. A.R. Suárez and M.R. Mazzieri. J. Org. Chem. **52**, 1145 (1987).
8. K.B. Yoon and J.K. Kochi. J. Org. Chem. **54**, 3028 (1989).
9. K. Eller. Coord. Chem. Rev. **126**, 93 (1993).
10. R.G. Pearson. Inorg. Chem. **27**, 734 (1988).
11. J. March. Advanced organic chemistry. Reactions, mechanisms and structure. 4th ed. John Wiley and Sons, New York. 1992. p. 280.
12. A. Vogel. Textbook of practical organic chemistry. 5th ed. Longmans Group, London. 1989.
13. F.E. Sheibley and C.F. Prutton. J. Am. Chem. Soc. **62**, 840 (1940).
14. D. Elmarch, S. Patai, and Z. Rappaport. J. Chem. Soc. (C), 3100 (1971).

Can. J. Chem. Downloaded from www.nrcresearchpress.com by 65.111.164.53 on 09/08/12
For personal use only.

Electron exchange kinetics in a tetrahedrally coordinated copper(II)/(I) couple

Peter D. Metelski, A. Scott Hinman, Hideo D. Takagi, and Thomas W. Swaddle

Can. J. Chem. Downloaded from www.nrcresearchpress.com by 65.111.164.53 on 09/08/12
For personal use only.

Abstract: The four-coordinate anion $Cu^{I}(dpym)_2^-$ (Hdpym = 3,3′,5,5′-tetramethyl-4,4′-dicarboethoxydipyrromethene) can be prepared in solution in acetone either by electrochemical reduction of the known tetrahedral complex $Cu^{II}(dpym)_2^0$ ($E^0 = -290$ mV vs. SCE) or by the quantitative reaction of 2Hdpym with $Cu(CH_3CN)_4^+$ in the absence of O_2. The latter reaction does not go to completion in solvents that bind relatively strongly to Cu^I or that are poor proton acceptors. Ligand exchange between $Cu^{I}(dpym)_2^-$ and excess Hdpym in acetone is "fast" in the ^1H NMR timeframe, with $k_1 = 1.4 \times 10^7$ L mol^{-1} s^{-1} at 298 K (first order in each reactant), $\Delta H_1^{\ddagger} = 3.4 \pm 0.6$ kJ mol^{-1}, and $\Delta S_1^{\ddagger} = -97 \pm 3$ J K^{-1} mol^{-1}. In the absence of excess Hdpym, dissociation of $Cu^{I}(dpym)_2^-$ in acetone remains negligible. Homogeneous electron exchange between $Cu^{I}(dpym)_2^-$ and $Cu^{II}(dpym)_2^0$ in acetone falls in the "slow" ^1H NMR timeframe, with $k_{ex} = 5.9 \times 10^3$ L mol^{-1} s^{-1}, $\Delta H_{ex}^{\ddagger} = 48.5 \pm 3.0$ kJ mol^{-1}, and $\Delta S_{ex}^{\ddagger} = -10 \pm 10$ J K^{-1} mol^{-1}, at ionic strength $I \approx 0.007$ mol L^{-1} and 298 K, while for the same self-exchange on a Pt electrode the heterogeneous rate constant $k_{el} = 0.16 \pm 0.04$ cm s^{-1} at $I \approx 0.1$ mol L^{-1} and 298 K, according to AC voltammetry. These values of k_{ex} and k_{el} are of the order expected for $Cu^{II/I}$ couples in which no significant change in coordination number or geometry accompanies electron transfer.

Key words: Electron transfer, copper complexes, ligand substitution kinetics, dynamic NMR.

Résumés : On peut préparer l'anion tétracoordiné $Cu^{I}(dpym)_2^-$ (Hdpym = 3,3′,5,5′-tétraméthyl-4,4′-dicarboéthoxydipyrrométhène) en solution dans l'acétone soit par une réduction électrochimique du complexe tétraédrique $Cu^{II}(dpym)^0$ ($E^0 = -290$ mV vs. SCE) ou par la réaction quantitative de 2Hdpym avec le $Cu(CH_3CN)_4^+$ en l'absence de O_2. La dernière réaction n'est pas complète dans des solvants qui se lient relativement fortement au Cu^I ou qui sont de pauvres accepteurs de proton. L'échange de coordinat entre le $Cu^{I}(dpym)_2^-$ et un excès de Hdpym dans l'acétone est rapide par rapport à la RMN du ^1H; $k_1 = 1{,}4 \times 10^7$ L mol^{-1} s^{-1} à 298 K (premier ordre par rapport à chaque réactif), $\Delta H_1^{\ddagger} = 3{,}4 \pm 0{,}6$ kJ mol^{-1} et $\Delta S_1^{\ddagger} = -97 \pm 3$ J K^{-1} mol^{-1}. En l'absence d'un excès de Hdpym, la dissociation du $Cu^{I}(dpym)_2^-$ dans l'acétone est négligeable. L'échange homogène d'électron entre le $Cu^{II}(dpym)^0$ dans l'acétone est lent à l'échelle de temps de la RMN du ^1H; $k_{éch} = 5{,}9 \times 10^3$ L mol^{-1} s^{-1}, $\Delta H_{éch}^{\ddagger} = 48{,}5 \pm 3{,}0$ kJ mol^{-1} et $\Delta S_{éch}^{\ddagger} = -10 \pm 10$ J K^{-1} mol^{-1}, à une force ionique d'environ 0,007 mol L^{-1} et à 298 K alors que, d'après la voltampérométrie CA, pour le même autoéchange sur une électrode de platine, $k_{él} = 0{,}16 \pm 0{,}04$ cm^{-1}, à une force ionique d'environ 0,1 mol L^{-1} et 298 K. Ces valeurs de $k_{éch}$ et $k_{él}$ sont de l'ordre de grandeur attendu pour les couples $Cu^{II/I}$ dans lesquels il ne se produit pas de changement significatif dans le nombre de coordination ou dans la géométrie qui accompagne le transfert d'électron.

Mots clés : transfert d'électron, complexes du cuivre, cinétique de substitution des coordinats, RMN dynamique.

[Traduit par le rédaction]

Introduction

According to the Vallee–Williams principle (1), the rates of outer-sphere electron transfer processes involving copper(II/I) couples will tend to be rather slow if the normally preferred coordination geometries (tetrahedral four-coordination for copper(I), tetragonal six- or five-coordination for copper(II)) prevail, as the extensive ligand rearrangement accompanying oxidation state change would then make a large Franck–Condon contribution to the free energy of activation $\Delta G^{\ddagger}$ (2). Thus, electron transfer in the $Cu(aq)^{2+/+}$ couple is extremely slow, with a self-exchange rate constant $k_{ex} \approx 5 \times 10^{-7}$ L mol^{-1} s^{-1} at 25°C in the absence of catalysis (e.g., by Cl^-) (3). Consequently, as Rorabacher and co-workers (4, 5) have shown, application of the Marcus cross relation to estimate $Cu^{II/I}$ self-exchange rate constants may give different results in oxidation and reduction modes, if conformational changes are rate limiting — the redox cycle follows a "square scheme"

Received July 27, 1994.

P.D. Metelski, A.S. Hinman, H.D. Takagi,[1] and T.W. Swaddle.[2] Department of Chemistry, The University of Calgary, Calgary, AB T2N 1N4, Canada.

[1] Present address: Department of Chemistry, Nagoya University, Nagoya 464-01, Japan.

[2] To whom correspondence should be addressed: tel.: (403) 220-5358, fax: (403) 289-9488, e-mail: swaddle@acs.ucalgary.ca.

Table 1. Proton chemical shifts δ/ppm[a] of dipyrromethene compounds at room temperature.

Compound	Solvent	≡C—H singlet	—CH_2—CH_3 quartet	≡C—CH_3[b] singlet	≡C—CH_3[c] singlet	—CH_2—CH_3 triplet
Hdpym	$CDCl_3$	7.03	4.31	2.60	2.49	1.39
	$(CD_3)_2CO$	7.34	4.26	2.54	2.43	1.34
$[H_2dpym]Cl$	$CDCl_3$	7.45	4.35	2.92	2.66	1.40
$Cu^{II}(dpym)_2^0$	$CDCl_3$	9.07(?)[d]	4.36[d]	1.60[d,e]	1.60[d,e]	1.38[d]
$Cu^{I}(dpym)_2^-$	$(CD_3)_2CO$	8.16	4.35	2.80	2.74	1.38
$Zn^{II}(dpym)_2^0$	CD_3CN	7.72	4.23	2.82, 2.78[f]	2.64	1.31

[a]Relative to tetramethylsilane.
[b]*cis* to N.
[c]*trans* to N.
[d]Broad.
[e]*cis* and *trans* coalesced.
[f]Two proton environments, believed due to distortion of complex.

in which the intermediate involved in the oxidation of Cu^I is different from that produced in the reduction of Cu^{II}.

If, however, the coordination environments of the Cu^I and Cu^{II} partners are constrained to be similar, the intermediates of the square scheme become virtually identical, the Marcus cross relationship (2) should be valid, and the $Cu^{II/I}$ self-exchange should be fast. In synthetic $Cu^{II/I}$ couples, this is most readily achieved when five-coordination is enforced in both the Cu^I and Cu^{II} partners ($k_{ex} > 10^4$ L mol^{-1} s^{-1}) (6). The efficacy of Cu-based biological redox reagents may be understood on this basis — except that in the case of the type I or "blue" copper proteins (azurins, plastocyanins, stellacyanins, etc.) the Cu centres are constrained to a *four*-coordinate, distorted tetrahedral environment, regardless of oxidation state, and their $Cu^{II/I}$ self-exchange in aqueous solution is fast ($k_{ex} \approx 10^5$–10^6 L mol^{-1} s^{-1}) unless strong electrostatic effects operate (7).

Synthetic couples in which the Cu^{II} as well as the Cu^I is known to be constrained to an approximately tetrahedral environment are few (8–13), and not all lend themselves to kinetic studies. For the couple $Cu(dmp)_2^{2+/+}$ (dmp = 2,9-dimethyl-1,10-phenanthroline), molecular models show that the methyl groups block the phenanthroline ligands from becoming coplanar when the Cu^I complex, which is known to be tetrahedral in its solid salts, is oxidized to Cu^{II}. It may therefore be *presumed* that the environment of Cu^{II} in $Cu(dmp)_2^{2+}$ is quasi-tetrahedral, although there is a possibility that one or both of the dmp complexes are five-coordinate (through acquisition of a solvent ligand) in solution (14). In any event, we found by direct NMR measurements that electron self-exchange in $Cu(dmp)_2^{2+/+}$ is indeed quite fast, with rate constant k_{ex} in triflate media at 25°C = 2.0×10^5, 4.9×10^3, and 3.1×10^3 kg mol^{-1} s^{-1} in D_2O, CD_3CN, and $(CD_3)_2CO$ at ionic strength $I \approx$ 0.002, 0.1, and 0.1 mol kg^{-1}, respectively (14). In contrast, Knapp et al. (11) found that electron exchange in the near-tetrahedral $CuL_2^{2+/+}$, where L = 2,2′-bis(2-imidazolyl)biphenyl, was surprisingly slow ($k_{ex} < 10^2$ L mol^{-1} s^{-1} in acetonitrile, −20 to +20°C). Furthermore, Lappin and Peacock (9) estimated k_{ex} for the self-exchange of aqueous 12-tungstocuprate(II/I), in which the Cu atom occupies a tetrahedral site, to be only 2.6 L mol^{-1} s^{-1} at 298 K — this result, however, came from application of the Marcus cross-relation (2) to the oxidation of $CuW_{12}O_{40}^{7-}$ by $Fe(CN)_6^{3-}$ rather than from direct measurement. Thus, there is a need for further kinetic data, particularly direct rate measurements, to assist in establishing the norm for $Cu^{II/I}$ exchanges.

In the present study, we have examined electron transfer kinetics in the $Cu^{II/I}(dpym)_2^{0/-}$ couple (Hdpym = 3,3′,5,5′-tetramethyl-4,4′-dicarboethoxydipyrromethene) in which the

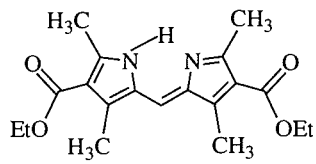

= Hdpym

coordination of Cu in $Cu(dpym)_2^0$ ("bis(dipyrromethene)copper(II)") is known from X-ray crystallography to be close to tetrahedral (8), at least in the solid state, again presumably because of the steric effects from the methyl groups. The Cu^{II} complex is interesting in that the ligands provide a porphyrin-like environment, but with tetrahedral rather than square-planar disposition of the N donor atoms about Cu. There are, however, special experimental difficulties — e.g., the uncharged $Cu^{II}(dpym)_2^0$ has very low solubility in polar solvents, its reduced form $Cu^{I}(dpym)_2^-$ has not hitherto been characterized, traces of oxidants must be excluded, and the rate of ligand exchange in the Cu^I complex can be fast on the redox timescale. Ligand exchange was found not to be competitive with electron transfer in the $Cu(dmp)_2^{2+/+}$ study reported previously (14), but Frei and Geier (15) have shown that ligand substitution in tetrahedral bis(diimine) complexes of Cu^I is generally rapid, and therefore we also examined the kinetics of the $Cu(dpym)_2^-$/Hdpym exchange in acetone.

Experimental

Preparation of Hdpym, $Cu(dpym)_2$, and $Zn(dpym)_2$

The deep red hydrochloride salt $[H_2dpym]Cl$ of the free ligand and the dark green bis(dipyrromethene)copper(II) were made by the method of Mellor and Lockwood (16), and gave good microanalyses for C, H, and N. The UV/visible spectrum of $[H_2dpym]Cl$ in acetonitrile showed a maximum at 467 nm (molar absorbance $\epsilon = 9780$ L mol^{-1} cm^{-1}) with shoulders near 440 and 410 nm, and the proton NMR spectrum in $CDCl_3$ is given in Table 1. The HCl-free ligand Hdpym was obtained by

Can. J. Chem. Downloaded from www.nrcresearchpress.com by 65.111.164.53 on 09/08/12
For personal use only.

Can. J. Chem. Downloaded from www.nrcresearchpress.com by 65.111.164.53 on 09/08/12
For personal use only.

Fig. 1. Potential-resolved spectra of $Cu^{II}(dpym)_2^0$ (0.360 mmol L^{-1}) acetone containing 0.1 mol L^{-1} $[TBA]BF_4$ at 21°C. The spectra at −200 mV and −400 mV correspond to unreduced and completely reduced $Cu^{II}(dpym)_2^0$, respectively.

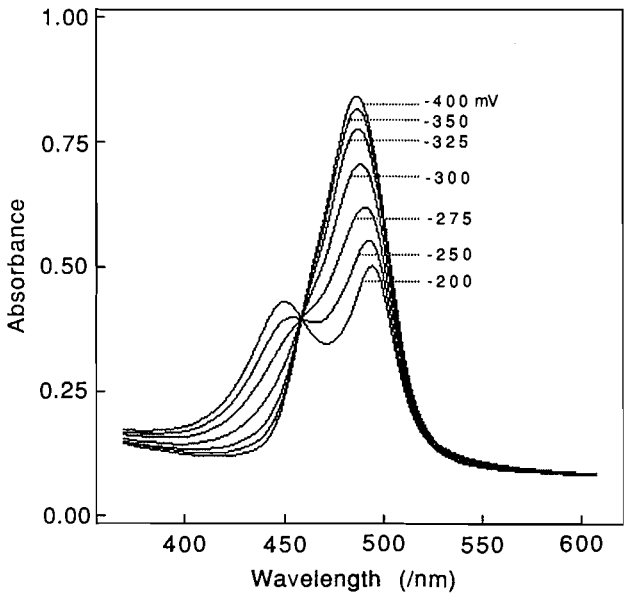

shaking a solution of $[H_2dpym]Cl$ (0.1 g) in dichloromethane (75 mL) with saturated aqueous $NaHCO_3$ (15 mL) for 1 min, drying the separated organic layer with anhydrous Na_2SO_4, evaporating off the solvent, and recrystallizing the bright orange solid twice from ethanol. Anal. calcd. for $C_{19}H_{24}O_4N_2$: C 66.26, H 7.02, N 8.13; found: C 66.18, H 7.04, N 8.00. The UV/visible spectrum in acetone showed a single absorbance maximum at 447 nm ($\epsilon = 6.28 \times 10^4$ L mol^{-1} cm^{-1}), while the fluorescence spectrum (with excitation at 447 nm) showed an emission maximum at 500 nm. The solubility of Hdpym in acetone at 25°C was determined spectrophotometrically to be 5.81×10^{-3} mol L^{-1}. The proton NMR spectrum in $CDCl_3$ is given in Table 1.

The UV/vis spectrum of $Cu(dpym)_2^0$ in ethanol (absorbance maxima at 496, 453, 263, and 225 nm, $\epsilon/10^4$ L mol^{-1} cm^{-1} = 10.6, 8.67, 2.93 and 5.57, respectively) agreed with that reported by Fergusson and Ramsay (17), and was the same in acetone (Fig. 1), acetonitrile, and CH_2Cl_2. The fluorescence spectrum in acetone showed maximum emission at 743 nm with excitation at 496 nm, and at 680 nm when excitation was at 453 nm.The solubility of $Cu(dpym)_2^0$ in acetone at 25°C was determined spectrophotometrically to be 3.60×10^{-4} mol L^{-1}. Its proton NMR spectrum in $CDCl_3$ is given in Table 1, along with that of $Zn(dpym)_2^0$ (17) which was prepared for comparison purposes in the same manner as $Cu(dpym)_2^0$. The major peaks of the ^1H NMR spectrum of $Cu(dpym)_2^0$ at 200 and 400 MHz were broadened by the paramagnetism of the copper(II) centre, but were readily identifiable after 16 transients. The resonance of the single methene proton on each ligand was greatly broadened resonance by virtue of the proximity of that proton to the Cu^{II} centre and weak because of its low relative abundance, but, with a saturated $Cu(dpym)_2^0$ solution in $CDCl_3$ at 0°C in a 10 mm sample tube, a broad singlet could be distinguished in a 400 MHz spectrum at 9.07 ppm after 10 000 transients.

Synthesis of the bis(dipyrromethene)copper(I) anion

Attempts to isolate pure, crystalline salts of $Cu^I(dpym)_2^-$ were unsuccessful, and this anion was characterized in solution following its preparation by alternative routes — reduction of $Cu^{II}(dpym)_2^0$ in solution:

[1] $Cu^{II}(dpym)_2^0 + e^- \rightarrow Cu^I(dpym)_2^-$

and displacement of acetonitrile in $(CH_3CN)_4Cu^+$ by Hdpym:

[2] $(CH_3CN)_4Cu^+ + 2Hdpym \rightarrow Cu^I(dpym)_2^- + 2H^+ + 4CH_3CN$

Solutions of $Cu^I(dpym)_2^-$ were found to oxidize to $Cu^{II}(dpym)_2^0$ over about an hour when exposed to the air, so all synthetic procedures were carried out in Schlenk glassware under dry N_2 or Ar.

In attempts to make $Cu^I(dpym)_2^-$ by direct reaction of a source of $dpym^-$ with $(CH_3CN)_4Cu^+$, chloride-free reagents (specifically, Hdpym rather than $[H_2dpym]Cl$) were necessary to prevent precipitation of CuCl, and solvents with a relatively strong affinity for Cu^I such as acetonitrile or dimethylsulfoxide were avoided as they gave mixtures of 1:1 and 2:1 dpym:Cu complexes, even with Hdpym in large excess. Since H^+ is formally produced in reaction [2], poor proton acceptor solvents such as alkanes, dichloromethane, chloroform, CCl_4, or nitromethane gave only reprecipitated starting materials. Methanol and ethanol caused slow oxidation of the $Cu(dpym)_2^-$ ion to $Cu(dpym)_2^0$. Although $Cu(dpym)_2^-$ appeared to form by reaction [2] in *N,N*-dimethylformamide and in propylene carbonate and seemed stable in these solvents over 24 h or longer, these high-boiling solvents were unsuited to the vacuum-line techniques described below. The only sufficiently volatile solvent that could be found that dissolved enough of the reagents required for this study without competing effectively with Hdpym for Cu^I or causing oxidation was acetone. For these experiments, acetone (BDH Assured) was dried over 4A molecular sieves, redistilled, and degassed by freeze–pump–thaw cycles at ca. 10 Pa before use; cyclic voltammetry with 0.1 mol L^{-1} tetrabutylammonium (TBA) perchlorate gave a clean sweep over the stability range of the solvent, −0.6 to +1.3 V vs. a saturated calomel electrode. It was established that, in acetone, dissociation of $Cu(dpym)_2^-$ was negligible, so that a 2:1 stoichiometric mixture of Hdpym and $[(CH_3CN)_4Cu]BF_4$ gave the desired $Cu(dpym)_2^-$ quantitatively. However, in order to remove all CH_3CN (from $(CH_3CN)_4Cu^+$) that might conceivably compete with Hdpym for Cu^I, a powdery product (presumably $H_2Cu^I(dpym)_2BF_4$) was first isolated by vacuum evaporation of the acetone and any remaining CH_3CN, then redissolved in acetone when required.

Tetra(acetonitrile)copper(I) tetrafluoroborate was made from Cu_2O (Fisher Certified) by the method of Kubas (18) and stored under dry nitrogen in the refrigerator. The Cu content was checked by standard methods (19). There were no absorbance bands in the visible spectrum , 350–700 nm, and the proton NMR spectrum showed a single methyl resonance at 2.22 ppm. Typically, stoichiometric amounts of $[(CH_3CN)_4Cu]BF_4$ (0.0234 mmol) and Hdpym (0.0467 mmol) were mixed in a 10 mm tube on a vacuum line and purged several times with argon before pumping at 7 Pa for 15 min to remove O_2, after which acetone (ca. 3 mL), purified as above, was

Can. J. Chem. Downloaded from www.nrcresearchpress.com by 65.111.164.53 on 09/08/12
For personal use only.

condensed onto the solids at low pressure with liquid N_2. The mixture was then kept at 25–30°C for about 10 min, so that the bright orange solids dissolved completely and reacted to form a brown solution. The solution was then frozen in liquid N_2 and the acetone was pumped away; the residue was warmed to about 30°C and pumped at 7 Pa for at least 15 min to remove any residual acetonitrile. The resulting powder was stable in air for up to one week, but was customarily stored under dry nitrogen and dissolved in purified acetone as required. Proton NMR of solutions in acetone-d_6 prepared in this way showed no trace of either residual CH_3CN or uncomplexed Hdpym; the observed resonances (Table 1) were as would be expected for $Cu(dpym)_2^-$ (cf. the isoelectronic $Zn^{II}(dpym)_2^0$). The UV/visible spectrum showed a single absorbance maximum at 488 nm (ϵ not accurately calculable), and excitation at 488 nm produced fluorescence with a sharp maximum at 732 nm.

The anionic nature of the brown complex was verified by electrophoresis of an acetone solution of ca. 10 μmol L^{-1} $Cu(dpym)_2^-$ and 0.1 mol L^{-1} $[TBA]BF_4$ through glass wool at 1.0 V; a single brown band migrated into the anode compartment, and the UV/visible spectrum of this band showed the single characteristic absorption maximum at 488 nm. The anionic character of the brown solute was further demonstrated by its absorption from acetone solution on dehydrated Dowex 1-X4 anion exchange resin (Cl^- form) and subsequent elution with 0.1 mol L^{-1} [TBA]Cl, although the UV/visible spectrum of the eluate did not match that of the original solution accurately, presumably because of dissolution of the resin by acetone or partial complexing of the Cu complex by chloride. The brown solute was not retained on the cation exchange resin Dowex 50W-X4 in a similar experiment. Neither $Cu^{II}(dpym)_2$ nor Hdpym were retained by Dowex 1-X4 or 50W-X4 under these conditions. FAB-MS of the powder in a nitrobenzylamine matrix gave a strong cluster of peaks centred at m/e = 749 as well as lighter fragments, as expected for $Cu(dpym)_2^-$. Thus, the brown solute was unquestionably $Cu(dpym)_2^-$, but attempts to precipitate it as a pure salt for structural analysis with Na^+, K^+, R_4N^+ (R = methyl, ethyl, and butyl), and tetraphenylarsonium cations were unsuccessful.

Attempts to make $Cu(dpym)_2^-$ in various solvents by chemical reduction of $Cu^{II}(dpym)_2^0$ with amalgamated Zn (which gave $Zn^{II}(dpym)_2^0$), hydroxylamine hydrochloride, hydrazine, dithionite, dithionate, thiosulfate, and sodium amalgam were unsuccessful. With $Cu(dpym)_2^0$ in acetone, potassium superoxide gave the characteristic 488 nm band of $Cu(dpym)_2^-$, but the reaction was not quantitative, and excess KO_2 destroyed the product. Electrochemical reduction methods, described below, were used to generate $Cu(dpym)_2^-$ in dilute solution, and to obtain definitive UV/visible spectra of it.

Electrochemistry and spectroelectrochemistry

Electrochemical measurements employed either acetone or dichloromethane containing 0.1 mol L^{-1} $[TBA]BF_4$ as supporting electrolyte. Dichloromethane was distilled from CaH_2. Spectroscopic grade acetone (BDH Assured) was dried over 4A molecular sieves and then fractionally distilled immediately before use. $[TBA]BF_4$ was recrystallized from isopropanol/water and dried in vacuo at 80°C. All solutions were purged with argon to remove O_2. Potential control in all experiments was accomplished with a HiTek model DT2101 potentiostat operating in conjunction with a HiTek model PPR1 waveform generator.

Cyclic voltammetry was carried out with a 125 μm diameter Pt disk working electrode positioned ca. 2 mm from the tip of a Luggin capillary. A home built aqueous saturated calomel electrode (SCE) was used as reference electrode, and a Pt wire helix served as counter electrode.

Thin-layer reflectance spectroelectrochemistry employed a 7 mm diameter Pt disk polished to a mirror finish, and a SCE as reference electrode. The details of the cell design, the rapid scanning spectrometer, and the experimental procedures have been published previously (20, 21).

The diffusion coefficient of $Cu(dpym)_2$ in acetone was determined by chronoamperometry. The cell employed a 7 mm diameter Pt disk working electrode fitted into a Teflon cell body. The electrode area was calibrated by chronoamperometry of $K_4Fe(CN)_6$ in 1 mol L^{-1} aqueous KCl, using the known (22) diffusion coefficient for $Fe(CN)_6^{4-}$. A Pt wire wound into a helix served as a counter electrode. For convenience, and to avoid contamination of nonaqueous solvents by the aqueous SCE, the cell was fitted with a silver wire quasi-reference electrode sealed into heat-shrink Teflon, with the exposed tip positioned ca. 1 mm from the edge of the Pt disk working electrode.

AC voltammetric measurements were used to determine the heterogeneous electron transfer rate constant of $Cu(dpym)_2^{0/-}$ in acetone. Phase angle data as a function of frequency (25–135 Hz) were measured at the experimentally observed half wave potential of the complex with a PAR model 124A lock-in amplifier. Phase angles were corrected for the influence of background current and uncompensated resistance, measured in the absence of Faradaic species, according to the procedures outlined by Smith (23). AC measurements were carried out in the same cell as was employed for chronoamperometric measurements.

NMR measurements

Proton NMR spectra were obtained on a Bruker AM-400 (9.4 T) spectrometer fitted with a N_2-flow temperature regulator.

For NMR studies of the rate of ligand exchange of $Cu(dpym)_2^-$ with Hdpym, an accurately weighed quantity of a stock acetone solution of Hdpym was evaporated to dryness on a vacuum line in a 5 mm NMR tube with a collar specially constructed for this purpose, so depositing 2.6–10.6 μmol of Hdpym. Freshly-dissolved $[(CH_3CN)_4Cu]BF_4$ (1.1–2.7 μmol) was introduced in acetone, whereupon the Hdpym dissolved to give a brown solution containing $Cu(dpym)_2^-$. The contents of the tube were then quickly frozen in liquid N_2, the tube was reattached to the vacuum line, and the tube was allowed to warm slowly while the solvent was pumped off at ca. 1 Pa (with care to avoid bumping of the evaporating solvent). The deposited solid was pumped for at least 15 min at 30°C and 1 Pa to remove all traces of acetonitrile, then a weighed amount of degassed acetone-d_6 that had been dried over 4A molecular sieves was distilled on to the solid, and the tube was sealed with a small flame. The NMR spectrum of the thawed solution in the vicinity of the methene resonance at chemical shift $\delta \approx$ 8.0 ppm was then recorded at descending temperatures from 300 to 230 K. At each temperature, 15 min were allowed for thermal equilibration, then the magnetic field was reshimmed.

Can. J. Chem. Downloaded from www.nrcresearchpress.com by 65.111.164.53 on 09/08/12
For personal use only.

Measurements below 230 K were rejected because of precipitation of the reactants and high solvent viscosity. The temperature readout was calibrated against the chemical shift difference of the methylhydroxyl protons of a methanol sample.

For NMR line-broadening measurements of the rate of electron transfer between $Cu(dpym)_2^0$ and $Cu(dpym)_2^-$ in acetone-d_6, a mixture of solid Hdpym and $[(CH_3CN)_4Cu]BF_4$ in 2:1 (±1.0%) molar ratio was prepared by the acetone evaporation technique outlined above — no excess of $[(CH_3CN)_4Cu]BF_4$ could be tolerated, as this was found to reduce $Cu(dpym)_2^0$, while excess Hdpym could cause line broadening through ligand exchange. The requisite amount of $Cu(dpym)_2^0$ was then added in acetone solution, and the solvent was evaporated as above. A weighed quantity of acetone-d_6 was then distilled on to the residue in a 10 mm NMR tube using the vacuum line. The amount of $Cu(dpym)_2^0$ was limited by its low solubility in acetone (vide supra). The linewidth of the methene proton line of $Cu^I(dpym)_2^-$ at 8.15 ppm was measured with careful exclusion of air. The temperature display was calibrated with neat methanol.

Results

Identity and characteristics of the reduced species

The cyclic voltammograms of 3.6×10^{-4} mol L^{-1} $Cu(dpym)_2^0$ in acetone and dichloromethane were fully reversible (peak-to-peak separation 60 mV at sweep rate 100 mV s^{-1}), implying that species formed by its electrochemical reduction did not undergo ligand loss (despite the high dilution) on the 10 s timescale of the CV experiments, and that the ligand was not irreversibly altered in the process. These facts suggest rapid electron transfer to and from the Cu centre, and, since it is shown below that the reduced compound is the same as the *labile* product of reaction [2], the reaction observed was [1] and the product $Cu^I(dpym)_2^-$ is very stable *thermodynamically* with respect to ligand loss. The half-wave potentials, which may be equated approximately to the electrode potential E^0, were −290 and −380 mV vs. SCE in acetone and dichloromethane, respectively, with 0.1 mol L^{-1} $[TBA]BF_4$ as the supporting electrolyte.

The reversibility and single-step nature of the reduction were confirmed by the potential-resolved spectra in Fig 1, in which there is a clean isosbestic point at 460 nm. Furthermore, a plot (Fig. 2) of $\log\{(A - A_O)/(A_R - A)\}$ vs. the applied potential ΔE_{appl},

$$[3] \quad \Delta E_{appl} = E^0 - (RT/nF) \ln \{(A - A_O)/(A_R - A)\}$$

where A is the absorbance of the solution at ΔE_{appl} and A_O and A_R are the absorbances initially and after complete reduction, respectively, gave an intercept E^0 = −285 mV vs. SCE (cf. −290 from the CV half-wave potential) and a slope $-0.0548 = -2.303RT/nF$, corresponding to a transfer of $n = 1.0_8$ electron. The limiting spectrum (at −400 mV in Fig. 1) as reduction in acetone progresses has an absorbance maximum at 488 ± 1 nm with $\epsilon = 1.44 \times 10^5$ L mol^{-1} cm^{-1}, and is identical in shape and position to that of the product of reaction [2]; it may be taken to be characteristic of $Cu^I(dpym)_2^-$. Spectroelectrochemical reduction of $Cu^{II}(dpym)_2^0$ in CH_2Cl_2 gave the same absorbance band, with maximum at 489 ± 1 nm, $\epsilon = 1.48 \times 10^5$ L mol^{-1} cm^{-1}; since the spectrum of $Cu^{II}(dpym)_2^0$ is also

Fig. 2. Nernst plot (equation [3]) for the spectroelectrochemical reduction of $Cu^{II}(dpym)_2^0$ in acetone. Conditions as in Fig. 1.

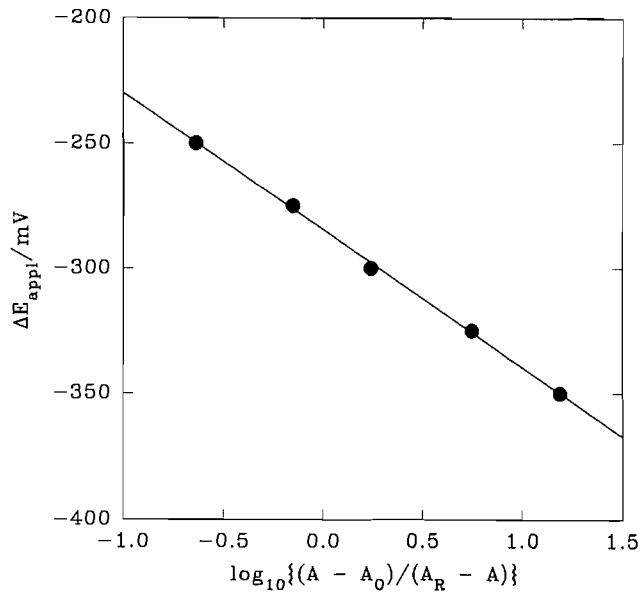

independent of solvent, this implies that neither $Cu^{II}(dpym)_2^0$ nor $Cu^I(dpym)_2^-$ has coordinated solvent in acetone or dichloromethane, and that both exist as four-coordinate, quasi-tetrahedral species in these solvents.

The proton NMR spectrum of the acetonitrile-free product of reaction [2] (Table 1) confirms that it is a dpym complex, different from the others listed but more closely resembling the isoelectronic $Zn^{II}(dpym)_2^0$ than its paramagnetic precursor $Cu^{II}(dpym)_2^0$, except that the minor splitting of the signal of the methyl group *cis* to the ring N atoms in $Zn^{II}(dpym)_2^0$ (suggesting a distorted tetrahedral coordination geometry) is absent. This confirms the identity of $Cu^I(dpym)_2^-$. The absence of Hdpym features from the proton NMR spectrum of solutions of $Cu^I(dpym)_2^-$ in acetone at concentrations of the order of 10^{-4} mol L^{-1} showed that $Cu^I(dpym)_2^-$ is less than 1% dissociated under those conditions. The methene resonance showed marked sensitivity to its chemical environment, and was broadened to the limit of detectability in the paramagnetic $Cu^{II}(dpym)_2^0$.

Kinetics of the exchange of dpym between bis(dipyrromethene)copper(I) and Hdpym in acetone

The methene proton spectrum of mixtures of $Cu^I(dpym)_2^-$ and Hdpym in acetone-d_6 consisted of a single peak that narrowed with increasing temperature or concentrations, indicating that chemical exchange of $dpym^-$ between Cu^I and H^+ sites was occurring on the "fast exchange" NMR timescale. Thus, the first-order rate constants k_A and k_B for the exchange of ligand on species A ($Cu(dpym)_2^-$, mole fraction p_A of total dpym pool) and B (Hdpym, mol fraction p_B of total dpym), respectively were related to the corresponding methene proton linewidths w_A and w_B by the expressions

$$[4] \quad k_A = 4\pi p_A p_B^2 (\delta\nu)^2 \{W - (p_A w_A + p_B w_B)\}^{-1}$$

$$[5] \quad k_B = 4\pi p_A^2 p_B (\delta\nu)^2 \{W - (p_A w_A + p_B w_B)\}^{-1}$$

in which $\delta\nu$ is the difference in chemical shift between the

Can. J. Chem. Downloaded from www.nrcresearchpress.com by 65.111.164.53 on 09/08/12
For personal use only.

Table 2. NMR data and rate constants k_1 for the exchange of Hdpym with $Cu^I(dpym)_2^-$ in acetone-d_6.[a]

[Hdpym]/ mmol L^{-1}	$[Cu^I(dpym)_2^-]$/ mmol L^{-1}	Temperature/ K	δ/ ppm	Linewidth/ Hz	k_1[b]/ 10^6 L mol^{-1} s^{-1}
2.41	1.54	300	7.83	5.42	15.5
		290	7.85	5.93	14.1
2.71	3.06	300	7.78	3.89	13.9
		290	7.80	4.11	13.5
		270	7.83	5.01	11.0
		250	7.86	6.77	7.9
		230	7.89	8.97	6.2
2.99	4.39	290	8.14	3.57	11.7
		270	8.18	4.09	10.8
		255	8.21	4.36	11.5
		240	8.24	5.93	7.7
		230	8.25	6.67	7.5
3.70	2.70	300	7.80	4.12	13.8
		295	7.81	3.99	14.9
		270	7.84	4.85	12.5
		250	7.87	5.45	12.0
		230	7.91	7.77	8.2
4.49	2.51	300	7.72	4.50	11.8

[a] $[H^+] = 2[Cu^I(dpym)_2^-]$, $[BF_4^-] = [Cu^I(dpym)_2^-]$.
[b] Calculated on basis that the exchange rate is first order with respect to both $Cu^I(dpym)_2^-$ and Hdpym.

methene singlets of A and B in separate solutions at the same temperature T, and W is the linewidth of the coalesced methene proton peak in the exchanging mixture (24). Since there are two methene protons in A but only one in B, the rate R of ligand exchange between A and B is then given by

$$[6] \quad R = 2k_A[A] = k_B[B] = 2k_1[A]^a[B]^b$$

where k_1 is the rate constant for the exchange reaction of order a in [A] and b in [B] (25). Details of the experimental conditions, chemical shifts δ and linewidths W of the coalesced line, and exchange rate data are given in Table 2. Over the temperature range of these experiments (300–230 K), δν increased monotonically from 328.5 to 336.0 Hz, w_A from 1.65 to 4.18 Hz, and w_B from 1.34 to 1.54 Hz, with most of the increases taking place at the lowest temperatures.

The ligand exchange rate data in Table 2 are presented as rate constants k_1 with the assumption that the exchange is first order with respect to each of $Cu(dpym)_2^-$ and Hdpym (i.e., $a = b = 1$ in eq. [6]). The useful ranges of Hdpym and $Cu(dpym)_2^-$ concentrations were limited on the one hand by the need to have enough solute to give accurately measurable spectra, and on the other by the narrowing of the linewidth with increasing concentrations when working at the fast exchange limit of the NMR linewidth technique. Given the rather large uncertainties arising from these limitations, it will be seen that k_1 is effectively constant at a given temperature. Thus, the foregoing assumption is vindicated, and k_1 can be identified with the process:

$$[7] \quad Cu(dpym)_2^- + Hdpym^* \rightarrow Cu(dpym)(dpym^*)^- + Hdpym$$

The k_1 values of Table 2 show only a slight temperature dependence which is obscured by the considerable scatter, but they may be summarized by the Eyring activation parameters $\Delta H_1^{\ddagger} = 3.4 \pm 0.6$ kJ mol^{-1} and $\Delta S_1^{\ddagger} = -97 \pm 3$ J K^{-1} mol^{-1}, corresponding to $k_1 = 1.4 \times 10^7$ L mol^{-1} s^{-1} at 298 K.

Kinetics of electron transfer between bis(dipyrromethene)copper(II) and -(I) in homogeneous solution in acetone

The rate of the self-exchange reaction of $Cu(dpym)_2^{0/-}$ in acetone-d_6 was well within the "slow exchange" region in the NMR timeframe, as shown by the constancy of the methene proton chemical shift of $Cu^I(dpym)_2^-$ at 8.15 ± 0.01 ppm, whether or not Cu^{II} was present, and by the increase in linewidth as the concentration of Cu^{II} increased. The rate constant k_{ex} was given by $\pi(W - W_0)/[Cu^{II}(dpym)_2^0]$, where W and W_0 are the Cu^I methene proton linewidths with and without the addition of $Cu^{II}(dpym)_2^0$, respectively. Because the solubility of $Cu^{II}(dpym)_2^0$ is low, the broadenings were less than 30% at 294 K, but Table 3 shows that the k_{ex} values so obtained were reproducible to about 10% over the accessible range of $Cu^{II}(dpym)_2^0$ concentrations, with an average of $(4.8 \pm 0.3) \times 10^3$ L mol^{-1} s^{-1} at 294.2 K and $I \approx 0.007$ mol L^{-1}. At 320.5 K, linewidths were broadened two- to three-fold by addition of $Cu^{II}(dpym)_2^0$ (Table 3), giving an average $k_{ex} = (2.25 \pm 0.08) \times 10^4$ L mol^{-1} s^{-1} from five measurements. Figure 3 is an Eyring plot for a single solution sample over the temperature range 294.2–320.5 K; the data are summarized by $\Delta H_{ex}^{\ddagger} = 48.5 \pm 3.0$ kJ mol^{-1} and $\Delta S_{ex}^{\ddagger} = -10.0 \pm 9.8$ J K^{-1} mol^{-1}, corresponding to $k_{ex} = 5.9 \times 10^3$ L mol^{-1} s^{-1} at 298 K.

Kinetics of heterogeneous electron transfer between bis(dipyrromethene)copper(II) and -(I) at a Pt electrode in acetone

The heterogeneous rate constant k_{el} for electron exchange in the $Cu(dpym)_2^{0/-}$ couple in acetone at a Pt electrode was determined by AC voltammetry using the relationship

Can. J. Chem. Downloaded from www.nrcresearchpress.com by 65.111.164.53 on 09/08/12
For personal use only.

Table 3. Rate constants for electron transfer in $Cu(dpym)_2^{0/-}$ in acetone-d_6.

Temperature/ K	$[Cu(dpym)_2^-]$/ mmol L^{-1}	$[Cu(dpym)_2^0]$/ mmol L^{-1}	Linewidth/ Hz	k_{ex}/ 10^3 L mol^{-1} s^{-1}
294.2	4.36	0.0	1.80 ± 0.01	—
	3.93	0.286	2.28 ± 0.02	5.3
	3.42	0.248	2.18 ± 0.03	4.8
		2.15 ± 0.03	4.4	
	3.06	0.222	2.13_5 ± 0.02	4.7
		2.13 ± 0.01	4.6	
320.5	4.53	0.0	0.85 ± 0.01	—
	2.78	0.196	2.17 ± 0.01	21.1
	3.08	0.218	2.48 ± 0.01	23.5
	4.53	0.0	2.82 ± 0.10[a]	—
	3.62	0.256	4.71 ± 0.15[a]	23.2
	3.31	0.234	4.49 ± 0.12[a]	22.4
			4.49 ± 0.12[a]	22.4

[a]Imperfect but consistent shimming of probehead.

Fig. 3. Eyring plot showing the temperature dependence of the rate constant k_{ex} for electron transfer between $Cu(dpym)_2^0$ (0.256 mmol L^{-1}) and $Cu(dpym)_2^-$ (3.62 mmol L^{-1}) in acetone-d_6.

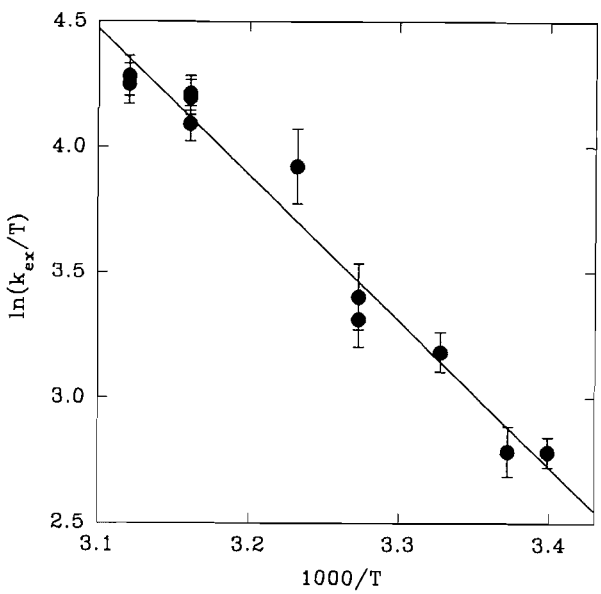

[8] $k_{el} = (2\pi fD/2)^{1/2}(\cot \phi - 1)^{-1}$

where f is the frequency of the current in Hz, D is the diffusion coefficient of the electroactive species (assumed to be the same for the oxidized and reduced forms), and ϕ is the phase angle (26). The diffusion coefficient for $Cu(dpym)_2^{0/-}$ (1.237×10^{-4} mol L^{-1}) was measured in acetone containing 0.1 mol L^{-1} [TBA]BF_4 using the Cottrell relation (26)

[9] $i_t = nFAC^*D^{1/2}(\pi t)^{-1/2}$

in which i_t is the current measured at time t during reduction of $Cu(dpym)_2^0$, C^* is the concentration of $Cu(dpym)_2^0$ in mol cm^{-3}, F = 96 487 C mol^{-1}, and A is the area of the working electrode in cm^2. Plots of i_t vs. $t^{-1/2}$ were accurately linear, as were those for an aqueous solution of 0.01 mol L^{-1} $K_4Fe(CN)_6$ in aqueous 1.0 mol L^{-1} KCl that was used as a calibrant to eliminate A (22). For $Cu(dpym)_2^0$, D was found to be 3.60×10^{-5} cm^2 s^{-1} in acetone at 25°C. Values of k_{el} obtained at various frequencies f are listed in Table 4. Since the heterogeneous electron transfer rates were near the upper limit accessible by AC voltammetry (i.e., near the time domain in which diffusion from the working electrode becomes rate-determining), the k_{el} values show considerable scatter, but the average value of 0.16 ± 0.04 cm s^{-1} is at least a semi-quantitative measure of the rate constant.

Table 4. Rate constant for heterogeneous electron transfer in $Cu(dpym)_2^{0/-}$ at a Pt surface in acetone at 25°C.[a]

Frequency f/Hz	k_{el}/cm s^{-1}
25.5	0.14
41.1	0.16
88.1	0.22
105.0	0.17
135.0	0.10

[a]From AC voltammetry. Supporting electrolyte 0.1 mol L^{-1} [TBA]BF_4. $[Cu(dpym)_2^0] = 1.237 \times 10^{-4}$ mol L^{-1}.

Discussion

We have shown that the species with light absorption maximum at 488 nm ($\epsilon = 1.44 \times 10^5$ L mol^{-1} cm^{-1}) prepared by electrochemical reduction of the known quasi-tetrahedral species $Cu(dpym)_2^0$ in acetone or dichloromethane is the same as that formed by reaction of Cu^I with Hdpym in acetone, that it carries one negative charge, and that its ^{1}H-NMR and mass spectra are consistent with the formulation $Cu(dpym)_2^-$. In acetone — a weak donor solvent — $Cu(dpym)_2^-$ forms quantitatively from Hdpym and Cu^I in a 2:1 molar ratio with no detectable free ligand, and the full reversibility of cyclic vol-

Can. J. Chem. Downloaded from www.nrcresearchpress.com by 65.111.164.53 on 09/08/12
For personal use only.

tammograms of $Cu(dpym)_2^{0/-}$ in acetone or CH_2Cl_2 confirms that ligand loss from $Cu(dpym)_2^-$ is negligible. Since the exchange of $Cu(dpym)_2^-$ with free Hdpym was shown to be fast, this stability of $Cu(dpym)_2^-$ is thermodynamic rather than simply kinetic. Since the UV/visible spectra of neither $Cu(dpym)_2^0$ nor $Cu(dpym)_2^-$ were solvent-dependent, neither species contains coordinated solvent, and therefore both are four-coordinate and quasi-tetrahedral, as $Cu(dpym)_2^0$ is known to be in the solid state (8).

The $Cu(dpym)_2^-$/Hdpym exchange in acetone is fast (k_1^{298} = 1.4×10^7 L mol^{-1} s^{-1}) because of the remarkably low enthalpy of activation (3.4 kJ mol^{-1}). Since the reaction seems to be first order with respect to both $Cu(dpym)_2^-$ and Hdpym, and since the dissociation of $Cu(dpym)_2^-$ is negligible, the simplest mechanism consistent with the very low $\Delta H^{\ddagger}$ is proton transfer from Hdpym to $Cu(dpym)_2^-$ followed by interchange of the newly-formed coordinated Hdpym and free $dpym^-$. An alternative possibility, attack of Hdpym on $Cu(dpym)_2^-$ followed by internal proton transfer and ligand loss, is less likely because steric hindrance would result in a substantial $\Delta H^{\ddagger}$.

Although the rate constants for homogeneous and heterogeneous electron transfer for $Cu(dpym)_2^{0/-}$ in acetone ($k_{ex} = 5.9 \times 10^3$ L mol^{-1} s^{-1} at I $\approx$ 0.007 mol L^{-1} and $k_{el} \approx 0.16$ cm s^{-1} at I = 0.1 mol L^{-1}, respectively, at 25°C) are dimensionally incompatible, they are mutually confirmatory in that they conform well to the $k_{ex} - k_{el}$ correlation demonstrated by Cannon (27) — Cannon's data, however, were for aqueous systems rather than acetone solutions. The value of k_{ex} is close to that found (14) for the $Cu(dmp)_2^{2+/+}$ exchange in the same solvent (3×10^3 kg mol^{-1} s^{-1} at I = 0.1 mol kg^{-1} and 25°C), ignoring possible minor effects of ionic strength. For $Cu(dpym)_2^{0/-}$, $\Delta H_{ex}^{\ddagger}$ is some 20 kJ mol^{-1} higher and $\Delta S_{ex}^{\ddagger}$ about 70 J K mol^{-1} more positive than for $Cu(dmp)_2^{2+/+}$, but these compensate in k_{ex} at near-ambient temperatures. This disparity in activation parameters might be supposed to indicate a difference in electron transfer mechanism, such as some sort of inner-sphere process for $Cu(dpym)_2^{0/-}$ as opposed to outer-sphere for $Cu(dmp)_2^{2+/+}$, and indeed we have shown that $Cu(dpym)_2^-$ is very labile. Under the conditions of our electron transfer rate measurements, however, the rate of ligand exchange on $Cu(dpym)_2^-$ was shown to be negligible, and an outer-sphere mechanism may be assumed for both couples.

The similarity in k_{ex} values for the two copper couples in acetone suggests that k_{ex} for the $Cu(dpym)_2^{0/-}$ exchange in water (which is inaccessible because of the insolubility of $Cu^{II}(dpym)_2^0$) might be about 3×10^5 L mol^{-1} s^{-1} at ca. 300 K, by analogy with $Cu(dmp)_2^{2+/+}$. Rorabacher et al. (28), however, point out that the presence of chloride ion during measurements on the latter aqueous system opens the possibility of a chloride-mediated electron transfer path in that case, so that the extrapolation may not be valid. Indeed, a change of solvent ordinarily has only a minor effect on outer-sphere electron transfer rates (29). Comparison of electron transfer rates in $Cu(dpym)_2^{0/-}$ or $Cu(dmp)_2^{2+/+}$, whatever the solvent, with those of the "blue" copper proteins in water (which are some two orders of magnitude faster) may not be entirely appropriate, since copper in the proteins is in a highly distorted but rigid N_2S_2 environment, whereas in the $dpym^-$ and dmp complexes the environment is N_4 with essentially tetrahedral geometry and some degree of flexibility. As noted elsewhere (30), such flexibility may lower electron transfer rates relative to those of encapsulating ligand systems by increasing the Franck–Condon barrier.

In any event, the $Cu(dpym)_2^{0/-}$ exchange may be considered to be at least moderately fast in the context of copper(II/I) electron transfer reactions, the values of k_{ex} and k_{el} being of the order expected for $Cu^{II/I}$ couples in which no significant change in coordination number or geometry accompanies electron transfer. The relative slowness of self-exchange in the bis(2,2′-bis(2-imidazolyl)-biphenyl)copper(II/I) exchange couple in acetonitrile is evidently an anomaly that reflects some special property of this system, as suggested by Knapp et al. (11). The self-exchange rate constant reported (9) for the aqueous $CuW_{12}O_{40}^{6-/7-}$ couple is also surprisingly low, but it was estimated indirectly from the Marcus cross relationship using a literature value of k_{ex} for the $Fe(CN)_6^{3-/4-}$ couple. Since this latter value depends strongly upon the cation concentration (31), and since the Coulombic work terms would be unusually large in the nominally 7-/3- cross reaction, the k_{ex} value estimated for the $CuW_{12}O_{40}^{6-/7-}$ self-exchange may be substantially in error.

Acknowledgements

We thank the Natural Sciences and Engineering Research Council of Canada for financial support, Dr. G. Liu for assistance with the fluorescence spectra, and Dr. D. B. Rorabacher and the reviewers for helpful suggestions.

References

1. B.L. Vallee and R.J.P. Williams. Proc. Natl. Acad. Sci. U.S.A. **59**, 498 (1968); J.J.R. Fraústo da Silva and R.J.P. Williams. The biological chemistry of the elements. Oxford University Press. 1993. pp. 182–184 and 388–399.
2. R.A. Marcus and N. Sutin. Biochim. Biophys. Acta, **811**, 265 (1985).
3. M.J. Sisley and R.B. Jordan. Inorg. Chem. **31**, 2880 (1992).
4. N.E. Meagher, K.L. Juntunen, M.J. Heeg, C.A. Salhi, B.C. Dunn, L.A. Ochrymowycz, and D.B. Rorabacher. Inorg. Chem. **33**, 670 (1994), and references therein.
5. A.M.Q. Vande Linde, B.C. Westerby, L.A. Ochrymowycz, and D.B. Rorabacher. Inorg. Chem. **32**, 251 (1993).
6. D.K. Coggin, J.A. González, A.M. Kook, C. Bergman, T.D. Brennan, W.R. Scheidt, D.M. Stanbury, and L.J. Wilson. Inorg. Chem. **30**, 1125 (1991), and references therein.
7. C. Dennison, P. Kyritsis, W. McFarlane, and A.G. Sykes. J. Chem. Soc. Dalton Trans. 1959 (1993), and references therein.
8. M. Elder and B.R. Penfold. J. Chem. Soc. A, 2556 (1969).
9. A.G. Lappin and R.D. Peacock. Inorg. Chim. Acta, **46**, L71 (1980).
10. R.D. Bereman, G.D. Shields, J. Bordner, and J.R. Dorfman. Inorg. Chem. **20**, 2165 (1981).
11. S. Knapp, T.P. Keenan, X. Zhang, R. Fikar, J.A. Potenza, and H.J. Schugar. J. Am. Chem. Soc. **112**, 3452 (1990).
12. V. Ravichandran, K.K. Chacko, A. Aoki, H. Yamazaki, J. Ruiz-Sanchez, J. Saurez-Verela, J.D. Lopez-Gonzalez,

J.M. Salas-Peregrin, and E. Colacio-Rodriguez. Inorg. Chim. Acta, **173**, 107 (1990)
13. N. Kitajima, K. Fujisawa, M. Tanaka, and Y. Moro-oka. J. Am. Chem. Soc. **114**, 9232 (1992).
14. H. Doine, Y. Yano, and T.W. Swaddle. Inorg. Chem. **28**, 2319 (1989).
15. U.M. Frei and G. Geier. Inorg. Chem. **31**, 187 (1992).
16. D.P. Mellor and W.H. Lockwood. Proc. R. Soc. New South Wales, **74**, 141 (1940).
17. J.E. Fergusson and C.A. Ramsay. J. Chem. Soc. 5222 (1965).
18. G.J. Kubas. Inorg. Synth. **19**, 90 (1979).
19. A.I. Vogel. A textbook of quantitative inorganic analysis. 3rd. ed. J. Wiley and Sons, New York. 1961. p. 358.
20. A.S. Hinman and B. Pavelich. Can. J. Chem. **65**, 919 (1987).
21. D.H. Jones and A.S. Hinman. Can. J. Chem. **68**, 2234 (1990).
22. M. von Stackelberg, M. Pilgram, and W. Toome. Z. Elektrochem. **57**, 342 (1953).
23. D.E. Smith. *In* Electroanalytical chemistry. Vol. 1. *Edited by* A.J. Bard. Marcel Dekker, New York. 1966. pp. 1–155.
24. J. Sandström. Dynamic NMR spectroscopy. Academic Press, New York. 1982. p. 17.
25. S.F. Lincoln. Prog. React. Kinet. **9**, 1 (1977).
26. A.J. Bard and L.R. Faulkner. Electrochemical methods. John Wiley and Sons, New York. 1980.
27. R.D. Cannon. Electron transfer reactions. Butterworths, London. 1980. p. 221.
28. B.C. Dunn, L.A. Ochrymowycz, and D.B. Rorabacher. Inorg. Chem. In press.
29. H. Doine and T.W. Swaddle. Inorg. Chem. **27**, 665 (1988); Can. J. Chem. **66**, 2763 (1988).
30. M.R. Grace and T.W. Swaddle. Inorg. Chem. **32**, 5597 (1993).
31. H. Takagi and T.W. Swaddle. Inorg. Chem. **31**, 4669 (1992).

Can. J. Chem. Downloaded from www.nrcresearchpress.com by 65.111.164.53 on 09/08/12
For personal use only.

Deprotonation energetics of some nucleosides in water from EMF measurements

Sonali Ganguly and Kiron K. Kundu

Abstract: The deprotonation constants of uridine (K_1 and K_2), thymidine (K_1 and K_2), cytidine (K_1 and K_2), guanosine (K_1, K_2, and K_3), and xanthosine (K_1, K_2, and K_3) have been obtained in water from EMF measurements of Harned-Ehler type cells comprising H_2 and Ag-AgI electrodes at different temperatures. The pK values were substituted in the temperature equation: $pK = AT^{-1} + B + CT$ and A, B, and C were obtained by the method of least squares. Related thermodynamic quantities viz. ΔG^0, $T\Delta S^0$, and ΔH^0 were obtained from coefficients A, B, and C of the respective nucleosides.

Key words: deprotonation energetics, uridine, thymidine, cytidine, guanosine, xanthosine.

Résumé : Faisant appel à des mesures de fém de cellules du type de Harned-Ehler et à des électrodes de Ag-AgI et opérant à diverses températures, on a mesuré les constantes de déprotonation de l'uridine (K_1 et K_2), de la thymidine (K_1 et K_2), de la cytidine (K_1 et K_2), de la guanosine (K_1, K_2 et K_3) et de la xanthosine (K_1, K_2 et K_3) en solution dans l'eau. On a introduit les valeurs des pK dans l'équation: $pK = AT^{-1} + B + CT$ et on a déterminé les valeurs de A, B et C par la méthode des moindres carrés. On a aussi déterminé les valeurs thermodynamiques correspondantes, à savoir le ΔG^0, $T\Delta S^0$ et ΔH^0 à partir des coefficients A, B et C des divers nucléosides.

Mots clés : énergies de déprotonation, uridine, thymidine, cytidine, guanosine, xanthosine.

[Traduit par la rédaction]

Introduction

As a continuation of our thermodynamic studies on deprotonation processes of pyrimidine bases and adenine and its derivatives in pure water (1) we now report the same for some nucleosides with a view to identifying the probable sites involved in the deprotonation steps of the various biochemical reactions.

A nucleoside is best defined as a unit composed of a purine or pyrimidine base and a sugar moiety (pentose or deoxypentose). The components are united by a β-glycosidic linkage between the carbon 1′ of the sugar and the nitrogen at position 9 in the purines or at position 1 in the pyrimidines (2) as shown in Fig. 1.

Among numerous publications on nucleoside deprotonation constants (K) in the literature (3*a*) only a few have reported data at zero ionic strength. The notable exceptions which provide data at zero ionic strength and 25°C are those of Izatt et al. (3*b*, 3*d*). However, data between 10^{-4} – 10^{-10} have been obtained mostly by half neutralization point method using glass (H^+) electrodes and aqueous saturated calomel electrodes SCE(w) cells with liquid junctions, while data above 10^{-4} and below 10^{-10} have been obtained by an indirect entropy titration method using calorimetry. In this paper, we report our findings on deprotonation constants of the different acidic sites and the related thermodynamic quantities, viz. ΔG^0, ΔS^0, and ΔH^0 of uridine (urd), thymidine (thd), cytidine (cyd), guanosine (guo), and xanthosine (xao) at zero ionic strength and 25°C by measuring the EMF's of the Harned-Ehler type (4) galvanic cells without liquid junctions, and comprised Pt, H_2 (g, 1 atm) and Ag-AgI electrodes and buffers of different ionic strengths at five equidisant temperatures from 15 to 35°C.

As in our previous papers (1), the Harned-Ehler type cells used for determining the pK's of the nucleosides and related energetics are [A]–[E].

For determining $(pK_1)_{H_2A}$ of urd and thd and $(pK_2)_{H_2A}$ of guo and xao, we used

Fig. 1. Structures of the different nucleosides.

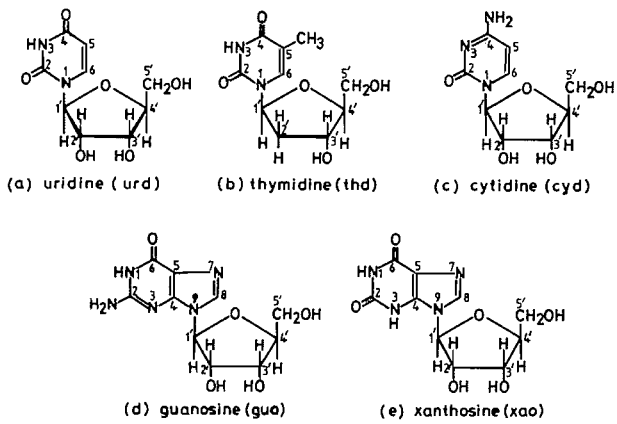

Received February 22, 1994.

S. Ganguly and K. K. Kundu.[1] Physical Chemistry Laboratories, Jadavpur University, Calcutta-700 032, India.

[1] To whom correspondence should be addressed.

Can. J. Chem. Downloaded from www.nrcresearchpress.com by 65.111.164.53 on 09/08/12
For personal use only.

Can. J. Chem. Downloaded from www.nrcresearchpress.com by 65.111.164.53 on 09/08/12
For personal use only.

[A] Pt, H_2(g, 1 atm)/$H_2A(m_1)$, $NaHA(m_2)$, $KI(m_3)$/AgI-Ag

For determining $(pK_2)_{HA^-}$ of urd and thd and $(pK_3)_{HA^-}$ of guo and xao, we used

[B] Pt, H_2(g, 1 atm)/$NaHA(m_1)$, $Na_2A(m_2)$, $KI(m_3)$/AgI-Ag

For determining $(pK_1)_{H_2A^+}$ of cyd, we used

[C] Pt, H_2(g, 1 atm)/$H_2A^+I^-(m_1)$, $HA(m_2)$, $KI(m_3)$/AgI-Ag

For determining $(pK_2)_{HA}$ of cyd, we used

[D] Pt, H_2(g, 1 atm)/$HA(m_1)$, NaA (m_2), KI (m_3)/AgI-Ag

For determining $(pK_1)_{H_3A^+}$ of guo and xao, we used

[E] Pt, H_2(g, 1 atm)/$H_3A^+I^-(m_1)$, $H_2A(m_2)$, $KI(m_3)$/AgI-Ag

Experimental

urd (grade U 3750), thd (grade T 9250), cyd (grade C 9505), guo (grade G 6752), and xao (grade X 0750) were obtained from Sigma Chemical Co. and were used as such after drying in a vacuum desiccator at 0–5°C. Purities of all chemicals were checked by UV spectroscopy (5, 6) and were found to be within 98–99%. Triple distilled CO_2-free water was used. Sodium hydroxide (GR), potassium iodide (GR), and hydroiodic acid (GR) were obtained from E. Merck.

Cell solutions of different ionic strengths were prepared by mixing appropriate weighed amounts of biochemicals, NaOH and KI of known molality, and triple distilled water in well stoppered Jena bottles. Appropriate amounts of standard NaOH solutions were used for stepwise neutralization of the acids in order to get the desired concentrations of the corresponding conjugate bases. For the determination of PK_1's of cyd, guo, and xao, HI acid was used instead of the alkali solution. The method of HI distillation was similar to that described earlier (7).

EMF method

The EMF's of the cells were measured using a Leeds and Northrup K_4-potentiometer fitted with a moving coil galvanometer (Cambridge Instrument Co.) as the null point detector. The preparation of Ag-AgI electrodes was described elsewhere (8). General experimental procedures including the preparation of H_2 (Pt) electrodes and the measurements of EMF were similar to those described earlier (7). As indicated in our previous papers (1), Ag-AgI electrodes were introduced after an hour's discharge of hydrogen gas through the cells. The equilibrium was attained in 3–4 h. A constant EMF reading to about ±0.1 mV for 1 h was taken as the criterion of equilibrium. The readings were first taken at 15°C and then successively at higher temperatures at 5°C intervals. The readings at 25°C when back checked after 35°C agreed to within ±0.1 mV.

Results

The measured EMF's of cells corrected to $p_{H_2} = 1$ atm gave the values of E. The emf data (E) of cells [A]–[E] at different temperatures and corresponding molalities of KI, H_2A, NaHA for cell [A], KI, NaHA, Na_2A for cell [B], KI, $H_2A^+I^-$, HA for cell [C], KI, HA, NaA for cell [D], and KI, $H_3A^+I^-$, H_2A for cell [E] for each of the cell solutions are given in Table 1.

Similar to our previous studies (1), the pK_1 and pK_2 values of urd, thd, cyd, guo, and xao and pK_3 of guo and xao were evaluated by using the functions pK_1', pK_2' and pK_3' defined by eqs [1]–[5].

$$pK_1(\text{urd, thd}) \text{ or } pK_2(\text{guo, xao}) = (E - E^0)/k + \log (m_{I^-} m_{H_2A}/m_{HA^-}) + \log (\gamma_{I^-}\gamma_{H_2A}/\gamma_{HA^-})$$

[1] $$pK_1'(\text{urd, thd}) \text{ or } pK_2'(\text{guo, xao}) = (E - E^0)/k + \log [m_3(m_1 + m_{OH^-})/(m_2 - m_{OH^-})] = pK_1(\text{urd, thd}) \text{ or } pK_2(\text{guo, xao}) + f(\mu)$$

[1′] $$\log m_{OH^-} = \log K_w + p_wH \text{ (Bates acidity function)} = -\log a_H \cdot \gamma_{OH^-} = -\log a_H \cdot \gamma_{I^-} = (E - E^0)/k + \log m_{I^-} \text{ (ref. 8).}$$

μ (ionic strength) $= m_2 + m_3$; $k = 2.3026RT/F$; m_{OH^-} stands for the molality of the hydroxyl ions that are formed from the hydrolysis of the conjugate bases where the pK's of the acids are greater than 9–10; K_w is the ionic product of water; m and γ denote the molality and molal activity coefficients of the species involved; E^0 is the standard electrode potential of the Ag-AgI electrodes in water (8); R, the universal gas constant; F, Faraday; T, absolute temperature in Kelvin; and $f(\mu)$ denotes a function of μ which is usually linear (1).

$$pK_2(\text{urd, thd}) \text{ or } pK_3(\text{guo, xao}) = (E - E^0)/k + \log (m_{I^-} m_{HA^-}/m_{A^{2-}}) + \log (\gamma_{I^-}\gamma_{HA^-}/\gamma_{A^{2-}})$$

[2] $$pK_1'(\text{urd, thd}) \text{ or } pK_3'(\text{guo, xao}) = (E - E^0)/k + \log [m_3(m_{1^-} + m_{OH^-})/(m_2 - m_{OH^-})] + 2S_f(\mu d_0)^{1/2} = pK_2(\text{urd, thd}) \text{ or } pK_3(\text{guo, xao}) + f(\mu)$$

where m_{OH^-} is given by eq. [1′], $\mu = m_1 + 3m_2 + m_3 - m_{OH^-}$, S_f (Debye-Hückel constant) $= 1.824 \times 10^6 (\epsilon_w T)^{-3/2}$, ϵ_w = the dielectric constant of water, and d_0 = density of water.

$$pK_1(\text{cyd} = \log (m_{H^+} m_{HA}/m_{H_2A^+}) - \log (\gamma_{H^+}\gamma_{HA}/\gamma_{H_2A^+})$$

[3] $$pK_1'(\text{cyd}) = -\log [m_{H^+}'(m_2 + m_{H^+}')/(m_1 - m_{H^+}')] = pK_1(\text{cyd}) + f(\mu)$$

where

[3′] $$-\log (m_{H^+}') = (E - E^0)/k + \log (m_{I^-}) - 2S_f(\mu d_0)^{1/2} \text{ (ref. 9)}$$

and $\mu = m_1 + m_3 \cdot m_{H^+}'$ denotes the apparent molality of hydrogen ion that results from significant deprotonation of the acid where pK is less than 3–4.

Table 1. EMF values at different temperatures for different cell solutions in pure water for deprotonation constant of urd, thd, cyd, guo, and xao.

μ	$m_1 \times 10^3$ (mol kg^{-1})	$m_2 \times 10^3$ (mol kg^{-1})	$m_3 \times 10^3$ (mol kg^{-1})	EMF (V) 15°C	20°C	25°C	30°C	35°C
			urd: $pK_1 = (pK_a)_{H_2A}$; $m_1 = m_{H_2A}$, $m_2 = m_{HA^-}$, $m_3 = m_{I^-}$					
0.0117	4.6	5.1	6.6	0.5208	0.5239	0.5291_5	0.5336	0.5383
0.0196	4.8	4.9	14.7	0.4991_5	0.5025	0.5065	0.5105	0.5152
0.0305	4.6	5.2	25.3	0.4885	0.4916	0.4957	0.4993	0.5038
0.0402	5.1	5.2	35.0	0.4779	0.4808	0.4848	0.4884_5	0.4926
0.0511	5.0	4.8	46.3	0.4701	0.4725	0.4763	0.4796	0.4837
0.0596	4.6	5.1	54.5	0.4700	0.4720	0.4761	0.4790	0.4835
0.0769	4.6	5.0	71.8	0.4627_5	0.4645	0.4691	0.4719	0.4759
0.0954	4.7	4.9	90.5	0.4565	0.4571	0.4627	0.4648	0.4690
			urd: $pK_2 = (pK_a)_{HA^-}$; $m_1 = m_{HA^-}$, $m_2 = m_{A^{2-}}$, $m_3 = m_{I^-}$					
0.0093	2.1	2.0	1.2	0.6804	0.6834	0.6859	0.6889	0.6919
0.0190	2.2	2.5	9.3	0.6345	0.6367	0.6384	0.6407	0.6425
0.0314	2.3	2.8	20.7	0.6169	0.6189	0.6203	0.6223	0.6240
0.0422	2.5	2.3	32.8	0.6005	0.6022	0.6034_5	0.6051	0.6066
0.0532	2.5	2.5	43.2	0.5955	0.5971	0.5982	0.5998	0.6013
0.0661	2.4	2.5	56.2	0.5889	0.5904	0.5914	0.5929	0.5942
0.0851	2.3	2.4	75.6	0.5804_5	0.5818	0.5826_5	0.5841	0.5856
			thd: $pK_1 = (pK_a)_{H_2A}$; $m_1 = m_{H_2A}$, $m_2 = m_{HA^-}$, $m_3 = m_{I^-}$					
0.0111	6.5	7.8	3.3	0.5689	0.5737	0.5794	0.5846_5	0.5892
0.0247	12.8	15.1	9.6	0.5422	0.5465	0.5518	0.5566_5	0.5608
0.0404	15.4	20.5	19.9	0.5271	0.5311_5	0.5362	0.5408	0.5447
0.0517	16.1	19.9	31.8	0.5136	0.5174_5	0.5223	0.5266	0.5303_5
0.0653	13.5	15.8	49.5	0.5012_5	0.5049	0.5045	0.5136	0.5171
0.0738	15.9	20.0	53.8	0.5010	0.5046	0.5092_5	0.5133	0.5168_5
0.0829	15.9	20.0	62.9	0.4971	0.5007	0.5052	0.5093	0.5127
0.0970	15.4	20.4	76.6	0.4935	0.4968	0.5015	0.5055	0.5088
			thd: $pK_2 = (pK_a)_{HA^-}$; $m_1 = m_{HA^-}$, $m_2 = m_{A^-}$, $m_3 = m_{I^-}$					
0.0113	2.5	2.6	1.0	0.6924	0.6954_5	0.6980	0.7010_5	0.7040
0.0250	2.1	2.2	16.3	0.6191	0.6209	0.6222	0.6238_5	0.6255_5
0.0390	2.6	2.7	28.3	0.6099	0.6115	0.6127	0.6143	0.6158
0.0482	3.1	3.3	35.2	0.6088_5	0.6105	0.6118	0.6133	0.6148
0.0574	2.6	2.7	46.7	0.5972_5	0.5987	0.5996_5	0.6011	0.6024
0.0731	2.3	2.4	63.5	0.5868_5	0.5880_5	0.5888_5	0.5901	0.5912
0.0881	2.4	2.5	78.2	0.5824_5	0.5837	0.5844	0.5856	0.5866
0.0990	3.0	3.2	86.4	0.5854_5	0.5867	0.5875	0.5887_5	0.5899
			cyd: $pK_1 = (pK_a)_{H_2A^+}$; $m_1 = m_{H_2A^+}$, $m_2 = m_{HA}$; $m_3 = m_{I^-}$					
0.0100	10.0	8.8	1.0	0.2065	0.2077	0.2083	0.2095	0.2103
0.0198	5.1	4.5	14.6	0.1918	0.1931	0.1934	0.1943	0.1948
0.0310	4.9	4.8	26.1	0.1848	0.1863	0.1862	0.1869	0.1876
0.0412	5.2	4.7	36.0	0.1772	0.1782	0.1783	0.1789	0.1793
0.0501	5.1	4.6	45.0	0.1734	0.1739	0.1741	0.1750	0.1750
0.0622	4.7	4.8	57.5	0.1919	0.1729	0.1727	0.1733	0.1736
0.0791	4.9	4.8	74.2	0.1660	0.1671	0.1669	0.1671_5	0.1673
0.0947	4.9	4.8	89.9	0.1626	0.1633_5	0.1633	0.1637	0.1638

Can. J. Chem. Downloaded from www.nrcresearchpress.com by 65.111.164.53 on 09/08/12
For personal use only.

Table 1. (*continued*)

μ	$m_1 \times 10^3$ (mol kg^{-1})	$m_2 \times 10^3$ (mol kg^{-1})	$m_3 \times 10^3$ (mol kg^{-1})	EMF (V) 15°C	20°C	25°C	30°C	35°C
cyd: $pK_2 = (pK_a)_{HA}$; $m_1 = m_{HA}$, $m_2 = m_{A^-}$, $m_3 = m_{I^-}$								
0.0102	4.6	5.2	5.0	0.6646	0.6677	0.6700	0.6731	0.6758
0.0249	4.9	4.8	20.1	0.6283	0.6307	0.6323	0.6347	0.6368
0.0396	4.5	5.2	34.4	0.6171_5	0.6193	0.6207_5	0.6229	0.6248
0.0523	4.6	5.2	47.1	0.6095	0.6113	0.6127	0.6147	0.6165
0.0637	4.1	5.6	58.1	0.6063	0.6081	0.6094	0.6113	0.6130
0.0761	4.7	5.0	71.1	0.5984	0.6001	0.6013	0.6031	0.6046
0.0870	5.0	4.7	82.3	0.5933	0.5949	0.5959_5	0.5977	0.5992
0.0960	4.5	5.2	90.8	0.5936	0.5951	0.5962	0.5980	0.5993
guo: $pK_1 = (pK_a)_{H_3A^+}$; $m_1 = m_{H_3A^+}$, $m_2 = m_{H_2A}$; $m_3 = m_{I^-}$								
0.0107	2.5	2.5	8.2	0.1268	0.1295	0.1321	0.1348_5	0.1375
0.0210	2.5	2.4	18.5	0.1120	0.1147	0.1062	0.1195	0.1220
0.0321	2.4	2.3	29.7	0.1042	0.1067	0.1090	0.1112_5	0.1136
0.0462	2.5	2.4	43.7	0.0963	0.0987_5	0.1009	0.1030	0.1052
0.0561	2.9	3.1	53.2	0.0904_5	0.0927	0.0945	0.0965_5	0.0986
0.0663	3.0	3.0	63.3	0.0865	0.0885_5	0.0904	0.0925	0.0944
0.0790	2.4	2.6	76.6	0.0878	0.0900	0.0918	0.0940	0.0960
0.0932	3.2	3.2	90.0	0.0795	0.0815	0.0830	0.0849_5	0.0867
guo: $pK_2 = (pK_a)_{H_2A}$; $m_1 = m_{H_2A}$, $m_2 = m_{HA^-}$, $m_3 = m_{I^-}$								
0.0090	1.2	1.4	7.6	0.5147	0.5197	0.5239	0.5284	0.5317
0.0191	1.1	1.2	17.9	0.4923	0.4966	0.5004	0.5045	0.5074_5
0.0302	2.0	2.3	27.9	0.4829	0.4873	0.4910	0.4947	0.4979
0.0398	2.4	2.3	37.5	0.4713_5	0.4753	0.4788	0.4827	0.4854
0.0520	1.5	1.3	50.7	0.4615	0.4655_5	0.4686	0.4722	0.4747
0.0623	2.5	2.5	59.8	0.4612	0.4652	0.6485	0.4722	0.4746_5
0.0732	1.9	2.2	71.0	0.4609	0.4647	0.4677	0.4716_5	0.4738
0.0984	1.8	1.9	96.5	0.4510	0.4549	0.4580	0.4618	0.4635_5
guo: $pK_3 = (pK_a)_{HA^-}$; $m_1 = m_{HA^-}$, $m_2 = m_{A^{2-}}$, $m_3 = m_{I^-}$								
0.0100	0.6	0.7	7.3	0.6101	0.6118	0.6130	0.6147	0.6162
0.0202	1.3	1.2	15.3	0.6034_5	0.6052	0.6064_5	0.6082	0.6097
0.0350	1.5	1.7	28.4	0.5954	0.5971	0.5982	0.5999_5	0.6014
0.0530	2.4	2.6	42.8	0.5928	0.5946	0.5960_5	0.5598	0.5994
0.0620	3.4	3.5	48.1	0.5948	0.5966	0.5983	0.6004	0.6022
0.0730	4.1	4.0	56.9	0.5921	0.5942	0.5958	0.5982	0.5999
0.0840	5.0	5.1	63.7	0.5932	0.5952	0.5970	0.5994	0.6015
0.0982	6.2	6.2	73.4	0.5918	0.5940	0.5962	0.5985	0.6008
xao: $pK_1 = (pK_a)_{H_3A^+}$; $m_1 = m_{H_3A^+}$, $m_2 = m_{H_2A}$; $m_3 = m_{I^-}$								
0.0103	2.5	2.3	7.8	0.1238	0.1271	0.1300	0.1330	0.1357
0.0198	2.3	2.4	17.5	0.1117	0.1147	0.1175_5	0.1203	0.1229
0.0317	2.6	2.5	29.1	0.0993	0.1022	0.1048	0.1073	0.1097
0.0420	2.6	2.4	39.4	0.0937_5	0.0965	0.0990	0.1015	0.1038
0.0523	3.2	3.2	49.1	0.0856	0.0881_5	0.0905	0.0928	0.0949
0.0608	3.0	3.1	57.8	0.0841	0.0867	0.0889	0.0913	0.0935
0.0717	2.7	2.8	69.0	0.0833	0.0859_5	0.0882	0.0906	0.0927
0.0923	2.8	3.0	89.5	0.0783_5	0.0809	0.0831	0.0853	0.0874

Can. J. Chem. Downloaded from www.nrcresearchpress.com by 65.111.164.53 on 09/08/12
For personal use only.

Table 1. (*concluded*)

μ	$m_1 \times 10^3$ (mol kg^{-1})	$m_2 \times 10^3$ (mol kg^{-1})	$m_3 \times 10^3$ (mol kg^{-1})	EMF (V) 15°C	20°C	25°C	30°C	35°C
xao: $pK_2 = (pK_a)_{H_2A}$; $m_1 = m_{H_2A}$, $m_2 = m_{HA^-}$, $m_3 = m_{I^-}$								
0.0110	2.2	2.7	8.3	0.3045	0.3082	0.3114	0.3149	0.3179
0.0212	2.2	2.7	18.5	0.2846	0.2880	0.2908	0.2942	0.2966_5
0.0311	2.5	2.4	28.7	0.2679	0.2710	0.2732	0.2763	0.2785
0.0397	2.3	2.6	37.1	0.2659	0.2686	0.2711	0.2739	0.2760
0.0511	2.2	2.7	48.4	0.2613	0.2640	0.2664	0.2691	0.2711
0.0692	2.3	2.7	66.5	0.2523	0.2551	0.2571	0.2596	0.2618
0.0784	2.5	2.4	76.0	0.2443	0.2466	0.2488	0.2509	0.2529
0.0901	2.6	2.5	87.6	0.2411	0.2431	0.2452	0.2475	0.2495
xao: $pK_3 = (pK_a)_{HA^-}$; $m_1 = m_{HA^-}$, $m_2 = m_{A^{2-}}$, $m_3 = m_{I^-}$								
0.0099	0.5	0.6	7.7	0.6026_5	0.6042_5	0.6055	0.6070	0.6084_5
0.0201	1.1	1.1	15.7	0.5988	0.6004	0.6017	0.6034	0.6049
0.0307	1.4	2.3	22.4	0.6050	0.6069	0.6084_5	0.6104	0.6125
0.0515	2.3	3.9	37.5	0.6007	0.6026	0.6041	0.6064	0.6081_5
0.0606	3.2	3.4	47.2	0.5901	0.5919	0.5932	0.5954	0.5973
0.0715	3.6	4.1	55.6	0.5888	0.5907	0.5920	0.5942	0.5961
0.0802	4.2	4.6	62.2	0.5869	0.5890	0.5902	0.5925	0.5946
0.0916	4.9	5.1	71.4	0.5840	0.5861	0.5875	0.5897	0.5919

$$pK_2(\text{cyd}) = (E - E^0)/k + \log (m_{I^-}m_{HA}/m_{A^-}) + \log (\gamma_{I^-}\gamma_{HA}/\gamma_{A^-})$$

[4] $$pK_2'(\text{cyd}) = (E - E^0)/k + \log [m_3(m_1 + m_{OH^-})/(m_2 - m_{OH^-})] = pK_2(\text{cyd}) + f(\mu)$$

where m_{OH^-} is given by eq. [1′] and $\mu = m_2 + m_3$

$$pK_1(\text{guo, xao}) = -\log (m_{H^+}m_{H_2A}/m_{H_3A^+}) - \log (\gamma_{H^+}\gamma_{H_3A^+})$$

[5] $$pK_1'(\text{guo, xao}) = -\log [m_{H^+}'(m_2 + m_{H^+}')/(m_1 - m_{H^+}')] = pK_1(\text{guo, xao}) + f(\mu)$$

where m_{H^+}' is given by eq. [3′] and $\mu = m_1 + m_3$.

In the above equations the required $E^0_{Ag\text{-}AgI}$ values at different temperatures were taken from the literature (8). The activity coefficients in water involved were obtained approximately from the Brønsted form of Debye–Hückel equation (9):

$$-\log \gamma_i = S_f Z_i^2 (\mu d_0)^{1/2} + b_i \mu.$$

where μ = molal ionic strength of the cell solutions, Z_i = charge of the species involved, S_f = Debye–Hückel constant, and b_i = constant for species i depending on the nature of the solvent and the temperature. Since in all cases pK_i' values were found to be linear with respect to μ, the pK values at different temperatures were obtained from the linear fit of the type $pK_i' = pK_i + b\mu$, where b stands for the algebraic sum of b_i for i species involved in the respective equations. The pK_i values along with the standard deviations are listed in Table 2.

For each acid, pK values at different temperatures were fitted into the Harned-Robinson type expression (10)

[6] $$pK = AT^{-1} + B + CT$$

using the method of least squares. The thermodynamic parameters ΔG^0, ΔS^0, and ΔH^0 accompanying deprotonation of the acids were evaluated using the same relations as described in our previous paper (1*a*). The values of ΔG^0, ΔS^0, and ΔH^0 so obtained and the values of the constants A, B, and C are presented in Table 3. The maximum uncertainties in ΔG^0, ΔS^0, and ΔH^0 as calculated by Please's method (11) are ±0.01 kJ mol^{-1}, ±1 J K^{-1} mol^{-1}, and 0.3 kJ mol^{-1}, respectively.

Discussion

The observed deprotonation constants for urd (K_1 and K_2), thd (K_1 and K_2), cyd (K_1 and K_2), guo (K_1, K_2, and K_3) and xao (K_1, K_2, and K_3) and related energetics at zero ionic strength and 25°C are compared in Table 4 with some literature data. The probable sites of ionization for all compounds studied are discussed below and the equilibria involved in the deprotonation processes are depicted in Schemes 1–5.

Scheme 1.

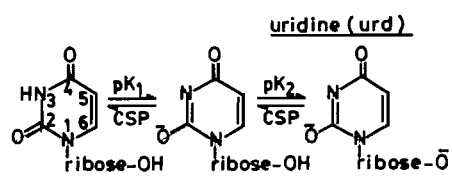

Scheme 2.

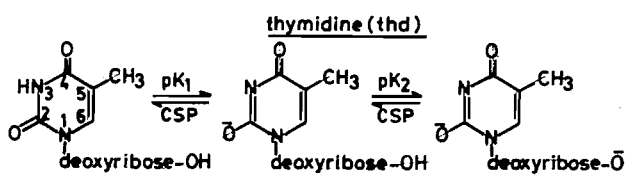

Can. J. Chem. Downloaded from www.nrcresearchpress.com by 65.111.164.53 on 09/08/12
For personal use only.

Can. J. Chem. Downloaded from www.nrcresearchpress.com by 65.111.164.53 on 09/08/12
For personal use only.

Table 2. pK values with standard deviation for the various nucleosides in pure water at different temperatures.[a]

Nucleosides	Parameter	Value				
		15°C	20°C	25°C	30°C	35°C
urd	pK_1	9.500 ± 0.002	9.390 ± 0.001	9.293 ± 0.001	9.207 ± 0.001	9.131 ± 0.001
	pK_2	12.900 ± 0.002	12.758 ± 0.002	12.626 ± 0.002	12.504 ± 0.002	12.392 ± 0.003
thd	pK_1	10.016 ± 0.001	9.909 ± 0.001	9.816 ± 0.001	9.727 ± 0.001	9.642 ± 0.001
	pK_2	13.181 ± 0.002	13.016 ± 0.001	12.865 ± 0.001	12.727 ± 0.002	12.601 ± 0.002
cyd	pK_1	4.182 ± 0.001	4.117 ± 0.002	4.053 ± 0.001	3.995 ± 0.001	3.940 ± 0.002
	pK_2	12.752 ± 0.003	12.604 ± 0.001	12.469 ± 0.002	12.345 ± 0.001	12.231 ± 0.002
guo	pK_1	2.000 ± 0.001	1.961 ± 0.001	1.924 ± 0.001	1.891 ± 0.001	1.860 ± 0.001
	pK_2	9.440 ± 0.001	9.350 ± 0.002	9.260 ± 0.002	9.170 ± 0.003	9.680 ± 0.001
	pK_3	12.583 ± 0.003	12.442 ± 0.003	12.309 ± 0.002	12.186 ± 0.001	12.070 ± 0.002
xao	pK_1	1.720 ± 0.001	1.700 ± 0.001	1.680 ± 0.001	1.660 ± 0.001	1.640 ± 0.001
	pK_2	5.770 ± 0.001	5.720 ± 0.001	5.673 ± 0.002	5.626 ± 0.002	5.581 ± 0.003
	pK_3	12.330 ± 0.003	12.180 ± 0.004	12.043 ± 0.004	11.917 ± 0.002	11.801 ± 0.002

[a]Correlation coefficient for $pK_{1,urd/thd/guo/xao} = pK_{2,urd/thd/guo/xao} = pK_{3,guo/xao} = 1$ at different temperatures.

Scheme 3.

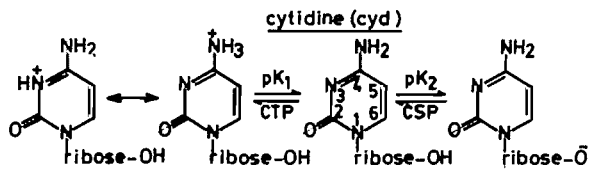

The fairly low magnitude of entropy change accompanying the first step deprotonation of cyd, guo, and xao indicates that the ionization processes involved were charge transfer processes (CTP) and the deprotonation sites were either $-\overset{+}{N}H-$ or $-\overset{+}{N}H_3$. The NMR spectrum of guanosine triphosphate in acidic D_2O (12) and IR studies of guanosine cation (13) confirm N_7 as the protonation site in guo. Based on the structural similarity between guo and xao Izatt et al. suggested N_7H^+ as the deprotonation site in protonated xao. Jardetzky et al.'s NMR data (12, 14) and calorimetric study (3*b*) favored N_3 protonation in cyd. However, as per Zana's ultrasonic studies of proton transfer reaction in the acidic range (15) and similar to cytosine as described in our previous paper (1*a*), the $-\overset{+}{N}H_3$ group can be considered the deprotonation site for protonated cyd.

Shapiro proposed that from UV and IR studies (16) N_1H- was the ionization site for uncharged guo. Similarity between the spectra of 1,7-dimethylxanthine and xao indicates ionization of the neutral xao to occur at the N_3H group. However, ultrasonic studies support the fact that the second step deprotonation of guo and xao are characterised by the formation of $C_6—O^-$ and $C_2—O^-$ groups, respectively (see Schemes 4 and 5).

For first step ionization of urd and thd, second step ionization of cyd, and second and third step ionizations of xao and guo, the accompanying entropy change is negative, indicating that the equilibria involved are charge separation processes (CSP) and the deprotonation sites are those shown in Schemes 1 to 5.

Similar to uracil and thymine (1*a*), in an alkaline solution two ionizations were detected for urd and thd. Ultrasonic studies indicate that pK_1 of urd and thd is characterised by 2-OH groups. The first step ionization of urd from 2-OH group is

Scheme 4.

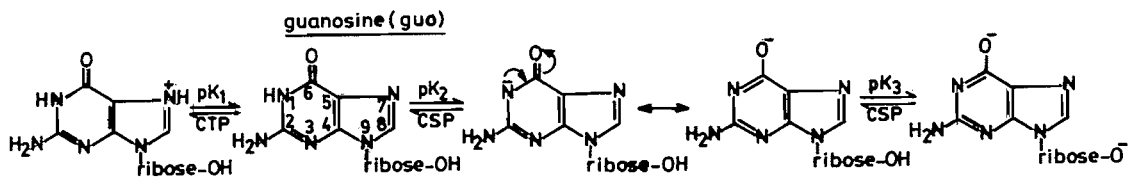

Scheme 5.

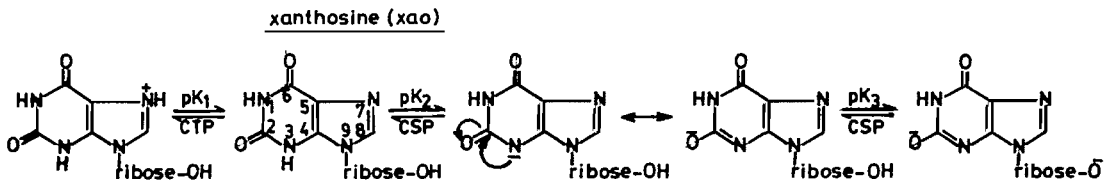

Table 3. Values of A, B, and C and relevant energetics $\Delta G°$, $\Delta S°$, and $\Delta H°$ (molal scale) for different nucleosides at 25°C.

Nucleosides	A/K	B	C/K^{-1}	$\Delta G°$/kJ mol^{-1}	$\Delta S°$/J K^{-1} mol^{-1}	$\Delta H°$/kJ mol^{-1}
urd			1st step dissociation			
	6073 (±9)	−25.98 (±0.07)	0.04998_5 (±0.00011)	53.04	−73.3	31.2
			2nd step dissociation			
	5294 (±1)	−15.33 (±0.06)	0.03421 (±0.00001)	72.06_5	−97.1	43.1
thd			1st step dissociation			
	2314 (±5)	−0.29 (±0.03)	0.00786 (±0.00005)	56.02	−84.2	30.9
			2nd step dissociation			
	6792 (±13)	−24.07 (±0.09)	0.04748 (±0.00015)	73.44	−81.2	49.2
cyd			1st step dissociation			
	1868 (±4)	-4.87_5 (±0.03)	0.00893 (±0.00005)	23.13	−8.6	20.6
			2nd step dissociation			
	6035 (±9)	−20.28 (±0.06)	0.04196 ($\pm 0.00010_5$)	71.19	−90.8	44.1
guo			1st step dissociation			
	1536 (±7)	−6.29 (±0.05)	0.01028 (±0.00008)	11.00	3.1	11.9
			2nd step dissociation			
	0 (±0)	14.62 (±0)	−0.01800 (±0)	52.81_5	−74.0	30.6
			3rd step dissociation			
	3767 (±6)	−5.40 (±0.05)	0.01702 (±0.00007)	70.22	−90.7	43.1_5
xoa			1st step dissociation			
	0 (±0)	2.87 (±0)	−0.00400 (±0)	9.57	−9.3	6.8
			2nd step dissociation			
	779 (±9)	3.25 (±0.07)	−0.00063 (±0.00010)	32.39	−55.0	16.0
			3rd step dissociation			
	6058 (±14)	−20.74 (±0.09)	0.04181_5 (±0.00016)	68.75	−80.3	44.8

[a]Values in parentheses are standard deviations.

also supported by the fact that the resulting anion is stabilized by intramolecular H-bond between 2-O$^-$ and 2′-OH group on the ribose. This is possible as nucleosides primarily exist in *anti* form in aqueous solutions (17).

The third step ionization of guo was demonstrated to occur at the ribose group (3*c*). Similarly the second step ionization of cyd and urd is assigned to the ribose moiety and for thd, to the dexyribose group (3*b*). By analogy with guo and other nucleosides, the third step ionization for xao is also expected to take place at the sugar group.

Interestingly enough, it is observed that the entropy of ionization accompanying the first step deprotonation of thd is less

Can. J. Chem. Downloaded from www.nrcresearchpress.com by 65.111.164.53 on 09/08/12
For personal use only.

Can. J. Chem. Downloaded from www.nrcresearchpress.com by 65.111.164.53 on 09/08/12
For personal use only.

Table 4. Comparison of pK_1, pK_2, and pK_3 values and related thermodynamic quantities for different nucleosides in water at 25°C.

	Method	pK_1	ΔG_1^0 (kJ mol^{-1})	ΔS_1^0 (J K^{-1} mol^{-1})	ΔH_1^0 (kJ mol^{-1})	pK_2	ΔG_2^0 (kJ mol^{-1})	ΔS_2^0 (J K^{-1} mol^{-1})	ΔH_2^0 (kJ mol^{-1})	pK_3	ΔG_3^0 (kJ mol^{-1})	ΔS_3^0 (J K^{-1} mol^{-1})	ΔH_3^0 (kJ mol^{-1})
						Uridine							
Present study	EMF method	9.29	53.0	−73.3	31.2	12.63	72.1	−97.1	43.1	—	—	—	—
Izatt et al. (*3b*)	pH, titration, calorimetry	9.30	53.1	−76.6	30.3	12.59	71.9	−87.9	44.3	—	—	—	—
						Thymidine							
Present study	EMF method	9.82	56.0	−84.2	30.9	12.86_5	73.4	−81.2	49.2	—	—	—	—
Izatt et al. (*3b*)	pH titration, calorimetry	9.79	55.9	−84.5	30.6	12.85	73.3	−72.8	51.9	—	—	—	—
						Cytidine							
Present study	EMF method	4.05	23.1	−8.6	20.6	12.47	71.2	−90.8	44.1	—	—	—	—
Izatt et al. (3bd)	pH titration calorimetry	4.08	23.3	−6.3	21.4	12.50	71.4	−95.8	43.1	—	—	—	—
						Guanosine							
Present study	EMF method	1.92	11.0	3.1	11.9	9.26	52.8	−74.0	30.6	12.31	70.2	−90.7	43.1
Izatt et al. (*3c*)	calorimetry	1.90	10.9	8.8	13.4	9.25	52.8	−69.9	32.0	12.33	70.4	−83.7	45.4
						Xanthosine							
Present study	EMF method	1.68	9.57	−9.3	6.8	5.67	32.4	−55.0	16.0	12.04	68.8	−80.3	44.8
Izatt et al. (*3c*)	calorimetry	—	—	—	—	5.67	32.4	−56.1	15.7	12.00	68.5	−79.1	45.4

than that for urd, i.e., $\Delta S^0_{1,thd} < S^0_{1,urd}$. This may be due to two reasons: First, in the thd anion, the water molecules solvate the 2-O^- group unlike the solvation of the urd anion where the 2-O^- forms intramolecular H-bond with the 2′-OH group. Second, in the case of the thd anion the water molecules are structured about the hydrophobic methyl group at 5-positions, causing more solvation for the thd conjugate base than for the urd conjugate base.

The entropy changes accompanying the second step ionization of urd ($\Delta S^0_{2,urd}$) and third step ionization of xao and guo ($\Delta S^0_{3,xao/guo}$) are less than that for the first step ionization of urd and second step ionizations of xao and guo, respectively. As discussed in our previous papers (1, 18, 19), the above observations can be explained by the nature of the equilibria and the accompanying entropy change. If H_2A denotes urd, xao, and guo and the equilibria were $H_2A + H_2O \; ^{\circ}HA^- + H_3O^+$ and $HA^- + H_2O \; ^{\circ}A^{2-} + H_3O^+$,

$$[7] \quad \Delta S_{HA^- — H_2A} = (\bar{S}^0_{H_3O^+} - \bar{S}^0_{H_2O}) + (\bar{S}^0_{HA^-} - \bar{S}^0_{H_2A})$$

and

$$[8] \quad \Delta S^0_{A^{2-} — H_2A} = (\bar{S}^0_{H_3O^+} - \bar{S}^0_{H_2O}) + (\bar{S}^0_{A^{2-}} - \bar{S}^0_{HA^-})$$

Since H_3O^+ carrying a charge must be solvated, resulting in more orderliness, there is a decrease in entropy of H_3O^+ relative to H_2O, i.e. $\bar{S}^0_{H_3O^+} < \bar{S}^0_{H_2O}$. For similar reason $\bar{S}^0_{HA^-} < \bar{S}^0_{H_2A}$ and $\bar{S}^0_{A^{2-}} < \bar{S}^0_{HA^-}$. But as the entropy of hydration of any ion is directly proportional to the square of ionic charge, it is expected that $(\bar{S}^0_{A^{2-}} - \bar{S}^0_{HA^-}) < (\bar{S}^0_{HA^-} - \bar{S}^0_{H_2A})$. In other words, $\Delta S_{A^{2-} — HA^-} < \Delta S^0_{HA — H_2A}$. This explains why $\Delta S^0_{2,urd}$ and $\Delta S^0_{3,xao/guo}$ are less than $\Delta S^0_{1,urd}$ and $\Delta S^0_{2,xao/guo}$, respectively.

Thus in conclusion it can be summarised that the generally good agreement of these precise deprotonation constant data and ionization energetics of the nucleosides obtained from our emf study and the earlier results serves to put the ionization thermodynamics of these important biomolecules on a relatively secure footing. Besides, these data also help to identify the possible sites of ionization in urd, thd, cyd, guo and xao. However, it is worth noting that we did not have data on the free energy of formation (ΔG^0_f) and enthalpy of formation (ΔH^0_f) for the nucleosides. We are therefore limited in our evaluation of energetics of formation in solution [$\Delta X^0_{f,soln}(A^-/HA^-)$] for the corresponding anions which otherwise should have provided a better insight towards the relative solvation behavior.

References

1. (*a*) S. Ganguly and K.K. Kundu. Can. J. Chem. **72**, 1120 (1994); (*b*) J. Solution Chem. In press.
2. B. Pullman and A. Pullmann. Quantum biochemistry. Interscience Publishers, New York. 1963.
3. R.M. Izatt, J.C. Christensen, and J.H. Rytting. (*a*) Chem. Rev. **71**, 439 (1971); (*b*) J. Chem. Soc. B, 1643 (1970); (*c*) Biochemistry, **9**, 4907 (1970); (*d*) J. Phys. Chem. **71**, 2700 (1967).
4. H.S. Harned and R.W. Ehlers. J. Am. Chem. Soc. **54**, 1350 (1932).
5. M. Windholz (*Editor*). The Merck index. 10th ed. Merck and Co., Rahway, N.J. 1983.
6. D. Shugar and J.J. Fox. Biochim. Biophys. Acta, **9**, 199 (1952).
7. (*a*) K.K. Kundu, D. Jana, and M.N. Das. Electrochim. Acta, **18**, 75 (1973); (*b*) K.K. Kundu and K. Majumder. J. Chem. Soc. Faraday Trans. I, **71**, 1422 (1975).
8. (*a*) H.B. Hetzer, R.A. Robinson, and R.G. Bates. J. Phys. Chem. **68**, 1929 (1964); (*b*) R.G. Bates. Electrometric pH

determination. John Wiley and Sons, New York. 1954. p. 25.
9. S. Glasstone. An introduction to electrochemistry. D. Van Nostrand Co. Inc., Princeton, N.J. 1942. p. 320.
10. H.S. Harned and R.A. Robinson. Trans. Faraday Soc. **36**, 973 (1940).
11. N.W. Please. Biochem. J. 196 (1954).
12. C.D. Jardetzky and O. Jardetzky. J. Am. Chem. Soc. **82**, 222 (1960).
13. J.T. Miles, F.B. Howard, and J. Frazier. Science, **142**, 1458 (1963).
14. O. Jardetzky, P. Pappas, and N.G. Wade. J. Am. Chem. Soc. **85**, 1557 (1963).
15. J. Lang, J. Strum, and R. Zana. (*a*) J. Phys. Chem. **77**, 2329 (1973); (*b*) J. Phys. Chem. **78**, 80 (1974); (*c*) Biopolymers, **10**, 2639 (1971).
16. R. Shapiro. Prog. Nucleic Acid Res. **8**, 73 (1968).
17. P.O.P. Ts'o. Basic principles in nucleic acid chemistry. Academic Press, London. 1974. p. 128.
18. K.K. Kundu, P.K. Chattopadhyay, and M.N. Das. J. Chem. Soc. B, 2034 (1972).
19. H. Talukdar, S.P. Rudra, and K.K. Kundu. Ind. J. Chem. **27A**, 764 (1988).

Can. J. Chem. Downloaded from www.nrcresearchpress.com by 65.111.164.53 on 09/08/12
For personal use only.

Completeness profiles of one-electron basis sets

Delano P. Chong

Abstract: The completeness profile is used to provide a visual assessment of the quality of one-electron basis sets. The approach is illustrated by examples of a number of basis sets for the carbon atom. New insight is gained regarding the superiority of spin density calculations using Chipman's basis sets.

Key words: One-electron basis sets.

Résumé : On utilise le profil du caractère complet pour obtenir une évaluation visuelle de la qualité des ensembles de base à un électron. On illustre cet approche par des exemples d'un certain nombre d'ensembles de base pour l'atome de carbone. On obtient une nouvelle compréhension concernant la supériorité des calculs de densité de spin en utilisant les ensembles de base de Chipman.

Mots clés : des ensembles de base à un électron.

[Traduit par la rédaction]

Can. J. Chem. Downloaded from www.nrcresearchpress.com by 65.111.164.53 on 09/08/12
For personal use only.

Introduction

In *ab initio* quantum chemical computations, the accuracy of variation methods depends on the completeness of both n-electron and one-electron spaces. In post-Hartree–Fock calculations, one is concerned with how well the n-electron space is represented by the truncated treatments. For example, configuration interaction (CI) computations with singly and doubly excited configurations are sometimes compared with full CI. On the other hand, in the independent particle approximation, self-consistent field molecular orbital (SCF-MO) computations with split-valence basis sets are often compared with results using more extensive basis sets. In this work, we are concerned only with the completeness of the one-electron space.

Different properties emphasize different regions of coordinate space of atoms or molecules. Accuracy of calculated *tight* properties, such as $\langle\delta(\mathbf{r})\rangle$ and the electric field gradient tensor at the nucleus (weighting approximately as r^{-3}), depends on the reliability of the wavefunction at or around the nucleus. Consequently, basis functions with high exponents are needed. Energy operators weight the wave function roughly as r^{-2} and r^{-1} and require completeness of basis a little less tight. Dipole moments and diamagnetic susceptibilities go as r and r^2, respectively, emphasizing the importance of correct representation of about the same region of space as normal bonds. Finally, diffuse basis functions are necessary for proper description of polarizabilities, long-range interactions, and weakly bonded complexes.

The quality of one-electron basis functions has received reviews from time to time (1–3). Furthermore, some workers focused their attention on the asymptotic behaviour (4), or concentrated on calculations of chemical shifts (5) and spin densities (6, 7), while others studied momentum space properties (8). Some recent investigations used information theory to examine the quality of one-electron basis sets (9–12). In contrast, the object of this work is to present a simple visual representation of the completeness of atomic orbital basis sets at different regions of space as tested by a scanning orbital (13). We call this the completeness profile of a basis set.

Received July 7, 1994.

D.P. Chong.[1] Department of Chemistry, 2036 Main Mall, University of British Columbia, Vancouver, BC V6T 1Z1, Canada.

[1] E-mail address: chong@theory.chem.ubc.ca

Theory

Suppose we are interested in a certain contracted Gaussian-type orbital (GTO) basis set

[1] $\phi_k = \Sigma\, \chi_j C_{jk}$ i.e., $\boldsymbol{\phi} = \boldsymbol{\chi}\mathbf{C}$

where χ_j represent the primitive GTO's. Let us first define a projection operator $\mathcal{P}$ by

[2] $\mathcal{P} = |\boldsymbol{\phi}\rangle\, \langle\boldsymbol{\phi}|\boldsymbol{\phi}\rangle^{-1}\langle\boldsymbol{\phi}|$

From the definition, it is easy to see that

[3] $\mathcal{P}^2 = \mathcal{P} = \mathcal{P}\dagger$

In terms of an orthonormalized basis set

[4] $\psi = \phi\mathbf{T}$, i.e., $\psi_m = \Sigma\phi_k T_{km}$

the projection operator is given by

[5] $\mathcal{P} = \Sigma|\psi_m\rangle\, \langle\psi_m|$

In this work, the transformation matrix $\mathbf{T}$ is chosen to be the popular Löwdin's symmetric orthonormalization matrix $\mathbf{S}^{-1/2}$. Now, we shall examine the completeness of the basis set in representing a normalized GTO $G(\alpha)$, with exponent α, as measured by how close

Can. J. Chem. Downloaded from www.nrcresearchpress.com by 65.111.164.53 on 09/08/12
For personal use only.

[6] $Y(\alpha) = \langle \mathcal{P}G(\alpha)|\mathcal{P}G(\alpha)\rangle = \langle G(\alpha)|\mathcal{P}G(\alpha)\rangle$

comes to unity. Substitution of eq. [5] into [6] gives

[7] $Y(\alpha) = \Sigma\langle G\alpha)|\psi_m\rangle\langle\psi_m|G(\alpha)\rangle$

The quantity $Y(\alpha)$ is nothing more than the sum of squares of the overlap of the test GTO $G(\alpha)$ with the orthonormalized basis $\{\psi\}$. We are free to choose the value of exponent α of the scanning GTO $G(\alpha)$. By the completeness profile, we mean $Y(\alpha)$ plotted against $x = \log \alpha$, as first introduced in our earlier paper (13).

For simplicity, we use $G(\alpha) = 1s(\alpha)$, $2p(\alpha)$, and $3d(\alpha)$ GTO's for $l = 0$, 1, and 2, respectively. If one uses a six-component d-shell, one introduces an extra $3s$ GTO. The effect is almost like adding an extra $1s$ GTO with exponent equal to $(3\ \alpha_d/7)$ (14). In the following calculations, we assume that five-component d-functions are being used.

Although GTO's have been used as the example, one can apply the same procedure to Slater-type orbitals equally well if one so desires.

Calculations

To illustrate our procedure, we have chosen a number of basis sets for the carbon atom. The popular STO-6G, 6-31G*, and 6-311G* basis sets have been well documented (15). The atomic natural orbitals (ANO) denoted by [321], [432], and [543] are due to Almlöf and Taylor (16). New correlation-consistent basis sets cc-pVnZ (n = D, T, Q) from Dunning and co-workers (17–20) are also included, as well as sample internal basis sets in the deMon density functional program (21, 22). Finally, the basis sets specially designed by Chipman (6, 7) for spin-density calculations are also studied. Table 1 summarizes the size of the primitive and contracted GTO sets as well as the contraction schemes.

The actual computation of $Y(\alpha)$ can be performed on a microcomputer. The program is easy to write or can be requested from the author.[2] In this work, we use $\log \alpha$ as the x-values and $Y(\alpha)$ for $l = 0$, 1, and 2 as the y-values. Eighty-one values of $x = \log \alpha$ ranging from -4.0 to $+4.0$ are preselected.

Results and discussion

Energy-optimization of basis sets has a tendency to overemphasize the tight region of space, at the expense of the bonding region. Conversely, higher completeness at high $x = \log \alpha$ tends to lead to a better energy. On the other hand, extension of adequate coverage towards the diffuse region (low x) tends to improve the description of bonding.

The results of our calculations are presented in Figs. 1 to 6, which display the completeness profile of each basis set for $x = -4$ to $+4$.

At first sight, many of the profiles appear rather similar. For example, it seems necessary for all basis sets to be fairly complete around $x = 1$ for carbon. Moreover, the completeness profiles of all split-valence basis sets show a dip about $x = 0.35$ (for carbon), indicating that there is less need for a basis set to be complete around the nodal region of the $2s$ orbital. To compare the completeness profiles in finer details, however, one needs to make a transparency of each completeness profile and to superimpose it on the other figures.

Let us first examine Fig. 1. For the minimal STO-6G basis, there is no d-function and hence no d-space completeness profile. The 6-31G* set extends the coverage of the valence region and 6-311G* improves the completeness over the tight region (high x). Comparison of Figs. 2 and 3 indicates that the completeness profiles of the ANO and cc-pVnZ basis sets are actually very similar in appearance. In Fig. 4, the two different valence double-ζ basis sets internal to the deMon program show almost identical completeness profiles, even though the DZVP3 was constructed from a much larger primitive space.

From these completeness profiles for the *Nl*-spaces, we see that the ANO basis sets appear to be slightly superior in every case for a given N, with two exceptions. For $4s$ and $5s$ contracted GTO, the correlation-consistent basis sets cc-pVTZ and cc-pVQZ seem better. In a recent paper, Schäfer *et al.* (23) proposed a new TZP basis set. For B to Ne, the contraction is from $11s6p$ primitives to $5s3p$ contracted GTO. Since the contracted s-space is larger than valence triple-ζ, the energy from this new basis set should not be directly compared (23) with that from the 6-311G basis. The completeness profiles of this new TZP basis for carbon (not shown) are actually slightly inferior to the $5s$ of cc-pVQZ and the $3p$ of [432] ANO, shown in Figs. 3 and 2, respectively.

In the completeness profiles in Fig. 5 for Chipman's basis sets, designed for spin density calculations, there are two features that stand out most of all. Firstly, $Y(\alpha)$ for s-space is

Table 1. Comparison of size[a] of primitive $\{\chi\}$ and contracted $\{\phi\}$ basis sets for carbon.

Group[b]	Name	$\{\chi\}$[c]	Contraction scheme[a]	$\{\phi\}$[c]
Gaussian	STO-6G	C60	66/6	210
	6-31G*	A41	631/31/1	321
	6-311G*	B51	6311/311/1	431
ANO	[321]	D86	DDD/88/6	321
	[432]	D86	DDDD/888/66	432
	[542]	D86	DDDDD/8888/666	543
cc-pVnZ	cc-pVDZ	941	991/41/1	321
	cc-pVTZ	A52	AA11/511/11	432
	cc-pVQZ	F63	FF111/6111/111	543
deMon	DZVP	951	621/41/1	321
	DZVP3	B81	821/71/1	321
	TZVP	A61	7111/411/1	431
Chipman	EPR521	951	51111/41/1	521
	EPR631	A61	511111/411/1	631
	EPR642	A62	511111/3111/11	642
Diffuse	[432f]	D87	DDDD/888/661	433
	[432] + 111	D86	DDDD1/8881/661	543
	aug-cc-pVTZ	B63	AA111/5111/111	543

[a]A to F represent 10 to 15, respectively.
[b]See text for references.
[c]Number of s-, p-, and d-type basis functions (f-type orbitals are not considered in this study).

[2] A copy of the executable codes for calculating the completeness profiles, with sample input, will be sent to any interested party who makes voluntary contribution to the cost of floppy and mailer.

Can. J. Chem. Downloaded from www.nrcresearchpress.com by 65.111.164.53 on 09/08/12
For personal use only.

Fig. 1. Completeness profiles of popular basis sets for carbon from Gaussian program (15). The completeness profiles are plotted in the following way: solid and dashed lines for the *s*- and *p*-spaces, respectively, while short dashes represent the polarization function *d*-space.

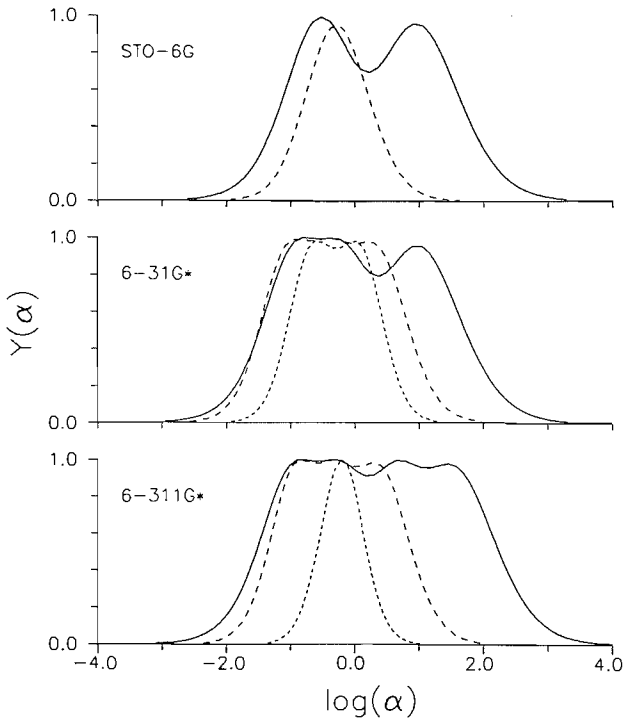

Fig. 2. Completeness profiles of atomic natural orbitals for carbon from Almlöf and Taylor (16). The completeness profiles are plotted in the following way: solid and dashed lines for the *s*- and *p*-spaces, respectively, while short dashes represent the polarization function *d*-space.

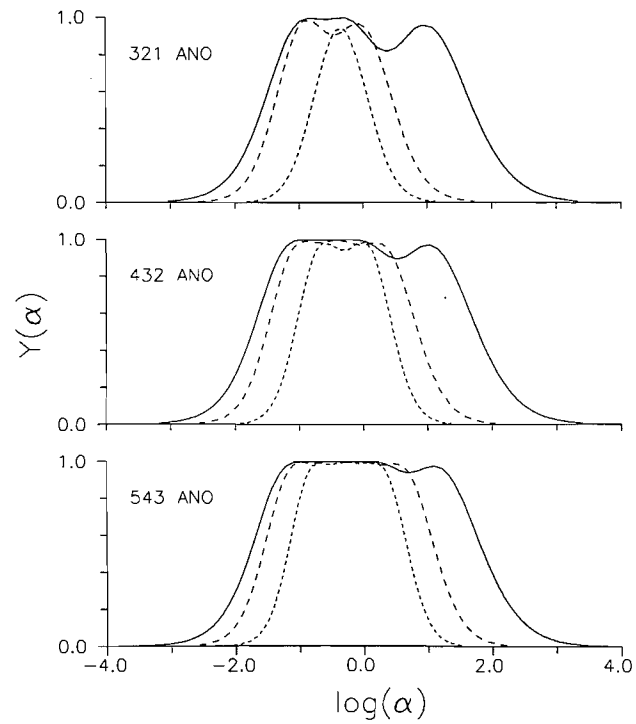

Fig. 3. Completeness profiles of new cc-pVnZ basis sets for carbon from Dunning and co-workers (17–20). The completeness profiles are plotted in the following way: solid and dashed lines for the *s*- and *p*-spaces, respectively, while short dashes represent the polarization function *d*-space.

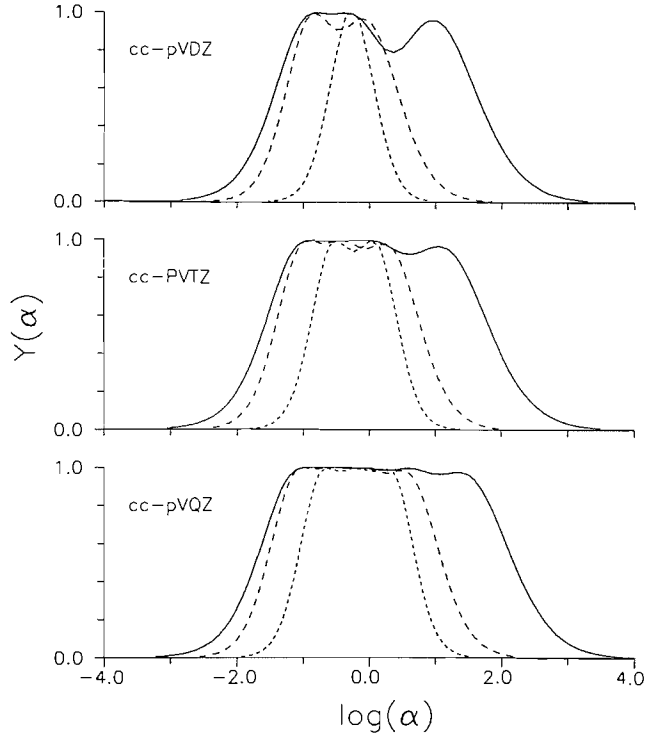

Fig. 4. Completeness profiles of some internal basis sets for carbon from the deMon program (21, 22). The completeness profiles are plotted in the following way: solid and dashed lines for the *s*- and *p*-spaces, respectively, while short dashes represent the polarization function *d*-space.

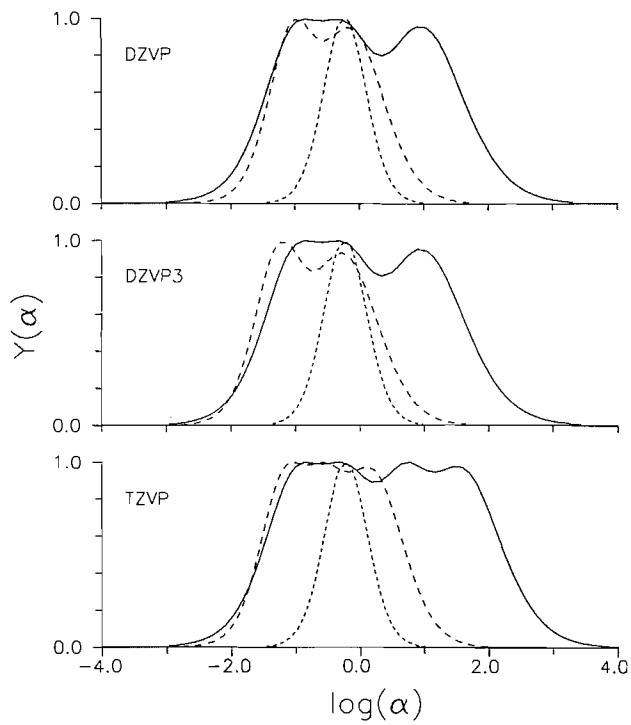

Can. J. Chem. Downloaded from www.nrcresearchpress.com by 65.111.164.53 on 09/08/12
For personal use only.

Fig. 5. Completeness profiles of basis sets for carbon designed by Chipman (6, 7) for spin density calculations. The completeness profiles are plotted in the following way: solid and dashed lines for the *s*- and *p*-spaces, respectively, while short dashes represent the polarization function *d*-space.

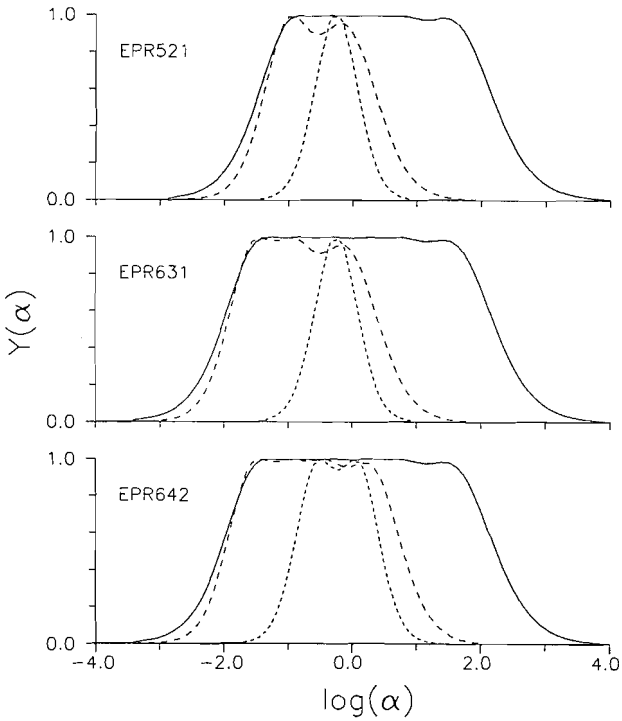

Fig. 6. Completeness profiles of basis sets for carbon containing diffuse functions. The completeness profiles are plotted in the following way: solid and dashed lines for the *s*- and *p*-spaces, respectively, while short dashes represent the polarization function *d*-space.

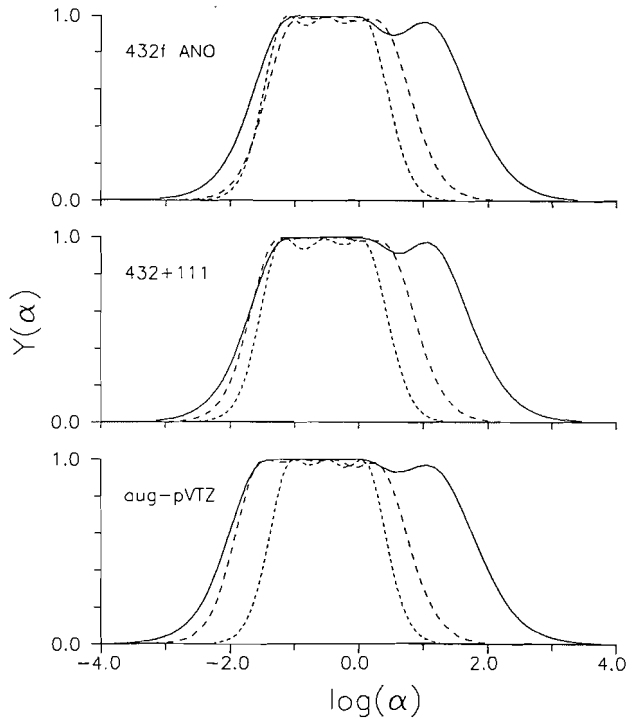

greater than 0.7 even at $x = 2$, confirming our expectation that tight properties require relatively high completeness in the tight region of coordinate space. The second special feature is the absence of the dip in the region of $0 < x < 1$. This also is not difficult to understand. The main source of many spin densities is spin polarization, largely taken into account by the UHF approach. In UHF calculations, the 2*s* nodes in the MO for α and β electrons occur at different *r* values and therefore higher completeness is needed throughout. From Fig. 5, it is not surprising to find that the smaller EPR521 basis set can give as reliable spin densities as the EPR631 set, chosen by Chipman himself (24) for larger radicals.

Except for Chipman's basis, we have been studying the quality of various general-purpose sets. However, it is well known that diffuse functions are necessary for a faithful description of anions and weak van der Waals complexes, as well as for the accurate computation of polarizabilities, hyperpolarizabilities, and theoretical momentum profiles (TMP) for electron momentum spetroscopy. In Fig. 6, we compare the completeness profiles of three basis sets containing diffuse functions, all starting with a comparable valence triple-ζ basis. In the [432*f*] basis, the set of [432] ANO was augmented by a single set of *d*-type field-induced polarization function (25–27). In the [432] + 111 basis, the set of [432] ANO was augmented by uncontracting the outermost primitive GTO in each type (28). Finally, the aug-cc-pVTZ basis includes one set of optimized diffuse functions of each type (19). Woon and Dunning (19) compared the results of calculated polarizabilities when they augmented the cc-pVnZ basis by several sets of diffuse functions. From Fig. 6, we can see that the completeness profiles are very similar for *d*-type functions. Consequently, we expect the three basis sets to lead to very similar polarizabilities. However, the [432f] basis lacks diffuse *p*-type functions. For anions and TMP, the aug-cc-pVNZ basis sets are therefore recommended.

Although we have selected the carbon atom as an example, other atoms can be studied in the same manner. Except for different numerical *x*-values, we expect the completeness profiles to show very similar qualitative behaviour.

In conclusion, a simple method has been proposed in this paper to provide a visual assessment of the completeness of one-electron basis sets. The quality of the completeness profile in different regions of coordinate space is expected to lead to new insight regarding the design and performance of different basis sets.

Acknowledgement

I thank Patrick Duffy, Dr. Michael Cohen, and Dr. Natalie Cann for valuable discussions.

References

1. S. Huzinaga. Comput. Phys. Rep. **2**, 279 (1985).
2. R. Ahlrichs and P.R. Taylor. J. Chim. Phys. **78**, 315 (1981).
3. E.R. Davidson and D. Feller. Chem. Rev. **86**, 681 (1986).
4. B. Tsapline. Chem. Phys. Lett. **21**, 32 (1973).
5. D.B. Chestnut and K.D. Moore. J. Comput. Chem. **10**, 648 (1989).

6. D.M. Chipman. Theor. Chim. Acta, **76**, 73 (1989).
7. D.M. Chipman. J. Chem. Phys. **91**, 5455 (1989).
8. A.M. Simas, A.J. Thakkar, and V.H. Smith, Jr. Int. J. Quantum Chem. **21**, 419 (1982).
9. A.M. Simas, A.J. Thakkar, and V.H. Smith, Jr. Int. J. Quantum Chem. **24**, 527 (1983).
10. P.E. Regier, J. Fisher, B.S. Sharma, and A.J. Thakkar. Int. J. Quantum Chem. **28**, 429 (1985).
11. D.D. Robertson, V.H. Smith, Jr., and A.J. Thakkar. Int. J. Quantum Chem. **32**, 427 (1987).
12. S.R. Gadre, S.A. Kulkarni, and I.H. Shirvastava. Chem. Phys. Lett. **166**, 445 (1990).
13. D.P. Chong and S.R. Longhoff. J. Chem. Phys. **93**, 570 (1990).
14. P. Chopra, L. Carlacci, H.F. King, and P.N. Prasad. J. Phys. Chem. **93**, 7120 (1989).
15. W.J. Hehre, L. Radom, P.v.R. Schleyer, and J.A. Pople. *Ab initio* molecular orbital theory. Wiley-Interscience, New York. 1986.
16. J. Almlöf and P.R. Taylor. J. Chem. Phys. **86**, 4070 (1987).
17. T.H. Dunning, Jr. J. Chem. Phys. **90**, 1007 (1989).
18. R.A. Kendall, T.H. Dunning, Jr., and R.J. Harrison. J. Chem. Phys. **96**, 6796 (1992).
19. D.E. Woon and T.H. Dunning, Jr. J. Chem. Phys. **98**, 1358 (1993).
20. D.E. Woon and T.H. Dunning, Jr. J. Chem. Phys. **100**, 2975 (1994).
21. A. St-Amant and D.R. Salahub. Chem. Phys. Lett. **169**, 387 (1990).
22. A. St-Amant. Ph.D. Thesis, University of Montreal. 1991.
23. A. Schäfer, C. Huber, and R. Ahlrichs. J. Chem. Phys. **100**, 5829 (1994).
24. D.M. Chipman. J. Chem. Phys. **94**, 6632 (1991).
25. G.D. Zeiss, W.R. Scott, N. Suzuki, D.P. Chong, and S.R. Langhoff. Mol. Phys. **37**, 1543 (1979).
26. D.P. Chong. J. Chin. Chem. Soc. **39**, 375 (1992).
27. J. Guan, P. Duffy, J.T. Carter, D.P. Chong, K.C. Casida, M.E. Casida, and M. Wrinn. J. Chem. Phys. **98**, 4753 (1993).
28. J.E. Rice, R.D. Amos, S.M. Colwell, N.C. Handy, and J. Sanz. J. Chem. Phys. **93**, 8828 (1990).

Can. J. Chem. Downloaded from www.nrcresearchpress.com by 65.111.164.53 on 09/08/12
For personal use only.

New extracellular fatty acids in culture filtrates of *Sporothrix flocculosa* and *S. rugulosa*

Streeti R. Choudhury, James A. Traquair, and William R. Jarvis

Abstract: Two new and rare unsaturated, extracellular fatty acids were identified in the culture filtrates of the biocontrol fungi, *Sporothrix flocculosa* and *S. rugulosa*. 16-Methyl-9*E*-nonadecenoic acid (**1**) and (*Z,Z*)-10,14-eicosadienoic acid (**2**) were characterized on the basis of infrared (IR) and nuclear magnetic resonance spectra (^{13}C and ^{1}N NMR), and gas chromatographic – mass spectrometric data (GC–MS). The structure of compounds **1** and **2** was confirmed by oxidative degradation to the known standards, dimethyl azelate, dimethyl succinate, dimethyl sebacate, and methyl caproate.

Key words: unsaturated fatty acids, fungi.

Résumé : On a identifié les nouveaux et peu abondants acides gras insaturés : les acides 16-méthyl-9*E*-nonadecénoique (**1**) et (*Z,Z*,)-10,14-eicosadiénoique (**2**) dans les filtrats de culture des champignons de biocontrôle, *Sporothrix flocculosa* et *S. rugulosa*, et on les a caractérisés par spectroscopie IR et de RMN du ^{13}C et du ^{1}H et par les données de chromatographie en phase gazeuse couplée à un spectromètre de masse (GC–MS). On a confirmé les structures des composés **1** et **2** par dégradation oxydante de standards connus : l'azélate de diméthyle, le succinate de diméthyle, le sébacate de diméthyle et la caproate de méthyle.

Mots clés : acides gras insaturés, champignons.

[Traduit par la rédaction]

Long-chained, unsaturated fatty acids with 14–24 carbon atoms and one or more double bonds are characteristic of the fungi, particularly the yeast and yeastlike species. The major unsaturated fatty acids associated with the cellular fractions of these fungi are oleic (C18:1) and linoleic (C18:2) acids (1, 2). A few rare and unusual fatty acids in the fungi include methyl-branched fatty acids and hydroxy fatty acids (1). Most studies deal with cellular fatty acids, which are involved in membrane structure and function. For example, linoleic acid is implicated in the structural integrity and activity of mitochondria (3). Linoleic acid has been reported as a morphogenetic factor in the sexual reproduction of the phytopathogens *Ophiostoma ulmi* (4) and *Nectria haematococca* (5). In general, fatty acids are also implicated in the synthesis of other secondary metabolites such as cyclopentanes, polyacetylenes, and polyketide aromatic compounds, which can be potent antibiotics and mycotoxins (1, 3). Four fungitoxic C18:2 hydroxy-unsaturated fatty acids have been identified in the stroma of the endophytic phytopathogen, *Epichloe typhina* (6). Little is known about extracellular fatty acids in the fungi, but acetylated and hydroxy fatty acids have been reported (1).

Recently, we identified a new antimicrobial, methyl-substituted C18:2, extracellular fatty acid in the culture filtrates of the yeastlike, biocontrol fungi, *Sporothrix flocculosa* and *S. rugulosa* (7). In the present report we describe two new and rare extracellular C20 fatty acids that are not antimicrobial.

Received May 25, 1994.

S.R. Choudhury and J.A. Traquair.[1] Agriculture and Agri-food Canada, Pest Management Research Center, 1391 Sandford Street, London, ON N5V 4T3, Canada.
W.R. Jarvis. Agriculture and Agri-food Canada, Research Station, Harrow, ON N0R 1G0, Canada.

[1] Author to whom correspondence may be addressed. Telephone (519) 645-4452. Fax: (519) 645-5476.

Results and discussion

The new unsaturated, C20 extracellular fatty acids were identified from filtrates of both *Sporothrix flocculosa* and *S. rugulosa* grown for 28 days on yeast–malt extract broth in static liquid culture. Compound **1** is an oil with molecular formula $C_{20}H_{38}O_2$. An FT-IR spectrum contained absorption bands at 3300 cm^{-1} (-OH stretch) and 1710 cm^{-1} (C=O stretch), indicating the presence of a spectrum -COOH group. The presence of this group was also revealed in the ^{1}H NMR spectrum at 11.65 ppm, while in the ^{13}C NMR spectrum resonances at 34.1 (C-2) and 180.0 ppm (C-1) were expected for attachment of this group to a methylene (8). The mass spectrum of compound **1** shows fragmentation at 293 [M – 17] and 266 [M – 44], which indicates the presence of an acid group at the terminal end in a chain (9). The ^{1}H NMR shows $\delta = 5.30$ ppm (t, 2H, $J = 17.1$ Hz, -CH=), indicating the presence of one double bond. Normally for *E* isomers the *J* values range between 12.0 and 18.0 Hz (10). We note that the coupling constant values thus indicate an *E* isomer, which was supported by ^{13}C NMR. The DEPT ^{13}C NMR showed two peaks at 130.35 and 130.45 ppm, which indicates the presence of a double bond. The position of the double bond was identified by following the technique given by Bus et al. (11), for the ^{13}C values of the neighbouring carbons of the double bonds. The *trans* unsaturations possess higher values in the range 29.5–38.0 ppm, whereas *cis* unsaturations have values of 26.0–28.5. The ^{13}C

Can. J. Chem. Downloaded from www.nrcresearchpress.com by 65.111.164.53 on 09/08/12
For personal use only.

Can. J. Chem. Downloaded from www.nrcresearchpress.com by 65.111.164.53 on 09/08/12
For personal use only.

values of compounds **1** are 32.6–32.65 for C-8 and C-11, which implies that the position of the *trans* unsaturation is between C-9 and C-10. This confirms the position of the double bond between C-9 and C-10.

The presence of two methyl groups was revealed by ^{13}C and ^{1}H NMR: one, at 14.5 (C-19), indicating a terminal methyl group that is shielded by methyl branching at the γ-position (^{1}H nmr δ = 0.9 (t, J = 6 Hz, 3H, -CH_3)) and another value at 19.8 (-CH_3 at C-16), indicating methyl branching at C-16 (ref. 8, p. 56). The triplet at 1.15 ppm (J = 6.3 Hz, 3H, -CH_3) is observed in ^{1}H NMR, and a singlet with a downfield shift in APT ^{13}C NMR indicating the presence of branching (12). In general, the APT ^{13}C NMR shows downfield shifts for both the CH_3 and CH, whereas in DEPT both CH_3 and CH give upfield shifts (ref. 10, p. 276). The ^{13}C NMR of the carbon bearing the methyl group shows resonance at 32.2 (C-16), which confirms the position of methyl branching at C-16 (13). The carbons next to the methyl branching show values 36.5 (C-15) and 38.7 (C-17). These values are deshielded by the methyl branching at C-16. The position of methyl branching was further supported by the fragmentation pattern of 16-methyl methylnonadecanoate **1***a*. Two large peaks are observed, one at 282 [M – 44] (50%) and the second at 255 (42%), with a small peak at 269 (5%) that carried the methyl group. The peaks at 251 and 233, observed by the loss of a methanol and a water molecule simultaneously from the fragment $^{+}CH(CH_3)(CH_2)_{14}$-$COOCH_3$, are also characteristic of the branching at C-16 (9).

To confirm the structure of compound **1** its methyl ester was oxidized using the Lemieux–von Rudloff reagent (14). This method was used to indicate the position of the double bond. Esterification of the acid fragments with HCl/MeOH after von Rudloff's oxidation gave two major components: one is 7-methyl methyldecanoate (Mol. Wt. 200). The *m/e* fragmentation pattern has two major peaks at 156 (40%) and 129 (45%) along with a small peak at 143 (7%). The smaller peak is the indication of the carbon bearing the methyl group; the peaks observed at 125 and 107 indicate the simultaneous loss of methanol and water from the fragment $^{+}CH(CH_3)(CH_2)_5$-$COOCH_3$. This confirms the methyl branching at C-7. The second major component is nonanedioic acid dimethyl ester (Mol. Wt. 216). The *m/e* fragmentation pattern shows the base peak at 98 (100%), which indicates the presence of dimethyl ester. This establishes the position of the double bond between C-9 and C-19. The catalytic hydrogenation of the methyl ester of compound **1** with PtO_2 resulted in formation of 16-methyl methylnonadecanoate **1***a*. From all these data it was concluded that this new fatty acid **1** is 16-methyl-9*E*-nonadecenoic acid.

Compound **2** is an oil with molecular formula $C_{20}H_{36}O_2$. An FT-IR spectrum contained broad absorption bands at 3310 cm^{-1} (-OH stretch) and 1710 cm^{-1} (-C=O). The ^{1}H NMR resonances at 11.60 (s, H, -COO*H*) as well as ^{13}C NMR signals at 180.1 (C-1) and 34.1 (C-2) indicate the presence of a -COOH group (8). The terminal acid group was also determined with the help of fragmentation patterns at 291 [M–17] and 264 [M – 44] (9). The ^{1}H NMR resonances at 5.32 (m, 4H, J = 10.2 Hz, -CH=) indicate the presence of two double bonds. Normally for *Z* isomers the range of J values is 6.0–12 Hz, but we have observed that the coupling constant of both the double bonds is 10.2 Hz, which indicates *Z,Z* isomers. The presence of two unsaturations in compound **2** was supported by the DEPT ^{13}C NMR (6), which gave four upfield signals at 129.30, 129.45, 130.22, and 130.35, indicating that double bonds are present between C-10 and C-11 and between C-14 and C-15. Compound **2** was reported previously as a principal component of corn oil, but without stereochemistry (15). The *cis* unsaturation of both the double bonds was confirmed in our study with the help of ^{13}C NMR, which shows a range of values between 27.2 and 27.5 for the neighboring carbons 9, 12, 13, and 16 (11).

Scheme 1

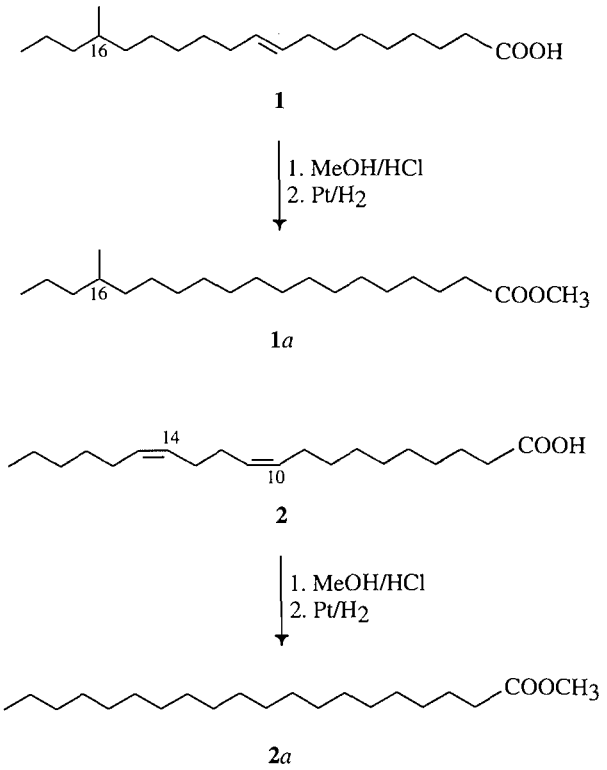

The lack of branching was confirmed by ^{1}H NMR. A triplet appeared for 3*H* at 0.8 ppm (J = 6.0 Hz) and DEPT ^{13}C NMR: 14.1 ppm (C-20) with an upfield shift indicating the presence of a terminal methyl group in the chain. Oxidation of compound **2** was done by Lemieux–von Rudloff's reagent (14) to establish the position of the double bonds. A mixture of three short-chain dimethyl esters was obtained, one of which was the dimethyl ester of succinic acid. Production of this ester indicates the presence of two -CH_2 groups between the two double bonds in the fatty acid **2**. The second dimethyl ester was decane-1,10-dioic acid dimethyl ester, whose formation located the position of the first double bond at Δ^{10}. The third ester was methyl hexanoate, whose formation indicated the position of a second double bond at Δ^{14}. On the basis of these data, compound **2** is *Z,Z*-10,14-eicosadienoic acid. Upon catalytic hydrogenation using PtO_2, the methyl ester derivative of this acid (2) gave eicosanoic acid methyl ester **2***a*. The ^{1}H NMR showed resonance at 3.6 ppm (s, 3H, -COOCH_3) and ^{13}C NMR signals were at 51.40 (-COOCH_3) and 174.45 (-$COOCH_3$).

Experimental

General experimental procedures

Proton nuclear magnetic resonance (^{1}H NMR) and ^{13}C (APT

Can. J. Chem. Downloaded from www.nrcresearchpress.com by 65.111.164.53 on 09/08/12
For personal use only.

and DEPT) spectra were recorded using $CDCl_3$ as solvent on a 200 MHz Varian XL-200 spectrometer with tetramethylsilane (TMS) as internal standard. All chemical shifts were recorded in ppm downfield from TMS. All infrared spectra were recorded on films using a Bruker FT-IR instrument with IBM FT-IR/32 software; intensities of all the bands are stated in cm^{-1}. UV spectra were obtained using $CHCl_3$ as solvent on a Shimadzu UV/VIS-160 spectrophotometer. Gas chromatographic (GC) analysis was carried out on a Varian 3400 GC fitted with a 10 m microbore glass column (0.53 mm diameter, 2.65 μm film thickness SE-30 stationary phase), using nitrogen (20 mL/min) as the carrier gas under temperature-programmed conditions (initial temperature of 140°C, final temperature 250°C, rate 5°C/min) or isothermally (200°C) and a flame ionization detector. For GC–MS analysis, gas chromatography on a Varian 3400 GC coupled with a MS Finnigan MAT-8230 mass spectrometer, with a mass selective detector fitted with a 12 m capillary glass column (0.2 mm internal diameter, 0.33 μm film thickness, cross-linked methyl silicone gum), and helium (ca. 2 mL/min) as a carrier gas were used under temperature-programmed conditions (initial temperature 140°C, final temperature 240°C, rate 5°C/min). Thin-layer chromatography (TLC) was performed on microscope glass plates coated with silica (about 0.1 mm thickness). A mixture of *n*-hexane–chloroform and *n*-hexane – ethyl acetate in various concentrations was used as developer. Preparative TLC was carried out on Kieselgel 60 F_{254} plastic sheets (Merck) coated with silica. Column chromatography was performed on Baker 60–200 mesh silica gel using gradient elution of mixtures of *n*-hexane–chloroform for compound **1** and *n*-hexane – ethyl acetate for compound **2**. Collected fractions were checked by TLC before pooling. Dimethyl succinate, methyl caproate, dimethyl azelate, and dimethyl sebacate acid (Aldrich Chemicals) were used as standards.

Growth of the fungi and extraction of free fatty acids

Voucher cultures are maintained in the Patent Depository at the American Type Culture Collection (ATCC), Rockville, Maryland, as ATCC 64874 (*S. flocculosa*) and ATCC 64875 (*S.rugulosa*). The fungi were grown on yeast–malt–potato–dextrose (0.5:1.0:2.0) broth (7) in 10 250-mL cotton-plugged Erlenmeyer flasks each containing 100 mL of broth. The mycelium from 28-day-old static liquid cultures grown at 23°C in the dark was filtered through a Buchner funnel using Whatman filter paper no. 2 to remove the mat. Remaining spores were removed by millipore filtration (0.22 μm) and then the cell-free filtrate was extracted seven times with $CHCl_3$ in a separatory funnel. The extracts were combined and dried over anhydrous Na_2SO_4 (1.89 g). Further purification was done by column chromatography on silica gel (60–200 mesh) using a procedure similar to that of Privett et al. (16). The two new fatty acids were investigated by preparative TLC using $CHCl_3$–hexane (3:7) as eluting solvent for compound **1** (yield 75 mg, 3.968%) and hexane–EtOAc (1:4) as eluting solvent for compound **2** (yield 82 mg, 4.33%).

*Compound **1** (oil)*: IR ν_{max}: 3300, 1710, 1660, 1410, and 920 cm^{-1}. ^1H NMR: 11.65 (s, 1H, COO*H*), 5.30 (5, 2H, J = 17.1 Hz, C*H*=), 2.3 (t, 2H, J = 6.5 Hz, CH_2COOH), 1.2–1.5 (m, 27H, CH_2), 1.15 (5, 3H, J = 6.3, CH_3, br), and 0.9 (t, 3H, J = 6 Hz, CH_3). ^{13}C NMR: 14.5 (C-19), 19.8 (C-20), 20.8 (C-18), 24.8 (C-3), 26.9 (C-14), 29.2 (C-6), 29.4 (C-5), 29.5 (C-4, 12), 29.6 (C-7), 29.8 (C-13), 32.2 (C-16), 32.60 (C-8), 32.65 (C-11), 34.1 (C-2), 36.5 (C-15), 38.7 (C-17), 130.35 (C-9), 130.45 (C-10), and 180.0 (C-1). HRFABMS *m/z* $\{M\}^+$ 310.2870 ($C_{20}H_{38}O_2$ requires 310.2871). EIMS, *m/z* $\{M^+\}$: 310(14), 295(22), 293(57), 281(17), 267(36), 266(28), 252(8), 250(10), 239(42), 236(40), 225(25), 222(47), 211(52), 209(38), 197(65), 195(55), 183(82), 181(75), 169(32), 167(30), 156(44), 154(32), 143(62), 141(15), 129(20), 127(34), 115(72), 112(56), 101(80), 98(76), 87(78), 74(100), 59(68), and 56(49).

*Compound **2** (oil)*: IR ν_{max}: 3300, 2650, 1710, 1665, 1412, 1230, and 920 cm^{-1}. ^1H NMR: 11.60 (s, H, COO*H*), 5.32 (m, 4H, J = 10.2 Hz, C*H*=), 2.3 (t, 2H, J = 6.8 Hz, CH_2COOH), 1.2–1.5 (m, 26H, CH_2), and 0.8 (t, 3H, J = 6 Hz, CH_3,). ^{13}C NMR: 14.1 (C-20), 22.7 (C-19), 24.9 (C-3), 29.4 (C-17), 27.3 (C-9), 27.45 (C-12), 27.5 (C-13), 27.2 (C-16), 29.2–29.8 (C-4–C-9), 31.6 (C-18), 34.1 (C-2), 129.30 (C-11), 129.45 (C-14), 130.20 (C-15), 130.35 (C-10), and 180.1 (C-1). HRFABMS *m/z* $\{M\}^+$ 308.2712, ($C_{20}H_{36}O_2$ requires 308.2715). EIMS, *m/z* $\{M^+\}$: 308(45), 293(24), 291(13), 264(42), 250(48), 236(20), 224(15), 220(18), 211(52), 207(38), 197(40), 194(42), 183(26), 179(41), 170(44), 165(70), 157(53), 151(68), 143(62), 138(27), 129(18), 125(56), 115(35), 111(74), 101(64), 98(72), 87(58), 84(34), 74(100), 60(77), and 57(60).

*16-Methyl-9*E*-nonadecenoic acid methyl ester*

A solution of **1** (31.0 mg, 0.01 mmol) in 10 mL of methanolic HCl was boiled under reflux for 60 min (17). The solvent was removed under reduced pressure and the pure methyl ester was obtained by column chromatography, using *n*-hexane and ethyl acetate (1:1) (25.0 mg, 77.1%). IR ν_{max}: 3010, 1725, 1680, 1375, and 996 cm^{-1}; ^1H NMR: 5.30(t, J = 17.2 Hz, 2H), 3.60(s, 3H), 2.33(t, J = 7 Hz, 2H), 1.3–1.5 (m, 27H), and 0.92(t, J = 6 Hz, 6H). HRFABMS *m/z* (rel. int.) $\{M\}^+$ 324.3019 ($C_{21}H_{40}O_2$ requires 324.3028). EIMS, *m/z* $\{M\}^+$: 324(6), 309(12), 306(24), 295(54), 293(22), 292(30), 281(58), 265(5), 253(60), 250(54), 240(32), 238(28), 225(57), 222(40), 211(46), 208(66), 196(25), 183(40), 181(76), 170(24), 168(35), 156(45), 153(52), 142(58), 141(85), 129(15), 127(77), 115(40), 113(68), 101(50), 98(44), 87(56), 84(70), 74(100), 59(80), and 43(52).

*16-Methyl methylnonadecanoate **1**a*

A catalytic amount of PtO_2 in MeOH was stirred in a stream of hydrogen. The methyl ester of compound **1** (32.4 mg, 0.01 mmol) was dissolved in MeOH (10 mL) and added to the reaction mixture. After 1 h this was filtered and evaporation of solvent gave 31.2 mg (95.75%) of pure compound **1***a*. IR ν_{max}: 2960, 1740, 1460, and 1340 cm^{-1}. ^1H NMR: 0.9 (m, 6H, CH_3), 1.2–1.8 (m, 31H, CH_2), 2.3 (t, *J = 6.1 Hz, 2H,* CH_2COOCH_3), and 3.66 (s, 3H, COOCH_3). ^{13}C NMR: 14.4 (C-19), 19.3 (C-20), 20.6 (C-18), 25.0 (C-3), 26.8 (C-14), 29.2–29.8 (C-4–C-13), 32.3 (C-16), 34.2 (C-2), 36.4 (C-15), 38.7 (C-17), 51.40 (OCH_3), and 174.35 (C-1). HRFABMS *m/z* (rel.int.) $\{M\}^+$ 326.3185 ($C_{21}H_{42}O_2$ requires 326.3184). EIMS, *m/z* $\{M\}^+$: 326(10), 311(32), 297(31), 295(12), 282(50), 269(5), 255(42), 253(30), 251(52), 241(42), 233(38), 227(20), 213(19), 199(15), 185(60), 171(45), 157(35), 143(32), 129(18), 115(24), 101(55), 87(80), 74(100), 71(86), 59(72), and 43(54).

Can. J. Chem. Downloaded from www.nrcresearchpress.com by 65.111.164.53 on 09/08/12
For personal use only.

(Z,Z)-10,14-Eicosadienoic acid methyl ester
A solution of **2** (30.8 mg, 0.01 mmol) in 10 mL of methanolic HCl was boiled under reflux for 60 min (17). The solvent was removed under reduced pressure and the pure methyl ester was obtained by column chromatography using *n*-hexane and ethyl acetate (1:2) (26.5 mg, 82.8%). IR ν_{max}: 2980, 2820, 1735, 1450, 1154, and 998 cm^{-1}. ^1H NMR: 5.34 (m, J = 10 Hz, 4H), 3.68 (s, 3H), 2.33 (t, J = 6.5 Hz, 2H), 1.3–1.5 (m, 26H), and 0.9 (t, J = 6 Hz, 3H). HRFABMS *m/z* (rel.int.) $\{M\}^+$ 322.2869 ($C_{21}H_{38}O_2$ requires 322.2871). EIMS, *m/z* $\{M\}^+$: 322(5), 307(10), 293(2.4), 291(8), 280(30), 265(27), 263(42), 251(39), 250(57), 249(40), 238(31), 235(23), 225(29), 221(44), 206(47), 197(28), 192(25), 184(15), 179(6), 172(46), 166(16), 157(16), 152(18), 142(28), 138(54), 130(32), 125(20), 115(40), 112(35), 101(74), 97(45), 88(58), 84(60), 74(100), 71(90), 59(85), 57(78), and 43(82).

Methyl eicosanoate **2**a
Compound **2** (32.2 mg, 0.01 mmol) was dissolved in MeOH (10 mL) and added to a catalytic amount of PtO_2 in MeOH and stirred in a stream of hydrogen for 1 h. The suspension was filtered and solvent was removed under reduced pressure to give **2***a* (29.7 mg, 91.1%). IR ν_{max}: 1740 and 1460 cm^{-1}. ^1H NMR: 0.8 (t, J = 6 Hz, 3H, CH_3), 1.2–1.8 (m, 34H, CH_2), 2.3 (t, J = 6.9 Hz, 2H, CH_2COOCH_3), and 3.6 (s, 3H, $COOCH_3$). ^{13}C NMR: 14.1 (C-20), 23.3 (C-19), 29.2–29.8 (C-3–C-17), 32.8 (C-18), 34.2 (C-2), 51.40 (OCH_3), and 174.45 (C-1). HRFABMS *m/z* (rel.int.) $\{M\}^+$ 326.3179 ($C_{21}H_{42}O_2$ requires 326.3184). EIMS, *m/z* $\{M\}^+$: 326(35), 311(20), 283(15), 255(6), 227(12), 198(42), 171(22), 143(8), 115(24), 87(38), 74(100), and 59(66).

Lemieux–von Rudloff oxidation
To establish the position of the double bonds a modified Lemieux–von Rudloff oxidation (14) was performed on the methyl esters. A stock oxidant solution of sodium metaperiodate (2.09 g) and $KMnO_4$ (0.04 g) in water (100 mL) was prepared. This solution (1 mL) together with K_2CO_3 solution (1 mL; 2.5 g/L) was added to the methyl ester (1 mg) in *t*-BuOH (1 mL) in a test tube and the mixture was shaken thoroughly at room temperature for 1 h. At the end of this time, the solution was acidified with one drop of concentrated sulphuric acid, and excess oxidant was destroyed with $NaHSO_3$. The solution was extracted with diethyl ether (3 × 4 mL). The organic layer was dried over sodium sulphate and removed in a stream of nitrogen at room temperature. The products were methylated with 1.2 N HCl/MeOH for GC–MS analysis. The oxidative compounds obtained from compound **1** are nonanedioic acid dimethyl ester (azelaic acid dimethyl ester) and 7-methyl methyldecanoate. Decane-1, 10-dioic acid dimethyl ester (sebacic acid dimethyl ester), succinic acid dimethyl ester, and methyl hexanoate (methyl caproate) are the oxidative products of compound **2**. The spectroscopic data were compared with authentic samples supplied by Aldrich Chemicals. The following MS data were collected for the oxidative compounds.

7-Methyl methyldecanoate: m/e (rel.int %): 200(44), 169(20), 157(30), 156(40), 143(7), 141(72), 129(45), 125(32), 107(22), 115(12), 101(25), 87(35), 74(100), and 59(42).

Dimethylazelate: m/e (rel.int %): 216(54), 185(32), 152(24), 143(55), 124(72), 111(60), 98(100), 92(42), 84(38), 73(40), 64(50), 55(35), and 41(22).

Dimethyl sebacate: m/e (rel.int %): 230(50), 199(34), 166(45), 157(62), 138(55), 124(40), 106(58), 98(100), 92(65), 73(44), 64(33), 55(28), and 41(60).

Dimethyl succinate: m/e (rel.int %): 146(65), 115(32), 98(100), 91(72), 86(54), 83(48), 73(40), 55(35), 63(58), and 60(54).

Methyl caproate: m/e (rel.int %): 130(35), 129(72), 115(45), 101(32), 99(62), 87(54), 74(100), 71(58), and 59(66).

Acknowledgements

We thank Mrs. Dorothy Drew for bibliographic assistance. This work was supported by operational (J.A.T.) and university–industry (J.A.T. and W.R.J.) grants from the Natural Sciences and Engineering Research Council of Canada.

References

1. J.D. Weete. Lipid biochemistry of fungi and other organisms. Plenum Press, New York. 1980.
2. C.W. Moss, T. Shinoda, and J.W. Samuels. J. Clin. Microbiol. **16**, 1073 (1982).
3. W.B.Turner and D.C. Aldridge, Fungal metabolites II. Academic Press, London. 1983. p. 124.
4. Y. Dalpé and P. Neumann. Eur. J. For. Pathol. **6**, 335 (1976).
5. P.S. Dyer, D.S. Ingram, and K. Johnston. Mycol. Res. **97**, 485 (1993).
6. H. Koshino, S. Togiya, T. Yoshihara, and S. Sakamura. Tetrahedron Lett. **28**, 73 (1987).
7. S.R. Choudhury, J.A. Traquair, and W.R. Jarvis. J. Nat. Prod. **57**, 700 (1994).
8. J.B. Stothers. Carbon-13 NMR spectroscopy. Academic Press, New York. 1972. p. 147.
9. G. Odham and E. Stenhagen. *In* Biochemical applications of mass spectrometry. *Edited by* G.R. Waller. Wiley–Interscience, New York. 1972.
10. R.M. Silverstein, G. Clayton Bassler, and T.C. Morrill. Spectrometric identification of organic compounds. 5th ed. Wiley–Interscience, New York. 1991. p. 221.
11. J. Bus, I. Sies, and M.S.F. Lie Ken Jie. Chem. Phys. Lipids, **17**, 501 (1976).
12. S.L. Patt and J.N. Shoolery. J. Magn. Reson. **46**, 539 (1982).
13. M.S.F. Lie Ken Jie and D.W.Y. Leung. Lipids, **25**, 1 (1990).
14. R.U. Lemieux and E. von Rudloff. Can. J. Chem. **33**, 1701 (1955).
15. R.T. Holman, F. Pusch, B. Svingen, and H.J. Dutton. Proc. Natl. Acad. Sci. U.S.A. **88**, 4830 (1991).
16. O.S. Privett, K.A. Dougherty, W.L. Erdahl, and A. Stolyhwo. J. Am. Oil Chem. Soc. **50**, 516 (1973).
17. J.P. Carreau and J.P. Dubacq. J. Chromatogr. **151**, 384 (1978).

On the purported axial preference in 2-methylthio and 2-methoxycyclohexanones: steric effects versus orbital interactions

Robert R. Fraser and Neil C. Faibish

Can. J. Chem. Downloaded from www.nrcresearchpress.com by 65.111.164.53 on 09/08/12
For personal use only.

Abstract: The value for the equilibrium constant representing the ratio of equatorial to axial conformers for 2-methylthio- and 2-methoxycyclohexanone has been measured in five solvents using 500 MHz ^{1}H nuclear magnetic resonance. In cyclohexane solvent, the methylthio group is found to have a large axial preference while that for the methoxy is negligible. For both compounds the equilibrium shows a strong solvent dependence. Comparison of these results with those known for the halo derivatives shows the amount of axial to increase in the order: fluoro, methoxy, chloro, bromo, and methylthio. With the aid of molecular mechanics calculations it is concluded that the order of conformational preference can be attributed to a variation in the van der Waals interaction between the substituent and the carbonyl group in the equatorial conformer.

Key words: α-substituted cyclohexanones, conformation, MMX calculations, steric and dipolar effects.

Résumé : Utilisant la résonance magnétique nucléaire du ^{1}H à 500 MHz et opérant dans cinq solvants, on a mesuré la valeur de la constante d'équilibre représentant le rapport des conformères équatorial et axial des 2-méthylthio- et 2-méthoxycyclohexanones. Dans le cyclohexane comme solvant, on trouve que le groupe méthylthio a une préférence axiale alors que celle du groupe méthoxy est négligeable. Pour les deux composés, l'équilibre dépend fortement du solvant. Une comparaison de ces résultats avec ceux connus pour les dérivés halogénés montre que la quantité de conformère axial augmente dans l'ordre : fluoro, méthoxy, chloro, bromo et méthylthio. En se basant sur des calculs de mécanique moléculaire, on conclut que l'ordre de préférences conformationnelles peut être attribué à une variation de l'interaction de van der Waals entre le substituant et le groupe carbonyle du conformère équatorial.

Mots clés : cyclohexanones α-substituées, conformation, calculs MMX, effets stériques et dipolaires.

[Traduit par la rédaction]

In the course of studies on the effects of α substituents on the rates of nucleophilic addition to a carbonyl group, we have made use of the conformationally fixed biaryl ketone, **1**(R = H), and a number of its derivatives (1). Each derivative consisted of two diastereomers whose relative stabilities varied widely. For the fluoro derivative, **1**(R = F) the equatorial isomer was strongly favored, while for the methylthio derivative, **1**(R = SCH_3) the axial isomer was the dominant component of an equilibrated mixture. To aid our understanding of the relative stabilities of these stereoisomers we sought, for comparison, the pertinent literature data on 2-substituted cyclohexanones. The latter compounds are conformational isomers that interconvert rapidly at room temperature as shown in equilibrium [1].

The conformations of cyclohexanones bearing a halogen substituent at the α carbon have been extensively studied (2). Infrared, dipole moment (3), and ^{1}Hmr (4) measurements all

[1] 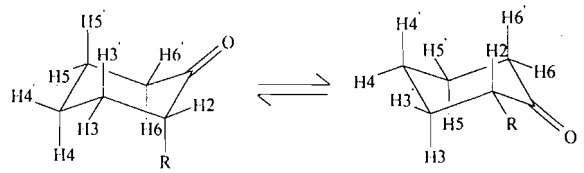

showed the bromo and chloro derivatives to exist mainly in the axial conformation in hydrocarbon solvent, with fluoro having no preference. In solvents of increasing polarity the proportion of equatorial increased, becoming dominant for the chloro and fluoro derivatives in acetonitrile (4). Three main factors, steric, dipole–dipole, and orbital interactions, have been proposed (2) to account for these changes in equilibrium [1] with structure and solvent.

For 2-methoxycyclohexanone the axial conformation seems to have earned a reputation for being dominant (2, 5–7), although there is but one piece of experimental evidence to that effect. Cantacuzene and Tordeux (8), using 60 MHz ^{1}Hmr, found 63% of the axial form in carbon tetrachloride, and 16% in acetonitrile. An earlier report described it as being mainly axial, regardless of solvent, although experimental details were not provided (9). However, considerable evidence from equilibration of diastereoisomers indicates an equatorial preference

Received July 11, 1994.

R.R. Fraser[1] **and N.C. Faibish.** Department of Chemistry, University of Ottawa, Ottawa, ON K1N 6N5, Canada.

[1] Author to whom correspondence may be addressed.

Can. J. Chem. Downloaded from www.nrcresearchpress.com by 65.111.164.53 on 09/08/12
For personal use only.

Fig. 1. The 500 MHz ^{1}Hmr spectrum of 2-methylthiocyclohexanone in $CDCl_3$. The insert shows an expansion of the octet for H6 at δ 2.94. The derived spectral parameters appear in Table 5.

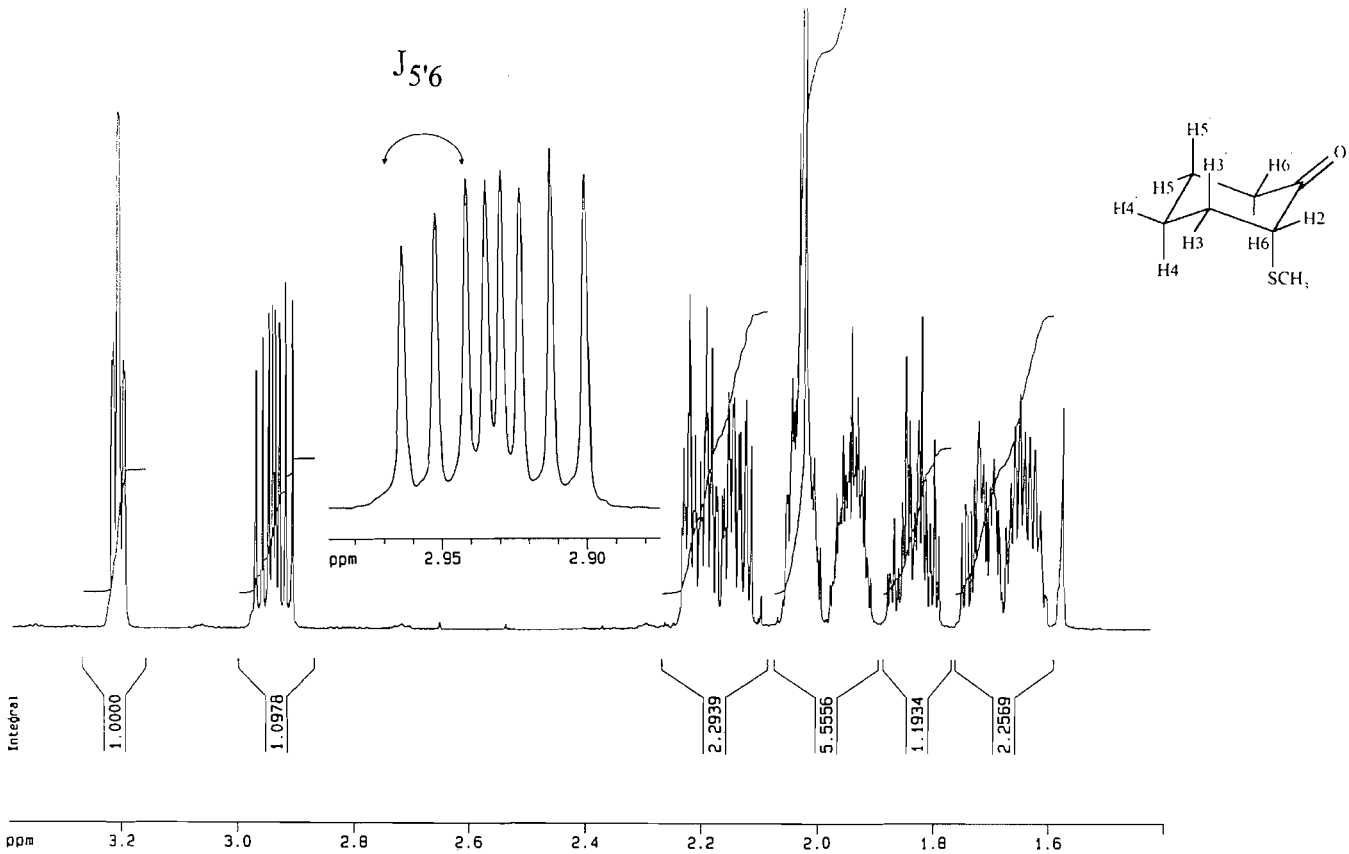

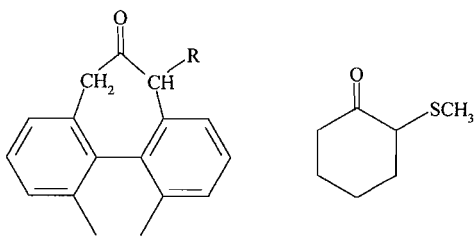

1

2

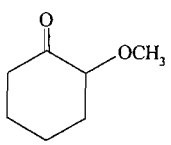

3

in polar solvents (10–12). And, very recently, a thorough study of this compound in deuterochloroform, using five separate nmr parameters for comparative assessment, reported it to be 28 ± 5% axial (13). In the same paper using the same criteria, 2-methylthiocyclohexanone was found to be 85% axial in deuterochloroform (13). Earlier, it has been estimated from infrared measurements (14) to contain 70% axial in carbon tetrachloride. In an independent study, equilibration of the 2-methylthio derivative of 4-*tert*-butylcyclohexanone in methanol was also reported to give 70% axial (15*a*).[2] To clarify the above inconsistencies we have determined the position of equilibrium [1] for both 2-methylthiocyclohexanone **2** and 2-methoxycyclohexanone **3** in five solvents from polar to nonpolar in character. Using 500 MHz ^{1}Hmr, the percent of axial methylthio conformer was found to vary from 94% in cyclohexane to 59% in acetonitrile. For methoxyl the range in percent axial was from 57 to 20. These results, combined with previous literature data on the halogens, offer further insight regarding the factors affecting K_{eq}.

Previous determinations of the conformational equilibrium [1] for cyclohexanones by ^{1}Hmr measurements relied upon either the chemical shift parameter (4) or the spin–spin splitting of the methine proton at C2 (4, 8). The latter method used the magnitude of the half bandwidth relative to that observed in model compounds to assess the proportion of equatorial conformer. When possible, direct measurement of a single coupling constant, (i.e., $J_{5',6}$), which represents a weighted average of the two conformations as in eq. [2], should provide

[2] For studies on the phenoxy, phenylthio, and phenylseleno derivatives, see refs. 15*b* and 15*c*.

Can. J. Chem. Downloaded from www.nrcresearchpress.com by 65.111.164.53 on 09/08/12
For personal use only.

Table 1. Equilibrium data for **2**.

Solvent	J_{obs} (Hz)	n_a	K	ΔG (kcal/mol)
C_6D_{12}	13.0	0.94	0.064	1.6
CCl_4	12.7	0.91	0.099	1.4
$CDCl_3$	11.2	0.78	0.28	0.7
CD_3COCD_3	9.9	0.67	0.5	0.4
CD_3CN	9.0	0.59	0.71	0.2

a more accurate evaluation of the mole fractions n_e, n_a and their ratio $n_e/n_a = K_{eq}$ (16).

[2] $J_{obs} = n_a J_{aa} + n_e J_{ee}$

The 500 MHz spectrum of **2** in $CDCl_3$ appears in Fig. 1. In the inset the protons are labeled to indicate their *cis* or *trans* (H′) relation to the *S*-methyl group. It is a first-order spectrum in that all nine ring protons are free from overlap with their neighbors.[3] The proton assignments were unambiguously determined by proton COSY and HMQC spectra. The triplet at δ 3.23 represents the methine proton at C2 whose small vicinal splitting clearly indicates its predominantly equatorial orientation. The predominantly axial proton at C6, δ 2.94, is strongly deshielded, in all likelihood by the axial *S*-methyl group (6) at C2. Its appearance as an octet provides values for the geminal coupling constant, $J_{6,6'}$, and the two vicinal couplings, $J_{5,6}$ and $J_{5',6}$. In the above spectrum we find J_{obs} for $J_{5',6} = 11.2$, which with the use of eq. [2] provides a value of 0.78 for n_a and thereby of 0.28 for K_{eq} in equilibrium [1]. In this calculation the values $J_{aa} = 13.7$ and $J_{ee} = 2.2$ were used for the purely diaxial and diequatorial coupling constants, as obtained from the splitting observed for the α protons in the spectrum of 4-*tert*-butylcyclohexanone.[4] These values are consistent with earlier measurements reported for cyclohexanone (17). In this way the values for J_{obs} were determined in five solvents, providing the data in Table 1 for equilibrium [1]. In carbon tetrachloride, 2-methylthiocyclohexanone shows a stronger bias towards the axial isomer than estimated by infrared (14). In deuterochloroform, our result agrees within experimental error with that reported by Basso et al. (13). The conformation changes markedly with increasing solvent polarity, from 94% axial in perdeuterated cyclohexane to 59% axial in the most polar solvent, acetonitrile. This solvent effect is very similar to that observed previously for the halo derivatives (3, 4). What is unique for the thiomethyl group is the magnitude of its axial preference, greater than that for any other heteroatom substituent.

[3] Using the program PCPMR (Serena Software, Box 3076, Bloomington, IN 47402), spectral simulation of the proton absorption in **2** using the observed splittings reproduced the experimental line positions to within 0.1 Hz.

[4] As described in the experimental, values for these two coupling constants were confirmed by simulation. By observing the sensitivity of the simulated spectra to the variations in input parameters we can estimate them to be reliable to within 0.2 Hz. As a result, eq. [2] should provide values for n_a accurate to ±0.02 in the middle of its range and to ±0.04 at either end of the range. ΔG will have consequent error limits of 0.1–0.4 kcal/mol.

Table 2. Equilibrium data for **3**.

Solvent	J_{obs} (Hz)	n_a	K	ΔG (kcal/mol)
C_6D_{12}	6.7	0.57(0.55)[a]	0.75	0.2
CCl_4	7.3	0.51(0.50)	0.96	0.0
$CDCl_3$	10.0	0.22(0.19)	3.5	−0.7
CD_3COCD_3	9.8	0.24	3.2	−0.7
CD_3CN	10.5	0.16	5.3	−1.0

[a]Values in parentheses were determined from $J_{5'6}$.

In assessing the position of the conformational equilibrium for 2-methoxycyclohexanone **3** it was not always possible to use the splittings in the absorption patterns for the protons at C6 due to overlapping shifts. To obtain a consistent set of data we used the splitting between the methine proton at C2 and the *trans* proton at C3 as J_{obs}. For this interaction it was necessary to modify the values for J_{aa} and J_{ee} to include the electronegativity effect of the methoxyl (18). Accordingly, the value for J_{aa} was reduced to 12.0 Hz and that for J_{ee} raised to 2.7 Hz. Application of eq. [2] led to the values appearing in Table 2. These results, in contrast to earlier assertions (2, 5–7, 9), show no axial preference for the methoxy substituent except in the least polar solvent, cyclohexane-d_{12}.

Factors affecting the conformational equilibrium [1]

Previous studies toward the understanding of substituent effects on this equilibrium have considered a variety of factors to explain the results (2). They can be divided into three main categories. The first of these, steric in nature, includes torsional and van der Waals interactions. In simple cyclohexanes, torsional effects are responsible for the increasing stability of the equatorial conformer in the series methyl, ethyl, and isopropyl for which the values of ΔG_{ea} are 1.7, 1.8, and 2.1 (19). However, in cyclohexanones there is an added steric factor, the 2-alkyl ketone effect, which favors the axial isomer. Its contribution to ΔG_{ea} is estimated at 0 for methyl, 1.0 for ethyl, and 1.7 kcal/mol for isopropyl (20). This trend has been explained by a repulsive interaction between the lone pair on the oxygen and the α substituent (a type of $A^{1,3}$ strain (21)). A second factor of importance is the greater repulsive interaction between the two dipoles in the equatorial conformer (22) that is diminished as the dielectric constant of the solvent increases. The third factor, a two-electron attractive orbital interaction involving either σ–π^* or n–π^* donation in the axial conformer, has frequently been cited to explain its unexpected stability. Orbital energies are expected to be more strongly influenced by the latter interaction (23).

To assess the relative importance of these factors, Table 3 presents data for the measurements in carbon tetrachloride and acetonitrile, the two solvents that are common to all present and previous ^{1}Hmr studies. For the sake of completeness, data on the phenoxy, phenylthio, and phenylseleno substituents (15*b*, 15*c*) are included. In carbon tetrachloride solution, the individual substituents exhibit conformational preferences from mainly axial (Br and SMe) to mainly equatorial (F). All show an appreciable increase in the amount of equatorial in acetonitrile. Calculations have shown (3, 4, 24) that the difference in dipole–dipole interactions for the two conformers is

Table 3. Solvent effects on 2-substituted cyclohexanones.

	% Axial		ΔG_{ea}		
Substituent	CCl_4	CH_3CN	CCl_4	CH_3CN	$\Delta\Delta G_{ea}$
F	36	13 (ref. 4)	−0.3	−1.1	0.8(1.4)[a]
Cl	72	35 (ref. 4)	0.6	−0.4	1.0(0.9)
Br	86	50 (ref. 4)	1.1	0.0	1.1(0.8)
OCH_3	51	16 (this work)	0.0	−1.0	1.0(0.9)
SCH_3	91	59 (this work)	1.4	0.2	1.2(1.1)
OC_6H_5	46	21 (ref. 15*b*)	−0.1	−0.8	0.7
SC_6H_5	72	47 (ref. 15*b*)	0.55	−0.1	0.65
SeC_6H_5	73	49 (ref. 15*b*)	0.6	0.0	0.60

[a]Numbers in parentheses calculated by MMX represent $\Delta\Delta E_T$.

effectively nullified by the change in dielectric constant of the solvent from 2.2 for carbon tetrachloride to 37.5 for acetonitrile. The magnitude of the dipole–dipole interaction energy can be estimated from the change in ΔG_{ea}, the conformational free energy difference, from solvent to solvent. This change, $\Delta\Delta G_{ea}$ appears in the last column. It is quite similar for most substituents and is a qualitative reflection of the group dipole moment of the substituent. Without the influence of dipole–dipole interactions, the data in acetonitrile (see column 2) represent equilibria that should reflect the influence of steric and orbital interactions only. To further probe the nature of these factors we carried out molecular mechanics calculations using the MMX program (25).[5]

Calculation of conformational energy differences using MMX

We have calculated the energies of the axial and equatorial conformers of methylthio-, methoxy-, bromo-, chloro-, and fluorocyclohexanone for media of dielectric constant 2.2 (carbon tetrachloride) and 37.5 (acetonitrile). The results appear in Table 4. In all cases the dipole/charge term[6] substantially favors the axial conformer in carbon tetrachloride, but has a negligible effect in acetonitrile, as was reported previously (3, 4, 24). For three of the substituents the calculated energy differences for ΔE_T are in reasonable agreement with experiment, overestimating ΔE by up to 0.7 kcal/mol. For the methoxyl and fluoro derivatives MMX gives poor results, the discrepancy with experiment averaging 2 kcal/mol. In all likelihood the torsional contributions to ΔE_T are the main source of error. Very recently it was concluded, on the basis of ab initio calculations and supporting infrared data, that the torsional parameters for the CCCO and CCCF fragments originally derived from the *A* values of cyclohexanes for use in MM2 need to be revised (26). What is impressive is the agreement obtained between the value for $\Delta\Delta E_T$ calculated for equilibrium [1] in CCl_4 and CD_3CN and that observed experimentally as $\Delta\Delta G$. This comparison appears in the last column of Table 3.

As previously suggested and confirmed by the above calculations, the percent axial conformer in acetonitrile will be free from the influence of dipole–dipole interactions. As seen in column 2 of Table 3 the amount of axial conformer increases in the order F, OCH_3, Cl, Br, SCH_3. Two aspects of this order require explaining: the large preference of fluorine for the equatorial position and the order of substituent preference. The preference shown by fluorocyclohexanone should be regarded as an intrinsic property of this ketone. There is no reason to anticipate its conformation based on the behavior of cyclohexanes. In more specific terms, we lack the model data from which to estimate the torsional parameter for a CC(O)CF fragment. We can only offer the observation that a stable conformation with bonds having electronegative substituents synperiplanar has precedence in olefins bearing vicinal halogens or methoxyl groups (27).

The increase in axial from 13% for F to 59% for SCH_3 represents a change in ΔG_{ea} of 1.3 kcal/mol. Qualitatively, this increase can be attributed to a change in the nonbonded interaction between the lone pair of electrons of the carbonyl oxygen and the equatorial substituent.[7] A numerical estimate is available from the difference in the van der Waals terms for the two conformers as calculated by MMX. In Table 4 this term changes by 0.9 kcal/mol from attractive, 0.3 for fluorine, to repulsive, 0.6 for the methylthio substituent. Clearly, the experimentally observed variation of 1.3 ± 0.4 kcal/mol can be accounted for entirely by the variation in van der Waals interactions. Consequently, consideration of an n–σ^* orbital interaction appears unnecessary. These conclusions regarding the relative importance of nonbonded interactions can be expected to apply to the derivatives of **1** (1).

Experimental

All spectra were measured using a Bruker AMX500 and an inverse detection probe with homogeneity optimized to give resolution to 0.4 Hz or less. Digital resolution of better than 0.1 Hz was used throughout. The ^1H–^1H COSY and HMQC spectra were obtained using the Bruker software. Deuterochloroform (99.96%) and acetone-d_6 (99.9%) were obtained from Merck, Sharp and Dohme. Acetonitrile (99.5%) was

[5] The MMX program, as part of PCMODEL, is available from Serena Software, Box 3076, Bloomington, IN.

[6] The MMX program calculates the dipole–dipole and other electrostatic interactions using the point-charge distributions obtained from MMPI and bond dipole moments as described in ref. 25.

[7] Evidence in support of such a steric effect has been reported in 2-alkoxycyclohexanones (8), where the percent of axial conformation was found to increase with the size of the alkoxy group.

Can. J. Chem. Downloaded from www.nrcresearchpress.com by 65.111.164.53 on 09/08/12
For personal use only.

Can. J. Chem. Downloaded from www.nrcresearchpress.com by 65.111.164.53 on 09/08/12
For personal use only.

Table 4. MMX calculations of steric energies.

	S^a	B	S–B	T	V	D/C	E_T	ΔE_T	(ΔG_{ea})
					X = SCH_3				
ε = 2.2									
Axial	0.34	0.88	0.11	4.20	2.48	−1.67	6.34	1.83	(1.4)
Equatorial	0.39	1.13	0.11	4.33	3.12	−0.91	8.17		
ε = 37.5									
Axial	0.36	0.89	0.12	4.19	2.44	−0.10	7.90	0.70[b]	(0.2)
Equatorial	0.40	1.07	0.11	4.38	3.09	−0.05	9.00		
					X = OCH_3				
ε = 2.2									
Axial	0.57	1.60	0.14	4.24	5.48	−2.15	9.87	2.02	(0.0)
Equatorial	0.60	1.49	0.16	4.61	5.78	−1.25	11.89		
ε = 37.5									
Axial	0.59	1.61	0.15	4.23	5.44	−0.13	11.89	1.16	(−1.0)
Equatorial	0.62	1.91	0.16	4.67	5.76	−0.07	13.05		
					X = Br				
ε = 2.2									
Axial	0.34	0.71	0.11	4.56	3.17	−2.07	6.81	1.12	(1.1)
Equatorial	0.37	0.95	0.11	4.08	3.75	−1.32	7.93		
ε = 37.5									
Axial	0.32	0.74	0.10	4.56	3.14	−0.12	8.74	0.42	(0.0)
Equatorial	0.36	0.87	0.11	4.08	3.83	−0.08	9.16		
					X = Cl				
ε = 2.2									
Axial	0.34	0.60	0.09	6.11	3.26	−2.51	7.89	0.45	(0.6)
Equatorial	0.34	0.80	0.09	5.10	3.53	−1.52	8.34		
ε = 37.5									
Axial	0.33	0.61	0.09	6.16	3.20	−0.15	10.23	−0.48	(−0.4)
Equatorial	0.33	0.71	0.09	5.11	3.61	−0.09	9.75		
					X = F				
ε = 2.2									
Axial	0.35	0.60	0.05	7.15	3.23	−3.43	7.95	−1.84	(−0.30)
Equatorial	0.30	0.58	0.06	4.18	2.98	−1.99	6.11		
ε = 37.5									
Axial	0.33	0.53	0.05	7.27	3.18	−0.20	11.16	−3.21	(−1.2)
Equatorial	0.28	0.48	0.06	4.19	3.04	−0.11	7.95		

[a]S = stretch, B = bend, S–B = stretch–bend, T = torsional, V = van der Waals, E_T = total steric energy, $\Delta E_T = E_{eq} - E_{ax}$, $\Delta G_{ea} = G_{eq} - G_{ax}$ (all in kcal/mol).

[b]Includes the entropy contribution due to two equivalent energy rotamers.

obtained from Cambridge Isotopes. 2-Methoxycyclohexanone was purchased from Aldrich. 2-Methylthiocyclohexanone was synthesized from cyclohexanone via reaction of its enolate with methyl methanethiolsulfonate (28).

The measured splittings reported as J_{obs} are estimated to be accurate to within 0.2 Hz or better as a consequence of line widths usually being between 0.8 and 1.0 Hz due to unresolved long-range couplings. The spectrum of **2** in $CDCl_3$ was reproduced by spectral simulation using PCPMR (13). Because this program's capacity is limited to eight nuclei, it was necessary to omit the proton at C2 from the calculations. Using input parameters based on the observed line spacings in each multiplet, the eight-line pattern calculated for H6 had line positions that agreed to within 0.1 Hz with those observed. Allowing for the absence of perturbation by H2, other multiplets showed similar agreement.

Can. J. Chem. Downloaded from www.nrcresearchpress.com by 65.111.164.53 on 09/08/12
For personal use only.

Fig. 2. A portion of the 500 MHz ^{1}Hmr spectrum for 4-*tert*-butylcyclohexanone in acetone-d_6: (*a*) the absorption for an axial (δ 2.3–2.4) and equatorial (δ 2.2–2.28) protons at C2; (*b*) the spectrum calculated by PCPMR using the parameters given in Table 5.

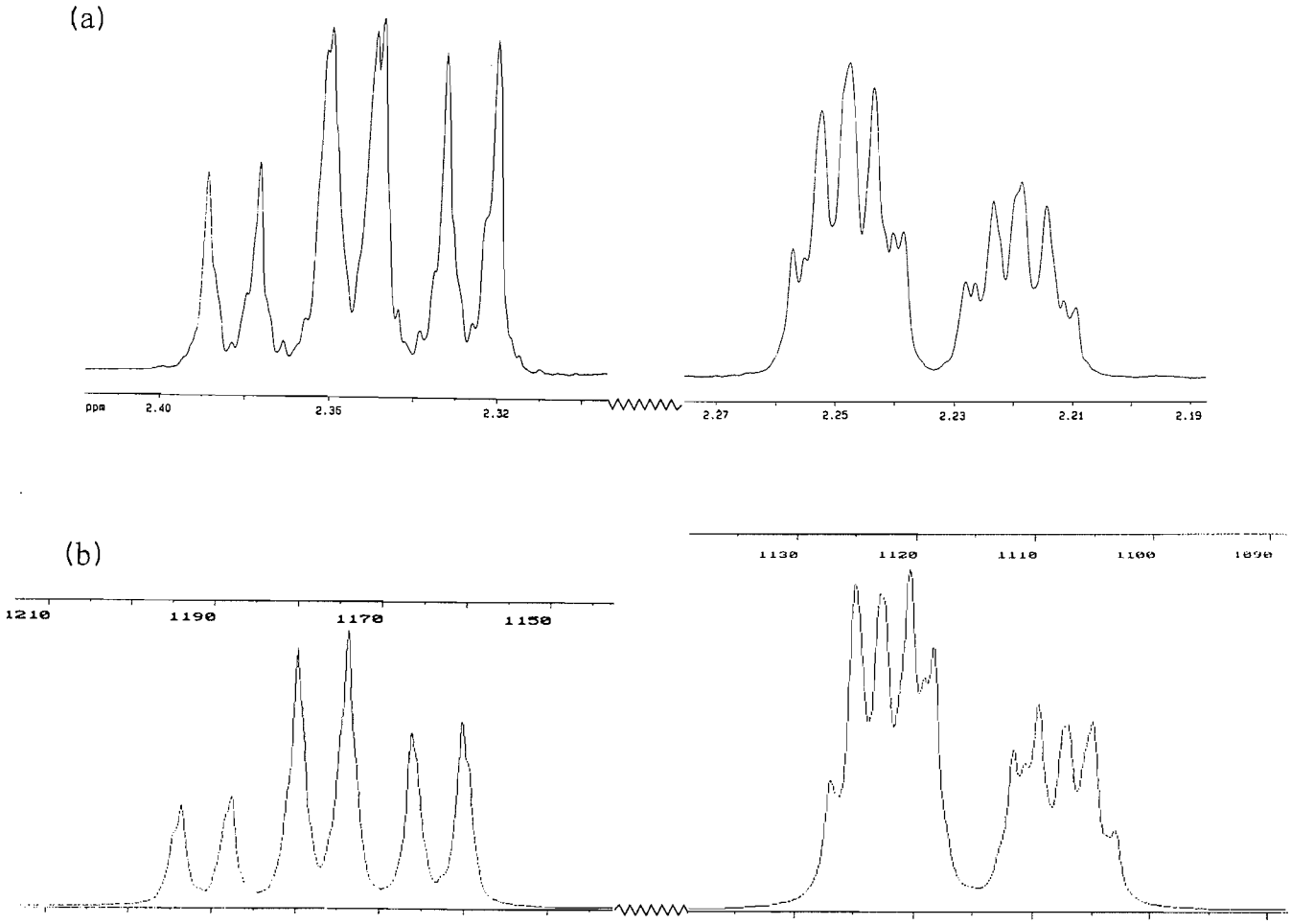

Table 5. Spectral parameters.

(*a*) 2-Methylthiocyclohexanone ($CDCl_3$)

Chemical shifts (Hz from TMS): H2 1615, H3 1030, H3′ 1083, H4 934, H4′ 837, H5 988, H5′ 875, H6 1485, H6′ 1119
Coupling constants (Hz): J_{35} = 1.6, $J_{4'6'}$ = 1.6, $J_{34'}$ = 4.9, J_{34} = 3.5, $J_{3'4'}$ = 3.8, $J_{3'4}$ = 10.1, $J_{33'}$ = −14.1, $J_{4'5'}$ = 3.8, $J_{4'5}$ = 4.9, $J_{45'}$ = 10.1, J_{45} = 3.5, $J_{44'}$ = −13.6, $J_{55'}$ = −13.2, $J_{56'}$ = 4.8, J_{56} = 5.8, $J_{5'6'}$ = 4.6, $J_{5'6}$ = 11.2, $J_{66'}$ = −14.5

(*b*) 4-*tert*-Butylcyclohexanone (acetone-d_6)

Chemical shifts (Hz from TMS): H_{2ax}, H_{6ax} 1176; H_{2eq}, H_{6eq} 1116; H_{3ax}, H_{5ax} 705; H_{3eq}, H_{5eq} 1040
Coupling constants (Hz): $J_{2ax2eq} = J_{6ax6eq}$ = −14.5, $J_{3ax3eq} = J_{5ax5eq}$ = −12.3, $J_{2ax3ax} = J_{5ax6ax}$ = 13.7, $J_{2eq3eq} = J_{5eq6eq}$ = 2.2, $J_{2ax3eq} = J_{5eq6ax}$ = 6.1, $J_{2eq3ax} = J_{5ax6eq}$ = 4.6, $J_{2eq6eq} = J_{3eq5eq}$ = 2, $J_{3eq5ax} = J_{3ax5eq}$ = 1, $J_{2eq6ax} = J_{2ax6eq}$ = 0.8

The spectrum of 4-*tert*-butylcyclohexanone in acetone-d_6 was chosen for determination of J_{aa} and J_{ee} for the protons at C2 and C6 as all ring protons were free from serious overlap in this solvent. The axial proton absorption pattern was reproduced by simulation using PCPMR, with omission of the axial proton at C4. Both proton patterns were difficult to reproduce, being sensitive to the long-range coupling constants, J_{35} and J_{26}, as well as to the vicinal and geminal interactions. A comparison of the experimental and simulated spectra for both α protons appears in Fig. 2. In view of the uncertainty associated with the absence of H4, the observed agreement is acceptable. The parameters used in the two simulations appear in Table 5.

All molecular mechanics calculations were carried out using the MMX program contained in PCMODEL (25). Energy minima were found for both conformational isomers and all three rotamers of the 2-substituent. In one case only, that for the equatorial isomer of **2** in acetonitrile, rotamers with the methyl *trans* to CH_2 and to CO were found to have the same minimum energy. Otherwise, a single rotamer, that with

methyl *trans* to CO, dominated regardless of the value for the dielectric constant.

Acknowledgments

The technical assistance of Dr. Glenn Facey and Mr. Raj Capoor is gratefully acknowledged. We wish to thank the Natural Sciences and Engineering Research Council of Canada for their financial support.

References

1. R.R. Fraser, C. Bensimon, F. Kong and X. Wu. Can. J. Chem. **71**, 685 (1993).
2. J.B. Lambert. *In* The conformational analysis of cyclohexenes, cyclohexadienes and related hydroaromatic compounds. *Edited by* P. Rabideau. VCH, Weinheim. 1989. Chap. 2.
3. E.L. Eliel, N.L. Allinger, S.J. Angyal, and G.A. Morrison. Conformational analysis. Interscience, New York. 1965. pp. 460–466.
4. Y.-H. Pan and J.B. Stothers. Can. J. Chem. **45**, 2943 (1967).
5. A.J. Kirby. The anomeric effect and related stereoelectronic effects at oxygen. Springer-Verlag, Berlin. 1983.
6. L.A. Paquette, B.M. Branan, D. Freidrich, S.D. Edmondson, and R.D. Rogers. J. Am. Chem. Soc. **116**, 506 (1994).
7. S.E. Denmark, M.S. Dappen, N.L. Sear, and R.T. Jacobs. J. Am. Chem. Soc. **112**, 3466 (1990).
8. D. Cantacuzene and M. Tordeux. Can. J. Chem. **54**, 2759 (1976).
9. M.J.T. Robinson. Tetrahedron, **30**, 1971 (1974).
10. J.-P. Battioni and W. Chodkiewicz. Bull. Soc. Chim. Fr. 320 (1977).
11. L. Mion, A. Casadevall, and E. Casadevall. Bull. Soc. Chim. Fr. 984 (1970).
12. H.O. House and H.W. Thompson. J. Org. Chem. **28**, 164 (1963).
13. E.A. Basso, C. Kaiser, R. Rittner, and J.B. Lambert. J. Org. Chem. **58**, 7865 (1993).
14. B. Wladislaw, H. Viertler, P.R. Olivato, I.C.C. Calagao, V.L. Pardini, and R. Rittner. J. Chem. Soc. Perkin Trans. **2**, 453 (1980).
15. (*a*) M.C. Carreno, E. Dominguez, J.L. Garcia-Ruano, and A. Rubio. J. Org. Chem. **52**, 3619 (1987); (*b*) H. Ozbal and W.W. Zajak, Jr. Tetrahedron Lett. 4821 (1979); (*c*) B.M. Trost, T.N. Salzmann, and K. Hiroi. J. Am. Chem. Soc. **98**, 4887 (1976).
16. F.A.L. Anet. J. Am. Chem. Soc. **84**, 1053 (1962).
17. J.B. Lambert, R.E. Carhart, P.W. Corfield, and J.E. Enemark. J. Chem. Soc. Chem. Commun. 999 (1968).
18. D. Hofner, S.A. Lesko, and G. Binsch. Org. Magn. Reson. **11**, 179 (1978).
19. J.A. Hirsch. Top. Stereochem. **1**, 119 (1967).
20. B. Rickborn. J. Am. Chem. Soc. **77**, 5418 (1955).
21. F. Johnson. Chem. Rev. **68**, 375 (968).
22. E.J. Corey and H.J. Burke. J. Am. Chem. Soc. **77**, 5418 (1955).
23. O. Eisenstein, N.T. Anh, Y. Jean, A. Devaquet, J. Cantacuzene, and L. Salem. Tetrahedron, **30**, 1717 (1974).
24. L. Dosen-Micovic, D. Jeremic, and N.L. Allinger. J. Am. Chem. Soc. **105**, 1723 (1983).
25. J.J. Gilbert, K.E. McKelvey, and J.J. Gajewski. Adv. Mol. Model. **2**, 69, (1990).
26. K.N. Houk, J.E. Eksterowicz, Y.D. Wu, C.D. Fugelsang, and D.B. Mitchell. J. Am. Chem. Soc. **115**, 4170 (1993).
27. R.C. Bingham. J. Am. Chem. Soc. **98**, 535 (1976).
28. D. Scholz. Synthesis, 944 (1983).

Can. J. Chem. Downloaded from www.nrcresearchpress.com by 65.111.164.53 on 09/08/12
For personal use only.

The synthesis, molecular and crystal structure of the 1:1 adduct of triphenyltin chloride with 2,3-diphenylthiazolidin-4-one

Frank E. Smith, Rosemary C. Hynes, John Tierney, Ying Z. Zhang, and George Eng

Can. J. Chem. Downloaded from www.nrcresearchpress.com by 65.111.164.53 on 09/08/12
For personal use only.

Abstract: The title compound was synthesized as part of an effort to produce a more effective fungicide to combat Dutch Elm Disease (DED), which is caused by the fungus *Ceratocystis ulmi*. A full X-ray structural analysis of the 1:1 adduct has been carried out and the results are reported along with the Mössbauer data for the compound. The crystals are monoclinic, space group $P2_1/a$ with $a = 19.240(3)$ Å, $b = 9.1463(24)$ Å, $c = 19.3512(24)$ Å, $\beta = 118.874(8)°$, $V = 2982.0(10)$ Å^3, $z = 4$, and $D_{calc} = 1.427$ Mg m^{-3}. The final discrepancy factors are $R_F = 0.056$ and $R_w = 0.058$ for 1915 significant reflections. The QS and IS values in the Mössbauer spectrum of the complex are 3.08 mm s^{-1} and 1.28 mm s^{-1}, respectively. The 2,3-diphenylthiazolidin-4-one behaves as a monodentate ligand and coordinates to the tin through the oxygen atom. The complex exhibits a trigonal bipyramidal configuration with the three phenyl groups in equatorial positions and the chloride and ligand oxygen occupying the apical sites.

Key words: triorganotin, fungicide, Dutch Elm Disease, thiazolidin-4-one.

Résumé : On a synthétisé le composé mentionné dans le titre dans un effort orienté vers la mise au point d'un fongicide plus efficace pour combattre la maladie des ormes qui est causée par le champignon *Ceratocystis ulmi*. Une analyse structurale complète par diffraction des rayons x de l'adduit 1 : 1 a été réalisée et on rapporte les résultats avec des données de Mössbauer du composé. Les cristaux sont monocliniques, groupe d'espace $P2_1/a$ avec $a = 19,240(3)$, $b = 9,1463(24)$ et $c = 19,3512(24)$ Å, $\beta = 118,874(8)°$, $V = 2982,0(10)$ Å^3, $z = 4$ et $D_{calc} = 1,427$ Mg m^{-3}. Les facteurs finaux de convergence sont $R_F = 0,056$ et $R_W = 0,058$ pour 1915 réflexions significatives. Les valeurs QS et IS du spectre de Mössbauer du complexe sont respectivement 3,08 mm s^{-1} et 1,28 mm s^{-1}. La 2,3-diphénylthiazolidin-4-one se comporte comme un coordinat monocoordinant; sa coordination à l'étain se fait par l'atome d'oxygène. Le complexe présente une configuration trigonale bipyramidale avec trois groupes phényles en positions équatoriales alors que le chlore et le coordinat oxygéné occupent des sites apicaux.

Mots cles : triorganoétain, fongicide, maladie des ormes, thiazolidin-4-one.

[Traduit par la rédaction]

Introduction

Organotin compounds have a wide range of biological applications depending on the number and species of the organic substituents present (1–3). The use of triphenyltin compounds as fungicides is well documented (1–6). However, when fungicides are to be used on living vegetation, the phytocidal properties of the compounds must also be taken into account.

Received February 15, 1994.

F.E. Smith.[1] Chemistry Department, Laurentian University, Sudbury, ON P3E 2C6, Canada.
R.C. Hynes. Biochemistry Department, University of Toronto, 1 King's College Circle, Toronto, ON M5S 1A8, Canada.
J. Tierney. Department of Chemistry, Pennsylvania State University, Delaware County Campus, Media, PA 19063, U.S.A.
Y.Z. Zhang and G. Eng. The Agricultural Experiment Station and the Department of Chemistry, The University of the District of Columbia, Washington, DC 20005, U.S.A.

[1] Author to whom all correspondence should be addressed. Telephone: (705) 675 1151; Fax: (705) 675 4844; e-mail: FSMITH@NICKEL.LAURENTIAN.CA

One class of triphenyltins that has been shown to possess a high fungicidal to phytocidal ratio is the triphenyltin chloride adducts (7). The title compound was synthesized as part of an effort to produce a more effective fungicide to combat Dutch Elm Disease (DED), which is caused by the fungus *Ceratocystis ulmi*. Earlier results have indicated that the triphenyltin moiety is effective in the inhibition of this fungus (8, 9). The 2,3-disubstituted thiazolidin-4-ones are compounds with known biological activity (10, 11), and so it was considered likely that an adduct of the two could well show increased fungicidal effects due to synergism. The ligand selected was 2,3-diphenylthiazolidin-4-one, whose structure is shown below:

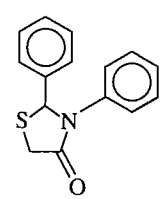

2,3-diphenylthiazolidin-4-one

Can. J. Chem. Downloaded from www.nrcresearchpress.com by 65.111.164.53 on 09/08/12
For personal use only.

While the adduct formed may have biological significance, it also presents an interesting structural problem since the ligand has three possible coordination sites, and no structural studies on complexes of this ligand have previously been reported. A full X-ray structural analysis of the 1:1 adduct has been carried out and the results are reported along with the Mössbauer data for the compound.

Experimental

Materials

Triphenyltin chloride was purchased from the Aldrich Chemical Co. and acetone obtained from Fisher Scientific. Both were used without further purification. The synthesis of 2,3-diphenylthiazolidin-4-one was carried out according to the literature method (10).

Preparation of complex

A solution of 2,3-diphenylthiazolidin-4-one (2.55 g, 10 mmol) in acetone (30 mL) was added dropwise to a solution of triphenyltin chloride (4.06 g, 10 mmol) in acetone (80 mL). The mixture was stirred at room temperature for 30 min and then allowed to stand for an additional 3 h. It was filtered and the filtrate was concentrated on a rotary evaporator, then dried in vacuum to give an oily residue. Scratching the sides of the flask resulted in solidification of the residue. The product was recrystallized from ligroin to yield needle-shaped crystals (5.60 g, 88% yield, mp 88–89°C). Anal. calcd. for $C_{33}H_{28}NOSClSn$: C 61.85, H 4.40, Sn 18.52; found: C 61.88, H 4.22, Sn 18.30.

Mössbauer spectroscopy

The Mössbauer spectra were measured at 80 K on a Ranger Scientific model MS-900 Mössbauer spectrometer in the acceleration mode with a moving source geometry using a liquid nitrogen cryostat (11). The sample was mounted in a Teflon holder. The source was 15 mCi $Ca^{119m}SnO_3$, and the velocity was calibrated at ambient temperature using a composition of $BaSnO_3$ and Sn foil (splitting = 2.52 mm s^{-1}). The resultant spectra were analyzed by a least-square fit to Lorenzian-shaped lines. All isomer shifts were calculated relative to $BaSnO_3$. The quadrupole splitting (QS) and isomer shift (IS) values for the complex are 3.08 ± 0.07 mm s^{-1} and 1.28 ± 0.02 mm s^{-1}, respectively.

X-ray analysis

Space group and cell dimensions

The crystals are monoclinic, space group $P2_1/a$ with a = 19.240(3) Å, b = 9.1463(24) Å, c = 19.3512(24) Å, β = 118.874(8)°, V = 2982.0(10) Å^3, z = 4, and D_{calc} = 1.427 Mg m^{-3}. Crystal dimensions: 0.40 × 0.15 × 0.05 mm. Empirical formula: $C_{33}H_{28}NOSClSn$. FW = 640.79. $F(000)$ = 1301.73, μ = 8.66 mm^{-1}.

Data collection, structure solution, and refinement

Cell dimensions were obtained from 12 reflections with 2θ in the range 60–70°. The intensity data were collected at 293 K on a Rigaku model AFC6S diffractometer run by the TEXRAY (12) diffractometer control program, using the θ/2θ scan mode and $Cu_{K\alpha}$ radiation (λ = 1.54056 Å). A total of 3125 reflections were measured, of which 3003 were unique. Of these, 1915 had $I_{net} > 2.5\sigma(I_{net})$ and R_{int} = 2.7%. The h, k and l ranges were −17 to 16, 0 to 9, and 0 to 19, respectively, and $2\theta_{max}$ was 100°. Absorption corrections were made with the NRC program ABSORB using ψ-scan data (13). The minimum and maximum transmission factors are 0.221 and 0.325. The structure was solved by direct methods, followed by a difference Fourier. All non-hydrogen atoms were refined with anisotropic thermal parameters. Hydrogen atoms were included in the calculated positions and not refined. Secondary extinction was refined (14) to 0.83(5). The refined parameter is the average length of a mosaic block in microns. Least-squares refinement was carried out on F. The final least-squares cycle was calculated with 66 atoms and 344 parameters. Weights based on counting-statistics were used. Final residuals are R_F = 0.056, R_W = 0.058 for data with $I_{net} > 2.5\sigma(I_{net})$, R_F = 0.126, R_W = 0.061 for all data. The goodness-of-fit was 2.07. Maximum shift/error was 0.098. In the last difference Fourier map, the top peak was 0.390 e/Å^3, and the deepest hole was −0.490 e/Å. Scattering factors were taken from the literature (15). Structure solution and refinement was performed using the NRCVAX system of crystal structure solving programs (16).

Discussion

Complexes of triphenyltin chloride are almost invariably five-coordinate with equatorial phenyl groups, even with potentially bi- or tridentate ligands (17–22). One spectroscopic tool that has been used for deducing the structural configuration of organotin compounds is Mössbauer spectroscopy. Mössbauer spectroscopy gives rise to two parameters, the isomer shift (IS) and the quadrupole splitting (QS). The isomer shift is related to the *s*-electron density at the tin nucleus, which can provide information as to its oxidation states and the bonding of the tin atom. The quadrupole splitting reflects the symmetry of the electronic environment around the tin nucleus and thus gives information concerning the arrangement of the ligands about the tin atom. Observed QS values in the range of 2.76–3.86 mm s^{-1} have been found for trigonal bipyramidal (TBP) organotin structures with axial ligand groups (1, 23, 24). Values of the parameter ρ, which is the QS/IS ratio, have been used to indicate the coordination number of the tin atom (23, 24). Although borderline ρ values are of questionable value, those falling well within the prescribed ranges can be very significant in structure identification (24). A ρ value of greater than 2.1 is indicative of a coordination number greater than four. The QS and IS values for the synthesized adduct are 3.08 mm s^{-1} and 1.28 mm s^{-1}, respectively. The observed ρ value of 2.41 would indicate that the adduct is greater than four coordinated. The ρ value, along with the observed QS value of 3.08 mm s^{-1}, would indicate that the triphenyltin chloride adduct is TBP with equatorial phenyl groups and the chloride atom and the ligand group occupying the axial positions. The TBP geometry of the molecule, with equatorial phenyl groups, predicted by the Mössbauer spectrum is confirmed by the X-ray structural investigation. An ORTEP (25) plot of the organotin complex is given in Fig. 1. A stereo pair showing the packing arrangement of the molecules in the unit cell is shown in Fig. 2. The final fractional coordinates of non-hydrogen atoms with equivalent isotropic thermal parameters are listed in Table 1, while the bond lengths and bond angles for the complex are presented in Tables 2 and 3, respectively. Cal-

Can. J. Chem. Downloaded from www.nrcresearchpress.com by 65.111.164.53 on 09/08/12
For personal use only.

Fig. 1. A stereo pair showing the packing in a unit cell.

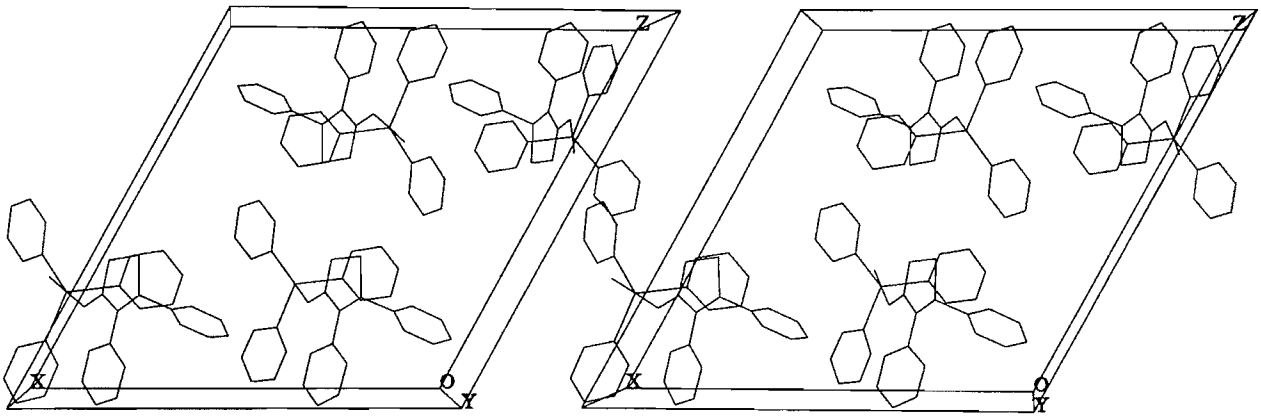

Table 1. Atomic parameters x, y, z and B_{eq}, esd refer to the last digit printed.

Atom	x	y	z	B_{eq} [a]
Sn	0.50379(6)	0.27790(11)	0.29383(6)	4.91(6)
Cl	0.54892(23)	0.0265(5)	0.33506(23)	6.3(3)
S	0.4025(3)	0.7911(5)	0.37702(24)	7.2(3)
O	0.4558(6)	0.5330(12)	0.2509(6)	6.0(7)
N	0.3791(7)	0.7302(14)	0.2361(7)	5.2(8)
C1	0.4325(9)	0.6296(18)	0.2789(9)	4.8(10)
C2	0.4591(9)	0.6467(19)	0.3652(9)	7.4(11)
C3	0.3521(10)	0.8441(16)	0.2723(8)	5.5(11)
C11	0.2628(10)	0.8439(20)	0.2379(8)	5.0(10)
C12	0.2195(12)	0.7328(18)	0.2468(10)	7.0(13)
C13	0.1374(14)	0.741(3)	0.2133(14)	8.7(17)
C14	0.0987(12)	0.864(3)	0.1700(12)	8.1(15)
C15	0.1407(14)	0.9736(22)	0.1609(11)	7.5(14)
C16	0.2224(12)	0.9681(18)	0.1937(10)	5.9(11)
C21	0.3553(9)	0.7472(16)	0.1525(9)	4.9(10)
C22	0.2939(9)	0.6633(18)	0.0981(10)	6.3(10)
C23	0.2735(10)	0.6779(21)	0.0167(11)	7.9(14)
C24	0.3141(12)	0.7717(24)	−0.0047(10)	7.5(14)
C25	0.3732(10)	0.8551(20)	0.0502(11)	6.9(12)
C26	0.3947(8)	0.8425(18)	0.1294(9)	5.9(10)
C31	0.4915(8)	0.2572(19)	0.1777(7)	5.1(10)
C32	0.4381(10)	0.3463(19)	0.1165(11)	6.9(12)
C33	0.4287(11)	0.3256(23)	0.0410(11)	8.2(14)
C34	0.4772(12)	0.226(3)	0.0291(10)	8.4(15)
C35	0.5309(11)	0.1451(20)	0.0918(12)	7.1(13)
C36	0.5378(8)	0.1571(18)	0.1654(9)	5.5(11)
C41	0.4017(9)	0.2683(18)	0.3085(10)	5.6(11)
C42	0.4088(11)	0.2051(21)	0.3779(12)	8.1(14)
C43	0.3444(18)	0.205(3)	0.3918(16)	11.5(22)
C44	0.2748(17)	0.269(4)	0.3372(21)	12.1(28)
C45	0.2646(14)	0.331(3)	0.2671(18)	10.8(21)
C46	0.3293(11)	0.3325(18)	0.2542(10)	6.8(12)
C51	0.6033(9)	0.3870(16)	0.3820(9)	4.7(10)
C52	0.6346(12)	0.3581(18)	0.4618(12)	7.4(14)
C53	0.6992(16)	0.432(3)	0.5179(11)	11.0(19)
C54	0.7353(11)	0.5348(23)	0.4989(13)	8.0(14)
C55	0.7068(14)	0.5650(22)	0.4200(14)	9.5(16)
C56	0.6421(11)	0.4882(22)	0.3644(9)	7.5(13)

[a] B_{eq} is the mean of the principal axes of the thermal ellipsoid.

Table 2. Bond distances in angstroms.

Bond	Distance	Bond	Distance
Sn—Cl	2.451(4)	C(23)—C(24)	1.35(3)
Sn—O	2.500(10)	C(24)—C(25)	1.36(3)
Sn—C(31)	2.151(12)	C(25)—C(26)	1.385(24)
Sn—C(41)	2.117(14)	C(31)—C(32)	1.396(25)
Sn—C(51)	2.101(14)	C(31)—C(36)	1.377(24)
S—C(2)	1.795(17)	C(32)—C(33)	1.39(3)
S—C(3)	1.840(14)	C(33)—C(34)	1.40(3)
O—C(1)	1.228(22)	C(34)—C(35)	1.37(3)
N—C(1)	1.329(21)	C(35)—C(36)	1.370(25)
N—C(3)	1.481(20)	C(41)—C(42)	1.41(3)
N—C(21)	1.462(19)	C(41)—C(46)	1.41(3)
C(1)—C(2)	1.501(23)	C(42)—C(43)	1.39(3)
C(3)—C(11)	1.514(24)	C(43)—C(44)	1.37(5)
C(11)—C(12)	1.38(3)	C(44)—C(45)	1.40(5)
C(11)—C(16)	1.41(3)	C(45)—C(46)	1.38(3)
C(12)—C(13)	1.39(3)	C(51)—C(52)	1.386(24)
C(13)—C(14)	1.39(4)	C(51)—C(56)	1.33(3)
C(14)—C(15)	1.35(4)	C(52)—C(53)	1.37(3)
C(15)—C(16)	1.38(3)	C(53)—C(54)	1.32(4)
C(21)—C(22)	1.375(23)	C(54)—C(55)	1.38(3)
C(21)—C(26)	1.364(23)	C(55)—C(56)	1.38(3)
C(22)—C(23)	1.43(3)		

culated hydrogen atom parameters and anisotropic thermal parameters have been deposited with the journal.[2]

The complex exhibits a trigonal bipyramidal configuration with the three phenyl groups in equatorial positions around the central tin atom, and the chloride and ligand oxygen occupying the apical sites. The principal axis is essentially linear, with a Cl—Sn—O(ligand) angle of 179.2°. The sum of the

[2] Complete sets of data may be purchased from: The Depository of Unpublished Data, Document Delivery, CISTI, National Research Council Canada, Ottawa, Canada K1A 0S2.

Calculated hydrogen atom parameters have also been deposited with the Cambridge Crystallographic Data Centre and can be obtained on request from The Director, Cambridge Crystallographic Data Centre, University Chemical Laboratory, 12 Union Road, Cambridge, CB2 1EZ, U.K.

Structure factor tables are no longer being deposited and may be obtained directly from the author.

Can. J. Chem. Downloaded from www.nrcresearchpress.com by 65.111.164.53 on 09/08/12
For personal use only.

Table 3. Bond angles in degrees.

Bonds	Angle	Bonds	Angle
Cl—Sn—O	179.2(3)	N—C(21)—C(26)	120.3(13)
Cl—Sn—C(31)	95.8(5)	C(22)—C(21)—C(26)	121.0(14)
Cl—Sn—C(41)	97.1(5)	C(21)—C(22)—C(23)	117.8(15)
Cl—Sn—C(51)	98.1(4)	C(22)—C(23)—C(24)	120.2(16)
O—Sn—C(31)	84.1(5)	C(23)—C(24)—C(25)	120.5(15)
O—Sn—C(41)	82.3(5)	C(24)—C(25)—C(26)	120.6(15)
O—Sn—C(51)	82.7(5)	C(21)—C(26)—C(25)	120.0(14)
C(31)—Sn—C(41)	119.7(6)	Sn—C(31)—C(32)	120.0(12)
C(31)—Sn—C(51)	119.2(5)	Sn—C(31)—C(36)	119.0(11)
C(41)—Sn—C(51)	116.8(6)	C(32)—C(31)—C(36)	120.9(13)
C(2)—S—C(3)	94.7(7)	C(31)—C(32)—C(33)	118.7(16)
Sn—O—C(1)	132.8(9)	C(32)—C(33)—C(34)	120.0(16)
C(1)—N—C(3)	122.3(12)	C(33)—C(34)—C(35)	118.8(16)
C(1)—N—C(21)	119.8(12)	C(34)—C(35)—C(36)	122.1(17)
C(3)—N—C(21)	117.0(11)	C(31)—C(36)—C(35)	119.2(15)
O—C(1)—N	124.1(14)	Sn—C(41)—C(42)	118.4(13)
O—C(1)—C(2)	124.4(14)	Sn—C(41)—C(46)	122.1(12)
N—C(1)—C(2)	111.5(15)	C(42)—C(41)—C(46)	119.3(15)
S—C(2)—C(1)	108.5(11)	C(41)—C(42)—C(43)	120.0(19)
S—C(3)—N	102.5(10)	C(42)—C(43)—C(44)	118.7(23)
S—C(3)—C(11)	111.4(10)	C(43)—C(44)—C(45)	123.4(22)
N—C(3)—C(11)	112.0(12)	C(44)—C(45)—C(46)	117.5(23)
C(3)—C(11)—C(12)	124.9(15)	C(41)—C(46)—C(45)	121.0(19)
C(3)—C(11)—C(16)	116.2(15)	Sn—C(51)—C(52)	123.4(12)
C(12)—C(11)—C(16)	118.8(16)	Sn—C(51)—C(56)	121.7(11)
C(11)—C(12)—C(13)	121.4(17)	C(52)—C(51)—C(56)	114.9(14)
C(12)—C(13)—C(14)	118.9(18)	C(51)—C(52)—C(53)	121.8(16)
C(13)—C(14)—C(15)	120.1(18)	C(52)—C(53)—C(54)	121.9(18)
C(14)—C(15)—C(16)	122.2(18)	C(53)—C(54)—C(55)	118.0(18)
C(11)—C(16)—C(15)	118.7(16)	C(54)—C(55)—C(56)	119.2(17)
N—C(21)—C(22)	118.8(14)	C(51)—C(56)—C(55)	124.1(15)

Fig. 2. The structure of the complex.

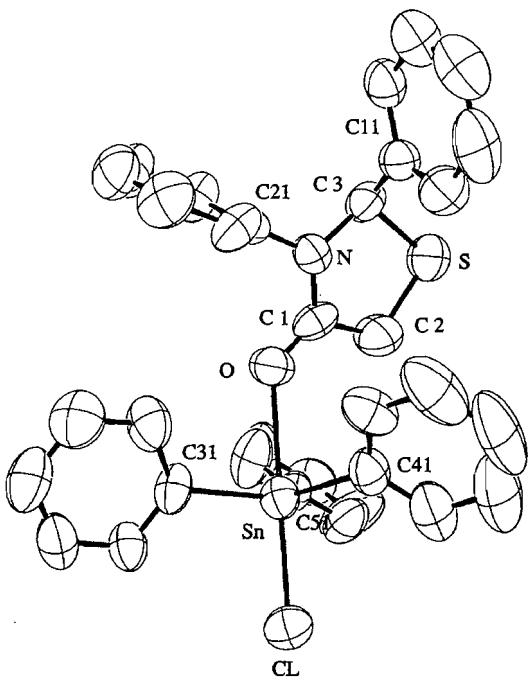

carbon–tin angles in the trigonal plane of the complex is 355.7° (116.8° + 119.7° + 119.2°), slightly less than the 358.2° value observed in triphenyltin *N*-salicylidene-6-aminohexanoate (26) and the 358.9° reported for terpyridyl-aquachlorotriphenyltin(IV) (19). This is probably a result of the relatively greater Cl—Sn—C(phenyl) angles observed in the present complex, indicating that the Sn atom is pulled slightly out-of-plane towards the Cl atom. The mean Cl—Sn—C(phenyl) angle for the title compound is 97.0° whereas for terpyridyl-aquachlorotriphenyltin(IV) the corresponding value is 93.6° (19). This increase in the Sn—Cl attraction is reflected in the shorter Sn—Cl bond length (2.45 Å) seen in the title complex, compared to that reported (2.52 Å) for the terpyridyl complex (19). In other respects, the coordination geometries about the tin atoms in these two complexes are very similar. The Sn—C(phenyl) distances are almost the same, showing average values of 2.12 Å for the title complex and 2.13 Å for the terpyridyl complex. The Sn—O bond distance in the title compound is 2.50 Å, within the range expected for a keto–oxygen interaction with tin (27). There are no short intermolecular contacts, and the packing in the unit cell appears to be controlled by the steric requirements of the five phenyl groups, which project in all directions from the complex.

References

1. A.G. Davies and P.J. Smith. *In* Comprehensive organometallic chemistry. Vol. 2. *Edited by* G. Wilkinson, F.G.A. Stone, and E.W. Abel. Pergamon Press, New York. 1982.
2. A.G. Davies and P.J. Smith. *In* Advances in inorganic chemistry and radiochemistry. Vol. 23. *Edited by* H.J. Emeleus and A.G. Sharpe. Academic Press, New York. 1980. p. 1.
3. S.J. Blunden and A. Chapman. *In* Organometallic compounds in the environment. *Edited by* P.J. Craig. John Wiley and Sons, New York. 1986. p. 111.
4. S. Nicklin and M.W. Robson. Appl. Organomet. Chem. **2**, 487 (1988).
5. M.H. Gitlitz. *In* Organotin compounds: new chemistry and applications. Vol. 157. *Edited by* J.J. Zuckerman. Am. Chem. Soc. Adv. Chem. Ser. 1976. p. 167.
6. A.J. Crowe. Appl. Organomet. Chem. **1**, 143 (1987).
7. R.C. Poller. *In* The chemistry of organotin compounds. Academic Press, New York. 1970. p. 271.
8. G. Eng, S.P. Coddington, L.L. Stockton, and A.D.W. Acholonu. Pestic. Sci. **26**, 117 (1989).
9. G. Eng, L.E. Khoo, L.L. Stockton, and S.P. Coddington. *In* Chemistry and technology of silicon and tin. *Edited by* V.G. Kumar Das, S.W. Ng, and M. Gielen. Oxford University Press, Oxford, England. 1991.
10. J. Tierney. J. Heterocycl. Chem. **26**, 997 (1989).
11. CYRO Industries of America, Inc., Salem, New Hampshire, U.S.A.
12. The Molecular Structure Corporation, Woodlands, Texas, U.S.A.
13. D.C. Phillips, A.C.T. North, and F.S. Mathews. Acta Crystallogr. **24**, 351 (1968).
14. A.C. Larson. *In* Crystallographic computing. *Edited by* F.R. Ahmed. Munksgaard, Copenhagen. 1970. p. 291.
15. International Tables for X-ray Crystallography. Vol. IV. 2nd ed. Kynoch Press, Birmingham, England. 1974. p. 99.
16. E.J. Gabe, Y. Le Page, J-P. Charland, F.L. Lee, and P.S. White. J. Appl. Crystallogr. **22**, 384 (1989).
17. F.E. Smith and L.E. Khoo. J. Inorg. Nucl. Chem. **43**, 1917 (1981).
18. L. Prasad and F.E. Smith. Acta Crystallogr. Sect. B: Struct. Crystallogr. Cryst. Chem. **B38**, 1815 (1982).
19. L. Prasad, F.L. Lee, Y. Le Page, and F.E. Smith. Acta Crystallogr. Sect. B: Struct. Crystallogr. Cryst. Chem. **B38**, 259 (1982).
20. F. Smith, L. Prasad, D. Povey, and M. Ladd. Experientia, **39**, 719 (1983).
21. M.F.C. Ladd, D.C. Povey, and F.E. Smith. J. Crystallogr. Spectrosc. Res. **14**, 249 (1984).
22. E.J. Gabe, F.L. Kee, and F.E. Smith. Inorg. Chim. Acta, **90**, L11 (1984).
23. J.J. Zuckerman. *In* Advances in organometallic chemistry. Vol. 9. *Edited by* F.G.A. Stone and R. West. Academic Press, New York. 1970. p. 22.
24. S.W. Ng, A.J. Kuthubutheen, Z. Arifin, Chen Wei, V.G. Kumar Das, B. Schulze, K.C. Molloy, W.H. Yip, and T.C.W. Mak. J. Organomet. Chem. **403**, 101 (1991).
25. C.K. Johnson. ORTEP-II. Report ORNL-5138, Oak Ridge National Laboratory, Tenn., U.S.A. 1976.
26. Y.C. Toong, S.P. Tai, M.C. Pun, F.E. Smith, Rosemary C. Hynes, and L.E. Khoo. Can. J. Chem. **70**, 2683 (1992).
27. E.R.T. Tiekink. Appl. Organomet. Chem. **5**, 1 (1991).

Can. J. Chem. Downloaded from www.nrcresearchpress.com by 65.111.164.53 on 09/08/12
For personal use only.

Novel O-C-C-O and C-O-C-C stereochemistry in crown ether analogs. X-ray crystal structure and NMR studies of dibenzo-20-crown-6

G.W. Buchanan, A. Moghimi, and C. Bensimon

Abstract: The X-ray crystal structure of the title material indicates that the molecule possesses a pseudo-centre of inversion. A pair of O-C-C-O bonds have a *trans* conformation in contrast to normal *gauche* stereochemistry for such units in crown ethers. For the C-O-C-C networks, which are normally *transoid* in crown ethers, all four such units involving methylene carbons of the 20-membered ring exhibit unusual geometries. Two units possess *gauche* conformations and the other two have torsion angles near 120°. Solution ^{1}H and ^{13}C NMR spectra have been recorded as a function of temperature and ^{13}C solid state spectra are included.

Key words: crown ether, solid state conformation.

Résumé : La structure cristalline du composé mentionné dans le titre, telle que déterminée par diffraction des rayons X, indique que la molécule possède un pseudo-centre d'inversion. Une paire de liaisons O-C-C-O existe dans une conformation *trans* alors que la stéréochimie normale de telles unités dans des éthers couronnes est *gauche*. Pour les réseaux C-O-C-C qui sont généralement transoïdes dans les éthers couronnes, les quatre unités impliquant les carbones méthyléniques du cycle à 20 chaînons présentent tous des géométries inhabituelles. Deux unités possèdent des conformations *gauche* et les deux autres ont des angles de torsion de 120°. On a déterminé les spectres RMN du ^{1}H du ^{1}H et du ^{13}C en fonction de la température et on a aussi inclus les spectres RMN du ^{13}C à l'état solide.

Mots clés : éther couronne, conformation à l'état solide.

[Traduit par la rédaction]

Introduction

The X-ray crystal structures of many dibenzo crown ethers are now available, including those for the dibenzo-18-crown-6 (1) and dibenzo-24-crown-8 (2) systems illustrated below. The conformations of C-O-C-C units are normally *transoid* in these structures, while O-C-C-O units where the carbons are not part of the aromatic ring adopt *gauche* geometries. The most substantial deviation from the *gauche* O-C-C-O stereochemistry occurs in the 24-crown-8 case where expansions of the torsional angle up to values of ca. 84° are found (2).

As part of our continuing program to examine structures and complexation features of novel crown ether analogs, we have now prepared the dibenzo-20-crown-6 system **1** shown below. Herein we report its X-ray structure as well as solution and solid state NMR spectral features. The solid phase ^{13}C shifts are discussed in terms of earlier ab initio shift calculations for constituent structural units.

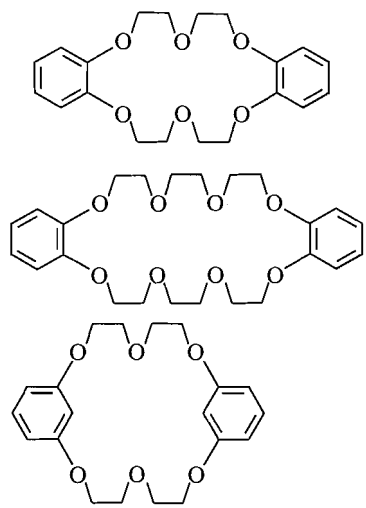

1

Received July 15, 1994.

G.W. Buchanan,[1] A. Moghimi, and C. Bensimon. Ottawa–Carleton Chemistry Institute, Department of Chemistry, Carleton University, 1125 Colonel By Drive, Ottawa, ON K1S 5B6, Canada.

[1] Author to whom correspondence may be addressed.

Results and discussion

The structure and numbering scheme for dibenzo-20-crown-6, **1**, is depicted in Fig. 1. The ORTEP plot for **1** is shown in Fig. 2, while the ^{13}C CPMAS spectra are depicted in Fig. 3. Table 1 contains bond lengths, Table 2 has bond angles, and torsion angles involving non-H atoms are presented in Table 3. Crystallographic data are listed in Table 4 and atomic parameters in

Can. J. Chem. Downloaded from www.nrcresearchpress.com by 65.111.164.53 on 09/08/12
For personal use only.

Can. J. Chem. Downloaded from www.nrcresearchpress.com by 65.111.164.53 on 09/08/12
For personal use only.

Fig. 1. Structure and numbering scheme for **1**.

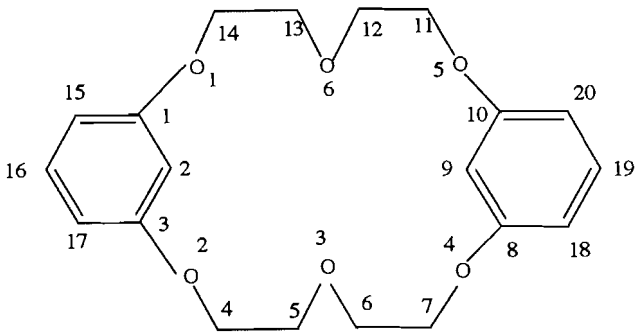

1

Table 1. Atomic bond distances in angstroms.

O1—C1	1.360(6)	C8—C9	1.382(6)
O1—C14	1.434(6)	C8—C18	1.402(7)
O2—C3	1.375(5)	C9—C10	1.395(7)
O2—C4	1.439(6)	C9—H9	0.94(5)
O3—C5	1.443(6)	C10—C20	1.394(7)
O3—C6	1.434(6)	C11—C12	1.518(7)
O4—C7	1.436(6)	C11—H11A	0.95(5)
O4—C8	1.375(6)	C11—H11B	1.08(5)
O5—C10	1.377(5)	C12—H12A	1.08(5)
O5—C11	1.438(6)	C12—H12B	0.97(5)
O6—C12	1.438(6)	C13—C14	1.492(7)
O6—C13	1.437(6)	C13—H13A	1.01(6)
C1—C2	1.398(7)	C13—H13B	0.98(5)
C1—C15	1.393(7)	C14—H14A	0.96(5)
C2—C3	1.390(7)	C14—H14B	0.95(5)
C2—H2	0.97(5)	C15—C16	1.373(7)
C3—C17	1.388(7)	C15—H15	0.96(5)
C4—C5	1.508(7)	C16—C17	1.386(7)
C4—H4A	1.05(6)	C16—H16	1.07(5)
C4—H4B	1.11(6)	C17—H17	0.92(5)
C5—H5A	1.12(5)	C18—C19	1.363(8)
C5—H5B	0.92(5)	C18—H18	0.97(4)
C6—C7	1.501(7)	C19—C20	1.392(7)
C6—H6A	0.98(5)	C19—H19	0.91(5)
C6—H6B	0.96(5)	C20—H20	0.99(5)
C7—H7A	1.01(5)		
C7—H7B	0.96(6)		

Table 5. In Table 6 are collected the ^{1}H NMR data while ^{13}C NMR chemical shifts are presented in Table 7.

X-ray crystal structure

The structure of **1**, as determined at −100°C, exhibits a pseudo-centre of inversion. Regarding the O-C-C-O networks, *gauche*-type geometries are present in the O2-C4-C5-O3 and O5-C11-C12-O6 units in accord with expectations based on "normal" preferred crown ether conformations (3, 4). In contrast, the torsion angles for the O3-C6-C7-O4 and O6-C13-C14-O1 units are 176.0° and −177.4°, respectively. Examination of molecular models indicates that these *trans* O-C-C-O geometries are adopted by the molecule in order to minimize a potentially repulsive steric interaction between the aromatic

Fig. 2. ORTEP diagram for **1**.

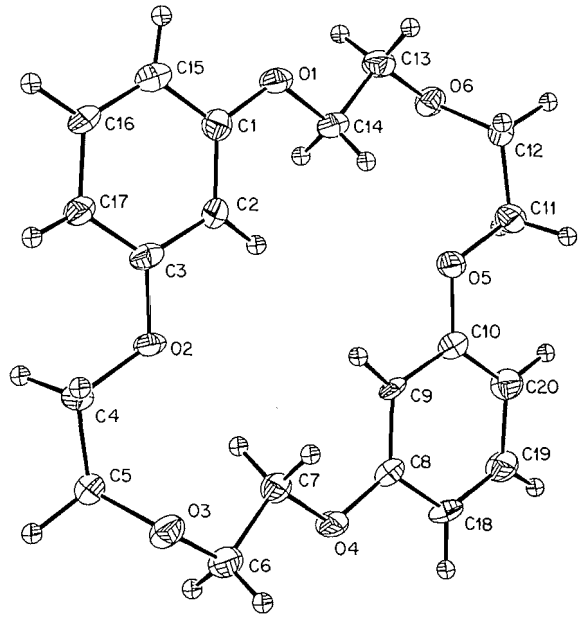

H's on C2 and C9. This minimization of inter-ring repulsion is also apparently more important than the maintenance of "normal" (3, 4) *trans* conformations in the C-O-C-C units. For example, the C5-O3-C6-C7 and C12-O6-C13-C14 units have torsion angles of 78.2° and −77.4°, respectively, while C6-O3-C5-C4 and C13-O6-C11-C12 exhibit angles of −127.5° and 126.6°, respectively. Hence all aliphatic C-O-C-C units of **1** have "abnormal" geometries.

With regard to the stereochemistry of the aryl-O-C units, there are two distinctly different types of geometries observed in crystalline **1**. For example, the C14-O1-C1-C15 unit and its pseudo-symmetry related counterpart C7-O4-C8-C18 are *transoid*, with torsion angles of −172.9° and 171.6°, respectively. In contrast, the C4-O2-C3-C17 unit and its counterpart C11-O5-C10-C20 are *cisoid*, with torsion angles of 1.5° and −1.2°, respectively. Such differences in environment between the terminal atoms of these units lead to very large ^{13}C chemical shifts between C15,18 and C17,20 in the solid state, while in solution these carbons exhibit one conformationally averaged resonance (*vide infra*).

Solution NMR spectra

The ^{1}H spectrum of **1** in $CDCl_3$ exhibits the expected A_2XY spin system for the aromatic protons and an AA'BB' type multiplet for the aliphatic hydrogens. Apart from minor temperature-dependent chemical shifts, both the ^{1}H and ^{13}C spectra are independent of temperature between 310 and 200 K, indicating fast conformational interchange on the NMR time scale throughout this temperature range.

First-order spectral analysis yielded the aromatic proton shifts and couplings collected in Table 6 while iterative computer analysis was employed for the aliphatic data. Assignment of the more deshielded half of the AA'BB' multiplet to protons on C4,7,11,14 was made on the basis of the observed nuclear Overhauser enhancement between the resonance centered at 4.150 ppm and the aromatic proton resonances on C2, 9 and C15,17,18,20.

Can. J. Chem. Downloaded from www.nrcresearchpress.com by 65.111.164.53 on 09/08/12
For personal use only.

Table 2. Atomic bond angles in degrees.

C1—O1—C14	118.6(4)	C9—C10—C20	120.7(4)
C3—O2—C4	117.9(4)	O5—C11—C12	107.8(4)
C5—O3—C6	113.1(4)	O5—C11—H11A	104(3)
C7—O4—C8	117.4(3)	O5—C11—H11B	106(3)
C10—O5—C11	117.8(4)	C12—C11—H11A	114(3)
C12—O6—C13	112.5(4)	C12—C11—H11B	103(3)
O1—C1—C2	123.2(4)	H11A—C11—H11B	120(4)
O1—C1—C15	117.0(4)	O6—C12—C11	109.8(4)
C2—C1—C15	119.8(5)	O6—C12—H12A	106.0(23)
C1—C2—C3	119.2(4)	O6—C12—H12B	109(3)
C1—C2—H2	120(3)	C11—C12—H12A	105.6(23)
C3—C2—H2	119(3)	C11—C12—H12B	114(3)
O2—C3—C2	114.1(4)	H12A—C12—H12B	111(4)
O2—C3—C17	124.8(4)	O6—C13—C14	111.1(4)
C2—C3—C17	121.1(4)	O6—C13—H13A	103(3)
O2—C4—C5	107.7(4)	O6—C13—H13B	109(3)
O2—C4—H4A	102(3)	C14—C13—H13A	108(3)
O2—C4—H4B	105(3)	C14—C13—H13B	111(3)
C5—C4—H4A	118(3)	H13A—C13—H13B	112(4)
C5—C4—H4B	100(3)	O1—C14—C13	106.7(4)
H4A—C4—H4B	121(4)	O1—C14—H14A	107(3)
O3—C5—C4	110.0(4)	O1—C14—H14B	109(3)
O3—C5—H5A	104.8(23)	C13—C14—H14A	109(3)
O3—C5—H5B	113(3)	C13—C14—H14B	114(3)
C4—C5—H5A	110.1(22)	H14A—C14—H14B	109(4)
C4—C5—H5B	115(3)	C1—C15—C16	119.8(4)
H5A—C5—H5B	102(4)	C1—C15—H15	113(3)
O3—C6—C7	110.4(4)	C16—C15—H15	126(3)
O3—C6—H6A	108(3)	C15—C16—C17	121.5(5)
O3—C6—H6B	101(3)	C15—C16—H16	121.6(24)
C7—C6—H6A	109(3)	C17—C16—H16	116.9(24)
C7—C6—H6B	110(3)	C3—C17—C16	118.6(5)
H6A—C6—H6B	114(4)	C3—C17—H17	124(3)
O4—C7—C6	107.0(4)	C16—C17—H17	117(3)
O4—C7—H7A	108(3)	C8—C18—C19	119.1(4)
O4—C7—H7B	114(3)	C8—C18—H18	120.9(24)
C6—C7—H7A	113(3)	C19—C18—H18	120.0(24)
C6—C7—H7B	110(3)	C18—C19—C20	122.0(5)
H7A—C7—H7A	104(4)	C18—C19—H19	122(3)
O4—C8—C9	123.6(4)	C20—C19—H19	115(3)
O4—C8—C18	115.8(4)	C10—C20—C19	118.4(5)
C9—C8—C18	120.6(5)	C10—C20—H20	118(3)
C8—C9—C10	119.2(4)	C19—C20—H20	122(3)
C8—C9—H9	126(3)		
C10—C9—H9	114(3)		
O5—C10—C9	114.1(4)		
O5—C10—C20	125.2(4)		

Table 3. Torsion angles (deg) involving non-H atoms.

C14-O1-C1-C2	5.7(3)	C14-O1-C1-C15	−172.9(5)
C1-O1-C14-C13	173.5(6)	C4-O2-C3-C2	−178.9(5)
C4-O2-C3-C17	1.5(3)	C3-O2-C4-C5	172.2(6)
C6-O3-C5-C4	−127.5(5)	C5-O3-C6-C7	78.2(4)
C8-O4-C7-C6	−170.1(6)	C7-O4-C8-C9	−7.6(3)
C7-O4-C8-C18	171.6(5)	C11-O5-C10-C9	178.9(5)
C11-O5-C10-C20	−1.2(3)	C10-O5-C11-C12	−174.6(6)
C13-O6-C12-C11	126.6(5)	C12-O6-C13-C14	−77.4(4)
O1-C1-C2-C3	−176.3(6)	O15-C1-C2-C3	2.2(3)
O1-C1-C15-C16	177.7(6)	C2-C1-C15-C16	−0.9(3)
C1-C2-C3-O2	177.8(6)	C1-C2-C3-C17	−2.6(3)
O2-C3-C17-C16	−178.8(6)	C2-C3-C17-C16	1.6(3)
O2-C4-C5-O3	68.5(4)	O3-C6-C7-O4	176.0(6)
O4-C8-C9-C10	177.4(6)	C18-C8-C9-C10	−1.7(3)
O4-C8-C18-C19	−178.6(6)	C9-C8-C18-C19	0.6(3)
C8-C9-C10-O5	−178.1(6)	C8-C9-C10-C20	2.0(3)
O5-C10-C20-C19	178.9(6)	C9-C10-C20-C19	−1.3(3)
O5-C11-C12-O6	−69.4(4)	O6-C13-C14-O1	−177.4(6)
C1-C15-C16-C17	−0.1(3)	C15-C16-C17-C3	−0.2(3)
C8-C18-C19-C20	0.2(3)	C18-C19-C20-C10	0.2(3)

Table 4. Crystallographic data.

Formula	$C_{20}H_{24}O_6$
fw	360.40
Crystal system	Monoclinic
Space group	*P* 21/*n*
a (Å)	6.980 (3)
b (Å)	12.781 (4)
c (Å)	20.089 (5)
β	93.12 (3)
V (Å^3)	1789.6 (10)
Z (molecules/unit cell)	4
D_c (g/cm^3)	1.338
Crystal dimensions (mm^3)	0.20 × 0.20 × 0.20
Radiation (λ, Å)	MoKα (0.70930)
Octants measured	*h*(−8 to 8), *k*(0 to 15), *l*(0 to 23)
Max. 2θ	49.9
Temperature	−110°C
No. of measured reflections	3413
No. of unique reflections	3140
No. of observed reflections with $I_{net} > 2.5\sigma I_{net}$	2274
R_f	0.081
R_w	0.104
Goodness of fit	2.76
No. of atoms	50
No. of parameters	332
Final-*D* map:	
deepest hole, e/Å^3	−0.520
highest peak, e/Å^3	0.450

It is of interest to compare the aliphatic vicinal coupling constants for **1**, having two *gauche* and two *trans* O-C-C-O networks, with those determined previously (5) for dibenzo-18-crown-6, which possesses four *gauche* O-C-C-O units. Both materials were examined in $CDCl_3$ solution. From the X-ray data, it is clear in the crystal that there will be two sets of *trans* vicinal protons and two sets of *gauche* vicinal protons in each O-C-C-O unit of **1**. By contrast, in crystalline dibenzo-18-crown-6, there will be one pair of *trans* vicinal protons and three pairs of *gauche* vicinal protons in each O-C-C-O moiety. Assuming that the preferred conformation in the crystal also exists in solution, one would anticipate substantially larger ^3J values for **1** than for dibenzo-18-crown-6. In reality there is a small increase observed. The ^3J values for dibenzo-18-crown-6 are 5.7 and 3.3 Hz (5), while those for **1** are 5.9 and 3.8 Hz. Hence conformational averaging in solution appears to render the vicinal couplings more nearly equal than would be expected based on crystal geometries alone.

Fig. 3. (*a*) 45.3 MHz ^{13}C CPMAS spectrum of **1**. (*b*) Dipolar dephased ^{13}C CPMAS spectrum of **1**.

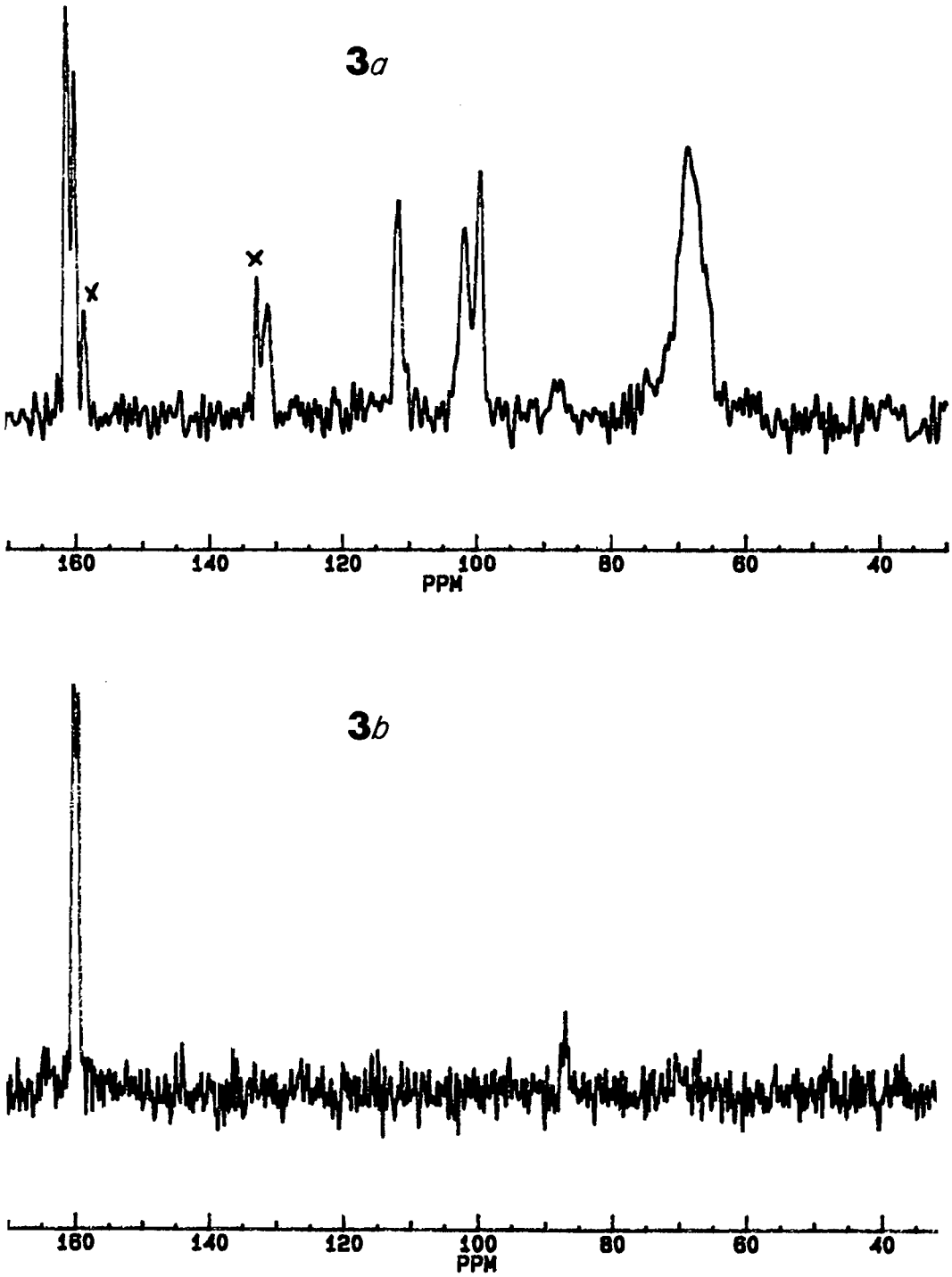

Can. J. Chem. Downloaded from www.nrcresearchpress.com by 65.111.164.53 on 09/08/12
For personal use only.

With respect to the solution ^{13}C NMR spectrum, the aromatic region can be readily assigned. Quaternary carbons 1, 3, 8, and 10 are the most deshielded, as expected (5) from early data on aromatic ethers. The known shielding effect (6) of *ortho* oxygen atoms is clearly operative here, giving rise to the resonance at 102.9 ppm for C2,9. The resonance at 107.4 is twice the intensity of that at 102.9, consistent with the assignment of the 107.4 peak to C15,17,18,20. The remaining CH resonance at 129.7 arises from C16,19. In the aliphatic region, the more shielded methylene carbon resonance at 67.8 ppm is attributed to C4,7,11,17 based on results of a ^{1}J HETCOR experiment and the known ^{1}H assignments for the methylene protons. This result is also consistent with trends found previously for dibenzo-15-crown-15 (7) and tetrabenzo-30-crown-10 (8) systems.

In the solid phase, the ^{13}C spectral multiplicity will reflect the asymmetric unit in the crystal if no unusual crystal packing effects or nonequivalent molecules in the unit cell are present

Can. J. Chem. Downloaded from www.nrcresearchpress.com by 65.111.164.53 on 09/08/12
For personal use only.

Table 5. Atomic parameters x, y, z, and B_{iso} (e.s.d.'s refer to the last digit printed).

	x	y	z	B_{iso}[a]
O1	0.5170(5)	0.3658(3)	0.43923(15)	2.25(15)
O2	0.1429(5)	0.2582(3)	0.24706(15)	2.23(15)
O3	0.1223(5)	0.1874(3)	0.11072(16)	2.21(14)
O4	0.4761(5)	0.3874(3)	0.07873(15)	2.26(15)
O5	0.8599(5)	0.4849(3)	0.27162(15)	2.21(15)
O6	0.8822(5)	0.5598(3)	0.40773(15)	2.13(14)
C1	0.3682(7)	0.3110(4)	0.40980(23)	2.00(20)
C2	0.3307(7)	0.3069(4)	0.34076(23)	1.88(20)
C3	0.1689(7)	0.2539(4)	0.31532(22)	1.81(19)
C4	−0.0231(8)	0.2070(5)	0.21649(23)	2.35(24)
C5	−0.0343(7)	0.2353(4)	0.14353(24)	2.06(21)
C6	0.2301(8)	0.2605(4)	0.0737(3)	2.30(22)
C7	0.3644(7)	0.3217(4)	0.11973(24)	2.03(21)
C8	0.6299(7)	0.4390(4)	0.10923(22)	1.88(20)
C9	0.6687(7)	0.4403(4)	0.17745(22)	1.70(20)
C10	0.8328(7)	0.4915(4)	0.20335(22)	1.86(20)
C11	1.0277(8)	0.5339(5)	0.30244(25)	2.32(22)
C12	1.0351(7)	0.5071(4)	0.37613(24)	2.00(22)
C13	0.7664(8)	0.4893(4)	0.44412(24)	2.22(22)
C14	0.6310(8)	0.4299(4)	0.39817(24)	2.10(23)
C15	0.2474(8)	0.2592(4)	0.45181(24)	2.22(23)
C16	0.0908(7)	0.2056(4)	0.42529(23)	2.13(21)
C17	0.0490(7)	0.2017(4)	0.35712(23)	2.05(20)
C18	0.7509(7)	0.4908(4)	0.06651(23)	2.07(23)
C19	0.9086(8)	0.5418(4)	0.0931(3)	2.49(22)
C20	0.9537(8)	0.5437(4)	0.16148(25)	2.33(22)
H2	0.410(7)	0.345(4)	0.3109(24)	2.7(11)
H4A	0.001(8)	0.128(4)	0.2295(24)	3.9(13)
H4B	−0.148(8)	0.251(4)	0.234(3)	4.0(13)
H5A	−0.167(7)	0.201(4)	0.1183(21)	2.3(11)
H5B	−0.049(7)	0.306(4)	0.1344(24)	2.7(12)
H6A	0.141(7)	0.308(4)	0.0496(22)	2.1(11)
H6B	0.301(7)	0.215(3)	0.0458(21)	1.7(10)
H7A	0.455(7)	0.276(4)	0.1476(23)	2.5(11)
H7B	0.293(8)	0.359(4)	0.152(3)	3.6(13)
H9	0.600(7)	0.405(4)	0.2093(25)	3.1(12)
H11A	1.009(6)	0.607(4)	0.2931(21)	1.5(10)
H11B	1.149(8)	0.493(4)	0.2841(25)	3.4(13)
H12A	1.167(7)	0.541(3)	0.3969(21)	1.8(10)
H12B	1.030(7)	0.433(4)	0.3856(23)	2.7(12)
H13A	0.688(7)	0.537(4)	0.472(3)	3.3(12)
H13B	0.851(7)	0.442(4)	0.7608(22)	2.0(10)
H14A	0.545(8)	0.477(4)	0.3748(24)	2.9(12)
H14B	0.692(7)	0.387(4)	0.3669(24)	2.8(12)
H15	0.287(7)	0.264(3)	0.4982(24)	2.4(11)
H16	−0.002(7)	0.163(4)	0.4562(22)	2.2(10)
H17	−0.053(7)	0.161(3)	0.3424(20)	1.6(10)
H18	0.727(6)	0.488(3)	0.0187(20)	0.8(9)
H19	0.985(7)	0.582(4)	0.0678(24)	3.3(13)
H20	1.067(7)	0.581(4)	0.1815(24)	3.3(13)

[a] B_{iso} is the mean of the principal axes of the thermal ellipsoid.

(9). For **1**, there is a pseudo-centre of inversion, which is apparent from examination of the torsion angle data in Table 3. Hence in the ^{13}C CPMAS spectrum (Fig. 3) one expects to observe 10 unique resonances in the absence of any peak overlap. Of the six anticipated aromatic resonances, all are resolved; however, the four aliphatic resonances appear as a broad singlet centered at 68.5 ppm.

Table 6. ^1H NMR data for **1** (0.01 M in $CDCl_3$).

Proton	δ(∓ 0.001)	^2J (Hz)	^3J (Hz)	^4J (Hz)
2,9	6.640			2.4
15,17,18,20	6.480		8.2	2.4
16,19	7.115		8.2	
4,7,11,14	4.150	−11.0	5.9	
			3.8	
5,6,12,13	3.891	−11.0	5.9	
			3.8	

Table 7. ^{13}C Chemical shifts for **1** (ppm from TMS ∓ 0.1)

Carbon	δ_C (solution)[a]	δ_C (solid)
1,8	160.0	159.9
2,9	102.9	99.4
3,10	160.0	161.1
4,11	67.8	68.5
5,12	70.1	68.5
6,13	70.1	68.5
7,14	67.8	68.5
15,18	107.4	111.5
16,19	129.7	131.1
17,20	107.4	101.6

[a] 0.1 M in $CDCl_3$.

The most shielded aromatic singlet at 99.4 ppm is assigned to C2,9 by analogy with the solution spectrum. Most interestingly, the resonance for C15,18,17,20, which is averaged to one line in solution with a chemical shift of 107.4 ppm, becomes a doublet in the solid phase, with components at 111.5 and 101.6 ppm, respectively. Due to the lack of conformational averaging in the solid phase, the resonance for the C15,18 pair is now distinct from the peak arising from C17,20. The more shielded resonance at 101.6 is attributed to the C17,20 pair. Examination of the torsion angles in the X-ray structure shows that both C17 and C20 are involved in essentially coplanar γ-interactions with aliphatic carbons C4 and C11, respectively. The interactions involved here are C4-O2-C3-C17 (θ = 1.5°) and C11-O5-C10-C20 (θ = −1.2°). By contrast, the C15, C18 pair experience nearly *trans*-coplanar γ-interactions with the aliphatic carbons C14 and C7, respectively. The pertinent torsion angles here are 172.9° for the C14-O1-C14-C15 network and 171.6° for the C7-O4-C8-C18 unit. It is well known (10) that *cis*-coplanar γ-interactions lead to substantially shielded terminal carbon resonances relative to the corresponding *trans* situations. Hence we are confident in the assignment of the more shielded line to C17, 20.

The resonance at 131.1 ppm is due to the pseudo-symmetry equivalent C16,19 pair and is within 2 ppm of the solution chemical shift. Finally, the C1,8 and C3,10 sites gives rise to resonances at 159.9 and 161.1 ppm. Subtle differences in the electronic environments at these pairs of carbons in the solid

Can. J. Chem. Downloaded from www.nrcresearchpress.com by 65.111.164.53 on 09/08/12
For personal use only.

may be responsible for the small chemical shift difference observed. The most effective conjugative electron release by the oxygen lone pairs into the aromatic ring (and hence more aryl C—O double bond character) is expected when the aliphatic carbon bonded to the oxygen is coplanar with the aromatic ring. Since these interactions are more nearly coplanar for the C3,10 pair than for C1,8 (vide supara), we assign these to the more deshielded resonance at 161.1 ppm to C3,10. The extra smaller absorption at ca. 158 ppm in the normal ^{13}C CPMAS spectrum disappears in the dipolar dephased version and henced is an impurity, since no aromatic CH in **1** would resonate in this region.

Experimental

Materials

Dibenzo-20-crown-6 was prepared according to the following procedure. A 2.0 L round-bottom flask was charged with resorcinol (Aldrich) (11.0 g, 0.1 mol), distilled water (200 mL), and $LiOH{\cdot}H_2O$ (2.1 g, 0.05 mol) and the mixture was stirred for 5 min. To this was added dropwise 1,5-dichloro-3-oxapentane (Aldrich) (7.2 g, 0.05 mol) and the reaction mixture was refluxed for 72 h. After cooling to 40°C, an additional 2.1 g of $LiOH{\cdot}H_2O$ was added, followed by another 7.2 g of the dichloride. Subsequent to dilution with 12 mL of distilled water, the mixture was refluxed for another 72 h. After cooling, the mixture was acidified to pH 2 by addition of dilute sulphuric acid and extracted with CH_2Cl_2 (4 × 15 mL). After washing with 5% NaOH (3 × 150 mL), saturated NaCl (4 × 150 mL), and water, the extracts were dried over anhydrous Na_2SO_4. Following solvent removal, the resultant crude solid was recrystallized from acetone to yield 1.5 g (4%) of dibenzo-20-C-6, mp 165–167°C. No attempt was made to optimize the yield.

Spectra

All solution NMR spectra were recorded using a Bruker AMX-400 spectrometer equipped with a 5 mm inverse probe and an Aspect X32 computer. An Aspect 3000 process controller was employed and all standard microprograms used are in the Bruker Software Library.

For the NOESY experiment, the mixing time used was selected to be consistent with the $1/T_1$ criterion (11), and in the present case it was set to 0.3 s. For the $^1H^{13}C$ HETCOR experiment, the free induction decays were acquired over 1024 data points for each of the 512 values of the evolution time, with a digital resolution of ca. 8 Hz/point in $F2$ and 4 Hz/point in $F2$. The raw data were zero filled in $F1$ prior to transformation using the qsine window function for both $F1$ and $F2$. The proton relaxation delays were set to 1 s. Delays were chosen to emphasize J values of 135–140 Hz.

The solid phase ^{13}C NMR spectra were recorded at 45.3 MHz using a Bruker CXP-180 spectrometer via techniques described previously (12). For the dipolar dephased spectrum, the ^1H decoupler was gated off for a period of 40 μs during the delay before the ^{13}C acquisition.

X-ray crystallographic measurements and structure solution

A summary of the crystallographic data is given in Table 4. Diffraction intensities were collected on a Rigaku diffractometer using MoKα radiation at −110°C. The Ω–2θ scan technique was used to a maximum 2θ value of 49.9°. The space group was determined by systematic absences. Unit cell parameters were obtained from least-squares refinement using the setting angles of 25 reflections in the range $40 < 2\theta < 50$. The data were corrected for Lorentz and polarization effects (13). No absorption correction was made. The structure was solved by direct methods plus Fourier maps and was refined by full-matrix least-squares analysis with weights based on counting statistics. Non-H atoms were refined anisotropically and H atoms isotropically. No crystal decay was noted during data collection. All calculations were performed using the NRC VAX Crystal Structure programs (14). Anisotropic temperature factors are available as supplementary data.[2]

Acknowledgements

G.W.B. is grateful to the Natural Sciences and Engineering Research Council of Canada (NSERC) for continued financial support. A.M. thanks the Iranian Ministry of Higher Education for a scholarship.

References

1. D. Bright and M.R. Truter. J. Chem. Soc. (B), 1544 (1970).
2. I.R. Hanson, D.L. Hughes, and M.R. Truter. J. Chem. Soc. Perkin Trans. 2, 972 (1976).
3. A.C. Coxon, D.A. Laidler, R.B. Pettman, and J.F. Stoddart. J. Am. Chem. Soc. **100**, 8260 (1978).
4. M.J. Bovill, D.J. Chadwick, and I.O. Sutherland. J. Chem. Soc. Perkin Trans. 2, 1529 (1980).
5. D. Live and S.I. Chan. J. Am. Chem. Soc. **98**, 3769 (1976).
6. J.D. Stothers. Carbon-13 NMR spectroscopy. Academic Press, New York. 1972.
7. G.W. Buchanan, S. Mathias, Y. Lear, and C. Bensimon. Can. J. Chem. **69**, 404 (1991).
8. G.W. Buchanan, A. Rodrigue, K. Bourque, A.C. Chiverton, I.R. Castleden, and S. Fortier. Can. J. Chem. **72**, 1218 (1994).
9. P.S. Belton, S.F. Tanner, K.M. Wright, M.P. Payne, M.R. Truter, and J.N. Wingfield. J. Chem. Soc. Perkin Trans. 2, 1307 (1985).
10. M. Barfield. *In* NMR shielding and molecular structure. *Edited by* J.A. Tossel. Kluwer Academic Publishers, Norwell, Mass. 1993.
11. A.E. Derome. Modern NMR techniques for chemistry research. Pergamon Press, Oxford. 1987.
12. G.W. Buchanan, A. Rodrigue, C. Bensimon, and C.I. Ratcliffe. Can. J. Chem. **70**, 1033 (1992).
13. D.F. Grant and E.J. Gabe. J. Appl. Crystallogr. **11**, 114 (1978).
14. E.J. Gabe, F.L. Lee, and Y. Lepage. J. Appl. Crystallogr. **22**, 384 (1989).

[2] This table can be purchased from: The Depository of Unpublished Data, Document Delivery, CISTI, National Research Council Canada, Ottawa, ON K1A 0S2, Canada. Structure factor amplitudes are no longer being deposited and may be obtained directly from the author.

Theoretical and experimental barriers to internal rotation in 2,6-difluorobenzaldehyde and 2,4,6-trifluorobenzaldehyde. Relatively low barriers

Ted Schaefer, Craig S. Takeuchi, Guy M. Bernard, and Frank E. Hruska

Can. J. Chem. Downloaded from www.nrcresearchpress.com by 65.111.164.53 on 09/08/12
For personal use only.

Abstract: The free energies of activation at 110 K for rotation about the exocyclic C—C bonds in 2,6-difluorobenzaldehyde and 2,4,6-trifluorobenzaldehyde, in dimethyl ether solutions, are 18.8 ± 0.5 and 20.0 ± 0.5 kJ mol^{-1}, respectively, as determined from $^{19}F\{^1H\}$ dynamic nuclear magnetic resonance measurements. For the parent compound $\Delta G^{\ddagger}$ is 32.2 kJ mol^{-1} in the same solvent. These free energy barriers, the lowest available for benzaldehyde derivatives, are likely a result of steric and electrostatic repulsions between the C^+—O^- and C^+—F^- bonds. Computations of the spectroscopic barrier in the 2,6-difluoro compound at various levels of molecular orbital theory imply that the barrier is predominantly twofold, with a fourfold component of opposite sign, whose magnitude is about 10% of the twofold component. A correlation-gradient computation, MP2/6-31G*, finds a barrier height of 18.6 kJ mol^{-1} for this compound, lower by 3.0 kJ mol^{-1} than found with the 6-31G* basis and 2.9 kJ mol^{-1} with 6-31G**. Similar computations are compared for the parent compound and the 4-fluoro, 2,4,6-trifluoro, and 3,5-difluoro derivatives. Linear relationships exist between the computed spectroscopic barriers (ΔE values at absolute zero for the free molecules) and the free energy barriers for benzaldehyde and the four fluoro derivatives; the theoretical barriers utilize 6-31G** and correlation-gradient MP2/6-31G* procedures. For the 2,6-difluoro derivative, the computed frequencies of the torsional motions about the exocyclic C—C bond yield spectroscopic twofold barriers. These barriers are much lower than the computed energy differences between the planar and perpendicular conformers, perhaps because the negative fourfold components flatten the potential at its minimum. A rough estimate of the relationship between $\Delta G^{\ddagger}$ and ΔE_0 for the 2,6-difluorobenzaldehyde suggests that the solvent increases the internal barrier by only about 3 kJ mol^{-1}. By way of contrast, the AM1 barriers, scaled by a factor of 1.9 (as previously recommended) range from 17.3 to 22.6 kJ mol^{-1}, the $\Delta G^{\ddagger}$ values from 18.8(5) to 34.4 kJ mol^{-1}, and the MP2/6-31G* (correlation-gradient) barriers span 18.6 to 36.8 kJ mol^{-1} for benzaldehyde and the four fluorine derivatives. It seems likely that the internal barrier in benzaldehyde is considerably larger than that modeled on torsional frequencies.

Key words: Free energies of activation, internal rotational barriers in 2,6-difluoro- and 2,4,6-trifluorobenzaldehyde; molecular orbital computations, internal rotational barriers in 2,6-difluoro- and 2,4,6-trifluorobenzaldehyde; correlation gradient computations on internal barriers in benzaldehyde and four of its fluorine derivatives.

Résumé : En se basant sur des mesures de résonance magnétique nucléaire dynamique du $^{19}F\{^1H\}$, on a établi que les énergies libres d'activation, à 110 K, pour la rotation autour des liaisons exocycliques C—C des 2,6-difluoro- et 2,4,6-trifluorobenzaldéhydes, en solutuions dans le méthoxyméthane, sont respectivement de 18,8 ± 0,5 et 20,0 ± 0,5 kJ mol^{-1}. Pour le composé parent, le $\Delta G^{\ddagger}$ est de 32,2 kJ mol^{-1}, dans le même solvant. Ces barrières d'énergies libres sont les plus basses disponibles pur des dérivés du benzaldéhyde et elles sont probablement le résultat de répulsions stériques et électrostatiques entre les liaisons C^+—O^- et C^+—F^-. Des calculs de barrière spectroscopique pour le composé 2,6-difluoré, à divers niveaux de la théorie des orbitales moléculaires, impliquent que la barrière est principalement binaire, qu'elle comporte une composante quaternaire de signe opposé dont l'amplitude est d'environ 10% de celle de la composante binaire. Un calcul de gradient de corrélation, MP2/6-31G*, a permis d'établir que, pour ce composé, la hauteur de la barrière est de 18,6 kJ mol^{-1}; cette valeur est respectivement 30 et 2,9 kJ mol^{-1} plus basse que celles trouvées avec des base 6-31G* et 6-31G**. On a comparé des calculs semblables pour le composé parent et les dérivés 4-fluoré, 2,4,6-trifluoré et 3,5-difluoré, Il existe des corrélations linéaires entre les barrières spectroscopiques calculées (valeurs de ΔE

Received August 9, 1994.

T. Schaefer,[1] C.S. Takeuchi, G.M. Bernard, and F.E. Hruska. Department of Chemistry, University of Manitoba, MN R3T 2N2, Canada.

[1] Author to whom correspondence may be addressed.

au zéro absolu, pour des molécules libres) et les barrières d'énergies libres du benzaldéhyde et les quatre dérivés fluorés; les barrières théoriques ont été obtenues à l'aide de procédures 6-31G** et des gradients de corrélation MP2/6-31G*. Pour le dérivé 2,6-difluoré, les fréquences calculées des mouvements de torsion autour de la liaison exocyclique C—C conduisent à des barrières binaires. Ces barrières sont beaucoup plus faibles que les différences d'énergie calculées entre les conformères plans et perpendiculaires; cette différence est peut-être causée par les composantes quaternaires qui aplatissent le potentiel à son minimum. Une évaluation grossière de la relation entre le $\Delta G^{\ddagger}$ et le ΔE_0 dans le cas du 2,6-difluorobenzaldéhyde suggère que le solvant augemente la barrière interne par environ 3 kJ mol^{-1}. Pour fins de comparaison, les barrières AM1 (ajustées par le facteur de 1,9 recommandé antérieurement) varient de 17,3 à 22,6 kJ mol^{-1} et les valeurs du $\Delta G^{\ddagger}$ varient de 18,8(5) à 34,4 kJ mol^{-1} alors que les barrières MP2/6-31G* (gradient de corrélation) varient de 18,6 à 36,8 kJ mol^{-1} pour le benzaldéhyde et ses quatre dérivés fluorés. Il semble probable que le barrière interne dans le benzaldéhyde soit considérablement plus élevée que celle dérivée du modèle des fréquences de torsion.

Mots clés : énergies d'activation, barrières à la rotation interne dans les 2,6-difluoro- et 2,4,6-trifluorobenzaldéhydes; calculs d'orbitales moléculaires, barrières à la rotation interne dans les 2,6-difluoro- et 2,4,6-trifluorobenzaldéhydes; calculs de gradients de corrélation sur les barrières internes dans le benzaldéhyde et quatre de ses dérivés fluorés.

[Traduit par la rédaction]

Introduction

The experimental and theoretical approaches to the barrier to rotation about the exocyclic Csp^2—Csp^2 bond in benzaldehyde have an interesting history. In the vapor, torsional frequencies assessed by various spectroscopic methods (1–3) imply a predominantly twofold barrier with a magnitude lying between 19 and 23 kJ mol^{-1}. Ab initio molecular orbital computations (4, 5) at the MP2/6-311G**//6-31G* level of approximation give a barrier height of 34.7 kJ mol^{-1}; whether correlation-gradient computations would alter this value substantially is not known. However, another approximation to the effect of electron correlation on the barrier, at the MCSCF level, yields 18–21 kJ mol^{-1} (6). The disagreement between the theoretical values has been discussed (7, 8). More theoretical and experimental work is needed (8).

One criticism (4) of the experimental value of the mainly twofold barrier derived from far-infrared data is that it also contains a positive fourfold component (3), whereas a negative component is found for related molecules (4). This criticism does not apply to the vibronic fluorescence results (2). Another might be that the torsion measurements imply a decrease in the barrier in the presence of a 4-fluoro substituent (9, 10), whereas theory (5) and intuition (the substituent increases the mobile bond order for the Csp^2—Csp^2 linkage) suggest the opposite. Another curious fact concerns the computation of the torsional frequency in benzaldehyde. For example, at the STO-3G level this frequency is computed as 111.1 cm^{-1} and is measured as 110.9 cm^{-1} in the vapor. Accordingly, the magnitudes of V_2, computed and experimental (torsion model), are essentially identical at 19.3 kJ mol^{-1}. The computed energy difference, ΔE_0 between the planar ground state and the perpendicular transition state is, however, 22.9 kJ mol. Similar comparisons hold for another basis set (5).

In solution, the internal barrier of benzaldehyde apparently increases to about 27 kJ mol^{-1} (9), as deduced from torsional frequencies. Dynamic nmr measurements have $\Delta G^{\ddagger}$ as 32.3 kJ mol^{-1} (11) and other nmr data yield $\Delta H^{\ddagger}$ as 30.5 kJ mol^{-1} (12). The apparent increase in the barrier in solution has been attributed (11) to the stabilization by the dielectric continuum of the polar ground state relative to the less polar transition state. Allowance for the zero-point energies of the planar and perpendicular conformers of benzaldehyde, estimated (5) at 1.3–2.0 kJ mol^{-1} (to be here subtracted from the theoretical barrier), yields about 33 kJ mol^{-1} as an approximation[2] to $\Delta H^{\ddagger}$. The rough agreement between the approximate, theoretical $\Delta H^{\ddagger}$ and the experimental $\Delta H^{\ddagger}$ is rather striking. It may be accidental; if not, the solvent effect on the barrier is relatively small. Similar remarks apply to 4-fluorobenzaldehyde and some other *para* derivatives (5).

If the barrier to internal rotation in benzaldehyde is closer to 30 kJ mol^{-1} than to 20 kJ mol^{-1}, it would be then interesting to know how the two kinds of experimental approaches compare to theoretical calculations in assessing rather lower barriers to rotation in appropriate benzaldehyde derivatives. Preliminary molecular orbital computations on 2,6-difluoro- and 2,4,6-trifluorobenzaldehyde implied barrier heights near 20 kJ mol^{-1}. Such a magnitude is perhaps just within the lowest range assessable by DNMR.

Accordingly, $^{19}F\{^1H\}$ experiments were performed on these molecules, with the result that reasonable magnitudes of $\Delta G^{\ddagger}$ became available. We here report on these results and compare them with molecular orbital computations of the barriers, including gradient-optimized post-Hartree–Fock estimates of the internal barrier height. In addition, the computations are compared with experimental results, previously reported (14), for 3,5-difluorobenzaldehyde. These are of interest because the barrier in this molecule is lower than in benzaldehyde, not immediately obvious from chemical intuition, and unlike the barrier in 4-fluorobenzaldehyde, which is higher than in benzaldehyde (according to DNMR but not according to torsional frequencies), as expected from a π-electron-donating *para* substituent.

Results

In dimethyl ether solution at 110 K, $\Delta G^{\ddagger}$ is 20.0 ± 0.5 kJ mol^{-1} for 2,4,6-trifluorobenzaldehyde and is 18.8 ± 0.5 kJ mol^{-1} for 2,6-difluorobenzaldehyde (see Experimental). The latter barrier is the smaller one, as expected from the additional presence of a π donor in the *para* position in the trifluoro derivative.

[2] A discussion of the relationship of a potential barrier to an activation energy is available (13).

Can. J. Chem. Downloaded from www.nrcresearchpress.com by 65.111.164.53 on 09/08/12
For personal use only.

Fig. 1. In (*b*) the equilibrium, planar, 6-31G* geometry is shown for 2,6-difluorobenzaldehyde; in (*a*) the correlation-gradient structure using MP2/6-31G* procedures. Although bond angles are different by up to only 0.3°, bond length differences are as large as 0.038 Å, the MP2 values being the larger ones and rather close to expectations (35).

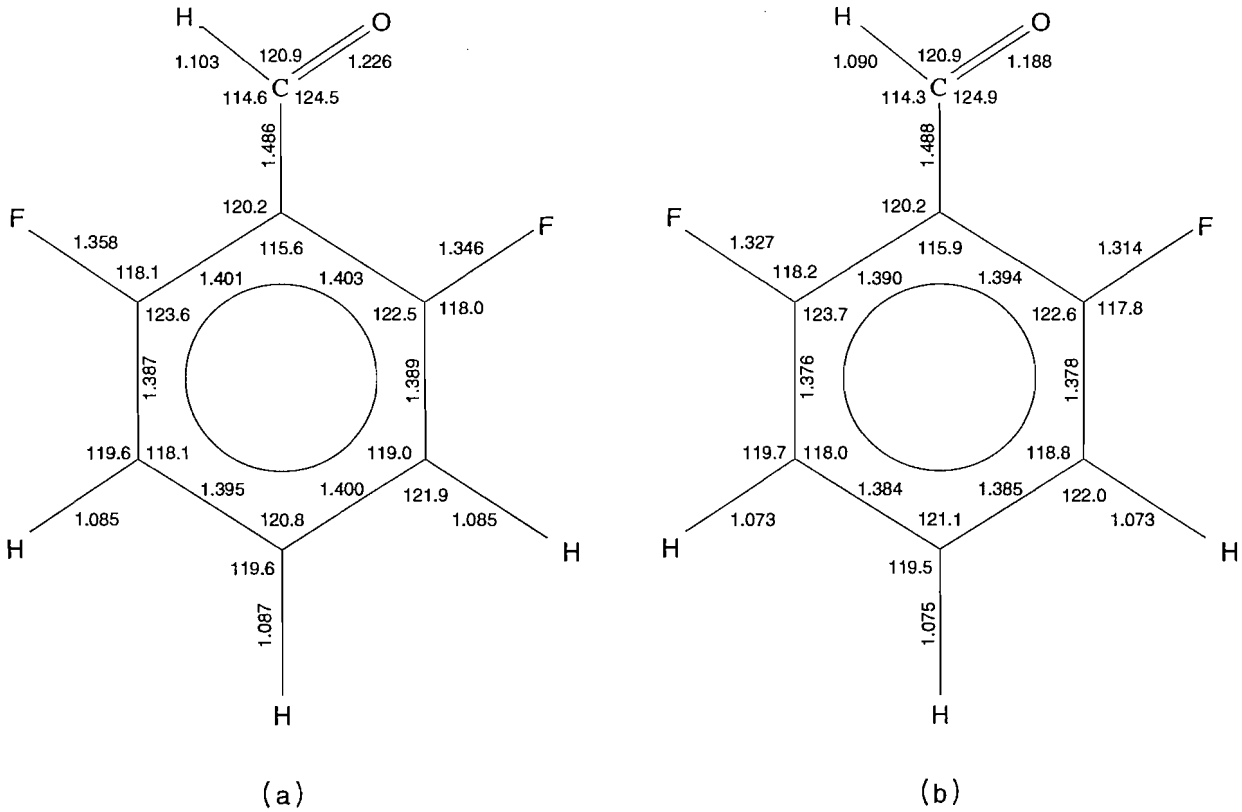

Table 1. Fourier components (in kJ mol^{-1}) of the computed barriers to internal rotation in 2,6-difluorobenzaldehyde.

Method	V_2[a]	V_4	V_6[d]	V_8	Standard error[e]
AM1	9.31	−0.59	−0.11	0.00	<0.01
STO-3G	20.09	−0.73	0.01	0.02	<0.01
3-21G	32.79	−2.02	0.43	−0.10	0.02
6-31G	19.55	−1.81	0.21	−0.06	0.01
6-31G*	21.27[b]	−2.10	0.21	−0.04	<0.01
6-31G**	21.29[c]	−2.03	0.19	−0.05	<0.01

[a]The total energies at 0° (planar) were −534.037 710, −538.152 867, −540.932 613, −541.126 702 and −541.133 864 au for bases STO-3G to 6-31G** in the order given in column 1.

[b]Geometry-optimized (correlation-gradient) MP2 (frozen core) computations of the conformers at 0° and 90° with the basis 6-31G* gave the barrier height, ΔE_0, as 18.56 kJ mol^{-1}; E_0 at 0° was −542.515 134 au.

[c]Computation of the zero-point energies for the planar and perpendicular conformers, as described in the text, gave ΔH_0 as 20.09 kJ mol^{-1}; the zero-point energy of the ground state is higher than that of the transition state by 1.39 kJ mol^{-1}.

[d]The barrier height is given by $V_2 + V_6$.

[e]In the fit to seven values of the relative computed energy, E_0, at 15° intervals in the torsion angle between 0° and 90°.

Table 2. V_2 values for 2,6-difluorobenzaldehyde as obtained[a] from the computed frequencies of torsion about the exocyclic C—C bond.

Method	υ_t(cm^{-1})	I_r(amu Å^2)	F[b]	V_2(kJ mol^{-1})
AM1	52.7	11.57	1.456	5.7
STO-3G	85.4	11.27	1.495	14.6
3-21G	100.5	10.84	1.555	19.4
6-31G	73.4	11.00	1.531	10.5
6-31G*	77.8	10.71	1.573	11.5
6-31G**	78.1	10.73	1.571	11.6

[a]V_2(cm^{-1}) = $\nu_t^2/4F$ where ν_t is given in cm^{-1}, I_r in amu Å^2, and F = 16.852/I_r.

[b]F is obtained from reduced moments of inertia based on the Pitzer formulation (15) and values are calculated with a locally written program using the computed geometries.

Table 1 presents the Fourier components of the computed internal rotational barriers of 2,6-difluorobenzaldehyde for various basis sets. In these computations, done at 15° intervals of the torsion angle, *all* other bond angles and lengths were optimized. An optimization was also performed with the 6-31G** basis in which all bond parameters, including the torsion angle, were allowed to vary. The result was that the torsion angle was zero (planar). Torsional frequencies were computed for the planar conformers, for which the "tight" option was chosen while computing the geometries. The torsional frequencies were used to compute V_2 values for the barriers (see Experimental); these are found in Table 2. Figure 1 presents the planar geometries found for 2,6-difluorobenzal-

Can. J. Chem. Downloaded from www.nrcresearchpress.com by 65.111.164.53 on 09/08/12
For personal use only.

Can. J. Chem. Downloaded from www.nrcresearchpress.com by 65.111.164.53 on 09/08/12
For personal use only.

Table 3. The AM1, 6-31G**, and correlation-gradient MP2/6-31G* internal barriers and the $\Delta G^{\ddagger}$ values[a] for benzaldehyde and four of its symmetrically substituted fluorine derivatives.

Compound	AM1[b]	6-31G**	MP2/6-31G*	$\Delta G^{\ddagger}$	μ[i]
C_6H_5CHO	11.2(21.3)	37.2[c]	35.4[d]	32.3(6)[f]	3.2[j]
4-F	11.9(22.6)	39.9	36.8	34.4(8)[g]	2.0[k]
3,5-di F	9.1(17.3)	32.8	34.6[e]	28.0(5)[h]	2.0[l]
2,4,6-tri F	9.9(18.8)	23.9	20.1	20.0(5)	~3.0[m]
2,6-di F	9.2(17.5)	21.5	18.6	18.8(5)	~4.2[m]

[a]In kJ mol^{-1}.

[b]Numbers in parentheses are greater by a factor of 1.9 (see text).

[c]The planar conformers have energies, in order down the column, of −343.444 137, −442.293 979, −541.139 250, −639.981 977, and −541.133 864 au.

[d]For these correlation gradient computations, the planar conformers have energies (down the column) of −344.486 360, −443.505 275, −542.521 821, −641.531 898, and −542.515 134 au.

[e]This number is of questionable quality. For the other four compounds the 6-31G* and 6-31G** barriers differ by less than 0.1 kJ mol^{-1} (see Table 1, for example). For 3,5-difluorobenzaldehyde, the 6-31G* barrier is 1.4 kJ mol^{-1} higher than that from the 6-31G** barrier and the correlation-gradient computation is higher yet, by 1.2 kJ mol^{-1} relative to the 6-31G* result.

[f]The mean of three values (16–18).

[g]The mean of two values (11–19).

[h]From ref. 14.

[i]The dipole moment in units of debye.

[j]From ref. 20.

[k]From ref. 21.

[l]Taken as the dipole moment of 3,5-dichlorobenzaldehyde (22); the dipole moments of the 4-fluoro and 4-chloro derivatives are equal (21, 22).

[m]Estimated from STO-3G and 6-31G calculations as described in the text.

dehyde with the 6-31G** basis and with *geometry-optimized* MP2/6-31G* computations (frozen core). MP2 computations yield bond lengths much nearer the accepted values than does the RHF calculation. Bond angles, however, are less sensitive to correlation effects.

The zero-point energies of the planar and perpendicular forms of this molecule were obtained by scaling the computed frequencies by 0.89; the basis set was 6-31G**. The ΔE_0 value (absolute zero), 21.50 kJ mol^{-1} and identified with $V_2 + V_6$, thereby became a ΔH_0 value of 20.09 kJ mol^{-1}. The ΔE_0 value for the correlation-gradient MP2 computations with the 6-31G* basis was 18.56 kJ mol^{-1}.

AM1, 6-31G**, and correlation-gradient MP2/6-31G* computations of ΔE_0 (spectroscopic barriers) are collected in Table 3 for benzaldehyde and four of its symmetrically fluorinated derivatives. $\Delta G^{\ddagger}$ values and dipole moments are also given for these molecules.

Discussion

The free energy barrier in 2,6-difluorobenzaldehyde

The $\Delta G^{\ddagger}$ of about 19 kJ mol^{-1} for 2,6-difluorobenzaldehyde at 110 K is roughly 13 kJ mol^{-1} lower than that of 32 kJ mol^{-1} at 160 K, also in dimethyl ether, for benzaldehyde (18). It is likely that dipole–dipole repulsion between $C^+{=}O^-$ and *ortho* C^+—F^- bonds accounts[3] for much of the decrease in $\Delta G^{\ddagger}$. In addition, steric repulsion between fluorine and oxygen atoms is also important, the interatomic distance of 2.5 Å being rather smaller than the sum of their van der Waals radii, 2.7$_6$ Å. This suggestion is in line with the observation that in 2,6-dichlorobenzaldehyde the barrier to internal rotation is much lower than in the fluoro analog and leads to a relatively large magnitude (23) of ^6J(H,CHO), an indicator of nonplanarity. Yet the C^+—Cl^- bond dipole is very nearly of the same magnitude as that of a C^+—F^- dipole and the O,Cl and O,F distances in the planar forms are almost exactly the same; the van der Waals radius of chlorine is, however, the larger. Repulsion between the C=O and C—F dipoles is also indicated by the free energy differences between the O-*cis* and O-*trans* conformers of 2-fluorobenzaldehyde (24); they are 7.6 ± 0.3 kJ mol^{-1} in CS_2 solution at 300 K and 4.5 ± 0.2 kJ mol^{-1} in acetone-d_6 solution, favoring the O-*trans* conformer. The two π donors in 2,6-difluorobenzaldehyde will stabilize the planar ground state, by how much is not known, countering the dipolar and steric destabilizations. Note that, to within experimental error, the increase in $\Delta G^{\ddagger}$ of 1.2 ± 1.0 kJ mol^{-1} caused by a 4-fluoro substituent, forming the 2,4,6-trifluoro derivative, is the same as the increase of 2.1 ± 1.4 kJ mol^{-1} in $\Delta G^{\ddagger}$ measured for 4-fluorobenzaldehyde relative to the parent compound.

As to the stabilization of the ground state by the solvent, at least the dipole moments of the planar and perpendicular conformers are needed for a first-order calculation in reaction field theory (25). The dipole moment of 2,6-difluorobenzaldehyde is not known. However, the experimental dipole moment of 2-fluorobenzaldehyde is reasonably well reproduced by the mean of the values calculated with the STO-3G and 6-31G bases (24). For the 2,6-difluoro derivative, the corresponding means is 4.15 D for the planar and 3.78 D for the perpendicular form. The dimethyl ether solution at 110 K is taken to have a dielectric constant of 12 (p. 567 of ref. 25), with the result that the ground state is stabilized by only 1.8 kJ mol^{-1}. A similar number would be calculated for benzaldehyde itself, indicating that a large second-order, quadrupolar, term would be needed to account for the large solvent effect (as indicated by the torsional frequencies) of about 6–8 kJ mol^{-1} on the barrier of this molecule.

Now, if the solvent stabilization of the ground state of the present two benzaldehyde derivatives is also large, as for benzaldehyde, then their internal barriers in the vapor should be some 6 kJ mol^{-1} less than in solution, a supposition to be addressed by the following discussion.

The theoretical barriers for 2,6-difluorobenzaldehyde

The theoretical barrier heights for the 2,6-difluoro compound (Table 1), ignoring the 3-21G result, range from 9.3 kJ mol^{-1} (AM1) to 21.5 kJ mol^{-1} (6-31G**) with the RHF geometry optimizations. An optimized MP2 calculation predicts the energy difference of planar and perpendicular forms as 18.6 kJ

[3] The dipolar repulsion is not sufficient to destroy the planarity of the molecule in its stable form, according to the molecular orbital calculations in the previous section. Also, a substantial deviation from planarity would have been manifested (23) by a measurable ^6J(H-4,CHO), whose magnitude, however, we find to be at <0.03 Hz (unpublished).

Can. J. Chem. Downloaded from www.nrcresearchpress.com by 65.111.164.53 on 09/08/12
For personal use only.

mol^{-1}. The barrier heights correspond to predominantly V_2 values; the V_4 components contribute not more than 10% to the barrier shape and not to the height. The V_6 terms do contribute to the height but are very small.

It has been suggested (6, 7) that an AM1 barrier for benzaldehydes should be scaled by a factor of 1.9. In the case it would yield 17.5 kJ mol^{-1}, not far from most of the values in Table 1 and close to the MP2 estimate of 18.6 kJ mol^{-1}. The implication would be (6, 7) that the internal barrier for the free molecule is also reasonably well given by the largest basis sets in Table 1. In the computations on benzaldehyde and some of its *para*-substituted derivatives, various basis sets were used to calculate υ_t, the fundamental torsional frequency about the C—CHO bond. For example, for benzaldehyde the STO-3G basis gave υ_t as 111.11 cm^{-1}, the measured value being 110.9 cm^{-1}. A V_2 then follows (footnote *a* in Table 2) in the manner employed by molecular spectroscopists. The curious result is that the computed V_2, while necessarily in agreement with the experimental value, is rather smaller than the energy difference between planar and perpendicular forms computed with the same basis.

Table 2 presents data bearing out this curious fact also for 2,6-difluorobenzaldehyde. The V_2 values entailed by the computed torsional frequencies are as much as 10 kJ mol^{-1} lower than the computed energy differences. Of course, the negative V_4 components in the theoretical potential curves somewhat alter the slope of the curve near the planar conformer and could account for part of the discrepancies. No experimental value of υ_t is available for the molecule in the vapor or liquid phase. Harrison and Green found 118 and 58 cm^{-1} for vibrations of the proper symmetry for υ_t in gaseous pentafluorobenzaldehyde, but state that there is no certain way of treating either of these modes as a purely torsional motion (26). Treatment of these modes as pure torsions yields V_2 values of 29.6 or 7.5 kJ mol^{-1}; it is suggested (26) that the true barrier lies between these extremes.

Comparison of $\Delta G^{\ddagger}$ and theoretical barriers for 2,6-difluorobenzaldehyde

A $\Delta G^{\ddagger}$ is not a V_2, of course, nor, equivalently, a ΔE_0, the computed energy difference at absolute zero. To obtain a ΔH_0, correction of ΔE_0 for zero-point energies is necessary. The latter were computed with the 6-31G** basis set for 2,6-difluorobenzaldehyde, giving ΔH_0 as 20.09 kJ mol^{-1}, smaller by 1.4 kJ mol^{-1} than ΔE_0; the computed frequencies had been scaled by a factor of 0.89. Now, an approximation to $\Delta H^{\ddagger}$ can be had (13, 27) by allowing for the loss of a vibrational degree of freedom in the transition state. In the presence case, one then has $\Delta H^{\ddagger}$ as ΔH_0–0.5 kJ mol^{-1}, or 19.6 kJ mol^{-1}. $\Delta H^{\ddagger}$ could not be measured by DNMR, obviously, so that an estimate of $T\Delta S^{\ddagger}$ is desirable. Use of eqs. 7.9d of ref. 27, assuming a υ_t of 85 cm^{-1} and that the transition state can be reached in two ways from the planar ground state, yields $\Delta G^{\ddagger}_{110} = \Delta H^{\ddagger} - T\Delta S^{\ddagger} = 19.6 - 0.6$ or 19.0 kJ mol^{-1}. The $\Delta S^{\ddagger}$ of 5.5 J mol^{-1} K^{-1} is rather smaller than the 15 J mol^{-1} K^{-1} obtained for benzaldehyde in dimethyl ether solution by DNMR; the range of temperature in this experiment was only 21°, however, so that a rather large error must be expected (18). Of course, had the MP2 result of 18.6 kJ mol^{-1} for ΔE_0 been used in this path towards $\Delta G^{\ddagger}$, assuming the same magnitudes of corrections, the estimated value of $\Delta G^{\ddagger}_{110}$ would be 16.1 kJ mol^{-1} for the free molecule. An error estimate is hardly reliable, that is, what the errors are in the approximations needed to arrive at $\Delta H^{\ddagger}$ and $\Delta S^{\ddagger}$ values from ΔE_0. Nevertheless, if this value of $\Delta G^{\ddagger}_{110}$ is taken as given, then the solvent causes an increase of 2.7 ± 0.5 kJ mol^{-1} in $\Delta G^{\ddagger}$; the dipole term in the reaction field model is estimated above as 1.8 kJ mol^{-1}. In these terms the MP2/6-31G* (a correlation-gradient calculation) value for ΔE_0, and therefore for V_2, of 18.6 kJ mol^{-1} would appear to be reasonably accurate. Such a barrier corresponds to a pure torsional frequency of 98.8 cm^{-1} for a twofold potential. Should a considerably lower frequency be found for a vibrational mode of 2,6-difluorobenzaldehyde in the vapor phase and a higher one in solution (see Table 2), the same situation as for benzaldehyde will arise: a large apparent solvent effect on the internal barrier, as indicated by υ_t, contrasting with a larger barrier calculated by present methods for the free molecule and therefore a closer agreement with (corrected) $\Delta G^{\ddagger}$ values as measured by DNMR in solution. In any event, the present experimental value of $\Delta G^{\ddagger}$ is less than 60% as large as that for benzaldehyde. It will be of interest to see how the various arguments (7, 8) about he proper approach to the computation of carbonyl group rotation will be resolved in the case of the difluoro derivative.

2,4,6-Trifluorobenzaldehyde and 3,5-difluorobenzaldehyde

The computed spectroscopic barriers for the trifluoro derivative are 9.9 kJ mol^{-1} (AM1) and 23.9 kJ mol^{-1} (6-31G**). The increase of 2.4 kJ mol^{-1} (6-31G**) relative to the 2,6-difluoro derivative is qualitatively consistent with the presence of the π-electron donor in the *para* position and with the difference in $\Delta G^{\ddagger}$ values measured for the two compounds. For the 3,5-difluoro compound the AM1 and 6-31G** spectroscopic barriers are 9.1 and 32.8 kJ mol^{-1}, respectively, and the latter is 4.4 kJ mol^{-1} lower than calculated for benzaldehyde (Table 3). The $\Delta G^{\ddagger}$ values also differ by 4.3 ± 1.0 kJ mol^{-1} (14).

Empirical relationship between ΔE_0 and $\Delta G^{\ddagger}$

Whatever the merits of the previous discussion of 2,6-difluorobenzaldehyde, the $\Delta G^{\ddagger}$ values in Table 3 correlate reasonably well with the ΔE_0 (spectroscopic barriers) values obtained from 6-31G** and MP2/6-31G* geometry-optimization procedures.[4] One has ΔE_0 (6-31G**) = 1.14 $\Delta G^{\ddagger}$ + 0.54 (r = 0.999) in units of kJ mol^{-1}. Also, ΔE_0 (MP2/6-31G*) = 1.19 $\Delta G^{\ddagger}$ – 3.8 (r = 0.999) if the numbers for 3,5-difluorobenzaldehyde are omitted (see footnote *e* in Table 3 for the difficulties encountered in the correlation-gradient computations for this compound).

The correlation-gradient MP2/6-316*spectroscopic barriers in Table 3 are 1.8 – 3.8 kJ mol^{-1} lower than those for the 6-31G** basis set (again ignoring the data for 3,5-difluorobenzaldehyde). For benzaldehyde the correlation-gradient procedure yields a barrier that is 0.6 kJ mol^{-1} lower in energy than the corresponding single-point computation (5). Further, a single-point calculation (5), MP2/6-311G*//6-31G*, at 34.7 kJ mol^{-1}, for the barrier is 0.7 kJ mol^{-1} lower than the 35.4 kJ

[4] Such correlations are not peculiar to fluorobenzaldehydes. For benzaldehyde and some 4-X derivatives, X = F, CN, OH, one has (5) that ΔE_0 (6-31G*) = 1.00 $\Delta G^{\ddagger}$ – 5.5 (r = 0.996) in units of kJ mol^{-1}.

Can. J. Chem. Downloaded from www.nrcresearchpress.com by 65.111.164.53 on 09/08/12
For personal use only.

mol^{-1} obtained in Table 3 for the geometry optimized MP2/6-31G* procedure. A correlation-gradient MP2 computation with the 6-311G* basis, not at present feasible with our computing resources, might therefore cause a further lowering of about 1 kJ mol^{-1} in the spectroscopic barrier that, however, is then still larger than $\Delta G^{\ddagger}$ and very much larger than the V_2 obtained from spectroscopic work.

The measured and estimated dipole moments in Table 3 imply that first-order solvent perturbations of the $\Delta G^{\ddagger}$ values are rather different fro the various molecules and would in any event not exceed about 2 kJ mol^{-1}. A solvent effect on the barrier, proportional to $\Delta G^{\ddagger}$, consistent with the linear correlation above, would therefore be unexpected. The AM1 barriers in parentheses, recommended (7) as reliable for the free molecules, illustrate, first, the large discrepancy between the various approaches to the barriers for the first three compounds and, second, that the recommendation (7), if correct for these compounds, cannot also be correct for the 2,6-difluoro derivatives.

Conclusion

The present experiments and (or) computations on benzaldehyde and four of its symmetrical fluorine derivatives suggest to us that the internal barrier to rotation in benzaldehyde is modified relatively little by the presence of solvent molecules and that, therefore, the barriers deduced from torsional frequencies are too small (8). In this connection, the comparison of computed barriers with those calculated form the computed torsional frequencies in Table 2 is important. Again, in our opinion the scaled (6) AM1 barriers in Table 3, having a range of only 5 kJ mol^{-1} for the five compounds, are inadequate.

Experimental

DNMR measurements

The $^{19}F\{^1H\}$ spectra of 2,6-difluorobenzaldehyde and 2,4,6-trifluorobenzaldehyde in dimethyl ether solutions at low temperatures were accumulated on Bruker AM 300 and WH 90 nmr spectrometers in a manner described previously for 4-bromo-2,6-difluoro-*N*-methylaniline (28). At 120 K the spectrum of the *para*-fluorine nucleus is a triplet (^4J = 11.0(1) Hz) while at lower temperatures the peaks broaden to essentially obscure the fine structure. At 110 K the *ortho*-fluorine nuclei give rise (84.7 MHz) to an incompletely separated doublet with a spacing of 350 Hz. At lower temperatures the signal disappears due to freezing or precipitation of solute. At 112 K the peaks coalesce to a singlet with a flat top and a width at half height of 550 Hz. The width of the signal from the *para*-fluorine nucleus is 41.0 Hz; this width includes 22 Hz from the $^4J(F_o,F_p)$ of 11 Hz, which also contributes to the line widths of the signal from the *ortho* fluorine nuclei. An analysis of the ^1H and ^{19}F nmr spectra of the compound at 300 K (CS_2/C_6D_{12} solution) showed that the coupling constant for the *ortho*-fluorine nuclei was 2.80 Hz. At coalescence, the width at half height for a simple, uncoupled AX system equals the chemical shift in the absence of exchange. Allowing for an error of 10% in the correct width at coalescence, and therefore in the rate constant, and 2° in T_c, yields $\Delta G^{\ddagger}_{110}$ as 20.0 ± 0.5 kJ mol^{-1} (eq. 7.13c of ref. 27).

Assessment of $\Delta G^{\ddagger}$ for 2,6-difluorobenzaldehyde depended on the reasonable assumption that the peak separation at slow exchange would be the same as for the trifluoro derivative. The coalescence temperature could not be reached in the sense that the sample "froze out" at 107 K. At 110 K the width at half height was 121 ± 2 Hz (84.7 MHz), whereas the reference compound, C_6F_6, had a width of 24 Hz. Measurements of this kind were also made at 120 and 130 K at 84.7 MHz and at 130 and 135 K at 284.3 MHz. Use of eq. 6.2d in ref. 27 and the assumption that the internal shift is 530 Hz for slow exchange gave $\Delta G^{\ddagger}110$ as 18.8 ± kJ mol^{-1}. This number reproduced the measured peak widths reasonably well at the different resonance frequencies and temperatures. For example, at 130 K and 84.7 MHz, $\Delta G^{\ddagger}$ values of 19.3 and 18.3 kJ mol^{-1} imply line widths of 9.3 and 3.7 Hz, respectively; the measured value is 7.7 Hz, corresponding actually to a $\Delta G^{\ddagger}$ of 19.0 kJ mol^{-1}. Again, because an analysis of the ^1H and ^{19}F nmr spectra of a CS_2/C_6D_{12} solution gave ^4J(F,F) as 3.2 Hz, its presence alters the analytical approach very little (compare 530 Hz for the internal shift in the absence of exchange). The coalescence temperature at 300 MHz is calculated as 112 ± 2 K; unfortunately such a temperature could not be reached on the AM 300.

Molecular orbital calculations

The program GAUSSIAN 92 (29) was used in all molecular orbital computations, employing the AM1 (30) parameterization, as well as the STO-3G (31), 3-21G (32), 6-31G (33), 6-31G* (34), and 6-31G** (34) basis sets in the ab initio procedure. The energy of the 2,6-difluorobenzaldehyde molecule was calculated at 15° intervals, between 0° and 90°, of the angle of torsion about the exocyclic C—C bond. During these optimizations *all* other bond angles and lengths were allowed to vary. These computations were performed with normal thresholds, as were the geometry-optimized MP2 computations (frozen core) with the 6-31G* basis. For purposes of computing vibrational frequencies the optimizations were done using the "tight" option, where final forces (hartrees Bohr^{-1} or hartrees radian^{-1}) and displacements (Bohr or radian) were all less than 0.00002.

Acknowledgment

We are grateful to the Natural Sciences and Engineering Research Council of Canada for financial assistance.

References

1. R.J. Kakar, E.A. Rinehart, C.R. Quade, and T. Kojima. J. Chem. Phys. **52**, 3803 (1970).
2. L.A. Glebova, Yu. A. Pentin, and V.I. Tyulin. Vestn. Mosk. Univ., Khim. Ser. **2**, 21 (1980).
3. J.R. Durig, H.D. Bist, K. Furic, J. Qui, and T.S. Little. J. Mol. Struct. **129**, 45 (1985).
4. M. Head-Gordon and J.A. Pople. J. Phys. Chem. **97**, 1147 (1993).
5. T. Schaefer, R. Sebastian, and F.E. Hruska. J. Mol. Struct. (Theochem), **281**, 269 (1993).
6. B. Coussens, K. Pierloot, and R.J. Meier. J. Mol. Struct. (Theochem), **259**, 331 (1992).
7. R.J. Meier. J. Phys. Chem. **97**, 10248 (1993).
8. M. Head-Gordon and J.A. Pople. J. Phys. Chem. **97**, 10250 (1993).

9. F.A. Miller, W.G. Fateley, and R.E. Witkowski. Spectrochim. Acta, Part A, **23**, 891 (1967).
10. H.C. Silver and J.L. Wood, Trans. Faraday Soc. **60**, 5 (1964).
11. T. Drakenberg, J. Sommer, and R. Jost. J. Chem. Soc. Perkin Trans. 2, 363 (1980).
12. D.M. Doddrell, M.R. Bendall, P.F. Barron, and T.D. Pegg. J. Chem. Soc. Chem. Commun. 77 (1979).
13. J. Kowalewski and T. Liljefors. Chem. Phys. Lett. **64**, 170 (1979).
14. T. Schaefer and C.S. Takeuchi. Can. J. Chem. **67**, 827 (1989).
15. K.S. Pitzer. J. Chem. Phys. **14**, 239 (1946).
16. F.A.L. Anet and M. Ahmad. J. Am Chem. Soc. **86**, 119 (1964).
17. T. Drakenberg, R. Jost, and J.M. Sommer. J. Chem. Soc. Chem. Commun. 1011 (1974).
18. L. Lunazzi, D. Maccientelli, and A. Boicelli. Tetrahedron Lett. 1205 (1975).
19. T.B. Grindley, A.R. Katritzky, and R.D. Topsom. J. Chem. Soc. Perkin Trans. 2, 443 (1975).
20. Y. Kawashima and K. Kozima. Bull. Chem. Soc. Jpn. **47**, 2879 (1974).
21. N.J. Leonard and L.E. Sutton. J. Am Chem. Soc. **70**, 1564 (1948).
22. R.A.Y. Jones, A.R. Katritzky, and A.V. Ochkin. J. Chem. Soc. B, 1795 (1971).
23. T. Schaefer, J. Peeling, G.H. Penner, A. Lemire, and R. Laatikainen. Can. J. Chem. **64**, 1859 (1986).
24. T. Schaefer and C.S. Takeuchi. Can. J. Chem. **68**, 339 (1990).
25. R.J. Abraham and E. Bretschneider. *In* Internal rotation in molecules. *Edited by* W.J. Orville-Thomas. J. Wiley and Sons, New York. 1974. Chap. 13.
26. J.H.S. Green and D.J. Harrison. J. Chem. Thermodyn. **8**, 529 (1976).
27. J. Sandström. Dynamic nmr spectroscopy. Academic Press, New York. 1982.
28. T. Schaefer, G.H. Penner, K. Marat, and R. Sebastian. Can. J. Chem. **62**, 2686 (1984).
29. M.J. Frisch, G.W. Trucks, M. Head-Gordon, P.M.W. Gill, M.W. Wong, J.B. Foresman, B.G. Johnson, H.B. Schlegel, M.A. Robb, E.S. Replogle, R. Gomperts, J.L. Andres, K. Raghavachari, J.S. Binkley, C. Gonzalez, R.L. Martin, D.J. Fox, D.J. Defrees, J. Baker, J.J.P. Stewart, and J.A. Pople. GAUSSIAN 92, Revision C. Gaussian, Inc., Pittsburg, Pa. 1992.
30. M.J.S. Dewar, E.J. Zoebisch, E.F. Healy, and J.J.P. Stewart. J. Am Chem. Soc. **107**, 3902 (1985).
31. W.J. Hehre, R.F. Stewart, and J.A. Pople. J. Chem. Phys. **51**, 2657 (1969).
32. J.S. Binkley, J.A. Pople, and W.J. Hehre. J. Am. Chem. Soc. **102**, 939 (1980).
33. W.J. Hehre, R. Ditchfield, and J.A. Pople. J. Chem. Phys. **56**, 2257 (1972).
34. P.C. Hariharan and J.A. Pople. Chem. Phys. Lett. **66**, 217 (1972).
35. O.L. Stiefvater. Z. Naturforsch. A: Phys. Phys. Chem. Kosmophys. **43A**, 155 (1988).

Can. J. Chem. Downloaded from www.nrcresearchpress.com by 65.111.164.53 on 09/08/12
For personal use only.

Stepwise synthesis of selenium coronands containing an odd number of selenium atoms: 1,5,9-triselenacyclododecane and 1,5,9,13,17-pentaselenacycloeicosane

Ivan Cordova-Reyes, Elizabeth VandenHoven, Ali Mohammed, and B. Mario Pinto

Can. J. Chem. Downloaded from www.nrcresearchpress.com by 65.111.164.53 on 09/08/12
For personal use only.

Abstract: The stepwise synthesis of two new selenium coronands containing an odd number of selenium atoms, starting from the fragments HO-$(CH_2)_3$-Cl, HO-$(CH_2)_3$-Br, HO-$(CH_2)_3$-SeCN, and NCSe-$(CH_2)_3$-SeCN, is described. The key diol containing one selenium atom, 4-selenaheptan-1,7-diol **4**, was obtained in 97% yield from the reaction of 3-bromo-1-propanol **3** and the selonolate anion derived from 3-selenocyanato-1-propanol **2** by sodium metal reduction in liquid ammonia. The ditosylate **5**, obtained from **4**, was then treated with the bisselenolate anion derived from 1,3-bisselenocyanatopropane **6** to give the target selenium coronand, 1,5,9-triselenacyclododecane [12Se3] **7**, in 96% yield. The ditosylate **5** was treated with two equivalents of the selenolate anion derived from **2** to give a second key acyclic diol **8** now containing three selenium atoms. The ditosylate **9**, obtained from **8**, was then treated with the bisselenolate anion derived from **6** to afford the second target coronand, 1,5,9,13,17-pentaselenacycloeicosane [20Se5] **11** in 44% yield.

Key words: selenium coronands, stepwise synthesis, macrocycles, heterocycles.

Résumé : Utilisant des fragments OH-$(CH_2)_3$-Cl, HO-$(CH_2)_3$-Br, HO-$(CH_2)_3$-SeCN et NCSe-$(CH_2)_3$-SeCN, on a réalisé la synthèse par étapes de deux nouveaux coronands du sélénium contenant un nombre impair d'atomes de sélénium. On a obtenu le diol clé contenant un atome de sélénium, le 4-sélénahepta-1,7-diol (**4**), avec un rendement de 97% par la réaction du 3-bromopropan-1-ol (**3**) avec l'anion sélénolate dérivé du 3-sélénocyanatopropan-1-ol (**2**) par réduction avec du sodium métallique dans l'ammoniac liquide. On traite alors le ditosylate **5**, obtenu à partir du composé **4**, avec l'anion bissélénolate dérivé du 1,3-bissélénocyanatopropane **6** pour obtenir le coronand sélénié désiré, le 1,5,9-trisélénacyclododécane [12Se3] (**7**), avec un rendement de 96%. On traite le ditosylate **5** avec deux équivalents de l'anion sélénolate obtenu à partir du composé **2**, pour obtenir le deuxième diol acyclique clé (**8**) qui contient maintenent trois atomes de sélénium. Le ditosylate **9**, obtenu à partir du produit **8**, est alors traité par l'anion bissélénolate dérivé du composé **6** pour fournir le deuxième coronand désiré, le 1,5,9,13,17-pentasélénacycloeicosane [20Se5] (**11**), avec un rendement de 44%.

Mots clés : coronands du sélénium, synthèse par étapes, macrocycles, hétérocycles.

[Traduit par la rédaction]

Introduction

There have been relatively few reports of the synthesis of selenium coronands. To the best of our knowledge, prior to our report of the serendipitous discovery of the simple selenium coronands in 1988 (1, 2), the only macrocyclic seleno ethers reported were the cyclic oligomers of selenaformaldehyde (3), diselenacyclophanes (4), and a selenium porphyrin derivative (5). Since our initial disclosure, we have reported the one-step syntheses of other prototype selenium coronands (6) and there have been reported syntheses of other macrocyclic diselena ethers (7), selenium porphyrin derivatives (8), tetraselena-3,4-benzocyclooctadecane, (9) mixed selena oxa macrocyclic ethers (9–12), and a tetraselenacyclohexadecine bis-naphthalene derivative (13).

It is also surprising, given the current interest in chalcogen macrocycles as models for metalloenzymes and metalloproteins and in the structure and bonding of metal–chalcogen macrocyclic complexes (see, for example, ref. 14), that there have not been more reports of the metal-ion complexes of these compounds. To date, we have reported the electron transfer reaction of the first metal-ion complex of a selenium coronand, the Cu(II) complex of 1,5,9,13-tetraselenacyclohexadecane (16Se4) (15), and Kelly et al. (16) have reported

Received August 17, 1994.

I. Cordova-Reyes, E. VandenHoven, A. Mohammed, and B.M. Pinto.[1] Department of Chemistry, Simon Fraser University, Burnaby, BC V5A 1S6, Canada.

[1] Author to whom correspondence may be addressed. Telephone: (604) 291-4327. FAX: (604) 291-3765. e-mail:

Can. J. Chem. Downloaded from www.nrcresearchpress.com by 65.111.164.53 on 09/08/12
For personal use only.

Scheme 1

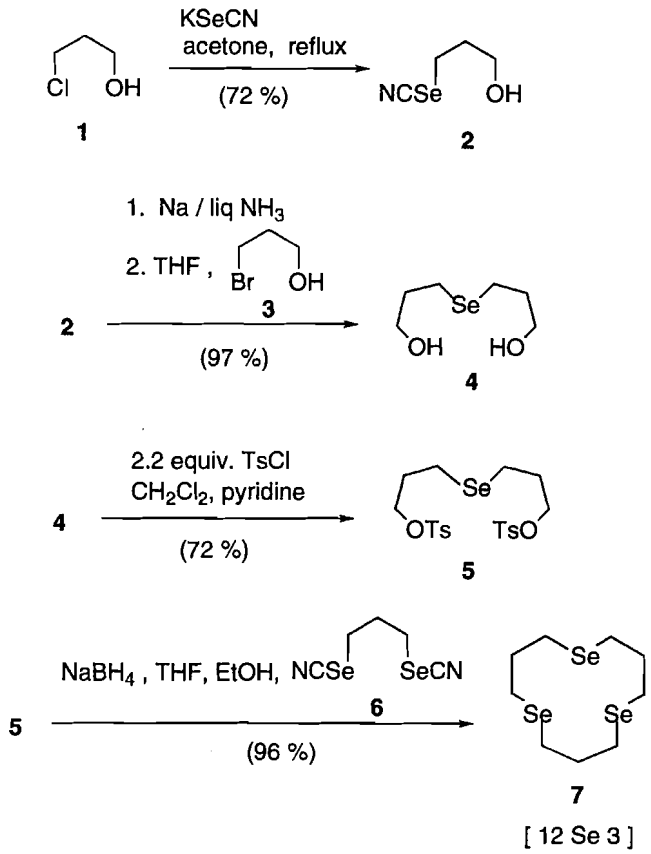

Scheme 2

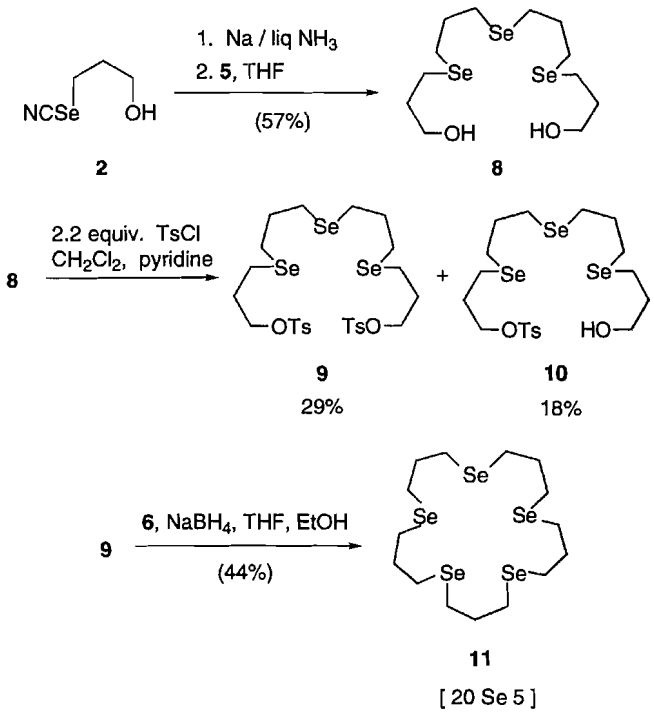

the synthesis of a Rh(III) complex of 16Se4. We have also reported the study of the adducts of 16Se4 with Cu(I) triflate and Hg(II) cyanide (17) and communicated our results on Cu(I), Cu(II), and Pd(II) complexes of the prototype selenium coronands (18). Three other reports of transition metal-ion complexation by macrocyclic selena ethers have also appeared (7, 9, 12).

The reported one-step synthesis of selenium coronands (1, 2, 6) is ideally suited to the synthesis of macrocycles containing an even number of constituent selenium atoms. To expand the repertoire of available selenium coronands and in the interest of developing more efficient synthetic routes, we chose to examine the stepwise synthesis of selenium coronands. We report herein the stepwise synthesis of two new selenium coronands containing an odd number of selenium atoms starting from the fragments HO-$(CH_2)_3$-Cl, HO-$(CH_2)_3$-Br, HO-$(CH_2)_3$-SeCN, and NCSe-$(CH_2)_3$-SeCN.

Results and discussion

3-Chloro-1-propanol **1** was converted to the key unit, 3-selenocyanato-1-propanol **2**, in 72% yield by treatment with potassium selenocyanate in refluxing acetone (Scheme 1). Reductive cleavage of the Se—CN bond in **2** with sodium in liquid ammonia then gave the selenolate anion, which was reacted with 3-bromo-1-propanol **3** to give 4-selenaheptan-1,7-diol **4** in 97% yield. Functionalization of the diol as the bis-*p*-toluenesulfonate gave **5** in 72% yield. Treatment of this unit with sodium propane-1,3-bisselenolate, derived from the borohydride reduction of propane-1,3-bisselenocyanate **6** (19), then afforded the target selenium coronand, 1,5,9-triselenacyclododecane [12Se3] **7** in 96% yield. The optimum conditions for the latter reaction consisted of the simultaneous addition of the ditosylate **5** and the bisselenocyanate **6** to a suspension of sodium borohydride in ethanol and THF over a period of 20 h.

The synthesis of the higher homologue containing five selenium atoms was executed in an analogous manner with common building units. Thus, treatment of the ditosylate **5** with 2 equivalents of the selenolate anion derived from 3-selenocyanato-1-propanol **2** afforded the acyclic derivative **8** containing three selenium atoms in 57% yield (Scheme 2). Tosylation of compound **8** proceeded in modest yield to give a mixture of the desired ditosylate **9** and the monotosylate **10**. Cyclization with sodium propane-1,3-bisselenocyanate, as described above for the case of **7**, then afforded the target coronand, 1,5,9,13,17-pentaselenacycloeicosane [20Se5] **11**, in 44% yield.

The syntheses described above represent the first examples of stepwise syntheses of selenium coronands from simple units and of selenium coronands containing an odd number of selenium atoms. The compounds will serve as new candidates for study of the metal-ion complexation behaviour of selenium coronands and their electron-transfer chemistry.

Experimental

Melting points were determined on a Fisher–Johns melting point apparatus and are uncorrected. ^{1}H NMR, ^{13}C NMR, and ^{77}Se NMR spectra were recorded on a Bruker AMX-400 NMR spectrometer at 400.13, 100.6, and 76.3 MHz, for proton, carbon, and selenium, respectively. All spectra were recorded in deuterochloroform and chemical shifts are given in ppm downfield from TMS. Chemical shifts and coupling constants were obtained from a first-order analysis of the spectra. For

Can. J. Chem. Downloaded from www.nrcresearchpress.com by 65.111.164.53 on 09/08/12
For personal use only.

the ^{77}Se NMR spectra, chemical shifts are given in ppm downfield from Me_2Se. Chemical ionization mass spectra were measured on a Hewlett–Packard HP-5985 mass spectrometer with isobutane as the reacting gas.

Analytical thin-layer chromatography (TLC) was performed on aluminum plates precoated with Merck silica gel 60F-254 as the adsorbent. The developed plates were air-dried, exposed to UV light and (or) sprayed with 5% sulfuric acid in ethanol, and heated at 150°C. Compounds were purified by flash chromatography on Kieselgel 60 (230–400 mesh).

Solvents were distilled before use and were dried, as necessary, by literature procedures. Solvents were evaporated under reduced pressure and below 40°C. Reactions performed under nitrogen were effected by means of standard Schlenk-tube techniques.

Microanalyses were performed by M.K. Yang of the Microanalytical Laboratory of Simon Fraser University.

3-Selenocyanato-1-propanol (2)

To a solution of 3-chloro-1-propanol (19.7 g, 0.208 mol) in spectral grade acetone (150 mL) was added potassium selenocyanate (30.0 g, 0.208 mol). The reaction mixture was refluxed overnight, filtered, and evaporated in vacuo to give a light yellow oil. Purification by silica gel flash chromatography (hexane:ethyl acetate (1:1)) gave **2** (24.5 g, 72%); ^1H NMR δ : 2.11 (2H, p, $CH_2(OH)CH_2CH_2SeCN$), 2.17 (1H, br s, $CH_2(OH)CH_2CH_2SeCN$), 3.20 (2H, t, $CH_2(OH)CH_2CH_2SeCN$), 3.77 (2H, t, $CH_2(OH)CH_2CH_2SeCN$); ^{13}C NMR δ : 26.4 ($CH_2(OH)CH_2CH_2SeCN$), 32.4 ($CH_2(OH)CH_2CH_2SeCN$), 60.4 ($CH_2(OH)CH_2CH_2SeCN$), 102.9 ($CH_2(OH)CH_2CH_2SeCN$). The compound was used in the next step without further characterization.

4-Selenaheptan-1,7-diol (4)

To 3-selenocyanato-1-propanol **2** (3.60 g, 21.95 mmol) in liquid ammonia (100 mL) and dry THF (40 mL) was added Na metal in small pieces until a colorless homogeneous solution was obtained. A solution of 3-bromo-1-propanol **3** (3.05 g, 21.95 mmol) in dry THF (30 mL + 3 × 5 mL rinse) was added dropwise. The ammonia was allowed to escape and the reaction mixture was diluted with water (250 mL) and extracted with methylene chloride (3 × 100 mL). The combined organic extracts were washed with water (100 mL), dried ($MgSO_4$), and evaporated in vacuo to yield a light yellow oil. Purification by silica gel chromatography (hexane:ethyl acetate (1:1)) gave **4** (4.1 g, 97%); ^1H NMR δ : 1.90 (4H, p, J = 6.2 Hz, $SeCH_2CH_2CH_2OH$), 2.65 (6H, t, J = 7.2 Hz, $SeCH_2CH_2CH_2OH$), 3.70 (4H, t, J = 6.1 Hz, $SeCH_2CH_2CH_2OH$); ^{13}C NMR δ : 20.2 ($SeCH_2CH_2CH_2OH$, J_{Se-C} = 55 Hz), 32.9 ($SeCH_2CH_2CH_2OH$), 61.8 ($SeCH_2CH_2CH_2OH$); CI MS, *m/e*: 198 (M^+ + 1 isotopic cluster). Anal. calcd. for $C_6H_{14}O_2Se$: C 36.56, H 7.16; found: C 36.38, H 7.21.

4-Selenaheptan-1,7-di-*p*-toluenesulfonate (5)

To a solution of **4** (6.21 g, 31.5 mmol) in CH_2Cl_2 (200 mL) and pyridine (17 mL, 220 mmol) was added dropwise a solution of *p*-toluenesulfonyl chloride (13.22 g, 69.3 mmol) in CH_2Cl_2 (50 mL). The reaction mixture was stirred at room temperature overnight, diluted to 300 mL with CH_2Cl_2, and washed with 10% HCl (3 × 200 mL), saturated $NaHCO_3$ (3 × 200 mL), water (300 mL), and brine (300 mL), dried ($MgSO_4$), and evaporated in vacuo to give a light yellow oil. Purification by silica gel flash chromatography (hexane:ethyl acetate (3:1)) gave **5** (11.50 g, 72%); ^1H NMR δ: 1.83–2.00 (4H, m, $SeCH_2CH_2CH_2OTs$), 2.44 (6H, s, Me), 2.49 (4H, t, J = 8.0 Hz, $SeCH_2CH_2CH_2OTs$), 4.07 (4H, t, J = 7.0 Hz, $SeCH_2CH_2CH_2OTs$), 7.33 (4H, d, J = 7.7 Hz, Ar), 7.77 (4H, d, J = 7.7 Hz, Ar); ^{13}C NMR δ: 18.9 ($SeCH_2CH_2CH_2OTs$), 21.3 (Me), 29.4 ($SeCH_2CH_2CH_2OTs$), 69.5 ($SeCH_2CH_2CH_2OTs$), 127.6 (C4′), 129.7 (C3′, C5′), 132.7 (C2′, C6′), 144.7 (C1′); CI MS, *m/e*: 506 (M^+ + 1 isotopic cluster). Anal. calcd. for $C_{20}H_{26}O_6S_2Se$: C 47.52, H 5.18; found: C 47.28, H 5.06.

1,5,9-Triselenacyclododecane (7)

To a suspension of $NaBH_4$ (0.15 g) in THF (100 mL) and EtOH (5 mL) was added simultaneously, via two separate dropping funnels, propane-1,3-bisselenocyanate **6** (19) (0.125 g; 0.5 mmol) and **5** (0.25 g; 0.5 mmol) each in THF:EtOH (80:20; 20 mL). The addition time was 20 h. The reaction mixture was filtered and evaporated in vacuo to give white crystals. These crystals were further purified by flash chromatography (hexane:ethyl acetate (3:1)) and recrystallized from hexane:ethyl acetate (3:1) to give long white needles **7** (0.175 g, 96%), mp 94–95.5°C; ^1H NMR δ: 2.01 (6H, p, J = 7.0 Hz, $SeCH_2CH_2CH_2Se$), 2.72 (12H, t, J = 7.0 Hz, $SeCH_2CH_2CH_2Se$); ^{13}C NMR δ: 22.5 ($SeCH_2CH_2CH_2Se$, J_{Se-C} = 31.4 Hz), 29.6 ($SeCH_2CH_2CH_2Se$); ^{77}Se NMR (76.3 MHz, $CDCl_3$) δ: 130; CI MS, *m/e*: 365 (M^++1 isotopic cluster). Anal. calcd. for $C_9H_{18}Se_3$: C 29.77, H 4.99; found: C 29.56, H 4.85.

4,8,12-Triselenapentadecan-1,15-diol (8)

To 3-selenocyanato-1-propanol **2** (325 mg, 1.98 mmol) in liquid ammonia (30 mL) was added Na metal in small pieces until a colorless homogeneous solution was obtained. Under a dry nitrogen environment, distilled THF (23 mL) was added to the reaction flask to dissolve the reduced selenium species. The liquid ammonia was removed under high vacuum until approximately 10 mL of THF solvent remained. Compound **5** (500 mg, 0.99 mmol) was dissolved in dry THF (2.5 mL) and then added dropwise to the oxygen-free system. The reaction mixture was stirred at room temperature overnight. The reaction mixure was then dissolved in distilled water (100 mL). The water layer was extracted with dichloromethane (3 × 45 mL). The CH_2Cl_2 layer was then washed once with distilled water (40 mL), dried over anhydrous $MgSO_4$, filtered, and evaporated in vacuo to yield a yellow oil. The yellow oil was further purified by flash chromatography (hexane:ethyl acetate (1:1)) to give **8** (248 mg, 57%); ^1H NMR δ: 1.84–1.96 (4H, m, $SeCH_2CH_2CH_2Se$), 1.96–2.05 (6H, m, $SeCH_2CH_2CH_2OH$), 2.59–2.69 (12H, m, $SeCH_2CH_2CH_2Se$, $SeCH_2CH_2CH_2OH$), 3.72 (4H, br t, J = 6.1 Hz, $SeCH_2CH_2CH_2OH$); ^{13}C NMR (100 MHz, $CDCl_3$) δ: 20.3 ($SeCH_2CH_2CH_2Se$), 23.7 ($SeCHCH_2CH_2OH$, J_{Se-C} = 31.4 Hz), 31.1 ($SeCH_2CH_2CH_2Se$), 33.0 ($SeCH_2CH_2CH_2OH$), 62.3 ($SeCH_2CH_2CH_2OH$); CI MS, *m/e*: 440 (M^+ + 1 isotopic cluster). Anal. calcd. for $C_{12}H_{26}O_2Se_3$: C 32.82, H 5.96; found: C 33.20, H 6.08.

4,8,12-Triselenapentadecane-1,15-di-*p*-toluenesulfonate (9) and 4,8,12-triselena-1-pentadecanol-15-*p*-toluenesulfonate (10)

To a solution of **8** (0.370 g, 0.842 mmol) in CH_2Cl_2 (15 mL)

Can. J. Chem. Downloaded from www.nrcresearchpress.com by 65.111.164.53 on 09/08/12
For personal use only.

was added dropwise a solution of p-toluenesulfonyl chloride (0.353 g, 1.85 mmol) in pyridine (0.47 mL, 5.89 mmol). The reaction mixture was stirred at room temperature for 17 h. The reaction mixture was diluted with CH_2Cl_2 (100 mL) and then washed with distilled water (3 × 40 mL), 10% HCl (3 × 40 mL), saturated $NaHCO_3$ (2 × 40 mL), and water (2 × 40 mL), dried (anhydrous $MgSO_4$), and evaporated in vacuo to give a light yellow oil. Purification by silica gel flash chromatography (hexane:ethyl acetate (3:1)) gave **9** (0.182 g, 0.244 mmol, 29%); R_f 0.27 in hexane:ethyl acetate (3:1), and **10** (0.090 g, 0.152 mmol, 18%); R_f 0.09 in hexane:ethyl acetate (3:1).

9. ^{1}H NMR δ: 1.85–2.00 (8H, m, $SeCH_2CH_2CH_2Se$, $SeCH_2CH_2CH_2OTs$), 2.44 (6H, s, Me), 2.50–2.70 (12H, m, $SeCH_2CH_2CH_2Se$, $SeCH_2CH_2CH_2$-OTs), 3.47 (4H, t, J = 6.0 Hz, $SeCH_2CH_2CH_2OTs$), 7.34 (4H, d, J = 8.1 Hz, Ar), 7.78 (4H, d, J = 8.1 Hz, Ar); ^{13}C NMR δ: 19.1 ($SeCH_2CH_2CH_2Se$), 21.6 ($SeCH_2CH_2CH_2OTs$), 23.6 ($SeCH_2CH_2CH_2Se$), 23.7 (Me), 29.8 ($SeCH_2CH_2CH_2Se$), 31.0 ($SeCH_2CH_2CH_2OTs$), 69.6 ($SeCH_2CH_2CH_2OTs$), 127.9 (C4′), 129.9 (C3′, C5′), 133.1 (C2′, C6′), 144.8 (C1′). Anal. calcd. for $C_{26}H_{38}O_6S_2Se_3$: C 41.77, H 5.12; found: C 41.59, H 4.99.

10. ^{1}H NMR δ: 1.85–2.00 (8H, m, $SeCH_2CH_2CH_2Se$, $SeCH_2CH_2CH_2OTs$), 2.44 (3H, s, Me), 2.50–2.70 (13H, m, $SeCH_2CH_2CH_2Se$, $SeCH_2CH_2$-CH_2OTs, $SeCH_2CH_2CH_2OH$), 3.47 (2H, t, J = 6.1 Hz, $SeCH_2CH_2CH_2OTs$), 3.72 (2H, t, J = 6.1 Hz, $SeCH_2CH_2CH_2OH$), 7.34 (2H, d, J = 8.0 Hz, Ar), 7.77 (2H, d, J = 8.3 Hz, Ar); ^{13}C NMR δ: 19.1 ($SeCH_2CH_2CH_2Se$), 20.3 ($SeCH_2CH_2CH_2Se$), 20.6 ($SeCH_2CH_2CH_2OH$), 21.6 ($SeCH_2CH_2CH_2OTs$), 23.6 ($SeCH_2CH_2CH_2Se$), 23.7 (Me), 29.8 ($SeCH_2CH_2CH_2Se$), 30.6 ($SeCH_2CH_2CH_2Se$), 31.0 ($SeCH_2CH_2CH_2$-OTs), 33.0 ($SeCH_2CH_2CH_2OH$), 62.4 ($SeCH_2$-CH_2CH_2OH), 69.6 ($SeCH_2CH_2CH_2OTs$), 127.9 (C4′), 129.9 (C3′, C5′), 133.1 (C2′, C6′), 144.8 (C_1′). Anal calcd. for $C_{19}H_{32}O_4SSe_3$: C 38.46, H 5.44; found: C 38.73, H 5.43.

1,5,9,13,17-Pentaselenacycloeicosane(11)

To a suspension of $NaBH_4$ (0.2 g) in THF:EtOH (80:20, 300 mL) was added, simultaneously in two separate dropping funnels, propane-1,3-bisselenocyanate **6** (19) (0.21 g, 0.83 mmol) and **9** (0.62 g, 0.83 mmol), each in THF:EtOH (80:20, 10 mL). The addition time was 20 h. The reaction mixture was filtered and evaporated in vacuo to give white crystals. Flash chromatography of the crude product with hexane:ethyl acetate (20:1) gave **11** (0.22 g, 44%) as white needles, mp 41–42°C; ^{1}H NMR δ: 2.03 (10H, p, J = 7.2 Hz, $SeCH_2CH_2$-CH_2Se), 2.69 (20H, t, J = 7.2 Hz, $SeCH_2CH_2CH_2Se$); ^{13}C NMR δ: 23.7 ($SeCH_2$-CH_2CH_2Se, $J_{^{13}C-Se}$ = 31 Hz), 31.3 ($SeCH_2CH_2CH_2Se$); ^{77}Se NMR δ: 152; CI MS, *m/e*: 606 (M^+ + 1 isotopic cluster). Anal. calcd. for $C_{15}H_{30}Se_5$: C 29.77, H 5.00; found: C 29.90, H 4.87.

Acknowledgments

We are grateful to the Natural Sciences and Engineering Research Council of Canada for financial support.

References

1. B.M. Pinto, B.D. Johnston, R.J. Batchelor, F.W.B. Einstein, and I.D. Gay. Can. J. Chem. **66**, 2956 (1988).
2. B.M. Pinto, R.J. Batchelor, B.D. Johnston, F.W.B. Einstein, and I.D. Gay. J. Am. Chem. Soc. **110**, 2990 (1988); B.M. Pinto, B.D. Johnston, R.J. Batchelor, and J.-H. Gu. J. Chem. Soc. Chem. Commun. 1087 (1988).
3. V.E. Weissflog. Z. Anorg. Allg. Chem. **488**, 60 (1982).
4. H. Higuchi and S. Misumi. Tetrahedron Lett. **23**, 5571 (1982); H. Higuchi, K. Tani, T. Otsubo, Y. Sakata, and S. Misumi. Bull. Chem. Soc. Jpn. **60**, 4027 (1987); R.H. Mitchell. Can. J. Chem. **58**, 1398 (1980); R.H. Mitchell, K.S. Weerawarna, and G.W. Bushnell. Tetrahedron Lett. **28**, 5119 (1987); R.H. Mitchell and K.S. Weerawarna. Tetrahedron Lett. **29**, 5587 (1988).
5. A. Ulman, J. Manassen, F. Frolow, and D. Rabinovitch. Tetrahedron Lett. 167 (1978).
6. R.J. Batchelor, F.W.B. Einstein, I.D. Gay, J.-H. Gu, B.D. Johnston, and B.M. Pinto. J. Am. Chem. Soc. **111**, 6582 (1989).
7. M. Hojjatie, S. Muralidharan, and H. Freiser. Tetrahedron, **45**, 1611 (1989).
8. E. Vogel, P. Rohrig, M. Sicken, B. Knipp, A. Herrmann, M. Pohl, H. Schmickler, and J. Lex. Angew. Chem. Int. Ed. Engl. **28**, 1651 (1989).
9. T. Kumagai and S. Akabori. Chem. Lett. 1667 (1989).
10. C.W. McDaniel, J.S. Bradshaw, K.H. Tarbet, B.C. Lindh, and R.M. Izatt. J. Inclusion Phenom. Mol. Recognit. Chem. **7**, 545 (1989).
11. A. Mazouz, J. Bodiguel, P. Meunier, and B. Gautheron. Phosphorus, Sulfur, Silicon, Relat. Elem. **61**, 247 (1991).
12. H. Xu, W. Li, and X. Liu. Youji Huaxue, **13**, 52 (1993).
13. H. Fujihara, M. Yabe, M. Ikemori, and N. Furukawa. J. Chem. Soc. Perkin Trans. 1, 2145 (1993).
14. D.B. Rorabacher. *In* Copper coordination chemistry: biochemical and inorganic perspectives. *Edited by* K.D. Karlin and J. Zubieta. Adenine, New York. 1983. pp. 167–202, S.R. Cooper and S.C. Rawle. Struct. Bonding (Berlin), **72**, 1 (1990); A.J. Blake and M. Schroder. *In* Adv. Inorg. Chem. **35**, 2 (1990).
15. R.J. Batchelor, F.W.B. Einstein, I.D. Gay, J.-H. Gu, B.M. Pinto, and X.M. Zhou. J. Am. Chem. Soc. **112**, 3706 (1990).
16. P.F. Kelly, W. Levason, G. Reid, and D.J. Williams. J. Chem. Soc. Chem. Commun. 1716 (1993).
17. R.J. Batchelor, F.W.B. Einstein, I.D. Gay, J.-H. Gu, and B.M. Pinto. J. Organomet. Chem. **411**, 147 (1991).
18. B.M. Pinto, R.J. Batchelor, F.W.B. Einstein, I.D. Gay, J. Gu, and X. Zhou. 76th Canadian Society for Chemistry Conference, Sherbrooke, Quebec. June, 1993. Abstr. 683.
19. B.M. Pinto, B.D. Johnston, and R. Nagelkerke. Heterocycles, **28**, 389 (1989).

Étude par radiolyse pulsée des propriétés spectrales et cinétiques de l'électron solvaté dans l'hexane-1,2,6-triol liquide

J.-P. Jay-Gerin, J. Chevrel, C. Ferradini, E. Ray, M.H. Klapper et M. Faraggi

Résumé : Le spectre d'absorption optique de l'électron solvaté (e_s^-) dans l'hexane-1,2,6-triol liquide a été mesuré par radiolyse pulsée nanoseconde à différentes températures (10–40°C) afin d'examiner l'influence de valeurs élevées de la viscosité du solvant sur les propriétés spectrales et cinétiques de e_s^-. En utilisant un accélérateur linéaire (durée de l'impulsion : 50 ns et dose par impulsion : 2,4–2,75 Gy), on observe un spectre dont le maximum d'absorption se situe à $\lambda_{max} = 560$ nm. La variation de cette longueur d'onde en fonction de la température, si elle existe dans la zone considérée, est inférieure aux erreurs expérimentales. À 20°C et 150 ns après le début de l'impulsion, le produit $G\epsilon_{max}$ du rendement en e_s^- et du coefficient d'extinction molaire à λ_{max} est égal à $2{,}55 \times 10^4$ molécule/(M cm 100 eV). Nous avons été amenés à comparer les résultats précédemment décrits avec ceux obtenus à l'aide d'un Febetron (durée de l'impulsion : 4 ns et dose par impulsion : 215 Gy). Cette comparaison nous a permis d'étendre les mesures vers les temps courts et d'évaluer l'influence des variations de la dose par impulsion. Dans le cas des expériences effectuées avec l'accélérateur linéaire, les absorbances décroissent en fonction du temps en suivant à toutes les longueurs d'onde une loi du premier ordre. Les courbes cinétiques obtenues avec le Febetron traduisent initialement une compétition en faveur d'une loi du second ordre. Celle-ci est remplacée, pour des temps plus longs, par une loi du premier ordre (ou du pseudo-premier ordre) dont la constante de vitesse (en s^{-1}) est comparable à celle déterminée à l'aide de l'accélérateur linéaire. Cette loi en fonction de la température implique, dans les deux cas, une énergie d'activation de ~45 kJ mol^{-1}. L'allure des spectres obtenus à l'aide de l'accélérateur linéaire et du Febetron diffère pour les doses par implusion étudiées, les différences observées croissant en fonction tu temps. Ces variations pourraient être attribuées au processus de second ordre mis en évidence uniquement dans le cas des forts débits de dose. Par ailleurs, le ralentissement de la vitesse de solvatation de l'électron dû à la viscosité ne semble pas être suffisamment important pour être décelable dans nos conditions expérimentales.

Mots clés : hexane-1,2,6-triol liquide, radiolyse pulsée, accélérateur linéaire et Febetron, électron solvaté, spectre d'absorption optique, propriétés cinétiques, viscosité du solvant, effets de dose et de température.

Abstract: The optical absorption spectrum of the solvated electron (e_s^-) in liquid hexane-1,2,6-triol has been measured by nanosecond pulse radiolysis at different temperatures (10–40°C) to investigate the influence of high solvent viscosity values on the spectral and kinetic properties of e_s^-. The wavelength at the absorption maximum, λ_{max}, is equal to 560 nm, and its variation with temperature, if it exists in the considered zone, is less than the experimental error. At 20°C and 150 ns, the value of the product $G\epsilon_{max}$ of the yield of e_s^- and the molar extinction coefficient at λ_{max} is 2.55×10^4 molecule/(M cm 100 eV). In the context of this work, we have compared results obtained with both a linear accelerator and a Febetron, a comparison that has allowed us to evaluate the influence of variations of the dose per pulse and to extend measurements to short times. In the case of experiments performed with the linear accelerator, e_s^- is found to decay at all wavelengths by a first-order reaction (or by a pseudo-first-order reaction) with an activation energy of ~45 kJ mol^{-1}. By contrast, kinetic curves obtained with the Febetron seem to show a competition in which a second-order law is followed at short

Reçu le 29 mars 1994. Révision reçue le 27 septembre 1994.

J.-P. Jay-Gerin,[1,2] **J. Chevrel et C. Ferradini.** Laboratoire de chimie-physique (Unité de recherche associée n° 400 au Centre national de la recherche scientifique), Université René Descartes, 45, Rue des Saints-Pères, 75270 Paris Cedex 06, France.
E. Ray et M.H. Klapper. Department of Chemistry, The Ohio State University, Columbus, OH 43210, U.S.A.
M. Faraggi. Nuclear Research Centre-Negev, P.O. Box 9001, Beer-Sheva 84190, Israel.

1. Adresse permanente : Groupe du Conseil de recherches médicales du Canada en sciences des radiations et Département de médecine nucléaire et de radiobiologie, Faculté de médecine, Université de Sherbrooke, Sherbrooke, QC J1H 5N4, Canada.
2. Auteur à qui adresser toute correspondance. Département de médecine nucléaire et de radiobiologie, Faculté de médecine, Université de Sherbrooke, Sherbrooke, QC J1H 5N4, Canada. Tél. : (819) 563-5555, poste : 4682. FAX : (819) 564-5442. Courrier électronique : JAYGERIN@VM1.SI.USHERB.CA

Can. J. Chem. Downloaded from www.nrcresearchpress.com by 65.111.164.53 on 09/08/12
For personal use only.

times. The fact that the shape of the spectra seems to vary as a function of the dose per pulse indicates the possible intervention of another species whose formation is favored by the use of high radiation doses. In other respects, the kinetics of electron solvation does not seem to be controlled by the viscosity of the solvent in our experimental conditions.

Key words: liquid hexane-1,2,6-triol, pulse radiolysis, linear accelerator and Febetron, solvated electron, optical absorption spectrum, kinetic properties, solvent viscosity, dose and temperature effects.

Can. J. Chem. Downloaded from www.nrcresearchpress.com by 65.111.164.53 on 09/08/12
For personal use only.

Introduction

De nombreux travaux de radiolyse, tant théoriques qu'expérimentaux, concernant le processus de solvatation de l'électron dans les liquides polaires, ont été développés (pour des revues d'ensemble récentes, voir, par exemple, réfs. 1–5). Le rôle de la viscosité (η) du solvant dans ce processus a été particulièrement étudié dans le cas des alcools liquides (voir, par exemple, réfs. 6 et 7). L'influence de valeurs élevées de η sur les propriétés spectrales et cinétiques des électrons en excès dans le milieu reste toutefois mal connue. On pourrait en effet envisager que le processus de solvatation soit ralenti et qu'il soit alors possible d'étudier celui-ci à l'échelle de la nanoseconde comme dans le cas des alcools liquides à basse température (8). Nous avons, dans ce but, caractérisé le spectre d'absorption de l'électron solvaté (e_s^-) dans l'hexane-1,2,6-triol ($HOCH_2$-$(CH_2)_3CH(OH)CH_2OH$), solvant de constante diélectrique statique $\epsilon_s = 29$ dont la viscosité est très élevée (2490 cP à 20°C) (9). Cette valeur de η à 20°C est plus de 500 fois supérieure à celles des alcools, plus de 20 fois à celles des diols et environ 2 fois celle du propane-1,2,3-triol (glycérol), donc supérieure à celles de tous les solvants déjà étudiés à ce point de vue à cette température (voir réf. 9).

Dans ce travail, nous nous sommes attachés à caractériser à différentes températures le spectre d'absorption de l'électron dans ce solvant et son évolution. Nous avons été amenés, dans ce cadre, à comparer les résultats obtenus à l'aide de deux accélérateurs. Le premier est un accélérateur linéaire pour lequel la dose par impulsion est comprise entre 2,4 et 2,75 Gy, la première mesure se situant 150 ns après le début de l'impulsion. Le second est un Febetron dont la dose moyenne par impulsion est de 215 Gy, la première mesure étant effectuée 4 ns après le début de l'impulsion. Cette comparaison nous a permis d'une part d'évaluer l'influence des variations de la dose par impulsion et d'autre part d'étendre les mesures vers les temps courts.

Matériel et méthodes

L'accélérateur linéaire utilisé (Varian V-7715A) est celui de l'Ohio State University à Columbus (10). Les électrons avaient une énergie de 4 MeV, la durée de l'impulsion était de 50 ns et la dose par impulsion était comprise entre 2,4 et 2,75 Gy. Le trajet optique était de 6 cm. La dosimétrie était effectuée par irradiation d'une solution aérée de KSCN 0,01 M et mesure à 480 nm du radical dithiocyanate $(SCN)_2^{\cdot -}$ en prenant pour le produit $G\epsilon[(SCN)_2^{\cdot -}]$ la valeur $2{,}1 \times 10^4$ molécule/(M cm 100 eV) (11).

Le Febetron 708 du Laboratoire de chimie-physique de l'Université Paris V (12) fournissait des impulsions d'électrons, de durée 4 ns à mi-hauteur et d'énergie 800 keV. Le trajet optique était égal à 1 cm. La dosimétrie était effectuée par microcalorimétrie. L'électron hydraté a été utilisé pour l'étalonnage de celle-ci en prenant à 400 nm un coefficient d'extinction molaire de 2000 M^{-1} cm^{-1} et un rendement à 20 ns de 3,2

Fig. 1. Spectres d'absorption de l'électron solvaté (e_s^-) dans l'hexane-1,2,6-triol pur, aéré, irradié à 10°C (□), 20°C (■), 30°C (○) et 40°C (●) à l'aide de l'accélérateur linéaire. Les absorbances ont été mesurées 150 ns après le début de l'impulsion. Durée de l'impulsion : 50 ns; dose par impulsion (en Gy) : 2,75 à 10°C, 2,65 à 20°C, 2,4 à 30°C et 2,5 à 40°C (l'influence de la densité électronique du solvant a été prise en compte); trajet optique : 6 cm. $\lambda_{max} = 560$ nm est la longueur d'onde correspondant au maximum des spectres observés. G est le nombre d'électrons solvatés présents à un instant donné pour 100 eV d'énergie absorbée et $\epsilon(e_s^-)$ est le coefficient d'extinction molaire exprimé en M^{-1} cm^{-1}. Rappelons que le produit $G\epsilon(e_s^-)$ est égal à $AN_{Av} \times 100/(ld \times \text{dose})$, où A est l'absorbance, N_{Av} est le nombre d'Avogadro, l est le trajet optique en cm, d est la densité en g L^{-1}, et où la dose est exprimée en eV g^{-1}.

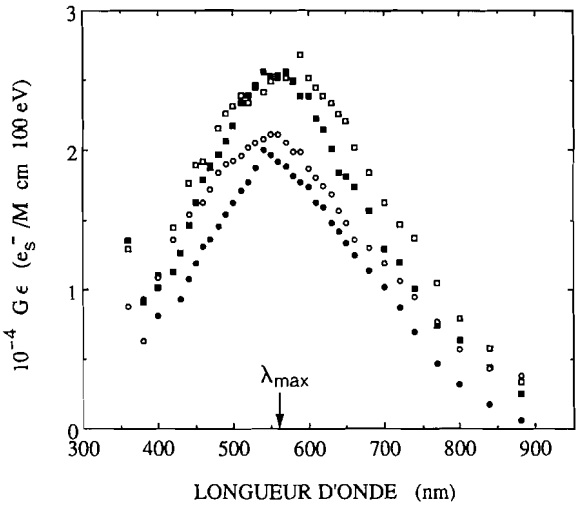

molécule/100 eV. L'influence de la densité électronique du solvant sur la valeur de la dose a été prise en compte. Les valeurs de l'absorbance ont été normalisées à une dose de $1{,}34 \times 10^{18}$ eV par gramme et par impulsion (215 Gy), les doses réelles par impulsion ne différant que peu de cette dose moyenne.

L'hexane-1,2,6-triol utilisé dans ce travail était, en ce qui concerne les expériences menées avec le Febetron, un produit Prolabo d'«usage courant», de pureté garantie à 97%, tandis que les expériences utilisant l'accélérateur linéaire portaient sur un produit Aldrich, de pureté 98%. Les deux produits étaient employés sans purification ultérieure ni dégazage préalable.

Résultats expérimentaux

La figure 1 donne les spectres de e_s^- obtenus à l'aide de l'accélérateur linéaire pour l'hexane-1,2,6-triol pur, aéré, irradié à 10, 20, 30 et 40°C, avec des doses respectivement de 2,75, 2,65, 2,4 et 2,5 Gy par impulsion. Les valeurs indiquées

Can. J. Chem. Downloaded from www.nrcresearchpress.com by 65.111.164.53 on 09/08/12
For personal use only.

Fig. 2. Comparaison des spectres d'absorption de l'électron solvaté dans l'hexane-1,2,6-triol pur, aéré, irradié à 10°C à l'aide de l'accélérateur linéaire avec une dose de 2,75 Gy par impulsion (□) et à (10,5 ± 0,5)°C à l'aide du Febetron avec une dose moyenne de 215 Gy par impulsion (●). (*A*) Dans le cas de l'accélérateur linéaire, les absorbances sont obtenues à 25 ns par extrapolation des courbes cinétiques. Dans le cas du Febetron, les absorbances ont été mesurées immédiatement après l'impulsion d'électrons dont la durée est de 4 ns à mi-hauteur. (*B*) Comparaison des spectres à 150 ns. Les barres d'incertitude indiquent, dans le cas du Febetron, les largeurs de bande spectrale associées aux largeurs de fente correspondantes du monochromateur utilisé.

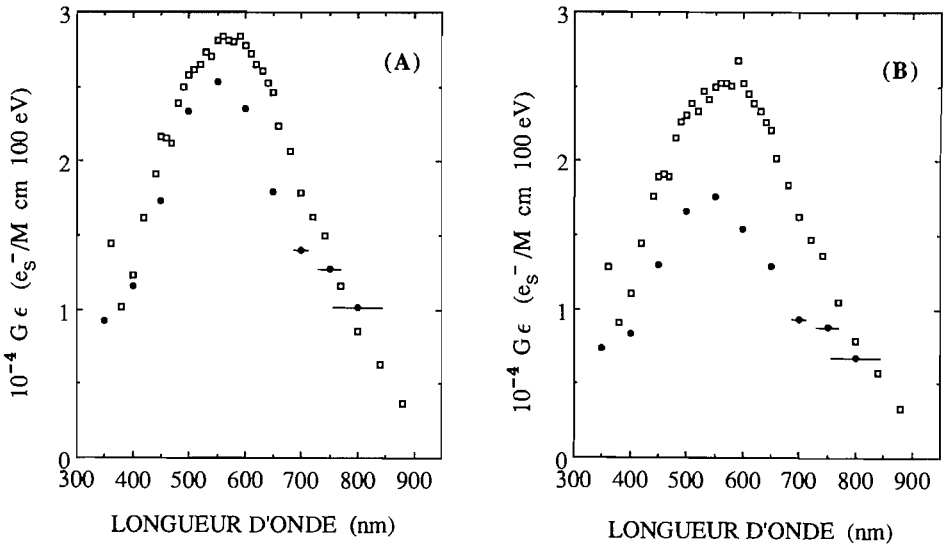

pour le produit $G\epsilon(e_s^-)$ sont celles obtenues à 150 ns après le début de l'impulsion. G dénote ici le nombre d'électrons solvatés présents par 100 eV d'énergie absorbée et $\epsilon(e_s^-)$ est le coefficient d'extinction molaire en unités M^{-1} cm^{-1}.

Les figures 2*A* et *B* montrent les comparaisons des spectres obtenus dans le cas de l'accélérateur linéaire à 25 ns, par extrapolation des courbes cinétiques, et à 150 ns, avec ceux obtenus à l'aide du Febetron dans les conditions déjà décrites, pour la température de 10°C. Les figures 3*A* et *B* montrent les mêmes comparaisons, mais à 20°C. Dans le cas du Febetron, la mesure des absorbances est effectuée à la fin de l'impulsion dont la durée est 4 ns à mi-hauteur, et les températures considérées sont respectivement de 10,5 (± 0,5)°C et 19 (± 1)°C. Dans ce cas également, l'addition d'un capteur d'électrons, le phénol en concentration 1 M, inhibe totalement l'absorbance à toutes les longueurs d'onde.

Les résultats obtenus avec l'accélérateur linéaire à 20°C nous permettent de déduire la longueur d'onde λ_{max} (ou l'énergie $E_{A_{max}}$(eV) = 1240/λ_{max}(nm)) correspondant au maximum des spectres observés et la largeur à mi-hauteur de ceux-ci : λ_{max} = 560 nm ($E_{A_{max}}$ = 2,21 eV) et $W_{1/2} \sim$ 1,25 eV. $W_{1/2}$ peut être divisé en une partie $W_b \sim$ 0,75 eV du côté haute énergie de $E_{A_{max}}$ et une partie $W_r \sim$ 0,50 eV du côté basse énergie. La variation de ces valeurs en fonction de la température, si elle existe dans la zone 10–40°C, est inférieure aux erreurs expérimentales.

Dans le cas des expériences effectuées avec l'accélérateur linéaire, les absorbances décroissent en fonction du temps en suivant à toutes les longueurs d'onde une loi exponentielle. Leur représentation semi-logarithmique est une droite dont la pente est fonction de la température. On obtient les valeurs suivantes (moyennes effectuées, à chaque température, sur environ 40 longueurs d'onde entre 400 et 700 nm) pour la constante de vitesse apparente du premier ordre (k) ainsi déterminée :

Température (°C)	Viscosité (réfs. 9 et 13) (cP)	k (10^6 s^{-1})
10	6154	0,88 ± 0,04
20	2490	1,5 ± 0,1
30	1011	5,1 ± 0,3
40	484	6,7 ± 0,3

Les courbes cinétiques obtenues avec le Febetron, donc à grandes doses et à temps courts, semblent traduire une compétition. La figure 4 donne, dans ce cas, en fonction du temps, la variation du logarithme de l'absorbance à 550 nm, et celle de son inverse pour les deux températures étudiées, à savoir, 10,5 et 19°C. On voit que, initialement, une loi du second ordre semble suivie. Elle est remplacée vers 300 ns à 19°C et vers 450 ns à 10,5°C par une loi du premier ordre dont la constante de vitesse apparente est comparable à celle observée dans le cas de l'accélérateur linéaire pour les deux mêmes températures et le même intervalle de temps. Une évolution similaire est obtenue aux autres longueurs d'onde.

L'ensemble des déterminations des constantes de vitesse du premier ordre a été reporté figure 5 sous forme d'un diagramme d'Arrhenius, ln(k) versus 1/T, où T est la température absolue. La pente de la droite représentative, obtenue à l'aide d'un ajustement direct sur les données brutes par une méthode de moindres carrés non-linéaire, conduit à une énergie d'activation de 45 (± 19) kJ mol^{-1}, la valeur entre parenthèses donnant l'intervalle de confiance à 95%.

Fig. 3. Comparaison des spectres d'absorption de l'électron solvaté dans l'hexane-1,2,6-triol pur, aéré, irradié à 20°C à l'aide de l'accélérateur linéaire avec une dose de 2,65 Gy par impulsion (□) et à (19 ± 1)°C à l'aide du Febetron avec une dose moyenne de 215 Gy par impulsion (●). (*A*) et (*B*) correspondent aux mêmes conditions expérimentales que celles des figures 2*A* et *B*. Les barres d'incertitude indiquent, dans le cas du Febetron, les largeurs de bande spectrale associées aux largeurs de fente correspondantes du monochromateur utilisé.

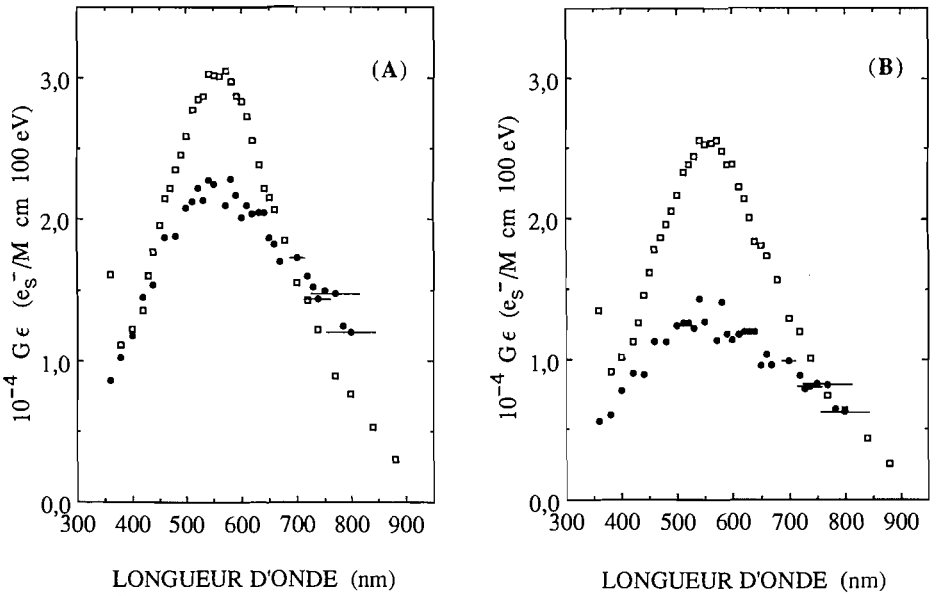

Discussion

Les spectres de e_s^- de la figure 1 ressemblent à ceux trouvés par d'autres auteurs (14–17) pour le glycérol et à ceux décrits pour les diols (18). On note qu'entre 10 et 40°C, dans la limite de la précision des mesures, leur forme n'est sensiblement pas affectée par la température. Pourtant la viscosité du solvant, dans cette gamme de température, varie de manière importante, passant de 6154 cP à 10°C à 484 cP à 40°C (13).

Comme le montre la figure 1, au maximum du spectre de e_s^-, correspondant à la température de 20°C (560 nm) et à un temps de 150 ns, $G\epsilon_{max}$ est égal à $2{,}55 \times 10^4$ molécule/(M cm 100 eV), valeur comparable à celles trouvées dans le glycérol (16, 17) ou dans les diols (18) à la température ambiante.

On peut tenter de calculer séparément chacune des deux grandeurs G et ϵ_{max} d'une manière approximative. En effet, il a été proposé (3, 19) la relation empirique suivante reliant ϵ_{max} à l'énergie $E_{A_{max}}$ correspondant au maximum du spectre de e_s^-:

$$\epsilon_{max} = \epsilon^0_{max} \exp(-\alpha E_{A_{max}})$$

avec $\epsilon^0_{max} = 5{,}54\ (\pm\ 0{,}89) \times 10^4\ M^{-1}\ cm^{-1}$ et $\alpha = 0{,}82\ (\pm\ 0{,}11)\ eV^{-1}$ (les valeurs entre parenthèses donnent les limites de confiance à 95% des paramètres). L'application de cette relation à l'hexane-1,2,6-triol ($E_{A_{max}} = 2{,}21$ eV) donne $\epsilon_{max} = 9015\ (\pm\ 3645)\ M^{-1}\ cm^{-1}$, ce qui conduit, en utilisant la valeur proposée ci-dessus pour le produit $G\epsilon_{max}$, à un rendement en e_s^-, immédiatement après l'impulsion (150 ns), égal à 2,7 (± 1,2) molécule/100 eV. Cette valeur est compatible avec celle du rendement en ions libres (G_{fi}), à $\sim 10^{-6}$ s, qui peut être estimée égale à 1,6 molécule/100 eV pour l'hexane-1,2,6-triol, à partir de la relation empirique (20)

Fig. 4. Comparaison des courbes cinétiques obtenues avec le Febetron à 550 nm, et à 10,5°C (+) et 19°C (×). La durée de l'impulsion d'électrons est de 4 ns à mi-hauteur. Les absorbances (*A*) sont normalisées à la dose moyenne de 215 Gy par impulsion. La figure donne en fonction du temps (en ns) la variation du logarithme de l'absorbance ln(*A*) et celle de son inverse 1/*A* pour les deux températures étudiées. Les droites en trait plein montrent une estimation des parts respectives en fonction du temps des deux lois d'évolution (voir texte).

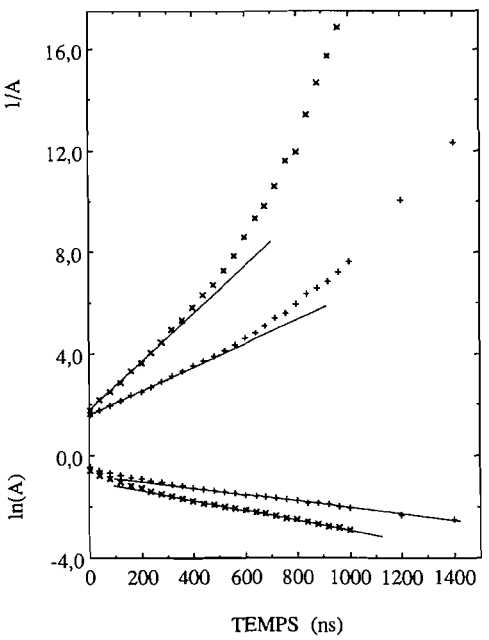

Can. J. Chem. Downloaded from www.nrcresearchpress.com by 65.111.164.53 on 09/08/12
For personal use only.

Can. J. Chem. Downloaded from www.nrcresearchpress.com by 65.111.164.53 on 09/08/12
For personal use only.

Fig. 5. Diagramme d'Arrhenius (en représentation semi-logarithmique) montrant la variation de k en fonction de $10^3/T$, où k est la constante de vitesse du premier ordre (en s^{-1}) de la disparition de e_s^- dans l'hexane-1,2,6-triol et T est la température absolue (en K). Les valeurs de k déterminées à 10, 20, 30 et 40°C (□) à l'aide de l'accélérateur linéaire sont indiquées dans le texte. Celles obtenues à l'aide du Febetron sont : $k = (1,9 \pm 0,2) \times 10^6$ s^{-1} à 19°C et $k = (1,2 \pm 0,1) \times 10^6$ s^{-1} à 10,5°C (●). La droite en trait plein passant par les points expérimentaux a été déterminée en utilisant un ajustement direct sur les données brutes par une méthode de moindres carrés non-linéaire. La pente de celle-ci, égale à $-E_a/R$, où E_a est l'énergie d'activation et R est la constante des gaz parfaits, conduit à $E_a = 45$ (± 19) kJ mol^{-1}, la valeur entre parenthèses correspondant aux limites de confiance à 95%. Le facteur pré-exponentiel s'élève à $2,2 \times 10^{14}$ s^{-1}.

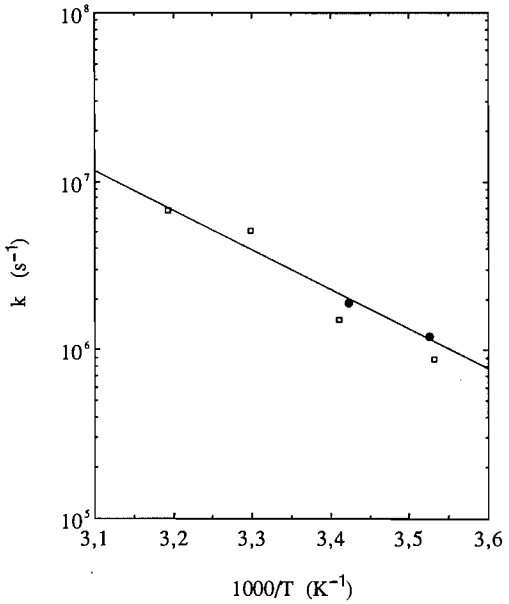

$$G_{fi} = G_{fi}^{\infty} \exp(-a/\epsilon_s)$$

où $G_{fi}^{\infty} = 3,7$ molécule/100 eV, $a = 25$ et $\epsilon_s = 29$ est la constante diélectrique statique du solvant (9). Elle est, de plus, du même ordre de grandeur que celle (2,27 molécule/100 eV) estimée à 10 ns pour le glycérol pur désaéré à 32°C en supposant $\epsilon_{max} = 12\,000$ M^{-1} cm^{-1} (16).

La largeur $W_r \sim 0,50$ eV des spectres de e_s^- dans l'hexane-1,2,6-triol du côté rouge de $E_{A_{max}}$ est très voisine de celles observées pour le glycérol (0,50 eV) (17) et pour les diols (0,54 ± 0,4 eV) (18). Le rapport $W_r/E_{A_{max}} \sim 0,23$ se compare également bien à ceux trouvés dans le glycérol (0,22 eV) (17) et dans les diols (0,23 ± 0,01 eV) (18). Le rapport W_b/W_r, qui donne une mesure de l'asymétrie des spectres, s'élève à ~1,5 pour l'hexane-1,2,6-triol; il est sensiblement inférieur à ceux trouvés pour le glycérol (1,8) (17) et pour les diols (1,6–2,1) (18).

Le fait de trouver, quelque soit le débit de dose, des valeurs similaires pour la constante de vitesse et l'énergie d'activation semble indiquer que la décroissance du premier ordre observée pour e_s^- correspond toujours à la même réaction. Il pourrait s'agir de la réaction de l'électron solvaté avec l'oxygène dissous qui conduit à une réaction du pseudo-premier ordre. Malheureusement, cette hypothèse n'a pas pu être vérifiée, la viscosité du solvant rendant très difficile sa désaération.

Pour expliquer la différence entre les spectres obtenus avec l'accélérateur linéaire et le Febetron (figs. 2 et 3), on peut se demander quelle est la nature de l'espèce (ou des espèces) transitoire(s) modifiant les spectres obtenus avec le Febetron. Comme cette espèce n'est pas formée dans le cas de l'accélérateur linéaire, sa production peut être favorisée par l'utilisation des hautes doses. Il est possible qu'elle apparaisse lors du processus de deuxième ordre survenant au début de l'évolution et impliquant l'électron solvaté (voir fig. 4). Ce processus pourrait être attribué à la réaction de celui-ci avec un des ions positifs présents. Ce serait les produits de cette réaction qui perturberaient le spectre.

Des expériences complémentaires seraient nécessaires pour obtenir une meilleure compréhension du comportement de l'électron en excès dans les milieux de grande viscosité. Il faudrait en particulier faire varier les paramètres dose et température dans de plus larges domaines.

Les présentes expériences semblent toutefois montrer que la viscosité est un paramètre moins important qu'on ne pouvait le penser *a priori* puisque nous n'avons pas observé de ralentissement de la vitesse de solvatation de l'électron dans nos conditions expérimentales.

Remerciements

Les auteurs remercient le Dr Bernard Hickel pour de fructueuses discussions. Cette étude a bénéficié de l'aide financière du Programme de subventions à la recherche coopérative de l'OTAN (subvention n° 91/0996) et du Programme de coopération franco-québécoise en recherche médicale. L'un de nous (J.-P. J.-G.) tient également à exprimer ses remerciements au Programme d'échanges INSERM–FRSQ en recherche en santé, ainsi qu'au Conseil de recherches médicales du Canada.

Bibliographie

1. E.M. Itskovitch, A.M. Kuznetsov et J. Ulstrup. *Dans* The chemical physics of solvation. Part C. Solvation phenomena in specific physical, chemical, and biological systems. *Éditeurs* : R.R. Dogonadze, E. Kálmán, A.A. Kornyshev et J. Ulstrup. Elsevier, Amsterdam. 1988. pp. 275–327.
2. T.R. Tuttle, Jr. et S. Golden. J. Phys. Chem. **95**, 5725 (1991).
3. J.-P. Jay-Gerin et C. Ferradini. *Dans* Excess electrons in dielectric media. *Éditeurs* : C. Ferradini et J.-P. Jay-Gerin. CRC Press, Boca Raton, Fla. 1991. pp. 259–285.
4. Y. Hirata et N. Mataga. Prog. React. Kinet. **18**, 273 (1993).
5. H. Abramczyk et J. Kroh. Radiat. Phys. Chem. **43**, 291 (1994).
6. W.J. Chase et J.W. Hunt. J. Phys. Chem. **79**, 2835 (1975).
7. G.A. Kenney-Wallace et C.D. Jonah. J. Phys. Chem. **86**, 2572 (1982) et références citées.
8. J.H. Baxendale et P. Wardman. Nature, **230**, 449 (1971).
9. J.-P. Jay-Gerin et C. Ferradini. J. Chim. Phys. **91**, 173 (1994).

10. W.D. Felix, B.L. Gall et L.M. Dorfman. J. Phys. Chem. **71**, 384 (1967).
11. G.E. Adams, J.W. Boag et B.D. Michael. Trans. Faraday Soc. **61**, 1674 (1965).
12. C. Houée-Levin, M. Gardès-Albert, C. Ferradini et J. Pucheault. Radiat. Res. **83**, 270 (1980).
13. R. Meister, C.J. Marhoeffer, R. Sciamanda, L. Cotter et T. Litovitz. J. Appl. Phys. **31**, 854 (1960).
14. S. Arai et M.C. Sauer, Jr. J. Chem. Phys. **44**, 2297 (1966).
15. D.C. Walker et S.C. Wallace. Chem. Phys. Lett. **6**, 111 (1970).
16. T. Kajiwara et J.K. Thomas. J. Phys. Chem. **76**, 1700 (1972).
17. F.-Y. Jou et G.R. Freeman. Can. J. Chem. **57**, 591 (1979).
18. K. Okazaki, K.M. Idriss-Ali et G.R. Freeman. Can. J. Chem. **62**, 2223 (1984).
19. J.-P. Jay-Gerin et C. Ferradini. Can. J. Chem. **68**, 553 (1990).
20. J.-P. Jay-Gerin et C. Ferradini. Radiat. Phys. Chem. **33**, 251 (1989).

Can. J. Chem. Downloaded from www.nrcresearchpress.com by 65.111.164.53 on 09/08/12
For personal use only.

Photoinduced addition of dioxygen molecules in the unsaturated sites of the $Pd_3(dppm)_3CO^{2+}$ catalyst

Pierre D. Harvey, Marielle Crozet, and Khin T. Aye

Abstract: The photoinduced addition of O_2 onto the unsaturated cluster $Pd_3(dppm)_3CO^{2+}$ (as a $CF_3CO_2^-$ salt) in acetonitrile is reported. The final product $Pd_3(dppm)_3(O_2)_2^{2+}$ ($\nu(O_2)$ = 838 and 866 cm^{-1}) is formed in a multistep fashion in which two photochemical intermediates are observed (presumably $Pd_3(dppm)_3(O_2)(CO)^{2+}$ and $Pd_3(dppm)_3(O_2)^{2+}$). No X-ray structure could be obtained, but numerous spectroscopic findings demonstrate that O_2 binds the Pd_3 center as a peroxo-O_2, and acts as a two-electron donor that triply bridges the metal atoms (forming a 44-electron cluster). The very small excited state lifetimes (between 25 and 35 ± 10 ps) obtained by picosecond flash photolysis indicate that the primary photoreaction is unimolecular, and demonstrate that the first photochemically added O_2 molecule must be preassembled in the excited state *prior* to any photoinduced transformation. This $Pd_3(dppm)_3CO^{2+}\cdots O_2$ ground state complex is responsible for the photoinduced production of the bisdioxygen compound and can be observed by UV–visible spectroscopy. The low efficiency of the photoreaction (quantum yield (Φ) = 0.033 ± 0.004) is explained by the very short excited state lifetime at 298 K, and the competition of O_2 with solvent molecules to occupy the unsaturated site of the empty cavity in $Pd_3(dppm)_3CO^{2+}$ (i.e., ground state guest–host chemistry). The binding constant for O_2 with $Pd_3(dppm)_3CO^{2+}$ is roughly estimated to range between 1 and 730 M^{-1} in the ground state and is considered to be weak.

Key words: clusters, photochemistry, guest–host, oxidation, dioxygen.

Résumé : Opérant dans l'acétonitrile, on a effectué l'addition photoinduite du O_2 sur le cluster insaturé $Pd_3(dppm)_3CO^{2+}$ (sous la forme d'un sel de $CF_3CO_2^-$). Le produit final, le $Pd_3(dppm)_3(O_2)^{2+}$($\nu(O_2)$ = 838 et 866 cm^{-1}) se forme en plusieurs étapes et on a observé deux intermédiaires photochimiques (probablement le $Pd_3(dppm)_3(O_2)(CO)^{2+}$ et le $Pd_3(dppm)_3(O_2)^{2+}$). On n'a pas pu obtenir de structures par diffraction des rayons X, mais plusieurs données spectroscopiques démontrent que le O_2 se lie au centre Pd_3 sous la forme d'un peroxo-O_2 et qu'il agit comme un donneur de deux électrons qui crée un triple pont avec les atomes métalliques (formant un cluster à 44 électrons). Les très faibles temps de vie de l'état excité (entre 25 et 35 ± 10 ps) obtenus par la photolyse éclair à la picoseconde indiquent que le photoréaction primaire est unimoléculaire et démontrent que la première molécule de O_2 qui s'additionne photochimiquement doit se préassembler dans l'état de transition *avant* toute transformation photoinduite. Ce complexe $Pd_3(dppm)_3CO^{2+}\cdots O_2$ dans l'état fondamental est responsable de la production photoinduite du composé bisdioxygène et on peut l'observer par spectroscopie UV–visible. On explique la faible efficacité de la photoréaction (rendement quantique (Φ) = 0,033 ± 0,004) par le très court temps de vie de l'état excité à 298 K et par la compétition entre le O_2 et les molécules de solvant pour occuper le site insaturé de la cavité de du $Pd_3(dppm)_3CO^{2+}$ (c'est-à-dire la chimie hôte–invité dans l'état fondamental). On évalue d'une façon approximative que la constante de liaison du O_2 pour le $Pd_3(dppm)_3CO^{2+}$ varie de 1 à 730 M^{-1} dans l'état fondamental et on la considère comme faible.

Mots clés : clusters, photochimie, hôte–invité, oxydation, dioxygène.

[Traduit par la rédaction]

Introduction

The catalytic oxidation of organics by palladium and platinum metals and their coordination complexes is of great importance with regard to a number of industrial applications such as the catalytic oxidation of ethylene and propene to form 1,2-diol products and ethylene oxide, and oxidation of formic acid, methanol, hydrazine, etc. in fuel cells (1–3). One of the key intermediates in these heterogeneous catalysis processes is the adsorbtion of dioxygen molecules at the catalytic metal surface (1). Surface studies have shown that dioxygen adsorbs molecularly (nondissociatively) onto Pt(111) while it adsorbs dissociatively ($T > 100$ K) and molecularly ($T < 100$ K) on Pd(111), Pd(110), and Pd(100) (4–11). Recently the chemistry of the coordinatively unsaturated tripalladium and triplatinum clusters ($M_3(dppm)_3CO^{2+}$; M = Pd, Pt; dppm = $((C_6H_5)_2P)_2CH_2$) has been reviewed (12), where it was proposed that these clusters be models for reactions on metal surfaces. The complexes are found to be catalysts for the

Received June 15, 1994.

P.D. Harvey,[1] M. Crozet, and K.T. Aye. Department of Chemistry, Université de Sherbrooke, QC J1K 2R1, Canada.

[1] Author to whom correspondence may be addressed. Telephone: (819) 821-7092. FAX: (819) 821-8017. e-mail: PHARVEY@STRUCTURE.CHIMIE.USHERB.CA

Can. J. Chem. Downloaded from www.nrcresearchpress.com by 65.111.164.53 on 09/08/12
For personal use only.

Can. J. Chem. Downloaded from www.nrcresearchpress.com by 65.111.164.53 on 09/08/12
For personal use only.

water–gas shift reaction (M = Pt)(12) and the electroreduction of CO_2 (M = Pd).[2] More relevant to this work, Puddephatt and co-workers also reported the dissociative addition of dioxygen to the cationic $[Pt_3(dppm)_3(\mu\text{-}Re(CO)_3)]^+$ cluster to form the μ^3-oxo complex $[Pt_3(\mu^3\text{-}O)_2(Re(CO)_3)(dppm)_3]^+$ (13). We now wish to report the first example of a stable (at room temperature) dioxygen complex of a trinuclear palladium cluster ($Pd_3(dppm)_3(O_2)_2^{2+}$), which can be considered as a potential oxidizing agent for organic molecules. According to picosecond flash photolysis spectroscopy, the primary photoinduced addition mechanism is found to pass through a unimolecular pathway via a preassembled complex in the ground state, $(Pd_3(dppm)_3CO^{2+})\cdots O_2$.

Experimental section

Materials

The complex $[Pd_3(dppm)_3CO](CF_3CO_2)_2$ was synthesized according to literature procedure (14). The solvents acetonitrile (Fisher), toluene (Fisher), and methanol (Fisher) were purified from procedures outlined in refs. 15 and 16.

Methodology

The photochemical reactions were performed in a homemade water-jacketed cylindrical container (20 cm × 7 cm), which was constantly stirred. Pure dioxygen was introduced (unless stated otherwise) at a constant rate of approximately one needle bubble per second. The bubbling was necessary to evacuate the excess pressure encountered when acetonitrile was slowly evaporated, and to eliminate CO. Two 200 W PTI Hg–Xe arc lamps and two LPS-250 power supplies (PTI) were used at both ends of the cylinder insuring that the solution was in the focal points (i.e., ~4 cm^{-1} from the cylinder). Two Oriel optical filters (cutoff at 450 nm) were placed in front of the lamps during irradiation. The optical density of the $Pd_3(dppm)_3CO^{2+}$–acetonitrile solution was adjusted to be ~1 in a 1 cm cell at 500 nm. These conditions were chosen for the best performance of the setup. The reactions were monitored by UV–visible spectroscopy. Typically the reactions were completed within 3 days (72 h) under constant stirring. The solutions were evaporated until dry, and the yellow product was recrystallized from acetonitrile–ether. The isolated yields were 85% or over. After spectroscopic and elemental analyses the yellow product was identified as $[Pd_3(dppm)_3(O_2)_2](CF_3CO)_2$: Anal. calcd.(%) for $C_{79}H_{66}P_6F_6O_8Pd_3$: C 53.83, H 3.77, P 10.54, F 6.47, O 7.26, Pd 18.11; found (%): C 54.77, H 3.61, P 9.91, O 7.54, Pd 18.03 (by difference F should analyse for 6.14%). It is crucial to keep a good flow of water to insure that the solution temperature stays below ~298 K, otherwise decomposition occurs. On many occasions unsatisfactory analyses were obtained when the temperature rose above ~310 K (i.e., insufficient water cooling).

$[Pd_3(dppm)_3(O_2)_2](CF_3CO_2)$: IR (KBr): $\bar{\nu}$ (cm^{-1}): 838 and 866 (O–O), 558, 542, 600 (Pd–O); UV–vis (CH_3OH, 77 K): λ_{max}(nm)(ϵ): 448 (1200); ^1H NMR (250 MHz, CDCN, 25°C) δ: 3.74 (t, ^2J(P,H) = 13 Hz, 6H, CH_2), 7.5 (complex, 60H, C_6H_5), ^{31}P NMR (120 MHz, CD_3CN, 25°C) δ: −4.62 (decoupled); MS (FAB, 70 kV) *m/z*: 1644 ($Pd_3(dppm)_3(O_2)_2(CF_3CO_2)$), 1600 ($Pd_3(dppm)_3O(CF_3CO_2)$), 1505 ($Pd_3(dppm)_3(O_2)$).

The photochemical quantum yield measurements were performed using the ferrioxalate actinometry method (17). The spectrometer used for monochromatic excitation was an Aminco–Bowman instrument equipped with a single monochromator and a 200-W Hg–Xe lamp (Hanovia). The slits were set at 0.5 mm, and excitation was 488 nm for all samples and standards ($\Phi_{standard}$ = 0.94). The absorbance of the complex solutions was adjusted to a value of 1 (at 488 nm) prior to the photochemical quantum yield measurements. This adjustment was done by weighing the samples and dissolving them in known amounts of solvent. Typical concentrations range from 3.4×10^{-5} to 4.0×10^{-5} M. The calibrations of the standard ferrioxalate actinometric solutions were performed carefully in the dark. The absorbance change at a given irradiation time was followed by UV–visible spectroscopy (Hewlett–Packard 8452A) at 476 nm (i.e., at λ_{max}). The measurements and calibration experiments were performed at least 3 times and made before 10% photoconversion. All the solutions were bubbled with pure O_2(g). At saturated conditions the concentration in acetonitrile for O_2 is $\sim 1 \times 10^{-2}$ M at room temperature (18).

Instrumentation

The FT-IR (4000–400 cm^{-1}) spectra were obtained on a Bomem (MB-102) spectrometer. Proton NMR spectra were measured at 250 MHz on a Bruker WM 250 spectrometer while ^{31}P NMR spectra were recorded at 300 MHz on a Varian spectrometer. Mass spectra were acquired with a Krator MS-50 TCTA spectrometer using an Iontech Saddle Field Source model FAB 11 NF operating at 70 kV with 2 mA current (at the Université de Montréal). The samples were in thioglycerol matrices. UV–visible spectra were obtained on a Hewlett Packard (HP 8452A) diode array spectrophotometer. The elemental analyses for C, H, and O were performed by Guelph Chemical Laboratories, Ltd. (Guelph, Ontario), and in our department using a KEVEX-700 X-ray emission spectrofluorometer operating at 60 kV for Pd and P. In these latter measurements, $PdCl_2$ (Aldrich) and dppm (Aldrich) were used as comparative standards.

Flash photolysis

Picosecond and nanosecond time-resolved measurements were carried out at the former Center for Fast Kinetic Research at Austin (CFKR). The setups were described previously (19).

Results and discussion

1. Photoaddition

The $Pd_3(dppm)_3CO^{2+}$ complex was originally prepared and described by Puddephatt and co-workers in 1983 (14), and was reported to be air stable. Under visible-light irradiation, the complex slowly reacts in the presence of O_2(g) to produce an unprecedented bis(dioxygen) palladium cluster:

$$[1]\quad Pd_3(dppm)_3CO^{2+} + O_2 \xrightarrow[\text{acetonitrile}]{h\nu > 450\text{ nm, 3 days}} Pd_3(dppm)_3(O_2)_2^{2+}$$

[2] I. Gauthier, I. Lognot, Y. Mugnier, K.T. Aye, K. Hierso, and P.D. Harvey. Manuscript in preparation.

Fig. 1. Typical UV–visible spectrocopic transformation during the irradiation of $Pd_3(dppm)_3CO^{2+}$ in acetonitrile saturated with $O_2(g)$ at 298 K. In a 1-cm cell and a concentration of $\sim 1 \times 10^{-5}$ M in cluster, the photochemical reaction is over in about 4 h.

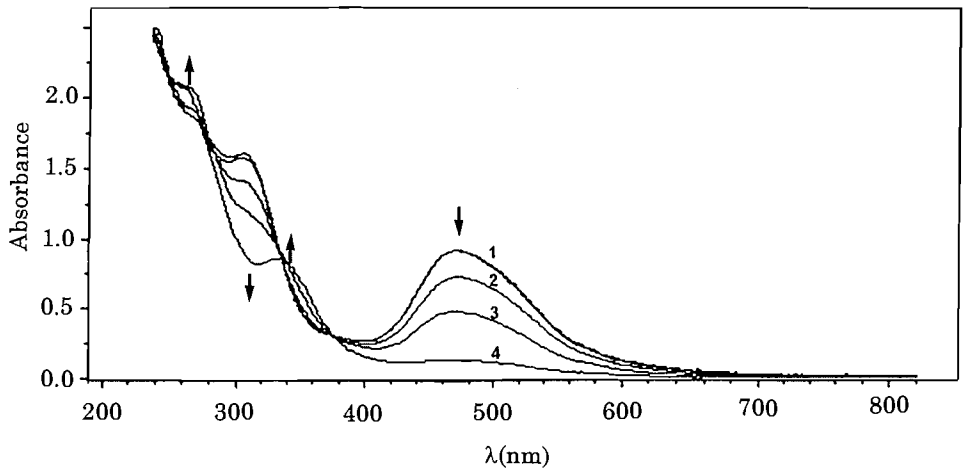

The reaction requires very precise experimental conditions of solvent, temperature, and light irradiation. Rapid photoinduced decomposition of the starting material is observed when benzene or THF solvents are used, when the solutions rise above room temperature, or when broadband irradiation techniques are employed. In the latter situation, the results are consistent with excitation to upper excited states, which are strongly Pd—CO antibonding (see for instance MO no. 19e) in the $Pd_3(\mu^3\text{-CO})$ frame (20). Irradiation using an optical filter with a 350 nm cutoff (instead of 450 nm) also produced photodegradation of the solutions, indicating that these excited states are not very energetic with respect to the lowest energy excited states. In the second case, the increase in heat (generated by the lamps) decomposed the bisdioxygen product or one of the photochemical intermediates in which dppm-oxide was readily observed (δ ^{31}P NMR = +25.37 ppm vs. H_3PO_4; IR: $\nu(P{=}O)$ = 1062 cm^{-1}, $\nu(C\text{-}P{=}O)$ = 512 cm^{-1}) along with the precipitation of a Pd/PdO black solid (identified by X-ray fluorescence). When an optical filter with a cutoff of 450 nm was used, no detectable photoinduced decomposition of the product was noted by NMR. The solvent dependence of the reactions indicates that the coordinating ability of the solvent stabilizes the photochemical intermediates during the transformations. When the conditions are appropriately set, the photoreaction proceeds cleanly. Clear isosbestic points are observed in the monitoring by UV–visible spectra, indicating that only one stable product is generated (Fig. 1). Occasionally the presence of phosphine oxide was detected but, generally, only as a minor product. The product can be isolated in a reasonably analytically pure state, and the identity of the photoproduct can easily be confirmed by Fast Atom Bombardement (FAB) spectrometry (and spectroscopy). The mass spectra were compared with computed spectra taking into account the natural abundance of the various isotopes. The comparison was adequate within the experimental uncertainties (due to the noise encountered in the spectra).

In theory, the structure of the bisdioxygen product can be determined by various methods including X-ray single crystal crystallography, ^{17}O NMR, and Raman spectroscopy (with ^{18}O-enriched samples), particularly when the binding modes of the oxygen atoms are concerned. Unfortunately all attempts to obtain crystals suitable for X-ray crystallography studies failed. The product also turned out to be very laser sensitive at 1064 nm (Nd: YAG laser) and at 514.5 nm ($Ar^+(g)$ laser) so that no Raman measurement was possible (including micro-Raman and FT-Raman). Finally, we have not been able to obtain $^{17}O_2$ as a reactant via commercial sources, and attempts to measure the ^{17}O NMR spectra based on the natural abundance of dioxygen samples also failed. Further, using enriched ^{17}O or ^{18}O samples appears to be unrealistic due to the large amount of material ($O_2(g)$) necessary to perform these experiments at constant purge.

Fortunately, there is available in the literature a large amount of vibrational data on the interactions of dioxygen at palladium and platinum surfaces, and for some complexes. The presence of the dioxygen molecules is readily demonstrated from the IR absorption spectra. The possibility of the presence of oxo groups (Pd-O-Pd) was quickly ruled out since the ν(PdO) peaks are generally found in the 450–475 cm^{-1} region (according to LEED studies of atomic oxygen chemisorbed onto Pd(100) surfaces, and because no such peak was observed in our spectra). These results are also supported by other results for Pt(111) surfaces (ν(PtO) for Pt-O-Pt is ~490 cm^{-1}) (4) and for Fe-O-Fe groups found in biologically related molecules; ν(FeO) = 486 cm^{-1} (22). On the other hand, the $\nu(O_2)$ frequencies are found at 871, 887, and 726 cm^{-1}, as measured by LEED spectroscopy for O_2 chemisorbed onto Pt(111), Pd(110) and Pd(100) surfaces, respectively (4, 5, 21). Similarly, in complexes of the type $Pt(L)_2O_2$ (L = phosphine or $CH_2{=}CH_2$), IR spectra also exhibit absorptions in the 814–828 cm^{-1} range associated with $\nu(O_2)$ (23). In biologically related Fe dimers bridged by O_2 (in a Fe-(μ^1-O_2)-Fe fashion), $\nu(O_2)$ and ν(FeO) are observed at 844 and 504 cm^{-1}, respectively (24). The IR spectra of the bisdioxygen product (Fig. 2) exhibit medium intensity absorptions at 838 and 866 cm^{-1}, and medium and larger intensity new signals in the 550 and 600 cm^{-1} regions, which are unambiguously assigned to $\nu(O_2)$ and ν(PdO), respectively. The peaks originally observed at 1815 (ν(CO)) and ~475 cm^{-1} (ν(PdC); doublet: a + e presumably in the C_{3v} point group) disappear during irradiation, which is consistent with the CO elimination. The fact that two stretches are observed for $\nu(O_2)$ (838 and 866 cm^{-1}), both in the solid

Can. J. Chem. Downloaded from www.nrcresearchpress.com by 65.111.164.53 on 09/08/12
For personal use only.

Can. J. Chem. Downloaded from www.nrcresearchpress.com by 65.111.164.53 on 09/08/12
For personal use only.

Fig. 2. Comparison of the FT-IR spectra (4 cm^{-1} resolution, 200 scans) for solid $Pd_3(dppm)_3CO^{2+}$ (starting materials, —) and $Pd_3(dppm)_3(O)_2^{2+}$ (pure final product, ...).

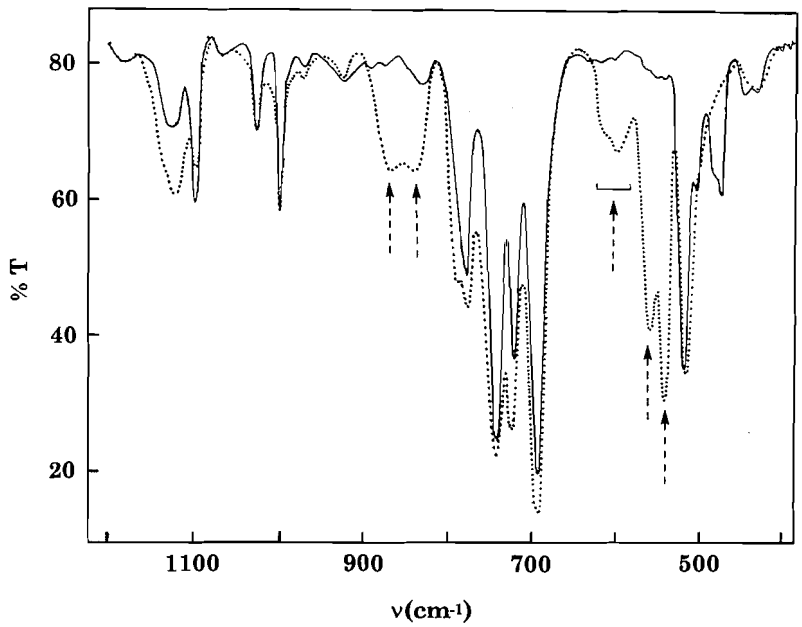

Scheme 1

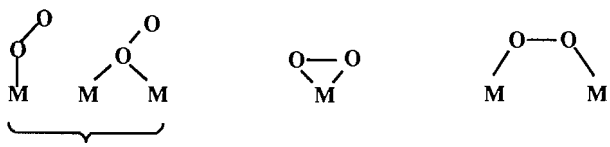

Type I Type II Type III

Scheme 2

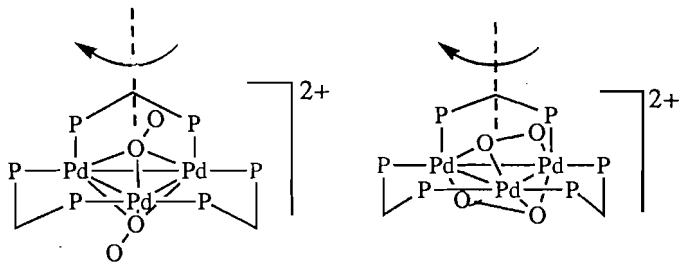

state and in solution, is consistent with the analytical results indicating the presence of two dioxygen ligands. The $\nu(O_2)$ and ν(PdO) values for $Pd^{II}(O_2)(t\text{-BuNC})_2$ are 893 and 484 cm^{-1} and for PdO_2 are 1024 and 427 cm^{-1}, respectively (25, 26), indicating that π back-bonding is (as expected) greater in the Pd_3^{2+} cluster with respect to the electron poorer Pd^{II} centers. However these data alone cannot distinguish between the three types of dioxygen adducts (Scheme 1: Type I, end-on; Type II, side-on; Type III, bridging).

Type II is not possible in this case due to steric hindrance with the *ortho*-hydrogen of the dppm-phenyl groups. This was verified by CPK models using computer modelings (SYBYL 5.5; Triphos Associates, St-Louis, Mo.) of the crystal structure of $[Pd_3(dppm)_3CO](CF_3CO_2)(PF_6)$ (27), in which the cavity is emptied from its $CF_3CO_2^-$ substrate, and replaced by O_2 sitting on one of the Pd atoms. The presence of a sharp and unique singlet in the ^{31}P-{H}-HNMR (–4.62 ppm) and a sharp triplet in the ^1H NMR spectra (3.74 ppm for the CH_2 groups, ^2J(P, H) = 13 Hz), and the relatively low complexity of the FT-IR spectra (Fig. 2), suggests that the molecule is symmetrical (i.e., type I, where one of the oxygens is triply bridging the Pd atoms). Literature data show that indeed linear molecules such as SCN^- and HC≡CH add to the M_3 centers (M = Pd, Pt) quasi-perpendicularly, when bridging in a triply bridging fashion (12).

The decrease in temperature (down to –60°C) did not change the ^1H NMR signal (i.e., in the CH_2 region). These experiments do not prove the true geometry since rapid equilibrum between the two (or more) structures may still be possible. Surface science studies (near-edge X-ray-absorption fine-structure studies) have recently demonstrated that the adsorbed O_2 molecules are oriented perpendicular (Type I) and parallel (Type III) to the bulk surface plane (i.e., Pt(110) surface; ref. 28), which somewhat improved the general idea that dioxygen binds the surface parallel to the surface plane (for instance for Pt(111) and Ag(110); refs. 29, 30). There has been no evidence of equilibrium between the two forms in this work but both are known to exist and must be considered. However the full width at half maximum for the proton signal is ≤6 Hz at 295 K, indicating that motion (or revolution) of the dioxygen molecules on top of the Pd_3 planes must be faster than the NMR time scale. The Type I structure appears to be more convenient for such motion as it does not involve the scission and formation of Pd—O bonds (see Scheme 2).

The O_2 ligands would then act as two-electron donors, and the product would fall in the 44-electron cluster category, a category that is generally encountered in the oxidatively added $M_3(dppm)_3CO^{2+}$ series (M = Pd, Pt). The ^{31}P NMR datum is consistent with the ^{31}P NMR data reported by Puddephatt and co-workers for a very large series of Pd_3 44-electron clusters; these values range from −6.7 to −12.7 ppm (with respect to H_3PO_4) (15, 31, 32), and suggest that no Pd—Pd bond scission occurred during the photoaddition. Further evidence for Pd_3

Scheme 3

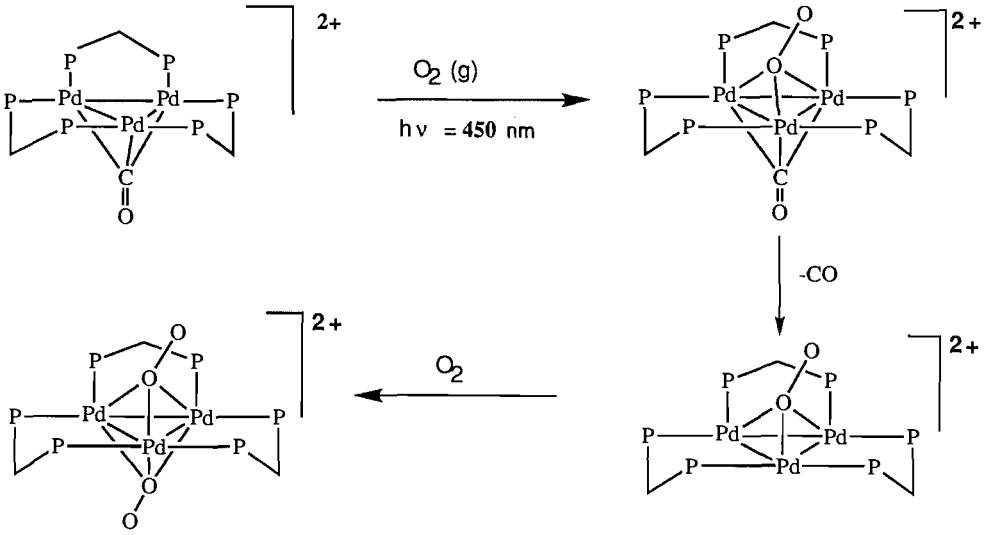

Fig. 3. ^{1}H NMR spectrum of the 4 ppm portion (vs. TMS) of the reaction mixture when the photoreaction vessel is purged with pure O_2(g) prior to photolysis, but not during photolysis. In this case the residue was collected after a few hours of irradiation, evaporated, then (without purification) dissolved in CD_2Cl_2 for NMR analysis. The scheme above the signal represents the coupling constant patterns for the two intermediates (1, 2) and the final product (3).

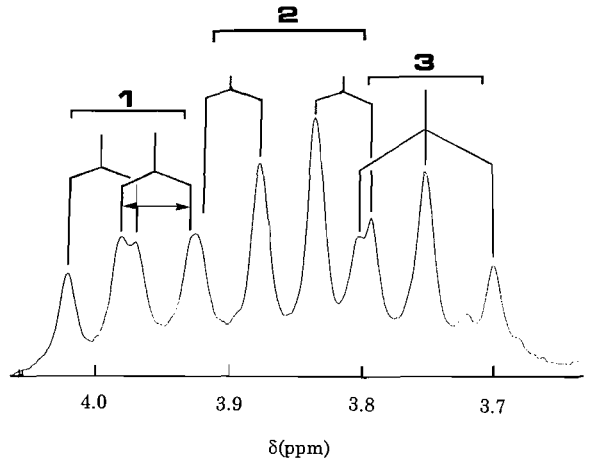

bonding is provided from emission spectroscopy. Typically λ_{emi}(monomer)<λ_{emi}(dimer)<λ_{emi}(trimer) for Pd^0L_4 monomers (~600–620 nm), Pd^I–Pd^I complexes (625–650 nm), and $Pd_3(dppm)_3CO^{2+}$ (720 nm), respectively (20, 33, 34). $Pd_3(dppm)_3(O_2)_2^{2+}$ exhibits an intense luminescence at 77 K centered at 760 nm (ethanol solutions) with a full width at half maximum (fwhm) of ~2800 cm^{-1} and a luminescence lifetime of 25 ± 3 μs. The data compare favorably with those of the $M_3(dppm)_3CO^{2+}$ complexes at 77 K (M = Pd, λ_{emi} = 720 nm, fwhm = 2400 cm^{-1}, τ_e = 2.4 μs (in 2MeTHF); M = Pt; λ_{emi} = 630 nm, fwhm = 2500 cm^{-1}, τ_e = 14 μs (2MeTHF); see ref. 14), and confirm the trinuclear bonding nature of the cluster product. Like $Pd_3(dppm)_3CO^{2+}$, $Pd_3(dppm)_3(O_2)_2^{2+}$ is not luminescent at room temperature. If a Type III structure occurs in which the O_2 molecule would act as a multielectron donor (more than two), then based upon the electron count, Pd—Pd bond scission would be expected. This is obviously not the case.

2. Photochemical intermediates and other properties

During continuous photolysis and O_2(g) bubbling, no photochemical intermediate was observed by ^{1}H NMR and IR during the monitoring. However, when the bubbling was stopped, leaving the rest of the dissolved O_2 to be slowly consumed upon continued irradiation, both ^{1}H NMR and IR spectra exhibited the growth of intermediate signals, followed by a disappearance or a decrease of these same signals upon further O_2(g) purging. By NMR, at the early stage of the irradiation, a first signal appears at 3.97 ppm with a coupling constant of 13 Hz. By IR, a new peak at 850 cm^{-1} is also readily noted (i.e., $\nu(O_2)$). A second signal subsequently appears at 3.85 ppm (coupling constant = 11 Hz) along with the final product signal (3.75 ppm, ^2J(P,H) = 13 Hz). Figure 3 shows a typical ^{1}H NMR spectrum in the 4 ppm region of the photochemical intermediates. The relative intensities of each of these signals depend upon whether further bubbling is provided to the solution; upon new additions of O_2, the first and second signals (3.98 and 3.83 ppm) successively disappeared. The final product signal (3.75 ppm) increased and remained. The two intermediates, the final product, and the starting materials exhibit identical R_f values, by thin-layer chromatography, and identical solubilities, so attempts to separate these were not successful. Upon prolonged irradiation, no new band appears in the IR, and the 850 cm^{-1} band remains as a broad signal (presumably a broad envelope including $\nu(O_2)$ of this intermediate along with those of the final product). Scheme 3 shows the proposed (and simplified) mechanism by which the bisdioxygen product must be formed. Intermediate 1 is assigned to $[Pd_3(dppm)_3(O_2)(CO)]^{2+}$ and Intermediate 2 is believed to be $[Pd_3(dppm)_3(O_2)]^{2+}$ (these are referred to as photochemical intermediates). The absence of efficient π back-bonding in the latter (i.e., 42e$^-$) intermediate implies that the complex is not a stable molecule (35). This is presumably why the acetonitrile solvent appears as a stabilizing agent in this case (by penetrating into the empty cavity and interacting with the Pd_3 center

Can. J. Chem. Downloaded from www.nrcresearchpress.com by 65.111.164.53 on 09/08/12
For personal use only.

Can. J. Chem. Downloaded from www.nrcresearchpress.com by 65.111.164.53 on 09/08/12
For personal use only.

(35), something that THF and benzene fail to do (i.e., decomposition is observed instead)). In this work, there was no evidence for oxo intermediates (from IR) as known for the $Fe(CO)_5$ and O_2 photoreaction (36). Surprisingly, addition of $(C_6H_5)_3P$ to $[Pd_3(dppm)_3(O_2)_2]^{2+}$ in solution did not lead to any reaction. It is suspected that steric hindrance plays, in part, a role in this inertness.

The quantum yield (Φ) for the photoreaction was 0.033 ± 0.004 based upon the disappearance of the 500 nm band in the UV–visible spectra. This quantum yield can be considered small with respect to other Φ values reported in the literature for inorganic compounds (see, for example, ref. 37) and, in particular, for Pd—Pd bonded complexes (38), but is the largest we have measured in the Pd_3 series. For example, both $M_3(dppm)_3CO^{2+}$ clusters (M = Pd,Pt) photoreact slowly with CH_2Cl_2 and $CHCl_3$ to produce the well-known $M(dppm)Cl_2$ complexes with no, or almost no, by-products for M = Pt and with ~50% yield for M = Pd (the other 50% of the products are uncharacterized). The Φ values in neat $CHCl_3$ and CH_2Cl_2 were in the order of 4×10^{-5} (!) (unpublished results). Photoinduced reactions of the clusters (M = Pd,Pt) with H_2(g), CO(g), and CO_2(g) were also observed but their reactivities were found to be very slow also ($\Phi \sim 0.002$!; unpublished results). In the latter cases the photoproducts are not identified. There are many reasons that could explain the low Φ values: (1) the excited state lifetimes are found to be extremely short ($\tau_1 < 40$ ps, M = Pd; $\tau_1 < 40$ ps, $70 < \tau_2 < 400$ ns, intensity ratio for $\tau_1/\tau_2 = 95/5$, M = Pt; ref. 39); (2) access to the lumophore is sterically hindered by another interacting substrate (i.e., $CF_3CO_2^-$ or CH_3CN) in the ground and excited states; and (3) the biradical-type excited state is delocalized over three metal centers, not localized as in the case of the $M_2(CO)_{10}$ dimers ($2 \times M(CO)_5$; M = Mn, Re; ref. 40). The second reason refers to the presence of guest–host chemistry involving the formation of weak preassembled ground-state complexes of the type cluster···substrates, and will be discussed further below.

Further irradiation (at 350–400 nm) of the bisdioxygen product in neat acetonitrile also led to decomposition similar to that described in the thermal reaction above (Pd/PdO and dppm-oxide). Photoinduced O—O and M—O_2 bond cleavages were previously observed at low-wavelength irradiation (230–330 nm) for the M(111) surfaces (M = Pd, Pt; refs. 41–43). In many ways, the unsaturated "$M_3(dppm)_3CO^{2+}$" clusters appear to behave very similarly to the bulk surfaces (12). Interestingly, photoinduced reaction between coadsorbed H_2 and O_2 on Pt(111) led to the formation of hydroxyls and water (43). Such an experiment has yet to be attempted on the $[Pd_3(dppm)_3(O_2)_2]^{2+}$ cluster.

3. Picosecond flash photolysis

The $Pd_3(dppm)_3CO^{2+}$ complex is nonluminescent at room temperature (20), so excited-state kinetics were followed by picosecond transient spectroscopy. The transient spectra (difference absorption) for $Pd_3(dppm)_3CO^{2+}$ in toluene (as well as in acetonitrile, Fig. 4) are characterized by a bleaching of the 490–500 nm band and the appearance of a broad transient band located at ~600 nm. Both kinetic traces of the bleached band recovery and transient decay (τ_e) are the same and short-lived (toluene, 35 ± 10 ps; acetonitrile 25 ± 10 ps). These lifetimes are in the same range as those reported for the $Pd_2(dmb)_2X_2$ and $Pd_2(tmb)_2X_2$ complexes (dmb = 1,8-diisocyano-*p*-menthane; tmb = 2,5-diisocyano-2′,5′-dimethylhexane; X = Cl, Br; ref. 34). In the latter cases, the low τ_e values are due to the rapid homolytic Pd^I—Pd^I bond scission followed by a rapid recombination. Such behavior is typical for $^1(d\sigma)^1(d\sigma^*)$ excited states generally encountered for d^7–d^7 and d^9–d^9 dimers (34). The lowest energy excited state for the $Pd_3(dppm)_3CO^{2+}$ complex is $a_1 \rightarrow a_2$ where the a_1 MO is weakly Pd—Pd bonding and the a_2 MO is Pd—Pd antibonding (20, 39). Such an excited state is somewhat similar to the $d\sigma d\sigma^*$ one in the M—M scheme. The difference is that the MO is delocalized over three Pd atoms. It is also reasonable to attribute the low τ_e value to homolytic Pd—Pd cleavage followed by the rapid formation of the M—M bond similar to that of the d^7–d^7 and d^9–d^9 dimers.

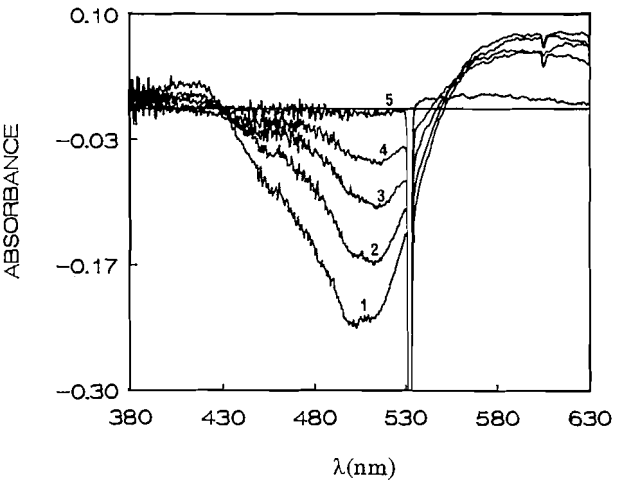

Fig. 4. Typical transient spectra of $Pd_3(dppm)_3CO^{2+}$ in acetonitrile at 298 K (λ_{exc} = 532 nm); delay time between the laser pulses: 1 = 45 ps, 2 = 55 ps, 3 = 65 ps, 4 = 95 ps, and 5 = 105 ps.

The weak solvent dependence on τ_e is associated with the $Pd_3(dppm)_3CO^{2+}$–solvent guest–host chemistry (27). Because the diffusion rate constants typically range between 10^9 and 10^{10} M^{-1} s^{-1} for common organic solvents (the data are taken from ref. 44; see footnote 12 of this reference) i.e., ~10^8–10^9 s^{-1} (by dividing the rate constants by the solvent concentration; pseudo-rate constant), the excited state deactivation rates ($(3–4) \times 10^{10}$ s^{-1}) appear to be too great to allow any efficient bimolecular process to occur in the excited state. Such an observation is also consistent with the relatively low quantum yields for the photoreaction and indicates that the cluster and the dioxygen molecule must be preassembled prior any photochemical event.

The most unusual result is the fact that no clear O_2 dependence on τ_e is observed, even at saturated conditions ($[O_2]_{sat'd}$ ~ 10^{-2} M in common organic solvents at 298 K, ref. 18). The experimental uncertainties are great (±10 ps) and may prevent the observation of any small decrease in τ_e upon bubbling. Also the concentration of O_2 bonded to the Pd_3 center within the cavity, which is in competition with ~10 M of neat solvent (blocking the cavity) prior to the laser pulse, may be rather low (i.e., 10^{-2} M = $[O_2]_{bonded}$ + $[O_2]_{free}$). The ground-state guest–host equilibrium constant has not been measured but can be estimated by using the following argument. Guest–host behavior is clearly seen from the UV–visible spectra upon light bubbling (Fig. 5). The ground-state

Fig. 5. Spectroscopic changes occurring upon bubbling O_2 into an acetonitrile solution of the unsaturated $Pd_3(dppm)_3CO^{2+}$ cluster in the dark (298 K).

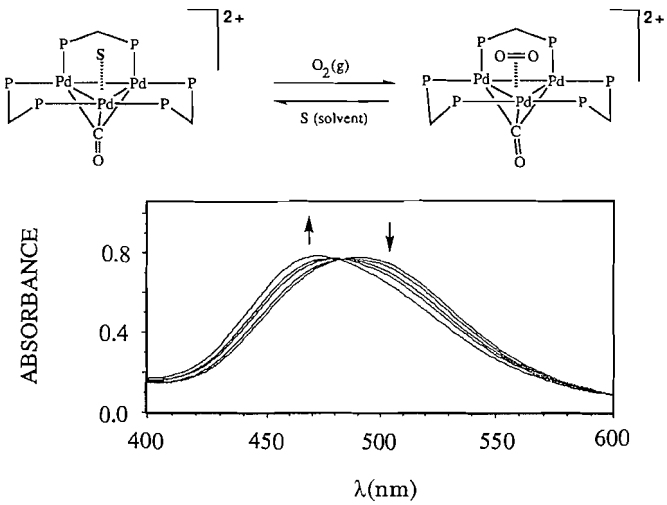

binding of O_2 induces the appearance of a new band located at ~464 nm. This binding is reversible (in the dark) by bubbling Ar(g), or any other gases (H_2, CO, CO_2 ...). The presence of spectroscopic transformation upon purging has been observed for all the solvents investigated, indicating that in the ground state O_2 competitively binds the Pd_3 center despite the fact that the $[O_2]$ at maximum can only be 10^{-2} M (by comparison with the neat solvents ~10 M). Based upon the binding equilibrum constants (K_{11}) measured for neutral organic molecules (including solvents), the lower limit for the K_{11} value for O_2 is ~1 M^{-1} (27). When sodium acetate is added to any of the solutions (toluene, methanol, dimethylformamide, etc.), bubbling O_2 does not induce a spectroscopic change, indicating that the acetate binds far more strongly than O_2, which in turn prevents O_2 from interacting strongly with the Pd_3 center. Because K_{11} for acetate is ~730 M^{-1} (27), the range for K_{11} for O_2 is between 1 and 730 M^{-1} (perhaps being much closer to the lower limit), at least in the ground state. Nonetheless, the ps flash photolysis experiments (i.e., lifetime measurements) indicate that O_2(g) must be close to the Pd_3 center prior to irradiation (preassembled reactants) in order to induce the net photoreaction, and that the solvent definitely plays an "inhibiting" role in the primary step of the phototransformation. The fact that both the spectra and kinetic traces were similar for the coordinating acetonitrile and noncoodinating toluene solvents indicates that the photoinduced decomposition observed for the THF and benzene solutions is not due to processes occurring in the early stage of the multistep photoaddition. This observation supports the model that suggests that acetonitrile must stabilize one of the photochemical intermediates. By facing the evidence that a preassembled ground-state cluster–dioxygen complex is formed, and that the excited state lifetimes are too low to allow efficient bimolecular reactions in the excited state, one has to modify Scheme 3 by adding an extra step as shown in a more detailed Scheme 4.

Final remarks

The (multistep) photoinduced addition of O_2 onto $Pd_3(dppm)_3CO^{2+}$ has been observed for the first time, which makes the reported air stability of the cluster somewhat conditional to photochemistry. Dioxygen binds the Pd_3 center in a peroxo fashion, which represents the first complex in which O_2 acts as a ligand in a trinuclear metal complex. Unfortunately, no crystal suitable for X-ray crystallography could be obtained. However, spectroscopy has provided much evidence for a Type I structure, which makes the product exhibit a 44-electron count. Prior to the photochemical event, uncomplexed O_2 must be very close to the Pd_3 center in order to interact in the particularly short-lived $^1(a_1)^1(a_2)$ excited state for the addition of the first O_2 molecule. The lack of apparent quenching of the transient by O_2(g) is unusual, but demonstrates the extremely low excited-state lifetimes (at 298 K), and the ground-state competitive binding of O_2 with the solvent inside the cavity of the $Pd_3(dppm)_3CO^{2+}$, explaining the low quantum yield of photoaddition of O_2. The $Pd_3(dppm)_3(O_2)_2^{2+}$ complex formed represents *one* model that can mimick the O_2 behavior adsorbed onto the bulk Pd surfaces; in many ways the complex exhibits similar properties including both thermally and photochemically induced O—O bond cleavage, which in this case produces, dppm-oxide among other by-products. In this respect, the use of $Pd_3(dppm)_3(O_2)_2^{2+}$ as an oxidizing agent for organic materials can easily be conceived. The fact that the cavities have a given dimension also implies that the oxidizing power of the cluster may be limited as experienced by the inertness toward $(C_6H_5)_3P$ (size selectivity). Clearly the methods of oxidation would have to be mild as the complex is both thermally and photochemically sensitive.

The photoinduced addition reactivity of O_2 onto $Pt_3(dppm)_3CO^{2+}$ has not been investigated. The preliminary results show that reactions are indeed observed but the rates of

Scheme 4

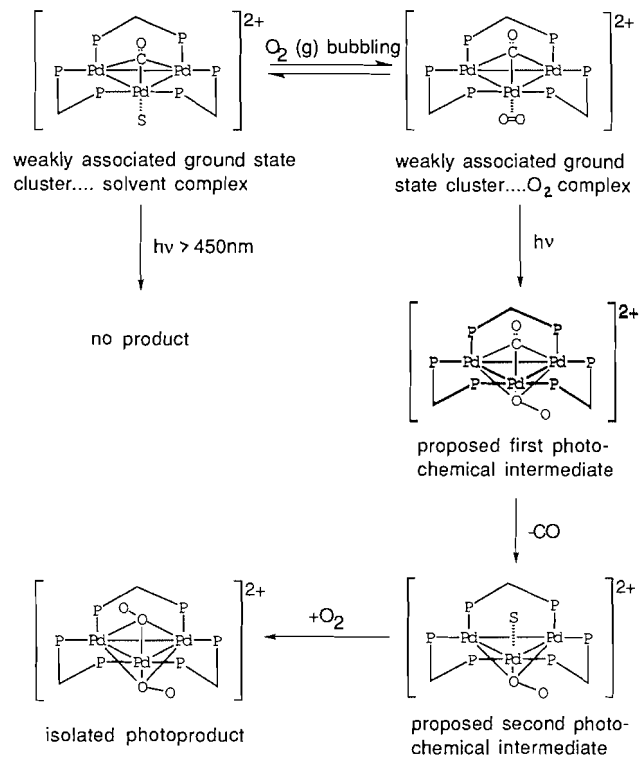

Can. J. Chem. Downloaded from www.nrcresearchpress.com by 65.111.164.53 on 09/08/12
For personal use only.

transformation are much slower than in the Pd case. Further, we have noticed that bubbling O_2 into a $Pt_3(dppm)_3CO^{2+}$ solution (in the dark) does not induce any spectroscopic changes normally associated with guest–host chemistry. This phenomenon has yet to be explained.

Acknowledgements

This research was supported by the Natural Sciences and Engineering Research Council of Canada and le Fonds pour la formation de chercheurs et l'aide à la recherche (Québec). P.D.H. thanks Dr. S.M. Hubig (University of Houston) for the measurements of the picosecond flash photolysis spectra at the former Fast Kinetic Research Center in Austin, Texas.

References

1. M.A. Benvenuto and A. Sen. J. Chem. Soc. Chem. Commun. 970 (1993), and references cited therein.
2. R.G. Austin, R.S. Michaelson, and R. S. Myers. Chem. Ind. **22**, 269 (1985).
3. K.A. Jorgensen. Chem. Rev. **89**, 431 (1989).
4. G.B. Fisher, B.A. Sexton, and J.L. Gland. J. Vacuum Sci. Technol. **17**, 144 (1980).
5. M. Nishijima, M. Jo, Y. Kuwahara, and M. Onchi. Solid State Commun. **60**, 257 (1980).
6. C. Nyberd and C.G. Tengstal. Solid State Commun. **44**, 251 (1982).
7. T. Matsushina. Surf. Sci. **157**, 297 (1985).
8. T. Matsushina. Surf. Sci. **217**, 155 (1989).
9. R. Imbihl and J. E. Demuth. Surf. Sci. **173**, 395 (1986).
10. J.L. Gland, B.A. Sexton, and G.B. Fisher. Surf. Sci. **95**, 587 (1980).
11. Steininger, S. Lehwald, and H. Ibach, Surf. Sci. **123**, 1 (1982).
12. R.J. Puddephatt, L. Manojlovic-Muir, and K.W. Muir, Polyhedron, **9**, 2767 (1990).
13. J. Xiao, J.J. Vittal, R.J. Puddephatt, L. Manojlovic-Muir. and K. W. Muir. J. Am. Chem. Soc. **115**, 7882 (1993).
14. L. Manojlovic-Muir, K.W. Muir, B.R. Lloyd, and J. Puddephatt. J. Chem. Soc. Chem. Commun. 1336 (1983).
15. D.D. Perrin and W.L.F. Armarego. *In* Purification of laboratory chemicals, 3rd ed. Oxford, U.K. 1988. pp. 65–310.
16. A.J. Gordon and R.A. Ford. *In* The chemist's companion. A handbook of practical data, techniques, and references. Wiley, New York. 1972. pp. 431–436.
17. J.G. Calvert and J.N. Pitts. *In* Photochemistry. Wiley, New York. 1966. pp. 783–795.
18. S.L. Murov, I. Carmichael, and G.L. Hug. *In* Handbook of photochemistry. 2nd ed. Marcel Dekker, New York. 1993. pp. 289–289.
19. S.M. Hubig, M. Drouin, A. Michel, and P.D. Harvey. Inorg. Chem. **30**, 3375 (1992).
20. R. Provencher and P.D. Harvey. Inorg. Chem. **127**, 163 (1993).
21. C. Nyberg and C.G. Tengstål. Surf. Sci. **127**, 163 (1983).
22. T.M. Loehr. *In* Oxygen complexes and oxygen activation by transition metals. *Edited by* A.E. Martell and D.T. Sawyer. Plenum Press, New York. 1987. pp. 17–33.
23. W.-S. Hwang. Polyhedron, **3**, 513 (1984).
24. I.M. Klotz and D.M. Kurtz, Jr. Acc. Chem. Res. **17**, 16 (1984).
25. A. Nakamura, Y. Tatsuno, M. Yamanoto, and S. Otsuka. J. Am. Chem. Soc. **93**, 6052 (1971).
26. H. Huber, W. Klotzbücher, G.A. Ozin, and A. Vander Voet. Can J. Chem. **51**, 2722 (1983).
27. R. Provencher, K.T. Aye, M. Drouin, J. Gagnon, N. Boudreault, and P.D. Harvey. Inorg. Chem. **33**, 3689 (1994).
28. Y. Ohno, T. Matsushima, S.-I. Tanaka, E. Yagasaki, and M. Kamada. Surf. Scien. **275**, 281 (1992).
29. J. Stöhr, J.L. Gland, W. Eberhardt, D. Outka, R.J. Madix, F. Sette, R.J. Madix, F. Sette, R.J. Koestner, and U. Doebler. Phys. Rev. Lett. **51**, 2414 (1983).
30. W. Wurth, J. Stöhr, P. Feulner, X. Pan, K.R. Bauchspiess, Y. Baba, E. Hudel, G. Rocker, and D. Menzel. Phys. Rev. Lett. **65**, 2426 (1990).
31. L. Manojlovic-Muir, K.W. Muir, B.R. Lloyd, and R.J. Puddephatt. J. Chem. Soc. Chem. Commun. 536 (1985).
32. M. Rahidi, E. Ksistof, J.J. Vittal, and R.J. Puddephatt. Inorg. Chem. **33**, 1497 (1994).
33. P.D. Harvey, W.P. Schaefer, and H.B. Gray. Inorg. Chem. **27**, 1101 (1988).
34. P.D. Harvey and Z. Murtaza. Inorg. Chem. **32**, 4721 (1993).
35. C. Mealli. J. Am. Chem. Soc. **107**, 2245 (1985).
36. P.D. Lyne, D.M.P. Mingos, T. Ziegler, and A.J. Downs. Inorg. Chem. **32**, 4785 (1993).
37. A.W. Adamson and P.D. Fleishauer (*Editors*). Concept of inorganic photochemistry. Wiley, New York. 1975. pp. 143–201.
38. D. Perreault, M. Drouin, A. Michel, and P.D. Harvey. Inorg. Chem. **31**, 2740 (1992).
39. P.D. Harvey, S.M. Hubig, and T. Ziegler. Inorg. Chem. **33**, 3700 (1994).
40. G.L. Geoffroy and M.S. Wrighton. *In* Organometallic photochemistry. Academic Press, New York. 1979. pp. 136–140.
41. X. Guo, L. Hanley, and J.T. Yates, Jr. J. Chem. Phys. **90**, 200 (1989).
42. X. -Y. Zhu, S.R. Hatch, A. Campion, and J.M. White. J. Chem. Phys. **91**, 5011 (1989).
43. T.A. Germer and W. Ho. J. Chem. Phys. **93**, 474 (1990).
44. P.D. Metcalf and C.P. Kubiak. J. Am. Chem. Soc. **108**, 4682 (1986).

Can. J. Chem. Downloaded from www.nrcresearchpress.com by 65.111.164.53 on 09/08/12
For personal use only.

Evidence of a solvent-mediated barrier to radiationless decay in the $\tilde{B}$ ($^1A_1$) state of thiophosgene in solution

Jieming Li and Ronald P. Steer

Abstract: Thiophosgene, Cl_2CS, has been excited in the near-uv and the resulting quantum yields of $\tilde{B}$–$\tilde{X}$ fluorescence and of Cl_2CS consumption have been measured as a function of solvent composition (perfluoro-*n*-hexane, *n*-hexane, CCl_4), temperature, and excitation wavelength. In agreement with previous work it is shown that (*i*) nonradiative processes dominate the decay of the $\tilde{B}$ state in solution, and (*ii*) perfluoroalkane solvents act as inert "heat baths". The process by which the $\tilde{B}$ state is apparently "quenched" by CCl_4 and *n*-hexane has been discovered. The nonradiative process leading to $\tilde{B}$'s decay involves activation and crossing a barrier, the height of which is a function of the nature and composition of the solvent. CCl_4 and *n*-hexane do not quench the excited state, but instead accelerate its rate of relaxation by lowering the barrier between the bound, radiative portion of the surface and a dark, unbound region. There is evidence that CCl_4 or *n*-hexane form clusters around a Cl_2CS solute molecule in mixed perfluoroalkane–CCl_4 or *n*-hexane solutions. Barrier crossing leads to photodecomposition via at least two parallel paths, one free radical (Cl + ClCS) and the other likely molecular (Cl_2 + CS), the relative contributions of which are a function of excitation wavelength.

Key words: thiophosgene, photochemistry, solvent-mediated barrier crossing.

Résumé : On a excité le thiophosgène, Cl_2CS, dans le proche-uv et on a mesuré les rendements quantiques de la fluorescence $\tilde{B}$–$\tilde{X}$ et de la consommation du Cl_2CS qui en résultent en fonction de la composition du solvant (perfluoro-*n*-hexane, *n*-hexane et CCl_4), de la température et de la longueur d'onde de l'excitation. En accord avec les travaux antérieurs, il est démontré que (*i*) les processus non dissociatifs dominent la dégénérescence de l'état $\tilde{B}$ en solution et (*ii*) les solvants perfluoroalcanes agissent comme des "bains de chaleur" inertes. On a découvert le processus par lequel l'état $\tilde{B}$ est apparemment désactivé par le CCl_4 et par le *n*-hexane. Le processus non radiatif conduisant à la dégénérescence de $\tilde{B}$ implique une activation et le passage d'une barrière dont la hauteur est une fonction de la nature et de la composition du solvant. Le CCl_4 et le *n*-hexane ne désactivent pas l'état excité, mais ils accélèrent plutôt sa vitesse de relaxation en abaissant la barrière entre la portion radiative liée de la surface et la région noire non liée. Il existe des indications à l'effet que le CCl_4 ou le *n*-hexane forment des agrégats autour d'une molécule de Cl_2CS en solution dans des mélanges de perfluoroalcane, CCl_4 ou *n*-hexane. Le passage d'une barrière conduit à une photodécomposition par le biais d'au moins deux voies parallèles, une impliquant un radical libre (Cl + ClCS) et l'autre étant probablement moléculaire (Cl_2 + CS); les contributions relatives des deux sont fonction de la longueur d'onde d'excitation.

Mots cles : thiophosgène, photochimie, passage de barrière déterminé par solvent.

[Traduit par la rédaction]

I. Introduction

Thiophosgene, Cl_2CS, has been studied extensively both in the gas phase and in solution because it offers insight into several important aspects of electronic spectroscopy, photophysics, and photochemistry (1–10). We have been particularly interested in the $\tilde{B}$ ($^1A_1$) state of Cl_2CS, which can relax by a relatively large number of possible parallel and sequential processes and therefore provides a challenging level of complexity. Fortunately, relatively strong $\tilde{B}$–$\tilde{X}$ fluorescence provides a convenient, sensitive experimental means of examining the dynamic behavior of this highly excited polyatomic species both in the isolated molecule and in a wide variety of condensed media.

Spectroscopic experiments on isolated Cl_2CS in cold supersonic expansions have been particularly useful in revealing the details of the $\tilde{B}$ state potential surface (2–4). The location of $\tilde{B}$–$\tilde{X}$ origin (λ = 291.75 nm; 34 277 cm^{-1}) and the wavenumbers of the upper state vibrations have now been established with some confidence as a result of recent optical–optical double resonance experiments (3). Previous studies have also shown that, in the isolated molecule, the quantum yield of emission from low-lying vibrational levels of the $\tilde{B}$ state approaches 1 (11), and a fluorescence-weakening surface crossing occurs with an onset at 1450 ± 50 cm^{-1} above the zero point level (4). Excitation at substantially higher energies (e.g., λ = 248 nm; 40 323 cm^{-1}) produces no observable fluorescence but does result in photodissociation of the molecule via at least two possible channels (10);

Received July 26, 1994.

J. Li and R.P. Steer.[1] Department of Chemistry, University of Saskatchewan, Saskatoon, SK S7N 0W0, Canada.

[1] To whom correspondence should be addressed.

Can. J. Chem. Downloaded from www.nrcresearchpress.com by 65.111.164.53 on 09/08/12
For personal use only.

Can. J. Chem. Downloaded from www.nrcresearchpress.com by 65.111.164.53 on 09/08/12
For personal use only.

[1] $Cl_2CS^v(\tilde{B}) \rightarrow Cl(^2P_{1/2,3/2}) + ClCS(\tilde{X}, \tilde{A}, \tilde{B})$

[2] $Cl_2CS^v(\tilde{B}) \rightarrow Cl_2(^1\Sigma_g^+) + CS(^1\Sigma)$

Both dissociation channels, including several electronically excited states of the radical products in channel [1], are energetically accessible at modest vibrational energies within the $\tilde{B}$ state, but their relative importance has yet to be established with certainty (1). For example, Okabe (9) has reported the quantum yield of Cl atom production is 1 at λ_{ex} = 253.7 nm (39 417 cm^{-1}), whereas Ondrey and Bersohn (10) report ϕ[1] = 0.2 and ϕ[2] = 0.8 for excitation at 248 nm (40 323 cm^{-1}).

In solution the formation of ground state van der Waals dimers of Cl_2CS (12) and the existence of a nearby very weak absorption, tentatively assigned to a "dark", doubly excited state (5), must be taken into account in order to model quantitatively the photophysical processes of the $\tilde{B}$ state (8, 13). When the relaxation of only monomeric Cl_2CS ($\tilde{B}$) is untangled from these complications, one finds that, in contrast to the isolated molecule, radiationless processes account for a very large fraction of decay events in solution at room temperature even when bound portions of the $\tilde{B}$ state are initially populated. More importantly, the radiationless decay rates of these low-lying, apparently bound, levels of the $\tilde{B}$ state are found to be strongly dependent on the nature of the solvent (6, 7). By measuring the decay rates of vibrationally thermalized $\tilde{B}$ states as a function of temperature in dilute, weakly interacting perfluoroalkane solutions we showed (7) that the nonradiative relaxation process exhibits an effective activation energy, E_a, of 1430 ± 80 cm^{-1} (17.1 ± 0.9 kJ mol^{-1}). This value is nearly identical to the vibrational energy of the $\tilde{B}$ state at the onset of the fluorescence weakening process seen in the isolated molecule. In more strongly interacting *n*-hexane or CCl_4 solutions, however, the quantum yields of $\tilde{B}$–$\tilde{X}$ fluorescence are much smaller (6), from which one may infer that the $\tilde{B}$ state lifetimes are much shorter than in perfluoroalkanes.

We have now completed experiments designed to understand more fully the behavior of monomeric Cl_2CS ($\tilde{B}$) in solution. The results demonstrate that solvents other than perfluoroalkanes increase the rate of nonradiative decay of the $\tilde{B}$ state primarily by lowering its effective activation barrier rather than by electronic quenching.

II. Experimental section

$\tilde{B}$–X fluorescence emission and excitation spectra and quantum yields were measured using a Spex, model 222 Fluorolog spectrofluorometer equipped with a "Datamate" computer. The procedure adopted for obtaining accurate values of emission quantum yields with this instrument have been described previously (14). Quinine hydrogen sulfate in 0.5 mol dm^{-3} H_2SO_4 (ϕ_f = 0.52 (15)) was employed as a fluorescence standard. Ultraviolet–visible absorption spectra were taken on a Cary, model 118 spectrophotometer.

Emission lifetimes were measured using a mode-locked Spectra-Physics model 2030 argon ion laser which synchronously pumped a cavity-dumped dye laser operating on rhodamine-6G. The 4 MHz output of the dye laser was frequency-doubled using an angle-tuned KDP crystal (Inrad) to obtain wavelengths in the 285–300 nm region with a maximum power of ca. 0.5 mW at 295 nm. To avoid rotational depolarization artefacts emission was observed at the magic polarization angle using a Zeiss M4QIII quartz prism monochromator and a Hamamatsu R2809 U-07 microchannel plate photomultiplier tube at the input end of a time-correlated single photon counting system. Further details of the laser excitation system, the detection equipment, and data processing methods have been given elsewhere (16).

When emission spectra or quantum yields were determined as a function of temperature, samples were placed in a thermostatted cell, the temperature of which was controlled to ±0.1°C by means of a circulating heat exchange fluid. When mixed perfluoroalkane–alkane or perfluoroalkane–CCl_4 solvents were employed, care was taken to ensure that bulk phase separation did not occur at any of the temperatures chosen for the study.

Thiophosgene (Aldrich) was purified by three trap-to-trap distillations in a glass vacuum line. The purified Cl_2CS was stored under vacuum in the dark at −20°C and was vacuum distilled again just prior to use. Perfluoro-*n*-hexane (PCR) was triply distilled through a one-meter glass column. No hydrogen-containing impurities could be detected by ^1H nmr in the resulting distillate, which was also essentially non-fluorescent. *n*-Hexane and CCl_4 solvents (BDH, Omnisolv) were purified using standard methods and also exhibited no significant fluorescence at the excitation wavelengths employed.

Samples were prepared by degassing the solvent by repeated free–pump–thaw cycles on a vacuum line, followed by condensation of Cl_2CS vapour into the solvent. A calibration curve of absorbance at λ_{max} (255 nm in perfluoro-*n*-hexane) vs. molar concentration of Cl_2CS was prepared by accurately weighing solute and solvent into a cell fitted for vacuum use. After this calibration curve had been established (ϵ_{max} = 4967 M^{-1} cm^{-1} for Cl_2CS in perfluoro-*n*-hexane), concentrations of Cl_2CS were determined routinely by absorbance measurements. In almost all experiments Cl_2CS concentrations were kept below ca. 4×10^{-4} M to minimize the effects of ground state van der Waals dimer formation known to be a problem at higher concentrations (12).

III. Results and discussion

Measurements of the quantum yields of $\tilde{B}$–$\tilde{X}$ fluorescence, ϕ_f, and the single exponential lifetimes, τ_f, of the $\tilde{B}$ state of Cl_2CS in solution permit one to calculate the first-order rate constant for $\tilde{B} \rightarrow \tilde{X}$ radiative decay and the sum of the first-order and pseudo-first-order rate constants for all parallel nonradiative decay process of the $\tilde{B}$ state using the relationships

[3] $k_r = \phi_f/\tau_f$

[4] $\Sigma k_{nr} = (1 - \phi_f)/\tau_f$

By making such measurements on Cl_2CS excited to various bound levels of the $\tilde{B}$ state in dilute perfluoro-1,3-dimethylcyclohexane as a function of temperature, we have previously shown (7) that: (*i*) $k_r = 2.1 \times 10^7$ s^{-1}, (*ii*) the only process contributing significantly to nonradiative decay is activation and barrier crossing leading, presumably, to dissociation, i.e., $\Sigma k_{nr} = k_{diss}$, (*iii*) the temperature dependence of the observed rate constant for nonradiative decay (dissociation) is given by $k_{diss} = k^0_{diss} \exp\{-E_a/RT\}$, and (*iv*) the value of E_a in perfluoro-

Fig. 1. $\tilde{B}$–$\tilde{X}$ fluorescence excitation spectra of 9.6×10^{-5} M Cl_2CS in perfluoro-*n*-hexane as a function of temperature. Emission was observed at a fixed wavelength of 400 nm. For clarity only spectra taken at six temperatures have been plotted.

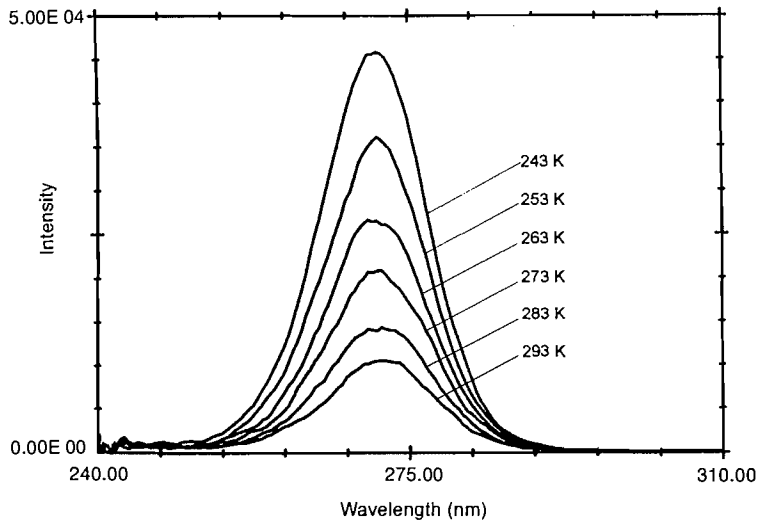

Can. J. Chem. Downloaded from www.nrcresearchpress.com by 65.111.164.53 on 09/08/12
For personal use only.

1,3-dimethylcyclohexane, 17.1 ± 0.9 kJ mol^{-1}, is identical to the vibrational energy of the $\tilde{B}$ state at the onset of fluorescence weakening as measured in the isolated molecule. On the basis of the observations (*ii*), (*iii*), and (*iv*) we previously concluded that the perfluoroalkane solvent in this system acts as a classical heat bath (17) by rapidly exchanging vibrational energy with the excited solute while causing only minimal perturbations of its electronic decay processes. We had also previously shown (6) that values of ϕ_f (and presumably τ_f) are much smaller in other common solvents such as *n*-hexane and CCl_4, and attributed this effect to solvent-assisted radiationless relaxation. The latter was further investigated (7) by determining the rates of apparent quenching of the fluorescent $\tilde{B}$ state when perfluoroalkane solutions were spiked with low concentrations of *n*-hexane and CCl_4. Although the data produced linear Stern–Volmer plots and near diffusion-limited second-order quenching rate constants, we were unable to identify the quenching mechanism.

The present work has been undertaken with the primary aim of determining the process(es) by which solvents assist the nonradiative decay of the $\tilde{B}$ state of Cl_2CS. To this end, we first sought to demonstrate that measurements of the relative intensities of the $\tilde{B}$–$\tilde{X}$ excitation spectra as a function of temperature in dilute ($<10^{-4}$ M) solution yield the same activation parameters as do the measurements of both ϕ_f and τ_f as a function of *T*. Figure 1 shows the $\tilde{B}$–$\tilde{X}$ excitation spectra of 9.6×10^{-5} M Cl_2CS in perfluoro-*n*-hexane for various temperatures between −30 and +20°C. Plotting the relative intensities of the emission, I_{em}, at the maximum of the excitation spectrum ($\lambda_{ex} = 272$ nm) in Arrhenius form reveals an excellent linear ln I_{em} vs. T^{-1} relationship (Fig. 2). The slope yields $E_a = 17.3 \pm 0.5$ kJ mol^{-1} (1446 ± 42 cm^{-1}) which, within experimental error, is identical to the value of $E_a = 17.1 \pm 0.9$ kJ mol^{-1} obtained in perfluoro-1,3-dimethylcyclohexane (7), and confirms that perfluoroalkanes act as inert heat baths in this system. Similar experiments in which Cl_2CS was excited to fluorescent levels of the $\tilde{B}$ state in other pure solvents or two-component solvent systems also yielded good linear Arrhenius plots from which apparent activation energies could be obtained.

The lifetime to the $\tilde{B}$ state is about 40 ns when Cl_2CS is excited to levels near $v = 0$ at low pressures in the gas phase (18). This lifetime diminishes to 4.2 ns in dilute perfluoroalkane solutions at room temperature when exciting at similar wavelengths (7). We have now attempted to measure the decay times of the very weak $\tilde{B}$–$\tilde{X}$ emission observed when Cl_2CS is excited near 290 nm in CCl_4 and *n*-hexane. The lifetimes are too short to measure with our system, which places an upper limit of ca. 10 ps on τ_f in these two solvents.

We also measured the $\tilde{B}$–$\tilde{X}$ fluorescence quantum yields for Cl_2CS as a function of substrate concentration in both CCl_4 and *n*-hexane in order to determine the values of ϕ_f at infinite dilution in these two solvents. The results showed that ϕ_f was only a weak function of Cl_2CS concentration in the 0.5×10^{-4} to 6×10^{-4} M range. Thus, only short extrapolations were required to obtain $\phi_f = 2.4 \times 10^{-4}$ in CCl_4 and $\phi_f = 1.9 \times 10^{-4}$ in *n*-hexane at infinite dilution where neither self-quenching nor self-association occur. The values of ϕ_f are much smaller in CCl_4 and *n*-hexane than those in perfluoroalkanes (6), and appear to scale in about the same proportions as the lifetimes. We therefore conclude that the difference is due to a much larger rate of nonradiative decay in media other than perfluoroalkanes. This conclusion is in full agreement with our previous inferences based on measurements of ϕ_f alone (6, 7). Embedding Cl_2CS in any solvent therefore induces radiationless decay of the $\tilde{B}$ state at rates which are much faster than those of its radiative decay and which are strongly solvent dependent.

When excitation wavelengths in the $272 < \lambda_{ex} < 292$ nm range are employed, the $\tilde{B}$ state will acquire an initial vibrational energy of 0 to ca. 2500 cm^{-1}. It is well-established that vibrational relaxation of polyatomic molecules such as these is essentially complete within a few picoseconds (19, 20) in most common liquid solvents. By measuring the subpicosecond

Can. J. Chem. Downloaded from www.nrcresearchpress.com by 65.111.164.53 on 09/08/12
For personal use only.

Fig. 2. Arrhenius plot of ln I_{em} vs. T^{-1} for the data presented in Fig. 1. Relative intensities were measured at the maximum of the excitation spectrum, 272 nm, and were normalized to 20°C for convenience.

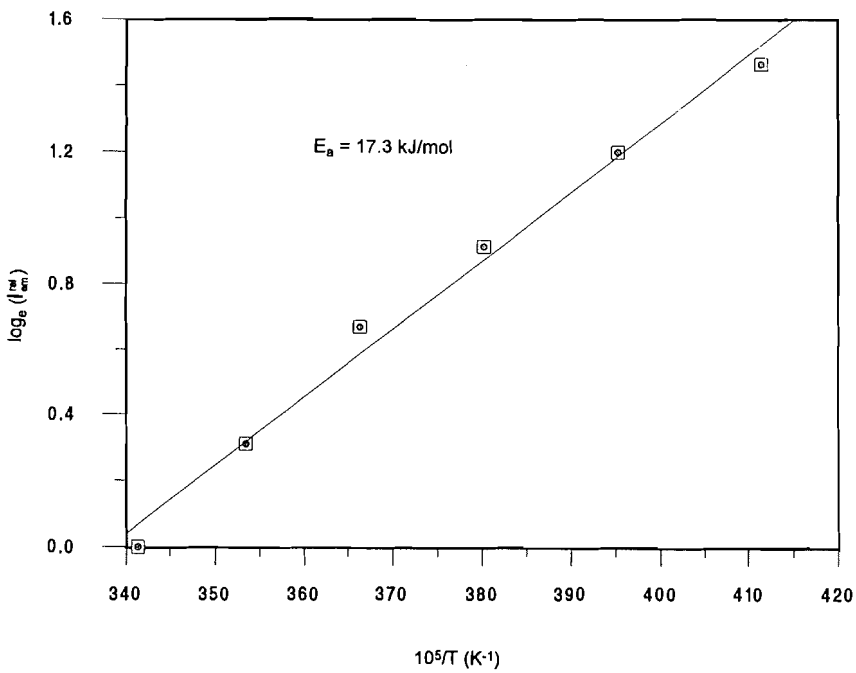

population relaxation times of the S_1 states of azulene and several of its derivatives as a function of initial vibrational energy content, we have recently demonstrated that perfluoroalkane solvents also behave in a similar fashion.[2] In previous work we had observed only a small (<30%) increase in the nonradiative decay rate when the initial vibrational energy of the $\tilde{B}$ state is increased from 0 to 2150 cm^{-1} (7). In the present work we observe no measurable changes in the shapes of the $\tilde{B}$–$\tilde{X}$ emission spectra of Cl_2CS in any solvent when λ_{ex} is varied in this same range. We therefore conclude that, even in CCl_4 and *n*-hexane where $\tau_f \leq 10$ ps, the electronically excited emitters are in vibrational equilibrium with their surroundings. It is therefore proper to consider quantitative relationships between the apparent activation energies whose measurement has been described previously and solution composition.

For this purpose we have measured the apparent activation energies, E_a, associated with the nonradiative decay of the $\tilde{B}$ state of Cl_2CS in solvents consisting of homogeneous mixtures of *n*-hexane with perfluoro-*n*-hexane and CCl_4 with perfluoro-*n*-hexane. The data are displayed graphically in Fig. 3. In both solvent systems E_a diminishes monotonically from a value of 17.3 kJ mol^{-1} in pure perfluoro-*n*-hexane to values of 1.7 ± 0.4 kJ mol^{-1} in pure *n*-hexane or 4.5 ± 0.4 kJ mol^{-1} in pure CCl_4.

In an attempt to determine the physical significance of the shapes of these E_a vs. mole fraction curves, a fit was sought between the data and values of E_a calculated using the following empirical equation

$$[5] \quad E_a^{calc} = \{E_a(PF) - E_a(S)\}(X)^n + E_a(S).$$

[2] D.T. Helbach-Helmrich and R.P. Steer. Unpublished results.

Fig. 3. Apparent activation energy, E_a, for the radiationless decay of the vibrationally equilibrated $\tilde{B}$ state of Cl_2CS as a function of solvent composition. The points are experimental data. The lines are calculated using eq. [5] with $n = 11$.

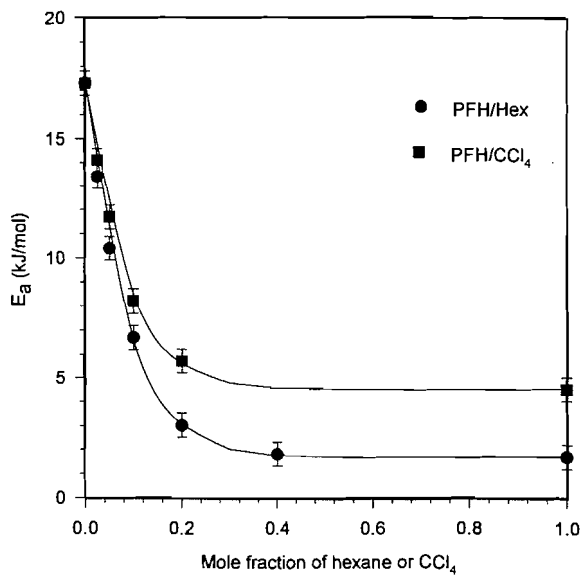

Here $E_a(PF) = 17.3$ kJ mol^{-1}, $E_a(S) = 1.7$ kJ mol^{-1} for S ≡ *n*-hexane or 4.5 kJ mol^{-1} for S ≡ CCl_4, X is the mole fraction of perfluoroalkane, and n is the only adjustable parameter. In both solvent systems the integer which provides the best fit between the values of E_a^{calc} calculated using eq. [5] and those observed by experiment is $n = 11$. When experimental error is accounted for, values of $n = 10$ or 12 would also be acceptable.

Can. J. Chem. Downloaded from www.nrcresearchpress.com by 65.111.164.53 on 09/08/12
For personal use only.

If one considers the perfluoroalkanes to be both chemically and physically inert, then the much faster rates of decay of the $\tilde{B}$ states in the presence of CCl_4 and *n*-hexane could be attributed to simple electronic quenching by the latter. The linear relationships previously obtained (7) when either the fluorescence intensities or the $\tilde{B}$ lifetimes are plotted in Stern–Volmer form as a function of CCl_4 or *n*-hexane concentration ($<10^{-1}$ M) in perfluoroalkane solvent support this interpretation. However, the data presented here provide strong evidence that the interaction between either CCl_4 or *n*-hexane and the *B* state of Cl_2CS does not involve simple electronic quenching via a 1:1 encounter complex or exciplex. First, there is no obvious single quenching "mechanism" which is consistent with all the data. Low-lying excited singlet states which could act as acceptors in an electronic energy transfer process are not available in either *n*-hexane or CCl_4. Quenching could also occur either by electron-transfer or by formation of a charge-transfer stabilized exciplex. However, if excited Cl_2CS were to act as an electron donor, the perfluoroalkanes with their large electron affinities should be the best acceptors, contrary to observation. On the other hand, if the $\tilde{B}$ state were to act as the electron acceptor in a charge-transfer complex then CCl_4 with its lower ionization energy should be a better "quencher" than *n*-hexane, again contrary to observation. Reactive chemical quenching might be possible for *n*-hexane (*vide infra*) but is not possible for CCl_4. Second, there appears to be no reasonable explanation for the fact that the activation energy associated with viscous flow is considerably higher in both CCl_4 (10.2 kJ mol^{-1}) and *n*-hexane (6.9 kJ mol^{-1}) than the values of E_a observed here. Diffusion limited quenching would therefore appear to be ruled out, although the "transient effect" complicates this interpretation when the lifetimes of the $\tilde{B}$ state are as short as they are in CCl_4 and *n*-hexane (21). Finally, the strongly nonlinear variation in E_a with solvent composition (Fig. 3) suggests that 1:1 molecular encounters between excited Cl_2CS and either CCl_4 or *n*-hexane are not responsible for the process which eventually results in fluorescence quenching. In fact, the large value of *n* required to give the best fit of eq. [5] to the data suggests that a process involving several CCl_4 or *n*-hexane molecules acting cooperatively may be operative here.

The onset of fluorescence weakening ca. 1430 cm^{-1} above the zero point level in the $\tilde{B}$ state (4) together with the observation of high yields of chemical decomposition products on excitation to higher levels in the vibrational manifold (9, 10) suggest that the $\tilde{B}$ state, described in zeroth order to be of $^1(\pi, \pi^*)$ configuration, is crossed by a second state which either is itself dissociative or is coupled to a dissociative state. Thus the potential energy hypersurface accessed by one-photon excitation in the near uv is expected to be complex and will exhibit either an avoided crossing if the intersecting state is of $^1A_1$ symmetry or a conical intersection if a state of different symmetry is involved. Irrespective of the nature of the intersecting state, the energy at which it crosses the $\tilde{B}$ surface will determine the height of the barrier between that portion of the surface which carries the oscillator strength and the rest of the surface which is "dark". The model is illustrated in Fig. 4.

We propose that the mechanism whereby species other than perfluoroalkanes increase the rate of nonradiative decay of the $\tilde{B}$ state in solution involves an interaction between excited

Fig. 4. Pictorial representation of a portion of the upper state hypersurface illustrating how the nature of the solvent can affect the height of the barrier to nonradiative decay of the fluorescent $\tilde{B}$ state. (*a*) The isolated molecule, (*b*) perfluoroalkane solvents, (*c*) more strongly interacting solvents.

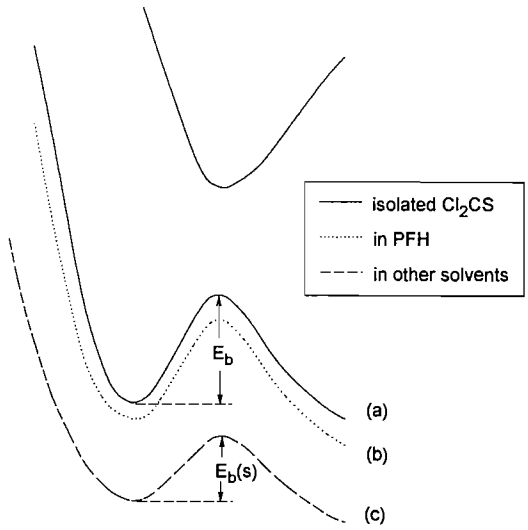

Cl_2CS and one or more "solvent" molecules which results in a lowering of the effective barrier between the fluorescent bound portion of the surface and a "dark" region (cf. Fig. 4). Since the rate of vibrational activation of bound excited species will be approximately independent of the nature of the solvent (and in any case is much faster than the nonradiative decay rate), a lower barrier will result in a faster rate of barrier crossing, an effective increase in the nonradiative decay rate, a lower fluorescence yield, and a shorter $\tilde{B}$ lifetime, as observed.

We further propose that the distinctly nonlinear variation of E_a with mole fraction of the solvent ($n = 11$ in eq. [5]) may be indicative of a preferential clustering of CCl_4 or *n*-hexane molecules around Cl_2CS in perfluoroalkane solutions. In effect, the assembly of a small number of CCl_4 or *n*-hexane molecules around a single solute species in homogeneous mixed perfluoroalkane solutions would cause the $\tilde{B}$ state to "experience" a primarily non-perfluoroalkane environment even when the mole fraction of perfluoro-*n*-hexane exceeds that of the second solvent component. Such a suggestion is not unreasonable since small aggregates of "solute" species are known to form in homogeneous solutions at temperatures not substantially removed from those at which bulk phase separation occurs (22, 23). Perfluoroalkanes are very "poor" solvents (24), so it is reasonable to assume that the energy gained through dispersive interactions among clustered CCl_4 or *n*-hexane molecules could offset the entropic deficit associated with their formation. Thiophosgene itself forms van der Waals dimers and oligomers at relatively low concentrations in perfluoroalkanes (12). It is also interesting to note that for systems such as mixed noble gas liquids in which dispersive interactions are responsible for solvation enthalpies, the coordination number of the "solute" by the "solvent" is found to be either somewhat greater or somewhat smaller than those of self-solvation (11–13), depending upon the relative sizes and polarizabilities of the species involved (22). A more precise

Can. J. Chem. Downloaded from www.nrcresearchpress.com by 65.111.164.53 on 09/08/12
For personal use only.

Fig. 5. Near-uv absorption spectra of dilute Cl_2CS in perfluoro-*n*-hexane as a function of photolysis time. Initial $[Cl_2CS] = 3.0 \times 10^{-4}$ M; $\lambda_{ex} = 255$ nm.

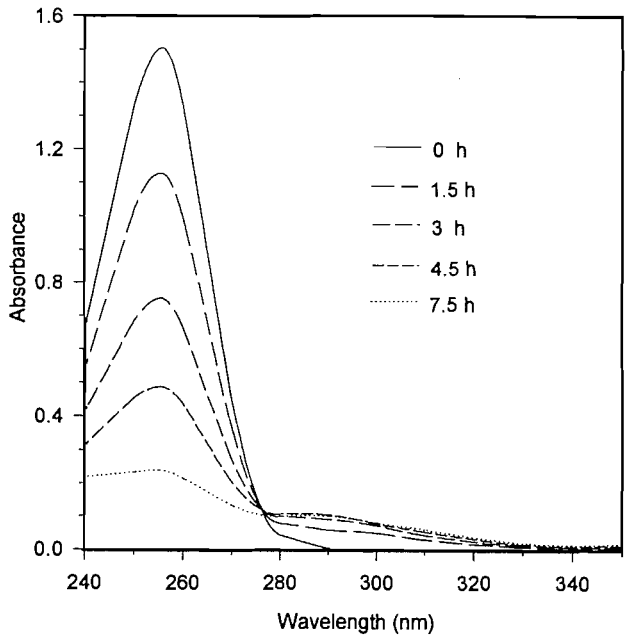

interpretation of the extremely non-linear variation of E_a with solvent composition awaits further investigation.

The effects of such clustering would be difficult to observe by standard spectroscopic means. The portion of the upper state which carries most of the oscillator strength is of $^1A_1$, $^1(\pi, \pi^*)$ character and is radiatively coupled to the $^1A_1$ ground state by an electric dipole allowed transition. Solvent effects on $\pi \rightarrow \pi^*$ transitions usually consist of a small red shift in more strongly interacting media. This red shift is a consequence of an increase in polarizability of the solute on excitation which results in a slightly greater dispersive stabilization of the excited species compared with the ground state. The uv absorption spectrum of Cl_2CS follows this pattern; $\lambda_{max} = 255$ nm in perfluoro-*n*-hexane and 257 nm in *n*-hexane. (λ_{max} is almost obscured in CCl_4 due to absorption by the solvent.) The fluorescence excitation spectra also exhibit similar shifts ($\lambda_{max} = 272$ nm in perfluoro-*n*-hexane, 274 nm in *n*-hexane, and 275 ± 1 nm in CCl_4). Because the rate of vibrational relaxation/activation is much faster than the rate of nonradiative electronic relaxation in these liquid solutions, a marked shift in the position of the excitation spectrum is not expected despite the fact that the activation barrier is considerably lower in both CCl_4 and *n*-hexane than in the perfluoroalkanes.

We suggest that the values of E_a are lower in more strongly interacting solvents because the dark state accessed on barrier crossing has a larger solvation energy than that of the radiative $^1(\pi, \pi^*)$ state (cf. Fig. 4). If this suggestion is correct, the dark state would need to have a greater polarizability than the radiative $^1(\pi, \pi^*)$ state since dispersive interactions dominate the solvation process. We have previously shown (5) that monomeric Cl_2CS exhibits a very weak, broad absorption in a region immediately to the red of the strong $\tilde{B}$–$\tilde{X}$ system. Excitation in this region produces no measurable fluorescence, so its upper state is not simply an extension of the bound, radiative $\tilde{B}$ surface into a region where the Franck–Condon factors for the $\tilde{B}$–$\tilde{X}$ transition are small. The dark state could be attributed to a triplet, for example of $^3(n_{Cl}, \pi_{CS}^*)$ or Rydberg character. However, a more interesting and more likely possibility is that the upper state is of primarily $^1A_1$, $^1(\pi^2, n^0, \pi^{*2})$ doubly excited character (25). Such a state is expected to have a larger polarizability than the neighboring $^1(\pi, \pi^*)$ state and would therefore exhibit the larger solvation energy required to produce the lower E_a observed in CCl_4 and *n*-hexane.

Additional strong support for the suggestion that barrier lowering (rather than than simple quenching) is responsible for the increased rate of nonradiative decay in CCl_4 and *n*-hexane can be obtained from an examination of the photochemistry of Cl_2CS in these two solvents compared with the perfluoroalkanes. Figure 5 shows how the near-uv spectra of a dilute solution of Cl_2CS in perfluoro-*n*-hexane change as a function of photolysis time when excited at $\lambda_{ex} = 255$ nm. As photolysis proceeds Cl_2CS is consumed and a broad new absorption feature with a maximum near 290 nm appears. An apparent isosbestic point is located at 276 nm. A detailed examination of these spectra, however, reveals that the isosbestic point is not "clean". This observation suggests that the weak absorption near 290 nm is due to a mixture of products, the composition of which is changing with time. This absorption also fades in the dark after photolysis, indicating that the products are not thermally stable. The identities of the products and their quantum yields are required if a detailed mechanism for the photolysis is to be enveloped. Unfortunately, having to employ only very dilute solutions to avoid the photolysis of ground state van der Waals dimers and problems of product instability made it impossible to accumulate sufficient material to permit analysis. Consequently, the photochemical behavior of uv-excited Cl_2CS had to be inferred from measurements of the quantum yields of consumption of the starting material, ϕ_C. Table 1 presents the value of ϕ_C as a function of the starting concentration of Cl_2CS in perfluoro-*n*-hexane for five different photolysis wavelengths from 285 to 255 nm. Table 2 shows how ϕ_C varies with temperature for one fixed, low concentration of Cl_2CS in perfluoro-*n*-hexane (5.8×10^{-5} M) at two of these wavelengths, 280 nm and 255 nm. We estimate the errors in ϕ_C to be ca. ± 10% at $\lambda_{ex} \leq 280$ nm for concentrations $> 5 \times 10^{-5}$ M and ±30% at $\lambda_{ex} = 285$ nm and at $\lambda_{ex} \leq 280$ nm for all concentrations $< 5 \times 10^{-5}$ M where the absorbance of these dilute solutions is extremely small. Despite these relatively large errors a number of important conclusions can be drawn from the data.

First, all of the quantum yields of Cl_2CS consumption are large. When one accounts for the fact that free radical recombination, reaction [6],

[6] $Cl + ClCS \rightarrow Cl_2CS$

will result in lower net consumption of Cl_2CS, one concludes that a large majority of the nonradiative decay events of the $\tilde{B}$ state either must involve direct bond scission (after barrier crossing) or must access a bound portion of the upper state which is itself strongly coupled to a dissociative state. Second, ϕ_C is significantly larger than 1 for excitation at 285 nm, and is marginally larger than 1 for excitation at $\lambda_{ex} = 280$ nm. This can only occur if Cl_2CS is consumed not only via the primary photolytic acts, reactions [1] and [2], but also in secondary reactions between ground state Cl_2CS and transient intermedi-

Can. J. Chem. Downloaded from www.nrcresearchpress.com by 65.111.164.53 on 09/08/12
For personal use only.

Table 1. ϕ_C for Cl_2CS in perfluoro-*n*-hexane as a function of concentration and excitation wavelength.[a]

λ_{ex} (nm)	$[Cl_2CS]$ (M)	ϕ_C
285	1.0×10^{-5}	1.1
	1.8×10^{-5}	1.6
	1.9×10^{-5}	1.5
	2.8×10^{-5}	1.7
	3.2×10^{-5}	2.1
	6.2×10^{-5}	2.1
	1.6×10^{-4}	2.0
	3.4×10^{-4}	2.4
280	4.0×10^{-6}	0.7
	2.0×10^{-5}	0.9
	2.7×10^{-5}	0.9
	3.3×10^{-5}	1.2
	5.3×10^{-5}	1.2
	2.0×10^{-4}	1.2
	3.8×10^{-4}	1.1
	4.5×10^{-4}	1.1
272	8.8×10^{-6}	0.6
	3.0×10^{-5}	0.8
	3.1×10^{-5}	0.8
	4.1×10^{-5}	0.8
	1.5×10^{-4}	0.8
	2.8×10^{-4}	0.8
	4.6×10^{-4}	0.8
	5.0×10^{-4}	0.8
265	3.1×10^{-6}	0.5
	1.8×10^{-5}	0.6
	2.0×10^{-5}	0.7
	2.6×10^{-5}	0.7
	5.9×10^{-5}	0.8
	2.6×10^{-4}	0.9
	3.1×10^{-4}	1.0
	4.8×10^{-4}	1.0
255	8.6×10^{-6}	0.8
	1.7×10^{-5}	0.8
	1.7×10^{-5}	0.8
	3.5×10^{-5}	0.9
	7.8×10^{-5}	1.1
	1.7×10^{-4}	1.1
	2.2×10^{-4}	1.0
	3.9×10^{-4}	1.2

[a]At room temperature.

ates. The most obvious such processes involve reactions Cl_2CS with Cl or ClCS produced in [1], but reactions between CS (produced in reaction [2]) and Cl_2CS cannot be ruled out. Third, ϕ_C generally *increases* with increasing Cl_2CS concentration up to ca. $4–5 \times 10^{-4}$ M, but levels out at an apparent plateau which is different for different excitation wavelengths. Finally, the profile of ϕ_C as a function of temperature at λ_{ex} = 280 nm is also different from that at λ_{ex} = 255 nm. We conclude that at least two primary photochemical processes are occurring, that the branching ratios among them are a function of λ_{ex}, and that the process which dominates at shorter λ_{ex}

Table 2. ϕ_C for Cl_2CS in perfluoro-*n*-hexane as a function of temperature for two excitation wavelengths.[a]

t(°C)	ϕ_C (λ_{ex} = 280 nm)	ϕ_C (λ_{ex} = 255 nm)
−20	0.6	1.0
−10	0.9	1.0
0	1.1	1.0
10	1.1	1.0
20	1.2	0.9
30	1.7	0.8

[a]$[Cl_2CS] = 5.8 \times 10^{-5}$ M for all experiments.

Table 3. Quantum yields of consumption of Cl_2CS in pure CCl_4 and a CCl_4/perfluoro-*n*-hexane mixture.[a]

Pure CCl_4		CCl_4/perfluoro-*n*-hexane	
$[Cl_2CS]$, M	ϕ_C	$[Cl_2CS]$, M	ϕ_C
1.6×10^{-5}	1.1	8.5×10^{-6}	0.8
2.2×10^{-5}	0.9	2.5×10^{-5}	1.0
2.8×10^{-5}	0.8	4.3×10^{-5}	1.1
7.6×10^{-5}	0.8	9.9×10^{-5}	1.1
		1.1×10^{-4}	1.1
		4.7×10^{-4}	0.7

[a]λ_{ex} = 280 nm. Room temperature. $X(CCl_4) = 0.05$.

results in a lower net consumption of Cl_2CS. Reactions [1] and [2] would appear to meet these requirements provided the branching ratio favors reaction [2] as λ_{ex} decreases. The recent observation by time-resolved infrared absorption of CS in the products of the flash photolysis of Cl_2CS in CD_3CN at 266 nm (footnote 3, ref. 26) support this suggestion. The general increases in ϕ_C with increasing Cl_2CS concentration likely reflect the competition between second-order radical recombination in bulk solution and pseudo-first-order reaction between the substrate and these intermediates. Diffusive self-quenching of the bound $\tilde{B}$ state ($k_{sq} = 2 \times 10^{10}$ M^{-1} s^{-1}, τ^0 = 4.2 ns (8)) is not important at these low concentrations. However, increasing absorption by ground state van der Waals dimer, whose absorbance constitutes ca. 20% of the total when the analytical concentration of Cl_2CS is 3×10^{-4} M (12), is a complicating factor.

In 1977 Okabe (9) showed that HCl ($\phi \sim 1$) is a major product of the uv photolysis of Cl_2CS in the presence of heptane in the gas phase, viz.,

[7] $Cl + C_7H_{16} \rightarrow HCl + C_7H_{15}$

This and other H-abstraction reactions are also expected when Cl_2CS is photolyzed in liquid *n*-hexane solutions. Such reactions produce alkyl free radicals which can themselves add to Cl_2CS in a manner which has parallel precedence in the photochemistry of aromatic and alicyclic thiones (27, 28). Because this series of reactions would influence ϕ_C in an

[3] B. Wagner. Private communications.

unpredictable way, we concluded that the determination of the quantum yields of Cl_2CS consumption in *n*-hexane solution would yield ambiguous results.

On the other hand, such reactions cannot occur in CCl_4 or in CCl_4–perfluoroalkane mixtures. We therefore reasoned that a comparison of the rates of Cl_2CS consumption in pure perfluoroalkane with those in CCl_4 or CCl_4–perfluoroalkane mixtures would provide valuable insight into the role of CCl_4 in these systems. Table 3 presents the results of photolyzing Cl_2CS at $\lambda_{ex} = 280$ nm in pure CCl_4 and in a mixture in which the mole fraction of CCl_4 in perfluoro-*n*-hexane is 0.05 (ca. 0.25 M). (Note that photolysis at $\lambda_{ex} < 280$ nm is not possible because the solvent is not transparent at these wavelengths.) The values of ϕ_C are comparable to those found when Cl_2CS is photolyzed in pure perfluoroalkane under similar conditions, clearly indicating that CCl_4 does not quench the $\tilde{B}$ state. These observations therefore support the suggestion that CCl_4 and *n*-hexane accelerate nonradiative decay by lowering the barrier between the fluorescent $\tilde{B}$ state and a dark portion of the upper state surface from which dissociation occurs. However, quantitative analyses of the products of the photolysis of Cl_2CS in these solvents are required before this mechanism can be proved conclusively.

IV. Conclusions

By measuring the intensities of $\tilde{B}$–$\tilde{X}$ fluorescence and the quantum yields of substrate consumption as a function of temperature, excitation wavelength, and solvent composition when Cl_2CS is electronically excited in solution we have shown that (*i*) nonradiative processes dominate the decay of the $\tilde{B}$ state, (*ii*) the nonradiative process(es) involve(s) activation and crossing a barrier whose height is a function of the composition of the solvent, (*iii*) perfluoroalkane solvents are inert and act as classical heat baths, (*iv*) CCl_4 and *n*-hexane do not quench the $\tilde{B}$ state, but instead accelerate the rate of its nonradiative decay by lowering the barrier between the bound, radiative portion of the surface and a dark region which is either unbound or strongly coupled to an unbound state, and (*v*) barrier crossing leads to photodecomposition via at least two parallel paths (likely reactions [1] and [2]), the relative importance of which is a function of excitation wavelength.

V. Acknowledgements

The authors gratefully acknowledge the continuing financial support of the Natural Sciences and Engineering Research Council of Canada. We are grateful to Dr. Brian Wagner, Steacie Institute for Molecular Sciences, National Research Council, Ottawa, for communicating the results of Cl_2CS photolysis experiments to us in advance of publication.

VI. References

1. A. Maciekewski and R.P. Steer. Chem. Rev. **93**, 67 (1993).
2. D.J. Clouthier and D.C. Moul. Top. Curr. Chem. **150**, 167 (1989).
3. B. Simard, V.J. MacKenzie, P.A. Hackett, and R.P. Steer. Can. J. Chem. **72**, 745 (1994).
4. M. Ludwiczak, D.R. Latimer, and R.P. Steer. J. Mol. Spectrosc. **147**, 414 (1991).
5. A. Maciejewski, M. Szymanski, and R.P. Steer. Chem. Phys. **165**, 101 (1992).
6. K.J. Falk, S.E. Sveinson, and R.P. Steer. Chem. Phys. Lett. **163**, 490 (1989).
7. M. Szymanski, S.E. Sveinson, and R.P. Steer. J. Phys. Chem. **95**, 5159 (1991).
8. A. Maciejewski, M. Szymanski, and R.P. Steer. J. Chem. Soc. Faraday Trans. **89**, 3251 (1993).
9. H. Okabe. J. Chem. Phys. **66**, 2058 (1977).
10. G.S. Ondrey and R. Bersohn. J. Chem. Phys. **79**, 175 (1983); M. Hachey, F. Grein, and R.P. Steer. Can. J. Chem. **71**, 112 (1993).
11. T. Oka, A.R. Knight, and R.P. Steer. J. Chem. Phys. **66**, 699 (1977).
12. A. Maciejewski, M. Szymanski, and R.P. Steer. Can. J. Chem. **71**, 1548 (1993).
13. M. Szymanski, A. Maciejeski, and R.P. Steer. Chem. Phys. **175**, 413 (1993).
14. A. Maciejewski and R.P. Steer. J. Photochem. **35**, 59 (1986).
15. S. Meech and D. Phillips. J. Photochem. **23**, 193 (1983).
16. D.R. James, D.R.M. Demmer, R.E. Verrall, and R.P. Steer. Rev. Sci. Instrum. **54**, 1121 (1983).
17. K.F. Freed and J. Jortner. J. Chem. Phys. **52**, 6272 (1970).
18. D.J. Clouthier, A.R. Knight, R.P. Steer, and P.A. Hackett. Chem. Phys. Lett. **70**, 89 (1980).
19. J. Keizer. Chem. Rev. **87**, 167 (1987) and references therein.
20. T. Elsaesser and W. Kaiser. Annu. Rev. Phys. Chem. **42**, 83 (1991) and references therein.
21. A. Maciejewski, M. Sikorski, M. Szymanski, W. Augustiniak, and R.P. Steer. Radiat. Phys. Chem. **39**, 155 (1992).
22. A. Ben-Naim. Solvation thermodynamics. Plenum Press, New York. 1987.
23. T. Kato. J. Phys. Chem. **89**, 5750 (1985).
24. A. Maciejewski. J. Photochem. Photobiol. A, **51**, 87 (1990).
25. M. Hachey, F. Grein, and R.P. Steer. Chem. Phys. Lett. **183**, 204 (1991).
26. G. Schallmoser, B.E. Wurfel, A. Thoma, N. Caspary, and V.E. Bondybey. Chem. Phys. Lett. **201**, 528 (1993).
27. J.R. Bolton, K.S. Chen, A.H. Lawrence, and P. de Mayo. J. Am. Chem. Soc. **97**, 1832 (1975).
28. V. Ramamurthy. Org. Photochem. **7**, 231 (1985).

Can. J. Chem. Downloaded from www.nrcresearchpress.com by 65.111.164.53 on 09/08/12
For personal use only.

Excess molar volumes of binary mixtures with 2-pentanone and 1-chloroalkanes at 298.15 and 308.15 K

José M. Pico, Consolación P. Menaut, Eulogio Jiménez, José L. Legido, Josefa Fernández, and M. Inmaculada Paz Andrade

Abstract: Excess molar volumes v^E at 298.15 and 308.15 K and normal atmospheric pressure for the binary mixtures 2-pentanone + 1-chloroalkane (from 1-chlorobutane to 1-chlorooctane) were obtained from measurements of the density with an Anton Paar densimeter. The v^E values for all mixtures were positive, and increase as the 1-chloroalkane length increases. Excess molar volumes depend slightly on the temperature. The same characteristics were found previously for the excess molar enthalpies of the same mixtures. Experimental v^E values are compared with theoretical results using the Prigogine–Flory–Patterson model.

Key words: thermodynamics, liquid mixtures, excess volumes, ketones, chloroalkanes.

Résumé : Utilisant des mesures de densité obtenues à l'aide d'un densimètre d'Anton-Paar, on a déterminé les volumes molaires d'excès, v^E, à 298,15 et 308,15 K et à pression atmosphérique normale pour des mélanges binaires de pentan-2-one + 1-chloroalcanes (allant du 1-chlorobutane au 1-chlorooctane). Les valeurs de v^E de chacun des mélanges sont toutes positives et elles augmentent avec une augmentation de la longueur de la chaîne des 1-chloroalcanes. Les volumes molaires d'excès ne dépendent que légèrement de la température. Antérieurement, on avait trouvé les mêmes caractéristiques pour les enthalpies molaires d'excès des mêmes mélanges. On a comparé les valeurs expérimentales des v^E avec les valeurs théoriques calculées en utilisant le modèle de Prigogine–Flory–Patterson.

Mots cles : thermodynamique, mélanges liquides, volumes d'excès, cetones, chloroalcanes.

[Traduit par la redaction]

Introduction

This work is part of a systematic study on the thermodynamic properties of mixtures of ketones with chloroalkanes. In a first paper (1) we measured excess molar enthalpies of 2-butanone and 2-pentanone with 1-chloroalkanes. We used these h^E values together with the literature values (2, 3) to redetermine new interaction parameters of the Tassios version of the UNIFAC group-contribution model (4, 5). Subsequently, we started to determine experimental excess molar volumes of this kind of mixtures, with an aim to perform, in future, quantitative treatment of these values with the Nitta–Chao group contribution model (6). In a recent paper we reported the v^E values of 3-pentanone or 3-heptanone with 1-chloroalkanes (7). To enlarge the data base needed to calculate the interaction parameters we report in the present paper the experimental excess molar volumes at 298.15 and 308.15 K of 2-pentanone with 1-chloroalkanes (from 1-chlorobutane to 1-chlorooctane). The influence of the position of the ketone group in the molecule of alkanone is analyzed by comparing the v^E values of both isomeric pentanones with 1-chloroalkanes.

The version of the Flory model (8, 9) due to Patterson and co-workers (10–12), named the Prigogine–Flory–Patterson (PFP) model, has been used often recently to correlate and to predict such thermodynamic properties of organic mixtures as h^E, v^E, c_P^E. The PFP model is very useful to analyze the influence of the size, shape, and momentum of the molecules on the behaviour of binary mixtures. In some cases, the differences between theoretical and experimental values have been used to show the occurrence of short-range order effect (13–15). In this paper we have applied this model by determining the interaction parameter X_{12} from excess molar enthalpies of the same mixtures.

Experimental

The sources and the purities of the chemicals were 2-pentanone (Fluka, puriss 99%), 1-chlorobutane (Fluka, puriss 99.5%), 1-chloropentane and 1-chlorohexane (Fluka, puriss 99%), 1-chloroheptane and 1-chlorooctane (Aldrich 99%). All liquids were used without purification, but prior to the measurements they were kept over Union Carbide 0.4 nm molecular sieves (Fluka) and partially degassed. Their densities agree well with the literature values, as can be seen in Table 1 (1, 7, 15–21).

Received April 7, 1994.

J.M. Pico, C.P. Menaut, and E. Jiménez. Departamento de Física, Universidad de La Coruña, E-15006 La Coruña, Spain.
J.L. Legido. Departamento de Física Aplicada, Facultad de Ciencias, Universidad de Vigo, E-31006 Vigo, Spain.
J. Fernández[1] and M.I. Paz Andrade. Departamento de Física Aplicada, Campus Universitario, Universidad de Santiago, E-15706 Santiago de Compostela, Spain.

[1] To whom correspondence should be addressed.

Can. J. Chem. Downloaded from www.nrcresearchpress.com by 65.111.164.53 on 09/08/12
For personal use only.

Can. J. Chem. Downloaded from www.nrcresearchpress.com by 65.111.164.53 on 09/08/12
For personal use only.

Table 1. Densities ρ of the pure liquids at 298.15 K.

Liquid	T (K)	ρ(exp.) (cm^3 mol^{-1})	ρ(lit.) (cm^3 mol^{-1})	
2-Pentanone	298.15	0.80135	0.80166(1)	0.8015(17)
	308.15	0.79161	0.7927[a]	
1-Chlorobutane	298.15	0.88079	0.88076(1)	0.88087(7)
	308.15	0.86962	0.86955(18)	0.8696[a]
1-Chloropentane	298.15	0.87700	0.87696(1)	0.87700(17)
	308.15	0.86692	0.8673[a]	
1-Chlorohexane	298.15	0.87311	0.87327(7)	0.87307(1)
	308.15	0.86376	0.8641[a]	
1-Chloroheptane	298.15	0.87115	0.87108(7)	0.87098(20)
	308.15	0.86230	0.8630[a]	
1-Chlorooctane	298.15	0.86876	0.86879(21)	0.86872(1)
	308.15	0.86028	0.8614[a]	

[a]Interpolated from ref. 19.

The measurements of densities were carried out with an Anton–Paar DMA 60/602 vibrating tube densimeter operating under static mode. A Haake F3 thermostat and a digital thermometer Anton–Paar DT 100-30 were used to regulate to better than 0.01 K the temperature inside the vibrating tube.

Before each series of measurements the apparatus was calibrated at atmospheric pressure with double-distilled and degassed water and *n*-heptane (Fluka >0.995). The excess molar volumes were calculated from the densities of the pure liquids and their mixtures. Binary mixtures were prepared by mass with a probable error in the mole fraction of less than 10^{-4}. All molar quantities are based on the IUPAC (22) relative atomic mass table.

Results

Excess molar volumes, v^E, for the five mixtures, (x 2-ketone + $(1 - x)$ 1-chloroalkane), measured at 298.15 and 308.15 K are listed in Tables 2 and 3. These data were fitted by unweighted least-squared polynomial regression to the equation

$$[1] \quad v^E/(cm^3\ mol^{-1}) = x(1 - x)\sum_{p=0}^{q} A_p(2x - 1)^p$$

The number of coefficients used in eq. [1] for each mixture was determined by applying an F test (22). The parameters A_p and their standard deviations s are given in Table 4 for all systems. A graphical representation of the experimental values together with the smoothing curves is shown in Fig. 1. We are not aware of any previous measurements of v^E for these mixtures.

Discussion

In all the mixtures studied the molar excess volumes are positive over the whole range of composition. The v^E–x curves are quite symmetrical, and their maximum is slightly skewed towards the region rich in ketone as the 1-chloroalkane length increases. The excess molar volumes increase slightly with temperature, presenting mean differences of about 1% between 298.15 and 308.15 K.

Fig. 1. Experimental excess molar volumes v^E at (*a*) 298.15 K and (*b*) 308.15 K of (x) 2-pentanone + $(1 - x)$ 1-chloroalkane. Experimental points: ○, 1-chlorobutane; □, 1-chloropentane; △, 1-chlorohexane; ◇, 1-chloroheptane; ●, 1-chlorooctane.

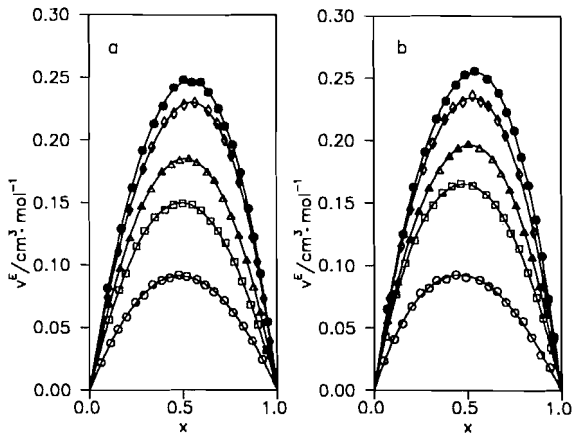

The equimolar excess volume $v^E(0.5)$ increases as the 1-chloroalkane chain grows in length, as can be seen in Fig. 2, where n is the number of the carbon atoms in the 1-chloroalkane. This behavior was found before for the excess enthalpies of the same mixtures (1) and for the excess molar volumes of 3-pentanone and 3-heptanone with 1-chloroalkane (7). However, while the variation in the excess molar enthalpies is almost linear with n, v^E increases more rapidly for smaller chloroalkanes. Similar differences between the dependence of h^E and v^E on n were also found by Lorenzana et al. for ester + *n*-alkane mixtures.

The behaviour of these mixtures in terms of efficient packing and formation and breaking of different interactions in the mixing process can be explained as in our previous paper (7) and references therein.

For binary mixtures of isomeric alkanone with 1-chlorohexadecane García et al. (2) have established that excess enthalpies are larger for the unsymmetrical *n*-alkanone than for the symmetrical *n*-alkanone. Figure 2 shows that this fact is

Can. J. Chem. Downloaded from www.nrcresearchpress.com by 65.111.164.53 on 09/08/12
For personal use only.

Table 2. Experimental excess molar volumes of (x) 2-pentanone + (1 − x) 1-chloroalkane at 298.15 K.

x	v^E / cm^3 mol^{-1}	x	v^E / cm^3 mol^{-1}	x	v^E / cm^3 mol^{-1}	x	v^E / cm^3 mol^{-1}
			2-Pentanone + 1-chlorobutane				
0.0611	0.0221	0.2916	0.0761	0.5208	0.0911	0.7676	0.0620
0.1124	0.0377	0.3370	0.0842	0.5756	0.0886	0.8209	0.0513
0.1516	0.0487	0.3858	0.0878	0.6192	0.0841	0.8665	0.0397
0.1963	0.0586	0.4300	0.0898	0.6659	0.0785	0.9200	0.0247
0.2442	0.0702	0.4785	0.0922	0.7211	0.0716		
			2-Pentanone + 1-chloropentane				
0.1038	0.0561	0.3515	0.1381	0.5975	0.1438	0.8150	0.0870
0.1568	0.0800	0.4048	0.1440	0.6476	0.1353	0.8612	0.0680
0.1923	0.0931	0.4514	0.1482	0.6876	0.1274	0.8998	0.0524
0.2533	0.1149	0.4983	0.1493	0.7272	0.1179	0.9421	0.0320
0.2975	0.1273	0.5518	0.1483	0.7746	0.1023		
			2-Pentanone + 1-chlorohexane				
0.1048	0.0689	0.3877	0.1746	0.6303	0.1745	0.8393	0.1040
0.1629	0.0976	0.4380	0.1804	0.6673	0.1681	0.8759	0.0827
0.2177	0.1221	0.4831	0.1839	0.7143	0.1537	0.9131	0.0626
0.2796	0.1474	0.5330	0.1855	0.7574	0.1398	0.9517	0.0340
0.3312	0.1609	0.5757	0.1823	0.7982	0.1243		
			2-Pentanone + 1-chloroheptane				
0.0960	0.0740	0.4019	0.2140	0.6836	0.2134	0.8955	0.1025
0.1540	0.1110	0.4529	0.2212	0.7225	0.2000	0.9291	0.0732
0.2146	0.1439	0.5091	0.2281	0.7566	0.1874	0.9638	0.0389
0.2881	0.1766	0.5661	0.2299	0.7987	0.1667		
0.3339	0.1940	0.6382	0.2236	0.8685	0.1224		
			2-Pentanone + 1-chlorooctane				
0.0958	0.0817	0.3946	0.2270	0.6385	0.2381	0.8491	0.1456
0.1706	0.1292	0.4535	0.2419	0.6922	0.2249	0.8779	0.1226
0.2302	0.1617	0.5052	0.2481	0.7253	0.2113	0.9124	0.0931
0.2839	0.1913	0.5495	0.2462	0.7667	0.1965	0.9511	0.0547
0.3461	0.2129	0.5976	0.2463	0.8059	0.1741		

also verified for excess molar volumes in the case of pentanone. The relative differences in v^E for both pentanones varies between 20% and 50%, depending on the 1-chloroalkane, and are bigger than the relative differences for excess enthalpies. The difference in the behaviour of the isomeric alkanones was attributed (2) to the steric hindrance of the adjacent alkyl groups. Our results confirm this hypothesis because in general excess volumes are more affected than excess enthalpies by steric hindrance.

According to the Prigogine–Flory–Patterson theory (10–12) h^E and v^E for binary mixtures are given by

$$[2]\quad \frac{v^E}{(x_1V_1^* + x_2V_2^*)} = \frac{(\tilde{V}^{1/3} - 1)\tilde{V}^{2/3}(\psi_1\theta_2\chi_{12})}{[(4/3)\tilde{V}^{1/3} - 1]P_1^*} - \frac{(\tilde{V}_1 - \tilde{V}_2)^2[(14/9)\tilde{V}^{1/3} - 1]\psi_1\psi_2}{[(4/3)\tilde{V}^{1/3} - 1]\tilde{V}} + \frac{(\tilde{V}_1 - \tilde{V}_2)(P_1^* - P_2^*)\psi_1\psi_2}{P_1^*\psi_1 + P_2^*\psi_2}$$

$$[3]\quad \frac{h^E}{(x_1P_1^*V_1^* + x_2P_2^*V_2^*)} = \frac{[(1/\tilde{V} + \tilde{T}/[(4/3)\tilde{V}^{1/3} - 1]](\psi_1\theta_2\chi_{12})}{P_1^*} - \frac{(1/\tilde{V}_1 - 1/\tilde{V}_2)^2[(2/9)\tilde{V}^{2/3}]\psi_1\psi_2}{[(4/3)\tilde{V}^{1/3} - 1]}$$

where all symbols have the same significance as in the original papers (10–12). The two first terms on right-hand side of eqs. [2]

Can. J. Chem. Downloaded from www.nrcresearchpress.com by 65.111.164.53 on 09/08/12
For personal use only.

Table 3. Experimental excess molar volumes of (x) 2-pentanone + ($1 - x$) 1-chloroalkane at 308.15 K.

x	v^E / cm^3 mol^{-1}	x	v^E / cm^3 mol^{-1}	x	v^E / cm^3 mol^{-1}	x	v^E / cm^3 mol^{-1}
			2-Pentanone + 1-chlorobutane				
0.0509	0.0235	0.2920	0.0820	0.5658	0.0884	0.7988	0.0555
0.1057	0.0408	0.3347	0.0881	0.6133	0.0835	0.8431	0.0427
0.1495	0.0532	0.3866	0.0894	0.6594	0.0796	0.8918	0.0287
0.1990	0.0672	0.4388	0.0926	0.7070	0.0709	0.9386	0.0190
0.2468	0.0780	0.4929	0.0905	0.7546	0.0624		
			2-Pentanone + 1-chloropentane				
0.0601	0.0430	0.3177	0.1487	0.5999	0.1567	0.8249	0.0946
0.1154	0.0767	0.3661	0.1587	0.6489	0.1489	0.8704	0.0747
0.1665	0.1018	0.4162	0.1638	0.6944	0.1383	0.9039	0.0583
0.2188	0.1202	0.4642	0.1660	0.7327	0.1260	0.9455	0.0346
0.2731	0.1387	0.5282	0.1638	0.7785	0.1136		
			2-Pentanone + 1-chlorohexane				
0.0717	0.0559	0.3508	0.1768	0.6349	0.1853	0.8461	0.1070
0.1247	0.0868	0.4026	0.1881	0.6798	0.1740	0.8852	0.0839
0.1901	0.1211	0.4502	0.1943	0.7267	0.1611	0.9180	0.0615
0.2406	0.1441	0.5052	0.1977	0.7610	0.1486	0.9559	0.0324
0.2947	0.1628	0.5642	0.1943	0.8044	0.1274		
			2-Pentanone + 1-chloroheptane				
0.0821	0.0737	0.3792	0.2172	0.6115	0.2282	0.9091	0.0844
0.1449	0.1156	0.4258	0.2266	0.6630	0.2165	0.9281	0.0696
0.1937	0.1452	0.4779	0.2314	0.7062	0.2043	0.9591	0.0406
0.2635	0.1773	0.5287	0.2363	0.7790	0.1735		
0.3141	0.1983	0.5735	0.2318	0.8554	0.1269		
			2-Pentanone + 1-chlorooctane				
0.0701	0.0652	0.3874	0.2322	0.6692	0.2386	0.8650	0.1372
0.1543	0.1252	0.4401	0.2448	0.7115	0.2231	0.8986	0.1082
0.2106	0.1630	0.4885	0.2530	0.7541	0.2083	0.9324	0.0741
0.2721	0.1912	0.5401	0.2560	0.7907	0.1872	0.9612	0.0433
0.3335	0.2178	0.6076	0.2497	0.8264	0.1646		

and [3] are the interactional and the curvature contributions to v^E and h^E, respectively. The third term in eq. [2] is the internal pressure contribution, v_p^E. The interactional terms, $v_{int.}^E$ and $h_{int.}^E$, are usually positive in the absence of hydrogen bond and other specific interactions. The curvature terms, $v_{cur.}^E$ and $h_{cur.}^E$, are always negative because $d^2\tilde{V}/dT^2$ is positive (12). The internal pressure contribution can be positive or negative depending on the sign of $(\tilde{V}_1 - \tilde{V}_2)(\tilde{P}_1 - \tilde{P}_2)$.

The parameters for the pure component liquids required in the calculations are given in Table 5. For 1-chlorobutane and 2-pentanone thermal expansion coefficient, α, and isothermal compressibility, κ_T, were taken from the literature (15, 17). For other pure liquids α was determined from the densities obtained in our laboratory and from those in ref. 19, and κ_T was determined using the McGowan method (23) and experimental data for surface tension (17, 24). From the values in Table 5 we conclude that the internal pressure contribution will be positive in all systems except for the 2-pentanone + 1-chlorobutane at both temperatures (12). The ratios s_1/s_2 were determined according to the original work of Abe and Flory (10).

The parameter X_{12} has been evaluated by using the experimental values of $h^E(0.5)$ for each system except in the case of the mixture with 1-chloroheptane, where $h^E(0.5)$ has been interpolated because of the absence of the experimental data. The theoretical values of both thermodynamic properties h^E and v^E together with their contributions using eqs. [2] and [3] are listed in Table 6.

The X_{12} parameter and the interactional terms of v^E and h^E

Can. J. Chem. Downloaded from www.nrcresearchpress.com by 65.111.164.53 on 09/08/12
For personal use only.

Table 4. Coefficients A_p for eq. [1] and standard deviations s determined by the method of least squares.

System	A_0	A_1	A_2	A_3	s
		T = 298.15 K			
2-Pentanone + 1-Chlorobutane	0.3655	−0.0243	−0.0101	—	0.0007
2-Pentanone + 1-Chloropentane	0.5997	−0.0170	−0.0149	—	0.0008
2-Pentanone + 1-Chlorohexane	0.7401	0.0355	0.0091	—	0.0010
2-Pentanone + 1-Chloroheptane	0.9128	0.1618	0.0930	−0.0200	0.0007
2-Pentanone + 1-Chlorooctane	0.9845	0.1548	0.0819	—	0.0015
		T = 308.15 K			
2-Pentanone + 1-Chlorobutane	0.3669	−0.0606	0.0238	−0.0298	0.0014
2-Pentanone + 1-Chloropentane	0.6612	−0.0525	0.0705	—	0.0008
2-Pentanone + 1-Chlorohexane	0.7870	0.0417	0.0423	−0.0595	0.0010
2-Pentanone + 1-Chloroheptane	0.9361	0.0928	0.0893	−0.0710	0.0009
2-Pentanone + 1-Chlorooctane	1.0132	0.1592	0.1087	−0.0575	0.0013

Table 5. Values of molar volumes, thermal expansion coefficient, isothermal compressibilities, and characteristic parameters for the pure liquids.

Liquid	T (K)	v (cm^3 mol^{-1})	$\alpha \times 10^3$ (K^{-1})	$\kappa_T \times 10^{-3}$ (MPa^{-1})	v^* (cm^3 mol^{-1})	$p^* \times 10^6$ (MPa)	T^* (K)
2-Pentanone	298.15	107.486	1.220	10.92	83.249	555.29	4715
	308.15	108.809	1.250	11.73	83.401	558.93	4739
1-Chlorobutane	298.15	105.194	1.269	12.13	80.826	527.44	4625
	308.15	106.445	1.290	12.84	81.115	533.13	4669
1-Chloropentane	298.15	121.575	1.119	10.93	95.607	493.57	4926
	308.15	122.960	1.132	11.81	95.946	485.10	4976
1-Chlorohexane	298.15	138.149	1.038	10.19	110.040	478.69	5126
	308.15	139.652	1.053	10.84	110.350	479.41	5165
1-Chloroheptane	298.15	154.563	1.009	9.74	124.453	467.07	5275
	308.15	156.153	1.023	10.28	124.595	460.01	5327
1-Chlorooctane	298.15	171.142	0.952	9.40	138.265	462.63	5377
	308.15	172.825	0.963	9.87	138.621	467.33	5421

are positive, increasing regularly with the chain length of the 1-chloroalkane in the mixture. This behaviour has been reported in the literature (15, 25, 26) with mixtures containing a polar molecule and a alkane. In this latter case X_{12} increases with the length of the alkane.

The interactional term is dominant in h^E, since the curvature contribution is negligible for short-chain 1-chloroalkanes, reaching only 4% for 1-chlorooctane. For the excess molar volume, although the interactional term is the greater contribution the curvature and internal pressure terms are important, especially for larger 1-chloroalkanes.

The PFP predictions are good for 1-chlorobutane and 1-

Table 6. Calculated contributions to the v^E and h^E at equimolar concentration using the PFP model.

T (K)	X_{12} (J cm^{-3})	$v^E_{exptl.}$	$v^E_{calcd.}$	$v^E_{int.}$ (cm^3 mol^{-1})	$v^E_{cur.}$	$v^E_{p.}$	$h^E_{int.}$ (J mol^{-1})	$h^E_{cur.}$ (J mol^{-1})
				2-Pentanone + 1-chlorobutane				
298.15	3.69	0.0914	0.0553	0.0676	−0.0026	−0.0097	80.40	−0.40
308.15	3.74	0.0917	0.0636	0.0728	−0.0018	−0.0074	82.27	−0.27
				2-Pentanone + 1-chloropentane				
298.15	6.93	0.1499	0.1686	0.1300	−0.0126	0.0514	158.91	−1.91
308.15	7.09	0.1653	0.1979	0.1423	−0.0177	0.0733	163.63	−2.63
				2-Pentanone + 1-chlorohexane				
298.15	9.96	0.1850	0.2710	0.1898	−0.0455	0.1266	273.78	−6.78
308.15	9.62	0.1967	0.2837	0.1945	−0.0546	0.1438	231.07	−8.07
				2-Pentanone + 1-chloroheptane				
298.15	12.92	0.2282	0.3316	0.2493	−0.0654	0.1477	318.74	−9.74
308.15	12.63	0.2340	0.3389	0.2574	−0.0778	0.1591	313.50	−11.50
				2-Pentanone + 1-chlorooctane				
298.15	15.85	0.2461	0.4556	0.3117	−0.1144	0.2583	402.60	−16.60
308.15	15.48	0.2533	0.4612	0.3204	−0.1345	0.2753	395.46	−19.46

Can. J. Chem. Downloaded from www.nrcresearchpress.com by 65.111.164.53 on 09/08/12
For personal use only.

Fig. 2. Plot of v^E of (0.5) 2-ketone + (0.5) 1-chloroalkane against n, the number of carbon atoms in 1-chloroalkane. Experimental values: ○, 2-pentanone at 298.15 K; □, 2-pentanone at 308.15 K; ●, 3-pentanone at 298.15 K (Lorenzana et al. (7)).

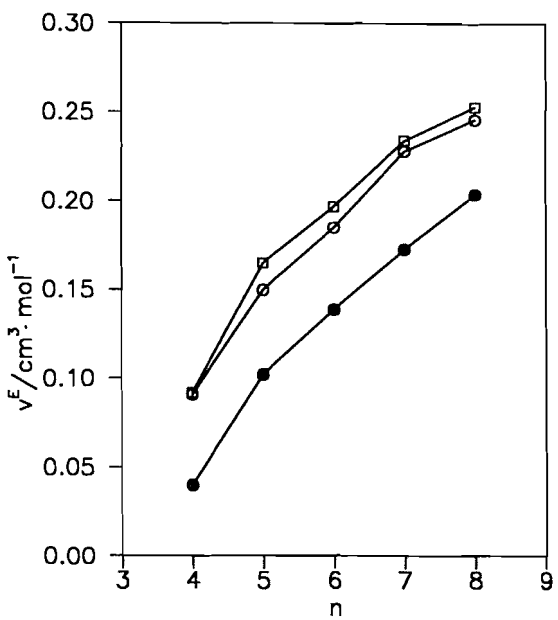

chloropentane, but not as good when the 1-chloroalkane length increases. The same observation has previously been made for mixtures containing alkanes (24, 25). It seems that when interactions are more important the PFP model predicts excess molar volumes that are larger than experimental values (27, 28).

References

1. J.M. Pico, C.P. Menaut, J. Fernández, J.L. Legido, and M.I. Paz Andrade. J. Solution Chem. **20**, 115 (1991).
2. I. García, J.C. Cobos, J.A. González, and C. Casanova. Thermochim. Acta, **128**, 209 (1988).
3. J.M. Lozano, S. Otin, and C. Gutierrez. Rev. Ciencias Zaragoza, **40**, 57 (1988).
4. W. Rupp, S. Hetzel, I. Ojini, and D. Tassios. Ind. Eng. Chem. Process Des. Dev. **23**, 391 (1984).
5. D. Dang and D. Tassios. Ind. Eng. Chem. Process Des. Dev. **25**, 22 (1986).
6. T. Nitta, E.A. Turek, R.A. Greenkorn, and K.C. Chao. AIChE J. **23**, 144 (1977).
7. T. Lorenzana, C. Franjo, E. Jimenez, J. Fernández, and M.I. Paz Andrade. J. Chem. Eng. Data, **39**, 172 (1994).
8. P.J. Flory. J. Am. Chem. Soc. **87**, 1833 (1965).
9. A. Abe and P.J. Flory. J. Am. Chem. Soc. **87**, 1838 (1965).
10. D. Patterson and G. Delmas. Discuss. Faraday Soc. **49**, 98 (1970).

11. M. Barbe and D. Patterson. J. Solution Chem. **9**, 753 (1980).
12. H.T. Van and D. Patterson. J. Solution Chem. **11**, 793 (1982).
13. S.N. Bhattacharyya and D. Patterson. J. Chem. Soc. Faraday Trans. I, **81**, 375 (1985).
14. M. Costas, H. Van Tra, D. Patterson, M. Cáceres, G. Tardajos, and E. Aicart. J. Chem. Soc. Faraday Trans. I, **84**, 1603 (1988).
15. A.D. Matilla, G. Tardajos, E. Junquera, and E. Aicart. J. Solution Chem. **20**, 8 (1991).
16. IUPAC. Pure Appl. Chem. **58**, 1677 (1986).
17. J.A. Riddick, W.B. Bunger, and T.K. Sakano. Organic solvents, techniques of chemistry. 4th ed. Vol. 2. Wiley–Interscience, New York. 1986.
18. A. Crespo Colin, M.R. Vigil, R.G. Rubio, A. Compostizo, and M. Diaz Peña. J. Chem. Soc. Faraday Trans. **87**, 93 (1991).
19. Selected values of properties of chemical compounds, TRC thermodynamic tables – non hydrocarbons, Thermodynamic Research Center: Texas A&M University, College Station, Texas. Tables 23-10-2-(1.0110)-d and 23-2-1(1.2000)-d. 1991.
20. J. Ortega. Ber. Bunsen-ges. Phys. Chem. **93**, 730 (1989).
21. J. Ortega and J.L. Legido. Fluid Phase Equilib. **86**, 21 (1993).
22. P. Bevington. Data reduction and error analysis for the physical sciences. McGraw-Hill, New York. 1969.
23. J.C. McGowan. Recl. Trav. Chim. Pays Bas, **76**, 155 (1957).
24. J.J. Jasper. J. Phys. Chem. Ref. Data, **1**, 841 (1972).
25. T. Kasprzycka-Guttman and H. Kurcínska. J. Solution Chem. **18**, 727 (1989).
26. A.M. Awwad and K.A. Jbara. Thermochim. Acta, **129**, 249 (1988).
27. J. Pouchly, A. Qin, and P. Munk. J. Solution Chem. **22**, 5 (1993).
28. M.E. Saint-Victor, A.J. Treszczanowicz, and D. Patterson. Fluid Phase Equilib. **46**, 295 (1989).

Can. J. Chem. Downloaded from www.nrcresearchpress.com by 65.111.164.53 on 09/08/12
For personal use only.

COMMUNICATION

A study of the vacuum pyrolysis of 1,2,3-benzotriazines. The HeI ultraviolet photoelectron spectra of benzazete and *o*-benzyne

Nick Henry Werstiuk, Chandra Deo Roy, and Jiangong Ma

Abstract: A CW CO_2 laser is used as a directed heat source to carry out the vacuum pyrolysis of 1,2,3-benzotriazine (**1***a*) and 4-methyl-1,2,3-benzotriazine (**1***b*). We report the first HeI photoelectron (pe) spectrum of benzazete (**2***a*), which correlates with ionization energies calculated with HAM/3 using an equilibrium geometry obtained at the ab initio HF/6-31G** level of the theory. The pe spectrum of *o*-benzyne (**3**) obtained in this study correlates with the spectrum published by Zhang and Chen, but not with the spectra reported in two earlier publications.

Key words: 1,2,3-benzotriazines, vacuum pyrolysis, HeI ultraviolet photoelectron spectra, benzazete, benzyne.

Résumé : On a utilisé un laser CW au CO_2 comme source dirigée de chaleur pour effectuer des pyrolyses sous vide des 1,2,3-benzotriazine (**1***a*) et 4-méthyl-1,2,3-benzotriazine (**2***b*). On a déterminé le premier spectre photoélectronqiue au HeI du benzazète (**2***a*) pour lequel il existe une bonne corrélation avec les énergies d'ionisation calculées avec HAM/3, en utilisant une géométrie d'équilibre obtenue par des calculs ab initio au niveau HF/6-31G** de la théorie. Le spectre photoélectronique du *o*-benzyne (**3**) obtenu au cours de ce travail est en bon accord avec le spectre publié par Zhang et Chen, mais il diffère de celui rapporté dans deux travaux antérieurs.

Mots clés : 1,2,3-benzotriazines, pyrolyse sous vide, spectre photoélectronique ultraviolet HeI, benzazète, benzyne.

[Traduit par la rédaction]

Ultraviolet photoelectron spectroscopy (pes) combined with semiempirical or ab initio calculations of equilibrium molecular geometries and molecular orbital (MO) eigenvalues, provides, within the limits of Koopmans theorem (1), a method for ordering the energies of MOs. As a result these studies give fundamental information about the bonding of stable compounds and transient species that is provided by no other technique. To this point, transient species studied with pes generally were prepared by vacuum pyrolysis of compounds with electrically heated furnaces centimetres in length (2, 3). To facilitate the preparation and detection of highly reactive transients in the gas phase, we developed a CW CO_2 laser/pes apparatus and used it successfully to study the vacuum pyrolysis of 6,6-dihalobicyclo[3.1.0]hexanes (4). In this communication we document the results of a study of the pyrolysis of 1,2,3-benzotriazine (**1***a*) and 4-methyl-1,2,3-benzotriazine (**1***b*) with this apparatus. We studied these compounds for three reasons (*a*) we wished to establish the general applicability of using the apparatus to prepare and study highly reactive transients; (*b*) there have been no reports of pe spectra of benzazetes, which appear to be highly reactive, nonisolable compounds (5); (*c*) previous studies produced three different pe spectra for *o*-benzyne (**3**) (6–8). We chose to study **1***a* and **1***b* because Rees and co-workers showed that these compounds decompose at relatively low temperatures (400–500°C) in a closed systems at 0.01 Torr (1 Torr = 133.3 Pa) and give good yields of biphenylene (**4**), the product of the dimerization of **3** (9, 10). Compounds **1***a* and **1***b* also are potential sources of benzazete (1-azabenzocyclobutene) (**2***a*) and 2-methylbenzazete (**2***b*) provided that the vacuum pyrolyses can be carried out under conditions where cyclization of the diradicals formed by extrusion of N_2 competes with fragmentation to **3** and HCN or CH_3CN (Scheme 1).

Received August 29, 1994.

N.H. Werstiuk,[1] C.D. Roy, and J. Ma. Department of Chemistry, McMaster University, Hamilton, ON L8S 4M1, Canada.

[1] Author to whom correspondence may be addressed.

Can. J. Chem. Downloaded from www.nrcresearchpress.com by 65.111.164.53 on 09/08/12
For personal use only.

Scheme 1

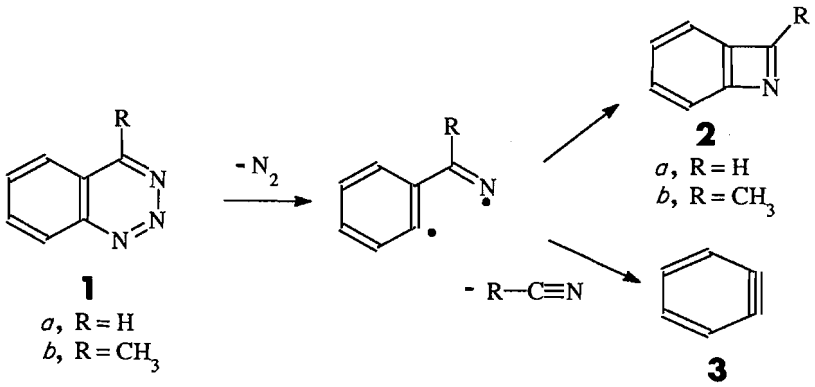

Fig. 1. (*a*) HeI pe spectrum of **1***a* obtained at a probe temperature of 112°C; (*b*) spectrum of the pyrolyzate of **1***a* obtained at a laser power of 40 W; (*c*) spectrum obtained by stripping spectrum 1(*a*) from spectrum 1(*b*); (*d*) spectrum of the pyrolyzate of **1***a* obtained at 54 W (*e*) spectrum of biphenylene (**4**) obtained at ambient temperature.

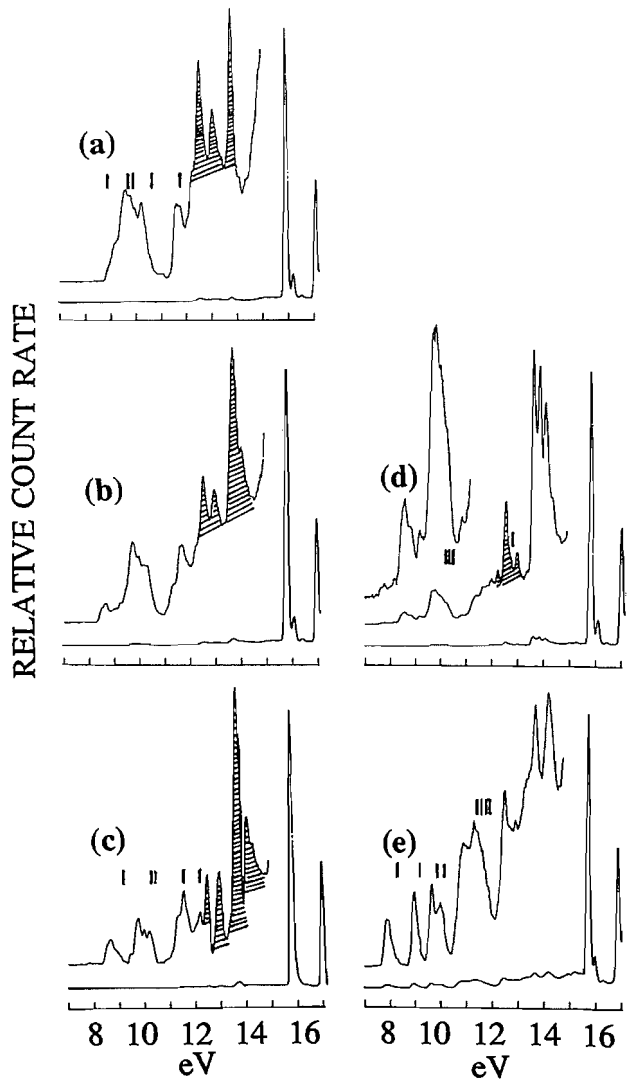

The pe spectra along with vertical expansions in the range 7–14 eV obtained for the pyrolysis of **1***a* and **1***b* at a number of laser power levels[2] are displayed in Figs. 1 and 2, respectively. In this study, N_2 introduced into the source as a make-up gas to maintain the total pressure in the source at around $(5–6) \times 10^{-3}$ Torr (the substrate base pressure was kept low at 10^{-4} Torr) greatly improved the quality of the spectra. The low-IP band of N_2, which has a much higher ionization cross section than the organic molecules, is seen at 15.6 eV in the spectra.[3] Figure 1(*a*) is the spectrum of **1***a* obtained at a probe temperature of 112°C. The solid bars on this spectrum show the five lowest ionization energies (IEs) (8.87, 9.70, 9.84, 10.55, 11.64 eV) of **1***a* calculated with HAM/3 (11) on the equilibrium geometry calculated at the HF/6-31G** level of theory with GAUSSIAN 92 (12). At a laser power of 40 W, there is a significant change in the pe spectrum (Fig. 1(*b*)); a peak appears at 8.8 eV and there is a change in the structure of the band(s) between 9 and 10.8 eV. Of significance is the fact that there is no band(s) between 13.5 and 14.5 eV corresponding to the low-IP band of HCN (13). This result indicates that **1***a* decomposes at a laser power of 40 W without extruding HCN. Figure 1(*c*) shows the result of stripping the

[2] The solid benzotriazine (10–20 mg) was placed in a bottle-shaped quartz reaction vessel that was inserted into a brass probe tip, which was electrically heated or cooled with circulating tap water. Quartz was used to fabricate the reaction vessel because it has a high melting point and, more importantly, it exhibits a very low lateral surface thermal conductivity. The main body of the reaction vessel made of 5 mm o.d. tubing is 1.5–2 cm long. The pyrolysis tube, which is 1.5 cm in length and made of 3 mm o.d. tubing, was constricted at the tip to an i.d. of approximately 1 mm after the sample was loaded. With the tip of the pyrolysis tube positioned 1 cm from the point of intersection with the ionizing photon beam, the 7 mm diameter laser beam was focused to a 1 mm diameter beam with a convex ZnSe lens and directed through a ZnSe window in the source housing to impinge on the tip of the quartz reaction vessel. In this configuration, the focused laser beam produces a hot zone that is approximately 2 mm in length. The pyrolysis reactions were carried out at a source pressure of $(6–7) \times 10^{-3}$ Torr with the fast-pumping valve partially open.

[3] The cross-hatched peaks are due to traces of oxygen (12–13 eV) in the N_2 used as the make-up gas, H_2O (12.6 eV) that is released from the quartz tubing when it is heated with the laser beam, and a shadow peak (13.6 eV) of N_2.

Can. J. Chem. Downloaded from www.nrcresearchpress.com by 65.111.164.53 on 09/08/12
For personal use only.

Can. J. Chem. Downloaded from www.nrcresearchpress.com by 65.111.164.53 on 09/08/12
For personal use only.

Fig. 2. (*a*) HeI photoelectron spectrum of **1***b*; (*b*) spectrum of the pyrolyzate of **1***b* obtained at 54 W.

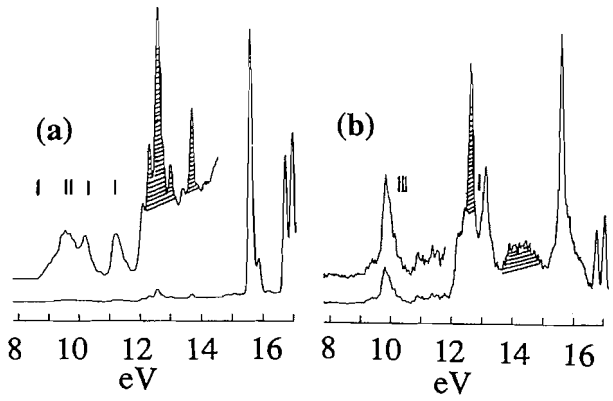

Fig. 3. Optimized equilibrium geometrical structure of benzazete (**2***a*) obtained at the HF/6-31G** level of theory.

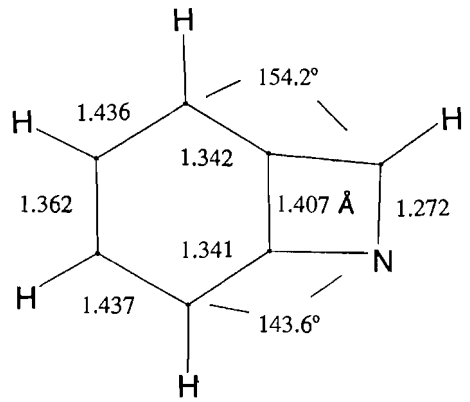

spectrum of **1***a* (Fig. 1(*a*)) from the 40-W spectrum 1(*b*) along with vertical bars that locate the five lowest IEs (9.11, 10.20, 10.26, 11.49, 12.09 eV) of benzazete (**2***a*) obtained with HAM/3 using the HF/6-31G** optimized equilibrium geometry calculated with GAUSSIAN 92. The surprisingly distorted optimized geometrical structure of **2***a* — it must be highly strained — exhibiting alternating long and short C—C bonds is displayed in Fig. 3. The localization of the π bonds means that **2***a* will not be stabilized by resonance to the same degree as benzene. Perhaps it is these factors which give rise to the high reactivity of **2***a*. We take good correlation between the calculated and experimental IEs[4] and the fact that HCN is not produced at 40 W as compelling evidence that Fig. 1(*c*) is the partial pe spectrum of **2***a*. At a laser power of 54 W, further changes occur in the low-IP region of the spectrum (Fig. 1(*d*)), and HCN, identified by the strong band exhibiting vibrational fine structure centered at 14 eV (13), is a product of the pyrolysis. Bars showing the four lowest IEs (10.20, 10.24, 10.35, 12.81 eV) of **3** calculated with HAM/3 using the HF/6-31G** equilibrium geometry are included in this spectrum. The outer valence Green function (OVGF) and extended two-particle-hole Tamm–Dancoff (extended 2ph-TDA) methods, which allow for orbital relaxation and correlation effects and which have successfully predicted the IEs of a range of organic molecules, have been used to calculate the IEs of **3** (14). The OVGF method yields values of 9.55, 9.57, and 9.77 eV for the three lowest IEs. The extended 2ph-TDA method yields values of 9.54, 9.54, and 9.65 eV. Thus the new band(s) between 9.3 and 10.5 eV correlate with the calculated three lowest IEs[5] of **3**. The peak at 8.8 eV corresponds to the lowest IE band of benzazete (Fig. 1(*c*)). Figure 1(*e*) is a display of the pe spectrum of an authentic sample of biphenylene (**4**) along with the eight lowest IEs calculated with HAM/3 on the 6-31G** optimized geometry. That there is only a very weak peak at 7.8 eV in spectrum 1(*d*) establishes that **3** does not dimerize to a significant extent under the experimental conditions used in this study. The spectrum of 4-methyl-1,2,3-benzotriazine (**1***b*) along with the five lowest IEs (8.59, 9.48, 9.60, 10.31, 11.64 eV) calculated at the HAM/3//6-31G** level of theory are shown in Fig. 2(*a*). Because **1***b* tended to decompose when warmed in the quartz reaction vessel for extended periods, the pyrolysis was carried out at 54 W in a short period of time (the temperature of the probe holding the reaction vessel was rapidly increased to 80°C) without N_2 being added as a make-up gas. Unlike the case of **1***a* where the spectrum was obtained by averaging 25 scans using a dwell time of 0.1 s/point, spectrum 2(*b*) was obtained in one scan utilizing a dwell time of 1 s/point. The calculated four lowest IEs of **3** are also shown on this spectrum. As was found in the pyrolysis of **1***a*, the band(s) centered at 9.7 eV correspond to the calculated first three IEs of **3** and as predicted by the calculations there are no additional well-defined bands between 10 and 12.5 eV. The group of bands (excluding the cross-hatched band at 12.6 eV due to H_2O[3]) between 12 and 13.5 eV are due to acetonitrile (13). Given that the calculated four lowest IEs (HAM/3 on the HF/6-31G** optimized geometry) of **2***b* are 8.71, 9.87, 9.93 and 11.05 eV, and there are no bands below 9 eV in spectrum 2(*b*), **1***b* decomposes without forming a significant amount of **2***b*. The low-IE region of spectrum 2(*b*) closely resembles the partial spectrum of **3** (it was generated by supersonic jet/flash vapour pyrolysis of benzocyclobutene-1,2-dione) published by Zhang and Chen (8), but not the spectra reported by two other research groups (6, 7). Thus **1***b* pyrolyzes cleanly to **3** and acetonitrile under the conditions employed in this study without forming significant amount of 2-methylbenzazete and biphenylene.

[4] The HAM/3 HOMO of **2***a* is a π-type MO with coefficients on N=C (0.437 and 0.299), the bridging C=C (–0.398 and –0.392), and on the remaining carbon atoms (–0.071, 0.423, 0.356, and –0.197). HOMO-1 is a π-type MO located predominantly on the phenyl ring (0.295, –0.365, 0.498, –0.164, 0.277, 0.505) with small coefficients being found on N=C (0.107 and –0.109). HOMO-2 is a σ-type in-plane orbital involving N (the lone pair), the carbons of the azete ring, and one of the benzene ring. HOMO-3 is a π-type MO with coefficients on N=C (–0.394 and –0.339), and four carbons of the benzene ring (0.304, 0.435, 0.420, 0.251) excluding the bridging C=C bond.

[5] According to the HAM/3 and HF/6-31G** calculations, the HOMO and HOMO-1 of **3** are π-type MOs and HOMO-2 is the in-plane orbital involving the carbons of the triple bond. Because ab initio calculations at the 4-31G level of theory have shown that the phenyl cation is highly distorted relative to benzene (15), is possible that the radical cation nominally derived from **3** by loss of an electron from this in-plane orbital may exhibit a broad Franck–Condon envelope. Perhaps this accounts for the shape, a relatively sharp peak overlapping a broad band, of the low-IP band(s) of **3**.

Acknowledgement

We thank the Natural Sciences and Engineering Research Council of Canada for financial support.

References

1. T.A. Koopmans. Physica, **1**, 104 (1933).
2. R. Schulz and A. Schweig. *In* Structure and reactivity. *Edited by* J.F. Liebman and A. Greenberg. VCH Publishers Inc., New York, 1988. Chap. 8.
3. N.P.C. Westwood. Chem. Soc. Rev. **18**, 317 (1989).
4. N.H. Werstiuk, C.D. Roy, and J. Ma. Can. J. Chem. **72**, (1994).
5. B.M. Adger, M. Keating, C.W. Rees, and R.C. Storr. J. Chem. Soc. Perkin Trans. 1, 41 (1975).
6. M.J.S. Dewar and T-P. Tien. J. Chem. Soc. Chem. Commun. 1243 (1985).
7. R. Schulz and A. Schweig. *In* Structure and reactivity. *Edited by* J.F. Liebman and A. Greenberg. VCH Publishers Inc., New York. 1988. Chap. 8. p. 335.
8. X. Zhang and P.J. Chen. J. Am Chem. Soc. **114**, 3147 (1992).
9. B.M. Adger, C.W. Rees, and R.C. Storr. J. Chem. Soc. Perkin Trans. 1, 45 (1975).
10. B.M. Adger, S. Bradbury, M. Keating, C.W. Rees, R.C. Storr, and M.T. Williams. J. Chem. Soc. Perkin Trans. 1, 31 (1975).
11. L. Asbrink, C. Fridh, and E. Lindholm. HAM/3. Quantum Chemistry Program Exchange (QCPE) Bulletin, **13**, 393 (1981).
12. M.J. Frisch, G.W. Trucks, M. Head-Gordon, P.M.W. Gill, M.W. Wong, J.B. Forseman, B.G. Johnson, H.B. Schlegel, M.A. Robb, E.S. Replogle, R. Gomperts, J.L. Andres, K. Raghavachari, J.S. Binkley, C. Gonzalez, R.L. Martin, D.J. Fox, D.J. Defrees, J. Baker, J.J.P. Stewart, and J.A. Pople. GAUSSIAN 92. Gaussian Inc., Pittsburgh, Pa. 1992.
13. K. Kimura, S. Katsumata, Y. Achiba, T. Yamazaki, and S. Iwata. The handbook of HeI photoelectron spectra of fundamental organic molecules: ionization energies, *ab initio* assignments and valence electronic structure of 200 molecules. Japan Scientific Societies Press, Tokyo. 1981.
14. I.H. Hiller, M.A. Vincent, M.F. Guest, and W. von Niessen. Chem. Phys. Lett. **134**, 403 (1987).
15. J.O. Noell and M.D. Newton. J. Am. Chem. Soc. **101**, 51 (1979)

Can. J. Chem. Downloaded from www.nrcresearchpress.com by 65.111.164.53 on 09/08/12
For personal use only.

Crystal chemistry of tetraradial species. Part 7. Lithium tetrakis(1-imidazolyl)-borate solvate, $Li^{iv}[Li^{iv}(H_2O)(MeOH)][B(C_3H_3N_2)_4]_2 \cdot MeOH$, a 3-dimensional polymer; with observations on the geometry of imidazole rings[1]

Osvald Knop and Pradip K. Bakshi

Abstract: The title compound is a 3-dimensional polymer with a completely ordered triclinic structure ($P\bar{1}$, a = 12.380(2) Å, b = 14.434(2) Å, c = 9.683(3) Å, α = 90.36(2)°, β = 105.44(2)°, γ = 90.75(2)°, Z = 2). Every B atom is tetrahedrally coordinated by N(1) atoms of the imidazole rings, every Li(1) atom is tetrahedrally coordinated by N(3) atoms, and every Li(2) atom is coordinated by two N(3) and two oxygen atoms, one from the H_2O molecule and one from a MeOH molecule. The imidazole rings connected by the B—N(1) and Li—N(3) bonds thus generate a 3-dimensional covalent polymeric network. The MeOH molecules of coordination are hydrogen-bonded to unengaged N(3) atoms, thereby supplementing the covalent bonding system. The H_2O molecules are hydrogen-bonded to the MeOH molecules of solvation to form centrosymmetric $[O_w...O_{MeOH}]_2$ rings, which in turn are connected to the covalent network by O_{MeOH}—H...N(3) bonds to the remaining unengaged N(3) atoms. Every atom in the structure except the H(C) hydrogens is thus involved in the 3-dimensional bond system. The excellent consistency of the bond lengths and endocyclic bond angles ϕ in the eight imidazole rings of the title compound has provided an opportunity for investigating the effect of substitution on the geometry of the imidazole ring in a sample of 17 substituted imidazoles. While the bond lengths have been found at most weakly correlated, the multilinear correlations of the ϕ in this sample are highly significant. Among the substituents the NO_2 group is the most *ipso*-ϕ-expanding and the anionic B (in the title compound) the most *ipso*-ϕ-contracting. Protonation or deprotonation at the N atoms affect the *ipso* C—N—C angles considerably. Limited comparisons are drawn with the results of the classical investigations by Domenicano et al. on the effect of substitution on the geometry of the benzene ring.

Key words: hydrogen bond, imidazole, lithium compounds, polymers, tetrahedral boron ions.

Résumé : Le composé mentionné dans le titre est un polymère tridimensionnel avec une structure triclinique complètement ordonnée ($P\bar{1}$, a = 12,380(2) Å, b = 14,434(2) Å, c = 9,683(3) Å, α = 90,36(2)°, β = 105,44(2)°, γ = 90,75(2)°, Z = 2). Chaque atome de bore est coordonné de façon tétraédrique par les atomes d'azote N(1) du cycle imidazole, chaque atome de lithium Li(1) est coordonné de façon tétraédrique par les atomes d'azote N(3) et chaque atome de lithium Li(2) est coordonné par deux atomes d'azote N(3) et par deux atomes d'oxygène, un provenant de l'eau et l'autre provenant de la molécule de MeOH. Les cycles imidazole reliés par les liaisons B—N(1) et Li—N(3) forment alors un réseau polymérique tridimensionnel. Les molécules de MeOH de coordination sont liées par des liaisons hydrogène aux atomes d'azote N(3) non engagés, renforçant ainsi les liaisons covalentes du système. Les molécules d'eau sont liées par des liaisons hydrogène aux molécules de MeOH de solvatation pour former des cycles centro-symétriques $[O_{eau}...O_{MeOH}]_2$ qui sont à leur tour reliés au réseau covalent par des liaisons O_{MeOH}—H...N(3) aux atomes de N(3) non engagés restants. Chaque atome de cette structure, à l'exception des hydrogènes H(C), est alors impliqué dans le système de liaison tridimensionnelle. L'excellente cohérence existant entre les longueurs de liaison et les angles de liaison endocycliques ϕ dans les huit cycles imidazoles du composé mentionné dans le titre fournit l'opportunité d'étudier l'effet de la substitution sur la géométrie du cycle imidazole dans un échantillon de 17 imidazoles substitués. Alors que les longueurs de liaisons tout au plus correspondent faiblement, les corrélations multilinéaires de l'angle ϕ dans cet

Received August 16, 1994.

O. Knop[2] and P.K. Bakshi.[3] Department of Chemistry, Dalhousie University, Halifax, NS B3H 4J3, Canada.

[1] The superscript iv indicates the coordination number of the Li atom. For Part 6 see ref. 1.

[2] To whom correspondence may be addressed (telephone: (902) 494-3317 or (902) 494-3305; facsimile: (902) 494-1310).

[3] Holder of a graduate scholarship, Canadian Commonwealth Scholarship and Fellowship Plan, and of a Killam Graduate Scholarship.

Can. J. Chem. Downloaded from www.nrcresearchpress.com by 65.111.164.53 on 09/08/12
For personal use only.

échantillon sont très fortement significatives. Parmi les substituants, le groupe NO_2 est le plus *ipso*-ϕ-dispersant et le groupe anionique B (dans le composé mentionné dans le titre) est le plus *ipso*-ϕ-contractant. La protonation ou la déprotonation des atomes d'azote affecte considérablement les angles *ipso* C—N—C. On établit des comparaisons limitées avec les résultats des études classiques effectuées par Domenicano et al. sur l'influence de la substitution sur la géométrie du cycle benzénique.

Mots clés : liaison hydrogène, imidazole, composés du lithium, polymères, anions bore tétraédriques.

[Traduit par la rédaction]

Can. J. Chem. Downloaded from www.nrcresearchpress.com by 65.111.164.53 on 09/08/12
For personal use only.

In Part 6 (1) we described the crystal structure of $[Li(H_2O)_4]BPh_4$, in which the four water molecules coordinating the Li^+ ion all form O—H...π hydrogen bonds to the phenyl groups and all the phenyl groups are H-bonded, thus giving rise to a 3-dimensional, completely H-bonded polymeric network. Curious to find out how the O—H...π bonding might compete with other possible interactions, we set out to prepare the Li salt of the tetrakis(1-imidazolyl)borate anion (TIB), $B(C_3H_3N_2)_4^-$, by metathesis of its Na salt (2, 3) with LiCl in aqueous methanol. The colourless crystals resulting from an exploratory experiment turned out to be neither the $Li(H_2O)_4^+$ nor the $Li(MeOH)_4^+$ salt of TIB but the title compound (TC). This has an interesting triclinic structure in which one Li atom is coordinated by four imidazole (Im) nitrogens and another by two nitrogens, an H_2O oxygen, and an MeOH oxygen. The composition of TC can thus be formulated as $Li^{iv}[Li^{iv}(H_2O)(MeOH)][B(C_3H_3N_2)_4]_2 \cdot MeOH$.[1] The basic structure motif corresponding to this formula is represented schematically in Fig. 1, which shows the coordination within the motif as well as the connectivity of the structure, and again in a crystallographic projection (Fig. 2), where the connectivities of the covalent (B—N, Li—N) and the H-bonding networks have been separated for clarity.

The crystal data of TC are assembled in the Experimental and the positional parameters of the nonhydrogen atoms in Table 1. The positional parameters and isotropic temperature factors of the hydrogens (Table A), the anisotropic thermal parameters of the nonhydrogen atoms (Table B), the interatomic distances and bond angles (Table C), and the deviations of the C and N atoms from the best planes through the Im ring skeletons (Table D) have been deposited.[4]

Organization of the structure

The distribution of the B and Li atoms in the TC structure does not lend itself to a simple description. The B atoms are attached exclusively to N(1) atoms[5] (rings 1—4 on B(1), rings 5–8 on B(2)), while the Li—N bonds involve only N(3) atoms, Li(1)—N(3) in rings 2, 3, 7 and 8, Li(2)—N(3) in rings 1 and 5.

Fig. 1. Schematic representation of the basic motif of the title compound. The heavy-line portion corresponds to the formula in text. The oxygen atoms O(w), O(m1), and O(m2) are, respectively, those of the H_2O molecule, the MeOH of coordination, and the MeOH of solvation. Small full circles represent H atoms. Small 1 and 3 stand for N(1) and N(3), respectively; the large numbers identify the imidazole rings.

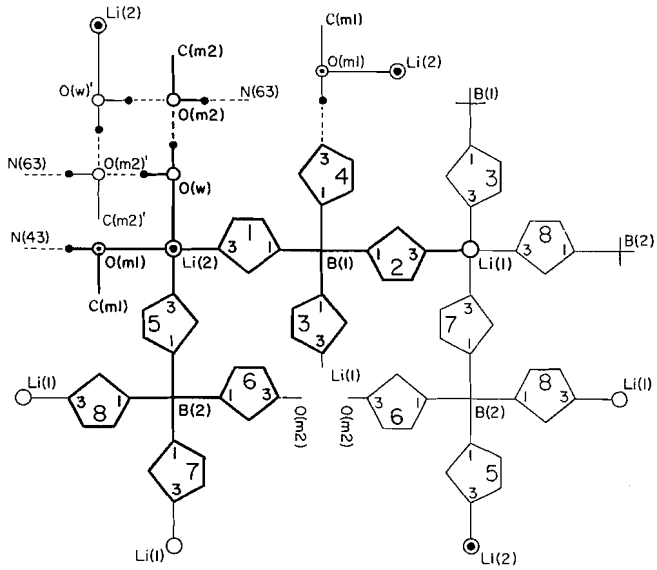

The N(3) atoms in rings 4 are H-bonded to MeOH molecules m1 coordinated to Li(2), and those in rings 6 are H-bonded to MeOH molecules m2 of solvation, as are the H_2O molecules w. The preferential formation of Li—N bonds on crystallization from MeOH–H_2O thus indicates that the Li—N rather than the Li—O interaction is dominant in these circumstances.

The O(w) and O(m1) atoms are 3-coordinate (Fig. 3), with the Li(2)—O(w) and Li(2)—O(m1) vectors roughly bisecting the angle between the two lone electron pairs on the oxygen atom. The O(m2) oxygen is 4-coordinate.

The anisotropic thermal parameters of all the nonhydrogen atoms are reasonable, with the exception of C(m1) of the coordinated MeOH molecule, for which the U_{ij} values are very large, with U_{ii} between 0.22 and 0.32 Å^2 (Table B). This is the only nonhydrogen atom in the otherwise completely ordered TC structure that shows positional disorder, very likely dynamic. The hypothesis that the large U_{ij} arise from a mixed MeOH,H_2O occupancy was rejected as only marginally probable, as it did not lead to a significant reduction of the U_{ij}(Cm1) and the refined occupancy factor for Cm1 was 0.83(2).

[4] This material can be purchased from: The Depository of Unpublished Data, Document Delivery, CISTI, National Research Council Canada, Ottawa, Canada, K1A 0S2. Tables A–C have also been deposited with the Cambridge Crystallographic Data Centre and can be obtained on request from The Director, Cambridge Crystallographic Data Centre, University Chemical Laboratory, 12 Union Road, Cambridge CB2 1EZ, U.K.

[5] *Housekeeping note.* The numbering of the Im ring atoms is standard, cf. Fig. 4. Crystallographic esd's are shown in parentheses. Standard deviations of means of distances, bond angles, etc. are shown in brackets; they do not include the esd's of the component values, and the means are computed with unit weights.

Fig. 2. Crystallographic projection of a portion of the structure of the title compound giving a relatively unobstructed view of the basic motif. (*Left*) Connectivity in the B,Li,Im system; MeOH of solvation (m2) omitted. (*Right*) The H-bonding system only. Both views correspond to the schematic of Fig. 1. Ring H atoms omitted for clarity. The numbers of atoms and rings attached to the B(1), B(2), Li(1), and Li(2) atoms correspond to the atom numbering of Table 1.

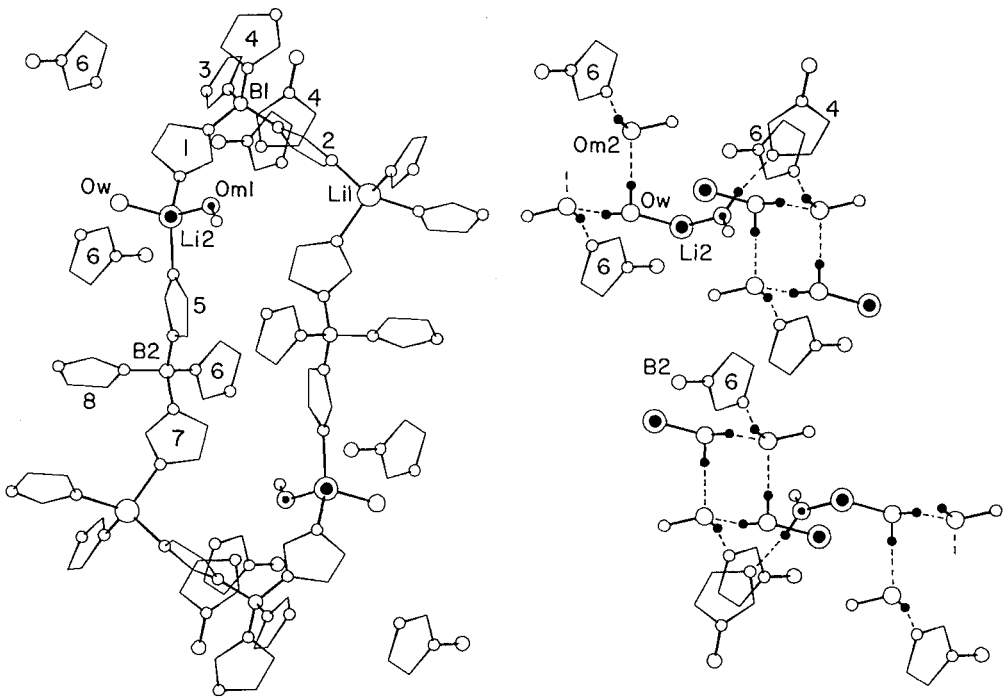

Bond lengths and angles

A detailed list of interatomic distances and bond angles in TC is given in Table C. The eight B—N bond lengths are closely similar, with a mean of 1.542[4] Å. The N—B—N valence angles range from 107.8(3)° to 111.6(3)°, with $\sigma = 1.2°$ on the tetrahedral 109.48° mean. There is no indication of a tendency of the BN_4 tetrahedron toward an S_4 symmetry, such as is often observed in the C—B—C valence angle α of the $BC(\alpha)_4$ tetrahedron in the tetraphenylborate anion (4, 5).

The d(Li—N) means for Li(1) and Li(2) are statistically indistinguishable, i.e. there is no observable effect of the mixed N, O coordination at Li(2) on d(Li—N). The mean Li—N bond length, 2.054[14] Å, is within 2σ of the Li—N bond lengths in $[Li^{iv}py_4]$ and in the $[Li^{iv}(Et_8\text{-porphyrin})]^+$ cation (Table 2). However, there seems to be no clear-cut separation between the $d(Li^{iv}—N)$ and the corresponding bond lengths with Li in 3- or 5-coordination in Table 2. With the exception of ring 5 the Li atom is significantly non-coplanar with its associated Im rings.

The Li(2)—O distances, to the H_2O and MeOH oxygens, respectively, fall in the general, broad range of Li^{iv}—O distances (Table 2; ref. 18).

The mean of the two O(w)...O(m2) distances in the planar $[O(w)...O(m2)]_2$ dimer is 2.854[7] Å, i.e. larger than the mean shortest O...O distance in ordinary ice, 2.76[1] Å (Fig. 3). The O...N distances O(m1)...N(43)″ = 2.718(5) Å and O(m2)...N(63)‴ = 2.681[4] Å (Table C) are comparable to the O...N distance in the O—H...N bond in $N_2H_4 \cdot 4MeOH$, 2.682(6) Å (19), but significantly shorter than similar distances in $N_2H_4 \cdot 2MeOH$, 2.730(6) Å (20), and $N_2H_4 \cdot H_2O$, 2.790(6) Å (21).

The imidazole rings

The variation in the (uncorrected) N—C and C—C bond lengths and in the endocylic bond angles ϕ in the eight Im rings of TC is remarkably small. The standard deviations of the means amount to 0.003–0.007 Å for the bond lengths and 0.3–0.4° for the angles (Table C), i.e. the sample populations for the five bond lengths and the five ϕ angles are very homogeneous. The ring skeletons are planar within 0.002[1] Å (Table D). The bond lengths and angles in TC are compared to those in Im, ImH^+, and a number of substituted imidazoles (sample **S**)[6] in Tables 3 and 4.

The d_{23} and d_{34} bond lengths in TC are the same as in unsubstituted Im; d_{12} and d_{51} in TC are increased, and d_{45} is decreased, but the changes are small compared to the respective overall bond-length variations in **S**: the largest difference, $d_{12}(TC) - d_{12}(Im) = 0.012$ Å, is at the limit of 3σ statistics.

While the data of Table 3 are informative in various ways, they also show the general difficulty of establishing a rationale for the sign and magnitude of the changes in d_{ij}(Im) on substitution, especially when more than one substituent is present. In this TC is no exception. The ranges of the individual (uncorrected) bond lengths in **S** are narrow, 0.044–0.058 Å, i.e., on the average ~4% of the bond length. An analysis along

[6] The sample **S** of Table 3 has been assembled mainly on the quality of the structure determinations retrieved from the Cambridge Structural Database, without regard to the nature of the substituents save for their simplicity. It does not include structures in which Im is a ligand to a (heavy) metal atom in a discrete coordination complex or in which the Im ring is part of a larger fused ring system.

Can. J. Chem. Downloaded from www.nrcresearchpress.com by 65.111.164.53 on 09/08/12
For personal use only.

Can. J. Chem. Downloaded from www.nrcresearchpress.com by 65.111.164.53 on 09/08/12
For personal use only.

Table 1. Positional parameters ($\times 10^4$) of nonhydrogen atoms in the title compound.[a]

Atom	x	y	z	Atom	x	y	z
B(1)	10137(4)	8448(3)	7223(4)	C(54)	4302(4)	6929(3)	8748(5)
N(11)	8845(2)	8460(2)	6697(3)	C(55)	3795(4)	6085(3)	8619(4)
C(12)	8096(3)	8187(3)	7426(4)	N(61)	4485(2)	4046(2)	6934(3)
N(13)	7040(3)	8338(2)	6742(3)	C(62)	4393(3)	3113(3)	6753(5)
C(14)	7100(3)	8744(3)	5472(4)	N(63)	5366(3)	2696(2)	7003(4)
C(15)	8190(3)	8827(3)	5437(4)	C(64)	6144(3)	3396(3)	7368(4)
N(21)	10513(2)	7699(2)	8383(3)	C(65)	5621(3)	4224(3)	7333(4)
C(22)	10521(3)	7750(3)	9792(4)	N(71)	2695(2)	4305(2)	7576(3)
N(23)	10797(3)	6961(2)	10479(3)	C(72)	1562(3)	4261(3)	7135(4)
C(24)	10973(4)	6366(3)	9453(4)	N(73)	1098(3)	3852(2)	8058(3)
C(25)	10806(4)	6801(3)	8175(4)	C(74)	1994(4)	3628(3)	9181(4)
N(31)	10613(2)	8215(2)	5946(3)	C(75)	2967(3)	3897(3)	8910(4)
C(32)	10166(3)	7639(3)	4822(4)	N(81)	2861(2)	4838(2)	5190(3)
N(33)	10844(3)	7479(2)	4004(3)	C(82)	2221(3)	5581(3)	4672(4)
C(34)	11804(3)	7982(3)	4653(4)	N(83)	1573(3)	5458(2)	3349(3)
C(35)	11677(3)	8429(3)	5838(4)	C(84)	1807(3)	4572(3)	2989(4)
N(41)	10594(2)	9398(2)	7863(3)	C(85)	2591(3)	4181(3)	4095(4)
C(42)	11600(4)	9575(3)	8819(4)	Li(1)	10551(5)	6506(4)	2373(6)
N(43)	11832(3)	10470(2)	9033(4)	Li(2)	5637(5)	8293(4)	7533(7)
C(44)	10942(4)	10901(3)	8150(4)	O(w)	4626(2)	9247(2)	6461(3)
C(45)	10179(3)	10262(3)	7433(4)	O(m1)	6184(3)	8734(2)	9525(3)
B(2)	3508(4)	4718(3)	6773(5)	C(m1)	5603(8)	8939(7)	10540(10)
N(51)	3936(2)	5680(2)	7393(3)	O(m2)	5879(2)	10938(2)	6573(3)
C(52)	4533(3)	6313(3)	6854(4)	C(m2)	6855(4)	10778(3)	7701(5)
N(53)	4774(3)	7083(2)	7631(3)				

[a]w, H_2O; m1, MeOH coordinated to Li(2); m2, MeOH of solvation.

Fig. 3. Details of the H-bonding in the title compound and of the coordination of the H_2O oxygen O(w), the O(m1) oxygen of the coordinated MeOH, and of the O(m2) oxygen of the MeOH of solvation. For esd's see Table C.

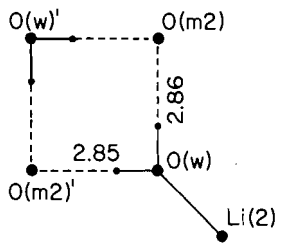

O(m2)-O(w)-O(m2)'	94.5°
Li(2)-O(w)-O(m2)	108.5°
Li(2)-O(w)-O(m2)'	114.5°
O(w)-O(m2)-O(w)'	85.5°

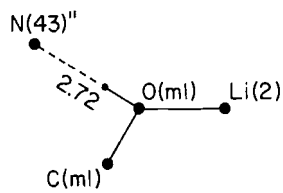

C(m1)-O(m1)-N(43)''	96.6°
Li(2)-O(m1)-N(43)''	131.3°
Li(2)-O(m1)-C(m1)	130.6°

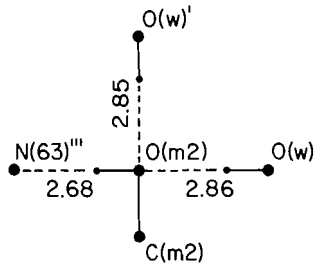

O(w)-O(m2)-O(w)'	85.5°
O(w)-O(m2)-N(63)'''	131.3°
O(w)-O(m2)-C(m2)	102.7°
O(w)'-O(m2)-N(63)'''	107.4°
O(w)'-O(m2)-C(m2)	129.3°
C(m2)-O(m2)-N(63)'''	103.7°

the lines of the classical investigations of Domenicano et al. (22–25) into the geometrical effects of substitution in benzene is precluded here partly because of the chemistry of **S** (multiple substitution, unsuitable combinations of substituents) in relation to its size, partly because of the heterocyclic nature of the Im ring. In benzene as reference the endocyclic angles are 120° by symmetry and only one skeletal bond length needs to be determined by experiment, whereas in Im as reference all five bond lengths and all five internal angles of this molecule must be supplied from experiment. It comes therefore as no surprise that such multilinear correlations as we have found to exist between the bond lengths in **S** are weak, although we do not know whether this is due to sampling deficiencies in **S** or to a real lack of correlation. For example, expressing d_{45} in terms of the other four bond lengths one obtains $d_{45} = 0.112 + 0.320d_{12} + 0.708d_{23} + 0.261d_{34} - 0.349d_{51}$ ($n = 18$, $r^2 = 0.56$, $\sigma = 0.009$ Å $\sim$ 20% of d_{45} range). The sums of the bond lengths in the ring range from 6.672 Å in **1** to 6.795 Å in **11** = TC. However, it is probable that this variability comes, like for benzene rings, from uncorrected thermal motion and sample inhomogeneity (25).

The ϕ_i angles offer more scope for informative data analysis. Because of geometrical constraints, and in contrast to the bond lengths, significant correlations can be expected and indeed are observed (see below). In a planar Im ring, $\Sigma\phi_i = 540°$. A change $\Delta\phi_i = \phi_i - \phi_i(\text{Im})$ produced by substitution at atom i will tend to be counteracted by attendant compensating changes of opposite sign in the angles at atoms adjacent to atom i, and $\Sigma\Delta\phi_i = 0$. The existence of such correlations is

Can. J. Chem. Downloaded from www.nrcresearchpress.com by 65.111.164.53 on 09/08/12
For personal use only.

Table 2. Selected Li—N and Li—O bond lengths (Å).[a]

Compound	*d*(Li—N)	*d*(Li—O)	Reference
Li in pure N coordination			
$\{[Li^{iii}N(iso\text{-}Pr)_2]_2[Me_2N(CH_2)_2NMe_2]\}_\infty$	2.017[14][b] 2.163[26][c]		6
TC, Li^{iv}	2.049[12]		This work
$[Li^{iv}py_4]$	2.066(7)		7
$(Li^{iv})^+$(phthalocyanine$^\cdot$)$^-$	1.942(5)		8
$[Li^{iv}(Et_8\text{-porphyrin})][Li^{iv}(thf)_4]_2$	2.037[5]	1.884[9]	9
$[Ph_2C{=}NLi^{iv}\cdot py]_4$	2.090[48][d] 2.105[37][e]		10
$[Li^{v}L]BPh_4$[f]	2.050[30][d] 2.015[2][g] 2.074[6][h]		11
$[Li^{v}L]ClO_4$[i]	2.040[27][d]		12
$[Li^{vi}L]BPh_4\cdot\frac{1}{2}Me_2CO$[j]	2.146[42][k] 2.273[19][m]		13
Li in mixed N,O or O coordination			
TC, Li^{iv} (2 N, 2 O)	2.065[13]	1.978(7)[n] 1.965(7)[p]	This work
Li^{iv}(3,5-dinitrobenzoate)(1,10-phenanthroline)$\cdot H_2O$ (2 N, 2 O)	2.135[5]	1.91(3)[n] 1.85(3)[q]	14
$Li^{iv}(NO_3)$(3,5-Me_2-py) (2 N, 2O)	2.12[2]	1.98[1]	15
$[Li^{iv}$(2-Me-py)$_2]ClO_4$ (2 N, 2O)	2.073[9]	2.003[9]	7
$[Li^{iv}$(2,6-Me_2-py)$_2]ClO_4$ (2 N, 2O)	2.136[1]	2.039[1]	7
$[Li^{iv}$(quinoline)$_2(H_2O)_2]Br\cdot$(quinoline)$_2$ (2 N, 2 O)	2.13[1]	1.925[50]	16
$Li^{iv}(SCN)_2(CH_2CH_2O)_6\cdot 2H_2O$ (3 O, 1 N)	2.005[7]	1.954[41][n] 2.020[38][r]	17
$[Li^{iv}(H_2O)_4]BPh_4$ (4 O)		1.933[7]	1
$Li^{iv}(ClO_4)(CH_2CH_2O)_6\cdot 2H_2O$ (4 O)		1.914[8][n] 2.097[27][r]	17

[a]Not corrected for thermal motion. Roman superscript, coordination number of the Li atom. Where *d* refers to a mean the standard deviation is in brackets.[5]
[b]Amide N.
[c]Diamine N.
[d]All Li—N.
[e]Li—N(py) only.
[f]L = 4,10,15-Me_3-1,4,7,10,15-pentaazabicyclo[5.5.5]heptadecane.
[g]Trigonal bipyramid, axial Li—N.
[h]Trigonal bipyramid, equatorial Li—N.
[i]L = 4,10-Me_2-1,4,7,10,15-pentaazabicyclo[5.5.5]heptadecane.
[j]L = 1,4,7-tris(pyrazol-1-ylmethyl)-1,4,7-triazacyclononane.
[k]Pyrazole N.
[m]Aminic N.
[n]Li—OH_2.
[p]Li—O(H)Me.
[q]Li—O(benzoate).
[r]Ether oxygen.

suggested by inspection of ϕ_i in Table 4. Indeed, the partial (pairwise) correlation coefficients r_{ij} for adjacent ϕ_i, ϕ_j angles in the Im rings of **S** range from −0.64 to −0.87, whereas for nonadjacent angles they are between −0.02 and +0.54 (Fig. 4). For TC specifically, the expected compensation (>2σ) in the adjacent angles is observed clearly for ϕ_1 and ϕ_2, less clearly for ϕ_3 and ϕ_5, and not for ϕ_5, although where ϕ_4 is involved the smallness and possibly a sign uncertainty of $\Delta\phi_4$ may be a factor:

	ϕ_1	ϕ_2	ϕ_3	ϕ_4	ϕ_5
$\Delta\phi_i$	−2.3(4)°	1.7(4)°	−0.9(5)°	0.5(4)°	1.1(4)°
ϕ_i range in **S**	7.6°	7.1°	6.0°	7.0°	8.1°
% of range	30(5)	24(4)	15(8)	7(6)	14(5)

Can. J. Chem. Downloaded from www.nrcresearchpress.com by 65.111.164.53 on 09/08/12
For personal use only.

Table 3. Bond lengths (Å) in selected imidazole rings (sample S).[a]

Compound	d_{12}	d_{23}	d_{34}	d_{45}	d_{51}	Reference
1 1-Me-Im	1.339(4)	1.288(4)	1.363(4)	1.335(5)	1.347(4)	26
2 ImH^{+}[b]	1.319[16]	1.319[16]	1.370[16]	1.344[11]	1.370[16]	27
3 1,5-dichloro-Im	1.331(10)	1.324(9)	1.345(9)	1.346(9)	1.347(9)	28
4 1-*A*-4-nitro-Im[c]	1.378(4)	1.301(4)	1.362(4)	1.348(4)	1.370(3)	29
5 2-Me-4-nitro-Im	1.357(3)	1.308(3)	1.360(2)	1.351(3)	1.344(3)	30
6 1,4-dinitro-Im	1.373(3)	1.300(3)	1.378(3)	1.354(3)	1.372(3)	31
7 1-*A*-2-Me-5-nitro-Im[d]	1.341(4)	1.343(5)	1.357(5)	1.355(5)	1.391(4)	32
8 1-*A*-2-Me-5-nitro-Im[e]	1.351(2)	1.334(2)	1.359(2)	1.356(2)	1.383(2)	33
9 1-*A*-2-nitro-Im[f]	1.359(3)	1.308(3)	1.366(3)	1.356(3)	1.362(3)	34
10 3-Ag-4-nitro-Im	1.340[6]	1.311[5]	1.364[3]	1.357[9]	1.351[9]	35
11 1-B-3-Li polymer (TC)	1.359[3]	1.322[3]	1.374[7]	1.359[5]	1.381[5]	This work
12 4-nitro-Im 100 K	1.357(2)	1.317(2)	1.367(2)	1.360(2)	1.355(2)	36
RT	1.348(3)	1.318(3)	1.363(3)	1.361(3)	1.349(3)	37
13 2,2′-biimidazole	1.351[1]	1.333[4]	1.365[7]	1.363[10]	1.349[6]	38
14 Im (n.d., 103 K)	1.347(1)	1.323(1)	1.375(1)	1.368(1)	1.369(1)	39
15 2-nitro-Im (105 K)	1.343(3)	1.318(3)	1.370(3)	1.376(3)	1.364(3)	40
16 [g]	1.347(3)	1.331(3)	1.334(3)	1.377(3)	1.349(3)	41
17 $(NH_4)_2(C_6N_8O_8)$[h]	1.345(3)	1.346(3)	1.346(3)	1.379(3)	1.347(3)	42
Mean	1.349[14]	1.319[15]	1.362[11]	1.358[11]	1.361[14]	
Range	0.058	0.058	0.044	0.044	0.047	
Range as % of mean	4.3	4.4	3.2	3.2	3.5	

[a]Uncorrected for thermal motion. Arranged in the increasing order of $d_{45} = d$(C═C). Im, imidazole; numbering as in Fig. 4. n.d., neutron diffraction.

[b]Means of 12 structures (27).

[c]*A* = —$S(O_2)$—(1-C_6H_2-2,4,6-Me_3).

[d]*A* = —CH_2CH_2NH—C(═S)OMe.

[e]*A* = —CH_2CH_2OH.

[f]*A* = —$CH_2CH(OH)$—CH_2OMe.

[g]4,4′,5,5′-Tetranitro-2,2′-biimidazole dihydrate.

[h]Diammonium salt of the 4,4′,5,5′-tetranitro-2,2′-biimidazolium anion.

The change $\Delta\phi_1$ produced by substituting the H atom on N(1) in Im by the anionic B atom is large, about a third of the ϕ_1 range, and negative. Both the sign and the order of magnitude of this $\Delta\phi_1$ are consistent with what is observed on similar substitution in benzene, e.g., in BPh_4^- or for —N—BPh_3 (mean ϕ, 115[1]°, refs. 4 and 5). It is not known whether the smaller $\Delta\phi_1$ in TC is attributable to the electronic difference between N and C or to the smaller local angle deformability of the Im ring compared with the larger 6-membered benzene ring.[7] The magnitude of the change in ϕ_3 associated with the cationic Li addition to N(3) is uncertain, but its sign appears to be correct: $\Delta\phi_3$ obtained from the correlation equation $\phi_3 = f(\phi_1, \phi_2, \phi_3)$ involving the ϕ_i with the three largest $|\Delta\phi_i|$ in TC (see below) is −1.1°, i.e., *statistically* in good agreement with observation.

To place these $\Delta\phi_i$ changes in an overall context of Im geometry and to relate them to the nature of the substituent, the ϕ_i at the substituted atom in **S** are plotted in Fig. 5 (left) against the corresponding ϕ_i in Im, as are also the *dependent* ϕ_i at the unsubstituted atoms (Fig. 5, right). From these plots one can draw the following conclusions:

(1) As seen in Fig. 5 (left), with the exception of ϕ_4(**17**) and ϕ_5(**16**) (cf. below), all the points for NO_2-substituted Im rings in **S** fall above the 45° ($x = y$) line, $\Delta\phi_i(NO_2) > 1.0(3)°$. This means that the NO_2 group expands (or at least does not contract) ϕ at its ring atom, regardless of other substitution(s) on the ring. This parallels the finding of ref. 24 for 1-NO_2-4-X-benzene derivatives: the powerful σ-electron-withdrawing nitro group opens up the *ipso* C—C—C angle by ~2°. The largest $\Delta\phi_i(NO_2)$ in **S** are $\Delta\phi_4$(**6**) = 4.3(3)° and $\Delta\phi_1$(**6**) = 2.8(3)° in 1,4-dinitro-Im, $\Delta\phi_4$(**4**) = 4.0(3)°, and $\Delta\phi_5$(**17**) = 3.7(3)°.

The two exceptions involve the highly substituted 4,4′,5,5′-tetranitro-2,2′-biimidazole **16** and its anion **17**. In the latter, each ring of the 2,2′-biimidazole system carries an anionic charge and has a C_{2v} symmetry, within the esd statistics. The effect of the σ-electron releasing deprotonation at N(1) is to decrease ϕ_1 by a significant amount: $\Delta\phi_1 = -4.8(3)°$. This ϕ_1 reduction requires a compensatory increase in the adjacent angles ϕ_2 and ϕ_5. However, the NO_2 substitution at C(5) causes an increase in ϕ_5 in its own right, and the synergetic

[7] The importance of steric strain (which may result from attaching four Im groups to the B atom) for the magnitude of ϕ_1 in TC is difficult to assess but is likely to be small. In ZPh_4 (Z = C to Pb) the internal angle at C(α) is, within experimental accuracy, the same regardless of the length of the Z—C(α) bond: the C(2)—C(1)—C(6) mean for the series is 117.4[4]°. If steric strain were a factor, this angle would be expected to increase with the Z—C(α) bond length, which increases from 1.55 Å for Z = C to 2.20 Å for Z = Pb (Borecka, Knop, and Cameron, to be published), a significant change.

Can. J. Chem. Downloaded from www.nrcresearchpress.com by 65.111.164.53 on 09/08/12
For personal use only.

Table 4. Endocyclic angles ϕ_i (deg) in selected imidazole rings.[a]

Compound	ϕ_1	ϕ_2	ϕ_3	ϕ_4	ϕ_5	Reference
2 ImH^{+}[b]	108.5[13]	108.9[12]	108.5[13]	107.1[10]	107.1[10]	27
6 1,4-dinitro-Im	109.9(2)	110.3(2)	104.1(2)	114.1(2)	101.6(2)	31
13 2,2′-biimidazole	108.2[1]	110.5[2]	105.2[1]	110.3[1]	105.8[1]	38
5 2-Me-4-nitro-Im	108.5(3)	110.9(3)	104.2(3)	112.2(3)	104.2(3)	30
3 1,5-dichloro-Im	107.0(6)	111.4(7)	104.9(6)	110.3(7)	106.3(7)	28
8 1-*A*-2-Me-5-nitro-Im[c]	105.5(1)	111.5(1)	106.2(1)	109.1(1)	107.6(1)	33
10 3-Ag-4-nitro-Im	108.2[2]	111.6[3]	104.3[2]	111.4[6]	104.6[5]	35
14 Im (n.d., 103 K)	107.1(1)	111.9(1)	105.1(1)	109.8(1)	106.0(1)	39
4 1-*A*-4-nitro-Im[c]	107.2(2)	111.9(2)	103.6(3)	113.8(2)	103.5(2)	29
12 4-nitro-Im 100 K	107.9(1)	111.9(1)	103.6(1)	112.4(1)	104.3(2)	36
12 4-nitro-Im RT	108.0(2)	112.0(2)	103.4(2)	112.1(2)	104.4(2)	37
7 1-*A*-2-Me-5-nitro-Im[d]	105.5(3)	112.1(3)	105.4(3)	109.9(3)	107.1(3)	32
1 1-Me-Im	106.6(3)	112.2(3)	104.9(3)	110.1(3)	106.2(3)	26
16 [g]	106.1(2)	112.6(2)	104.3(2)	111.0(2)	106.0(2)	41
9 1-*A*-2-nitro-Im[f]	104.5(2)	113.8(2)	104.2(2)	110.0(2)	107.6(2)	34
11 1-B-3-Li polymer (TC)	104.8[3]	113.6[3]	104.2[4]	110.3[3]	107.1[3]	This work
15 2-nitro-Im (105 K)	105.3(2)	114.3(2)	103.8(2)	110.0(2)	106.6(2)	40
17 $(NH_4)_2(C_6N_8O_8)$[h]	102.3(2)	116.0(2)	102.5(2)	109.5(2)	109.7(2)	42
Mean	106.7[18]	112.1[16]	104.6[13]	110.7[17]	105.9[18]	
Range	7.6	7.1	6.0	7.0	8.1	
Range as % as mean	7.1	6.3	5.7	6.3	7.6	

[a]Arranged in the order of increasing ϕ_2 = N(1)—C(2)—N(3). For footnotes see Table 3.

Fig. 4. Atom numbering in the imidazole ring and the pairwise correlation coefficients $r_{ij} = r(\phi_i,\phi_j)$ for the endocyclic ϕ angles in the imidazole rings of sample **S** (Table 4).

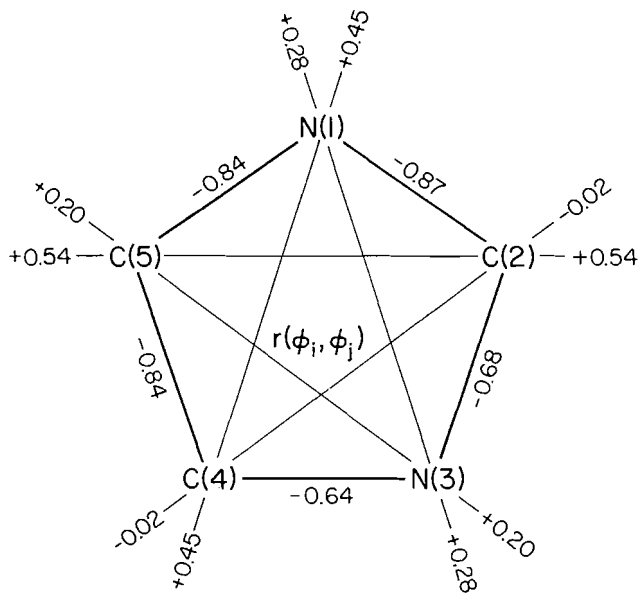

effect of the two interventions results in a large $\Delta\phi_5$, 3.7(3)°. The angle ϕ_2, which is expected to increase in consequence of the reduction in ϕ_1, is also affected by the partner-ring substitution at C(2), the combined effect being $\Delta\phi_2$ = 4.1(3)°. The three changes $\Delta\phi_1 + \Delta\phi_2 + \Delta\phi_5$ thus require a total compensation at ca −3.0°, which leaves no scope for a significant *positive* $\Delta\phi_4$ at C(4), the site of the other NO_2 substitution; in fact, $\Delta\phi_4$ = −0.3(3)°. In **16**, $\Delta\phi_4$ = 1.2(3)° and $\Delta\phi_5$ = 0.0(3)°. In contrast to **17**, $\Delta\phi_2$ is only 0.7(3)°. It is thus probable that the unusually large ϕ_2 in **17** is mainly the consequence of the deprotonation at N(1). This, however, does not explain the smallness of $\Delta\phi_2$(**16**).

(2) In TC = **11**, $\Delta\phi_1$ = −2.3(3)°, a significant contraction. This again parallels the substitution in benzene, where the σ-electron-releasing anionic $-BPh_3^-$ group was found (24) to be the most powerful contractor of the *ipso* C—C—C internal angle.[7] Here again the decrease in ϕ_1 (TC) is only about half that observed in BPh_4^- (cf. above). The negative sign of $\Delta\phi_3$ on Li^+ addition is consistent with the electronegativity of Li.

(3) Protonation at N(3) in Im to give ImH^+ (**2**) is associated with a substantial increase in the *ipso* angle, ~3.4°, and with large corresponding changes in the adjacent angles ϕ_2 and ϕ_4. This compares with the change observed in **17** for the opposite process, deprotonation at N(1), for which $\Delta\phi_1$ = −4.8(3)°.

(4) As seen in Fig. 5 (right), large $\Delta\phi$ changes at substituted atoms are compensated, mostly unequally, by corresponding opposite changes at the adjacent atoms. The points in the plot are redistributed accordingly.

Multilinear correlations of ϕ_i

For a sample as diverse as **S** the pairwise correlation coefficients r_{ij} for adjacent angles (Fig. 4) are sufficiently large to make one look for possible *multilinear* interdependence of the ϕ_i. The condition $\Sigma\phi_i$ = 540° reduces the multilinear regression to a four-parameter problem, $\phi_j = a_0 + \Sigma_{mnp} a_i\phi_i$. Indeed, the correlations obtained in the individual regressions are high: $0.88 < r^2 < 0.98$ (Table 5). For example, for the angle ϕ_2 = N(1)—C(2)—N(3) (facing the C=C bond in Im), $\phi_2 = 282.1 - 0.485\phi_1 - 0.859\phi_3 - 0.257\phi_4$ (n = 18, r^2 = 0.972, σ = 0.3° ~ 4% of ϕ_2 range). This high correlation confirms, statistically, the existence of asymmetric compensation of a change in ϕ_2 by changes in the adjacent angles ϕ_1 and ϕ_3, but it also reveals the extent of involvement of angles at second-

Fig. 5. Effect of substitution on the endocyclic angles ϕ_i in imidazole. (*Left*) The endocyclic angle ϕ_i at the substituted atom in the Im rings of Table 4 plotted against the corresponding angle in unsubstituted Im. Code numbers as in Tables 3 and 4. The vertical width of the 45° band is 2°, corresponding approximately to ±3(esd) on ϕ_i. (*Right*) The corresponding plot of ϕ_i at the unsubstituted ring atoms. The rings represented by the small black circles contain at least one NO_2 substituent.

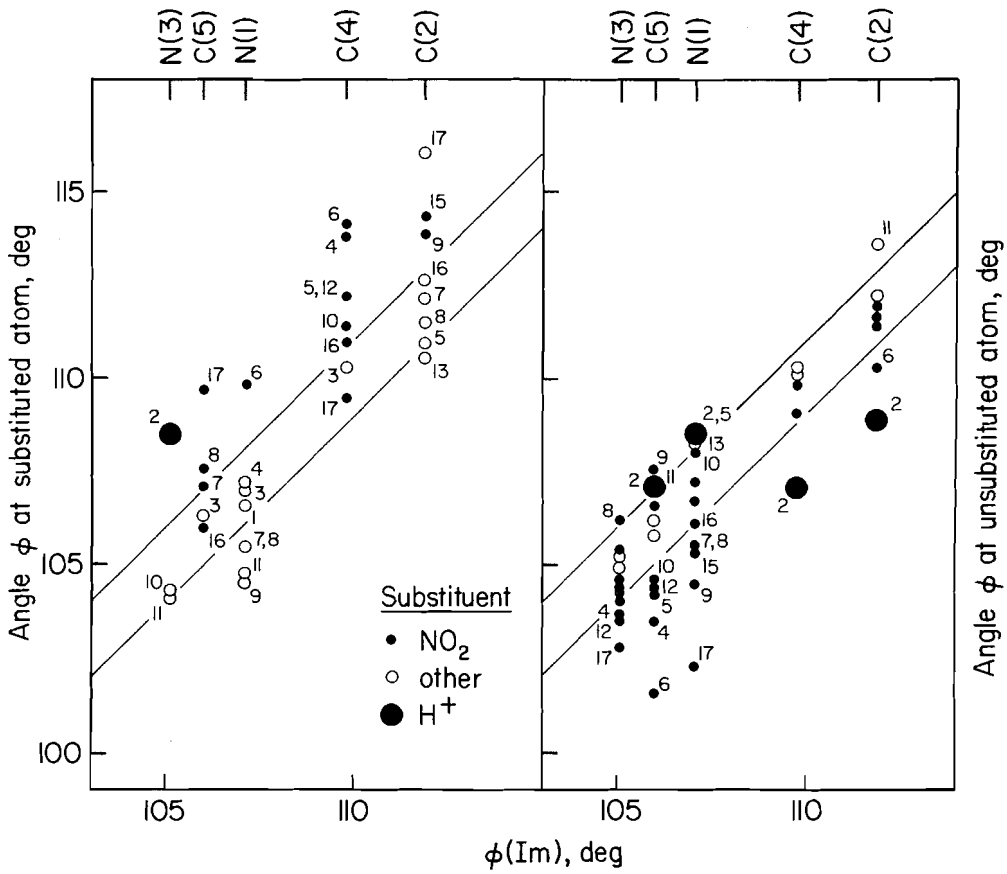

nearest neighbours of C(2). In general, a change in ϕ_i induced by substitution at atom *i* cannot always be accompanied by changes of the opposite sign in the angles at *both* adjacent atoms (Table 4). This is due to the impossibility of satisfying cyclic sign alternation of $\Delta\phi_i$ in an odd-membered planar ring. In this respect the effects of substitution on the ϕ_i in Im differ from those in benzene, investigated by Domenicano et al. (22–25).

While we have not investigated *mixed* ϕ_i,d_{ij} correlations in detail, it seems that they do not add to the information obtained from the angle correlations alone. For ϕ_2, for example, regression on the length d_{45} of the bond opposite ϕ_2 and on the adjacent angles ϕ_1 and ϕ_3 resulted in $r^2 = 0.963$, $\sigma = 0.3° \sim 4\%$ of ϕ_2 range, while a regression of ϕ_2 on ϕ_1 and ϕ_3 alone gave $r^2 = 0.961$, $\sigma = 0.3°$. The contribution of the d_{45} term to ϕ_2 in the regression equation is only of the order of 0.1–0.2°, i.e. comparable to the experimental esd's. A ϕ_2 regression on ϕ_4, ϕ_5, and d_{45} gave $r^2 = 0.83$, $\sigma = 0.7° \sim 10\%$ of ϕ_2 range, with the d_{45} term accounting for only ~0.2% of the combined contribution from the two angles.

Although further statistical inferences could probably be obtained by identifying additional angle correlations in **S** (e.g. possibly concerning π electron involvement), these have not been attempted for fear of *Quis nimis probat nihil probat.*

Conclusions

The title compound is, to our knowledge, a 3-dimensional polymer of a novel type. Its structure is made up of two networks. The primary, covalent network consists of imidazole rings connected by B—N(1) and Li—N(3) bonds in tetrahedral arrays. The secondary, H-bonded network connects the remaining N(3) atoms, uninvolved in the covalent network, to the H_2O and MeOH molecules coordinated to Li(2), with the MeOH molecule of solvation acting as a H-bonding intermediary between the H_2O molecule and an N(3) atom (Fig. 1). The H_2O molecules and the MeOH molecules of solvation form centrosymmetric H-bonded dimer pairs. The Li—N interaction dominates the structure in spite of the ample opportunity for Li—O bonds to form, preferentially, during crystallization.

The homogeneity of the skeletal bond lengths and endocy-

Can. J. Chem. Downloaded from www.nrcresearchpress.com by 65.111.164.53 on 09/08/12
For personal use only.

Table 5. Endocyclic angles ϕ_j in the imidazole rings of sample **S** regressed linearly on ϕ_i ($i = m, n, p$): $\phi_j = a_0 + \Sigma a_i\phi_i$.

				Regression coefficients					
j	*mnp*	r^2	σ	a_0	a_1	a_2	a_3	a_4	a_5
1	234	0.932	0.5°	392.62°		−1.5368	−0.9770	−0.1044	
	235	0.953	0.4°	271.35°		−0.8837	−0.2354		−0.3869
	245	0.968	0.3°	313.96°		−0.4024		−0.4893	−1.0196
	345	0.943	0.5°	412.71°			−0.0844	−1.0930	−1.6636
2	134	0.972	0.3°	282.10°	−0.4850		−0.8590	−0.2570	
	135	0.960	0.3°	230.43°	−0.5666		−0.6350		0.0805
	145	0.881	0.6°	256.61°	−1.1247			0.1300	−0.3673
	345	0.921	0.4°	184.37°			−1.0837	−0.1228	0.5161
3	124	0.955	0.3°	283.50°	−0.3222	−0.8982		−0.3961	
	125	0.898	0.4°	205.18°	−0.2502	−1.0527			0.4164
	145	0.820	0.5°	284.92°	0.1243			−1.1369	−0.6395
	245	0.934	0.3°	229.70°		−0.5883		−0.5290	~0
4	123	0.881	0.6°	449.59°	−0.1552	−1.2096	−1.7854		
	125	0.943	0.4°	329.02°	−0.7246	0.0689			−1.4042
	135	0.966	0.3°	308.82°	−0.4297		−0.3634		−1.0788
	235	0.946	0.4°	264.82°		−0.0929	−0.7371		−0.6289
5	123	0.903	0.5°	77.10°	−0.8086	0.2625	0.8188		
	124	0.979	0.3°	253.54°	−0.6588	−0.0849		−0.6126	
	134	0.981	0.3°	257.88°	−0.5112		−0.1414	−0.7463	
	234	0.937	0.4°	142.28°		0.5489	−0	−0.8843	

clic bond angles ϕ in the eight imidazole rings of the title compound invites comparison with the geometries of other such rings. A sample of imidazole rings in seventeen compounds (including unsubstituted imidazole as reference) was analyzed for correlations between the bond lengths and between the ϕ angles. While the bond lengths in a ring are not correlated or at most weakly so, multilinear correlations between the ϕ angles are highly significant and reveal the extent of involvement of changes in the angles at the adjacent as well as nonadjacent ring atoms. Among the substituents represented in the sample the NO_2 group is the most powerful expander and the anionic B atom the most powerful contractor of the *ipso* angle in the ring. The general conclusions parallel those formulated for substitutions in benzene by Domenicano et al. (22–25), but important differences arise from the heterocyclic and odd-member character of the imidazole ring.

Experimental

Preparation

Methanolic solutions of LiCl and the commercially available $NaB(C_3H_3N_2)_4$ were combined in a 1:1 molar ratio, a small amount of water was added to reduce the evaporation rate, and the resulting solution was allowed to crystallize by evaporation at room temperature. No effort was made to protect the solution from contact with atmospheric CO_2, a precaution recommended in ref. 2.

Crystallographic data

$B_2C_{26}H_{34}Li_2N_{16}O_3$, fw 654.2. Crystal size, 0.35 × 0.25 × 0.25 mm^3, $\mu_{Mo} = 0.84$ cm^{-1}; Rigaku AFC5R single-crystal diffractometer, λ = 0.71069 Å; θ-range, 2–23°; unit-cell dimensions and orientation matrices from 23 carefully centred reflections; $T \sim 21$°C. Space group $P\bar{1}$ (no. 2); a = 12.380(2) Å, b = 14.434(2) Å, c = 9.683(3) Å, α = 90.36(2)°, β = 105.44(2)°, γ = 90.75(2)°, V = 1668(1) Å^3, Z = 2, ρ_c = 1.303(1) g/cm^3, $F(000)$ = 684. Total reflections measured, 4901; unique reflections, 4648, R_{merg} = 3.2%; unique reflections used ($I > 3\sigma(I)$), 2620. No absorption correction. Although α and γ are very close to 90°, the symmetry is unambiguously triclinic: the three monoclinic space groups with no systematic absences, viz. *Pm*, *P*2, and *P*2/*m*, were ruled out by the unacceptably high $R_{merg}(F^2)$ values, ~90% compared to 3.2% for $P\bar{1}$.

Structure solved by direct methods (43) and refined by TEXSAN-TEXRAY (44), using the $w = 4F_o^2/\sigma^2(F_o^2)$ weighting scheme. Anisotropic temperature factor, exp $[-2\pi^2(U_{11}h^2a^{*2} + U_{22}k^2b^{*2} + U_{33}l^2c^{*2} + 2U_{23}klb^*c^* + 2U_{13}hla^*c^* + 2U_{12}hka^*b^*)]$. The nonhydrogen atoms were refined without constraints. The H(C) atoms were placed geometrically at C—H = 1.08 Å. The H(O) atoms were located from a difference map and then constrained (O—H = 1.00 Å). The H(X) were assigned isotropic temperature factors, $U_{iso} = 1.2U_{eq}$(X); their positions were not refined, R = 3.9%, R_w = 4.0%, G.O.F. = 2.02; d/p = 5.9. Residual electron density in final difference map, −0.20/+0.17 e/Å^3.

Acknowledgments

We thank Drs. D.C. Hamilton, T.S. Cameron, and S.V. Sereda for having contributed in various ways to the completion of this investigation. A research grant from the Natural Sciences

Can. J. Chem. Downloaded from www.nrcresearchpress.com by 65.111.164.53 on 09/08/12
For personal use only.

and Engineering Research Council of Canada to O.K. is acknowledged.

References

1. P.K. Bakshi, S.V. Sereda, O. Knop, and M. Falk. Can. J. Chem. **72**, 2144 (1994).
2. S. Chao and C.E. Moore. Anal. Chim. Acta, **100**, 457 (1978).
3. D.C. Hockman, C.E. Moore, J.L. Huston, and S. Chao. Anal. Lett. **14**, 719 (1981).
4. P.K. Bakshi, A. Linden, B.R. Vincent, S.P. Roe, D. Adhikesavalu, T.S. Cameron, and O. Knop. Can. J. Chem. **72**, 1273 (1994).
5. O. Knop, T.S. Cameron, P.K. Bakshi, A. Linden, and S.P. Roe. Can. J. Chem. **72**, 1870 (1994).
6. M.P. Bernstein, F.E. Romesberg, D.J. Fuller, A.T. Harrison, D.M. Collum, Q.-Y. Liu, and P.G. Willard. J. Am. Chem. Soc. **114**, 5100 (1992).
7. S. Harvey, J.D. Kildea, B.W. Skelton, and A.H. White. Aust. J. Chem. **45**, 1135 (1992).
8. H. Sugimoto, M. Mori, H. Masuda, and T. Taga. J. Chem. Soc. Chem. Commun. 962 (1986).
9. J. Arnold. J. Chem. Soc. Chem. Commun. 976 (1990).
10. D. Barr, R. Snaith, W. Clegg, R.E. Mulvey, and K. Wade. J. Chem. Soc. Dalton, 2141 (1987).
11. A. Bencini, A. Bianchi, S. Chimichi, M. Ciampolini, P. Dapporto, E. Garcia-España, M. Micheloni, N. Nardi, P. Paoli, and B. Valtancoli. Inorg. Chem. **30**, 3687 (1991).
12. A. Bencini, A. Bianchi, A. Borselli, S. Chimichi, M. Ciampolini, P. Dapporto, M. Micheloni, N. Nardi, P. Paoli, and B. Valtancoli. Inorg. Chem. **29**, 3282 (1990).
13. M. Di Vaira, B. Cosimelli, F. Mani, and P. Stoppioni. J. Chem. Soc. Dalton, 331 (1991).
14. M.S. Hundal, G. Sood, P. Kapoor, and N.S. Poonia. J. Crystallogr. Spectrosc. Res. **21**, 395 (1991).
15. C.L. Raston, C.R. Whitaker, and A.H. White. Aust. J. Chem. **41**, 1917 (1988).
16. C.L. Raston, B.W. Skelton, C.R. Whitaker, and A.H. White. Aust. J. Chem. **41**, 409 (1988).
17. P. Groth. Acta Chem. Scand. **A36**, 109 (1982).
18. W.N. Setzer and P. von R. Schleyer. Adv. Organomet. Chem. **24**, 353 (1985).
19. R. Liminga and A.M. Sørensen. Acta Chem. Scand. **21**, 2669 (1967).
20. R. Liminga. Acta Chem. Scand. **21**, 1206 (1967).
21. R. Liminga and I. Olovsson. Acta Crystallogr. **17**, 1523 (1963).
22. A. Domenicano, A. Vaciago, and C.A. Coulson. Acta Crystallogr. Sect. B, **31**, 221 (1975).
23. A. Domenicano, A. Vaciago, and C.A. Coulson. Acta Crystallogr. Sect. B, **31**, 1630 (1975).
24. A. Domenicano, P. Mazzeo, and A. Vaciago. Tetrahedron Lett. 1029 (1976).
25. A. Domenicano, P. Murray-Rust, and A. Vaciago. Acta Crystallogr. Sect. B, **39**, 457 (1983).
26. A.C. Wang and B.M. Craven. Acta Crystallogr. Sect. B, **35**, 510 (1979).
27. G. Levasseur and A.L. Beauchamp. Acta Crystallogr. Sect. C, **47**, 547 (1991).
28. S.-Q. Dou and A. Weiss. Z. Naturforsch. **47a**, 177 (1992).
29. Z. Taira and J. Uchi. Acta Crystallogr. Sect. C, **44**, 2002 (1988).
30. A. Kálmán, F. van Meurs, and J. Tóth. Cryst. Struct. Commun. **9**, 709 (1983).
31. M.R. Grimmet, S.-T. Hua, K.-C. Chang, S.A. Foley, and J. Simpson. Aust. J. Chem. **42**, 1281 (1989).
32. N.M. Blaton, O.M. Peeters, and C.J. De Ranter. Acta Crystallogr. Sect. B, **35**, 753 (1979).
33. N.M. Blaton, O.M. Peeters, and C.J. De Ranter. Acta Crystallogr. Sect. B, **35**, 2465 (1979).
34. C. Jenkins and A.R. Walton. Acta Crystallogr. Sect. C, **44**, 1095 (1988).
35. I. Ségalas and A.L. Beauchamp. Can. J. Chem. **70**, 943 (1992).
36. H.L. De Bondt, E. Ragia, N.M. Blaton, O.M. Peeters, and C.J. De Ranter. Acta Crystallogr. Sect. C, **49**, 693 (1993).
37. I. Ségalas, J. Poitras, and A.L. Beauchamp. Acta Crystallogr. Sect. C, **48**, 295 (1992).
38. D.T. Cromer, R.R. Ryan, and C.B. Storm. Acta Crystallogr. Sect. C, **43**, 1435 (1987).
39. R.M. McMullan, J. Epstein, J.R. Ruble, and B.M. Craven. Acta Crystallogr. Sect. B, **35**, 688 (1979).
40. I.K. Larsen. Acta Crystallogr. Sect. C, **40**, 285 (1984).
41. D.T. Cromer and C.B. Storm. Acta Crystallogr. Sect. C, **46**, 1957 (1990).
42. D.T. Cromer and C.B. Storm. Acta Crystallogr. Sect. C, **46**, 1959 (1990).
43. G.M. Sheldrick. SHELXS-86. *In* Crystallographic computing *Edited by* G.M. Sheldrick, C. Kruger, and R. Goddard. Oxford University Press. 1985.
44. TEXSAN-TEXRAY single crystal structure analysis package. Molecular Structure Corporation, The Woodlands, Tex. 1989.

Can. J. Chem. Downloaded from www.nrcresearchpress.com by 65.111.164.53 on 09/08/12
For personal use only.

Synthèse de divers types d'hétérocycles fonctionnels par décomposition de peroxydes insaturés : réactions compétitives

E. Montaudon, L. Lemée et M-J. Bourgeois

Résumé : La décomposition de peroxydes γ-insaturés substitués dans un solvant bon donneur d'hydrogène peut conduire à deux oxétanes isomères de configuration. La substitution homolytique intramoléculaire consécutive à la première étape d'addition peut être concurrencée par un transfert intramoléculaire d'hydrogène 1,5 suivi d'une cyclisation. Les facteurs influençant cette compétition, non signalée à notre connaissance, sont déterminés.

Mots clés : peroxydes insaturés, oxétanes, substitution homolytique intramoléculaire, transfert d'hydrogène intramoléculaire 1,5.

Abstract: Decomposition of γ-unsaturated substituted peroxides in a good hydrogen donor solvent can lead to two diastereoisomeric oxetans. An intramolecular 1,5 hydrogen shift followed by a cyclization may compete with the homolytic intramolecular substitution following the first addition step. The factors governing this never-reported competition are determined.

Key words: unsaturated peroxides, oxetans, homolytic intramolecular substitution, intramolecular 1,5 hydrogen shift.

Can. J. Chem. Downloaded from www.nrcresearchpress.com by 65.111.164.53 on 09/08/12
For personal use only.

Lors d'études antérieures (1), nous avons montré que la décomposition induite de peroxydes insaturés dans un solvant donneur d'hydrogène conduit avec de bons rendements à des hétérocycles fonctionnels, parfois accompagnés de peroxydes adduits. Le peroxyde de 1-allylcycloheptyle et de *tert*-butyle présente un comportement différent puisque, à côté des produits précités, il apparaît un nouveau composé, en quantité non négligeable. La détermination de la structure de ce dernier a entraîné une hypothèse de mécanisme de réaction originale, compétitive de celles habituelles. Ce travail décrit les résultats obtenus lors de cette décomposition et la démonstration du mécanisme proposé.

1. Décomposition du peroxyde de 1-allylcycloheptyle et de *tert*-butyle

La décomposition du peroxyde de 1-allylcycloheptyle et de *tert*-butyle, **1***a*, est effectuée dans les conditions définies précédemment (1), à savoir : chauffage à 100°C durant 12 h d'un mélange constitué de dichlorométhane, peroxyde, peracétate de *tert*-butyle, carbonate de sodium anhydre dans les rapports molaires 100/1/0,5/2. Le dichlorométhane est choisi pou sa simplicité de mise en œuvre; le peracétate de *tert*-butyle joue le rôle d'amorceur radicalaire et le carbonate de sodium est garant de la stabilité de l'oxétane, susceptible de se former, dans les conditions de réaction. À côté du 2-(2,2-dichloroéthyl)-1-oxa-spiro[3,6]décane, **2***a* (30%), et du peroxyde de *tert*-butyle et de 1-(4,4-dichlorobutyl)cycloheptyle, **4***a* (6%), normalement attendus (figure 1), un autre composé, X, est isolé par chromatographie liquide–solide sur alumine (20%).

1.1. Détermination de la structure de X

Le spectre de masse de X, en ionisation chimique, présente un amas isotopique à 236–238–240 dénonçant la présence de 2 atomes de chlore; il s'agit donc d'un composé de formule brute $C_{11}H_8OCl_2$, isomère de **2***a*.

Le spectre infrarouge montre l'absence de fonction OH et de double liaison; X est donc un éther bicyclique.

Dans le spectre RMN ^{13}C, il apparaît un atome de carbone quaternaire, deux tertiaires et huit secondaires. Les déplacements chimiques des carbones tertiaires (C_t) et quaternaire (C_q) (73,5–75,3 et 86,2) suggèrent la présence des motifs C_q-

Fig. 1

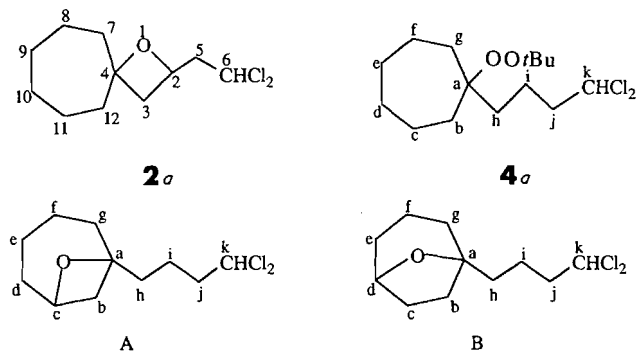

Reçu le 27 avril 1994.

E. Montaudon,[1] **L. Lemée et M-J. Bourgeois.** Institut du Pin, Université Bordeaux I, 351, cours de la Libération, F 33405 Talence Cedex, France.

1. Auteur à qui adresser toute correspondance. Téléphone : 56 84 64 20. Télécopie : 56 84 64 22.

Tableau 1. Estimation des déplacements chimiques des atomes de carbone de A et B.

	a	b	c	d	e	f	g	h	i	j	k
4*a*	84,8 q	35,9 s	22,9 s	30,8 s	30,8 s	22,9 s	35,9 s	36,8 s	20,0 s	44,1 s	73,7 t
A	81 q	41 s	74 t	36 s	27 s	23 s	36 s	37 s	20 s	44 s	74 t
B	85 q	32 s	28 s	82 t	36 s	19 s	36 s	37 s	20 s	44 s	74 t
obs.	86,2 q	41,5 s	75,3 t	[a]	24,2 et	23,4 s	[a]	[a]	20,0 s	43,7 s	73,5 t

[a]33,5 ou 33,9 ou 37,9 s.

O-C_t et -$CHCl_2$. Ces informations amènent à imaginer pour X les structures A ou B (figure 1). Les spectres ^{13}C de A et B sont calculés à partir de celui du peroxyde de *tert*-butyle et de 1-(4,4-dichlorobutyl)cycloheptyle, **4***a*. Le substituant «O-Ca» est assimilé à un groupe OR introduit sur les carbones c ou d; les perturbations empiriques induites sont de l'ordre de +51, +5 et −4 sur les positions α, β et γ respectivement (2). Les estimations et les valeurs observées sont rassemblées dans le tableau 1. La comparaison avec le spectre réel indiquerait un meilleur accord avec la structure A : 23,4 et 24,2 ppm (C_e ou C_f); 33,5–33,9 et 37,9 (C_d, C_g ou C_h); 41,5 (C_b).

Le spectre RMN ^1H à 250 MHz comporte trois séries de signaux : un triplet à 5,7 ppm (1 H appartenant à $CHCl_2$), un massif entre 4,6 et 4,5 ppm (1 H) et un autre entre 2,7 et 1,4 ppm (16 H). Le signal observé entre 4,6 et 4,5 ppm est attribuable à un proton situé en α d'un atome d'oxygène. Or on sait que le déplacement chimique de ce type de proton dépend de la taille du cycle auquel il appartient : 3,3–2,8 ppm dans un oxirane, 4,8–4,5 ppm dans un oxétane et 4,2–3,9 ppm dans un tétrahydrofurane (1). X présente donc une structure oxétane.

L'ensemble des techniques spectroscopiques plaide en faveur d'une structure du type oxétanique bicyclique.

Un argument supplémentaire par voie chimique a été recherché. Les oxétanes et tétrahydrofuranes ne présentent pas la même stabilité : l'ouverture des cycles à 4 chaînons est très facile, contrairement à celle de leurs homologues supérieurs (3). Nous avons étudié le comportement d'oxétanes et de tétrahydrofuranes bicycliques (1) (figure 2), lors de leur chauffage à 110°C durant 10 h dans le dichlorométhane, en présence ou non de carbonate de sodium (rapports molaires CH_2Cl_2/hétérocycle/Na_2CO_3 : 100/0,3/2 ou 100/0,3/0). Si les tétrahydrofuranes restent intacts dans les deux cas, les oxétanes, stables en milieu basique, disparaissent en absence de base, se transformant en alcools monocycliques insaturés (figure 2). Un mécanisme de réaction a déjà été proposé (1).

Un échantillon de X, chauffé à 110°C dans le dichlorométhane, disparaît presque totalement (il en reste moins de 5%). De même, lorsque **1***a* est décomposé dans le dichlorométhane en absence de carbonate de sodium, ni **2***a* ni le composé X ne sont observés. Ceci confirme donc l'appartenance de X à la famille des oxétanes.

C'est donc bien la structure A qu'il faut retenir pour le composé X : il s'agit du 1-(4,4 dichlorobutyl)-7-oxa[4.1.1]bicyclooctane, **3***a*.

1.2. Mécanisme de la réaction

La formation des composés **2***a* et **4***a* met en jeu des réactions déjà décrites (1). L'addition d'un radical issu du solvant à la double liaison du peroxyde conduit à un radical adduit. Celui-ci peut évoluer par substitution homolytique intramoléculaire, S_Hi, ou par transfert d'hydrogène issu du solvant. Ce même radical adduit est probablement responsable de la formation de **3***a* : il se réarrangerait par transfert d'hydrogène intramoléculaire 1,5 en un radical isomère qui subirait à son tour les réactions habituelles, à savoir la S_Hi et l'arrachement d'hydrogène au solvant (figure 3). Il est logique d'imaginer que ce transfert 1,5 est réversible.

L'éventualité d'un transfert d'hydrogène 1,6, beaucoup moins souvent observé que le transfert 1,5 (4–6), ne doit pas être retenue car celui-ci donnerait lieu à la formation du composé cyclique B. Or, seuls deux composés hétérocycliques, **2***a* et **3***a*, ont été isolés.

Une telle compétition entre une substitution intramoléculaire et un transfert d'hydrogène intramoléculaire 1,5 condui-

Fig. 2

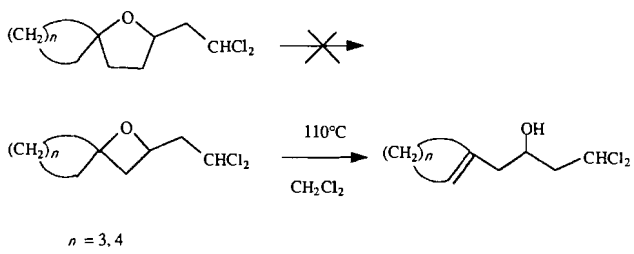

Fig. 3

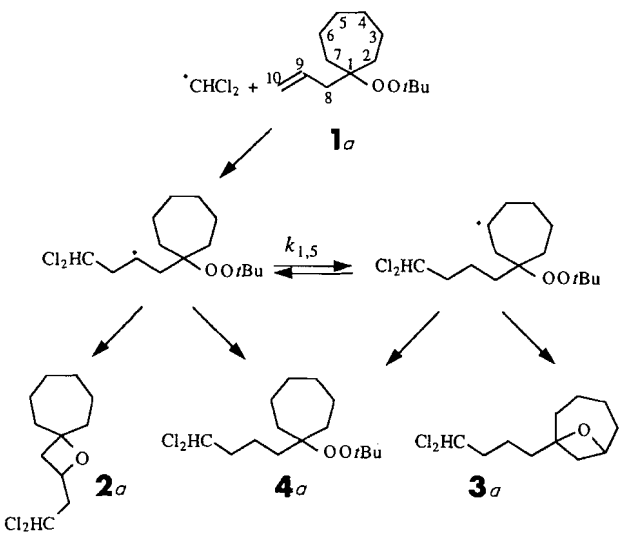

Can. J. Chem. Downloaded from www.nrcresearchpress.com by 65.111.164.53 on 09/08/12
For personal use only.

Tableau 2. Décomposition induite[a] de **1***a* dans le dichlorométhane. Influence de la température sur les rendements.[b]

Température (°C)[c]	**2***a*	**3***a*	**4***a*
60	5	5	Traces
80	23	27	3
110	32	25	6
140	32	17	—

[a]Rapports molaires CH_2Cl_2/**1***a*/Am/Na_2CO_3 : 100/1/0,5/2 à 110°C et 60°C; 100/1/0,5/4 à 80°C; 100/1/0/2 à 140°C.

[b]Déterminés par CPG sur le mélange réactionnel brut.

[c]Am, durée : 110°C, PA, 12 h ; 80°C, peroxyde de benzoyle (PB), 24 h ; 60°C, perdicarbonate de diéthyle (PDCE), 10 h ; 140°C, pas d'amorceur, 10 h.

sant à deux cycles différents n'a, à notre connaissance, jamais été signalée dans la littérature.

1.3. Influence de la température

L'influence de la température sur le cours de la réaction a été recherchée en réalisant la décomposition de **1***a* à 60, 80 et 140°C. La stabilité des oxétanes **2***a* et **3***a* dans les conditions opératoires a été testée. Les résultats sont rassemblés dans le tableau 2.

On observe que, à 140, 110 et 80°C, la quantité d'hétérocycles est la même (~50%), mais que le rapport **2***a*/**3***a* diminue nettement, le peroxyde adduit **4***a* restant très minoritaire. À 60°C où le phénomène devrait s'amplifier, la réaction est malheureusement très ralentie. Puisque la réaction de transfert d'un atome d'hydrogène du solvant intervient faiblement, ceci signifie, concernant les réactions unimoléculaires, que le transfert 1,5 est favorisé par rapport à la S_Hi par un abaissement de la température.

1.4. Comparaison avec nos travaux antérieurs

Lors de nos travaux sur les homologues à 6 et 5 chaînons du peroxyde **1***a* (1), un oxétane de type **3***a* a été vainement recherché. Son absence pourrait s'expliquer de deux manières : soit le radical adduit initialement formé ne donne pas lieu à un transfert d'hydrogène intramoléculaire 1,5, soit le radical isomère du radical initial ne peut subir la S_Hi.

L'examen des modèles moléculaires montre que, aussi bien à partir de **1***a* que du peroxyde de 1-allylcyclohexyle et de *tert*-butyle, **1***b*, le transfert semble possible. En effet, dans les deux cas, on peut obtenir l'alignement de la liaison C—H qui va se rompre et de l'orbitale atomique du centre radicalaire initial, indispensable dans l'état de transition (5) (figure 4). Par contre, à partir de l'homologue cyclopentyle, cette géométrie est difficile à envisager.

En ce qui concerne la deuxième étape régie par l'alignement de la liaison O—O et de l'orbitale du carbone radicalaire (7), si elle semble facile avec **1***a*, elle paraît probable quoique plus difficile avec **1***b* (figure 4), mais impossible avec l'homologue cyclopentyle.

Afin d'essayer de rechercher la bonne hypothèse, nous avons décomposé **1***b* dans le tétrachlorure de carbone.

Fig. 4

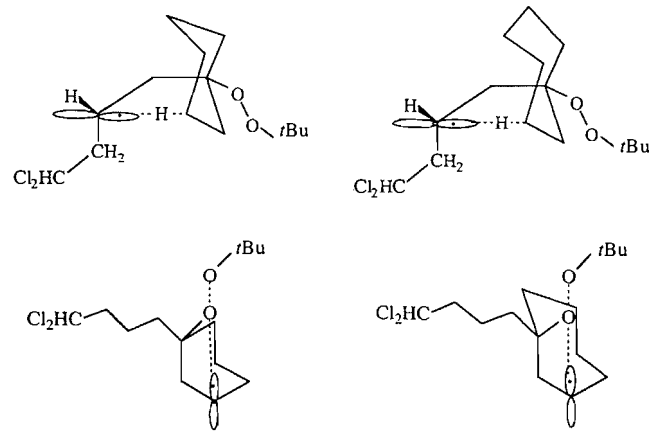

Fig. 5

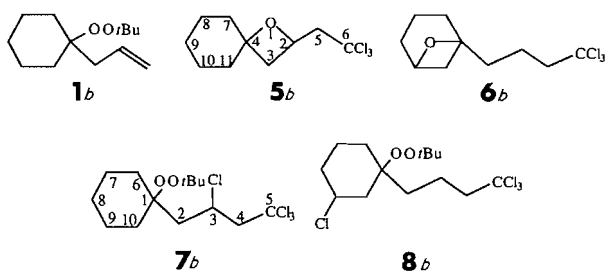

L'atome transféré du solvant au(x) radical(aux) est alors un chlore. Si le transfert 1,5 a lieu, les deux peroxydes adduits susceptibles de se former sont différenciables (figure 5). Cependant, le transfert d'un atome de chlore à partir de CCl_4 étant plus rapide que celui d'un atome d'hydrogène à partir de CH_2Cl_2, la réaction intermoléculaire peut exclure totalement celles intramoléculaires. Afin d'essayer de pallier cette difficulté, nous avons donc diminué la concentration du solant en utilisant un cosolvant, le benzène, relativement inerte dans les conditions de réaction (rapport molaire CCl_4/benzène : 20/80). Après réaction, nous avons isolé et vérifié la formation exclusive de 17% de 2-(2,2,2-trichloroéthyl)-1-oxa-spiro-[3,5]nonane, **5***b*, et de 39% de peroxyde de *tert*-butyle et de 1-(2,4,4,4-tétrachlorobutyl)cyclohexyle, **7***b*.

La présence de **5***b* indique que le transfert de chlore conduisant à **7***b* n'est pas suffisamment rapide pour inhiber d'autres évolutions du radical adduit, et en particulier la S_Hi. Le radical adduit ne semble pas évoluer par transfert d'hydrogène intramoléculaire : en effet, l'oxétane **6***b* et le peroxyde **8***b* qui en seraient issus ne sont pas mis en évidence. Or, si la stabilité dans le milieu de **6***b* (composé particulièrement tendu) n'est pas connue, il n'y a aucune raison pour que **8***b*, de structure très proche de **7***b*, se forme et se décompose dans les conditions de réaction. C'est essentiellement l'absence de **8***b* qui laisse penser que le radical adduit isomère ne s'est pas formé.

Il semble donc que, des deux hypothèses formulées, il faille retenir la première : la conformation du radical adduit serait telle qu'un transfert intramoléculaire 1,5 est impossible dans une structure cyclique à six chaînons, et donc a fortiori à cinq

Can. J. Chem. Downloaded from www.nrcresearchpress.com by 65.111.164.53 on 09/08/12
For personal use only.

chaînons, contrairement à ce qui est observé avec les homologues à sept chaînons.

2. Étude de la compétition S_Hi / transfert d'hydrogène 1,5

Une confirmation des résultats obtenus avec **1***a* et une meilleure connaissance du mécanisme passent par l'étude de modèles plus simples. Notre choix s'est porté sur les peroxydes acycliques indiqués ci-dessous. Nous nous sommes également intéressés au peroxyde de *tert*-butyle et de 1-méthallylcycloheptyle, **1***g*.

	$CH_2{=}C(R_a)\text{-}CH_2\text{-}C(R_b)\ (OOtBu)\text{-}CH_2\text{-}CH(R_c)CH_3$		
1*c*	$R_a = H$	$R_b = H$	$R_c = H$
1*d*	$R_a = H$	$R_b = H$	$R_c = Me$
1*e*	$R_a = Me$	$R_b = H$	$R_c = H$
1*f*	$R_a = H$	$R_b = Me$	$R_c = H$

2.1. Décompositions induites dans le dichlorométhane

Les composés susceptibles de se former lors de la décomposition des différents peroxydes acycliques dans le dichlorométhane sont présentés dans la figure 6 (Z-X = Cl_2CH-H). L'ensemble des résultats est consigné dans le tableau 3. Tous les produits sont isolés et leur structure déterminée grâce à leur spectre RMN ^{13}C, à l'exception de **4***d* et **4***e* identifiés par couplage CPG-SM dans le mélange réactionnel.

Quelques commentaires peuvent être faits :

(*i*) Les proportions d'oxétane(s) formé(s) sont toujours très supérieures à celles de peroxyde adduit, sauf dans le cas du peroxyde **1***c*. Ces oxétanes sont trisubstitués, sauf ceux issus de **1***c* qui ne sont que disubstitués. Nous avions déjà observé que les hétérocycles à quatre chaînons se forment d'autant mieux qu'ils portent plus de substituants (8). Cette différence avait été attribuée à l'intervention d'un effet Thorpe–Ingold.

(*ii*) La composition de la fraction oxétanique dépend de la classe de l'atome de carbone radicalaire. Lorsque les deux sites dans R et R′ sont secondaires (**1***c*, **1***f* ou **1***a*), les deux oxétanes sont présents, dans des proportions sensiblement voisines. Par contre, lorsqu'un site est secondaire et l'autre tertiaire, le seul oxétane mis en évidence correspond à une S_Hi au sein du radical le plus stable : **3** à partir de **1***d* et **2** à partir de **1***e* et **1***g*.

(*iii*) Lorsque l'oxétane peut se présenter sous deux formes diastéréoisomères, celles-ci sont observées (**2***c*, **3***c*, **2***e*, **2***f* et **3***f*).

2.2. Décompositions induites dans le tétrachlorure de carbone

Le peroxyde **1***f* a été décomposé dans le tétrachlorure de carbone. Les produits attendus sont indiqués dans la figure 6 (Z-X = Cl_3C-Cl).

Dans les conditions habituelles, seuls les peroxydes adduits **7***f* et **8***f* ont été obtenus (tableau 4); le transfert d'un atome de chlore aux radicaux adduit et isomère est trop rapide par rapport aux S_Hi. L'emploi de benzène comme cosolvant inerte a permis de ralentir cette étape et de mettre en évidence simultanément la présence des quatre partenaires, lorsque les proportions molaires CCl_4/benzène sont égales à 5/95. Les peroxydes adduits **7***f*, **8***f* et l'oxétane **5***f* ont été isolés et identifiés à partir de différents mélanges; l'oxétane **6***f* a été identifié par couplage CPG-SM.

Fig. 6

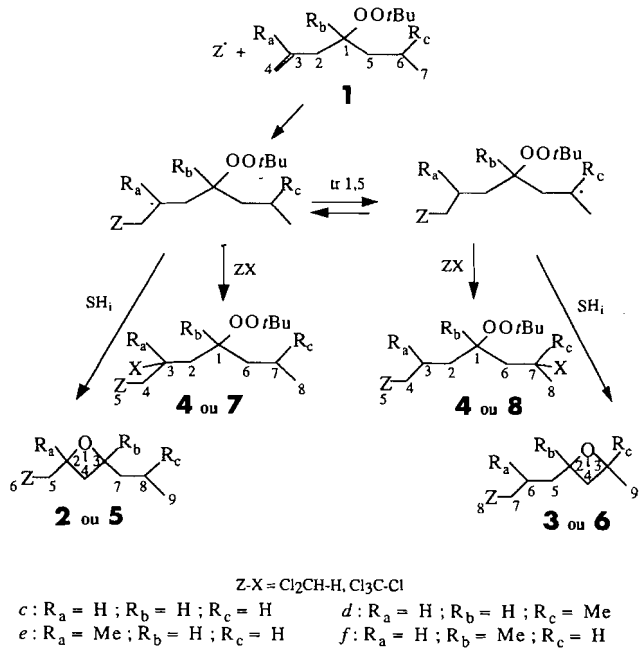

Cet ensemble de résultats confirme l'hypothèse de mécanisme initialement avancé.

Conclusion

La décomposition de peroxydes γ-insaturés substitués dans un solvant donneur d'hydrogène peut conduire à deux types d'oxétanes isomères de constitution. L'un provient de l'addition d'un radical issu du solvant à l'insaturation du peroxyde, suivie d'une substitution homolytique intramoléculaire. L'autre met en jeu une réaction concurrente de cette dernière, à savoir un transfert intramoléculaire d'hydrogène 1,5 réversible, lui-même suivi d'une substitution homolytique intramoléculaire. La compétition est gouvernée par la classe des sites radicalaires isomères susceptibles de se former. Signalons qu'une telle compétition, génératrice de deux cycles différents, n'a pas, à notre connaissance, été signalée dans la littérature.

Partie expérimentale

Techniques analytiques

Les analyses en CPG ont été effectuées sur un appareil de type Delsi DI 200 (ionisation de flamme, gaz vecteur : azote), équipé de colonnes capillaires — CPSIL 5 B (longueur 25 m, diamètre intérieur 0,32 mm), OV 1 (longueur 15 m, diamètre intérieur 0,31 mm), BP 20 (longueur 25 m, diamètre intérieur 0,22 mm) — et associé à un intégrateur Intersmat ICR-1B.

Les dosages ont été effectués par la méthode de l'étalon interne. En l'absence des produits de référence, après vérification de la pureté des produits par CPG, les techniques spectroscopiques ont permis de confirmer la structure des composés.

Les spectres RMN ^1H ont été enregistrés sur des appareils

Can. J. Chem. Downloaded from www.nrcresearchpress.com by 65.111.164.53 on 09/08/12
For personal use only.

Tableau 3. Décomposition induite[a] de peroxydes γ-insaturés dans le dichlorométhane. Produits obtenus et rendements.[b]

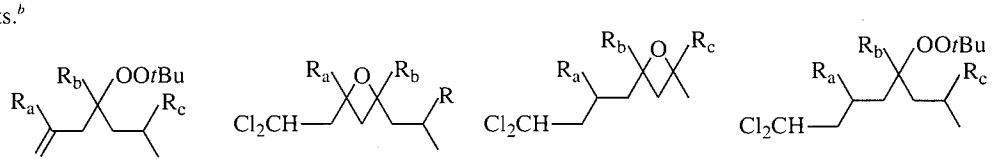

N°	R_a	R_b	R_c	**2**[c]	**3**[c]	**4**
1*c*	H	H	H	**2***c* : 12 (40/60)	**3***c* : 6 (35/65)	**4***c* : 32
1*d*	H	H	Me	—	**3***d* : 42	**4***d* : 7
1*e*	Me	H	H	**2***e* : 65 (52/48)	—	**4***e* : 1
1*f*	H	Me	H	**2***f* : 19 (45/55)	**3***f* : 23 (45/55)	**4***f* : 9
	1*g*			**2***g* : 66		

[a]Rapports molaires CH_2Cl_2/**1**/PA/Na_2CO_3 : 100/1/0,5/2; 110°C, 12 h.
[b]Déterminés par CPG sur le mélange réactionnel brut.
[c]Les deux formes diastéréoisomères sont présentes.

Tableau 4. Décomposition induite[a] de **1***f* dans le tétrachlorure de carbone. Produits obtenus et rendements.[b]

Rapports molaires CCl_4/benzène	**1***f*	**5***f*	**6***f*	**7***f*	**8***f*
100/0	—	—	—	24 (58/42)	10 (56/44)
15/85	3	10	—	12	38
5/95	8	11	5	4	25

[a]Rapports molaires CCl_4 + benzène/**1**/PA/Na_2CO_3 : 100/1/0,5/2; 110°C, 12 h.
[b]Déterminés par CPG sur le mélange réactionnel brut, en utilisant les coefficients théoriques calculés selon réf. 9.

Perkin–Elmer R 24B fonctionnant à 60 MHz et Bruker AC 250 fonctionnant à 250 MHz.

Les spectres RMN ^{13}C ont été effectués sur un appareil Bruker 250 fonctionnant à 62,9 MHz. Les spectres «théoriques» des produits susceptibles de se former sont calculés à partir des spectres de produits très voisins en utilisant une méthode d'incrémentation. Les variations moyennes du déplacement chimique sont estimées selon ref. 2 dans le cas d'introduction d'un atome de chlore ou d'un groupe méthyle en extrémité ou milieu de chaîne; selon ref. 10 dans le cas d'introduction d'un groupe méthyle sur un cycle oxétanique.

Les spectres de masse ont été réalisés sur des appareils VG Micromass 16 F (ionisation par impact électronique) et Fisons VG-autospec (ionisation chimique : NH_3) couplés à un chromatographe en phase gazeuse.

Techniques réactionnelles

Les réactions de décomposition des différents composés peroxydiques sont effectuées sur des mélanges constitués par le dichlorométhane, le peroxyde, l'amorceur et le carbonate de sodium dans les rapports molaires 100/1/0,5/2. La durée et la température des réactions dépendent de la nature de l'amorceur (Am) : perdicarbonate de diéthyle (PDCE) : 60°C, 10 h; peroxyde de benzoyle (PB) : 80°C, 24 h; peracétate de *tert*-butyle (PA) : 110°C, 12 h.

Les conditions propres à chaque expérience sont rappelées dans les tableaux de la partie théorique.

Études analytiques : 2 mL sont introduits dans une ampoule de 10 mL. Celle-ci, fermée hermétiquement, est placée dans un bain d'huile thermostaté posé sur une agitateur magnétique. Les produits de réaction sont identifiés par comparaison des temps de rétention en CPG avec ceux d'échantillons isolés et éventuellement par couplage CPG-SM. Les rendements sont déterminés par CPG directement sur le mélange réactionnel selon la méthode de l'étalon interne.

Études préparatives : 90 mL de solution sont introduits dans un autoclave en acier de 125 mL que l'on place dans le bain thermostaté d'un agitateur magnétique chauffant. Après élimination du solvant, les produits de réaction sont isolés par chromatographie liquide–solide sur alumine neutre désactivée avec 5% d'eau.

Matières premières

Le peracétate de *tert*-butyle est préparé par action de l'hydroperoxyde de *tert*-butyle sur le chlorure d'acétyle en présence de pyridine (11).

Le perdicarbonate de diéthyle est préparé par action du chloroformiate d'éthyle sur le peroxyde de sodium (12).

Les peroxydes proviennent de l'alkylation de l'hydroperoxyde de *tert*-butyle au moyen des alcools correspondants, via leur trichloroacétimidate (méthode A) (13) ou leur mésylate (méthode B) (14). Les alcools sont formés par condensation organomagnésienne (15) du bromure d'allyle et du bromure de méthallyle sur les dérivés carbonylés convenables.

Peroxyde de 1-allylcycloheptyle et de tert-*butyle,* ***1***a : méthode A; rdt = 42%; $Eb_{0,01}$ = 48°C; n_D^{20} = 1,4550. RMN ^1H : 5,9–5,7 (m, 1 H, H9), 5,0–4,8 (m, 2 H, H10), 2,3 (m, J = 7 Hz, 2H, H8), 1,8–1,2 (m, 12 H, autres H), 1,1 (s, 9 H, *t*Bu). RMN ^{13}C : 135,3 (C9), 116,5 (C10), 84,6 (C1), 77,7 (CMe_3), 43,2 (C8), 35,6 (C2, C7), 30,6 (C4, C5), 26,5 (CMe_3), 22,6 (C3, C6).

Can. J. Chem. Downloaded from www.nrcresearchpress.com by 65.111.164.53 on 09/08/12
For personal use only.

Can. J. Chem. Downloaded from www.nrcresearchpress.com by 65.111.164.53 on 09/08/12
For personal use only.

Peroxyde de 1-allylcyclohexyle et de tert-*butyle,* ***1***b : déjà décrit (13).

Peroxyde de tert-*butyle et de 1-propylbut-3-ényle,* ***1***c : méthode B; rdt = 10%; purifié sur silice; n_D^{20} = 1,4231. RMN ^{1}H : 5,9–5,7 (m, 1 H, H3), 5,1–4,9 (m, 2 H, H3, H4), 3,8 (qt, J = 6 Hz, 1 H, H1), 2,5–2,1 (m, 2 H, H2), 1,5–1,3 (m, 4 H, H5, H6), 1,2 (s, 9 H, *t*Bu), 0,8 (t, J = 7 Hz, 3 H, H7). RMN ^{13}C : 134,9 (C3), 116,7 (C4), 82,6 (C1), 79,7 (*C*Me$_3$), 37,2 (C2), 34,2 (C5), 26,4 (C*Me*$_3$), 18,8 (C6), 14,1 (C7).

Peroxyde de tert-*butyle et de 1-isobutylbut-3-ényle,* ***1***d : méthode B; rdt = 10%; purifié sur silice; n_D^{20} = 1,4262. RMN ^{1}H : 5,9–5,6 (m, 1 H, H3), 5,1–4,9 (m, 2 H, H4), 4,1–3,9 (m, 1 H, H1), 2,5–2,1 (m, 2 H, H2), 1,8–1,6 (m, 1 H, H6), 1,5–1,2 (m, 2 H, H5), 1,2 (s, 9 H, *t*Bu), 0,8 (2 d, J = 7 Hz, 6 H, H7 et Hc). RMN ^{13}C : 134,8 (C3), 116,7 (C4), 80,9 (C1), 79,5 (*C*Me$_3$), 41,3 (C2), 37,8 (C5), 26,5 (C*Me*$_3$), 24,7 (C6), 23,3 et 22,5 (C7 et C$_c$).

Peroxyde de tert-*butyle et de 3-méthylbut-3-ényle,* ***1***e : méthode B; rdt 10% purifié sur silice; n_D^{20} = 1,4384. RMN ^{1}H : 4,8–4,6 (m, 2 H, H4), 4,1–3,9 (m, 1 H, H1), 2,5–2,0 (m, 2 H, H2), 1,7 (s, 3 H, H$_a$), 1,5–1,3 (m, 4 H, H5, H6), 1,2 (s, 9 H, *t*Bu), 0,9 (t, J = 7 Hz, 3 H, H7). RMN ^{13}C : 142,8 (C3), 112,5 (C4), 81,8 (C1), 79,7 (*C*Me$_3$), 41,2 (C2), 34,6 (C5), 26,5 (C*Me*$_3$), 22,9 (C$_a$), 18,9 (C6), 14,2 (C7).

Peroxyde de tert-*butyle et de 1-méthylbut-3-ényle,* ***1***f : méthode A; rdt 38%; purifié sur silice; n_D^{20} = 1,4187. RMN ^{1}H : 5,9–5,7 (m, 1 H, H3), 5,0–4,9 (m, 2 H, H4), 2,2 (m, 2 H, H2), 1,5–1,2 (m, 4 H, H5, H6), 1,1 (s, 9 H, *t*Bu), 1,0 (s, 3 H, H$_b$), 0,8 (t, J = 7 Hz, 3 H, H7). RMN ^{13}C : 135,0 (C3), 116,8 (C4), 81,5 (C1), 78,0 (*C*Me$_3$), 42,2–39,6 (C2 et C5), 26,6 (C*Me*$_3$), 22,1 (C$_b$), 16,7 (C6), 14,6 (C7).

Peroxyde de tert-*butyle et de 1-méthallylcycloheptyle,* ***1***g : méthode A; rdt = 10%; purifié sur silice; n_D^{20} = 1,4610. RMN ^{1}H : 4,7–4,5 (m, 2 H, H10), 2,2 (s, 2 H, H8), 1,7 (s, 3 H, Me), 1,6–1,2 (m, 12 H, autres H), 1,1 (s, 9 H, *t*Bu). RMN ^{13}C : 143,7 (C9), 113,9 (C10), 85,8 (C1), 78,1 (*C*Me$_3$), 45,7 (C8), 36,2 (C2, C7), 31,2 (C4, C5), 26,8 (C*Me*$_3$), 24,2 (Me), 23,1 (C3, C6).

Produits de réactions

Oxétanes

2-(2,2-Dichloroéthyl)-1-oxa-spiro[3.6]décane, ***2***a : n_D^{20} = 1,4895. RMN ^{1}H : 5,8–5,7 (m, 1 H, H6), 4,7–4,6 (m, 1 H, H2), 2,6–2,0 (m, 4 H, H3, H5), 1,9–1,4 (m, 12 H, autres H). RMN ^{13}C : 86,1 (C4), 70,7 et 69,7 (C2 et C6), 52,4 (C5), 43,8–41,5 et 39,0 (C3, C7 et C$_{12}$), 28,1 (C9, C10), 21,3 et 20,8 (C8 et C11). SM (IE), *m/z* (*I*%) : 236 (2) M$^{+\cdot}$, 2Cl, 112 (45), 95 (31), 84 (47), 82 (24), 69 (32), 68 (100), 67 (29), 56 (34), 55 (85), 54 (20), 41 (50). Analyse centésimale calc. pour $C_{11}H_{18}OCl_2$: C 55,71, H 7,65, O 6,75, Cl 29,90%; exp. : C 55,39, H 7,99, O 6,48, Cl 29,16%.

1-(4,4-Dichlorobutyl)-7-oxa [4.1.1] bicyclooctane, ***3***a (ou A) : RMN ^{1}H : 5,7 (t, J = 6 Hz, 1 H, H$_k$), 4,6–4,5 (m, 1 H, H$_c$), 2,7–1,4 (m, 16 H, autres H). RMN ^{13}C : 86,2 (C$_a$), 75,3 (C$_c$), 73,5 (C$_k$), 43,7 (C$_j$), 41,5 (C$_b$), 37,9–33,9 et 33,5 (C$_d$, C$_g$ et C$_h$), 24,2 et 23,4 (C$_e$ et C$_f$), 20,0 (C$_i$). SM (IE), *m/z* (*I* %) : 236 (5) M$^{+\cdot}$, 2 Cl, 192 (36), 168 (24), 155 (64), 153 (100), 117 (29), 111 (53), 93 (24), 89 (38), 83 (43), 55 (33), 41 (20).

2-(2,2,2-Trichloroéthyl)-1-oxa-spiro[3.5]nonane, ***5***b : n_D^{20} = 1,5082. RMN ^{1}H : 4,9 (AB*X* et MN*X*, 1 H, H2), 3,1 et 3,0 (*MN*X, J_{MN} = 14,7 Hz, J_{MX} = 4,4 Hz et J_{NX} = 7,0 Hz, 2 H, H5), 2,5 et 2,2 (*AB*X, J_{AB} = 11 Hz, J_{AX} = 8,1 Hz, J_{BX} = 6,5 Hz, 2 H, H3), 1,9–1,1 (m, 10 H, autres H). RMN ^{13}C : 96,1 (C6), 83,8 (C4), 71,7 (C2), 62,4 (C5), 40,3 (C3), 39,1 et 37,9 (C7 et C11), 24,9 (C9), 22,7 et 22,2 (C8 et C10). SM (IC, NH_3), *m/z* : 274 MNH_4^+, 3 Cl; 257 MH^+, 3 Cl. Analyse centésimale calc. pour $C_{10}H_{15}OCl_3$: C 46,63, H 5,87, O 6,21, Cl 41,29%; exp. : C 46,99, H 5,49, O 6,95, Cl 40,98%.

2-(2,2-Dichloroéthyl)-4-propyloxétane, ***2***c : n_D^{20} = 1,4702. RMN ^{1}H : 5,8–5,7 (m, 1 H, H6), 4,9–4,7 (2 m, 2 H, H2, H4), 2,8–2,3 (m, 4 H, H3, H5), 2,2–1,1 (m, 4H, H7, H8), 0,9 (t, J = 7 Hz, 3 H, H9). RMN ^{13}C, *cis* : 78,7 et 73,7 (C2 et C4), 69,2 (C6), 52,1 (C5), 40,6 (C7), 33,1 (C3), 17,2 (C8), 13,8 (C9); *trans* : 79,3 et 74,7 (C2 et C4), 69,5 (C6), 51,0 (C5), 39,6 (C7), 31,9 (C3), 17,3 (C8), 13,8 (C9). SM (IC, NH_3), *m/z* : 214 MNH_4^+, 2 Cl; 197 MH^+, 2 Cl.

2-(4,4-Dichlorobutyl)-4-méthyloxétane, ***3***c : RMN ^{1}H : 5,7 (t, J = 6 Hz, 1 H, H8), 4,8–4,5 (2 m, 2 H, H2, H4), 2,4–2,0 (m, 4 H, H3, H7), 1,9–1,5 (m, 4 H, H5, H6), 1,4 et 1,3 (2 d, J = 6 Hz, 3 H, H9). RMN ^{13}C, *cis* : 77,0 et 74,6 (C2 et C4), 73,5 (C8), 43,4 (C7), 37,6 et 35,0 (C3 et C5), 24,8 (C9), 21,1 (C6); *trans* : 77,7 et 75,4 (C2 et C4), 73,5 (C8), 43,4 (C7), 36,5 et 33,9 (C3 et C5), 23,9 (C9), 21,3 (C6). SM (IC, NH_3), *m/z* : 214 MNH_4^+, 2 Cl; 197 MH^+, 2 Cl.

2-(4,4-Dichlorobutyl)-4,4-diméthyloxétane, ***3***d : RMN ^{1}H : 5,7 (t, J = 6 Hz, 1 H, H8), 4,6–4,4 (m, 1 H, H2), 2,5–1,5 (m, 8 H, autres H), 1,4 et 1,3 (2 s, 6 H, H9 et H$_c$). RMN ^{13}C : 80,0 (C4), 73,4 (C2 et C8), 43,3 et 39,4 (C3 et C7), 37,5 (C5), 31,1 et 29,1 (C9 et C$_c$), 21,3 (C6). SM (IC, NH_3), *m/z* : 228 MNH_4^+, 2 Cl; 211 MH^+, 2 Cl; 85 $[M - (CH_2)_3CHCl_2]^+$.

2-(2,2-Dichloroéthyl)-2-méthyl-4-propyloxétane, ***2***e : RMN ^{1}H : 5,9–5,7 (m, 1 H, H6), 4,7–4,4 (m, 1 H, H4), 2,8–2,3 (m, 4 H, H3, H5), 1,8–1,5 (m, 2 H, H7), 1,4 (2 s, 3 H, H$_a$), 1,3–1,1 (m, 2 H, H8), 0,9 (t, J = 7 Hz, 3 H, H9). RMN ^{13}C, 1° diast. : 79,8 (C2), 75,2 (C4), 69,5 (C6), 54,4 (C5), 40,4 et 38,5 (C3 et C7), 28,8 (C$_a$), 17,6 (C8), 13,9 (C9); 2° diast. : 80,7 (C2); 75,6 (C4), 69,2 (C6), 55,8 (C5), 40,7 et 39,1 (C3 et C7), 26,3 (C$_a$), 17,6 (C8), 13,9 (C9). SM (IC, NH_3), *m/z* : 228 MNH_4^+, 2 Cl; 211 MH^+, 2 Cl; 113 $[M - CH_2CHCl_2]^+$.

2-(2,2-Dichloroéthyl)-4-méthyl-4-propyloxétane, ***2***f : n_D^{20} = 1,4620. RMN ^{1}H : 5,8–5,6 (m, 1 H, H6), 4,9–4,5 (m, 1 H, H2), 2,7–2,0 (m, 4 H, H3, H5), 1,7–1,4 (m, 2 H, H7), 1,4–1,0 (m et 2 s, 5 H, H8 et H$_b$), 1,0–0,7 (m, 3 H, H9). RMN ^{13}C, 1° diast. : 83,3 (C4), 70,5 et 69,6 (C2 et C6), 51,9 (C5), 45,8 (C7), 37,6 (C3), 26,6 (C$_b$), 16,8 (C8), 14,4 (C9); 2° diast. : 83,3 (C4), 70,5 et 69,6 (C2 et C6), 52,4 (C5), 44,1 (C7), 37,4 (C3), 28,9 (C$_b$), 16,9 (C8), 14,3 (C9). SM (IC, NH_3), *m/z* : 228 MNH_4^+, 2 Cl; 211 MH^+, 2 Cl; 167 $[M - Pr]^+$, 2 Cl. Analyse centésimale

Can. J. Chem. Downloaded from www.nrcresearchpress.com by 65.111.164.53 on 09/08/12
For personal use only.

calc. pour $C_9H_{16}OCl_2$: C 51,20, H 7,64, O 7,58, Cl 33,58%; exp. : C 51,19, H 7,11, O 8,08, Cl 33,17%.

2-(4,4-Dichlorobutyl)-2,4-diméthyloxétane, ***3***f : n_D^{20} = 1,4668. RMN ^{1}H : 5,7 (t, *J* = 6 Hz, 1 H, H8), 4,8–4,5 (m, 1 H, H4), 2,5–1,0 (m, 14 H, autres H). RMN ^{13}C, 1° diast. : 80,8 (C2), 73,4 (C8), 70,7 (C4), 43,6 (C7), 42,5 et 39,2 (C3 et C5), 26,3 (C_b), 24,7 (C9), 20,3 (C6); 2° diast. : 81,0 (C2), 73,4 (C8), 70,7 (C4), 43,6 (C7), 40,5 et 39,3 (C3 et C5), 28,9 (C_b), 24,2 (C9), 20,2 (C6). SM (IC, NH_3), *m/z* : 228 MNH_4^+, 2 Cl; 211 MH^+, 2 Cl; 85 $[M - (CH_2)_3CHCl_2]^+$. Analyse centésimale calc. pour $C_9H_{16}OCl_2$: C 51,20, H 7,64, O 7,58, Cl 33,58%; exp. : C 51,02, H 7,60, O 7,80, Cl 33,51%.

2-(2,2,2-Trichloroéthyl)-4-méthyl-4-propyloxétane, ***5***f : RMN ^{1}H : 5,0–4,8 (m, 1 H, H2), 3,3–2,9 (m, 2 H, H5), 2,7–2,1 (m, 2 H, H3), 1,7–1,2 (m et 2 s, 7 H, H7, H8, H_b), 1,0–0,8 (m, 3 H, H9). RMN ^{13}C, 1° diast. : 96,2 (C6), 84,0 (C4), 71,2 (C2), 62,4 (C5), 43,9 (C7), 39,0 (C3), 28,9 (C_b), 17,1 (C8), 14,4 (C9); 2° diast. : 96,1 (C6), 83,9 (C4), 71,2 (C2), 62,0 (C5), 45,6 (C7), 39,1 (C3), 26,5 (C_b), 16,9 (C8), 14,3 (C9). SM (IC, NH_3), *m/z* : 262 MNH_4^+, 3 Cl; 245 MH^+, 3 Cl; 201 $[M - Pr]^+$, 3 Cl; 113 $[M - CH_2CCl_3]^+$.

2-(4,4,4-Trichlorobutyl)-2,4-diméthyloxétane, ***6***f : SM (IC, NH_3), *m/z* : 262 MNH_4^+, 3 Cl; 245 MH^+, 3 Cl; 85 $[M - (CH_2)_3CCl_3]^+$.

2-(2,2-Dichloroéthyl)-2-méthyl-1-oxa-spiro[3.6]décane, ***2***g : n_D^{20} = 1,4915. RMN ^{1}H (250 MHz) : 5,7 (AB*X*, 1 H, H6), 2,6 et 2,5 (*AB*X, J_{AB} = 14,4 Hz, J_{AX} = 9,1 Hz, J_{BX} = 4,5 Hz, 2 H, H5), 2,4 et 2,1 (*AB*, J_{AB} = 24,3 Hz, 2 H, H3), 1,9–1,2 (m et s, 15 H, autres H). RMN ^{13}C : 82,3 (C4), 76,3 (C2), 69,5 (C6), 56,1 (C5), 44,8 (C3), 43,2 (C7 et C12), 28,0 (C9 et C10), 27,9 (Me), 21,1 (C8 et C11). SM (IC, NH_3), *m/z* : 286 MNH_4^+, 2 Cl; 251 MH^+, 2 Cl. Analyse centésimale calc. pour $C_{12}H_{20}OCl_2$: C 57,38, H 8,03, O 6,37, Cl 28,23%; exp. : C 57,03, H 8,28, O 6,74, Cl 28,38%.

Peroxydes adduits

Peroxyde de tert-*butyle et de 1-(4,4-dichlorobutyl)cycloheptyle,* ***4***a : RMN ^{1}H : 5,8 (t, *J* = 6 H, 1 H, H_k), 2,2 (q, *J* = 6 Hz, 2 H, H_j), 1,8–1,5 (m, 16 H, autres H), 1,2 (s, 9 H, *t*Bu). RMN ^{13}C : 84,8 (C_a), 78,0 (*C*Me$_3$), 73,7 (C_k), 44,1 (C_j), 36,8 (C_h), 35,9 (C_b, C_g), 30,8 (C_e, C_d), 26,7 (C*Me*$_3$), 22,9 (C_c, C_f), 20,0 (C_i). SM (IE), *m/z* (I %) : 221 (23), 2 Cl; 185 (22), 165 (21), 149 (23), 95 (27), 89 (24), 83 (100), 81 (27), 73 (32), 69 (91), 57 (49), 55 (60), 43 (27), 41 (56). Analyse centésimale calc. pour $C_{15}H_{28}O_2Cl_2$: 57,88, H 9,07, O 10,28, Cl 22,78%; exp. : C 58,06, H 9,42, O 9,98, Cl 22,54%.

Peroxyde de tert-*butyle et de 1-(2,4,4,4-tétrachlorobutyl)cyclohexyle,* ***7***b : n_D^{20} = 1,5148, RMN ^{1}H : 4,4 (AB*X* et MN*X*, 1 H, H3), 3,5 et 3,0 (*MN*X, J_{MN} = 16 Hz, J_{MX} = 2,5 Hz, J_{NX} = 8,2 Hz, 2 H, H4), 2,3 et 1,9 (*AB*X, J_{AB} = 15,2 Hz, J_{AX} = 6,7 Hz, J_{BX} = 5,7 Hz, 2 H, H2), 1,9–1,2 (m, 10 H, autres H), 1,15 (s, 9 H, *t*Bu). RMN ^{13}C : 97,7 (C5), 80,5 et 78,8 (C1 et *C*Me$_3$), 62,0 (C4), 53,3 (C3), 45,8 (C2), 34,7 et 32,8 (C6 et C10), 26,9 (C*Me*$_3$), 23,9 (C8), 22,1 (C9, C7). SM (1C, NH3), *m/z* : 382 MNH_4^+, 4 Cl.

Peroxyde de tert-*butyle et de 5,5-dichloro 1-propylpentyle,* ***4***c : n_D^{20} = 1,4547. RMN ^{1}H : 5,7 (t, *J* = 6 Hz, 1 H, H5), 3,9–3,8 (m, 1 H, H1), 2,2–2,1 (m, 2 H, H4), 1,6–1,3 (m, 8 H, autres H), 1,2 (s, 9 H, *t*Bu), 0,9 (t, *J* = 7 Hz, 3 H, H8). RMN ^{13}C : 82,8 (C1), 79,8 (*C*Me$_3$), 73,6 (C5), 43,8 (C4), 34,8 (C6), 31,5 (C2), 26,6 (C*Me*$_3$), 22,0 (C3), 19,0 (C7), 14,4 (C8). SM (IC, NH_3), *m/z* : 288 MNH_4^+, 2 Cl. Analyse centésimale calc. pour $C_{12}H_{24}O_2Cl_2$: C 53,14, H 8,92, O 11,80, Cl 26,14%; exp. : C 52,75, H 8,40, O 11,50, Cl 27,54%.

Peroxyde de tert-*butyle et de 5,5-dichloro-1-isobutylpentyle,* ***4***d : SM (IC, NH_3), *m/z* : 302 MNH_4^+, 2 Cl; 285 MH^+, 2 Cl.

Peroxyde de tert-*butyle et de 5,5-dichloro-3-méthyl-1-propylpentyle,* ***4***e : SM (IC, NH_3), *m/z* : 302 MNH_4^+, 2 Cl.

Peroxyde de tert-*butyle et de 5,5-dichloro-1-méthyl-1-propylpentyle,* ***4***f : n_D^{20} = 1,4547. RMN ^{1}H : 5,7 (t, *J* = 6 Hz, 1 H, H5), 2,2–2,1 (m, 2 H, H4), 1,6–1,2 (m, 8 H, autres H), 1,1 (s, 9 H, *t*Bu), 1,0 (s, 3 H, H_b), 0,8 (t, *J* = 7 Hz, 3 H, H8). RMN ^{13}C : 81,6 (C1), 78,2 (*C*Me$_3$), 73,7 (C5), 44,1 (C4), 39,6 et 35,8 (C2 et C6), 26,7 (C*Me*$_3$), 22,2 (C_b), 20,3 (C3), 17,0 (C7), 14,8 (C8). SM (IC, NH_3), *m/z* : 302 MNH_4^+, 2 Cl.

Peroxyde de tert-*butyle et de 3,5,5,5-tétrachloro-1-méthyl-1-propyl pentyle,* ***7***f, *identifié à partir d'un mélange* ***7***f–***8***f : RMN ^{13}C, 1° diast. : 61,3 (C4), 53,6 (C3), 45,8 (C2), 38,5 (C6), 26,7 (C*Me*$_3$), 23,8 (C_b), 17,0 (C7), 14,7 (C8); 2° diast. : 61,8 (C4), 53,7 (C3), 46,2 (C2), 41,6 (C6), 26,7 (C*Me*$_3$), 22,7 (C_b), 17,2 (C7), 14,7 (C8). SM (IC, NH_3), *m/z* : 370 MNH_4^+, 4 Cl.

Peroxyde de tert-*butyle et de 5,5,5-trichloro-1-méthyl-1-(2-chloropropyl)pentyle,* ***8***f, *identifié à partir d'un mélange enrichi en* ***8***f : RMN ^{1}H : 4,3–4,1 (m, 1 H, H7), 2,7–2,5 (m, 2 H, H4), 2,2–1,6 (m, 6 H, H2, H3, H6), 1,5 (d, *J* = 7 Hz, 3 H, H8), 1,2 (s, 3 H, H_b), 1,1 (s, 9 H, *t*Bu). RMN ^{13}C, 1° diast. : 100,1 (C5), 81,1 (C1), 78,6 (*C*Me$_3$), 55,5 (C4), 54,3 (C7), 47,5 (C6), 36,9 (C2), 27,4 (C8), 26,7 (C*Me*$_3$), 21,3 (C_b), 20,7 (C3); 2° diast. : 100,1 (C5), 81,2 (C1), 78,6 (*C*Me$_3$), 55,5 (C4), 54,0 (C7), 47,5 (C6), 34,9 (C2), 27,4 (C8), 26,7 (C*Me*$_3$), 23,2 (C_b), 21,0 (C3). SM (IC, NH_3), *m/z* : 370 MNH_4^+, 4 Cl.

Bibliographie

1. E. Montaudon, R. Kappes, L. Lemée, M. Campagnole et M.J. Bourgeois. Bull. Soc. Chim. Fr. **131**, 253 (1994).
2. E. Breitmaier et W. Voelter. Carbon-13 NMR spectroscopy. 3° ed. VCH, Weinheim. 1987. Chap. 4, p. 315.
3. W.L.F. Armarego. Stereochemistry of heterocyclic compounds. Part 2. Wiley and Sons, New York. 1977, p. 36 et réf. citées.
4. J.W. Wilt. Free radicals. Vol. 1. *Édité par* J.K. Kochi. Wiley Interscience, New York. 1973. Chap. 8, p. 333.
5. A.L.J. Beckwith et K.U. Ingold. Rearrangements in ground and excited states. Vol. 1. *Édité par* P. de Mayo. Academic Press, New York. 1980. Chap. 4, p. 181.
6. E.I. Heiba et R.M. Deissau. J. Am. Chem. Soc. **89**, 3772 (1967).
7. N.A. Porter et J.R. Dixon. J. Am. Chem. Soc. **100**, 7116

(1978); N.A. Porter, M.A. Cudd, R.W. Miller et A.T. McPhail. J. Am. Chem. Soc. **102**, 414 (1980).
8. M. Agorrody, M. Campagnole, E. Montaudon et B. Maillard. Tetrahedron, **43**, 3429 (1987).
9. J. Tranchant. Manuel pratique de chromatographie en phase gazeuse. Masson, Paris. 1982. Chap. 3, p. 69.
10. X. Lubeigt, F. Flies, M.J. Bourgeois, E. Montaudon et B. Maillard. Can. J. Chem. **69**, 1320 (1991).
11. P.D. Bartlett et R.R. Hiatt. J. Am. Chem. Soc. **80**, 1398 (1958).
12. F. Strain, W.E. Bissinger, W.R. Dial, H. Rudoff, B.J. Dewitt, H.C. Stevens et J.H. Langston. J. Am. Chem. Soc. **72**, 1254 (1950).
13. M.J. Bourgeois, E. Montaudon et B. Maillard. Tetrahedron, **49**, 2477 (1993).
14. M.J. Bourgeois, E. Montaudon et B. Maillard. Synthesis, 700 (1989).
15. O. Grumitt, E.P. Budewitz et C.C. Chudd. Org. Synth. **36**, 60 (1956).

Can. J. Chem. Downloaded from www.nrcresearchpress.com by 65.111.164.53 on 09/08/12
For personal use only.

Formation of methyl 2-arylhydrazono-3-oxobutanoates and 2-arylhydrazono-3-oxobutanenitriles during the coupling reaction of arenediazonium ions with methyl 3-aminocrotonate and 3-aminocrotononitrile

D. Sean Brown, Jason V. Jollimore, Marcus P. Merrin, Keith Vaughan, and Donald L. Hooper

Abstract: Reaction of aryldiazonium salts with methyl 3-aminocrotonate (**1**) affords high yields of the methyl 2-arylhydrazono-3-oxobutanoates (**4**); analogous diazonium coupling with 3-aminocrotononitrile (**2**) gives the 2-arylhydrazono-3-oxobutanenitriles (**5**). The hydrazones are the product of diazonium coupling at the C2-vinylic carbon, concomitant with hydrolysis of the 3-amino substituent to the 3-oxo derivative; there is no evidence for the formation of a triazene (**6**), which would be the product of N-coupling. All hydrazones (**4***a–e* and **5***a–d*) have been fully characterized by IR and ^{1}H and ^{13}C NMR spectroscopy; the NMR spectra of the methyl 2-arylhydrazono-3-oxobutanoates (**4**) suggest the presence of two isomeric intramolecularly H-bonded forms in solution. Selected compounds were further characterized by elemental analysis and mass spectrometry. A mechanism is proposed for the conversion of **1** or **2** into **4** or **5**, and these observations are compared with previously reported observations of diazonium coupling reactions with unsaturated systems.

Key words: hydrazone, diazonium, aminocrotonate, aminocrotononitrile, hydrogen bonding.

Résumé : La réaction des sels aryldiazoniums avec le 3-aminocrotonate de méthyle (**1**) conduit avec d'excellents rendements aux 2-arylhydrazono-3-oxobutanoates de méthyle (**4**); des couplages analogues de diazoiques avec le 3-aminocrotonitrile (**2**) donne les 2-arylhydrazono-3-oxobutanenitriles (**5**). Les hydrazones sont les produits du couplage des diazoiques au niveau du carbone vinylique C2, suivi de l'hydrolyse du substituant 3-amino qui conduit au dérivé 3-oxo; il n'y a pas de preuve de la formation d'un triazène (**6**) qui pourrait être le produit du couplage avec l'azote. On a caractérisé complètement toutes les hydrazones (**4***a–e* et **5***a–d*) par la spectroscopie IR et de RMN du ^{1}H et du ^{13}C. Les spectres de RMN des 2-arylhydrazono-3-oxobutanoates de méthyle (**4**) suggèrent la présence de deux formes isomères en solution liées par des liaisons hydrogènes intramoléculaires. On a de plus caractérisé les composés choisis par l'analyse élémentaire et par la spectrométrie de masse. On propose un mécanisme pour la transformation du composé **1** ou **2** en composé **4** ou **5** et on a comparé ces observations avec les observations rapportées antérieurement sur le couplage des diazoiques avec les systèmes insaturés.

Mots clés : hydrazone, diazonium, aminocrotonate, aminocrotononitrile, liaisons hydrogènes.

[Traduit par la rédaction]

Introduction

1-Aryl-3-alkyltriazenes (Ar-N=N-NHR), often referred to as "monoalkyltriazenes," are produced by the coupling reaction of the arene diazonium ion, ArN_2^+, with an alkylamine, RNH_2 (1). Monoalkyltriazenes with a reactive functional group incorporated in the alkyl moiety, e.g., Ar-N=N-NH-CH_2-CO_2Et, are useful synthons for a variety of heterocyclic molecules (2). As part of our continuing interest in the search for new triazene synthons, we were interested in extending our studies to the vinylic triazenes (**6**), which would be useful precursors for monocyclic 1,2,3-triazines. The vinylic triazene (**6**) is formally the product expected from coupling an arenediazonium ion with the amino nitrogen atom of a 3-aminocrotonic acid derivative (e.g., **1** or **2**). However, when we attempted such a synthesis of triazenes of type **6**, we obtained different products, which arise from C-coupling at the C2 vinylic carbon in preference to N-coupling. These products have been identified as the 2-arylhydrazono-3-oxobutanoates

Received August 5, 1994.

D.S. Brown, J.V. Jollimore, M.P. Merrin, and K. Vaughan.[1] Department of Chemistry, Saint Mary's University, Halifax, NS B3H 3C3, Canada.
D.L. Hooper. Department of Chemistry, Dalhousie University, Halifax, NS B3H 4J3, Canada.

[1] Corresponding author. Telephone: (902) 420-5650. Fax: (902) 420-5261.

Can. J. Chem. Downloaded from www.nrcresearchpress.com by 65.111.164.53 on 09/08/12
For personal use only.

Table 1. Physical data for the methyl 2-arylhydrazono-3-oxobutanoates (**4**) and the 2-arylhydrazono-3-oxobutanenitriles (**5**).

Compound	X	Yield (%)	Melting point (°C)	Solvent	IR(cm^{-1})
4*a*	CO_2Et	86	100.5–102	EtOAc	3140(NH), 1700(C=O), 1690(C=O), 1650(C=O)
4*b*	CN	72	180–181	EtOAc	3140(NH), 2195(C≡N), 1680(C=O), 1655(C=O)
4*c*	$CONH_2$	97	210–211.5	EtOAc	3360/3300 (NH_2), 3120(NH), 1680(C=O), 1665(C=O)
4*d*	NO_2	88	189–191	EtOAc	3160(NH), 1690(C=O), 1660(C=O)
4*e*	Br	78	128–131	EtOAc	3180(NH), 1675(C=O)
5*a*	CO_2Et	90	230–231	Toluene	3200(NH), 2190(C≡N), 1700(C=O), 1660(C=O)
5*b*	CO_2Me	80	220–221	Hexane–EtOAc	3195(NH), 2180(C≡N), 1710(C=O), 1650(C=O)
5*c*	NO_2	86	260–264	Hexane–$CHCl_3$	3200(NH), 2180(C≡N), 1650(C=O)
5*d*	Br	84	213–214	Hexane–EtOAc	3205(NH), 2180(C≡N), 1655(C=O)
5*e*	CN	93	270–273	EtOAc	3220(NH), 2190(C≡N), 1655(C=O)

Can. J. Chem. Downloaded from www.nrcresearchpress.com by 65.111.164.53 on 09/08/12
For personal use only.

(**4**) from **1** and the 2-arylhydrazonocrotononitriles (**5**) from **2** and in this paper we report the synthesis and identification of both series of hydrazones.

Experimental

All reagents were reagent grade materials purchased from the Aldrich Chemical Co. Ltd., and were used without further purification. Melting points were determined on a Reichert hot-stage microscope and are uncorrected. Infrared spectra were obtained using Nujol mulls, unless otherwise indicated, on a Perkin Elmer 299 spectrophotometer. ^1H and ^{13}C NMR spectra were obtained on the Bruker 250 MHz spectrophotometer of the Atlantic Region Magnetic Resonance Centre at Dalhousie University. Unless otherwise noted, chemical shifts were recorded in $CDCl_3$ solutions at 20°C, and are relative to TMS (1%) internal standard. Mass spectral analysis was performed at the Institute of Marine Biosciences (NRC, Halifax) on a Finnigan Quadrupolar 4500 GC-MS with a temperature-programmed solids probe.

Methyl 2-Arylhydrazono-3-oxobutanoates (4 *a–e*) and 2-arylhydrazono-3-oxobutanenitriles (5*a–d*)

General procedure

The appropriate arylamine (0.01 mol) was dissolved, with gentle warming if necessary, in 2 M hydrochloric acid (30 mL) and diazotized at −5°C to 0°C with sodium nitrite (0.011 mol, 0.76 g) in water (5 mL). The mixture was stirred at −5°C for 0.5 h, and then filtered where necessary, to afford a clear solution of the diazonium salt, which was then treated with a solution of either (*a*) methyl 3-aminocrotonate (**1**) (1.3 g) in 2 M hydrochloric acid (5 mL), or (*b*) 3-aminocrotononitrile (**2**) (1.6 g) in 2 M hydrochloric acid (2 mL). The mixture was again stirred for 0.5 h at 0°C, and then neutralized carefully with either (*a*) sodium acetate trihydrate (20 g) in water, or (*b*) saturated sodium carbonate, respectively. The solid hydrazone formed was isolated by filtration, dried under vacuum, and recrystallized to constant melting point from an appropriate solvent. Yields and physical data of the hydrazones are given in Table 1, and spectroscopic data are shown in Tables 2–5. Mass spectral fragmentation data are given in Tables 6–7.

Results and discussion

The diazonium salt, $Ar\text{-}N_2^+Cl^-$, was prepared in the conventional manner by reaction of the appropriate arylamine in hydrochloric acid with sodium nitrite at low temperature, and then coupled with either methyl 3-aminocrotonate (**1**) or 3-aminocrotonitrile (**2**). Neutralization of the resulting solution gave a high yield of a single yellow product, which could be readily purified by recrystallization. Analysis of the IR, NMR, and mass spectra of these products results in the unequivocal assignment of the hydrazone structure **4** or **5**, rather than the 3-amino-2-arylazo structure **3**, which does not appear to be present even as a minor product of the coupling reaction mixture.

The key to this structural identification is found in the mass spectra of the products. The molecular ions are found to have a *m/z* in agreement with the expected molar mass of the hydrazone, **4** or **5**. The molar mass of the hydrazone is one mass unit higher than the molar mass of the analogous triazene (**6**); furthermore, elemental analysis showed a lower nitrogen content

Can. J. Chem. Downloaded from www.nrcresearchpress.com by 65.111.164.53 on 09/08/12
For personal use only.

Scheme 1

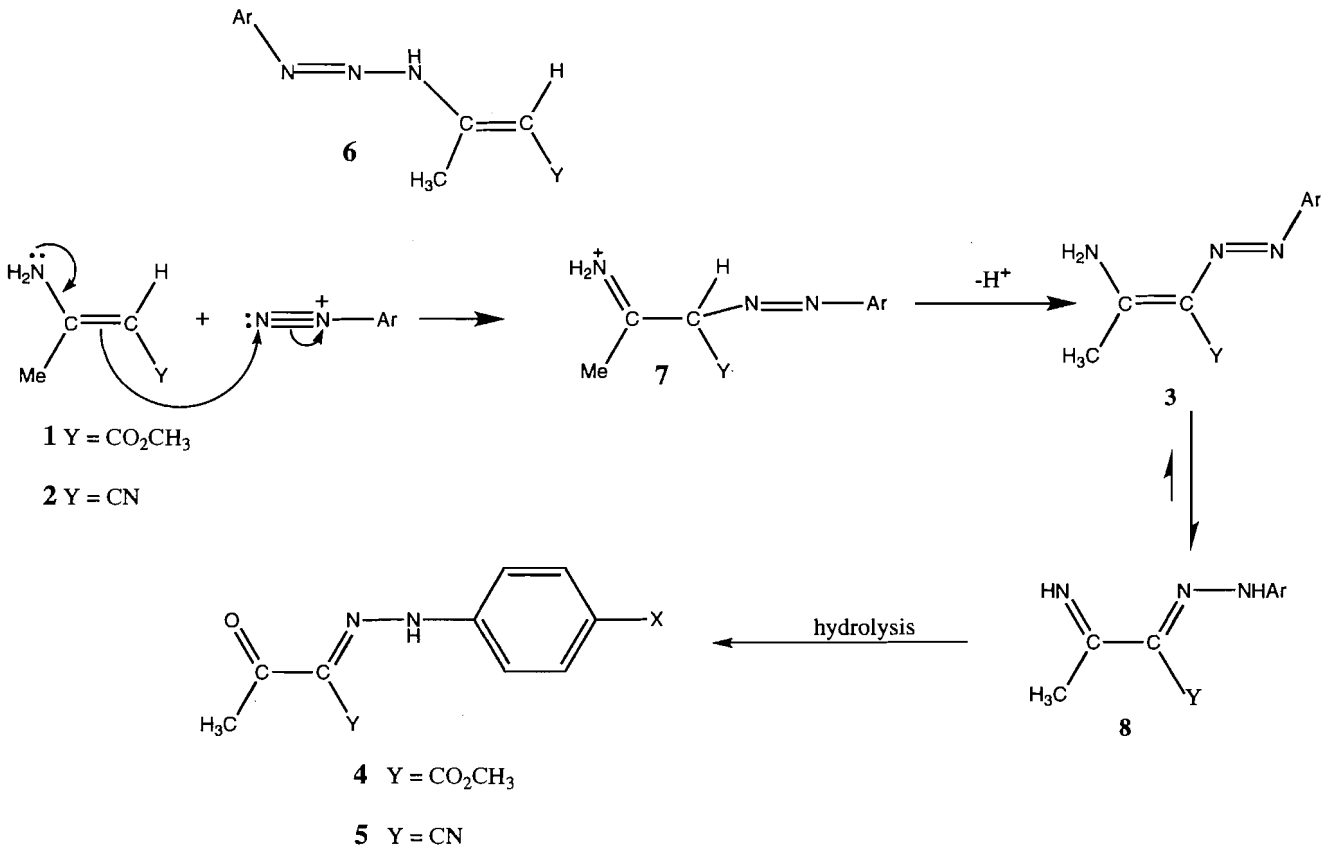

Table 2. Methyl 2-arylhydrazono-3-oxobutanoates (**4**): ^{1}H NMR chemical shifts[a] in ppm relative to TMS (1%) at 20°C.

Compound	X	N-H	Aromatic (AA'BB')	O-CH_3	C-CH_3	X
4*a*	CO_2Et	12.76(br s) (14.68)	8.07, 8.10, 7.35, 7.39 (8.05, 8.08, 7.43, 7.46)	3.92(s) (3.89)	2.52(s) (2.61)	1.40 (t, CH_3), 4.39 (q, CH_2)
4*b*	CN	12.71(br s) (14.57)	7.67, 7.70, 7.39, 7.43 (7.66, 7.69, 7.47, 7.51)	3.92(s) (3.90)	2.52(2) (2.62)	—
4*c*	$CONH_2$	12.80(br s) (14.71)	7.85, 7.89, 7.38, 7.42	3.93(s) (3.90)	2.53(s) (2.62)	5.89(br s, NH_2) (5.71)
4*d*	NO_2	12.76(br s) (14.59)	8.28, 8.31, 7.41, 7.45 (8.26, 8.29, 7.49, 7.53)	3.94(s) (3.92)	2.41(s) (2.63)	—
4*e*	Br	12.77(br s) (14.77)	7.48, 7.51, 7.21, 7.23 (7.47, 7.50, 7.27, 7.30)	3.90(s) (3.87)	2.49(s) (2.60)	—

[a]Chemical shifts in parentheses are assigned to the minor component of the mixture.

than that expected for the triazene, but was consistent with the hydrazone structure. All of the other spectroscopic features of the products are consistent with the hydrazone structure, rather than the triazene structure. Of particular note is the absence of the vinylic proton that should be present in the ^{1}H NMR spectra of **6**.

The methyl 2-arylhydrazono-3-oxobutanoates (**4***a–e*) are obtained in high yield from diazonium coupling with methyl 3-aminocrotonate (**1**). The hydrazones of this series all recrystallize readily from ethyl acetate. The IR spectra of these hydrazones (Table 1) all show the common features of a hydrazone NH at 3140–3180 cm^{-1}, a ketone carbonyl at 1650–1675 cm^{-1}, and the ester carbonyl band at 1680–1690 cm^{-1}. The functional groups present in the *para* position of the aryl moiety are also evident. Three representative examples of this hydrazone series, **4***b*, **4***d*, and **4***e*, were analysed for elemental composition with excellent fit to the expected percentages (Table 8).

The assignment of the hydrazone structure (**4**) is also supported by the ^{1}H NMR spectra (Table 2) and the observed chemical shifts agree very well with those reported by Elguero et al. (3*a*) for the unsubstituted arylhydrazone (**4**, X = H). The

Table 3. Methyl 2-arylhydrazono-3-oxobutanoates (**4**): ^{13}C NMR chemical shifts in ppm relative to TMS (1%) at 20°C.

Compound	X	Aromatic[a]	Ester C=O	Ketone C=O	C=N	O-CH_3	C-CH_3	X
4*a*	CO_2Et	145.0(C1) 114.9(C2,6) 131.4(C3,5) 115.8(C4)	163.9 (165.9)	194.4 (197.0)	126.6	52.3	26.8 (30.9)	14.35(CH_3) 61.0(OCH_3) 165.9(C=O)
4*b*	CN	144.9(C1) 115.7(C2,6) 133.9(C3,5) 116.5(C4)	163.7	194.15	129.1	52.5	26.8 (30.9)	118.7(C≡N)
4*c*	$CONH_2$	144.8(C1) 114.5(C2,6) 132.3(C3,5) 115.6(C4)	162.9	193.9	129.1	52.3	25.4	167.4($CONH_2$)
4*d* (in DMSO-d_6)	NO_2	148.2(C1) 114.9(C2,6) 125.7(C3,5) 142.2(C4)	162.6	194.1	135.3	52.6	26.9 (31.0)	—
4*e*	Br	140.6(C1) 117.0(C2,6) 132.6(C3,5) 117.85(C4)	164.2	194.3 (197.2)	126.0	52.2	26.8 (30.8)	—

[a]Aromatic: C4 is the carbon atom adjacent to the substituent X.

^{13}C NMR spectra (Table 3) of the hydrazone series (**4**) give further corroboration of the assigned structures. Of particular note is the presence in all five compounds of the keto-carbon atom, which has a resonance of ca. 194 ppm. Other features of the ^{13}C NMR spectra are as expected.

The ^1H NMR spectra of the methyl 2-arylhydrazono-3-oxobutanoates (**4**) all show a doubling of peaks, with a major and a minor component. The composition of the mixture does not change after repeated purification, indicating that these hydrazones exist as an equilibrium mixture. Some doubling of signals is also observed in the ^{13}C NMR spectra. A similar equilibrium was observed with the unsubstituted hydrazone (**4**, X = H) by Elguero et al. (*3a*), who attributed the phenomenon to the existence of two isomeric H-bonded forms (**4***A* and **4***B*):

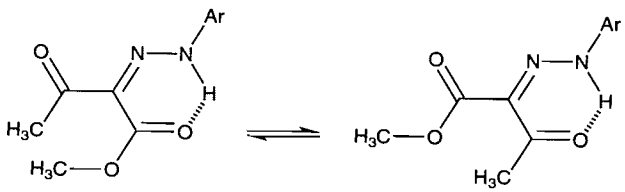

4*A* **4***B*

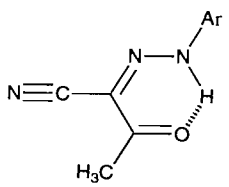

5*A*

By analogy with this reported example, it is evident that the major component of the mixtures of H-bonded forms of **4***a–e* is the ketone-carbonyl H-bonded form **4***B*, which is consistent with the NH chemical shift being at higher field. Measurement of the NMR integrals affords the following percent composition (%**4***A*:%**4***B*) for each compound in the series: **4***a*, 20:80%; **4***b*, 15:85%; **4***c*, 40:60%; **4***d*, 28:72%; **4***e*, 30:70%.

The 2-arylhydrazono-3-oxobutanenitriles (**5***a–d*) are obtained in high yield from diazonium coupling with 3-aminocrotononitrile (**2**); physical data of these compounds are presented in Table 1. The IR spectra show the expected hydrazone NH at ca. 3200 cm^{-1}, the keto-carbonyl at ca. 1655 cm^{-1}, and a weak cyano peak at 2180 or 2190 cm^{-1}. The mass spectra of three examples, **5***b*, **5***c*, and **5***d*, were recorded and showed the correct molecular ion mass for the hydrazone structure. Table 4 shows the ^1H NMR data for the cyano-hydrazone series. The spectra are consistent with the presence of a single species, the intramolecularly H-bonded hydrazone **5***A*.

The ^{13}C NMR spectra of the cyano-hydrazones (**5**) are recorded in Table 5. All spectra exhibit the expected chemical shifts: (*a*) cyano-group carbon at ca. 116 ppm; (*b*) keto-carbonyl carbon at ca. 192 ppm, (*c*) a methyl carbon at *ca.* 24 ppm; (*d*) two singlet and two doublet aromatic resonances, and (*e*) the carbon signals of the carbonyl and alkyl groups in the ester function of **5***a* and **5***b*. The imino-group carbon of the hydrazone moiety is observed universally at ca. 110 ppm, which is consistent with the chemical shift reported in the range 103–109 ppm for the imino-carbon atom of a series of ethyl cyano-(arylhydrazono)acetates, Ar-NH-N=C(CN)CO_2Et (3b). The chemical shift of the imino-carbon of the methyl 2-arylhydrazono-3-oxobutanoates (**4**) is observed in the range 126–135 ppm.

Can. J. Chem. Downloaded from www.nrcresearchpress.com by 65.111.164.53 on 09/08/12
For personal use only.

Can. J. Chem. Downloaded from www.nrcresearchpress.com by 65.111.164.53 on 09/08/12
For personal use only.

Table 4. 2-Arylhydrazono-3-oxobutanenitriles (**5**): ^{1}H NMR chemical shifts in ppm relative to TMS (1%) at 20°C in DMSO-d_6.

Compound	X	Aromatic (AA'BB')	C-CH_3	NH	X
5a	CO_2ET	8.10, 8.06, 7.70, 7.66	2.43	12.39	1.13 (t, CH_3), 4.29 (q, CH_2)
5b	CO_2Me	8.05, 7.99, 7.64, 7.58	2.58	12.43	3.89 (O—CH_3)
5c	NO_2	8.28, 8.24, 7.73, 7.69	2.55	12.55	—
5b	Br	7.60, 7.56, 7.49, 7.45	2.39	12.26	—
5e	CN	7.89, 7.80, 7.68, 7.60	2.52	12.41	—

Table 5. 2-Arylhydrazono-3-oxobutanenitriles (**5**): ^{13}C NMR chemical shifts in ppm relative to TMS (1%) at 20°C in DMSO-d_6.

Compound	X	Aromatic	*C*=N	*C*=O	*C*H_3	*C*≡N	X
5a	CO_2Et	145.71(s) C1 130.75(d) C3,5 125.58(s) C4 115.91(d) C2,6	110.59(s)	192.50(s)	24.70(q)	115.91(s)	165.19 (s, *C*=O) 60.62 (t, O-*C*H_2) 14.19 (q, C-*C*H_3)
5d	CO_2Me	145.68(s) C1 130.80(d) C3,5 125.31(s) C4 115.88(d) C2,6	110.55(s)	192.67(s)	24.64(q)	115.44(s)	165.69 (s, *C*=O) 52.06 (q, O-*C*H_3)
5c	NO_2	147.21(s) C1 143.29(s) C4 125.51(d) C3,5 116.20(d) C2,6	110.32(s)	192.63(s)	24.68(q)	116.83(s)	—
5d	Br	141.33(s) C1 132.30(d) C3,5 118.21(d) C2,6 114.34(s) C4	110.85(s)	192.65(s)	24.65(q)	116.95(s)	—
5e	CN	145.44 C1 133.80 C4 118.90 C3,5 116.84 C2,6	110.45	192.64	24.68	116.70	106.34 (C≡N)

Scheme 2

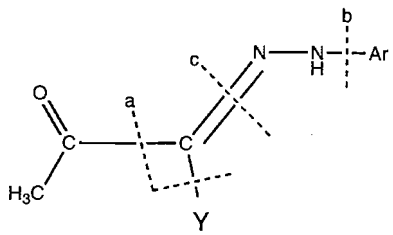

Table 6 shows details of the fragments observed in the mass spectra of the hydrazones **4***a* and **4***e*, with assignments of the major fragments. Table 7 shows a summary of the mass spectral information for the second series of hydrazones, **5***b*, **5***c*, and **5***d*. Both sets of data support the hydrazone structures and have some features in common. However, the major fragmentation pathway is somewhat different for hydrazones of type **4**, which afford an intense fragment corresponding to the moiety ArNHN=C$^+$. This fragment arises from cleavage of both bonds indicated by line "a" in Scheme 2. On the other hand,

Table 6. Mass spectral data of two examples of the methyl 2-arylhydrazono-3-oxobutanoates (**4***a* and **4***e*)

	4*a* (X = CO_2Et)		**4***e* (X = Br)	
Peak assignment	*m/z*	%	*m/z*	%
$M^{+\cdot}$	292	92	298/300	100
$M^{+\cdot}$ – $CH_3\cdot$	277	<1%	—	
$M^{+\cdot}$ – $OCH_3\cdot$	261	3	—	
$M^{+\cdot}$ – $OC_2M_5\cdot$	247	13	—	
$M^{+\cdot}$ – $HCO_2CH_3\cdot$	232	6	238/240	40
C=NNHAr$^{+\cdot}$	190	100	196/198	90
ArNH$^{+\cdot}$	—		170/172	51
ArN$^{+\cdot}$	163	54	—	
Ar$^{+\cdot}$	—		155/157	26
$M^{+\cdot}$ – Ar·	143	14	143	39
$CH_3COCNCO_2CH_3^{+\cdot}$	128	2	128	10

Table 7. Mass spectral data of the 2-arylhydrazono-3-oxobutanenitriles.

	5*b* (X = CO_2Me)		5*c* (X = NO_2)		5*d* (X = Br)	
Peak assignment	*m/z*	%	*m/z*	%	*m/z*	%
$M^{+\cdot}$	245	79	232	79	265/267	100
$M^{+\cdot} - CH_3CO\cdot$	202	5	189	2	222/224	3
$M^{+\cdot} - NCCOCH_3\cdot$	171	4	163	3	196/198	8
ArN_2^+	163	10	150	29	183/185	35
$Ar^{+\cdot}$	135	100	122	60	155/157	83
$ArNH_2^{+\cdot}$	151	4	138	3	171/173	17
$ArNH^{+\cdot}$	150	4	137	<1	170/172	6
CH_3CO^+	43	51	43	47	43	52

Table 8. Elemental analysis of representative hydrazones.

		Analysis (%)							
		Calculated				Found			
Compound	Formula	C	H	N	Br	C	H	N	Br
4*b*	$C_{12}H_{11}N_3O_3$	58.77	4.52	17.14	—	58.81	4.49	17.20	—
4*d*	$C_{11}H_{11}N_3O_5$	49.81	4.18	15.85	—	49.85	4.18	15.78	—
4*e*	$C_{11}H_{11}N_2O_3Br$	44.17	3.71	9.37	26.7	44.08	3.72	9.37	27.2

Can. J. Chem. Downloaded from www.nrcresearchpress.com by 65.111.164.53 on 09/08/12
For personal use only.

hydrazones of type **5** give major fragments arising from cleavage at bonds "b" and "c", producing respectively the $Ar^{+\cdot}$ and $ArN_2^{+\cdot}$ fragments.

Scheme 1 shows a proposed pathway to explain the formation of the hydrazones (**4** and **5**) from the diazonium coupling reaction. The reaction is initiated by electrophilic attack by the diazonium ion on the π electrons of the alkene; attack at C2 is preferred over attack at C3 because of the anchimeric assistance to the electron flow from the electron lone-pair on the amino-nitrogen atom. The initial attack leads to the intermediate iminium ion (**7**), which deprotonates to give the aylazo-compound (**3**). Isomerization of **3** affords the hydrazone **8**, which hydrolyses rapidly at the imino group in the acidic reaction medium to give the observed product **4** or **5**.

The hydrazonocrotonic acid derivatives (**4** and **5**) formed in the reactions described here are formally the products of diazonium coupling with the carbanion of either methyl acetoacetate or acetoacetonitrile, respectively (reaction [1]):

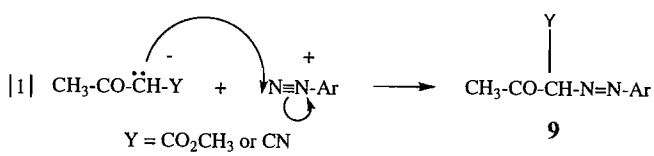

9

The reaction of aryldiazonium salts with carbanions of β-dicarbonyl compounds has been reported by several workers (4), and it was found that the initially formed azo compounds, such as **9**, always isomerize to the preferred hydrazone tautomer. However, no physical data, such as melting points, were reported in these papers. Chattaway and Ashworth (5) and Gasteiger and Strauss (6) reported the formation of keto-hydrazones of type **4** from diazonium coupling with alkyl-acetoacetates, but again no physical data were given; apparently, the ketohydrazones were generated *in situ* for reaction with ammonia to afford the 2-arylazo-3-aminocrotonate (**10**). Similar coupling reactions with β-keto-nitriles, e.g., CH_3COCH_2CN, have been reported for the synthesis of α-arylhydrazono-β-ketonitriles (7).

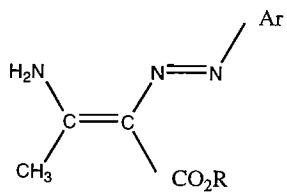

10

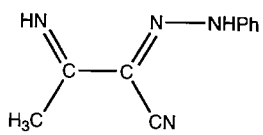

11

One of the original and more elegant examples of diazonium coupling to reactive methylene compounds is the work of Meyer (8), in which the diazonium ion was coupled with β-iminobutyronitrile to give the 2-arylhydrazono-3-ketiminobutanenitrile (**11**). In more recent work, Elnagdi et al. (9) reported further synthetic applications of the 2-arylhydrazono-3-ketiminobutanenitrile (**11**), which is formally the deprotonated form of the hydrazone tautomer of the intermediate (**7**) in our proposed mechanism (Scheme 1).

The reaction of enamines with diazonium salts can follow a different pathway, also leading to hydrazone formation, but via a different mode of attack by the diazonium ion at the α-carbon of an activated alkyl side chain. Thus reaction of 3-amino-2-cyano-2-pentene-1,5-dicarboxylate (**12**) with diazonium ions results in coupling at C4 to afford the hydrazone

(**14**) (10), and in similar fashion diazonium coupling with the tricyano-enamine (**13**) affords the hydrazone (**15**) (11).

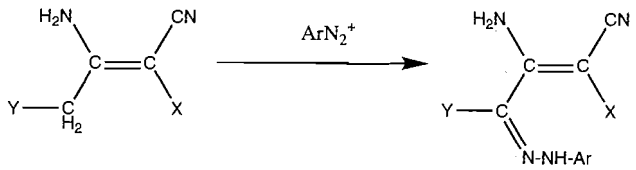

12 X=Y=CO_2Et **14** X=Y=CO_2Et

13 X=Y=CN **15** X=Y=CN

Thus the reactions of enamines with diazonium ions can occur by several different options, but none of those reported appear to give rise to a triazene via N-coupling. Furthermore, the reactions reported here represent a different variation on the theme of C-coupling involving hydrazone formation, concomitant with removal of the amino residue by hydrolysis. Further studies will be undertaken to assess the synthetic potential of this reaction in heterocyclic chemistry.

Acknowledgements

We gratefully acknowledge the contribution of the Atlantic Regional Magnetic Resonance Centre for providing NMR spectra, and we thank the National Research Council of Canada for making the mass spectral facility at the Institute for Marine Biosciences (Halifax) available. None of this work would have been possible without the generous financial assistance of the Natural Sciences and Engineering Research Council of Canada, supplemented by a research grant from the Saint Mary's University Senate Research Committee.

References

1. T.P. Ahern, H. Fong, and K. Vaughan. Can. J. Chem. **55**, 1701 (1977).
2. K.M. Baines, T.W. Rourke, K. Vaughan, and D.L. Hooper. J. Org. Chem. **46**, 856 (1981); K.M. Baines, K. Vaughan, D.L. Hooper, and L.F. Leveck. Can. J. Chem. **61**, 1549 (1983).
3. (*a*) J. Elguero, R. Jacquier, and G. Tarrago. Bull. Soc. Chim. Fr. 2981 (1966); (*b*) D. Prasad, N. Prasad, R.H. Prasad, R.J. Ferrier, and S.M. Milgate. J. Chem. Soc. Perkin Trans. 1, 1397 (1984).
4. R. Pichon, J. Le Saint, and P. Courtot. Bull. Soc. Chim. Fr. (Pt 2), 449 (1980); H.C. Yao. J. Org. Chem. **29**, 2959 (1964).
5. F.D. Chattaway and D.R. Ashworth. J. Chem. Soc. 475 (1933).
6. J. Gasteiger and U. Strauss. Chem. Ber. **114**, 2336 (1981).
7. J. Quilico. Gazz. Chim. Ital. **70**, 11 (1940); M.H. Elnagdi, M.R.H. Elmoghayar, and D.H. Fleita. J. Prakt. Chem. **316**, 975 (1974).
8. E.v. Meyer. J. Prakt. Chem. **52**, 94 (1958).
9. M.H. Elnagdi, M.M.M. Sallam, H.M. Fahmy, S.A-M. Ibrahim, and M.A.M. Elias. Helv. Chim. Acta, **59**, 551 (1976).
10. S.M. Fahmy, N.M. Abed, R.M. Mohareb, and M.H. Elnagdi. Synthesis, 490 (1982).
11. M.H. Elnagdi, K.U. Sadek, N.M. Taha, and Y. M. Yassin. Collect. Czech. Chem. Commun. **55**, 734 (1990).

Can. J. Chem. Downloaded from www.nrcresearchpress.com by 65.111.164.53 on 09/08/12
For personal use only.

Electrochemical investigations on some potential antibacterials, I

Rajeev Jain and M. Damodharan

Abstract: Electrochemical behaviour of the medicinally important 4-(4′-sulphonamoyl)hydrazono-1-phenyl-3-methyl-2-pyrazolin-5-ones has been studied at d.m.e. and glassy carbon electrodes. At d.m.e., all six compounds exhibited a single, well-defined, four-electron wave in the pH range 2.5–12.0. Polarographic four-electron wave was found to be diffusion-controlled and irreversible. Similarly, cyclic voltammetry of these compounds at glassy carbon electrode exhibited a single peak. Peak potential shows shifts towards negative potential with pH, with linear segments up to pH 8.2 and are practically pH independent at higher pH values. An anodic peak at far-off positive potential was observed in the reverse scan, indicating the irreversible nature of the electrode process. Controlled potential electrolysis and coulometric studies gave the value of n as 4.0 ± 0.1 in the pH range 2.5 to 10.0. Out of the two major end products formed, one was identified as sulphanilamide and the other as 1-phenyl-3-methyl-4-amino-2-pyrazolin-5-one on the basis of IR and NMR studies. On the basis of DCP, LSV, CV, CPE, coulometry and spectral analysis, a mechanism has been postulated for the reduction of these compounds at d.m.e. and glassy carbon electrodes.

Key words: polarography, cyclic voltammetry, antibacterials, pyrazolin-5-ones.

Résumé : On a étudié le comportement électrochimique de 4-(4′-sulfonamoyl)hydrazono-1-phényl-3-méthyl-2-pyrazolin-5-ones au niveau d'électrodes d.m.e. et de carbone vitreux. Avec les électrodes d.m.e., à des pH allant de 2,5 à 12,0, les six composés choisis présentent tous une seule vague, bien définie, de quatre électrons. On a établi que cette vague polarographique est contrôlée par la diffusion et qu'elle est irréversible. De la même manière, la voltampérométrie cyclique de ces composés au niveau d'une électrode de carbone vitreux présente un seul pic. Le potentiel du pic présente un déplacement vers le potentiel négatif avec une variation du pH; les segments sont linéaires à des pH allant jusqu'à 8,2 et ils sont pratiquement indépendants du pH à des valeurs de pH plus élevées. Lors du balayage inverse, on a observé un pic anodique à un potentiel extrêmement positif; ceci suggère une nature irréversible pour le processus. Une électrolyse à potentiel contrôlé et des études coulométriques indiquent que, à des pH allant de 2,5 à 10,0, la valeur de n est égale à 4,0 ± 0,1. En se basant sur des études de rmn et d'ir, on a identifié les deux products formés au cours des réactions; l'un est le sulfanilamide et l'autre est la 1-phényl-3-méthyl-4-amino-2-pyrazolin-5-one. En se basant sur les DCP, LSV, CV, CPE, la coulométrie et les analyses spectrales, on propose une mécanisme pour la réduction de ces composés aux électrodes de d.m.e. et de carbone vitreux.

Mots cles : polarographie, voltampérométrie cyclique, antibactériens, pyrazolin-5-ones.
[Traduit par la rédaction]

A review (1, 2) of the electrochemistry of some biologically important organic molecules illustrates very well how modern electrochemical techniques can provide biologically significant information. Electrochemical studies of hydrazones have attracted many workers (3–7) because of their medicinal importance (8, 9). The reduction of hydrazones has been reviewed in detail by Turyan (10). Fundamental contribution in this field has been made by Lund (11) and Kitajev et al. (12–14). The reduction mechanism has been reviewed by Kitajev and Buzykin (15). A four-electron reduction is usually observed in an acidic solution (11–14) involving breaking the N—N bond during the reduction. More recently a four-electron reduction of the hydrazones has been reported (16–18) in acidic as well as in alkaline media with the formation of amino compounds. On the other hand, Zuhri et al. (5) have found a two-electron reduction followed by a hydrolysis that resulted in the formation of the corresponding carbonyl compound. Hydrolysis of the reduced product has also been observed by Lund (7) for similar hydrazones. However, Fahmy et al. (19) have reported further reduction of the amino compound formed after the four-electron reduction to ammonia and ketone in a two-electron wave. However, only a few reports are available on the electroreduction of hydrazones at solid electrodes (20, 21).

An underlying rationale for our studies on the electrochemical reduction of biologically important *N*-heterocyclic molecules is that such studies can lead to information on the reaction routes and mechanisms of biological redox reactions. One of the reasons to investigate the electrochemical behaviour of biologically important compounds is the development of possible correlation based on the mechanistic paths involved and the associated characteristic potentials; e.g., half-wave potentials are a function of electron density and other factors, which are simply related to some biological,

Received April 22, 1994.
R. Jain[1] and M. Damodharan. Chemistry Department, Jiwaji University, Gwalior-474 011, India.

[1]To whom correspondence should be addressed.

Can. J. Chem. Downloaded from www.nrcresearchpress.com by 65.111.164.53 on 09/08/12
For personal use only.

Table 1. Electrochemical characteristics of 4-(4'-sulphonamoyl) hydrazono-1-phenyl-3-methyl-2-pyrazolin-5-ones, concentration 1.0×10^{-4} M, at pH 6.5.

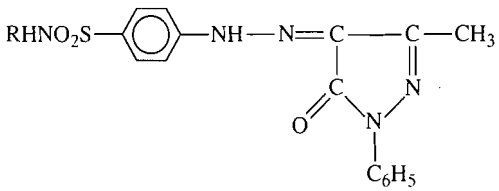

S.No.	R	$-E_{1/2}$, V	i_d, μA	E_p, V	i_p, μA
1	H—	0.93	1.22	0.93	14.4
2	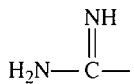	1.02	1.04	0.95	11.2
3	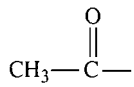	1.06	1.04	0.98	10.02
4		1.06	1.04	1.04	16.20
5	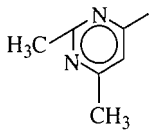	1.10	1.00	1.05	10.52
6	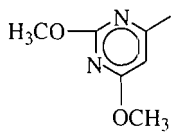	1.10	1.06	1.00	10.4

clinical, physical, or chemical property and activity. Furthermore, to broaden our knowledge on electrochemistry and to probe the possibilities of electroanalytical assays, we thought it worthwhile to study in a comprehensive manner the electroreduction behaviour of the medicinally important (22) 4-(4'-sulphonamoyl)hydrazono-1-phenyl-3-methyl-2-pyrazolin-5-ones at d.m.e. and glassy carbon electrodes.

Experimental

Polarographic curves were recorded on an ELICO DC CL 25 polarograph with capillary characteristics $m^{2/3}t^{1/6}$, 3.62 $mg^{2/3}$ $s^{1/2}$, drop time 3.20 s^{-1} at h = 65 cm in 1.0 M KCl solution (0.0 V SCE). Saturated calomel electrode was used as the reference electrode. Temperature coefficient was determined by Nejedly's (23) method. Triply distilled mercury was used for the d.m.e. All the polarograms were recorded at 298 ± 0.1 K.

Voltammograms were recorded on a cyclic voltammograph (BAS, CV-27) with an *x–y/t* recorder (Digital, Model Omnigraph). A three-electrode system was used, glassy carbon as the working electrode, Ag/AgCl in 1.0 M KCl as the referenced electrode, and a platinum wire as the counter electrode. The GC electrode was polished with fine grade emery paper followed by polishing alumina (0.5 μm), washed, and activated by triangular voltage sweeps from +1.0 to −1.4 V at the rate of 5 and 200 mV/s for 15 min. The activated electrode was tested (24) for its activity in ferricyanide–ferrocyanide in 0.1 M KCl solution.

The compounds listed in Table 1 were prepared by the reported (22) procedure. Britton-Robinson buffers (25) were used throughout the electrochemical study. pH of the solutions were measured with a glass electrode. In a typical electrochemical study, e.g., when studying the influence of pH on the cyclic voltammetric behaviour, 1.0×10^{-4} M solutions of these compounds were prepared by mixing 1.0 mL compound (1.0×10^{-3} M in DMF), 3.0 mL DMF (which was necessary to keep the compound in solution), 5.0 mL appropriate buffer, and 1.0 mL (1.0 M) KCl as the supporting electrolyte. Polarograms and voltammograms were recorded after removal of oxygen.

As the products of controlled potential electrolysis (CPE) have been known to differ depending on the nature of the electrode employed (26), controlled potential electrolysis (CPE) was done at d.m.e. and GC electrodes in a microcell (27). For coulometric determination (27) of the number of electrons transferred in the electrode process 2.0 mL of the solution of the depolarizer (1.0×10^{-3}) having 4.0 mL of buffer, 3.0 mL of dimethyl formamide, and 1.0 mL of potassium chloride was electrolysed by applying a potential corresponding to the limiting current of the polarographic wave. From the decrease in current with time during electrolysis, the number of electrons transferred was calculated. Progress of the electrolysis was monitored by recording the polarograms at different intervals of time, until only the background current is attained. Coulometry was done at the GC electrode, using a BAS CV-27 coulometer, the value of Q was directly read, and by applying

$$Q = nFN$$

n was calculated; here N is the number of moles.

Results and discussion

Polarographic behaviour

All 4-(4'-sulphonamoyl)hydrazono-1-phenyl-3-methyl-2-pyrazolin-5-ones (Table 1) exhibited a single, well-defined, four-electron wave in the pH range 2.5–12.0. A comparison of limiting currents of different pyrazolin-5-ones indicates that most of the compounds studied are reduced by the same number of electrons. The nature of the wave was established by recording the polarograms at various heights of mercury reservoir (55 to 95 cm) as well as by studying the effect of concentration ($(1.0–5.0) \times 10^{-4}$ M) on the limiting current. It was observed that the limiting current is directly proportional to the square root of the mercury reservoir height and the concentration of the depolarizer. These facts confirmed that the waves are controlled by diffusion (28). The half-wave potentials were dependent on pH and shifted towards more negative potentials with an increase in pH. The plots of $E_{1/2}$ vs. pH were (Fig. 1) linear up to 8.2 and after that there was a little change in $E_{1/2}$.

Cyclic voltammetry

Cyclic voltammograms of 4-(4'-sulphonamoyl)hydrazono-1-phenyl-3-methyl-2-pyrazolin-5-ones in buffer solutions of pH 2.5–12.0, at different scan rates (50–200 mV/s) and concen-

Can. J. Chem. Downloaded from www.nrcresearchpress.com by 65.111.164.53 on 09/08/12
For personal use only.

Can. J. Chem. Downloaded from www.nrcresearchpress.com by 65.111.164.53 on 09/08/12
For personal use only.

Fig. 1. Plot of $-E_{1/2}$ vs. pH (*1*) 4-[4′-sulphonamoyl]-, (*2*) 4-[4′-guanylsulphonamoyl]-, (*3*) 4-[4′-(4″,6″-dimethylpyrimidinyl)sulphonamoyl]hydrazono-1-phenyl-3-methyl-2-pyrazolin-5-ones at concentration 1.0×10^{-1} M.

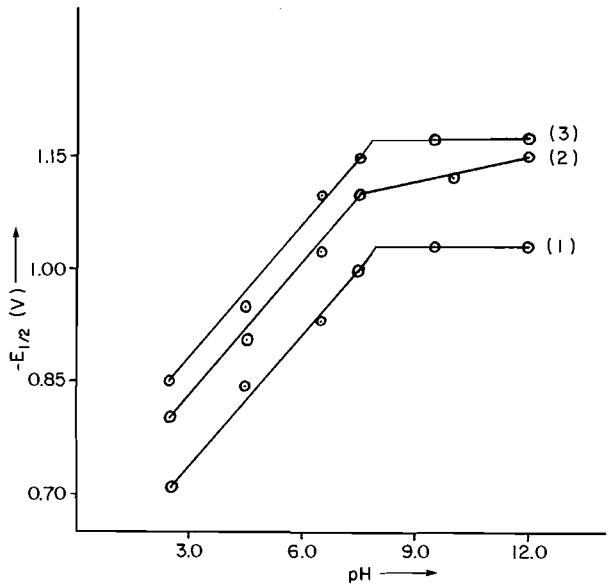

trations ((1.0–5.0) $\times 10^{-4}$ M), exhibited not very well-defined, single four-electron peaks. Some typical voltammograms are shown in Fig. 2. This behaviour is in agreement with that observed from polarographic measurements. Peak potentials show shifts towards negative potential with pH, with linear segments up to pH 8.2, and are practically pH independent at higher pH values. An anodic peak at far off positive potential was observed in the reverse scan indicating the irreversible (29) nature of the electrode process. The values of peak potential and peak currents are given in Table 1.

Coulometry and product analysis

Controlled potential electrolysis of these compounds at the plateau potential (−1.0 V) using the mercury pool cathode consumed 4.0 ± 0.2 electrons. The dark yellow colour of the starting solution almost disappeared at the end of the electrolysis. Coulometric studies at slightly more negative potential than the peak potential I_c, using GC electrodes, also gave the value of n as 4.0 ± 0.1 in the pH range 2.5–10.0. A cyclic voltammogram of the solution after exhaustive electrolysis did not exhibit any reduction peak. To characterise the major end products, electrolysis was carried out at pH 2.5, 6.5, and 10.0. The electrolysis resulted in two products on separation by TLC. One of the products was identified as sulphanilamide by comparison with the authentic sample. The other product was identified as 1-phenyl-3-methyl-4-amino-2-pyrazolin-5-one on the basis of IR and NMR studies (ν_{max}^{Nuzol} 3320 (NH_2), 1665 (C=O cyclic), 1600 (C=N), 1650 (heterocyclic five-membered 2-pyrazolin-5-one), δ ($CDCl_3$): 2.1 (1H, CH), 3.17 (3H, CH_3), 4.2 (2H, NH_2), and 7.0–8.0 (5H′, C_6H_5)).

Mechanism

Keeping in view the results of DCP, LSV, CV, CPE, and coulometry, the scheme on the facing page may be proposed for the reduction of these compounds at d.m.e. and GC electrodes.

Fig. 2. Cyclic voltammograms of 4-[4′-sulphonamoyl]hydrazono-1-phenyl-3-methyl-2-pyrazolin-5-one at (*1*) pH 4.5, (*2*) pH 2.5; concentration 1.0×10^{-4} M.

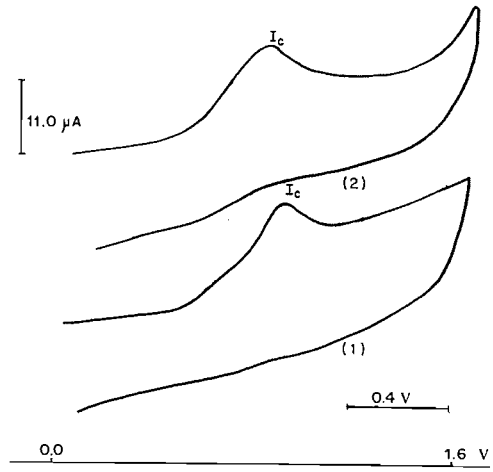

Alternatively, the radical (**I**) could also combine with an electron instead of a proton, but this possibility is ruled out by the fact that such a reduction would involve only two electrons, whereas polarographic data clearly indicate a four electron transfer reaction at the d.m.e.

The above mechanism is supported by a shift of $E_{1/2}$ towards more negative values with pH as protons are consumed in the reduction. As the equilibrium shifts towards the unprotonated form, the $E_{1/2}$ tends to become constant. Dependence of $E_{1/2}$ on pH is described by the equation (28):

$$E_{1/2} = \text{constant} + \frac{RT}{\alpha nF} \ln\left[1 + \frac{[H^+]}{K_a}\right]$$

The plot of $E_{1/2}$ vs. pH is composed of two intersecting linear segments and the pH at the point of intersection of its two linear parts is $\approx pK_1$. Similar steps of the reduction of the hydrazono group involving cleavage of the —N—N— bond have also been proposed by other workers (30–33). Due to an acid–base equilibrium between the structural forms of the compound (NH—N=C— ⇌ NH—NH=C—),[+] the wave height remains pH independent as long as the formation of the acidic form from the basic form is fast enough. As the pH increases and the rate of the protonation decreases, the wave height decreases as well. Ultraviolet–visible spectra of the solution during electrolysis were recorded at different time intervals; at 425 nm the peak due to —NH—N=C— grouping showed a decrease in the peak height after each interval of time and finally the peak disappeared, confirming the above reduction mechanism. The value of P is determined in the usual manner (28).

It was observed that the half-wave potential shifted to more negative potential (34) with increasing concentration of DMF, whereas the limiting current decreases.

Acknowledgement

The authors thank The University Grants Commission, New Delhi, for financial assistance to carry out this work.

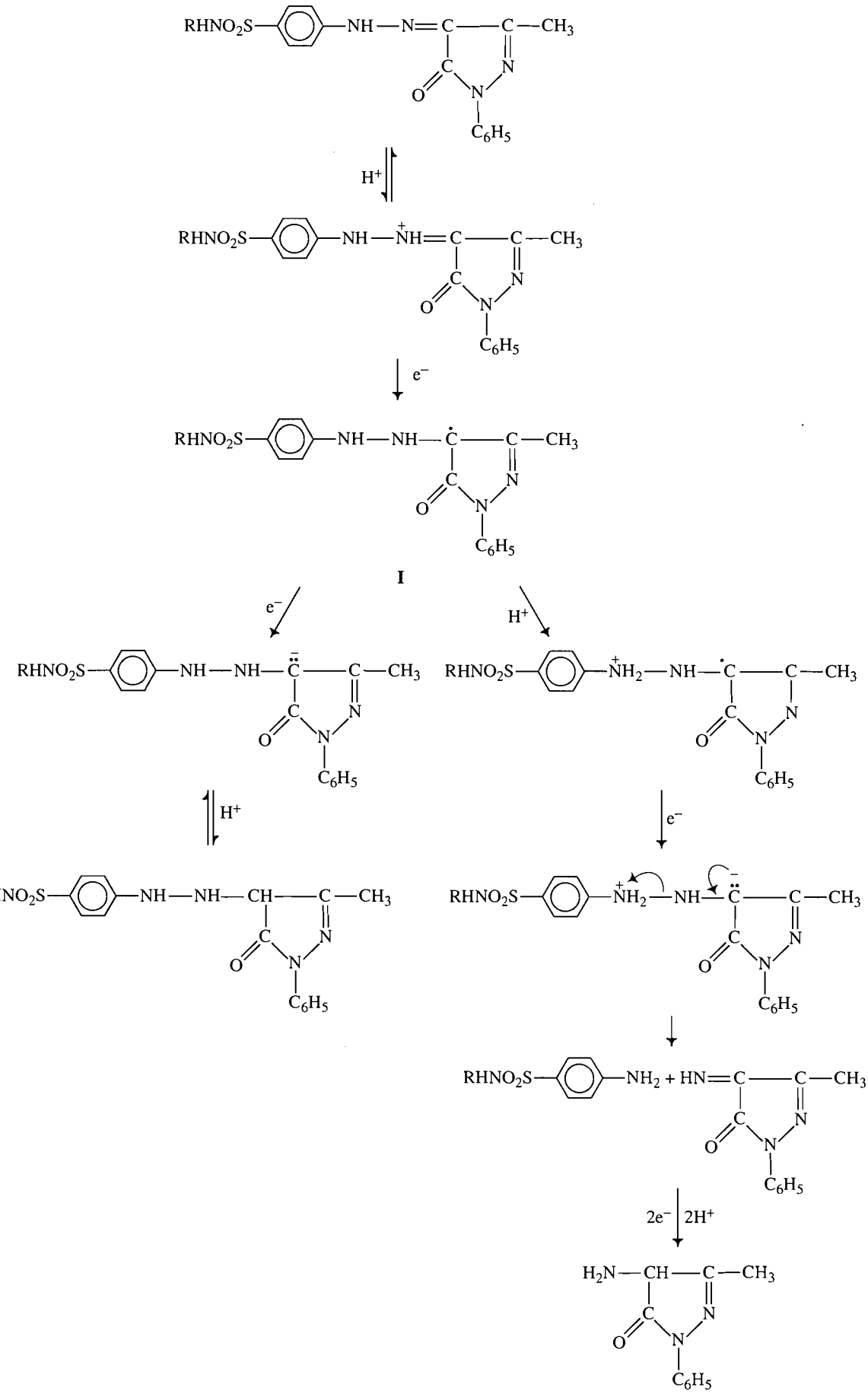

I

Can. J. Chem. Downloaded from www.nrcresearchpress.com by 65.111.164.53 on 09/08/12
For personal use only.

References

1. D. Dryhurst. *In* Comprehensive treatise on electrochemistry. *Edited by* S. Srinivasan and V. Chizmadjev. Plenum Press, New York. 1979. p. 325.
2. G. Dryhurst. *In* Electrochemistry of biological molecules. Academic Press, New York. 1977.
3. R. Jain, D.D. Agarwal, and R.K. Shrivastava. J. Chem. Soc. Perkin Trans. II, 1353 (1990).
4. N.C. Mathur, R.N. Goyal, and W.U. Malik. Indian J. Chem. **29A**, 765 (1990).
5. A.Z.A. Zuhri and J.S. Shalabi. J. Chem. Soc. Perkin Trans. 499 (1985).
6. M.A. Gomez Neoto, M.D. Lugue, D. Castro, and M. Valcarcel. Electrochim. Acta, **28**, 1725 (1983).
7. H. Lund. Electrochim. Acta, **28**, 395 (1983).
8. K. Shyam, L.A. Cosby, and A.C. Sartorelli. J. Med. Chem. **28**, 149 (1985).
9. H.G. Garg and C. Prakash. J. Pharm. Sci. **60**, 323 (1971).
10. Ya. I. Turyan. Usp. Khim. **46**, 1725 (1977); Russian Chem. Rev. **46**, 925 (1977).
11. H. Lund. Tetrahedron Lett. 3651 (1968).
12. Yu. P. Kitajev and G.K. Budnikov. Zh. Obshch. Khim. **33**, 1396 (1963).
13. Yu. P. Kitajev and I.M. Skrebkova. Zh. Obshch. Khim. **37**, 1204 (1967).
14. Yu. P. Kitajev, G.K. Budnikov, T.V. Trojepolskaya, and I.M. Skrebkova. Zh. Obshch. Khim. **37**, 437 (1967).
15. Yu. P. Kitajev, and B.I. Buzykin. Hydrazones. Izdat. Nauka, Moscow. 1974.
16. R.N. Goyal, R. Bushan, and A. Agarwal. J. Electroanal. Chem. **171**, 281 (1981).
17. R.N. Goyal. J. Indian Chem. Soc. **64**, 281 (1987).
18. R.N. Goyal and R. Jain. J. Electroanal. Chem. **84**, 141 (1977).
19. H.M. Fahmy, H.A.A. Ead, and M.A. Wahab. J. Chem. Soc. Perkin Trans. II, 45 (1985).
20. N.C. Mathur, R.N. Goyal, and W.U. Malik. Indian J. Chem. **29A**, 765 (1990).
21. W.U. Malik, R.N. Goyal, and M. Rajeshwari. Bull. Chem. Soc. France. I, 78 (1987).
22. R. Jain, D.D. Agarwal, and M. Damodharan. Indian J. Heterocycl. Chem. **2**, 265 (1993).
23. V. Nejedly. Collect. Czech. Chem. Commun. **1**, 319 (1929).
24. M. Noel and P.N. Anantharaman. Analyst, **110**, 1095 (1985).
25. H.T.S. Britton-Robinson. *In* Hydrogen ions. Vol. 2. D. Van Nostrand, New York. 1956.
26. H. Lund. Lecture at XIX Congress of Pure and Applied Chemistry, London. 1963.
27. O. Manousek, O. Exner, and P. Zuman. Collect. Czech. Chem. Commun. **33**, 3988 (1968).
28. L. Meites. *In* Polarographic techniques. Interscience, New York. 1967.
29. R.S. Nicholson and I. Shain. Anal. Chem. **36**, 722 (1984).
30. R. Jain and A. Dixit. Croat. Chem. Acta, **59**, 463 (1986).
31. Y.P. Kitajev, G.K. Budnikov, and L.I. Malsova. Izv. Acad. Nauk SSSR, Ser. Khim. **9**, 1911 (1967).
32. H. Lund. Acta Chem. Scand. **13**, 249 (1959).
33. W.U. Malik, R.N. Goyal, and R. Jain. J. Electroanal. Chem. **105**, 349 (1979).
34. S.G. Mairanovskii. Talanta, **12**, 1299 (1965).

Can. J. Chem. Downloaded from www.nrcresearchpress.com by 65.111.164.53 on 09/08/12
For personal use only.

Étude de la stéréochimie de la réaction de cycloaddition dipolaire-1,3 de quelques 5-phényl-3,6-dihydro-2*H*-1,4-oxazin-2-ones avec les *N*-méthyl et *N*-phénylmaléimides

Karin Monnier, Gérard Schmitt, Bernard Laude, Marie-France Mercier, Marek M. Kubicki et Michel Jannin

Résumé : La synthèse de six 5-phényl-3,4-dihydro-2*H*-1,4-oxazin-2-ones **1** à partir d'acides aminés est décrite. Ces composés sont des précurseurs d'ylures d'azométhine cycliques hexagonaux comportant un stéréocentre. Ces produits à caractère dipolaire réagissent avec les *N*-phényl et *N*-méthylmaléimides pour donner diastéréospécifiquement des cycloadduits pour lesquels l'approche du dipolarophile s'effectue sur la face la moins encombrée du dipôle et avec le reste maléimido en position *exo*. Malheureusement, on observe une racémisation lors de la réaction de cycloaddition, probablement par suite d'une tautomérie imine–ènamine du dipôle.

Mots clés : α-aminoacides, ylures d'azométhine cycliques, diastéréospécificité.

Abstract: Six derivatives of 5-phenyl-3,4-dihydro-2*H*-1,4-oxazin-2-ones **1** were synthetized from α-amino acids. These compounds are precursors of six-membered cyclic azomethine ylids involving one stereocenter. The 1,3-dipolar species react with *N*-methyl and *N*-phenylmaleimides, leading diastereospecifically to cycloadducts where the approach of the dipolarophile occurs from the less hindered side of the 1,3-dipole and with the maleimido moiety in an *exo* position. Unfortunately, racemization was observed during the cycloaddition reaction, presumably owing to reversible imine–enamine transformation.

Key words: α-amino acids, cyclic azomethine ylids, diastereospecificity.

Introduction

La synthèse asymétrique faisant appel à des réactions de cycloaddition dipolaires-1,3 des ylures d'azométhine a mobilisé l'attention de plusieurs équipes (1–9) qui ont eu recours à des auxiliaires chiraux sur le dipolarophile (1, 2), sur le dipôle (3, 4, 9), ou comme catalyseur (6). Récemment, Harwood et coll. (7, 8) ont décrit l'utilisation d'acides α-aminés qui sont des précurseurs bien connus des ylures d'azométhine (10–16), mais qui sont incapables d'exprimer la chiralité originale car cette information est nécessairement perdue lors de la formation de l'ylure d'azométhine par suite de la prototropie. L'idée mise en œuvre par ces auteurs consiste à condenser un composé prochiral avec un acide α-aminé pour créer un nouveau centre de chiralité, dont la configuration sera imposée par celle du carbone asymétrique de l'acide α-aminé précurseur.

Schéma 1

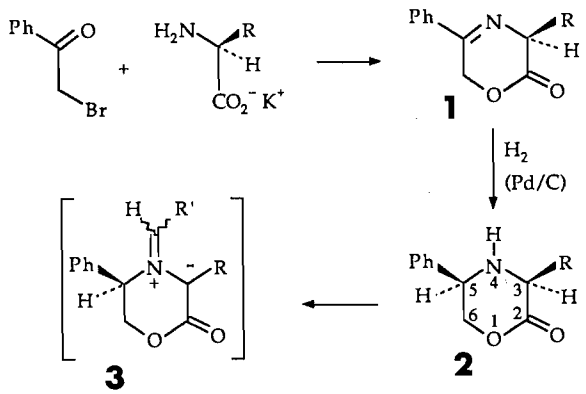

L'auxiliaire prochiral utilisé est la bromacétophénone qui par condensation avec un acide α-aminé conduit à une 3,6-dihydro-2*H*-1,4-oxazin-2-one **1** dont l'hydrogénation asymétrique permet d'obtenir de façon hautement stéréosélective la morpholinone **2** (schéma 1). Cette hydrogénation asymétrique a été étudiée par Caplar et al. (17). Elle s'accompagne du transfert total de la chiralité de l'α-aminoacide sur le centre benzylique formé en position 5. C'est ce nouveau stéréocentre en C-5 qui peut ensuite contrôler la stéréosélectivité de la

Reçu le 19 avril 1994.

K. Monnier, G. Schmitt, B. Laude[1] et M.-F. Mercier. Laboratoire de chimie organique, Université de Franche-Comté, 16 Route de Gray, 25030 Besançon, France.
M.M. Kubicki. Laboratoire de synthèse et d'électrosynthèse orgnométalliques (Unité de recherche associé n° 1685), Université de Bourgogne, 6 Boulevard Gabriel, 21000 Dijon, France.
M. Jannin. Laboratoire de physique des solides, Université de Bourgogne, 6 Boulevard Gabriel, 21000 Dijon, France.

1. Auteur correspondant : B. Laude. Tél. : 81 66 62 70. Fax : 81 66 62 30.

Can. J. Chem. Downloaded from www.nrcresearchpress.com by 65.111.164.53 on 09/08/12
For personal use only.

Can. J. Chem. Downloaded from www.nrcresearchpress.com by 65.111.164.53 on 09/08/12
For personal use only.

Schéma 2

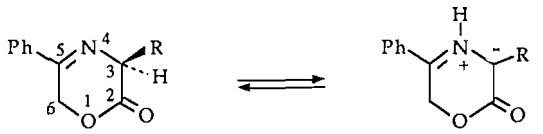

1

cycloaddition à partir de l'ylure d'azométhine **3** dérivé de la morpholinone **2**.

L'examen de la structure **1** montre qu'on a également affaire à un ylure d'azométhine potentiel dans lequel le dipôle et le groupement activant, ici une fonction lactone, sont tous deux complètement insérés dans un cycle (schéma 2). Certains d'entre nous (18) ont récemment montré que pour ce type de dipôle-1,3 cyclique, l'approche dipôle–dipolarophile est diastéréospécifique et qu'elle conduit uniquement au cycloadduit de structure *exo*, à la différence de ce qui se passe lorsque le dipôle n'est pas complètement inséré (7, 8) dans le cycle, comme dans **3**, où on observe une diastéréosélectivité majoritaire en faveur du cycloadduit *endo*.

L'objectif du présent travail a été de créer un deuxième centre de chiralité sur le modèle de type **1**, et il est évident que seul le carbone 6 pouvait tenir ce rôle (schéma 3). Si au cours de la synthèse de ces ylures d'azométhine ou de leurs précurseurs, on peut séparer les deux épimères résultant de l'introduction de ce nouveau carbone asymétrique, on disposera alors d'un dipôle-1,3 dont l'élément chiral sera le carbone-6. Du fait de la double diastéréospécificité de la réaction (en *anti* du groupe R^1 d'une part et en donnant le cycloadduit *exo* d'autre part), on pouvait espérer obtenir une cycloaddition [3 + 2] conduisant à un seul énantiomère.

Nous avons donc entrepris la synthèse de divers dérivés de la 5-phényl-3,6-dihydro-2*H*-1,4-oxazin-2-one **1** et étudié la stéréosélectivité de leur approche sur les *N*-méthyl et *N*-phénylmaléimides en cycloaddition dipolaire-1,3. Il faut signaler dès à présent que si nous avons bien observé la diastéréospécificité de la réaction, nous n'avons pas réussi à atteindre la pureté optique.

Synthèse des 3,6-dihydro-2*H*-1,4-oxazin-2-ones 1

Nous avons préparé les six composés résultant de la combinaison des substituants R^1 et R^2 indiqués sur le schéma 3. Pour les obtenir, nous avons adapté la séquence des réactions (schéma 3), déjà mises en œuvre par d'autres auteurs (17, 19) pour d'autres substances.

Esters α-cétoliques des acides *N*-(benzyloxycarbonyl)-α-aminés 4

Les α-bromoalkylphénones utilisées sont l'α-bromoacétophénone, l'α-bromopropiophénone et la bromodésoxybenzoïne. Les acides aminés sont la glycine et la L-alanine protégées. Les rendements de ces condensations sont bons ou même excellents (70–97%).

Lorsque R^1 et R^2 sont différents de H (**4***d* et **4***f*), on obtient un mélange de deux épimères. Nous avons pu séparer l'épimère majoritaire par cristallisation fractionnée uniquement dans le cas de **4***f* (R^1 = Ph, R^2 = CH_3). Pour ce qui concerne **4***d*, l'existence des deux diastéréoisomères est mise en évidence par rmn protonique, mais nous n'avons jamais réussi à les isoler ni par cristallisation fractionnée, ni par chromatographie.

Les propriétés physiques et les paramètres spectroscopiques de tous les composés **4** sont décrits en partie expérimentale.

Bromhydrates des esters α-cétoliques de la glycine et de la L-alanine 5

Les composés **4** précédents sont traités par une solution d'HBr à 40% dans l'acide acétique, méthode classique de déprotection des acides *N*-(benzyloxycarbonyl)-α-aminés. Ce traitement permet d'obtenir avec un rendement quasi-quantitatif les bromhydrates **5**. Seuls quatre d'entre eux (**5***a*, *b*, *e*, *f*) ont été isolés à l'état solide. Les deux autres (**5***c*, *d*) sont restés huileux. À partir de l'épimère majoritaire de **4***f*, on pouvait espérer obtenir un seul diastéréoisomère **5***f*. En fait, nous avons obtenu un mélange des deux épimères. Le spectre de rmn ^1H de ce mélange montre que leurs proportions relatives sont de 82 : 18.

Schéma 3

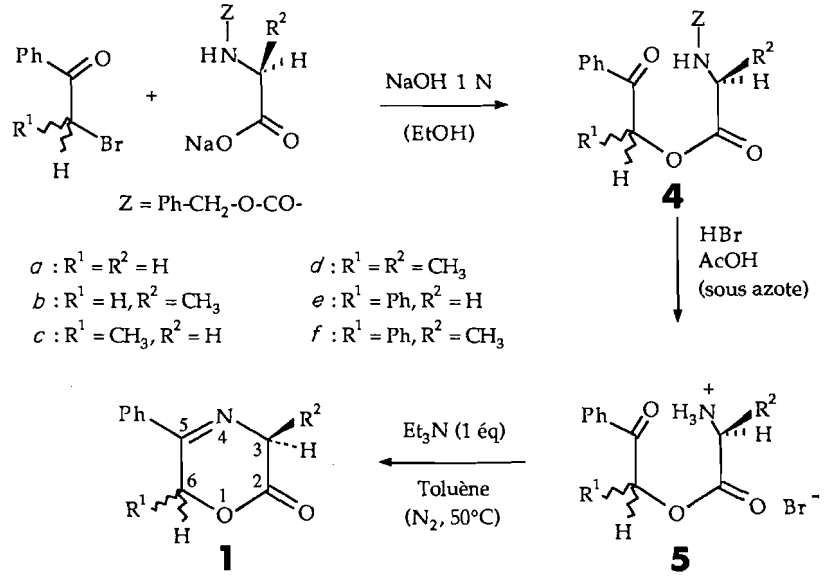

4 **1** **5**

Schéma 4

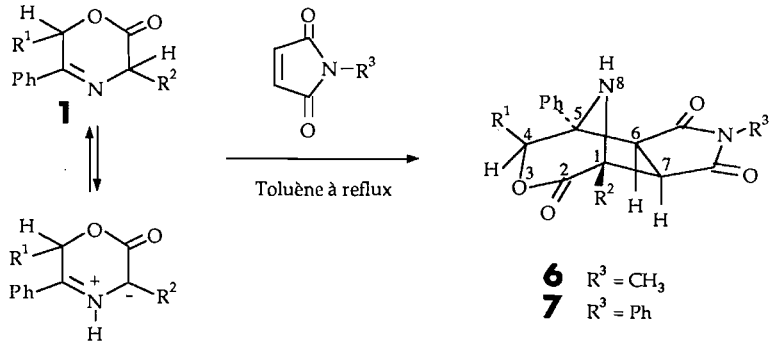

Fig. 1. Approche *endo* des deux réactants.

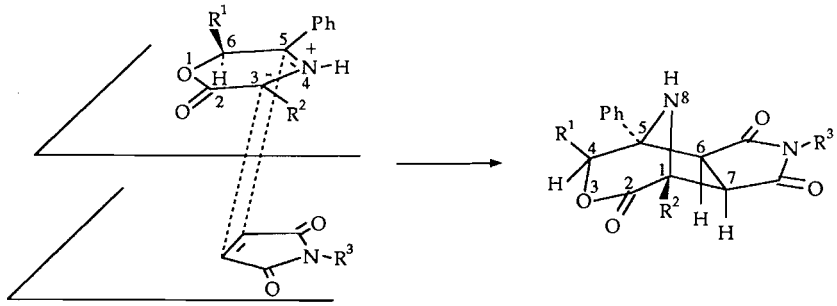

Ces composés sont instables et doivent être immédiatement engagés dans la réaction de cyclisation décrite ci-après.

Les paramètres de rmn ^1H et ^{13}C des bromhydrates qui ont cristallisé sont décrits en partie expérimentale.

Cyclisation des bromhydrates 5. Obtention des 3,6-dihydro-2*H*-1,4-oxazin-2-ones 1

En suivant le mode opératoire décrit dans la partie expérimentale, nous avons préparé les six oxazinones **1**. Les rendements sont relativement médiocres (de 30 à 50%), tout en étant comparables à celui déjà signalé pour le composé **1***a* (19). Ces composés **1** sont très peu stables sauf si, isolés à l'état solide (**1***a* et **1***c*), on les conserve au réfrigérateur. Cette fragilité ne permet pas de les purifier par une technique d'analyse immédiate comme la chromatographie ou la distillation au four tubulaire sous pression réduite lorsqu'ils sont huileux. Nous n'avons donc pas pu séparer les éventuels épimères issus de **4***d* et **4***f*. Cette fragilité avait déjà été signalée par Schulz et Steglich (19) pour des composés du même type. Les composés **1** doivent donc être engagés rapidement dans les réactions de cycloaddition dipolaire-1,3 décrites plus loin.

Malgré leur instabilité, il est possible de tracer les spectres de rmn ^1H en solution dans $CDCl_3$ (cf. partie expérimentale). Seul le produit **1***d* n'a pu être correctement analysé en rmn ^1H, mais la présence de l'ylure d'azométhine potentiel est néanmoins attesté par sa réaction ultérieure de cycloaddition. Parmi les autres composés **1**, seule l'oxazinone **1***f* (R^1 = Ph, R^2 = CH_3) pouvait exister sous forme de deux épimères *cis* et *trans*. L'examen du spectre de rmn ^1H du brut réactionnel huileux montre que l'un des épimères est largement majoritaire (>95%), les signaux de l'autre épimère étant difficilement accessibles dans le «bruit de fond» du spectre. Mais cet isomère majoritaire est peut-être totalement ou partiellement racémisé puisque les réactions de cycloaddition qui ont été engagées avec **1***f* ont conduit à un cycloadduit racémisé. On peut donc légitimement supposer que cet isomère majoritaire n'est pas énantiomériquement pur ou que la racémisation intervient lors de la réaction de cycloaddition.

Réactions de cycloaddition des oxazinones 1 sur les *N*-méthyl et *N*-phénylmaléimides

Ce sont les seuls dipolarophiles qui ont conduit à un cycloadduit. Les esters acrylique, fumarique et maléique ainsi que le diméthylacétylène dicarboxylate n'ont donné aucune réaction. Sur les six ylures d'azométhine potentiels **1**, seul le composé **1***e* n'a pas réagi et quels que soient les essais nous avons toujours observé sa décomposition avant la réaction de cycloaddition. Les cinq autres ont conduit aux cycloadduits **6** et **7** avec des rendements variant entre 20 et 50% (schéma 4).

Diastéréospécificité des réactions de cycloaddition

Toutes ces réactions sont diastéréospécifiques et la stéréochimie est de type *exo* à la fois pour le reste maléimido et pour le substituant R^1 lorsque ce dernier est différent de H.

La disposition stéréochimique du reste maléimido est déterminée à l'aide de la rmn ^1H lorsque R^2 = H. Dans ce cas les spectres de rmn ^1H présentent un signal singulet pour le proton H1. L'absence de couplage entre ce proton H1 et le proton H7 indique que l'angle dièdre H1-C1-C7-H7 est proche de 90°, ce qui impose une disposition *exo* du groupement maléimido. Cela peut sembler étonnant puisque les travaux de Harwood et coll. (7, 8) décrivent l'obtention du mélange *exo/endo* avec une plus grande proportion de ce dernier. Mais il s'agit d'un dipôle-1,3 qui n'est pas complètement inséré dans le cycle hexagonal (schéma 1). Ce résultat avait déjà été observé par Grigg et al. (20), Mkhairi et Hamelin (21) et Lakhlifi et al. (18,

Can. J. Chem. Downloaded from www.nrcresearchpress.com by 65.111.164.53 on 09/08/12
For personal use only.

Can. J. Chem. Downloaded from www.nrcresearchpress.com by 65.111.164.53 on 09/08/12
For personal use only.

Fig. 2. Structure moléculaire du cycloadduit **6***d*.

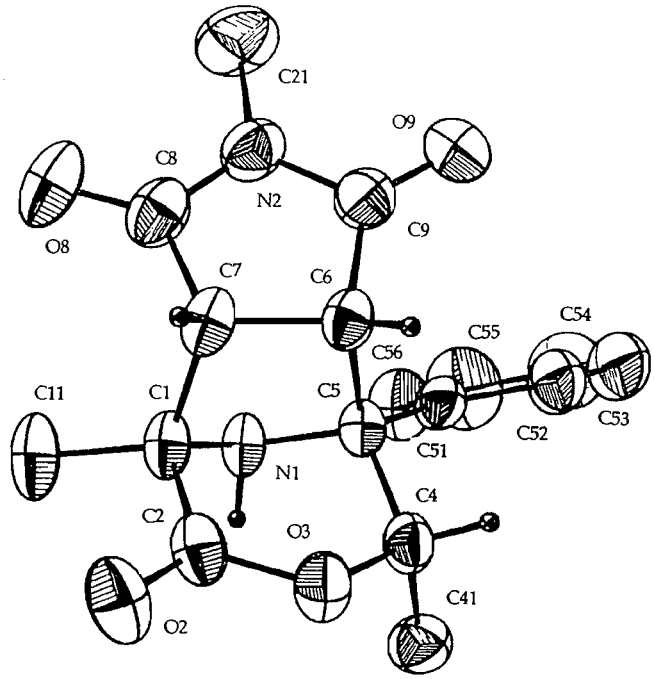

22, 23) pour des réactions analogues. Il n'est nullement contradictoire avec la règle «*endo*» puisque, comme le montre la figure 1, la disposition relative du dipôle et du dipolarophile permet une interaction maximale entre le système π du dipôle et celui du groupement maléïmido (18).

La formation des produits **6** et **7** est donc favorisée de deux façon : (*i*) cinétiquement, puisque l'approche est celle qui conduit à l'état de transition le plus stabilisé; (*ii*) thermodynamiquement, puisqu'elle conduit au stéréoisomère le moins encombré.

Dans ces conditions, il n'est pas surprenant que nous n'ayons jamais décelé, dans les bruts réactionnels, la présence d'un composé résultant de l'approche *endo*.

Sur cette même figure 1 nous avons aussi représenté l'approche du dipôle en *anti* par rapport au substituant R^1 ce qui a été prouvé par l'analyse radiocristallographique du cycloadduit **6***d* ($R^1 = R^2 = R^3 = CH_3$). La structure moléculaire de **6***d* est représentée sur la figure 2 et les distances et les angles interatomiques sont rassemblés dans les tableaux 1 et 2 respectivement. Il est raisonnable de penser que tous les cycloadduits **6** et **7** ont la même stéréochimie et que l'approche dipôle–dipolarophile s'est bien effectuée sur le demi-espace le moins encombré du dipôle cyclique.

Nous espérions réussir une synthèse asymétrique par cycloaddition du dipôle **1***f* (R^1 = Ph; $R^2 = CH_3$) où l'un des épimères est largement majoritaire. En fait, on obtient un mélange racémique du cycloadduit comme le montre le dédoublement des signaux des protons H6 et H7 sur le spectre de rmn ^{1}H du composé **6***f* enregistré dans $CDCl_3$ en présence de l'auxiliaire chiral (+)Eu(TFC)$_3$. Il apparaît donc que même si l'on pouvait obtenir un épimère énantiomériquement pur du précurseur **1***f* de l'ylure d'azométhine potentiel, la configuration absolue du carbone asymétrique C-6 est transformée en deux configurations *R* et *S* lors de la réaction de cycloaddition, probablement via deux prototropies ayant lieu lors du chauffage de l'oxazinone **1** (schéma 5). Cette racémisation peut également avoir lieu lors de la formation de **1***f* par traitement du bromhydrate **5***f* à l'aide de triéthylamine. Tout se passe donc comme s'il existait un équilibre entre les deux formes énantiomères de l'ylure d'azométhine, qui conduiront aux deux énantiomères de **6***f* ou **7***f* par cycloaddition sur le *N*-méthyl ou *N*-phénylmaléimide.

Les paramètres spectroscopiques des différents cycloadduits **6** et **7** sont rassemblés en partie expérimentale.

En conclusion, ce travail confirme la diastéréospécificité de l'approche dipôle–dipolarophile lorsque le dipôle-1,3 est complètement inséré dans un cycle, diastéréospécificité conduisant au cycloadduit de structure *exo*. Si le cycle comporte un stéréocentre, l'approche intervient également sur la face la moins encombrée du dipôle. Mais avec le présent modèle la double prototropie qui intervient au cours de la réaction empêche une éventuelle synthèse asymétrique.

Tableau 1. Distances (Å) interatomiques pour **6***d*.

N1	C1	1,466(3)	C6	C9	1,516(4)
N1	C5	1,464(3)	C7	C8	1,520(4)
N1	H1	0,90(3)	C8	O8	1,211(4)
C1	C11	1,524(4)	C9	O9	1,208(4)
C1	C2	1,526(5)	C9	N2	1,384(4)
C1	C7	1,538(4)	N2	C21	1,459(5)
C2	O2	1,207(3)	N2	C8	1,376(5)
C2	O3	1,339(4)	C51	C52	1,385(4)
O3	C4	1,470(3)	C51	C56	1,375(4)
C4	C41	1,514(4)	C52	C53	1,394(5)
C4	C5	1,538(4)	C53	C54	1,359(6)
C5	C6	1,572(4)	C54	C55	1,364(7)
C5	C51	1,521(4)	C55	C56	1,389(5)
C6	C7	1,541(4)			

Tableau 2. Angles (°) interatomiques pour **6***d*.

C1	N1	C5	104,4(2)	C7	C6	C9	104,5(2)
N1	C1	C11	112,2(2)	C1	C7	C6	104,0(2)
N1	C1	C2	114,0(2)	C1	C7	C8	114,0(2)
N1	C1	C7	99,4(3)	C6	C7	C8	104,4(2)
C11	C1	C2	109,3(2)	C9	N2	C21	123,3(3)
C11	C1	C7	117,8(2)	C9	N2	C8	113,9(3)
C2	C1	C7	103,9(2)	C21	N2	C8	122,6(3)
C1	C2	O2	123,1(3)	C7	C8	N2	108,1(2)
C1	C2	O3	118,3(2)	N2	C8	O8	124,1(3)
O2	C2	O3	118,3(3)	C7	C8	O8	127,7(3)
C2	O3	C4	122,0(2)	O9	C9	N2	123,9(3)
O3	C4	C41	107,2(2)	C6	C9	N2	107,9(2)
O3	C4	C5	111,1(2)	C6	C9	O9	128,1(3)
C41	C4	C5	114,6(2)	C5	C51	C56	121,1(3)
N1	C5	C4	109,6(2)	C5	C51	C52	120,2(2)
N1	C5	C6	101,0(3)	C52	C51	C56	118,6(3)
N1	C5	C51	113,3(2)	C51	C52	C53	120,5(4)
C4	C5	C6	109,6(3)	C52	C53	C54	120,0(4)
C4	C5	C51	109,0(2)	C53	C54	C55	120,1(3)
C7	C5	C51	114,3(2)	C54	C55	C56	120,5(4)
C5	C6	C7	104,3(3)	C51	C56	C55	120,4(4)
C5	C6	C9	114,5(2)				

Can. J. Chem. Downloaded from www.nrcresearchpress.com by 65.111.164.53 on 09/08/12
For personal use only.

Schéma 5

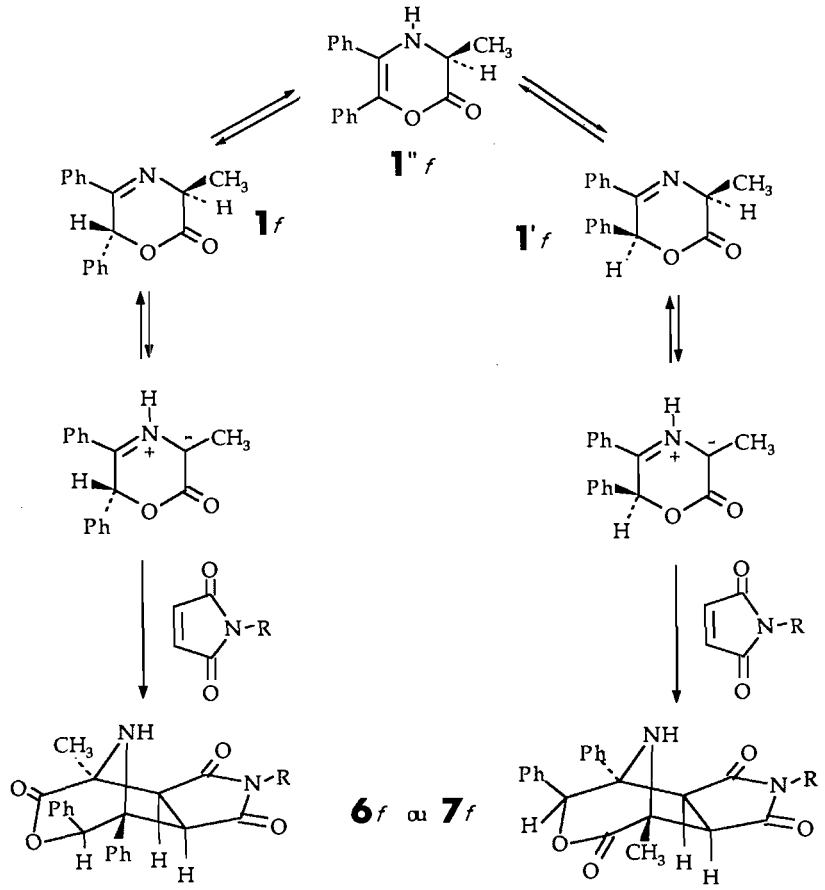

Partie expérimentale

Les points de fusion déterminés sur banc Kofler ne sont pas corrigés. Les spectres d'absorption ir ont été obtenus avec un spectrophotomètre Beckman IR 33, les produits étant pastillés dans KBr. Les spectres de rmn ^{1}H ont été obtenus avec un spectromètre Bruker-Spectrospin AC 200, les échantillons étant dissous dans $CDCl_3$ ou DMSO-d_6 avec le tétraméthylsilane comme référence interne. Les microanalyses ont été assurées par le Service d'Analyses du CNRS à Vernaison.

1. Synthèse des 5-phényl-3,6-dihydro-2*H*-1,4-oxazin-2-one 1

1.1. Préparation des esters α-cétoliques d'acides N-*(benzyloxycarbonyl)-aminés 4*

Les acides aminés *N*-protégés sont des produits commerciaux.

Mode opératoire général : Dans un réacteur de 250 mL muni d'un agitateur et d'un réfrigérant à reflux, on prépare une solution de 0,10 mol d'acide *N*-(benzyloxycarbonyl)-aminé dans 100 mL de NaOH 1 N et 70 mL d'éthanol. On y ajoute 0,10 mol d'α-bromoalkylphénone. Le mélange est porté à reflux de 1 à 3 h selon les cas. On laisse revenir le milieu réactionnel à température ambiante, puis on effectue les traitements suivants :

Avec R^1 = H, Ph et R^2 = H, CH_3 :

On additionne de l'éthanol jusqu'à ce que la solution devienne claire et limpide. La solution est placée 1 nuit au réfrigérateur. Le produit solide obtenu est filtré, séché et recristallisé dans l'éthanol. Dans le cas où R^1 = Ph et R^2 = CH_3, on obtient deux diastéréoisomères que l'on sépare par cristallisation fractionnée dans l'éthanol.

Avec R^1 = CH_3 et R^2 = H, CH_3 :

La solution est concentrée sous vide afin d'éliminer une partie de l'éthanol, puis on l'extrait à l'éther. La phase organique est lavée plusieurs fois à l'eau, séchée sur Na_2SO_4, puis évaporée sous pression réduite. Le résidu obtenu est huileux. Dans le cas ou R^1 = CH_3 et R^2 = CH_3, on obtient aussi deux diastéréoisomères que nous n'avons pas pu séparer par chromatographie.

N-*Benzyloxycarbonylglycinate de benzoylméthyle 4*a *(R^1 = R^2 = H)* : Durée de la réaction : 1 h, *F* = 96°C, Rdt. 97%; ir : ν(NH) = 3349 cm^{-1}, ν(C=O) = 1760, 1697 cm^{-1}; rmn ^{1}H ($CDCl_3$) : 4,20 (d, 2H, $J_{CH_2\text{-}NH}$ = 6), 5,14 (s, 2H, Ph-CH_2-O), 5,40 (sl, 1H, NH), 5,42 (s, 2H, -O-CH_2-CO), 7,30–7,92 (m, 10 H ar.); rmn ^{13}C ($CDCl_3$) : 42,50 (t, *J* = 140, CH_2-N), 66,50 (t, *J* = 147, CH_2), 67 (t, *J* = 148, CH_2), 127,60–136 (8 signaux des C ar.), 156,10 (s, C=O carbamate), 169,50 (s, C=O ester), 191,20 (s, C=O cétone). Anal. calc. (%) pour $C_{18}H_{17}NO_5$: C66,04, H 5,24, N 4,28; tr. (%) : C 65,93, H 5,32, N 4,17.

N-*Benzyloxycarbonyl-L-alanate de benzoylméthyle 4*b *(R^1 = H, R^2 = CH_3)* : Durée de la réaction : 3 h, *F* = 146°C, Rdt. 88%; ir : ν(NH) = 3367 cm^{-1}, ν(C=O) = 1756, 1689 cm^{-1}; rmn ^{1}H ($CDCl_3$) : 1,55 (d, 3H, *J* = 7, CH_3-CH), 4,55 (dq, 1H, $J_{CH_3\text{-}CH}$ = 7; $J_{CH\text{-}NH}$ = 7, Me-C*H*-NH-), 5,12 (s, 2H, Ph-CH_2-

Can. J. Chem. Downloaded from www.nrcresearchpress.com by 65.111.164.53 on 09/08/12
For personal use only.

O), 5,25 (d, 1H, J = 16, 20, -CO-HC*H*-O), 5,29 (sl, 1H, NH), 5,44 (d, 1H, J = 16, 20, -CO-*H*CH-O), 7,30–7,93 (m, 10 H ar.); rmn ^{13}C ($CDCl_3$) : 18,70 (q, J = 130, *C*H_3), 49,80 (d, J = 133, CH), 66,40 (t, J = 139, *C*H_2), 66,90 (t, J = 140, -*C*H_2), 127,70–136,30 (8 signaux des C ar.), 156,30 (s, C=O carbamate), 172,50 (s, C=O ester), 191,40 (s, C=O cétone). Anal. calc. (%) pour $C_{19}H_{19}NO_5$: C 66,85, H 5,61, N 4,10; tr. (%) : C 67,02, H 5,55, N 4,22.

N-*Benzyloxycarbonylglycinate de 1-benzoyléthyle* **4**c (R^1 = CH_3, R^2 = *H*) : Durée de la réaction : 3 h, huile, Rdt. 70%; ir : ν(NH) = 3368 cm^{-1}, ν(C=O) = 1757, 1700 cm^{-1}; rmn ^1H ($CDCl_3$) : 1,54 (d, 3H, J = 6,90, *C*H_3-CH-O), 3,96–4,22 (système AB dédoublé avec J_{AB} = 17, $J_{CH_2\text{-}NH}$ = 6, *C*H_2-NH), 5,10 (s, 2H, *C*H_2-O), 5,38 (t mal défini, 1H, NH), 6,05 (q, 1H, J = 6,90, O-C*H*-CH_3), 7,30–8,02 (m, 10 H ar.); rmn ^{13}C ($CDCl_3$) : 16,30 (q, J = 129, *C*H_3), 41,90 (t, J = 141, *C*H_2-N), 66,10 (t, J = 146, *C*H_2O), 71,70 (d, J = 154, *C*H-O), 127,60–135,80 (8 signaux des C ar.), 156,10 (s, C=O carbamate), 169,20 (s, C=O ester), 195,80 (s, C=O cétone). Anal. calc. (%) pour $C_{19}H_{19}NO_5$: C 66,85, H 5,61, N 4,10; Tr. (%) : C 67,16, H 5,42, N 4,37.

N-*Benzyloxycarbonyl-L-alanate de 1-benzoyléthyle* **4**d (R^1 = R^2 = CH_3) : Mélange des deux épimères non séparés. Durée de la réaction : 3 h, huile, Rdt. 86%; ir : ν(NH) = 3349 cm^{-1}, ν(C=O) = 1752, 1700 cm^{-1}; rmn ^1H ($CDCl_3$) : 1,44–1,57 (quatre doublets imbriqués correspondant aux 6 protons des groupes méthyle de chaque épimère), 4,50 (m, 1H, -C*H*-NH- des deux épimères), 5,12 (sl, 2H, CH_2-O), 5,35 (deux doublets élargis pour les groupes NH de chaque épimère), 6,02 (m, pour le groupe CH_3-C*H*-O de chaque épimère), 7,30–7,95 (m, 10 H ar.); rmn ^{13}C ($CDCl_3$) : 16,90 et 17 (deux signaux correspondant aux groupes *C*H_3-CH-NH de chaque épimère), 18,30 et 18,50 (deux signaux correspondant aux groupes *C*H_3-CH-O de chaque épimère), 49,40 et 49,60 (deux signaux correspondant aux groupes CH_3-*C*H-NH de chaque épimère), 66,80 (un signal correspondant aux groupes *C*H_2-O de chaque épimère), 72,10 et 72,20 (deux signaux correspondant aux groupes CH_3-*C*H-O de chaque épimère), 127,90–136,10 (11 signaux des C ar. des deux épimères), 155,50 et 155,60 (deux signaux correspondant aux C=O carbamate de chaque épimère), 172 et 172,50 (deux signaux correspondant aux C=O ester de chaque épimère), 196 et 196,20 (deux signaux correspondant aux C=O cétoniques de chaque épimère).

N-*Benzyloxycarbonylglycinate de désyle* **4**e (R^1 = *Ph*, R^2 = *H*) : Durée de la réaction : 3 h, F = 122°C, Rdt. 80%; ir : ν(NH) = 3357 cm^{-1}, ν(C=O) = 1751, 1694 cm^{-1}; rmn ^1H ($CDCl_3$) : 4,05–4,28 (système AB dédoublé avec J_{AB} = 17 et ^3J = 6,50, 2H, -CH_2-NH), 5,11 (s, 2H, CH_2-O), 5,31 (t élargi, 1H, NH), 6,92 (s, 1H, Ph-C*H*-O), 7,30–7,98 (m, 15 H ar.); rmn ^{13}C ($CDCl_3$) : 42,60 (t, J = 140,80, *C*H_2-N), 67 (t, J = 146, *C*H_2-O), 78,30 (d, J = 149,50, *C*H-O), 127,90–136,10 (122 signaux pour 18 C ar.), 156,40 (s, C=O carbamate), 169,60 (s, C=O ester), 193 (s, C=O cétone). Anal. calc. (%) pour $C_{24}H_{21}NO_5$: C 71,45, H 5,25, N 3,47; tr. (%) : C 71.67, H 5,12, N 3,52.

N-*Benzyloxycarbonyl-L-alanate de désyle* **4**f (R^1 = *Ph*, R^2 = CH_3) : Durée de la réaction : 3 h, Rdt. global 80%.
Epimère majoritaire, F = 110°C; ir : ν(NH) = 3379 cm^{-1}, ν(C=O) = 1760, 1701 cm^{-1}; rmn ^1H ($CDCl_3$) : 1,56 (d, 3H, J = 7,20, *C*H_3-CH), 4,54 (dq, 1H, $J_{CH_3\text{-}CH}$ = $J_{CH\text{-}NH}$ = 7,20), 5,10 (système AB fortement couplé centré à 5,10 ppm, 2H, CH_2-O), 5,29 (d, 1H, J = 7,20, NH), 6,90 (s, 1H, Ph-C*H*-O), 7,30–7,97 (m, 15 H ar.); rmn ^{13}C ($CDCl_3$) : 18,60 (q, J = 140, *C*H_3-CH), 49,50 (d, J = 145,90, *C*H-CH_3), 66,90 (t, J = 139,50, *C*H_2-O), 78,30 (d, J = 149, *C*H-O), 128,10–136,20 (10 signaux pour 15 C ar.), 155,60 (s, C=O carbamate), 172,60 (s, C=O ester), 193,10 (s, C=O cétone). Anal. calc. (%) pour $C_{25}H_{23}NO_5$: C 71,93, H 5,55, N 3,36; tr. (%) : C 72,12, H 5,41, N 3,27.
Epimère minoritaire, F = 112°C; ir : ν(NH) = 3379 cm^{-1}, ν(C=O) = 1739, 1690 cm^{-1}; rmn ^1H ($CDCl_3$) : 1,44 (d, 3H, J = 7,10, *C*H_3-CH), 4,56 (dq, 1H, $J_{CH_3\text{-}CH}$ = $J_{CH\text{-}NH}$ = 7,10), 5,08 (système AB fortement couplé centré à 5,08 ppm, 2H, *C*H_2-O), 5,26 (d, 1H, J = 7,10, NH), 7,30–7,97 (m, 15 H ar.); rmn ^{13}C ($CDCl_3$) : 18,60 (q, J = 140, *C*H_3-CH), 49,80 (d, J = 145, *C*H-CH_3), 66,90 (t, J = 139,50, *C*H_2-O), 78,20 (d, J = 147, *C*H-O), 128,10–136,20 (10 signaux pour 15 C ar.), 155,50 (s, C=O carbamate), 172,20 (s, C=O ester), 193,20 (s, C=O cétone).

1.2. Synthèse des bromhydrates des esters α-cétoliques d'acides aminés **5**

Mode opératoire général : La préparation et le traitement se font sous atmosphère d'azote. Dans un erlenemeyer bicol de 250 mL, surmonté d'un réfrigérant muni d'une arrivée d'azote, on place 10 g d'ester α-cétolique d'acide *N*-(benzyloxycarbonyl)-aminé. À l'aide d'une ampoule à brome, on additionne goutte à goutte 50 mL d'HBr–CH_3COOH à 40%.

On remarque un dégagement de CO_2 et la réaction est légèrement exothermique. Après 15 min d'agitation, on chauffe le mélange dans un bain d'huile à T = 50°C pendant 5 min. On laisse revenir le milieu réactionnel à température ambiante, puis on lui ajoute 150 mL d'éther anhydre. La solution est placée dans un bain de glace.

Pour R^1 = R^2 = H; R^1 = H, R^2 = CH_3; R^1 = Ph, R^2 = H; R^1 = Ph, R^2 = CH_3, le bromhydrate précipite avec un rendement quantitatif. Le solide est filtré sur verre fritté sous atmosphère d'azote, lavé plusieurs fois à l'éther anhydre et essoré. Ces produits incolores sont très hygroscopiques. Ils sont directement utilisés pour la réaction suivante.

Pour R^1 = CH_3 et R^2 = H, CH_3, le bromhydrate reste à l'état pâteux. On aspire la solution éthérée surnageante à l'aide d'une trompe à eau, et rince plusieurs fois à l'éther anhydre, tout en restant sous atmosphère d'azote. Ces produits pâteux sont utilisés directement pour la réaction suivante.

Les bromhydrates **5** n'ont pas été soumis à l'analyse élémentaire quantitative. Paramètres de rmn ^1H et ^{13}C des bromhydrates **5** isolés à l'état solide (dans D_2O) sont comme suit.

Bromhydrate du glycinate de benzoylméthyle **5**a (R^1 = R^2 = *H*) : rmn ^1H : 4,20 (s, 2H, CH_2-$\overset{+}{N}$), 5,76 (s, 2H, O-CH_2-O), 7,61 (t, 2 H ar.), 7,78 (d, 1H ar.), 7,97 (d, 2 H ar.); rmn ^{13}C : 42,90 (t, J = 146, *C*H_2-$\overset{+}{N}$), 70,90 (t, J = 149,50, *C*H_2-O), 129,40–137,90 (4 signaux des C ar.), 170,60 (s, C=O ester), 198 (s, C=O cétone).

Bromhydrate du L-alanate de benzoylméthyle **5**b (R^1 = *H*, R^2 = CH_3) : rmn ^1H : 1,73 (d, 3H, J = 7,20, *C*H_3-CH-$\overset{+}{N}$), 4,45 (q,

Can. J. Chem. Downloaded from www.nrcresearchpress.com by 65.111.164.53 on 09/08/12
For personal use only.

1H, J = 7,20, C*H*-CH_3), 5,70 (système AB fortement couplé centré à 5,70 ppm), 7,41 (t, 2 H ar.), 7,58 (t, 1 H ar.), 7,76 (d, 2 H ar.); rmn ^{13}C : 16,40 (q, J = 139, CH_3-CH-$\overset{+}{N}$), 49,80 (d, J = 146, -CH-$\overset{+}{N}$), 69,10 (t, J = 149, CH_2-O), 129–136,10 (4 signaux des C ar.), 178–40 (s, C=O ester), 196 (s, C=O cétone).

Bromhydrate du glycinate de désyle **5**e *(R^1 = Ph, R^2 = H)* : rmn ^{1}H : 4,29 (système AB centré à 4,29 ppm, J_{AB} = 17,50, CH_2-$\overset{+}{N}$), 7,42 (s, 1H, Ph-CH-O), 7,45–8,11 (m, 10 H ar.); rmn ^{13}C : 39,70 (t, J = 146, CH_2-$\overset{+}{N}$), 79 (d, J = 152, CH-O), 128,30–134,50 (8 signaux pour 10 C ar.), 167 (s, C=O ester), 195,30 (s, C=O cétone).

Bromhydrate du L*-alanate de désyle* **5**f *(R^1 = Ph, R^2 = CH_3), deux épimères* : rmn ^{1}H : 1,83 (d, 3H, J = 7,20, CH_3 épimère minoritaire), 1,96 (d, 3H, J = 7,20, CH_3 épimère majoritaire), 4,58 (q, 1H, J = 7,20, CH épimère majoritaire), 4,67 (q, 1H, J = 7,20, CH épimère minoritaire), 7,30–8,20 (m, 11H, Ph-CH-O et H ar. des deux épimères); rmn ^{13}C : 15,80 (q, J = 138, CH_3-CH-$\overset{+}{N}$ de l'épimère minoritaire), 16,10 (q, J = 139, CH_3-CH-N de l'épimère majoritaire), 49,40 (d, J = 147, CH-$\overset{+}{N}$ pour les deux épimères), 80 (d, J = 153, CH-O pour les deux épimères), 129,30–135,40 (8 signaux pour les 10 C ar. des deux épimères), 170,40 et 170,70 (s, C=O ester), 196 et 196,20 (s, C=O cétone).

*1.3. Préparation des 3,6-dihydro-2*H*-1,4-oxazin-2-ones* **1**

Mode opératoire général : Sous atmosphère d'azote, dans un erlenmeyer bicol surmonté d'un réfrigérant, on place 5 g du bromhydrate dans 50 mL de toluène anhydre. La solution est chauffée dans un bain d'huile à 50°C pendant 5 min. À ce mélange, on ajoute goutte à goutte un équivalent de triéthylamine en solution dans deux fois son volume de toluène anhydre. Après addition, le mélange est agité 15 min à 50°C. La solution laisse apparaître un précipité blanc qui est filtré. On concentre le filtrat à 20% de son volume sous pression réduite.

Le résidu est additionné d'éther anhydre pour faire précipiter le sel de triéthylammonium encore dissout. On filtre ce sel et réévapore la solution à l'évaporateur rotatif. On obtient un produit solide ou huileux directement utilisé pour les réactions de cycloaddition. Les solides sont purifiés par cristallisation dans l'éthanol pour les analyses spectroscopiques.

*5-Phényl-3,6-dihydro-2*H*-1,4-oxazin-2-one* **1**a *(R^1 = R^2 = H) (19)* : Rdt. 40%, F = 95°C; ir : ν(C=O) = 1739 cm^{-1}; rmn ^{1}H ($CDCl_3$) : 4,55 (t, 2H, J = 2, CH_2-N), 5,39 (t, 2H, J = 2, CH_2-O), 7,40–7,80 (m, 5 H ar.); rmn ^{13}C ($CDCl_3$) : 50,40 (t, J = 142,60, CH_2-N), 67,20 (t, J = 149,80, CH_2-O), 125,90, 128,70, 131,40 et 134 (4 signaux pour 6 C ar.), 162,90 (s, C=N), 166,60 (s, C=O).

*3-Méthyl-5-phényl-3,6-dihydro-2*H*-1,4-oxazin-2-one* **1**b *(R^1 = H; R^2 = CH_3)* : Rdt. 35%, F = 58°C; ir : ν(C=O) = 1757 cm^{-1}; rmn ^{1}H ($CDCl_3$) : 1,69 (d, 3H, J = 7,20, CH_3), 4,29 (qdd, 1H, J = 7,20, ^5J = 2,80, ^5J = 1,10, H^3), 5,23 (dd, 1H, ^2J = 16, ^5J = 2,80, H6), 5,46 (dd, 1H, ^2J = 16, ^5J = 1,10, H6′), 7,30–7,90 (m, 5 H ar.); rmn ^{13}C ($CDCl_3$) : 18 (q, J = 130, CH_3-CH), 55,20 (d, J = 137, CH-N), 66,60 (t, J = 149, CH_2-O), 126,10–134,10 (4 signaux pour 6 C ar.), 163,40 (s, C=N), 170,30 (s, C=O). Anal. calc. (%) pour $C_{11}H_{11}NO_2$: C 69,82, H 5,86, N 7,40; tr. (%) : C 70,01, H 5,76, N 7,32.

*6-Méthyl-5-phényl-3,6-dihydro-2*H*-1,4-oxazin-2-one* **1**c *(R^1 = CH_3; R^2 = H)* : Rdt. 50%, F = 54°C; ir : ν(C=O) = 1762 cm^{-1}; rmn ^{1}H ($CDCl_3$) : 1,60 (d, 3H, ^3J = 7,10, CH_3 en 6), 4,34 (dd, 1H, ^2J = 21,50, ^5J = 1,50, H3), 4,80 (dd, 1H, ^2J = 21,50, ^5J = 1,30, H3′), 5,75 (qdd, ^3J = 7,10, ^5J = 1,50, ^5J = 1,30, H6), 7,45–7,85 (m, 5 H ar); rmn ^{13}C ($CDCl_3$) : 19,20 (qd, ^1J = 129, ^2J = 5, CH_3 en 6), 50 (dd, ^1J = 148, ^1J = 136, CH_2-N), 74,60 (d, ^1J = 153, CH-O), 126,40, 128,90, 131,30 et 134,20 (4 signaux pour 6 C ar.), 166,40 (s, C=N), 167,30 (s, C=O lactone). Anal. calc. (%) pour $C_{11}H_{11}NO_2$: C 69,82, H 5,86, N 7,40; tr. (%) : C 69,76, H 5,93, N 7,51.

*5,6-Diphényl-3,6-dihydro-2*H*-1,4-oxazin-2-one* **1**e *(R^1 = Ph; R^2 = H)* : Rdt. 30%, huile non soumise à l'analyse élémentaire; ir : ν(C=O) = 1743 cm^{-1}; rmn ^{1}H ($CDCl_3$) : 4,11 (dd, 1H, ^2J = 20,90, ^5J = 1,10, H3), 4,83 (dd, 1H, ^2J = 20,90, ^5J = 0,75, H3′), 6,64 (signal élargi, 1H, H6), 7,30–7,90 (m, 10 H ar.).

*3-Méthyl-5,6-diphényl-3,6-dihydro-2*H*-1,4-oxazin-2-one* **1**f *(R^1 = Ph; R^2 = CH_3)* : Rdt. 30%, huile non soumise à l'analyse élémentaire, épimère majoritaire; ir : ν(C=O) = 1741 cm^{-1}; rmn ^{1}H ($CDCl_3$) : 1,72 (d, 3H, ^3J = 7,10, CH_3), 3,90 (q, 1H, ^3J = 7,10, H3), 6,65 (s, 1H, H6), 7,30–7,90 (m, 10 H ar.).

2. Cycloaddition des 3,6-dihydro-2*H*-1,4-oxazin-2-ones sur les *N*-méthyl et *N*-phénylmaléimides

Mode opératoire général

La réaction est effectuée sous atmosphère d'azote. On dissout 10 mmol du précurseur de dipôle dans 40 mL de toluène anhydre. À cette solution, on ajoute 12 mmol de dipolarophile et le mélange est porté à reflux pendant une durée variable.

Pour R^1 = R^2 = H, R^3 = CH_3 ou Ph et R^1 = CH_3, R^2 = H, R^3 = CH_3 ou Ph, on obtient un précipité lorsque la solution revient à température ambiante. Le solide est filtré et recristallisé dans l'éthanol.

Pour tous les autres cas, le solvant est évaporé à l'évaporateur rotatif et on obtient une huile à laquelle on ajoute 1 mL d'éthanol et 1 mL de toluène. Un solide cristallise après 24 h au réfrigérateur, il est filtré et lavé à l'éthanol.

*1,5-Imino-3-oxa-5-phénylcycloheptan-2-one-*exo*-6,7-(*N*-méthyldicarboximide)* **6**a *(R^1 = R^2 = H; R^3 = CH_3)* : Durée de la réaction : 4 h, Rdt. 30%, F = 260°C; ir : ν(NH) = 3317 cm^{-1}, ν(C=O) = 1747, 1703 cm^{-1}; rmn ^{1}H (CD_3COCD_3) : 2,65 (s, 3H, N-CH_3), 3,56 (d, 1H, J = 7,30, H6 ou H7), 3,80 (d, 1H, J = 7,30, H7 ou H8), 3,87 (sl, 1H, NH), 4,15 (s, 1H, H1), 4,27 (d, 1H, J = 11, H4), 4,98 (d, 1H, J = 11, H4′), 7,20–7,55 (m, 5 H ar.); rmn ^{13}C (CD_3COCD_3) : 24,50 (q, J = 141, N-CH_3), 51 (d, J = 144, d, C6 ou C7), 51,30 (d, J = 144, C7 ou C8), 59,80 (d, J = 155, C1), 64,80 (s, C5), 79,30 (t, J = 150, C4), 126–136,80 (4 signaux pour 6 C ar.), 167,20 (s, C=O), 174,30 (s, C=O), 175,90 (s, C=O). Anal. calc. (%) $C_{15}H_{14}N_2O_4$: C 62,93, H 4,93, N 9,78; tr. (%) : C 63,09, H 4,78, N 9,87.

*1,5-Imino-3-oxa-5-phénylcycloheptan-2-one-*exo*-6,7-(*N-

Can. J. Chem. Downloaded from www.nrcresearchpress.com by 65.111.164.53 on 09/08/12
For personal use only.

phényldicarboximide) **7**a *(R^1 = R^2 H; R^3 = Ph)* : Durée de la réaction : 4 h, Rdt. 28%, *F* = 246°C; ir : ν(NH) = 3299 cm^{-1}, ν(C═O) = 1748, 1716 cm^{-1}; rmn ^1H (DMSO-d_6) : 3,80 (d, 1H, *J* = 6,70, H6 ou H7), 3,95 (d, 1H, *J* = 6,70, H7 ou H6), 4,18 (s, 1H, H1), 4,28 (d, 1H, *J* = 10,70, H4), 4,57 (sl, 1H, NH), 5,20 (d, 1H, *J* = 10,70, H4′), 7,05–7,60 (m, 10 H ar.); rmn ^{13}C (DMSO-d_6) : 50,70 (d, *J* = 144, C6 ou C7), 50,90 (d, *J* = 144, C7 ou C6), 59,40 (d, *J* = 155, C1), 64,10 (s, C5), 78,60 (t, *J* = 153, C4), 125,80–136,70 (8 signaux pour 12 C ar.), 167,80 (s, C═O), 173,90 (s, C═O), 175,50 (s, C═O). Anal. calc. (%) pour $C_{20}H_{16}N_2O_4$: C 68,95, H 4,63, N 8,04; tr. (%) : C 68,79, H 4,72, N 8,16.

*1,5-Imino-1-méthyl-3-oxa-5-phénylcycloheptan-2-one-*exo-*6,7-(*N*-méthyldicarboximide)* **6**b *(R^1 = H; R^2 = R^3 = CH_3)* : Durée de la réaction : 18 h, Rdt. 25%, *F* = 220°C; ir : ν(VH) = 3306 cm^{-1}, ν(C═O) = 1736, 1705 cm^{-1}; rmn ^1H (DMSO-d_6) : 1,50 (s, 3H, CH_3 en 1), 2,72 (s, 3H, N-CH_3), 3,39 (d, 1H, *J* = 7,10, H6 ou H7), 3,90 (d, 1H, *J* = 7,10, H7 ou H6), 4,17 (d, 1H, *J* = 10,60, H4), 4,41 (sl, 1H, NH), 5,05 (d, 1H, *J* = 10,60, H4′), 7,25–7,55 (m, 5 H ar.); rmn ^{13}C (DMSO-d_6) : 18,10 (q, *J* = 129, CH_3 en −1), 24,70 (q, *J* = 140,50, N-CH_3), 52,10 (d, *J* = 144, C6 ou C7), 52,30 (d, *J* = 144, C7 ou C6), 63,10 (s, C1), 64 (s, C5), 79,50 (t, *J* = 152, C4), 125,90–136,80 (4 signaux pour 6 C ar.), 170,20 (s, C═O), 174,20 (s, C═O), 174,50 (s, C═O). Anal. calc. (%) pour $C_{16}H_{16}N_2O_4$: C 63,99, H 5,37, N 9,33; tr. (%) : C 64,21, H 5,27, N 9,26.

*1,5-Imino-1-méthyl-3-oxa-5-phénylcycloheptan-2-one-*exo-*6,7-(*N*-phényldicarboximide)* **7**b *(R^1 = H; R^2 = CH_3; R^3 = Ph)* : Durée de la réaction : 18 h, Rdt. 20%, *F* = 192°C; ir : ν(NH) = 3257 cm^{-1}, ν(C═O) = 1730, 1715 cm^{-1}; rmn ^1H (DMSO-d_6) : 1,61 (s, 3H, CH_3 en 1), 3,54 (d, 1H, *J* = 7,50, H6 ou H7), 4,02 (d, 1H, *J* = 7,50, H7 ou H6), 4,27 (d, 1H, *J* = 10,50, H4), 4,54 (sl, 1H, NH), 5,18 (d, 1H, *J* = 10,50, H4′), 7,10–7,70 (m, 10 H ar.); rmn ^{13}C (DMSO-d_6 : 18,20 (q, *J* = 129, CH_3 en 1), 52,30 (d, *J* = 150, C6 ou C7), 52,50 (d, *J* = 150, C7 ou C6), 63,50 (s, C1), 64,10 (s, C5), 79,30 (t, *J* = 156, C4), 125,90–136,90 (8 signaux pour 12 C ar.), 170,20 (s, C═O), 173,40 (s, C═O), 173,60 (s, C═O). Anal. calc. (%) pour $C_{21}H_{18}N_2O_4$: C 69,60, H 5,00, N 7,73; tr. (%) : C 69,73, H 4,87, N 7,89.

*1,5-Imino-*exo-*4-méthyl-3-oxa-5-phénylcycloheptan-2-one-*exo-*6,7-(*N*-méthyldicarboximide)* **6**c *(R^1 = CH_3; R^2 = H; R^3 = CH_3)* : Durée de la réaction : 5 h, Rdt. 36%, *F* > 260°C; ir : ν(NH) = 3321 cm^{-1}; ν(C═O) = 1740, 1704 cm^{-1}; rmn ^1H (DMSO-d_6) : 0,93 (d, 3H, *J* = 6,50, CH_3 en 4), 2,68 (s, 3H, N-CH_3), 3,59 (d, 1H, *J* = 7,30, H6 ou H7), 3,90 (d, 1H, *J* = 7,30, H7 ou H6), 4,02 (s, 1H, H1), 4,52 (sl, 1H, NH), 5,29 (q, 1H, *J* = 6,50, H4), 7,15–7,65 (m, 5 H ar.); rmn ^{13}C (DMSO-d_6) : 17,40 (q, *J* = 128, CH_3 en 4), 24,80 (q, *J* = 143, N-CH_3), 50,50 (d, *J* = 137,50, C6 ou C7), 51,60 (d, *J* = 146, C7 ou C6), 59,20 (s, C1), 67,30 (s, C5), 84,50 (d, *J* = 154, C4), 124,20–136,70 (5 signaux pour 6 C ar.), 167,80 (s, C═O), 174,50 (s, C═O), 176,60 (s, C═O). Anal. calc. (%) pour $C_{17}H_{18}N_2O_4$: C 64,95, H 5,77, N 8,91; tr. (%) : C 65,12, H 5,63 N 8,99.

*1,5-Imino-*exo-*4-méthyl-3-oxa-5-phénylcycloheptan-2-one-*exo-*6,7-(*N*-phényldicarboximide)* **7**c *(R^1 = CH_3; R^2 = H; R^3 = Ph)* : Durée de la réaction : 18 h, Rdt. 50%, *F* = 220°C; ir : ν(NH) = 3320 cm^{-1}; ν(C═O) = 1750, 1712 cm^{-1}; rmn ^1H (DMSO-d_6) : 1,02 (d, 3H, *J* = 6,20, CH_3 en −4), 3,75 (d, 1H, *J* = 7,10, H6 ou H7), 3,97 (d, 1H, *J* = 7,10, H7 ou H6), 4,12 (sl, 1H, NH), 5,39 (q, 1H, *J* = 6,20, H4), 6,95–7,65 (m, 10 H ar.); rmn ^{13}C (DMSO-d_6) : 17,30 (q, *J* = 127, CH_3 en 4), 50,90 (d, *J* = 149, C6 ou C7), 52 (d, *J* = 149, C7 ou C6), 59,60 (d, *J* = 155, C1), 67,50 (s, C5), 84,60 (d, *J* = 154, C4), 124, 10–136,90 (8 signaux pour 12 C ar.), 167,80 (s, C═O), 173,80 (s, C═O), 175,40 (s, C═O). Anal. calc. (%) pour $C_{21}H_{18}N_2O_4$: C69,60, H 5,00, N 7,73; tr. (%) : C 69,51, H 5,13, N 7,86.

*1,5-Imino-1-méthyl-*exo-*4-méthyl-3-oxa-5-phénylcycloheptan-2-one-*exo-*6,7-(*N*-méthyldicarboximide)* **6**d *(R^1 = R_2 = R^3 = CH^3)* : Durée de la réaction : 18 h, Rdt. 20%, *F* = 188°C; ir : ν(NH) = 3336 cm^{-1}; ν(C═O) = 1737, 1704 cm^{-1}; rmn ^1H (DMSO-d_6) : 0,93 (d, 3H, *J* = 6,50, CH_3 en 4), 1,54 (s, 3H, CH_3 en −1), 2,68 (s, 3H, N-CH_3), 3,38 (d, 1H, *J* = 7,30, H6 ou H7), 3,96 (d, 1H, *J* = 7,30, H7 ou H6), 4,43 (sl, 1H, NH), 5,28 (q, 1H, *J* = 6,50, H4), 7,25–7,70 (m, 5 H ar.); rmn ^{13}C (DMSO-d_6) : 17,30 (q, *J* = 127, CH_3 en 1 ou 4), 17,50 (q, *J* = 129, CH_3 en 4 ou 1), 24,80 (q, *J* = 141, N-CH_3), 52,80 (d, *J* = 141, C6 ou C7), 53,40 (d, *J* = 146, C7 ou C6), 63,50 (s, C1), 67,60 (s, C5), 85,20 (d, *J* = 153, C4), 124,60–137 (5 signaux pour 6 C ar.), 170,30 (s, C═O), 174,20 (s, C═O), 174,50 (s, C═O). Anal. calc. (%) pour $C_{18}H_{20}N_2O_4$: C 65,84, H 6,14, H 7,73; tr. (%) : C 66,02, H 6,07, N 7,82.

*1,5-Imino-1-méthyl-*exo-*4-méthyl-3-oxa-5-phénylcycloheptan-2-one-*exo-*6,7-(*N*-phényldicarboximide)* **7**d *(R^1 = R^2 = CH_3; R^3 = Ph)* : Durée de la réaction : 18 h, Rdt. 30%, *F* = 210°C; ir : ν(NH) = 3320 cm^{-1}, ν(C═O) = 1736, 1712 cm^{-1}; rmn ^1H (DMSO-d_6) : 1,08 (d, 3H, *J* = 6,40, CH_3 en 4), 1,69 (s, 3H, CH_3 en 1), 3,56 (d, 1H, *J* = 7,30, H6 ou H7), 4,10 (d, 1H, *J* = 7,30, H7 ou H6), 4,60 (sl, 1H, NH), 5,44 (q, 1H, *J* = 6,40, H4), 7,10–7,75 (m, 10 H ar.); rmn ^{13}C (DMSO-d_6) : 17,30 (q, *J* = 128, CH_3 en 1 ou 4), 17,60 (q, *J* = 129, CH_3 en 4 ou 1), 53 (d, *J* = 140, C6 ou C7), 53,70 (d, *J* = 145, C7 ou C6), 63,90 (s, C1), 67,80 (s, C5), 85,40 (d, *J* = 156, C4), 124,60–137 (8 signaux pour 12 C ar.), 170,30 (s, C═O), 173,30 (s, C═O), 173,60 (s, C═O). Anal. calc. (%) pour $C_{22}H_{20}N_2O_4$: C 70,20, H 5,36, N 7,44; tr. (%) : C 70,31, H 5,23, N 7,37.

*1,5-Imino-1-méthyl-3-oxa-*exo-*4-phényl-5-phénylcycloheptan-2-one-*exo-*6,7-(*N*-méthyldicarboximide)* **6**f *(R^1 = Ph; R^2 = R^3 = CH_3)* : Durée de la réaction : 18 h, Rdt. 25%, *F* > 260°C; ir : ν(NH) = 3320 cm^{-1}, ν(C═O) = 1742, 1707 cm^{-1}; rmn ^1H (DMSO-d_6) : 1,70 (s, 3H, CH_3 en 1), 2,71 (s, 3H, N-CH_3), 3,59 (d, 1H, *J* = 7,10, H6 ou H7), 4,29 (d, 1H, *J* = 7,10, H7 ou H6), 4,34 (sl, 1H, NH), 6,11 (s, 1H, H4), 6,75–7,90 (m, 12 H ar.); rmn ^{13}C (DMSO-d_6) : 17,20 (q, *J* = 129, CH_3 en 1), 24,90 (q, *J* = 141, N-CH_3), 54,20 (d, *J* = 142,50, C6 ou C7), 54,50 (d, *J* = 144, C7 ou C6), 65,10 (s, C1), 70,90 (s, C5), 89,50 (d, *J* = 155, C4), 125,10–137,10 (8 signaux pour 12 C ar.), 170 (s, C═O), 173,90 (s, C═O), 174,20 (s, C═O). Anal. calc. (%) pour $C_{21}H_{18}N_2O_4$: C 69,60, H 5,00, N 7,73; tr. (%) : C 69,77, H 4,93, N 7,82.

*1,5-Imino-1-méthyl-3-oxa-*exo-*4-phényl-5-phénylcycloheptan-2-one-*exo-*6,7-(*N*-phényldicarboximide)* **7**f *(R^1 = Ph; R^2 = CH^3; R^3 = Ph)* : Durée de la réaction : 18 h, Rdt. 40%, *F* > 260°C; ir : ν(NH) = 3288 cm^{-1}, ν(C═O) = 1742, 1704 cm^{-1};

Can. J. Chem. Downloaded from www.nrcresearchpress.com by 65.111.164.53 on 09/08/12
For personal use only.

Tableau 3. Données cristallographiques pour **6***d*.

Formule $C_{17}H_{18}N_2O_4$	fw 314,34
a = 6,734(1) Å	groupe d'espace $P2_1/n$ (No. 14)
b = 8,824(3) Å	d_{calc} = 1,324 g cm^{-3}
c = 26,556(4) Å	λ(MoKα) = 0,71073 Å
β = 92,48(1)°	μm = 0,891 cm^{-1}
V = 1576,5 Å^3	R(F) = 0,043
Z = 4	GOF = 2,447

Tableau 4. Coordonées atomiques des atomes non-hydrogène pour **6***d*.

Atom (Å^2)[a]	x	y	z	B_{eq}
N1	0,1971(3)	0,6880(3)	0,89635(8)	3,12(5)
N2	0,5908(4)	0,9276(3)	0,8906(1)	4,22(6)
O2	0,1896(3)	0,5875(3)	1,02800(7)	4,46(5)
O3	0,2994(3)	0,4536(2)	0,96570(7)	3,58(4)
O8	0,4006(4)	1,0532(2)	0,94645(9)	5,53(6)
O9	0,7729(3)	0,7518(3)	0,84913(9)	4,89(5)
C1	0,2246(4)	0,7230(3)	0,9501(1)	3,25(6)
C2	0,2300(4)	0,5835(4)	0,9842(1)	3,48(6)
C4	0,3328(4)	0,4336(3)	0,9118(1)	3,26(6)
C5	0,3627(4)	0,5871(3)	0,8858(1)	2,91(5)
C6	0,5411(4)	0,6736(3)	0,9130(1)	3,06(5)
C7	0,4418(4)	0,7771(3)	0,9512(1)	3,31(6)
C8	0,4681(5)	0,9361(4)	0,9306(1)	4,00(6)
C9	0,6499(4)	0,7816(4)	0,8794(1)	3,77(6)
C11	0,0680(5)	0,8331(4)	0,9680(1)	4,66(7)
C21	0,6660(6)	1,0618(4)	0,8656(2)	6,8(1)
C41	0,1616(5)	0,3405(4)	0,8897(1)	4,22(7)
C51	0,3866(4)	0,5605(3)	0,8298(1)	3,45(6)
C52	0,5406(5)	0,4712(4)	0,8137(1)	4,67(7)
C53	0,5583(6)	0,4411(5)	0,7625(1)	6,15(9)
C54	0,4246(7)	0,5000(6)	0,7281(1)	7,6(1)
C55	0,2737(7)	0,5897(6)	0,7535(1)	7,4(1)
C56	0,2534(5)	0,6196(5)	0,7944(1)	5,27(8)

[a] B_{eq} = (4/3)*[$a2$*B(1,1) + $b2$*B(2,2) + $c2$*B(3,3) + ab(cos γ)*B(1,2) + ac(cos β)*B(1,3) + bc(cos α)*B(2,3)]

rmn ^{1}H (DMSO-d_6) : 1,69 (s, 3H, CH_3 en 1), 3,75 (d, 1H, J = 7,30, H6 ou H7), 4,42 (d, 1H, J = 7,30, H7 ou H6), 4,53 (sl, 1H, NH), 6,24 (s, 1H, H4), 6,90–7,90 (m, 15 H ar.); rmn ^{13}C (DMSO-d_6) : 17,30 (q, J = 129, CH_3 en 1), 54,50 (d, J = 141, C6 ou C7), 54,80 (d, J = 145, C7 ou C6), 65,60 (s, C1), 71,30 (s, C5), 89,50 (d, J = 155, C4), 124,90–137 (11 signaux pour 18 C ar.), 170 (s, C═O), 173 (s, C═O), 173,30 (s, C═O). Anal. calc. (%) pour $C_{27}H_{22}N_2O_4$: C 73,95, H 5,06, N 6,39; tr. (%); C 74,12, H 5,11, N 6,27.

3. Analyse radiocristallographique du cycloadduit 6*d*

Les monocristaux incolores de morphologie irrégulière de **6***d* ont été obtenus par recristallisation dans l'éthanol. Le cristal de dimensions approximatives 0,40 × 0,30 × 0,15 mm a été monté sur un diffractomètre CAD4 d'Enraf–Nonius. Les paramètres de la maille élémentaire ont été calculés à partir de 25 réflexions sélectionnées par le programme SEARCH et centrées par SETANG de la bibliothèque SDP. Les extinctions systématiques ($h0l$, $h + l = 2n$; $0k0$, $k = 2n$) ont indiqué le groupe d'espace unique $P2_1/n$ du système monoclinique. Les intensités mesurées ont été conventionnellement corrigées pour les effets de Lorentz et de polarisation. Les données cristallographiques sont rassemblées dans le tableau 3. La structure de **6***d* a été résolue par les méthodes directes (MULTAN de SDP) qui ont permis la localisation des atomes non-hydrogène. Les coordonnées des ces atomes ont été affinées avec les facteurs thermiques anisotropes. Les positions des atomes d'hydrogène ont été calculées à l'aide du programme HYDRO, à l'exception de l'atome H1 (porté par N1) qui a été localisé sur la carte de Fourier-différence. Les atomes d'hydrogène ont été introduits dans les calculs finaux avec les paramètres thermiques isotropes. Les coordonnées des atomes non-hydrogène sont données dans le tableau 4.

Tableaux des données cristallographiques complètes (S1), facteurs thermiques anisotropes (S2), atomes d'hydrogène (S3), distances (S4) et angles (S5) interatomiques (5 pages), ont été déposés comme matériel supplémentaire.[2]

Bibliographie

1. A.G.H. Wee. J. Chem. Soc. Perkin Trans. 1, 1363 (1989).
2. D.A. Barr, M.J. Dorrity, R. Grigg et J.F. Malone. Tetrahedron Lett. **31**, 6569 (1990).
3. J. Rouden, J. Royer et H.P. Husson. Tetrahedron Lett. **30**, 5133 (1989).
4. P. Deprez, J. Royer et H.P. Husson. Tetrahedron: Asymmetry, **2**, 1189 (1991).
5. A. Padwa, Y.Y. Chen, U. Chiacchio et U. Dent. Tetrahedron, **41**, 3529 (1985).
6. T. Coulter, R. Grigg, J.F. Malone et V. Sridharan. Tetrahedron Lett. **32**, 5417 (1991).
7. A.S. Anslow, L.M. Harwood, H. Phillips et D. Watkin. Tetrahedron: Asymmetry, **2**, 169 (1991); **2**, 997 (1991).
8. A.S. Anslow, L.M. Harwood, H. Phillips, D. Watkin et L.F. Wong. Tetrahedron: Asymmetry, **2**, 1343 (1991).
9. R.M. Williams, W. Zhai, D.J. Aldous et S.C. Aldous. J. Org. Chem. **57**, 6527 (1992).
10. M. Joucla et J. Mortier. J. Chem. Soc. Chem. Commun. 1566 (1985) et références citées.
11. M. Joucla, J. Mortier, J. Hamelin et L. Toupet. Bull. Soc. Chim. Fr. 143 (1988).
12. O. Tsuge, S. Kanemasa, M. Ohe et S. Takenaka. Chem. Lett. 973 (1986).
13. H. Ardiil, R. Grigg, V. Sridharan et S. Surendrakumar. Tetrahedron, **44**, 4953 (1988).
14. P. Armstrong, R. Grigg, M.W. Jordan et J.F. Malone. Tetrahedron, **41**, 3547 (1985).
15. R. Grigg et P. Armstrong. Tetrahedron, **45**, 7581 (1989).
16. R. Grigg, L.M. Duffy, M.J. Dorrity, J.F. Malone, S. Rajviroongit et M. Thornton-Pett. Tetrahedron, **46**, 2213 (1990).

2. Cette série complète de tableaux peut être achetée de : Dépôt des données non publiées, Service de fourniture de documents, ICIST, Conseil national de recherches Canada, Ottawa, ON K1A 0S2, Canada. Les facteurs de structure observés et calculés sont disponibles auprès de l'auteur correspondant.

Les tableaux des données cristallographiques, des atomes d'hydrogène, des distances et des angles ont aussi été déposés au Cambridge Crystallographic Data Centre, University Chemical Laboratory, 12 Union Road, Cambridge, CB2 1EZ, U.K.

17. V. Caplar, A. Lisini, F. Kajfez, D. Kolba et V. Sunsic. J. Org. Chem. **43**, 1355 (1978).
18. T. Lakhlifi, A. Sedqui, T. Fathi, B. Laude et J.F. Robert. Can. J. Chem. **72**, 1417 (1994).
19. G. Schulz et W. Steglich. Chem. Ber. **110**, 3615 (1977).
20. R. Grigg, L.D. Basanagoudar, D.A. Kennedy, J.F. Malone et S. Thianpatanagul. Tetrahedron Lett. 2803 (1982).
21. A. Mkhairi. Thèse de Doctorat de l'Université de Rennes (1986); A. Mkhairi et J. Hamelin. Tetrahedron Lett. **28**, 1397 (1987).
22. T. Lakhlifi. Thèse de Doctorat ès Sciences Physiques, Besançon (1989).
23. T. Lakhlifi, A. Sedqui, B. Laude, Nguyen Dinh An et J. Vebrel. Can. J. Chem. **69**, 1156 (1991).

Can. J. Chem. Downloaded from www.nrcresearchpress.com by 65.111.164.53 on 09/08/12
For personal use only.

Cyclobutene photochemistry. Substituent effects on the photochemistry of 1-phenylcyclobutene

William J. Leigh and J. Alberto Postigo

Can. J. Chem. Downloaded from www.nrcresearchpress.com by 65.111.164.53 on 09/08/12
For personal use only.

Abstract: The photochemistry and photophysics of 1-phenylcyclobutene and five aryl-substituted derivatives have been studied in various solvents at room temperature. All six compounds fluoresce with quantum yields in the 0.2–0.3 range in cyclohexane and acetonitrile solution. 1-Phenylcyclobutene undergoes [2+2]-cycloreversion ($\phi = 0.09$) to yield phenylacetylene upon photolysis in either hydrocarbon or acetonitrile solution, and undergoes (Markovnikov) solvent addition upon irradiation in methanol solution ($\phi = 0.08$) in addition to cycloreversion. Triplet sensitization and quenching experiments indicate that cycloreversion and methanol addition are both excited singlet state processes. None of the six compounds studied undergo ring opening to the corresponding 2-aryl-1,3-butadiene in detectable yield. Quantum yields for cycloreversion in cyclohexane, acetonitrile, and methanol solution and methanol addition have been determined for the six compounds, along with excited singlet state lifetimes. The quantum yields and rate constants for cycloreversion and methanol addition are both enhanced by substitution with electron-donating groups. The variation in the rate constant for [2+2]-cycloreversion with substituent indicates that there is substantial dipolar character developed in the cyclobutenyl σ-bond framework during the reaction, in almost exact correspondence with that developed in the π system during photoprotonation. No deuterium scrambling is observed in 1-phenylcyclobutene-2,4,4-d_3 after photolysis in pentane solution to ca. 80% conversion, indicating that skeletal rearrangements leading to cyclopropyl carbenes do not occur in the direct photolysis of arylcyclobutene derivatives. A pericyclic mechanism for the photocycloreversion reaction is suggested. Triplet–triplet absorption spectra and triplet lifetimes of 1-phenyl-, 1-(*para*-methylphenyl)-, and 1-(*para*-trifluoromethylphenyl)cyclobutene in hydrocarbon solution are also reported.

Key words: photochemistry, cyclobutene, fluorescence, [2+2]-cycloreversion, substituent effects, nanosecond laser flash photolysis, lifetime, triplet state, styrene, photoaddition

Résumé : On a étudié, dans différents solvants et à différentes températures, la photochimie et la photophysique du 1-phenylcyclobutène et de cinq dérivés aryles substitués. Tous ces six composés entrent en fluorescence avec des rendements quantiques de l'ordre de 0,2 à 0,3 en solution dans le cyclohexane et dans l'acétonitrile. Le 1-phénylcyclobutène subit une cycloélimination [2+2] ($\phi = 0{,}09$) pour conduire au phénylacétylène par photolyse en solution dans un hydrocarbure ou dans l'acétonitrile, avec en plus une addition de solvant (de type Markovnikov) par irradiation dans une solution de méthanol ($\phi = 0{,}08$). Les expériences de sensibilisation du triplet et de désactivation indiquent que la cycloélimination et l'addition de méthanol sont toutes deux des états singulets excités. Aucun des six composés étudiés ne conduit par ouverture du cycle au 2-aryl-1,3-butadiène en quantité décelable. On a déterminé, pour les six composés, les rendements quantiques de la cycloélimination dans des solutions de cyclohexane, d'acétonitrile et de méthanol et de l'addition de méthanol ainsi que les temps de vie de l'état singulet excité. La présence de substituants électrodonneurs augmente les rendements quantiques et les constantes de vitesse de la cycloélimination et de l'addition de méthanol. La variation de la constante de vitesse de la cycloélimination [2+2] indique qu'il se développe un caractère dipolaire très marqué dans les liaisons σ du squelette du groupe cyclobutényle au cours de la réaction et cela correspond presqu'exactement au caractère qui se développe dans les systèmes π au cours de la photoprotonation. On n'observe pas de brouillage du au deutérium dans le 1-phénylcyclobutène-2,4,4-d_3 après la photolyse en solution dans le pentane avec une conversion de 80% environ; ceci indique que le réarrangement du squelette conduisant au carbènes du type cyclopropyle ne se produit pas lors de la photolyse directe des dérivés arylcyclobutènes. On suggère un mécanisme péricyclique pour la réaction de photocycloélimination. On rap-

Received August 28, 1994.

W.J. Leigh[1] and J.A. Postigo. Department of Chemistry, McMaster University, Hamilton, ON L8S 4M1, Canada.

[1] Author to whom correspondence may be addressed. Telephone: (905) 525-9140, ext. 23715/23485. Fax: (905) 522-2509. e-mail: LEIGH@McMAIL.CIS. McMaster.CA

porte également les spectres d'absorption triplet–triplet et les durées de vie du triplet du 1-phenyl-, du 1-(*para*-méthylphényl)- et du 1-(*para*-trifluorométhylphényl) cyclobutène en solution dans un hydrocarbure.

Mots clés : photochimie, cyclobutène, fluorescence, cycloélimination [2+2], effets de substituants, photolyse du laser, durée de vie, l'état triplet, styrène, photoaddition.

[Traduit par le rédaction]

Introduction

The photochemistry of alkyl- and arylcyclobutenes appears to differ in many respects (1, 2). Alkyl-substituted derivatives undergo competing ring opening and [2+2]-cycloreversion upon photolysis in solution. Ring opening is nonstereospecific in most simple cyclobutenes (3, 4), while cycloreversion takes place stereospecifically (5, 6). The quantum yields of these processes vary according to the relative energies of the cyclobutene Rydberg and valence states. Substitution with nonconjugative electron-withdrawing substituents results in a substantial reduction in the quantum yield for cycloreversion and a significant increase in that for ring opening (4). From this it has been concluded that ring opening is a π,π^* singlet

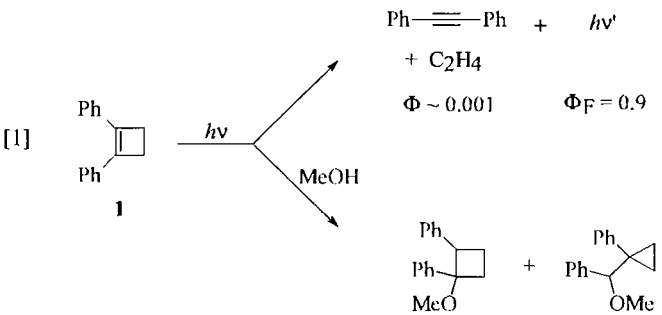

state process, while cycloreversion arises from an excited singlet state with substantial (π,R(3*s*)) Rydberg character. The observation of skeletal rearrangements in the photochemistry of asymmetrically substituted, monocyclic alkylcyclobutenes suggests that cycloreversion may proceed via cyclopropyl carbene intermediates formed by ring contraction (7–9).

While arylcyclobutenes have not been as extensively studied as alkylated derivatives, 1,2-diphenylcyclobutene (**1**) is known to fluoresce efficiently and undergo formal [2+2]-cycloreversion upon photolysis in hydrocarbon solution (see eq. [1]), to the exclusion of ring opening (9–11). This contrasts the behaviour of benzocyclobutenes and Dewar aromatics, which both undergo efficient ring opening upon photolysis in condensed media (12–15). It has been suggested that the failure of arylcyclobutenes to undergo excited state ring opening may be due to simple energetic considerations; the π,π^* singlet state energy is too low to enable cleavage of the cyclobutene C3—C4 bond (1, 2). A second possibility is that the lack of reactivity towards ring opening is for some reason due to polarization of the styrenic C=C bond in the π,π^* excited singlet state. In acyclic and other cyclic phenylalkenes, this polarization is reflected in enhanced basicity and nucleophilicity in the excited state compared to that in the ground state (16–19). This appears to hold true for arylcyclobutenes as well, since photolysis of **1** in alcohol solution results in the formation of ethers consistent with initial protonation of the lowest excited singlet state by the solvent (18).

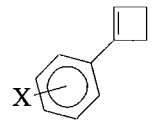

a: X = 4-OCH_3 *d*: X = 4-OCF_3
b: X = 4-CH_3 *e*: X = 4-CF_3
c: X = H *f*: X = 3-CF_3

2

1-Phenylcyclobutene (**2***c*) fluoresces ($\Phi_F = 0.27$) in solution (20) and in the gas phase (21, 22), and affords the styrenic triplet state by intersystem crossing (20, 23, 24). To our knowledge, however, no information on the photochemistry of this molecule exists in the literature. In this paper, we report the results of a study of the effects of aryl substituents on the photochemical and photophysical behavior of 1-phenylcyclobutene, using the series of compounds **2***a–f*. The study of **2***a–f*, which were chosen so as to systematically alter the basicity and polarization of the π,π^* singlet state, was undertaken with several goals in mind. Our primary goals were to determine whether ring opening might become an important mode for excited state decay in phenylated cyclobutenes when the polarization of the C=C bond is altered through appropriate substitution, and to what degree [2+2]-cycloreversion is affected by such alterations in the electronic character of the lowest excited singlet state. The possibility that photocycloreversion proceeds via a similar mechanism to that of alkylcyclobutenes has been investigated with 1-phenylcyclobutene-2,4,4-d_3 (**2***c*–d_3), in which the involvement of a cyclopropylcarbene intermediate should be revealed by scrambling of deuteriums between C4 and C3 in reisolated material after photolysis.

We also wished to examine the effects of substituents on the efficiency of the photoaddition of alcohols to the molecule, as 1-phenylcyclobutene is a rigid analog of styrene, for which the photoaddition of water and alcohols has been studied in detail (19, 25, 26). Styrenes substituted with electron-withdrawing substituents do not undergo photohydration in solution in detectable yield (19, 25, 26). The process involves initial protonation of the excited singlet state, a property that makes electron-donor substituted styrenes useful as precursors for the corresponding 1-phenylethyl cations in time-resolved studies of carbenium ion reactivity (27–29). Presumably, photoprotonation is inefficient in electron-poor analogs because their relatively low excited state basicities render the process too slow to compete effectively with free-rotor excited state relaxation. Thus, arylcyclobutenes may also be potentially suitable as precursors for the study of electron-acceptor substituted benzylic carbenium ions by time-resolved methods. We have studied the photoaddition of methanol to **2***a–f* and have examined the effect of the alcohol on their excited singlet state lifetimes, in order to lay the groundwork for future studies of this type.

Finally, we report the triplet–triplet absorption spectra of 1-phenylcyclobutene (**2***c*) and the 4-methyl- (**2***b*) and 4-trifluo-

Can. J. Chem. Downloaded from www.nrcresearchpress.com by 65.111.164.53 on 09/08/12
For personal use only.

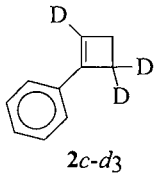

2c-d_3

romethyl- (**2*d***) analogs in cyclohexane solution at room temperature, along with rate constants for triplet–triplet energy transfer to *trans*-piperylene, obtained using nanosecond laser flash photolysis (NLFP) techniques. The triplet states of a wide variety of cyclic and acyclic arylalkenes have already been characterized by such methods (23, 30, 31), but that of 1-phenylcyclobutene has not.

Results

Compounds **2*a–f*** were synthesized by addition of the corresponding aryllithium reagent to cyclobutanone, followed by acid-catalyzed dehydration of the intermediate 1-arylcyclobutanol (**3**; see eq. [2]). The cyclobutanols were also methylated to provide authentic samples of the ethers (**4**) anticipated from the photolysis of the arylcyclobutenes in methanol solution.

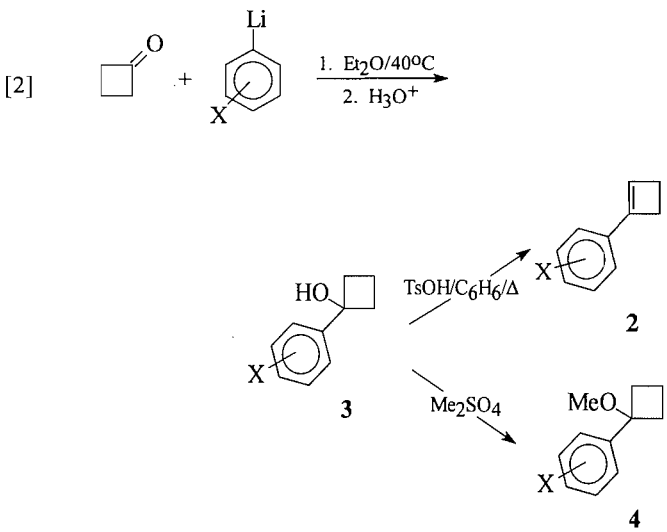

[2]

Compound **2*c*–d_3** was synthesized from cyclobutanone-2,2,4,4-d_4 using a similar procedure to that employed for the synthesis of the parent compound (**2*c***). ^{1}H NMR analysis of the compound indicated it to be ca. 93% deuterated at positions 2 and 4 of the cyclobutenyl ring.

Direct irradiation of deoxygenated ~0.002 M solutions of **2*a–f*** in pentane or dried acetonitrile results in the formation of the corresponding arylacetylenes **5*a–f*** in high chemical yield (eq. [3]). In one case (**2*f***), the photolysates also contained substantial amounts of two dimeric compounds. The dimers were not isolated, but were tentatively identified as such on the basis of their mass spectra. The yields of the dimers were significant even when the concentration of **2*f*** was lowered to 2×10^{-4} M. Irradiation of a pentane solution of **2*f*** (2×10^{-4} M) containing 0.02 M 1,3-cyclohexadiene had no effect on the yield of arylacetylene **5*f***, but led to substantial quenching of the formation of the dimeric products.

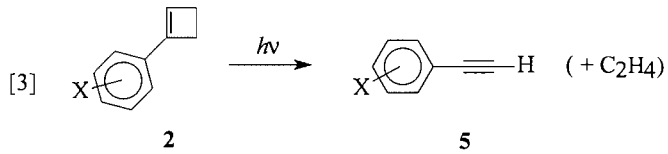

[3]

Photolysis of a deoxygenated 0.05 M solution of **2*c*–d_3** in acetonitrile-d_3 under similar conditions to those above resulted in the formation of phenylacetylene-*d* (**5*c*–*d***), as verified by GC–MS analysis. Integration of the ^{1}H NMR spectrum of the crude mixture after photolysis to ca. 50% conversion afforded a H3/H4 ratio in the remaining starting material which was indistinguishable from that measured in the unphotolyzed material.

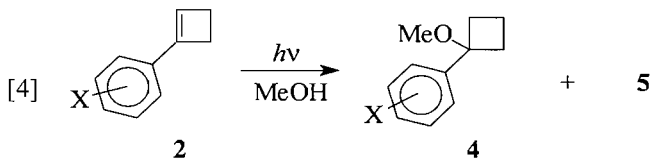

[4]

Direct irradiation of deoxygenated ~0.002 M solutions of **2** in methanol results in the formation of the corresponding 1-aryl-1-methoxycyclobutane **4** (eq. [4]), with substantial quenching of the formation of **5** in each case. No other products were observed to be formed in significant yield from photolysis of any of the compounds studied, so long as the conversions were kept below ca. 30%. At higher conversions, small amounts of reduction products of **2** could be detected in the photolysates; these were tentatively identified as the corresponding arylcyclobutanes by GC–MS. Photolysis of similar solutions in the presence of *trans*-1,3-pentadiene (0.01 M) yielded the same products in approximately the same quantum yields as those carried out in the absence of diene.

Quantum yields for formation of **5** (ϕ_5) and **4** (ϕ_4) from direct irradiation of **2** (to ca. 5% conversion) in deoxygenated pentane and methanol solutions, respectively, were determined by potassium ferrioxalate actinometry and are collected in Table 1. Included in this table are quantum yields for the formation of **5** in acetonitrile solution, which were determined for each compound using the quantum yields in pentane as secondary standards. Quantum yields for formation of **5** in methanol solution were estimated based on the relative yields of **5** and **4** obtained upon photolysis of **2** (to 5–12% conversion) in that solvent.

Photolysis of deoxygenated 0.008 M solutions of **2*c*** in acetonitrile containing varying amounts of methanol between 0 and 16 M were carried out in a merry-go-round apparatus, and product formation was monitored by GC after ca. 2% conversion. Figure 1(*a*) shows the Stern–Volmer plot for quenching of the formation of phenylacetylene (**5*c***) by the alcohol. The slope yields a Stern–Volmer constant of $k_q\tau = 0.046 \pm 0.003$ M^{-1}. Figure 1(*b*) shows a reciprocal plot of the yield of **4*c*** obtained in these experiments as a function of methanol concentration. The data were corrected for the formation of a small amount of a product (presumably the alcohol **3*c***) that has the same retention time as the ether under the GC conditions employed, and which is formed in significant yields in acetonitrile in the absence of methanol. The intercept/slope

Can. J. Chem. Downloaded from www.nrcresearchpress.com by 65.111.164.53 on 09/08/12
For personal use only.

Table 1. Quantum yields for arylacetylene (**5**) formation from photolysis of **2***a–f* in pentane, acetonitrile, and methanol solution, and for methyl ether (**4**) formation from photolysis of **2***a–f* in methanol solution at 23°C.[a]

2	Substituent	$\phi_5^{pentane}$	ϕ_5^{MeCN}	ϕ_4^{MeOH}	ϕ_5^{MeOH}
a	4-OMe	0.20 ± 0.02	0.18 ± 0.02	0.13 ± 0.02	0.05 ± 0.02
b	4-Me	0.15 ± 0.02	0.12 ± 0.05	0.10 ± 0.02	0.03 ± 0.02
c	H	0.09 ± 0.01	0.09 ± 0.02	0.08 ± 0.01	0.010 ± 0.005
d	4-CF_3	0.07 ± 0.01	0.08 ± 0.01	0.05 ± 0.01	0.016 ± 0.003
e	4-OCF_3	0.022 ± 0.003	0.035 ± 0.009	0.024 ± 0.007	0.005 ± 0.002
f	3-CF_3	0.0045 ± 0.0006	0.0090 ± 0.0006	0.0006 ± 0.0001	0.0001 ± 0.0001

[a]Determined by electronic actinometry, calibrated with ferrioxalate. ϕ_5^{MeOH} values were estimated from the relative yields of **5** and **4** in methanol solution and the corresponding ϕ_4^{MeOH} values.

Table 2. Fluorescence emission maxima, quantum yields and lifetimes for **2***a–f* in pentane and acetonitrile and fluorescence lifetimes in methanol.[a]

		Pentane			Acetronitrile			Methanol
2	X	λ_F^{max}	ϕ_F[b]	τ_F (ns)[c]	$\lambda_F$max	ϕ_F[b]	τ_F (ns)[c]	τ_F (ns)[c]
a	4-OMe	330	0.20	12.9	331	0.20	10.2	5.6
b	4-Me	335	0.21	12.1	319	0.22	9.7	6.6
c	H	309	0.25	12.2	320	0.24	9.0	7.4
d	4-CF_3	309	0.25	12.1	322	0.27	11.8	11.5
e	4-OCF_3	335	0.30	12.5	337	0.31	11.6	10.8
f	3-CF_3	337	0.31	6.7	331	0.18	7.5	7.0

[a]Determined at 23 ± 1°C.
[b]Errors in fluorescence quantum yields are ca. 20%.
[c]Errors in lifetimes are ca. 10%.

ratio calculated by least-squares analysis of these data affords $k_q\tau = 0.02 \pm 0.01$ M^{-1}; this value should be considered to be a lower limit owing to the poor precision of the data at lower methanol concentrations.

Steady state fluorescence emission spectra of the six compounds were recorded in deoxygenated acetonitrile and pentane solutions at 25°C, as well as in methanol in the cases of **2***b–d*. The emission bands showed minor fine structure in pentane, but were approximately Gaussian in acetonitrile and methanol, with maxima centred at 320–330 nm. Fluorescence quantum yields were determined using naphthalene as a standard ($\phi_F = 0.23$ (32)) (33), and are listed in Table 2.

The phosphorescence emission spectrum of **2***c* was measured in a methylcyclohexane glass at 77 K. The spectrum (not shown) is similar in position and fine structure to that reported by Ramamurthy et al. for the same compound in thallium-exchanged zeolites (24). The phosphorescence lifetime was determined to be 4.1 ± 0.2 ms in methylcyclohexane at 77 K.

Fluorescence lifetimes were determined for **2***a–f* in deoxygenated pentane, acetonitrile, and methanol solutions using the time-correlated single photon counting technique, and are also included in Table 2. The fluorescence of carefully purified samples of **2***b–f* (monitored at the emission maxima) exhibited single exponential decay kinetics, so long as the number of counts acquired for decay acquisition was kept below 5000. In the case of **2***a*, it was necessary to limit acquisition to less than 2000 counts. GC analysis verified that sample photodecomposition was negligible (i.e., <1%) over the course of these experiments in each case. Oxygen quenches the fluorescence of **2***a–c* efficiently; for example, the lifetime of **2***b* in air-saturated acetonitrile is $\tau_s = 6.0$ ns. This allows a rough estimate of $k_q \sim 2 \times 10^{10}$ M^{-1} s^{-1} for the rate constant for quenching of the excited singlet state of this compound by oxygen in this solvent. On the other hand, there is less than a 10% difference in the lifetimes of **2***d,e* and no difference in those of **2***f* in air- and nitrogen-saturated acetonitrile.

Table 3 contains rate constants for fluorescence (k_F^0) and cycloreversion (k_5) in pentane and acetonitrile solution and cycloreversion and methanol addition (k_4) in methanol, calculated using the quantum yield and lifetime data collected in Tables 1 and 2.

Addition of methanol (0–2 M) to deoxygenated solutions of **2***c* in acetonitrile results in a slight reduction in singlet lifetime: ca. 10% over the concentration range studied. Least-squares analysis of a plot of $1/\tau_s$ vs. methanol concentration over the 0–2 M range (Fig. 1(*c*)) affords a slope of $k_q = (5.1 \pm 1.4) \times 10^6$ M^{-1} s^{-1}. Over a larger concentration range, a plot of $1/\tau_s$ vs. [MeOH] is curved, levelling off to a value of 1.35×10^8 s^{-1} ($\tau_s = 7.4$ ns) for the neat alcohol.

Nanosecond laser flash photolysis (NLFP) experiments employed the pulses (248 nm, 16 ns, 40–80 mJ) from a Kr/F_2 excimer laser and a microcomputer–controlled detection system. Flash photolysis of continuously flowing, extensively deoxygenated isooctane solutions of **2***c* (ca. 6×10^{-5} M) gave

Can. J. Chem. Downloaded from www.nrcresearchpress.com by 65.111.164.53 on 09/08/12
For personal use only.

Table 3. Rate constants for fluorescence (k_F^0) in cyclohexane and acetonitrile solution, [2+2]-cycloreversion (k_5) in pentane, acetonitrile, and methanol solution, and photoaddition of methanol in neat methanol (k_4).[a]

		Hydrocarbon[b]		Acetonitrile		Methanol	
2	X	k_F^0 ($\times 10^{-7}$ s)	k_5 ($\times 10^{-7}$ s)	k_F^0 ($\times 10^{-7}$ s)	k_5 ($\times 10^{-7}$ s)	k_5 ($\times 10^{-7}$ s)	k_4 ($\times 10^{-7}$ s)
a	4-OMe	1.6 ± 0.2	1.6 ± 0.2	2.2 ± 0.3	2.0 ± 0.2	0.88 ± 0.08	2.3 ± 0.3
b	4-Me	1.7 ± 0.2	1.2 ± 0.2	2.4 ± 0.3	1.3 ± 0.5	0.46 ± 0.05	1.5 ± 0.2
c	H	2.0 ± 0.2	0.74 ± 0.07	2.6 ± 0.3	1.0 ± 0.2	0.14 ± 0.02	1.1 ± 0.2
d	4-CF_3	2.4 ± 0.2	0.58 ± 0.08	3.0 ± 0.4	0.7 ± 0.1	0.14 ± 0.02	0.4 ± 0.1
e	4-OCF_3	3.4 ± 0.3	0.18 ± 0.2	3.6 ± 0.4	0.3 ± 0.1	0.046 ± 0.006	0.2 ± 0.1
f	3-CF_3	4.6 ± 0.5	0.07 ± 0.01	2.9 ± 0.3	0.14 ± 0.02	0.0014 ± 0.003	0.009 ± 0.001

[a]Calculated from quantum yield and lifetime data in Tables 1 and 2.
[b]Fluorescence lifetimes were determined in cyclohexane solution; cycloreversion was determined in pentane solution.

rise to readily detectable transient absorptions in the 300–340 nm region (λ_{max} = 310 nm), which decayed with clean pseudo-first-order kinetics and a lifetime of about 2 μs. Figure 2 shows the transient absorption spectrum obtained from this solution; the insert shows a transient decay trace measured at a monitoring wavelength of 320 nm. Decay traces were collected by signal averaging of four to five separate decays, with correction for the substantial prompt fluorescence emitted by the sample. The presence of oxygen (either added intentionally or due to incomplete deoxygenation) results in substantial reductions in both the initial yield and the lifetime of the transient. The transient is quenched by *trans*-piperylene ($k_q = (1.6 \pm 0.1) \times 10^9$ M^{-1} s^{-1}), and can thus be assigned to the triplet state of **2***c*.

Similar experiments were carried out for 1-(*para*-methylphenyl)- and 1-(*para*-trifluoromethylphenyl)cyclobutene. The triplet–triplet absorption spectrum of **2***b* exhibited λ_{max} = 310 nm, while that of **2***d* was shifted to 320 nm. The triplet lifetimes of both compounds were similar to that of **2***c* in deoxygenated isooctane solution. The triplet–triplet absorptions of **2***b* and **2***d* exhibited similar sensitivities to the presence of oxygen and similar rate constants for quenching by *trans*-piperylene as those from **2***a*. NLFP of extensively deoxygenated solutions containing varying concentrations of **2***d* between 5×10^{-5} and 2×10^{-4} M allowed us to estimate an upper limit of 1×10^9 M^{-1} s^{-1} for the self-quenching rate constant for **2***d*.

Flash photolysis of a deoxygenated, 0.02 M solution of 4-methoxyacetophenone in acetonitrile with a nitrogen laser (337 nm, 6 ns, 4–5 mJ) afforded readily detectable transient absorptions at 385 nm due to formation of the ketone triplet state. The lifetime of the triplet state is quenched upon addition of **2***c* to the solution, with a bimolecular rate constant of $k_q = (2.4 \pm 0.1) \times 10^9$ M^{-1} s^{-1}.

Discussion

The values of ϕ_F (= 0.24) and τ_s (= 12.2 ns) reported here for **2***c* in pentane solution at room temperature are both in reasonable agreement with those reported by Zimmerman et al. for the same compound in methylcyclohexane–isopentane solution at 27°C (ϕ_F = 0.27; τ_s = 15.9 ± 0.9 ns) (20). These workers also reported a value of ϕ_{ISC} = 0.004 for the quantum yield of intersystem crossing in **2***c*, determined by the biacetyl phosphorescence sensitization method (34, 35). Thus, intersystem crossing is over an order of magnitude less efficient than either fluorescence or reaction via [2+2]-cycloreversion (ϕ_{5c} = 0.09), and the combination of these three processes accounts for only about 40% of excited state decay events. Presumably, nonproductive radiationless decay processes account for the rest.

The fluorescence emission maxima of **2***a–f* vary slightly between 320 and 330 nm, but show no regular variation with substituent or solvent throughout the series. On the other hand, the fluorescence quantum yields increase throughout the series in both solvents while the singlet lifetimes decrease, resulting in a fourfold variation in the radiative rate constant k_F^0 (Table 3). The singlet lifetimes are consistently shorter in acetonitrile solution than in pentane for **2***c* and those derivatives bearing electron-donating substituents (**2***a*, *b*). This may be due to the presence of small amounts of water in the polar solvent. Oxygen quenches the lowest excited singlet state of **2***a–c* efficiently ($k_q \sim 2 \times 10^{10}$ M^{-1} s^{-1} for **2***b*), presumably by an electron transfer mechanism (36, 37). In agreement with this, the fluorescence lifetimes of **2***d–f* are approximately the same in air- and nitrogen-saturated solution.

1-Phenylcyclobutene (**2***c*) exhibits readily detectable phosphorescence in a hydrocarbon glass at 77 K, but detection of the triplet in solution at room temperature by nanosecond laser flash photolysis (NLFP) techniques is difficult unless the solutions are *thoroughly* deoxygenated. Presumably, this reflects the rapid quenching of the excited singlet state of **2***c* by molecular oxygen. The triplet–triplet absorption spectrum reported here for **2***c* is similar to that reported previously for 1-phenylcyclopentene (23). The lifetime and UV absorption spectrum of the triplet state of **2***c* appears to be relatively insensitive to substituents on the aryl ring or to solvent polarity. The rate constants for triplet quenching by dienes (e.g., *trans*-piperylene) are significantly slower than the diffusion-controlled rate in both acetonitrile and isooctane, presumably because the triplet energy of **2***c* (ca. 60 kcal/mol (24)) is approximately isothermal with the diene triplet energy. The triplet state of **2***d* is reactive toward dimerization ($k_{sq} \sim 1 \times 10^9$ M^{-1} s^{-1}), but this process proceeds in significant chemical yield only when population of the triplet by intersystem crossing competes

Can. J. Chem. Downloaded from www.nrcresearchpress.com by 65.111.164.53 on 09/08/12
For personal use only.

Can. J. Chem. Downloaded from www.nrcresearchpress.com by 65.111.164.53 on 09/08/12
For personal use only.

Fig. 1. Quenching of 1-phenylcyclobutene (2*c*) excited singlets by methanol in deoxygenated acetonitrile solution at 23°C: (a) Stern–Volmer plot for the quenching of phenylacetylene (**5***c*) formation; (b) Reciprocal plot for the formation of methyl phenylcyclobutyl ether (**4***c*); (c) quenching of singlet lifetime.

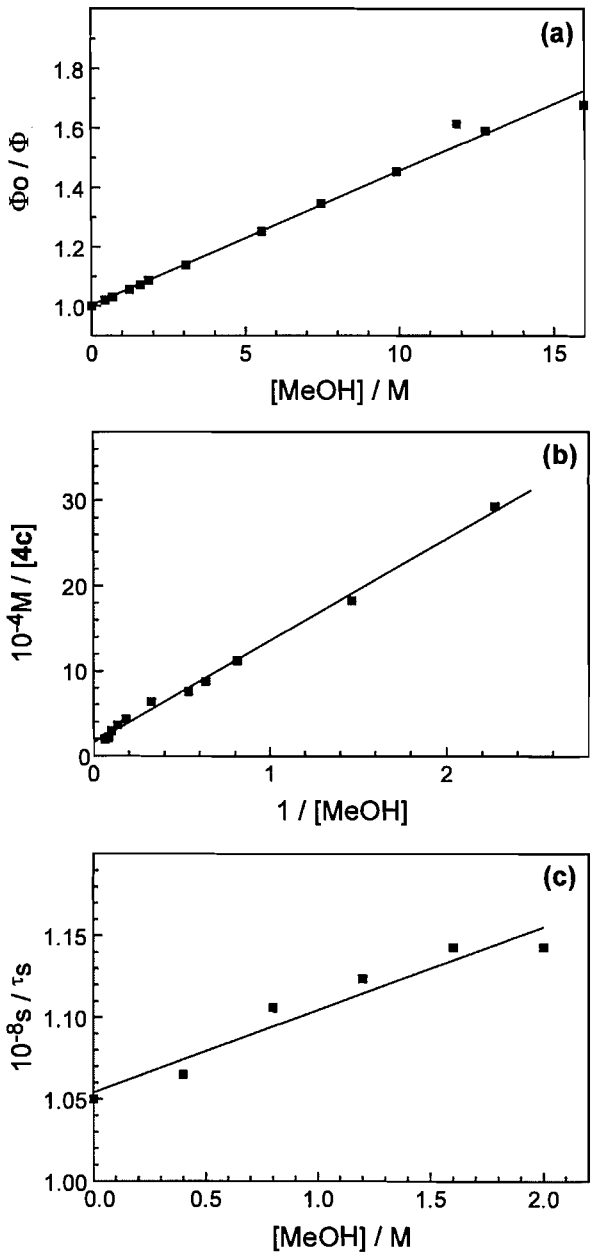

effectively with excited singlet state cycloreversion, as in those derivatives bearing strong electron-withdrawing substituents on the phenyl ring.

Direct irradiation of **2** in aprotic solvents results in the formation of the corresponding phenylacetylene (**5**) in high chemical yield. The reaction is singlet derived, as evidenced by the lack of observable quenching of the formation of **5***c* from photolysis of **2***c* in the presence of diene, and the fact that **5***c* is not formed under triplet sensitization conditions. While there is no significant solvent effect on the quantum yield for cycloreversion for any of the compounds studied (except perhaps for **2***f*), the quantum yields (Table 1) and rate constants (Table 3) for the process decrease markedly throughout the series with increasing substituent electron-withdrawing power.

Fig. 2. The triplet–triplet absorption spectrum of 1-phenylcyclobutene (**2***c*) in deoxygenated isooctane solution, obtained by nanosecond laser flash photolysis techniques. The insert shows a representative decay trace, monitored at 320 nm.

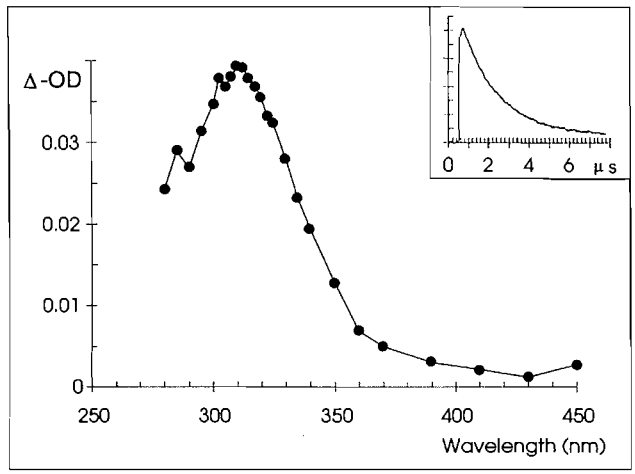

The rate constants for cycloreversion of **2** show only a very qualitative correlation with ground-state substituent constants ($\rho = -1.2 \pm 0.5$ ($r^2 = 0.60$) for the data in pentane solution). That of the *meta*-trifluoromethyl substituted derivative **2***f* correlates particularly poorly with the rest of the compounds in the series. The general inadequacy of ground state substituent constants, particularly for *meta* substituents, in describing substituent effects on excited-state reactions of aromatic compounds is well documented (16, 26, 38–43). The cycloreversion rate constants for **2***a–d,f* correlate somewhat better with the σ_{ex} values of Baldry (which are based on the excited state pK_a values of substituted phenols (38)), but still only qualitatively; $\rho_{ex} = -0.9 \pm 0.4$ ($r^2 = 0.69$). Correlation with the $\sigma^{h\nu}$ scale of McEwen and Yates (based on the photoprotonation of substituted styrenes and phenylacetylenes (26)) is not possible owing to the absence of data for electron-withdrawing substituents other than 4-fluoro.

Electrocyclic ring opening to the corresponding 2-aryl-1,3-butadiene does not occur in detectable yield with any of the compounds studied in this work. From this it can be concluded that efficient ring opening requires that the energy of the lowest excited singlet state be significantly higher than the cyclobutenyl C3—C4 bond energy.

Photolysis of **2** in methanol solution results in the formation of the corresponding Markovnikov addition product **4** in high chemical yield. The reaction occurs from the lowest excited singlet state, as evidenced by the lower fluorescence lifetimes observed for **2***a–d* in methanol compared to those in acetonitrile, the substantial quenching of the formation of cycloreversion products in methanol and methanolic acetonitrile, and the fact that the reaction is not quenched by dienes. In the case of **2***c*, the Stern–Volmer constant obtained from the quenching of phenylacetylene formation by methanol in acetonitrile (Fig. 1(*a*)) agrees with that obtained from the reciprocal plot for the formation of cyclobutyl ether **4***c* (Fig. 1(*b*)) within experi-

[5] 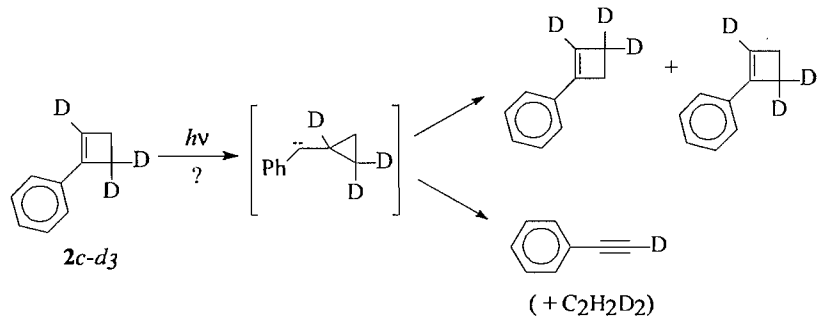

mental error. The Stern–Volmer constant ($k_q\tau = 0.046 \pm 0.003$ M^{-1}) obtained from least-squares analysis of the data in Fig. 1(*a*) affords a quenching rate constant $k_q = 5.1 \times 10^6$ M^{-1} s^{-1}, in satisfactory agreement with the rather imprecise value measured by single photon counting techniques ($k_q = (5.1 \pm 1.4) \times 10^6$ M^{-1} s^{-1}). It is noteworthy that the rate of quenching of the excited singlet state of **2***c* in acetonitrile, as measured by the above techniques, is approximately an order of magnitude faster than that determined in neat methanol solution (4.4×10^5 M^{-1} s^{-1}; from the Φ_{4c} and τ_s-values for **2***c* in methanol). While we cautiously ascribe this to a simple solvent effect, the difference *should* result in curvature in quenching plots taken over the full range of concentrations between neat acetonitrile and neat methanol.

Most aspects of the excited singlet state quenching of **2** by methanol appear to be analogous to those observed for the quenching of the excited singlet states of acyclic and other cyclic styrene derivatives by water and alcohols (16, 25, 44). As anticipated, however, addition to **2** occurs with measurable efficiency even in the derivatives bearing reasonably strong electron-withdrawing groups. As noted previously for styrene, the regiochemistry and substituent effect on the rates of photoaddition of methanol are consistent with significant π-polarization of the C=C bond in the lowest excited singlet state of 1-phenylcyclobutene. Electron-withdrawing substituents on the phenyl ring reduce the polarization of the C=C bond, lowering its basicity and reducing its reactivity toward photoprotonation. In spite of this qualitative similarity to styrene photoadditions, the magnitude of the substituent effect on the process appears to differ significantly in 1-phenylcyclobutene. This can be seen by comparing the span in the rate constants for methanol addition in **2** to those reported by McEwen and Yates for the rates of water-catalyzed photohydration of substituted styrenes in neutral aqueous solution. These were reported to be 1.86×10^4 M^{-1} s^{-1} for styrene itself, 3.80×10^4 M^{-1} s^{-1} for 4-methylstyrene, and 2.45×10^5 M^{-1} s^{-1} for 4-methoxystyrene (26). The corresponding parameters in the present study are the k_4-values calculated from the ϕ_4 and τ_s^{MeOH} values for **2***a–c* in methanol solution (Table 3), after conversion to second-order rate constants by correcting for the solvent concentration (they vary by only a factor of about two throughout the series of three compounds). For the parent compound, the rate of methanol addition to **2***c* in methanol is ~25 times faster than the rate of water addition to styrene in water. The much less pronounced substituent effect on the rates of methanol photoaddition to **2***c* compared to that on the rates of water photoaddition to styrene may be the result of this substantial difference in absolute reactivity, although it will clearly be necessary to study the photochemistry of the two sets of compounds under more similar sets of conditions before reliable conclusions can be made in this regard.

The mechanism of [2+2]-photocycloreversion in arylcyclobutenes is expected to differ from that in alkylcyclobutenes. In the latter case, previous work has led to the conclusion that cycloreversion derives from a π,R(3*s*)-like state (4) and may involve the intermediacy of cyclopropyl carbene intermediates (7). The π,R(3*s*) state in **2** is expected to be substantially higher in energy than the π,π* singlet state (45), and is thus not expected to play a role in the photochemistry of phenylated systems. Indeed, while there is substantial precedent for Rydberg-derived [1,2]-shifts in the photochemistry of aliphatic alkenes and cycloalkenes (17, 46), there appear to be few examples (47) of such processes (yielding carbenes) in phenylalkene photochemistry. Although the excited singlet state behaviour of most of the phenylalkenes that have been studied is dominated by torsional relaxation (so that carbene-derived products might be difficult to detect in significant yield, particularly when the carbene intermediate can revert to the starting olefin), rearrangements of this type have not been observed even in the torsionally constrained phenylcycloalkenes that have been investigated in detail (44, 48).

Nevertheless, it is interesting to note that the efficiency of photocycloreversion in **2** is subject to a similar polar substituent effect as that observed previously for alkylcyclobutene derivatives (4). We thus felt it was important to study the mechanism of the formal [2+2]-cycloreversion reaction of **2** in greater detail. The photochemistry of 2,4,4-trideuterio-1-phenylcyclobutene (**2***c–d*$_3$) in acetonitrile solution was investigated in order to probe for skeletal rearrangements that might be indicative of the intermediacy of a cyclopropyl carbene in the [2+2]-cycloreversion process. If cycloreversion proceeds via such an intermediate (see eq. [5]), then one would expect to observe scrambling of deuterium between positions 3 and 4 of the cyclobutenyl ring, since carbenes of this type are known to undergo ring expansion to the corresponding cyclobutene in addition to fragmentation to alkene and alkyne (49–51). Examination of the ^{1}H NMR spectrum of an irradiated 0.02 M solution of **2***c–d*$_3$ after ca. 50% conversion offers no evidence for significant scrambling of the label between the two positions. We thus conclude that cyclopropyl carbene intermediates are not formed in the direct photolysis of phenylcyclobutenes to a significant extent; the similarity in the substituent effect on the quantum yield of the process to that in alkylcyclobutenes appears to be coincidental.

The substituent effect on k_5 indicates that there is substantial dipolar character developed in the σ-bond framework dur-

Can. J. Chem. Downloaded from www.nrcresearchpress.com by 65.111.164.53 on 09/08/12
For personal use only.

Can. J. Chem. Downloaded from www.nrcresearchpress.com by 65.111.164.53 on 09/08/12
For personal use only.

Fig. 3. Log–log plot of the rates of methanol addition (k_4) versus photocycloreversion (k_5) in methanol solution for **2***a–f*.

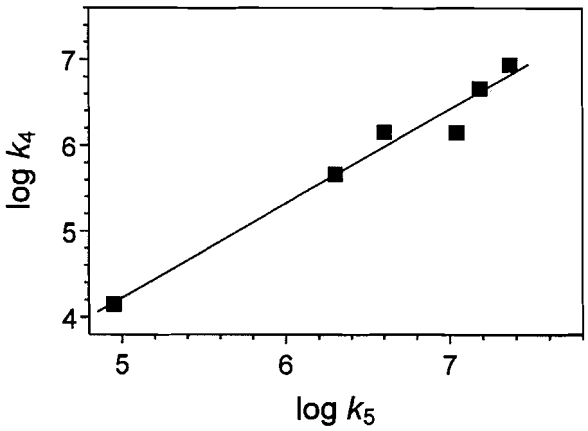

ing the formal [σ_{2s} + σ_{2s}]-cycloreversion reaction, with positive charge developing at C1 of the cyclobutene ring. This is similar to the polarization experienced in the π-bond framework during photoprotonation; a log–log plot of the rate constants for photocycloreversion (in methanol) versus those for solvent photoaddition (Fig. 3) has a slope of 1.1 ± 0.2 (r^2 = 0.970), indicating an almost exact correspondence between the substituent effects on the two processes. It is reasonable to conclude that the photochemical [2+2]-cycloreversion of phenylcyclobutenes is a concerted process, which proceeds through a transition state of considerable dipolar character in the cyclobutenyl σ-bond framework (eq. [6]). In fact, theory predicts that polar factors should have a pronounced effect on the dynamics of singlet [2+2]-cycloreversion and -cycloaddition when the diagonals of the four-atom array are unequal (52, 53). To our knowledge, this is the first experimental verification of this in excited singlet [2+2]-cycloreversion reactions. In contrast to the substantial effect of polar substituents on the rate of the process, there is little variation in rate with solvent polarity in aprotic solvents (Table 3). Surprisingly, there is a substantial reduction in the rates of cycloreversion of all six compounds in methanol compared to acetonitrile; the origins of this intriguing solvent effect are the subject of continued study.

The substantial photoreactivity that **2***a–f* exhibit towards methanol holds considerable promise for studies of the effects of electron-withdrawing substituents on the kinetics of alkene photoprotonation and on the reactivity of the corresponding benzylic carbenium ions. Further work in this area will be directed at more detailed studies of the photoaddition of alcohols to arylcyclobutenes, and toward establishing a more precise comparison between the reactivity of phenylcyclobutenes and simple styrenes toward excited singlet state protonation.

Experimental

^{1}H NMR spectra were recorded on Bruker AC200 (200 MHz) or AC300 (300 MHz) spectrometers in deuteriochloroform solution, and are reported in parts per million downfield from tetramethylsilane. ^{13}C NMR spectra were recorded on the AC200 spectrometer, and ^{19}F NMR spectra were recorded on the AC300; they are reported in parts per million relative to tetramethylsilane and trichlorofluoromethane, respectively. Infrared spectra were recorded in the gas phase using a GC–FTIR system consisting of a Hewlett-Packard 5890 gas chromatograph (equipped with a 5 m × 0.53 mm HP-1 megabore capillary column (Hewlett–Packard, Inc.)) connected through a Biorad GC/C 32 interface to a Biorad FTS-40 FTIR spectrometer. Ultraviolet absorption spectra were recorded on a Perkin Elmer Lambda 9 spectrometer interfaced to an IBM PS/2-286 microcomputer, or on a Hewlett–Packard HP8451 UV spectrometer. Fluorescence emission and excitation spectra were recorded on a Perkin Elmer LS-5 spectrofluorometer, which is also interfaced to the IBM PS/2-286 and controlled by software supplied by the manufacturer. Gas chromatographic analyses were carried out using a Hewlett–Packard 5890 gas chromatograph equipped with a flame ionization detector, a Hewlett–Packard 3396 integrator, and a HP-1 megabore capillary column (12 m × 0.53 mm; Hewlett–Packard, Inc.) or a DB-1 megabore capillary column (30 m × 0.53 mm, Chromatography Specialties). GC–MS analyses were carried out using a Hewlett–Packard 5890 gas chromatograph equipped with a HP-5971A mass selective detector and a DB-1 microbore capillary column (12 m × 0.2 mm; Chromatographic Specialties, Inc.). Exact Masses were determined on a VGH ZABE mass spectrometer and employed a mass of 12.000 000 for carbon. Semipreparative VPC separations employed a Varian 3300 gas chromatograph equipped with 6 ft × 0.25 in. stainless steel columns consisting of (*a*) 5% OV-101 on Supelcoport or (*b*) 10% QF-1 on 80/100 Chromosorb (Supelco, Inc.).

n-Pentane (Baker Photrex), cyclohexane (BDH Omnisolv),

[6]

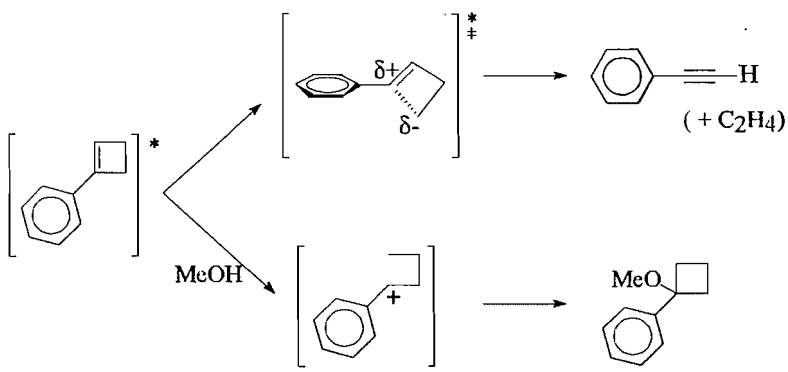

Can. J. Chem. Downloaded from www.nrcresearchpress.com by 65.111.164.53 on 09/08/12
For personal use only.

and barium oxide (Mallinckrodt) were used as received from the suppliers. Acetonitrile (Omnisolv) was dried over calcium hydride and distilled under dry nitrogen. Benzene (Baker Analyzed) was purified by several extractions with concentrated sulfuric acid, followed by distillation through a Vigreux column. Tetrahydrofuran (Baker Analyzed) was refluxed over sodium–benzophenone and distilled immediately prior to use. Dimethyl sulfoxide (Caledon) was dried over potassium hydroxide and distilled under reduced pressure. *p*-Toluenesulfonic acid monohydrate was used as received from Matheson. Bromobenzene, 4-bromotoluene, 4-bromoanisole, 4-bromobenzotrifluoride, 4-trifluoromethoxybromobenzene, 3-bromobenzotrifluoride, cyclobutanone, *n*-butyllithium, and *n*-decane were all used as received from Aldrich Chemical Co. Phenylacetylene and 4-tolylacetylene were used as received from Lancaster Chemicals, Inc.

Preparation of compounds

The cyclobutenes **2***a–f* were prepared by acid-catalyzed dehydration of the corresponding 1-arylcyclobutanol (**3**) (54), which was prepared by addition of the appropriate aryllithium to cyclobutanone in anhydrous ether at −40°C. The aryllithium reagents were prepared as solutions in ether from the corresponding bromoarene by lithium exchange using *n*-butyllithium. In the syntheses of **3***a,b,e*, the exchange was accelerated by sonication of the solutions at room temperature. A typical procedure is described below for the preparation of 1-(4-trifluoromethylphenyl)cyclobutene (**2***d*).

*1-(4-Trifluoromethylphenyl)cyclobutene (***2**d)

In an oven-dried 50 mL 2-neck roundbottom flask equipped with a dropping funnel, magnetic stirrer, rubber septum, and nitrogen inlet were placed 4-bromobenzotrifluoride (3.43 g, 0.015 mol) and anhydrous ether (10 mL). The flask was cooled under an atmosphere of dry nitrogen to −40°C with a dry ice – acetone bath, and a 1.6 M hexane solution of *n*-butyllithium (9.5 mL, 0.015 mol) was added dropwise over 1 h. The bath and contents of the flask were then allowed to warm to 0°C over ca. 1 h. The temperature of the resulting yellow solution was again lowered to −40°C, and a solution of cyclobutanone (0.47 g, 0.0067 mol) in anhydrous ether (10 mL) was added dropwise over 1 h. The resulting yellow solution was then allowed to warm to room temperature over a further 1 h. The dark red mixture that resulted was quenched by slow addition of water (20 mL) and then extracted with ether (3 × 10 mL). The combined ether extracts were dried over anhydrous sodium sulfate and filtered. Evaporation of the solvent on a rotary evaporator yielded an orange liquid (1.23 g), which was distilled under vacuum. The major fraction (0.75 g, 0.0035 mol, 70%; bp 87°C (0.3 Torr; 1 Torr = 133.3 Pa); mp 52–54°C), was identified as *1-(4-trifluoromethylphenyl)cyclobutanol* (**3***d*) on the basis of the following spectral data. IR: 3632 (w), 2996 (m), 1328 (s), 1286 (w), 1232 (w), 1172 (m), 1149 (s), 1076 (m), 1017 (w), 846 (w). ^{1}H NMR: δ: 1.55 (br s, 1 H), 1.76 (cplx m, 1 H), 2.08 (brs, 1 H), 2.36 (cplx, m, 2 H), 2.54 (cplx, m, 2 H), 7.62 (s, 4 H). ^{13}C NMR; δ: 12.96, 37.18, 79.60, 125.51, 125.42, 125.36, 125.27, 126.88, 129.0 (q), 156.39. ^{19}F NMR; δ: −62.67. MS, *m/e* (I): 197 (17), 188 (98), 173 (100), 151 (35), 147 (42), 145 (96), 125 (33), 91 (75), 69 (33). Exact Mass, calcd. for $C_{11}H_{11}F_3O$: 216.0762; found: 216.0750.

Significantly higher isolated yields of the cyclobutanols can be obtained using column chromatography (neutral alumina, hexane–ether mixtures) to purify the crude reaction mixtures in the above step.

A solution of **3***d* (0.50 g, 0.0023 mol) and a few crystals of *p*-toluenesulfonic acid in dry benzene (25 mL) was stirred under reflux for 6 h, in a 50 mL roundbottom flask equipped with a glass tube that contained a small thimble filled with granulated calcium chloride and was topped with a reflux condenser. The resulting light brown solution was cooled to room temperature, water (25 mL) was added, and the mixture was extracted with pentane (3 × 10 mL). The combined extracts were washed with saturated aqueous sodium bicarbonate, dried over anhydrous magnesium sulfate, and the solvent was evaporated to yield a light yellow liquid (0.40 g). The product was isolated as a colourless liquid (0.20 g, 0.001 mol, 43%; bp 77°C (1 Torr); mp 20–22°C) by vacuum distillation. Better yields can be obtained by purification of the crude product by column chromatography (neutral alumina; 10% ether in hexane). The product was further purified by semi-preparative gas chromatography, and identified as *1-(4-trifluoromethylphenyl)cyclobutene* (**2***d*) on the basis of the following data. IR: 3056 (w), 2962 (m), 2935 (m), 2852 (m), 1330 (s), 1176 (m), 1149 (s), 1073 (s), 1043 (w), 1019 (w), 900 (w), 846 (m), 765 (w). UV (MeCN), λ_{max}: 260 nm (ε 14 800 M^{-1} cm^{-1}). ^{1}H NMR, δ: 2.40 (m, 2 H), 2.65 (t, J = 4 Hz, 2 H), 6.25 (br s, 1 H), 7.25 (d, J = 8.2 Hz, 2 H), 7.39 (d, J = 8.2 Hz, 2 H). ^{13}C NMR, δ: 26.44, 28.65, 124.32, 125.15, 130.27, 137.89, 145.14, 129.10 (q, CF_3). ^{19}F NMR, δ: −62.70. MS, *m/e* (*I*): 198 (15), 179 (21), 177 (22), 151 (28), 145 (21), 129 (100), 128 (50), 120 (15), 75 (27), 63 (20), 51 (16). Exact Mass, calcd. for $C_{11}H_9F_3$: 198.0656; found: 198.0688.

Cyclobutenes **2***a–c,e,f* were prepared in similar fashion to 2*d*, except that the initial lithium exchange in the cyclobutanol synthesis required less or more vigorous conditions depending on substituent. The yields of the intermediate 1-arylcyclobutanols ranged from 50 to 90% after chromatography, and those of the cyclobutenes from 70 to 90% after isolation by alumina column chromatography. The latter were all subjected to additional purification (>99% by GC) by semipreparative gas chromatography. Spectral and analytical data for the remaining 1-arylcyclobutanols and 1-arylcyclobutenes in the series are listed below.

*1-(4-Methoxyphenyl)cyclobutanol (***3**a): IR: 3576 (m), 2966 (s), 2941 (s), 2883 (m), 1610 (m), 1513 (s), 1472 (m), 1298 (m), 1253 (s), 1224 (m), 1175 (m). ^{1}H NMR, δ: 1.66 (cplx m, 1 H), 1.98 (cplx m, 1 H), 2.36 (m, 2 H), 2.55 (m, 2 H), 3.78 (s 3 H), 7.42 (dd, 2 H), 7.77 (dd, 2 H). MS, *m/e* (*I*): 178 (27), 177 (38), 147 (31), 135 (100), 121 (11), 105 (7), 91 (9), 65 (7).

*1-(4-Methoxyphenyl)cyclobutene (***2**a): IR: 3009 (w), 2956 (m), 2932 (m), 2851 (m), 1605 (m), 1424 (w), 1300 (m), 1258 (s), 1174 (m), 1056 (w), 1038 (w), 835 (m), 760 (w). UV (pentane), λ_{max}: 261 nm (ε 17 900 M^{-1} cm^{-1}). ^{1}H NMR, δ: 2.50 (m, 2 H), 2.77 (t, 2 H), 3.81 (s, 3 H), 6.13 (t, 1 H), 6.84 (dd, J = 2.2, 6.8 Hz, 2 H), 7.26 (dd, J = 2.2, 6.8 Hz, 2 H). ^{13}C NMR, δ: 26.02, 55.29, 113.74, 124.57, 125.55. MS, *m/e* (*I*): 160 (65), 159 (31), 145 (27), 129 (42), 117 (91), 115 (100), 102 (21), 91 (42), 89 (64), 77 (11), 51 (15). Exact Mass, calcd. for $C_{11}H_{12}O$: 160.0888; found: 160.0904.

*1-(4-Methylphenyl)cyclobutanol (***3**b). IR: 3634 (m), 3032 (m),

Can. J. Chem. Downloaded from www.nrcresearchpress.com by 65.111.164.53 on 09/08/12
For personal use only.

2994 (s), 2958 (s), 2883 (m), 1621 (w), 1517 (m), 1342 (m), 1243 (m), 1136 (m), 1055 (m), 1021 (m), 818 (m), 720 (m). ^{1}H NMR, δ: 1.66 (cplx m, 2 H), 1.98 (br s, 2 H), 2.37 (s, 3 H), 2.37 (br s, 2 H), 2.54 (br s, 2 H), 7.17 (d, 0.7 Hz, 2 H), 7.37 (d, 0.7 Hz, 2 H). ^{13}C nmr, δ: 12.93, 21.02, 36.80, 109.22, 124.92, 129.09, 136.90, 143.29. MS, *m/e* (*I*): 147 (26), 134 (71), 119 (100), 92 (37), 91 (63), 77 (10), 65 (16). Exact Mass, calcd. for $C_{11}H_{14}O$: 162.1045; found: 162.1037.

1-(4-Methylphenyl)cyclobutene (**2**b): IR: 3057 (m), 3030 (m), 2957 (s), 2932 (s), 2883 (m), 2853 (m), 1510 (m), 1317 (w), 1291 (w), 1241 (w) , 1183 (w), 1117 (w), 899 (w), 822 (m), 754 (m). UV (MeCN), λ_{max}: 258 nm (ε 15 500 M^{-1} cm^{-1}). ^{1}H NMR, δ: 2.27 (s, 3 H), 2.46 (br t, 2 H), 2.72 (t, J = 3.3 Hz, 2 H), 6.15 (br s, 1 H), 7.05 (d, 2 H), 7.18 (d, 2 H). ^{13}C NMR, δ: 21.30, 26.15, 28.75, 102.86, 124.12, 125.96, 128.95, 137.14. MS, *m/e* (*I*): 144 (24), 129 (100), 128 (59), 115 (90), 90 (9), 89 (11), 63 (18), 51 (12). Exact Mass, calcd. for $C_{11}H_{12}$: 144.0939; found: 144.0930.

1-Phenylcyclobutanol (**3**c: mp 40–41°C (54)). IR: 3633 (m), 3073 (m), 3041 (m), 2995 (s), 2960 (s), 1448 (m), 1342 (m), 1242 (m), 1177 (w), 1139 (m), 1026 (m), 899 (m), 761 (m). ^{1}H NMR, δ: 1.68 (cplx m , 1 H), 2.01 (cplx m, 1 H), 2.36 (cplx m, 2 H), 2.56 (cplx m, 2 H), 7.27 (m, 1 H), 7.36 (m, 2 H), 7.49 (m, 2 H). ^{13}C NMR, δ: 12.99, 36.83, 124.93, 127.24, 128.44. MS, *m/e* (*I*): 148 (8), 147 (7), 130 (12), 120 (58), 115 (18), 105 (100), 102 (15), 91 (63), 78 (89), 77 (99), 74 (21), 63 (16), 51 (48).

1-Phenylcyclobutene (**2**c): IR: 3069 (m), 3041 (m), 2958 (s), 2933 (s), 2888 (w), 2852 (m), 1580 (w), 1491 (w), 1244 (w), 1070 (w), 901 (w), 850 (w), 729 (s). ^{1}H NMR (55), δ: 2.51 (m, 2 H), 2.79 (t, 2 H), 6.27 (t, 1 H), 7.31 (m, 5 H). ^{13}C NMR (56), δ: 26.18, 28.72, 124.16, 127.13, 127.36, 128.07, 128.28, 128.64, 135.04, 146.40.

1-(4-Trifluoromethoxyphenyl)cyclobutanol (**3**e): IR: 3630 (w), 2996 (m), 2965 (w), 1513 (m), 1273 (s), 1229 (m), 1186 (m), 1142 (w), 1020 (m), 851 (w). ^{1}H NMR, δ: 1.18 (cplx m, 1 H), 1.63 (br s, 1 H), 1.97 (cplx m, 2 H), 2.11 (cplx m., 2 H), 6.82 (m, 2 H), 7.13 (m, 2 H). ^{13}C NMR, δ: 12.88, 37.06, 76.56, 120.6 (q), 120.83, 127.08, 134.71, 144.92. ^{19}F NMR, δ: −94.59. MS, *m/e* (*I*): 204 (74), 189 (100), 175 (7), 162 (23), 147 (15), 95 (22), 69 (15). Exact Mass, calcd. for $C_{11}H_{11}F_3O_2$: 232.0711; found: 232.0695.

1-(4-Trifluoromethoxyphenyl)cyclobutene (**2e**): IR: 3036 (w), 2968 (m), 2911 (w), 1794 (m), 1597 (m), 1502 (m), 1274 (s), 1226 9s), 1187 (s), 1112 (m), 1023 (w), 901 (m), 836 (m), 790 (m). UV (pentane), λ_{max}: 255 nm (ε 17 400 M^{-1} cm^{-1}). ^{1}H NMR, δ: 2.52 (br d, 2 H), 2.79 (t, 2 H), 6.35 (br s, 1 H), 7.25 (br q, 4 H). ^{13}C NMR, δ: 25.37, 34.94, 118.50, 127.38, 129.56, 130.43, 134.75, 147.80. ^{19}F NMR, δ: −59.08. MS, *m/e* (*I*): 214 (50), 199 (11), 186 (23), 175 (4), 145 (7), 130 (14), 129 (100), 128 (36), 127 (38), 117 (21), 115 (29), 102 (7), 89 (21), 69 (21), 63 (14), 51 (7). Exact Mass, calcd. for $C_{11}H_9F_3O$: 214.0605; found: 214.0593.

1-(3-Trifluoromethylphenyl)cyclobutanol (**3**f): IR: 3633 (w), 3080 (w), 2996 (m), 2956 (m), 2889 (w), 1441 (w), 1330 (s), 1272 (m), 1178 (s), 1147 (s), 1077 (m), 1019 (w), 902 (w), 838 (w), 804 (w), 703 (m). ^{1}H NMR, δ: 1.55 (br s, 1 H), 1.73 (cplx m, 1 H), 2.04 (cplx m, 1 H), 2.34 (cplx m, 2 H), 2.48 (cplx m, 2 H), 7.61 (m, 4 H). ^{13}C NMR, δ: 12.98, 37.15, 76.73, 121.81, 123.98, 124.06, 128.37, 128.92, 130.0 (q), 147.32. ^{19}F NMR, δ: −62.71. MS, *m/e* (*I*): 197 (13), 188 (94), 173 (100), 159 (6), 145 (56), 127 (7), 91 (19), 75 (6). Exact Mass, calcd. for $C_{11}H_{11}F_3O$: 216.0762; found: 216.0750.

1-(3-Trifluoromethylphenyl)cyclobutene (**2**f): IR: 2955 (m), 2816 (m), 1601 (w), 1444 (m), 1348 (m), 1327 (s), 1282 (m), 1256 (m), 1181 (s), 1151 (s), 1076 (m), 981 (w), 891 (w), 799 (m). UV (MeCN), λ_{max}: 254 nm (ε 15 100 M^{-1} cm^{-1}). ^{1}H NMR, δ: 2.54 (m, 2 H), 2.81 (t, J = 4.0 Hz, 2 H), 6.38 (t, J = 1.2 Hz, 1 H), 7.43 (m, 4 H). ^{13}C NMR, δ: 26.38, 28.72, 120.93, 123.89, 127.34, 128.74, 129.36, 146.20. ^{19}F NMR, δ: −63.01. MS, *m/e* (*I*): 198 (23), 179 (11), 177 (46), 151 (40), 129 (100), 128 (40), 120 (9), 75 (9), 63 (4), 51 (5). Exact Mass, calcd. for $C_{11}H_9F_3$: 198.0656: found: 198.0649.

2,4,4-Trideuterio-1-phenylcyclobutene (**2**c–d_3) was prepared from cyclobutanone-2,2,4,4-d_4 by a similar procedure to that employed for the parent compound. A mixture of cyclobutanone (1.0 g, 0.014 mol), triglyme (15 mL), deuterium oxide (5.0 mL), and potassium carbonate (5.0 g) was stirred for 24 h at 70°C. After cooling, the resulting solution was extracted with ether (5 × 10 mL). The combined organic extracts were dried with anhydrous sodium sulfate, and then distilled through a short Vigreux fractionating column at atmospheric pressure. Once the ether had distilled off, the receiving flask was cooled to −78°C and attached to two consecutive traps immersed in dry ice – isopropanol, and the temperature of the still was allowed to increase gradually. Deuterated cyclobutanone (0.5 g, 51 % yield) and traces of ethyl ether collected in the receiving flask and the traps. ^{1}H NMR analysis of the distillate indicated that the ketone was ca. 80% tetradeuterated. The material was subjected to a second deuteration cycle as described above, after which the α-proton resonances in the ^{1}H NMR spectrum of the isolated material were undetectable by ^{1}H NMR spectroscopy. A solution of the deuterated ketone (0.29 g, 0.0039 mol) in tetrahydrofuran (10 mL) was cooled at −78°C and treated dropwise with phenyllithium (0.0039 mol). The solution was stirred for 30 min at −78°C, allowed to warm to room temperature, and then quenched by dropwise addition of deuterium oxide (3.0 mL). Work-up as described above afforded a slightly yellow oil (0.505 g), which was purified by silica gel column chromatography and tentatively identified as *1-phenylcyclobutanol-2,2,4,4-*d_4 (mp 43–46°C) on the basis of its mass spectrum: MS, *m/e* (*I*): 152 (0.5), 151 (0.8), 150 (0.2), 122 (48), 105 (100), 93 (26), 78 (81), 77 (68), 51 (33), 30 (5), 29 (4), 28 (3), 27 (1).

1-Phenylcyclobutene-2,4,4-d_3 (**2**c–d_3) was prepared by refluxing a solution of the alcohol from above (0.4 g) in benzene-d_6 (5.0 mL) containing traces of deuterium oxide and *p*-toluenesulfonic acid monohydrate (recrystallized thrice from D_2O) for 5 h. After cooling to room temperature, the solution was washed with a small amount of 5% aqueous sodium hydroxide and dried over anhydrous magnesium sulfate. The solvent was removed on the rotary evaporator to yield a colourless oil (0.35 g), from which **2**c–d_3 was isolated by semi-preparative VPC after bulb-to-bulb distillation. ^{1}H NMR analysis indicated the compound to be >95% deuterated at the

Can. J. Chem. Downloaded from www.nrcresearchpress.com by 65.111.164.53 on 09/08/12
For personal use only.

C2 and C4 positions of the cyclobutene ring. IR: 3074 (m), 3039 (m), 2035 (s), 2291 (w), 2226 (m), 2154 (w), 1954 (w), 1798 (w), 1606 (w), 1493 (m), 1447 (w), 1291 (w), 1019 (w), 753 (s). ^{1}H NMR (CD_3CN), δ: 2.48 (s, 2H), 2.81 (m, 0.12 H), 6.32 (t, 0.05 H), 7.31 (m, 5H). MS, *m/e* (*I*): 133 (81), 132 (100), 131 (79), 119 (9), 118 (21), 117 (45), 116 (44), 103 (81), 79 (11), 78 (12), 77 (30), 76 (26), 75 (21), 67 (11), 66 (12), 65 (14), 52 (16) 51 (36), 50 (18), 39 (13).

The 1-methoxy-1-arylcyclobutanes (**4***a–f*) were prepared by stirring a mixture of the corresponding 1-arylcyclobutanol (0.0009 mol), barium oxide (0.005 mol), iodomethane (0.002 mol), and dry dimethyl sulfoxide (10 mL) for 24 h at room temperature. After addition of 5% aqueous hydrochloric acid, extraction with ether, drying and evaporation of the ether extracts, and finally alumina column chromatography (20% ether in hexane), the compounds were isolated as colourless oils in 75–85% yield. They were identified on the basis of their NMR, IR, and mass spectral data, which are listed below.

1-Methoxy-1-(4-methoxyphenyl)cyclobutane (**4**a): IR: 2995 (m), 2953 (m), 1652 (m), 1616 (m), 1558 (m), 1517 (m), 1510 (s), 1305 (m), 1252 (s), 1178 (m), 1135 (m), 1047 (w), 972 (w), 833 (m), 777 (w). ^{1}H NMR, δ: 1.80 (cplx m, 1H), 1.99 (cplx m, 1 H), 2.46 (cplx m, 2 H), 2.55 (cplx m, 2 H), 2.85 (s, 3 H), 3.76 (s, 3 H), 6.89 (d, 2 H), 7.32 (d, 2 H). MS, *m/e* (*I*): 192 (4), 191 (4), 177 (2), 164 (42), 163 (100), 149 (8), 133 (42), 121 (12), 119 (42), 105 (8), 91 (25), 77 (17), 63 (9). Exact Mass, calcd. for $C_{12}H_{16}O_2$: 192.1150: found: 192.1127.

1-Methoxy-1-(4-methylphenyl)cyclobutane (**4**b): IR: 3031 (m), 2995 (s), 2950 (s), 2885 (m), 2830 (m), 1621 (w), 1516 (m), 1296 (m), 1249 (m), 1137 (s), 1090 (m), 1056 (m), 815 (m), 786 (w). ^{1}H NMR, δ: 1.68 (cplx m, 1 H), 1.97 (cplx m, 1 H), 2.36 (s, 3 H), 2.36 (m, 4 H), 2.92 (s, 3 H), 7.15 (d, J = 7.9 Hz, 2 H), 7.28 (d, J = 7.9 Hz, 2 H). ^{13}C NMR, δ: 12.99, 21.06, 32.88, 50.34, 81.34, 126.29, 128.92, 136.78, 140.10. MS, *m/e* (*I*): 162 (5), 161 (36), 148 (22), 147 (39), 133 (100), 117 (55), 115 (28), 105 (22), 91 (33), 77 (11), 65 (17), 51 (5). Exact Mass, calcd. for $C_{12}H_{16}O$: 176.1201; found: 176.1190.

1-Methoxy-1-phenylcyclobutane (**4**c): IR: 3071 (m), 3037 (m), 2884 (s), 2952 (s), 2914 (m), 2831 (m), 1449 (m), 1289 (m), 1248 (m), 1136 (s), 1090 (m), 1046 (m), 759 (m). ^{1}H NMR, δ: 1.58 (cplx m, 1 H), 1.87 (cplx m, 1 H), 2.32 (cplx m, 4 H), 2.86 (s, 3 H), 7.30 (m, 5 H). ^{13}C NMR, δ: 13.01, 32.80, 50.47, 126.28, 127.14, 128.24. MS, *m/e* (*I*): 161 (3), 134 (37), 133 (100), 115 (6), 104 (31), 91 (34), 77 (35). MS/CI (NH_3), *m/e* (*I*): 131 (100), 148 (50), 162 (4), 180 (5). MS/CI (CH_4); *m/e* (*I*): = 61 (9), 79 (28), 85 (34), 131 (100), 163 (11). HRMS ($M^+ - 1$), calcd. for $C_{11}H_{13}O$: 161.0966; found: 161.0944.

1-Methoxy-1-(4-trifluoromethylphenyl)cyclobutane (**4**d): IR: 2997 (m), 2951 (m), 2834 (w), 1620 (w), 1408 (w), 1323 (s), 1300 (w), 1173 (s), 1147 (s), 1087 (m), 1072 (m), 1018 (m), 842 (s). ^{1}H NMR, δ: 1.67 (m, 1 H), 1.96 (m, 1 H), 2.36 (d, 2 H), 2.39 (double sextet, 2H), 2.92 (s, 3 H), 7.57 (q, J = 8.4 Hz, 4 H). ^{13}C NMR, δ: 12.90, 32.80, 50.67, 81.26, 125.28, 125.36, 125.42, 126.55, CF_3 not observed. ^{19}F NMR, δ: −62.67. MS, *m/e* (*I*): 202 (27), 210 (61), 182 (11), 172 (27), 161 (28), 151 (25), 145 (42), 133 (100), 103 (22), 75 (8). Exact Mass, calcd. for $C_{12}H_{13}F_3O$: 230.0918; found: 230.0900.

1-Methoxy-1-(4-trifluoromethoxyphenyl)cyclobutane (**4**e): ^{1}H NMR, δ: 1.65 (m, 1 H), 1.98 (m, 1 H), 2.40 (d, 2 H), 2.42 (m, 2 H), 2.93 (s, 3 H), 7.02 (m, 4 H). ^{13}C NMR, δ: 12.86, 32.70, 50.63, 78.60, 120.90, 127.14, 134.90, 144.60. MS, *m/e* (*I*): 245 (3), 230 (6), 218 (48), 217 (100), 188 (45), 175 (15), 161 (15), 133 (36), 119 (18), 91 (9), 77 (6), 69 (15). Exact Mass, calcd. for $C_{13}H_{13}F_3O_2$: 246.0868; found: 246.0901.

1-Methoxy-1-(3-trifluoromethylphenyl)cyclobutane (**4**f): IR: 3080 (w), 2997 (m), 2952 (m), 2833 (w), 1489 (w), 1439 (w), 1335 (s), 1270 (s), 1177 (s), 1145 (s), 1100 (m), 1077 (m), 1042 (w), 901 (w), 802 (w). ^{1}H NMR, δ: 1.65 (cplx m, 1 H), 1.95 (cplx m, 1 H), 2.36 (d, 2 H), 2.39 (m, 2 H), 2.92 (s, 3 H), 7.60 (m, 4 H). ^{13}C NMR, δ: 12.88, 32.71, 50.62, 81.23, 122.92, 124.05, 128.82, 129.62, 144.49. ^{19}F NMR, δ: −62.69. MS, *m/e* (*I*): 215 (8), 202 (58), 201 (98), 172 (40), 159 (25), 151 (40), 145 (33), 133 (100), 103 (22). Exact Mass, calcd. for $C_{12}H_{13}F_3O$: 230.0918; found: 230.0901.

Irradiations were carried out on a 0.5 mL scale in 3 in. × 5 mm quartz tubes, in a Rayonet reactor containing one RPR-254 lamp. For the purposes of product identification, photolyses were taken to ca. 40% conversion, and the products identified by GC–MS, GC–FTIR, and GC coinjection with authentic samples in the cases of phenylacetylene (**5***c*), 4-tolylacetylene (**5***b*), and 4-trifluoromethylphenylacetylene (**5***d*). (57) Identification of the other substituted phenylacetylenes was based on their GC retention times, the prominent parent ion and characteristic fragmentation patterns in their mass spectra (58), and their characteristic IR spectra (obtained by GC–FTIR analyses of the crude photolysis mixtures). Mass and gas phase infrared spectral data for the five substituted phenylacetylenes are given below.

4-Methoxyphenylacetylene (**5**a) *(59)*: IR: 3318 (s), 3083 (w), 3031 (w), 2957 (w), 2925 (w), 2838 (w), 2110 (m), 1650 (w), 1598 (m), 1581 (m), 1508 (s), 1489 (s), 1461 (m), 1443 (m), 1290 (m), 1245 (m), 1180 (m), 1103 (w). MS (58); *m/e* (*I*): 132 (80), 131 (75), 117 (27), 101 (39), 90 (20), 50 (20).

4-Methylphenylacetylene (**5**b) *(59)*: IR: 3317 (s), 3084 (w), 3031 (w), 2962 (m), 2925 (m), 2866 (w), 2111 (m), 1508 (s), 1261 (s), 1215 (m), 1103 (m), 1020 (m), 826 (m), 650 (s), 603 (s), 529 (s). MS, *m/e* (*I*):= 116 (75), 115 (100), 89 (40), 74 (20), 63 (35), 50 (29).

4-Trifluoromethylphenylacetylene (**5**d) *(57)*: IR: 3314 (s), 3083 (m), 3060 (w), 3035 (w), 2928 (w), 2112 (m), 1601 (m), 1575 (w), 1489 (s), 1444 (m), 1401 (w), 1325 (m), 1223 (m), 1172 (m), 1132 (m), 1102 (w), 1071 (m). MS: *m/e* (*I*): 170 (100), 169 (25), 151 (40), 120 (40), 99 (10), 75 (20), 74 (20).

4-Trifluoromethoxyphenylacetylene (**5**e): IR: 3314 (s), 2980 (s), 2828 (s), 2869 (m), 2855 (m), 2112 (w), 1671 (w), 1597 (w), 1574 (w), 1489 (m), 1445 (m), 1380 (w), 1261 (s), 1227 (m), 1100 (s), 1070 (m), 1025 (s). MS, *m/e* (*I*): 186 (100), 167 (30), 120 (17), 117 (15), 99 (20), 85 (15), 75 (25), 74 (31).

3-trifluoromethylphenylacetylene (**5**f) *(57)*: IR: 3314 (s), 3076 (m), 3035 (w), 2923 (w), 2114 (w), 1602 (w), 1579 (s), 1485 (s), 1430 (s), 1348 (s), 1272 (s), 1223 (m), 1174 (s), 1131 (s),

1088 (s), 914 (m). MS: *m/e* (*I*): 170 (100), 169 (30), 151 (40), 120 (42), 99 (10), 75 (20), 74 (30), 69 (10).

Quantum yields were determined by electronic actinometry using a system similar to that described previously (60), and 260 nm excitation. The system was calibrated daily with potassium ferrioxalate. Samples were contained in round (1 cm × 2.54 cm) Suprasil UV cells, which were sealed with rubber septa and deoxygenated with a stream of dry nitrogen prior to photolysis. Quantum yields were calculated from the slopes of plots of product concentration versus accumulated photon counts. Product concentrations were determined by GC relative to an internal standard (*n*-decane) and were corrected for relative FID response factors using working curves.

Relative quantum yield determinations and Stern–Volmer studies were carried out using a Rayonet reactor equipped with a merry-go-round and one 253.7 nm Hg lamp. Relative yields of methyl phenylcyclobutyl ether (**4***c*) from photolysis of **2***c* in methanolic acetonitrile solution were corrected for a small amount of dark reaction for each methanol concentration studied, and for the formation of a product (with identical retention time to **4***c*) in runs carried out in the absence of methanol.

Fluorescence lifetimes were measured at ambient temperature (22–25°C) using a PTI LS-100 single photon counting system and a hydrogen flash lamp. Cuvettes were constructed from 1 cm × 1 cm square Suprasil tubing (Vitro Dynamics Ltd.) and were constricted to 7 mm round tubing at the top of the cell. The cuvettes were sealed using a rubber septum, and the solutions, 0.001–0.005 M in **2**, were deoxygenated with a stream of dry nitrogen for at least 60 min prior to the experiment. Fluorescence decays were recorded using 260 nm excitation and a monitoring wavelength corresponding to the emission maximum of the cyclobutene in the particular solvent being studied. Decays were recorded with 5000–10 000 counts in the maximum channel, and were deconvoluted and analysed using the software provided by the manufacturer. In general, the decays were fit to single or double exponential functions in order to obtain the best possible fit. In cases where the data fit best to a two exponential function, the second component comprised less than ca. 10% of the decay. In each case, the lifetimes reported are the average of at least two independent determinations, the results of which invariably differed by less than 5%. The solutions were checked by GC immediately after determination of the lifetime to verify that no appreciable photodecomposition of the sample occurred during the experiment.

Nanosecond laser flash photolysis experiments employed the pulses (248 nm, ca. 16 ns) from a Lumonics 510 excimer laser filled with F_2/Kr/He mixtures or those (337 nm, ca. 6 ns) from a Lumonics 761M excimer laser filled with N_2/He mixtures, and a microcomputer-controlled detection system (61, 62). Solutions of **2***b–d* were prepared at concentrations such that the absorbance at the excitation wavelength (248 nm) was ca. 0.3 (6×10^{-5} M), and were made to flow continuously from a calibrated 100 mL capacity reservoir through a 3 × 7 Suprasil flow cell. The solutions were deoxygenated with a stream of dry nitrogen in the reservoir for 45 min prior to and continuously throughout flash photolysis experiments. Quenchers were added directly to the reservoir by microlitre syringe as aliquots of standard solutions. Quenching rate constants were calculated by linear least-squares fits of decay rate versus quencher concentration data using Inplot 4.0 (Graphpad, Inc.). Errors are reported as twice the standard deviations obtained from these analyses.

Can. J. Chem. Downloaded from www.nrcresearchpress.com by 65.111.164.53 on 09/08/12
For personal use only.

Acknowledgements

We wish to thank P. Venneri, Z. Musa, B. Sayer, and D. Hughes for technical assistance, the McMaster Regional Center for Mass Spectrometry for Exact Mass determinations, and Dr. V. Bonacic-Koutecky for helpful discussions. The financial support of the Natural Sciences and Engineering Research Council of Canada is also gratefully acknowledged.

References

1. W.J. Leigh. Chem. Rev. **93**, 487 (1993).
2. W.J. Leigh. Can. J. Chem. **71**, 147 (1993).
3. K.B. Clark and W.J. Leigh. J. Am. Chem. Soc. **109**, 6086 (1987).
4. W.J. Leigh, K. Zheng, N. Nguyen, N.H. Werstiuk, and J. Ma. J. Am. Chem. Soc. **113**, 4993 (1991).
5. J. Saltiel and L.S. Ng Lim. J. Am. Chem. Soc. **91**, 5404 (1969).
6. W.J. Leigh, K. Zheng, and K.B. Clark. Can. J. Chem. **68**, 1988 (1990).
7. K.B. Clark and W.J. Leigh. Can. J. Chem. **66**, 1571 (1988).
8. W. Adam, T. Oppenlander, and G. Zang. J. Am. Chem. Soc. **107**, 3921 (1985).
9. Y. Inoue, M. Sakae, and T. Hakushi. Chem. Lett. 1495 (1983).
10. E.H. White and J.P. Anhalt. Tetrahedron Lett. 3937 (1965).
11. C.D. DeBoer and R.H. Schlessinger. J. Am. Chem. Soc. **90**, 803 (1968).
12. G. Quinkert, W.-W. Wiersdorff, M. Finke, K. Opitz, and F.-G. von der Haar. Chem. Ber. **101**, 2302 (1968).
13. G. Quinkert, M. Finke, J. Palmowski, and W.-W. Wiersdorff. Mol. Photochem. **1**, 433 (1969).
14. R.V. Carr, B. Kim, J.K. McVey, N.C. Yang, W. Gerhartz, and J. Michl. Chem. Phys. Lett. **39**, 57 (1976).
15. N.C. Yang, R.V. Carr, E. Li, J.K. McVey, and S.A. Rice. J. Am. Chem. Soc. **96**, 2297 (1974).
16. P. Wan and K. Yates. Rev. Chem. Intermed. **5**, 157 (1984).
17. P.J. Kropp. Org. Photochem. **4**, 1 (1979).
18. M. Sakuragi and M. Hasegawa. Chem. Lett. 29 (1974).
19. S.S. Hixson. Tetrahedron Lett. 277 (1973).
20. H.E. Zimmerman, K.S. Kamm, and D.P. Werthemann. J. Am. Chem. Soc. **97**, 3718 (1975).
21. K.P. Ghiggino, K. Hara, G.R. Mant, D. Phillips, K. Salisbury, R.P. Steer, and M.D. Swords. J. Chem. Soc. Perkin Trans. 2, 88 (1978).
22. G.R. Mant and K. Salisbury. J. Chem. Soc. Faraday Trans. 2, **77**, 1487 (1981).
23. R. Bonneau. J. Am. Chem. Soc. **104**, 2921 (1982).
24. V. Ramamurthy, J.V. Caspar, D.F. Eaton, E.W. Kuo, and D.R. Corbin. J. Am. Chem. Soc. **114**, 3882 (1992).
25. P. Wan, S. Culshaw, and K. Yates. J. Am. Chem. Soc. **104**, 2509 (1982).
26. J. McEwen and K. Yates. J. Phys. Org. Chem. **4**, 193 (1991).

27. R.A. McClelland, V.M. Kanagasabapathy, and S. Steenken. J. Am. Chem. Soc. **110**, 6913 (1988).
28. R.A. McClelland, F. Cozens, and S. Steenken. Tetrahedron Lett. **31**, 2821 (1990).
29. R.A. McClelland, C. Chan, F. Cozens, A. Modro, and S. Steenken. Angew. Chem. Int. Ed. Engl. **30**, 1337 (1991).
30. R.A. Caldwell and C.V. Cao. J. Am. Chem. Soc. **104**, 6174 (1982).
31. T. Ni, R.A. Caldwell, and L.A. Melton. J. Am. Chem. Soc. **111**, 457 (1989).
32. I.B. Berlman. Handbook of fluorescence spectra of aromatic molecules. Academic Press, London. 1965.
33. D.F. Eaton. *In* CRC handbook of organic photochemistry, Vol. I. *Edited by* J.C. Scaiano. CRC Press, Boca Raton, Fla. 1989. p. 231.
34. F. Wilkinson and J.T. Dubois. J. Chem. Phys. **39**, 377 (1963).
35. K. Sandros. Acta Chem. Scand. **23**, 2815 (1969).
36. M. Kojima, H. Sakuragi, and K. Tokumaru. Tetrahedron Lett. **22**, 2889 (1981).
37. K. Onodera, G.-I. Furusawa, M. Kojima, M. Tsuchiya, S. Aihara, R. Akaba, H. Sakuragi, and K. Tokumaru. Tetrahedron, **41**, 2215 (1985).
38. P.J. Baldry. J. Chem. Soc. Perkin Trans. 2, 951 (1979).
39. H.E. Zimmerman and V.R. Sandel. J. Am. Chem. Soc. **85**, 915 (1963).
40. H.E. Zimmerman and S. Somasekhara. J. Am. Chem. Soc. **85**, 922 (1963).
41. H. Shizuka and S. Tobita. J. Am. Chem. Soc. **104**, 6919 (1982).
42. W. Brandon, A.L. Pincock, J.A. Pincock, P. Redden, and C. Sehmbey. J. Am. Chem. Soc. **109**, 2181 (1987).
43. J.A. Pincock and P.R. Redden. Can. J. Chem. **67**, 227 (1989).
44. P.J. Kropp. J. Am. Chem. Soc. **95**, 4611 (1973).
45. M.B. Robin. *In* Higher excited states of polyatomic molecules. Vol. II. Academic Press, New York. 1975. p. 209.
46. M.G. Steinmetz. Org. Photochem. **8**, 67 (1987).
47. S.S. Hixson. J. Am. Chem. Soc. **97**, 1981 (1975).
48. R.J. Duguid and H. Morrison. J. Am. Chem. Soc. **113**, 3519 (1991).
49. R.A. Moss, W. Liu, and K. Krogh-Jespersen. J. Phys. Chem. **97**, 13413 (1993).
50. W.R.I. White and M.S. Platz. J. Org. Chem. **57**, 2841 (1992).
51. L. Friedman and H. Shechter. J. Am. Chem. Soc. **82**, 1002 (1960).
52. V. Bonacic-Koutecky, J. Koutecky, and J. Michl. Angew. Chem. Int. Ed. Engl. **26**, 170 (1987).
53. J. Michl and V. Bonacic-Koutecky. Electronic aspects of organic photochemistry. John Wiley & Sons, New York. 1990. Chap. 5.
54. A. Burger and R. Bennett. J. Med. Pharm. Chem. **2**, 687 (1960).
55. J.W. Wilt, J.M. Kosturik, and R.C. Orlowski. J. Org. Chem. **30**, 1052 (1965).
56. R.L. Trace and W.M. Jones. J. Organomet. Chem. **376**, 103 (1989).
57. K. Kodaira and K. Okuhara. Bull. Chem. Soc. Jpn. **61**, 1625 (1988).
58. S. Safe. J. Chem. Soc. (B), 962 (1971).
59. C. Laurence, M. Berthelot, L.L. Leveson, and C.W. Thomas. Spectrochim. Acta, Part A: **38A**, 487 (1982).
60. W.J. Leigh and D.R. Arnold. Can. J. Chem. **59**, 3061 (1981).
61. G.W. Sluggett and W.J. Leigh. J. Am. Chem. Soc. **114**, 1195 (1992).
62. W.J. Leigh, M.S. Workentin, and D. Andrew. J. Photochem. Photobiol. A: **57**, 97 (1991).

Can. J. Chem. Downloaded from www.nrcresearchpress.com by 65.111.164.53 on 09/08/12
For personal use only.

Nascent $HF^{\dagger}$ and $HSO(^2A')$ formations in the elementary reactions of $F + H_2S$ and $HS + O_3$ and the internal energy distributions

Yasunori Yoshimura, Toshio Kasai, Hiroshi Ohoyama, and Keiji Kuwata

Abstract: Chemiluminescence of the vibrationally excited $HF^{\dagger}$ and of the electronically excited HSO* in the $^2A'$ state were observed in the elementary reactions of $F + H_2S$ and $HS + O_3$. In the $F + H_2S$ reaction, the vibrational populations of $HF^{\dagger}$ in $v = 3$ and 4 were found to be nonstatistical but the rotational distribution in the $v = 4$ state was found to be Boltzmann-like with a rotational temperature of 700 K, confirming similar data obtained by different methods. The HSO* emission was observed in the $HS + O_3$ elementary reaction. The spectrum of HSO* characterized by broad vibrational bands indicates nonstatistical excitation for the rotational and vibrational states.

Key words: chemiluminescence, internal energy distribution, $F + H_2S$, $HS + O_3$, $HF^{\dagger}$, HSO^*.

Résumé : On a observé la chimiluminescence de l'excitation vibrationnelle du $HF^{\dagger}$ et de l'excitation électronique du HSO* dans l'état $^2A'$ dans les réactions élémentaires : $F + H_2S$ et $HS + O_3$. On a trouvé dans la réaction $F + H_2S$ que les populations de $HF^{\dagger}$ dans les états $v = 3$ et $v = 4$ ne sont pas statistiques mais que la distribution rotationnelle dans l'état $v = 4$ est du type Boltzmann avec une température rotationnelle de 700 K, confirmant ainsi des données similaires obtenues par différentes méthodes. On a observé l'émission HSO* dans la réaction élémentaire $HS + O_3$. Le spectre du HSO* caractérisé par une large bande vibrationnelle indique une excitation non statistique des états rotationnel et vibrationnel.

Mots clés : chimiluminescence, distribution de l'énergie interne, $F + H_2S$, $HS + O_3$, $HF^{\dagger}$, HSO^*.

[Traduit par la rédaction]

1. Introduction

Sulfur-containing molecules, such as hydrogen sulfide, mercaptans, and sulfur dioxide, are known to be easily oxidized by oxygen and ozone because of the multi-valency of the sulfur atom ranging from S(I) to S(VI). Those compounds have received significant attention because they are relevant to global problems of environmental chemistry (1–6). In the $H_2S + O_3$ reaction, SO_2 and H_2O were observed as the final products and HSO, HS, and SO were estimated as the reaction intermediates (3, 4, 7). There has been an extensively accumulated body of valuable data on these chemical species using the flow method, the flame method (8–11), and the arrested relaxation method (12–14). Practically, these methods afford a relaxation-free environment during the reaction. On the other hand, the use of molecular beams provides us complementary data, which are useful for confirming the available experimental results.

Received April 5, 1994.

Y. Yoshimura,[1] T. Kasai,[2] H. Ohoyama, and K. Kuwata.
Department of Chemistry, Faculty of Science, Osaka University, Toyonaka, Osaka 560, Japan.

[1] Present address: Sumitomo Sitix Co. Ltd., 1-banchi, Higashihama-cho, Amagasaki, Hyogo 660 Japan.

[2] To whom correspondence should be addressed: tel.: +81-6-850-5401; fax.: +81-6-850-5403; e-mail: a61680a@center.osaka-u.ac.jp

The reaction of $F + H_2S$ is a typical hydrogen extraction with a fast rate of $k = \sim 10^{-11}$ cm^3 molecule^{-1} s^{-1} (15–19). This reaction is 186.6 kJ mol^{-1} exothermic at 0 K and the total available energy is ~197 kJ mol^{-1} (20). This means that the product HF in the ground state can be excited up to $v = 4$. Chang et al. have investigated the HF infrared chemiluminescence for the fundamental and the first overtone and determined the relative populations in the $v = 1 \sim 4$ states. Several experiments using a fast-flow reactor or arrested relaxation have also been carried out (21, 22). The rotational lines of the fundamental emission bands of HF concentrates near 3 μm, thus these bands tend to overlap. These overlaps make it difficult to analyze the rotational distribution. In the present work, we observed the HF chemiluminescence in the visible region for the second overtone ($3 \rightarrow 0$) and the third overtone ($4 \rightarrow 0$). These overtone emissions appear separately in the 670 nm and 860 nm wavelength regions. For the overtone emission measurements, one must also take into account a very small probability of transition if it is compared with the fundamental one. In the vibrationally excited HF, marked as $HF^{\dagger}$, the probability for the $4 \rightarrow 3$ transition is larger than that for the $4 \rightarrow 0$ transition by $\sim 10^6$. Nevertheless, the high sensitivity for photon count detection with a photomultiplier would be able to compensate for the losses.

[1] $HS + O_3 \rightarrow HSO^* + O_2$

Can. J. Chem. Downloaded from www.nrcresearchpress.com by 65.111.164.53 on 09/08/12
For personal use only.

Can. J. Chem. Downloaded from www.nrcresearchpress.com by 65.111.164.53 on 09/08/12
For personal use only.

Fig. 1. Cross-sectional view of the reaction chamber and a block diagram for the chemiluminescence measurements. For $HF^{\dagger}$ measurement, the F atoms were directly used without the H_2S flow at the Teflon nozzle (1 mm ϕ in tubing and 3 mm ϕ in nozzle head). For HSO* measurement, the HS radicals were prepared by merging the H_2S flow at the Teflon nozzle and the target molecule O_3 was replaced by H_2S.

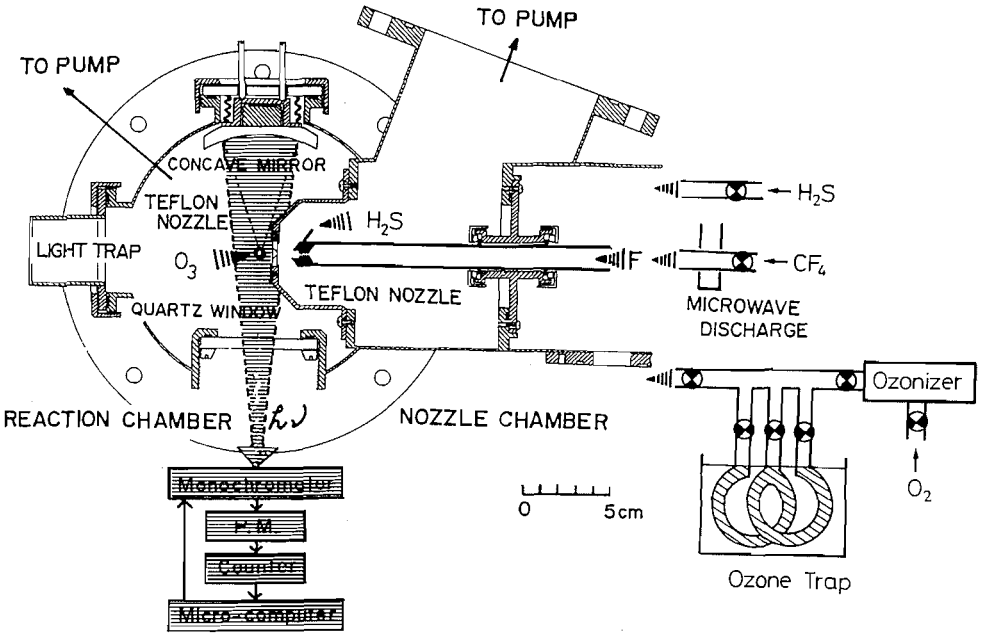

This reaction is known to be 295 kJ/mol exothermic (20). In the $H_2S/O/O_3$ reaction at a total pressure of 1 Torr, Schurath et al. observed the HSO chemiluminescence with vibrational structures in the 550–850 nm region, which was assigned to the S—O stretching mode (23(*a*)). They proposed that reaction [1] could be extracted as an elementary reaction. The laser irradiation study of the HSO* emission in the HS/O_3 system at 1 mTorr was done by Kendall et al. and the rotational temperature of HSO* was estimated to be as low as 700 K (23(*b*)).

Direct observations of the reaction using the HS radical beam would be worthwhile to carry out, since it is desirable to decouple the reaction from other possible secondary reactions by utilizing the single collision conditions. The $HSO^* + O_3 \rightarrow HS + 2O_2$ reaction might follow reaction [1] if the O_3 pressure is high (24). In this study, we reinvestigated the $F + H_2S$ reaction under single collision conditions to characterize the HF product, and the co-product HS was utilized as a radical beam in the $HS + O_3$ elementary reaction. The HSO* chemiluminescence was studied to determine the initial distribution of internal energy, and comparison was made with other results to learn more about product energy partition and possible reaction mechanisms.

2. Experimental

Figure 1 shows the cross-sectional view of the reaction chamber and a block diagram for the chemiluminescence measurement. The reaction chamber and the fore-chamber were differentially pumped by a 6-in. (~1300 L/s) and a 4-in. (~580 L/s) diffusion pump, respectively. A liquid nitrogen trap was used in the reaction chamber when necessary, but for safety reasons no trap was used when we used ozone. The background pressure during a run was 8×10^{-3} Pa and the ultimate pressure was $\sim 1 \times 10^{-4}$ Pa. A typical nozzle pressure of a reactant was 0.4–5 Torr (1 Torr = 133 Pa).

For the $HF^{\dagger}$ measurement, the F atoms, generated by microwave discharge of CF_4, effuse from the Teflon nozzle and enter the reaction chamber through a 2-mm ϕ collimator (26, 27). H_2S directly effuses into the reaction chamber and reaction [2] takes place in the reaction volume (the beam intersection). Typical flow rates at the nozzles are 0.5 μmol s^{-1} for CF_4 and 1.1 μmol s^{-1} for H_2S.

[2] $H_2S + F \rightarrow HS + HF^{\dagger}$

For the HSO* measurement, the target H_2S molecule was replaced by O_3 and the HS radicals were prepared by merging the H_2S flow at the Teflon nozzle in the fore-chamber. The F atoms or the HS radical beam cross a diverging beam of reagent molecules at 5 mm above the target nozzle in the reaction chamber. The HS radicals were prepared as in reaction [2] by merging a flow of H_2S with a flow of F atoms at the Teflon nozzle. The beam intensity of HS is estimated by measuring the $HF^{\dagger}$ emission intensity at 670 nm (30). Ozone, produced by an ozonizer and concentrated at a dry-ice ethanol ozone-trap, directly effused into the reaction chamber (27, 31).

Though the target molecules were not collimated in this study, the angular distribution measurement using a nude ion-gauge showed a typical directional profile as a diverging beam similar to the case of the O + NO reaction, where the flux intensity of NO was estimated to be $\sim 10^{17}$ molecules s^{-1} in reaction volume (25). We express the beam intensity here as the unit of flow rate (μmol s^{-1}) at a nozzle, since beam intensity should be proportional to flow rate under the present nozzle conditions (28, 29). Judging from the number density of

Can. J. Chem. Downloaded from www.nrcresearchpress.com by 65.111.164.53 on 09/08/12
For personal use only.

Fig. 2. Emission spectrum of HF with the spectral resolution of 3 nm. The flow rate of CF_4 is 0.5 μmol s^{-1} for producing the F atoms, and the flow rate of H_2S is 1.1 μmol s^{-1}. R and P stand for the R- and P-branches.

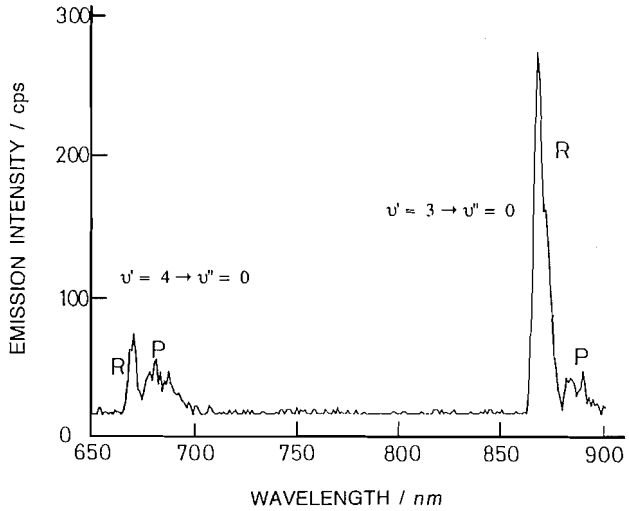

Fig. 3. Dependence of the $HF^{\dagger}$ emission intensity on the flow rate of H_2S at 670 nm (i.e., the R-head of the third overtone band).

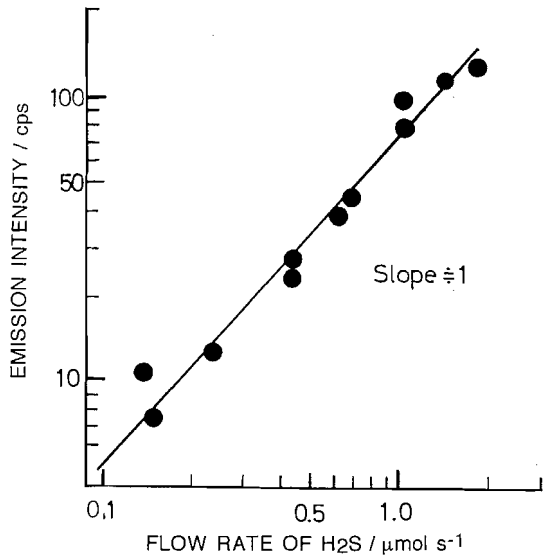

reagents in the reaction volume, the collisional deactivation of products needs to be considered carefully. Thus, the linear relationship between the signal intensity for product emission and the reagent densities has to be checked very carefully if one hopes for reliable data. It is also expected that a directional encounter of the reagents at a right angle will reduce the chance of collisional deactivation in this study. A more detailed characterization of reagent beams is described elsewhere, and the reaction volume was estimated to be a few mm in radius (25).

The product chemiluminescence in the reaction zone is collected by a concave mirror (focal length, 5 cm) in the third direction and focused onto the entrance slit of a monochromator (focal length, 30 cm), followed by a photon count unit. The optical setup confined the detector view as shown in Fig. 1, except that the cone of view of the monochromator was overstated and drawn too widely. In an exact setup, the collimator walls were set out of sight. Any walls of the chamber should be away from the line of sight of the detection, otherwise products would be partly deactivated at the walls and they could be observed. This was tested by inserting various sizes of the view-confine aperture on the quartz window and we indeed observed preferentially an emission from the reaction volume at beam intersection. In addition, we could see the emission signal only if the concave mirror was properly adjusted to the point of the reaction volume. We therefore concluded that the emission we observed came mostly from the crossed beam region. The signal count (cps) was recorded as a function of the monochromator wavelength. The wavelength scan was repeated and the signal counts were accumulated by a microcomputer to improve the signal-to-noise ratio. The background signal was subtracted from our data.

3. Results

3.1 F + H_2S reaction

Figure 2 shows the chemiluminescence spectrum of $HF^{\dagger}$ from 650 to 900 nm, where two overtone bands of $v' = 4 \rightarrow v'' = 0$ and $v' = 3 \rightarrow v'' = 0$ appear. The spectral resolution was 3 nm and we measured each point at 1 nm intervals for 10 s on each point. Since the spectrum is not calibrated for the photomultiplier sensitivity and the efficiency of monochromator transmission in the figure, the apparent intensity in the figure does not reflect the ratio of the $(3 \rightarrow 0)$ and $(4 \rightarrow 0)$ overtones (32). After we corrected for wavelength efficiencies in our detection, we obtained a relative population ratio of 1:1 for $v = 3{:}4$, which includes experimental error and analysis error (>10%). For analysis, we used the rotationally averaged values of the square of the transition matrix elements taken from the experimental values from Sileo and Cool (32). This procedure might bring on some uncertainty, which will be discussed in a later section.

Figure 3 shows the dependence of emission intensity of the $HF^{\dagger}$ third overtone on the H_2S flow rate. The relationship was found to be linear within the uncertainty as the figure shows. This linear relationship confirms the single collision conditions for the H_2S reactant molecule. Because the change in the CF_4 flow rate affected the microwave discharge conditions, it was not possible to examine the dependence of $HF^{\dagger}$ emission on the flow rate of F atoms. Therefore, the CF_4 flow rate was used a constant at an optimum condition for the discharge (0.4 Torr of CF_4 pressure). Since the fluorine atom beam intensity is estimated to be very small, signal linearity with respect to the F atoms would be preserved.

Figure 4 shows the emission spectrum of the third overtone of $HF^{\dagger}$. The spectrum was taken with a 1.2 nm resolution and measured at a 0.2 nm interval. The largest band at 670 nm was assigned the R-head and a series of P-branches, from P(1) to P(9), in the direction of longer wavelengths (33). The rotational distribution of $HF^{\dagger}$ in $v = 4$ was determined by spectral simulation of this spectrum.

Spectral simulation and the rotational distribution of $HF^{\dagger}$ in v = 4

The spectral simulation was carried out via a standard method using eq. [2] (34(*a*)).

Can. J. Chem. Downloaded from www.nrcresearchpress.com by 65.111.164.53 on 09/08/12
For personal use only.

Fig. 4. Emission spectrum of the third overtone of $HF^{\dagger}$ (shown with the dotted area). The flow rate of CF_4 is 0.4 μmol s^{-1}, and the flow rate of H_2S is 1.1 μmol s^{-1}. The resolution was 1.2 nm at the 0.2 nm scan interval. The assignment of the bands is the R-head from left and the series of the P-branches to the longer wavelengths as shown from P(1) to P(9). The broken line shows the simulated spectrum (see the text).

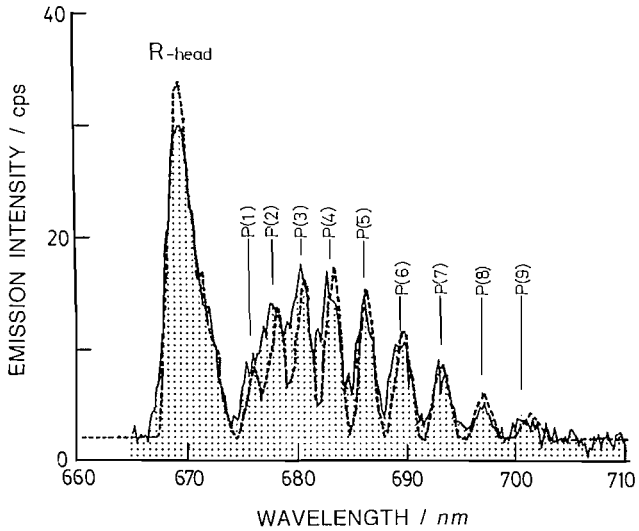

$$[3]\quad I^{v'J'}_{v''J''} \propto \nu^3 \cdot |R^{v'J'}_{v''J''}|^2 \cdot (hcBv'/kT) \cdot N_{v'} \times \exp\,[-F(v', J')/kT]$$

where ν is the wave number, and $B_{v'}$ and $N_{v'}$ are the rotational constant and the population in the v' vibrational state, respectively. $|R^{v'J'}_{v''J''}|^2$ represents the square of the dipole transition matrix element for $(v', J') \rightarrow (v'', J'')$, and $F(v', J')$ is the term value of the vibrating rotator in the Dunham expression as shown by the following relation (34(*b*)). The third overtone transition of HF corresponds to $(4, J') \rightarrow (0, J'')$ and the term value includes the correction due to the $v = 4$ vibration.

$$F(v, J) = \sum_{i,m} Y_{im}(v + \tfrac{1}{2})[J(J+1)]^m$$

The allowed transitions are the ones with $\Delta J = J' - J'' = +1$ for the R branch, and the one with $\Delta J = -1$ for the P branch. The triangle function was used as the slit function for the monochromator. The rotational temperature, T_R, was systematically varied to determine the best fit with a minimum χ^2. The best fit was obtained with T_R = 700 K, and the simulated spectrum is shown by the dotted line in Fig. 4. Figure 5 represents the initial rotational distribution for $HF^{\dagger}$ in the $v = 4$ thus obtained.

3.2. HS + O_3 reaction

Figure 6 shows the emission spectrum from the reaction volume in the HS + O_3 reaction. The flow rate of O_3 at the nozzle was 1.5 μmol s^{-1}. The spectral resolution was 3 nm. We measured each point at 1 nm intervals for 10 seconds. Even though the signal-to-noise ratio was unavoidably weak under the single collision conditions, the emission profile appears to be very broad when it is compared with the HSO spectra reported earlier (23(*b*)). For confirmation of the single collision conditions, the linearity of the emission intensity with respect to the reagent flow rate was tested.

Fig. 5. Initial rotational distribution for the levels J = 0–8 of $HF^{\dagger}$ in the $v = 4$ state (shown with the filled circles). The open circles are the relative populations for J = 0–7 measured by Chang et al. (cited from ref. 21).

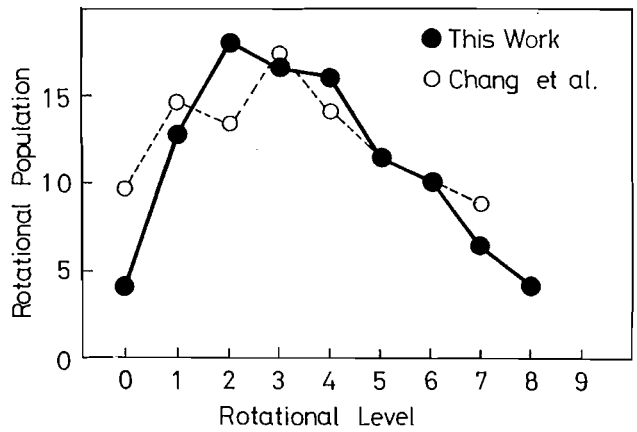

Fig. 6. Emission spectrum from the beam reaction of HS + O_3 with the spectral resolution of 3 nm. The flow rates of CF_4, H_2S, and O_3 are 0.5, 0.3, and 1.5 μmol s^{-1}, respectively. The spectrum of Kendall et al. is shown for reference (cited from ref. 23(*b*)).

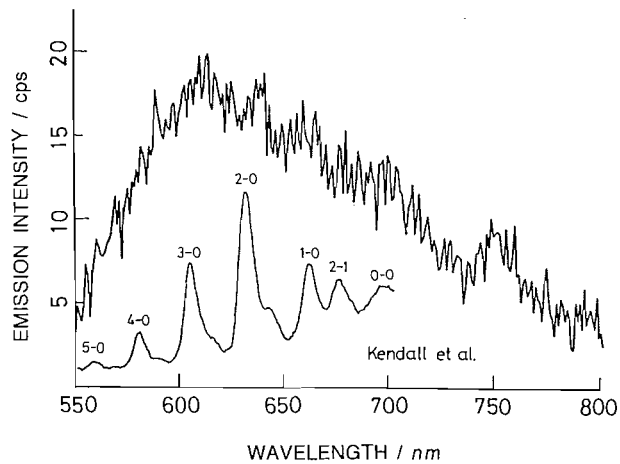

Figure 7 shows the logarithmic plot of peak emission intensity at 600 nm vs. O_3 flow rate. The log–log plot was used to cover a wider range of flow rate. The dependence was found to be linear, with a slope of ~1. The $HF^{\dagger}$ emission at the Teflon nozzle is regarded to be a good measure for the HS beam intensity, since reaction [2] provides an equal number of HS radicals to $HF^{\dagger}$. The emission intensity in the H_2S + O_3 reaction was found to be approximately linear to the $HF^{\dagger}$ emission. Thus, these linear relationships for both reactants confirm that the chemiluminescence shown in Fig. 6 was due to a single collision of HS and O_3, which leads to the HSO* formation.

There remain some ambiguities as to how unreacted reagents of F atoms might keep traveling and react with O_3 in the reaction chamber. This possibility, however, was refuted by experiments because neither the F + O_3 nor the H_2S + O_3 reaction gave any chemiluminescence. Another possibility may be that the vibrationally excited $HF^{\dagger}$ (which is the coproduct of HS at the Teflon nozzle) might react with O_3 to give emissive products like HFO*. But no chemiluminescence was

Can. J. Chem. Downloaded from www.nrcresearchpress.com by 65.111.164.53 on 09/08/12
For personal use only.

Fig. 7. Dependence of the emission intensity at 600 nm in Fig. 6 on the flow rate of O_3.

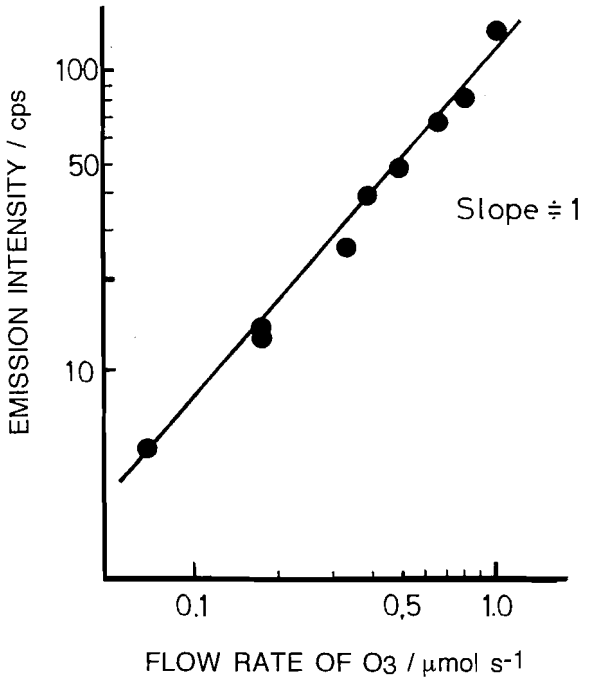

Fig. 8. Emission spectrum from gas–beam reaction of HS + O_3 with the spectral resolution of 3 nm. The flow rates of CF_4, H_2S are 0.5, and 0.4 μmol s^{-1}, respectively. Ozone at the flow rate of 0.9 μmol s^{-1} was confined in the target region of the reaction chamber. The spectrum of Kendall et al. is shown for reference (cited from ref. 23(*b*)).

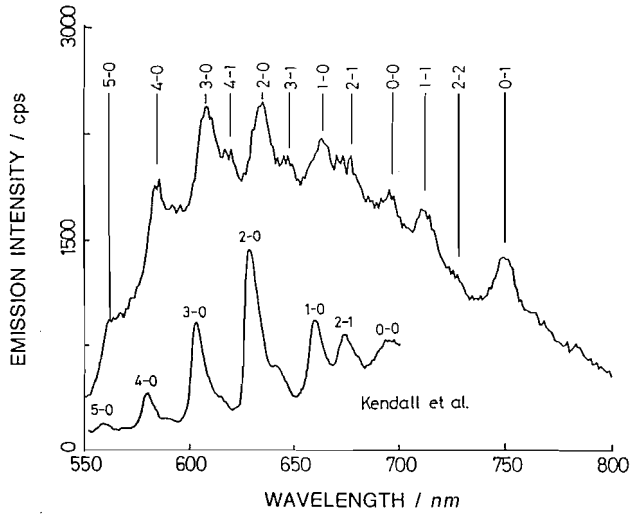

expected judging from the available energy in the $HF^{\dagger}$ + O_3 reaction (20).

To substantiate the hypothesis that the chemiluminescence in Fig. 6 is indeed due to the reaction product HSO*, a gas–beam experiment was carried out by increasing the total pressure of the reactants up to ~1 Pa in the reaction chamber. The HSO* emission intensity increased by a factor of ten. Figure 8 shows the spectrum obtained under such conditions. Since rotational relaxation of the reactant collisions tends to make each vibrational band narrower, the vibrational bands can be assigned, as already reported in ref. 23, to the progression of the S—O stretching mode of HSO* in the $^2A'$ electronic state, which is indicated by the vibrational quantum numbers in Fig. 6.

Fig. 9. Estimated initial distributions of the HSO($^2A'$) vibration. The circles and the squares are obtained by the spectral simulations of Figs. 6 and 8, respectively. The distribution with the triangles is cited from ref. 23(*b*). The three distributions are normalized at $v = 2$.

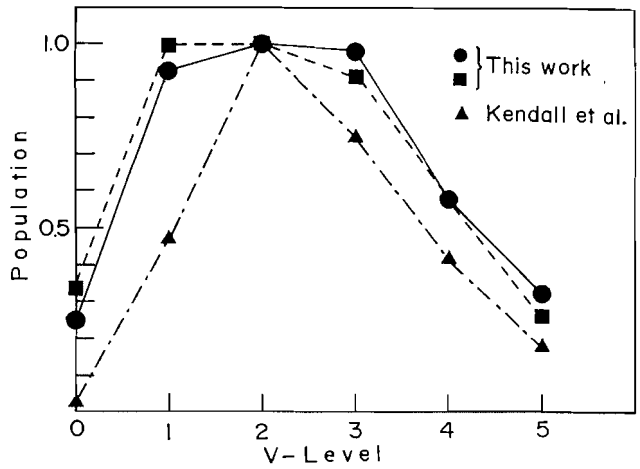

The cause of the significant broadness of the HSO* emission spectrum in Fig. 6 needs to be considered next. A broadening could happen if more than one vibrational mode is excited together with the S—O stretching mode, and (or) extremely high excitation of the HSO* rotation. First, we carried out the spectral simulation, assuming that the S—O mode of HSO* was preferentially excited. The effects of rotational excitation of HSO* were then tested.

Figure 9 shows the vibrational distribution obtained by simulating the spectrum in either Fig. 6 or Fig. 8. If the energy of reaction is preferentially released in the S—O vibrational mode, HSO* in the $^2A'$ state could be excited up to $v = 15$ (35). Radiative lifetimes from all levels (v', J') can be obtained from the reciprocals of the total Einstein $A_{v',J'}$ coefficient, which is given below, and is proportional to the squared dipole transition moments (36).

$$A_{v',J'} = \left[\frac{1}{2J'+1}\right]\left[(J')\sum_{v''} A_{v',J';v'',J'-1} + (J'+1) \times \sum_{v''} A_{v',J';v'',J'+1}\right]$$

The relative population of v' (after averaging for J') is given by the emission intensity divided by the squared dipole transition moments, which include the Franck–Condon factors. We estimated the Franck–Condon factors from radiative lifetimes for individual vibrational levels observed by Kawasaki and co-workers (37). The spectroscopic parameters for the $^2A' \rightarrow {}^2A''$ transition and the molecular constants were taken from the literature (23(*a*)). Table 1 lists the calculated relative Franck–Condon factors (38–40). We then carried out the spectral simulation to estimate the HSO* rotational distribution. In a sim-

Can. J. Chem. Downloaded from www.nrcresearchpress.com by 65.111.164.53 on 09/08/12
For personal use only.

Table 1. Estimated Franck–Condon factors for the vibronic transitions $(v', 2A') \rightarrow (v'', {}^2A'')$ of HSO

$v' \rightarrow v''$	Relative Franck–Condon factors
$7 \rightarrow 0$	2.16
$6 \rightarrow 0$	1.76
$5 \rightarrow 0$	1.46
$4 \rightarrow 0$	1.31
$3 \rightarrow 0$	1.08
$2 \rightarrow 0$	1.00[a]
$1 \rightarrow 0$	0.91
$0 \rightarrow 0$	0.82

[a]The $(2 \rightarrow 0)$ transition is set as 1.00 for normalization purpose.

Fig. 10. Simulated spectra of $HSO(^2A')$ with the estimated rotational temperatures of 3000 K (the solid line) and 700 K (the shaded area). The bandwidths become broad as the temperature increases, but the observed spectrum of Fig. 6 was found to be too broad to simulate.

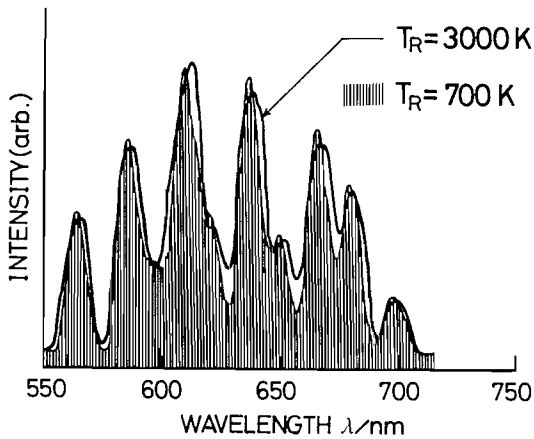

ulation process, a single rotational temperature and the same band shape of (030) – (000) were assumed for all vibrational bands.

Figure 10 shows the simulated spectra with two estimated temperatures, 3000 K (the solid line) and 700 K (the shaded area). There is a general tendency that the vibrational band becomes broad as the rotational temperature increases. As seen in the figure, neither simulated spectra agrees with the observed one, if we assume that the rotational distribution is Boltzmann. The observed spectrum may reflect a nonstatistical rotational distribution of the HSO* product.

4. Discussion

4.1. F + H_2S reaction

Earlier studies give the relative $HF^\dagger$ vibrational population for $v = 3$ and $v = 4$. Chang and co-workers reported a value of 1:0.75, and the fast-flow reactor experiment done by Agrawalla and Setser gave a value of 1:0.33. The arrested relaxation by Dill et al. yielded 1:0.52. The present work gives a relatively larger population with the ratio of 1.0:~1 (21, 22). As mentioned in the previous section, the uncertainty in our work (>10%) does not make our result superior to the previously reported values. On the other hand, our result is in excellent agreement with those obtained by other methods, confirming the reliability of our data.

The solid circles in Fig. 5 show the rotational distribution of HF in $v = 4$ obtained in this work and the open circles show the one measured by Chang et al. (21(*a*)). This result indicates that the two distributions show a similar tendency on the whole except for a smaller population in the $J = 0$ level in the present study. The fast-flow reactor and the arrested relaxation studies also gave similar HF rotational distributions which extend to the thermochemical limit for several vibrational levels (21(*c*), 22). The present result seems to be in better agreement with the distribution in the arrested relaxation method than the one in the fast-flow reactor.

Energy partition among the products' rotation and translation

The energetics shows that ~90% of the reaction energy is released as vibrational freedom of HF when the molecule is excited up to $v = 4$. The remaining ~3% of the available energy appears in the rotation of HF characterized as $T_R = 700$ K, and the corresponding average rotational energy of HF is ~5 kJ mol^{-1}. The quantity, g_r, defined by eq. [4], is known to be a good measure to test whether or not a rotational distribution is statistical (41, 42).

$$[4] \quad g_r = f_{rot}/(1 - f_{vib}) = 0.03/(1 - 0.9) = 0.3$$

where f_{rot} stands for the fraction of the energy released to the HF rotation, i.e., equal to 0.03 in the present case for $HF^\dagger$ ($v = 4$), and f_{vib} is the fraction of the vibrational excitation, i.e., $f_{vib} = 0.9$. Equation [4] calculates g_r to be 0.3.

If we suppose the energy partitioning is statistical among all freedoms of HF and HS, g_r can be calculated by eq. [5].

$$[5] \quad g_r = N_{rot}(HF)/[(N_{trans} + N_{rot}(HF) + N_{rot}(HS)] = 2/(3 + 2 + 2) = 0.28$$

where N_{rot} represents the degree of rotational freedom, and N_{trans} is the degree of freedom for the relative translation of the products. The expected g_r becomes 0.28 as previously shown. Good agreement is seen between 0.3 and 0.28; the former is the experimentally observed value using eq. [4] and the latter is the calculated value using eq. [5]. This result suggests that the energy partition in the F + H_2S reaction statistically occurs among the relative translation and rotations of HF and HS. On the other hand, this reaction does not seem to occur in a statistical way for the HF vibrational excitation as already seen in Sect. 3.1.

4.2. HS + O_3 reaction

We have shown that the HSO* spectrum of Fig. 6 observed under the single collision conditions is significantly broad and it is indeed different from the ones in the earlier studies using various methods (1–6, 23(*b*)). Kendall et al. suggested that the rotational relaxation in the reaction system is probably very

Fig. 11. Simulated rotational structure of the $A'(003) \rightarrow A''(000)$ overtone spectrum of HSO.

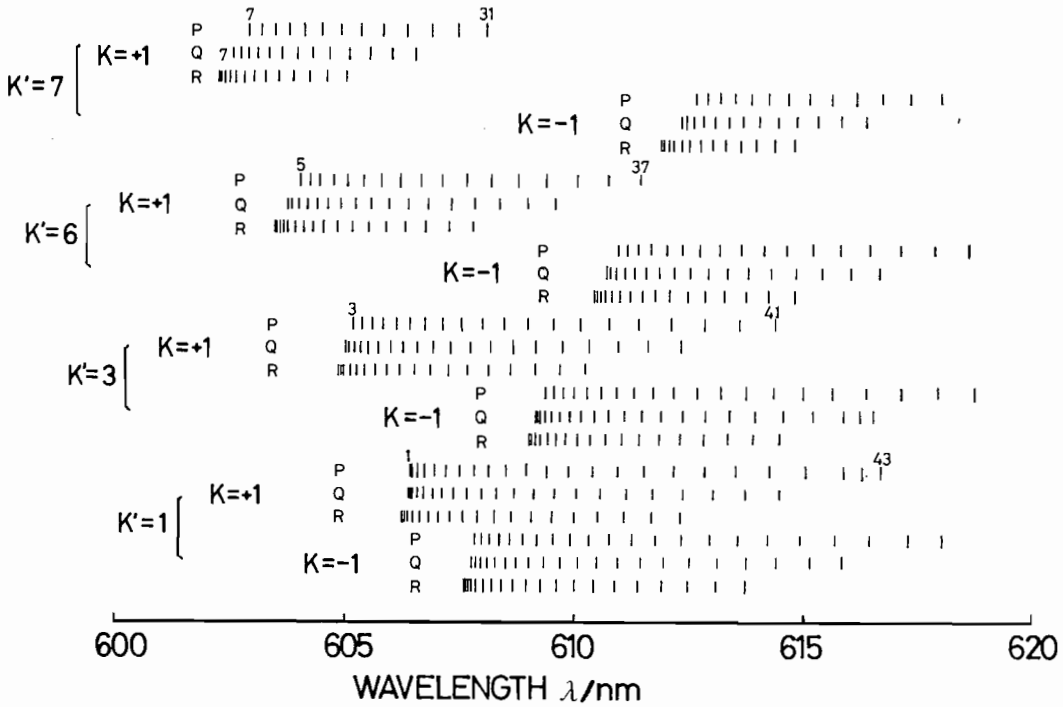

fast (23(*b*)). If this is the case, the single collision conditions in the present study may enable us to observe such nascent HSO* radicals which are free from rotational relaxation.

Figure 11 shows a simulated structure of rotation for the $A'(003) \rightarrow A''(000)$ overtone spectrum of HSO. K' and K represent the rotational quantum numbers of HSO in the upper and the lower electronic states, respectively. The rotational lines with the higher K tend to extensively populate apart from these band-origins, because the molecular constants of HSO for the $^2A'$ excited state and the $^2A''$ ground state are known to be similar (38–40). This broadening tendency would tell us that a non-Boltzmann distribution of rotation with higher K' levels should be considered in simulating the observed spectrum of HSO* in the elementary reaction [1] (43). The feasibility of excitation in other vibrational modes remains as an open question. It is hoped that future studies can clarify molecular-level mechanisms of such nonstatistical reactions under either the well-defined collisional geometry using the oriented HS radical beam or the well-defined initial states of the reactant molecules using laser excitation and detection (42, 44, 45).

References

1. K.H. Becker, M.A. Inocencio, and U. Schurath. Int. J. Chem. Kinet. **1S**, 205 (1975).
2. I.R. Schurath, R.E. Graham, and D. Gutman. Int. J. Chem. Kinet. **8**, 451 (1976).
3. S.W. Benson. Chem. Rev. **78**, 23 (1978).
4. I.R. Slagle, F. Baiocchl, and D. Gutman. J. Phys. Chem. **82**, 1333 (1978).
5. (*a*) N.S. Wang, E.R. Lovejoy, and C.J. Howard. J. Phys. Chem. **91**, 5743 (1987); (*b*) N.S. Wang and C.J. Howard. J. Phys. Chem. **94**, 8787 (1990).
6. K. Ravichandran, R. Williams, and T.R. Fletcher. Chem. Phys. Lett. **217**, 375 (1994).
7. S. Glavas and S. Toby. J. Phys. Chem. **79**, 779 (1975).
8. C.A. Parr, J.C. Polanyi, and W.H. Wong. J. Chem. Phys. **58**, 5 (1973).
9. A.G. Gaydon. The spectroscopy of flames. Chapman and Hall, London. 1974; D.W. Setser. Reactive intermediates in the gas phase. Academic Press, New York. 1979.
10. K.H. Becker, W. Groth, and D. Thran. Chem. Phys. Lett. **6**, 583 (1970).
11. M.J.Y. Clement and D.A. Ramsay. Can. J. Phys. **39**, 205 (1961).
12. D.H. Maylotte, J.C. Polanyi, and K.B. Woodall. J. Chem. Phys. **57**, 1547 (1972).
13. J.C. Polanyi and K.B. Woodall. J. Chem. Phys. **57**, 1574 (1972).
14. K.G. Anlauf, D.S. Horne, R.G. Macdonald, J.C. Polanyi, and K.B. Woodall. J. Chem. Phys. **57**, 1561 (1972).
15. R.R. Friedl, Wm. H. Brune, and J.G. Anderson. J. Chem. Phys. **79**, 4227 (1983).
16. D.A. Whytock, R.B. Timmons, J.H. Lee, J.V. Michael, W.A. Payne, and L.J. Stief. J. Chem. Phys. **65**, 2052 (1976).
17. M.J. Kurylo, N.C. Peterson, and W. Braun. J. Chem. Phys. **54**, 943 (1971).
18. R.R. Friedl, W.H. Brune, and J.G. Anderson. J. Chem. Phys. **79**, 4227 (1983).
19. R.R. Friedl, W.H. Brune, and J.G. Anderson. J. Phys. Chem. **89**, 5505 (1985).
20. H. Okabe. Photochemistry of small molecules. John Wiley, New York. 1978. p. 379.
21. (*a*) H.W. Chang, D.W. Setser, M.J. Perona, and R.L. Johnson. Chem. Phys. Lett. **9**, 587 (1971); (*b*) W.H. Duewer and D.W. Setser. J. Chem. Phys. **58**, 2310

Can. J. Chem. Downloaded from www.nrcresearchpress.com by 65.111.164.53 on 09/08/12
For personal use only.

(1973); (*c*) B.S. Agrawalla and D.W. Setser. J. Phys. Chem. **90**, 2450 (1986); (*d*) E. Arunan, D. Raybone, and D.W. Setser. J. Chem. Phys. **97**, 6348 (1992).
22. B. Dill and H. Heydtmann. Chem. Phys. **35**, 161 (1978).
23. (*a*) T. Schurath, M. Weber, and K.H. Becker. J. Chem. Phys. **67**, 110 (1977); (*b*) D.J. Kendall, J.J.A. O'Brien, J.J. Sloan, and R.G. Macdonald. Chem. Phys. Lett. **110**, 183 (1984).
24. J. Espinosa-Garcia and J.C. Corchado. Chem. Phys. Lett. **218**, 128 (1994).
25. (*a*) T. Kasai, T. Masui, H. Nakane, I. Hanazaki, and K. Kuwata. Chem. Phys. Lett. **56**, 84 (1978); (*b*) T. Kasai. Ph.D. Thesis, Osaka University. 1979; (*c*) Y. Yoshimura, H. Ohoyama, T. Hamada, T. Kasai, and K. Kuwata. Chem. Phys. Lett. **106**, 271 (1984); (*d*) H. Ohoyama, T. Kasai, Y. Yoshiomura, H. Kimura, and K. Kuwata. Chem. Phys. Lett. **118**, 263 (1985); (*e*) T. Kasai, T. Fukawa, T. Matsunami, D.-C. Che, K. Ohashi, H. Ohoyama, and K. Kuwata. Rev. Sci. Instrum. **64**, 1150 (1993).
26. C.E. Kolb and M. Kaufmann. J. Phys. Chem. **76**, 947 (1972).
27. H. Ohoyama, T. Kasai, Y. Yoshimura, H. Kimura, and K. Kuwata. Chem. Phys. Lett. **118**, 263 (1985).
28. J.A. Giordmaine and T.C. Wang. J. Appl. Phys. **31**, 463 (1960).
29. H. Pauly. Atomic and molecular beam methods. Vol. 1. *Edited by* G. Scoles. Oxford University Press, New York/ Oxford. 1988. p. 83.
30. R.L. Spellicy, R.E. Meredith, and F.G. Smith. J. Chem. Phys. **57**, 5119 (1972).
31. G.A. Cook, A.D. Kiffer, C.V. Klumpp, A.H. Malik, and L.A. Spence. Ozone chemistry and technology, advances in chemistry series. American Chemical Society, Washington, D.C. 1959.
32. R.N. Sileo and T.A. Cool. J. Chem. Phys. **65**, 117 (1976).
33. D.U. Webb and K.N. Rao. J. Mol. Spectrosc. **28**, 121 (1968).
34. (*a*) G. Herzberg. Molecular spectra and molecular structure. I. Spectra of diatomic molecules. 2nd ed. Van Nostrand Reinhold, New York. 1950. p. 106; (*b*) E. Arunan, D.W. Setser, and J.F. Ogilvie. J. Chem. Phys. **97**, 1734 (1992).
35. F.E. Davidson, A.R. Clemo, C.L. Duncan, R.J. Browett, J.H. Hobson, and R. Grice. Chem. Phys. **46**, 33 (1982).
36. W.T. Zemke, W.C. Stwalley, S.R. Langhoff, G.L. Valderrama, and M.J. Berry. J. Chem. Phys. **95**, 7846 (1991).
37. (*a*) M. Kawasaki, K. Kasatani, S. Tanahashi, and H. Sato. Chem. Phys. Lett. **75**, 128 (1980); (*b*) M. Kawasaki, K. Kasatani, S. Tanahashi, H. Sato, and Y. Fujimura. J. Chem. Phys. **78**, 7146 (1983).
38. A.B. Sannigrahi, K.H. Thunemann, S.D. Peyerimhoff, and R.J. Buenker. Chem. Phys. **20**, 25 (1977).
39. G. Hancock and I.W.M. Smith. Appl. Opt. **10**, 1827 (1971).
40. M. Kakimoto, S. Saito, and E. Hirota. J. Mol. Spectrosc. **80**, 334 (1980).
41. K. Tamagake and D.W. Setser. State-to-state chemistry. *Edited by* P.R. Brooks and E.F. Hayes. ACS. Symp. Ser. **56**, 124 (1977).
42. R.D. Levine and R.B. Bernstein. Molecular reaction dynamics. Oxford University Press, London. 1974.
43. H.W. Chang, D.W. Setser, M.J. Perona, and R.L. Johnson. Chem. Phys. Lett. **9**, 587 (1971).
44. T. Kasai, K. Ohashi, H. Ohoyama, and K. Kuwata. Chem. Phys. Lett. **127**, 581 (1986).
45. (*a*) D.-C. Che, T. Kasai, H. Ohoyama, K. Ohashi, T. Fukawa, and K. Kuwata. J. Phys. Chem. **95**, 8159 (1991); (*b*) D.-C. Che, T. Kasai, H. Ohoyama, and K. Kuwata. J. Phys. Chem. **98**, 132 (1994).

Can. J. Chem. Downloaded from www.nrcresearchpress.com by 65.111.164.53 on 09/08/12
For personal use only.

Adamantane-based nitrile sulfides: the generation of the synthetic equivalent of the first bis(nitrile sulfide)

John N. Bridson, Melbourne J. Schriver, and Shuguang Zhu

Abstract: The reaction of 1,3-adamantanedicarbonamide with chlorocarbonylsulfenyl chloride in hot toluene gives two new oxathiazolone derivatives that have had their structures confirmed crystallographically: 1,3-bis(1,3,4-oxathiazol-2-on-5-yl)-adamantane and 1-cyano-3-(1,3,4-oxathiazol-2-on-5-yl)-adamantane. (Crystal data: $C_{10}H_{14}(COC(O)SN)_2$: $P2_1/m$, $a = 10.447(2)$, $b = 7.119(3)$, $c = 10.684(2)$ Å, $\beta = 112.98(1)°$, $V = 731.5(3)$ Å^3, $z = 2$, $D_c = 1.536$ g cm^{-3}, $R = 0.034$, $R_w = 0.029$; $(NC)C_{10}H_{14}(COC(O)SN)$: $P2_1/c$, $a = 9.153(2)$, $b = 19.134(2)$, $c = 7.130(3)$ Å, $\beta = 105.38(2)°$, $V = 1204(1)$ Å^3, $z = 4$, $D_c = 1.447$ g cm^{-3}, $R = 0.038$, $R_w = 0.035$.) The reaction of the precursor with dimethyl acetylenedicarboxylate (DMAD) in refluxing chlorobenzene gave a mixture that was resolved into pure compounds by Kugelrohr sublimation; these were shown to be sulfur, tetramethyl thiophenetetracarboxylate, 1,3-adamantanedinitrile, 1,3-bis(4,5-bis(methoxycarbonyl)-isothiazol-3-yl)-adamantane, and 1-cyano-3-(4,5-bis(methoxycarbonyl)-isothiazol-3-yl)-adamantane. The structures of the two new isothiazole derivatives were confirmed crystallographically. (Crystal data: $C_{10}H_{14}(CNS{\cdot}DMAD)_2$: $Pca2_1$, $a = 15.857(4)$, $b = 11.562(4)$, $c = 13.602(4)$ Å, $V = 2494(2)$ Å^3, $z = 4$, $D_c = 1.424$ g cm^{-3}, $R = 0.057$, $R_w = 0.038$; $C_{10}H_{14}(CN)(CNS{\cdot}DMAD)$: $P2_1/c$, $a = 19.683(2)$, $b = 11.566(3)$, $c = 7.727$ (3) Å, $\beta = 93.30(2)°$, $V = 1756(1)$ Å^3, $z = 4$, $D_c = 1.363$ g cm^{-3}, $R = 0.079$, $R_w = 0.076$.) The pattern of reactivity indicates that the *synthetic equivalent* of the bis(nitrile sulfide) may be present in solution but has a very short lifetime and failed to react at all with 1,3-adamantanedinitrile.

Key words: oxathiazolone, nitrile sulfide, cycloaddition, isothiazole.

Résumé : La réaction du adamantane-1,3-dicarbonamide avec le chlorure de chlorocarbonylsulfényle dans du toluène chaud donne deux nouveaux dérivés oxathiazolone dont les structures ont été confirmées par cristallographie : 1,3-bis(1,3,4-oxathiazol-2-on-5-yl)-adamantane et 1-cyano-3-(1,3,4-oxathiazol-2-on-5-yl)-adamantane. (Les données cristallines du composé $C_{10}H_{14}(COC(O)SN)_2$ sont : $P2_1/m$, avec $a = 10,447(2)$, $b = 7,119(3)$, $c = 10,684(2)$ Å, $\beta = 112,98(1)°$, $V = 731,5(3)$ Å^3, $z = 2$, $D_c = 1,536$ g cm^{-3}, $R = 0,034$, $R_w = 0,029$ et celles du composé $(NC)C_{10}H_{14}(COC(O)SN)$ sont : $P2_1/c$, avec $a = 9,153(2)$, $b = 19,134(2)$, $c = 7,130(3)$ Å, $\beta = 105,38(2)°$, $V = 1204(1)$ Å^3, $z = 4$, $D_c = 1,447$ g cm^{-3}, $R = 0,038$, $R_w = 0,035$.) La réaction du précurseur avec l'acétylènedicarboxylate de méthyle (DMAD) dans le chlorobenzène au reflux donne un mélange que l'on a séparé en composés purs par la sublimation de Kugelrohr pour obtenir : le soufre, le thiophènetétracarboxylate de méthyle, le 1,3-adamantanedinitrile, le 1,3-bis(4,5-bis(méthoxycarbonyl)-isothiazol-3-yl)-adamantane et le 1-cyano-3-(4,5-bis(méthoxycarbonyl)-isothiazol-3-yl)-adamantane. On a confirmé, par cristallographie, les structures des deux nouveaux dérivés de l'isothiazole. (Les données cristallines du composé $C_{10}H_{14}(CNS{\cdot}DMAD)_2$ sont : $Pca2_1$, avec $a = 15,857(4)$, $b = 11,562(4)$, $c = 13,602(4)$ Å, $V = 2494(2)$ Å^3, $z = 4$, $D_c = 1,424$ g cm^{-3}, $R = 0,057$, $R_w = 0,038$ et celles du composé $C_{10}H_{14}(CN)(CNS{\cdot}DMAD)$ sont : $P2_1/c$, avec $a = 19,683(2)$, $b = 11,566(3)$, $c = 7,727$ (3) Å, $\beta = 93,30(2)°$, $V = 1756(1)$ Å^3, $z = 4$, $D_c = 1,363$ g cm^{-3}, $R = 0,079$, $R_w = 0,076$.) L'allure de la réactivité indique que l'*équivalent synthétique* du bis(sulfure de nitrile) peut être présent en solution mais qu'il a un temps de vie très court et qu'il ne réagit pas du tout avec tous les 1,3-adamantanedinitriles.

Mots clés : oxathiazolone, sulfide de nitrile, cycloaddition, isothiazole.

[Traduit par la rédaction]

Introduction

Synthesis of heterocyclic systems via the 1,3-dipolar cycloaddition reaction is a well-established protocol in synthetic chemistry (1). The nitrile sulfides ($R\text{-}C{\equiv}N^+\text{-}S^-$) are a relatively new family of 1,3-dipoles that are typically generated in solution by the thermal decarboxylation of an oxathiazolone derivative (2). These synthetically useful 1,3-dipoles have been shown to be unstable with respect to decomposition to sulfur and the corresponding nitrile. We recently described the generation of the first adamantane-based nitrile sulfide and reported the reaction of these 1,3-dipoles with the C≡C and S≡N triple bonds to give isothiazoles and dithiadiazoles, respectively (3).

The chemistry of carbon–sulfur–nitrogen heterocycles has

Received September 19, 1994.

J.N. Bridson, M.J. Schriver,[1] and S. Zhu. Department of Chemistry, Memorial University of Newfoundland, St. John's, NF A1B 3X7, Canada.

[1] Author to whom correspondence may be addressed. Telephone: (709) 737-8744. Fax: (709) 737-3702. E-mail: mschriver@kean.ucs.mun.ca

Can. J. Chem. Downloaded from www.nrcresearchpress.com by 65.111.164.53 on 09/08/12
For personal use only.

Can. J. Chem. Downloaded from www.nrcresearchpress.com by 65.111.164.53 on 09/08/12
For personal use only.

recently been an area of intense research. The electron-rich cations and radicals described by Banister and Rawson (4), Oakley and co-workers (5), and Parsons and Passmore (6) that have been generated in the search for new conductive materials have clearly delineated the potential of these systems. Their most recent efforts have focused on the preparation of molecules that contain multiple heterocyclic moieties, usually substituted on aromatic or π-delocalized systems. We are interested in the use of saturated hydrocarbon cages as substrates to stabilize reactive π systems. We have concentrated on the adamantane moiety in this role because there are multiple tertiary carbon atoms in the carbon cage and the substitution of these centres with reactive π systems may provide access to new oligomeric materials. Indeed, recent work on the thermal polymerization of adamantyl alkynes has indicated that useful polymers can be prepared from such systems (7).

Few molecules have been reported that bear more than one site capable of 1,3-dipolar cycloaddition via the nitrile sulfides (1). There were early reports of molecules that bore two of the precursor heterocycles but there is no indication that they were ever used to generate the nitrile sulfides (8). More recently, a polymer backbone substituted with the precursor oxathiazolone heterocycles has been reported and indications of reaction as nitrile sulfides were observed (9).

We have prepared for the first time an adamantane-based molecule that contains two oxathiazolone heterocycles. The reaction of this molecule with an electron-deficient alkyne to give a bis(isothiazole) derivative confirms that the *synthetic equivalent* of a bis(nitrile sulfide) has been generated if not the actual bis(1,3-dipole) itself (the reaction gives the desired products even though the actual identity of the intermediates may be uncertain). The new oxathiazolone and isothiazole derivatives were identified by spectroscopic and analytical techniques and the structures were confirmed by X-ray crystallography. The solid state structures of the oxathiazolone derivatives show limited π delocalization in the heterocycles whilst the isothiazole derivatives are clearly extensively delocalized and the observed distortions from planarity are a result of the steric effect of the adjacent adamantyl group.

Experimental

General procedures

1,3-Adamantanedicarboxylic acid, chlorocarbonylsulfenyl chloride, and dimethyl acetylenedicarboxylate were purchased commercially (Aldrich) and used without further purification. The 1,3-adamantanedicarbonamide was prepared from the dicarboxylic acid following standard procedures given in ref. 10. Toluene (Na) and chlorobenzene (CaH_2) were dried by refluxing with the given drying agent under nitrogen. Reactions involving chlorocarbonylsulfenyl chloride were performed under nitrogen. The reaction mixtures were resolved by fractional sublimation using a Büchi GKR-50 Kugelrohr apparatus operating at 10^{-3} Torr (1 Torr = 133.3 Pa). Melting points were determined on a Mel-Temp II melting point apparatus and are uncorrected. Elemental analyses were carried out at Canadian Microanalytical Service Ltd., Delta, British Columbia, Canada. IR spectra were recorded from Nujol mulls on KBr plates using a Mattson Polaris FT-IR instrument. NMR spectra were recorded on a General Electric 300 MHz instrument (^1H, ^{13}C). Chemical shifts are reported in ppm (high-frequency positive) relative to internal standards (^1H, ^{13}C: TMS). Mass spectra were recorded on a VG Micromass 7070HS double focusing spectrometer. Molecular orbital calculations were made using the HyperChem (Autodesk, version III) suite of semi-empirical programs operating on a 80486 based IBM-compatible computer. Molecules were subjected to a full geometry optimization (Polak–Ribiere conjugate gradient) prior to the single point calculations.

Reaction of $C_{10}H_{14}[C(O)NH_2]_2$ with ClC(O)SCl

Neat chlorocarbonylsulfenyl chloride, ClC(O)SCl (9.4 g, 72 mmol), was added to a mixture of toluene (70 mL) and 1,3-adamantane dicarbonamide, $C_{10}H_{14}[C(O)NH_2]_2$ (4.0 g, 18 mmol), under nitrogen to give a clear yellow solution over a white solid. The solution was heated to 95 ± 5°C for 11 h. The resulting clear orange solution was subjected to rotary evaporation (60°C water bath) to remove the excess ClC(O)SCl and solvent, and a wet yellow solid (6.8 g) was obtained. The mixture was dissolved in $CHCl_3$ and passed through a column (silica gel, 60 mesh) to give a white solid $C_{10}H_{14}[\overline{COC(O)SN}]_2$ (2.9 g, 8.6 mmol, 47.6%). This solid was recrystallized from a 5:1 EtOH:$CHCl_3$ solvent mixture to give clear colourless needle-shaped crystals, mp 134–140°C (dec.); IR (cm^{-1}): 1959w, 1934w, 1896w, 1873w, 1815m, 1803m, 1769ms, 1743ms, 1596 ms, 1262 ms, 1222 ms, 1085 m, 973ms, 921ms. NMR (δ in ppm), ^1H δ(no. of H): 2.315 (m, 2H), 2.222 (s, 2H), 2.066 (m, 2H), 2.024 (m, 2H), 1.980(m, 2H), 1.937(m, 2H), 1.782(2H). ^{13}C δ(assign.): 174.0 (C=O), 165.5 (C=N), 39.7 (C_{quat}), 38.5 (CH_2), 37.8 (CH_2), 34.6 (CH_2), 27.2 (CH). Mass spectrum (EI, 70 eV) *m/z* (%, assign.): 338 (7, M^+), 294 (0.3, $[NS(O)COC]C_{10}H_{14}$ − CNS), 262 (2, $[NS(O)COC]C_{10}H_{14}$ − CN), 236 (46, $C_{10}H_{14}$−[COC(O)SN]), 160 (73, $C_{10}H_{14}$ − CN). Anal. calcd. for $C_{14}H_{14}N_2O_4S_2$: C 49.7, H 4.2, N 8.3, S 19.0%; found: C 49.8, H 4.3, N 8.2, S 19.1%.

From the original column a second white solid [CN]-$C_{10}H_{14}$-[COC(O)SN] (1.1 g, 4.2 mmol, 23.3%) was recovered and recrystallized from acetone to give clear colourless plate-shaped crystals, mp 104–120°C (dec.); IR (cm^{-1}): 2230 w, 1958w, 1895w, 1841w, 1802m, 1764 ms, 1740ms, 1588m, 1247m, 1109m, 1033w, 976ms, 920ms. NMR, ^1H δ(no. of H): 2.196 (m, 4H), 2.04–1.85 (m, 8H), 1.691 (t, 2H). ^{13}C δ(assign.): 173.7 (C=O), 164.7 (C=N), 123.5 (C≡N), 40.3 (C_{quat}), 38.5(C_{quat}), 37.7 (CH_2), 37.3 (CH_2), 34.1 (CH_2), 30.1 (CH), 26.5 (CH_2). Mass spectrum (EI, 70 eV) *m/z* (%, assign.): 262 (7, M^+), 186 (32, $C_{10}H_{14}(CN)_2$), 160 (100, $C_{10}H_{14}$ − CN). Anal. calcd. for $C_{13}H_{14}N_2O_2S$: C 59.5, H 5.4, N 10.7%; found: C 58.5, H 5.3, N 10.6%.

The column yielded a third white solid, which was identified as the 1,3-adamantane-dinitrile, $C_{10}H_{14}(CN)_2$ (0.7 g, 3.7 mmol, 20.9%), which was recrystallized from ethyl acetate to give clear colourless plate-shaped crystals, mp 186–187°C; IR (cm^{-1}): 2233m. NMR, ^1H δ(no. of H): 2.304 (s, 2H), 2.195 (m, 2H), 2.039 (d, 8H), 1.729 (m, 2H). ^{13}C δ(assign.): 122.9 (C≡N), 40.9 (C_{quat}), 38.0 (CH_2), 33.6 (CH), 29.5 (CH_2), 26.0 (CH_2). Mass spectrum (EI, 70 eV) *m/z* (%, assign.): 186 (43, M^+), 159 (100, M^+ − HCN), 118(30).

Reaction of $C_{10}H_{14}[\overline{COC(O)SN}]_2$ with $CH_3OC(O)$-C≡C-C(O)OCH_3 (DMAD)

1,3-Bis(1,3,4-oxathiazol-2-on-5-yl)-adamantane, $C_{10}H_{14}$-

Table 1. Crystallographic data.

	1*a*	**1***b*	**1***c*	**1***d*
Formula	$C_{14}H_{14}N_2O_4S_2$	$C_{13}H_{14}N_2O_2S$	$C_{24}H_{26}N_2O_8S_2$	$C_{18}H_{20}N_2O_4S$
fw	338.40	262.33	534.60	360.43
Space group	$P2_1/m$ (no. 11)	$P2_1/c$ (no. 14)	$Pca2_1$ (no. 29)	$P2_1/c$ (no. 14)
Reflections used for unit cell (2θ range, deg)	21 (40.3–47.2)	21 (36.5–41.0)	17 (21.8–28.1)	24 (20.0–22.9)
a, Å	10.447(2)	9.153(2)	15.857(4)	19.683(2)
b, Å	7.119(3)	19.134(2)	11.562(4)	11.566(3)
c, Å	10.682(2)	7.130(3)	13.602(4)	7.727(3)
β, deg	112.98(1)	105.38(2)		932.30(2)
V, Å^3	731.5(3)	1204(1)	2492(2)	1756(1)
Z	2	4	4	4
F(000)	352	552	1120	760
D_{calcd}, Mg m^{-3}	1.536	1.447	1.424	1.363
Size, mm	0.40 × 0.20 × 0.20	0.40 × 0.40 × 0.08	0.40 × 0.35 × 0.20	0.30 × 0.25 × 0.15
μ, cm^{-1}	3.67	2.52	2.53	1.99
Max 2θ, deg	50.0	50.1	50.1	45.1
Reflections:				
Measured	1478	2393	2529	2656
Unique	1400	2211		2447
Observed	1125[a]	1577[a]	1724[b]	1675[a]
Parameters	122	164	275	227
R	0.034	0.038	0.057	0.079
R_w	0.029	0.035	0.038	0.076
GoF	2.37	1.92	1.69	4.20
Largest feature in final difference map e$^-$/Å^3	0.31	0.22	0.31	0.52

$R = \Sigma \| F_o | - | F_c \| / \Sigma | F_o |$
$R_w = [\Sigma(w (| F_o | - | F_o |)^2 / \Sigma(w | F_o |)^2]^{1/2}$
[a] $I_o > 2.00\sigma(I_o)$
[b] $I_o > 1.00\sigma(I_o)$

$[\overline{COC(O)SN}]_2$ (2.3 g, 6.8 mmol), and DMAD (4.9 g, 34.5 mmol) were dissolved in 50 mL chlorobenzene. The slightly yellow, clear solution turned brown and evolved a gas while it was heated to reflux. The heating was stopped after 12 h at which point the solution was a clear dark red-brown. An oily dark-brown solid (6.1 g) was obtained by solvent evaporation. The solid was dissolved in $CHCl_3$ and passed through a column (silica gel, 60 mesh) to give an oily orange solid (5.5 g). The material was loaded on Kugelrohr distillation apparatus, and heated up to 110°C to remove the by-products: tetramethyl thiophenetetracarboxylate and S_8 (total mass: 0.2 g). The temperature was then raised to 165°C to give the white solid, 1,3-adamantane-dinitrile (0.6 g, 3.0 mmol, 44%), in the outer bulb and a purple sticky solid, 1-cyano-3-(4,5-bis(methoxycarbonyl)-isothiazol-3-yl)-adamantane **1***d* (1.1 g, 3.0 mmol, 44%), in the inner bulb. The mononitrile **1***d* was recrystallized from ethyl acetate to give clear colourless plate-shaped crystals, mp 87–88°C; IR (cm^{-1}): 2232w, 1737ms, 1706ms, 1528m, 1286s, 1252s, 1145m, 1052m, 915w, 809w, 773w; NMR, ^{1}H δ(no. of H): 3.974 (s, 3H), 3.915 (s, 3H), 2.366 (s, 2H), 2.220 (m, 2H), 2.053 (m, 8H), 1.741 (m, 2H). ^{13}C δ(assign.): 172.7 (C═O), 165.9 (C═O), 159.3 (C_{het}), 155.4 (C_{het}), 132.4 (C═N), 124.3 (C≡N), 53.1 and 52.9 (OCH_3), 42.4 (CH_2), 39.6 (C_{quat}), 39.0 (CH_2), 38.7 (CH_2), 34.5 (C_{quat}), 30.7 (CH_2), 27.3 (CH). Mass spectrum (EI, 70 eV) *m/z* (%, assign.): 360 (49, M$^+$), 345 (100, M − CH_3), 328 (31, M − MeOH), 300 (26, M − $HC(O)OCH_3$), 270 (46, NC − $C_{10}H_{14}$ − [CCCSN] − C≡O), 186 (2, NC − $C_{10}H_{14}$ − CN), 160 (4, $C_{10}H_{14}$ − CN). Anal. calcd. for $C_{18}H_{20}N_2O_4S$: C 60.0, H 5.6, N 7.8%; found: C 59.9, H 5.6, N 7.9%.

The brown sticky solid residue was shown to be 1,3-bis(3,4-methoxycarbonylisothiazol-3-yl)-adamantane **1***c* (0.45 g, 0.8 mmol, 12%). Clear colourless parallelepiped crystals were recrystallized from ethyl acetate, mp 149–150°C; IR (cm^{-1}): 1972 w, 1933 w, 1896 w, 1871 w, 1803 m, 1772 ms, 1742 ms, 1595 ms, 1262 ms, 1221 ms, 1084 m, 973 ms, 919 ms. NMR, ^{1}H δ(no. of H): 3.974 (s, 6H), 3.905 (s, 6H), 2.431 (s, 2H), 2.255 (m, 2H), 2.117–1.999 (m, 8H), 1.758 (m, 2H). ^{13}C δ(assign.): 174.1 (C═O), 165.9 (C═O), 159.2 (C_{het}), 154.7 (C_{het}), 132.6 (C═N), 53.0/52.8 (OCH_3), 43.8 (CH_2), 40.9 (C_{quat}), 39.6 (CH_2), 35.1 (CH_2), 28.5 (CH). Mass spectrum (EI, 70 eV) *m/z* (%, assign.): 534 (100, M$^+$), 519 (M − CH_3), 503 (24, M − OCH_3), 502 (12, M − MeOH), 487 (17, M − MeOH, CH_3), 470 (13, M − 2S), 416 (14, M − 2$COOCH_3$). Anal. calcd. for $C_{24}H_{26}N_2O_8S_2$: C 53.9, H 4.9, N 5.2%; found: C 53.7, H 4.9, N 5.2%.

Can. J. Chem. Downloaded from www.nrcresearchpress.com by 65.111.164.53 on 09/08/12
For personal use only.

Decomposition of $C_{10}H_{14}[COC(O)SN]_2$ in DMSO monitored by ^{13}C NMR

A solution of 50 mg $C_{10}H_{14}[COC(O)SN]_2$ and 2 mL DMSO (insoluble at room temperature but soluble above 80°C) was placed in a 5 mm o.d. NMR tube. The reaction was carried out at 135°C and followed by ^{13}C NMR. Spectra ($200 > \delta_C > 100$ ppm) were recorded at 20 min, 1 h, 2 h, and 3 h. The spectra showed that the peaks assignable to the heterocycle (172.99 ppm, 164.43 ppm) decrease and the peak assignable to the nitrile (122.62 ppm) increases as the decomposition reaction proceeds. Only a peak assignable to the nitrile (122.62 ppm) was observed after 1 h.

Reaction of 1,3-bis(1,3,4-oxathiazol-2-on-5-yl)-adamantane and 1,3-adamantane-dinitrile in chlorobenzene

A solution of $C_{10}H_{14}[COC(O)SN]_2$ (0.27 g, 0.8 mmol) and $C_{10}H_{14}(CN)_2$ (0.15 g, 0.8 mmol) in 6 mL of chlorobenzene was placed in a flask fitted with a condenser. The solution was heated to reflux (135°C). The initially clear colourless solution turned to yellow, then brown while it was evolving a gas. The heating was stopped after 4 h and the solvent was evaporated by rotary evaporation. Two NMR samples in $CDCl_3$ were made: (*a*) 1:1 molar ratio starting materials in $CDCl_3$ and (*b*) the residue from the reaction. ^{13}C NMR spectra of the two samples showed that 13 peaks (10 for two adamantane moieties and 3 for C=O, C=N, C≡N) of the starting materials were converted to 6 peaks (5 for adamantane and 1 for C≡N). The product of the reaction was recovered: 1,3-adamantyldinitrile, 0.30 g (1.6 mmol), and S, 0.05 g (1.6 mmol).

X-ray data collection, solution and refinement

Crystals of $C_{10}H_{14}(COC(O)SN)_2$ **1***a* were obtained from a 1:1 solvent mixture of $CHCl_3$ and hexanes. Crystals of $(NC)C_{10}H_{14}(COC(O)SN)$ **1***b*, $C_{10}H_{14}(CNS{\cdot}DMAD)_2$ **1***c*, and $(NC)C_{10}H_{14}(CNS{\cdot}DMAD)$ **1***d* were obtained from ethyl acetate. Unit cell parameters were obtained from the setting angles of accurately centered reflections. The choice of space group was based on systematically absent reflections, packing considerations, and a statistical analysis of intensity distribution and was confirmed by the successful solution and refinement of the structure. All pertinent crystallographic data are summarized in Table 1. Data were collected at room temperature on a Rigaku AFC6S diffractometer (MoKα, λ = 0.71069 Å, graphite monochromator) using the ω–2θ scan technique. The intensities of three representative reflections, which were measured after every 150 reflections, remained constant throughout data collection, indicating crystal and electronic stability. Data were corrected for Lorentz and polarization effects and empirical absorption correction was applied based on DIFABS. Scattering factors were taken from Cromer and Waber (11) and anomalous dispersion effects were included in F_c.

The structures were solved using direct methods (12) to find the heavier elements and the remaining non-hydrogen atoms were located from a series of difference Fourier maps. Hydrogen atoms were included assuming ideal positions (with bond lengths of 0.95 Å) with isotropic thermal parameters 20% greater than the bonded partner. The data set for **1***c* was weak and precluded fully anisotropic refinement of the non-hydrogen atoms. It was clear from the refinement values that the adamantane moiety is sufficiently rigid to permit these atoms to be left isotropic. To improve the data to refined parameters ratio the cutoff of $F^2/\sigma F^2$ was set at 1.00. The analysis of the data from **1***d* revealed that it was not single and several peaks were poorly shaped and (or) had asymmetric and large background counts. These peaks were removed and a list is included in the supplementary material.[2]

All calculations for the structures of **1***a*, **1***b*, **1***c*, and **1***d* were performed using the TEXSAN crystallographic software package (13) and a VAX 3100 work station. Fractional atomic coordinates and isotropic thermal parameters for the non-hydrogen atoms for **1***a*, **1***b*, **1***c*, and **1***d* are given in Tables 2, 3, 4, and 5, respectively, and selected bond lengths and angles for **1**a, **1**b, **1**c and **1**d are given in Table 6. Supplementary material (atomic positional parameters, anisotropic thermal parameters, bond lengths and angles) is available.[2]

Table 2. Positional parameters and *B*(eq) for $C_{10}H_{14}(COC(O)SN)_2$ **1***a*.

Atom	*x*	*y*	*z*	*B*(eq)
S(1)	0.3524 (1)	1/4	0.31112(8)	4.36(4)
S(2)	0.77618(9)	1/4	−0.1809 (1)	4.63(4)
O(1)	0.0809 (3)	1/4	0.2642 (2)	6.0(1)
O(2)	0.1457 (2)	1/4	0.0852 (2)	3.9(1)
O(3)	0.6943 (3)	1/4	−0.4526 (2)	6.2(1)
O(4)	0.5322 (2)	1/4	−0.3612 (2)	4.2(1)
N(1)	0.3836 (2)	1/4	0.1670 (2)	3.6(1)
N(2)	0.6410 (2)	1/4	−0.1305 (2)	3.9(1)
C(1)	0.1710 (4)	1/4	0.2231 (3)	4.2(1)
C(2)	0.2680 (3)	1/4	0.0644 (3)	3.2(1)
C(3)	0.6667	1/4	−0.3549 (3)	4.5(2)
C(4)	0.5273 (3)	1/4	−0.2343 (3)	3.3(1)
C(5)	0.2516 (3)	1/4	−0.0816 (3)	3.1(1)
C(6)	0.3975 (3)	1/4	−0.0833	3.0(1)
C(7)	0.3841 (3)	1/4	−0.2336 (3)	3.1(1)
C(8)	0.3039 (2)	0.0729(3)	−0.3066 (2)	4.1(1)
C(9)	0.1591 (2)	0.0746(4)	−0.3026 (2)	4.5(1)
C(10)	0.1717 (2)	0.0731(3)	−0.1546 (2)	4.1(1)
C(11)	0.0798 (3)	1/4	−0.3750	5.4(2)

[2] The supplementary material can be purchased from: The Depository of Unpublished Data, Document Delivery, CISTI, National Research Council Canada, Ottawa, Canada K1A 0S2.

Tables of atomic positional parameters, and bond distances and bond angles for $C_{14}H_{14}N_2O_4S_2$, $C_{13}H_{14}N_2O_2S$, $C_{24}H_{26}N_2O_8S_2$, and $C_{18}H_{20}N_2O_4S$ have also been deposited with the Cambridge Crystallographic Data Centre, and can be obtained on request from The Director, Cambridge Crystallographic Data Centre, University Chemistry Laboratory, 12 Union Road, Cambridge, CB2 1EZ, U.K.

Structure factor amplitudes are no longer being deposited and may be obtained directly from the author.

Can. J. Chem. Downloaded from www.nrcresearchpress.com by 65.111.164.53 on 09/08/12
For personal use only.

Table 3. Positional parameters and B(eq) for $(NC)C_{10}H_{14}(\overline{COC(O)SN})_2$ **1***b*.

Atom	x	y	z	B(eq)
S(1)	0.68693(8)	0.78463(4)	0.6209(1)	3.35(3)
O(1)	0.6298 (2)	0.65522(8)	0.5933(2)	3.13(7)
O(2)	0.8756 (2)	0.6777 (1)	0.7438(3)	4.5(1)
N(1)	0.5086 (2)	0.7591 (1)	0.5065(3)	2.90(9)
N(2)	0.3179 (3)	0.4559 (1)	−0.0366(4)	5.9(1)
C(1)	0.5013 (3)	0.6926 (1)	0.5069(3)	2.6(1)
C(2)	0.7540 (3)	0.6988 (1)	0.6673(4)	3.1(1)
C(3)	0.3632 (3)	0.6492 (1)	0.4223(3)	2.4(1)
C(4)	0.2351 (3)	0.6960 (1)	0.3046(4)	2.9(1)
C(5)	0.0931 (3)	0.6522 (1)	0.2184(4)	3.2(1)
C(6)	0.0423	0.6171 (1)	0.3833(4)	4.0(1)
C(7)	0.1688 (3)	0.5696 (1)	0.4979(4)	3.6(1)
C(8)	0.3117 (3)	0.6122 (1)	0.5875(3)	3.1(1)
C(9)	0.3980 (3)	0.5933 (1)	0.2843(4)	2.8(1)
C(10)	0.2554 (3)	0.5492 (1)	0.1984(3)	2.7(1)
C(11)	0.1282 (3)	0.5968 (1)	0.0826(4)	3.2(1)
C(12)	0.2041 (3)	0.5133 (1)	0.3642(4)	3.5(1)
C(13)	0.2907 (3)	0.4962 (1)	0.0666(4)	3.7(1)

Table 4. Positional parameters and B(eq) for $C_{10}H_{14}(CNS{\cdot}DMAD)_2$ **1***c*.

Atom	x	y	z	B(eq)
S(1)	0.0632(1)	0.4480(2)	0.2680	3.45(8)
S(2)	0.1704(1)	−0.0402(2)	−0.0885(2)	4.1(1)
O(1)	0.3098(3)	0.4985(4)	0.4330(4)	3.9(3)
O(2)	0.3389(4)	0.6092(5)	0.3024(4)	5.8(3)
O(3)	0.1706(3)	0.6767(4)	0.4397(5)	5.4(3)
O(4)	0.0360(3)	0.6329(4)	0.4071(4)	4.3(3)
O(5)	0.4702(3)	0.0141(4)	−0.0868(4)	4.8(3)
O(6)	0.4087(3)	0.1016(4)	−0.2152(4)	4.9(3)
O(7)	0.3575(4)	−0.1500(5)	−0.2477(5)	6.8(4)
O(8)	0.2180(4)	−0.1492(4)	−0.2765(4)	5.2(3)
N(1)	0.1306(3)	0.3669(5)	0.2070(5)	3.1(3)
N(2)	0.1976(3)	0.0575(5)	−0.0060(5)	3.7(3)
C(1)	0.2086(4)	0.3960(5)	0.2288(5)	2.6(3)
C(2)	0.2170(4)	0.4876(6)	0.3010(5)	2.8(3)
C(3)	0.1388(4)	0.5257(6)	0.3294(5)	2.8(3)
C(4)	0.2769(4)	0.0872(6)	−0.0171(5)	2.8(3)
C(5)	0.3196(4)	0.0298(5)	−0.0947(6)	2.8(3)
C(6)	0.2676(4)	−0.0458(6)	−0.1424(5)	3.2(3)
C(7)	0.3148(4)	0.1766(6)	0.0523(5)	2.6(1)
C(8)	0.2438(4)	0.2436(5)	0.1045(5)	2.5(1)
C(9)	0.2811(4)	0.3323(5)	0.1780(5)	2.5(1)
C(10)	0.3369(4)	0.4177(6)	0.1194(5)	3.3(1)
C(11)	0.4068(4)	0.3552(6)	0.0675(5)	3.6(2)
C(12)	0.3687(4)	0.2657(6)	−0.0040(6)	3.6(2)
C(13)	0.3699(4)	0.1141(6)	0.1275(5)	3.2(1)
C(14)	0.4079(4)	0.2031(6)	0.2001(6)	3.5(2)
C(15)	0.3368(4)	0.2682(6)	0.2543(6)	3.5(1)
C(16)	0.4611(4)	0.2900(7)	0.1415(6)	4.3(2)
C(17)	0.2958(5)	0.5390(7)	0.3434(6)	3.7(4)
C(18)	0.3750(5)	0.5576(8)	0.4880(7)	5.9(5)
C(19)	0.1202(5)	0.6209(6)	0.3995(6)	3.5(4)
C(20)	0.0066(5)	0.7249(7)	0.4724(7)	6.0(5)
C(21)	0.4090(5)	0.0454(6)	−0.1292(6)	3.7(4)
C(22)	0.4891(6)	0.1182(8)	−0.2634(8)	8.1(6)
C(23)	0.2871(5)	−0.1204(6)	−0.2282(7)	4.2(4)
C(24)	0.2308(7)	−0.2176(7)	−0.3642(7)	8.1(6)

Can. J. Chem. Downloaded from www.nrcresearchpress.com by 65.111.164.53 on 09/08/12
For personal use only.

Can. J. Chem. Downloaded from www.nrcresearchpress.com by 65.111.164.53 on 09/08/12
For personal use only.

Table 5. Positional parameters and B(eq) for (NC)$C_{10}H_{14}$(CNS·DMAD) **1***d*.

Atom	*x*	*y*	*z*	*B*(eq)
S(1)	0.3505(1)	0.2008(2)	0.4816(2)	3.92(9)
O(1)	0.3525(3)	0.6179(4)	0.5091(6)	5.0(3)
O(2)	0.3302(2)	0.5399(4)	0.7653(6)	4.0(2)
O(3)	0.4834(2)	0.2477(4)	0.6718(7)	5.2(3)
O(4)	0.4670(2)	0.4390(4)	0.6965(6)	4.8(3)
N(1)	0.2776(3)	0.2565(5)	0.4013(7)	3.7(3)
N(2)	0.0121(4)	0.2719(7)	0.043(1)	6.7(4)
C(1)	0.2741(3)	0.3648(6)	0.4347(8)	3.4(3)
C(2)	0.3320(3)	0.4137(6)	0.5313(8)	3.4(3)
C(3)	0.3795(3)	0.3284(6)	0.5630(8)	3.2(3)
C(4)	0.2128(3)	0.4340(6)	0.3594(9)	3.7(3)
C(5)	0.1603(3)	0.3495(6)	0.2728(9)	4.1(4)
C(6)	0.0992(3)	0.4199(7)	0.187(1)	4.4(4)
C(7)	0.1243(4)	0.5013(7)	0.052(1)	4.8(4)
C(8)	0.1750(4)	0.5856(7)	0.137(1)	4.5(4)
C(9)	0.2361(3)	0.5163(6)	0.218(1)	4.1(4)
C(10)	0.1771(3)	0.5030(6)	0.500(1)	4.4(4)
C(11)	0.1174(4)	0.5727(7)	0.416(1)	4.6(4)
C(12)	0.1423(4)	0.6553(7)	0.279(1)	5.5(4)
C(13)	0.0650(3)	0.4882(7)	0.331(1)	4.8(4)
C(14)	0.3397(3)	0.5344(6)	0.593(1)	3.4(3)
C(15)	0.3394(4)	0.6525(6)	0.842(1)	5.0(4)
C(16)	0.4493(4)	0.3328(6)	0.653(1)	3.9(4)
C(17)	0.5344(4)	0.4485(8)	0.788(1)	6.0(5)
C(18)	0.0494(4)	0.3362(7)	0.108(1)	4.9(4)

Table 6. Selected bond lengths (Å) and angles (deg).

1*a*		**1***b*		**1***c*		**1***d*	
				Bond lengths			
S1—N1	1.694(2)	S1—N1	1.691(2)	S1—N1	1.646(6)	S1—N1	1.659(5)
S2—N2	1.697(3)			S2—N2	1.650(6)		
S1—C1	1.756(3)	S1—C2	1.753(3)	S1—C3	1.716(7)	S1—C3	1.692(7)
S2—C3	1.762(3)			S2—C6	1.709(7)		
O1—C1	1.184(3)	O2—C2	1.174(3)	N1—C1	1.315(7)	N1—C1	1.281(7)
O3—C3	1.186(4)			N2—C4	1.312(7)		
O2—C1	1.391(3)	O1—C2	1.396(3)	C1—C2	1.451(8)	C1—C2	1.441(9)
O4—C3	1.379(2)			C1—C9	1.531(8)	C1—C4	1.536(9)
O4—C4	1.377(3)	O1—C1	1.374(3)	C2—C3	1.371(8)	C2—C3	1.371(8)
N1—C2	1.276(3)	N1—C1	1.276(3)	C4—C5	1.419(9)		
N2—C4	1.269(3)	N2—C13	1.139(3)	C4—C7	1.523(9)	C6—C18	1.49(1)
C2—C5	1.500(4)	C1—C3	1.499(3)	C5—C6	1.365(9)	N2—C18	1.142(9)
C4—C7	1.499(4)	C10—C13	1.474(4)				
				Angles			
N1—S1—C1	93.6(1)	N1—S1—C2	93.8(1)	N1—S1—C3	95.1(3)	N1—S1—C3	93.8(3)
N2—S2—C3	93.2(1)			N2—S2—C6	94.7(3)		
C1—O2—C3	111.5(2)	C1—O1—C2	111.9(2)	S1—N1—C1	110.6(5)	S1—N1—C1	111.1(5)
C3—O4—C4	112.4(2)			S2—N2—C4	110.6(5)		
S1—N1—C2	109.1(2)	S1—N1—C1	109.4(2)	N1—C1—C2	115.2(6)	N1—C1—C2	116.0(6)
S2—N2—C4	109.5(2)			N1—C1—C9	118.8(6)	N1—C1—C4	118.9(6)
S1—C1—O1	130.5(3)	S1—C2—O2	130.7(2)	C1—C2—C3	110.0(6)	C2—C1—C4	124.9(6)
S1—C1—O2	106.6(2)	S1—C2—O1	106.2(2)	S1—C3—C2	109.1(5)	C1—C2—C3	108.7(6)
S1—C1—O2	122.9(3)			N2—C4—C5	114.8(6)	S1—C3—C2	110.4(5)
O2—C2—N1	119.1(3)	O1—C1—N1	118.8(2)	N2—C4—C7	119.0(6)		
				C5—C4—C7	126.2(6)		
		N2—C13—C10	179.3(3)	C4—C5—C6	111.4(6)	N2—C18—C6	178.2(9)
				S2—C6—C5	108.4(5)		

Can. J. Chem. Downloaded from www.nrcresearchpress.com by 65.111.164.53 on 09/08/12
For personal use only.

Scheme 1

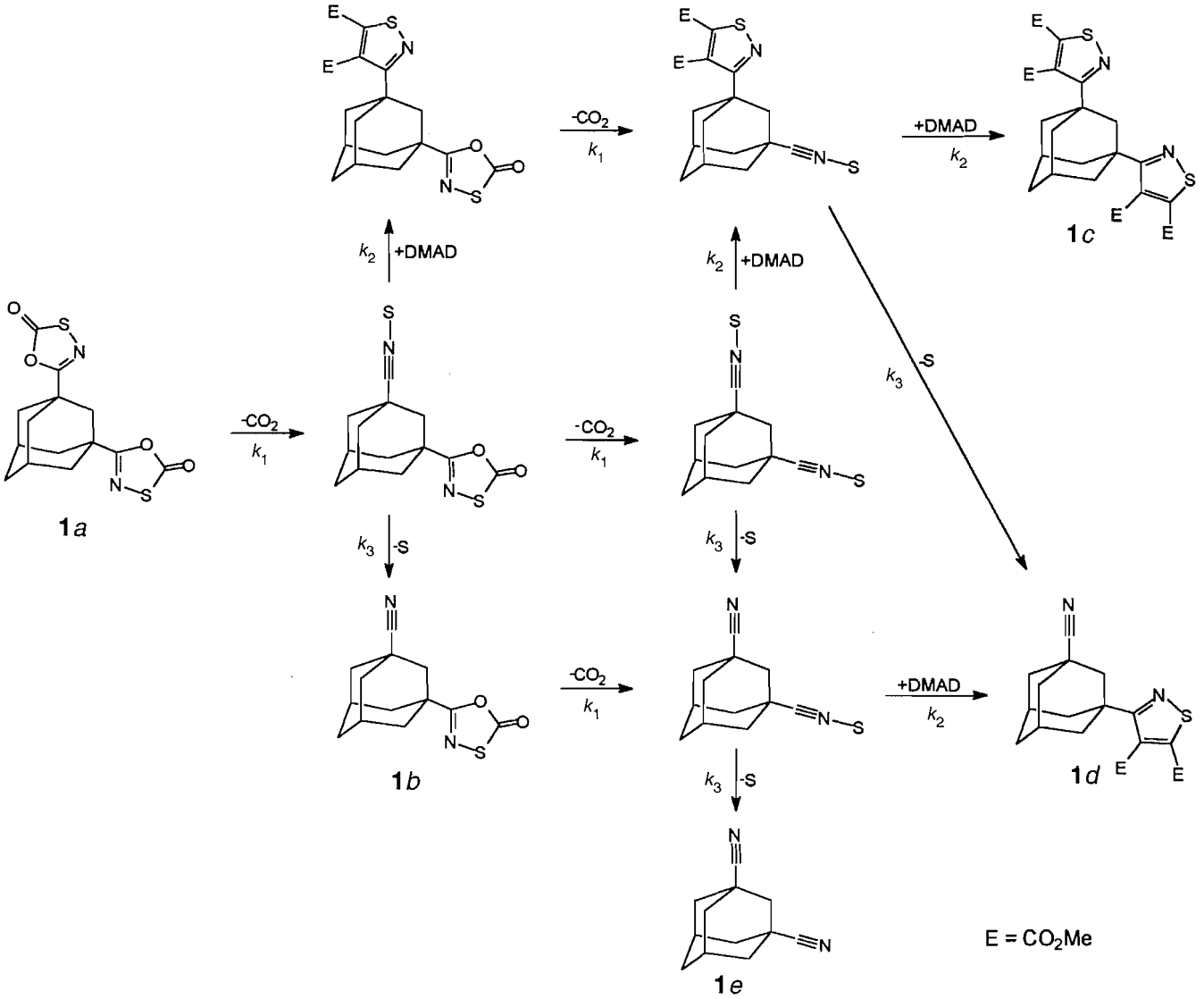

Results and discussion

Preparation of $C_{10}H_{14}[\overline{COC(O)SN}]_2$ and $C_{10}H_{14}(CN)$-$[\overline{COC(O)SN}]$

Reactions of organic amides with chlorocarbonylsulfenyl chloride [ClC(O)SCl] in hot toluene solutions have been reported to give oxathiazolone derivatives [R-$\overline{COC(O)SN}$] in varying yields (2). These compounds are widely used as precursors for the thermal generation of derivatives of the nitrile sulfides (R-C≡N^+-S^-), a family of propargyl allenyl-type 1,3-dipoles (A≡B-C) that have been shown to have an extensive cycloaddition chemistry. Reaction of the 1,3-adamantanedicarbonamide ($C_{10}H_{14}[(C(O)NH_2]_2$) with ClC(O)SCl under N_2 gave two heterocyclic products containing the oxathiazolone heterocycle. The expected bis(oxathiazolone) derivative (**1***a* $C_{10}H_{14}[\overline{COC(O)SN}]_2$) was isolated in 48% recovered yield by column chromatography while a second derivative, which was determined to be the mono(oxathiazolone) (**1***b* $(NC)C_{10}H_{14}$-$[\overline{COC(O)SN}]$), was also isolated in 23% yield. The remaining adamantane species that was obtained from the chromatographic separation was the dinitrile (**1***e* $C_{10}H_{14}(CN)_2$), which was recovered in 21% yield (total recovery of the adamantane-based compounds was approximately 92%). The compounds were clearly identified as oxathiazolone derivatives by the observation of distinctive ^{13}C resonances in the regions 174.2 ± 0.6 ppm (**1***a* 174.0 ppm, **1***b* 173.7 ppm, assigned to C=O) and 162 ± 5.2 ppm (**1***a* 165.5 ppm, **1***b* 164.7 ppm, assigned to C=N). Both compounds were fully characterized spectroscopically and their structures were confirmed by X-ray crystallographic methods.

It is known that the oxathiazolone heterocycles will give the unstable nitrile sulfides in solution, which, if not immediately trapped, will decompose to the corresponding nitrile and sulfur. These experiments indicate that the initial condensation reaction is nearly quantitative to give the desired bis(oxathiazolone) **1***a*. Unfortunately, under the reaction conditions a sig-

Fig. 1. An ORTEP (21) view of $C_{10}H_{14}(\overline{COC(O)SN})_2$ **1***a*.

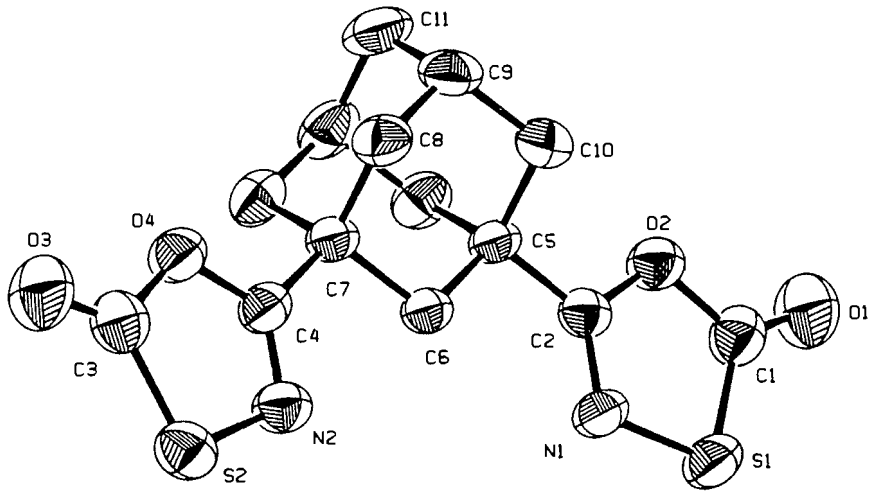

nificant fraction of the product goes through a stepwise decomposition (loss of CO_2 followed by loss of S) to the mono(oxathiazolone) **1***b* and ultimately to the dinitrile **1***e*. Lower reaction temperatures did not improve the yield of the reaction and left unreacted starting materials. The chemistry of the mono(oxathiazolone) **1***b* will be the subject of future research.

Reaction of $C_{10}H_{14}[\overline{COC(O)SN}]_2$ with DMAD

The reaction of oxathiazolone derivatives with electron-deficient alkynes has been reported to give isothiazole derivatives in high yield (14). Based on the reactivity pattern observed above, it was expected that the reaction of the bis(oxathiazolone) **1***a* with dimethyl acetylenedicarboxylate (DMAD) in refluxing chlorobenzene would give the bis(isothiazole) **1***c*, the mono(isothiazole) **1***d*, and the dinitrile **1***e*. The reaction mixture was resolved by chromatography and Kugelrohr sublimation to give **1***c* in 12% yield, **1***d* in 44% yield, and **1***e* in 44% yield. Unexpectedly, a fourth product (which was usually contaminated with elemental sulfur) was obtained in small amounts and was shown to be tetramethylthiophene tetracarboxylate (S·(DMAD)$_2$). This compound was also isolated and identified by X-ray crystallography (15). The presence of this thiophene derivative is obviously a product of the well-known reaction of DMAD with sulfur and has been reported as one of the products of similar reactions (16). The heterocyclic compounds **1***c* and **1***d* were fully characterized spectroscopically and identified by comparison with the data from the previously reported monosubstituted adamantane derivatives. Analysis of the ^{13}C NMR spectra of these compounds allowed clear identification of the adamantane, methylacetyl ($\delta_{C=O}$ = 173.5 ± 1.0 and 169 ppm; δ_{OMe} = 52.9 ± 0.1 ppm), and isothiazole (δ_{Chet} = 159.2 ± 0.1, 154.6 ± 0.2, and 132.5 ± 0.1 ppm) moieties in **1***c* and **1***d*. The spectroscopic data are fully consistent with the presence of symmetric or asymmetric disubstituted adamantane groups and the appropriate heterocycle or nitrile. The structures of **1***c* and **1***d* were unambiguously determined by X-ray crystallographic methods.

The pattern of products determined for this reaction indicates that under the reaction conditions of concentration and temperature, the decomposition reactions of the nitrile sulfides (k_3) in Scheme 1 are competitive with the cycloaddition reactions (k_2). Indeed, 88% of the isolated adamantane-based products are the result of nitrile sulfide decomposition reactions and only 56% of the isolated adamantane-based products are the result of cycloaddition reactions. These results are consistent with earlier reports on the kinetics of cycloaddition and decomposition of the nitrile sulfides (17). It has been shown that the desulfuration reaction of the nitrile sulfides is a bimolecular process, therefore the extent of decomposition should decrease with dilution (17). These reactions may provide higher yields at lower concentrations and subsequent investigations on the reaction of **1***a* with inorganic π systems will examine this possibility. The recovered yield of the reaction of a monosubstituted adamantane with DMAD was reported to be 27% (3). If the two heterocycles in **1***a* react completely independently, then the percent yield of the total reaction would be expected to be the square of the yield of an individual cycloaddition reaction (predicted yield ~7%). The isolated yield of **1***a* (12%) is higher than expected but this is undoubtedly due to the separation difficulties experienced in the earlier work (3). The pattern of products from this reaction is consistent with totally independent cycloaddition reactions of approximately equal rates and decomposition reactions of approximately equal rates. The high recovered yield of **1***d* may indicate that several routes to the dinitrile **1***d* are possible.

The presence of the bis(nitrile sulfide) is not proven by the presence of the bis(isothiazole) **1***c*. A possible reaction sequence for the separate carbon dioxide extrusion, desulfuration, and cycloaddition reactions is given in Scheme 1. The actual reaction pathway may in fact go through individual nitrile sulfide intermediates with the other oxathiazolone heterocycle intact. Partial confirmation of this thesis may lie in the actual isolation of the nitrile-oxathiazolone **1***b*. The presence of **1***c* in the product mixture does indicate, however, that **1***a* can be used to generate the *synthetic equivalent* of the bis(nitrile sulfide).

Structural features

The solid state structures of **1***a*, **1***b*, **1***c*, and **1***d* have been determined by X-ray crystallography and views of the compounds are presented in Figs. 1, 2, 3, and 4, respectively. The weak-

Can. J. Chem. Downloaded from www.nrcresearchpress.com by 65.111.164.53 on 09/08/12
For personal use only.

Can. J. Chem. Downloaded from www.nrcresearchpress.com by 65.111.164.53 on 09/08/12
For personal use only.

Fig. 2. An ORTEP (21) view of $(NC)C_{10}H_{14}(\overline{COC(O)SN})$ **1***b*.

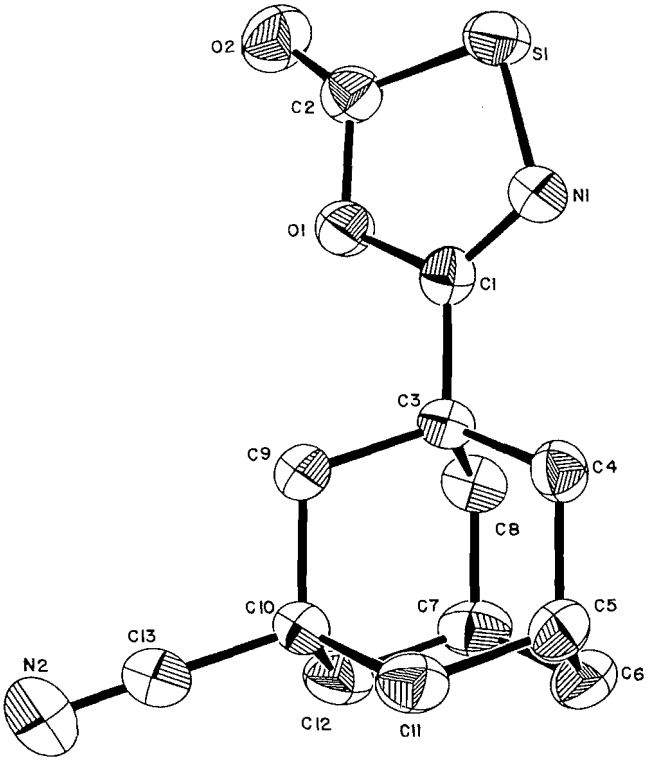

ness of the data set for **1***c* did not allow a fully isotropic refinement of all the non-hydrogen atoms but fully confirms the presence of the two heterocycles bound to the adamantane moiety. No significant intermolecular contacts are observed in the structures.

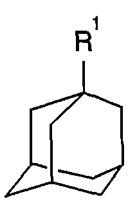

2*a* - $\overline{COC(O)SN}$

2*b* - CNS•DMAD

2*c* - C≡N

There are no significant differences in the adamantane frameworks of the compounds **1***a*, **1***b*, **1***c*, and **1***d*. The heterocycles are planar, partially delocalized (**1***a* and **1***b*) or fully delocalized (**1***c* and **1***d*) π systems as described previously (3). The nitrile substituents in **1***b* and **1***d* have C—N bond distances consistent with the range expected for alkyl nitriles (*d* C≡N = 1.16 Å (18)). The ester groups in **1***c* and **1***d* are planar and have bond distances and angles consistent with those reported for methylacetyl groups in similar compounds (3). It is noted, however, that in **1***c*, **1***d*, and **2**b the plane of the ester group next to the adamantane moiety is twisted out of the plane of the heterocycle to which it is attached, while the second ester group, which is more distant from the adamantane moiety, essentially lies in the plane of the heterocycle. This twisting is consistently accompanied by a lengthening of the C—C bond (**2***b*: 1.494(6) vs. 1.491(6) Å (3); **1***c*: 1.504(9)\1.500(9) vs. 1.48(1)\ 1.49(1) Å; and **1***d*: 1.509(9) vs. 1.482(9) Å); however, these

Fig. 3. An ORTEP (21) view of $C_{10}H_{14}(CNS{\cdot}DMAD)_2$ **1***c*.

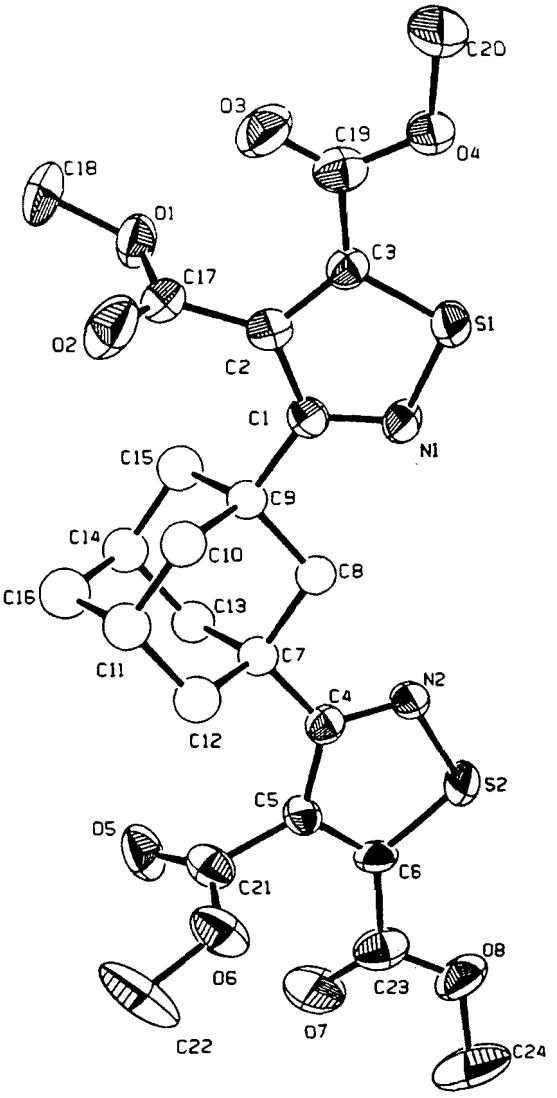

differences are well below the usual test for significance ($\delta > 3\sigma$). In addition, similar observations were made concerning the positioning of the methoxycarbonyl substituents of tetramethyl thiophenetetracarboxylate (15). If the pattern of bond lengthening that is observed is real, then it may be due to the loss of π-bond delocalization that would occur when the methylacetyl group twists out of the plane of the heterocycle. The observed angles by which the proximal ester groups are twisted from the plane of the heterocycles are: **1***c* 87.6/80.9°, **1***d* 75.1°, and **2***b* 89.0° (3). The explanation for the observed geometries of these molecules may be provided by a simple model where the fully planar geometry, which optimizes π-bond delocalization, is not possible because of the steric influence of the adjacent adamantane group. It is noted, however, that geometry optimization calculations (semi-empirical: PM3) indicate that the fully planar isomer of the parent isothiazole heterocycle (H-CNS·DMAD) is the *least* favoured energetically (E_{total} = −2099.9 kcal). Indeed, the isomers of this heterocycle where the proximal methoxycarbonyl (E_{total} = −2104.5 kcal) or both methoxycarbonyl groups (E_{total} = −2105.4 kcal) are twisted 90° from the heterocyclic plane, are

Fig. 4. An ORTEP (21) view of $(NC)C_{10}H_{14}$(CNS·DMAD) **1***d*.

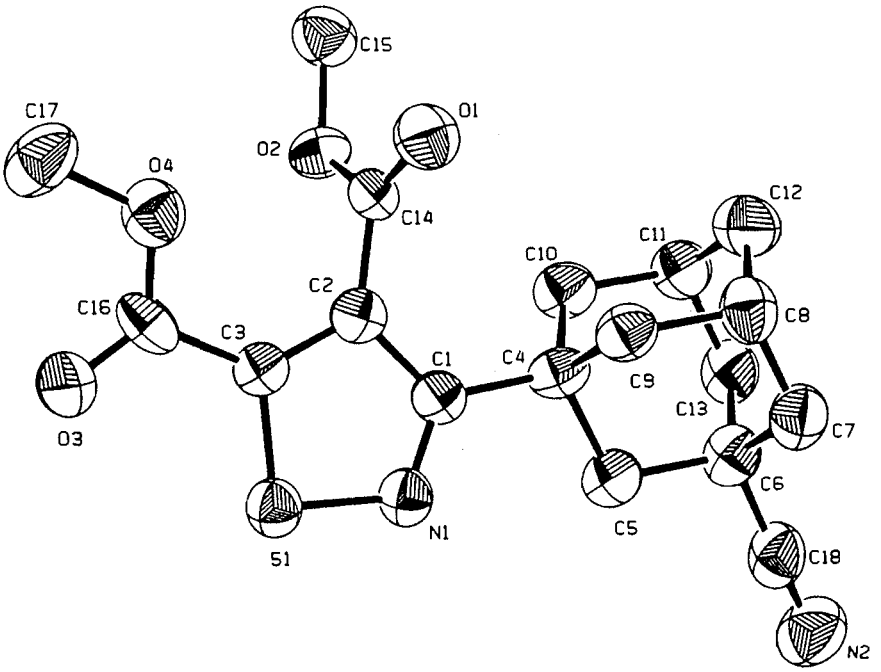

significantly more stable. That the more distant methoxycarbonyl group adopts a geometry in which it is essentially coplanar with the isothiazole heterocycle may be due to the methoxy oxygen atom making contact with the heterocyclic sulfur atom. The oxygen atom would roughly lie on the sulfur–nitrogen bond axis so that the sulfur atom adopts a distorted trigonal bipyramidal geometry. The calculated atomic charges (PM3) on the sulfur (+0.375) and the oxygen (OCH_3: −0.259) atoms are consistent with this type of contact within the molecule. Long-range contacts between sulfur and oxygen atoms in the same molecules were observed previously (19).

The angles subtended by the two substituent groups on the adamantane moieties are close to the ideal expected for a tetrahedral arrangement (ideal: 109.5°; **1***a*: 107.2(2)°, **1***b*: 109.4(2)°, **1***c*: 108.0(5)°, **1***d*: 107.6(6)°), indicating that the adamantane moiety is not strained by substitution with the sterically demanding heterocycles. Indeed, the molecules **1***a* and **1***c* have a molecular C_{2v} symmetry in the solid state with the heterocycle atoms of **1***a* lying on a crystallographic mirror plane.

Table 6 contains the bond distances and angles from the common parts of **1***a* and **1***b* and also compares **1***c* and **1***d*. The data clearly show that the heterocycles do not differ significantly ($\delta > 3\sigma$) regardless of the nature of the second substituent. Indeed, the complete independence of the two heterocyclic centres that was assumed from the experimental data above is confirmed by the data in the table. The oxathiazolone heterocycles in **1***a* and **1***b* have localized C—N π bonds (accepted for C_{sp^2}=N_{sp^2}: 1.28 Å (18); observed: **1***a* 1.276(3)/1.269(3) Å, **1***b* 1.276(3) Å; accepted for C_{sp^2}—S_{sp^3}: 1.75 Å (18), observed: **1***a* 1.756(3)/1.7623 Å, **1***b* 1.753(3) Å) while the isothiazole heterocycles in **1***c* and **1***d* have more delocalized π bonding, with the C—N π bond weaker and the C—S bond stronger (C=N, observed: **1***c* 1.315(7)/1.312(7) Å, **1***d* 1.281(7) Å; C—S, observed: **1***c* 1.716(7)/1.709(7) Å, **1***d* 1.692(7) Å).

Scheme 2

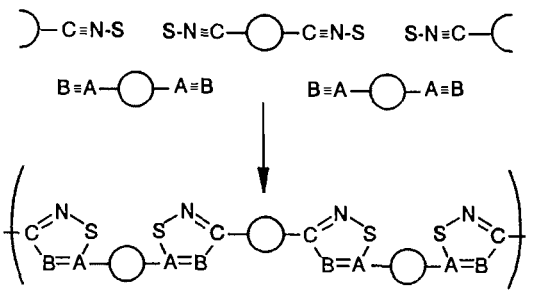

Cycloaddition and polymerization reactions of bis(nitrile sulfides)

The generation of molecules with multiple heterocyclic moieties and the potential for the generation of oligomeric or polymeric systems are crucial areas of new chemistry for the bis(nitrile sulfides). The generation of oligomeric materials by sequential symmetry-allowed cycloaddition reactions has been an area of intense research (20). We have now established that bis(oxathiazolone) molecules can be used to generate molecules bearing multiple heterocyclic systems. Therefore systems such as the bis(1,2,3,5-dithiadiazolyl)-alkyl radicals, which cannot be prepared by current preparative techniques (4–6), may be prepared by reaction of the bis(oxathiazolone) with N≡S-Cl as described in ref. 3. The generation of a series of heterocyclic compounds by reaction of **1***a* with inorganic π systems is now practical. The prerequisites for generating chain molecules from such bis(1,3-dipoles) would be the reactivity and stability of the bis(1,3-dipoles) and the reactivity of the bis(π bonds) according to Scheme 2.

This study has focused on the generation of the *synthetic equivalent* of the first bis(nitrile sulfide) and the reaction of this species with monomeric π systems to establish the pattern of reactivity. It was initially considered possible by the authors

Can. J. Chem. Downloaded from www.nrcresearchpress.com by 65.111.164.53 on 09/08/12
For personal use only.

that the nitrile sulphides generated from **1***a* might undergo premature cycloaddition reactions with the nitrile π bonds in the decomposition products **1***b*, **1***c*, and **1***e*, leading to complex mixtures. The NMR studies reported here and the analysis of the quantitative decomposition reactions of **1***a* clearly indicate that few if any intermediates are observed in the decomposition reaction and that no cycloaddition reaction occurs between the nitrile sulfides and the nitriles generated by decomposition. Indeed, the actual reaction of **1***a* and **1***e* gives a quantitative yield of **1***e* and S_8 and is in agreement with previous studies that indicated that nitrile sulfides, while highly reactive to nitrile π systems, give higher yields with aromatic nitriles or those bearing strongly electron-withdrawing substituents (17). In previous work it was shown by theoretical calculations and the established pattern of reactivity that the aromatic nitrile sulfides have extensively delocalized π systems that may stabilize the 1,3-dipole (3). If this is a reliable analysis, then an aromatic ring may be a more suitable platform for the generation of bis(nitrile sulfides) in polymerization reactions. Indeed, this work indicates that the reaction of an aromatic bis(nitrile sulfide) with an electron-deficient alkyne may provide a better route to the desired polymeric systems.

The compound **1***a* is therefore a useful compound for the generation of a synthetic equivalent to the first bis(nitrile sulfide). The facile and rapid decomposition of the intermediate(s), however, means that the synthetic utility of this compound may be limited to the preparation of mono- and bisheterocyclic compounds as described above.

Acknowledgements

We thank the Natural Sciences and Engineering Research Council of Canada and Memorial University for financial support and Dr. J. Burnell for helpful discussions.

References

1. A. Padwa (*Editor*). 1,3-Dipolar cycloaddition chemistry. John Wiley and Sons, New York. 1984.
2. R.M. Paton. Chem. Soc. Rev. **18**, 33 (1989); C. Wentrup and P. Kambouris. Chem. Rev. **91**, 365 (1991).
3. J.N. Bridson, S.B. Copp, M.J. Schriver, S. Zhu, and M.J. Zaworotko. Can. J. Chem. **72**, 1143 (1994).
4. A.J. Banister and J.M. Rawson. *In* The chemistry of inorganic ring systems. *Edited by* R. Steudel. Elsevier Science Publishers, Amsterdam. 1992. Chap. 17.
5. A.W. Cordes, R.C. Haddon, and R.T. Oakley. *In* The chemistry of inorganic ring systems. *Edited by* R. Steudel. Elsevier Science Publishers, Amsterdam. 1992. Chap. 16.
6. S. Parsons and J. Passmore. Acc. Chem. Res. **27**, 101 (1994).
7. T.G. Archibald, A.A. Malik, K. Baum, and M.R. Unroe. Macromolecules, **24**, 5261 (1991).
8. F.B. Islam and H. Kwart. J. Chem. Eng. Data, **30**, 507 (1985).
9. R.M. Mortier, R.M. Paton, G. Scott, and I. Stobie. Br. Polym. J. **19**, 303 (1987).
10. B.S. Furniss, A.J. Hannaford, P.W.G. Smith, and A.R. Tatchell. Vogel's textbook of practical organic chemistry. 5th ed. John Wiley and Sons, New York. 1989.
11. D.T. Cromer and J.T. Waber. *In* International tables for X-ray crystallography. Vol. IV. Kynoch Press, Birmingham, England. 1974 (Present distributer: Kluwer Academic Publishers, Dordrecht and Boston.)
12. C.J. Gilmore. J. Appl. Crystallogr. **17**, 42 (1984); P.T. Beurskens, DIRDEF: Direct Methods for Difference Structures, Technical Report 1984/1, Crystallography Laboratory, Toernooiveld, 6525 Ed Nijmegen, The Netherlands.
13. TEXSAN–TEXRAY Structure Analysis Package, Molecular Structure Corporation, Woodlands, Tex. 1985.
14. R.K. Howe, T.A. Gruner, L.G. Carter, L.L . Black, and J.E. Franz. J. Org. Chem. **43**, 3736 (1978).
15. J.N. Bridson, M.J. Schriver, and S. Zhu. J. Chem. Crystallogr. In press.
16. J.E. Franz and L.L. Black. Tetrahedron Lett. 1381 (1970).
17. M.C. McKie. Ph.D. Thesis, University of Edinburgh. 1988.
18. J. March. Advanced organic chemistry. 3rd ed. John Wiley and Sons, New York. 1984. Chap. 1, pp. 18–20, and references therein.
19. R.E. Rosenfield, R. Parthasarathy, and J.D. Dunitz. J. Am. Chem. Soc. **99**, 4860 (1977); J.G. Angyan, R.A. Poirier, A. Kucsman, and I.G. Csizmadia. J. Am. Chem. Soc. **109**, 2237 (1987).
20. M. Pollmann and K. Müllen. J. Am. Chem. Soc. **116**, 2318 (1994); P.R. Ashton, G.R. Brown, N.S. Isaacs, D. Guiffrida, F.H. Kohnke, J.P. Mathais, A.M.Z. Slawin, D.R. Smith, J.F. Stoddart, and D.J. Williams. J. Am. Chem. Soc. **114**, 6330 (1992).
21. C.K. Johnson. ORTEPII. Report ORNL-5138, Oak Ridge National Laboratory, Oak Ridge, Tenn. 1976.

Can. J. Chem. Downloaded from www.nrcresearchpress.com by 65.111.164.53 on 09/08/12
For personal use only.

Kinetic study of the reactions of methoxy-substituted phenacyl radicals

S.V. Jovanovic, J. Renaud, A.B. Berinstain, and J.C. Scaiano

Abstract: The photochemistry of various mono- and dimethoxy-substituted α-bromoacetophenones has been investigated by laser flash photolysis in organic solvents. The short-lived excited singlet states cleave to yield bromine atoms and the corresponding methoxyphenacyl radicals with quantum yields ranging from 0.13 to 0.35. With the exception of 4-methoxy-α-bromoacetophenone (**6**), all other substrates yield readily detectable triplet states; these have π,π^* character and are very poor hydrogen abstractors. Triplet decay does not contribute to methoxyphenacyl radical formation. While methoxyphenacyl radicals may have a spin density as high as 0.3 at the carbonyl oxygen, which accounts for the alkoxy-like visible band in their absorption spectrum, their chemical reactivity is dominated by the radical character at the carbon site. Methoxyphenacyl radicals are modest hydrogen abstractors; for example, reaction of **6** with 1,4-cyclohexadiene occurs with a rate constant of 2.6×10^5 M^{-1} s^{-1}, while for addition to the double bond in 1,1-diphenylethylene the rate constant is 9.4×10^7 M^{-1} s^{-1}. Additions to other double bonds are likely to be slower (e.g., **12** + 1,3-cyclohexadiene, $k \leq 10^5$ M^{-1} s^{-1}). In contrast, reaction with oxygen occurs with $k_q = 2.5 \times 10^9$ M^{-1} s^{-1}. Under the conditions relevant for their participation in paper yellowing, the methoxyphenacyl radicals will be converted to peroxyl radicals. These probably play a key role in the oxidative photodegradation of lignin.

Key words: methoxyphenacyl radicals, α-bromoacetophenones, laser flash photolysis.

Résumé : Faisant appel à la photolyse laser éclair, on a étudié la photochimie de diverses mono- ou diméthoxy-α-bromoacétophénones dans des solvants organiques. Les états singulets excités de courte durée de vie se brisent pour donner des atomes de brome et les radicaux méthoxyphénacyles correspondants, avec des rendements quantiques allant de 0,13 à 0,35. À l'exception de la 4-méthoxy-α-bromoacétophénone (**6**), tous les autres substrats fournissent des états triplets facilement détectables; ils possèdent un caractère π,π^* et une très mauvaise habilité à enlever des hydrogènes. La dégénérescence de l'état triplet ne contribue pas à la formation du radical méthoxyphénacyle. Alors que les radicaux méthoxyphénacyles peuvent posséder une densité de spin allant jusqu'à 0,3 au niveau de l'oxygène du carbonyle, ce qui explique la bande semblable à celle des alcoxy dans leur spectre d'absorption, leur réactivité chimique est dominée par le caractère radicalaire au site carboné. L'habilité des radicaux méthoxyphénacyles à enlever des hydrogènes est modeste; par exemple, la réaction du composé **6** avec le cyclohexa-1,4-diène se produit avec une constante de vitesse de $2{,}6 \times 10^5$ M^{-1} s^{-1}, alors que, pour l'addition à la double liaison du 1,1-diphényléthylène, la constante de vitesse est de $9{,}4 \times 10^7$ M^{-1} s^{-1}. Il est probable que les additions sur d'autres doubles liaisons seront plus lentes (par exemple, pour **12** + cyclohexa-1,3-diène, $k \leq 10^5$ M^{-1} s^{-1}). Par ailleurs, la réaction avec l'oxygène se produit avec une $k_q = 2{,}5 \times 10^9$ M^{-1} s^{-1}. Dans des conditions semblables à celles par lesquelles ils participient au jaunissement du papier, les radicaux méthoxyphénacyles sont transformés en radicaux peroxyles. Ces derniers jouent probablement un rôle dans la photodégradation oxydante de la lignine.

Mots clés : radicaux méthoxyphénacyles, α-bromoacétophénones, photolyse laser éclair.

[Traduit par le rédaction]

Introduction

Photoinduced yellowing of papers manufactured from ultra-high-yield pulps limits their use to low-grade paper products, such as newsprint, catalog, and advertising products. The yellowing process results largely from photoinduced reactions involving the chromophores in lignin; among these, mono- and dimethoxyphenols, methoxyacetophenones, and aryloxyanisoles are believed to play an important role (1). The absorption of light leads to various unstable intermediates, such as aromatic ketone singlets and triplets, phenoxyl, phenacyl, and peroxyl radicals, and presumably singlet oxygen. Ultimately, yellow products such as quinones, oligomers, and other degradation products are formed (1).[2] The knowledge of the kinetics and mechanisms of the reactions of unstable intermediates should advance our understanding of lignin photochemistry in general and lead to rational strategies to inhibit the photoyellowing of paper.

A variety of radical mechanisms are believed to play a role in the photodegradation of lignin. These include the direct

Received August 24, 1994.

S.V. Jovanovic, J. Renaud, A.B. Berinstain, and J.C. Scaiano.[1] Department of Chemistry, University of Ottawa, Ottawa, ON K1N 6N5, Canada.

[1] Author to whom correspondence may be addressed. Telephone: (613) 562-5170. Fax: (613) 564-6793.

[2] A recent book summarizes the research in this area (2).

Can. J. Chem. Downloaded from www.nrcresearchpress.com by 65.111.164.53 on 09/08/12
For personal use only.

Chart 1

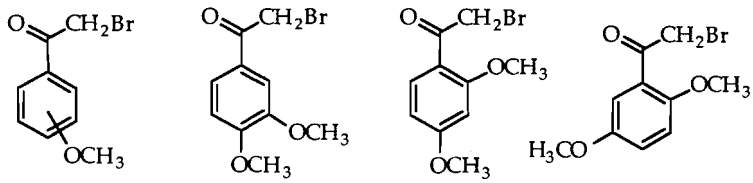

4, 2-CH_3O
5, 3-CH_3O
6, 4-CH_3O

7 8 9

photodecomposition of phenols to yield phenoxyl radicals, the abstraction of phenolic hydrogens to yield also phenoxyl radicals, the cleavage of excited states of substituted α-phenoxyacetophenones to produce phenacyl and phenoxyl radicals, and the cleavage of aromatic ketyl radicals (1, 3, 4).

The complexity of lignin is such that studies on native lignin are difficult and their interpretation is frequently inconclusive. Several research groups have employed "designer" model compounds in their studies. These molecules tend to include some of the key features of lignin and, therefore, their behavior can be taken to represent a modest fraction of the reactions that may occur in native lignin. Among these model compounds, α-guaiacoxyacetoveratrone (**1**) has been the subject of numerous studies (3, 5–10).

1

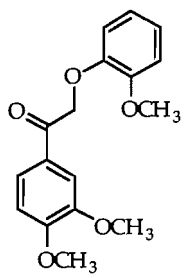

Of the various radicals mentioned above, phenacyl radicals are probably the least understood, yet they may be very important species in the chain of events leading to the oxidative degradation of lignin. In pulp, phenacyl radicals are probably produced by photoinduced cleavage of β-ether bonds in a process resembling the mechanism of decomposition of **1**, reaction [1].

[1] **1** $\xrightarrow{h\nu}$ **2** + **3**

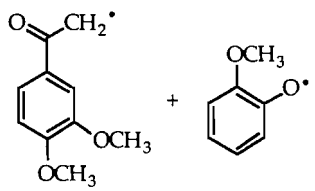

While radical **2** has been written as a carbon-centered species, it can also be written in its canonical form, as an oxygen-centered radical (11), i.e.,

[2]

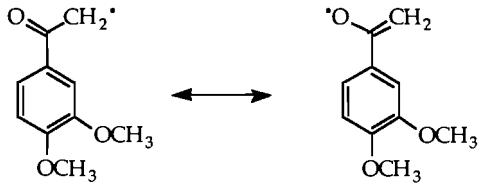

Recent work has suggested that the "oxy" form of **2** may account for its absorption properties (11), which are reminiscent of those recently reported for cumyloxyl radicals (12, 13). Product studies on the addition of phenacyl radicals to olefins show that these reactions lead to C—C bond formation, thus showing carbon-centered radical behavior (14, 15).

This study was undertaken in an attempt to learn about the kinetics and spectroscopy of **2** and related phenacyl radicals. In our search for spectroscopically "clean" sources of phenacyl radicals, we concluded that substituted α-bromoacetophenones were a convenient source of these radicals. A similar reaction is known in the case of phenacyl sulfides (16). In this report, we have employed laser flash photolysis techniques to study several α-bromoacetophenones and the phenacyl radicals produced in their photodecomposition.

Experimental section

The various substituted α-bromoacetophenones were obtained from either Lancaster or Aldrich and were recrystallized from hexane before use. The same applies to 4-methoxyphenol and 2,6-dimethoxyphenol used in several experiments. Chart 1 illustrates the structures of the phenacyl precursors employed in this study. Ascorbic acid, 1,4-cyclohexadiene, and triethylamine were Aldrich products; sorbic acid was from Sigma. Solvents were Omnisolv grade from BDH.

Laser flash photolysis experiments were carried out using a Lumonics EX-510 excimer laser for excitation (Xe–HCl–He mixtures, 308 nm, ~ ns, 20–80 mJ/pulse). The signals from a monochromator–photomultiplier detector system were initially captured by a Tektronix 2440 digital oscilloscope interfaced to a Macintosh-IIcx computer that provided facilities for experiment control and data capture and processing (11). Nitrogen-saturated samples were flowed through a quartz cell constructed of 7 mm × 7 mm Suprasil square tubing. This ensured that a fresh portion of solution was irradiated by each laser pulse, thus avoiding problems related to sample depletion

Can. J. Chem. Downloaded from www.nrcresearchpress.com by 65.111.164.53 on 09/08/12
For personal use only.

Scheme 1

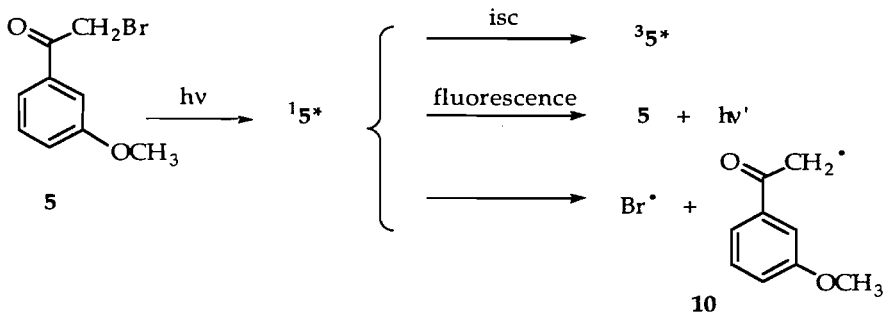

or product accumulation. Software for the laser system was written in the LabVIEW 2.2 programming environment from National Instruments.

Molecular modeling calculations were performed on a Tektronix CAChe workstation (software version 3.5) using the AM1 UHF semiempirical method, as part of the MOPAC program version 6.1.

Results

Laser excitation (308 nm) of substituted α-bromoacetophenones leads to two detectable transients. These can be characterized as the excited triplet state (detectable in most, but not all cases) and phenacyl radicals. Bromine atoms, produced concurrently with phenacyl radicals, are not detectable in the spectral region of interest; their presence can be readily established by complexation with either benzene or bromide ions (17, 18). Formation of phenacyl radicals competes with intersystem crossing (isc) to the triplet manifold, and in some systems with fluorescence emission, as illustrated for **5** in Scheme 1.

We will show below that the triplet states of these molecules do not yield any significant amounts of phenacyl radicals. These appear to be derived exclusively from the singlet state.

Characterization of the triplet states from ketones 4–9

Laser excitation of deaerated solutions of the ketones in Chart 1 leads, in most cases, to the detection of a reaction intermediate that can be characterized as the ketone triplet state (see Fig. 1). A notable exception is the case of **6**, where the triplet state has not been detected in spite of numerous attempts to do so. Interestingly, no triplet state has been detected in the photochemistry of the parent α-bromoacetophenone (17).

The triplet states were identified through their characteristic behavior toward various quenchers. In particular, conjugated dienes are well-established quenchers of triplet states (19–21). In our case, we employed sorbic acid, **11**, to help identify the triplet states; quenching is expected to involve energy transfer.

For example, in the case of **5**, the triplet state has a lifetime of 2.2 μs in 2-propanol, and was quenched by sorbic acid with a rate constant of 2.2×10^9 M^{-1} s^{-1} at 20°C. For **8** the rate constant was 2.1×10^9 $M^{-1}s^{-1}$. This rate constant is derived from a

11 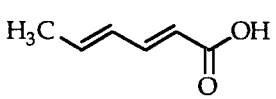

Table 1. Rate constants for the quenching of carbonyl triplets by various quenchers in 2-propanol at 20°C.

Triplet	Quencher	k_q (M^{-1} s^{-1})	τ (μs)
4	Sorbic acid	2.2×10^9	2.0
5	Sorbic acid	2.2×10^9	2.2
8	Sorbic acid	2.1×10^9	4.5
9	Sorbic acid	1.6×10^9	1.8
5	Triethylamine	1.8×10^8	2.2
7	Triethylamine	6.5×10^6	5.6

plot of the first-order rate constant for triplet decay as a function of the quencher concentration, i.e.,

[3] $k_{decay} = \tau^{-1} + k_q[\mathbf{11}]$

Representative plots according to eq. [3] are shown in Fig. 2, and the lifetime and quenching data have been summarized in Table 1. The triplet states were also readily quenched by oxygen, as expected.

The monomethoxy-substituted triplet states were readily quenched by triethylamine; for example, in the case of **5**, $k_q = 1.8 \times 10^8$ M^{-1} s^{-1} in 2-propanol as solvent. In contrast, the rate constant for **7** is 6.5×10^6 M^{-1} s^{-1} (Et_3N). It is interesting to note that the molecules in Table 1 do not photoreduce appreciably in alcohols, with $k_q < 5 \times 10^4$ M^{-1} s^{-1} for 2-propanol. The inability to photoreduce in alcohols is characteristic of ketones with low-lying π,π* states, a situation frequently encountered in methoxy-substituted acetophenones (22, 23).

The triplet states (Fig. 1) show maxima around 380 nm for the monosubstituted derivatives, and around 420 nm for the disubstituted ones (compounds **7–9**). A small blue shift (~20 nm) is observed in nonpolar solvents such as hexane.

We were surprised by the failure to detect the triplet state of **6**. Some sensitization experiments were carried out to determine if this was due to the involvement of a very short-lived triplet, or a low yield for its formation.

Xanthone is a convenient sensitizer, since its triplet state is readily detectable and is relatively long-lived in many organic solvents (24). Xanthone was excited at either 355 or 308 nm and the triplet state monitored at 600 nm; its lifetime under our experimental conditions (0.3 mM) was ~6 μs in acetonitrile. Addition of **6** led to efficient quenching with rate constants of $(1.1 \pm 0.1) \times 10^{10}$ M^{-1} s^{-1} and $(4.0 \pm 0.6) \times 10^9$ M^{-1} s^{-1} in ace-

Can. J. Chem. Downloaded from www.nrcresearchpress.com by 65.111.164.53 on 09/08/12
For personal use only.

Can. J. Chem. Downloaded from www.nrcresearchpress.com by 65.111.164.53 on 09/08/12
For personal use only.

Fig. 1. Triplet spectra recorded in 2-propanol following 308 nm laser excitation of ketones **4**, **5**, **8**, and **9**.

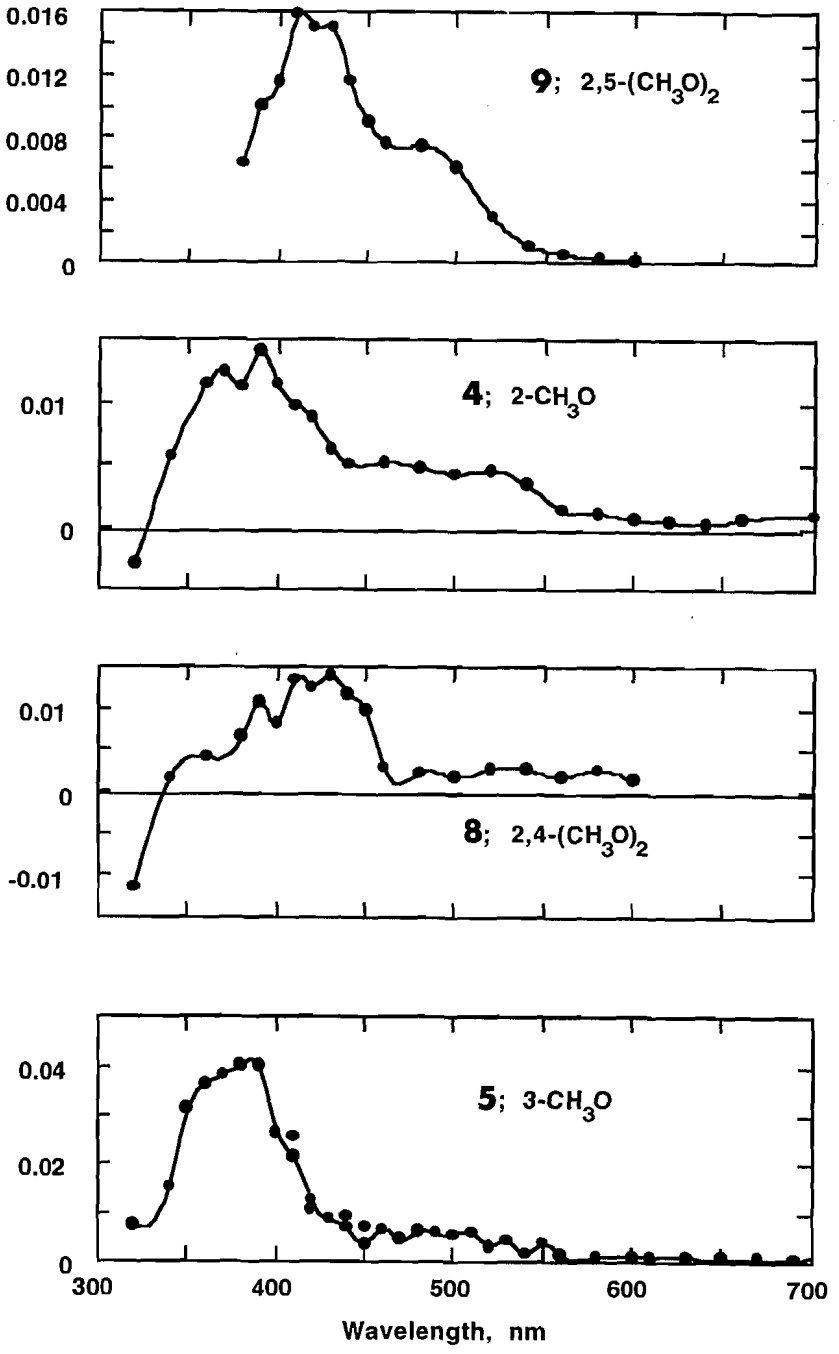

tonitrile and 2-propanol, respectively. These near-diffusion-controlled rate constants suggest efficient energy transfer. However, our attempts to detect the triplet state of **6** were unsuccessful, since no other transient could be detected following decay of the xanthone triplet, under conditions where >90% of the xanthone triplets were quenched by **6**. Given the dynamics of energy transfer for the highest concentration of **6** employed (0.12 mM), this allows us to set an upper limit of 0.5 μs for the triplet lifetime. Clearly, the failure to detect triplet **6** in the direct or sensitized photolysis is due to its short triplet lifetime. Another important observation is that triplet energy transfer from xanthone to **6** does not lead to the formation of the corresponding phenacyl radical. Thus, phenacyl radical formation is a singlet state process.

The yields of phenacyl radicals (vide infra) were not influenced by quenching of the triplet states by sorbic acid, suggesting that, just as in the case of **6**, radicals are normally derived from the singlet state. Similar conclusions have been reached in related systems using CIDNP spectroscopy (8, 9).

To our surprise, the lifetime of the triplet states of the monomethoxy derivatives **4** and **5** showed an unexpected solvent dependence. Thus, the triplet lifetime of **5** was 2.2 μs in 2-propanol (η = 2.2 cP), 500 ns in methanol (η = 0.55 cP), and 400 ns in hexane (η = 0.29 cP). The triplet lifetime was insen-

Can. J. Chem. Downloaded from www.nrcresearchpress.com by 65.111.164.53 on 09/08/12
For personal use only.

Fig. 2. Quenching of the triplet states of **3** and **8** by sorbic acid in 2-propanol at 20°C, following 308 nm laser excitation.

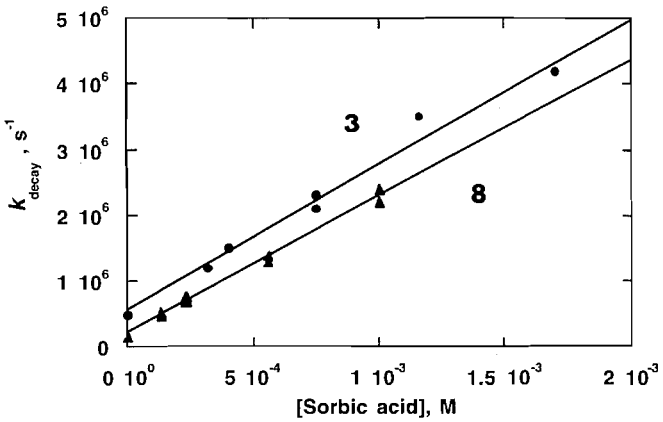

sitive to changes in the concentration of **5** from 0.08 to 0.3 mM, thus ruling out possible influence of impurity quenching in the ketone as the source of the observed viscosity dependence. The effect may be related to an unusually slow bond rotation. Chlorine influences strongly rates of bond rotation in reaction intermediates derived from chloroacetophenones (25). If this assumption is correct for the bromoacetophenones, it would imply that radiationless triplet deactivation and bond rotation are coupled processes.

Table 2. Yield of bromine atoms (measured as $Br_2^{\bullet}$) produced upon laser photolysis at 308 nm in oxygen saturated methanol containing 2% water.

Substrate	Φ
α-Bromoacetophenone	(0.41)[a]
4	0.28
5	0.35
6	0.35
7	0.18
8	0.23
9	0.13

[a]Used as a standard, see ref. 17.

Characterization and reactivity of methoxy-substituted phenacyl radicals

The transient spectra of methoxyphenacyl radicals produced by photodecomposition of the substrates in Chart 1 are all rather similar (see Fig. 3), featuring one band in the 320–420 nm region and a weaker one in the 520–600 nm range in polar solvents such as methanol and acetonitrile. The absorption bands for the monomethoxy-substituted derivatives are blue shifted by ca. 20 nm in hexane. The radicals decay by a mixture of first- (or pseudo-first) and second-order processes. Typical half-lives under our experimental conditions for the

Fig. 3. Transient spectra from phenacyl radicals in 2-propanol following 308 nm laser excitation. Top: **5**, □; **6**, ●; **9**, ▲. Bottom: **4**, ■; **8**, ○.

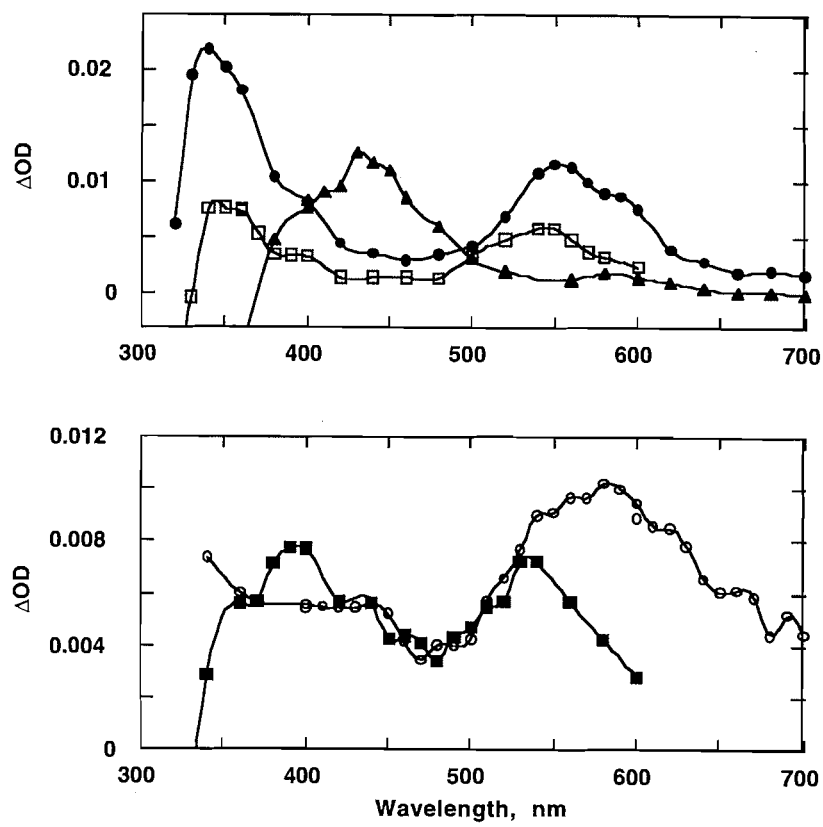

Fig. 4. Plot of k_{decay} against oxygen concentration for the reaction of radical **12** in acetonitrile. Laser excitation at 308 nm. Insert shows a representative trace, monitored at 520 nm.

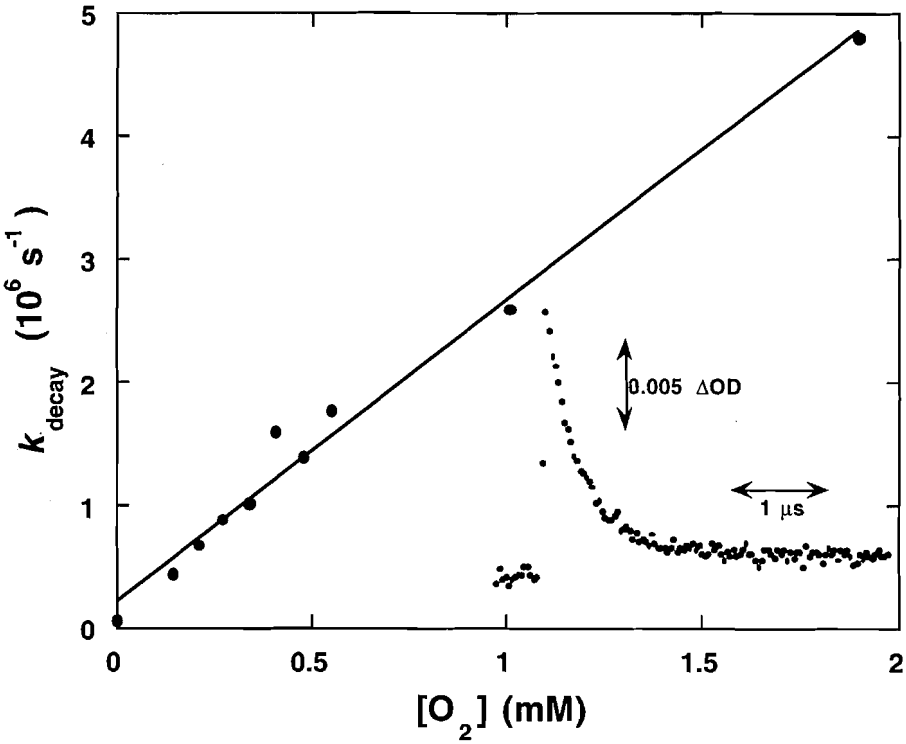

radical from **6** in solvents such as methanol, ethanol, 2-propanol, and acetonitrile are in the neighborhood of 10 μs.

The yields of phenacyl radicals from the various precursors in Chart 1 can be readily determined by scavenging the bromine atoms with bromide, to give the readily detectable $Br_2^{\bullet-}$. Bromide was added as NaBr and the concentration of 0.08 M was chosen to ensure that >98% of the bromine atoms would be trapped by bromide (26, 27). The yields obtained are given in Table 2; these were quantified by using α-bromoacetophenone ($\Phi = 0.41$) as a standard (17).

Most experiments were carried out with monomethoxy-substituted phenacyl radicals, particularly those from ketone **6**. Phenacyl radicals react readily with oxygen. A series of measurements were carried out at various oxygen concentrations; these were adjusted by bubbling the samples with oxygen–nitrogen mixtures of known composition. The pseudo-first-order rate constant for radical decay follows eq. [4].

[4] $k_{decay} = k_o + k_{ox}[O_2]$

Figure 4 shows a plot of k_{decay} against oxygen concentration for the reaction of **12**, the radical from **6**, in acetonitrile. From the slope, we obtain $k_{ox} = 2.4 \times 10^9$ M^{-1} s^{-1}; essentially the same number was obtained in methanol. The value is in line with typical reactivities of stabilized carbon-centered free radicals toward oxygen (28). While we did not measure rate constants for other radicals derived from the molecules in Chart 1, experiments in air or oxygen-saturated solution showed that all react readily with oxygen.

1,1-Diphenylethylene is a well-established free radical scavenger (29). Radical addition (reaction [5]) leads to a resonance-stabilized and readily detectable radical, with a characteristic intense absorption in the 330 nm region.

Reaction [5] can be studied by monitoring the decay of the phenacyl radical in the 500-600 nm region, or the formation of the product radical at or around 330 nm. Figure 5 shows a plot of k_{decay} (monitored at 520 nm) against the concentration of $Ph_2C{=}CH_2$ and a representative trace (insert). Monitoring of the reaction by following the phenacyl radical (rather than **13**)

[5]

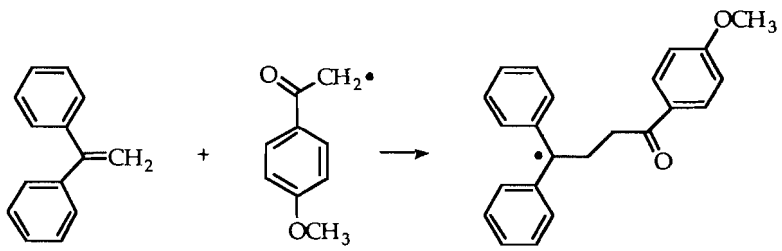

12 **13**

Can. J. Chem. Downloaded from www.nrcresearchpress.com by 65.111.164.53 on 09/08/12
For personal use only.

Can. J. Chem. Downloaded from www.nrcresearchpress.com by 65.111.164.53 on 09/08/12
For personal use only.

Fig. 5. Plot of k_{decay} against the concentration of $Ph_2C{=}CH_2$ in acetonitrile. Laser excitation at 308 nm. Insert shows a representative trace monitored at 520 nm.

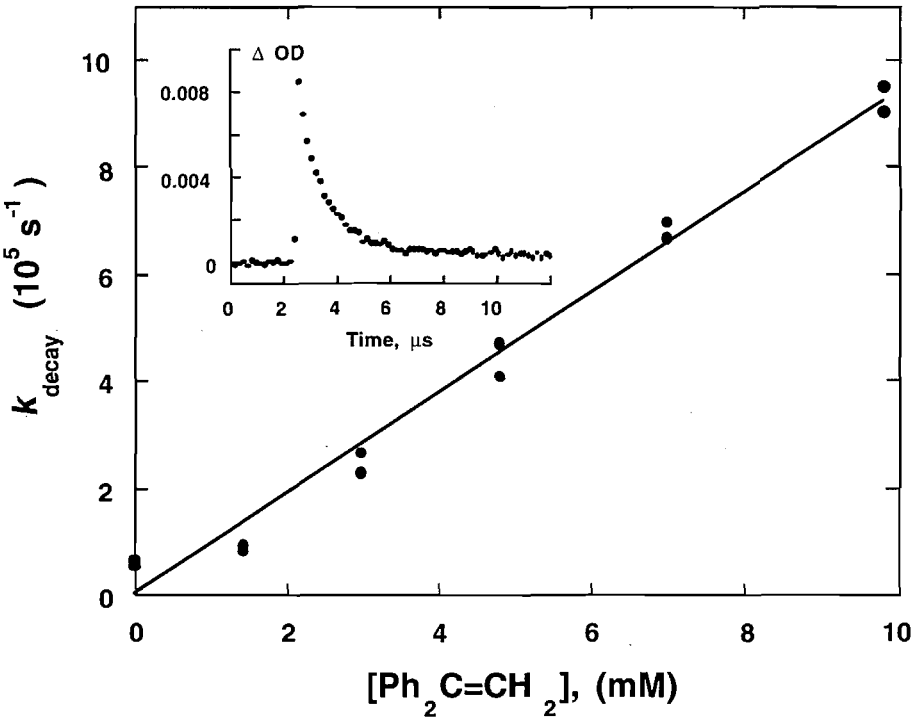

Fig. 6. Spectrum of the product (**13**) from reaction [5] in acetonitrile, 308 nm laser excitation, 480 ns after laser pulse.

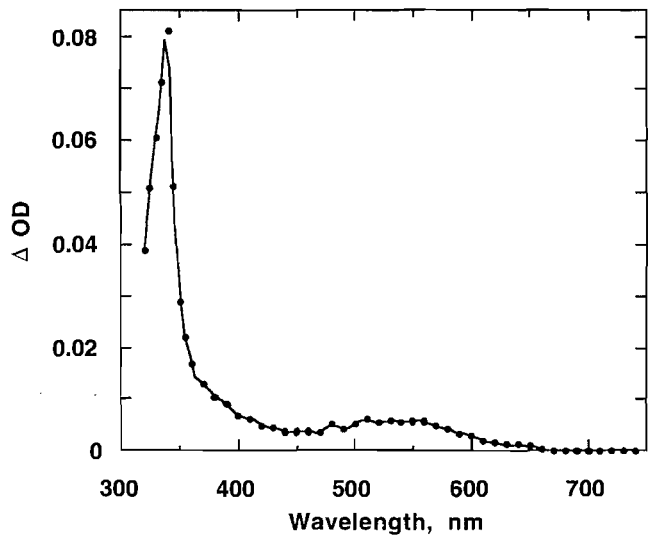

was preferred since it should not be subject to interference by possible addition of Br˙ to 1,1-diphenylethylene. The spectrum of the product is shown in Fig. 6. The plot leads to a surprisingly high rate constant of 9.4×10^7 M^{-1} s^{-1} for reaction of the radical from **6** in acetonitrile. For comparison, *n*-nonyl radicals add with a rate constant of $\sim 3.0 \times 10^5$ M^{-1} s^{-1} at 20°C (29). While these experiments do not provide direct evidence of the mode of attack, we assume that reaction occurs at the carbon center to give **13**, since most of the spin density is at this site (30); the assumption is also consistent with product studies in related systems (14, 15).

Table 3. Rate constants for the reactions of substituted phenacyl radicals with 2-mercaptoethanol.

Phenacyl precursor	k (M^{-1} s^{-1})[a]
4	1.8×10^5
5	1.4×10^5
6	2.8×10^5
8	2.9×10^5
9	1.4×10^5

[a]In methanol at 20°C following 308 nm laser excitation. Errors estimated as ±20%.

To explore the possibility of efficient scavenging of the methoxyphenacyl radicals, which could shut down the phenacyl route of the paper yellowing, we measured the reactivities of the methoxyphenacyl radicals with well-known radical inhibitors; the results are summarized in Table 3.

Several results in the last few years have suggested that mercaptans may be viable compounds as brightness stabilizers for TMP products (31). In view of this, it seemed important to examine the reactivity of phenacyl radicals toward the S—H bond. The substrate selected for these tests was 2-mercaptoethanol, $HOCH_2$-CH_2SH. The corresponding rate constants in methanol (see Table 1) are in the $(1.4–2.9) \times 10^5$ M^{-1} s^{-1} range. The highest rates of H-abstraction from 2-mercaptoethanol are measured for 4-methoxy- and 2,4-dimethoxyphenacyl radicals. However, the difference between the lowest and highest rate is only a factor of ~2, which suggests that the effect of the methoxy substitution on the benzene ring on the reactivity of the phenacyl radical is indeed very small.

The rate constants for reaction of 4-methoxyphenacyl radi-

Can. J. Chem. Downloaded from www.nrcresearchpress.com by 65.111.164.53 on 09/08/12
For personal use only.

Table 4. Rate constants for the reactions of 4-methoxyphenacyl radical (**12**) derived from **6** at room temperature.

Substrate	k, M^{-1} s^{-1} [a]	Solvent
2-Propanol	$\sim 4 \times 10^3$	Acetonitrile
2-Mercaptoethanol	2.8×10^5	Methanol
Triethylamine	1.2×10^4	Methanol
1,4-Cyclohexadiene	2.6×10^5	Methanol
Oxygen	2.5×10^9	Methanol or acetonitrile
4-Methoxyphenol	$<1 \times 10^6$	Methanol or hexane
Ascorbate	$<5 \times 10^6$	Methanol
Sorbic acid	$<5 \times 10^6$	Methanol
1,1-Diphenylethylene	9.4×10^7	Acetonitrile

[a]Accurate within ± 20%.

Fig. 7. Calculated bond orders for radical **6**. Results from AM1 calculations.

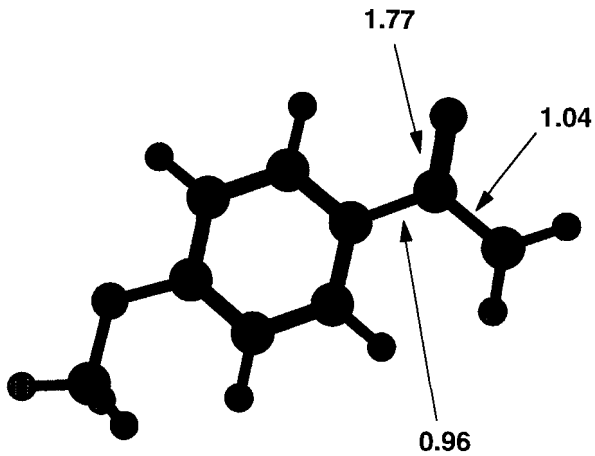

cal (**12**) with various potential hydrogen donors that could act as "repair agents" are given in Table 4.

Semiempirical calculations (AM1) on the structure of methoxyphenacyl radicals suggest some oxygen-centered radical character. Thus, in the case of **6**, Fig. 7 shows the key bond orders; these are consistent with ESR data (30) on the radicals (vide infra). Calculated spin densities at the oxygen center are about 0.3; surprisingly this arises largely at the expense of spin density elsewhere in the ring, since the spin density at the carbon radical site remains close to one. Calculations on the ketones that would result from hydrogen abstraction by phenacyl radicals show that the enol tautomer lies generally ca. 10 kcal/mol above the ketone form. Thus, we expect reactions at the oxygen center to be thermodynamically less favorable than those at the carbon center.

Earlier calculations on **6** have already shown that a visible band should be expected for radicals of this type (11).

Discussion

Photodecomposition of substituted α-bromoacetophenones such as those in Chart 1 leads to the rapid and relatively efficient (see Table 2) formation of phenacyl radicals and bromine atoms. The former are readily detectable with laser flash photolysis techniques, while the bromine atoms become "visible" in the presence of suitable complexing agents such as bromide ions or aromatic molecules. Bromine atom elimination occurs from the singlet state of the ketones. If there is any triplet contribution, it must be sufficiently small (<5%) to be undetectable under our experimental conditions. The result is in line with analogous observations in the case of similarly substituted α-phenoxyacetophenones (8–10). Typical aromatic ketones (e.g., benzophenone) undergo intersystem crossing with near-quantitative efficiency to yield a triplet state that is responsible for much of their photochemistry (19); in this sense methoxy-substituted acetophenones are unusual in that the singlet state plays a dominant role in their photochemistry. Phenyl ω-dialkylaminoalkyl ketones provide another example of aromatic ketones where the singlet state is important (32). The triplet states of methoxy-substituted α-bromoacetophenones show typical π,π^* characteristics, and are unreactive in hydrogen abstraction reactions towards typical hydrogen donors such as alcohols. The triplets can be quenched with amines, although with rates significantly below the diffusion-controlled limit. For example, triplet **7** is quenched by triethylamine with a rate constant of only 6.5×10^6 M^{-1} s^{-1}, reflecting the electron-rich characteristics of methoxy-substituted aromatic ketones.

Phenacyl radicals have an electron distribution leading to some radical character at the oxygen center, but mostly at the carbon site. This leads to the calculated bond orders of Fig. 7. The visible absorption band of these radicals is believed to reflect their "oxy" (or n,π^*) characteristic, which makes this particular resonance structure similar to that of cumyloxyl radicals; these have recently been shown to also have an absorption band in the visible region (13).

The spectroscopy and reactivity of phenacyl radicals is consistent with their ESR parameters (30). Thus, the α-hydrogen coupling constants for $C_6H_5COCH_2^{\cdot}$ are approximately 19.6 gauss, compared with 22.3 gauss for the ethyl radical.

While the presence of unpaired electron density at the oxygen center influences the ESR parameters and absorption spectroscopy of the radicals, their reactivity is clearly a reflection of their carbon-centered properties, as reported in recent work by Russell and Kulkarui, and Khanna (14, 15), who showed that phenacyl addition to alkenes occurs with C—C bond formation.

The reaction rate constants of methoxyphenacyl with various "repair agents" appear to be very low (Table 4). The rates with well-known H-atom donors, such as 2-mercaptoethanol and 1,4-cyclohexadiene, $k = 2.8$ and 2.4×10^5 M^{-1} s^{-1}, are two orders of magnitude lower than typical H-atom transfer rates of either simple alkyl, e.g., $k(^{\cdot}CH_3$ + glutathione) = 5×10^7 M^{-1} s^{-1} (33), or alkoxyl radicals (34, 35). The enthalpy change for S-H abstraction by phenacyl from simple aliphatic thiols should be around −2 kcal/mol (BDE[3] ($C_6H_5COCH_2$—H) ~93 kcal/mol and BDE (RS—H) ~91 kcal/mol) (36). The reactions of 4-methoxyphenacyl radicals with well-known electron donors, such 2,6-dimethoxyphenol, 4-methoxyphenol, and ascorbate are slow, $k < 10^6$ M^{-1} s^{-1}. These slow rates of electron transfer suggest that the methoxyphenacyl radicals react mainly as nucleophiles and more like C-centered alkyl than like O-centered alkoxyl radicals. Given the high reactivity towards oxygen, we anticipate that in the context of the photoyellowing of lignin-rich pulp and paper, the fate of phen-

[3] BDE = bond dissociation energy.

acyl radicals will be the formation of the corresponding peroxyl radical, $ArCOCH_2OO^{\cdot}$, which may further contribute to the oxidative degradation of lignin. It would therefore be important to learn more about the reactivity of peroxyl radicals of this type.

Acknowledgment

This work was supported by the Natural Sciences and Engineering Research Council of Canada and the Canadian Network of Centres of Excellence through the Mechanical and Thermomechanical Wood Pulps Network.

References

1. G. J. Leary. J. Pulp Paper Sci. **20**, J154 (1994).
2. C. Heitner and J.C. Scaiano (*Editors*). Photochemistry of lignocellulosic materials. ACS Symp. Ser. **531** (1993).
3. A.B. Berinstain, M.K. Whittlesey, and J.C. Scaiano. *In* Photochemistry of lignocellulosic materials. *Edited by* C. Heitner and J.C. Scaiano. American Chemical Society, Washington. 1993. p. 111.
4. J.A. Schmidt and C. Heitner. J. Wood Chem. Technol. **11**, 397 (1991).
5. J.A. Schmidt, E. Goldsmidt, C. Heitner, J.C. Scaiano, A.B. Berinstain, and L.J. Johnston. *In* Photochemistry of lignocellulosic materials. *Edited by* C. Heitner and J.C. Scaiano. American Chemical Society, Washington. 1993. p. 122.
6. J.C. Scaiano, A.B. Berinstain, M.K. Whittlesey, P.R.L. Malenfant, and C. Bensimon. Chem. Mater. **5**, 700 (1993).
7. A. Castellan, N. Colombo, C. Vanucci, P. Fornier de Violet, and H. Bouas-Laurent. J. Photochem. Photobiol. A: **51**, 451 (1990).
8. W.U. Palm and H. Dreeskamp. J. Photochem. Photobiol. A: **52**, 439 (1990).
9. W. U. Palm, H. Dreeskamp, H. Bouas-Laurent, and A. Castellan. Ber. Bunsen-ges. Phys. Chem. **96**, 50 1992).
10. J.A. Schmidt, A.B. Berinstain, F. de Rege, C. Heitner, L.J. Johnston, and J.C. Scaiano. Can. J. Chem. **69**, 104 (1991).
11. J.C. Scaiano, M.K. Whittlesey, A.B. Berinstain, P.R.L. Malenfant, and R.H. Schuler. Chem. Mater. **6**, 836 (1994).
12. J.T. Banks and J.C. Scaiano. J. Am. Chem. Soc. **115**, 6409 (1993).
13. D.V. Avila, J. Lusztyk, and U. Ingold. J. Am. Chem. Soc. **114**, 6576 (1992).
14. G.A. Russell and S.V. Kulkarni, J. Org. Chem. **58**, 2678 (1993).
15. G.A. Russell, S.V. Kulkarni, and R.K. Khanna. J. Org. Chem. **55**, 1080 (1990).
16. P.J. Wagner and M.J. Lindstrom. J. Am. Chem. Soc. **109**, 3062 (1987).
17. W.G. McGimpsey and J.C. Scaiano. Can. J. Chem. **66**, 1474 (1988).
18. J.C. Scaiano, B.R. Arnold, and W.G. McGimpsey. J. Phys. Chem. **98**, 5431 (1994).
19. N.J. Turro. Modern molecular photochemistry. Benjamin/Cummings Publishing Co., Menlo Park, Calif. 1978.
20. P.J. Wagner and I. Kochevar. J. Am. Chem. Soc. **90**, 2232 (1968).
21. J.C. Scaiano, W.L. Leigh, M.A. Meador, and P.J. Wagner. J. Am. Chem. Soc. **107**, 5806 (1985).
22. P.J. Wagner and T. Nakahira. J. Am. Chem. Soc. **95**, 8474 (1973).
23. N.C. Yang, D.S. McClure, S.L. Murov, J.J. Houser, and R. Dosenbery. J. Am. Chem. Soc. **89**, 5466 (1967).
24. J.C. Scaiano. J. Am. Chem. Soc. **102**, 7747 (1980).
25. J.C. Netto-Ferreira and J.C. Scaiano. J. Am. Chem. Soc. **113**, 5800 (1991).
26. V. Nagarajan and R.W. Fessenden. J. Phys. Chem. **89**, 2330 (1985).
27. J.C. Scaiano, M. Barra, M. Krzywinski, R. Sinta, and G. Calabrese. J. Am. Chem. Soc. **115**, 8340 (1993).
28. B. Maillard, K.U. Ingold, and J.C. Scaiano. J. Am. Chem. Soc. **105**, 5095 (1983).
29. J. Chateauneuf, J. Lusztyk, and K.U. Ingold. J. Org. Chem. **53**, 1629 (1988).
30. G. Brunton, H.C. McBay, and K.U. Ingold. J. Am. Chem. Soc. **77**, 4447 (1977).
31. S.R. Daneault and M. Levesque. **17**, 187 (1991).
32. P.J. Wagner and T. Jellinek. J. Am. Chem. Soc. **93**, 7328 (1971).
33. S.V. Jovanovic and M.G. Simic. *In* Anticarcinogenesis and radiation protection. *Edited by* O.F. Nygaard and A.C. Upton. Plenum Press, New York. 1991. p. 229.
34. H. Paul, R.D. Small, Jr., and J.C. Scaiano. J. Am. Chem. Soc. **100**, 4520 (1978).
35. V. Malatesta and J.C. Scaiano. J. Org. Chem. **47**, 1455 (1982).
36. D.F. McMillen and D.M. Golden. Annu. Rev. Phys. Chem. **33**, 493 (1982).

Can. J. Chem. Downloaded from www.nrcresearchpress.com by 65.111.164.53 on 09/08/12
For personal use only.

Polarographic studies of indium(III) in aqueous medium of sodium azide

Roberto Tokoro, Mauro Bertotti, and Lúcio Angnes

Abstract: In this paper, some aspects of the polarography of indium(III) in azide/hydrazoic acid buffer are presented. The electrode process is mostly governed by diffusion in the complexing medium. Nevertheless, for controlled-potential coulometry (involving a large time window) a catalytic process was observed, ascribed to the reaction of the hydrazoic acid and indium amalgam. The stability of azide complexes of In(III) was studied polarographically, and the formation of four mononuclear species was confirmed by computational analysis of data obtained from polarograms of In(III) in different azide concentrations. The values of the global constants obtained are: $\beta_1 = 3.7 \times 10^3\ M^{-1}$, $\beta_2 = 8.6 \times 10^5\ M^{-2}$, $\beta_3 = 5.0 \times 10^7\ M^{-3}$, $\beta_4 = 2.1 \times 10^9\ M^{-4}$, in a constant ionic strength medium held at 2.0 M with $NaClO_4$. These data are in good agreement with those obtained by potentiometry. The value found for $E^{0'}$ of the In(III)/In couple was -512.2 mV vs. calomel electrode (3 M NaCl), the mean diffusion coefficient of the complex being $(6.1 \pm 0.2) \times 10^{-6}\ cm^2\ s^{-1}$ in perchlorate medium ($T = 25°C$).

Key words: polarography, indium(III), azide, stability constants, catalytic wave.

Résumé : Dans ce travail, on présente quelques aspects de la polarographie de l'indium(III) dans un tampon d'azoture/acide hydrazoïque. Le processus à l'électrode est principalement déterminé par la diffusion dans le milieu complexant. Toutefois, pour la coulométrie à potentiel contrôlé (impliquant une large fenêtre de temps), on a observé un processus catalytique attribué à la réaction de l'acide hydrazoïque avec l'amalgame d'indium. Faisant appel à la polarographie, on a étudié la stabilité des complexes d'azoture avec le In(III) et on a confirmé la formation de quatre espèces mononucléaires par une analyse mathématique des données obtenues à partir de polarogrammes du In(III) à diverses concentrations d'azoture. Les valeurs des constantes globales obtenues sont : $\beta = 3{,}7 \times 10^3\ M^{-1}$, $\beta_2 = 8{,}6 \times 10^5\ M^{-2}$, $\beta_3 = 5{,}0 \times 10^7\ M^{-3}$ et $\beta_4 = 2{,}1 \times 10^9\ M^{-4}$, à une force ionique constante maintenue à 2,0 M par du $NaClO_4$. Ces données sont en bon accord avec celles obtenues par potentiométrie. La valeur trouvée pour $E^{0'}$ dans le couple In(III)/In est de $-512{,}2$ mV vs. électrode au calomel (3 M NaCl) alors que le coefficient moyen de diffusion du complexe est $(6{,}1 \pm 0{,}2) \times 10^{-6}\ cm^2\ s^{-1}$ dans un milieu de perchlorate ($T = 25°C$).

Mots clés : polarographie, indium(III), azoture, constantes de stabilité, vague catalytique.

[Traduit par la rédaction]

Introduction

The study of the chemistry of the azide anion, N_3^-, was introduced in our institute by Senise (1), and afterwards developed by Senise and Neves (2), who observed for the first time the catalytic reduction of hydrazoic acid in the presence of cobalt and zinc cations. This observation led to the work of Tokoro and Neves (3). Thenceforth, attempts were directed towards finding other metal ions that would play a similar role in the reduction of hydrazoic acid, as well as to investigate reactions where the azide anion acts as a catalyst for the reduction of a variety of metals. For this later study, indium(III) seemed very promising. Polarographic studies of the thiocyanate of indium(III) appear in the literature (4–12), whereas the electrochemical behavior of the corresponding isosteric azide complex remains practically unexplored. The pseudo-halides of both the thiocyanate and azide are isosteric and thus the purpose of the present work is the search for and verification of such similarities.

In this paper, electrochemical studies on the In(III) + N_3^- system were carried out in order to investigate the formation of complexes in aqueous solution. Several electrochemical methods have been employed to determine the stability constants of equilibria involving a metallic ion and a ligand, but one of the most widely used is based on polarographic determinations when reversibility conditions are attained. The electrode process was characterized, the suitable parameters were obtained, and finally the dependence of half-wave potential on azide concentration provided data for evaluation of the stability constants.

Experimental

Reagents

A standard solution of indium(III) perchlorate was prepared from pure metallic indium (Fisher Scientific Co. certified reagent) dissolved in an excess of perchloric acid (Merck, PA). Gentle heating was necessary to complete the dissolution of the metal. The excess of acid was used to prevent the for-

Received April 11, 1994.

R. Tokoro,[1] M. Bertotti, and L. Angnes. Instituto de Química da Universidade de São Paulo, P. O. Box 20780, CEP 01498-970, São Paulo, Brazil.

[1] Author to whom correspondence maybe addressed. Fax: 815-5579. Telex: 1180 902 USPO BR.

Can. J. Chem. Downloaded from www.nrcresearchpress.com by 65.111.164.53 on 09/08/12
For personal use only.

Can. J. Chem. Downloaded from www.nrcresearchpress.com by 65.111.164.53 on 09/08/12
For personal use only.

mation of hydroxo complexes of indium(III). This solution was diluted with bidistilled water to a final volume of 500.0 mL. The final concentration of indium(III) in this solution was calculated according to the weight of the metallic form, and the final acidity was determined by a potentiometric standard addition method (13). Sodium perchlorate and sodium azide solutions (prepared from Merck PA grade salts) were standardized gravimetrically by drying a known volume of the solutions to constant weight. For microscopic observations, active charcoal purchased from Merck was employed. All the other reagents were used as available commercially. Purity of all the solutions was checked through polarographic determinations.

Apparatus

Polarographic studies were performed with a Metrohm Polarecord 506 and a Tacussel Polaropulse PRG 5. For some preliminary runs, a Leeds and Northup Electrochemograph was also used. Metrohm EA 874 or a EA 876-5 cells were used in most of the polarographic experiments. A dropping mercury electrode, a calomel electrode, and a platinum wire, used as auxiliary electrode, were hermetically sealed in the covers of the cells. The characteristics of the capillary were m = 2.427 mg s^{-1} and τ = 3.33 s at −0.7 V and h = 97 cm, in 2.0 M $NaClO_4$. When tast and pulse techniques were used, the drop time was mechanically controlled; the typical measuring time t_m was 40 ms. Coulometry at controlled potential was carried out with a PAR 173 potentiostat coupled with a PAR 179 integrator. The experiments were carried out in a Metrohm 20 mL cell, equipped with a Fischer magnetic stirrer and a Teflon-coated stirring bar. The working electrode was a mercury pool (5.5 cm^2 area) and a 3 M NaCl calomel electrode was used as reference. It made contact with the solution via a Luggin capillary filled with 2.0 M $NaClO_4$. As auxiliary electrode, a platinum wire was utilized. Microscopic observation were made with an Olympus SZIII-BR-SIT zoom microscope. The pH measurements were carried out with a Micronal B 375 potentiometer and a Metrohm EA 121 combined glass electrode. A Metrohm 274 (5 mL) piston burette with a thin capillary was employed for precise volume additions. All the measurements were run at 25.0 ± 0.5°C, maintained with a Haake ultra-thermostat.

Calibration of instruments

The polarographic measurement systems were calibrated using a standard 0.977 mM cadmium perchlorate solution in 0.1 M $NaClO_4$ supporting electrolyte. The apparatus for the controlled-potential coulometry was calibrated using a standard cadmium(II) solution, and the n value obtained was very close to 2 (deviations in consecutive experiments were not larger than 5%).

Microscopic observations

To perform the microscopic observations of the movement of the solution around the mercury drop surface, small particles of active charcoal were used. To obtain particles of the desired size, 2 g of active charcoal were added to 1 L of bidistilled water, stirred, and were allowed to stand for 10 min. Then the supernatant was transferred to another vessel and the water was gently evaporated. The amount of charcoal obtained was around 50 mg, to be used as contrast.

Fig. 1. Polarographic behavior of 0.7892 mM In(III) in perchlorate medium (I = 2.0 M) as a function of pH (○ limiting current and ■ half-wave potential).

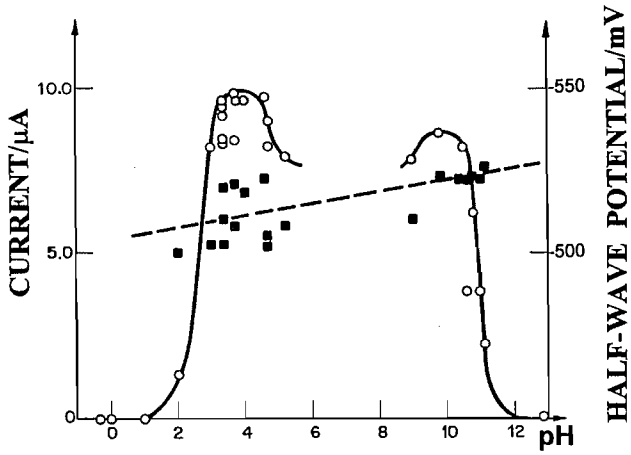

Working conditions

Two distinct solutions, the first (A) containing the metallic ion plus an N_3^-/HN_3 buffer, and the second (B) the metallic ion and hydrazoic acid, were used as previously described in a potentiometric study involving the formation of indium(III) azide complexes (14). Both solutions A and B were prepared directly inside the piston burette and in the polarographic cell, respectively, to avoid exposure to open air and consequently the loss of HN_3 by volatilization. Also, to minimize recontamination of the solutions with oxygen, these two vessels were "washed out" with a flow of nitrogen during 15 min. The composition of solution A (in the piston burette) was 0.300 M NaN_3, 0.100 M HN_3, 7.892×10^{-4} M In(III) at an ionic strength of 2.0 M, maintained with $NaClO_4$. Solution B (prepared directly in the polarographic cell) reached a final volume of 10.00 mL, and had the following composition: 0.100 M HN_3, 7.892×10^{-4} M In(III) at an ionic strength of 2.0 M, also maintained with $NaClO_4$. Both solutions, A and B, were prepared adding suitable volumes of reagents and adjusting with water to the final volume. All the components of the A and B solutions were previously saturated with nitrogen. In the preparation of both solutions, sodium azide was the last to be added, in order to minimize the loss of hydrazoic acid. The small amount of oxygen that could contaminate all the solutions during mixing was shown to be negligible when the polarograms were recorded. The adopted procedure consisted in the addition of known volumes of solution A to the solution B contained in the cell, with the aid of a thin polyethylene capillary adapted to the burette. After each addition, gentle micro bubbling with nitrogen ensured homogeneity, and then the corresponding polarogram was recorded and a precise value for $E_{1/2}$ was determined. Each experiment consisted of a large number of additions so that the analytical concentration of azide in the solution varied from 0.9 to 82.6 mM.

Results and discussion

Preliminary studies

Figure 1 shows that at a pH around 3.8 the polarographic current reaches its maximum intensity for indium(III) in perchlo-

Table 1. Polarographic behavior of 1.578 mM In(III) in different supporting electrolytes.

Supporting electrolyte	Wave at ~−0.6V	Observations
0.1 M $HClO_4$ + 2.0 M $NaClO_4$	No	Discharge of H^+ ~−1.4 V
0.1 M H_2SO_4 + satd. Na_2SO_4	No	Discharge of H^+ ~−1.4 V
0.1 M HNO_3 + 2.0 M $NaNO_3$	No	Slight outline of wave
0.1 M HCl + 2.0 M NaCl	Yes	Well defined, without minimum
2.0 M HCl	Yes	Well defined
2.0 M $HClO_4$	No	Discharge of H^+ ~−1.4 V
0.01 M $HClO_4$ + 2.0 M $NaClO_4$	No	Slight outline of wave
0.001 M $HClO_4$ + 2.0 M $NaClO_4$	Yes	Small height of wave
4.6×10^{-4} M $HClO_4$ + 2.0 M $NaClO_4$	Yes	Well defined, without minimum
1 mM N_3^- + 20 mM HN_3 + 2 M $NaClO_4$	Yes	Well defined
20 mM HN_3 + 2.0 M $NaClO_4$	Yes	Well defined

rate medium. Using the stability constants of the indium(III) + OH^- system (15) (log β_1 = 10.89, log β_2 = 21.34, and log β_3 = 30.88) to construct the distribution diagram of the species, it is possible to conclude that at pH 3.8 a species with two ligands predominates, the $In(OH)_2^+$ form. These observations agree with the work of Lawson and Aikens (16), who suggested that a dihydroxo-indium(III) complex is the electroactive form in solution.

In noncomplexing medium, In(III) is present as the aquo complex $In(H_2O)_6^{3+}$ and the polarographic wave is absent. From an electrochemical viewpoint, In(III) should behave similarly to the first-row transition metals for which electron transfer from the electrode to the metallic ion occurs through a ligand bridge (17–19). In this respect, the water molecule is not a good bridge for electron transfer. The reduction wave of indium(III) at the dropping mercury electrode is irreversible and very much drawn out in strongly acidified noncomplexing aqueous media such as $NaNO_3$ or $NaClO_4$. The presence of a small amount of certain ligands accelerates the electroreduction of the metallic ion, resulting in the appearance of the polarographic wave. According to data from Table 1, In(III) is electroactive in acidic medium containing chloride ions, where chloro-complex species are formed. The presence of the polarographic wave for In(III) is also observed in acidic HN_3 solutions. This wave can be attributed to the reduction of an In(III)/azide species, which is formed in this acidic medium despite the relatively low pK_a value for the dissociation constant of HN_3 ($K_a = 2.4 \times 10^{-5}$ M) (20).

Complexation processes involve more stable chemical species that require a more negative potential for reduction to occur. Normally a shift of the polarographic wave toward more negative potentials is observed. In the system considered in the present comunication, when a small amount (less than 1 mM) of azide is present in solution, the complexation with indium(III) begins to occur and the polarographic wave appears. Further additions of azide shift the polarographic wave to the expected negative potential side, making studies on the complexing effect possible.

Characterization of the electrode process

To obtain information about the nature of the electrode process, a study involving the variation of the mercury column height was made. The classical relation between the dc polarographic current (along different regions on the wave) and the square root of the height of the mercury column is the origin of the group of straight lines presented in Fig. 2. The linear response shown in this figure, for different potentials picked out along the polarographic wave, gives evidence that the electrode process is controlled by diffusion. In more negative potentials of the limiting region, a minimum appears (between −1.0 and −1.4 V), and in this potential range the current is almost independent of the height of the mercury column. Preliminary studies showed that the deepest current region was achieved at 2.0 M NaN_3, and microscopic observation around the mercury drop showed an upward movement of the solution at −1.2 V. Gas evolution was also observed. The addition of 0.002% Triton X-100 stopped the movement, but the polarographic minimum was still there. Further studies on this subject were not carried out.

Fig. 2. Dependence of dc polarographic current on different heights of the mercury column for a solution containing 1.578 mM In(III) + 0.50 M N_3^- + 0.020 M HN_3, (I = 2.0 M). The currents were measured at different potentials along the polarographic waves: ● −0.850 V (limiting region); ○ −0.760 V ($E_{3/4}$); Δ −0.750 V ($E_{1/2}$); Δ −0.740 V ($E_{1/4}$).

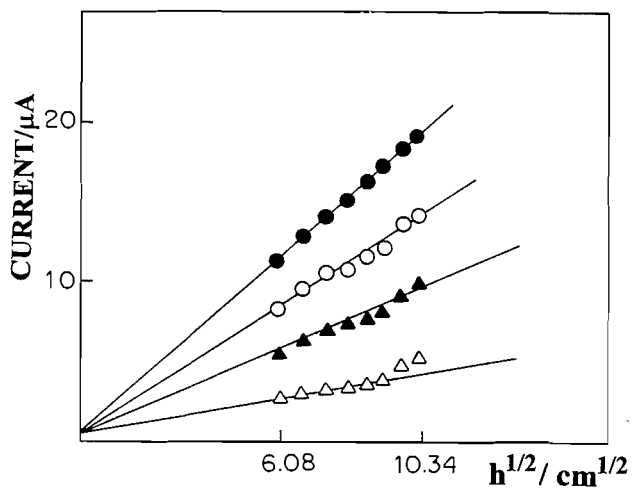

Figure 3 shows the dependence of the normal pulse polarographic current along the wave on the square root of reciprocal pulse widths. A family of straight lines was obtained, demon-

Can. J. Chem. Downloaded from www.nrcresearchpress.com by 65.111.164.53 on 09/08/12
For personal use only.

Can. J. Chem. Downloaded from www.nrcresearchpress.com by 65.111.164.53 on 09/08/12
For personal use only.

Fig. 3. Dependence of the current on $t_m^{-1/2}$ (t_m = measuring time), the current values being measured at different potentials along the normal-pulse polarograms. Working solution: 0.7892 mM In(III) + 0.1 M N_3^- + 0.020 M HN_3 (I = 2.0 M).

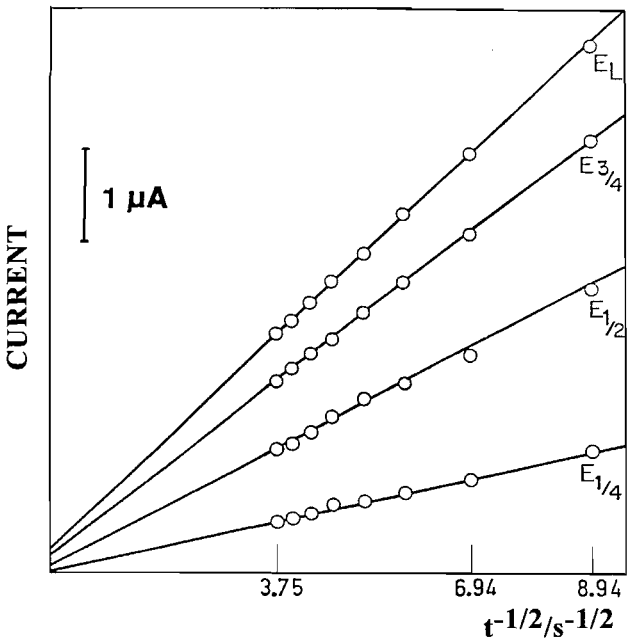

Fig. 4. Normal- and reverse-pulse polarograms of 0.7892 mM In(III) + 0.10 M N_3^- + 0.10 M HN_3 solution (I = 2.0 M). The initial potentials (E_i) for both scans are indicated .

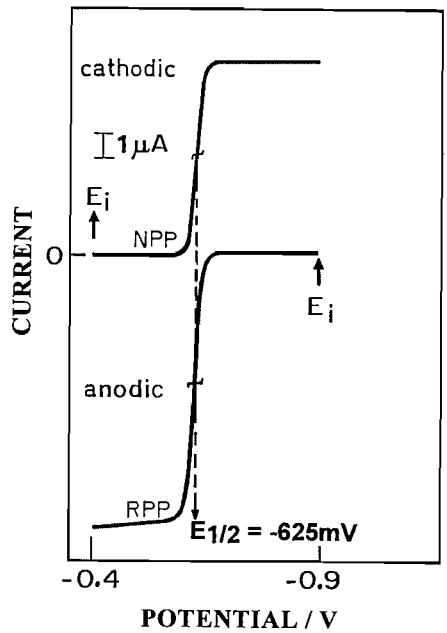

strating that the process is primarily governed by diffusion. The intercepts (up to 8% of the full scale) apparently are not a simple instrumental artifact or due to the back pressure, since previous calibration tests using a known reversible system (iron(III) in saturated ammonium oxalate medium) led to an intercept of only 1–2%. Another means of characterizing the reversibility of an electrode process consists in the comparison of the normal- and reverse-pulse polarographic waves (21–23). The coincidence of $E_{1/2}$ values obtained for the present system in these two runs and the ratio between the cathodic and anodic currents being close to the unity are unequivocal proof of the reversibility of the process. Figure 4 shows the normal- and the reverse-pulse polarograms. The larger anodic current in comparison to the cathodic current can be explained in the light of Galvez's expanding spherical electrode theory (24). Two additional pieces of evidence support of the reversibility of In(III) electroreduction when azide ions are present in solution: (*i*) The tast polarogram run with a 2.0 mM indium amalgam dropping electrode in a solution containing 0.5 M sodium azide and 1.5 mM indium (III) showed a combined wave with the same $E_{1/2}$ value (−680 ± 5 mV) as one obtained with a mercury dropping electrode in a 1.5 mM indium(III) + 0.5 M azide solution. (*ii*) Finally, the dependence of the polarographic current (tast mode) along the wave on the fifth root of the drop time, which varied from 0.4 to 6.0 s, was linear, indicating that the process is predominantly controlled by diffusion transport (25).

The experimental results agree with the study of Moussa et al. (26), in which $k_s = 5.3 \times 10^{-2}$ cm s^{-1} was found for the exchange $In^{3+} + 3\ e^- \rightleftharpoons In(Hg)$ in azide medium, showing that the electron transfer is not the determining step for the electroreduction of In(III) in the complexing medium.

Determination of n and $E_{1/2}$

Since electrochemical reversibility was proven for the In(III)/N_3^- system, the reversible polarographic equation was used to calculate the characteristic parameters n and $E_{1/2}$. These values are presented in Table 2, and were obtained in azide/hydrazoic acid buffers. In all the experiments, the analytical concentrations of the two components (of the buffers) were calculated to maintain the pH around 3, thus hindering the hydrolysis of indium(III). The $E_{1/2}$ values (included in Table 2) changed with the variation of azide concentration, as predicted, and the n value was always slightly smaller than 3.

Coulometric studies

The value of n previously found in polarographic experiments was lower than 3, therefore controlled potential coulometry studies were carried out in the indium(III)/azide system. During electrolysis, the concentration of the remaining electroactive species was monitored by polarographic measurements. A plot of the limiting current against the charge applied, extrapolated to the zero current, yielded experimental values of both Q and n. Several experiments were performed using 0.8 and 1.5 mM In(III) solutions in 0.1 M N_3^- + $x$$HN_3$ buffers, where x was varied from 0.006 to 0.1 M. Potential was applied at the plateau of the polarographic waves. The graphical extrapolation of the data obtained in these experiments provided an n value of 3.5, which increased gradually by increasing the HN_3 concentration in the buffer. The experimental data led to the conclusion that indium(III) is chemically regenerated from the amalgam, due to the oxidative characteristics of hydrazoic acid. This statement was experimentally proven through the detection of ammonium ions in the electrolyzed solutions, as a product of the chemical step reduction of hydrazoic acid. Further coulometric experiments at controlled potential (−0.9 V) in the Cd(II) + 0.1 M N_3^- + 0.05 M HN_3 solution reinforced the

Table 2. Half-wave potential and limiting current data from the polarograms recorded for 0.7890 mM In(III) solutions in different azide/hydrazoic acid buffers (I = 2.0 M maintained with $NaClO_4$). The n values were calculated from the reversible polarographic equation.

$C_{N_3^-}$-(mM)	C_{HN_3}(mM)	pH for buffer without In^{3+}	pH for buffer with In^{3+}	$-E_{1/2}$/(mV)	i_d/(μA)	n
0	20[a]	1.68	1.58	No wave	—	—
0	20	2.32	2.12	512.1	8.30	2.62
1	20	2.47	2.70	519.6	8.81	2.71
2	40	3.40	2.80	526.3	9.11	2.64
3	60	3.00	2.86	538.7	8.87	2.71
4	80	2.96	2.87	540.7	9.15	2.61
6	120	3.15	3.07	558.7	9.15	2.71
7	140	3.10	3.03	560.1	9.19	2.73
8	160	3.01	2.85	555.2	9.31	2.73
9	180	3.00	2.95	562.5	9.11	2.68
10	200	2.95	2.88	560.0	9.11	2.72
12	240	3.21	3.12	581.1	9.44	2.83
14	280	3.13	3.00	571.1	9.27	2.70
16	320	3.05	2.96	578.5	9.27	2.72
18	360	3.04	2.96	581.9	9.27	2.73
20	400	2.98	2.85	582.1	9.31	2.73

[a]$HClO_4$ (5 mM) was added to restrain the dissociation of HN_3.

oxidizing power of HN_3, since the n values obtained were also larger than the expected value (n = 2). Regarding this subject, the formation of ammonium as a HN_3 reduction product has been reported in other electrochemical systems such as Co(II)/HN_3 (3) and Mo(VI)/HN_3 (27).

Table 1 shows that a small polarographic wave appears in the In(III) + 0.001 M $HClO_4$ system in $NaClO_4$ medium. Coulometric experiments were carried out under these experimental conditions. After the application of 10% of the total charge required for exhaustive electroreduction of In(III), the polarogram of the remaining solution showed a higher limiting current than the initial solution. The explanation for this interesting observation could be related to a pH increasing during the electrolysis, since the electroreduction of the $In(OH)_2^+$ species gives rise to displacement of two hydroxide ions. Further, parallel oxidation of the indium amalgam by protons is probably going to occur, contributing to the rise in pH. The equilibrium concentration of the $In(OH)_2^+$ species can be increased after the partial electrolysis in this less acidic medium. According to Fig. 1, the polarographic limiting current depends on the concentration of this species (predominating at pH around 4). Therefore, the current is higher than that obtained for the starting solution (pH around 3), despite the decrease of the analytical concentration of In(III) due to partial electrolysis.

Determination of the stability constants of the complexes

Azide acts as a catalytic ligand under polarographic conditions in which In(III) is electroactive (12). When the azide concentration increases, the half-wave potential shifts to the more negative side, this displacement being due to the complexing effect (Table 2) . The validity of the determination of stability constants by polarography is questionable if certain requirements are not satisfied (28). In our case, the indium(III)/azide complexes are electroactive, the reduction at the electrode is controlled by diffusion, and the complexes are labile (29). Experimental ac polarograms showed no adsorption of complex species at potentials less negative than $E_{1/2}$ and a similar behavior was previously reported for the In(III)/SCN^- system (30). In addition, experiments using different drop times generated polarograms with the same $E_{1/2}$, confirming the absence of coupled chemical reactions and the predominance of diffusive behavior. The kinetic contribution, significant in the coulometric studies, is less critical for the polarographic experiments, as Table 2 demonstrates. Such complicating steps should be fast enough for the overall electrode process to be governed by diffusion. In this way, the study of complex formation could be performed by polarography (31).

To confirm the absence of polynuclear complexes, polarograms in the presence of three different concentrations of indium(III) (0.789 mM, 1.578 mM, and 4.000 mM) in 0.480 M NaN_3 + 0.020 M HN_3 (I = 2.0 M) were recorded and the same $E_{1/2} = -679 \pm 3$ mV was found. This constant value of the half-wave potential shows the formation of only mononuclear species, as was also verified in previous potentiometric studies (14).

Studies of complex formation require knowledge of the conditional potential of the couple In(III)/In in the absence of the ligand, at a given ionic strength. Preliminary studies were carried out to determine this formal potential taking into account some literature information: indium amalgam is sensitive to In^{3+} aquo ions (32, 33); the exact determination of the potential of the reversible couple is difficult due to the reaction between metallic indium and In(III) ions, producing unstable In(I) ions ($K = 1.3 \times 10^{-11}$ M^2) that affect the equilibrium potential (34); In(I) is easily oxidized by protons (35); finally, measurements of the potential in non-acidic or weakly acidic solutions can be affected by the hydrolysis of In(III) (36). Preliminary measurements of the standard potential were carried out using an indium amalgam dropping electrode (~1% w/w), in In(III) solutions. In spite of the relatively good stability of the potentiometric measurements, the standard potential cal-

Can. J. Chem. Downloaded from www.nrcresearchpress.com by 65.111.164.53 on 09/08/12
For personal use only.

Can. J. Chem. Downloaded from www.nrcresearchpress.com by 65.111.164.53 on 09/08/12
For personal use only.

culated for different concentrations of metallic ion in these solutions was not constant, probably due to the oxidation of the amalgam. Three series of measurements afforded the following values: $E^{0'} = -464.6$ mV, $E^{0'} = -494.1$ mV, and $E^{0'} = -503.6$ mV.

The evaluation of the conditional potential of the In(III)/In couple was made using data for the dependence of the half-wave potential of the polarograms on the analytical concentration of azide, two sets of experimental measurements being obtained. The azide concentration in the solution was evaluated taking into account the azide resulting from dissociation of the hydrazoic acid. The experimental data were plotted and the curve smoothed. Extrapolation to zero azide concentration led to $E^{0'} = -(512.0 \pm 0.5)$ mV. Using this value and the experimental data for $E_{1/2}$, the corresponding values of $F_0(L)$ (Leden's function (37)) were calculated for each analytical concentration of the ligand, L.

$$[1] \quad F_0(L) = \text{antilog}\left(\frac{E_{1/2(L)} - E^{0'}}{0.01972}\right)$$

A nonlinear regression algorithm (38–40) was employed to calculate in an iterative form the stability constants of the complexes from the following equation:

$$[2] \quad F_0(L) = 1 + \beta_1[L] + \beta_2[L]^2 + \ldots + \beta_n[L]^n$$

where β_i corresponds to a global constant for species ML_i and n is the maximum number of species formed.

In a first step, the global constants were calculated by considering the concentration of azide ions as equal to the total concentration of this pseudo-halide in the cell. A first group of stability constants was obtained and used to subtract the amount of azide consumed in the complexation, using Bjerrum's function (41). With the new concentrations of azide ions, a new set of constants was determined. The process was repeated until the equilibrium concentration of the constituents of the system remained unchanged, thus yielding the required equilibrium concentrations.

The plot of the dependence of $E_{1/2}$ values on the equilibrium concentrations of azide is shown in Fig. 5. After a magnification of the scale, the extrapolation to the zero equilibrium concentration yielded $E^{0'} = -(512.2 \pm 0.5)$ mV. This value agrees with that obtained using a computational method of data analysis ($E^{0'} = -511.4$ mV), in which a polynomial regression was employed. With the $F_0(L)$ data, calculated for different azide equilibrium concentrations, the following group of four successive stability constants was found:

$$\beta_1 = 3.7 \times 10^3 \text{ M}^{-1}$$
$$\beta_2 = 8.6 \times 10^5 \text{ M}^{-2}$$
$$\beta_3 = 5.0 \times 10^7 \text{ M}^{-3}$$
$$\beta_4 = 2.1 \times 10^9 \text{ M}^{-4}$$

To evaluate the effect of the error in the determination of the value for the formal potential of the In(III)/In system (due to the graphic extrapolation), a variation of 1 mV was ascribed to the $E^{0'}$. The two new groups of β found were in agreement with the first group of constants, the maximum deviation being 25% for β_1.

Fig. 5. Dependence of the half-wave potential for the 7.892×10^{-4} M indium(III) polarograms on azide equilibrium concentrations.

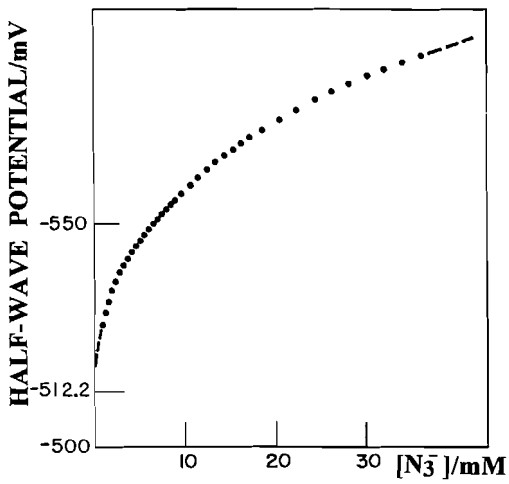

Fig. 6. Distribution diagram for the In(III) and the azide species as a function of free azide concentration.

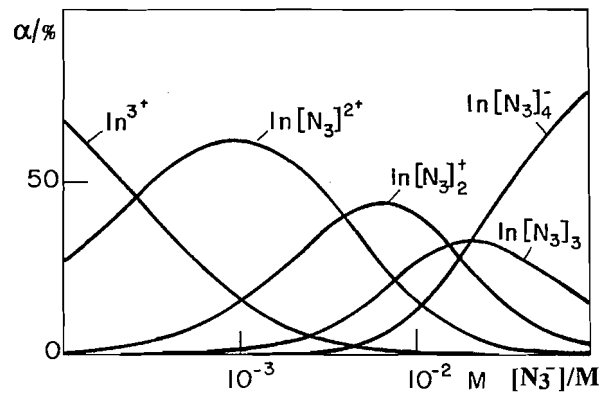

The distribution curve of the complex species, shown in Fig. 6, was calculated using the set of constants presented above ($E^{0'} = -512.2$ mV). The formation of tetra-coordinated species was confirmed according to the following equation, considering the range of concentration up to 100 mM in azide:

$$[3] \quad \frac{\Delta E_{1/2}}{\Delta \log [N_3^-]} = p \times \frac{0.05916}{n}$$

where p corresponds to the coordination number and n to the number of electrons involved in the In(III) reduction.

The formation of mono-azide indium(III) species in solutions containing only hydrazoic acid is favored more than the hydrolysis reaction of the metallic ion, where a mono-hydroxy species could be formed. This assertion is proved considering the equilibria involving the species:

$$HN_3 + In^{3+} \rightleftharpoons In(N_3)^{2+} + H^+ \qquad (\beta_1 . K_{HN_3})$$
$$In(OH)^{2+} + H^+ \rightleftharpoons In^{3}+ + H_2O \qquad (1/K_w . 1/K_{hl})$$
$$In(OH)^{2+} + HN_3 \rightleftharpoons In(N_3)^{2+} + H_2O$$

Table 3. Formal potential data for the In(III)/In couple in different media as reported in the literature.

$-E^{0'}$(V)	Experimental conditions	References
0.511	vs. SCE, I = 1.0 M KNO_3 (30°C)	16
0.485[a]	I = 2.0 M $NaClO_4$	44
0.4833[a]	vs. SCE, I = (1.98 M $NaClO_4$ + 0.02 M $HClO_4$) (30°C)	45
0.5138	vs. SCE, I = 2.0 M (25°C)	46
0.531[b]	vs. SCE, I = 0.1 M KNO_3	47
0.4833[b]	vs. SCE, I = (1.9 M $NaClO_4$ + 0.1 M $HClO_4$) (30°C)	48
0.516[c]	vs. SCE, I = 2.0 M $NaClO_4$ (25°C)	14
0.521[d]	vs. Ag/AgCl (0.025 M NaCl), I = 1.0 M $NaClO_4$ (25°C)	49
0.474	vs. SCE, I = 4.0 M $NaClO_4$	50
0.44	vs. Ag/AgCl (5.0 M NaCl), I = 3.0 M $NaClO_4$ (30°C)	51
0.717[e]	vs. SCE, I = 1.0 M KSCN	52
0.4977[f]	vs. SCE (NaCl), I = 2.0 M $NaClO_4$ (25°C)	53
0.5142[g]	vs. SCE (NaCl), I = 2.0 M $NaClO_4$ (25°C) (SCN^-)	53
0.5043[g]	vs. SCE (NaCl), I = 2.0 M $NaClO_4$ (25°C) (Br^-)	53
0.5122	vs. SCE, I = 2.0 M $NaClO_4$ (25°C)	Present work

[a]Values discussed by Lawson and Aikens (16)

[b]Values discussed by Narusawa et al. (46)

[c]Estimated $E^{0'}$ value using the global constants obtained by the authors (14) and the present experimental data.

[d]Estimated $E^{0'}$ value using the global constants obtained by the authors of ref. 49 and the present experimental data, without the proper correction for the reference electrode used.

[e]Value corresponding to $E_{1/2}$ in a solution with the ionic strength maintained with KSCN as discussed by Kondziela and Biernat (50).

[f]Values calculated from graphical extrapolation of potentials measured after additions of bromide, according to ref. 53.

[g]Values recalculated for $E^{0'}$ using the experimental data (Tables II and IV from ref. 53) and our polynomial regression program.

Can. J. Chem. Downloaded from www.nrcresearchpress.com by 65.111.164.53 on 09/08/12
For personal use only.

where β_1 corresponds to the global constant for the mono-azide indium(III) complex, K_{HN_3} the dissociation constant of hydrazoic acid, K_w the dissociation constant of water, and K_{h1} the hydrolysis constant for the mono-hydroxy complex of indium(III).

Using data from the literature (15) and the value for β_1 found in this paper, the global constant for the equilibrium between the hydroxo and azide indium(III) species is 116 M^{-1}. Thus, it is concluded that in the equilibria relating to this study, formation of the hydroxo indium(III) species can be disregarded in the N_3^-/HN_3 buffers. The existence of mixed species at low azide concentrations was not taken into account, since the kinetics of the hydrolysis reaction is slow and the $E_{1/2}$ value for each addition of ligand was reproducible. In addition, when the metallic ion is complexed with azide, the probability of formation of hydroxo complexes is even smaller.

In the formation of complexes, numerous parameters are involved, but those that generally predominate are both the statistical and the ligand effects (41). This latter is the sum of the electrostatic factor and a remaining portion called the "rest effect," which consolidates all the other effects. When the rest effect is negligible, the ligand effect can be represented by the electrostatic factor. The work that must be realized by moving an electrically charged ligand from ML_i to ML_{i+1} represents this factor. The stepwise constants ($K_i = \beta_i/\beta_{i+1}$) of the present system are

$$K_1 = 3.7 \times 10^3\ M^{-1}$$
$$K_2 = 2.3 \times 10^2\ M^{-1}$$
$$K_3 = 5.9 \times 10^1\ M^{-1}$$
$$K_4 = 4.2 \times 10^1\ M^{-1}$$

and they agree with the statistical model for successive complex formation, since $K_i/K_{i+1} > 1$ for $i = 1, 2$, and 3. The importance of the ligand effect can be estimated using eq. [4], proposed by Bjerrum (42) and discussed by Sen (43):

$$[4] \quad \frac{K_i}{K_{i+1}} = \left[\frac{(n - i + 1)(i + 1)}{(n - i)i}\right]x^2$$

where n and i correspond, respectively, to the coordination number and the number of ligands coordinated to metal. When the influence of electrostatic forces in complexation reactions is negligible, the x values according to eq. [4] are unity. However, the calculation of x for $i = 1$, 2, and 3 in the indium(III)/azide system leads, respectively, to 2.44, 1.31, and 0.72. In this way, the contribution of the electrostatic factor in the formation of complexes between In(III) and N_3^- ions cannot be disregarded.

Diffusion coefficient of the complexes

The mean diffusion coefficient of the complexes for the

indium(III)/azide system was calculated using the Ilkovic equation. Polarograms of 0.789 mM indium(III) were recorded over the entire range of azide concentration (0–100 mM), and the height of the waves was used to calculate the corresponding diffusion coefficient assuming $n = 3$. A value of $(6.1 \pm 0.2) \times 10^{-6}$ cm^2 s^{-1} was obtained, and it is in agreement with the value reported in a previous paper (30) for the indium (III)/thiocyanate system.

Conclusions

Analysis of the observed evidence confirms a predominantly diffusion-controlled process on the electrode along the entire wave, as well as in the limiting region, for the electroreduction of In(III) in complexing azide medium. A kinetic contribution was also verified. In the potentials corresponding to the so-called "polarographic minimum," the process is no longer governed predominantly by diffusion.

The determination of the formal potential, $E^{0'}$, for the In(III)/azide system led to the value −512.2 mV, obtained by graphical extrapolation to a condition where the azide was absent. This $E^{0'}$ agrees fairly well with the values from Lawson and Aikens (16) and Naruzawa et al. (46). Good results are also obtained by calculation of this formal potential using the global constants for the system, determined by Bertotti and Tokoro (14), Avsar (49), and Momoki and Ogawa (53) (see Table 3).

Computational analysis of the experimental polarographic data obtained in the present study showed that in this system four successive complexes of indium(III)/azide are formed when the ligand concentration is increased up to 100 mM. This concentration of ligand is sufficiently high to cover the whole range in which the four complexes are formed. The values of the global constants obtained agree with those reported in the literature where other techniques than polarography are described.

The polarographic data also allow the evaluation of the mean diffusion coefficient of the In(III)/azide complexes. The value found is in agreement with the diffusion coefficient for the thiocyanate complex of In(III), reinforcing the evidence regarding the similarity between the azide and thiocyanate pseudo halides.

Acknowledgements

The authors are grateful to the Conselho Nacional de Pesquisa (CNPq) and the Fundação de Amparo à Pesquisa do Estado de São Paulo (FAPESP) for financial support. We also thank Professor Paschoal Senise for reading this manuscript.

References

1. P. Senise. J. Am. Chem. Soc. **81**, 4196 (1959).
2. P. Senise and E.F.A. Neves. J. Am. Chem. Soc. **83**, 4146 (1961).
3. R. Tokoro and E.F.A. Neves. J. Electroanal. Chem. **125**, 115 (1981).
4. T. Takahashi and H. Shirai. Rep. Inst. Ind. Sci. Univ. Tokyo, **10**, 10 (1961).
5. P. Sakellaridis. C.R. Seances Acad. Sci. Ser. C, **255**, 127 (1962).
6. N. Tanaka, T. Takeuchi, and R. Tamamushi. Bull. Chem. Soc. Jpn. **37**, 1435 (1964).
7. A.J. Engel, J. Lawson, and D.A. Aikens. Anal. Chem. **37**, 203 (1965).
8. M. Sluyters-Rehbach, B. Timmer, and J.H. Sluyters. Z. Phys. Chem. **52**, 89 (1967).
9. M.A. Loshkarev and A.A. Kazarov. Sov. Electrochem. (Engl. Transl.), **3**, 31 (1967).
10. R. de Levie and A. A. Husovsky. J. Electroanal. Chem. **22**, 29 (1969).
11. L. Pospisil and R. de Levie. J. Electroanal. Chem. **25**, 245 (1970).
12. O.E. Ruvinskii and Ya. I. Tur'yan. J. Anal. Chem. USSR (Engl. Transl.), **31**, 460 (1976).
13. E.F.A. Neves and T.V. Silva. Simp. Bras. Eletroquim. Eletroanal. An. 4th, 63 (1984).
14. M. Bertotti and R. Tokoro. Talanta, **36**, 424 (1989).
15. E.A. Biryuk, V.A. Nazarenko, and R.V. Ravitskaya. IUPAC Chem. Data Ser. no. 21. Pergamon Press, Oxford. 1982. p. 47.
16. J.G. Lawson and D.A. Aikens. J. Electroanal. Chem. **15**, 193 (1967).
17. W. Beck and W.P. Fehlhammer. MTP Int. Rev. Sci.: Inorg. Chem. Ser. One, **2**, 253 (1972).
18. F.C. Anson. Acc. Chem. Res. **8**, 400 (1975).
19. A.J. Motheo, E.R. Gonzalez, and L.A. Avaca. Can. J. Chem. **64**, 413 (1986).
20. E.F.A. Neves, R. Tokoro, and M.E.V. Suarez. J. Chem. Res. Miniprint, 401 (1979); J. Chem. Res. Synop. 376 (1979).
21. K.B. Oldham and E.P. Parry. Anal. Chem. **42**, 229 (1970).
22. I. Ruzic. J. Electroanal. Chem. **75**, 25 (1977).
23. J. Osteryoung and E. Kirowa-Eisner. Anal. Chem. **52**, 62 (1980).
24. J. Galvez. Anal. Chem. **57**, 585 (1985).
25. A.A. Vlcek. Prog. Inorg. Chem. **5**, 211 (1963).
26. A.A. Moussa, M.M. Abou. Romia, and F. El-Taib Heakal. Eletrochim. Acta, **15**, 1391 (1970).
27. M. Bertotti and R. Tokoro. J. Electroanal. Chem. **377**, 287 (1994).
28. A.M. Bond and G. Hefter. J. Electroanal. Chem. **31**, 477 (1971).
29. H. Taube. Chem. Rev. **50**, 69 (1952).
30. B. Timmer, M. Sluyters-Rehbach, and J.H. Sluyters. J. Electroanal. Chem. **15**, 343 (1967).
31. M. Sluyters-Rehbach and J.H. Sluyters. J. Electroanal. Chem. **39**, 339 (1972).
32. N. Sunden. Z. Elektrochem. **57**, 100 (1953).
33. J.N. Butler. J. Phys. Chem. **68**, 1828 (1964).
34. V.V. Losev and A.P. Pchel'nikov. Sov. Electrochem. (Engl. Transl.), **4**, 230 (1968).
35. R.E. Visco. J. Phys. Chem. **69**, 202 (1965).
36. R. Piercy and N.A. Hampson. J. Appl. Electrochem. **5**, 1 (1975).
37. I. Leden. Z. Phys. Chem. **188**, 160 (1941).
38. J. Rydberg. Acta Chem. Scand. **15**, 1723 (1961).
39. W.E. Wentworth. J. Chem. Educ. **42**, 96 (1965).
40. G. Boratto. Basic para Cientistas e Engenheiros. Livros Técnicos e Científicos, Rio de Janeiro. 1984. p. 109.
41. N. Bjerrum. Z. Anorg. Allg. Chem. **119**, 179 (1921).

Can. J. Chem. Downloaded from www.nrcresearchpress.com by 65.111.164.53 on 09/08/12
For personal use only.

42. J. Bjerrum. Metal ammine formation in aqueous solution. P. Haase & Son, Copenhagen. 1987.
43. B. Sen. Anal. Chim. Acta, **27**, 515 (1962).
44. D. Cozzi and S. Vivarelli. Z. Elektrochem. **58**, 907 (1954).
45. N. Sunden. Sven. Kem. Tidskr. **66**, 20 (1954).
46. Y. Narusawa, J. Hashimoto, and H. Hamagushi. Bull. Chem. Soc. Jpn. **38,** 234 (1965).
47. E.D. Moorhead and W.M. MacNevin. Anal. Chem. **34**, 269 (1962).
48. T.P. Radhakrishnan and A.K. Sundaram. J. Electroanal. Chem. **5**, 124 (1963).
49. E. Avsar. Acta Chem. Scand. Ser. A: **A36**, 627 (1982).
50. P. Kondziela and J. Biernat. J. Electroanal Chem. **61**, 281 (1975).
51. A.M. Bond. J. Electrochem. Soc. **119**, 1503 (1972).
52. J.W. Grenier and L. Meites. Anal. Chim. Acta, **14**, 482 (1956).
53. K. Momoki and H. Ogawa. Anal. Chem. **43**, 1664 (1971).

Can. J. Chem. Downloaded from www.nrcresearchpress.com by 65.111.164.53 on 09/08/12
For personal use only.

A detailed shape characterization of regular polypeptide conformations

Gustavo A. Arteca

Abstract: Regular polypeptide conformations include secondary structural motifs such as α-helices and β-strands. The occurrence of some regular conformation is usually deduced from a local analysis of dihedral angles. However, the value of a dihedral angle in itself does not provide any information on the conformation's "shape." This drawback can be circumvented with global, rather than local, macromolecular shape descriptors. Recently, fractal exponents have been proposed as a source of such descriptors. Yet, this approach does not fully capture all essential shape features, since protein backbones are *not* fractal. In this work, we deal instead with a more "natural" characterization of the polymer's global shape that uses both the chain's geometry and "topology." For the geometry, we study the behaviour of molecular size and anisometry. For the chain's folding features, we study the self-entanglements in a polymer fold. We compute these descriptors for all relevant secondary structural motifs. By using self-entaglements and molecular geometry, we provide a view of secondary structure that is both conceptually appealing and also more discriminating than previous ones in the literature.

Key words: molecular shape analysis, protein secondary structure, self-entanglements.

Résumé : Les conformations régulières des polypeptides incluent des motifs de structure secondaire connus comme «hélices α» et «filaments β». Ces conformations sont souvent deduites à partir d'une analyse locale des angles dihédriques. Cependant, la valeur d'un angle dihédrique par elle-même ne donne aucune information sur la forme d'une conformation. Ce problème peut être éliminé si l'on emploie des descripteurs globaux, au lieu de locaux. Récemment, les exposants fractaux ont été introduits à ce propos. Mais cette méthode ne décrit pas bien la forme, car les protéines ne sont pas rigoureusement fractales. Nous suivons ici une voie plus «naturelle», qui utilise la géométrie et la «topologie» de la chaîne polymérique. Pour la description de la forme géométrique, nous étudions la taille et l'anisométrie moléculaires. Pour les caractéristiques des pliements, nous calculons la complexité des enchevêtrements d'une polymère. Tous ces descripteurs sont calculés pour les motifs les plus importants de la structure secondaire. En étudiant les enchevêtrements et la géométrie moléculaire, nous obtenons une description des structures secondaires, laquelle est au même temps intéressant du point de vue conceptuel et aussi plus discriminatoire que d'autres proposées dans la littérature.

Mots clés : analyse de forme moléculaire, structure secondaire des protéines, enchevêtrements.

Can. J. Chem. Downloaded from www.nrcresearchpress.com by 65.111.164.53 on 09/08/12
For personal use only.

Introduction

Native protein conformations exhibit well-known hierarchical levels of spatial organization, from primary to tertiary structure (1). On a large scale, a peptide conformation often exhibits entire arrays of atoms that rigidly maintain their spatial positions relative to one another (2, 3). These well-organized, stable ensembles are known as supersecondary structures. These structures are a key element in understanding protein stability and function. Despite the variety of primary sequences, the number of supersecondary structures appears to be limited (4, 5). This observation sustains the modern viewpoint that polypeptide chains with variable composition are "naturally selected" on the basis of their capability to achieve rapidly some specific structural features (6). That is, structural features would appear to be preserved with priority over primary sequences. For this reason, our ability to characterize and recognize the occurrence of specific protein folds has become a central issue in structural biology (7). A number of computational techniques have been developed to classify such features and compare protein architectures. (For reviews on recent work, see refs. 7 and 8.) Yet, there is still a need for efficient methods that account for all relevant aspects of macromolecular shape. In this work we deal with this latter task.

Regular polypeptide conformations correspond to relatively short, periodic three-dimensional (3D) arrays of amino acid residues stabilized by hydrogen bonding. These include the familiar *secondary structural motifs*, such as α-helices and β-strands (9). Other structures do occur, although less frequently (1, 10). These latter include polyglycine and polyproline helical strands, and other types of helices, such as the 3_{10}-helix. The organization of these secondary motifs in specific spatial arrays relative to each other defines the supersecondary structure. In this work, we deal with a novel, detailed characterization of global molecular shape in all the regular conformations that make up a protein's secondary structure.

The occurrence of regular conformations within a protein structure is usually deduced from a *local* analysis of dihedral angles (1, 11). The values of such angles depend on the

Received August 26, 1994.

G.A. Arteca. Département de chimie et biochimie, Laurentian University, Ramsey Lake Road, Sudbury, ON P3E 2C6, Canada.

Can. J. Chem. Downloaded from www.nrcresearchpress.com by 65.111.164.53 on 09/08/12
For personal use only.

peptide's composition and they vary with local deformations in the motifs. Moreover, the value of a dihedral angle is simply a "label" for a regular conformation. By itself, it does not provide any information on shape or folding features. This latter information can, of course, be retrieved by visually inspecting the molecular backbone on a computer screen. However, any efficient, unbiased analysis will require the use of mathematical tools to quantify molecular shape. The use of *global*, rather than local, descriptors can circumvent the above drawbacks. This is the point of view we adopt in this work.

There are a number of possible global, single-number descriptors that convey aspects of molecular shape. The most obvious are descriptors of molecular size, such as the radius of gyration (12). These parameters depend only on the molecular geometry. They make no explicit use of the sequence in which the atoms are connected (from now on referred to as the "molecular connectivity"). A detailed characterization of molecular shape must incorporate both pieces of information within appropriate global descriptors.

Recently, fractal theory (13) has been used to provide this type of descriptor (14–17). The fractal dimension of a curve is related to some of its some essential shape features. In the case of a protein backbone with n residues, a "fractal exponent" D can be defined from the following scaling relationship (14, 15):

$$[1] \qquad L(m) \sim m^{1-D}$$

where $L(m)$ is the length of the backbone measured with the "scale" of $m \leq n$ residues. When $m = 1$ we find the actual length of the backbone as a sequence of straight-line segments joining the α-carbons. When $m = n$, we find the end-to-end distance of the backbone. In actual fractal curves (i.e., those exhibiting *self-similarity* at each scale considered (13)), the slope in a graph of ln $L(m)$ vs. ln m will provide the fractal dimension D. However, protein backbones are *not* self-similar and the relation between ln L and ln m is poorly linear (15, 16). Therefore D is only an *apparent, approximate* exponent somewhat related to the protein's shape features. Moreover, as shown in ref. 16, the results for D depend strongly on the method used for its computation, and alternative definitions of fractal exponents provide different results (17). Despite these deficiencies, the fractal exponents derived in ref. 16 distinguish between some secondary structural motifs. Strands in β-sheets appear as one-dimensional objects ($D \approx 1.07 \pm 0.05$), whereas α-helices have larger mean fractal exponents ($D \approx 1.4 \pm 0.1$) (16). The discriminating power of these global descriptors is limited, however, by the fact that a self-avoiding random walk in 3D space also has dimensionality $D = 1.4$ (17). Clearly, there is a need for other types of shape descriptors, which, while using the same type of input information, provide a more meaningful characterization of secondary structure.

In this work, we deal with a more natural characterization of the polymer's global shape that also uses its molecular geometry and chain topology. Regarding the chain's folding features, we employ a new approach to studying self-entanglements in a polymer (18, 19). The method, based on the probability of observing double-points ("crossings") in all possible two-dimensional projections of a molecular backbone, measures quantitatively the nature of the polymer fold. In this work, we compute this descriptor for all relevant secondary structural motifs in polypeptides. Its behaviour in terms of number of residues is also determined. The analysis is complemented by comparing the description of self-entanglements with that provided by purely geometrical descriptors. In addition to the familiar radius of gyration, we present here for the first time a characterization of secondary structure in terms of asphericity. By using a joint description of self-entanglements and molecular geometry, we provide a new and concise classification of secondary structure.

The organization is as follows. The next two sections briefly discuss the geometric definition of the secondary structures and the nature of the shape description. The detailed shape characterization is given in a following section. The interpretation of the results and their value for recognition of protein folding features are discussed at the end.

Regular polypeptide conformations

Regular conformations of secondary structural motifs are specified by a single set of Ramachandran dihedral angles φ, ψ, and ω defined from the protein backbone (11). These are model conformations. Actual protein secondary structure may deviate from these ideal angles, while maintaining their overall shape.

Seven secondary structures are studied in this work. Three of them are helices: the (right-handed) α-helix, the 3_{10}-helix, and the π-helix. Two structures are "helicoidal strands," known as polyglycine II and polyproline II conformations. Finally, we consider pure strands, namely, those found in parallel and antiparallel β-sheets.

For all the motifs considered here, the amino acids are found in *trans* conformations. (Otherwise stated, we have $\omega = 180°$.) The following pairs of dihedral angles (ϕ, ψ) define the motifs (1): (*a*) the α-helix: (−58°, −47°); (*b*) the 3_{10}-helix: (−49°, −26°); (*c*) the π-helix: (−57°, −70°); (*d*) the polyglycine II "helical strand": (−80°, 150°); (*e*) the polyproline II "helical strand": (−78°, 149°); (*f*) the strand for an antiparallel β-sheet: (−139°, 135°) (and $\omega = -178°$); (*g*) the strand of a parallel β-sheet: (−119°, 113°).

The first two helices are found in proteins (1, 20), although long 3_{10}-helices are not known. Even though π-helices have not been found experimentally, they are included here because of their interesting shape features. This latter structure is a compact helix with fourfold symmetry. The 3_{10}-helix has threefold symmetry and is the least compact. The α-helix has intermediate properties.

Polyproline does not form α-helices but can be found in a different conformation known as polyproline II. This conformation exhibits threefold symmetry, and comprises small compact loops elongated in a strandlike fashion. For this reason, we refer to it as a "helicoidal strand." Polyglycine, because of the absence of side chains, can appear in a larger number of stable conformations than other polypeptides. The conformation polyglycine II is comparable to polyproline II.

The two β-strands considered here are qualitatively different. The β-strand found in antiparallel sheets is an almost planar ribbonlike structure. The one found in parallel sheets is "pleated," appearing as a twisted ribbon. (These two *strands* are often referred to loosely in the literature as antiparallel and parallel "β-sheets." Properly, a *sheet* comprises several

Can. J. Chem. Downloaded from www.nrcresearchpress.com by 65.111.164.53 on 09/08/12
For personal use only.

strands. Nonetheless, we shall use both terminologies interchangeably.)

In addition to the angles ϕ, ψ, and ω, other geometrical properties are frequently associated with the α-carbon backbone of regular secondary structures. Two common local parameters are τ, the axial translation per residue, and n_T, the number of residues "per turn." The product $p = \tau n_T$, known as the *pitch* of the motif, is a property used mostly for helices, where the notion of "turn" is meaningful. Two other parameters used for helices are their radius ρ, and the rotation per residue γ (1, 20). This set of local parameters is derived from special features in regular conformations. They cannot be defined for other folds and, thus, they do not constitute a tool to compare shapes of arbitrary conformations. More appropriate descriptors are dealt with in the next section.

Regular conformations model more accurately the stable secondary structures of polypeptides with a single type of amino acids. In our case, we have used *n*-polyalanine to describe all helical and β-strand motifs, where n is the number of residues. (For *regular* conformations, the results are expected to depend little on most chosen single amino acids.) The other two secondary motifs were modelled with *n*-polyglycine and *n*-polyproline. All molecular structures were built by adding residues sequentially, using the dihedral angles quoted above and a standard molecular modeling program (21). The α-carbon backbones derived from these "frozen" conformations are studied in the rest of this work. The conclusions should also be valid if the backbone regular conformation is allowed to relax to an actual energy minimum, within the framework of some standard molecular force field.

Molecular size and shape descriptors

Two groups of global descriptors have been computed for the motifs discussed above. One group of parameters describes molecular size and geometric shape. The second group corresponds to descriptors of entanglement complexity in the protein backbone.

As a classic descriptor of molecular size, we use the radius of gyration R_G (12). The basic properties of R_G for some secondary motifs are well known (1). We include here a quantitative analysis for the sake of comparison with other shape descriptors. The radius of gyration measures the compactness of the backbone, in addition to size. Size parameters scale *linearly* with the number of amino acid residues for the secondary motifs studied here. (In the case of random polymers, the conformationally averaged radius of gyration, $\langle R_G \rangle$, scales as $\langle R_G \rangle \sim cn^{\nu}$, with $\nu < 1$ (12).)

The geometric shape can be conveyed by the chain's *anisometry* (i.e., the deviation from a spherical distribution of atoms). An appropriate parameter is the *asphericity* (22–24):

$$[2] \qquad \Omega = \frac{(I_2 - I_1)^2 + (I_3 - I_2)^2 + (I_3 - I_1)^2}{2(I_3 + I_2 + I_1)^2}$$

where $\{I_i\}$ are the principal moments of inertia of the backbone. This function has been applied to study multidimensional random walks (23, 24). (Equation [2] is used in ref. 22. The parameter defined in refs. 23 and 24 is equivalent to 4Ω, for 3D chains.) For spherical and highly prolate objects, we find $\Omega = 0$ and $\Omega = \frac{1}{4}$, respectively. As far as we know, the asphericity has not been used to characterize secondary structural features, even though it provides a simple descriptor. For regular conformations, Ω varies nonlinearly with the number of residues and tends asymptotically to the limit value of $\frac{1}{4}$. In the Appendix, we deduce the quantitative behaviour of Ω for large n in some secondary structures.

The radius of gyration and the asphericity provide complementary information on size, compactness, and shape derived from the backbone geometry. However, a detailed characterization must include shape descriptors that depend explicitly on the geometry *and* connectivity. Therefore, the third aspect of macromolecular shape that we analyze is the "degree of folding" or the "complexity of self-entanglements" in the chain. In a previous work, we introduced a new shape descriptor to this purpose: the probability distribution of overcrossings (the overcrossing spectrum) (18).

This overcrossing spectrum is defined by the probabilities $\{A_N(n)\}$ of observing an n-atom chain as a projected curve with N bond–bond crossings. We refer to these "double points" resulting from a 2D-projection as *overcrossings*. An actual evaluation of overcrossing probabilities is performed as follows (18): (*a*) the backbone is enclosed by the smallest sphere centred at the centre of mass; (*b*) an arbitrary point $\boldsymbol{r}$ over the sphere is chosen, and the backbone is projected to a plane which is tangent to the surface at $\boldsymbol{r}$. For this projection, we evaluate a number of overcrossings $N(\boldsymbol{r})$; (*c*) the same procedure is repeated for a large number of points randomly distributed over the sphere; (*d*) the probability of observing a given number N of overcrossings is simply computed as the number of projections yielding N crossings divided by the total number of random projections. Details of the algorithm, and applications to several real protein structures, can be found in ref. 18. The overcrossing spectrum uses *all* possible "views" of a backbone. The resulting description is invariant under rigid rotations and translations.

The probability distribution $\{A_N(n)\}$ is in itself a global shape descriptor. The type of overcrossings in a polymer conformation depends not so much on its size or geometric shape, *but on the twists, turns, and various convolutions of the chain*. We refer to these features as "self-entanglements." The main features of the distribution are summarized by two parameters: (1) A^*, the probability of the most probable number of overcrossings N^* (i.e., the maxima of the distribution); (2) $\bar{N}$, the mean number of overcrossings, given by

$$[3] \qquad \bar{N} = \sum_{N=0}^{\max N} N A_N(n)$$

where $\max N = (n-3)(n-2)/2$, for a *nonbranched* chain with n residues (18). The nature of the self-entanglements is expressed quantitatively by the descriptors A^* and $\bar{N}$. The more convoluted and entangled the backbone, the larger $\bar{N}$ and the smaller A^*. In contrast, one finds $\bar{N} \to 0$ and $A^* = A_0 \to 1$ for swollen and disentangled chains. In ref. 18, the overcrossing spectra of some rigid protein structures are discussed in some detail. As well, the values of A^* for a number of real (irregular) α-helices found in proteins are compared. Here, we extend this work by carrying out a detailed analysis for all relevant regular secondary motifs using A^* and $\bar{N}$ as shape descriptors.

Typical results for overcrossing spectra of regular con-

Can. J. Chem. Downloaded from www.nrcresearchpress.com by 65.111.164.53 on 09/08/12
For personal use only.

Fig. 1. Comparison of overcrossing spectra for polyalanine α-helices of variable lengths. (Note that in all cases the maximum probability of overcrossings is associated with $N^* = 0$, and it remains approximately constant at $A^* = 0.41$. In contrast, the position of the second maximum in A_N increases with n.)

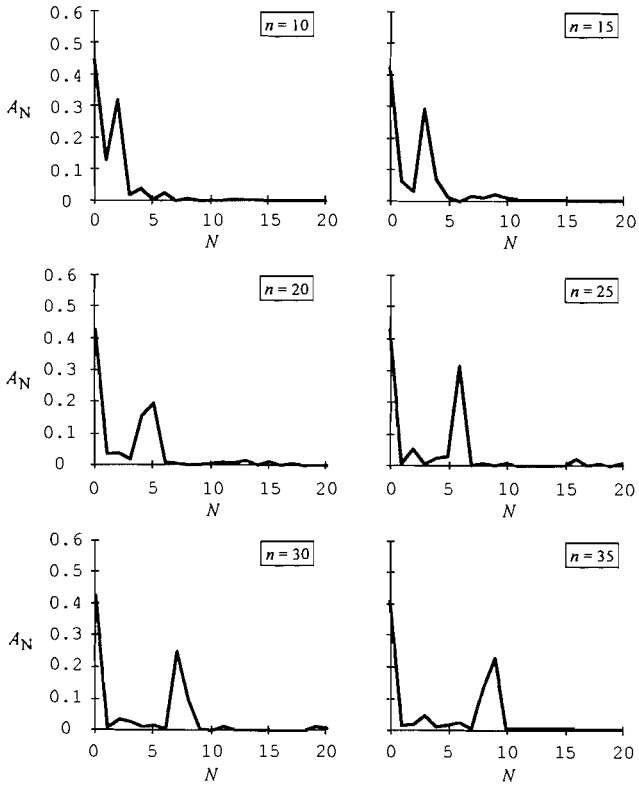

formations are illustrated in Fig. 1. The figure displays the probabilities of observing $N \leq 20$ overcrossings in regular n-polyalanine α-helices, with $n = 10$, 15, 20, 25, 30, and 35. These spectra (and all others in this work) are derived by averaging the results of 4 different randomizations, with a number of projections ranging between 10 000 and 60 000. The six spectra in Fig. 1 exhibit two large maxima. One is always centred at $N^* = 0$ and corresponds to the maximum probability A^*. This probability appears to change little with n (18). The position of the second maximum, in contrast, increases almost linearly with n. As a result, it is found that the mean number of overcrossings $\bar{N}$ also increases linearly with n. The same trend is found for $\bar{N}$ in all secondary structures, although the $\bar{N}$ values depend on the entanglement complexity. On the other hand, the behaviour of A^* depends strongly on the motif considered, and it can provide a greater discrimination among shapes (see below). (Note that each conformation is characterized in *absolute* terms, and not relative to an (arbitrary) reference structure.)

The four descriptors R_G, Ω, A^*, and $\bar{N}$ are used in a detailed analysis of a given conformation. Intuitively, these descriptors could be related. For instance, one would expect a small radius of gyration, a large mean number of overcrossings, and a spheroid with small anisometry in the case of a compact backbone. However, actual conformations exhibit much richer features. The various aspects of molecular

Fig. 2. Dependence of the mean number of overcrossings $\bar{N}$ on the length of the polypeptide chain, for three types of helices. (The different box sizes represent the error bars due to the numerical evaluation of overcrossing probabilities by averaging the results from various randomizations of the 2D projections.)

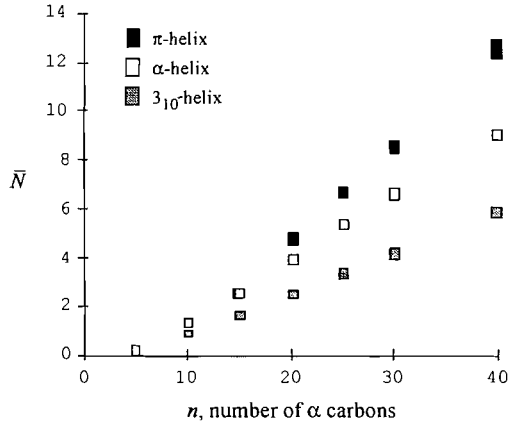

shape in regular secondary structures can only be captured when using the above descriptors simultaneously. In the next section the results obtained are discussed in detail.

The shape of secondary structural motifs with variable chain length

The results presented below have been derived from computations on n-polypeptides with $5 \leq n \leq 40$. Longer chains have been considered only in selected cases. Since the chains are in regular conformations, $n = 40$ is large enough to reach the asymptotic limit. The behaviour for large n depends on the shape descriptor considered.

It is found that radius of gyration and the mean overcrossing number increase linearly with n for *all* secondary structural motifs. Therefore, molecular size and entanglement complexity can be characterized by two coefficients c and a:

$$[4] \qquad R_G \approx cn, \qquad \bar{N} \approx n/a$$

The quality of the two correlations in eq. [4] is comparable. For instance, in α-helices:

$$[5a] \qquad R_G \approx (0.41 \pm 0.01)n + (0.7 \pm 0.2) \text{ in Å}, \qquad C_c = 0.99992, \ 10 \leq n \leq 40$$

$$[5b] \qquad \bar{N} \approx n/(3.7 \pm 0.3) + (-1.5 \pm 0.2), \qquad C_a = 0.9997, \ 10 \leq n \leq 40$$

with 95% confidence errors. (C_c and C_a are the corresponding correlation coefficients.) The results for $\bar{N}$ are less accurate than those for R_G due to the algorithm based on averaging over random projections. The individual values of $\bar{N}$ have, at best, an accuracy of 3 significant figures.

Figure 2 compares the mean overcrossing numbers for the three helical secondary structures. The asymptotic behaviour (cf. eq. [4]) requires at least ca. 15 residues to set in. The results allow one to make two observations in com-

Table 1. Characteristic coefficients of molecular size (c) and molecular shape (a) for various secondary structural motifs. The coefficients quantify the linear dependence of the radius of gyration R_G (in Å) and mean number of overcrossings $\bar{N}$ with the number of amino acid residues n. (The errors correspond to 95% confidence intervals. The correlations coefficients for R_G vs. n and $\bar{N}$ vs. n are C_c and C_a, respectively. See text for discussion.)

Motif	R_G coefficient (c, in Å)	C_c	$\bar{N}$ coefficient (a)	C_a
π-Helix	0.268 ± 0.012	0.9995	2.63 ± 0.23	0.9980
α-Helix	0.408 ± 0.007	0.9999	3.68 ± 0.27	0.9997
3_{10}-Helix	0.567 ± 0.004	0.9999	6.10 ± 0.19	0.9998
Polyproline II	0.8951 ± 0.0007	0.9999	24.50 ± 0.41	0.9999
Polyglycine II	0.9008 ± 0.0005	0.9998	24.54 ± 0.49	0.9998
Parallel β-sheet	0.9438 ± 0.0001	0.9999	179 ± 6	0.9998
Antiparallel β-sheet	1.0008 ± 0.0004	0.9999	1900 ± 700	0.9801

paring the helical folds: (a) from the point of view of self-entanglements, all types of helices with 5 or fewer amino acid residues exhibit the same shape features; (b) longer helices are clearly distinct, with π-helices and α-helices resembling each other more closely than the 3_{10}-helices. The latter have the simplest folding (i.e., the least entangled), because of their smaller overcrossing numbers.

The results for the coefficients c and a are collected in Table 1 for all secondary structures. The dimensionless parameter a is a single number that conveys important information on the folding shape. We shall regard it as the *self-entanglement length* of a regular polypeptide conformation. It represents the mean number of residues needed to increase by 1 the average overcrossing numbers in 2D projections. The larger the a value, the less complex the entanglement nature of a conformation, regardless of its size. For a planar conformation we expect $a \to \infty$ (i.e., a regular structure with no entanglements).

From Table 1, we observe that "antiparallel sheets" are the least entangled of all secondary structural motifs. Their very large a value is consistent with an almost planar conformation. Strands in parallel sheets exhibit a marginal degree of folding, since ca. 200 residues are needed to observe one overcrossing. Nevertheless, our approach distinguishes the two motifs, reflecting the fact that the β-strands in parallel sheets are *twisted* ("pleated"), and thus not equivalent to the strands in antiparallel sheets. In contrast, the two strands appear equivalent to other global descriptors, such as the fractal dimension (16).

On the other extreme of the complexity scale, the π-helix is found to be the most entangled of the motifs. This result is consistent with it being the most compact of all structures, i.e., the one with the smallest c coefficient. The polyglycine II and polyproline II motifs have exactly the same self-entanglement length a, and occupy an intermediate position between helices and strands. Since over 20 residues are needed in polyglycine II and polyproline II conformations to produce an average of one overcrossing, these motifs will mostly resemble strands whenever found in actual protein structures.

The interpretation of a as a self-entanglement length is appropriate for *regular* conformations, because of the linear scaling of $\bar{N}$ with n. In medium-size random polymers and in actual proteins, the conformational average of $\bar{N}$ scales as $\langle \bar{N} \rangle \sim n^{\beta}$, with $\beta \approx 1.4$ (19). Hence, within our approach, secondary *and* tertiary structure are distinguished by their different scaling behaviour. A global descriptor such as the fractal dimension produces the same result for a regular α-helix and for an entire globular protein.

The previous analysis can be supplemented by using the descriptors A^* and Ω. The asphericity is derived from the same information used to compute R_G, whereas A^* is extracted from the overcrossing spectra that yielded $\bar{N}$. These descriptors are nonlinear functions of n. As shown below, they allow a greater discrimination in shape features.

Figure 3 shows the maximum overcrossing probabilities for the helical motifs as a function of n. (For completeness, the graph includes the *exact* result $A^* = 1$ for $n = 3$.) As expected, the least entangled 3_{10}-helices exhibit the largest A^* values. The asymptotic behaviour sets in at $n > 15$, where one finds a probability of observing *no overcrossings* in ca. 65% of the projections ($A_0 = A^*$). The α-helices show a similar behaviour, with an almost constant asymptotic probability $A_0 = A^* \approx 0.40$ for large n.

The behaviour of A^* in π-helices (the most entangled motif) is peculiar: it oscillates as a function of n. Overcrossing spectra for π-helices resemble those in Fig. 1, but here the two maxima are closer in height. Hence, the most probable number of overcrossings is not always "0". The oscillations in A^* correspond to helices where $N^* \neq 0$.

Figure 3 summarizes the expected pattern for A^* in helices: a rapid decrease from $A^* \approx 1$ at small n values, reaching either a constant or small oscillating values for larger n. Figure 4 summarizes the results for the asphericity Ω. To reveal more clearly the asymptotic behaviour of Ω, we have added helices with length up to $n = 100$. The asphericity increases rapidly from small values, corresponding to quasi-spherical chains, up to the limit for highly prolate chains. As we show in the Appendix, this limit is reached with a law $\Omega \sim \frac{1}{4} - (\text{const} \times n^{-2})$. Note that the asphericity for π-helices has a minimum at approximately $n \approx 7$. For polypeptides shorter than seven residues, the α-helical conformation is more spherical than the π-helix.

Figures 3 and 4 provide a complementary description of the helices. From the point of view of self-entanglements, long α-helices are closer to π-helices than to 3_{10}-helices. In contrast, from the point of view of anisometry, a long α-helix is almost as prolate as a 3_{10}-helix. This result indicates that

Can. J. Chem. Downloaded from www.nrcresearchpress.com by 65.111.164.53 on 09/08/12
For personal use only.

Can. J. Chem. Downloaded from www.nrcresearchpress.com by 65.111.164.53 on 09/08/12
For personal use only.

Fig. 3. Dependence of the maximum probability of overcrossings A^* on the length of the polypeptide chain, for three types of helices. (The exact limit $A^* = 1$ for $n = 3$ has been added for completeness. See text for a discussion of the irregular behaviour of A^* in the π-helix.)

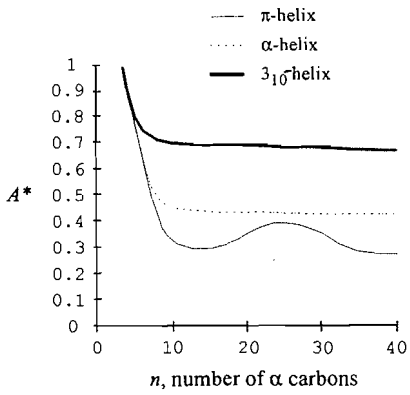

Fig. 4. Dependence of the asphericity Ω with the length of the polypeptide chain, for three types of helices.

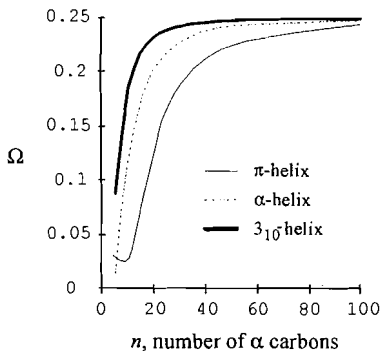

a single global descriptor cannot capture all shape features. By using the present set of properties, we can achieve a more complete characterization of secondary structure.

Figure 5 and 6 show the full shape description in the remaining motifs. The polyproline II and polyglycine II conformations are compared in Fig. 5, whereas Fig. 6 compares the parallel and antiparallel β-sheets.

The comparison of polyproline II and polyglycine II is a critical test since these two conformations are very similar in terms of common local measures (1). The results in Fig. 5 for R_G and Ω indicate that these two motifs are virtually coincident in terms of size, compactness, and anisometry. Similarly, their corresponding mean numbers of overcrossings $\bar{N}$ cannot be distinguished within our computational error (cf. Table 1 for the self-entanglement lengths). Only the maximum probability of overcrossings A^* indicates a small difference in shape features between the two conformations. With this property, we observe that polyglycine II and polyproline II backbones have the same shapes for $n < 20$. Yet, as the probability of no overcrossings $A_0(= A^*)$ decreases faster in polyglycine II chains, we conclude that the latter are slightly more entangled. This difference may stem from the local differences in fold caused by the smaller amino acid residue. This result suggests that A^* can be used as a *discriminating*

Fig. 5. Shape descriptors for regular polyproline II and polyglycine II motifs with variable number of residues. (Only the descriptor A^* indicates small differences between their shapes, in the case of long chains. See Fig. 2 with respect to the error bars.)

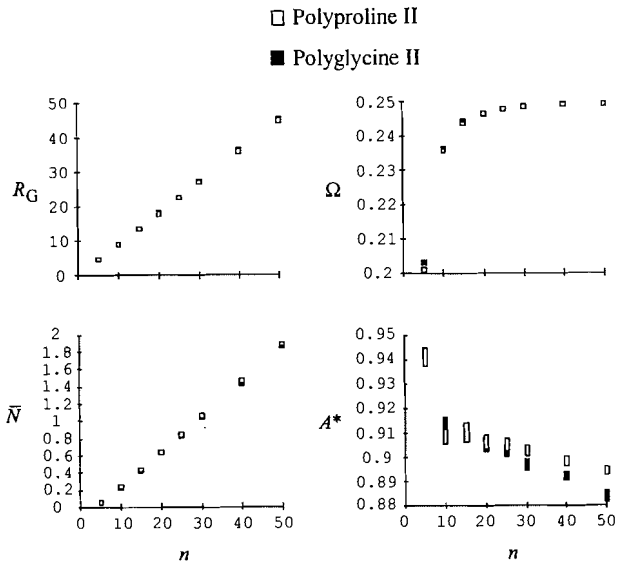

Fig. 6. Shape descriptors for the regular strands in antiparallel and parallel β-sheets with a variable number of residues. (The fact that the parallel strand is nonplanar and twisted ("pleated") is only reflected by the shape descriptors $\bar{N}$ and A^*. The antiparallel strand is almost planar and therefore less entangled. The large error bars for $\bar{N}$ are typical of the computation of overcrossings in objects that are close to planar. See Fig. 2 with respect to the error bars.)

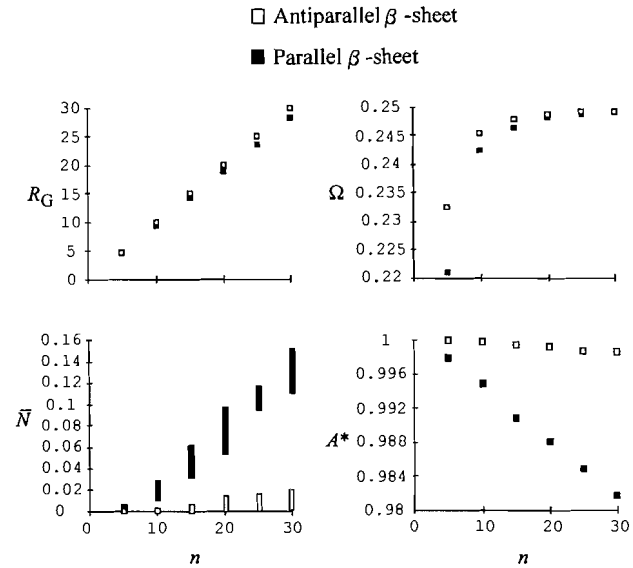

tool, sensitive enough to detect changes of global shapes in polymers with similar conformations but different compositions.

The comparison of β-strands is another critical test, since they have very similar local (1) and global (16) descriptors. From Fig. 6, we make the following observations:

(*a*) the radius of gyration magnifies the size difference for long strands. While strands with $n < 10$ are virtually indistinguishable, long parallel β-sheets are smaller (cf. Table 1); (*b*) the asphericity magnifies the difference in geometric shape for small n. Strands with $n > 20$ have virtually the same anisometry, whereas short parallel β-sheets are less prolate; (*c*) only the descriptors of self-entanglements provide a clear distinction between the two β-sheet motifs. The larger $\bar{N}$ and smaller A^* values for parallel β-sheets imply that the latter are more entangled. (Both objects are, of course, little "entangled" in *absolute* terms, as the A^* and $\bar{N}$ values indicate.)

Summarizing, the difference in structure caused by the "twist" in parallel β-sheets is reflected in the global shape descriptors A^* and $\bar{N}$. This difference cannot be noted when using only geometrical descriptors.

Further comments and conclusions

In conclusion, we have shown that a thorough characterization of secondary structures can be achieved with the use of several descriptors, focusing on different aspects of molecular shape. Our results indicate that descriptors of self-entanglements are "natural" and efficient tools to monitor folding features in regular conformations.

Other properties have been used in the literature to study secondary motifs. With respect to *global* descriptors (16), we believe that our approach discriminates better between similar conformations. As well, it has a conceptual advantage, since self-entanglements can be defined rigorously for any 3D curves. In contrast, a global descriptor such as the fractal dimension assumes a behaviour that is only an approximation for polypeptides (16).

The present analysis goes beyond the information provided by a *local* property. In fact, some familiar local parameters, such as the number of residues per turn n_T, do not describe molecular shape (1). For example, if one stretches a helix elastically, n_T may be conserved. However, the molecular shape would change as the helix becomes less entangled. The present shape descriptors recognize this difference. Other parameters, such as the pitch p or the axial translation τ, only make sense if there is a preferential axis, as in regular conformations. They become meaningless for arbitrary polymers. In contrast, the shape descriptors A^* and $\bar{N}$ can be used in all instances.

From our results, two important observations can be made for A^* and $\bar{N}$. First, the self-entanglement length a (eq. [4]) is a better property than D (eq. [1]) as a single number to represent the global shape of secondary motifs. Second, the dependence of A^* upon n appears to be a discriminating function for motifs, and it allows one to study the effect that a change in amino acids has over the shapes of similar conformations.

This improved analysis of secondary structure contributes to our understanding of protein shapes at their various levels of structural organization. A better representation of protein folding features is a much needed component in the current research to predict tertiary structure from primary sequence (25, 26), develop *de novo* proteins (the "inverse folding problem") (27), and recognize intermediates during folding dynamics (28, 29).

In closing, it should be noted that the methodology presented here is not restricted to the analysis of regular conformations in chain molecules. As shown in ref. 30, we can extend the characterization of self-entanglements to the study of ensembles of several chains. Therefore, our procedure can also be applied to periodic multichain arrays, such as those found for nucleic acids. Work on these systems is underway and will be presented elsewhere.

Acknowledgment

This work has been supported by an individual operating grant from the Natural Sciences and Engineering Research Council (NSERC) of Canada. I would like to thank Prof. S. Fraga (Edmonton) for sending a copy of the manuscript of ref. 26 prior to publication.

References

1. T.E. Creighton. Proteins: structures and molecular principles. Freeman, New York. 1984.
2. M. Levitt and C. Chothia. Nature, **261**, 552 (1976).
3. (*a*) J.S. Richardson. Adv. Protein Chem. **34**, 167 (1981); (*b*) Methods Enzymol. **115**, 349 (1985).
4. C. Chothia. Nature, **357**, 543 (1993).
5. T.L. Blundell and M.S. Johnson. Protein Eng. **2**, 877 (1993).
6. E.I. Shakhnovich. Phys. Rev. Lett. **72**, 3907 (1994).
7. J.M. Thornton. Curr. Opinion Struct. Biol. **2**, 888 (1992).
8. C. Orengo. Curr. Opinion Struct. Biol. **4**, 429 (1994).
9. (*a*) L. Pauling, R.B. Corey, and H.R. Branson. Proc. Natl. Acad. Sci. U.S.A. **37**, 205 (1951); (*b*) L. Pauling and R.B. Corey. Proc. Natl. Acad. Sci. U.S.A. **37**, 729 (1951).
10. C. Chothia and A.G. Murzin. Structure, **1**, 217 (1993).
11. G.N. Ramachandran and V. Sasisekharan. Adv. Protein Chem. **23**, 283 (1968).
12. P.J. Flory. Statistical mechanics of chain molecules. Interscience, New York. 1969.
13. B.B. Mandelbrot. The fractal geometry of nature. Freeman, New York. 1982.
14. Y. Isogai and T. Itoh. J. Phys. Soc. Jpn. **53**, 2162 (1984).
15. C.-X. Wang, Y.-Y. Shi, and F.-H. Huang. Phys. Rev. A: Gen. Phys. **41**, 7043 (1990).
16. Y. Xiao. Phys. Rev. E: Stat. Phys. Plasmas, Fluids, Relat. Interdiscip. Top. **49**, 5903 (1994).
17. G.C. Wagner, J.T. Colvin, J.P. Allen, and H.J. Stapleton. J. Am. Chem. Soc. **107**, 5589 (1985).
18. G.A. Arteca. Biopolymers, **33**, 1829 (1993).
19. G.A. Arteca. Phys. Rev. E: Stat. Phys. Plasmas, Fluids, Relat. Interdiscip. Top. **49**, 2417 (1994).
20. C. Toniolo and E. Benedetti. Trends Biochem. Sci. **16**, 350 (1991).
21. HyperChem (Release 4), Hypercube Inc., Waterloo, Ontario, 1994.
22. A. Baumgärtner. J. Chem. Phys. **98**, 7496 (1993).
23. J. Rudnick and G. Gaspari. Science, **237**, 384 (1987).
24. H.W. Diehl and E. Eisenriegler. J. Phys. A: Math. Gen. **22**, L 87 (1989).
25. P. Bork, C. Ouzounis, and C. Sander. Curr. Opinion Struct. Biol. **4**, 393 (1994).

Can. J. Chem. Downloaded from www.nrcresearchpress.com by 65.111.164.53 on 09/08/12
For personal use only.

26. S. Fraga and J.M.R. Parker. Amino Acids, **7**, 175 (1994).
27. J.S. Richardson and D.C. Richardson. *In* Proteins: form and function. *Edited by* R.A. Bradshaw and M. Purton. Elsevier, Cambridge. 1990. pp. 173–182.
28. M. Karplus and E. Shakhnovich. *In* Protein folding. *Edited by* T.E. Creighton. Freeman, New York. 1992. pp. 127–195.
29. O.B. Ptitsyn. *In* Protein folding. *Edited by* T.E. Creighton. Freeman, New York. 1992. pp. 243–300.
30. G.A. Arteca. J. Comput. Chem. **15**, 633 (1994).

Appendix

We show here the asymptotic behaviour of the asphericity Ω for helicoidal conformations in terms of n, the number of amino acid residues. Let I_3 be the principal moment of inertia associated with the helical axis. If we now consider regular, perfectly cylindrical helices, the conformations become prolate symmetric tops and the principal moments of inertia associated with the axes perpendicular to the helical axis coincide, i.e., $I_1 = I_2$. In this case, the asphericity becomes (cf. eq. [2]):

$$[A.1] \quad \Omega = \frac{(1 - I_3/I_1)^2}{4(1 + I_3/2I_1)^2}$$

In the asymptotic limit of very long helices, $I_3 \ll I_1$. Expanding eq. [A.1] in power series up to the first order in (I_3/I_1), we obtain:

$$[A.2] \quad \Omega \approx \frac{1}{4} - \frac{3I_3}{4I_1}$$

The limit $\Omega \rightarrow 1/4$ corresponds to the maximum value of asphericity in prolate objects. To obtain the asymptotic behaviour in terms of the number of monomers n, we can estimate the two principal moments of inertia in eq. [A.2] in terms of familiar helical parameters. Let ρ be the radius of the helix, τ the axial translation per residue (i.e., the "helical pitch" divided by the number of residues per turn), and γ the rotation per residue. The values of these parameters can be found in refs. 1 and 20. Since all the main chain atoms in the present model of a helix are identical and lie on the surface of a cylinder, we obtain:

$$[A.3] \quad I_3 \approx n\rho^2$$

For the remaining moment of inertia we proceed as follows. Using centre of mass as the origin, the atoms can be labelled by an index $|i| \leq n/2$, where $i > 0$ corresponds to the positions with positive coordinate along the helical axis. With this notation, the position of each atom along the helical axis becomes $i\tau$. For the same atom, the position along an axis perpendicular to the helical one can be estimated as $\rho \cos(i\gamma)$. Therefore, in the limit of long helices (i.e., where the main contributions come from large $|i|$ values), we have

$$[A.4] \quad I_1 \approx 2\sum_{i=1}^{n/2}[(i\tau)^2 + \rho^2\cos^2(i\gamma)] \approx 2\tau^2\sum_{i=1}^{n/2} i^2 \approx \frac{\tau^2 n^3}{12}$$

where only the largest contribution to a power of n has been retained. Introducing eqs. [A.3] and [A.4] in eq. [A.2], we deduce that the asymptotic behaviour of Ω follows a n^{-2} law:

$$[A.5] \quad \Omega \approx \frac{1}{4} - 9\left(\frac{\rho}{\tau}\right)^2 n^{-2}$$

As an example, for an α-helix we have $\rho \approx 2.5$ Å, $\tau \approx 1.6$ Å, which gives $9(\rho/\tau)^2 \approx 22.0$. This result can be checked numerically by considering polyalanine α-helices of variable length. Using the results for $n = 20$, 25, 30, 35, 50, and 100 polyalanines (see discussion in the article), a least-squares fitting of $\ln(\frac{1}{4} - \Omega)$ vs. $\ln n$ produces:

$$[A.6] \quad \ln\left(\frac{1}{4} - \Omega\right) \approx (-2.02 \pm 0.10)\ln n + (3.1 \pm 0.4)$$

with 95% confidence intervals and a correlation coefficient of 0.9994. Equation [A.6] translates into the asymptotic result: $\Omega \approx \frac{1}{4} - (22 \pm 9)n^{-2.0\pm0.1}$, $n \gg 1$, in good agreement with the prediction [A.5] for α-helices. The anisometry of other helices and secondary structural motifs can be analyzed in a similar fashion.

Can. J. Chem. Downloaded from www.nrcresearchpress.com by 65.111.164.53 on 09/08/12
For personal use only.

Single-crystal absorption spectroscopy of binuclear complexes of iron(III) and manganese(III) with the μ-oxo-bis(μ-acetato)dimetal core

Yanick Pelletier and Christian Reber

Can. J. Chem. Downloaded from www.nrcresearchpress.com by 65.111.164.53 on 09/08/12
For personal use only.

Abstract: Single-crystal absorption spectroscopy at variable temperature is used to determine exchange couplings between transition metal centers in both the electronic ground and excited states in two new homobimetallic complexes with the formula $[LM(\mu\text{-}O)(\mu\text{-}CH_3CO_2)_2ML'](ClO_4)_2$, where M is iron(III) or manganese(III). L and L' denote 1,4,7-triazacyclononane and 1,4,7-trimethyl-1,4,7-triazacyclononane, respectively. Values for the ground state exchange coupling constant J are -295 cm^{-1} and $+10$ cm^{-1} for the iron and manganese compounds, respectively, using $H_{ex} = -JS_1 \cdot S_2$. Exchange interactions in excited states are qualitatively analyzed, indicating that a spin-forbidden transition of the Fe–Fe binuclear unit occurs with significant intensity by the single-ion mechanism, and not as expected by the Tanabe pair intensity mechanism for spin-forbidden transitions, the dominant mechanism for isoelectronic complexes of manganese(II).

Key words: absorption spectra, exchange interaction, magnetic properties, bimetallic complexes of iron(III), bimetallic complexes of manganese(III)

Résumé : La spectroscopie d'absorption de cristaux à température variable est utilisée pour déterminer quantitativement des constantes de couplage d'échange entre les deux centres métalliques de nouveaux complexes binucléaires du fer(III) et du manganèse(III) ayant comme ligands pontants un ligand oxo et deux groupes acétato. Les constantes de couplage J sont de -295 cm^{-1} et $+10$ cm^{-1} pour les composés du fer et du manganèse avec l'opérateur $H_{ex} = -JS_1 \cdot S_2$. L'interaction d'échange dans les états excités est analysée de façon qualitative, indiquant que le mécanisme d'intensité pour transitions d'une unité binucléaire de Tanabe n'est pas effectif dans le composé du fer, contrairement aux observations pour des composés binucléaires du manganèse(II) qui sont isoélectroniques au complexe du fer(III) dans cette étude.

Mots clés: spectroscopie d'absorption, interaction d'échange, propriétés magnétiques, composés binucléaires du fer(III), composés binucléaires du manganèse(III)

1. Introduction

Binuclear complexes of iron and manganese with oxo and carboxylato bridging ligands are important constituents of the active sites in metalloproteins and have been shown to be catalytically active (1–6). A large number of model compounds have been synthesized recently, among them a series of triply bridged binuclear compounds with the μ-oxo-bis(μ-acetato) bridging geometry (5, 7). We present absorption spectra of two homobimetallic compounds of this type with the formula $[LM(\mu\text{-}O)(\mu\text{-}CH_3CO_2)_2ML'(ClO_4)_2$. The metal centers M are either iron(III) or manganese(III). L and L' denote 1,4,7-triazacyclononane and 1,4,7-trimethyl-1,4,7-triazacyclononane, respectively. The manganese compound contains one water molecule per formula unit in the crystal. The structure and a variety of physical properties of both compounds are reported in ref. 7. We abbreviate them as {MnMn} and {FeFe} in the following.

The detailed absorption spectra of crystals of {FeFe} and {MnMn} as a function of temperature are used to determine effects of the exchange coupling both in the ground and some excited electronic states, providing new insight into the detailed electronic structure of these compounds. The comparison with existing spectroscopic data on isoelectronic systems shows a large variation of spectroscopic and magnetic properties and therefore considerable potential for the tuning of these properties by chemical variation of the ligand systems and oxidation states of the metal centers. The wide variety of spectroscopic observations and excited state behavior has been extensively studied for binuclear compounds of chromium(III), where a variety of absorption and luminescence techniques can be applied (8, 9). Binuclear complexes of copper(II) have been investigated in detail because of their simple d^1–d^1 hole configuration, making them ideal model systems for experimental and theoretical studies. (8, 10–12) Other metals, such as iron(III) and manganese(III) in this work, have received much less attention (8). The work on

Received, October 5, 1994.

Y. Pelletier and C. Reber.[1] Département de chimie, Université de Montréal, C.P. 6128, Succursale Centre-Ville, Montréal, QC H3C 3J7, Canada.

[1] Author to whom correspondence may be addressed. Telephone (514) 343-7332. Fax: (514) 343-7586. e-mail: reber@ere.umontreal.ca

Can. J. Chem. Downloaded from www.nrcresearchpress.com by 65.111.164.53 on 09/08/12
For personal use only.

compounds containing Fe^{3+}-O-Fe^{3+} units is summarized in refs. 6 and 13.

2. Experimental

The compounds were obtained as powders from the laboratory of Karl Wieghardt (7). Thin crystalline samples of {FeFe} and {MnMn} used for optical absorption spectroscopy were obtained by slow evaporation of saturated solutions in methanol on quartz plates at room temperature. The samples with typical areas of 0.5 mm^2 were mounted in a helium cryostat (Oxford Instruments CF 1204). The quality of the sample crystals was examined under a microscope between crossed polarizers and extinction directions were determined. Only unpolarized spectra are reported because the polarization direction had no significant effects on band intensities and positions, most likely due a structure with multiple inequivalent sites for the chromophore in the crystal, leading to bimetallic units with different orientation relative to the polarization directions. The crystal structure of {FeFe} and {MnMn} was not determined, but structures with eight formula units per unit cell are reported in ref. 7 for the analogous {FeMn} and {FeCr} compounds. All the spectra were measured with a Varian Cary 5E spectrometer. Commercial computer software was used for conversion of the spectra to a wave-number scale and for the least-squares fits.[2]

3. Spectroscopic Results

The absorption spectrum of {FeFe} is shown in Fig. 1 as a function of temperature. The band positions in the overall spectrum, shown in the inset, are typical for Fe^{3+} compounds in a distorted octahedral coordination with nitrogen and oxo ligands (6, 14). The band positions and estimated molar absorptivities of the room temperature spectrum in Fig. 1 are similar to those of the solution spectrum in ref. 7, with the high molar absorptivities indicating the importance of exchange coupling between the two metal centers. The transitions can be assigned with the Tanabe–Sugano diagram for d^5 systems and by analogy with the detailed assignments of the high-resolution spectra reported for pairs of Fe^{3+} ions in sapphire (14, 15). The unstructured band at 13 000 cm^{-1} corresponds to the $^6A_1 \rightarrow {}^4T_1$ transition in the O point group. Its shape and overall intensity show very little change with temperature. The next band system is the superposition of the $^6A_1 \rightarrow {}^4T_2$ and $^6A_1 \rightarrow {}^2T_2$ transitions, shown in detail in the main part of Fig. 1. We identify four bands with distinct temperature dependencies. The most intense band is centered at 21 230 cm^{-1}, denoted by a square, and shows a decrease in intensity with increasing temperature. The intensity of the band at 19 340 cm^{-1}, denoted by a circle, strongly increases with temperature. Two weak bands at 17 990 cm^{-1} and 23 360 cm^{-1} (triangle in Fig. 1) show a slight increase in intensity with temperature. The different temperature dependencies are caused by exchange interaction between the metal centers and will be discussed in Sect. 4(a). In isoelectronic compounds of manganese(II) the corresponding transitions are weak and at higher energy than for {FeFe},

[2] Igor Pro, by Wavemetrics, Inc., Lake Oswego, OR 97035, U.S.A. Technical Notes 7 and 22. 1994.

Fig. 1. Single-crystal absorption spectra of {FeFe} as a function of temperature. Main figure: $^6A_1 \rightarrow {}^4T_2$, $^2T_2$ band with intensities determined by thermal population of different levels of the exchange-split ground state of the binuclear system. Bands used for the determination of the exchange coupling parameter J are denoted by the square, circle, and solid triangle symbols. Temperatures for the measurements are 15, 80, 120, 180, 200, 250, and 300 K, top to bottom at the band maximum denoted by the circle. The order is inverted at the band maximum denoted by the square. Inset: overall absorption spectrum at 80 K.

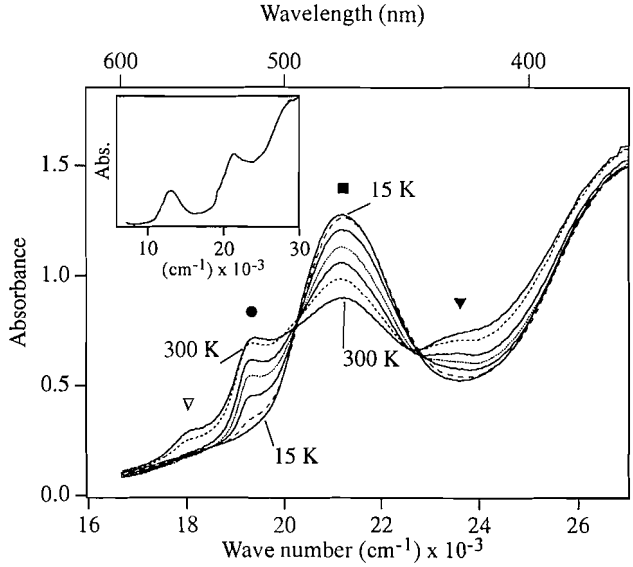

often hidden by the sharp bands corresponding to the $^6A_1 \rightarrow {}^4A_1, {}^4E$ transitions, where initial and final states of the transition arise from the same electron configuration. These are the transitions that were used in the literature to determine exchange coupling constants (14, 16, 17). Their widths are smaller than 50 cm^{-1}, narrower by almost an order of magnitude than the transitions in Fig. 1. From the positions of the $^6A_1 \rightarrow {}^4T_1$ and $^6A_1 \rightarrow {}^4T_2$, $^2T_2$ bands we estimate a value of Dq/B of 1.6 for {FeFe} from the ligand-field diagrams in ref. 18. This value is considerably higher than for manganese(II) compounds due to the trivalent metal ion and it is higher than for iron(III) pairs in sapphire due to the stronger ligand field created by the triazacyclononane ligands.

Figure 2 shows single crystal absorption spectra of the {MnMn} compound as a function of temperature. As for the {FeFe} compound, the band positions and intensities at 300 K are similar to those reported in solution (7). We observe a hot band at 19 230 cm^{-1} superimposed on a more intense band at 20 620 cm^{-1}. This is the only band that changes significantly with temperature and we will use it to determine the ground-state exchange coupling constant for this compound in Sect. 4(b). The band system shown in Fig. 2 is assigned to the spin-allowed $^5E \rightarrow {}^5T_2$ transition of a d^4 transition metal center, split by low-symmetry crystal-field components and vibronic effects. This assignment leads to a Dq/B value of 1.8 (15, 18), very similar to the value of 1.6 determined for {FeFe} and thus supporting our assignment. The temperature dependence of the spectra in Fig. 2 shows evidence for a broad cold band centered at 21 500 cm^{-1}. Its intensity is too low to be quantitatively determined at each temperature. A weak, broad

Can. J. Chem. Downloaded from www.nrcresearchpress.com by 65.111.164.53 on 09/08/12
For personal use only.

Fig. 2. Single crystal absorption spectra of {MnMn} as a function of temperature. The hot band used to determine the exchange coupling parameter in Fig. 6 is denoted by a circle. The spectra are vertically offset for clarity by 0.06 absorbance units in order of increasing temperature.

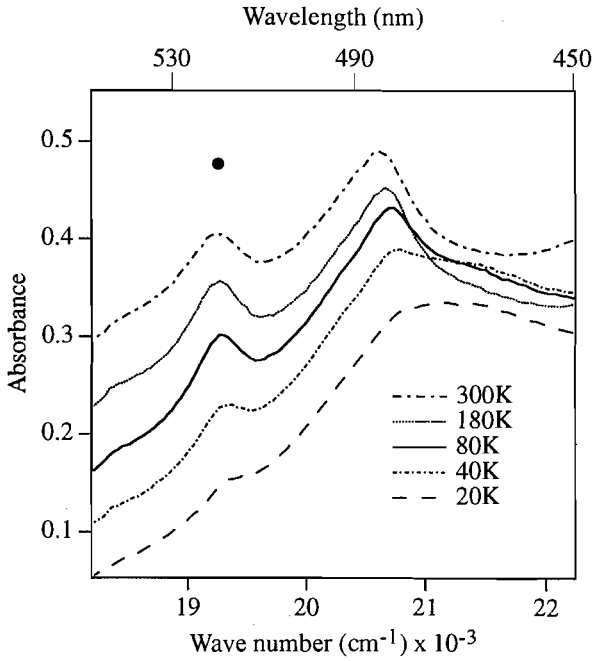

shoulder centered at 17 500 cm^{-1} in the absorption spectrum of {MnMn} is assigned as the spin-forbidden $^5E \rightarrow {}^3T_1$ band, the lowest energy transition at the crystal field strength of this compound. Comparison of the spectra of {MnMn} and {FeFe} therefore allows an assignment of the observed bands despite the lack of highly resolved fine structure in the spectra.

4. Discussion

(a) Temperature dependence of the spectrum of {FeFe}

The absorption spectrum in Fig. 1 shows a pronounced temperature dependence of the absorption intensities in the system of bands between 17 200 cm^{-1} and 24 200 cm^{-1}. We determine the intensities of individual bands by fitting a sum of Gaussians to the experimental spectra. The variation of the intensities with temperature allows us to quantitatively determine the exchange coupling parameter J in this new binuclear compound. In the following analysis and for all comparisons with literature values we use the exchange Hamiltonian

$$[1] \quad H_{ex} = -JS_1 \cdot S_2$$

The same operator is used in ref. 7 and we can therefore directly compare the numerical values for the ground state coupling constant J obtained from magnetic measurements with the value from absorption spectra in this work.

We first discuss the temperature-dependent absorption intensities in terms of ground state exchange splittings in the binuclear molecular unit. The absorption bands showing a change of intensity with temperature originate from different levels of the electronic ground state, split by exchange interaction. For the case of a binuclear Fe^{3+} complex, the ground state

Fig. 3. Fit of the absorption spectra in Fig. 1 to a sum of four Gaussians. The experimental spectrum is shown as a dotted line, the best fit as a solid line. The individual Gaussians are denoted by dot-dashed lines. The bottom trace of the graph shows the difference between experiment and fit on the right-hand ordinate scale enlarged by a factor of four. Vertical bars denote the region used for fitting the linear base line.

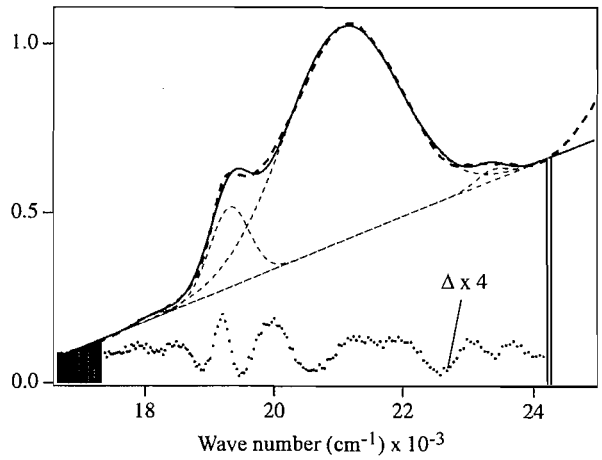

splits into six levels with total spins ranging from 0 to 5. The energy separations of the levels are J, $2J$, $3J$, $4J$, and $5J$, with increasing pair spin quantum number S. The compound is reported to be antiferromagnetic, therefore the level with $S = 0$ is lowest in energy (7).

To separate the intensities of the overlapping bands forming the absorption spectrum in Fig. 1, we fitted a sum of four Gaussians to the experimental spectrum. The result of this fit is illustrated in Fig. 3 for the spectrum measured at 200 K, a temperature where all four bands have significant intensities. In a first step, we determined a linear base line from the areas of the spectrum denoted by vertical bars, then we fitted the sum of four Gaussians to the spectrum, using the previously determined linear base line. The base line and the four Gaussians are included in Fig. 3. The residuals of the fit, also included in Fig. 3, show the limits of the model based on Gaussians for an accurate description of the bandshape. The largest differences are found in the region of overlap between bands, and are caused by the assumption of Gaussian bandshapes. It is important to notice that the discrepancies in these regions of low intensity of each Gaussian do not have a large influence on the calculated band intensities. The Gaussians are integrated to calculate the intensity of each transition as a function of temperature, shown in Fig. 4. The band maxima obtained from the fit change by 300 cm^{-1} between 15 and 300 K. This small shift to lower energy indicates that no structural phase transition occurs in the temperature range studied.

The integrated intensities $I(S)$ of absorption transitions from the ground state levels with pair spins S of 0 and 1 are given by eqs. [2] and [3], respectively.

$$[2] \quad I(S=0) = C_0(1 + 3e^{J/kT} + 5e^{3J/kT} + 7e^{6J/kT} + 9e^{10J/kT} + 11e^{15J/kT})^{-1}$$

$$[3] \quad I(S=1) = C_1(3e^{JkT})(1 + 3e^{J/kT} + 5e^{3J/kT} + 7e^{6J/kT} + 9e^{10J/kT} + 11e^{15J/kT})^{-1}$$

Fig. 4. Relative intensities of the absorption bands of {FeFe} originating from ground state levels with pair spin S as a function of temperature. The symbols denote experimental intensities determined from the absorption spectra in Fig. 1. The solid lines are fits to eqs. [2] and [3] for the transitions originating from the ground state levels with pair spins S of 0 and 1, respectively, with a value of -295 cm^{-1} for the exchange coupling parameter J in eq. [1]. The dotted lines denote curves calculated using the literature value of -207 cm^{-1} for J (7).

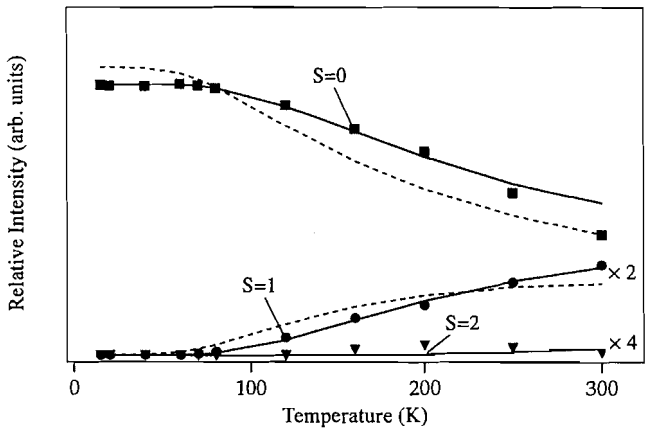

The scaling factors C_0 and C_1 are necessary because no reliable absolute oscillator strengths can be determined due to the large uncertainties in estimating the thickness of our crystals. Three parameters, J, C_0, and C_1, were adjusted by a least-squares method.[2] The calculated intensities are in very good agreement with the experimental data, as shown in Fig. 4. An average value of -295 ± 8 cm^{-1} was obtained for J, and values of 1904 ± 11 A cm^{-1} and 716 ± 33 A cm^{-1} are obtained for the factors C_0 and C_1, respectively. In a separate step, we fitted the temperature dependence of the high-energy band at 23 530 cm^{-1}, denoted by the solid triangle in Fig. 1. These low intensities were not included in the first stage of the fit because their relative errors are much larger than those of the more intense bands. The value of J was held constant and we adjusted only the parameter C_3 in a fit equation analogous to eq. [3], but for the ground state level with $S = 2$. A value of 312 ± 148 A cm^{-1} was obtained for the scaling constant C_3. The large error reflects the low absolute intensity of the band denoted by the solid triangle in Fig. 1 and is the reason why these intensities were not included in the fit used to determine J. The fit is shown in Fig. 4 and agrees well with the experimental intensities, confirming the J value found from the more intense bands. We conclude that transitions from three of the five ground state levels, those with pair spins of 0, 1, and 2, to different excited states are observed. The coupling constant J obtained from the absorption spectra is in reasonable agreement with the value of -207 cm^{-1} determined from magnetic susceptibility data (7). The difference between the two values is most likely due to the influence of paramagnetic impurities on the magnetic measurements, evident from Fig. 5 of ref. 7 and uncertainties in our Gaussian fitting procedure of the optical spectra. We include in Fig. 4 relative intensities for the two most intense transitions, calculated from eqs. [2] and [3] with the literature value of -207 cm^{-1} for the coupling constant J and by refining the constants C_0 and C_1. This comparison shows that the intensities obtained with both values are reasonable, especially for the band originating from the level with a pair spin S of 1. An underlying assumption to the analysis both in this work and in ref. 7 is that J is considered independent of temperature. This has been shown to be problematic for a bimetallic compound of chromium(III), leading to errors of more than 30% for the J value determined from temperature-dependent measurements (19). Magnetic measurements and optical spectra are expected to be affected in different ways by the temperature dependence of J, causing the discrepancy observed between the two values of J. In view of the fundamentally different physical effects used by the two methods and the underlying assumptions, we conclude that the agreement between our value of J and the literature result is satisfactory and illustrates the potential of optical spectroscopy as an alternative method for the determination of magnetic properties.

The exchange interaction in the ground state of {FeFe} is an order of magnitude larger than for triply bridged Fe^{3+} pairs in sapphire, where an antiferromagnetic interaction with a value of -25 cm^{-1} for J was determined (14). It is interesting to note that the opposite order of the J values is observed for similar systems containing Cr^{3+} ions: a strong antiferromagnetic coupling with values of -115 cm^{-1} (20) and -128 cm^{-1} (21) in the triply-bridged nearest neighbor pairs in ruby and tris-μ-hydroxo-bridged molecular compounds, respectively, and a much weaker coupling of -29 cm^{-1} (22) in a binuclear compound with μ-hydroxo-bis-μ-acetato-bridged chromium ions, similar to {FeFe}. This comparison shows that the prediction of the value of the exchange constant based simply on comparisons of bridging geometries or electron configurations is very difficult.

The {FeFe} compound with its d^5–d^5 electron configuration is a particularly interesting system for a study of the dominant intensity mechanism of the observed absorption transitions. Two mechanisms can contribute to the intensity: the single-ion mechanism and the pair mechanism described by Tanabe and co-workers (9). The spectroscopic signatures of the two mechanisms are different because of their different spin selection rules: $\Delta S = 0, \pm 1$ for the former (23, 24) and $\Delta S = 0$ for the latter mechanism (25, 26). In the {FeFe} compound, a transition with $\Delta S = 0$ is not possible at very low temperature because there exists no excited state with a pair spin of 0 in a d^5–d^5 system. The cold band at 21 230 cm^{-1} therefore gains its intensity by the single-ion mechanism and the spin of the final state of the absorption transition is $S = 1$, most likely a component of the $^6A_1{}^4T_2$ pair state. It is interesting to note that for pairs of manganese(II) ions the corresponding transition is not observed, but the hot bands arising from the $S = 1,2$ ground state components are intense, indicating a Tanabe mechanism, analyzed in detail for a series of fluoride lattices doped with manganese(II) (17, 27). Possible reasons for the efficiency of the single-ion mechanism in {FeFe} compared to the highly symmetrical host lattices doped with manganese(II) are the considerable odd-parity crystal field components in the {FeFe} compound and the larger spin-orbit coupling of iron(III) compared to manganese(II) (28). The Tanabe mechanism could contribute to the intensity of the hot bands observed in {FeFe}, but their intensity, as illustrated for the most intense hot band by the value of C_1, is not higher than the intensity of the cold band, indicating very weak or no contributions by the Tanabe mechanism. This is surprising, because

Can. J. Chem. Downloaded from www.nrcresearchpress.com by 65.111.164.53 on 09/08/12
For personal use only.

Can. J. Chem. Downloaded from www.nrcresearchpress.com by 65.111.164.53 on 09/08/12
For personal use only.

Fig. 5. Energy levels and observed transitions used for the determination of exchange coupling constants in {FeFe} and {MnMn}. The assignments of pair spin quantum numbers are discussed in the text.

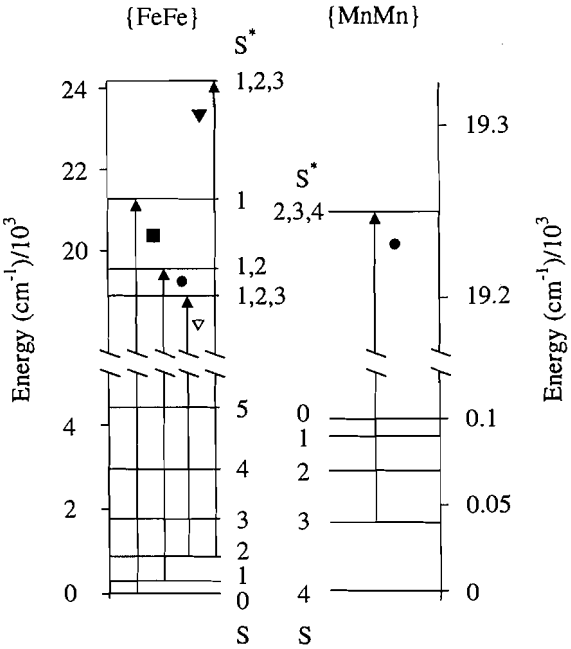

the title compound does not have a center of inversion in the point group of the binuclear molecular unit and therefore fulfills the symmetry requirements of the Tanabe mechanism (9).

The unresolved absorption spectra do not allow us to quantitatively determine excited state exchange coupling constants J^*, but we can nevertheless compare our spectroscopic results to the energetic order of the excited states arising from the $^2T_2$-$^4T_2$ region of the d^5 Tanabe–Sugano diagram (15). Literature assignments of similar spectra of bimetallic compounds of iron(III) include low-energy charge-transfer bands, (6) but we limit our qualitative discussion to *d–d* transitions, based on the similar intensities and widths of all the bands in Fig. 1. All the transitions are schematically illustrated in Fig. 5. The excited state at 21 230 cm^{-1}, determined from the maximum of the cold band, must have a pair spin S^* of 1 and therefore arises from a $^6A_1{}^4T_2$ pair state. Using the selection rules for the single-ion mechanism leads to possible values of 1, 2 or 3 for the pair spins of the final states of the hot bands. They could thus arise both from $^6A_1{}^4T_2$ or from $^6A_1{}^2T_2$ pair states. The Tanabe–Sugano diagram shows that the $^4T_2$ and $^2T_2$ excited states are close in energy for {FeFe}. The interactions between these two states make it impossible to determine a ferromagnetic or antiferromagnetic ordering of the spin levels of the two excited states from our spectra, but the pair spins and single-ion parent state assignments of the bands observed for {FeFe} are confirmed.

(b) Temperature dependence of the spectrum of {MnMn}

The {MnMn} compound shows only one absorption band with a distinct temperature dependence: the hot band centered at 19 230 cm^{-1}. This is the only band that can be used for the calculation of the ground state exchange coupling constant J. It is remarkable to notice that {MnMn} provides a rare example of

Fig. 6. Intensity of the hot band of {MnMn} at 19 230 cm^{-1} in Fig. 2 as a function of temperature. The solid line is a fit to eq. [4] leading to an exchange coupling constant J of +10 cm^{-1}.

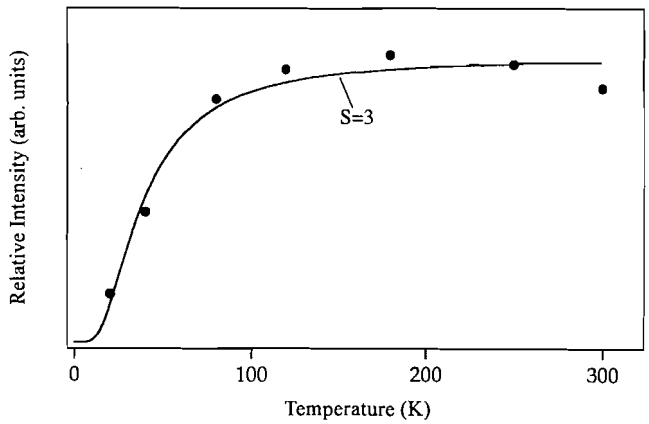

a spin-allowed *d–d* transition that is strongly affected by exchange effects. (9) The intensity of the hot band was determined and integrated in the same way as described for {FeFe} and is shown in Fig. 6. The pair spin of a d^4–d^4 system can range from $S = 0$ to $S = 4$, and it is not obvious which of these levels is the initial state of the transition. The comparison with magnetic measurements in ref. 7 shows that a ferromagnetic coupling is expected for this compound, i.e., the level with $S = 4$ is lowest in energy. It is reasonable to assume that the hot band originates from the $S = 3$ level. Its intensity is then given by:

$$[4]\quad I(S=3) = C_3(7e^{-4J/kT})(9 + 7e^{-4J/kT} + 5e^{-7J/kT} + 3e^{-9J/kT} + e^{-10J/kT})^{-1}$$

From the fit of eq. [4] to the experimental intensities we obtained a value of +10 ± 1 cm^{-1} for J, in very good agreement with the literature value of +14 cm^{-1} (7), and a value of 93 ± 3 A cm^{-1} for C_3. The calculated relative intensity is compared to the experimental intensities in Fig. 6. The combination of magnetic measurements and optical spectra of {MnMn} confirms the ferromagnetic coupling, leads to consistent values for the magnitude of the exchange interaction in this compound, and confirms the pair spin of 3 for the initial state of the transition shown schematically in Fig. 5. The pair spin S^* of its final state is 2, 3, or 4 with the intensity mechanisms discussed for {FeFe}.

Acknowledgements

We thank Professor Karl Wieghardt (Ruhr-Universität, Bochum, Germany) for the gift of the compounds used in this study. This work was made possible by operating and equipment grants from the Natural Sciences and Engineering Research Council of Canada (NSERC) and Fonds pour la formation de chercheurs et l'aide à la recherche (FCAR) (Province of Quebec). Y. P. acknowledges the award of an undergraduate research fellowship by NSERC.

References

1. V. J. DeRose, K. E. Liu, D. M. Kurtz, Jr., B. M. Hoffmann, and S. J. Lippard. J. Am. Chem. Soc. **115**, 6440 (1993).

2. R. M. Buchanan, S. Chen, J. F. Richardson, M. Bressan, L. Forti, A. Morvillo, and R. H. Fish. Inorg. Chem. **33**, 3208 (1994).
3. R. Hage, J. E. Iburg, J. Kerschner, J. H. Koek, E. L. M. Lempers, R. J. Martens, U. S. Racherla, S. W. Russell, T. Swarthoff, M. R. P. van Vliet, J. B. Warnaar, L. van der Wolf, and B. Krijnen. Nature, **369**, 637 (1994).
4. K. Wieghardt. Angew. Chem. Int. Ed. Engl. **28**, 1153 (1989).
5. J. R. Hartman, R. L. Rardin, P. Chaudhuri, K. Pohl, K. Wieghardt, B. Nuber, J. Weiss, G. C. Papaefthymiou, R. B. Frankel, and S. J. Lippard. J. Am. Chem. Soc. **109**, 7387 (1987).
6. E. I. Solomon, F. Tuczek, D. E. Root, and C. A. Brown. Chem. Rev. **94**, 827 (1994).
7. R. Hotzelmann, K. Wieghardt, U. Flörke, H.-J. Haupt, D. C. Weatherburn, J. Bonvoisin, G. Blondin, and J.-J. Girerd. J. Am. Chem. Soc. **114**, 1681 (1992).
8. P. J. McCarthy and H. U. Güdel. Coord. Chem. Rev. **88**, 69 (1988).
9. H. U. Güdel. Comments Inorg. Chem. **5**, 189 (1984).
10. A. E. Hansen and C. J. Ballhausen. Trans. Faraday Soc. **61**, 631 (1965).
11. E. I. Solomon, K. W. Penfield, and D. E. Wilcox. Struct. Bonding (Berlin), **53**, 1 (1983).
12. S. R. Desjardins, D. E. Wilcox, R. L. Musselman, and E. I. Solomon. Inorg. Chem. **26**, 288 (1987).
13. E. I. Solomon and D. E. Wilcox. *In* Magneto-structural correlations in exchange-coupled systems. *Edited by* R. D. Willett, D. Gatteschi, and O. Kahn. Reidel, Dordrecht. 1983.
14. J. Ferguson and P. E. Fielding. Aust. J. Chem. **25**, 1371 (1972).
15. S. Sugano, Y. Tanabe, and H. Kamimura. Multiplets of transition metal ions in crystals. Academic Press, New York and London. 1970.
16. J. Ferguson. Progr. Inorg. Chem. **12**, 159 (1970).
17. J. Ferguson, H. U. Güdel, E. R. Krausz, and H. J. Guggenheim. Mol. Phys. **28**, 893 (1974).
18. E. König and S. Kremer. Ligand field energy diagrams. Plenum Press, New York and London. 1977.
19. H. Riesen and H. U. Güdel. Chem. Phys. Lett. **133**, 429 (1987).
20. G. F. Imbusch and W. M. Yen. *In* Lasers, spectroscopy and new ideas. Vol. 54. *Edited by* W. M. Yen and M. D. Levenson. Springer, Berlin. 1987; pp 248–267.
21. H. Riesen and H. U. Güdel. Mol. Phys. **60**, 1221 (1987).
22. C. Reber, H. U. Güdel, M. Buijs, K. Wieghardt, and P. Chaudhuri. Inorg. Chem. **27**, 2115 (1988).
23. M. Naito. J. Phys. Soc. Jpn. **34**, 1491 (1973).
24. S. Decurtins and H. U. Güdel. Inorg. Chem. **21**, 3598 (1982).
25. Y. Tanabe, T. Moriya, and S. Sugano. Phys. Rev. Lett. **15**, 1023 (1965).
26. J. Ferguson, H. J. Guggenheim, and Y. Tanabe. J. Phys. Soc. Jpn. **21**, 692 (1966).
27. J. Ferguson, H. J. Guggenheim, and Y. Tanabe. Phys. Rev. Lett. **14**, 737 (1965).
28. A. Abragam and B. Bleaney. Electron paramagnetic resonance of transition metal ions. Clarendon Press, Oxford. 1970. Tables 7.6, 7.7.

Can. J. Chem. Downloaded from www.nrcresearchpress.com by 65.111.164.53 on 09/08/12
For personal use only.

Stereospecific reactions of aryltellurium(IV) trichlorides with 3-cyclohexene-1-methanol and 3-cyclohexene-1,1-dimethanol: the X-ray crystal structure of 2′,4′-dimethoxyphenyl(*trans*-6-oxabicyclo[3.2.1]oct-4-yl)tellurium(IV) dichloride

Bozena Borecka, T. Stanley Cameron, M. Azad Malik, and Barry C. Smith

Abstract: Aryltellurium(IV) trichlorides react with 3-cyclohexene-1-methanol and 3-cyclohexene-1,1-dimethanol to give aryl(*trans*-6-oxabicyclo[3.2.1]oct-4-yl)tellurium(IV) dichlorides and aryl(*cis*-1-hydroxymethyl-*trans*-6-oxabicyclo[3.2.1]oct-4-yl)tellurium(IV) dichlorides. The structure of 2′,4′-dimethoxyphenyl(*trans*-6-oxabicyclo[3.2.1]oct-4-yl)tellurium(IV) dichloride has been determined by single crystal X-ray analysis. The compound $C_{15}H_{20}Cl_2O_3Te$, M_r = 446.8, crystallizes in the monoclinic space group $P2_1/c$ with a = 9.626(2) Å, b = 15.768(5) Å, c = 11.176(3) Å, β = 92.08(1)°, V = 1695.2(5) Å^3, and D(calc) = 1.751 for Z = 4. Tellurium is bonded axially to two chlorines and equatorially to aryl carbon and carbon from the cyclohexyl portion of oxabicyclo[3.2.1]oct-4-yl in a pseudo-trigonal–bipyramidal arrangement having an equatorial lone pair of electrons. Bond lengths are Te—Cl(1) = 2.492(3) Å, Te—Cl(2) = 2.539(3) Å, Te—C(4) = 2.175(10) Å, and Te—C(9) = 2.090(10) Å.

Key words: organotellurium(IV), 3-cyclohexene-1-methanol, 3-cyclohexene-1,1-dimethanol.

Résumé : Les trichlorures d'aryltellure(IV) réagissent avec le 3-cyclohexène-1-méthanol et avec le 3-cyclohexène-1,1-diméthanol pour donner les dichlorures d'aryl (*trans*-6-oxabicyclo[3.2.1]oct-4-yl)tellure(IV) et d'aryl (*cis*-1-hydroxyméthyl-*trans*-6-oxabicyclo[3.2.1] oct-4-yl)tellure(IV). On a déterminé la structure du dichlorure de 2′,4′-diméthoxyphényl (*trans*-6-oxabicyclo[3.2.1]oct-4-yl)tellure(IV) par cristallographie de rayons X sur un cristal unique. Le composé $C_{15}H_{20}Cl_2O_3Te$, M_r = 446,8, cristallise dans le groupe d'espace monoclinique $P2_1/c$ avec a = 9,626 (2) Å, b = 15,768(5) Å, c = 11,176(3) Å, β = 92,08(1)°, V = 1695,2(5) Å^3 et $D_{(calc)}$ = 1,751 pour Z = 4. Le tellure est lié en position équatoriale à deux chlorures et en position axiale au carbone du groupe aryle et à celui de la portion cyclohexyle du groupe oxabicyclo[3.2.1]oct-4-yl dans une configuration pseudo-bipyramidale–trigonale ayant un doublet libre en position équatoriale. Les longueurs de liaison sont : Te—Cl(1) = 2,492(3) Å, Te—Cl(2) = 2,539(3) Å, Te—C(4) = 2,175(10) Å et Te—C(9) = 2,090(10) Å.

Mots clés : organotellure(IV), 3-cyclohexène-1-méthanol, 3-cyclohexène-1,1-diméthanol.

[Traduit par la rédaction]

Introduction

Aryltellurium(IV) trichlorides undergo addition reactions with cycloalkenes to give aryl(*trans*-2-chloro-1-cycloalkyl)tellurium(IV) dichlorides (1–3). Similar reactions in the presence of an alcohol give aryl(*trans*-2-alkoxy-1-cycloalkyl)tellurium(IV) dichlorides as the result of electrophilic addition by aryldichlorotellurium(IV) and nucleophilic attack by alkoxy on the cyclic telluronium intermediates (3, 4). This paper describes reactions of aryltellurium(IV) trichlorides with 3-cyclohexene-1-methanol and 3-cyclohexene-1,1-dimethanol (Fig. 1), which contain alcoholic groups capable of intramolecular nucleophilic attack. The heterotricyclic[3.2.1]- nature of the products is established by NMR spectroscopy and by an X-ray crystallographic investigation of 2′,4′-dimethoxyphenyl(*trans*-6-oxabicyclo[3.2.1]oct-4-yl)-tellurium(IV) dichloride.

Received June 21, 1994.

B. Borecka and T.S. Cameron.[1] Department of Chemistry, Dalhousie University, Halifax, NS B3H 4J3, Canada.
M.A. Malik and B.C. Smith. Department of Chemistry, Birkbeck College (University of London). Gordon House, 29 Gordon Square, London WC1H 0PP, England.

[1] Author to whom correspondence may be addressed. Telephone: (902) 494-3305. Fax: (902) 494-1310.

Can. J. Chem. Downloaded from www.nrcresearchpress.com by 65.111.164.53 on 09/08/12
For personal use only.

Table 1. Aryl(*trans*-6-oxabicyclo[3.2.1]oct-4-yl)tellurium(IV) dichlorides and aryl(*cis*-1-hydroxymethyl-*trans*-6-oxabicyclo[3.2.1]oct-4-yl)tellurium(IV) dichlorides.

Compound	Yield (%)	Melting point (°C)	Found (%)			Formula	Calculated (%)		
			C	H	Cl		C	H	Cl
p-$MeOC_6H_4(C_7H_{11}O)TeCl_2$	72	Oil	40.63	4.29	17.35	$C_{14}H_{18}Cl_2O_2Te$	40.34	4.35	17.01
p-$EtOC_6H_4(C_7H_{11}O)TeCl_2$	61	Oil	42.18	4.64	16.69	$C_{15}H_{20}Cl_2O_2Te$	41.82	4.68	16.46
p-$PhOC_6H_4(C_7H_{11}O)TeCl_2$	71	108–110	48.12	4.39	15.24	$C_{19}H_{20}Cl_2O_2Te$	47.66	4.21	14.81
2′,4′-$(MeO)_2C_6H_3(C_7H_{11}O)TeCl_2$	67	180	39.90	4.58	15.80	$C_{15}H_{20}Cl_2O_3Te$	40.32	4.51	15.87
3′,4′-$(MeO)_2C_6H_3(C_7H_{11}O)TeCl_2$	67	113–115	40.19	4.48	15.90	$C_{15}H_{20}Cl_2O_3Te$	40.32	4.51	15.87
p-$MeOC_6H_4(C_8H_{13}O_2)TeCl_2$	42	Oil	40.53	4.49	16.03	$C_{15}H_{20}Cl_2O_3Te$	40.32	4.51	15.87
p-$EtOC_6H_4(C_8H_{13}O_2)TeCl_2$	65	124	42.39	4.78	16.42	$C_{16}H_{22}Cl_2O_3Te$	41.70	4.68	15.39
2′,4′-$(MeO)_2C_6H_3(C_8H_{13}O_2)TeCl_2$	67	164	40.10	4.54	14.90	$C_{16}H_{22}Cl_2O_4Te$	40.30	4.65	14.87
3′,4′-$(MeO)_2C_6H_3(C_8H_{13}O_2)TeCl_2$	60	167	40.27	4.64	15.15	$C_{16}H_{22}Cl_2O_4Te$	40.30	4.65	14.87

Fig. 1. 3-Cyclohexene-1-methanol and 3-cyclohexene-1,1-dimethanol.

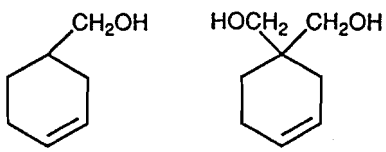

Experimental

In a typical reaction, a mixture of 2,4-dimethoxyphenyltellurium(IV) trichloride (1.50 g, 4.0 mmol) and 3-cyclohexene-1-methanol (0.45 g, 4.0 mmol) in chloroform (50 cm^3) was boiled under reflux (3 h). The red mixture was filtered, shaken with charcoal, and refiltered. The colourless filtrate was evaporated under reduced pressure. Crystallization from light petroleum (bp 40–60°C) gave 2′,4′-dimethoxyphenyl(*trans*-6-oxabicyclo[3.2.1]oct-4-yl)tellurium(IV) dichloride (1.19 g, 2.7 mmol, 67%), mp 180°C. The colourless products are stable at room temperature and are soluble in organic solvents. Yields, melting points, and analytical data are summarized in Table 1.

Data collection, structural analysis, and refinement

A suitably sized crystal of 2′,4′-dimethoxyphenyl(*trans*-6-oxabicyclo[3.2.1]oct-4-yl)tellurium(IV) dichloride was mounted on a glass fibre. An Enraf–Nonius CAD4 four-circle diffractometer, λ(MoKα) = 0.70926 Å with an ω–2θ scan at 291 K was used to measure the unit cell dimensions and collect the data. The crystal and data collection parameters are listed in Table 2. The unit cell constants were obtained by a least-squares analysis of the diffractometer setting angles of 25 well-centered reflections in the range 2θ = 20–30°. The intensities were reduced to a standard scale using routine procedures (5). Lorentz and polarization corrections were applied and absorption corrections (6) were performed. Scattering factors for neutral atoms (7) were corrected for the real part of anomalous dispersion. All calculations and refinements were performed by SHELX-76 (8).

The systematically absent reflections confirmed the space group as $P2_1/c$. Positions of tellurium were determined from a Patterson map and the remaining non-hydrogen atoms were located in subsequent difference-Fourier syntheses. The structure was refined initially by a full-matrix least-squares procedure with independent isotropic temperature factors on the non-hydrogen atoms. Hydrogen atoms were placed in their geometrically calculated positions, d(C—H) = 1.08 Å. Absorption corrections were then applied. The final refinements with anisotropic temperature factors on the non-hydrogen atoms and individual isotropic temperature factors on the hydrogen atoms gave $R = 0.0462$ and $R_w = 0.0475$ for 1548 unique observed reflections, $I > 3.00\sigma(I)$. A 2-block matrix least-squares method was employed. The function minimized was $\Sigma(\omega|F_o| - |F_c|)^2$ where ω is the weight. No correction for extinction was applied. The final difference map had no recognisable features (maximum peak 0.57 e $Å^{-3}$). The figures were produced with CHEMGRAPH (9). The fractional atomic positional parameters and temperature factors of non-hydrogen atoms are listed in Table 3. Anisotropic thermal parameters for non-hydrogen atoms, a diagram showing thermal ellipsoids, and a table of atomic parameters for hydrogen atoms are available as supplementary material.[2]

Results

Aryltellurium(IV) trichlorides, $ArTeCl_3$ (Ar = *p*-$MeOC_6H_4$, *p*-$EtOC_6H_4$, *p*-$PhOC_6H_4$, 2,4-$(MeO)_2C_6H_3$, and 3,4-$(MeO)_2C_6H_3$), react with 3-cyclohexene-1-methanol or 3-cyclohexene-1,1-dimethanol in chloroform. Analyses and mass spectra of the products are consistent with addition followed by the elimination of hydrogen chloride and the formation of

[2] Copies of material on deposit can be purchased from: The Depository of Unpublished Data, Document Delivery, CISTI, National Research Council Canada, Ottawa, Canada K1A 0S2.

The diagram showing thermal ellipsoids and the table of atomic parameters for hydrogen atoms have also been deposited with the Cambridge Crystallographic Data Centre, and can be obtained on request from The Director, Cambridge Crystallographic Data Centre, University Chemical Laboratory, 12 Union Road, Cambridge, CB2 1EZ, U.K.

Structure factor amplitudes are no longer being deposited and may be obtained directly from the author.

Can. J. Chem. Downloaded from www.nrcresearchpress.com by 65.111.164.53 on 09/08/12
For personal use only.

Can. J. Chem. Downloaded from www.nrcresearchpress.com by 65.111.164.53 on 09/08/12
For personal use only.

Table 2. Parameters for data collection and refinement. Crystal data.

Formula	$C_{15}H_{20}Cl_2O_3Te$
Molecular weight	445.81
Crystal class	Monoclinic
Space group	$P2_1/c$
a (Å)	9.626(2)
b (Å)	15.768(5)
c (Å)	11.176(3)
β (deg)	92.08(1)
Volume (Å^3)	1695.2(5)
Z	4
D(calc)	1.751
F(000)	880.0
μ (cm^{-1})	20.81
Crystal dimensions (mm)	0.1 × 0.2 × 0.4
Temperature (K)	291.0
Diffractometer	CAD4
λ(MoKα)	0.70926
hkl range	*h*: −10 10
	k: 0 17
	l: 0 12
θ range	3.0–23.0
Sin (θ)/λ	0.55
Take off angle (deg)	6.0
Detector width (mm) variable slit:	4(1.4 + tan θ)
Scan speed (deg/min)	Variable 1.6–3.3
Scan type	ω/2θ
Scan width (deg)	1.0 + 0.35 tan θ
Standards	−2, −7 1; 3 −4 4; −5 −1 1
Variation	0.0
No. of measured reflections	2588
No. of unique reflections	2347
R_m (merging R)	0.04
No. of observed reflections	1548 ($I > 3.00\sigma(I)$)
Transmission coefficients from absorption correction	1.0 to 0.740
Weighting scheme	$w = 1.9266/[\sigma^2F + 0.0005F^2]$
Highest peak in final diff. Fourier (e Å^{-3})	0.57
Agreement factors:	
R	0.0472
Rw	0.0487
GOF	2.0043

Table 3. Fractional atomic positional parameters and equivalent isotropic temperature factors (Å^2) for $C_{15}H_{20}Cl_2O_3Te$ with esd's in parentheses.

Atom	*x/a*	*y/b*	*z/c*	U_{eq}[a]
Te1	0.13223(7)	0.01458(4)	0.14925(7)	0.0410
Cl1	0.1236(3)	0.1494(1)	0.2651(2)	0.0625
Cl2	0.1536(3)	−0.1229(1)	0.0329(2)	0.0578
C1	0.3544(10)	0.2138(7)	−0.0487(10)	0.0520
C2	0.3940(12)	0.2082(6)	0.0825(10)	0.0560
C3	0.4211(10)	0.1162(6)	0.1254(9)	0.0455
C4	0.3244(9)	0.0487(6)	0.0648(8)	0.0373
C5	0.2811(10)	0.0730(7)	−0.0652(9)	0.0448
O6	0.4075(7)	0.0800(4)	−0.1296(6)	0.0574
C7	0.4553(12)	0.1668(7)	−0.1272(11)	0.0605
C8	0.2211(11)	0.1613(6)	−0.0708(10)	0.0510
O1	−0.0208(7)	−0.0686(5)	0.3400(6)	0.0584
O2	0.3464(7)	−0.1558(5)	0.6198(7)	0.0627
C9	0.2109(9)	−0.0457(6)	0.3039(8)	0.0368
C10	0.3534(11)	−0.0524(7)	0.3342(10)	0.0512
C11	0.3934(11)	−0.0888(7)	0.4401(9)	0.0482
C12	0.2964(10)	−0.1212(6)	0.5185(10)	0.0462
C13	0.1565(11)	−0.1162(6)	0.4875(10)	0.0510
C14	0.1137(10)	−0.0798(6)	0.3790(10)	0.0461
C15	−0.1264(11)	−0.1069(8)	0.4060(10)	0.0642
C16	0.2516(13)	−0.1799(8)	0.7098(10)	0.0659

[a] U_{eq} is calculated as: $\{U_{11}(a^*.a)^2 + U_{22}(b^*.b)^2 + U_{33}(c^*.c)^2 + 2(U_{12}.a^*.b^*.a.b.\cos(\gamma) + U_{13}.a^*.c^*.a.c.\cos(\beta) + U_{23}.b^*.c^*.b.c.\cos(\alpha))\}/3$.

condensation products. NMR evidence indicates that the products are aryl(*trans*-6-oxabicyclo[3.2.1]oct-4-yl)tellurium(IV) derivatives. No traces of [2.2.2] heterotricyclic products were detected.

Mass spectra

The mass spectra of aryl(*trans*-6-oxabicyclo[3.2.1]oct-4-yl)tellurium(IV) dichlorides and aryl(*cis*-1-hydroxymethyl-*trans*-6-oxabicyclo[3.2.1]oct-4-yl)tellurium(IV) dichlorides are characterized by base peaks at M_r 111 and 141, respectively, and molecular ion peaks at the relative molecular mass minus the relative atomic mass of one chlorine atom. Other peaks show the loss of a second chlorine atom and fragments

Fig. 2. Diagrammatic representation of aryl(*cis*-1-hydroxymethyl-*trans*-6-oxabicyclo[3.2.1]oct-4-yl)tellurium(IV) dichloride with letters A–H assigned to cyclohexyl hydrogen atoms.

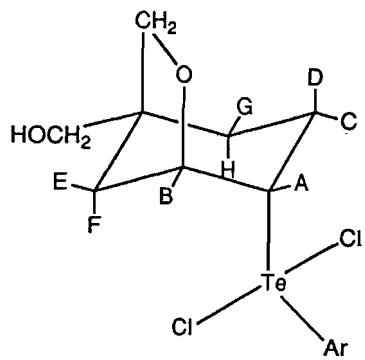

corresponding to ArTeCl, ArTe, ArCl, and Ar groups. The data are summarized in Table 4.

Proton NMR spectra

NMR spectra were recorded on a Varian VXR 400 spectrometer. Letters are assigned to the cyclohexyl hydrogens of aryl(*cis*-1-hydroxymethyl-*trans*-6-oxabicyclo[3.2.1]oct-4-yl)tellurium(IV) dichloride in Fig. 2 in order to assist the discussion of NMR spectra. Cyclohexyl H-CTe and H-CO protons are labelled A and B, respectively. Neighbouring geminal cyclohexyl methylene protons are C (*cis* to Te), D

Table 4. Mass spectra of aryl(*trans*-6-oxabicyclo[3.2.1]oct-4-yl)tellurium(IV) dichlorides and aryl(*cis*-1-hydroxymethyl-*trans*-6-oxabicyclo[3.2.1]oct-4-yl)tellurium(IV) dichlorides.

Compound	R	Ar	RCl	ArCl	ArTe	ArTeCl	$ArTeCl_2$	ArTeR	ArTeClR	$ArTeCl_2R$
p-$MeOC_6H_4(C_7H_{11}O)TeCl_2$	111	107	146	142	237	270	—	348	383	—
p-$EtOC_6H_4(C_7H_{11}O)TeCl_2$	111	121	146	156	251	286	321	362	397	432
p-$PhOC_6H_4(C_7H_{11}O)TeCl_2$	111	170	—	204	299	334	369	408	445	481
2′,4′-$(MeO)_2C_6H_3(C_7H_{11}O)TeCl_2$	111	138	—	172	267	302	337	378	413	447
3′,4′-$(MeO)_2C_6H_3(C_7H_{11}O)TeCl_2$	111	138	—	172	267	302	337	378	413	447
p-$MeOC_6H_4(C_8H_{13}O_2)TeCl_2$	141	107	176	142	237	270	—	378	413	—
p-$EtOC_6H_4(C_8H_{13}O_2)TeCl_2$	141	121	—	156	251	286	321	392	427	462
2′,4′-$(MeO)_2C_6H_3(C_8H_{13}O_2)TeCl_2$	141	138	—	172	267	302	337	406	443	477
3′,4′-$(MeO)_2C_6H_3(C_8H_{13}O_2)TeCl_2$	141	138	—	172	267	302	338	406	443	478

[a]R = $C_7H_{11}O$ or $C_8H_{13}O_2$.

Table 5. Chemical shifts and coupling constants 400 MHz for H-CTe (A) and H-CO (B) protons in aryl(*trans*-6-oxabicyclo[3.2.1]oct-4-yl)tellurium(IV) dichlorides and aryl(*cis*-1-hydroxymethyl-*trans*-6-oxabicyclo[3.2.1]oct-4-yl)tellurium(IV) dichlorides in chloroform.

Compound	H-CTe δ(A) (ppm)	H-CO δ(B) (ppm)	^3J(A–B) (Hz)	^3J(B–F) (Hz)
p-$MeOC_6H_4(C_7H_{11}O)TeCl_2$	4.19	5.10	3.2	6.2
p-$EtOC_6H_4(C_7H_{11}O)TeCl_2$	4.17	5.10	3.1	6.2
p-$PhOC_6H_4(C_7H_{11}O)TeCl_2$	4.20	5.10	[a]	[a]
2′,4′-$(MeO)_2C_6H_3(C_7H_{11}O)TeCl_2$	4.37	5.15	3.3	6.0
3′,4′-$(MeO)_2C_6H_3(C_7H_{11}O)TeCl_2$	4.17	5.11	3.1	6.2
p-$MeOC_6H_4(C_8H_{13}O_2)TeCl_2$	4.20	5.16	3.3	6.2
p-$EtOC_6H_4(C_8H_{13}O_2)TeCl_2$	4.18	5.16	3.1	5.9
2′,4′-$(MeO)_2C_6H_3(C_8H_{13}O_2)TeCl_2$	4.46	5.26	3.2	6.0
3′,4′-$(MeO)_2C_6H_3(C_8H_{13}O_2)TeCl_2$	4.20	5.17	3.2	6.0

[a]Coupling constants could not be measured accurately.

Fig. 3. Cyclohexyl H-CTe (A) and H-CO (B) proton signals at 400 MHz for 2′,4′-dimethoxyphenyl(*cis*-1-hydroxymethyl-*trans*-6-oxabicyclo[3.2.1]oct-4-yl)tellurium(IV) dichloride in $CDCl_3$.

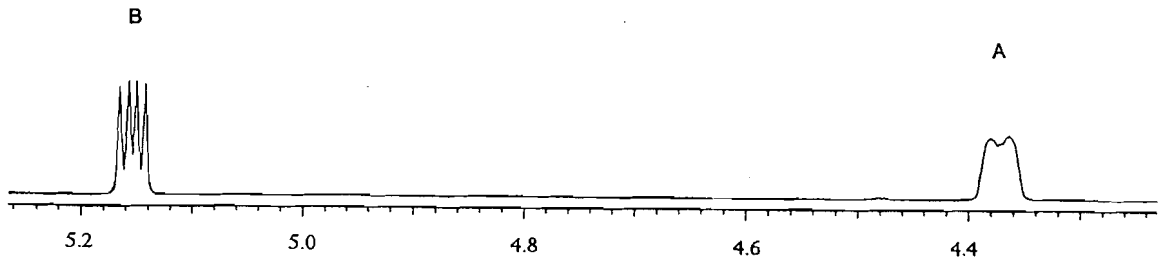

(*trans* to Te), E (*cis* to bridging OCH_2), and F (*trans* to bridging OCH_2). The remaining geminal cyclohexyl methylene protons are G (*cis* to bridging CH_2O) and H (*trans* to bridging OCH_2).

The signals for cyclohexyl H-CTe (A) and H-CO (B) protons differ in appearance from the well-resolved six- or eight-line multiplets in aryl(*trans*-2-alkoxy-1-cycloalkyl)tellurium(IV) dihalides (3) caused by strong coupling between *trans*-diaxial protons (^3J 10–12 Hz). Cyclohexyl A and B signals from 2′,4′-dimethoxyphenyl(*cis*-1-hydroxymethyl-*trans*-6-oxabicyclo[3.2.1]oct-4-yl)tellurium(IV) dichloride are illustrated in Fig. 3. The H-CTe (A) signal appears as two unresolved bands through equatorial–axial coupling, ^3J(A–D) ca.7 Hz, that are broadened by diequatorial coupling, ^3J(A–B) 3.2 Hz, ^3J(A–C) ca. 1 Hz. COSY spectra (described below) indicate further weak coupling with protons F and H. The cyclohexyl H-CO (B) protons appear as four lines through equatorial–axial coupling, ^3J(B–F) 6.0 Hz, and diequatorial coupling, ^3J(A–B) 3.2 Hz; diequatorial coupling with eclipsed proton E is not observed.

Chemical shifts and coupling constants for cyclohexyl A and B protons in aryl(*trans*-6-oxabicyclo[3.2.1]oct-4-yl)tellu-

Can. J. Chem. Downloaded from www.nrcresearchpress.com by 65.111.164.53 on 09/08/12
For personal use only.

Fig. 4. Resolution-enhanced cyclohexyl methylene proton signals C–H at 400 MHz for 2′,4′-dimethoxyphenyl(*cis*-1-hydroxymethyl-*trans*-6-oxabicyclo[3.2.1]oct-4-yl)tellurium(IV) dichloride in $CDCl_3$.

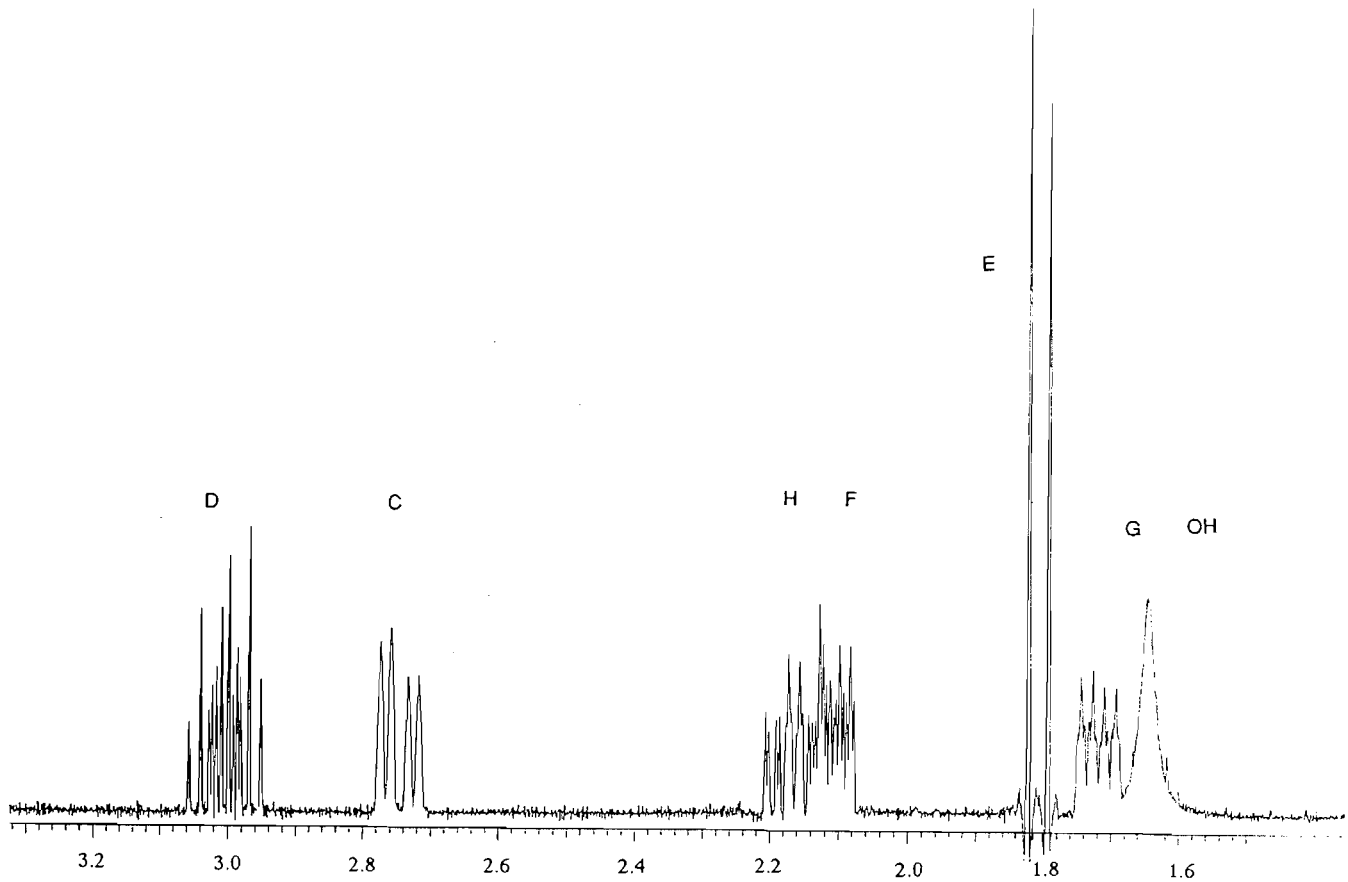

rium(IV) dichlorides and aryl(*cis*-1-hydroxymethyl-*trans*-6-oxabicyclo[3.2.1]oct-4-yl)tellurium(IV) dichlorides are summarized in Table 5. Chemical shifts of A protons are similar to those in aryl(*trans*-2-chlorocyclohexyl)tellurium(IV) dichlorides but B protons appear at lower field than those in aryl(*trans*-2-chloro-1-cyclohexyl)tellurium(IV) dichlorides or aryl(*trans*-2-alkoxy-1-cycloalkyl)tellurium(IV) dichlorides (3). The coupling constants establish that A and B protons occupy *trans*-diequatorial positions and confirm that tellurium and oxygen occupy *trans*-diaxial positions in aryl(*trans*-6-oxabicyclo[3.2.1]oct-4-yl)tellurium(IV) dichlorides and aryl(*cis*-1-hydroxymethyl-*trans*-6-oxabicyclo [3.2.1]oct-4-yl)tellurium(IV) dichlorides.

Resolution-enhanced signals from the three pairs of cyclohexyl geminal methylene protons C to H of 2′,4′-dimethoxyphenyl(*cis*-1-hydroxymethyl-*trans*-6-oxabicyclo[3.2.1]oct-4-yl)tellurium(IV) dichloride in Fig. 4 confirm the [3.2.1] bridging structure with a cyclohexyl chair conformation in solution. Equatorial proton C appears as four lines through geminal, ^2J(C–D) 16 Hz, and equatorial–axial coupling, ^3J(C–H) 7 Hz, broadened by weak diequatorial coupling, ^3J(A–C) ~ ^3J(C–G) 1 Hz. Axial proton D gives a 12-line signal (triplets of doublets of a doublet) through geminal, ^2J(C–D) 16 Hz, diaxial, ^3J(D–H) 12 Hz, and axial–equatorial coupling, ^3J(A–D) ~ ^3J(D–G) 7 Hz. The simplest signal is the doublet from equatorial proton E, which couples geminally, ^2J(E–F) 12 Hz, but not with eclipsed equatorial proton B. Axial proton F appears as four triplets through geminal, ^2J(E–F) 12 Hz, and axial–equatorial coupling, ^3J(B–F) 6 Hz, and diequatorial coupling with distant protons A and G, ^4J ca. 2 Hz. Equatorial proton G exhibits four lines through geminal, ^2J(G–H) 14 Hz, and axial–equatorial coupling, ^3J(D–G) 7 Hz, that are split into triplets through weaker coupling with equatorial proton C and distant proton F. Axial proton H undergoes geminal, ^2J(G–H) 14 Hz, diaxial, ^3J(D–H) 12 Hz, and axial–equatorial coupling, ^3J(C–H) 6 Hz, to appear as doublets of a broad-centred triplet. Further coupling with one bridging methylene proton, ^4J ca. 2 Hz, causes splitting of the four outer lines and broadening of the two inner bands.

Methylene proton signals from free $HOCH_2$ and bridging OCH_2 groups in the spectrum of *p*-ethoxyphenyl(*cis*-1-hydroxymethyl-*trans*-6-oxabicyclo[3.2.1]oct-4-yl)tellurium (IV) dichloride are illustrated in Fig. 5. Free methanolic methylene protons give the expected four-line signal, ^2J 11 Hz. One bridging OCH_2 methylene proton appears as a doublet, ^2J 8 Hz; the other appears as two pairs of doublets through further coupling with proton H, ^4J 2 Hz. Proton signals from aryl groups and their substituents resemble those in aryl(*trans*-2-chloro-1-cycloalkyl)tellurium(IV) dichlorides and aryl(*trans*-2-ethoxy-1-cycloalkyl)tellurium(IV) dichlorides (3).

A two-dimensional homonuclear shift correlated (COSY) spectrum of 2′,4′-dimethoxyphenyl(*cis*-1-hydroxymethyl-*trans*-6-oxabicyclo[3.2.1]oct-4-yl)tellurium(IV) dichloride confirms that the H-CTe (A) proton couples with cyclohexyl

Can. J. Chem. Downloaded from www.nrcresearchpress.com by 65.111.164.53 on 09/08/12
For personal use only.

Table 6. Cyclohexyl and methanolic carbon-13 NMR chemical shifts for aryl(*trans*-6-oxabicyclo[3.2.1]oct-4-yl)tellurium(IV) dichlorides and aryl(*cis*-1-hydroxymethyl-*trans*-6-oxabicyclo[3.2.1]oct-4-yl)tellurium(IV) dichlorides in chloroform.

Compound	δ(ppm)							
	C-Te	C-O	Other cycloalkyl carbons				CH_2O	CH_2OH
p-$MeOC_6H_4(C_7H_{11}O)TeCl_2$	75.76	72.68	35.24	34.51	27.96	21.90	64.44	
p-$EtOC_6H_4(C_7H_{11}O)TeCl_2$	75.71	72.66	35.21	34.51	27.92	21.85	64.43	
p-$PhOC_6H_4(C_7H_{11}O)TeCl_2$	75.60	72.52	35.22	34.40	27.84	21.87	64.36	
2′,4′-$(MeO)_2C_6H_3(C_7H_{11}O)TeCl_2$	75.75	72.80	35.74	34.49	28.24	22.00	57.73	
3′,4′-$(MeO)_2C_6H_3(C_7H_{11}O)TeCl_2$	75.80	72.71	35.19	34.54	28.00	21.93	64.82	
p-$MeOC_6H_4(C_8H_{13}O_2)TeCl_2$	77.07	74.40	45.73	37.42	30.46	22.39	63.96	66.85
p-$EtOC_6H_4(C_8H_{13}O_2)TeCl_2$	76.98	74.41	45.73	37.42	30.46	22.39	64.00	66.94
2′,4′-$(MeO)_2C_6H_3(C_8H_{13}O_2)TeCl_2$	77.04	74.61	45.71	37.93	30.84	22.53	57.52	67.07
3′,4′-$(MeO)_2C_6H_3(C_8H_{13}O_2)TeCl_2$	77.16	74.52	45.79	37.38	30.66	22.44	64.52	67.03

Can. J. Chem. Downloaded from www.nrcresearchpress.com by 65.111.164.53 on 09/08/12
For personal use only.

Fig. 5. Bridging OCH_2 and free $HOCH_2$ methylene proton signals at 400 MHz from *p*-ethoxyphenyl(*cis*-1-hydroxymethyl-*trans*-6-oxabicyclo[3.2.1]oct-4-yl)tellurium(IV) dichloride in $CDCl_3$.

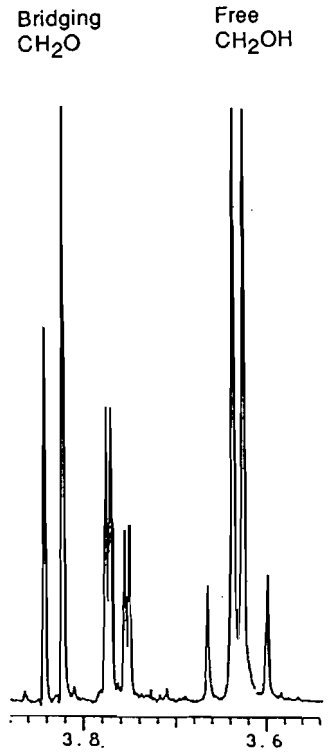

B, C, D, F, and H protons, that the H-CO (B) proton couples only with protons A and F, and that proton C couples with protons A, G, and H. The free $HOCH_2$ methylene protons couple only with each other. The bridging OCH_2 protons couple with each other and one couples also with proton H.

Carbon-13 NMR spectra

Aryl C-Te signals appear at lowest field with carbons *ortho* to tellurium at next lowest field followed by other aryl carbons. Carbons that were alkenic originally appear in midfield with

Table 7. Interactomic distances (Å) for $C_{15}H_{20}Cl_2O_3Te$.

Atoms	Distance
Te—Cl(1)	2.492(3)
Te—Cl(2)	2.539(3)
Te—C(4)	2.175(10)
Te—C(9)	2.090(10)
C(1)—C(2)	1.50 (2)
C(1)—C(7)	1.52 (2)
C(1)—C(8)	1.54 (2)
C(2)—C(3)	1.55 (2)
C(3)—C(4)	1.554(14)
C(4)—C(5)	1.545(14)
C(5)—O(6)	1.441(13)
C(5)—C(8)	1.51 (2)
O(6)—C(7)	1.444(14)
O(1)—C(14)	1.363(13)
O(1)—C(15)	1.413(14)
O(2)—C(12)	1.331(13)
O(2)—C(16)	1.434(15)
C(9)—C(10)	1.404(15)
C(9)—C(14)	1.388(14)
C(10)—C(11)	1.36 (2)
C(11)—C(12)	1.40 (2)
C(12)—C(13)	1.38 (2)
C(13)—C(14)	1.39 (2)

C-Te slightly lower than C-O as shown in Table 6. Chemical shifts for cycloalkyl C-Te are similar to those in aryl(*trans*-2-chloro-1-cyclohexyl)tellurium(IV) dichlorides (3). The OCH_2 methylene carbons appear below bridging methylene carbons and free methanolic carbons. Cyclohexyl methylene carbons appear at high field.

Discussion

Mechanism

The proposed mechanism for reaction of an aryltellurium(IV) trichloride with 3-cyclohexene-1-methanol is illustrated diagrammatically in Fig. 6. Electrophilic attack by aryldichloro-

Fig. 6. Proposed scheme for reaction of aryltellurium(IV) trichloride with 3-cyclohexene-1-methanol.

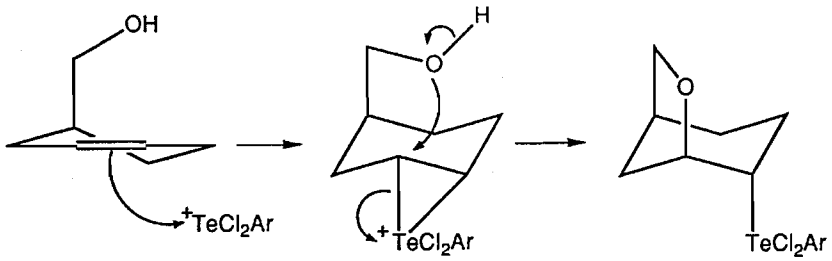

Fig. 7. Crystal structure of 2′,4′-dimethoxyphenyl(*trans*-6-oxabicyclo[3.2.1]oct-4-yl)tellurium(IV) dichloride.

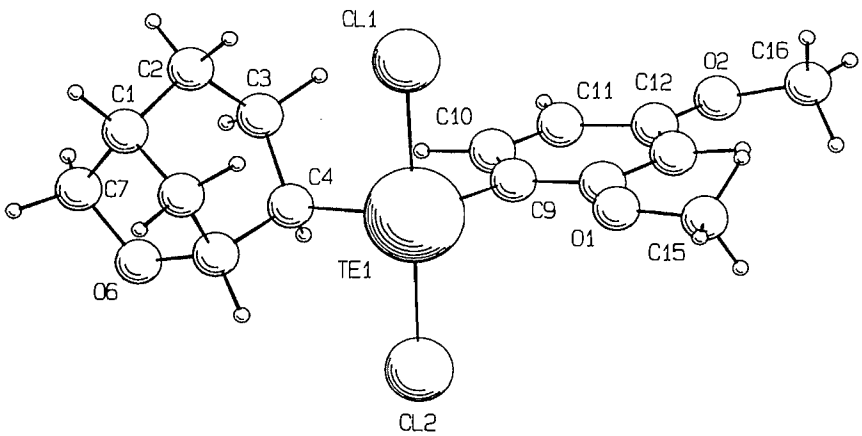

Fig. 8. (*a*) Packing diagram and (*b*) details of long contacts in 2′,4′-dimethoxyphenyl(*trans*-6-oxabicyclo[3.2.1]oct-4-yl)tellurium(IV) dichloride.

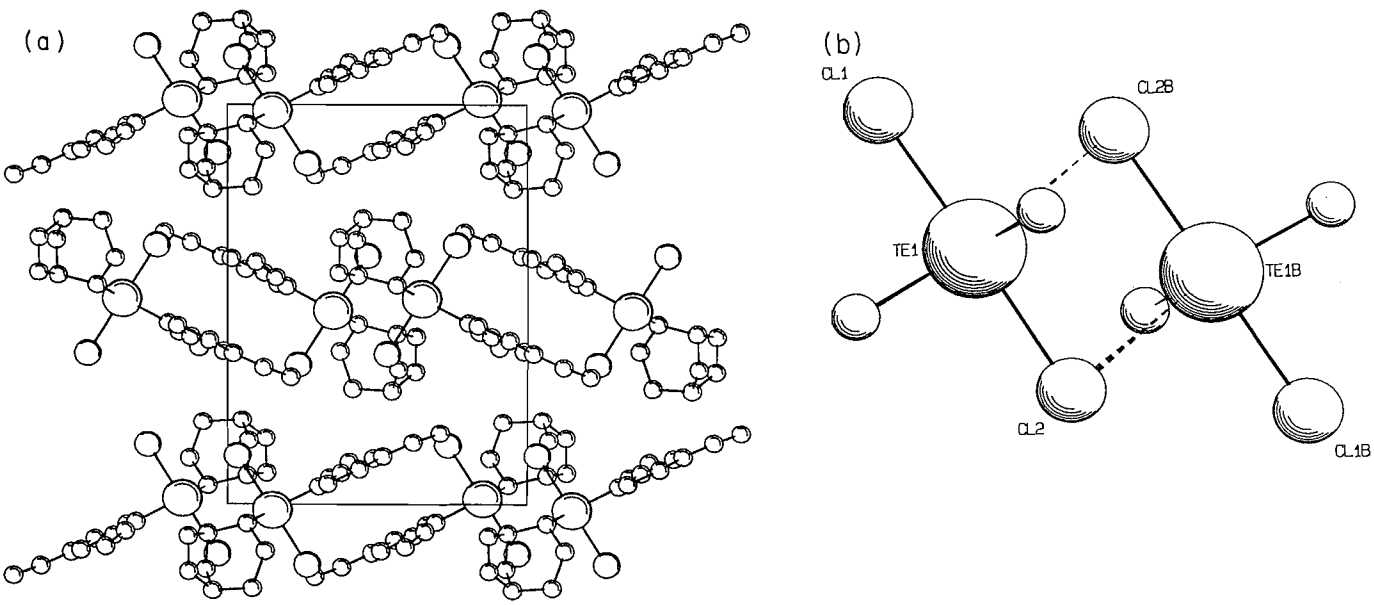

Can. J. Chem. Downloaded from www.nrcresearchpress.com by 65.111.164.53 on 09/08/12
For personal use only.

Can. J. Chem. Downloaded from www.nrcresearchpress.com by 65.111.164.53 on 09/08/12
For personal use only.

Table 8. Interbond angles (deg) for $C_{15}H_{20}Cl_2O_3Te$.

Atoms	Angle
Cl(1)—Te—C12	177.25(10)
Cl(1)—Te—C(4)	93.4(3)
Cl(1)—Te—C(9)	88.6(3)
Cl(2)—Te—C(4)	84.4(3)
Cl(2)—Te—C(9)	90.1(3)
C(4)—Te—C(9)	100.5(4)
C(2)—C(1)—C(7)	112.9(9)
C(2)—C(1)—C(8)	107.8(9)
C(7)—C(1)—C(8)	101.0(9)
C(1)—C(2)—C(3)	113.0(9)
C(2)—C(3)—C(4)	114.6(9)
Te—C(4)—C(3)	119.1(7)
Te—C(4)—C(5)	105.3(6)
C(3)—C(4)—C(5)	112.1(8)
C(4)—C(5)—O(6)	106.5(8)
C(4)—C(5)—C(8)	111.0(8)
O(6)—C(5—C(8)	103.7(8)
C(5)—O(6)C(7)	109.7(8)
C(1)—C(7)—O(6)	105.2(9)
C(1)—C(8)—C(5)	100.0(9)
C(14)—O(1)—C(15)	118.1(8)
C(12)—O(2)—C(16)	119.0(9)
Te—C(9)—C(10)	123.7(7)
Te—C(9)—C(14)	116.4(7)
C(10)—C(9)—C(14)	119.9(9)
C(9)—C(10)—C(11)	119.0(10)
C(10)—C(11)—C(12)	121.7(10)
O(2)—C(12)—C(11)	117.0(10)
O(2)—C(12)—C(13)	123.8(10)
C(11)—C(12)—C(13)	119.2(10)
C(12)—C(13)—C(14)	119.9(10)
O(1)—C(14)—C(9)	114.2(9)
O(1)—C(14)—C(13)	125.5(10)
C(9)—C(14)—C(13)	120.2(10)

Table 9. Torsional angles (deg) for $C_{15}H_{20}Cl_2O_3Te$.

Atoms	Angle
Cl(1)—Te—C(4)—C(3)	21.9(7)
Cl(1)—Te—C(4)—C(5)	−104.9(6)
Cl(1)—Te—C(9)—C(10)	−90.2(8)
Cl(1)—Te—C(9)—C(14)	89.4(8)
Cl(2)—Te—C(4)—C(3)	−156.4(7)
Cl(2)—Te—C(4)—C(5)	76.7(6)
Cl(2)—Te—C(9)—C(10)	87.4(8)
Cl(2)—Te—C(9)—C(14)	−93.0(8)
C(4)—Te—C(9)—C(10)	3.1(9)
C(4)—Te—C(9)—C(14)	−177.4(8)
C(9)—Te—C(4)—C(3)	−67.4(8)
C(9)—Te—C(4)—C(5)	165.8(6)
C(2)—C(1)—C(7)—O(6)	85.6(9)
C(7)—C(1)—C(2)—C(3)	−51.1(11)
C(2)—C(1)—C(8)—C(5)	−75.8(9)
C(8)—C(1)—C(2)—C(3)	59.6(10)
C(7)—C(1)—C(8)—C(5)	42.8(9)
C(8)—C(1)—C(7)—O(6)	−29.3(10)
C(1)—C(2)—C(3)—C(4)	−36.3(11)
C(2)—C(3)—C(4)—Te1	−92.0(8)
C(2)—C(3)—C(4)—C(5)	31.6(10)
Te—C(4)—C(5)—O(6)	−169.2(5)
Te—C(4)—C(5)—C(8)	78.5(8)
C(3)—C(4)—C(5)—O(6)	59.9(9)
C(3)—C(4)—C(5)—C(8)	−52.4(10)
C(4)—C(5)—O(6)—C(7)	−92.9(8)
C(4)—C(5)—C(8)—C(1)	72.6(8)
O(6)—C(5)—C(8)—C(1)	−41.5(9)
C(8)—C(5)—O(6)—C(7)	24.3(9)
C(5)—O(6)—C(7)—C(1)	3.7(10)
C(15)—O(1)—C(14)—C(9)	175.3(8)
C(15)—O(1)—C(14)—C(13)	−9.2(14)
C(16)—O(2)—C(12)—C(11)	172.0(9)
C(16)—O(2)—C(12)—C(13)	−8.3(14)
Te—C(9)—C(10)—C(11)	176.5(7)
Te—C(9)—C(14)—O(1)	0.0(10)
Te—C(9)—C(14)—C(13)	−175.8(8)
C(10)—C(9)—C(14)—O(1)	179.6(8)
C(10)—C(9)—C(14)—C(13)	3.8(13)
C(14)—C(9)—C(10)—C(11)	−3.1(14)
C(9)—C(10)—C(11)—C(12)	1.1(14)
C(10)—C(11)—C(12)—O(2)	179.9(8)
C(10)—C(11)—C(12)—C(13)	0.2(14)
O(2)—C(12)—C(13)—C(14)	−179.2(8)
C(11)—C(12)—C(13)—C(14)	0.5(14)
C(12)—C(13)—C(14)—O(1)	−177.8(9)
C(12)—C(13)—C(14)—C(9)	−2.4(13)

tellurium(IV) at the double bond produces a three-membered cyclic telluronium intermediate. Nucleophilic attack by methanolic oxygen with Walden inversion at carbon bonded to axial hydrogen is expected from the Furst–Plattner rule (see, for example, ref. 10). Ring opening gives the observed [3.2.1] tricyclic structure with tellurium and oxygen in adjacent diaxial positions. Postulated intermediates in reactions of aryltellurium(IV) trichlorides with 3-methylcyclohexene have tellurium and chlorine in similar diaxial positions, but ring inversion occurs so that tellurium and chlorine occupy diequatorial positions in aryl(*trans*-2-chloro-*trans*-3-methyl-1-cycloalkyl)tellurium(IV) dichlorides (11).

Structure

The molecule of 2′,4′-dimethoxyphenyl(*trans*-6-oxabicyclo-[3.2.1]oct-4-yl)tellurium(IV) dichloride is shown in Fig. 7. Tellurium has a pseudo-trigonal–bipyramidal configuration with four-coordinate tellurium bonded axially to two chlorines and equatorially to carbons from dimethoxyphenyl and oxabicyclo[3.2.1]oct-4-yl. Nonbonding contacts with tellurium avoid regions of equatorial nonbonding electrons. Long-range interactions between tellurium and chlorine from different asymmetric units, Te...Cl(2B) ($-x$, $-y$, $-z$) 3.771 Å, tie the molecules into the trigonal–bipyramidal arrangements of Fig. 8b.

Tellurium–chlorine bond lengths are Te—Cl(1) 2.492(3) Å and Te—Cl(2) 2.539(3) Å. The Cl(1)—Te—Cl(2) angle is

177.3(1)°. Tellurium–carbon bond lengths are Te—C(4) 2.175(10) Å and Te—C(9) 2.090(10) Å with Te—C(alkyl) longer than Te—C(aryl) (12). The C(4)—Te—C(9) angle is 100.5(4)°. These values are close to corresponding distances and angles in other diorganotellurium(IV) dichlorides (see, for example, ref. 13). The average cyclohexyl C—C bond length is 1.533 Å. The ring has a distorted chain conformation with C(3) at 0.439 Å above and C(8) at 0.899 Å below the plane through C(1), C(2), C(4), and C(5), which forms an angle of 109.26° with the plane through C(1), C(7), O(6), and C(5). Bridging distances are C(1)–C(7) 1.52(2) Å and O(6)–C(7) 1.444(14) Å. The average cyclohexyl C—C—C angle of 109.7°, smaller than 111.3° in cyclohexane (14), and the mean torsional angle of 54.7° are consistent with some flattening of the cyclohexyl ring caused by substituents (15). Selected interatomic distances, interbond angles, and torsional angles are given in Tables 7, 8, and 9, respectively.

Acknowledgements

We thank the Natural Sciences and Engineering Research Council of Canada for support to T.S.C.

References

1. M.M. Campos and N. Petragnani. Tetrahedron Lett. **6**, 11 (1959); Tetrahedron, **18**, 521 (1962).
2. T.S. Cameron, R.B. Amero, and R.E. Cordes. Cryst. Struct. Commun. **9**, 539 (1980).
3. M.A. Malik, M.E.S. Ali, F.J. Berry, J. Kaur, M. Rowshani, and B.C. Smith. Inorg. Chim. Acta, **180**, 251 (1991).
4. S. Uemura, S.-I. Fukuzawa, and A. Toshimitsu. J. Organomet. Chem. **250**, 203 (1983).
5. T.S. Cameron and R.E. Cordes. Acta Crystallogr. Sect. B. Struct. Crystallogr. Cryst. Chem. **B35**, 749 (1979).
6. N. Walker and D. Stuart. Acta Crystallogr. Sect. A: Found. Crystallogr. **A39**, 158 (1983).
7. D.T. Cromer and J.T. Waber. *In* International tables for X-ray crystallography. Vol IV. Kynoch Press, Birmingham, U.K. 1974.
8. G.M. Sheldrick. *In* SHELX-76. Program for crystal structure determination. University of Cambridge, Cambridge, U.K. 1976.
9. E.K. Davies. *In* The CHEMGRAPH suite. Chemical Crystallography Laboratory, University of Oxford, Oxford, U.K. 1983.
10. S.J. Angyal. Chem. Ind. (London), 1230 (1954); R.J. Ferrier and P.M. Collins. Monosaccharide chemistry. Penguin Books Ltd., Harmondsworth, U.K. 1972.
11. B. Borecka, T.S. Cameron, M.A. Malik, and B.C. Smith. Can. J. Chem. **72**, 1844 (1994).
12. O. Bastiansen and M. Traetteberg. Tetrahedron, **17**, 147 (1962).
13. T.S. Cameron, R.B. Amero, C. Chan, and R.E. Cordes. Cryst. Struct. Commun. **9**, 543 (1980); R.K. Chada and J.M. Miller. J. Chem. Soc. Dalton Trans. 117 (1982); R.K. Chada and J.E. Drake. J. Organomet. Chem. **268**, 141 (1984); S. Husebye, E.A. Meyers, R.A. Zingaro, J.V. Comasseto, and N. Petragnani. Acta Crystallogr. Sect. C: Cryst. Struct. Commun. **C43**, 1147 (1987).
14. M. Davis and M. Hassel. Acta Chem. Scand. **17**, 1181 (1963).
15. C. Altona and M. Sundaralingam. Tetrahedron, **26**, 925 (1970).

Can. J. Chem. Downloaded from www.nrcresearchpress.com by 65.111.164.53 on 09/08/12
For personal use only.

Studies on the mechanism of chelate degradation in iron-based, liquid redox H_2S removal processes

Dian Chen, Arthur E. Martell, and Derek McManus

Abstract: Available data on the oxidation of nitrilotriacetic acid (NTA), ethylenedinitrilotetraacetic acid (EDTA), *N*-hydroxyethylethylenediaminetriacetic acid (HEDTA), and other aminopolycarboxylate chelating agents are reviewed and the intermediates and products of the oxidative degradation of each chelating agent are described and compared. The oxidation of these chelating agents occurs during the reoxidation of the ferrous chelate to the ferric chelate, during which a Fenton type side reaction occurs in which hydrogen peroxide is formed and which in turn generates the hydroxyl radical by reaction with ferrous ion. The site of oxidative attack by the hydroxyl radical on these ligands seems to be the $-CH_2-$ groups α to the carboxylate groups, as well as the $-CH_2-$ groups in the ethylene bridges between the nitrogens. The evidence for the implication of the hydroxyl radical as the active oxidant is discussed, and the use of phenyl-*tert*-butylnitrone (PBN) as the trapping agent for the hydroxyl radical is described. The use of chelating agents as Fe^{3+}/Fe^{2+} redox catalysts for the oxidation of H_2S to sulfur that are less reactive toward the hydroxyl radical is recommended.

Key words: chelate degradation, H_2S oxidation, nitrilotriacetic acid (NTA), ethylenedinitrilotetraacetic acid (EDTA), *N*-hydroxyethylethylenediaminetriacetic acid (HEDTA).

Résumé : On passe en revue les données disponibles sur l'oxydation des acides nitrilotriacétique, éthylènedinitrilotétraacétique et *N*-hydroxyéthyléthylènediaminetriacétique ainsi que d'autres agents aminopolycarboxyliques chélatants; dans chaque cas, on décrit et on compare les intermédiaires et les produits de la dégradation oxydante de chacun des agents chélatants. L'oxydation de ces agents chélatants se produit lors de la réoxydation du chélate ferreux en chélate ferrique alors qu'il se produit une réaction secondaire du type de Fenton au cours de laquelle il se forme du peroxyde d'hydrogène qui, à son tour, génère la formation du radical hydroxyle par réaction avec l'ion ferreux. Le site de l'attaque oxydante du radical hydroxyle sur ces coordinats semble être les groupes $-CH_2-$ en α des groupes carboxylates ainsi que les groupes $-CH_2-$ des ponts éthylènes entre les azotes. On discute des données suggérant l'implication du radical hydroxyle comme oxydant actif et on décrit l'utilisation de la phényl-*tert*-butylnitrone (PBN) comme agent de piégeage du radical hydroxyle. Pour l'oxydation du H_2S en soufre, il est recommandé d'utiliser, comme catalyseurs rédox Fe^{3+}/Fe^{2+}, des agents chélatants qui sont moins réactifs vis-à-vis des radicaux hydroxyles.

Mots clés : chélate dégradation, H_2S oxydation, acide nitrilotriacétique, acide éthylènedinitrilotétraacétique, acide *N*-hydroxyéthyléthylènediaminetriacétique.

[Traduit par la rédaction]

Introduction

The oxidation of H_2S to S_8 by oxygen may be represented by the overall reaction

$$[1] \quad H_2S + \tfrac{1}{2}O_2 \rightarrow \tfrac{1}{8}S_8\downarrow + H_2O$$

The oxygen also oxidizes H_2S further, resulting in the formation of soluble products such as thiosulfate and sulfate, which are not as conveniently separated as elemental sulfur. Formation of these undesirable products is to a large extent avoided by carrying out the reaction in two steps with an Fe(III), Fe(II) chelate as a redox catalyst. With the 2:1 nitrilotriacetic acid (NTA, H_3L)–Fe(III) as the catalyst system the reaction sequence would be as follows:

H_2S absorption and oxidation

$$[2] \quad H_2S + 2FeNTA \rightarrow \tfrac{1}{8}S_8 + 2FeNTA^- + 2H^+$$

Reoxidation of the chelate

$$[3] \quad 2FeNTA^- + \tfrac{1}{2}O_2 + H_2O \rightarrow 2FeNTA + 2OH^-$$

In practice the process is usually carried out industrially in two compartments, an absorber and an oxidizer, so that the H_2S and oxygen (or air) do not come into contact. Some mixing is unavoidable since the solution of the oxidized iron(III) chelate

Received July 12, 1994.

D. Chen and A.E. Martell.[1] Department of Chemistry, Texas A & M University, College Station, TX 77843-3255, U.S.A.
D. McManus. Director, R & D, Wheelabrator Clean Air Systems, Inc., 2 West Main St., Plainfield, IL 60544, U.S.A.

[1] Author to whom correspondence may be addressed. Telephone: (904) 845-5055. Fax: (904) 845-4719. E-mail: MARTELL@CHEMVX.TAMU.EDU

Can. J. Chem. Downloaded from www.nrcresearchpress.com by 65.111.164.53 on 09/08/12
For personal use only.

Can. J. Chem. Downloaded from www.nrcresearchpress.com by 65.111.164.53 on 09/08/12
For personal use only.

is pumped into the absorber (along with a little dissolved oxygen) to be used over again.

The use of the Fe(III)–NTA chelate as a catalyst for the oxidation of H_2S to S_8 has recently been described (1). Since the data in the literature on the iron(III), (II)–NTA chelates was incomplete, a thorough investigation of this concentration-dependent chelate system was carried out, and the interrelationships of the 1:1 normal and hydroxy iron(III) complexes with the 2:1 chelate have now been described (2).

In this paper the investigation of other Fe(III, II) chelate systems as catalysts for the oxidation of H_2S are described. Since the main problem with the use of NTA is degradation of the ligand, similar considerations apply to the use of substitute ligands in place of NTA. The use of several stabilizers that slow the rate of NTA degradation is explored. Also, the possible role of hydroxyl radical in the oxidation of the organic ligands is described.

Experimental

Materials

The following materials were obtained in the highest purity available and were used without further purification: nitrilotriacetic acid trisodium salt (99%, Aldrich); H_2S (99.5%, Gas Analytical Service); catalase (Biomedicals, Inc., bovine liver, E.C. 1.11.1.6; sterile aqueous solution, activity, 40 000 units per milligram solid, unit definition, one unit decomposes one micromole of H_2O_2 per minute, 25°C, pH 7.0, approx. 30 000 units per millilitre); (ethylenedinitrilo)tetraacetic acid disodium salt (EDTA) (Reagent A.C.S., Matheson, Coleman & Bell); *N*-hydroxyethylethylenediaminetriacetic acid (HEDTA) (98%, GFS Co.); 2,6-pyridinedicarboxylic acid (99%, Aldrich); 2,6-pyridinedimethanol (98%, Aldrich); iminodiacetic acid, disodium salt monohydrate (reagent ACS, Aldrich); *N*-(2-hydroxyethyl)iminodiacetic acid (98%, Aldrich).

2,6-Pyridinediacetic acid (PDA) was synthesized by a modification of the method of Couturier and Petitfaux (3).

2,6-Di(bromomethyl)pyridine

This compound was synthesized by a modification of the method of Baker et al. (4). A 25.0 g sample of 2,6-pyridinedimethanol and 250 mL 48% HBr were refluxed for 18 h. The solvent was removed by vacuum distillation. The residue was refluxed with 120 mL 48% HBr for another 18 h. The solvent was again removed by vacuum distillation and the product was dried at 120°C under vacuum for 2 h. NMR measurement of the product showed it to be pure. The yield is quantitative. ^{1}H NMR (D_2O, ppm): 8.0 (t, 1H, pyridine), 7.5 (d, 2H, pyridine), 4.3 (s, 4H, CH_2).

2,6-Di(cyanomethyl)pyridine

This compound was synthesized by following the method of Baker et al. (4). A mixture of 2,6-di(bromomethyl)pyridine hydrobromide (10.0 g), potassium cyanide (8.5 g), and water (105 mL) was heated at 80–90°C for 5 h. After the mixture was cooled, 50 mL of water was added and the product was extracted with $CHCl_3$. The organic phase was dried with anhydrous $MgSO_4$. The solvent was removed under reduced pressure and the residue was dried at 50°C under vacuum for 2 h. The product was recrystallized from ethanol to give a final yield of 2.8 g (56%). ^{1}H NMR ($CDCl_3$): 7.82 (t, 1H, pyridine), 7.45 (d, 2H, pyridine), 3.96 (s, 4H, CH_2). ^{13}C NMR ($CDCl_3$): 150.7, 138.6, 121.5 (pyridine), 116.7 (CN), 26.3 (CH_2).

2,6-Pyridinediacetic acid

A mixture of 2,6-di(cyanomethyl)pyridine (10.0 g) and concentrated HCl (12 M, 160 mL) was refluxed for 24 h. The excess HCl and solvent were removed and the residue was dissolved in 120 mL water. Activated carbon (2 g) was added to the solution and the mixture was heated to 50°C with stirring for 30 min. It was then filtered and the pH was adjusted to 2.1 by the addition of HCl. White crystals formed after the solution was allowed to stand near 0°C for 4 h. The product, 2,6-pyridinediacetic acid, was filtered off and washed with water until no chloride remained in the filtrate. The product was dried over P_2O_5 under vacuum for 48 h. The weight of the white product obtained was 9.1 g (73%). ^{1}H NMR (D_2O): 8.34 (t, 1H, pyridine), 7.76 (d, 2H, pyridine), 4.08 (m, 1.6 H, CH_2). The proton NMR measurements show that the integration of the H in CH_2 gives only about 1.6 H, far less than 4, which is the theoretical number of H atoms. This does not mean that the product is impure, because in the D_2O solution the hydrogen of the CH_2 groups slowly exchanges with deuterium, so that the integration of hydrogen is less than 4. This interpretation was confirmed by a kinetic investigation. The peak at 4.08 (CH_2) almost disappears after the D_2O solution is allowed to stand for 24 h.

^{13}C NMR (D_2O): 171.4, 148.4, 147.4, 127.5 ppm. The results of the ^{13}C NMR measurements show that there is no single peak for carbon in the CH_2 group. Because the deuterium exchanged with the hydrogen and the deuterium couples with the carbon in the CH_2 group, the ^{13}C resonance of the latter appears only as a small multiple peak. Since no CN peak (carbon in the CN group) was found in the ^{13}C NMR, the hydrolysis of 2,6-(cyanomethyl)pyridine to 2,6-pyridinediacetic acid was considered to be complete. Anal. calcd. for $C_9H_9NO_4 \cdot 0.5H_2O$: C 52.95, H 4.94, N 6.86; found: C 53.00, H 5.02, N 6.80.

Redox reaction equipment and conditions

The redox reaction was carried out in a two-chambered glass apparatus described previously (1), and the pH and redox potential in both the absorber and oxidizer were monitored. The H_2S flow rate was maintained at 2.0 mL min^{-1} and the air flow rate was regulated at 1.0 L min^{-1}. The temperature was maintained at 25.0 ± 1.0°C throughout.

HPLC equipment

An IBM L.C. pump No. 771008 equipped with a chromatography accessory, an UV–visible spectro monitor 3100 (LDC Analytical), and a chart recorder 6885 (Kipp and Zonen) were used.

NMR spectra

The proton and ^{13}C NMR spectra were recorded with a Varian X1-200 NMR spectrometer, and chemical shifts are reported in ppm. The internal standard used for NMR measurements in $CDCl_3$ is TMS (tetramethylsilane) and in D_2O is HOD. The ESR spectra were obtained from a Bruker ESR 300 spectrometer.

HPLC analysis and operating conditions

The concentrations of all ligands and intermediates were ana-

Fig. 1. Ten millimolar $[Fe(III)]_0$ (10 mM) and $[NTA]_0$ (20 mM) species as a function of p[H] with % based on total Fe(III) present. Only metal-ion-containing species are plotted. H_{-n} represents $(OH)_n$.

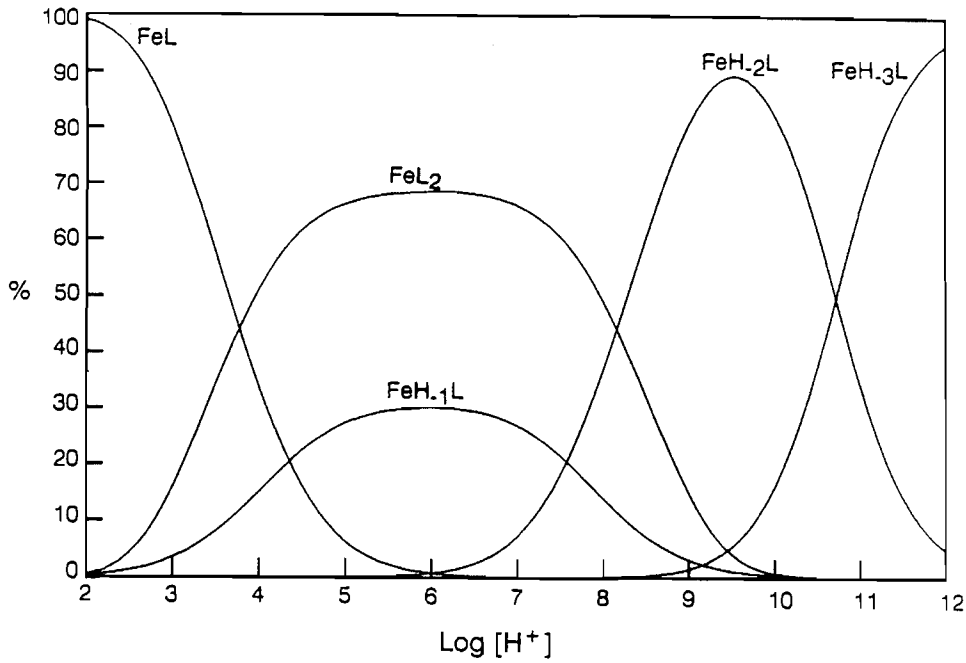

lyzed by HPLC by the method previously described for NTA (1).

The procedure for the preparation of an iron-free sample of pyridine is the same as previously described for NTA (1). The operating conditions used are as follows: column: 250 mm, 4.1 mm; packing, Versapack C_{18}, 10 μm; mobile phase, 18% methanol, 77% water, 4.1% acetic acid; flow rate 1.5 mL min^{-1}; detector UV 260 nm, sample 20 mL, recorder 20 mV full scale, chart speed 0.5 cm min^{-1}.

Calibration of HPLC analysis

The quantitative calibrations for the HPLC analysis of all ligands and intermediates were carried out with varying amounts of known samples of these compounds. The peak heights at the indicated amplification settings were plotted vs. concentration of the species. The linear nature of these plots indicated accurate HPLC determinations of these molecular species over a considerable range of concentration.

Results and discussion

On the basis of the stability constants, and metal chelate constants described previously (2), the distribution curves in Fig. 1 may be derived for the Fe(III)–NTA chelate system for the concentrations employed (0.018 M Fe(III) and 0.036 M NTA). From Fig. 1 it is seen that the ferric–NTA system at the operating pH of 8.5 is quite complex, consisting of about 6% $FeOHL^-$, 64% $Fe(OH)_2L^{2-}$, and 30% FeL_2^{3-} (where NTA is H_3L). Under these conditions the degradation scheme proposed for NTA is represented by the following sequence:

Sequence 1

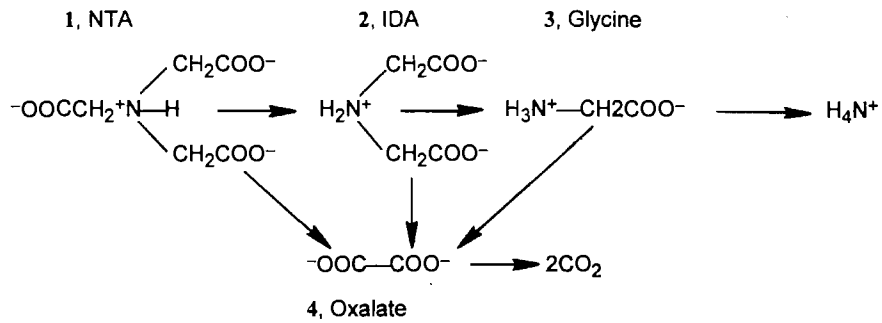

Can. J. Chem. Downloaded from www.nrcresearchpress.com by 65.111.164.53 on 09/08/12
For personal use only.

Fig. 2. Degradation of Fe(III)–EDTA at pH 8.5 and 25.0°C; H_2S flow rate 2.0 mL/min (EDTA 0.036 M, Fe(III) 0.018 M).

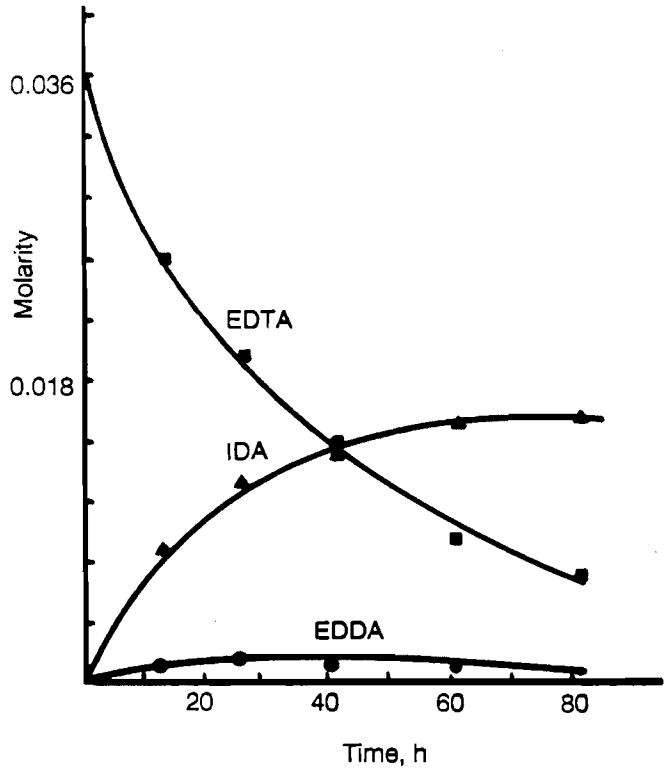

All of the intermediates shown above, and NTA itself, were quantitatively analyzed by HPLC. The degradation was slow but progressive, with about 80% of the NTA being oxidized in 100 h.

Degradation of EDTA

The degradation of EDTA, illustrated in Fig. 2, shows that over 80% of the EDTA was oxidized in 80 h, and that iminodiacetic acid (IDA) and ethylenediaminediacetic acid (EDDA) were quantitatively determined by HPLC as intermediates in the oxidation process. The following degradation scheme represents a reasonable sequence of oxidation products.

All of the oxidation intermediates shown in sequence 2 equations below are reasonable, being formed by hydroxylation of one of the CH_2 groups, either on the ethylene bridge or side-chain acetate groups. Following hydroxylation, the aldehyde formed by hydrolytic cleavage (not shown) is rapidly converted to the corresponding carboxylate, NTA, or oxalate anions. The NTA would be expected to degrade in turn, as described above. The oxidation and cleavage of each acetate group would be expected to form oxalate ion but, for reasons of clarity, are not shown in the above scheme. The intermediates found and measured quantitatively by HPLC are IDA and symmetrical ethylenediaminediacetic acid (S-EDDA), as indicated by Fig. 2. No NTA was found. The end products of degradation, CO_2 and NH_4^+, are not shown.

The degradation of HEDTA and the rate of formation of IDA are shown in Fig. 3. The formation of IDA can occur by oxidation of HEDTA to EDTA, followed by degradation as described above, or by direct oxidative cleavage of the ethyl-

Sequence 2

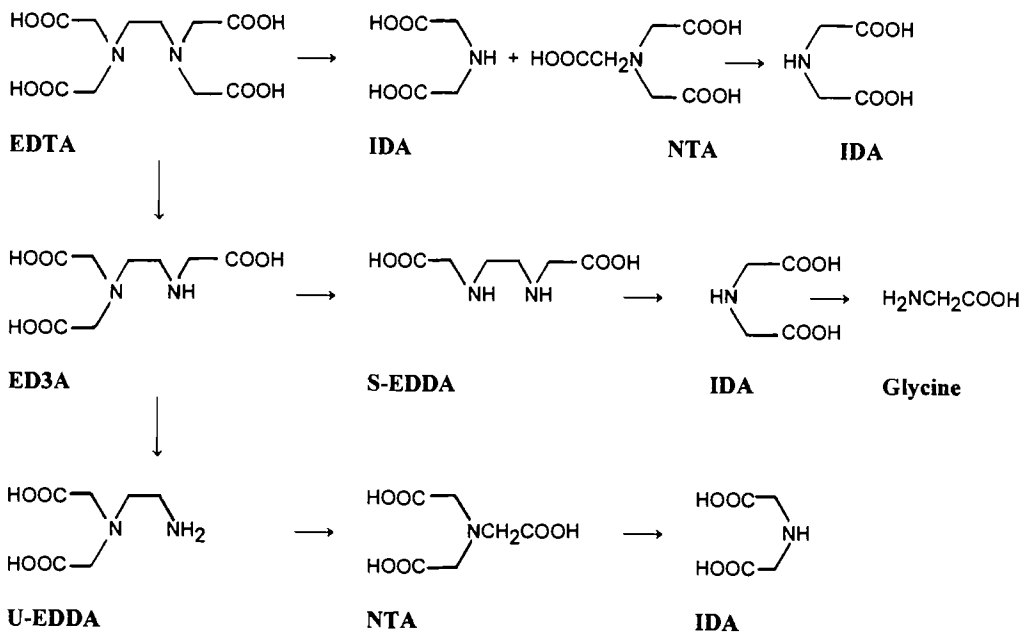

Can. J. Chem. Downloaded from www.nrcresearchpress.com by 65.111.164.53 on 09/08/12
For personal use only.

Can. J. Chem. Downloaded from www.nrcresearchpress.com by 65.111.164.53 on 09/08/12
For personal use only.

Fig. 3. Degradation of Fe(III)–HEDTA at pH 8.5 and 25.0°C; H_2S flow rate 2.0 mL/min (HEDTA 0.036 M, Fe(III) 0.018 M).

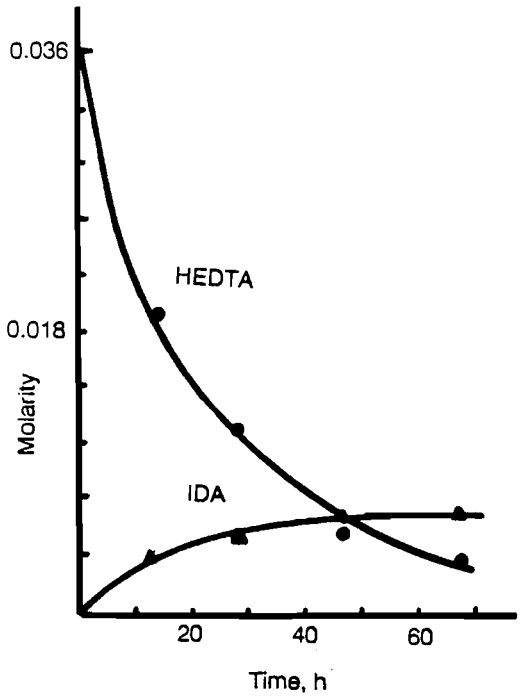

Fig. 4. Degradation of Fe(III)–NTA, Fe(III)–EDTA, and Fe(III)–HEDTA at pH 8.5 and 25.0°C; H_2S flow rate 2.0 mL/min; % is mol% of species based on initial concentration of NTA, EDTA, and HEDTA; 0.036 M = 100%.

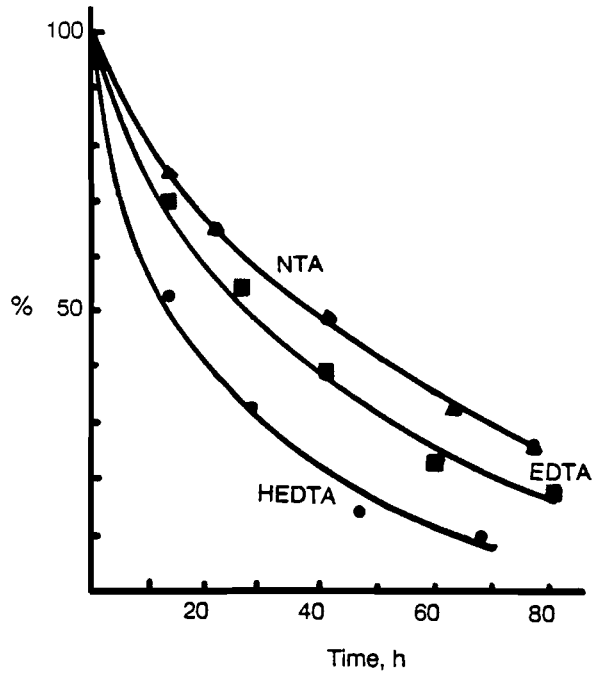

ene bridge, as indicated by the following sequence of reactions. (sequence 3)

As indicated by Fig. 3, the oxidative degradation of HEDTA is relatively rapid with only 10% of the ligand left after 70 h. A comparison of the relative rates of degradation of NTA, EDTA, and HEDTA, under the operating conditions of pH 8.5 and 0.018 M Fe(III) concentration, is illustrated in Fig. 4. From the plots presented it is apparent that NTA is by far the superior ligand. Since it is also the least expensive, it is the ligand of choice now being used to form the Fe(III), Fe(II) catalytic system for the oxidation of H_2S to S_8.

The 2:1 Fe(III) chelate of 2,6-pyridinedicarboxylic acid (dipicolinic acid) was used as the catalyst for the oxidation of H_2S to S_8 by air, under conditions similar to the tests on NTA, EDTA, and HEDTA, described above, except the pH had to be kept at 6.0 or lower. No measurable degradation was found to occur in a 100 h period. (There is the possibility that the pyridine ring was hydroxylated during this time period but no appreciable effect on the redox reaction was observed.) The lack of oxidative degradation was considered remarkable; however, dipicolinic acid does not form a sufficiently stable iron(III) chelate to keep it from precipitating as $Fe(OH)_3$ at pH

Sequence 3

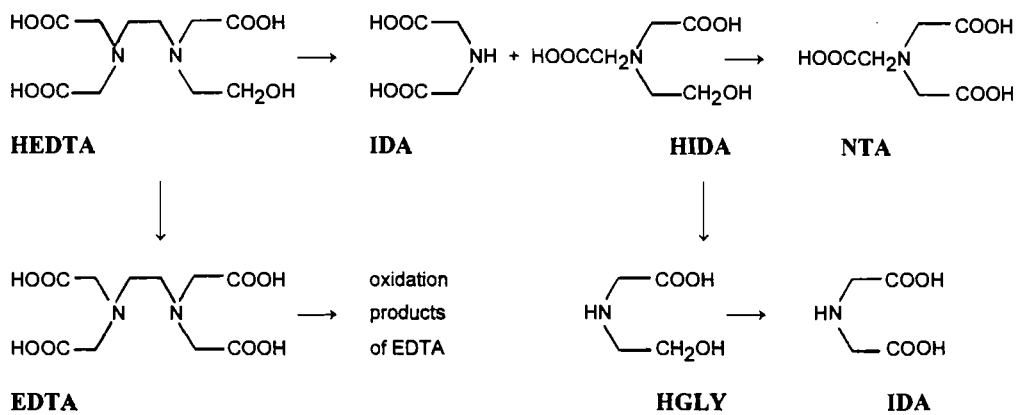

Can. J. Chem. Downloaded from www.nrcresearchpress.com by 65.111.164.53 on 09/08/12
For personal use only.

Fig. 5. Degradation of Fe(III) – 2,6-pyridinediacetic acid at pH 7.0. H_2S flow rate 2.00 mL/min. 100% 2,6-pyridinediacetic acid = 0.041 M (Fe(III) 0.0205 M).

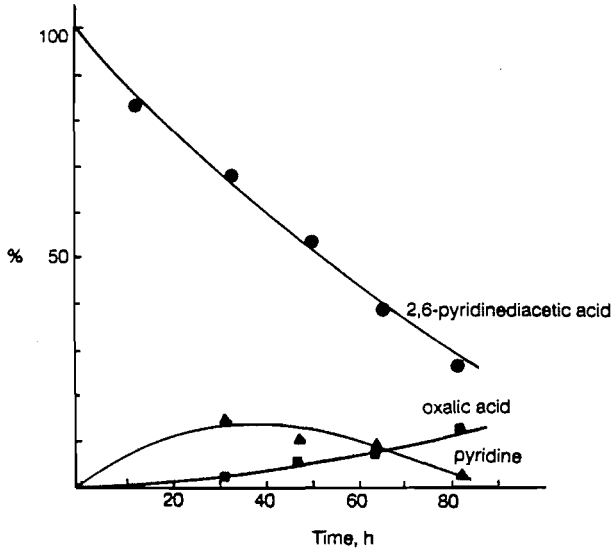

Fig. 6. Degradation of Fe(III) – *N*-(2-hydroxyethyl)iminodiacetic acid at pH 8.5. H_2S flow rate 2.0 mL/min. 100% *N*-(2-hydroxyethyl)iminodiacetic acid = 0.036 M (Fe(III) 0.018 M).

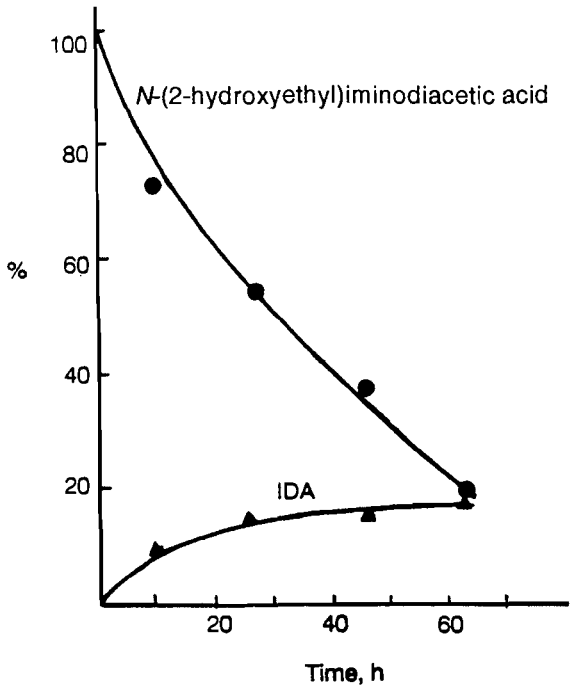

8.5. Therefore the absorption of H_2S gas into the aqueous system would be slowed down and this catalyst system was thus considered unsatisfactory.

Because 2,6-pyridinedicarboxylic acid does not degrade, but does not form a stable enough iron(III) chelate, we decided to investigate a closely related pyridine-containing ligand, which forms more stable Fe(III) chelates: 2,6-pyridinediacetic acid. This new chelating agent has been synthesized and it forms a 2:1 iron(III) chelate that does not precipitate at pH 7.0. The degradation run was therefore made at pH 7.0, and is illustrated in Fig. 5. The rate of degradation is seen to be fairly rapid, with the formation of both pyridine and oxalate in the oxidation process. Oxidative degradation of the ligand probably involves the following sequences of reactions. It is noted that the pyridine ring is also probably hydroxylated.

In the oxidative degradation sequence shown below for EDTA and HEDTA, two of the intermediates are chelating agents that form stable iron(III) complexes, *N*-hydroxyethyliminodiacetic acid (HIDA) and IDA. In fact HIDA has been used as a sequestering agent for Fe(III) in alkaline solution. Figures 6 and 7 show that these chelating agents also undergo oxidative degradation at rates comparable to those indicated above for chelating agents such as NTA, EDTA, and HEDTA.

The use of radical scavengers

A number of additives that function as radical scavengers have been used to slow down (or prevent) radical-induced oxidative degradation. The added material reacts with free radicals, thus preventing them from attacking, hydroxylating, and thus

Sequence 4

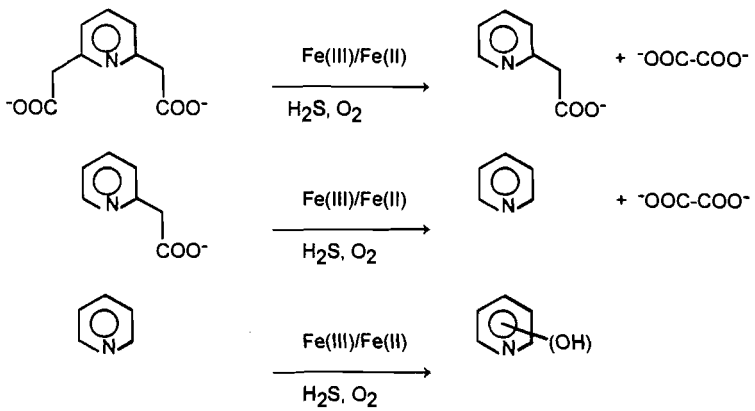

Can. J. Chem. Downloaded from www.nrcresearchpress.com by 65.111.164.53 on 09/08/12
For personal use only.

Fig. 7. Degradation of Fe(III)–IDA at pH 8.5, 25.0°C; H_2S flow rate 2.0 mL/min (IDA 0.036 M, Fe(III) 0.018 M).

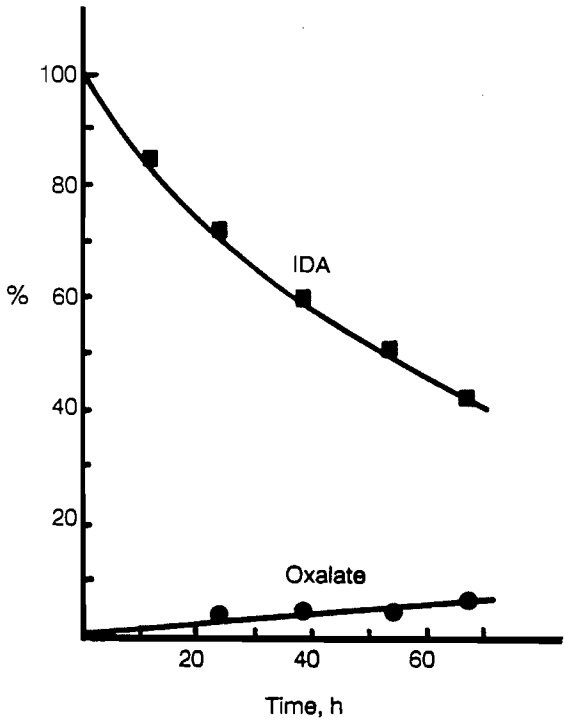

Fig. 8. Degradation of Fe(III)–NTA at pH 8.5 with 1.0 M NaCl and degradation of Fe(III)–NTA under comparable conditions (NTA 0.036 M, Fe(III) 0.018 M).

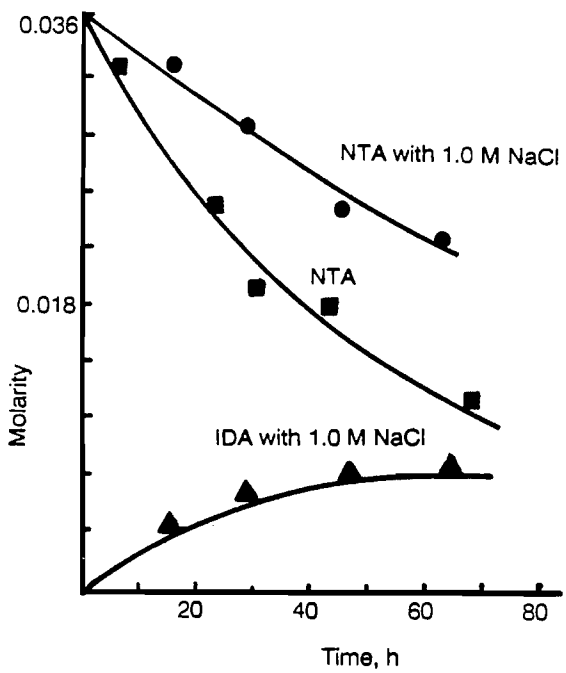

Fig. 9. Degradation of Fe(III)–NTA at pH 8.5 with 0.0362 M imidazole, 25.0°C; H_2S flow rate 2.0 mL/min (NTA 0.036 M, Fe(III) 0.018 M).

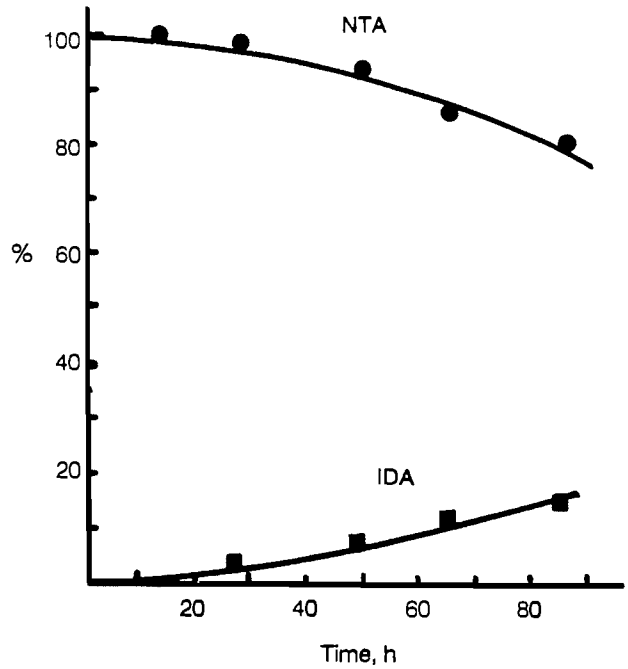

Fig. 10. Degradation of Fe(III)–NTA at pH 8.5 with 0.036 M benzoic acid (NTA 0.036 M, Fe(III) 0.018 M).

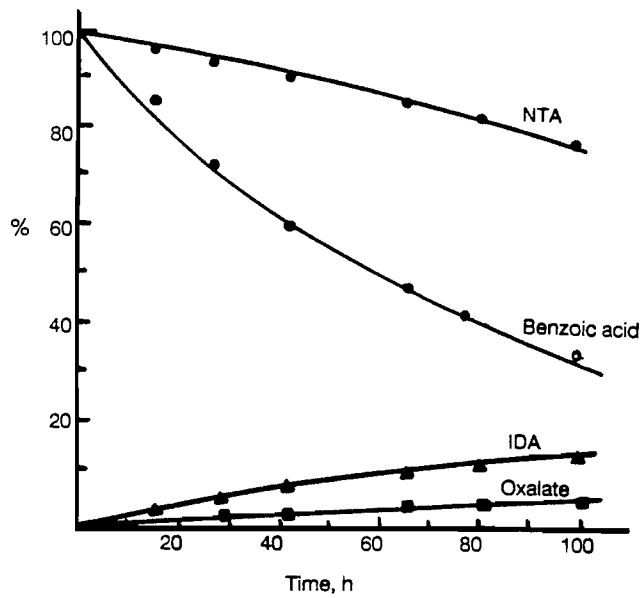

degrading the organic ligand. There are many such additives that may be used. One of the simplest of all is the chloride ion. Figure 8 shows the beneficial effect of sodium chloride on the rate of degradation of NTA. Even more dramatic effects can be achieved with imidazole and benzoic acid, as Figs. 9 and 10 indicate. (Benzoic acid is discussed in more detail below.) A very effective and inexpensive free radical scavenger is thiosulfate ion, usually supplied as sodium thiosulfate. Figure 11 shows that thiosulfate reduces the rate of degradation of NTA dramatically — almost by an order of magnitude. In the intro-

Can. J. Chem. Downloaded from www.nrcresearchpress.com by 65.111.164.53 on 09/08/12
For personal use only.

Fig. 11. Degradation of Fe(III)–NTA at pH 8.5 with 5% $Na_2S_2O_3 \cdot 5H_2O$. % is mol% of species based on initial concentration of NTA; 0.036 M = 100% (Fe(III) 0.018 M).

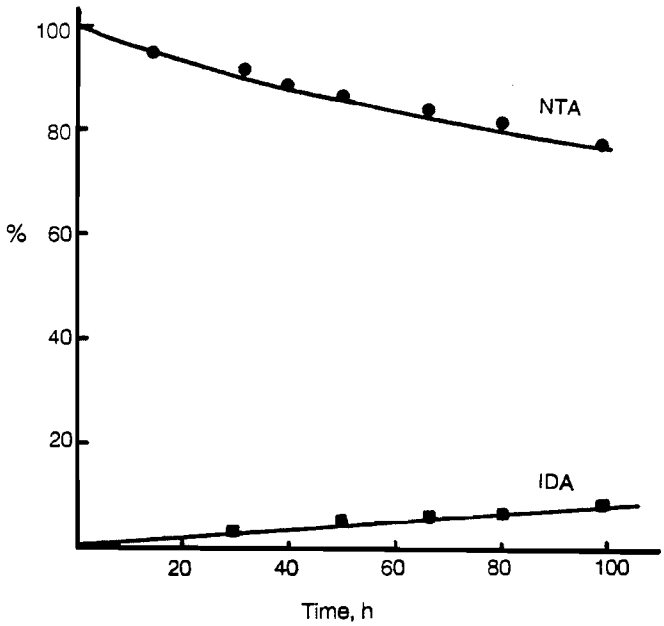

duction it was indicated that some thiosulfate is generated as a by-product of the H_2S oxidation process, and this would further slow down NTA degradation. Alkali metal thiosulfate is very widely added as a radical scavenger to protect the NTA (or other chelating agent) used as a catalyst for the oxidation of H_2S to S_8 by air (5).

Implication of hydroxyl radical

The radical scavengers described above react with many free radical intermediates and thus slow down the free radical attack on the chelating agent employed. While they would certainly react with hydroxyl radical, they are for the most part nonspecific reagents and their protective effects do not demonstrate the involvement of the hydroxyl radical. The use of catalase is somewhat different, since its function is simply to destroy H_2O_2 by disproportion to oxygen and water, thus slowing down or preventing the formation of hydroxyl radical. Figure 12 shows that catalase does slow down the oxidative degradation of NTA, thus indicating that the hydroxyl radical (6) is the active oxygen species responsible for the oxidation degradation of NTA.

Benzoic acid was used as a probe to explore the role of the hydroxyl radical in the degradation process. Figure 10 shows that not only does the benzoic acid greatly slow the degradation of NTA, but that the benzoic acid degrades much more rapidly (due to hydroxylation) than does NTA. Hydroxylation of benzoic acid produces a mixture of *o*-, *m*-, and *p*-hydroxybenzoic acids (sequence 5), and as indicated by the HPLC

Fig. 12. Degradation of Fe(III)–NTA with catalase (catalase solution added at a dilution of 1:100) at pH 7.0 and 25.0°C; H_2S flow rate 2.0 mL/min (NTA 0.036 M, Fe(III) 0.018 M).

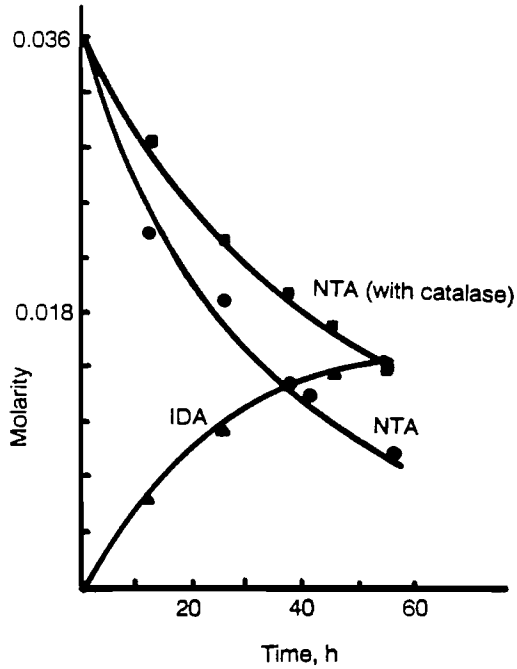

Fig. 13. HPLC analysis of a mixture of *o*-, *m*-, *p*-hydrobenzoic acids and benzoic acid (C_{18}-column) at 235 nm. Mobile phase: 18% methanol, 77.9% water, 4.1% acetic acid.

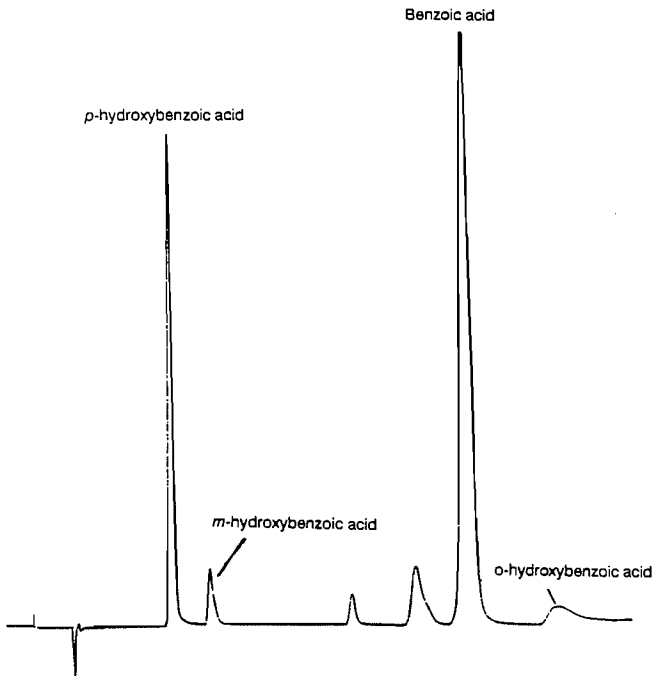

Sequence 5

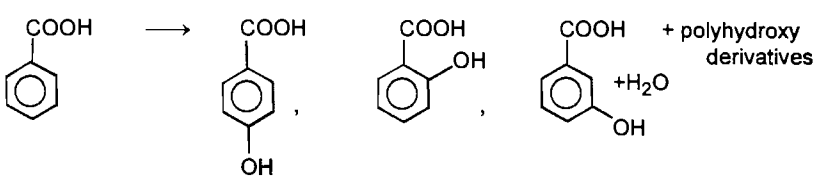

Fig. 14. ESR spectrum of the reaction product of Fe(II)–NTA with H_2O_2 at pH 8.5.

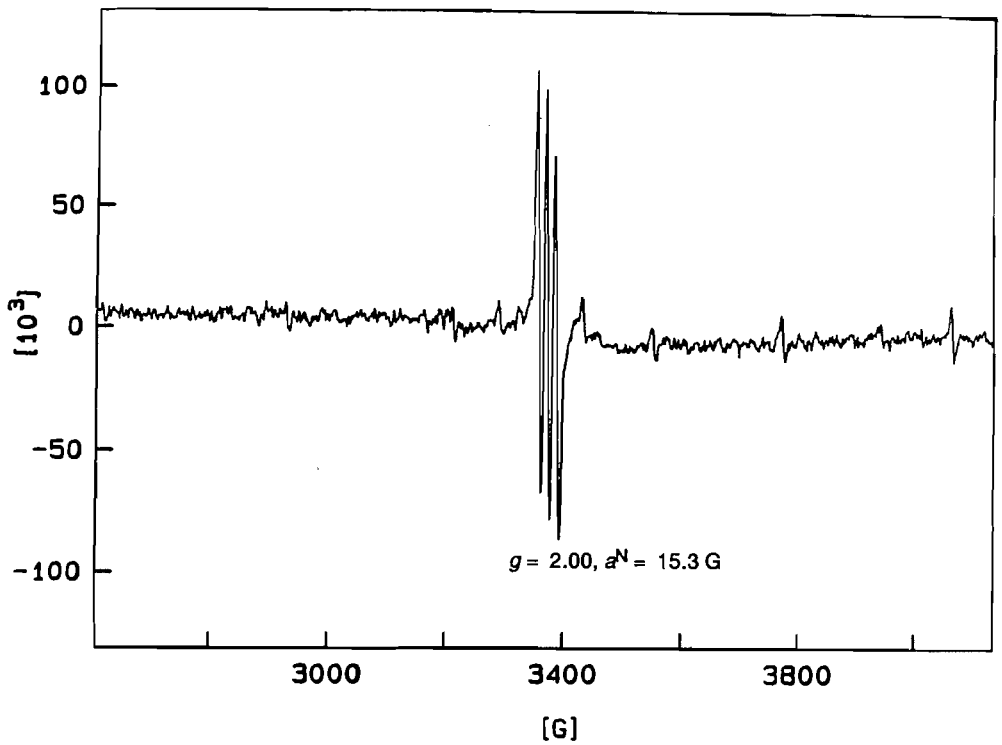

analysis illustrated by Fig. 13. The formation of these hydroxylation products is taken as evidence for the involvement of the hydroxyl radical, as was done by Grinstead (7). There was also evidence for further hydroxylation of benzoic acid in the TLC analysis of reaction products, showing that 2,5- and 2,3-dihydroxybenzoic acids were also formed.

ESR measurements

To further confirm the formation of the hydroxyl radical, phenyl-*tert*-butylnitrone was used as a spin trap and the radical that it generated by hydroxylation by the ·OH radical was detected by its ESR spectrum.

PBN

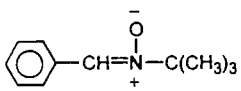

phenyl-*tert*-butylnitrone (PBN)

The control experiment was carried out on a solution of Fe(II)–NTA (Fe(II) 0.030 M, NTA 0.060 M) (5 mL) mixed with a small amount of 30% H_2O_2 and 30 mg PBN. The pH of the solution was adjusted to 8.5 and the ESR spectra of this solution measured immediately at room temperature gave the ESR spectrum illustrated in Fig. 14. The results show that the Fe(II)–NTA reacts with H_2O_2 to form a radical that reacts with PBN to give rise to ESR peaks at $g = 2.00$ and $a^N = 15.3$ G ($g = 2.006$, $a^N = 15.3$ G) (8). To probe the role of ·OH in the degradation of NTA, a solution of Fe(III)–NTA (Fe(III) 0.030 M, NTA 0.060 M) and PBN (saturated solution) was treated with H_2S and air for 60 min at pH 8.5. The ESR measurement of the reaction solution at room temperature showed that an ESR peak appeared at $g = 2.00$ and $a^N = 15.3$ G (Fig. 15). The new ESR peak had the same characteristics as the one described in the control experiment, and is taken as evidence that the hydroxyl radical was generated during the redox reaction.

Assuming that the oxidative degradation of the chelating agent is initiated by the hydroxyl radical, the following sequence of reactions is now proposed, with the use of NTA as the chelating agent:

[4] $2FeNTA^- + O_2 + 2H_2O \rightarrow 2FeNTA + H_2O_2 + 2OH^-$

[5] $FeNTA^- + H_2O_2 \rightarrow FeNTA + OH^- + {}^{\cdot}OH$

[6] $R^1R^2\overset{+}{N}HCH_2COO^- + {}^{\cdot}OH \rightarrow R^1R\overset{+}{N}H\dot{C}HCOO^- + H_2O$

[7] $R^1R^2\overset{+}{N}H\dot{C}HCOO^- + H_2O + FeNTA \rightarrow R^1R^2\overset{+}{N}H\underset{\displaystyle OH}{\underset{|}{C}}HCOO^- + FeNTA^- + H^+$

[8] $R^1R^2\overset{+}{N}H\underset{\displaystyle OH}{\underset{|}{C}}HCOO^- \rightarrow R^1R^2\overset{+}{N}H_2 + OHCCOO^-$

[9] $OHCCOO^- + \frac{1}{2}O_2 \rightarrow {}^-OOCCOO^- + H^+$

[10] ${}^-OOCCOO^- + 2H^+ + \frac{1}{2}O_2 \rightarrow 2\,CO_2 + H_2O$

$R^1 = R^2 = CH_2COO^-$ NTA

$R^1 = H, R^2 = CH_2COO^-$ IDA

$R^1 = R^2 = H$ glycine

Can. J. Chem. Downloaded from www.nrcresearchpress.com by 65.111.164.53 on 09/08/12
For personal use only.

Fig. 15. ESR spectrum of the reaction product of Fe(III)–NTA with H_2S and air at pH 8.5.

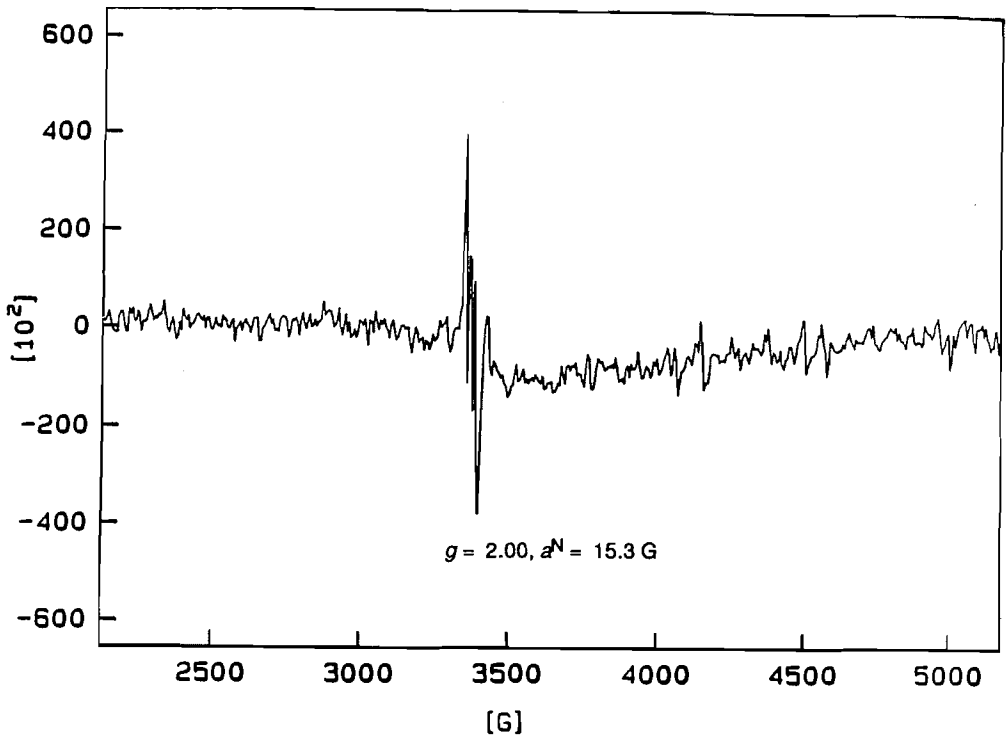

Can. J. Chem. Downloaded from www.nrcresearchpress.com by 65.111.164.53 on 09/08/12
For personal use only.

Other chelating agents described in this paper are presumed to undergo similar degradation reactions, the point of initial attack being the CH_2 groups in the acetate side chain or in the ethylene bridge. It is noted that dipicolinic acid, which does not have such methylene groups, degrades at a much slower rate (or not at all). Apparently degradation of the ligand by hydroxylation of the aromatic ring occurs at a much slower rate than does a ligand with readily hydroxylated methylene groups.

The activation of H_2O_2 by Fe(II) chelates (Fenton chemistry) in aqueous solution has been described (9, 10).

$$Fe(II)L^- + H_2O_2 \rightarrow Fe(III)L + OH^- + OH^{\cdot}$$

Such solutions have been shown to react as oxidants with various substrates in the same way as does the hydroxyl radical generated from Fe^{2+} and H_2O_2 without a chelating agent present. In this work the formation of H_2O_2 is indicated as an intermediate by noting that catalase reduced the rate of degradation of NTA. As explained above, H_2O_2 is an intermediate that is required to produce the hydroxyl radical.

Sugimoto and Sawyer (11) reported that in nonaqueous solution the activation of H_2O_2 by Fe(II) for the catalytic and selective oxygenation of hydrocarbon substrates may occur via non-Fenton chemistry pathways. Numerous studies have proposed high-valent iron-oxo intermediates, such as FeO^{3+} (formally Fe^{V}), ferryl complexes, $(L)Fe^{IV}{=}O$ or $(L^{\cdot+})Fe^{IV}{=}O$ (12–16), and $(L)_nFe^{IV}(OH)(OOH)$ (17).

The oxidant that is responsible for the degradation of NTA and other ligands is tentatively considered to be the hydroxyl radical and not a high-valent iron-oxo species. The following factors were considered in coming to this conclusion: (1) The Fe(III)–NTA redox reaction takes place in aqueous media. (2) The oxidation product of H_2S is S_8. If the oxidizing species were an iron-oxo complex, the oxidation product of H_2S would be H_2SO_4, not S_8. (3) The hydroxylation products of benzoic acid are the same as those produced by the $^{\cdot}OH$ radical generated without a chelating agent present (18, 19). (4) The addition of free radical scavengers ($Na_2S_2O_3$, benzoic acid, etc.) slows down the degradation of NTA while there is no effect of these scavengers when the oxidizing species are high-valent iron-oxo compounds (14). (5) ESR measurement of the degradation of Fe(III)–NTA with the trapping agent shows that a new peak appears at $g = 2.00$ and $a^N = 15.3$ G. A similar ESR spectrum generated by Fe(II)–NTA and H_2O_2 is considered due to the hydroxyl radical. (6) The fact that the rate of degradation of NTA increases as the pH is lowered correlates with increased rate of generation of hydroxyl radical as the pH is lowered.

Further work on the development of iron chelate systems as catalysts for the oxidation of H_2S to S_8 will focus on ligands that do not have methylene groups that undergo facile oxidative attack, and on the possible elimination of the hydroxyl radical, which has been identified as the active oxidant in the degradation of the chelating agent.

Acknowledgement

This research was supported by Wheelabrator Clean Air Systems, Inc.

References

1. D. Chen, D.R.J. Motekaitis, A.E. Martell, and D. McManus. Can. J. Chem. **71**. 1524 (1993).
2. A.E. Martell and R.J. Motekaitis. J. Coord. Chem. **31**, 67 (1994).
3. Y. Couturier and C. Petitfaux. J. Chem. Research (M), 4701 (1979).
4. W. Baker, K.M. Buggle, J.F.W. McOmine, and D.A.M. Watkins. J. Chem. Soc. 3594 (1958).
5. D. McManus and F.R. Kin. U.S. Patent No. 4,622,212, Nov. 11, 1986.
6. T.J. Egan, S.R. Barthakur, and P. Aisen. J. Inorg. Biochem. **48**, 241 (1992).
7. R.R. Grinstead. J. Am. Chem. Soc. **82**, 3472 (1960).
8. J.R. Harbour, V. Chow, and J.R. Bolton. Can. J. Chem. **52**, 3549 (1974).
9. D.I. Metelitsa. Russ. Chem. Rev. **40**, 563 (1971).
10. N.A. Vysotkaya. Russ. Chem. Rev. **42**, 851 (1973).
11. H. Sugimoto and D.T. Sawyer. J. Am. Chem. Soc. **106**, 4283 (1984).
12. J.D. Rush and W.J. Koppenol. J. Biol. Chem. **261**, 6739 (1986).
13. L. Yamazaki and L.H. Piette. J. Biol. Chem. **265**, 13589 (1990).
14. S. Rahhal and H.W. Richter. J. Am. Chem. Soc. **110**, 3126 (1988).
15. J.T. Groves. *In* Cytochrome P-450: structure, mechanism and biochemistry. *Edited by* P. Ortiz de Montellano. Planum, New York. 1985. Chap. 1.
16. J.T. Groves and Y. Watanabe. J. Am. Chem. Soc. **108**, 7834 (1986).
17. H.C. Tung, C. Kang, and D.T. Sawyer. J. Am. Chem. Soc. **114**, 3445 (1992).
18. M. Anbar, D. Meyerstein, and P. Neta. J. Phys. Chem. **8**, 2660 (1966).
19. G.W. Klein, K. Bhatia, V. Madhavan, and R.H. Schuler. J. Phys. Chem. **17**, 1767 (1975).

Glossary

S-EDDA	*N*,*N*′-ethylenediaminediacetic acid
U-EDDA	*N*,*N*-ethylenediaminediacetic acid
EDTA	ethylenediaminetetraacetic acid
HEDTA	*N*-hydroxyethyl-*N*,*N*э,*N*э-ethylenediaminetriacetic acid
HGLY	*N*-hydroxyethylglycine
HIDA	*N*-hydroxyethyliminodiacetic acid
IDA	iminodiacetic acid
NTA	nitrilotriacetic acid
PBN	phenyl-*tert*-butylnitrone
PDA	2,6-pyridinediacetic acid
PDCA	2,6-pyridinedicarboxylic acid

Can. J. Chem. Downloaded from www.nrcresearchpress.com by 65.111.164.53 on 09/08/12
For personal use only.

Antiferromagnetism and metamagnetism in 1,4-diazine and pyridine complexes of nickel(II)

Tom Otieno and Robert C. Thompson

Abstract: Several nickel(II) complexes containing pyridine (py), pyrazine (pyz) or methylpyrazine (mepyz) have been synthesized and characterized by vibrational and electronic spectroscopy, differential scanning calorimetry, and magnetic susceptibility studies to cryogenic temperatures. A comparison of the magnetic properties of the polymeric diazine-bridged complexes, $Ni(pyz)_2X_2$ (X = Cl or NO_3), $Ni(pyz)(p\text{-}CH_3C_6H_4SO_3)_2$, $Ni(mepyz)(NO_3)_2$, and $Ni(pyz)_3(CH_3SO_3)_2.CH_3OH$ with those of the related monometallic systems, $Ni(py)_4X_2$ (X = Cl, $p\text{-}CH_3C_6H_4SO_3$ or CH_3SO_3) and $Ni(mepyz)_4(NO_3)_2.H_2O$ provides evidence for weak antiferromagnetic coupling between metal centers mediated by bridging diazine ligands in the former group of compounds. The magnetic properties were analyzed employing a model for $S = 1$ which takes into account zero-field splitting and employs a molecular field term to account for weak magnetic exchange. The compounds $Ni(pyz)Cl_2$ and $Ni(py)Cl_2$ show metamagnetic behaviour with critical fields of 13 and 2 kOe, respectively, at 2 K. In these compounds nickel ions, linked in chains by bridging chlorides, exhibit intrachain ferromagnetic and interchain antiferromagnetic exchange. In $Ni(pyz)Cl_2$ bridging pyrazine ligands are considered to provide the pathway for the antiferromagnetic coupling resulting in a high critical field.

Key words: nickel(II), pyrazine, pyridine, complexes, metamagnetism, antiferromagnetism.

Résumé : On a synthétisé plusieurs complexes de nickel contenant la pyridine (py), la pyrazine (pyz), la méthylpyrazine (mepyz) et on les caractérisés par spectroscopie vibrationnelle et électronique, par calorimétrie à balayage différentiel et par des études de susceptibilité magnétique à des températures cryogéniques. Une comparaison des propriétés magnétiques des complexes polymères avec la diazine en position de pont, $Ni(pyz)_2X_2$ (X = Cl ou NO_3), $Ni(pyz)(p\text{-}CH_3C_6H_4SO_3)_2$, $Ni(mepyz)(NO_3)_2$, et $Ni(pyz)_3(CH_3SO_3)_2.MeOH$ avec ceux des systèmes monométalliques apparentés $Ni(py)_4X_2$ (X = Cl, $p\text{-}CH_3C_6H_4SO_3$ ou CH_3SO_3) et avec $Ni(mepyz)_4(NO_3)_2,H_2O$, indique dans le premier groupe de composés, l'existence d'un faible couplage antiferromagnétique entre les centres métalliques par l'intermédiare des ligands diazine en position de pont. On a analysé les propriétés magnétiques en utilisant un modèle $S = 1$ qui tient compte du dédoublement au champ zéro et qui utilise un terme de champ moléculaire pour tenir compte du faible échange magnétique. Les composés $Ni(pyz)Cl_2$ et $Ni(py)Cl_2$ présentent un comportement métamagnétique à des champs critiques de 13 et de 2 respectivement à 2 K. Dans ces composés les ions nickel, liés en chaîne par les chlorures en position de pont, subissent un échange ferromagnétique entre les chaînes voisines et un échange antiferromagnétique à l'intérieur d'une chaîne. On pense que dans le composé $Ni(pyz)Cl_2$, les ligands pyrazines en position de pont fournissent une voie d'accès au couplage antiferromagnétique provoquant un champ critique élevé.

Mots cles : nickel(II), pyrazine, pyridine, complexes, métamagnétisme, antiferromagnétisme.

[Traduit par la rédaction]

Introduction

Extensive studies on 1,4-diazine complexes of copper(II) (1–9) and more recently iron(II) (10–13) have demonstrated the potential of pyrazine (pyz), and its C-substituted derivatives, to bridge metal centres and form one-dimensional linear chains and two-dimensional square lattice extended arrays. Two-dimensional hexagonal and three-dimensional diamond-like lattices have also been observed in copper(I) complexes (14). Of particular interest is the ability of these ligands to mediate magnetic exchange in complexes where the metal is in a paramagnetic ground state. The copper, d^9, and iron, d^6, studies have provided several examples of systems in which the metals are coupled antiferromagnetically. The magnitude of the coupling has been related to structural features such as metal–ligand distance and the orientation of the plane of the bridging ligand with respect to the metal/ligand chromophore, the latter affecting the degree of overlap between the ligand π-orbitals and the magnetic orbital(s) on the metal (2, 4, 7).

A better appreciation of the extent to which 1,4-diazine ligands mediate magnetic exchange in extended arrays

Received August 25, 1994.

T. Otieno and R.C. Thompson.[1] Department of Chemistry, University of British Columbia, 2036 Main Mall, Vancouver, BC V6T 1Z1, Canada.

[1] Author to whom correspondence may be addressed. Tel: (604) 822 4979, fax: (604) 822 2847, e-mail: robert.c.thompson@mtsg.ubc.ca.

Can. J. Chem. Downloaded from www.nrcresearchpress.com by 65.111.164.53 on 09/08/12
For personal use only.

Can. J. Chem. Downloaded from www.nrcresearchpress.com by 65.111.164.53 on 09/08/12
For personal use only.

requires the investigation of other d^n configurations and we report here our studies on some nickel(II), d^8, complexes. Previous studies on such systems include a low-temperature magnetic susceptibility study on $Ni(pd)_2(dmpyz)$ (pd = $CH_3COCHOCCH_3$, dmpyz = 2,5-dimethylpyrazine) which revealed weak antiferromagnetic exchange (15) and high temperature only susceptibility studies on $Ni(pyz)_2Cl_2$ (16). To extend the range of known and characterized compounds of this type we examined the magnetic properties of the complexes formed in the solid state from reactions of pyrazine and methylpyrazine (mepyz) with nickel(II) nitrate, methanesulphonate, and *p*-toluenesulphonate.These particular polyatomic anions were chosen, in part, because earlier work had established infrared spectral criteria for coordination modes of these anions. Hence it was anticipated that infrared data together with electronic spectral data on these complexes could be used profitably in their structural characterization. This is an important consideration in view of the difficulties encountered here and in previous work in obtaining nickel(II) 1,4-diazine complexes in single crystal form suitable for X-ray diffraction studies. Further characterization of the previously studied $Ni(pyz)_2Cl_2$ and $Ni(pyz)Cl_2$, including susceptibility measurements to cryogenic temperatures, are also reported here. In addition, an examination of the low-temperature magnetic behaviour of the related chloro-bridged pyridine complex, $Ni(py)Cl_2$ (17), was prompted by our studies on $Ni(pyz)Cl_2$ which indicated that bridging chloro ligands are mediating magnetic exchange in this compound.

Zero-field splitting of the $^3A_{2g}$ ground term in octahedral nickel(II) complexes can significantly affect the magnetic properties, particularly at very low temperatures (18). To assess the magnitude of this effect in complexes of the type being studied here, magnetic studies are required on monometallic systems in which the probability of intermolecular exchange is minimized. For this purpose we measured low-temperature susceptibilities of the pyridine complexes, $Ni(py)_4X_2$ (where X = Cl, CH_3SO_3, and p-$CH_3C_6H_4SO_3$).

Experimental

Syntheses

All chemicals were at least reagent grade quality and were used without further purification. Although $Ni(pyz)Cl_2$ and $Ni(py)Cl_2$ are sufficiently air-stable that manipulations can be carried out in the atmosphere, samples were stored in vials in a desiccator. The rest of the complexes are hygroscopic and were handled and stored in a nitrogen atmosphere glove box. Since all the metal salts used as reactants were hydrates the dehydrating agent 2,2-dimethoxypropane (2,2-dmp) was routinely added to the solvents.

Nickel(II)-methanesulfonate and -paratoluenesulfonate are not available commercially and were prepared as hydrated salts from nickel(II) chloride hexahydrate and the corresponding silver(I) sulfonate following the literature procedure for the preparation of $Cu(p\text{-}CH_3C_6H_4SO_3)_2$ (19). Heating the solid products to temperatures of up to 140°C for several hours resulted in only partial dehydration, as indicated by the decreased intensity of the infrared bands assigned to OH vibrations. $Ni(py)_4Cl_2$ and $Ni(pyz)_2Cl_2$ were prepared by literature methods (20, 21) and had satisfactory microanalytical results.

Many of the complexes were prepared by a general method in which the appropriate binary nickel(II) salt dissolved in 4–12 mL of methanol containing about 10% v/v 2,2-dmp was added to an excess of the ligand. In the case of pyrazine, the addition was to ligand dissolved in about 5 mL of the methanol/2,2-dmp solvent. The solid products that resulted were isolated by filtration and then washed and dried as described below.

Tetrakis(pyridine)nickel(II) methanesulfonate, $Ni(py)_4(CH_3SO_3)_2$

Prepared by the general method using hydrated nickel(II) methanesulfonate (0.639 g, ~2.6 mmol) and 50 mmol pyridine. The blue precipitate was washed with small amounts of diethylether and dried *in vacuo* for 1.75 h. Anal. calcd. for $NiC_{22}H_{26}N_4S_2O_6$: C 46.74, H 4.64, N 9.91; found: C 46.63, H 4.77; N 10.01.

Tris(pyrazine)nickel(II) methanesulfonate, methanol solvate, $Ni(pyz)_3(CH_3SO_3)_2.CH_3OH$

Prepared by the general method using hydrated nickel(II) methanesulfonate (0.544 g, ~2.2 mmol) and 23.4 mmol pyrazine. The blue precipitate was washed with small amounts of the solvent containing some pyrazine and then dried for 5 h *in vacuo*. Anal. calcd. for $NiC_{15}H_{22}N_6S_2O_7$: C 34.57, H 4.25, N 16.12; found: C 34.50, H 4.50, N 15.88.

Tetrakis(pyridine)nickel(II) p-*toluenesulfonate, $Ni(py)_4$(p-$CH_3C_6H_4SO_3)_2$*

Prepared by the general method using hydrated nickel(II) *p*-toluenesufonate (0.868 g, ~2.2 mmol) and 124 mmol pyridine. The blue precipitate was washed with small quantities of the solvent and diethylether and then dried for 3.5 h *in vacuo*. Anal. calcd. for $NiC_{34}H_{34}N_4S_2O_6$: C 56.92, H 4.78, N 7.81; found: C 57.12, H 4.94, N 7.85.

Mono(pyrazine)nickel(II) p-*toluenesulfonate, $Ni(pyz)$(p-$CH_3C_6H_4SO_3)_2$*

Prepared by the general method using hydrated nickel(II) *p*-toluenesufonate (0.963 g, ~2.4 mmol) and 24.5 mmol pyrazine. The blue precipitate was dried, *in vacuo*, for 2.5 h at room temperature and then for 13 h at 85°C and finally for 6 h at 100°C to give a pale green product. Anal. calcd. for $NiC_{18}H_{18}N_2S_2O_6$: C 44.93, H 3.77, N 5.82; found: C 45.00, H 3.75, N 6.01.

Bis(pyrazine)nickel(II) nitrate, $Ni(pyz)_2(NO_3)_2$

Prepared by the general method using 7.05 mmol nickel(II) nitrate hexahydrate and 38.6 mmol pyrazine. The blue precipitate was dried *in vacuo* for 6 h. Anal. calcd. for $NiC_8H_8N_6O_6$: C 28.02, H 2.35, N 24.51; found: C 27.78, H 2.57, N 24.70.

Tetrakis(methylpyrazine)nickel(II) nitrate monohydrate, $Ni(mepyz)_4(NO_3)_2.H_2O$

A solution of 4.22 mmol nickel(II) nitrate hexahydrate in 5 mL of ethanol containing about 10% v/v 2,2-dmp was added to 39 mmol of methylpyrazine and the mixture allowed to sit. After several days a blue precipitate formed. The supernatant liquid was decanted off and the solid washed with small amounts of the solvent and then dried *in vacuo* for 3 h. Anal. calcd. for $NiC_{20}H_{26}N_{10}O_7$: C 41.62, H 4.54, N 24.27; found: C 41.75, H 4.74, N 24.14.

Can. J. Chem. Downloaded from www.nrcresearchpress.com by 65.111.164.53 on 09/08/12
For personal use only.

Mono(methylpyrazine)nickel(II) nitrate, Ni(mepyz)$(NO_3)_2$
This light blue complex was prepared by thermolysis of $Ni(mepyz)_4(NO_3)_2.H_2O$ at 90°C, *in vacuo*, for 13 h. Anal. calcd. for $NiC_5H_6N_4O_6$: C 21.69, H 2.18, N 20.24; found: C 21.81, H 2.26, N 20.45.

Mono(pyridine)nickel(II) chloride, Ni(py)Cl_2
A sample of $Ni(py)_4Cl_2$ was heated *in vacuo* at 140°C for 5 h during which time the color changed from blue to yellow. Anal. calcd. for $NiC_5H_5NCl_2$: C 28.77, H 2.41, N 6.71; found: C 28.97, H 2.51, N 6.62.

Mono(pyrazine)nickel(II) chloride, Ni(pyz)Cl_2
A sample of $Ni(pyz)_2Cl_2$ was heated at 255–258°C for 3 h under a stream of nitrogen gas to give a pale yellow product. Anal. calcd. for $NiC_4H_4N_2Cl_2$: C 22.91, H 1.92, N 13.36; found: C 22.89, H 1.91, N 13.47.

Physical measurements

Differential scanning calorimetry (DSC) studies in the 35–450°C temperature range were made using equipment and procedures previously described (22). For the current studies the measuring cell atmosphere was nitrogen gas at a flow rate of 50 mL min^{-1}. Infrared spectra in the range 4 000 – 250 cm^{-1} were recorded on a Perkin-Elmer Model 598 spectrometer using samples mulled in Nujol or hexachlorobutadiene and pressed between KRS-5 plates (Harshaw Chemical Co.). Calibration was achieved using polystyrene; band frequencies are considered accurate to ±3 cm^{-1}. Electronic spectra in the 25 000 – 5 000 cm^{-1} range were recorded on either a Cary 14 or a Cary 5 UV-VIS-NIR spectrophotometer. Samples were mulled in Nujol and sandwiched between quartz glass plates with a second set of plates containing only Nujol placed in the reference beam. Magnetic susceptibilities over the temperature range ~2 to ~82 K were measured for all compounds at an applied field of 9 225 Oe using a P.A.R Model 155 vibrating sample magnetometer as previously described (23). This instrument was also used to obtain the 2549, 5251, and 7501 Oe data reported here for $Ni(py)Cl_2$. Samples were held in Kel-F capsules. A Quantum Design (MPMS) SQUID magnetometer was used to obtain the magnetization data for field dependence studies on $Ni(py)Cl_2$ and $Ni(pyz)Cl_2$. Procedures involving the use of this instrument were described previously (24). Magnetic susceptibilities were corrected for diamagnetism of all atoms (nickel, −11; $CH_3SO_3^-$, −35; p-$CH_3C_6H_4SO_3^-$, −89; NO_3^-, −20; water, −13; methanol, −34; pyridine, −49; pyrazine, −45; methylpyrazine, −57) and temperature independent paramagnetism of nickel, 200. All corrections are in units of 10^{-6} cm^3 mol^{-1}. Carbon, hydrogen, and nitrogen analyses were performed by P. Borda of this department.

Results

Synthesis and Thermoanalysis

Addition of excess pyrazine or methylpyrazine to a methanol/2,2-dmp solution of the appropriate nickel salt led to the isolation of complexes of composition $Ni(pyz)_3(CH_3SO_3)_2.CH_3OH$, $Ni(pyz)(p\text{-}CH_3C_6H_4SO_3)_2$, $Ni(pyz)_2(NO_3)_2$, and $Ni(mepyz)_4(NO_3)_2.H_2O$. Attempts to obtain methylpyrazine complexes of the sulphonates by this general method failed to yield analytically pure samples.The general method was used successfully, however, to obtain the pyridine complexes $Ni(py)_4(CH_3SO_3)_2$ and $Ni(py)_4(p\text{-}CH_3C_6H_4SO_3)_2$. Thermoanalysis studies indicated sequential loss of neutral ligands for many of the complexes (Table 1) and suggested the possibility of obtaining bulk samples of some intermediate species by thermolysis. Thus it was possible to obtain a bulk sample of the compound $Ni(mepyz)(NO_3)_2$ by the thermolysis of $Ni(mepyz)_4(NO_3)_2.H_2O$. Thermoanalysis data for the former compound are included in Table 1. Attempts to obtain bulk samples of intermediates of the other complexes by thermolysis were not successful except in the case of the chloride derivatives. $Ni(py)_4Cl_2$ and $Ni(pyz)_2Cl_2$ were prepared by literature methods (20, 21) and the thermolysis of bulk samples of these was used to obtain $Ni(py)Cl_2$ and $Ni(pyz)Cl_2$. Thermochemical studies on all four of these chloro complexes have been reported previously (25–28) and our thermoanalysis data are in agreement with the earlier work.

Spectroscopic studies

The UV-VIS-NIR spectra of $Ni(py)_4Cl_2$ and $Ni(pyz)_2Cl_2$ obtained in this work were in agreement with reported spectra (20, 29, 30); data for the other complexes have been deposited as supplementary material.[2] The spectra are consistent with pseudo- octahedral geometry. Evidence for lower than O_h symmetry is seen in the splitting of the band assigned to the $^3A_{2g} \rightarrow {}^3T_{2g}$ transition. This is clearly observed in all of the spectra except those of $Ni(pyz)Cl_2$ and $Ni(mepyz)(NO_3)_2$ where the band is, nonetheless, very broad.

Selected anion and neutral ligand bands with assignments, obtained from the infrared spectra of the complexes, have also been deposited.[2] A careful examination of the infrared spectra gave no evidence for non-coordinated neutral ligand in any of the complexes. The absorptions that occur at 405, 605, and 1 583 cm^{-1} in free pyridine are shifted to higher frequencies in the complexes, as expected (31–33). In pyrazine complexes, the infrared band which occurs at 417 cm^{-1} in the free ligand shows significant shifts on coordination (11–13, 34). Shifts of this band to ~450 cm^{-1} usually indicate monodentate coordination, whereas shifts to significantly higher frequencies generally indicate a bridging mode of coordination (35). $Ni(pyz)_2(NO_3)_2$, $Ni(pyz)_2Cl_2$, $Ni(pyz)Cl_2$, and $Ni(pyz)(p\text{-}CH_3C_6H_4SO_3)_2$ exhibit bands consistent with bridging pyrazine, whereas the spectrum of $Ni(pyz)_3(CH_3SO_3)_2.CH_3OH$ suggests the presence of both bridging and terminal pyrazines. It has been noted that bands at 410 and 472 cm^{-1} in free methylpyrazine show significant shifts to higher frequencies on coordination (36). Such shifts are observed in both $Ni(mepyz)(NO_3)_2$ and $Ni(mepyz)_4(NO_3)_2.H_2O$, with larger shifts in the former complex relative to those in the latter, possibly reflecting bridging and terminal diazine ligands respectively.

Monodentate or bidentate coordination of a sulfonate group is expected to result in a splitting of the SO_3 asymmetric stretching mode, υ_4 (33). Significant band splitting of this type is seen in all of the sulfonate complexes studied here and, based on previous work on related complexes (1, 11), the mag-

[2] Supplementary material mentioned in the text may be purchased from: The Depository of Unpublished Data, Document Delivery, CISTI, National Research Council Canada, Ottawa, Canada K1A 0R6.

Can. J. Chem. Downloaded from www.nrcresearchpress.com by 65.111.164.53 on 09/08/12
For personal use only.

Table 1. Thermal parameters.[a]

Compound	Temperature °C	ΔH^b kJ mol^{-1}	Accumulated weight loss[b] % calcd.	obs.	Accumulated number and type of species lost
$Ni(py)_4(CH_3SO_3)_2$	198–215	184	42	42	3 py
	273	72	56	56	4 py
$Ni(py)_4(p\text{-}CH_3C_6H_4SO_3)_2$	180–216	—	44	46	4 py
$Ni(pyz)_3(CH_3SO_3)_2.CH_3OH$	113–147	147	22	25	pyz + CH_3OH
	250	27	37	37	pyz
	375	75	52	53	pyz
$Ni(pyz)_2(NO_3)_2$	240	61	23	26	pyz
	300[c]				
$Ni(pyz)(p\text{-}CH_3C_6H_4SO_3)_2$	311	75	17	18	pyz
$Ni(mepyz)_4(NO_3)_2.H_2O$	93	116	19	18	mepyz + H_2O
	139	127	52	50	3 mepyz + H_2O
	280[c]				
$Ni(mepyz)(NO_3)_2$	270[c]				

[a]Estimated error limits: peak temperature ±5°C, ΔH ±5%, weight loss ±5%.
[b]Was determined only when the thermal events were clearly separated.
[c]Onset of decomposition.

nitude of the splitting is consistent with bidentate sulfonate coordination in $Ni(pyz)(p\text{-}CH_3C_6H_4SO_3)_2$ and monodentate coordination in the others. Analysis of the infrared bands assigned to internal vibrations of the nitrate ion (37) may also be used to distinguish between monodentate and bidentate coordination (38). The spectra of the nitrates studied here support bidentate anion coordination in $Ni(mepyz)(NO_3)_2$ and monodentate coordination in the other complexes.

Magnetic properties

Complete magnetic data have been deposited as supplementary material.[2] Of the complexes studied here the four of the type NiL_4X_2 exhibit the smallest temperature dependence in μ_{eff} values. A plot of μ_{eff} versus temperature for $Ni(py)_4Cl_2$ is shown in Fig. 1. The μ_{eff} versus temperature behavior of $Ni(pyz)(p\text{-}CH_3C_6H_4SO_3)_2$ is similar to that of the above group while the complexes $Ni(pyz)_2Cl_2$, $Ni(mepyz)(NO_3)_2$, and $Ni(pyz)_3(CH_3SO_3)_2.CH_3OH$ show greater decreases in μ_{eff} below 25 K. The magnetic moment of $Ni(pyz)_2(NO_3)_2$ shows a significant decrease with temperature over the whole temperature range studied; in addition, the magnetic susceptibility of this compound exhibits a maximum at 3 K.

The magnetic properties of $Ni(pyz)Cl_2$ and $Ni(py)Cl_2$ are dramatically different from those of the other complexes. At an applied field of 9 225 Oe the magnetic moments of

Fig. 1. Magnetic moment versus temperature plots for (*a*) $Ni(py)Cl_2$, (*b*) $Ni(pyz)Cl_2$, and (*c*) $Ni(py)_4Cl_2$. The moments were calculated from susceptibility data obtained at a magnetic field strength of 9 225 Oe.

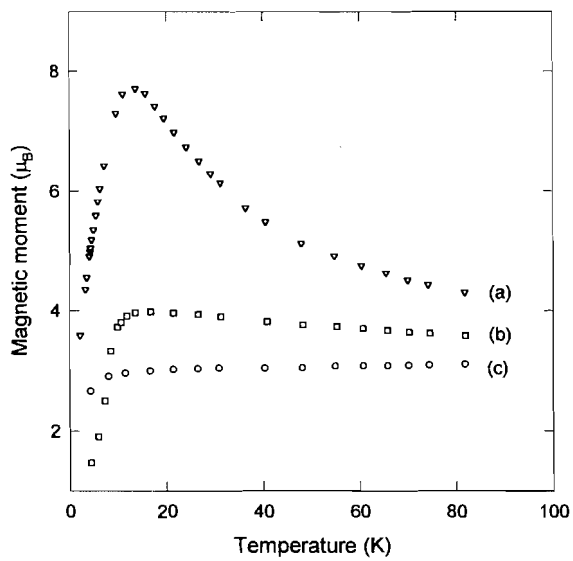

Can. J. Chem. Downloaded from www.nrcresearchpress.com by 65.111.164.53 on 09/08/12
For personal use only.

Fig. 2. Selected magnetization isotherms for $Ni(pyz)Cl_2$: ○ (2 K), ∇ (8 K), □ (20 K).

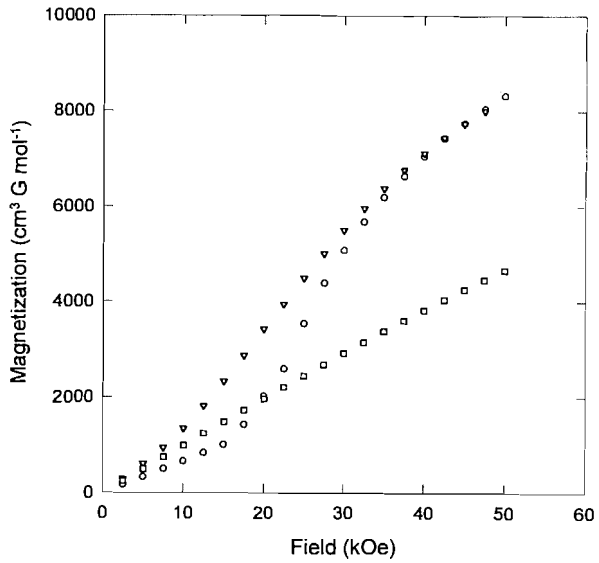

Fig. 3. Selected magnetization isotherms for $Ni(py)Cl_2$: ○ (2 K), ∇ (10 K), □ (20 K), Δ (35 K).

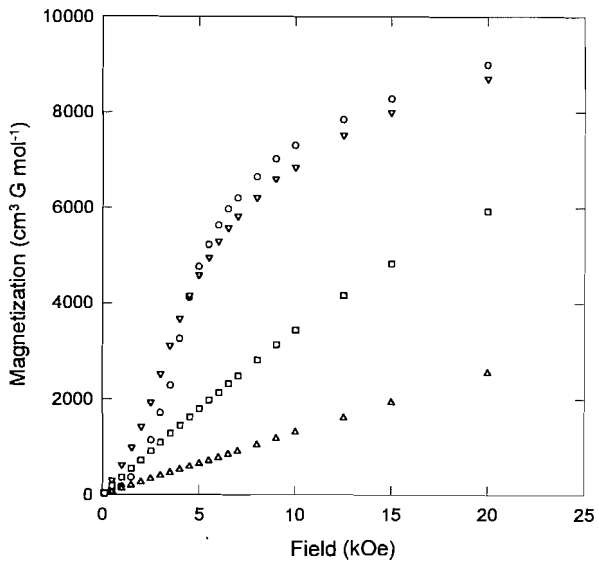

$Ni(pyz)Cl_2$ and $Ni(py)Cl_2$ exhibit maxima of 3.99 and 7.72 μ_B at 17 and 14 K, respectively (Fig. 1). The susceptibility of $Ni(pyz)Cl_2$, which shows no measurable field dependence between 2 549 and 9 225 Oe, passes through a maximum at 10 K. At field strengths above 12 000 Oe and at low temperatures the susceptibility of this complex is field dependent; magnetization versus applied field plots for selected temperatures are displayed in Fig. 2. Of all the complexes studied here, only $Ni(py)Cl_2$ shows a field dependence of the susceptibility between 2 549 and 9 225 Oe over the temperature range studied. As the temperature is lowered below 80 K, the susceptibility increases and is essentially field independent until ~15 K.

Fig. 4. Proposed structures: **A** = $M(pyz)_2X_2$, **B** = $M(pyz)X_2$, **C** = $Ni(py)Cl_2$

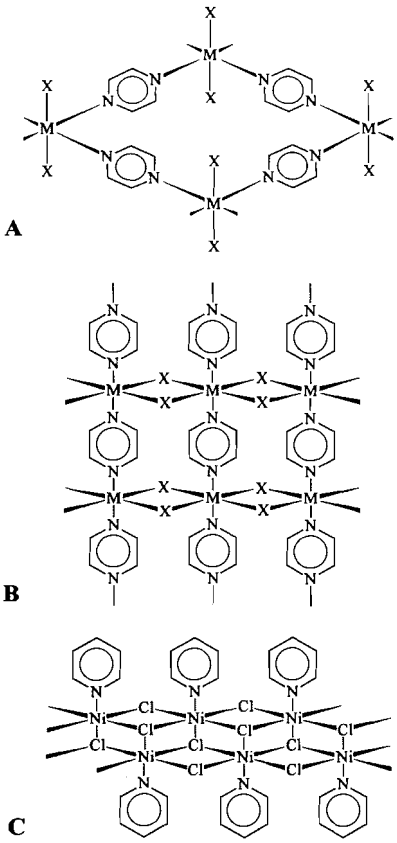

Below this temperature it becomes field dependent with the susceptibility leveling off below ~5 K at values of 0.734, 0.827, and 0.918 $cm^3 mol^{-1}$ for fields of 9 225, 7 501, and 5 252 Oe, respectively. At 2 549 Oe, however, the susceptibility passes through a maximum of 0.830 $cm^3 mol^{-1}$ at 11 K and decreases to 0.460 $cm^3 mol^{-1}$ at 2.1 K. Magnetization versus applied field plots for selected temperatures are displayed in Fig. 3.

Discussion

$Ni(pyz)_2X_2$ and $Ni(py)_4X_2$ complexes

On the the basis of spectroscopic evidence, Goldstein et al. (16, 39) proposed an extended sheet structure for $Ni(pyz)_2Cl_2$ in which nickel ions are bridged in a two-dimensional square lattice array by pyrazine ligands and six-coordination about the metal ion is achieved by axially bonded chloride ions. This type of structure, shown in Fig. 4, has been confirmed by single crystal X-ray structural determinations in a number of related bis(pyrazine) complexes, namely: $Co(pyz)_2Cl_2$, $Cu(pyz)_2(ClO_4)_2$, $Cu(pyz)_2(CH_3SO_3)_2$, and $Fe(pyz)_2(NCS)_2$ (2, 4, 10, 39). Our spectroscopic results are in agreement with the earlier studies on $Ni(pyz)_2Cl_2$ and are consistent with a similar sheet structure for the analogous $Ni(pyz)_2(NO_3)_2$. On the basis of high-temperature magnetic susceptibility studies, Goldstein et al. (16) had concluded that $Ni(pyz)_2Cl_2$ is mag-

Can. J. Chem. Downloaded from www.nrcresearchpress.com by 65.111.164.53 on 09/08/12
For personal use only.

Table 2. Magnetic parameters.[a]

Compound	D (cm^{-1})	$-zJ$ (cm^{-1})	g	F
$Ni(py)_4Cl_2$	4.7	0.038	2.19	0.0073
$Ni(py)_4(CH_3SO_3)_2$	7.3	0.041	2.24	0.0085
$Ni(py)_4(p\text{-}CH_3C_6H_4SO_3)_2$	8.8	0.006	2.11	0.0069
$Ni(mepyz)_4(NO_3)_2.H_2O$	6.3	0.021	2.20	0.0045
$Ni(pyz)_3(CH_3SO_3)_2.CH_3OH$	10.0	0.067	2.15	0.0073
$Ni(mepyz)(NO_3)_2$	9.3	0.094	2.21	0.0102
$Ni(pyz)(p\text{-}CH_3C_6H_4SO_3)_2$	7.5	0.036	2.19	0.0060
$Ni(pyz)_2Cl_2$	5.5	0.135	2.17	0.0064
$Ni(pyz)_2(NO_3)_2$	7.2	0.520	2.16	0.0197

[a]Estimated uncertainties: $D \pm 10\%$, $-zJ \pm 10\%$, $g \pm 2\%$.

netically dilute. The low-temperature studies reported here reveal weak magnetic concentration effects. In these $Ni(pyz)_2X_2$ complexes the metal chromophore is NiN_4X_2 and before discussing their magnetic properties in detail it is appropriate to consider first the monometallic $Ni(py)_4X_2$ analogues.

$Ni(py)_4Cl_2$ is known to have a *trans*-octahedral structure (40) and, on the basis of similarities in their electronic spectra, the compounds.$Ni(py)_4X_2$ (X = CH_3SO_3 and p-$CH_3C_6H_4SO_3$) and $Ni(mepyz)_4(NO_3)_2.H_2O$ likely exhibit the same geometry. This conclusion is supported by evidence from infrared spectroscopy that the anions involved are coordinated in a monodentate fashion. The *trans*-octahedral structure has been confirmed for the iron analogues of the methanesulfonate and p-toluenesulfonate compounds (33).

In view of the monometallic nature of these complexes any intermolecular exchange would be expected to be very weak. The measured moments at the higher temperatures studied are relatively temperature independent and of a magnitude normally observed for magnetically dilute nickel(II) complexes of this type (41). The decrease in magnetic moments at the lower temperatures studied is caused by the effects of zero-field splitting, ZFS (18), accompanied possibly by very weak exchange effects. Accordingly, we examined fits of the magnetic susceptibility employing the previously published equation for the susceptibility, χ_m, of an $S = 1$ system including ZFS (42), with χ_m modified by the molecular field approximation to include the effects of weak spin interactions (43). The equation employed for the exchange-corrected susceptibility, χ'_m, is:

$$\chi'_m = (\chi_m/[1 - (2zJ/Ng^2\mu_B{}^2)\chi_m])$$

where J is the exchange coupling constant, z is the number of interacting nearest neighbors, and the remaining terms have their usual meaning. In the fitting procedure D, the zero-field splitting parameter, g, and zJ were employed as variable parameters and best fit values of these are given in Table 2. Fits of experimental data to the model were made using a nonlinear least-squares procedure with the following function minimized:

$$F = \left[\frac{1}{n}\sum_{i=1}^{n}\left(\frac{\chi^i_{calc} - \chi^i_{obs}}{\chi^i_{obs}}\right)^2\right]^{1/2}$$

where n is the number of data points. The F value provides a measure of the goodness of fit between experiment and theory. Excellent fits as judged visually and by the the value of F were obtained for all four compounds. In all cases $|D| >> |zJ|$, a necessary requirement for applying the molecular field approximation (18). Values of D are in the range 5–9 cm^{-1}; this compares with the reported values of $D = 4.35$ cm^{-1} for $[Ni(C_5H_5NO)_6][ClO_4]_2$, -19 cm^{-1} for $Ni(py)_2Cl_2$, and -23 cm^{-1} for $Ni(pyrazole)_2Br_2$ (44). Ignoring intermolecular exchange (setting $J = 0$) gives poorer agreement between experiment and theory and generates D values ranging from 2% higher for the tosylate complex to 40% higher for the chloride derivative. The very small values of $|zJ|$ confirm that any exchange in these complexes is extremely weak.

The magnetic properties of the two $Ni(pyz)_2X_2$ complexes studied here indicate that there is stronger antiferromagnetic exchange in comparison to that present in the tetrakis(ligand) complexes. In view of the proposed sheet structures for these pyrazine complexes, attempts were made to analyze their magnetic data using Lines high-temperature series expansion for a two-dimensional square-lattice $S = 1$ antiferromagnetic system in the Heisenberg limit (45). Satisfactory agreement between experiment and this theory was not obtained for $Ni(pyz)_2(NO_3)_2$. A satisfactory fit of the data for $Ni(pyz)_2Cl_2$ to this model was obtained with the parameters $J = -0.38$ cm^{-1} and $g = 2.17$ ($F = 0.0066$); however, since the model ignores ZFS effects and since $|D|$ is likely to be significantly greater than the $|J|$ determined, we consider the fit to be fortuitous. Assuming ZFS is significantly larger than the exchange in these complexes, we analyzed the data according to the ZFS model modified to include the effects of weak spin interactions as described above. Excellent fits were obtained for both compounds (Table 2) and although the $|zJ|$ values are significantly greater than those obtained for the tetrakis(ligand) complexes, they are still less than 10% of the $|D|$ values making the application of the molecular field approximation appropriate. It should be noted that, as would be expected, the D values are very comparable to those of the monometallic complexes with similar chromophores, namely $Ni(py)_4Cl_2$ and $Ni(mepyz)_4(NO_3)_2.H_2O$. The stronger antiferromagnetic coupling in $Ni(pyz)_2(NO_3)_2$ may be a consequence of the weaker coordinating strength of the nitrate compared to chloride. This could yield stronger metal–pyrazine interactions resulting in enhanced exchange effects.

The ability of pyrazine to mediate antiferromagnetic ex-

Can. J. Chem. Downloaded from www.nrcresearchpress.com by 65.111.164.53 on 09/08/12
For personal use only.

change between nickel(II) centers is demonstrated by these results; however, the magnitude of the exchange appears to be quite weak when comparisons are made with iron and copper $M(pyz)_2X_2$ systems previously studied. To compare complexes with different d^n configurations it is appropriate to compare values of $4S^2J$ (where S is the total spin) rather than J (46). For the two $Ni(pyz)_2X_2$ complexes studied here, taking $z = 4$, the value of $-4S^2J$ is 0.14 cm^{-1} for X = Cl and 0.52 cm^{-1} for $X = NO_3$. These are an order of magnitude smaller than the values of $-4S2J$ determined for $Cu(pyz)_2(ClO_4)_2$ (5.2 cm^{-1}) and for $Fe(pyz)_2X_2$, where $X = CH_3SO_3$, CF_3SO_3, and NCS (2.9, 3.2 and 5.8 cm^{-1}, respectively) (4, 11, 12). It had been suggested earlier that the exchange in $Fe(pyz)_2(NCS)_2$ is weaker than in $Cu(pyz)_2(ClO_4)_2$ (10); however, the $4S^2J$ data do not support this. More important perhaps is the fact that the exchange is very similar in the two compounds, in spite of the fact that, as was pointed out previously (10), the canting of the pyrazine rings with respect to the MN_4 chromophore is almost identical in the two compounds, while the Fe—N distances are greater than the Cu—N distances. This might have been expected to lead to weaker exchange in the Fe case. It was suggested in the earlier work that the unpaired electron density in the t_{2g} orbital set of the iron compound is providing additional pathways for antiferromagnetic exchange and this is offsetting the effect of the longer Fe—N distances. In the complexes studied in the current work, the Ni—N bond distances are also likely to be greater than the corresponding distances in the copper complexes. In the case of nickel, however, the effect of long M—N bonds is not offset by unpaired t_{2g} electron density and this may account for the weak coupling in the nickel complexes. The canting of the pyrazine rings with respect to the NiN_4 chromophore is also an important factor in determining the strength of magnetic exchange; however, this aspect cannot be explored further in the absence of more detailed structural information.

Ni(diazine)X_2 complexes and $Ni(pyz)_3(CH_3SO_3)_2.CH_3OH$

Goldstein and Unsworth (47) suggested a structure for $Ni(pyz)Cl_2$ in which chains of nickel ions, doubly-bridged by chloride ions, are cross-linked by bidentate bridging pyrazine molecules to form an overall extended sheet structure. Our spectroscopic data are in agreement with the earlier work and support such a structure, shown in Fig. 4. This type of structure has been observed in $Cu(pyz)Cl_2$ and $Cu(pyz)Br_2$ (9). Spectroscopic evidence in this study supports six-coordinate structures involving bridging 1,4-diazine ligands and bidentate anions for $Ni(pyz)(p\text{-}CH_3C_6H_4SO_3)_2$ and $Ni(mepyz)(NO_3)_2$. Likely structures involve chains of 1,4-diazine bridged metal ions which are either isolated with six-coordination achieved by bidentate chelating anions or are cross-linked by bidentate bridging anion groups to form a sheet structure like that proposed for $Ni(pyz)Cl_2$. An example of the former structural type is provided by $Cu(pyz)(NO_3)_2$ (5) while the latter structural type has been proposed previously for $Fe(pyz)(p\text{-}CH_3C_6H_4SO_3)_2$ (11). The electronic and infrared spectra of $Ni(pyz)_3(CH_3SO_3)_2.CH_3OH$ are consistent with a structure involving a linear chain of pyrazine-bridged nickel ions with six-coordination completed by the other two pyrazine ligands and the methanesulfonate ions.

A qualitative comparison of the magnetic properties of $Ni(pyz)(p\text{-}CH_3C_6H_4SO_3)_2$, $Ni(mepyz)(NO_3)_2$, and $Ni(pyz)_3(CH_3SO_3)_2.CH_3OH$ with those of the bis(pyrazine) derivatives discussed above, indicates the magnitude of exchange is comparable or slightly smaller in the complexes being considered here. In view of the comments made above regarding the relative magnitudes of exchange coupling and ZFS we consider it inappropriate to analyze the magnetic properties of these complexes employing one-dimensional or two-dimensional models which ignore ZFS effects (45, 48, 49). Analysis of the data employing the ZFS model modified to account for weak exchange as described above results in good agreement between experiment and theory (Table 2). The values of the ZFS parameter, D, are comparable to those of the bis(pyrazine) complexes and the values of $|zJ|$ are smaller, again validating the use of the molecular field approximation. Assuming that any weak exchange in these compounds is being mediated primarily by bridging pyrazine ligands and setting z = 2 yields $-J$ values in the range 0.018 – 0.047 cm^{-1} for the monopyrazine bridged complexes compared to the $-J$ values of 0.035 and 0.13 cm^{-1} for the bis(pyrazine) bridged compounds. In summary, antiferromagnetic exchange in nickel(II) complexes containing bridging 1,4-diazine ligands is very weak and is little affected by the number of bridging diazines.

In a conference report (50) on the low-temperature magnetic properties of $Ni(pyz)Cl_2$ it was stated that the complex exhibits a Néel temperature of ~10 K and ferromagnetic behavior above this temperature. The maximum observed in the magnetic susceptibility versus temperature data at 10 K in the present work indicates antiferromagnetic coupling. That the behaviour is not simple antiferromagnetic, however, is evident from the magnetic moment data (Fig. 1). At ~80 K the moment is greater than that of $Ni(py)_4Cl_2$ and rises to even higher values as the temperature is lowered, indicative of ferromagnetic exchange. The moment goes through a maximum as the temperature is lowered further. We interpret this result as follows. The nickel ions are coupled ferromagnetically in chains via the bridging chloride ions and there is interchain antiferromagnetic coupling via bridging pyrazine ligands. Magnetic behaviour of this type is exhibited in a number of linear chain metamagnetic materials such as NiL_2X_2 (X is Cl or Br and L is pyrazole or pyridine) (51) and $M(py)_2Cl_2$ (M is Co, Fe, or Ni) and $Fe(py)_2(NCS)_2$ (52, 53). Unlike the situation described for $Ni(pyz)Cl_2$, however, in these complexes the interchain antiferromagnetism is mediated by non-bonding interactions. In order to examine $Ni(pyz)Cl_2$ for metamagnetic behavior, we examined the field-dependence of its magnetization at low temperatures (Fig. 2). Metamagnetic transitions were clearly observed below 10 K. The critical field, H_c, defined as the extrapolation of the linear portion of the magnetization, M, vs. field curve to the $M = 0$ axis (52), is 13 kOe at 2 K for $Ni(pyz)Cl_2$. A measure of the strength of intrachain ferromagnetic coupling may be obtained by extrapolation of the high-temperature portion of a Curie–Weiss (χ^{-1} versus T) plot to low temperatures (51). Such an analysis gives $J = 4$ cm^{-1} for $Ni(pyz)Cl_2$. Interesting comparisons can be made with $Ni(py)_2Cl_2$, a metamagnetic compound which exhibits ferromagnetic coupling with $J = 4$ cm^{-1} and a critical field, $H_c = 3$ kOe (51). The similarity in the two J values is consistent with the fact that in both compounds the ferromagnetic coupling is thought to take place along -$NiCl_2$- chains, in other words by identical pathways.The critical field is affected

by the strength of the antiferromagnetic interaction between the ferromagnetically coupled chains. The stronger the interaction the higher is H_c. In $Ni(py)_2Cl_2$ the Ni atoms in the $-NiCl_2-$ chains are capped by pyridine ligands and the interchain coupling is through space (non-bonding interactions) and the critical field is 3 kOe. In $Ni(pyz)Cl_2$ the $-NiCl_2-$ chains are cross-linked by pyz ligands and the higher H_c observed (13 kOe) is consistent with these ligands providing a significant antiferromagnetic pathway for exchange.

$Ni(py)Cl_2$

Our work on $Ni(pyz)Cl_2$ prompted a more detailed investigation of the magnetic behaviour of $Ni(py)Cl_2$. For this pyridine compound Goldstein and Hughes (17) proposed a double-strand halide-bridged polymeric chain structure in which each metal ion is surrounded by one pyridine ligand, two bicoordinate halide ions, and three tricoordinate halide ions, as depicted in Fig. 4. Each nickel ion is bonded to four nickel neighbours by bridging chlorides with the potential for ferromagnetic coupling within the double strand chains and interchain antiferromagnetic coupling through non-bonding interactions leading to metamagnetic behaviour. Earlier high-temperature magnetic susceptibility studies (300–90 K) had indicated the presence of ferromagnetic exchange. (54), and our cryomagnetic studies confirm metamagnetism. Qualitatively, the behaviour is similar to that of $Ni(pyz)Cl_2$. The magnetic moment versus temperature plot shows a maximum (Fig. 1) and the magnetization data (Fig. 3) show metamagnetic transitions below 10 K. As a consequence, perhaps, of the fact that each nickel is chlorine-bridged to four nearest neighbour nickels in $Ni(py)Cl_2$, the ferromagnetic interactions are stronger in this system compared to the interactions in the pyrazine analogue. This is evidenced by the higher magnetic moment values (Fig. 1) and larger value of J (8 cm^{-1}, determined as described above). The magnetization data indicate a critical field, H_c, of 2 kOe at 2 K for $Ni(py)Cl_2$, a value much smaller than that in $Ni(pyz)Cl_2$ but similar to that reported for $Ni(py)_2Cl_2$ (52). This is consistent with the fact that, as in the latter compound, the antiferromagnetic interchain effects are mediated by non-bonding interactions.

Summary and conclusions

This work has shown that in complexes of the type Ni(1,4-diazine)$_x$X$_2$, in which nickel(II) ions are linked by bridging diazine ligands in extended chains (for $x = 1$) or sheets (for $x = 2$), and in which the X anions are not involved significantly in mediating exchange, the diazine ligands are capable of transmitting antiferromagnetic interactions between metal centers. The magnitude of the interaction is significantly weaker than that seen in analogous copper(II) systems. It is suggested that this is a consequence of longer metal—N bond lengths which are not compensated for by the existence of additional antiferromagnetic pathways via t_{2g} unpaired electron density as is present in analogous iron(II) compounds. The ability of pyrazine to transmit antiferromagnetic interactions between nickel(II) ions was further demonstrated in the analysis of the metamagnetic behaviour of $Ni(pyz)Cl_2$. The relatively high critical field observed for this compound compared to those found for $Ni(py)_2Cl_2$ and $Ni(py)Cl_2$ is interpreted as a direct result of significant antiferromagnetic interactions mediated by the bridging pyrazine ligands.

Acknowledgements

Financial support from the Natural Sciences and Engineering Research Council of Canada is gratefully acknowledged.

References

1. J.S. Haynes, S.J. Rettig, J.R. Sams, J. Trotter, and R.C. Thompson. Inorg. Chem. **27**, 1237 (1988).
2. J.S. Haynes, S.J. Rettig, J.R. Sams, R.C. Thompson, and J. Trotter. Can. J. Chem. **65**, 420 (1987).
3. E. Coronado, M. Drillon, and D. Beltran. Inorg. Chim. Acta, **82**, 13 (1984).
4. J. Darriet, M.S. Haddad, E.N. Duesler, and D.N. Hendrickson. Inorg. Chem. **18**, 2679 (1979).
5. A. Santoro, A.D. Mighell, and C.W. Reimann. Acta Crystallogr. **B26**, 979 (1970).
6. H.W. Richardson, J.R. Wasson, and W.E. Hatfield. Inorg. Chem. **16**, 484 (1977).
7. H.W. Richardson and W.E. Hatfield. J. Am. Chem. Soc. **98**, 835 (1976).
8. G.W. Inman, Jr. and W.E. Hatfield. Inorg. Chem. **11**, 3085 (1972).
9. T. Fetzer, A. Lentz, and T. Debaerdemaeker. Z. Naturforsch. **44B**, 553 (1989).
10. J.A. Real, G. De Munno, M.C. Munoz, and M. Julve. Inorg. Chem. **30**, 2701 (1991).
11. J.S. Haynes, J.R. Sams, and R.C. Thompson. Can. J. Chem. **66**, 2079 (1988).
12. J.S. Haynes, A. Kostikas, J.R. Sams, A. Simopoulos, and R.C. Thompson. Inorg. Chem. **26,** 2630 (1987).
13. J.S. Haynes, J.R. Sams, and R.C. Thompson. Inorg. Chem. **25**, 3740 (1986).
14. T. Otieno, S.J. Rettig, R.C. Thompson, and J. Trotter. Inorg. Chem. **32**, 1607 (1993).
15. A.B. Blake and W.E. Hatfield. J. Chem. Soc. Dalton Trans. 868 (1978).
16. M. Goldstein, F.B. Taylor, and W.D. Unsworth. J. Chem. Soc. Dalton Trans. 418. (1972).
17. M. Goldstein and R.J. Hughes. Inorg. Chim. Acta, **37**, 71 (1979).
18. C.J. O'Connor. *In* Progress in inorganic chemistry. Vol. 29. *Edited by* S.J. Lippard. Interscience, New York. 1982. p. 203.
19. A.L. Arduini, M. Garnett, R.C. Thompson, and T.C.T. Wong. Can. J. Chem. **53**, 3812 (1975).
20. D.A. Rowley and R.S. Drago. Inorg. Chem. **6**, 1092 (1967).
21. A.B.P. Lever, J. Lewis, and R.S. Nyholm. J. Chem. Soc. 5042 (1963).
22. J.S. Haynes, K.W. Oliver, and R.C. Thompson. Can. J. Chem. **63**, 1111 (1985).
23. J.S. Haynes, K.W. Oliver, S.J. Rettig, R.C. Thompson, and J. Trotter. Can. J. Chem. **62**, 891 (1984).
24. M.K. Ehlert, S.J. Rettig, A. Storr, R.C. Thompson, and J.Trotter. Can. J. Chem. **70**, 2161 (1992).

Can. J. Chem. Downloaded from www.nrcresearchpress.com by 65.111.164.53 on 09/08/12
For personal use only.

25. G. Liptay, K. Burger, E. Mocsari-Fulop, and I. Porubszky. J. Therm. Anal. **2**, 25 (1970).
26. I.G. Murgulescu, E. Segal, and D. Fatu. J. Inorg. Nucl. Chem. **27**, 2677 (1965).
27. I.G. Murgulescu, E. Segal, and D. Fatu. Rev. Roum. Chim. **11**, 291 (1966).
28. G. Beech and C.T. Mortimer. J. Chem. Soc. Sect. A, 1115 (1967).
29. O. Bostrup and C.K. Jurgensen. Acta Chem. Scand. **11**, 1223 (1957).
30. A.B.P. Lever, J. Lewis, and R.S. Nyholm. J. Chem. Soc. 4761 (1964).
31. J.K. Wilmshurst and H.J. Bernstein. Can. J. Chem. **35**, 1183 (1957).
32. N.S. Gill, R.H. Nuttall, D.E. Scaife, and D.W.A. Sharp. J. Inorg. Nucl. Chem. **18**, 79 (1961).
33. J.S. Haynes, S.J. Rettig, J.R. Sams, R.C. Thompson, and J. Trotter. Can. J. Chem. **64**, 429 (1986).
34. R.C. Lord, A.L. Marston, and F.A. Miller. Spectrochim. Acta, **9**, 113 (1957).
35. T. Otieno, S.J. Rettig, R.C. Thompson, and J. Trotter. Can. J. Chem. **67**, 1964 (1989).
36. T. Otieno, S.J. Rettig, R.C. Thompson, and J. Trotter. Inorg. Chem. **32**, 4384 (1993).
37. G. Herzberg. Infrared and Raman spectra of polyatomic molecules. D. Van Nostrand, New York. 1945.
38. N.F. Curtis and Y.M. Curtis. Inorg. Chem. **4**, 804 (1965).
39. P.W. Carreck, M. Goldstein, E.M. McPartlin, and W.D. Unsworth. Chem. Commun. 1634 (1971).
40. G.J. Long and P.J. Clarke. Inorg. Chem. **17**, 1394 (1978).
41. L. Sacconi. *In* Transition metal chemistry, a series of advances. Vol. 4. *Edited by* R.L. Carlin. Marcel Dekker, New York. 1968. p. 199.
42. R.L. Carlin. J. Chem. Educ. **43**, 521 (1966).
43. R.L. Carlin. C.J. O'Connor, and S.N. Bhatia, J. Am. Chem. Soc. **98**, 3523 (1976).
44. R.L. Carlin. Magnetochemistry. Springer-Verlag, Berlin. 1986.
45. M.E. Lines. J. Phys. Chem. Solids, **31**, 101 (1970).
46. S.L. Lambert and D.N. Hendrickson. Inorg. Chem. **18**, 2683 (1979).
47. M. Goldstein and W.D. Unsworth. Inorg. Chim. Acta, **4**, 342 (1970).
48. W. Hiller, J. Strahle, A. Datz, M. Hanack, W.E. Hatfield, L.W. Haar, and P. Gutlich. J. Am. Chem. Soc. **106**, 329 (1984).
49. G.R. Wagner and S.A. Friedberg. Phys. Lett. **9**, 11 (1964).
50. E. Witten, C. Torardi, N. Scoville and W. Reiff. Abstracts of Papers, ACS/CSJ Chemical Congress, Honolulu, Hawaii. 1979. PHYS 221.
51. H.T. Witteveen, W.L.C. Rutten, and J. Reedijk. J. Inorg. Nucl. Chem. **37**, 913 (1975).
52. S. Foner, R.B. Frankel, W.M. Reiff, B.F. Little, and G.J. Long. Solid State Commun. **16**, 159 (1975).
53. S. Foner, R.B. Frankel, E.J. McNiff, Jr., W.M. Reiff, B.F. Little, and G.J. Long. AIP Conf. Proc. **24**, 363 (1975).
54. D.M.L. Goodgame, M. Goodgame, and M.J. Weeks. J. Chem. Soc. 5194 (1964).

Can. J. Chem. Downloaded from www.nrcresearchpress.com by 65.111.164.53 on 09/08/12
For personal use only.

Solvent effects on the reactivity of solvated electrons with $NO_{3,s}^-$ in C_1 to C_4 alcohols

Yixing Zhao and Gordon R. Freeman

Abstract: The rate constants $k_2(e_s^- + NO_{3,s}^-)$ in pure C_1 to C_4 alcohol solvents at 298 K increase with *increasing* viscosity and *decreasing* permittivity. Thus the reactivity increases with decreasing diffusivity and increasing coulombic repulsion, so the Debye–Smoluchowski model does not apply. The effective reaction radius κR_r increases with decrease of effective trap depth E_r/τ of the electrons in the solvent: $\kappa R_r = C_\tau(E_r/\tau)^{p_\tau}$. Values of κR_r and E_r/τ change with temperature, and values of p_τ fall in four categories: ~0.0 for water and methanol; ~1.3 for primary alcohols; 0.6 for secondary alcohols; 1.8 for *tert*-butanol. The C—H groups participate in the $e_s^- + NO_{3,s}^-$ reaction.

Key words: alcohol solvents, solvated electron, nitrate ion, reactivity, solvent effects.

Résumé : Les constantes de vitesse $k_2(e_s^- + NO_{3,s}^-)$ dans des alcools allant de C_1 à C_4 comme solvants à 298 K augmentent lorsque la viscosité augmente et lorsque la permittivité diminue. Ainsi la réactivité augmente lorsque la diffusivité diminue et lorsque la répulsion coulombienne augmente de telle sorte que le modèle de Debye–Smoluchowski ne s'applique pas. Le rayon effectif de la réaction κR_r augmente avec la diminution de la profondeur du piège effectif E_r/τ des électrons dans le solvant. $\kappa R_r = C_\tau(E_r/\tau)^{p_\tau}$. Les valeurs de κR_r et de E_r/τ varient avec la température, et les valeurs de p_τ diminuent pour les quatre catégories: ~0,0 pour l'eau et le méthanol; ~1,3 pour les alcools primaires; 0,6 pour les alcools secondaires; 1,8 pour le *tert*-butanol. Les groupes C—H participent dans la réaction $e_s^- + NO_{3,s}^-$.

Mots clés : solvants alcooliques, électron solvaté, ion nitrate, réactivité, effets des solvants.

[Traduit par la rédaction]

Introduction

Elucidation of the reactivity of e_s^- with $NO_{3,s}^-$ in water and in alcohol solvents is a long-standing problem (1–11). The reaction rate constant k_2 of e_s^- with many solutes in a series of alcohols follows the Smoluchowski–Debye model, and increases with increasing fluidity ($1/\eta$) of the solvent (11, 12). By contrast, the rate constant $k_2(e_s^- + NO_{3,s}^-)$ increases approximately linearly with *decreasing* fluidity in a series of alcohol solvents at 298 K (11). This increase in reaction rate accompanied by a decrease in diffusion rate points to the behavior of a reactant encounter pair. The value of $k_2(e_s^- + NO_{3,s}^-)$ also increases with decreasing trap depth of e_s^-, as represented by the optical absorption energy E_r (13, 14). However, there is lack of overall correlation in all C_1 to C_4 alcohols, including secondary and tertiary alcohols (9, 10). Therefore, in this paper we bring together data to advance the understanding of the reaction in all C_1 to C_4 alcohols.

Received June 20, 1994.

Y. Zhao and G.R. Freeman.[1] Chemistry Department, University of Alberta, Edmonton, AB T6G 2G2, Canada.

[1] Author to whom all correspondence should be addressed; tel. (403) 492 3468, fax. (403) 492 8231, email: knp@dept.chem.ualberta.ca.

Data

Values of k_2 in the different solvents were taken from refs. 3, 4, 6, 7, 9–11 and are listed for 298 K in Table 1.

Kinetic properties of the solvents are viscosity η (15–17) and dielectric relaxation (electric dipole rotation) time (18–22). Values are collected in Table 1.

The tenacity with which an electron is held in a solvation site is assumed to be related to the e_s^- optical absorption energy (23). Electrons with lower optical absorption energies tend to be more reactive (13, 14, 24), so the energy E_r half way up the low energy side of the absorption band is chosen for correlations with reaction rate constants (Table 1).

Discussion

Transport properties

Figure 1*A* shows correlations of k_2 ($e_s^- + NO_{3,s}^-$) with solvent viscosity η. The rate constants in the primary alcohols *increase* with η; those in the secondary alcohols are higher but have a similar tendency; k_2 is higher in the tertiary alcohol, and the highest in water. This indicates chemical participation of solvent molecules in the reaction (9). The higher the η value, the more difficult it is for the reactants in an encounter pair to diffuse apart, giving more time for reaction to occur. The probability of reaction during an encounter must increase as η^m with $m \approx 2$, because the encounter frequency decreases approximately as η^{-1}.

Can. J. Chem. Downloaded from www.nrcresearchpress.com by 65.111.164.53 on 09/08/12
For personal use only.

Can. J. Chem. Downloaded from www.nrcresearchpress.com by 65.111.164.53 on 09/08/12
For personal use only.

Table 1. Reaction rates and parameters for e_s^- + $NO_{3,s}^-$ in C_1 to C_4 alcohols at 298 K.

Alcohol	k_2 (10^6 m^3/mol·s)	E_r (zJ)[h]	η (mPa·s)	ε[i]	τ (ps)[j]	E_r/τ (zJ/ps)
Water[a]	9.4[7], 9.8[10]	219	0.89	78.5	8.3	26.4
MeOH[b]	0.026	237	0.557	32.6	46	5.2
EtOH[b]	0.068	210	1.10	24.3	125	1.68
1-PrOH[c]	0.09	229	1.96	20.1	372	0.616
2-PrOH[c]	0.65	173	2.08	18.4	370*	0.468
1-BuOH[d]	0.19	232	2.60	17.4	479	0.484
i-BuOH[e]	0.25	224	3.40	17.6	480*	0.467
2-BuOH[f]	0.75	179	3.05	16.7	510*	0.293
t-BuOH[g]	3.2	104[k]	4.45	12.4	420	0.247

[a]References 7, 10.
[b]Reference 3.
[c]Reference 4.
[d]Reference 9.
[e]Reference 11.
[f]Reference 6.
[g]Reference 10.
[h]Energy at A/A_{max} = 0.5 on the low energy side of the optical absorption band of e_s^-; ref. 23.
[i]Static permittivity.
[j]Dielectric relaxation time τ_1, for water to 2-butanol from ref. 15 (*extrapolated value), and *tert*-butanol from ref. 21.
[k]Authors' unpublished work.

Fig. 1. Correlations of k_2 with η (*A*) and E_r (*B*) in C_1 to C_4 alcohols and water at 298 K (Table 1).

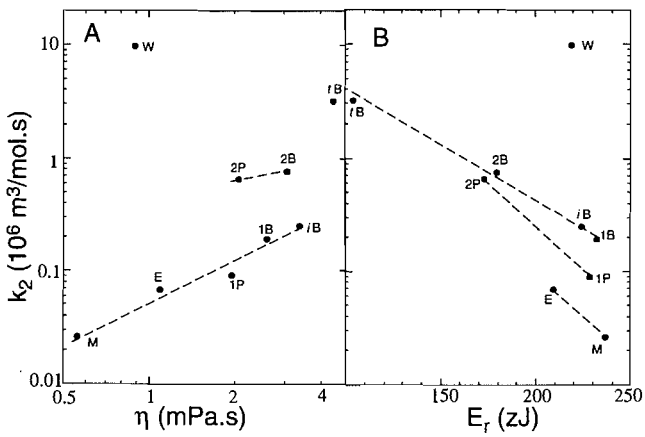

Trap-depth model and modification

The Smoluchowski model is used to investigate the transport properties in diffusion-controlled reactions. However, reactivity is also often dependent on the solvation energy of the reactants, especially of e_s^- (13, 14, 24). The mean free energy of solvation of electrons in water, −162 kJ/mol at 298 K (25), is similar to the optical absorption energy E_{Amax} = 166 kJ mol (26). This supports the search for correlations of k_2 with optical absorption energy E_r.

Figure 1*B* shows correlations of $k_2(e_s^- + NO_{3,s}^-)$ with E_r at 298 K. Among the butanols k_2 decreases with an increase in E_r. The values of k_2 also decrease with decreasing number of carbons, from 4 to 1. However, k_2 is largest in water.

The dielectric relaxation times τ of the series of alcohols (excluding *tert*-butanol) at different temperatures vary approximately linearly with η (Fig. 2). The equation of the line in Fig. 2 is:

[1] $\tau(ps) = 195[\eta(mPa \cdot s) - 0.30]$

The reported values of τ for *tert*-butanol at 298 K (20–22) are much smaller than eq. [1] indicates for η = 4.45 mPa·s, and those at 323 K and 343 K were obtained by extrapolation from lower temperatures (21, 22). The smaller ratio of τ/η for *tert*-butanol probably has to do with the sphere-like structure of the molecules, which can rotate and reorient faster than the chain-like butanols.

Correlations of electron solvation times with the intermediate dielectric relaxation time τ_2 (27), and of electron transfer reaction rate constants with the longitudinal relaxation τ_L (28) have been made. However, we use the longest relaxation time $\tau_1 = \tau$ for our general correlation with $k_2(e_s^- + NO_{3,s}^-)$, because τ_1 data are more complete.

The layered structures of Figs. 1*A* and *B* suggest that a more basic correlation might be found. From the Smoluchowski–Debye model (6, 9, 10) one can get:

[2] $k_2 = 4\pi N_A(D_e + D_s)\kappa R_r f$

where N_A is Avogadro's constant, D_i is the diffusion coefficient of *i*, R_r is the center-to-center reactant separation when reaction occurs, and κ is the probability that reaction occurs during one encounter and equals unity for diffusion-controlled reactions. The quantity κR_r is called an effective reaction radius; values have been estimated from the values of k_2 by factoring out the Debye coulombic factor *f* and approximate values of the diffusion coefficients (conductances) of the ionic reactants:

Can. J. Chem. Downloaded from www.nrcresearchpress.com by 65.111.164.53 on 09/08/12
For personal use only.

Fig. 2. Correlation of viscosity η and dielectric relaxation time τ of C_1 to C_4 alcohols and water at 298, 323, and 343 K. Some of the values of τ are extrapolated from those at lower temperatures. The symbol for each solvent is followed by the references for η; τ. Water, ○, 12; 15. Methanol, +, 12; 15,16. Ethanol, ×, 12; 15,16. 1-Propanol, △, 12; 15,16. 2-Propanol, ▲, 13; 15,16. 1-Butanol, □, 12; 15,17. *i*-Butanol, ■, 14; 15,17. 2-Butanol, ◇, 14; 15,17. *tert*-Butanol, ◆, 14; 17–19. The line through all data (except those for water and *tert*-butanol) represents eq. [1].

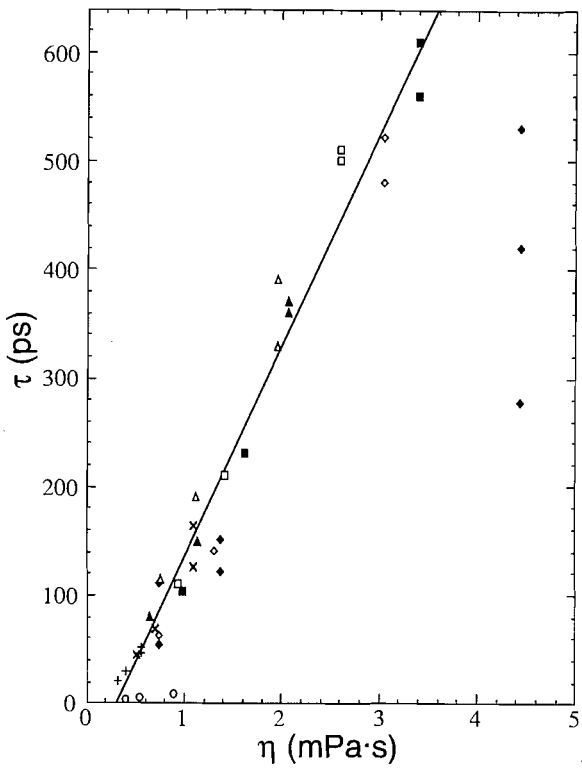

$$[3] \quad \kappa R_r(m) \approx 1 \times 10^{-16} k_2/fT\Lambda_0$$

where Λ_0 (S·m^2/mol) is the molar conductance of the reactant electrolyte solutions. To obtain accurate values of κR_r we would require accurate values of conductance of solvated electrons in the alcohols, but they are not available. At this stage we are looking for trends. A log–log plot of apparent κR_r values against E_r/τ at 298 K provides a better overall correlation of the reactivities in the C_1 to C_4 alcohols (black circles and full line in Fig. 3) than did the plots in Fig. 1. The value of κR_r at 298 K decreases with increasing trap depth of e_s^- and with decreasing relaxation time in the series of solvents. The value of κR_r in water is $\sim 10^2$ times higher than that extrapolated for an alcohol at the same value of E_r/τ (Fig. 3), which implies that the reaction is different in water.

A plot of κR_r against E_r/η shows a correlation similar to that in Fig. 3, as expected because of the linear relationship between τ and η.

In the C_1 to C_4 alcohol series at 298 K, if (*1*) the alcohol has a longer carbon chain, (*2*) the chain is more branched, or (*3*) the branch point is closer to the hydroxyl group, then E_r/τ is lower and κR_r is higher. This correlation might indicate that a longer and more branched chain alcohol has more difficulty to

Fig. 3. Correlation of apparent κR_r values and E_r/τ in C_1 to C_4 alcohols and water at 298 K (●), 323 K (□), and 343 K (△). The label of each dashed line identifies the solvent and the slope.

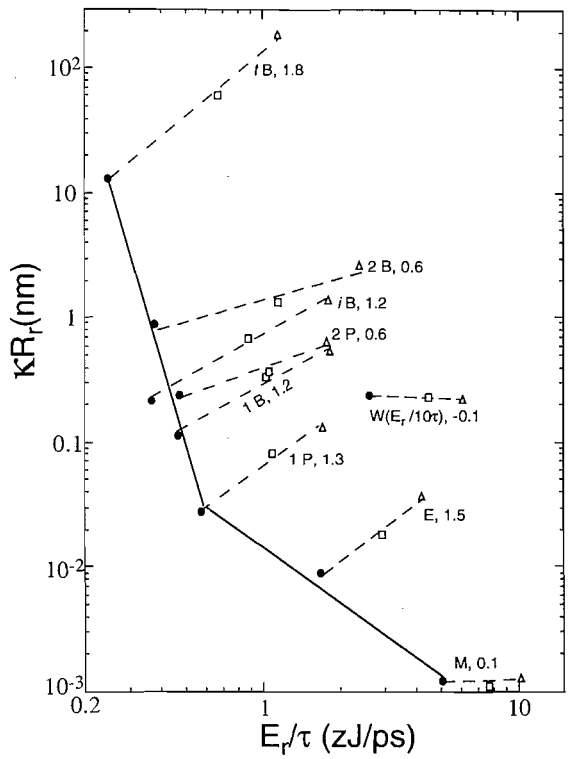

orient its —O—H dipole in the field of the electron or ion to solvate them, and that slower or less exoergic solvation results in a higher reaction rate constant with NO_3^-. The quantity E_r/τ can be understood as an effective trap-depth, since E_r is approximately equal to the binding energy of the e_s^- to its solvent site, and τ is related to the time during which the electron remains in a higher-than-equilibrium energy state after jumping to a new site. Similar correlations might be obtained with E_r/τ_2 or E_r/τ_L, but sufficient data are not available.

The values of κR_r and E_r/τ in a given alcohol usually increase with temperature (Fig. 3), and can be expressed by the empirical equation

$$[4] \quad \kappa R_r = C_\tau (E_r/\tau)^{p_\tau}$$

The slope of the line for a given alcohol in Fig. 3 equals p_τ, and the value of κR_r at $E_r/\tau = 1$ zJ/ps gives C_τ. There are four groups of p_τ values: ~0.0 for water and methanol, 0.6 for secondary alcohols, ~1.3 for primary alcohols, and 1.8 for *tert*-butanol. We do not understand the step size of 0.6.

Correlations of C_τ with τ are shown in Fig. 4. The four groups of p_τ probably indicate four different types of solvation structure in alcohols: *tertiary* alcohols, *secondary* alcohols, *primary* alcohols, and methanol. Water remains an exception.

It has been suggested that solvent molecules participate chemically in the reaction $e_s^- + NO_{3,s}^-$ in water and alcohols (4, 9). Reactivity in *tert*-butanol is highest; it has a relatively long dielectric relaxation time, and it has the maximum number of —CH_x groups attached to the α-carbon atom of the alcohol.

Can. J. Chem. Downloaded from www.nrcresearchpress.com by 65.111.164.53 on 09/08/12
For personal use only.

Fig. 4. Correlation of C_τ (eq. [4]) with τ (298 K) of C_1 to C_4 alcohols and water. The dashed lines connect species having same p_τ values.

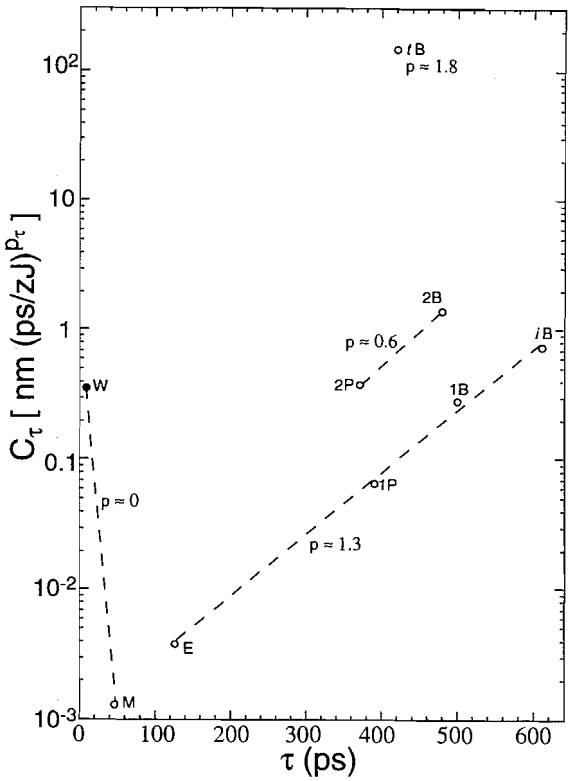

On the other hand, methanol has the lowest reactivity, the shortest dielectric relaxation time and no —CH_x groups attached to the α-carbon atom.

The correlations in Fig. 4 suggest two aspects of the solvent effect on the reaction: (*1*) solvation structure (packing form), and (*2*) solvent reorientation time. The reactivity in *tert*-butanol is higher than in the secondary alcohols. On the one hand, the solvation structure in *tert*-butanol results in a relatively high mobility of electrons in that alcohol (29); the mobility might be higher than it is in secondary alcohols. On the other hand, as e_s^- approaches $NO_{3,s}^-$ the C—H's of the three groups on the $HOC(CH_3)_3$ molecules that solvate the electron are accessible to the NO_3^- and product NO_3^{2-}, so there are more chances for reaction to occur than in secondary alcohols, and more chances in secondary than in primary alcohols. Methanol has no far reaching β-C—H's, so it has the lowest reactivity in this series.

In a given group of alcohols in Fig. 4 (for example, in primary or secondary alcohols), reactivity increases with solvent molecular reorientation time τ. This is because after the reaction

[5] $e_s^- + NO_{3,s}^- \rightarrow NO_3^{2-}$

the O—H dipole of the in-between molecule that solvated the electron tends to rotate in the field of the new NO_3^{2-} ion. The longer the relaxation time (τ, τ_2, or τ_L), the higher is the chance for the NO_3^{2-} ion to react with a C—H of the alcohol that was associated with e_s^-.

Fig. 5. Correlation of p_τ (●) and E_2–$E_{\Lambda 0}$ (□) with $k_2(e_s^- + NO_{3,s}^-)$ in C_1 to C_4 alcohols and water at 298 K.

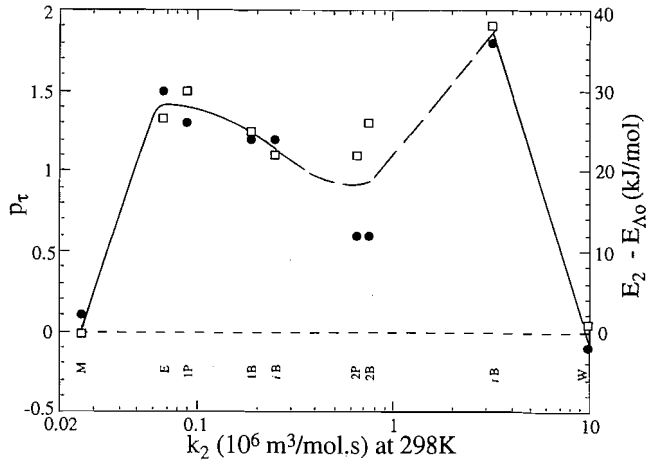

[6] $NO_3^{2-} + RR'CHOH \rightarrow NO_2^- + OH^- + RR'\dot{C}OH$

Therefore, from 2-propanol to 2-butanol and from ethanol to *i*-butanol, the reactivity increases with an increase in τ (Fig. 4). It is not clear why methanol falls into a group with water ($p_\tau \approx 0$).

Figure 5 shows plots of p_τ and $E_2 - E_{\Lambda 0}$ against k_2, where E_2 is the Arrhenius activation energy of the reaction (e_s^- + $NO_{3,s}^-$) in a pure alcohol, and $E_{\Lambda 0}$ is the Arrhenius activation energy of molar conductivity of lithium nitrate in the same alcohol. Both p_τ and $E_2 - E_{\Lambda 0}$ are temperature coefficients; p_τ is from apparent values of κR_r (Fig. 3) whereas $E_2 - E_{\Lambda 0}$ contains the Debye *f* factor. Both contain any non-ion-like mobility of e_s^-. Methanol and water are at opposite ends of the curve, which indicates that the reaction e_s^- + $NO_{3,s}^-$ in methanol has a different mechanism from that in water. The latter is a nearly diffusion-controlled reaction and the former is entropy-controlled (30). Throughout the series the variations of p_τ and $E_2 - E_{\Lambda 0}$ are similar. The peak at *tert*-butanol seems to be associated with a high mobility of e_s^- in that solvent (29).

Acknowledgments

We thank the Natural Sciences and Engineering Research Council of Canada for financial assistance, and the personnel of the Radiation Research Center for maintaining the accelerator and electronic equipment.

References

1. B. Hickel. J. Phys. Chem. **82**, 1005 (1978).
2. A.J. Elliott, D.R. McCracken, G.V. Buxton, and N.D. Wood. J. Chem. Soc. Faraday Trans. **86**, 1539 (1990).
3. C.C. Lai and G.R. Freeman. J. Phys. Chem. **94**, 4891 (1990).
4. S.A. Peiris and G.R. Freeman. Can. J. Phys. **68**, 940 (1990).
5. G. Duplâtre and C.D. Jonah. J. Phys. Chem. **95**, 897 (1991).
6. S.A. Peiris and G.R. Freeman. Can. J. Chem. **69**, 884 (1991).

7. G.V. Buxton and S.R. Mackenzie. J. Chem. Soc. Faraday Trans. **88**, 2833 (1992).
8. T.B. Kang and G.R. Freeman. Can. J. Chem. **71**, 1297 (1993).
9. R. Chen. and G.R. Freeman. Can. J. Chem. **71**, 1303 (1993).
10. Y. Zhao and G.R. Freeman. Can. J. Chem. In press.
11. R. Chen, Y. Avotinsh, and G.R. Freeman. Can. J. Chem. **72**, 1083 (1994).
12. M.S. Tunuli and Farhataziz. J. Phys. Chem. **90**, 6587 (1986).
13. A.M. Afanassiev, K. Okazaki, and G.R. Freeman. J. Phys. Chem. **83**, 1244 (1979).
14. P.C. Senanayake and G.R. Freeman. J. Chem. Phys. **87**, 7007 (1987).
15. R.C. Weast (ed). Handbook of chemistry and physics. 70th ed. CRC Press, Boca Raton, Fla. 1989. pp. F41–44.
16. W. Weber. Rheol. Acta, **14**, 1012 (1975).
17. P.C. Senanayake, N. Gee, and G.R. Freeman. Can. J. Chem. **65**, 2441 (1987).
18. F. Buckley and A.A. Maryott. Table of dielectric dispersion data for pure liquids and dilute solutions. National Bureau of Standards Circular 589. Washington, D.C. 1958.
19. J. Barthel, K. Bachhuber, R. Buchner, and H. Hetzenauer. Chem. Phys. Lett. **165**, 369 (1990).
20. H. Sato, H. Nakamura, K. Itoh, and K. Higasi. Chem. Lett. Chem. Soc. Jpn. 1167 (1985).
21. M. Tabellout, P. Lanceleur, J.R. Emery, D. Hayward, and R.A. Pethrick. J. Chem. Soc. Faraday Trans. **86**, 1493 (1990).
22. S.M. Puranik, A.C. Kumbharkhane, and S.C. Mehrotra. Indian J. Pure Appl. Phys. **29**, 47 (1991).
23. A.D. Leu, K.N. Jha, and G.R. Freeman. Can. J. Chem. **60**, 2342 (1982).
24. K. Okazaki and G.R. Freeman. Can. J. Chem. **56**, 2313 (1978).
25. H.A. Schwarz. J. Phys. Chem. **95**, 6697 (1991).
26. K.H. Schmidt, P. Han, and D.M. Bartels. J. Phys. Chem. **96**, 199 (1992).
27. W.J. Chase and J.W. Hunt. J. Phys. Chem. **79**, 2835 (1975).
28. M.J. Weaver. Chem. Rev. **92**, 463 (1992).
29. Y. Zhao and G.R. Freeman. Can. J. Chem. In press.
30. A.M. Afanassiev, K. Okazaki, and G.R. Freeman. Can. J. Chem. **57**, 839 (1979).

Can. J. Chem. Downloaded from www.nrcresearchpress.com by 65.111.164.53 on 09/08/12
For personal use only.

Ironcyclopentadienyl mediated 2-alkyl-2-arylphenylsulphonylacetonitrile synthesis

Alaa S. Abd-El-Aziz, Christine R. de Denus, and Harold M. Hutton

Abstract: A unique route to the synthesis of 2-alkyl-2-arylphenylsulphonylacetonitriles via the nucleophilic aromatic substitution (S_NAr) of chloroarene cyclopentadienyliron complexes with 2-alkyl phenylsulphonylacetonitriles has been investigated. Reactions of chloroarene complexes (**1***a–d*) with 2-alkyl phenylsulphonylacetonitrile (**2***a,b*) in the presence of K_2CO_3 in DMF at room temperature led to the formation of complexes **3***a–d* and **4***a,c,d* in good yields. The use of alkylated phenylsulphonylacetonitriles as nucleophiles in the reactions with the *p*-dichlorobenzene complex (**1***e*) allowed the formation of the disubstituted complexes (**5**, **6**). Photolytic demetallation provided an efficient route to the liberation of the arylated phenylsulphonylacetonitriles **7***a–d*, **8***a,c,d*, **9**, and **10**.

Key words: chloroarene, phenylsulphonylacetonitrile, nucleophilic substitution.

Résumé : On explore une méthode originale de synthèse des 2-alkyl-2-arylphénylsulphonylacétonitriles via la substitution aromatique nucléophile (S_NAr) des complexes du chloroarènecyclopentadiényl de fer avec les 2-alkylphénylsulphonylacétonitriles. Les réactions des complexes de choroarènes (**1***a–d*) avec le 2-alkylphénylsulphonylacétonitrile (**2***a,b*) en présence de K_2CO_3 dans le DMF à la température ambiante conduisent, avec de bons rendements, à la formation des complexes **3***a–d* et **4***a,c,d*. L'emploi des phénylsulphonylacétonitriles alkylés comme nucléophiles dans la réaction avec le complexe de *p*-dichlorobenzène (**1***e*) permet la formation de complexes disubstitués (**5**, **6**). La démétallation photolytique fournit une excellente voie d'accès à la libération des phénylsulphonylacétonitriles **7***a–d*, **8***a,c,d*, **9** et **10**.

Mots cles : chloroarène, phénylsulphonylacétonitrile, substitution nucléophile.

[Traduit par la rédaction]

Introduction

Since the displacement of the chloro group in the η^6-chlorobenzene-η^5-cyclopentadienyliron complex by a number of nucleophiles was first reported (1), numerous publications have appeared describing the use of these complexes in the synthesis of various organic molecules (2–10). Other metal moieties such as chromium tricarbonyl ($Cr(CO)_3$), manganese tricarbonyl ($Mn(CO)_3^+$), and cyclopentadienylruthenium ($CpRu^+$) have been used in the activation of the haloarene ring towards nucleophilic substitution reactions (11–18). In a recent review, Astruc has shown the flexibility of such systems as well as the advantages for the use of $CpFe^+$ over the above metal moieties (19). The advantage of using the $CpFe^+$ moiety is primarily due to the activating ability of this group towards displacement reactions. This was demonstrated clearly by the kinetic study carried out by Knipe et al. (20, 21). As well, the low toxicity and cost of this type of $FeCp^+$ complexation makes this route attractive in the synthesis of substituted aromatic compounds. Our research interest is focused on the use of the $CpFe^+$ complexes of chloroarenes in the synthesis of potentially biologically active molecules (2–5). We recently reported that chloroarene complexes can undergo nucleophilic aromatic substitution (S_NAr) with ethyl cyanoacetate or phenylsulphonylacetonitrile, leading to carbon–carbon bond formation (4, 5). In these studies, we demonstrated that photolysis of these arylated ethyl cyanoacetate or phenylsulphonylacetonitrile complexes led to the liberation of the compounds from their metal moieties in very high yields. These compounds are very valuable precursors to alkanoic acids and heterocyclic compounds that are known for their great importance in the pharmaceutical industry (22–28). One of the most important alkanoic acids is 2-(4-isobutylphenyl)propanoic acid, which is widely known as Ibuprofen. This compound exhibits anti-inflammatory and antipyretic activity and has been used successfully in the treatment of general muscle pain and stiffness, as well as in the treatment of patients with rheumatoid arthritis (29–32).

There are a number of routes to the synthesis of alkanoic acids that involve the conversion of alkyl aryl ketones into esters using thallium-promoted rearrangement followed by hydrolysis (33, 34). Other routes include Darzen's condensation reaction or the conversion of alkyl aryl ketones to aldehydes followed by oxidation to give the alkanoic acids (35, 36). One of the most interesting routes to the synthesis is the

Received November 3, 1994.

A.S. Abd-El-Aziz,[1] C.R. de Denus, and H.M. Hutton. Department of Chemistry, University of Winnipeg Winnipeg, MB R3B 2E9, Canada.

[1] Author to whom correspondence may be addressed.

Can. J. Chem. Downloaded from www.nrcresearchpress.com by 65.111.164.53 on 09/08/12
For personal use only.

Can. J. Chem. Downloaded from www.nrcresearchpress.com by 65.111.164.53 on 09/08/12
For personal use only.

arylation of phenylsulphonylacetonitriles, which are converted to alkanoic acids via alkylation and reductive desulphonation, followed by hydrolysis (25). This synthesis allows for the introduction of alkyl groups after the arylation of phenylsulphonylacetonitrile. To date there are few reports on the synthesis of arylated phenylsulphonylacetonitriles that have been shown to be converted to alkanoic acids (25, 37, 38). Suzuki et al. have shown that arylation of phenylsulphonylacetonitrile could be achieved via the displacement of an iodo group of an aryl iodide using a carbon nucleophile (25). This nucleophile was generated from the reaction of phenylsulphonylacetonitrile and sodium hydride in the presence of a copper salt as catalyst and HMPA as solvent. In a recent report Sakamoto et al. demonstrated that arylation could also be possible using either aryl iodide or aryl bromide in the presence of palladium(0) catalyst and DME as solvent (38). The harsh experimental conditions as well as the unreactivity of aryl chlorides, and the difficulty of introducing various substituents in the benzene ring, indicates that the new method we developed in the arylation of phenylsulphonylacetonitrile via the aid of the $CpFe^+$ moiety is a practical route to the synthesis of these compounds (4).

As an extension of our previous study, we carried out the alkylation process prior to the arylation step, which gives rise to a more flexible route to the synthesis of alkanoic acids. As well, the alkylation of phenylsulphonylacetonitrile allows for the possibility of dinucleophilic substitution reactions with dichlorobenzene complexes.

Results and discussion

Among the most important synthetic routes to carbon–carbon bond formation are the reactions of cyclopentadienyliron complexes of chloroarenes with various carbon nucleophiles. In our recent report on the synthesis of arylated phenylsulphonylacetonitriles, we presented a novel method for the preparation of a large number of these compounds. In the present work, we would like to demonstrate further the flexibility and efficiency of our cyclopentadienyliron-mediated methodology. In this paper, we present our recent investigation of the alkylation of phenylsulphonylacetonitrile prior to the substitution reactions with arene complexes. The alkylation allows for variation in the length of the carbon chain of the phenylsulphonylalkane nitrile as well as for the possibility of double nucleophilic substitution with dichlorobenzene complexes.

Alkylation of phenylsulphonylacetonitrile was conducted by generating the carbon nucleophile using sodium ethoxide, followed by the reaction with either ethyl bromide or *n*-butyl bromide to give **2***a* and **2***b*, respectively, as described in the experimental section. These two compounds were previously prepared by Lamm and Ankner using ion-pair alkylation (39). The yields of these reactions were slightly higher than the literature values. The ^1H NMR of these compounds are in agreement with those reported in the literature. Full characterization of **2***a* and **2***b* is reported in the experimental section.

The reactions of 1.0 mmol of complexes **1***a–d* with 1.05 mmol of compounds **2***a* or **2***b* in the presence of potassium carbonate in DMF, at room temperature, gave rise to the displacement of the chloro group by the carbon nucleophiles. The products were isolated as yellow solids in yields ranging from 69 to 96%. It is important to note that the reaction of compound **2***a* with *o*-chlorotoluene complex (**1***b*) gave the desired complex with lowest yield. On the other hand, reaction of compound **2***b* with *o*-chlorotoluene complex (**1***b*) failed to give the substituted complex; instead, decomposition of the starting complex took place.

Scheme 1

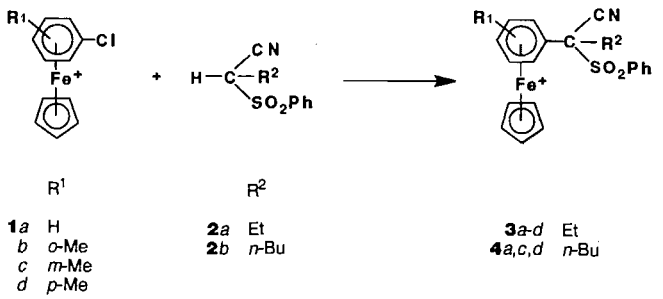

Complexes **3***a-d* and **4***a,c,d* were characterized using ^1H and ^{13}C NMR as well as IR and elemental analysis. In all the ^1H NMR spectra (200 MHz) of the product complexes, **3***a–d* and **4***a,c,d*, a very distinct singlet appeared in the range 5.29–5.36 ppm, which is evidence of the cyclopentadienyl (Cp) resonance. In some cases, where the complexed arene contains a methyl group in the *ortho* or *meta* position, **3***b*, **3***c*, **4***c*, we observed the presence of two Cp resonances of equal intensity. This result is in agreement with our recent work in which we observed preferential orientation of the arene substituent, allowing for different magnetic environments for the possible rotamers (40). This behavior was also observed with the arene methyl group. It is important to note that the methylene group in the α-position of the alkylphenylsulphonylacetonitrile group appears as an AB system. The splitting pattern and the coupling constant are given in the detailed experimental section. ^{13}C NMR (50 MHz) lends evidence in support of the ^1H NMR evaluation. For example, the carbon spectra of complex **3***b* was quite complex, showing two Cp resonances at 79.35 and 79.43 ppm and two arene methyl resonances at 21.39 and 22.03 ppm. The arene carbons also appeared as 12 resonances, further demonstrating the presence of two conformers of equal populations (see Scheme 1).

In the reactions of dichlorobenzene complexes with phenylsulphonylacetonitrile, disubstitution reactions could take place provided that a different nucleophile, such as an oxygen- or sulphur-containing nucleophile, could be used prior to the arylation step (4). In that study, we displaced a chloro group using an oxygen-containing nucleophile, followed by substitution with the carbon nucleophile generated from phenylsulphonylacetonitrile. We would like also to note that no disubstituted materials were obtained, owing to the deprotonation of the resulting arylated phenylsulphonylacetonitrile complex. This phenomenon is of course due to the basic reaction conditions, which allow for the deprotonation of the methine proton from the complex and the formation of a neutral zwitterion cyclohexadienyliron complex as shown in Scheme 2. This zwitterion would thus be more electron rich than the starting dichlorobenzene complex (**1***e*), and hence the second chlorine atom would be rendered incapable of undergoing a second substitution.

The alkylation of phenylsulphonylacetonitrile prior to nucleophilic aromatic substitution allows for the displacement

Can. J. Chem. Downloaded from www.nrcresearchpress.com by 65.111.164.53 on 09/08/12
For personal use only.

Scheme 2

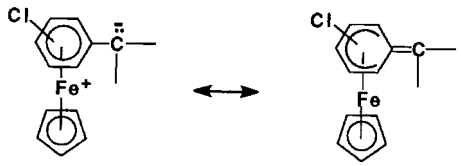

of one or two chlorine groups in the dichlorobenzene complexes. In this study, we would like to demonstrate that by alkylating the phenylsulphonylacetonitrile, the reaction could proceed under similar conditions to give the disubstituted products. As an example, we carried out the reaction of the *p*-dichlorobenzene complex (**1***e*), with an excess of either nucleophile **2***a* or **2***b*, in the presence of potassium carbonate and DMF. In these reactions, it was noted that longer reaction times were necessary in order to produce the disubstituted complexes (**5**, **6**) in good yields (Scheme 3). This is in agreement with our previous results on double nucelophilic substitution using alkylated diethyl malonate (8). The *p*-disubstituted complexes were chosen because of the importance of many *p*-disubstituted alkanoic acid esters that exhibit some form of biological activity. The disubstituted complexes (**5**, **6**) were obtained in good yields and were fully characterized. It is very important to note that in these spectra the splitting patterns became much simpler due to the plane of symmetry possessed by the complexes.

Decomplexation of the arylated alkylphenylsulphonylacetonitrile complexes led to the liberation of the free substituted arenes in very high yields. One of the most efficient methods of obtaining the free arenes from their complexes is photolytic demetallation (41–44) (Scheme 4). By dissolving the complex in a mixture of acetonitrile and dichloromethane and irradiating it with a Xenon lamp for a short period of time, it is possible to isolate the desired organic compounds (**7***a–d*, **8***a,c,d*, **9**, **10**) via column chromatography. The monosubstituted compounds were obtained as oils or solids, while the disubstituted compounds were isolated as white solids. The identities of all products were confirmed by ^{1}H and ^{13}C NMR, IR, and MS spectroscopy, as well as by melting points. The major differences in the NMR spectra of these compounds from those of the complexes were the absence of the cyclopentadienyl peak(s) and the shift of the arene peaks to a lower field. As well, we no longer observed any evidence of isomers in the compounds, which allows for simpler spectral patterns. In conclusion, this methodology demonstrates our ability to prepare 2-alkyl-2-arylphenylsulphonylacetonitriles under mild conditions and very high yields. As well, aryl di(alkylphenylsulphonylacetonitrile) could be synthesized via the proposed reaction schemes.

Experimental

^{1}H and ^{13}C NMR spectra were recorded at 200 and 50 MHz, respectively, on a Varian Gemini 200 NMR spectrometer, with chemical shifts (ppm) being calculated from the solvent signals. Deuteroacetone and deuterochloroform were used as solvents for the complexed and free 2-alkyl-2-aryl-phenylsulphonylacetonitriles, respectively. Coupling constants were calculated in hertz (Hz). MS were obtained on a Hewlett–Packard 5970 Series mass selective detector, by electron impact (70 V). Signal positions are given in *m/z* units. IR were recorded on a Perkin–Elmer model 781 spectrophotometer. Melting points were measured in a capillary using a Mel-Temp II and are uncorrected. All new compounds gave satisfactory elemental analyses.

Starting materials

Starting complexes **1***a–e* were prepared by ligand exchange reactions (45). Anhydrous aluminum chloride, aluminum powder, ferrocene, chloroarenes, reagent grade solvents, and ammonium hexafluorophosphate are commercially available and were used without further purification. Silica gel 60–100 mesh was used in the column chromatographic purification of the liberated arenes.

Synthesis of ethyl or butylphenylsulphonylacetonitrile (**2***a,b*)

In a flame-dried 250 mL 3-necked flask, equipped with a stir bar and condenser fitted with a calcium chloride tube, was placed 30 mL of absolute ethanol. Sodium (0.780 g; 34 mmol) was added to the ethanol over a period of 30 min. After all the sodium reacted with the ethanol, 5.44 g (30 mmol) of phenylsulphonylacetonitrile was added to the warm solution of the sodium ethoxide. Without delay, 3.2 mL (43 mmol) of ethyl bromide or 4.6 mL (43 mmol) of butyl bromide was added slowly to the solution, upon which it turned a slightly yellow color. The reaction mixture was refluxed for 8 h and left to sit in a dark place for 1 week, during which time a white precipitate formed. The mixture was then filtered, the reaction flask washed with ethanol, and the solution also filtered. To this mixture, 25 mL of distilled water and 0.5 mL of concentrated hydrochloric acid were added. The mixture was then transferred to a separatory funnel and the aqueous sodium bromide solution was drawn off. Following drying over magnesium sulphate, the ethanol was removed using a rotary evaporator to

Scheme 3

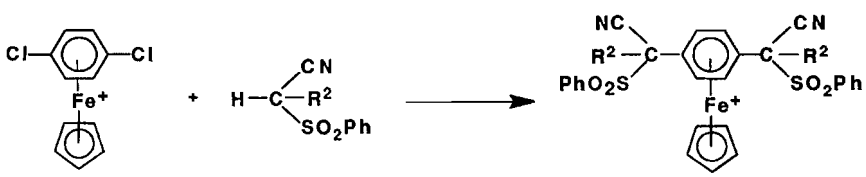

	R^2
1*e*	
2*a*	Et
2*b*	*n*-Bu
5	Et
6	*n*-Bu

Scheme 4

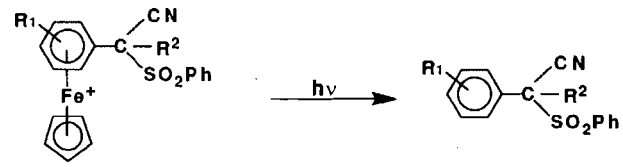

Complex	R^1	R^2	compound
3*a*	H	Et	**7***a*
3*b*	*o*-Me	Et	**7***b*
3*c*	*m*-Me	Et	**7***c*
3*d*	*p*-Me	Et	**7***d*
4*a*	H	*n*-Bu	**8***a*
4*c*	*m*-Me	*n*-Bu	**8***c*
4*d*	*p*-Me	*n*-Bu	**8***d*
5	*p*-CCN(Et)SO_2Ph	Et	**9**
6	*p*-CCN(*n*-Bu)SO_2Ph	*n*-Bu	**10**

produce a yellow oil. Purification of this oil using column chromatography gave unreacted phenylsulphonylacetonitrile, and monalkylated and dialkylated products.

2-Ethylphenylsulphonylacetonitrile **2**a
Colorless oil, 2.28 g (36.3%); ν_{max} (KBr) (cm^{-1}): 1158, 1340 (SO_2), 2340 (CN): ^1H NMR: 1.10 (3H, t, *J* 7.2 Hz, CH_3), 1.90 (1H, m, CH_2), 2.22 (1H, m, CH_2), 3.87 (1H, dd, *J* 4.6, 10.5 Hz, CH), 7.96 (4H, m, SO_2Ph), 8.00 (1H, m, SO_2Ph); ^{13}C NMR: 11.06 (CH_3), 20.68 (CH_2), 58.77 (CH), 113.76 (CN), 129.50 (4C, SO_2Ph), 135.14 (SO_2Ph), 135.50 (quaternary SO_2Ph); *m/z*: 209 (M^+, 6%).

2-Butylphenylsulphonylacetonitrile **2**b
Colorless oil, 2.25 g (31.6%); ν_{max} (KBr) (cm^{-1}): 1160, 1340 (SO_2), 2340 (CN); ^1H NMR: 0.90 (3H, t, *J* 7.2, CH_3), 1.35 (2H, m, CH_2CH_3), 1.89 (2H, m, $CH_2CH_2CH_3$), 2.22 (2H, m, $CH_2CH_2CH_2CH_3$), 3.87 (1H, dd, *J* 4.6, 10.5, CH), 7.59–7.67 (4H, m, SO_2Ph), 7.80–8.02 (1H, m, SO_2Ph); ^{13}C NMR: 13.54 (CH_3), 22.65 (CH_2CH_3), 26.81 ($CH_2CH_2CH_3$), 31.59 ($CH_2CH_2CH_2CH_3$), 57.56 (CH), 113.90 (CN), 129.58 (4C, SO_2Ph), 135.21 (SO_2Ph), 135.58 (quaternary SO_2Ph); *m/z*: 237 (M^+, 4.5%).

Nucleophilic substitution reactions

Monosubstitution
A mixture of 1.0 mmol of starting chloroarene complex, 2.5 mmol of potassium carbonate, 1.05 mmol of **2***a* or **2***b*, and 10 mL of *N,N*-dimethyl formamide was stirred at room temperature, under a nitrogen atmosphere, for 7 h. The resulting red reaction mixture was then filtered into 10 mL of 10% hydrochloric acid, the reaction flask washed with acetone, and the washings were also filtered. The acetone was then removed under reduced pressure and a concentrated aqueous solution of ammonium hexafluorophosphate was added to the filtrate, at which time the product precipitated as a yellow solid. After 10 min the product was collected by filtration, and washed with water followed by diethyl ether.

η^5-*Cyclopentadienyl*[η^6-*ethylphenyl(phenylsulphonylacetonitrile)]iron(II) hexafluorophosphate* (**3**a): 0.435 g, 79%; ν_{max} (KBr) (cm^{-1}): 1158, 1335 (SO_2), 2340 (CN); ^1H NMR: 1.50 (3H, t, *J* 7.4, CH_3), 2.76 (1H, m, CH_2), 2.97 (1H, m, CH_2), 5.36 (5H, s, Cp), 6.29 (2H, d, *J* 6.4, ArH), 6.57 (1H, m, ArH), 6.72 (2H, m, ArH), 7.64 (4H, m, SO_2Ph), 7.89 (1H, m, SO_2Ph); ^{13}C NMR: 11.20 (CH_3), 26.71 (CH_2), 71.60 (quaternary C-CH_2CH_3), 79.07 (5C, Cp), 88.15, 88.76, 88.80, 88.92, 90.51 (5C, ArC), 98.49 (quaternary ArC), 115.04 (CN), 130.61, 131.65 (4C, SO_2Ph), 133.13 (quaternary SO_2Ph), 137.65 (SO_2Ph).

η^5-*Cyclopentadienyl*[η^6-*ethyl* (o-*tolyl*)*phenylsulphonylacetonitrile]iron(II) hexafluorophosphate* (**3**b): 0.389 g, 69%. ν_{max} (KBr) (cm^{-1}): 1160, 1340 (SO_2), 2350 (CN); ^1H NMR 1.29, 1.47 (3H, t, *J* 7.3, CH_3), 2.68, 2.79 (3H, s, $ArCH_3$), 2.88 (2H, m, CH_2), 5.31, 5.33 (5H, s, Cp), 6.40 (1H, d, *J* 6.8, ArH), 6.52–6.62 (2H, m, ArH), 6.71 (1H, t, *J* 6.2, ArH), 7.62–7.95 (5H, m, SO_2Ph); ^{13}C NMR: 11.02, 11.69 (CH_3), 21.39, 22.03 ($ArCH_3$), 29.55 (CH_2), 70.64 (quaternary C-CH_2CH_3), 79.35, 79.43 (5C, Cp), 87.66, 87.99, 88.18, 89.59, 90.17, 90.56, 92.49, 92.54 (4C, ArC), 97.32 (1C, quaternary ArC), 103.90, 104.39 (1C, quaternary ArC), 115.46 (CN), 130.77, 131.80 (4C, SO_2Ph), 133.72 (quaternary SO_2Ph), 137.34 (SO_2Ph).

η^5-*Cyclopentadienyl*[η^6-*ethyl* (m-*tolyl*)*phenylsulphonylacetonitrile]iron(II) hexafluorophosphate* (**3**c): 0.481 g, 85%. ν_{max} (KBr) (cm^{-1}): 1160, 1335 (SO_2), 2240 (CN); ^1H NMR: 1.49, 1.51 (3H, t, *J* 7.4, CH_3), 2.46, 2.62 (3H, s, $ArCH_3$), 2.73 (1H, m, CH_2), 2.95 (1H, m, CH_2), 5.30, 5.32 (5H, s, Cp), 6.53 (2H, m, ArH), 6.63 (2H, m, ArH), 7.61 (4H, m, SO_2Ph), 7.68 (1H, m, SO_2Ph); ^{13}C NMR: 11.25 (CH_3), 20.19, 20.53 ($ArCH_3$), 26.58 (CH_2), 71.75 (quaternary C-CH_2CH_3), 79.39 (5C, Cp), 85.90, 86.55, 87.90, 87.97, 88.13, 88.34, 90.86, 90.93 (4C, ArC), 99.00, 105.16 (2C, quaternary ArC), 115.40 (CN), 130.61, 131.83 (4C, SO_2Ph), 134.80 (quaternary SO_2Ph), 137.26 (SO_2Ph).

η^5-*Cyclopentadienyl*[η^6-*ethyl* (p-*tolyl*)*phenylsulphonylacetonitrile]iron(II) hexafluorophosphate* (**3**d): 0.444 g, 79%. ν_{max} (KBr) (cm^{-1}): 1160, 1335 (SO_2), 2240 (CN); ^1H NMR: 1.47 (3H, t, *J* 7.4, CH_3), 2.60 (3H, s, $ArCH_3$), 2.70 (1H, m, CH_2), 2.96 (1H, m, CH_2), 5.31 (5H, s, Cp), 6.24 (1H, d, *J* 6.7, ArH), 6.53 (3H, m, ArH), 7.62 (4H, m, SO_2Ph), 7.67 (1H, m, SO_2Ph); ^{13}C NMR: 11.21 (CH_3), 20.40 ($ArCH_3$), 26.74 (CH_2), 71.38 (quaternary C-CH_2CH_3), 79.35 (5C, Cp), 86.99, 87.61, 88.95, 89.18 (4C, ArC), 96.92, 106.84 (2C, quaternary ArC), 115.14 (CN), 130.65, 131.75 (4C, SO_2Ph), 133.19 (quaternary SO_2Ph), 137.23 (SO_2Ph).

η^5-*Cyclopentadienyl*[η^6-*butyl (phenyl)phenylsulphonylacetonitrile]iron(II) hexafluorophosphate* (**4***a*): 0.412 g, 71%. ν_{max} (KBr) (cm^{-1}): 1158, 1342 (SO_2), 2350 (CN); ^1H NMR: 1.01 (3H, t, *J* 7.3, CH_3), 1.56 (2H, m, CH_2CH_3), 1.90 (2H, m, $CH_2CH_2CH_3$), 2.63–2.89 (2H, m, $CH_2CH_2CH_2CH_3$), 5.35 (5H, s, Cp), 6.52–6.74 (5H, m, ArH), 7.54 (4H, m, SO_2Ph), 7.88 (1H, m, SO_2Ph); ^{13}C NMR: 13.89 (CH_3), 23.07 (CH_2CH_3), 29.04 ($CH_2CH_2CH_3$), 32.64 ($CH_2CH_2CH_2CH_3$), 71.01 (quaternary, C-C_4H_9), 79.14 (5C, Cp), 87.96, 88.26, 88.86, 89.04, 90.57 (5C, ArC), 98.64 (quaternary ArC), 115.30 (CN), 130.69, 131.79 (4C, SO_2Ph), 133.28 (quaternary SO_2Ph), 137.30 (SO_2Ph).

η^5-*Cyclopentadienyl*[η^6-*butyl* (m-*tolyl*)*phenylsulphonylace-*

Can. J. Chem. Downloaded from www.nrcresearchpress.com by 65.111.164.53 on 09/08/12
For personal use only.

Can. J. Chem. Downloaded from www.nrcresearchpress.com by 65.111.164.53 on 09/08/12
For personal use only.

*tonitrile]iron(II) hexafluorophosphate (**4**c):* 0.569 g, 96%. ν_{max} (KBr) (cm^{-1}): 1157, 1340 (SO_2), 2240 (CN); ^1H NMR: 1.01 (3H, m, CH_3), 1.56 (2H, m, CH_2CH_3), 1.89 (2H, m, $CH_2CH_2CH_3$), 2.47, 2.60 (3H, s, $ArCH_3$), 2.89 (2H, m, $CH_2CH_2CH_2CH_3$), 5.28, 5.29 (5H, s, Cp), 6.46–6.62 (4H, m, ArH), 7.58–7.93 (5H, m, SO_2Ph); ^{13}C NMR: 13.84 (CH_3), 20.10, 20.38 ($ArCH_3$), 22.96 (CH_2CH_3), 28.98 ($CH_2CH_2CH_3$), 32.45 ($CH_2CH_2CH_2CH_3$), 70.87, 70.96 (quaternary, C-C_4H_9), 79.24 (5C, Cp), 86.01, 86.42, 87.79, 87.86, 87.88, 88.00, 88.21, 90.79 (4C, ArC), 97.97, 98.09 (quaternary ArC), 104.82, 105.11 (quaternary ArC), 115.24 (CN), 130.52, 131.78 (4C, SO_2Ph), 133.12 (quaternary SO_2Ph), 137.17 (SO_2Ph).

*η^5-Cyclopentadienyl[η^6-butyl (p-tolyl)phenylsulphonylacetonitrile]iron(II) hexafluorophosphate (**4**d):* 0.444 g, 75%. ν_{max} (KBr) (cm^{-1}): 1160, 1340 (SO_2), 2250 (CN); ^1H NMR: 0.98 (3H, t, *J* 7.3, CH_3), 1.53 (2H, m, CH_2CH_3), 1.85 (2H, m, $CH_2CH_2CH_3$), 2.64 (3H, s, $ArCH_3$), 2.84 (2H, m, $CH_2CH_2CH_2CH_3$), 5.31 (5H, s, Cp), 6.26 (1H, d, *J* 6.2 , ArH), 6.48 (1H, d, *J* 6.2 , ArH), 6.59 (2H, s, ArH), 7.61–7.73 (4H, m, SO_2Ph), 7.89–7.92, 7.61–7.73 (1H, m, SO_2Ph); ^{13}C NMR: 13.61 (CH_3), 20.13 ($ArCH_3$), 22.71 (CH_2CH_3), 28.73 ($CH_2CH_2CH_3$), 32.27 ($CH_2CH_2CH_2CH_3$), 70.49 (quaternary, C-C_4H_9), 79.04 (5C, Cp), 86.93, 87.26, 88.66, 88.89 (4C, ArC), 96.59 (quaternary ArC), 106.54 (quaternary ArC), 115.04 (CN), 130.37, 131.47 (4C, SO_2Ph), 132.86 (quaternary SO_2Ph), 136.99 (SO_2Ph).

*η^5-Cyclopentadienyl[p-di-{η^6-ethyl (phenyl)phenylsulphonylacetonitrile]iron(II) hexafluorophosphate (**5**):* 0.590 g, 78%. ν_{max} (KBr) (cm^{-1}): 1158, 1338 (SO_2), 2240 (CN); ^1H NMR: 1.34 (6H, t, *J* 7.3, CH_3), 2.75 (2H, m, CH_2), 2.91 (2H, m, CH_2), 5.54 (5H, s, Cp), 6.65–6.94 (4H, m, ArH), 7.76–7.79 (8H, m, SO_2Ph), 8.04 (2H, m, SO_2Ph); ^{13}C NMR: 11.05 (2C, CH_3), 26.79 (2C, CH_2), 71.22 (2C, quaternary C-CH_2CH_3), 80.81 (5C, Cp), 87.75 (4C, ArC), 100.06 (2C, quaternary ArC), 114.94 (2C, CN), 130.98, 131.80 (8C, SO_2Ph), 133.35 (2C, quaternary SO_2Ph), 137.63 (2C, SO_2Ph).

*η^5-Cyclopentadienyl[p-di-{η^6-butyl phenyl(phenylsulphonylacetonitrile)}]iron(II) hexafluorophosphate (**6**):* 0.590 g, 75%. ν_{max} (KBr) (cm^{-1}): 1158, 1338 (SO_2), 2242 (CN); ^1H NMR: 0.93 (6H, t, *J* 7.2, CH_3), 1.49 (4H, m, CH_2CH_3), 1.82 (4H, m, $CH_2CH_2CH_3$), 2.73 (4H, m, $CH_2CH_2CH_2CH_3$), 5.52 (5H, s, Cp), 6.65–6.79 (4H, m, ArH), 7.77–7.80 (8H, m, SO_2Ph), 8.01 (2H, m, SO_2Ph); ^{13}C NMR: 13.74 (2C, CH_3), 22.80 (2C, CH_2CH_3), 28.83 (2C, $CH_2CH_2CH_3$), 32.59 (2C, $CH_2CH_2CH_2CH_3$), 70.57 (2C, quaternary, C-C_4H_9), 80.68 (5C, Cp), 87.40, 87.61 (4C, ArC), 100.02 (2C, quaternary ArC), 115.01(2C, CN), 130.94, 131.69 (8C, SO_2Ph), 133.24 (2C, quaternary SO_2Ph), 137.63 (2C, SO_2Ph).

Photolytic demetallation. General procedure for photolysis

Samples (0.5 mmol) of each of the complexes **3***a–d*, **4***a*, *c*, *d*, **5**, and **6**, were separately dissolved in a mixture of dichloromethane and acetonitrile (30 mL: 10 mL) in a Pyrex tube. The solution was deoxygenated by bubbling nitrogen through it after which the reaction tube was fitted into a photochemical apparatus equipped with a Xenon lamp and irradiated at room temperature for 4 h. The solvent was concentrated to a volume of 1–2 mL using rotary evaporation. The residue was applied to a silica gel column, which was then washed with hexane and eluted with chloroform. Removal of the solvent from the eluate gave the expected liberated arenes with the following yields and spectral data.

*Ethyl phenyl(phenylsulphonylacetonitrile) (7*a*):* isolated as a light cream-colored solid; 0.114 g, 80%; mp 89–91°C. ν_{max} (KBr) (cm^{-1}): 1158, 1340 (SO_2), 2340 (CN); ^1H NMR: 1.02 (3H, t, *J* 7.3, CH_3), 2.63 (2H, m, CH_2), 7.34 (6H, m, ArH and SO_2Ph), 7.63 (4H, m, ArH and SO_2Ph); ^{13}C NMR: 9.21 (CH_3), 25.02 (CH_2), 73.20 (quaternary C-CH_2CH_3), 116.31 (CN), 128.21 (quaternary ArC), 128.49, 128.52, 128.53, 128.65, 128.73 (5C, ArC), 129.98, 130.50 (4C, SO_2Ph), 133.81 (quaternary SO_2Ph), 134.69 (SO_2Ph); *m/z*: 285 (M^+, 1.0%).

*Ethyl (o-tolyl)phenylsulphonylacetonitrile (7*b*):* isolated as a colorless oil; 0.136 g, 91%. ν_{max} (KBr) (cm^{-1}): 1156, 1355 (SO_2), 2305 (CN); ^1H NMR: 1.07 (3H, t, *J* 7.3, CH_3), 2.31 (3H, s, $ArCH_3$), 2.57 (1H, m, CH_2), 2.90 (1H, m, CH_2), 7.08–7.69 (9H, m, ArH and SO_2Ph); ^{13}C NMR: 9.24 (CH_3), 21.76 ($ArCH_3$), 26.98 (CH_2), 67.09 (quaternary C-CH_2CH_3), 117.64 (CN), 125.10 (quaternary ArC), 126.38, 128.84 (3C, ArC), 130.08, 130.79 (4C, SO_2Ph), 133.31 (ArC), 134.20 (quaternary SO_2Ph), 134.87 (SO_2Ph), 140.34 (quaternary ArC); *m/z*: 299 (M^+, 1.0%).

*Ethyl (m-tolyl)phenylsulphonylacetonitrile (7*c*):* isolated as a light cream-colored solid; 0.127 g, 85%; mp 84–85.5°C. ν_{max} (KBr) (cm^{-1}): 1158, 1330 (SO_2), 2300 (CN); ^1H NMR: 1.05 (3H, t, *J* 7.4, CH_3), 2.28 (3H, s, $ArCH_3$), 2.68 (2H, m, CH_2), 7.20 (4H, m, ArH), 7.44 (2H, m, SO_2Ph), 7.57 (3H, m, SO_2Ph); ^{13}C NMR: 9.23 (CH_3), 21.29 ($ArCH_3$), 24.91 (CH_2), 73.22 (quaternary C-CH_2CH_3), 116.43 (CN), 125.54 (ArC), 127.99 (quaternary ArC), 128.57(2C, ArC), 129.23 (ArC), 130.59, 130.72 (4C, SO_2Ph), 133.85 (quaternary SO_2Ph), 134.68 (SO_2Ph), 138.62 (quaternary ArC); *m/z*: 299 (M^+, 1.0%).

*Ethyl (p-tolyl)phenylsulphonylacetonitrile (7*d*):* isolated as a light cream-colored solid; 0.120 g, 80%; mp 90–92°C. ν_{max} (KBr) (cm^{-1}): 1160, 1330 (SO_2), 2305 (CN); ^1H NMR: 1.04 (3H, t, *J* 7.4, CH_3), 2.37 (3H, s, $ArCH_3$), 2.67 (2H, m, CH_2), 7.14 (2H, d, *J* 6.4, ArH), 7.26 (2H, d, *J* 6.3, ArH), 7.42 (2H, m, SO_2Ph), 7.60 (3H, m, SO_2Ph); ^{13}C NMR: 9.21 (CH_3), 21.13 ($ArCH_3$), 25.05 (CH_2), 73.03 (quaternary C-CH_2CH_3), 116.48 (CN), 125.05 (quaternary ArC), 128.47, 128.65 (4C, ArC), 129.47, 130.62 (4C, SO_2Ph), 133.66 (quaternary SO_2Ph), 134.66 (SO_2Ph), 140.29 (quaternary ArC); *m/z*: 299 (M^+, 1.0%).

n-*Butyl phenyl(phenylsulphonylacetonitrile) (8*a*):* isolated as a yellowish oil; 0.143 g, 91%. ν_{max} (KBr) (cm^{-1}): 1158, 1340 (SO_2), 2240 (CN); ^1H NMR: 0.87 (3H, t, *J* 7.0, CH_3), 1.19 (2H, m, CH_2CH_3), 1.40 (2H, m, $CH_2CH_2CH_3$), 2.59 (2H, m, $CH_2CH_2CH_2CH_3$), 7.24–7.62 (10H, m, ArH and SO_2Ph); ^{13}C NMR: 13.62 (CH_3), 22.39 (CH_2CH_3), 26.96 ($CH_2CH_2CH_3$), 30.80 ($CH_2CH_2CH_2CH_3$), 72.50 (quaternary, C-C_4H_9), 116.52 (CN), 128.39, 128.63, 128.73 (5C, ArC), 129.55, 130.54 (4C, SO_2Ph), 133.79 (quaternary SO_2Ph), 134.67 (SO_2Ph), 139.05 (quaternary ArC); *m/z*: 313 (M^+, 1.0%).

n-*Butyl (*m-*tolyl)phenylsulphonylacetonitrile (**8**c):* isolated as a yellowish oil; 0.136 g, 83%. ν_{max} (KBr) (cm^{-1}): 1158, 1335 (SO_2), 2240 (CN); ^1H NMR: 0.86 (3H, t, *J* 7.1, CH_3), 1.18 (2H, m, CH_2CH_3), 1.40 (2H, m, $CH_2CH_2CH_3$), 2.24 (3H, s, $ArCH_3$), 2.56 (2H, m, $CH_2CH_2CH_2CH_3$), 7.16–7.62 (9H, m, ArH and SO_2Ph), ^{13}C NMR: 13.58 (CH_3), 21.26 ($ArCH_3$), 22.36 (CH_2CH_3), 26.92 ($CH_2CH_2CH_3$), 30.69 ($CH_2CH_2CH_2CH_3$), 72.47 (quaternary, C-C_4H_9), 116.61 (CN), 125.35, 128.51, 128.55, 129.10 (4C, ArC), 130.55, 130.65 (4C, SO_2Ph), 133.77 (quaternary SO_2Ph), 134.58 (SO_2Ph), 138.56 (quaternary ArC); *m/z*: 327 (M^+, 1.0%).

n-*Butyl (*p-*tolyl)phenylsulphonylacetonitrile (**8**d):* isolated as a yellowish oil; 0.136 g, 83%. ν_{max} (KBr) (cm^{-1}): 1158, 1342 (SO_2), 2240 (CN); ^1H NMR: 0.86 (3H, t, *J* 7.1, CH_3), 1.19 (2H, m, CH_2CH_3), 1.40 (2H, m, $CH_2CH_2CH_3$), 2.33 (3H, s, $ArCH_3$), 2.55 (2H, m, $CH_2CH_2CH_2CH_3$), 7.09 (2H, d, *J* 8.4, ArH), 7.22 (2H, d, *J* 8.4, ArH), 7.34–7.42 (2H, m, SO_2Ph), 7.51–7.63 (3H, m, SO_2Ph); ^{13}C NMR: 13.66 (CH_3), 21.14 ($ArCH_3$), 22.43 (CH_2CH_3), 26.98 ($CH_2CH_2CH_3$), 30.86 ($CH_2CH_2CH_2CH_3$), 72.31 (quaternary, C-C_4H_9), 116.70 (CN), 128.36, 128.63 (4C, ArC), 129.45, 130.65 (4C, SO_2Ph), 133.92 (quaternary SO_2Ph), 134.64 (SO_2Ph), 140.26 (quaternary ArC); *m/z*: 327 (M^+, 1.0%).

p-*Diethyl phenyl(phenylsulphonylacetonitrile) (**9**):* isolated as a white solid; 0.192 g, 78%; mp 168–172°C (dec.). ν_{max} (KBr) (cm^{-1}): 1160, 1330 (SO_2), 2240 (CN); ^1H NMR: (DMSO-d_6): 0.90 (6H, t, *J* 7.1, CH_3), 2.43 (2H, m, CH_2), 2.75 (4H, m, CH_2), 7.43 (4H, s, ArH), 7.48–7.63 (8H, m, SO_2Ph), 7.82 (2H, t, *J* 7.1, SO_2Ph); ^{13}C NMR: 9.16 (2C, CH_3), 24.88 (2C, CH_2), 72.54 (2C, quaternary C-CH_2CH_3), 115.92 (2C, CN), 129.11 (4C, ArC), 129.34 (4C, SO_2Ph), 129.86 (2C, quaternary ArC), 130.15 (4C, SO_2Ph), 132.97 (2C, quaternary SO_2Ph), 135.74 (2C, SO_2Ph); *m/z*: 492 (M^+, 0.6%).

p-*Dibutyl phenyl(phenylsulphonylacetonitrile) (**10**):* isolated as a white solid; 0.195 g, 71%; mp 145–148°C (dec.). ν_{max} (KBr) (cm^{-1}): 1158, 1342 (SO_2), 2240 (CN); ^1H NMR: 0.90 (6H, t, *J* 7.1, CH_3), 1.19 (4H, m, CH_2CH_3), 1.42 (4H, m, $CH_2CH_2CH_3$), 2.55 (4H, m, $CH_2CH_2CH_2CH_3$), 7.37 (4H, s, ArH), 7.38–7.46 (8H, m, SO_2Ph), 7.51–7.68 (2H, m, SO_2Ph); ^{13}C NMR: 13.70 (2C, CH_3), 22.37 (2C, CH_2CH_3), 27.05 (2C, $CH_2CH_2CH_3$), 31.09 (2C, $CH_2CH_2CH_2CH_3$), 71.95 (2C, quaternary, C-C_4H_9), 116.13 (2C, CN), 128.92, 128.98 (4C, ArC), 130.63, 130.71 (8C, SO_2Ph), 130.90 (2C, quaternary ArC), 133.55 (2C, quaternary SO_2Ph), 135.21 (2C, SO_2Ph); *m/z*: 548 (M^+, 0.6%).

Acknowledgments

Financial support for this work provided by the University of Winnipeg and the Natural Sciences and Engineering Research Council of Canada (NSERC) is gratefully acknowledged. C.R.D. (graduate student, University of Manitoba) thanks NSERC for a postgraduate scholarship.

References

1. A.N. Nesmeyanov, N.A. Vol'Kenau, and I.N. Bolesova. Dokl. Akad. Nauk SSSR, **175**, 606 (1967).
2. A.S. Abd-El-Aziz, D.C. Schriemer, and C.R. de Denus. Organometallics, **1**, 374 (1994).
3. A.S. Abd-El-Aziz, S. Tesfalidet, C.R. de Denus, and K. Lezynska. Synth. Commun. **23**, 1415 (1993).
4. A.S. Abd-El-Aziz and C.R. de Denus. J. Chem. Soc. Perkin Trans. 1, 293 (1993).
5. A.S. Abd-El-Aziz and C.R. de Denus. Synth. Commun. **22**, 581 (1992).
6. R.C. Cambie, S.J. Janssen, P.S. Rutledge, and P.D. Woodgate. J. Organomet. Chem. **434**, 97 (1992).
7. A.J. Pearson, J.G. Park, S.H. Yang, and Y.H. Chuang. J. Chem. Soc. Chem. Commun. 1363 (1989).
8. A.S. Abd-El-Aziz, C.C. Lee, A. Piorko, and R.G. Sutherland. J. Organomet. Chem. **348**, 95 (1988).
9. A. Piorko, A.S. Abd-El-Aziz, C.C. Lee, and R.G. Sutherland. J. Chem. Soc. Perkin Trans. 1, 469 (1989).
10. R.M. Moriarty and U.S. Gill. Organometallics, **5**, 253 (1986).
11. S.G. Davies. Organotransition metal chemistry: applications to organic synthesis. Pergamon Press, Oxford, U.K. 1982.
12. M.F. Semmelhack, G.R. Clark, J.L. Garcia, J.J. Harrison, Y. Thebtaranonth, W. Wulff, and A. Yamashita. Tetrahedron, **37**, 3957 (1981).
13. F. Hossner and M. Voyle. J. Organomet. Chem. **347**, 365 (1988).
14. P. Del Buttero, S. Maiorana, and A. Papagni. J. Chem. Soc. Chem. Commun. 1181 (1985).
15. V. Percec and S. Okita. J. Polym. Sci. Part **A**: Polym. Chem. **31**, 923 (1993).
16. R.M. Moriarty, U.S. Gill, and Y.Y. Ku. J. Organomet. Chem. **350**, 157 (1988).
17. J.A. Segal. J. Chem. Soc. Chem. Commun. 1338 (1985).
18. A.A. Dembek, P.J. Fagan, and M. Marsi. Macromolecules, **26**, 2992 (1993).
19. D. Astruc. Top. Curr. Chem. **180**, 48 (1991).
20. A.C. Knipe, S.J. McGuinness, and W.E. Watts. J. Chem. Soc. Chem. Commun. 842 (1979).
21. A.C. Knipe, S.J. McGuinness, and W.E. Watts. J. Chem. Soc. Perkin Trans 2, 193 (1981).
22. K. Matsui and M. Motoi. Bull. Chem. Soc. Jpn. **46**, 1755 (1973).
23. T. Hirayama, M. Kamanda, H. Tsurumi, and M. Mimura. Chem. Pharm. Bull. **24**, 26 (1976).
24. Y. Shih and J. Wang. Heterocycles, **22**, 2799 (1984).
25. H. Suzuki, Q. Yi, J. Inoue, K. Kusume, and T. Ogawa. Chem. Lett. 887 (1987).
26. T.Y. Shen. Angew. Chem. Int. Ed. Engl. **11**, 6 (1972).
27. D.I. Barron, A.R. Copley, and D.K. Vallance. Br. J. Pharmacol. Chemother. **33**, 396 (1968).
28. T. Y. Shen. *In* Handbook of experimental pharmacology. Vol. 50/II. Springer-Verlag, Berlin, Heidelberg, New York. 1979. p. 305.
29. D.J. Drain, M.J. Daly, M. Horlington, J.G.B. Howes, J.M. Scruton, and R.A. Selway. J. Pharm. Pharmacol. **22**, 684 (1970).
30. S.S. Adams, K.F. McCullough, and J.S. Nicholson. Arch. Int. Pharmacodyn. **178**, 115 (1969).
31. M.K. Jasani, W.W. Downie, B.M. Samuels, and W.W. Buchanan. Ann. Rheum. Dis. **27**, 457 (1968).
32. T.M. Chalmers. Ann. Rheum. Dis. **28**, 513 (1969).

Can. J. Chem. Downloaded from www.nrcresearchpress.com by 65.111.164.53 on 09/08/12
For personal use only.

33. S. Tanaka and K. Hashimoto. Chem. Abstr. **85**, 142843f (1976).
34. A. McKillop, B.P. Swann, and E.C. Taylor. J. Am. Chem. Soc. **93**, 4919 (1971).
35. C.F.H. Allen and J. Van Allan. Org. Synth. Coll. Vol. III, 725 (1955).
36. J. Pataki, M. Konieczny, and R.G. Harney. J. Org. Chem. **47**, 1133 (1982).
37. H. Suzuki, T. Kobayashi, and A. Osuka. Chem. Lett. 589 (1983).
38. T. Sakamoto, E. Katoh, Y. Kondo, and H. Yamanka. Chem. Pharm. Bull. **36**, 1664 (1988).
39. B. Lamm and K. Ankner. Acta. Chem. Scand. B, **38**, 2 (1978).
40. A.S. Abd-El-Aziz, P. Hazendonk, C.R. de Denus, and H.M. Hutton. Inorg. Chim. Acta, **219**, 221 (1994).
41. A.N. Nesmeyanov, N.A. Vol'Kenau, and L.S. Shilovtseva. Dokl. Nauk. Akad. SSSR, **190**, 857 (1970).
42. R.G. Sutherland, W.J. Pannekoek, and C.C. Lee. Can. J. Chem. **56**, 1782 (1978).
43. J.R. Hamon, J.Y. Saillard, A. LeBeuze, and M.G. McGlinchy. D. Astruc, J. Am. Chem. Soc. **104**, 7549 (1982).
44. T.P. Gill, and K.R. Mann. Inorg. Chem. **22**, 1986 (1983).
45. I.U. Khand, P.L. Pauson, and W.F. Watts. J. Chem. Soc. C, 2261 (1968).

Can. J. Chem. Downloaded from www.nrcresearchpress.com by 65.111.164.53 on 09/08/12
For personal use only.

Spectrophotometric determination of free, ionized, metal ion concentrations in solution by an indicator increment method. Application to the determination of free Mg^{2+} with calmagite

Hongji Ren, Byron Kratochvil, and Xiwen He

Can. J. Chem. Downloaded from www.nrcresearchpress.com by 65.111.164.53 on 09/08/12
For personal use only.

Abstract: A spectrophotometric method, called the Indicator Increment Method, is described in which varying amounts of a complexing indicator are added to a sample and the visible spectra recorded after each addition. Through multiple equilibrium calculations the free metal ion concentration, as well as total metal and total ligand concentrations, can be estimated in systems that contain a single metal ion and one ligand. The technique was tested successfully for the determination of free magnesium in the presence of NTA, phosphate, or oxalate using calmagite as indicator. The method requires the approximate conditional stability constant of the metal–ligand complex to be known beforehand.

Key words: ionized magnesium, indicator increment method, spectrophotometry.

Résumé : On décrit une méthode spectrophotométrique, appelée méthode de l'incrément d'indicateur, dans laquelle on ajoute des quantités variables d'un indicateur complexant à un échantillon et on détermine son spectre visible après chaque addition. Utilisant des calculs d'équilibres multiples, on peut évaluer la concentration de l'ion métallique libre ainsi que les concentrations totales du métal et du coordinat dans des systèmes contenant un seul ion métallique et un seul coordinat. On a évalué la technique avec succès pour la détermination du magnésium libre, en présence de NTA, de phosphate ou d'oxalate, en utilisant de la calmagite comme indicateur. La méthode nécessite de connaître à l'avance la constante de stabilité conditionnelle approximative du complexe métal–coordinat.

Mots cles : magnésium ionisé, méthode de l'incrément d'indicateur, spectrophotométrie.

[Traduit par la rédaction]

Introduction

The measurement of uncomplexed metal ion concentrations in solutions containing bound or complexed metal is of biological and environmental interest because it is usually the free, or hydrated, form that more readily undergoes reaction. Knowledge of free ion levels in solution is needed in, for example, industrial applications in metallurgy, electroplating, and food processing (1), clinical measurement of physiologically important ionic calcium and magnesium in serum and urine (2–5), biomedical investigations of mechanisms such as formation of kidney stones (6–9), and environmental studies (10, 11). The major methods in use at this time for these determinations are ion selective electrode potentiometry and spectrophotometry, although other techniques have been described, including ion exchange, voltammetry, dialysis, and multiple equilibria calculations from total analysis.

Spectrophotometric methods have been especially useful in the determination of metal ions in biological systems. An example is the determination of calcium with Arsenazo III (12). A modification of the general technique, called the Sample Ion Increment Method (SIIM) (13), gives improved sensitivity over a broader range of sample concentrations. With the SIIM method, a known quantity of indicator is added to the sample and the absorbance measured, then a known increment of the species to be determined is added and the absorbance remeasured. The second measurement determines the extent of "species buffering" in the original sample and permits correction for complexation by the indicator. We describe here a different approach, called the Indicator Increment Method (IIM), which uses equilibrium calculations based on absorbance measurements following addition of varying amounts of indicator rather than metal ion. Like the SIIM method, the IIM method is useful for metal–ligand systems with low metal ion buffer capacity, a situation where the simple spectrophotometric method is not applicable. For a system containing a single metal ion and ligand, the method allows the estimation

Received October 21, 1994.

H. Ren and B. Kratochvil.[1] Department of Chemistry, University of Alberta, Edmonton, AB T6G 2G2, Canada.
X. He. Department of Chemistry, Nankai University, Tianjin, People's Republic of China 300071.

[1] Author to whom correspondence may be addressed.

Can. J. Chem. Downloaded from www.nrcresearchpress.com by 65.111.164.53 on 09/08/12
For personal use only.

Fig. 1. Visible spectra of calmagite and magnesium–calmagite complex. A: spectrum of 1.6×10^{-5} M calmagite in 0.1 M KNO_3 at pH 10. Water used as reference. B: spectrum of 6.0×10^{-4} M $Mg(NO_3)_2$ and 1.6×10^{-5} M calmagite in 0.1 M KNO_3 at pH 10. Water again used as reference. C: Difference spectrum of B and A. The maximum in the difference spectrum occurs at 512 nm and the minimum at 616 nm.

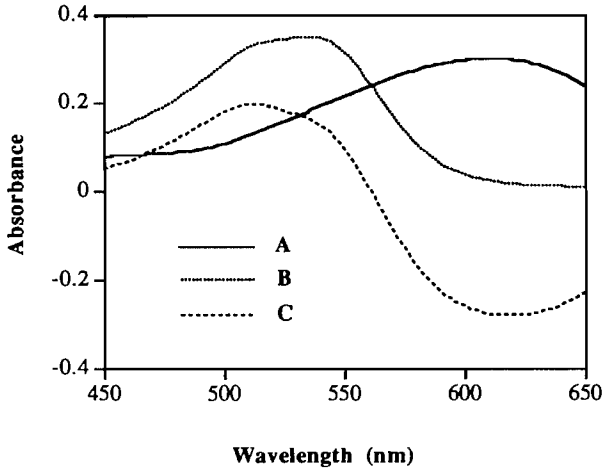

of not only the free metal ion concentration but also the total metal and total ligand concentrations.

Experimental

Reagents and chemicals

A 5×10^{-3} M solution of $Mg(NO_3)_2$ was prepared by dissolving 0.6410 g of $Mg(NO_3)_2 \cdot 6H_2O$ (Baker Analyzed Reagent) in 500 mL pure water. Commercial calmagite (Terochem Laboratories, Edmonton, Canada) was found by spectrophotometric titration with a standard solution of $Mg(NO_3)_2$ to have a purity of 69%, a level adequate for the two-wavelength method used in this study. Concentrations of calmagite solutions (1 mM) were calculated on the basis of this purity. Solutions were adjusted to an ionic strength of 0.1 by addition of 1.0 M KNO_3 (BDH analytical reagent), which had been passed through a column of Dowex® Chelating Resin (Sigma) to remove polyvalent cations (14). All other chemicals were analytical grade and were used without further purification. Distilled water was passed through a Barnstead NANOpure water purification system before use.

Instrumentation

All pH measurements were made with a Fisher Accumet® model 520 pH/ion meter and a glass–calomel electrode pair calibrated with commercial buffers (Fisher). Spectrophotometric measurements were made in a constant temperature room thermostated at 25 ± 1°C on a Hewlett–Packard model 8451A diode array spectrophotometer with 1-cm silica cells; the spectra were stored on 3.5 in. floppy disks for later processing.

Procedure

The molar absorptivity values of calmagite at 512 and 616 nm were determined by measuring the absorbance of a series of solutions at pH 10 and ionic strength 0.1. These wavelengths were chosen because the difference between the molar absorptivities of the Mg^{2+}–calmagite complex and the free indicator was largest at these values (see Fig. 1). Absorption coefficients for the Mg^{2+}–calmagite complex at these wavelengths were determined by measuring the absorbances of a series of solutions containing varying excess amounts of Mg^{2+} and a constant calmagite concentration. Incomplete complexation of calmagite was estimated and corrected for by an iteration method using an estimated initial conditional stability constant for the complex. The actual conditional stability constant of the Mg^{2+}–calmagite complex was determined by measuring, at 512 and 616 nm, a second series of solutions containing differing amounts of Mg^{2+} and calmagite; a value of 2.56×10^5 M^{-1} was found under the experimental conditions used. This compares satisfactorily with a reported value of 4.87×10^5 M^{-1}, measured using the continuous variation method in 0.1 M potassium chloride (15).

For each magnesium – nitrilotriacetic acid (Mg^{2+}–NTA) experiment, 0.4, 0.6, and 0.8 mL increments of 1.06×10^{-3} M calmagite solution were added to a set of three 25-mL volumetric flasks containing 20 mL of a magnesium–NTA solution. Sufficient 1.0 M KNO_3 was added to each of the flasks to adjust the final ionic strength to 0.1 after dilution to 25 mL. The pH of each solution was adjusted to near 10 by addition of dilute NaOH, followed by a small amount of pH 10 NH_3–NH_4NO_3 buffer. Absorbances were measured at 512 and 616 nm for each of the solutions after dilution to 25 mL with pure water. Two additions of indicator provide sufficient information to solve the equations, but we usually added indicator solution three times so that three pairs of results (termed 1,2; 1,3; and 2,3) could be used in the calculation of $[M_T]_0$, $[F_L]_0$, and $[M]_0$ in each solution.

A similar procedure was followed for the other systems with the exception of the Mg^{2+}–K_2HPO_4 study, where phosphate provided adequate buffering on its own.

Theory

Equations for calculation of free metal ion concentrations by the Indicator Increment Method (IIM) are developed here for three systems, one consisting of a metal ion M and a ligand H_nL that react to form a single metal–ligand complex ML, a second the same but including formation of complexes of the type ML, MHL, MH_2L, ... , and a third including formation of both ML and ML_2.

Case 1. Determination of free metal ion concentration in a solution containing metal ion, protonated ligand, and metal–ligand complex

The free metal ion concentration $[M]_0$ in an unknown solution is determined by adding a known amount of an indicator H_nI that forms a 1:1 colored complex, $[MI]_i$, with the metal. First $[MI]_i$ is calculated, then $[M]_i$, as follows (charges on the ions have been omitted for simplicity):

The absorbance A_0 of a sample solution of volume V_0 in a cell of pathlength b is measured at two wavelengths; here 512 nm (A_0^{512nm}) and 616 nm (A_0^{616nm}) were selected. A known quantity of indicator ligand H_nI is added to the solution and a new absorbance A_i measured (as A_i^{512nm} and A_i^{616nm}) at the two wavelengths in the new volume V_i. The difference in absorbance values between the two wavelengths is used for the calculations ($A_0 = A_0^{512nm} - A_0^{616nm}$, $A_i = A_i^{512nm} - A_i^{616nm}$).

Can. J. Chem. Downloaded from www.nrcresearchpress.com by 65.111.164.53 on 09/08/12
For personal use only.

Then

$$[1] \quad A_i - A_0 \frac{V_0}{V_i} = \epsilon_{MI} b[MI]_i + \Sigma\epsilon' b([F_I]_i - [MI]_i)$$

where

$$\Sigma\epsilon' = \alpha_{H_nI}\epsilon_{H_nI} + \alpha_{H_{n-1}I}\epsilon_{H_{n-1}I} + \ldots + \alpha_I\epsilon_I$$

The α terms are the fractions of uncomplexed indicator in each of its protonated forms; the ϵ terms are the corresponding absorption coefficient differences at the two wavelengths of the subscript species. $[F_I]_i$ is the total indicator concentration in the solution being measured. Once $[MI]_i$ has been measured, $[M]_i$ can be obtained from the relation

$$[2] \quad [MI]_i = \frac{[MI]_i}{K'_{MI}\{[F_I]_i - [MI]_i\}}$$

where K'_{MI} is the conditional stability constant for the metal–indicator complex. The free metal ion concentration in the initial solution $[M]_0$ may be calculated from the stability constant expression K'_{ML} once $[M_T]_0$ and $[F_L]_0$ have been determined. Their values are obtained by use of the expressions described in the next section.

(i) Determination of total metal $[M_T]_0$ and total ligand $[F_L]_0$ concentration in a solution containing M, H_nL, and ML

Consider a sample solution containing a metal ion M and an auxiliary ligand H_nL for which ML is the only major metal ligand complex formed. The species present under these conditions are M, L, ML, HL, H_2L, ... , H_nL. An indicator H_nI that forms only the single colored complex MI is now added to the sample solution. The total concentration of auxiliary ligand $[F_L]$ is given by

$$[F_L] = [L] + [HL] + \ldots + [H_nL] + [ML]$$

and the fraction of uncomplexed auxiliary ligand α_L by

$$\alpha_L = \frac{[L]}{[F_L] - [ML]}$$

The conditional stability constant K'_{ML} for formation of ML is the product of the thermodynamic stability constant K_{ML} and α_L:

$$K'_{ML} = K_{ML}\alpha_L = \frac{[ML]}{[M]\{[F_L] - [ML]\}}$$

Rearranging gives

$$[3] \quad [ML] = \frac{K'_{ML}[F_L][M]}{1 + K'_{ML}[M]}$$

If now a solution containing indicator H_nI is added to an original sample solution having a total metal ion concentration of $[M_T]_0$ and a total ligand concentration of $[F_L]_0$, both complexation of metal by the indicator and dilution occurs. Under these conditions $[F_L]_i = [F_L]_0\, V_0/V_i$ and $[M_T]_i = [M_T]_0\, V_0/V_i = [M]_i + [ML]_i + [MI]_i$. Then

$$[4] \quad [ML]_i = [M_T]_0\,(V_0/V_i) - [M]_i - [MI]_i$$

From eq. [3], $[ML]_i$ can also be written as

$$[5] \quad [ML]_i = \frac{V_0}{V_i}\,\frac{K'_{ML}[F_L]_0[M]_i}{1 + K'_{ML}[M]_i}$$

Combining eqs. [4] and [5] and rearranging,

$$[6] \quad [M_T]_0(V_0/V_i) + (V_0/V_i)\,[M]_iK'_{ML}\{[M_T]_0 - [F_L]_0\} - \{[M]_i([M]_i + [MI]_i)K'_{ML} + ([M]_i + [MI]_i)\} = 0$$

Separating terms in $[M_T]_0$ and $[F_L]_0$,

$$[7] \quad (V_0/V_i) + [M]_iK'_{ML}V_0/V_i)[M_T]_0 - ([M]_iK'_{ML}V_0/V_i)[F_L]_0 - ([M]_i + [MI]_i)(1 + K'_{ML}[M]_i) = 0$$

If $[MI]_i$, $[M]_i$, V_0, V_i, and K'_{ML} are known, eq. [7] becomes an expression of the form

$$[8] \quad a_i[M_T]_0 + b_i[F_L]_0 + c_i = 0$$

where

$$a_i = (V_0/V_i) + [M]_iK'_{ML}V_0/V_i$$

$$b_i = -\,[M]_iK'_{ML}V_0/V_i$$

and

$$c_i = -\,([M]_i + [MI]_i)(1 + K'_{ML}[M]_i)$$

If indicator solution is added twice and absorbance measurements are made after each addition, two equations of the form of eq. [8] can be written, from which values of $[M_T]_0$ and $[F_L]_0$ can be obtained.

(ii) Calculation of $[M]_0$

The value of $[M]_0$ may now be obtained from the K'_{ML} expression

$$[9] \quad K'_{ML} = \frac{[ML]_0}{[M]_0([F_L]_0 - [ML]_0)} = \frac{[M_T]_0 - [M]_0}{[M]_0([F_L]_0 - [M_T]_0 + [M]_0)}$$

By rearrangement to quadratic form,

$$[10] \quad K'_{ML}[M]_0^2 + \{K'_{ML}([F_L]_0 - [M_T]_0) + 1\} \times [M]_0 - [M_T]_0 = 0$$

Solution of this equation gives the free metal ion concentration in the original system $[M]_0$.

Case 2. Determination of $[M_T]_0$, $[F_L]_0$, and $[M]_0$ when protonated metal complexes of the type ML, MHL, MH_2L, ... form

If a series of soluble metal complexes form that contain protons or hydroxyl ions, and the conditional overall stability constants are known for each complex, then a modification of the

Can. J. Chem. Downloaded from www.nrcresearchpress.com by 65.111.164.53 on 09/08/12
For personal use only.

previously described approach can be used. For the simplest case, when the only additional species is MHL, the mass balance equations for the original solution are

$$[11] \quad [M_T]_0 = [M]_0 + [ML]_0 + [MHL]_0$$

and

$$[12] \quad [F_L]_0 = [L]_0 + [HL]_0 + [ML]_0 + [MHL]_0$$

For ML in this system,

$$[13] \quad K'_{ML} = K_{ML}\alpha_L = \frac{[ML]_0}{[M]_0\{[F_L]_0 - ([ML]_0 + [MHL]_0)\}}$$

while for MHL

$$[14] \quad K'_{MHL} = K_{MHL}\alpha_{HL} = \frac{[MHL]_0}{[M]_0\{[F_L]_0 - ([ML]_0 + [MHL]_0)\}}$$

Combining eqs. [13] and [14] gives

$$[15] \quad [ML]_0 + [MHL]_0 = \frac{[M]_0[F_L]_0(K'_{ML} + K'_{MHL})}{1 + [M]_0(K'_{ML} + K'_{MHL})}$$

For the more general case where polyprotonated metal ligand complexes of the type MH_2L or MH_3L form in significant concentrations, eq. [15] becomes

$$[16] \quad [ML]_0 + [MHL]_0 + [MH_2L]_0 \ldots = \frac{[M]_0[F_L]_0(K'_{ML} + K'_{MHL} + K'_{MH_2L} + \ldots)}{1 + [M]_0(K'_{ML} + K'_{MHL} + K'_{MH_2L} + \ldots)} = \frac{[M]_0[F_L]_0K'_\Sigma}{1 + [M]_0K'_\Sigma}$$

A similar expression can be written to take into account the formation of complexes containing hydroxyl ions of the type $M(OH)_xL$.

When indicator is added as described in Case 1, solution conditions are shifted from "0" to "i", giving $[F_L]_i = V_0/V_i[F_L]_0$ and $[M_T]_i = V_0/V_i\,[M_T]_0$. From eq. [16]

$$[17] \quad [ML]_i + [MHL]_i + [MH_2L]_i \ldots = \frac{V_0}{V_i}\,\frac{[M]_i[F_L]_0K'_\Sigma}{1 + [M]_iK'_\Sigma}$$

and from mass balance

$$[18] \quad [ML]_i + [MHL]_i + [MH_2L]_i \ldots = \frac{V_0}{V_i}\,[M_T]_0 - [M]_i - [MI]_i$$

Combining eqs. [17] and [18], and rearranging, gives

$$[19] \quad \left\{\frac{V_0}{V_i}(1 + [M]_iK'_\Sigma)\right\}[M_T]_0 - \left\{\frac{V_0}{V_i}[M]_iK'_\Sigma\right\}[F_L]_0 - \{([M]_i^2 + [M]_i[MI]_i)K'_\Sigma + [M]_i - [MI]_i\} = 0$$

This is an equation of the form

$$[20] \quad a_1[M_T]_0 + b_1[F_L]_0 + c_1 = 0$$

Addition of a second increment of indicator and remeasurement gives a second equation

$$[21] \quad a_2[M_T]_0 + b_2[F_L]_0 + c_2 = 0$$

which when solved simultaneously with eq. [20] gives values for $[M_T]_0$ and $[F_L]_0$. A value for $[M]_0$ can then be obtained from eqs. [11] and [15].

Case 3. Estimation of $[M_T]_0$, $[F_L]_0$, and $[M]_0$ when metal–ligand complexes ML and ML_2 form

When both 1:1 and 1:2 metal–ligand complexes form, the relationships are

$$[M_T]_0 = [M]_0 + [ML]_0 + [ML_2]_0$$

and

$$[F_L]_0 = [L]_0 + [HL]_0 + [H_2L]_0 + \ldots + [H_nL]_0 + [ML]_0 + 2[ML_2]_0$$

Let

$$[F_L]_0^* = [L]_0 + [HL]_0 + [H_2L]_0 + \ldots + [H_nL]_0$$

Then

$$[22] \quad [F_L]_0 = [F_L]_0^* + [ML]_0 + 2[ML_2]_0$$

Since

$$\beta'_{ML} = \frac{[ML]_0}{[M]_0\,[F_L]_0^*} \quad \text{and} \quad \beta'_{ML_2} = \frac{[ML_2]_0}{[M]_0[F_L]_0^{*2}}$$

then

$$[23] \quad [ML]_0 + [ML_2]_0 = \beta'_{ML}[M]_0[F_L]_0^* + \beta'_{ML_2}[M]_0[F_L]_0^{*2}$$

On addition of indicator H_nI,

$$[24] \quad [ML]_i + [ML_2]_i = \beta'_{ML}[M]_i[F_L]_i^* + \beta'_{ML2}[M]_i[F_L]_i^{*2}$$

and, from mass balance for $[M_T]$,

$$[25] \quad [ML]_i + [ML_2]_i = \frac{V_0}{V_i}\,[M_T]_0 - [M]_i - [MI]_i$$

When $[F_L]_0 >> [M_T]_0$, then $[F_L]_0^* \approx [F_L]_0$, and $[F_L]_i^* \approx [F_L]_0^*(V_0/V_i)$ Substituting into eq. [24], and combining with [25], gives upon rearrangement

$$[26] \quad \frac{V_0}{V_i}\,[M_T]_0 - \frac{V_0}{V_i}\,\beta'_{ML}[M]_i[F_L]_i^* - \left(\frac{V_0}{V_i}\right)^2\beta'_{ML_2}[M]_i[F_L]_i^{*2} - [M]_i - [MI]_i = 0$$

Table 1. Determination of total magnesium, total NTA, and ionic magnesium by the indicator increment method.

	$pM_{T\,0}$			$pF_{L\,0}$			$pM_{\,0}$		
	1,2	1,3	2,3[a]	1,2	1,3	2,3[a]	1,2	1,3	2,3[a]
Solution 1									
Found	4.34	4.37	4.39	3.92	3.96	4.00	5.56	5.55	5.53
Average		4.37			3.96			5.55	
Taken		4.30			4.00			5.38[b]	
Solution 2									
Found	4.47	4.33	4.14	3.97	3.79	3.52	5.68	5.72	5.79
Average		4.31			3.76			5.73	
Taken		4.30			3.90			5.53[b]	
Solution 3									
Found	4.34	4.31	4.29	3.70	3.68	3.65	5.84	5.85	5.85
Average		4.31			3.68			5.85	
Taken		4.30			3.82			5.64[b]	

[a]Combinations of increments used in calculation.
[b]Theoretical value for free magnesium calculated from initial total metal and total NTA concentrations.

Can. J. Chem. Downloaded from www.nrcresearchpress.com by 65.111.164.53 on 09/08/12
For personal use only.

Upon addition of another increment of indicator solution and measurement of [MI] after the addition, values of V_0, V_1, V_2, $[M]_1$, $[M]_2$, $[MI]_1$, and $[MI]_2$ can be obtained. With knowledge of β'_{ML} and β'_{ML_2}, the pairs of equations

$$a_1[M_T]_0 + b_1[F_L]_0^* + c_1[F_L]_0^{*2} + d_1 = 0$$

and

$$a_2[M_T]_0 + b_2[F_L]_0^* + c_2[F_L]_0^{*2} + d_2 = 0$$

can be solved to obtain $[M_T]_0$ and $[F_L]_0^*$. Then $[M]_0$ can be found from

$$[27] \quad [M]_0 = \frac{[M_T]_0}{1 + \beta'_{ML}[F_L]_0^* + \beta'_{ML_2}[F_L]_0^{*2}}$$

Results and Discussion

Application of Case 1 to the Mg^{2+} – nitrilotriacetic acid system

The ligand NTA (nitrilotriacetic acid), which is reported to form only a 1:1 complex with magnesium (16), was selected to test the applicability of Case 1. The conditional stability constant of the Mg^{2+}–NTA complex in concentration terms (log $K' = 5.31$) was obtained from the literature (16) by multiplying the literature value by the fraction α of unprotonated ligand (L^{-3}) present ($\alpha_{L^{-3}} = 0.69$ at pH 10).

Possible formation of $MgOH^+$ at pH 10 was considered. A stability constant for this species at ionic strength 0.1 is not available, but a log K value of 2.1 was calculated from the value reported at infinite dilution, 2.58 (17), and the extended Debye–Hückel equation. Using this value, the fraction of magnesium present as $MgOH^+$ at pH 10 was estimated to be 0.012, a level sufficiently small to be neglected for the purpose of this work. Another possible competing ligand was NH_3 coming from the small amount of NH_3 buffer used. The final concentration of NH_3 in the solution, 3×10^{-3} M, was so small, however, that formation of a magnesium–ammonia complex was considered to be negligible.

To reduce measurement uncertainty in the IIM method it is important to select the appropriate amount of indicator to be added in each increment. The amount should be sufficient to cause a significant equilibrium shift in the original system, since the larger the shift the more accurate the results. It should not be too large, however, or the initial ionic strength of the solution may be shifted enough to affect the conditional stability constants of metal–indicator and metal – auxiliary ligand complexes.

An equilibrium shift means that the free metal ion concentration is reduced when indicator is added. Such a shift will only be seen in solutions where the metal ion buffer capacity is low. For systems with high metal ion buffer capacity, the free metal ion concentration will not be affected by indicator addition. In this situation a simple direct spectrophotometric method can be used. Thus the IIM method offers a complimentary tool for conventional spectrophotometric free metal ion determinations.

A summary of the results, calculated on a Macintosh computer using a BASIC program written for the purpose,[2] is shown in Table 1. It can be seen that agreement between experimental and calculated values is acceptable considering the low concentrations being measured.

Application of Case 2 to magnesium–K_2HPO_4 system

The ligand K_2HPO_4 at a total concentration of 2.5 mM was selected to verify Case 2 because it forms magnesium complexes mainly in the form of $MgPO_4^-$ and $MgHPO_4$. At pH 10, 98.2% of the phosphate is in the form of HPO_4^{2-}, with the

[2] A listing of the computer program may be purchased from: The Depository of Unpublished Data, Document Delivery, CISTI, National Research Council Canada, Ottawa, Canada K1A 0S2.

Table 2. Determination of total magnesium, total K_2HPO_4, and ionic magnesium by the indicator increment method.

	$pM_{T\,0}$			$pF_{L\,0}$			$pM_{\,0}$		
	1,2	1,3	2,3[a]	1,2	1,3	2,3[a]	1,2	1,3	2,3[a]
Solution 1									
Found	5.08	5.06	5.04	1.91	1.85	1.76	5.57	5.60	5.64
Average		5.06			1.84			5.60	
Taken		4.90			1.60			5.63[b]	
Solution 2									
Found	4.69	4.68	4.68	1.67	1.65	1.63	5.36	5.37	5.38
Average		4.68			1.65			5.37	
Taken		4.60			1.60			5.35[b]	
Solution 3									
Found	4.38	4.39	4.39	1.65	1.66	1.66	5.06	5.06	5.06
Average		4.39			1.66			5.06	
Taken		4.30			1.60			5.02[b]	

[a]Combinations of increments used in calculation.
[b]Theoretical value for free magnesium calculated from initial total metal and total phosphate concentrations.

Table 3. Determination of total magnesium, total $H_2C_2O_4$, and ionic magnesium by the indicator increment method.

	$pM_{T\,0}$			$pF_{L\,0}$			$pM_{\,0}$		
	1,2	1,3	2,3[a]	1,2	1,3	2,3[a]	1,2	1,3	2,3[a]
Solution 1									
Found	4.64	4.60	4.55	2.12	2.06	1.97	5.44	5.46	5.51
Average		4.60			2.05			5.47	
Taken		4.60			2.00			5.53[b]	
Solution 2									
Found	4.26	4.24	4.23	2.01	1.99	1.97	5.18	5.18	5.19
Average		4.24			1.99			5.18	
Taken		4.30			2.00			5.23[b]	
Solution 3									
Found	4.19	4.12	4.04	2.13	2.04	1.93	4.98	5.00	5.04
Average		4.12			2.03			5.01	
Taken		4.12			2.00			5.02[b]	

[a]Combinations of increments used in calculation.
[b]Theoretical value for free magnesium calculated from initial total metal and total oxalate concentrations.

remainder present as PO_4^{3-}. The conditional stability constants for the $MgPO_4^-$ and $MgHPO_4$ species in concentration terms were calculated from literature values (18) corrected to pH 10. Also, potassium ion complexation was taken into account through the relation $K_{MgL} = K'_{MgL}(1 + K_{KL}[K^+])$. Ionic strength effects were corrected for using the Davies equation; a log K'_Σ value of 2.23 was obtained at ionic strength 0.1 and pH 10. The wavelengths used, as well as all other experimental conditions, were as in Case 1. The results, Table 2, show the measured values of $[M]_0$ to agree well with the calculated ones. Values for $[M_T]_0$ and $[F_L]_0$ also agree well with the initial amounts taken.

Application of Case 3 to the magnesium–oxalic acid system

Oxalate forms two relatively stable complexes with magnesium, ML and ML_2. At pH 10, nearly 100% of oxalate is in the $C_2O_4^{2-}$ form. The conditional stability constants at pH 10, calculated from literature data (19), are 575 for K_{ML} and 17 400 for K_{ML_2}. A small amount of NH_3 (final $C_{NH_3} = 3 \times 10^{-3}$ M) was added to buffer the system after initial adjustment to near pH 10 with NaOH. All other conditions were the same as in Case 1. The results, shown in Table 3, indicate quite satisfactory agreement.

Effect of K'_{ML} value on results

For all three cases discussed above, values of the metal–auxiliary ligand conditional stability constants are needed in order to carry out the calculations. The effect of the values chosen for these conditional stability constants on the results found

Can. J. Chem. Downloaded from www.nrcresearchpress.com by 65.111.164.53 on 09/08/12
For personal use only.

Fig. 2. Effect of variation in value of K'_{MgNTA} used on calculated free metal ion concentrations (plotted as calculated value $\times 10^6$), and on calculated total ligand and total metal ion concentrations (plotted as log values).

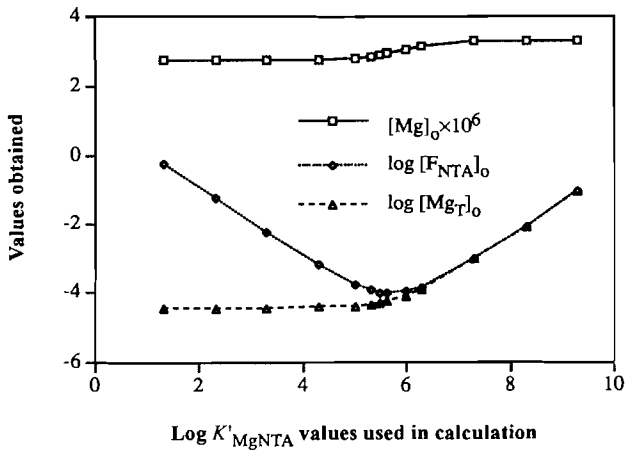

for the free metal ion, total ligand, and total metal ion concentrations was studied using the experimental data for solution 1 of Case 1. Changing $K'_{Mg\text{-}NTA}$ from the calculated literature value of 2.0×10^5 shows that the free magnesium ion concentration shifts from −4% of the original value for a 10 000 times smaller $K'_{Mg\text{-}NTA}$ to +16% of the original for a 10 000 times larger $K'_{Mg\text{-}NTA}$ (see Fig. 2). This means that estimation of free metal ion concentrations is still possible even though the conditional stability constant of the metal–ligand complex is not known precisely.

On the other hand, calculated values for total ligand concentrations are unacceptably large when $K'_{Mg\text{-}NTA}$ is made 10 000 times smaller, and they decrease as $K'_{Mg\text{-}NTA}$ increases until $K'_{Mg\text{-}NTA}$ is close to $K'_{Mg\text{-}calmagite}$ (2.6×10^5), then increase with further increases in $K'_{Mg\text{-}NTA}$. Calculated values for total metal ion concentrations do not change much when $K'_{Mg\text{-}NTA}$ is smaller than $K'_{Mg\text{-}calmagite}$, but increase as $K'_{Mg\text{-}NTA}$ becomes close to $K'_{Mg\text{-}calmagite}$, and become essentially identical to calculated total ligand concentrations when $K'_{Mg\text{-}NTA}$ is larger than $K'_{Mg\text{-}calmagite}$. This suggests that accurate estimation of total ligand and total metal ion concentrations is not feasible unless the conditional stability constant of the metal–ligand complex is known in advance with reasonable accuracy.

Similar results were obtained when both free and total species concentrations were evaluated for Cases 2 and 3.

Conclusions

An advantage of the IIM method is that both total metal ion and total ligand concentrations can be obtained in addition to the concentration of free metal ion. Also, the method is especially useful for metal–ligand systems with low metal ion buffer capacity, a situation where the traditional simple spectrophotometric method is not applicable. A disadvantage is that preliminary information on the ligand and its conditional stability constant with the metal must be available or determined beforehand, although an estimation of the free metal ion concentration is still possible when the conditional stability constant is not known. Also, the magnesium–calmagite system used here requires measurements to be made at a known pH near 10 and at constant ionic strength. Other metals that form complexes with calmagite, such as calcium, may interfere by competing with magnesium for the indicator. However, the approach is suitable for situations where species concentrations in a defined metal–ligand system are to be monitored. The precision and accuracy of the free magnesium measurements can be considered to be satisfactory, in light of the limited availability of alternative methods.

Acknowledgments

Financial support from the Natural Sciences and Engineering Research Council of Canada and the University of Alberta is gratefully acknowledged.

References

1. Orion Research, Analytical Methods Guide, 8th ed. Orion Research Corporation, Cambridge, Mass. 1977.
2. M. Walser. Anal. Chem. **32**, 711 (1960).
3. J. H. Ladenson and G.N. Bowers, Jr. Clin. Chem. **19**, 565 (1973).
4. B.E. Cham. Clin. Chim. Acta, **37**, 5 (1972).
5. G.A.Rose. Clin. Chim. Acta, **37**, 343 (1972).
6. T.A. Borden and E. S. Lyon. Invest. Urol. **6**, 412 (1969).
7. H. Fleisch, W.G. Robertson, L.H. Smith, W. Vahiensieck (*Editors*). Urolithiasis research. Plenum Press, New York. 1976.
8. R.W. Marshall, M. Cochran, W.G. Robertson, A. Hodgkinson, and B.E.C. Nordin. Clin. Sci. **43**, 433 (1972).
9. B.E.C. Nordin (*Editor*). Calcium, phosphate and magnesium metabolism: clinical physiology and diagnostic procedures. Churchhill Livingstone, Edinburgh. 1976.
10. R. Jasinski, I. Trachtenberg, and D. Andrychuk. Anal. Chem. **46**, 364 (1974).
11. J.R. Donat, K.A. Lao, and K.W. Bruland. Anal. Chim. Acta, **284**, 547 (1994).
12. B. Kratochvil and X. He. Can. J. Chem. **68**, 1932 (1990).
13. R.B. Fulton and B. Kratochvil. Anal. Chem. **52**, 546 (1980).
14. J.S. Nielsen. Ph.D. Thesis, Department of Civil Engineering, University of Alberta, Edmonton. 1982.
15. F. Lindstrom and H. Diehl. Anal. Chem. **32**, 1123 (1960).
16. A.E. Martell and R.M. Smith. Critical stability constants. Vol. 1. Amino acids. Plenum, New York. 1974.
17. R.M. Smith and A.E. Martell. Critical stability constants. Vol. 4. Inorganic complexes. Plenum, New York. 1976.
18. C.W. Childs. Inorg. Chem. **9**, 2465 (1970).
19. A.E. Martell and R.M. Smith. Critical stability constants. Vol. 3. Other organic ligands. Plenum, New York. 1977.

Can. J. Chem. Downloaded from www.nrcresearchpress.com by 65.111.164.53 on 09/08/12
For personal use only.

COMMUNICATION

Subpicosecond vibrational relaxation of the S_1 states of azulene and guaiazulene in solution

Dietrich Tittelbach-Helmrich, Brian D. Wagner, and Ronald P. Steer

Abstract: The S_1 population decay times of azulene and 1,4-dimethyl-7-isopropylazulene (guaiazulene) in solution have been determined as a function of their initial vibrational energy content, E^i_{vib}, using a pump–probe experiment with subpicosecond time resolution. The S_1 lifetime of azulene does not depend on E^i_{vib} for energies up to 1760 cm^{-1}, whereas the lifetime of the shorter-lived S_1 state of guaiazulene is independent of E^i_{vib} only for energies up to ~1000 cm^{-1}. At higher energies, the lifetime decreases with increasing E^i_{vib}, and exhibits the same behavior in two structurally different solvents. It is suggested that internal conversion to the electronic ground state from a vibrationally unrelaxed S_1 state is responsible for the effects observed in guaiazulene, and that intramolecular vibrational redistribution occurs with a time constant of several hundred femtoseconds.

Key words: pump–probe spectroscopy, azulene, femtosecond processes.

Résumé : Utilisant une expérience de pompe–sonde avec un temps de résolution inférieur à la picoseconde, on a déterminé les temps de dégénérescence de la population S_1 de l'azulène et du 1,4-diméthyl-7-isopropylazulène (guaïazulène) en solution en fonction de leur contenu énergétique vibrationnel initial, E^i_{vib}. Le temps de vie de l'état S_1 de l'azulène ne dépend pas de E^i_{vib} pour les énergies allant jusqu'à 1760 cm^{-1} alors que celui de l'état S_1 du guaïazulène, qui est beaucoup plus court, n'est indépendant de E^i_{vib} que jusqu'à des énergies d'environ 1000 cm^{-1}. À des énergies plus élevées, le temps de vie diminue avec une augmentation de E^i_{vib} et il présente le même comportement dans deux solvants de structures différentes. Il est suggéré que la conversion interne d'un état S_1 qui n'a pas subi de relaxation vibrationnelle vers l'état électronique fondamental est responsable pour les effets observés avec le guaïazulène et qu'une redistribution vibrationnelle intramoléculaire se produit avec une constante de temps de plusieurs centaines de femtosecondes.

Mots clés : spectroscopie pompe–sonde, azulène, processus femtosecond.

[Traduit par la rédaction]

1. Introduction

Picosecond pump–probe methods have been used for 20 years to investigate the fast relaxation processes of the first excited singlet state (S_1) of azulene and related molecules in condensed media (1–8). In these experiments the pump pulse populates S_1 and the probe pulse, after appropriate variable temporal delay, probes S_1 by exciting fluorescence from S_2. When these experiments are carried out in solution the amount of vibrational energy deposited in the molecule by the probe laser is not critical because the fluorescent S_2 state is photostable and relatively long-lived (ca. 1–2 ns for azulene in several solvents (9)) whereas vibrational thermalization occurs in a much shorter period (for a review, see ref. 10). Emission is therefore always observed from the vibrationally relaxed S_2 state. On the other hand, the amount of vibrational energy deposited in the molecule by the pump laser may be important because the S_1 states have population decay times that are much shorter, of the order of 0.5–5 ps (1–8).

Several previous experiments employed a single pulsed laser to generate both pump and probe beams, and one such experiment examined the effect of the initial vibrational energy, E^i_{vib}, on the lifetime of S_1 (11). The latter investigation

Received August 15, 1994.

D. Tittelbach-Helmrich, B.D. Wagner,[1] and R.P. Steer.[2]
Department of Chemistry, University of Saskatchewan, Saskatoon, SK S7N 0W0, Canada.

[1] Present address: Steacie Institute for Molecular Sciences, National Research Council of Canada, Ottawa, ON K1A 0R6, Canada.

[2] Author to whom correspondence may be addressed. Telephone: (306) 966-4654. Fax: (306) 966-4730.

Can. J. Chem. Downloaded from www.nrcresearchpress.com by 65.111.164.53 on 09/08/12
For personal use only.

Can. J. Chem. Downloaded from www.nrcresearchpress.com by 65.111.164.53 on 09/08/12
For personal use only.

reported no measurable change in the picosecond decay rate of the S_1 state of azulene in dichloroethane or methylcyclohexane solution at $E^i_{vib} \leq 4800\ cm^{-1}$, but was conducted with equipment that only permitted the observation of variations greater than a factor of 2 or 3. Very recently, however, Matsumoto et al. (6) reported that they had measured the vibrational relaxation time within the S_1 state of azulene in ethylene glycol and found it to decrease from 300 fs at $E^i_{vib} = 850\ cm^{-1}$ to 50 fs at $E^i_{vib} = 1630\ cm^{-1}$. The fact that in the same experiment they measured an S_1 population decay time that was a factor of ca. 2 too long (8) could cast some doubt on these results.

We have developed a two-photon fluorescence experiment with subpicosecond time resolution and have determined the effect of E^i_{vib} on the population decay rates of azulene and 1,4-dimethyl-7-isopropylazulene (guaiazulene) in several solvents. The results indicate that the S_1 population decay of guaiazulene may be used as a fast internal clock against which the rates of its vibrational thermalization may be calibrated.

2. Experimental section

The sub-picosecond pump–probe laser system used in this work was described in detail previously (7). Briefly, the output of a mode-locked Spectra-Physics Nd:YAG laser is passed through a fibre optic pulse compressor and an SHG crystal to generate 532 nm light, which synchronously pumps a Spectra-Physics dye laser operating on DCM. The dye laser produces approximately 70–100 mW of average power, consisting of trains of mode-locked pulses having a $sech^2$ shape and a FWHM of ca. 0.5 ps, as measured using an autocorrelation technique (7). The dye laser output is split into two beams of approximately equal intensity, generating pump and probe beams. The pump beam is mildly focussed onto the contents of a 0.1 mm path length quartz cell, while the probe beam is passed through an optical delay line before being focussed onto the same cell in a colinear, counterpropagating fashion. Fluorescence in the near-uv–visible is collected, passed through band-pass filters to remove scattered exciting light, and detected with a single photon counting photomultiplier tube.

The instrument response function (IRF) is measured by determining the intensity of two-photon excited fluorescence from the S_1 state of an ultraviolet laser dye (e.g., α-NPO) as a function of the pump–probe delay time. The IRF is typically near Gaussian in shape with a FWHM of ca. 1.3 ps, due principally to jitter between the two trains of pulses. This FWHM is an improvement by a factor of nearly 2 over our previous two-color (two dye-laser) pump–probe experiments (7), and allows the measurement of shorter lifetimes than previously possible in the two-color mode. The excited state population decay constant of the sample is obtained by deconvolution of the measured $S_2 \rightarrow S_0$ fluorescence intensity vs. optical delay profile and the IRF measured under identical conditions. Deconvolution was effected using the standard Marquardt algorithm, assuming a single exponential population decay function for the S_1 state, as previously described (7). A recent, detailed analysis of two-photon, one- and two-color, pump–probe, laser–molecule interactions using a semi-analytic perturbative approach has shown that reliable population decay constants can be obtained with the procedures used here (12). The precision of the lifetime measurements in the present experiments is typically ca. 80 fs.

Azulene and guaiazulene (Aldrich), acetonitrile (BDH, Omnisolv), and perfluoro-*n*-hexane (PCR) were all used as received. Cyclohexane (BDH, Omnisolv) was fractionally distilled before use. The solutions were ca. 6×10^{-3} M in concentration. All experiments were conducted at room temperature, 20 ± 1°C.

3. Results and discussion

We previously measured the population decay times of the S_1 states of azulene, guaiazulene, and several other substituted azulenes in solvents of varying polarity, viscosity, and structure (7, 8). Variations in the population decay times (of the vibrationally relaxed S_1 states) were found to be governed exclusively by the Franck–Condon factors for the $S_1 \rightsquigarrow S_0$ radiationless transition, which decrease approximately exponentially with increasing S_1–S_0 electronic energy spacing, $\Delta E(S_1–S_0)$. No effect of changing the excitation wavelength, and hence E^i_{vib}, was observed on the S_1 lifetime of azulene. However, the temporal resolution of our experiment is now significantly better than when these measurements were first carried out, and we therefore redetermined the S_1 lifetimes of azulene in cyclohexane for pump wavelengths from 685 to 620 nm, which provide between 230 and 1760 cm^{-1} of excess vibrational energy in the nascent excited state. Again, no effect was observed, and a constant value of $\tau = 1.00 \pm 0.08$ ps was determined, in perfect agreement with our previous result (7). This indicates that the rate of vibrational relaxation within S_1 is faster than the rate of internal conversion from S_1 to S_0, so that excited state depopulation occurs from the vibrationally relaxed S_1 state. Such behavior is typical of polyatomic molecules in condensed phase (Vavilov's law). However, for guaiazulene, whose S_1–S_0 energy gap is smaller and which therefore has a shorter S_1 lifetime, a significant increase in the rate of population decay was observed with increasing E^i_{vib}. The results are shown in Fig. 1 where $\log(\tau^{-1}) = \log(\Sigma k_{nr})$ is plotted vs. E^i_{vib}.

The following observations are significant and form the basis for further comment. (*i*) The global average values of $\tau(S_1)$ for guaiazulene at low E^i_{vib} are 0.53 ± 0.08 and 0.52 ± 0.03 ps in perfluoro-*n*-hexane and cyclohexane, respectively. (*ii*) The values of $\tau(S_1)$ for guaiazulene in both cyclohexane and perfluoro-*n*-hexane decrease (apparently exponentially) with increasing E^i_{vib}, in contrast to azulene itself. (*iii*) No significant difference is found between the profiles of $\tau(S_1)$ (or $\log_{10}(\Sigma k_{nr})$, Fig. 1) vs. E^i_{vib} for guaiazulene in two structurally different solvents.

The values of $\tau(S_1)$ obtained when guaiazulene is excited to low E^i_{vib} ($\lesssim 1000\ cm^{-1}$) yield values of $\log(k_{nr})$ that fall squarely on the plot of the energy-gap law constructed previously from data taken for six azulene derivatives in six different solvents (Fig. 2) (7, 8). We note that $\Delta E(S_1–S_0)$ for guaiazulene is almost identical in both perfluoro-*n*-hexane and cyclohexane, so identical lifetimes of the thermalized S_1 states are to be expected in these two solvents if the energy-gap law (13) accurately describes the rates of radiationless decay in these systems. We therefore conclude that (*i*) the energy-gap law does model the $S_1 \rightsquigarrow S_0$ radiationless process reasonably well, at least over the limited range of $\Delta E(S_1–S_0)$ examined here (Fig. 2); (*ii*) the S_1 state of guaiazulene cannot be distinguished from a vibrationally relaxed excited state when $E^i_{vib} <$

Can. J. Chem. Downloaded from www.nrcresearchpress.com by 65.111.164.53 on 09/08/12
For personal use only.

Fig. 1. Plot of $\log_{10}(\Sigma k_{nr})$ vs. E^i_{vib} for the S_1 population decays of azulene in cyclohexane, chx, and guaiazulene in cyclohexane and perfluoro-*n*-hexane, pfh. The sets of data were taken in three independent series; the value for guaiazulene in cyclohexane at low E^i_{vib} is therefore not exactly the same as the global average value referred to in the text and shown in Fig. 2.

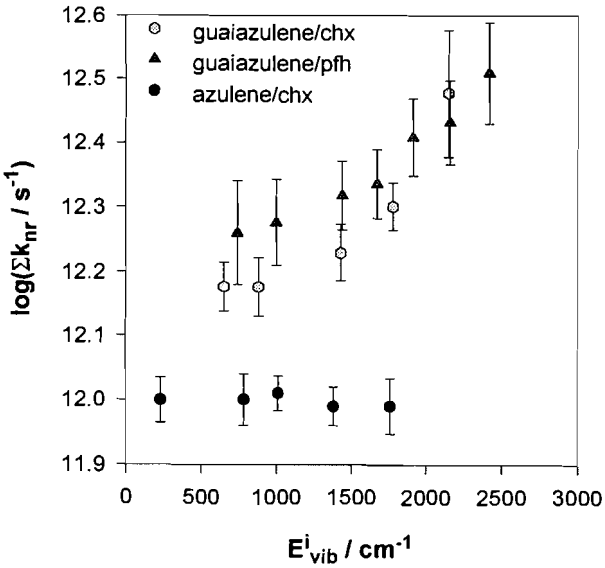

Fig. 2. Plot of $\log(\Sigma k_{nr})$ vs. S_1–S_0 energy gap for azulene and five derivatives in several solvents of different polarity at room temperature. The initial vibrational energy content of S_1 is less than 1000 cm^{-1} in all cases.

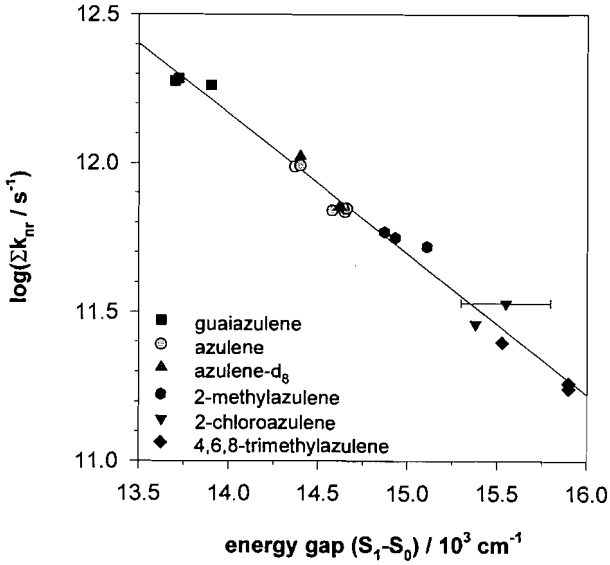

1000 cm^{-1}; and (*iii*) when $E^i_{vib} > 1000$ cm^{-1} the S_1 state of guaiazulene must be undergoing population decay from a vibrationally unrelaxed ensemble with more favorable Franck–Condon factors for $S_1 \rightsquigarrow S_0$ relaxation since at these excitation energies $\log_{10}(\Sigma k_{nr})$ values fall well above the line for the energy-gap law correlation.

An increase in k_{nr} with increasing E^i_{vib} is often observed when a polyatomic molecule retains its initial vibrational energy (as, for example, in the isolated molecule), and this behavior has been accounted for in the theory of radiationless transitions (14, 15). Such increases in k_{nr} (decrease in $\tau(S_1)$) have been observed in supersonically expanded azulene; increases by factors of about 2 at $E^i_{vib} = 1394$ cm^{-1} (16) and 3.5 at $E^i_{vib} = 2417$ cm^{-1} (17) compared with $E^i_{vib} = 0$ are found. Because we see no change in k_{nr} for azulene in cyclohexane at $0 < E^i_{vib} \leq 1760$ cm^{-1}, vibrational relaxation must occur on a time scale that is significantly faster than the population decay time, 1 ps in this case. This result does not provide a definitive check on the vibrational relaxation measurements of Matsumoto et al. (6), however, because differences in $\tau(S_1)$ measurable by us are expected only when E^i_{vib} is relatively large, i.e., >1000 cm^{-1}, whereas at such E^i_{vib} Matsumoto et al. find vibrational relaxation times that are faster than the temporal resolution of our equipment.

On the other hand, the observation of an increase in k_{nr} with E^i_{vib} for guaiazulene shows that, for this trialkyl-substituted derivative, vibrational relaxation is not complete in solution during its subpicosecond S_1 lifetime. This increase in k_{nr} with E^i_{vib} can therefore be used as a fast internal clock with which the rate of vibrational relaxation can be timed. For guaiazulene in either cyclohexane or perfluoro-*n*-hexane this rate is of the order of a few hundred femtoseconds at $E^i_{vib} \sim$ 1000–2000 cm^{-1}. Measurement of the precise relaxation rates and a determination of whether they are due to intramolecular or intermolecular relaxation must await a determination, from linewidth measurements, of the lifetimes of the isolated guaiazulene molecule as a function of E^i_{vib}. The lack of effect when cyclohexane, which has high-frequency C–H oscillators, is replaced by perfluoro-*n*-hexane, which does not, tends to suggest that the effects of a finite rate of intramolecular vibrational redistribution in guaiazulene are being observed here.

4. Acknowledgements

The authors are grateful to the Natural Sciences and Engineering Research Council of Canada and the Centers of Excellence in Molecular and Interfacial Dynamics (CEMAID) for financial support.

References

1. E.P. Ippen and C.V. Shank. Appl. Phys. Lett. **27**, 488 (1975).
2. J.P. Heritage and A. Penzkofer. Chem. Phys. Lett. **44**, 76 (1976).
3. E.P. Ippen, C.V. Shank, and R.L. Woerner. Chem. Phys. Lett. **46**, 20 (1977).
4. C.V. Shank, E.P. Ippen, O. Teschke, and R.O. Fork. Chem. Phys. Lett. **57**, 433 (1978).
5. D. Schwarzer, J. Troe, and J. Schroeder. Ber. Bunsen-ges. Phys. Chem. **95**, 933 (1991).
6. T. Matsumoto, K. Ueda, and M. Tomita. Chem. Phys. Lett. **191**, 627 (1992).
7. B.D. Wagner, M. Szymanski, and R.P. Steer. J. Chem. Phys. **98**, 301 (1993).
8. D. Tittelbach-Helmrich, B.D. Wagner, and R.P. Steer. Chem. Phys. Lett. **209**, 464 (1993).
9. B.D. Wagner, D. Tittelbach-Helmrich, and R.P. Steer. J. Phys. Chem. **96**, 7904 (1992).

10. T. Elsaesser and W. Kaiser. Annu. Rev. Phys. Chem. **42**, 83 (1991).
11. D. Huppert, J. Jortner, and P.M. Rentzepis. Isr. J. Chem. **16**, 277 (1977).
12. P. Tran, W.J. Meath, B.D. Wagner, and R.P. Steer. J. Chem. Phys. **100**, 4165 (1994).
13. R. Englman and J. Jortner. Mol. Phys. **18**, 145 (1970).
14. P. Avouris, W.M. Gelbart, and M.A. El-Sayed. Chem. Rev. **77**, 793 (1977).
15. A.L. Sobolewski. Chem. Phys. **115**, 469 (1987).
16. A. Amirav and J. Jortner. J. Chem. Phys. **81**, 4200 (1984).
17. S.K. Kulkarni and J.E. Kenny. J. Chem. Phys. **89**, 4441 (1988).

Can. J. Chem. Downloaded from www.nrcresearchpress.com by 65.111.164.53 on 09/08/12
For personal use only.

The effect of *meta*- or *para*-cyano substitution on the reactivity of the radical cations of arylalkenes and alkanes. Radical ions in photochemistry, Part 34[1]

Donald R. Arnold, Xinyao Du, and Jing Chen

Can. J. Chem. Downloaded from www.nrcresearchpress.com by 65.111.164.53 on 09/08/12
For personal use only.

Abstract: The effect of electron-withdrawing substituents, *meta*- or *para*-cyano, on the reactivity of the radical cation of arylalkenes and alkanes has been determined. The radical cations were generated by single electron transfer (set) to an electron-accepting photosensitizer. Three reactions were studied: (*i*) the addition of nucleophile to the radical cation of arylalkenes, (*ii*) cleavage of the benzylic carbon–carbon bond of the radical cation of arylalkanes; and (*iii*) the deprotonation of the benzylic carbon–hydrogen bond of the radical cation of arylalkanes. The radical cations of 4-(1-phenylethenyl)benzonitrile (**1***b*), 3-(1-phenylethenyl)benzonitrile (**1***c*), 4-(2-methoxy-1-phenylethyl)benzonitrile (**2***b*), 3-(2-methoxy-1-phenylethyl)benzonitrile (**2***c*), *cis*- and *trans*-5-cyano-2-methoxy-1-phenylindane (**6***b-cis* and *-trans*), and 6-cyano-3-phenylindene (**7***b*) were generated, by single electron transfer to the lowest excited singlet state of 1,4-dicyanobenzene (**3**), in acetonitrile–methanol. The radical cations of **1***b*, **1***c*, and **7***b* react with methanol to yield the *anti*-Markovnikov adducts (**2***b*, **2***c*, and **6***b-cis* and **6***b-trans*). The radical cations of **2***b*, **2***c*, and **6***b-trans* cleave at the benzylic carbon–carbon bond to give products derived from the radical and carbocation fragments. The radical cation of **6***b-cis* deprotonates from the benzylic position with subsequent formation of the diastereomer, **6***b-trans*. This behaviour can be explained/predicted on the basis of the proposed mechanisms for these reactions. Molecular orbital calculations (AM1) support the conclusions.

Key words: photosensitized, electron transfer, radical ions, radicals, molecular orbital calculations (AM1).

Résumé : On a déterminé l'effet de substituants électroattracteur, les groupes *méta*- et *para*-cyano, sur la réactivité de cations radicaux d'arylalcènes et alcanes. On a généré les cations radicaux par le transfert d'un seul électron à un photosensibilisateur accepteur d'électron. On a étudié trois réactions : (*i*) l'addition d'un nucléophile sur le cation radical des arylalcènes; (*ii*) le clivage de la liaison carbone–carbone benzylique du cation radical des arylalcanes et (*iii*) la déprotonation de la liaison carbone–hydrogène benzylique du cation radical des arylalcanes. On a généré les cations radicaux des 4-(1-phényléthényl)benzonitrile (**1***b*), 3-(1-phényléthényl)-benzonitrile (**1***c*), 4-(2-méthoxy-1-phényléthyl)benzonitrile (**2***b*), 3-(2-méthoxy-1-phényléthyl)benzonitrile (**2***c*), *cis*- et *trans*-5-cyano-2-méthoxy-1-phénylindane (**6***b-cis* et *-trans*) et 6-cyano-3-phénylindène (**7***b*) par un transfert d'un seul électron à l'état singulet excité le plus bas du 1,4-dicyanobenzène (**3**), en solution dans l'acétonitrile–méthanol. Les cations radicaux des composés **1***b*, **1***c* et **7***b* réagissent avec le méthanol pour donner des adduits *anti*-Markovnikov (**2***b*, **2***c* et **6***b-cis* et **6***b-trans*). Les radicaux cations **2***b*, **2***c* et **6***b-trans* se clivent au niveau de la liaison carbone–carbone benzylique pour donner des produits dérivés des fragments radicalaires et carbocationiques. Le cation radical **6***b-cis* se déprotone en position benzylique avec la formation subséquente de son diastéréoisomère, le composé **6***b-trans*. On peut expliquer/prédire ce comportement en se basant sur les mécanismes proposés pour ces réactions. Des calculs d'orbitales moléculaires (AM1) sont en accord avec ces conclusions.

Mots cles : transfert d'électron, ions radicaux, radicaux, calculs d'orbitales moléculaires (AM1).

[Traduit par la rédaction]

Received August 5, 1994.

D.R. Arnold[2], X. Du, and J. Chen. Department of Chemistry, Dalhousie University, Halifax, NS B3H 4J3, Canada.

[1] The preceding publications in this series are ref. 1.

[2] Author to whom correspondence may be addressed. Telephone: (902) 494-3714. Fax: (902) 494-1310. E-mail: arnold@ac.dal.ca.

Introduction

It is becoming increasingly evident that reactions of radical ions, generated by photo-induced single electron transfer (set), have significant synthetic utility (2). Three reactions that are of particular interest to us are (*i*) the addition of nucleophiles to the radical cation of arylalkenes, a reaction that can yield the *anti*-Markovnikov addition product; (*ii*) the carbon–carbon bond cleavage of radical cations, which ultimately yields products derived from the radical and carbocation fragments; (*iii*) the deprotonation of the radical cation, a reaction that can be used to invert the configuration at a saturated carbon centre. Archetypical examples of these processes are illustrated in reactions [1]–[3] (3–5).

Reaction [1] (3)

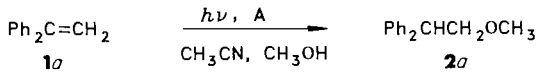

A = 1,4-dicyanobenzene (**3**, an electron-accepting photosensitizer)

Reaction [2] (4)

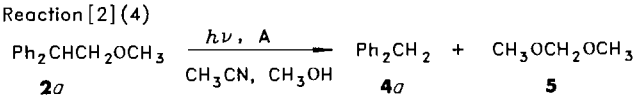

Reaction [3] (5)

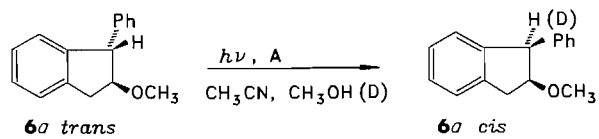

6a trans *6a cis*

Full appreciation of the utility of these reactions is dependent upon establishing their scope and limitations. This understanding is usually couched in terms of the reaction mechanism. The effects of variation in structure and the effects of substitution by electron-donating and electron-withdrawing groups must be understood, for each step of the reaction mechanism, before reactivity will be predictable. We have made some progress; the mechanisms proposed for reactions [1]–[3] are summarized in Schemes 1–3 (3–5). A previous publication in this series describes the effects of an electron-donating group, *meta*- or *para*-methoxy (6). This study has now been extended; we report here upon the influence of an electron-withdrawing group, *meta*- or *para*-cyano substitution, on these reactions.

Scheme 1. The mechanism for the photosensitized (electron transfer) nucleophilic (methanol) addition to arylalkenes (reaction [1]) (3).

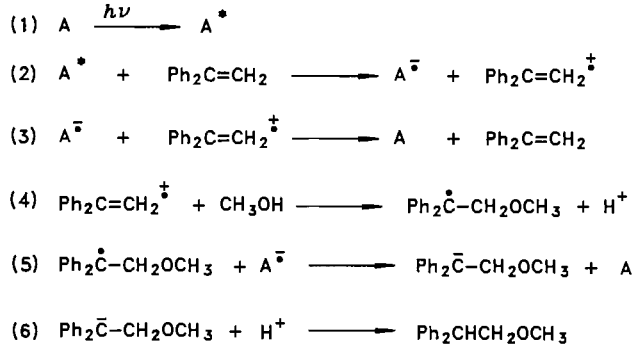

A = 1,4-dicyanobenzene (an electron-accepting photosensitizer)

Scheme 2. The mechanism for the photosensitized (electron transfer) carbon–carbon bond cleavage (reaction [2]) (4).

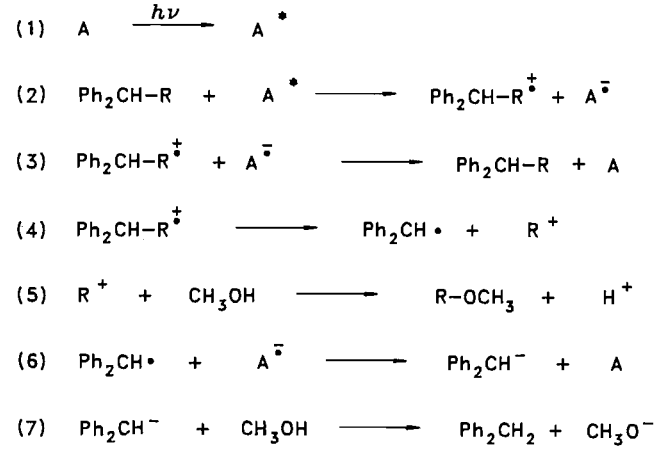

Scheme 3. The mechanism for the photosensitized (electron transfer) isomerization involves deprotonation of the radical cation, reduction of the resulting radical, and reprotonation of the anion (reaction [3]) (5).

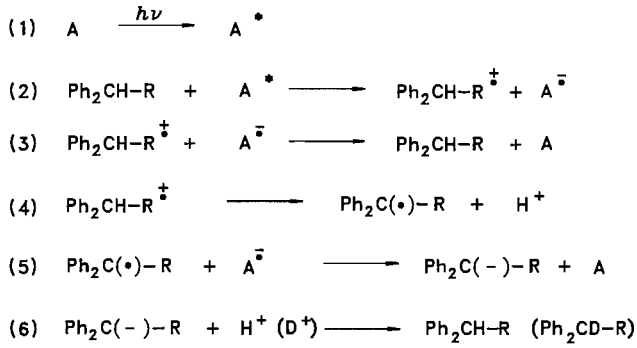

Results

The compounds chosen for study are shown in Fig. 1; all except 4- and 3-(1-phenylethenyl)benzonitrile (**1***b*, **1***c*) are new compounds. The alkenes (**1***b*, **1***c*, and **7***b*) were prepared by dehydration of the alcohols obtained from the Grignard reaction. The procedure used for the preparation of 6-cyano-3-phenylindene (**7***b*) is summarized in Scheme 4.

The irradiation conditions were similar to those used in previous studies; hence, the results can be compared. Acetonitrile–methanol (3:1) solutions of the arylalkene or alkane (0.1 M) and 1,4-dicyanobenzene (**3**) (0.05 M) were irradiated, through Pyrex, with a 1 kW medium-pressure mercury vapour lamp. The temperature was held at 10°C. Progress of the reaction was followed by capillary column gas chromatography with a mass selective detector (gc/ms). Products were gener-

Can. J. Chem. Downloaded from www.nrcresearchpress.com by 65.111.164.53 on 09/08/12
For personal use only.

Can. J. Chem. Downloaded from www.nrcresearchpress.com by 65.111.164.53 on 09/08/12
For personal use only.

Fig. 1. Compounds chosen for study.

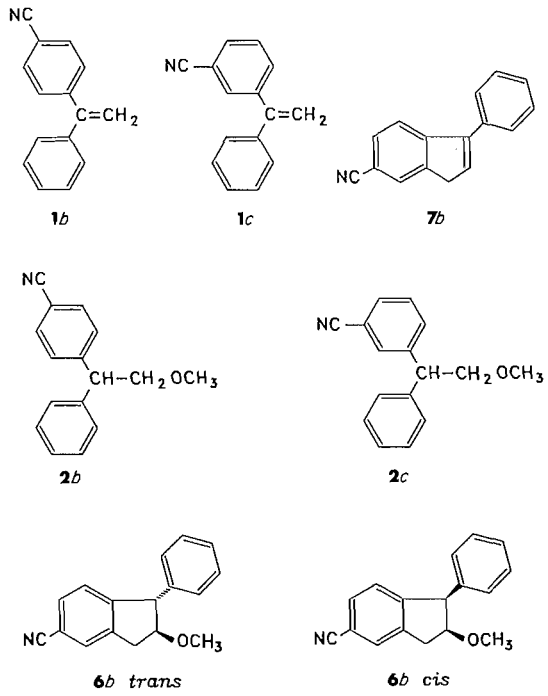

Scheme 4

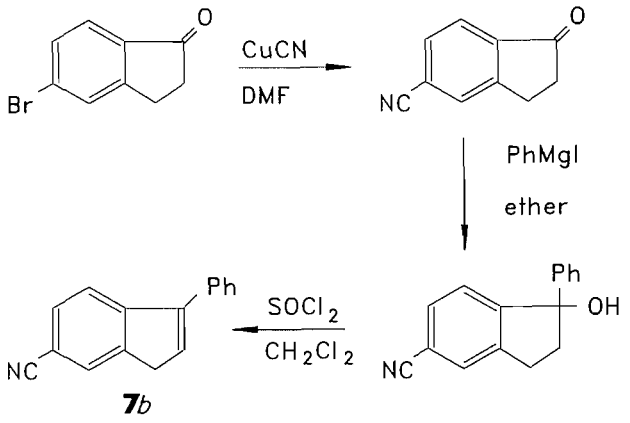

ally isolated by dry-column flash chromatography (dcfc) on silica gel or by preparative gas chromatography (prep gc).

The major products formed upon irradiation of 4-(1-phenylethenyl)benzonitrile (**1***b*) and 3-(1-phenylethenyl)benzonitrile (**1***c*) were the *anti*-Markovnikov addition products, 4-(2-methoxy-1-phenylethyl)benzonitrile (**2***b*) and 3-(2-methoxy-1-phenylethyl)benzonitrile (**2***c*) (reactions [4] and [5]). The structures assigned to these products were based upon analysis of the ^1H and ^{13}C nmr and mass spectra. The first evidence for these structures (**2***b* and **2***c*) was the observation of the molecular ions at *m/z* 237 ($M^{+\cdot}$) and base-peaks at *m/z* 192 ($M^{+\cdot}$ − 45, indicative of the loss of a methoxy methylene group) in the mass spectrum. The ^1H nmr spectra have the characteristic ABX patterns for the alkyl hydrogens and singlets for the methoxy methyl groups.

The *anti*-Markovnikov adducts, *cis*-**6***b* and *trans*-**6***b*, were formed from 6-cyano-3-phenylindene (**7***b*) under these conditions (reaction [6]). The *cis* and *trans* isomers were obtained in almost equal amounts (*cis*-**6***b*:*trans*-**6***b*, 4:3). The structures assigned to these isomers were also based upon an analysis of ^1H nmr spectra. The ^1H nmr spectra of the *cis* and *trans* isomers of **6***a*, and of the *para*-methoxy-substituted derivatives (**6***d*), show vicinal coupling between the bis-benzylic proton (X) and the proton adjacent to the methoxy group (Y) as part of an ABXY pattern in the aliphatic region. In every case, the observed coupling constant (J_{XY}) is slightly larger for the *trans* than for the *cis* isomer. For the parent system (**6***a*), J_{XY}: *trans*, 6.3; *cis*, 6.2 Hz. The stereochemistry of *trans*-**6***b* (J_{XY}:

Reaction [4]

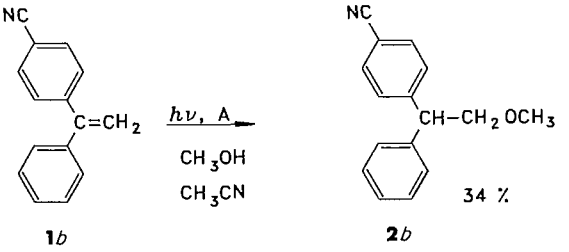

A = 1,4-dicyanobenzene (**3**)

Reaction [5]

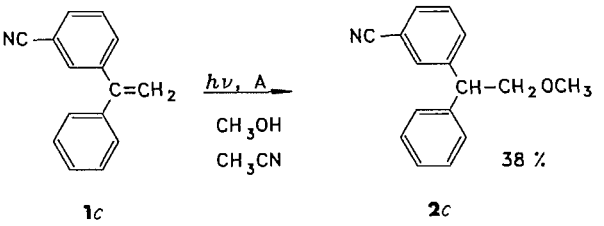

Reaction [6]

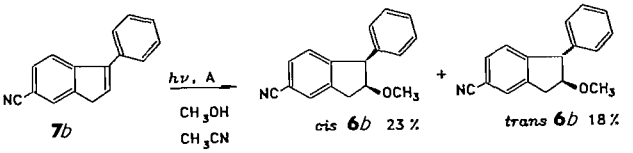

Reaction [7]

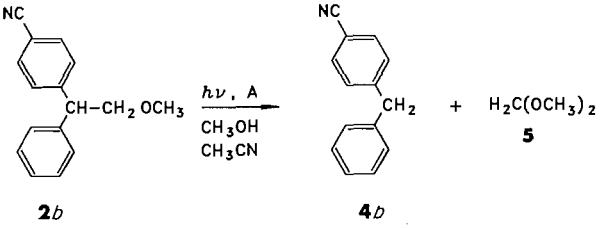

Reaction [8]

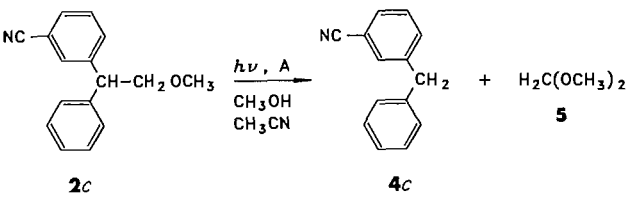

Can. J. Chem. Downloaded from www.nrcresearchpress.com by 65.111.164.53 on 09/08/12
For personal use only.

5.80 Hz) and *cis*-**6***b* (J_{XY}: 5.55 Hz) was assigned on this basis.

Both 4-(2-methoxy-1-phenylethyl)benzonitrile (**2***b*) and 3-(2-methoxy-1-phenylethyl)benzonitrile (**2***c*) cleave upon irradiation under these conditions (reactions [7] and [8]). The products, 4-benzylbenzonitrile (**4***b*) and 3-benzylbenzonitrile (**4***c*), were positively identified by comparison (^{1}H nmr, ir spectra) with authentic samples.

Irradiation of acetonitrile–methanol solutions of 1,4-dicyanobenzene (**3**) and *cis*-**6***b* leads to isomerization, formation of *trans*-**6***b*; no cleavage product was observed until a significant concentration of the *trans* isomer was attained (reaction [9]). When this irradiation was carried out in acetonitrile–methanol-O-*d* (3:1) deuterium was incorporated at the bis-benzylic position of the *trans*-**6***b* formed. In marked contrast, starting with *trans*-**6***b*, irradiation leads to formation of the cleavage product, 4-benzyl-3-(2,2-dimethoxy)ethyl benzonitrile (**8**), and to isomerization to the *cis* isomer (reaction [10]). The structure of the cleavage product (**8**) was established by analysis of the ^{1}H nmr spectrum. The crystalline 2,4-dinitrophenylhydrazone derivative of **8** was also fully characterized (^{1}H nmr and combustion analysis).

When the irradiation of *trans*-**6***b* was carried out in acetonitrile–methanol-O-*d* (3:1) solution, the mass spectrum of the cleavage product (**8**) indicated essentially quantitative incorporation of one deuterium atom. The ^{1}H nmr spectrum of **8**, isolated from this reaction mixture, showed that the deuterium is incorporated exclusively at the bis-benzylic position (4.11 ppm).

Reaction [9]

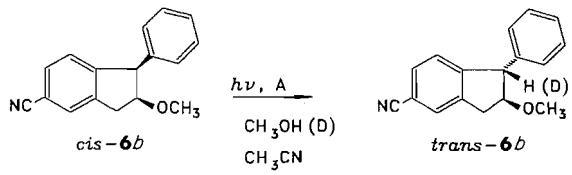

Reaction [10]

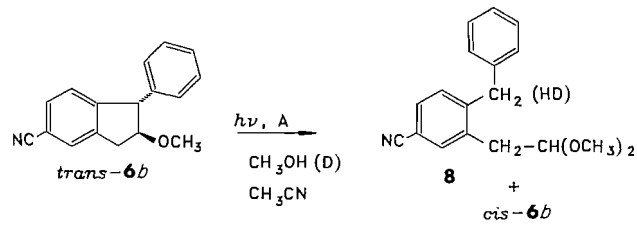

Molecular orbital calculations (AM1 (7)) were carried out to provide information regarding the structures and the spin and charge distribution on the radical cations of the arylalkenes, **1***a*–*e*$^{+\cdot}$. These results are summarized in Fig. 2.

Table 1. The oxidation potentials of some aryl alkenes and alkanes and the free energy change (ΔG_{ET}, calculated) for the electron transfer process from these potential donors to the excited singlet state of 1,4-dicyanobenzene (**3**).

Compound	$E_{1/2}^{OX}$ (*V*)[a]	ΔG_{ET} (kcal mol^{-1})[b]
1,1-Diphenylethylene (**1***a*)	1.82[c]	−18.6
4-(1-Phenylethenyl)benzonitrile (**1***b*)	2.03	−13.8
3-(1-Phenylethenyl)benzonitrile (**1***c*)	2.22	−9.4
1-(4-Methoxyphenyl)-1-phenylethylene (**1***d*)	1.32[d]	−30.2
1-(3-Methoxyphenyl)-1-phenylethylene (**1***e*)	1.53[d]	−25.3
3-Phenylindene (**7***a*)	1.53[d]	−25.3
6-Cyano-3-phenylindene (**7***b*)	1.64	−22.8
3-(4-Methoxyphenyl)indene (**7***d*)	1.24[d]	−32.0
3-(3-Methoxyphenyl)indene (**7***e*)	1.44[d]	−27.4
1,1-Diphenylethane	2.13[c]	−11.5
Methyl 2,2-diphenylethyl ether (**2***a*)	2.15[c]	−11.0
4-(2-Methoxy-1-phenylethyl)benzonitrile (**2***b*)	2.55	−1.8
3-(2-Methoxy-1-phenylethyl)benzonitrile (**2***c*)	2.50	−3.0
Methyl 2-(4-methoxyphenyl)-2-phenylethyl ether (**2***d*)	1.57[d]	−24.4
Methyl 2-(3-methoxyphenyl)-2-phenylethyl ether (**2***e*)	1.67[d]	−22.1
trans-2-Methoxy-1-phenylindane (**6***a-trans*)	2.01	−14.3
cis-5-Cyano-2-methoxy-1-phenylindane (**6***b-cis*)	2.11	−12.0
trans-5-Cyano-2-methoxy-1-phenylindane (**6***b-trans*)	2.11	−12.0
trans-2-Methoxy-1-(4-methoxyphenyl)indane (**6***d-trans*)	1.62[d]	−23.3
trans-2-Methoxy-1-(3-methoxyphenyl)indane (**6***e-trans*)	1.64[d]	−22.8

[a]Oxidation potentials measured by cyclic voltammetry at a platinum electrode relative to the saturated calomel electrode (sce) using tetraethylammonium perchlorate (0.1 M TEAP) as electrolyte in acetonitrile. The anodic wave was irreversible, so the oxidation potentials were taken as 0.028 V less than the anodic peak potential (ref. 8).

[b]Based on the Weller equation; $E_{0,0}$ (**3**) 97.6 kcal mol^{-1}, $E_{1/2}^{red}$ (**3**) −1.66 V, the Coulombic attraction term was taken to be 1.29 kcal mol^{-1} (ref. 9).

$$\Delta G_{ET} = 23.06\,[E_{1/2}^{OX}(D/D^{+\cdot}) - E_{1/2}^{red}(A^{\cdot-}/A) - e/a\varepsilon] - E_{0,0}$$

[c]Reference 4.

[d]Reference 6.

Fig. 2. Calculated (AM1) structure and spin and charge distribution on the radical cations of (*a*) 1,1-diphenylethylene (**1***a*$^{+\cdot}$); (*b*) 4-(1-phenylethenyl)benzonitrile (**1***b*$^{+\cdot}$); (*c*) 3-(1-phenethenyl)benzonitrile (**1***c*$^{+\cdot}$); (*d*) 1-(4-methoxyphenyl)-1-phenylethylene (**1***d*$^{+\cdot}$); and (*e*) 1-(3-methoxyphenyl)-1-phenylethylene (**1***e*$^{+\cdot}$).

(a)

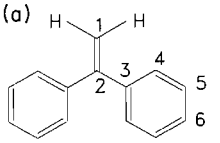

	Spin density	Charge density
1	0.801	0.277
2	−0.091	0.122
3	−0.085	−0.131
4	0.229	0.109
5	−0.230	0.039
6	0.304	0.143

Dihedral angle
1,2,3,4 = 29.4°
Bond length
2–3 = 1.43 Å

(b)

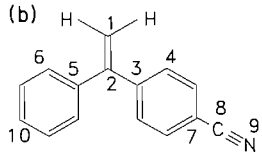

	Spin density	Charge density
1	0.772	0.292
2	−0.099	0.101
3	−0.163	−0.132
4	0.237	0.081
5	−0.018	−0.095
6	0.250	0.102
7	0.278	0.066
8	−0.075	−0.102
9	0.076	0.016
10	0.373	0.169

Dihedral angle
1,2,3,4 = 36.9°
1,2,5,6 = 22.8°
Bond length
2–3 = 1.45 Å
2–5 = 1.42 Å

(c)

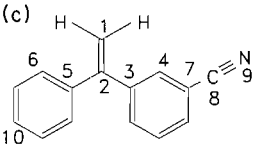

	Spin density	Charge density
1	0.780	0.286
2	−0.112	0.102
3	−0.114	−0.150
4	0.200	0.127
5	−0.001	−0.089
6	0.250	0.104
7	−0.191	−0.007
8	0.049	−0.095
9	−0.048	0.000
10	0.382	0.174

Dihedral angle
1,2,3,4 = 37.2°
1,2,5,6 = 22.4°
Bond length
2–3 = 1.45 Å
2–5 = 1.42 Å

(d)

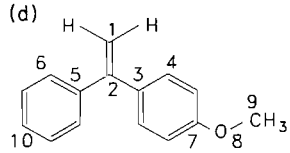

	Spin density	Charge density
1	0.789	0.209
2	−0.385	0.018
3	0.395	−0.043
4	−0.044	0.162
5	0.299	−0.131
6	−0.285	0.051
7	0.187	0.224
8	0.112	−0.177
9	−0.009	0.303
10	−0.277	0.072

Dihedral angle
1,2,3,4 = 13.9°
1,2,5,6 = 48.9°
Bond length
2–3 = 1.42 Å
2–5 = 1.46 Å

(e)

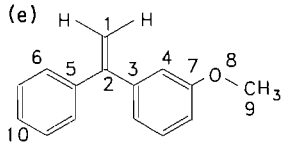

	Spin density	Charge density
1	0.772	0.288
2	−0.093	0.105
3	−0.133	−0.074
4	0.227	0.063
5	−0.090	−0.133
6	0.214	0.087
7	−0.262	0.099
8	−0.028	−0.231
9	0.001	0.249
10	0.280	0.135

Dihedral angle
1,2,3,4 = 28.8°
1,2,5,6 = 30.4°
Bond length
2–3 = 1.44 Å
2–5 = 1.44 Å

Oxidation potentials of several compounds of interest, measured by cyclic voltammetry in acetonitrile solution, are reported in Table 1.

Discussion

Generation of the radical ions

The first three steps in the proposed mechanisms for reactions [1]–[3] are the same. The arylalkenes and arylalkanes are essentially transparent to irradiation of wavelengths longer than 280 nm, the short-wavelength cutoff of the Pyrex filter. The long-wavelength absorption of 1,4-dicyanobenzene (**3**) extends beyond 280 nm. Excitation leads to the first excited singlet state, the ^1L_b state, of **3**. This singlet state has a sufficiently long lifetime (9.73 ns (4)) to allow bimolecular quenching, by a rapid single electron transfer mechanism, by prospective donors.

The free energy changes associated with the electron transfer processes (ΔG_{ET}), calculated by the Weller equation, are listed in Table 1. The rate of the electron transfer process is expected to be diffusion controlled when the oxidation potential of the donor is <2.4 V (sce), that is, when ΔG_{ET} is more negative than ca. −5 kcal mol^{-1} (9).[3] Rate constants measured by the fluorescence quenching technique are consistent with this expectation (4). All of the arylalkenes studied have oxidation potentials less than 2.4 V; therefore, step 2, Scheme 1, should occur at the diffusion-controlled rate. The only compounds studied that have oxidation potentials above this limit are the *meta*- and *para*-cyanophenyl-substituted ethers **2***b* and **2***c*. Still, in these cases, electron transfer is exergonic; radical ion formation can, and obviously does, occur.

Back-electron transfer, step 3, Schemes 1–3, is favourable in every case. This process is exergonic by >3 V; this is sufficient to retard the process, i.e., the rate of back-electron trans-

[3] All of the oxidation and reduction potentials mentioned in this paper are referenced against the saturated calomel electrode (sce).

Can. J. Chem. Downloaded from www.nrcresearchpress.com by 65.111.164.53 on 09/08/12
For personal use only.

Can. J. Chem. Downloaded from www.nrcresearchpress.com by 65.111.164.53 on 09/08/12
For personal use only.

fer falls within the Marcus inverted region (10). Rapid reactions, including solvent separation of the radical-ion pair, can compete with this mode of deactivation (11).

The addition of nucleophiles to the radical cations of arylalkenes

Step 4 of Scheme 1, addition of nucleophile (i.e., methanol) to the arylalkene radical cation, requires positive charge density on the terminal alkene carbon. The rate of addition of methanol to the radical cation $\mathbf{1}a^{+\cdot}$, within the methanol-solvation cage of the radical-ion pair, has been measured (3×10^9 s^{-1} (12)). Methoxy substitution greatly retards this reaction; the addition of methanol to the radical cation of 1,1-dianisylethylene has been estimated to be 10^7 M^{-1} s^{-1}, almost two orders of magnitude slower than the addition to $\mathbf{1}a^{+\cdot}$ (12–14). This is clearly a reflection of the reduced positive charge density on the terminal carbon of the alkene; the positive charge is largely associated with the *para*-methoxy groups.

In previous publications we have described the application of (relatively) high-level *ab initio* molecular orbital calculations (UHF/STO-3G) to explain/predict radical cation reactivity (6, 15). The calculated spin and charge distributions on the radical cations of the model compounds, 3- and 4-vinylanisole, are consistent with the proposed mechanism for the reactions of **1***d* and **1***e* (6). This type of calculation becomes computer-time prohibitive for large molecules and we have now applied semi-empirical molecular orbital calculations (AM1) to the problem. The calculated structure and spin and charge distribution for the radical cations $\mathbf{1}a$–$e^{+\cdot}$ are summarized in Fig. 2.

The unsubstituted 1,1-diphenylethylene radical cation ($\mathbf{1}a^{+\cdot}$) is symmetric (C_2); the spin and charge are distributed equally over both phenyl rings and the dihedral angles between the planes of the rings and the alkene are identical (30°). There is significant spin and charge density on the terminal carbon of the alkene. This is consistent with the observed reactivity, nucleophilic (methanol) attack at this position (reaction [1]).

The fully optimized structure of the *para*-methoxy derivative ($\mathbf{1}d^{+\cdot}$) is not symmetric; the dihedral angle between the plane of the *para*-methoxy-substituted ring and the alkene is significantly smaller than that for the unsubstituted ring (14° vs. 49°). *para*-Methoxy substitution of the radical cation increases the interaction between the methoxy-substituted ring and the alkene. This increased interaction is also reflected in the bond length between the methoxy-substituted ring and the alkene. The calculations show that the charge density on the terminal carbon of the double bond of $\mathbf{1}d^{+\cdot}$ is the lowest of the derivatives studied. Furthermore, the ratio (spin density)/(charge density) at the terminal carbon is greatest (3.8) with this derivative. These calculations are consistent with the observed reactivity of $\mathbf{1}d^{+\cdot}$, a slower rate of nucleophilic attack at the terminal carbon relative to radical addition initiated by attack of the terminal carbon on the neutral molecule (6).

The conjugative interaction between the *meta*-methoxy-substituted ring and the double bond is not as dominant as in the *para*-methoxy derivative. The dihedral angles between the planes of the two aryl rings and the alkene are now nearly identical (29° vs. 30°), and are essentially the same as that calculated for the unsubstituted case. The charge density on the terminal carbon of the alkene is again high on the radical cation of the *meta*-methoxy derivative, the ratio of (spin density)/(charge density) (2.7) is decreased, and nucleophilic attack at the terminal position is observed (6).

The calculations indicate that the structures and the spin and charge distribution for the *para*- and *meta*-cyano-substituted derivatives are similar to one another. The dihedral angles and bond lengths indicate that conjugative interaction between the unsubstituted phenyl ring and the double bond is greater than with the cyano-substituted ring. The positive charge density on the terminal carbon of the alkene is even greater in the radical cation of these cyano derivatives than it is in the unsubstituted case. The observed reactivity is consistent: nucleophilic attack on the terminal carbon (reactions [4] and [5]).

Step 5, Scheme 1, reduction of the bis-benzylic radical to the anion by the radical anion $\mathbf{3}^{-\cdot}$, should be favourable in the unsubstituted case and for the *para*- and *meta*-cyano derivatives. The reduction potentials of the 1,1-diphenylethyl, the 1-(3-cyanophenyl)-1-phenylethyl, and the 1-(4-cyanophenyl)-1-phenylethyl radicals are −1.34, −1.1, and −0.9 V (16). The reduction potential of 1,4-dicyanobenzene (**3**) is significantly more negative (−1.66 V) (4). This step is favourable even in the case of the *para*-methoxy- (−1.5 V) and *meta*-methoxy- (−1.3 V) substituted derivatives (6).

Step 6, Scheme 1, protonation of the bis-benzylic anion, will be favourable and rapid in every case. The ratio of stereoisomers (*cis*-**6***b*/*trans*-**6***b*, 4:3) initially formed in reaction [6] reflects differences in the rate of protonation; there is a preference for protonation from the less hindered side of the bis-benzylic anion.

The observations regarding the addition of nucleophile (methanol) to the radical cations of these arylalkenes are nicely accounted for on the basis of these mechanistic considerations.

The carbon–carbon bond cleavage of radical cations

Carbon–carbon bond cleavage of a radical cation yields the radical and carbocation fragments; that fragment radical having the lower oxidation potential becomes the carbocation (step 4, Scheme 2) (17). In consideration of the cleavage of the radical cations $\mathbf{2}b^{+\cdot}$ and $\mathbf{2}c^{+\cdot}$, the oxidation potential of the (3-cyanophenyl)phenylethyl and (4-cyanophenyl)phenylethyl radicals will be significantly greater than that of the methoxymethyl radical (−0.24 V) (16). Cleavage occurs (reactions [7] and [8]), as expected, to give the diarylethyl radical and the α-oxy carbocation.

The fact that the *para*- and *meta*-methoxy-substituted derivatives (**2***d* and **2***e*) do not cleave can be attributed to unfavourable thermodynamic factors. Thermochemical data determine an activation energy greater than 100 kJ mol^{-1} for cleavage of the *para*-methoxy derivative (**2***d*). Cleavage of the radical cation of the unsubstituted methyl 2,2-diphenylethyl ether ($\mathbf{2}a^{+\cdot}$) requires significantly less energy, ca. 45 kJ mol^{-1}, and cleavage of the radical cations of the *para*- and *meta*-cyano derivatives ($\mathbf{2}b^{+\cdot}$ and $\mathbf{2}c^{+\cdot}$) require even less (7 kJ mol^{-1}) (Fig. 3). These differences can be attributed largely to the effect of the substituent on the oxidation potential of the ether (**2***a*–*e*). The oxidation potentials, listed in Table 1, show the expected trend: methoxy substitution lowers the oxidation potential by ca. 0.5 V, cyano substitution increases the oxidation potential by ca. 0.4 V. Previous studies have defined the practical limit

Fig. 3. Thermochemical cycles useful for estimating the bond dissociation energy of the radical cations of (*a*) methyl 2,2-diphenylethyl ether (**2***a*); (*b*) 4-(2-methoxy-1-phenylethyl)benzonitrile (**2***b*).

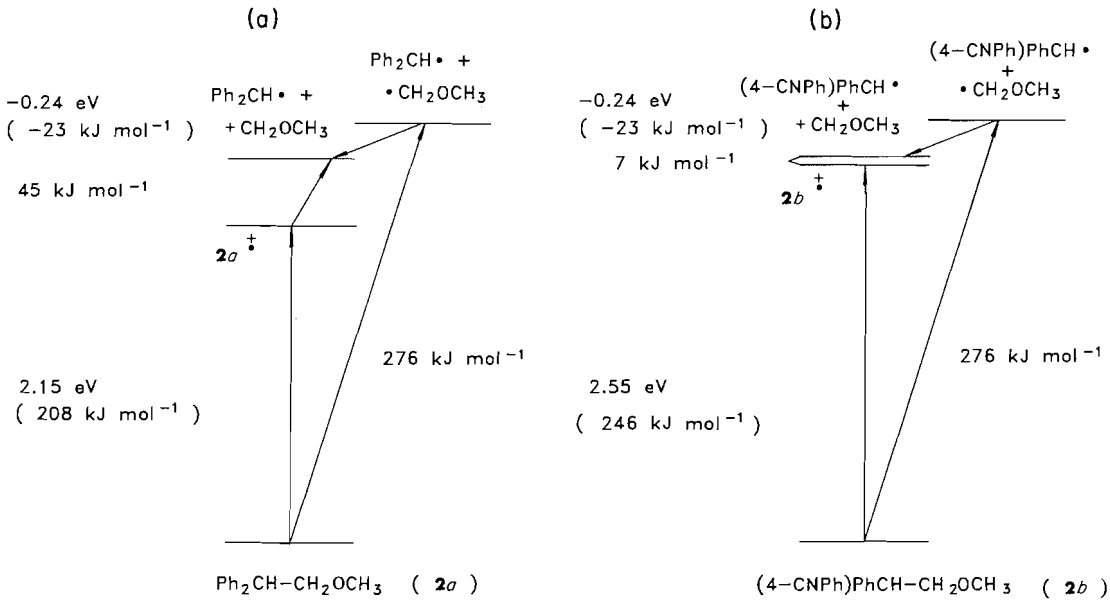

for this step, less than ca. 60 kJ mol^{-1}, in order for cleavage to be competitive with deactivation by back-electron transfer (17, 18).

There is an additional reason why the radical cation of the *meta*-methoxy derivative, $\mathbf{2e}^{+\cdot}$, does not cleave. The singly occupied molecular orbital (SOMO) has the *para*-quinoidal structure, with high charge density associated with the methoxy group; there is little spin or charge density on the *ipso* position attached to the benzylic carbon–carbon bond. The SOMO of the unsubstituted derivative, $\mathbf{2a}^{+\cdot}$, and of the cyano derivatives, $\mathbf{2b}^{+\cdot}$ and $\mathbf{2c}^{+\cdot}$, will have the *para*-quinoidal configuration, largely involving the unsubstituted phenyl ring, with high spin and charge density on the *ipso* position.

Deprotonation of the radical cation

The increase in the acidity of radical cations relative to the neutral molecules is well recognized (19). The pK_a of the bis-benzylic hydrogen of the radical cation of methyl 2,2-diphenylethyl ether ($\mathbf{2a}^{+\cdot}$) may be as low as −14, certainly acidic enough to deprotonate in this solvent mixture (acetonitrile–methanol) (6). This dramatic increase in acidity, quantitatively estimated with thermochemical cycles similar to those in Fig. 3, is largely associated with the oxidation potential of the neutral molecule. The effect of substituents on the stability of the 1,1-diarylethyl radical is relatively small. For compounds with similar carbon–hydrogen bond dissociation energies, an increase of 0.1 V in the oxidation potential corresponds to an increase of 2 pK_a units in the acidity of the radical cation (19). While deprotonation is exergonic in every case ($\mathbf{2a}$–$\mathbf{e}^{+\cdot}$), this process is kinetically slow. The labile hydrogen is not hydrogen bonded in the neutral molecule and there is a significant solvent reorganization required upon deprotonation.

The importance of conformation influencing radical cation reactivity

The reactivity of the diastereomeric indane derivatives, *cis*-**6** and *trans*-**6**, is of particular interest. In the parent system, the radical cations of both *cis*-**6***a* and *trans*-**6***a* undergo deprotonation and subsequent isomerization; no carbon–carbon bond cleavage was observed. The spin and charge density, delocalized in the singly occupied molecular orbital (SOMO), is largely distributed over the fused aryl ring. The vulnerable bis-benzylic carbon–carbon bond is almost orthogonal to the SOMO and cleavage is not observed. On the other hand, the bis-benzylic carbon–hydrogen bond is favourably orientated for overlap with the SOMO and the bis-benzylic proton is therefore acidic. Deprotonation, reduction of the resulting bis-benzylic radical to the anion by the 1,4-dicyanobenzene radical anion ($\mathbf{3}^{-\cdot}$), followed by protonation/deuteration, can account for the observed isomerization and deuterium incorporation (reaction [3]).

Table 2 summarizes the results of molecular mechanics calculations (MM3 (20)) identifying conformers of *cis*-**6***a* and *trans*-**6***a*. All of the minima within 4 kJ mol^{-1} of the global minimum are listed. We make the logical assumptions that the optimum conformation for benzylic bond cleavage will have a 90° dihedral angle between the plane of the aryl ring bearing the SOMO and the bond to break, and that the conformations of the neutral molecule and the radical cation are similar, at least with respect to the benzylic bonds (21). Furthermore, cleavage of the benzylic carbon–carbon bond, with formation of the α-oxy carbocation, requires overlap of a nonbonding pair of electrons on the oxygen with the vulnerable carbon–carbon anti-bonding orbital (σ*) (Fig. 4). The optimum dihedral angle between the methoxy-methyl group and the vulnerable carbon–carbon bond will be 60° in the starting conformation, increasing up to 90° at the transition state; the α-oxy carbocation is planar. Deviation of the dihedral angle, away from the optimum, will increase the barrier for cleavage as a function of $\cos^2\theta$.

For the unsubstituted derivative $\mathbf{6a}^{+\cdot}$, the SOMO will be largely associated with the fused aryl ring. The dihedral angle is favourable for deprotonation, particularly for the *trans* isomer (85°, 99% effective overlap), and is unfavourable for car-

Can. J. Chem. Downloaded from www.nrcresearchpress.com by 65.111.164.53 on 09/08/12
For personal use only.

Table 2. Conformers of 2-methoxy-1-phenylindane (**6***a*).

Above global minimum (kJ mol^{-1})	Fused ring		Unfused ring		
	Ar–CH	Ar–CH	Ph–CH	Ph–CC	CC–OCH$_3$
			(Dihedral angle)		
cis					
4.1	84	18	20	80	103
2.9	85	19	19	80	160
0.59	46	19	6	64	79
0.0	44	21	26	83	171
trans					
4.1	45	18	26	83	85
0.67	85	19	2	61	80
0.0	85	20	12	70	170
Optimum	90	90	90	90	60–90

Fig. 4. The importance of conformation for radical cation carbon–carbon bond cleavage.

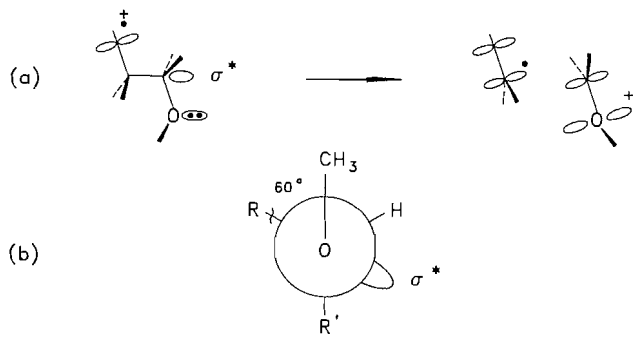

bon–carbon bond cleavage (20°, 10%). *para*-Methoxy substitution moves the SOMO to the unfused ring. Carbon–carbon bond cleavage might now occur, there are low-energy conformers that have nearly optimum dihedral angles; however, as described above, the energy barrier for cleavage is too great. Deprotonation can compete, even though a 26° dihedral angle allows only 20% effective overlap.

Differences in the reactivity of the diastereomers, *cis*-**6***b* and *trans*-**6***b*, can now be explained. Cyano substitution on the fused ring moves the SOMO out onto the unfused phenyl ring. The SOMO will have the *para*-quinoidal structure with high spin and charge density on the *ipso* position. The oxidation potentials of both *cis* and *trans* isomers are high enough (2.1 V) to render carbon–carbon bond cleavage energetically feasible. *cis*-**6***b*$^{+\cdot}$ deprotonates but does not cleave (reaction [9]); *trans*-**6***b*$^{+\cdot}$ deprotonates *and* cleaves (reaction [10]). The global minimum of the *cis* isomer is oriented favourably (26°, 20% effective overlap) for deprotonation; neither of the low-energy conformers of the *trans* isomer is in a favourable orientation for deprotonation (12°, 4% effective overlap). The conformation of the methoxy methyl group is poorly oriented (170°) for carbon–carbon bond cleavage in the global minimum of both isomers; however, the next higher conformer of both isomers should be reactive. *cis*-**6***b*$^{+\cdot}$ deprotonates from the global minimum; *trans*-**6***b*$^{+\cdot}$ cannot; instead, *trans*-**6***b*$^{+\cdot}$ cleaves from the next higher energy conformer. Deprotonation of the *trans* isomer may involve the third, higher energy, conformer.

Experimental

General methods

The ^{1}H and ^{13}C nmr spectra were recorded on either a Nicolet 360 NB (361.1 or 90.8 MHz) or a Bruker AC 250 (250.1 or 62.9 MHz) nmr spectrometer, and are reported in parts per million (ppm) downfield from tetramethylsilane. Infrared spectra (ir) were recorded on either an air-purged Perkin–Elmer 180 or on a Nicolet 205 infrared spectrometer and are reported in wavenumbers (ν) relative to the 1602 cm^{-1} absorption of polystyrene film. Mass spectra (ms) were recorded on a Hewlett–Packard 5970 series mass selective detector and are reported as *m/z* (relative intensity). Exact Mass determinations were carried out using a ZAB-E spectrometer. Elemental analyses were performed by Canadian Microanalytical Services Inc., Delta, B.C., and agreed to within ±0.3 of the calculated values. Melting points were determined using a Cybron Corporation Thermolyne melting point apparatus linked to a digital thermocouple, and were corrected.

The photochemical reactions were followed by gas chromatography (gc) using either an HP 5890 GC, fitted with a 5% phenyl methyl silicone fused silica WCOT column (25 × 0.20 mm, 0.33 μm film thickness), coupled to an HP 5970 mass selective detector (gc/ms); or an HP 5890 GC, fitted with a DB-1701 fused silica WCOT column (30 m × 0.25 mm, 0.25 μm film thickness), with a flame ionization detector (gc/fid).

The photoproducts were usually isolated by dry column flash chromatography (dcfc) on thin-layer chromatography (tlc) grade silica gel (Merck) eluting with an ethyl acetate – hexane solvent gradient (22). Preparative gas chromatography (prep gc) was carried out using a Varian Aerograph 90-P, fitted with a 3/8 in. × 6 ft aluminum column packed with 5% SE-30 on Chromosorb W 60/80 NAW.

Can. J. Chem. Downloaded from www.nrcresearchpress.com by 65.111.164.53 on 09/08/12
For personal use only.

Can. J. Chem. Downloaded from www.nrcresearchpress.com by 65.111.164.53 on 09/08/12
For personal use only.

Materials

Solvents were fractionally distilled. Acetonitrile (Fisher, ACS grade) was distilled successively from sodium hydride and phosphorus pentoxide, and was then passed through a column of basic alumina, refluxed over calcium hydride for 24 h under a nitrogen atmosphere, and fractionally distilled. The 1,4-dicyanobenzene (**3**) (Aldrich) was purified by treatment with Norite in methylene chloride, followed by recrystallization from 95% ethanol. Acetylbenzonitrile (3- and 4-), iodobenzene, and cyanobenzyl bromide (3- and 4-) were also obtained from Aldrich Chemical Co. 5-Bromo-1-indanone was obtained from MTM Research Chemicals.

Cyclic voltammetric measurements

Oxidation potentials were measured by cyclic voltammetry using an apparatus similar to that previously described (23). The working electrode was a platinum sphere (1 mm diameter), while the counter electrode was a platinum wire. The reference electrode was a saturated calomel electrode (sce), which was connected to the solution by a Luggin capillary. The electrolyte was tetraethylammonium perchlorate (0.1 M TEAP) and the solvent was acetonitrile. Substrate concentrations were typically 5 mM. As the anodic waves were irreversible, the half-wave potentials were taken as 0.028 V before the anodic peak potentials, using a 200 mV s^{-1} sweep rate (8).

Irradiations

Irradiations were carried out using a CGE 1 kW medium-pressure mercury vapour lamp contained in a water-cooled quartz immersion well. The temperature was generally maintained at 10°C. The solvent was acetonitrile–methanol (3:1 by volume) at a typical concentration of 1,4-dicyanobenzene (**3**) 0.05 M and reactant 0.1 M. Solutions were placed in 2 cm i.d. Pyrex tubes or 5 mm Pyrex nmr tubes, degassed by ebullition with dry nitrogen, and sealed.

Preparation of compounds

*3-(1-Phenylethenyl)benzonitrile (**1**c)*

The phenyl Grignard reagent was prepared from iodobenzene (20.4 g, 0.1 mol) and magnesium metal turnings (2.43 g, 0.1 mol) in anhydrous diethyl ether (40 mL). This solution of phenylmagnesium iodide was added dropwise to a solution of 3-acetylbenzonitrile (5.0 g, 0.034 mol) in diethyl ether:benzene (2:1 by volume, 350 mL) and the mixture was stirred overnight at room temperature. The reaction mixture was poured into cold saturated aqueous ammonium chloride (200 mL) and the product was extracted with ether. The combined ether extract was washed with water and then dried over magnesium sulphate. Evaporation of the solvent give a light yellow oil, which was dissolved in dichloromethane (100 mL). A solution of thionyl chloride (12.2 g, 0.102 mol) in dichloromethane (70 mL) was added and this mixture was refluxed for 6 h. The solvent and excess thionyl chloride were evaporated, the residue was dissolved in ether, and the resulting solution was washed with saturated aqueous sodium bicarbonate, saturated aqueous sodium chloride, and was then dried over magnesium sulphate. Evaporation of the solvent gave the crude alkene (**1***e*), which was purified by chromatography (dcfc) using a hexane – ethyl acetate solvent gradient (0–10%, gradually increasing the concentration of ethyl acetate until the eluent was 10% ethyl acetate in hexane). The purified alkene was isolated as a colourless oil (3.56 g, 50% yield). 3-(1-Phenylethenyl)benzonitrile (**1***c*); ir (neat film, P.-E.), ν: 2225 (CN); ^{1}H nmr ($CDCl_3$, 360NB) δ: 7.62–7.25 (m, 9H), 5.56 (s, 1H), 5.49 (s, 1H); ^{13}C nmr ($CDCl_3$, 360NB) δ: 148.11 (s), 142.67 (s), 140.10 (s), 132.47 (d) , 131.72 (d), 131.14 (d), 129.01 (d), 128.43 (d), 128.23 (d), 128.03 (d), 118.72 (s), 116.09 (t), 112.39 (s); ms *m/z*: 205 ($M^{+\cdot}$, 90), 204 (100), 190 (88), 178 (21), 177 (19), 77 (24), 76 (22), 75 (19), 51 (29). This compound has been reported previously (24).

*4-(1-Phenylethenyl)benzonitrile (**1**b)*

Phenylmagnesium iodide was prepared by slowly adding iodobenzene (24.4 g, 0.120 mol), with stirring, to magnesium turnings (2.91 g, 0.120 mol) and anhydrous diethyl ether (80 mL) in a cooled, nitrogen-purged flask. The resulting solution was added dropwise, with stirring, into a solution of 4-acetylbenzonitrile (6.0 g, 0.041 mol) in anhydrous diethyl ether (350 mL). This mixture was stirred overnight at room temperature. The crude reaction mixture was poured into a cold, saturated, aqueous solution of ammonium chloride (200 mL). The product was extracted into diethyl ether. The combined ether extract was washed with water and then dried over magnesium sulphate. Evaporation of the solvent gave the alcohol, an oil, which was not fully characterized, but was used directly in the next step. 4-(1-Phenyl-1-hydroxyethyl)benzonitrile; ms, *m/z*: 223 ($M^{+\cdot}$, 5), 208 ($M^{+\cdot} - CH_3$, 100), 205 (24), 190 (27), 130 (82), 102 (35), 77 (38), 51 (33).

Thionyl chloride (7.52 g, 0.063 mol) was added to a solution of the alcohol dissolved in dichloromethane (100 mL). This mixture was heated, under reflux, overnight. The solvent and excess thionyl chloride were evaporated. The crude product was taken up in diethyl ether (70 mL), washed with water, and dried over magnesium sulphate. Evaporation of the solvent gave the alkene (**1***b*), which was purified by chromatography (dcfc), eluting with a hexane – ethyl acetate solvent gradient (0–10%), to a colourless oil. 4-(1-Phenylethenyl)benzonitrile (**1***b*) (4.2 g, 49% from the ketone); ir (neat film, P.-E.): 3080(w), 3020(w), 2220(s, CN), 1650(m), 1600–1480(s); uv: λ_{max} = 234 nm, log e = 4.29; ^{1}H nmr ($CDCl_3$, 360NB)) δ: 7.57 (d, 2H, 8.3 Hz), 7.39 (d, 2H, 8.3 Hz), 7.33–7.24 (m, 5H), 5.56 (s, 1H), 5.52 (s, 1H); ^{13}C nmr ($CDCl_3$, AC250) δ: 148.71 (s), 146.09 (s), 140.21 (s), 132.10 (d), 128.87 (d), 128.49 (d), 128.28 (d), 128.18 (d), 118.90 (s), 116.77 (t), 111.34 (s); ms *m/z*: 205 ($M^{+\bullet}$, 100), 204 (92), 190 (93), 177 (19), 102 (17), 77 (26), 51 (49). The observed spectra (ir, ^{1}H nmr) are similar to those previously reported for this compound (25).

*6-Cyano-3-phenylindene (**7**b)*

This alkene was prepared by a three-step procedure starting with 5-bromo-1-indanone (Scheme 4). A mixture of 5-bromo-1-indanone (8.5 g, 0.04 mol), cuprous cyanide (4.12 g, 0.05 mol), and dimethylformamide (10 mL) was refluxed under nitrogen for 4 h. The resulting brown mixture was poured into a solution of hydrated ferric chloride (19 g) and concentrated hydrochloric acid (10 mL) in water (60 mL); this mixture was kept at 60–70°C for 15 min. The organic layer was separated and the aqueous layer was extracted with toluene (2 × 25 mL). The extracts were combined with the organic layer, filtered, washed with dilute hydrochloric acid (4 × 25 mL), water, and

saturated aqueous sodium bicarbonate (3 × 20 mL), and dried with sodium sulphate. Evaporation of the solvent gave 5-cyano-1-indanone as a solid (4.5 g, 70%), mp 128.9–130.1°C. 5-Cyano-1-indanone; ir (KBr, Nic.), ν: 3050 (w), 2925 (w), 2361 (m), 1690 (m), 1615 (m), 1500 (s); ^{1}H nmr ($CDCl_3$, AC250) δ: 7.65–7.86 (m, 3H), 3.23 (2H, AA′ part 3.50, 8.50 Hz), 2.78 (2H, XX′ part, 3.50, 8.50 Hz); ^{13}C nmr ($CDCl_3$, AC250) δ: 205.32 (s), 154.85 (s), 140.02 (s), 131.04 (d), 130.93 (d), 124.47 (d), 118.00 (s), 117.64 (s), 36.18 (t), 25.70 (t); ms *m/z*: 157 (68), 156 (32), 129 (100), 128 (34), 102 (39), 101 (26), 75 (26), 51 (76).

Phenylmagnesium iodide prepared from iodobenzene (12.45 g, 0.061 mol) and magnesium metal turnings (1.48 g, 0.061 mol) in anhydrous diethyl ether (80 mL) was added dropwise to a solution of 5-cyano-1-indanone (4.5 g, 0.029 mol) in the solvent mixture benzene (150 mL) – anhydrous ether (100 mL). The resulting solution was heated under reflux for 7 h, cooled, and poured into saturated aqueous ammonium chloride (150 mL). The product was extracted into diethyl ether, dried, and the solvent was evaporated. The residue was then added to a stirred cold solution of thionyl chloride (6.8 g) in dichloromethane (80 mL), and the resulting solution was refluxed for 14 h. The solvent and excess thionyl chloride were evaporated and the residue was dissolved in ether, washed with saturated aqueous sodium bicarbonate, saturated aqueous sodium chloride, and was then dried over magnesium sulphate. Evaporation of the solvent gave the crude alkene (**7***b*), which was purified by chromatography (dcfc), eluting with a hexane – ethyl acetate solvent gradient (0–3%), to give 6-cyano-3-phenylindene (**7***b*) as a colourless solid (2.95 g, 48%, mp 71.5–72.1°C); ir (KBr, Nic.), ν: 3050 (w), 2226 (s), 1665 (m), 1609 (m), 1487 (m), 1449 (s), 832 (s), 759 (s), 699 (s); ^{1}H nmr ($CDCl_3$, AC250) δ: 7.75–7.24 (m, 8H), 6.78 (t, 1H, 1.9 Hz), 3.54 (d, 2H, 1.9 Hz); ^{13}C nmr ($CDCl_3$, AC250) δ: 148.4 (s), 145.2 (s), 144.9 (s), 135.0 (d), 134.8 (s), 130.8 (d), 128.9 (d), 128.2 (d), 127.7 (d), 127.4 (d), 120.9 (d), 120.0 (s), 108.0 (s), 38.3 (t); ms *m/z*: 217 (100), 216 (38), 214 (11), 190 (11), 189 (11). Exact Mass, calcd. for $C_{16}H_{11}N$: 217.0891; found: 217.0886.

*Irradiation of 3-(1-phenylethenyl)benzonitrile (**1**c) and 1,4-dicyanobenzene (**3**) in acetonitrile–methanol (reaction [5])*

A solution of 3-(1-phenylethenyl)benzonitrile (**1***c*) (0.75 g, 3.7 mmol) and 1,4-dicyanobenzene (**3**) (0.5 g, 3.7 mmol) in acetonitrile–methanol (3:1, 40 mL) was degassed by nitrogen ebullition for 5 min and irradiated through Pyrex until the alkene was consumed (>90%). The volatile components of the photolysate were removed on a rotary evaporator and the residue was chromatographed (dcfc), eluting with a hexane – ethyl acetate solvent gradient. The ether, 3-(2-methoxy-1-phenylethyl)benzonitrile (**2***c*), was obtained as a light yellow oil (330 mg, 38%). The analytical sample was purified by prep gc, ir (neat film, P.-E.), ν: 3029 (w), 2926 (m), 2898 (m), 2228 (s), 1607 (m), 1500 (m), 1496 (m), 1453 (m), 1112 (s), 700 (s); ^{1}H nmr ($CDCl_3$, AC250) δ: 7.55–7.17 (m, 9H), 4.30 (dd, 1H, 7.15, 7.15 Hz), 3.92 (dd, 1H, 7.15, 10.30 Hz), 3.82 (dd, 1H, 7.15, 10.30 Hz), 3.37 (s, 3H); ^{13}C nmr ($CDCl_3$, AC250) δ: 143.82 (s), 140.77 (s), 133.11 (d), 131.96 (d), 130.29 (d), 129.25 (d), 128.83 (d), 128.21 (d), 127.14 (d), 119.07 (s), 112.50 (s), 75.39 (t), 59.05 (q), 50.60 (d); ms *m/z*: 237 ($M^{+\bullet}$, 44), 207 (25), 192 (100, $M^{+\bullet} - 45$ ($-CH_2OCH_3$)), 190 (49), 165 (43), 102 (5), 77 (10), 51 (13). Anal. calcd. for $C_{16}H_{15}NO$: C 80.98, H 6.37, N 5.90; found: C 80.61, H 6.35, N 5.88.

*Irradiation of 4-(1-phenylethenyl)benzonitrile (**1**b) and 1,4-dicyanobenzene (**3**) in acetonitrile–methanol (reaction [4])*

A solution of 4-(1-phenylethenyl)benzonitrile (**1***b*) (1.2 g, 6.0 mmol) and 1,4-dicyanobenzene (**3**) (0.5 g, 3.8 mmol) in acetonitrile–methanol (3:1, 80 mL) was degassed by nitrogen ebullition for 5 min and irradiated through Pyrex until the alkene was consumed (>90%). The volatile components of the photolysate were removed on a rotary evaporator and the residue was chromatographed (dcfc), eluting with a hexane – ethyl acetate solvent gradient. The ether, 4-(2-methoxy-1-phenylethyl)benzonitrile (**2***b*), was obtained as a light yellow oil (482 mg, 34%). A sample for analysis was purified by prep gc; ir (neat film, P.-E.) ν: 2920(s), 2230(s), 1609(s), 1500(s), 1498(s), 1457(s), 1110(s), 700(s); ^{1}H nmr ($CDCl_3$, 360NB) δ: 7.58 (d, 2H, 8.22 Hz), 7.36 (d, 2H, 8.22 Hz), 7.33–7.17 (m, 5H), 4.32 (dd, 1H, 7.15, 7.15 Hz), 3.93 (dd, 1H, 10.30, 7.15), 3.89 (dd, 1H, 10.30, 7.15 Hz), 3.37 (s, 3H); ^{13}C nmr ($CDCl_3$, AC250) δ: 147.84 (s), 140.72 (s), 132.28 (d), 129.23 (d), 128.81 (d), 128.22 (d), 127.13 (d), 119.01 (s), 110.37 (s), 75.33 (t), 59.05 (q), 51.08 (d); ms *m/z*: 237 ($M^{+\bullet}$, 42), 207 (24), 192 (100, $M^{+\bullet} - 45$ ($-CH_2OCH_3$)), 190 (57), 165 (50), 102 (6), 51 (21). Anal. calcd. for $C_{16}H_{15}NO$: C 80.98, H 6.37, N 5.90; found: C 81.02, H 6.35, N 5.77.

*The photosensitized (electron transfer) cleavage of 3-(2-methoxy-1-phenylethyl)benzonitrile (**2**c), reaction [8]*

A solution of 3-(2-methoxy-1-phenylethyl)benzonitrile (**2***c*) (23.7 mg, 0.10 mmol) and 1,4-dicyanobenzene (**3**) (10 mg, 0.08 mmol) in acetonitrile–methanol (3:1, 1 mL) was degassed by nitrogen ebullition and irradiated through Pyrex. Progress of the reaction was followed by gc/fid; at 50% conversion, the yield of 3-benzylbenzonitrile (**4***c*) was 70%. The structure of this product was established by comparison (gc/fid, gc/ms, retention time, and fragmentation pattern) with an authentic sample.

*The photosensitized (electron transfer) cleavage of 4-(2-methoxy-1-phenylethyl)benzonitrile (**2**b), reaction [7]*

When a solution of 4-(2-methoxy-1-phenylethyl)benzonitrile (**2***b*) and 1,4-dicyanobenzene (**3**) in acetonitrile–methanol (3:1) was irradiated through Pyrex, as described above for the *meta* isomer, carbon–carbon bond cleavage also occurred. The yield of 4-benzylbenzonitrile (**4***b*), estimated by gc/fid, was 75% at 50% conversion.

*Preparation of 3-benzylbenzonitrile (**4**c)*

Anhydrous aluminium chloride (0.17 g, 1.28 mmol) was added, in small portions, with stirring, to a benzene (70 mL) solution of 3-cyanobenzyl bromide (5 g, 0.025 mol), cooled in an ice bath. The resulting mixture was refluxed for 10 h, then cooled in an ice bath, and ice (10 g) was cautiously added, followed by water (100 mL). The organic layer was separated and washed with dilute hydrochloric acid and with water, and then dried over anhydrous calcium chloride. The solvent was evaporated and the residue distilled; 3-benzylbenzonitrile (**4***c*) (4.22 g, 86%) was obtained in the fraction boiling between 138 and 144°C (0.1 Torr; 1 Torr = 133.3 Pa), which crystallized to colourless crystals: ir (neat film, Nic.), ν: 3025 (w),

Can. J. Chem. Downloaded from www.nrcresearchpress.com by 65.111.164.53 on 09/08/12
For personal use only.

Can. J. Chem. Downloaded from www.nrcresearchpress.com by 65.111.164.53 on 09/08/12
For personal use only.

2920 (w), 2229 (s), 1599 (m), 1582 (m), 1495 (s), 1483 (s), 1454 (m), 1436 (w), 1075 (w), 1030 (w), 786 (s), 759 (m), 715 (s), 700 (s), 688 (s); ^{1}H nmr ($CDCl_3$, AC250) δ: 7.51–7.19 (m, 9H), 4.03 (s, 2H); ^{13}C nmr ($CDCl_3$, AC250) δ: 142.74 (s), 139.57 (s), 133.55 (d), 132.41 (d), 130.00 (d), 129.36 (d), 129.03 (d), 128.89 (d), 126.77 (d), 119.05 (s), 112.53 (s), 41.46 (t); ms *m/z*: 193 ($M^{+\bullet}$, 100), 190 (15), 165 (28), 91 (13). This compound has been reported previously (26).

*Preparation of 4-benzylbenzonitrile (**4**b)*

The procedure used for the preparation of the *meta* isomer (**4***c*), described above, was used for the preparation of this isomer. Starting with 4-cyanobenzyl bromide (5 g, 0.025 mol) and aluminium chloride (0.17 g, 1.28 mmol) in dry benzene (70 mL), 4-benzylbenzonitrile (**4***b*) (3.85 g, 78%) was obtained from the distillation fraction boiling at 142–144°C (0.1 Torr). This sample solidified, mp 49.0–50.0°C; ir (neat film, Nic.), ν: 2927 (w), 2861 (w), 2222 (s), 1602 (s), 1483 (s), 1448 (s), 1414 (s), 1176 (s), 860 (s), 797 (s), 729 (s), 706 (s); ^{1}H nmr ($CDCl_3$, AC250) δ: 7.56 (d, 2H, 7.93 Hz), 7.34–7.14 (m, 7H), 4.02 (s, 2H); ^{13}C nmr ($CDCl_3$, AC250) δ: 146.80 (s), 139.38 (s), 132.33 (d), 129.68 (d), 129.01 (d), 128.81 (d), 126.72 (d), 119.06 (s), 110.04 (s), 42.00 (t); ms *m/z*: 193 ($M^{+\bullet}$, 100), 190 (14), 165 (24), 91 (10). This compound has been reported previously (26).

*Irradiation of 6-cyano-3-phenylindene (**7**b) and 1,4-dicyanobenzene (**3**) in acetonitrile–methanol (reaction [6])*

A solution of 6-cyano-3-phenylindene (**7***b*) (506 mg, 2.33 mmol) and 1,4-dicyanobenzene (**3**) (236 mg, 1.84 mmol) in acetonitrile–methanol (3:1) (23 mL) was irradiated through Pyrex with the 1 kW mercury vapour lamp. Analysis of the ^{1}H nmr spectrum of the reaction mixture indicated **7***b* was consumed and gc/ms showed two new peaks, with similar retention times and mass spectral fragmentation patterns, attributed to the ethers, *cis*-**6***b* and *trans*-**6***b*. The solvent was evaporated and the crude reaction mixture was separated by chromatography (dcfc) using a solvent gradient of 2–5% ethyl acetate in hexane as the eluent. A colourless oil (100 mg, 18%), obtained in the earlier fractions, was assigned the *trans* isomer (*trans*-**6***b*). Another colourless oil (127 mg, 23%), in later fractions, was assigned the *cis* isomer (*cis*-**6***b*).

trans-**6***b*: ir (neat film, Nic.), ν: 3093 (w), 2929 (w), 2828 (w), 2228 (s), 1602 (m), 1494 (s), 1454 (m), 1115 (s), 811 (m), 753 (m), 701 (s), 632 (m); ^{1}H nmr ($CDCl_3$, AC250) δ: 7.55–7.01 (m, 8H), 4.36 (d, 1H, $J_{1,2}$ = 5.8 Hz, H-1), 4.19 (ddd, 1H, $J_{1,2}$ = $J_{2,3}$ ≃ 5.8 Hz, $J_{2,3'}$ = 6.40 Hz, H-2), 3.38 (dd, 1H, $J_{3,3'}$ = 16.4, $J_{2,3'}$ = 6.40Hz, H-3′), 3.36 (s, 3H), 2.99 (dd, 1H, $J_{3,3'}$ = 16.4 Hz, $J_{2,3}$ = 5.8 Hz, H-3); ^{13}C nmr ($CDCl_3$, AC250) δ: 149.76 (s), 141.93 (s), 141.40 (s), 131.26 (d), 128.89 (d), 128.34 (d), 128.24 (d), 127.19 (d), 126.28 (d), 119.26 (s), 110.95 (s), 89.90 (d), 57.91 (d), 57.58 (q), 37.49 (t); ms *m/z*: 249 ($M^{+\cdot}$, 34), 217 (100, $M^{+\cdot}$ − 32 (CH_3OH)), 216 (26), 204 (17), 190 (13). Exact Mass calcd. for $C_{17}H_{15}NO$: 249.1154; found: 249.1152.

cis-**6***b*: ir (neat film, Nic.), ν: 3065 (w), 2920 (w), 2820 (w), 2228 (s), 1600 (m), 1490 (m), 1454 (m), 1271 (m), 1095 (m), 702 (s); ^{1}H nmr ($CDCl_3$, AC250) δ: 7.59-7.09 (m, 8H), 4.46 (d, 1H, $J_{1,2}$ = 5.7 Hz, H-1), 4.27 (dt, 1H, $J_{1,2}$ = 5.7 Hz, $J_{2,3}$ = 4.3 Hz, H-2), 3.18 (d, 2H, $J_{2,3}$ = 4.3 Hz, H-3), 3.06 (s, 3H); ^{13}C nmr ($CDCl_3$, AC250) δ: 150.26 (s), 142.76 (s), 137.56 (s), 131.06 (d), 130.00 (d), 128.46 (d), 128.25 (d), 127.21 (d), 126.01 (d), 119.37 (s), 110.66 (s), 84.91 (d), 57.33 (d), 56.18 (q), 38.00 (t); ms *m/z*: 249 ($M^{+\cdot}$, 34), 217 (100, $M^{+\cdot}$ − 32 (CH_3OH)), 216 (26), 204 (17), 190 (13). Exact Mass calcd. for $C_{17}H_{15}NO$: 249.1154; found: 249.1152.

*Photosensitized irradiation of 5-cyano-2-methoxy-1-phenylindane (*cis- *and* trans-**6**b*) and 1,4-dicyanobenzene (**3**) in acetonitrile–methanol*

A solution of 5-cyano-2-methoxy-1-phenylindane (1:2.5, *cis*-**6***b*:*trans*-**6***b*) (170 mg, 0.7 mmol) and 1,4-dicyanobenzene (**3**) (130 mg, 1 mmol) in acetonitrile–methanol (3:1, 10 mL) was irradiated through Pyrex at 10°C. Progress of the reaction was followed by gc/ms and gc/fid. The *cis*/*trans* ratio remained unchanged. After 61% conversion, the acetal, 4-benzyl-3-(2,2-dimethoxy)ethyl benzonitrile (**8**) (51 mg, 43%), was isolated by chromatography (dcfc) using an ethyl acetate – hexane solvent gradient (0–20%): 4-benzyl-3-(2,2-dimethoxy)-ethyl benzonitrile (**8**): ir (neat film, Nic.), ν: 3027 (w), 2937 (s), 2832 (m), 2228 (s), 1602 (m), 1495 (s), 1450 (s), 1121 (s), 1071 (s), 701 (m): ^{1}H nmr ($CDCl_3$, AC250) δ: 7.56–7.08 (m, 8H), 4.30 (t, 1H, 5.47 Hz), 4.11 (s, 2H), 3.28 (s, 6H), 2.91 (d, 2H, 5.47 Hz); ^{13}C nmr ($CDCl_3$, AC250) δ: 145.03 (s), 139.14 (s), 137.05 (s), 134.32 (d), 131.03 (d), 130.18 (d), 128.73 (d), 128.66 (d), 126.49 (d), 119.02 (s), 110.28 (s), 104.65 (d), 53.90 (q, two OCH_3 groups), 39.18 (t), 36.22 (t); ms *m/z*: 249 (9), 218 (11), 217 (13), 204 (5), 190 (5), 75 ($-CH(OCH_3)_2$, 100).

4-Benzyl-3-(2,2-dimethoxy)ethyl benzonitrile (**8**) was converted into the crystalline 2,4-dinitrophenylhydrazone derivative by the standard method (27). Recrystallization from ethanol – ethyl acetate gave the 2,4-dinitrophenylhydrazone, mp 212.2–213.2°C; ^{1}H nmr ($CDCl_3$, AC250) δ: 10.87 (s, 1H), 9.12 (d, 1H, 2.60 Hz), 8.31 (dd, 1H, 9.61, 2.60 Hz), 7.78 (d, 1H, 9.61 Hz), 7.59 (dd, 1H, 7.78, 1.68 Hz), 7.55 (d, 1H, 1.68 Hz), 7.34 (d, 1H, 7.78 Hz), 7.17 (t, 1H, 5.3 Hz, the imine hydrogen), 7.29–7.20 (3H, overlap with solvent ($CHCl_3$) peak), 7.07–7.02 (m, 2H), 4.14 (s, 2H), 3.74 (d, 2H, 5.3 Hz, the methylene hydrogens next to the imine). When the ^{1}H nmr was taken in C_6D_6 solution, the imine hydrogen was shifted to 6.07 (t, 1H, 5.4 Hz), coupled to the methylene hydrogens at 3.28 (d, 2H, 5.4 Hz). Anal. calcd. for $C_{22}H_{17}N_5O_4$: C 63.61, H 4.12, N 16.86; found: C 63.44, H 4.11, N 17.15.

When a small sample of pure *trans* isomer (*trans*-**6***b*) was irradiated under the conditions described above, the acetal (**8**) was formed immediately; the *cis* isomer (*cis*-**6***b*) was formed more slowly. When a small sample of pure *cis* isomer (*cis*-**6***b*) was irradiated, formation of the *trans* isomer (*trans*-**6***b*) was observed immediately; no acetal (**8**) was detected until an appreciable amount of the *trans*-**6***b* was present.

Photosensitized irradiation of trans-*5-cyano-2-methoxy-1-phenylindane (*trans-**6**b*) in acetonitrile–methanol-O-d (3:1).*

A solution of *trans*-5-cyano-2-methoxy-1-phenylindane (*trans*-**6***b*) and 1,4-dicyanobenzene (**3**) in acetonitrile–methanol-O-*d* (3:1) was irradiated. Progress of the reaction was followed by gc/ms (single-ion monitoring) and gc/fid. After 60% conversion, ms indicated deuterium incorporation in the *cis* and *trans* isomers (5% and 3%, $M^{+\cdot}$) and in the acetal (**8**)

(>90%, $M^{+\cdot} - 32$ (CH_3OH)). The mixture was separated by chromatography (dcfc), eluting with an ethyl acetate – hexane (0–8%) solvent gradient. Analysis of the ^1H nmr spectra of **8** indicated nearly quantitative incorporation of one deuterium at the bis-benzylic position. There was no indication of deuterium incorporation at the mono-benzylic position.

Acknowledgements

This work was supported by a grant from the Natural Sciences and Engineering Research Council of Canada. We thank Dr. D.L. Hooper at the Atlantic Regional Magnetic Resonance Centre at Dalhousie University for the 360 MHz nmr spectra and for help in the preparation of the manuscript.

References

1. (*a*) K.A. McManus and D.R. Arnold. Can. J. Chem. **72**, 2291 (1994); (*b*) D.R. Arnold, K.A. McManus, and X. Du. Can. J. Chem. **72**, 415 (1994); (*c*) D.R. Arnold and X. Du. Can. J. Chem. **72**, 403 (1994).
2. (*a*) H.D. Roth. Topics Curr. Chem. **163**, 131 (1992); (*b*) J. Mattay. Synthesis, 233 (1989); (*c*) M.A. Fox. Adv. Photochem. **13**, 237 (1986).
3. R.A. Neunteufel and D.R. Arnold. J. Am. Chem. Soc. **95**, 4080 (1973).
4. D.R. Arnold and A.J. Maroulis. J. Am. Chem. Soc. **98**, 5931 (1976).
5. D.R. Arnold, B.J. Fahie, L.J. Lamont, J. Wierzchowski, and K.M. Young. Can. J. Chem. **65**, 2734 (1987).
6. D.R. Arnold, X. Du, and K. Henseleit. Can. J. Chem. **69**, 839 (1991).
7. M.J.S. Dewar, E.G. Zoebisch, E.F. Healy, and J.J.F. Stewart. J. Am. Chem. Soc. **107**, 3902 (1985).
8. (*a*) R.S. Nicholson and I. Shain. Anal. Chem. **36**, 706 (1964); (*b*) Anal. Chem. **37**, 178 (1965).
9. (*a*) D. Rehm and A. Weller. Israel J. Chem. **8**, 259 (1970); (*b*) H. Leonhardt and A. Weller. Ber. Bunsen-ges. Phys. Chem. **63**, 791 (1963).
10. R.A. Marcus. Discuss. Faraday Soc. **29**, 21 (1960).
11. (*a*) I.R. Gould, D. Ege, S.L. Mattes, and S. Farid. J. Am. Chem. Soc. **109**, 3794 (1987); (*b*) I.R. Gould, D. Ege, J.E. Moser, and S. Farid. J. Am. Chem. Soc. **112**, 4290 (1990); (*c*) S.L. Mattes and S. Farid. Org. Photochem. **6**, 233 (1983).
12. S.L. Mattes and S. Farid. J. Am. Chem. Soc. **108**, 7356 (1986).
13. (*a*) M.S. Workentin, N.P. Schepp, L.J. Johnston, and D.D.M. Wayner. J. Am. Chem. Soc. **116**, 1141 (1994); (*b*) L.J. Johnston and N.P. Schepp. J. Am. Chem. Soc. **115**, 6564 (1993).
14. R.A. McClelland, V.M. Kanagasabapathy, N.S. Banait, and S. Steenken. J. Am. Chem. Soc. **111**, 3966 (1989).
15. X. Du, D.R. Arnold, R.J. Boyd, and Z. Shi. Can. J. Chem. **69**, 1365 (1991).
16. (*a*) B.A. Sim, P.H. Milne, D. Griller, and D.D.M. Wayner. J. Am. Chem. Soc. **112**, 6635 (1990); (*b*) D.D.M. Wayner, D.J. McPhee, and D. Griller. J. Am. Chem. Soc. **110**, 132 (1988).
17. R. Popielarz and D.R. Arnold. J. Am. Chem. Soc. **111**, 3068 (1990).
18. (*a*) L.J. Lamont and D.R. Arnold. Can. J. Chem. **68**, 390 (1990); (*b*) A. Okamoto, M.S. Snow, and D.R. Arnold. Tetrahedron, **42**, 6175 (1986).
19. (*a*) A.M. de P. Nicholas and D.R. Arnold. Can. J. Chem. **60**, 2165 (1982); (*b*) F.G. Bordwell, J.-P. Cheng, and M.J. Bausch. J. Am. Chem. Soc. **110**, 2867 (1988); (*c*) M.M. Green, S.L. Mielke, and T. Mukhopadhyay. J. Org. Chem. **49**, 1276 (1984); (*d*) J.M. Masnovi, S. Sankararaman, and J.K. Kochi. J. Am. Chem. Soc. **111**, 2263 (1989); (*e*) V.D. Parker, Y. Chao, and B. Reitstoen. J. Am. Chem. Soc. **113**, 2336 (1991).
20. N.L. Allinger, Y.H. Yuh, and J.-H. Lii. J. Am. Chem. Soc. **111**, 8551 (1989).
21. (*a*) A.L. Perrott and D.R. Arnold. Can. J. Chem. **70**, 272 (1992); (*b*) D.R. Arnold and S.A. Mines. Can. J. Chem. **65**, 2312 (1987).
22. (*a*) W.C. Still, M. Kahn, and A. Mitra. J. Org. Chem. **43**, 2925 (1978); (*b*) L.H. Harwood. Aldrichchimica Acta, **18**, 25 (1985).
23. A. Okamoto, M.S. Snow, and D.R. Arnold. Tetrahedron, **42**, 6175 (1986).
24. H. Yamada, Y. Tsuno, and Y. Yukawa. Bull. Chem. Soc. Jpn. **43**, 1459 (1970).
25. M. Tada, K. Inoue, and M. Okabe. Bull Chem. Soc. Jpn. **56**, 1420 (1983).
26. (*a*) O. Exner and K. Bocek. Collect. Czech. Chem. Commun. **38**, 50 (1973); (*b*) O. Exner and M. Budesinsky. Magn. Reson. Chem. **27**, 27 (1989).
27. R.L. Shriner, R.C. Fuson, and D.Y. Curtin. The systematic identification of organic compounds: 4th ed. J. Wiley & Sons, New York. 1956.

Can. J. Chem. Downloaded from www.nrcresearchpress.com by 65.111.164.53 on 09/08/12
For personal use only.

Design and synthesis of near-infrared absorbing pigments. I. Use of Pariser–Parr–Pople molecular orbital calculations for the identification of near-infrared absorbing pigment candidates

Denis Désilets, Peter M. Kazmaier, and Richard A. Burt

Abstract: The usefulness of the Pariser–Parr–Pople molecular orbital method for the identification of near-infrared absorbing pigment candidates for photogenerator applications is outlined. Several pigments based on the well-known class of photogenerators *N,N'*-dialkyl-3,4,9,10-perylenetetracarboxylic diimides were investigated and pigments of the dibenzoperylene, bisanthene, and zethrene classes were identified as the most promising candidates of the series. On the basis of the predictions, 7,8,15,16-dibenzo[*a*, *j*]perylenetetracarboxylic diimide was prepared and the validity of the calculations was verified.

Key words: photoconductor, near-infrared, Pariser–Parr–Pople calculations, polycyclic aromatic hydrocarbon, aceanthrene green.

Résumé : On présente des données montrant l'utilité de la méthode des orbitales moléculaires Pariser–Parr–Pople pour l'identification de pigments pouvant être des candidats pour une absorption dans le proche infrarouge pour des applications comme photogénérateurs. On a étudié plusieurs pigments dérivés de la classe bien connue de photogénérateurs des diimides de l'acide *N,N'*-dialkylpérylène-3,4,9,10-tétracarboxylique et on a identifié des pigments des classes du dibenzopérylène, du bisanthène et du zéthrène comme les candidats les plus prometteurs de la série. Sur la base de ces prédictions, on a préparé le diimide de l'acide dibenzo-[*a*, *j*]pérylène-7,8,15,16-tétracarboxylique et on a vérifié la validité des calculs.

Mots clés : photoconducteur, proche infrarouge, calculs Pariser–Parr–Pople, hydrocarbure polycyclique aromatique, acéanthrene vert.

[Traduit par la rédaction]

Introduction

Diimide (**1**) and bis(benzimidazole) (**2**) derivatives of 3,4,9,10-perylenetetracarboxylic dianhydride (Scheme 1) are well-known pigments and have been used in a wide variety of applications (1–5). These compounds have proven to be photogenerating materials with high photosensitivity in the visible, low dark decay, and excellent cyclic stability (6–9). Because of the increased interest in near-infrared photosensitive materials for laser printing applications, it would be highly desirable to design photogenerators with these properties and which would be photosensitive at the gallium aluminium arsenide (GaAlAs) diode laser wavelength around 780 nm. The preparation of polycyclic aromatic imides and benzimidazole derivatives is expected to be difficult because of the insolubility of these pigments and also because the available synthesis methodology for polycyclic aromatics is very substrate specific. In view of these constraints, it is essential to have a calculational method that would predict the spectral response of a pigment prior to embarking on a lengthy synthesis process.

Scheme 1

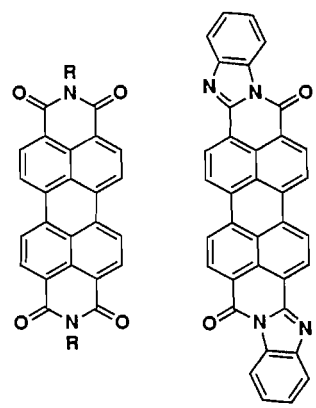

1 **2**

Pariser–Parr–Pople (PPP) calculations have been shown to be a useful method for the colour prediction of organic dye

Received August 16, 1994.

D. Désilets,[1,2] P.M. Kazmaier,[1] and R.A. Burt. Xerox Research Centre of Canada, 2660 Speakman Drive, Mississauga, ON, L5K 2L1, Canada.

[1] Authors to whom correspondence may be addressed. Telephone: (905) 823-7091. Fax: (905) 822-7022.

[2] Present address: Apotex Research Inc., 400 Ormont Drive, Toronto, ON M9L 1N9, Canada. Telephone: (416) 749-9300. Fax: (416) 745-5038.

Can. J. Chem. Downloaded from www.nrcresearchpress.com by 65.111.164.53 on 09/08/12
For personal use only.

Can. J. Chem. Downloaded from www.nrcresearchpress.com by 65.111.164.53 on 09/08/12
For personal use only.

Fig. 1. Normalized electronic absorption spectra and xerographic spectral response of the perylene diimide **1**, R = Me (6).

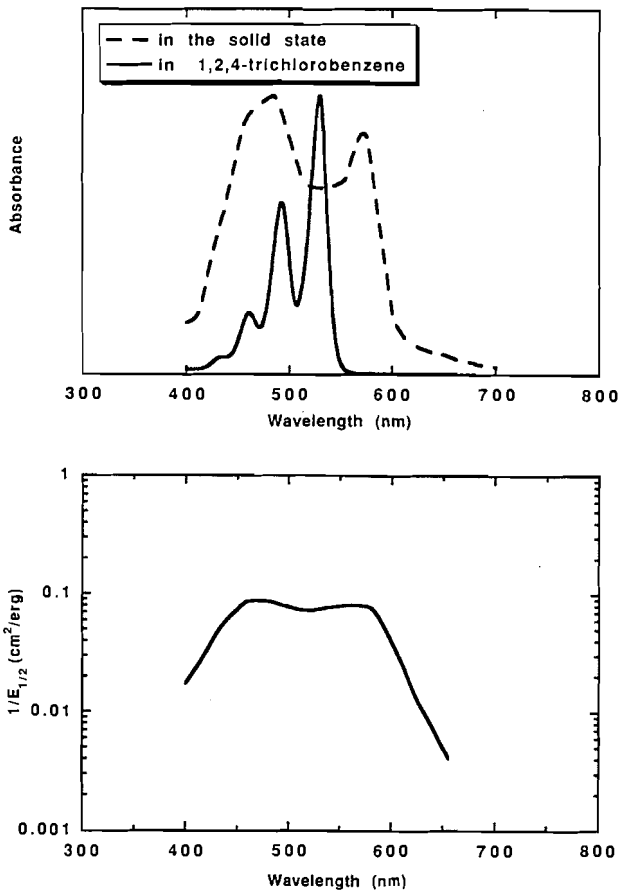

molecules such as azos, quinone, and cyanine-type dyes in the visible region (10–12). This paper will report on the application of this method to the identification of near-infrared absorbing polycyclic aromatic imide pigment candidates.

Results and discussion

Description of the method

In optoelectronic devices such as photoreceptors, the photogenerator pigment is used in the form of a dispersion in a polymer matrix. An ideal method for screening potential near-infrared photogenerator pigments would identify derivatives possessing the required absorptivity in the near-infrared, for the pigment as a solid state dispersion in a binder polymer. Unfortunately, calculations of solid state spectra are beyond the scope of the PPP method and of any other currently available molecular orbital program since these programs have been parameterized to reproduce solution or gas phase results.

To circumvent this problem, a solution absorption maximum has been calculated for candidate near-infrared photogenerator pigment structures and these solution absorption values with the corresponding oscillator strengths (a measure of the area under the absorption peak) were compared to a known, benchmark photogenerator of the polycyclic pigment class with a photosensitivity in the visible. The solid state absorption maximum was estimated by assuming that aggregation for the candidate compound would be comparable to that observed for the benchmark compound. Fortunately, the correct prediction of a red shift in the molecular absorption is far more important than the accurate prediction of the solid state absorption maximum of the candidate pigment because the absorption broadens considerably in the solid state and the candidate pigment will function in a device as long as the absorption maximum has been shifted far enough into the infrared to provide a region of uniform light absorption for the diode laser. Furthermore, because of the high loadings in the devices, the useful range extends beyond the pigment solid state absorption maximum. For example, *N,N*-dimethyl-3,4,9,10-perylenetetracarboxylic diimide, with absorption maxima at 461, 493, and 530 nm in solution and at 485 and 575 nm in the solid state, still provides a flat xerographic spectral response from 445 to 580 nm (Fig. 1). The xerographic spectral response curve is a standard test to measure the panchromaticity of a photoreceptor (7). It is obtained by plotting the inverse of the exposure energy required to reduce the surface potential by half versus the wavelength of the light source. Similarly, the bis(benzimidazole) derivative (**2**) has absorptions at 545 and 665 nm in the solid state and provides flat xerographic spectral response from 490 to 710 nm (6).

Scheme 2

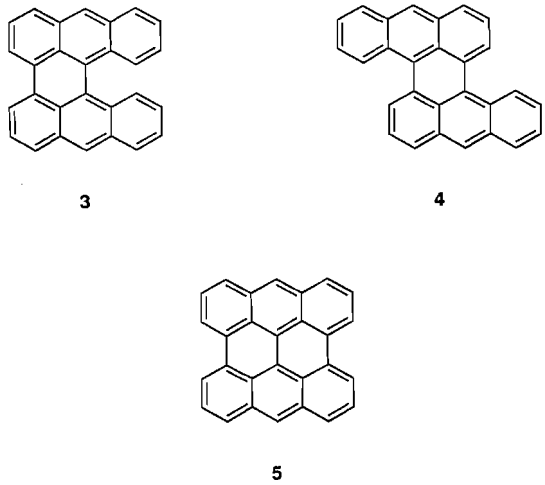

PPP calculations are designed to handle planar systems. For our purposes polycyclic aromatic pigments are assumed to be planar and all rings have been approximated by regular hexagons or pentagons. This approximation is a reasonable assumption since the calculated values have been shown to be much more dependent on the PPP parameters required for the calculations than on the molecular bond angles and bond lengths (11). This can be demonstrated by comparing dibenzo[*a,o*]perylene (**3**) and dibenzo[*a,j*]perylene (**4**) to bisanthene (**5**) (Scheme 2). In the case of the dibenzoperylenes, molecular mechanics calculations as well as CPK models indicate that the two anthracene units should be distorted from planarity on the order of 20°–30° whereas bisanthene is planar. The results of Table 1 show that the predictive power of the PPP calculations is not seriously compromised by assuming a planar system for the dibenzoperylenes.

In addition to the absorption maximum, PPP calculations provide an estimate of the oscillator strength (*f*), which is

Can. J. Chem. Downloaded from www.nrcresearchpress.com by 65.111.164.53 on 09/08/12
For personal use only.

Scheme 3

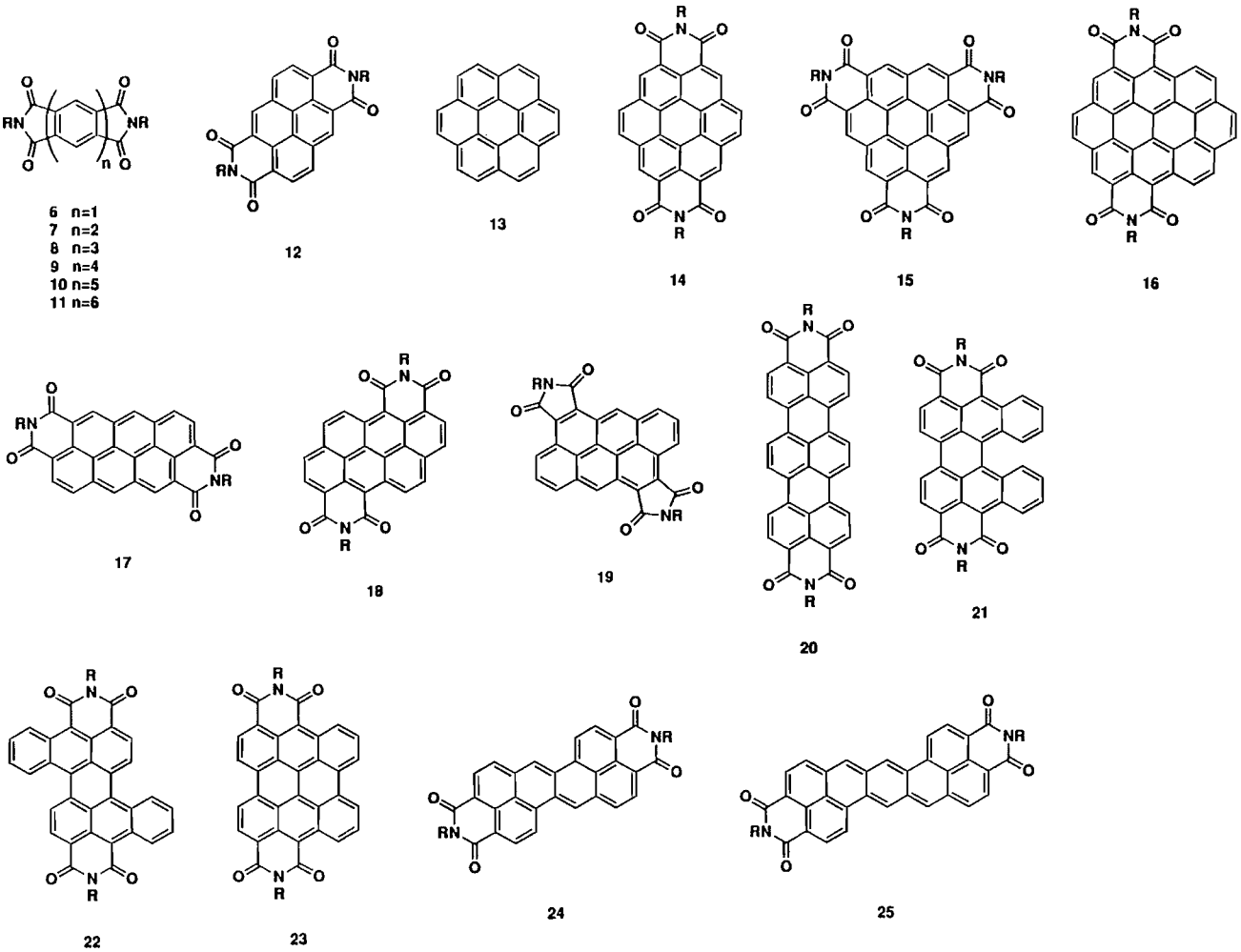

Table 1. Comparison between the calculated and experimental absorptions of dibenzoperylenes and bisanthene.

Compound	Calculated absorption (nm)	Experimental absorption[a] (nm)
Dibenzo[*a*,*o*]perylene	533	516
Dibenzo[*a*,*j*]perylene	524	516
Bisanthene	563	603

[a]In benzene. Data taken from refs. 13 (p. 49) and 14.

related to the area under the absorption band. Since the extinction coefficient is related to the height of the band, the two quantities are linearly related only if the band widths are the same and if the bands are symmetrical. Since high absorption is a prerequisite for achieving high photosensitivity, the oscillator strengths are useful in determining the extinction coefficients and, therefore, the photosensitivity of a pigment. However, since PPP parameters have been selected to provide the correct estimates for dye and pigment absorption maxima, the parameterization is necessarily non-optimal vis-a-vis the oscillator strength. Thus, oscillator strength estimates often lead to poor correlation within a particular compound class (11) and they can only be used as a qualitative tool.

In the examples studied in this paper, we selected *N,N'*-dialkyl-3,4,9,10-perylenetetracarboxylic diimides (**1**) as the benchmark compounds and, therefore, we need a shift of the order of 200 nm to extend the 580 nm photosensitivity limit of these photogenerator pigments to 780 nm. Ideally, since the calculated absorption of the benchmark diimide is at 469 nm, suitable near-infrared absorbing candidates should have their calculated absorption near 670 nm on the basis of this 200 nm shift or near 590 nm on the basis of a constant energy shift (15) calculated from the difference between the calculated absorption and the observed absorption in the solid state for the benchmark perylene pigment. On the other hand, if we extend the conjugation by using a bis(benzimidazole) derivative instead of a diimide, the required shift to extend the 710 nm photosensitivity limit of the bis(benzimidazole) perylene towards the desired 780 nm wavelength is now only 70 nm. Thus, diimides with a calculated absorption maxima around 540 nm (wavelength shift) or 500 nm (energy shift (15)) become good candidates.

The calculations were done on a wide variety of polycyclic diimides (Scheme 3) and the results are presented in Table 2. The following observations can be made.

Table 2. Pariser–Parr–Pople calculated absorptions and oscillator strengths in cyclohexane for the compounds of Scheme 3.

Compound	Calculated absorption (nm)	Calculated oscillator strength
1	469	1.77
6	300, 297, 296	0.30, 1.02, 0.00
7	327	0.42
8	361	0.21
9	427	0.32
10	485	0.41
11	537	0.46
12	396	1.65
13	373	0.00
14	441	0.20
15	407	0.00
16	485	1.34
17	466	2.06
18	505	1.94
19	470	1.10
20	576	2.47
21	615	1.80
22	605	1.76
23	643	1.83
24	601	2.27
25	687	3.29

Polyarenes

One simple concept for achieving infrared photosensitivity would be to increase conjugation by extending the aromatic structure in a linear sense. Consequently, linear polyarenes were investigated and a series is represented by compounds **6–11**. These pigments were not found to be good candidates for near-infrared activity for two reasons. First, to obtain a red shift of the absorption vis-a-vis the benchmark, one needs to go to five or six fused rings as in **10** and **11**. For very long annelated systems like this, imide substitution imparts very little *n*-character (acceptor) to the kernel. Therefore since higher polyacenes are unstable (16), the same behavior is expected for the diimide derivatives. Second, the low oscillator strengths associated with these compounds suggest they would not have high enough extinction coefficients to be usable pigments.

Simple polycyclic arenes

Another approach would be to take a known photogenerator such as **1** and simply extend the conjugation by fusing benzene rings to the chromophore. Initially calculations were done on some simple polycyclic arenes in which the conjugation of the perylene nucleus was extended by merging with extra aromatic rings in the bay region of the chromophore. As seen by the results for compounds **12–16**, this class does not seem very promising. Extension of the conjugation as in the coronene case (**14**) does in fact shift the absorption maximum in a hypsochromic sense rather than the bathochromic shift intuitively expected. Furthermore, the oscillator strength is low, being identically zero for those compounds with 3-fold symmetry. Extraordinary extension of the conjugation, as in the ovalene case (**16**), brings very little improvement of the values, indicating that the difficult synthesis of the material should not be attempted. An interesting observation highlighting the usefulness of the PPP method can be made when comparing compounds **14** and **15** to the coronene nucleus **13**. One can see that the introduction of two imide units on coronene increases the maximum absorption wavelength from 373 to 441 nm but that one cannot further increase the position of the absorption by adding one more unit. The introduction of this supplementary unit in fact decreases the position of the absorption to 407 nm. These examples indicate that simple intuition based on the principle of the efficacy of extended conjugation without a detailed analysis of the excitation process does not provide a reliable guide for predicting the impact of structural change on the absorption maximum and oscillator strength of these materials.

Anthanthrenes

The importance of using PPP calculations in the design of new near-infrared photogenerator materials can be illustrated by a consideration of anthanthrenes. Diimides and bis(benzimidazole) derivatives of anthanthrene in which the substitution of the nucleus is the same as that in compound **17** have been reported in the literature (17–20). Calculations predict that there would be no substantial advantage if such derivatives were prepared. However, the calculations predict that a shift of the absorption could be achieved if the anthanthrene nucleus were substituted as in **18**. On the other hand, replacing the two six-membered ring anhydrides in **18** with two five-membered ring units as in **19** gives no wavelength advantage. The ability to predict which isomeric anthanthrenes provide the optimum absorption maximum shift again shows the usefulness of the PPP method for pigment design.

Perylenes

Extending the conjugation of perylene diimide **1** by inserting an extra naphthalene ring between the two naphthalene rings of perylene as in the terrylene **20** leads to a substantial improvement over the perylene derivative. Since the preparation of tetraalkyl-substituted terrylene and related derivatives has been reported recently in the literature (21–24), the synthesis of the corresponding diimides can be considered. Calculations indicate that dibenzoperylene or bisanthene derivatives **21–23** would lead to much better candidates for near-infrared absorbing diimide pigments. The expected shift of the absorption towards the near-infrared is of the order of 140–170 nm compared to the benchmark diimide **1**. However, deviation from planarity that might affect photosensitivity of these derivatives is expected in the case of compounds **21** and **22**, but compound **23** is predicted to be planar.

Zethrenes

Zethrenes are an interesting class of pigments that are predicted by PPP calculations to have substantial near-infrared shifts. The quinoid bond fixation leads to long-wavelength absorption for the corresponding hydrocarbons (ref. 13, pp. 447–466). With relatively small increase in molecular weight, zethrene derivatives such as **24** and **25** are predicted to experience a considerable shift towards the near-infrared as well as a large increase of the extinction coefficient. Their calculated oscillator strength values are among the highest of the series

Can. J. Chem. Downloaded from www.nrcresearchpress.com by 65.111.164.53 on 09/08/12
For personal use only.

Can. J. Chem. Downloaded from www.nrcresearchpress.com by 65.111.164.53 on 09/08/12
For personal use only.

Fig. 2. Normalized solid state absorption spectra of the perylene diimide **1**, R = H, and of the dibenzoperylene **22**, R = H.

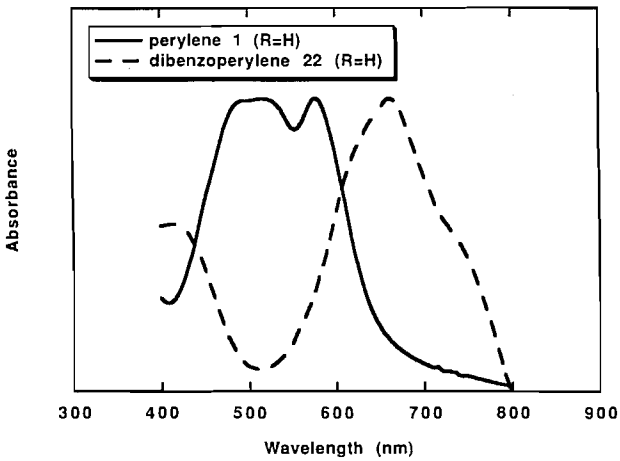

and they are predicted to give highly absorbing near-infrared pigments.

Experimental verification

To verify the reliability of the PPP method for predicting potential infrared photogenerating candidates, the synthesis of 7,8,15,16-dibenzo[*a,j*]perylenetetracarboxylic diimide (**22**, R = H) was undertaken and will be reported in the following paper. The absorption spectrum in a vinyl acetate binder is shown in Fig. 2 and compared with that of the benchmark 3,4,9,10-perylenetetracarboxylic diimide (**1**, R = H). As one can see, the calculations provided a reliable guide for the prediction of the absorption maximum. The observed 160 nm bathochromic shift is larger than the 136 nm shift calculated on the basis of a simple wavelength shift but smaller than the 220 nm shift calculated on the basis of a constant energy shift (15).

Conclusion

PPP calculations provide an important tool for predicting the absorption maxima of potential near-infrared photogenerator pigments. Intuition, based on the principle of extended conjugation, is an unreliable guide for predicting the impact of ring fusion to the chromophore and cannot determine which isomeric diimide derivative has the longest absorption maximum combined with the highest oscillator strength.

Compounds with 3-fold symmetry such as coronene derivative **15** have a forbidden low-energy transition. Furthermore, the effect of extended conjugation is offset by ground stabilization as shown in resonance structure **26** (Scheme 4). In contrast, bond fixation can favorably impact the absorption maximum as in dibenzoperylenes (**21–23**) and zethrenes (**24, 25**). The identification and preparation of the dibenzoperylene derivative **22** (R = H) verifies the efficacy of this methodology.

Scheme 4

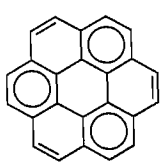

26

Computational

Pariser–Parr–Pople calculations were performed using parameters based on the ones published by Griffiths (11). Molecular mechanics calculations were done using the MMX parameters reported by Gajewski et al. (25).

Experimental

Preparation of 7,8,15,16-dibenzo[*a, j*]perylenetetracarboxylic diimide 22 (R = H)

The dibenzoperylene **22** (R = H) was prepared as reported by Kardos (26). The structure was determined as described in the following paper.

Preparation of the pigment films and measurement of the absorption spectra

The absorption spectra of the pigments were obtained by following the protocol of Loutfy (27). The pigment (180–200 mg) was suspended in a solution of poly(vinyl acetate) in methylene chloride (1.5% by weight, 10 mL) and ball-milled for 24 h with 1/8 in. stainless steel shot. The film was prepared by draw-down coating using a wire-wound rod (No. 6). The absorption spectrum was measured using a Cary 5 UV–Vis–NIR spectrophotometer.

Acknowledgments

The authors wish to thank Dr. T. I. Martin for helpful discussions and support throughout the near-infrared polycyclic aromatic photogenerator project. We would also like to express our sincerest appreciation to Professor J. Griffiths (University of Leeds) for providing a copy of the PPP program and for helpful comments. We also thank B. Keoshkerian for obtaining a copy of the program and P. Blaney for translating it into Fortran.

References

1. W. Herbst and K. Hunger. *In* Industrielle Organische Pigmente, Herstellung, Eigenschaften, Anwendung. VCH Verlagsgesellschaft, Weinheim. 1993. pp. 472–481.
2. P.F. Gordon. *In* The chemistry and application of dyes. *Edited by* D.R. Waring and G. Hallas (Topics in Applied Chemistry. *Edited by* A.R. Katritzky and G.J. Sabongi). Plenum Press, New York. 1990. Chap. 8.
3. A.T. Peters and H.S. Freeman (*Editors*). *In* Colour chemistry, the design and synthesis of organic dyes and pigments (advances in colour chemistry). Elsevier Applied Science, London. 1991. pp. 198 and 207–208.
4. H. Zollinger. *In* Color chemistry, syntheses, properties and applications of organic dyes and pigments. VCH Verlagsgesellschaft, Weinheim. 1987. pp. 184–185.
5. R.L.M. Allen. *In* Colour chemistry. Appleton–Century–Crofts, New York. 1971. p. 256.
6. R.O. Loutfy, A.M. Hor, P. Kazmaier, and M. Tam. J. Imaging Sci. **33**, 151 (1989).

7. R.O. Loutfy, A.M. Hor, C.K. Hsiao, G. Baranyi, and P. Kazmaier. Pure Appl. Chem. **60**, 1047 (1988).
8. K.C. Nguyen and D.S. Weiss. Denshi Shashin Gakkaishi, **27**, 2 (1988).
9. K.C. Nguyen and D.S. Weiss. J. Imaging Technol. **15**, 158 (1989).
10. J. Griffiths. *In* Colour and constitution of organic molecules. Academic Press, London. 1976. Chap. 2.
11. J. Griffiths. Dyes Pigm. **3**, 211 (1982).
12. M. Adachi and S. Nakamura. Dyes Pigm. **17**, 287 (1991).
13. E. Clar. *In* Polycyclic hydrocarbons. Vol. 2. Academic Press, London. 1964.
14. E. Clar and H. Frömmel. Chem. Ber. **82**, 46 (1949).
15. J.R. Dias. *In* Handbook of polycyclic hydrocarbons, part A, benzenoid hydrocarbons (physical sciences data). Elsevier, New York. 1987. p. 103.
16. E. Clar. *In* Polycyclic hydrocarbons. Vol. 1. Academic Press, London. 1964. pp. 423–465.
17. G.N. Vorozhtsov, N.S. Dokunikhin, and N.B. Feldblum. Zh. Org. Khim. **11**, 1517 (1975).
18. N.S. Dokunikhin, G.N. Vorozhtsov, F.I. Kichina, and N.B. Feldblum. Ger. Patent 2,318,285 (1974).
19. N.S. Dokunikhin, G.N. Vorozhtsov, F.I. Kichina, and N.B. Feldblum. Brit. Patent 1,385,596 (1975).
20. N.S. Dokunikhin, G.N. Vorozhtsov, F.I. Kichina, and N.B. Feldblum. U.S. Patent 4,166,181 (1979).
21. U. Anton, C. Göltner, and K. Müllen. Chem. Ber. **125**, 2325 (1992).
22. K. H. Koch and K. Müllen. Chem. Ber. **124**, 2091 (1991).
23. A. Bohnen, K. H. Koch, W. Lüttke, and K. Müllen. Angew. Chem. Int. Ed. Engl. **29**, 525 (1990).
24. Y. Nagao, Y. Abe, and T. Misono. Dyes Pigm. **16**, 19 (1991).
25. J.J. Gajewski, K.E. Gilbert, and J. McKelvey. *In* Advances in molecular modeling. Vol. 2. *Edited by* D. Liotta. JAI Press, New York. 1990. pp. 65–92.
26. M. Kardos. Ber. Dtsch. Chem. Ges. **46**, 2086 (1913).
27. R.O. Loutfy. Can. J. Chem. **59**, 549 (1981).

Can. J. Chem. Downloaded from www.nrcresearchpress.com by 65.111.164.53 on 09/08/12
For personal use only.

Design and synthesis of near-infrared absorbing pigments. II. Structure determination of aceanthrene green and derivatives

Denis Désilets, Peter M. Kazmaier, Richard A. Burt, and Gordon K. Hamer

Abstract: The reported structure of aceanthrene green, a pigment prepared by potassium hydroxide fusion of 1,9-anthracenedicarboxylic imide, was found to be incorrect. The structure of the pigment is reassigned to 7,8,15,16-dibenzo[*a,j*]perylenetetracarboxylic diimide on the basis of COSY, NOESY, and inversion–recovery ^{1}H NMR experiments. *N*-Alkyl- or *N*-phenyl-1,9-anthracenedicarboxylic imides, aceanthryleno[1,2-*b*]quinoxaline, and a benzimidazole derivative of 1,9-anthracenedicarboxylic anhydride were found to give the same dibenzo[*a,j*]perylene structure when reacted in potassium hydroxide. The electronic spectra of these derivatives is reported and it is shown that, as predicted by Pariser–Parr–Pople calculations, they absorb in the near-infrared. Finally, a mechanistic outline for the fusion is proposed on the basis of AM1 and frontier molecular orbital calculations.

Key words: photoconductor, near-infrared, aceanthrene green, alkalifusion, polycyclic aromatic hydrocarbon.

Résumé : On a trouvé que la structure proposée antérieurement pour l'acéanthrène vert, un pigment préparé par fusion de l'imide de l'acide anthracène-1,9-dicarboxylique avec de l'hydroxyde de potassium, est incorrecte. En se basant sur des expériences COSY, NOESY et d'inversion–récupération en RMN du ^{1}H on lui a réattribué la structure du diimide de l'acide dibenzo[*a,j*]pérylène-7,8,15,16-tétracarboxylique. On a trouvé que par réaction, par fusion avec de l'hydroxyde de potassium, les *N*-alkyl- ou *N*-phénylimides de l'acide anthracène-1,9-di- carboxylique, l'acéanthryléno[1,2-*b*]quinoxaline et un dérivé benzimidazole de l'anhydride de l'acide anthracène-1,9-dicarboxylique conduisent tous à la même structure dibenzo[*a,j*]pérylène. On rapporte les spectres électroniques de ces dérivés et il est montré, tel que prédit par des calculs de type Pariser–Parr–Pople, qu'ils absorbent dans le proche infrarouge. Enfin, en se basant sur des calculs d'orbitales moléculaires AM1 et frontières, on propose un aperçu du mécanisme pour la fusion.

Mots cles : photoconducteur, proche infrarouge, acéanthrène vert, fusion alcaline, hydrocarbure polycyclique aromatique.

[Traduit par la rédaction]

Introduction

Pigments absorbing in the near-infrared, at the gallium aluminium arsenide (GaAlAs) or indium phosphide (InP) diode laser wavelengths, have become the subject of an increasing number of studies. For example, near-infrared absorbing pigments are required for applications in xerographic printing, optical recording, and laser filters (1–4). As reported in the previous paper (5), diimide **1** (Scheme 1) or bis(benzimidazole) **2** derivatives of 1,6,7,16-dibenzo[*a,o*]perylenetetracarboxylic dianhydride are interesting candidates as near-infrared absorbing pigments for laser printing applications. Although no structure determination was ever published, the pigment aceanthrene green was reported by Chemical Abstract (6), Color Index (7) and other authors (8–10) as having the 1,6,7,16-dibenzo[*a,o*]perylenetetracarboxylic diimide structure **3**. Aceanthrene green was prepared by Kardos (11) in 1913 using a potassium hydroxide fusion on 1,9-anthracenedicarboxylic imide followed by an air oxidation. It has been considered industrially but has never achieved commercial importance (8, 9, 12–24). However, Kardos proposed structure **4** for the compound on the basis of elemental analysis and most probably from mechanistic considerations (10). It is worth mentioning that the stoichiometry of structure **3** agrees more closely with the reported elemental analysis than does that of structure **4**.

This paper will report on the structure of aceanthrene green and on some of its derivatives prepared by potassium hydroxide fusion. Studies directed towards an understanding of the mechanism of the fusion reaction will also be presented.

Received August 16, 1994.

D. Désilets,[1] P.M. Kazmaier, R.A. Burt, and G.K. Hamer. Xerox Research Centre of Canada, 2660 Speakman Drive, Mississauga, ON L5K 2L1, Canada.

[1] Author to whom correspondence may be addressed. Telephone: (416) 749-9300. Fax: (416) 745-5038. Present address: Apotex Research Inc., 400 Ormont Drive, Toronto, ON M9L 1N9, Canada.

Can. J. Chem. Downloaded from www.nrcresearchpress.com by 65.111.164.53 on 09/08/12
For personal use only.

Can. J. Chem. Downloaded from www.nrcresearchpress.com by 65.111.164.53 on 09/08/12
For personal use only.

Scheme 1

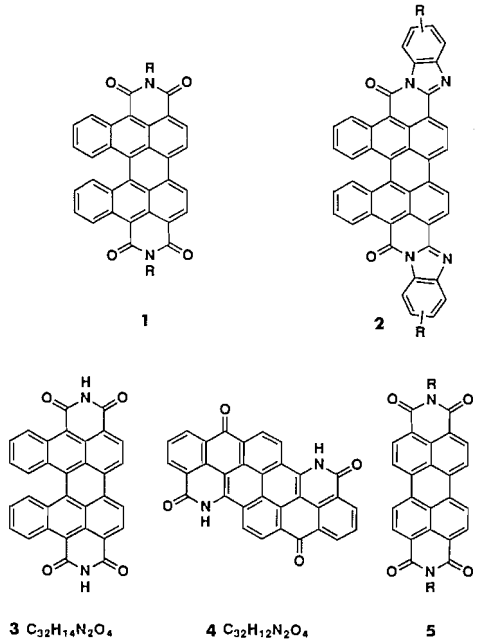

Scheme 2

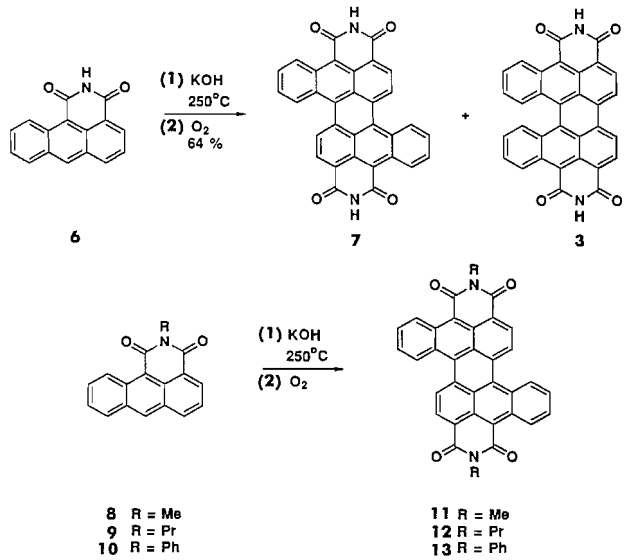

Results and discussion

Preparation and structure determination of aceanthrene green and derivatives

With the help of Pariser–Parr–Pople calculations (25, 26) it was found that aceanthrene green, as represented by structure **3** (Scheme 1), should absorb near 615 nm (5). This represents a bathochromic shift of 145 nm compared with the calculated absorption of the well-known diimide perylene pigment **5** at 470 nm. One can therefore envision derivatives of perylene pigments such as **1** or **2** that would be near-infrared absorbing.

The synthesis of aceanthrene green was repeated as originally described by Kardos (11). After preparing the imide **6** (Scheme 2), the fusion was carried out in molten potassium hydroxide at 250°C and it was followed by an air oxidation. The dark-green solid obtained after the reaction was found to be a mixture composed of the *trans*-dibenzoperylene[2] **7** and of the *cis*-dibenzoperylene[2] **3**, reported in the literature as aceanthrene green, in a ratio of 6.8:1. The assignment of the structure was done with the help of COSY (27, 28), NOESY (29, 30), and inversion–recovery (31) ^{1}H NMR experiments after the material was found to be soluble in a mixture of chloroform and trifluoroacetic acid. The COSY experiment (Fig. 1) shows the presence of a two-spin (H2 and H3 of the anthracene unit[3]) and a four-spin system (H5, H6, H7, and H8 of the anthracene unit) in both components, indicating that the position of the fusion is indeed at C4 and C9 in both isomers. A NOESY experiment showed an interaction between H3 and H5′ in the major isomer, but not in the minor one. This allows for the assignment of the *trans* structure to the major isomer. Furthermore, the inversion–recovery experiment (Fig. 2) shows that there are two slow- and two fast-relaxing protons for the major component, and one fast- and three slow-relaxing protons for the minor component. AM1 and PCMODEL calculations show that, for the *trans* isomer, the distance between H3 of one of the anthracene units and H5′ of the other unit is around 2.13–2.37 Å, which is less than the 2.48–2.46 Å distance between two vicinal protons. On the other hand, in the *cis* isomer, the distance between H5 and H5′ is calculated to be 2.74–3.05 Å, which is larger than the 2.48–2.46 Å distance between two adjacent protons. H3 and H3′ of this isomer were found to be 2.03–2.19 Å apart, which is shorter than the vicinal distance. Therefore, the major isomer can again be assigned to the *trans* structure with the fast-relaxing H3 and H5 and the slow-relaxing, isolated H2 and H8. The minor structure can be assigned to the *cis* isomer with the fast-relaxing H3 and the slow-relaxing H2, H5, and H8. The complete assignment of the ^{1}H NMR peaks can then be done in the following way. In the *trans* isomer, the COSY experiment leaves only one possibility for the assignment of the fast-relaxing protons at 8.74 ppm in a two-spin system and at 8.81 ppm in a four-spin system, and of the slow-relaxing protons at 9.05 ppm in a two-spin system and at 10.03 ppm in a four-spin system. These peaks can be assigned to H3, H5, H2, and H8, respectively. The remaining peaks at 7.97 and 8.10 can then be assigned to H6 and H7, respectively, with the help of the COSY spectrum. In the *cis* isomer, the fast-relaxing proton at 8.94 ppm and the slow-relaxing proton at 9.11 ppm, both in a two-spin system, can be assigned to H3 and H2, respectively. However, since both H5 and H8 are slow-relaxing in the *cis* isomer, the assignment of the peaks has to be done on the basis of the similar environment for H8, H7, and H6 and of the different environment for H5 in both isomers. Therefore, the peak at 7.53 ppm can be assigned to H6 (7.97 ppm for the *trans* isomer), the one at 7.98 ppm to H7 (8.10 ppm for the *trans* isomer), the one at 9.87 ppm to H8 (10.03 ppm for the

[2] Throughout this discussion, we will refer to *trans*-dibenzoperylene instead of dibenzo[*a,j*]perylene and to *cis*-dibenzoperylene instead of dibenzo[*a,o*]perylene.

[3] For simplicity, we will refer to the anthracene nucleus numbering for the explanation of the NMR results.

Fig. 1. 400 MHz ^{1}H–^{1}H COSY spectrum of aceanthrene green with NOESY insert. COSY mixing pulse, 45°; NOESY mixing time, 800 ms (ca. $1.4 \times t_1$).

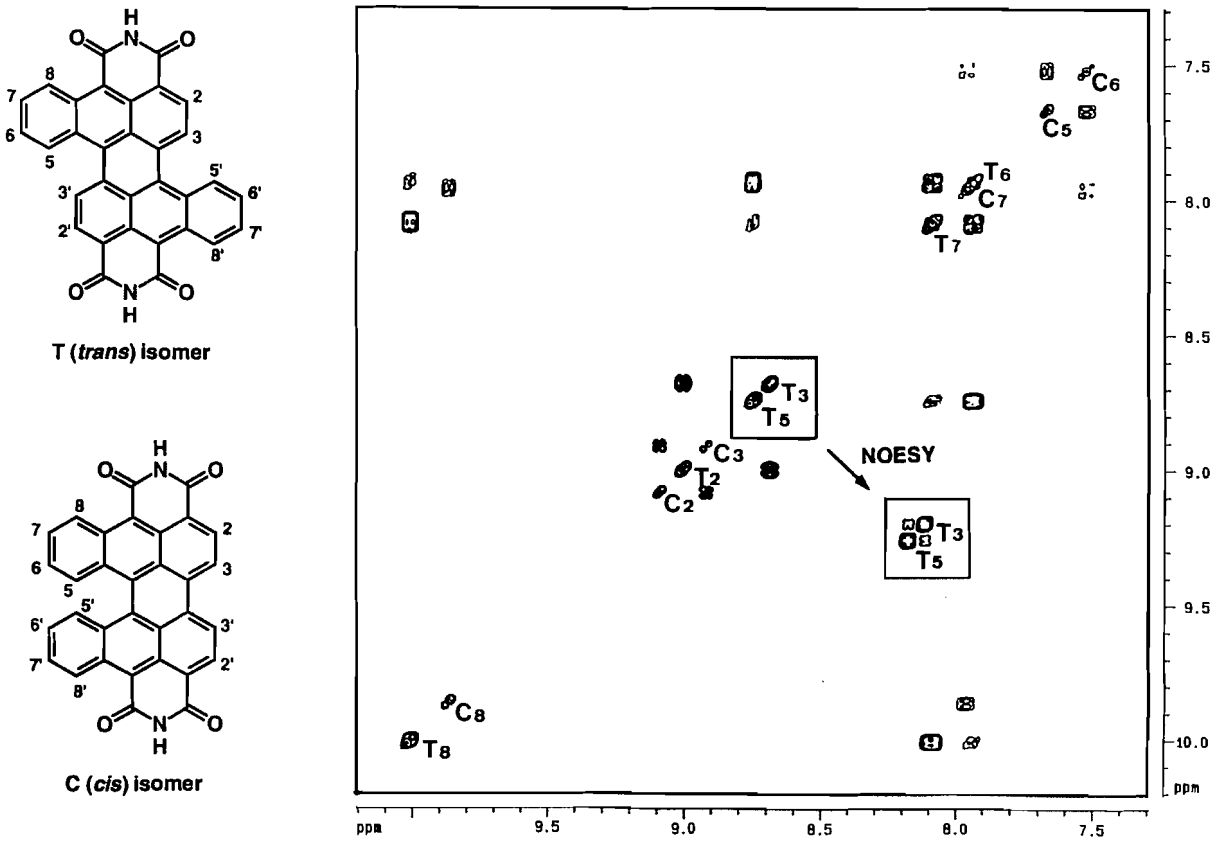

Fig. 2. 400 MHz ^{1}H NMR spectrum (bottom) and inversion–recovery (top; recovery delay, 600 ms) spectrum of aceanthrene green.

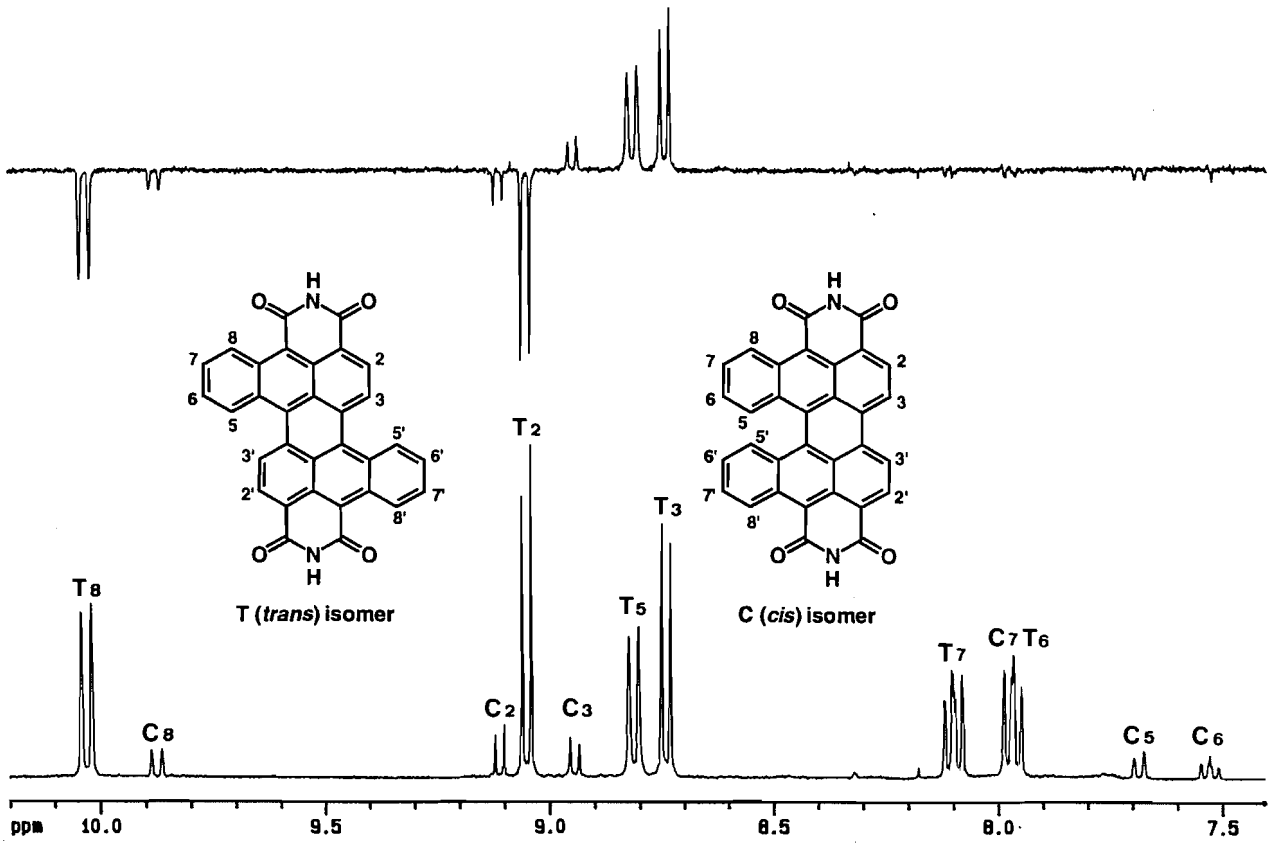

Can. J. Chem. Downloaded from www.nrcresearchpress.com by 65.111.164.53 on 09/08/12
For personal use only.

Scheme 3

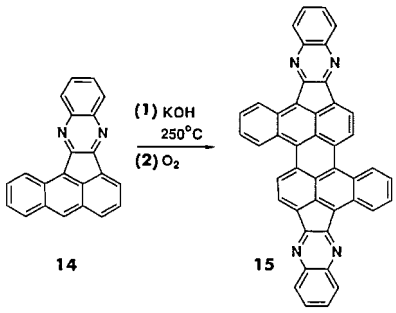

trans isomer), and the one at 7.68 ppm to H5 (8.81 ppm for the *trans* isomer). This assignment is further supported by the fact that H5 is expected to be faster relaxing than H8 due to the presence of an extra H5 proton from the other anthracene unit. The inversion–recovery experiment shows that this is indeed the case. The material was also characterized by mass spectrometry and infrared spectroscopy. The yield of the reaction was calculated to be 64% based on the assigned structure.

The reaction was also carried out on the *N*-methyl, *N*-propyl, and *N*-phenyl derivatives of 1,9-anthracenedicarboxylic imide (**8**–**10**). In contrast with the results obtained for the fusion of the simple imide, it was found that these derivatives give only the *trans* isomer with traces of impurities that could not be assigned to the *cis* isomer.

Potassium hydroxide fusion of anthracene derivatives is known elsewhere in the literature. In 1954, Bradley and Pexton reported their results on the fusion of the quinoxaline **14** (Scheme 3) (32) and, after obtaining the same material by fusion of the quinoxaline derivative brominated at position 10 of the anthracene moiety, they concluded that the compound was a dibenzo derivative having either the *cis* or the *trans* regiochemistry. After reinvestigating this reaction, it was found that, here again, only the *trans* isomer **15** is obtained. The structure of the fused quinoxaline was determined by the same series of experiments that were used for the structure determination of the diimides.

The COSY experiment (Fig. 3) showed the presence of two four-spin systems and one two-spin system. The two-spin system was assigned to H2 and H3 of the anthracene unit. The NOESY experiment showed an interaction between H3 and H5′, enabling the assignment of the *trans* structure to the material and of the two four-spin systems. As a matter of fact, both the two-spin and the four-spin systems of the anthracene unit were found in an almost identical position as those of the diimide derivative. The total assignment of the structure was done with the help of inversion–recovery experiments, as in the case of the diimide. Both H3 and H5 were found to be fast relaxing and H8 was found to be slow relaxing. However, in contrast with the results obtained for the diimide, H2 was found to be fast relaxing and this can be explained by the presence of a deuterium (from the deuterated trifluoroacetic acid) on the closest nitrogen of the quinoxaline ring. The protona-

Fig. 3. 400 MHz ^{1}H–^{1}H COSY spectrum of the quinoxaline **15** with NOESY insert. COSY mixing pulse, 45°; NOESY mixing time, 600 ms (ca. $1.2 \times t_1$)

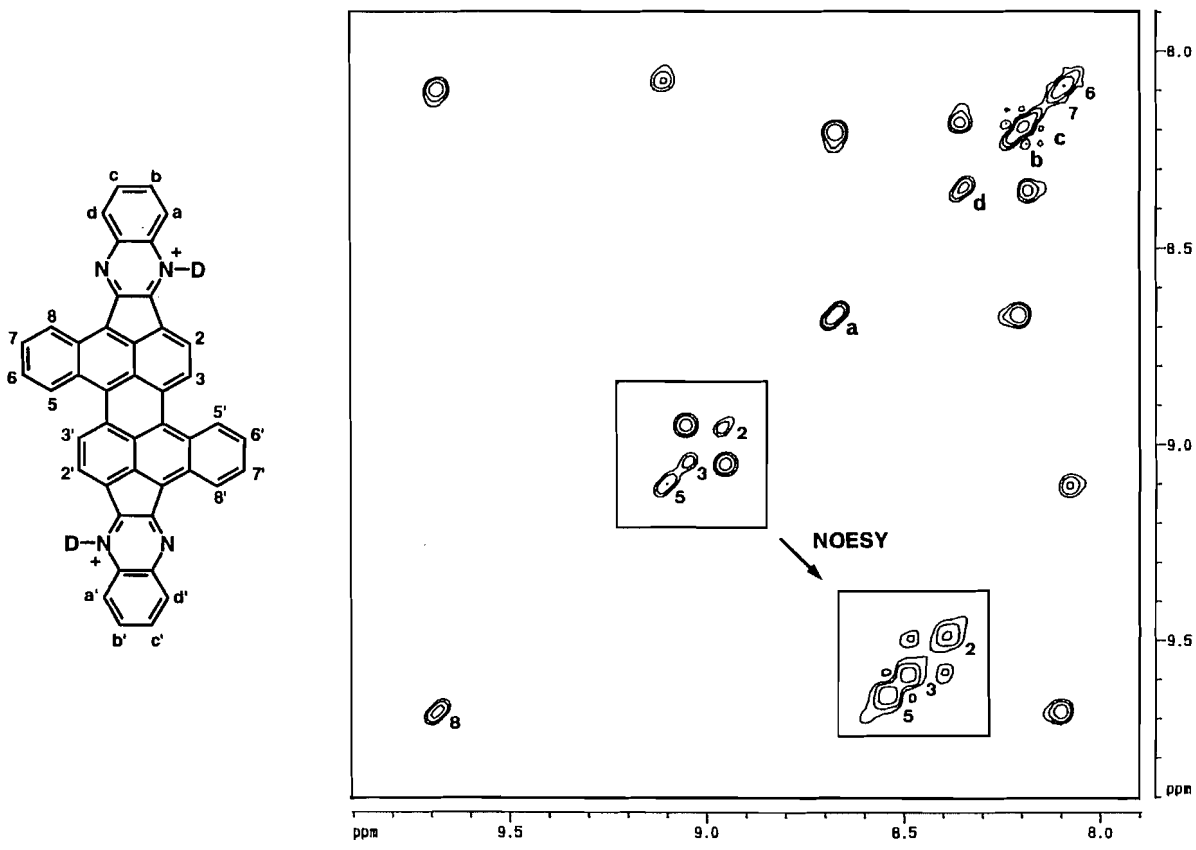

Can. J. Chem. Downloaded from www.nrcresearchpress.com by 65.111.164.53 on 09/08/12
For personal use only.

Can. J. Chem. Downloaded from www.nrcresearchpress.com by 65.111.164.53 on 09/08/12
For personal use only.

Scheme 4

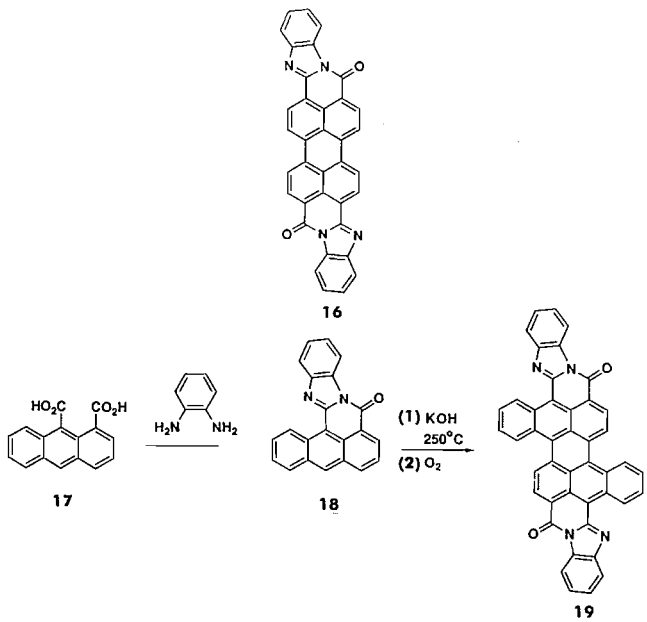

tion occurs at this position because protonation on the other nitrogen would lead to a severe interaction with the peri proton (H8) of the anthracene unit. This protonation allowed for the assignment of the protons on the benzene ring since the fast-relaxing doublet at 8.68 ppm could then be assigned to Ha (Fig. 3) of the benzene ring and the slow-relaxing one at 8.35 ppm to Hd.

The preparation of the bis(benzimidazole) derivative of *trans*-dibenzoperylenetetracarboxylic dianhydride, the near-infrared absorbing analog of the bis(benzimidazole) perylene pigment **16** (Scheme 4), required the synthesis of the benzimidazole derivative of 1,9-anthracenedicarboxylic anhydride. Although two regioisomers were expected on reaction with 1,2-phenylenediamine, surprisingly, only one isomer was obtained. The compound was identified as having structure **18** after characterization by ^{1}H NMR. The assignment was done in the following way. First, the H2 proton was identified at 8.90 ppm on the basis that it is the only doublet with only one minor coupling constant and also on the basis of similarity of the chemical shift when compared with the simple diimides. The carbonyl carbon was then identified in the ^{13}C NMR at 160.75 ppm, the imine carbon being at 150.06 ppm. The correlation between H2 and the carbonyl carbon was then demonstrated by a selective INAPT experiment (33, 34), thus showing that the carbonyl carbon is two atoms away from C2. With one isomer in hand, it was then possible to prepare the bis(benzimidazole) derivative of *trans*-dibenzoperylene by a route that yields one and only one regioisomer. This contrasts with the mixture of "*cis*" and "*trans*" bis(benzimidazole) perylenes obtained when 3,4,9,10-perylenetetracarboxylic dianhydride is reacted with 1,2-phenylenediamine in the industrial preparation of this pigment.

The benzimidazole derivative **18** was fused in molten potassium hydroxide as described earlier but, unfortunately, it was not possible to satisfactorily purify the bis(benzimidazole) derivative of *trans*-dibenzoperylene (**19**) due to its very low solubility. Solvent washes and extractions proved to be inadequate while attempts at purification by means of train sublimation (35) proved unsuccessful. However, TLC and doping ^{1}H NMR experiments showed that no starting material was present in the mixture. ^{1}H NMR in a mixture of trifluoroacetic acid and chloroform showed a complex spectrum, not only because the additional protons of the benzene ring showed a complex AA'BB' system but because of additional components in the mixture. Since overlapping of the peaks also seems to be more extensive than in the case of the other dibenzoperylenes, attempts were made to shift the position of the peaks with the addition of another cosolvent. Thus, addition of benzene was found to give the peak separation required for the structure determination. With the help of a COSY experiment in a mixture of trifluoroacetic acid, chloroform, and benzene (1:1:4) (Fig. 4), the *trans*-dibenzoperylene structure could again be assigned to the major component by the same process as described earlier.

A tentative assignment of the protons of the phenyl ring was done in the following way. It was assumed that, as in the case of the quinoxaline, a deuteration occurred on the heterocyclic benzimidazole ring, enabling a fast relaxation of the neighbouring protons at positions 8 and d. Inversion–recovery experiments showed that H8 was indeed fast relaxing and H2 was slow relaxing as opposed to both being slow relaxing as in the case of the diimides. The multiplet at 8.65 ppm, which was found to be slow relaxing, was assigned to Ha and the multiplet at 7.93 ppm, which was found to be fast relaxing, was assigned to Hd. This enabled the assignment of the lower field part of the multiplet at 7.45 ppm to Hc and the high-field part to Hb.

The material was also characterized by mass spectrometry and only the fused material was detected. The infrared spectrum of the material was very closely related to that of the starting material, further confirming the structure.

Electronic absorption spectra of the dibenzoperylene derivatives

As discussed earlier, the electronic absorption of the dibenzoperylene derivatives is predicted to be shifted towards the near-infrared when compared to that of simple perylene derivatives. For example, Pariser–Parr–Pople calculations (5, 25, 26) predict that the *trans*-dibenzoperylenetetracarboxylic diimide derivative should absorb near 605 nm whereas the calculated absorption of the perylene analog is near 470 nm. This represents a calculated shift of 135 nm towards the near-infrared. The electronic spectra of the *trans*-dibenzoperylene derivatives were measured in 1,2,4-trichlorobenzene. The spectra of the *N,N'*-dipropyl diimide and of the bis(benzimidazole) *trans*-dibenzoperylene derivatives are presented in Fig. 5 and compared with that of *N,N'*-diethyl-3,4,9,10-perylenetetracarboxylic diimide (**5**, R = Et). The extinction coefficient of the *N,N'*-dipropyl derivative at 701 nm was found to be 35 300 L mol^{-1} cm^{-1}, which is very similar to the value for the 546 nm band of the corresponding hydrocarbon, *trans*-dibenzoperylene, reported as 31 600 L mol^{-1} cm^{-1} in MeOH (36). This value of the extinction coefficient is considerably lower than those reported for simple perylene diimide derivatives. For example, the value for the 524 nm peak of *N,N'*-dipropyl-3,4,9,10-perylenetetracarboxylic diimide is 78 730 L mol^{-1} cm^{-1} when measured in chlorofom (37). These lower values reflect the fact that the dibenzoperylene nucleus is distorted

Fig. 4. 400 MHz ^1H–^1H COSY spectrum of the bis(benzimidazole) **19** with NOESY insert. COSY mixing pulse, 45°; NOESY mixing time, 500 ms (ca. $1.2 \times t_1$).

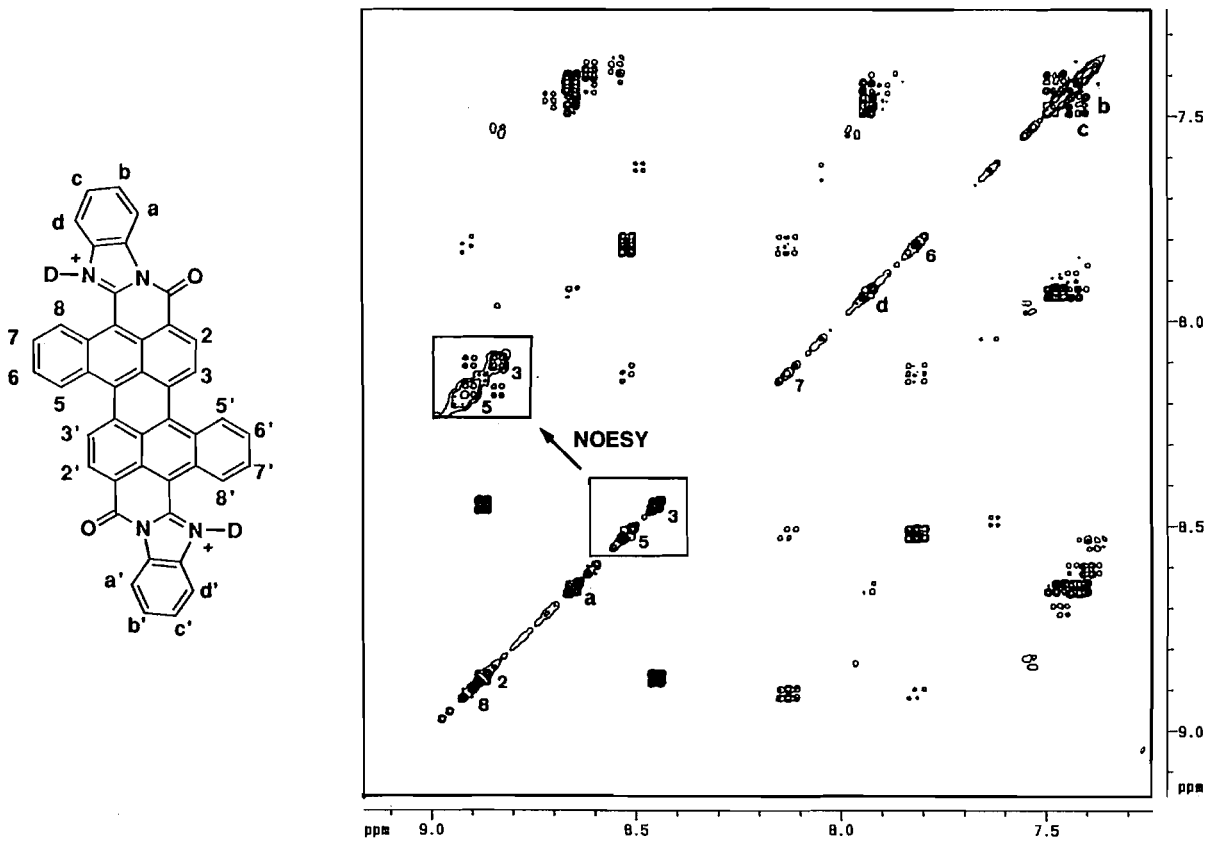

from planarity, therefore having a reduced amount of overlap between the two π-systems of the individual anthracene units. The *N,N'*-dimethyl and *N,N'*-diphenyl diimide derivatives had spectra that were almost identical to that of the *N,N'*-dipropyl derivative whereas the simple diimide derivative was found to be insoluble in 1,2,4-trichlorobenzene. As predicted by the calculations, the absorption of the *trans*-dibenzoperylene derivatives is shifted towards the near-infrared, compared to that of the perylene derivative, as seen in Fig. 5. The experimental bathochromic shift of the absorption around 170 nm is larger than the 135 nm shift calculated on the basis of a simple wavelength shift, but very close to the 180 nm shift calculated on the basis of a constant energy shift (38) obtained from the difference between the calculated absorption and the experimental absorption in 1,2,4-trichlorobenzene of the perylene diimide analog. There is an additional 85 nm shift towards the near-infrared for the absorption of the bis(benzimidazole) derivative of *trans*-dibenzoperylene **19** at 785 nm. This absorption is now well within the emission wavelength spectrum of the gallium aluminium arsenide semiconductor laser.

Fig. 5. Comparison of the electronic absorption spectrum of a perylene diimide with those of the dibenzoperylene derivatives (normalized spectra).

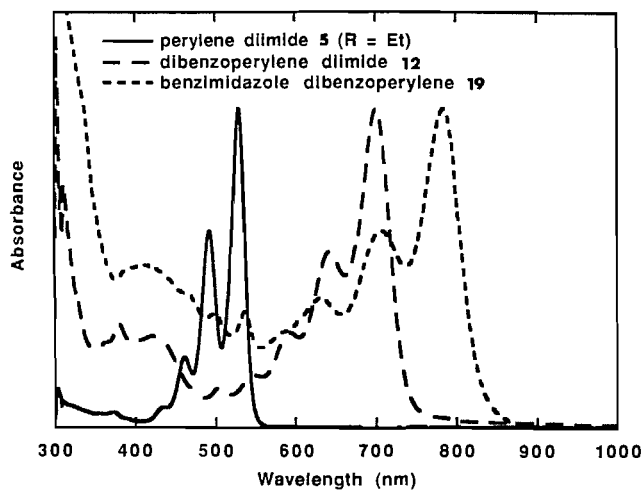

Theoretical studies on the mechanism of the reaction

The preferential formation of the *trans* isomer over the *cis* analog deserves some comment. Even though the *cis* isomer of dibenzoperylene looks more hindered than the *trans* isomer, molecular mechanics and AM1 calculations show that they are of comparable stability and that one is not significantly more strained than the other. If one accepts this evidence for comparable thermodynamic stability then the answer to the variable selectivity in the fusion reaction must have its origin in kinetic control.

With the help of molecular orbital calculations, an attempt was made to develop a mechanistic outline for the reaction that would account for the preferential formation of the *trans*-

Can. J. Chem. Downloaded from www.nrcresearchpress.com by 65.111.164.53 on 09/08/12
For personal use only.

Table 1. Value of the heats of formation for the different arylides obtained from AM1 calculations.

Position of the anion	H_f (imide **6**) (kcal/mol)	H_f (*N*-methyl imide **8**) (kcal/mol)	H_f (quinoxaline **14**) (kcal/mol)	H_f (benzimidazole **18**) (kcal/mol)
C2	74.3	19.0	166.4	124.4
C3	63.6	18.9	167.8	125.2
C4	61.7	14.1	164.2	120.9
C5	61.4	22.0	169.8	130.4
C6	61.3	26.6	173.5	135.3
C7	66.0	25.9	172.8	134.7
C8	76.0	31.3	177.3	137.8
C10	58.2	9.92	159.2	117.8
Ca	—	—	173.3	143.6
Cb	—	—	171.5	139.6
Cc	—	—	171.6	142.2
Cd	—	—	172.9	139.2

Fig. 6. (*A*) AM1-generated HOMO of the 10-arylide derivative of *N,N'*-dimethyl-*trans*-dibenzoperylene **8**. (*B*) AM1-generated LUMO of *N,N'*-dimethyl-*trans*-dibenzoperylene **8**.

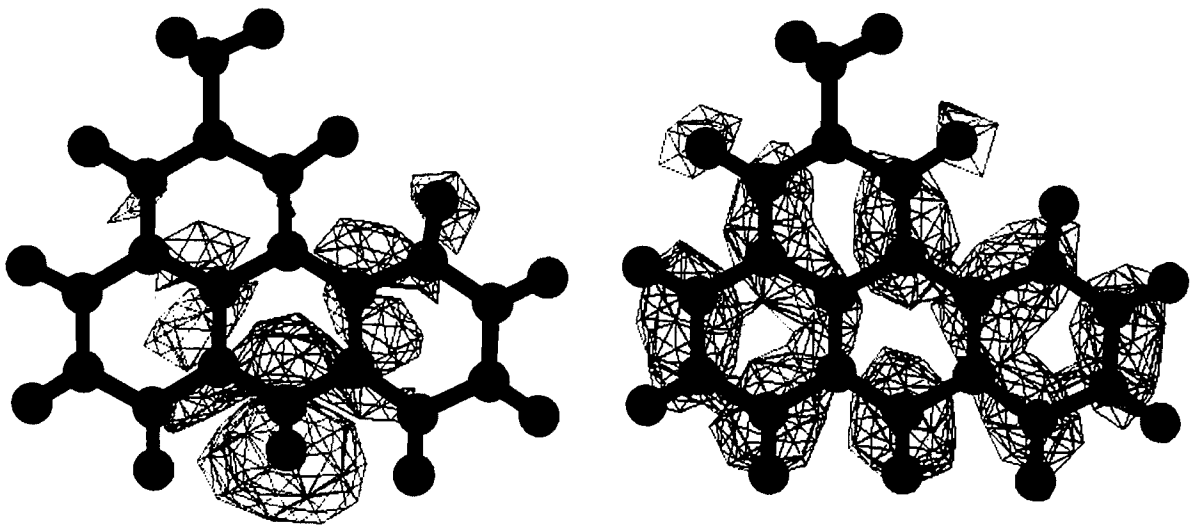

dibenzoperylene. As the first step of the reaction, it is reasonable to consider the formation of an arylide. To locate the site of proton abstraction on the ring, the heats of formation of each of the different arylides for the three systems studied were calculated. The calculations were performed using the AM1 parameters (39) and the results are presented in Table 1. In the case of the imide, the formation of a dianion was considered because of the higher acidity of the imide proton.

The results show that proton abstraction at position 10 is favored in all cases, followed by abstraction at position 4. Furthermore, in all cases, the difference is large enough (greater or equal than 3.1 kcal/mol) to account for proton abstraction at position 10 as a major reaction even at 250°C.

It was then assumed that the next step in the reaction would involve an attack of the HOMO of the anion on the LUMO of a neutral anthracene unit. Figure 6 shows the HOMO of the arylide and the LUMO of the neutral unit of the *N*-methyl derivative calculated using the semiempirical AM1 scheme in MOPAC. As expected, the HOMO of the anion is highly localized at position 10, which is the site of formation of the anion. As can be seen by looking at the LUMO, position 4 of the anthracene is favored over position 10 for a vinylogous Michael-type addition. Carbon 4 is connected to the carbonyl carbon through carbons 4a, 9a, and 1 whereas carbon 10 is isolated. The atomic orbitals situated on carbons 4, 4a, 9a, 1, and the C=O moiety are the most significant contributors to the LUMO orbital of the anthracene imide derivative. A mechanistic outline such as the one presented in Scheme 5 can then be proposed to explain the formation of the *trans* isomer. Similar results are obtained when the calculations are performed on the bis(benzimidazole) and bis(quinoxaline) derivatives.

If the anion were to form at position 4 instead of position 10, then the *cis* isomer would be obtained. This is probably why a larger amount of the *cis* isomer is formed when the simple

Can. J. Chem. Downloaded from www.nrcresearchpress.com by 65.111.164.53 on 09/08/12
For personal use only.

Scheme 5

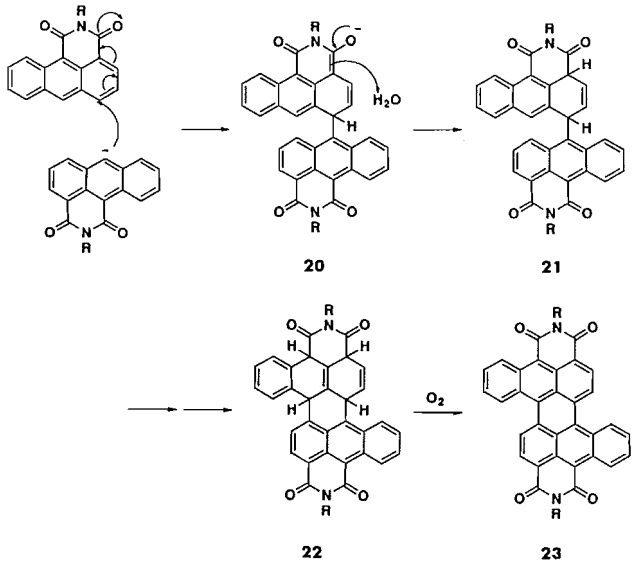

anthracene imide is fused, since the difference in heats of formation of the anion between positions 10 and 4 is smaller compared with the other anthracene derivatives, as shown in Table 1 (3.5 kcal/mol for the imide derivative vs. 4.2 kcal/mol for the methyl derivative and 5.0 kcal/mol for the bis(quinoxaline) derivative). This smaller difference in the heats of formation favouring the anion at position 10 can also be used to explain the less selective formation of the bis(benzimidazole) derivative **19** since the value is 3.1 kcal/mol in favor of the anion formation at position 10.

Conclusion

Potassium hydroxide fusions have been used extensively in the dye and pigment field. With the advent of mass spectrometry and powerful NMR techniques, it is now possible to reinvestigate the structure of the materials obtained. Since the reaction described in this paper leads to reasonably pure products, it might be useful to reinvestigate previously obtained materials that were not considered useful at the time because of an unknown structure. One might gain a more profound understanding of the mechanism of the fusion and apply these principles to the preparation of highly complex pigments. Presently, synthetic routes leading to these types of pigments are limited due to the low solubility of the intermediates obtained, which inhibits further manipulation. The advantage of the potassium hydroxide fusion route is that one deals with simple, soluble intermediates up to the last step, which then gives a reasonably pure product. The results of this work show that this methodology is useful for the preparation of near-infrared-absorbing perylene type of pigments. Although it was not possible to prepare the analytically pure bis(benzimidazole) derivative of *trans*-dibenzoperylenetetracarboxylic dianhydride, ^{1}H NMR analysis, mass spectrometry, and infrared spectroscopy show that the material is present as a major component in the mixture.

Finally, the results on the investigation of the mechanism of the reaction demonstrate that theoretical calculations can be applied to the determination of a mechanistic outline. However, since these are preliminary studies, more elaborate calculations taking into effect the high temperature and polarity of the molten potassium hydroxide media have to be done in order to confirm the theory.

Computational

AM1 calculations were performed using the parameters reported by Dewar et al. (39). Pariser–Parr–Pople calculations were performed using parameters based on those published by Griffiths (26). Molecular mechanics calculations were done using the MMX parameters reported by Gajewski et al. (40).

Experimental

Melting points were determined using a Thomas–Hoover or an Electrothermal capillary melting point apparatus and are uncorrected. Mass spectrometry was carried out with a Finnigan 4500 MAT instrument by the electron impact method. IR spectra were recorded on a Nicolet 20DX FT-IR spectrophotometer. Electronic spectra measurements were acquired using a Cary 5 UV–Vis–NIR spectrophotometer. NMR spectra were recorded at ambient temperature (27°C) on a Bruker AMX-400 spectrometer operating at 400.14 MHz for ^{1}H and 100.62 MHz for ^{13}C using a 5 mm ^{1}H/^{13}C dual probe. Samples (4–8 mg/mL) were prepared in $CDCl_3$ or CF_3COOD–$CDCl_3$, 1:1 v/v, containing a small amount of TMS as an internal chemical shift reference; C_6D_6 was used as a cosolvent for **19**. The ^{1}H spectra were measured at a digital resolution of 0.08–0.16 Hz/point with a 45° pulse and a 5 s recycle time. Recovery times between 100 ms and 1.2 s with a recycle delay of 10 s were employed for inversion–recovery (31) relaxation experiments. The ^{13}C–{^{1}H} selective INEPT (INAPT) spectra were recorded using a pulse sequence adapted from Bax et al. (33, 34); the ^{1}H selective excitation was provided by a rectangular pulse of 25 Hz nominal width (90° pulse, 10 ms). Standard pulse sequences and phase cycling schemes (41) were used to record ^{1}H–^{1}H COSY (27, 28) and phase-sensitive (TPPI) NOESY (29, 30) spectra. The COSY mixing pulse was 45° (28) and the NOESY mixing time was 500–800 ms, depending on the T_1 values of the sample; the recycle delay was 3 s. For compounds **7** and **15**, a total of 256 1K FIDs of 4 (COSY) or 16 scans each (NOESY) were acquired; for **19**, 512 2K FIDs of 16 scans each were acquired for both COSY and NOESY. The data sets were multiplied in both t_1 and t_2 dimensions by a cosine-bell squared (COSY) or sine-bell squared (NOESY) function and zero-filled once in t_1. The COSY matrix was processed in magnitude mode and the NOESY-TPPI matrix in phase-sensitive mode. The contour plots shown in Fig. 1,3, and 4 have been symmetrized for clarity of presentation.

1,9-Anthracenedicarboxylic imide (6)

1,9-Anthracenedicarboxylic anhydride (11) (5.00 g), ammonium acetate (250 g), and water (25 mL) were slowly heated to 110°C under an ammonia atmosphere. Heating was continued for 2 h and the melt was cooled to room temperature. The solid mass was added to 1 L of water. The resulting solid was filtered and washed with water. Train sublimation (35) of the crude material gave the imide **6** (3.98 g, 80%) as orange needles; mp 302–304°C (lit. (11) mp 293–294°C). IR (KBr) ν_{max}: 3181, 3067, 1688, 1674, 1564, 1532, 1399, 1368, 1318, 1235,

Can. J. Chem. Downloaded from www.nrcresearchpress.com by 65.111.164.53 on 09/08/12
For personal use only.

Can. J. Chem. Downloaded from www.nrcresearchpress.com by 65.111.164.53 on 09/08/12
For personal use only.

909, 860, 799, 733, 500 cm^{-1}. ^1H NMR ($CDCl_3$; the assignment was done by decoupling and inversion–recovery (31) experiments) δ: 7.68 (ddd, 1H, J = 8.4, 6.6, and 0.9 Hz, H6), 7.78 (dd, 1H, J = 8.4 and 7.1 Hz, H3), 7.88 (ddd, 1H, J = 9.1, 6.7, and 1.4 Hz, H7), 8.16 (d, 1H, J = 8.5 Hz, H5), 8.44 (dd, 1H, J = 8.4 and 0.9 Hz, H4), 8.77 (dd, 1H, J = 7.0 and 1.3 Hz, H2), 8.92 (s, 1H, H10), 10.01 (dd, 1H, J = 9.2 and 0.8 Hz, H8) ppm.

N-Methyl-1,9-anthracenedicarboxylic imide (8)

A suspension of 1,9-anthracenedicarboxylic acid (42) (4.58 g, 17.2 mmol) in 1-methyl-2-pyrrolidinone (90 mL) under nitrogen was heated to 125°C for 30 min to enable complete conversion to the anhydride. The mixture was cooled to 30°C and 40% aqueous methylamine (8.9 mL, 105 mmol) was added dropwise. The solution was heated to 75°C for 45 min and poured into 750 mL water with stirring. After filtration, the solid was washed with water and dried. Recrystallization from acetone yielded the imide **8** (2.33 g, 52%) as orange needles; mp 229–230°C. IR (KBr) ν_{max}: 1690, 1651, 1563, 1534, 1437, 1408, 1318, 1279, 1098, 897, 799, 745, 731, 525 cm^{-1}. ^1H NMR ($CDCl_3$) δ: 3.61 (s, 3H, NCH_3), 7.62 (ddd, 1H, J = 8.4, 6.6, and 0.8 Hz, H6), 7.68 (dd, 1H, J = 8.3 and 7.1 Hz, H3), 7.80 (ddd, 1H, J = 9.1, 6.7, and 1.4 Hz, H7), 8.06 (d, 1H, J = 8.4 Hz, H5), 8.28 (dd, 1H, J = 8.4 and 0.9 Hz, H4), 8.71 (dd, 1H, J = 7.0 and 1.2 Hz, H2), 8.73 (s, 1H, H10), 9.93 (dd, 1H, J = 9.1 and 0.5 Hz, H8) ppm.

N-Propyl-1,9-anthracenedicarboxylic imide (9)

A suspension of 1,9-anthracenedicarboxylic acid (42) (6.50 g, 24.4 mmol) in 1-methyl-2-pyrrolidinone (200 mL) under nitrogen was heated to 125°C for 15 min to enable complete conversion to the anhydride. A solution of *n*-propylamine (8.80 g, 149 mmol) in 1-methyl-2-pyrrolidinone (70 mL) was slowly added and heating was continued for 45 min. The mixture was then cooled to room temperature and diluted with 600 mL water while stirring. The pH was adjusted to 3 with 2 M hydrochloric acid and the resulting solid was filtered, washed with water, and dried. Recrystallization from ethanol yielded the imide **9** (6.73 g, 95%) as orange needles; mp 170–171°C. IR (KBr) ν_{max}: 1684, 1647, 1564, 1435, 1402, 1372, 1352, 1217, 1109, 895, 795, 739 cm^{-1}. ^1H NMR ($CDCl_3$) δ: 1.07 (t, 1H, J = 7.4 Hz, CH_3), 1.84 (sextet of multiplet, 2H, J = 7.5 and <1.8 Hz, CH_2), 4.24 (m, 2H, NCH_2), 7.61 (ddd, 1H, J = 8.4, 6.6, and 1.1 Hz, H6), 7.71 (dd, 1H, J = 8.4 and 7.1 Hz, H3), 7.81 (ddd, 1H, J = 9.2, 6.6, and 1.5 Hz, H7), 8.08 (doublet of quintet, 1H, J = 8.4 and 0.7 Hz, H5), 8.31 (ddd, 1H, J = 8.4, 1.3, and 0.6 Hz, H4), 8.73 (dd, 1H, J = 7.1 and 1.3 Hz, H2), 8.77 (s, 1H, H10), 9.98 (ddd, 1H, J = 9.1, 1.8, and 0.9 Hz, H8) ppm.

N-Phenyl-1,9-anthracenedicarboxylic imide (10)

A suspension of 1,9-anthracenedicarboxylic acid (42) (4.50 g, 16.9 mmol) in 1-methyl-2-pyrrolidinone (180 mL) under nitrogen was heated to 125°C for 15 min to enable complete conversion to the anhydride. Aniline (9.60 g, 103 mmol) was slowly added and the solution was stirred at 180°C. Two additional portions of aniline (9.60 g, 103 mmol) were added after 7 h and 23 h. After 28 h of heating, the mixture was cooled, poured into 600 mL water, and the pH was adjusted to 3 with 6 M hydrochloric acid. The solid was filtered, washed with water, and dissolved in 800 mL dichloromethane. The dichloromethane was extracted with 0.5 M sodium hydroxide (2 × 250 mL), water (3 × 250 mL), 0.5 M hydrochloric acid (1 × 250 mL), and water (3 × 250 mL). The dichloromethane fraction was dried over magnesium sulfate and evaporated. The solid obtained was recrystallized from acetone to give the imide **10** (3.07 g, 56%) as greenish-yellow needles; mp 272–274°C. IR (KBr) ν_{max}: 1694, 1647, 1563, 1370, 1319, 1217, 735, 706 cm^{-1}. ^1H NMR ($CDCl_3$) δ: 7.40 (m, 2H, phenyl), 7.52 (m, 1H, phenyl), 7.61 (m, 2H, phenyl), 7.65 (ddd, 1H, J = 8.3, 6.7, and 1.1 Hz, H6), 7.79 (dd, 1H, J = 8.4 and 7.0 Hz, H3), 7.81 (ddd, 1H, J = 9.2, 6.6, and 1.4 Hz, H7), 8.16 (doublet of quintet, 1H, J = 8.4 and 0.7 Hz, H5), 8.44 (ddd, 1H, J = 8.4, 1.3, and 0.5 Hz, H4), 8.82 (dd, 1H, J = 7.1 and 1.3 Hz, H2), 8.92 (s, 1H, H10), 9.96 (ddd, 1H, J = 9.2, 1.9, and 0.9 Hz, H8) ppm.

Benzimidazole derivative of 1,9-anthracenedicarboxylic anhydride (18)

1,9-Anthracenedicarboxylic acid (42) (16.2 g, 60.8 mmol) was refluxed in acetic acid (700 mL) for 15 min under argon. 1,2-Phenylenediamine (19.7 g, 183 mmol) was added. After refluxing for 4 h, another portion of 1,2-phenylenediamine (19.7 g, 183 mmol) was added, followed by another (10.0 g, 9.25 mmol) after 22 h. The reaction mixture was cooled after 24 h and most of the acetic acid was evaporated. The residue was dissolved in 1.5 L dichloromethane and extracted with 1 M hydrochloric acid (3 × 350 mL), water (2 × 250 mL), saturated sodium bicarbonate (3 × 250 mL), brine (2 × 250 mL), and finally water (250 mL). The dichloromethane phase was dried on magnesium sulfate and evaporated to give the crude material (15.8 g). Purification by flash chromatography yielded the desired benzimidazole derivative **18** (10.6 g, 54%) as orange-red needles; mp 233–234°C. IR (KBr) ν_{max}: 1690, 1559, 1520, 1451, 1402, 1360, 1329, 750, 714 cm^{-1}. ^1H NMR ($CDCl_3$) δ: 7.51 (m, 2H, phenylene), 7.64 (ddd, 1H, J = 8.4, 6.6, and 1.1 Hz, H6), 7.75 (dd, 1H, J = 8.3 and 7.0 Hz, H3), 7.88 (ddd, 1H, J = 9.1, 6.6, and 1.4 Hz, H7), 7.98 (m, 1H, phenylene), 8.09 (doublet of quintet, 1H, J = 8.4 and 0.7 Hz, H5), 8.39 (ddd, 1H, J = 8.4, 1.3, and 0.6 Hz, H4), 8.64 (m, 1H, phenylene), 8.68 (s, 1H, H10), 8.90 (dd, 1H, J = 7.1 and 1.3 Hz, H2), 10.62 (ddd, 1H, J = 9.1, 1.8, and 0.9 Hz, H8) ppm. ^{13}C NMR ($CDCl_3$) δ: 114.80, 116.05, 120.23, 123.09, 125.30, 125.48, 125.72, 126.30, 126.73, 127.94, 129.46, 129.54, 130.46, 131.02, 131.44, 132.49, 133.40, 133.64, 136.52, 144.10, 150.06, 160.75 ppm.

Aceanthrene green (7) (7,8,15,16-dibenzo[*a*,*j*]perylenetetracarboxylic diimide; *trans* isomer) contaminated with 1,6,7,16-dibenzo[*a*,*o*]perylenetetracarboxylic diimide (3) (*cis* isomer)

Potassium hydroxide (12.0 g, 214 mmol) was mixed with water (1.80 g, 100 mmol) to form a thick paste. The imide **6** (3.00 g, 12.1 mmol) was added and the mixture was heated to 250–260°C in a zirconium crucible using a sand bath. The mixture was stirred with a spatula every 15 min and after 90 min of heating, it was slowly added to water (60 mL). Air was bubbled into the suspension while stirring. After 6 h, the mixture was neutralized and filtered. The resulting solid was slurried several times in water and then acetone to yield aceanthrene green (1.91 g, 64%); mp >300°C. IR (KBr) ν_{max}: 1680,

Can. J. Chem. Downloaded from www.nrcresearchpress.com by 65.111.164.53 on 09/08/12
For personal use only.

1584, 1564, 1535, 1427, 1385, 1331, 1279, 1262, 1235 cm^{-1}. UV–Vis–NIR (H_2SO_4) λ_{max} (ϵ): 867 (26 700), 494 (14 900), 420 (10 800), 269 (45 000) 211 nm (61 000 L mol^{-1} cm^{-1}). ^1H NMR (CF_3CO_2D–$CDCl_3$ 1:1), the ratio of the *trans* (**7**) to *cis* (**3**) isomer was found to be 6.8:1, δ: 7.53 (ddd, 2H, J = 8.7, 6.7, and 1.1 Hz, H10, H13 of *cis* isomer), 7.68 (doublet of multiplet, 2H, J = 8.7 Hz, H11, H12 of *cis* isomer), 7.97 (ddd, 2H, J = 8.7, 6.8, and 1.2 Hz, H3, H11 of *trans* isomer), 7.98 (2H, hidden under H3, H11 of *trans* isomer, H9, H14 of *cis* isomer), 8.10 (ddd, 2H, J = 9.1, 6.8, and 1.3 Hz, H2, H10 of *trans* isomer), 8.74 (d, 2H, J = 7.8 Hz, H5, H13 of *trans* isomer), 8.81 (d, 2H, J = 8.5 Hz, H4, H12 of *trans* isomer), 8.94 (d, 2H, J = 8.0 Hz, H3, H4 of *cis* isomer), 9.05 (d, 2H, J = 7.9 Hz, H6, H14 of *trans* isomer), 9.11 (d, 2H, J = 7.9 Hz, H2, H5 of *cis* isomer), 9.87 (d, 2H, J = 8.9 Hz, H8, H15 of *cis* isomer), 10.03 (d, 2H, J = 9.1 Hz, H1, H9 of *trans* isomer) ppm. MS *m/z* (%): 490 (100, M^+), 475 (1, M^+−NH). Anal. calcd. for $C_{32}H_{14}N_2O_4$: C 78.36, H 2.88, N 5.71%; found: C 79.38, H 3.08, N 5.49%; Kardos (11): C 78.52, H 3.14, N 5.75%.

N,N'-Dimethyl-7,8,15,16-dibenzo[*a,j*]perylenetetracarboxylic diimide (11)

A process similar to that described for the preparation of aceanthrene green was used for the fusion of the imide **8**, and the diimide **11** was obtained in 28% yield; mp >300°C. IR (KBr) ν_{max}: 1682, 1645, 1564, 1537, 1433, 1385, 1339, 1289, 1100, 775 cm^{-1}. UV–Vis–NIR (1,2,4-trichlorobenzene) λ_{max}: 701, 642, 418 nm. ^1H NMR (CF_3CO_2D–$CDCl_3$ 1:1) δ: 3.83 (s, 6H, 2 × NCH_3), 7.91 (ddd, 2H, J = 8.7, 6.8, and 1.0 Hz, H3, H11), 8.05 (ddd, 2H, J = 9.1, 6.8, and 1.1 Hz, H2, H10), 8.70 (d, 2H, J = 7.9 Hz, H5, H13), 8.78 (d, 2H, J = 8.4 Hz, H4, H12), 8.99 (d, 2H, J = 7.9 Hz, H6, H14), 9.93 (d, 2H, J = 8.9 Hz, H1, H9) ppm.

N,N'-Dipropyl-7,8,15,16-dibenzo[*a,j*]perylenetetracarboxylic diimide (12)

A process similar to that described for the preparation of aceanthrene green was used for the fusion of the imide **9** and the diimide **12** was obtained in 29% yield; mp >300°C. IR (KBr) ν_{max}: 1684, 1647, 1564, 1433, 1387, 1325, 1109, 775 cm^{-1}. MS *m/z* (%): 574 (67, M^+), 532 (10, M^+ − $CH_3CH{=}CH_2$), 490 (24, M^+ − $(CH_3CH{=}CH_2)_2$). An analytical sample can be obtained in 60% yield after purification by flash chromatography using chloroform. UV–Vis–NIR (1,2,4-trichlorobenzene) λ_{max} (ϵ): 701 (35 300), 642 (19 400), 592 (10 500), 549 (5700), 503 (4300), 422 (10 100), 380 (11 400), 312 nm (26 900 L mol^{-1} cm^{-1}). ^1H NMR (CF_3CO_2D–$CDCl_3$ 1:1) δ: 1.17 (t, 6H, J = 7.4 Hz, 2 × CH_3), 1.96 (sextet of multiplet, 4H, J = 7.7 and <2 Hz, 2 × CH_2), 4.41 (m, 4H, 2 × NCH_2), 7.91 (ddd, 2H, J = 8.6, 6.8, and 1.1 Hz, H3, H11), 8.05 (ddd, 2H, J = 9.1, 6.7, and 1.2 Hz, H2, H10), 8.69 (d, 2H, J = 7.9 Hz, H5, H13), 8.77 (d, 2H, J = 8.4 Hz, H4, H12), 8.98 (d, 2H, J = 7.9 Hz, H6, H14), 9.92 (d, 2H, J = 8.6 Hz, H1, H9) ppm. Anal. calcd. for $C_{38}H_{26}N_2O_4$: C 79.43, H 4.56, N 4.88, O 11.14%; found: C 78.89, H 4.51, N 4.47, O 11.20%.

N,N'-Diphenyl-7,8,15,16-dibenzo[*a,j*]perylenetetracarboxylic diimide (13)

A process similar to that described for the preparation of aceanthrene green was used for the fusion of the imide **10**. Purification of the crude, slightly soluble material by flash chromatography using chloroform gave the diimide **13** in 8% yield; mp >300°C. IR (KBr) ν_{max}: 1692, 1657, 1564, 1420, 1387, 1331, 1211, 745 cm^{-1}. UV–Vis–NIR (1,2,4-trichlorobenzene) λ_{max}: 704, 645, 593, 548, 504, 430, 381 nm. ^1H NMR (CF_3CO_2D–$CDCl_3$ 1:1) δ: 7.44 (m, 4H, phenyl), 7.64 (m, 6H, phenyl), 7.95 (ddd, 2H, J = 8.7, 6.8, and 1.2 Hz, H3, H11), 8.04 (ddd, 2H, J = 9.1, 6.7, and 1.3 Hz, H2, H10), 8.75 (d, 2H, J = 7.8 Hz, H5, H13), 8.85 (d, 2H, J = 8.6 Hz, H4, H12), 9.08 (d, 2H, J = 7.9 Hz, H6, H14), 9.93 (doublet of multiplet, 2H, J = 9.1 and <0.6 Hz, H1, H9) ppm.

Preparation of the bis(quinoxaline) derivative of 7,8,15,16-dibenzo[*a,j*]perylenetetracarboxylic dianhydride (15)

The compound was prepared as described by Bradley and Pexton (32). IR (KBr) ν_{max}: 1599, 1560, 1432, 1415, 1280, 1272, 1224, 1176, 1113, 761 cm^{-1}. ^1H NMR (CF_3CO_2D–$CDCl_3$ 1:1) δ: 8.07 (ddd, 2H, J = 8.4, 6.8, and 1.2 Hz, H3, H11), 8.12 (ddd, 2H, J = 8.3, 6.8, and 1.0 Hz, H2, H10), 8.17 (ddd, 2H, J = 8.2, 7.1, and 1.4 Hz, H4, H4′ of phenylene), 8.23 (ddd, 2H, J = 8.3, 7.0, and 1.4 Hz, H3, H3′ of phenylene), 8.35 (dd, 2H, J = 8.1 and 1.4 Hz, H5, H5′ of phenylene), 8.68 (dd, 2H, J = 8.1 and 1.4 Hz, H2, H2′ of phenylene), 8.95 (d, 2H, J = 7.9 Hz, H6, H14), 9.06 (d, 2H, J = 7.9 Hz, H5, H13), 9.10 (d, 2H, J = 8.7 Hz, H4, H12), 9.67 (dd, 2H, J = 8.7 and 1.0 Hz, H1, H9) ppm. MS *m/z*: 604 (100 M^+), 302 (98, $M^+/2$). Anal. calcd. for $C_{44}H_{20}N_4$: C 87.40, H 3.33, N 9.27%; found: C 87.16, H 3.32, N 9.03%.

Preparation of the bis(benzimidazole) derivative of 7,8,15,16-dibenzo[*a,j*]perylenetetracarboxylic dianhydride (19)

A process similar to that described for the preparation of aceanthrene green was used for the fusion of the benzimidazole derivative of 1,9-anthracenedicarboxylic anhydride **18** to yield the crude bis(benzimidazole) derivative **19** in 44% yield. Partial purification was achieved by dissolving a portion of the crude material (500 mg) in trifluoroacetic acid (50 mL) and heating at 70°C. Acetic acid (80 mL) was slowly added to the solution while maintaining the temperature at 70°C. After cooling to room temperature, the suspension was filtered. The resulting solid was washed with trifluoroacetic acid–acetic acid (1:3) and slurried several times in acetone. Drying under high vacuum yielded the impure bis(benzimidazole) derivative **19** (310 mg, 62%); mp >300°C. IR (KBr) ν_{max}: 1690, 1564, 1518, 1449, 1383, 1356, 1343, 1267, 764, 747 cm^{-1}. UV–Vis–NIR (1,2,4-trichlorobenzene) λ_{max}: 785, 708, 632, 537, 499, 411 nm. ^1H NMR (CF_3CO_2D–$CDCl_3$–benzene-d_6 1:1:4) δ (major peaks only): 7.45 (m, H3, H3′, H4, H4′ of benzene ring), 7.81 (t, J = 7.7 Hz, H3, H11), 7.93 (m, H5, H5′ of benzene ring), 8.13 (t, J = 7.7 Hz, H2, H10), 8.45 (d, J = 7.9 Hz, H5, H13), 8.52 (d, J = 8.7 Hz, H4, H12), 8.65 (m, H2, H2′ of benzene ring), 8.87 (d, J = 7.9 Hz, H6, H14), 8.96 (d, J = 8.4 Hz, H1, H9) ppm. MS *m/z* (%): 636 (100, M^+), 318 (39 $M^+/2$). Anal. calcd. for $C_{44}H_{20}N_4O_2$: C 83.01, H 3.17, N 8.80%; found: C 81.23, H 3.19, N 8.58%.

Acknowledgment

The authors would like to thank Dr. T. I. Martin for his support throughout the near-infrared polycyclic aromatic photogenerator project and for helpful discussions.

References

1. J. Fabian, H. Nakazumi, and M. Matsuoka. Chem. Rev. **92**, 1197 (1992).
2. P.F. Gordon. *In* The chemistry and application of dyes. *Edited by* D.R. Waring and G. Hallas (Topics in applied chemistry. *Edited by* A.R. Katritzky and G.J. Sabongi). Plenum Press, New York. 1990. Chap. 8.
3. M. Matsuoka. *In* Colour chemistry, the design and synthesis of organic dyes and pigments. *Edited by* A.T. Peters and H.S. Freeman (Advances in colour chemistry). Elsevier Applied Science, London. 1991. Chap. 3.
4. P. Gregory. *In* Colour chemistry, the design and synthesis of organic dyes and pigments. *Edited by* A.T. Peters and H.S. Freeman (Advances in colour chemistry). Elsevier Applied Science, London. 1991. Chap. 9.
5. D. Désilets, P.M. Kazmaier, and R.A. Burt. Can. J. Chem. **73**, 325 (1995).
6. Chem. Abstr. [6424-79-9]; Dibenzo[*h,h'*]phenanthro-[2,1,10-*def*:7,8,9-*d'e'f'*]diisoquinoline-1,3,8,10(2*H*,9*H*)-tetrone; aceanthrene green.
7. Society of Dyers and Colourists. *In* Colour index. 3rd ed. Vol. 4. Society of Dyers and Colourists, Bradford. 1971. CI No. 71125, p. 4589.
8. H.R. Schweizer. *In* Künstliche Organische Farbstoffe und ihre Zwischenprodukte. Springer-Verlag, Berlin. 1964. p. 385.
9. H.E. Fierz-David. *In* Künstlische Organische Farbstoffe Technologie der Textilfasern. Vol. III. *Edited by* R.O. Herzog. Julius Springer, Berlin. 1926. pp. 621–623.
10. E. de B. Barnett. *In* Anthracene and anthraquinone. Baillière, Tindall and Cox, London. 1921. pp. 330 and 384.
11. M. Kardos. Ber. Dtsch. Chem. Ges. **46**, 2086 (1913).
12. Badische Anilin & Soda Fabrik. Fr. Patent 458,949 (1913).
13. M. Kardos. Ger. Patent 275,220 (1913).
14. M. Kardos. Ger. Patent 278,660 (1913).
15. Badische Anilin & Soda Fabrik. Ger. Patent 280,092 (1913).
16. M. Kardos. Ger. Patent 280,839 (1913).
17. M. Kardos. Ger. Patent 282,711 (1913).
18. M. Kardos. Ger. Patent 284,210 (1913).
19. M. Kardos. Ger. Patent 286,096 (1914).
20. Badische Anilin & Soda Fabrik. Brit. Patent 12,584 (1913).
21. Badische Anilin & Soda Fabrik. Brit. Patent 1,425 (1914).
22. M. Kardos. Badische Anilin & Soda Fabrik. U.S. Patent 1,216,134 (1917).
23. M. Kardos and P. Nawiasky. Badische Anilin & Soda Fabrik. U.S. Patent 1,253,252 (1918).
24. F.O. Robitschek. *In* FIAT final report 764, dyestuffs manufacturing processes of I.G. Farbenindustrie, A.G. Vol. 1. Library of Congress, Washington. 1947. p. 11.
25. J. Griffiths. *In* Colour and constitution of organic molecules. Academic Press, London. 1976. Chap. 2.
26. J. Griffiths. Dyes Pigm. **3**, 211 (1982).
27. W.P. Aue, E. Bartoldi, and R.R. Ernst. J. Chem. Phys. **64**, 2229 (1976).
28. A. Bax and R. Freeman. J. Magn. Reson. **44**, 542 (1981).
29. J. Jeener, B.H. Meier, P. Bachmann, and R.R. Ernst. J. Chem. Phys. **71**, 4546 (1979).
30. G. Bodenhausen, H. Kogler, and R.R. Ernst. J. Magn. Reson. **58**, 370 (1984).
31. R.L. Vold, J.S. Waugh, M.P. Klein, and D.E. Phelps. J. Chem. Phys. **48**, 3831 (1968).
32. W. Bradley and F.W. Pexton. J. Chem. Soc. 4436 (1954).
33. A. Bax. J. Magn. Reson. **51**, 314 (1984).
34. A. Bax, C.H. Niu, and D. Live. J. Am. Chem. Soc. **106**, 1150 (1984).
35. H.J. Wagner, R.O. Loutfy, and C.K. Hsiao. J. Mater. Sci. **17**, 2781 (1982).
36. E. Clar and H. Frömmel. Chem. Ber. **82**, 46 (1949).
37. H. Langhals, S. Demmig, and T. Potrawa. J. Prakt. Chem. **333**, 733 (1991).
38. J.R. Dias. *In* Handbook of polycyclic hydrocarbons, part A, benzenoid hydrocarbons (physical sciences data). Elsevier, New York. 1987.
39. M.J.S. Dewar, E.G. Zoebisch, E.F. Healy, and J.J.P. Stewart. J. Am. Chem. Soc. **107**, 3902 (1985).
40. J.J. Gajewski, K.E. Gilbert, and J. McKelvey. *In* Advances in molecular modeling. Vol. 2. *Edited by* D. Liotta. JAI Press, New York. 1990. pp. 65-92.
41. W.E. Hull. *In* Two-dimensional NMR spectroscopy: applications for chemists and biochemists. *Edited by* W.R. Croasmun and R.M. K. Carlson. VCH Publishers, New York. 1987.
42. E.D. Bergmann and R. Ikan. J. Org. Chem. **23**, 907 (1958).

Can. J. Chem. Downloaded from www.nrcresearchpress.com by 65.111.164.53 on 09/08/12
For personal use only.

Generation of oxindole-2-thiones (thiols) via dilithiated *N-tert*-Boc-anilines. Synthesis of a sulfur analog of MK886[1]

Alicia Cervantes, Claudia A. Contreras, Angel Guzman, Elena E. Vale, Esperanza Velarde, Sylvie L. Berthiaume, and Joseph M. Muchowski

Abstract: The N,C-dilithiated derivatives of the *N-tert*-butoxycarbonyl-2-alkylthiomethylanilines **5***a–c* and the *N-tert*-butoxycarbonyl-2-alkoxycarbonylmethylanilines **11***a*, *b* were converted into the *N-tert*-butoxycarbonyloxindole-2-thiones(thiols) **7***a–c* and **14***a*, *b*, respectively, by sequential reaction with carbon disulfide and methyl iodide. Compound **7***b* was converted into **10***d*, the sulfur analog of MK886.

Key words: *N-tert*-butoxycarbonyl-2-alkylthiomethylanilines, dilithiation, *N-tert*-butoxycarbonyl-2-alkoxycarbonylmethylanilines, *N-tert*-butoxycarbonyloxindole-2-thiones.

Résumé : Utilisant une séquence de réactions impliquant le disulfure de carbone et l'iodure de méthyle, on a transformé les dérivés N,C-dilithiés des *N-tert*-butoxycarbonyl-2-alkylthiométhylanilines (**5***a–c*) et des *N-tert*-butoxycarbonyl-2-alkoxycarbonylméthylanilines (**11***a*, *b*) en *N-tert*-butoxycarbonyloxindole-2-thiones (**7***a–c*) et 2-thiols (**14***a*, *b*) respectivement. On a transformé le produit **7***a* en **10***d*, l'analogue sulfuré du MK886.

Mots clés : *N-tert*-butoxycarbonyl-2-alkylthiométhylanilines, dilithiation, *N-tert*-butoxycarbonyl-2-alkoxycarbonylméthylanilines, *N-tert*-butoxycarbonyloxindole-2-thiones.

[Traduit par la rédaction]

MK886 (**1**, Scheme 1) is a potent and specific inhibitor of leukotriene biosynthesis by virtue of its ability to block (and reverse) the translocation of 5-lipoxygenase from the cytosol to the cellular membrane (1). Replacement of the methylene carbon in the C-2 side chain of **1** by a sulfur atom, as in **2**, would lengthen this chain by about 0.5 Å (2), a change that was not expected to have a significant impact on the biological activity. This paper describes the synthesis of 3-alkylthiooxindole-2-thiones and the use of one of these compounds to prepare the direct sulfur analog of MK886.

Compound **1** has been prepared (3) by saponification of the corresponding ester, which in turn was prepared by a Fischer indole synthesis from 1-(4-chlorobenzyl)-1-(4-isopropylphenyl)hydrazine hydrochloride and methyl 2,2-dimethyl-5-(*tert*-butylthio)-4-oxopentanoate. Application of the Fischer method to the generation of **2** would be synthetically difficult.

Scheme 1

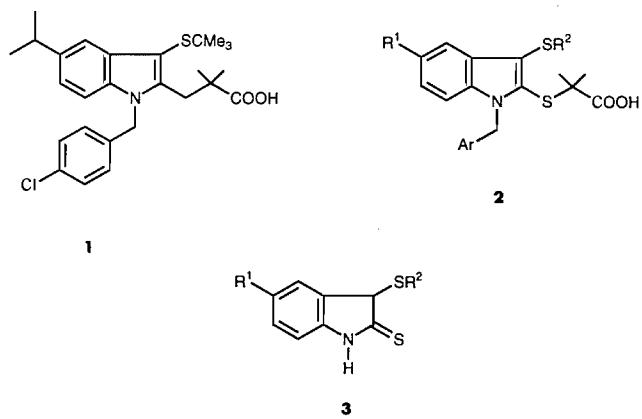

A particularly attractive route to this class of compounds appeared to be sequential S- and N-alkylation of the appropriate 3-alkylthiooxindole-2-thiones **3**. Although **3** is, in principle, available by the thioalkylation of oxindole-2-thione dianion, we chose to study an approach to these compounds based on the consecutive reaction of *N*-(*tert*-butoxycarbonyl)-*o*-toluidine dianions (4) with a dialkyl disulfide and carbon disulfide.

To establish the viability of the above concepts, *tert*-Boc-*o*-toluidine (**4***a*) was converted into the dianion with *s*-butyllithium (−40°C/THF) and treated with di-*tert*-butyldisulfide. The sulfide **5***a* (Scheme 2) obtained in this way was converted into the dianion (*s*-BuLi) and reacted with 3 equivalents of carbon disulfide. Work-up of the reaction mixture at this stage gave a mixture of several products that was not studied. If, however,

Received September 29, 1994.

A. Cervantes, C.A. Contreras, A. Guzman, E.E. Vale,[2] and E. Verlarde. Syntex S.A. de C.V., División de Investigación, Apartado Postal 272-CIVAC, 62500 Jiutepec, Morelos, México.
S.L. Berthiaume and J.M. Muchowski.[3] Synthex Research, Institute of Organic Chemistry, 3401 Hillview Avenue, Palo Alto, CA 94304, U.S.A.

[1] Contribution no. 884 from the Syntex Institute of Organic Chemistry.
[2] A portion of this work was carried out by E.E.V. in partial fulfullment of the requirements for the degree of Quimico Bacteriologo Parasitologo at the Universidad Autonoma de Chihuahua, Facultad de Ciencias Quimicas, Chihuahua, Chihuahua, Mexico.
[3] Author to whom correspondence may be addressed.

Can. J. Chem. Downloaded from www.nrcresearchpress.com by 65.111.164.53 on 09/08/12
For personal use only.

Can. J. Chem. Downloaded from www.nrcresearchpress.com by 65.111.164.53 on 09/08/12
For personal use only.

Scheme 2

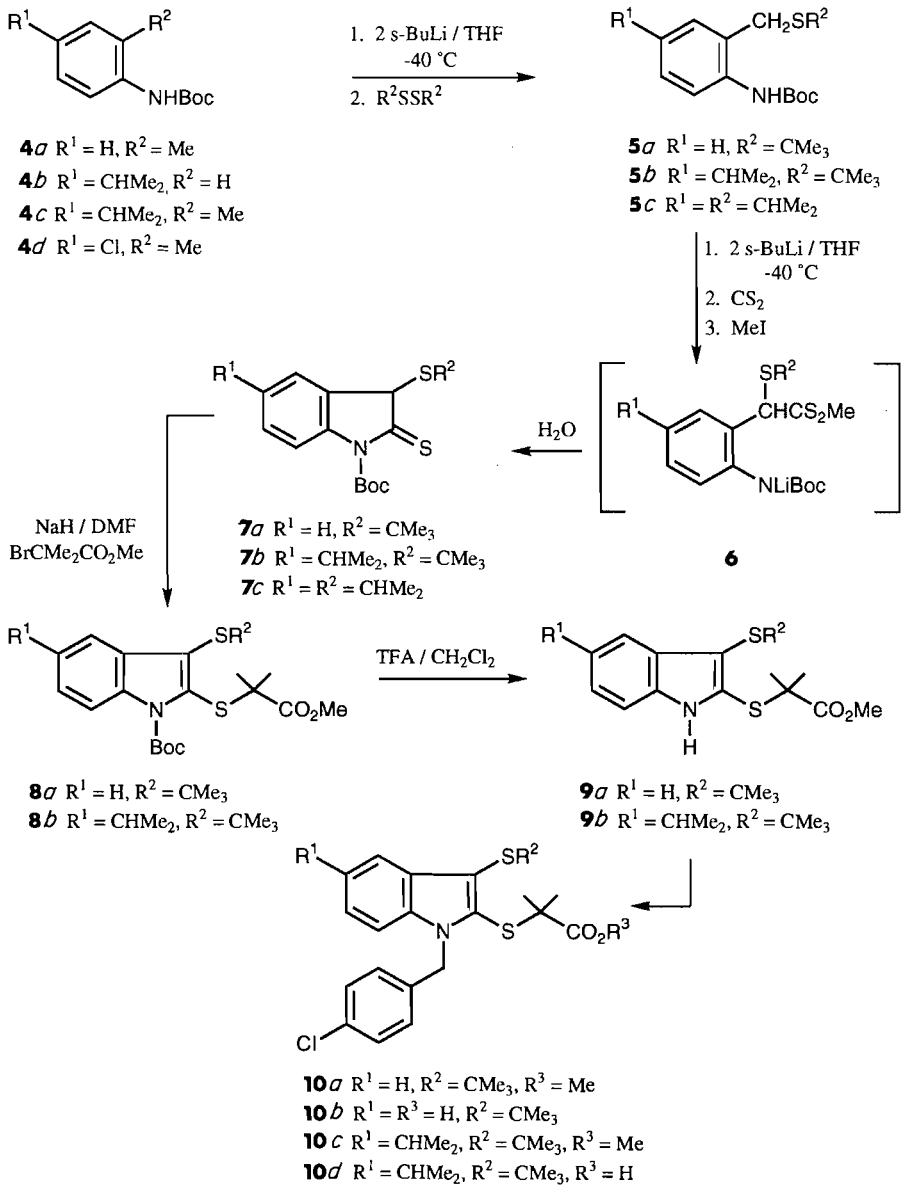

methyl iodide (1.1 equiv.) was added to the dianion – carbon disulfide reaction mixture, work-up after 1 h gave 1-*tert*-Boc-3-*tert*-butylthiooxindol-2-thione (**7***a*) directly. Obviously, cyclization of the intermediate lithiated dithio ester **6** occurred spontaneously in the reaction mixture or during the course of the work-up procedure. The conversion of **7***a* into the MK886 analog **10***b* was then effected by a four-step sequence beginning with S-alkylation of the sodium salt of **7***a* with methyl 2-bromo-2-methylpropionate followed by removal of the *tert*-Boc group, N-alkylation of the sodium salt of **9***a* with 4-chlorobenzyl bromide, and finally saponification.

To prepare the direct analog **10***d* of MK886, 4-isopropyl-*tert*-Boc-aniline (**4***b*) was lithiated with 2.5 equivalents of *tert*-butyllithium at −10°C and then treated with 1 equivalent of methyl iodide. The crude *o*-tolyl compound **4***c* was then converted into the sulfides **5***b* and **5***c* in 33 and 44% overall yields, respectively, based on **4***b*.[4] Both **5***b* and **5***c* were converted into the corresponding oxindoles **7***b* and **7***c*, and the former

[4] This difficult lithiation, which occurred in >65% yield based on isolated **5***c*, was effected under the conditions reported (5) for the generation of dilithio-*tert*-Boc-aniline. It has recently been alleged (6) that the degree of *o*-lithiation reported by us for *tert*-Boc-aniline could not be repeated. We have reproduced the reported yields of electrophile-trapped products on numerous occasions but, as has been pointed out by us (7), it is important that the THF–pentane ratio originally reported (ca. 2:1; *tert*-butyllithium is sold in pentane solution) be adhered to. When this precaution is taken, even complex, enolizable electrophiles give acceptable product yields on quite substantial scales (8). The report of Stanetty et al. (6) indicates that the lithiation of *tert*-Boc-aniline is much less sensitive to the conditions using diethyl ether as the solvent, and we concur with their observations.

Scheme 3

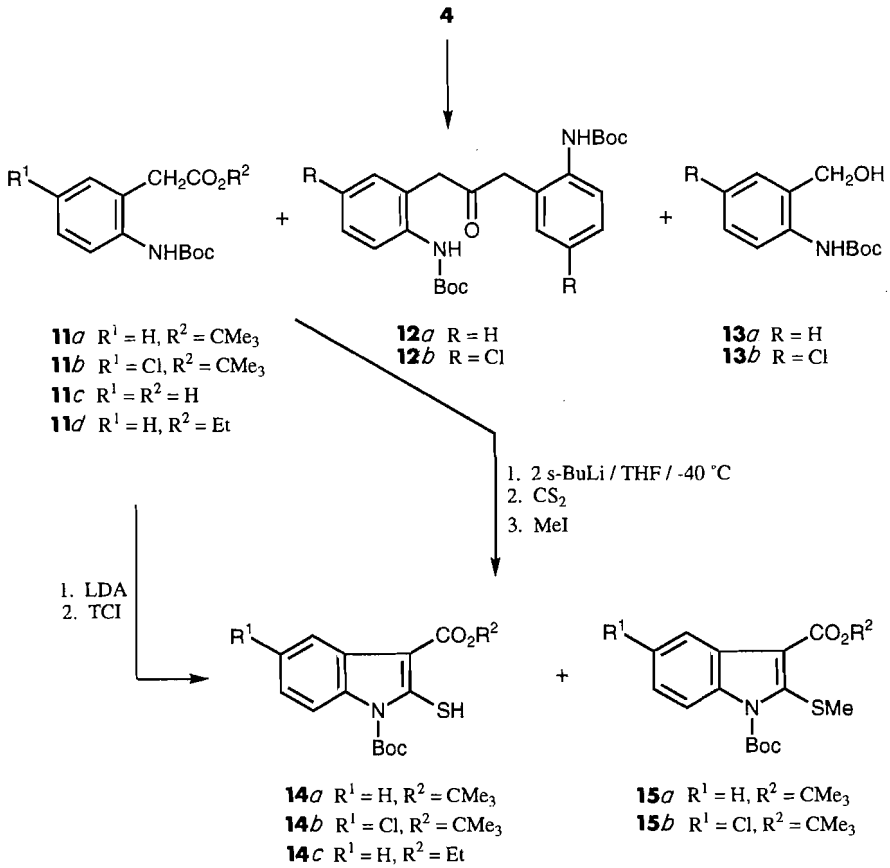

was transformed into **10***d* by the reaction sequence used to prepare **10***b*.

Compound **10***d* inhibited ionophore-stimulated leukotriene synthesis in human leukocytes with a potency ca. 1/3 of that reported (IC_{50} = 102 nm) for MK886(1).[5] Since the bioavailability in animals (e.g., rats) was quite poor, no attempt was made to establish if this inhibition was due to 5-lipoxygenase translocation blockade.

The ease of synthesis of **7***a–c* prompted us to determine if this route to oxindole-2-thiones had a broader applicability than that embodied by these compounds. Therefore the dianion of the *tert*-Boc-*ortho*-toluindine (**4***a*) was subjected to the reaction conditions that successfully generated **7***a–c* from **5***a–c*. A very complex mixture of products was obtained that was not studied. Based on the plausible assumption that the anion-stabilizing alkylthio moiety in **5***a–c* contributes to the success of the above process, the acetic acid esters **11** are also logical substrates. The *tert*-butyl esters **11***a, b* were prepared (40–50% yield) by the addition of the dianions of **4***a* and **4***d* to di-*tert*-butyl dicarbonate[6] at low temperature. Small amounts of the ketones **12***a, b* and the alcohols **13***a, b* (derived from adventitious oxygen) were also produced in these reactions. Generation of the dianions corresponding to **11***a, b* and subsequent reaction with carbon disulfide and methyl iodide gave a mixture of products from which the expected thiols **14***a, b* (15–30%) and the S-methyl compounds **15***a, b* (5–30%) derived therefrom were separated by column chromatography. To eliminate the inconvenience of preparing the *tert*-butyl esters and to the obviate S-methylthio ether formation, the dianion of **4***a* was carboxylated, and the carboxylic **11***c* was converted into the ethyl ester **11***d*. The dianion of **11***d*, generated in this case with LDA, was treated with thiocarbonyldiimidazole.[7] The thiol **14***c* was indeed obtained as the major product, but only in 35% yield. This reaction nevertheless deserves further examination.

Compounds **14***a–c* apparently exist in the thiol form as indicated by the low-field position (δ 8,3–8.4) of the exchangeable proton in the nmr spectrum. By comparison, compounds **7***a–c* show a sharp singlet at δ 5.7–5.8 clearly consistent with the thione form.

Experimental

The physical constants of the compounds reported herein were obtained as described previously (9).

4-Isopropyl-*N*-*tert*-butoxycarbonylaniline (**4***b*)

This compound was prepared by the general method described previously (4, 5). The crude product was purified by column chromatography on silica gel using hexane – ethyl acetate

[5] We thank M. Ernest and S. Panah, Institute of Biological Sciences, for providing us with this data.

[6] The normal mode of addition gave **12** as a major product.

[7] We thank Professor L.E. Overman, University of California, Irvine, for this suggestion

Can. J. Chem. Downloaded from www.nrcresearchpress.com by 65.111.164.53 on 09/08/12
For personal use only.

Can. J. Chem. Downloaded from www.nrcresearchpress.com by 65.111.164.53 on 09/08/12
For personal use only.

(97:3) as the eluting solvent. The pure material was obtained as a solid (97% yield) that, after crystallization from hexane, had mp 104–105°C; ir (KBr): 3313, 1696, 1609, 1598 cm^{-1}; nmr (200) δ: 1.21 (d, 6H, J = 7.0 Hz, Me_2CH), 1.51 (s, 9H, Me_3CO), 2.86 (sept, 1H, J = 7.0 Hz, Me_2CH), 6.42 (bs, 1H, NH), 7.20 (q, 4H, J = 8.7 Hz, H-2, 3, 5, 6). Anal. calcd. for $C_{14}H_{21}NO_2$: C 71.45, H 8.99, N 5.95; found: C 71.74, H 8.96, N 5.94.

2-Methyl-4-chloro-*N-tert*-butoxycarbonylaniline (*4d*)

Although this compound has been reported previously (4), its physical properties have not. It was obtained in 98% yield by the reported method (4) as a solid that, after trituration with ether and drying, had mp 95.5–97°C; nmr (300) δ: 1.51 (s, 9H, Me_3CO), 2.22 (s, 3H, Me), 6.20 (bs, 1H, NH), 7.13 (m, 1H, H-5), 7.16 (d, 1H, J = 2.5 Hz, H-3), 7.75 (d, 1H, J_o = 8.4 Hz, H-6). Anal. calcd. for $C_{12}H_{16}ClNO_2$: C 59.62, H 6.67, N 5.80; found: C 59.77, H 6.53, N 5.74.

2-*tert*-Butylthiomethyl-*N-tert*-butoxycarbonylaniline (*5a*)

A solution of *s*-butyllithium in cyclohexane (1.17 M, 72 mL, 84.2 mmol) was added to a stirred solution of **4***a* (7.0 g, 33.6 mmol; prepared in 96% yield from *o*-toluidine by the standard procedure (4, 5) in dry THF (120 mL) cooled to −40°C (N_2 atmosphere). After 20 min, a solution of di-*tert*-butyldisulfide (6.0 g, 33.6 mmol) in dry THF (50 mL) was added, and stirring at −40°C was continued for 30 min. The solution was diluted with water, the product was extracted into ethyl acetate, the extract was dried over sodium sulfate, and the solvent was removed in vacuo. Crystallization of the solid residue from hexane gave **5***a* (8.57 g, 86% yield), mp 104–105°C; ir ($CHCl_3$): 3356, 1728, 1593 cm^{-1}; nmr (90) δ: 1.39 (s, 9H, Me_3CS), 1.53 (s, 9H, Me_3CO), 3.74 (s, 2H, CH_2S), 7.25–7.35 (m, 3H), 7.44 (bs, 1H, NH), 7.82 (d, 1H, J_o = 8.1 Hz). Anal. calcd. for $C_{16}H_{25}NO_2S$: C 65.04, H 8.53, N 4.74, S 10.86; found: C 65.33, H 8.31, N 4.81, S 10.83.

Generation of the sulfides 5*b* and 5*c*

A 1.9 M solution of *tert*-butyllithium in pentane (23.7 mL, 45 mmol) was added to a stirred solution of **4***b* (4.7 g, 20 mmol) in dry THF (60 mL), and cooled to −70°C in a nitrogen atmosphere, at a rate such that the temperature stayed below −65°C. After 15 min, the temperature was raised to −20°C where it was maintained for 2 h. At this time, methyl iodide (2.84 g, 20 mmol) was added, and after 30 min at −20°C the solution was diluted with water and worked up as described for the synthesis of **5***a*. The crude product consisted of the starting material and **4***c* in a ca. 7:3 ratio as ascertained by the nmr spectrum; nmr (90) δ: 1.22 (d, 6H, J = 6.7 Hz, Me_2CH), 1.52 (s, 9H, Me_3CO), 2.23 (s, 3H, 2-Me), 2.82 (sept, 1H, J = 6.7 Hz, Me_2CH), 6.14 (bs, 1H, NH), 6.96–7.29 (m, 2H, H-3, 5), 7.61 (d, 1H, J_o = 9.1 Hz, H-6). The crude product was used without purification for the synthesis of **5***b* and **5***c*, using the technique described above for the synthesis of **5***a*.

2-tert-*Butylthiomethyl-4-isopropyl*-N-tert-*butoxycarbonylaniline (*5b*)*

Obtained as a solid (33% overall based on **4***b*) after purification by tlc on silica gel using hexane – ethyl acetate (94:6) as the developing solvent. After crystallization from hexane, it had mp 74–75°C; ir (KBr): 3369, 3334, 1725, 1590 cm^{-1}; nmr (200) δ: 1.21 (d, 6H, J = 6.9 Hz, Me_2CH), 1.42 (s, 9H, Me_3CS), 1.52 (s, 9H, Me_3CO), 2.85 (sept, 1H, J = 6.9 Hz, Me_2CH), 3.73 (s, 2H, CH_2S), 7.06 (d, 1H, J_m = 2.1 Hz, H-3), 7.12 (dd, 1H, J_o = 8.2 Hz, J_m = 2.1 Hz, H-5), 7.30 (bs, 1H, NH), 7.64 (d, 1H, J_o = 8.2 Hz, H-6). Anal. calcd. for $C_{19}H_{31}NO_2S$: C 67.61, H 9.26, N 4.14, S 9.50; found: C 67.73, H 9.12, N 4.09, S 9.45.

2-Isopropylthiomethyl-4-isopropyl-N-tert-*butoxycarbonylaniline (*5c*)*

Obtained in 44% yield overall (based on **4***b*) after purification by preparative tlc on silica gel using hexane – ethyl acetate (99:1) as the developing solvent; ir ($CHCl_3$): 3434, 3360, 1722, 1590 cm^{-1}; nmr (200) δ: 1.20 (d, 6H, J = 6.9 Hz, Me_2CH), 1.28 (d, 6H, J = 6.9 Hz, Me_2CHS), 1.52 (s, 9H, Me_3CO), 2.72–3.00 (m, 2H, Me_2CH, Me_2CHS), 3.74 (s, 2H, CH_2S), 6.99 (d, 1H, J_m = 2.1 Hz, H-3), 7.12 (dd, 1H, J_o = 8.3 Hz, J_m = 2.1 Hz, H-5), 7.29 (bs, 1H, NH), 7.67 (d, 1H, J_o = 8.3 Hz, H-6). Anal. calcd. for $C_{18}H_{29}NO_2S$: C 66.84, H 9.04, N 4.33, S 9.89; found: C 66.80, H 8.92, N 4.28, S 9.85.

Synthesis of the oxindole-2-thiones 7*a*–7*c*

The synthesis of **7***a* was typical. A solution of *s*-butyllithium in cyclohexane (23 mL of a 1.17 M solution; 27 mmol) was added to a solution of **5***a* (3.2 g, 10.8 mmol) in dry THF (40 mL) cooled to −40°C in a nitrogen atmosphere. After 20 min, carbon disulfide (1.95 mL, 2.46 g, 32.4 mmol) was added at −30°C, followed 10 min thereafter by methyl iodide (1.69 g, 11.9 mmol). The solution was stirred at −30°C for 1 h, water was added, and the mixture was worked up as described for **5***a*. The crude product was purified by column chromatography on silica gel using hexane – ethyl acetate (98.5:1.5) to elute the desired material as an oil (2.77 g, 76% yield); ir ($CHCl_3$): 1733 cm^{-1}; nmr (200) δ: 1.38 (s, 9H, Me_3CS), 1.74 (s, 9H, Me_3CO), 5.81 (s, 1H, H-3), 7.16–7.29 (m, 1H, H-4), 7.60–7.65 (m, 2H, H-5, 6), 8.02–8.07 (m, 1H, H-7); MS (EI) *m/z*: 337 (M^+, 14), 281 (27), 225 (100), 181 (22), 57 (76). This compound was not characterized further.

3-tert-*Butylthio-5-isopropyl*-N-tert-*butoxycarbonyloxindole-2-thione (*7b*)*

Obtained in 64% yield as an oil after purification by column chromatography on silica gel using hexane – ethyl acetate (95:5) as the eluting solvent; ir ($CHCl_3$): 1729 cm^{-1}; nmr (200) δ: 1.29 (d, 6H, J = 6.9 Hz, Me_2CH), 1.37 (s, 9H, Me_3CS), 1.72 (s, 9H, Me_3CO), 3.02 (sept, 1H, J = 6.9 Hz, Me_2CH), 5.78 (s, 1H, H-3), 7.1 (m, 1H, J_o = 8.6 Hz, J_m = 2.0 Hz, $J_{3,6}$ = 0.4 Hz, H-6), 7.48 (d, 1H, J_m = 2.0 Hz, H-4), 7.94 (d, 1H, J_o = 8.6 Hz, H-7). Anal. calcd. for $C_{20}H_{29}NO_2S_2$: C 63.30, H 7.70, N 3.68, S 16.86; found: C 63.21, H 7.65, N 3.52, S 16.75.

3-Isopropylthio-5-isopropyl-N-tert-*butoxycarbonyloxindole-2-thione (*7c*)*

Obtained in 65% yield as an oil after purification by column chromatography on silica gel using hexane – ethyl acetate (99:1) to elute the product; ir ($CHCl_3$): 1729, 1611 cm^{-1}; nmr (200) δ: 1.28 (d, 6H, J = 6.7 Hz, Me_2CH), 1.31 (d, 6H, J = 6.9 Hz, Me_2CHS), 1.72 (s, 9H, Me_3CO), 3.02 (sept, 1H, J = 6.9 Hz, Me_2CHS), 3.24 (sept, 1H, J = 6.7 Hz, Me_2CH), 5.66 (s, 1H, H-3), 7.12 (dd, 1H, J_o = 8.7 Hz, J_m = 1.8 Hz, H-6), 7.43 (d,

Can. J. Chem. Downloaded from www.nrcresearchpress.com by 65.111.164.53 on 09/08/12
For personal use only.

1H, J_m = 1.8 Hz, H-4), 7.94 (d, 1H, J_o = 8.7 Hz, H-7). Anal. calcd. for $C_{19}H_{27}NO_2S_2$: C 62.42, H 7.44, N 3.83, S 17.54; found: C 62.37, H 7.19, N 3.87, S 17.62.

Synthesis of the indoles 8*a* and 8*b* by alkylation of the oxindole-2-thiones 7*a* and 7*b*

The synthesis of **8*a*** was typical. A solution of **7*a*** (2.7 g, 8 mmol) in dry DMF (30 mL) was added to a stirred suspension of 50% sodium hydride in mineral oil (0.422 g, 8.8 mmol) in dry DMF (30 mL) in a nitrogen atmosphere at room temperature. When hydrogen evolution had ceased, methyl 2-bromo-2-methylpropionate (1.45 g, 8 mmol) was added, and the solution was stirred for 20 min. The reaction mixture was then worked up as for **5*a*** to give solid **8*a***, which, after crystallization from hexane (63% yield), had mp 89–90°C; ir (KBr): 1741, 1723, 1603 cm^{-1}; nmr (200) δ: 1.29 (s, 9H, Me_3CS), 1.44 (s, 6H, $SCMe_2$), 1.72 (s, 9H, Me_3CO), 3.67 (s, 3H, OMe) 7.24–7.41 (m, 2H, H-5, 6), 7.80–7.85 (m, 1H, H-4), 8.00–8.04 (m, 1H, H-7). Anal. calcd. for $C_{22}H_{31}NO_4S_2$: C 60.38, H 7.14, N 3.20, S 14.65; found: C 60.47, H 6.97, N 3.13, S 14.87.

Compound **8*b*** was obtained as an oil (76% yield) after purification by tlc on silica gel using hexane – ethyl acetate (9:1) as the developing solvent; ir ($CHCl_3$): 1748, 1728 cm^{-1}; nmr (200) δ: 1.29 (s, 9H, Me_3CS), 1.31 (d, 6H, J = 6.8 Hz, Me_2CH), 1.71 (s, 9H, Me_3CO), 3.03 (sept, 1H, J = 6.8 Hz, Me_2CH), 3.68 (s, 3H, OMe), 7.26 (dd, 1H, J_o = 8.7 Hz, J_m = 1.9 Hz, H-6), 7.66 (d, 1H, J_m = 1.9 Hz, H-4), 7.93 (d, 1H, J_o = 8.7 Hz, H-7). Anal. calcd. for $C_{25}H_{37}NO_4S_2$: C 62.61, H 7.77, N 2.92, S 13.34; found: C 62.58, H 7.70, N 3.12, S 13.08.

Synthesis of the indoles 9*a* and 9*b* by N-deprotection of 8*a* and 8*b*

A solution of the *N-tert*-butoxycarbonyl compound in dry dichloromethane (10–20 mL/g indole derivative) containing trifluoroacetic acid (1 mL/g of indole derivative) was stirred at room temperature for 3 h. The solution was diluted with dichloromethane, washed with 5% sodium bicarbonate solution, dried over sodium sulfate, and evaporated in vacuo. The solid residue was crystallized from hexane.

Compound **9*a*** obtained in 80% yield, had mp 119–121°C; ir ($CHCl_3$): 3461, 3358, 1718 cm^{-1}; nmr (200) δ: 1.28 (s, 9H, Me_3CS), 1.53 (s, 6H, $SCMe_2$), 3.82 (s, 3H, OMe), 7.13–7.28 (m, 2H), 7.36–7.41 (m, 1H), 7.74–7.78 (m, 1H), 9.61 (bs, 1H, NH). Anal. calcd. for $C_{17}H_{23}NO_2S_2$: C 60.52, H 6.87, N 4.15, S 18.97; found: C 60.69, H 6.75, N 4.09, S 18.99.

Compound **9*b***, obtained in 88% yield, had mp 106–107°C; ir (KBr): 3306, 1706 cm^{-1}; nmr (200) δ: 1.28 (s, 9H, Me_3CS), 1.30 (d, 6H, J = 6.8 Hz, Me_2CH), 1.52 (s, 6H, $SCMe_2$), 3.02 (sept, 1H, J = 6.8 Hz, Me_2CH), 3.81 (s, 3H, OMe), 7.13 (dd, 1H, J_o = 7.5 Hz, J_m = 2.0 Hz, H-6), 7.32 (d, 1H, J_o = 7.5 Hz, H-7), 7.60 (d, 1H, J_m = 2.0 Hz, H-4), 9.48 (bs, 1H, NH). Anal. calcd. for $C_{20}H_{29}NO_2S_2$: C 63.28, H 7.70, N 3.69, S 16.89; found: C 63.52, H 7.65, N 3.68, S 16.73.

Synthesis of the *N-p*-chlorobenzylindoles 10*a* and 10*c* by N-alkylation of 9*a* and 9*b*

The synthesis of **10*a*** was typical. A solution of the indole compound **9*a*** (0.340 g, 1 mmol) in dry DMF (4 mL) was added to a stirred suspension of 50% sodium hydride in mineral oil (0.053 g, 1.1 mmol) in dry DMF (3 mL) maintained in a nitrogen atmosphere at room temperature. When hydrogen evolution had cease, *p*-chlorobenzyl bromide (0.205 g, 1 mmol) was added, and stirring was continued for 30 min. The reaction solution was then worked up as described for the synthesis of **8*a*** and **8*b***. The crude product was purified by preparative tlc on silica gel using hexane – ethyl acetate (85:15) as the developing solvent.

Compound **10*a*** was obtained as a foam in 75% yield; ir ($CHCl_3$): 1725 cm^{-1}; nmr (200) δ: 1.28 (s, 9H, Me_3CS), 1.47 (s, 6H, $SCMe_2$), 3.67 (s, 3H, OMe), 5.58 (s, 2H, CH_2), 6.87 (d, 1H, J = 8.5 Hz), 7.15–7.26 (m, 5H), 7.83–7.88 (m, 1H). Anal. calcd. for $C_{24}H_{28}ClNO_2S_2$: C 62.38, H 6.10, Cl 7.67, N 3.03, S 13.87; found: C 62.46, H 6.08, Cl 7.63, N 2.96, S 13.80.

Compound **10*c*** was isolated in 64% yield as a foam after purification by preparative tlc on silica gel using hexane – ethyl acetate (9:1) as the eluting solvent; ir ($CHCl_3$): 1725 cm^{-1}; nmr (200) δ: 1.28 (s, 9H, Me_3CS), 1.29 (d, 6H, J = 6.9 Hz, Me_2CH), 1.46 (s, 6H, $SCMe_2$), 3.01 (sept, 1H, J = 6.9 Hz, Me_2CH), 3.68 (s, 3H, OMe), 5.52 (bs, 2H, CH_2), 6.89 (d, 2H, J = 8.5 Hz, H-2′,6′), 7.08–7.26 (m, 4H, H-6, 7, 3′, 5′), 7.68 (s, 1H, H-4). Anal. calcd. for $C_{27}H_{34}ClNO_2S_2$: C 64.32, H 6.79, Cl 7.03, N 2.77, S 12.72; found: C 64.27, H 6.72, Cl 6.90, N 2.61, S 12.58.

Synthesis of the carboxylic acids 10*b* and 10*d* by saponification of 10*a* and 10*c*

A solution of the methyl ester in methanol (10–15 mL/mmol ester) containing sodium hydroxide (1.2–2 mmol/mmol ester) and water (1–2 mL/mmol ester) was stirred at room temperature overnight or heated at reflux for 4 h. The solvent was removed in vacuo, water was added to the residue, and the solution was made acidic with 6 N hydrochloric acid. The product was extracted with ethyl acetate, and the extract was washed with water, dried over sodium sulfate, and evaporated in vacuo. The solid residue was crystallized from hexane.

Compound **10*b***, obtained in 88% yield, had mp 174–176°C; ir ($CHCl_3$): 2664, 2584, 1703 cm^{-1}. Anal. calcd. for $C_{23}H_{26}ClNO_2S_2$: C 61.65, H 5.85, Cl 7.91, N 3.12, S 14.31; found: C 61.52, H 5.71, Cl 7.98, N 3.00, S 14.26.

Compound **10*d***, isolated in 89% yield, had mp 155–156°C; ir ($CHCl_3$): 2651, 2547, 1703 cm^{-1}. Anal. calcd. for $C_{26}H_{32}ClNO_2S_2$: C 63.71, H 6.58, Cl 7.23, N 2.85, S 13.08; found: C 63.67, H 6.65, Cl 7.35, N 2.81, S 13.01.

tert*-Butyl 2-*tert*-butoxycarbonylaminophenyl acetate 11*a

A −40°C solution of the dianion of **4*a***, prepared as described for the synthesis of **5*a*** from **4*a*** (5.00 g, 24.0 mmol) in THF (85 mL) and 1.34 M *s*-butyllithium in cyclohexane (45.0 mL, 60.3 mmol), was cannulated into a stirred solution of di-*tert*-butyldicarbonate (5.8 mL, 5.50 g, 25.2 mmol) in dry THF (21 mL) at −70°C (N_2 atmosphere) at a rate such that the reaction temperature did not exceed −70°C. Within 5 min of the addition, the solution was poured into an excess of aqueous ammonium chloride solution. The products were extracted into ethyl acetate, the extract was dried over magnesium sulfate, and the solvent was removed in vacuo. The residual mixture was separated by column chromatography on silica gel using hexane – ethyl acetate (95:5) to elute the products.

Compound **11*a*** was obtained as a solid (3.70 g, 50.0% yield based on **4*a***) that had mp 82–85°C after crystallization from hexane; ir ($CHCl_3$): 3396, 1723, 1591 cm^{-1}; nmr (200) δ: 1.45 (s, 9H, Me_3CO), 1.53 (s, 9H, Me_3CO), 3.52 (s, 2H, CH_2), 7.03

Can. J. Chem. Downloaded from www.nrcresearchpress.com by 65.111.164.53 on 09/08/12
For personal use only.

(td, 1H, J_o = 7.6 Hz, J_m = 1.5 Hz, H-4 or H-5), 7.20 (td, 1H, J_o = 7.6 Hz, J_m = 1.5 Hz, H-5 or H-4), 7.29 (dd, J_o = 7.6 Hz, J_m = 1.5 Hz, H-6), 7.71 (bs, 1H, NH), 7.81 (bd, 1H, J_o = 7.6 Hz, H-3). Anal. calcd. for $C_{17}H_{25}NO_4$: C 66.42, H 8.19, N 4.55; found: C 66.53, H 8.20, N 4.60.

In addition, a small amount of **12***a* (0.331 g, 6.7%) was isolated as a solid that, after crystallization from hexane, had mp 128–130°C; ir ($CHCl_3$): 3426, 3368, 1719, 1590 cm^{-1}; nmr (200) δ: 1.50 (s, 18H, Me_3CO), 3.80 (s, 4H, CH_2), 6.98–7.12 (m, 4H), 7.03 (bs, 2H, NH), 7.24–7.30 (m, 2H), 7.68 (bd, 2H, J_o = 8.1 Hz, H-3, 3′); MS (EI) *m/z*: 440 (M^+). Anal. calcd. for $C_{24}H_{32}N_2O_4$: C 68.15, H 7.32, N 6.36; found: C 68.15, H 7.39, N 6.40.

There was also isolated a much more polar material (0.250 g, 4.6%), which, on the basis of its spectroscopic properties, was assumed to be 2-*tert*-butoxycarbonylaminobenzyl alcohol (**13***a*), as an oil; ir ($CHCl_3$) 3601, 3396, 1723, 1525 cm^{-1}; nmr (200) δ: 1.53 (s, 9H, Me_3CO), 1.80 (bs, 1H, OH), 4.69 (s, 2H, CH_2), 7.02 (td, 1H, J_o = 7.6 Hz, J_m = 1.5 Hz, H-4 or H-5), 7.18 (dd, 1H, J_o = 7.6 Hz, J_m = 1.5 Hz, H-6), 7.65 (bs, 1H, NH), 7.82 (td, 1H, J_o = 7.6 Hz, J_m = 1.5 Hz, H-5 or H-4); MS(EI) *m/z*: 223 (M^+). This compound was not characterized further.

tert-Butyl 2-*tert*-butoxycarbonylamino-4-chlorophenyl acetate 11*b*

This compound was prepared in a manner similar to **11***a* except that *tert*-butyllithium was used to generate the dianion of **4***d* (8), and that the crude product was separated into **11***b* and a mixture of **12***b* and **13***b* by column chromatography on silica gel using hexane – ethyl acetate (95:5) as the eluting solvent.

Compound **11***b* was obtained in 38–43% yield (based on **4***d*) as a solid that had mp 90–91°C after crystallization from dichloromethane; ir ($CHCl_3$): 3395, 1723 cm^{-1}; nmr (200) δ: 1.45 (s, 9H, Me_3CO), 1.52 (s, 9H, Me_3CO), 3.48 (s, 2H, CH_2), 7.19 (dd, 1H, J_o = 8.4 Hz, J_m = 2.5 Hz, H-5), 7.25 (d, 1H, J_m = 2.5 Hz, H-3), 7.70 (bs, 1H, NH), 7.77 (bd, 1H, J_o = 7.5 Hz, H-6). Anal. calcd. for $C_{17}H_{24}ClNO_4$: C 59.72, H 7.07, Cl 10.37, N 4.09; found: C 59.80, H 7.11, Cl 10.55, N 4.11.

The mixture of **12***b* and **13***b* was separated by tlc on silica gel using toluene–acetone (98:2) as the developing solvent. This gave **12***b* and **13***b* as solids in ca. 4% and 10–13% yields, respectively.

Compound **12***b* had mp 192–193.5°C after crystallization from dichloromethane–methanol. Anal. calcd. for $C_{25}H_{30}Cl_2N_2O_5$: C 58.92, H 6.25, Cl 13.75, N 5.43; found: C 58.62, H 5.81, Cl 13.71, N 5.61.

Compound **13***b* had mp 89–90°C after crystallization from hexane; ir ($CHCl_3$): 3601, 3394, 1723 cm^{-1}; nmr (200) δ: 1.52 (s, 9H, Me_3CO), 2.03 (t, 1H, J = 5.8 Hz, OH), 4.65 (d, 2H, J = 5.8 Hz, CH_2O), 7.16 (d, 1H, J_m = 2.3 Hz, H-6), 7.43 (dd, 1H, J_o = 8.7 Hz, J_m = 2.3 Hz, H-4), 7.59 (bs, 1H, NH), 7.89 (d, 1H, J_o = 8.7 Hz, H-3). Anal. calcd. for $C_{12}H_{16}ClNO_3$: C 55.92, H 6.25, Cl 13.75, N 5.43; found: C 56.10, H 6.30, Cl 13.86, N 5.48.

tert-Butyl 1-*tert*-butoxycarbonyl-2-mercaptoindole-3-carboxylate 14*a* and *tert*-butyl 1-*tert*-butoxycarbonyl-2-methylthioindole-3-carboxylate 15*a*

A solution of 1.08 M *s*-butyllithium in cyclohexane (18.6 mL, 20 mmol) was added to a stirred solution of compound **11***a* (3.0 g, 9.76 mmol) in dry THF (150 mL) at −40 to −35°C in an argon atmosphere. The solution was stirred for 45 min at −40°C and then carbon disulfide (1.76 mL, 2.23 g, 29 mmol) dissolved in THF (10 mL) was added, followed after 20 min by methyl iodide (0.66 mL, 1.50 g, 10.6 mmol). The reaction temperature was raised to 0°C, and after 45 min the reaction mixture was worked up as for **11***a*. The crude product was separated by column chromatography on silica gel into **14***a* and **15***a* using hexane – ethyl acetate (98:2) as the eluting solvent.

Compound **14***a* was obtained as a yellowish-green solid (1.113 g, 33% yield) that, after crystallization from hexane, had mp 92–94°C; ir ($CHCl_3$): 1738, 1702, 1657 cm^{-1}; nmr (200) δ: 1.68 (s, 9H, Me_3CO), 1.73 (s, 9H, Me_3CO), 7.22 (td, 1H, J_o = 7.5 Hz, J_m = 2.2 Hz, H-5 or H-6), 7.27 (td, 1H, J_o = 7.5 Hz, J_m = 2.2 Hz, H-6 or H-5), 7.95–8.09 (m, 2H, H-4, 7), 8.40 (s, 1H, SH); MS(EI) *m/z*: 349 (M^+). Anal. calcd. for $C_{18}H_{23}NO_4S$: C 61.87, H 6.63, N 4.00; found: C 61.86, H 6.70, N 4.11.

Compound **15***a* was obtained (1.130 g, 32% yield) as an oil; ir ($CHCl_3$): 1741, 1698 cm^{-1}; nmr (200) δ: 1.68 (s, 9H, Me_3CO), 1.71 (s, 9H, Me_3CO), 2.55 (s, 3H, SMe), 7.27 (td, J_o = 7.7 Hz, J_m = 2.3 Hz, H-5 or H-6), 7.31 (td, 1H, J_o = 7.7 Hz, J_m = 2.3 Hz, H-6 or H-5), 7.90–8.04 (m, 2H, H-4, 7); MS (EI) *m/z*: 363 (M^+). Anal. calcd. for $C_{19}H_{25}NO_4S$: C 62.78, H 6.93, N 3.85; found: C 62.18, H 6.75, N 3.98.

tert-Butyl 1-*tert*-butoxycarbonyl-2-mercapto-5-chloroindole-2-carboxylate 14*b* and *tert*-butyl 1-*tert*-butoxycarbonyl-2-methylthio-5-chloroindole-2-carboxylate 15*b*

This mixture was obtained in the same manner as described for **14***a* and **15***a* except that it was separated into its components by flash column chromatography using hexane – ethyl acetate (95:5) as the eluting solvent. Compounds **14***b* and **15***b* were obtained in 15 and 5% yields, respectively.

Compound **14***b* was a solid that had mp 75–77°C after crystallization from hexane; ir ($CHCl_3$): 1742, 1660, 1608 cm^{-1}; nmr (200) δ: 1.68 (s, 9H, Me_3CO), 1.72 (s, 9H, Me_3CO), 7.19 (dd, 1H, J_o = 9.0 Hz, J_m = 2.1 Hz, H-6), 7.96–8.00 (m, 2H, H-4, 7), 8.40 (s, 1H, SH). Anal. calcd. for $C_{18}H_{22}ClNO_4S$: C 56.31, H 5.77, N 3.65; found: C 56.30, H 5.80, N 3.76.

Compound **15***b* was obtained as an oil; ir ($CHCl_3$): 1725 cm^{-1}; nmr (300) δ: 1.68 (s, 9H, Me_3CO), 1.70 (s, 9H, Me_3CO), 2.55 (s, 3H, SMe), 7.26 (dd, 1H, J_o = 8.9 Hz, J_m = 2.2 Hz, H-6), 7.87 (d, 1H, J_o = 8.9 Hz, H-7), 7.99 (d, 1H, J_m = 2.2 Hz, H-4). This compound was not characterized further.

Ethyl 2-*tert*-butoxycarbonylaminophenyl acetate 11*d*

Potassium carbonate (1.41 g, 10.2 mmol) was added to a stirred solution of the crude carboxylic acid **11***c* (2.35 g, 9.3 mmol), prepared as described by Clark et al. (8), in DMF (25 mL), and after 0.5 h ethyl iodide (0.82 mL, 1.62 g, 10.2 mmol) was added. After a further 2 h, the reaction mixture was poured into water and extracted with ethyl acetate; the extract was washed with water and dried over magnesium sulfate. Removal of the solvent in vacuo gave an oily residue that was purified by column chromatography on silica gel using hexane – ethyl acetate (95:5) as the eluting solvent. Compound **11***d* was obtained as an oil (2.14 g, 82% yield); ir ($CHCl_3$): 3377, 1725, 1603, 1585 cm^{-1}; nmr (200) δ: 1.29 (t, 3H, J = 7.1 Hz, OCH_2CH_3), 1.60 (s, 9H, Me_3CO), 3.63 (s, 2H,

CH_2), 4.13 (q, 2H, J = 7.1 Hz, OCH_2CH_3), 7.07–7.33 (m, 3H), 7.68 (bs, 1H, NH), 7.80 (d, 1H, J_o = 8.1 Hz). Anal. calcd. for $C_{15}H_{21}NO_4$: C 64.49, H 7.57, N 5.01; found: C 64.53, H 7.61, N 4.98.

Ethyl 1-*tert*-butoxycarbonyl-2-mercaptoindole-3-carboxylate 14*c*

A solution of compound **11***d* (0.459 g, 1.64 mmol) in dry THF (10 mL) was added to a stirred solution of lithium diisopropylamide, prepared from diisopropylamine (0.5 mL, 0.36 g, 3.6 mmol(and 1.3 M *n*-butyllithium in hexane (2.78 mL) in dry THF (15 mL), cooled to −78°C, at a rate such that the reaction temperature did not exceed −70°C. After 0.5 h, thiocarbonyldiimidazole (0.87 g, 4.9 mmol) was added and stirring at −78°C was continued for 2 h, followed by 0.67 h at −40°C. The reaction mixture was diluted with water and extracted with hexane. The extract was dried over magnesium sulfate and evaporated in vacuo. The residue was purified by column chromatography on silica gel using hexane – ethyl acetate (95:5) to give the product as a solid (0.175 g, 33% yield) that had mp 66°C after crystallization from ether–hexane; ir ($CHCl_3$): 1740, 1664 cm^{-1}; nmr (200) δ: 1.50 (t, 3H, J = 7.1 Hz, Me), 1.75 (s, 9H, Me_3CO), 4.47 (q, 2H, J = 7.1 Hz, CH_2), 7.19–7.35 (m, 3H, H-5-7), 8.01–8.12 (m, 1H, H-4), 8.26 (s, 1H, SH). Exact Mass calcd. (*m/z*) for $C_{16}H_{19}NO_4S$: 321.1035; found: 321.1032.

References

1. C.A. Rouzer, A.W. Ford-Hutchinson, H.E. Morton, and J.W. Gillard. J. Biol. Chem. **265**, 1436 (1990).
2. J. March. *In* Advanced organic chemistry. Reactions, mechanism, and structure. 3rd ed. John Wiley and Sons, New York. 1985. p. 19.
3. J.W. Gillard, H.E. Morton, R. Fortin, and Y. Guindon. European Patent Application 0 275 667 (1987).
4. R.D. Clark, J.M. Muchowski, L.E. Fisher, L.A. Flippin, D.B. Repke, and M. Souchet. Synthesis, 871 (1991).
5. J.M. Muchowski and M.C. Venuti. J. Org. Chem. **45**, 4798 (1980).
6. P. Stanetty, H. Koller, and M. Mihovilovic. J. Org. Chem. **57**, 6833 (1992).
7. I-S. Cho, L. Gong and J.M. Muchowski. J. Org. Chem. **56**, 7288 (1991).
8. R.D. Clark, J.M. Caroon, A.F. Kluge, D.B. Repke, A.P. Roszkowski, A.M. Strosberg, S. Baker, S.M. Bitter, and M.D. Okada. J. Med. Chem. **26**, 657 (1983).
9. A. Guzman, C. Quintero, and J.M. Muchowski. Can. J. Chem. **69**, 2059 (1991).

Can. J. Chem. Downloaded from www.nrcresearchpress.com by 65.111.164.53 on 09/08/12
For personal use only.

Preparation of diversely protected 2-azido-2-deoxyglycopyranoses from glycals

Stanislas Czernecki and Ebtissam Ayadi

Abstract: A new and efficient preparation of diversely protected 2-azido-2-deoxyglycopyranosides from the corresponding glycals is described. The glycals are first transformed into protected phenyl 2-azido-2-deoxyselenoglycopyranosides by azido-phenylselenylation. Two procedures were employed according to the protecting groups present: sodium azide and diphenyldiselenide in the presence of (diacetoxyiodo)benzene for peracetylated glycals (Procedure A) or trimethylsilyl azide and tetra-*n*-butylammonium fluoride in the presence of *N*-phenylselenophthalimide for perbenzylated glycals (Procedure B). A *gluco–manno* mixture (90%) is obtained from protected D-glucal whereas only the *galacto* isomer is formed from protected D-galactal (75%). The compatibility of the second procedure with one free hydroxyl group and a variety of protecting groups was verified with 1,5-anhydro-2-deoxy-3,4-*O*-isopropylidene-D-*lyxo*-hex-1-enitol and its 6-*O*-acetyl, 6-*O*-allyl, 6-*O*-benzyl, and 6-*O*-*tert*-butyldimethylsilyl derivatives as well as with 1,5-anhydro-4,6-*O*-benzylidene-2-deoxy-D-*lyxo*-hex-1-enitol and its 3-*O*-acetyl and 3-*O*-benzyl derivatives, which were transformed into phenyl 2-azido-2-deoxy-α-D-selenogalactopyranoside derivatives in good yield. In the second step, hydrolysis of these selenoglycosides afforded diversely protected glycopyranoses in high yield. Peracetylated derivatives were hydrolyzed in the presence of *N*-iodosuccinimide, whereas mercury trifluoroacetate was employed for 3,4-*O*-isopropylidene, 4,6-*O*-benzylidene, and perbenzylated derivatives. In some cases the two steps can be carried out without isolation of the intermediate selenoglycoside.

Key words: glycals, 2-azido-2-deoxygalactopyranose, 2-azido-2-deoxyglucopyranose, selenoglycosides.

Résumé : On décrit une nouvelle préparation efficace de divers 2-azido-2-désoxyglycopyranosides protégés de diverses manières à partir des glycals correspondants. Dans la première étape, on transforme les glycals en 2-azido-2-désoxysélénoglycopyranosides de phényle protégés par azidophénylsélénylation. On a utilisé deux méthodes suivant la nature des groupes protecteurs présents : azoture de sodium et diphényldisélénure en présence de (diacétoxyiodo)benzène avec les glycals peracétylés (méthode A) ou azoture de triméthylsilyle et fluorure de tétra-*n*-butylammonium en présence de *N*-phénylsélénophtalimide avec les glycals perbenzylés (méthode B). On obtient un mélange *gluco–manno* (90%) à partir du D-glucal alors que l'on obtient uniquement l'isomère *galacto* à partir du D-galactal (75%). Utilisant le 1,5-anhydro-2-désoxy-3,4-*O*-isopropylidène-D-*lyxo*-hex-1-énitol et ses dérivés 6-*O*-acétyl-, 6-*O*-allyl-, 6-*O*-benzyl- et 6-*O*-*tert*-butyldiméthylsilyl- ainsi que le 1,5-anhydro-4,6-*O*-benzylidène-2-désoxy-D-*lyxo*-hex-1-énitol et ses dérivés 3-*O*-acétyl- et 3-*O*-benzyl- qui ont été transformés en dérivés du 2-azido-2-désoxy-α-galactopyranoside de phényle avec de bons rendements, on a vérifié la compatibilité de la deuxième méthode avec la présence d'un groupe hydroxyle libre et de divers groupes protecteurs. Dans la deuxième étape, l'hydrolyse de ces sélénoglycosides fournit divers glycopyranoses protégés avec des rendements élevés. On a hydrolysé les dérivés peracétylés en présence de *N*-iodosuccinimide alors que l'on a utilisé du trifluoroacétate de mercure pour les dérivés 3,4-*O*-isopropylidène, 4,6-*O*-benzylidène et perbenzylés. Dans certains cas, on a effectueé les deux étapes sans isoler les sélénoglycosides intermédiaires.

Mots clés : glycals, 2-azido-2-désoxygalactopyranose, 2-azido-2-désoxyglucopyranose, sélénoglycosides.

[Traduit par la rédaction]

Introduction

Protected 2-azido-2-deoxy derivatives of galactose and glucose are extensively used for the synthesis of biologically important 2-amino-2-deoxygalactose- (and glucose-) containing oligosaccharides (1, 2). Due to the small size of the azido group, 2-azido-2-deoxyglycopyranosyl donors are generally used as reactive intermediates. Depending on the leaving group and the promotor used, they can induce either a 1,2-*cis* or a 1,2-*trans* stereochemistry (2) and regeneration of the amino function is possible under mild conditions. They are generally prepared in two steps from the corresponding glycals: azidonitration followed by transformation of the obtained 2-azido-1-nitrate adducts into various glycosyl donors by displacement of the anomeric nitrate by halide ions as described by Lemieux and Ratcliffe (3) or by using potas-

Received July 20, 1994.

S. Czernecki[1] and E. Ayadi. Laboratoire de chimie des glucides, Université Pierre et Marie Curie, 4, place Jussieu, 75005 Paris, France.

[1] Author to whom correspondence may be addressed. Telephone: 033-1-4427 5557. Fax: 033-1-4427 5513.

Can. J. Chem. Downloaded from www.nrcresearchpress.com by 65.111.164.53 on 09/08/12
For personal use only.

Table 1. Synthesis of diversely protected 2-azido-2-deoxy glycopyranosides.

Entry	Glycal	Azido-phenylselenylation			Hydrolysis			Yield from glycal (%)
		Procedure	Compound	Yield (%)	Procedure	Compound	Yield (%)	
1	**1***a*	A[a]	(**5***a* + **6***a*)[c]	91	C[d]	(**11***a* + **12***a*)[c]	90	82
2	**1***b*	B[b]	(**5***b* + **6***b*)[c]	82	D[e]	(**11***b* + **12***b*)[f]	93	76
3	**2***a*	A	**7***a*	92	C	**13***a*	87	80
4	**2***b*	B	**7***b*	75	D	**13***b*	87	65
5	**3***a*	B	**9***a*	59				
6	**3***b*	B	**9***b*	91	D	**14***a*	79	72
7	**3***b*	A	**9***b*	50				
8	**3***c*	B	**9***c*	84	D	**14***b*	87	73
9	**3***d*	B	**9***d*	66				
10	**3***e*	B	**9***e*	74	D	**14***c*	88	65
11	**4***a*	B	**10***a*	68				
12	**4***b*	B	**10***b*	73	D	**15***a*	86	63
13	**4***c*	B	**10***c*	76	D	**15***b*	82	62

[a]Procedure A: $(PhSe)_2$ (0.6 equiv.), NaN_3 (2.4 equiv.), $PhI(OAc)_2$ (1.4 equiv.), CH_2Cl_2, 48 h rt.
[b]Procedure B: *N*-PSP (2 equiv.), $(CH_3)_3SiN_3$ (2 equiv.), $(n-Bu)_4NF$ (0.2 equiv.), CH_2Cl_2, 48 h rt.
[c]Inseparable mixture.
[d]Procedure C: NIS (5 equiv.), THF–H_2O, 12 h rt.
[e]Procedure D: $(CF_3COO)_2Hg$ (1.5 equiv.), THF–H_2O, CH_2Cl_2, 30 min rt.
[f]66% *gluco*, 12% *manno*, and 15% of a *gluco–manno* mixture.

sium *O*-ethyl dithiocarbonate (4). Efficient glycosyl donors such as trichloroacetimidates (5) and fluorides (6) can also be prepared after hydrolysis of the anomeric *O*-nitrate. Several methods were reported for the latter transformation (5, 7, 8).

We recently disclosed a new route to protected 2-azido-2-deoxyglycopyranoses in which azido-phenylselenylation of protected glycal afforded a phenyl 2-azido-2-deoxyselenoglycoside that was readily hydrolyzed (9). We now report full details with extension of this methodology to several diversely protected glycals to demonstrate its compatibility with a variety of protecting groups employed in oligosaccharide synthesis.

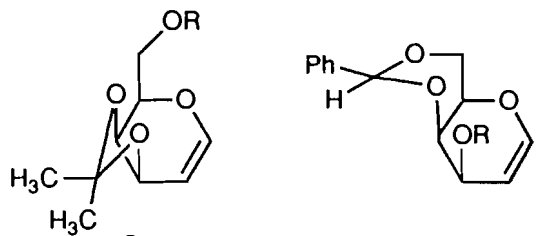

3*a* R=H
3*b* R=Ac
3*c* R=Bn
3*d* R=TBDMS
3*e* R=Allyl

4*a* R=H
4*b* R=Ac
4*c* R=Bn

TBDMS= $Si(Me)_2CMe_3$
Allyl = CH_2-CH=CH_2

Results and discussion

Treatment of 3,4,6-tri-*O*-acetyl-d-glucal (**1***a*) and 3,4,6-tri-*O*-acetyl-d-galactal (**2***a*) with (diacetoxyiodo)benzene (1.4 equiv.) and sodium azide (2.4 equiv.) in the presence of diphenyldiselenide (0.6 equiv.) in methylene chloride at room temperature afforded phenyl 3,4,6-tri-*O*-acetyl-2-azido-2-deoxy-1-seleno-α-d-glycopyranosides in good yield (Table 1, entries 1 and 3). From **1***a* the *gluco* (**5***a*) and *manno* (**6***a*) isomers were obtained in 91% yield as an inseparable mixture. From the integration of H1 signals in the ^1H NMR spectrum of the mixture, the proportion was found to be 3:2. Interestingly, only the α anomers were formed, as indicated by the values of the H1,H2 coupling constants (5.3 Hz for the *gluco* isomer and ≈0 Hz for the *manno* isomer). From **2***a*, only one compound, the α-*galacto* isomer **7***a*, was formed and isolated in crystalline form (92%). No *talo* isomer **8***a* could be detected in the ^1H NMR spectrum of the crude mixture, although it is known that some *talo* azidonitrate (4–8%) is formed in azidonitration of protected d-galactal (3, 4). The regio- and the stereochemistry of this reaction can be rationalized by addition of an electrophilic azido radical (10) formed in situ by oxidation of azide ion (11) to C2 of the electron-rich double bond of the glycal, generating an anomeric radical by the anomeric effect in the α configuration. Further reaction with diphenyldiselenide affords the α-selenoglycosides.

When perbenzylated glycals **1***b* (12) and **2***b* (13) were reacted under the same conditions, perbenzylated phenyl 2-azido-2-deoxy-1-seleno-α-d-glycopyranosides were obtained in low yield, in agreement with recent results (14). This could be due to oxidative cleavage of the benzyl group under reaction conditions. Interestingly, when **1***b* and **2***b* were reacted with azidotrimethylsilane (2 equiv.), tetra-*n*-butylammonium fluoride (0.2 equiv.), and *N*-phenylselenophthalimide (*N*-PSP, 2 equiv.) in methylene chloride, phenyl 2-azido-3,4,6-tri-*O*-benzyl-2-deoxy-1-seleno-α-d-glycopyranosides were obtained in good yield. As above, a mixture of *gluco* (**5***b*) and

Can. J. Chem. Downloaded from www.nrcresearchpress.com by 65.111.164.53 on 09/08/12
For personal use only.

Can. J. Chem. Downloaded from www.nrcresearchpress.com by 65.111.164.53 on 09/08/12
For personal use only.

manno (**6***b*) isomers was obtained (82%) with low diastereoselectivity (70:30) from the *glucal* derivative **1***b*, whereas complete diastereocontrol was observed and the α-*galacto* selenoglycoside **7***b* was obtained as the sole product (75%) from **2***b*. The regio- and diastereochemical outcome of the reaction was verified by ^{1}H NMR spectroscopy. The chemical shifts of H1 of **5***b*, **6***b*, and **7***b* (5.95, 5.85, and 5.93 ppm, respectively) are in agreement with the values already reported for selenoglycosides (15–17) and azido sugars (18). the presence of the phenylseleno group of C1 was further confirmed by hydrolysis leading to 2-azido-2-deoxyglycopyranose derivatives (vide infra). Transformation of **7***a* into **7***b* by deacetylation and benzylation (see Experimental) definitively confirmed that the regioselectivity of the reaction was the same as above.

Although more work is necessary to understand and to rationalize these results, similar changes in regioselectivity in azido-phenylselenylation have already been observed with exocyclic alkenes (19).

The compatibility of this methodology with many protecting groups was further demonstrated with diversely protected D-galactal derivatives, which are often employed in oligosaccharide synthesis: 1,5-anhydro-2-deoxy-3,4-*O*-isopropylidene-D-*lyxo*-hex-1-enitol (**3***a*) (20) and its 6-*O*-acetylated (**3***b*) (20), 6-*O*-benzylated (**3***c*) (20), and 6-*O*-*tert*-butyldimethylsilylated (**3***d*) derivatives. The compatibility with the benzylidene group, which is very sensitive to oxidation and to radical reactions, was also demonstrated with 1,5 anhydro-4,6-*O*-benzylidene-2-deoxy-D-*lyxo*-hex-1-enitol (**4***a*) (20) and its 3-*O*-acetyl (**4***b*) (4) and 3-*O*-benzyl (**4***c*) (20) derivatives.

Azido-phenylselenylation of acetylated derivative **3***b* according to procedure A was very slow, but the same diastereocontrol was observed and the α-*galacto* selenoglycoside **9***b* was obtained (Table 1, entry 7). Better results were obtained with procedure B, which was employed for the transformation of **3***b*, **3***c*, **3***d*, **4***b*, and **4***c* into protected 2-azido-2-deoxy-1-seleno-α-D-galactopyranosides in good yield (see Table 1). For **3***d*, in which a *tert*-butyldimethylsilyl group was present, tetra-*n*-butylammonium fluoride was omitted, the reaction time was longer than with other glycals, and the yield of **9***d* slightly lower (66%). Transformation of **9***d* into **9***b* by desilylation and acetylation further confirmed that the regioselectivity was the same with both methods. The *galacto* configuration of the resulting 2-azido-2-deoxyselenoglycosides was confirmed by ^{1}H NMR spectroscopy. For **9***b*, **9***c*, **9***d*, and **9***e*, the values of coupling constants of H2 with H1 (≈5 Hz indicating a *cis* relationship) and with H3 (6–7 Hz) were in agreement with values already reported for such 3,4-*O*-isopropylidene *galacto* derivatives (20). For **10***b* and **10***c* the corresponding coupling constants ($J_{1,2}$ = 5.2 Hz and $J_{2,3}$ = 10.5 Hz) clearly indicated the α-D-*galacto* configuration.

Interestingly, azido-phenylselenylation by procedure B was also possible in the presence of one unprotected hydroxyl group and compounds **3***a* and **4***a* were transformed into **9***a*[2] and **10***a* (Table 1, entries 5 and 11). Although the reaction was not as clean and the yield was lower, this possibility is interesting because **9***a* and **10***a* could eventually serve as glycosyl acceptors as well as glycosyl donors.

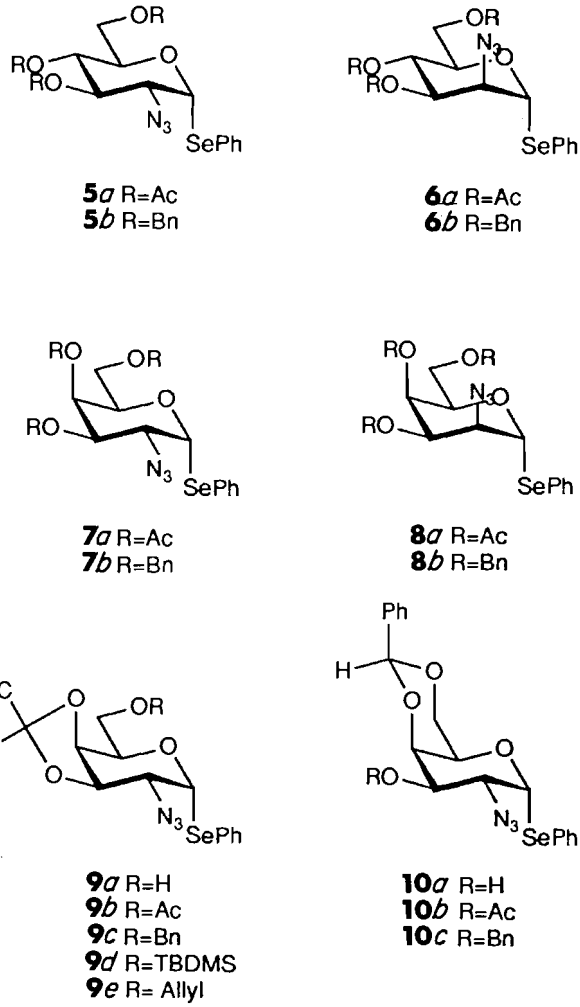

Furthermore, it was verified that the reaction can be successfully carried out in the presence of an *O*-allyl ether. For that purpose, 6-*O*-allyl-1,5-anhydro-2-deoxy-3,4-*O*-isopropylidene-D-*lyxo*-1-enitol **3***e* was prepared from **3***a*. Azido-phenylselenylation of **3***e* according to procedure B was highly selective and protected 2-azido-2-deoxy-1-seleno-α-D-galactopyranoside **9***e* was obtained in 74% yield. The product formed by double azido-phenylselenylation was isolated (3%) and characterized by ^{1}H NMR.[3]

These easily obtained 2-azido-2-deoxyselenoglycosides were subjected to hydrolysis to generate the anomeric hydroxyl. Owing to the *soft* nature of the selenium atom, *soft* catalysts such as heavy metal salts were evaluated.

When ether-oxides or acetals were present as protecting group, hydrolysis was complete in 30 min at room temperature in the presence of mercury trifluoroacetate in wet tetrahydrofuran and the protected 2-azido-2-deoxyglycopyranoses were obtained in good yield (see Table 1). When mercury acetate was employed, some 1-*O*-acetyl derivative was also

[2] In this case the regioselectivity was not complete and a small amount (7%) of 3,4-*O*-isopropylidene-2-phenylseleno-β-D-galactopyranosyl azide was also formed, isolated, and characterized by analysis and spectroscopic methods (see experimental).

[3] ^{1}H NMR (200 MHz, $CDCl_3$) δ: 1.20 (s, 3H, CH_3), 1.40 (s, 3H, CH_3), 3.10-3.80 (m, 6H), 3.90-4.30 (m, 4H), 4.50 (m, 1H, $J_{2,3}$ = 7.2 Hz, H2), 5.80 (d, 1H, $J_{1,2}$ = 5 Hz, H1), 7.10-7.70 (m, 10 H, aromatic).

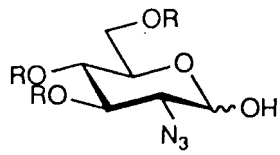

11*a* R=Ac
11*b* R=Bn

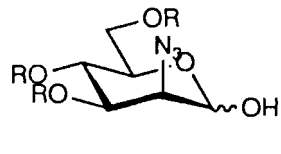

12*a* R=Ac
12*b* R=Bn

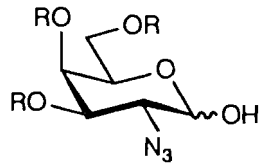

13*a* R=Ac
13*b* R=Bn

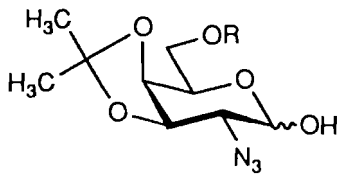

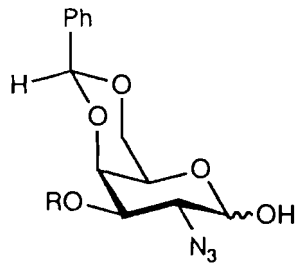

14*a* R=Ac
14*b* R=Bn
14*c* R=Allyl

15*a* R=Ac
15*b* R=Bn

formed. Hydrolysis of the *gluco–manno* mixture of **5***b* and **6***b* afforded a mixture of **11***b* and **12***b* that could be separated by flash chromatography, and **11***b* was obtained in crystalline form (66%).

Under these conditions, the hydrolysis of acetylated derivatives **5***a*, **6***a*, and **7***a* was very slow, presumably because the electron-withdrawing effect of the acetoxy group does not favor the formation of the carbenium ion. When *N*-iodosuccinimide (5 equiv.) was employed instead of mercury trifluoroacetate, the reaction was complete in 12 h at room temperature. From **5***a*–**6***a*, an inseparable mixture of **11***a* and **12***a* was obtained, whereas the *galacto* azido-selenoglycoside **7***a* was transformed into **13***a* (87%).

The complete stereocontrol obtained in the *galacto* series makes this procedure very useful. For convenience, it was verified with **2***b* that the two steps can be carried out without purification of the intermediate azido-selenoglycoside **7***b*. In this case, after azido-phenylsenylation, the precipitate was filtered off and the solvent evaporated. Hydrolysis of the crude **7***b* afforded **13***b* after flash chromatography (72% overall yield).

Conclusion

The presently described transformation of protected glycals into 2-azido-2-deoxyglycopyranosides represents a new and very efficient method for the preparation of these important intermediates in oligosaccharide synthesis (21). The overall yield obtained for the preparation of these 2-azido-2-deoxyglycopyranoses compares favorably with yields previously reported for azidonitration followed by hydrolysis. The success of the process in the case of D-galactal derivatives is particularly remarkable because only the *galacto* isomer is obtained in high yield, affording an easy access to galactosamine donors. Another advantage of this methodology is its compatibility with a variety of protecting groups including acetates, acetals, allyl ethers, benzyl ethers, benzylidene groups, and silyl ethers as well as with one nonprotected hydroxyl group. The mild conditions employed would also allow extension of this methodology to glycals derived from disaccharides.

Experimental

General procedures

Melting points were measured with a Thomas–Hoover apparatus and are uncorrected. IR spectra were recorded with a Unicam spectrometer. ^{1}H NMR spectra were recorded on a Bruker AM 200 spectrometer. Optical rotations were measured on a Perkin–Elmer 141 polarimeter in a 10 cm cell at 22°C. Analytical TLC was performed on Merck aluminum precoated plates of silica gel 60 F-254 with detection by UV and by spraying with 6 N H_2SO_4 and heating about 2 min at 300°C. For flash chromatography, Merck silica gel 60 (230–400 mesh) and anhydrous solvents were employed. Solvents were evaporated under reduced pressure in a rotary evaporator below 30°C.

Microanalyses were performed at the Service de Microanalyse de l'Université Pierre et Marie Curie.

N-Phenylselenophthalimide (*N*-PSP) was prepared according to Nicolaou et al. (22).

*1,5-Anhydro-2-deoxy-3,4-*O*-isopropylidene-6-*O*-tert-butyldimethylsilyl-*D*-lyxo-hex-1-enitol* **3***d*

To a solution of **3***a* (20) (500 mg, 2.68 mmol) and imidazole (456 mg, 6.7 mmol) in DMF (5 mL), *tert*-butyldimethylsilylchloride (505 mg, 3.35 mmol) was added. The reaction was stirred at 46°C for 48 h. The solvent was evaporated and the residue partitioned between H_2O and Et_2O (20 mL, 1:1) and

Can. J. Chem. Downloaded from www.nrcresearchpress.com by 65.111.164.53 on 09/08/12
For personal use only.

Can. J. Chem. Downloaded from www.nrcresearchpress.com by 65.111.164.53 on 09/08/12
For personal use only.

the aqueous phase extracted with ether (2 × 10 mL). The combined Et_2O layer was washed with H_2O (2 × 10 mL) and dried ($MgSO_4$). After evaporation, the residue was purified by flash chromatography. Elution with CH_2Cl_2–hexane (1:4 and 3:7) afforded ***3d*** (677 mg, 84%), solid, mp 38–40°C; R_f 0.77 (EtOAc–hexane 1:9); $[\alpha]_D$ −2.6 (*c* 1, CH_2Cl_2); ^{1}H NMR (200 MHz, $CDCl_3$) δ: 0.10 (s, 6H, $2CH_3$, silyl), 0.90 (s, 9H, $3CH_3$, silyl), 1.40 (s, 3H, CH_3), 1.45 (s, 3H, CH_3), 3.90 (m, 3H, H5, H6, H6′), 4.35 (ddd, 1H, $J_{3,4}$ = 6 Hz, H4), 4.60 (dd, 1H, $J_{2,3}$ = 2.7 Hz, H3), 4.75 (ddd, 1H, $J_{1,2}$ = 6.2 Hz, $J_{2,4}$ = 1.6 Hz, H2), 6.30 (d, 1H, H1). Anal. calcd. for $C_{15}H_{28}O_4Si$: C 59.96, H 9.39; found: C 60.27, H 9.12.

*6-O-Allyl-1,5-anhydro-2-deoxy-3,4-O-isopropylidene-*d*-lyxo-hex-1-enitol* ***3e***

Sodium hydride (60%, 146 mg, 3.48 mmol) was added in small portions to a solution of ***3a*** (590 mg, 3.17 mmol) in DMF (10 mL) under stirring and cooling in ice-water. The mixture was then stirred for 30 min at room temperature, allyl bromide (304 μL, 3.48 mmol) was added dropwise, and the mixture was stirred overnight at room temperature. Excess NaH was destroyed with MeOH and the reaction mixture partitioned between H_2O and CH_2Cl_2 (30 mL, 1:1). The aqueous layer was reextracted with CH_2Cl_2 (2 × 5 mL). The combined organic phase was washed with H_2O until the pH was neutral and then dried ($MgSO_4$). Evaporation afforded a residue, which was chromatographed on silica gel. Elution with EtOAc–hexane (1:10) afforded ***3e***: 584 mg (81%) as an oil. R_f 0.63 (EtOAc–hexane 1:9); $[\alpha]_D$ 14.2 (*c* 1, CH_2Cl_2); ^{1}H NMR (200 MHz, $CDCl_3$) δ: 1.30 (s, 3H, CH_3), 1.50 (s, 3H, CH_3), 3.65–3.85 (2dd, 2H, $J_{5,6}$ = 5 Hz $J_{5,6'}$ = 7.6 Hz, $J_{6,6'}$ = 10.2 Hz, H6, H6′), 4.10 (m, 1H, H4), 4.20 (m, 3H, CH_2 allyl, H5), 4.7 (dd, 1H, $J_{3,4}$ = 6.2 Hz, H3), 4.80 (m, 1H, $J_{2,4}$ = 1.5 Hz, $J_{2,3}$ = 2.8 Hz, H2), 5.30 (m, 2H, CH=*CH*$_2$), 5.90 (m, 1H, *CH*=CH$_2$), 6.40 (d, 1H, $J_{1,2}$ = 6.3 Hz, H1). Anal. calcd. for $C_{12}H_{18}O_4$: C 63.69, H 8.01; found: C, 63.43, H 8.16.

Typical procedures for azido-phenylselenylation

Procedure A

To a stirred solution of glycal (1 mmol), diphenyldiselenide (0.6 mmol), and sodium azide (2.4 mmol) in dichloromethane (4 mL) under argon, (diacetoxyiodo)benzene (1.4 mmol) was added. The mixture was stirred at room temperature during 48 h until TLC indicated completion of the reaction. The solution was diluted with dichloromethane (20 mL) and washed with 5% aqueous $NaHCO_3$ (2 × 8 mL). The aqueous layer was reextracted with dichloromethane (2 × 5 mL), the organic layer was washed until neutral pH, dried over $MgSO_4$, filtered, and evaporated. The crude product was purified by column chromatography on silica gel.

Procedure B

To a stirred solution of glycal (1 mmol), azidotrimethylsilane (2 mmol), and tetra-*n*-butylammonium fluoride (0.2 mmol) in dichloromethane (10 mL) under argon, was added *N*-PSP (2 mmol). The mixture was stirred at room temperature during 48 h. The solvent was evaporated, toluene (15 mL) was added, the precipitated salts were filtered off, and the crude mixture was concentrated and purified by column chromatography on silica gel. The following 2-azido-2-deoxy-1-seleno-α-d-glycopyranosides were prepared using one of these procedures.

*Phenyl 3,4,6-tri-*O*-acetyl-2-azido-2-deoxy-1-seleno-*α*-*d*-glucopyranoside* ***5a*** *and* α-d-*mannopyranoside* ***6a***

Procedure A: yield (91%), oil; R_f 0.75 (CH_2Cl_2–Et_2O 9:1); IR (neat): 2119 (N_3), 1757 (OAc) cm^{-1}; ^{1}H NMR (200 MHz, $CDCl_3$) *gluco* isomer δ: 2.00–2.20 (3s, 9H, OAc), 3.90–4.00 (dd, 1H, $J_{6',6}$ = 12.21 Hz, $J_{6,5}$ = 1.96 Hz, H6), 4.00–4.10 (dd, 1H, $J_{2,3}$ = 10.15 Hz, H2), 4.25–4.35 (dd, 1H, $J_{6',5}$ = 4.89 Hz, H6′), 4.50 (m, 1H, $J_{5,4}$ = 10.4 Hz, H5), 5.20–5.50 (m, 2H, H3, H4), 5.95 (d, 1H, $J_{1,2}$ = 5.39 Hz, H1), 7.15–7.20 (m, 5H, aromatic); *manno* isomer δ: 2.10–2.30 (3s, 9H, OAc), 4.20 (2dd, 2H, $J_{6,6'}$ = 12.24 Hz, $J_{6,5}$ = 2.16 Hz, $J_{6',5}$ = 5.15 Hz, H6, H6′), 4.37 (dd, 1H, $J_{2,3}$ = 2.95 Hz, H2), 4.45 (m, 1H, H5), 5.25–5.45 (m, 2H, H3, H4), 5.80 (d, 1H, $J_{1,2}$ = 1.27 Hz, H1), 7.20–7.70 (m, 5H, aromatic). Anal. calcd. for $C_{18}H_{21}O_7N_3Se$: C 45.96, H 4.50, N 8.93; found: C 46.35, H 4.47, N 9.00.

*Phenyl 3,4,6-tri-*O*-acetyl-2-azido-2-deoxy-1-seleno-*α*-*d*-galactopyranoside* ***7a***

Procedure A: yield (92%), solid, mp 104–105°C; R_f 0.75 (CH_2Cl_2–Et_2O 9:1); $[\alpha]_D$ +170 (*c* 1, CH_2Cl_2); IR (KBr): 2119 (N_3), 1757 (OAc) cm^{-1}; ^{1}H NMR (200 MHz, $CDCl_3$) δ: 2.20 (3s, 9H, OAc), 4.05 (2dd, 2H, $J_{6,5}$ = 7.1 Hz, $J_{6,6'}$ = 11.4 Hz, H6, H6′), 4.30 (dd, 1H, $J_{2,3}$ = 10.8 Hz, H2), 4.70 (bt, 1H, H5), 5.15 (dd, 1H, $J_{3,4}$ = 3.2 Hz, H3), 5.50 (dd, 1H, $J_{4,5}$ = 1.1 Hz, H4), 6.00 (d, 1H, $J_{1,2}$ = 5.4 Hz, H1), 7.20–7.70 (m, 5H, aromatic). Anal. calcd. for $C_{18}H_{21}O_7N_3Se$: C 45.96, H 4.50, N 8.93; found: C 46.06, H 4.50, N 9.08.

*Phenyl 2-azido-3,4,6-tri-*O*-benzyl-2-deoxy-1-seleno-*α*-*d*-glucopyranoside* ***5b*** *and* -α-d-*mannopyranoside* ***6b***

Procedure B: yield (82%), oil; R_f 0.75 (CH_2Cl_2–hexane 9:1); IR (neat): 2119 (N_3) cm^{-1}; ^{1}H NMR (200 MHz, $CDCl_3$) δ: 3.50–4.30 (m, 6H, H2, H3, H4, H5, H6, H6′), 4.40–5.00 (m, 6H, $3CH_2$ benzyl), 5.85 (bs, 0.3H, H1 *manno*), 5.95 (d, 0.7 H, $J_{1,2}$ = 4.98 Hz, H1 *gluco*), 7.00–7.70 (m, 20H, aromatic). Anal. calcd. for $C_{33}H_{33}O_4N_3Se$: C 64.49, H 5.41, N 6.83; found: C 64.43, H 5.48, N 7.00.

*Phenyl 2-azido-3,4,6-tri-*O*-benzyl-2-deoxy-1-seleno-*α*-*d*-galactopyranoside* ***7b***

Procedure B: yield (75%), oil; R_f 0.75 (CH_2Cl_2–hexane 9:1); $[\alpha]_D$ +157 (*c* 1, CH_2Cl_2); IR (neat): 2119 (N_3) cm^{-1}; ^{1}H NMR (200 MHz, $CDCl_3$) δ: 3.40–3.65 (m, 3H, H5, H6, H6′), 3.75 (dd, 1H, $J_{3,2}$ = 10.48 Hz, $J_{3,4}$ = 2.65 Hz, H3), 4.05 (d, 1H, H4), 4.30–5.00 (m, 7H, $3CH_2$ benzyl, H2), 5.93 (d, 1H, $J_{1,2}$ = 5.22 Hz, H1) 7.10–7.70 (m, 20H, aromatic) Anal. calcd. for $C_{33}H_{33}O_4N_3Se$: C 64.49, H 5.41, N 6.83; found: C 64.59, H 5.59, N 7.02.

*Phenyl 6-*O*-acetyl-2-azido-2-deoxy-3,4-*O*-isopropylidene-1-seleno-*α*-*d*-galactopyranoside* ***9b***

Procedure B: yield (91%), solid, mp 86–88°C; R_f 0.59 (EtOAc–hexane 1:4); $[\alpha]_D$ +237.7 (*c* 1, CH_2Cl_2); IR (KBr): 2119 (N_3), 1750 (CO) cm^{-1}; ^{1}H NMR (200 MHz, $CDCl_3$) δ: 1.15 (1s, 3H, CH_3), 1.25 (1s, 3H, CH_3), 2.00 (1s, 3H, OAc), 4.00 (t, 1H, $J_{4,5}$ = 1.65 Hz, $J_{5,6}$ = 5.5 Hz, $J_{5,6'}$ = 4.91 Hz, H5), 4.10–4.20 (m, 4H, H3, H4, H6, H6′), 4.30 (dd, 1H, $J_{2,3}$ = 6.05

Can. J. Chem. Downloaded from www.nrcresearchpress.com by 65.111.164.53 on 09/08/12
For personal use only.

Hz, H2), 5.90 (d, 1H, $J_{1,2}$ = 4.95 Hz, H1), 7.10–7.80 (m, 5H, aromatic). Anal. calcd. for $C_{17}H_{21}O_5N_3Se$: C 47.89, H 4.96, N 9.86; found: C 47.98, H 4.96, N 9.99.

*Phenyl 2-azido-6-*O*-benzyl-2-deoxy-3,4-*O*-isopropylidene-1-seleno-*α*-*D*-galactopyranoside* **9**c

Procedure B: yield (84%), oil; R_f 0.57 (EtOAc–hexane 1:9); $[\alpha]_D$ +202.8 (*c* 1, CH_2Cl_2); IR (neat): 2119 (N_3) cm^{-1}; ^1H NMR (200 MHz, $CDCl_3$) δ: 1.40 (1s, 3H, CH_3) 1.55 (1s, 3H, CH_3), 3.70–3.90 (m, 2H, $J_{5,6}$ = 6.61 Hz, $J_{5,6'}$ = 5.11 Hz, $J_{6,6'}$ = 12.3 Hz, H6, H6′), 4.00 (t, 1H, $J_{4,5}$ = 1.4 Hz, H5), 4.05–4.45 (m, 2H, H3, H4), 4.60 (dd, 2H, CH_2 benzyl), 4.70 (1H, $J_{2,3}$ = 6.91 Hz, H2), 5.9 (d, 1H, $J_{1,2}$ = 4.95 Hz, H1), 7.00–7.60 (m, 10H, aromatic). Anal. calcd. for $C_{22}H_{25}O_4N_3Se$: C 55.69, H 5.31, N 8.86; found: C 55.62, H 5.28, N 9.00.

*Phenyl 2-azido-2-deoxy-3,4-O-isopropylidene-6-*O*-tert-butyldimethylsilyl-1-seleno-*α*-*D*-galactopyranoside* **9***d*

Procedure B: yield (66%), oil; R_f 0.56 (EtOAc–hexane 1:12); $[\alpha]_D$ +170.3 (*c* 1, CH_2Cl_2); IR (neat): 2119 (N_3) cm^{-1}; ^1H NMR (200 MHz, $CDCl_3$) δ: 0.00 (1s, 6H, $2CH_3$, silyl), 0.80 (1s, 9H, $3CH_3$, silyl) 1.35 (1s, 3H, CH_3), 1.50 (1s, 3H, CH_3), 3.65–3.95 (m, 3H, $J_{6,6'}$ = 10.2 Hz, $J_{5,6}$ = 6.6 Hz, $J_{5,6'}$ = 6.4 Hz, H6, H6′, $J_{2,3}$ = 7.7 Hz, H2), 4.10–4.30 (m, 2H, $J_{3,4}$ = 5.3 Hz, H3, $J_{4,5}$ = 2.36 Hz, H4), 4.45 (m, 1H, H5), 5.75 (d, 1H, $J_{1,2}$ = 5.02 Hz, H1), 7.1–7.7 (m, 5H, aromatic). Anal. calcd. for $C_{21}H_{33}O_4N_3SeSi$: C 50.59, H 6.67, N 8.42; found: C 50.33, H 6.77, N 8.34.

*Phenyl 2-azido-3,4,6-tri-O-benzyl-2-deoxy-1-seleno-*α*-*D*-galactopyranoside* **7**b *from* **7**a

A solution of **7***a* (235 mg, 0.5 mmol) and NaOMe (1 M, 0.8 mL) in MeOH (1 mL) was stirred at room temperature until deacetylation was complete (15 h). After neutralization with Amberlite resin IRN 77 (H^+ form) and filtration, evaporation of the solvent afforded a crude product (197 mg), which was dissolved in DMF (2.5 mL). After cooling at 0°C, NaH (60%, 80 mg, 2 mmol) was added. After stirring 1 h, benzyl bromide (200 μL, 1.65 mmol) was added and the mixture stirred at room temperature until TLC indicated completion of the reaction (15 h). Excess NaH was destroyed with MeOH and the reaction mixture partitioned between H_2O and CH_2Cl_2 (30 mL, 1:1). The aqueous layer was reextracted with CH_2Cl_2 (2 × 5 mL). The combined organic phase was washed with H_2O until neutral pH, and dried ($MgSO_4$). Evaporation afforded a residue, which was chromatographed on silica gel. Elution with CH_2Cl_2–hexane (1:1) afforded **7***b*: 253 mg (82%) as an oil identical to **7***b* prepared by azido-phenylselenylation of **2***b*.

*Phenyl 6-*O*-acetyl-2-azido-2-deoxy-3,4-*O*-isopropylidene-1-seleno-*α*-*D*-galactopyranoside* **9**b *from* **9**d

To a solution of **9***d* (20 mg, 0.04 mmol) in THF (100 μL) was added *n*-Bu_4NF (1.1 M THF solution, 35 mL). Completion of the reaction was observed after stirring 30 min at room temperature. After evaporation, the residue was dissolved in pyridine (25 μL), and Ac_2O (12 μL, 0.12 mmol) was added. After stirring overnight at room temperature, evaporation and coevaporation with toluene afforded a residue, which was chromatographed on silica gel. Elution with EtOAc–hexane (1:16) afforded crude **9***b* (12 mg, 70%). Recrystallization from absolute EtOH afforded an analytical sample identical to **9***b* prepared by azido-phenylselenylation of **3***b*.

*Phenyl 2-azido-2-deoxy-3,4-*O*-isopropylidene-1-seleno-*α*-*D*-galactopyranoside* **9**a

Procedure B: yield (59%), oil; R_f 0.79 (EtOAc–hexane 1:9); $[\alpha]_D$ +167.7 (*c* 1, CH_2Cl_2); IR (neat): 2119 (N_3), 3400 (OH) cm^{-1}, ^1H NMR (200 MHz, $CDCl_3$) δ: 1.38 (1s, 3H, CH_3), 1.55 (1s, 3H, CH_3), 1.78 (1s, 1H, OH), 3.70–3.90 (m, 2H, H6, H6′), 3.90–4.00 (dd, 1H, $J_{2,3}$ = 7.5 Hz, H2), 4.15–4.35 (m, 2H, $J_{3,4}$ = 5.34 Hz, H3, H4), 4.40–4.60 (m, 1H, H5), 5.80 (d, 1H, $J_{1,2}$ = 5.15 Hz, H1), 7.10–7.60 (m, 5H, aromatic). Anal. calcd. for $C_{15}H_{19}O_4N_3Se$: C 46.88, H 4.98, N 10.93; found: C 46.86, H 5.28, N 10.93.

*3,4-*O*-Isopropylidene-2-phenylseleno-*β*-*D*-galactopyranosyl azide*

Procedure B: yield (7%), oil; R_f 0.56 (EtOAc–hexane 1:9); $[\alpha]_D$ +31.4 (*c* 1, CH_2Cl_2); IR (neat): 2119 (N_3), 3400 (OH) cm^{-1}; ^1H NMR (200 MHz, $CDCl_3$) δ: 1.30 (1s 3H, CH_3), 1.40 (1s, 3H, CH_3), 2.50 (1s, 1H, OH), 3.40 (dd, 1H, $J_{1,3}$ = 6.7 Hz, H2), 3.70–4.20 (m, 5H, H3, H4, H5, H6, H6′), 4.60 (d, 1H, $J_{1,2}$ = 10.5 Hz, H1), 7.10–7.80 (m, 5H, aromatic). Anal. calcd. for $C_{15}H_{19}O_4N_3Se$: C 46.88, H 4.98, N 10.93; found: C 47.82, H 5.27, N 10.66.

*Phenyl 6-*O*-allyl-2-azido-2-deoxy-3,4-*O*-isopropylidene-1-seleno-*α*-*D*-galactopyranoside* **9**e

Procedure B: yield (74%), oil; R_f 0.42 (EtOAc–hexane 1:12); $[\alpha]_D$ +223.8 (*c* 1, CH_2Cl_2); IR (neat): 2119 (N_3) cm^{-1}; ^1H NMR (200 MHz, $CDCl_3$) δ: 1.30 (1s, 3H, CH_3), 1.50 (1s, 3H, CH_3), 3.50–3.80 (2dd, 2H, $J_{5,6}$ = 7.10 Hz, $J_{5,6'}$ = 5 Hz, $J_{6,6'}$ = 10.5 Hz, H6, H6′), 3.85–4.00 (m, 3H), 4.15 (m, 2H, CH_2 allyl), 4.60 (m, 1H), 5.05–5.25 (m, 2H, CH=CH_2), 5.75 (d, 1H, $J_{1,2}$ = 5.1 Hz, H1), 5.80–5.90 (m, 1H, CH=CH_2), 7.10–7.70 (m, 5H, aromatic). Anal. calcd. for $C_{18}H_{23}O_4N_3Se$: C 50.94, H 5.46, N 9.90; found: C 51.15, H 5.29, N 9.93.

*Phenyl 2-azido-4,6-*O*-benzylidene-2-deoxy-1-seleno-*α*-*D*-galactopyranoside* **10**a

Procedure B: yield (68%), solid; mp 116–117°C; R_f 0.57 (ether–hexane 1:4); $[\alpha]_D$ +155.8 (*c* 1, CH_2Cl_2); IR (KBr): 2119 (N_3), 3400 (OH) cm^{-1}; ^1H NMR (200 MHz, $CDCl_3$) δ: 1.6 (1s, 1H, OH), 4.00 (dd, 1H, $J_{5,6}$ = 3.41 Hz, $J_{6,6'}$ = 10 Hz, H6), 4.05 (m, 3H H3, H5, H6′), 4.20 (d, 1H, $J_{4,5}$ = 1 Hz, H4), 5.55 (s, 1H, PhCH), 4.30 (dd, 1H, $J_{2,3}$ = 10.05 Hz, H2), 6.05 (d, 1H, $J_{1,2}$ = 5.03 Hz, H1), 7.20–7.60 (m, 10H, aromatic). Anal. calcd. for $C_{19}H_{19}O_4N_3Se$: C 52.78, H 4.43, N 9.72; found: C 52.93, H 4.45, N 9.46.

*Phenyl 3-*O*-acetyl-2-azido-4,6-*O*-benzylidene-2-deoxy-1-seleno-*α*-*D*-galactopyranoside* **10**b

Procedure B: yield (73%), solid; mp 135–137°C; R_f 0.50 (EtOAc–hexane 1:4); $[\alpha]_D$ +307.9 (*c* 1, CH_2Cl_2); IR (KBr): 2119 (N_3), 1750 (OAc) cm^{-1}; ^1H NMR (200 MHz, $CDCl_3$) δ: 2.20 (1s, 3H, OAc), 4.00–4.30 (m, 3H, $J_{5,6}$ = 1.8 Hz, $J_{5,6'}$ = 1.45 Hz, $J_{6,6'}$ = 12.75 Hz, H5, H6, H6′), 4.40–4.60 (m, 2H, H2, H4), 5.10 (dd, 1H, $J_{2,3}$ = 10.8 Hz, $J_{3,4}$ = 3.38 Hz, H3), 5.60 (1s, 1H, PhCH), 6.10 (d, 1H, $J_{1,2}$ = 5.2 Hz, H1), 7.20–7.70 (m, 10H, aromatic). Anal. calcd. for $C_{21}H_{21}O_5N_3Se$: C 53.16, H 4.46, N 8.85; found: C 53.18, H 4.55, N 8.88.

Can. J. Chem. Downloaded from www.nrcresearchpress.com by 65.111.164.53 on 09/08/12
For personal use only.

Phenyl 2-azido-3-O-benzyl-4,6-O-benzylidene-2-deoxy-1-seleno-α-D-galactopyranoside ***10***c

Procedure B: yield (76%), solid; mp 141–143°C; R_f 0.63 (EtOAc–hexane 1:4); $[\alpha]_D$ +143.3 (*c* 1, CH_2Cl_2); IR (KBr): 2119 (N_3) cm^{-1}; ^1H NMR (200 MHz, $CDCl_3$) δ: 3.80 (dd, 1H, $J_{2,3}$ = 10.37 Hz, $J_{3,4}$ = 3.35 Hz, H3), 3.95–415 (m, 3H, H5, H6, H6′), 4.25 (d, 1H, H4), 4.40 (dd, 1H, H2), 4.80 (dd, 2H, *J* = 12.08 Hz, $PhCH_2$), 5.50 (1s, 1H, PhCH), 6.05 (d, 1H, $J_{1,2}$ = 5.20 Hz, H1), 7.20–7.60 (m, 15H, aromatic). Anal. calcd. for $C_{26}H_{25}O_4N_3Se$: C 59.77, H 4.82, N 8.04; found: C 60.01, H 4.97, N 7.82.

Typical procedures for hydrolysis

Procedure C

A solution of the protected phenyl 2-azido-2-deoxy-α-D-selenoglycopyranoside (1 mmol) in THF–H_2O (2 mL, 1:1) was treated at room temperature with *N*-iodosuccinimide (5 mmol). After 12 h the mixture was diluted with EtOAc (10 mL), and washed with saturated K_2CO_3 (10 mL). The aqueous layer was reextracted with EtOAc (2 × 5 mL). The organic layer was washed until neutral pH, dried over $MgSO_4$, filtered, and evaporated. The crude product was purified by column chromatography on silica gel.

Procedure D

A solution of the protected phenyl 2-azido-2-deoxy-α-D-selenoglycopyranoside (1 mmol) in THF–H_2O (2 mL, 1:1), was treated at room temperature with mercury trifluoroacetate (1.5 mmol). After 30 min the mixture was diluted with EtOAc (10 mL), and washed with saturated K_2CO_3 (10 mL). The aqueous layer was reextracted with EtOAc (2 × 5 mL). The combined EtOAc layer was washed with 5% aqueous Na_2S (10 mL). The aqueous layer was reextracted with EtOAc (2 × 10 mL), the organic layer was washed until neutral pH, dried over $MgSO_4$, filtered, and evaporated. The crude product was purified by column chromatography on silica gel.

3,4,6-Tri-O-acetyl-2-azido-2-deoxy-D-glucopyranose ***11***a *and mannopyranose* ***12***a

Procedure C was applied to the mixture of **5***a* and **6***a* to give a mixture of **11***a* and **12***a* (5) in 90% yield. Anal. calcd. for $C_{12}H_{17}O_8N_3$: C 43.50, H 5.17, N 12.68; found: C 43.68, H 4.98, N 12.66.

3,4,6-Tri-O-acetyl-2-azido-2-deoxy-D-galactopyranose ***13***a

Procedure C was applied to **7***a* to give known **13***a* (5) in 87% yield. Anal. calcd. for $C_{12}H_{17}O_8N_3$: C 43.50, H 5.17, N 12.68; found: C 43.59, H 5.32, N 12.69.

2-Azido-3,4,6-tri-O-benzyl-2-deoxy-D-glycopyranose ***11***b *and mannopyranose* ***12***b

Procedure D was applied to the mixture of **5***b* and **6***b* to give a mixture of **11***b* and **12***b*, which was chromatographed on silica gel. The first fraction gave known **11***b* (23) (66%) as a solid; mp 97°C. Anal. calcd. for $C_{27}H_{29}O_5N_3$: C 68.19, H 6.14, N 8.83; found: C 67.99, H 6.14, N 8.95.

The second fraction afforded **12***b* (12%) as a syrup, R_f 0.52 (ether–hexane 2:1); IR (neat): 2119 (N_3), 3400 (OH) cm^{-1}; ^1H NMR (200 MHz, $CDCl_3$) δ: 3.40 (m, 1H), 3.50–3.95 (m, 7H), 4.00–4.30 (m, 4H, $J_{2,3}$ = 3.56 Hz, $J_{3,4}$ = 9.12 Hz, H4), 4.45–5.00 (m, 9H, $J_{1,2}$ = 1.63 Hz, H2), 5.15 (s, 1H, H2), 7.10–7.60 (15H, aromatic). Anal. calcd. for $C_{27}H_{29}O_5N_3$: C 68.19, H 6.14, N 8.83; found: C 68.62, H 6.16, N 8.79.

A mixture of **11***b* and **12***b* was obtained in 15% yield.

2-Azido-3,4,6-tri-O-benzyl-2-deoxy-D-galactopyranose ***13***b

Procedure D was applied to **7***b* to give known **13***b* (5) in 87% yield. Anal. calcd. for $C_{27}H_{29}O_5N_3$: C 68.19, H 6.14, N 8.83; found: C 68.17, H 6.10, N 8.68.

6-O-Acetyl-2-azido-2-deoxy-3,4-O-isopropylidene-D-galactopyranose ***14***a

Procedure D was applied to **9***b* to give known **14***a* (8) in 79% yield. Anal. calcd. for $C_{11}H_{17}O_6N_3$: C 45.98, H 5.82, N 14.62; found: C 46.12, H 5.82, N 14.63.

2-Azido-6-O-benzyl-2-deoxy-3,4-O-isopropylidene-D-galactopyranose ***14***b

Procedure D was applied to **9***c* to give known **14***b* (7) in 87% yield. Anal. calcd. for $C_{16}H_{21}O_5N_3$: C 57.30, H 6.31, N 12.53; found: C 57.45, H 6.42, N 12.66.

3-O-Acetyl-2-azido-4,6-O-benzylidene-2-deoxy-D-galactopyranose ***15***a

Procedure D was applied to **10***b* to give known **15***a* (7) in 87% yield. Anal. calcd. for $C_{15}H_{17}O_6N_3$: C 57.73, H 5.11, N 12.53; found: C 57.62, H 5.17, N 12.52.

2-Azido-3-O-benzyl-4,6-O-benzylidene-2-deoxy-D-galactopyranose ***15***b

Procedure D was applied to **10***c* to give **15***b* in 82% yield as a syrup; R_f 0.52 (EtOAc–hexane 2:3); IR (neat): 2119 (N_3), 3400 (OH) cm^{-1}; ^1H NMR (200 MHz, $CDCl_3$) δ: 2.90 (1s, 1H, OH), 3.35 (1s, 1H, OH), 3.40 (dd, 1H, $J_{2,3}$ = 10.2 Hz, $J_{1,2}$ = 3.45 Hz, H2), 3.80–4.40 (m, 11H), 4.50 (1H, d, $J_{1,2}$ = 8.01 Hz, H1β), 1.75 (1s, 4H, $PhCH_2$), 5.40 (1s, 1H, H1α), 5.50 (1s, 2H, PhCH), 7.20–7.60 (m, 20H, aromatic). Anal. calcd. for $C_{20}H_{21}O_5N_3$: C 62.65, H 5.52, N 10.96; found: C 62.62, H 5.36, N 11.09.

6-O-Allyl-2-azido-2-deoxy-3,4-O-isopropylidene-D-galactopyranose ***14***c

Procedure D was applied to **9***e* to give **14***c* in 88% yield as a syrup; R_f 0.53 (EtOAc–hexane 1:3); IR (neat): 2119 (N_3), 3400 (OH) cm^{-1}; ^1H NMR (200 MHz, $CDCl_3$) δ: 1.20–1.30 (2s, 6H, 2 CH_3), 1.50–1.70 (2s, 6H, $2CH_3$), 2.50 (s, 1H, OH), 3.20–4.20 (m, 14 H), 4.30–4.45 (m, 3H), 4.50 (d, 1H, $J_{1,2}$ = 8.2 Hz, H1β), 5.20 (m, 4H, $2CH{=}CH_2$), 5.25 (d, 1H, $J_{1,2}$ = 3.3 Hz, H1α), 5.8 (m, 2H, $2CH{=}CH_2$). Anal. calcd. for $C_{12}H_{19}O_5N_3$: C 50.51, H 6.71, N 14.72; found: C 50.33, H 6.86, N 14.79.

Note added in proof

Since the submission of this paper the separation of **5***b* and **6***b* was made possible by using a less polar eluent (ether–hexane 1:11) for column chromathography on silica gel. From **1***b* (1.248 g, 3 mmol), **6***b* was obtained as a syrup (518 mg, 28%), oil; R_f 0.60 (ether–hexane 1:4); $[\alpha]_D$ +83 (*c* 1, $CHCl_3$); IR (neat): 2119 (N_3) cm^{-1}; ^1H NMR (250 MHz, $CDCl_3$) δ: 3.75 (dd, 1H, $J_{5,6}$ = 1.75 Hz, $J_{6,6'}$ = 10.9 Hz, H6), 3.85 (dd, 1H $J_{5,6'}$ = 4.5 Hz, H6′), 4.00–4.15 (m, 3H, H3, H4, H5), 4.21 (dd, 1H,

$J_{2,3}$ = 3Hz, H2), 4.60–4.79 (m, 6H, $3CH_2$ benzyl), 5,85 (d, 1H, $J_{1,2}$ = 1.4 Hz, H1), 7.10–7.50 (m, 20H, aromatic) and **5***b* as crystals (1.135 g, 61.6%), mp 86–89°C; R_f 0.45 (ether–hexane 1:4); $[\alpha]_D$ +99 (*c* 1, $CHCl_3$); IR (KBr): 2119 (N_3) cm^{-1}; ^1H NMR (250 MHz, $CDCl_3$) δ: 3.88 (dd, 1H, $J_{5,6}$ = 2 Hz, $J_{6,6'}$ = 10.1 Hz, H6), 4.05–4.25 (m, 4H, H2, H3, H4, H6′), 4.58 (m, 1H, H5), 4.88–5.3 (m, 6H, $3CH_2$ benzyl), 5.95 (d, 1H, $J_{1,2}$ = 5 Hz, H1), 7.20–7.70 (m, 20H, aromatic).

Acknowledgments

We are grateful to Doctor J.M. Valéry for recording the ^1H NMR spectra.

References

1. H. Paulsen. Chem. Soc. Rev. **13**, 15 (1984).
2. J. Banoub, P. Boullanger, and D. Lafont. Chem. Rev. **34**, 243 (1992).
3. R.V. Lemieux and R.M. Ratcliffe. Can. J. Chem. **57**, 1244 (1979).
4. A. Marra, F. Gauffeny, and P. Sinaÿ. Tetrahedron, **47**, 5149 (1991).
5. G. Grunder and R.R. Schmidt. Liebigs Ann. Chem. 1826 (1984).
6. W. Rosenbrook, Jr., D.A. Riley, and P. A. Lartey. Tetrahedron Lett. **26**, 5 (1985).
7. F. Gauffeny, A. Marra, L.K.S. Shun, P. Sinaÿ, and C. Tabeur. Carbohydr. Res. **219**, 237 (1991).
8. T. Toyokuni, S. Cai, and B. Dean. Synthesis, 1236 (1992).
9. S. Czernecki, E. Ayadi, and D. Randriamandimby. J. Chem. Soc. Chem. Commun. 35 (1994).
10. F. Minisci and R. Galli. Tetrahedron Lett. **12**, 553 (1962).
11. M. Tingoli, M. Tiecco, D. Chianelli, R. Balducci, and A. Temperini. J. Org. Chem. **56**, 6809 (1991).
12. I.D. Blackburne, P.M. Fredericks, and R.D. Guthrie. Aust. J. Chem. **29**, 381 (1976).
13. N.V. Bovin, S.E. Zarabyan, and A.Y. Khorlin. Carbohydr. Res. **98**, 25 (1981).
14. F. Santoyo-Gonzalez, F.G. Calvo-Flores, P. Garcia-Mendoza, F. Hernandez Mateo, J. Isac-Garcia, and R. Robles-Diaz. J. Org. Chem. **58**, 6122 (1993).
15. R. Benhaddou, S. Czernecki, and D. Randriamandimby. Synlett, 967 (1992).
16. H.M. Zuurmond, P.H. Van der Meer, P.A.M. Van der Klein, G.A. Van der Marel, and J.H. Van Boom. J. Carbohydr. Chem. **12**, 1091 (1992).
17. D.M. Gordon and S.J. Danishefsky. Carbohydr. Res. **206**, 361 (1990).
18. J.M. Be Miller, V.J. Blazis, and G.W. Myers. J. Carbohydr. Chem. **9**, 39 (1990).
19. R. M. Giuliano and F. Duarte. Synlett, 419 (1992).
20. A. Fernandez-Majoralas, A. Marra, A. Trumtel, A. Veyrières, and P. Sinaÿ. Carbohydr. Res. **188**, 81 (1989).
21. B. Ferrari and A. Pavia. Tetrahedron, **41**, 1939 (1985).
22. K.C. Nicolaou, D.A. Claremon, W.E. Barnette, and S.P. Seitz. J. Am. Chem. Soc. **101**, 3704 (1979).
23. W. Kinzy and R.R. Schmidt. Liebigs Ann. Chem. 1537 (1985).

Can. J. Chem. Downloaded from www.nrcresearchpress.com by 65.111.164.53 on 09/08/12
For personal use only.

Order–disorder effects in clathrates. A crystallographic and ^{35}Cl NQR spectroscopic study of CCl_3X guest molecules (X = Cl, Br, CH_3, CN, NO_2, H) in hexakis(phenylthio)benzene

L. Pang, F. Brisse, and E.A.C. Lucken

Abstract: X-ray crystallography and NQR spectroscopy have been jointly used to study CCl_3X-hexakis(phenylthio)benzene (HPTB) (X = Cl, Br, CH_3, CN, NO_2, H) clathrates. The crystal of the non-clathrated HPTB is triclinic, $P\bar{1}$, $a = 9.5614(7)$, $b = 10.2088(13)$, $c = 10.6193(11)$ Å, $\alpha = 68.45(1)°$, $\beta = 76.98(1)°$, $\gamma = 65.62(1)°$, $Z = 1$; crystals of the clathrates with CCl_3CH_3, CCl_3Br, CCl_3NO_2, and CCl_3CN are isostructural and trigonal, $R\bar{3}$, $a = 14.18$–14.32, $c = 20.47$–20.62 Å, $Z = 3$. The trigonal host cavity of HPTB clathrates contains two CCl_3X guest molecules, and the X group occupies either the axial or one of the equatorial positions and thus undergoes a molecular order/disorder depending upon its nature. Dipole–dipole interactions between host and guest molecules are considered here to explain this order/disorder effect quantitatively.

Key words: clathrates, crystal structures, NQR, hexakis(phenylthio)benzene.

Résumé : On a utilisé conjointment la cristallographie des rayons X et la spectroscopie RQN pour étudier les clathrates CCl_3X-hexakis(phénylthio)benzène (HPTB) (X = Cl, Br, CH_3, CN, NO_2 et H). Les cristaux du HPTB qui n'est pas sous la forme de clathrate sont tricliniques, $P\bar{1}$, $a = 9,5614(7)$, $b = 10,2088(13)$ et $c = 10,6193(11)$ Å, $\alpha = 68,45(1)°$, $\beta = 76,98(1)°$ et $\gamma = 65,62(1)°$, $Z = 1$; les cristaux sous la forme de clathrate avec du CCl_3CH_3, CCl_3Br, CCl_3NO_2 et CCl_3CN sont isostructuraux et trigonaux, groupe d'espace $R\bar{3}$, $a = 14,18$–$14,32$, $c = 20,47$–$20,62$ Å, $Z = 3$. La cavité trigonale hôte des clathrates de HPTB contient deux molécules invitées de CCl_3X et les groupes X occupent soit la position axiale ou l'une des positions équatoriales et ils subissent donc un ordre/désordre moléculaire dépendant de leur nature. On considère que dans ces cas, les interactions dipôle–dipôle entre les molécules hôtes et invitées peuvent expliquer quantitativement cet effet ordre/désordre.

Mots clés : clathrates, structures cristallines, RQN, hexakis(phénylthio)benzène.

[Traduit par la rédaction]

Introduction

Order–disorder phenomena are usually observed in inclusion compounds or clathrates (1). It is generally agreed that the guest molecules are disordered in the host cavity because of the weak intermolecular host–guest interactions occurring at the level of van der Waals forces (2). The guest molecules can easily adopt many molecular orientations associated with different but undistinguished local potential minima. In a clathrate where the guest molecule and the host cavity do not have the same symmetry, the guest molecules are statistically distributed over a large number of molecular orientations, so that the orientational disorder is always present in the crystals. However, in a clathrate where the guest molecule has the same symmetry as that of the host cavity, the order and disorder effects are controlled by the two factors: (1) intermolecular interactions, and (2) steric effect.

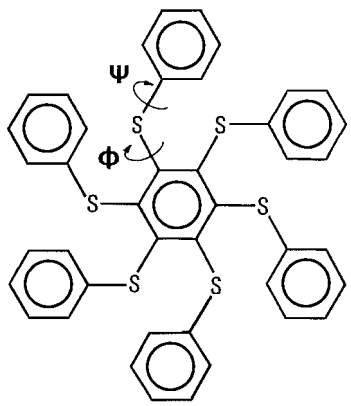

1

2 = **1**·CCl_4 (1:2)
3 = **1**·CCl_3CH_3 (1:2)
4 = **1**·CCl_3Br (1:2)
5 = **1**·CCl_3NO_2 (1:2)
6 = **1**·CCl_3CN (1:2)
7 = **1**·CCl_3H (1:2)

Received August 19, 1994.

L. Pang and F. Brisse.[1] Département de Chimie, Université de Montréal, C.P. 6128, Succ. A, Montréal, QC H3C 3J7, Canada.
E.A.C. Lucken. Département de Chimie Physique, Université de Genève, 30 quai E. Ansermet, 1211 Genève, Switzerland.

[1] Author to whom correspondence may be addressed.

Can. J. Chem. Downloaded from www.nrcresearchpress.com by 65.111.164.53 on 09/08/12
For personal use only.

Can. J. Chem. Downloaded from www.nrcresearchpress.com by 65.111.164.53 on 09/08/12
For personal use only.

Table 1. Summary of crystal data.

Compound	**1**	**3**	**4**	**5**	**6**
Formula	$C_{42}H_{30}S_6$	$C_{42}H_{30}S_6$ $2(CCl_3CH_3)$	$C_{42}H_{30}S_6$ $2(CCl_3Br)$	$C_{42}H_{30}S_6$ $2(CCl_3NO_2)$	$C_{42}H_{30}S_6$ $2(CCl_3CN)$
Crystal size (mm)	0.60 × 0.41 × 0.35	0.38 × 0.36 × 0.36	0.38 × 0.34 × 0.34	0.57 × 0.52 × 0.42	0.46 × 0.46 × 0.41
Crystal system	Triclinic	Trigonal	Trigonal	Trigonal	Trigonal
Space group	$P\bar{1}$	$R\bar{3}$	$R\bar{3}$	$R\bar{3}$	$R\bar{3}$
Refls. determining lattice	25	25	25	25	25
2θ range (deg)	$40 \leq 2\theta \leq 44$	$40 \leq 2\theta \leq 45$	$40 \leq 2\theta \leq 45$	$40 \leq 2\theta \leq 44$	$40 \leq 2\theta \leq 45$
Unit-cell dimension					
a(Å)	9.5614(7)	14.203(2)	14.184(2)	14.207(5)	14.321(4)
b(Å)	10.2088(13)				
c(Å)	10.6193(11)	20.571(5)	20.623(4)	20.606(8)	20.474(6)
α(deg)	68.45(1)				
β(deg)	76.98(1)				
γ(deg)	65.62(1)				
V(Å^3)	874.8(2)	3594(1)	3592.9(12)	3560(2)	3640(2)
Z^a	1	3	3	3	3
Host:guest ratio		1:2	1:2	1:2	1:2
Molecular weight (g mol^{-1})	727.06	993.87	1123.61	1055.81	1015.84
F(000)	378	1530	1686	1614	1554
D_c(g cm^{-3})	1.38	1.38	1.56	1.46	1.39
D_m(g cm^{-3})	1.28	1.33	1.54	1.38	1.38
μ(mm^{-1})	3.79	6.01	8.00	6.11	5.97

[a]Number of the host molecules in the unit cell.

Hexakis(phenylthio)benzene (HPTB) has been shown to form clathrates with small organic solvents (3). An early crystallographic investigation (4) revealed that the clathrate of CCl_4 crystallizes in the space group $R\bar{3}$ and has a host cavity with threefold symmetry similar to that of Dianin's compound (5). A comparison with Dianin's compound indicates that the HPTB molecules form a cage-type clathrate whose cavity is slightly longer and can thus imprison two guest molecules of the size of CCl_4, giving a host:guest ratio of 1:2. In fact, the HPTB molecule does also form clathrates with CCl_3CH_3, CCl_3Br, CCl_3CN, CCl_3NO_2, and CCl_3H (3).

Pang et al. studied some chlorine-containing guest molecules in different inclusion compounds. It was shown that specific host–guest dipole–dipole interactions play a role in the order–disorder effects for the twofold symmetric guest molecules CX_2Cl_2 (X = Cl, Br, CH_3, H) in the cavities of the Werner complexes $Ni(SCN)_2$(3-methylpyridine)$_4$ (6). The authors also showed that a steric effect predominates in the order–disorder effect in the case of threefold symmetric guest molecules CCl_3X (X = F, Cl, Br, I, CH_3, CN, NO_2, H) in the cavities of Dianin's compound (7). We report here the results of a crystallographic and NQR spectroscopic study of HPTB clathrates with CCl_4, **2**, CCl_3CH_3, **3**, CCl_3Br, **4**, CCl_3NO_2, **5**, CCl_3CN, **6**, CCl_3H, **7**, as guest molecules. The structure of HPTB in its nonporous phase **1** is also reported.

Results and discussion

X-Ray crystallography

Crystal data of compounds **1** and **3–6** are summarized in Table 1. Molecule **1** (HPTB) and the atomic numbering adopted are shown in Fig. 1. A selection of the geometrical parameters of these compounds is given in Tables 2 and 3.

Fig. 1. ORTEP drawing of the HPTB with the atomic numbering adopted for all the compounds.

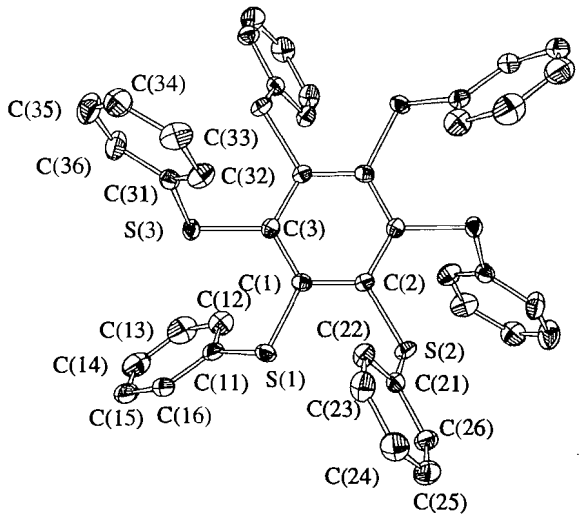

Description of the host molecule and cavity

Crystals of compound **1**, the nonporous form or the non-clathrated phase, crystallize in a triclinic unit cell of space group $P\bar{1}$. Since there is only one HPTB molecule per unit cell, its centre must coincide with a crystallographic centre of symmetry. The HPTB molecule has normal bond lengths and bond angles (see Table 2). The central benzene ring and the six side benzene rings are nearly planar and the sulphur atoms are displaced, on the average, by 0.036 Å from the central benzene ring but deviate by an average of 0.17 Å from the side rings. The six side rings are alternatively up and down from the central ring. The orientations of the side rings with respect to the

Can. J. Chem. Downloaded from www.nrcresearchpress.com by 65.111.164.53 on 09/08/12
For personal use only.

central ring are characterized by the ϕ and ψ torsion angles (see Table 2). The values taken by the ϕ angle are in the range 52°–68°. The ψ angle is around 28° in **3–6**. In **1**, however, two of the ψ angles have values of ~35° while the third one is 5°.

The clathrates **3–6**, for which the host:guest ratio is 1:2, are isostructural (space group $R\bar{3}$) with the CCl_4–HPTB clathrate (4) and have essentially the same host cavity. The host molecules in these clathrates have similar conformations to that of the non-clathrated phase. Their geometrical parameters are compared in Table 2. The cavity formed by HPTB molecules is a trigonal, centrosymmetric, hourglass-shaped cage. Two HPTB molecules at $z = 0$ and 1 form the top and bottom of the cage while molecules at $z = \frac{1}{3}$ and $\frac{2}{3}$ build the sides of the cage. The largest regions of the cavity (diameter ~6.9 Å) are at $z = \frac{1}{3}$ and $\frac{2}{3}$. The cavity, with a volume of about 297 Å^3 (8), can accommodate two molecules of CCl_4 (88 Å^3), CCl_3CH_3 (88 Å^3), CCl_3Br (93 Å^3), CCl_3NO_2 (90 Å^3), CCl_3CN (90 Å^3), CCl_3H (68 Å^3) (7).

A stereo pair of clathrate **3** is shown in Fig. 2. The two ordered CCl_3CH_3 molecules are disposed in such a way that the equatorial chlorine atoms are located in the larger region of the cavity while the methyl groups on the C_3 axis face one another and point towards the centre of the cavity.

Order–disorder effects of CCl_3X in the trigonal cavity

The clathrates **3–6** have a rigid host cavity that accommodates two CCl_3X molecules. Each of these may adopt any of three possible orientations: the X group is in the axial position and points toward the centre (orientation I) or to the top (or the bottom) of the cavity (orientation III); the X group is in one of the three equatorial positions (orientation II). Under the threefold symmetry of the cavity, these orientations are triply degenerate. The combination of two of the three orientations yields six distinct situations for the two CCl_3X guest molecules present in the cavity (see Fig. 3). It is clear that under the threefold symmetry and the centrosymmetry only the structures *a* (I + I) and *f* (III + III) are ordered whereas the structures *b–e* are disordered because of the presence of substructures. The above-mentioned orientations are *on symmetry* since the axial atoms are on the C_3 axis and the other atoms, in the equatorial positions, are equivalent. However, it is possible that the guest molecules are *off symmetry* when the axial atoms are not on the C_3 axis and the axial bond does not coincide with the rotation axis. As a consequence, the atoms in the equatorial positions are no longer equivalent. It is because of these *off-symmetry* orientations that the clathrates often present many molecular-disordered situations. The molecular orientations of the guests in clathrates **2–6** and their relative occupancy factors as obtained in this X-ray study are shown in Fig. 4.

Clathrate **3** has an ordered structure because the CCl_3CH_3 molecule is only *on symmetry* in orientation I. The two methyl groups face one another and point towards the centre of the cavity, while the chlorine atoms occupy the equatorial positions so that the guest molecules are in the ordered structure *a* (Fig. 3).

Clathrate **4** has two molecular orientations, I and II, with respective occupancy factors of 25 and 75%. This clathrate may be represented by the three situations, *a*, *b*, and *d* of Fig. 3. Orientation I is *off symmetry* since the C—Br bond does not coincide with the C_3 axis. Furthermore, the bromine atoms of the two molecules in the cage cannot point towards each other since the C—Br bond is longer than the C—Cl bond and because of the larger van der Waals radius of Br compared to that of Cl. Consequently, structure *a* is unlikely and the clathrate is assumed to be 50% in structure *b* and 50% in structure *d*. In structure *d* the molecules are *on symmetry* in orientation II; thus there are two chlorine sites: axial and equatorial sites that are in a ratio of 1 to 2; in structure *b* the molecules are half *on symmetry* in orientation II and half *off symmetry* in orientation I so that there is one axial site and four slightly different equatorial sites for the chlorine atoms.

Clathrate **5**, observed in three orientations, I, II, and III with respective occupancy factors of 50, 35, and 15%, is disordered. The three orientations of the guest, CCl_3NO_2, are all *off symmetry*, and the guest may be present in all six situations *a–f* in any proportion. Since each of them has six chlorine sites, the molecular structure is completely disordered.

The CCl_3CN molecule in clathrate **6** has also three *off-symmetry* orientations, I, II, and III with occupancy factors of 45, 20, and 35%. As the C-C≡N group is longer (2.58 Å) and C—Cl (1.77 Å) it would be difficult for the two neighboring CCl_3CN molecules to have the cyano groups pointing towards one another (as in structure *a*). Thus, only structures *b–f* are possible. The major orientation I (45%) indicates that the cyano groups are preferably located in the axial position pointing towards the end of the cavity (structure *f*).

^{35}Cl NQR spectroscopy

The NQR spectra of clathrates **2–4** obtained at 77 K are shown in Fig. 5. Two close and intense lines of intensity ratio 1:3 were observed for clathrate **2**. This is consistent with the observed crystal structure for CCl_4–HPTB in which the molecule is *on symmetry* with one axial and three identical equatorial chlorine atoms (structure *a*).

The strong single NQR line of **3** implies that CCl_3CH_3 is also in the ordered structure *a*, thus the chlorine atoms can only be located at the equivalent equatorial positions, and the methyl groups are preferably in the axial position pointing towards the centre of the cavity. This interpretation is confirmed by the above X-ray work.

From the NQR point of view, when molecules adopt different molecular orientations, the chemical environment or the electric-field-gradient tensors around the resonant nucleus is slightly changed from one orientation to another, so that the NQR lines spread over a wide region of frequency. If the separation between NQR lines is smaller than or nearly equal to the line width, only a broad band consisting of many closed lines is observed. This is the case for clathrate **4**.

The spectrum of **4** consists of two weak and broad signals, which give unambiguous proof that CCl_3Br is present in different molecular orientations. Thus, the two signals of intensity ratio about 1:2 reveal the existence of two distinct chlorine sites but the weak intensities and large line widths imply that these sites are perturbed by a small molecular disorder effect. As established in the X-ray work, the CCl_3Br molecule has a major (75%) orientation II *on symmetry*. In this case, the axial and the two equatorial chlorine sites yield an intensity ratio of 1:2. However, the minor (25%) orientation I is *off symmetry*. This affects the electronic gradient field of the major molecules and acts as an impurity causing the weakening and broadening of the signals.

The clathrates **5–7** did not show any NQR signals at 77 K.

Table 2. Bond lengths (Å), bond angles (deg), and torsion angles (deg) of HPTB host moleucule in compounds **1**, and 3–6.

	Distance				
Bond	**1**	**3**	**4**	**5**	**6**
S(1)—C(1)	1.770(2)	1.770(1)	1.769(2)	1.772(2)	1.768(3)
S(1)—C(11)	1.770(2)	1.773(1)	1.775(2)	1.768(2)	1.770(3)
S(2)—C(2)	1.775(2)				
S(2)—C(21)	1.771(2)				
S(3)—C(3)	1.770(2)				
S(3)—C(31)	1.774(2)				
C(11)—C(12)	1.387(3)	1.389(2)	1.390(3)	1.385(4)	1.381(5)
C(11)—C(16)	1.393(3)	1.387(2)	1.387(3)	1.388(4)	1.386(6)
C(12)—C(13)	1.397(3)	1.388(2)	1.392(2)	1.391(4)	1.389(6)
C(13)—C(14)	1.387(4)	1.377(3)	1.376(4)	1.378(5)	1.367(7)
C(14)—C(15)	1.371(4)	1.387(3)	1.383(4)	1.359(6)	1.370(7)
C(15)—C(16)	1.385(3)	1.389(3)	1.387(4)	1.392(5)	1.392(5)
C(21)—C(22)	1.387(3)				
C(21)—C(26)	1.395(3)				
C(22)—C(23)	1.387(3)				
C(23)—C(24)	1.381(4)				
C(24)—C(25)	1.383(3)				
C(25)—C(26)	1.385(3)				
C(31)—C(32)	1.387(3)				
C(31)—C(36)	1.388(3)				
C(32)—C(33)	1.384(3)				
C(33)—C(34)	1.380(3)				
C(34)—C(35)	1.387(4)				
C(35)—C(36)	1.380(3)				
C(1)—C(2)	1.407(2)	1.409(2)	1.412(3)	1.405(2)	1.409(3)
C(1)—C(3)	1.407(2)	1.409(3)	1.412(3)	1.405(3)	1.409(3)
C(2)—C(3)′	1.411(2)				
			Angle		
C(1)—S(1)—C(11)	106.2(1)	103.0(1)	103.4(1)	103.4(1)	102.9(1)
C(2)—S(2)—C(21)	104.6(1)				
C(3)—S(3)—C(31)	104.0(1)				
S(1)—C(11)—C(12)	124.1(2)	124.1(1)	124.4(2)	124.3(2)	123.9(2)
S(1)—C(11)—C(16)	115.6(2)	115.8(1)	115.7(2)	115.9(2)	116.1(3)
C(12)—C(11)—C(16)	120.0(2)	120.0(1)	119.7(2)	119.7(2)	119.9(3)
C(11)—C(12)—C(13)	119.3(2)	119.6(2)	119.4(2)	119.4(3)	119.7(4)
C(12)—C(13)—C(14)	120.2(2)	120.6(2)	120.9(3)	120.6(3)	120.2(5)
C(13)—C(14)—C(15)	120.3(2)	119.8(2)	119.7(3)	119.9(4)	120.5(5)
C(14)—C(15)—C(16)	120.2(2)	120.2(2)	120.1(3)	120.6(4)	120.0(4)
C(11)—C(16)—C(15)	120.1(2)	119.9(2)	120.3(2)	119.7(3)	119.7(3)
S(2)—C(21)—C(22)	126.5(1)				
S(2)—C(21)—C(26)	113.7(1)				
C(22)—C(21)—C(26)	119.7(2)				
C(21)—C(22)—C(23)	120.6(2)				
C(22)—C(23)—C(24)	120.2(2)				
C(23)—C(24)—C(25)	119.8(2)				
C(24)—C(25)—C(26)	119.7(2)				
C(21)—C(26)—C(25)	120.0(2)				
S(3)—C(31)—C(32)	123.8(1)				
S(3)—C(31)—C(36)	116.0(1)				
C(32)—C(31)—C(36)	120.0(2)				
C(31)—C(32)—C(33)	119.6(2)				
C(32)—C(33)—C(34)	120.6(2)				

Can. J. Chem. Downloaded from www.nrcresearchpress.com by 65.111.164.53 on 09/08/12
For personal use only.

Table 2 (*concluded*).

Bond	Angle 1	3	4	5	6
C(33)—C(34)—C(35)	119.4(2)				
C(34)—C(35)—C(36)	120.6(2)				
C(31)—C(36)—C(35)	119.7(2)				
C(2)—C(1)—C(3)	120.0(1)	119.9(1)	119.9(2)	120.0(1)	119.9(2)
C(1)—C(2)—C(3)′	120.4(1)				
C(2)′—C(3)—C(1)	119.5(1)				
S(1)—C(1)—C(2)	117.4(1)	119.0(1)	118.7(2)	118.9(2)	119.0(3)
S(1)—C(1)—C(3)	122.5(1)	121.1(1)	121.3(2)	121.1(2)	121.1(3)
S(2)—C(2)—C(1)	121.3(1)				
S(2)—C(2)—C(3)′	118.3(1)				
S(3)—C(3)—C(1)	118.8(1)				
S(3)—C(3)—C(2)′	121.7(1)				
	Torsion angle				
C(3)—C(1)—C(2)—C(3)′	−4.5(1)				
C(1)—S(1)—C(11)—C(12)	33.7(2)	28.5(1)	26.0(2)	27.6(2)	32.7(3)
C(1)—S(1)—C(11)—C(16)	−152.3(2)	−156.1(1)	−159.1(2)	−156.6(2)	−151.9(3)
C(11)—S(1)—C(1)—C(2)	−132.0(2)	−125.2(2)	−125.0(2)	−125.0(2)	−126.3(2)
C(11)—S(1)—C(1)—C(3)	52.5(1)	55.8(1)	56.6(2)	55.6(2)	53.8(2)
S(1)—C(1)—C(2)—C(3)′	179.9(2)	176.1(1)	176.3(2)	176.0(2)	174.9(2)
C(2)—S(2)—C(21)—C(26)	−4.7(1)				
C(2)—S(2)—C(21)—C(22)	179.7(2)				
C(21)—S(2)—C(2)—C(1)	−68.4(1)				
C(21)—S(2)—C(2)—C(3)′	113.4(2)				
S(2)—C(2)—C(1)—C(3)′	−177.5(2)				
C(3)—S(3)—C(31)—C(36)	−39.5(1)				
C(3)—S(3)—C(31)—C(32)	145.7(2)				
C(31)—S(3)—C(3)—C(1)	125.9(2)				
C(31)—S(3)—C(3)—C(2)′	−55.3(1)				
S(3)—C(3)—C(1)—C(2)	176.8(2)				

The absence of NQR signals may be due to both statistical and dynamical disorder effects. Thus, the quasi 3-fold symmetric molecule CCl_3NO_2 in **5** may not only adopt different structures but the NO_2 group may also rotate around the C—N bond. This intermolecular rotation produces a fluctuation on the electric-field-gradient tensors (or a significant molecular inhomogeneity) of the resonant nuclei on the same and neighbouring guest molecules, so that the relaxation time T_2* is too short for the resonances to be observable.

The CCl_3CN guest molecule occupies roughly the same molecular volume as CCl_3CH_3. However, its slightly longer C-C≡N group has greater oscillation amplitudes, thus causing a dynamical effect. As shown in the X-ray work, the CCl_3CN molecule is statistically disordered. This is the main reason for the disappearance of the NQR signals.

The guest molecule in clathrate **7** has the smallest molecular volume. It is evident that, in the cavity, the $CHCl_3$ molecules can undergo a molecular reorientation by interchanging three orientations within the various possible structures. Consequently, for the clathrates **5**–**7**, both the statistical disorder effect and the high-amplitude motion are responsible for the disappearance of the NQR signals at relatively low temperatures.

Host–guest interaction

The nonbonded van der Waals forces are usually considered to be responsible for the host–guest interactions in organic inclusion compounds although, in some particular cases, electrostatic interactions and hydrogen bonding are also important factors. It is expected that the dipole–dipole interactions do exist and play an important role in the host–guest interactions when both the host cavity and the guest molecules have significant dipole moments.

Table 4 contains dipole moments for the CCl_3X guest molecules and the HPTB host molecule calculated by semi-empirical methods (see Experimental). An excellent agreement with the experimental results is observed for the CCl_3CH_3 (1.76 debye (14)) and CCl_3Br (0.21 debye) (15)) molecules.

Since the HPTB host cavity is of the trigonal symmetry, the x and y components of its dipole moment should be zero, so that only the z component needs to be considered. The sign and the magnitude of the z-component dipole moment of the

Can. J. Chem. Downloaded from www.nrcresearchpress.com by 65.111.164.53 on 09/08/12
For personal use only.

Table 3. Bond length (Å) and bond angles (deg) of CCl_3X guest molecule in compounds **1** and **3–6**.

Bond	3	4	5	6
		Distance		
Guest molecule I				
CG(IA)—CL(IA)	1.766(2)	1.78(1)	1.78(2)	1.77(2)
CG(IA)—CL(IB)		1.78(1)	1.78(1)	1.77(2)
CG(IA)—CL(IC)			1.79(1)	1.77(2)
CG(IA)—BR(I)		1.92(1)		
CG(IA)—CG(IB)	1.492(7)			1.46(1)
CG(IA)—NG(IA)			1.46(1)	
NG(IA)—OG(IA)			1.22(2)	
NG(IA)—OG(IB)			1.22(2)	
CG(IB)—NG(IB)				1.16(2)
Guest molecule II				
CG(IIA)—CL(IIA)		1.77(2)	1.77(1)	1.77(2)
CG(IIA)—CL(IIB)		1.77(2)	1.77(1)	1.77(3)
CG(IIA)—CL(IIC)		1.77(3)	1.77(2)	1.77(2)
CG(IIA)—BR(II)		1.90(2)		
CG(IIA)—CG(IIB)				1.45(3)
CG(IIA)—NG(IIA)			1.46(2)	
NG(IIA)—OG(IIA)			1.22(2)	
NG(IIA)—OG(IIB)			1.22(2)	
CG(IIB)—NG(IIB)				1.15(3)
Guest molecule III				
CG(IIIA)—CL(IIIA)			1.78(3)	1.76(3)
CG(IIIA)—CL(IIIB)			1.78(2)	1.76(2)
CG(IIIA)—CL(IIIC)			1.78(3)	1.76(3)
CG(IIIA)—NG(IIIA)			1.46(2)	
NG(IIIB)—OG(IIIA)			1.22(4)	
NG(IIIB)—OG(IIIB)			1.22(4)	
CG(IIIA)—CG(IIIB)				1.45(2)
CG(IIIB)—NG(IIIB)				1.17(2)
		Angle		
Guest molecule I				
CL(IA)—CG(IA)—CL(IB)	108.7(1)	112.3(5)	111.(1)	115.(1)
CL(IA)—CG(IA)—CL(IC)			110.(1)	108.(1)
CL(IB)—CG(IA)—CL(IC)			110.(1)	112.(1)
BR(I)—CG(IA)—CL(IA)		109.6(4)		
BR(I)—CG(IA)—CL(IB)		108.5(6)		
CL(IA)—CG(IA)—CG(IB)	110.2(1)			106.(1)
CL(IB)—CG(IA)—CG(IB)				109.(1)
CL(IC)—CG(IA)—CG(IB)				107.(1)
NG(IA)—CG(IA)—CL(IA)			107.(1)	
NG(IA)—CG(IA)—CL(IB)			110.(1)	
NG(IA)—CG(IA)—CL(IC)			109.(1)	
CG(IA)—NG(IA)—OG(IA)			120.(2)	
CG(IA)—NG(IA)—OG(IB)			120.(1)	
OG(IA)—NG(IA)—OG(IB)			120.(2)	
CG(IA)—CG(IB)—NG(IB)				179.(3)
Guest molecule II				
CL(IIA)—CG(IIA)—CL(IIB)		112.(1)	108.(1)	110.(2)
CL(IIA)—CG(IIA)—CL(IIC)		110.(1)	111.(1)	111.(2)
CL(IIB)—CG(IIA)—CL(IIC)		112.(1)	113.(1)	110.(1)
BR(II)—CG(IIA)—CL(IIA)		101.(1)		

Can. J. Chem. Downloaded from www.nrcresearchpress.com by 65.111.164.53 on 09/08/12
For personal use only.

Table 3 (*concluded*).

Bond	Angle 3	4	5	6
BR(II)—CG(IIA)—CL(IIB)		112.(1)		
BR(II)—CG(IIA)—CL(IIC)		109.(1)		
NG(IIA)—CG(IIA)—CL(IIA)			109.(1)	
NG(IIA)—CG(IIA)—CL(IIB)			108.(1)	
NG(IIA)—CG(IIA)—CL(IIC)			109.(1)	
CG(IIA)—NG(IIA)—OG(IIA)			119.(2)	
CG(IIA)—NG(IIA)—OG(IIB)			119.(2)	
OG(IIA)—NG(IIA)—OG(IIB)			120.(2)	
CL(IIA)—CG(IIA)—CG(IIB)				108.(2)
CL(IIB)—CG(IIA)—CG(IIB)				109.(2)
CL(IIC)—CG(IIA)—CG(IIB)				109.(2)
CG(IIA)—CG(IIB)—NG(IIB)				179.(5)
Guest molecule III				
CL(IIIA)—CG(IIIA)—CL(IIIB)			111.(1)	110.(1)
CL(IIIA)—CG(IIIA)—CL(IIIC)			110.(1)	108.(1)
CL(IIIB)—CG(IIIA)—CL(IIIC)			111.(1)	109.(1)
NG(IIIA)—CG(IIIA)—CL(IIIA)			108.(2)	
NG(IIIA)—CG(IIIA)—CL(IIIB)			109.(2)	
NG(IIIA)—CG(IIIA)—CL(IIIC)			108.(2)	
CG(IIIA)—NG(IIIA)—OG(IIIA)			119.(3)	
CG(IIIA)—NG(IIIA)—OG(IIIB)			120.(3)	
OG(IIIA)—NG(IIIA)—OG(IIIB)			120.(3)	
CL(IIIA)—CG(IIIA)—CG(IIIB)				108.(2)
CL(IIIB)—CG(IIIA)—CG(IIIB)				111.(2)
CL(IIIC)—CG(IIIA)—CG(IIIB)				110.(2)
CG(IIIA)—CG(IIIB)—NG(IIIB)				178.(3)

Can. J. Chem. Downloaded from www.nrcresearchpress.com by 65.111.164.53 on 09/08/12
For personal use only.

Fig. 2. Stereo pair showing the CCl_3CH_3 molecules in the HPTB cage (clathrate **3**).

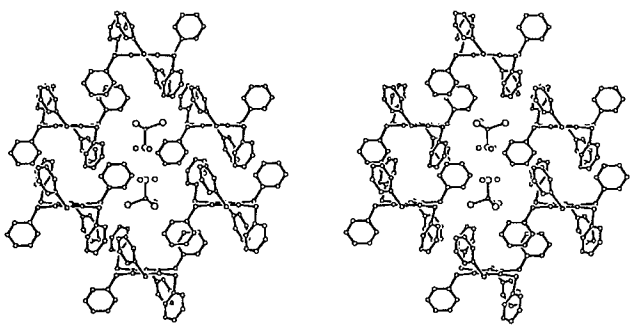

CCl_3X guest molecule depend upon its molecular orientation. Thus, when the CCl_3X guest molecules are in orientation I or III, that is, when the X group is located in the axial position and pointing towards either the centre or the ends of the cavity, each guest molecule has a *z*-component dipole moment of the same magnitude but of opposite sign. Thus, because the symmetry axis of the guest molecule coincides with the *z* axis, these orientations correspond to the largest *z* component. The positive and negative signs of the dipole moment are associated with a vector oriented from X to the trichloromethyl group (or vice versa) when the molecules are in orientation I. This description is reversed when the molecules are in orientation III. When the guest molecules are in orientation II, e.g., when the X group is in the equatorial position, the *z* component has a smaller magnitude and is of the opposite sign with respect to orientation I, because the molecular axis does not coincide with the *z* axis.

Table 4. Calculated *z* component and total electric dipole moment (debye) of the CCl_3X guest molecules (in orientations I, II, and III) and of the HPTB host molecule.

Molecule	Orientation I	II	III	Total
CCl_4	0.00	0.00	0.00	0.00
CCl_3CH_3	1.75	−0.59	−1.75	1.75
CCl_3Br	0.22	−0.07	−0.22	0.22
CCl_2NO_2	−2.55	0.60	2.55	2.55
CCl_3CN	1.16	−0.52	−1.16	1.16
CCl_3H	1.16	−0.52	−1.16	1.16
HPTB	0.00			0.00
HPTB (half)	0.72			0.72

Since the HPTB molecule is centrosymmetric, its dipole moment is zero. However, each "half HPTB molecule" has a dipole moment of 0.72 debye along the *z* axis. The evidence for a multiple moment in the host cavity can be visualized in Fig. 6. The crystallographic analysis reveals that one CCl_3X

Can. J. Chem. Downloaded from www.nrcresearchpress.com by 65.111.164.53 on 09/08/12
For personal use only.

Fig. 3. The six possible molecular structures CCl_3X within three orientations in the HPTB trigonal cavity.

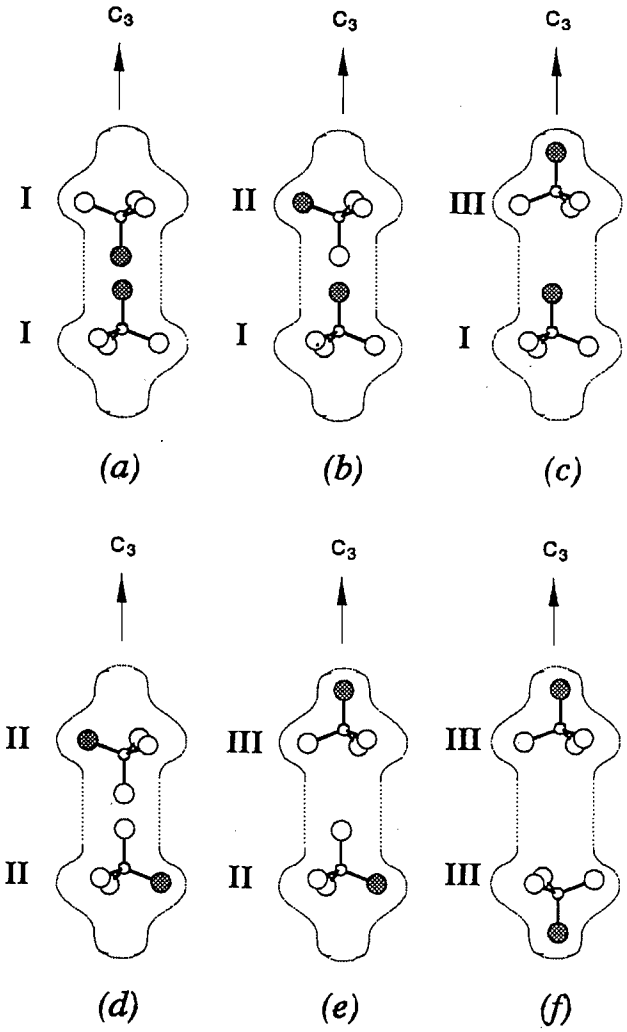

guest molecule may occupy only half of the cavity at $z = 0.2$–0.5 (or at $z = 0.5$–0.8). Only the four closest HPTB molecules (numbered 1–4 Fig. 6; three at $z = \frac{1}{3}$ and one at $z = 0$) contribute to the dipole moment of half the host cavity, consisting of two dipole moments whose vectors go from $z = \frac{1}{2}$ and $\frac{1}{6}$ to $z = \frac{1}{3}$.

When the CCl_3CH_3 guest molecule is in orientation I or III, its dipole moment vector is parallel to that of the host cavity, so that the dipole–dipole interaction is favourable. Since the methyl group has higher nonbonded energy when it is pointing to the bottom than when it is pointing towards the centre of the cavity, orientation III is not observed. The CCl_3CH_3 guest molecule in orientation II has smaller and opposite dipole moment (relative to orientation I), which results in an unfavourable dipole–dipole interaction. Consequently, the CCl_3CH_3 guest molecule can only be present in orientation I *on symmetry*, which gives the ordered structure *a*.

The situation is different for the CCl_3Br guest molecule. There is a weakly favourable dipole–dipole interaction because of the small dipole moment of the guest molecule in orientations I and III. However, because of its high nonbonded energy (steric factor), orientation III cannot be considered. Orientation II has a nearly zero dipole–dipole interaction

Fig. 4. Summary of the observed orientations and disorder of the CCl_3X guest molecules in the HPTB trigonal cavity.

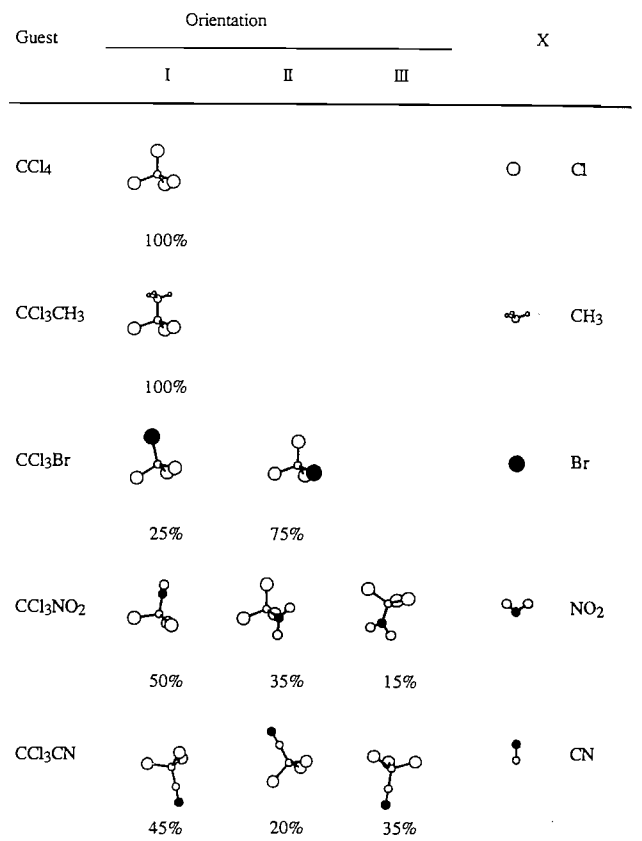

because the CCl_3Br guest molecule has a *z*-component dipole moment of only -0.07 debye. In the absence of a strongly favourable dipole–dipole interaction, orientations I and II are all possible for the CCl_3Br molecule. Thus results in a disorder and may give structures *a*, *b*, and *d*.

Although CCl_3NO_2 and CCl_3CN are slightly polar guest molecules, they cannot give favourable dipole–dipole interactions in any of the three orientations because their dipole moment vectors are all in the opposite direction to that of the host cavity, so that the three molecular orientations may be present and disordered structures are to be expected for these guest molecules.

The smaller $CHCl_3$ guest molecule has two possible orientations, I and III, that give favourable dipole–dipole interactions, whereas orientation II is unlikely due to its slightly unfavourable dipole–dipole interactions.

Experimental

Sample preparation

Hexakis(phenylthio)benzene (HPTB) was prepared according to MacNicol et al. (9), mp 178–179°C; *M* (mass spectrum) 726; τ (NMR in $CDCl_3$) 2.7–3.2 (30H, complex, aromatic). The crystals of **1**, the stable non-clathrated phase, were grown from its solution in CCl_3CN. The crystals appeared after the solution was heated and quickly cooled. The clathrates **2**–**7** were prepared by a slow recrystallization from a solution of the host molecule in the corresponding guest solvents. The

Can. J. Chem. Downloaded from www.nrcresearchpress.com by 65.111.164.53 on 09/08/12
For personal use only.

Fig. 5. ^{35}Cl NQR spectra at 77 K of the clathrates (*a*) **2**, (*b*) **3**, and (*c*) **4**.

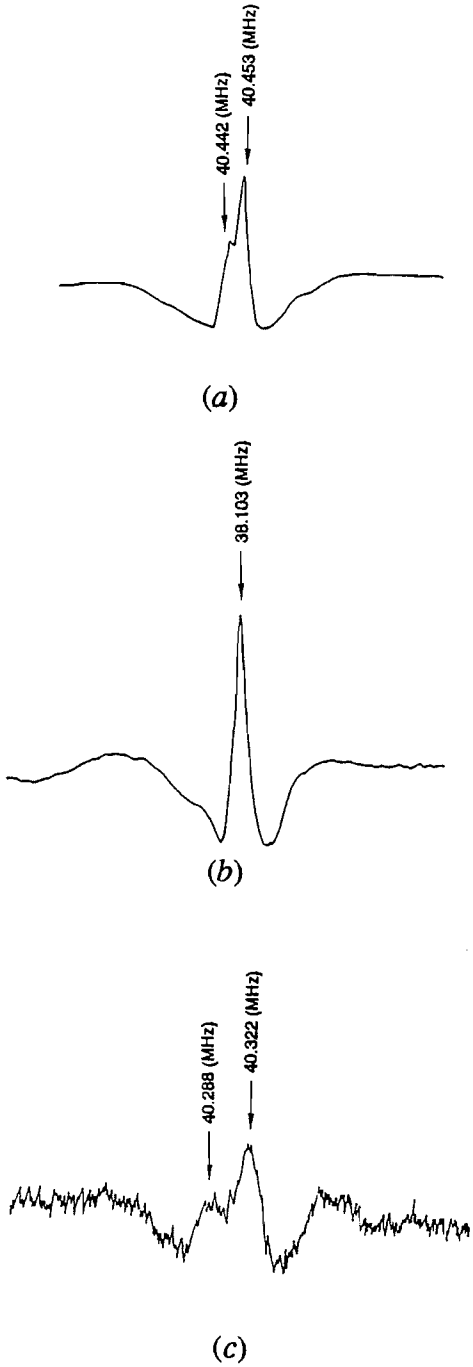

host:guest ratio was obtained for clathrates **2–7**, using either ^1H NMR analysis, crystal density measurement, or thermogravimetry,[2] which confirms the previously published results except for clathrate **5** (3) (mp 179°C, **2**; 183°C, **3**; 178°C, **4**; 180°C, **5**; 179°C, **6**; 180°C, **7**).

Fig. 6. Multiple moment of the HPTB host cavity; (*a*) view perpendicular to the *c* axis; (*b*) view down the *c* axis.

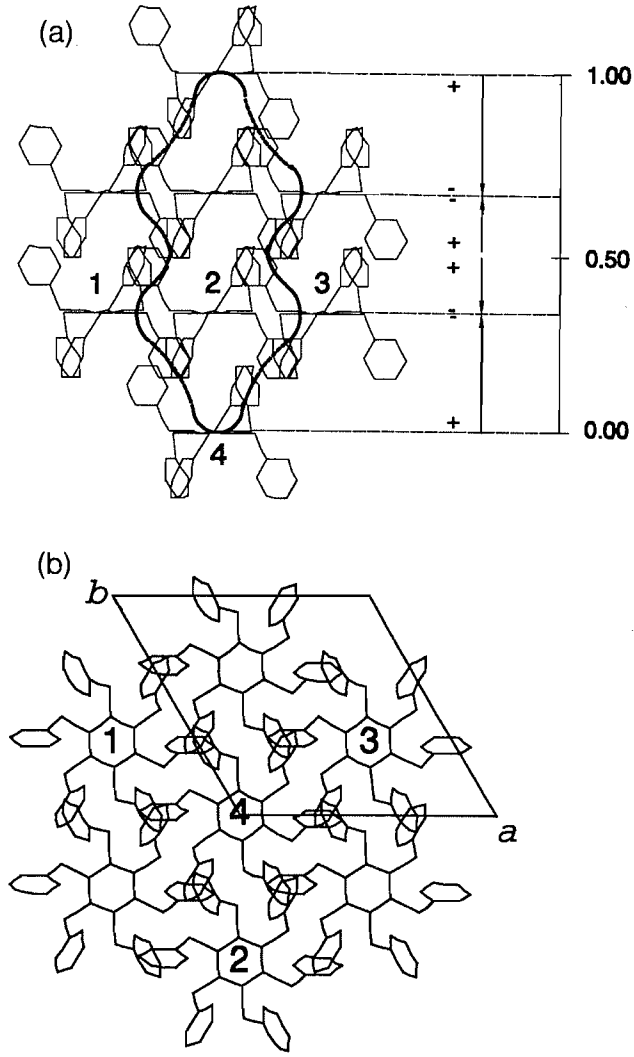

Crystal structure determination of compounds 1–6

The single crystals were selected and removed from the mother liquor, quickly mounted on a glass fibre, and cooled for the X-ray intensity data collection at low temperature. The crystal densities were obtained by pycnometry using cyclohexane–CCl_3Br mixtures.

The unit-cell parameters were established and the reflection intensities were collected at 220 K on a Nonius CAD4 diffractometer using graphite-monochromatized Cu*K*α radiation (λ = 1.54178 Å). A summary of the crystal data, intensity mea-

[2] The error of the host to guest ratio of the clathrates **2–7** determined by NMR analysis and crystal density measurements is within 5%. However, only the nearest integer values were taken as the host:guest ratio for the clathrates. Thermogravimetry gives a more precise method to determine the host:guest ratio; for example, **3** forms 1:2 (host:guest) clathrate (found: loss of CCl_3CH_3 after 4 h at 50–70°C/25 Torr, 26.76 (1 Torr = 133.3 Pa); $C_{42}H_{30}S_6{\cdot}2CCl_3CH_3$ requires 26.84); **4** forms 1:2 (host:guest) clathrate (found: loss of CCl_3Br after 4 h at 50–70°C/25 Torr, 35.24; $C_{42}H_{30}S_6{\cdot}2CCl_3Br$ requires 35.29); **5** forms 1:2 (host:guest) clathrate (found: loss of CCl_3NO_2 after 12 h open air at room temperature, 31.15; $C_{42}H_{30}S_6{\cdot}2CCl_3NO_2$ requires 31.14).

Table 5. Summary of experimental data and structure refinement.

Compound	1	3	4	5	6
Guest molecule		CCl_3CH_3	CCl_3Br	CCl_3NO_2	CCl_3CN
Temperature (K)	220	220	220	220	220
Technique	Diffractometer: Enraf–Nonius CAD-4, single crystal Graphite crystal monochromator: Cu Kα, λ = 1.54178 Å ω–2θ scan				
θ_{max} (deg)	70	70	70	70	70
Number of reflections					
Measured	6227	8613	8322	7906	8541
Independent	3315	1520	1520	1522	1532
Observed ($3\sigma(I)$ criterion)	3207	1412	1375	1328	1375
R_{int}	0.024	0.041	0.055	0.061	0.059
Standard reflection/60 mm	4	4	4	5	4
h	−11 → 11	−17 → 17	−17 → 17	−17 → 17	−17 → 17
k	−12 → 12	−17 → 17	−17 → 17	−17 → 17	−17 → 17
l	−12 → 12	−24 → 24	−25 → 25	−25 → 25	−24 → 24
Absorption correction					
Difabs	0.23 → 0.40	0.14 → 0.29	0.08 → 0.23	0.06 → 0.23	0.08 → 0.25
Solution and refinement					
Solution	Direct method				
Refinement	Full-matrix least-squares on F				
Number of variables	278	113	145	177	168
Final ΔF/(e Å^{-3})	0.43, −0.55	0.28, −0.21	0.31, −0.45	0.29, −0.54	0.55, −0.78
Weight scheme	$\Sigma w(F_o - F_c)^2$, $w = 1/[\sigma^2(F_o) + gF_o^2]$ with $\sigma(F_o)$ from counting statistics				
g	0.0002	0.0002	0.0002	0.0002	0.0002
Final shift/error	0.013	0.12	0.26	0.28	0.13
Final R and R_w	0.036, 0.056	0.028, 0.044	0.035, 0.045	0.049, 0.076	0.052, 0.068
S	3.24	2.42	2.29	0.98	3.01
Computer and programs	Macro VAX-3400, SHELXS86 (10), SHELX76 (11), NRCVAX (12)				
Scattering factors	International tables for X-ray crystallography (13)				

surements, structure determinations, and refinements is given in Tables 1 and 5.[3]

Refinement of ordered and disordered structures

The structures of the host HPTB in the non-clathrated phase and in the clathrate compounds are all ordered and can be refined without difficulty. The non-hydrogen atoms of HPTB were refined anisotropically. In the course of the refinement, the following constraints were applied: C—Cl = 1.77 ± 0.02 Å, C—Br = 1.90 ± 0.02 Å, C—N = 1.45 ± 0.02 Å, N—O = 1.22 ± 0.02 Å, C—C′ = 1.44 ± 0.02 Å, C′≡N = 1.13 ± 0.02 Å, Cl...Cl = 2.93 ± 0.02 Å, and Cl...Br = 3.00 ± 0.02 Å. The evidence for the molecular disorder can be immediately seen from high atomic thermal parameters ($U_{eq} > 0.25$ Å^2). Difference Fourier syntheses, calculated after the refinement had converged, revealed some strong new residual peaks that correspond to the guest molecule in another orientation. These new peaks were added to the refinement. To determine the occupancy factors, the isotropic thermal parameters were kept at fixed values while an overall occupancy factor was refined for each partial molecule. When the R index improved significantly, the model was accepted; otherwise, the same procedure was repeated until a satisfactory solution was obtained. After convergence, the occupancy factors were kept constant, while the atomic thermal parameters were allowed to vary individually. During the last cycle, the atomic thermal parameters and the occupancy factors were slightly adjusted.

In our work, two or three models were required to describe the disorder of the guest molecules inside the HPTB host cavities. The residual electron density differences indicate that these are sufficient. Thus, clathrate **3** was refined with one model without constraining the CCl_3CH_3 molecule; clathrate **4** was refined with two models; clathrates **5** and **6** were refined with three models.

The guest molecule in **3** and that with the 75% occupancy in **4** were refined anisotropically. All other disordered molecules in **4**, **5**, and **6** were given isotropically.

^{35}Cl NQR spectroscopy

Freshly prepared samples for NQR spectroscopy were briefly

[3] Tables of atomic coordinates, bond lengths and angles, and thermal parameters for compounds **1** and **3–6** can be purchased from: The Depository of Unpublished Data, Document Delivery, CISTI, National Research Council Canada, Ottawa, Canada K1A 0S2.

The tables of atomic coordinates and bond lengths and angles have also been deposited with the Cambridge Crystallographic Data Centre, and can be obtained on request from The Director, Cambridge Crystallographic Data Centre, University Chemical Laboratory, 12 Union Road, Cambridge, CB2 1EZ, U.K.

Structure factor amplitudes are no longer being deposited and may be obtained directly from the author.

Can. J. Chem. Downloaded from www.nrcresearchpress.com by 65.111.164.53 on 09/08/12
For personal use only.

sucked dry and immediately sealed in glass vials. The NQR spectra at 77 K were measured on a Decca superregenerative spectrometer, frequencies being compared to harmonics from an internal crystal-controlled oscillator. Temperatures were measured with a Hewlett–Packard 2802A digital thermometer by using a platinum thermocouple (precision ±0.5°C).

Electric dipole moment calculation

The electric dipole moments of the guest molecules and of the HPTB molecule were calculated using AM1 semi-empirical quantum mechanics (16) with HyperChem™ Release 2 package[4] running on an 80486 50 Hz IBM-compatible personal computer.

The geometries of the guest molecule were constructed manually and minimized with the molecular mechanics force field (17). Two molecular orientations were considered in the calculation: X groups are located on either the axial or equatorial position, which does not change the total dipole moments but, rather, their components along the x, y, and z axes. The geometry of the HPTB molecule was taken from our crystallographic study; the total and the half of the HPTB molecule were calculated, respectively. The guest molecules were finally minimized with AM1 semi-empirical quantum mechanics, which employed the Polak–Ribiere conjugate gradient technique. The minimizations were terminated when the maximum derivative of all atoms was less than a value of 0.1 kcal mol^{-1} $Å^{-1}$. The dipole moment of the HPTB host molecule was determined with the AM1 method using single point calculation. The results obtained are shown in Table 4. The calculated total energies, atomic coordinates and charges, and dipole moments of the molecules under consideration have been deposited (see footnote 3).

Acknowledgments

The Natural Sciences and Engineering Research Council of Canada and the Swiss National Research Fund support this work. We thank Dr. Michel Simard and Mme Francine Bélanger-Gariépy for their assistance in the crystallographic work.

References

1. J.L. Atwood, J.E.D. Davies, and D.D. MacNicol. Inclusion Comp. **1–5** Academic Press, London. 1984.
2. A.I. Kitaigorodsky. Molecular crystals and molecules. Academic Press, New York. 1973. p. 134.
3. D.D. MacNicol. Inclusion Comp. **2**, 123, (1984).
4. D.D. MacNicol, A.D.U. Hardy, and D.R. Wilson. J. Chem. Soc. Perkin Trans. 2, 1011 (1979).
5. J.L. Flippen, J. Karle, and I.L. Karle. J. Am. Chem. Soc. **93**, 3749 (1970).
6. L. Pang, E.A.C. Lucken, and G. Bernardinelli. J. Inclusion Phenom. **13**, 63 (1992).
7. L. Pang and M.A. Whitehead. J. Mol. Struc. (Theochem), **257**, 143 (1992).
8. L. Pang, E.A.C. Lucken, and G. Bernardinelli. J. Am. Chem. Soc. **112**, 8754 (1990).
9. D.D. MacNicol, P.R. Mallinson, A. Murphy, and G.J. Sym. Tetrahedron Lett. **23**, 4131 (1982).
10. G.M. Sheldrick. SHELXS86. Program for the solution of crystal structures. University of Göttingen, Germany. 1985.
11. G.M. Sheldrick. SHELX76. A program for crystal structure determination. Cambridge University, England. 1976.
12. E.J. Gabe, Y. LePage, J.-P. Charland, F.L. Lee, and P.S. White. J. Appl. Crystallogr. **22**, 384 (1989).
13. International tables for X-ray crystallography. Vol. IV. Kynoch, Birmingham, U.K. 1974.
14. CRC handbook of chemistry and physics. 73rd ed. CRC Press, Inc., Boca Raton, Fla. 1992–1993. pp. 9–45.
15. M. Smyth. J. Chem. Phys. **24**, 814 (1956).
16. M.J.S. Dewar, E.G. Zoebisch, E.F. Healy, and J.J.P. Stewart. J. Am. Chem. Soc. **108**, 3902 (1985).
17. U. Berkert and N.L. Allinger. Molecular mechanics. American Chemical Society Monograph 177, Washington, D.C. 1982.

[4] HyperChem™ program, AutoDesk Inc., Scientific Modeling Division, 2320 Marinship Way, Sausalito, CA 94965-9910, U.S.A.

Can. J. Chem. Downloaded from www.nrcresearchpress.com by 65.111.164.53 on 09/08/12
For personal use only.

Electrochemical behavior of amidine hydrochlorides and amidines

Benoit Daoust and Jean Lessard

Abstract: The electrochemical behavior of *N,N*-dimethyl-*N'*-phenylformamidine hydrochloride was studied on a platinum electrode. The oxidation peak at +0.90 V vs. Ag/Ag^+ 0.01 M (in CH_3CN – 0.1 M $LiClO_4$) was assigned to the oxidation of the chloride anion. *N,N*-Dimethyl-*N'*-(4-chlorophenyl)formamidine and *N,N*-dimethyl-*N'*-(2-chlorophenyl)formamidine were isolated from the preparative electrolysis of this amidine hydrochloride. The electrochemical behavior of *N*-phenylbenzamidine hydrochloride and *N*-phenylcyclohex-3-enecarboxamidine hydrochloride was also studied at platinum and at vitreous carbon. Cyclic voltammetry of a number of amidines was performed. Only *N*-arylbenzamidines showed a reduction peak at potentials less negative than −3.0 V vs. Ag/Ag^+ 0.01 M (discharge potential of the medium at vitreous carbon). Preparative electrooxidations of all amidines studied were unsuccessful because of strong and rapid passivation of the anode.

Key words: amidine, electrochemical oxidation, chloride, amidine hydrochloride.

Résumé : Le comportement électrochimique du chlorhydrate de la *N,N*-diméthyl-*N'*-phénylformamidine a été étudié sur une électrode de platine. Le pic d'oxydation à +0.90 V vs. Ag/Ag^+ 0.01 M (dans CH_3CN – 0.1 M $LiClO_4$) a été attribué à l'oxydation de l'anion chlorure. La *N,N*-diméthyl-*N'*-(4-chlorophényl)formamidine et la *N,N*-diméthyl-*N'*-(2-chlorophényl)formamidine ont été isolées de l'électrolyse préparative de ce chlorhydrate d'amidine. Le comportement électrochimique du chlorhydrate de la *N*-phénylbenzamidine et du chlorhydrate de la *N*-phénylcyclohex-3-ènecarboxamidine a également été étudié sur platine et sur carbone vitreux. Plusieurs amidines ont été étudiées par voltammétrie cyclique. Seules les *N*-arylbenzamidines ont donné un pic de réduction à un potentiel supérieur à −3.0 V vs. Ag/Ag^+ 0.01 M (potentiel de décharge du milieu sur carbone vitreux). Il n'a pas été possible d'effectuer l'électrooxydation préparative des amidines à cause d'une forte et rapide passivation de l'anode.

Mots clés : amidine, oxydation électrochimique, chlorure, chlorhydrate d'amidine.

[Traduit par la rédaction]

Introduction

Amidines have been studied mainly as precursors of the synthesis of biologically active compounds (1) but have been the subject of few electrochemical studies (2–5). In 1977, Barbey and Caullet (2) studied the electrochemical behavior of an amidine hydrochloride, *N,N*-dimethyl-*N'*-phenylformamidine hydrochloride (**1**HCl). They assigned the anodic wave at $E_{½}$ = 0.89 V vs. Ag/Ag^+ 0.01 M in the voltammogram of **1**HCl in CH_3CN – 0.1 M $LiClO_4$ at a rotating platinum disc electrode to the oxidation of the imino nitrogen of the amidine group. By means of cyclic voltammetry and preparative electrolyses, we have reassigned this wave to the oxidation of the chloride anion. We have extended the electrochemical study to two other amidine hydrochlorides and have also looked at the cyclic voltammetric behavior of a number of amidines.

Received September 9, 1994.

B. Daoust and J. Lessard.[1] Laboratoire d'électrochimie et d'électrocatalyse, Département de chimie, Université de Sherbrooke, Sherbrooke, QC J1K 2R1, Canada.

[1] Author to whom correspondence may be addressed. Telephone: (819) 821-7091. Fax: (819) 821-8017.

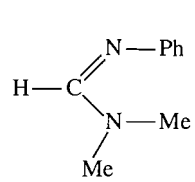

1

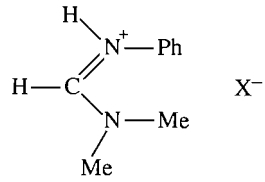

1 HCl X = Cl
1 $HClO_4$ X = ClO_4

Electrochemical behavior of amidine hydrochlorides. *N,N*-Dimethyl-*N'*-phenylformamidine hydrochloride (1HCl)

Oxidation behavior

In their study of the electrochemical behavior of **1**HCl, in CH_3CN – 0.1 M $LiClO_4$, Barbey and Caullet (2) showed that the oxidation wave at $E_{½}$ = +0.89 V vs. Ag/Ag^+ 0.01 M in the linear sweep voltammogram (LSV) at platinum corresponds to a one-electron process. Considering that the amino nitrogen was protonated (see $\mathbf{1}H^+$ in Scheme 1), they assigned this wave to the oxidation of the electron pair of the imino nitrogen of $\mathbf{1}H^+$ to give the dication radical **2** (Scheme 1). Upon adding 1 mole of $HClO_4$ per mole of **1**HCl, they observed the disappearance of the oxidation wave and explained this loss of elec-

Can. J. Chem. Downloaded from www.nrcresearchpress.com by 65.111.164.53 on 09/08/12
For personal use only.

Scheme 1 (Proposition of Barbey and Caullet (2))

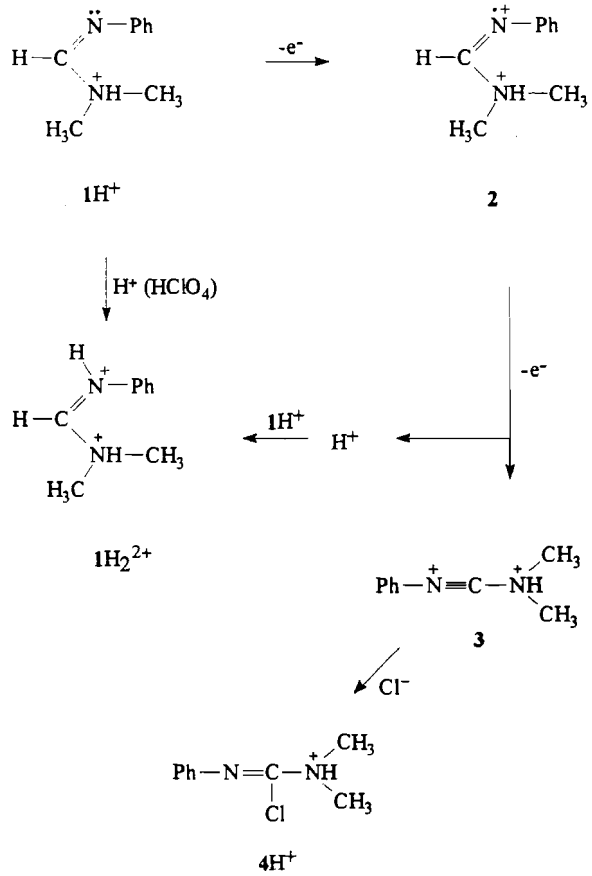

troactivity by protonation of the imino nitrogen to form the dication $\mathbf{1}H_2^{2+}$ (Scheme 1). During the potentiostatic preparative electrolysis of **1**HCl (+1.0 V vs. Ag/Ag^+ 0.01 M), the authors noted the disappearance of the oxidation wave and the appearance of a reduction wave at $E_{1/2}$ = +0.55 V in the LSV. They attributed this new wave to the reduction of the dication **3** (Scheme 1). After the electrolysis, they isolated a product which they assumed was the perchlorate of the chloroamidine **4** (**4**$HClO_4$) and proposed the mechanism shown in Scheme 1 for its formation. It is noteworthy that this mechanism corresponds to a two-electron process while coulometric experiments indicated a one-electron process. The authors explained this result by the fact that half of **1**HCl molecules would be eliminated from the oxidation process by protonation of the imino nitrogen with the protons formed in the oxidation of **2** to **3** (Scheme 1).

We decided to reinvestigate the electrochemical behaviour of **1**HCl on the basis that the observed oxidation potential (+0.90 V vs. Ag/Ag^+ 0.01 M) appeared too low for the oxidation of a protonated amidine. Furthermore, the oxidation of the protonated amidine cannot involve the electron pair of the imino nitrogen as suggested by Barbey and Caullet (2) since it is the most basic of the two nitrogens due to charge delocalization (stabilization) of the conjugate acid, and it is the nitrogen that is protonated (6, 7). As shown below, the anodic wave at +0.90 V is due to the oxidation of the chloride anion.

Voltammetric behavior of 1HCl

The cyclic voltammogram of **1**HCl on platinum (CH_3CN – 0.1 M $LiClO_4$) is presented in Fig. 1*A*. An oxidation peak at $E_p(ox1)$ = +0.90 V vs. Ag/Ag^+ 0.01 M corresponding to the oxidation wave reported by Barbey and Caullet (2) is observed (Table 1, entry 1). This oxidation peak is also present in the voltammogram of LiCl (Fig. 1*C*) (Table 1, entry 13). According to literature data (8), the voltammogram of LiCl on a platinum rotating disc electrode in CH_3CN – Et_4NClO_4 0.1 M shows two oxidation waves at $E_{1/2}(ox1)$ = +1.1 V and $E_{1/2}(ox2)$ = +1.7 V vs. SCE, which would correspond to +0.8 V and +1.4 V vs. Ag/Ag^+ 0.01 M. These two oxidation waves were attributed to reactions [1] and [2], respectively. Thus, the oxidation

[1] $3Cl^- - 2e^- \rightleftharpoons Cl_3^-$

[2] $2Cl_3^- - 2e^- \rightleftharpoons 3Cl_2$

peak at $E_p(ox1)$ = +0.90 V must be ascribed to the oxidation of the chloride anion. The absence of the second oxidation peak at ca. +1.4 V in Fig. 1*C* is not due to strong ion pairing between Cl_3^- and the lithium cation ($LiClO_4$ as supporting electrolyte) because it was absent also in the cyclic voltammogram of LiCl and that of Et_3NHCl in CH_3CN – 0.1 M Et_4NClO_4 using the same platinum electrode as that used in Fig. 1*C*. The discrepancy between our results and those published by Kolthoff and Coetzee (8) could be due to a difference in the state of the electrode surface resulting from a different electrode pretreatment.

The cathodic peak at +0.58 V in Fig. 1*C* is due to the reduction of Cl_3^- (reverse of reaction [1]) so the cathodic peak at +0.57 V ($E_p(red1)$) in Fig. 1*A* must be due also to the reduction of Cl_3^- and not to the reduction of the dication **3** (Scheme 1) as proposed by Barbey and Caullet (2). The fact that the peak is much smaller in Fig. 1*A* than in Fig. 1*C* suggests that some Cl_3^- does react with the protonated amidine (**1**H^+), as shown by the preparative oxidation (see below).

The cyclic voltammogram of **1**$HClO_4$ (Fig. 1B) does not show any anodic peak at ca. +0.90 V nor any cathodic peak at ca. +0.58 V. The disappearance of those two peaks upon changing the counter anion from Cl^- (Fig. 1*A*) to ClO_4^- (Fig. 1*B*) provides further evidence that they are really due to the oxidation of Cl^- and the reduction of Cl_3^-, respectively, and not to the oxidation of the protonated amidine **1**H^+ and the reduction of the dication **3** (Scheme 1).

Upon adding perchloric acid to the electrolytic solution of **1**HCl, the oxidation peak at +0.90 V decreases in intensity (Fig. 2*B*) and disappears completely when 1 equivalent has been added (Fig. 2*C*). As mentioned above, Barbey and Caullet (2) reported a similar observation for the linear sweep voltammogram of **1**HCl in the presence of $HClO_4$. Furthermore, as shown in Figs. 2*B* and 2*C*, the addition of $HClO_4$ to **1**HCl gives rise to a new oxidation peak, a shoulder at ca. +1.4 – 1.5 V, and to a small reduction peak at +0.70 V. The addition of a second equivalent of $HClO_4$ does not cause any further change in the cyclic voltammogram (voltammogram identical to that of Fig. 2*C*) except for the appearance of the reduction peak of $HClO_4$ at –0.39 V. The same behavior is observed in the cyclic voltammogram of Et_3NHCl upon adding $HClO_4$: disappearance of the oxidation peak at +0.90 V, appearance of the shoulder at +1.4–1.5 V, and appearance of a reduction peak at

Can. J. Chem. Downloaded from www.nrcresearchpress.com by 65.111.164.53 on 09/08/12
For personal use only.

Fig. 1. Cyclic voltammetry on a Pt electrode: (*A*) **1**HCl (6.0 mM); (*B*) **1**$HClO_4$ (4.5 mM); (*C*) LiCl (18 mM) in CH_3CN – 0.1 M $LiClO_4$. Sweep range: 0–+2.2 V vs. Ag/Ag^+ 0.01 M; sweep rate: 100 mV/s.

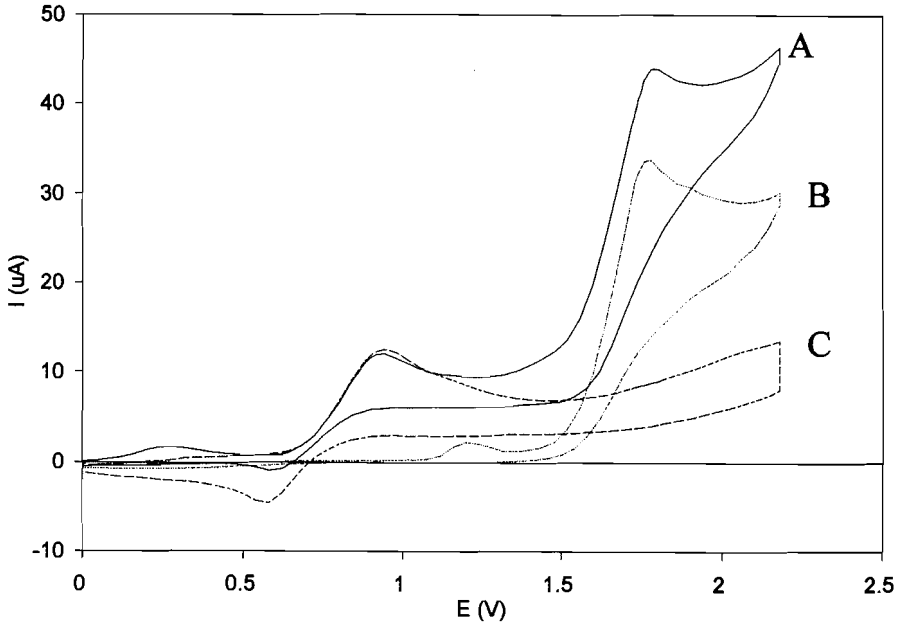

Table 1. Cyclic voltammetric data for amidine hydrochlorides in CH_3CN – 0.1 M[a] $LiClO_4$.

				Scan I[c]						Scan II[c]			
Entry	Salt	Conc. ($\times 10^3$M)	Working electrode[b]	E_p(ox1) (V)	(*i* ox1) (μA)	E_p(red1) (V)	(*i* red1) (μA)	E_p(ox2) (V)	(*i* ox2) (μA)	E_p(red2) (V)	(*i* red2) (μA)	E_p(red3) (V)	(*i* red3) (μA)
1	**1**HCl	6.0	Pt	+0.90	(12)	+0.58	(1)	+1.78	(40)	−1.33	(40)	—	—
2	**1**HCl	9.0	VC	+1.12	(103)	—	—	+1.89	(447)	−1.99	(111)	—	—
3	**1**$HClO_4$	4.5	Pt	—	—	—	—	+1.78	(33)	−1.43	(8)	—	—
4	**1**$HClO_4$	7.5	VC	—	—	—	—	+1.97	(155)	−2.14	(77)	—	—
5	**10**HCl	10	Pt	+0.84	(12)	+0.56	(4)	+1.28	(17)	−1.20	(8)	—	—
6	**10**HCl	10	VC	+1.55	(60)	—	—	+2.03	(60)[d]	−1.82	(176)	−2.66	(220)
7	**10**$HClO_4$	7.0	Pt	—	—	—	—	+2.06	(39)	−1.16	(13)	—	—
8	**10**$HClO_4$	7.0	VC	—	—	—	—	+1.97	(545)	−1.78	(181)	−2.87[e]	—
9	**11**HCl	7.5	Pt	+0.90	(10)	—	—	+1.45	(10)	−1.43	(18)	—	—
10	**11**HCl	7.5	VC	+1.54	(40)	—	—	+2.06	(40)[d]	−2.24	(160)	—	—
11	**11**$HClO_4$	7.0	Pt	—	—	—	—	—	—	−1.72	(10)	—	—
12	**11**$HClO_4$	7.0	VC	—	—	—	—	+1.92	(67)	−2.31	(125)	—	—
13	LiCl	18	Pt	+0.92	(12)	+0.57	(4)	—	—	—	—	—	—
14	LiCl	8.0	VC	+1.00	(21)	—	—	—	—	—	—	—	—
15	Et_3NHCl	5.0	Pt	+0.90	(10)	+0.65	(3)	—	—	—	—	—	—

[a]Auxiliary electrode: vitreous carbon rod; reference electrode: Ag/Ag^+ 0.01 M; scan rate: 100 mV s^{-1}.
[b]VC: vitreous carbon.
[c]Scan I: between 0 and +2.0–+ 2.5 V; scan II: between 0 and −2.0–−3.0 V.
[d]Broad peak (approximate value of E_p).
[e]The peak potential was too close to the discharge potential to measure the cathodic current.

−0.39 V when more than 1 equivalent of $HClO_4$ is added. Thus, only 1 equivalent of $HClO_4$ reacts with **1**HCl and Et_3NHCl. The identical behavior of **1**HCl and Et_3NHCl suggests that the amidine moiety is not involved in the disappearance of the oxidation peak for the chloride anion. Indeed, the disappearance of the oxidation peak at +0.90 V is due to protonation of the chloride anion by $HClO_4$ (eq. [3]), which is a stronger acid than HCl ($pK_{a\ HClO_4\ (H_2O)} = -10$; $pK_{a\ HCl\ (H_2O)} = -7$) and the appearance of the peak at +1.4–1.5 V is due to the oxidation of the undissociated HCl formed (eq. [3]), as con-

Can. J. Chem. Downloaded from www.nrcresearchpress.com by 65.111.164.53 on 09/08/12
For personal use only.

Fig. 2. Cyclic voltammetry of **1**HCl (5 mM) in CH_3CN – 0.1 M $LiClO_4$ on a Pt electrode: (*A*) **1**HCl alone; (*B*) plus 0.5 equivalent of $HClO_4$; (*C*) plus 1 equivalent of $HClO_4$. Sweep range: 0–+2.2 V vs. Ag/Ag^+ 0.01 M; sweep rate: 100 mV/s.

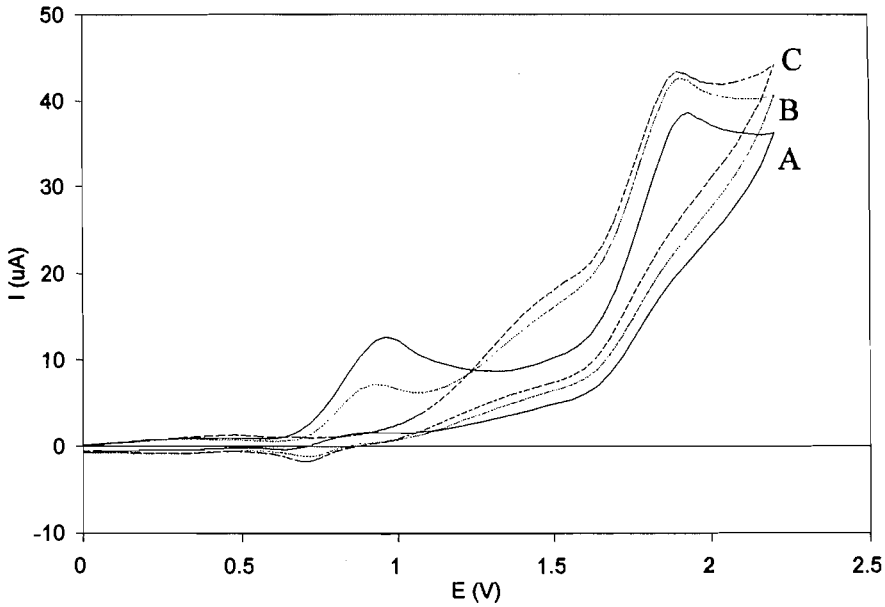

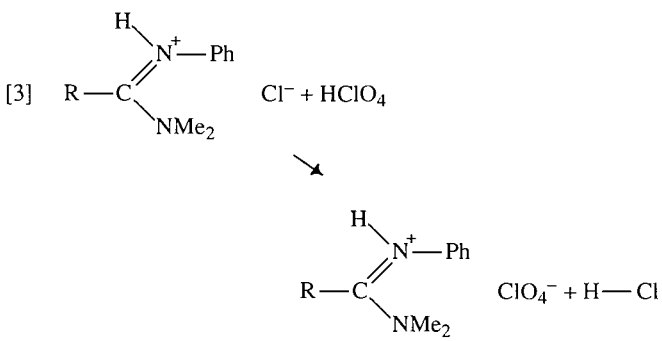

firmed by the absence of an oxidation peak at +0.90 V and the presence of a broad peak at +1.4–1.5 V in the cyclic voltammogram of anhydrous HCl in CH_3CN – 0.1 M $LiClO_4$. Upon adding water, the broad peak changes to a narrower peak at +0.90 V due to regeneration of the chloride anion since H_3O^+ ($pK_{a\,(H_2O)} = -1.75$) is a weaker acid than HCl: $HCl + H_2O \rightarrow H_3O^+Cl^-$. These results show clearly that the amidinium cation $\mathbf{1}H^+$ is not protonated to the dication $\mathbf{1}H_2^{2+}$ contrarly to Barbey and Caullet's hypothesis (2) (see Scheme 1). As with **1**HCl, the addition of 1 equivalent of $HClO_4$ to a solution of **10**HCl and **11**HCl in CH_3CN – 0.1 M $LiClO_4$ resulted in a shift of the oxidation peak of Cl^- from +0.84 to +1.20 V for **10**HCl and from +0.90 to +1.32 V for **11**HCl.

The second oxidation peak at $E_p(ox2) = +1.78$ V vs. Ag/Ag^+ 0.01 M in the voltammograms of both the hydrochloride **1**HCl (Fig. 1*A*) and the perchlorate **1**$HClO_4$ (Fig. 1*B*) could be attributed to the oxidation of the protonated amidine. The preparative oxidation of these salts at +1.7 V consumed 2 moles of electrons per mole of salt. However no product (starting material or reaction products) could be recovered or detected from these oxidations after the usual basic work-up and extraction.

Preparative electrooxidation of 1HCl

The potentiostatic preparative electrolysis of **1**HCl (see the Experimental) carried out under the same conditions as those used by Barbey and Caullet (2) (E_w = +0.75 V, CH_3CN – 0.1 M $LiClO_4$), consumed 1.5 moles of electrons per mole of **1**HCl and gave 72% of the parent amidine **1** and 14% of two chlorinated products after alkaline work-up and ether extraction. The major chlorinated product (13%) was identified as *N,N*-dimethyl-*N'*-(4-chloro)phenylformamidine (**5**) and the minor one (≤1%) as *N,N*-dimethyl-*N'*-(2-chloro)phenylformamidine (**6**) (see Scheme 2) by comparison (^1H and ^{13}C NMR, IR and mass spectra) with authentic samples synthesized as described by Pedersen (9). It is noteworthy that neither the chloroamidine **4**, which Barbey and Caullet (2) claimed to have isolated as the perchlorate salt (**4**$HClO_4$), nor its hydrolysis product, *N,N*-dimethyl-*N'*-phenylurea (**9**), were detected.

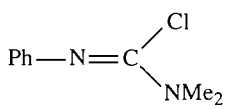

4

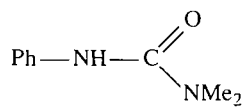

9

Reaction of amidine 1 with electrogenerated chlorine

Since the oxidation of **1**HCl at +0.75 V (Table 2, entry 1) generates chlorine according to reaction [1], the chlorinated products **5** and **6** must arise from the electrophilic chlorination of the protonated amidine during the electrolysis and (or) of the amidine (which should be a better nucleophile than the protonated form) during the basic work-up. When chlorine was generated by electrolyzing LiCl at platinum in CH_3CN – 0.1 M $LiClO_4$ (E_w = +0.75 V, 1 mole of electrons per mole of salt), then the circuit was opened and 0.16 equivalent of **1**$HClO_4$ was added to the electrolysis medium (Table 2, entry 2); the

Can. J. Chem. Downloaded from www.nrcresearchpress.com by 65.111.164.53 on 09/08/12
For personal use only.

Can. J. Chem. Downloaded from www.nrcresearchpress.com by 65.111.164.53 on 09/08/12
For personal use only.

Scheme 2

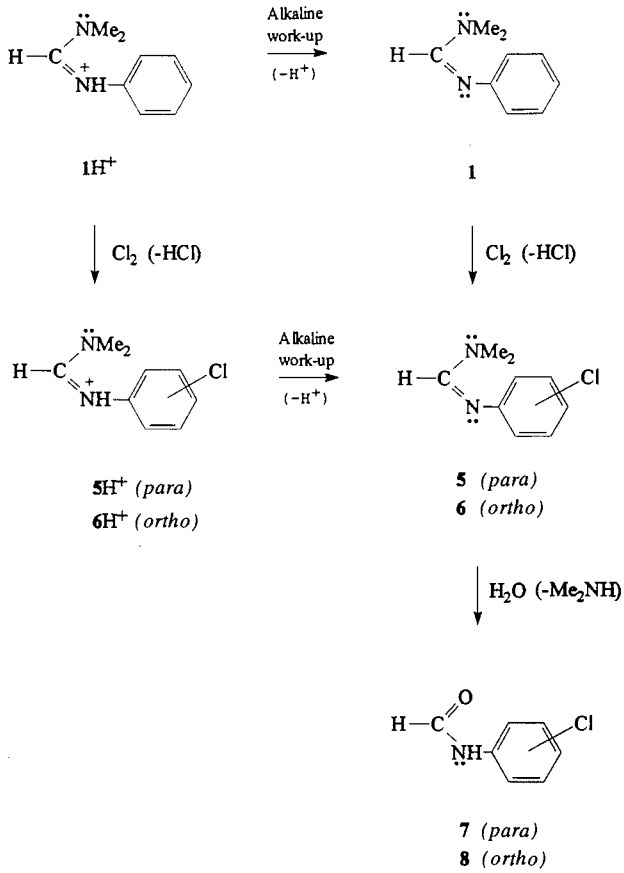

products obtained after the usual work-up, separation, and analysis were the parent amidine **1** (90%) and the *para*-chloro derivative **5** (10%). Adding amidine **1** to chlorine electrogenerated as above also led, after the same isolation procedure, to the chlorinated amidines **5** (11%) and **6** (≤1%). Only 8% of amidine was recovered. In addition, the products of hydrolysis of **5** and **6**, 4-chloroformanilide (**7**)(~10%) and 2-chloroformanilide (**8**)(~1%), respectively (see Scheme 2), and some dichlorinated amidines (5%) were detected by GLC in the crude reaction mixture and identified by GC–MS.

Reduction behavior

To complete the electrochemical study of **1**HCl, its reduction was studied both by cyclic voltammetry and preparative electrolysis. The cyclic voltammogram of a solution of **1**HCl in CH_3CN – 0.1 M $LiClO_4$ at platinum (Fig. 3*A*) shows a reduction peak at −1.33 V (see E_p(red2) in entry 1, Table 1)[2]. After the addition of 1 equivalent of $HClO_4$, the cyclic voltammogram shows a new reduction peak at −0.62 V in addition to the peak at −1.33 V (compare Fig. 3*B* and 3*A*).[2] The preparative reduction of the latter solution at −0.62 V consumed 1 mole of electrons per mole of substrate and gave, after the usual basic work-up and ether extraction, the parent amidine **1** in a quantitative yield. Coulometric measurements on this same solution at −1.33 V (second reduction peak) revealed a two-electron process and the preparative electrolysis gave the amidine **1** in a 94% yield. Based on the oxidation results, the electrochemical behavior just described can be readily explained by eqs. [4] and [5]. The addition of 1 equivalent of $HClO_4$ to a solution of **1**HCl gives **1**$HClO_4$ and HCl (eq. [3]), as already pointed out. Reduction of the latter gives rise to the reduction peak at −0.62 V (eq. [4]), the current of which indeed increases upon addition of anhydrous HCl. The reduction peak at −1.33 V corresponds to the reduction of the proton of the monoprotonated amidine **1**H^+ to hydrogen and amidine **1** (eq. [5]). Upon adding more than 1 equivalent of $HClO_4$ to the electrolytic solution of **1**HCl, a third reduction peak appears at −0.39 V and increases with the amount of $HClO_4$ added (Fig. 4). This peak corresponds to the reduction of $HClO_4$ as mentioned above (see Oxidation behavior) and as confirmed by the cyclic voltammogram of a 4.5 mM solution of $HClO_4$ in CH_3CN – 0.1 M $LiClO_4$. The presence of this peak in Fig. 4 shows clearly that only 1 equivalent of $HClO_4$ reacts with **1**HCl and that $HClO_4$ is not an acid strong enough to further protonate the monoprotonated amidine **1**H^+, as already pointed out (see Oxidation behavior).

[4] $H—Cl + e^- \longrightarrow \frac{1}{2}H_2 + Cl^-$

[5] 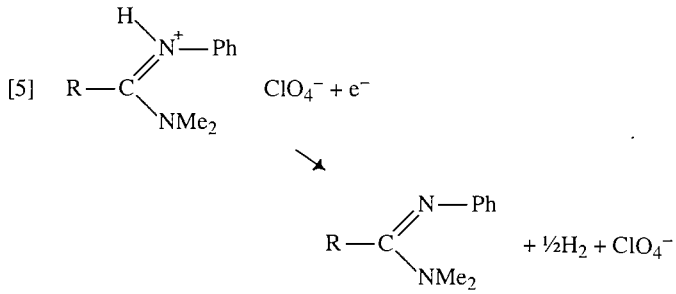

Hydrochlorides of amidines 10 (10HCl) and 11 (11HCl)

Oxidation behavior

At platinum

When compared to the cyclic voltammogram of **1**HCl, the voltammograms of *N*-phenylbenzamidine hydrochloride (**10**HCl) and *N*-phenylcyclohex-3-enecarboxamidine hydrochloride (**11**HCl) at platinum in CH_3CN – 0.1 M $LiClO_4$ also exhibit an anodic peak at ca. +0.90 V, which corresponds to the oxidation of the chloride anion (eq. [1]) (see E_p(ox1) in Table 1, entries 5 and 9). In the case of **10**HCl, the cathodic peak corresponding to the reduction of electrogenerated chlorine is also observable at +0.56 V (E_p(red 1), entry 5). However, for **11**HCl, this reduction peak is absent in the voltammogram, probably as a result of reaction of the electrogenerated chlorine with the cyclohexene ring to give dichlorides and (or)

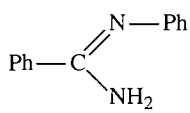

10

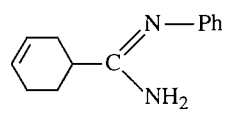

11

[2] The origin of the weak anodic peaks at −0.80 V in Fig. 3*A* and −0.33 and −0.93 V in Fig. 3*B* can be attributed to the oxidation of chemisorbed hydrogen.

Table 2. Preparative electrolysis of **1**HCl and LiCl at platinum.[a]

Entry	Compound (c = 0.02 M)	E_{app}[b] (V)	Moles of e⁻ per mole of salt	Yield of products[c] (%)				
				5	**6**	**7**[d]	**8**[d]	**1**
1	**1**HCl	+0.75	1.5	13	≤1	—	—	72
2	LiCl + **1**$HClO_4$[e]	+0.90	1	10	—	—	—	90
3[f]	LiCl + **1**[e]	+0.84	1	11	≤1	~10	<1	8

[a]In CH_3CN – 0.1 M $LiClO_4$, platinized Pt as auxiliary electrode.
[b]Applied potential vs Ag/Ag^+ 0.01 M.
[c]Yield of isolated products unless otherwise indicated.
[d]Not isolated, detected by GLC and identified by GC–MS in the crude product mixture.
[e]The solution of LiCl was electrolyzed first. The electrolysis was stopped after a charge corresponding to 1 mole of electrons per mole of LiCl. Then, 0.16 mole of **1**$HClO_4$ (entry 2) or 0.33 mole of amidine **1** (entry 3) per mole of LiCl was added and the mixture was stirred at room temperature for 12 h.
[f]We also detected, by GLC (identified by GC–MS), 5% of dichlorinated products and traces of succinonitrile.

Can. J. Chem. Downloaded from www.nrcresearchpress.com by 65.111.164.53 on 09/08/12
For personal use only.

Fig. 3. Cyclic voltammetry on a Pt electrode: (*A*) **1**HCl (6.8 mM); (*B*) **1**HCl (6.8 mM) plus 1 equivalent of $HClO_4$ in CH_3CN – 0.1 M $LiClO_4$. Sweep range: 0–−2.5 V vs. Ag/Ag^+ 0.01 M; sweep rate: 100 mV/s.

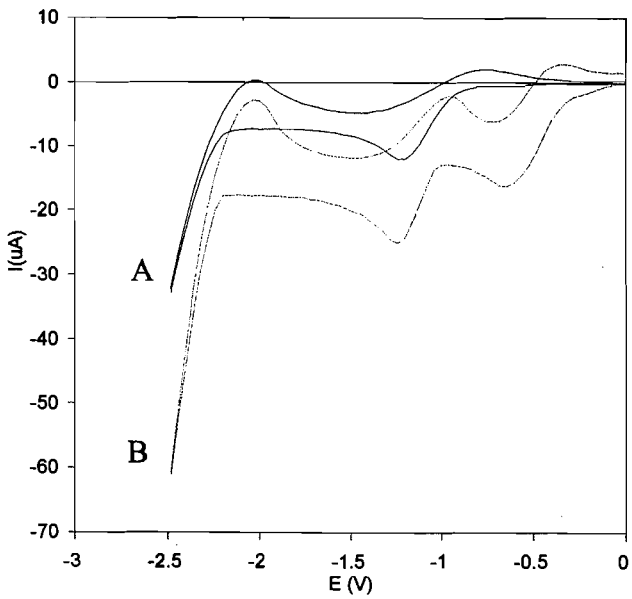

Fig. 4. Cyclic voltammetry of **1**HCl (6.8 mM) in CH_3CN – 0.1 M $LiClO_4$ on a Pt electrode: (*A*) plus 1.5 equivalents of $HClO_4$; (*B*) plus 2.0 equivalents of $HClO_4$; (*C*) plus 3.0 equivalents of $HClO_4$. Sweep range: 0–+2.5 V vs. Ag/Ag^+ 0.01 M; sweep rate: 100 mV/s.

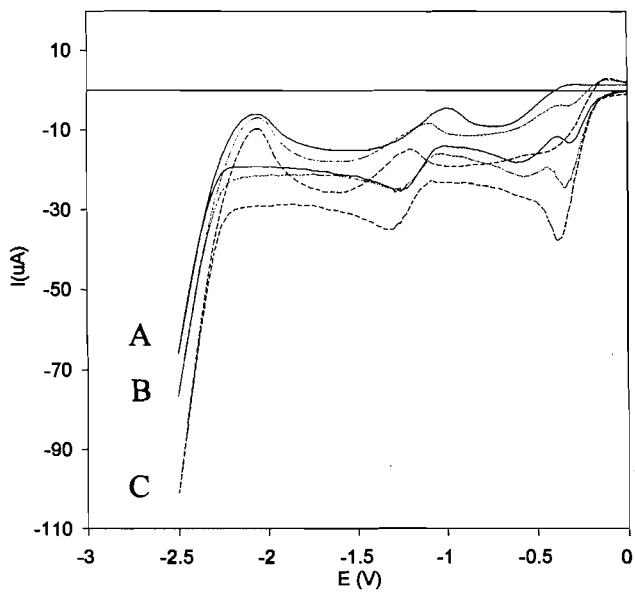

allylic chlorides. Attempts to isolate such chlorinated derivatives from preparative electrolyses of **11**HCl were, however, unsuccessful. Controlled potential oxidations of **11**HCl at +0.90 V or +1.0 V using a charge corresponding to 1 mole of electrons per mole of salt led to only the partial recovery (35–75%) of the parent amidine **11** after basic work up. The recovery of the parent amidine **10** in the preparative oxidation of **10**HCl after basic work up was even lower (0–40%). In addition to the peak at +0.90 V (E_p(ox1)), the voltammograms of **10**HCl and **11**HCl at platinum also show a second oxidation peak (E_p(ox2)) but at a less positive potential (+1.28 V and +1.45 V, respectively, see Table 1, entries 5 and 9) than that of **1**HCl (E_p(ox2) = +1.78 V, entry 1 and Fig. 1*A*). In the case of **1**HCl (entry 1), E_p(ox2) was tentatively attributed to the oxidation of the protonated amidine (**1**H^+) (see above), the same peak being present also in the voltammogram of **1**$HClO_4$ (entry 3). However, the potential of the second oxidation peak differs for **10**HCl (E_p(ox2) = +1.28 V, entry 5) and **10**$HClO_4$ (E_p(ox2) = +2.06 V, entry 7). Furthermore, a second oxidation

Can. J. Chem. Downloaded from www.nrcresearchpress.com by 65.111.164.53 on 09/08/12
For personal use only.

peak is present in the voltammogram of **11**HCl (E_p(ox2) = +1.45 V, entry 9) but is absent in the voltammogram of **11**$HClO_4$ (entry 11). Therefore, the origin of E_p(ox2) in the voltammograms of the amidine hydrochlorides is not known. The preparative oxidations of **10**HCl and **11**HCl at a potential corresponding to E_p(ox2) consumed 2 moles of electrons per mole of hydrochlorides. No product nor any parent amidine could be isolated after the usual basic work-up followed by extraction with ether.

At vitreous carbon

The potential of the first oxidation peak is the same for both hydrochlorides (E_p(ox2) = +1.54 V for **10**HCl and +1.55 V for **11**HCl) and is absent in the voltammograms of **10**$HClO_4$ and **11**$HClO_4$ (entries 8 and 12, respectively). Therefore, it can most probably be attributed to the oxidation of the chloride anion. Interestingly, LiCl is oxidized at a more positive potential (E_p(ox1) = +1.00 V, entry 14) at vitreous carbon than the chloride ion of **10**HCl and **11**HCl, whereas the oxidation potential (E_p(ox1)) at platinum is the same for LiCl, **10**HCl, and **11**HCl (see entries 13, 5, and 9, respectively), as already mentioned. The chloride anion of amine hydrochlorides is also oxidized at more positive potentials on vitreous carbon than LiCl but at less positive potentials than the chloride ion of **10**HCl and **11**HCl, and the oxidation potential depends on the structure of the amine: E_p(ox1) = +1.12, +1.13 and +1.25 V for $Et_2NH{\cdot}Cl$, $(CH_3)_2NH{\cdot}HCl$, and pyridine hydrochloride, respectively. The more difficult oxidation of the chloride ion of amidine and amine hydrochlorides when compared to LiCl as well as the differences in the oxidation potential with the structure of the amidine/amine moiety could be attributed to the adsorption of the protonated (or unprotonated) amidine/amine. The controlled potential oxidation at vitreous carbon of **10**HCl and **11**HCl at the potential of the first anodic peak (E_w = +1.5 V) consumed 2 moles of electrons per mole of salt and not 1 mole as in the preparative oxidation at platinum at +0.90 V. These oxidations led to the complete destruction of the organic moiety since no product nor parent amidine could be detected after the usual basic work-up and extraction with ether.

The second oxidation peak in the voltammograms of **10**HCl and **11**HCl at vitreous carbon appears at potentials (E_p(ox2) = ca. +2.05 V, Table 1, entries 6 and 10) similar to those of the oxidation peak observed in the voltammograms of **10**$HClO_4$ and **11**$HClO_4$ at both vitreous carbon (E_p(ox2) = ca. +1.95 V, entries 8 and 12) and platinum (E_p(ox2) = +2.06 V for **10**$HClO_4$, entry 7). Again, no product or parent amidine could be isolated from the preparative oxidations at a potential (+2.0 V) corresponding to that of the second oxidation peak.

Reduction behavior

The electrochemical reduction of the hydrochlorides and perchlorates of amidines **10** and **11** was studied by cyclic voltammetry in the 0 to ca. −3 V range and by preparative electrolysis. The voltammetric data are recorded in Table 1. At platinum, the voltammograms of **10**HCl, **10**$HClO_4$, **11**HCl, and **11**$HClO_4$ show only one irreversible reduction peak (entries 5, 7, 9, and 11), as in the cyclic voltammograms of **1**HCl and **1**$HClO_4$ (entries 1 and 3). As in the case of **1**HCl and **1**$HClO_4$, this reduction peak corresponds to the reduction of the proton of the protonated amidines **10**H^+ and **11**H^+ since the preparative electrolysis at the peak potential consumed 1 mole of electrons per mole of salt to give the parent amidine in high yield (95–100%).

At vitreous carbon (Table 1, entries 6, 8, 10, and 12), the cyclic voltammograms of **10**HCl, **10**$HClO_4$, **11**HCl, and **11**$HClO_4$ also show a peak corresponding to the reduction of H^+ of the protonated amidine, as confirmed by the preparative electrolysis at the peak potentials: Q = 1 mole of electrons per mole of salt, parent amidine as the sole product isolated in 88–90% yield. The reduction potentials are more negative at vitreous carbon (E_p(red 1) = −1.78 to −2.31 V) than at platinum (E_p(red 1) = −1.16 to −1.72 V), as expected for the reduction of protons since the overpotential for proton reduction is known to be higher at vitreous carbon than at platinum (10).

The structure of the amidine to which the proton is attached has a definitive influence on the reduction potential of the proton. Both at platinum and at vitreous carbon, the peak potential and hence the ease of proton reduction increase in the order **11**H^+, **1**H^+, and **10**H^+: E_p(red2) = −1.43, −1.33, and −1.20 V, respectively for the hydrochlorides at Pt (entries 9, 1, and 5); −1.72, −1.43 , and −1.16 V, respectively, for the perchlorates at Pt (entries 11, 3, and 7); −2.24, −1.99, and −1.82 V, respectively, for the hydrochlorides at vitreous carbon (entries 10, 2, and 6); −2.31, −2.14, and −1.78 V, respectively, for the perchlorates at vitreous carbon (entries 12, 4, and 8).

The voltammograms of **10**HCl and **10**$HClO_4$ at vitreous carbon exhibit a second reduction peak at −2.66 V and −2.87 V, respectively (E_p(red3) in Table 1, entries 6 and 8). This second peak should correspond to the reduction of the parent benzamidine **10** liberated after reduction of the acidic proton, which occurs at *ca.* −1.2 V as seen above. Indeed, the voltammetric reduction of *N*-phenylbenzamidine (**10**) at vitreous carbon in the same medium gives a peak at −2.81 V (see Table 3, entry 3) and addition of benzamidine **10** to a solution of **10**HCl or **10**$HClO_4$ causes an increase of the current of the second reduction peak.

Amidines

Oxidation behavior

The oxidation and reduction peak potentials of amidine **1** and of amidines **10–20**, determined by cyclic voltammetry, are reported in Table 3. At platinum, the voltammograms of the *N*-phenylamidine **1** and the *N*-phenylamidines **10–18** all show two irreversible oxidation peaks, a first peak between +0.70 and +0.84 V vs. Ag/Ag^+ 0.01 M and a second peak in the range of +1.83–+2.40 V. At vitreous carbon, the voltammograms of the *N*-phenylamidines **10–17** show only the first oxidation peak between +0.60 and +0.80 V whereas the second oxidation peak is present at +1.92 V (entry 20) in the voltammogram of the *N,N'*-diphenylamidine **18**. The voltammograms of the *N*-cyclohexylamidines **19** and **20** differ from those of the other amidines in showing an anodic peak at +1.26–+1.34 V at both platinum (entries 21 and 23) and vitreous carbon (entries 22 and 24). It is noteworthy that, according to the ^1H NMR spectra and to Prevorsek (11), the *N*-phenylamidines **1** and **10–18** exist as the tautomer possessing the phenyl group on the imino nitrogen (even if the phenyl ring is out of the plane and thus not fully conjugated with the amidine moiety (12)) whereas the prefered tautomer of the *N*-cyclohexylamidines **19** and **20** has the cycloalkyl substituent on the amino nitro-

Table 3. Cyclic voltammetric data of amidines.

				Scan I[c]						Scan II[e]			
Entry	Amidine[a]	Working electrode[b]	Conc. ($\times 10^3$)	E_p(ox1) (V)	i(ox1) (μA)	E_p(ox2)[d] (V)	i(ox2) (μA)	E_p(ox3) (V)	i(ox3) (μA)	E_p(red1) (V)	i(red1) (μA)	E_p(red2) (V)	i(red2) (μA)
1	**1**	Pt	10	+0.78	(24)	—	—	+1.84	(57)	—	—	—	—
2	**10**	Pt	7.0	+0.71	(3)	—	—	+2.19	—	—	—	—	—
3		VC	7.5	+0.67	(30)	—	—	—	—	−2.81	(76)	—	—
4[f]		VC[g]	7.5	—	—	—	—	—	—	−2.69	(110)	—	—
5	**11**	Pt	5.0	+0.78	(4)	—	—	+1.83	—	—	—	—	—
6		VC	5.0	+0.80	(84)	—	—	—	—	—	—	—	—
7	**12**	Pt	5.0	+0.73	(10)	—	—	+1.93	—	—	—	—	—
8		VC	7.5	+0.63	(160)	—	—	—	—	—	—	—	—
9	**13**	Pt	5.0	+0.74	(5)	—	—	+1.90	—	—	—	—	—
10		VC	7.5	+0.68	(70)	—	—	—	—	—	—	—	—
11	**14**	Pt	5.0	+0.70	(11)	—	—	+2.40	—	—	—	—	—
12		VC	10	+0.65	(175)	—	—	—	—	—	—	—	—
13	**15**	Pt	10	+0.75	(10)	—	—	+2.15	—	—	—	—	—
14		VC	10	+0.69	(58)	—	—	—	—	−2.60	(87)	−2.84	(130)
15	**16**	Pt	5.0	+0.84	(3)	—	—	+1.92	—	—	—	—	—
16		VC	7.5	+0.68	(44)	—	—	—	—	—	—	—	—
17	**17**	Pt	5.0	+0.70	(5)	—	—	+1.87	—	—	—	—	—
18		VC	7.5	+0.60	(39)	—	—	—	—	—	—	—	—
19	**18**	Pt	8.0	+0.73	(13)	—	—	+1.93	(10)	—	—	—	—
20		VC	7.0	+0.74	(110)	—	—	+1.91	(208)	−2.46[h]	(85)	—	—
21	**19**	Pt	8.0	+0.65	(3)	+1.34	(9)	+1.93	(7)	—	—	—	—
22		VC	11	+0.75[i]	(21)	+1.29[i]	(15)	—	—	—	—	—	—
23	**20**	Pt	9.0	+0.72	(4)	+1.29	(7)	+1.94	(7)	—	—	—	—
24		VC	12	+0.73	(36)	+1.26	(60)	—	—	—	—	—	—

[a]All waves are irreversible; experimental conditions are: CH_3CN – 0.2 M Bu_4NBF_4, auxiliary electrode Pt, reference electrode Ag/Ag^+ 0.01 M, scan rate 100 mV/s.
[b]VC = vitreous carbon.
[c]Oxidation scan: 0—+2.2 V.
[d]The oxidation current could not be measured for peaks that were too close to the bulk discharge.
[e]Reduction scan at Pt: 0—2.5 V; reduction scan at VC: 0 to −3.0 V.
[f]0.1 M $LiClO_4$ as supporting electrolyte.
[g]Only the 0 to −3.0 V region was scanned.
[h]In the backward scan, there was a small reduction peak (20 μA) at −0.40 V.
[i]Broad waves (approximate E_p).

gen. Thus, an amidine with an alkyl substituent on the amino nitrogen and an unsubstituted imino nitrogen gives an additionnal oxidation peak at ca. +1.3 V when compared to a *N*-phenylamidine.

On the other hand, the structure of the amidine has little influence on the first anodic peak potential. At platinum, *N*-cyclohexylamidine (**19**) is the easiest to oxidize (+0.65 V, Table 3, entry 21) and *endo N*-phenylnorborn-5-ene-2-carboxamidine (**16**) the most difficult to oxidize (+0.84 V, entry 15). At vitreous carbon, the easiest amidine to oxidize is *exo N*-phenylnorborn-5-ene-2-carboxamidine (**17**) (+0.60 V, entry 18) and the most difficult to oxidize is *N*-phenylcyclohex-3-ene carboxamidine (**11**) (+0.80 V, entry 6). So there is no particular trend. There is also no particular trend for the second oxidation peak at platinum but the range of oxidation potentials is wider, with +1.83 V for the amidine **11** (entry 5) and +2.40 V for the amidine **14** (entry 11).

The cyclic voltammograms of all the amidines, scanning from 0 V to +2.2 or +2.5 V, showed clearly the passivation of the anode both at platinum and at vitreous carbon. On platinum, the formation of a golden layer was easily seen and this layer could be destroyed only with nitric acid (≥1 M). This passivation was such that it was impossible to carry out any coulometric determination or any preparative oxidation at potentials corresponding to the peak potentials of the cyclic voltammograms. The passivation is not due to the polymeriza-

Can. J. Chem. Downloaded from www.nrcresearchpress.com by 65.111.164.53 on 09/08/12
For personal use only.

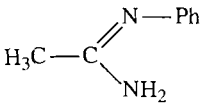

12

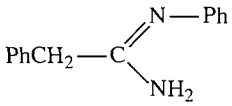

13

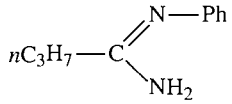

14

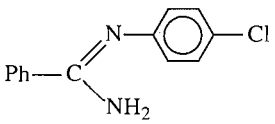

15

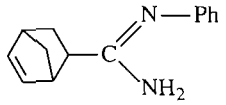

16 (*endo*)
17 (*exo*)

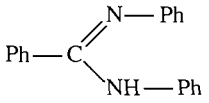

18

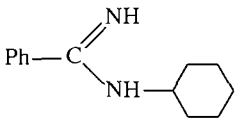

19

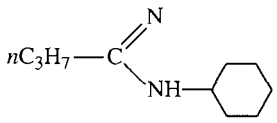

20

tion of acetonitrile that was reported to occur when oxidizing amines in that solvent (13) since passivation occurred also when the electrooxidation was carried out in dichloromethane or DMF. The passivation has to be attributed to polymerization of the amidine initiated by its oxidation.

Reduction behavior

We also studied the voltammetric reduction of the amidines at platinum and at vitreous carbon. As can be seen from Table 3 (entries 3, 4, 14, and 20), only the *N*-arylbenzamidines **10, 15,** and **18** with at least one phenyl group on one of the amidine nitrogens were reducible at potentials less negative than −3.0 V vs. Ag/Ag^+ 0.01 M, the discharge potential of the solvent or supporting electrolyte at vitreous carbon. None were reducible at platinum, the discharge potential being −2.5 V. The peak potentials vary from −2.81 V for amidine **10** (entry 3) to −2.46 V for amidine **18** (entry 20). As expected, the benzamidine **18** with two phenyl rings attached to the amidine nitrogens (one on each nitrogen) is easier to reduce than the benzamidines **10** and **15** with only one phenyl group on one of the amidine nitrogens. Even if one of the two phenyl groups on the amidine nitrogens in **18** is twisted out of the plane of the amidine moiety, it still exerts an electron-withdrawing effect. *N*-(4-Chlorophenyl)benzamidine (**15**) is easier to reduce (−2.60 V, entry 14) than *N*-phenylbenzamidine (**10**) (−2.81 V, entry 3) because of the electronwithdrawing (inductive) effect of the chlorine. In the voltammogram of *N*-(4-chlorophenyl)benzamidine (**15**), the second reduction peak at −2.84 V is due to *N*-phenylbenzamidine (**12**), as confirmed by an increase of the current of that peak when adding **10** to the electrolytic solution of **15**. *N*-Phenylbenzamidine (**10**) results from the reduction of the C—Cl bond of **15** and is most probably reduced to *N*-benzylaniline and ammonia at −2.84 V through a four electron – four-proton process. The reduction of benzamidines to benzylamines has already been reported by Heb and Bluemcke (14).

Conclusion

We have shown that the oxidation peak at +0.90 V vs. Ag/Ag^+ 0.01 M in the voltammogram of *N,N*-dimethyl-*N'*-phenylformamidine hydrochloride (**1**HCl) at a platinum electrode is not due to the oxidation of the protonated amidine cation ($\mathbf{1}H^+$) as proposed by Barbey and Caullet (2) but to the oxidation of the chloride anion. This same peak is also present in the voltammograms of *N*-phenylbenzamidine hydrochloride (**10**HCl) and *N*-phenylcyclohex-3-enecarboxamidine hydrochloride (**11**HCl). Preparative oxidations of **1**HCl at +0.75 V gave, after basic work-up, the parent amidine (72%) together with some 14% of products resulting from electrophilic chlorination of the aromatic ring. No chlorinated products were detected from the controlled potential oxidation of **10**HCl and of **11**HCl, and the recovery of the parent amidine was low.

All *N*-phenylamidines investigated (see **1**, and **10–18**) gave two irreversible oxidation peaks (at ca. +0.7–0.8 V and +1.9 V) at platinum and only one (at ca. +0.7 V) at vitreous carbon while the *N*-cyclohexylamidines **19** and **20** gave three irreversible oxidation peaks (at ca. +0.7, +1.3, and +1.9 V) at platinum and two (at ca. +0.7 and +1.3 V) at vitreous carbon. Strong passivation of the anode attributed to the deposition of an amidine polymer or oligomer on the electrode (formation of a golden layer) was observed in the preparative oxidations of each and every one of the amidines studied in CH_3CN–Bu_4NBF_4 as well as in CH_2Cl_2–Bu_4NBF_4. Only the *N*-arylbenzamidines gave a reduction peak before the discharge of the medium at vitreous carbon.

Experimental

General

Melting points were determined on a Buchi apparatus and are uncorrected. Infrared (IR) spectra were recorded on a Perkin Elmer 1600 Series FTIR. Proton and ^{13}C nuclear magnetic resonance (NMR) spectra were obtained on a Bruker AC-300 instrument. Mass spectra were obtained with a Hewlett Packard (HP) 5971 mass selective detector coupled with a HP 5890 Series II gas chromatograph. Exact Masses were determined with a VG Micromass ZAB-2F instrument.

Solvent and electrolyte

Technical grade acetonitrile was purified as described in ref. 15. Technical grade dichloromethane was distilled over CaH_2 and kept under argon. Tetrabutylammonium tetrafluoroborate (Bu_4NBF_4) prepared from tetrafluoroboric acid and tetrabutylammonium bromide (15) was recrystallized from 95% ethanol or acetonitrile. It was then dried in vacuum at 100°C for 12 h. Commercially available $LiClO_4$ (BDH) was dried in the same manner.

Electrochemical instrumentation and methods

For all voltammetric analyses as well as preparative electrolyses, solutions were deoxygenated with dry and oxygen-free nitrogen. A nitrogen atmosphere was maintained over the solution throughout the experiments. The cyclic voltammetry experiments were performed with a Princeton Applied Research (PAR) 173 potentiostat coupled to a PAR 175C

Can. J. Chem. Downloaded from www.nrcresearchpress.com by 65.111.164.53 on 09/08/12
For personal use only.

Can. J. Chem. Downloaded from www.nrcresearchpress.com by 65.111.164.53 on 09/08/12
For personal use only.

function generator in a two-compartment cell containing 3 mL of electrolyte solution or with a PAR 273 potentiostat in a two-compartment cell containing 8 mL of electrolyte solution. The working electrode was either a 1 mm^2 platinum disk or a 7.45 mm^2 vitreous carbon disk. The auxiliary electrode was a platinum wire or a vitreous carbon rod. Platinum and vitreous carbon electrodes were polished using 0.3 μm micropolish alumina (Buehler) before each use. Potentials were measured with respect to an Ag/Ag^+ 0.01 M (in acetonitrile) electrode.

The preparative electrolyses were carried out with an Electrosynthesis Company (ESC) 410 potentiostat having an ESC 640 coulometer and an ammeter connected in series within the auxiliary circuit; a two compartment glass H-cell (volume of each compartment = 12.5 or 25 mL) having a Nafion-324 (E-I du Pont de Nemours & Co) membrane as separator was used. The working electrode was either a 2 cm^2 platinum grid or 3.18 cm^2 vitreous carbon rod. The auxiliary electrode was a 2 cm^2 platinized platinum grid. The reference electrode was an Ag/Ag^+ 0.01 M electrode.

Amidines

N,N-*Dimethyl* N′-*phenylformamidine* (***1***)
Compound **1** was prepared according to the method described by Pedersen (9). *N,N*-dimethylformamide (50 mL, 47 g, 0.64 mol), P_2O_5 (15 g, 0.11 mol), and acetanilide (10.12 g, 0.075 mol) were refluxed for 2 h. The reaction mixture was cooled to ambient temperature and 400 mL of 1 M NaOH was added slowly. Extraction with ether yielded 6.75 g (61%) of **1**: bp 100°C/1.5 Torr (lit. (9) bp 70–72°C/0.1 Torr) (1 Torr = 133.3 Pa); IR ($CHCl_3$) cm^{-1}: 3010 (C-H arom.), 2930 (C-H aliph.), 1636 (C=N), and 1103 (C-N); ^1H NMR ($CDCl_3$) δ: 2.94 (s,6H), 6.98 (m,3H), 7.25 (m,2H), 7.46 (s,1H) ppm; ^{13}C NMR ($CDCl_3$) δ: 34.1 (CH_3), 39.7 (CH_3), 120.9 (CH), 122.0 (CH), 128.6 (CH), 151.6 (C), 153.0 (N-C=N) ppm; HMRS, *m/z*: 148.0998; calcd. for $C_9H_{12}N_2$: 148.1000.

N-*Phenylbenzamidine* (***10***)
Compound **10** was prepared according to the method described by Cooper and Partridge (16). Aniline (9.3 g, 0.1 mol) was dissolved in 25 mL of toluene and $NaNH_2$ (4 g, 0.1 mol) was added. After refluxing for 2 h, benzonitrile (10.3 g, 0.1 mol) was added, reflux was maintained overnight, then 125 mL of 2 N HCl was added slowly. The solution was extracted with 4 portions (100 mL) of ether to give 7.3 g of **10** (37%): mp 115–117°C (lit. (16) mp 114–115°C); IR (KBr) cm^{-1}: 3510 and 3404 (NH_2) and 1049 (C-N); ^1H NMR ($CDCl_3$) δ: 1.7 (broad peak, 1H), 6.99 (d, J = 7.8 Hz, 2H), 7.13 (t, J = 7.5 Hz, 1H), 7.32 (t, J = 7.5 Hz, 2H), 7.47 (m, 5H) ppm; ^{13}C NMR ($CDCl_3$) δ: 121.5 (CH), 122.9 (CH), 126.7 (CH), 128.5 (CH), 129.4 (CH), 130.5 (CH) ppm; HRMS, *m/z*: 196.0994; calcd. for $C_{13}H_{12}N_2$: 196.1000.

N-*Phenylcyclohex-3-enecarboxamidine* (***11***)
11 was prepared by the method described by Cooper and Partridge (16), with cyclohex-3-enecarbonitrile instead of benzonitrile. The yield was 46%: mp 88–90°C; IR ($CHCl_3$) cm^{-1}: 3518 and 3409 (NH_2), 3029 and 3012 (C-H arom. and C-H alkene), 2926 (C-H aliph.), 1643 (N-C=N), and 1589 (C-N); ^1H NMR ($CDCl_3$) δ: 1.73 (m,1H), 2.10 (m,2H), 2.30 (m,1H), 2.51 (m,1H), 4.04 (broad peak, 1H), 5.72 (m,2H), 6.87 (d, J = 7.9 Hz, 2H), 7.00 (t, J = 7.4 Hz, 1H), 7.29 (t, J = 7.8 Hz, 2H ppm); ^{13}C NMR ($CDCl_3$) δ: 24.9 (CH_2), 26.7 (CH_2), 29.3 (CH_2), 40.2 (CH), 121.8 (CH), 122.8 (CH), 125.6 (CH), 126.9 (CH), 129.4 (CH), 149.1 (C), 162.0 (N-C=N) ppm; HRMS, *m/z*: 200.1314; calcd. for $C_{13}H_{16}N_2$: 200.1313.

N-*Phenylacetamidine* (***12***)
12 was prepared by the same method as that used to obtain **10**, with acetonitrile instead of benzonitrile. The yield was 22%: mp 62–64°C; IR (KBr) cm^{-1}: 3527 and 3412 (NH_2), 3020 (C-H arom.), 2979 (C-H aliph.), 1663 (N-C=N), 1597 (NH_2), and 1050 (C-N); ^1H NMR ($CDCl_3$) δ: 2.03 (s,3H), 4.47 (broad peak, 1H), 6.86 (d, J = 7.5 Hz, 2H), 7.01 (t, J = 7.8 Hz, 1H), 7.29 (t, J = 7.8 Hz, 2H) ^{13}C NMR ($CDCl_3$)δ: 77.2 (CH_3), 121.8 (CH), 122.6 (CH), 129.2 (CH), 149.6 (C), 155.3 (N-C=N) ppm; HRMS, *m/z*: 134.0843; calcd. for $C_8H_{10}N_2$: 134.0844.

N-*Phenylphenylacetamidine* (***13***)
13 was prepared by the same method as that used to obtain **10**, with phenylacetonitrile instead of benzonitrile. The yield was 45%: mp 136–138°C; IR (KBr) cm^{-1}: 3510 and 3404 (NH_2), 3020 (C-H arom.), 2979 (C-H aliph.), 1655 (N-C=N), 1597 (NH_2), and 1050 (C-N); ^1H NMR (C_6D_6) δ: 3.4 (s,2H), 3.6-3.8 (broad peak, 1H), 6.98 (t, J = 7.5 Hz, 1H), 7.05 (d, J = 7.8 Hz, 2H), 7.21 (s,5H), 7.25 (t, J = 7.8 Hz, 2H) ppm; ^{13}C NMR ($CDCl_3$) δ: 43.0 (CH_2), 121.7 (CH), 122.8 (CH), 127.1 (CH), 128.9 (CH), 129.0 (C-H), 129.4 (C-H), 136.5 (C), 149.0 (C), 157.5 (N-C=N) ppm; HRMS, *m/z*: 210.1155; calcd. for $C_{14}H_{14}N_2$: 210.1157.

N-*Phenylbutanamidine* (***14***)
Compound **14** was prepared by the same method as that used to obtain **10**, with butyronitrile instead of benzonitrile. The yield was 14%: mp 66–67°C; IR (KBr) cm^{-1}: 3527 and 3412 (NH_2), 3020 (C-H arom.), 2971 (C-H aliph.), 1665 N-C=N), 1597 (NH_2), and 1050 (C-N); ^1H NMR ($CDCl_3$) δ: 1.01 (t, J = 7.4 Hz, 3H), 1.72 (6 peaks, J = 7.5 Hz, 2H), 2.33 (t, J = 7.7 Hz, 2H), 4.59 (broad peak, 1H), 6.92 (d, J = 7.2 Hz, 2H), 7.07 (t, J = 7.5 Hz, 1H), 7.32 (t, J = 7.8 Hz, 2H) ppm; ^{13}C NMR ($CDCl_3$) δ: 13.6 (CH_3), 20.6 (CH_2), 38.2 (CH_2), 121.7 (CH), 122.6 (CH), 129.3 (CH), 149.6 (C), 158.2 (N-C=N) ppm; HRMS, *m/z*: 162.1153; calcd. for $C_{10}H_{14}N_2$: 162.1157.

N-*(4-chlorophenyl)benzamidine* (***15***)
15 was prepared according to the method described by Cooper and Partridge (16) with a 22% yield: mp 101–106°C (lit. (16) mp 103–106°C); IR ($CHCl_3$) cm^{-1}: 3513 and 3405 (NH_2), 3000 (C-H arom.), 1640 (N-C = N), and 1578 (NH_2); ^1H NMR ($CDCl_3$) δ: 4.85 (broad peak, 1H), 6.93 (d, J = 8.6 Hz, 2H), 7.33 (d, J = 8.6 Hz, 2H), 7.45 (m,3H), 7.84 (br d, 2H) ppm; ^{13}C NMR ($CDCl_3$) δ: 123.1 (CH), 126.8 (CH), 128.2 (CH), 128.6 (CH), 129.1 (CH), 129.5 (C), 130.7 (C), 135.29 (C), 148.1 (N-C=N) ppm; HRMS, *m/z*: 230.0608; calcd. for $C_{13}H_{11}N_2Cl$: 230.0611.

N-*Phenylnorborn-5-enyl-2-carboxamidines* (***16+17***)
These compounds were prepared by the same method as that used to obtain **10**, with norborn-5-ene-2-carbonitrile (as a mixture of *endo* and *exo* epimers) instead of benzonitrile. The yield was 39%. The two epimeric amidines, *endo* **16** and *exo*

17, were easily separated by flash chromatography on silica gel (ethanol as eluent). *endo* **16**: mp 95–97°C; IR ($CHCl_3$) cm^{-1}: 3507 and 3404 (NH_2), 3000 (C-H arom. and alkene), 2975 (C-H aliph.), 1639 (N-C=N), 1586 (NH_2), and 1048 (C-N); ^1H NMR ($CDCl_3$)δ: 1.3–1.5 (m,3H), 2.03 (m,1H), 2.95 (s,1H), 3.10 (m,1H), 3.18 (s,1H), 4.47 (broad peak, 1H), 6.08 (m,1H), 6.31 (m,1H), 6.83 (d, J = 7.1 Hz, 2H), 6.99 (t, J = 7.4 Hz, 1H), 7.28 (t, J = 7.8 Hz, 2H) ppm; ^{13}C NMR ($CDCl_3$) δ: 30.6 (CH_2), 42.9 (CH_2), 43.7 (CH), 47.0 (CH), 50.5 (CH), 121.9 (CH), 122.9 (CH), 129.3 (CH), 132.2 (CH), 138.2 (CH), 148.7 (C), 160.7 (N-C=N) ppm; HRMS, *m/z*: 212.1308; calcd. for $C_{14}H_{16}N_2$: 212.1313. *exo* **17**: mp 83–85°C; IR ($CHCl_3$) cm^{-1}: 3516 and 3407 (NH_2), 3062 and 3012 (C-H arom. and alkene), 1642 (N-C=N), 1589 (NH_2), and 1047 (C-N); ^1H NMR ($CDCl_3$) δ: 1.44 (m,2H), 1.72 (d, J = 8.4 Hz, 1H), 2.09 (t of d, J = 11.6 and 4.0 Hz, 1H), 2.23 (m,1H), 2.94 (s,1H), 3.08 (s,1H), 4.5–5.0 (broad peak, 1H), 6.14 (m,2H), 6.89 (d, J = 7.5 Hz, 2H), 7.04 (t, J = 7.4 Hz, 1H), 7.30 (t, J = 7.8 Hz, 2H) ppm; ^{13}C NMR ($CDCl_3$) δ: 30.8 (CH_2), 41.6 (CH_2), 43.6 (CH), 46.5 (CH), 46.7, 122.1 (CH), 123.2 (CH), 129.4 (CH), 136.1 (CH), 138.3 (CH) ppm; HRMS, *m/z*: 212.1308; calcd. for $C_{14}H_{16}N_2$: 212.1313.

N,N′-*Diphenylbenzamidine* (***18***)
18 was prepared according to the method described by Khanolkar et al. (17) with a 23% yield: mp 146–148°C; IR ($CHCl_3$) cm^{-1}: 3434 and 3382 (NH), 3062 and 3011 (C-H arom.), 1632 (N-C=N), and 1590 (NH); ^1H NMR ($CDCl_3$) δ: 6.48 (s,1H), 6.68 (m,1H), 6.9–7.4 (m,12H), 7.65 (m,1H) ppm; ^{13}C NMR ($CDCl_3$) δ: 121.4 (CH), 122.1 (CH), 122.2 (CH), 123.3 (CH), 123.5 (CH), 128.4 (CH), 128.6 (CH), 129.1 (CH), 129.4 (CH), 129.7 (C), 130.1 (C) ppm; HRMS, *m/z*: 272.1311; calcd. for $C_{19}H_{16}N_2$: 272.1313.

N-*Cyclohexylbenzamidine* (***19***)
19 was prepared according to the method described by Partridge et al. (16). Aluminum trichloride (12 g, 0.09 mol) was added very slowly to benzonitrile (10.3 g, 0.1 mol) and cyclohexylamine (9.9 g, 0.1 mol) in order to maintain the reaction temperature below 100°C. Then, 100 mL of cold water was added. After filtration, 3.98 g (22% yield) of **19** was obtained: mp 116–118°C; IR ($CHCl_3$) cm^{-1}: 3443 and 3323 (NH), 3000 (C-H arom.), 2934 (C-H aliph.), 1608 (N-C=N), and 1049 (C-N); ^1H NMR ($CDCl_3$) δ: 1.1–1.3 (m,4H), 1.3–1.5 (m,2H), 1.61 (m,1H), 1.73 (m,1H), 2.08 (m,2H), 3.6–3.9 (broad peak, 1H), 7.36 (m,3H), 7.50 (m,2H) ppm; ^{13}C NMR ($CDCl_3$) δ: 24.9 (CH_2), 25.8 (CH_2), 33.1 (CH_2), 49.7 (CH), 125.9 (CH), 128.6 (CH), 129.8 (CH), 138.7 (C) ppm; HRMS, *m/z*: 202.1464; calcd. for $C_{13}H_{18}N_2$: 202.1470.

N-*Cyclohexylbutanamidine* (***20***)
20 was prepared according to the procedure used for the preparation of **19** by substituting benzonitrile with butyronitrile. The yield was 8%: mp between 0 and 20°C; IR ($CHCl_3$) cm^{-1}: 3448 (NH), 2965 and 2934 (C-H aliph.), 1613 (N-C=N), and 1050 (C-N); ^1H NMR ($CDCl_3$) δ: 0.92 (t, J = 7.8 Hz, 3H), 1.10 (m,4H), 1.33 (t of q, J = 12.0 and 3.0 Hz, 2H), 1.60 (m,5H), 1.93 (m,2H), 2.07 (t, J = 7.8 Hz, 2H), 3.52 (broad peak, 1H) ppm; ^{13}C NMR ($CDCl_3$) δ: 13.5 (CH_3), 20.4 (CH_2), 24.9 (CH_2), 25.8 (CH_2), 33.2 (CH_2), 39.7 (CH_2), 49.1 (CH) ppm; HRMS, *m/z*: 168.1625; calcd. for $C_{10}H_{20}N_2$: 168.1626.

Amidine salts

N,N-*Dimethyl* N′-*phenylformamidine hydrochloride* (***1HCl***)
The corresponding amidine **1** (622 mg, 4.2 mmol) was added to 10 mL of water and 0.1 N HCl was added until everything dissolved. After the water was evaporated, 581 mg (75% yield) of the desired hydrochloride was obtained: mp 238–240°C; IR (KBr) cm^{-1}: 3018 (C-H arom.), 2975 (C-H aliph.), 1697 (C=N), and 1137 (C-N); ^1H NMR (CD_3OD) δ: 4.49 (s,3H), 4.62 (s,3H), 8.50 (t, J = 7.1 Hz, 1H), 8.60 (m,4H), 9.78 (s,1H) ppm; ^{13}C NMR (CD_3OD) δ: 37.5 (CH_3), 44.4 (CH_3), 120.8 (CH), 128.0 (CH), 130.9 (CH), 155.3 (C) ppm.

N-*Phenylbenzamidine hydrochloride* (***10HCl***)
This compound was prepared according to the procedure used for the preparation of **1**HCl, with 85% yield: mp 230°C (dec.); IR (KBr) cm^{-1}: 3033 (C-H arom.) and 1659 (N-C=N); ^1H NMR (CD_3OD) δ: 7.52 (t, J = 7.7 Hz, 3H), 7.61 (d, J = 7.6 Hz, 2H), 7.69 (t, J = 7.7 Hz, 2H), 7.81 (t, J = 7.6 Hz, 1H), 7.93 (d, J = 8.4 Hz, 2H) ppm; ^{13}C NMR (CD_3OD)δ: 126.6 (CH), 129.4 (CH), 130.3 (CH), 130.6 (CH), 131.6 (CH), 135.4 (C), 166.2 (N-C=N) ppm.

N-*Phenylcyclohex-3-enecarboxamidine hydrochloride* (***11HCl***)
11HCl was prepared according to the procedure used for the preparation of **1**HCl, with 100% yield: mp 190–194°C; IR (KBr) cm^{-1}: 3030 (C-H arom. and C-H alkene), 2820 (C-H aliph.), and 1676 (N-C=N); ^1H NMR (D_2O) δ: 2.0 (m,1H), 2.12 (m,1H), 2.25 (m,2H), 2.45 (m,2H), 2.9 (m,1H), 5.80 (m,2H), 7.35 (d, J = 7.8 Hz, 2H), 7.45 (t, J = 7.5 Hz, 1H), 7.50 (t, J = 7.8 Hz, 2H) ppm; ^{13}C NMR (CD_3OD) δ: 25.8 (CH_2), 26.8 (CH_2), 29.7 (CH_2), 40.6 (CH), 125.2 (CH), 126.8 (CH), 127.9 (CH), 130.3 (CH), 131.5 (CH), 135.0 (C), 173.3 (N-C=N) ppm.

N,N-*Dimethyl*-N′-*phenylformamidine perchlorate* (***1HClO$_4$***)
The corresponding amidine **1** (600 mg, 2.4 mmol) was added to 10 mL of water and 0.1 N $HClO_4$ was added until everything was dissolved. The water was evaporated, after which 474 mg (47% yield) of the desired perchlorate was obtained: mp 154–155°C; IR (KBr) cm^{-1}: 3060 (C-H arom.), 2976 (C-H aliph.), 1701 (N-C=N), and 1136 (C-N); ^1H NMR (CD_3OD) δ: 3.20 (s,3H), 3.36 (s,3H), 7.34 (m,3H), 7.47 (d of t, J = 7.6 and 2.0 Hz, 2H), 8.20 (s,1H ppm); ^{13}C NMR (CD_3OD)δ: 37.3 (CH_3), 44.1 (CH_3), 119.8 (CH), 127.2 (CH), 130.3 (CH), 153.7 (C) ppm.

Authentic samples

N,N-*Dimethyl*-N′-*(4-chlorophenyl)formamidine* (***5***)
5 was prepared according to the procedure used for the preparation of **1** by substituting acetanilide by 4-chloroacetanilide. The yield was 86%: bp 140–150°C/2–3 Torr; IR ($CHCl_3$) cm^{-1}: 3000 (C-H arom.), 2924 (C-H aliph.), 1637 (N-C=N), and 1103 (C-N); ^1H NMR, ($CDCl_3$) δ: 2.94 (s,6H), 6.83 (m,2H), 7.15 (m,2H), 7.41 (s,1H) ppm; ^{13}C NMR ($CDCl_3$) δ: 34.2 (CH_3), 40.0 (CH_3), 122.2 (CH), 127.1 (CH), 128.7 (C), 150.6 (C), 153.3 (N-C=N) ppm; HMRS, *m/z*: 182.0610; calcd. for $C_9H_{11}N_2Cl$: 182.0611.

Can. J. Chem. Downloaded from www.nrcresearchpress.com by 65.111.164.53 on 09/08/12
For personal use only.

Can. J. Chem. Downloaded from www.nrcresearchpress.com by 65.111.164.53 on 09/08/12
For personal use only.

N,N-*Dimethyl* N′-*(2-chlorophenyl)formamidine (6)*
6 was prepared according to the procedure used for the preparation of amidine **1** by substituting acetanilide by 2-chloroacetanilide. The yield was 85%: bp 166–168°C/2–3 Torr; IR ($CHCl_3$) cm^{-1}: 3010 (C-H arom.), 2930 (C-H aliph.), 1634 (N-C=N), and 1104 (C-N); ^1H NMR ($CDCl_3$) δ: 3.04 (s,6H), 6.87 (m,2H), 7.13 (d of t, J = 7.6 and 1.5 Hz, 1H), 7.34 (d of d, J = 7.9 and 1.5 Hz, 1H), 7.45 (s,1H) ppm; ^{13}C NMR ($CDCl_3$) δ: 34.4 (CH_3), 40.2 (CH_3), 121.3 (CH), 121.4 (CH), 123.0 (CH), 127.3 (CH), 129.6 (C), 153.5 (N-C=N) ppm; HRMS, *m/z*: 182.0610; calcd. for $C_9H_{11}N_2Cl$: 182.0611.

Preparative electrolyses

Electrooxidation of N-N-*dimethyl*-N′-*phenylformamidine hydrochloride (1HCl) (Entry 1, Table 2)*
Hydrochloride **1**HCl (62 mg, 0.34 mmol), in CH_3CN – 0.1 M $LiClO_4$, was electrolyzed on a platinum electrode in a two compartment H-cell at an anodic potential of +0.75 V until the current was 10% of its starting value (2 moles of electrons per mole of **1**HCl). The anolyte was evaporated to dryness in vacuo and 20 mL of 5% $NaHCO_3$ was added to the residue. Extraction with ether (3 × 20 mL) yielded 50 mg of a yellowish solid. The three products detected by TLC (ethanol as eluent) were separated by flash chromatography on silica gel (ethanol as eluent). The less polar fraction consisted of *N,N*-dimethyl-*N′*-(2-chlorophenyl)formamidine (**6**) (<1 mg, <1% yield), identical (^1H and ^{13}C NMR, MS) to an authentic sample. The second fraction consisted of *N,N*-dimethyl-*N′*-(4-chlorophenyl)formamidine (**5**) (8 mg, 13% yield), identical (^1H and ^{13}C NMR, MS) to an authentic sample. The more polar fraction consisted of *N,N*-dimethyl-*N′*-phenylformamidine (**1**) (36 mg, 72% yield).

Electrooxidation of LiCl followed by the addition of 1HClO$_4$ (entry 2, Table 2)
LiCl (60 mg, 1.415 mmol), in CH_3CN – 0.1 M $LiClO_4$, was electrolyzed on a platinum electrode in a two-compartment H-cell at an anodic potential of +0.90 V until the current was 10% of its starting value (1 mole of electrons per mole of LiCl). The electrodes were disconnected and **1**$HClO_4$ (56 mg, 0.23 mmol) was added. After 12 h, work-up of the solution was carried out as above and two spots were observed on TLC (ethanol as eluent). Amidines **5** (4 mg, 10% yield) and **1** (31 mg, 90% yield) were isolated by flash chromatography on silica gel (ethanol as eluent).

Electrooxidation of N-*phenylbenzamidine hydrochloride (10HCl)*
Compound **10**HCl (58 mg, 0.25 mmol), in CH_3CN – 0.1 M $LiClO_4$, was electrolyzed on a platinum electrode in a two compartment H-cell. Two electrolyzes were carried out, one at an anodic potential of +0.90 V and the other at +1.40 V, until the current was 10% of its starting value. A third electrolysis was carried out at a constant current of 2 mA. The charge passed corresponded to 2 moles of electrons per mole of **10**HCl. After the usual work-up, only the parent amidine **10** (0–40% yield) was observed in all cases (identified and quantified by GLC using an authentic sample).

Electrooxidation of N-*phenylcyclohex-3-enecarboxamidine hydrochloride (11HCl)*
Three electrolyses were carried out exactly as above. After the usual work-up, only the corresponding amidine **11** (35–75% yield) was observed in all cases.

Electroreduction of N-*phenylbenzamidine hydrochloride (10HCl)*
Compound **10**HCl (13 mg, 0.055 mmol), in CH_3CN – 0.1 M $LiClO_4$, was electrolyzed on a vitreous carbon electrode in a two compartment H-cell, at a cathodic potential of −1.8 V, until the current was 10% of its starting value (1 mole of electrons per mole of **10**HCl). After the usual work-up, only the parent amidine **10** was obtained (11 mg, 100% yield).

Compound **10**HCl (16 mg, 0.069 mmol), under the same conditions as above, was also electrolyzed three times at −2.6 V until the current was 10% of its starting value (5–8 moles of electrons per mole of **10**HCl). After the usual work-up, the major product was again the parent amidine **10** (25–50% yield). However, in one of these experiments, *N*–benzylaniline was detected by GC–MS.

Electroreduction of N-*phenylcyclohex-3-enecarboxamidine hydrochloride (11HCl)*
Compound **11**HCl (10 mg, 0.042 mmol), in CH_3CN – 0.1 M $LiClO_4$, was electrolyzed on a vitreous carbon electrode in a two compartment H-cell, at a cathodic potential of −2.2 V, until the current was 10% of its starting value (1 mole of electrons per mole of **11**HCl). After the usual work-up, only the parent amidine **11** was obtained (7 mg, 90% yield).

Acknowledgements

We are grateful to Professor Zdenek Valenta for fruitful discussions. The financial support of the Natural Sciences and Engineering Research Council of Canada and the Fonds pour la formation de chercheurs et l'aide à la recherche (FCAR) du Québec is gratefully acknowledged.

References

1. (*a*) A.D. Broom, J.I. Skin, and G.L. Anderson. J. Org. Chem. **41**, 1095 (1976); (*b*) B. Koren, F. Kovac, A. Petric, B. Stranovnik, and M. Tisler. Tetrahedron, **32**, 493 (1976); (*c*) M.H. Elnagdi, M.R.H. Elmoghayer, D.H. Fleita, E.A. Hafez, and S.M. Fahmy. J. Org. Chem. **41**, 3781 (1976).
2. G. Barbey and C. Caullet. Tetrahedron Lett. **45**, 3937 (1977).
3. R.A. Fulton and F.W. Bergstrom. J. Am. Chem. Soc. **56**, 167 (1934).
4. G. Cauquis, H.M. Fahmy, G. Pierre, and M.H. Elnagdi. J. Heterocycl. Chem. **16**, 413 (1979).
5. J.A. Squella, L.J. Nunez-Vergara, H. Rodriguez, A. Marquez, J.M. Rodriguez-Mellado, M. Blasquez, E. Roldan, and M. Dominguez. Collect. Czech. Chem. Commun. **56**, 2791 (1991)
6. J. Oszczapowicz and K. Ciszkowski. J. Chem. Soc. Perkin Trans. 2, 663 (1987).
7. (*a*) I.D. Cunningham, J. Llor, and L. Munoz. J. Chem. Soc. Perkin Trans. 2, 1747 (1991); (*b*) I.D. Cunningham,

J.S. Blanden, J. Llor, L. Munoz, and A.P. Sharatt. J. Chem. Soc. Perkin Trans. 2, 1751 (1991).
8. I.M. Kolthoff and J.F. Coetzee. J. Am. Chem. Soc. **79**, 1852 (1957).
9. E.B. Pedersen. Synthesis, 546 (1979).
10. K.J. Vetter. Angew. Chem. **73**, 277 (1961).
11. D.C. Prevorsek. J. Phys. Chem. **66**, 769 (1962).
12. S. Patai. *In* The chemistry of amidines and imidates. Wiley Interscience, New York. 1975. p. 17.
13. K.K. Barnes and C.K. Mann. J. Org. Chem. **32**, 1474 (1967).
14. U. Heb and C.-O. Bluemcke. Z. Chem. **28**, 144 (1988).
15. Y. Huang. Ph.D. Thesis, Université de Sherbrooke (1991).
16. F.C. Cooper and M.W. Partridge. J. Chem. Soc. 255 (1953).
17. S.P. Joshi, A.P. Khanolkar, and T.S. Wheeler. J. Chem. Soc. 793 (1936).

Can. J. Chem. Downloaded from www.nrcresearchpress.com by 65.111.164.53 on 09/08/12
For personal use only.

Dependence upon temperature of the excess molar volumes of tetrahydropyran + *n*-alkane mixtures

R. Bravo, M. Pintos, and A. Amigo

Abstract: Excess molar volumes V^E, at 288.15 and 308.15 K and normal atmospheric pressure, are reported for the binary mixtures tetrahydropyran + *n*-alkanes (C_7–C_9). From the results, the differential coefficient $(\partial V^E/\partial T)_p$ was estimated over the entire range of mole fractions. The Prigogine–Flory–Patterson theory and its applicability in predicting V^E is tested.

Key words: Excess molar volumes, digital densimeter, tetrahydropyran, *n*-heptane, *n*-octane, *n*-nonane, Prigogine–Flory–Patterson theory.

Résumé : On a déterminé les volumes molaires d'excès, V^E, de mélanges binaires de tétrahydropyrane et de *n*-alcanes (C_7–C_9), à 288,15 et 308,15 K et à la pression atmosphérique normale. À partir de ces résultats, on a évalué le coefficient différentiel, $(\partial V^E/\partial T)_p$, pour tout l'ensemble des fractions molaires. On a évalué la théorie de Prigogine–Flory–Patterson et son utilité à prédire V^E.

Mots clés : volumes molaires d'excès, densimètre digital, tétrahydropyrane, *n*-heptane, *n*-octane, *n*-nonane, théorie de Prigogine–Flory–Patterson.

[Traduit par la rédaction]

Can. J. Chem. Downloaded from www.nrcresearchpress.com by 65.111.164.53 on 09/08/12
For personal use only.

1. Introduction

This work is part of an extensive study of excess thermodynamic properties for a large number of solvent pairs. As a complement to previous work (1–3) we report here the excess molar volumes V^E of binary mixtures of tetrahydropyran + *n*-alkanes (*n*-heptane, *n*-octane, and *n*-nonane) at 288.15 and 308.15 K and atmospheric pressure, over the entire range of mole fractions. The results were used to calculate the differential coefficient describing the variation of the excess molar volume with isobaric changes of temperature.

The aim of the present study was also to investigate the effect on the excess molar volumes V^E of the variation of temperature and hydrocarbon chain length of the alkane molecule. We found that the symmetry and magnitude of V^E curves are influenced mainly by structural factors.

Thermodynamic excess properties of liquid mixtures containing molecules of different size and shape have been very successfully discussed on the basis of molecular statistics using the Prigogine–Flory–Patterson (PFP) theory (4–11). In the present investigation, the PFP theory is applied to the binary mixtures analyzed and the predicted V^E are compared to the experimental values.

Received June 15, 1993.

R. Bravo,[1] M. Pintos, and A. Amigo. Departamento de Física Aplicada, Facultad de Física, Universidad de Santiago de Compostela, 15706 Santiago de Compostela, Spain.

[1] Author to whom correspondence may be addressed. Telephone: 34-81-563100, ext. 4041.

2. Experimental

The sources and purities of the chemicals used were as follows: tetrahydropyran (THP), Fluka, puriss. p.a. 99.5%; *n*-heptane, Fluka, puriss. p.a. 99.5%; *n*-octane, Fluka, puriss. p.a. 99.5%; and *n*-nonane, Fluka, purum 99%. All liquids were used without further purification, and before use were stored in the dark over molecular sieves (Union Carbide Type 4A) and were partially degassed.

Mixtures were prepared by mass using a Mettler H51 (precision of 1×10^{-5} g) and air-tight stoppered bottles. Conversion to molar quantities was based on the 1985 table issued by IUPAC (12). The possible error in the molar fractions is estimated to be $<10^{-4}$. The densities were measured by an Anton Paar digital precision densimeter (model DMA 60/602) operated in the static mode and capable of a precision of better than 3×10^{-3} kg m^{-3}. A Heto circulating thermostat (type 04 PT 623) maintained the temperature constant to within 0.01 K. Bidistilled degassed water and dry air were used as calibrating substances (13, 14).

Densities of the pure liquids at the temperature of interest in this work, together with some values from the literature (3, 15–18), are given in Table 1.

3. Theory

The excess volumes of THP + *n*-alkanes can be understood reasonably well on the basis of the Prigogine–Flory–Patterson theory of mixtures. In this theory the excess molar volume can be expressed as the sum of three terms: an interactional term that is proportional to the Flory χ_{12} parameter, a free volume contribution that originates from a difference in the degree of thermal expansion between the two compo-

Can. J. Chem. Downloaded from www.nrcresearchpress.com by 65.111.164.53 on 09/08/12
For personal use only.

Table 1. Experimental densities (ρ) of pure components.

Liquid		ρ/(g.cm^{-3}) Expt.	Lit.
n-Heptane	288.15	0.68785	0.68775[b]
	298.15	0.67949[a]	0.67956[b]
	308.15	0.67112	0.67129[b]
n-Octane	288.15	0.70656	0.70657[c]
	298.15	0.69848[a]	0.69861[d]
	308.15	0.69047	0.69054[d]
n-Nonane	288.15	0.72183	0.72155[c]
	298.15	0.71365[a]	0.71411[d]
	308.15	0.70624	0.70633[d]
THP	288.15	0.88892	—
	298.15	0.87886[a]	0.8772[e]
	308.15	0.86880	—

[a]Reference 3.
[b]Reference 14.
[c]Reference 15.
[d]Reference 16.
[e]Reference 17.

nents, and a P^* contribution that arises from the differences in the internal pressures and reduces the volumes of the components.

The following brief sketch of the model is intended to make clear the physical meaning of its parameters.

Van and Patterson's approximate expression of V^E (9) in terms of the three contributions is

$$[1] \qquad \frac{V^E_{\text{Interactional}}}{(xV^*)_1 + (xV^*)_2} = \frac{(\tilde{V}^{1/3} - 1)\tilde{V}^{2/3}\psi_1\theta_2\chi_{12}}{[(4/3)\tilde{V}^{-1/3} - 1]\tilde{V}}$$

$$[2] \qquad \frac{V^E_{\text{Curvature}}}{(xV^*)_1 + (xV^*)_2} = -\frac{(\tilde{V}_1 - \tilde{V}_2)^2((14/9)\tilde{V}^{-1/3} - 1)\psi_1\psi_2}{[(4/3)\tilde{V}^{-1/3} - 1]\tilde{V}}$$

$$[3] \qquad \frac{V^E_{P^*\text{effect}}}{(xV^*)_1 + (xV^*)_2} = \frac{(\tilde{V}_1 - \tilde{V}_2)(P^*_1 - P^*_2)\psi_1\psi_2}{P^*_2\psi_1 + P^*_1\psi_2}$$

where the contact energy fraction ψ_i is given by

$$[4] \qquad \psi_1 = (1 - \psi_2) = (\Phi P^*)_1/[(\Phi P^*)_1 + (\Phi P^*)_2]$$

The reduction parameters of the components or solutions are obtained through the relationships of the Flory model (6), i.e., eqs. [5]–[10].

The reduced volume for pure substance i is defined in terms of the thermal expansion coefficients α_i

$$[5] \qquad \tilde{V}_i = \left[\frac{[1 + (4/3)\alpha_i T]}{(1 + \alpha_i T)}\right]^3$$

At zero pressure, the reduced volume and temperature satisfy the reduced equation of state

$$[6] \qquad \tilde{T}_i = (\tilde{V}_i^{1/3} - 1)/(\tilde{V}_i^{4/3})$$

Table 2. Parameters for the pure components.

Liquid	V^* (cm^3 mol^{-1})	P^* (J cm^{-3})
Heptane	113.65[a]	431[a]
Octane	127.89[a]	439[a]
Nonane	142.24[b]	435[b]
THP	77.12[c]	663[c]

[a]Reference 19.
[b]Reference 20.
[c]Reference 21.

where the reduced temperature for a mixture is defined as

$$[7] \qquad \tilde{T} = \frac{(\Phi P^* \tilde{T})_1 + (\Phi P^* \tilde{T})_2}{(\Phi P^*)_1 + (\Phi P^*)_2 - \Phi_1\theta_2\chi_{12}}$$

and the characteristic pressure is

$$[8] \qquad P^*_i = (\alpha_i/\kappa_i)T(\tilde{V}_i)^2$$

The segment fraction ϕ_i and the site fraction θ_i are defined as

$$[9] \qquad \Phi_1 = (1 - \Phi_2) = (xV^*)_1/[(xV^*)_1 + (xV^*)_2]$$

and

$$[10] \qquad \theta_1 = (1 - \theta_2) = \Phi_1/[\Phi_1 + (\Phi s)_2/s_1]$$

The parameter s_1/s_2 is the ratio of the surface contact sites per segment for the respective components.

Table 2 contains, for all pure components used in this work, the characteristic parameters necessary for the application of the PFP theory. The reducing parameters for the *n*-alkanes have been obtained from refs. 19 and 20. To calculate these parameters for THP, the dependence of the density upon temperature and pressure must be known. This dependence was estimated using the Lydersen–Greenkorn–Hougen method (21). In both cases the reducing parameters determined are taken to be constant within the temperature and pressure range considered here. The ratio s_1/s_2 has been approximated (22) by

$$[11] \qquad s_1/s_2 = (V^*_2/V^*_1)^{1/3}$$

where V^*_i is the hard core volume.

As in Flory's original theory of nonpolar molecules, χ_{12} is an adjustable mixing parameter and it was calculated from the experimental V^E data. χ_{12} is supposed to be a constant parameter independent of temperature.

4. Results and discussion

The experimental values of V^E at the temperatures 288.15 and 308.15 K are summarized in Table 3.

All mixtures exhibit positive V^E values, increasing with the length of the hydrocarbon chain of the alkane. The x vs. V^E curves are almost symmetrical about $x = 0.5$. The plot of V^E at 308.15 K for the binary mixture THP + *n*-heptane,

Can. J. Chem. Downloaded from www.nrcresearchpress.com by 65.111.164.53 on 09/08/12
For personal use only.

Table 3. Experimental excess molar volumes V^E for the binary systems: x THP + (1-x) n-alkane.

x	V^E (cm^3 mol^{-1})	x	V^E (cm^3 mol^{-1})	x	V^E (cm^3 mol^{-1})	x	V^E (cm^3 mol^{-1})
			x THP + (1-x) n-heptane				
T = 288.15 K							
0.0480	0.0492	0.3367	0.2106	0.6541	0.2131	0.9513	0.0474
0.1042	0.0949	0.4224	0.2281	0.7220	0.1910		
0.2002	0.1588	0.5050	0.2302	0.7958	0.1576		
0.2786	0.1942	0.5761	0.2282	0.8645	0.1177		
T = 308.15 K							
0.0515	0.0595	0.3378	0.2433	0.6389	0.2450	0.9390	0.0655
0.1067	0.1122	0.4141	0.2507	0.7201	0.2170		
0.1870	0.1736	0.4922	0.2660	0.7971	0.1766		
0.2575	0.2132	0.5623	0.2618	0.8670	0.1294		
			x THP + (1-x) n-octane				
T = 288.15 K							
0.0637	0.0784	0.3527	0.3287	0.6475	0.3479	0.9608	0.0631
0.1145	0.1351	0.4211	0.3569	0.7202	0.3111		
0.1938	0.2138	0.5027	0.3689	0.8016	0.2502		
0.2703	0.2739	0.5656	0.3662	0.8670	0.1862		
T = 308.15 K							
0.0540	0.0775	0.3582	0.3628	0.6509	0.3790	0.9531	0.0785
0.1134	0.1522	0.4207	0.3916	0.7176	0.3436		
0.1909	0.2354	0.5018	0.4050	0.8017	0.2763		
0.2749	0.3086	0.5675	0.4053	0.8675	0.1997		
			x THP + (1-x) n-nonane				
T = 288.15 K							
0.0467	0.0790	0.3494	0.4000	0.6469	0.4310	0.9514	0.1049
0.1133	0.1738	0.4210	0.4240	0.7257	0.3894		
0.1916	0.2665	0.4997	0.4428	0.7973	0.3292		
0.2731	0.3437	0.5715	0.4477	0.8668	0.2390		
T = 308.15 K							
0.0446	0.0757	0.2628	0.3548	0.5519	0.4843	0.7953	0.3458
0.0657	0.1092	0.3246	0.4060	0.6235	0.4701	0.8585	0.2639
0.1214	0.1913	0.4083	0.4555	0.6957	0.4341	0.9366	0.1324
0.1951	0.2846	0.4706	0.4768	0.7332	0.4066	0.9802	0.0436

given in Fig. 1, is a typical example of the results obtained in this work. As can be seen from Table 3, the excess molar volume increases with the temperature.

A function of the form

$$[12] \quad V^E/(\text{cm}^3\ \text{mol}^{-1}) = x(1-x) \times \sum_{i=1}^{n}\sum_{j=1}^{3} A_{ij}(T-T_0)^{j-1}(2x-1)^{i-1}$$

where T_0 is the reference temperature (T_0 = 298.15 K), was fitted to the results for each mixture using the ordinary (unweighted) least-squares method. In this fit we include our experimental results obtained for the same binary mixtures at the temperature 298.15 K (3). The parameters A_{ij} and the standard deviation s of the fit are listed in Table 4. These parameters were used to calculate the solid curves in Figs. 1 and 2.

Values of $(\partial V^E/\partial T)_p$ calculated using eq. [12] for the system THP + n-heptane at 308.15 K are plotted in Fig. 2. Curves for the excess partial molar quantities V_i^E and $(\partial V_i^E/\partial T)_p$ of component i (i = 1 for THP, i = 2 for n-heptane) at 308.15 K are also included in Figs. 1 and 2.

The predictions of V^E using the PFP theory are excellent for the mixtures analyzed, as shown by Fig. 1. This can be seen by considering the results in Table 5. For all the mixtures studied the interactional term was found to be positive, being the most important contribution. The magnitude and sign of

Can. J. Chem. Downloaded from www.nrcresearchpress.com by 65.111.164.53 on 09/08/12
For personal use only.

Fig. 1. Excess molar volumes V^E and excess partial molar volumes V_i^E for x THP + $(1 - x)$ n-heptane at 308.15 K. (———) Curves calculated from eq. [12]. (– – –) Curves calculated from PFP theory.

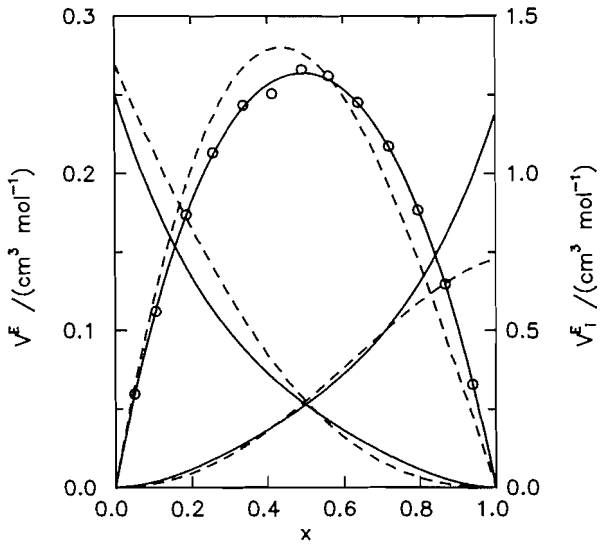

Fig. 2. $(\partial V^E/\partial T)_p$ and $(\partial V_i^E/\partial T)_p$ for x THP + $(1 - x)$ n-heptane at 308.15 K. (———) Curves calculated from eq. [12]. (– – –) Curves calculated from PFP theory.

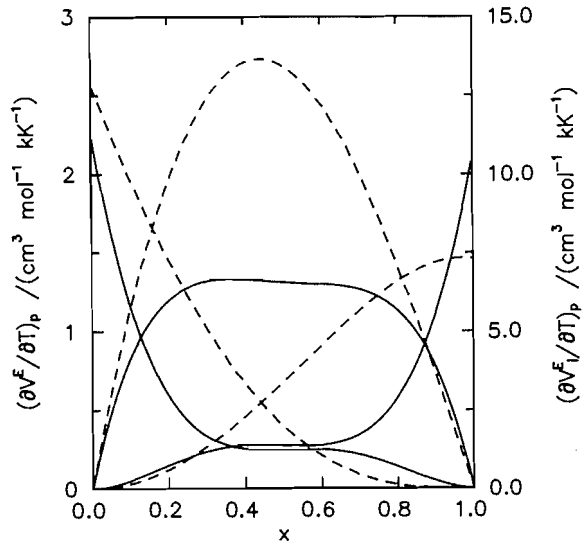

Table 4. Coefficients A_{ij} and standard deviations s for least-squares representation of V^E by eq. [12].

	THP + n-heptane	THP + n-octane	THP + n-nonane
A_{11}	0.99668	1.5707	1.8685
A_{12}	0.006333	0.007327	0.007228
A_{13}	−0.0000543	−0.000196	−0.000101
A_{21}	−0.2181	0.17599	0.26719
A_{22}	−0.000854	−0.000382	0.000649
A_{23}	0.0000266	−0.000116	−0.000114
A_{31}	0.13480	−0.004995	0.11088
A_{32}	0.0009408	0.001023	−0.007403
A_{33}	0.0002355	0.0000487	0.000697
s	0.0020	0.0020	0.0020

the free volume term are dependent on the relative magnitude of the thermal expansion coefficient of the components and it also makes a significant contribution to the excess molar volume.

Predicted values of $(\partial V^E/\partial T)_p$ and of the excess partial molar quantities V_i^E and $(\partial V_i^E/\partial T)_p$, calculated for the system THP + n-heptane at 308.15 K, are given in Figs. 1 and 2 (broken lines).

Acknowledgements

This work was supported by the Xunta de Galicia, promoción xeral do coñecemento (XUGA 8040289) and the Universidad de Santiago de Compostela (programa de subvencions para a adquisición de material científico), Spain.

Table 5. Experimental and predicted excess molar volumes at $x_1 = 0.5$ using the Prigogine–Flory–Patterson theory.

THP +	T (K)	χ_{12} (J cm^{-3})	$V^E_{exp.}$ (cm^3 mol^{-1})	$V^E_{cal.}$ (cm^3 mol^{-1})	$V^E_{int.}$ (cm^3 mol^{-1})	$V^E_{curv.}$ (cm^3 mol^{-1})	$V^E_{fv.}$ (cm^3 mol^{-1})
n-heptane	288.15	28.25	0.2320	0.2227	0.5029	−0.0227	−0.2574
	298.15	28.25	0.2492[a]	0.2487	0.5450	−0.0251	−0.2712
	308.15	28.25	0.2636	0.2753	0.5901	−0.0280	−0.2868
n-octane	288.15	24.83	0.3691	0.3557	0.4367	−0.0022	−0.0788
	298.15	24.83	0.3925[a]	0.3892	0.4727	−0.0024	−0.0811
	308.15	24.83	0.4064	0.4251	0.5108	−0.0025	−0.0832
n-nonane	288.15	20.19	0.4465	0.4320	0.3530	−0.0022	0.0811
	298.15	20.19	0.4671[a]	0.4618	0.3823	−0.0022	0.0816
	308.15	20.19	0.4827	0.5056	0.4119	−0.0031	0.0968

References

1. M. Pintos, R. Bravo, M.I. Paz Andrade, and V. Pérez Villar. J. Chem. Thermodyn. **14**, 951 (1982).
2. A. Amigo, R. Bravo, and M. Pintos. J. Chem. Eng. Data, **38**, 141 (1993).
3. M. Pintos, R. Bravo, and A. Amigo. J. Chem. Thermodyn. **25**, 337 (1993).
4. I. Prigogine. The molecular theory of solutions. North Holland, Amsterdam. 1957.
5. P.J. Flory, R.A. Orwoll, and A. Vrij. J. Am. Chem. Soc. **86**, 3509 (1964).
6. P.J. Flory. J. Am. Chem. Soc. **87**, 1833 (1965).
7. D. Patterson and G. Delmas. Discuss. Faraday Soc. **49**, 98 (1970).
8. M. Barbe and D. Patterson. J. Solution Chem. **9**, 753 (1980).
9. H.T. Van and D. Patterson. J. Solution Chem. **11**, 793 (1982).
10. M. Costas and D. Patterson. J. Solution Chem. **11**, 807 (1982).
11. T.M. Letcher and R.C. Baxter. J. Solution Chem. **18**, 65 (1989).
12. Pure Appl. Chem. **58**, 1677 (1986).
13. H. Wagenreth and W. Blanke. PBT-Mitteilungen, **81**, 412 (1971).
14. R.C. Weast (*Editor*). Handbook of chemistry and physics. 61st ed. CRC Press, Boca Ratón, Fla. 1981.
15. F. Kimura, A.J. Treszczanowicz, C.J. Halpin, and G.C. Benson. J. Chem Thermodyn. **15**, 503 (1983).
16. B.D. Smith and R. Srivastava. Thermodynamic data for pure compounds. Part A. Elsevier Science Publishing, Amsterdam. 1986.
17. M. Diaz Peña and G. Tardajos. J. Chem. Thermodyn. **10**, 19 (1978).
18. J.A. Riddick, W.B. Burger, and T.K. Sakano. Organic solvents. 4th ed. Wiley–Interscience, New York, 1986.
19. A. Heintz and R.N. Lichtenthaler. Ber. Bunsen-ges. Phys. Chem. **84**, 890 (1980).
20. A.M. Awwad and M.A. Salman. Fluid Phase Equilib. **31**, 105 (1986).
21. J. Ocón and G. Tojo. Quím. Ind. (Madrid), **8**, 116 (1961).
22. A. Abe and P.J. Flory. J. Am. Chem. Soc. **87**, 1838 (1965).

Can. J. Chem. Downloaded from www.nrcresearchpress.com by 65.111.164.53 on 09/08/12
For personal use only.

Evaluation of thermodynamic parameters on highly correlated chemical systems: a spectrophotometric study of the 1:1 and 1:2 equilibria between I_2 and R_4todit = 4,5,6,7-tetrathiocino[1,2-*b*:3,4-*b*′]diimidazolyl-1,3,8,10-tetraalkyl-2,9-dithione; (R = Bu, Me (new data); Et, Ph (reinvestigation)). Crystal and molecular structure of the charge-transfer complex Bu_4todit·$2I_2$

Francesco Bigoli, Paola Deplano, Maria Laura Mercuri, Maria Angela Pellinghelli, Antonio Sabatini, Emanuele F. Trogu, and Alberto Vacca

Abstract: The reactions between Bu_4todit and I_2 in $CHCl_3$ solution have been investigated by spectrophotometry at different temperatures. Evidence for the stepwise formation of the 1:1 and 1:2 charge-transfer complexes has been obtained by computer analysis of the experimental data. The stability constants of both complexes and the corresponding standard enthalpy and entropy changes have been calculated. The 1:2 complex has been characterized in the solid state by an X-ray structural study: the crystals of Bu_4todit·$2I_2$ are monoclinic, space group $C2/c$, $a = 16.352(6)$, $b = 9.376(5)$, $c = 23.470(7)$ Å, $\beta = 99.78(2)°$, $Z = 4$, $R = 0.0579$. The molecular structure shows that the two thionic sulfur atoms coordinate two diiodine molecules, the bond distances and angles being similar to those observed previously in Et_4todit·$2I_2$. On the contrary, the solution studies disagree with the previous investigations on Et_4todit and Ph_4todit, where the absorbance data were explained assuming the formation of the 1:1 complex only. A new calculation procedure for the least-squares minimization of spectrophotometric data, based on Powell's direct search method, has been developed. This procedure allows for the refinement of the standard enthalpy and entropy changes from a set of absorbance data at different temperatures. Convergence has been attained for the reaction of diiodine with Bu_4todit and Me_4todit (new data) and also for Et_4todit and Ph_4todit (old data).

Key words: equilibrium constants, charge-transfer complexes, Fourier transform–Raman, X-ray, I_2-thioamides.

Résumé : Faisant appel à la spectrophotométrie, on a étudié les réactions entre le Bu_4todit et le I_2, en solution dans le chloroforme, à diverses températures. En se basant sur une analyse par ordinateur des données expérimentales, on a obtenu des données suggérant une formation par étapes de complexes de transfert de charge 1 : 1 et 1 : 2. On a calculé les constantes de stabilité des deux complexes ainsi que les changements correspondants d'enthalpie et d'entropie standard. On a caractérisé les complexes 1 : 2 à l'état solide par diffraction des

Received May 27, 1994. Revision received December 8, 1994.

F. Bigoli and M.A. Pellinghelli. Dipartimento di Chimica Generale ed Inorganica, Chimica Analitica, Chimica Fisica, Università degli Studi di Parma, Centro di Studio per la Strutturistica Diffrattometrica del Consiglio Nazionale delle Ricerche, Viale delle Scienze 78, I-43100 Parma, Italy.
P. Deplano,[1] **M.L. Mercuri, and E.F. Trogu.** Dipartimento di Chimica e Tecnologie Inorganiche e Metallorganiche, via Ospedale 72, I-09124 Cagliari, Italy.
A. Sabatini and A. Vacca. Dipartimento di Chimica dell'Università, via Maragliano 77, I-50144, Firenze, Italy.

[1] Author to whom correspondence may be addressed: Telephone: 70-662975. Fax: 70-668797.

Can. J. Chem. Downloaded from www.nrcresearchpress.com by 65.111.164.53 on 09/08/12
For personal use only.

rayons X : les cristaux de Bu_4todit·$2I_2$ sont monocliniques, groupe d'espace *C2/c*, *a* = 16.352(6), *b* = 9.376(5), *c* = 23,470(7) Å, β = 99,78(2)°, *Z* = 4, *R* = 0,0579. Les structures moléculaires montrent que les deux atomes de soufre thionique sont coordonnés à deux molécules d'iode et que les longueurs et les angles des liaisons sont semblables à ceux observés antérieurement pour le Et_4todit·$2I_2$. Par contre, les études en solution sont en désaccord avec les résultats des études antérieures sur le Et_4todit et le Ph_4todit dans lesquelles des données d'absorbance ont été expliquées en faisant l'hypothèse qu'il n'existait que des complexes 1 : 1. On a mis au point une nouvelle méthode de calcul pour la minimisation, par la technique des moindres carrés, des données spectrophotométriques; elle est basée sur la méthode de recherche directe de Powell. Cette procédure permet de raffiner les changements d'enthalpie et d'entropie standard à partir d'un ensemble de données d'absorbance à diverses températures. On a pu obtenir une convergence pour la réaction du diiode avec le Bu_4todit et le Me_4todit (nouvelles données) ainsi que pour le Et_4todit et le Ph_4todit (données antérieures).

Mots clés : constantes d'équilibre, complexes de transfert de charge, Raman par transformation de Fourier, rayons X, I_2-thioamides.

[Traduit par la rédaction]

Introduction

The new series of heterocycles R_4todit = 4,5,6,7-tetrathiocino[1,2-*b*:3,4-*b'*] diimidazolyl-1,3,8,10-tetraalkyl-2,9-dithione, which is depicted below for clarity (1), is a class of polyfunctional donors containing two equivalent thiocarbonyl groups located in positions far apart in the molecule.

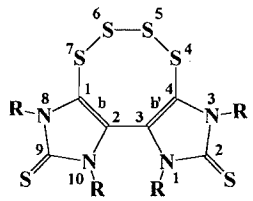

R_4todit

Consequently, these molecules may act as bridging ligands in the preparation of polynuclear metal complexes, and indeed a variety of metal–sulfur polymers have been characterized (2–4). Also, these molecules react with diiodine to produce molecular complexes. In the case of R = Et, the expected 1:2 complex was isolated in the solid state, and characterized by X-ray diffractometric studies. In $CHCl_3$ solutions, instead, only the 1:1 complex seemed to exist in the concentration range explored (5), as was also found in the case of the R = Ph derivative (6). These results were unexpected since, due to the structural and electronic features of the ligand, the coordination at one thionic sulfur should not significantly affect the donor capability of the other.

Both the equilibrium constants and the molar absorptivities of the 1:1 complex had been calculated simultaneously from spectrophotometric data using the computer program SUPERSPEC (7) derived from SUPERQUAD. Despite many attempts it was not possible to fit the experimental data by means of models different from the 1:1 case. We tentatively explained these intriguing results by assuming that "complexes of stoichiometry higher than 1:1 exist in solution at oversaturation or incipient precipitation conditions" (5). However, another reason for the failure to identify the 1:2 complex may be related to the procedure used in analysing the spectrophotometric data. Such procedures, including the one used by SUPERSPEC, are all based on the assumption that the following equation, derived from the well known Lambert–Beer law, is valid:

$$[1] \quad A = l\Sigma c_i\epsilon_i$$

where A is the absorbance of the solution at a given wavelength, l is the optical path length, and c_i and ϵ_i, are, respectively, the molar concentrations and molar absorptivities (at the same wavelength) of the absorbing species. These methods allow the simultaneous determination of both molar absorptivities and equilibrium constants β. In fact, the concentrations of the absorbing species are a function of the equilibrium constants, $c_i = f_i(\beta)$, and, as a consequence, the absorbances A are also β dependent:

$$[2] \quad A = \Sigma f_i(\beta)\epsilon_i$$

This equation is nonlinear with respect to the parameters β and ϵ_i, and even contains the product of these quantities. This introduces a strong correlation between the parameters and, in some cases, the least-squares minimization process may fail, as the matrix of the normal equations may be nearly singular. Such a correlation may be resolved if the spectra of solutions that contain the various absorbing species in a wide range of mutual molar ratios are available. Another source of correlation may derive from the greater or lesser proximity of the molar absorptivity values of the different species; if these values are identical any method of refinement will fail.

Recently, the synthesis of R_4todit molecules of varying R substituents was stimulated by the fact that they show anticancer activity, which depends on the alkyl substituents (8). Among these the *n*-butyl derivative showed higher solubility than others previously investigated. Hence we decided to perform an extensive solution study on the Bu_4todit compound. The formation of 1:1 and 1:2 complexes was clearly shown using the computer program SUPERSPEC, although a similar attempt to solve the Me_4todit–diiodine system in the same concentration range by considering the formation of both the 1:1 and 1:2 species was unsuccessful. The discrepancy between these results prompted us to develop a new refinement strategy for the analysis of this type of experimental data, which could solve, coherently and satisfactorily, both the systems described above (R = Bu and Me) and those previously reported (R = Et and Ph).

Experimental

Synthesis

Twice sublimed I_2, and $CHCl_3$ (stored over molecular sieves) were Carlo Erba ACS grade. The donors Me_4todit and

Can. J. Chem. Downloaded from www.nrcresearchpress.com by 65.111.164.53 on 09/08/12
For personal use only.

Can. J. Chem. Downloaded from www.nrcresearchpress.com by 65.111.164.53 on 09/08/12
For personal use only.

Bu_4todit were prepared according to ref. 1. Anal. calcd. for Bu_4todit ($C_{22}H_{36}N_4S_6$): C 48.58, H 6.69, N 10.53, S 35.32; found: C 48.14, H 6.61, N 10.21, S 35.05.

When mixed with I_2 in $CHCl_3$, in ratios varying between 1:2 and 1:10 (ligand:I_2), the analytical and spectroscopic results on the solids obtained by slow evaporation of the reagent solution are always the same according to the formulation R_4todit·$2I_2$ (R = Me, Bu). In the R = Bu case, the 1:2 complex was isolated in the form of lustrous red-brown crystals suitable for X-ray diffraction studies.

Anal. calcd. for Me_4todit·$2I_2$ ($C_{10}H_{12}N_4S_6I_4$): C 13.45, H 1.36, N 6.30, S 21.66; found: C 12.90, H 1.09, N 6.11, S 20.80.

Anal. calcd for Bu_4todit·$2I_2$ ($C_{22}H_{36}N_4S_6I_4$): C 25.01, H 3.43, N 5.30, S 18.21; found: C 24.83, H 3.32, N 5.61, S 17.95.

Spectroscopic measurements

IR spectra (cm^{-1}) were recorded on a Perkin Elmer model 983 spectrophotometer as KBr pellets.

Me_4todit·$2I_2$: 2923vw, 1518m, 1445s, 1367s, 1332m, 1223w, 1154s, 1101w, 1079w, 1035ms 861m, 829m, 762w, 728w, 707w, 617w, 533m, 418ms, 381w, 300w, 273m, 242w, 219w.

Bu_4todit: 2960s, 2940ms, 2878ms, 1437s, 1405vs, 1335s, 1360s, 1337m, 1295m, 1220vs, 1197w, 1155w, 1118w, 938w, 900w, 860vw, 830vw, 737vw, 640vw, 432w, 420w.

Bu_4todit·$2I_2$: 2956w, 2925w, 2857w, 1518m, 1461w, 1448s, 1405*vs*, 1390s, 1344m, 1310m, 1295m, 1251w, 1217s, 1176w, 1151s, 1117mw, 1069w, 948w, 937mw, 919w, 814m, 763w, 736w, 696w, 562w, 496w, 412w.

FT–Raman spectra (resolution ±4 cm^{-1}) were recorded on a Bruker RFS 100 Fourier Transform Raman spectrophotometer, operating with an exciting frequency of 1064 nm (Nd:YAG laser). The power level of the laser source was 300 mW for the solution samples, and varied between 10 and 30 mW for the solid samples. The detection of the signal was made with an indium–gallium–arsenide detector operating at room temperature. The $CHCl_3$ solutions and the solid samples were introduced, respectively, into a suitable cell (Suprasil 300, HELLMA cell of 0.5 cm thickness) and into a capillary tube and then fitted into the compartment designed for 180° scattering geometry. Five solutions having constant concentration of the donor and increasing concentrations of I_2 in the ratios 1:0.5, 1:1, 1:2, 1:4, and 1:6 for each derivative were prepared. Due to the different solubility of the adducts, the concentrations of the donors were as follows: [Me_4todit] = 1.65×10^{-3} mol dm^{-3}; Bu_4todit = 1.25×10^{-2} mol dm^{-3}; [Et_4todit] = 6.25×10^{-3} mol dm^{-3}; [Ph_4todit] = 2.50×10^{-3} mol dm^{-3}.

Solution studies

Electronic spectra were measured at different temperatures in the 10–35°C range in $CHCl_3$ solutions with a Cary 5 spectrophotometer equipped with a temperature probe accessory connected to a thermostatable multicell block.

Me_4todit: a set of eight solutions containing a fixed I_2 concentration (5.00×10^{-4} mol dm^{-3}) and variable Me_4todit concentrations ranging from 2.50×10^{-4} to 5.00×10^{-3} mol dm^{-3} (in the ratios [I_2]:[Me_4todit] = 1:0.5; 1:1; 1:1.5; 1:2; 1:3; 1:4; 1:6; 1:10) was prepared, and the spectra were recorded in the 450–550 nm range using 1 cm silica cells. Three other sets of solutions were prepared with a fixed Me_4todit concentration ((a) 2.50×10^{-4} mol dm^{-3}; (b) 6.04×10^{-5} mol dm^{-3}) and variable I_2 concentrations ranging from (a) 5.00×10^{-4} to 1.00×10^{-2} mol dm^{-3} (in the ratios [Me_4todit]:[I_2] = 1:2; 1:4; 1:8; 1:12; 1:20; 1:32; 1:40); (b) 1.21×10^{-4} to 6.04×10^{-3} mol dm^{-3} (in the ratios [Me_4todit]:[I_2] = 1:2; 1:4; 1:10; 1:20; 1:40, 1:60; 1:80; 1:100), and their spectra were measured in the range 260–450 nm in 1 mm silica cells. In the third set of solutions, the donor concentration was 2.50×10^{-4} mol dm^{-3} and I_2 concentrations ranged from 5.00×10^{-5} to 5.00×10^{-4} mol dm^{-3} (in the ratios [Me_4todit]:[I_2] = 1:0.2; 1:0.4; 1:0.6; 1:0.8; 1:1; 1:1.4; 1:1.8; 1:2) and their spectra were recorded between 550 and 270 nm.

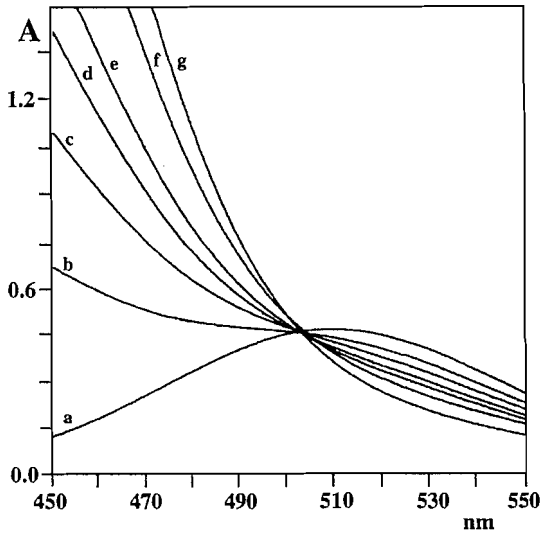

Fig. 1. Visible spectra at 293 K in a 1.0 cm cell of $CHCl_3$ solutions containing constant amounts of I_2 ($c = 5.0 \times 10^{-4}$ mol dm^{-3}) and variable Bu_4todit concentrations in the ratios: (a) 1:0; (b) 1:0.25; (c) 1:0.5; (d) 1:1; (e) 1:1.5; (f) 1:2; (g) 1:10.

Bu_4todit: a set of seven solutions containing fixed I_2 concentration (5.00×10^{-4} mol dm^{-3}) and variable Bu_4todit concentrations ranging from 1.25×10^{-4} to 5.00×10^{-3} mol dm^{-3} (in the ratios [I_2]:[Bu_4todit] = 1:0.25; 1:0.5; 1:1; 1:1.5; 1:2; 1:4; 1:10; see Fig. 1) was prepared, and the spectra were recorded in the 450–550 nm range in 1 cm silica cells. Another set of 13 solutions was prepared with a fixed Bu_4todit concentration (2.50×10^{-4} mol dm^{-3}) and variable I_2 concentrations ranging from 2.50×10^{-4} to 1.00×10^{-2} mol dm^{-3} (in the ratios [Bu_4todit]:[I_2] = 1:0.2; 1:0.4; 1:0.6; 1:0.8; 1:1; 1:1.4; 1:1.8; 1:2; 1:4; 1:8; 1:12; 1:20; 1:40; see Fig. 2), and their spectra were measured in the range 260–550 nm in 1 mm silica cells. In a third set of solutions, the donor concentration was 5.00×10^{-5} mol dm^{-3} and I_2 concentrations ranged from 1.25×10^{-4} to 5.00×10^{-3} mol dm^{-3} (in the ratios [Bu_4todit]:[I_2] = 1:2.5; 1:5; 1:10; 1:20; 1:40; 1:60; 1:80; 1:100), and their spectra were recorded between 500 and 270 nm. The previously reported data were used to reinvestigate the cases of the R = Et and Ph derivatives (5, 6). In addition, for R = Et, a set of 13 solutions was prepared with a fixed Et_4todit concentration (2.50×10^{-4} mol dm^{-3}) and variable I_2 concentrations ranging from 2.50×10^{-4} to 1.00×10^{-2} mol dm^{-3} (in the ratios [Et_4todit]:[I_2] = 1:0.2; 1:0.4; 1:0.6; 1:0.8; 1:1; 1:1.4; 1:1.8; 1:2; 1:4; 1:8; 1:12; 1:20; 1:40), and the absorbances were monitored in the 260–550 nm range, using 0.1 cm quartz cells.

Can. J. Chem. Downloaded from www.nrcresearchpress.com by 65.111.164.53 on 09/08/12
For personal use only.

Fig. 2. UV–visible spectra at 293 K in a 0.1 cm cell of $CHCl_3$ solutions containing fixed amounts of Bu_4todit ($c = 2.5 \times 10^{-4}$ mol dm^{-3}) and variable I_2 concentrations in the ratios: (1) 1:0; (2) 1:0.4; (3) 1:0.8; (4) 1:1.4; (5) 1:2; (6) 1:4; (7) 1:8; (8) 1:12; (9) 1:20; (10) 1:40.

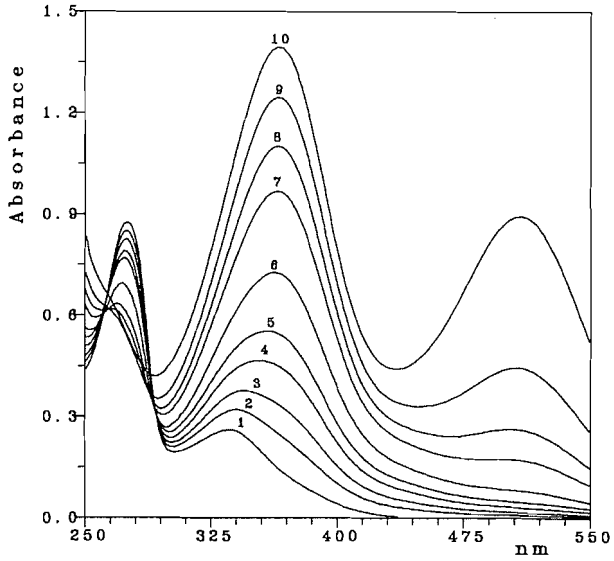

Calculations

The program SUPERSPEC derived from SUPERQUAD has previously been described (7). It was used to refine simultaneously the equilibrium constants and the molar extinction coefficients from the experimental absorbances every ten nanometers in the 250–550 nm range at six different temperatures. The total number of experimental points was: Me_4todit = 2078, Bu_4todit = 2115, Ph_4todit = 871, Et_4todit = 1260. The values of $\Delta H°$ and $\Delta S°$ were calculated by least-squares fitting of the corresponding ln β versus $1/T$ according to the van't Hoff equation.

The same experimental data were used to calculate $\Delta H°$, $\Delta S°$, and the molar extinction coefficients by POWELSPEC, a new program that uses Powell's direct search minimization method (9). The assumption was made that molar absorptivity values ϵ_i do not vary in the temperature range explored. Schemes 1 and 2 demonstrate the main differences between the two programs.

X-ray crystallography

Crystal data are as follows:

$C_{22}H_{36}N_4S_6I_4$; MW = 1056.531; monoclinic, space group $C2/c$, a = 16.352(6), b = 9.376(5), c = 23.470(7) Å, β = 99.78(2)°(by least-squares refinement from the θ values, in the range 8°–17°, of 30 reflections accurately measured), U = 3546(3) $Å^3$, D_c = 1.979 Mg m^{-3}, Z = 4, $F(000)$ = 2016, Mo-Kα radiation (λ = 0.71073 Å), μ= 38.38 cm^{-1}. Crystal dimensions: 0.13 × 0.21x × 0.26 mm^3.

Data collection and processing

Data collection was made on a Siemens AED diffractometer with Nb-filtered Mo-Kα radiation using the θ–2θ scan mode. Of a total of 4231 measured reflections ($\pm h$, $\pm k$, $\pm l$), 1393 having $I \geq 2\sigma(I)$ were considered as observed and were employed in the analysis. The recorded intensities were corrected for the Lorentz polarization factor, for absorption (maximum and minimum values 1.23820, 0.79242), and extinction (maximum and minimum values 1.22639, 0.86078) following the empirical method of Walker and Stuart (10*a*).[2]

Scheme 1

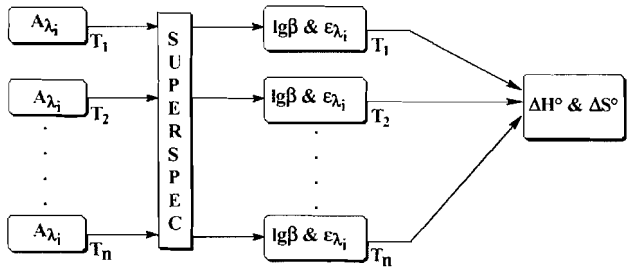

Scheme 2

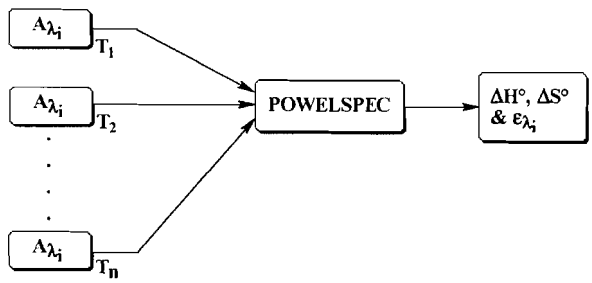

Structure analysis and refinement

The structure was solved by Patterson and Fourier methods and refined by full-matrix least squares, with anisotropic thermal parameters for all non-hydrogen atoms excluding those of the substituents groups, using the SHELX-76 program (11).

The coordinates of the hydrogen atoms placed at their geometrically calculated positions were not refined, but introduced in the final structure factor calculation with a single-refined isotropic thermal parameter (U = 0.1939(252) $Å^2$).

The scattering factors and corrections for anomalous dispersion effects were those from ref. 12. The weighting scheme used in the final cycles was $w = 0.8921(\sigma^2(F_o) + 0.001719F_o^2)^{-1}$. Final convergence was reached at an R value of 0.0579 (R' = 0.0697). The final electron density difference synthesis showed no peaks >0.94 and <−1.05 e $Å^{-3}$. The programs ABSORB (10*b*), PARST (13), PLUTO (14), and ORTEP (15) were used. Calculations were carried out on the Gould-Sel 32/77 computer of the C.N.R. Centro di Studio per la Strutturistica Diffrattometrica. Final atomic coordinates are in Table 1, bond distances and angles in Table 2.[3]

[2] The program ABSORB (10*b*) was used.

[3] Tables of fractional atomic coordinates for the H atoms and anisotropic thermal parameters have been deposited. Copies of these tables may be purchased from: The Depository of Unpublished Data, Document Delivery, CISTI, National Research Council Canada, Ottawa, Canada K1A 0S2.

The table of fractional atomic coordinates has also been deposited with the Cambridge Crystallographic Data Centre, and can be obtained on request from The Director, Cambridge Crystallographic Data Centre, University Chemical Laboratory, 12 Union Road, Cambridge, CB2 1EZ, U.K.

Structure factor amplitudes are no longer being deposited and may be obtained directly from the author.

Can. J. Chem. Downloaded from www.nrcresearchpress.com by 65.111.164.53 on 09/08/12
For personal use only.

Table 1. Fractional atomic coordiantes ($\times 10^4$) and isotropic thermal parameters (Å $\times 10^4$).

	x/a	*y/b*	*z/c*	*U*
I(1)	2479.9(7)	1787.5(13)	947.9(5)	641(4)[a]
I(2)	3962.7(8)	3312.5(17)	885.5(6)	913(6)[a]
S(1)	1061(3)	144(5)	940(2)	710(19)[a]
S(2)	−897(3)	4049(5)	1804(2)	691(18)[a]
S(3)	−122(4)	5749(5)	2063(3)	1015(26)[a]
N(1)	564(6)	706(12)	1966(4)	365(41)[a]
N(2)	135(8)	2269(14)	1302(5)	547(50)[a]
C(1)	570(9)	1051(17)	1405(7)	509(61)[a]
C(2)	−204(8)	2652(16)	1796(7)	483(57)[a]
C(3)	82(8)	1670(17)	2203(5)	455(51)[a]
C(4)	980(9)	−533(17)	2271(6)	527(41)
C(5)	1899(10)	−340(19)	2444(7)	743(50)
C(6)	2128(12)	905(22)	2851(9)	907(60)
C(7)	3020(13)	977(27)	3087(10)	1224(79)
C(8)	−42(10)	3033(20)	728(7)	728(50)
C(9)	−842(13)	2585(26)	398(9)	1017(68)
C(10)	−1028(16)	3691(31)	−110(11)	1494(101)
C(11)	−1938(16)	3883(43)	−369(15)	2590(196)

[a]Equivalent isotropic *U* defined as one-third of the trace of the orthogonalized U_{ij} tensor.

Table 2. Bond distances (Å) and angles (deg) with esd's in parentheses.

I(1)—I(2)	2.840(2)	N(2)—C(2)	1.41(2)
I(1)—S(1)	2.783(5)	N(2)—C(8)	1.51(2)
S(2)—S(3)	2.064(7)	C(2)—C(3)	1.35(2)
S(3)—S(3′)	2.020(9)	C(3)—C(3′)	1.47(2)
S(1)—C(1)	1.69(2)	C(4)—C(5)	1.50(2)
S(2)—C(2)	1.73(2)	C(5)—C(6)	1.51(3)
N(1)—C(1)	1.36(2)	C(6)—C(7)	1.47(3)
N(1)—C(3)	1.38(2)	C(8)—C(9)	1.46(3)
N(1)—C(4)	1.47(2)	C(9)—C(10)	1.57(4)
N(2)—C(1)	1.35(2)	C(10)—C(11)	1.52(4)

I(2)—I(1)—S(1)	175.3(1)	S(2)—C(2)—N(2)	123.2(11)
I(1)—S(1)—C(1)	101.8(6)	N(2)—C(2)—C(3)	105.7(13)
S(3)—S(2)—C(2)	102.5(5)	S(2)—C(2)—C(3)	130.9(12)
S(2)—S(3)—S(3′)	107.7(3)	N(1)—C(3)—C(2)	108.4(12)
C(3)—N(1)—C(4)	124.9(11)	C(2)—C(3)—C(3′)	125.1(14)
C(1)—N(1)—C(4)	125.6(11)	N(1)—C(3)—C(3′)	126.5(13)
C(1)—N(1)—C(3)	109.5(11)	N(1)—C(4)—C(5)	113.4(13)
C(2)—N(2)—C(8)	124.7(13)	C(4)—C(5)—C(6)	113.1(14)
C(1)—N(2)—C(8)	125.4(13)	C(5)—C(6)—C(7)	113.3(17)
C(1)—N(2)—C(2)	109.6(13)	N(2)—C(8)—C(9)	110.8(15)
N(1)—C(1)—N(2)	106.7(13)	C(8)—C(9)—C(10)	104.6(18)
S(1)—C(1)—N(2)	127.3(12)	C(9)—C(10)—C(11)	115.6(22)

Key to symmetry operations: (′) −x, y, (1/2 − z).

Results and Discussion

The spectrophotometric data concerning the reactions of Bu_4todit and I_2 were analysed using the computer program SUPERSPEC (see Experimental). Assuming that both complexes Bu_4todit·I_2 and Bu_4todit·$2I_2$ are present at equilibrium, convergency is attained for all temperatures, the root-mean-square error on the absorbances being less than 0.01. The values of the complex formation constants are listed in Table 3. The values of the enthalpy and entropy changes interpolated from the van't Hoff plot (correlation coefficients 0.999 and 0.991 for the 1:1 (**I**) and 1:2 (**II**) complexes, respectively) are also reported in Table 3.

It must be noted that the agreement between $\Delta H^\circ_{\mathbf{I}}$ and $\Delta S^\circ_{\mathbf{II}}$ obtained for this complex and the corresponding values of the previously investigated complexes (4, 5) is very poor. Moreover, further results (see solution FT–Raman studies) suggested similar interaction strengths between the donors and I_2. This poor agreement seems to indicate that the old results are questionable.

These conflicting results induced us to study another compound of the R_4todit class, namely, the R = Me derivative. The reaction of this ligand with diiodine was investigated spectrophotometrically, using concentration ranges of the reagents as close as possible to those used in the Bu_4todit investigation. The computer refinement of these data, using SUPERSPEC, converged at all temperatures for the equilibrium model consisting of the 1:1 and 1:2 complex species. Unfortunately, the fit of experimental and calculated data was less satisfactory and the dependence of the ln β values versus $1/T$ was far from being linear. In fact, in this system high values of the correlation coefficients among the parameters (equilibrium constants and molar absorptivities) were found. In addition, the values of the calculated molar absorptivities of the Me_4todit complexes were quite different at the different temperatures, whereas this behaviour was found neither for the ligand Me_4todit nor for Bu_4todit or its complexes.

For this reason we thought it advisable to carry out a refinement using the spectrophotometric data of Me_4todit at all temperatures simultaneously, and assuming that (*i*) the equilibrium model is that of the stepwise addition of two diiodine molecules to the ligand, (*ii*) the molar absorptivities are constant quantities within the temperature range investigated, and (*iii*) the values of the formation constants follow the van't Hoff equation. In this procedure the function to be minimized is the sum of the weighted squared residuals between experimental and calculated absorbances, *U*, and the refinable parameters are the ΔH°, ΔS° values and the molar absorptivities of the two complexes. The equilibrium constants are calculated using the formula:

$$[3] \quad -RT \ln \beta = \Delta H^\circ - T\Delta S^\circ$$

The calculation was performed with a new program, POWELSPEC, which uses Powell's direct search minimization method (9). The ΔH° and ΔS° values obtained are reported in Table 4. They appear realistic when compared with those previously obtained for Bu_4todit using SUPERSPEC.

A POWELSPEC refinement of Bu_4todit yielded ΔH° and ΔS° values close enough to the SUPERSPEC results. The small differences, which are, however, significant even considering the error limits of the parameters, can be ascribed to the different assumptions of the two minimization methods. In particular, the standard deviations of the parameters are significantly smaller in the POWELSPEC refinement. This is due both to the constraints regarding temperature dependence of the formation constants and constancy of the molar absorptivity and to

Table 3. Logarithms of the equilibrium constants (standard deviations in parentheses) calculated by means of SUPERSPEC, and standard enthalpy and entropy changes for the 1:1 (**I**) and 1:2 (**II**) complexes between Bu_4todit and I_2 in $CHCl_3$ solutions.

	log β						$\Delta H°$	$\Delta S°$
	10°C	15°C	20°C	25°C	30°C	35°C	(kcal mol^{-1})	(cal K^{-1} mol^{-1})
$\mathbf{I}_{Bu}$	3.73(3)	3.60(2)	3.41(2)	3.35(2)	3.25(2)	3.14(2)	−9.3(6)	−16(2)
$\mathbf{II}_{Bu}$	6.44(6)	6.19(5)	5.94(3)	5.72(5)	5.51(5)	5.29(5)	−18.2(1)	−35(1)

Table 4. Standard enthalpy and entropy changes (standard deviations in parentheses) for the 1:1 (**I**) and 1:2 (**II**) complexes between R_4todit (R = Me, Et, *n*-Bu, Ph) and I_2, in $CHCl_3$ solutions, calculated by means of POWELSPEC.

R	$\Delta H°_I$ (kcal mol^{-1})	$\Delta H°_{II}$ (kcal mol^{-1})	$\Delta S°_I$ (cal K^{-1} mol^{-1})	$\Delta S°_{II}$ (cal K^{-1} mol^{-1})
Me	−7.3(1)	−15.4(1)	−11.2(2)	−29.0(3)
Et	−7.4(1)	−16.8(1)	−11.5(2)	−34.7(5)
n-Bu	−8.5(1)	−17.4(1)	−13.1(3)	−32.1(3)
Ph	−6.0(1)	−13.7(1)	−7.1(3)	−24.1(5)

Table 5. Comparison of the standard enthalpy and entropy changes (standard deviations in parentheses) for the 1:1 (**I**) and 1:2 (**II**) equilibria between R_4todit (R = Et, Ph) and I_2, in $CHCl_3$ solutions, calculated by means of POWELSPEC (P) (this work) and SUPERSPEC (S) (previous results).

R	$\Delta H°_I$ (kcal mol^{-1})	$\Delta H°_{II}$ (kcal mol^{-1})	$\Delta S°_I$ (cal K^{-1} mol^{-1})	$\Delta S°_{II}$ (cal K^{-1} mol^{-1})
Et (S)	−4.4(5)	—	−2(2)	—
Et (P)	−7.4(1)	−16.8(1)	−11.5(2)	−34.7(5)
Ph (S)	−3.9(2)	—	−1(1)	—
Ph (P)	−6.0(1)	−13.7(1)	−7.1(3)	−24.1(5)

the higher value of the ratio between experimental data and parameters to be refined.

These encouraging results induced us to also reconsider the equilibria between diiodine and the Et_4todit and Ph_4todit ligands, on the basis of the model consisting of the two complexes. After processing the old data with POWELSPEC, convergency was attained, and the $\Delta H°$ and $\Delta S°$ values of the refined parameters are close to the corresponding values obtained for the other two systems. Once convergence is reached, the standard deviations of the parameters and their correlation coefficient were calculated by inversion of the matrix of the second derivatives of the function U, the derivatives being obtained by numerical differentiation. With these values, the estimated errors in the log β values are calculated using the standard procedure for the propagation of variance. This method of calculating errors is derived from the method first used in LETAGROP (16). The whole set of results is summarized in Table 4 and a comparison of values obtained previously and in this work is reported in Table 5.

The calculated spectra of the 1:1 and 1:2 complexes of diiodine and Bu_4todit are reported as an example in Fig. 3. The new strong bands at 370 nm are attributed to the charge-transfer transitions, while the characteristic band of I_2 is blue-shifted and appears as a shoulder at 450 nm. The characteristic free ligand band is blue-shifted and does not appear in the wavelength range explored. The main features of the spectra of the other complexes are similar.

The new calculation procedure used by the program POWELSPEC is significantly more time consuming than that used by SUPERSPEC. However, it appears to be more reliable, robust, and stable, as convergence was reached for all systems under investigation. The occasional failures of SUPERSPEC are ascribed to the critical step of inversion of the normal equations matrix, which may be ill-defined and nearly singular, when the parameters are highly correlated. On the contrary,

Fig. 3. Calculated UV–visible spectra of the 1:1(**I**) and 1:2 (**II**) complexes between Bu_4todit (**L**) and I_2 at 283 K in $CHCl_3$ solutions. The spectrum of the free ligand is reported for comparison.

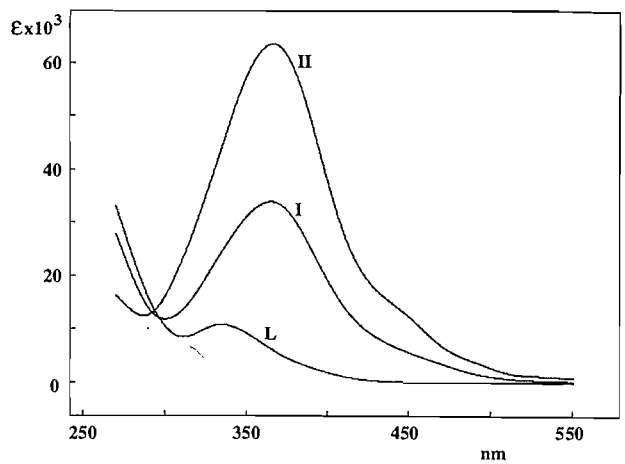

Powell's method does not require inversion of any matrix for direct search of the minimum.

It is noteworthy that all systems have been solved in terms of the same equilibrium model (which includes the 1:2 complex species isolated both previously and now in the solid state) and that the corresponding values of the thermodynamic functions fall in the range of medium-strong adducts. In particular, the values of $\Delta H°_I$ and $\Delta S°_I$ are comparable to those previously determined for the reaction of diiodine with the corresponding monothiones (17). This supports our results.

Fourier transform – Raman spectroscopy

The FT–Raman spectra of $CHCl_3$ solutions obtained by addition of increasing amounts of I_2 to the R_4todit being investigated show the same features in the characteristic region of the

Can. J. Chem. Downloaded from www.nrcresearchpress.com by 65.111.164.53 on 09/08/12
For personal use only.

Can. J. Chem. Downloaded from www.nrcresearchpress.com by 65.111.164.53 on 09/08/12
For personal use only.

Fig. 4. FT–Raman spectra in a 0.5 cm cell of $CHCl_3$ solutions of Bu_4todit ($c = 1.25 \times 10^{-2}$ mol dm^{-3}) and variable I_2 concentrations in the ratios: (1) 1:0.5; (2) 1:1; (3) 1:2; (4) 1:4.

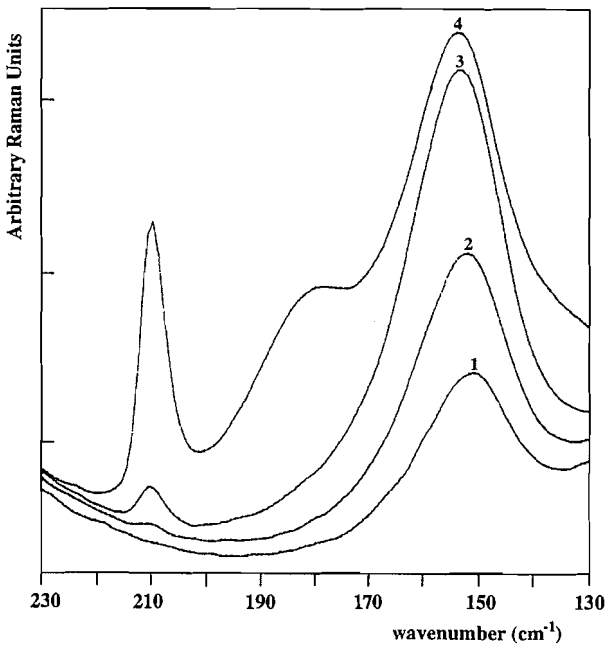

I–I vibrations, and the Bu_4todit+I_2 case is reported as an example in Fig. 4. One peak at 152 cm^{-1}, which is neither present in the spectrum of the donors nor in that of I_2, arises on addition of diiodine to the donors. This peak is attributed to the stretching vibration of coordinated I_2. Uncoordinated I_2, instead, shows the peak due to the stretching vibration at 210 cm^{-1} (18). A negative shift of the ν(I–I) vibration, and therefore a lowering of the force constant, is expected when I_2 interacts with a donor, since the formation of a complex leads to a decrease in I—I bond order, in agreement with a MO description that shows that the HOMO has some σ^* I—I antibonding character (19). Stronger interaction leads to larger negative shifts of the ν(I–I) peak. This was verified in a series of I_2 complexes for which structural data were available (20).

An identical position for the ν(I–I) peak in all adducts, therefore, suggests that the interaction between I_2 and the R_4todit is of the same strength. The sequence found in the series investigated (Ph < Et≈Me < *n*-Bu) suggests an increase in interaction strength on increasing the electrodonation power of the R substituents; this seems to contrast with the FT–Raman results. However, solution Raman studies seem to be more informative in determining the interaction strength, since thermodynamic functions may contain large contributions due to solvation effects.

The shoulder at 180 cm^{-1}, which appears in the more concentrated solutions ($[I_2] > 5.0 \times 10^{-2}$ mol dm^{-3}), is also present in the spectrum of free iodine solutions at the same concentration, falls at the same position as in solid I_2 (21), and is attributed to autoassociated I_2.

The FT–Raman spectra of the solid complexes (R_4todit·$2I_2$) show the characteristic ν(I–I) vibrations at 146 cm^{-1} (R = Et), 157 cm^{-1} (R = Bu), 167–146 cm^{-1} (R = Me), 171 cm^{-1} (R = Ph). Solid state effects could be invoked to explain the differences found in the position of this peak in solution and in the solid state. However, a comparison of the R = Et and R = Bu complexes of known X-ray structures shows that while a greater reduction of the I—I distance is found in the R = Bu case, an unexpectedly lower shift is observed in the ν(I–I) band.

Crystal structure of Bu_4todit·$2I_2$

The molecular structure of this neutral molecular compound, which, like Et_4todit·$2I_2$(5) and bis(morpholinothiocarbonyl)–bis(diiodine)(22), belongs to a series with two S heteroatoms in the donor and two diiodine molecules as acceptors, is shown in Fig. 5 together with the atomic numbering scheme. Excluding the substituents, the structural data of the ligand molecule are similar to those observed in the uncomplexed molecules of the corresponding tetraethyl (1) and tetraphenyl

Fig. 5. Perspective view of the Bu_4todit·$2I_2$ molecule with a non-hydrogen atom numbering scheme.

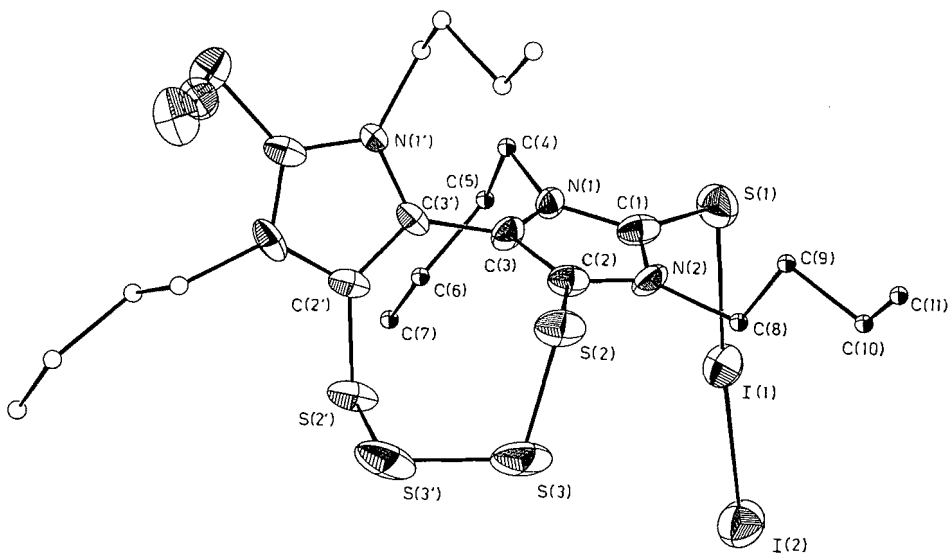

Fig. 6. Projection of the structure viewed along *b*.

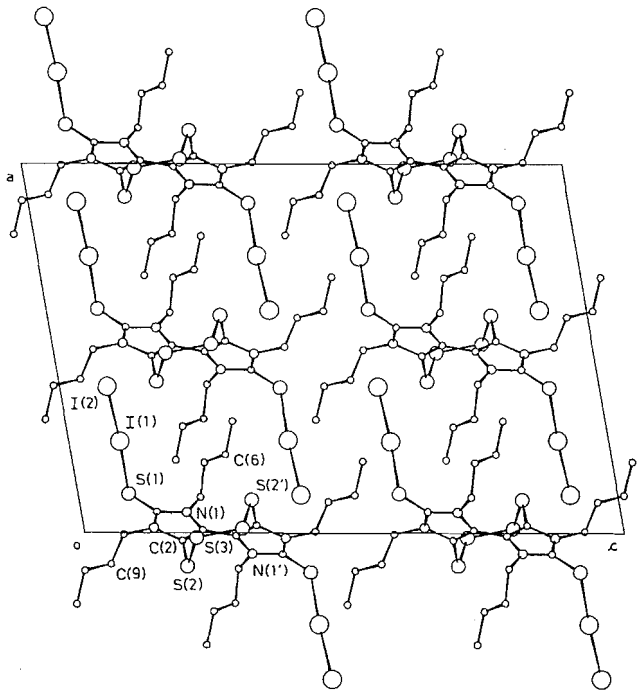

(6) derivatives in the bis-diiodine adduct and in the complexes of the tetraethyl derivative with $CuCl_2$ (3), $CdCl_2$ (2), and CuI (4). The analogies include the presence of a twofold axis, the orientation of the two imidazoline rings (N1-C3-C3′-N1′: −70(2)°) determined by the mutually opposite disposition of the butyl groups, and the chair conformation of the eight-membered ring. The imidazoline ring is not exactly planar (maximum deviation 0.027(15) Å for C(1)). The two butyl groups show different conformations, as a consequence of the minimum hindrance, since only the C(8)-C(9)-C(10)-C(11) moiety is in the extended shape. In fact, C(6) is +syn-clinal with respect to N(1) (N(1)-C(4)-C(5)-C(6); 61(2)°) and C(7) is anti-periplanar with respect to C(4) (C(4)-C(5)-C(6)-C(7): 172(2)°), both C(10) and C(11) are anti-periplanar with respect to N(2) and C(8), respectively (N(2)-C(8)-C(9)-C(10); 168(2)°, C(8)-C(9)-C(10)-C(11); −156(2)°). In the C(1)-S(1)-I(1)-I(2) moiety, which is roughly planar (maximum deviation 0.018(16) Å for C(1)) and roughly perpendicular to the imidazoline ring (I(1)-S(1)-C(1)-N(1): −101(1)°; I(1)-S(1)-C(1)-N(2): 77(1)°), the bond distances and angles are similar to those observed in the corresponding adduct $Et_4todit \cdot 2I_2$.

As shown in Fig. 6, here interactions of type $I_2 \cdots I_2$ are not present, owing to the hindrance of the substituents. The most relevant contacts determining the packing are: I(2)···S(3) (1/2+*x*, *y*−1/2, *z*) 3.775(6) Å; S(2)···S(3)(−*x*, *y*, 1/2−*z*) 3.299(7) Å; S(3)···C(7)(1/2−*x*, 1/2+*y*, 1/2−*z*) 3.52(2) Å; C(5)···C(7)(1/2−*x*, *y*−1/2, 1/2−*z*) 3.68(3) Å; C(7)···C(11) (1/2+*x*, 1/2−*y*, 1/2+*z*) 3.61(4) Å; and C(11)···C(11) (−1/2−*x*, 1/2−*y*, −*z*) 3.77(5) Å.[3]

Conclusions

The results of this investigation show that systems that could not be refined using the conventional SUPERSPEC program have been solved satisfactorily with POWELSPEC. However, it should be remembered that two hard constraints have been imposed in this algorithm: *(i)* the temperature independence of the molar absorptivities and *(ii)* the validity of the van't Hoff equation in the temperature range investigated. Moreover, this computer program is remarkably slower and does not directly provide standard deviation values for the parameters. In our opinion, SUPERSPEC should be employed whenever possible, and POWELSPEC is to be considered a valid alternative when the correlation among parameters produces a nearly singular matrix of the normal equations, and precludes the convergence of most of Newton's minimization methods. By applying POWELSPEC it was possible to solve the case of the equilibrium reaction of R_4todit (R = Et,Ph) with diiodine, for which SUPERSPEC gave wrong results involving a 1:1 model, as well as that of R_4todit (R = Me, *n*-Bu), in terms of the stepwise addition of two I_2 molecules to the ligand. The $\Delta H°$ sequence found with the R substituents is not confirmed by FT–Raman results, which suggest a very similar I_2–R_4todit interaction strength for all R derivatives investigated. This discrepancy is ascribed to solvation effects that affect the $\Delta H°$ values. Structural data on Bu_4todit are similar to those previously obtained in the bis-diiodine complex of the corresponding tetraethyl derivative.

On the basis of these results, there is no doubt that both the equilibrium model and the thermodynamic functions obtained here for Et_4todit and Ph_4todit must replace the corresponding results reported previously.

Acknowledgements

We acknowledge the support of the Consiglio Nazionale delle Ricerche of Rome (Progetto Finalizzato Chimica Fine) in this research.

References

1. D. Atzei, F. Bigoli, P. Deplano, M.A. Pellinghelli, and E.F. Trogu. Phosphorus Sulfur, **37**, 189 (1988).
2. F. Bigoli, P. Deplano, M.A. Pellinghelli, and E.F. Trogu. Inorg. Chim. Acta, **170**, 245 (1990).
3. F. Bigoli, P. Deplano, M.A. Pellinghelli, A. Sabatini, E.F. Trogu, and A. Vacca. Inorg. Chim.Acta, **180**, 201 (1991).
4. F. Bigoli, P. Deplano, M.A.Pellinghelli, and E.F. Trogu. Inorg. Chim. Acta, **182**, 33 (1991).
5. D. Atzei, F. Bigoli, P. Deplano, M.A. Pellinghelli, A. Sabatini, E.F. Trogu, and A. Vacca. Can. J. Chem. **67**, 1416 (1989).
6. F. Bigoli, P. Deplano, M.L. Mercuri, M.A. Pellinghelli, E.F. Trogu, and A. Vacca. Phosphorus, Sulfur, Silicon, **62**, 53 (1991).
7. P. Gans, A. Sabatini, and A. Vacca. J. Chem. Soc. Dalton Trans. 1195 (1985).
8. P. Deplano, E.F. Trogu, and P. La Colla. Patent Application Milano, 93A002377 (9-11-1993) and Department of Health and Human Services NSC Number: 633113-Y.
9. M.J.D. Powell. Comput. J. **7**, 155 (1964).
10. (*a*) N. Walker and D. Stuart. Acta Crystallogr. Sect. A: Found. Crystallogr. **A39**, 158 (1983); (*b*) F. Ugozzoli. Comput. Chem. **11**, 109 (1987).
11. G.M. Sheldrick. SHELX-76. A program for crystal structure determination. University of Cambridge, England. 1976.

Can. J. Chem. Downloaded from www.nrcresearchpress.com by 65.111.164.53 on 09/08/12
For personal use only.

12. International tables for X-ray crystallography. Vol. 4. Kynoch Press, Birmingham, England. 1974. pp. 99, 149.
13. M. Nardelli. Comput. Chem. **7**, 95 (1987).
14. W.D.S. Motherwell. PLUTO, University of Cambridge, U.K. 1976.
15. C.K. Johnson. ORTEP, Rep ORNL-3794, revised, Oak Ridge National Laboratory, Tennessee. 1965.
16. D. Dryssen, N. Ingri, and L.G. Sillèn. Acta Chem. Scand. **15**, 694 (1961).
17. A. Suszka. J. Chem. Soc. Perkin Trans. 2, 531 (1985).
18. P. Klaboe, J. Am. Chem. Soc. **89**, 3667 (1967).
19. K. Purcell and J.C.Kotz. Inorganic chemistry. Sanders, Philadelphia. 1977.
20. P. Deplano, F.A. Devillanova, J.A. Ferraro, F. Isaia, V. Lippolis, and M.L. Mercuri, Appl. Spectrosc. **46**, 1625 (1992).
21. A. Anderson and T.S. Sun. Chem. Phys. Lett. **6**, 611 (1970).
22. D. Atzei, F. Bigoli, P. Deplano, M.A. Pellinghelli, E.F. Trogu, and A. Vacca. Can. J. Chem. **66**, 1483 (1988).

Can. J. Chem. Downloaded from www.nrcresearchpress.com by 65.111.164.53 on 09/08/12
For personal use only.

Solvated electron mobility in liquid *tert*-butanol

Yixing Zhao and Gordon R. Freeman

Abstract: The mobility μ_e of solvated electrons in liquid *tert*-butanol was estimated from the measured rate constant of the diffusion-controlled reaction $e_s^- + H_s^+ \rightarrow H_s$, combined with the measured molar conductivities of perchloric acid and ammonium perchlorate solutions; T = 300–330 K. The values $\mu_e = 4.1 \times 10^{-8}$ m^2 V^{-1} s^{-1} at 300 K and $E_\mu = 41$ kJ mol^{-1} indicate that electrons migrate by a hopping mechanism in liquid *tert*-butanol. This contrasts with the ion-like diffusion mechanism of e_s^- in methanol and ethanol.

Key words: *tert*-butanol, solvated electron, activation energy, mobility.

Résumé : On a évalué la mobilité μ_e des électrons solvatés dans le *tert*-butanol liquide à partir de la constante mesurée pour la réaction contrôlée par diffusion $e_s^- + H_s^+ \rightarrow H_s$ combinée aux conductivités molaires mesurées de solutions d'acide perchlorique et de perchlorate d'ammonium, à des températures allant de 300 à 330 K. Les valeurs de $\mu_e = 4{,}1 \times 10^{-8}$ m^2 V^{-1} s^{-1}, à 300 K et $E_\mu = 41$ kJ mol^{-1} indiquent que, dans le *tert*-butanol liquide, les électrons migrent par un mécanisme de saut. Ce comportement contraste avec le mécanisme de diffusion ressemblant aux ions qui l'on observe pour les e_s^- dans le méthanol et l'éthanol.

Mots clés : *tert*-butanol, électron solvaté, énergie d'activation, mobilité.

[Traduit par la rédaction]

Introduction

The mobilities of electrons in alcohols are difficult to measure directly, for two reasons: (*i*) proton transfer reactions (acid–base autodissociation) of alcohols produce a relatively high intrinsic conductivity, which means that relatively high concentrations of e_s^- must be used to obtain a sufficiently high e_s^- conductance signal above the background conductance; (*ii*) the large radiation pulse dose needed to produce the high, uniform e_s^- concentration in the sample requires equipment that is available at only two or three labs in the world (1–5).

The accurate interpretation of measured rates of reactions of e_s^- requires knowledge of the values of their diffusion coefficients D_e (or the mobilities μ_e) and activation energies. Values of μ_e and E_μ in water are well established (5). Values of μ_e in alcohols are less certain, and the E_μ values have not been measured (1–3, 6).

Values of μ_e in water, methanol, and ethanol are similar to those of the hydroxide (5) and respective alkoxide (1) ions. In mixed methanol/water and ethanol/water solvents this similarity appears to persist, judging from the solvent composition dependences of rate constants of diffusion-controlled reactions (7–9). However, in isopropanol (3) and larger alcohols (2, 3) μ_e appears to be larger than the mobility of a normal anion or alkoxide ion. These measurements have not been repeated, and must therefore be viewed with caution. In support of them, our study of e_s^- reactivity in *tert*-butanol (10) provides evidence that μ_e in *tert*-butanol is about 10 times higher than the mobility of a normal anion in this alcohol. The relevant data are presented below.

Received April 26, 1994.

Y. Zhao and G.R. Freeman.[1] Department of Chemistry, University of Alberta, Edmonton, AB T6G 2G2, Canada.

[1] Author to whom correspondence should be addressed. Tel.: (403) 492-3468; fax.: (403) 492-8231; e-mail: knp@dept.chem.ualberta.ca

Experimental and results

The purified alcohol contained 5×10^{-4} mole fraction of water (10). Up to 1×10^{-5} mole fraction more water was added with the $HClO_4$ to measure the rate constant and molar conductance.

The experimental techniques are described in the following paper (10).

The sum of the mobilities of e_s^- and H_s^+, $(\mu_e + \mu_{H^+})$, in *tert*-butanol was estimated from the measured rate constant k_2 of the diffusion controlled reaction $e_s^- + H_s^+ \rightarrow H_s$ (10). A rearranged version of the Smoluchowski–Debye–Nernst–Einstein equation was used (11):

$$[1] \qquad \mu_e + \mu_{H^+} = 1.48 \times 10^{-16} k_2 / f T \mathcal{F} \kappa R_r$$

where f is the Debye coulombic interaction factor, T is the temperature, $\mathcal{F}$ is the Faraday, κ is the probability of reaction per encounter and is near unity for $e_s^- + H_s^+$ in alcohols (12), and R_r is the center-to-center encounter radius of $e_s^- + H_s^+$ and is taken as 1.6 nm in *tert*-butanol (10). The Debye factor is given by

$$[2] \qquad f = \frac{x}{e^x - 1}$$

$$[3] \qquad x = -\xi^2 / 4\pi\varepsilon_0 \varepsilon R_r k_B T$$

Can. J. Chem. Downloaded from www.nrcresearchpress.com by 65.111.164.53 on 09/08/12
For personal use only.

Can. J. Chem. Downloaded from www.nrcresearchpress.com by 65.111.164.53 on 09/08/12
For personal use only.

Fig. 1. Arrhenius plots. □, $k_2(e_s^- + H_s^+)$; ×, Debye f; ○, μ_{H^+}; ●, μ_e; in pure *tert*-butanol solvent.

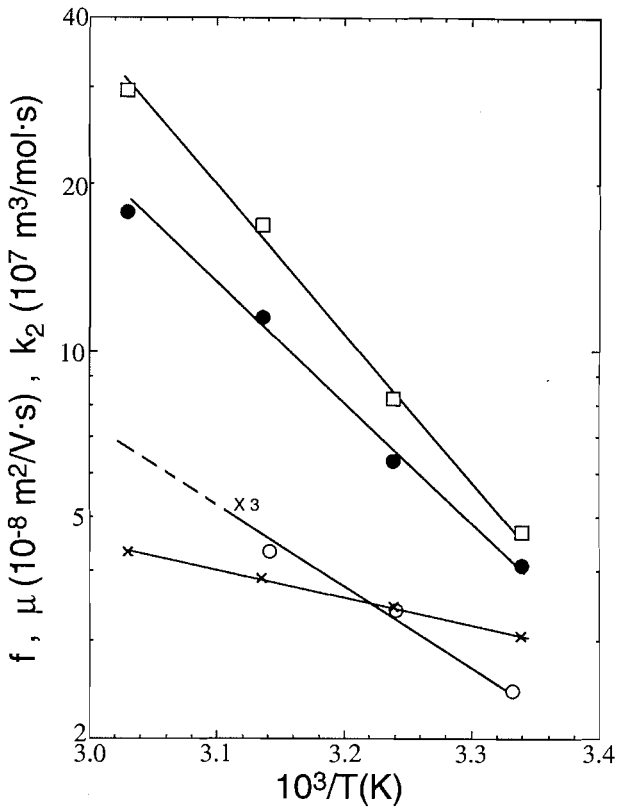

where ξ is the proton charge, ε is the relative permittivity of the medium between the proton and electron at R_r, and k_B is Boltzmann's constant.

An Arrhenius plot of $k_2(e_s^- + H_s^+)$ is shown in Fig. 1, for temperatures 299.5–330.0 K; E_2 = 50 kJ mol^{-1}. The value of κR_r was taken as constant at 1.6 nm (10). The values of the Debye factor f calculated from known values of ε (Table 1) are included in Fig. 1; E_f = 10 kJ mol^{-1}.

From the measured molar conductances of dilute solutions of $HClO_4$ and NH_4ClO_4 (Table 2), we estimated the ratio $\mu_{H^+}/\mu_{ClO_4^-}$ and hence μ_{H^+}; $\mu = \lambda/\mathcal{F}$. In ethanol at 298 K the mobility of ClO_4^- is near the geometric mean of those of NH_4^+ and H^+ (Table 3). For lack of better information we assumed the same to apply in *tert*-butanol solvent, and subdivided the conductances of $NH_4^+ClO_4^-$ and $H^+ClO_4^-$ in this way. The geometric factor is given by $\Lambda_0(HClO_4)/\Lambda_0(NH_4ClO_4)$. The values of μ_{H^+} are included in Fig. 1; $E_{\mu H^+} \approx 28$ kJ mol^{-1}.

The derived values of μ_e are listed in Table 1 and plotted in Fig. 1; $E_{\mu_e} = 41$ kJ mol^{-1}.

Table 2. Measured conductivities of $HClO_4$ and NH_4ClO_4; estimated ionic conductivity of H_s^+ in *tert*-butanol.

T (K)	$\Lambda_0(HClO_4)^a$ (10^{-4} S m^2 mol^{-1})	T (K)	$\Lambda_0(NH_4ClO_4)^b$ (10^{-4} S m^2 mol^{-1})
300.1	11.4	300.9	5.25
308.5	15.5	308.3	6.18
318.3	19.4	318.3	7.42

T_{ave} (K)	300.5	308.4	318.3
$\frac{\lambda_{ClO_4^-}}{\lambda_{NH_4^+}} \approx \frac{\lambda_{H^+}}{\lambda_{ClO_4^-}}$	2.2	2.5	2.6
$\lambda_{NH_4^+}$ (10^{-4} S m^2 mol^{-1})	1.7	1.8	2.0
$\lambda_{ClO_4^-}$ (10^{-4} S m^2 mol^{-1})	3.6	4.4	5.4
λ_{H^+} (10^{-4} S m^2 mol^{-1})	7.8	11.1	14.0
μ_{H^+} (10^{-8} m^2 V^{-1} s^{-1})	0.81	1.15	1.45

[a]Concentration: 2–10 mmol m^{-3}.
[b]Concentration: 6–30 mmol m^{-3}.

Discussion

Protons diffuse by a Grotthus (H^+ exchange) mechanism in alcohols, which allows H^+ to migrate 4.8 times faster than NH_4^+ and 2.2 times faster than ClO_4^- in *tert*-butanol at about 300 K (Table 2). The 5×10^{-4} mole fraction of water in the alcohol evidently did not quench the Grotthus mechanism. The activation energy of the H^+ exchange mechanism (28 kJ mol^{-1}) is 1.6 times larger than that of normal ion transport (17 kJ mol^{-1} for NH_4^+ and ClO_4^- (10)).

Electrons migrate even faster than protons in *tert*-butanol, and the activation energy is larger (41 kJ mol^{-1}, Table 3). The mobility ratio e_s^-/H_s^+ is 5 at 300 K and 8 at 330 K (Fig. 1). The high mobility and high activation energy indicate that electrons in *tert*-butanol migrate by a hopping mechanism.

The value of E_{μ_e} = 41 kJ mol^{-1} is only slightly larger than E_τ = 39 kJ mol^{-1} for molecular electric dipole rotation (Table 3). We suggest that thermally agitated dipole rotation of the solvating molecules is the process that activates the electron hopping.

Table 1. Estimation of mobility of e_s^- in *tert*-butanol.[a]

T (K)	ε	f	k_2 (10^6 m^3 mol^{-1} s^{-1})[b]	$\frac{\lambda_{H^+}}{\lambda_{ClO_4^-}}$	μ_{H^+} (10^{-8} m^2 V^{-1} s^{-1})	μ_e (10^{-8} m^2 V^{-1} s^{-1})	$\mu_e + \mu_{H^+}$ (10^{-8} m^2 V^{-1} s^{-1})
299.5	12.1	3.05	47	2.2	0.8	4.1	4.9
308.7	10.2	3.44	82	2.5	1.15	6.3	7.4
318.9	8.6	3.89	168	2.6	1.6	11.4	13.0
330.0	7.4	4.33	295	3.1	~2.3	17.5	19.8

[a]Using eq. [1], $\kappa R_r = 1.6 \times 10^{-9}$ m, $\mathcal{F}$ = 96 500 C mol^{-1}.
[b]$HClO_4$ concentrations 1–6 mmol m^{-3}.

Table 3. Comparison of mobilities of ions and solvated electrons with parameters in alcohols and water at 298 K.

Solvent	η^{-1} [a] (mPa s)$^{-1}$	μ (10^{-8} m^2 V^{-1} s^{-1}) [b,c]				$\Lambda_0(HClO_4)$ [d] (10^{-4} S m^2 mol^{-1})	Λ_0 ratio ($e_s^-/HClO_4$)	Activation E (kJ mol^{-1})			
		$NH_{4,s}^+$	$ClO_{4,s}^-$	H_s^+	e_s^-			η	τ [e]	μ_e [f]	$\Lambda_0(HClO_4)$
Water	1.12[13]	7.6	7.0	36.2	19[5]	417[16]	0.44	17	19	20	12[g]
MeOH	1.8[13]	6.0	7.3	14.7	6[1,6 b]	214[16]	0.27	11	16		9.4[h]
EtOH	0.9[13]	2.0	3.5	6.0	3[1,6 b]	93[16]	0.31	14	18		13[h]
2-PrOH	0.5[14]		0.86	1.7	5[3]	25[17]	1.9	22	27		21[d]
1-BuOH	0.4[13]		0.50	1.0	8[3]	14.6	5.3	19	26		21[d]
i-BuOH	0.29[15]		0.49	0.97	7[3]	14.1[12]	4.8	24	28		24[d]
tert-BuOH[i]	0.22[15]	0.16	0.35	0.76	~4	10.6	~4	31	39	~41	27[d]

[a]Fluidity of solvent; reference numbers are superscripts.

[b]Mobility of ions in water, MeOH, and EtOH, ref. 16; in EtOH the conductivity ratios of $NH_{4,s}^+$:$ClO_{4,s}^-$ and $ClO_{4,s}^-$:H_s^+ are approximately 1:2 and 1:2, respectively. The same ratios are assumed for the other alcohols (except *tert*-BuOH) to estimate the ionic conductivities of $NH_{4,s}^+$, $ClO_{4,s}^-$, and H_s^+ from the measured electrolyte molar conductivities; for *tert*-BuOH, ionic conductivities estimated from corresponding electrolyte conductivities and self-consistance gives ratios $NH_{4,s}^+$:$ClO_{4,s}^-$ and $ClO_{4,s}^-$:H_s^+ equal to 1:2.2 and 1:2.2, respectively.

[c]Mobility of electrons; *tert*-BuOH, present work.

[d]Molar conductivity of $HClO_4$; 1-BuOH, R. Chen's unpublished data; *tert*-BuOH, present work.

[e]Dielectric relaxation time: ref. 18, except *tert*-BuOH, ref. 19.

[f]Electron mobility in water, ref. 5; *tert*-BuOH, present work.

[g]Present work.

[h]Calculated from data in ref. 20.

[i]All values extrapolated from measurements at 300 K and higher temperatures; freezing point is 298.7 K.

By comparing μ_e with the fluidity η^{-1} of the various solvents (Table 3), and the conductance ratio $e_s^-/HClO_4$, one might suggest that electron hopping also occurs in 2-propanol and in all the butanols.

References

1. P. Fowles. Trans. Faraday Soc. **67**, 428 (1971).
2. A.V. Vannikov, E.I. Mal'tzev, V.I. Zolotarevsky, and A.V. Rudnev. Int. J. Radiat. Phys. Chem. **4**, 135 (1972).
3. A.V. Rudnev, A.V. Vannikov, and N.A. Bakh. High Energy Chem. **6**, 416 (1972).
4. K.H. Schmidt. Int. J. Radiat. Phys. Chem. **4**, 439 (1972).
5. K.H. Schmidt, P. Han, and D.M. Bartels. J. Phys. Chem. **96**, 199 (1992).
6. J.-P. Dodelet and G.R. Freeman. Can. J. Chem. (*a*) **50**, 2667 (1972); (*b*) **50**, 2729 (1972).
7. F. Barat, L. Gilles, B. Hickel, and B. Lesigne. J. Phys. Chem. **77**, 1711 (1973).
8. O.I. Micic and B. Cercek. J. Phys. Chem. **81**, 833 (1977).
9. Y. Maham and G.R. Freeman. J. Phys. Chem. **92**, 1506 (1988).
10. Y. Zhao and G.R. Freeman. Can. J. Chem. **73**, 392 (1995).
11. R. Chen and G.R. Freeman. Can. J. Chem. **71**, 1303 (1993).
12. R. Chen, Y. Avotinsh, and G.R. Freeman. Can. J. Chem. **72**, 1083 (1994).
13. R.C. Weast (*Editor*). Handbook of chemistry and physics. 59th ed. CRC Press, Boca Raton, Fla. 1979. p. F-52.
14. W. Weber. Rheol. Acta, **14**, 1012 (1975).
15. P.C. Senanayake, N. Gee, and G.R. Freeman. Can. J. Chem. **65**, 2441 (1987).
16. D. Dobos. Electrochemical data. Elsevier Scientific Publishing, New York. 1975. pp. 88–89.
17. S.A. Peiris and G.R. Freeman. Can. J. Chem. **69**, 884 (1991).
18. F. Buckley and A.A. Maryott. Table of dielectric dispersion data for pure liquids and dilute solutions. National Bureau of Standards Circular 589.1958.
19. M. Tabellout, P. Lanceleur, J.R. Emery, D. Hayward, and R.A. Pethrick. J. Chem. Soc. Faraday Trans. **86**, 1493 (1990).
20. G.J. Janz and R.P.T. Tomkins, Nonaqueous electrolytes handbook. Vol. 1. Academic Press, New York. 1972. pp. 299–301.

Can. J. Chem. Downloaded from www.nrcresearchpress.com by 65.111.164.53 on 09/08/12
For personal use only.

Solvent effects on the reactivity of solvated electrons with ions in *tert*-butanol/water mixtures

Yixing Zhao and Gordon R. Freeman

Abstract: Reactions of e_s^- with the ions $NO_{3,s}^-$, $NH_{4,s}^+$, and H_s^+ showed different variations of rate with solvent composition in *tert*-butanol/water mixtures from 0 to 100 mol% water. In pure *tert*-butanol solvent at 298 K the respective values of k_2 (10^6 m^3 mol^{-1} s^{-1}) are 3.2, 13, and 42. The estimated value of reaction radius R_r depends on the minimum number of solvent molecules needed between e_s^- and the reactant ion to attain the static values of ε of the bulk solvent used in the calculation of the Debye factor f; R_r is assumed to be larger in the alcohol-rich region than in the water-rich region, because the solvent molecules are larger. The Smoluchowski–Debye–Nernst–Einstein model is used to evaluate the effective reaction radius κR_r, where κ is the probability of reaction per encounter; κR_r decreases from pure *tert*-butanol to pure water. In the water-rich region the activation energies E_2 of the efficient reactions, 11–24 kJ mol^{-1}, are similar to $E_{\Lambda 0}$ of the reactant electrolyes, 12–23 kJ mol^{-1}. For the inefficient reactant NH_4^+ ClO_4^-, E_2 = 30 kJ mol^{-1}. The high values of E_2 = 43–53 kJ mol^{-1} in pure *tert*-butanol solvent are attributed to a high activation energy for diffusion of e_s^- in this solvent.

Key words: *tert*-butanol/water solvents, solvated electron, ions, reactivity, solvent effects.

Résumé : Les vitesses de réaction des e_s^- avec les ions $NO_{3,s}^-$, $NH_{4,s}^+$ et H_s^+ présentent des variations différentes avec la composition des mélanges de solvant *tert*-butanol/eau en allant de 0 à 100% en eau. Dans le *tert*-butanol pur, à 298 K, les valeurs relatives de k_2 (10^6 m^2 mol^{-1} s^{-1}) sont 3,2, 13 et 42. La valeur estimée du rayons de réaction R_r dépend du nombre minimal de molécules de solvant requis entre le e_s^- et l'ion réactif pour atteindre les valeurs statiques de ε de l'ensemble du solvant utilisée par le facteur f de Debye; comme les molécules de solvant sont plus volumineuses que celles de l'eau, on considère que R_r est plus élevé dans la région riche en alcool que dans la région riche en eau. On a utilisé le modèle de Smoluchowski–Debye–Nernst–Einstein pour évaluer le rayon réactionnelle efficace, κR_r, dans lequel κ est la probabilité de réaction par rencontre; κR_r diminue en allant du *tert*-butanol pur à l'eau pure. Dans la région riche en eau, les énergies d'activation E_2 des réactions efficaces, 11–24 kJ mol^{-1}, sont semblables aux valeurs de $E_{\Lambda 0}$ des électrolytes qui réagissent, 12–23 kJ mol^{-1}. Pour le réactif inefficace NH_4^+ ClO_4^-, E_2 = 30 kJ mol^{-1}. On attribue les valeurs élevées de E_2 = 43–53 kJ mol^{-1} observées dans le *tert*-butanol à une énergie élevée d'activation de la diffusion des e_s^- dans ce solvant.

Mots clés : solvants *tert*-butanol/eau, électron solvaté, ions, réactivité, effets de solvants.

[Traduit par la rédaction]

Introduction

The reactivity of solvated electrons e_s^- depends mainly on the natures of the coreactant and solvent (1–5). The study of rates of reaction of e_s^- with solutes in different solvents provides useful information about solvent effects, which helps us understand the behaviour of electrons and the nature of solvents. The reaction rates in single component and mixed solvents are related to transport properties, as in Smoluchowski-type models for diffusion-controlled reactions (1, 3, 4, 6–8), and relative energy levels of the reactants, as in the electron trap-depth model (2, 7, 8*a*). Electron reaction rates with inefficient capturers are larger when the electron solvation energy, represented by the optical absorption energy E_r (2), is smaller.

The physical properties of *tert*-butanol/water mixed solvents vary markedly with composition (9, 10). The present paper reports a continuation of the study of e_s^- reaction rates in this solvent system (11).

Experimental

The *tert*-butanol was obtained from BDH (Assured grade, 98%), and later from Fluka (>99.7%). The purification method was similar to that in ref. 11*a*. *tert*-Butanol was dried at 304 K for at least one week on Davison 3Å molecular sieves, then bubbled with UHP argon (99.999%, Liquid Carbonic Canada) and treated with sodium borohydride (2 g

Received June 16, 1994.

Y. Zhao and G.R. Freeman.[1] Department of Chemistry, University of Alberta, Edmonton, AB T6G 2G2, Canada.

[1] Author to whom correspondence should be addressed: tel.: (403) 492-3468; fax.: (403) 492-8231; e-mail: knp@dept.chem.ualberta.ca

Can. J. Chem. Downloaded from www.nrcresearchpress.com by 65.111.164.53 on 09/08/12
For personal use only.

Can. J. Chem. Downloaded from www.nrcresearchpress.com by 65.111.164.53 on 09/08/12
For personal use only.

L^{-1}) under argon at 323 K for 24 h. Then the alcohol was fractionally distilled under argon through an 80 × 2.3 cm column packed with glass beads (6 mm). The first 20–25% of the distillate was discarded; distillate was collected after there was no further reduction in optical absorption between 260 and 280 nm, which is due to carbonyl compounds (12). The middle 50% portion was collected and stored in a flask under argon positive pressure. The water content, measured by Karl–Fisher titration, was 0.05 mol%. The solvated electron half-life after a 100 ns pulse of 340 fJ (2.1 MeV) electrons (4 J kg^{-1}) at 300 K was over 10 μs.

Perchloric acid (70 wt% in water, reagent) was obtained from Fisher Scientific. $LiNO_3$ (99.999% Gold label), NH_4NO_3 (99.999%), $LiClO_4$ (reagent grade), and NH_4ClO_4 (99.8%) were from Aldrich.

Techniques of sample solution preparation, irradiation, and optical measurements were the same as described in ref. 13. Conductance measurement was as in ref. 14.

Results and discussion

tert-BuOH/water mixed solvents

tert-Butanol is completely miscible with water. The following mol% of water in *tert*-butanol were used for rate constant measurements of all solutes: 0, 5, 10, 30, 50, 70, 90, 97, 100. Measurements of electrical conductance were done in the same solvents, except 5 mol%.

Rate constants

The reactions are

$$[1] \qquad e_s^- + ROH_s \rightarrow RO_s^- + H_s \qquad k_1$$

$$[2] \qquad e_s^- + S_s \rightarrow \text{Products} \qquad k_2$$

The observed first-order decay rate constant k_{obs} ($= k_1 + k_2$ [S]) in a given solvent was measured for the pure solvent and six concentrations of solute S. The value of k_1 might include a contribution from trace impurities in the solvent: $k_1 = k_1' + k_i$[I]. The value of the second-order rate constant k_2 was obtained from the slope of a plot of k_{obs} against solute concentration. The values of k_2 for each solvent were measured at temperatures from 273 to 343 K, except in pure *tert*-butanol whose mp is 298.7 K.

Arrhenius plots of k_2 for the four solutes ($Li_s^+ + NO_{3,s}^-$), ($NH_{4,s}^+ + NO_{3,s}^-$), ($NH_{4,s}^+ + ClO_{4,s}^-$), and ($H_s^+ + ClO_{4,s}^-$) are given in Figs. 1–4. Table 1 contains the symbols for these figures. The reaction parameters are listed in Table 2.

The value of k_2 for the reaction of $e_s^- + (Li_s^+ + ClO_{4,s}^-)$ is very small, being 110 m^3 mol^{-1} s^{-1} in water and 660 m^3 mol^{-1} s^{-1} in *tert*-butanol at 298 K (Table 2). Thus the large value of k_2 of ($Li_s^+ + NO_{3,s}^-$) is due to $NO_{3,s}^-$, of ($H_s^+ + ClO_{4,s}^-$) is due to H_s^+, and of ($NH_{4,s}^+ + ClO_{4,s}^-$) is due to $NH_{4,s}^+$ (Table 2).

The solvent composition dependence of k_2 at 298 K is shown in Fig. 5. Values of the optical absorption energy E_T (15), relative permittivity (16), and viscosity (10) are shown for comparison.

The value of k_2 of ($NH_{4,s}^+ + NO_{3,s}^-$) in the water-rich region is due to $NO_{3,s}^-$, and in the alcohol-rich region is due to $NH_{4,s}^+$. This conclusion agrees with earlier work (14). In the alcohol-rich solvents the rate constants for $NH_{4,s}^+$ are about

Fig. 1. Arrhenius plots of k_2 for the reaction of e_s^- with $Li_s^+ + NO_{3,s}^-$ in *tert*-butanol/water mixed solvents. Refer to Table 1 for symbols.

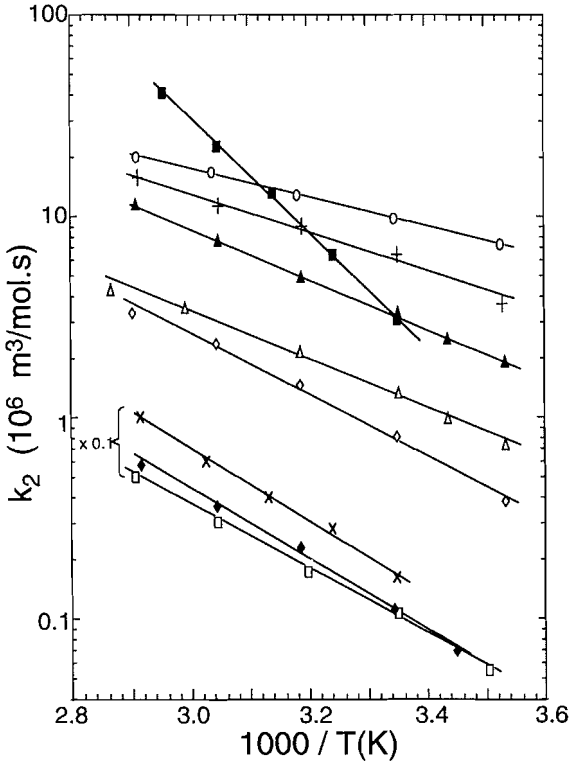

Fig. 2. Arrhenius plots of k_2 for the reaction of e_s^- with $NH_{4,s}^+ + NO^-{}_{3,s}$ in *tert*-butanol/water. Refer to Table 1 for symbols.

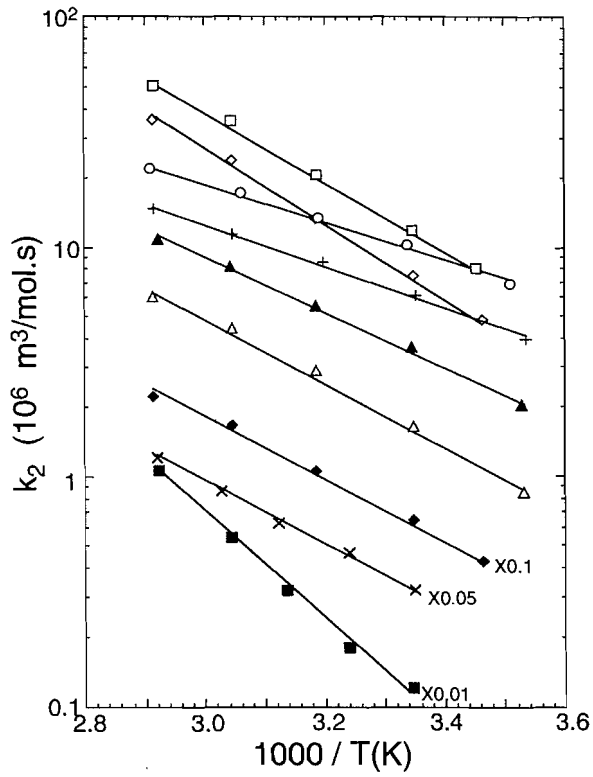

Can. J. Chem. Downloaded from www.nrcresearchpress.com by 65.111.164.53 on 09/08/12
For personal use only.

Fig. 3. Arrhenius plots of k_2 for the reaction of e_s^- with $NH_{4,s}^+ + ClO_{4,s}^-$ in *tert*-butanol/water. Refer to Table 1 for symbols. The data for 100, 97, and 90 mol% of water have been corrected for the contribution of the reaction of e_s^- with H_s^+. Refer to ref. 14 for the correction method.

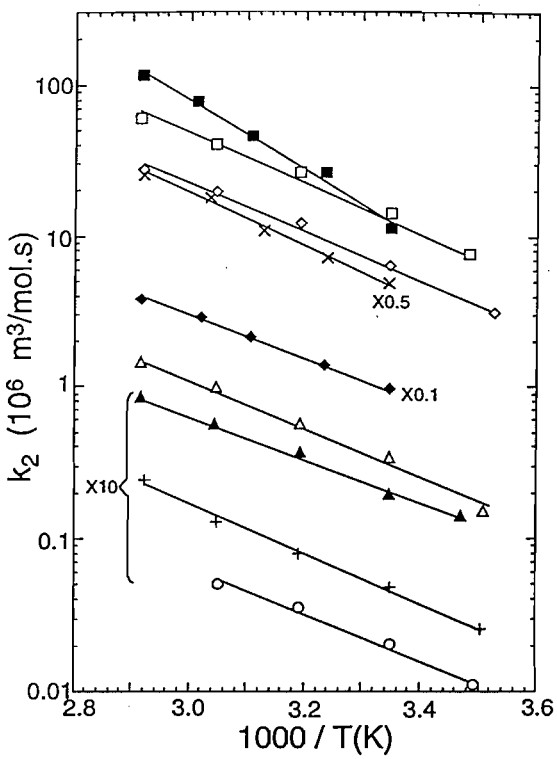

Fig. 4. Arrhenius plots of k_2 for the reaction of e_s^- with $H_s^+ + ClO_{4,s}^-$ in *tert*-butanol/water. Refer to Table 1 for symbols.

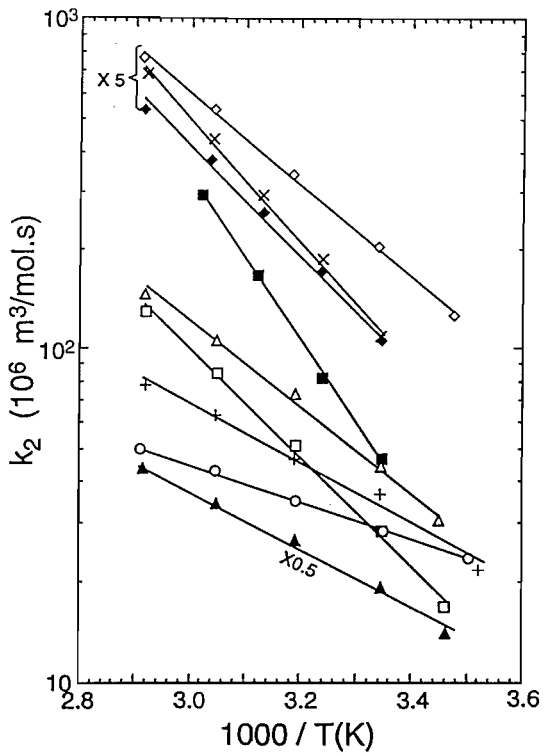

Table 1. Symbols in Fig. 1–4.

Symbol	mol% water	Symbol	mol% water
■	0	△	70
×	5	▲	90
◆	10	+	97
□	30	○	100
◇	50		

10 times higher than those for $NO_{3,s}^-$ (Fig. 5). The Coulombic attraction of the opposite charges ($NH_{4,s}^+ + e_s^-$) and repulsion of the like charges ($e_s^- + NO_{3,s}^-$) is the main cause of this difference (see Debye factor f in Table 2).

The value of k_2 ($e_s^- + H_s^+$) stays $\geq 2 \times 10^7$ m^3 mol^{-1} s^{-1} at all solvent compositions. It is higher than those of the other three reactions. In the region of 30–100 mol% water, the variation of the k_2 of H_s^+ is very different from those of the reactions with $NO_{3,s}^-$ and $NH_{4,s}^+$ (Fig. 5).

Addition of 5–10 mol% of water to *tert*-butanol decreases the rate constant of each reaction by a factor of 0.5 to 0.3 (Fig. 5). We attribute this to a decrease in mobility of e_s^-, which is unusually high in pure *tert*-butanol (17).

The variation of k_2 with solvent composition between 50 and 100 mol% of water is different for each of the four solutes (Fig. 5). The variation of k_2 ($NO_{3,s}^-$) varies in the expected way with viscosity η and relative permittivity ε, but not with e_s^- trap depth E_r (2). In the water-rich region (100–70 mol%), values of k_2 for $NO_{3,s}^-$ and ($NH_{4,s}^+ + NO_{3,s}^-$, mainly due to $NO_{3,s}^-$) increase as diffusion rates increase (viscosity decreases). In the alcohol-rich region (0–50 mol% water), k_2 for $NO_{3,s}^-$ increases as the viscosity *increases*, indicating a change of reaction mechanism.

Reaction radius and Debye factor f

For a diffusion-controlled reaction of e_s^- with a solute of charge $z\xi$ the Smoluchowski–Debye equation (18) is

$$[3] \qquad k_2 = 4\pi N_A (D_e + D_s) R_r f$$

where N_A is Avogadro's constant, D_i is the diffusion coefficient of i, and R_r is the average center-to-center reactant separation when reaction occurs. The Debye factor f is given by

$$[4] \qquad f = \frac{x}{(e^x - 1)}$$

$$[5] \qquad x = -\frac{z\xi^2}{4\pi\varepsilon_0\varepsilon R_r k_B T}$$

where x is the ratio of the coulombic energy of the reactants at R_r to the thermal agitation energy $k_B T$, and ε is the relative permittivity of the medium between the reactants at separation R_r. The factor f reflects the effect of the coulombic interaction between the two reactants on the probability that they will approach each other to within the distance R_r at which reaction can occur.

Values of R_r are not well defined and can be quite different for different solutes and solvents; the estimated value

Can. J. Chem. Downloaded from www.nrcresearchpress.com by 65.111.164.53 on 09/08/12
For personal use only.

Table 2. Reaction rate parameters in *tert*-BuOH/water solvents at 298 K.

E_t(zJ)[a]	η[b] (mPa s^{-1})	ε[c]	H_2O mol %	f[d]	k_2 (10^6 m^3 mol^{-1}s^{-1})	k_2/f (10^6 m^3 mol^{-1}s^{-1})	E_2 (kJ mol^{-1})	Λ_o[e]	$E_{\Lambda o}$[e]
				$NO_{3,s}^-$((1.5–42) × 10^{-2} mol m^{-3} for k_2)					
104	4.45	12.4	0	0.283	3.2	11	53	1.9[f]	15
	4.33	12.0	5	0.229	1.7	7.3	34		
171	4.20	11.5	10	0.195	1.2	6.2	32	4.6	18
	4.41	12.9	30	0.193	0.96	5.0	31	8.2	24
215	4.76	17.6	50	0.288	0.76	2.6	29	14.0	26
	4.98	27.2	70	0.465	1.3	2.7	26	19.6	25
	3.23	53.2	90	0.69	3.3	4.8	22	38.0	23
223	1.60	70.0	97	0.76	6.2	8.2	18	80	20
219	0.89	78.4	100	0.78	9.8	13	14	113	13
				$NH_{4,s}^+$((0.3–900) × 10^{-2} mol m^{-3} for k_2)					
			0	3.00	13	4.3	43	4.9	17
			5	3.47	9.2	2.7	34		
			10	3.83	9.2	2.4	29	6.0	21
			30	4.02	14	3.4	29	8.9	24
			50	3.33	6.0	1.8	30	15.2	26
			70	2.36	0.32	0.14	30	22.5	25
			90	1.62	0.02[g]	0.012	30	48.5	22
			97	1.45	0.0045[g]	0.0031	31	90	18
			100	1.40	0.0019[g]	0.0014	30	140	14
				$NH_{4,s}^+NO_{3,s}^+$((0.25–12.0) × 10^{-2} mol m^{-3} for k_2)					
			0	3.00	11	3.8	43	2.37	19
			5	3.47	6.5	1.9	27		
			10	3.83	6.2	1.6	28	4.6	21
			30	4.02	11	2.7	29	8.3	25
			50	3.33	7.1	2.1	30	16.6	26
			70	0.465	1.6	3.4	28	25.0	26
			90	0.690	3.5	5.1	24	56	23
			97	0.757	6.1	8.1	17	118	18
			100	0.779	10	13	15	150	17
				H_s^+ + ((0.1–3.0) × 10^{-2} mol m^{-3} for k_2)					
			0	3.00	42	14	50	10.6	27
			5	3.47	23	6.6	36		
			10	3.83	20	5.3	33	12.7	25
			30	4.02	28	7.0	30	17.0	25
			50	3.33	38	11	28	30.0	25
			70	2.36	44	18	24	66	24
			90	1.62	39	24	19	170	22
			97	1.45	35	24	15	345	14
			100	1.40	29	20	11	400	12
				Li_s^+ + $ClO_{4,s}^-$((100–6000) mol m^{-3} for k_2)					
			0		6.6 × 10^{-4}			3.9	14
			10					6.6	19
			30					9.0	23
			50					12.4	25
			70					18.3	25
			90					37.0	21
			97					74	18
			100		1.1 × 10^{-4}			105	15

[a]Reference 15, except *tert*-butanol is from the authors' unpublished work.
[b]Reference 10.
[c]Reference 16.
[d]Debye factor, see text.
[e]Molar conductivity, 10^{-4} S m^2 mol^{-1}; activation energy, kJ mol^{-1}.
[f]Estimated value, to be discussed in a later paper.
[g]Corrected for $NH_{4,s}^+ \rightleftharpoons NH_{3,s}^+$, as in ref. 14.

Can. J. Chem. Downloaded from www.nrcresearchpress.com by 65.111.164.53 on 09/08/12
For personal use only.

Fig. 5. Solvent composition dependence of k_2 in *tert*-butanol/water mixtures at 298 K. The solutes are ●, $Li_s^+ + NO_{3,s}^-$; ○, $NH_{4,s}^+ + NO_{3,s}^-$; ▲, $NH_{4,s}^+ + ClO_{4,s}^-$; □, $H_s^+ + ClO_{4,s}^-$. Physical parameter reference lines are ×, E_r (15); - · - relative permittivity ε (16); - - - viscosity, η (10).

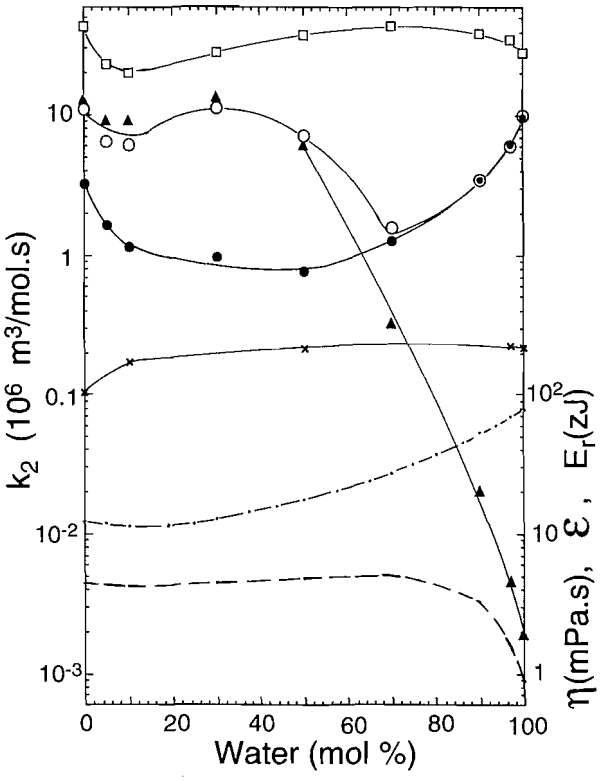

also depends on the method of estimation. Sometimes R_r estimated from the Smoluchowski–Debye equation [3] is called the effective reaction radius (R_{eff}) to distinguish it from the real reaction radius R_r. Milosavljevic and Micic (6) estimated R_{eff} for reactions of e_s^- with several solutes in methanol or ethanol mixed with water, using the Smoluchowski equation and estimated values of diffusion coefficients. For nitrobenzene in methanol/water solvents they obtained $R_{eff} = 0.8$ nm in pure water solvent, 0.9 nm in 20 mol% methanol, and 1.2 nm in pure methanol. For nitrobenzene in ethanol/water solvents they obtained $R_{eff} = 0.9$ nm in water, 0.7 nm in 20 mol% ethanol, and 1.3 nm in pure ethanol. However, Lai and Freeman (8*a*) used $R_r = 0.8$ nm for nitrobenzene over the whole range of water mixtures with methanol or ethanol.

Tunuli and Farhataziz (19) applied equation [3] to the reaction of e_s^- with Ag_s^+ in C_{1-10} alcohols. They used different methods to estimate R_r and obtained $R_r = 1.22$–1.28 nm for methanol, 1.42–1.48 nm for ethanol, 1.52–1.74 nm for 1-propanol, and 1.54–2.0 nm for 1-butanol.

Schwarz and Gill (1) calculated effective reaction radii r_r in the study of the diffusion-controlled reactions of e_s^- with $NH_{4,s}^+$, Ag_s^+ and other solutes in ethanol. For charged solutes, they used eqs. [6] and [7] to calculate r_r:

$$[6] \qquad r_r = r_c/[1 - \exp(-r_c/r_0)]$$

$$[7] \qquad r_c = -\frac{z\xi^2}{4\pi\varepsilon_0\varepsilon k_B T}$$

where r_c is the distance at which the coulombic interaction between the ions equals the thermal agitation energy $k_B T$, and r_0 is the center-to-center separation of the solvated reactant ions in contact. Schwarz used $r_0 = 1.1$ nm and the static value of ε of the bulk solvent in eqs. [6] and [7]. The reactants (electron and ion) are solvated, which means each reactant is surrounded by a layer of ethanol molecules oriented by the charge–dipole interaction. The average diameter of an ethanol molecule is about 0.4 nm, which with the radii of the electron cavity and the solute ion gives $r_0 \approx 1.1$ nm. Since there are only two solvent molecules between the two charged reactants and they cannot reorient freely, the relative permittivity ε of these two molecules is less than the static value of bulk ethanol. The static value of ε probably requires at least one more solvent molecule between those that solvate the reactant ions, or a minimum of $r \approx 1.5$ nm. The value of r_c in ethanol is 2.3 nm at 298 K, for $z = 1$ and $\varepsilon = 24.3$. The use of the simple ratio r_c/r_0 in eq. [6] requires that the same value of ε be applicable for both r_0 and r_c. This is improbable for $r_0 = 1.1$ nm in ethanol. If we release the "contact" restriction and replace r_0 in eq. [6] by R_r of eq. [3] then r_r in eq. [6] equals $R_r f$ in eq. [3].

For neutral solutes, eq. [8] was used (1).

$$[8] \qquad k_1' r_r = r_0 + \left(\frac{2}{b}\right)(\ln Z_0 + 0.57)$$

where $Z_0 = 2v^{1/2}/b(D_e + D_s)^{1/2}$, v and b are from the fitted reaction probability $\beta(r)$ based on electron transfer through overlapping wavefunctions ("tunneling", refs. 1, 20):

$$[9] \qquad \beta(r) = \gamma \exp[-b(r - r_0)]$$

where $v \approx 10^{15}$ cycles/s is the orbital oscillation frequency of the solvated electron, and $b^{-1} \approx 10^{-10}$ m is the separation distance $(r - r_0)$ where the reaction probability is decreased by a factor of 1/3 from the value v at contact $(r - r_0 = 0)$.

For mixed solvents the values of the diffusion coefficient of e_s^- are not known, so it is difficult to estimate the reaction radius. Therefore, for the reactions of e_s^- with $NO_{3,s}^-$ and H_s^+ in propanols (21) and butanols (13, 14, 21*b*), fixed values of R_r were used for f factor calculation in eqs. [4] and [5], namely, $R_r(e_s^- + NO_{3,s}^-) = 1.5$ nm, $R_r(e_s^- + H_s^+) = R_r(e_s^- + NH_{4,s}^+) = 1.0$ nm. Then κ, the probability that reaction occurs during one encounter, was inserted into [3] (21):

$$[10] \qquad k_2 = 4\pi N_A(D_e + D_s) f \kappa R_r$$

where κR_r can be considered as an effective reaction radius.

One might expect R_r to be larger when the solvating molecules are larger, hence larger for alcohol solvation than for water solvation. In most *tert*-butanol/water mixtures, from 30–100 mol% of water, e_s^- is preferentially solvated by water (15), so $R_r(e_s^- + NO_{3,s}^-) = 1.5$ nm and $R_r(e_s^- + NH_{4,s}^+) = 1.0$ nm are still used. This implies that there are, including the solvating molecules, about four water molecules between e^- and NO_3^-, and about three between e^- and NH_4^+ when reaction occurs. In pure *tert*-butanol, there could be about three and a half *tert*-butanol molecules between e^- and NO_3^-, and three between e^- and NH_4^+ to attain the bulk, static value of ε between the charges. The diameter of *tert*-butanol is about 0.5 nm, which gives a center-to-center $R_r(e_s^- + NO_{3,s}^-) = 2.1$

Can. J. Chem. Downloaded from www.nrcresearchpress.com by 65.111.164.53 on 09/08/12
For personal use only.

Table 3. Estimated values of R_r (nm) in *tert*-BuOH/water mixtures.[a]

Water (mol%)	$R_r(e_s^- + NO_{3,s}^-)$ (nm)	$R_r(e_s^- + NH_{4,s}^+)$ (nm)
0	2.1	1.6
5	1.9	1.4
10	1.8	1.3
30	1.6	1.1
50–100	1.5	1.0

[a] R_r is assumed to be relatively insensitive to temperature.

nm and $R_r(e_s^- + NH_{4,s}^+) = 1.6$ nm by the replacement of water molecules whose van der Waals diameter is 0.29 nm.[2] In the solvent region 0–30 mol% of water, the relative numbers of *tert*-butanol and water molecules between the reactants gradually change and the values of R_r gradually decrease. The values of R_r are listed in Table 3, and are assumed to be relatively insensitive to temperature. The corresponding values of f are in Table 2; the values of f for H_s^+ are the same as for $NH_{4,s}^+$.

The value of k_2 is dependent on both R_r and the factor f (eq. [10]), while f is dependent on R_r, the charge of the reactant ion, and the ε of the solvent between the electron and ion (eqs. [4] and [5]). Figure 6 shows the solvent composition dependence of εR_r and hence f for the reactions $e_s^- + NO_{3,s}^-$ and $e_s^- + NH_{4,s}^+$ (or H_s^+). As εR_r increases the coulombic interaction becomes weaker; f decreases towards unity for e_s^- reaction with a cation, and increases toward unity for reaction with an anion.

Normalized rate constants k_2/f

Equation [10] can be rearranged to eq. [11]:

$$[11] \qquad k_2/f = 4\pi N_A(D_e + D_s)\kappa R_r$$

where k_2/f normalizes the rate constant for the coulombic effect. Figure 7 shows the changes of k_2/f with solvent composition for different solutes in *tert*-butanol/water mixtures at 298 K. The method described in ref. 13 was used to calculate k_2/f for $e_s^- + (NH_{4,s}^+ + NO_{3,s}^-)$. The k_2/f curves for different solutes are closer together than are the k_2 curves in Fig. 5.

Molar conductivity of solutes

The solvent composition dependences of molar conductivities of all four solutes at 298 K are shown in Fig. 8 and listed in Table 2. The concentration ranges used in conductance measurements were close to those used to determine rate constants. The measured value of Λ for $LiNO_3$ in *tert*-butanol is about 0.46×10^{-4} S m^2 mol^{-1}, compared to 3.86×10^{-4} S m^2 mol^{-1} for $LiClO_4$. This indicates that (Li_s^+ $NO_{3,s}^-$) ion pairs form in *tert*-butanol. The value of $\Lambda_0 = 1.9$

[2] Reference 22. $r_{vdW} = \left(\frac{3}{4\pi N_A} \cdot \frac{b}{4}\right)^{1/3} = 4.63 \times 10^{-9} b^{1/3}$.

Fig. 6. Dependence of Debye f on εR_r for $Li_s^+ + NO_{3,s}^-$ (●) and $NH_{4,s}^+ + ClO_{4,s}^-$ (▲) in *tert*-butanol/water mixtures at 298 K. The numbers on the curves are mol% of water.

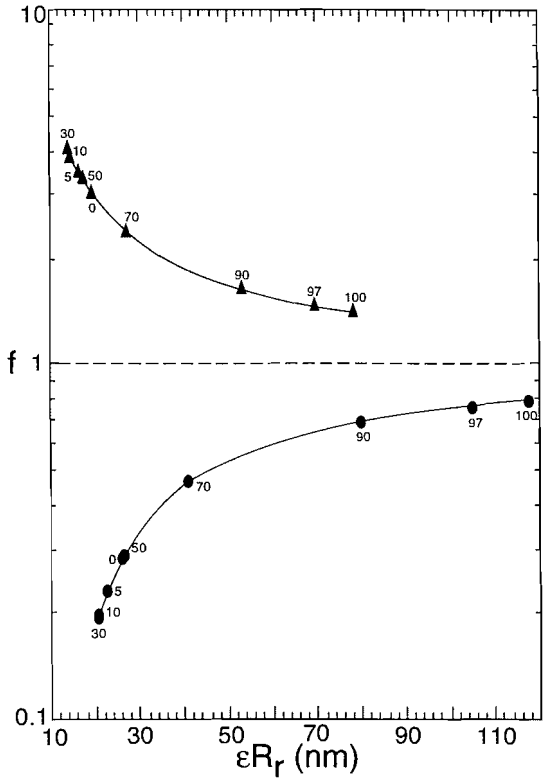

Fig. 7. k_2/f in *tert*-butanol/water mixtures at 298 K. Symbols are as in Fig. 5.

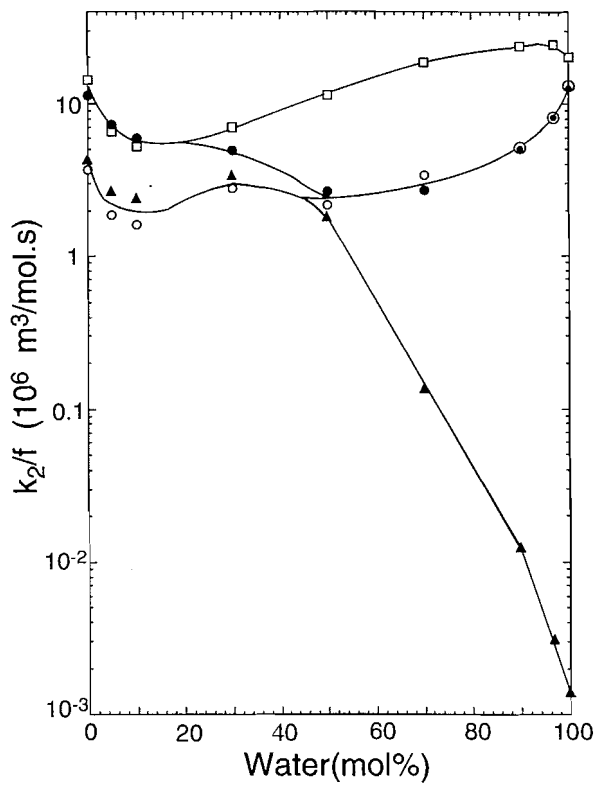

Can. J. Chem. Downloaded from www.nrcresearchpress.com by 65.111.164.53 on 09/08/12
For personal use only.

Fig. 8. Composition dependence of Λ_0 in *tert*-butanol/water at 298 K. Symbols are as in Fig. 5.

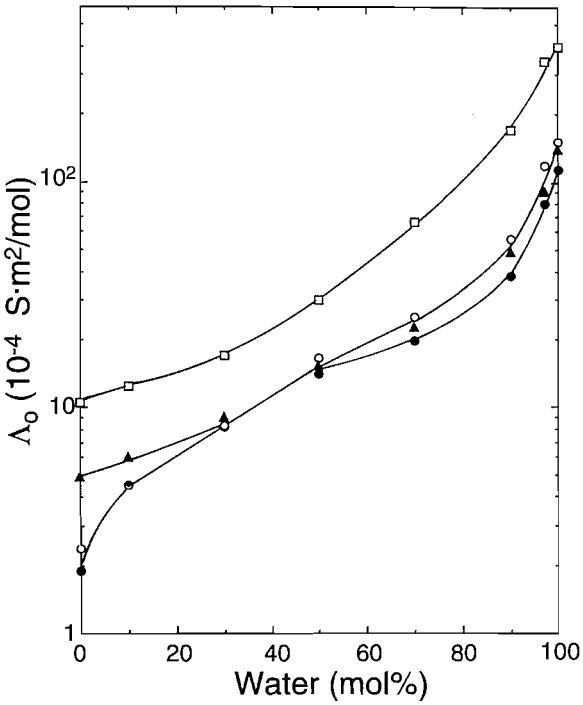

Fig. 9. Solvent composition dependence of r_d of *tert*-butanol/water mixtures at 298 K. Symbols are as in Fig. 5. - - - represents η (10).

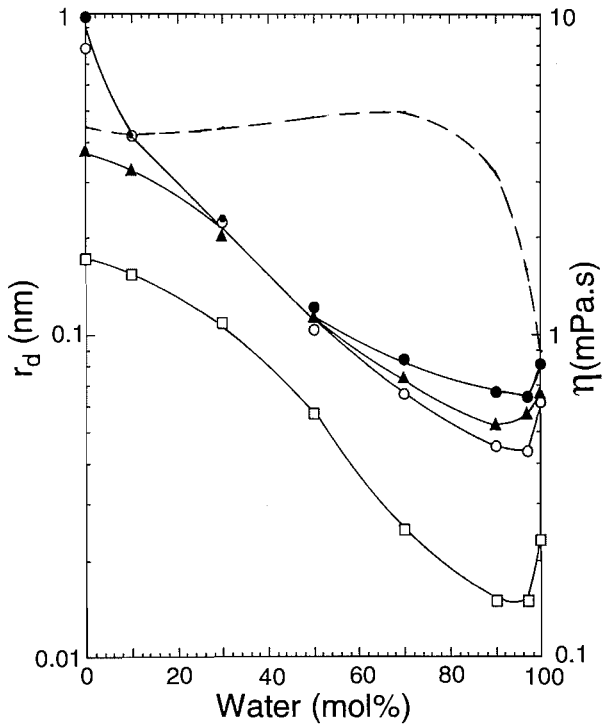

$\times 10^{-4}$ S m^2 mol^{-1} for $Li^+_s + NO^-_{3,s}$ in *tert*-butanol is estimated from the values of the other three solutes $Li^+_s + ClO^-_{4,s}$, $NH^+_{4,s} + ClO^-_{4,s}$, and $NH^+_{4,s} + NO^-_{3,s}$ (Table 2, Fig. 8). The ion pairing will be discussed in a later paper.

The values of Λ_0 are proportional to the mobilities μ_i of the ions (23):

$$[12] \qquad \Lambda = \nu_+\lambda_+ + \nu_-\lambda_-$$

where ν_+ is the number of cations and ν_- is the number of anions in a formula of the electrolyte, and

$$[13] \qquad \lambda_i = z_i\mu_i F = \frac{z_i^2 D_i F^2}{RT}$$

where λ_i is the molar conductivity of ion i, z_i is the number of charges of the ion, F is the Faraday constant, and R is the gas constant. Substitution of D_i by the Stokes–Einstein relation (23),

$$[14] \qquad D_i \approx \frac{k_B T}{6\pi\eta r_{di}}$$

where r_{di} is the effective hydrodynamic radius of the solvated ion, gives

$$[15] \qquad \lambda_i \approx \frac{z_i^2 F^2}{N_A 6\pi\eta r_{di}}$$

For the 1:1 electrolytes ($z = 1$) in the present study, the effective radius r_d for mutual diffusion of the positive and negative ions is

$$[16] \qquad r_d \approx \frac{F^2}{N_A 6\pi\eta\Lambda_0} = 8.2 \times 10^{-16}/\eta\Lambda_0$$

where $r_d^{-1} = (r_{d+}^{-1} + r_{d-}^{-1})$ (21*c*).

The values of r_d decrease as the water content of the solvent increases up to 90–97 mol%, pass through a minimum and increase somewhat toward pure water solvent (Fig. 9). The decrease of D_i on going from water to *tert*-butanol is due to the increasing viscosity of the solvent and the larger size of the molecules that solvate the ions. The reason for the apparent decrease of r_d upon addition of a few percent of alcohol to water is that the viscosity of the bulk solvent increases considerably, due to a more ordered structure of the mixed solvent (24), while the ions are selectively solvated by the water and presumably remain in lower viscosity microzones (21*c*). Use of the bulk viscosity in eq. [16] makes r_d appear to decrease.

Smoluchowski–Debye–Nernst–Einstein model

Diffusion coefficients from eq. [13] can be substituted in eq. [11]:

$$[17] \qquad k_2/f = \frac{4\pi k_B T}{\xi^2}(\lambda_e + \lambda_i/z_i^2)\kappa R_r$$

which can be rearranged to

$$[18] \qquad \kappa R_r = 1.48 \times 10^{-16} k_2/(\lambda_e + \lambda_i/z_i^2) f\, T$$

where λ_e is the molar conductivity of e^-_s. For the solutes studied in his work, $z_i = \pm 1$. In water, the diffusion of e^-_s dominates the relative motion of each pair except that with H^+_s (21*b*). The values of the individual ionic conductivities in the mixed solvents are unknown, so an approximation is

Can. J. Chem. Downloaded from www.nrcresearchpress.com by 65.111.164.53 on 09/08/12
For personal use only.

Fig. 10. Solvent composition dependence of apparent values of κR_r in *tert*-butanol/water mixtures at 298 K. Symbols are as in Fig. 5.

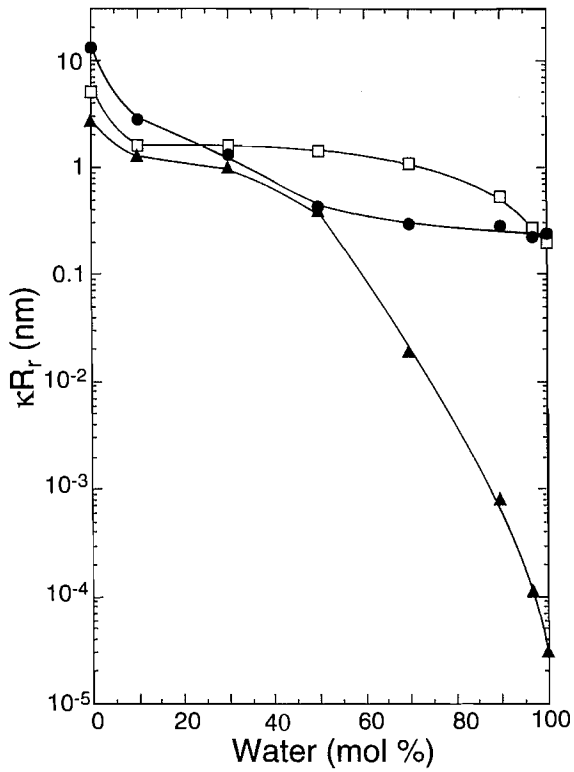

made in order to estimate κR_r from measured molar conductivities of the electrolytes. In water:

$[\lambda_e + \lambda(H_s^+)]/\Lambda_0(H_s^+, ClO_{4,s}^-) = 1.3$ (21b), so $\kappa R_r = 1.1 \times 10^{-16}\ k_2/\Lambda_0(H_s^+, ClO_{4,s}^-)fT$; $[\lambda_e + \lambda(NO_{3,s}^-)]/\Lambda_0(Li_s^+, NO_{3,s}^-) = 2.3$ (21b), so $\kappa R_r = 0.6 \times 10^{-16}\ k_2/\Lambda_0(Li_s^+, NO_{3,s}^-)fT$; $[\lambda_e + \lambda(NH_{4,s}^+)]/\Lambda_0(NH_{4,s}^+, ClO_{4,s}^-) = 1.6$ (14), so $\kappa R_r = 0.9 \times 10^{-16}\ k_2/\Lambda_0(NH_{4,s}^+, ClO_{4,s}^-)fT$. For the lack of anything better, these equations were used for all solvent compositions to estimate κR_r.

The estimated values of κR_r are plotted in Fig. 10. The curves are again different from those in Figs. 5 and 7. The value of κR_r for each solute increases continuously with increasing *tert*-butanol content. This indicates that the reactivity of e_s^- with all solutes gradually increases on going from water to *tert*-butanol solvent.

For all solutes in pure *tert*-butanol solvent the apparent values of κ are much larger than unity, in spite of the large values of R_r chosen, 2.1 nm for $NO_{3,s}^-$ and 1.6 nm for $NH_{4,s}^+$ and H_s^+. The true value of κ can not be greater than unity. The apparent values of κ for the reaction $e_s^- + H_s^+$ in 10–70 mol% water are slightly larger than 1 (Table 4), but they are within the uncertainty of the approximations. From $k_2(e_s^- + H_s^+)$ in *tert*-butanol the mobility of e_s^- in this solvent is estimated to be $\mu(e_s^-) \approx 4 \times 10^{-8}$ m^2 V^{-1} s^{-1} at 298 K, and $E_{\mu e} \approx 41$ kJ mol^{-1} (17).

E_2 and $E_{\Lambda 0}$

The solvent dependences of the Arrhenius activation energies E_2 of reaction and $E_{\Lambda 0}$ of mobility for all four solutes are

Table 4. Apparent κ values in *tert*-butanol/water mixtures at 298 K.

Water (mol%)	$\kappa(NO_{3,s}^-)$	$\kappa(NH_{4,s}^+)$	$\kappa(H_s^+)$
100	0.16	3.1×10^{-5}	0.20
97	0.15	1.1×10^{-4}	0.27
90	0.19	7.9×10^{-3}	0.53
70	0.20	0.019	1.07
50	0.27	0.37	1.45
30	0.82	0.88	1.42
10	1.4	0.95	1.24
0	6.1	1.7	3.3

Fig. 11. Solvent composition dependence of E_2 and $E_{\Lambda 0}$ in *tert*-BuOH/water mixtures. Symbols are as in Fig. 5.

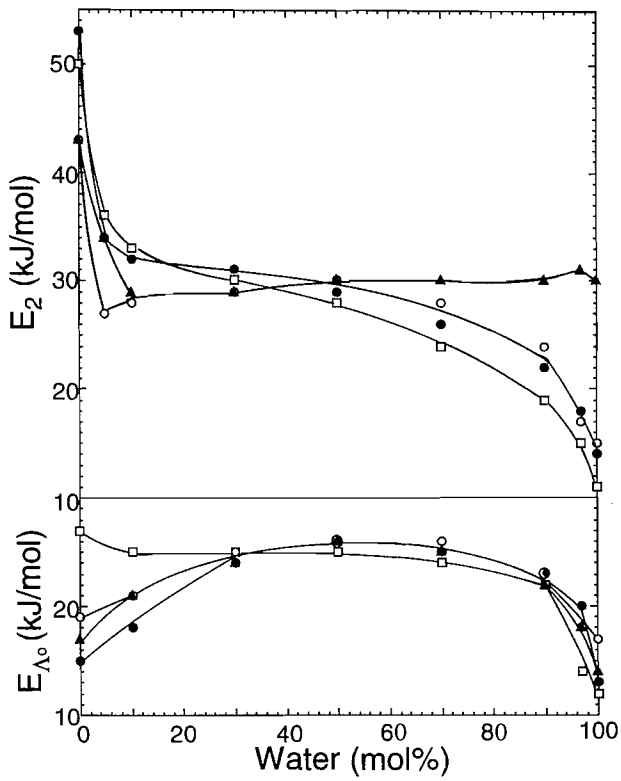

plotted in Fig. 11. The values of E_2 increase from water to alcohol, whereas $E_{\Lambda 0}$ for the salts have a maximum at 50 mol% water.

For reaction [2] to occur, the reactants e_s^- and $S^{\pm 1}$ must diffuse together

[19] $\quad e_s^- + S^{\pm 1} \rightleftharpoons [e_s^-, S^{\pm 1}] \qquad k_d, k_{-d}$

then react

[20] $\quad [e_s^-, S^{\pm 1}] \rightarrow P \qquad k_{20}$

From the steady-state approximation one obtains

$$[21] \qquad k_2 = \frac{k_d k_{20}}{k_{-d} + k_{20}}$$

If $k_{20} > k_{-d}$, then $k_2 \approx k_d$ and E_2 should be close to $E_{\Lambda 0}$. For the reactions $e_s^- + NO_{3,s}^-$ and $e_s^- + H_s^+$ in the water-rich region of 100–70 mol% of water, the reactions are not far from diffusion-controlled and E_2 and $E_{\Lambda 0}$ are similar (Tables 2 and 4). For $NH_{4,s}^+$ in 100–70 mol% of water the rate constants are low, and the values of E_2 are much higher than $E_{\Lambda 0}$.

In the alcohol-rich region from 50 to 10 mol% water, the values of E_2 do not change much, while $E_{\Lambda 0}$ decreases somewhat. In the solvents 10 to 0% water E_2 increases greatly, while $E_{\Lambda 0}$ for the salts decrease and that for $HClO_4$ remains constant. The increase of E_2 is attributed to a large temperature coefficient of diffusion of e_s^-, which reaches 41 kJ mol^{-1} in pure *tert*-butanol (17).

Acknowledgements

We thank the Natural Sciences and Engineering Research Council of Canada for financial assistance, and the personnel of the Radiation Research Center for maintaining the accelerator and electronic equipment.

References

1. H.A. Schwarz and P.S. Gill. J. Chem. Phys. **81**, 22 (1977).
2. A.M. Afanassiev, K. Okazaki, and G.R. Freeman. J. Phys. Chem. **83**, 1244 (1979).
3. Farhataziz, S. Kalachandra, and M.S. Tunuli. J. Phys. Chem. **88**, 3837 (1984).
4. A.J. Elliot, D.R. McCracken, G.V. Buxton, and N.D. Wood. J. Chem. Soc. Faraday Trans. **86**, 1539 (1990).
5. G.V. Buxton and S.R. Mackenzie. J. Chem. Soc. Faraday Trans. **88**, 2833 (1992).
6. B.H. Milosavljević and O.I. Mićić. J. Phys. Chem. **82**, 1359 (1978).
7. P.C. Senanayake and G.R. Freeman. J. Chem. Phys. **87**, 7007 (1987).
8. C.C. Lai and G.R. Freeman. J. Phys. Chem. (*a*) **94**, 302 (1990); (*b*) **94**, 4891 (1990).
9. A.K. Covington and P. Jones (*Editors*). Hydrogen-bonded solvent systems. Taylor & Francis, London. 1986. (*a*) D.N. Gloew, H.D. Mak, and N.S. Rath. p. 195; (*b*) M.C.R. Symons and M.J. Blandamer. p. 211.
10. P.C. Senanayake, N. Gee, and G.R. Freeman. Can. J. Chem. **65**, 2441 (1987).
11. P.C. Senanayake and G.R. Freeman. J. Phys. Chem. (*a*) **91**, 2123 (1987); (*b*) **92**, 5142 (1988).
12. R.M. Silverstein, G.C. Bassler, and T.C. Morrill. Spectrometric identification of organic compounds. 4th ed. Wiley, New York. 1981. p. 315.
13. R. Chen, Y. Avotinsh, and G.R. Freeman. Can. J. Chem. **72**, 1083 (1994).
14. R. Chen and G.R. Freeman. Can. J. Chem. **71**, 1303 (1993).
15. A.D. Leu, K.N. Jha, and G.R. Freeman. Can. J. Chem. **60**, 2342 (1982).
16. Y.Y. Akhadov. Dielectric properties of binary solutions. Pergamon Press, New York. 1980. p. 475.
17. Y. Zhao and G.R. Freeman. Can. J. Chem. **73**, 389 (1995).
18. P. Debye. Trans. Electrochem. Soc. **82**, 265 (1942).
19. M.S. Tunuli and Farhataziz. J. Phys. Chem. **90**, 6587 (1986).
20. J.R. Miller. J. Phys. Chem. **79**, 1070 (1975).
21. S.A. Peiris and G.R. Freeman. (*a*) Can. J. Phys. **68**, 940 (1990); (*b*) Can. J. Chem. **69**, 884 (1991); (*c*) Can. J. Chem. **69**, 157 (1991).
22. R.C. Weast (*Editor*). Handbook of chemistry and physics. 70th ed. CRC Press, Boca Raton, Fla. 1989. p. D-190.
23. W.P. Atkins. Physical chemistry. 4th ed. Freeman, New York. 1990, Chap. 25.
24. F. Franks and D.J.G. Ives. Q. Rev. (London), **20**, 1 (1966).

Can. J. Chem. Downloaded from www.nrcresearchpress.com by 65.111.164.53 on 09/08/12
For personal use only.

An NMR study of mixed, tartrate-containing Ti^{IV} complexes

Pierre G. Potvin and Benjamin G. Fieldhouse

Can. J. Chem. Downloaded from www.nrcresearchpress.com by 65.111.164.53 on 09/08/12
For personal use only.

Abstract: The reactions of amines and amino alcohols with diisopropyl or diethyl *R,R*- or *S,S*-tartrate and $Ti(O^iPr)_4$ were examined by ^1H and ^{13}C NMR to obtain and characterize nonfluxional complexes with the tartrate units in novel binding modes. The mildly acidic 8-hydroxyquinoline and *N*-phenyl-*N*-benzoylhydroxylamine selectively formed the products of a double O^iPr substitution, $Ti_2(tartrate)_2(ligand)_2(O^iPr)_2$, and the products of double tartrate substitution, $Ti(ligand)_2(O^iPr)_2$, while 2,4-pentanedione formed only the latter. Basic amino alkanols formed diastereomerically pure $Ti_2(tartrate)_2(aminoalkoxide)(O^iPr)_3$ species. *N,N*-Dimethyl-2-aminoethanol (H*dmae*) also and uniquely formed monomeric $Ti(tartrate)_2(Hdmae)_2$ species that could be described as doubly zwitterionic. Secondary or tertiary amines formed triply C_2-symmetric $Ti_3(tartrate)_4(amine)_2(O^iPr)_4$ assemblies. Some minor components were believed to be μ-O^iPr species. All mixed complexes except $Ti(tartrate)_2(Hdmae)_2$ contained chelating and bridging tartrate units, without coordination by ester carbonyls. A nonchelating, nonbridging tartrate unit was also present in the amino alcohol cases. Primary amines, aromatic amines, and hydrazines all failed to provide identifiable complexes. As well, *N,N*-dibenzylhydroxylamine failed to generate in solution the complex that had previously been characterized by X-ray crystallography. Amidst the rich chemistry of Ti^{IV}-tartrate systems, the evident selectivities in product formation were ascribed to macro-ring closures that are specifically directed by the electronic nature of the addend. Transient O^iPr-bridged intermediates were also implicated.

Key words: mixed Ti^{IV} alkoxides, chiral Ti^{IV} alkoxides, enantiospecific complexation.

Résumé : Dans le but d'obtenir et de caractériser des complexes qui ne sont pas en fluxion d'unités tartrates dans de nouveaux modes de liaison, on a étudié les réactions des amines et des aminoalcools avec les *R,R*- ou *S,S*-tartrates de diisopropyle ou de diéthyle, en présence de $Ti(O^iPr)_4$, en faisant appel à la RMN du ^1H et du ^{13}C. Les 8-hydroxyquinoléine et *N*-phényl-*N*-benzoylhydroxylamine qui sont légèrement acides forment sélectivement les produits d'une double substitution, $Ti_2(tartrate)(ligand)_2(O^iPr)_2$ et les produits d'une double substitution du tartrate, $Ti(ligand)_2(O^iPr)_2$; par ailleurs, la pentane-2,4-dione ne donne que ce dernier type de composé. Les aminoalcools basiques forment des espèces $Ti_2(tartrate)_2(aminoalcoolate)(O^iPr)_3$ qui sont diastéréomériquement pures. Le *N,N*-diméthyl-2-aminoéthanol (H*dmae*) réagit de la même manière et ne forme que l'espèce monomère $Ti(tartrate)_2(Hdmae)_2$ que l'on peut décrire comme zwitterionique. Les amines secondaires ou tertiaires forment des assemblées $Ti_3(tartrate)_4(amine)_2(O^iPr)_4$ de symétrie C_2. On croit que quelques composants mineurs sont des espèces μ-O^iPr. Tous les complexes, à l'exception du $Ti(tartrate)_2(Hdmae)_2$, contiennent des unités tartrates chélatantes servant de pont sans coordination par les groupes carbonyles des esters. Une unité tartrate non chélatante ne servant pas de pont est aussi présente dans les cas des aminoalcools. Les amines primaires, les amines aromatiques et les hydrazines n'ont donné lieu à aucun complexe identifiable. De la même manière, la *N,N*-dibenzylhydroxylamine, en solution, n'a pas donné lieu à la formation du complexe qui a été caractérisé antérieurement par cristallographie à l'aide de rayons X. Dans la riche chimie des systèmes du Ti^{IV}-tartrate, les sélectivités évidentes dans la formation de produits est attribuée à des fermetures de macrocyles qui sont dirigés spécifiquement par la nature électronique du produit additionné. Des intermédiaires transitoires comportant des ponts O^iPr sont aussi impliqués.

Mots clés : alcoolates mixtes du Ti^{IV}, alcoolates chiraux du Ti^{IV}, complexation énantiospécifique.

[Traduit par la rédaction]

Introduction

Our interest in Ti^{IV} complexes of chiral dialkoxide ligands (diolates) is rooted in the usefulness of the tartrate ester complexes in chiral catalysis (1). The motive of our work (2–5) has been to understand the origins of that success in order to develop new catalysts. While drawing upon the large base of knowledge concerning reactivity and selectivity (1), our efforts have been directed at the characterization, mainly by NMR, of the structures of the catalysts in solution, both directly and by contrast with those of numerous analogues. A set of observational criteria has evolved that allows one to distinguish between chelating and non-

Received September 30, 1994.

P.G. Potvin[1] and B.G. Fieldhouse. Department of Chemistry, York University, 4700 Keele Street, North York, ON M3J 1P3, Canada.

[1] Author to whom correspondence may be addressed. Telephone: (416) 736-2100, ext. 66140. Fax: (416) 736-5936.

Can. J. Chem. Downloaded from www.nrcresearchpress.com by 65.111.164.53 on 09/08/12
For personal use only.

chelating diolate units and to decide if the side-chain groups are coordinated (3).

The Katsuki–Sharpless catalysts (1) are fluxional because the side-chain ester groups are reversibly and weakly bound, complicating the study of their structures and their interactions with substrates. We recently undertook to examine certain mixed complexes for two reasons: Firstly, the loosely bound ester groups could be supplanted by more stably bound groups from companion ligands, permitting an easier characterization. Two existing X-ray structures (6) were to serve as controls. Secondly, acting as "proxies" for the catalytic substrates, companion ligands could provide mixed species that model the catalytic intermediates.

A rich chemistry has emerged, which this paper assembles and discusses. As well as presenting more complete details of the mixed ligand species already communicated (4, 5), many new examples and an entirely new and unique tartrate binding mode are reported for the first time. Overall, the products were formed with surprising selectivity, providing three new tartrate binding modes and evidence of transient O^{i}Pr bridges. Further insights have also been gained into reactivity, the Katsuki–Sharpless catalyst structure, and new catalyst designs.

Experimental section

General

Diisopropyl *R,R*- or *S,S*-tartrate, diethyl *R,R*-tartrate, and titanium tetraisopropoxide were freshly distilled. $CDCl_3$ was dried over $Mg(ClO_4)_2$. Unless otherwise stated, NMR spectra were obtained at 19–20°C on a Bruker AM-300 instrument operating at 300 MHz for ^1H or 75.1 MHz for ^{13}C, using pulse sequences from the Bruker library. Integration was performed digitally, at times after digital enhancement of the resolution, which was achieved by zeroing the last half of a 16-kbyte-long FID and zero-filling an additional 48 kbytes before Fourier transformation. Baseline correction was at times used to integrate AB quartets. Spectra were also obtained with simultaneous irradiation of the CH_3 region to simplify the OC*H* region and to establish the numbers and positions of OC*H* heptets. Single-frequency homo-decoupling (^1H–^1H) and hetero-decoupling (^1H–^{13}C) and 2-dimensional shift correlation experiments were used to establish connectivities. ^1H–^{13}C couplings were measured by gated decoupling. Chemical shifts are reported in ppm from TMS and coupling constants are in hertz (Hz). For AB quartets, the J_{AB} and calculated $\Delta\delta$ values are reported. Abbreviations include v for very, b for broad, h for heptet, and m for multiplet. J_{app} denotes apparent couplings. Mass spectrometry was performed by Dr. B. Khouw on a VG instrument (York) or on a ZAB-80 instrument at the McMaster Regional Centre for Mass Spectroscopy. EI experiments were conducted at 70 eV. CI experiments with NH_3 and FAB in various matrices were less informative.

Unless specifically indicated in the results section, reaction mixtures were obtained in one or more ways, depending on which reagent, if any, needed to be added last or whether the proportion of a reagent was to be varied. Solutions 37–42 mM in Ti_2*dipt*$_2$(O^{i}Pr)$_4$ were prepared in $CDCl_3$, with due care to exclude moisture, by mixing appropriate amounts of reagents in volumetric flasks. Such solutions were useful for a few days. Weighed amounts of solid addends were then added, as such or diluted in $CDCl_3$, to 0.4 mL aliquots. Liquid materials were measured by microsyringe and added neat or diluted in some $CDCl_3$. Equivalently, 0.4 mL of a 0.16 M stock $CDCl_3$ solution of H_2*dipt* or H_2*det* was treated with 18 μL of Ti(O^{i}Pr)$_4$ (1 equiv.) by microsyringe, then with successive aliquots of addends (solid or liquid). In reverse order, 18 μL of neat Ti(O^{i}Pr)$_4$ were diluted with 0.4 mL of $CDCl_3$, treated with appropriate amounts of addend as above, whence the simple binary reactions could be analyzed, and then with various aliquots of the stock tartrate solutions. Alternatively, weighed or volumetrically measured addends were diluted with the tartrate stock solution, then treated with aliquots of neat Ti(O^{i}Pr)$_4$. In some cases, additional amounts of reagents could be added later. Most reaction mixtures were reexamined after several days.

cis-*Ti*(acac)$_2$(*O^{i}Pr*)$_2$: ^1H NMR: δ 5.51 (s, 2H, *acac* C*H*), 4.78 (h, 2H, OC*H*), 2.03, 1.92 (2s, 12H, *acac* CH_3), 1.25 (bd, OCCH_3); ^{13}C NMR: δ 191.2 (*C*O), 102.6 (*acac* *C*H), 78.6 (O*C*H), 26.86, 25.86 (*acac* *C*H$_3$), 25.30 (OC*C*H$_3$).

cis-*Ti*(Oq)$_2$(*O^{i}Pr*)$_2$: ^1H NMR: δ 8.52 (d, 2H, *J* = 4.4, H-2′), 7.98 (d, 2H, *J* = 7.6, H-4′), 7.47 (dd, 2H, *J* = 8.0, 8.0, H-6′), 7.12 (dd, 2H, *J* = 4.7, 8.3, H-3′), 7.07 (d, 2H, *J* = 7.0, H-5′ or H-7′), 7.05 (d, 2H, *J* = 7.5, H-7′ or H-5′), 4.61 (h, 2H, *J* = 6.1, TiOC*H*Me$_2$), 1.13, 0.91 (2d, 12H, *J* = 6.1, TiOCHCH_3); ^{13}C NMR: δ 162.54, 141.45 (Ar *C*), 144.97, 137.48, 129.62, 121.18, 113.99, 111.09 (Ar *C*H), 78.18 (O*C*H), 25.26 (*C*H$_3$).
Ti(O bpa)$_2$(*O^{i}Pr*)$_2$: ^1H NMR: δ 7.42–7.21 (m, 10H), 4.99 (h, 2H), 1.32 (d, 12H). ^{13}C NMR: δ 163.40 (*C*=O), 140.94, 130.56, 129.19, 129.02, 128.89, 128.59, 128.17, 128.06, 127.88, 125.66 (Ph), 77.36 (O*C*H), 25.43 (*C*H$_3$).

Ti$_2$dipt$_2$(Oq)$_2$(*O^{i}Pr*)$_2$ (***1***): ^1H NMR: δ 8.52 (d, 2H, *J* = 4.4, H-2′), 8.01 (d, 2H, *J* = 8.2, H- 4′), 7.48 (t, 2H, *J* = 7.7, H-6′), 7.14 (dd, 2H, *J* = 4.5, 8.3, H-3′), 7.07 (d, 4H, *J* = 7.7, H-5′, H-7′), 5.58, 4.68 (2d, 4H, *J* = 9.3, diolate OC*H*), 5.26, 4.98 (2h, 4H, *J* = 6.0, ester OC*H*), 4.70 (h, 2H, *J* = 6.0, TiOC*H*Me$_2$), 1.57, 1.31 (2d, 24H, *J* = 6.0, 6.0, ester CH_3), 1.13, 0.92 (2d, 12H, *J* = 6.0, 6.6, TiOCH$_3$); ^{13}C NMR: δ 170.09, 169.39 (*C*=O), 147.85, 137.83, 129.39, 120.79, 116.34, 110.53 (Ar), 89.55, 84.22 (diolate O*C*H), 81.39 (TiO*C*HMe$_2$), 68.91, 68.46 (ester O*C*H), 25.06, 25.01, 24.67, 21.68, 21.61, 21.36 (*C*H$_3$).

Ti$_2$dipt$_2$(O bpa)$_2$(*O^{i}Pr*)$_3$ (***3***): ^1H NMR: δ 7.53-7.20 (m, 20H), 5.22 (ABq, 2H, *J* = 9.05, Δδ = 0.204 , diolate OC*H*), 5.16, 5.04 (2h, 4H, ester OC*H*), 4.45 (h, 2H, TiO^{i}Pr OC*H*), 1.44-0.73 (m, OCHCH_3). ^{13}C NMR: δ 171.09, 169.65 (ester *C*=O), 164.63 (hydroxamate *C*=O), 140.46, 130.53, 129.37, 128.97, 128.54, 128.07, 128.01, 127.94, 127.85, 125.61, 125.48 (Ph), 88.85 ($^1J_{HC}$ = 155.64), 84.63 ($^1J_{HC}$ = 147.51), (diolate O*C*H), 79.81 (TiO*C*HMe$_2$), 68.11, 67.50 (ester O*C*H), 25.37, 21.64, 21.58 (*C*H$_3$).

Ti$_2$dipt$_2$(Oep)(*O^{i}Pr*)$_3$ (***6***): ^1H NMR: δ 8.89 (d, 2H, *J* = 4.6, H-6′), 7.81 (m, 1H), 7.30 (m, 2H), 5.67 (d, 1H, *J* = 8.0, diolate OC*H*), 5.22 (ABq, 2H, *J* = 9.1, Δδ = 0.097, diolate OC*H*), 5.03 (d, 1H, *J* = 7.4, diolate OC*H*), 5.1–4.9, 4.85, 4.74 (m+2h, 7H, OC*H*Me$_2$), 4.48, 4.32 (AB portion of ABXY system, 1H+1H, OCH_2), 3.48, 3.13 (XY portion of ABXY system, 1H+1H, OCH$_2$CH_2), 1.20–0.99 (m, 42H, OCHCH_3). ^{13}C NMR: δ 171.55, 170.89, 170.31, 170.01 (*C*=O), 161.28, 151.40,

Can. J. Chem. Downloaded from www.nrcresearchpress.com by 65.111.164.53 on 09/08/12
For personal use only.

139.59, 125.45, 121.31 (pyridine C), 86.05, 85.96, 85.02, 84.65 (diolate OCH), 79.85, 79.68, 78.25 (TiO*C*HMe$_2$), 69.39 (O*C*H$_2$), 67.92, 67.82, 67.36 (ester OCH), 39.05 (OCH$_2$*C*H$_2$), 25.59, 25.49, 25.26, 21.65 (*C*H$_3$).

Ti(dmae)(*O*^{i}*Pr*)$_3$: ^{1}H NMR: δ 4.68 (bh, 3H, OC*H*), 4.20 (t, 2H, *J* = 5.7, OC*H*$_2$), 2.74 (t, 2H, *J* = 5.7, NC*H*$_2$), 2.44 (s, 6H, NC*H*$_3$), 1.24 (d, 24H, *J* = 5.9, CC*H*$_3$); ^{13}C NMR: δ 76.17 (O*C*H), 67.63 (O*C*H$_2$), 61.81 (N*C*H$_2$), 46.49 (N*C*H$_3$), 26.49 (C*C*H$_3$).

Ti$_2$dipt$_2$(dmae)(*O*^{i}*Pr*)$_3$ (**7**): ^{1}H NMR: δ 5.62 (d, 1H, *J* = 7.2, diolate OC*H*), 5.21 (ABq, 2H, *J* = 9.3, Δδ = 0.130, diolate OC*H*), 5.07 (d, 1H, *J* = 7.2, diolate OC*H*), 5.04, 5.02, 4.98, 4.97 (4h, 5H, OC*H*Me$_2$), 4.81, 4.80 (2h, 2H, OC*H*Me$_2$), 4.54, 4.27 (AB portion of ABXY system, 1H+1H, OC*H*$_2$), 2.93, 2.80 (XY portion of ABXY system, 1H+1H, NC*H*$_2$), 2.71, 2.67 (2s, 6H, NC*H*$_3$), 1.36–1.20 (m, 48H, OCHC*H*$_3$); ^{13}C NMR: δ 172.28, 171.02, 170.12, 169.88 (*C*=O), 85.95 ($^1J_{HC}$ = 147.5, $^2J_{HC}$ = 3.05), 85.44, 85.40, 84.22 ($^1J_{HC}$ = 152.6, $^2J_{HC}$ = 6.1) (diolate O*C*H), 79.93, 79.80, 78.45 (TiO*C*HMe$_2$), 68.56 (O*C*H$_2$), 67.94, 67.90 (ester O*C*H), 63.98 (N*C*H$_2$), 50.74, 48.77 (N*C*H$_3$), 26.09, 25.88, 25.74, 25.71, 25.64, 21.79, 21.70, 21.61, 21.59 (CH*C*H$_3$).

Ti$_2$dipt$_2$(dmap)(*O*^{i}*Pr*)$_3$ (**8**): ^{1}H NMR: δ 5.60 (d, 1H, *J* = 7.3, diolate OC*H*), 5.20 (ABq, 2H, *J* = 9.15, Δδ = 0.061, diolate OC*H*), 5.08 (d, 1H, *J* = 7.3, diolate OC*H*), 5.05, 5.02, 5.01, 4.99, 4.97 (5h, 5H, ester OC*H*, 4.80, 4.79 (2h, 2H, TiOC*H*Me$_2$), 4.76–4.68 (m, 1H, TiOC*H*CH$_3$), 2.77 (dd, 1H, *J* = 11.3, NC*H*$_2$), 2.73, 2.66 (2s, 6H, NC*H*$_3$), 2.39 (dd, 1H, *J* = 2.9, 11.3, NC*H*$_2$), 1.37–1.20 (m, 78H incl. HO^{i}Pr, CC*H*$_3$); ^{13}C NMR: δ 171.89, 170.98, 170.03 (*C*=O), 85.87 ($^1J_{HC}$ = 147.82, $^2J_{HC}$ = 3.81), 85.59 ($^1J_{HC}$ = 152.6, $^2J_{HC}$ = 2.86), 85.22 ($^1J_{HC}$ = 149.73, $^2J_{HC}$ = 4.77), 84.45 ($^1J_{HC}$ = 152.59, $^2J_{HC}$ = 5.72) (diolate O*C*H), 79.73, 79.61, 78.24 (TiO*C*HMe$_2$), 73.64 (OCHCH$_3$), 69.86 (NCH$_2$), 67.89, 67.82, 67.73, 67.69 (ester O*C*H), 51.47, 47.81 (N*C*H$_3$), 26.18, 25.83, 25.75, 25.71, 25.58, 21.68, 21.56, 20.22 (C*C*H$_3$).

Ti(dmac)(*O*^{i}*Pr*)$_3$: ^{1}H NMR: δ 4.70 (bm, 2H, TiOC*H*CH$_3$), 3.97 (bm+m, 3H, TiO^{i}Pr + HO^{i}Pr + *dmac* O*C*H), 2.62 (m, 1H, NC*H*), 2.37 (s, 6H, NC*H*$_3$), 1.94 (bs, O*H*), 1.77, 1.70 (m+m, 4H), 1.40–1.20 (m+d, 28H, C*H*$_2$, HO^{i}Pr + TiO^{i}Pr C*H*$_3$); ^{13}C NMR: δ 80.85, 76.00 (O*C*H), 72.08 (N*C*H), 41.61 (N*C*H$_3$), 35.65, 26.37, 24.53, 21.29 (*C*H$_2$, C*C*H$_3$).

Ti$_2$dipt$_2$(dmac)(*O*^{i}*Pr*)$_3$ (**9**): ^{1}H NMR: δ 5.60 (d, 1H, *J* = 7.3, diolate OC*H*), 5.19 (ABq, 2H, *J* = 9.25, Δδ = 0.082, diolate O*C*H), 5.09 (d, 1H, *J* = 7.2, diolate OC*H*), 5.02, 5.00, 4.96 (3h, 5H, OC*H*Me$_2$), 4.79 (2h, 2H, OC*H*Me$_2$), 4.20 (m, 1H, *dmap* O*C*H, 3.33 (m, 1H, *dmac* NC*H*), 2.67, 2.58 (2s, 6H, NC*H*$_3$), 2.27 (bs, 5H, OH), 1.87–1.70 (m, 8H, C*H*$_2$), 1.38–1.19 (m, 48H incl. HO^{i}Pr, CC*H*$_3$); ^{13}C NMR: δ 172.09, 171.09, 170.08, 170.05 (*C*=O), 85.91, 85.57, 85.32, 84.39 (diolate O*C*H), 80.76, 79.64, 78.17 (TiO*C*HMe$_2$, *dmac* O*C*H), 73.42 (*C*H), 67.88, 67.85, 67.74, 67.70 (ester O*C*H), .06, 41.24 (N*C*H$_3$), 26.19, 25.80, 25.72, 25.57, 24.97, 24.11, 21.78, 21.71, 21.59, 20.40 (*C*H$_2$, C*C*H$_3$).

Ti[(+)-*O*eph](*O*^{i}*Pr*)$_3$ *or* *Ti*[(−)-Oeph](*O*^{i}*Pr*)$_3$: ^{1}H NMR: δ 7.38 (d, 2H, H-2'), 7.30 (dd, 2H, H-3'), 7.24 (t, 1H, H-4'), 5.39 (d, 1H, *J* = 5.1, OC*H*Ph), 4.76 (bm, 3H, OC*H*Me$_2$), 3.27 (m, 1H, NC*H*), 2.54 (d, 3H, *J* = 6.1, NC*H*$_3$), 2.28 (m, 1H, NH), 1.25 (bd, 18H, OCHC*H*$_3$), 0.83 (d, 3H, *J* = 6.7, NCHC*H*$_3$). ^{13}C NMR: δ 142.20, 127.78, 126.78, 126.44 (Ph), 85.07 (O*C*HPh), 61.93 (N*C*H), 34.60 (NCH*C*H$_3$), 25.35 (b, OCH*C*H$_3$), 13.79 (NCH*C*H$_3$).

Ti$_2$(R,R-dipt)$_2$[(−)-Oeph](*O*^{i}*Pr*)$_3$ *and* *Ti*$_2$(S,S-dipt)$_2$[(+)-*O*eph](*O*^{i}*Pr*)$_3$ (**10**) : ^{1}H NMR: δ 7.48–7.16 (m, 5H, Ph), 5.82 (d, 1H, *J* = 4.2, PhC*H*), 5.65 (d, 1H, *J* = 8.6, diolate OC*H*), 5.31 (wide ABq, 2H, *J* = 9.4, Δδ = 0.275, diolate O*C*H), 5.10 (m, 6H, NH, OC*H*Me$_2$), 4.93 (d, 1H, *J* = 8.6, diolate OC*H*), 4.81, 4.07 (2h, 2H, OC*H*Me$_2$), 3.39 (dq, 1H, *J* = 4.0, NC*H*), 2.68 (d, 3H, *J* = 6.1, NC*H*$_3$), 1.40–1.24 (m, 39H, OCHCC*H*$_3$), 0.88 (d, 3H, *J* = 6.8, NCHC*H*$_3$), 0.80, 0.68 (2d, 6H, *J* = 6.1, OCHC*H*$_3$); ^{13}C NMR: δ 173.45, 170.44, 170.06 (*C*=O), 141.83, 127.82, 126.19, 125.90 (Ph), 86.08, 85.54, 84.78, 84.50 (diolate O*C*H), 82.30 (O*C*HPh), 80.21, 79.67, 78.40 (TiO*C*HMe$_2$), 68.42, 68.09, 67.94, 67.64 (ester O*C*HMe$_2$), 63.60 (N*C*H), 36.55 (N*C*H$_3$), 26.26, 25.98, 25.66, 24.63, 24.49, 21.80, 21.71 (OCH*C*H$_3$), 10.44 (NCH*C*H$_3$).

Ti[(+)-*O*cin](*O*^{i}*Pr*)$_3$: ^{1}H NMR (incomplete): δ 8.88 (d, 1H, H-2'), 8.10 (d, 1H, H-3'), 7.89 (d, 1H, H-8'), 7.76 (d, 1H, H-5'), 7.62, 7.48 (2 dd, 2H, H-6', H-7'), 6.38 (d, 1H, *cin* OC*H*), ~4.8 (m, 1H, C*H*=CH$_2$), 4.50 (d, 1H, CH=C*H*$_{trans}$), 3.85 (dd, 1H), 3.51 (t, 1H), 3.29 (t, 1H), 2.88–2.69 (m, 2H), 2.08 (dd, 1H), 1.68–1.44 (m), 1.08 (m); ^{13}C NMR: δ 150.14 (*C*-2'), 138.87, 130.27, 128.55, 125.81, 123.63, 119.82 (Ar *C*, *C*H=CH$_2$), 114.72 (CH=*C*H$_2$), 80.35 (*cin* O*C*H), 62.58 (N*C*H), 51.35, 50.63 (NCH$_2$), 39.91 28.64 (*C*H), 26.24, 25.17 (*C*H$_2$, *C*H$_3$).

Ti$_2$S,S-dipt$_2$[(+)-*O*cin](*O*^{i}*Pr*)$_3$ (**11**): ^{1}H NMR: δ 8.90 (d, 1H, *J* = 4.3, H-2'), 8.71 (d, 1H, *J* = 4.4, H-3'), 8.15 (d, 1H, *J* = 8.2, H-8'), 7.74 (d, 1H, *J* = 8.4, H-5'), 7.68, 7.49 (2dd, 2H, J_{app} = 7.1, 7.5, H-6', H-7'), 6.93 (d, 1H, *J* = 7.6, *cin* O*C*H), 5.79 (d, 1H, *J* = 6.48, diolate O*C*H), 5.34 (wide ABq, 2H, *J* = 9.26, Δδ = 0.276, diolate O*C*H), 5.08 (h, 4H, *J* = 6.2, ester O*C*H, 4.87, 4.82 (2h, 4H, TiOC*H*Me, C*H*=CH$_2$), 4.60 (m, 1H, NC*H*), 4.52 (d, 1H, *J* = 10.4, CH=C*H*$_{cis}$), 4.26 (d, 1H, *J* = 17.1, CH=C*H*$_{trans}$), 3.87 (m, 2H, C*H*$_2$CH$_2$), 3.04 (≈d, 2H, *J* = 8.9, NC*H*$_2$CH), 2.85 (m, 1H, NCH$_2$C*H*'), 0.20 (m, 1H, NCH$_2$C*H*), 2.12 (bs, 5H, OH), 1.90–1.60 (3m, 3H, NCH$_2$CH*H*', NCH-C*H*H', NCHCH$_2$C*H*), 1.64–1.10 (m + d (HO^{i}Pr), C*H*$_3$, NCH-CH*H*'); ^{13}C NMR: δ 172.87, 170.95, 169.96, 169.09 (*C*=O), 149.68 (*C*-2'), 148.86, 147.69 (*C*-4', *C*-8a'), 137.19, 130.33, 128.52, 125.85, 123.56, 121.23 (*C*H, *C*H=CH$_2$), 127.17 (*C*-4a'), 115.28 (CH=*C*H$_2$), 86.93, 86.26, 85.58, 85.38 (diolate O*C*H), 81.96 (*cin* O*C*H), 80.52, 80.42, 78.32 (TiO*C*HMe), 68.22, 68.17, 68.01, 67.85 (ester O*C*H), 63.92 (N*C*H), 54.45, 54.08 (NCH$_2$), 39.47, 27.61 (*C*H), 26.36, 26.25, 26.19, 25.94, 25.84, 25.67, 25.10, 21.81, 21.76, 21.64, 21.57 (*C*H$_2$, *C*H$_3$).

Ti$_2$det$_2$(dmap)(*O*^{i}*Pr*)$_3$ (**12**): ^{1}H NMR: δ 5.72 (d, 1H, *J* = 5.35, diolate OC*H*), 5.26 (ABq, 2H, *J* = 9.16, Δδ = 0.156, diolate O*C*H), 5.11 (d, 1H, *J* = 5.29, diolate OC*H*), 5.00 (h, 1H, *J* = 6.11, TiOC*H*Me$_2$), 4.83–4.72 (m, 3H, TiOC*H*Me$_2$ + OC*H*CH$_3$CH$_2$), 4.26–4.08 (m, 8H, OC*H*$_2$), (dd, 1H, *J* = 11.5, NC*H*$_2$), 2.72, 2.67 (2s, 6H, NC*H*$_3$), 2.39 (dd, 1H, *J* = 3.15, 11.6, NC*H*$_2$), 1.77 (OH), 1.36–1.12 (m, 66H incl. HO^{i}Pr,

Can. J. Chem. Downloaded from www.nrcresearchpress.com by 65.111.164.53 on 09/08/12
For personal use only.

CCH_3); ^{13}C NMR: δ 173.05, 170.56 (*C*=O), 85.80 ($^1J_{HC}$ = 145.8, $^2J_{HC}$ = 3.05), 85.13 ($^1J_{HC}$ = 150.6, $^2J_{HC}$ = 4.1), 85.06 ($^1J_{HC}$ = 151.1, $^2J_{HC}$ = 3.2), 83.92 ($^1J_{HC}$ = 153.6, $^2J_{HC}$ = 7.1) (diolate O*C*H), 79.96, 79.66, 78.63 (TiO*C*HMe$_2$), 73.66 (O*C*HCH$_3$), 69.95 (N*C*H$_2$), 60.76, 60.35, 60.26 (O*C*H$_2$), 51.59, 47.92 (N*C*H$_3$), 26.20, 25.90, 25.77, 25.73, 25.48, 25.46 (TiOCH(*C*H$_3$)$_2$), 20.28 (OCH*C*H$_3$CH$_2$), 14.15, 14.10, 13.96, 13.92 (CH$_2$*C*H$_3$).

Ti$_2$det$_2$(dmac)*(O^{i}Pr)$_3$* ***(13)***: ^1H NMR: δ 5.74 (d, 1H, *J* = 5.00, diolate O*CH*), 5.23 (ABq, 2H, *J* = 9.13, Δδ = 0.165, diolate O*C*H), 5.10 (d, 1H, *J* = 4.97, diolate O*CH*), 5.01 (h, 1H, *J* = 6.12, TiOC*H*Me$_2$, 4.79, 4.75 (2h, 2H, *J* = 7.33, TiOC*H*Me$_2$), 427–3.98 (m, 14H, O*C*H$_2$ + *dmac* O*C*H + HO^{i}Pr O*C*H), (m, 1H, *dmac* N*CH*), 2.68, 2.58 (2s, 6H, N*C*H$_3$), 2.27 (bs, 5H, OH), 1.84–1.70 (m, 8H, C*H*$_2$), 1.38–1.10 (m, 60H incl. HO^{i}Pr, C*C*H$_3$); ^{13}C NMR: δ 173.16, 172.32, 170.75, 170.48 (*C*=O), 85.76 ($^1J_{HC}$ = 145.5, $^2J_{HC}$ = 3.05), 85.02 ($^1J_{HC}$ = 150.6, $^2J_{HC}$ = 6.1), 84.96 ($^1J_{HC}$ = 151.6, $^2J_{HC}$ = 3.05), 83.78 ($^1J_{HC}$ = 153.6, $^2J_{HC}$ = 6.1) (diolate O*C*H), 80.64, 79.80, 79.58, 78.46 (TiO*C*HMe$_2$, *dmac* O*C*H), 73.44 (N*C*H), 60.71, 60.25, 60.19, 60.16 (ester O*C*H$_2$), 48.05, 41.31 (N*C*H$_3$), 34.29, 26.09, 25.31, 24.89, 21.76, (*C*H$_2$, C*C*H$_3$), 14.08, 14.01, 13.88, 13.81 (ester *C*H$_3$).

*Ti*det$_2$*(H*dmae*)*$_2$ ***(14)***: ^1H NMR: δ 11.52 (bs, 2H), 5.32 (ABq with b A portion, 4H, *J* = 8.22, Δδ = 0.248, diolate O*C*H), 5.25 (m, 2H, O*C*H$_2$), 4.51 (m, 2H, O*C*H$_2$), 4.14 (2q, O*C*H$_2$), 3.90–3.93 (bm, N*C*H$_2$), 3.39 (bm, 2H, N*C*H$_2$), 3.05, 2.81 (2d, 12H, N*C*H$_3$), 1.25 (t, 12H, CH$_2$*C*H$_3$); ^{13}C NMR: δ 172.45, 172.11 (*C*=O), 86.49 (diolate O*C*H), 68.07 (*C*H$_2$), 64.28 (N*C*H$_2$), 61.59, 60.27 (ester O*C*H$_2$), 43.93, 43.32 (N*C*H$_3$), 14.09 (CH$_2$*C*H$_3$).

Ti$_3$dipt$_4$*(NEt$_3$)$_2$(O^{i}Pr)$_4$* ***(16)***: ^1H NMR: δ 5.24 (AB q, 8H, O*CH*, *J* = 9.34, Δδ = 0.184, diolate O*CH*), 4.99 (2h, 8H, *J* = 0.32, ester O*CH*), 4.83 (h, 4H, *J* = 5.91, TiOC*H*CH$_3$), 3.28 (b, 12H, NC*H*$_2$), 1.69 (bs, 8H, OH), 1.30–1.12, 1.07 (m+t, 138H incl. HO^{i}Pr, C*H*$_3$); ^{13}C NMR: δ 171.28, 170.79 (*C*=O), 85.64 ($^1J_{HC}$ = 155.64, $^2J_{HC}$ = 6.1), 85.06 ($^1J_{HC}$ = 149.54, $^2J_{HC}$ = 5.09) (diolate O*C*H), 77.28 (TiO*C*HCH$_3$), 67.82, 67.36 (ester O*C*H), 46.18 (N*C*H$_2$), 26.00, 25.64, 21.87, 21.70, 21.65, (*C*H$_3$).

Ti$_3$dipt$_4$*(NHEt$_2$)$_2$(O^{i}Pr)$_4$* ***(17)***: ^1H NMR: δ 8.7 (vb, 2H, NH), 5.23 AB q, 8H, O*CH*, *J* = 9.06, Δδ = 0.148, diolate O*CH*), 5.00, 4.99 (2h, 8H, *J* = 6.05, ester O*CH*), 4.81 (h, 4H, *J* = 6.32, TiOC*H*CH$_3$), 3.19, 3.12 (2bm, 8H, NC*H*$_2$), 2.74 (bs, 8H, OH), 1.30–1.13 (m, 132H incl. HO^{i}Pr, C*H*$_3$). ^{13}C NMR: δ 171.62, 171.89 (*C*=O), 86.10 ($^1J_{HC}$ = 155.6, $^2J_{HC}$ = 5.09), 84.97 ($^1J_{HC}$ = 150.5, $^2J_{HC}$ = 4.07) (diolate O*C*H), 77.21 (TiO*C*HCH$_3$), 68.18, 67.73 (ester O*C*H), 41.59 (N*C*H$_2$), 26.02, 25.69, 25.29, 21.71 (*C*H$_3$), 11.28 (Et *C*H$_3$).

Ti$_3$dipt$_4$*(NH^{i}Pr$_2$)$_2$(O^{i}Pr)$_4$* ***(18)***: ^1H NMR: δ 8.4 (vb, 2H, NH), 5.23 (AB q, 8H, O*CH*, *J* = 9.07, Δδ = 0.196, diolate O*CH*), 4.99, 4.98 (2 h, 8H, ester O*CH*), 4.83 (h, 4H, TiOC*H*CH$_3$), 2.80 (h, 4H, N*CH*), 1.30–1.12, 1.06 (m+d, 144H incl. HO^{i}Pr, C*H*$_3$) m; ^{13}C NMR: δ 171.28, 170.94 (*C*=O), 85.80 ($^1J_{HC}$ = 155.6, $^2J_{HC}$ = 6.1), 85.04 ($^1J_{HC}$ = 150.5, $^2J_{HC}$ = 6.1) (diolate O*C*H), 77.21 (TiO*C*HCH$_3$), 68.05, 67.66 (ester O*C*H), 45.28 (N*C*H), 26.04, 25.68, 23.23, 21.89, 21.74 (*C*H$_3$).

Ti$_3$det$_4$*(NEt$_3$)$_2$(O^{i}Pr)$_4$* (**20**): ^1H NMR: δ 5.28 (AB q, 8H, O*CH*, *J* = 9.33, Δδ = 0.092, diolate O*CH*), 4.75 (h, 4H, *J* = 6.05, TiOC*H*CH$_3$), 4.31–3.99 (m. 24H, O*C*H$_2$, HO^{i}Pr O*C*H), 3.28 (b, 12H, NC*H*$_2$), 1.73 (b, 8H, OH), 1.35–1.21 (m, 114H incl. HO^{i}Pr, C*H*$_3$); ^{13}C NMR: δ 171.70, 171.40 (*C*=O), 85.52 ($^1J_{HC}$ = 154.4, $^2J_{HC}$ = 6.1), 84.60 ($^1J_{HC}$ = 148.5, $^2J_{HC}$ = 3.1) (diolate O*C*H), 77.26 (TiO*C*HCH$_3$), 60.37, 59.90 (ester O*C*H$_2$), 45.72 (N*C*H$_2$), 25.91, 25.55, (O^{i}Pr *C*H$_3$), 14.09, 14.01 (Et *C*H$_3$).

Ti$_3$det$_4$*(NHEt$_2$)$_2$(O^{i}Pr)$_4$* ***(21)***: ^1H NMR: δ 8.74 (vb, 2H, NH), 5.27 (AB q, 8H, O*CH*, *J* = 8.25, Δδ = 0.087, diolate O*CH*), 4.74 (h, 4H, *J* = 6.32, TiOC*H*CH$_3$), 4.29–4.01 (m, 24H, ester O*C*H$_2$, HO^{i}Pr O*C*H), 3.19, 3.12 (2m, 8H, N*CH*), 1.74(bs, 8H, OH), 1.37–1.12 (m, 108H incl. HO^{i}Pr, C*H*$_3$); ^{13}C NMR: δ 172.00, 171.79 (*C*=O), 85.82 ($^1J_{HC}$ = 154.6, $^2J_{HC}$ = 6.1), 84.55 ($^1J_{HC}$ = 148.5, $^2J_{HC}$ = 3.06, diolate O*CH*), 77.29 (TiO*C*HCH$_3$), 60.59, 60.07 (ester O*C*H$_2$), 41.45 (N*C*H$_2$), 25.90, 25.57, 25.27 (*C*H$_3$), 14.08, 14.02 (OEt *C*H$_3$), 10.94 (NEt *C*H$_3$).

Ti$_3$det$_4$*(NH^{i}Pr$_2$)$_2$(O^{i}Pr)$_4$* ***(22)***: ^1H NMR: δ 8.4 (vb, 2H, NH), 8.26 (AB q, 8H, O*CH*, *J* = 8.79, Δδ = 0.106, diolate O*CH*), 4.73 (h, 4H, TiOC*H*CH$_3$), 4.32–4.01 (m, 24H, ester O*C*H$_2$, HO^{i}Pr O*C*H), 3.38 (b, 4H, N*CH*), 1.90 (bs, 8H, OH), 1.43–1.12 (m, 120H incl. HO^{i}Pr, C*H*$_3$); ^{13}C NMR: δ 171.70, 170.48 (*C*=O), 85.54, 84.46 (diolate O*C*H), 77.32 (TiO*C*HCH$_3$), 60.45, 59.97 (ester O*C*H$_2$), 47.33 (N*C*H), 25.91, 25.55, 25.27, 20.08, 19.38 (*C*H$_3$), 14.09, 14.03 (Et *C*H$_3$).

Ti$_3$det$_4$*(Me$_4$*en*)$_2$(O^{i}Pr)$_4$* ***(23)***: ^1H NMR: δ 5.28 (AB q, 8H, O*CH*, *J* = 9.08, Δδ = 0.072, diolate O*CH*), 4.74 (h, 4H, *J* = 6.05, TiOC*H*CH$_3$), 4.32–3.89 (m, 24H, ester O*C*H$_2$, HO^{i}Pr O*C*H), 2.70 (vbm, 8H, NC*H*$_2$), 2.48 (vb, 24H, N*CH*) 1.36–1.12 (m, 96H incl. HO^{i}Pr, C*H*$_3$); ^{13}C NMR: δ 171.68, 171.35 (*C*=O), 85.57, 84.53 (diolate O*C*H), 77.36 (TiO*C*HCH$_3$), 60.48, 59.97 (ester O*C*H$_2$), 45.20 (N*C*H$_2$), 25.90, 25.57, 25.28 (*C*H$_3$), 14.09, 14.03 (OEt *C*H$_3$), 30.83 (N*C*H$_3$).

Results

The reactions reported here were essentially instantaneous. The products were often many. They often participated in equilibria and were all, to various degrees, sensitive to moisture. Our experimental approach has therefore been to analyze reaction mixtures in situ by NMR, with corroboration by mass spectrometry whenever possible. (Only EI experiments with relatively stable molecules of moderate size have ever been fruitful.) Aside from assisting the elucidation of product structures, this approach has allowed us to rapidly examine a large number of reaction mixtures, to vary the reactant ratios and the order of mixing at will, to quantitate the product ratios, to detect minor products and transesterification, to assess ligand exchange reactivity, to monitor equilibria, and to look for longer-term changes in product composition.

8-Hydroxyquinoline

With 0.5 equivalent of Ti(O^{i}Pr)$_4$, 8-hydroxyquinoline (HO*q*) produced the bright yellow Ti(O*q*)$_2$(O^{i}Pr)$_2$ according to eq. [1]. As with Ti(*acac*)$_2$(O^{i}Pr)$_2$ (7), diastereotopic pairs of C*H*$_3$ signals in the ^1H NMR spectra confirmed the *cis* geometry in

Fig. 1. Aromatic and OC*H* regions of the ^{1}H NMR spectrum of a 3:3:4 mixture of $Ti(O^iPr)_4$, H_2*dipt*, and HO*q* in $CDCl_3$. Unmarked peaks are assigned to complex **1**. The OC*H* and O*H* signals from unreacted H_2*dipt* are coupled.

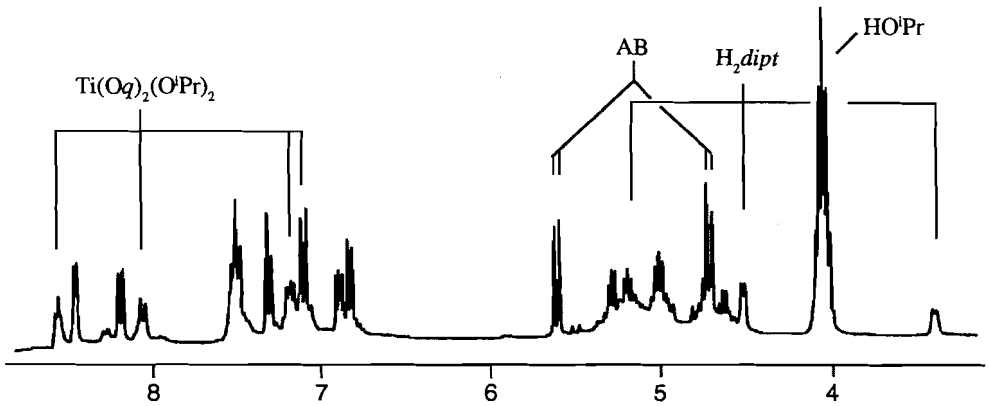

$Ti(Oq)_2(O^iPr)_2$ (8). At 1:1 reaction ratios, the same products were produced but with half of the $Ti(O^iPr)_4$ left unreacted. As was surmised in regard to the reaction of 2,4-pentanedione (H*acac*) (9), the first equivalent of HO*q* reacted more slowly with tetracoordinate $Ti(O^iPr)_4$ than did the second equivalent with the putative pentacoordinate intermediate. As would be expected of hexacoordinate complexes, both $Ti(Oq)_2(O^iPr)_2$ and $Ti(acac)_2(O^iPr)_2$ were completely inert toward additional amounts of either reactant and toward diisopropyl *R,R*-tartrate (H_2*dipt*).

[1] $Ti(O^iPr)_4 + 2\ HOq \rightarrow [Ti(Oq)(O^iPr)_3 + HOq + HO^iPr]$

$\rightarrow Ti(Oq)_2(O^iPr)_2 + 2\ HO^iPr$

The reverse reaction, i.e., using preformed $Ti_2dipt_2(O^iPr)_4$, was more fruitful. With H*acac*, the tendency to form $Ti(acac)_2(O^iPr)_2$ was so pronounced that no well-defined mixed complex could be detected. With HO*q*, the results of numerous experiments led to eq. [2].

[2] $3\ Ti_2dipt_2(O^iPr)_4 + 8\ HOq \rightarrow 2\ Ti_2dipt_2(Oq)_2(O^iPr)_2$

$+ 2\ Ti(Oq)_2(O^iPr)_2 + 2\ H_2dipt + 4\ HO^iPr$

All reactions produced both $Ti(Oq)_2(O^iPr)_2$ and a new product, $Ti_2dipt_2(Oq)_2(O^iPr)_2$, whose structural assignment is detailed below. With ≤4/3 equivalents of HO*q* present per Ti, they were formed in about equal amounts with the liberation of an equal amount of H_2*dipt*, according to integration ratios in the ^{1}H NMR spectra. With >4/3 equivalents, free HO*q* was also present and relatively more $Ti(Oq)_2(O^iPr)_2$ was produced. With < 4/3 equivalents, there was unused $Ti_2dipt_2(O^iPr)_4$, which was indirectly detected: it reacted with the liberated H_2*dipt* to give an ill-defined, fluxional but reproducible, mixture of products, with recognizable NMR signal patterns, that we call "tartrate-excessive material" for convenience. This mixture arises whenever H_2*dipt* and $Ti(O^iPr)_4$ are mixed in >1:1 ratios. As with that mixture, samples with <4/3 HO*q* equivalents per Ti were also more sensitive to hydrolysis by adventitious H_2O than were samples with ≥4/3 equivalents, confirming the presence of the moisture-sensitive $Ti_2dipt_2(O^iPr)_4$. (Such hydrolysis produces white flocculent Ti-containing solids and free H_2*dipt*. $Ti_2dipt_2(Oq)_2(O^iPr)_2$ was more resistant but, over a few days, gave way to the more robust $Ti(Oq)_2(O^iPr)_2$. This too later partially decomposed, probably to μ-oxo dimeric species (10)). Samples with exactly 4/3 equivalents of HO*q* per Ti had neither free HO*q* nor unreacted $Ti_2dipt_2(O^iPr)_4$ (Fig. 1).

Given that some H_2*dipt* was liberated, one could attempt to preclude it by increasing the Ti:H_2*dipt* ratio. Unfortunately, mixtures of $Ti_2dipt_2(O^iPr)_4$ and $Ti(O^iPr)_4$ form $Ti_2dipt(O^iPr)_6$ only partially (2). Without a complete conversion, a subsequent reaction with HO*q* will be more complicated as all three species can react separately with HO*q*. Indeed, a 3:2:4 mixture, from $Ti_2dipt_2(O^iPr)_4$ + $Ti(O^iPr)_4$ + 4 HO_q, and all other mixtures with <1 equivalent of H_2*dipt* per Ti, produced more $Ti(Oq)_2(O^iPr)_2$, less $Ti_2dipt_2(Oq)_2(O^iPr)_2$, and more of the tartrate-excessive material.

The new product was evidently unreactive toward H_2*dipt*, HO*q*, or HO^{i}Pr, as was true of $Ti(Oq)_2(O^iPr)_2$. This inertness, along with its sharp NMR signals, suggested hexacoordination. The NMR spectra indicated a single, new type of tartrate moiety because of an AX pattern ($\Delta\delta = 0.90$, $J = 9.3$) that correlated to well separated O*C*H peaks ($\Delta\delta = 5.33$) in the ^{13}C NMR spectra. This contrasted with the singlets produced by the fluxional $Ti_2dipt_2(O^iPr)_4$ (2) but resembled the AX system (J_{AX} = 8.3) produced by $[Cp_2Zrdipt]_2$ at 233 K (11). There were two distinct ester O*C*H heptets with a corresponding pair of O*C*H peaks and two *C*=O peaks, but both of these lay near the position of the *C*=O signal from free H_2*dipt*. This contrasted with the widely separated ester signals produced by $Ti_2(tartrate)_2(O^tBu)_4$ (5, 12), $Ti_2dipt_2(O^iPr)_4$, and $Ti_2dipt(O^iPr)_6$ (2) that were attributed to the presence of one Ti-bound side chain with downfield-shifted signals, and one that remained free with relatively stationary signals. Clearly, the *dipt* unit in the new product was asymmetrically and rigidly bound but neither of its ester carbonyls was coordinating, as in the Zr complex. Also present were one new TiO^{i}Pr O*C*H heptet, the corresponding O*C*H peak, and one new set of quinoline resonances. Signal integration matched a 1:1:1 ratio of these new quinoline, tartrate, and TiO^{i}Pr moieties.

These observations were consistent with a C_2-symmetric dimer of $Ti(dipt)(Oq)(O^iPr)$, with a Ti_2O_2 core, hexacoordination, rigidity, and inertness. Structure **1** was drawn by analogy with crystalline **2** (6) and because tartrate units are prone to bridge (6, 13). The orientation of the O*q* units drawn in **1**

Can. J. Chem. Downloaded from www.nrcresearchpress.com by 65.111.164.53 on 09/08/12
For personal use only.

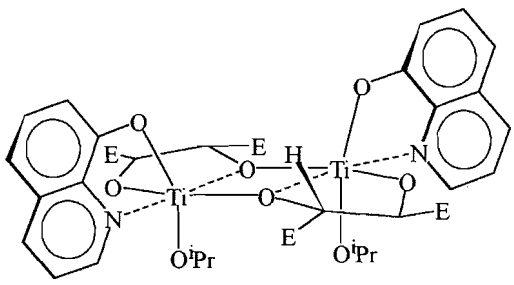

1 E = COO^iPr

was suggested by other observations: one tartrate OC*H* signal was, according to experience, unusually upfield in the ^1H NMR spectrum, at 4.68 ppm *vs.* 5.11 ppm for $Ti_2dipt_2(O^iPr)_4$, and the TiO*C*HMe_2 signal was downfield by ≈3 ppm from its more usual position near 78 ppm in the ^{13}C NMR spectrum. Accordingly, **1** places the TiO^iPr group in a deshielding region of the aromatic moiety while the bridging OC*H* finds itself in the shielding region of the O*q* attached to the other metal.

N-Benzoyl-*N*-phenylhydroxylamine

To verify that the solid-state structure reported for **2** (6) could be reproduced in solution, analogous reactions with the hydroxamic acid *N*-benzoyl-*N*-phenylhydroxylamine (HO*bpa*) were undertaken. With $Ti(O^iPr)_4$ alone, HO*bpa* had a lesser tendency to form the 2:1 complex than did HO*q* or H*acac* and a 1:1 reactant ratio produced a *ca.* 3:1 mixture of $Ti(Obpa)_2(O^iPr)_2$ and $Ti(Obpa)(O^iPr)_3$ according to eq. [3]. This left some unreacted $Ti(O^iPr)_4$.

[3] $7\ Ti(O^iPr)_4 + 7\ HObpa \rightarrow 3\ Ti(Obpa)_2(O^iPr)_2 + Ti(Obpa)(O^iPr)_3 + 3\ Ti(O^iPr)_4$

$Ti(Obpa)_2(O^iPr)_2$ was readily identified. More of it was produced when less $Ti(O^iPr)_4$ or more HO*bpa* was initially present and it was inert toward added HO*bpa* or H_2dipt. In contrast, $Ti(Obpa)(O^iPr)_3$ was reactive. It gave rise to very broad TiO^iPr and HO^iPr OC*H* signals due to rapid alcohol–alkoxide exchanges, a behaviour ascribable to pentacoordination. A second equivalent of HO*bpa* per Ti converted the $Ti(Obpa)(O^iPr)_3$ and the free $Ti(O^iPr)_4$ to $Ti(Obpa)_2(O^iPr)_2$. However, the treatment with H_2dipt was complicated by the presence of the large amount of free $Ti(O^iPr)_4$.

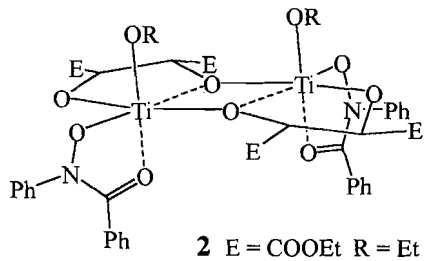

2 E = COOEt R = Et
3 E = COO^iPr R = ^{i}Pr
4 E = COOEt R = ^{i}Pr

A clearer picture emerged when preformed $Ti_2dipt_2(O^iPr)_4$ was treated with HO*bpa*. In analogy with the HO*q* case, a new product arose that was assigned the formula $Ti_2dipt_2(Obpa)_2(O^iPr)_2$. This was accompanied by $Ti(Obpa)_2(O^iPr)_2$ and some free H_2dipt but, at a starting Ti:HO*bpa* ratio of 1:1, the ratio of $Ti_2dipt_2(Obpa)_2(O^iPr)_2$ to $Ti(Obpa)_2(O^iPr)_2$ was about 3:1. The reaction was approximately described by eq. [4], with the quantitation being complicated by several overlaps in the ^1H NMR spectra and the presence of the aforementioned tartrate-excessive material, which resulted from the H_2dipt and $Ti(O^iPr)_4$ side-products. Equation [4] suggests that a 7:8 Ti:HO*bpa* ratio should avoid the liberation of $Ti(O^iPr)_4$. This was not entirely successful as the rate of mixing and dissolution of the solid HO*bpa* probably influenced the exact outcome.

[4] $4\ Ti_2dipt_2(O^iPr)_4 + 8\ HObpa \rightarrow 3\ Ti_2dipt_2(Obpa)_2(O^iPr)_2 + Ti(Obpa)_2(O^iPr)_2 + 2\ H_2dipt + Ti(O^iPr)_4 + 4\ HO^iPr$

The NMR signals were similar to those of $Ti_2dipt_2(Oq)_2(O^iPr)_2$ and included a wide AB system ($\Delta\delta$ = 0.204, J = 9.05) from the single tartrate unit. Overall, the spectra were entirely consistent with **3**, the isopropoxy analogue of **2** (6), and provided the first link between solution-state and solid-state structures.

An attempt was made to cleanly produce the 2:2:2 complex and to clarify the OC*H* region by adding $Ti(O^iPr)_4$ to a 1:1 mixture of H_2det and (dissolved) HO*bpa*. This was not completely successful as much alkoxy scrambling (OEt ↔ O^iPr) took place through transesterification and subsequent alcohol–alkoxide exchange. The mixed complex could not be fully characterized but a new AB system (J_{AB} = 8.8), consistent with structure **4**, was readily discerned.

N,N-Dibenzylhydroxylamine

This ligand was of interest because of the reported crystal structure **5** (6) and because it is a stable analogue of ^{t}BuOOH,

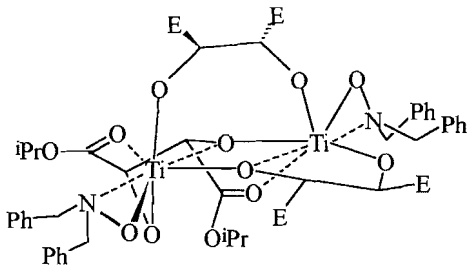

5 E = COO^iPr

the oxidant used in the Katsuki–Sharpless asymmetric epoxidation (1). However, only complex spectra with broad signals resulted from the addition of *N,N*-dibenzylhydroxylamine ($HONBn_2$) to preformed $Ti_2dipt_2(O^iPr)_4$. A 2:3:2 Ti:H_2 *dipt*:$HONBn_2$ mixture was somewhat cleaner, showing two AB quartets (J = 13.2 and 14.9) due to benzylic methylenes, but the tartrate signals were all broad and much free H_2dipt was still present. The ^{13}C NMR spectrum was not very informative: pairs of CH_2 peaks due to Ti-bound $ONBn_2$ were found, but the Ti-bound tartrate signals were broad and weak and resembled those in the parent $Ti_2dipt_2(O^iPr)_4$ (2). These disappointing reactions served to remind us that crystalline samples are not necessarily representative of reaction mixtures.

Can. J. Chem. Downloaded from www.nrcresearchpress.com by 65.111.164.53 on 09/08/12
For personal use only.

Can. J. Chem. Downloaded from www.nrcresearchpress.com by 65.111.164.53 on 09/08/12
For personal use only.

Alkanolamines

In a previous communication (4), it was reported that alkanolamines (denoted generically as H*AA*) formed single diastereomers of $Ti_2dipt_2(AA)(O^iPr)_3$ complexes. These were obtained by treatment of the preformed $Ti_2dipt_2(O^iPr)_4$ with 0.5 equivalent per Ti of an achiral or a homochiral H*AA* or with 1 equivalent of a racemic H*AA*, in which case one H*AA* enantiomer remained unreacted. They were also produced by treatment of the preformed $Ti(AA)(O^iPr)_3$ complexes with H_2dipt, in which case half or one antipode of the H*AA* was liberated. Thus, compounds **6** and **7** were from the achiral 2-(2-hydroxyethyl)pyridine (HO*epy*) and *N,N*-dimethyl-2-aminoethanol (H*dmae*), respectively, while the racemic *N,N*-dimethyl-1-amino-2-propanol (H*dmap*) and *N,N*-dimethyl-*trans*-2-aminocyclohexanol (H*dmac*) provided **8** and **9**, respectively, as

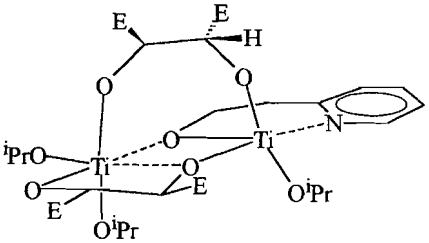

6 E = COO^iPr

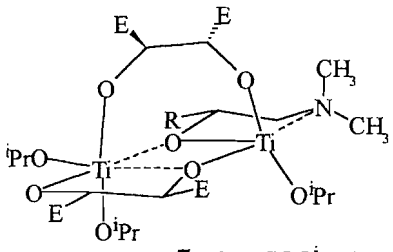

7 E = COO^iPr R = H
8 E = COO^iPr R = CH_3
12 E = COOEt R = CH_3

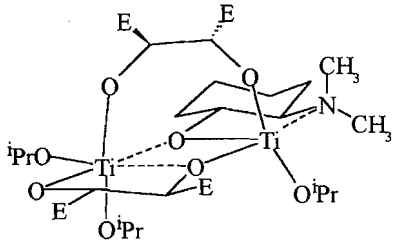

9 E = COO^iPr
13 E = COOEt

single diastereomers. As evidence of the enantiospecificity, free *S,S*-H*dmac* was separated from the reaction of *rac* material by size-exclusion chromatography (4). Further, (−)-(1*R*,2*S*)-ephedrine [(−)-H*eph*] similarly formed **10** but (+)-(1*S*,2*R*)-ephedrine [(+)-H*eph*] gave only complex, undecipherable spectra. Instead, (+)-H*eph* reacted with $Ti_2(S,S\text{-}dipt)_2(O^iPr)_4$ to afford *ent*-**10**.

Mass spectroscopy of the H*dmac* mixture showed peaks

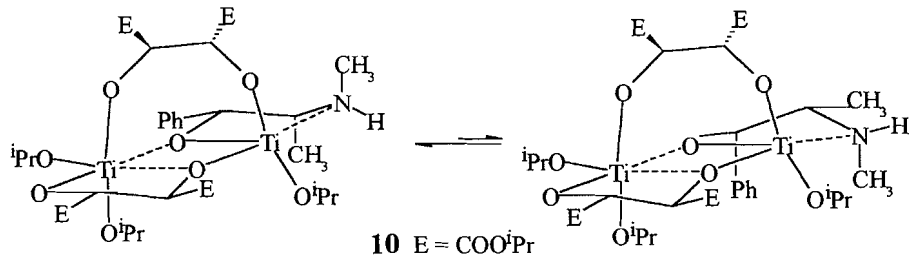

10 E = COO^iPr

attributable to **9** and to $Ti_2dipt_2(R,R\text{-}dmac)(S,S\text{-}dmac)(O^iPr)_2$ (4). As there was no sign of the latter product in solution, a substitution of O^iPr by the free *S,S*-H*dmac* must have occurred during evaporation of the sample on the EI probe. This also occurred during an attempted isolation of the 2:2:1 species. The stoichiometry has since been confirmed by mass spectrometry of a sample of $Ti_2dipt_2(dmae)(O^iPr)_3$ (*m/z* 826) generated without excess H*dmae*.

Reference 4 presents a sample ^1H NMR spectrum. In all cases, the patterns were as follows. Two equally intense sets of skeletal OC*H* and O*CH* signals indicated two distinct *dipt* units. There was no sign of ester carbonyl coordination and, given the stoichiometry of reaction, this implied that one metal was pentacoordinate. One tartrate unit resembled those in **1** and **3**, producing an AB quartet with J_{AB} consistently in the 9.1–9.4 Hz range, and modest chemical shift differences between O*CH* peaks. These signals were therefore assigned to the rigid, chelating, and bridging *dipt* units depicted in **6–10**. The second set of signals was an AX system with more variability in J_{AX} (7.2–8.6 Hz). This set was therefore assigned to a relatively flexible *dipt* that lacked the chelation feature. The A doublet was unusually far downfield, near 5.6 ppm. This was attributed to the OC*H* attached to the pentacoordinate Ti (explicitly drawn in **6**) suffering a deshielding by the nearby ester carbonyl on the other, chelating, tartrate unit. Pentacoordination was manifested as broadened signals for HO^iPr and any unreacted or liberated H*AA*, as was the case with the $Ti(dmae)(O^iPr)_3$ and $Ti(dmap)(O^iPr)_3$, which were known to be monomeric and therefore pentacoordinate (14), and with $Ti(Oeph)(O^iPr)_3$, which is also monomeric according to mass spectrometry. The bridging by the amino alkoxide oxygens depicted in **6–10** is reasonable given that those oxygens are more basic than those in the tartrate and less hindered than in O^iPr. Such bridges would spatially fix the carbinol centres and allow for enantiospecific complexation.

The ephedrine case had some peculiarities. Firstly, one $TiOCH(CH_3)_2$ heptet was unusually upfield, nearly overlapping that of HO^iPr, and was coupled to two far upfield CH_3

Can. J. Chem. Downloaded from www.nrcresearchpress.com by 65.111.164.53 on 09/08/12
For personal use only.

doublets. Shielding by the phenyl group might be responsible. Secondly, minor peaks (visible most clearly in the aromatic region and at the benzylic position) suggested the coexistence of the conformational isomer depicted, probably arising in relief of steric interactions involving the *N*-CH_3, which, in turn, would attempt to avoid 1,2-interactions with the *C*-CH_3.

These 2:2:1 mixed complexes were invoked to explain the oxidative resolution of *N,N*-1-trisubstituted H*AA* reported by Miyano et al. (15), whereby the complexation, and not the oxidation, is enantioselective. It was also proposed that the absolute stereochemistry of a homochiral H*AA* could be assigned according to which tartrate antipode will give rise to the characteristic NMR patterns (4). To illustrate the operational simplicity and the generality of the method, even with a complex H*AA*, consider the case of (+)-cinchonine (H*cin*), whose absolute stereochemistry leads one to expect a well-defined mixed complex only with *S,S*-tartrate. A small sample (17.8 mg) of the sparingly soluble free base was suspended in $CDCl_3$ and treated with 2 equivalents of $Ti(O^iPr)_4$ in $CDCl_3$ solution, whereupon it dissolved with shaking and formed the 1:1 complex, leaving half the $Ti(O^iPr)_4$ unreacted. Half of that solution was transferred to a fresh NMR tube and each tube was treated with one or the other antipode of H_2*dipt* in $CDCl_3$ solutions such that each tube had a 2:2:1 Ti:*dipt*:*AA* ratio. The tube with *R,R-dipt* displayed a complicated, undecipherable spectrum of broad signals, while that with *S,S-dipt* showed a clean spectrum of a single species (**11**) with the characteristic patterns. Thus, without special precautions with regard to atmospheric moisture, the prediction was quickly borne out. Even smaller samples could have been used with dilute solutions of the reagents. Small excesses of either reagent are tolerated and the amino alcohols are, in principle, recoverable.

The spectra of the H*cin* complexes were fairly easy to analyse because of the shifts induced by complexation. Each of the quinoline resonances, the olefinic and carbinol OC*H* signals were readily found. After the first reaction with $Ti(O^iPr)_4$, the OC*H* signal shifted downfield and the olefinic signals shifted upfield, presumably owing to the influence of the *syn* quinoline portion brought into proximity by chelation. This situation persisted after the addition of the tartrate, confirming that the cinchonine remained chelated. Several aliphatic multiplets were also shifted downfield. Unlike the H*eph* case, however, which is also a *cis* substituted amino alcohol, no isomerism was found in this case, probably due to a lack of flexibility at the amino end.

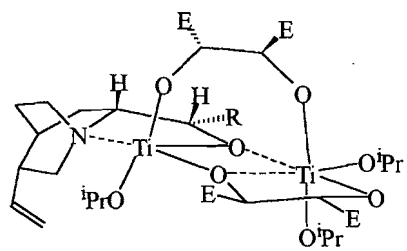

11 E = COO^iPr R = 4-quinolinyl

We now report that diethyl *R,R*-tartrate (H_2*det*) formed analogous mixed complexes **12** and **13** in reactions with $Ti(O^iPr)_4$ *without transesterification*. This confirms the absence of carbonyl coordination. By adding the H_2*det* or the $Ti(O^iPr)_4$ last, to avoid transesterification, a 2:2:2 H_2*det*:Ti$(O^iPr)_4$:H*dmap* mixture afforded a clear spectrum fitting structure **12**, in which the ester OCH_2 signals were well removed from the OC*H* region. The same occurred with H*dmac* to give **13**, but not with H*dmae* (*vide infra*). With **12** and **13**, the AB quartets had a large J_{AB} as before (9.1 and 9.2 Hz), but the AX system exhibited smaller J_{AX} values (5.0 and 5.3 Hz) than with **8** or **9**. This provided further support for the assignment of this AX system to a more flexible, nonchelated, and nonbridging tartrate unit.

The special case of 2-*N,N*-dimethylaminoethanol

When a sample of **7** had been allowed to stand for 4 days, signals from a new species emerged. The unusual appearance and positions of these signals promised an interesting origin. These same new signals also arose as a minor contaminant of **7** when H*dmae* had been added immediately after mixing H_2*dipt* with $Ti(O^iPr)_4$. The possibility of a transesterification involving H*dmae* could be ruled out since the mixing time was short and because there was no spectral evidence of that exchange. The new species could be prepared directly by adding $Ti(O^iPr)_4$ to mixtures of H_2*det* or H_2*dipt* and H*dmae*. Depending on the reactant ratio used, this was at times accompanied by various amounts of **7** and (or) free H*dmae* and (or) free tartrate. The reactions with H_2*det* were cleanest and their ^1H NMR spectra had a relatively uncluttered OC*H* region that allowed more complete signal assignments (see Fig. 2).

Most notable were new, downfield-shifted NCH_3 (diastereotopic) pairs of peaks but there were also a pair of upfield-shifted NCH_3 peaks, a broad signal at 11.5–12 ppm, likely due to an exchangeable H, and a new AB quartet in which the (downfield) A portion was significantly broader than the B portion. The latter suggested a chelating tartrate unit but with weaker coupling than in the previously described cases (J_{AB} = 8.22 with H_2*det*, 8.80 with H_2*dipt*). There was only one new tartrate OCH peak, but the ester *C*=O and OCH_2 peaks were paired. Their positions and the absence of transesterification suggested that neither carbonyl was coordinated. There were no new TiO^iPr signals at all and, therefore, no new TiO^iPr groups. New pairs of OCH_2 and NCH_2 multiplets were also found. Irradiation of the broad 11.5–12 ppm signal produced a collapse of both NCH_3 pairs into two singlets and a simplification of at least one NCH_2 multiplet (the other overlapped the HO^iPr heptet). This suggested the presence of *protonated amino groups*, where the N*H* (at very low field) was coupled to NCH_2 and to both kinds of NCH_3. The downfield positions of the OCH_2 multiplets clearly indicated that the *dmae* units were attached to the metal but the upfield positions of the NCH_3 peaks indicated that the N was not. Integration revealed a 1:1 *det*:*dmae* ratio in the new product, but the Ti content could only be estimated at <1 equivalent by examining several reaction stoichiometries. From the generic formula Ti_x-det_y(H*dmae*)$_y$, the equation $4x-2y = 0$ leads to $x = y/2$. With bidentate *det* and monodentate *dmae*, even the simplest formula (x = 1 and y = 2) affords hexacoordination.

To fit the available information, the two new species were drawn as **14** and **15**. They could be described as doubly zwitterionic and H-bonded. The H-bonding depicted would maintain diastereotopic NCH_3 groups and account for the broadness of both the N*H* and the downfield tartrate OC*H* signals. (The irradiation of the low-field N*H* did not sharpen the

Fig. 2. OC*H* region of the ^{1}H NMR spectrum of a 1:2:2 mixture of Ti(O^{i}Pr)$_4$, H$_2$*det*, and H*dmae* in $CDCl_3$, assigned to complex **14**.

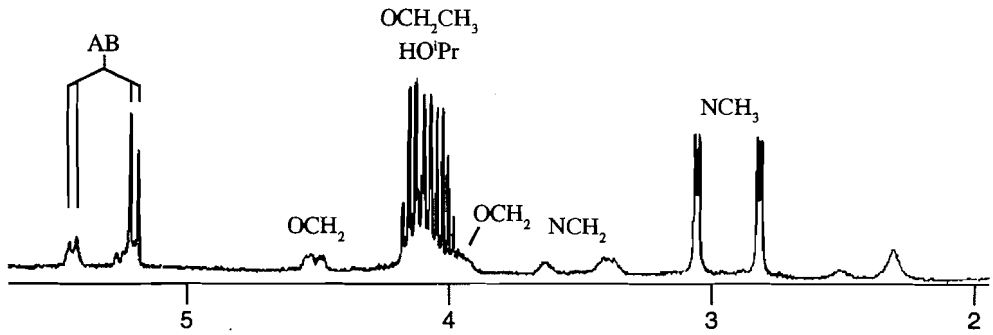

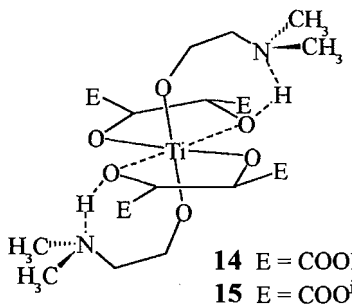

14 E = COOEt
15 E = COO^{i}Pr

downfield (A) portion of the tartrate AB system.) Severe broadening would also account for the visible presence of only one tartrate skeletal OC*H* peak. These are the first instances of well-defined species bearing two tartrate units per Ti. The basicity at N and the absence of strong steric repulsions were key, as neither H*epy*, which was probably insufficiently basic, nor H*dmap*, which was probably too bulky, showed any trace of analogous species.

Simple amines

The reactions with simple amines were initially explored in anticipation that they would form either analogues of the amino alcohol complexes with a novel, bridging O^{i}Pr group (**A**) or analogues of the HO*q* and HO*bpa* complexes (**B**). Analogues of **14** and **15** were also possible.

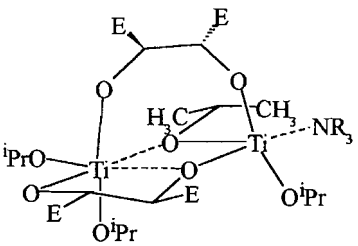

A

E = COO^{i}Pr or COOEt

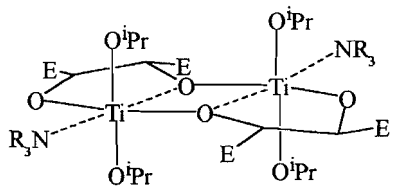

B

As communicated earlier (5), NEt_3 and NH^iPr_2 were found to instead produce the 3:4:2 mixed complexes **16** and **18**, using NMR signal integration and many titration experiments to decide the stoichiometry. We now report that $NHEt_2$ and *N,N,N′,N*-tetramethyl-1,2-diaminoethane (Me_4en) will form analogous complexes **17** and **19**, respectively, and that H$_2$*det* can also be used, affording **20**–**23**. Clean spectra resulted from mixing H$_2$*dipt*, Ti(O^{i}Pr)$_4$, and amine at 3:4:2 ratios or by treating 2:1 H$_2$*det*–amine mixtures with 3/4 equivalents of Ti(O^{i}Pr)$_4$ per tartrate without fear of transesterification. With <4/3 equivalents of tartrate per Ti present, the parent Ti$_2$(tartrate)$_2$(O^{i}Pr)$_4$ was also present (with transesterification, if using H$_2$*det*). With >4/3 equivalents of tartrate or <2/3 equivalents of amine per Ti, the complex set of signals typical of tartrate-excessive material appeared. No amide formation was ever detected.

As illustrated in Fig. 3, the adducts were characterized by single, sharp, AB quartets, entirely similar to those previously described and assigned to chelating and bridging tartrate units

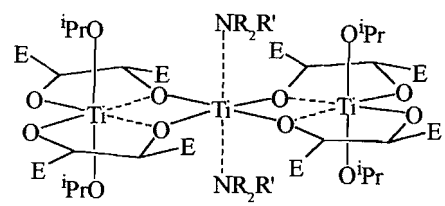

16 E = COO^{i}Pr R = R′ = Et
17 E = COO^{i}Pr R = Et R′ = H
18 E = COO^{i}Pr R = ^{i}Pr R′ = H
19 E = COO^{i}Pr R = Me R′ = $CH_2CH_2NMe_2$
20 E = COOEt R = R′ = Et
21 E = COOEt R = Et R′ = H
22 E = COOEt R = ^{i}Pr R′ = H
23 E = COOEt R = Me R′ = $CH_2CH_2NMe_2$

Can. J. Chem. Downloaded from www.nrcresearchpress.com by 65.111.164.53 on 09/08/12
For personal use only.

Fig. 3. OC*H* region of the ^{1}H NMR spectrum of a 3:4:2 mixture of $Ti(O^iPr)_4$, H_2*det*, and NH^iPr_2 in $CDCl_3$, assigned to complex **22**. Note the minor doublets above 5 ppm.

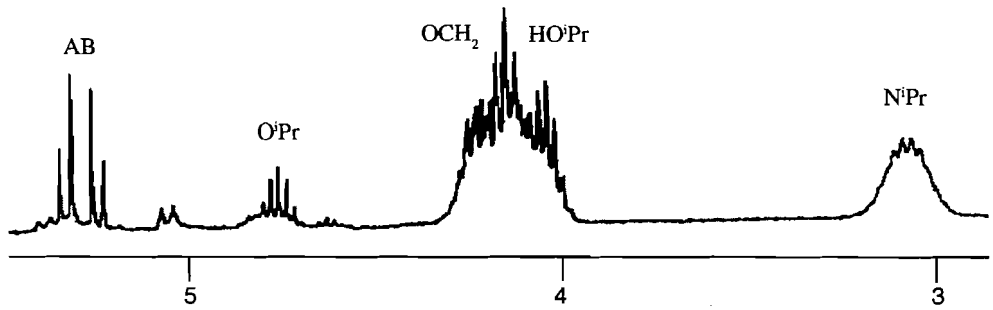

(J_{AB} = 9.1–9.4 with H_2*dipt*, 8.2–9.3 with H_2*det*), along with two new, sharp and closely spaced, ester OC*H* heptets (or OCH_2 quartets) and one sharp O^{i}Pr heptet. ^{13}C NMR concurred and also confirmed the absence of ester coordination. The amine signals were also interesting: in the $NHEt_2$ case, for instance, two broad CH_2 quintets appeared some 0.5 ppm downfield of the position where the quartet from free $NHEt_2$ appears, and the N*H* signal was very broad and near 8.7 ppm. This indicated a single type of amine coordinated to a metal in a chiral environment, with diastereotopic CH_2 groups coupled to the NH. With progressive additions of further amine, the quintets melded, shifted upfield, and eventually became the quartet of free $NHEt_2$. Thus, bound and free amine were rapidly exchanging. Using H_2*det* greatly simplified the OC*H* region. Thus, the ratio of the AB quartet to the TiO^{i}Pr heptet could be fairly accurately measured at about 2:1 from a 1:1 *det*:O^{i}Pr ratio. Hence, from the generic formula $Ti_x det_y(O^iPr)_{4x-2y}(amine)_n$, $y/(4x-2y) = 1$ leads to $y/x = 4/3$, which concurred with the results of the titration experiments. To place four equivalent but asymmetrically bound tartrate units and four equivalent O^{i}Pr groups about three Ti centres requires that n be 2. Structures **16**–**23** could then be drawn.

These complexes were labile and involved in equilibria with the parent $Ti_2(tartrate)_2(O^iPr)_4$ species, the tartrate-excessive material, and the free amines. Indeed, heating a 1:1:1 mixture to 50°C and recooling demonstrated that $Ti_2 dipt_2(O^iPr)_4$ and the free amine were favoured at higher temperatures.

Two other phenomena were noted with the two secondary amines. Firstly, when these were added to preformed $Ti_2 dipt_2(O^iPr)_4$, a second, more minor, product was also present. They gave rise to AX systems that included a doublet far downfield (at 5.4–5.5 ppm), reminiscent of those in the amino alcohol complexes. Due to overlaps, the partner doublet was found only in the $NHEt_2$ case, at 4.6 ppm. These AX systems may signal the partial formation of the O^{i}Pr-bridged analogues **A** originally predicted. Secondly, 2:3:1 Ti:tartrate:$NHEt_2$ or NH^iPr_2 mixtures produced another minor product whose tartrate unit gave rise to a broad and much weaker doublet of doublets with $J \approx 8.25$ (confirmed by decoupling and correlation spectroscopy), which partially overlapped the sharp AB quartet of the major, 4:3:2 product (see Fig. 3). However, no additional ^{13}C signals could be detected to attribute to these minor products. We speculate that they were analogues of **14** and **15**.

The weaker base morpholine produced only broad ^{1}H NMR signals when added to H_2*dipt*–$Ti(O^iPr)_4$ mixtures, but when $Ti(O^iPr)_4$ was added to a 2:1 H_2*det*:morpholine mixture, an analogous 4:3:2 product (J_{AB} = 8.8) seemed to form; however, its signals overlapped a large amount of broad resonance in the OC*H* region, and it could not be fully characterized. Reactions with *n*-propylamine, *tert*-butylamine, phenylhydrazine, 2-hydroxyethylhydrazine, pyridine, 4-dimethylaminopyridine, and 2,2′-bipyridine all failed to produce well-defined species, giving complex spectra or only broadened signals. Perhaps fast *O*-to-*N* transacylation took place with the primary amines and hydrazines while the pyridines were perhaps too poorly basic.

H-C coupling constants

In many cases, the tartrate $^1J_{HC}$ (145.5–155.6 Hz) and $^2J_{HC}$ (3.1–7.1 Hz) values could be measured from ^{1}H-coupled ^{13}C NMR spectra. In other cases, this was not possible (weak signals, signal overlaps, and ambiguities in assignment). The general observation was that, for every OCH pair suspected to belong to a chelating tartrate unit, one was always associated with a stronger $^1J_{HC}$ and a stronger $^2J_{HC}$. The nonchelated tartrate units of the tartrate–amino alcohol mixed complexes also gave rise to paired O*C*H signals of differing $^1J_{HC}$ values (though the $^2J_{HC}$ values were more similar).

The significance of the $^2J_{HC}$ values is not clear but $^1J_{HC}$ values are associated with the hybridization and *s* character at C. We postulate that these differences in $^1J_{HC}$ arise from π-type donation by O in the bridging OCH, on the one hand, or in a terminal OCH at pentacoordinate Ti, on the other. Among other changes, both kinds of π donation are associated with a lengthening of the O—C bond (7, 12, 16).

Discussion

Tartrate esters adopt a variety of binding modes in the solid state (6, 7) but, until part of the present work was recently communicated (4, 5), only two had been identified in solution. One is tridentate coordination, with chelation by the diol part, bridging of two Ti by one of the two diolate oxygens, and coordination by an ester or amide carbonyl group. This is adopted by $Ti_2(dipt)(O^iPr)_6$ and its analogue from *meso*-H_2*dipt*, by $Ti_2(tartrate)_2(O^iBu)_4$ species, and by a crystalline tartramide complex (6). The second binding mode differs from the first only in that it lacks the chelation feature. It is adopted by $Ti_2 dipt_2(O^iPr)_4$, the Katsuki–Sharpless asymmetric epoxidation catalyst (1), by two $Ti_3(tartramide)_2(O^iPr)_8$ complexes in solution (2, 5), and by the crystalline tartrate salts of transition metals (17). Of the three new binding modes seen here, the most prevalent is that in which the side-chain

Can. J. Chem. Downloaded from www.nrcresearchpress.com by 65.111.164.53 on 09/08/12
For personal use only.

Can. J. Chem. Downloaded from www.nrcresearchpress.com by 65.111.164.53 on 09/08/12
For personal use only.

Scheme 1

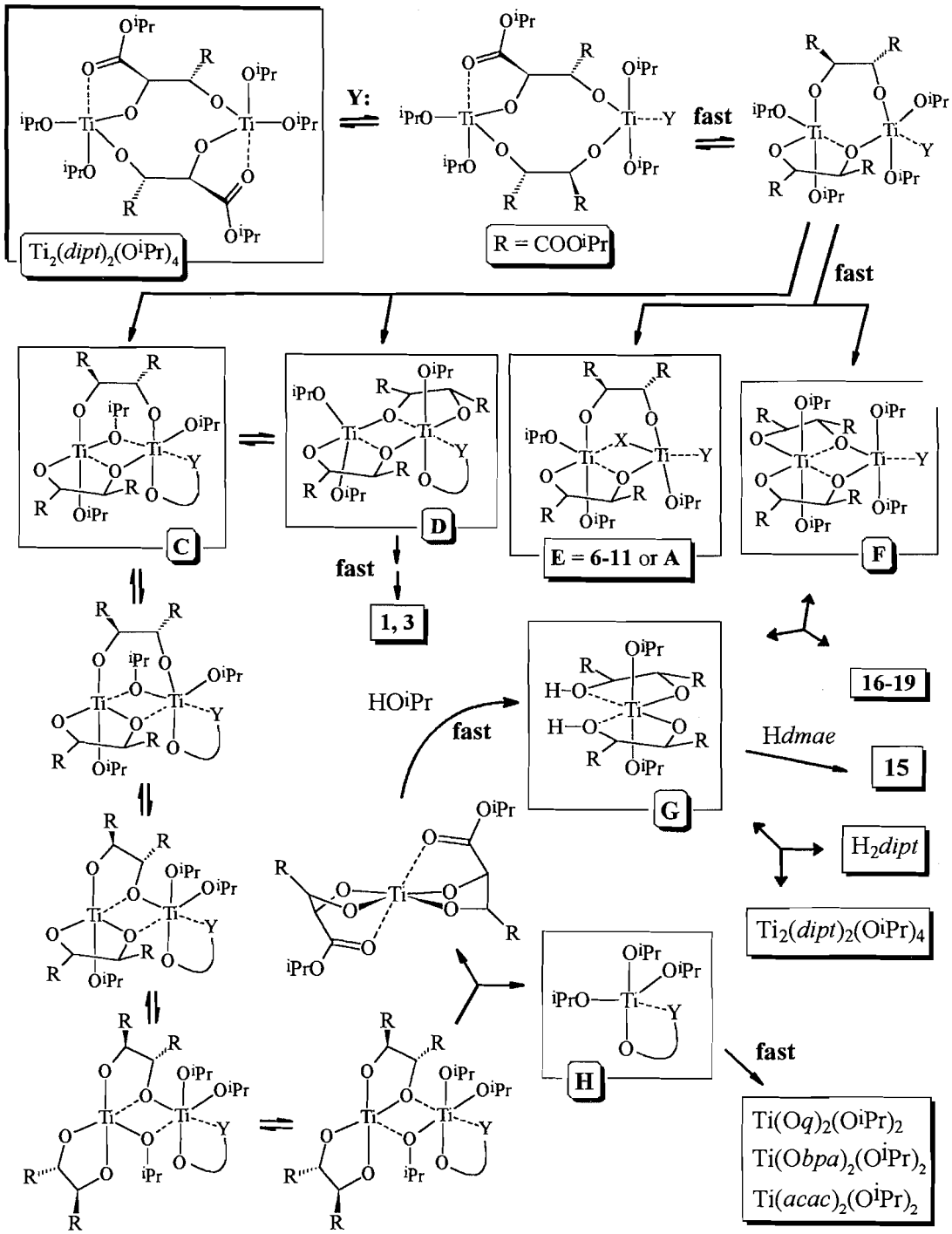

coordination is simply replaced by that of another group of external origin. This mode has also been found several times in the solid state (6, 7). The fourth mode, found in solution in the amino alcohol complexes and present in the crystalline **5** (6), involves only terminal ligation with the spanning of two metal centres. The fifth, involving mononuclear species **14** and **15**, is unprecedented.

The reactions described herein were selective in that other, plausible products did not form: with HO*q* and HO*bpa*, no product of the simultaneous replacements of O^{i}Pr and tartrate were apparent. The reactions with amino alcohols were enantiospecific. In the reactions with amines, other products (**A** and **B**) were anticipated.

Scheme 1 attempts to assemble and rationalize most of our observations in the reactions of $Ti_2dipt_2(O^iPr)_4$. Though the geometries at Ti, the ligand positions, and the sequence of events may not be exactly correct, it describes a likely origin of the observed selectivities: the various products observed can all be viewed as resulting from an initial macro-ring closure triggered by the binding of an addend Y onto the reactive

Can. J. Chem. Downloaded from www.nrcresearchpress.com by 65.111.164.53 on 09/08/12
For personal use only.

$Ti_2dipt_2(O^iPr)_4$. The architecture of the condensed adducts **C–F** then depends on which metal contributes the second bridge, and this in turn depends on the electron-donating ability and the bulk of the addend.

Consider the reactions of HO*q*, HO*bpa*, and H*acac*. They substitute an electron-rich group, O^iPr, with a poorer one. The second bridge should therefore originate at the other metal, favouring hexacoordination at the electron-poor metal in **D** and (or) **C**. (The closure sequence may in fact be the opposite of that drawn.) Though not depicted, the pentacoordinate centres in **C**, **D**, and structures following **C** may be partially stabilized by the binding of a tartrate ester group but this would be strenuous, weak, and reversible (3). The conversion of **D** to the observed products **1** and **3** is self-evident. The further reaction of **C** is depicted economically, but other routes are possible. Through fast, intramolecular ligand reorganizations, this effects a net exchange of tartrate and O^iPr substituents between metals so as to place the relatively more electron-rich O^iPr groups on the electron-poorer metal. Once the segregation is accomplished, we speculate that dissociation produces a pentacoordinate intermediate **H**, which is rapidly trapped by a second equivalent of the addend (eqs. [1] and [3]), and $Ti(dipt)_2$, which can be quenched by ambient HO^iPr to give **G** and take its place in the fluxional mixture we call tartrate-excessive material. This dissociation could instead be triggered by an external attack by HO^iPr, H_2dipt or something else to produce **G** directly or other members of the family of tartrate-excessive materials. That mixture partly liberates H_2dipt while regenerating $Ti_2dipt_2(O^iPr)_4$. As required by eq. [2], the intermediacy of equal amounts of **C** and **D** from HO*q* will ensure that one of every three *dipt* units initially available will be liberated as H_2dipt and that equal amounts of **1** and $Ti(Oq)_2(O^iPr)_2$ will be produced. Similarly, eq. [4] corresponds to a 3:1 preference for **D** over **C**. The reaction with H*acac* apparently proceeded exclusively through **C**.

On the other hand, the bulky and electron-rich aminoalcohols and amines add electron density and the second bridge should originate from the electron-rich metal. Closure to **F** and (or) **E** then favours hexacoordination at the electron-poorer metal. (With amino alcohols, the opposite closure sequence may occur.) When an amino alkoxide O is available as a relatively compact and electron-rich bridge, **E** (i.e., **6–11**) is favoured over **F**. With amines, this electronic preference is offset by steric congestion and the less electron-rich tartrate O is used to form the bridge in **F**, though **E** (i.e., the minor products **A**) can also form with the less bulky secondary amines. In the absence of excess H_2dipt, the reaction of amines can go no further and can only revert to starting materials. (Only with amines are the reactions entirely reversible.) The presence of excess tartrate produces tartrate-excessive material, probably including **G**, which can react reversibly with **F** to give the dominant amine adducts **16–19** in the presence of sufficient amine. Finally, the unusual H*dmae* adduct **15** can be formed from **G** by simple substitutions.

Scheme 1 also explains other observations. Firstly, the absence of **B**-type amine adducts is logical since the electron-donating ability of amino-type N disfavours the intermediacy of a **D**-like precursor to **B**. Secondly, the "wrong" antipode combinations in the amino alcohol reactions would be expected to give a fluxional mixture of adducts resulting from (reversible) formation of **F** and (or) O^iPr-bridged **E**, with the additional possibility of oligomeric assemblies. Complex, undecipherable spectra were in fact obtained. Finally, it is not too surprising that $HONBn_2$ produced complex reaction mixtures. As a bidentate, the Lewis basicity of $HONBn_2$ is probably closer to that of HO*q* than to that of amino alcohols. Both **C**- and **D**-derived products can be expected. (The crystallized product **5** can be viewed as a **D**-derived architecture, whether this came from $Ti_2dipt_2(O^iPr)_4$ or from a 3:2 *dipt*:Ti assembly.) But $ONBn_2$ is probably a poor, facultative bidentate and much of it may be monodentate, simply involved in exchanges with HO^iPr. With excess H_2dipt, it may end up scrambled among the components of the tartrate-excessive material. Further, the small "bite" of bidentate $ONBn_2$ enables the binding of other groups, including HO^iPr and ester carbonyls, to produce heptacoordination. This too may be a fluxional affair.

While the details of Scheme 1 remain uncertain, three conclusions seem inevitable. Firstly, Scheme 1 requires that $Ti_2dipt_2(O^iPr)_4$ have the 10-membered macrocyclic form depicted, a structure that has been the subject of some controversy (5); it would be very difficult to account for the products otherwise. In particular, the condensed, **D**-like form preferred by the Sharpless group (1, 6, 12) would be expected to give products with only **D**-derived architectures.

Secondly, the reactions that require internal reorganizations or ligand exchanges must be fast. Indeed, because H_2det can be used in the reactions with amines and amino alcohols, they evidently proceeded faster than could transesterification. Most of the steps depicted involve pentacoordination (or strained hexacoordination if ester carbonyls are allowed to coordinate) while the observed end products are relatively inert thermodynamic sinks (**6–13** retain some ligand exchange reactivity). In regard to the design of new catalysts for asymmetric reactions, it is interesting to note that $Ti_2dipt_2(O^iPr)_4$ itself is fluxional, not "well-defined," and its structure was indirectly deduced (2, 3, 5). Much of its success in catalyzing the Katsuki–Sharpless asymmetric epoxidation of allylic alcohols (1) can be ascribed to its avoidance of a thermodynamic sink (3, 5). A successful catalyst therefore need not be well-defined but should possess this same ability. Accordingly, **C–G** all have desirable architectures.

Finally, it would be difficult to account for the selective formation of $Ti(Oq)_2(O^iPr)_2$, $Ti(Obpa)_2(O^iPr)_2$, and $Ti(acac)_2(O^iPr)_2$ without invoking transient O^iPr bridges. As well, O^iPr-bridged **A**-type complexes from amines are an undeniable possibility. Such bridging has only once been directly observed, by low-temperature ^{13}C NMR spectroscopy of $Ti(O^iPr)_4$ (18), but their presence has been invoked in several cases, such as $Ti_2dipt(O^iPr)_6$ (2, 3). Only steric congestion seems to impede their more ready formation, for structures **1–13**, **16–23**, and others (6, 7) all involve bridging by secondary carbinol oxygens, and O^iPr is more Lewis basic than tartrate. The significance of such bridges is that they may well play a role in the Katsuki–Sharpless catalytic system, serving to rigidify the reaction template. During that reaction, the allylic alcohol substrate and the oxidant are initially loaded onto $Ti_2dipt_2(O^iPr)_4$ by exchange with O^iPr groups. The subsequent enantioselective O transfer was earlier rationalized on a **D**-like template (1, 6, 19). If, like $ONBn_2$, ^tBuOO is considered a relatively electron-poor bidentate (20), then both **C**- and **D**-like assemblies are possible. Bridging O^iPr or allyloxide groups (**C**) would in fact be electronically preferred over a second tar-

trate bridge (**D**), and the small "bite" of ^{t}BuOO (20) might well accommodate any additional steric demands.

Scheme 1 is but one window on the rich chemistry manifested by Ti^{IV}-tartrate systems and much of it, undoubtedly, is yet unexposed.

Acknowledgements

The authors thank Steven Balsky and Stephen Bianchet for assistance, and the Natural Sciences and Engineering Research Council of Canada for continued funding.

References

1. T. Katsuki and K. B. Sharpless. J. Am. Chem. Soc. **102**, 5974 (1980); M. G. Finn and K. B. Sharpless. *In* Asymmetric synthesis. Vol. 5. *Edited by* J. D. Morrison. Academic Press, New York. 1985. p. 247.
2. P. G. Potvin, R. Gau, P. C. C. Kwong, and S. Bianchet. Can. J. Chem. **67**, 1523 (1989).
3. S. Bianchet and P. G. Potvin. Can. J. Chem. **70**, 2256 (1992).
4. P. G. Potvin. J. Org. Chem. **57**, 3272 (1992).
5. P. G. Potvin and S. Bianchet. J. Org. Chem. **57**, 6629 (1992).
6. I. D. Williams, S. F. Pedersen, K. B. Sharpless, and S. J. Lippard. J. Am. Chem. Soc. **106**, 6430 (1984).
7. D. C. Bradley and C. E. Holloway. J. Chem. Soc. (A), 282 (1969).
8. H. H. Takimoto and J. B. Rust. J. Org. Chem. **26**, 2467 (1961).
9. C. Holloway and A. E. Sentek. Can. J. Chem. **49**, 519 (1971).
10. G. D. Smith, C. N. Caughlan, and J. A. Campbell. Inorg. Chem. 11, 2989 (1972).
11. G. Erker, S. Dehnicke, M. Rump, C Krüger, S. Werner, and M. Nolte. Angew. Chem. Int. Ed. Engl. **30**, 1349 (1991).
12. M. G. Finn and K. B. Sharpless. J. Am. Chem. Soc. **113**, 113 (1990).
13. S. F. Pedersen, J. C. Dewan, R. R. Eckman, and K. B. Sharpless. J. Am. Chem. Soc. **109**, 1279 (1987).
14. E. Alyea and P. H. Merrell. Inorg. Nucl. Chem. Lett. **9**, 69 (1973).
15. S. Miyano, L. D.-L. Lu, S. M. Viti, and K. B. Sharpless. J. Org. Chem. **48**, 3608 (1983); **50**, 4350 (1985); M. Kihara, K. Ohnishi, and S. Kobayashi. J. Heterocycl. Chem. **25**, 161 (1988).
16. J. C. Huffman, K. G. Moloy, and K. G. Caulton. Inorg. Chem. **27**, 2190 (1988).
17. R. E. Tapscott, R. L. Bedford, and I. C. Paul. Coord. Chem. Rev. **4**, 323 (1969); R. E. Tapscott and G. L. Robbins. Inorg. Chem. **15**, 154 (1976); S. K. Hahs, R. B. Ortega, R. E. Tapscott, C. F. Campana, and B. Morosin. Inorg. Chem. **21**, 664 (1982); R. B. Ortega, R. E. Tapscott, and C. F. Campana. Inorg. Chem. **21**, 672 (1982).
18. M. Marsi and D. C. Roe. Am. Chem. Soc. Nat. Meet. Los Angeles, Sept. 1988.
19. K. A. Jorgensen, R. A. Wheeler, and R. Hoffman. J. Am. Chem. Soc. 109, 3240 (1987).
20. H. Mimoun, P. Chaumette, M. Mignard, L. Saussine, J. Fisher, and R. Weiss. Nouv. J. Chim. **7**, 467 (1983).

Can. J. Chem. Downloaded from www.nrcresearchpress.com by 65.111.164.53 on 09/08/12
For personal use only.

Manifestations of noncovalent bonding in the solid state. 6.[1] $[H_4(cyclam)]^{4+}$ (cyclam = 1,4,8,11-tetraazacyclotetradecane) as a template for crystal engineering of network hydrogen-bonded solids

S. Subramanian and Michael J. Zaworotko

Abstract: A series of salts of composition $[H_4(cyclam)]X{\cdot}nH_2O$, where cyclam = 1,4,8,11-tetraazacyclotetradecane and X = $4Cl^-$ (**1**, $n = 4$), $4Br^-$ (**2**, $n = 4$), $4I^-$ (**3**, $n = x$), $4ClO_4^-$ (**4**, $n = 2$), $4CNS^-$ (**5**, $n = 2$), $2SO_4^{2-}$ (**6**, $n = 6$), and (p-$CH_3C_6H_4SO_3^-$) (**7**, $n = 0$) have been prepared and crystal structures of **1**, **2**, **4**, **5**, **6**, and **7** have been determined by single crystal X-ray crystallography. **1**, **2**, **3**, **4**, and **7** were prepared by crystallizing cyclam with a large excess of the corresponding acid whereas the thiocyanate, **5**, and the sulphate, **6**, salts were prepared by metathesis of the perchlorate salt, **4**, with KCNS and K_2SO_4, respectively. Crystal data: **1**: orthorhombic, *Pnnb*, $a = 7.7962(16)$, $b = 14.278(4)$, $c = 17.787(4)$ Å, $V = 1979.9(8)$ Å^3, $Z = 4$, $D_c = 1.39$ Mg m^{-3}, $R_f = 0.051$, and $R_w = 0.069$ for 1176 reflections with $I > 3\sigma(I)$. **2**: triclinic, $P\bar{1}$, $a = 7.6860(8)$, $b = 7.8848(9)$, $c = 9.6385(11)$ Å, $\alpha = 105.111(16)°$, $\beta = 95.495(18)°$, $\gamma = 102.464(17)°$, $V = 543.43(12)$ Å^3, $Z = 1$, $D_c = 1.82$ Mg m^{-3}, $R_f = 0.034$, and $R_w = 0.041$ for 1530 reflections with $I > 3\sigma(I)$. **4**: monoclinic, $P2_1/n$, $a = 8.4519(11)$, $b = 15.9248(12)$, $c = 9.2981(17)$ Å, $\beta = 106.243(18)°$, $V = 1201.5(3)$ Å^3, $Z = 2$, $D_c = 1.76$ Mg m^{-3}, $R_f = 0.052$, and $R_w = 0.068$ for 1902 reflections with $I > 3.0\sigma(I)$. **5**: triclinic, $P\bar{1}$, $a = 8.2996(7)$, $b = 9.0061(15)$, $c = 9.2015(15)$ Å, $\alpha = 107.60(3)°$, $\beta = 97.738(14)°$, $\gamma = 108.863(9)°$, $V = 599.44(15)$ Å^3, $Z = 1$, $D_c = 1.309$ Mg m^{-3}, $R_f = 0.038$ and $R_w = 0.049$ for 1856 reflections with $I > 4\sigma(I)$. **6:** triclinic, $P\bar{1}$, $a = 7.8687(5)$, $b = 8.8396(12)$, $c = 9.0405(25)$ Å, $\alpha = 68.547(16)$, $\beta = 85.332(9)$, $\gamma = 78.473(7)°$, $V = 573.43(18)$ Å^3, $Z = 1$, $D_c = 1.693$ Mg m^{-3}, $R_f = 0.053$ and $R_w = 0.076$ for 1441 reflections with $I > 3\sigma(I)$. **7**: triclinic, $P\bar{1}$, $a = 8.533(3)$, $b = 9.110(3)$, $c = 15.3605(21)$ Å, $\alpha = 82.475(17)°$, $\beta = 74.307(20)°$, $\gamma = 73.26(3)°$, $V = 1099.0(5)$ Å^3, $Z = 1$, $D_c = 1.343$ Mg m^{-3}, $R_f = 0.042$ and $R_w = 0.052$ for 2460 reflections with $I > 2.5\sigma(I)$. **1**, **2**, **4**, **5**, **6**, and **7** exhibit extensive network hydrogen bonding between the anions, cations, and, if appropriate, water molecules of crystallization. The dimensionality of the hydrogen-bonded networks is dependent upon the nature of the anion and the number of water molecules of crystallization since the cation adapts a centrosymmetric exodentate conformation in all six salts.

Keywords: crystal engineering, cyclams, network hydrogen bonding.

Résumé : On a préparé une série de sels de composition $[H_4(cyclam))]X{\cdot}nH_2O$, dans lesquels cyclam = 1,4,8,11-tétraazacyclotétradécane et X = $4\,Cl^-$ ($n = 4$), $4\,Br^-$ (**2**, $n = 4$), $4I^-$ (**3**, $n = x$), $4\,ClO_4^-$ (**4**, $n = 2$), $4CNS^-$ (**5**, $n = 2$), $2\,SO_4^{2-}$ (**6**, $n = 6$) et $4(p$-$CH_3C_6H_4SO_3^-)$ (**7**, $n = 0$) et on a déterminé les structures cristallines des composés **1, 2, 4, 5, 6** et **7** par diffraction des rayons X. On a préparé les composés **1, 2, 3, 4** et **7** par cristallisation du cyclame avec un grand excès de l'acide correspondant alors que l'on a préparé les sels de thiocyanate, **5,** et de sulfate, **6**, par métathèse du perchlorate, **4**, avec respectivement du KCNS et du K_2SO_4. Les données cristallines sont les suivantes. **1** : orthorhombique, *Pnnb*, $a = 7{,}7962(16)$, $b = 14{,}278(4)$ et $c = 17{,}787(4)$ Å, $V = 1979{,}9(8)$ Å^3, $Z = 4$, $D_c = 1{,}39$ Mg m^{-3}, $R_f = 0{,}051$ et $R_w = 0{,}069$ pour 1176 réflexions avec $I > 3\sigma(I)$; **2** : triclinique, $P\bar{1}$, $a = 7{,}6860(8)$, $b = 7{,}8848(9)$ et $c = 9{,}6385(11)$ Å, $\alpha = 105{,}111(16)°$, $\beta = 95,495\ (18)°$ et $\gamma = 102{,}464(17)°$, $V = 543.43(12)$ Å^3, $Z = 1$, $D_c = 1{,}82$ Mg m^{-3}, $R_f = 0{,}034$, and $R_w = 0{,}041$ pour 1530 réflexion avec $I > 3\sigma(I)$. **4** : monoclinique, $P2_1/n$, $a = 8.4519(11)$, $b = 15.9248(12)$ et $c = 9{,}2981(17)$ Å, $\beta = 106{,}243(18)°$, $V = 1201{,}5(3)$ Å^3, $Z = 2$, $D_c = 1{,}76$ Mg m^{-3}, $R_f = 0{,}052$, and $R_w = 0{,}068$ for 1902 réflexions with $I > 3.0\sigma(I)$; **5** : triclinque, $P\bar{1}$, $a = 8{,}2996(7)$, $b = 9{,}0061(15)$, et $c = 9{,}2015(15)$ Å, $\alpha = 107{,}60(3)°$, $\beta = 97{,}738(14)°$, $\gamma =$

Received June 30, 1994.

S. Subramanian and M.J. Zaworotko.[2] Department of Chemistry, Saint Mary's University, Halifax, NS B3H 3C3, Canada.

[1] For parts 1–5 see ref. 14*b* and refs. therein.

[2] Author to whom correspondence may be addressed. Telephone: (902) 420-5661. Fax: (902) 420-5261. E-mail: mzaworot@science.stmarys.ca

Can. J. Chem. Downloaded from www.nrcresearchpress.com by 65.111.164.53 on 09/08/12
For personal use only.

108,863(9)°, V = 599,44(15) Å^3, Z = 1, D_c = 1,309 Mg m^{-3}, R_f = 0,038 and R_w = 0,049 pour 1856 réflexions avec $I > 4\sigma(I)$. **6** : triclinique, $P\bar{1}$, a = 7,8687(5), b = 8,8396(12), c = 9,0405(25) Å, α = 68,547(16)°, β = 85,332(9)°, γ = 78,473(7)°, V = 573,43(18) Å^3, Z = 1, D_c = 1,693 Mg m^{-3}, R_f = 0,053 and R_w = 0,076 pour 1441 réflexions avec $I > 3\sigma(I)$. **7**: triclinique, $P\bar{1}$, a = 8,533(3), b = 9,110(3), c = 15,3605(21) Å, α = 82,475(17)°, β = 74,307(20)°, γ = 73,26(3)°, V = 1099,0(5) Å^3, Z = 1, D_c = 1,343 Mg m^{-3}, R_f = 0,042 et R_w = 0,052 pour 2460 réflexions avec $I > 2{,}5\sigma(I)$. Les composés **1**, **2**, **4**, **5**, **6**, et **7** présentent tous un réseau important de liaisons hydrogènes entre les anions, les cations et, dans les cas appropriés, avec les molécules d'eau de cristallisation. Puisque le cation adopte une conformation exodentate centrosymétrique dans chacun de ces six sels, les dimensions des réseaux des liaisons hydrogènes dépendent de la nature de l'anion et du nombre de molécules d'eau de cristallisaiton.

Mots clés : genie de cristaux, cyclams, réseaux des liaisons hydrogènes.

[Traduit par la rédaction]

Introduction

Exploitation of noncovalent interactions between molecular or ionic components for the rational design of solid state structures that might exhibit interesting electrical, magnetic, and optical properties, i.e., crystal engineering, is a current theme of solid state research (1–3). A fundamental principle of crystal engineering is that a given set of structural units (neutral molecules or, in the case of salts, cations and anions) will form networks defined by the spatial orientation of the moieties that engage in noncovalent bonding. In particular, it is becoming increasingly evident that the specificity, directionality, and predictability (4) of intermolecular hydrogen bonding can be utilized to assemble supramolecular structures of, at the very least, controlled dimensionality, if not predictable bulk physical properties. Indeed, hydrogen bonding has been exploited to design and construct one- (4–7), two- (8–11), or three- (12–14) dimensional solid state structures. However, this should not imply that all molecules or ions are suitable candidates for crystal engineering purposes. One has to carefully examine the functionality and geometry of molecules or ions before one attempts to exploit them for crystal engineering purposes. For example, carboxylic acid (12) and pyridone (13) functional groups are exploitable since they contain both hydrogen bond donor and hydrogen bond acceptor moieties that are geometrically disposed towards *self-assembly* (i.e., they are self-complementary). On the other hand, moieties such as the ammonium cation and oxyanions are incapable of self-assembly in the absence of a second complementary component since they are multifunctional hydrogen bond donors and acceptors, respectively. However, they would be complementary with each other, so salts that contain such moieties would be expected to engage in *strict* or *modular self-assembly* (15). Cocrystals can also represent examples of strict self-assembly.

There are several potential applications for crystal engineers to focus upon and a particularly topical application concerns design of solids that exhibit second-order nonlinear optical properties such as second harmonic generation, SHG. SHG activity is possible in as wide an array of compounds as inorganics (KH_2PO_4, $LiNbO_3$), organics (nitroanilines) (16), organometallics (ferrocene derivatives and acetylides) (17, 18), and organic cation salts (7, 19–24). The aforementioned examples represent single-component self-assembly. Self-assembly of two components of a salt requires that both the cation and the anion must be multifunctional, rigidly exodentate, and complementary. In our attempts to identify and utilize structural units that would lead to the formation of 1D, 2D, or 3D solids, we embarked upon a structural investigation of salts of the macrocyclic tetracation $[H_4(cyclam)]^{4+}$, which adapts an *exodentate* conformation. This observation is in contrast to that of cyclam itself (25), in which an *endodentate* conformation exists (see Scheme 1), facilitating coordination to transition metal cations (26). Surprsingly, very few salts of cyclam have been structurally characterized and those known are limited to its dication, $[H_2(cyclam)]^{+2}$ (27, 28). A dioxalate salt of the tetracation $[H_4(cyclam)]^{+4}$ has been reported, but it was not subjected to X-ray crystallographic study (27). In this study, we report full details of an X-ray structure we have communicated (29), along with the X-ray structures of five new simple $[H_4(cyclam)]^{4+}$ salts. The focus of the present study concerns whether or not $[H_4(cyclam)]^{4+}$ can act as a reliable template for crystal engineering and how the number and spatial orientation of hydrogen bond acceptors (i.e., counterions and (or) solvent molecules) influences crystal packing.

Scheme 1. Conformations of cyclam, $[H_2(cyclam)]^{2+}$, and $[H_4(cyclam)]^{4+}$.

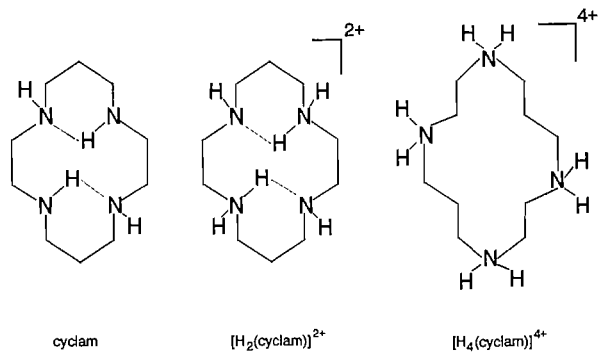

Experimental

Cyclam, purchased from Strem Chemicals, Inc., perchloric acid (75%) and KCNS, purchased from Fisher Scientific Co., and all the other chemicals, purchased from Aldrich Chemical Co., were used without further purification. IR spectra were recorded on a Perkin–Elmer 1600 series FTIR using solid state reflectance technique (oven dried KBr crystals). Melting points were recorded on a Fisher–Johns apparatus and were not corrected.

Caution! Perchlorate salts are potentially explosive and should not be dried in an oven or over a hot plate. It is advis-

Can. J. Chem. Downloaded from www.nrcresearchpress.com by 65.111.164.53 on 09/08/12
For personal use only.

Can. J. Chem. Downloaded from www.nrcresearchpress.com by 65.111.164.53 on 09/08/12
For personal use only.

able to prepare them in small quantities and filter them using fritted funnels and store them wet.

Preparation of $[H_4(cyclam)]Cl_4 \cdot 4H_2O$ (1)
Cyclam (0.200 g, 0.998 mmol) was dissolved in 20 mL of 4 M HCl and the solution was allowed to evaporate slowly at room temperature, affording large colourless crystals of $[H_4(cyclam)]Cl_4 \cdot 4H_2O$. Yield: 0.406 g (0.970 mmol, 97.2%); mp: melts sharply at 284°C with decomposition. IR (cm^{-1}): 3775 (weak), 3547, 3439, 3027, 2953, 2795, 2714, 2631, 2495, 2421 (all strong); 2150, 2008, 1882, 1784 (all very weak), 1650 (N-H asym), 1580, 1450, 1367(C-H); 1308, (all strong) 1270, 1210, 1154, 1107 (all medium); 1066 (strong), 1049, 984, 909, 858, 816, 768, 747 (all medium)

Preparation of $[H_4(cyclam)]Br_4 \cdot 4H_2O$ (2)
Cyclam (0.100 g, 0.499 mmol) was dissolved in 8 mL of 4 M HBr and the solution was allowed to evaporate slowly at room temperature to form large colourless crystals of the title compound. Yield 0.250 g (0.419 mmol, 84.1%); mp: melts at 281°C with decomposition. IR (cm^{-1}): 3458 (N-H); 2986, 2745 (C-H); 2413, (NH_2^+); 1614, 1569, 1474, 1443, 1363, 1297, 1122, 1082, 1012, 901, 856, 821, 750.

Preparation of $[H_4(cyclam)]I_4 \cdot xH_2O$ (3)
Solid cyclam (0.400 g, 2.00 mmol) was added in small portions to 10 mL of 48% hydroiodic acid. A copious white precipitate formed instantaneously. Water (15 mL) was added to a suspension of this precipitate and the mixture was boiled until a clear solution was formed. Upon cooling to room temperature, colourless clusters of transparent crystals that lose moisture rapidly to form an opaque anhydrous solid were afforded. Yield: 1.31 g (1.84 mmol, 92.2% (anhydrous)); mp: melts at 265°C and turns brown. IR (cm^{-1}): 3394 (N-H); 2954 (C-H); 2519 ($>NH_2^+$); 1625, 1616, 1570, 1558, 1540, 1521, 1506, 1474, 1438, 1414, 1368, 1298, 1116, 1078, 1010, 903, 893, 844, 754, 742. The anhydrous salt was observed to be soluble in boiling methanol, affording a colorless solution. However, upon storage this solution was observed to turn brown and deposit dark brown crystals, presumably of a triiodide salt.

Preparation of $[H_4(cyclam)](ClO_4)_4 \cdot 2H_2O$ (4)
Cyclam (0.200 g, 0.998 mmol) was dissolved in 5 mL of water and 5 mL of 70% perchloric acid was added dropwise. A white crystalline precipitate formed instantaneously. The mixture was stirred well, cooled in an ice bath, filtered under suction, and washed successively with methanol and ether. Yield: 0.76 g. The wet precipitate was not dried for safety reasons. About 0.200 g of the salt was dissolved in 15 mL of water and diluted with 70% perchloric acid for a final concentration of approximately 30–35% acid. This solution was cooled at 5°C for several days at which point large blocks of colourless crystals had formed. mp: turned slightly brown at 185°C and melted into a dark liquid above 285°C. IR (cm^{-1}): 3929, 3562, 3485 (water/H-bonds), 3166, 3086 (C-H), 2855, 2745, 2674 (H-bonds), 2342, 2002 ($>NH_2^+$, ammonium cation), 1619, 1579 (N-H, asym), 1478, 1428, 1393 (C-C), 1302, 1207, 1096 (broad, ClO_4^-), 1007, 936, 896, 841, 745.

Preparation of $[H_4(cyclam)](CNS)_4 \cdot 2H_2O$ (5)
4 (0.500 g, 0.783 mmol) was dissolved in 6 mL of water and to this 0.330 g (3.4 mmol) of KCNS in 6 mL of water was added. On standing in an ice bath, most of the $KClO_4$ precipitated and was removed by filtration. The mother liquor was cooled at 5°C for 2 days until the final traces $KClO_4$ crystallized. The solution was again filtered and the mother liquor was concentrated slowly (at 40°C) on a warm hot plate until the solution was reduced to less than 2 mL. The solution was allowed to cool and left to stand overnight, at which point long colourless crystals were obtained. Yield: 0.328 g (0.694 mmol, 88.6%); mp: melts sharply at 154°C with decomposition. IR (cm^{-1}): 3448, 3367, 3025, 2965, 2764, 2393, 2072 (CNS), 1614 (N-H), 1569, 1456, 1418, 1383, 1312, 1278, 1147, 1112, 1077, 981, 931, 861, 770, 735.

Preparation of $[H_4(cyclam)](SO_4)_2 \cdot 6H_2O$ (6)
To a solution of 0.218 g (1.25 mmol) of K_2SO_4 in 5.0 mL of water, a solution of 0.400 g (0.626 mmol) of wet **4** in 5.0 mL of water was added. A crystalline white precipitate of $KClO_4$ formed instantaneously. The mixture was cooled in an ice bath for 1 h to ensure complete precipitation of $KClO_4$ and was then filtered. The resulting filtrate was left to evaporate at room temperature, affording colourless crystals of **6**. Yield: 0.280 g (0.555 mmol, 88.0%); mp: melts at 244–245°C with decomposition. IR (cm^{-1}): 3458, 3317 (broad, strong, water); 3016 (C-H); 2694, 2523 ($>NH_2^+$ cation); 1624, 1574, 1499, 1458, 1378, 1333, 1297, 1273, 1217 (all sharp, medium); 1132, 1062 (broad, strong, sulphate); 986, 906, 786, 750 (sharp, medium).

Preparation of $[H_4(cyclam)](tosylate)_4$ (7)
To a solution of 0.200 g (0.998 mmol) of cyclam in 10 mL of methanol was added a solution of 0.760 g (4.00 mmol) of *p*-$CH_3C_6H_4SO_3H \cdot H_2O$ in 10 mL of water. The resulting homogeneous solution was layered with tetrahydrofuran and left to stand at room temperature. Large crystals of $[H_4(cyclam)](p\text{-}CH_3C_6H_4SO_3)_4$ were obtained. A second crop of crystals was obtained from the mother liquor. Yield: 0.830 g (0.934 mmol, 93.6%); mp: melts into a clear liquid at 264°C without decomposition. IR (cm^{-1}): 3659, 3471 (v weak, moisture), 3253, 3018, 2845, 2496 (strong), 1949 (v weak), 1626 and 1606 (C=C), 1460, 1426 (medium strong), 1315, 1284 (weak), 1218, 1172 & 1122 (sulphonate), 1037, 1006, 976, 861, 810, 780, 740, 705, 680.

X-ray crystallography
Single crystals suitable for X-ray crystallography were mounted and sealed in thin-walled glass capillaries and optically centred on the goniometer of an Enraf–Nonius CAD4 diffractometer. The experimental parameters used for data collection and structure refinement are presented in Table 1. Listings of atomic positional coordinates for all non-hydrogen atoms for compounds **1**, **2**, **4**, **5**, **6**, and **7** are presented in Tables 2–7. All structures were solved by direct methods using the PC version of the NRCVAX (30) programme package locally implemented on IBM-compatible 80486 computers. Values of $R = \Sigma(F_o - F_c)/(F_o)$, $R_w = [(\Sigma w((F_o - F_c)^2/\Sigma w F_o^2]^{1/2}$, and GOF = $[(\Sigma w((F_o - F_c)^2/(\text{no. of reflns.} - \text{no. of parameters})]^{1/2}$ were determined. Weights based on counting statistics were used, the weight modifier, k, being determined empirically via statistical analysis of the variation in intensity of the standard reflections. All the non-hydrogen atoms were refined anisotropically.

Can. J. Chem. Downloaded from www.nrcresearchpress.com by 65.111.164.53 on 09/08/12
For personal use only.

Table 1. Crystal data and summary of intensity data collection and structure refinement for compounds **1**, **2**, **4**, **5**, **6**, and **7**.

Compound	**1**	**2**	**4**	**5**	**6**	**7**
Formula	$C_{10}H_{32}N_4O_4Cl_4$	$C_{10}H_{36}N_4O_4Br_4$	$C_{10}H_{32}N_4O_{18}Cl_4$	$C_{14}H_{32}N_8O_2S_4$	$C_{10}H_{40}N_4O_{14}S_2$	$C_{38}H_{52}N_4O_{12}S_4$
Formula wt.	418.13	595.89	638.09	472.49	504.39	888.45
Crystal system	Orthorhombic	Triclicnic	Monoclinic	Triclinic	Triclinic	Triclinic
Space group	*Pnnb*	$P\bar{1}$	$P2_1/n$	$P\bar{1}$	$P\bar{1}$	$P\bar{1}$
Temp. °C	17	17	17	17	17	17
Cell constants[a]						
a, Å	7.7962(16)	7.6860(8)	8.4519(11)	8.2996(7)	7.8687(5)	8.533(3)
b, Å	14.278(4)	7.8848(9)	15.9248(12)	9.0061(15)	8.8396(12)	9.110(3)
c, Å	17.787(4)	9.6385(11)	9.2981(17)	9.2015(15)	9.040(2)	15.3605(21)
α, deg		105.111(16)	107.6(3)	68.547(16)	82.475(17)	
β, deg		95.495(18)	106.243(18)	97.738(14)	85.332(9)	74.307(20)
γ, deg		102.464(17)	108.863(9)	78.473(7)	73.26(3)	
Cell volume, $Å^3$	1979.9(8)	543.43(12)	1201.5(3)	599.44(15)	573.43(18)	1099.0(5)
F(000)	848	296	664	252	304	472
Z	4	1	2	1	1	1
D_{calc}, g cm^{-3}	1.39	1.82	1.76	1.309	1.693	1.343
μ_{calc}, cm^{-1}	5.9	73	0.31	0.40	0.48	0.27
Scan type	ω/2θ	ω/2θ	ω/2θ	ω/2θ	ω/2θ	ω/2θ
Radiation	Graphite monochromated Mo, K_α(λ = 0.70930 Å) used for all compounds					
Max. crystal dimension, mm	0.4 × 0.6 × 0.8	0.15 × 0.25 × 0.75	0.6 × 0.7 × 0.8	0.2 × 0.4 × 0.6	0.5 × 0.6 × 0.7	0.4 × 0.6 × 0.8
Scan width	0.8 + 0.35 tan θ	0.8 + 0.35 tan θ	0.8 + 0.35 tan θ	0.8 + 0.35 tan θ	0.8 + 0.35 tan θ	0.8 + 0.35 tan θ
Transmission range	0.789, 0.999	0.593, 0.997	0.886, 0.998	0.873, 1.000	0.841, 0.998	0.766, 1.000
Decay of standards	±2%	±2%	±2%	±2%	±2%	±2%
Reflections measured	1307	2048	2234	2101	1613	2992
2θ range, deg	44.9	49.8	49.8	49.8	44.9	49.8
Unique reflections	1307	1922	2104	2101	1498	2863
Reflections observed[b]	1176($I > 3\sigma(I)$)	1530($I > 3\sigma(I)$)	1902($I > 3\sigma(I)$)	1856($I > 4\sigma(I)$)	1441($I > 3\sigma(I)$)	2460($I > 2.5\sigma(I)$)
Number of parameters	104	100	163	127	136	262
Weight modifier, *k*	0.00005	0.0001	0.00002	0.00005	0.00001	0.00005
G.O.F.	6.08	2.48	8.27	4.12	13.59	4.09
R_f	0.051	0.034	0.052	0.038	0.053	0.042
R_w	0.069	0.041	0.068	0.049	0.076	0.052
Final diff. map(max) ($e/Å^3$)	0.35	0.45	0.58	0.27	0.33	0.22

[a]Least-squares refinement of $((\sin\theta)/\lambda)^2$ for 24 reflections $\theta > 16°$.

[b]Corrections: Lorentz polarization and absorption (empirical ψ scan).

Can. J. Chem. Downloaded from www.nrcresearchpress.com by 65.111.164.53 on 09/08/12
For personal use only.

Table 2. Atomic parameters x,y,z and B_{iso} for $[H_4(cyclam)]Cl_4{\cdot}4H_2O$.

	x	y	z	B_{iso}
Cl1	0.22074(12)	0.64772(6)	0.04257(6)	2.72(5)
Cl2	0.49714(14)	0.51365(8)	0.30829(6)	3.44(5)
N1	0.4239 (4)	0.49381(20)	0.13976(16)	2.11(13)
N2	0.2006 (4)	0.86460(21)	0.06630(18)	2.14(13)
C1	0.5947 (5)	0.5106 (3)	0.10580(23)	2.56(17)
C2	0.3585 (5)	0.8864 (3)	0.11170(21)	2.27(16)
C3	0.2008 (5)	0.8948 (3)	−0.01486(21)	2.22(16)
C4	0.3509 (5)	0.35244(25)	0.05805(21)	2.14(15)
C5	0.3689 (5)	0.3919 (3)	0.13751(21)	2.42(17)
Ow1	0.6450 (6)	0.3035 (3)	0.3116 (3)	8.3 (3)
Ow2*	1/4	0.707 (4)	1/4	14.3 (18)
Ow3*	0.065 (3)	0.7459 (14)	0.2070 (11)	8.5 (7)
Ow4*	0.155 (8)	0.7233 (21)	0.2357 (19)	11.4 (12)

B_{iso} is the mean of the principal axes of the thermal ellipsoid.
* = partial occupancy.

Table 3. Atomic parameters x,y,z and B_{iso} for $[H_4(cyclam)]Br_4{\cdot}4H_2O$.

	x	y	z	B_{iso}
Br1	0.25255(7)	0.21859(7)	0.11388(6)	3.17(3)
Br2	0.68552(7)	0.90564(7)	0.40466(6)	3.02(3)
OW1	0.9842 (6)	0.2723 (5)	0.3769 (5)	3.71(20)
OW2	0.6029 (8)	0.3669 (9)	0.4347 (7)	7.8 (4)
N1	1.2825 (5)	0.8592 (5)	0.2074 (4)	2.22(19)
N2	0.8751 (6)	0.5614 (5)	0.2978 (4)	2.32(19)
C1	1.0934 (7)	0.8023 (6)	0.2371 (6)	2.23(20)
C2	1.0690 (7)	0.6324 (7)	0.2849 (5)	2.29(23)
C3	0.7433 (6)	0.4911 (7)	0.1578 (6)	2.41(22)
C4	0.7845 (8)	0.3266 (8)	0.0546 (6)	3.4 (3)
C5	0.6576 (7)	0.2746 (7)	−0.0904 (6)	2.52(23)

B_{iso} is the mean of the principal axes of the thermal ellipsoid.

Methylene, aromatic C-H, and ammonium hydrogen atoms were calculated (d_{C-H} = 1.08 Å) and the methyl hydrogen atoms of the tosylate anion in salt **7** were located from difference Fourier map inspection and fixed during the refinement. In compound **1**, water molecules were observed to be disordered; 3.75 molecules of water were found per cation and they were refined with isotropic temperature factors and site occupancy as a variable. In compound **7**, the final difference Fourier map revealed a peak worth 1 e/Å^3 that was assumed to be a water oxygen atom. Refinement of site occupancy afforded a site occupancy value of 0.095. Final fractional coordinates for all atoms, selected interatomic distances and angles, and thermal parameters are available as supplementary material.[3]

[3] Listings of complete atomic positional parameters, anisotropic thermal parameters, and interatomic distances for **1, 2, 4, 5, 6,** and **7** have been deposited and may be purchased from: The Depository of Unpublished Data, Document Delivery, CISTI, National Research Council Canada, Ottawa, Canada K1A 0S2.

Tables of atomic positional parameters and interatomic distances have also been deposited with the Cambridge Crystallographic Data Centre, and can be obtained on request from The Director, Cambridge Crystallographic Data Centre, University Chemical Laboratory, 12 Union Road, Cambridge, CB2 1EZ, U.K.

Structure factor amplitudes are no longer being deposited and may be obtained directly from the author.

Table 4. Atomic parameters x,y,z and B_{iso} for $[H_4(cyclam)](ClO_4)_4{\cdot}2H_2O$.

	x	y	z	B_{iso}
Cl1	0.89831(10)	0.82673(5)	0.01949(9)	2.37(4)
O1	0.7857 (4)	0.82142(24)	0.1067 (4)	5.84(19)
O2	1.0443 (4)	0.78234(20)	0.0947 (4)	5.25(16)
O3	0.8291 (6)	0.78961(25)	−0.1215 (4)	7.69(24)
O4	0.9405 (4)	0.91183(17)	0.0009 (4)	4.50(15)
Cl2	1.26903(11)	0.87824(5)	0.79541(10)	2.66(4)
O5	1.3686 (4)	0.88591(19)	0.6947 (4)	4.69(16)
O6	1.2046 (4)	0.95822(19)	0.8158 (5)	5.99(20)
O7	1.1286 (4)	0.82438(21)	0.7303 (4)	5.24(16)
O8	1.3549 (5)	0.8391 (3)	0.9309 (4)	6.42(19)
Ow	1.0351 (3)	0.84034(17)	0.4029 (3)	3.37(12)
N1	0.6851 (3)	0.84064(16)	0.4109 (3)	2.30(12)
N2	0.8468 (3)	1.00281(19)	−0.2796 (3)	2.54(12)
C1	0.7341 (4)	0.87516(20)	−0.4331 (4)	2.32(14)
C2	0.8169 (4)	0.96045(21)	−0.4290 (4)	2.13(13)
C3	0.6962 (4)	1.02692(23)	−0.2305 (4)	2.55(15)
C4	0.5898 (4)	1.08806(24)	−0.3402 (4)	2.96(16)
C5	0.5633 (4)	0.89013(22)	0.2926 (4)	2.29(14)

B_{iso} is the mean of the principal axes of the thermal ellipsoid.

Table 5. Atomic parameters x,y,z and B_{iso} for $[H_4(cyclam)](SCN)_4{\cdot}2H_2O$.

	x	y	z	B_{iso}
S1	0.55750(8)	0.19423(8)	0.27233(7)	3.79(3)
C11	0.6540 (3)	0.3272 (3)	0.19201(23)	2.58(10)
N11	0.7204 (3)	0.41999(24)	0.13369(24)	3.68(11)
S2	0.32330(8)	0.15690(8)	0.61115(7)	3.50(3)
C21	0.2356 (3)	0.2516 (3)	0.5161 (3)	3.23(11)
N21	0.1712 (3)	0.3156 (3)	0.4481 (3)	4.95(14)
O	0.24550(22)	0.03023(21)	0.94310(20)	4.08(9)
N1	0.73098(22)	0.43053(21)	0.67136(19)	2.66(8)
N2	1.11430(21)	0.26464(20)	0.90422(19)	2.36(8)
C1	0.8533 (3)	0.3377 (3)	0.67414(23)	2.61(10)
C2	0.8059 (3)	0.2192 (3)	0.76348(24)	2.62(10)
C3	0.9412 (3)	0.14229(25)	0.78580(24)	2.65(10)
C4	0.9013 (3)	0.6605 (3)	0.93278(23)	2.76(10)
C5	0.7193 (3)	0.5367 (3)	0.82706(24)	2.67(10)

B_{iso} is the mean of the principal axes of the thermal ellipsoid.

Results and discussion

The salts were prepared by various methods depending upon the nature of the anion. Salts **1**, **2**, **3**, **4**, and **7** were prepared by direct crystallization of cyclam from concentrated aqueous solutions of these acids. The thiocyanate, **5**, and sulphate, **6**,

Can. J. Chem. Downloaded from www.nrcresearchpress.com by 65.111.164.53 on 09/08/12
For personal use only.

Table 6. Atomic parameters x,y,z and B_{iso} for $[H_4(cyclam)](SO_4)_2 \cdot 6H_2O$.

	x	y	z	B_{iso}
S1	0.33890(12)	0.80505(11)	0.22807(11)	1.95(5)
O1	0.2238 (3)	0.8969 (3)	0.0904 (3)	2.74(13)
O2	0.3560 (4)	0.9154 (3)	0.3134 (3)	2.80(13)
O3	0.5110 (4)	0.7473 (4)	0.1726 (4)	4.32(17)
O4	0.2630 (4)	0.6663 (4)	0.3362 (3)	4.12(16)
N1	0.3235 (4)	0.2479 (4)	0.2739 (4)	2.11(14)
N2	0.3260 (4)	0.9674 (4)	−0.2164 (4)	2.18(15)
C1	0.5185 (5)	0.6958 (5)	−0.1845 (5)	2.48(19)
C2	0.3482 (5)	0.8095 (5)	−0.2472 (5)	2.37(18)
C3	0.1694 (5)	1.0951 (5)	−0.2918 (5)	2.64(18)
C4	0.1640 (5)	1.1473 (5)	0.5279 (5)	2.55(19)
C5	0.3215 (5)	0.2213 (5)	0.4460 (4)	2.24(18)
Ow1	0.0653 (4)	0.2181 (4)	0.0966 (4)	3.79(16)
Ow2	0.0671 (4)	0.5320 (3)	0.1937 (4)	3.29(14)
Ow3	0.7551 (4)	0.4786 (4)	0.3367 (4)	3.85(15)

B_{iso} is the mean of the principal axes of the thermal ellipsoid.

were prepared by metathesis of $[H_4(cyclam)](ClO_4)_4$ with KCNS and K_2SO_4, respectively. The latter reactions proceed because $KClO_4$ is sparingly soluble. The filtrates were concentrated to give the required salts in crystalline form. Attempts to prepare crystals of $[H_4(cyclam)][HSO_4]_4 \cdot xH_2O$ based on a similar reaction between $KHSO_4$ and **4** yielded crystals of **5** only. Therefore, it does not appear that the hydrogen sulphate salt can be obtained by this method.

Cyclam and its derivatives have been extensively used in the study of coordination chemistry of transition metal ions in different oxidation states and many of these complexes have been characterized by single crystal X-ray crystallography (26). However, only two of its dicationic salts, $[H_2(cyclam)](ClO_4)_2$ (27) and $[H_2(cyclam)](CF_3SO_3)_2$ (28), have been characterized by X-ray crystallography. These studies indicate that $[H_2(cyclam)]^{2+}$ adapts an *endodentate* conformation (see Scheme 1) with the nitrogen atoms oriented towards the center of the macrocyclic cavity. A similar conformation is observed in the structure of cyclam itself (25). The stabilization of such a conformation can be attributed to strong intraionic hydrogen bonding (31). Differences in networking between the two salts can be attributed to the poor polarizability and hydrogen-accepting tendencies of perchlorate compared to that of trifluoromethanesulphonate.

It is known that all four nitrogen atoms of cyclam can be protonated under strongly acidic conditions (32) and the preparation of $[H_4(cyclam)][(COO)_2]_2$ has been described. However, no X-ray structural studies of the tetracation salts were reported until we began our studies. Unlike cyclam and its dication, $[H_2(cyclam)]^{2+}$, the tetracation, $[H_4(cyclam)]^{4+}$, adapts an *exodentate* conformation in the structures of salts we reported previously (24, 29) and in all six structures described herein. In other words, the nitrogen atoms are oriented away from the ring cavity, occupying positions as far away as possible from each other on the ring periphery (Scheme 1). The ORTEP (33) perspective view presented in Fig. 1, which could represent any of the six salts, reveals that the ethylene bridges are *transoid* and the propylene bridges ($^{N}\backslash/\backslash/^{N}$) adapt a "w"

Table 7. Atomic parameters x,y,z and B_{iso} for $[H_4(cyclam)][p\text{-}MeC_6H_4SO_3]_4$.

	x	y	z	B_{iso}
S1	0.22841(9)	0.18194(8)	0.63645(5)	2.49(4)
O1	0.1767 (3)	0.34285(23)	0.60952(16)	3.79(12)
O2	0.2184 (3)	0.08310(24)	0.57079(14)	3.40(11)
O3	0.38897(25)	0.13510(24)	0.66039(15)	3.30(11)
C1	0.0788 (4)	0.1465 (3)	0.73613(20)	2.55(14)
C2	0.1135 (4)	0.0089 (4)	0.78555(24)	3.80(17)
C3	−0.0062 (5)	−0.0216 (4)	0.8615 (3)	4.97(21)
C4	−0.1622 (5)	0.0839 (5)	0.8884 (3)	4.51(20)
C5	−0.1938 (4)	0.2197 (4)	0.8375 (3)	4.09(18)
C6	−0.0749 (4)	0.2544 (4)	0.76252(22)	3.23(16)
C7	−0.2943 (6)	0.0484 (6)	0.9691 (3)	7.5 (3)
S2	0.51573(10)	0.59738(9)	0.66993(6)	3.10(4)
O11	0.4423 (3)	0.5387 (3)	0.61139(15)	3.97(12)
O12	0.6957 (3)	0.52293(25)	0.65469(16)	3.77(11)
O13	0.4779 (3)	0.76321(24)	0.66651(17)	4.47(13)
C11	0.4202 (4)	0.5398 (4)	0.78144(23)	3.33(17)
C12	0.4131 (6)	0.6181 (4)	0.8540 (3)	5.18(24)
C13	0.3394 (7)	0.5712 (5)	0.9407 (3)	6.3 (3)
C14	0.2710 (6)	0.4479 (5)	0.9580 (3)	5.29(23)
C15	0.2799 (6)	0.3712 (5)	0.8845 (3)	6.0 (3)
C16	0.3526 (5)	0.4160 (4)	0.7970 (3)	4.87(22)
C17	0.1944 (7)	0.3969 (6)	1.0536 (3)	7.6 (3)
N1	0.2185 (3)	−0.3548 (3)	0.50714(17)	2.67(13)
N2	0.2779 (3)	0.0274 (3)	0.39048(16)	2.40(11)
C31	0.3047 (4)	−0.2279 (3)	0.47356(21)	2.62(15)
C32	0.2219 (4)	−0.1179 (3)	0.40565(22)	3.10(16)
C33	0.1917 (4)	0.1447 (4)	0.32807(21)	2.90(15)
C34	0.0037 (4)	0.2099 (3)	0.36708(22)	2.93(16)
C35	−0.0339 (4)	0.3087 (3)	0.44676(22)	2.70(15)

B_{iso} is the mean of the principal axes of the thermal ellipsoid.

Fig. 1. ORTEP perspective view of the tetracation $[H_4(cyclam)]^{4+}$.

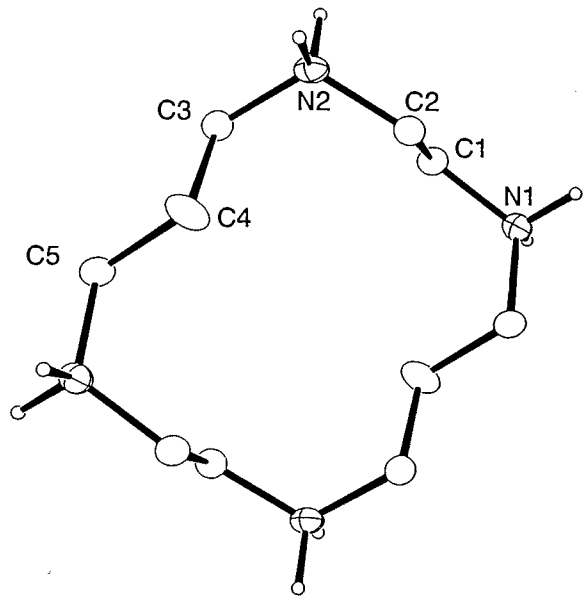

Can. J. Chem. Downloaded from www.nrcresearchpress.com by 65.111.164.53 on 09/08/12
For personal use only.

conformation. Electrostatic repulsion between the positive charges on the secondary ammonium centers makes observation of such a conformation reasonable. The most salient feature from the perspective of crystal engineering is that all eight protons of $[H_4(cyclam)]^{4+}$ are accessible for interionic hydrogen bonding and are spatially oriented in a manner that approximates 4-fold symmetry. Of course, $[H_4(cyclam)]^{4+}$ is unable to self-assemble since it is incapable of functioning as a hydrogen bond acceptor. However, it will be complementary with molecules or anions that are capable of acting as hydrogen bond acceptors . $[H_4(cyclam)]^{4+}$ is therefore functionally related to the cubanes ($[M(CO)_3(\mu_3\text{-}OH)]_4$, M = Mn, Re) we have utilized for strict self-assembly of 3D diamondoid solids (14). It is clearly capable of not only forming 1D and 2D networks, but also 3D networks. The precise nature of networks sustained by $[H_4(cyclam)]^{4+}$ will be determined by the number of available hydrogen bond acceptors from the anions and (or) the solvents of crystallisation and their spatial orientation. The remainder of this discussion focusses upon the nature of hydrogen bonding in salts of $[H_4(cyclam)]^{4+}$ and how the functionality of the anions influences the crystal architecture. The structural features of the salts are discussed individually below. Intracation and intraanion distances and angles are within expected ranges and the analysis focusses upon hydrogen bonding. It is assumed that hydrogen bonds are present for X—H···Y if the X···Y distance is within the sum of the van der Waals radii of atoms X and Y (34).

$[H_4(cyclam)]Cl_4 \cdot 4H_2O$ (1)

Preliminary details concerning 1 have been communicated (29). The cation lies around a crystallographic inversion center and is hydrogen bonded to eight adjacent cations via N—H···Cl···H—N bridges (N···Cl 3.065(3)–3.242(3) Å). The ability of the chloride anions to hydrogen bond obtusely (N···Cl···N angles are 128.98(8)° and 144.45(9)°) facilitates the formation of a 3D network. As Fig. 2 reveals, cations on adjacent layers eclipse each other and there are two microchannels, (*i*) and (*ii*), that run parallel to the *a*-axis. Each channel contains two molecules of water per cation. In microchannel (*ii*) the water molecules are disordered so it cannot be determined if they self-assemble as oligomers or as a polymer. This is a common observation in solids that contain microchannels that are filled with water molecules (35). However, microchannel (*i*) has the requisite diameter and placement of hydrogen bond acceptors to allow ordering of the water molecules, which exist as symmetrical 1D polymers. Such ordering of water molecules is to our knowledge unique and is presumably facilitated by hydrogen bonding of water oxygen O—H moieties to chloride ions along the walls of the microchannels. The hydrogen atoms that bridge water molecules could not be located since crystallographic symmetry requires that they must be disordered, but those that are hydrogen bonded to chloride anions could be located (O—H···Cl(2), 2.27 Å; 176°). The O···O distances within this water polymer are 2.728(10) and 2.736(10) Å, which compare closely with the O···O distances in ice (2.750–2.793 Å) (36, 37) and a water dimer that was encountered in a host–guest complex (2.805 Å) (38).

$[H_4(cyclam)]Br_4 \cdot 4H_2O$ (2)

One half of the cation, anions, and water molecules constitute the asymmetric unit because once again the cation lies around a crystallographic inversion center. All the anions and the water molecules are involved in network hydrogen bonding with the cation such that cations on successive layers eclipse one another. However, no microchannels were observed in this structure since, although the stoichiometry is the same as that for **1**, the nature of the networking is entirely different. The bromide anions bridge both cations and water molecules. A portion of the network involving the bromide anions, water molecules, and the $[H_4cyclam]^{4+}$ nitrogen atoms is shown in Fig. 3. All four lone pairs of Br2 are involved in hydrogen bonding interactions between adjacent cations through N1—H···Br2···H—N2 bridges. Thus, N1 of one cation is bridged through Br2 (Br2···N1, 3.371(4) Å) to N2 of an adjacent cation (Br2···N2, 3.330(4) Å). Br2 also shows interactions with O1 and O2 (O1···Br2, 3.370(4) Å; O2···Br2, 3.502(5) Å). Br1 exhibits three prominent hydrogen bonding interactions, bridging both water molecules and linking to N1. The hydrogen bond distances are Br1···O1, 3.417, Br1···O2, 3.653, and Br1···N1, 3.236(4) Å, respectively. Presumably, the larger size of bromide ions and their involvement in bridging water molecules precludes formation of microchannels and water polymers.

Fig. 2. ORTEP perspective view of the *bc* plane in **1**. Microchannels *i* and *ii* are parallel to the *a*-axis and microchannel *i* contains the ordered polymer of water molecules.

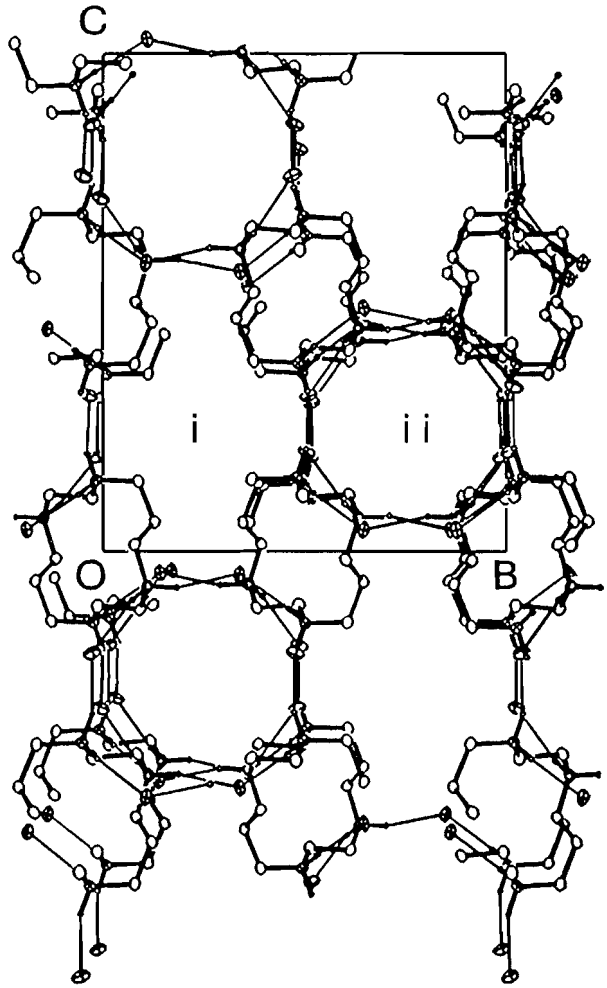

Can. J. Chem. Downloaded from www.nrcresearchpress.com by 65.111.164.53 on 09/08/12
For personal use only.

Fig. 3. ORTEP perspective view of the polymeric chain formed by bromide anions and water molecules in **2**. NH_2^{2+} moieties hydrogen bond to bromide anions.

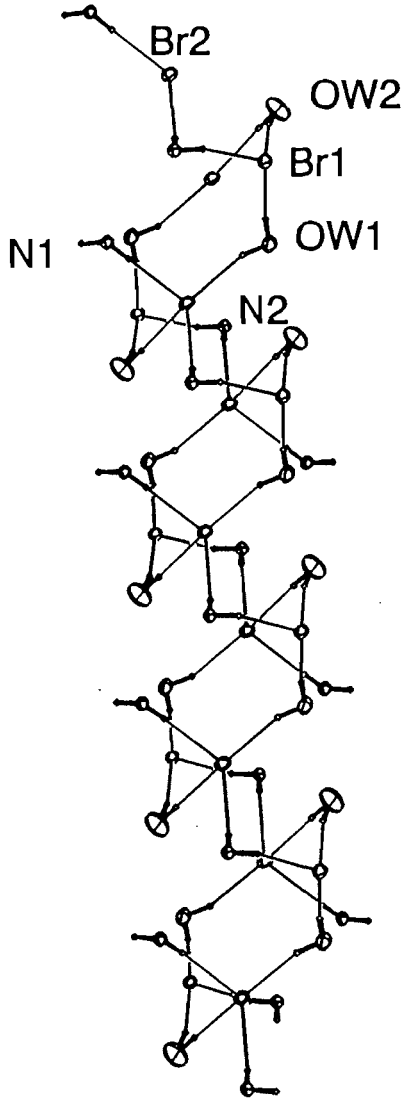

Fig. 4. ORTEP perspective view of a portion of the network in **4**.

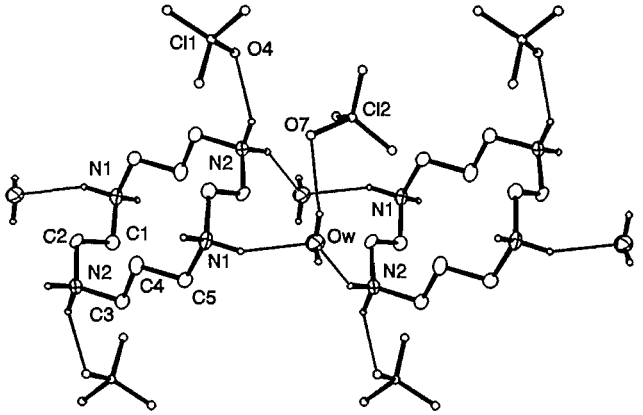

Fig. 5. ORTEP perspective view of a portion of the network in **5**.

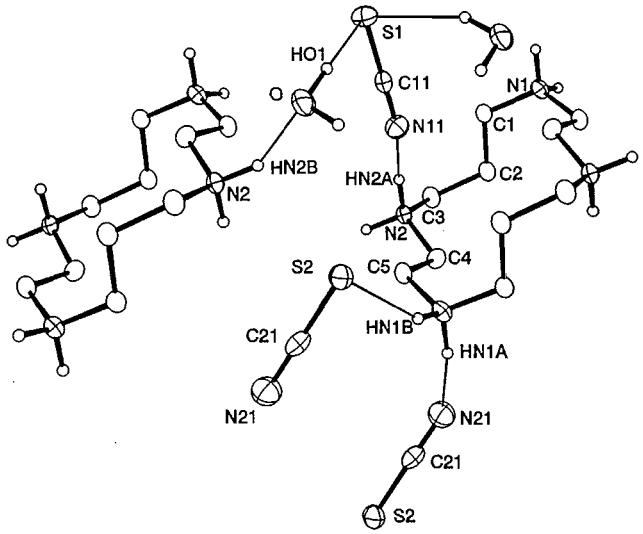

$[H_4(cyclam)](ClO_4)_4 \cdot 2H_2O$ (4)

An ORTEP perspective of the network hydrogen bonding in **4** is shown in Fig. 4. The perchlorate anion is generally regarded as being a weak hydrogen bond acceptor and it does not act as a strong hydrogen bond acceptor in the network. Neighbouring cations are joined sidewise through two N1—H···Ow···H—N2 (N2···Ow, 3.032(4) Å; N1···Ow, 2.979(4) Å) hydrogen bonds that manifest themselves as linear tapes. There are only two crystallographically independent perchlorate anions because the cation lies around a crystallographic inversion centre and they are terminally bound. Though terminally bound, the perchlorates show multiple points of contact, to NH_2^+ moieties as well as to water molecules: N1···O2, 3.051(4) Å; N1···O7, 3.083(4) Å; N2···O6, 2.989(4) Å between perchlorate oxygen atoms and nitrogen atoms; O_w···O1, 2.979(5) Å, Ow···O2, 3.033(4) Å, and Ow···O7, 2.934(4) Å between perchlorate oxygen atoms and water molecules. These interactions are much stronger than those observed (<3.5 Å) in $[H_2$-(cyclam)$](ClO_4)_2$ (31) and can be attributed to the higher charge on the tetracation.

$[H_4(cyclam)](CNS)_4 \cdot 2H_2O$ (5)

An ORTEP perspective of the network hydrogen bonding in **5** is illustrated in Fig. 5. One half of the cation, two anions, and one water molecule constitute the asymmetric unit since the cation once again lies around a crystallographic inversion center. The two crystallographically independent thiocyanate ions are linear (N-C-S, 179.16(19)° and 178.77(22)°) and both are involved in hydrogen bonding, but in different modes. One set of thiocyanate ions generates a bridging N1—H···S2—CN2···H—N1 motif and two such motifs link adjacent cations. Because both hydrogen atoms of N1 on neighbouring cations are involved (N1···S2, 3.326(19) Å; N1···N21, 2.766(3) Å) a 12-membered centrosymmetric hydrogen bond stabilized macrocyclic ring motif is formed. This 12-membered ring motif and the 14-membered ring $[H_4(cyclam)]^{4+}$ cation alternate to form 1D strands in which N1 is the spiro atom common to both rings. These strands are cross-linked by the second set of thiocyanate ions and the water molecules. N11 is linked to HN2A of the cations (N2···N11, 2.877(3) Å) while HN2B is bonded to S1 of the anion through a molecule of water

Fig. 6. ORTEP perspective view of a portion of the network in **6**. The arrow is parallel to the sheets formed by sulphate anions and water molecules.

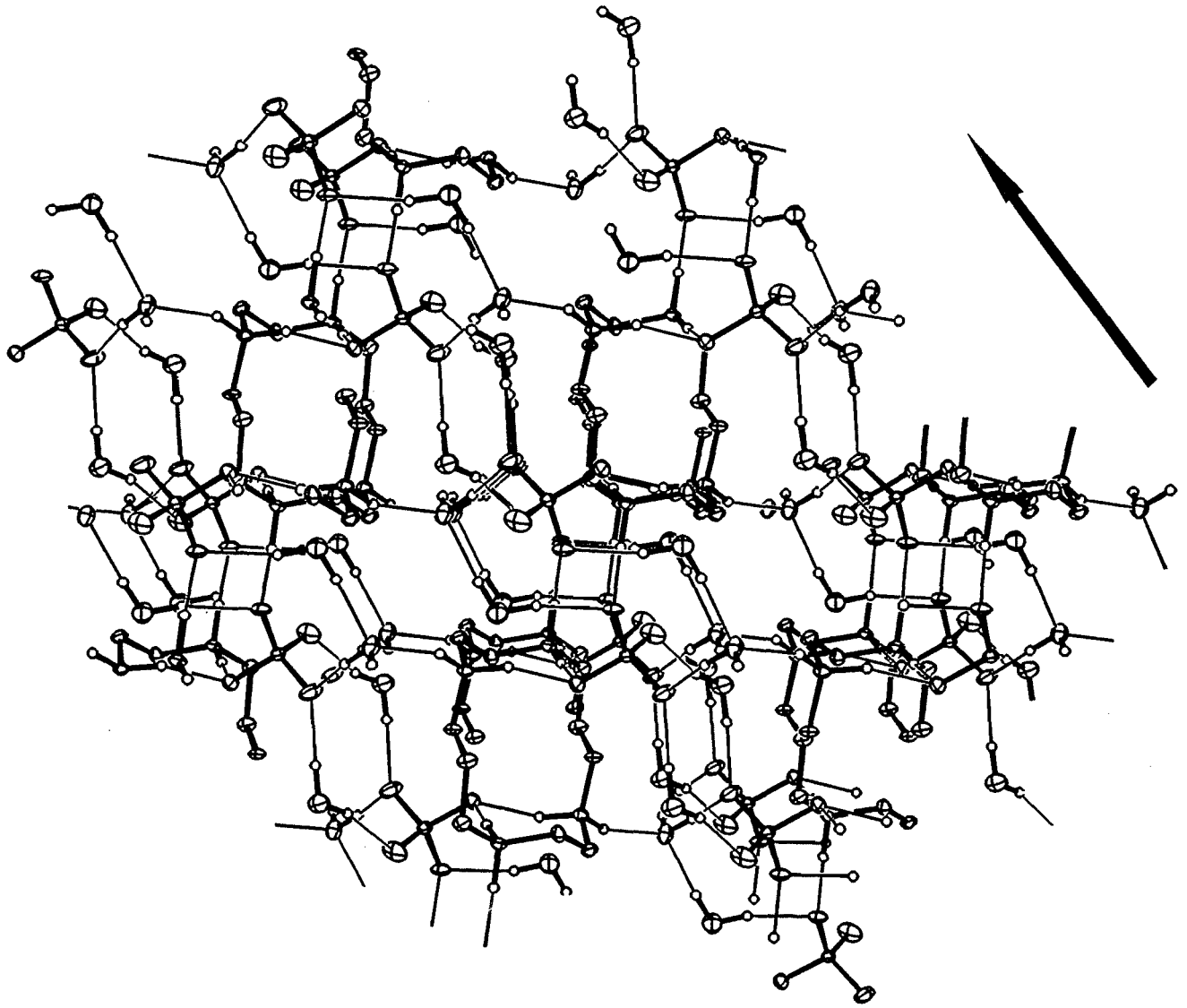

(N2···O, 2.758(2) Å; O···S1, 3.282(2) and 3.358(2) Å). A 2D network is therefore afforded.

$[H_4(cyclam)](SO_4)_2 \cdot 6H_2O$ (6)

An ORTEP perspective of the networking in **6** is shown in Fig. 6. The cation lies around an inversion center and hence the asymmetric unit is defined by one half of the cation, one anion, and three water molecules. Sulphate anions are good hydrogen bond acceptors and the structure can be regarded as 3D since there are sheets of sulphate anions and water molecules cross-linked by $[H_4(cyclam)]^{4+}$ cations. Adjacent $[H_4(cyclam)]^{4+}$ cations are cross-linked through two N2—H···O1—S—O2···H—N1 bridges (O1···N2, 2.702(4) Å; O2···N1, 2.788(4) Å). O2 also interacts with N2 (O2···N2, 2.849(3) Å). The other two oxygen atoms of the sulphate anion do not interact with the cation. Rather, they interact with water molecules. Each water molecule is hydrogen bonded to a sulphate oxygen atom (O1··· Ow1, 2.883(4); O3···Ow3, 2.756(4) Å; O4···Ow2, 2.760(4) Å). The oxygen atoms of the water molecules Ow1 and Ow2 also show hydrogen bonding interactions with N1 (N1···Ow1, 2.796(4) Å; N1···Ow2, 2.790(4) Å).

$[H_4(cyclam)](p\text{-tosylate})_4$ (7)

The cation once again lies around a crystallographic inversion center so there are only two independent anions. Figure 7 presents an ORTEP view of the cation and illustrates how the anions are hydrogen bonded to the NH_2^+ moieties. All the hydrogen atoms of the cation and two of the oxygen atoms of the *p*-toluenesulfonate anions are engaged in hydrogen bonding. NH_2^+ moieties are linked to crystallographically equivalent NH_2^+ groups on neighbouring cations through N—H··· O—S—O···N—H bridges (N2···O2, 2.765(3) Å; O3···N2, 2.749(3); N1···O11, 2.708(3) Å; N1···O12, 2.903(3) Å). Thus, the networking generates a 2D sheet of cations bridged by *p*-toluenesulfonate anions. The hydrophobic toluene rings project outwards on both sides of the 2D sheet. Hence, the overall crystal structure can be described as layers of ionic networks separated by hydrophobic regions (Fig. 8). The hydrogen bond

Can. J. Chem. Downloaded from www.nrcresearchpress.com by 65.111.164.53 on 09/08/12
For personal use only.

Can. J. Chem. Downloaded from www.nrcresearchpress.com by 65.111.164.53 on 09/08/12
For personal use only.

Fig. 7. ORTEP plot of the cation and the two unique *p*-tosylate anions.

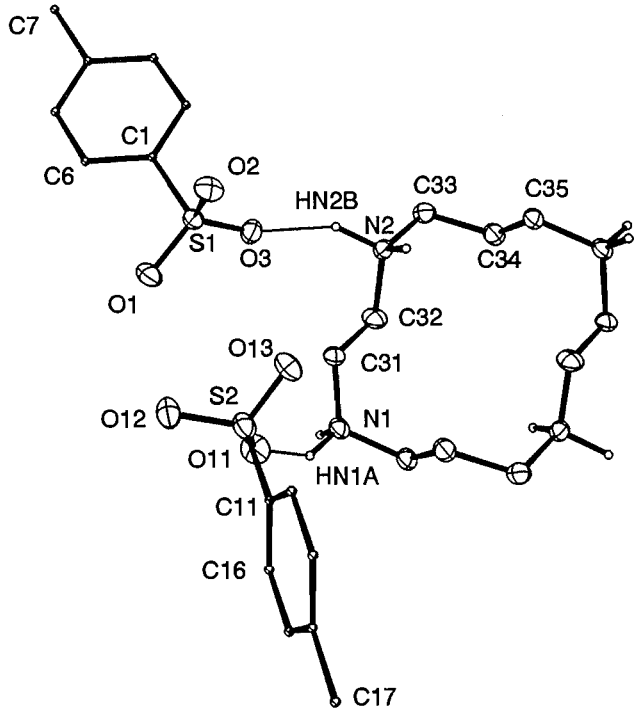

angles vary in the range of 144.7°–167.8°. The N—H···O—S—O··· N—H bridges involve both hydrogen atoms of each NH_2^+ moiety and therefore form 12-membered rings similar to those found in the thiocyanate salt. Although there are no water molecules involved in the hydrogen bonding network there appears to be one solvent water molecule that partially occupies a hydrophobic cavity (see experimental section).

The salts reported herein possess many common structural features. The symmetric tetracation lies around an inversion center in all the structures and adapts the same *exo*-dentate conformation irrespective of the dimensionality of the network. The anions play a significant role in the network hydrogen bonding. All six structures clearly conform to the hydrogen bonding rules delineated by Etter (31). Water plays a dominant role in bridging the cations only when the anions are nominally weak hydrogen bond acceptors. In the absence of water and in the presence of surplus hydrogen bond acceptors, as in **7**, all the strong hydrogen bond donors are utilized. It is perhaps surprising that the halide salts adapt dramatically different solid state structures. The observation of a 1D water polymer in **1** is serendipitous but can be rationalized. That the iodide salt, **3**, loses moisture so readily suggests that it possesses an architecture more similar to **1** than to **2**. If so, the microchannels would be expected to be larger and not bind the water molecules as strongly. This would explain the observed behaviour. The ionic nature of these salts demands aqueous media for the formation of single crystals and hence competition from water as a hydrogen bond donor/acceptor is unavoidable. The absence of water molecules in **7** is presumably a reflection of the relatively high strength of the hydrogen bond accepting capabilities of sulfonate anions (28) and the hydrophobic tolyl groups.

In summary, it is clear that $[H_4(cyclam)]^{4+}$ consistently adapts a centrosymmetric exodentate conformation that facilitates network hydrogen bonding. The nature of the resulting network can be 1D, 2D, or 3D depending upon the nature of the counterion (i.e., its hydrogen bond accepting capabilities and geometry) and the number of solvent molecules. Unfortunately, none of the six new structures is polar. This is because the center of inversion present in $[H_4(cyclam)]^{4+}$ manifests itself crystallographically. Derivatives of cyclam that possess no center of symmetry would be expected to be much more predisposed to crystallize in polar space groups and would therefore be worthy of further study.

Fig. 8. ORTEP view of a portion of the network in **7** that illustrates how the tolyl moieties orient themselves to form hydrophobic regions above and below the hydrogen bonded sheet.

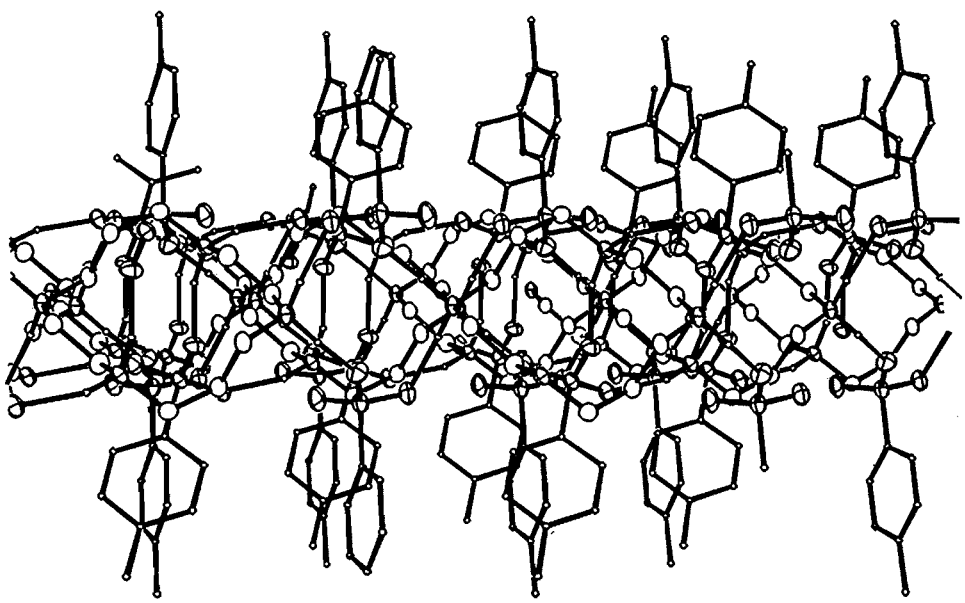

Acknowledgements

We thank the Natural Sciences and Engineering Research Council of Canada (NSERC) for a research grant to M.J.Z. and Saint Mary's University for purchasing the X-ray diffractometer.

References

1. G.R. Desiraju. *In* Crystal engineering; the design of organic solids. Elsevier Science Publishing Company, Inc., New York. 1989.
2. P.J. Fagan and M.D. Ward. Sci. Am. **267**, 48 (1992).
3. C. B. Aakeroy and K. R. Seddon. Chem. Soc. Rev. 397 (1993).
4. J.-M. Lehn, M. Mascal, A. Decian, and J. Fischer. J. Chem. Soc. Perkin Trans. 2, 461 (1992).
5. M. Gallant, M.T.P. Viet, and J. D. Wuest. J. Org. Chem. **56**, 2284 (1991).
6. K. Kondo, S. Ochiai, K. Takemoto, Y. Kai, and N. Kasai. Chem. Phys. Lett. **188**, 282 (1992).
7. S.J. Geib, S C. Hirst, C. Vincent, and A.D. Hamilton. J. Chem. Soc. Chem. Commun. 1283 (1991).
8. L. Lieserowitz and A.T. Hagler. Proc. R. Soc. London. A: **388**, 133 (1983).
9. D. Tanner, J.A. Fitzgerald, and B.R. Philips. Angew. Chem. Int. Ed. Engl. Adv. Mater. **28**, 649 (1989).
10. Y.-L. Chang, M.-A. West, F.W. Fowler, and J.W. Lauher. J. Am. Chem. Soc. **115**, 5991 (1993).
11. S.B. Copp, S. Subramanian, and M.J. Zaworotko. Angew. Chem. Int. Ed. Engl. **32**, 706 (1993).
12. O. Ermer. J. Am. Chem. Soc. **110**, 3747 (1990).
13. M. Simard, D. Su, and J.D. Wuest. J. Am. Chem. Soc. **113**, 4696 (1991).
14. (*a*) S.B. Copp, S. Subramanian, and M.J. Zaworotko. J. Am. Chem. Soc. **114**, 8719 (1992); (*b*) J. Chem. Soc. Chem. Commun. 1078 (1993).
15. J.S. Lindsey. New J. Chem. **15**, 153 (1991).
16. R.A. Hahn and D. Bloor (*Editors*). Organic materials for nonlinear optics. Royal Society of Chemistry, London. 1989.
17. M.L.H. Green, S.R. Marder, M.E. Thompson, J.A. Bandy, D. Bloor, P.V. Kolinsky, and R.J. Jones. Nature, 330 (1987); 360 (1987).
18. S.R. Marder, J.E. Sohn, and G.D. Stucky (*Editors*). Materials for nonlinear optics; chemical perspectives. ACS Symp. Ser. American Chemical Society, Washington, D.C. 1991.
19. C.B. Aakeroy, P.B. Hitchcock, B.D. Moyle, and K.R. Seddon. J. Chem. Soc. Chem. Commun. 1856 (1989).
20. C.B. Aakeroy, G.S. Bahra, P.B. Hitchcock, Y. Patell, and K.R. Seddon. J. Chem. Soc. Chem. Commun. 152 (1993).
21. C.B. Aakeroy, P.B. Hitchcock, and K.R. Seddon. J. Chem. Soc. Chem. Commun. 553 (1992).
22. C.B. Aakeroy and P.B. Hitchcock. J. Mater. Chem. **3**, 1129 (1993).
23. J. Pecaut, Y. Le Fur, and R. Masse. Acta Crystallogr. Sect. B: Struct. Sci. **B49**, 535 (1993).
24. S. Subramanian and M.J. Zaworotko. Can. J. Chem. **71**, 433 (1993).
25. G.A. Melson (*Editor*). Coordination chemistry of macrocyclic compounds. Plenum Press, New York. 1979. Chap. 4. p. 237.
26. L.F. Lindoy. *In* The chemistry of macrocyclic ligand complexes. Cambridge University Press, Cambridge. 1989.
27. C. Nave and M. R. Truter. J. Chem. Soc. Dalton Trans. 2351 (1974).
28. G. Bandoli, A. Dolmella, and S. Gatto. J. Crystallogr. Spectrosc. Res. **23(9)**, 755 (1993).
29. S. Subramanian and M. J. Zaworotko. J. Chem. Soc. Chem. Commun. 952 (1993).
30. E.J. Gabe, Y. Le Page, J-P. Charland, F.L. Lee, and P.S. White. J. Appl. Crystallogr. **22**, 384 (1989).
31. M. C. Etter. Acc. Chem. Res. **23**, 120 (1990).
32. M. Micheloni, A. Sabatini, and P. Paoletti. J. Chem. Soc. Perkin Trans. 2, 828 (1978).
33. C.K. Johnson. ORTEP, a Fortran thermal ellipsoid plot program. Technical Report ORNL-5138, Oak Ridge, Tenn. 1976.
34. S.N. Vinogradov and R.H. Linnell. Hydrogen bonding. Van Nostrand Reinhold, Toronto. 1971.
35. I.R. Hanson and M.R. Truter. Biosci. Rep. **2**, 521 (1982).
36. S.J. La Placa, W.C. Hamilton, B. Kamb, and A. Prakash. J. Chem. Phys. **66**, 498 (1977).
37. A.H. Narten, C.G. Venkatesh, and S.A. Rice. J. Chem. Phys. **64**, 1106 (1976).
38. P.J. Dutton, F.R. Fronczek, T.M. Fyles, and R.D. Gandour. J. Am. Chem. Soc. **112**, 166 (1990).

Can. J. Chem. Downloaded from www.nrcresearchpress.com by 65.111.164.53 on 09/08/12
For personal use only.

Thermochemistry of the liquid bismuth(III) oxide – boron oxide: a new solvent for oxide melt solution calorimetry

Jacques Rogez and Jean Claude Mathieu

Abstract: In solution calorimetry, the choice of solvent is important. Some criteria for this choice for oxide melt solution calorimetry are reviewed. A new solvent is proposed and the corresponding physicochemical study is presented. Some structural interpretations are suggested for these Bi_2O_3–B_2O_3 melts.

Key words: thermochemistry, calorimetry, high temperature, oxide melt.

Résumé : En calorimétrie de dissolution le choix du solvant est important. Quelques éléments de ce choix sont revus. On propose un nouveau solvant et son étude physicochimique est présentée. Des interprétations structurales sont suggérées pour ces liquides Bi_2O_3–B_2O_3.

Mots clés : thermochimie, calorimétrie, température élevée, oxyde fondu.

[Traduit par la rédaction]

Can. J. Chem. Downloaded from www.nrcresearchpress.com by 65.111.164.53 on 09/08/12
For personal use only.

Introduction

The determination of the enthalpic quantities corresponding to the formation of solid compounds, and liquid or solid solutions, is the aim of calorimetry. For oxide systems, within the temperature range where measurements may be done (typically up to 1700 K), direct reaction between the reactants is always difficult and often even impossible due to the low reaction rates (slow diffusion processes of the elements, slow interface reactions or high viscosities). As a result, for such studies, solution calorimetry, which consists in comparing the destruction energies of the networks of products and reagents, has rapidly become indispensable where the choice of solvent is difficult.

From a very early stage the curiosity of scientists has been attracted to dissolution phenomena. In alchemic tradition all the liquids that dissolve certain solids were called "menstrui." The origin of this word stems from the revolution period of the moon, and refers to the generally long duration of this process. In the seventeenth century the chemist Boerhaave defined a "menstruum" as a substance that, "if it were applied to another, following the rules of the art, would break it so finely that the particles of the solvent would nearly completely mingle with those of the solute" (1).

In oxide solution calorimetry, the original idea was to perform the dissolution in the temperature range where the calorimetric experiments are the easiest and also the most accurate, i.e., around ambiant temperature. For a recent example see ref. 2. Acidic and basic aqueous solvents are commonly used. An important drawback to this method is the generally great difference between the measured thermal effects of the dissolution reactions and the expected enthalpy, which can be some percentage of the former. Moreover, the enthalpy of the reaction of formation is calculated from at least two different solution reactions, which further increases the inaccuracy.

To overcome this difficulty, it was proposed to use a solvent the chemical nature of which is quite similar to that of the solute, even if the experimental setup imposes a ticklish problem. The final expected enthalpy and the dissolution energy should be of about the same magnitude. One of the main constraints of this choice is the need to carry out the measurements at high temperature. The studies are generally performed between 500 and 1200 K in a fluxmeter.

Nevertheless, these two measurement methods complement one another well. By means of thermodynamic cycles it is possible to verify the agreement between the measured and estimated quantities such as heat capacities and, in particular, the melting and transition enthalpies.

During the last 20 years, only a few groups of researchers have ventured and persevered in the difficult technology of high-temperature solution calorimetry in molten oxide melts. The aim has very often been the study of compounds of geological interest. O.J. Kleppa and co-workers at the University of Chicago were the pioneers in this technique (3). Later, A. Navrotsky at Princeton University and two groups in Grenoble (France) and in Moscow (CEI) used this method. Such equipment has already enabled the authors to perform thermochemical studies of, for example, the albite–orthoclase and the Na_2O–K_2O–SiO_2 systems (4, 5).

Various solvents have been investigated by the different groups; in most cases the $2PbO$–B_2O_3 melt has been used. The aim of this paper is to propose a new solvent, and the corresponding thermochemical study is presented.

The choice of a solvent

The choice of a solvent is crucial for successful solution calorimetry. This paper is restricted to studies of oxide systems.

Received June 6, 1994. Revision received December 14, 1994.

J. Rogez[1] **and J.C. Mathieu.** Centre de Thermodynamique et Microcalorimétrie du Centre National de la Recherche Scientifique, 26 rue du 141ème R.I.A., 13331 Marseille Cédex 3, France.

[1] Author to whom correspondence may be addressed. Telephone: 33-91-28-20-50. Fax: 33-91-50-38-29.

Can. J. Chem. Downloaded from www.nrcresearchpress.com by 65.111.164.53 on 09/08/12
For personal use only.

The particular conditions the solvent must satisfy have been distinguished from the restricting conditions imposed by the calorimetric setup.

(*i*) The solvent must obviously dissolve the constituents of the systems under consideration. Calorimetric dissolution experiments are long and tedious, and the price to be paid, in time, for a measurement is heavy. For this reason, the chosen melt should be able to dissolve a large number of acid and basic constituents without showing a great difference between the dissolution enthalpies. Thus, the results obtained for various systems can be compared and corroborated. This last condition is satisfied when the solvent presents a buffer character in the sense of the acid-basic reactions in oxide systems as defined by Flood and Förland (6). Generally speaking, the main problem of the experimental investigations is the reproducibility of the measurements. In oxide solution calorimetry it often amounts to a few percent, for example, 4% for SiO_2 in the $2PbO–B_2O_3$ melt at 970 K (7). In some cases it may be worse, as stated by Shearer and Kleppa for the dissolution of MgO in $2PbO–B_2O_3$ (±20%) (8). We have also observed such a discrepancy in a previous study of the $MgO–Cr_2O_3$ system by solution calorimetry in the same solvent. The choice of solvent is always a compromise between fast dissolution kinetics, which induces the use of a strong reagent, and a measured energy that is not too high. In aqueous solvents this dilemma is neatly solved by varying the solvent concentration.

The vapor pressure of the solvent must remain very low within the temperature range investigated. During the runs the quantity of solvent must not significantly change and, in the case of a multicomponent melt, the composition must not vary by differential vaporization. From this viewpoint, those simple oxides whose melting points are very low, such as OsO_4, Re_2O_7, or, to a lesser degree, TeO_2, are not suitable. In most cases the sample is thermally stabilized above the melt surface before the dissolution. If the equilibrium pressure above the melt is too high, the sample may react with the solvent vapor before the expected dissolution in the liquid state.

The solvent must present a low viscosity in order to keep the dissolution rate relatively high. Pure boron oxide, for example, has too high a viscosity at 1070 K. The stirring that is necessary in most cases must be mechanically possible without damaging the stirring setup. If the basic constituent is a network former melt, the other constituents have to include some network modifiers in order to diminish the viscosity, which depends on the degree of polymerization.

The solvent is commonly prepared outside the calorimeter by melting the various oxides or by thermal decomposition of the corresponding carbonates. Toxicity is then a significant factor in the choice of solvent. Some oxides, such as B_2O_3, Sb_2O_3, MoO_3, and Bi_2O_3 are not known as toxic reagents. The cations or the metallic atoms of other oxides are toxic after ingestion or inhalation (As_2O_3, V_2O_5, PbO, with cumulative effect). In this sense the handling of the solvent must be easy. A melt that is insensitive to moisture is more suitable for extended storage.

Generally, the enthalpies of formation or the enthalpies of transition are deduced from the partial dissolution enthalpies at infinite dilution. Extrapolation to zero concentration is easier the less the dissolution enthalpy varies with composition. Indeed, a linear dependence with a low or zero slope has been observed in many systems. Though perfect chemical homogeneity in the liquid is sometimes difficult to obtain when, for example, partial crystallizations or vitrifications inducing chemical segregations occur during the quench; the values are generally not sensitive to small concentration differences between batches coming from the same primary melt.

Table 1. The melting temperatures T_f (in K) of simple oxides whose melting points are less than 1400 K (10–12).

Chemical formula	T_f (K)
OsO_4	313
Re_2O_7	570
As_2O_3	585
B_2O_3	723
TeO_2	660
Sb_2O_3	929
V_2O_5	943
MoO_3	1075
Bi_2O_3	1098
PbO	1170
GeO_2	1389

Most of these conditions are satisfied when the solvent presents some buffer properties with respect to the acid and basic oxides. A discussion of this point has been already given by Kleppa (9). The choice of $PbO–B_2O_3$ as solvent has been mainly justified by the low variation of the partial enthalpy in the composition range $x_{PbO} = 0.45$ to $x_{PbO} = 0.8$. In addition, the phase diagram presents a wide liquid zone around the eutectic composition close to the compound $2PbO·B_2O_3$. When a new solvent is selected this characteristic should be a criterion in the choice of the best composition.

(*ii*) The calorimetric configuration imposes some conditions on the choice of solvent.

The melting point must be sufficiently low to be within the temperature range of the calorimeters, which generally offer a maximum temperature of about 1300 K. At higher temperature technological problems appear in the mechanical behaviour of the setup. As shown in Table 1 very few single oxides are convenient. Polyconstituent oxides, which present lower melting points as eutectics, are more suitable. It can be mentioned that in oxide systems very low euctectics are not common and most systems show binary or ternary high-melting-point compounds. At present, the greatest number of dissolution experiments with various solvents have been performed between 950 and 1250 K.

The solvent must not interact with the measurement cell atmosphere, which is generally air. The chosen oxide or mixture of oxides will then be stable under a 0.21 atm partial pressure of oxygen (1 atm = 101.3 kPa).

Another important consideration is the reactivity of the solvent with respect to the material constituting the crucible and the stirring equipment. For good heat transfer to the fluxmeter, a metallic crucible having high thermal conductivity is necessary. Pure gold and silver, which are oxide melt resistant, are generally chosen. The dissolution time is important as the metal of the crucible may be exposed to attack of the solvent for long periods. The kinetics of this dissolution reaction must remain very slow. Even if the dissolution rate is low, mechan-

Can. J. Chem. Downloaded from www.nrcresearchpress.com by 65.111.164.53 on 09/08/12
For personal use only.

ical damage may occur. For example, during local remelting for strengthening some parts of a platinum crucible, some bubbles of alkaline metal or oxide were observed on the crucible walls, which had been previously exposed to $NaBO_2$–$LiBO_2$ solvent. The presence of lithium in the melt may induce a diffusion of this alkaline element into the grain boundaries of the metal and may then cause it to become brittle. The break may occur during further handling of the crucible at ambiant temperature when renewing the solvent between two dissolutions. Diffusion into the grain may also occur if the solubility of the foreign element in the crucible metal is high enough. Tin with respect to platinum is a good example of this phenomenon. If a compound is formed, the diffusion process can be stopped. If the melting point of the corresponding compound is quite near the dissolution temperature, the brittleness at high temperature may increase. Our experience gives a lifetime for platinum crucibles of about 50 runs in $2PbO$–B_2O_3 melt and 10 runs in $NaBO_2$–$LiBO_2$ melt. Finally, the cost of the crucible, which is mainly a labour cost even for precious metals, must be taken into account.

The kinetics of the dissolution reaction must be fast compared to the characteristic time for stability of the calorimeter. Typically, the dissolution time should not be greater than 1 h. This rate depends greatly on transport phenomena in the liquid state, interface reactions during the dissolution being generally rapid. The liquidus slope of the solute–solvent phase diagram gives an indication of the dissolution rate. Thus, most experiments are performed by stirring in the melt, which homogenizes the liquid and also increases the dissolution rate. This kind of setup imposes a measurement of the stirring energy by performing a blank run after each dissolution; this then doubles the experimental time.

In conclusion, it seems that pure oxides cannot satisfy these constraints. The solution lies in multicomponent melts including acidic and basic oxides. Because of the toxicity of PbO a new solvent was sought. Solvents based on B_2O_3 are good candidates, as boron oxide is the lowest melting oxide that satisfies the criteria of toxicity, vapor pressure, and cost. Alkaline earth – boron oxide melts present too high vapor pressures. The alkaline earth – boron oxide systems show phase separations in the liquid phases and the eutectics are very close to those of the pure oxides. Finally, bismuth oxide – boron oxide melts were selected; as the Bi_2O_3–B_2O_3 and PbO–B_2O_3 phase diagrams are similar, it may be expected that the two melts behave similarly. In the following, the thermodynamic study of the Bi_2O_3–B_2O_3 melt is presented.

Physicochemical study of the system Bi_2O_3–B_2O_3 at 1023 K

The thermochemical properties of the $Bi_2O_{3(1-x)}$–B_2O_{3x} system in the liquid state have been investigated in the composition range $0.1 < x < 0.8$.

Preparation of the solvent

The starting materials are Extra Pure bismuth(III) oxide and Pro Analysi boric acid as provided by Merck. For each composition, about 80 g of solvent are prepared by reacting boric acid with bismuth oxide in a platinum crucible. The two weighed powders are carefully mixed and introduced into an open-air furnace whose temperature is electronically controlled. At the beginning of the reaction, the temperature is raised slowly in order to control the thermal decomposition of the boric acid. As a final stage of the process, the melt is kept at 1123 K during 1 h. After quenching on a stainless steel plate, the ground solid is melted again at the same final temperature for homogenization.

Measurements of the partial mixing enthalpies

The starting materials for the solute samples are anhydrous boron trioxide provided by Merck (Pro Analysi quality) and the same bismuth(III) oxide as that used for the solvent. As mentioned in Table 2, about 0.08 mole of solvent is used for each melt composition.

The calorimetric measurements are performed in a twin Tian–Calvet-type calorimeter at 1023 K in air. The experimental high-temperature equipment has been described previously (4). The inner diameter of the heat flux sensor is 17 mm and the pure platinum crucible as 70 mm in height and 14 mm in inner diameter. Before dissolution the ground sample (typically <100 μm) is thermally equilibrated on a platinum cup just above the free surface of the melt inside the calorimetric cell. Hence, the solute and the solvent are at the same temperature before the reaction. Dissolution begins when the cup is introduced into the liquid by a vertical motion of the calorimetric equipment. Automatic vertical shaking of the cup increases the global dissolution rate. Thermal effects due to the transfer of the cup into the measurement cell and the stirring motion are measured just after completion of the reaction by carrying out the same experiment without a sample. The reproducibility of this blank run is about 95%; it represents about 20% of the overall thermal effect. The thermogram is automatically integrated by a microcomputer.

Results

In Table 2 and Fig. 1 the partial mixing enthalpies of Bi_2O_3 and B_2O_3 referred to solid Bi_2O_3 and liquid B_2O_3 are reported for the various concentrations. The inaccuracy is about ±4 kJ mol^{-1} except for $x_{B_2O_3} = 0.2$ where the discrepancy between the Bi_2O_3 partial enthalpies is higher. The partial enthalpies do not vary within the error margin in the solute composition ranges $0 < y_{Bi_2O_3} < 0.004$ and $0 < y_{B_2O_3} < 0.011$. It may then be expected that these values represent the partial mixing enthalpies. For the B_2O_3-rich composition only one value is available because of the too-high viscosity of the melt and the close proximity of this concentration to the phase separation curve in the liquid state, which induces a lower dissolution rate. In only one run did the molten sample not remain stacked in the cup without dissolution.

The curves in Fig. 1 fit the results, taking into account the Gibbs–Duhem relation. The integrating pole is $x_{B_2O_3} = 0.4$, $\Delta H_{B_2O_3} = -48.7$ kJ mol^{-1}. The Bi_2O_3 partial enthalpy at $x = 0$ corresponds to the melting enthalpy given by Robie et al. (10); $\Delta H_f = 16.74$ kJ mol^{-1}.

In the concentration range $0.2 < x_{B_2O_3} < 0.75$ the partial enthalpies do not vary significantly. Consequently this behaviour induces a flat curve for the integral mixing enthalpy referred to the two liquids at around −45 kJ mol^{-1}.

After each run and for each melt composition, the resulting liquid was quenched on a stainless steel plate. Because of the heterogeneity of the sample temperature, the mean cooling rate can be estimated at 10 K s^{-1} in the liquidus temperature

Table 2. Partial mixing enthalpies of Bi_2O_3 and B_2O_3 in B_2O_3–Bi_2O_3 melts at 1023 K. The quantities $N_{B_2O_3}$ or $N_{Bi_2O_3}$ per μmol represent the amounts of solute dissolved in each run. The quantity N_s per mmol of the solvent is reported for each bath.

$N_{Bi_2O_3}$/μmol	$\Delta_{mix}H_{Bi_2O_3}$ (kJ mol^{-1})	$N_{B_2O_3}$/μmol	$\Delta_{mix}H_{B_2O_3}$ (kJ mol^{-1})
	0.1 B_2O_3 – 0.9 Bi_2O_3 (N_s/mmol = 64.5)		
47	−8.82	193	−105.0
39	−5.29	187	−104.8
47	−3.63	140	−100.1
	0.2 B_2O_3 – 0.8 Bi_2O_3 (N_s/mmol = 72)		
67	−25.5	239	−62.0
110	−8.62	366	−62.9
72	−35.0	156	−62.6
	0.4 B_2O_3 – 0.6 Bi_2O_3 (N_s/mmol = 91)		
75	−35.7	152	−51.7
92	−34.6	355	−46.6
47	−32.0	127	−47.7
88	−28.6		
	0.6 B_2O_3 – 0.4 Bi_2O_3 (N_s/mmol = 122)		
	−42.5	127	−47.6
29	−46.0	395	−47.9
44	−42.9	93	−48.1
42	−32.7		
	0.8 B_2O_3 – 0.2 Bi_2O_3 (N_s/mmol = 72)		
		101	−33.3

range. For the composition $x_{B_2O_3} = 0.1$ the solid phase is a dark crystal without an apparent glassy phase. At $x = 0.2$ and 0.4, quenching results in a mixture of a glass with crystals (dark for 0.2 and yellow for 0.4). For $x_{B_2O_3} = 0.6$–0.8 a yellow-orange glass without a crystalline phase was always observed. An X-ray analysis was performed on the $x = 0.1$–0.2–0.4 crystalline phases. The two former samples include the α Bi_2O_3 and the $2Bi_2O_3{\cdot}B_2O_3$ compounds. At $x = 0.2$ the percentage of this compound is more important than in the $x = 0.1$ sample. The presence of the $12Bi_2O_3{\cdot}B_2O_3$ compound cannot be ensured in the $x = 0.2$ crystalline phase. This latter compound is not observed in the $x = 0.4$ sample, which contains only the $2Bi_2O_3{\cdot}B_2O_3$ compound.

Discussion

A comparison between the physicochemical properties of the liquids Bi_2O_3–B_2O_3 and PbO–B_2O_3 is attempted.

First, the liquid PbO–Bi_2O_3 is stable enough to form an eutectic whose melting point is 190 K lower than the lowest melting point of the constituent oxides ($T_{fBi_2O_3}$ = 1098 K; T_{fPbO} = 1159 K). In the solid state the respective solubilities are weak. However, the existence of a large intermediate high-temperature b.c.c. solid solution indicates that the two elements are compatible with oxygen in a single lattice (13).

Considering the various solid bismuth and lead oxides, it appears that these elements differ in the possible valence states. Assuming that oxygen adopts in all cases the −2 valency, Pb may present the 2, 8/3, 3, and 4 valencies and Bi the 2, 3, and 5. Comparison of the thermodynamic properties of these compounds shows that the more stable oxides (from 900 K to higher temperatures) are PbO (valency +2) and Bi_2O_3 (valency +3). All the other Bi oxides decompose at low temperature and sometimes before the hypothetic melting points. These two valence states may be considered to be the only ones present in the liquid. If the melting point is an indication of the stability of a compound, PbO and Bi_2O_3 resemble each other closely.

A greater similarity is found between the Bi_2O_3–B_2O_3 and PbO–B_2O_3 phase diagrams if the lead oxide is written as Pb_2O_2. In the two systems a wide liquid domain is observed at 1000 K, which indicates a greater stability of these phases. The minima of the integral mixing enthalpies are −47 kJ mol^{-1} in the Bi_2O_3–B_2O_3 system and −26 kJ mol^{-1} for the PbO–B_2O_3 melt. These values indicate a higher stability of the former liquid. In the Pb_2O_2–B_2O_3 system the minimum of the liquidus is about 750 K as compared to 900 K in the other system. In both cases a phase separation in the liquid state is observed on the boron-rich side.

Designating the $a Bi_2O_3{:}b B_2O_3$ and $a Pb_2O_2{:}b B_2O_3$ solid compounds by $a{:}b_{Bi}$ and $a{:}b_{Pb}$, the 1:4 and 2:1 ratios are common to both systems. Corresponding to the $3{:}5_{Bi}$ composition, three lead compounds that melt peritectically are mentioned ($5{:}8_{Pb}$, $9{:}16_{Pb}$, and $1{:}16_{Pb}$). The phase diagrams differ with respect to the $3{:}5_{Bi}$, $12{:}1_{Bi}$, and the $1{:}1_{Pb}$, which have no corresponding $3{:}5_{Pb}$, $12{:}1_{Pb}$, and $1{:}1_{Bi}$. Among these three compounds only the $3{:}5_{Bi}$ melts congruently. Assuming a partial ionic decomposition of the corresponding melts, the borate

Can. J. Chem. Downloaded from www.nrcresearchpress.com by 65.111.164.53 on 09/08/12
For personal use only.

Can. J. Chem. Downloaded from www.nrcresearchpress.com by 65.111.164.53 on 09/08/12
For personal use only.

Fig. 1. Integral and partial mixing enthalpies in the B_2O_3–Bi_2O_3 liquid system at 1023 K referred to liquid B_2O_3 and solid Bi_2O_3. Dotted lines: partial mixing enthalpies; ●: $\Delta_{mix}H_{Bi_2O_3}$; ▲: $\Delta_{mix}H_{B_2O_3}$. Solid line: integral mixing enthalpy.

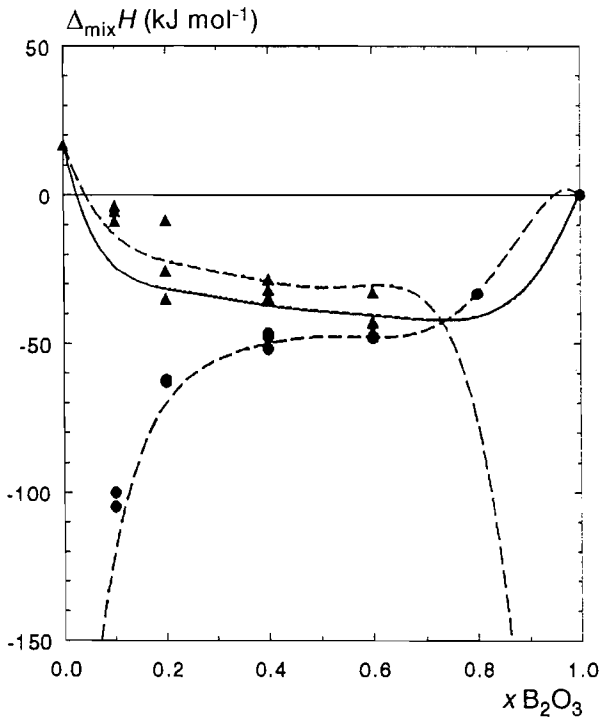

entities corresponding to these particular compositions may be expected in the presence of three-coordinated boron. Table 3 shows that the linear borate anions may be $(B_4O_7)^{-2}$ or $(B_4O_7\text{-}O\text{-}B_4O_7)^{-6}$, which present a double oxygen–boron bonding (-B═O) at each end of the chains; BO_2^-, which presents only one -B═O entity; and $(B_2O_5)^{-4}$, which has no double bonding between B and O. The more acid the melt, the more probable are anions with a double bond. Such behaviour has been observed in silicate melts where the following reaction is favoured by an increase in temperature, i.e., when the acidity of melt also increases:

$$(Si_2O_5)^{-2} = (SiO_3)^{-2} + SiO_2$$

In the two systems studied it is necessary to call upon cationic entities such as $(Pb_2O)^{+2}$, $(Bi_3O_2)^{+5}$, $(Bi_2O_2)^{+2}$, or $(BiO)^+$ in the basic composition range. It appears in this scheme that the polymerization of the cation arises in the Bi_2O_3–B_2O_3 system at a greater boron concentration than in the PbO–B_2O_3 system.

As an acid–base function can be defined with respect to the proton in the aqueous milieu, in molten oxide chemistry an acid will be any compound containing one or several particles able to accept an oxygen anion. The basic reaction can be written as (6):

$$\text{base} = \text{acid} + O^{-2}$$

The basicity of a melt is measured via the oxygen activity in the liquid or the value of the constant of the former equilibrium. An oxide is all the more acidic the weaker its dissociation and the lower the oxygen anion concentration in the melt. The corresponding element is then all the more electronegative. As the temperature rises the acidity of the melt increases. For example, SiO_2 behaves as an acid at 1300 K but decomposes as a basic compound into Si^{+4} and $2O^{-2}$ at higher temperature. An amphoteric oxide is a compound that is able either to give or to retain an oxygen anion.

Table 3. Possible ionic decompositions of some solid compounds (Bi_2O_3 or Pb_2O_2)$_a$(B_2O_3)$_b$ written *a*:*b*, in systems Bi_2O_3–B_2O_3 and Pb_2O_2–B_2O_3.

a:*b*	Bi_2O_3–B_2O_3 system	Pb_2O_2–B_2O_3 system
1:4	$2Bi^{+3}(B_4O_7\text{-}O\text{-}B_4O_7)^{-6}$	$Pb^{+2}(B_4O_7)^{-2}$
1:3	$Bi^{+3}\,3(BO_2)^-$	
1:2		$Pb^{+2}\,2(BO_2)^-$
3:5	$(Bi_3O_2)^{+5}\,5(BO_2)^-$	
1:1		$2Pb^{+2}(B_2O_5)^{-4}$
2:1	$2(Bi_2O_2)^{+2}(B_2O_5)^{-4}$	$2(Pb_2O)^{+2}(B_2O_5)^{-4}$
12:1	$10(Bi_2O_3)\,4(BiO)^+(B_2O_5)^{-4}$	

Lead oxide is a moderately strong base, as Pb^{+2} is a weak acid. Boron oxide acts as a strong acid. On the electronegativity scale O is at 3.5 whereas B is at 2.0, Bi is at 1.9 and Pb at 1.8 (14). It can be assumed that boron oxide and bismuth oxide present about the same acidity and the acid–base behaviour in the Bi_2O_3–B_2O_3 system will be different from that in the PbO–B_2O_3 system. The Bi—O bonding will probably present a less ionic character than that of Pb—O, and will approach the nature of the B—O bonding.

The integral and partial mixing Gibbs free energies corresponding to such an acid–base melt will show some particularities. The Darken function will exhibit some maxima at compositions corresponding to stable entities in the melt (15). In other words, a sharp dependence of the partial thermodynamic functions upon composition will be observed around these particular concentrations. In the present case and to a first approximation, the partial mixing enthalpies will determine the most probable acidic or basic entities that take part in the acid–base reaction of the two oxides. In the concentration regions where the acidity does not vary significantly, the partial thermodynamic function will exhibit a plateau. The solution will then show a buffer character.

Such an analysis was performed by Holm and Kleppa on the previously measured partial mixing enthalpies in PbO–B_2O_3 melts (16). Some sharp variations of these thermodynamic functions are observed around the compositions $x_{B_2O_3} = 0.16$–0.2 and $x_{B_2O_3} = 0.55$–0.6. Assuming that lead is in the Pb^{+2} state, these concentrations correspond to oxygen/boron ratios of 4–3.5 and of 1.91–1.83, respectively. The authors attribute these anomalies to the appearance of some borate anions: BO_4^{-5}, $B_2O_7^{-8}$ corresponding to the same O/B ratios 4–3.5, and $(B_8O_{15})^{-6}$ or $(B_4O_7\text{-}O\text{-}B_4O_7)^{-6}$ (O/B = 1.88). These suggestions are founded on the possible bonding of boron and oxygen atoms in borate glasses. A buffer region lies between these two concentrations.

In the Bi_2O_3–B_2O_3 liquid, such anomalies are observed at $x_{B_2O_3} = 0.05$–0.15 (O/B = 10–30) and $x_{B_2O_3} = 0.75$–0.85 (O/B = 1.77–2). The buffer conditions are realized for $0.4 < x_{B_2O_3} < 0.6$. As in the PbO–B_2O_3 melt, the O/B = 1.77–2 ratio may be

attributed to the formation of borate anions $(B_8O_{15})^{-6}$ or $(B_4O_7\text{-}O\text{-}B_4O_7)^{-6}$. This assumption is confirmed by the great stability of the solid compound $1{:}4_{Bi}$ (O/B = 1.88; T_f = 988 K). For the former entity the high O/B ratio cannot be explained with only a boron-polymerized anion. At this concentration oxygen-bismuth cations are formed.

From analyses of the crystalline phases of the quenching products, it may be thought that, as in the $12{:}1_{Bi}$ compound, some Bi_2O_3, $(BiO)^+$ or $(Bi_2O_3)^{+2}$, and $(B_2O_5)^{-4}$ entities appear in the melt for an O/B ratio of about 10–30. The nature of the cation cannot be described precisely from enthalpic measurements alone but it can be established that oxygen–boron cationic entities are present. From this viewpoint further structural characterizations would be of great interest.

$Bi_2O_{3(1-x)}$–B_2O_{3x} melts as solvents

To verify the ability of these melts to dissolve various solutes, dissolutions of simple oxides such as SiO_2 in the quartz and glassy form, and of Cr_2O_3, MgO, $FeO_{1.132}$, and some glassy melts of MgO–SiO_2 have been carried out in the $8Bi_2O_3$–$2B_2O_3$ melt at 923 K. The dissolution enthalpies lie between 0 and −40 kJ mol^{-1}. No significant variations as a function of solute concentration in the melt were observed. These dissolution enthalpies remain in all cases about 20–30 kJ mol^{-1} lower than those obtained in 2PbO–B_2O_3.

The thermodynamic study of the carnegieite crystal – glassy nepheline transition in $4Bi_2O_3$–$6B_2O_3$ liquid was successfully performed at 1023 K (17).

All the experiments were carried out in a platinum crucible of 0.3 mm thickness. No chemical attack or weight variations were observed during the runs. For the composition richest in B_2O_3 the diameter of the crucible became larger during the cooling, producing some mechanical damage. Such phenomena were not observed for lower $x_{B_2O_3}$ contents. For experiments of long duration, a diffusion of Bi in the crucible metal may occur. On the platinum-rich side of the Bi–Pt phase diagram a eutectic at 1003 K is mentioned, between the pure Pt and the Bi:Pt compound whose melting point is 1038 K (18). For previously mentioned reasons, experiments of long duration at temperatures higher than 1000 K will perhaps be difficult.

It seems that for $0.4 < x_{Bi_2O_3} < 0.6$ the buffer conditions are realized.

Considering the dissolution experiments, it appears that the viscosities of the PbO–B_2O_3 and Bi_2O_3–B_2O_3 melts are very similar.

Although indications regarding the toxicity of chemicals are very scarce, it has been established that the Bi compounds are less toxic than the Pb compounds.

Form these remarks it can be concluded that Bi_2O_3–B_2O_3 melts are good solvents for oxide melt solution calorimetry.

Can. J. Chem. Downloaded from www.nrcresearchpress.com by 65.111.164.53 on 09/08/12
For personal use only.

Acknowledgments

We are grateful to R. Depeyre for assistance in the dissolution experiments.

References

1. M. Goupil. *In* Du flou au clair. Histoire de l'affinité chimique. Édition du Comité des Travaux Historiques et Scientifiques, Paris. 1991. p. 99.
2. M. Ganteaume, M. Coten, and M. Decressac. Thermochim. Acta, **178**, 81 (1991).
3. T. Yokokawa and O.J. Kleppa. J. Inorg. Chem. **5–7**, 954 (1964).
4. J. Rogez, R. Chastel, C. Bergman, C. Brousse, R. Castanet, and J.C. Mathieu. Bull. Mineral. **106**, 119 (1983).
5. J. Rogez and J.C. Mathieu. Phys. Chem. Liq. **3–7**, 954 (1985).
6. H. Flood and T. Förland. Acta Chemica Scand. **1**, 592 (1947).
7. R.C. Newton, T.V. Charlu, and O.J. Kleppa. Geochim. Cosmochim. Acta, **44**, 933 (1980).
8. J.A. Shearer and O.J. Kleppa. J. Inorg. Nucl. Chem. **35**, 1073 (1973).
9. O.J. Kleppa. NATO Adv. Study Inst. Proc. Newcastle, England. 1974. pp. 369–387.
10. L.B. Pankratz, J.M. Stuve, and N.A. Gokcen. Thermodynamic data for mineral technology. Bureau of Mines, Bulletin 677. 1984.
11. R.A. Robie, B.S. Hemingway, and J.R. Fisher. Thermodynamic properties of minerals and related substances at 298.15 K and 1 bar pressure and at higher temperatures. Geological Survey Bulletin 1452, U.S. Government Printing Office, Washington. 1978.
12. R.C. Weast (*Editor*). Handbook of chemistry and physics. CRC Press, Boca Raton, Fla. 1984.
13. E.M. Levin, C.R. Robbins, and H.F. McMurdie. Phase diagrams for ceramists. Vol. I. *Edited by* M.K. Reser. The American Ceramic Society, Ohio. 1964. pp. 115, 125, 126.
14. A.N. Bloch and G.C. Schatteman. *In* Structure and bonding in crystals. Vol. 1. *Edited by* M. O'Keeffe and A. Navrotsky. Academic Press, New York. 1981. p. 58.
15. L.S. Darken. Trans. Metall. Soc. AIME, **239**, 80 (1967).
16. J.L. Holm and O.J. Kleppa. Inorg. Chem. **6–4**, 645 (1967).
17. P. Richet, R.A. Robie, J. Rogez, B.S. Hemingway, P. Courtial, and C. Tequi. Phys. Chem. Miner. **17**, 385 (1990).
18. F.A. Shunk. Constitution of binary alloys. 2nd suppl. McGraw–Hill Book Company, New York. 1969.

Densities, viscosities, and refractive indexes of *tert*-butyl methyl ether + butyl alcohols at 298.15 K

Roque Riggio, Hector E. Martinez, Norma Z. de Salas, and Juan F. Ramos

Abstract: Densities, viscosities, and refractive indexes of three binary systems, *tert*-butyl methyl ether + *n*-butanol, + *sec*-butanol, + isobutanol, have been determined at 298.15 K and atmospheric pressure over the complete composition range. We also report calculated excess properties including molar volume, viscosity, and Gibbs free energy for the activation of flow for these systems.

Key words: binary systems, excess properties.

Résumé : On a déterminé les densités, les viscosités et les indices de réfraction de trois systèmes binaires de l'oxyde de *tert*-butyle et de méthyle + *n*-butanol (ou + *sec*-butanol ou + isobutanol) à 298,15 K et à la pression atmosphérique à concentrations couvrant toutes les compositions. On rapporte aussi les propriétés en excès qui ont été calculées, y compris le volume molaire, la viscosité et l'énergie libre de Gibbs pour l'activation de l'écoulement de ces systèmes.

Mots clés : systèmes binaires, propriétés en excès.

[Traduit par la rédaction]

Can. J. Chem. Downloaded from www.nrcresearchpress.com by 65.111.164.53 on 09/08/12
For personal use only.

Introduction

The present work forms part of our programme on the measurement of transport properties of electrolyte and non-electrolyte solutions containing alcohols as one of the components (1–4).

In this contribution we report on the measured values of densities, viscosities, and refractive indexes, at 298.15 K and atmospheric pressure, of binary mixtures of *tert*-butyl methyl ether (MTB) + *n*-butanol (B_1), + *sec*-butanol (B_2), + isobutanol (B_3).

From the above-mentioned properties we compute several excess properties including: molar volume (V^E), viscosity (η^E), and Gibbs free energy for activation of flow (G^{*E}).

Experimental

Materials

All chemicals (Merck-Darmstadt p.a) were dried over anhydrous K_2CO_3 and fractionally distilled under a nitrogen atmosphere. The middle fraction was collected and stored over molecular sieves (0.3 nm for alcohols and 0.4 nm for ether) in order to prevent water absorption. The mixtures were prepared by using a Mettler H11 balance and then stored in air-tight stoppered bottles.

Density (ρ)

Densities of both the pure components and their mixtures were determined by an Anton Paar DMA46 calculating density meter with a built-in thermostat. The accuracy was estimated to be ± 0.1 kg m^{-3}.

Viscosity (η)

Viscosities of both the pure components and their mixtures were determined by a Cannon–Feske viscosimeter, which was calibrated with doubly distilled water and benzene. The accuracy was estimated to be $\pm 0.5\%$.

Refractive index (n_D)

Refractive indexes of both the pure components and their mixtures (sodium D line) were measured with a Bausch–Lomb Abbé-3L refractometer. The accuracy was estimated to be ± 0.0001. For both viscosity and refractive index, a thermostatically controlled bath, constant to ± 0.01°C, was used.

Results

The experimental data for the pure liquids investigated in this work are reported in Table 1, along with the literature values for comparison. Experimental data of densities, viscosities, and refractive indexes of the binary mixtures at 298.15 K are given in Table 2.

The excess functions for these binary systems were computed by using the following Redlich–Kister–Kind equation:

$$[1] \quad X^E = x_i x_j \sum_{k=0}^{n} a_k (2x_i - 1)^k$$

Received June 11, 1994.

R. Riggio,[1] **H.E. Martinez, N.Z. de Salas.** Facultad de Ciencias Naturales, Universidad Nacional de Salta, Buenos Aires 177, 4400 Salta, Republica Argentina.

J.F. Ramos. Facultad de Ciencias Exactas, Universidad Nacional de Salta, Buenos Aires 177, 4400 Salta, Republica Argentina.

[1] Author to whom correspondence may be addressed. Telephone: 087-251008. Fax: 087-251021.

Table 1. Experimental physical properties of the pure liquids at 298.15 K.[a]

	ρ		η		n_D	
Component	Expt.	Lit. (13)	Expt.	Lit. (13)	Expt.	Lit. (13)
MTB	735.7	—	0.348	—	1.3667	—
B_1	805.7	806.0	2.580	—	1.3974	1.3973
B_2	802.4	802.6	3.030	3.018(13)	1.3950	1.3950
B_3	798.2	797.8	3.380	—	1.3938	1.3939

[a]Units: ρ, kg m^{-3}; η, mPa s.

Can. J. Chem. Downloaded from www.nrcresearchpress.com by 65.111.164.53 on 09/08/12
For personal use only.

Table 2. Experimental values of density, viscosity, and refractive index for the MTB + B_1, MTB + B_2, and MTB + B_3 systems at 298.15 K.[a]

MTB + B_1				MTB + B_2				MTB + B_3			
X_{MTB}	ρ	η	n_D	X_{MTB}	ρ	η	n_D	X_{MTB}	ρ	η	n_D
0.0000	805.7	2.580	1.3974	0.0000	802.4	3.030	1.3950	0.0000	798.2	3.380	1.3938
0.1020	799.1	1.940	1.3954	0.0999	795.2	2.160	1.3934	0.1007	792.4	2.390	1.3922
0.2000	792.7	1.480	1.3932	0.1992	788.0	1.570	1.3912	0.2009	786.3	1.720	1.3902
0.2998	786.2	1.140	1.3908	0.2992	780.9	1.160	1.3886	0.2996	780.2	1.270	1.3880
0.3995	779.6	0.902	1.3881	0.3976	774.1	0.910	1.3859	0.3951	774.2	0.987	1.3856
0.5111	772.1	0.719	1.3850	0.5030	767.0	0.725	1.3828	0.5020	767.5	0.776	1.3828
0.6008	765.9	0.613	1.3822	0.6017	760.5	0.609	1.3798	0.6038	761.1	0.637	1.3799
0.6996	758.9	0.529	1.3788	0.6989	754.3	0.518	1.3768	0.7002	755.1	0.536	1.3770
0.7994	751.5	0.460	1.3752	0.7986	748.0	0.443	1.3736	0.8022	748.6	0.449	1.3738
0.9005	743.7	0.401	1.3711	0.8979	741.9	0.384	1.3703	0.9008	742.3	0.385	1.3704
1.0000	735.7	0.348	1.3667	1.0000	735.7	0.348	1.3667	1.0000	735.7	0.348	1.3667

[a]Units: ρ, kg m^{-3}; η, mPa s.

Table 3. Coefficients a_k from eq. [1] and standard deviations for the binary systems at 298.15 K.[a]

Systems	Coefficients	$V^E \times 10^6$	η^E	G^{*E}
	a_0	−3.7021	−0.8617	−602.18
	a_1	−0.8386	0.9688	91.99
MTB + B_1	a_2	−0.1274	−0.2645	241.22
	σ_y	3.47×10^{-3}	2.73×10^{-3}	0.147
	a^0	−1.3517	−3.8387	−783.39
	a_1	0.0813	2.5529	257.13
MTB + B_2	a_2	−0.2216	−1.2544	10.02
	a_3	—	—	−394.77
	σ_y	4.53×10^{-3}	3.60×10^{-3}	0.226
	a_0	−2.5620	−1.2254	−765.60
	a_1	−0.1087	1.6992	224.47
MTB + B_3	a_2	−0.4793	−1.1071	−25.23
	a_3	—	—	−409.08
	σ_y	3.55×10^{-3}	1.98×10^{-3}	0.222

[a]Units: V^E, m^3 mol^{-1}; η^E, mPa s.

where X^E denotes either V^E, η^E, or G^{*E}, x_i and x_j are the molar fractions of components i and j, respectively, the a_k denotes polynomial coefficients. In each case, the optimum number of coefficients was ascertained through an examination of the variation of the standard error of estimate with n:

$$[2] \quad \sigma_y = [E(X^E_{obs} - X^E_{calc})^2/(n_{obs} - n)^{1/2}$$

where n_{obs} is the number of measurements.

In turn, the excess properties were calculated by using the following equations:

Can. J. Chem. Downloaded from www.nrcresearchpress.com by 65.111.164.53 on 09/08/12
For personal use only.

Fig. 1. Molar excess volumes of the systems at 298.15 K.

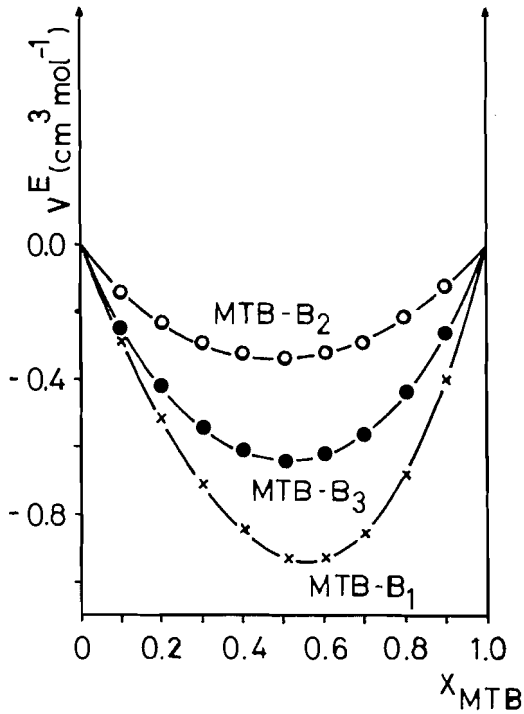

Fig. 2. Excess viscosities of the systems at 298.15 K.

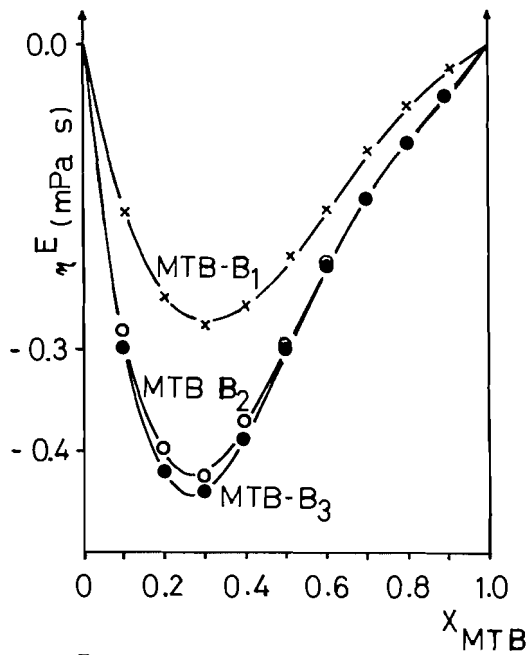

[3] $V^E = [(x_1M_1 + x_2M_2)/\rho] - (x_1V_1 + x_2V_2)$

[4] $\eta^E = \eta - \eta^{id} = \eta - \exp(x_1 \ln \eta_1 + x_2 \ln \eta_2)$

[5] $G^{*E} = RT[\ln \eta V - (x_1 \ln \eta_1 V_1 + x_2 \ln \eta_2 V_2)]$

where M_1 and M_2 are the molecular weights of the pure components, V, V_1, and V_2 are the molar volumes of each mixture and its pure components, η, η_1, and η_2 are the viscosities of each mixture and its pure components, respectively, and η^{id} is the viscosity of ideal mixture.

Fig. 3. Molar excess free energies of viscous flow activation by the systems at 298.15 K.

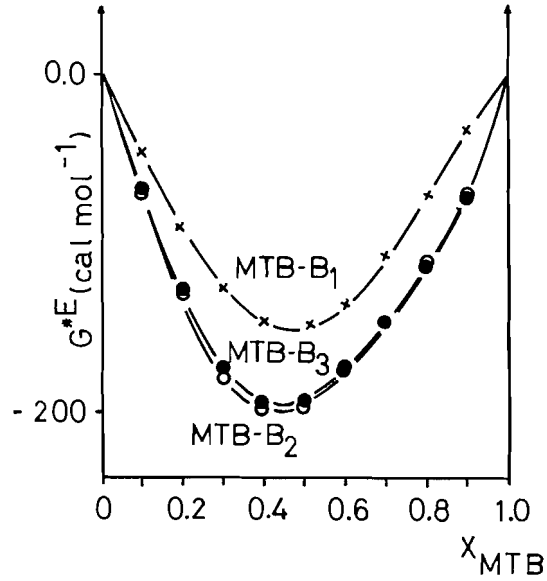

In Table 3 we report the a_k coefficients for the excess functions of eq. [1] as well as the corresponding standard deviations for each one of the binary systems mentioned before.

Discussion

It is well known that the alcohols involved in this research are substances associated by hydrogen bonding (5, 6). When alcohols are mixed with polar solvents some specific interactions occur due to breakdown of the hydrogen bonds (7). Here we report on the determination of the following excess properties: molar volumes (V^E), viscosities (η^E), and free energies of viscous flow (G^{*E}).

The excess volumes calculated at 298.15 K are plotted against composition in Fig. 1. We note that negative values are obtained for all cases. The increments for the V^E's are in the following order:

$$MTB + B_1 < MTB + B_3 < MTB + B_2$$

Usually, this behaviour is expected for mixtures in which positive contributions caused by disruption of the hydrogen-bonded-alcohol structure are dominated by the geometrical fitting of the ether into the remaining alcohol structure, and by specific interactions due to formation of multimers of alcohol and ether molecules. The lower values for B_1 followed by the B_3 and B_2 mixtures are in good agreement with the slight possibility of a geometric ordering due to the restructuring of the alcohol and the position of the alcohol function at the secondary carbon (8).

Figure 2 shows that for all systems η^E is negative over the whole composition range. The shapes of the viscosity–composition curves are characteristic for those systems containing a component capable of molecular association (9). It can be observed that viscosity decreases to a greater extent on the initial addition of ether to alcohols. Negative deviations occur when dispersion forces are responsible, which is in complete agreement with the conclusions reached for the V^E's.

In Fig. 3 we show the variation of G^{*E} values with compo-

sition for all three systems. According to previous reports (10, 11), this parameter can be considered as a valid measure of molecular interaction. In our case, the negative G^{*E} values lead us to conclude that repulsive forces are dominant.

The almost linear variation of the refractive indexes for the three systems in terms of the composition is in agreement with the conclusion of Loiselier (12) for a large number of ideal and nonideal systems. Neither the polar characteristic of the MTB nor the existence of hydrogen bonding in alcohols seems to have any important effect on the linear dependence of this property upon concentration.

Acknowledgement

We wish to express our thanks to Hernán E. Campos y Carlos A. Saravia for experimental assistance. This work was supported by INENCO-CONICET-UNSa, Republica Argentina.

References

1. H.N. Solimo, R. Riggio, and H.E. Martinez. J. Solution Chem. **15**, 283 (1986).
2. R. Riggio, J.F. Ramos, M. Hernandez Ubeda, and J.A. Espindola. Can. J. Chem. **59**, 3305 (1981).
3. R. Riggio, M. Hernandez Ubeda, J.F. Ramos, and H.E. Martinez. J. Chem. Eng. Data, **25**, 318 (1980).
4. R. Riggio, H.E. Martinez, J.A. Espidola, and J.F. Ramos. J. Chem. Eng. Data, **29**, 11 (1984).
5. H.C. Van Ness, J. Van Winkle, H.H. Richtol, and H.E. Hollinger. J. Phys. Chem. **71**, 1483 (1967).
6. G.C. Pimentel and A.L. McClellan. The hydrogen bond. W.H. Freeman and Co., San Francisco. 1960.
7. J.E. House. J. Trans. Ill. Acad. Sci. 123 (1966).
8. N.L. Allinger et al. Organic chemistry. Worth Publishers, Inc., New York. 1971.
9. M. Liler and D. Kosanovic. Hydrogen bonding. Pergamon Press, London. 1959.
10. T.M. Reed and T.E. Taylor. J. Phys. Chem. **63**, 58 (1959).
11. R. Meyer, M. Meyer, J. Metzer, and A. Poneloux. J. Chem. Phys. **62**, 405 (1971).
12. H. Loiselier. These de Doctorat-es-Sciences, Lyon. 1965. p. 80.
13. J.A. Riddic and W.B. Bunger. Organic solvents. Vol. II. 3rd ed. Wiley–Interscience, New York. 1970.

Can. J. Chem. Downloaded from www.nrcresearchpress.com by 65.111.164.53 on 09/08/12
For personal use only.

Multisubstituted phthalonitriles, naphthalenedicarbonitriles, and phenanthrenetetracarbonitriles as precursors for phthalocyanine syntheses

Clifford C. Leznoff, Dmitri S. Terekhov, Colin R. McArthur, Steven Vigh, and Jing Li

Can. J. Chem. Downloaded from www.nrcresearchpress.com by 65.111.164.53 on 09/08/12
For personal use only.

Abstract: Electrophilic aromatic nitration under mild conditions of 4-hydroxyphthalonitrile gave 4-hydroxy-3-nitrophthalonitrile and 4-hydroxy-5-nitrophthalonitrile, while bromination yielded 3-bromo-4-hydroxyphthalonitrile, 4-bromo-5-hydroxyphthalonitrile, and 3,5-dibromo-4-hydroxyphthalonitrile. Iodination gave 4-hydroxy-5-iodophthalonitrile and 4-hydroxy-3,5-diidophthalonitrile. Coupling of 4-iodophthalonitrile, 3-iodophthalonitrile, and 5-iodo-2,3-dicyanonaphthalene with *trans*-1,2-bis(tri-*n*-butylstannyl)ethene gave *trans*-1,2-bis(3,4-dicyanophenyl)ethene, *trans*-1,2-bis(2,3-dicyanophenyl)ethene, and *trans*-1,2-bis(6,7-dicyanonaphthyl)ethene. Photocyclization of a dilute solution of *cis*- or *trans*-1,2-bis(3,4-dicyanophenyl)ethene in dioxane gave a 1:1 mixture of 2,3,6,7- and 2,3,5,6-tetracyanophenanthrenes separable by chromatography.

Key words: phthalonitriles, naphthalenedicarbonitriles, phenanthrenetetracarbonitriles, electrophilic substitution.

Résumé : La nitration électrophile aromatique du 4-hydroxyphtalonitrile, dans des conditions douces, conduit au 4-hydroxy-3-nitrophtalonitrile et au 4-hydroxy-5-nitrophtalonitrile alors que sa bromation fournit du 3-bromo-4-hydroxyphtalonitrile, du 4-bromo-5-hydroxyphtalonitrile, et du 3,5-dibromo-4-hydroxyphtalonitrile. L'iodation fournit du 4-hydroxy-5-iodophtalonitrile et du 4-hydroxy-3,5-diiodophtalonitrile. Le couplage des 4-iodophtalonitrile, 3-iodophtalonitrile et 5-iodo-2,3-dicyanonaphtalène avec du *trans*-1,2-bis(tri-*n*-butylstannyl)éthène fournit du *trans*-1,2-bis(3,4-dicyanophényl)éthène, du *trans*-1,2-bis(2,3-dicyanophényl)éthène et du *trans*-1,2-bis(6,7-dicyanonaphtyl)éthène. La photocyclisation d'une solution diluée des isomères *cis*- et *trans*-1,2-bis(3,4-dicyanophényl)éthène dans le dioxane fournit un mélange 1 : 1 des 2,3,6,7- et 2,3,5,6-tétracyanophénanthrènes que l'on peut séparer par chromatographie.

Mots clés : phtalonitriles, naphtalènedicarbonitriles, phénanthrènetétracarbonitriles, substitution électrophile.

[Traduit par la rédaction]

Some substituted aromatic *o*-dinitriles are widely used in the synthesis of phthalocyanines (1), polymers, and intermediates in organic syntheses (2). Most common methods of their synthesis include cyanation of aromatic halides (2) or more recently triflates (3), nucleophilic substitution of nitrophthalonitriles (4–6), aromatic coupling using, for example, 4-iodophthalonitriles mediated by palladium catalysts (7, 8), Diels–Alder addition of fumaronitrile or dicyanoacetylene to substituted dienes and furans (9), and multistep synthesis involving the transformation of aromatic *o*-diacids via imides and diimides (10) to dinitriles (11–13). Direct electrophilic aromatic substitution of aromatic *o*-dinitriles is generally not used owing to the presence of the two deactivating electron-withdrawing nitrile groups and the fact that these groups are susceptible to hydrolysis during the strongly acidic conditions of these reactions. Our interests in phthalocyanine synthesis led us to prepare a variety of multisubstituted phthalonitriles, bisaromatic-*o*-dinitriles, naphthalenedicarbonitriles (5-substituted-2,3-dicyanonaphthalenes), and phenanthrenetetracarbonitriles, using a wide variety of methods including rarely used electrophilic aromatic substitution reactions and photocyclization.

Received November 11, 1994.

C.C. Leznoff,[1] D.S. Terekhov, C.R. McArthur, S. Vigh, and J. Li. Department of Chemistry, York University, North York (Toronto), ON M3J 1P3, Canada.

[1] Author to whom correspondence my be addressed.

Iodination, nitration, and bromination of 4-hydroxyphthalonitrile (1)

A recent paper by Gaude et al. (14) described the direct iodination of phenols by iodine nitrate and we thought that this procedure could be successful in the direct iodination of 4-hydroxyphthalonitrile (**1**)(15) as the two nitrile groups may not sufficiently deactivate phenol **1** towards electrophilic aromatic substitution. Thus, treatment of **1** with iodine nitrate in acetonitrile for 2 h at room temperature gave a mixture, separable by flash chromatography, of 4-hydroxy-3,5-diiodophthalonitrile (**2**) and 4-hydroxy-5-iodophthalonitrile (**3**) in 5 and 2.5% yield, respectively (Scheme 1).

The poor yields of **2** and **3** (probably as a result of the electron-deactivating cyano groups of **1**) and the possibility of converting nitro groups into diazonium salts and iodo groups

Can. J. Chem. Downloaded from www.nrcresearchpress.com by 65.111.164.53 on 09/08/12
For personal use only.

Scheme 1

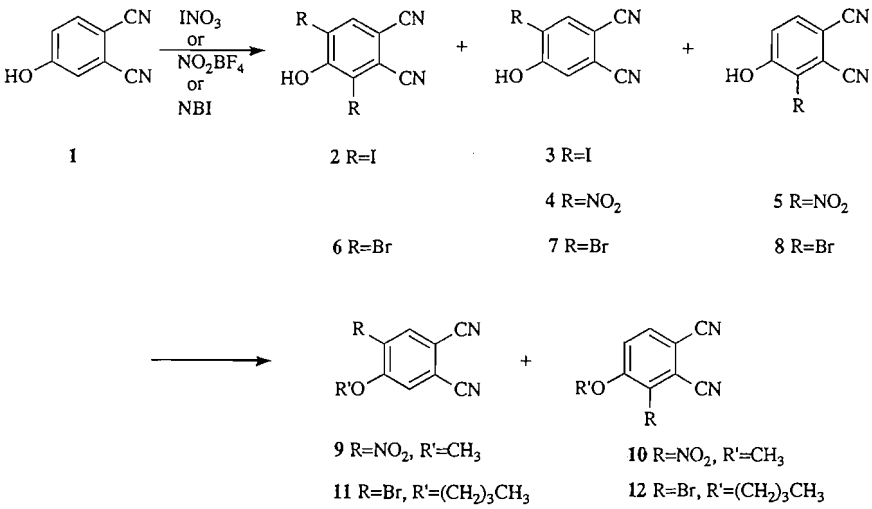

Scheme 2

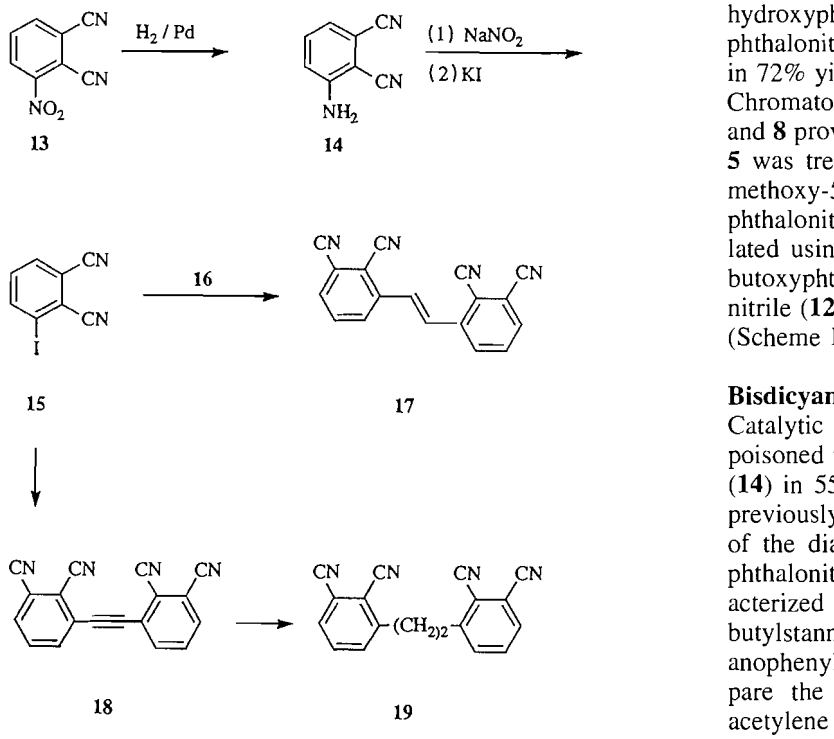

led us to consider direct nitration of **1**, using the mild nitrating reagent nitronium tetrafluoroborate (16). Nitration of **1** with nitronium tetrafluoroborate in acetic acid at room temperature, followed by flash chromatography (17) and vacuum liquid chromatography (18) of the reaction mixture, gave 4-hydroxy-5-nitrophthalonitrile (**4**) and 4-hydroxy-3-nitrophthalonitrile (**5**) in 15 and 13% yield, respectively (Scheme 1).

Since the yields of **4** and **5** were still unsatisfactory, we decided to try a rarely used brominating agent, *N,N*-dibromoisocyanuric (NBI) acid (19, 20) known to brominate aromatic compounds containing both activating and deactivating substituents. Although sulfuric acid is used in this procedure, the reaction time is short and the temperature low. Hence, **1** was reacted with NBI in concentrated sulfuric acid for 10 min at room temperature to give 3,5-dibromo-4-hydroxyphthalonitrile (**6**) and a mixture of monobromo-4-hydroxyphthalonitriles consisting of 4-bromo-5-hydroxyphthalonitrile (**7**) and 3-bromo-4-hydroxyphthalonitrile (**8**) in 72% yield that was inseparable by flash chromatography. Chromatography of the product mixtures of **4** and **5** and of **7** and **8** proved to be quite tedious. Hence the mixture of **4** and **5** was treated with diazomethane to give the less polar 4-methoxy-5-nitrophthalonitrile (**9**) and 4-methoxy-3-nitrophthalonitrile (**10**), while the mixture of **7** and **8** was alkylated using K_2CO_3 and 1-bromobutane to give 4-bromo-5-butoxyphthalonitrile (**11**) and 3-bromo-4-butoxyphthalonitrile (**12**) in 30 and 34% overall yield from **1**, respectively (Scheme 1).

Bisdicyanoarylethenes from dicyanoiodoarenes

Catalytic reduction of 3-nitrophthalonitrile (**13**) (21) with a poisoned palladium catalyst (22) gave 3-aminophthalonitrile (**14**) in 55–83% yields, which are considerably higher than previously reported (23). Diazotization of **14** and treatment of the diazonium salt with potassium iodide gave 3-iodophthalonitrile (**15**), only mentioned in an article but not characterized (24). Coupling of **15** with *trans*-1,2-bis(tri-*n*-butylstannyl)ethene (**16**) (25) gave *trans*-1,2-bis(2,3-dicyanophenyl)ethene (**17**) in 59% yield. In an attempt to prepare the *cis* isomer of **17**, iodo **15** was coupled with acetylene and a palladium catalyst (7, 8) to give 1,2-bis(2,3-dicyanophenyl)ethyne (**18**). Catalytic hydrogenation of **18** over a Lindlar catalyst as previously described did not result in semi-hydrogenation and only starting material was recovered. Hydrogenation over palladium on charcoal afforded the fully saturated 1,2-bis(2,3-dicyanophenyl)ethane (**19**) (Scheme 2).

Bromination (9) of 2,3-dimethyl–1-nitrobenzene (**20**) gave 2-bromomethyl-3-dibromomethyl–1-nitrobenzene (**21**), which on treatment (9) with sodium iodide in *N,N*-dimethylformamide and fumaronitrile (**22**) yielded the known 5-iodo-2,3-dicyanonaphthalene (**23**), prepared by a different route (26). Reduction of **23** (26), gave 5-amino-2,3-dicyanonaphthalene (**24**) (26), which upon diazotization and treatment with potassium iodide gave the unknown 5-iodonaphthalene-2,3-dicarbonitrile (**25**). Coupling of **25** with **16** gave *trans*-1,2-bis(6,7-dicyanonaphthyl)ethene (**26**) (Scheme 3). Both

Can. J. Chem. Downloaded from www.nrcresearchpress.com by 65.111.164.53 on 09/08/12
For personal use only.

Scheme 3

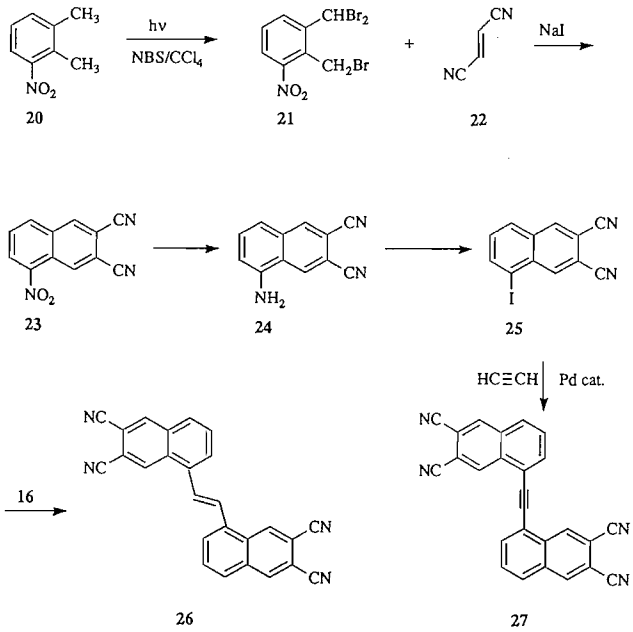

arylethenes **17** and **26** were extremely insoluble compounds, which likely caused attempts at subsequent reactions to fail. In an attempt to make a more soluble *cis* isomer of **26**, compound **25** was coupled with acetylene in the presence of copper iodide and bis(triphenylphosphine)palladium dichloride (7, 8) to give 1,2-bis(6,7-dicyanonaphthyl) ethyne (**27**) in 54% yield (Scheme 3). This highly insoluble compound also proved resistant to semi-hydrogenation.

2,3,6,7-Tetracyanophenanthrene (31) and 2,3,5,6-tetracyanophenanthrene (32)

Attempts to induce photocyclization (27–29) of **17** and **26** to give exclusively one isomer of tetracyanoarenes failed, probably because of their extreme insolubility. In a search for more soluble precursors, 4-iodophthalonitrile (**28**) (8) was coupled with **16** to give *trans*-1,2,bis(3,4-dicyanophenyl)ethene (**29**) in 94% yield. The *cis* isomer (**30**) has previously been made in our laboratory (26). Although **29** and **30** were both highly insoluble in most solvents, photocyclization of **29** and **30** was effected in a dilute solution of dioxane to afford a 1:1 mixture of 2,3,6,7-tetracyanophenanthrene (**31**) and 2,3,5,6-tetracyanophenanthrene (**32**) in 60–75% yield (Scheme 4). Regioselectivity in stilbene-like photocyclization reactions can vary, depending on the substituent (30).

The separation of this mixture was finally achieved using flash chromatography and slow elution with ethyl acetate – hexane (1:3) over 12 days to give pure **31** and **32**. A third possible isomer, namely 3,4,5,6-tetracyanophenanthrene, was not detected in any of the photocyclization experiments.

Spectroscopic analysis

All nitriles exhibited typical nitrile absorption at 2220–2240 cm^{-1} in their infrared spectra. The NMR spectra of all compounds were consistent with their structures. The structure of the tribromo derivative **21**, however, was determined by the fact that long-range coupling occurred between the proton at C-4 and the $CHBr_2$ group to give a doublet of doublets (see

Scheme 4

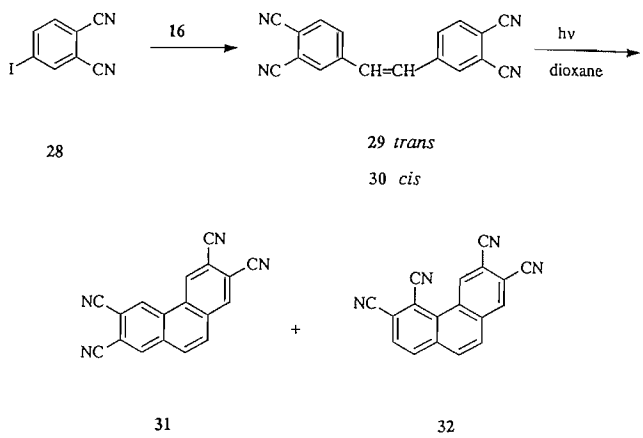

Experimental), and hence the $CHBr_2$ group is at the 3 position.

A NOESY spectrum of compound **25** exhibited long-range coupling between the singlet at 8.88 ppm (H-C1) and the doublet at 8.20 ppm (H-C8). Thus, the other singlet at 8.61 ppm is H-C4, the doublet at 8.49 is H-C6, and the triplet at 7.62 is H-C7. The HH-COSY and NOESY spectra of **32** (Figs. 1 and 2) clearly exhibited a singlet at 9.03 ppm (H-C1) coupled to a doublet at 8.31 ppm (H-C10), while the singlet at 10.03 ppm is uncoupled and is ascribed to H-C9, which shows long-range coupling to H-C8 at 8.65 ppm, leaving the remaining doublet at 8.47 ppm for H-C7. All new compounds exhibited parent ions in their mass spectra and satisfactory elementary analysis or high-resolution mass spectra (HRMS).

The ready availability of multisubstituted phthalonitriles, bisphthalonitriles, and tetracyanophenanthrenes will enable the preparation of unusual phthalocyanines.

Experimental

Matheson high-purity argon was used to maintain inert atmosphere conditions. Infrared (IR) spectra were recorded on a Pye Unicam SP1000 infrared spectrophotometer using KBr discs. Nuclear magnetic resonance (NMR) spectra for proton and carbon were recorded on a Bruker AM300 NMR spectrometer unless otherwise stated. TMS was used as the internal standard. The positions of the signals are reported in δ units. The splittings of the signal are described as singlets (s), doublets (d), triplets (t), quartets (q), pentets (p), hextets (h) doublets of doublets (dd), broad (br), or multiplets (m). The ultraviolet–visible spectra (UV–VIS) were recorded on a Varian CARY 2400 spectrophotometer UV–VIS–NIR. Mass spectra (MS) were recorded at 70 eV using a VG Micromass 16F mass spectrometer for molecules less than 900 amu or a Kratos Profile in the EI mode. The number in parentheses after the indicated ion shows the percentage of the base peak represented by that ion. The high-resolution mass spectra (HRMS) were obtained at 70 eV of a DEI model using a ZAB-E double focusing spectrometer of BE geometry. Melting points (mp) were determined using a Kofler hot stage melting point apparatus and are uncorrected. Flash chromatography was performed using silica gel of particle size 20–45 μm. All reactions were stirred with a magnetic stirrer. Ultrasound activation was carried out using a Branson 1200 sonicator. All

Fig. 1. The ^1H–^1H COSY NMR spectrum of 2,3,5,6-tetracyanophenanthrene (**32**) in DMSO-d_6.

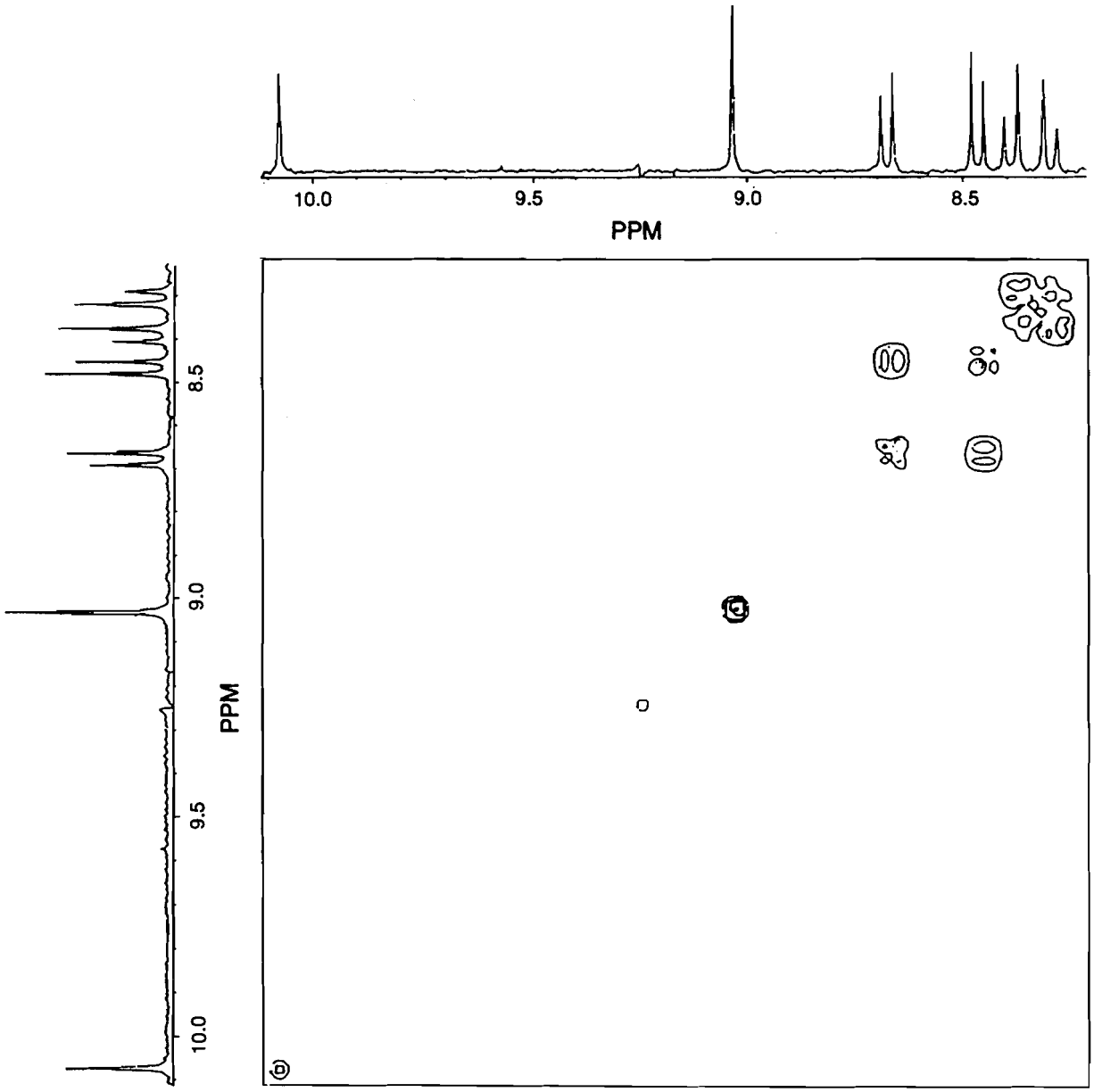

Can. J. Chem. Downloaded from www.nrcresearchpress.com by 65.111.164.53 on 09/08/12
For personal use only.

solvents were freshly distilled before use. Microanalysis were performed by Guelph Chemical Laboratory Ltd., Guelph, Ontario. Thin-layer chromatography (TLC) was performed using silica gel G as the absorbent.

4-Hydroxy-3,5-diiodophthalonitrile (2) and 4-hydroxy-5-iodophthalonitrile (3)

Silver nitrate (0.85 g, 5 mmol) in 15 mL of acetonitrile was added dropwise to a solution containing 1.27 g of iodine (5 mmol) in 30 mL of acetonitrile, while the solution was stirred at 0°C. After 5 min, the precipitate of silver iodide (about 2.5 mmol) was filtered off and then compound **1** (0.72 g, 5 mmol) in 10 mL of acetonitrile was added to the filtrate. The resulting solution was stirred at room temperature for 2 h. An additional precipitate of silver iodide (about 2.5 mmol) was filtered off. The filtrate was washed with a solution of sodium bisulfite. The organic layer was dried over anhydrous magnesium sulfate for 2 h. The crude product was chromatographed on silica gel with petroleum ether and toluene (1:1). The first fraction gave a small amount of a yellow band. The second fraction was collected to give, in 5% yield, 70 mg of compound **3**; mp 237–239°C; IR (KBr, cm^{-1}): 3320 (OH), 3070, 2950, 2900, 2850, 2230 (CN), 1570, 1550, 1480, 1330, 1280, 1170, 1120, 900; ^1H NMR (DMSO-d_6) δ: 9.50 (s, 1H, O*H*), 8.52 (s, 1H, *H*-C6 or *H*-C3), 8.48 (s, 1H, *H*-C3 or *H*-C6); MS *m/z*: 270 (M^+, 100). Exact Mass calcd. for $C_8H_3N_2IO$: 269.9289; found: 269.9289. Further elution gave, in 2–3% yield, 52 mg of compound **2**; mp 290°C (dec.); IR (KBr, cm^{-1}): 3360(O-H), 2240(C≡N), 1550, 1552, 1440, 1380, 1302, 1240, 1130, 920; ^1H NMR (DMSO-d_6) δ: 8.43 (s, 1H, *H*-C6), 4.3 (br, s, 1H, O*H*). Exact Mass calcd. for $C_8H_2N_2I_2O$: 395.8255; found: 395.8255.

Fig. 2. The ^1H–^1H NOESY NMR spectrum of 2,3,5,6-tetracyanophenanthrene (**32**) in DMSO-d_6.

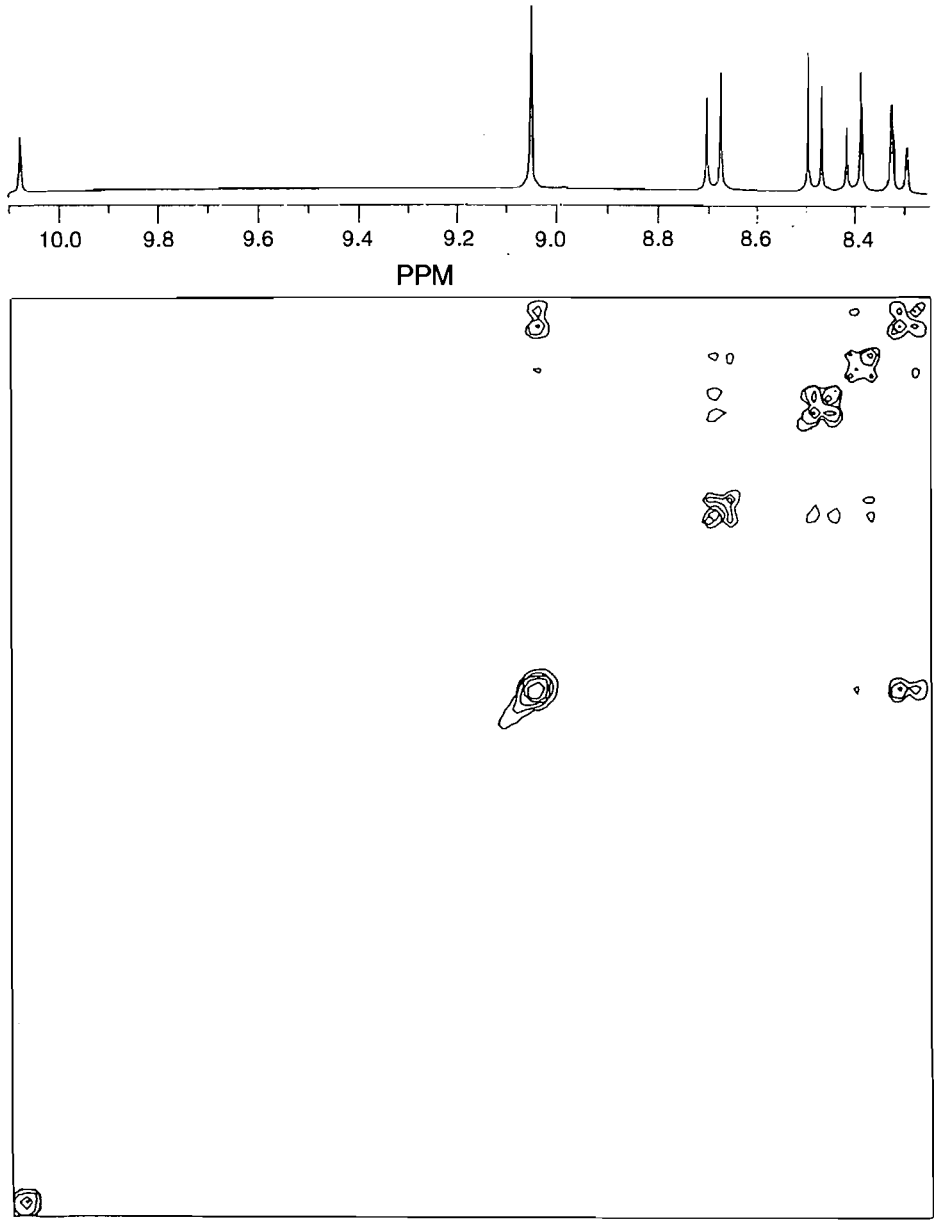

Can. J. Chem. Downloaded from www.nrcresearchpress.com by 65.111.164.53 on 09/08/12
For personal use only.

*4-Hydroxy-5-nitrophthalonitrile (**4**) and 4-hydroxy-3-nitrophthalonitrile (**5**)*

To a 50 mL round-bottomed flask, compound **1** (1 g, 6.9 mmol), nitronium tetrafluoroborate (1.37 g, 10.35 mmol) (from Aldrich Chemical Company Ltd.), and 30 mL of acetic acid were added. The mixture was stirred at room temperature for 6 h and then poured into 100 mL of water. The resulting solution was extracted with ethyl acetate. The combined organic layer was washed with water and sodium bicarbonate solution and then dried over anhydrous magnesium sulfate. Magnesium sulfate was filtered off. The filtrate was chromatographed on a flash silica gel column by elution with ethyl acetate and hexane (v/v = 2:1). The first fraction was collected to give, in 15–16% conversion, 200 mg of compound **4** as a yellow solid; mp 182–184°C; IR (KBr, cm^{-1}): 3280 (OH), 2250 (C≡N), 1630, 1565 (NO_2), 1320 (NO_2), 1280, 1120, 740; ^1H NMR (DMSO-d_6) δ: 8.64 (s, 1H, *H*-C6), 7.62 (s, 1H, *H*-C3), 4.3 (br, s 1H, O*H*); MS *m/z*: 189 (M+, 100). Anal. calcd. for $C_8H_3N_3O_3$: C 50.81, H 1.60, N 22.22; found: C 50.84, H 1.28, N 21.98. Continuous elution with the same eluant gave 500 mg of the unreacted starting material **1**. Further elution with ethyl acetate gave, in 13–14% conversion, 180 mg of compound **5**, also as a yellow solid; mp >320°C; IR (KBr, cm^{-1}): 3400(OH), 2230 (C≡N), 1590, 1530 (NO_2), 1475, 1380, 1340 (NO_2), 1270, 840, 690; ^1H NMR (DMSO-d_6) δ: 7.75 (d, J = 9 Hz, 1H, *H*-C6), 7.04 (d, J = 9 Hz, 1H, *H*-C5); MS *m/z*: 189 (M+, 100). Exact Mass calcd. for $C_8H_3N_3O_3$: 189.0174; found: 189.0180.

*3,5-Dibromo-4-hydroxyphthalonitrile (**6**), 4-bromo-5-hydroxyphthalonitrile (**7**), and 3-bromo-4-hydroxyphthalonitrile (**8**)*

A solution of 10 g (35.2 mmol) of *N,N*-dibromoisocyanuric

Can. J. Chem. Downloaded from www.nrcresearchpress.com by 65.111.164.53 on 09/08/12
For personal use only.

acid (NBI) (16) in 100 mL of concentrated H_2SO_4 was added in one portion to a solution of 7.8 g (54.2 mmol) of 4-hydroxyphthalonitrile (**1**) (12) in 100 mL of conc. H_2SO_4 at room temperature. The mixture was stirred for 10 min and then poured onto 800 g of ice. The resulting precipitate was filtered and the filtrate extracted three times with ethyl acetate. The extract was washed with water, a 2% solution of $NaHCO_3$, water, and dried over anhydrous $MgSO_2$. Evaporation of the solvent gave a mixture of products. Flash chromatography on silica gel and elution with ethyl acetate gave in the early fractions, in 12% yield, 2.0 g of 3,5-dibromo-4-hydroxyphthalonitrile (**6**) as a yellow-white solid, mp 269–271°C, IR (KBr, cm^{-1}): 3280 (OH), 2214 (CN); ^1H NMR (DMSO-d_6) δ: 11.16 (s, 1H, O-H), 8.38 (s, 1H, *H*-C6); MS *m/z*: 302 (M+, 100). Anal. calcd. for $C_8H_2Br_2N_2O$: C 31.83, H 0.67, N 9.28; found: C 31.82, H 0.65, N 9.00.

Further elution with ethyl acetate and evaporation of the solvent gave 2.1 g of a mixture of monobromo compounds. The original precipitate was extracted four times with ethyl acetate (leaving a residue of isocyanuric acid) and the extract dried, filtered, and evaporated as above to give an additional 6.6 g for an overall yield of 72% of an inseparable mixture of 4-bromo-5-hydroxyphthalonitrile (**7**) and 3-bromo-4-hydroxyphthalonitrile (**8**); 1H NMR (DMSO-d_6) δ: 11.16 (s, O-*H*), 8.39 (s, *H*-C6 (**7**)), 8.08 (s, *H*-C3 (**7**), 7.81 (d, *H*-C6) (**8**)), 7.30 (d, *H*-C3 (**8**)).

*4-Methoxy-5-nitrophthalonitrile (**9**)*

To 30 mg of compound **4** (0.16 mmol) in 20 mL of anhydrous ether, diazomethane (300 mg) in 30 mL of anhydrous ether was added dropwise at room temperature during a 30 min period. The evaporation of the ether gave, in 92% yield, 30 mg of compound **9**; mp 94–96°C; IR (KBr, cm^{-1}): 3060, 2940, 2220 (C≡N), 1900, 1600, 1550, 1520 (NO_2), 1390, 1350, 1190, 1100, 980, 750; ^1H NMR ($CDCl_3$) δ: 8.2 (s, 1H, *H*-C6), 7.5 (s, 1H, *H*-C3), 4.1 (s, 3H, C*H*$_3$); MS *m/z*: 203 (M^+, 100). Anal. calcd. for $C_9H_5N_3O_3$: C 53.21, H 2.48, N 20.68; found: C 53.49, H 2.29, N 20.53.

*4-Methoxy-3-nitrophthalonitrile (**10**)*

To 30 mg of compound **5** (0.16 mmol) in 20 mL of anhydrous ether, diazomethane (300 mg) in 30 mL of anhydrous ether was added dropwise at room temperature during a 30 min period. The solution was continuously stirred for 30 min. The evaporation of the ether gave, in 89% yield, 29 mg of compound **10**; mp 110–112°C; IR (KBr, cm^{-1}): 3090, 2980, 2240 (C≡N), 1920, 1600, 1540 (NO_2), 1480 1360, 1280, 1060, 850, 780; ^1H NMR ($CDCl_3$) δ: 7.91 (d, *J* = 8.9 Hz, 1H, *H*-C6), 7.41 (d, *J* = 8.9 Hz, 1H, *H*-C5), 4.07 (s, 3H, C*H*$_3$); MS *m/z*: (M^+, 100). Anal. calcd. for $C_9H_5N_3O_3$: C 53.21, H 2.48, N 20.68; found: C 53.30, H 2.30, N 20.73.

*4-Bromo-5-butoxyphthalonitrile (**11**) and 3-bromo-4-butoxyphthalonitrile (**12**)*

To 50 mL of *N,N*-dimethylformamide (DMF) were added 4.0 g (18 mmol) of the mixture of **7** and **8**, 4.7 g of K_2CO_3, and 4.5 g of 1-bromobutane. The mixture was stirred at 90°C for 2 h and then poured into 200 mL of water. The mixture was extracted twice with benzene and the extract washed twice with water and dried over anhydrous $MgSO_4$. The solvent was evaporated to give 7.6 g of a solid mixture. The mixture was separated by flash chromatography on silica gel using benzene–hexane (1:1) as eluant to give, in the first fractions, in 34% yield, 4-bromo-5-butoxyphthalonitrile (**11**); mp 117–119°C; IR (KBr, cm^{-1}): 2230 (CN); ^1H NMR ($CDCl_3$) δ: 7.93 (s, 1H, *H*-C6), 7.18 (s, 1H, *H*-C3), 4.13 (t, *J* = 4.2 Hz, 2H, OC*H*2), 1.88 (m, 2H, OCH$_2$C*H*$_2$), 1.56 (m, 2H, CH$_3$C*H*$_2$), 1.01 (t, *J* = 4.9 Hz, 3H, C*H*$_3$); MS *m/z*: 278 (M^+, 31). Anal. calcd. for $C_{12}H_{11}BrN2O$: C 51.64, H 3.97, N 10.04; found: C 52.04, H 4.03, N 10.02.

Further elution gave 3-bromo-4-butoxyphthalonitrile (**12**) in 30% yield; mp 116–117°C; IR (KBr, cm^{-1}): 2235 (CN); ^1H NMR ($CDCl_3$) δ: 7.79 (d, *J* = 5.8 Hz, 1H, *H*-C6), 7.11 (d, *J* = 5.8 Hz, *H*-C3), 4.14 (t, *J* = 4.2 Hz, 2H, C*H*$_2$), 1.87 (m, 2H, OCH$_2$C*H*$_2$), 1.55 (m, *J* = 3.7 Hz, 2H, CH$_3$C*H*$_2$), 1.00 (t, *J* = 4.9 Hz, 3H, C*H*$_3$); MS *m/z*: 278 (M^+, 76). Anal. calcd. for $C_{12}H_{11}BrN_2O$: C 51.64, H 3.97, N 10.04; found: C 51.76, H 3.86, N 9.95.

*3-Aminophthalonitrile (**14**)*

Nitrophthalonitrile (**13**) (21) was prepared using the procedure of Campagna et al. (12, 13) in 95% yield. The selective reduction of **13** was facilitated using a poisoned catalyst (22, 23). A mixture of 2.5 g of 5% palladium on barium sulfate and 5 mg of thiourea in 2.5 mL of methanol was shaken for 1 h. The solvent was evaporated and the brown residue homogenized.

A suspension of 4.5 g (26 mmol) of **13** in 100 mL of dry dioxane–ethanol (3:1) containing 750 mg of the poisoned catalyst was hydrogenated at 30 psi (1 psi = 6.9 kPa) in a Parr hydrogenation bottle for 1 h at room temperature. The yellow solution was concentrated and purified by flash chromatography using toluene–acetonitrile (5:1) as eluant to give 3.1 g (83% yield) of **14** as a yellow powdery solid, mp 210–212°C (lit. (31) mp 195–198°C).

*3-Iodophthalonitrile (**15**)*

Compound **14** (3.1 g, 21.7 mmol) was mixed with concentrated hydrochloric acid (62 mL) and ice (155 g), and sodium nitrite (2.35 g, 34.1 mmol) in water (20 mL) was added in one portion. After 1.5 h at 5°C, the solution was filtered. The diazonium salt solution was added dropwise to a stirred cool solution of potassium iodide in 30 mL of water. The resulting dark brown mixture was stirred for 0.5 h. This mixture was added to benzene and the solution was washed with cold water, cold 5% $NaHCO_3$, cold water, cold saturated $Na_2S_2O_3$, and again with cold water. The benzene solution was dried over anhydrous magnesium sulfate, filtered, and concentrated to a small volume. Chromatography on 200 g of normal grade silica gel and elution with benzene gave, in 62% yield, 3.3 g of pure **15** as white crystals, mp 167–169°C; IR (KBr, cm^{-1}): 3090, 2240 (CN), 1580, 1550, 1450, 1430, 1210, 1130, 810, 730; ^1H NMR ($CDCl_3$) δ: 8.16 (d, *J* = 8 Hz, 1H, Ar*H*-6), 7.78 (d, *J* = 8 Hz, 1H, Ar*H*-4), 7.40 (t, *J* = 8 Hz, 1H, Ar*H*-5); MS *m/z*: 254 (M^+), 202, 127, 100. Anal. calcd. for $C_8H_3N_2I$: C 37.82, H 1.19, N. 11.03, I 49.95; found: C-38.36, H 1.10, N 11.20, I 49.81.

trans-*1,2-Bis(2,3-dicyanophenyl)ethene (**17**)*

To a 50 mL round-bottomed flask equipped with a magnetic stirrer were added 3-iodophthalonitrile (**15**) (132 mg, 0.52 mmol), compound **16** (157.6 mg, 0.26 mmol), toluene (25.0 mL), and tetrakis(triphenylphosphine) palladium(0) (18.6 mg, 0.016 mmol). The resulting mixture was deoxygenated with a

Can. J. Chem. Downloaded from www.nrcresearchpress.com by 65.111.164.53 on 09/08/12
For personal use only.

stream of argon for 5 min. The reaction flask was placed in an oil bath at 100–120°C and stirred under argon at this temperature until TLC analysis indicated that **15** was consumed (10 h). The reaction mixture was allowed to cool to room temperature and kept under argon overnight. The precipitate was filtered off and washed with toluene and diethyl ether to give, in 59% yield, 45 mg of compound **17** as an off-white solid; mp >330°C; IR (KBr, cm^{-1}): 3080, 2230 (C≡N), 1580, 1470, 1440, 1270, 1200, 1160, 801, 740. MS *m/z*: 280 (M^+, 100). Anal. calcd. for $C_{18}H_8N_4$: C 77.14, H 2.86, N 20.00; found: C 77.24, H 2.39, N 20.27.

*1,2-Bis-(2,3-dicyanophenyl)ethyne (**18**)*

By a procedure previously described (7, 8), 3.0 g (11.8 mmol) of **15**, 80 mL of dry, freshly distilled diethylamine, and 25 mg (0.133 mmol) of bis(triphenylphosphine) palladium dichloride was placed into a 250 mL two-necked flask, equipped with a magnetic stirrer, a condenser, and a gas inlet tube. The flask was flushed with argon and a moderate stream of dry acetylene was passed through the solution for 9 h at room temperature. A pale pink precipitate was observed. This mixture was evaporated and the remaining residue was washed with water, methanol, and diethyl ether. The crude product was extracted with methanol in a Soxhlet extractor for 12 h until the extract was almost clear. This process removed brown impurities. The pale pink compound was dried to give, in 88% yield, 1.44 g of **18**, mp >300°C. This product is sufficiently pure that it can be used directly without further purification. Two recrystallizations of a small sample of **18** from acetonitrile gave white crystals of pure **18**, mp >300°C; IR (KBr, cm^{-1}): 3090, 2240 (CN), 1590, 1480, 1450, 1340,1290, 1190, 810, 710; ^{1}H NMR (DMSO-d_6, 300 MHz) δ: 8.25 (d, J = 8 Hz, 2H, Ar*H*-6), 8.16 (d, J = 8 Hz, 2H, Ar*H*-4), 8.01 (t, J = 8 Hz, 2H, Ar*H*-50; MS *m/z*: 278(M^+), 251, 224, 200, 176, 139. Anal. calcd. for $C_{18}H_6N_4$: C 77.69, H 2.17, N 20.13; found: C 77.42, H 2.08, N 20.78.

*1,2-Bis-(2,3-dicyanophenyl)ethane (**19**)*

A suspension of 0.200 g (0.72 mmol) of **18** in 150 mL of acetonitrile containing 50 mg of 10% palladium on charcoal was hydrogenated at 65 psi in a Parr hydrogenation bottle for 4 h at room temperature. The clear solution was filtered from the catalyst and concentrated. The compound was purified by flash chromatography using acetonitrile as eluant to give 0.190 g (94% yield) of **19** as yellow needles, mp 246–248°C; IR (KBr, cm^{-1}): 3090–2920, 2230 (CN), 1590, 1480, 820, 750; ^{1}H NMR (DMSO-d_6, 300 MHz) δ: 8.01 (d, J = 8 Hz, 2H, Ar*H*-6), 7.81 (t, J = 8 Hz, 2H, Ar*H*-5), 7.72 (d, J = 8 Hz, 2H, Ar*H*-4), 3.28 (s, 4H, CH_2CH_2O; MS *m/z*: 282(M^+), 255, 226, 201, 141. Anal. calcd. for $C_{18}H_{10}N_4$: C 76.58, H 3.57, N. 19.84; found: C 76.32, H 3.69, N 19.99.

*2-Bromomethyl-3-dibromomethylnitrobenzene (**21**)*

To a 1000 mL one-necked round-bottomed flask, charged with 500 mL of carbon tetrachloride, 3-nitro-*o*-xylene (**20**) (10 g, 66 mmol) (from Aldrich Chemical Company Ltd), *N*-bromosuccinimide (70.88 g, 396 mmol), and 200 mg of benzoyl peroxide were added. The mixture was irradiated using a 270 W sun lamp for 12 h or until TLC analysis indicated that the 3-nitro-*o*-xylene (**20**) was consumed. A precipitate was formed and the hot solution was filtered. The filtrate was concentrated, preabsorbed on a small amount of flash silica gel, and then loaded on a 5 cm diameter column containing flash silica gel and eluted with cyclohexane. The second fraction was collected to give 17 g of compound **21** in 83% yield; mp 67–68°C: IR (KBr cm^{-1}): 3080, 3020, 1520 (NO2), 1440, 1380 (NO2), 1255, 1230, 1140, 930, 850, 820, 780, 745, 680, 640; ^{1}H NMR ($CDCl_3$) δ: 8.28 (d, J = 7.3 Hz, 1H, *H*-C_6), 7.86 (dd, J = 7.3, 1.0 Hz, 1H, *H*-C4), 7.59 (t, J = 8 Hz, 1H, *H*-C5), 7.12 (brs, 1H, C*H*Br_2), 4.72 (s, 2H, CH_2Br); ^{13}C NMR ($CDCl_3$) δ: 143.0, 135.0, 131.2, 130.2, 126.5, 125.9, 34.4, 21.4; MS *m/z*: 306 (M^+−79), 308, 310, 384 (M^+−1), 386, 388, 390. Exact Mass calcd. for $C_8H_6Br_3NO_2$: 383.7871 (M^+−H); found 383.7873.

*5-Aminonaphthalene-2,3-dicarbonitrile (**24**)*

Nitronaphthalene-2,3-dicarbonitrile (**23**), prepared from **19** and fumaronitrile (**22**) by the procedure of Kovshev et al. (*9a*), gave, upon hydrogenation as for the preparation of **13** above, the known **24**, mp 256–258°C (lit. (26) mp 257–258°C).

*5-Iodonaphthalene-2,3-dicarbonitrile (**25**)*

A solution of concentrated H_2SO_4 (12 mL) and ice (50 g) was cooled to 0°C on a salt–ice bath. Compound **24** (300 mg, 1.6 mmol) was added to this solution followed by an aqueous solution of sodium nitrite (176.5 mg, 2.56 mmol). The resulting solution was stirred for 1 h at 0°C and then added dropwise to 20 mL of an aqueous solution of sodium iodide (5 g), which was vigorously stirred and kept below 3°C. After 0.5 h at 3°C, the dark brown solution was allowed to slowly warm to room temperature. Benzene (50 mL) was added to the dark brown solution. After stirring for 10 min, the resulting mixture was filtered. The organic layer was separated and washed with cold water, 10% $NaHCO_3$, cold water, a cold saturated solution of $Na_2S_2O_3$, again with cold water, and then dried over anhydrous magnesium sulfate for 2 h. The magnesium sulfate was filtered off. The filtrate was concentrated to a small volume and chromatographed on a column containing regular grade silica gel using toluene as the eluant to give, in 46% yield, 270 mg of compound **25** as a yellow solid; mp 243°C; IR (KBr, cm^{-1}): 3080, 2240, (C≡N), 1540, 1430, 918, 900, 800; ^{1}H NMR (DMSO-d_6) δ: 8.88 (s, 1H, *H*-Cl), 8,61 (s, 1H, H-C4), 8.48 (d, J = 8 Hz, 1H, *H*-C6), 8.19 (d, J = 8 Hz, 1H, *H*-C8), 7.62 (t, J = 8 Hz, 1H, *H*-C7): ^{13}C NMR (DMSO)-d_6) δ: 142.3, 139.4, 137.5, 134.0, 133.0, 132.0, 129.8, 116.0, 115.9, 110.8, 109.9, 100.3; MS *m/z*: 304 (M^+, 100). Anal. calcd. for $C_{12}H_8N_2$: C 47.40, H 1.66, N 9.21; found: C 47.76, H 1.55, N 8.94.

trans-*1,2-Bis(6,7-dicyanonaphthyl)ethene (**26**)*

To a 50 mL round-bottom flask equipped with a magnetic stirrer, 5-iodonaphthalene-2,3-dicarbonitrile (**25**) (300 mg, 0.96 mmol), compound **16** (290 mg, 0.48 mmol), toluene (25.0 mL), and tetrakis(triphenylphosphine)palladium(0) (33.5 mg, 0.029 mmol) were added. The resulting mixture was deoxygenated with a stream of argon for 5 min. The reaction flask was placed in an oil bath at 100–120°C and stirred under argon at this temperature until TLC analysis indicated that **25** was consumed (about 10 h). The reaction mixture was allowed to cool to room temperature and remained under argon overnight. The precipitate was filtered and washed with toluene and diethyl ether to give, in 80% yield, 150 mg of compound

Can. J. Chem. Downloaded from www.nrcresearchpress.com by 65.111.164.53 on 09/08/12
For personal use only.

26 as a green-yellow solid; mp >330°C; IR (KBr, cm^{-1}): 3050, 2220 (C≡N), 1450, 1370, 1360, 1340, 960, 901, 801, 750. Exact Mass calcd. for $C_{26}H_{12}N_4$: 380.1061; found: 380.1064.

1,2-Bis(6,7-dicyanonaphthyl)ethyne (27)

Compound **25** (265 mg, 0.87 mmol), 25 mL of dry, freshly distilled diethylamine, 25 mg of copper(I) iodide (0.133 mmol), and 20 mg of bis(triphenylphosphine)palladium dichloride (0.028 mmol) were added to a 100 mL two-necked round-bottomed flask, which was equipped with a magnetic stirrer, a condensor, and a gas inlet tube. The flask was first flushed with argon and then a moderate stream of dry acetylene was bubbled though the solution for 6 h at room temperature. A brown precipitate was produced. The precipitate was filtered off and extracted continuously with methanol in a Soxhlet apparatus for about 12 h, or until the extract was colourless. The precipitate in the thimble was dried in an oven at 100°C for 2 h, to give, in 54% yield, 178 mg of compound **27** as a brown solid; mp >330°C; IR (KBr, cm^{-1}): 3060, 2230 (C≡N), 1580, 1260, 1180, 900, 800, 750; MS *m/z*: 378 (M^+, 100). Exact Mass calcd. for $C_{26}H_{10}N_4$: 378.0905; found: 378.0917.

trans-*1,2-Bis(3,4-dicyanophenyl)ethene (29)*

To a 50 mL round-bottomed flask equipped with a magnetic stirrer, 4-iodophthalonitrile (**28**) (517 mg, 1.96 mmol), compound **16** (594 mg, 0.98 mmol), toluene (5.0 mL, freshly distilled over sodium), and tetrakis(triphenylphosphine)palladium(0) (21.7 mg, 0.018 mmol) (from Aldrich Chemical Company Ltd) were added. The resulting mixture was deoxygenated with a stream of argon for 5 min. The reaction flask was placed in an oil bath at 100–120°C and stirred under argon at this temperature until TLC analysis indicated that **28** was consumed (about 10 h). The reaction mixture was allowed to cool to room temperature and remained under argon overnight. The precipitate was filtered off and washed with toluene and diethyl ether to give, in 98% yield, 279 mg of compound **29**; mp >330°C; IR (KBr, cm^{-1}): 3050, 2220 (C≡N), 1590, 1490, 1415, 1325, 960, 910, 840, 725; ^{1}H NMR (DMSO-d_6) δ:8:41 (s, 2H, *H*-C2), 8.17 (d, J = 8.2, *H*-C5), 8.07 (br, d, J = 8.2, 2H, *H*-C6), 7.71 (s, 2H, *HC*=C*H*); MS *m/z*: 280 (M^+, 100). Anal. calcd. for $C_{18}H_8N_4$: C 77.13, H 2.88, N 19.95; found: C 76.96, H 2.57, N 19.64.

2,3,6,7-Tetracyanophenanthrene (31) and 2,3,5,6-tetracyanophenanthrene (32)

To 90 mL of dioxane in a Pyrex tube (40 x 5 cm), *trans*-**29** (40 mg, 0.14 mmol) or *cis*-**30** (26) (40 mg, 0.14 mmol) and iodine (25 mg, 0.19 mmol) were added. The suspension was sonicated until all particulates were dissolved. The tube was placed in a Rayonet photochemical reactor and irradiated for 9 h (the wavelength emitted by the lamps used was in the range of 257–350 nm). In the irradiation of **29** a trace amount of precipitate was removed by filtration. The solution was washed with a saturated solution of sodium bisulfite and then with ethyl acetate. The organic layer was separated and dried over anhydrous $MgSO_4$. After filtering the $MgSO_4$, the solution was concentrated. The concentrated solution was preadsorbed on a small amount of flash silica gel, then loaded on a column containing TLC grade silica gel G and eluted slowly over a 12 day period with hexane – ethyl acetate (3:1). The first fraction gave, in 31 and 40% yield from **29** and **30**, respectively, 12.2 and 15.9 mg of compound **31**; mp >330°C; IR (KBr, cm^{-1}): 3065, 3040, 2240 (C≡N), 1595, 1245, 920; 1H NMR (DMSO-d_6) δ: 9.86 (s, 2H, *H*-C1, *H*-C8), 8.99 (s, 2H, *H*-C4, *H*-C5), 8.33 (s, 2H, *H*-C9, *H*-C10); ^{13}C NMR (DMSO-d_6) δ: 136.1, 134.2, 132.1, 130.6, 130.3, 116.1, 115.9, 112.6, 111.7; MS *m/z*: 278 (M^+, 100). Anal. calcd. for $C_{18}H_6N_4$: C 77.69, H 2.17, N 20.13; found: C 77.33, H 2.34, N 19.88.

Further elution with the same solvents gave, in 28 and 36% yields from **29** and **30**, respectively, 11.0 and 14.2 mg of compound **32**; mp >330°C; IR (KBr, cm^{-1}): 3395, 2220 (C≡N), 1585, 925, 870; ^{1}H NMR (DMSO-d_6) δ: 10.07 (s, 1H, *H*-C4), 9.03 (s, 1H, *H*-C1), 8,67 (d, J = 8.4, 1H, *H*-C8), 8.47 (d, J = 8.4, 1H, *H*-C7), 8.39 (d, J = 8.9, 1H, *H*-C9), 8.31 (d, J = 8.9, 1H, *H*-C10); ^{13}C NMR (DMSO-d_6) δ: 136.4, 125.9, 135.5, 134.8, 131.4, 131.1, 130.5, 128.9, 127.4, 118.5, 117.8, 116.4, 116.2, 115.6, 112.6, 112.0, 111.1; MS *m/z*: 278 (M^+, 100). Anal. calcd. for $C_{18}H_6N_4$: C 77.69, H 2.17, N 20.13; found: C 77.20, H 2.33, N 19.91.

Acknowledgement

We are grateful to the Natural Sciences and Engineering Research Council of Canada for financial support of this research.

References

1. C.C. Leznoff. *In* Phthalocyanines; properties and applications. Vol. 1. *Edited by* C.C. Leznoff and A.B.P. Lever. VCH, New York. 1989. p.1.
2. G.P. Ellis and T.M. Romney-Alexander. Chem. Rev. **87**, 779 (1987).
3. M.R.I. Chambers and D.A. Widdowson. J. Chem. Soc. Perkin Trans. I, 1365 (1989); K. Takagi and Y. Sakakibara. Chem. Lett. 1957 (1989).
4. T.M. Keller, T.R. Price, and J.R. Griffith. Synthesis, 613 (1980); N.P. Marullo and A.W. Snow. ACS Symp. Ser. **14**, 325 (1982).
5. W.O. Siegl. J. Heterocycl. Chem. **18**, 1613 (1981).
6. C.C. Leznoff, S.M. Marcuccio, S. Greenberg, A.B.P. Lever, and K.B. Tomer. Can. J. Chem. **63**, 623 (1985).
7. S. Takahashi, Y. Kuroyama, K. Sonogashira, and N. Hagihara. Synthesis, 627 (1980); K. Sonogashira, Y. Tohoa, and H. Haginara. Tetrahedron Lett. 4467 (1975).
8. S.M. Marcuccio, P.I. Svirskaya, S. Greenberg, A.B.P. Lever, C.C. Leznoff, and K.B. Tomer. Can. J. Chem. **63**, 3057 (1985).
9. (*a*) E.I. Kovshev, V.A. Puchnova, and E.A. Luk'yanets. Zh. Org. Khim. **7**, 369 (1971), (*b*) M.J. Cook, M.F. Daniel, K.J. Harrison, N.B. McKeown, and A.J. Thomson. J. Chem. Soc. Chem. Commun. 1086 (1987).
10. R.A. McClelland, N.E. Seaman, J.M. Duff, and R.E. Branston. Can. J. Chem. **63**, 121 (1985).
11. H.D.K. Drew and D.B. Kelly. J. Chem. Soc. 637 (1941); C.R. Rasmussen, J.F. Gardocki, J.N. Plampin, B.L. Twardzik, B.E. Reynolds, A.J. Molinari, N. Schwartz, W.W. Bennetts, B.E. Price, and J. Marakowski. J. Med. Chem. **21**, 1044 (1978).
12. F. Campagna, A. Carotti, and G. Cassini. Tetrahedron Lett. 1813 (1977).
13. T.W. Hall, S. Greenberg, C.R. McArthur, B. Khouw and C.C. Leznoff. Nouv. J. Chim. **6**, 653 (1982).

14. D. Gaude, G. Gellon, R. le Goaller, and J. Pierre. Can. J. Chem. **67**, 104 (1989).
15. V. A. Ustinov, V. V. Plakhtinskii, G. S. Mironov, and N. S. Ryabukhina. Zh. Org. Khim. **15**, 1775 (1979).
16. S. J. Kuhn and G. A. Olan. J. Am. Chem. Soc. **83**, 4564 (1961).
17. W. C. Still, M. Kahn, and A. Mitra. J. Org. Chem. **43**, 2923 (1978).
18. N. M. Targett, J. P. Kilcoyne, and B. Green. J. Org. Chem. **44** 4692, (1979).
19. W. Gottardi. Monatsh. Chem. **99**, 815 (1968); **100**, 42, (1969).
20. J. Rosevear and J. F. K. Wilshire. Aust. J. Chem. **33**, 1561 (1977).
21. S. A. Mikhalenki, V. M. Derkacheva, and E. A. Luk'yanets. Zh. Obshch. Khim. **51**, 1650 (1981).
22. H. Musso and H. Schroeder. Ber. Dtsch. Chem. Ges. **98**, 1562 (1965).
23. J. Griffiths and B. Roozpeikar. J. Chem. Soc. Perkin Trans. 1, 42 (1976).
24. Yu. M. Osipov, G.P. Shaposhnikov, V.P. Kulinich, and R.P. Smirnov. Khim. Geterosikl. Soedin. 74 (1989).
25. J.C. Bottaro, R.N. Hanson, and D.E. Seitz. J. Org. Chem. **46**, 5221 (1981); A. N. Nesmeyanov and A. E. Borisov. Dokl. Akad. Nauk SSSR, **174**, 96 (1967).
26. E.I. Kovshev and E.A. Luk'yanets. Zh. Obshch. Khim. **42**, 1593 (1972).
27. P. Hugelshofer, J. Kalvoda, and K. Schaffner. Helv. Chim Acta, **43**, 1322 (1960).
28. F.B. Mallory, J.T. Gordon, and C.S. Wood. J. Am. Chem. Soc. **85**, 829 (1963).
29. C.C. Leznoff and R.J. Hayward. Can. J. Chem. **48**, 1842 (1970).
30. W.H. Laarhoven, Th. J.H.M. Cuppen, and R.J.F. Nivard. Tetrehedron, **26**, 4865 (1970).
31. S. Vigh, H. Lam, P. Janda, A.B.P. Lever, C.C. Leznoff, and R.L. Cerny. Can. J. Chem. **69**, 1457 (1991).

Can. J. Chem. Downloaded from www.nrcresearchpress.com by 65.111.164.53 on 09/08/12
For personal use only.

Sulfonyl esters 6. Elucidation of the first sequence in the Trithioorthoformate Reaction

James Clayton Baum, Bradley Eugene Black, Laura Precedo, John Edward Goehl, and Richard Francis Langler

Abstract: The one-pot conversion of a mercaptan and an aryl methanesulfonate into a trithioorthoformate is described. The intermediacy of a sulfide-sulfonate ester is firmly established. Experimental and computational results permit the formulation of a possible pathway for the formation of the intermediate sulfide-sulfonate ester.

Key words: single electron transfer, sulfonate esters, sulfide-sulfonate esters.

Résumé : On décrit une conversion unipotique d'un mercaptan et d'un méthanesulfonate d'aryle en un trithioorthoformate. On a établi sans ambiguïté qu'un ester sulfure-sulfonate agit comme intermédiaire. Les résultats expérimentaux et les calculs permettent de formuler une voie réactionnelle possible pour la formation de l'intermédiaire sulfure-sulfonate.

Mots clés : transfert d'un seul électron, esters sulfonates, esters sulfure-sulfonate.

[Traduit par la rédaction]

Introduction

Some time ago (1), we reported the sulfonyl transfer reaction shown in eq. [1].

[1] $CF_3CH_2OSO_2CH_3 + PhCH_2SH \xrightarrow{CH_3ONa} [CH_3SO_2OCH_3] + PhCH_2SCH_3$ (27%)

Recent work (2–4) employed sodium hydride as the base and hexamethyl phosphoramide (HMPA) as the solvent. We now report the results shown in eq. [2].

[2] 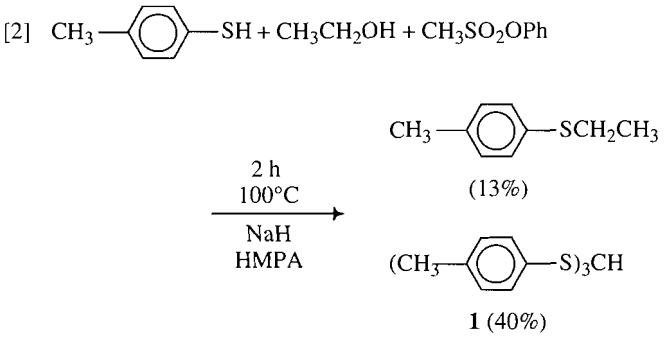

This reaction we have dubbed the Trithioorthoformate Reaction. The present report discloses our findings and conclusions about the processes that introduce the first thio *p*-tolyl group.

Results and discussion

When phenyl methanesulfonate was replaced by phenyl ethanesulfonate, no trithioorthoformate **1** was formed, suggesting that the methine carbon is more likely to come from phenyl methanesulfonate than from HMPA. The failure of the reactions shown in eqs. [4] and [5] to produce any trithioorthoformates containing simple thiophenyl groups suggests that the phenoxysulfonyl group is the last to be replaced in the conversion of phenyl methanesulfonate into **1**.

[3] 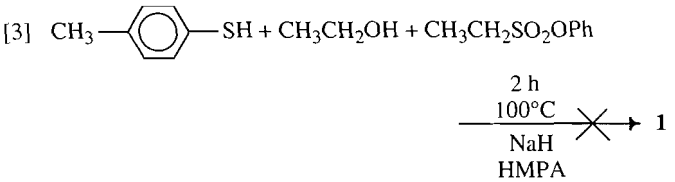

[4] 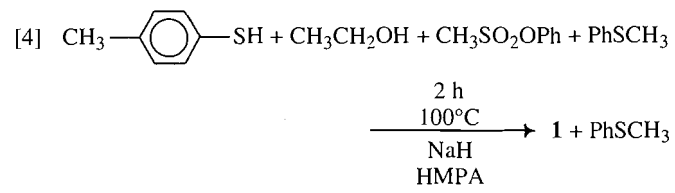

[5] 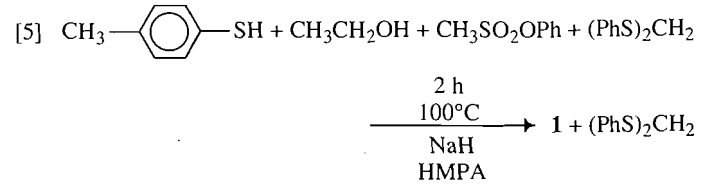

Received October 10, 1994.

J.C. Baum, B.E. Black, and L. Precedo. Department of Chemistry, Florida Institute of Technology, Melbourne, FL 32901-6988, U.S.A.

J.E. Goehl and R.F. Langler.[1] Department of Chemistry, Mount Allison University, Sackville, NB E0A 3C0, Canada.

[1] Author to whom correspondence may be addressed. Telephone + Fax: (506) 364-2361.

Can. J. Chem. Downloaded from www.nrcresearchpress.com by 65.111.164.53 on 09/08/12
For personal use only.

Can. J. Chem. Downloaded from www.nrcresearchpress.com by 65.111.164.53 on 09/08/12
For personal use only.

To improve the chances of isolating one or more of the intermediates, we carried out reactions at room temperature and varied the sulfonate ester structure. Equation [6] shows the general reaction and Table 1 presents our results.

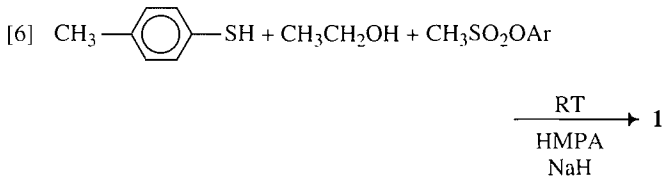

Because signals for a potential intermediate were observed in the ^{1}H nmr spectrum of the crude when the reaction was carried out with *p*-chlorophenyl methanesulfonate, further exploration employed that sulfonate ester. Ethanol was shown to be a spectator species by the results in eq. [7].

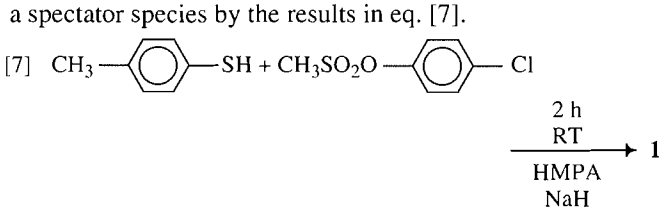

The trithioorthoformate reaction occurs between the mercaptan and the sulfonate ester, proceeding by sequential replacement of two protons and the aryloxysulfonyl group initially attached to the methanesulfonate methyl carbon.

When the crude product from eq. [6] (Table 1, case 2) was repeatedly chromatographed, a sulfonyl-containing product with ^{1}H nmr δ: 7.33 (8H), 4.40 (2H, s), and 2.33 (3H, s) was isolated in 6% yield. Structure **2** was assigned to this compound.

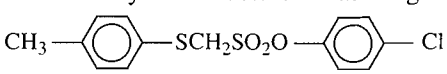

2

An unambiguous, independent synthesis of **2** from *p*-chlorophenyl chloromethanesulfonate was completed (4), thus lending support to our initial pathway conclusions (eqs. [2]–[7]). Compound **2** was also oxidized to the corresponding sulfone-sulfonate ester, which was fully characterized.

The yield[2] of **2** was raised to 27% in HMPA by varying eq. [8] conditions.

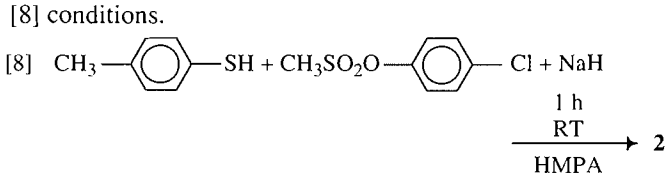

The intermediacy of **2** in the trithioorthoformate reaction was confirmed by the results shown in eq. [9] (cf. results on CH_3SO_2O-◯-Cl in Table 1)

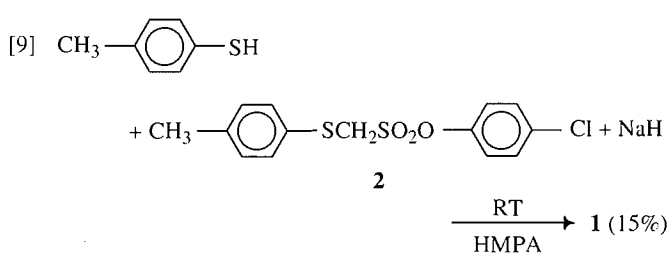

[2] Routine production of **2** was less costly and faster (reaction time: 0.5 h) when the reaction was conducted in DMSO (yield: 29%).

Table 1. Reaction of *p*-toluenethiol with various aryl methanesulfonates — the Trithioorthoformate Reaction. Correlation of yields of *p*-tolyl trithioorthoformate (**1**) with the LUMO eigenvalues of the sulfonates.

Methanesulfonate ester	LUMO[a] eigenvalue (eV)	Yield **1** (%)
CH_3SO_2O—◯	0.3516	0
CH_3SO_2O—◯—Cl	−0.0201	4
CH_3SO_2O—◯—SO_2CH_3	−0.6193	30
CH_3SO_2O—◯(Br, Br)—Br	−1.0038	0[b]
CH_3SO_2O—◯—NO_2	−1.9839	0[b]

[a]LUMO eigenvalues were calculated using the ZINDO program (3, 5).
[b]Complete discussions of the reactions of the tribromophenyl and nitrophenyl sulfonates have been presented in refs. 2 and 3, respectively.

It is now clear that eq. [8] represents an overview of the first sequence when the reaction is conducted with *p*-chlorophenyl methanesulfonate.

The most perplexing feature of the mechanism associated with eq. [8] can be formulated as shown below:

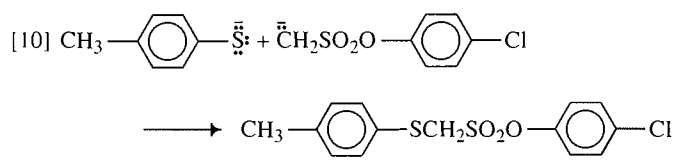

The oxidizing agent in this reaction must selectively oxidize at least one of the reactants in the presence of a substantial excess of sodium hydride.[3]

A priori, the plethora of established oxidizing agents for the conversion of mercaptans to disulfides (6) makes it likely that the mercaptide anions would be oxidized in preference to the sulfonate-stabilized carbanions. In accord with that supposition, eq. [6] reactions in which we used *p*-tolyl mercaptan as a reactant afforded *p*-tolyl disulfide (yields up to 63%). Equation [11] provides good support for the intermediacy of the disulfide in the formation of trithioorthoformate **1**.

It is noteworthy that both intermediates **2** and *p*-tolyl disulfide increase the yield of trithioorthoformate **1** (5%, Table 1), when they are introduced as starting materials (**1**, 15%, eq. [9], and **1**, 23%, eq. [11]).

An overview of the first sequence of the trithioorthoformate reaction is presented in Scheme 1.

The principal oxidizing agent might be atmospheric oxy-

[3] Sodium hydride may act as a reducing agent: see ref. 4 and references therein.

Can. J. Chem. Downloaded from www.nrcresearchpress.com by 65.111.164.53 on 09/08/12
For personal use only.

Scheme 1

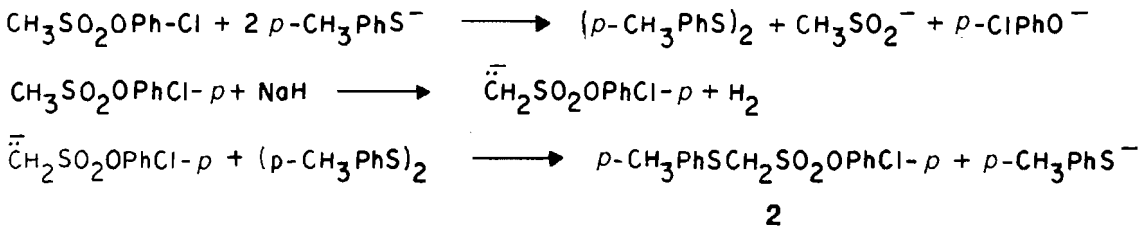

[11] CH_3SO_2O—C$_6$H$_4$—Cl + (CH$_3$—C$_6$H$_4$—S)$_2$ + NaH

RT, HMPA ⟶ **1** (23%) + **2** (17%) + CH_3SO_2O—C$_6$H$_4$—Cl (0%)

gen. However, (*i*) the eq. [8] reaction proceeds normally under a nitrogen atmosphere and (*ii*) a HMPA solution of *p*-tolyl mercaptide anions furnishes *p*-tolyl disulfide in only 27% yield after exposure to air at room temperature for 1 h 5 min.

Recently published results (2), eq. [12], make it very likely that the sulfonate esters themselves serve as the principal oxidizing agents.

[12] CH_3SO_2O—C$_6$H$_2$(Br)$_2$—Br + CH$_3$—C$_6$H$_4$—SH + NaH

RT, HMPA ⟶ (CH$_3$—C$_6$H$_4$—S)$_2$ (98%)

In accord with previous discussions (2, 4), we propose that a likely redox mechanism would involve single electron transfer (SET).[4] The facility of such processes should vary with the LUMO energy of the oxidant.

Equations [13] and [14] contrast with the corresponding results for *p*-chlorophenyl methanesulfonate (eqs. [8] and [11]), which can be readily rationalized from the LUMO eigenvalues provided in Table 1.

[13] CH_3SO_2OPh + CH$_3$—C$_6$H$_4$—SH + NaH

RT, HMPA ⟶ (CH$_3$—C$_6$H$_4$—SCH_2SO_2OPh **3** (7%) + CH_3SO_2OPh (59%)

[14] CH_3SO_2OPh + (CH$_3$—C$_6$H$_4$—S)$_2$ + NaH

RT, HMPA ⟶ **3** (7%) + **1** (24%) + CH_3SO_2OPh (37%)

First, consider the reactions that employ the mercaptan. The relatively high-lying phenyl methanesulfonate LUMO leads to slow oxidation (SET), a low yield of sulfide-sulfonate ester **3**, and a very substantial amount of unchanged phenyl methanesulfonate (59%). In contrast, the lower lying *p*-chlorophenyl methanesulfonate LUMO leads to more facile oxidation (SET), quadruple the yield of sulfide-sulfonate ester **2**, and only 7% recovered sulfonate ester (eq. [8]).

Reactions with disulfide alleviate the need for an oxidation step in order to form trithioorthoformate **1**. Both phenyl methanesulfonate and *p*-chlorophenyl methanesulfonate should have methyl protons with comparable acidity so that carbanion formation (as assumed in eq. [10]) would proceed smoothly in both cases. These reactions give low yields of sulfide–sulfonate esters **2** or **3** and comparable yields of the trithioorthoformate **1** (eqs. [11] and [14]). Note the complete consumption of the chloroester (eq. [11]) versus the recovery of a third of the phenyl methanesulfonate (eq. [14]).

The results in equations [8], [11], [13], and [14] suggest an interesting series of experiments. Assume that the sulfide-sulfonate esters **2** and **3** are formed as shown in eq. [15].

[15] CH_3SO_2OAr + NaH ⟶ $\bar{C}H_2SO_2OAr$ + (*p*-$CH_3PhS)_2$

S_N2 ↓

p-$CH_3PhSCH_2SO_2OAr$ + *p*-CH_3PhS^-

If the reaction shown in eq. [15] were a simple S_N2 substitution, then the yield of sulfide-sulfonate ester **2** should decrease as the amount of disulfide is decreased in consecutive runs. *But*, if the sulfonate ester is a redox reagent that can oxidize mercaptide anions back to disulfide then the outcome should be very different.

Initially, a decrease in the amount of disulfide would produce fewer mercaptide anions. In turn, the amount of methanesulfonate consumed by mercaptide anions[5] would be

[4] Note the earlier proposal by Wenkert et al. (7) that the β-chlorination of indole anions proceeds by SET from the indole anion to benzenesulfonyl chloride.

[5] *p*-Chlorophenyl methanesulfonate and **2** should accept an electron with comparable facility based on the ZINDO calculated eigenvalues for their LUMOs, which are −0.0201 and +0.0207 eV, respectively.

Can. J. Chem. Downloaded from www.nrcresearchpress.com by 65.111.164.53 on 09/08/12
For personal use only.

Scheme 2

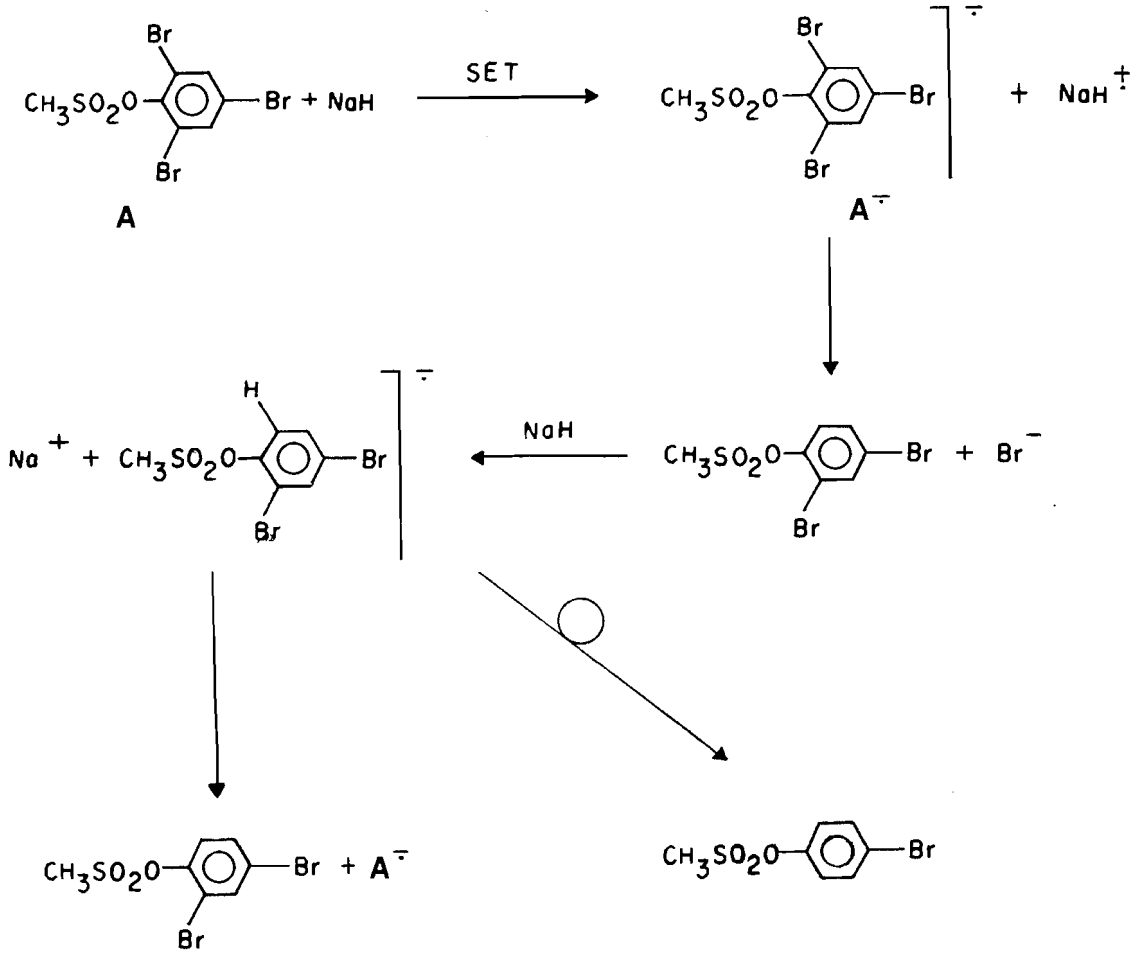

reduced and more methanesulfonate carbanions should be available to carry out the substitution that produces sulfide-sulfonate **2**. Thus, initially, the yield of sulfide-sulfonate ester would *increase* when the amount of disulfide is *decreased*. Of course the yield of **2** will ultimately have to decrease as the amount of added disulfide nears zero. Analysis of eq. [15], assuming that all mercaptide anions produced would reduce any sulfonate ester present, leads to the conclusion that the sulfide-sulfonate ester yield should reach a maximum for the reaction in which the *p*-chlorophenyl sulfonate/*p*-tolyl disulfide ratio is approximately 1:0.5.

This series of reactions was conducted in the same manner and on the same scale as described in the experimental section under "Reaction of *p*-chlorophenyl methanesulfonate with *p*-tolyl disulfide" (except the amount of disulfide was reduced from run to run). Our results follow the form: ratio methanesulfonate/disulfide (grams of sulfide-sulfonate ester **2** isolated), 1:1 (0.765 g), 1:0.5 (1.297 g), 1:0.4 (1.068 g), 1:0.3 (0.843 g). Note that simple S_N2 substitution uncomplicated by redox chemistry should have given the following results: 1:1 (0.765 g), 1:0.5 (0.382 g), 1:0.4 (0.306 g), and 1:0.3 (0.229 g). In our view, these results offer very strong support for the role of *p*-chloromethanesulfonate as oxidant and virtually eliminate any other oxidant from consideration.

Are mercaptide anions the exclusive reductants in these reactions or can sodium hydride also initiate SET reactions with aryl methanesulfonates? A recently reported study (4) of reactions between aryl methanesulfonates and sodium hydride established routine formation of two products.

$$[16]\quad CH_3SO_2OAr + NaH \xrightarrow[HMPA]{RT} CH_3SO_2CH_2SO_2OAr + ArOH$$

Reactions described in the present report that employed either *p*-tolyl mercaptan or *p*-tolyl disulfide (e.g., eqs. [6], [7], [11]) failed to furnish any sulfone-sulfonate esters. Apparently sulfonate-stabilized carbanions sulfenylate more rapidly than they decompose to form sulfene[6] and phenoxide ions. We proposed that eq. [16] reactions, which produced phenols exclusively, were proceeding by SET from sodium hydride to the aryl methanesulfonate (LUMO eigenvalues ≤ -1 eV).

As part of the present work, we subjected 2,4,6-tribromophenyl methanesulfonate to reaction with sodium hydride. Given the LUMO eigenvalue (Table 1) for 2,4,6-tribromophenyl methanesulfonate, the high yield of the tribromophenol and the absence of a product sulfone-sulfonate ester are expected results. The selective displacement of *ortho* bromine atoms is entirely inconsistent with the formation of a Meisenheimer complex (3). Such behaviour is consistent with

[6] Reference 4 concludes that sulfene is an intermediate in the formation of aryl sulfone–sulfonates as depicted in eq. [16].

Can. J. Chem. Downloaded from www.nrcresearchpress.com by 65.111.164.53 on 09/08/12
For personal use only.

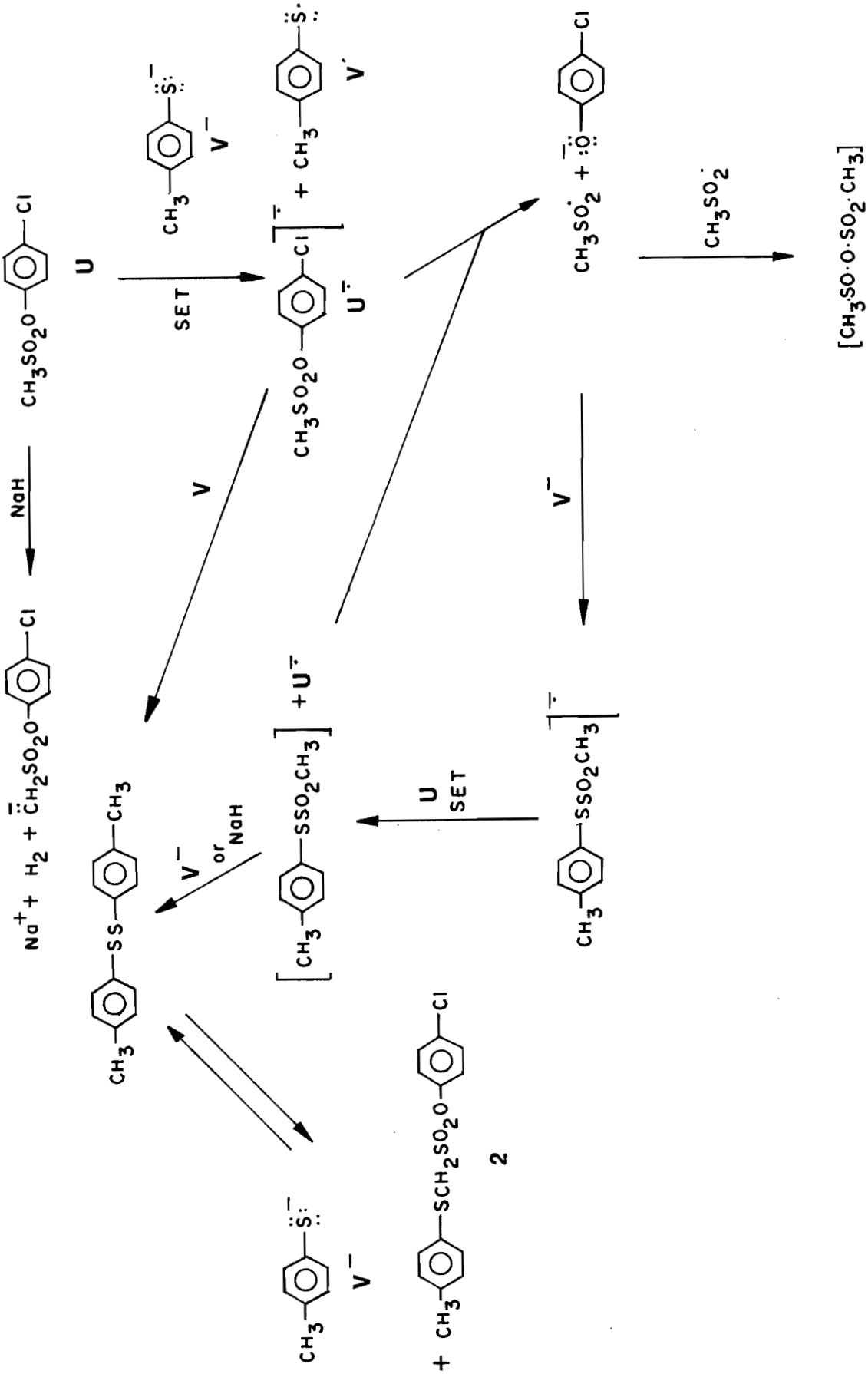

Scheme 3. The first sequence of the trithioorthoformate reaction.

Can. J. Chem. Downloaded from www.nrcresearchpress.com by 65.111.164.53 on 09/08/12
For personal use only.

[17] 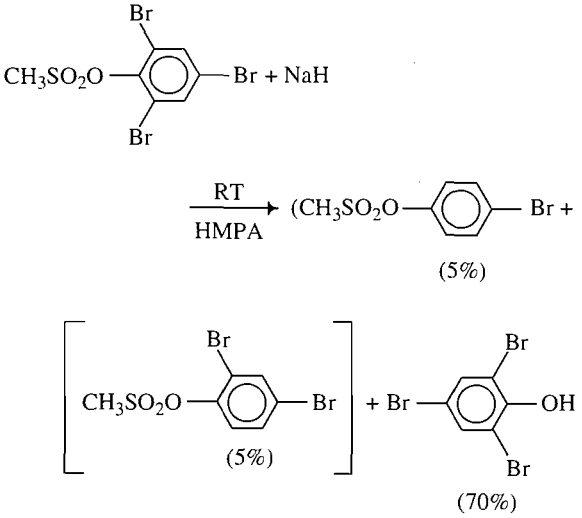

SET-induced dechlorination of *p*-chlorophenyl methanesulfonate (8).

At the suggestion of a referee, we repeated the eq. [17] reaction in the presence of *m*-dinitrobenzene. No debrominated sulfonate esters were formed, suggesting that debromination was accomplished by a radical-anion chain SET mechanism (8*b*–8*e*) as depicted in Scheme 2.

The failure of the tribromophenyl sulfonate ester in Table 1 to produce any trithioorthoformate **1**, despite its obvious ability to oxidize mercaptide anions (LUMO eigenvalue −1.0038 eV) may now be attributed to its facile reduction by NaH. The nitrosulfonate ester (LUMO eigenvalue −1.9839 eV) undergoes nucleophilic aromatic substitution with mercaptide anions (3).

From the time that the eq. [11] results were obtained, we were interested in the possibility that sulfonate-stabilized carbanion sulfenylation might be reversible. Reversibility would not be surprising in view of Trost's results showing that carboxylic ester sulfenylation in THF–HMPA is reversible (9). Reversibility of sulfonate ester sulfenylation under our conditions was established by the following results:

Scheme 3 provides a complete proposal for the first sequence of the Trithioorthoformate Reaction and accounts for all of our experimental results. Note that the intermediacy of thiolsulfonates was considered in detail in an earlier paper (2).

The sulfide-sulfonate ester **3** was produced in only 7% yield under our optimized conditions (see eq. [13]). A significant improvement in the yield of **3** was realized when we carried out the following reaction:

[19] 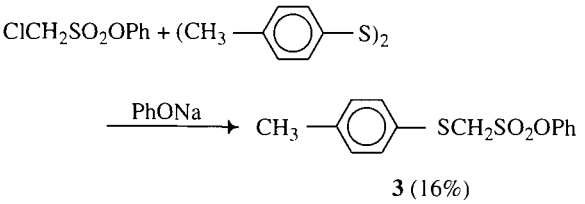

Methods

Details for ZINDO computations have been given earlier (3, 5).

[18] 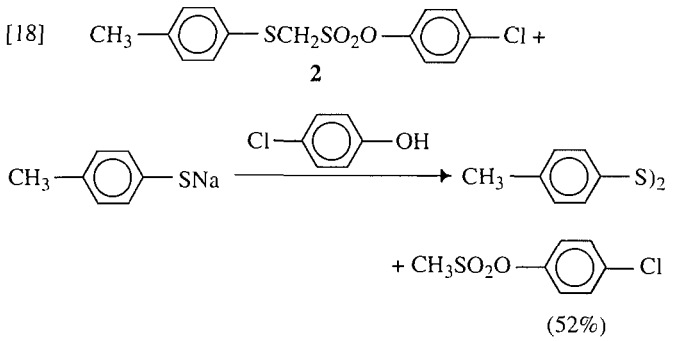

Experimental

General

The ir spectra were recorded on a Perkin–Elmer 237B grating spectrophotometer. Ultraviolet spectra were run on a Beckman DU-2 spectrophotometer. The nmr spectra were obtained on a Varian EM360A instrument using TMS as the internal standard. Melting points were determined on a Gallenkamp MFB-595 capillary melting point apparatus and are uncorrected. Gas–liquid chromatographic analyses were carried out with a He flow rate of 70 mL/min through a column of 8% Carbowax on Chromosorb W. Column temperatures were 130°C for *p*-tolyl mercaptan analysis and 210°C for *p*-tolyl disulfide analysis.

Sodium hydride was purchased as a dry solid (97%). It was repackaged under N_2 into 1-g lots. Sample vials were sealed with beeswax. Sodium hydride for experiments was weighed from the sample vials into flasks that were sealed with ground-glass stoppers.

Standard work-up

The crude reaction mixture was poured into water (400 mL) and 10% HCl (10 mL). The resultant mixture was washed with diethyl ether (3 100-mL aliquots). The combined ether layers were concentrated and the residue poured into water (100 mL). The resultant mixture was extracted with diethyl ether (3 100-mL aliquots). The combined ether layers were washed with 2.5% NaOH (100 mL), dried ($MgSO_4$), and concentrated.

Formation of p-*tolyl ethyl sulfide and trithioorthoformate* ***1*** *at elevated temperature*

A solution of absolute ethanol (0.636 g, 13.8 mmol) in HMPA[7] (10 mL) was added dropwise to a suspension of sodium hydride (0.659 g, 27.4 mmol) in HMPA (50 mL). A solution of *p*-tolyl mercaptan (1.705 g, 13.8 mmol) in HMPA (10 mL) was added dropwise over 5 min. Phenyl methanesulfonate (2.370 g, 13.8 mmol) was added and the reaction mixture maintained at 100–120°C for 2 h.[8] Standard work-up furnished a crude sample.

The crude product was chromatographed on silica gel

[7] HMPA (hexamethylphosphoramide) is toxic and carcinogenic (10).

[8] Upon completion of mixing the reactants, a significant portion of the sodium hydride was still unreacted. The reaction of ethanol with sodium hydride in HMPA is extremely slow, presumably due to the very high pK_a's of simple alcohols in very polar aprotic solvents, e.g., methanol has a pK_a of 29.0 in DMSO (11).

Can. J. Chem. Downloaded from www.nrcresearchpress.com by 65.111.164.53 on 09/08/12
For personal use only.

(200 g) employing chloroform elution (100-mL fractions). Fractions 5–7 were combined to give a mixture of nonpolar compounds (1.635 g).

The nonpolar mixture was chromatographed on silica gel (150 g) employing mixed hexanes for elution (100-mL fractions). Fractions 6–10 were combined and concentrated, affording a mixture of *p*-tolyl ethyl sulfide (0.272 g, 1.78 mmol, 13%) and *p*-tolyl methyl sulfide (0.101 g, 0.73 mmol, 5%). The mixture was analyzed quantitatively by nmr as outlined elsewhere (12). Each component was identified by the addition of authentic material, which induced an increase in intensity for the appropriate signals in the proton nmr of the mixture.

Fractions 22–35 were combined and concentrated, furnishing clean trithioorthoformate **1** (0.708 g, 1.85 mmol, 40%). Chromatographed **1** was shown to be identical to authentic material prepared as described previously (13).

Reaction of phenyl ethanesulfonate and p-*tolyl mercaptide ions*

The reaction "Formation of *p*-tolyl ethyl sulfide and trithioorthoformate **1** at elevated temperature" was rerun on the same scale but phenyl ethanesulfonate (13.8 mmol) was substituted for the methanesulfonate. Standard work-up furnished crude product that showed no trithioorthoformate **1** by nmr or tlc. Column chromatography (200 g silica gel) employing chloroform for elution (30 100-mL fractions) resolved the product mixture. The principal product was *p*-tolyl disulfide (0.835 g, 3.39 mmol) from fractions 5 and 6. No trithioorthoformate **1** was found in any column fractions.

Trithioorthoformate reaction in the presence of phenyl methyl sulfide

The reaction "Formation of *p*-tolyl ethyl sulfide and trithioorthoformate **1** at elevated temperature" was rerun on the same scale but phenyl methyl sulfide (0.865 g, 6.8 mmol) in HMPA[7] (10 mL) was also added. Standard work-up furnished a semicrystalline crude residue. Recrystallization from methanol furnished the trithioorthoformate **1** (0.263 g, 0.68 mmol), which was identical to authentic material by nmr, ir, and mp. The mother-liquor concentrate was chromatographed on silica gel (150 g) employing carbon tetrachloride for elution (100-mL fractions). Fraction 5 furnished *p*-tolyl disulfide (0.242 g, 0.98 mmol). Fraction 6 yielded unchanged phenyl methyl sulfide (0.192 g, 1.5 mmol). Fractions 7–10 were combined and concentrated, giving impure trithioorthoformate **1**. Recrystallization from methanol furnished a crop of clean **1** (0.111 g, 0.29 mmol).

Trithioorthoformate reaction in the presence of bis(thiophenyl)methane

This reaction was carried out in the same manner as "Formation of *p*-tolyl ethyl sulfide and trithioorthoformate **1** at elevated temperature" employing the following chemicals: phenyl methanesulfonate (0.741 g, 4.30 mmol), sodium hydride (0.106 g, 4.41 mmol), *p*-tolyl mercaptan (0.536 g, 4.32 mmol), bis(thiophenyl)methane (0.996 g, 4.29 mmol), and HMPA[7] (40 mL).

Standard work-up furnished crude product (1.193 g), which was chromatographed on silica gel (100 g) employing carbon tetrachloride for elution (100 mL fractions). Fraction 4 gave unchanged bis(thiophenyl)methane (0.353 g, 1.52 mmol). Fractions 5 and 6 were combined, affording bis(thiophenyl)methane (0.333 g, 1.43 mmol) and the trithioorthoformate **1** (0.131 g, 0.34 mmol).

Reaction of aryl methanesulfonates with sodium hydride and p-*tolyl mercaptan in the presence of ethanol*

The series of reactions represented by eq. [6] was set up in HMPA[7] on the same scale as just outlined under "Formation of *p*-tolyl ethyl sulfide and trithioorthoformate **1** at elevated temperature." Reactions were run at ambient temperature. The reaction on *p*-chlorophenyl methanesulfonate was run for 1 h while the others were all run for 2 h.

Column chromatography as described for the previous experiment furnished the trithioorthoformate **1** and *p*-tolyl disulfide. Yields for these products from each aryl methanesulfonate were: sulfonate (% **1**, % disulfide), phenyl methanesulfonate (0, 0), *p*-chlorophenyl methanesulfonate (4, 4), *p*-methylsulfonylphenyl methanesulfonate (30, 10), 2,4,6-tribromophenyl methanesulfonate[9] (0, 63), and *p*-nitrophenyl methanesulfonate[9] (0, 4).

Optimized preparation of the sulfide-sulfonate ester **2** *in HMPA*[7]

The reactions represented by eq. [8] were all conducted in the manner outlined below.

A solution of *p*-tolyl mercaptan (4.254 g, 34.3 mmol) in HMPA[7] (25 mL) was added dropwise to a suspension of sodium hydride (1.651 g, 68.7 mmol) in HMPA[7] (75 mL). Upon completion of the addition, the reaction mixture was stirred at ambient temperature for 5 min. *p*-Chlorophenyl methanesulfonate (2.828 g, 13.7 mmol) was added, and the reaction mixture stirred for 1 h at ambient temperature.

The reaction mixture was subjected to standard work-up. Crude product was chromatographed on silica gel (200 g) employing carbon tetrachloride elution (100-mL fractions). Fractions 7–10 were combined and concentrated, affording clean trithioorthoformate **1** (0.287 g, 0.75 mmol, 5.5%). Fractions 21–45 were combined and concentrated, affording homogeneous sulfide-sulfonate ester **2** (4) (1.221 g, 3.72 mmol, 27%). After collecting 60 fractions of carbon tetrachloride, the eluting solvent was changed to chloroform. Fractions 65–67 were combined to give unchanged *p*-chlorophenyl methanesulfonate (0.195 g, 7%).

Peroxidation of the sulfide–sulfonate ester **2**

A solution of the sulfide–sulfonate ester **2** (0.510 g, 1.55 mmol) in chloroform (50 mL) was cooled in an ice–water bath. *m*-Chloroperoxybenzoic acid (85%, 0.699 g, 3.45 mmol peracid) was added to the reaction mixture in small portions. The ice was allowed to melt and the reaction to return to room temperature. The reaction was stirred for 48 h upon completion of peracid addition.

The reaction mixture was poured into chloroform and the resultant mixture extracted with 2.5% NaOH (3 50-mL portions). Crude sulfone-sulfonate ester was chromatographed on silica gel (50 g) employing 1:1 methylene chloride/carbon tetrachloride for elution (5-mL fractions). Fractions 5–7 were combined and concentrated, furnishing clean sulfone-sulfonate ester (0.384 g, 1.06 mmol, 68%). Recrystallized sul-

[9] See Table 1, footnote *b*.

Can. J. Chem. Downloaded from www.nrcresearchpress.com by 65.111.164.53 on 09/08/12
For personal use only.

fone-sulfonate ester had mp 76.3–77.1°C; ir ($CHCl_3$); 1398, 1340, and 1155 cm^{-1}; nmr ($CDCl_3$) δ: 7.93 (2H, d), 7.43 (2H, d), 7.36 (4H, br s), 4.73 (2H, s), and 2.46 (3H, s); ms *m/e*: M^+ +2, 362 (13%), 360 (29%), 155 (100%), and 91 (57%). Anal. calcd. for $C_{14}H_{13}ClO_5S_2$: C 46.60, H 3.63; found: C 46.97, H 3.40.

Routine preparation of **2**

A solution of *p*-tolyl mercaptan (4.250 g, 34.2 mmol) in dimethyl sulfoxide (DMSO) (25 mL) was added dropwise to a slurry of sodium hydride (1.668 g, 69.5 mmol) in DMSO (75 mL) over 30 min. The reaction mixture was stirred at ambient temperature for 10 min to permit complete evolution of H_2. *p*-Chlorophenyl methanesulfonate (2.824 g, 13.7 mmol) was added and the reaction mixture stirred at ambient temperature for 35 min.[10]

Standard work-up furnished crude product (2.170 g), which was chromatographed on silica gel (220 g) employing carbon tetrachloride elution (20 100-mL fractions) followed by chloroform elution (100-mL fractions). Fractions 25–27 were combined and concentrated, giving clean sulfide-sulfonate ester **2** (1.292 g, 3.93 mmol, 29%).

Reaction of the sulfide-sulfonate ester **2** *with* p-*tolyl mercaptan*

A solution of *p*-tolyl mercaptan (0.943 g, 7.60 mmol) in HMPA[7] (25 mL) was added dropwise to a suspension of sodium hydride (0.368 g, 15.3 mmol) in HMPA[7] (75 mL). The sulfide-sulfonate ester **2** (1.004 g, 3.06 mmol) was added and the reaction mixture stirred at ambient temperature for 1 h 10 min.

Standard work-up with routine column chromatography (80 g silica gel, carbon tetrachloride elution) furnished a mixture of *p*-tolyl disulfide and the trithioorthoformate **1** (0.362 g). Preparative thick-layer chromatography on this mixture (three 20 cm × 20 cm plates, developed 3 times with hexanes) furnished clean **1** (0.181 g, 0.47 mmol, 15%). The initial column also provided unchanged **2** (0.221 g).

Reaction of p-*chlorophenyl methanesulfonate with* p-*tolyl disulfide*

A solution of *p*-tolyl disulfide (3.375 g, 13.7 mmol) in HMPA[7] (10 mL) was added to a suspension of sodium hydride (1.013 g, 42.2 mmol) in HMPA[7] (80 mL). *p*-Chlorophenyl methanesulfonate (2.825 g, 13.7 mmol) was added and the reaction mixture stirred for 1 h 10 min.

Standard work-up furnished a crude mixture (3.424 g). Crude product was chromatographed on silica gel (350 g) employing 0.5% methanol in carbon tetrachloride (40 100-mL fractions) followed by 0.5% methanol in chloroform (100-mL fractions) for elution. Fractions 12 and 13 provided a mixture that was recrystallized from methanol to give the trithioorthoformate **1** (0.502 g). Fractions 14–17 gave clean **1** (0.694 g). Total trithioorthoformate **1** obtained was 3.13 mmol (23%).

Fractions 49–55 were combined, poured into 2.5% NaOH (50 mL), and the resultant mixture was washed with chloroform (3 50-mL aliquots). The organic solution was dried ($MgSO_4$) and concentrated, yielding sulfide-sulfonate ester **2** (0.765 g, 2.33 mmol, 17%).

Reaction of p-*tolyl mercaptide ions with air*

p-Tolyl mercaptan (0.477 g, 3.6 mmol) in HMPA[7] (3 mL) was added to a slurry of sodium hydride (0.155 g, 6.4 mmol) in HMPA[7] (9 mL). The reaction mixture was stirred for 1 h 5 min. Standard work-up afforded a crude residue that contained *p*-tolyl disulfide (0.122 g, 0.49 mmol) as established by gas chromatography.

Reaction of phenyl methanesulfonate and p-*tolyl mercaptan*

A solution of *p*-tolyl mercaptan (4.250 g, 34.2 mmol) in HMPA[7] (25 mL) was added dropwise to a suspension of sodium hydride (1.680 g, 70.0 mmol) in HMPA[7] (75 mL). Phenyl methanesulfonate (2.346 g, 13.6 mmol) was added and the reaction mixture stirred at ambient temperature for 1 h 10 min.

Crude product (1.897 g), obtained by standard work-up, was subjected to column chromatography on silica gel (190 g) employing carbon tetrachloride (60 100-mL fractions) followed by chloroform (100-mL fractions) for elution. Fractions 8 and 9 were combined and concentrated, providing trithioorthoformate **1** (0.463 g, 0.121 mmol, 0.9%). Fractions 38–51 were combined and concentrated, yielding the sulfide-sulfonate ester **3** (4) (0.270 g, 0.918 mmol, 6.7%). Fractions 53–66 were combined and concentrated, furnishing unchanged phenyl methanesulfonate (1.388 g, 59%).

Reaction of phenyl methanesulfonate with p-*tolyl disulfide*

Phenyl methanesulfonate (2.342 g, 13.6 mmol), sodium hydride (0.687 g, 28.6 mmol), and *p*-tolyl disulfide (2.804 g, 11.3 mmol) were reacted and worked-up as described for the reactants under "Reaction of phenyl methanesulfonate and *p*-tolyl mercaptan."

Crude product was chromatographed on silica gel (300 g) employing carbon tetrachloride (150 100-mL fractions) followed by chloroform (100-mL fractions) for elution.

Fractions 11–19 yielded clean trithioorthoformate **1** (1.374 g, 3.59 mmol, 24%).

Fractions 85–113 furnished the sulfide-sulfonate ester **3** (4) (0.266 g, 0.904 mmol, 6.6%).

Fractions 117–162 were combined and added to 2.5% NaOH (50 mL). The resultant mixture was extracted with chloroform (3 50-mL aliquots). The combined organic layers were dried ($MgSO_4$) and concentrated, furnishing phenyl methanesulfonate (0.873 g, 37%).

Preparation of 4-bromophenyl methanesulfonate

Bromophenol was condensed with methanesulfonyl chloride following the procedure described earlier for the preparation of 2,4,6-tribromophenyl methanesulfonate (2). 4-Bromophenyl methanesulfonate had mp 81.9–83.2°C; ir ($CHCl_3$): 1165 and 1360 cm^{-1}; nmr ($CDCl_3$) δ: 7.70 (2H, d, J = 9.5 Hz), 7.20 (2H, d, J = 9.5 Hz), and 3.11 (3H, s); ms *m/e*: M^+ +2, 252 (100%), 250 (88%), 175 (11%), 174 (54%), 173 (73%), 172 (81%), and 171 (55%). Anal. calcd. for $C_7H_7BrO_3S$: C 33.48, H 2.80; found: C33.57, H 2.89.

Reaction of 2,4,6-tribromophenyl methanesulfonate with sodium hydride

A solution of 2,4,6-tribromophenyl methanesulfonate (2)

[10] Reaction time is critical: shorter times prevent accumulation of **2** and longer periods lead to consumption of **2**.

Can. J. Chem. Downloaded from www.nrcresearchpress.com by 65.111.164.53 on 09/08/12
For personal use only.

(5.009 g, 12.2 mmol) in HMPA[7] (10 mL) was added dropwise to a slurry of sodium hydride (0.582 g, 24.2 mmol) in HMPA (20 mL). Upon completion of the addition, the reaction mixture was stirred at ambient temperature for 1 h 5 min.

Standard work-up furnished crude material from the organic layer and a solution of aqueous base. The aqueous base was first acidified with concentrated hydrochloric acid, then 10% HCl (100 mL) was added. The aqueous acid solution was extracted with diethyl ether (5 100-mL portions), yielding 2,4,6-tribromophenol (2.825 g, 8.54 mmol, 70%).

The original organic layer was concentrated and chromatographed on silica gel (100 g) employing carbon tetrachloride (31 100-mL fractions) followed by chloroform (100-mL fractions) for elution. Fractions 18–28 were combined and concentrated, furnishing a mixture of the tribromophenyl methanesulfonate and 2,4-dibromophenyl methanesulfonate[11] (0.452 g). Further attempts to resolve this mixture by column chromatography and thick-layer preparative chromatography were unsuccessful. Fractions 33–40 were combined and concentrated, giving clean 4-bromophenyl methanesulfonate (0.142 g, 0.562 mmol, 4.6%). The 4-bromophenyl methanesulfonate so obtained was identical to authentic material by nmr, ir, mp, and mixture mp.

Reaction of 2,4,6-tribromophenyl methanesulfonate with sodium hydride in the presence of 1,3-dinitrobenzene

The reaction described under "Reaction of 2,4,6-tribromophenyl methanesulfonate with sodium hydride" was rerun on the same scale in the presence of 1,3-dinitrobenzene (4.049 g, 24.1 mmol). The same work-up furnished the same yield of tribromophenol and a mixture of neutrals containing 1,3-dinitrobenzene (3.453 g) and 2,4,6-tribromophenyl methanesulfonate (0.906 g). No dibromophenyl or monobromophenyl methanesulfonate was detectable (nmr).

*Reaction of **2** with sodium* p*-tolyl mercaptide in the presence of p-chlorophenol*

A solution of *p*-tolyl mercaptan (0.441 g, 3.55 mmol) in HMPA[7] (10 mL) was added to a slurry of sodium hydride (0.085 g, 3.54 mmol) in HMPA[7] (11 mL) and the reaction mixture stirred at room temperature for 10 min. *p*-Chlorophenol (0.455 g, 3.55 mmol) in HMPA[7] (4 mL) was added. The sulfide-sulfonate ester **2** (1.003 g, 3.05 mmol) was added and the reaction mixture stirred at ambient temperature for 1 h 5 min.

Crude product (1.125 g), obtained by standard work-up, was subjected to column chromatography on silica gel (150 g) employing carbon tetrachloride (67 100-mL fractions) followed by chloroform (100-mL fractions) for elution.

Fractions 4–6 furnished *p*-tolyl disulfide (0.321 g, 1.30 mmol, 73%). Fractions 7–10 yielded trithioorthoformate **1** (0.138 g, 0.361 mmol, 10%). Fractions 39–51 gave unchanged **2** (0.060 g, 6%). Fractions 67–73 furnished *p*-chlorophenyl methanesulfonate (0.326 g, 1.58 mmol, 52%). Recrystallized methanesulfonate was identical to authentic material by mp, mixture mp, ^{1}H nmr, ir, and double spotted tlc.

*Preparation of the sulfide-sulfonate ester **3***

A solution of phenol (0.921 g, 9.79 mmol) in HMPA[7] (8 mL) was added dropwise to a suspension of sodium hydride (0.230 g, 9.58 mmol) in HMPA[7] (5 mL). Upon completion of the addition, the reaction mixture was stirred at ambient temperature for 10 min. Phenyl chloromethanesulfonate (4) (2.014 g, 9.77 mmol) and *p*-tolyl disulfide (1.190 g, 4.83 mmol) were added. The reaction mixture was stirred at ambient temperature for 45 min.

Crude product, obtained by standard work-up, was subjected to column chromatography on silica gel (200 g) employing carbon tetrachloride elution (100-mL fractions). Fractions 107–166 were combined and concentrated, giving the sulfide-sulfonate ester **3** (0.466 g, 1.58 mmol, 16%).

[11] The structural assignment for the dibromomethanesulfonate rests entirely on the proton nmr obtained by subtraction of the tribromomethanesulfonate signals from the ^{1}H nmr of the mixture.

Acknowledgements

The authors acknowledge some technical assistance from J.S. Quick, D.C. Stone, and K.A. Ginigé. Mass spectra were run by D. Drummond at the University of New Brunswick. We are grateful to the Florida Institute of Technology and Mount Allison University for financial support.

References

1. R.F. Langler and N.A. Morrison. Can. J. Chem. **65**, 2385 (1987).
2. K.A. Durkin, R.F. Langler, and N.A. Morrison. Can. J. Chem. **66**, 3070 (1988).
3. J.C. Baum, J. Bolhassan, R.F. Langler, P.J. Pujol, and R.K. Raheja. Can. J. Chem. **68**, 1450 (1990).
4. J.C. Baum, K.A. Durkin, L. Precedo, S.B. O'Blenes, J.E. Goehl, R.F. Langler, G.K. MacCormack, and L.L. Smith. Can. J. Chem. **69**, 2127 (1991).
5. J. Ridley and M. Zerner. Theor. Chim. Acta, **32**, 111 (1973).
6. L. Field. *In* Organic chemistry of sulfur. *Edited by* S. Oae. Plenum Press, New York. 1977. p. 316.
7. E. Wenkert, P.D.R. Moeller, and S.R. Piettre. J. Org. Chem. **52**, 3404 (1987).
8. (*a*) J.C. Carnahan, Jr., W.D. Closson, J.R. Ganson, D.A. Juckett, and K.S. Quall. J. Am. Chem. Soc. **98**, 2526 (1976); (*b*) J.F. Bunnett. Acc. Chem. Res. **11**, 413 (1978); (*c*) N. Kornblum. Angew. Chem. Int. Ed. Engl. **14**, 734 (1975); (*d*) M. Julliard and M. Chanon. Chem. Rev. **83**, 425 (1983); (*e*) M. Chanon and M.L. Tobe. Angew. Chem. Int. Ed. Engl. **21**, 1 (1982).
9. B.M. Trost. *In* Organic sulfur chemistry: structure, mechanism and synthesis. *Edited by* C.J.M. Stirling. Butterworths, London. 1975. p. 255.
10. N.I. Sax. Dangerous properties of industrial materials. Van Nostrand–Rheinhold, New York. 1979. p. 721.
11. F.G. Bordwell. Acc. Chem. Res. **12**, 456 (1988).
12. J.S. Grossert and R.F. Langler. Can. J. Chem. **55**, 407 (1977).
13. A.L. Kramzfelder and R.R. Vogt. J. Am. Chem. Soc. **60**, 1714 (1938).

Peroxydation de l'acide linolénique en présence des fibres d'amiante ou de némalite. Résultats préliminaires avec des cellules épithéliales

Germaine Levasseur-Acker, Roger Zalma, Edith Copin, Jeanine Fournier, Henri Pezerat et Roger Jankowski

Résumé : La peroxydation de l'acide linolénique (LH), en milieu aqueux aéré, a été étudiée en présence de fibres de chrysotile (UICC A et B), de crocidolite UICC et de némalite. Des études préliminaires sur la peroxydation des membranes des cellules épithéliales des voies aériennes ont également été réalisées. Les radicaux ($L^{\cdot}$, $LOO^{\cdot}$) issus de la peroxydation sont détectés en RPE à l'aide d'un piégeur de radicaux, le POBN. L'activité de ces minéraux contenant du fer(II) est liée à la formation d'espèces activées de l'oxygène et en particulier de certaines d'entre elles très électrophiles ($^{\cdot}OH$ ou entités perferryles et ferryles). Leur mise en évidence en RPE par l'intermédiaire d'un piégeur de radicaux, le DMPO, est réalisée en absence et en présence de certains complexants du fer(II) tels que les ions phosphate, l'ADP, l'ATP, l'AMP et l'EDTA. La formation et la nature des entités activées de l'oxygène est fonction non seulement de la nature du matériau inorganique mais aussi de la nature des complexants du milieu. L'extrapolation des résultats obtenus à partir de l'acide linolénique à la peroxydation des membranes des cellules épithéliales ne peut se faire directement.

Mots clés : amiante, peroxydation, complexants du fer, espèces activées de l'oxygène, RPE.

Abstract: Linolenic acid (LH) peroxidation in aqueous medium is studied in the presence of fibers of chrysotile (UICC A and B), crocidolite UICC, and némalite. Preliminary studies on the peroxydation of epithelial cell membranes were also performed. Radicals ($L^{\cdot}$, $LOO^{\cdot}$) formed from the peroxidation process are detected by EPR with a spin trapping agent, POBN. The activity of these iron(II)-containing fibers is related to the formation of activated oxygen species, particularly of some highly electrophilic species ($^{\cdot}OH$ or perferryl and ferryl entities). The presence of these species is shown by EPR with a spin trapping agent, DMPO, in the presence or in the absence of certain iron(II) chelators (phosphate ions, ADP, ATP, AMP, EDTA). The formation and the nature of activated oxygen species depend on the nature both of the inorganic material and of the chelator. It is not possible to directly extrapolate the results obtained with linolenic acid to the peroxidation of epithelial cell membranes.

Key words: asbestos, peroxidation, iron chelators, activated oxygen species, EPR.

Introduction

La toxicité des fibres d'amiante et de némalite a été examinée par de nombreux auteurs. Un certain nombre d'entre eux (1) ont montré que ces matériaux présentant un caractère donneur d'électrons dû à l'existence de sites réducteurs (Fe(II)) sont capables d'activer, en milieu aqueux aéré, l'oxygène moléculaire dissous pour conduire à la formation d'espèces activées de l'oxygène (EAO). Ces sites réducteurs Fe(II) peuvent éventuellement être formés par réduction de sites Fe(III) en présence d'un réducteur. Les espèces activées de l'oxygène, susceptibles de participer à des processus de stress oxydant (2), peuvent être de diverse nature et se différencier par leur pouvoir oxydant. En effet nos études récentes (3, 4) ont permis de distinguer deux sous-ensembles parmi l'ensemble des EAO. Le premier, appelé A*, regroupe des espèces très oxydantes (par exemple des radicaux $^{\cdot}OH$, ou des espèces ferryles $Fe^{IV}{=}O$, et (ou) perferryles $Fe^{V}{=}O$ (5)), capables d'arracher un atome d'hydrogène à une grande variété de molécules cibles (RH) telles le DMSO, l'alcool ou l'anion formiate, pour donner un radical $R^{\cdot}$. Le second sous-ensemble, appelé P*, correspond à des espèces moins électrophiles que les A* (par exemple les entités superoxo Fe^{III}-$O_2^{-\cdot}$ (6)) qui sont incapables d'extraire un atome d'hydrogène aux molécules cibles (RH) citées ci-dessus mais par contre sont aptes à attaquer un

Reçu le 29 juillet 1994.

G. Levasseur-Acker. Laboratoire de physiologie respiratoire, Faculté de Médecine Cochin-Port Royal, 24 rue du Faubourg Saint-Jacques, 75014 Paris, France.
R. Zalma, E. Copin, J. Fournier[1] et H. Pezerat. Laboratoire de réactivité de surface, Centre national de la recherche scientifique, Unité de recherche associée n° 1106, Université Pierre et Marie Curie, Tour 54, 4 place Jussieu, 75252 Paris Cédex 05, France.
R. Jankowski. Hôpital Central de Nancy, Service d'oto-rhino-laryngologie (ORL), 29 avenue de Lattre de Tassigny, 54037 Nancy, France.

[1] Auteur à qui adresser toute correspondance. Téléphone : 33 (1) 44 27 55 33. Fax : 33 (1) 44 27 60 33.

Can. J. Chem. Downloaded from www.nrcresearchpress.com by 65.111.164.53 on 09/08/12
For personal use only.

hydrogène plus labile sur un lipide polyinsaturé (LH) et ainsi de déclencher la peroxydation. A fortiori les espèces A* sont aussi capables d'initier la peroxydation des lipides.

Bien que le mécanisme de la peroxydation lipidique apparaisse très complexe, il est généralement admis (7) que la peroxydation s'effectue selon une succession de réactions radicalaires réparties en trois étapes principales : initiation, propagation et terminaison.

Par abstraction d'un atome d'hydrogène la première étape (initiation) conduit à la formation d'un radical L·

$$[1] \quad LH \xrightarrow{-H^{\cdot}} L^{\cdot}$$

La seconde étape (propagation) en milieu aéré, fait apparaître des radicaux peroxyles (LOO·) et des hydroperoxydes :

$$[2] \quad L^{\cdot} + O_2 \longrightarrow LOO^{\cdot}$$

$$[3] \quad LOO^{\cdot} + LH \longrightarrow LOOH + L^{\cdot}$$

La dernière étape (terminaison) correspond à la combinaison des radicaux L· et LOO· pour donner des produits non radicalaires.

La présente étude a pour but de mettre en évidence le rôle des EAO dans l'initiation de la peroxydation de l'acide linolénique, grâce à la détection des radicaux L· ou LOO· formés. Certaines de ces entités activées de l'oxygène (A* et P*) sont dans le cas présent générées par des fibres minérales d'amiante (chrysotile, crocidolite) ou de némalite, matériaux contenant du Fe(II), après réaction avec l'oxygène moléculaire dissous dans un milieu aqueux. Plusieurs types de fer(II) peuvent être à l'origine de l'apparition des EAO (8, 9) : les ions Fe^{2+} liés au réseau solide, les ions Fe^{2+} passés en solution se retrouvant soit à l'état hydraté soit à l'état complexé par des ligands appropriés. La production de ces EAO peut être aussi liée à la présence de fer(III) pouvant présenter les mêmes types de coordination que le fer(II), à condition que les ions Fe^{3+} puissent être préalablement réduits en ions Fe^{2+} par des molécules réductrices telles la NADPH. Les différences de réactivité du fer vis-à-vis de l'oxygène moléculaire sont fonction de ses divers états du cation de transition.

Dans le cadre de l'étude de la peroxydation de l'acide linolénique, nous avons été amenés à étudier l'influence de certaines molécules complexantes susceptibles d'extraire le fer des fibres minérales (10), ce processus pouvant contribuer à la formation de ces espèces A* ou P* en solution. Une étude de la peroxydation des membranes de cellules épithéliales en présence des fibres minérales est également abordée et nous exposerons les résultats préliminaires obtenus avec ou sans ajout de complexants.

Matériaux et méthodes

Fibres minérales

L'étude a porté sur trois échantillons d'amiante qui nous ont été fournis par l'Union Internationale contre le Cancer (UICC) : deux échantillons de chrysotiles A (Rhodésie) et B (Canada) et un échantillon de crocidolite. Nous avons choisi également d'examiner une brucite fibreuse, la némalite, de la mine d'Asbestos (Québec). La némalite est un contaminant fréquent des chrysotiles canadiens (11). La crocidolite et la némalite ont été broyées 2 min à la main dans un mortier en agate juste avant la réalisation des tests.

Réactifs

L'éthylènediamine tétraacétique disodique dihydraté (EDTA, 99%) et quatre nucléotides adényliques ont été utilisés : l'adénosine 5′-diphosphate sodique (ADP, 97%), l'adénosine 5′-monophosphate sodique (AMP, 99%), l'adénosine 5′-triphosphate disodique (ATP, 99%) et la nicotinamide adénine diphosphate tétrasodique (NADPH, 96%). Tous ces réactifs ainsi que l'agent mouillant, le CHAPS ou 3-[(3-cholamidopropyl)-diméthylammoniol]-1-propanesulfonate, le DMPO ou 5-5′-diméthyl-1-pyrroline-*N*-oxyde (99%) et l'acide linolénique ou acide 9-12-15-octadécatriènoïque (98%) viennent de chez Sigma. Le DMPO a été purifié par filtration sur charbon actif suivant la méthode préconisée par Buettner et Oberley (12). Le POBN ou α-(4-pyridyl 1-oxyde)-*N*-*tert*-butylnitrone (99%) provient de chez Jansen Chimica. Le dihydrophosphate de potassium et le monohydrophosphate de potassium permettant de préparer la solution tampon (pH 7,4) et le formiate de sodium proviennent de chez Merck. Le milieu de culture utilisé pour la culture cellulaire est le «Dulbecco modified Eagle's medium» (DME) provenant de chez Gibco. La pronase provient de chez Sigma Chemical Co.

Cultures cellulaires

L'expérimentation a été menée sur des cellules provenant de 15 polypes du nez obtenus par chirurgie chez des sujets atteints de polypose nasale. Dès l'ablation les tissus sont rincés dans le milieu de culture DEM stérile puis incubés pendant 16 h à 4°C dans ce milieu de culture contenant 0,1% de pronase (enzyme protéolytique qui digère les tissus enrobant les cellules, ce qui conduit ainsi à leur dissociation). Les cellules dissociées obtenues sont comptées et mises en culture selon la technique décrite par Levasseur-Acker et al. (13). Lorsque les cultures cellulaires arrivent à confluence (6–8 jours de culture), elles sont utilisées pour le test de peroxydation lipidique.

Test de peroxydation

Le test de peroxydation est effectué dans un réacteur à l'abri de la lumière à 37°C. Les fibres (45 mg) sont mises en suspension dans 2 mL d'une solution aqueuse (tamponnée ou non en milieu phosphate; 0,1 M; pH 7,4) contenant un piégeur de radicaux le POBN (0,1 M). À cette solution sont ajoutés 25 μL d'acide linolénique pur (23 mM) auxquels on additionne, pour faciliter sa mise en suspension, un surfactant, le CHAPS à la concentration de 0,8 mM. Lorsque le test est réalisé en présence des complexants, la quantité ajoutée correspond à des concentrations variant de 1 à environ 7 mM selon la nature du complexant. Des parties aliquotes du milieu réactionnel sont prélevées à des temps déterminés, filtrées et examinées en RPE (Bruker ESP 300 E) afin de mettre en évidence et d'évaluer la quantité d'adduits radicalaires formés. Lorsque le test est effectué sur des cellules, la quantité de fibres est seulement de 20 mg et l'acide linolénique est remplacé par les cellules (1×10^6). Suivant les cas, l'expérience est menée dans le milieu de culture DEM, dans l'eau ou le sérum physiologique (solution saline à 9‰). Le temps de vie des radicaux R· (L· ou LOO·) formés lors de la peroxydation est trop court pour per-

Can. J. Chem. Downloaded from www.nrcresearchpress.com by 65.111.164.53 on 09/08/12
For personal use only.

Can. J. Chem. Downloaded from www.nrcresearchpress.com by 65.111.164.53 on 09/08/12
For personal use only.

Fig. 1. Spectre RPE de l'adduit radicalaire (POBN,R)˙. Conditions : champ central : 3480 G; fréquence : 9,7693 GHz; puissance : 10 mW; constante de temps: 0,128 s; modulation d'amplitude: 2,043 G; gain : 4×10^4.

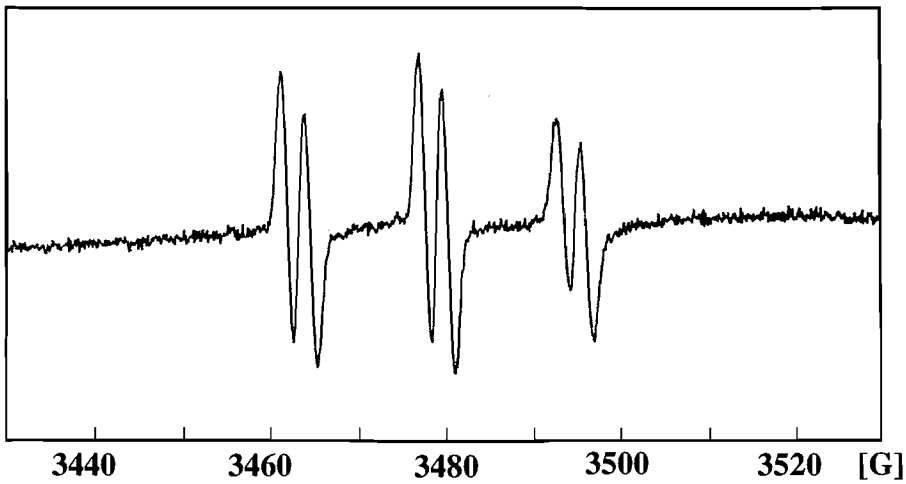

Schéma 1. Formation de l'adduit radicalaire (POBN,R)˙.

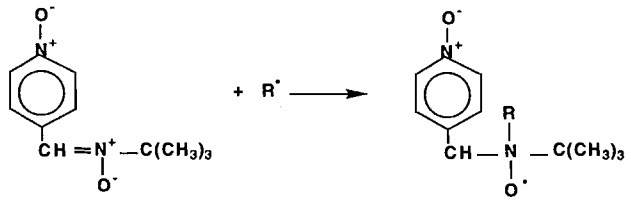

mettre leur étude. C'est la raison pour laquelle on ajoute un piégeur de radicaux le POBN, conduisant à la formation d'un adduit radicalaire suffisamment stable pour être mis en évidence par RPE (Schéma 1).

Cette derniére réaction peut être représentée plus simplement sous la forme :

[4] $\text{POBN} + \text{R}^{\cdot} \longrightarrow (\text{POBN,R})^{\cdot}$

Mise en évidence des entités A*

Certaines espèces oxydantes A*, radicalaires telles ˙OH, peuvent être mises en évidence par RPE en présence d'un piégeur de radicaux, le DMPO (14), grâce à la formation d'un adduit plus stable :

[5] $\text{DMPO} + {}^{\cdot}\text{OH} \longrightarrow (\text{DMPO,OH})^{\cdot}$

D'autres espèces A* telles les entités ferryles, perferryles, etc. ne peuvent être détectées directement par l'intermédiaire du DMPO. Cependant, ces entités oxydantes à l'égal des radicaux ˙OH sont capables d'arracher un atome d'hydrogène à une molécule RH tel l'ion formiate HCO_2^- (15) :

[6] $HCO_2^- + \text{A}^* \longrightarrow CO_2^{-\cdot} + \text{AH}$

Le radical carboxylate $CO_2^{-\cdot}$ en présence de DMPO conduit à la formation d'un adduit radicalaire détecté en RPE.

[7] $CO_2^{-\cdot} + \text{DMPO} \longrightarrow (\text{DMPO,}CO_2^-)^{\cdot}$

Pour la mise en évidence des radicaux ˙OH, 45 mg du solide testé sont mis en suspension dans 2 mL d'une solution aqueuse aérée de DMPO (50 mM). Après incubation à 37°C à l'abri de la lumière pendant des temps déterminés, des parties aliquotes sont prélevées et examinées en RPE. Le même protocole réalisé en présence du formiate de sodium permet de mettre en évidence les adduits radicalaires $(\text{DMPO,}CO_2^-)^{\cdot}$. Les conditions d'obtention et les caractéristiques de ce spectre ainsi que celui de $(\text{DMPO,OH})^{\cdot}$ ont été précédemment détaillées dans diverses études (16).

Les intensités des adduits radicalaires $(\text{POBN,LOO})^{\cdot}$, $(\text{DMPO,}CO_2^-)^{\cdot}$ et $(\text{DMPO,OH})^{\cdot}$ mentionnées dans les tableaux de résultats présentés ci-dessous sont exprimées en unités arbitraires (u.a.).

Résultats et discussion

Les tests de peroxydation de l'acide linolénique réalisés avec chacun des quatre échantillons de fibres minérales en présence de POBN conduit à la formation d'adduits radicalaires $(\text{POBN,R})^{\cdot}$ où R˙ serait LOO˙ plutôt que L˙ en milieu aqueux aéré (17). Le spectre RPE, traduisant la présence de ces adduits, est constitué de 6 raies (Figure 1) et les constantes de couplage évaluées à partir du spectre ont pour valeur a_N = 15,8 G et a_H = 2,8 G. Ces valeurs sont conformes à celles trouvées par Rosen et Rauckman (17).

Les intensités du signal RPE obtenues après piégeage par le POBN des radicaux formés au cours de la peroxydation de l'acide linolénique sont rassemblées dans le tableau 1. On observe pour les quatre matériaux testés que l'intensité des spectres après un temps d'incubation de 30 min varie suivant la nature de la fibre minérale testée et qu'elle est nettement supérieure à celle du contrôle obtenu sans fibres.

L'activité vis-à-vis de la peroxydation de l'acide linolénique est du même ordre pour la némalite et la crocidolite et elle est nettement plus importante que celles des chrysotiles A et B. Le fait que l'activité du chrysotile B soit plus importante que celle de son homologue A peut sans doute s'expliquer par la présence de la némalite dans l'échantillon B. L'activité observée traduit le degré de peroxydation de l'acide linolénique (18) et elle est due aux espèces activées de l'oxygène formées à partir du Fe^{2+} accessible en surface de la fibre minérale et (ou) en solution. Cette activité ne peut être due

Can. J. Chem. Downloaded from www.nrcresearchpress.com by 65.111.164.53 on 09/08/12
For personal use only.

Tableau 1. Peroxydation de l'acide linolénique en présence des différentes fibres minérales.

Matériaux	Intensité (POBN,R)·[a] après incubation 30 min
Némalite[b]	11000
Crocidolite UICC[b]	9900
Chrysotile UICC (B)	7100
Chrysotile UICC (A)	5100
Contrôle[c]	750

Conditions expérimentales : 45 mg de fibres en suspension dans 2 mL d'une solution aqueuse contenant : acide linolénique (23 mM), tampon phosphate pH 7,4 (0,1 M), POBN (0,1 M) et CHAPS (0,8 mM).

[a]Intensité exprimée en unités arbitraires (u.a.).

[b]Echantillon broyé 2 min à la main.

[c]Test effectué en absence de fibres minérales.

Tableau 2. Peroxydation des cellules épithéliales en présence de différentes fibres minérales.

Matériaux	Intensité (POBN,R)·[a] après incubation 60 min
Némalite[b]	1000
Crocidolite UICC[b]	0
Chrysotile UICC (A)	0
Chrysotile UICC (B)	0
Contrôle[c]	0

Conditions expérimentales : les cellules en culture sont soumises à l'action de 20 mg de fibre minérale mis en suspension dans 2 mL d'une solution aqueuse comprenant 0,5 mL de sérum physiologique. Cette solution contient du tampon phosphate pH 7,4 (0,1 M), du POBN (0,1 M) et du CHAPS (0,8 mM).

[a]Intensité exprimée en unités arbitraires (u.a.).

[b]Echantillon broyé 2 min à la main.

[c]Test effectué en absence de fibres minérales.

seulement à des espèces A* puisque le chrysotile A ne conduit qu'à la formation d'une très faible quantité d'adduits radicalaires (DMPO, CO_2^-)· (4, 18), elle serait donc liée à des espèces A* et P*.

Ces premiers résultats permettent d'envisager une possible attaque des membranes cellulaires en milieu biologique selon des mécanismes semblables à ceux de l'oxydation de l'acide linolénique. Le tableau 2 révéle l'intensité du signal (POBN,R)· lors du test de peroxydation des membranes de cellules épithéliales nasales humaines en culture primaire en présence des différentes fibres minérales. Les résultats obtenus sont assez surprenants puisque seule la némalite présente une activité alors que la crocidolite active dans la peroxydation de l'acide linolénique (tableau 1) ne présente alors aucune activité. Ces résultats nous amènent à envisager le rôle de plusieurs facteurs : (*i*) activité oxydante en surface des fibres et (ou) activité en solution; (*ii*) nature des espèces oxydantes A* (·OH et (ou) ferryle et perferryle) et (ou) P* (Fe^{III} superoxo).

Il est à priori probable que l'activité de surface, sur des temps aussi courts qu'une heure, ne permettra que difficilement une interaction entre les entités oxydantes à l'interface fibre–milieu et les zones sensibles des lipides organisés au sein de la double couche des membranes cellulaires. Cette interaction ne peut guère se produire que pendant les processus d'internalisation des particules au sein des cellules, ou suite à la rupture de la membrane (cytotoxicité). Il n'est pas impossible que la différence entre némalite et crocidolite soit due à des cinétiques de ces phénomènes plus rapides avec le premier minéral qu'avec le second.

La nature et la charge des espèces oxydantes en solution vont jouer également un rôle car la diffusion au sein de la double couche des espèces non chargées comme ·OH est probablement plus aisée que celle des ferryles et perferryles, entités existant principalement sous forme anionique (19).

Des études précédentes (20) ayant montré qu'en milieu phosphate aéré la némalite, à la différence de la crocidolite, générait des ·OH en quantité importante, il est plausible de considérer à titre d'hypothèse que cette différence de nature dans les espèces oxydantes formées joue également un rôle dans le phénomène de la peroxydation des membranes cellulaires.

Pour essayer d'approfondir cette interprétation, nous avons étudié plus particulièrement la crocidolite UICC active en présence de l'acide linolénique (tableau 1) mais totalement inactive en présence des cellules épithéliales (tableau 2).

Sachant que l'activité oxydante des fibres minérales étudiées est due à l'accessibilité du fer(II) dans les matériaux (8), nous avons tenté de modifier cette accessibilité par ajout de complexants ce qui a aussi pour conséquence de changer le potentiel rédox du couple Fe^{3+}/Fe^{2+}. Les tests ont été réalisés en présence d'un certain nombre de complexants solubles du fer tels l'AMP, l'ADP, l'ATP, l'EDTA et des ions phosphate, ces derniers pouvant jouer également un rôle important dans le phénomène de lixiviation des fibres minérales (18). En premier lieu, nous avons recherché si les complexants avaient une influence sur la formation des entités hautement électrophiles du type A*. Rappelons que ces entités sont capables en présence de DMPO et d'ions formiate de former des adduits radicalaires (DMPO,CO_2^-)·.

Les résultats obtenus à partir de la crocidolite UICC, préalablement broyée 2 min à la main (tableau 3), montrent l'influence des complexants sur l'intensité du signal de l'adduit radicalaire (DMPO,CO_2^-)·, donc sur l'activité oxydante du matériau suite à la formation d'espèces activées de l'oxygène de type A*.

Par rapport au milieu eau distillée, l'ajout de complexants permet une augmentation de l'intensité du signal et mis à part le cas de l'EDTA, le signal croît avec le temps d'incubation. Il apparaît donc que la présence d'un complexant ou du phosphate dans le milieu favorise la formation d'espèces A*. Cette augmentation pourrait s'expliquer soit par une meilleure accessibilité de l'oxygène aux Fe^{2+} du réseau solide du fait d'une cinétique de lixiviation du solide favorisée par la présence de ces complexants, soit par un renforcement du caractére réducteur du Fe^{2+} à l'état complexé, soit encore par ces deux phénomènes intervenant simultanément. Par ailleurs il est probable que l'encombrement stérique du complexe influence le pouvoir oxydant du système. Dans le cas de l'EDTA, le signal à 60 min n'est pas significatif de toutes les espèces A* formées, car il diminue en fonction du temps d'incubation. Ce phénomène est probablement du à une diminution du temps de vie des adduits radicalaires (DMPO,CO_2^-)·, observé dans le

Can. J. Chem. Downloaded from www.nrcresearchpress.com by 65.111.164.53 on 09/08/12
For personal use only.

Tableau 3. Influence des complexants sur l'intensité du signal $(DMPO,CO_2^-)^{\bullet}$ obtenus à partir de la crocidolite UICC.

Complexant	Intensité du signal $(DMPO,CO_2^-)^{\bullet}$[a] 15 min[a]	30 min[b]	60 min[b]
AMP	3500	8000	9180
ADP	10900	14000	16360
ATP	4930	9450	12670
Phosphate	7540	12700	17000
EDTA	13300		8200
Sans complexant[c]	3700	5000	6050

Conditions expérimentales : 45 mg de crocidolite préalablement broyée 2 min en suspension dans 2 mL d'une solution aqueuse contenant du formiate de sodium et du DMPO (0,05 M). Cette solution contient suivant les cas soit du tampon phosphate pH 7,4 (0,1 M), soit 5 mg de complexant AMP (7,2 mM), ADP (5,8 mM), ATP (4,5 mM), soit 0,75 mg d'EDTA (1 mM).

[a]Intensité exprimée en unités arbitraires (u.a.).

[b]Temps d'incubation (à 37°C à l'abri de la lumière).

[c]Test effectué en présence de la crocidolite en milieu eau distillée.

Tableau 4. Influence de complexants sur l'intensité des spectres $(DMPO,OH)^{\bullet}$ obtenus avec la crocidolite UICC.

Complexant	Intensité du signal $(DMPO,OH)^{\bullet}$[a] 60 min d'incubation
AMP	1480
ADP	0
ATP	0
Phosphate	0
EDTA	1120
Sans complexant[b]	1830

Conditions expérimentales : 45 mg de crocidolite préalablement broyée 2 min en suspension dans 2 mL d'une solution aqueuse de DMPO (0,05 M). Cette solution contient suivant les cas soit du tampon phosphate pH 7,4 (0,1 M), soit 5 mg de complexant AMP (7,2 mM), ADP (5,8 mM), ATP (4,5 mM), soit 0,75 mg d'EDTA (1 mM).

[a]Intensité exprimée en unités arbitraires (u.a.).

[b]Test effectué en présence de la crocidolite en milieu eau distillée.

cas où des espèces très réductrices sont présentes en solution (21).

Afin d'examiner dans quelle mesure les entités oxydantes présentes en solution aqueuse sont des radicaux $^{\cdot}OH$, les tests ont été refaits en présence de DMPO à partir de la crocidolite en suspension dans l'eau contenant les complexants sans adjonction de formiate de sodium (tableau 4). Les résultats de ce tableau montrent l'influence des complexants sur la formation des radicaux $^{\cdot}OH$ mis en évidence sous la forme de l'adduit radicalaire $(DMPO,OH)^{\cdot}$. On note que le test réalisé avec la crocidolite, sans phosphate et sans complexant, permet la génération de radicaux $^{\cdot}OH$. On remarque aussi que la présence de certains complexants (ATP, ADP) et des ions phosphate ne permet pas la formation de radicaux $^{\cdot}OH$. Il apparaît donc que les radicaux $(DMPO,CO_2^-)^{\cdot}$ observés (tableau 3) sont dus à des mécanismes faisant intervenir des entités

Tableau 5. Intensité du signal $(DMPO,CO_2^-)^{\bullet}$ obtenus à partir de filtrats de suspensions de la crocidolite UICC en présence de complexants.

Complexant	Intensité $(DMPO,CO_2^-)^{\bullet}$[a] après incubation 60 min
AMP	2000
ADP	2400
ATP	3600
Phosphate	0
EDTA	5100
Sans complexant[b]	0

Conditions expérimentales : la solution aqueuse étudiée contient 0,5 mL de filtrat, de la NADPH (1 mM), du formiate de sodium (1M) et du DMPO (0,05 M). Le filtrat est obtenu après 3 h d'incubation de 45 mg de crocidolite broyée dans 1 mL d'une solution contenant suivant les cas soit du tampon phosphate pH 7,4 (0,1 M), soit 5 mg de complexant AMP (7,2 mM), ADP (5,8 mM), ATP (4,5 mM), soit 0,75 mg d'EDTA (1 mM).

[a]Intensité exprimée en unités arbitraires (u.a.).

de type ferryle ou perferryle capables d'arracher un hydrogène à l'ion formiate. Par contre dans les autres cas (AMP, EDTA et sans complexant), l'intensité des signaux $(DMPO, OH)^{\cdot}$ d'une part (tableau 4) et $(DMPO,CO_2^-)^{\cdot}$ d'autre part (tableau 3) montrent que les entités oxydantes A* comportent en grande majorité des espèces oxydantes de type ferryle ou perferryle et pour une partie moindre des radicaux $^{\cdot}OH$. En effet les étalonnages en nombre de radicaux par litre effectués dans nos conditions d'évaluation permettent de considérer que pour une même intensité en unités arbitraires (u.a.) le rapport entre le nombre d'adduits $(DMPO, CO_2^-)^{\cdot}$ et celui des adduits $(DMPO, OH)^{\cdot}$ est approximativement de l'ordre de 2 (20).

Afin d'évaluer l'apport maxima des complexes du fer(II) en solution dans le système réactionnel, nous avons étudié l'oxydation du formiate sur des filtrats issus des suspensions contenant la crocidolite broyée et incubée 3 h avec les différents complexants utilisés ci-dessus. Le fer(II) en solution s'oxydant facilement en fer(III) du fait de la présence de l'oxygène dissous dans le milieu aqueux, il est probable qu'une partie du fer précipite sous forme d'hydroxyde ferrique qui sera éliminé lors de la filtration. En ajoutant au filtrat un réducteur comme la NADPH, le fer(III) complexé pourra éventuellement être réduit à l'état de fer(II) susceptible de former des espèces activées de l'oxygène.

Le test d'oxydation de l'anion formiate sur les filtrats a conduit aux résultats exposés dans le tableau 5. D'après les valeurs de l'intensité du signal de l'adduit radicalaire $(DMPO,CO_2^-)^{\cdot}$, on observe que la présence en solution des complexes du fer et des ligands, AMP, ATP, ADP et EDTA, contribuent à la formation des radicaux $^{\cdot}OH$ et $CO_2^{\cdot -}$. En milieu eau distillée ou en présence de phosphate on n'observe pas de signal $(DMPO,CO_2^-)^{\cdot}$. Deux raisons peuvent expliquer ce fait : en effet, soit l'essentiel du fer oxydé lors des trois heures d'incubation a pu précipiter (par exemple sous forme d'un phosphate de fer(III) insoluble) puis a été éliminé par filtration, soit il est possible que des ligands comme HPO_4^{2-}, $H_2PO_4^-$ ou HCO_2^- confèrent aux ions Fe^{3+} un potentiel rédox qui ne permet pas leur réduction en Fe^{2+} par la NADPH.

L'activité constatée (valeur de 6050 u.a., tableau 3) de la

Can. J. Chem. Downloaded from www.nrcresearchpress.com by 65.111.164.53 on 09/08/12
For personal use only.

Tableau 6. Intensité du signal (POBN,R)$^{\cdot}$ lors de la peroxydation de l'acide linolénique en présence de la crocidolite UICC et de différents complexants.

Complexant	Intensité du signal (POBN,R)$^{\cdot}$[a] après incubation 30 min
AMP	9100
ADP	9230
ATP	12100
Phosphate	9900
EDTA	22000
Sans complexant[b]	9900

Conditions expérimentales : 45 mg de fibres dans 2 mL d'une solution aqueuse contenant : acide linolénique (23 mM), POBN (0,1 M), CHAPS (0,8 mM) et suivant les cas soit du tampon phosphate pH 7,4 (0,1 M), soit 5 mg de complexant AMP (7,2 mM), ADP (5,8 mM), ATP (4,5 mM), soit 0,75 mg d'EDTA (1 mM).

[a]Intensité exprimée en unités arbitraires (u.a.).

[b]Test effectué en présence de la crocidolite en milieu eau distillée.

crocidolite en suspension en milieu eau distillée en absence de complexant par comparaison à l'inactivité du filtrat correspondant (tableau 5) permet de penser que cette activité est liée à l'apparition de radicaux $^{\cdot}$OH et d'espèces du type ferryle ou perferryle liées au solide. Les radicaux $^{\cdot}$OH ne peuvent être présents dans le filtrat au bout de 3 h d'incubation du fait de leur temps de vie très court (22) et les autres espèces sont probablement éliminées par filtration.

La comparaison des données des tableaux 3 et 5 révèle une activité oxydante en présence de complexant plus faible pour les filtrats que pour les suspensions, bien que l'activité oxydante des filtrats soient dues pour partie à des Fe(III) du solide mis en solution sous forme de complexe puis réduits par la NADPH, processus qui ne joue pas de rôle dans les résultats du tableau 3. Il semble probable que même en présence de complexes la majorité de l'activité oxydante due à la crocidolite apparaît à la surface du solide suite à l'interaction des Fe(II) encore liés au réseau solide avec l'oxygène .

Le tableau 6 répertorie les résultats des tests de peroxydation de l'acide linolénique effectués en présence de crocidolite UICC broyée et de différents complexants. Parmi les complexants seul l'EDTA augmente nettement l'activité, l'ATP donnant une augmentation moins significative. Les autres complexants (AMP, ADP, phosphate) n'ont pas d'influence sur l'activité. Il ne semble pas que l'on puisse établir une corrélation entre l'activité due aux entités oxydantes A* (test d'oxydation de l'anion formiate, tableau 3) et celle mise en évidence au cours de la peroxydation de l'acide linolénique (tableau 6). Il est très probable que les mécanismes de peroxydation de l'acide linolénique dépendent non seulement des espèces A* mais aussi des entités superoxo (P*). On peut envisager aussi l'intervention d'autres facteurs comme, par exemple, l'adsorption de l'acide linolénique sur la surface du solide. Cette adsorption plus ou moins importante suivant la nature du milieu peut perturber les cinétiques de lixivation et les réactions de peroxydation.

À partir de ces données, des tests préliminaires de peroxydation ont été réalisés avec des cellules, en présence de crocidolite broyée et différents complexants. Les résultats obtenus, exprimés par l'intensité des adduits radicalaires (POBN,R)$^{\cdot}$, sont présentés dans le tableau 7. Des tests de contrôle effectués sans cellules en présence du milieu de culture ou de sérum physiologique ou d'eau ne donnent pas de signaux alors que l'on constate la présence de l'adduit radicalaire (POBN,R)$^{\cdot}$ avec l'EDTA et l'ATP dans ces divers milieux. Ce résultat semble conforme à l'activité observée dans le tableau 6 où l'EDTA et l'ATP sont les plus actifs dans la peroxydation de l'acide linolénique. On remarque aussi dans le tableau 7 qu'en présence de l'ATP en milieu tampon phosphate il n'apparaît pas de signal en RPE et qu'en présence de l'AMP et de l'ADP, l'activité de la crocidolite est nulle quelle que soit la nature du milieu étudié (eau ou sérum physiologique en présence de tampon ou non).

Tableau 7. Influence de complexants sur l'intensité du signal (POBN,R)$^{\cdot}$ obtenu à partir de la crocidolite UICC en présence des cellules épithéliales

Complexant	Intensité du signal (POBN,R)$^{\cdot}$[a] 60 min d'incubation	Conditions
EDTA	700	Milieu de culture sans TP
EDTA	960	Milieu eau sans TP
AMP	0	Milieu eau sans TP
ADP	0	Sérum physiologique sans TP
ADP	0	Sérum physiologique avec TP
ATP	840	Milieu de culture sans TP
ATP	0	Sérum physiologique avec TP

Conditions expérimentales : les cellules en culture sont soumises à l'action de 20 mg de fibres mis en suspension dans 2 mL d'une solution aqueuse comprenant éventuellement 0,5 mL de sérum physiologique ou 0,5 mL de milieu de culture. Cette solution contient du POBN (0,1 M) et du CHAPS (0,8 mM) et suivant les cas soit du tampon phosphate (TP) pH 7,4 (0,1 M), soit 5 mg de complexant AMP (7,2 mM), ADP (5,8 mM), ATP (4,5 mM), soit 0,75 mg d'EDTA (1 mM).

[a]Intensité exprimée en unités arbitraires (u.a.).

Conclusion

La présente étude permet de confirmer que les fibres d'amiante et de némalite sont à même de peroxyder les lipides polyinsaturés suite à la formation de diverses espèces activées de l'oxygène (EAO). Dans ce processus de peroxydation la formation d'espèces A* très électrophiles (ferryles, perferryles, $^{\cdot}$OH) joue le rôle principal, mais des EAO du type P* à caractére moins électrophile (Fe^{III} superoxo) peuvent également participer au processus.

Dans le cas de la crocidolite, la présence de complexants dans le milieu permet d'augmenter sensiblement (surtout pour l'EDTA) l'oxydation du formiate par les espèces A*, et la peroxydation de l'acide linolénique (seulement pour l'EDTA et l'ATP) par des espèces A* et P*.

Les espèces A* sont très majoritairement des ferryles et des perferryles dans le cas de la crocidolite, la formation d'·OH n'étant pas favorisée par l'ajout de complexant et même inhibée par la présence de phosphate, d'ADP et d'ATP. Enfin on note que les espèces A*, pour la crocidolite, sont en grande majorité générées à partir de la réaction avec l'oxygène d'entités en surface du solide, même en présence de complexant.

La comparaison de l'activité de divers matériaux dans la peroxydation de l'acide linolénique et dans celle des membranes de cellules en culture, ne révèle pas un strict parallélisme dans la formation des radicaux peroxydes issus des lipides polyinsaturés.

Plusieurs phénomènes peuvent être à l'origine du fait que, dans nos conditions expérimentales, les EAO générées en présence de némalite soient capables de peroxyder les membranes cellulaires alors que celles générées en présence de chrysotile ou de crocidolite ne le permettent pas. La peroxydation des membranes cellulaires va dépendre en effet de l'accessibilité des EAO aux sites sensibles sur les molécules d'acide gras organisées en double-couche. Or cette accessibilité va être fonction de la cinétique de divers phénomènes comme l'internalisation des particules au sein des cellules et la rupture de la membrane cellulaire (cytotoxicité), tous facteurs qui ne dépendent pas uniquement de la production des EAO. Il est bien connu par exemple que la crocidolite est moins cytotoxique que le chrysotile.

De plus il est nécessaire de noter que nous n'avons pas étudié comparativement la némalite et la crocidolite dans le rôle respectif des activités de surface et des activités en solution. L'importance relative de ces deux types d'activité pourrait expliquer la différence constatée entre ces deux matériaux fibreux dans la peroxydation des membranes cellulaires.

Enfin il est possible également que la nature des EAO formées (qui varie en fonction de la nature du solide) joue un rôle dans les différences observées lors de la peroxydation des membranes des cellules. On note par exemple qu'en présence d'ions phosphate la némalite, et non la crocidolite, génère des ·OH, mais la présence d'EDTA peut favoriser la formation de ces radicaux avec la crocidolite, ce qui montre l'importance de la nature du milieu.

La complexité des facteurs conditionnant la vie cellulaire ne permet pas toujours d'extrapoler directement les phénomènes observés dans des milieux chimiques simples aux différents systèmes organisés des milieux biologiques.

Bilbliographie

1. L. Bonneau, H. Suquet, C. Malard et H. Pezerat. Environ. Res. **41**, 251 (1986).
2. H. Sies. *Dans* Oxidative stress. *Editeur* : H. Sies. Academic Press, London. 1985.
3. H. Pezerat. *Dans* Mechanisms in fibre carcinogenesis. A223. *Editeurs* : R.C. Brown, J.A. Hoskins et N.F. Johnson. Plenum Press, New York. 1991. pp. 387–396.
4. J. Fournier, J. Guignard, A. Nejjari et H. Pezerat. *Dans* Mechanisms in fibre carcinogenesis. A223. *Editeurs :* R.C. Brown, J.A. Hoskins et N.F. Johnson. Plenum Press, New York. 1991. pp. 407–414.
5. K. Yamaguchi, Y. Takahara et T. Fueno. *Dans* The role of oxygen in chemistry and biochemistry. Studies in organic chemistry. Vol. 33. *Editeur* : W. Ando. Elsevier. 1988. pp. 263–268.
6. B. Halliwell et J.M. Gutteridge. Biochem. J. **219**, 1 (1984).
7. B. Halliwell et J.M. Gutteridge. *Dans* Free radicals in biology and medicine. *Editeurs* : B. Halliwell et J.M. Gutteridge. Clarendon Press, Oxford Science Publication, London. 1985.
8. R. Zalma, J. Guignard, H. Pezerat et M. C. Jaurand. *Dans* Effects of mineral dusts on cells. Vol. H 30. *Editeurs* : B.T. Mossman et R.O. Begin. NATO ASI Ser. 1989. pp. 257–264.
9. S. Chouchane, J. Guignard et H. Pezerat. *Dans* Cellular and molecular effects of mineral and synthetic dusts and fibres. Vol. 85. *Editeurs* : J.M.G. Davis et M.-C. Jaurand. NATO ASI Ser. 1994. pp. 397–402.
10. L.G. Lund et A.E. Aust. Arch. Biochem. Biophys. **278**, 60 (1990).
11. W.J. Murphy et R.A. Ross. Clays Clay Miner. **25**, 78 (1977).
12. G.R. Buettner et L.W. Oberley. Biochem. Biophys. Research Commun. **83**, 69 (1978).
13. G.M. Levasseur-Acker, M. Molimard, J. Regnard, E. Naline, Ch. Freche et A. Lockhart. Am. J. Respir. Cell Mol. Biol. **10**, 378 (1994).
14. E. Finkelstein, G.M. Rosen et E.J. Rauckman. Arch. Biochem. Biophys. **200**, 1 (1980).
15. K. Makino, M.M. Mossoba et P. Riesz. J. Phys. Chem. **87**, 1369 (1979).
16. R. Zalma, L. Bonneau, J. Guignard, H. Pezerat et M.C. Jaurand. Can. J. Chem. **65**, 2338 (1987).
17. G.M. Rosen et E. J. Rauckman. Proc. Natl. Acad. Sci. U.S.A **78**, 7346 (1981).
18. A. Nejjari. Thèse de l'Université P. et M. Curie, Paris. 1992.
19. B.H.J. Bielski. Ann. Neurol. **32**, S28 (1992).
20. R. Zalma. Thèse d'État, Paris. (1988).
21. D. Costa. Thèse de l'Université P. et M. Curie, Paris. 1989.
22. M. Anbar et P. Neta. J. Phys. Chem. **74**, 3199 (1970).

Can. J. Chem. Downloaded from www.nrcresearchpress.com by 65.111.164.53 on 09/08/12
For personal use only.

COMMUNICATION

Experimental and AM1 calculational studies of the deprotonation of bicyclo[2.2.2]octane-2,5-dione and bicyclo[2.2.2]octane-2,6-dione: a study of homoconjugation, inductive, and steric effects on the rates and diastereoselectivities of α enolization

Nick Henry Werstiuk and Chandra Deo Roy

Abstract: The kinetics of NaOD-catalyzed H/D exchange (enolization) at C3 α to the carbonyl group of bicyclo[2.2.2]octane-2,5-dione (**1**) and bicyclo[2.2.2]octane-2,6-dione (**2**) have been studied in 60:40 (v/v) dioxane–D_2O at 25.0°C. The second-order rate constants for exchange are $(9.7 \pm 1.5) \times 10^{-1}$ and $(3.4 \pm 1.2) \times 10^{-5}$ L mol^{-1} s^{-1} for **1** and **2**, respectively. Thus, **1**, exchanges 76 times faster than bicyclo[2.2.2]octan-2-one (**3**) ($k = (1.27 \pm 0.02) \times 10^{-2}$ L mol^{-1} s^{-1}), but the 2,6-dione **2** unexpectedly is much less reactive (2.7×10^{-3}) than the monoketone. Unlike the large *exo* selectivity of 658 observed in the case of bicyclo[2.2.1]heptan-2-one, small and opposite selectivities, *exo* (1.2) for **1** and *endo* (2.1) for **2**, are found for the isomeric [2.2.2] ketones. The results indicate that the incipient enolate of **1** is stabilized by a polar effect of the β carbonyl group at C5, not by homoconjugation. The source of the surprising low reactivity of **2** is unknown at this stage. The small diastereoselectivities, *exo* (1.2) for **1** and *endo* (2.1) for **2**, correlate with relative energies of the diastereomeric pyramidal enolates calculated with AM1.

Key words: enolization, bicyclo[2.2.2]octane-2,5-dione, bicyclo[2.2.2]octane-2,6-dione, AM1, thermodynamic acidities.

Résumé : Opérant à 25,0°C, dans des solutions 60 : 40 (v/v) de dioxane–D_2O, on a étudié la cinétique de l'échange (énolisation) H/D, catalysé par le NaOD, au niveau du C3 en α du groupe carbonyle de la bicyclo[2.2.2]octane-2,5-dione (**1**) et de la bicyclo[2.2.2]octane-2,6-dione (**2**). Les constantes de vitesse d'échange du deuxième ordre sont de $(9,7 \pm 1,5) \times 10^{-1}$ et $(3,4 \pm 1,2) \times 10^{-5}$ L mol^{-1} s^{-1} respectivement pour **1** et **2**. Le composé **1** s'échange donc 76 fois plus rapidement que la bicyclo[2.2.2]octan-2-one (**3**) ($k = (1,27 \pm 0,02) \times 10^{-2}$ L mol^{-1} s^{-1}; toutefois, la 2,6-dione (**2**) est beaucoup moins réactive ($2,7 \times 10^{-3}$ fois moins réactif) que la monocétone. Par opposition à la forte sélectivité de 658 observée dans le cas de la bicyclo[2.2.1]heptan-2-one, on a observé de faibles sélectivités opposées, *exo* (1.2) pour **1** et *endo* (2.1) pour **2**, pour les cétones [2.2.2] isomères. Les résultats indiquent que l'énolate qui se forme dans le composé **1** est stabilisé par un effet polaire du groupe carbonyle β en C5 et non pas par homoconjugaison. La cause de cette faible réactivité surprenante du composé **2** est pour l'instant inconnue. Les faibles diastéréosélectivités, *exo* (1,2) pour **1** et *endo* (2,1) pour **2**,

Received August 29, 1994.

N.H. Werstiuk[1] **and C.D. Roy.** Department of Chemistry, McMaster University, Hamilton, ON L8S 4M1, Canada.

[1] Author to whom correspondence may be addressed. Telephone: (905) 525-9140. Fax: (905) 522-2509.

Can. J. Chem. Downloaded from www.nrcresearchpress.com by 65.111.164.53 on 09/08/12
For personal use only.

offrent une bonne corrélation avec les énergies relatives calculées par AM1 pour les énolates pyramidaux diastéréomères.

Mots clés : énolisation, bicyclo[2.2.2]octane-2,5-dione, bicyclo[2.2.2]octane-2,6-dione, AM1, acidités thermodynamiques.

[Traduit par la rédaction]

Can. J. Chem. Downloaded from www.nrcresearchpress.com by 65.111.164.53 on 09/08/12
For personal use only.

Over the past two decades a great deal of research has been carried out on the α and β (homoenolization) enolization of ketones (1–4) to determine the role of various factors such as orbital alignment, steric effects, homoconjugation, and hyperconjugation in determining the kinetic and thermodynamic acidities of this very important class of compounds. Our long-standing interest in this field (5, 6), specifically in establishing how remote polar groups stabilize enolates, and our developing interest in using semiempirical calculations with AM1 to predict and rationalize variations in the kinetic and thermodynamic acidities of carbon and oxygen acids (6–9) motivated us to undertake experimental and computational studies on the isomeric diones bicyclo[2.2.2]octane-2,5-dione (**1**) and bicyclo[2.2.2]octane-2,6-dione (**2**). Because the C3 methylene hydrogens of **1** and **2** are diastereotopic[2] and exhibit distinct ^{1}H nmr resonances (6), which is not the case for bicyclo[2.2.2]octan-2-one, the diastereoselectivities of exchange can be determined in the absence of differential steric effects for *exo* and *endo* approach of the base at C3. This is an important point because it is possible that a differential steric effect between the methano and ethano bridges gives rise to the large *exo* selectivity of 658 found for enolization at C3 of bicyclo[2.2.1]heptan-2-one (5). Our goal was to use the diastereoselectivities of H/D exchange and AM1 calculations to establish the importance of homoconjugative stabilization of an incipient enolate by a carbonyl group located β to the enolizable center as in [2.2.2] ketones. If α enolization at C3 of **1** is assisted by homoconjugation, then the *exo/endo* rate ratio should be substantially greater than 1, a consequence of the fact that *exo* deprotonation leads to development of the back-lobe of a *p*-orbital *syn* to the π-system of the carbonyl group at C5; this is not the case for *endo* deprotonation. On the other hand, if the incipient enolate is stabilized solely by a polar effect and differential steric effects are small or negligible (this also holds for the enolization of **2**) the *exo/endo* diastereoselectivity should be near 1. A study of **1** and **2** also provided us with an opportunity to establish whether AM1 is useful for predicting the relative rates and diastereoselectivities of enolization reactions in solution. In this communication we report the rates and the *exo/endo* preferences for NaOD-catalyzed H/D exchange of **1** and **2** along with the results of an AM1 calculational study.

To check our experimental method, the H/D exchange of bicyclo[2.2.2]octan-2-one (**3**) was studied in 0.04 M NaOD – 60:40 dioxane–D_2O at 25.0°C. The second-order rate constant ($(1.27 \pm 0.02) \times 10^{-2}$ L mol^{-1} s^{-1}) compares reasonably well with the rate constant (3.03×10^{-2} L mol^{-1} s^{-1}) obtained in another study (10), with the difference possibly arising from the fact that slightly different dioxane/D_2O ratios were used in the two studies. Under identical conditions, the 2,5-dione **1** ($k = (9.7 \pm 1.5) \times 10^{-2}$), which we synthesized recently (6), underwent exchange 76 times faster[3] than **3** and 2.8×10^4 times faster than **2** ($k = (3.4 \pm 1.2) \times 10^{-5}$), which was prepared by the method described by Gerlach and Muller (11). Analysis of several incompletely exchanged (30%) samples of **1** with ^{2}H nmr established that exchange of the *exo* hydrogen is preferred by a factor of 1.2. Because the differential steric effect for approach of hydroxide ion *exo* or *endo* at C3 is expected to be small, the results establish that the incipient enolate anion at C3 is stabilized through a polar effect, not by homoconjugation. Unlike **1**, the 2,6-dione **2** is much less reactive (2.7×10^{-3}) than **3**. The low rate of exchange of **2** is not due to a hydroxide ion-depleting ring-opening reaction; **2** was recovered in 80% yield (there was 5.03% H/D exchange at C3(C5)) from a 4 h reaction in 0.04 M NaOD – dioxane–D_2O at 25°C. Some time ago Bartlett and Forrest Woods found that **2** did not give the positive $FeCl_3$ test that is exhibited by enolizable 1,3-diketones, but they did not carry out base-catalyzed H/D exchange studies (12). Our work shows that H/D exchange at the bridgehead carbon C1 does not occur at a detectable rate in a medium that induces rapid H/D exchange of acyclic and monocyclic 1,3-diketones; there is no detectable signal with the chemical shift expected for the bridgehead deuteron in the ^{2}H spectrum of **2**, which was isolated from a 4 h exchange reaction. Under identical conditions, the hydrogens at C3 and C6 of the 2,5-dione **1** are equilibrated with the deuterium pool (97% exchange) within 1 min. The reason for the low reactivity of **2** relative to monoketone **3** is presently unknown. That this low reactivity is not due to the formation of a cyclic hydrate involving the carbonyl groups at C2 and C6 was established by ^{1}H nmr spectroscopy. The exchange solution of **2** exhibits only signals that exactly match the nmr spectrum obtained in $CDCl_3$. Possibly, a through-space interaction of the carbonyl π-systems at C2 and C6, a decrease in the electrophilicity of carbonyl groups, and angle strain resulting from the introduction of a second carbonyl group at C6 combine to

[2] The *exo* hydrogens are *syn* to the ethano bridges of **1** and **2**; the *endo* hydrogens are *anti* to the ethano bridges. As in the case of **1** (6), nuclear Overhauser difference spectroscopy was used to assign the resonances of the C3 *exo* and *endo* hydrogens of **2**.

[3] The exchange solutions (60:40 dioxane–D_2O) were 0.12 M in ketone and 0.02 or 0.04 M in NaOD. Uptake of deuterium was monitored with 200 MHz ^{1}H nmr spectroscopy by integrating the appropriate resonances and using the bridgehead protons as internal standards. In some cases the results were checked mass spectrometrically. Because **1** and **2** exhibited significant variations in the rates of H/D exchange as the base concentration was decreased, we used a one-point kinetic method to obtain the rate constants, which are the mean of three determinations. That the variability in the rate was not due to the intrusion of an acid–base equilibrium involving **1** and its enolate was established by obtaining a 200 MHz ^{1}H nmr spectrum of the exchange solution; within the detection limits of nmr, no signals other than those due to **1** were found in the spectrum.

Can. J. Chem. Downloaded from www.nrcresearchpress.com by 65.111.164.53 on 09/08/12
For personal use only.

Table 1. AM1-calculated enthalpies of formation and ionization.

Ketone	ΔH_f[a] ketone	ΔH_f C1-enolate	ΔH_f C3-enolate	ΔH_i C1	ΔH_i C3	$\Delta\Delta H_i$ C3	Relative rate
1	−85.75	−68.03	−94.96	381.9	355.1	−8.1	76
2	−85.34	−67.94	−93.99	381.6	355.6	−0.5	0.0027
3	−61.51	−33.14	−60.47	392.6	363.2	0.0	1

[a]The values are in kcal/mol.
[b]ΔH_i = (ΔH_f(enolate) − ΔH_f(ketone)) − $\Delta H_f(H^+)$; $\Delta H_i(H^+)$ taken as 365.4 kcal/mol.

Table 2. AM1-calculated enthalpies of formation of pyramidal enolates and experimentally observed diastereoselectivities.

Ketone	ΔH_f[a] *exo* enolate	ΔH_f *endo* enolate	ΔH_f*exo* − ΔH_f*endo*	*exo/endo* Diastereoelectivity
1	−85.52	−85.39	−0.13	1.2
2	−84.36	−84.87	+0.51	0.48

[a]The values in kcal/mol.

reduce the kinetic acidity of **2**. Additional experimental and computational studies are needed to determine the source(s) of the unexpected low reactivity of **2**. Analysis of partially labelled **2** (6%) with ^2H nmr established that deprotonation at C3 occurs with *an* endo *diastereoselectivity of 2.1.*

Two sets of AM1 calculations (the keyword PRECISE was used to tighten the convergence criteria) were carried out on the 2,5-dione **1**, the 2,6-dione **2**, **3**, and their enolates and the results are given in Tables 1 and 2. The gas phase enthalpies of ionization of **1**, **2**, and **3** calculated from the ΔH_f's of the ketones and their planar enolates are given in Table 1. The geometrical structures of the optimized geometries of **1** and **2** are given in Fig. 1. The AM1-calculated C(3) ΔH_i's (ΔH_i (**1**) − ΔH_i (**3**) = −8.1 kcal/mol), which are a measure of the relative thermodynamic acidities of **1** and **3**, correlate with the kinetic acidities. But **2** is much less reactive kinetically than **3**, not what would be expected on the basis of the calculational ΔH_i's. Yet the calculated ΔH_i of the C1 bridgehead hydrogen of **2** is 18.4 and 26.0 kcal/mol higher than the C3 ΔH_i's of **3** and **1**, respectively, in keeping with the fact that this hydrogen does not undergo H/D exchange under normal enolization conditions (vide supra). Most surprising is the finding that the calculated C1 ΔH_i's of **1** and **2** are virtually identical. That the C1 ΔH_i's of **1** and **2** are 10.7 and 11.0 kcal/mol lower than the C1 ΔH_i of **3** establishes two important points: (*a*) the inductive stabilization of a carbanion by an α carbonyl group is reproduced in the AM1 calculations, and (*b*) α and β carbonyl groups evidently stabilize a bridgehead enolate of a [2.2.2] ketone to the same degree.[4] To establish whether AM1 calculations are useful for estimating the relative reactivities of diastereotopic hydrogens α to a carbonyl group and to provide new insights into the factors that determine the diastereoselectivities, we calculated the ΔH_f's (Table 2) of *exo* and *endo* pyramidal C3 enolates of **1** (**1**-*exo*-enolate and **1**-*endo*-enolate) and **2** (**2**-*exo*-enolate and **2**-*endo*-enolate). The AM1-optimized geometrical structures of the pyramidal enolates obtained by deleting the *exo* or *endo* hydrogens and fixing the H-C3-C2-O torsional angle of the remaining hydrogen at the value calculated for the ketone are displayed in Fig. 1. While

Fig. 1. Displays of AM1-optimized geometrical structures of ketones and pyramidal enolates.

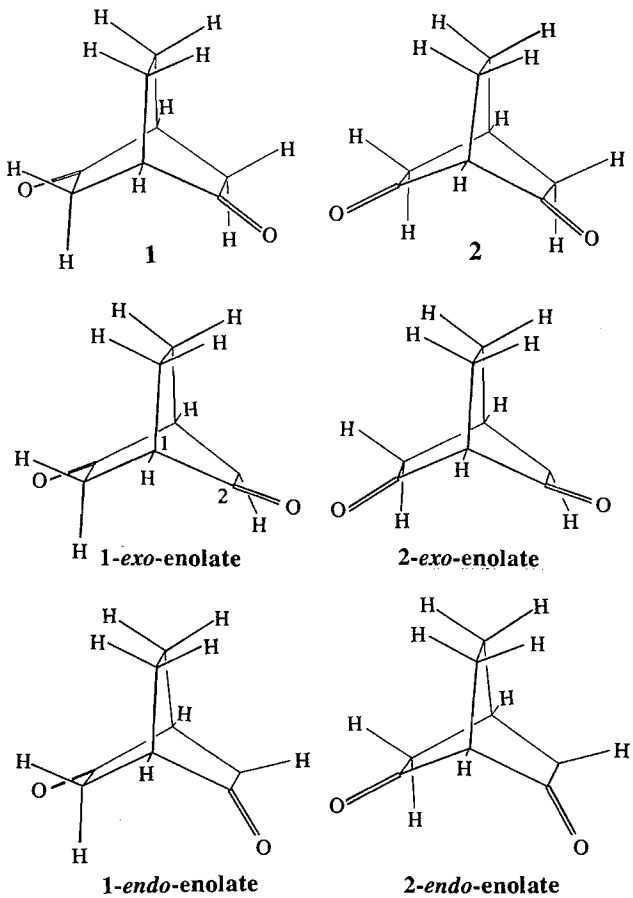

[4] We plan to determine the rates of bridgehead exchange of 3,3,6,6-tetramethylbicyclo[2.2.2]octane-2,5-dione and 3,3,5,5-tetramethylbicyclo[2.2.2]octane-2,6-dione with *t*-BuOK/*t*-BuOD to test the results of the AM1 calculations.

1-*exo*-enolate is slightly more stable than **1**-*endo*-enolate, the order of stability is reversed for the pyramidal enolates derived from **2** (Table 2). Because the transition states for OH^- induced α enolization undoubtedly have pyramidal character, we expected that the experimental diastereoselectivities would correlate with the $\Delta\Delta H_f$'s of the pyramidal enolates. The data given in Table 2 confirm this expectation. We expect that $\Delta\Delta H_f$'s of the pairs of pyramidal enolates will decrease to bring the values in line with the experimental diastereoselectivities as the α carbons approach the triangular planar configuration of the planar enolates. It is also noteworthy that the relative magnitudes of the $\Delta\Delta H_f$'s correlate with the relative magnitudes of the diastereoselectivities. It is possible that better orbital alignment — the *endo* H-C3-C=O torsional angle is 2° larger than the *exo* H-C3-C2-O angle — and a through-space polar effect differentially stabilize the *endo* pyramidal enolate of **2** relative to the *exo* diastereomer. In going from **1** to **1**-*exo*-enolate, C3 bends slightly towards the carbonyl carbon at C5: the C3-C4-C5 angle decreases from 108.6° to 106.9° and the C3,C5 internuclear distance decreases from 2.46 to 2.42 Å. And, there is a surprisingly large increase in the C1—C2 bond lengths when the ketones are converted to the pyramidal enolates (**1**, 1.517 Å; **1**-*exo*-enolate, 1.555 Å; **1**-*endo*-enolate, 1.555 Å; **2**, 1.518 Å; **2**-*exo*-enolate, 1.567 Å; **2**-*endo*-enolate, 1.565 Å). According to the AM1 calculations (Tables 1 and 2), the pyramidal enolates are 9–10 kcal/mol higher in energy than the planar enolates (the *exo* enolates of **1** and **2** by 9.44 and 9.63 kcal/mol, respectively; the *endo* enolates of **1** and **2** by 9.57 and 9.12 kcal/mol, respectively). Even so, there must be a substantial interaction between the anionic carbon and the carbonyl group of the pyramidal enolates because the AM1-calculated enolate C2—C3 bond lengths (**1**-*exo*-enolate, 1.402 Å; **1**-*endo*-enolate, 1.398 Å; **2**-*exo*-enolate, 1.399 Å; **2**-*endo*-enolate, 1.397 Å) are much shorter than the corresponding C—C bonds of **1** and **2** (1.507 and 1.506 Å, respectively).

Can. J. Chem. Downloaded from www.nrcresearchpress.com by 65.111.164.53 on 09/08/12
For personal use only.

Acknowledgement

We thank the Natural Sciences and Engineering Research Council of Canada for financial support.

References

1. S. Forsen and N.M. Nilsson. *In* The chemistry of the carbonyl group. Vol. II. *Edited by* S. Patai. John Wiley and Sons, Inc., New York. 1970. pp. 157–240.
2. E. Buncel. *In* Carbanions: mechanistic and isotopic aspects. Monograph 9. *Edited by* C. Eaborn and N.B. Chapman. Elsevier Scientific Publishing Col., Amsterdam. 1975. pp. 69–93.
3. J. Toullec. *In* Advances in physical organic chemistry. Vol. 18. *Edited by* V. Gold and D. Bethell. Academic Press, London. 1982. pp. 1–77.
4. N.H. Werstiuk. Tetrahedron Report Number 141, Tetrahedron, **39**, 205 (1985).
5. N.H. Werstiuk and S. Banerjee. Can. J. Chem. **63**, 534 (1985), and references therein.
6. N.H. Werstiuk, S. Yeroushalmi, and H. Guan-Lin. Can. J. Chem. **70**, 974 (1991), and references therein.
7. N.H. Werstiuk. Can. J. Chem. **66**, 2958 (1988).
8. N.H. Werstiuk and D. Andrew. Can. J. Chem. **68**, 1467 (1990).
9. N.H. Werstiuk and C.D. Roy. Can. J. Chem. **72**, 2348 (1994).
10. G.A. Abad, S.P. Jindal, and T.T. Tidwell. J. Am. Chem. Soc. **95**, 6326 (1973).
11. H. Gerlach and W. Muller. Angew. Chem. Int. Ed. Engl. **11**, 1030 (1972).
12. P.D. Bartlett and G. Forrest Woods. J. Am. Chem. Soc. **62**, 2933 (1940).

1994 E.W.R. Steacie Award Lecture Application of natural products chemistry to a biological problem[1]

William A. Ayer

Abstract: Aspen that bear a certain type of black gall have a lower incidence of heartwood rot (caused by the fungus *Phellinus tremulae*) than do nearby non-gall trees. Efforts to determine the chemical nature of this black gall effect are described. The metabolites of some fungi associated with the black gall (*Phoma etheridgei, Stachybotrys cylindrospora*), and of the rotting fungus *Phellinus tremulae*, are described. Extracts of the black gall tissue have a very high concentration of benzoic acid and it is suggested that the benzoic acid may play a role in the protection of the galled trees.

Key words: fungal metabolites, aspen, benzoic acid, salicylic acid, black galls on aspen, *Phellinus tremulae*.

Résumé : Les trembles qui portent un certain type de galle noire sont moins susceptible à la pourriture du coeur du bois (causée par le champignon *Phellinus tremulae*) que les arbres avoisinants ne portant pas de galle. On décrit les efforts faits pour déterminer la nature chimique de cet effet de la galle noire. On décrit les métabolites de quelques champignons associés à la galle noire (*Phoma etheridgei, Strachybotrys cylindrospora*) et du champignon causant la pourriture, le *Phellinus tremulae*. Les extraits du tissu de la galle noire contiennent une grande concentration d'acide benzoïque et on suggère que cet acide peut jouer un rôle dans la protection des arbres qui portent la galle.

Mots clés : métabolites de champignons, tremble, acide benzoïque, acide salicylique, galles noires sur le tremble, *Phellinus tremulae*.

[Traduit par la rédaction]

Introduction

When I entered graduate school at the University of New Brunswick in 1953 the nature of natural products chemistry was quite different from what it is today, both in its methods and in its objectives. It was sufficient then to study a particular compound just because "it was there," and it often took years of painstaking chemical degradation to determine the structure of a relatively small molecule. At the time I started my studies, others in the laboratory began work on the elucidation of the structure of the Lycopodium alkaloid annotinine. In my final year in Fredericton, I was part of the team that arrived at the correct structure, **1**, for this unique 16-carbon alkaloid (1). During this period, U.N.B. acquired its first infrared spectrometer and we began to hear of a new physical method, nuclear magnetic resonance spectroscopy! Nowadays, the determination of the structure of a new natural product often requires only a few days, sometimes only a few hours. By the late 60s it was apparent that if one were to continue with isolation and structure determination studies, there should be a purpose other than the discovery of a new structural class of natural products. The study of the "black gall effect" of aspen will be used to provide an example of how natural products chemistry may be applied to provide knowledge that perhaps will be useful to the forestry sector in our country.

Decay and stain of aspen

Aspen (*Populus tremuloides* Michx.) is the most widely distributed tree species in North America (2). In this country, aspen represents more than one half of the merchantable hardwood timber and 11% of our entire timber resource (3). The utilization of aspen has increased substantially in recent years. The introduction of oriented strand board (OSB), prepared by compacting thin strands of aspen with resins under heat and pressure, and the development of new pulp and paper technologies such as chlorine-free chemothermomechanical pulping (CTMP) have been important factors in the increased use of this previously neglected resource (2, 4). Because of its natural light weight and its colorless, tasteless, and odorless properties, aspen is also used extensively in the production of chopsticks and popsicle sticks (2).

A serious limitation to the utilization of aspen results from the fact that it is very susceptible to decay and stain caused by fungi (5). Heartwood decay, caused by *Phellinus tremulae*, is often present in a high percentage of trees in a mature stand (5). Stored logs of aspen are extremely susceptible to blue stain fungi (6).

Received January 5, 1995.

This lecture is dedicated to Dorothy K. Ayer and to the memory of Rueben Sandin and John Hooz.

W.A. Ayer. Department of Chemistry, University of Alberta, Edmonton, AB T6G 2G2, Canada.

[1] The E.W.R. Steacie Award Lecture was delivered at the Annual Conference of the Canadian Society for Chemistry, Winnipeg, Manitoba, June 1, 1994.

Can. J. Chem. Downloaded from www.nrcresearchpress.com by 65.111.164.53 on 09/08/12
For personal use only.

Fig. 1. The tremulane family of sesquiterpenes.

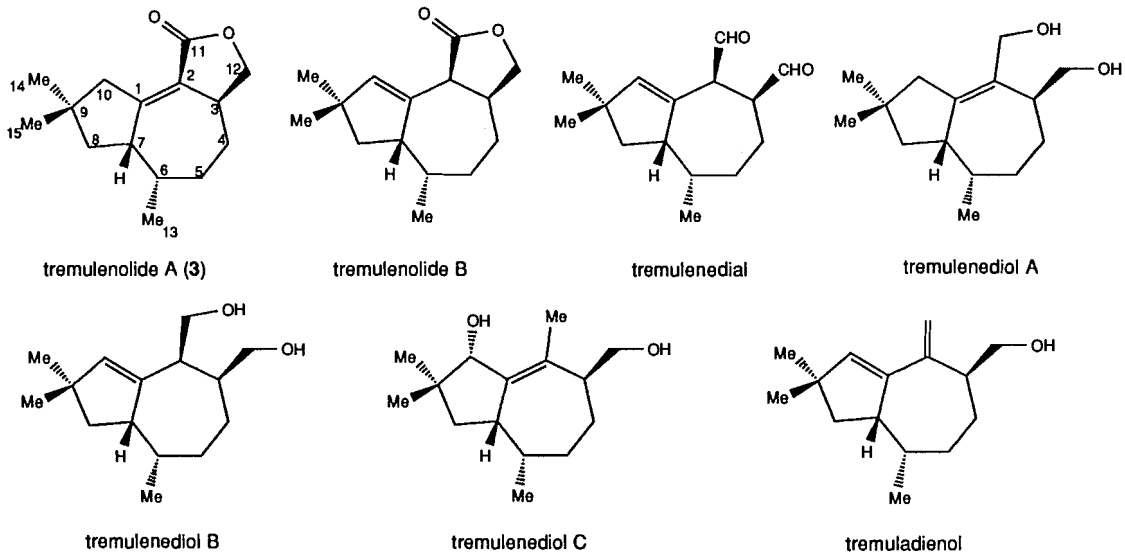

Can. J. Chem. Downloaded from www.nrcresearchpress.com by 65.111.164.53 on 09/08/12
For personal use only.

It has been discovered that aspen with a certain type of black gall occurring as a stem deformitory have a lower incidence of decay caused by *Ph. tremulae* than do nearby non-gall trees (7). The cause of these galls is still under investigation.[2] This exciting discovery by Hiratsuka, communicated to us several years ago, encouraged us, with the cooperation of Dr. Hiratsuka and his colleagues, and L. Sigler, curator of the University of Alberta Microfungus Herbarium, to examine the chemistry of the black galls, and of fungi associated with the black galls, to see if we could discover a chemical cause of this black gall effect.

Chemistry of the decay fungi and micro-organisms related to the black galls

We have approached this problem in several ways. One approach was to study the chemical constituents of the black galls themselves. Another was to examine the metabolites of fungi associated with the black galls which our collaborators had shown to be antagonistic to the decay-causing *Phellinus tremulae*. It has also been observed (5, 8) that when the decay fungus *Peniophora polygonia* is also present in *Phellinus* infected aspen, there is a sharp demarcation between the *Peniophora* rot and the *Phellinus* rot. This mutual antagonism is also observed in agar cultures (8). Thus the metabolites of the two decay-causing fungi were of interest in an attempt to determine the chemical basis of the antagonism.

The presence of the decay fungus *Ph. tremulae* in aspen can usually be detected by the appearance of the distinctive fruiting bodies, or conks (pictured in ref. 2, p. 75), on the main stem of the tree. The fungus causes rotting of the heartwood of the tree. The rotted heartwood (also shown in ref. 2, p. 75) often has a distinctive odor of wintergreen, due to the presence of methyl salicylate (9). When the fungus is grown in liquid culture on 2% malt extract broth, methyl salicylate is one of the metabolites produced. More interestingly, when the fermentation is carried out in the presence of beads of DIAION HP 20®, a highly porous styrene–divinylbenzene resin useful in removing nonpolar metabolites from aqueous media (10), we isolate not only methyl salicylate, but also its biogenetic precursor, the valence tautomer 2-carbomethoxyoxepin:1-carbomethoxybenzene 1,2 oxide (**2**) (11). In the presence of traces of acid, **2** undergoes facile rearrangement to methyl salicylate. It was suggested some time ago that the biosynthesis of salicylic acid (and methyl salicylate) involves monooxidase oxidation of benzoic acid (methyl benzoate) to the arene oxide followed by NIH shift of the carboxyl or carbomethoxyl group (12), but the arene oxide had not previously been isolated from natural sources. To demonstrate that *Ph. tremulae* could indeed carry out this transformation, we added ^{13}C-carboxyl-labelled benzoic acid to the growing culture and were able to isolate the appropriately labelled oxepin **2** as well as labelled methyl salicylate and labelled methyl benzoate (13). The significance of these observations in relation to the black gall effect will be discussed later. *Phellinus tremulae* also produces a new family of sesquiterpenes, which we call the tremulanes, shown in Fig. 1 (14). The structures were determined by NMR techniques (^{1}H–^{1}H COSY, HMQC, HMBC) and other methods including in the case of tremulenolide A (**3**), X-ray crystallography. Chemical correlations among the tremulenes also played an important role in the structural studies. For example, manganese dioxide oxidation of tremulenediol A (Fig. 1) provided tremulenolide A (**3**). Presumably, oxidation of the diol selectively oxidized the allylic alcohol to provide the α,β-unsaturated aldehyde, which, after hemiacetal formation, gave the allylic hemiacetal, and this in turn was oxidized to the unsaturated lactone **3** (14).

The tremulane (**4**) family does not obey the biogenetic isoprene rule. It is positionally isomeric with the lactarane (**5**) and the recently reported (15) merulane (**6**) perhydroazulene sesquiterpenes. It was, therefore, of interest to study the biosynthesis of this unique sesquiterpene skeleton. *Phellinus tremulae* was cultivated in shake cultures that were periodically supplemented with injections of sodium [1-^{13}C]-, [2-$^{13}C_2$]-, and [1,2-$^{13}C_2$]acetate (16). Since tremulenediol A (Fig. 1) can be isolated in reasonable amounts and is readily puri-

[2] Y. Hiratsuka, Northern Forestry Centre, Forestry Canada, private communication.

Can. J. Chem. Downloaded from www.nrcresearchpress.com by 65.111.164.53 on 09/08/12
For personal use only.

Scheme 1

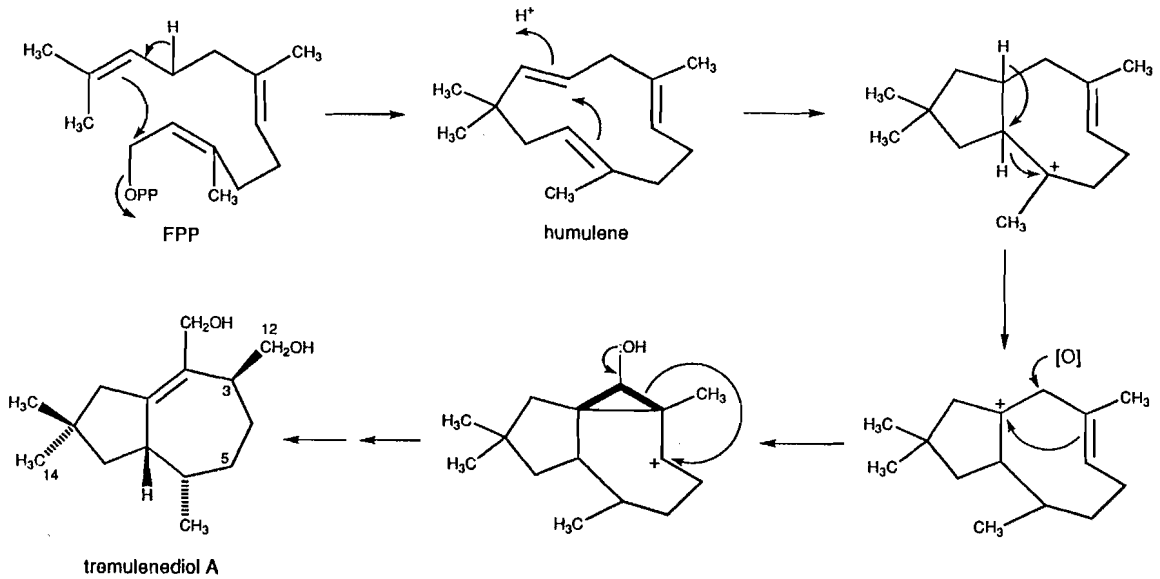

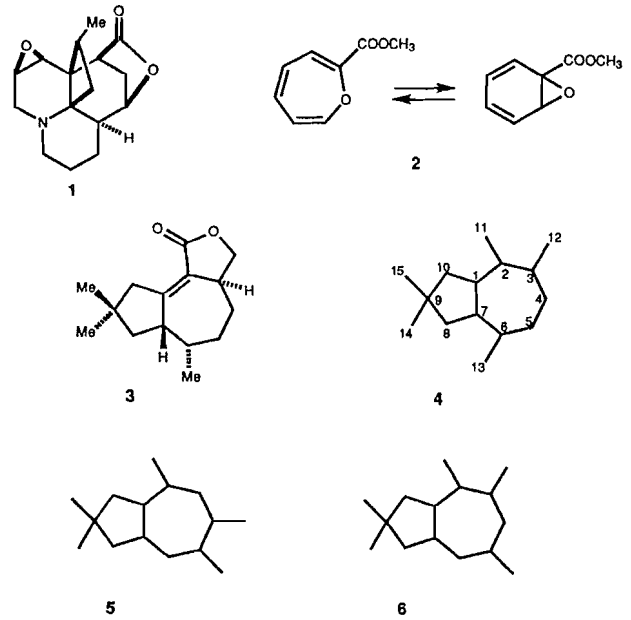

Fig. 2. ^{13}C-acetate labelling results.

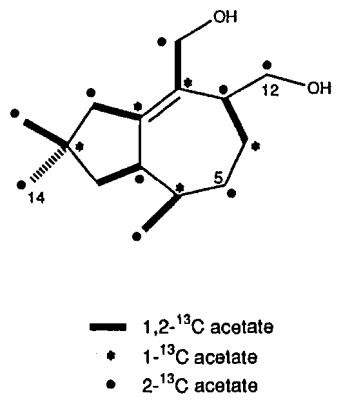

fied as its di-*p*-bromobenzoate, it was chosen for ^{13}C NMR analysis of the labelling patterns. The labelling results are summarized in Fig. 2. A 2D-INADEQUATE experiment on the material from the [1,2-$^{13}C_2$]acetate-labelling experiment clearly confirmed the spin-coupled pairs and showed that carbons 5, 12, and 14 do not give rise to cross peaks. The lactarane skeleton **5** and, presumably, the merulane skeleton **6** are formed from farnesyl pyrophosphate (FPP) via humulene (see Scheme 1) (17). A possible route from FPP, via humulene, to the tremulane skeleton that is in accord with the labelling results is shown in Scheme 1.[3] In order that the C-2 to C-11 bond originate from the same acetate unit, it is necessary that the oxygenated carbon in the cyclopropyl intermediate (Scheme 1) be the group that migrates to C-3, rather than the methyl group. An alternative pathway involving the head-to-tail addition of geranyl pyrophosphate to dimethylallyl pyrophosphate (14, 16) also accounts for the observed labelling pattern, but since we are not aware of any sequiterpenes that are not derived via FPP, we favor the pathway shown in Scheme 1.

None of the metabolites produced by *Ph. tremulae* showed antifungal activity against *Peniophora polygonia*, and we turned our attention to the metabolites of this latter fungus. A number of new drimane sesquiterpenes (e.g., peniopholide (**7**)) as well as some known members of this class were isolated (18), along with a number of benzenoid compounds (19). Bioassays revealed that *Pe. polygonia* also produces some volatile acids and alcohols that inhibit the grown of *Ph. tremulae* (8). These were identified by gas chromatography (gc), gc–ir, and gc–ms (20). The most active of the volatile compounds were 2-phenylethanol and benzoic acid and these proved to be the most active of all the metabolites examined, but complete inhibition required concentrations of 1000 μg/mL. Several commercially available analogs of the aromatic acids were also tested and it was discovered that 4-phenyl-3-butenoic acid (**8**), a known enzyme hydroxylase inhibitor (21),

[3] We thank Professor David Cane for first suggesting this pathway.

causes complete inhibition of the growth of *Ph. tremulae* at 10 μg/mL (20). We conclude that it is *Pe. polygonia* which is responsible for the antagonism observed between the two decay fungi, but that the metabolites are not sufficiently active to be of practical value. However, further testing of compound **8** and analogs thereof is being conducted.

The investigation of the fungi associated with the black galls has led to the isolation of several fungi that are antagonistic to *Ph. tremulae* or to *Ophiostoma crassivaginatum*, the most common of the blue stain fungi that cause stain in stored logs of aspen (6). Among these antagonistic fungi is a newly discovered fungus, *Phoma etheridgei*, which is consistently present on the surface of the galls (22). This fungus shows antagonistic activity against both *Ph. tremulae* and *O. crassivaginata*.

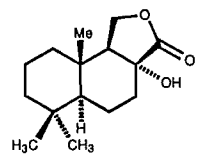

7

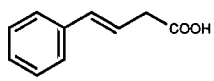

8

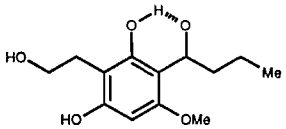

9

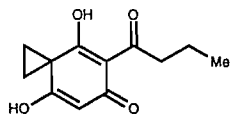

10

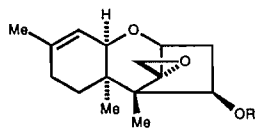

11 R = Ac
12 R = H

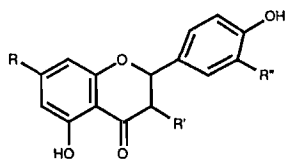

13 R = OH, R' = R" = H
14 R = OCH_3, R' = OH, R" = H
15 R = R' = OH, R" = H
16 R = R' = R" = OH

It was difficult to obtain liquid cultures of the *Phoma* species that consistently produced bioactive material until we discovered that spore (pycnidia) suspensions of the fungus should be used as inoculum for the liquid cultures rather than mycelia suspensions (23). Bioassay (against *Ph. tremulae*) -guided separation of the metabolites (again DIAION HP 20® was used to facilitate the isolation process) led to the isolation of a new natural product that we have named phomalone, and which has been shown to possess structure **9** (23). Phomalone is an unusual hexaketide, which labelling studies have shown is derived by condensation of two triketide chains and further elaborated via a cyclopropylcyclohexadienone intermediate such as **10**. Phomalone completely inhibits the growth of *Ph. tremulae* at a concentration of 250 μg/mL, but has no effect at 25 μg/mL. Since phomalone cannot be detected in the tissue of aspen bearing the black galls, it appears unlikely that it is responsible for the black gall effect (23). However, the potential use of *Phoma etheridgei* as a bioprotectant against *Ph. tremulae* is being studied (22).

Other fungi being explored by the forest scientists as possible bioprotectants include two fungi obtained from healthy aspen, *Lecythophora hoffmannii* (24) and *Stachybotrys cylindrospora* (25). The nature of the antifungal agents(s) produced by *L. hoffmannii* has not yet been determined, but we have shown that the compounds responsible for the antifungal activity of *S. cylindrospora* are the trichothecene mycotoxins trichodermin (**11**) and trichodermol (**12**) (26). The known toxicity of the latter type of compound mitigates against use of this fungus as a bioprotectant.

The chemistry of the black galls

We hesitated to begin studying the chemistry of the galls themselves. The wood and bark of aspen had already been examined and a variety of compounds, from triterpenes (27), to glycosides (28), to flavanoids and aromatic acids (29), have been reported. I felt it might be an unrewarding experience to try to sort out the normal products from those induced by the black galls. However, we decided that we would at least extract some sawdust from black gall tissue and compare the bioassay (against *Ph. tremulae*) of the extract with the bioassay of an extract of "clean" aspen from a non-gall healthy tree. We extracted with several solvents, including water, and found that ethyl acetate provided us with the largest amount of extract. The extract was divided into acidic and non-acidic fractions and these were then subjected to bioassay. The acidic portion of the black gall tissue inhibited the growth of *Ph. tremulae* in agar cultures! The extracts from the healthy tissue showed no activity. A similar result was obtained when dichloromethane was the extraction solvent. The aqueous extract gave a faintly positive result.

The acidic portion of the ethyl acetate fraction (5 g of acidic material was obtained from 500 g of air-dried sawdust) was separated into its components by a combination of column chromatography, flash chromatography, and preparative tlc. The major component (0.8 g!) was benzoic acid. Other components identified include *trans*-cinnamic acid, *p*-hydroxybenzoic acid, *p*-hydroxycinnamic acid, and the known flavanoids naringenin (**13**), 7′-methyl-3-hydroxynaringenin (**14**), aromandendrin (**15**), and taxifolin (**16**) (30). Benzoic acid was the only compound that showed activity against *Ph. tremulae* (1000 ppm shows complete inhibition of growth on carrot agar). Benzoic acid is known to have weak antimicrobial activity and is widely used as a food preservative, often in the form of its more soluble sodium salt (31). To determine whether benzoic acid might be acting as the protective agent in the black gall trees, we next studied the benzoic acid level in these trees in an area well removed from the site of the gall. Since dichloromethane is as effective a solvent as ethyl acetate in extracting the benzoic acid from sawdust and it is more volatile, it was chosen as the solvent for the subsequent studies. This has the added advantage that dichloromethane extracts less of the more polar materials present in the wood. As a control, it was necessary to examine the benzoic acid level in healthy, non-galled trees. Sawdust prepared from black gall tissue, from wood removed 25 cm above the gall, and from wood of a healthy tree (the trees were adjacent to one another and harvested on the same day near Blue Ridge, Alberta, in July, 1993) was extracted with dichloromethane. *p*-Toluic acid was added to the sawdust to serve as an internal standard to measure the extraction efficiency. The acids were removed from the dichloromethane by extraction with aqueous sodium

Can. J. Chem. Downloaded from www.nrcresearchpress.com by 65.111.164.53 on 09/08/12
For personal use only.

Can. J. Chem. Downloaded from www.nrcresearchpress.com by 65.111.164.53 on 09/08/12
For personal use only.

bicarbonate, then back-extracted, after acidification, into dichloromethane. Phenylacetic acid was added to the concentrated extract to serve as a further internal standard. The acids were esterified by addition of diazomethane and the amount of benzoic acid (as methyl benzoate) was determined by gas chromatography, using the methyl *p*-toluate and methyl phenylacetate peaks for comparison. The black gall tissue contained 1700 ppm of benzoic acid, the wood from the gall-bearing tree contained 90 ppm, and the wood from the non-galled tree contained only 14 ppm. Several duplicate experiments were carried out and the results were reproducible to ±5% (30).

Our bioassays on agar plates indicate that the minimum inhibitory concentration (mic) of benzoic acid against *Ph. tremulae* is in the range of 800–1000 ppm; mic values ranging between 120 and 500 ppm are reported against some other fungi (31). It is difficult to quantitatively relate the level of benzoic acid in the tree tissue to that obtained by adding benzoic acid to an agar preparation. It is also known that the antifungal activity of benzoic acid is pH dependent (31). It is clear that further work is necessary before we can state whether or not benzoic acid is responsible for the black gall effect.

I noted earlier that the decay fungus *Ph. tremulae* is capable of transforming benzoic acid to methyl benzoate and methyl salicylate. It has previously been reported that the bark of aspen contains benzoylated and salicyloylated glycosides (32, 33). In recent years it has been established that salicylic acid plays an important role in the induction of systemic acquired resistance (SAR) in many plants (34–36). Salicylic acid (in the form of its glycoside, salicin) was one of the first natural products to be isolated (1828) and its acetyl derivative, aspirin, is the most widely used pharmaceutical product (37). Although the many beneficial effects of salicylic acid in human medicine are well studied and much is known (37), the question as to why plants make salicylic acid has not been widely addressed. It appears that this so-called secondary metabolite plays an important role in defending plants, as well as humans, against disease!

Salicylic acid is produced in plants by the monooxygenase oxidation of benzoic acid (38, 39). Benzoic acid is biosynthesized from phenylalanine via cinnamic acid (38), one of the minor acids isolated from black gall tissue. Salicylic acid was not isolated directly from the black galls but it was detected, along with benzoic acid, in the form of glycosides (which are not soluble in dichloromethane), by extraction with butyl alcohol of the sawdust remaining after dichloromethane extraction and hydrolysis of this extract. It has been suggested that the glycosides provide a mechanism by which plants may store salicylic acid for rapid deployment during SAR (35). It is possible to speculate that the black gall effect may not be directly due to the antifungal activity of benzoic acid, but that the excess benzoic acid serves as a ready precursor of salicylic acid, the SAR signal molecule. In tobacco, it has been demonstrated that the hydroxylase required for the oxidation of benzoic acid to salicylic acid (presumably via the carboxyl form of oxepin **2**) is activated by the pathogen (38).

As mentioned above, *Ph. tremulae* is capable of methylating benzoic acid and then transforming it into methyl salicylate (oil of wintergreen), a molecule that does not induce SAR (34). Analysis of the benzoic acid level in *Phellinus* infected aspen reveals a concentration of benzoic acid intermediate between the healthy trees and the galled trees (30). Thus the methylating ability of *Phellinus* species (40) may be a factor in their ability to successfully invade host plants.

It is clear that much remains to be done in the study of the black gall effect and that the hypotheses advanced herein are only that, hypotheses. I do hope, however, that this lecture does illustrate some of the ways in which natural products chemistry may make some contribution in the study of biological problems.

Acknowledgements

I am deeply indebted to my co-workers and collaborators on the "aspen project" for the support they have provided. In particular, I wish to acknowledge the leading role that Dr. Yasuyuki Hiratsuka of the Northern Forestry Centre in Edmonton has played in this work. Yasu's observation that aspen with black galls seem to be resistant to rot reminds me of Svent-Györgyis' observation on the mark of a great scientist: "to see what everyone sees, to think what no one has thought." Hiratsuka's co-workers, Dr. P. (Chak) Chakravarty and Dr. Leonard Hutchison, contributed much to the project as did Patricia Crane and Gabriele Herger. The insightful comments and critiques of Lynn Sigler of the U. of A. Microfungus Herbarium have been of great value. I am immensely grateful to the members of my own research group who worked so diligently and enthusiastically on this project, and who provided many of the ideas. The details of the work I've discussed are provided in refs. 11, 13, 14, and 16 with Elizabete Cruz (who introduced the use of DIAION HP 20), refs. 18, 19, and 20 with Latchezar Trifonov (who coordinated much of the work), ref. 23 with Luis Jimenez (who persisted with the reluctant *Phoma* species), refs. 25 and 26 with Shichang Miao, and ref. 30 with Gabrielle Pausler (who cheerfully carried out the sawdust extractions). Katarzyna Ptaszynska carried out valuable preliminary studies on *Lecythophora hoffmannii*, a fungus reluctant to provide consistent bioactivity. I would also like to express my appreciation to members of the Chemistry Department staff who have provided strong support over the years, especially Erica Schamedatus, Lois Browne, Tom Nakashima, Alan Hogg, Tony Schnautz, and Avron Levine. It has been a privilege to work with all of these people.

The financial assistance of the Natural Sciences and Engineering Research Council in the form of operating grants (W.A.A.) and a Strategic Grant (with Y. Hiratsuka and L. Sigler) is gratefully acknowledged.

References

1. K. Wiesner, Z. Valenta, W.A. Ayer, and C. Bankiewicz. Chem. Ind. 1019 (1956).
2. E.B. Peterson and N.M. Peterson. Ecology, management, and use of aspen and balsam poplar in the prairie provinces. For. Can. North. For. Cent., Spec. Rep. 1. 1992.
3. K. Hunt, J.T. Basham, and J.A. Kemperman. Can. J. For. Res. **8**, 181 (1978).
4. D.A. Cheyne. *In* Aspen Symposium 1989. *Edited* by R.D. Adams. USDA For. Gen. Tech. Rep. NC-140. 1990. pp. 275–281.
5. Y. Hiratsuka, D.A. Gibbard, O. Bakowsky, and G.B. Maier. Classification and measurement of aspen decay

and stain in Alberta. For. Can. North. For. Cent., Inf. Rep. NOR-X-314. 1990.
6. Y. Hiratsuka. Forest tree diseases of the prairie provinces. Northern For. Centre, Can. For. Serv., Info. Rep. NOR-X-286. 1987. p. 142.
7. P.E. Crane, P.V. Blenis, and Y. Hiratsuka, Can. J. For. Res. **24**, 2240 (1994).
8. P. Chakravarty and Y. Hiratsuka. Eur. J. For. Path. **22**, 354 (1992).
9. R.P. Collins and A.F. Halim. Can. J. Microbiol. **18**, 65 (1972).
10. Y. Tokiwa, M. Miyoshi-Saitoh, H. Kobayashi, R. Sunaga, M. Konishi, T. Oki, and S. Iwasaki. J. Am. Chem. Soc. **114**, 4107 (1992).
11. W.A. Ayer and E.R. Cruz. Tetrahedron Lett. **34**, 1589 (1993).
12. D.R. Boyd and G.A. Berchtold. J. Am. Chem. Soc. **101**, 2470 (1979).
13. W.A. Ayer and E.R. Cruz. J. Nat. Prod. In press.
14. W.A. Ayer and E.R. Cruz. J. Org. Chem. **58**, 7529 (1993).
15. M. Jonassohn, H. Anke, O. Sterner, and C. Svensson. Tetrahedron Lett. **35**, 1593 (1994).
16. E.R. Cruz. Ph.D. thesis, University of Alberta, Edmonton. 1993. pp. 80–93.
17. W.A. Ayer and L.M. Browne, Tetrahedron, **37**, 2199 (1981).
18. W.A. Ayer and L.S. Trifonov. J. Nat. Prod. **55**, 1454 (1992).
19. W.A. Ayer and L.S. Trifonov. J. Nat. Prod. **56**, 85 (1993).
20. L.S. Trifonov, P. Chakravarty, Y. Hiratsuka, and W.A. Ayer. Eur. J. For. Path. **22**, 441 (1993).
21. A.F. Bradbury, J. Mistry, B.A. Roos, and D.G. Smyth. Eur. J. Biochem. **189**, 363 (1990).
22. L.J. Hutchison, P. Chakravarty, L.M. Kawchuk, and Y. Hiratsuka. Can. J. Bot. **72**, 1424 (1994).
23. W.A. Ayer and L.D. Jimenez. Can. J. Chem. **72**, 2326 (1994).
24. P. Chakravarty and Y. Hiratsuka. Z. Pflanzenkr. Pflanzenschutz, **101**, 74 (1994).
25. Y. Hiratsuka, P. Chakravarty, S. Miao, and W.A. Ayer. Can. J. For. Res. **24**, 174 (1994).
26. W.A. Ayer and S. Miao. Can. J. Chem. **71**, 487 (1993).
27. R.A. Abramovitch and R.G. Micetich. Can. J. Chem. **41**, 2362 (1963).
28. T.P. Clausen, T.P. Evans, P.B. Reichardt, and J.P. Bryant. J. Nat. Prod. **52**, 207 (1989).
29. S. English, W. Greenway, and F.R. Whatley. Can. J. Bot. **69**, 2291 (1991).
30. G. Pausler, W.A. Ayer, and Y. Hiratsuka. Can. J. For. Res. Submitted.
31. K. Lueck. Antimicrobial food additives. Springer-Verlag, Berlin. 1980. pp. 210–218.
32. M. Hubbes. Can. J. Bot. **47**, 1295 (1969).
33. S.F. Darling. Tappi, **50**, 193 (1967).
34. N. Yalpani and I. Raskin. Trends Microbiol. **1**, 88 (1993).
35. D.A. Dempsey and D.F. Klessig. Trends Cell Biol. **4**, 335 (1994).
36. D.M. Horvath and N.H. Chua. Curr. Opin. Biotechnol. **5**, 131 (1994).
37. G. Weissman. Sci. Am. **264**, 84 (1991).
38. N. Yalpani, J. Leon, M.A. Lawton, and I. Raskin. Plant Physiol. **103**, 315 (1993).
39. J. Leon, N. Yalpani, I. Raskin, and M.A. Lawton. Plant Physiol. **103**, 323 (1993).
40. D.B. Harper, J.T.G. Hamilton, J.T. Kennedy, and K.J. McNally. Appl. Environ. Microbiol. **55**, 1981 (1989).

Can. J. Chem. Downloaded from www.nrcresearchpress.com by 65.111.164.53 on 09/08/12
For personal use only.

^{1}H NMR study of the solvolysis of the paramagnetic tetrachloro-bis(imidazole)ruthenium(III) anion in water, methanol, and dimethyl sulfoxide

Craig Anderson and André L. Beauchamp

Can. J. Chem. Downloaded from www.nrcresearchpress.com by 65.111.164.53 on 09/08/12
For personal use only.

Abstract: The ^{1}H NMR signals of the Ru(III) species present in solution are considerably broadened and shifted by paramagnetism, but they can be used to follow chloride displacement in the *trans*-$[RuCl_4Im_2]^-$ ion. This anion remains predominant for several hours at room temperature in D_2O, but its signals are progressively replaced by those of a monoaqua $[RuCl_3(D_2O)Im_2]$ complex. Over a period of days, two new sets of peaks appear, corresponding to two isomers of $[RuCl_2(D_2O)_2Im_2]^+$. The same behaviour is observed for the 1-methyl- and 4-methylimidazole analogues. These reactions can be driven backwards by addition of KCl, but $[RuCl_4Im_2]^-$ is not quantitatively regenerated in solution even for 6 M NaCl. Within several months, the $[RuCl_2(D_2O)_2Im_2]^+$ isomers further aquate to a single species $[RuCl(D_2O)_3Im_2]^{2+}$. In CD_3OD, displacement of the first chloride of $[RuCl_4Im_2]^-$ takes place faster, over several hours, but substitution stops at the $[RuCl_3(CD_3OD)Im_2]$ stage. In DMSO, substitution occurs very slowly. The $[RuCl_3(DMSO)Im_2]$:$[RuCl_4Im_2]^-$ mixture (1:2) obtained after 12 days starts to show very slow reduction to two Ru(II) species, one of which precipitates as yellow crystals. From X-ray diffraction work (monoclinic, $P2_1/n$, $a = 9.951$, $b = 8.564$, $c = 10.527$ Å, $\beta = 92.95°$, $R = 0.033$), the compound was identified as $[RuCl_2(DMSO\text{-}d_6)_2Im_2]$, where the metal has a *trans-trans-trans* coordination and the DMSO ligands are S-bonded.

Key words: paramagnetic ruthenium anion, solvolysis, chloro complexes.

Résumé : Les signaux RMN ^{1}H des espèces de Ru(III) présentes en solution sont fortement élargis et déplacés par le paramagnétisme, mais on peut les utiliser pour suivre le déplacement des chlorures dans l'ion *trans*-$[RuCl_4Im_2]^-$. Cet anion demeure prédominant durant quelques heures à température ambiante dans D_2O, mais ses signaux sont progressivement remplacés par ceux du complexe monoaqua $[RuCl_3(D_2O)Im_2]$. Sur une période de quelques jours apparaissent deux séries de nouveaux pics correspondant à deux isomères de $[RuCl_2(D_2O)_2Im_2]^+$. On observe le même comportement pour les complexes analogues du 1-methyl- et du 4-methylimidazole. On peut déplacer l'équilibre en sens inverse par addition de KCl, mais $[RuCl_4Im_2]^-$ n'est pas regénéré quantitativement en solution même pour 6 M NaCl. En quelques mois, les isomères de $[RuCl_2(D_2O)_2Im_2]^+$ subissent une aquation supplémentaire pour donner l'unique espèce $[RuCl(D_2O)_3Im_2]^{2+}$. Dans CD_3OD, le déplacement du premier chlorure de $[RuCl_4Im_2]^-$ se produit plus rapidement, en quelques heures, mais la substitution s'arrête à l'étape de $[RuCl_3(CD_3OD)Im_2]$. Dans DMSO, la substitution a lieu très lentement. Dans le mélange $[RuCl_3(DMSO)Im_2]$:$[RuCl_4Im_2]^-$ (1:2) obtenu après 12 jours commence une très lente réduction en deux espèces de Ru(II), dont l'une précipite sous forme de cristaux jaunes. Au moyen d'une étude par diffraction des rayons X (monoclinique, $P2_1/n$, $a = 9{,}951$, $b = 8{,}564$, $c = 10{,}527$ Å, $\beta = 92{,}95°$, $R = 0{,}033$), ce composé a été identifié comme étant $[RuCl_2(DMSO\text{-}d_6)_2Im_2]$, où le métal possède une coordination *trans-trans-trans* et les ligands DMSO sont liés par le soufre.

Mots clés : paramagnétisme, ruthénium, solvolyse, complexes chloro.

Introduction

Several ruthenium complexes have attracted attention as potential non-platinum antitumour agents (1, 2). To this series were recently added chloro-ruthenium(III) complexes with imidazoles and related N-heterocyclic ligands, whose promising antitumour properties are presently being evaluated (3). Considering that related ruthenium(II) compounds with nitroimidazoles are known to be efficient radiosensitizers (4, 5), it appears that important chemotherapeutic applications are to be associated with ruthenium–imidazole systems.

The chloro-Ru(III)-imidazole compounds have been well characterized as solids (6, 7), but their behaviour in solution is complicated. A good understanding of solution chemistry is important, first, to identify the species actually responsible for

Received July 18, 1994.

C. Anderson and A.L. Beauchamp.[1] Département de chimie, Université de Montréal, C.P. 6128, Succ. centre-ville, Montréal, QC H3C 3J7, Canada.

[1] Author to whom correspondence may be addressed. Telephone: (514) 343-6446. Fax: (514) 343-7586. E-Mail: beauchmp@ere.umontreal.ca

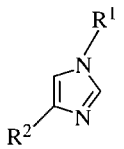

Im	$R^1 = R^2 = H$
1-MeIm	$R^1 = CH_3$, $R^2 = H$
4(5)-MeIm	$R^1 = H$, $R^2 = CH_3$

the therapeutic activity. In addition, the presence of imidazole makes these compounds attractive as models to unravel complex processes involving metallobiomolecules, where the imidazole unit is present as such in the histidine residue or as one of the purine rings in nucleic acids.

The binding of (ImH)[$RuCl_4Im_2$] (**1**) to biological substrates has been shown to take place slowly, over several hours, in fresh aqueous solutions (8, 9), suggesting that a chloro ligand must first be replaced by water, as in the case of $PtCl_2(NH_3)_2$. Other Ru(III) systems have, so far, been considered as substitution inert in physiological conditions (10), and activation by in situ reduction to a more labile Ru(II) species has been assumed to take place (11). This Ru(II) species would then be able to interact with the target molecules after dissociation of a Cl^- ligand, a step considered to be of paramount importance. This mechanism has been proposed to explain the radiosensitizer ability of [$RuCl_2(4\text{-}NO_2Im)_2(DMSO)_2$] (5), where a Cl^- ligand is quickly released and replaced by a water molecule in aqueous medium. Therefore, whether interactions with biomolecules involve the Ru(III) centre itself or a reduced Ru(II) species is still unclear, but the presence of a readily displaced aqua ligand in the active species seems to be widely accepted.

The solution chemistry of Ru(III) compounds is still difficult to study, because NMR techniques are not routinely applicable to such paramagnetic species: the unpaired electron in these low-spin d^5 complexes causes line broadening and large chemical shifts, making spectra difficult to obtain and interpret (12). When this work was undertaken, ^1H NMR spectra had been reported for aqueous solutions of [$Ru(NH_3)_5Im]Cl_3$, used as a model for ruthenium–histidyl protein complexes (13). More recently, the spectra of (ImH)[$RuCl_4Im_2$] in DMSO (10) and of Na[$RuCl_4$(DMSO)Im] in D_2O (14) were reported.

In the present paper, ^1H NMR spectroscopy is used to follow the behaviour of (ImH)[$RuCl_4Im_2$] and the analogues with 1-MeIm and 4(5)-MeIm[2] in three solvents. Very recently, on the basis of HPLC and other experiments, Keppler et al. (3) gave a description of the earlier aquation steps for the Im complex, which are generally in good agreement with our results described here.

Experimental

Instruments and reactants

^1H NMR spectra were recorded on Varian XL-300 or Bruker AMX-300 spectrometers. No particular precautions were taken to protect the solutions from the atmosphere. Sweep-widths of 50 or 100 kHz were used at pulse rates of 0.04 s. The peaks were referenced to residual solvent peaks (D_2O, δ = 4.80; CD_3OD, δ = 3.30; $(CD_3)_2SO$, δ = 2.50 ppm) and given with respect to Me_4Si, downfield being positive. Infrared spectra (4000–220 cm^{-1}) were recorded on a Perkin–Elmer 1600 FTIR apparatus as either KBr or CsI pellets.

The imidazole ligands were used as received from Aldrich. $RuCl_3 \cdot 3H_2O$ (Aldrich) was "activated" by refluxing in an ethanol – aqueous HCl mixture for several hours prior to each synthesis.

Preparative work

The (LH)[$RuCl_4L_2$] compounds were prepared by variations of known methods (6, 7). Pure samples were found to be obtained only if acidity, temperature, and reaction time were carefully controlled. Activation of $RuCl_3$ was necessary, but various procedures commonly used in the literature were equally efficient. The reactions proceeded normally with HCl ~1 M. In the absence of acid, extremely insoluble green products precipitated, which remain uncharacterized, but are thought to be chloride-bridged polymeric materials of the type described earlier (15).

(ImH)[$RuCl_4Im_2$], 1

Commercial $RuCl_3$ (0.94 g) was dissolved in a mixture of concentrated HCl (2 mL), H_2O (12 mL), and EtOH (12 mL). This solution was refluxed for 3 h at which time its volume was reduced by half. It was filtered while hot and added to a solution of imidazole (3.0 g) in 6 N HCl (5 mL). The mixture was heated gently for 15 min and allowed to cool. Within 24 h, an orange powder had precipitated, which was filtered, washed with copious amounts of cold methanol, then dried under high vacuum. Yield: 10–20%.

The red-brown powder often contained red crystals, whose cell parameters and space group are those of (ImH)[$RuCl_4Im_2$] (6). The powder and the crystals gave identical IR spectra, where the low-frequency bands (cm^{-1}) correspond with those reported: 334 (s), 294 (w), 249 (m). The ^1H spectra of fresh solutions showed a single set of signals with the expected intensity ratio for ImH^+ and [$RuCl_4Im_2$]$^-$. The samples were free of $(ImH)_2$[$RuCl_5Im$], as evidenced from the absence of the characteristic signals for this species (−27.0, −15.2, and −6.7 ppm) (16).

(4-MeImH)[$RuCl_4$(5-MeIm)$_2$], 2

A solution containing concentrated HCl (2.1 mL), EtOH (24 mL), water (24 mL), and $RuCl_3$ (0.95 g) was refluxed for 2.5 h. The volume was reduced to 8 mL and cooled to room temperature. To this solution was added 4-MeIm (2.1 g) in 6 M HCl (2.5 mL). The resulting solution was stirred for 5 min and then held at 8°C for 4 days, at which time a red powder appeared. This solid was filtered and washed with EtOH. Yield: 20%. IR (cm^{-1}): 385 (w), 335 (m), 314 (s), 290 (vs), 274 (sh). The ^1H spectra of fresh solutions showed a single set of signals with the expected intensities (see next section). Anal. calcd. for $C_{12}H_{19}Cl_4N_6Ru$: C 29.40, H 3.91, N 17.14, Cl 28.93; found: C 29.79, H 4.01, N 17.06, Cl 29.09.

(1-MeImH)[$RuCl_4$(1-MeIm)$_2$]·H_2O, 3

This complex was prepared similarly to the 4-MeIm product and isolated as the monohydrate. Yield: 20%. IR (cm^{-1}): 398 (w), 350 (vw), 319 (vs), 280 (m), 268 (m), 254 (w), 248 (w).

[2] Conventional ring numbering starting with the N-H(R) position is used. The two tautomeric forms are designated as 4-MeIm (4-methyl-1*H*-imidazole) and 5-MeIm (5-methyl-1*H*-imidazole), respectively. The equilibrium mixture is represented by 4(5)-MeIm.

Can. J. Chem. Downloaded from www.nrcresearchpress.com by 65.111.164.53 on 09/08/12
For personal use only.

Can. J. Chem. Downloaded from www.nrcresearchpress.com by 65.111.164.53 on 09/08/12
For personal use only.

Table 1. Crystal data and conditions of data collection for $[RuCl_2(DMSO)_2Im_2]$.

Formula	$C_{10}H_{20}Cl_2N_4O_2S_2Ru$
Formula weight	464.39
Crystal system	Monoclinic
Space group	$P2_1/n$
a, Å	9.951(1)
b, Å	8.564(1)
c, Å	10.527(1)
β, deg	92.95(1)
V, Å^3	895.9(2)
D_{calc}, g cm^{-3}	1.721
Z	2
Radiation, λ (Å)	CuKα, 1.54056
$F(000)$	468
μ, cm^{-1}	123.2
Crystal size, mm	0.053 × 0.074 × 0.33
$2\theta_{max}$, deg	140
Scan technique	ω/2θ
Scan width, Δω, deg	1.00 + 0.14 tan θ
Scan speed, deg(ω) min^{-1}	3.30
No. unique reflections measured	1693
No. observed reflections	1450
Rejection criterion, $I/\sigma_I <$	2.5
T, K	293
R^a	0.033
$R_w{}^a$	0.036
Goodness-of-fit	2.50

$^aR = \Sigma \| F_o \| - \| F_c \| / \Sigma | F_o |$, $R_w = [\Sigma w(| F_o | - | F_c |)^2 / \Sigma w | F_o |^2]^{1/2}$.

Fresh solutions showed a single set of ^{1}H NMR signals with the expected intensities (see next section). Anal. calcd. for $C_{12}H_{21}Cl_4N_6ORu$: C 28.36, H 4.16, N 16.54, Cl 27.90; found: C 28.45, H 3.99, N 16.38, Cl 28.00.

trans,trans,trans-*[$RuCl_2$(DMSO-d_6)$_2Im_2$]*

Complex **1** (37 mg) was dissolved in DMSO-d_6 (3 mL) and acetone (25 mL) was added. This solution was heated gently for 15 min. The initial orange-yellow precipitate of **1** was filtered and the mother liquor was allowed to rest. In 2 days, the product precipitated as elongated yellow crystals, whose X-ray structure has been determined. Low-frequency IR data (cm^{-1}): 392 (s), 362 (m), 351 (s), 302 (vw), 279 (vw), 248 (w), 241 (m).

Crystal structure of $[RuCl_2(DMSO\text{-}d_6)_2Im_2]$

X-ray diffraction data were obtained with an Enraf–Nonius CAD-4 diffractometer. A reduced cell was determined from 25 reflections on a rotation photograph and final cell parameters were calculated by least-squares refinement on 25 higher angle reflections ($20° < \theta < 25°$) obtained from a quick pre-collection. The Niggli parameters clearly identified a monoclinic reduced cell. Space group $P2_1/n$ was determined unambiguously from the systematic absences (h0l, $l \neq 2n$; 0k0, $k \neq 2n$) in the intensity data set. Crystal data are given in Table 1.

Four standards were used to monitor intensity every hour and orientation every 200 measurements. Variations remained within ±2.0% during data collection. A whole sphere of data (6331 reflections) was collected by the ω/2θ scan technique. They were averaged to 1693 independent hk$l$ and hk$\bar{l}$ reflections, of which 1450 where above background ($I > 2.5\ \sigma_I$). The usual corrections for the effects of Lorentz and polarization were finally applied.

From the Patterson map, the Ru atom was found to lie on a crystallographic inversion centre and the origin was arbitrarily chosen. The remaining atoms were located from structure-factor and ΔF calculations. The structure was refined on $|F|$ by full-matrix least squares. The function minimized was $\Sigma w(|F_o| - |F_c|)^2$ with individual weights w based on counting statistics ($w = 1/[\sigma^2(F_o) + 0.00005\ F_o{}^2]$). All non-hydrogen atoms were refined anisotropically. The hydrogens were fixed at idealized positions (C(N)—H = 0.95 Å, U_{iso} = 0.075 Å^2). The general background in the final ΔF map was below ±0.3 e Å^{-3}. A few residuals of ±|0.9–1.2| e Å^{-3} remained near the Ru atom. The refined coordinates of the non-hydrogen atoms are given in Table 2. The temperature factors are available as supplementary material.[3] All calculations were done with the NRCVAX package (17).

Preliminary crystallographic results on (ImH)[$RuCl_4Im_2$]·2DMSO

The orthorhombic crystals ($Pbcm$, a = 7.873(2), b = 15.404(6), c = 19.913(4) Å, Z = 4) were obtained by adding acetone to a fresh solution of **1** in DMSO at 5°C (see text). Most of them were twinned. Intensities were collected on two apparently good specimens, as for the previous structure, but at −100°C. The data set used consisted of 2352 independent hk$l$ reflections, of which 1278 with $I > 3\ \sigma_I$ were retained and corrected for Lorentz and polarization effects. The Ru atom was readily found from the Patterson map. The remaining non-hydrogen atoms in the ImH^+ and $[RuCl_4Im_2]^-$ ions were located in the next ΔF map. Peaks for lattice solvent molecules were then found, but they defined a highly disordered DMSO molecule, in which the oxygen atom and the methyl groups could not be distinguished. These atomic positions were refined isotropically to R = 0.114. Small electron density residuals in the solvent region suggested partial replacement of DMSO by acetone in the structure. A similar problem has been encountered for related compounds (14). The coordinates and interatomic distances are given as supplementary material.[3] So far, we have been unable to grow better crystals. Despite the crystallographic disorder encountered, the presence of ImH^+ and $[RuCl_4Im_2]^-$ in this crystal is unambiguously established.

[3] The supplementary material includes four sets of ^{1}H NMR spectra, a table of data for the equilibrium constants, complete crystallographic data (anisotropic temperature factors, hydrogen coordinates, least-squares plane calculations, geometry of hydrogen bonds) for $[RuCl_2(DMSO\text{-}d_6)_2Im_2]$, and partial crystallographic data (coordinates and geometry) for (ImH)[$RuCl_4Im_2$]·2DMSO (12 pages). Copies of material on deposit may be purchased from: The Depository of Unpublished Data, Document Delivery, CISTI, National Research Council Canada, Ottawa, Canada K1A 0S2.

Tables of hydrogen coordinates, and distances and angles for $[RuCl_2(DMSO\text{-}d_6)_2Im_2]$, have also been deposited with the Cambridge Crystallographic Data Centre and can be obtained on request from the Director, Cambridge Crystallographic Data Centre, University Chemical Laboratory, 12 Union Road, Cambridge, CB2 1EZ, U.K.

Can. J. Chem. Downloaded from www.nrcresearchpress.com by 65.111.164.53 on 09/08/12
For personal use only.

Table 2. Refined coordinates for $[RuCl_2(DMSO)_2Im_2]$.

Atom	x	y	z	B_{eq}
Ru	0.00000	0.00000	0.00000	1.95(2)
Cl	0.05325(12)	–0.02748(14)	0.22543(11)	2.93(5)
S	0.2242(1)	0.2251(1)	0.0075(1)	2.86(5)
O	0.1258(4)	0.3241(4)	–0.1064(4)	4.7(2)
N(1)	–0.3332(4)	0.2422(5)	0.1389(4)	3.5(2)
N(3)	–0.1695(4)	0.1349(4)	0.0398(4)	2.3(2)
C(2)	–0.2319(5)	0.1388(6)	0.1472(5)	3.0(2)
C(4)	–0.2356(5)	0.2391(6)	–0.0401(5)	3.2(2)
C(5)	–0.3369(5)	0.3059(7)	0.0216(5)	3.9(3)
C(6)	0.0809(6)	0.3518(6)	0.1354(6)	3.8(3)
C(7)	0.2955(6)	0.1859(8)	0.0570(7)	5.3(3)

Results

Aqueous solutions of $(ImH)[RuCl_4Im_2]$, 1

The red complex **1** could be obtained, as described earlier (6), by reacting commercial $RuCl_3$ with several equivalents of imidazole in ethanol–HCl. The cell parameters of the crystals matched perfectly those already reported, as did the ν(Ru–Cl) (334 and 294 cm^{-1}) and ν(Ru–N) (249 cm^{-1}) IR bands. Splitting (614/622 and 1046/1063 cm^{-1}) due to the presence of both imidazolium counterion and coordinated imidazole (18) was also noted. Although the samples appeared to be pure from these criteria, the ^1H NMR spectra of fresh D_2O solutions often showed small spurious peaks, which were eventually found to be predominant in fresh solutions of $(ImH)_2[RuCl_5Im]$ (16). Starting materials free of $(ImH)_2$ $[RuCl_5Im]$ could be obtained by carefully adjusting heating, acidity, and reaction time (see experimental section).

Complex **1** is quite soluble in water and ^1H spectra could be recorded in spite of paramagnetism. Coordinated imidazole gives rise to three broad, but well-defined, peaks (Fig. 1*a* and Table 3), shifted to very high field by coordination to the paramagnetic Ru(III) centre. Two extra peaks are found in the normal region, at 7.4 (H2) and 8.6 ppm (H4/H5), for the imidazolium counterion. The N-H protons are seen for neither the coordinated ligand nor the imidazolium ion, due to rapid exchange with D_2O. As in the case of $[Ru(NH_3)_5Im]Cl_3$ (13), the relatively narrow signal of coordinated imidazole at -5.7 ppm is assigned to H5, that is, the proton furthest away from the metal centre. The peaks at -16.0 and -21.4 ppm are assigned to H4 and H2, respectively, on the basis of data from reactions using C2-deuterated imidazole, to be published later (16).

This spectrum is consistent with the *trans*-$[RuCl_4Im_2]^-$ structure determined for the solid (6), in that a single set of peaks is seen for the two equivalent coordinated imidazoles. However, the *cis* isomer and aquation products could produce a similar spectrum. As a check, complex **1** was dissolved in water and acetone was added after 15 min. The IR spectrum of the precipitate was superimposable with that of **1** and its ^1H NMR spectrum showed only the original set of peaks, thereby making the possibility of isomerization, aquation, or imidazole loss during this period of time very unlikely.

Over a period of several hours, the signals of $[RuCl_4Im_2]^-$ decreased, while a set of peaks appeared for a new complex

Fig. 1. ^1H NMR spectra of complex **1** in D_2O immediately after dissolution *(a)*, after 22 h *(b)*, after 21 days *(c)*, and after 8.5 months *(d)*. Sharp peaks at 7.4 and 8.6 ppm for the ImH^+ ion not shown.

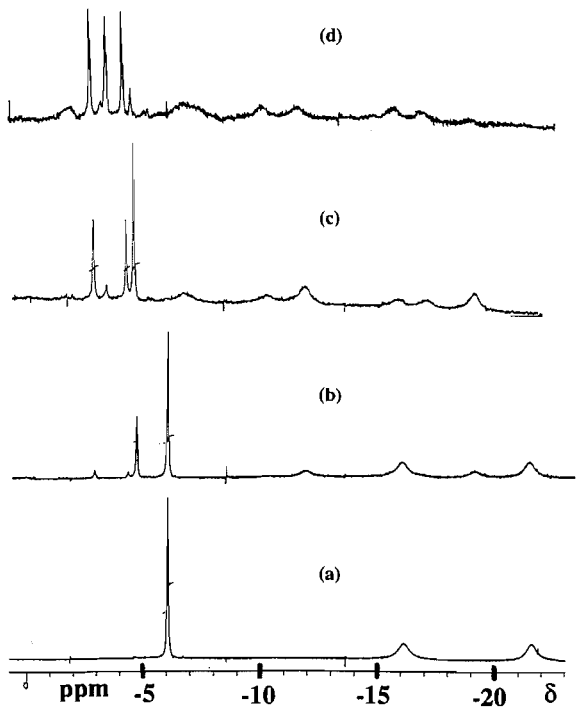

1a[4] (Fig. 1*b*). Both imidazole ligands should be retained, since the Ru—N bond with N-heterocycles is usually regarded as kinetically inert (19). Therefore, this single set of three peaks is attributable to two equivalent coordinated imidazole ligands. The narrowest peak (–4.7 ppm) is assigned to the remote H5 proton, whereas the other two broad peaks (–19.2 and –12.0 ppm) are assigned to the H2 and H4 protons, respectively, from deuteration experiments.

This new species is either *cis*-$[RuCl_4Im_2]^-$ or a $[RuCl_3$-

[4] This and all other "aqua" species discussed in this paper can behave as weak acids and they exist at equilibrium as a mixture of the Ru-OH and Ru-OH_2 forms.

Can. J. Chem. Downloaded from www.nrcresearchpress.com by 65.111.164.53 on 09/08/12
For personal use only.

Table 3. ^{1}H NMR data

Complex	H2	H4	H5	N1-CH_3
		(ImH)[$RuCl_4Im_2$] (1)		
D_2O solution				
1	−21.4	−16.0	−5.7	
1a	−19.2	−12.0	−4.7	
1b	−17.1	−10.4	−4.4	
	−16.0	−6.9	−3.1	
1c	−11.7	−7.0	−3.7	
CD_3OD solution				
1	−19.6	−18.1	−6.9	
1d	−14.7	−14.4	−5.1	
DMSO-d_6 solution				
1	−18.5	−17.2	−7.6	−2.6 (N–H)
1e	−17.5	−13.5	−2.0	0.6 (N–H)
		(4-MeImH)[$RuCl_4$(5-MeIm)$_2$] (2)		
D_2O solution				
2	−24.1	−14.2	−0.2 (CH_3)	
2a	−22.2	−9.6	2.3 (CH_3)	
2b	−20.5	−7.9	2.1 (CH_3)	
	−18.8	−3.8	2.0 (CH_3)	
		(1-MeImH)[$RuCl_4$(1-MeIm)$_2$] (3)		
D_2O solution				
3	−21.2	−16.7	−6.6	1.4
3a	−18.6	−12.4	−5.3	3.80
3b	−15.0	−7.2	−3.3	3.85
	−16.1	−10.4	−4.6	3.90

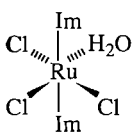

1a

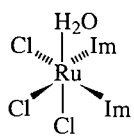

1a1

(D_2O)Im_2] molecule, resulting from the substitution of a chloro ligand by water. The latter possibility is preferred on the basis of experiments in the presence of KCl described below. There exist three possible isomers of [$RuCl_3(D_2O)Im_2$], but only **1a** and **1a1** are consistent with the presence of a single set of NMR signals for coordinated imidazole. No direct evidence for a particular geometry could be obtained. Addition of acetone at this or a later stage gave no precipitate. When the solvent was removed in vacuo at ~60°C, only (ImH)[$RuCl_4Im_2$] (**1**) was obtained. Solubility was not high enough to obtain good solution Raman data. Considering that the conversion of **1a** leads only to **1** when solvent is removed or KCl is added and that no extra signals are detected for a hypothetical *cis*-[$RuCl_4Im_2$]$^-$ species, for instance, the *trans* form **1a** is preferred. Keppler et al. (3) monitored the appearance of this species by HPLC and they also proposed the *trans* structure, which has been observed in the crystal structure of the related [$RuCl_3(H_2O)$(1-methylindazole)$_2$] complex.

After several days, the spectrum (Fig. 1*c*) contains two new sets of three peaks associated with coordinated imidazole (Table 3). Those at −16.0, −6.9, −3.1 ppm are assigned to one type of Im ligands and those at −17.1, −10.4, −4.4 ppm to another type, although some of the signals could be interchanged, since both sets have the same intensity and grow at the same rate. They likely correspond to new substitution products [$RuCl_2(D_2O)_2Im_2$]$^+$, of which two isomers **1b1** (*trans,cis,cis*) and **1b2** (*trans,trans,trans*) contain *trans* imidazoles (Scheme 1).[5] Formation of two species at the same rate is surprising, but a similar case has recently been found with a Ru(III) complex of 9-methylhypoxanthine (20). Keppler et al. (3) noted the formation of a diaqua species, but stereoisomers were not mentioned. These authors also found that **1a** is attacked by free imidazole to generate *mer*-[$RuCl_3Im_3$]. The latter species, which contains two nonequivalent coordinated imidazoles in a 2:1 ratio, is not detected in our conditions.

Over a period of months, a new species **1c** progressively

[5] **Noted added in proof:** The first two aquation steps in Scheme 1 have also been observed for (ImH)[$RuCl_4Im_2$](**1**) in a very recent study by Dhubhgaail et al.(41).

Can. J. Chem. Downloaded from www.nrcresearchpress.com by 65.111.164.53 on 09/08/12
For personal use only.

Scheme 1

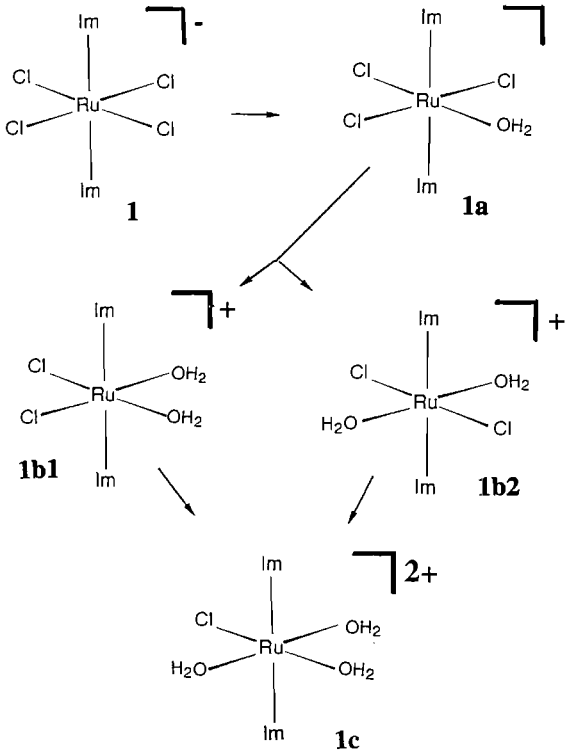

appears. After 8.5 months (Fig. 1*d*), **1a**, **1b1**, and **1b2** are still present, but **1c** accounts for ~30% of the intensity in the paramagnetic region. Complex **1c** gives a sharp H5 signal at −3.7 ppm. The corresponding signals for H2 and H4 probably occur at −7.0 and −11.7. The new species **1c** containing only one type of imidazole should be $[RuCl(D_2O)_3Im_2]^{2+}$, produced by further aquation of both **1b1** and **1b2**. In the meantime, some decomposition has occurred, producing a few black particles and a small amount of Ru(II) species giving sharp low-intensity peaks in the diamagnetic region.

A comment should be made here concerning the control of pH in these experiments. Buffers were not used, in order to prevent any interference by coordination of the buffer material to the metal centre over the long periods of time the systems were monitored. The pH of a fresh 0.01 M solution of **1** decreased from 5.0 to ~3.2 during the first few days and then remained constant indefinitely. Thus, the system buffered itself to ~3.2 as the initial aquation process was taking place. Since N-H groups of coordinated imidazole are very weakly acidic (pK_a of 8.9 for $[Ru(NH_3)_5Im]^{3+}$) (21), this acidity must originate from partial conversion of coordinated water molecules into hydroxo groups. The proportions of the Ru-OH_2 and Ru-OH forms cannot be established at the present time, since the two forms are in fast exchange on the NMR time scale and individual pK_a values were not determined. From the observed pH, the behavior of the **1a+1b1+1b2** mixture can be regarded as similar to that of a weak acid of pK_a ~4.4, which is consistent with the acidities found for related aqua-Ru(III) species (5, 22).

Methylated imidazoles

Literature methods, adjusted as above for complex **1**, were used to prepare the analogues with 1-MeIm and 4(5)-MeIm. Both complexes showed the usual ν(Ru–Cl) and ν(Ru–N) absorptions (6) at ~317(s)/~285(m) and ~250(w) cm^{-1}, respectively. In both cases, extra bands appear for the methyl groups. For (1-MeImH)$[RuCl_4(1\text{-MeIm})_2]$, a weak band at 398 cm^{-1} probably originates from the δ(N–CH_3) mode in the coordinated ligand, which is known to shift from 355 cm^{-1} in free 1-MeIm to ~385 cm^{-1} in $CuCl_2(1\text{-MeIm})_2$ (23) and $[ReO_2(1\text{-MeIm})_4]^+$ (24). Since this vibration is not sensitive to protonation (25), the very weak component at ~350 cm^{-1} should be due to the $(1\text{-MeImH})^+$ counter ion. In the 4(5)-MeIm compound, the low-frequency ν(Ru–Cl) band at 290 cm^{-1} should include a contribution of the γ(C–CH_3) mode, which occurs at this frequency for the $[ReO_2L_4]^+$ complex (24) and the protonated form (25). The δ(C–CH_3) mode of the 4-MeImH^+ ion shows at 335 cm^{-1}, where it is expected, whereas the weak peak at 385 cm^{-1} is likely due to the same mode shifted from ~350 cm^{-1} by coordination as in the previous case.

The aqueous solution chemistry of (4-MeImH)$[RuCl_4(5\text{-MeIm})_2]$ (**2**) and (1-MeImH)$[RuCl_4(1\text{-MeIm})_2]$ (**3**) mimics that of complex **1** exactly as described above: the same pattern and progression was seen in the NMR spectra over a period of weeks (Figs. S1-1 and S1-2).[3] The chemical shifts are listed in Table 3. The absence of extra sets of peaks for the 4(5)-MeIm system is interesting, since it shows that the ligand is always coordinated as the same tautomer, that is, the 5-MeIm form found in the solid state (6).

Reaction of 1 in the presence of KCl

A fresh solution of complex **1** (0.015 M) in the presence of 0.12 M KCl gave the same spectrum as in pure D_2O and the subsequent steps leading to **1a**, **1b1**, and **1b2** were not inhibited by KCl. They took place along exactly the same pattern, at a slightly slower rate than in the absence of KCl, but the **(1b1+1b2)/1a** ratio after 2 weeks was somewhat lower than in the KCl-free solution after the same time. As expected, this ratio progressively decreased as the KCl (or NaCl) concentration increased to 1.5 M and 6 M.

The reaction is reversible and can be driven in the opposite direction by increasing the chloride concentration. When KCl was added to an aged KCl-free solution or the KCl concentration was increased in an equilibrated solution, the final mixture was the same as when all the KCl had been added to the fresh solution. From a set of four solutions containing **1** (0.005–0.015 M) and NaCl (1–6.3 M) under equilibrium conditions, an "apparent" constant K_1, valid at the equilibrium pH of 3.2, could be determined for the first aquation step (eq. [1]) (Table S1-1).[3] Equilibrium constants for the next steps could not be obtained, because months are sometimes needed to reach equilibrium and, by that time, side reactions have occurred.

[1] $\mathbf{1} \rightleftharpoons \mathbf{1a} + Cl^-$

$K_1 = [\mathbf{1a}][Cl^-]/[\mathbf{1}] = 3.4 \pm 0.4\ M^{-1}$

Thus, as mentioned earlier (10), no appreciable change is noted in physiological saline solution after 1 h, but, a few hours after dissolution, aquation of **1** has taken place to a significant extent and it cannot be prevented even in 6 M NaCl. Reversibility to Cl^- supports the above interpretation in terms of successive aquation reactions with Cl^- displacement, thereby ruling out simple isomerization.

Can. J. Chem. Downloaded from www.nrcresearchpress.com by 65.111.164.53 on 09/08/12
For personal use only.

Fig. 2. ^{1}H NMR spectra of complex **1** in CD_3OD solution immediately after dissolution *(a)* and after 24 h *(b)*; * = solvent, water, and impurity (~1 ppm).

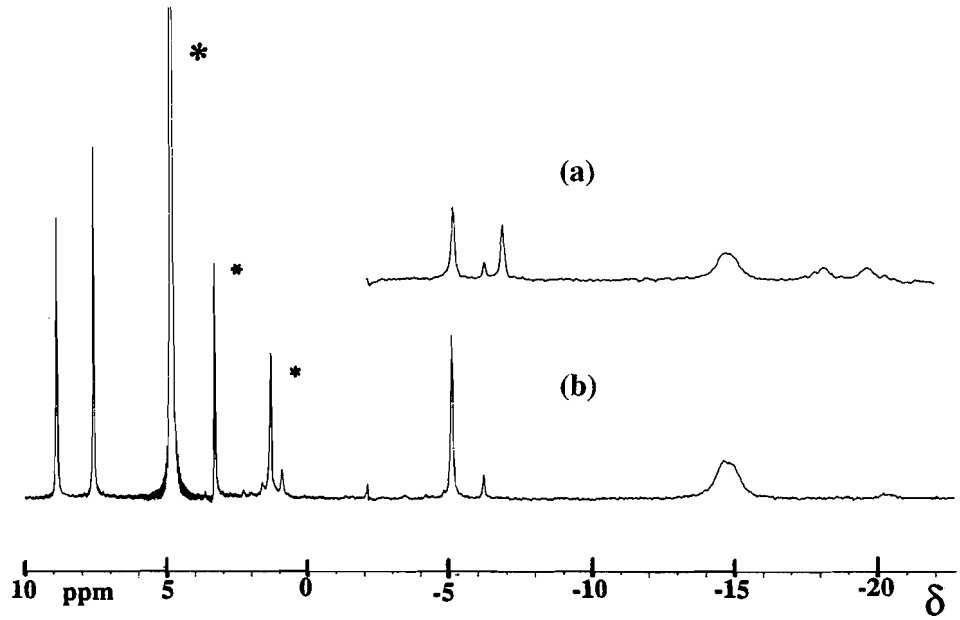

Solutions of 1 in CD_3OD

Besides the sharp signals at 8.9 and 7.6 ppm for the imidazolium ion, two unequal sets of high-field imidazole peaks are initially observed at room temperature (Fig. 2 and Table 3), corresponding to two species each containing equivalent imidazole ligands. One species is derived from the other, as evidenced from one set (−5.1, −14.7, and −14.4 ppm) increasing with time at the expense of the other (−6.9, −18.1, and −19.6 ppm). For the earlier peaks, the chemical shifts are not very different from those of **1** in water and they are assigned to $[RuCl_4Im_2]^-$. By analogy with water solutions, the other set of peaks is assumed to be due to the monosolvent species $[RuCl_3(CD_3OD)Im_2]$, **1d**, corresponding to the monoaqua complex **1a**. Examples of Ru(III) complexes containing coordinated methanol are known (20, 26).

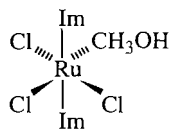

1d

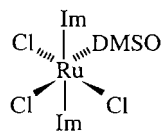

1e

Conversion into **1d** was complete within 24 h at room temperature and the spectrum remained unchanged over a period of several days. At low temperature, conversion was much slower. A solution of **1** was prepared at −50°C and spectra were taken as it was progressively allowed to warm up to 40°C over a period of 4 h. The signals showed a regular downfield shift with temperature (Fig. S1-3), as commonly found in paramagnetic systems (12), but signal correspondence with earlier results was readily made via the spectrum at 25°C. The fresh solution at −50°C showed only the peaks for **1**. The second species **1d** began to appear at 0°C and, as the solution was heated up further to 40°C, it kept growing while **1** disappeared. After allowing the reaction to go to completion (1 day), cooling this sample down to 0°C did not regenerate **1**. Therefore, higher temperature increased the rate of conversion, but did not affect appreciably the equilibrium position.

When the solution of **1** was left at room temperature for 7 days, two very weak peaks (<5%) appeared at −6 and −8 ppm, respectively. They increased only very slowly during the next 2 weeks, while the colour of the solution changed from yellow to dark orange because of decomposition to unidentified products. Therefore, any subsequent reaction is slow at this temperature in methanol.

Attempts were made to isolate solids from fresh or aged solutions. Adding acetone gave no precipitate. When the solvent was removed in vacuo at room temperature or by mild heating, reconversion to **1** took place, even if the solution had aged for several days. The ^{1}H NMR spectra both in D_2O and in CD_3OD were identical with those initially found for **1** in these solvents.

Thus, solvolysis in methanol is faster than in water, but it stops at an earlier stage: conversion of **1d** into a $[RuCl_2(CD_3OD)_2Im_2]^+$ species similar to **1b** could not be observed.

Solutions of 1 in DMSO

The ^{1}H NMR spectrum of **1** in DMSO has been reported, but has been neither thoroughly analyzed, nor fully assigned (10). Figure 3*a* shows three imidazolium peaks with the expected 2:1:2 ratio: 14.3 ppm (N-H), 9.1 ppm (H2), and 7.7 ppm (H4/H5). Four peaks attributed to coordinated imidazole are assigned by analogy to the spectrum in D_2O: −7.6 ppm (narrowest, H5), −2.6 ppm (N-H, not seen in D_2O), −17.2 ppm (H4), and −18.5 ppm (H2).

To make sure that the initial species was the unchanged $[RuCl_4Im_2]^-$ ion, a solution of **1** was prepared at −5°C and its ^{1}H NMR spectrum was recorded at this temperature, where any solvolysis or isomerization processes should be retarded, as noted in CD_3OD. Spectra were also taken while the temper-

Fig. 3. ^{1}H NMR spectra of complex **1** in DMSO-d_6 solution immediately after dissolution *(a)* and after 6 days *(b)*; * = solvent and water.

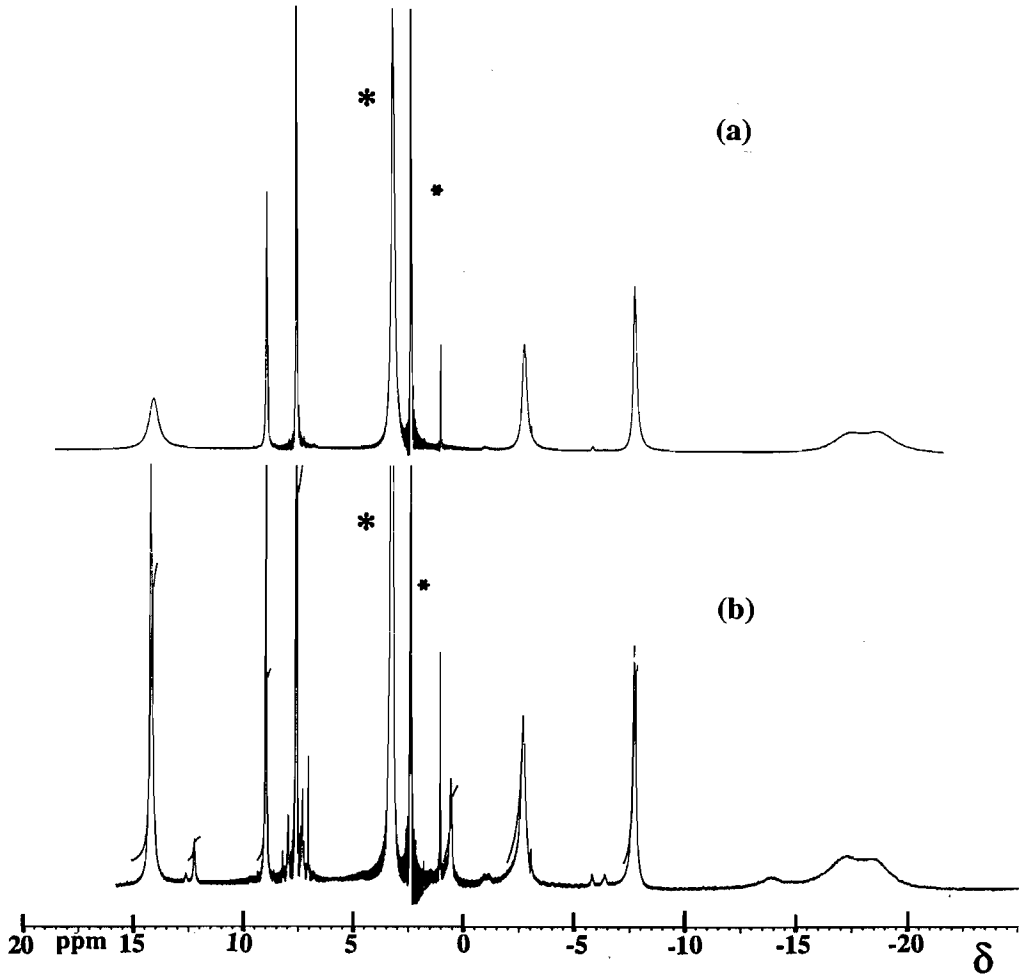

Can. J. Chem. Downloaded from www.nrcresearchpress.com by 65.111.164.53 on 09/08/12
For personal use only.

ature was raised over a period of 4 h to 25°C by steps of 5°. The peaks showed the regular shift as temperature increased, typical of this paramagnetic system, but the same single set of peaks was seen at all temperatures (Fig. S1-4).[3] An orange-brown powder precipitated when acetone was added to a fresh solution. Single crystals of the same material appeared within several hours when a layer of acetone was poured onto the solution and the system was left at 5°C. They were shown by X-ray diffraction (see experimental section) to be $(ImH)[RuCl_4Im_2]\cdot$ 2DMSO containing the same *trans*-$[RuCl_4Im_2]^-$ and ImH^+ ions as the solvent-free crystals (6). When lattice solvent was removed by extensive pumping in high vacuum, both the powder and the crystals gave the same IR spectrum and the same ^{1}H NMR spectra in DMSO-d_6 and D_2O, which were also identical with those of the starting material **1**. Therefore, the species initially present in DMSO is *trans*-$[RuCl_4Im_2]^-$.

This species has a good kinetic stability, since it remains dominant for several days at room temperature. After 6 days (Fig. 3*b*), it still accounts for 75% of the spectral intensity. A new species **1e** gives peaks (20%) in the paramagnetic region, at −13.5 (H4) and 0.6 ppm (probably N-H). Its H5 resonance likely contributes to the peak of **1** at −17.2 ppm, which has become stronger than the −18.5 ppm component. According to the integration, the N-H resonance of **1** at −2.6 ppm includes a contribution from **1e** (probably H2). This new product **1e** is believed to be $[RuCl_3(DMSO)Im_2]$, where a Cl^- ligand has been substituted by a probably S-bonded DMSO molecule. This species is assumed to be similar to the corresponding $[RuCl_3(D_2O)Im_2]$ complex **1a** formed in water. The spectrum also shows very small peaks (< 5%) for the imidazole protons of a diamagnetic species **1f** at 12.5 (well resolved, N-H), 8.05, 7.41, and 7.13 ppm (tails of strong imidazolium peaks at 7.7 ppm). Any DMSO present in the complex would not be detected, since the reaction takes place in DMSO-d_6.

After 12 days, **1** and **1e** represent 51 and 25% of the intensity, respectively. The contribution of **1f** has increased to 15%, whereas another diamagnetic species **1g** (δ 12.9 (N-H), 8.25, 7.45, and 7.28 ppm), barely visible in the previous spectrum, has become more significant (9%). Within ~2 weeks, yellow crystals of *trans,trans,trans*-$[RuCl_2(DMSO)_2Im_2]$ (see X-ray diffraction work below) became visible. The peaks due to both Ru(III) products were still present over many weeks, indicating that the overall conversion to the diamagnetic products **1f** and **1g** is very slow. The crystals did not redissolve readily in DMSO: stirring for 1–2 weeks gave a solution whose very weak ^{1}H NMR signals matched exactly those of **1g**.

These observations can be reasonably explained by the fol-

Can. J. Chem. Downloaded from www.nrcresearchpress.com by 65.111.164.53 on 09/08/12
For personal use only.

lowing pathway. The first step would be a reduction of $[RuCl_3(DMSO)Im_2]$ (**1e**) to $[RuCl_3(DMSO)Im_2]^-$ (which would be **1f**), followed by substitution of a Cl^- ligand by DMSO to give $[RuCl_2(DMSO)_2Im_2]$ (to be labelled **1g**), which would then crystallize out. Reduction of Ru(III) to Ru(II) in DMSO is well documented: $[RuCl_2(DMSO)_4]$ is thought to be formed via $[RuCl_4(DMSO)_2]^-$ and $[RuCl_3(DMSO)_3]$, reduction being effected by the solvent itself oxidizing to the sulfone (27). Reduction of Ru(III) to Ru(II) is known to take place readily when more than one π-accepting sulfoxide ligand is coordinated, and the complex becomes increasingly reducible with each new DMSO ligand introduced in the coordination sphere. Owing to the large *trans* effect of DMSO, the Cl^- ligand displaced in $[RuCl_3(DMSO)Im_2]^-$ should be *trans* to the DMSO already present, leading to the *trans-trans-trans* geometry observed in the solid.

An alternate scenario cannot be totally ruled out. Compound **1e** could first undergo a second solvolysis and form $[RuCl_2(DMSO)_2Im_2]^+$, which would be immediately reduced to $[RuCl_2(DMSO)_2Im_2]$ (which would be **1f**) crystallizing out slowly. Several possibilities would then exist for the other diamagnetic species **1g** derived from **1f**: further solvolysis to $[RuCl(DMSO)_3Im_2]^+$, isomerization to a species with imidazoles and (or) DMSO in *cis* arrangements (a geometry reported to be more stable for $RuCl_2(DMSO)_4$) (28)), or even aquation with water slowly leaking into the NMR tube. This pathway is believed to be less likely, since unusual dissolution kinetics would have to be assumed to explain that the above saturated solution of the crystals in DMSO gives no ^1H NMR signals for $[RuCl_2(DMSO)_2Im_2]$ itself, but only those of the derived species. Furthermore, $[RuCl_2(DMSO)_2Im_2]^+$would have to reduce so quickly as to not be detected in solution: reduction is much slower in related systems (27).

The crystals of *trans,trans,trans*-$[RuCl_2(DMSO)_2Im_2]$ are not very soluble in D_2O. Overnight stirring gives a solution whose NMR spectrum shows imidazole peaks at 7.26, 7.30, and 8.04 ppm, in the range previously published for Ru(II)–imidazole complexes (29). The DMSO resonance expected at 2.7–3.4 ppm is not visible because the sample has been obtained from DMSO-d_6. No peaks are seen outside the 0–10 ppm range, thus confirming the absence of Ru(III) products here. The species actually present in solution is probably not intact $[RuCl_2(DMSO)_2Im_2]$, but the aquation product $[RuCl(H_2O)(DMSO)_2Im_2]^+$, since aquation is relatively fast for similar systems containing *trans* DMSO (5, 29).

Crystal structure of $[RuCl_2(DMSO\text{-}d_6)_2Im_2]$

$(ImH)[RuCl_4Im_2]$ (**1**) was dissolved in a DMSO-d_6–acetone mixture by gently heating for 15 min. The yellow rectangular prisms, which were used for X-ray work, appeared within 2 days. The same crystals were obtained only after several weeks from pure DMSO solution.

The unit cell contains two approximately octahedral *trans,trans,trans*-$[RuCl_2(DMSO)_2Im_2]$ molecules (Fig. 4). Related $RuCl_2(DMSO)_2L_2$ complexes have been isolated from reaction of *cis*-$RuCl_2(DMSO)_4$ with 1-MeIm or 2-MeIm, but they are believed to be of the all-*cis* configuration (30).[6]

Since the metal is sitting on crystallographic inversion centres, all *trans* angles in the present compound are within 2.5°

[6] Also, B.R. James, private communication.

Fig. 4. ORTEP drawing of *trans,trans,trans*-$[RuCl_2(DMSO)_2Im_2]$. The Ru atom occupies a crystallographic inversion centre. Ellipsoids correspond to 50% probability. Hydrogens are omitted for simplicity.

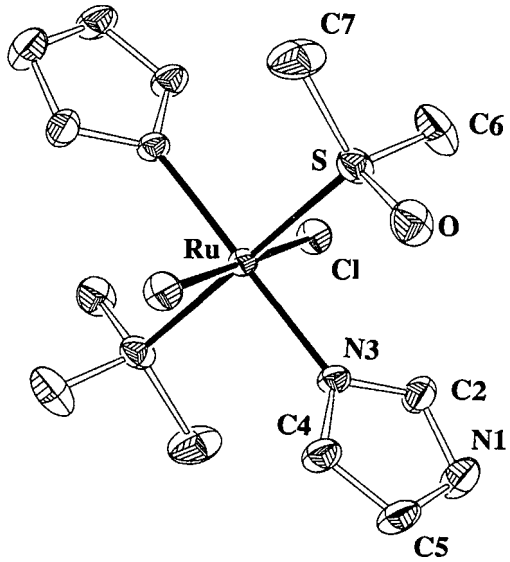

of the ideal 90° value (Table 4). DMSO is S-bonded and its Ru—S bond length (2.290(1) Å) is slightly shorter than observed in $RuX_2(DMSO)_4$ (2.353(1) Å for X = Cl (31), 2.352(2) Å for X = Br (28)), probably because two of the DMSO ligands are replaced here by less sterically demanding imidazoles. Our Ru—Cl distance (2.416(1) Å) compares well with those found for mutually *trans* Ru—Cl bonds in Ru(II) compounds (2.40–2.43 Å) (28, 29, 31), this bond being ~0.06 Å shorter in Ru(III) compounds (6, 27, 31, 32). The Ru-N distance of 2.105(4) Å is somewhat longer than found in the $[RuCl_4Im_2]^-$ ion (2.079(3) Å), which reflects the change in oxidation state and greater steric demand of DMSO. The geometry of the DMSO and imidazole ligands is normal. The imidazole ring is planar within 0.005 Å (1σ), but the Ru—N bond does not lie exactly in this plane (Ru-to-plane distance = 0.056(8) Å).

Each imidazole N-H proton forms a bifurcated hydrogen bond with a chlorine and a DMSO oxygen of a neighbouring molecule in the unit cell (Fig. 5). The N···Cl and N···O separations (3.323(4) and 2.790(6) Å, respectively) are typical of these types of interactions (33). The molecule participates in four such hydrogen bonds as donor or as acceptor. Other intermolecular contacts correspond to normal van der Waals interactions.

The infrared spectrum of *trans,trans,trans*-$[RuCl_2(DMSO)_2Im_2]$ is distinctly different from those of the complexes discussed above. Peak doubling due to the presence of both coordinated and protonated imidazoles is no longer present. The ν(S–O) mode of DMSO is identified at 1057 cm^{-1}, in agreement with S-bonding (27, 31). A hydrogen-bonded ν(N–H) band is also seen at 3242 cm^{-1}. In the 600–200 cm^{-1} region, the spectrum is assigned with the aid of data for Ru(III) compounds (6) and the related Ru(II) complex *trans,cis,cis*-$[RuCl_2(DMSO)_2Im_2]$ (29). The Ru–N and Ru–S stretching modes are assigned at 240 and 392 cm^{-1}, respec-

Can. J. Chem. Downloaded from www.nrcresearchpress.com by 65.111.164.53 on 09/08/12
For personal use only.

Table 4. Interatomic distances and bond angles in $[RuCl_2(DMSO)_2Im_2]$

Atoms	Distance (Å)	Atoms	Distance (Å)
Ru–Cl	2.416(1)	N(1)–C(2)	1.341(6)
Ru–N(3)	2.105(4)	N(1)–C(5)	1.350(7)
Ru–S	2.290(1)	C(2)–N(3)	1.319(6)
S–O	1.470(4)	N(3)–C(4)	1.370(6)
S–C(6)	1.798(5)	C(4)–C(5)	1.355(7)
S–C(7)	1.790(6)		
Atoms	**Angles (deg)**	**Atoms**	**Angle (deg)**
Cl–Ru–S	87.55(4)	C(6)–S–C(7)	99.1(3)
Cl–Ru–N(3)	89.76(11)	Ru–N(3)–C(2)	126.9(3)
S–Ru–N(3)	88.16(11)	Ru–N(3)–C(4)	126.8(3)
Ru–S–O	119.0(2)	C(2)–N(3)–C(4)	106.2(4)
Ru–S–C(6)	112.6(1)	N(1)–C(2)–N(3)	110.2(5)
Ru–S–C(7)	110.8(2)	C(2)–N(1)–C(5)	108.3(4)
O–S–C(6)	106.0(3)	N(3)–C(4)–C(5)	109.1(5)
O–S–C(7)	107.4(3)	N(1)–C(5)–C(4)	106.3(5)

Fig. 5. Hydrogen bonds (thin lines) between the *trans,trans,trans*-$[RuCl_2(DMSO)_2Im_2]$ in the unit cell. Atoms can be identified by comparison with Fig. 4. Hydrogen atoms are omitted for simplicity.

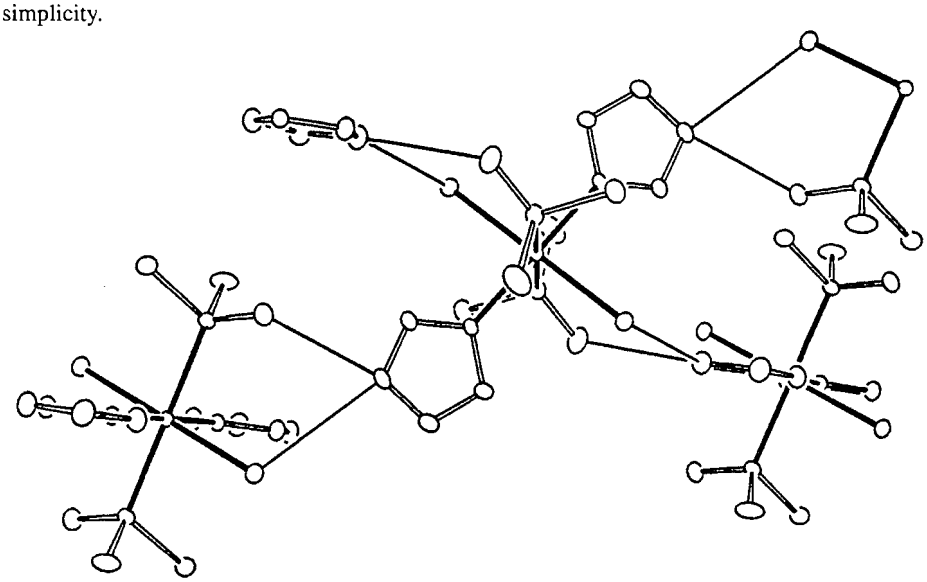

tively, whereas the ν(Ru–Cl) bands at 351 and 362 cm^{-1} occur at relatively high frequency.

Discussion

Solvolysis of $[RuCl_4Im_2]^-$ could be followed by means of ^1H NMR spectroscopy in water, methanol, and DMSO, in spite of the presence of the paramagnetic Ru(III) centre. The imidazole peaks are broad but not exaggeratedly so, the various resonances are spread over a large but limited range, and the chemical shifts of the various species are sufficiently different to allow the appearance and disappearance of successive species to be followed. The present complexes make a homogeneous series and the signals are found to undergo regular downfield shifts as the Cl^- ligands are successively replaced by solvent molecules.

The initial species observed in the NMR spectra has half-lives of 1–2 h in CD_3OD, ~3 days in D_2O, and ~2 weeks in DMSO. Ru(III) complexes are generally regarded as kinetically inert, especially compared to the Ru(II) analogues (19). However, chloride-rich systems are expected to react relatively quickly, since the low position of Cl^- in the spectrochemical series decreases the barrier for substitution (34). For instance, $[RuCl_6]^{3-}$ and $[RuCl_5(H_2O)]^{2-}$, which are thermodynamically stable only at very high Cl^- concentrations, aquate in seconds when dissolved in H_2O (35). Considering that these species are very labile, it was first checked that the complex initially observed in our NMR spectra was still the $[RuCl_4Im_2]^-$ ion present in the solid. This was confirmed by reprecipitation from solution in which later signals had not yet appeared. In the three solvents, the precipitate obtained was the initial $(ImH)[RuCl_4Im_2]$ salt (isolated as a solvate for

Can. J. Chem. Downloaded from www.nrcresearchpress.com by 65.111.164.53 on 09/08/12
For personal use only.

DMSO), thereby confirming that chloride is not lost instantaneously in these solvents.

Our results in D_2O indicate that replacing two water molecules by imidazole in the coordination sphere does not drastically affect the behaviour of the remaining coordinated chlorides. Indeed, from the equilibrium constants available (35, 36), it can be predicted that a solution $[RuCl_6]^{3-}$ should undergo successive aquation reactions and, at the concentration level used for our NMR work ($\sim 5\times10^{-3}$ M), $[RuCl(H_2O)_5]^{2+}$ should be the major component at equilibrium. The rate of aquation decreases regularly as chlorides are displaced: $[RuCl_4(H_2O)_2]^-$ (for which kinetic data are still missing) should aquate relatively quickly; the half-life of $[RuCl_3(H_2O)_3]$ has been found to be ~45 days and that of $[RuCl(H_2O)_5]^{2+}$ has been estimated to be >1 year (35). A similar pattern is found here for the Im system: the half-lives increase regularly from $[RuCl_4Im_2]^-$ (~3 days) to $[RuCl_3(H_2O)Im_2]$ (~21 days) to $[RuCl_2(H_2O)_2Im_2]^+$ (~4 months), and the final product is again the monochloro ion $[RuCl(H_2O)_3Im_2]^{2+}$. For the first aquation process, the rate observed here corresponds well with that reported by Keppler et al. (3), who related the slow binding to biological substrates in fresh solutions of (ImH)$[RuCl_4Im_2]$ to the formation of the monoaqua species, which would actually be the active form.

Although the composition of the various species in solution has been identified, their stereochemistry is less certain. For instance, the *cis,fac*-$[RuCl_3(H_2O)Im_2]$ isomer would also be consistent with the single set of resonances observed for **1a**, whereas the two equal sets of signals, assigned to different isomers **1b1** and **1b2**, could also arise from nonequivalent imidazoles in the *cis,cis,cis*-$[RuCl_2(H_2O)_2Im_2]$ isomer. Such possibilities cannot be ruled out, but their formation in the **1**–**1a**–**1b** interconversion sequence, which is reversible to Cl^-, would imply that a change of configuration takes place quantitatively and reversibly at one step. This model appears to be unlikely, considering that equilibrium and kinetic data on the chloro-aqua system indicate that both isomers of $[RuCl_3(H_2O)_3]$ and of $[RuCl_2(H_2O)_4]^+$ have comparable stabilities and are not quickly interconverted (35). Unfortunately, we were unable to isolate the solvolyzed Ru(III) compounds as solids. Only in the case of DMSO was it possible to isolate suitable crystals of a final Ru(II) product, in which the *trans* imidazole arrangement present in the starting product was found to have been retained.

Aquation under nonbasic conditions is generally assumed to occur by a predominantly dissociative mechanism, which is thought to be followed in the case of $[Ru(NH_3)_5Cl]^{2+}$ (37). Relatively slow solvolysis observed for the related $[RuCl_4(5\text{-nitroimidazole})_2]^-$ ion (38), where the nitro group reduces electron density at the Ru(III) centre, would be consistent with this assumption. A dissociative process normally takes place via a five-coordinate intermediate, and a square-pyramidal intermediate is predicted for the present low-spin d^5 system since the loss of ligand–field stabilization is less than for a trigonal-bipyramidal intermediate (39). A square-pyramidal transition state should lead to retention of configuration, which is what is suggested by our study.

All species observed contain two coordinated imidazole ligands. No evidence for significant loss of coordinated imidazole could be obtained: none of the signal sets found for species derived from $[RuCl_5Im]^{2-}$ (16) were observed here and the imidazolium resonances did not show the shifts and (or) intensity changes expected if imidazole was liberated. Similarly, there is no evidence for the formation of the *mer*-$[RuCl_3Im_3]$ complex reported by Keppler et al. (3) to form concurrently with $[RuCl_2(H_2O)_2Im_2]^+$. This tris-imidazole complex would contain two nonequivalent Im ligands and give rise to two sets of signals (2:1 ratio). However, this complex has recently been detected during reactions run in the presence of excess imidazole (16). The absence of this species here could be ascribed to our relatively low pH. Our experiments were carried out without buffer and the pH was found to stabilize to ~3.2 early in the aquation process. Therefore, at this pH, imidazole is actually quenched in the protonated form (pK_a ~7) (40), making the amount of neutral Im ligand available to attack on the Ru(III) centre very small. Buffered solutions of higher pH, such as those used by Keppler (pH = 7.0–7.4, carbonate buffer) should provide more favourable conditions for the appearance of this compound.

Acknowledgments

We wish to thank M. Simard and F. Bélanger-Gariépy for assistance with the crystallographic part of this work, as well as J.D. Wuest and J. Vaugeois for access to the FTIR instrument. The financial support of the Natural Sciences and Engineering Research Council of Canada is gratefully acknowledged.

References

1. M.J. Clarke. Met. Ions Biol. Syst. **11**, 231 (1980).
2. M.J. Clarke. Platinum, gold and other chemotherapeutic agents. ACS Symp. Ser. **209**, 335 (1983).
3. B.K. Keppler, K.-G. Lipponer, B. Stenzel, and F. Kratz. *In* Metal complexes in cancer chemotherapy. *Edited by* B.K. Keppler. VCH, Weinheim. 1993. p. 187.
4. N. Farrell. Transition metal complexes as drugs and chemotherapeutic agents. Kluwer Academic, Dordrecht. 1989. Chap. 6.
5. P.K.L. Chan, P.K.H. Chan, D.C. Frost, B.R. James, and K.A. Skov. Can. J. Chem. **66**, 117 (1988).
6. B.K. Keppler, W. Rupp, U.M. Juhl, H. Endres, R. Niebl, and W. Balzer. Inorg. Chem. **26**, 4366 (1987); B.K. Keppler, D. Wehe, H. Endres, and W. Rupp. Inorg. Chem. **26**, 844 (1987).
7. J. Souček. Collect. Czech. Chem. Commun. **27**, 960 (1962).
8. E. Holler, W. Schaller, and B. Keppler. Arzneim.-Forsch. **41**, 1065 (1991).
9. F. Kratz, M. Hartmann, B. Keppler, and L. Messori. J. Biol. Chem. **269**, 2581 (1994).
10. B.K. Keppler, M. Henn, U.M. Juhl, M.R. Berger, R. Niebl, and F.E. Wagner. Prog. Clin. Biochem. Med. **10**, 41 (1989).
11. M.J. Clarke. Prog. Clin. Biochem. Med. **10**, 25 (1989).
12. I. Bertinti and C. Luchinat. NMR of paramagnetic molecules in biological systems. Benjamin-Cummings, Menlo Park, Calif. 1986; G.N. La Mar. NMR of paramagnetic molecules. *Edited by* W. De Horricks, Jr. and R.H. Holm. Academic Press, New York. 1973.
13. H. Toi, G.N. La Mar, R. Margalit, C.M. Che, and H.B. Gray. J. Am. Chem. Soc. **106**, 6213 (1984).

14. E. Alessio, G. Balducci, A. Lutman, G. Mestroni, M. Calligaris, and W.M. Attia. Inorg. Chim. Acta, **203**, 205 (1993).
15. T. Bora, M. Devi, and P.K. Gogoi. Transition Met. Chem. (Weinheim, Ger.) **11**, 467 (1986).
16. C. Anderson and A.L. Beauchamp. Inorg. Chem. Submitted.
17. E.J. Gabe, Y. Le Page, J.P. Charland, and F.L. Lee. J. Appl. Crystallogr. **22**, 384 (1989).
18. F. Králík and J. Vřeštál. Collect. Czech. Chem. Commun. **26**, 1298 (1961).
19. E.A. Seddon and K.R. Seddon. The chemistry of ruthenium, Elsevier, Amsterdam. 1984.
20. M. Leduc and A.L. Beauchamp. In preparation.
21. M.F. Hoq and R.E. Shepherd. Inorg. Chem. **23**, 1851 (1984).
22. Z. Harzion and G. Navon. Inorg. Chem. **19**, 2236 (1980).
23. C. Perchard and A. Novak. J. Chim. Phys. **65**, 1964 (1968).
24. S. Bélanger and A.L. Beauchamp. In preparation.
25. A.M. Bellocq and C. Garrigou-Lagrange. J. Chim. Phys. **66**, 1511 (1969); **67**, 951 (1970).
26. J. Dehand and J. Rose. Inorg. Chim. Acta, **37**, 249 (1979).
27. E. Alessio, G. Balducci, M. Calligaris, G. Costa, W.M. Attia, and G. Mestroni. Inorg. Chem. **30**, 609 (1991).
28. E. Alessio, G. Mestroni, G. Nardin, W.M. Attia, M. Calligaris, G. Sava, and S. Zorzet. Inorg. Chem. **27**, 4099 (1988).
29. M. Henn, E. Alessio, G. Mestroni, M. Calligaris, and W.M. Attia. Inorg. Chim. Acta, **187**, 39 (1991).
30. P.K.L. Chan. Ph.D. Dissertation, University of British Columbia, Vancouver. 1988.
31. J.S. Jaswal, S.J Rettig, and B.R. James. Can. J. Chem. **68**, 1808 (1990).
32. A.A. Batista, L.R.V. Olmo, G. Oliva, E.E. Castellano, and O.R. Nascimento. Inorg. Chim. Acta, **202**, 37 (1992).
33. G.H. Stout and L.H. Jensen. X-ray structure determination, a practical guide. MacMillan, London. 1968.
34. F. Basolo and R.G. Pearson. Mechanism of inorganic reactions. 2nd ed. Wiley, New York. 1967; J.D. Atwood. Inorganic and organometallic reaction mechanisms. Brooke/Cole Publishers, Monterey, Calif. 1985, and references therein.
35. R.E. Connick. *In* Advances in the chemistry of the coordination complexes. *Edited by* S. Kirschner. Macmillan, New York. 1961. p. 15.
36. M.M.T. Khan, G. Ramachandraiah, and A.P. Rao. Inorg. Chem. **25**, 665 (1986).
37. L.A.P. Kane-Maguire and G. Thomas. J. Chem. Soc. Dalton Trans. 1324 (1975).
38. C. Anderson and A.L. Beauchamp. Inorg. Chim. Acta. In press.
39. K.F. Purcell and J.C. Kotz. Inorganic chemistry. Saunders, Philadelphia. 1977. Chap. 13.
40. M.R. Grimmett. *In* Comprehensive heterocyclic chemistry. Vol. 5. *Edited by* A.R. Katritzki and C.W. Rees. Pergamon Press, Oxford. 1984. Chap. 4.06.
41. O.M.N. Dhubhghaill, W.R. Hagen, B.K. Keppler, K.-G. Lipponer, and P.J. Sadler. J. Chem. Soc. Dalton Trans. 3305 (1994).

Can. J. Chem. Downloaded from www.nrcresearchpress.com by 65.111.164.53 on 09/08/12
For personal use only.

Family-independent relationships between computed molecular surface quantities and solute hydrogen bond acidity/basicity and solute-induced methanol O–H infrared frequency shifts

Helena Hagelin, Jane S. Murray, Tore Brinck, Michel Berthelot, and Peter Politzer

Abstract: Family-independent relationships between computed molecular surface properties and solute hydrogen bond acidity/basicity and solute-induced methanol O–H infrared frequency shifts are presented. The molecular surface quantities, computed at the ab initio HF/6-31G* level, are primarily related to the electrostatic potential of the molecule, but also include the average local ionization energy on its surface.

Key words: hydrogen bond acidity/basicity, O–H frequency shifts, molecular electrostatic potential.

Résumé : On présente des relations indépendantes des familles entre d'une part les propriétés de surface moléculaire calculées et d'autre part l'acidité/basicité de la liaison hydrogène du soluté et les déplacements induits par le soluté de la fréquence infrarouge du O–H. Les quantités de surface moléculaire, calculées ab initio au niveau HF/6-31G*, sont principalement reliées au potentiel électrostatique de la molécule; elles comprennent toutefois la moyenne de l'énergie d'ionisation locale sur sa surface.

Mots clés : l'acidité/basicité de la liaison hydrogène, déplacements de la fréquence du O–H, potentiel électrostatique de la molécule.

[Traduit par la rédaction]

Can. J. Chem. Downloaded from www.nrcresearchpress.com by 65.111.164.53 on 09/08/12
For personal use only.

Introduction

In view of the well-established importance of the electrostatic component in hydrogen bonding (1–6), it is not surprising that the molecular electrostatic potential $V(\boldsymbol{r})$ has been found to be an effective means for analyzing and correlating such interactions (2, 7–9). In particular, we have shown that the hydrogen-bond-accepting tendencies (basicities) of solutes and solvents can be related to the most negative values of their electrostatic potentials, V_{min} (10, 11). Analogously, good relationships exist between solute and solvent hydrogen-bond-donating tendencies (acidities) and the most positive values of the potential on their molecular surfaces, $V_{S,max}$ (11, 12). However, these correlations are family dependent; different types of compounds (e.g., alcohols, azines, ethers, etc.) must be treated separately.

Our present objective is to demonstrate that this family dependence can be eliminated by improving the quality of the wave functions used to compute the electrostatic potential and, in the case of hydrogen bond acceptor molecules, by using surface electrostatic potential minima instead of spatial minima. We will also show that a general representation of the infrared O–H frequency shift, $\Delta\nu_{OH}$, which occurs when hydrogen bond acceptors complex with methanol, can be obtained using our General Interaction Properties Function (GIPF) approach (13, 14).

The GIPF provides a unified approach to correlating and predicting a variety of physicochemical properties that reflect molecular interactions (13, 14). The procedure involves representing each property in terms of some subset of a group of computed molecular quantities. Each resulting relationship is viewed as a special case of the GIPF described by eq. [1]:

$$[1] \qquad \text{Property} = f[\text{area}, \bar{I}_{S,min}, V_{S,max}, V_{S,min}, V_{min}, \Pi, \sigma^2_{tot}, \nu]$$

The quantities in brackets in eq. [1] are measures of various aspects of a molecule's interactive behavior; except for

Received September 20, 1994.

H. Hagelin, J.S. Murray, and P. Politzer.[1] Department of Chemistry, University of New Orleans, New Orleans, LA 70148, U.S.A.

T. Brinck. Department of Physical Chemistry, Royal Institute of Technology. 100 44 Stockholm, Sweden.

M. Berthelot. Laboratoire de spectrochimie moléculaire, Faculté des sciences et des techniques, Université de Nantes, 2, rue de la Houssinière, 44072 Nantes Cédex 03, France.

[1] Author to whom correspondence may be addressed. Telephone: (504) 286-6850. Fax: (504) 286-6860. Internet: papcm@uno.edu

Can. J. Chem. Downloaded from www.nrcresearchpress.com by 65.111.164.53 on 09/08/12
For personal use only.

surface area and $\bar{I}_{S,min}$, they are defined in terms of the electrostatic potential $V(\boldsymbol{r})$. The quantities relevant to the present study will be introduced and discussed in the next section.

Methods and procedures

The electrostatic potential $V(\boldsymbol{r})$ created in the space around a molecule by its nuclei and electrons is an effective tool for interpreting and predicting chemical reactive behavior, and has been found to be particularly well suited for the analysis of noncovalent interactions such as hydrogen bonding (9, 15–19). $V(\boldsymbol{r})$ is defined rigorously by eq. [2],

$$[2] \qquad V(\boldsymbol{r}) = \sum_{A} \frac{Z_A}{|\boldsymbol{R}_A - \boldsymbol{r}|} - \int \frac{\rho(\boldsymbol{r}')d\boldsymbol{r}'}{|\boldsymbol{r}' - \boldsymbol{r}|}$$

where Z_A is the charge on nucleus A, located at $\boldsymbol{R}_A$, and $\rho(\boldsymbol{r})$ is the molecular electronic density function. The sign of $V(\boldsymbol{r})$ in any particular region depends upon whether the effects of the nuclei or the electrons are dominant there. An approaching electrophile, such as a hydrogen to be donated in a hydrogen bond, will initially be attracted to those regions where $V(\boldsymbol{r})$ is negative, and particularly to the points where $V(\boldsymbol{r})$ has its most negative values (the local minima, V_{min}).

The use of the electrostatic potential to predict sites susceptible to nucleophilic attack is not as straightforward as for electrophilic attack, due to the fact that $V(\boldsymbol{r})$ maxima are found only at the positions of the nuclei (20). These reflect the magnitudes of the nuclear charges and cannot be assumed to indicate relative reactivities toward nucleophiles. However, we have demonstrated that the electrostatic potential maxima on the molecular surface ($V_{S,max}$), which are significantly removed from the nuclei, do reflect relative affinities for nucleophiles (12, 21, 22), and identify hydrogen-bond-accepting atoms.

The average local ionization energy, $\bar{I}(\boldsymbol{r})$, is defined in eq. [3] (23):

$$[3] \qquad \bar{I}(\boldsymbol{r}) = \sum_{i} \frac{\rho_i(\boldsymbol{r})|\varepsilon_i|}{\rho(\boldsymbol{r})}$$

$\rho_i(\boldsymbol{r})$ is the electronic density of the ith molecular orbital at the point $\boldsymbol{r}$, ε_i is its orbital energy, and $\rho(\boldsymbol{r})$ is the total electronic density function. We interpret $\bar{I}(\boldsymbol{r})$ as the energy required, on average, to remove an electron from a point $\boldsymbol{r}$ in the space of an atom or molecule (23–26). In particular, we have found that the positions where $\bar{I}(\boldsymbol{r})$ has its lowest values on the molecular surface, the $\bar{I}_{S,min}$, are indicative of the sites that are most susceptible to charge transfer with electrophiles (23, 24, 26). For example, for a group of 40 anionic conjugate bases of carbon, oxygen, and nitrogen acids, we have shown that a very good correlation exists between the measured pK_a of the acid and the calcuated $\bar{I}_{S,min}$ of the conjugate base (24).

In accordance with the suggestion of Bader et al. (27), we define the molecular surface as the 0.001 au contour of the electronic density. Our surface areas are obtained by means of grids of equidistant points, converted to units of Å^2.

Four of the quantities in eq. [1] are site-specific: $\bar{I}_{S,min}$, $V_{S,max}$, $V_{S,min}$, and V_{min}. They are indicative of the tendencies for charge transfer ($\bar{I}_{S,min}$) or electrostatic interaction ($V_{S,max}$, $V_{S,min}$, and V_{min}) occurring at specific points. (Note that $V_{S,min}$ refers to minima on the molecular surface, while the V_{min} can be anywhere in the space of the molecule.)

The other four quantities in eq. [1] are global: area, Π, σ^2_{tot}, and ν. These are representative of the entire molecular surface. Π, σ^2_{tot}, and ν are statistically based quantities, which we introduced in earlier work in an effort to develop quantitative measures of key aspects of the overall surface potentials of molecules (13, 14, 28–34). Π, as expressed by eq. [4], is the average deviation of the electrostatic potential on the molecular surface. $V(\boldsymbol{r}_i)$ is the value of $V(\boldsymbol{r})$ at point $\boldsymbol{r}_i$ on the surface, and $\bar{V}_S$ is the average value of the potential on the surface:

$$[4] \qquad \Pi = \frac{1}{n}\sum_{i=1}^{n} |V(\boldsymbol{r}_i) - \bar{V}_S|$$

$$\bar{V}_S = \frac{1}{n}\sum_{i=1}^{n} V(\boldsymbol{r}_i)$$

Π can be viewed as a measure of the local polarity that is present in a molecule, even one having zero dipole moment. We have demonstrated its relationship to several empirical polarity/polarizability parameters and also to the dielectric constant (13, 28). The values of Π for organic molecules typically fall in the range from 2 to 15 kcal/mol (13, 28, 29).

The other global quantities in eq. [1] are σ^2_{tot}, which is the total variance of the electrostatic potential on the molecular surface, and ν, an electrostatic balance parameter. These do not enter into the present analysis, and accordingly will not be discussed further. Applications of these quantities are described in detail elsewhere (13, 14, 29–34).

In this work, GAUSSIAN 88 (35) was used to optimize geometries and to compute $\rho(\boldsymbol{r})$ and $V(\boldsymbol{r})$. All of this was done at the HF/6-31G* level. While all of the quantities in eq. [1] were computed for each molecule of interest, only the four site-specific properties ($\bar{I}_{S,min}$, $V_{S,max}$, $V_{S,min}$, and V_{min}) and one global property, Π, are needed for the correlations presented in this article. These relationships were developed using the SAS statistical analysis program.[2]

Results

In developing our earlier correlations between hydrogen bond acidity and $V_{S,max}$ (11, 12) and between hydrogen bond basicity and V_{min} (10, 11), we used experimentally derived measures of relative hydrogen-bonding tendencies. For solvents, these are the solvatochromic parameters α and β for acidity and basicity, respectively, obtained from linear solvation energy relationships (36). For solutes, the corresponding parameters are α_2^H for acidity and β_2^H for basicity, which were defined to be linearly related to the equilibrium constants for forming 1:1 complexes between the solute molecule and a given reference hydrogen bond donor or acceptor, in CCl_4 (37–39). In this study, we have focused on α_2^H and β_2^H, since these are currently more frequently used than α and β.

Hydrogen bond acidity

We computed the quantities in our GIPF (eq. [1]) for a group of 18 hydrogen-bond-donating molecules of a variety of types, including CH, NH, and OH donors. These com-

[2] SAS Institute Inc., Cary, NC 27511, U.S.A.

Can. J. Chem. Downloaded from www.nrcresearchpress.com by 65.111.164.53 on 09/08/12
For personal use only.

Table 1. Properties of some hydrogen bond donors.[a]

Molecule	α_2^H	Corrected α_2^H (predicted)	$V_{S,max}$ (kcal/mol)
CH_3COCH_3	0.04 (–0.13)	–0.12	22.3
CH_3CN	0.09 (–0.01)	–0.01	27.8
CH_3NO_2	0.12 (0.02)	0.10	33.5
CH_2Cl_2	0.13 (0.07)	0.04	30.2
$CHCl_3$	0.20	0.16	36.7
$C_6H_5NH_2$	0.26 (0.20)	0.15	36.3
CH_3CH_2OH	0.33	0.36	47.0
CH_3OH	0.37	0.38	47.8
Pyrrole	0.41	0.39	48.3
Indole	0.44	0.41	49.6
CH_3COOH	0.55	0.55	56.4
CF_2CH_2OH	0.57	0.66	62.1
C_6H_5OH	0.60	0.59	58.4
2-Naphthol	0.61	0.61	59.7
p-$C_6H_4(Cl)OH$	0.67	0.70	64.1
p-$C_6H_4(OH)NO_2$	0.82	0.86	72.5
$(CF_3)_3COH$	0.86	0.82	70.1
CF_3COOH	0.95	0.88	73.3

[a]The α_2^H values were obtained by R.W. Taft. A statistical correction has been applied to some of the α_2^H values, as indicated by parentheses.

Fig. 1. Plot of experimentally derived α_2^H (corrected) versus calculated $V_{S,max}$ for the molecules in Table 1. The linear correlation coefficient is 0.991.

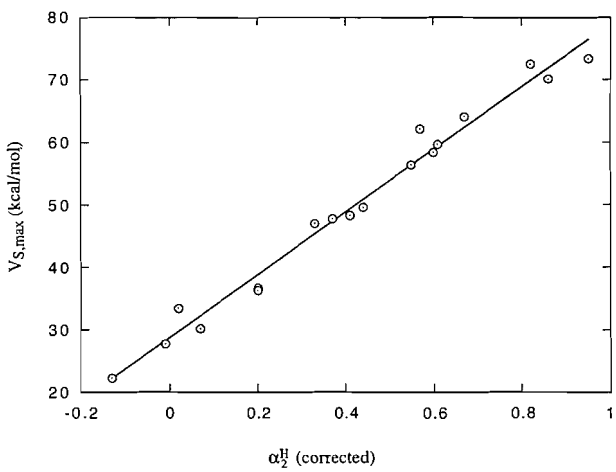

pounds are listed in Table 1 along with their experimentally derived but statistically corrected[3] α_2^H values and our calculated $V_{S,max}$. We found that at the HF/6-31G* level, the key variable correlating with α_2^H is $V_{S,max}$, which is invariably associated with the hydrogen(s) to be donated in the hydrogen bond. No other quantity, site-specific or global, is needed to obtain a family-independent relationship with α_2^H.

[3] The statistical correction to α_2^H is applied to those molecules having N similar hydrogens available for hydrogen bonding. α_2^H is defined by: $\alpha_2^H = (\log K_a + 1.1)/4.636$, where K_a is the equilibrium constant for a 1:1 complex of the donor and a reference acceptor. Then $K_a = \sum_{i=1}^{N} K_{ai} = NK'_a$, where K'_a is the corrected value. Accordingly, $\log K_a = \log N + \log K'_a$ and α_2^H (corrected) $= \alpha_2^H - (\log N)/4.636$.

Table 2. Properties of some hydrogen bond acceptors.

Molecule	log K_{HB}[a]	Corrected log K_{HB} (predicted)	$V_{S,min}$ (kcal/mol)
Benzene	–0.50	–0.53	–20.1
Cl_3CCN	–0.26[b]	0.29	–29.1
$(CH_3CH_2S)_2$	–0.10 (–0.40)	–0.17	–24.0
$(CH_3CH_2)_2S$	0.11[c]	0.08	–26.9
Dithiane	0.24 (–0.06)	–0.26	–23.0
Tetramethylsulfide	0.30	0.14	–27.5
ClH_2CCN	0.39[b]	0.87	–35.6
HCO_2CH_3	0.69[d]	1.58	–43.4
$F_3CCH_2NH_2$	0.72	0.39	–30.3
(3,5-Cl_2)pyridine	0.80[e]	0.41	–30.5
C_6H_5CHO	0.80[e]	1.27	–40.0
CH_3OH	0.82[f]	1.27	–40.0
CH_3CN	0.91[b]	1.45	–42.0
$CH_3CO_2CH_3$	1.00[d]	1.32	–40.5
$(CH_3CH_2)_2O$	1.01[e]	0.91	–36.0
CH_3CH_2OH	1.02[f]	1.29	–40.2
Dioxane	1.03[e] (0.73)	0.73	–34.0
CH_3COCH_3	1.18[g]	1.38	–41.2
Tetrahydrofuran	1.26[c]	1.33	–40.7
Pyrimidine	1.35[c] (1.05)	0.88	–35.7
$(CH_3CH_2)_3P{=}S$	1.46	1.00	–37.0
$(CH_3)_2NCN$	1.56	1.88	–46.8
Cyclopropylamine	1.64[c]	1.25	–39.8
NH_3	1.68	1.98	–47.8
Pyridine	1.88[c]	1.37	–41.1
(4-CH_3)pyridine	2.03[c]	1.51	–42.6
$(CH_3)_2NCHO$	2.10[h]	2.02	–48.3
CH_3NH_2	2.15	1.69	–44.6
$CH_3(CH_2)_3NH_2$	2.17	1.70	–44.7
$(CH_3)_2NCOCH_3$	2.44[h]	2.07	–48.8
$(CH_3)_2S{=}O$	2.53[c]	2.85	–57.5
(1-CH_3)imidazole	2.60[i]	2.20	–50.3
Pyridine N-oxide	2.76[g]	2.42	–52.7

[a]The log K_{HB} values were obtained from M. Berthelot, unless otherwise indicated. A statistical correction has been applied to obtain the vlues in parentheses.
[b]Reference 51.
[c]Reference 47.
[d]Reference 52.
[e]Reference 48.
[f]Reference 54.
[g]Reference 50.
[h]Reference 53.
[i]Reference 49.

The resulting excellent linear correlation between $V_{S,max}$ and the statistically corrected α_2^H values is given in eq. [5] and is shown in Fig. 1. The correlation coefficient is 0.991 and the standard deviation is 0.04.

$$[5] \qquad \alpha_2^H(\text{corrected}) = 0.0196\ V_{S,max} - 0.556$$

Hydrogen bond basicity

For a group of 33 hydrogen-bond-accepting molecules of a variety of types, we chose to seek correlations directly with the equilibrium constant, K_{HB}, for 1:1 complexation of

Can. J. Chem. Downloaded from www.nrcresearchpress.com by 65.111.164.53 on 09/08/12
For personal use only.

Table 3. Properties of some hydrogen bond acceptors.[a]

Molecule	$\Delta\nu_{OH.}$ exp. (cm^{-1})	$\Delta\nu_{OH.}$ pred. (cm^{-1})	V_{min} (kcal/mol)	$\bar{I}_{S,min}$ (eV)	Π (kcal/mol)
ClCCN	23	41	−39.1	15.20	7.31
C_6H_6	28	14	−20.7	11.88	9.06
ClH_2CCN	48.5	43	−48.6	14.50	16.86
HCO_2CH_3	54	45	−58.3	15.00	22.22
C_6H_5CHO	65	95	−55.8	15.16	12.70
$(CH_3CH_2S)_2$	75	98	−31.5	10.88	9.01
CH_3CN	75.5	77	−57.8	13.94	21.09
$CH_3CO_2CH_3$	77	100	−56.6	15.06	12.88
CH_3OH	116	126	−59.9	14.85	12.59
$(CH_3)_2NCN$	117.5	149	−64.4	13.33	18.15
CH_3CH_2OH	120	143	−61.4	14.77	11.58
Dithiane	121	107	−33.1	10.43	10.62
Dioxane	126	95	−53.7	15.15	11.03
$(CH_3CH_2)_2S$	146	173	−39.3	10.05	7.45
$(CH_3CH_2)_2O$	150	147	−55.8	14.86	6.37
$(CH_3)_2NCHO$	150	158	−67.6	14.36	15.60
Tetramethylsulfide	154	167	−39.4	10.04	8.40
Tetrahydrofuran	158	162	−62.0	14.50	8.93
$(CH_3)_2NCOCH_3$	179	180	−68.8	14.30	13.73
$(CH_3CH_2)_3P{=}S$	195	183	−47.7	9.64	13.85
(3,5-Cl_2)pyridine	200	169	−55.1	13.45	7.77
$(CH_3)_2S{=}O$	205	242	−85.8	12.83	23.22
Pyrimidine	213	184	−62.8	13.14	12.78
$F_3CCH_2NH_2$	250	223	−66.7	12.36	12.97
$(CH_3)_3P{=}O$	266	254	−79.0	12.75	16.58
NH_3	275	310	−87.9	11.83	18.90
Pyridine *N*-oxide	278	234	−77.9	12.90	18.13
Pyridine	286	249	−70.9	12.62	11.65
(4-CH_3)pyridine	304	267	−73.0	12.51	11.10
Cyclopropylamine	310	335	−79.6	11.63	9.67
(1-CH_3)imidazole	313	278	−82.1	12.41	16.85
CH_3NH_2	344	353	−84.4	11.52	11.25
$CH_3(CH_2)_3NH_2$	354	379	−83.8	11.50	7.21

[a]The experimentally determined $\Delta\nu_{OH}$ values were obtained from M. Berthelot.

Fig. 2. Plot of experimentally determined log K_{HB} (corrected) versus calculated $V_{S,min}$ for the molecules in Table 2. The linear correlation coefficient is 0.902.

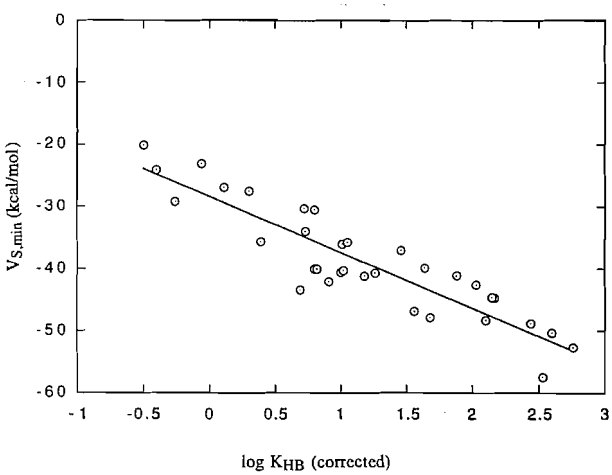

the acceptors with *p*-fluorophenol. We are using K_{HB} rather than β_2^H because the data, listed in Table 2, are from several different sources and accordingly it seemed preferable to use the actual measured quantity (K_{HB}) rather than one defined in terms of it (β_2^H).

As in the case of the hydrogen bond acidity correlations, we have listed the statistically corrected[4] values of log K_{HB} in Table 2, along with the calculated $V_{S,min}$ for each molecule. Only four acceptors need statistical corrections; these are $(CH_3CH_2S)_2$, dithiane, dioxane, and pyrimidine. These each have two identical hydrogen-bond-accepting heteroatoms per molecule.

Upon applying SAS to the data set of corrected log K_{HB} values, we find a reasonable linear relationship between $V_{S,min}$

[4] The statistical correction to log K_{HB} is applied to those molecules having N indistinguishable atoms that can accept a hydrogen bond. Then $K_{HB} = \sum_{i=1}^{N} K_{HBi} = NK'_{HB}$ where K'_{HB} is the corrected value, and log K'_{HB} = log K'_{HB} − log N.

Can. J. Chem. Downloaded from www.nrcresearchpress.com by 65.111.164.53 on 09/08/12
For personal use only.

Fig. 3. Plot of experimentally determined versus predicted $\Delta\nu_{OH}$ values for the molecules in Table 3. The linear correlation coefficient is 0.966.

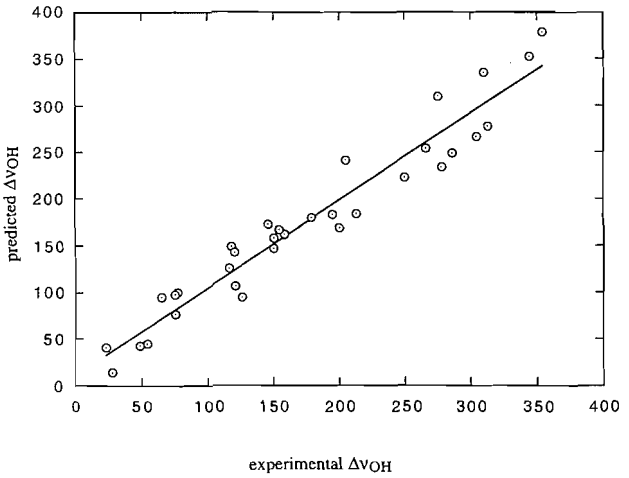

and log K_{HB}, given in eq. [6] and Fig. 2.

$$[6] \qquad \log K_{HB}(\text{corrected}) = -9.030 \times 10^{-2}\, V_{S,min} - 2.341$$

The correlation coefficient and standard deviation are 0.902 and 0.39, respectively. This correlation is of lower quality than that between α_2^H and $V_{S,max}$. This may be due in part to the fact that $V_{S,max}$ is always on a hydrogen, while $V_{S,min}$ is on a variety of acceptor heteroatoms.

Methanol infrared O–H frequency shift

Berthelot and Laurence have developed an experimentally accessible means of quantitating hydrogen-bond-accepting tendencies through the measurement of the IR frequency shift of the methanol O–H peak when the hydrogen is complexed with a hydrogen-bond-accepting molecule (40–46). This O–H frequency shift is designated $\Delta\nu_{OH}$.

Table 3 lists 33 molecules with their experimentally determined $\Delta\nu_{OH}$ values[5] and some calculated quantities: V_{min}, $\bar{I}_{S,min}$, and Π. The molecules in Table 3 represent a variety of types of compounds, including some with second-row hydrogen-bond-accepting atoms.

We have found a good three-parameter correlation, given in eq. [7], between $\Delta\nu_{OH}$ and the quantities V_{min}, $\bar{I}_{S,min}$, and Π. The linear correlation coefficient is 0.966 and the standard deviation is 26 cm^{-1}. Figure 3 presents a plot of experimentally determined $\Delta\nu_{OH}$ values vs. those predicted from eq. [7]. The dominant term in eq. [7] is V_{min}, followed by $\bar{I}_{S,min}$ and Π.

$$[7] \qquad \Delta\nu_{OH} = -5.427\, V_{min} - 25.48\, \bar{I}_{S,min} - 7.113\, \Pi + 268.3$$

In looking back at eq. [6], it is interesting to point out that the addition of either $\bar{I}_{S,min}$ and (or) Π does not statistically improve the quality of the log K_{HB} versus $V_{S,min}$ relationship. That eqs. [6] and [7] are indeed different is consistent with the known lack of family-independent correlation between log K_{HB} and $\Delta\nu_{OH}$.

[5] M. Berthelot, private communication.

Summary and conclusion

We have demonstrated that family-independent correlations can be obtained for solute hydrogen bond acidity and basicity, as quantitated by α_2^H and log K_{HB}, respectively, and for the methanol infrared O–H frequency shift, $\Delta\nu_{OH}$, that occurs upon the complexation of methanol with hydrogen-bond-accepting molecules. Our results show that α_2^H and log K_{HB} can be well represented by an electrostatic potential term alone, $V_{S,max}$ and $V_{S,min}$, respectively. $\Delta\nu_{OH}$, on the other hand, requires a term reflecting charge transfer contributions as well as electrostatic potential terms.

Acknowledgement

We greatly appreciate the support provided by ARPA/ONR Contract No. N00014-91-J-1987, administered by ONR. T.B. acknowledges support by the Swedish Natural Sciences Research Council (NFC).

References

1. H. Umeyama and K. Morokuma. J. Am. Chem. Soc. **99**, 1316 (1977).
2. P. Kollman. J. Am. Chem. Soc. **99**, 4875 (1977).
3. M.A. Benzel and C.E. Dykstra. J. Chem. Phys. **78**, 4052 (1983).
4. A.D. Buckingham and P.W. Fowler. Can. J. Chem. **63**, 2018 (1985).
5. S. Lin and C.E. Dykstra. Chem. Phys. **107**, 343 (1986).
6. A.C. Legon and D.J. Millen. Acc. Chem. Res. **20**, 39 (1987).
7. P. Kollman, J. McKelvey, A. Johansson, and S. Rothenberg. J. Am. Chem. Soc. **97**, 955 (1975).
8. G. Leroy, G. Louterman-Leloup, and P. Ruelle. Bull. Soc. Chim. Belg. **85**, 205 (1976); **85**, 219 (1976); **85**, 229 (1976).
9. P. Politzer and K.C. Daiker. *In* The force concept in chemistry. *Edited by* B.M. Deb. Van Nostrand Reinhold, New York. 1981. Chap. 6.
10. J.S. Murray, S. Ranganathan, and P. Politzer. J. Org. Chem. **56**, 3734 (1991).
11. J.S. Murray and P. Politzer. J. Chem. Res. S, 110 (1992).
12. J.S. Murray and P. Politzer. J. Org. Chem. **56**, 6715 (1991).
13. J.S. Murray, T. Brinck, P. Lane, K. Paulsen, and P. Politzer. J. Mol. Struct. (Theochem), **307**, 55 (1994).
14. J.S. Murray and P. Politzer. *In* Quantitative treatments of solute solvent interactions. Vol. 1. *Edited by* P. Politzer and J.S. Murray. Elsevier, Amsterdam. 1994. Chap. 8.
15. E. Scrocco and J. Tomasi. Adv. Quantum Chem. **11**, 115 (1978).
16. P. Politzer and D.G. Truhlar (*Editors*). Chemical applications of atomic and molecular electrostatic potentials. Plenum Press, New York. 1981.
17. P. Politzer, P.R. Laurence, and K. Jayasuriya. Environ. Health Perspect. **61**, 191 (1985).
18. P. Politzer and J.S. Murray. *In* Theoretical biochemistry and molecular biophysics: A comprehensive survey. Vol. 2. *Edited by* D.L. Beveridge and R.

Lavery. Adenine Press, Schenectady, N.Y. 1991. Chap. 13.
19. P. Politzer and J.S. Murray. *In* Reviews in computational chemistry. Vol. 2. *Edited by* K.B. Lipkowitz and D.B. Boyd. VCH Publishers, New York. 1991. Chap. 7.
20. R.K. Pathak and S.R. Gadre. J. Chem. Phys. **93**, 1770 (1993).
21. P. Sjoberg and P. Politzer. J. Phys. Chem. **94**, 3959 (1990).
22. J.S. Murray, P. Lane, T. Brinck, P. Politzer, and P. Sjoberg. J. Phys. Chem. **95**, 844 (1991).
23. P. Sjoberg, J.S. Murray, T. Brinck, and P. Politzer. Can. J. Chem. **68**, 1440 (1990).
24. T. Brinck, J.S. Murray, and P. Politzer. J. Org. Chem. **56**, 5012 (1991).
25. M. Haeberlein, J.S. Murray, T. Brinck, and P. Politzer. Can. J. Chem. **70**, 2209 (1992).
26. T. Brinck, J.S. Murray, and P. Politzer. Int. J. Quantum Chem. **48**, 73 (1993).
27. R.F.W. Bader, M.T. Carroll, J.R. Cheeseman, and C. Chang. J. Am. Chem. Soc. **109**, 7968 (1987).
28. T. Brinck, J.S. Murray, and P. Politzer. Mol. Phys. **76**, 609 (1992).
29. J.S. Murray, P. Lane, T. Brinck, and P. Politzer. J. Phys. Chem. **97**, 5144 (1993).
30. P. Politzer, P. Lane, J.S. Murray, and T. Brinck. J. Phys. Chem. **96**, 7938 (1992).
31. P. Politzer, J.S. Murray, P. Lane, and T. Brinck. J. Phys. Chem. **97**, 729 (1993).
32. J.S. Murray, P. Lane, T. Brinck, K. Paulsen, M.E. Grice, and P. Politzer. J. Phys. Chem. **97**, 9369 (1993).
33. J.S. Murray, T. Brinck, and P. Politzer. J. Phys. Chem. **97**, 13807 (1994).
34. T. Brinck, J.S. Murray, and P. Politzer. J. Org. Chem. **58**, 7070 (1993).
35. M.J. Frisch, M. Head-Gordon, H.B. Schlegel, K. Raghavachari, J.S. Binkley, C. Gonzalez, D.J. Defrees, D.J. Fox, R.A. Whiteside, R. Seeger, C.F. Melius, J. Baker, R. Martin, L.R. Kahn, J.J.P. Steward, E.M. Fluder, S. Topiol, and J.A. Pople. GAUSSIAN 88, Gaussian Inc., Pittsburgh, Pa. 1988.
36. M.J. Kamlet, J.-L. M. Abboud, M.H. Abraham, and R.W. Taft. J. Org. Chem. **48**, 2877 (1983).
37. M.H. Abraham, P.L. Grellier, D.V. Prior, J.J. Morris, P.J. Taylor, C. Laurence, and M. Berthelot. Tetrahedron Lett. **30**, 2571 (1989).
38. M.H. Abraham, P.L. Grellier, D.V. Prior, P.P. Duce, J.J. Morris, and P.J. Taylor. J. Chem. Soc. Perkin Trans. 2 699 (1989).
39. M.H. Abraham, P.L. Grellier, D.V. Prior, J.J. Morris, and P.J. Taylor. J. Chem. Soc. Perkin Trans. 2, 521 (1990).
40. C. Laurence, M. Berthelot, M. Helbert, and K. Sraïdi. J. Phys. Chem. **93**, 3799 (1989).
41. J.-Y. Le Questel, C. Laurence, A. Lachkar, M. Helbert, and M. Berthelot. J. Chem. Soc. Perkin Trans. 2, 2091 (1992).
42. F. Besseau, C. Laurence, and M.J. Berthelot. J. Chem. Soc. Perkin Trans. 2, 485 (1994).
43. C. Laurence, M. Berthelot, M. Lucon, and D.G. Morris. J. Chem. Soc. Perkin Trans. 2, 491 (1994).
44. C. Laurence, M. Helbert, and A. Lachkar. Can. J. Chem. **71**, 254 (1993).
45. E.D. Raczyinska, C. Laurence, and M. Berthelot. Can. J. Chem. **70**, 2203 (1992).
46. M. Berthelot, M. Helbert, C. Laurence, and J.Y. LeQuestel. J. Phys. Org. Chem. **6**, 302 (1993).
47. D. Gurka and R.W. Taft. J. Am. Chem. Soc. **91**, 4794 (1969).
48. L. Joris, J. Mitsky, and R.W. Taft. J. Am. Chem. Soc. **94**, 3438 (1972).
49. S. Bogaerts, M.-C. Haulait-Pirson, and Th. Zeeger-Huyskens. Bull. Soc. Chim. Belg. **88**, 1003 (1979).
50. R.W. Taft, D. Gurka, I. Joris, P.v.R. Schleyer, and J.W. Rakshys. J. Am. Chem. Soc. **91**, 4801 (1969).
51. M. Berthelot, M. Helbert, C. Laurence, and J.-Y. Le Questel. J. Phys. Org. Chem. **6**, 302 (1993).
52. F. Besseau, C. Laurence, and M. Berthelot. J. Chem. Soc. Perkin Trans. 2, 485 (1994).
53. J.-Y. Le Questel, C. Laurence, A. Lachkar, M. Helbert, and M. Berthelot. J. Chem. Soc. Perkin Trans. 2, 2091 (1992).
54. C. Laurence, M. Berthelot, M. Helbert, and K. Sraïdi. J. Phys. Chem. **93**, 3799 (1989).

Can. J. Chem. Downloaded from www.nrcresearchpress.com by 65.111.164.53 on 09/08/12
For personal use only.

Condensation reactions between vanadate and small functionalized peptides in aqueous solution

Alan S. Tracey, Jaswinder S. Jaswal, Fikile Nxumalo, and Sarah J. Angus-Dunne

Abstract: The role that histidyl, seryl, tyrosyl, and other side chains of small peptides play in the formation of vanadate complexes has been investigated using ^{1}H, ^{13}C, and ^{51}V nuclear magnetic resonance spectroscopy. Formation constants of product complexes in aqueous solution have been determined and the influence of pH on the equilibria established. The results revealed that, in histidine-containing compounds, the protonation state of the imidazole ring of the free ligand strongly influences product formation. The results unequivocally showed that no vanadium-to-imidazole bond was formed for any of the histidine-containing complexes studied. However, imidazole and other aromatic side-chain residues have an effect on product stability via their influence on the protonation state (pK_a) of the products. Aliphatic side-chains, such as those in asparagine or glutamate, do not appear to play a significant role in the formation of products. This is not true, however, of serine or threonine where the side-chains readily generate vanadium–oxygen bonds.

Key words: vanadate, vanadium, 51-V NMR, peptides, complexes, aqueous equilibria.

Résumé : Utilisant la RMN du ^{1}H, du ^{13}C et du ^{51}V, on a étudié le rôle joué par des chaînes latérales histidyle, séryle, tyrosyle et autres de petits peptides dans la formation de complexes du vanadate. On a déterminé les constantes de formation des complexes en solution aqueuse et on a établi l'influence du pH sur l'équilibre. Les résultats révèlent que, dans les composés contenant de l'histidine, l'état de protonation du noyau imidazole du coordinat libre influence fortement la formation du produit. Les résultats montrent sans équivoque qu'il ne se forme pas de liaison vanadium–imidazole dans aucun des complexes étudiés contenant de l'histidine. Toutefois, à cause de leur influence sur l'état de protonation (pK_a) des produits, l'imidazole et d'autres résidus aromatiques dans les chaînes latérales ont un effet sur la stabilité des produits. Les chaînes latérales aliphatiques, telles que celles rencontrées dans l'asparagine ou le glutamate, ne semblent pas jouer de rôle significatif dans la formation des produits. Toutefois, ceci n'est pas vrai pour la sérine ou la thréonine avec lesquelles les chaînes latérales génèrent facilement des liaisons vanadium–oxygène.

Mots clés : vanadate, vanadium, RMN du ^{51}V, peptides, complexes, équilibre aqueux.

[Traduit par la rédaction]

Introduction

The past few years have seen a remarkable surge of interest in the aqueous chemistry of the oxovanadium(V) ion, vanadate. In large part, this interest has been generated because vanadate can influence the function of a large number of phosphate-utilizing enzymes by entering directly into metabolic processes (for recent reviews of much of the chemistry and biochemistry of vanadate the readers are referred to the two compendiums, refs. 1 and 2). In addition to this, vanadium is contained in the prosthetic group of some nitrogen-fixing enzymes (3–5) and in a number of haloperoxidases of marine algae (6–8).

Much of the metabolism of phosphate involves tyrosyl, histidyl, seryl, or other residues in the active site of the protein. It is of interest, therefore, to develop an understanding of the interactions between the side-chain substituents and vanadate.

Recent studies have revealed some of the chemistry associated with the reactions between vanadate and amino acids or peptides (9–12). This work has been limited in scope, in part because of the complexity of the interactions involved, particularly when the peptides contain functionalized side chains. The involvement of histidine in complex formation with vanadate has been studied (13), as has that of asparagine (11), tyrosine (14), aspartic acid (9, 15), and serine (11).

In this study, the reaction of a number of di- and tripeptides with vanadate is reported. In one series of reactants, at least one amino acid residue of the peptide had a functionalized side chain. In a second series, both amino acid residues in a number of dipeptides were functionalized. A previous report detailed the interactions between vanadate and peptides with no func-

Received September 27, 1994.

A.S. Tracey,[1] J.S. Jaswal,[2] F. Nxumalo, and S.J. Angus-Dunne. Department of Chemistry, Simon Fraser University, Burnaby, BC V5A 1S6, Canada.

[1] Author to whom correspondence may be addressed. Telephone: (604) 291-4464. Fax: (604) 291-3765. E-mail: tracey@sfu.ca

[2] Present address: Department of Chemistry, Washington State University, Pullman, WA 99164-4660, U.S.A.

Can. J. Chem. Downloaded from www.nrcresearchpress.com by 65.111.164.53 on 09/08/12
For personal use only.

tionalized side chains (11) and that information is necessary for understanding these more complex systems.

Experimental

Materials

The peptides used in this study were obtained from Sigma Chemical Company. In some cases the purity of the peptides was checked by ^{1}H NMR spectroscopy but all were used as supplied. The buffer *N*-(2-hydroxyethyl)piperazine-*N'*-ethane sulfonic acid (HEPES) was purchased from Boehringer Mannheim GmbH and used as provided, as was the vanadium pentoxide (99.99%) purchased from Aldrich Chemical Company.

Ligands

The pK_a values for a number of ligands were required. They were obtained by a sequential titration of the particular dipeptide, first from a pH 13.5 solution with HCl until well below the pK_a (pH 2), then with NaOH until back to pH 13.5. The pK_a values were taken from the titration curve of pH vs. volume of added acid or base. The values obtained were as follows: for terminal NH_3–hisser 8.0; hisgly 8.1; glyhis 8.1: for imidazolium–hisser 7.0; hisgly 6.6; glyhis 7.0. The pK_a values for trptrp (7.7), trptyr (8.1), and tyrgly (8.1) were taken from ref. 16.

Solutions

Stock solutions of sodium vanadate were prepared in distilled water by adding 0.5 mol equivalent of V_2O_5 to a 1.0 M solution of NaOH and stirring until the solution became colourless (generally overnight). The concentration was adjusted to provide a 0.1 M stock solution.

1.0 M HEPES and 2.0 M KCl stock solutions were individually prepared in distilled water. Stock solutions of 0.05–0.08 M tryptophyltryptophan and tryptophyltyrosine were prepared by warming the appropriate amounts of dipeptide in distilled water. The peptides, tyrosylglycine, glycylhistidylglycine, tryptophylglycylglycine, and N-CBz-histidylglycine were weighed and added directly to the sample solutions. The remaining stock solutions were prepared at concentrations varying from 0.06 to 0.3 M, depending on the solubility, in distilled water.

The final solutions were prepared by adjusting the pH of the stock solutions to appropriate values so that, on combining them into the final solution, the pH was not less than 6.2. The volume was adjusted to near the final volume; the pH was then adjusted upward with NaOH to the desired value and final volume adjustments made. This procedure prevented the formation of decavanadate. The final solutions contained 20 mM HEPES buffer and the appropriate amounts of vanadate and peptide, and the ionic strength was 1.0 M with KCl. Freshly opened standard buffers at pH 4.0 and pH 10.0 were used for pH calibration.

For ^{1}H and ^{13}C NMR spectroscopic studies of the histidylserine–vanadate equilibria, the solutions were prepared in D_2O and pD adjustments made using DCl or NaOD.

Equilibration of the reactant solutions frequently required many hours. Solutions were normally allowed to stand 1 day at room temperature before obtaining the final NMR spectra. Spectra were again obtained after several additional days to ensure all systems had been in equilibria. Rates of equilibration were found to vary for different peptides but no detailed kinetic study was made.

Spectroscopy

All NMR spectra were obtained from a Bruker AMX-400 NMR spectrometer operating at ambient temperature (21 ± 1°C). ^{51}V chemical shifts are given relative to an external $VOCl_3$ reference at 0.0 ppm. Base-line corrections were applied to all spectra before integrals were obtained.

Methods

The equilibrium equations, derived on the basis of concentration and pH studies, were put into the appropriate linear form, as outlined in the text, and the results were analyzed using standard least-squares techniques. The quoted errors are for the 95% confidence level.

Results and discussion

In this study, the reactions of vanadate with six dipeptides (glyhis, hisgly, hisser, pheglu, tyrgly, and trptyr) were selected for detailed analysis. Extensive concentration and pH studies were carried out for these systems. An additional 14 peptides were studied in a more cursory fashion at pH 7.0.

Glycylhistidine

In the initial studies with glycylhistidine, the total vanadate concentration was maintained at 3.0 mM and the glycylhistidine concentration was varied from 10 to 50 mM. For the 40 mM peptide concentration, additional spectra were obtained for 5.0 and 7.0 mM total vanadate. Under these conditions a single product signal, at −511 ppm, was observed. This signal is close to that (−519 ppm) previously reported for the product of the condensation with alanylhistidine (13). To ascertain the stoichiometry of this product, it is first necessary to know whether additional products are formed.

In addition to the major product, there is possibly a product arising from condensation at the terminal NH_2 group that gives overlapping signals with monomeric vanadate, perhaps because of rapid exchange. To investigate this possibility it is necessary to consider the predominant oligomerization reactions of vanadate as expressed in eqs. [1]–[3]. It frequently happens that the tetramer, V_4, gives a well-defined NMR signal and therefore provides a useful reference for defining the concentration of the vanadate monomer.

$$[1] \quad 2V_1 \underset{}{\overset{K_{12}}{\rightleftharpoons}} V_2, \qquad [V_1]^2K_{12} = [V_2]$$

$$[2] \quad 4V_1 \underset{}{\overset{K_{14}}{\rightleftharpoons}} V_4, \qquad [V_1]^4K_{14} = [V_4]$$

$$[3] \quad 5V_1 \underset{}{\overset{K_{15}}{\rightleftharpoons}} V_5, \qquad [V_1]^5K_{15} = [V_5]$$

The formation of the rapidly exchanging product is written as eq. [4], where V_1 is monomeric vanadate, P is the peptide, and VP is the product. K_{14} and K_1 can be determined simultaneously by combining eq. [2] with eq. [4] and rearranging to give eq. [5]

Can. J. Chem. Downloaded from www.nrcresearchpress.com by 65.111.164.53 on 09/08/12
For personal use only.

Can. J. Chem. Downloaded from www.nrcresearchpress.com by 65.111.164.53 on 09/08/12
For personal use only.

[4] $V_1 + P \underset{}{\overset{K_1}{\rightleftharpoons}} VP, \qquad [V_1][P]K_1 = [VP]$

[5] $$\frac{[V_1] + [VP]}{[V_4]^{1/4}} = K_{14}^{-1/4} + K_1 K_{14}^{-1/4}[P]$$

When the data were plotted, a linear relationship was obtained but the slope of the line was indistinguishable from zero. From the scatter in the points it was estimated that K_1 was not larger than about 1 M^{-1}. Reported values of K_1 for other dipeptides under similar conditions are about 0.4 M^{-1} (11). From the *Y*-intercept, a value of $(2.1 \pm 0.3) \times 10^{10}$ M^{-3} was calculated for K_{14}. This value is very close to those previously reported for the formation of the vanadate tetramer at this pH (17).

Initial studies of the data for the −511 ppm product suggested that this product contained a single glycylhistidine and a single vanadate and was formed as described by eq. [4]. Figure 1 shows the results of plotting the experimental data. The good linear relationship that was obtained yielded a formation constant of $(1.01 \pm 0.06) \times 10^2$ M^{-1} for K_1. The absence of upward curvature in the experimental data indicated that the −511 ppm NMR signal was not a composite signal deriving from products of VP and V_2P stoichiometry in the fashion recently reported for the −519 ppm product formed from the reaction of alanylhistidine with vanadate (13). However, reanalysis of the alanylhistidine data given in Tables 2 and 3 of ref. 13, according to eq. [4], gave two excellent linear relationships with no upward curvature, as shown in Figs. 2*A* and 2*B*, respectively. There is no indication, from these graphs, that a V_2P product is formed. Earlier studies of other peptides also provided no evidence for formation of a V_2P product (11). It is not impossible that such products are formed; however, the information presently available does not provide evidence for the occurrence of such a product under the conditions of these various studies. The monopeptide monovanadium product, VP, is the only discernible product.

In previous studies of peptidovanadate complex formation it was found that the products giving rise to ^{51}V NMR signals near −510 ppm were formed from $VO_4H_2^-$ and the neutral (zwitterionic) peptide without gaining or losing a proton at pH 7. The products, however, had pK_a values near 10 (11). This value differs considerably from those of the uncomplexed peptides (see experimental section). When an attempt was made to analyze the results of the pH variation study of the glycylhistidine system (pH 6.52–9.61) it was found that the pK_a values both of the terminal nitrogen and of the imidazole nitrogen had to be considered in order to interpret the results. This indicated very clearly that the imidazole ring played an important role in the complexation reaction.

From the pK_a values for the terminal amino group and the imidazole ring of glycylhistidine (see experimental section), the concentration of the positively charged dipeptide can be calculated for all the pH values of this study. As a consequence, product formation can be written according to the top line of eq. [6]. However, a plot of [VP] vs. $[VO_4H_2^-][P^+]$ was not linear as expected. This demonstrated that
it was necessary to consider the pH dependence of the charge state of the product, as in the completed eq. [6]. The concentration of $VO_4H_2^-(V_1^-)$ for this equation is given directly by its pK_{a2} (=8.2) and the pH of the individual solutions. Equation

Fig. 1. A graphical representation of the formation of the −511 ppm product of the reaction of glycylhistidine with vanadate. Conditions of the experiments: pH, 7.0; HEPES buffer, 20 mM; ionic strength, 1.0 M with KCl; variable total glycylhistidine concentration, 10–50 mM; variable total vanadate concentration, 3.0–7.0 mM.

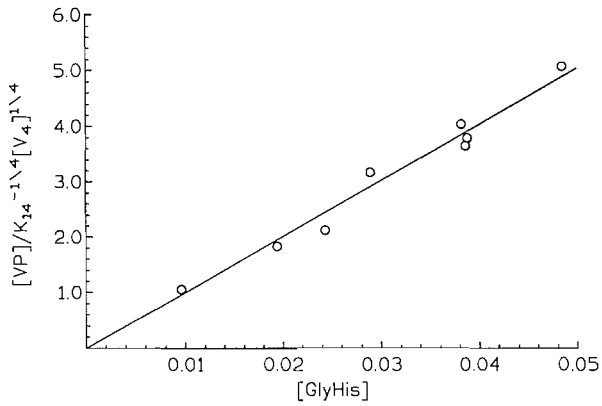

Fig. 2. The formation of the −519 ppm product of the reaction of alanylhistidine with vanadate is shown. The data are (*A*) from Table 2 and (*B*) from Table 3 of ref. 13. For these experiments the total vanadate concentration was varied between 1 and 17 mM and the total peptide concentration between 1 and 52 mM. The data were obtained at pH 7.2 under conditions of 0.2 M ionic strength with NaCl.

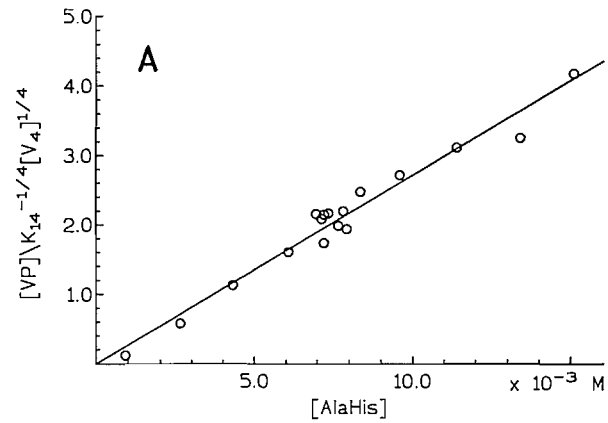

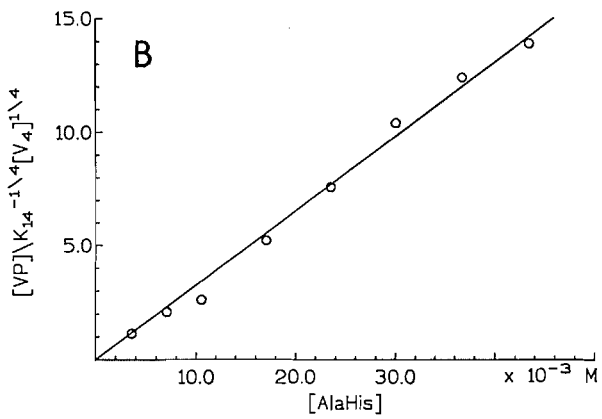

Can. J. Chem. Downloaded from www.nrcresearchpress.com by 65.111.164.53 on 09/08/12
For personal use only.

Fig. 3. The formation of the −511 ppm products ([VP] = [VP^0] + [VP^-]) of the reaction of monoanionic vanadate with cationic glycylhistidine is shown as a function of the inverse of the hydrogen ion concentration. The upward slope of the line is consistent with a pK_a for the product. The conditions of the experiments were as follows: total vanadate, 3.0 mM; total glycylhistidine, 40 mM; HEPES buffer, 20 mM; KCl, 1.0 M; pH, variable, pH 6.52–8.73.

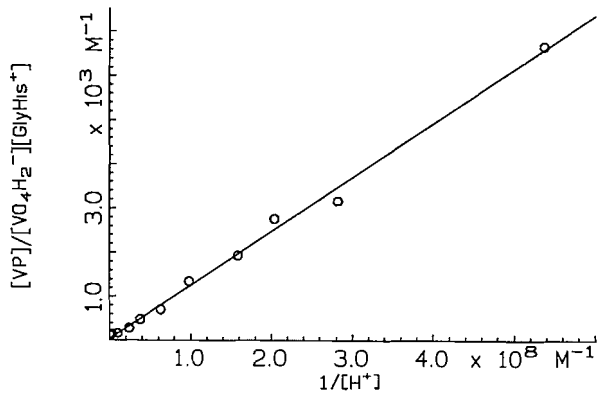

[6] $VO_4H_2^- + P^+ \overset{K_2'}{\rightleftharpoons} VP$

$VP \overset{K_a}{\rightleftharpoons} H^+ + VP^{1-}$

[6] can then be reformulated in linear form as eq. [7] where a plot of 1/[H^+] vs. the term on the left of eq. [7] should give a line of slope, $K_2'K_a$, and intercept, K_2'.

$$[7] \qquad \frac{([VP^0] + [VP^-])}{[VO_4H_2^-][P^+]} = K_2'\left(1 + \frac{K_a}{[H^+]}\right)$$

The experimental results are displayed in Fig. 3. Although the slope is well determined, the *Y*-intercept, and therefore K_2' (= 29 ± 66 M^{-1}), is not very well defined because its value is small compared to the scatter in the experimentally determined *Y*-values, which range from 140 to 6700 M^{-1}.

Further information can be gleaned from the experimental results by reformulating eq. [6] as eq. [8] to give eq. [9], then replotting the data. The slope and intercept from this plot gave values

$VP \overset{K_a}{\rightleftharpoons} H^+ + VP^-$

[8] $VO_4H_2^- + P^+ \overset{K_2''}{\rightleftharpoons} VP^- + H^+$

$$[9] \qquad \frac{([VP^0] + [VP^-])[H^+]}{[VO_4H_2^-][P^+]} = K_2'' + [H^+]K_2''/K_a$$

of (1.1 ± 0.2) × 10^{-5} for K_2'' and a pK_a of about 7 (Table 1). This pK_a value, although not well defined, is similar to that of the imidazole ring in glycylhistidine and its value seemingly suggests that the imidazole ring is directly involved in product stability. If the pK_a value is correctly attributed, its occurrence means that no vanadium–imidazole nitrogen bond is formed. If the imidazole ring is not directly involved in product stability, the formation constant of the product would not be sensitive to the overall charge state of the product unless the pK_a that is measured does not arise from loss of a proton from the imidazole but rather from the vanadate core. In two cases where the peptides have no aromatic side chains, the products have a pK_a of about 9 or 10 (11). No evidence for loss of an additional proton from VP^- at the high pH values of this study was obtained.

Histidylglycine

The reactions of histidylglycine are not very different from those of glycylhistidine and again only one product was observed. This product gave a ^{51}V NMR signal at −513 ppm and is formed with a formation constant of 67 ± 4 M^{-1} at pH 7.0.

The pH variation study clearly showed that here, as for glycylhistidine, it was necessary to consider the product charge state when interpreting the results of the experiments. When the results were plotted according to eq. [9], a value of (2.0 ± 0.3) × 10^{-5} was obtained for K_2'' and a value of 6.7 for the pK_a of the product. As for glycylhistidine, the pK_a was not well determined, but its value supports the previous suggestion that there is no bond formed from the vanadium to the imidazole nitrogen of the histidine side chain. The value for K_2'', in this case, is twice that for the glycylhistidine ligand. This indicates the presence of slightly more favourable interactions leading to product stability but the difference is not large.

Neither N-CBz-histidylglycine (30 mM) nor glycyclglycylhistidine (60 mM) gave significant amounts of any product. This suggests that vanadium – imidazole nitrogen bonds are not easily formed in this type of complex. Either of the above ligands could complex in a tridentate fashion without requiring a terminal amino group adjacent to the peptide nitrogen and the terminal carboxylate group but such products were not observed.

The complexes observed here are, apparently, not very different from those formed with simpler dipeptides such as glycylglycine where complexation requires the N-terminal amino group, the N-H of the peptide linkage, and a terminal unprotected carboxylate group (9, 11).

Histidylserine

At pH 7.0, the major product of the reaction gave a vanadium NMR signal at −517 ppm. A second product with a ^{51}V chemical shift of −503 ppm was also formed, but at a low relative concentration of about 5% of that of the major product. The formation constant for the major product, as described by eq. [4], was (3.2 ± 0.2) × 10^2 M^{-1} while that of the minor product was (0.2 ± 0.1) × 10^2 M^{-1}, both for pH 7.0.

When the pH variation study was carried out, it became obvious that the two products had a different proton stoichiometry. The −503 ppm product became increasingly favoured relative to the −517 ppm product with increase in pH. This behaviour is similar to that previously reported for glycylserine (11) and is ascribed to the involvement of the terminal carboxylate in complex formation for the −517 ppm product and the hydroxyl group of the hydroxymethyl of

Table 1. ^{51}V chemical shifts and the formation constants for the products of the equilibrium reactions between vanadate and a number of simple peptides.[a]

Peptide	^{51}V Chemical Shift (ppm)	K_1 (pH 7.0) (M^{-1})	K_2'' (variable pH)	pK_a[b]
Formation constants from concentration and pH variation studies				
GlyHis	−511	101 ± 6	$(1.1 \pm 0.2) \times 10^{-5}$	7.0 ± 0.2
HisGly	−513	67 ± 4	$(2.0 \pm 0.3) \times 10^{-5}$	6.7 ± 0.3
HisSer[c]	−517	320 ± 20	$(1.5 \pm 0.4) \times 10^{-5}$	7.5 ± 0.2
HisSer[c]	−503	20 ± 10	$(4.8 \pm 1.9) \times 10^{-5}$	7.8 ± 0.2
Formation constants from spectra obtained at pH 7.0				
GlyThr[d]	−511	28		
GlyThr[d]	−497	17		
GlyGlu	−508	23		
GluGlu	−516	45		
GluLys	−513	93		
AlaHis[e]	−519	270 ± 10		
No products were observed, under the reaction conditions, with up to 30 mM N-CBz-HisGly, 60 mM GlyHisGly, 100 mM GlyGlySar				

[a]All formation constants were obtained for aqueous solutions with 20 mM HEPES buffer and an ionic strength of 1.0 M maintained with KCl.

[b]The pK_a values are for the product complexes and were determined from the variation of the product formation constant as a function of pH.

[c,d]The −517,−511 ppm signals arise from reaction at the carboxylate group; the −503,−497 ppm signals from reaction involving the hydroxyl group of the side chain. The formation constants of the −517,−503 ppm and −511,−497 ppm pairs should not be compared as they are for different types of equilibrium reactions.

[e]The formation constant is for pH 7.2 and 0.2 M NaCl, calculated from the data in Table 2 of ref. 13 as discussed in the text.

Can. J. Chem. Downloaded from www.nrcresearchpress.com by 65.111.164.53 on 09/08/12
For personal use only.

serine for the −503 ppm product. The loss of a proton from the hydroxyl group in the second case means there is no difference in charge state at the vanadium nucleus of the two products; both can be designated as VP^-. Overall, then, the −517 ppm product is a complex that can take up, but not release, a proton as described by eq. [8]. The −503 ppm product is also ionizable but, since the loss of the initial proton is from the CH_2OH group when the product is formed, this complex can lose, but not gain, an additional proton. Equation [10] describes this latter type of behaviour.

$$[10] \quad VO_4H_2^- + P^+ \underset{}{\overset{K_2'''}{\rightleftharpoons}} VP^- + H^+$$

$$K_a \Big\| \Big\downarrow H^+$$

$$VP^{2-}$$

Figure 4*A* shows a plot of the experimental results for the −517 ppm product according to eq. [9]. The graph is similar to those obtained for glycylhistidine and for histidylglycine. The intercept gave a value of $(1.5 \pm 0.4) \times 10^{-5}$ for K_2''. The upward slope of this graph is consistent with a pK_a for the product ($pK_a = 7.5$). Figure 4*B* shows a similar plot, but based on eq. [10], for the −503 ppm product. The intercept, $K_2''' = (4.8 \pm 1.9) \times 10^{-6}$, gives the formation constant for the monoanionic product. This value is about a factor of 10 larger than the analogous value for glycylserine (11). In the case of glycylserine, a third component was observed and assigned to an isomeric product of reaction at the hydroxyl group. A third product was not observed here. This is consistent with the previous assignment, since in the present case steric interactions involving the imidazole ring could selectively discriminate against one of the isomers. Proton NMR spectra from D_2O solution also showed that there was formation of only two products.

The upward slope of the graph shown in Fig. 4*B* arises because of the pK_a of the −503 ppm product ($pK_a = 7.8$). The pK_a values for the −517 and −503 ppm products, 7.5 and 7.8 (Table 1), respectively, are significantly larger than those of the histidine in the free ligand, $pK_a = 7.0$ (experimental section). It was possible to show that a proton was being lost from the imidazole ring by carrying out a pD variation study in D_2O solution. This study revealed an almost identical pD dependence of the histidyl ^1H NMR signals from the histidylserine ligand and the −517 ppm product complex, suggesting an insignificant difference in pK_a between the imidazole in the product and in the free ligand. Over the pD range of 6.22–8.49, the C1 proton of the imidazole ring (see Scheme 1) of the free ligand underwent a chemical shift change of −0.57 ppm, while the chemical shift of the corresponding imidazole proton in the product changed in a corresponding manner by −0.53 ppm. These results clearly showed that the imidazole ring was not complexed and, in addition, indicated that the pK_a measured from the pH dependence of the formation constant of the product is not the same parameter as the pK_a of the imidazole ring. This means, therefore, that at the vanadium centre

Fig. 4. The dependence on hydrogen ion concentration of the formation of the two major products of the reaction of histidylserine with vanadate is shown. *A* is consistent with the uptake of a single proton by a −517 ppm monoanionic product with increasingly acidic conditions. *B* indicates the loss of a proton from a −503 ppm monoanionic product under increasingly basic conditions. The conditions of the experiments were as follows: total vanadate, 3.0 mm; total histidylserine, 9.0 mM; KCl, 1.0 M; HEPES buffer, 20 mM; pH variable, pH 6.45–9.46.

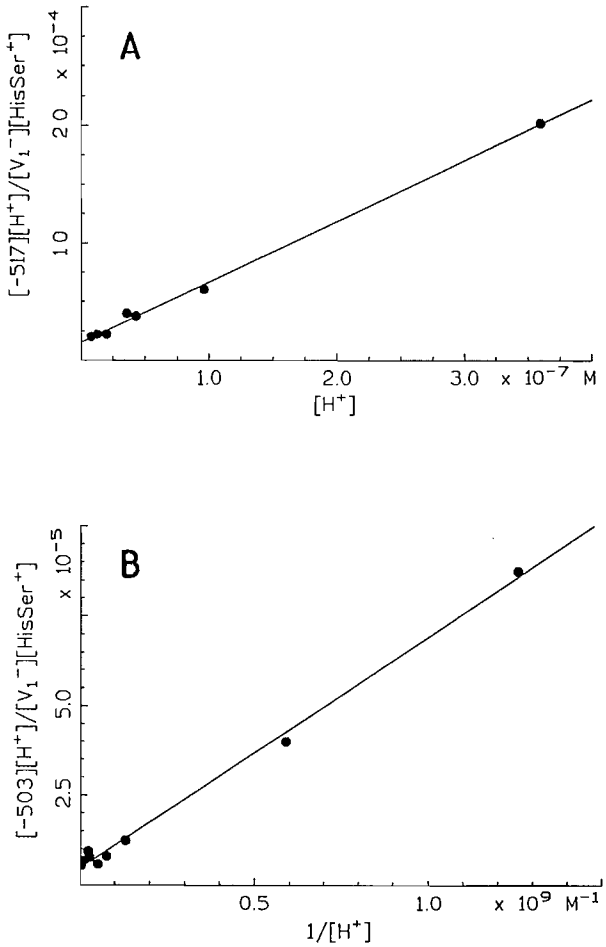

the charge state remains constant at −1 as the product is formed. Clearly, however, an additional proton can be given up from the vanadium centre and, of course, also from imidazolium but in independent reactions.

Additional information about the product complexes was obtained from ^{13}C NMR spectra. Table 2 gives the carbon chemical shifts, for both the ligand and the product complexes, for a selection of pD values. The coordination-induced shifts are also given.

The −517 ppm product, the product favoured by lower pH, shows significant coordination shifts only for the backbone carbons. This is consistent with a tridentate complexation involving the terminal nitrogen, terminal carboxyl, and peptidp nitrogen as proposed earlier for simpler peptides with nonfunctionalized side chains (9, 11). For the −503 ppm product there is a large complexation shift for the carbon of the serine hydroxymethyl group. This supports the pH study that revealed the loss of a single proton as this product is formed. In

Scheme 1

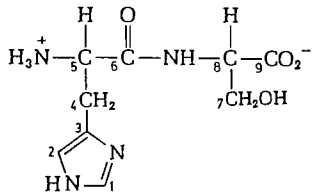

this case a $-CH_2O^-$ rather than a $-CO_2^-$ is the ligating group. No large coordination shifts were observed for the imidazole carbons, reinforcing the view that no vanadium–imidazole bond is generated as the complex is formed.

The fact that an additional proton can be lost from the vanadium centre of either complex almost certainly means that the products are not five-coordinate. If they were, the proton being lost in the subsequent deprotonation reaction would originate from the ammonium group ($V\text{-}NH_2$-) of the complex since there are no other protons. There is no evidence from this work that the terminal amino functionality is complexed as other than an amino group when either of the products is formed. The $-O^-$ of monoanionic vanadate ($VO_2(OH)_2^-$) might form a hydroxo ligand in the early stages of product formation, possibly by the ammonium changing to amino during the initial stages of complex formation. Following this formalism, an aquo ligand would subsequently be formed by incorporating the hydrogen from the peptide nitrogen into one of the hydroxo ligands as the reaction proceeds, with elimination of water, to form products. Loss of any protons would have been revealed in the pH variation study. The only alternative is that there is proton transfer from the NH_2 group to a hydroxo group to form an aquo ligand. This seems unlikely, but it is possible and might account for the slow formation of these products. The two possibilities are depicted in Scheme 2. (Note that a five-coordinate product would be formed if water was released from **A**.) A reviewer has suggested that the ^{13}C coordination-induced shift of the carbon 5 (~11 ppm) is not large enough to account for the formation of a product such as **B**. This argument has merit since, for **B**, the bonding about nitrogen would, in essence, go from that of a primary ammonium functionality in the free ligand to a secondary amino group in the product. In product **A** the ammonium-type functionality is retained as the product is formed.

Phenylglutamate

Experimental results from a detailed study of the reaction of this dipeptide with vanadate have been reported (17). These results were interpreted to mean that in addition to the expected mononuclear monoligand product, VP, an additional binuclear bisligand product (V_2P) was formed. In view of the complications that can arise from competing interactions and the conclusions drawn from the original work, reevaluation of the published data might provide some useful insights. It has previously been shown that vanadate undergoes a condensation reaction with carboxylates to form a product that is in rapid equilibration with its precursors (18). It is then necessary to analyze the original data in accordance with eq. [5]. When the data were plotted as appropriate for eq. [5], the intercept was $(3.1 \pm 0.3) \times 10^{-3}\ M^{3/4}$, which corresponds to $(1.1 \pm 0.4) \times 10^{10}\ M^{-3}$ for K_{14}. This intercept can be used in conjunction with the concentrations of tetravanadate to ascertain the concentration of monovanadate for all ligand concentrations

Can. J. Chem. Downloaded from www.nrcresearchpress.com by 65.111.164.53 on 09/08/12
For personal use only.

Table 2. ^{13}C chemical and coordination shifts for the products of the reaction of histidylserine with vanadate obtained as a function of pH.[a]

	pH 7.14			pH 7.80					pH 8.63				
	Chemical shift		Coordination shift	Chemical shift			Coordination shift		Chemical shift			Coordination shift	
		Product			Product					Product			
Carbon	Ligand	−517[b]	−517[b]	Ligand	−517[b]	−503[b]	−517[b]	−503[b]	Ligand	−517[b]	−503[b]	−517[b]	−503[b]
1	138.6	138.6	0.0	138.7	139.0	0.3			138.9	[c]	139.2	[c]	0.3
2	120.9	120.1	−0.8	121.0	119.9	120.2	−1.1	−0.8	121.1	120.0	120.2	−1.1	−0.9
3	132.6	134.4	1.8	133.8	135.2		1.4		134.7	135.4	135.7	0.7	1.0
4	31.8	32.3	0.5	33.0	32.7	31.6	−0.3	−1.4	33.8	32.8	31.7	−1.0	−1.9
5	60.1	70.6	10.5	59.8	70.6	72.5	10.8	12.7	59.7	70.6	72.6	10.9	12.9
6	174.2	182.3	8.1	176.4	182.5		6.1		178.0	182.7	183.6	4.7	5.6
7	64.7	65.4	0.7	64.7	65.3	78.2	0.6	13.5	64.9	65.5	78.3	0.5	13.4
8	56.2	60.3	4.1	56.7	60.5	61.3	3.8	4.6	57.2	60.5	61.4	3.3	4.6
9	178.6	185.6	7.0	178.6	185.6		7.0		178.7	185.7	182.5	7.0	4.2

[a]All ^{13}C NMR shifts are for 90 mM total vanadate and 100 mM histidylserine in D_2O solution at the indicated pH except for the ligand spectra where 90 mM KCl was added as an electrolyte to repalce the vanadate in the solution. The shifts quoted are for the numbering system shown in Scheme 1.

[b]Product complexes are identified by their ^{51}V chemical shifts.

[c]No signal was observed for this carbon. The signal is expected to lie under those of the free ligand and the −517 ppm product.

Can. J. Chem. Downloaded from www.nrcresearchpress.com by 65.111.164.53 on 09/08/12
For personal use only.

of the study, an important factor for further analysis of the data.

Examination of the data for the major product of the reaction (−515 ppm, pH 7.6) was carried out according to eq. [4]. For this analysis, the concentration of monovanadate was determined from that of tetravanadate and its formation constant. This allowed the formation of the carboxylate-derived product, described above, which is in rapid equilibration with V_1, to be accounted for. Under these conditions, the downward curvature in the graph that was previously reported from the ligand concentration study was not observed (Fig. 5*A*). This result, therefore, is not consistent with the formation of a binuclear monoligand product, as previously reported from analysis of these data (18). The formation constant obtained from this analysis for VP (−515 ppm), obtained from the ligand concentration study, was $(2.4 \pm 0.2) \times 10^2$ M^{-1} (Fig. 5*A*) and $(2.1 \pm 0.1) \times 10^2$ M^{-1}(Fig. 5*B*) from the vanadate ion concentration study (all data from ref. 15). There is no evidence, in Fig. 5*B*, of upward curvature. Therefore, this second graph also provides no evidence for formation of a monoligand bisvanadate product.

Tyrosylglycine

Reaction of tyrosylglycine with vanadate at pH 7.0 revealed the formation of a single product with a vanadium chemical shift of −513 ppm. A vanadate ester formed at the phenolic hydroxyl group will also have formed (14) but it was not observed at the rather low peptide concentrations of this study, maximum 15 mM. The measured formation constant was 34 ± 3 M^{-1} for pH 7.0. The pH variation study did not reveal the formation of any additional products. It did, however, show that the observed product carried a single negative charge and that this product had a pK_a of about 9. The broad product signal could not be accurately integrated at the high pH values, where the signal was of low intensity. As a consequence the pK_a value was only poorly defined.

The reaction of glycyltyrosine with vanadate was not studied in detail. The spectra that were obtained gave a formation constant of about 70 M^{-1} for the product at pH 7.0. A rather detailed study of this system, carried out at pH 7.2, has been reported (18). The reported data give a value of $(1.1 \pm 0.1) \times 10^2$ M^{-1} for K_1.

No product was observed to form with 60 mM tyrosylglycylglycine. Similarly 60 mM tryptophylglycylglycine did not yield an observable product. However, products were formed with tryptophylglycine, glycyltryptophan, tyrosyltyrosine, and similar ligands. Table 3 lists the compounds studied and the product formation constants.

A study of glycyltyrosine has reported the formation of products that are different from those described above and that are formed after several days of incubation (16). Such products were also observed here but they have not been studied in detail. Because of the long incubation times it is possible that an oxidative reaction occurs to give these products. Vanadate is known to oxidize phenolic materials and any V(IV) produced in the oxidation would quickly recycle to V(V) by air oxidation. This could account for the observed NMR spectra.

Tryptophyltyrosine

Only one product was observed from the reaction of tryptophyltyrosine with vanadate. The product observed gave a ^{51}V NMR signal at −520 ppm. This chemical shift is close to that observed for the products formed with other peptides. As for tyrosylglycine, no product of reaction at the hydroxyl group was observed because of the low concentrations employed in the study. When the experimental results were correlated according to eq. [4], a good linear relationship was observed as is shown in Fig. 6. The product formation constant, K_1, obtained from this graph was $(5.7 \pm 0.3) \times 10^2$ M^{-1}.

A pH variation study was carried out for a total ligand concentration of 9.0 mM. The results provided no evidence for additional products. The linear correlation obtained when the

Can. J. Chem. Downloaded from www.nrcresearchpress.com by 65.111.164.53 on 09/08/12
For personal use only.

Scheme 2

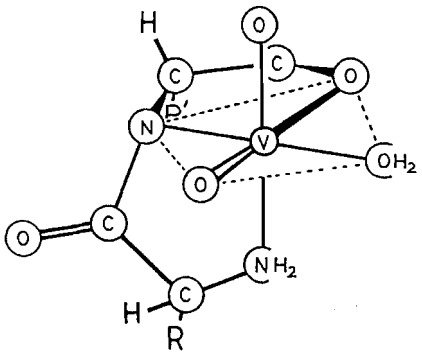

A

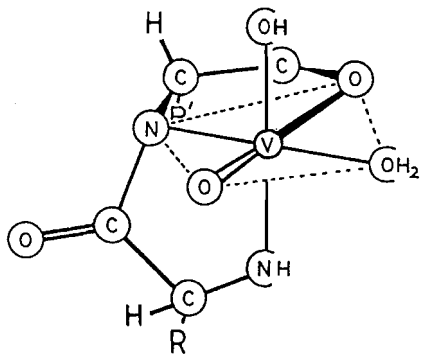

B

reaction was written according to eq. [11] gave a pK_{a2} of 8.5 for the product and a value for K_1' of $(2.1 \pm 0.7) \times 10^2\ M^{-1}$.

[11] $H_2VO_4^- + \text{trptyr} \overset{K_1'}{\rightleftharpoons} VP^-$

K_{a2}' H^+ K_a H^+ K_{a2} H^+

HVO_4^{2-} trptyr^- VP^{2-}

Tryptophyltryptophan

The only observed product of the reaction of tryptophyltryptophan with vanadate gave a −518 ppm NMR signal. A product formation constant of $(1.8 \pm 0.4) \times 10^2\ M^{-1}$ was determined for this ligand. The pH variation study, carried out at 7 mM total ligand, did not reveal the formation of any additional products but gave a value for K_1' of $(2.2 \pm 0.3) \times 10^2\ M^{-1}$ and of 8.1 for the pK_{a2} of the product. This pK_{a2} can be compared with the value of 8.5 obtained for the tryptophyltyrosine product, those in the order of about 7 for the histidine-derived products, and those of about 10 for other dipeptides that have aliphatic side chains (11).

In addition to the preceding two dipeptides, several others with aromatic side chains were studied in a cursory fashion at pH 7.0 and formation constants were estimated by ignoring possible complicating factors such as those already discussed. The results are presented in Table 3.

Fig. 5. The formation of the −515 ppm product of the reaction of phenylglutamate with vanadate is shown. The data for Fig. 5*A* are taken from the ligand concentration study portion of Table 1, ref. 18 while the data for Fig. 5*B* are from the vanadate concentration study section of the same table. The conditions for the experiments were (*A*) total vanadate, 10.0 mM; variable phenylglutamate, 10–90 mM; pH, 7.5; ionic strength, 1.0 M with NaCl; (*B*) total phenylglutamate, 30 mM; variable added vanadate, 3.0–27 mM; pH, 7.5; ionic strength, 1.0 M with NaCl.

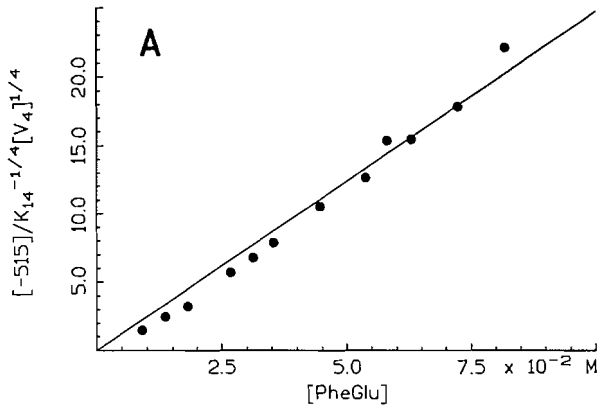

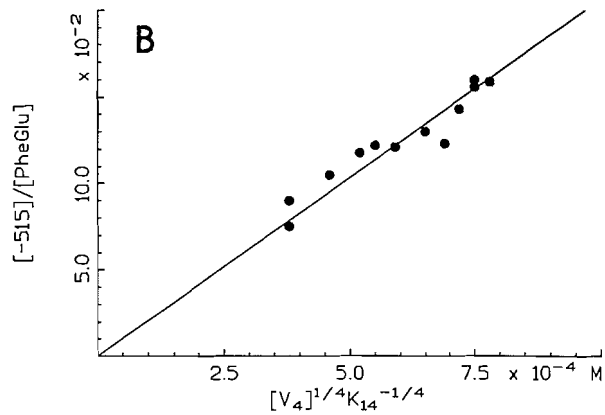

Discussion

Product formation, in all the systems studied here, involves tridentate complexation through the peptide nitrogen, the N-terminal nitrogen, and a C-terminal oxygen, as for dipeptides containing nonfunctionalized side chains (9, 11). For the histidine-containing ligands, the formation of the product is quite sensitive to the protonation state of the imidazole ring in free ligand. Presumably this, to a large extent, reflects conformational changes associated with the varying protonation states. ^1H NMR studies of the histidine signals of histidylserine showed that the pK_a values of the imidazolium in the free ligand and in the vanadium complex are not much different from each other. It is expected that this finding also applies to the other histidine-containing ligands of this study (Table 1).

Table 3. Formation constants and ^{51}V chemical shifts for the products of the reaction of a number of dipeptides with vanadate.

Dipeptide	^{51}V chemical shift (ppm)	K_1 (pH 7.0) (M^{-1})	pK_a
TrpTyr	−520	570 ± 30	8.5 ± 0.3
TrpTrp	−518	180 ± 40	8.1 ± 0.3
TrpPhe[a]	−519	47	
TyrTyr[a]	−519	140	
TyrGly	−511	34 ± 3	
GlyTyr[a,b]	−510	125	
GlyTrp[a]	−510	144	
TrpGly[a]	−511	101	
PheGlu[a,b]	−515	252	
No chelate products were observed under the reaction conditions for 60 mM TyrGlyGly,[c] 80 mM TrpGlyGly			

[a]Values for K_1 were estimated for a small number of spectra obtained at pH 7.0 for each ligand.

[b]The reported value was obtained from the pH 7.2 data in ref. 18 and corrected to pH 7.0.

[c]Reaction at the hydroxyl group of the tyrosine ring was observed, as expected (14).

Fig. 6. A graphical representation of the formation of the −522 ppm product of the reaction of tryptophyltyrosine with vanadate is shown. The graph is consistent with the formation of a monoligand monovanadium product. The conditions of the experiments were as follows: total vanadate, 6.2 mM; total tryptophyltyrosine, variable, 3.0–30 mM; pH, 7.0; ionic strength, 1.0 M with KCl.

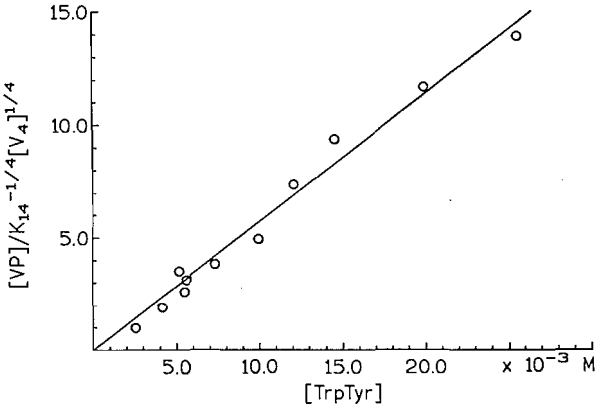

The presence of significant electrostatic or hydrogen-bonding interactions between the vanadium centre and the imidazole ring in the product would be expected to have a large effect on the pK_a of the imidazole, compared to that of the free ligand. Since any such effect must be small, it is evident that the pK_a of the imidazole is not the same parameter as the pK_a determined from the pH dependence of the formation constant. They need not be the same because product formation is not necessarily influenced by the charge on a remote group. As previously mentioned, with such dipeptides as glycylglycine, the second pK_a of the product is about 10 (11). There is no apparent reason why this value should drop to near 7 because of the presence of a histidine rather than a glycine. However, other complexes with dipeptides that have an aromatic side chain, tryptophyltryptophan and tryptophyltyrosine, also had reduced pK_a values (Table 3). It seems evident, therefore, that aromatic side chains, including that of histidine, have a significant effect on the stability of vanadate complexes of dipeptides, even though there is no evidence for vanadium – aromatic group bond formation. In the case of histidine, the evidence clearly shows there is no vanadium–imidazole bond formation. A recent X-ray study of a histidine-containing complex also did not show a vanadium – imidazole nitrogen bond (19) although, in other systems, such bond formation does occur as, for example, in a salicylidene – ethyl imidazole complex (20). It is possible that products with imidazole–vanadium bonds also form here but, if they do, they are comparatively disfavoured products.

Dipeptides containing other aromatic side chains such as those of tyrosine or tryptophan do not appear to react much differently with vanadate than do nonfunctionalized peptides. The product formation constants tend to be somewhat larger for the aromatic systems but this may, to a large extent, simply reflect changes in the population density of the various rotomeric isomers of the uncomplexed dipeptides. Clearly, however, electronic influences of the aromatic rings cannot be ignored.

Side chains such as those of glutamate or lysine apparently have little influence on formation of dipeptide–vanadate complexes, although the side-chain carboxylate group of glutamate will react to form an anhydride similar to those formed with acetate and other carboxylic acids (21).

Only seryl and threonyl side chains have been observed to coordinate to vanadate and do so by substituting a terminal carboxylate oxygen of the dipeptide by the oxygen of the hydroxyl group. In the latter case, a proton is released as products are formed (this work, and ref. 11).

With only a few exceptions, in the examples that have been studied, the major products have ^{51}V chemical shifts between −510 and −520 ppm with the frequency shifting to about −500 ppm when a hydroxyl replaces a carboxyl group in the product complex. In this regard, it is interesting to note that vanadate complexes with a number of multidentate ligands related to the peptides of this study had chemical shifts varying from −507 to −521 ppm when the ligand contained a carboxylate group and below 500 ppm for hydroxyl-containing derivatives. A six-coordinate geometry was proposed for these materials (10). A crystalline material prepared from the tetradentate ligand, tris(2-hydroxyethyl)amine, has been characterized by X-ray diffraction studies (22). This material is pentacoordinate but the ^{51}V chemical shift (−483 ppm, ref. 10) is outside the range of chemical shifts observed for the complexes studied here. Overall, for the peptide complexes, the evidence strongly supports a coordination of the form displayed in Scheme 2(**A**) but, for the reasons discussed earlier, a pentacoordinate geometry cannot be unequivocally ruled out.

Acknowledgements

The support of the Natural Sciences and Engineering Research Council of Canada in the form of an operating grant to A.S.T. is gratefully acknowledged.

Can. J. Chem. Downloaded from www.nrcresearchpress.com by 65.111.164.53 on 09/08/12
For personal use only.

References

1. N.D. Chasteen (*Editor*). Vanadium in biological systems. Kluwer Academic Publishers, Dordrecht, Boston, London. 1990.
2. H. Sigel and A. Sigel (*Editors*). Metal ions in biological systems. Vol. 31: Vanadium and its role for life. Marcel Dekker, Inc., New York. 1995.
3. R.E. Eady. Tetrahedron, **8**, 1695 (1989).
4. B.J. Hales, E.E. Case, J.E. Morningstar, M.F. Dzeda, and L.A. Mauterer. Biochemistry, **25**, 7251 (1986).
5. R.L. Robson, R.E. Eady, T.H. Richardson, R.W. Miller, M. Hawkins, and J.R. Postgate. Nature, **322**, 388 (1986).
6. E. de Boer, Y. van Kooyk, M.G.M. Tromp, H. Plat, and R. Wever. Biochim. Biophys. Acta, **869**, 48 (1986).
7. H.S. Soedjak and A. Butler. Biochim. Biophys. Acta, **1079**, 1 (1991).
8. R. Wever and B.E. Krenn. *In* Vanadium in biological systems. *Edited by* N.D. Chasteen. Kluwer Academic Publishers, Dordrecht, Boston, London. 1990. pp. 81–97.
9. D. Rehder. Inorg. Chem. **27**, 4312 (1988).
10. D.C. Crans and P.K. Shin. J. Am. Chem. Soc. **116**, 1305 (1994).
11. J.S. Jaswal and A.S. Tracey. Can. J. Chem. **69**, 1600 (1991).
12. A.S. Tracey and J.S. Jaswal. Inorg. Chem. **32**, 4235 (1993).
13. M. Fritzsche, V. Vergopoulos, and D. Rehder. Inorg. Chim. Acta, **211**, 11 (1993).
14. A.S. Tracey and M.J. Gresser. Proc. Natl. Acad. Sci. (U.S.A.), **83**, 609 (1986).
15. D.C. Crans, R.L. Bunch, and L.A. Theisen. J. Am. Chem. Soc. **111**, 7597 (1989).
16. D.D. Perrin and W.L.F. Armarego. *In* Purification of laboratory chemicals. 3rd ed. Pergamon Press, Oxford, New York. 1988.
17. A.S. Tracey, M.J. Gresser, and S. Liu. J. Am. Chem. Soc. **110**, 5869 (1988).
18. D. Rehder, H. Holst, W. Priebsch, and H. Vilter. J. Inorg. Biochem. **41**, 171 (1991).
19. V. Vergopoulos, W. Priebsch, M. Fritzsche, and D. Rehder. Inorg. Chem. **32**, 1844 (1993).
20. C.R. Cornman, J. Kampf, and V.L. Pecoraro. Inorg. Chem. **31**, 1981 (1992).
21. A.S. Tracey, H. Li, and M.J. Gresser. Inorg. Chem. **29**, 2267 (1990).
22. D.C. Crans, H. Chen, O.P. Anderson, and M.M. Miller. J. Am. Chem. Soc. **115**, 6769 (1993).

Can. J. Chem. Downloaded from www.nrcresearchpress.com by 65.111.164.53 on 09/08/12
For personal use only.

Structure – activity relationships in antagonist and inverse agonist ligands for the benzodiazepine receptor

Penelope W. Codding, Aleksander W. Roszak, Maria B. Szkaradzinska, James M. Cook, Timothy J. Hagen, and Michael S. Allen

Can. J. Chem. Downloaded from www.nrcresearchpress.com by 65.111.164.53 on 09/08/12
For personal use only.

Abstract: The X-ray crystal and molecular structures of the three benzodiazepine (BZD) receptor ligands are presented and the electronic character of inverse agonist ligands is probed through molecular orbital calculations. Two of the ligands have a 6-benzylamino substituent: 6-benzylamino-β-carboline-3-carboxylic acid methyl ester, **1**, which is a high affinity antagonist with IC_{50} = 10 nM, and 6-benzylamino-β-carboline, **2**, which is a moderate affinity inverse agonist with IC_{50} = 106 nM. The third compound, 3-ethoxy-β-carboline hydrochloride, **3**, displays partial inverse agonist activity with an IC_{50} of 24 nM. Intermolecular interactions, including extensive hydrogen bonding involving both the pyridyl nitrogen atom and the indole N—H as well as π stacking of aromatic rings, are characteristic of β-carbolines and are found in these three structures. In addition, two of these compounds are protonated in the crystalline state, thereby providing a model for interactions in the absence of the 3-carboxylic acid ester function. Electronic calculations show that (1) the partial inverse agonist ligand has the highest charge on the N(2) atom and (2) high affinity β-carbolines possess two neighboring sites that have high electrostatic attraction for a hydrogen atom in an intermolecular interaction. These findings suggest that modifications to the 3-position side chain to enhance the charge on the pyridyl N atom and provide a hydrogen bond acceptor site will facilitate the development of *partial* inverse agonist ligands.

Key words: β-carbolines, benzodiazepine receptor, crystallography, structure–activity relationships.

Résumé : Faisant appel à la diffraction des rayons X, on a déterminé les structures cristallines et moléculaires de trois coordinats récepteurs de benzodiazépine (BDZ) et on a évalué le caractère électronique des coordinats agonistes inverses à l'aide de calculs d'orbitales moléculaires. Deux des coordinats portent un substituant 6-benzylamino, soit l'ester méthylique de l'acide 6-benzylamino-β-carboline-3-carboxylique (**1**), un antagoniste de grande affinité avec IC_{50} = 10 nM, et la 6-benzylamino-β-carbonlin (**2**), un agoniste inverse d'affinité modérée avec IC_{50} = 106 nM. Le troisième composé, le chlorhydrate de la 3-éthoxy-β-carboline (**3**), présente une activité agoniste inverse partielle avec IC_{50} = 24 nM. Les interactions intermoléculaires, comprenant des ponts hydrogènes importants impliquant l'atome d'azote du pyridyle ainsi que le N—H de l'indole de même que l'empilement π des noyaux aromatiques, sont caractéristiques des β-carbolines et on les retrouve dans les trois structures. De plus, deux de ces composés, protonés à l'état cristallin, peuvent servir de modèles pour les interactions en l'absence de la fonction ester de l'acide 3-carboxylique. Les calculs électroniques montrent que (1) le coordinat avec une activité agoniste inverse partielle porte la charge la plus importante sur l'atome N(2) et (2) que les β-carbolines de plus grande affinité possèdent deux sites voisins qui ont une grande attraction électrostatique pour un atome d'hydrogène dans une interaction intermoléculaire. Ces observations suggèrent que des modifications à la chaîne latérale en position 3 augmentent la charge sur l'atome d'azote du pyridyle et qu'elles fournissent un site accepteur de liaisons hydrogènes qui facilite le développement de coordinats possédant une activité agoniste inverse *partielle*.

Mots cles : β-carbolines, récepteur de benzodiazépine, cristallographie, relations structure–activité.

[Traduit par la rédaction]

Received June 28, 1994.

P.W. Codding,[1] A.W. Roszak,[2] and M.B. Szkaradzinska. Departments of Chemistry and of Pharmacology and Therapeutics, University of Calgary, Calgary, AB T2N 1N4, Canada.
J.M. Cook, T.J. Hagen, and M.S. Allen. Department of Chemistry, University of Wisconsin–Milwaukee, Milwaukee, WI 53201, U.S.A.

[1] Author to whom correspondence may be addressed. Telephone: (403) 220-5340. Fax: (403) 284-1372.
[2] Current address: Department of Chemistry, Queen's University, Kingston, Ont., Canada.

Can. J. Chem. Downloaded from www.nrcresearchpress.com by 65.111.164.53 on 09/08/12
For personal use only.

Introduction

The benzodiazepine (BZD) receptor found in brain is part of a ligand-gated ion channel that contains the γ-amino butyric acid (GABA) receptor and the chloride ionophore (1, 2). Ligands for the central nervous system BZD receptor allosterically modulate responses to GABA and mediate anticonvulsant, anxiolytic, hypnotic, and sedative effects (3). Agonist ligands for the receptor elicit these responses, antagonists bind and elicit no response, and inverse agonist ligands elicit opposite responses (convulsant, etc.). In addition to useful properties, the drugs often induce unwanted effects, like amnesia, and tolerance is rapidly developed. Recently the focus has been on the design of ligands that elicit a *partial* response: partial agonists show fewer side effects and partial inverse agonists may be useful as cognition enhancers. Efforts to develop more effective ligands have been advanced by recent progress toward understanding the molecular composition of the receptor complex. The receptor complex has been cloned and functional multisubunit complexes have been expressed; however, the exact stoichiometry of the functional complex in the central nervous system is not known (4). The receptor complex shows extensive heterogeneity, including six forms of the α subunit, three forms of the β subunit, three forms of the γ subunit, and a δ subunit (4). The presence of three types of subunit, α, β, and γ, is required for a functional ion channel controlled by GABA and modulated by BZDs. BZD ligands appear to interact with the α subunit but only behave as modulators of GABA when the γ subunit is also present. Structure–function studies (5–7) on reconstituted channels suggest that different subtypes recognize ligands with different effects, although this information is neither unequivocal or sufficiently broadly tested to be conclusive. Tests on reconstituted complex with a small set of ligands (agonist benzodiazepines and inverse agonist β-carbolines) suggest that the binding sites of agonists and inverse agonists may be in different domains and may be modulated by the specific combination of types of α and γ subunit. Unfortunately, different chemical species (β-carboline inverse agonists and benzodiazepine agonists) were tested, which prevents simple deductions from the evidence; however, these results open the possibility that separate sites for positive and negative efficacy ligands may exist and may require reconceptualization of many of the current models (see ref. 8 for a review) for the BZD binding site.

The structural features that favor binding of a β-carboline at the BZD receptor have been established (9–15). They include a planar, unsaturated ring system, a basic pyridyl N atom, an unobstructed indole N-H group, and at least one additional substituent: either (*a*) a side chain in position 3 that contains a carbonyl oxygen atom or is electron releasing, or (*b*) a hydrophobic group in position 5 or 6, or (*c*) an oxygen-containing side chain in position 4. The binding affinity and specific activity of the β-carbolines seems to be determined by recognition of each of these different types of side chain and a balance among the recognition sites. Many β-carbolines have been synthesized and tested in an effort to develop effective agonist ligands for the BZD receptor. Predicting the balance between the effects of the side chains (*a*)–(*c*), as described above, is challenging. Compound ZK93423, 6-benzyloxy-4-methoxymethyl-β-carboline-3-carboxylic acid ethyl ester, is a potent BZD receptor agonist (IC_{50} = 1.0 nM) (16). When a 6-benzylamino group (17) is added to position 6 of either of the

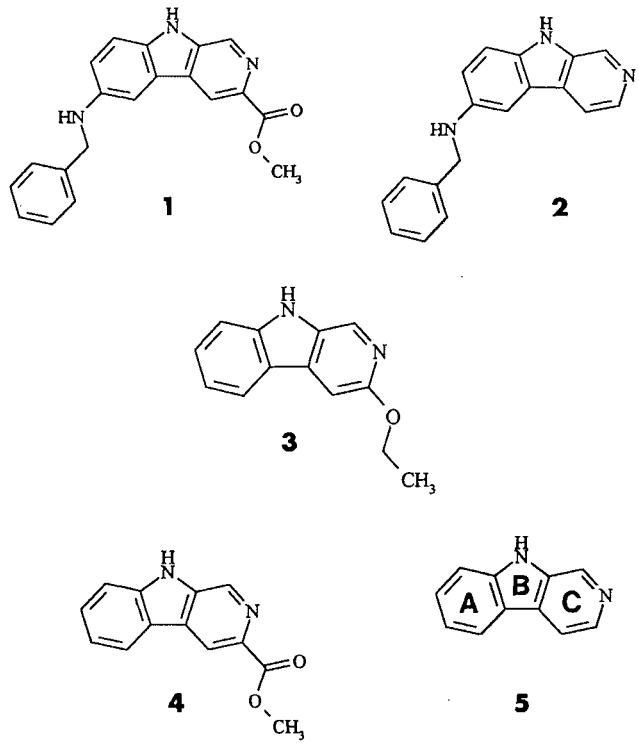

β-carbolines **4** and **5**, as an isostere for the benzyloxy group, the compounds do not have agonist activity. The addition of the 6-benzylamino to the inverse agonist βCCM (**4**) produces an antagonist, 6-benzylamino-β-carboline-3-carboxylic acid methyl ester, **1**. The same substitution in norharmane, **5**, a compound that has no detectable activity, produces 6-benzylamino-β-carboline, **2**, which is an inverse agonist (17). It appears that substituents in all three positions, (*a*)–(*c*), may be required to achieve agonist activity (18).

In addition to the goal of understanding the components dictating specific activity, a detailed understanding of the features that determine affinity is needed to design partial agonists (19), which are the preferred therapeutic targets because they induce fewer side effects. Thus, exercising precise control over the efficacy of BZD ligands is required. The compounds presented here present some of the issues related to understanding affinity and hence efficacy. The addition of the 6-benzylamino group greatly enhances the affinity of **2** over norharmane (**5**) and may suggest that there is an additional binding site on the receptor, perhaps hydrophobic in nature, which interacts with the benzylamino groups of **1** and **2**. However, compound **1** does not bind more effectively than the related compound βCCM, compound **4**, which has an IC_{50} = 1 nM, even though **1** possesses both the hydrophobic side chain in position 6 and the 3-methyl ester of compound **4**. This difference suggests either that the side chains produce complex electronic effects or that molecular size (in particular, molecular length) is an important criterion for binding. To further investigate the electronic effects of ligands, we studied compound **3**, 3-ethoxy β-carboline, which has an IC_{50} value of 24 nM and an activity profile similar to βCCM and compound **2**, which has an electron-releasing group in position 3. The profiles of the three compounds (**2**, **3**, and **4**) suggest that reasonable affinity and inverse (or partial inverse) agonist activity

Can. J. Chem. Downloaded from www.nrcresearchpress.com by 65.111.164.53 on 09/08/12
For personal use only.

Table 1. Crystal data.

Compound	1	2	3
Formula	$C_{20}H_{17}N_{30}O_2 \cdot 1/2\ (C_4H_8O_{20})$	$C_{18}H_{15}N_31 \cdot 3/2\ (C_2H_4O_2) \cdot 1/2\ (H_2O)$	$C_{13}H_{12}N_2O \cdot HCl$
FW	375.43	372.43	248.71
Crystal dimensions (mm)	0.40 × 0.38 × 0.14	0.38 × 0.16 × 0.12	0.34 × 0.32 × 0.27
System and space group	Triclinic, $P\bar{1}$	Triclinic, $P\bar{1}$	Triclinic, $P\bar{1}$
a(Å)	11.052(1)	6.1118(7)	7.3883(3)
b(Å)	11.500(2)	18.753(2)	8.3839(2)
c(Å)	16.400(2)	19.802(2)	10.1130(3)
α(°)	69.622(9)	61.29(1)	105.485(2)
β(°)	81.838(9)	79.32(1)	99.352(3)
γ(°)	82.23(1)	83.00(1)	93.670(3)
V(Å)	1925.9(5)	1954.7(4)	591.85(3)
Z	4	4	2
F(000)	792	788	260
ρ_c (g cm^{-3})	1.295	1.265	1.398
μ (cm^{-1})	7.22	7.24	27.35
h, k, l ranges	0,13; −13,14; −19,19	0,6; −19,19; −19,21	0,9; −10,10; −12,12
Max. (sin Θ) / λ (Å^{-1})	0.6090	0.5310	0.6262
No. of unique reflections	7278	4924	2442
No. of observed reflections ($I > 2.5\ \sigma_I$)	5184	2806	2410
No. of reflections used in refinement[a]	6346	4256	2413
No. of parameters refined	620	592	207
k value/weighting: $w^{-1} = \sigma_F^2 + k(F_o^2)$	0.0001	0.0001	0.0001
Final R	0.067	0.066	0.037
R_w	0.071	0.061	0.048
S (goodness of fit)	1.48	1.12	1.15
Max. shift/error (final cycle)	0.06	0.04	0.01
Max. residual density in ΔF map (e Å^{-3})	0.48	0.26	0.34
Min. residual density in ΔF map (e Å^{-3})	−0.20	−0.18	−0.24
Isotropic extinction parameter	1.42(6) × 10^{-3}	Not used	Not used

[a]The reflections used in the refinement included the observed reflections and those unobserved reflections for which $F_c^2 > 2.5\ \sigma(F_o^2)$.

can be achieved by either an electron-withdrawing or electron-releasing group in the 3-position or by no substituent at the 3-position and a substituent at the 6-position, whereas the presence of both substituents (at 3 and at 6) produces an antagonist of high affinity (**1**).

We report the results of crystal structure determinations of compounds **1**, **2**, and **3**, which establish their preferred intermolecular interactions, along with the results of molecular orbital calculations on the inverse agonists (compounds **2**, **3**, and **4**), which establish the electronic effects of their side chains. This study seeks to provide explanations for the complex structure–activity profile of β-carbolines.

Experimental section

X-ray crystallography

Samples were crystallized in the Wisconsin laboratory from an ethyl acetate – ethanol mixture (**1**), from acetic acid (**2**), and from an ethanol–hydrochloride mixture (**3**) by a slow evaporation. X-ray intensity data were collected at room temperature on an Enraf–Nonius CAD-4F automated diffractometer with Ni-filtered CuK_α radiation (λ = 1.54178 Å) using an ω/2θ scan mode. The cell parameters and orientation matrices were determined by least-squares refinement of the angular positions of 25 reflections with θ-values in the range 41°–67° for **1**, 24°–31° for **2**, and 36°–39° for **3**. During the data collection the intensities of three standard reflections were measured every 2000 s of exposure; they showed no significant variation. All intensities were corrected for Lorentz and polarization effects; absorption corrections were not applied. A summary of crystal data and details of the structure refinements are given in Table 1.

All three structures were solved by direct methods, structures **1** and **2** using MULTAN78 (20*a*) and structure **3** using SHELXS86 (20*b*). Structures 1 and 2 were found to contain two independent β-carboline molecules per asymmetric unit together with several solvent molecules: one molecule of ethyl acetate in **1**, and three acetic acid molecules and one water molecule in **2**. Structure **3** contained one protonated β-carboline and one chloride ion in the asymmetric unit.

All H atoms, except for those of the carboxyl groups in the acetic acid molecules of **2**, were located in difference Fourier syntheses after isotropic refinement. In **2**, subsequent cycles of anisotropic refinement revealed the positions of two of the acetic acid carboxyl H atoms that were hydrogen bonded to the pyridyl nitrogen atoms of the two β-carboline molecules. In molecule **2***a*, the pyridyl N atom was fully protonated. In molecule **2***b*, a ΔF map contained two peaks between the

Can. J. Chem. Downloaded from www.nrcresearchpress.com by 65.111.164.53 on 09/08/12
For personal use only.

pyridyl N atom and one of the acetic acid carboxyl oxygen atoms. One of these peaks was located 1.23 Å from the nitrogen atom, the other 1.28 Å from the oxygen atom. The peaks were of equal height, indicating that the pyridyl N atom of molecule **2***b* is protonated in 50% of the molecules and that the H atom is bonded to the acetic acid molecule in the other half of the molecules. Both H atoms were included in the refinement with fixed coordinates, occupancy factors of 50%, and isotropic thermal parameters equal to 120% of the U_{eq} values of the appropriate N and O atoms. The H atom of the carboxyl group of the third acetic acid molecule (A3) was not located. In contrast to the complex pattern in the crystal structure of compound **2**, in **3** the difference Fourier synthesis indicated that the pyridyl N atom was fully protonated; this difference is probably due to the difference in strength of the acids used in formation of the β-carboline salts.

In structures **1** and **2**, blocked least-squares refinement was performed with the two independent β-carboline molecules in separate blocks and the parameters of the solvent molecules in one (for structure **1**) or two (for structure **2**) blocks. Refinement was done on *F*. In the final cycles of all three structural refinements, the coordinates and anisotropic thermal parameters of all the non-hydrogen atoms and the coordinates and isotropic thermal parameters of most of the H atoms, including all those involved in the hydrogen bonding to β-carboline molecules, were varied. The remaining H atoms were held in fixed positions with U_{iso} equal to the average U_{iso} of the neighboring refined hydrogen atoms.

The reflections used in the refinements included the observed reflections ($I > 2.5\ \sigma(I)$), and those unobserved reflections that had $F_c^2 > 2.5\ \sigma(I)$. Non-hydrogen atom scattering factors and anomalous dispersion corrections were from Cromer and Mann (21) and the H-atom scattering factors from Stewart et al. (22) The isotropic extinction correction used is based on the method of Larsen (23) and Zachariasen (24). All of the calculations except structure solution were done with the XRAY76 system of programs (25) implemented on a Honeywell computer; drawings of the individual β-carboline molecules were prepared with the program ORTEPII (26); the least-squares superpositions of molecules were calculated with the program PROFIT (27) and drawn with the program PLUTO (28).

The atomic coordinates and equivalent isotropic thermal parameters for the non-H atoms are given in Table 2. The conformations of the β-carboline molecules and the atom labeling schemes are shown in Figures 1, 2, and 3. The bond distances and bond angles for the non-H atoms are listed in Table 3.[3]

[3] The anisotropic thermal parameters for the non-hydrogen atoms; coordinates, thermal parameters, bond lengths and angles for H atoms and for all atoms of solvent molecules; and the REFCODES of the Cambridge Structural Database search may be purchased from: The Depository of Unpublished Data, Document Delivery, CISTI, National Research Council Canada, Ottawa, Canada, K1A 0S2.

Tables of atomic coordinates, bond lengths and angles, and the REFCODES have also been deposited with the Cambridge Crystallographic Data Centre, and can be obtained on request from The Director, Cambridge Crystallagraphic Data Centre, University Chemical Laboratory, 12 Union Road, Cambridge, CB2 1EZ, U.K.

Structure factor amplitudes are no longer being deposited and may be obtained directly from the author.

Fig. 1. Molecular structures and atomic labeling schemes for (*a*) molecule **1***a* and (*b*) molecule **1***b*.

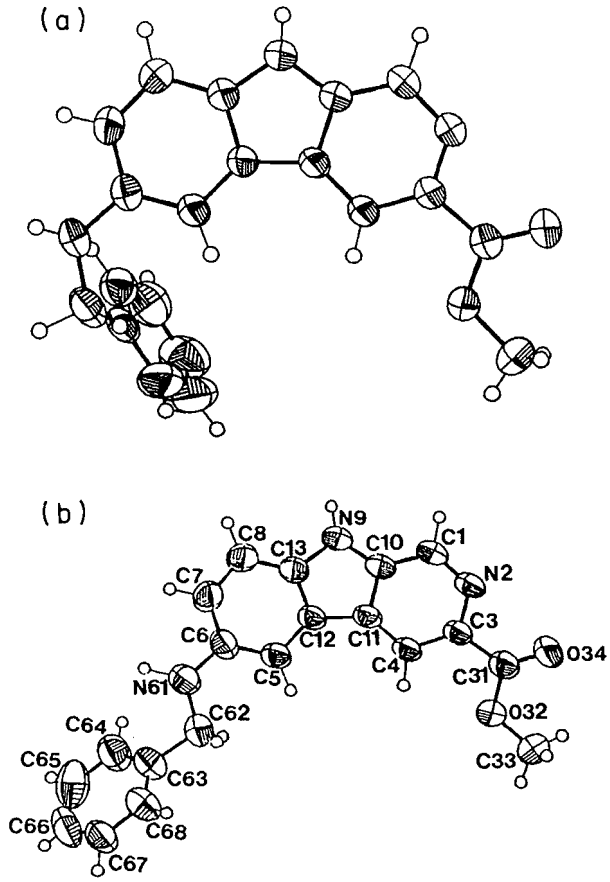

Computational methods

Molecular mechanics calculations were performed using the MM2 force field and extensions to it as provided in the program Macromodel (29) implemented on an IBM RISC/6000 computer. Usage-directed Monte Carlo searching of conformational space was used to examine 3000 conformers with tabulation of those conformers within 50 kJ mol^{-1} of the lowest energy structure.

Ab initio molecular orbital calculations were done by using the GAUSSIAN90 program (30) implemented on an IBM RISC/6000 computer. All calculations were conventional closed-shell molecular orbital calculations wherein equilibrium values of the geometrical parameters were obtained by minimizing the molecular energy. The geometry of each molecular structure was fully optimized using the STO-3G basis set and a stationary point calculation of electronic properties was done with the 3-21G basis set. The 3-21G basis set was used with the SPARTAN program[4] to evaluate the electrostatic potential at attraction energies of -5, -10, -30, -50, and -70 kcal mol^{-1}. Calculations on the 6-benzylamino compounds (**1** and **2**) were done on a model that replaced the phenyl ring with a methyl group and, in all cases, the conformation of the 3-position side chain was restricted to the most common conformation observed in the crystal structure.

[4] SPARTAN, Version 1.0, Wavefunction Inc., 18401 von Karman, Irvine, CA 92715, U.S.A. (1991).

Table 2(*a*). Fractional coordinates ($\times 10^4$) and equivalent isotropic thermal parameters ($Å^2 \times 10^2$) for non-H atoms of β-carboline **1** with esd's in parentheses.

$$B_{eq} = (8\pi^2/3)\Sigma_i\Sigma_j U_{ij} a_i^* a_j^* \boldsymbol{a}_i \cdot \boldsymbol{a}_j$$

	x	*y*	*z*	B_{eq}
Molecule A				
C(1)	9163(3)	7417(3)	2760(2)	512(15)
N(2)	8005(2)	7691(2)	3000(1)	502(12)
C(3)	7672(3)	7576(3)	3857(2)	461(13)
C(4)	8488(3)	7192(3)	4489(2)	439(13)
C(5)	11056(3)	6108(3)	5554(2)	489(14)
C(6)	12234(3)	5639(3)	5757(2)	525(15)
C(7)	13139(3)	5462(3)	5109(2)	565(17)
C(8)	12907(3)	5741(3)	4254(2)	535(16)
N(9)	11252(2)	6605(2)	3245(1)	508(12)
C(10)	10048(3)	6993(3)	3356(2)	458(13)
C(11)	9699(3)	6888(2)	4243(2)	426(13)
C(12)	10804(3)	6418(3)	4676(2)	432(13)
C(13)	11733(3)	6241(3)	4053(2)	466(14)
C(31)	6348(3)	7884(3)	4049(2)	532(15)
O(32)	6052(2)	7893(2)	4864(1)	658(12)
C(33)	4769(3)	8169(4)	5118(2)	808(22)
O(34)	5594(2)	8105(3)	3544(1)	837(15)
N(61)	12619(2)	5350(3)	6595(2)	667(15)
C(62)	11733(3)	5475(3)	7263(2)	625(18)
C(63)	12333(3)	5113(3)	8125(2)	613(18)
C(64)	11798(3)	4313(3)	8871(2)	648(19)
C(65)	12264(4)	4028(3)	9658(2)	661(19)
C(66)	13288(5)	4522(4)	9701(3)	862(26)
C(67)	13898(4)	5309(4)	8935(4)	975(29)
C(68)	13395(4)	5568(4)	8146(2)	793(23)
Molecule B				
C(1)	4385(2)	7387(3)	2080(2)	435(13)
N(2)	3384(2)	7100(2)	1858(1)	425(10)
C(3)	3286(2)	7364(2)	990(2)	390(12)
C(4)	4164(2)	7913(2)	333(2)	374(11)
C(5)	6721(2)	9225(2)	−806(2)	384(11)
C(6)	7848(2)	9704(2)	−1053(2)	406(12)
C(7)	8523(2)	9766(3)	−400(2)	465(13)
C(8)	8122(2)	9344(3)	474(2)	469(13)
N(9)	6381(2)	8345(2)	1542(1)	441(10)
C(10)	5314(2)	7956(2)	1454(2)	379(11)
C(11)	5206(2)	8222(2)	555(1)	352(11)
C(12)	6291(2)	8791(2)	84(2)	352(11)
C(13)	6997(2)	8847(2)	717(2)	379(11)
C(31)	2107(2)	7079(2)	813(2)	416(12)
O(32)	2068(2)	7308(2)	−45(1)	516(9)
C(33)	944(3)	7063(3)	−287(2)	620(17)
O(34)	1261(2)	6707(2)	1351(1)	551(10)
N(61)	8346(2)	10169(2)	−1920(1)	503(12)
C(62)	7773(3)	10042(3)	−2618(2)	496(15)
C(63)	7717(3)	8723(3)	−2597(2)	457(14)
C(64)	6809(3)	8447(4)	−2985(2)	736(21)
C(65)	6742(5)	7263(5)	−2970(3)	1001(30)
C(66)	7561(5)	6312(4)	−2561(3)	896(27)
C(67)	8462(3)	6556(3)	−2174(2)	673(20)
C(68)	8544(3)	7743(3)	−2192(2)	554(16)

Can. J. Chem. Downloaded from www.nrcresearchpress.com by 65.111.164.53 on 09/08/12
For personal use only.

Table 2(*b*). Fractional coordinates ($\times 10^4$) and equivalent isotropic thermal parameters ($Å^2 \times 10$) for the non-H atoms of β-carboline **2**.

	x	*y*	*z*	B_{eq}
Molecule A				
C(1)	2336(9)	8877(3)	5838(3)	52(3)
N(2)	323(8)	9032(2)	6125(2)	50(2)
C(3)	−1200(9)	8442(3)	6550(3)	51(3)
C(4)	−676(8)	7659(3)	6679(3)	45(3)
C(5)	1910(8)	5936(3)	6740(2)	42(2)
C(6)	3455(10)	5378(3)	6651(3)	49(3)
C(7)	5599(9)	5620(3)	6243(3)	57(3)
C(8)	6185(8)	6406(3)	5904(3)	59(3)
N(9)	4875(7)	7798(2)	5727(2)	54(2)
C(10)	2941(9)	8100(3)	5963(3)	44(3)
C(11)	1393(8)	7473(3)	6391(3)	40(2)
C(12)	2542(8)	6751(3)	6397(2)	40(2)
C(13)	4658(8)	6976(3)	5988(3)	46(3)
N(61)	3061(8)	4561(2)	6971(2)	65(3)
C(62)	883(11)	4243(3)	7326(3)	66(3)
C(63)	153(10)	4106(3)	8161(3)	49(3)
C(64)	−1881(12)	3790(4)	8536(4)	71(4)
C(65)	−2576(12)	3649(4)	9281(5)	80(5)
C(66)	−1246(17)	3821(4)	9669(4)	80(5)
C(67)	805(13)	4136(4)	9297(4)	75(4)
C(68)	1500(10)	4275(3)	8548(3)	57(3)
Molecule B				
C(1)	7020(11)	1048(3)	9523(4)	74(4)
N(2)	6880(8)	1676(3)	8825(3)	67(3)
C(3)	5035(12)	2184(3)	8672(3)	65(4)
C(4)	3204(11)	2064(3)	9246(3)	68(4)
C(5)	−310(9)	1392(3)	10950(3)	54(3)
C(6)	−1256(8)	967(3)	11713(3)	52(3)
C(7)	−69(9)	291(3)	12218(3)	55(3)
C(8)	1951(9)	8(3)	12011(3)	60(3)
N(9)	4986(7)	283(2)	10897(2)	56(2)
C(10)	5193(10)	875(3)	10152(3)	59(3)
C(11)	3248(10)	1407(3)	10011(3)	56(3)
C(12)	1810(9)	1107(3)	10714(3)	51(3)
C(13)	2882(8)	429(3)	11246(3)	54(3)
N(61)	−3291(7)	1176(2)	12031(2)	57(2)
C(62)	−4912(9)	1748(3)	11581(3)	61(3)
C(63)	−5094(9)	2566(3)	11568(3)	49(3)
C(64)	−6856(9)	3095(3)	11244(3)	64(3)
C(65)	−7107(12)	3850(4)	11220(4)	84(4)
C(66)	−5562(15)	4095(4)	11489(4)	90(5)
C(67)	−3857(13)	3579(4)	11804(3)	83(4)
C(68)	−3575(9)	2813(3)	11842(3)	62(3)

Can. J. Chem. Downloaded from www.nrcresearchpress.com by 65.111.164.53 on 09/08/12
For personal use only.

Results

In compound **1**, the conformation of the side chain in the 3 position places an oxygen atom in the plane of the β-carboline skeleton and *cis* to the pyridyl nitrogen atom. The coplanar conformation of the ester side chain in **1** allows formation of an extended π system over the side chain and the polycycle; the dihedral angle between the plane of the β-carboline and the plane defined by five side-chain atoms is 8.2(5)° in **1***a* and 5.6(5)° in **1***b*. The torsion angle N(2)-C(3)-C(31)-O(34), which determines the orientation of the carbonyl oxygen atom, is 6.6(5)° and 3.5(4)° in **1***a* and **1***b*, respectively. Although compound **3** does not have a 3-ester substituent, the side chain adopts a conformation that orients one of the lone pairs of electrons on the ether O atom toward N(2), a position similar to the orientation of the lone pairs on the carbonyl oxygen atom of

Can. J. Chem. Downloaded from www.nrcresearchpress.com by 65.111.164.53 on 09/08/12
For personal use only.

Table 2(*c*). The fractional coordinates ($\times 10^4$ and $\times 10^5$ for Cl) and equivalent isotropic thermal parameters ($Å^2 \times 10^2$) for the non-H atoms of β-carboline **3**.

Atom	*x/a*	*y/b*	*z/c*	B_{eq}
C(1)	3413(2)	1895(2)	4495(2)	286(5)
N(2)	2894(2)	1417(1)	3094(1)	273(5)
C(3)	2150(2)	2409(2)	2346(2)	265(5)
C(4)	1886(2)	4027(2)	3007(2)	266(5)
C(5)	1798(2)	7662(2)	5430(2)	330(6)
C(6)	2002(2)	8920(2)	6659(2)	387(7)
C(7)	2745(2)	8662(2)	7944(2)	377(7)
C(8)	3296(2)	7158(2)	8044(2)	334(6)
N(9)	3540(2)	4266(2)	6604(1)	308(5)
C(10)	3160(2)	3475(2)	5198(1)	260(5)
C(11)	2392(2)	4569(2)	4456(1)	246(5)
C(12)	2360(2)	6113(2)	5495(2)	264(5)
C(13)	3099(2)	5875(2)	6796(2)	280(5)
O(31)	1752(2)	1613(1)	979(1)	347(5)
C(32)	714(2)	2383(2)	27(2)	340(6)
C(33)	1948(3)	3457(3)	−493(2)	481(9)
Cl	36103(5)	−22030(4)	20991(4)	362(2)

Fig. 2. Molecular structures and atomic labeling schemes for the protonated forms of (*a*) molecule **2***a* and (*b*) molecule **2***b*.

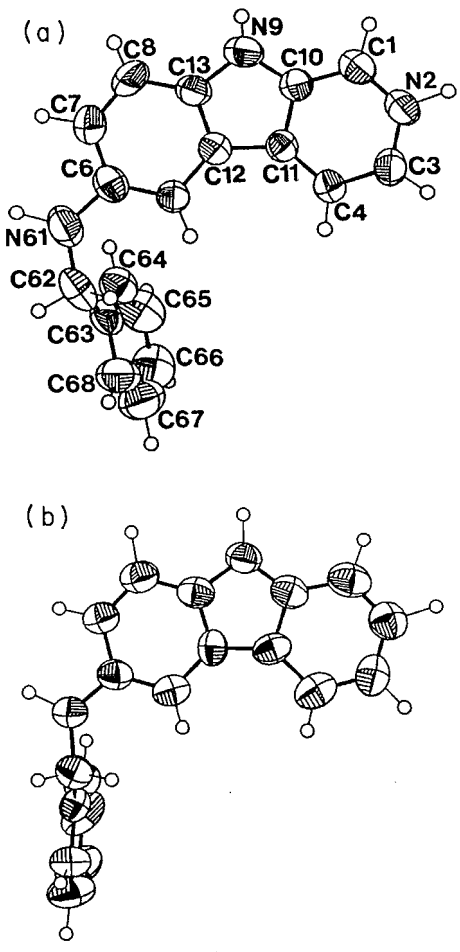

Fig. 3. Molecular structures and atomic labeling schemes for molecule 3.

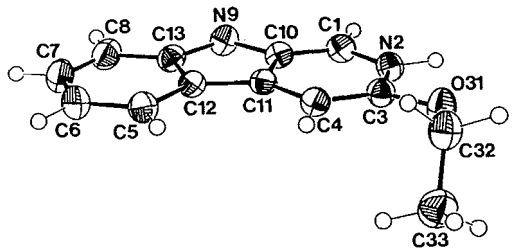

the ester side chain in **1** and related compounds. The ether oxygen atom and the first carbon atom of the ethyl group are in the plane of the polycycle; the torsion angle N(2)-C(3)-O(31)-C(32) is 171.5(2)°.

Compound **1** displays three-center hydrogen bonding, which involves both the ester side chain and the N(2) nitrogen function of the β-carboline. In each unique molecule, the indole N(9)-H donates a hydrogen atom to a neighboring molecule; this H atom is bonded to both the pyridyl N atom and to the carbonyl oxygen atom. The other two structures do not have an ester side chain and, thus, have different hydrogen-bonding patterns (all hydrogen bonds are tabulated in Table 4 and shown for structures **1** and **2** in Figs. 4 and 5). Both compounds **2** and **3** show protonation of the pyridyl nitrogen atom; protonation may be the result of either the acidic crystallization conditions or the greater basicity of the pyridyl nitrogen atom in the absence of the ester side chain. In molecule **2***a*, there is complete transfer of the proton from acetic acid molecule A1 to the pyridyl N atom; this transfer produces delocalization of the π electrons in the carboxyl group of the donor acetic acid molecule so that the two C—O bonds have similar bond lengths, 1.232(7) and 1.240(7) Å. About 50% of the pyridyl N atoms in molecule **2***b* are protonated, so the ob-

Table 3(*a*). Bond distances (Å) and bond angles (°) for the non-hydrogen atoms of β-carbolines **1** and **2**.

	Compound **1**		Compound **2**	
	Molecule **1***a*	Molecule **1***b*	Molecule **2***a*	Molecule **2***a*
Bond				
C(1)—N(2)	1.314(4)	1.328(4)	1.315(7)	1.327(7)
C(1)—C(10)	1.400(4)	1.397(3)	1.371(8)	1.445(8)
N(2)—C(3)	1.366(3)	1.365(3)	1.366(6)	1.363(8)
C(3)—C(4)	1.387(4)	1.377(3)	1.370(8)	1.393(8)
C(4)—C(11)	1.377(4)	1.381(4)	1.365(7)	1.423(7)
C(5)—C(6)	1.380(4)	1.381(4)	1.376(7)	1.371(7)
C(5)—C(12)	1.418(4)	1.401(3)	1.412(6)	1.424(8)
C(6)—C(7)	1.402(4)	1.415(4)	1.405(7)	1.401(6)
C(6)—N(61)	1.411(4)	1.392(3)	1.381(6)	1.387(7)
C(7)—C(8)	1.380(5)	1.371(4)	1.356(8)	1.355(8)
C(8)—C(13)	1.383(4)	1.387(4)	1.383(8)	1.372(6)
N(9)—C(10)	1.352(4)	1.358(4)	1.351(7)	1.348(6)
N(9)—C(13)	1.402(4)	1.388(3)	1.385(6)	1.405(6)
C(10)—C(11)	1.418(4)	1.417(3)	1.419(7)	1.433(8)
C(11)—C(12)	1.445(4)	1.436(3)	1.386(6)	1.386(6)
C(12)—C(13)	1.389(4)	1.408(4)	1.386(6)	1.386(6)
N(61)—C(62)	1.395(4)	1.443(3)	1.437(8)	1.441(6)
C(62)—C(63)	1.546(5)	1.514(5)	1.531(9)	1.513(9)
C(63)—C(64)	1.361(4)	1.387(6)	1.364(9)	1.393(7)
C(63)—C(68)	1.357(6)	1.385(4)	1.378(10)	1.379(10)
C(64)—C(65)	1.373(5)	1.364(7)	1.359(13)	1.384(10)
C(65)—C(66)	1.355(7)	1.364(6)	1.373(15)	1.384(13)
C(66)—C(67)	1.409(6)	1.362(7)	1.372(12)	1.352(10)
C(67)—C(68)	1.401(7)	1.370(6)	1.368(10)	1.392(10)
C(3)—C(31)	1.474(4)	1.476(4)		
C(31)—O(32)	1.334(4)	1.344(3)		
C(31)—O(34)	1.199(4)	1.203(3)		
O(32)—C(33)	1.446(4)	1.446(4)		
Angle				
N(2)—C(1)—C(10)	122.1(2)	121.9(2)	119.4(5)	120.7(5)
C(1)—N(2)—C(3)	118.2(2)	118.0(2)	122.3(4)	121.8(5)
N(2)—C(3)—C(4)	123.8(2)	123.8(3)	120.2(5)	121.2(4)
C(3)—C(4)—C(11)	118.2(2)	118.7(2)	119.4(4)	120.0(5)
C(6)—C(5)—C(12)	118.0(3)	119.1(3)	117.9(4)	117.9(4)
C(5)—C(6)—C(7)	120.4(3)	118.9(2)	120.0(5)	118.4(5)
C(5)—C(6)—N(61)	123.6(3)	123.3(3)	123.5(5)	124.5(4)
C(7)—C(6)—N(61)	116.0(3)	117.7(2)	116.2(5)	117.0(4)
C(6)—C(7)—C(8)	122.5(3)	123.0(2)	121.7(5)	125.0(4)
C(7)—C(8)—C(13)	116.7(3)	117.7(3)	118.9(4)	116.4(4)
C(10)—N(9)—C(13)	108.5(2)	108.8(2)	108.5(4)	105.5(4)
C(1)—C(10)—N(9)	130.6(3)	131.0(2)	130.2(5)	130.6(5)
C(1)—C(10)—C(11)	119.3(3)	119.7(3)	120.0(5)	118.6(4)
N(9)—C(10)—C(11)	110.0(2)	109.3(2)	109.8(4)	110.8(5)
C(4)—C(11)—C(10)	118.4(2)	117.9(2)	118.7(5)	117.7(5)
C(4)—C(11)—C(12)	136.2(2)	135.5(2)	135.9(4)	136.3(5)
C(10)—C(11)—C(12)	105.4(2)	106.6(2)	105.4(4)	106.0(4)
C(5)—C(12)—C(11)	132.9(2)	133.3(3)	132.5(4)	132.5(4)
C(5)—C(12)—C(13)	119.8(3)	120.5(2)	120.8(4)	120.6(4)

Can. J. Chem. Downloaded from www.nrcresearchpress.com by 65.111.164.53 on 09/08/12
For personal use only.

Can. J. Chem. Downloaded from www.nrcresearchpress.com by 65.111.164.53 on 09/08/12
For personal use only.

Table 3(*a*) (*concluded*).

	Compound 1		Compound 2	
	Molecule 1*a*	Molecule 1*b*	Molecule 2*a*	Molecule 2*a*
C(11)—C(12)—C(13)	107.3(2)	106.2(2)	106.8(4)	106.8(4)
C(8)—C(13)—N(9)	128.6(3)	130.1(3)	130.0(4)	127.3(4)
C(8)—C(13)—C(12)	122.7(3)	120.8(2)	120.5(4)	121.7(5)
N(9)—C(13)—C(12)	108.7(2)	109.1(2)	109.5(5)	110.9(4)
C(6)—N(61)—C(62)	117.6(3)	121.3(2)	122.2(4)	124.4(4)
N(61)—C(62)—C(63)	109.7(3)	116.1(2)	115.8(6)	115.3(5)
C(62)—C(63)—C(64)	119.6(3)	120.4(3)	118.7(7)	117.6(6)
C(62)—C(63)—C(68)	121.0(3)	122.7(3)	122.1(5)	123.1(5)
C(64)—C(63)—C(68)	119.4(3)	116.9(3)	119.2(6)	119.3(6)
C(63)—C(64)—C(65)	121.2(4)	121.3(4)	120.4(8)	120.0(7)
C(64)—C(65)—C(66)	120.3(3)	120.8(5)	120.6(7)	120.2(6)
C(65)—C(66)—C(67)	120.0(4)	119.2(5)	119.4(7)	119.5(7)
C(66)—C(67)—C(68)	117.7(4)	120.5(3)	119.8(8)	121.5(8)
C(63)—C(68)—C(67)	121.2(3)	121.4(3)	120.6(6)	119.5(5)
N(2)—C(3)—C(31)	113.2(2)	113.5(2)		
C(4)—C(3)—C(31)	123.0(2)	122.5(2)		
C(3)—C(31)—O(32)	112.7(3)	111.6(2)		
C(3)—C(31)—O(34)	125.2(3)	125.7(3)		
O(32)—C(31)—O(34)	122.1(3)	122.6(3)		
C(31)—O(32)—C(33)	116.7(3)	115.9(2)		

served geometry is an average over an ensemble of both protonated and deprotonated states. For **2***b*, the hydrogen-bonded acetic acid molecule (A2) has dissimilar C—O bond lengths of 1.345(7) and 1.225(6) Å. In each structure, the indole N(9)-H group acts as a hydrogen atom donor. In compound **3**, the electron-donating characteristics of the ether side-chain oxygen atom may help to stabilize the proton on N(2); in this structure, the chloride ions link molecules by hydrogen bonding to the protonated N atom and the indole N-H group. In both **1** and **2**, the benzylamino group participates in hydrogen bonding with solvent molecules, as shown in Figs. 4 and 5.

Stacking interactions between the aromatic systems are present in all three of the reported structures. The β-carboline skeletons of all five unique molecules in the three structures are planar; the standard deviations for the least-squares planes of the 13 non-H atoms are in the range 0.012–0.035 Å. In structures **1** and **2**, the π stacking interactions are limited by the out-of-plane conformation of the 6-benzylamino substituent in three of the four unique molecular conformations. Molecules **1***a* form pairs related by a center of symmetry as do molecules **1***b*, to produce a partial overlap of ring A with ring C. The distance between the parallel β-carboline skeletons is 3.459 Å in **1***a* and 3.406 Å in **1***b*. Molecules **2***b* form a close pair related by a center of symmetry; the molecules are 3.371 Å apart with overlap of rings A and B. Extensive overlap of aromatic rings occurs in structure **3** even though the terminus of the side chain is perpendicular to the β-carboline plane; centrosymmetric dimers stack in pairs separated by 3.292 Å.

Compounds **1** and **2** each have a 6-benzylamino substituent; however, as shown in Figs. 1 and 2, molecule **1***a* displays one conformation and molecules **1***b*, **2***a*, and **2***b* display another. In **1***a*, the torsion angle C(6)-N(61)-C(62)-C(63) is 179.8(3)°; the angle ranges in value from −63.4(3)° to −106.0(6)° in the other molecules. To establish the conformational properties of this side chain, the Cambridge Structural Database (31) was searched to identify the crystallographically observed conformations, and molecular mechanics calculations were used to evaluate the energy differences between these conformations. The database search revealed only three fragments with a ben-

Fig. 4. The hydrogen-bonding pattern in **1** with hydrogen bonds shown as broken lines. The two unique molecules are labeled *A* and *B* and the solvent ethyl acetate molecule is labeled EA.

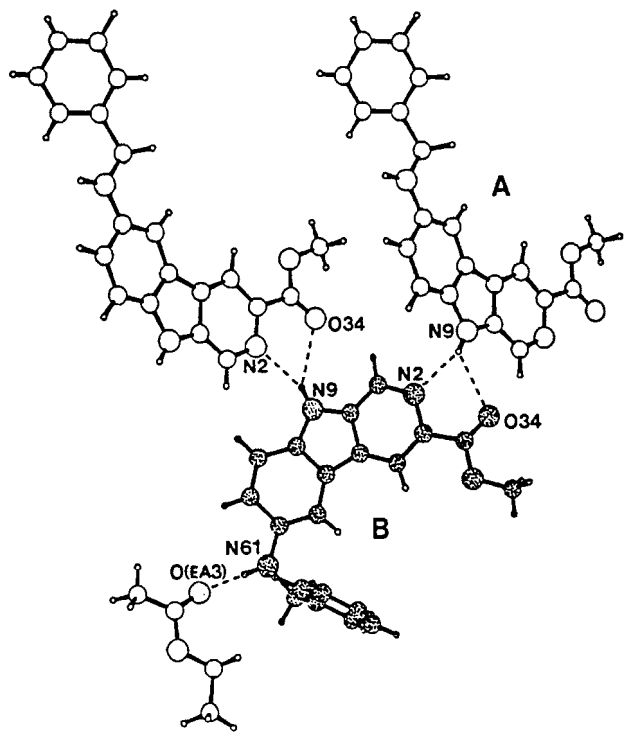

Can. J. Chem. Downloaded from www.nrcresearchpress.com by 65.111.164.53 on 09/08/12
For personal use only.

Table 3(*b*). The bond distances (Å) and bond angles (°) for the non-hydrogen atoms of β-carboline **3**.

Atoms	Distance
C(1)—N(2)	1.348(2)
C(1)—C(10)	1.367(2)
N(2)—C(3)	1.351(2)
C(3)—C(4)	1.384(2)
C(3)—O(31)	1.339(2)
C(4)—C(11)	1.392(2)
C(5)—C(6)	1.379(2)
C(5)—C(12)	1.403(2)
C(6)—C(7)	1.404(2)
C(7)—C(8)	1.373(2)
C(8)—C(13)	1.402(2)
N(9)—C(10)	1.372(2)
N(9)—C(13)	1.378(2)
C(10)—C(11)	1.422(2)
C(11)—C(12)	1.437(2)
C(12)—C(13)	1.411(2)
O(31)—C(32)	1.445(2)
C(32)—C(33)	1.491(3)
Atoms	**Angle**
N(2)—C(1)—C(10)	117.8(1)
C(1)—N(2)—C(3)	123.9(1)
N(2)—C(3)—C(4)	120.5(1)
N(2)—C(3)—O(31)	111.3(1)
C(4)—C(3)—O(31)	128.2(1)
C(3)—C(4)—C(11)	117.5(1)
C(6)—C(5)—C(12)	118.2(2)
C(5)—C(6)—C(7)	121.0(2)
C(6)—C(7)—C(8)	122.2(2)
C(7)—C(8)—C(13)	117.1(2)
C(10)—N(9)—C(13)	108.2(1)
C(1)—C(10)—N(9)	129.9(1)
C(1)—C(10)—C(11)	120.3(1)
N(9)—C(10)—C(11)	109.8(1)
C(4)—C(11)—C(10)	119.9(1)
C(4)—C(11)—C(12)	134.3(1)
C(10)—C(11)—C(12)	105.8(1)
C(5)—C(12)—C(11)	133.4(1)
C(5)—C(12)—C(13)	120.0(1)
C(11)—C(12)—C(13)	106.6(1)
C(8)—C(13)—N(9)	128.8(1)
C(8)—C(13)—C(12)	121.6(1)
N(9)—C(13)—C(12)	109.6(1)
C(3)—O(31)—C(32)	119.5(1)
O(31)—C(32)—C(33)	111.6(1)

zylamino group attached to a phenyl ring; one of these has the extended conformation observed in **1***a* (with a C_{ph}-N-C-C torsion angle of 178.9°) while the two other have a bent conformation (with C_{ph}-N-C-C angles of −88.5° and −79.2°). A Monte Carlo search of 3000 conformations calculated by molecular mechanics (29) for the benzylaminophenyl fragment produced two highly populated, minimized conformations with torsion angles ±67.7° and 179.5°. The energies of the bent and the extended conformations are the same and the ratio of the populations (2.5:1) favors the bent conformer for statistical reasons due to the symmetry of the fragment (the (+) and (−) torsion angles have the same energy in the calculation). These findings indicate that the distribution of conformers found in the crystal (bent:extended = 5:2) is statistical. The torsion angle C(5)-C(6)-N(61)-C(62) is similar in all four molecular conformations presented here and the three conformations found in the database; this angle is always less than 15°, thereby placing the *p* orbital on the amino nitrogen atom perpendicular to the plane of the phenyl ring (ring A in the β-carbolines) and in position to interact with the aromatic system. In contrast to the benzylamino side chain present in these antagonist and inverse agonist ligands, *agonist* β-carbolines have a 6-benzyloxy side chain. Monte Carlo searching for the low-energy conformations of the benzyloxyphenyl fragment shows a slight difference in energy between the bent and extended conformers with the extended conformer favored by 1 kcal/mol; the distribution of extended to bent conformers is not statistical (1:1) and indicates that the extended conformation is slightly favored.

Fig. 5. The hydrogen-bonding pattern in **2** with hydrogen bonds shown as broken lines. The two unique molecules are labeled A and B and the solvent molecules are labeled A*n* for the *n*th molecule of acetic acid and W for the water molecule. Hydrogen bonds between solvent molecules are not shown but are listed in Table 4. Molecule B is partially protonated in its interaction with acetic acid molecule A2.

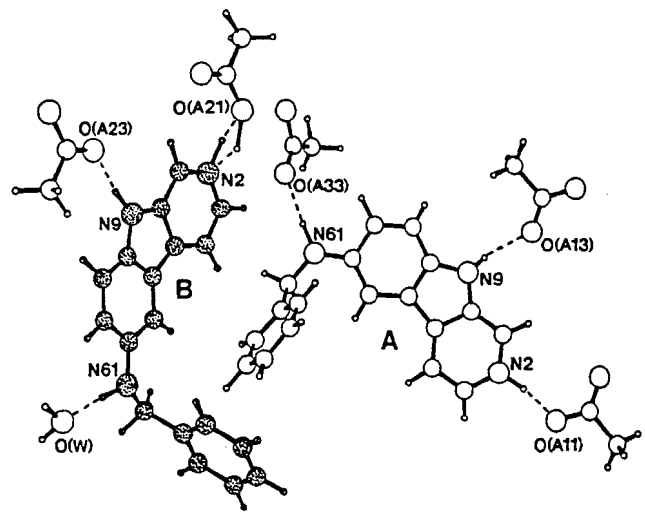

A comparison of the geometry found in **1** with that of the carboxylic acid methyl ester, βCCM (compound **4**, ref. 10), shows that the electron-releasing benzylamino group has an influence on the geometry of the β-carboline, with the greatest effect on the two indole C—N bonds that are across the A ring from the benzylamino group. The average C(13)—N(9) bond in **1** is significantly longer (1.395(9) Å), while the average N(9)—C(10) bond is shorter (1.352(4) Å). A similar difference between the two indole C—N bonds is observed in the geometry of **2**. Although the 3-ethoxy side chain is also electron releasing and across the C ring from N(9), the two C—

Table 4. Hydrogen bond geometry. EA represents a solvent molecule of ethyl acetate in the structure of **1**, A*n* represents the *n*th molecule of acetic acid that cocrystallized with compound **2**, and W represents a solvent water molecule in the structure of **2**. The positions assigned to hydrogen atom H(2) and H(1,A2) were only 50% occupied; the parameters of these atoms were not refined.

Hydrogen bond	D···A (Å)	D—H (Å)	H···A (Å)	∠(D—H···A) (°)	Symmetry operator	Molecules donor → acceptor
N(9)—H(9)···N(2)	2.998(3)	0.87(2)	2.18(2)	155(3)	1 + *x*, *y*, *z*	**1***a*–**1***b*
N(9)—H(9)···O(34)	3.066(3)	0.87(2)	2.44(3)	129(2)	1 + *x*, *y*, *z*	**1***a*–**1***b*
N(9)—H(9)···N(2)	3.018(3)	0.85(3)	2.21(2)	160(2)	*x*, *y*, *z*	**1***b*–**1***a*
N(9)—H(9)···O(34)	3.200(3)	0.85(2)	2.58(0)	131(2)	*x*, *y*, *z*	**1***b*–**1***a*
N(61)—H(61)···O(3,EA)	3.090(3)	0.87(2)	2.29(2)	155(2)	1 + *x*, *y*, *z* − 1	**1***b*–EA
N(9)—H(9)···O(3,A1)	2.734(5)	0.79(4)	1.96(4)	167(4)	1 − *x*, 1 − *y*, 1 − *z*	**2***a*–A1
N(61)—H(61)···O(3,A3)	2.952(7)	1.09(5)	1.87(5)	171(4)	1 − *x*, 1 − *y*, 2 − *z*	**2***a*–A3
N(2)—H(2)···O(1,A1)	2.623(6)	1.05(5)	1.58(5)	169(4)	*x*, 1 + *y*, *z*	**2***a*–A1
N(9)—H(9)···O(3,A2)	2.754(5)	1.05(3)	1.72(3)	172(2)	*x*, *y* − 1, 1 + *z*	**2***b*–A2
N(61)—H(61)···O(W)	2.965(5)	1.07(3)	1.91(4)	169(5)	*x*, *y* − 1, 1 + *z*	**2***b*–W
N(2)—H(2)···O(1,A2)	2.577(6)	1.23	1.38	163	2 − *x*, 1 − *y*, 1 − *z*	**2***b*–A2
O(1,A2)—H(1,A2)···N(2)	2.577(6)	1.28	1.56	130	2 − *x*, 1 − *y*, 1 − *z*	A2–**2***b*
O(W)—H(1W)···O(3,A1)	2.754(6)	1.00(7)	1.77(8)	167(9)	− *x*, 1 − *y*, 1 − *z*	W–A1
O(W)—H(2W)···O(1,A1)	2.670(6)	1.04(7)	1.68(6)	157(6)	− *x* − 1, 1 − *y*, 1 − *z*	W–A1
N(2)—H(2)···Cl	3.053(1)	0.99(2)	2.09(2)	164(2)	*x*, *y*, *z*	**3**–**3**
N(9)—H(9)···Cl	3.150(2)	0.84(2)	2.38(2)	154(2)	1 − *x*, − *y*, 1 − *z*	**3**–**3**

Can. J. Chem. Downloaded from www.nrcresearchpress.com by 65.111.164.53 on 09/08/12
For personal use only.

N(9) bonds are nearly the same length in compound **3**: 1.372(2) and 1.378(2) Å, suggesting that the presence of N(2) in the C ring attenuates the effect of the ethoxy group. In the case of an electron-withdrawing group attached to C(3), as present in compound 4, the C—N(9) bonds are almost equal in length: averages over two observations are 1.374(3) and 1.376(6) Å; and, for comparison, these C—N bonds in an unsubstituted β-carboline, norharmane **5** (32), are equal and are 1.371(4) Å.

Comparison of geometries of the pyridine rings (C) shows that the protonation of the atom N(2) in **2** and **3** causes significant changes in the endocyclic bond angles. The C(1)-N(2)-C(3) angle increases from an average of 118.1(1)° for the unprotonated molecules in **1** to an average of 123.1(8)° for the fully protonated molecules **2***a* and **3**. The adjacent angles, C(10)-C(1)-N(2) and N(2)-C(3)-C(4), decrease by approximately 2.5°. Consistent with the partial protonation of atom N(2) in molecule **2***b*, these structural changes are slightly smaller in molecule **2***b* than in the fully protonated structures. These differences, which are due to protonation, are also evident in comparisons between these molecules and the unsubstituted and unprotonated structure, norharmane (32).

The atomic charges on the pyridyl N(2) atom show trends that are related to the electronic character of the side chain on C(3). Structures without a side chain, norharmane and compound **2**, have a charge of −0.648 on N(2). Structures with an electron-withdrawing group, the methyl ester, compound **1**, and βCCM, have smaller charges, of −0.638, on N(2). The highest charge on N(2), −0.686, is calculated for compound **3**, which has an electron-releasing substituent on C(3). The dipole moments of these compounds show an interesting trend. Norharmane has the lowest dipole moment at 3.116 debye and the antagonist, compound **1**, has the highest (5.827 debye). For the three inverse agonists, the trend in the values of the dipole moment follows the IC_{50} values. The lowest affinity compound, **2**, has the lowest dipole moment of 3.749 debye and the highest affinity compound, βCCM, has the highest value of 5.043 debye, with compound **3** falling in between with a dipole moment of 4.156 debye.

Discussion

Intermolecular contacts in crystals serve as models for the molecular interactions that determine recognition of a ligand at a receptor. Extensive crystallographic studies of β-carboline BZD receptor ligands (9, 11–14) have identified three characteristic interactions and proposed that they are important for recognition. The crystal structures of compounds **1**, **2**, and **3** display these interactions.

One interaction is a three-center hydrogen bond in which both the pyridyl nitrogen atom (N(2)) and the carbonyl oxygen atom of the ester side chain act as acceptors. Compounds **1** and **2** differ only in the presence or absence of the ester side chain that allows formation of the three-center hydrogen bond; the difference in the affinity of **1** (IC_{50} = 10 nM) vs. **2** (IC_{50} = 106 nM) suggests the additional interaction of a hydrogen atom with the carbonyl oxygen atom, as well as the pyridyl N atom, is important. As shown in Fig. 4, both unique conformations of compound **1** form this hydrogen bond. The *cis* conformation of the sp^2 hybridized N atom and the carbonyl oxygen atom facilitates formation of this three-center bond; this conformation is found in the crystal structures of most of the ester-containing BZD receptor ligands, regardless of the chemical type or the biological effect of the ligand (9, 11–14). The ethoxy conformation that is observed in crystals of structure **3** could also facilitate a three-center hydrogen bond; the protonation of N(2) represents complete proton transfer to one acceptor and is undoubtedly stabilized by the lone pairs on the ether oxygen atom. This hydrogen-bonding pattern may explain mutation experiments on the BZD binding subunit, α_1,

Can. J. Chem. Downloaded from www.nrcresearchpress.com by 65.111.164.53 on 09/08/12
For personal use only.

Fig. 6. Maps of the electrostatic potential surface for the three inverse agonist ligands, βCCM, molecule **2,** and molecule **3**. The mesh surface shows the area for an attractive interaction of −50 kcal/mol and the solid surface shows the −70 kcal/mol binding area.

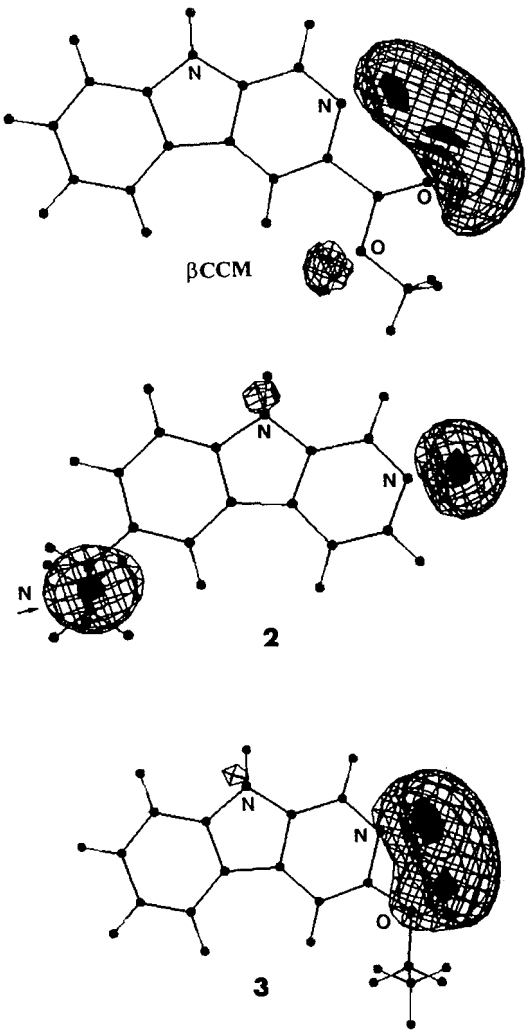

which show that a histidine residue is important for binding agonists and antagonist ligands. Mutant α_1(Arg-101)$\beta_2\gamma_2$ receptors, wherein histidine was replaced with arginine, showed reduced affinity for agonists and the antagonist Ro15-1788 (33). The three-center hydrogen bond with an N-H group imbedded in a five-membered ring, as is observed in β-carboline crystal structures, is a good model for an interaction with histidine and could be formed by the antagonist Ro15-1788 (11); it would be useful if this α_1 mutant was tested against agonist β-carbolines to establish if the His is required for recognition of this type of agonist.

A second intermolecular interaction typical of β-carbolines is the stacking of aromatic rings and coplanar ester side chains. The stacking may model receptor interactions because fully aromatic β-carbolines display high affinity for the BZD receptor, in contrast to their saturated derivatives, which have low affinity for the receptor (9, 14). All of the structures reported here display close stacking of aromatic rings despite the bulk, and out-of-plane conformations, of the side chains in the structures.

The third intermolecular interaction found in inverse agonist β-carbolines is a hydrogen bond donated by the indole N(9)-H group. Methyl substitution at N(9) drastically reduces ligand affinity from IC_{50} = 5 nM for the β-carboline-3-carboxylic acid methyl ester (βCCM) to IC_{50} > 50 000 nM for its 9-methyl derivative (34), thereby suggesting the importance of this hydrogen bond. Even though the hydrogen-bonding patterns are quite different in the three structures reported here, in each case the indole N(9)-H participates in a hydrogen bond (see Table 4), which provides evidence that this group forms a hydrogen bond with the receptor.

The protonated β-carbolines in the structures of **2** and **3** provide a model for the type of interaction with the receptor that could arise for ligands lacking an ester side chain. Theoretical calculations by Loew et al. (35) have shown that protonation is less favored for 3-ester derivatives, by as much as 4.5 kcal/mol for βCCM (**4**) vs. norharmane (**5**). Our calculations of atomic charges, both with semiempirical methods (14) and with *ab initio* methods as reported herein, show that the electronic character of the side chain at position 3 influences the charge on N(2). Compounds **2** and **3** have the highest charge on N(2) and are observed as protonated molecules in the crystal. The absence of an ester side chain in structure **2** increases the basicity of the nitrogen atom and contributes to stabilization of the protonated form (as is true for norharmane in comparison to its methyl ester (36). βCCM and compound **1**, in contrast, have the lowest charges on N(2). A balance between these two extremes is achieved in compound **3** where the electron-releasing group at position 3 produces the largest negative charge at N(2) (see Results) and the protonated form is observed in the crystal.

Proton transfer to the pyridyl N atom and three-centre hydrogen bond formation are possible models for the ligand receptor interaction that can be deduced from the intermolecular interactions observed in the crystals. High charge on N(2) (which may result in proton transfer) seems to be correlated to the desired efficacy, that of *partial* inverse agonist, because compound **3** has reasonable affinity and the highest negative charge on N(2). Binding affinity seems to be better correlated with the presence of an oxygen atom in the 3-position side chain, since the two ester compounds, βCCM and compound **1**, have significantly higher affinity than the related compounds, norharmane and **2**, respectively, which lack a side chain in the 3 position. In addition, compound **3** has an ether side chain and high affinity. Examination of the electrostatic potential surfaces for **2**–**4** for the position of highest attraction for a proton reveals that the three inverse agonists differ in this respect and the difference is due to the side chain, see Fig. 6. The two high-affinity compounds have two positions with >70 kcal attraction energy for a proton; these positions are near N(2) and the O atom in the 3 side chain. Compound **2** has 10-fold lower affinity for the receptor and has only one position of >70 kcal attraction.

The results presented here suggest that a *partial* inverse agonist can be designed by choosing a side chain at position 3, which facilitates the three-center interaction with a proton or hydrogen bond donor and at the same time increases the charge on the N(2) atom. This suggestion for the side chain is supported by the computational results that find the highest charge on N(2) for compound **3** and the presence of two neigh-

Can. J. Chem. Downloaded from www.nrcresearchpress.com by 65.111.164.53 on 09/08/12
For personal use only.

boring sites of attraction for a proton in the high-affinity ligands, and by the crystallographic results, which strongly indicate a particular side chain conformation and a three-center hydrogen bond interaction. These results suggest that the ester side chain common to β-carboline ligands is an unfortunate choice for *partial* efficacy because it serves to reduce the charge on N(2) and, indeed, may shift the preferred position for the hydrogen atom in the intermolecular interaction toward the O atom and away from the N(2) atom. Interestingly, although the ester side chain lowers the charge on N(2), this side chain confers highest affinity on the β-carboline ligands.

The antagonist activity of compound **1** is not explained by these findings. We hypothesize that the molecule is too large to fit into the binding site to the same extent as do the inverse agonists, and thus adopts a different geometry in the critical hydrogen bond interaction. This hypothesis is supported by the fact that β-carboline-3-carboxylic acid *tert*-butyl ester is also an antagonist. It may be that these larger ligands form hydrogen bonds with only the O atom of the side chain due to a restriction in access to the binding site.

In conclusion, the preponderance of crystallographic data on conformations and intermolecular interactions provides a working model for the shape of β-carbolines when bound to a receptor and for the bonds formed. Molecular orbital calculations show that the ligands with desirable effects and high affinity have identifiable electronic properties: desirable effect is found in the ligand with highest charge on N(2) and high affinity is found in the inverse agonist with the highest dipole moment. Taken together, these data suggest that modifications to the 3-position side chain to enhance the charge on the pyridyl N atom and provide an hydrogen bond acceptor site will facilitate the development of *partial* inverse agonist ligands.

References

1. W. Haefley and P. Polc. Receptor biochemistry and methodology. Vol. 5. Alan R. Liss, Inc., New York. 1986. p. 97.
2. S.H. Snyder. J. Med. Chem. **26**, 1667 (1983).
3. C. Brown, I. Martin, B. Jones, and N. Oakley. Eur. J. Pharmacol. **103**, 139 (1984).
4. P.H. Seeburg, W. Wisden, T.A. Verdoorn, D.B. Pritchett, P. Werner, A. Herb, H. Lüddens, R. Sprengel, and B. Sakmann. Cold Spring Harbor Symposia on Quantitative Biology. Vol. LV. 1990. p. 29.
5. C. Kleingoor, M. Ewert, G. von Blankenfeld, P.H. Seeburg, and H. Kettenmann. Neurosci. Lett. **130**, 169 (1991).
6. S. Ymer, A. Draguhn, W. Wisden, P. Werner, K. Keinänen, P.R. Schofield, R. Sprengel, D.B. Pritchett, and P.H. Seeburg. EMBO J. **9**, 3261 (1990).
7. G. Puia, S. Vicini, P.H. Seeburg, and E. Costa. Mol. Pharmacol. **39**, 691 (1991).
8. H.O. Villar, M.F. Davies, G.H. Loew, and P.A. Magguire. Life Sci. **48**, 593 (1991).
9. A.K.S. Muir and P.W. Codding. Can. J. Chem. **62**, 1803 (1984).
10. A.K.S.Muir and P.W. Codding. Can. J. Chem. **63**, 2752 (1985).
11. P.W. Codding and A.K.S. Muir. Mol. Pharmacol. **28**, 178 (1985).
12. P.W. Codding, M.B. Szkaradzinska, A.W. Roszak, L.J. Aha, T.J. Hagen, and J.M. Cook. Can. J. Chem. **66**, 2981 (1988).
13. P.W. Codding, A.W. Roszak, M.B. Szkaradzinska, J.M. Cook, and L.J. Aha. *In* Trends in medicinal chemistry '88. *Edited by* H. Van der Goot, G. Domány, L. Pallos, and H. Timmerman. Elsevier Science, Amsterdam. 1989. p 109.
14. P.W. Codding, A.W. Roszak, M.B. Szkaradzinska, P.A. Fleitz, and R.R. Birge. Frontiers in drug research, crystallographic and computational methods. *Edited by* B. Jensen, F.S. Jørgensen, and H. Kofod. Alfred Benzon Symp. 28, Munksgaard, Copenhagen. 1990. pp. 78–90.
15. M.S. Allen, Y.-C. Tan, M.L. Trudell, K. Narayanan, L.R. Schindler, M.J. Martin, C. Schultz, T.J. Hagen, K.F. Koehler, P.W. Codding, P. Skolnick, and J.M. Cook. J. Med. Chem. **33**, 2343 (1990).
16. D.N. Stephens, W. Kehr, H.H. Schneider, and R. Schmiechen. Neurosci. Lett. **47**, 333 (1984).
17. T.J. Hagen, P. Skolnick, and J.M. Cook. J. Med. Chem. **30**, 750 (1987).
18. S.P. Hollinshead, M.L. Trudell, P. Skolnick, and J.M. Cook. J. Med. Chem. **33**, 1062 (1990).
19. W. Haefely, J.R. Martin, and P. Schoch. Trends Pharmacol. Sci. **11**, 452 (1990).
20. (*a*) P. Main, S.E. Hall, L. Lessinger, G. Germain, J.-P. Declercq, and M.M. Woolfson. MULTAN78. A system of computer programs for the automatic solution of crystal structures from X-ray diffraction data. Universities of York, England, and Louvain, Belgium. 1978; (*b*) G.M. Sheldrick. Acta Crystallogr. Sect. A: Found. Crystallogr. **A46**, 467 (1990).
21. D.T. Cromer and J.B. Mann. Acta Crystallogr. Sect. A: Cryst. Phys. Diffr. Theor. Gen. Crystallogr. **A24**, 321 (1968).
22. R.F. Stewart, E.R. Davidson, and W.T. Simpson. J. Chem. Phys. **42**, 3175 (1965).
23. A.C. Larson. Acta Crystallogr. **23**, 664 (1967).
24. W.H. Zachariasen. Acta Crystallogr. **23**, 558 (1967).
25. J.M. Stewart. XRAY76. The X-ray system of crystallographic programs. Computer Science Center, University of Maryland, College Park, Md. 1976.
26. C.K. Johnson. ORTEP-II. Report ORNL-5138, Oak Ridge National Laboratory, Oak Ridge, Tenn. 1976.
27. G.D. Smith. PROFIT. A molecular fitting program. Medical Foundation of Buffalo, Buffalo, N.Y. 1983.
28. S. Motherwell. PLUTO. University Chemical Laboratory, Cambridge, England. 1979.
29. F. Mohamdi, N.G.J. Richards, W.C. Guide, M.L. Liskamp, C. Caufield, G. Chang, T. Chandrickson, and W.C. Still. J. Comput. Chem. **11**, 440 (1990).
30. M.J. Frisch, M. Head-Gordon, G.W. Trucks, J.B. Foresman, H.B. Schlegel, K. Raghavachari, M. Robb, J.S. Binkley, C. Gonzalez, D.J. Defrees, D.J. Fox, R.A. Whiteside, R. Seeger, C.F.Melius, J. Baker, R.L. Martin, L.R. Kahn, J.J.P. Stewart, S. Topiol, and J.A. Pople. GAUSSIAN90, Version I. Gaussian Inc., Pittsburgh, Pa. 1990.

31. F.H. Allen, S. Bellard, M.D. Brice, B.A. Cartwright, A. Doubleday, H. Higgs, T. Hummelink, B.G. Hummelink-Peters, O. Kennard, W.D.S. Motherwell, J.R. Rodgers, and D.G. Watson. Acta Crystallogr. Sect. B: Struct. Crystallogr. Cryst. Chem. **B35**, 2331 (1979).
32. S. Roychowdhury and P. Roychowdhury. Collected Abstracts. XIIth Congress and General Assembly of the International Union of Crystallography. Ottawa, Ont. 1981. p. C-205.
33. H.A. Wieland, H. Lüddens, and P.H.Seeburg. J. Biol. Chem. **267**, 1426 (1992).
34. M.S. Allen, T.J. Hagen, M.L. Trudell, P.W. Codding, P. Skolnick, and J.M. Cook. J. Med. Chem. **31**, 1854 (1988).
35. G.H. Loew, J. Nienow, J.A. Lawson, L. Toll, and E.T. Uyeno. Mol. Pharmacol. **28**, 17 (1985).
36. H. Konschin, H. Tylli, J. Gynther, and J. Rouvinen. J. Mol. Struct. (Theochem), **153**, 307 (1987).

Can. J. Chem. Downloaded from www.nrcresearchpress.com by 65.111.164.53 on 09/08/12
For personal use only.

Crystal structure and thermal expansion of hexakis(phenylthio)benzene and its CBr_4 clathrate

Darek Michalski, Mary Anne White, Pradip K. Bakshi, T. Stanley Cameron, and Ian Swainson

Can. J. Chem. Downloaded from www.nrcresearchpress.com by 65.111.164.53 on 09/08/12
For personal use only.

Abstract: The crystal structures of hexakis(phenylthio)benzene (HPTB) and its CBr_4 clathrate have been determined by single crystal X-ray diffraction data collected at $T = 18°C$ and refined to final R_w of 0.036 and 0.047, respectively. Pure HPTB is triclinic, space group $P\bar{1}$ (No. 2), with $a = 9.589(2)$ Å, $b = 10.256(1)$ Å, $c = 10.645(2)$ Å, $\alpha = 68.42(1)°$, $\beta = 76.92(2)°$, $\gamma = 65.52(1)°$, and $Z = 1$. The CBr_4 clathrate of HPTB is rhombohedral, space group $R\bar{3}$ (No. 148), with $a = 14.327(4)$ Å, $b = 20.666(8)$ Å, and $Z = 3$. The host–guest mole ratio of HPTB–CBr_4 is 1:2. Neutron powder diffraction was carried out on powders of both compounds in the temperature range $25 K < T < 295 K$. Thermal expansion coefficients were determined for HPTB and HPTB–CBr_4 over this temperature range.

Key words: thermal expansion, crystal structure, clathrate.

Résumé : On a déterminé les structures cristallines de l'hexakis(phénylthio)benzène (HPTB) et de son clathrate CBr_4 à partir de données de diffraction des rayons X par un cristal unique, obtenues à 18°C et affinées jusqu'à des valeurs finales de R_w de 0,036 et de 0,047, respectivement. Le HPTB pur est triclinique, groupe d'espace $P\bar{1}$ (No. 2), avec $a = 9,589(2)$, $b = 10,256(1)$ et $c = 10,645(2)$ Å, $\alpha = 68,42(1)°$, $\beta = 79,92(2)°$ et $\gamma = 65,52(1)°$ et $Z = 1$. Le clathrate CBr_4 du HPTB est rhomboédrique, groupe d'espace $R\bar{3}$ (No. 148), avec $a = 14,327(4)$ et $b = 20,666(8)$ Å et $Z = 3$. Le rapport molaire hôte/invité dans le clathrate est de 1:2. On a effectué une diffraction de neutron par des poudres des deux composés, à des températures allant de 25 K à 295 K. On a déterminé les coefficients d'expansion thermique de HPTB et du HPTB–CBr_4 sur l'ensemble de ces températures.

Mots clés : coefficients d'expansion thermique, structure cristalline, clathrate.

[Traduit par la rédaction]

Introduction

Inclusion compounds are systems in which one type of chemical species (the "guest") is spatially confined in non-rigorously defined cavities distributed within another species (the "host") (1). Clathrates are a subset of inclusion compounds, distinguished either on the basis of the host–guest interaction criteria or by the topology of the host–guest system; the guest molecules in clathrates are held by steric barriers developed within the lattice composed of the host molecules (2, 3). The intermolecular interaction between host and guest molecules in a clathrate is weak in comparison with chemical bonds (4), and the host–guest relationship in clathrates is determined by the steric compatibility of the host lattice voids with the guest molecules. The architecture of clathrates allows studies of the effects of the restricted geometry on the behaviour of individual guest species, their clusters, or even their whole assembly. In addition, the effect of the guest species on the properties of the host structure can be studied. The latter is more formidable since there are not many compounds which yield both a clathrate and a clathrand (i.e., an empty clathrate). This is due to instability of the polymorph of the host lattice, which is isostructural with the clathrate; this structure usually can exist only when buttressed by guest molecules (4).

We have initiated investigations of thermal properties of clathrates to get insight into the aforementioned aspects of molecular behaviour (5–12). Thermal expansion is one of these properties. The driving force for thermal expansivity is brought about by a strain-dependent entropy that creates the elastic response of the solid phase. It is a bulk property that does not have an atomic or molecular counterpart. Thermal expansion reveals the anharmonicity of a crystal lattice and knowledge of it is indispensable in thermodynamic studies for its essential role in analysis of the volume-dependent crystal properties (13).

We report here crystal structures (determined for single crystals) and the thermal expansivity (determined for powders) of systems based on hexakis(phenylthio)benzene, **1**, (HPTB for short). This compound is an archetypal example of one of the first premeditated, engineered clathrates (14, 15). The hexagonal arrangement of six hydrogen-bonded host molecules of clathrates as in hydroquinone or Dianin's systems (1) was the

Received November 1, 1994.

D. Michalski, M.A. White,[1] P.K. Bakshi, and T.S. Cameron. Dalhousie University, Department of Chemistry, Halifax, NS B3H 4J3, Canada
I. Swainson. AECL Research, Chalk River Laboratories, Chalk River, ON K0J 1J0, Canada

[1] Author to whom correspondence should be addressed; telephone: 902-494-3894; fax: 902-494-1310; E-MAIL: MAWHITE@AC.DAL.CA

Can. J. Chem. Downloaded from www.nrcresearchpress.com by 65.111.164.53 on 09/08/12
For personal use only.

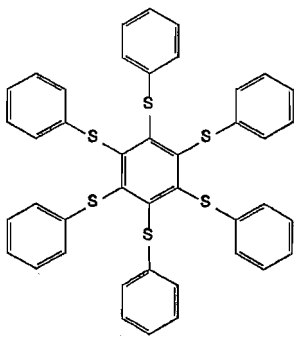

1

basis for the proposal and realization of the design of HPTB and related systems (15). In HPTB systems the hydrogen-bonded hexamer is replaced by a single host molecule with a permanent consolidated structure (15) (also *vide infra*). The structures of HPTB and its inclusion compounds are of particular interest in light of the proposal that the unusual thermal conductivity observed for clathrate hydrates and Dianin's clathrate is ascribable to resonant scattering of acoustic modes by the localized optic modes brought about by an intrinsic motion of the molecular moieties (7, 11). Examination of the thermal properties of the HPTB system will provide further information on the potential topological and (or) dynamical origin of the unusual thermal behaviour of clathrates.

Experimental procedure

HPTB was prepared by a literature route involving the reaction of C_6Cl_6 with C_6H_5SNa (15). All single crystals prepared here were obtained by slow evaporation: yellow transparent molecular crystals of HPTB were grown from chloroform; yellow (with orange hue) transparent HPTB–CBr_4 crystals were grown from a solution of chloroform with excess CBr_4 (3:1, CBr_4-to-HPTB mole ratio). Powders of HPTB and HPTB–CBr_4 for the neutron powder diffraction were obtained from the same solutions by rapid recrystallization.

Single crystal diffraction data was collected on CAD4/Rigaku AFC5R four-circle diffractometers at room temperature (18 ± 1°C). The crystals were sealed in thin-walled glass capillaries to prevent crystal decomposition caused by possible guest escape during data collection. The intensities were reduced and corrected for Lorentz and polarization effects; empirical absorption corrections were applied (16). Scattering factors for neutral atoms and anomalous dispersion corrections were taken from the literature (17). Positions of the non-hydrogen atoms were obtained from direct methods (18). The H(C) atoms were placed in their geometrically calculated positions (C—H = 1.08 Å) and not refined (U_{iso}(H) = 1.2 B_{eq}(C) of the attached carbon atom). The structure was refined by full-matrix least squares.[2] The function minimized was $\Sigma w(\Delta|F|)$ (17), where w is the weight derived from the counting statistics. The anisotropic temperature factors were defined as exp $[-2\pi(U_{11}h^2a^{*2} + U_{22}k^2b^{*2} + U_{33}l^2c^{*2} + 2U_{23}klb^*c^* + 2U_{13}hla^*c^* + 2U_{12}hka^*b^*)]$. Experimental details are given in

[2] Observed and calculated structure factors are available from the corresponding author.

Fig. 1. An ORTEP (30) drawing of an HPTB molecule in pure HPTB.

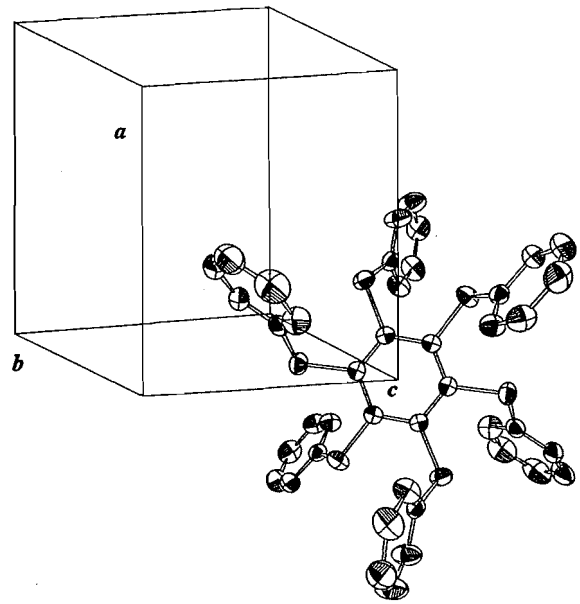

Table 1. The computer programs TEXAN (19) and SHELX (20) were used in the crystallographic investigation.

Thermal expansion measurements were performed by determination of the lattice parameters of powder samples of HPTB and HPTB–CBr_4 within the temperature range 25 K < T < 295 K, using the C2 neutron powder diffractometer in the NRU reactor of AECL Research, Chalk River, Canada. The instrument consists of an 800-wire detector spanning 80° in 2θ, giving 0.1° channel interval. During the measurements the detector was stepped once so that the measured step size for the profile refinements was 0.05°. The samples were loaded into cylindrical vanadium cans with an internal diameter of 4 mm and placed in an open cycle He cryostat. The sample was rotationally centred photographically in the beam before the experiment began. The cryostat was continuously rotated by 90° during the measurement in order to improve the powder averaging in the spectra. The temperature stability was ±1 K during each measurement. The experiment used the reflection from a Si531 monochromator at a take-off angle of approximately 110°. The calibration was performed using a standard Si powder. The wavelength was determined by Rietveld fitting the Si profile and found to be 1.50506(3) Å. The incident collimation used during the experiment was 0.4° and a cooled sapphire filter was used to reduce second-order contamination of the beam. The spectrum was fitted using the GSAS program (21) from 6° to 36°. Three parameters were used to fit the angle-dependent Gaussian line width of the peaks.

Results and discussion

Structure of pure HPTB

The hexakis(phenylthio)benzene molecule is highly symmetrical in the solid state (Fig. 1); phenyl groups are situated alternatively above and below the plane of the central phenyl ring. This compound crystallizes in the space group $P\bar{1}$. The crystallographic axis passes through the C(20)—S(1) bond, so that

Can. J. Chem. Downloaded from www.nrcresearchpress.com by 65.111.164.53 on 09/08/12
For personal use only.

Table 1. Physical properties and parameters for data collection and refinement of HPTB and the CBr_4 clathrate of HPTB.

Parameter	Value	
	HPTB	CBr_4–HPTB
Formula	$C_{42}H_{30}S_6$	$C_{44}H_{30}S_6Br_8$
Formula weight	727.1	1390.3
Crystal size (mm^3)	0.4 × 0.3 × 0.3	0.3 × 0.3 × 0.15
θ range, deg[a]	12.0–14.0/25	25.0–33.3/21
Crystal system	triclinic	trigonal
Space group	$P\bar{1}$ (No. 2)	$R\bar{3}$ (no. 148)
a (Å)	9.589(2)	14.327(4)
b (Å)	10.256(1)	14.327(4)
c (Å)	10.645(2)	20.666(8)
α(°)	68.42(1)	90
β(°)	76.92(2)	90
γ(°)	65.52(1)	120
V ($Å^3$)	883(1)	3674(2)
Z	1	3
ρ_{calc} (g/cm^3)	1.368(2)	1.885(1)
ρ_{exp} (g/cm^3)[b]	1.365 ± 0.005	1.863 ± 0.005
Melting point (°C)[c]	180.0 ± 0.5	165.5 ± 0.5 (decomp)
F(000) (e)	378	2010
Diffractometer[d]	CAD4	RIGAKU
μ (cm^{-1})	4.01	67.63
θ range (°)	2–30	2–25
Reflections		
Total measured	5556	1624
Total unique	5138	1440
Unique used[e]	3373	642
Parameters; *d/p*	218; 15.5	91, 7.1
Absorption		
corrections (min, max)	0.60, 1.11	0.91, 1.20
$100R$, $100R_w$	4.44, 3.60	5.56, 4.73
G.O.F.	2.38	2.32
Residual		
e.d. (min, max)	−0.37, 0.35	−1.15, 0.91
T (°C)	18	18

[a] $\theta_{min} < \theta < \theta_{max}/n$. The lattice parameters and orientation matrices were obtained by least squares from the setting angles θ of n suitable reflections.

[b] The density was found at T = 22°C by matching the crystal density with aqueous RbI solutions; the density of the clathrate corresponds to 98% of the guest occupancy.

[c] Determined by differential scanning calorimetry.

[d] CAD4, MoKα (graphite monochromator), λ = 0.70926 Å; Rigaku AFC5R, MoKα (graphite monochromator), λ = 0.71069 Å.

[e] $I > 3\sigma(I)$.

half of the molecule is unique and the other half is related by the centre of symmetry. The C—S bond lengths are not unusual, mean 1.768(2) Å. The central and side chain phenyl rings are almost planar. The ability of HPTB to form clathrates stems from the very open molecular topology. The packing coefficient, i.e., the ratio of the van der Waals volume of the molecular content of the unit cell to the volume of the unit cell itself, determined by molecular mechanics (22) is 0.60. Organic molecular crystals typically have packing coefficients in the range 0.65–0.77 (23). Relevant values are presented in Tables 2–4.

Structure of HPTB–CBr_4

The CBr_4 clathrate of HPTB crystallizes in a trigonal crystal system, space group $R\bar{3}(h)$. Its structure is similar to its CCl_4 analogue (15). A cavity, in the zone of the crystallographic c-axis, is formed by eight host HPTB molecules. The guest molecules close the top and the bottom of the cage. The effective

Fig. 2. (*a*) A view of HPTB–CBr_4 showing the placement of the guest and host molecules. The *c*-axis is vertical. For clarity, one HPTB molecule above the plane and one HPTB molecule below the plane are omitted. (*b*) An ORTEP (30) drawing of HPTB and CBr_4 molecules in the clathrate of HPTB.

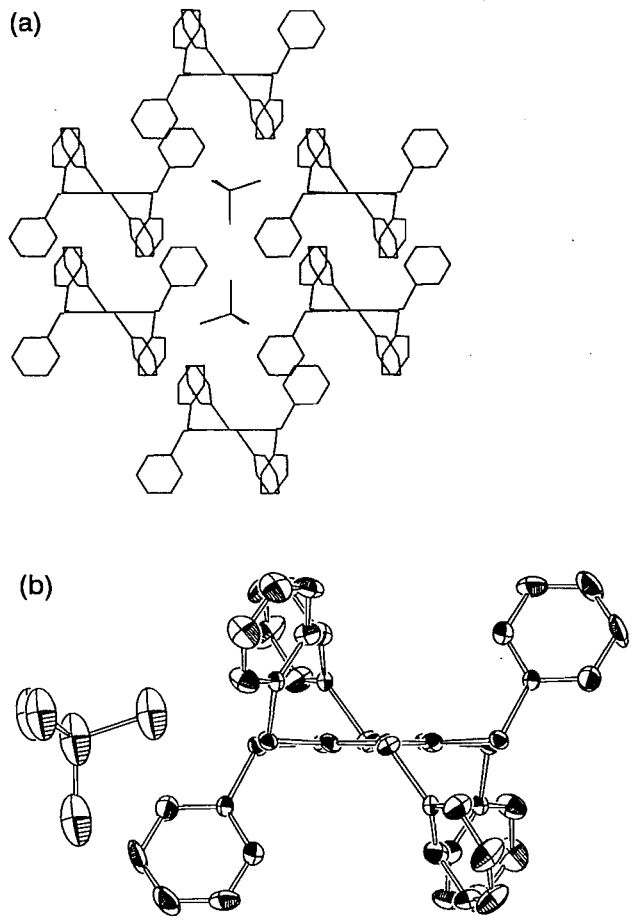

Table 2. Positional parameters and *B*(eq) for HPTB.

Atom	*x/a*	*y/b*	*z/c*	*B*(eq) in Å^2
S(1)	0.0007(1)	0.2287(1)	0.7025(1)	3.3(1)
S(2)	0.3147(1)	0.0336(1)	0.8470(1)	3.3(1)
S(3)	−0.3078(1)	0.1872(1)	0.8520(1)	3.1(1)
C(1)	0.4377(2)	−0.1526(2)	0.8510(2)	2.8(2)
C(2)	0.5912(3)	−0.1881(3)	0.8582(3)	4.8(3)
C(3)	0.6976(3)	−0.3240(3)	0.8445(4)	5.9(3)
C(4)	0.6519(3)	−0.4259(3)	0.8285(3)	5.0(3)
C(5)	0.4988(3)	−0.3932(3)	0.8274(3)	4.8(3)
C(6)	0.3903(3)	−0.2552(3)	0.8367(3)	3.8(2)
C(7)	0.0932(2)	0.3461(2)	0.7013(2)	3.1(2)
C(8)	0.1648(3)	0.4055(3)	0.5773(3)	4.1(2)
C(9)	0.2256(3)	0.5110(4)	0.5626(4)	5.8(3)
C(10)	0.2193(4)	0.5559(4)	0.6703(5)	6.5(4)
C(11)	0.1521(4)	0.4955(4)	0.7940(4)	5.9(4)
C(12)	0.0875(3)	0.3907(3)	0.8105(3)	4.4(3)
C(13)	−0.2795(2)	0.1163(2)	0.7162(2)	2.6(2)
C(14)	−0.1532(3)	−0.0039(3)	0.6899(2)	3.3(2)
C(15)	−0.1520(3)	−0.0539(3)	0.5847(3)	4.0(3)
C(16)	−0.2743(3)	0.0132(3)	0.5080(3)	4.6(3)
C(17)	−0.3996(3)	0.1327(3)	0.5339(3)	4.6(3)
C(18)	−0.4028(3)	0.1849(3)	0.6373(2)	3.5(2)
C(19)	0.1403(2)	0.0148(2)	0.0339(2)	2.4(2)
C(20)	0.0039(2)	0.1022(2)	0.8693(2)	2.4(2)
C(21)	−0.1356(2)	0.0848(2)	0.9332(2)	2.3(2)

Table 3. Intramolecular distances in Å involving the nonhydrogen atoms for HPTB.

Atom	Atom	Distance	Atom	Atom	Distance
S(1)	—C(7)	1.762(3)	C(8)	—C(9)	1.376(6)
S(1)	—C(20)	1.770(2)	C(9)	—C(10)	1.366(7)
S(2)	—C(1)	1.770(2)	C(10)	—C(11)	1.372(5)
S(2)	—C(19)	1.768(2)	C(11)	—C(12)	1.390(6)
S(3)	—C(13)	1.767(3)	C(13)	—C(14)	1.389(3)
S(3)	—C(21)	1.766(2)	C(13)	—C(18)	1.388(3)
C(1)	—C(2)	1.376(4)	C(14)	—C(15)	1.389(5)
C(1)	—C(6)	1.372(5)	C(15)	—C(16)	1.366(4)
C(2)	—C(3)	1.382(4)	C(16)	—C(17)	1.379(4)
C(3)	—C(4)	1.362(6)	C(17)	—C(18)	1.379(5)
C(4)	—C(5)	1.366(5)	C(19)	—C(21)	1.412(3)
C(5)	—C(6)	1.390(4)	C(19)	—C(20)	1.404(3)
C(7)	—C(8)	1.389(3)	C(21)	—C(20)	1.408(3)
C(7)	—C(12)	1.380(5)			

length of the cavity occupied by two guest species is ca. 18 Å (Fig. 2). The elongated cavity is of the closed cage type. The gaps in the cage wall (determined using van der Waals radii) are smaller than the effective sizes of the guest molecules. The enclathrated guests are oriented such that the axial C—Br bond of CBr_4 molecule is along the 3-fold axis. The geometry of CBr_4 is tetrahedral, the mean Br—C—Br angle is 109.5(12)°. The axial C—Br distance (1.92(2) Å) is not significantly longer than the other C—Br distances (mean 1.904(1) Å). The corrected mean values for C—Br distances and Br—C—Br angles obtained after thermal motion analysis (24) are 1.945(14) Å and 109.5(11)°, respectively.

The anisotropic thermal parameters of the nonhydrogen atoms are ordinary, with the exception of U_{33}[Br(1)] and U_{11} and U_{22}[Br(2)]. The large temperature factors of Br atoms are not unexpected since CBr_4 is a non-bonded guest molecule. The TLS analysis of the thermal motion of the CBr_4 molecule reveals a surprising degree of compliance with the rigid body model, $R(U_{ij})$ = 2.74%, $R_w(U_{ij})$ = 2.58%, rms(U_{ij}) = 0.0020 and rms[esd(U_{ij})] = 0.0014. The mean librational amplitudes about the three principle axes of libration are L_1, 3.9°; L_2, 9.4°, and L_3, 9.4°. The translation motion is essentially isotropic, with mean principal displacement of ~0.24 Å. However, significant screw motion along the S_2 and S_3 directions is also apparent in the screw tensor:

$$\begin{matrix} -0.50 & 0.00 & 0.00 \\ 0.00 & 0.25 & 0.00 \\ 0.00 & 0.00 & 0.25 \end{matrix}$$

The intermolecular Br...Br distance of 3.310(7) Å is shorter

Can. J. Chem. Downloaded from www.nrcresearchpress.com by 65.111.164.53 on 09/08/12
For personal use only.

Can. J. Chem. Downloaded from www.nrcresearchpress.com by 65.111.164.53 on 09/08/12
For personal use only.

Table 4. Intramolecular bond angles involving the nonhydrogen atoms for HPTB.

Atom	Atom	Atom	Angle	Atom	Atom	Atom	Angle
C(7)	—S(1)	—C(20)	106.2(1)	C(7)	—C(12)	—C(11)	119.4(3)
C(1)	—S(2)	—C(19)	104.0(1)	S(3)	—C(13)	—C(14)	126.0(2)
C(13)	—S(3)	—C(21)	105.1(1)	S(3)	—C(13)	—C(18)	114.1(2)
S(2)	—C(1)	—C(2)	116.0(2)	C(14)	—C(13)	—C(18)	119.7(3)
S(2)	—C(1)	—C(6)	124.0(2)	C(13)	—C(14)	—C(15)	119.5(2)
C(2)	—C(1)	—C(6)	119.8(2)	C(14)	—C(15)	—C(16)	120.6(2)
C(1)	—C(2)	—C(3)	119.7(3)	C(15)	—C(16)	—C(17)	119.9(3)
C(2)	—C(3)	—C(4)	120.8(3)	C(16)	—C(17)	—C(18)	120.5(3)
C(3)	—C(4)	—C(5)	119.3(3)	C(13)	—C(18)	—C(17)	119.8(2)
C(4)	—C(5)	—C(6)	120.8(4)	S(2)	—C(19)	—C(21)	121.4(2)
C(1)	—C(6)	—C(5)	119.4(3)	S(2)	—C(19)	—C(20)	119.0(1)
S(1)	—C(7)	—C(8)	115.9(2)	C(21)	—C(19)	—C(20)	119.7(2)
S(1)	—C(7)	—C(12)	124.4(2)	S(3)	—C(21)	—C(19)	118.6(2)
C(8)	—C(7)	—C(12)	119.4(3)	S(3)	—C(21)	—C(20)	121.5(1)
C(7)	—C(8)	—C(9)	120.2(3)	C(19)	—C(21)	—C(20)	119.9(2)
C(8)	—C(9)	—C(10)	120.4(3)	S(1)	—C(20)	—C(19)	122.3(2)
C(9)	—C(10)	—C(11)	119.9(4)	S(1)	—C(20)	—C(21)	117.3(2)
C(10)	—C(11)	—C(12)	120.6(4)	C(19)	—C(20)	—C(21)	120.3(2)

Table 5. Positional parameters and B(eq) for HPTB–CBr_4.

Atom	*x/a*	*y/b*	*z/c*	B(eq) in Å^2
Br(1)	0.5461(1)	0.3439(1)	0.0350(1)	7.35(9)
Br(2)	2/3	1/3	−0.0866(2)	11.5(3)
S(1)	0.1101(2)	0.8545(2)	0.0031(1)	1.8(1)
C(1)	0.0541(7)	0.7721(7)	0.0718(5)	1.5(4)
C(2)	0.0598(9)	0.6793(8)	0.0736(6)	3.3(5)
C(3)	0.027(1)	0.6143(8)	0.1289(6)	4.3(6)
C(4)	−0.013(1)	0.641(1)	0.1797(6)	4.2(6)
C(5)	−0.0226(8)	0.731(1)	0.1796(5)	3.3(5)
C(6)	0.0138(8)	0.7979(8)	0.1263(5)	2.6(5)
C(7)	0.0459(7)	0.9333(7)	0.0002(5)	1.5(2)
C(8)	0.6667	0.3333	0.006(1)	4(2)

Table 6. Intramolecular distances in Å involving the nonhydrogen atoms for HPTB–CBr_4.

Atom	Atom	Distance	Atom	Atom	Distance
Br(1)	—C(8)	1.904(7)	C(1)	—C(6)	1.40(1)
Br(1)	—C(8)	1.904(7)	C(2)	—C(3)	1.40(1)
Br(1)	—C(8)	1.904(7)	C(3)	—C(4)	1.34(2)
Br(2)	—C(8)	1.92(2)	C(4)	—C(5)	1.37(2)
S(1)	—C(1)	1.76(1)	C(5)	—C(6)	1.38(1)
S(1)	—C(7)	1.778(8)	C(7)	—C(7)	1.405(8)
C(1)	—C(2)	1.37(1)	C(7)	—C(7)	1.405(8)

than the shortest intermolecular distance between Br atoms found in the structure of pure CBr_4 (3.78(2) Å) (25) but is comparable to that observed in the CBr_4 clathrate of the seleno analogue of HPTB, hexakis(phenylseleno)benzene (26). The same type of shortening for the Cl...Cl contact with respect to the phase II of pure CCl_4 (27) was also observed in the case of the previously reported structure of the CCl_4 clathrate of HPTB (15). The origin of this effect is not clear.

A crystallographic axis passes through the centre of the central phenyl ring. The sulphur atom is displaced by 0.064 and 0.137 Å from the centres of the phenyl substituent and central phenyl rings, respectively. Yet both the central and the side chain phenyl rings are considered to be satisfactorily planar. The bond lengths and angles are comparable with those of HPTB and its CCl_4 clathrate (15). Relevant values are presented in Tables 5–7.

Thermal expansion of HPTB and HPTB–CBr_4

The results of the room-temperature single crystal X-ray measurement of the CBr_4 clathrate of HPTB at T = 291 K (see Table 1) agree very well with the values extracted from neutron diffraction experiment at T = 295 K: a = 14.328(3) Å, c = 20.663(6) Å, and V = 3674(1) Å^3.

There is satisfactory correspondence for the values obtained for HPTB (see Table 1) at T = 295 K with a = 9.565(9) Å, b = 10.279(7) Å, c = 10.629(10) Å, α = 68.46(6)°, β = 77.09(9)°, γ = 65.81(7)°, and V = 883.0(6) Å^3 as determined by neutron powder diffraction, compared with values (see Table 1) from single crystal X-ray measurements.

Three factors might contribute to slight differences between the X-ray and neutron diffraction results. First, neutrons are scattered by the atomic nuclei, whereas X-rays are scattered by the average electron cloud around the nucleus. Secondly, the compound consists of a significant number of hydrogen atoms, which results in a high background in the neutron diffraction pattern. Third, an intrinsic feature of organic molecular crystals is weak intermolecular interactions, which, with the low symmetry of the HPTB crystal and its open structure, makes the structure susceptible to easy distortion by thermal and mechanical effects. For example, it is known that the structure of powdered samples of the

Can. J. Chem. Downloaded from www.nrcresearchpress.com by 65.111.164.53 on 09/08/12
For personal use only.

Fig. 3. (*a*) HPTB–CBr_4 *a*-axis as a function of temperature. ○, neutron results (most error bars are smaller than the data circles); ●, X-ray result. The solid line is the least-squares fit to the data, used to calculate thermal expansion (Fig. 4). (*b*) HPTP-CBr_4 *c*-axis as a function of temperature. ○, neutron results; ●, X-ray result. The solid line is the least-squares fit to the data, used to calculate thermal expansion (Fig. 4). (*c*) HPTP–CBr_4 unit cell volume as a function of temperature. ○, neutron results (error bars are smaller than the data circles); ●, X-ray result. The solid line is the least-squares fit to the data, used to calculate thermal expansion (Fig. 6).

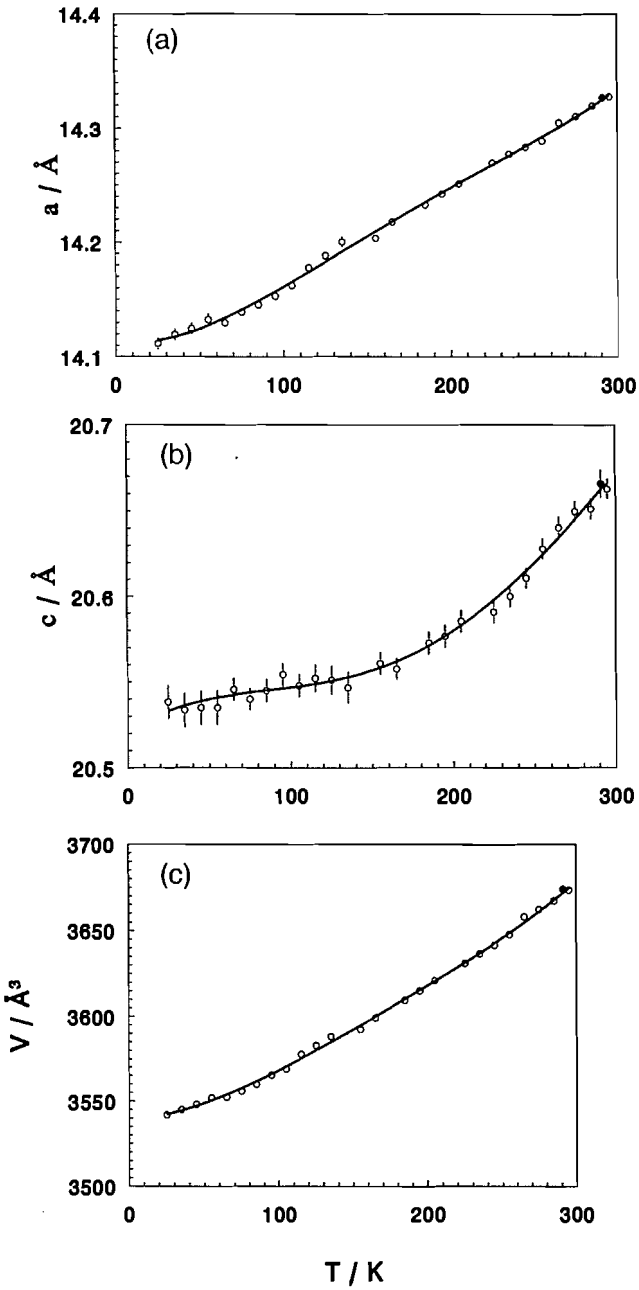

CCl_4 clathrate of Dianin's compound is easily disturbed on grinding (9).

The changes in the unit cell dimensions and volume of the CBr_4 clathrate of HPTB with temperature are shown in Fig.

Fig. 4. (*a*) HPTB–CBr_4 thermal expansion along the *a*-axis as a function of temperature, as determined from the least-squares fit to the lattice parameter (Fig. 3). (*b*) HPTB–CBr_4 thermal expansion along the *c*-axis as a function of temperature, as determined from the least-squares fit to the lattice parameter (Fig. 3).

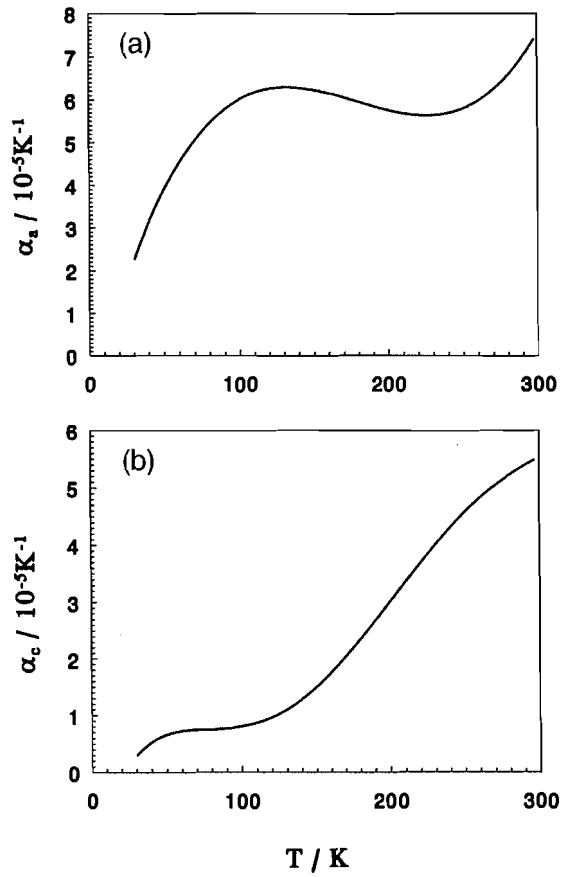

Table 7. Intramolecular bond angles involving the nonhydrogen atoms for HPTB–CBr_4.

Atom	Atom	Atom	Angle
Br(1)	—C(8)	—Br(1)	110.7(6)
Br(1)	—C(8)	—Br(1)	110.7(6)
Br(1)	—C(8)	—Br(2)	108.2(6)
Br(1)	—C(8)	—Br(1)	110.7(6)
Br(1)	—C(8)	—Br(2)	108.3(6)
Br(1)	—C(8)	—Br(2)	108.2(6)
C(1)	—S(1)	—C(7)	104.2(4)
S(1)	—C(1)	—C(2)	116.2(8)
S(1)	—C(1)	—C(6)	125.6(7)
C(2)	—C(1)	—C(6)	117.9(9)
C(1)	—C(2)	—C(3)	120(1)
C(2)	—C(3)	—C(4)	120(1)
C(3)	—C(4)	—C(5)	122(1)
C(4)	—C(5)	—C(6)	118(1)
C(1)	—C(6)	—C(5)	122(1)
S(1)	—C(7)	—C(7)	122.7(7)
S(1)	—C(7)	—C(7)	117.3(7)
C(7)	—C(7)	—C(7)	120.00(2)

Fig. 5. (*a*) HPTP *a*-axis as a function of temperature. ○, neutron results; ●, X-ray result. The temperature dependence is too weak for an accurate least-squares fit. (*b*) HPTP *b*-axis as a function of temperature. ○, neutron results (error bars are smaller than the data circles); ●, X-ray result. The temperature dependence is too weak for an accurate least-squares fit. (*c*) HPTP *c*-axis as a function of temperature. ○, neutron results; ●, X-ray result. The temperature dependence is too weak for an accurate least-squares fit. (*d*) HPTP unit cell volume as a function of temperature. ○, neutron results (error bars are smaller than the data circles); ●, X-ray result. The line indicates the least-squares fit used to determine thermal expansion (Fig. 6).

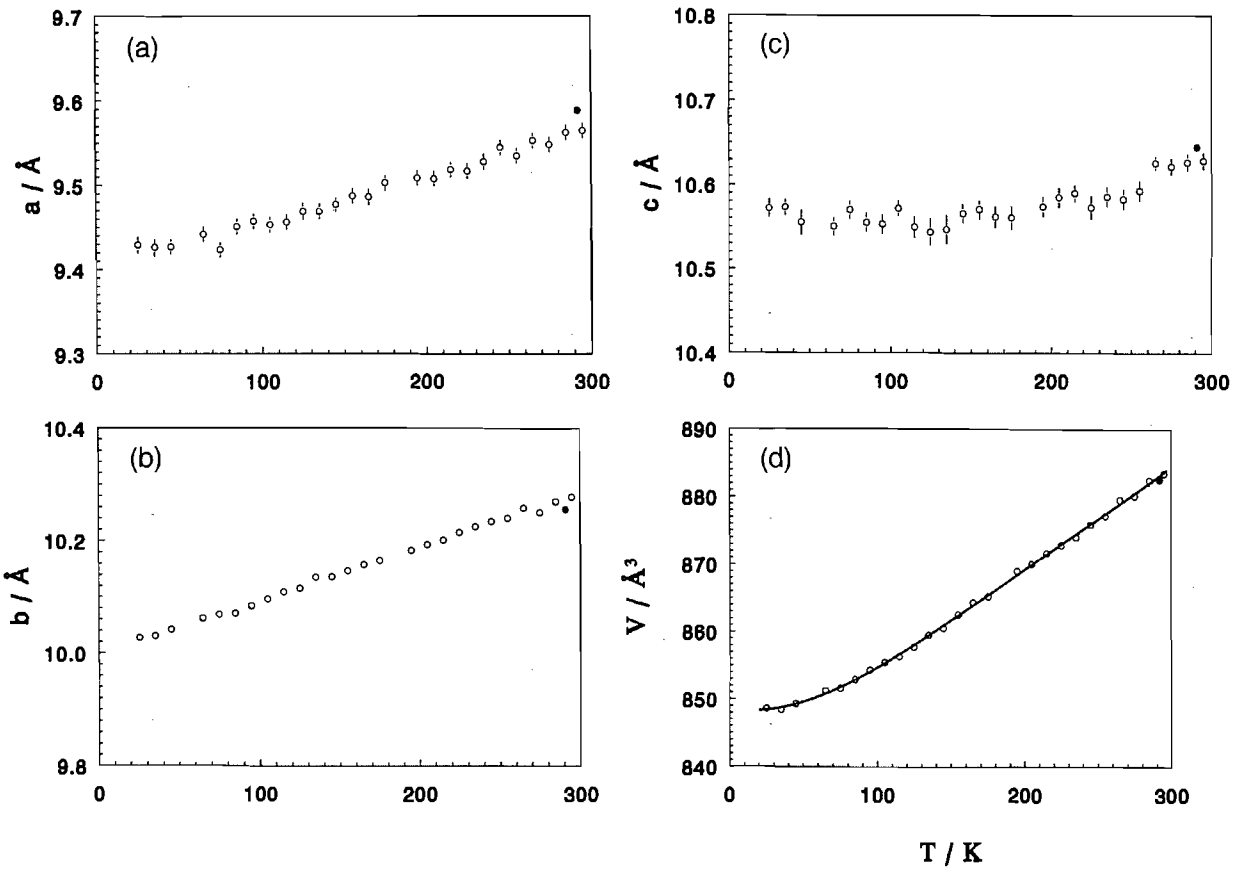

Can. J. Chem. Downloaded from www.nrcresearchpress.com by 65.111.164.53 on 09/08/12
For personal use only.

3. The value of the *a*-axis decreases monotonically with decreasing temperature. For the *c*-axis, two regions can be distinguished; above and below ca. 200 K (Fig. 3*b*). Similar behaviour was observed for Dianin's clathrates (9, 10), which have the same space group. The stronger effect of temperature on the *a*-axis than the *c*-axis can be attributed to more accessible space in the cavity in the *a*-direction than in the *c*-direction. Knowledge of the temperature dependence of the unit cell dimensions of HPTB–CBr_4 allows for the determination, through smooth fitting, of the values of the thermal expansion tensor as a function of temperature. Due to the symmetry of the system the tensor for HPTB–CBr_4 has only two non-zero independent components defined as $\alpha_a = a^{-1}da/dT$ and $\alpha_c = c^{-1}dc/dT$, i.e., $\alpha_{11} = \alpha_{22} = \alpha_a$ and $\alpha_{33} = \alpha_c$, respectively (Fig. 4).

In the case of the pure HPTB the largest temperature-dependence in the unit cell dimension is for the *b*-axis. (See Fig. 5 for unit cell dimensions and volume as functions of temperature.) The values of *a* and *c* change only very slowly with temperature. It is difficult to interpret this on the basis of the topological features of the crystal because of the very low symmetry of the structure.

Although both HPTB and HPTB–CBr_4 have anisotropic thermal expansivity neither displays any anomalous behaviour (e.g., negative thermal expansion).

The volume thermal expansivities, i.e. $\alpha_v = V^{-1}dV/dT$, of HPTB and HPTB–CBr_4 are similar in character (Fig. 6) with slightly higher values for pure HPTB. This contrasts with results for clathrate hydrates and Dianin's clathrates, which showed enhanced thermal expansion of the clathrates with respect to the host compound (i.e., ice or the clathrand of Dianin's compound) (9, 10, 28, 29). This was ascribed to the extra pressure exerted by the host molecules on the walls of the cages; molecular dynamics simulations corroborated this view for clathrate hydrates (28). In our opinion the absence of this effect for HPTB and HPTB–CBr_4 stems from differences between their structures and those of the clathrate hydrates and Dianin's clathrates. All three systems conform to the afore-mentioned topological definition of a clathrate compound, i.e., a structure based on lattice lacunae. Yet a subtle,

Fig. 6. (*a*) HPTB volume thermal expansion as a function of temperature, as determined from the least-squares fit to the volume (Fig. 5*d*). (*b*) HPTB–CBr_4 volume thermal expansion as a function of temperature, as determined from the least-squares fit to the volume (Fig. 3*c*).

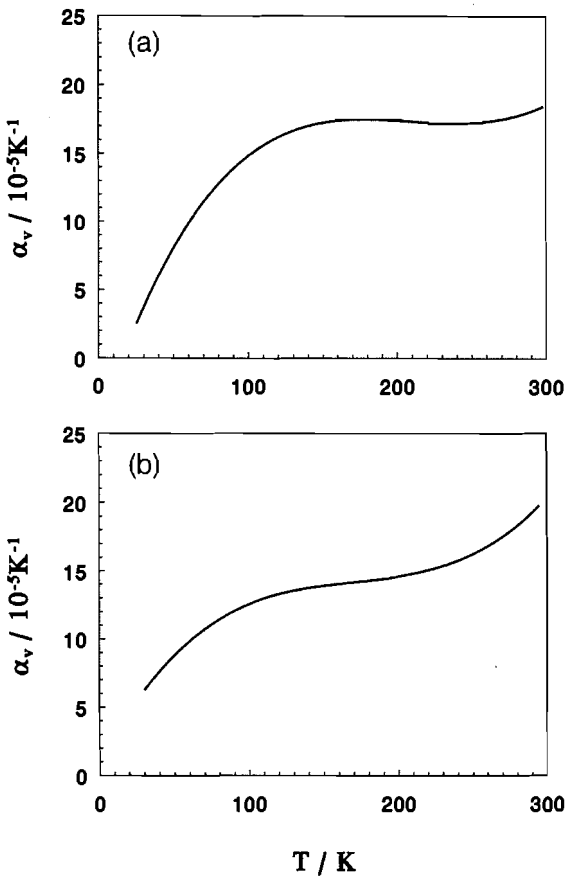

but most significant, distinction lies in the constitution of these assemblies. Dianin's clathrate and clathrate hydrates form better defined cavities. The clathrate edifice is composed of the host molecules associated through hydrogen bonds, and the steric barriers that limit the volume of the voids are tight; this lets the guest have noticeable impact on the thermal expansion. In contrast, the HPTB clathrates are more open. The guests can be considered as space fillers that are loosely retained in the lattice; although the thermal parameters of CBr_4 are small, the CBr_4 guest molecules can easily be pumped away with destruction of the lattice. This also explains why volatile guests such as CCl_4 and CH_3CCl_3 are easily lost from HPTB (15).

Acknowledgements

This work was financially supported by the Natural Sciences and Engineering Research Council of Canada (grants to M.A.W. and T.S.C., scholarship to D.M.), the Killam Trust Fund (scholarship to D.M. and P.K.B.), the Commonwealth Scholarship Fund (P.K.B.), and the Canadian Institute for Neutron Scattering. The assistance of B.M. Powell is also gratefully acknowledged.

References

1. D.D. MacNicol, J.J. McKendrick, and D.R. Wilson. Chem. Soc. Rev. **7**, 65 (1978).
2. H.M. Powell. J. Chem. Soc. 61 (1948).
3. E. Weber and H.-P. Josel. J. Inclusion Phenom. **1**, 79 (1983).
4. H.M. Powell. *In* Inclusion compounds. Vol. 1. *Edited by* J.L. Atwood, J.E.D. Davies, and D.D. MacNicol. Academic Press, London. 1984. pp. 1–28.
5. M.A. White and M.T. MacLean. J. Phys. Chem. **89**, 1380 (1985).
6. M.A. White. J. Phys. (Les Ulis, Fr.) **C1**, 565 (1987).
7. J.S. Tse and M.A. White. J. Phys. Chem. **92**, 5006 (1988).
8. M.A. White and M. Zakrzewski. J. Inclusion Phenom. **8**, 215 (1990).
9. W. Abriel, A. du Bois, M. Zakrzewski, and M.A. White. Can. J. Chem. **68**, 1352 (1990).
10. M. Zakrzewski, M.A. White, and W. Abriel. J. Phys. Chem. **94**, 2203 (1990).
11. M. Zakrzewski and M.A. White. Phys. Rev. B: Solid State, **45**, 2809 (1992).
12. M.A. White and R.T. Perry. Chem. Mater. **6**, 603 (1994).
13. R.S. Krishnan, R. Srinivasan, and S. Devanarayan. *In* Thermal expansion of crystals. Pergamon Press, Oxford. 1979.
14. D.D. MacNicol and D.R. Wilson. J. Chem. Soc. Commun. 494 (1976).
15. A.D. Hardy, D.D. MacNicol, and D.R. Wilson. J. Chem. Soc. Perkin Trans. 2, 1011 (1979).
16. N. Walker and D. Stuart. Acta Crystallogr. Sect. A: Cryst. Phys. Diffr. Theor. Gen. Crystallogr. **A39**, 158 (1983).
17. International tables for crystallography. Vol. IV. The Kynoch Press, Birmingham, England. 1974.
18. G.M. Sheldrick. SHELXS 86. *In* crystallographic computing. *Edited by* G.M. Sheldrick, C. Kruger, and R. Goddard. Oxford University Press, Oxford. 1985. pp. 175–189.
19. TEXAN-TEXRAY. Single crystal structure analysis package. Version 5.0. Molecular Structure Corporation, The Woodlands, Tex.
20. G.M. Sheldrick. SHELX 76. Program for crystal structure determination. University of Cambridge, Cambridge, England. 1976.
21. A.C. Larson and R.B. Von Dreele. GSAS—general structure analysis system. Los Alamos National Laboratory. 1990.
22. CHEM-X, Chemical Design Ltd., Oxford, England. 1990.
23. A.I. Kitaigorodsky. *In* Molecular crystals and molecules. Academic Press, New York. 1973.
24. V. Schomaker and K.N. Trueblood. Acta Crystallogr. Sect. B: Struct. Crystallogr. Cryst. Chem. **B24**, 63 (1968).
25. M. More, F. Baert, and J. Lefebvre. Acta Crystallogr. Sect. B: Struct. Crystallogr. Cryst. Chem. **B33**, 3681 (1977).

Can. J. Chem. Downloaded from www.nrcresearchpress.com by 65.111.164.53 on 09/08/12
For personal use only.

26. C.J. Gilmore, D.D. MacNicol, P.R. Mallison, and A. Murphy. J. Incl. Phenom. **1**, 295 (1984).
27. S. Cohen, R. Powers, and R. Rudman. Acta Crystallogr. Sect. B: Struct. Crystallogr. Cryst. Chem. **B34**, 1670 (1979).
28. J.S. Tse and W.R. McKinnon. J. Phys. Chem. **91**, 4188 (1987).
29. J.S. Tse. J. Inclusion Phenom. **8**, 25 (1990).
30. C.K. Johnson. ORTEPII. Report ORNL-5138. Oak Ridge National Laboratory, Oak Ridge, Tenn. 1976.

Can. J. Chem. Downloaded from www.nrcresearchpress.com by 65.111.164.53 on 09/08/12
For personal use only.

The photochemical nucleophile–olefin combination, aromatic substitution (photo-NOCAS) reaction. Part 8: methanol–2-carene, and 1,4-dicyanobenzene[1]

Donald R. Arnold, Xinyao Du, and Huub J.P. de Lijser

Can. J. Chem. Downloaded from www.nrcresearchpress.com by 65.111.164.53 on 09/08/12
For personal use only.

Abstract: The structure and reactivity of the radical cation of (+)-2-carene ((1*S*,6*R*)-3,7,7-trimethyl-*cis*-bicyclo[4.1.0]hept-2-ene (**3**)) have been studied. The radical cation was generated by photoinduced single electron transfer to the first electronically excited singlet state of 1,4-dicyanobenzene in acetonitrile–methanol (3:1). The 1:1:1 (methanol:2-carene:1,4-dicyanobenzene) adducts were formed: *trans*-3-(4-cyanophenyl)-4-(1-methoxy-1-methylethyl)-1-methylcyclohexene (**14**), and *cis*- (**15**) and *trans*-3-(4-cyanophenyl)-6-(1-methoxy-1-methylethyl)-3-methylcyclohexene (**16**) in a combined yield of 80%. The efficiency of the reaction and the yield of products were increased by the addition of biphenyl, serving as a codonor. These photo-NOCAS adducts formally result from cleavage of the three-membered ring of the 2-carene radical cation, at the C1—C7 bond, forming the tertiary carbocation and allylic radical. Reaction of the cation with methanol and coupling of the allylic radical with the 1,4-dicyanobenzene radical anion at the *ipso* position, followed by loss of cyanide ion, completes the sequence. There was no evidence for cleavage of the C1—C6 bond under these conditions; however, when the irradiation was carried out in acetonitrile (no methanol) the (+)-2-carene was partially racemized. Racemization is indicative of C1—C6 bond cleavage. The results of *ab initio* molecular orbital calculations (STO-3G) provide insight into the extent of C1—C7 bond cleavage in the radical cation. The calculated spin and charge distribution, on the 2-carene radical cation global minimum (**3***a*$^{+\cdot}$), is consistent with the observed regiospecificity of adduct formation.

Key words: photoinduced electron transfer, radical ions, molecular orbital calculations, bond cleavage, 2-carene.

Résumé : On a étudié la structure et la réactivité du cation radical du (+)-2-carène ((1*S*,6*R*)-3,7,7-triméthyl-*cis*-bicyclo[4.1.0]hept-2-ène (**3**)). On a généré le cation radical par un transfert photoinduit d'un seul électron vers le premeir état singulet électroniquement excité du 1,4-dicyanobenzène, dans un mélange acétonitrile–méthanol (3 : 1). Il se forme des adduits 1 : 1 : 1 (méthanol : 2-carène : 1,4-dicyanobenzène) : les *trans*- et *cis*-3-(4-cyanophényl)-4-(1-méthoxy-1-méthyléthyl)-1-méthylcyclohexène (**14** et **15**) et le *trans*-3-(4-cyanophényl)-6-(1-méthoxy-1-méthyléthyl)-3-méthylcyclohexène (**16**) avec un rendement combiné de 80%. L'efficacité de la réaction et le rendement sont augmentés par l'addition de biphényle qui agit comme condonneur. Ces adduits photo-NOCAS sont formellement le résultat d'un clivage du cycle à trois chaînons du cation radical du 2-carène, au niveau de la liaison C1—C7, conduisant à la formation du carbocation tertiaire et d'un radical allylique. La réaction du cation avec le méthanol et le couplage du radical allylique avec l'anion radical du 1,4-dicyanobenzène en position *ipso*, suivi de la perte de l'ion cyanure, complète la séquence de réactions. Dans ces conditions, on n'a pas observé de données suggérant un clivage de la liaison C1—C6; toutefois, si l'on effectue l'irradiation dans l'acétonitrile (sans méthanol), le (+)-2-carène se racémise partiellement. La racémisation indique qu'il se produit un clivage en C1—C6. Les résultats de calculs *ab initio* d'orbitales moléculaires (STO-3G) fournissent des indications sur l'importance du clivage de la liaison C1—C7 du cation radical. La distribution de spin et de charge calculées sur le minimum global du cation radical du 2-carène (**3***a*$^{+\cdot}$) est en accord avec la régiosélectivité observée pour la formation des adduits.

Mots clés : transfert photoinduit d'électron, ions radicaux, calculs d'orbitales moléculaires, clivage de la liaison, 2-carène.

[Traduit par la rédaction]

Received October 20, 1994.

D.R. Arnold,[2] X. Du, and H.J.P. de Lijser. Department of Chemistry, Dalhousie University, Halifax, NS B3H 4J3, Canada.

[1] This is also Part 35 of the series Radical Ions in Photochemistry; see refs. 1 and 2 for preceding parts of these series.

[2] Author to whom correspondence may be addressed. Telephone: (902) 494-3714. Fax: (902) 494-1310. E-mail: arnold @ ac.dal.ca

Can. J. Chem. Downloaded from www.nrcresearchpress.com by 65.111.164.53 on 09/08/12
For personal use only.

Introduction

Interesting results from the study of the reactions of the radical cations of the vinylcyclobutane derivatives, α- and β-pinene (**1** and **2**, reactions [1] and [2] (1*c*, *d*)), have promoted us to extend our examination to the vinylcyclopropane analog, (+)-2-carene ((1*S*,6*R*)-3,7,7-trimethyl-*cis*-bicyclo[4.1.0]hept-2-ene, **3**) (reaction [3]). This naturally occurring chiral terpene has often been used to test reaction mechanisms involving the more common intermediates (3).[3] The radical cation has received less attention (4). Results of this investigation, incorporating (+)-2-carene (**3**) in the photo-NOCAS reaction, are relevant to the broader understanding of the nature of vinyl cyclopropyl, and other substituted cyclopropyl, radical cations (5, 6). Results of a study of the related radical cation of sabinene (**17**) have recently been reported (5*e*).

Results

Irradiation of an acetonitrile–methanol (3:1) solution of 1,4-dicyanobenzene (**4**), biphenyl (**5**), and (+)-2-carene (**3**), at 10°C through a Pyrex filter, with a medium-pressure mercury vapour lamp, leads to formation of the photo-NOCAS adducts (reaction [3]). *trans*-3-(4-Cyanophenyl)-4-(1-methoxy-1-methylethyl)-1-methylcyclohexane (**14**), and *cis*- (**15**) and *trans*-3-(4-cyanophenyl)-6-(1-methoxy-1-methylethyl)-3-methylcyclohexene (**16**) were isolated from the photolysate by dry-column flash (dcfc) and medium-pressure liquid (mplc) chromatography. The combined yield of these 1:1:1 adducts was 80%, based upon 1,4-dicyanobenzene (**4**) consumed.

Adducts **14**, **15**, and **16** are chiral; presumably, the original configuration at C6 (*R*) of (+)-2-carene (**3**) has been maintained. 2-Carene (**3**) recovered from the photolysate showed no loss of optical activity. The addition of the codonor biphenyl (**5**), to the reaction mixture, increased the efficiency and yield of the reaction; however, reaction does occur upon irradiation in the absence of **5**, and the ratio of photo-NOCAS products formed under these conditions was the same.

An acetonitrile solution of 2-carene (**3**), 1,4-dicyanobenzene (**4**), and biphenyl (**5**), without added methanol, was irradiated under similar conditions. No products analogous to the imines **9** and **13**, formed in reactions [1] and [2], were detected (gc/ms, gc/fid); however, the observed optical rotation of the

Reaction [1] (1)

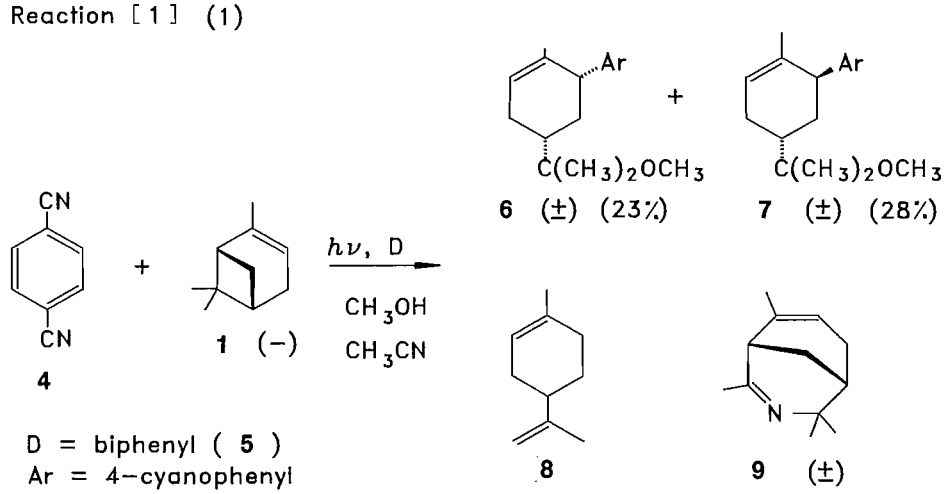

Reaction [2] (1)

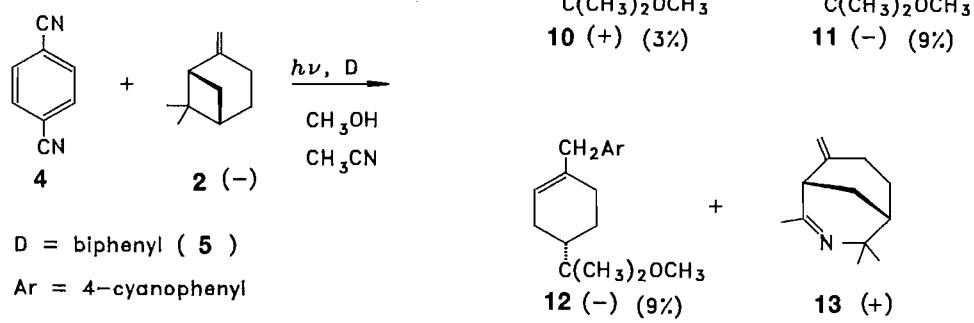

[3] For example: reaction with singlet oxygen (3*a*); reaction with ozone (3*b*); reaction with HO˙ and NO_3 (3*c*); the ene-reaction with *N*-phenyltriazolenedione (3*d*); hydroboration (3*e*); the ene-reaction with *N*-sulphinylbenzene sulphonamide (3*f*); epoxidation with *meta*-chloroperbenzoic acid (3*g*); cyclopropanation (3*h*); reaction with iron tricarbonyl (3*i*); reaction with *n*-butyllithium–tetramethylethylenediamine complex (3*j*); and reaction with palladium(II) (3*k*, *l*, *m*).

Can. J. Chem. Downloaded from www.nrcresearchpress.com by 65.111.164.53 on 09/08/12
For personal use only.

Reaction [3]

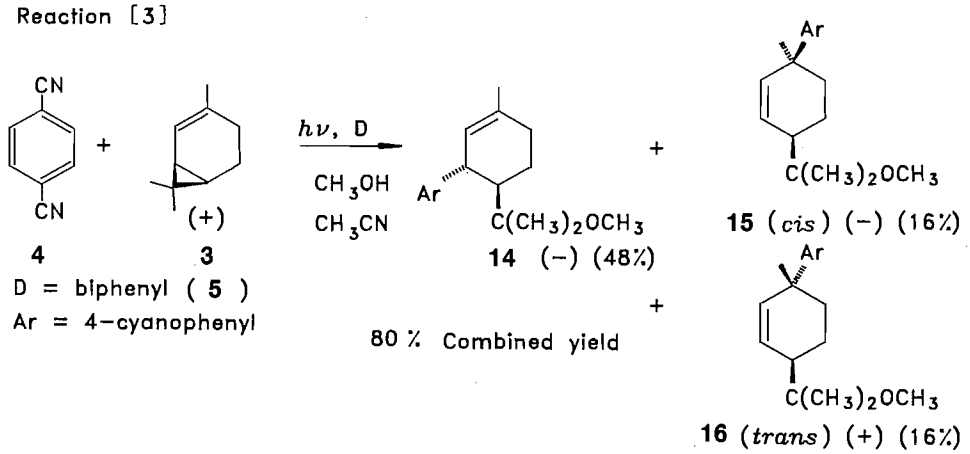

Reaction [4]

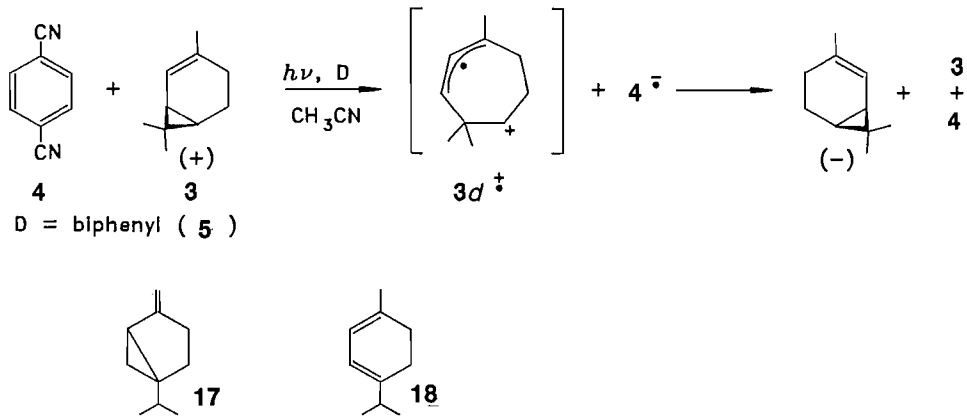

Table 1. The oxidation potentials of some compounds of interest and the calculated free energy change (ΔG_{ET}) for the electron transfer process to the excited singlet state of 1,4-dicyanobenzene (**4**) as the acceptor.

Donor	$E_{1/2}^{ox}$ (V)[a]	(ΔG_{ET} kJ mol^{-1})[b]
α-Pinene (1)	1.75	−84.8
β-Pinene (2)	2.20	−41.4
2-Carene (3)	1.39	−119.5
Biphenyl (5)	1.85	−75.1
1-Methylcyclohexene	1.93	−67.4

[a]Oxidation potentials, estimated as 0.028 V before the peak potential measured at a platinum electrode, relative to the saturated calomel electrode (SCE) using tetraethylammonium perchlorate (0.1 M TEAP) as the electrolyte in acetonitrile (ref. 7).

[b]Based on the Weller equation (ref. 8); $E_{0,0}$ (**4**) = 408.4 kJ mol^{-1}, $E_{1/2}^{red}$ (**4**) = −1.66 V. The Coulombic attraction term was taken to be 5.40 kJ mol^{-1} (ref. 9).

The Weller equation: ΔG_{ET} (kJ mol^{-1}) = 96.48 [$E_{1/2}^{ox}$ (D/D$^{\cdot+}$) − $E_{1/2}^{red}$ (A/A$^{\cdot-}$) − $e/a\varepsilon$] − $E_{0,0}$.

2-carene (**3**) recovered from this photolysate was significantly decreased (reaction [4]).

The oxidation potentials of several compounds of interest, determined by cyclic voltammetry, are summarized in Table 1.

Structure determination

Structural assignments for the new compounds were based primarily on analysis of the ^{1}H and ^{13}C nmr spectra. The overall connectivity was easily established; assigning configuration was more demanding. Details are given in the experimental section. The spectra for the *cis* and *trans* isomers, **15** and **16**, were very similar. In the proton nmr spectrum of the isomer assigned the *cis* configuration (**15**), the signal due to the axial hydrogen (H5) is at lower frequency (0.94 ppm) than the axial hydrogen (H5) (1.58 ppm) of the other isomer (**16**) assigned the *trans* configuration. We attribute this difference to a shielding effect of the aromatic ring that is in the pseudo-axial position of the cyclohexene in the *cis* isomer. Comparison of the ^{13}C nmr spectra of the two isomers provides additional support for this assignment. In the ^{13}C nmr spectrum of **15**, the *cis* isomer, the half-width of the central lines of the quartet corresponding to the carbon of the methyl group at δ 30.31 is relatively narrow (8.2 Hz). This is attributed to relatively small equatorial–equatorial and equatorial–axial $^3J_{C-H}$ couplings. The ^{13}C nmr spectrum of **16**, the *trans* isomer, displays a quartet at δ 26.62 with each line having a half-width of 13.5 Hz. Such a broad signal is indicative of larger axial–axial coupling of the methyl carbon to the axial H4 (at ca. 1.68 ppm) plus other small $^3J_{C-H}$ couplings (10).

Computational details

Ab initio molecular orbital calculations were carried out with the GAUSSIAN 92/DFT series of programmes (11). Open-shell species were treated in the unrestricted Hartree–Fock (UHF) formalism; closed-shell species were treated in the restricted

Table 2. The calculated (*ab initio*) total energies for the neutral 2-carene (**3**), in two conformations, and for several alternative structures of the 2-carene radical cation ($3^{+\cdot}$).

	HF/STO-3G (au)
2-Carene (**3***a*, pseudo-boat conformation)	−383.371 780 (−383.366 190)[a]
2-Carene (**3***b*, pseudo-chair conformation)	−383.372 767 (−383.368 076)[a]
3,7,7-Trimethyl-*trans*-bicyclo[4.1.0]hept-2-ene	−383.303 648
2-Carene radical cation ($3a^{+\cdot}$, pseudo-boat conformation)	−383.175 591
2-Carene radical cation ($3b^{+\cdot}$, pseudo-chair conformation)	−383.169 356
2-Carene radical cation ($3c^{+\cdot}$, ring-cleaved, six-membered)	−383.170 128
2-Carene radical cation ($3d^{+\cdot}$, ring-cleaved, seven-membered)	−383.119 489

[a]Previously reported (STO-3G) (12). The variation in these two numbers can be attributed to differences in conformation involving the methyl groups C8 and C9.

Scheme 1

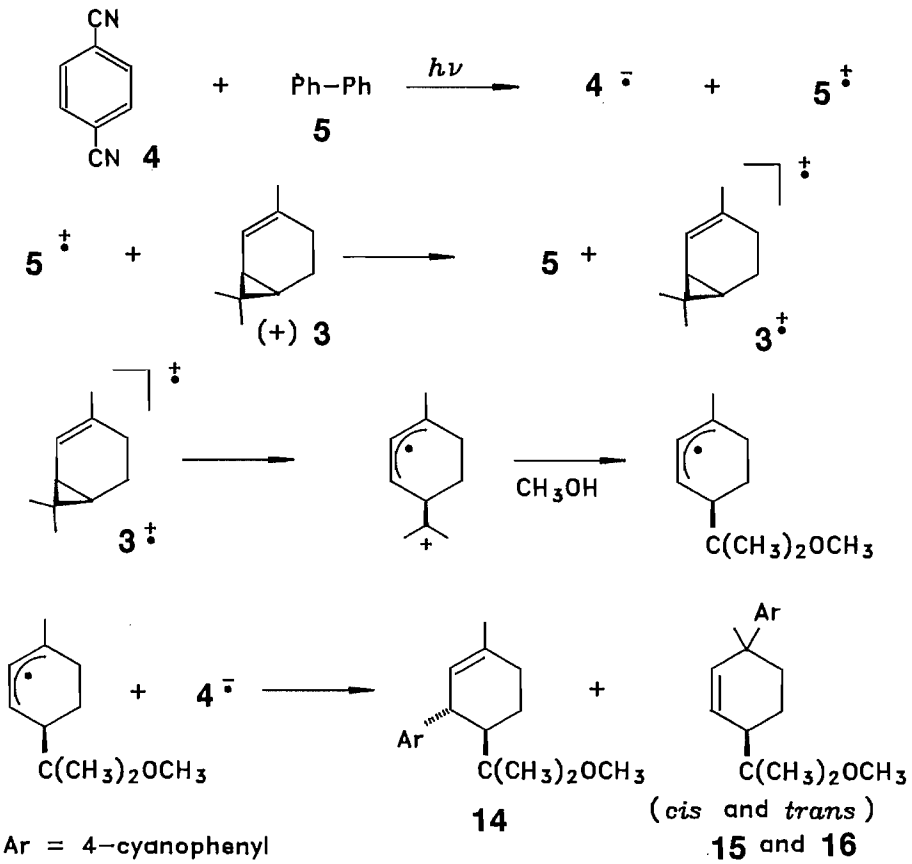

Hartree–Fock (RHF) formalism. All of the optimized structures were confirmed to be minima by frequency calculations. The charge and spin distributions were calculated by Mulliken population analysis. The calculated (STO-3G) total energies for fully optimized structures are summarized in Table 2.

The calculated total energies for the neutral 2-carene in two conformations, pseudo-boat (**3***a*) and pseudo-chair (**3***b*), indicate a slight preference (2.6 kJ mol^{-1}) for the pseudo-chair conformer. This order is reversed in the radical cations, the pseudo-boat conformer ($3a^{+\cdot}$) is more stable (16 kJ mol^{-1}) than the pseudo-chair conformer ($3b^{+\cdot}$). The distonic, ring-cleaved, six-membered ring radical cation ($3c^{+\cdot}$), formed upon cleavage of the C1—C7 bond, is only 14 kJ mol^{-1} less stable than the global minimum ($3a^{+\cdot}$). The alternative structure, cleavage of the C1—C6 bond ($3d^{+\cdot}$), is significantly (147 kJ mol^{-1}) less stable. These fully optimized structures are shown in Figs. 1–6; charge and spin distribution on the radical cations are summarized in Tables 3–6.

Molecular orbital calculations on 2-carene (3) have been reported previously (12). The differences between the published energies and those reported here can be attributed to variation in conformation of the methyl groups, C8 and C9.

The calculations indicate that the *trans*-fused configurational isomer of the neutral 2-carene (3) is significantly (182 kJ mol^{-1}) less stable than the naturally occurring *cis* isomer.

Discussion

The mechanism proposed for reaction [3] is summarized in Scheme 1.

Can. J. Chem. Downloaded from www.nrcresearchpress.com by 65.111.164.53 on 09/08/12
For personal use only.

Can. J. Chem. Downloaded from www.nrcresearchpress.com by 65.111.164.53 on 09/08/12
For personal use only.

Fig. 1. The fully optimized (STO-3G) structure of 2-carene (*3a*), pseudo-boat conformation).

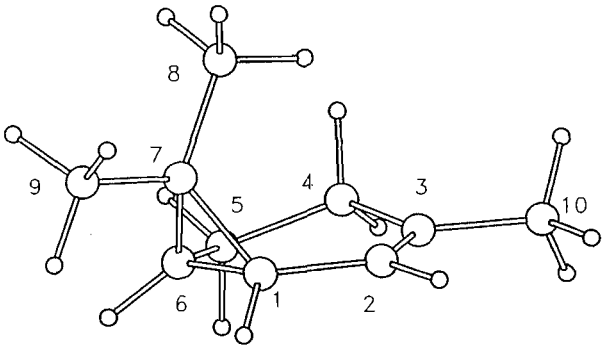

Bond length (pm)		Bond angle (°)		Dihedral angle (°)	
C_1-C_2	150.3	$C_1C_2C_3$	123.9	$C_1C_2C_3C_4$	2.3
C_2-C_3	131.6	$C_2C_3C_4$	122.6	$C_7C_1C_2C_3$	-62.7
C_1-C_6	150.7	$C_2C_1C_6$	117.4	$C_6C_1C_2C_3$	7.2
C_1-C_7	152.4	$C_2C_1C_7$	121.9	$C_8C_7C_9C_6$	147.1
		$C_1C_6C_7$	60.6		

Fig. 2. The fully optimized (STO-3G) structure of 2-carene (*3b*, pseudo-chair conformation).

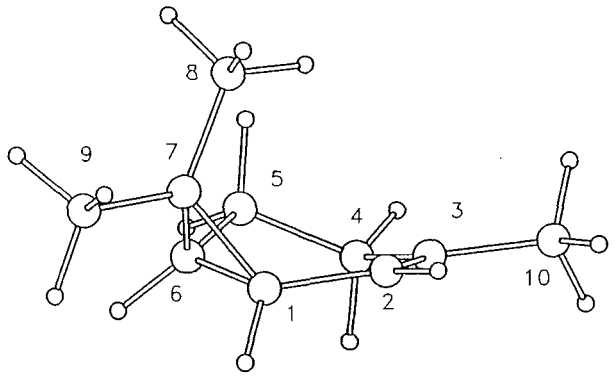

Bond length (pm)		Bond angle (°)		Dihedral angle (°)	
C_1-C_2	150.6	$C_1C_2C_3$	122.4	$C_1C_2C_3C_4$	-0.2
C_2-C_3	131.5	$C_2C_3C_4$	121.0	$C_7C_1C_2C_3$	-87.9
C_1-C_6	150.7	$C_2C_1C_6$	117.2	$C_6C_1C_2C_3$	-17.9
C_1-C_7	151.8	$C_2C_1C_7$	121.6	$C_8C_7C_9C_6$	146.7
		$C_1C_6C_7$	60.3		

The oxidation potential of 2-carene (**3**), 1.39 V (vs. sce), is relatively low.[4] Using the Weller equation, we calculate that electron transfer from **3** to the first electronically excited singlet state of 1,4-dicyanobenzene (**4**) is exergonic (−120 kJ mol^{-1}) by an amount sufficient that electron transfer will be diffusion controlled (8). Electron transfer from biphenyl (**5**) (oxidation potential, 1.85 V) to the excited state of **4** is also diffusion controlled (step 1, Scheme 1) (9, 13). Electron transfer from **3** to the radical cation of the codonor ($\mathbf{5}^{+\cdot}$) is exergonic (step 2, Scheme 1). The increase in efficiency of the reaction in the presence of the codonor is attributed to a greater ratio of the rates of radical ion pair cage escape, versus back electron transfer, for the pair ($\mathbf{4}^{-\cdot}$–$\mathbf{5}^{+\cdot}$) relative to the pair ($\mathbf{4}^{-\cdot}$–$\mathbf{3}^{+\cdot}$). This difference is the result of a slower rate of back-electron transfer in the former pair due to a relatively smaller reorganizational energy for $\mathbf{5}^{+\cdot}$ returning to **5** (9, 13).

Analysis of the photoelectron spectra of vinylcyclopropane has provided convincing evidence for a stabilizing conjugative interaction between the π-bond of the alkene and the Walsh "π-type" orbital of cyclopropane in the vinylcyclopropane radical cation (5*c*, *d*). The relatively low ionization potential (8.26 V (4*d*)) and oxidation potential (1.39 V (Table 1)) of 2-carene (**3**) indicate this interaction is also occurring in this radical cation. The molecular orbital calculations lend support to this conclusion. The dihedral angle $C_7C_1C_2C_3$ of the pseudo-boat conformation of the neutral molecule (*3a*) (−62.7°) is favourable for overlap between the π-bond of the alkene linkage C2—C3 and the Walsh "π-type" orbital of the cyclopropane on C1 (Fig. 1). Ionization from the HOMO of this structure gives the global minimum for the radical cation, $3a^{+\cdot}$, which has a long (186.6 pm) C1–C7 bond; the dihedral angle $C_6C_1C_2C_3$ is now almost planar (−0.8°); and bonding at C7 is also almost planar (170°) (Fig. 3).

Carbons C7, C8, and C9 bear 43% of the positive charge density while the spin density is highest (0.837) on C3 (Table 3). Clearly, methanol should (and does) attack this radical cat-

Fig. 3. The fully optimized (STO-3G) structure of 2-carene radical cation ($3a^{+\cdot}$, pseudo-boat conformation).

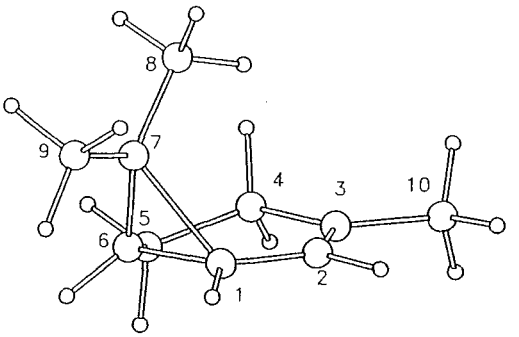

Bond length (pm)		Bond angle (°)		Dihedral angle (°)	
C_1-C_2	141.2	$C_1C_2C_3$	123.0	$C_1C_2C_3C_4$	0.5
C_2-C_3	139.7	$C_2C_3C_4$	121.8	$C_7C_1C_2C_3$	-60.2
C_1-C_6	153.0	$C_2C_1C_6$	120.7	$C_6C_1C_2C_3$	-0.8
C_1-C_7	186.6	$C_2C_1C_7$	110.9	$C_8C_7C_9C_6$	170.2
		$C_1C_6C_7$	76.2		

Fig. 4. The fully optimized (STO-3G) structure of 2-carene radical cation ($3b^{+\cdot}$, pseudo-chair conformation).

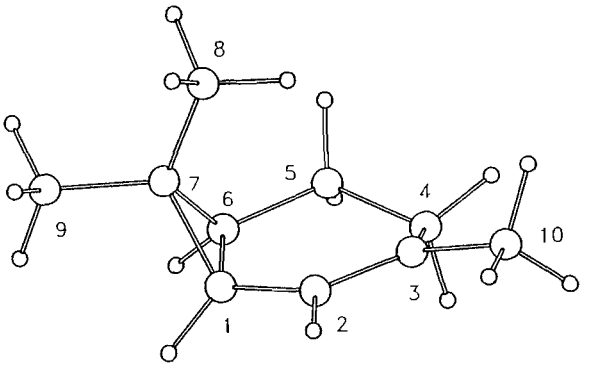

Bond length (pm)		Bond angle (°)		Dihedral angle (°)	
C_1-C_2	144.8	$C_1C_2C_3$	122.7	$C_1C_2C_3C_4$	-14.9
C_2-C_3	142.5	$C_2C_3C_4$	118.8	$C_7C_1C_2C_3$	-72.3
C_1-C_6	152.9	$C_2C_1C_6$	119.0	$C_6C_1C_2C_3$	-5.2
C_1-C_7	157.9	$C_2C_1C_7$	119.9	$C_8C_7C_9C_6$	152.0

[4] All of the oxidation and reduction potentials mentioned in this manuscript are referenced against the saturated calomel electrode (SCE).

Can. J. Chem. Downloaded from www.nrcresearchpress.com by 65.111.164.53 on 09/08/12
For personal use only.

Fig. 5. The fully optimized (STO-3G) structure of 2-carene radical cation ($3c^{+\cdot}$, ring-cleaved, six-membered).

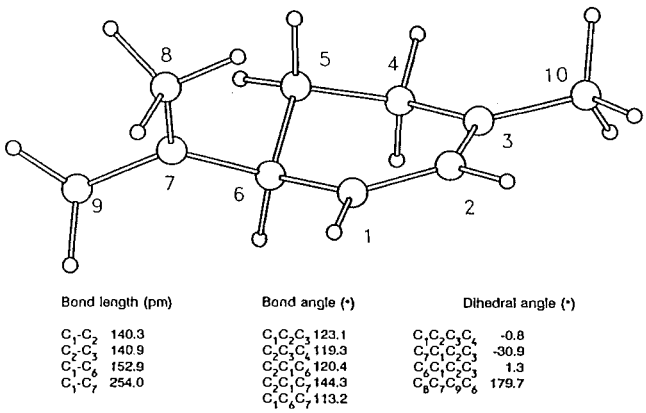

Fig. 6. The fully optimized (STO-3G) structure of 2-carene radical cation ($3d^{+\cdot}$, ring-cleaved, seven-membered).

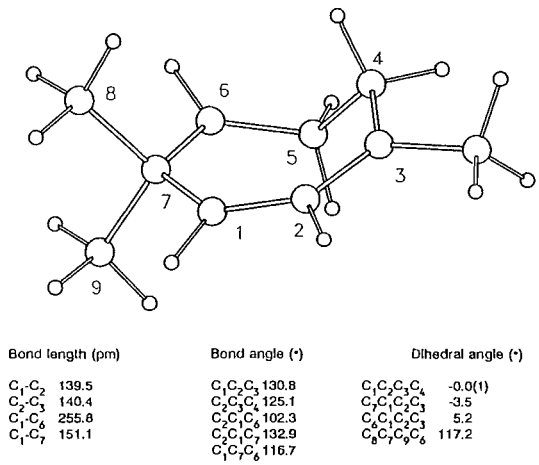

ion at C7, generating the allylic radical. Products resulting from attack of methanol on the original alkene linkage (C2) were not observed. The charge density at C2 is only 7%.

This regioselectivity is predicted from the simple rule: The regioselectivity of radical cation cleavage depends upon the relative oxidation potentials of the fragment radicals; the fragment with the lower oxidation potential will react preferentially as the carbocation (9*b*, 14). The oxidation potential of the *tert*- butyl radical (0.09 V) is significantly lower than that of the relevant allyl radical (ca. 0.15 V) (15).[5]

The difference in energy between the global minimum for the radical cation ($3a^{+\cdot}$) and the distonic ring-cleaved species ($3c^{+\cdot}$) is not significant (14 kJ mol^{-1}). Differences in solvation energy of these two species may in fact reverse this order of stability. It is not clear from the structure of the photo-NOCAS adducts, nor from these *ab initio* calculations, whether methanol attack occurs on the ring-closed ($3a^{+\cdot}$) or ring-cleaved distonic ($3c^{+\cdot}$) radical cation. In reactions [1] and [2], formation of the imines 9 and 13 was attributed to reaction of the ring-cleaved distonic radical cations of α- and β-pinene. This type of product was not observed in reaction [3]; nor was the imine

[5] Also, D.D.M. Wayner. Unpublished results.

Table 3. The charge and spin distribution calculated (STO-3G) for the radical cation of 2-carene ($3a^{+\cdot}$, pseudo-boat conformation).

			Spin			
No.[a]	Group	Charge[b]	Carbon	Hydrogen(s)		
1	CH	0.102	0.490	−0.033		
2	CH	0.069	−0.570	0.040		
3	C	0.072	0.837			
4	CH_2	0.064	−0.101	0.019	0.030	
5	CH_2	0.092	0.038	−0.005	−0.004	
6	CH	0.091	−0.129	0.028		
7	C	0.153	0.432			
8	CH_3	0.137	−0.050	0.021	0.002	0.013
9	CH_3	0.139	−0.049	0.021	0.007	0.005
10	CH_3	0.082	−0.102	0.026	0.028	0.006

[a]Numbering of carbon atoms in Fig. 3.
[b]Atomic charges, hydrogens summed with carbon atom.

Table 4. The charge and spin distribution calculated (STO-3G) for the radical cation of 2-carene ($3b^{+\cdot}$, pseudo-chair conformation).

			Spin			
No.[a]	Group	Charge[b]	Carbon	Hydrogen(s)		
1	CH	0.003	−0.040	0.010		
2	CH	0.229	0.393	−0.026		
3	C	0.157	0.568			
4	CH_2	0.103	−0.067	0.011	0.025	
5	CH_2	0.089	0.014	−0.000(3)	0.001	
6	CH	0.060	0.004	0.004		
7	C	0.067	0.128			
8	CH_3	0.081	−0.011	0.006	0.001	0.002
9	CH_3	0.059	−0.006	0.003	0.002	−0.001
10	CH_3	0.151	−0.070	0.004	0.021	0.023

[a]Numbering of carbon atoms in Fig. 4.
[b]Atomic charges, hydrogens summed with carbon atom.

formed upon irradiation of 2-carene (**3**) in acetonitrile in the absence of added methanol (reaction [4]). The distonic radical cation $3c^{+\cdot}$ has a more localized positive charge; carbons C7, C8, and C9 bear 70% of the positive charge. Therefore $3c^{+\cdot}$ would be expected to be more reactive at C7, less selective toward nucleophilic attack, with consequent reaction with acetonitrile and imine formation. We take this as evidence that the reactive radical cation has the delocalized/stabilized three-membered bridged structure ($3a^{+\cdot}$). Previous studies have provided convincing evidence that some substituted cyclopropane radical cation ring cleavages are nucleophilic assisted (5*e*, 6).

The results of photo-induced CIDNP and mass spectral studies are in complete agreement with these results. The observed CIDNP polarization was consistent with the radical cation of 2-carene (3) having structure $3a^{+\cdot}$ in which spin and charge are delocalized over the olefinic group and the C1—C7 bond (4*a*). The mass spectral behaviour (metastable ion characteristics and collision-induced dissociation) of 2-carene (**3**)

Can. J. Chem. Downloaded from www.nrcresearchpress.com by 65.111.164.53 on 09/08/12
For personal use only.

Table 5. The charge and spin distribution calculated (STO-3G) for the radical cation of 2-carene ($3c^{+\cdot}$, ring-cleaved, six-membered ring).

			Spin			
No.[a]	Group	Charge[b]	Carbon	Hydrogen(s)		
1	CH	0.025	1.014	−0.076		
2	CH	0.021	−0.839	0.058		
3	C	0.036	1.000			
4	CH_2	0.058	−0.119	0.035	0.017	
5	CH_2	0.065	0.032	−0.004	−0.003	
6	CH	0.041	−0.110	0.030		
7	C	0.301	0.021			
8	CH_3	0.203	−0.002	0.000(2)	0.000(4)	0.000(1)
9	CH_3	0.206	−0.000(2)	0.000(4)	−0.001	0.000(3)
10	CH_3	0.044	−0.124	0.008	0.032	0.031

[a]Numbering of carbon atoms in Fig. 5.
[b]Atomic charges, hydrogens summed with carbon atom.

Table 6. The charge and spin distibution calculated (STO-3G) for the radical cation of 2-carene ($3d^{+\cdot}$, ring-cleaved, seven-membered ring).

			Spin			
No.[a]	Group	Charge[b]	Carbon	Hydrogen(s)		
1	CH	0.128	0.654	−0.050		
2	CH	0.009	−0.598	0.042		
3	C	0.104	0.658			
4	CH_2	0.098	−0.066	0.015	0.013	
5	CH_2	0.099	−0.081	0.002	0.008	
6	CH	0.228	0.654	−0.049		
7	C	0.003	−0.123			
8	CH_3	0.109	−0.018	0.004	0.001	0.000(2)
9	CH_3	0.126	−0.035	0.002	0.005	0.001
10	CH_3	0.097	−0.081	0.004	0.018	0.020

[a]Numbering of carbon atoms in Fig. 6.
[b]Atomic charges, hydrogens summed with carbon atom.

and α-terpinene (**18**) are similar. This observation led to the suggestion that the long-lived molecular ion of 2-carene ($3^{+\cdot}$) cleaves the C1—C7 bond giving a radical cation identical with that of α-terpinene ($18^{+\cdot}$) prior to fragmentation (4*b*, *c*).

When the irradiation was carried out in acetonitrile (without added methanol) the (+) 2-carene (**3**) recovered, after prolonged irradiation, had undergone partial racemization (reaction [4]). It seems reasonable that under these conditions, i.e., no nucleophile, racemization is the result of competitive, less efficient, cleavage of the fused carbon–carbon bond (C1—C6); that is, reversible formation of $3d^{+\cdot}$. We found no evidence of isomerization of 2-carene, i.e., formation of the *trans* isomer. This is not surprising in view of significantly higher calculated total energy of this isomer (Table 2).

An interesting example of this dichotomy, C1—C7 versus C1—C6 bond cleavage depending upon solvent polarity/nucleophilicity, was observed previously (3*l*). The palladium(II)-induced ring opening of 2-carene (**3**), leading to chloro- or oxypalladation, is remarkably solvent dependent. Reaction of **3** with $PdCl_2(MeCN)_2$ in methanol gives a good yield (80%) of the (π-allyl)palladium complexes **19** and **20** resulting from C1—C7 bond cleavage (reaction [5]) (3*l*). When this reaction is carried out in less polar, less nucleophilic, solvent (chloroform) some product resulting from C1—C6 bond cleavage, **21**, is observed (reaction [6]) (3*l*). Furthermore, cleavage of the C1—C6 bond becomes the dominant mode when the solvent is nonpolar (benzene) (3*l*). This reaction is an oxidative addition of the Pd(II); it is perhaps not surprising that factors influencing the reactivity of the radical cation also effect this reaction.

The regio- and stereochemistry of the (next to) last step in the proposed mechanism, coupling of the allylic radical with

Reaction [5] (3l)

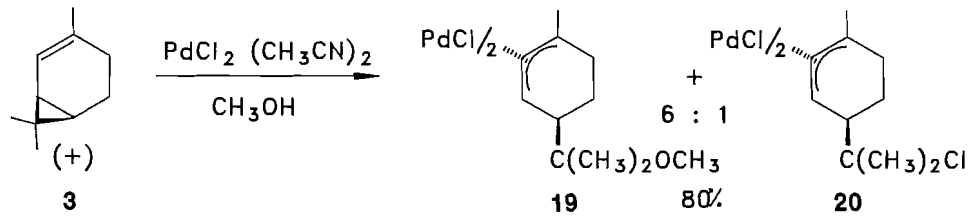

Reaction [6] (3l)

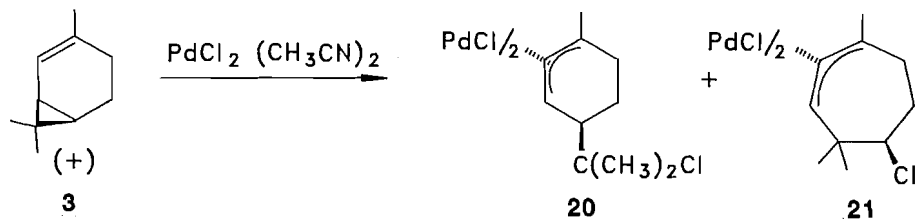

Solvent: C_6H_6 1 : 6.1
$CHCl_3$ 3.4 : 1

Can. J. Chem. Downloaded from www.nrcresearchpress.com by 65.111.164.53 on 09/08/12
For personal use only.

the radical anion ($4^{-\cdot}$), deserves comment. Equal amounts of the *cis* and *trans* isomers, **15** and **16**, indicate no steric influence of the remote bulky alkyl substituent; coupling occurs from both the pseudo-axial and pseudo-equatorial positions. When coupling occurs at the carbon adjacent to the alkyl substituent only the less hindered *trans* product (**14**) is formed. The fact that coupling occurs preferentially at the carbon adjacent to the bulky alkyl substituent results from the fact that this is the more reactive, less sterically hindered, *secondary* end of the ambident allylic radical.

We found none of the ethers that could result from reduction of the intermediate allylic radical, followed by protonation. This is consistent with the expected reduction potential of this radical, i.e., more negative than the reduction potential of 1,4-dicyanobenzene (**4**) (−1.66 V).

Experimental

General methods

The ^{1}H and ^{13}C NMR spectra were recorded on a Nicolet 360 NB nmr spectrometer coupled to an Oxford Instruments superconducting magnet and a Nicolet 192 kword data acquisition system, or an EM-360L spectrometer, and are reported in parts per million (ppm) to high frequency from tetramethylsilane (TMS). Elemental analyses were performed by Canadian Microanalytical Services Inc., Delta, B.C. The optical rotations of the starting material and products were determined with a Perkin–Elmer model 141 polarimeter.

The reactions were followed by gas chromatography (gc) using either an HP 5890 gas chromatography, fitted with a 5% phenyl methyl silicone fused silica WCOT column (25 m × 0.20 mm, 0.33 μm film thickness), coupled to an HP 5970 mass selective detector (ms), or an HP 5890 gas chromatography, fitted with a DB-1701 or DB-225 fused silica WCOT column (30 m × 0.25 mm, 0.25 μm film thickness), with a flame ionization detector (fid), coupled to a HP 3392A integrator. Mass spectra (ms) were recorded on a HP 5970 series mass selective detector and are reported as *m/z* (relative intensity).

Materials

Solvents were fractionally distilled. Acetonitrile (Fisher ACS grade) was distilled successively from sodium hydride and phosphorus pentoxide, and was then passed through a column of basic alumina, refluxed over calcium hydride for 24 h under a nitrogen atmosphere, and fractionally distilled. The 1,4-dicyanobenzene (**4**) (Aldrich) was purified by treatment with Norite in methylene chloride, followed by recrystallization from 95% ethanol. Biphenyl (**5**) (Aldrich) was recrystallized from methanol. (+)-2-Carene (**3**) was also obtained from Aldrich Chemical Co. and was used as received.

Cyclic voltammetric measurements

Oxidation potentials were obtained by cyclic voltammetry using an apparatus similar to that previously described (16). The working electrode was a platinum sphere (1 mm diameter), while the counter electrode was a platinum wire. The reference electrode was a saturated calomel electrode (SCE), which was connected to the solution by a Luggin capillary. The electrolyte was tetraethylammonium perchlorate (TEAP, 0.1 M) and the solvent was acetonitrile. Substrate concentrations were typically 0.005 M. If the anodic wave was not reversible, the half-wave potential was taken as 0.028 V before the anodic peak potential (7).

Formation of photo-NOCAS adducts from methanol, 2-carene (3), and 1,4-dicyanobenzene (4) (reaction [3])

A solution of 2.18 g (16 mmol) (+)-2-carene (**3**), 1.31 g (8.5 mmol) biphenyl (**5**), and 1.03 g (8 mmol) 1,4-dicyanobenzene (**4**) in 160 mL acetonitrile–methanol (3:1) was degassed by nitrogen ebullition for 5 min and irradiated through Pyrex for 140 h. The temperature was maintained at 10°C. The volatile components of the photolysate, including unreacted **3**, were removed by distillation. The nonvolatile residue was treated with 10% ethyl acetate in hexane and unreacted **4** (100 mg) was recovered by filtration. The remaining solution was separated by dcfc, eluting with an ethyl acetate – hexane solvent gradient. Most of the biphenyl (**5**) (91%) was recovered. The photo-NOCAS adducts eluted as a mixture (oil, 1.57 g), which accounts for 80% of the 1,4-dicyanobenzene (**4**) consumed. The photo-NOCAS adducts were separated by repetitive mplc using two different solvent systems, 6% ethyl acetate in toluene and 6% ethyl acetate in hexane. The specific rotation of the starting 2-carene (**3**) was $[\alpha]_D^{20}$ +97.1 (c 1%, $CHCl_3$). A sample isolated from the volatile components of the irradiation mixture, by prep-gc (40% SE-30 on Chromosorb W 60/80), had $[\alpha]_D^{20}$ +97.7 (c 1%, $CHCl_3$).

trans-*3-(4-Cyanophenyl)-4-(1-methoxy-1-methylethyl)-1-methylcyclohexene (**14**):* $[\alpha]_D$ −240.0 (*c* 1%, $CHCl_3$). ^{1}H nmr (361 MHz, $CDCl_3$) δ: 7.54 (d, 2H, J = 8.4 Hz), 7.29 (d, 2H, J = 8.4 Hz), 5.13 (s, br, 1H, coupled to the proton at 3.46 ppm), 3.46 (m, 1H, $w_{1/2}$ = 16 Hz, coupled to the proton at 1.95 ppm), 2.82 (s, 3H), 2.12–2.07 (m, 1H), 2.03 (dd, 1H, J = 4.8, 0.5 Hz), 1.95 (ddd, 1H, J = 3.6, 7.7, 10.3 Hz), 1.83 (dddd, 1H, J = 3.6, 4.9, 4.8, 13.3 Hz), 1.70 (s, br, 3H), 1.49 (dddd, 1H, J = 5.2, 9.9, 10.3, 13.3 Hz), 1.11 (s, 3H), 1.01 (s, 3H); ^{13}C nmr (90.79 MHz, $CDCl_3$) δ: 154.23 (s), 134.67 (s), 131.78 (d, 160.5), 129.17 (d, 158.5), 124.53 (d, 155.5), 119.26 (s), 109.03 (s), 76.88 (s), 48.29 (q, 141.7), 47.38 (d, 124.0), 44.30 (d, 127.2), 29.68 (t, 126.0), 23.58 (q, 125.7), 23.44 (q, 123.1), 23.34 (q, 127.6), 23.32 (q, 123.7); ms *m/z*: 254 (0.2), 237(14.5), 222(9.8), 209(7.2), 194(13.9), 169(7.0), 154(19.3), 73(100). Anal. calcd. for **14**, $C_{18}H_{23}NO$: C 80.25, H 8.61, N 5.20; found: C 80.45, H 8.69, N 5.17.

cis-*3-(4-Cyanophenyl)-6-(1-methoxy-1-methylethyl)-3-methylcyclohexene (**15**):* $[\alpha]_D$ −47.9 (*c* 1%, $CHCl_3$). ^{1}H nmr (361 MHz, $CDCl_3$) δ: 7.58 (d, 2H, J = 8.6 Hz), 7.47 (d, 2H, J = 8.6 Hz), 5.98 (ddd, 1H, J = 1.4, 2.2, 10.2 Hz), 5.74 (ddd, 1H, J = 1.8, 2.5, 10.2 Hz), 3.21 (s, 3H), 2.38 (dddd, 1H, J = 2.2, 2.5, 5.6, 11.1 Hz), 2.01 (dddd, 1H, J = 1.4, 1.9, 3.2, 13.3 Hz), 1.71 (ddd, 1H, J = 2.7, 13.0, 13.3 Hz), 1.51 (ddddd, 1H, J = 1.8, 1.9, 2.7, 5.6, 12.5 Hz), 1.36 (s, 3H), 1.07 (s, 3H), 1.06 (s, 3H), 0.94 (dddd, 1H, J = 3.2, 11.1, 12.5, 13.0 Hz); ^{13}C nmr (90.78 MHz, $CDCl_3$) δ: 154.89 (s), 134.49 (d, 155.3), 131.75 (d, 165.2), 129.54 (d, 150.5), 127.78 (d, 160.8), 119.13 (s), 109.41 (s), 76.82 (s), 48.86 (q, 140.3), 44.02 (d, 124.8), 40.16 (s), 38.71 (t, 129.1), 30.31 (q, 127.9, $w_{1/2}$ = 8.2 Hz), 22.31 (q, 125.0), 22.03 (q, 125.2), 20.93 (q, 127.4); ms *m/z*: 254 (0.2), 237(1.5), 222(1.9), 194(1.4), 140(0.6), 73(100). Anal. calcd. for **15**, $C_{18}H_{23}NO$: C 80.25, H 8.61, N 5.20: found: C 80.59, H 8.73, N 5.10.

trans-*3-(4-Cyanophenyl)-6-(1-methoxy-1-methylethyl)-3-methylcyclohexene (**16**):* $[\alpha]_D$ 89.1° (*c* 1%, $CHCl_3$). ^1H nmr (361 MHz, $CDCl_3$) δ: 7.58 (d, 2H, *J* = 8.6 Hz), 7.46 (d, 2H, *J* = 8.6 Hz), 5.89 (ddd, 1H, *J* = 0.7, 2.2, 10.3 Hz), 5.74 (ddd, 1H, *J* = 1.6, 2.7, 10.3 Hz), 3.23 (s, 3H), 2.37 (dddd, 1H, *J* = 2.2, 2.7, 5.7, 11.0 Hz), 1.87–1.80 (m, 1H), 1.64–1.72 (m, 2H), 1.63–1.54 (m, 1H), 1.41 (s, 3H), 1.16 (s, 3H), 1.15 (s, 3H); ^{13}C nmr (90.78 MHz, $CDCl_3$) δ: 156.12 (s), 135.27 (d, 159.6), 132.02 (d, 165.1), 128.29 (d, 151.3), 126.93 (d, 160.8), 119.13 (s), 109.44 (s), 76.87 (s), 48.92 (q, 140.2), 43.30 (d, 123.9), 39.99 (d, 127.2), 38.9 (t, 124.0), 26.62 (q, 125.6), 22.40 (q, 125.1), 22.09 (q, 125.0), 21.46 (q, 126.9); ms *m/z*: 254 (0.2), 237(3.8), 222(3.8), 194(2.7), 116(4.1), 79(4.8), 73(100). Anal. calcd. for **16**, $C_{18}H_{23}NO$: C 80.25, H 8.61, N 5.20; found: C 79.90, H 8.61, N 5.16.

Acknowledgements

This work was supported by a grant from the Natural Sciences and Engineering Research Council of Canada. We thank Dr. D.L. Hooper at the Atlantic Regional Magnetic Resonance Centre at Dalhousie University for the high-field NMR spectra and for help in the preparation of the manuscript.

References

1. (*a*) K.A. McManus and D.R. Arnold. Can. J. Chem. **72**, 2291 (1994); (*b*) D.R. Arnold, K.A. McManus, and X. Du. Can. J. Chem. **72**, 415 (1994); (*c*) D.R. Arnold and X. Du. Can. J. Chem. **72**, 403 (1994); (*d*) D.R. Arnold and X. Du. J. Am. Chem. Soc. **111**, 7666 (1989).
2. (*a*) D.R. Arnold, X. Du, and J. Chen. Can. J. Chem. **73**, 307 (1995); (*b*) A.L. Perrott and D.R. Arnold. Can. J. Chem. **70**, 272 (1992).
3. (*a*) K.H. Schulte-Elte and V. Rautenstrauch. J. Am. Chem. Soc. **102**, 1738 (1980); (*b*) R. Atkinson, D. Hasegawa, and S.M. Aschmann. Int. J. Chem. Kinet. **22**, 871 (1990); (*c*) S.B. Corchnoy and R. Atkinson. Environ. Sci. Technol. **24**, 1497 (1990); (*d*) W. Adam, O. De Lucchi, and K. Hill. Chem. Ber. **115**, 1982 (1982); (*e*) H.C. Brown, J.V.N.V. Prasad, and M. Zaidlewicz. J. Org. Chem. **53**, 2911 (1988); (*f*) G. Deleris, J. Dunogues, and A. Gadras. Tetrahedron, **44**, 4243 (1988); (*g*) B.C. Clark, T.C. Chafin, P.L. Lee, and G.L.K. Hunter. J. Org. Chem. **43**, 519 (1978); (*h*) E.C. Friedrich and E.J. Lewis. J. Org. Chem. **55**, 2491 (1990); (*i*) P. Eslbracht and I. Winkels. Chem. Ber. **124**, 191 (1991); (*j*) M. Andrianome and B. Delmond. Tetrahedron Lett. **26**, 6341 (1985); (*k*) J.-E. Backvall and E.E. Bjorkman. J. Chem. Soc. Chem. Commun. 693 (1982); (*l*) D. Wilhelm, J.-E. Backvall, R.E. Nordberg, and T. Norin. Organometallics, **4**, 1296 (1985); (*m*) R.C. Larock, H. Song, S. Kim, and R.A. Jacobsin. J. Chem. Soc. Chem. Commun. 834 (1987).
4. (*a*) H.D. Roth and T. Herbertz. J. Am. Chem. Soc. **115**, 9804 (1993); (*b*) J.J. Brophy and A. Maccoll. Org. Mass Spectrom. **27**, 1042 (1992); (*c*) C. Basic and A.G. Harrison. Can. J. Appl. Spectrosc. **36**, 33 (1991); (*d*) V.A. Chuiko, E.N. Manukov, Yu.V. Chizhov, and M.M. Timoshenko. Khim. Prir. Soedin. 639 (1985); Chem Abstr. **104**, 88869q (1986).
5. (*a*) C. Dass, D.A. Peake, and M.L. Gross. Org. Mass. Spectrom. **21**, 741 (1986); (*b*) L.T. Scott, I. Erden, W.R. Brunsvold, T.H. Schultz, K.N. Houk, and M.N. Paddon-Row. J. Am. Chem. Soc. **104**, 3659 (1982); (*c*) Y. Harada, K. Seki, A. Suzuki, and H. Inokucki. Chem. Lett. 893 (1973); (*d*) P. Bruckmann and M. Klessinger. Chem. Ber. **107**, 1108 (1974); (*e*) H. Weng, V. Sethuraman, and H.D. Roth. J. Am. Chem. Soc. **116**, 7021 (1994).
6. (*a*) J.P. Dinnocenzo, W.P. Todd, T.R. Simpson, and I.R. Gould. J. Am. Chem. Soc. **112**, 2462 (1990); (*b*) J.P. Dinnocenzo and M. Schmittel. J. Am. Chem. Soc. **109**, 1561 (1987); (*c*) J.P. Dinnocenzo and D.A. Conlon. J. Am. Chem. Soc. **110**, 2324 (1988); (*d*) J.P. Dinnocenzo, D.R. Lieberman, and T.R. Simpson. J. Am. Chem. Soc. **115**, 366 (1993); (*e*) V.R. Rao and S.S. Hixson. J. Am. Chem. Soc. **101**, 6458 (1979); (*f*) D.D.M. Wayner, R.J. Boyd, and D.R. Arnold. Can. J. Chem. **63**, 3283 (1985).
7. (*a*) R.S. Nicholson and I. Shain. Anal. Chem. **36**, 706 (1964); (*b*) Anal. Chem. **37**, 178 (1965).
8. D. Rehm and A. Weller. Isr. J. Chem. **8**, 259 (1970).
9. (*a*) R.M. Borg, D.R. Arnold, and T.S. Cameron. Can. J. Chem. **62**, 1785 (1984); (*b*) D.R. Arnold and M.S. Snow. Can. J. Chem. **66**, 3012 (1988).
10. J.L. Marshall. Carbon–carbon and carbon–proton NMR coupling: application to organic stereochemistry and conformational analysis. Verlag Chemie International, Deerfield Beach, Fla. 1983.
11. M.J. Frisch, G.W. Trucks, H.B. Schlegel, P.M.W. Gill, B.G. Johnson, M.W. Wong, J.B. Foresman, M.A. Robb, M. H.-Gordon, E.S. Replogle, R. Gomperts, J.L. Andres, K. Raghavachari, J.S. Binkley, C. Gonzalez, R.L. Martin, D.J. Fox, D.J. Defrees, J. Baker, J.J.P. Stewart, and J.A. Pople. GAUSSIAN 92/DFT, Revision F.2. Gaussian, Inc., Pittsburgh, Pa. 1993.
12. H. Tylli. J. Mol. Struct. (Theochem), **181**, 11 (1988).
13. (*a*) A.P. Schaap, L. Lopez, and S.D. Gagnon. J. Am. Chem. Soc. **105**, 663 (1983); (*b*) T. Majima, C. Pac, A. Nakasone, and H. Sakurai. J. Am. Chem. Soc. **103**, 4499 (1981); (*c*) S. Mattes and S. Farid. Org. Photochem. **6**, 233 (1983).
14. R. Popielarz and D.R. Arnold. J. Am. Chem. Soc. **112**, 3068 (1990).
15. D.D.M. Wayner, D.J. McPhee, and D. Griller. J. Am. Chem. Soc. **110**, 132 (1988).
16. A. Okamoto, M.S. Snow, and D.R. Arnold. Tetrahedron, **42**, 6175 (1986).

Can. J. Chem. Downloaded from www.nrcresearchpress.com by 65.111.164.53 on 09/08/12
For personal use only.

Thermodynamic characteristics of NADH/NAD$^+$ analogues in acetonitrile: 2-methyl, 4-methyl and 2,4-dimethyl 1-benzyl-dihydronicotinamides and the corresponding pyridinium species

Agnès Anne and Jacques Moiroux

Abstract: Procedures were elaborated for the syntheses of the title compounds. The thermodynamic changes brought about by each methyl substitution were then determined quantitatively. In acetonitrile, the respective one-electron oxidation and one-electron reduction potentials of the NADH and NAD$^+$ analogues were obtained by means of direct and indirect (using ferrocene mediators) cyclic voltammetry. The redox potentials of formal hydride transfers were deduced from the studies of equilibrated reactions occurring between the analogues. The pK_a's of the cation radicals ensued.

Key words: NADH/NAD$^+$ methylated analogues, one-electron transfers, hydride transfer, thermodynamics.

Résumé : On a mis au point des méthodes de synthèse des composés mentionnés dans le titre. On a ensuite déterminé quantitativement les changements thermodynamiques provoqués par chaque substitution par un groupe méthyle. Faisant appel à la voltampérométrie cyclique directe et indirecte (à l'aide de médiateurs ferrocène), on a déterminé les potentiels respectifs de l'oxydation à un électron et de la réduction par un électron des analogues de NADH et NAD$^+$ dans l'acétonitrile. Les potentiels rédox des transferts formels d'hydrure ont été déduits des études sur des réactions équilibrées se produisant entre les analogues. Les pK_a des radicaux cations en découlent.

Mots clés : analogues méthylés de NADH/NAD$^+$, transferts monoélectroniques, transfert d'hydrure, thermodynamique.

[Traduit par la rédaction]

Introduction

Efficient asymmetric reductions of prochiral ketones by NADH analogues, reacting in the absence of enzyme, have been reported using an approach that mimics the selective shielding of one of the diastereotopic C-4 hydrogens of NADH in the enzyme cavity by introducing a methyl substituent at C-4 of a 1,4-dihydronicotinamide (1–4). However, in general, such a modification was accompanied by other changes in the structure. In most cases a second methyl substituent was present at the C-2 position of 1,4-dihydronicotinamide and one or both hydrogens of the amide were substituted by various alkyl groups in order to hinder its free rotation (1, 2, 4).

While the introduction of multiple substituents brings about steric constraints, electronic effects are also involved. Both of these steric and electronic parameters must be taken into account for a careful analysis of the observed changes in reactivity resulting from the substitutions. It is inherent to the electronic effects to affect the reducing strength of the NADH analogue ($\mathbf{A}_i\mathbf{H}$), particularly its overall hydride affinity. For instance, efficient enantioselective hydride transfer can be achieved with a given $\mathbf{A}_i\mathbf{H}$ but only toward highly activated keto or imino substrates due to its poor reducing power (4). In previous studies (5) the redox abilities of a series of $\mathbf{A}_i\mathbf{H}/\mathbf{A}_i^+$ couples, $\mathbf{A}_i^+$ being the corresponding NAD$^+$ analogue, have been characterized by the thermodynamic features of the following [1]–[4] equilibria:

$$[1]\quad \mathbf{A}_i\mathbf{H} \rightleftharpoons \mathbf{A}_i^+ + \underbrace{\mathrm{H}^+ + 2\mathrm{e}}_{\text{or } \mathrm{H}^-} \qquad E^\circ_{i1}$$

$$[2]\quad \mathbf{A}_i\mathbf{H} \rightleftharpoons \mathbf{A}_i\mathbf{H}^{\bullet+} + \mathrm{e} \qquad E^\circ_{i2}$$

$$[3]\quad \mathbf{A}_i\mathbf{H}^{\bullet+} \rightleftharpoons \mathbf{A}_i^\bullet + \mathrm{H}^+ \qquad \mathrm{p}K_{ai3}$$

$$[4]\quad \mathbf{A}_i^\bullet \rightleftharpoons \mathbf{A}_i^+ + \mathrm{e} \qquad E^\circ_{i4}$$

E°_{i1}, the standard potential of the $\mathbf{A}_i\mathbf{H}/\mathbf{A}_i^+$ redox couple, is of straightforward interest for the thermodynamic characterization of the direct hydride transfer. E°_{i2} and E°_{i4} are one-elec-

Received October 24, 1994

A.Anne and J. Moiroux.[1] Laboratoire d'électrochimie moléculaire de l'Université de Paris, 7 - Denis Diderot, Unité Associée au Centre national de la recherche scientifique no. 438, 2 place Jussieu, 75231 Paris Cédex 05, France.

[1] Author to whom correspondence may be addressed.

Can. J. Chem. Downloaded from www.nrcresearchpress.com by 65.111.164.53 on 09/08/12
For personal use only.

Scheme 1

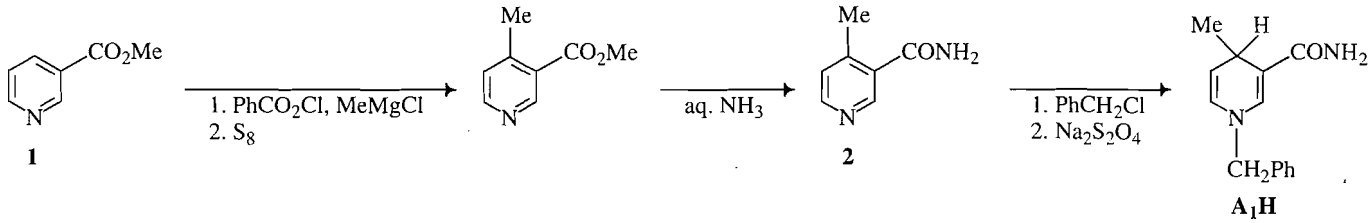

1 2 A_1H

tron standard potentials relevant for overall hydride transfers initiated by electron transfers. In the present paper, all potentials are expressed in mV vs. the aqueous KCl saturated calomel electrode (SCE). pK_{ai3} measures the thermodynamic acidity of the intermediate cation radical. In particular, the behavior of 1-benzyl-1,4-dihydronicotinamide (BNAH = A_4H in the following), the most widely used among the closest analogues of NADH, was thus investigated (*5b*, *d*, *e*).

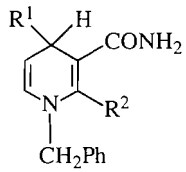

A_1H R^1 = Me; R^2 = H
A_2H R^1 = H; R^2 = Me
A_3H R^1 = Me; R^2 = Me
A_4H R^1 = H; R^2 = H

As part of a step-by-step study starting with BNAH we undertook to determine quantitatively the thermodynamic changes caused by incremental introductions of methyl substituents first at the C-4 position of the 1,4-dihydronicotinamide ring, second at the C-2 position, third at both the C-2 and C-4 positions, the amido group at C-3 remaining unsubstituted. In the following, the corresponding derivatives are denoted A_1H, A_2H, and A_3H, respectively. The early stages of the procedures previously reported in the literature for the synthesis of A_1H are rather tedious (6). Therefore we developed a more convenient approach followed by the classical route to obtain A_1H. The same classical route was adopted for the preparation of A_2H, a new BNAH derivative. The more elaborate novel compound A_3H was synthesized in a one-step procedure with A_2^+ as the starting material.

Preparation of the A_iH and A_i^+ analogues

Preparation of the A_1^+/A_1H and A_2^+/A_2H couples

We adopted a classical route, i.e., quaternarization of the appropriate nicotinamide, to afford the desired pyridinium A_i^+, followed by dithionite reduction to give the 1,4-dihydronicotinamide A_iH. However, all the reported procedures for the synthesis of the 4-methylnicotinamide **2** needed for the A_1^+/A_1H system involved the drastic and time-consuming preparation of the special intermediate 4-methyl-3-cyanopyridine (6). Therefore, to circumvent this problem, we devised a simple and handy method starting with the commercially available methylnicotinate **1** (Scheme 1). Compound **1** activated by reaction with phenyl chloroformate was converted into its corresponding methyl 4-methylnicotinate according to a very convenient two-step procedure described in the literature (7). The copper-catalyzed regioselective addition of the methyl Grignard reagent to the phenoxycarbonyl salt of **1** followed by aromatization of the crude 4-methyl-1,4-dihydropyridine afforded, at the 0.1 mol scale, the 4-methylated ester in an overall yield of 40%. The desired amide **2** was readily obtained as a pure compound by the action of saturated aqueous ammonia on the crude ester and was then easily alkylated with benzyl bromide in acetonitrile into its pyridinium A_1^+ bromide (*8a*). The reduction of A_1^+ with sodium dithionite has been reported to yield exclusively and quantitatively the 1,4 isomer A_1H (*8b*). Actually, we found that the above mentioned procedure gave a mixture of 1,6 and 1,4 isomers in a ratio of 20 to 80, with a total yield of 40% as reported for slightly different reduction conditions (*8a*). Purification of A_1H by recrystallization was unsuccessful but could be achieved by column chromatography on neutral aluminium oxide.

The commercially available ester methyl 2-methylnicotinate **3** was converted into the 2-methyl nicotinamide **4** (83% yield), followed by alkylation to the pyridinium A_2^+ in a moderate yield (30%). The lower reactivity of **4** compared to that of **2** towards N-benzylation probably results from steric shielding due to the 2-methyl substituent. The dithionite reduction of A_2^+ was carried out at 100°C in a biphasic aqueous alkaline buffer–toluene mixture to give readily, in 20% yield, the desired 1,4 isomer (A_2H) with no apparent formation of the 1,6 isomer.

Preparation of the A_3^+/A_3H system

On the one hand, attempts at ammonolyzing the ethyl 2,4-dimethylnicotinate, a commercially available but sterically hindered ester, failed even at high temperatures and (or) long reaction time, or *via* the use of the ammonia dimethylaluminium-amide reagent (9). On the other hand, the pyridinium A_3^+ once obtained, was tested for reduction with dithionite, and showed poor reactivity with no spectroscopic evidence of formation of a 4-methylated-1,4-dihydropyridine system. Therefore we sought an alternate route that could afford directly the 2,4-dimethyl-1,4-dihydronicotinamide A_3H.

Unhindered alkyl Grignard reagents have been shown to react with N-alkylated pyridinium salts to give predominantly the 1,6- and 1,2-dihydro isomers in a low to moderate yield, and the reaction is apparently of limited interest for preparation of 4-alkylated-1,4-dihydropyridine derivatives. However, we anticipated in light of previous reports that, in the presence of a catalytic amount of cuprous iodide (9), the addition of the methyl Grignard reagent to pyridinium A_2^+, which exhibits a C-2 blocked position (10), would be directed preferentially to the C-4 position (Scheme 2). Low reactivity was observed and some of the starting pyridinium was found unchanged even after long reaction time. Despite this fact, the isolation of the compound of interest, A_3H, was readily achieved by precipitation from the reaction mixture (26% overall yield). No attempt was made at isolation and identification of products other than A_3H.

Can. J. Chem. Downloaded from www.nrcresearchpress.com by 65.111.164.53 on 09/08/12
For personal use only.

Scheme 2

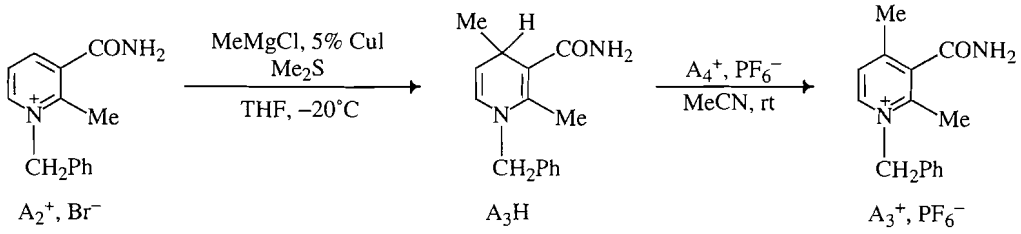

Table 1. Thermodynamic characteristics of the $\mathbf{A}_i\mathbf{H}/\mathbf{A}_i^+$ redox couples. Standard potentials of hydride transfer ($E°_{i1}$), one-electron oxidation of $\mathbf{A}_i\mathbf{H}$ ($E°_{i2}$), one-electron reduction of $\mathbf{A}_i^+$ ($E°_{i4}$), and pK_a of the cation radical $\mathbf{A}_i\mathbf{H}^{\cdot+}$ (pK_{ai3}).[a,b]

$\mathbf{A}_i\mathbf{H}/\mathbf{A}_i^+$	$E°_{i1}$(mV)[c]	$E°_{i2}$(mV)	$E°_{i4}$(mV)	pK_{ai3}
$\mathbf{A}_1\mathbf{H}/\mathbf{A}_1^+$	−22 ± 36	836 ± 8	−1260 ± 25	6.5 ± 1.8
$\mathbf{A}_2\mathbf{H}/\mathbf{A}_2^+$	−43 ± 35	709 ± 8	−1205 ± 25	7.1 ± 1.8
$\mathbf{A}_3\mathbf{H}/\mathbf{A}_3^+$	−59 ± 32	732 ± 8	−1395 ± 25	9.4 ± 1.7
$\mathbf{A}_4\mathbf{H}/\mathbf{A}_4^+$	−22 ± 29[d]	786 ± 8[e]	−1105 ± 10[e]	4.7 ± 1.3

[a]In acetonitrile at 20°C.
[b]All potentials are referred to the SCE.
[c]At pH = 0, anchoring value. The main uncertainty occurs in the case of $\mathbf{A}_4\mathbf{H}/\mathbf{A}_4^+$ (*5a, b*).
[d]From ref. *5b*.
[e]From ref. *5e*.

For the preparation of the pyridinium $\mathbf{A}_3^+$, we utilized the quantitative hydride transfer reaction that occurs from the 2,4-dimethyl dihydronicotinamide $\mathbf{A}_3\mathbf{H}$ to the 4-position of the sterically unhindered pyridinium $\mathbf{A}_4^+$. The reaction was carried out in acetonitrile at room temperature and proceeded cleanly, affording, after column chromatography, the pyridinium $\mathbf{A}_3^+$ in 80% yield.

Determination of the one-electron reduction potentials ($E°_{i4}$) of the $\mathbf{A}_i^+$ cations

Starting at 0 mV toward negative potentials, the cyclic voltammogram of a solution of $\mathbf{A}_i^+$ in acetonitrile, plus 0.1 M supporting electrolyte, exhibits an irreversible cathodic peak whatever the potential scan rate v ($v \leq 400$ V s^{-1}). The features of the voltammogram do not depend on the nature of the electrode material. The cathode may be either a platinum, or gold, or glassy carbon disk. The peak height i_p corresponds to a one-electron transfer. At slow potential scan rate ($v \leq 1$ V s^{-1}), the other peak characteristics, $E_p - E_{p/2} = 39 \pm 2$ mV, $dE_p/d \log v = -20 \pm 2$ mV, ascertain that we are then dealing with a Nernstian heterogeneous electron transfer producing the neutral radical $\mathbf{A}_i^{\cdot}$ (reaction [4]) followed by fast and irreversible dimerization of $\mathbf{A}_i^{\cdot}$ (11), as already observed for $\mathbf{A}_4^+$ and other NAD^+ analogues under the same conditions (*5a, d, e*). E_p is the peak potential, $E_{p/2}$ is the potential at half-peak height. Then, for $v \leq 1$ V s^{-1}, $E_p = E°_{i4} - 57.2 + 19.4 \log(k_{dim}C°_{A_i+}/v)$ (*11a*), k_{dim} being the dimerization rate constant ($-dC_{A_i}/dt = k_{dim}C_{A_i}^2$, with $C_{A_i} = \mathbf{A}_i^{\cdot}$ concentration) and $C°_{A_i+}$ the $\mathbf{A}_i^+$ bulk concentration. The lack of observable reversibility in the cyclic voltammogram for potential scan rates up to 400 V s^{-1} shows that the rate of dimerization of the neutral radical $\mathbf{A}_i^{\cdot}$ is fast indeed. It is probably not very different from that of $\mathbf{A}_4^{\cdot}$ ($k_{dim} = 10^9$ M^{-1} s^{-1}) (*5d*), i.e., the presence of the methyl substituents at positions C-2 and (or) C-4 of the 1,4-dihydronicotinamide ring does not cause any dramatic decrease in the rate of dimerization. Actually the radical–radical coupling may occur at any of the C-2, C-4, or C-6 (unsubstituted) positions and it is probably not slower than that of the neutral radical derived from 10-methylacridinium ($k_{dim} = 10^{7.5}$ M^{-1} s^{-1}) (*5d*). Therefore it seems reasonable to assume that $10^{7.5} \leq k_{dim} \leq 10^9$ M^{-1} s^{-1}. As a result, the measurements of the E_p's, at $v = 0.1$ V s^{-1} and $C°_{Ai+} = 1$ mM, provide the means of calculating the values of the $E°_{i2}$'s reported in Table 1.

Determination of the one-electron oxidation potentials ($E°_{i2}$) of the $\mathbf{A}_i\mathbf{H}$ analogues

Presently, it is well established that the oxidation of $\mathbf{A}_i\mathbf{H}$ proceeds along a DISP 1 mechanism when it is initiated by heterogeneous one-electron abstraction, reaction [2] occurring at the electrode–solution interface in direct electrochemistry (*5a, c, e*). Because the cation radical $\mathbf{A}_i\mathbf{H}^{\cdot+}$ is thermodynamically a strong acid (*5e*), its deprotonation in the presence of base B, reaction [5], is irreversible. Typically, B is a pyridine derivative added in at least 10-fold excess over the $\mathbf{A}_i\mathbf{H}$ concentration. Because the standard potential of the $\mathbf{A}_i\mathbf{H}/\mathbf{A}_i\mathbf{H}^{\cdot+}$ redox couple is much greater than that of the $\mathbf{A}_i^{\cdot}/\mathbf{A}_i^+$ redox couple, the disproportionation reaction, reaction [6], is irreversible. Its driving force is so large that its rate constant is

[2] $\mathbf{A}_i\mathbf{H} \underset{k_{-2}}{\overset{k_2}{\rightleftharpoons}} \mathbf{A}_i\mathbf{H}^{\cdot+} + e \qquad E°_{i2}$

[5] $\mathbf{A}_i\mathbf{H}^{\cdot+} + B \xrightarrow{k_H} \mathbf{A}_i^{\cdot} + BH^+$

[6] $\mathbf{A}_i\mathbf{H}^{\cdot+} + \mathbf{A}i^{\cdot} \xrightarrow{k_6} \mathbf{A}_i\mathbf{H} + \mathbf{A}i^+$

Can. J. Chem. Downloaded from www.nrcresearchpress.com by 65.111.164.53 on 09/08/12
For personal use only.

Can. J. Chem. Downloaded from www.nrcresearchpress.com by 65.111.164.53 on 09/08/12
For personal use only.

close to the diffusion limit (5*a*,*e*,*c*). With the BNAH analogues, reaction [5] is so fast compared to backward reaction [2] that the determination of $E°_{i2}$ cannot be achieved practically by means of cyclic voltammetry in direct electrochemistry, i.e., when A_iH^+ is generated by the heterogeneous electron transfer of reaction [2] (5*e*). Homogeneous redox catalysis, an indirect electrochemical approach, can be used instead. Cyclic voltammetry is still the excitation and measurement technique. Then the reaction sequence of the catalytic process is as follows:

$$[7] \quad P \rightleftharpoons Q + e \qquad E°_{PQ}$$

$$[8] \quad Q + A_iH \underset{k_{-e}}{\overset{k_{+e}}{\rightleftharpoons}} P + A_iH^{\cdot+}$$

$$[5] \quad A_iH^{\cdot+} + B \xrightarrow{k_H} A_i^{\cdot} + BH^+$$

$$[9] \quad Q + A_i^{\cdot} \xrightarrow{k_9} P + A_i^+$$

The reduced form P of the P/Q mediator couple is introduced in the solution and Q is generated reversibly at the solution–electrode interface. In the presence of the substrate A_iH, the anodic current increases. The value of the ratio $i_p/i_p°$ of the oxidation peak currents in the presence and absence of A_iH, respectively, is a reflection of the kinetics of the reactions following step [7]. The mediators used were selected so that their standard potentials were close enough to the oxidation potential of A_iH to obtain an appreciable increase in current and not too close, so as to avoid overlapping of the catalytic and direct oxidation waves (5*e*, 12). Under these conditions the kinetics of the catalytic process are controlled by the homogeneous, reversible, and uphill electron transfer of reaction [8] and by the irreversible deprotonation of reaction [5]. Two limiting situations can be reached depending on the value of the competition parameter $k_{-e}C°_P/k_HC°_B$ (11*b*, 12*b*, 13), $C°_P$ and $C°_B$ being the respective bulk concentrations of the mediator P and the base B. When it is sufficiently small, the kinetic control is entirely by forward reaction [8]. When it is sufficiently large, the kinetic control passes to reaction [5] with reaction [8] acting as a preequilibrium whose equilibrium constant $K_8 = k_{+e}/k_{-e}$ is given by $RT \ln K_8 = F(E°_{PQ} - E°_{i2})$. The experimental diagnostic criterium ascertaining that the former situation is reached is twofold: $i_p/i_p°$ must be $C°_P$ dependent and $C°_B$ independent. In such circumstances k_{+e} can be derived from the measured $i_P/i°_P$ using appropriate working curves (13*a*, *b*). The most precise results were obtained with P = dimethylferrocene ($E°_{PQ}$ = 317 ± 2 mV) as the mediator for the monoelectronic oxidation of A_1H and P = vinylferrocene ($E°_{PQ}$ = 420 ± 2 mV) for the oxidations of A_2H and A_3H. In each case, measurements were performed successively with pyridine and 3,5-dimethylpyridine as the base B. Identical results were observed. Thus we found 2.9 ± 0.1, 3.3 ± 0.1, 2.9 ± 0.1 for the log k_{+e}'s involved in the experiments carried out with A_1H, A_2H, and A_3H. The value of k_{-e} has been shown to equal the diffusion limit of $10^{9.9}$ M^{-1} s^{-1} provided that $E°_{i2} - E°_{PQ}$ is ca. 400 mV or more (5*c*). Attributing such a value to each of the k_e's needed for the computations of the $E°_{i2}$'s through the use of the set of equations $K_8 = k_{+e}/k_{-e}$ and $RT \ln K_8 = F(E°_{PQ} - E°_{i2})$, we obtained, for the $E°_{i2}$'s, the data reported in Table 1.

These data confirm, a posteriori, the validity of the assumption formulated above concerning the values of the k_{-e}'s.

Determination of the standard potentials ($E°_{i1}$) of hydride transfer of the A_iH/A_i^+ redox couples

The standard potential $E°_{i4}$, determined previously (5*b*), was taken as the anchoring point for the evaluation of the $E°_{i1}$'s (i = 1–3). The experimental determination of a relevant set of equilibrium constants K_{ij} (reaction [10]) was then required since $E°_{i1} = E°_{j1} + 29.61 \log K_{ij}$. To do so we followed the kinetics of reaction [10] starting with A_i^+ and A_jH, until equilibrium. At each time of measurement, the composition of an aliquot of the reaction mixture was analyzed quantitatively by means of UV–visible absorption spectrophotometry after suitable dilution, if necessary.

$$[10] \quad A_i^+ + A_jH \underset{k_{-10}}{\overset{k_{10}}{\rightleftharpoons}} A_iH + A_j^+ \qquad K_{ij} = k_{10}/k_{-10}$$

Then:

$$-\frac{da(1-x)}{dt} = k_{10}a^2(1-x)(n-x) - k_{-10}a^2x^2$$

a and *na* being the respective initial concentrations of A_i^+ and A_jH, and *x* the fraction of A_i^+ transformed at time *t*. That gives:

$$\ln\left(\frac{x_1}{x_2}\frac{x-x_1}{x-x_2}\right) = k_{10}a\frac{K_{ij}-1}{K_{ij}}(x_1 - x_2)t$$

x_1 and x_2 being the solutions of the quadratic equation:

$$\frac{K_{ij}-1}{K_{ij}}x^2 - (n+1)x + n = 0$$

Knowing the experimental *x* vs. *t* data, both k_5 and K_{ij} were adjusted to reach the best linearity for the $\ln([x^2/x^1][(x - x_1)/(x - x_2)])$ vs. *t* plot. The kinetic and thermodynamic data thus obtained are gathered together in Table 2. That $K_{43} = K_{42} \times K_{23}$, within experimental uncertainty, shows the coherence of the data. The ensuing $E°_{i1}$'s, at pH 0, are reported in Table 1. The main uncertainty occurs in the case of A_4H/A_4^+ (5*a*,*b*). The other determinations are made by reference to A_4H/A_4^+ with smaller additional error. Thus, the relative values in the series are known with better accuracy than the absolute values. The same is true for the pK_{ai3}'s calculated below.

The knowledge of $E°_{i1}$, $E°_{i2}$ and $E°_{i4}$ for each derivative enabled us to calculate the pK_{ai3} of the corresponding cation radical since $pK_{ai3} = (2E°_{i1} - (E°_{i2} + E°_{i4}))/58.15$. The values found for the pK_{ai3}'s are given in Table 1.

Discussion

The data gathered in Table 1 show how substitutions at the 2 and (or) 4 positions of the dihydronicotinamide ring affect quantitatively some of the thermodynamic characteristics of the A_iH/A_i^+ redox couple.

As all substituents are electron donating methyl groups, one would expect similar trends in the changes brought about by

Table 2. Determinations of the rate constants (k_5) and equilibrium constants (K_{ij}) of hydride transfers occurring between some $\mathbf{A}_i^+$ and $\mathbf{A}_j\mathbf{H}$.[a]

$\mathbf{A}_i^+$ (initial concentration) (mM)	$\mathbf{A}_j\mathbf{H}$ (initial concentration) (mM)	λ(nm)[b] ε (M^{-1} cm^{-1})[c]	k_5 (M^{-1} s^{-1})	K_{ij}
$\mathbf{A}_4^{+d}$ (46.78) or (81)	$\mathbf{A}_1\mathbf{H}$ (4.66) or (6.5)	360[e] ε_{A_4H} = 4850 ε_{A_1H} = 3350	0.66 ± 0.12	1.0 ± 0.5
$\mathbf{A}_4^{+d}$ (17.05)	$\mathbf{A}_2\mathbf{H}$ (15.49)	348[e] ε_{A_4H} = 6020 ε_{A_2H} = 4030	16.2 ± 1.2	5 ± 2
$\mathbf{A}_4^{+d}$ (12.67) or (1.925)	$\mathbf{A}_3\mathbf{H}$ (13.33) or (1.931)	360[e] ε_{A_4H} = 4850 ε_{A_3H} = 840	42 ± 6	18 ± 4
$\mathbf{A}_2^{+f}$ (2.196)	$\mathbf{A}_3\mathbf{H}$ (2.207)	360[e] ε_{A_3H} = 840 ε_{A_2H} = 3000	0.90 ± 0.06	4 ± 2

[a]In acetonitrile at 20°C.
[b]Wavelength at which the absorbance was measured.
[c]Molar absorbance at wavelength λ.
[d]PF_6^- as counterion.
[e]$\varepsilon_{A_i^+} = \varepsilon_{A_j^+} = 0$.
[f]Br^- as counterion.

substitution, i.e., increases in the reducing powers of the $\mathbf{A}_i\mathbf{H}$'s and concomitant decreases in the oxidizing powers of the $\mathbf{A}_i^+$'s with increasing degree of substitution. Accordingly, the standard potentials $E°_{i4}$ show that the oxidizing power of $\mathbf{A}_i^+$ is decreased upon replacing H by CH_3 at C-2 (by 100 mV when there is no CH_3 at C-4, by 135 mV when there is a CH_3 at C-4) and at C-4 (by 155 mV when there is no CH_3 at C-2, by 190 mV when there is a CH_3 at C-2). The introduction of a second methyl group suggests some synergistic effect. However, its apparent magnitude (35 mV) is within experimental uncertainty. Thus a CH_3 at C-2 or C-4 contributes to a greater extent to the stabilization of $\mathbf{A}_i^+$ than to the stabilization of $\mathbf{A}_i^{\cdot}$. This can be explained by stabilization through C—H hyperconjugation (electron donation), the $\sigma_{C-H} \rightarrow \pi$ overlap being larger for $\mathbf{A}_i^+$ than for $\mathbf{A}_i^{\cdot}$.

The standard potentials $E°_{i2}$ show clearly that the reducing power of $\mathbf{A}_i\mathbf{H}$ is increased by introducing a CH_3 at C-2 (by 77 mV when there is no CH_3 at C-4, by 54 mV when there is a CH_3 at C-4). Thus a CH_3 at C-2 stabilizes $\mathbf{A}_i\mathbf{H}^{\cdot+}$ more than it stabilizes $\mathbf{A}_i\mathbf{H}$. This can be explained once more by a difference in $\sigma_{C-H} \rightarrow \pi$ overlaps (C—H hyperconjugation). On the other hand, the introduction of a CH_3 at C-4 decreases the reducing power of $\mathbf{A}_i\mathbf{H}$ by 50 mV when there is no CH_3 at C-2 and the effect is somewhat smaller (27 mV) when there is a CH_3 at C-2 stabilizing $\mathbf{A}_i\mathbf{H}^{\cdot+}$. $\mathbf{A}_i\mathbf{H}$ and $\mathbf{A}_i\mathbf{H}^{\cdot+}$ are not planar and the substituent at C-4 (out of plane) should prefer the pseudo axial orientation to avoid eclipsing the $CONH_2$ group. One possible explanation for the decrease of reducing power by a substituent at C-4 is that $\mathbf{A}_i\mathbf{H}^{\cdot+}$ would be stabilized, again more so than $\mathbf{A}_i\mathbf{H}$, by C_{4-H} hyperconjugation involving the hydrogen in the pseudo-axial orientation in the unsubstituted derivative, whereas such $\sigma_{C4-H} \rightarrow \pi$ overlap would be negligible in the C-4 substituted derivative because the H at C-4 is then in a pseudo-equatorial orientation.

For the standard potential for hydride transfer ($E°_{i1}$), steric effects have an influence on a substituent at C-4, but not at C-2, because steric compression is introduced in going from the nonplanar $\mathbf{A}_i\mathbf{H}$ to the planar $\mathbf{A}_i^+$. This steric compression effect more or less offsets the stabilization of $\mathbf{A}_i^+$ by electron donation (hyperconjugation): $E°_{11} = E°_{41}$ (no substituent at C-2); $E°_{21} > E°_{31}$ by 16 mV (CH_3 at C-2). It would be interesting to compare $E°_{11}$ with $E°_{i1}$ for a *tert*-butyl substituent at C-4, unfortunately we have not been able to determine the latter (12*b*, 14).

Concerning pK_{ai3}, the introduction of a CH_3 at C-2 makes $\mathbf{A}_i\mathbf{H}^{\cdot+}$ less acidic by 2.4–2.9 pK_a units suggesting that a CH_3 at C-2 should stabilize $\mathbf{A}_i\mathbf{H}^{\cdot+}$ more than it stabilizes $\mathbf{A}_i^{\cdot}$. Although not stabilized by C-4 substitution (see above), $\mathbf{A}_i\mathbf{H}^{\cdot+}$ also becomes less acidic by 1.8–2.3 pK_a units when a CH_3 is present at C-4. Within the framework of the tentative explanations put forward in the present discussion it would then require that, in going from the nonplanar $\mathbf{A}_i\mathbf{H}^{\cdot+}$ to the planar $\mathbf{A}_i^{\cdot}$, the contribution of the steric compression would prevail over the electronic effects.

Experimental section

All chemicals were Aldrich Chemical Co. commercial products except methyl 2-methylnicotinate, which was from Lancaster Synthesis Ltd. They were of the highest purity available and used as received. Spectroscopic and electrochemical instruments were the same as previously described (5, 12, 14).

Can. J. Chem. Downloaded from www.nrcresearchpress.com by 65.111.164.53 on 09/08/12
For personal use only.

Can. J. Chem. Downloaded from www.nrcresearchpress.com by 65.111.164.53 on 09/08/12
For personal use only.

Compounds cited without reference are under current study in our laboratory and were prepared according to well-described procedures (5*b*). Spectral data are given only for compounds that were not previously described or were isolated as impure samples.

Elaboration of the A_1^+/A_1H system

4-Methylnicotinamide **2**

The nicotinamide **2** was prepared from methylnicotinate **1** following a three-step procedure (see Scheme 1). A mixture of **1** (12.1 g, 88 mmol), cuprous iodide (762 mg, 3.8 mmol), and methyl sulfide (17.6 mL) was treated with phenyl chloroformate (10.4 mL, 80 mmol) in 200 mL of THF at −20°C (Dry Ice – CCl_4) followed by addition of a 3 M solution of methyl magnesium chloride (90 mmol) in 30 mL of THF. Details of the reaction and work-up of the solution were similar to those reported in the literature (7). The crude methyl 1-phenacyl-4-methyl-1,4-dihydronicotinate was aromatized with sulfur (3 g, 171 mmol) in refluxing decalin (110 mL, 3 h). Work-up of the solution was analogous to that described in ref. 7. The isolated crude methyl 4-methylnicotinate (5.1 g), obtained as a brown oil, was reacted with concentrated aqueous ammonia (20 mL, 4 days) in a classical manner (15). The pale blond crystals that appeared were collected, washed with acetone, then ether, and dried at 70°C to give 1.9 g of pure 4-methylnicotinamide **2** (overall yield, based on starting **1** and including the second crop, 26%): mp 165°C (lit. (6*b*) mp 147°C), (6*c*) 167°C); ^{1}H NMR (DMSO-d_6) δ (ppm): 8.51 (s, 1 H), 8.40 (d, 1 H, J = 5.0 Hz), 7.88 and 7.47 (2 × bs, 2 × 1H), 7.19 (d, 1H, J = 5.0 Hz), 2.39 (s, 3H). Anal. calcd. (%) for $C_7H_8N_2O$: C 61.75, H 5.92, N 20.57; found: C 62.09, H 6.02, N 20.63. A second crop of **2** (1.2 g) of sufficient purity for the preparation of A_1^+ was obtained as follows: after concentration of the filtrate under vacuum, the residue was taken up in warm MeOH (30–40°C), and acetone was added until solid began to appear. After a while in the refrigerator, the precipitate was collected and recrystallized from a 30% methanol – acetone mixture to afford **2** (mp 164–165°C).

1-Benzyl-4-methyl-3-carbamoylpyridinium A_1^+ *chloride*

The general procedure and relative quantities of reactants were as described previously (8*a*). Typically 1.26 g (70% yield) of the pyridinium A_1^+ chloride (mp 206–209°C) was obtained starting from 1.2 g of **2**. Anal. calcd. (%) for $C_{14}H_{15}ClN_2O$: C 64.00, H 5.75, N 10.68; found: C 63.98, H 5.60, N 10.68.

1-Benzyl-4-methyl-1,4-dihydronicotinamide A_1H

A_1^+ chloride (454 mg, 1.73 mmol) was dissolved in 50 mL of 1 M aqueous sodium hydrogen carbonate and mixed with 80 mL of chloroform under vigorous stirring. The mixture was cooled to 0°C and carbon dioxide was passed through the solution for 10 min. Subsequently, sodium dithionite (2.41 g, 13.8 mmol) was added in small quantities during 30 min. The reaction was run for 20 h at room temperature and the chloroform layer was then separated from the water layer. The organic phase was washed three times with water, dried over sodium sulfate, and concentrated under vacuum. The resulting yellow residue (150 mg, 40% yield) was shown by ^{1}H NMR analysis in $CDCl_3$ to contain the 1,4- and 1,6-dihydronicotinamide isomers in a typical ratio of 80:20. Such a ratio was measured by means of the ^{1}H NMR signals of the methyl protons, respectively found in the 1,4 and 1,6 isomers at δ 1.14 (d, J = 6.5 Hz) and δ 1.98 ppm (d, J = 1.48 Hz) (8). An identical ratio was obtained following either the procedure claimed by the authors to afford only the desired A_1H (8b), or the procedure of ref. 8a. Purification of the residue by recrystallization from aqueous methanol as proposed was unsuccessful. Therefore, a collection of residues isolated from a number of reductions was subjected to preparative LC on a column of neutral aluminium oxide (active neutral, 70–230 mesh, Merck) with ethyl acetate – ethanol (10:1.6) as the eluent. 1-Benzyl-4-methyl-1,4-dihydronicotinamide A_1H was obtained as a yellow solid (overall yield, 15%), contaminated, as judged by ^{1}H NMR, by less than 1% of the undesired 1,6 isomer: mp 119°C (lit. (8*a*) mp 117°C); UV–vis, λ_{max} (nm) (ϵ_{max} (M^{-1} cm^{-1})) in MeCN: 334 (5750). Anal. calcd. (%) for $C_{14}H_{16}N_2O$: C 73.66, H 7.06, N 12.27; found: C 73.43, H 7.02, N 12.43. The 1,6 isomer, 1-benzyl-4-methyl-1,6-dihydronicotinamide, was prepared by borohydride reduction of A_1^+ in a classical manner. The purity of the product was confirmed by ^{1}H NMR. Its melting point (mp 145°C) was identical to that given in ref. 8*a*, while it could not be compared to the quite dubious value of 113°C reported later (8*b*).

Elaboration of the A_2^+/A_2H system

2-Methylnicotinamide **4**

Methyl 2-methylnicotinate **3** (25 g, 0.165 mol) was reacted with concentrated aqueous ammonia (42 mL, 5 days) in the same way as **2**. The white crystals that appeared were filtered, washed with ether, and dried at 70°C to afford 18.6 g (83% yield) of pure 2-methylnicotinamide **4**: mp 161°C; ^{1}H NMR ($CDCl_3$) δ (ppm): 8.57 (dd, 1H, J = 4.9 Hz, J = 1.8 Hz), 7.75 (dd, 1H, J = 7.7 Hz, J = 1.8 Hz), 6.45 (dd, 1H, J = 7.7Hz, J = 4.9 Hz), 5.84 (bs, 2H), 2.73 (s, 3H). Anal. calcd. (%) for $C_7H_8N_2O$: C 61.75, H 5.92, N 20.57; found: C 61.95, H 5.87, N 20.46.

1-Benzyl-2-methyl-3-carbamoylpyridinium A_2^+ *bromide*

In a flask equipped with a $CaCl_2$-protected reflux condenser, a solution of **4** (4.8 g, 35 mmol) and benzyl bromide (18 mL, 4.4-fold excess) in dimethylformamide (100 mL) was heated under reflux at 100°C with vigorous stirring for 24 h. After concentration under vacuum to ca. one half of the initial volume, the resulting white solid was filtered off and washed with acetone. Recrystallization from 60% methanol – ether gave 3.2 g (30% yield) of 1-benzyl-2-methyl-3-carbamoylpyridinium A_2^+ bromide: mp 215°C; UV–vis, λ_{max} (nm) (ϵ_{max} (M^{-1} cm^{-1})) in MeCN: 272 (4570); ^{1}H NMR (DMSO-d_6) δ (ppm): 9.22 (dd, 1H, J = 6.0 Hz, $J_{6,4}$ = 1.3 Hz), 8.62 (dd, 1H, J = 5.9 Hz, J = 1.4 Hz), 8.36 (bs, 1H), 8.14 (app m, 2H), 7.5–7.25 (m, 5H), 5.99 (s, 2H), 2.75 (s, 3H). Anal. calcd. (%) for $C_{14}H_{15}BrN_2O$: C 54.74, H 4.92, N 9.12; found: C 54.80, H 4.87, N 9.06.

1-Benzyl-2-methyl-1,4-dihydronicotinamide A_2H

To a degassed biphasic solution of toluene (6 mL) and water (6.6 mL) containing sodium dithionite (1.2 g, 6.9 mmol) and sodium carbonate (0.71 g, 67 mmol) (16), was added a degassed solution of the pyridinium A_2^+ bromide (334 mg,

Can. J. Chem. Downloaded from www.nrcresearchpress.com by 65.111.164.53 on 09/08/12
For personal use only.

1.09 mmol) in water (1.5 mL). The orange color that appeared instantaneously upon mixing turned pale yellow. The mixture was vigorously stirred for 15 min at 100°C under nitrogen. Upon cooling, a pale yellow precipitate formed in the organic phase; the fluffy solid was filtered off, washed with water, and recrystallized from aqueous methanol to afford pure 1-benzyl-2-methyl-1,4-dihydronicotinamide **A_2H** (70% yield): mp 146°C; UV–vis, λ_{max} (nm) (ϵ_{max} (M^{-1} cm^{-1})) in MeCN: 340 (4700); ^1H NMR ($CDCl_3$) δ (ppm): 7.40–7.20 (m, 5H), 5.80 (dt, 1H, J = 7.9 Hz, J = 1.5 Hz), 5.23 (bs, 2H), 4.72 (dd, 1H, J = 7.6 Hz, J = 3.7 Hz), 4.48 (s, 2H), 3.21 (m, 2H), 2.25 (d, 3H, J = 0.78 Hz). Anal. calcd. (%) for $C_{14}H_{16}N_2O$: C 73.66, H 7.06, N 12.27; found: C 73.39, H 7.09, N 12.02.

Elaboration of the A_3^+/A_3H system

1-Benzyl-2,4-dimethyl-1,4-dihydronicotinamide A_3H

A stirred suspension of A_2^+ bromide (2.5 g, 8.1 mmol) in 24 mL of dry THF containing cuprous iodide (81 mg, 0.4 mmol) and methyl sulfide (2 mL, 30 mmol) was cooled to −20°C (Dry Ice – CCl_4) under nitrogen. A 3 M solution of methyl magnesium chloride in 3.8 mL (11.4 mmol) of THF was added dropwise over 20 min. The yellow mixture was stirred at −20°C for 10 min and then at room temperature for 1 h. Quenching of the reddish solution with 5% aqueous sodium hydrogen carbonate (60 mL) precipitated the magnesium salts as a paste, leaving a clear solution that was separated. Addition of ether (20 mL) under stirring afforded a white precipitate in the ether phase, which was filtered off and washed copiously with water. Recrystallization from MeOH–H_2O afforded a pure sample of **A_3H** (0.48 g, 26% yield): mp 182°C; UV–vis, λ_{max} (nm) (ϵ_{max} (M^{-1} cm^{-1})) in MeCN: 322 (3930); ^1H NMR ($CDCl_3$) δ (ppm): 7.40–7.15 (m, 5H), 5.87 (d, 1H, J = 7.6 Hz), 5.38 (bs, 2H), 4.74 (dd, 1H, J = 7.6 Hz, J = 5.1 Hz), 4.57 (AB q, 2H, J_{AB} = 17 Hz), 3.27 (m, 1H), 2.15 (s, 3H), 1.12 (d, 3H, J = 6.5 Hz). Anal. calcd. (%) for $C_{15}H_{18}N_2O$: C 74.35, H 7.49, N 11.56; found: C 74.26, H 7.47, N 11.46.

1-Benzyl-2,4-dimethyl-3-carbamoylpyridinium A_3^+ hexafluorophosphate

A_3H (106 mg, 0.44 mmol) was placed in a 50 mL flask with 30 mL of MeCN and nitrogen gas was bubbled through the solution. Then 1-benzyl-3-carbamoylpyridinium A_4^+ hexafluorophosphate (150 mg, 0.42 mmol) was added to the solution with stirring and the flask was sealed immediately with a serum cap. The mixture was allowed to react for 16 h at room temperature in the dark under a nitrogen atmosphere. The solvent was evaporated, leaving a residue that was shown by ^1H NMR analysis to contain equal amounts of the dihydronicotinamide **A_4H** and the pyridinium A_3^+ (95% yield). The crude mixture was column chromatographed on neutral alumina: the dihydronicotinamide was first eluted with a mixture of $CHCl_3$–MeOH (80:20) and the 1-benzyl-2,4-dimethyl-3-carbamoylpyridinium A_3^+ hexafluorophosphate was then eluted with methanol and isolated as a white solid (75% yield): mp 146°C; UV–vis, λ_{max} (nm) (ϵ_{max} (M^{-1} cm^{-1})) in MeCN: 270 (5050); ^1H NMR (CD_3CN) δ (ppm): 8.47 (d, 1H, J = 6.6 Hz), 7.76 (d, 1H, J = 6.6 Hz), 7.5–7.25 (m, 5H), 6.72 (bs, 2H), 5.66 (s, 2H), 2.65 (s, 3H) 2.57 (s, 3H). Anal. calcd. (%) for $C_{15}H_{17}N_2OPF_6$: C 46.64, H 4.44, N 7.25; found: C 46.82, H 4.48, N 7.20.

The three pyridinium A_1^+, A_4^+ chloride, and A_2^+ bromide salts were converted into their corresponding hexafluorophosphate salts for experiments that required concentrations higher than ca. 3 mM in MeCN. They were obtained as follows: approximately 2 mmol of the starting pyridinium salt was dissolved in 10–20 mL H_2O, depending on its solubility. To each of these solutions, a 4-fold mol excess of NH_4PF_6 (1.08 g) dissolved in 2.5 mL of water was added dropwise. The white products, which separated promptly, were collected and washed with cold water. Yields were between 60 and 90%. A_1^+, PF_6^-: mp 134°C. Anal. calcd. (%) for $C_{14}H_{15}N_2OPF_6$: C 45.19, H 4.06, N 7.53; found: C 45.33, H 4.02, N 7.57. A_2^+, PF_6^-: mp 167°C. Anal. calcd. (%) for $C_{14}H_{15}N_2OPF_6$: C 45.17, H 4.06, N 7.53; found: C 45.30, H 3.96, N 7.39. A_4^+, PF_6^-: mp 139°C. Anal. calcd. (%) for $C_{13}H_{13}N_2OPF_6$: C 43.59, H 3.66, N 7.82; found: C 43.62, H 3.63, N 7.81.

References

1. (*a*) A. Ohno, M. Ikeguchi, T. Kimura, and S. Oka. J. Am. Chem. Soc. **101**, 7036 (1979); (*b*) A. Ohno, T. Goto, J. Nakai, and S. Oka. Bull. Chem. Soc. Jpn. **54**, 3478 (1981); (*c*) A. Ohno, J. Nakai, K. Nakamura, T. Goto, and S. Oka. Bull. Chem. Soc. Jpn. **54**, 3482 (1981); (*d*) Bull. Chem. Soc. Jpn. **54**, 3486 (1981); (*e*) A. Ohno, M. Kashiwagi, Y. Ishihara, S. Ushida, and S. Oka. Tetrahedron, **42**, 961 (1986); (*f*) S. Yasui and A. Ohno. Bioorg. Chem. **14,** 70 (1986); (*g*) A. Ohno, M. Ogawa, and S. Oka. Tetrahedron Lett. **29**, 1951 (1988); (*h*) A. Ohno, M. Ogawa, Y. Mikata, and T. Goto. Bull. Chem. Soc. Jpn. **63**, 813 (1990); (*i*) M. Okamura, T. Kashiwagi, Y. Mikata, T. Maruyama, and A. Ohno. Tetrahedron Lett. **32**, 1475 (1991); (*j*) A. Ohno, Y. Mikata, T. Goto, T. Kashiwagi, T. Tanaka, and M. Sawada. Bull. Chem. Soc. Jpn. **64**, 81 (1991); (*k*) A. Ohno, T. Goto, Y. Mikata, T. Kashiwagi, and T. Maruyama. Bull. Chem. Soc. Jpn. **64**, 87 (1991); (*l*) M. Okamura, T. Kashiwagi, Y. Mikata, N. Yamazaki, and A. Ohno. Chem. Lett. 1247 (1992); (*m*) M. Okamura, Y. Mikata, T. Kashiwagi, A. Tsutsumi, and A. Ohno. Bull. Chem. Soc. Jpn. **66**, 1191 (1993); (*n*) M. Okamura, Y. Mikata, N. Yamazaki, A. Tsutsumi, and A. Ohno. Bull. Chem. Soc. Jpn. **66**, 1197 (1993).
2. A.I. Meyers and T. Oppenlaender. J. Am. Chem. Soc. **108**, 1989 (1986).
3. D.D. Tanner and A. Kharrat. J. Am. Chem. Soc. **110**, 2068 (1988).
4. J.P. Versleijen, M.S. Sanders-Hovens, S.A. Vanhommerig, J.A. Vekemans, and E.M. Meijer. Tetrahedron, **35**, 7793 (1993).
5. (*a*) P. Hapiot, J. Moiroux, and J.M. Savéant. J. Am. Chem. Soc. **112**, 1337 (1990); (*b*) A. Anne and J. Moiroux. J. Org. Chem. **55**, 4608 (1990); (*c*) A. Anne, P. Hapiot, J. Moiroux, P. Neta, and J.M. Savéant. J. Phys. Chem. **95**, 2370 (1991); (*d*) A. Anne, P. Hapiot, J. Moiroux, and J.M. Savéant. J. Electroanal. Chem. Interfacial Electrochem. **331**, 959 (1992); (*e*) A. Anne, P. Hapiot, J. Moiroux, P. Neta, and J.M. Savéant. J. Am. Chem. Soc. **114**, 4694. (1992).
6. (*a*) S.M. McElvain and M.A. Goese. J. Am. Chem. Soc. **65**, 2233 (1943); (*b*) J.L. Webb and A.H. Corwin. J. Am. Chem. Soc. **66**, 1456 (1944); (*c*) J.M. Bobbit and D.A. Scola. J. Org. Chem. **25**, 560 (1960).

7. D.L. Comins, E.D. Stroud, and J.J. Herrick. Heterocycles, **22**, 151 (1984).
8. (*a*) J.F. Biellmann and H.J. Callot. Bull. Soc. Chim. 1159 (1968); (*b*) A.C. Lovesey and W.C.J. Ross. J. Chem. Soc. B, 192 (1969).
9. (*a*) D.L. Comins and S. O'Connor. Adv. Heterocycl. Chem. **44**, 199 (1988); (*b*) T. Holm. Acta Chem. Scand. **45**, 276 (1991).
10. (*a*) A.R. Katrizky, J.G. Keay, and M.P. Sammes. J. Chem. Soc. Perkin Trans. 1, 668 (1981); (*b*) K-Y. Akiba, Y. Iseki, and V Wada. Bull. Chem. Soc. Jpn. **57**, 1994 (1984).
11. (*a*) J.M. Savéant and E. Vianello. Electrochim. Acta, **12**, 1545 (1967); (*b*) C.P. Andrieux and J.M. Savéant. *In* Investigations of rates and mechanisms of reactions. Vol. 6. *Edited by* C.F. Bernasconi. Wiley, New York. 1986. 4/E. Part 2. pp. 305–390.
12. (*a*) C.P. Andrieux, A. Anne, J. Moiroux, and J.M. Savéant. J. Electroanal. Chem. Interfacial Electrochem. **307**, 17 (1991); (*b*) A. Anne, J. Moiroux, and J.M. Savéant. J. Am. Chem. Soc. **115**, 10224 (1993).
13. (*a*) C.P. Andrieux, C. Blocman, J.M. Dumas-Bouchiat, and J.M. Savéant. J. Electroanal. Chem. Interfacial Electrochem. **87**, 55 (1978); (*b*) C.P. Andrieux, C. Blocman, J.M. Dumas-Bouchiat, F. M'Halla, and J.M. Savéant. J. Electroanal. Chem. Interfacial Electrochem. **113**, 19 (1980); (*c*) J. Am. Chem. Soc. **102**, 3806 (1980); (*d*) C. P. Andrieux and J. M. Savéant. J. Electroanal. Chem. Interfacial Electrochem. **205**, 43 (1986).
14. A. Anne. Heterocycles, **34**, 2331 (1992).
15. A.I. Vogel. *In* A text book in practical organic chemistry. 3rd ed. Longman, London. 1970. p. 850.
16. (*a*) Y. Combret, J. Duflos, G. Dupas, J. Bourguignon, and G. Queguinier. Tetrahedron, **49**, 5237 (1993); (*b*) Y.S. Wong, C. Marazano, D. Gnecco, and B.C. Das. Tetrahedron Lett. **35**, 707 (1994).

Can. J. Chem. Downloaded from www.nrcresearchpress.com by 65.111.164.53 on 09/08/12
For personal use only.

The hydration of mesitylketene in aqueous solution: detection of acid catalysis for an aromatic ketene

J. Andraos, A.J. Kresge, and N.P. Schepp

Can. J. Chem. Downloaded from www.nrcresearchpress.com by 65.111.164.53 on 09/08/12
For personal use only.

Abstract: Mesitylketene was generated flash photolytically in aqueous solution by the photo-Wolff reaction of 2,4,6-trimethyldiazoacetophenone and also by rearrangement of mesitylynol obtained through photodecarbonylation of mesitylhydroxycyclopropenone, and rates of hydration of this ketene were measured in dilute perchloric acid, sodium perchlorate, and sodium hydroxide solutions as well as in concentrated sodium perchlorate and perchloric acid solutions. In dilute solution only an uncatalyzed reaction and a sodium-hydroxide-catalyzed process were observed, both of which could be attributed to nucleophilic attack, by water and by hydroxide ion, respectively, at the ketene carbonyl carbon atom. In concentrated sodium perchlorate solutions, a mild decrease in reaction rate with increasing salt concentration was observed, as expected on the basis of decreasing water activity and a consequent slowing of the uncatalyzed reaction. A similar mild decrease was found in perchloric acid solutions up to $[HClO_4] \cong 1$ M, but this then gave way to a rate increase that became dominant above $[HClO_4] \cong 2$ M. This appearance of acid catalysis indicates a change in reaction mechanism from nucleophilic attack of water to an electrophilic process involving rate-determining protonation on the β-carbon atom of the ketene group. Analysis of the acid-catalyzed reaction rate by the Cox–Yates method gives the catalytic coefficient $k_{H^+} = 4.7\ M^{-1}\ s^{-1}$. This, when compared with $k_{H^+} = 1.01 \times 10^4\ M^{-1}\ s^{-1}$ for ketene itself, shows that the mesityl group retards acid-catalyzed hydration by a factor of 2200, and consequently the acid-catalyzed reaction of this, and other aromatic ketenes as well, becomes apparent only under strongly acidic conditions.

Key words: mesitylketene, ketene hydration, acid catalysis, Cox–Yates excess acidity correlation.

Résumé : On a généré le mésitylcétène par photolyse éclair en solution aqueuse à l'aide d'une réaction de photo-Wolff de la 2,4,6-triméthyldiazoacétophénone ainsi que par un réarrangement du mésitylynol obtenu par photodécarbonylation de la mésitylhydroxycyclopropénone et on a mesuré ses vitesse d'hydratation en solution diluée d'acide perchlorique, de perchlorate de sodium et d'hydroxyde de sodium ainsi que dans des solutions concentrées de perchlorate de sodium et d'acide perchlorique. En solutions diluées, on n'a observé qu'une réaction qui n'est pas catalysée et un processus catalysé par l'hydroxyde de sodium; les deux peuvent être attribués à une attaque nucléophile, respectivement par l'eau et l'ion hydroxyde, au niveau du carbone du carbonyle du cétène. En solutions concentrées d'acide perchlorique, on a observé une légère diminution de la vitesse de réaction avec une augmentation de la concentration de sel, tel qu'on peut s'y attendre en se basant sur une diminution de l'activité de l'eau accompagnant un ralentissement de la réaction qui n'est pas catalysée. On a aussi observé une légère diminution semblable dans les solutions d'acide perchlorique jusqu'à des concentrations de $HClO_4$ d'environ 1 M; toutefois, au-delà de cette valeur, il y a une augmentation de la vitesse qui devient dominante au-dessus de $[HClO_4] \equiv 2$ M. Cette catalyse acide apparente indique qu'il se produit un changement de mécanisme de réaction qui passe d'une attaque nucléophile de l'eau à un processus électrophile impliquant une protonation du carbone en β du groupe cétène dans l'étape qui détermine la vitesse. Une analyse de la vitesse de réaction acidocatalysée par la méthode de Cox–Yates fournit un coefficient catalytique $k_{H^+} = 4{,}7\ M^{-1}\ s^{-1}$. Cette valeur, comparée à celle observée avec le cétène non substitué ($k_{H^+} = 1{,}01 \times 10^4\ M^{-1}\ s^{-1}$) montre que le groupe mésityle retarde la réaction d'hydratation acidocatalysée par un facteur de 2200 et que la réaction acidocatalysée de ce cétène ainsi que celles d'autres cétènes aromatiques ne deviennent apparentes que dans des conditions fortement acides.

Mots clés : mésitylène, hydratation de cétène, catalyse acide, corrélation d'acidité en excès de Cox–Yates.

[Traduit par la rédaction]

Received November 4, 1994.

J. Andraos, A.J. Kresge,[1] and N.P. Schepp. Department of Chemistry, University of Toronto, Toronto, ON M5S 1A1, Canada.

[1] Author to whom correspondence may be addressed. Telephone: (416) 978-7259. Fax: (416) 978-8775. E-mail: akresge@alchemy.chem.utoronto.ca

Can. J. Chem. Downloaded from www.nrcresearchpress.com by 65.111.164.53 on 09/08/12
For personal use only.

Introduction

The hydration of ketenes in neutral and basic aqueous solution occurs by nucleophilic attack of water or hydroxide ion at the carbonyl carbon atom of the ketene functional group; this is then followed by ketonization of the carboxylic acid enolate ion thus formed, eq. [1] (1).

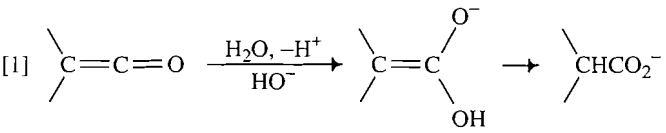

There is also an acid-catalyzed reaction that takes place by a different mechanism: rate-determining protonation of the β-carbon atom followed by reaction of the ensuing acylium ion with water, eq. [2] (2).

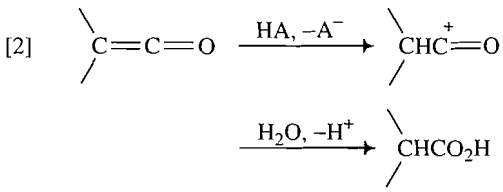

Acid catalysis, however, is generally weak and has until now not been reported for ketenes with aromatic substituents attached directly to the ketene functional group. It is believed that this is so because aromatic substituents stabilize the initial state of the hydration reaction through conjugation with the carbon–carbon double bond of the ketene group; this double bond is destroyed in the rate-determining step of the acid-catalyzed reaction and the stabilization is lost, making the energy difference between initial state and transition state larger, and the reaction consequently slower, than it would otherwise be. In the reaction of ketenes with nucleophiles, on the other hand, the ketene carbon–carbon double bond is retained and conjugative stabilization by aromatic substituents is not lost in the transition state of this process; aromatic substituents, moreover, provide additional transition state stabilization by interaction with the negative charge being generated on the substrate by the nucleophilic attack. Aromatic substituents thus retard acid-catalyzed hydration but accelerate the uncatalyzed nucleophilic attack of water, and this makes a characteristically weak acid catalysis difficult to detect against a strengthened background water reaction.

It follows from these considerations that acid catalysis of aromatic ketene hydration might become detectable in concentrated aqueous solutions of strong mineral acids where the superacidity and decreased water activity of such media would slow the water reaction and accelerate the acid-catalyzed process. We have found this to be the case for the hydration of mesitylketene, **2**,[2] in perchloric acid solutions more concentrated than 2 M.

[2] Mesityl = 2,4,6-trimethylphenyl.

Mesitylketene is quite labile, and fast-reaction methods must be used to study its hydration in aqueous solution. We have employed flash photolytic techniques, generating the ketene for the most part by photo-Wolff reaction of 2,4,6-trimethyldiazoacetophenone, **1**, eq. [3] (3). This method, however, could not be used in the more concentrated perchloric acid solutions we employed because of a facile acid-catalyzed

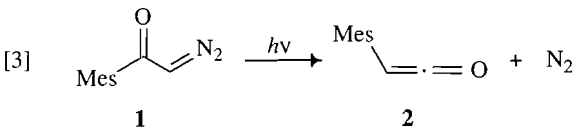

decomposition of the diazo compound, and we consequently supplemented this source of mesitylketene with generation by rearrangement of the corresponding ynol, **4**, produced by photodecarbonylation of mesitylhydroxycyclopropenone, **3**, eq. [4] (4).

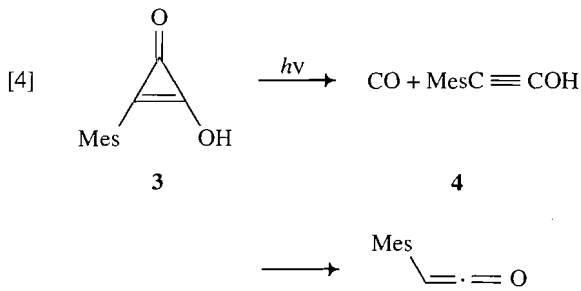

Experimental section

Materials

2,4,6-Trimethyldiazoacetophenone (**1**) was prepared by diazo transfer from methanesulfonyl azide to 2,4,6-trimethylacetophenone activated as the formyl derivative (5); the melting point and infrared spectrum of the product were consistent with those reported in the literature (6). Mesitylhydroxycyclopropenone (**3**) was a sample that had been prepared before (4) by Friedel–Crafts reaction of mesitylene with tetrachlorocyclopropene followed by hydrolysis of the trichloride product (7). All other materials were best available commercial grades.

Kinetics

Rates of hydration of mesitylketene were determined spectrophotometrically by monitoring the decrease in ketene absorbance at λ = 260 nm. The ketene was generated flash photolytically using a conventional flash system that has already been described (8). The temperature of the reaction mixtures was controlled at 25.0 ± 0.05°C. All of the kinetic data conformed well to the first-order rate law, and observed first-order rate constants were obtained by nonlinear least-squares fitting of an exponential function.

Results

Rates of hydration of mesitylketene were measured in dilute aqueous solutions of sodium perchlorate using both H_2O

Can. J. Chem. Downloaded from www.nrcresearchpress.com by 65.111.164.53 on 09/08/12
For personal use only.

and D_2O as the solvent and a fixed sodium perchlorate concentration of 0.10 M. The data are summarized in Table S1.[3] Fourteen separate determinations in H_2O gave $k = 135 \pm 1$ s^{-1} as the average value for that solvent, and ten determinations in D_2O gave the average $k = 90 \pm 2$ s^{-1}. These results provide the solvent isotope effect $k_{H_2O}/k_{D_2O} = 1.50 \pm 0.04$.[4]

Rates of hydration of mesitylketene were also measured in dilute perchloric acid and sodium hydroxide solutions. The acid or base concentrations were varied, from 0.005 to 0.1 M for the perchloric acid solutions and from 0.002 to 0.01 M for sodium hydroxide, but the ionic strength was kept constant at 0.10 M by adding $NaClO_4$ as required. Six to twelve replicate measurements were made at each concentration. The data are summarized in Tables S2 and S3.[3]

Observed first-order rate constants showed no systematic variation with $[HClO_4]$ over the concentration range employed for these dilute solutions. Linear least-squares analysis gave an expression, $k/s^{-1} = (137 \pm 1) + (0.93 \pm 25.1)$ $[HClO_4]$, whose slope was undetermined and whose intercept agrees well with the value obtained in sodium perchlorate solutions, $k/s^{-1} = (135 \pm 1)$. Observed rate constants determined in sodium hydroxide solutions, on the other hand, increased regularly with increasing [NaOH], and least-squares analysis gave the relationship $k/s^{-1} = (133 \pm 27) + (1.01 \pm 0.04) \times 10^5$ [NaOH]; the intercept of this expresson also agrees well with the result obtained in sodium perchlorate solutions.

In addition to these studies performed in dilute solutions at a fixed ionic strength of 0.10 M, rate measurements of mesitylketene hydration were also made in concentrated aqueous sodium perchlorate and perchloric acid solutions. One series of determinations was performed in sodium perchlorate solutions over the concentration range $[NaClO_4] = 0.4$–4 M and another in perchloric acid solutions over the concentration range $[HClO_4] = 0.1$–4 M; in both series the solutions contained no additional electrolyte and the ionic strength was consequently equal to $[NaClO_4]$ or $[HClO_4]$. The data are summarized in Tables S4 and S5,[3] and are displayed in Fig. 1; the various relationships between rate and concentration shown by these data are discussed below.

Discussion

The present results demonstrate that the hydration of mesitylketene occurs by "uncatalyzed" and hydroxide-ion-catalyzed routes but does not show acid catalysis in dilute aqueous solution. This behavior is characteristic of aromatic ketenes. The hydration of phenylketene, for example, also takes place by uncatalyzed and hydroxide-ion-catalyzed routes and is not acid catalyzed (*2a*); the solvent isotope effects on the uncatalyzed reactions of these two substrates, moreover, are also quite similar: $k_{H_2O}/k_{D_2O} = 1.50$ for mesitylketene and 1.44 for phenylketene (*2a*).

The two ketenes do differ in reactivity, but that is in keeping with the expected reaction mechanism of eq. [1]. In this mechanism the substrate is taking on negative charge, and

[3] Tables S1–S5 of rate data may be purchased from: The Depository of Unpublished Data, Document Delivery, CISTI, National Research Council Canada, Ottawa, Canada K1A 0S2.

[4] Uncertainties cited are standard deviations of mean values.

Fig. 1. Relationship between rates of hydration of mesitylketene and electrolyte concentration in aqueous $HClO_4$ and $NaClO_4$ solutions at 25°C; (○) $HClO_4$, ketene generated from diazo precursor; (□) $HClO_4$, ynol precursor; (Δ) $NaClO_4$, diazo precursor.

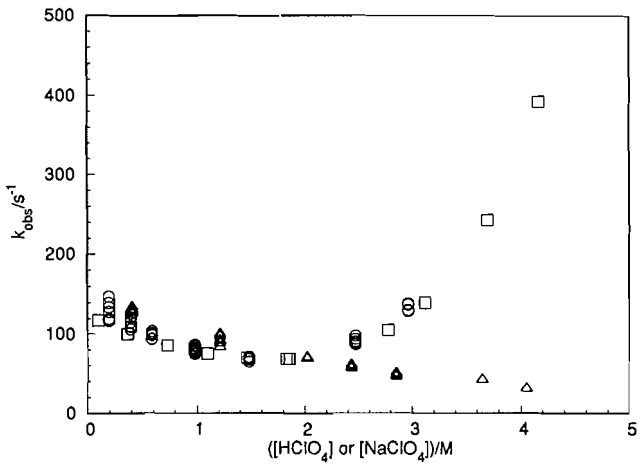

electron-donating substituents such as the methyls in the mesityl group should hinder this process and lower the reaction rate. The data summarized in Table 1 show retardations of 35-fold for the uncatalyzed reaction and 12-fold for the hydroxide-ion catalyzed process. The smaller retardation for the hydroxide-ion-catalyzed reaction is consistent with the greater reactivity and consequent expected lower selectivity of that process.

As Fig. 1 illustrates, the hydration of mesitylketene does show acid catalysis in concentrated aqueous perchloric acid solutions. The rate of reaction first decreases with increasing acid concentration, but a similar retardation also occurs in concentrated sodium perchlorate solutions, and it may be reasonably attributed to a decrease in water activity and a consequent slowing of the uncatalyzed reaction. The rate retardation in sodium perchlorate solutions continues over the entire concentration range investigated, but in perchloric acid solutions it begins to diminish at $[HClO_4] \cong 1$ M and then gives way to a rate acceleration that becomes clearly dominant above $[HClO_4] \cong 2$ M.

The rate retardation in sodium perchlorate solutions can be expressed as a linear relationship between $\log(k_{obs})$ and electrolyte concentration over the entire range examined, as can also the retardation in perchloric acid solutions up to $[HClO_4] = 1.1$ M. Figure 2 demonstrates these relationships; it also shows a steeper dependence upon concentration for the perchloric acid solutions than for the sodium perchlorate solutions, which is consistent with the expected stronger hydration of the H^+ ion than of the Na^+ ion and the consequent lower amount of "free" water in perchloric acid than in sodium perchlorate solutions of the same molar concentration.

The persistence of the linear relationship between $\log(k_{obs})$ and $[NaClO_4]$ up to a concentration of 4 M suggests that the rate retardation in perchloric acid solutions might be similarily related to $[HClO_4]$ up to 4 M as well, and this then pro-

Can. J. Chem. Downloaded from www.nrcresearchpress.com by 65.111.164.53 on 09/08/12
For personal use only.

Fig. 2. Dependence of log (k_{obs}) for the hydration of mesitylketene upon [$HClO_4$] and [$NaClO_4$] in aqueous solution at 25°C; (○) $HClO_4$ solutions; (Δ) $NaClO_4$ solutions.

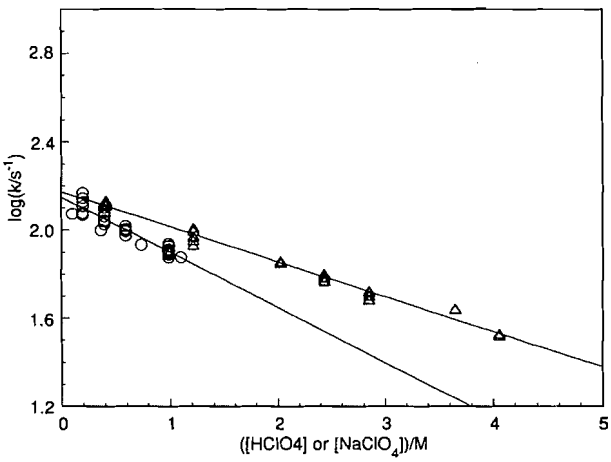

Fig. 3. Cox–Yates plot for the hydration of mesityketene in aqueous $HClO_4$ solutions at 25°C.

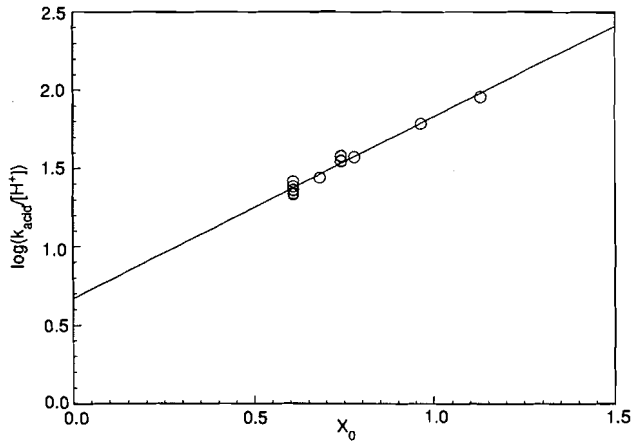

Table 1. Summary of rate constants for the hydration of mesitylketene and phenylketene in aqueous solution at 25°C.[a]

Rate constant	MesCH=C=O	PhCH=C=O[b]
k_{H_2O}(s^{-1})	135	4770
k_{D_2O}(s^{-1})	90	3150
k_{H_2O}/k_{D_2O}	1.50	1.44
k_{HO^-} (M^{-1} s^{-1})	101 000	1 220 000
k_{H^+} (M^{-1} s^{-1})	4.67[c]	—

[a]Ionic strength = 0.10 M unless specified otherwise.
[b]Reference 2*a*.
[c]Extrapolated from concentrated acid solutions to an "infinitely dilute" standard state.

vides a means of subtracting out the retardation from observed rate constants measured in perchloric acid solutions in the region of clear acid catalysis, [$HClO_4$] = 2–4 M. When this is done, rate constants for acid catalysis are obtained that increase more rapidly than in direct proportion to [$HClO_4$]. But this is commonly the case for reactions proceeding by rate-determining proton transfer to carbon, such as the present process, and the situation is usually handled by using an acidity function to correlate the data. The Cox–Yates X_0 function (9) appears to be the best scale available for this purpose (10), and the correlating function that applies to the present situation is given in eq. [5] (11). Figure 3 shows that the data conform well to this relationship; least-squares analysis gives the result $\log(k/[H^+]) = (0.669 \pm 0.040) + 1.16 \pm 0.05\ X_0$, which provides the hydronium-ion catalytic coefficient $k_{H^+} = 4.67 \pm 0.43\ M^{-1}\ s^{-1}$.

$$[5] \quad \log (k/[H^+]) = \log (k_{H^+}) + mX_0$$

Comparison of this result with $k_{H^+} = 1.01 \times 10^4\ M^{-1}\ s^{-1}$ for ketene itself (2*b*) gives a mesityl group rate retardation of 2200-fold, which corresponds to a substituent effect of $\delta\Delta G^{\neq} = 4.6$ kcal mol^{-1}. This is not unlike rate-retarding phenyl-group substituent effects found for other reactions that proceed by rate-determining proton transfer to carbon, e.g., $\delta\Delta G^{\neq} = 3.4$ and 4.1 kcal mol^{-1} for the hydrolysis of *cis*- and *trans*-β-methoxystyrene (12) and $\delta\Delta G^{\neq} = 3.1$ and 3.6 kcal mol^{-1} for the ketonization of the *cis* and *trans* enols of phenylacetaldehyde (13).

Acknowledgement

We are grateful to the Natural Sciences and Engineering Research Council of Canada and the Donors of the Petroleum Research Fund, administered by the American Chemical Society, for financial support of this work.

References

1. (*a*) T.T. Tidwell. Acc. Chem. Res. **23**, 273 (1990); (*b*) A.D. Allen, J. Andraos, A.J. Kresge, M.A. McAllister, and T.T. Tidwell. J. Am. Chem. Soc. **114**, 1878 (1992), J. Andraos and A.J. Kresge. J. Am. Chem. Soc. **114**, 5643 (1992).
2. (*a*) A.D. Allen, A.J. Kresge, N.P. Schepp, and T.T. Tidwell. Can. J. Chem. **65**, 1719 (1987), (*b*) J. Andraos and A.J. Kresge. J. Photochem. Photobiol. A: **57**, 165 (1991).
3. M. Regitz and G. Mass. Diazo compounds, properties and synthesis. Academic Press, New York. 1986. pp. 185–195.
4. Y. Chiang, A.J. Kresge, R. Hochstrasser, and J. Wirz. J. Am. Chem. Soc. **111**, 2355 (1989).
5. D.F. Taber, R.E. Ruckle, Jr., and M.J. Hennessy. J. Org. Chem. **51**, 4077 (1986).
6. H. Morrison, S. Danishefsky, and P. Yates. J. Org. Chem. **26**, 2617 (1961).
7. J.S. Chickos, E. Patton, and R. West. J. Org. Chem. **39**, 1647 (1974).
8. Y. Chiang, M. Hojatti, J.R. Keeffe, A.J. Kresge, N.R. Schepp, and J. Wirz. J. Am. Chem. Soc. **109**, 4000 (1987).
9. R.A. Cox and K. Yates. Can. J. Chem. **59**, 2116 (1981).

10. A.J. Kresge, H.J. Chen, G.L. Capen, and M.F. Powell. Can. J. Chem. **61**, 249 (1983).
11. R.A. Cox and K. Yates. Can. J. Chem. **67**, 2944 (1979).
12. Y. Chiang, A.J. Kresge, and C.I. Young. Can. J. Chem. **56**, 461 (1978).
13. Y. Chiang, A.J. Kresge, P.A. Walsh, and Y. Yin. J. Chem. Soc. Chem. Commun. 869 (1989).

Can. J. Chem. Downloaded from www.nrcresearchpress.com by 65.111.164.53 on 09/08/12
For personal use only.

Theoretical evidence for P—S and P—N $p\pi$—$p\pi$ bonding within the heterocyclopentadienyl framework

Martin T. MacLennan and Katherine Valenta Darvesh

Abstract: SCF and Møller–Plesset calculations have been carried out for systems containing P—S and P—N $p\pi$—$p\pi$ bonds: namely, the 1,3,2-dithiaphospholium cation, the 1,3,2-diazaphospholium cation, and the 1,3,2-azathiaphospholium cation. The computed geometries are reported, along with Mulliken atomic charges and selected vibrational frequencies. ΔH^0 values for heterolytic P—H bond dissociation and for isodesmic bond separation reactions provide information on the energetics and stabilization of the P—S and P—N $p\pi$—$p\pi$ bonds.

Key words: SCF and MP2 calculations, third period $p\pi$—$p\pi$ bonding, bond separation reactions.

Résumé : On a effectué des calculs de champ autocohérent et de Møller–Plesset sur des systèmes contenant des liaisons $p\pi$—$p\pi$ P—S et P—N, soit les cations 1,3,2-dithiaphospholium, 1,3,2-diazaphospholium et 1,3,2-azathiaphospholium. On rapporte les géométries calculées ainsi que les charges atomiques de Mulliken et des fréquences vibrationnelles choisies. Les valeurs des ΔH^0 pour la dissociation de la liaison P—H et pour les réactions de séparation isodesmique de la liaison fournissent de l'information sur les énergies et la stabilisation des liaisons $p\pi$—$p\pi$ P—S et P—N.

Mots clés : calculs SCF et MP2, liaison $p\pi$—$p\pi$ de la troisième période, réactions de séparation de liaison.

[Traduit par la rédaction]

Introduction

There has been renewed interest over the past decade in the ability of third-period elements to form $p\pi$—$p\pi$ bonds (for example, refs. 1, 2). The supposed nonexistence of such compounds has been explained by insufficient overlap, and by the relative weakness of the π bond as compared to the σ bond (Schmidt et al., ref. 1 and references therein). Recently, $p\pi$—$p\pi$ bonding has been experimentally achieved between the group 15 elements and sulfur (2–5). This bonding has been facilitated by the adoption of a template containing a $(4n + 2)$ number of π electrons, namely, the heteroindenyl framework, with heteroatoms replacing C at the 1, 2, and 3 positions. An example is shown:

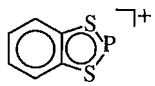

namely, the 1,3,2-benzodithiaphospholium cation. Experimental evidence suggesting $p\pi$—$p\pi$ bonding came from planarity as noted in the crystal structure, and from the bond lengths (4). For example, in the above cation, the mean sulfur—phosphorus bond length was found to be 2.016 Å, which is considerably shorter than the single P—S bond length of 2.122 Å found in $(PhS)_3P$ (6). Preliminary theoretical studies confirmed the Hückel nature of the compounds (2). While experimental results can be interpreted in terms of $p\pi$—$p\pi$ bonding, experiment cannot show definitively that it occurs. The present work represents a closer theoretical look at these heteroaromatic systems, with a view to explore further the role of $p\pi$—$p\pi$ bonding.

The phenomenon of $p\pi$—$p\pi$ bonding involving third period elements is under active study. It has been reviewed by numerous authors (7–9). In his review of compounds of group 14 and 15 elements involving $p\pi$—$p\pi$ multiple bonding, Norman describes how steric protection can be an effective experimental technique to stabilise the bond (9). In this approach, sterically bulky substituents are bonded to the heteroatom. The chemistry of diphosphenes has been extensively reviewed by Weber (7). On the computational side, Schmidt et al. have established a theoretical table of A=B π bond strengths for C, N, O, Si, P, and S (1). The ability of silicon and other group 4 elements to participate in aromatic bonding has been investigated theoretically (10, 11). Substantial delocalization was found to exist in these structures although there is a drop in "aromaticity" (delocalization energy) between carbon and silicon, when comparing benzene with silabenzene. Theoretical work directly related to this study has been carried out on the carbon heterocycles. A ZDO study of thiazolium and dithiolium reported atomic charge densities (12). A survey of theoretical work on sulfur heterocycles has been carried out (13). These references report many instances where double bonding involving elements of the third period or greater can occur.

Received October 3, 1994.

M.T. MacLennan and K.V. Darvesh.[1] Department of Chemistry, Mount St. Vincent University, Halifax, NS B3M 2J6, Canada.

[1] To whom correspondence should be addressed. Tel: (902) 457-6544; fax: (902) 457-0579; email: kdarvesh@linden.msvu.ca.

Can. J. Chem. Downloaded from www.nrcresearchpress.com by 65.111.164.53 on 09/08/12
For personal use only.

Can. J. Chem. Downloaded from www.nrcresearchpress.com by 65.111.164.53 on 09/08/12
For personal use only.

Our model has been restricted to the

framework for computational simplicity. Our objective is to quantify the extent of the $p\pi$—$p\pi$ bonding as much as possible, using current *ab initio* computational techniques.

We initially outline the computational methods used. This is followed by a presentation of the theoretically obtained geometries, molecular orbitals, and charge distributions. A section on the relevant vibrational frequencies follows. Finally, thermochemical cycle results are analyzed.

Computational methods

All calculations were performed using GAUSSIAN 90 (14) on a Stellar GS 2500 system. Geometries were fully optimized at the SCF level using the 6-31G* basis set (15, 16), starting with 3-21G optimized structures. SCF force field calculations were carried out, using analytical energy second derivatives. Single point MP2 calculations (17, 18) were also performed at the SCF optimized geometries of the phosphorus systems in order to carry out the thermochemical analysis. These are referred to as MP2/6-31G*//6-31G* calculations.

Results and discussion

A. Geometries

The cationic systems studied were all based on the following framework:

For simplicity, the following shorthand will be used, consistent with previous experimental work on related compounds

	X	Y	Z	Name	Reference[a]
1[S_2P]	S	P	S	1,3,2-Dithiaphospholium cation	4
1[N_2P]	NH	P	NH	1,3,2-Diazaphospholium cation	19
1[NSP]	NH	P	S	1,3,2-Azathiaphospholium cation	2
1[NSC]	NH	CH	S	1,3-Thiazolium cation	20
1[S_2C]	S	CH	S	1,3-Dithiolium cation	21

[a]Experimental references refer to the benzo-substituted cation.

Neutral systems required for the thermochemical cycles were based on the following framework:

	X	Y	Z	Reference
2[S_2P]	S	PH	S	2
2[N_2P]	NH	PH	NH	22
2[NSP]	NH	PH	S	2

A table of geometrical data is shown (Table 1). A glance at the theoretical P—S distance (2.015 Å) in 1[S_2P] confirms that it is shorter than the P—S single bond length of 2.122 Å found in $(PhS)_3P$ (6). However, it is somewhat longer than the P=S bond length in HPS calculated by Schmidt et al. of 1.903 Å obtained at the 3-21G* level (1). 1[S_2P] can be thought of as a 6π resonance hybrid, using similar structures as for 1,3-dithiolium (23, 24).

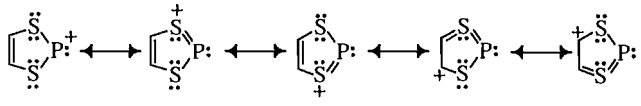

A **B** **C** **D** **E**

These structures can certainly account for the shortness of the sulfur–phosphorus bond. The sulfur–carbon distance in 1[S_2P] is also intermediate between an experimentally determined single bond (1.819 Å) and a double bond (1.611 Å) (25). The carbon—carbon bond length of 1.336 Å is more of a pure double bond (typically 1.34 Å). This tends to suggest that the structures **D** and **E** have little weight. The P—N and N—C bond distances in 1[N_2P] and 1[NSP] also appear to show partial double bond character.

The bond distances of the carbon heterocycles 1[S_2C] and 1[NSC] serve to confirm the similar behaviour of the phosphorus compounds. C4—S distances are similar for carbon and phosphorus heterocycles. The C2—S and C2—N distances display considerable evidence of π character due to their similarity with $H_2C{=}S$ (1.611 Å) and $H_2C{=}NH$ (1.273 Å), respectively. For comparison purposes, experimental data on related compounds are included in Table 1. Good agreement is observed between theory and experiment. The only major difference is in the C—C bond, which is longer in the substituted compounds, since it is part of a benzene ring. Apart from that, the maximum deviation from experiment is the S—P bond in 1[NSP], which is 2.0337 Å experimentally for the benzo-derivative, giving a deviation of 0.018 Å. This could be due to the absence of electron correlation, which typically lengthens the bonds.

All systems are planar. This has been verified by force field calculations performed at the optimized geometries, which do not reveal imaginary frequencies.

B. Orbitals and charges

The π energy levels and orbitals for the 5 cationic systems are shown in Fig. 1. A better understanding of the bonding comes from the π orbitals shown. The partial double bond character

Can. J. Chem. Downloaded from www.nrcresearchpress.com by 65.111.164.53 on 09/08/12
For personal use only.

Table 1*a*. Geometrical data.[a,b]

	1[S_2P]	1[N_2P]	1[NSP]	1[S_2C]	1[NSC]	2[S_2P]	2[N_2P]	2[NSP]
P—S	2.015		2.016			2.118		2.131
P—N		1.644	1.645				1.730	1.719
C2—S				1.660	1.677			
C2—N					1.304			
C5—S	1.723		1.721	1.723	1.728	1.775		1.781
C4—N		1.370	1.371		1.384		1.426	1.413
C4—C5	1.336	1.346	1.341	1.337	1.336	1.317	1.322	1.320

[a]All bond lengths in angstroms and all bond angles in degrees.
[b]Theoretical results, this work.

Table 1*b*. Geometrical data.[a,b]

	1[S_2P][c]	1[N_2P][d]	1[NSP][e]	2[S_2P][f]
P—S	2.016(3)		2.0337(14)	2.110(2)
	2.015(3)			2.102(2)
P—N		1.643(6)	1.643(3)	
C5—S	1.728(5)		1.732(4)	1.761(5)
	1.711(6)			1.765(6)
C4—N		1.379(9)	1.387(4)	
C4—C5	1.383(7)	1.378(10)	1.394(5)	1.401(6)

[a]All bond lengths in angstroms and all bond angles in degrees.
[b]Previously determined experimental results on related compounds.
[c]1,3,2-Benzodithiaphospholium cation, ref. 4.
[d]1,3,2-Benzodiazaphospholium cation, ref. 19.
[e]1,3,2-Benzazathiaphospholium cation, ref. 2.
[f]The derivative parent phosphine, 5-methyl-2-phenyl-1,3,2-benzodithiaphosphole, ref. 4.

observed in the structures is seen in the orbitals, which bear a strong resemblance to the cyclopentadienyl anion (11). The π-LUMO is located primarily at the 2 position (P or CH), consistent with studies of the benzo-derivatives at the STO-3G level (2). Nucleophilic attack would be expected to occur at the 2 position.

The atomic charges for the cations are given in Table 2. These were obtained via Mulliken population analysis. While the charge partitioning scheme can be argued to be somewhat arbitrary (ref. 26, p. 28), it is expected that some qualitative insight may stem from these results. As Mulliken charges for ions are especially unrealistic, the values for the neutral species calculated are included in the table. The charges relative to the neutral species serve as a guide to the location of the positive charge.

For 1[S_2P] the positive charge is borne by the phosphorus (0.49) and by the two sulfurs (0.28 each). This is confirmed by comparison with 2[S_2P]. In contrast, the 1[S_2C] carbon at the 2 position bears a summed charge of −0.13, and sulfur carries the only positive charge. In 1[NSP] and 1[N_2P], phosphorus bears a positive charge but nitrogen, unlike the sulfur in 1[S_2P] and 1[NSP], is negative, consistent with the higher electronegativity of nitrogen.

The Mulliken overlap population matrix was used to compare the extent of π-overlap between atoms. Results are reported in Table 3. The absolute numbers have little meaning. However, for 1[S_2P] it is immediately obvious there is significant sulfur—phosphorus $p\pi$—$p\pi$ bonding. If the C4—C5 π bond order is placed at 1, then the P—S π bond order appears

Fig. 1. Molecular orbital energy levels for π orbitals.

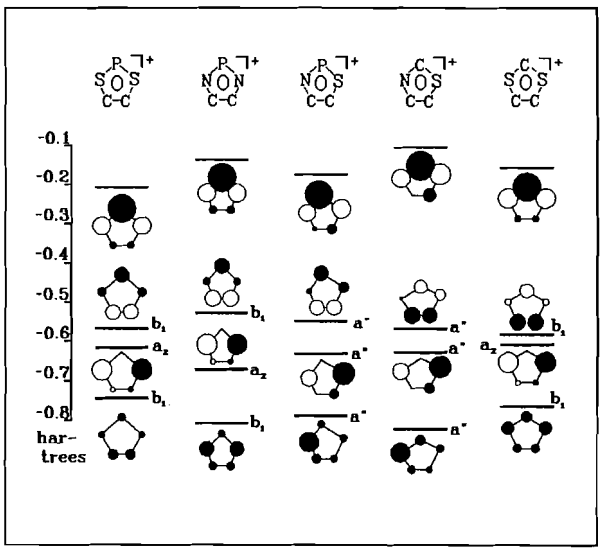

to be 0.5 and the C—S π bond order is just 0.2. It appears, once again, that structures **D** and **E** of the resonance hybrid have little weight for all five systems studied. The P—N π bond in 1[N_2P] appears to be comparable in strength to the P—S π bond in 1[S_2P], and the results for the mixed species 1[NSP] show that the P—S and P—N π bonds have essentially equal bond orders.

C. Vibrational frequencies

Results for selected computed molecular vibrational frequencies are reported in Table 4. The labels for the vibrations were obtained by sketching the normal mode output of the frequency calculations. It is interesting to note the 1[S_2P] P—S symmetric and asymmetric stretching frequencies. Their values are intermediate to the P—S and P=S frequencies computed by Schmidt et al. (522 and 791 cm^{-1}, respectively) (1). Burford has reported peaks at 525 and 665 cm^{-1} and proposed that they were due to the S—P—S moiety. Our findings are consistent with that view. The P—N stretching frequencies in 1[N_2P] are also intermediate to computed P—N and P=N frequencies (1). The C—S and C—N frequencies in 1[S_2P] and in 1[N_2P], respectively, lie between their respective single and double bond frequencies, but the values fall closer to single bond frequencies. For example, the computed C—S and C=S frequencies reported by Schmidt et al. are 778 and 1196 cm^{-1}, respectively (1).

Can. J. Chem. Downloaded from www.nrcresearchpress.com by 65.111.164.53 on 09/08/12
For personal use only.

Table 2. Atomic charges.

Atom	1[S_2P]	1[N_2P]	1[NSP]	1[NSC]	1[S_2C]	2[S_2P]	2[N_2P]	2[NSP]
P	0.49	0.90	0.73	—	—	0.22 (0.22)	0.69 (0.63)	0.49 (0.46)
C2	—	—	—	−0.05 (0.29)	−0.49 (0.13)			
H[a]	—	—	—	0.34	0.36			
S	0.28	—	0.23	0.54	0.61	−0.01		−0.07
N[b]	—	−0.78 (−0.31)	−0.78 (−0.30)	−0.62 (−0.14)	—		−0.88(−0.51)	−0.88 (−0.49)
H[c]	—	0.47	0.48	0.48	—		0.37	0.39
C4[b]	−0.36 (−0.02)	0.04 (0.35)	−0.44 (−0.11)	−0.46 (−0.13)	−0.37 (0.04)	−0.34 (−0.10)	−0.02 (+0.19)	−0.42 (−0.19)
H1[d]	0.33	0.31	0.33	0.33	0.33	0.24	0.21	0.23
C5[b]	−0.36 (−0.02)	0.04 (0.35)	0.13 (0.44)	0.16 (0.43)	−0.37 (0.04)	−0.34 (−0.10)	−0.02 (+0.19)	0.08 (0.29)
H2	0.33	0.31	0.32	0.32	0.33	0.24	0.21	0.22

[a]H on C2, 1[NSC], 1[S_2C].
[b]Numbers in parentheses represent values of charge with hydrogen atom summed in.
[c]H on N.
[d]H1 and H2 are on C4 and C5.

Table 3. Mulliken π-overlap[a].

	1[S_2P]	1[N_2P]	1[NSP]	1[S_2C]	1[NSC]
P—S[b]	0.213		0.220		
P—N		0.230	0.222		
C2—S				0.135	0.242
C2—N					0.267
C5—S	0.091		0.086	0.058	0.092
C4—N		0.085	0.088		0.095
C4—C5	0.437	0.438	0.436	0.434	0.445

[a]Summed for all pairs of inner and outer functions.
[b]$3p_xP$–$3p_xS$ overlap, for example.

Table 4. Selected molecular vibrational frequencies.[a]

1[S_2P]	1[N_2P]	1[NSP]
ω_4 (b_2)	ω_8 (b_2)	ω_4 (a')
608.6 (25.55)	970.6 (9.39)	630.1 (18.53)
asymmetric P—S	asymmetric P—N	P—S
ω_5 (a_1)	ω_9 (a_1)	ω_5 (a')
629.4 (13.81)	972.1 (10.04)	791.5 (11.90)
symmetric P—S	symmetric P—N	C—S
ω_7 (a_1)	ω_{11} (a_1)	ω_9 (a')
783.4 (2.25)	1153.4 (44.13)	954.1 (2.97)
symmetric C—S	symmetric C—N	P—N
ω_9 (b_2)	ω_{12} (b_2)	ω_{11} (a')
927.6 (7.97)	1216.5 (14.29)	1180.2 (5.22)
asymmetric C—S	asymmetric C—N	C—N
ω_{13} (a_1)	ω_{17} (a_1)	ω_{15} (a')
1647.7 (54.85)	1745.9 (164.54)	1712.6 (116.42)
symmetric C—C	symmetric C—C	C—C

[a]All frequency values are in cm^{-1}, followed by IR intensities in KM/mol in parentheses.

D. Thermochemical cycles

A measure of the energy involved in $p\pi$—$p\pi$ bonding would be the most useful contribution of our study, since geometries and frequencies represent extensions of the benzo-substituted experimental results. We have devised an isogyric reaction (i.e., the number of electron pairs is conserved) to evaluate the π bond strength. The reaction resembles the dehydrogenation cycle of Schmidt et al. (1).

The scheme is drawn for 1[S_2P] as an example:

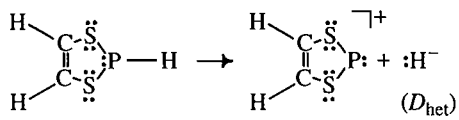

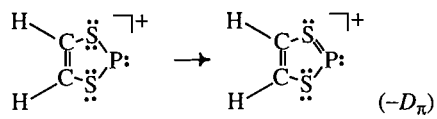

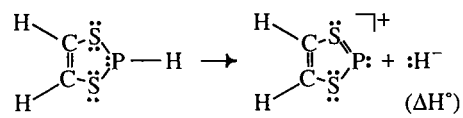

$$2[S_2P] \longrightarrow 1[S_2P] + H^-$$

The heat of the reaction ΔH^0 can be calculated via our *ab initio* methods, and then the heterolytic bond dissociation energy can be estimated. This gives a direct measure of the π bond strength:

$$D_\pi = D_{het} - \Delta H^0$$

We estimated the heterolytic bond dissociation energy to be 330.4 kcal/mol. This estimate came from MP2 calculations for the species in the following process:

$$PH_3 \longrightarrow PH_2^+ + H^-$$

These values were corrected for zero point vibrational effects.

Table 5. Total energies.

	SCF/6-31G*	MP2/6-31G*//6-31G*	ZPE[b]
1[S_2P]	−1212.38487	−1212.99424	0.04074
2[S_2P]	−1213.21628	−1213.81317	0.04987
1[N_2P]	−527.46785	−528.15058	0.07433
2[N_2P]	−528.23102	−528.90836	0.08213
1[NSP]	−869.92759	−870.57362	0.05760
2[NSP]	−870.72562	−871.36237	0.06596
PH_3	−342.44795	−342.55151	0.02618
PH_2^+	−341.50655	−341.58623	0.01509
H^-	−0.42244	−0.42891	0.0

[a]All energies in hartress, E_h.
[b]Zero-point vibrational energy computed at the SCF/6-31G* level.

Table 6. D_π results.[a]

	Corrected[b] MP2 ΔH^0
[S_2P]	90.7
[NSP]	109.2
[N_2P]	128.4

[a]All values in kcal/mol.
[b]Corrected for zero-point vibrational effects using SCF/6-31G* zero point energies, scaled by 0.89 (27).

Tables 5 and 6 report energies and D_π values. Note that the D_π results amount to 90.7, 109.2, and 128.4 kcal/mol for reactions leading to 1[S_2P], 1[NSP], and 1[N_2P], respectively. These numbers are extremely large when compared with the recommended values of 40 and 44 kcal/mol for the P═S and P═N π bond strengths of Schmidt et al. (1). A possible explanation is the fact that the hydride ion is unbound at the MP2 level with the basis set used. However, it should be noted that by applying the formula $D_\pi = D_{het} - \Delta H^0$, the energy of the hydride is subtracted out anyway. It is proposed that the aromaticity of the cationic species accounts at least in part for the extra stabilization. The contribution of the aromaticity to the stabilization was explored by looking at isodesmic bond separation reactions of the type used by Baldridge and Gordon in their study of the aromaticity of metal-substituted benzene and cyclopentadiene (10). The type of reaction shown is only one of the types used by theoreticians in their attempts to quantify aromaticity. Baldridge and Gordon outline several other types (10). In the present work, the bond separation reaction for 1[S_2P] is the following:

Table 7. Total energies for bond separation reactions.[a,b]

	SCF/6-31G*	MP2/6-31G*//6-31G*	ZPE[c]
CH_4	−40.19517	−40.33244	0.04778
SH_2	−398.66732	−398.78821	0.01645
SH_3^+	−398.94184	−399.06253	0.02897
CH_3—SH	−437.70032	−437.95234	0.04963
S═PH	−738.78851	−739.01111	0.00980
CH_2═CH_2	−78.03172	−78.28434	0.05477
HS—PH_2	−739.97316	−740.19260	0.02960
NH_3	−56.18436	−56.35371	0.03700
NH_4^+	−56.53077	−56.69954	0.05328
CH_3—NH_2	−95.20983	−95.50583	0.06891
HN═PH	−396.27954	−396.54915	0.02458
H_2N—PH_2	−397.48164	−397.74719	0.04746

[a]All energies in hartrees, E_h.
[b]Energies of some species reported in Table 5.
[c]Zero-point vibrational energy computed at the SCF/6-31G* level.

$$1[S_2P] + PH_3 + 2CH_4 + 3SH_2 \rightarrow SH_3^+ + 2CH_3—SH + S═PH + CH_2═CH_2 + HS—PH_2$$

This reaction satisfies the isodesmic criterion in that the number of bonds of each formal type is conserved. An extra sulfur-containing species was included on both sides to be the bearer of the positive charge on the product side. The energetics of the bond separation reactions are presented in Tables 7 and 8. Note that the ΔH^0 shown suggests that 1[S_2P] is more aromatic than benzene, whose equivalent bond separation reaction

$$C_6H_6 + 6CH_4 \rightarrow 3H_3C—CH_3 + 3H_2C═CH_2$$

has a ΔH^0 of 61 kcal/mol at the SCF/3-21G* level (10). The more appropriate companion to our species is the cyclopentadienyl anion. The ΔE for the bond separation reaction of the cyclopentadienyl anion is 87 kcal/mol, computed at the SCF/3-21G level (11). Our MP2 values are very similar to this result. Comparing ΔH^0 values for 1[S_2P] and 1[N_2P], delocalization stabilization is less for 1[S_2P], in accord with the observation that a larger heteroatom tends to decrease the stabilization (10).

Conclusion

Bond lengths, molecular orbitals, and vibrational frequencies all indicate the presence of $p\pi$—$p\pi$ bonding to the phosphorus in 1[S_2P], 1[N_2P], and 1[NSP]. The D_π values suggest that sta-

Can. J. Chem. Downloaded from www.nrcresearchpress.com by 65.111.164.53 on 09/08/12
For personal use only.

bilization comes from the aromaticity of the species. Bond separation values for ΔH^0 confirm this. The D_π results and the bond separation ΔH^0 values follow the same trends, with their respective maxima at 1[N_2P]. the large ΔH^0 values found in the bond separation reactions highlight the role of delocalization in the viability of these species.

Acknowledgements

The financial support of the Natural Sciences and Engineering Research Council of Canada in the form of an undergraduate student award to M.T.M. and a research grant to K.V.D. is gratefully acknowledged. The financial support of Mount Saint Vincent University in the form of an internal grant is also gratefully acknowledged. Many thanks to Dalhousie University for making available the Stellar GS 2500, and for their library facilities. K.V.D. acknowledges the helpful comments of the referees with gratitude. Finally, many thanks to Neil Burford and his group for helpful comments and support.

References

1. M.W. Schmidt, P.N. Truong, and M.S. Gordon. J. Am. Chem. Soc. **109**, 5217 (1987).
2. N. Burford, A.I. Dipchand, B.W. Royan, and P.S. White. Inorg. Chem. **29**, 4938 (1990).
3. N. Burford, B.W. Royan, J.M. Whalen, J.F. Richardson, and R.D. Rogers. J. Chem. Soc. Chem. Commun. **18**, 1273 (1990).
4. N. Burford, B.W. Royan, A. Linden, and T.S. Cameron. Inorg. Chem. **28**, 144 (1989).
5. N. Burford, B.W. Royan, and P.S. White. J. Am. Chem. Soc. **111**, 3746 (1989).
6. N. Burford, B.W. Royan, and P.S. White. Acta Crystallogr. Sect. C: Cryst. Struct. Commun. **C46**, 274 (1990).
7. L. Weber. Chem. Rev. **92**, 1839 (1992).
8. A.H. Cowley and N.C. Norman. Prog. Inorg. Chem. **34**, 1 (1986).
9. N.C. Norman. Polyhedron, **12**, 2431 (1993).
10. K.K. Baldridge and M.S. Gordon. J. Am. Chem. Soc. **110**, 4204 (1988).
11. M.S. Gordon, P. Boudjouk, and F. Anwari. J. Am. Chem. Soc. **105**, 4972 (1983).
12. H.C. Sorensen and L.L. Ingraham. J. Heterocycl. Chem. **8**, 551 (1971).
13. R. Zahradnik. Adv. Heterocycl. Chem. **5**, 1 (1985).
14. M.J. Frisch, M. Head-Gordon, G.W. Trucks et al. GAUSSIAN 90, Gaussian Inc., Pittsburgh, Pa. 1990.
15. M.M. Francl, W.J. Pietro, W.J. Hehre, J.S. Binkley, M.S. Gordon, D.J. DeFrees, and J.A. Pople. J. Chem. Phys. **77**, 3654 (1982).
16. P.C. Hariharan and J.A. Pople. Chem. Phys. Lett. **16**, 217 (1972).
17. C. Moller and M.S. Plesset. Phys. Rev. **46**, 618 (1934).
18. J.A. Pople, J.C. Binkley, and R. Seeger. Int. J. Quantum Chem. Symp. **10**, 1 (1976).
19. N. Burford, A.L. Dipchand, B.W. Royan, and P.S. White. Acta Crystallogr. Sect. C: Cryst. Struct. Commun. **C45**, 1485 (1989).
20. T. Matsumoto, H. Yamamoto, and S.J. Inoue. J. Am. Chem. Soc. **106**, 4829 (1984).
21. G.A. Olah and J.L. Grant. J. Org. Chem. **42**, 2237 (1977).
22. N. Burford, A.L. Dipchand, B.W. Royan, and P.S. White. Acta Crystallogr. Sect. C: Cryst. Struct. Commun. **C45**, 1345 (1989).
23. H. Gotthardt. *In* Comprehensive heterocyclic chemistry. Vol. 6. *Edited by* A.R. Katritzky and C.W. Rees. Pergamon Press Ltd., Oxford. 1984. pp. 813–850.
24. H. Prinzbach and E. Futterer. Adv. Heterocycl. Chem. **7**, 39 (1966).
25. M.D. Harmony et al. J. Phys. Chem. Ref. Data, **8**, 619 (1979).
26. W.J. Hehre, L. Random, P.v.R. Schleyer, and J.A. Pople. *In Ab initio* molecular orbital theory. John Wiley and Sons, Inc., New York. 1985. p. 174.
27. J.A. Pople, B.T. Luke, M.J. Frisch, and J.S. Binkley. J. Phys. Chem. **89**, 2198 (1985).

Can. J. Chem. Downloaded from www.nrcresearchpress.com by 65.111.164.53 on 09/08/12
For personal use only.

Structure–activity relationship study of synthetic hydrazines as ecdysone agonists in the control of spruce budworm (*Choristoneura fumiferana*)

Anmar K. Mohammed-Ali, Tak-Hang Chan, Anthony W. Thomas, George M. Strunz, and Brent Jewett

Can. J. Chem. Downloaded from www.nrcresearchpress.com by 65.111.164.53 on 09/08/12
For personal use only.

Abstract: A quantitative structure–activity relationship study was performed for a number of aroylhydrazine compounds with respect to their biological activity against spruce budworm. It was found that the biological activity can be modulated by substituents on the aromatic rings. Substituents with high π value and small L value lead to increase in biological activity. Molecular mechanics calculations were used to explain how the active compounds may mimic the strong-binding Y region of ecdysone.

Key words: spruce budworm, ecdysone, agonist, hydrazines, quantitative structure–activity relationship.

Résumé : On a effectué une étude de la relation quantitative structure–activité d'un certain nombre de composés aroylhydrazines par rapport à leur activité biologique contre tordeuse d'épinette. On a trouvé que l'activité peut être modulée par les substituants attachés au noyaux aromatiques. Les substituants avec des valeurs élevées de π et des valeurs de L faibles augmentent l'activité biologique. On a utilisé des calculs de mécanique moléculaire pour expliquer comment les composés actifs peuvent mimer la région Y de forte liaison de l'ecdysone.

Mots clés : tordeuse d'épinette, ecdysone, agoniste, hydrazines, relation quantitative structure–activité.

[Traduit par la rédaction]

Introduction

The spruce budworm (*Choristoneura fumiferana*) is an insect pest that inflicts severe damage to the spruce-fir forest in North America (1). This insect poses a threat to over 150 million acres of susceptible forest in the Eastern United States and Canada, threatening the wood supply from large areas of forest in eastern Canada. The spruce budworm can be found from Virginia to Newfoundland and west across Canada throughout the boreal forest region. Efforts to control the spruce budworm up to now have relied on the spraying of chemical insecticides such as the organophosphate Fenitrothion or the microbial insecticide *Bacillus thuringiensis* (Bt) (2). The widespread use of synthetic broad-spectrum chemical pesticides is a matter of public concern. Furthermore, insect resistance to Bt in the laboratory has recently been reported (3). There is therefore a need to search for alternative, environmentally acceptable, approaches for forest protection against spruce budworm.

We recently reported that azadirachtin (**1**), in the form of an emulsion, is an effective growth regulator and antifeedant for spruce budworm (4). Because of the structural complexity of **1**, structure–activity relationship studies based on **1** will be a considerable challenge (5). The compound specionin (**2**), isolated from the leaves of *Catalpa speciosa* Warder (Bignoniaceae), was reported to deter feeding by spruce budworm at about 50–100 ppm concentration (6). While a number of syntheses of specionin have been reported (7, 8), its biological activity remains to be confirmed (8). Another approach to control of insects is based on the critical role of ecdysone (**3**) in their molting and development (9). In 1988, Wing et al. reported the effect of a non-steroidal ecdysone agonist, 1,2-dibenzoyl-1-*tert*-butylhydrazine (**4**, RH-5849), which mimics the action of 20-hydroxyecdysone (10). The hydrazine **4** was found to be extraordinary potent at promoting molting in larvae of the tobacco hornworm (*Manduca sexta*). We have since reported the X-ray structure of **4** and its effect against spruce budworm (LD_{50} = 0.31 μg) (11). Because of the relative simplicity of its chemical structure and its potency, we have undertaken a structure–activity relationship study of analogues of **4** with respect to their effect on spruce budworm.

Received October 12, 1994.

A. Mohammed-Ali, T.-H. Chan.[1] Department of Chemistry, McGill University, Montreal, QC H3A 2K6, Canada
A.W. Thomas, G.M. Strunz, and B. Jewett. Canadian Forest Service, P.O. Box 4000, Fredericton, NB E3B 5P7, Canada.

[1] Author to whom correspondence may be addressed. Telephone: (514) 398-6932. Fax: (514) 398-3797.

Experimental

General

Melting points (mp) were determined on a Gallenkamp block and were uncorrected. Proton nuclear magnetic resonance (^{1}H NMR) spectra were taken on Varian-200, XL-300, and XL-500 instruments. The data are reported in parts per million (ppm) relative to the TMS reference line with the multiplicity

Can. J. Chem. Downloaded from www.nrcresearchpress.com by 65.111.164.53 on 09/08/12
For personal use only.

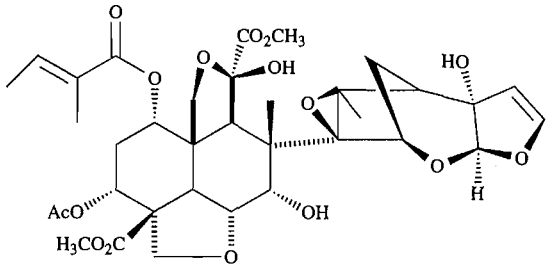

1

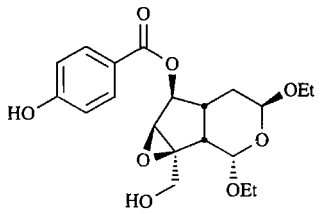

2

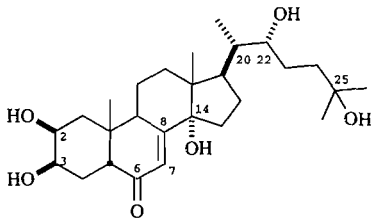

3

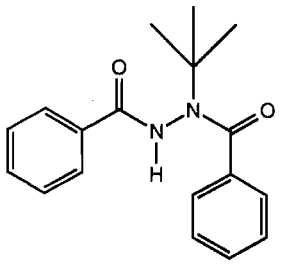

4

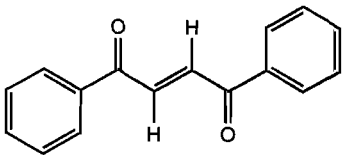

5

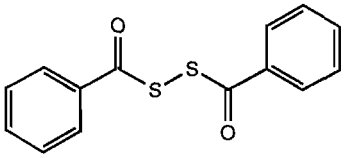

6

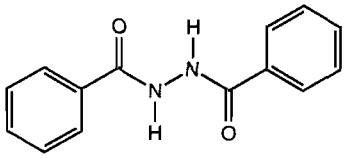

7

(s, singlet; d, doublet; t, triplet; q, quartet, m, multiplet; b, broad), coupling constants in hertz and the number of protons also given. Carbon-13 nuclear magnetic resonance (^{13}C NMR) spectra were recorded on Varian XL-300 and XL-200 instruments. Mass spectra (MS) were recorded using ammonia chemical ionization (CI) on a Hewlett–Packard 5890A mass spectrometer, or on a Kratos 25 mass spectrometer operating at an ionization potential of 70 eV (EI) and are reported as *m/z* relative intensity %). Exact Mass (HRMS) values were determined on the Kratos instrument. Molecular mechanics calculations were performed with PCMODEL from Serena Software.

Synthesis

Compounds **5** and **7** were obtained commercially from Aldrich. All the hydrazine compounds were synthesized following the general procedure. Compound **4** was reported previously (10). For compounds **8**, **9**, **10**, and **11**, the corresponding chloroformates were used instead of the acid chlorides. Compound **6** was prepared by treating thiobenzoic acid with an equivalent amount of potassium hexacyanoferrate (III) in aqueous sodium hydroxide solution.

1,2,-Dibenzoyl disulfide ***6***: mp 129–129.5°C; ^1H NMR ($CDCl_3$): 7.63 (m); ^{13}C NMR ($CDCl_3$): 128.1, 128.9, 134.3, 186.0; MS (CI): 275 (5.9), 152 (25), 138 (54), 122 (32), 104 (100); HRMS calcd. for $C_{14}H_{10}O_2S_2$: 274.0122; found: 274.0104.

General procedures for tert-butyl aroyl hydrazines

The appropriate acid chloride (8 mmol) was added dropwise to a cooled (0°C) solution of *tert*-butylhydrazine hydrochloride (4 mmol) in aqueous sodium hydroxide (12 mmol) solution. A white precipitate was formed in 30 min. The mixture was filtered after 2 h. The product was recrystallized from ethanol–water (1:1) to give the desired compound in good yield, generally in the range of 60–90%.

1-tert-Butyl-1,2-difuroylhydrazine ***14***: mp 203–204°C; ^1H NMR (DMSO-d_6): 1.46 (s, 9H), 6.51 (5, J = 1.2 Hz, 1H), 6.71 (t, J = 1.2 Hz, 1H), 6.91 (d, J = 2.2 Hz, 1H), 7.31 (d, J = 2.2 Hz, 1H), 7.74 (s, 1H), 7.97 (s, 1H); ^{13}C NMR (DMSO-d_6): 27.3, 61.0, 111.2, 112.0, 114.9, 115.3, 144.9, 145.7, 146.3, 147.2, 157.8, 159.9; MS (EI): 276 (1), 221 (11), 220 (76), 152 (2), 125 (7), 95 (100); HRMS, calcd. for $C_{14}H_{16}N_2O_4$: 276.1110; found: 276.1116.

1-tert-Butyl-1,2-dicyclohexanecarbonylhydrazine ***12***: mp 205–205.5°C; ^1H NMR (DMSO-d_6): 1.18 (m, 10H), 1.29 (s, 9H), 1.69 (m, 10H), 2.24 (m, 2H); ^{13}C NMR (DMSO-d_6): 25.0, 25.1, 25.2, 25.3, 25.5, 25.6, 27.5, 28.5, 28.6, 28.9, 29.3, 41.3, 42.0, 59.2, 174.7, 176.7; MS (EI): 308 (0.3), 252 (4), 198 (100), 183 (44), 142 (39), 111 (29), 88 (26), 83 (67); HRMS: calcd. for $C_{18}H_{32}N_2O_2$: 308.2464; found: 308.2473.

1-tert-*Butyl-1,2-di-2-naphthoylhydrazine* ***15***: mp 248.5–249°C; ^{1}H NMR (DMSO-d_6): 1.56 (s, 9H), 7.44–8.08 (m, 14H); ^{13}C NMR (DMSO-d_6): 27.5, 60.4, 123.5, 124.3, 126.2, 126.4, 126.7, 126.8, 127.4, 127.5, 127.8, 128.0, 128.1, 128.5, 129.5, 131.7, 131.9, 132.9, 134.1, 135.2, 166.0, 171.8; MS (EI): 396 (4), 340 (25), 172 (6), 155 (100), 127 (44); HRMS, calcd. for $C_{26}H_{24}N_2O_2$: 396.1838; found: 396.1830.

1-tert-*Butyl-1,2-dimethoxycarbonylhydrazine* ***8***: mp 80–80.5°C; ^{1}H NMR (DMSO-d_6): 1.31 (s, 9H), 3.55 (s, 3H), 3.61 (s, 3H); ^{13}C NMR (DMSO-d_6): 27.6, 51.9, 52.2, 59.1, 155.2, 156.8; MS (CI): 222 (48, M − 17), 205 (100), 166 (41), 149 (40).

1-tert-*Butyl-1,2-diethoxycarbonylhydrazine* ***9***: oil; ^{1}H NMR (DMSO-d_6): 1.30 (s, 9H), 1.13 (t, J = 4.6 Hz, 3H), 1.17 (t, J = 4.6 Hz, 3H), 4.03 (m, 4H), 9.1 (s, 1H); ^{13}C NMR (DMSO-d_6): 14.3, 14.5, 27.7, 58.9, 60.4, 60.6, 154.9, 156.5; MS (EI): 232 (0.3), 176 (100), 130 (32), 104 (61); HRMS, calcd. for $C_{10}H_{20}N_2O_4$: 232.1423; found: 232.1421.

1-tert-*Butyl-1,2-diphenylacetylhydrazine* ***13***: mp 323.5–324°C; ^{1}H NMR (DMSO-d_6): 1.26 (s, 9H), 3.51 (s, 2H), 3.54 (s, 2H), 7.00–7.31 (m, 10H); ^{13}C NMR (DMSO-d_6): 27.4, 40.1, 40.5, 59.8, 126.1, 126.7, 128.0, 128.3, 129.1, 129.2, 134.9, 135.7, 170.0, 171.9; MS (EI): 324 (0.2), 268 (1), 206 (100), 191 (40), 150 (44), 136 (5), 118 (41), 91 (67); HRMS, calcd. for $C_{20}H_{24}O_2N_2$: 324.1838; found: 324.1831.

1-tert-*Butyl-1,2-diphenoxycarbonylhydrazine* ***10***: mp 160–160.5°C; ^{1}H NMR (DMSO-d_6): 1.42 (s, 9H), 7.27 (m, 10H); ^{13}C NMR (DMSO-d_6): 27.6, 60.0, 121.4, 121.7, 125.4, 129.4, 129.5, 129.6, 150.6, 150.9, 154.1, 154.8; MS (CI): 346 (100, M – 17), 329 (56), 290 (90).

1-tert-*Butyl-1,2-dibenzoxycarbonylhydrazine* ***11***: mp 95.5–96°C; ^{1}H NMR (DMSO-d_6): 1.31 (s, 9H), 5.07 (m, 4H), 7.29 (m, 10H); ^{13}C NMR (DMSO-d_6): 27.7, 59.2, 65.9, 66.2, 127.1, 127.2, 127.5, 127.6, 127.9, 128.2, 128.3, 136.6, 154.6, 156.5; MS (CI): 375 (21), 374 (M – 17), 357 (59), 318 (76), 314 (21), 313 (100), 257 (38); HRMS, calcd. for $C_{20}H_{24}N_2O_4$: 356.1736; found: 356.1720.

1-tert-*Butyl-1,2-di*-p-*hexyloxybenzoylhydrazine* ***16***: mp 153–154°C; ^{1}H NMR ($CDCl_3$): 0.88 (m, 6H), 1.30 (m, 16H), 1.56 (s, 9H), 3.92 (m, 4H), 6.77 (m, 4H), 7.38 (m, 4H); ^{13}C NMR (DMSO-d_6): 13.9, 22.5, 25.0, 25.6, 27.8, 29.0, 29.1, 31.4, 31.5, 61.4, 67.9, 68.2, 113.5, 114.0, 121.6, 124.0, 128.6, 129.7, 130.5, 132.2, 159.9, 161.9, 163.5, 166.6, 170.7, 173.5; MS (CI): 498 (40), 497 (97), 479 (42), 442 (32), 441 (100).

1-tert-*Butyl-1,2*-m-*methylbenzoylhydrazine* ***17***: mp 138.5–139°C; ^{1}H NMR (DMSO-d_6): 1.47 (s, 9H), 2.25 (s, 3H), 2.26 (s, 3H), 7.10–7.30 (m, 8H); ^{13}C NMR (DMSO-d_6): 20.8, 27.4, 60.1, 123.5, 124.1, 127.0, 127.2, 127.5, 128.2, 129.6, 132.2, 132.5, 136.4, 137.6, 137.7, 166.1, 171.9; MS (CI): 325 (8), 269 (44), 192 (100), 136 (56), 119 (42). HRMS, calcd. for $C_{20}H_{24}N_2O_2$: 324.1838; found: 324.1830.

1-tert-*Butyl-1,2*-p-*methylbenzoylhydrazine* ***18***: mp 324–324.5°C; ^{1}H NMR (DMSO-d_6): 1.47 (s, 9H), 2.22 (s, 3H), 2.29 (s, 3H), 7.05–7.44 (m, 8H), 10.52 (s, 1H); ^{13}C NMR (DMSO-d_6): 20.7, 20.8, 27.4, 60.2, 126.6, 127.1, 127.8, 128.9, 129.4, 134.9, 138.6, 141.7, 165.6, 171.9; MS (CI): 325 (12), 268 (62), 193 (20), 192 (100), 136 (33), 135 (76), 133 (22), 118 (57); HRMS, calcd. for $C_{20}H_{24}N_2O_2$: 324.1838; found: 324.1832.

1-tert-*Butyl-1,2*-m-*methoxybenzoylhydrazine* ***19***: mp 170–170.5°C; ^{1}H NMR (DMSO-d_6): 1.50 (s, 9H), 3.72 (s, 3H), 3.74 (s, 3H), 6.85–7.55 (m, 8H); ^{13}C NMR (DMS0-d_6): 27.4, 55.1, 55.2, 60.2, 111.6, 112.1, 114.9, 117.5, 118.7, 119.2, 133.7, 139.1, 158.2, 159.0, 165.8; 171.5; MS (CI): 357 (0.4), 208 (24), 153 (100), 152 (34); HRMS, calcd. for $C_{20}H_{24}N_2O_4$: 356.1736; found: 356.1731.

1-tert-*Butyl-1,2-di*-p-*methoxybenzoylhydrazine* ***20***: mp 174.5–175°C; The compound was unstable in DMSO solution. ^{1}H NMR (DMSO-d_6): 1.30 (s, 9H), 3.80 (s, 6H), 7.00 (m, 4H), 7.87 (m, 4H); MS (CI): 357 (48), 301 (81), 283 (100).

1-tert-*Butyl-1,2-di*-m-*cyanobenzoylhydrazine* ***21***: mp 198.5–199.5°C; ^{1}H NMR (DMSO-d_6): 1.50 (s, 9H), 7.52–8.02 (m, 8H); ^{13}C NMR (DMSO-d_6): 27.3, 60.7, 110.6, 118.8, 117.8, 118.1, 129.1, 129.9, 130.0, 130.4, 131.1, 131.6, 132.7, 132.9, 135.5, 138.4, 164.2, 169.8; MS (EI): 346 (0.6), 290 (48), 130 (100), 102 (37), 57 (38); HRMS, calcd. for $C_{20}H_{18}N_4O_2$: 346.1430; found: 346.1433.

1-tert-*Butyl-1,2-di*-p-*cyanobenzoylhydrazine* ***22***: mp 228–229°C; ^{1}H NMR (DMSO-d_6): 1.48 (s, 9H), 7.53–8.09 (m, 8H); ^{13}C NMR (DMSO-d_6): 27.2, 60.8, 111.8, 114.4, 117.9, 118.2, 127.0, 127.7, 131.7, 132.7, 135.7, 135.8, 141.8, 141.9, 164.9, 170.2; MS (CI): 347 (13), 203 (100), 147 (29), 145 (47), 130 (26); HRMS, calcd. for $C_{20}H_{18}N_4O_2$: 346.1430; found: 346.1427.

1-tert-*Butyl-1,2-di*-m-*bromobenzoylhydrazine* ***23***: mp 215°C; ^{1}H NMR (DMSO-d_6): 1.45 (s, 9H), 7.26–8.02 (m, 8H); ^{13}C NMR (DMSO-d_6): 27.3, 60.5, 120.5, 121.7, 125.4, 126.2, 128.9, 129.4, 130.0, 130.8, 132.0, 134.2, 134.7, 139.6, 164.6, 170.0; MS (CI): 452 (4), 400 (49), 399 (28), 398 (100), 397 (34); 396 (51), 257 (69), 255 (72), 201 (51), 199 (53), 184 (68), 182 (68), 178 (44), 122 (44), 105 (58).

1-tert-*Butyl-1,2-di*-p-*bromobenzoylhydrazine* ***24***: mp 251.5–252.5°C; ^{1}H NMR (DMSO-d_6): 1.45 (s, 9H), 7.33–7.65 (m, 8H); ^{13}C NMR (DMSO-d_6): 27.3, 60.5, 122.5, 125.8, 128.5, 129.0, 130.4, 131.0, 131.5, 136.8, 165.0, 170.8; MS (CI): 454 (2), 452 (8), 398 (21), 257 (27), 255 (26), 178 (100), 122 (55), 85 (23).

1-tert-*Butyl-1,2-di*-m-*nitrobenzoylhydrazine* ***25***: mp 220–221°C; ^{1}H NMR (DMSO-d_6): 1.52 (s, 9H), 7.57–8.29 (m, 8H); ^{13}C NMR (DMSO-d_6): 27.2, 60.9, 121.0, 121.5, 124.2, 126.7, 129.6, 130.5, 133.0, 133.4, 138.9, 146.8, 147.6, 164.0, 169.5; MS (CI): 387 (5), 330 (100), 222 (53), 166 (22).

1-tert-*Butyl-1,2-di*-p-*nitrobenzoylhydrazine* ***26***: mp 385.5–386°C; ^{1}H NMR (DMSO-d_6): 1.51 (s, 9H), 7.67 (d, J = 7.8 Hz, 4H), 8.21 (m, 4H); ^{13}C NMR (DMS0-d_6): 27.2, 60.9, 122.9, 123.4, 123.5, 123.7, 127.6, 128.6, 128.8, 130.5, 137.3, 138.9,

Can. J. Chem. Downloaded from www.nrcresearchpress.com by 65.111.164.53 on 09/08/12
For personal use only.

Can. J. Chem. Downloaded from www.nrcresearchpress.com by 65.111.164.53 on 09/08/12
For personal use only.

147.5, 149.4, 164.6, 169.9; MS (CI): 330 (22), 300 (5), 167 (9), 150 (100).

1-tert-*Butyl-1,2-di*-m-*chlorobenzoylhydrazine* ***27***: mp 199–200°C; ^{1}H NMR ($CDCl_3$): 1.57 (s, 9H), 7.25 (m, 8H); ^{13}C NMR (DMSO-d_6): 27.7, 61.9, 124.3, 124.7, 126.2, 127.0, 129.5, 129.7, 130.1, 132.3, 133.7, 133.9, 134.9, 139.1, 165.7, 171.6; MS (CI): 365 (1.4), 214 (34), 212 (100), 156 (48), 155 (26), 140 (24), 138 (27), 138 (60); HRMS, calcd. for $C_{18}H_{18}N_2Cl_2$: 364.0745; found: 364.0728.

1-tert-*Butyl-1,2-di*-p-*chlorobenzoylhydrazine* ***28***: mp 201–201.5°C; ^{1}H NMR (DMSO-d_6): 1.47 (s, 9H), 7.32–8.00 (m, 8H); ^{13}C NMR (DMSO-d_6): 27.3, 60.5, 127.6, 128.3, 128.7, 129.0, 130.7, 133.8, 136.4, 136.8, 164.8, 170.8; MS (CI): 366 (0.02), 158 (22), 156 (65), 141 (31), 139 (100), 111 (39), 75 (20).

1-tert-*Butyl-1,2-di*-m-*fluorobenzoylhydrazine* ***29***: mp 164.5–165°C; ^{1}H NMR (DMSO-d_6): 1.47 (s, 9H), 7.18–7.45 (m, 8H); ^{13}C NMR (DMSO-d_6): 27.3, 60.5, 113.2 (d, J = 23 Hz), 113.8 (d, J = 23 Hz), 116.1 (d, J = 21 Hz), 118.9 (d, J = 21 Hz), 122.5 (d, J = 2.2 Hz), 123.1 (d, J = 3.3 Hz), 129.7 (d, J = 8.8 Hz), 130.8 (d, J = 8.8 Hz), 134.3 (d, J = 6.6 Hz), 139.8 (d, J = 6.6 Hz), 159.6 (d, J = 42 Hz), 163.2 (d, J = 43 Hz), 164.7 (d, J = 3.3 Hz), 170.3 (d, J = 2.2 Hz); MS (CI): 333 (9), 277 (100), 276 (22), 196 (86), 140 (52), 123 (58). HRMS, calcd. for $C_{18}H_{18}N_2O_2F_2$: 332.1336; found: 332.1343.

1-tert-*Butyl-1,2-di*-p-*fluorobenzoylhydrazine* ***30***: mp 167.5–168°C; ^{1}H NMR (DMSO-d_6): 1.48, (s, 9H), 7.08–8.04 (m, 8H); ^{13}C NMR (DMSO-d_6): 27.4, 60.4, 114.4 (d, J = 21 Hz), 115.5 (d, J = 22 Hz), 128.6 (d, J = 3.3 Hz), 129.0 (d, J = 8.8 Hz), 129.7 (d, J = 8.8 Hz), 134.1 (d, J = 3.3 Hz), 161.3 (d, J = 124 Hz), 165.0 (d, J = 129 Hz), 164.9, 170.9; MS (CI): 333 (10), 277 (48), 196 (100), 140 (55), 123 (22); HRMS, calcd. for $C_{18}H_{18}N_2O_2F_2$: 332.1336; found: 332.1331.

1-tert-*Butyl-1,2-di*-p-*ethylbenzoylhydrazine* ***31***: mp 143.5–144.5°C; ^{1}H NMR (DMSO-d_6): 1.13 (m, 6H), 1.48 (s, 9H), 2.60 (m, 4H), 7.36 (m, 8H); ^{13}C NMR (DMSO-d_6): 15.9, 16.0, 28.1, 28.5, 28.6, 60.8, 127.4, 127.8, 128.4, 128.6, 130.0, 130.5, 135.9, 145.5, 148.5, 166.5, 172.6; MS (CI): 353 (51), 297 (100); MS (EI): 352 (0.6), 296 (11), 150 (6), 133 (100), 105 (14); HRMS, calcd. for $C_{22}H_{28}N_2O_2$: 352.2151; found: 352.2147.

Bioassay methods

1. Type 1 bioassays

Diet preparation: Standard McMorran diet (12) was lyophilized and powdered to pass through a 40-mesh screen (425 μm openings). This powdered diet was diluted with cellulose powder (Alphacel) in a proportion of 1 part of diet to 1.5 parts of Alphacel to give 40% McMorran diet. At this concentration of nutrients, the dry weight of the amount eaten by 6th instar larvae approximates the dry weight of host-tree foliage normally consumed (13). Diet containing the desired concentration of the test compound was prepared by treating the powdered 40% McMorran diet with a solution of the compound in methylene chloride and then completely removing the solvent at 30°C in a rotary evaporator. A total of 18 g of the residual powder was hydrated to 75% water content with 54 mL of 0.6% aqueous potassium sorbate solution and mixed into a paste. This potassium sorbate retards the growth of fungus (14). The amount of test compound added to the powdered diet was such as to give a concentration of 10, 50, or 100 ppm in the hydrated diet. Control diets were prepared in a similar way, but with only solvent.

Experimental procedure: Each 72 g of diet paste was divided into 50 aliquots and loaded into fibrin cups. One cup of diet plus one recently moulted, unfed, 6th instar larva was placed in a petri dish (35 × 10 mm). A bioassay consisted of 50 replicates (25 males, 25 females) per concentration per compound. Larvae were reared at 21°C, 17-h photoperiod, and examined daily. The bioassay was terminated when all larvae had either died or pupated. Mortality was recorded. The dishes were examined visually and the amount of diet eaten, relative to the solvent-only control, was estimated. A reduction of about >33% in the amount eaten was obvious. When this occurred, the frass was dried (60°C) and weighed. Frass weight is an accurate measure of the amount of food eaten. (4) Up to 6 bioassays (300 larvae) could be run at one time as a group. Compound **4** was included in seven of these groups as a treatment reference.

2. Type 2 bioassays

The 40% McMorran diet powder was prepared as for the type 1 bioassays and then made into wafers of ca. 1 cm diameter and 1 mm thick and weighing ca. 20 mg (15). These diet wafers were treated with the test compound in methylene chloride solvent and the solvent evaporated in a fume hood. Using this method, the amount of compound in each wafer could be controlled. The wafers were hydrated and fed to recently-moulted unfed 6th instar larvae as in type 1 bioassays. When a larva had eaten all its treated wafer (i.e., ingested the full dose of the test compound), usually within 24 h, it was given non-treated 40% McMorran paste. Solvent-only wafers were used as controls. Mortality was recorded as the failure of a larva to moult to a pupa. This bioassay was used to determine the LD_{50} of 10 compounds, using the SAS probit procedure (16). Two series of dosages were used, 0.025, 0.05, 0.10, 0.15, 0.20 micrograms per larva and 0.2, 0.4, 0.5, 0.6, 0.8 micrograms per larva. These dosages gave concentrations that ranged between ca. 0.3–10 ppm in the hydrated wafers. Each dosage per compound was replicated with 40 larvae (20 males, 20 females).

Results

Type 1 bioassays were conducted with 28 compounds including **4**. At 10 ppm, compound **4** invariably resulted in 100% larval mortality and very high feeding reduction; i.e., in three bioassays when feeding reduction was measured, values of 93.4, 94.0 and 94.4% were obtained. Of the other 27 compounds, **15** and **31** resulted in 22 and 54% larval mortality, respectively, and 43 and 44% feeding reduction, respectively (Table 1). Compounds **17**, **18**, **19**, **23**, **28**, **29**, and **30**, were as active as **4** (Table 1). Compound **27** gave 100% mortality at 10 ppm but feeding reduction was not measured. The other 16 compounds (**5–14**, **16**, **20–22**, **25–26**) were inactive, in that larval mortality never exceeded 6% and there was no obvious effect on amount of diet consumed at 10 ppm concentration for

Can. J. Chem. Downloaded from www.nrcresearchpress.com by 65.111.164.53 on 09/08/12
For personal use only.

Table 1. Compounds showing biological activity against 6th instar spruce budworm larvae when incorporated into artificial diet at 10 ppm of the wet weight (Type 1 bioassay).

Compound	Mortality, %	Feeding reduction, %
15	22	43
17	100	95
18	100	94
19	100	93
23	100	90
27	100	Not recorded
28	100	92
29	100	94
30	100	93
31	54	44

5, **12**, **13**, **16**, **20**, **21**, **22**, **25**, **26**; at 50 ppm concentration for **8**, **9**, **10**, **11**, **14**; and at 100 ppm concentration for **6** and **7**.

The LD_{50} values for 10 compounds are given in Table 2 and ranged from 0.120 micrograms (μg) for **24** and 0.311 (μg) for **4**, to an estimated 1.003 μg for **19**. The low LD_{50} values for **4**, **17**, **18**, **23**, **27**, **28**, **29**, and **30** were to be expected from the Type 1 bioassays as the average amount of compound ingested was <0.5 micrograms per larva and resulted in 100% mortality. For **19**, mortality was influenced by the rate of its ingestion rather than the total amount ingested. At concentration of 2–4 ppm, the larvae ingested more compound and suffered lower mortality than when they fed on diets containing 6–10 ppm. The LD_{50} value of 1.003 μg for **19** refers to a diet concentration of 3 ppm; at 10 ppm the LD_{50} value is <0.5 μg. Note that the values for **17**, **18**, and **19** were estimated from the probit analysis as they were outside the range of the concentrations tested, i.e., 0.2–0.8 micrograms per larva. The LD_{50} values for **20**, **21**, **22**, **25**, **26**, and **31** were not determined as they showed no, or attenuated, biological activity at 10 ppm concentration.

Discussion

Preliminary studies

We examined first the effects of the changes of gross structure on the biological activity. Compounds **5–31** were compared with **4** using a feeding bioassay (Type 1 bioassay). All the compounds were tested using sixth instar larvae. The newly moulted sixth instar larvae were maintained on artificial diet containing 10 ppm (wet weight) of the test compound, with untreated diet as the control. At pupation, when feeding inhibition exceeded 33%, the frass was dried (60°C) and weighed, the weights indicating the amount of diet consumed.

Compounds **5** and **6** were designed to probe the effect of replacing the hydrazine linkage by another functionality. It is

Table 2. The physical parameters and LD_{50} values (Type 2 bioassay) of substituted **4**.

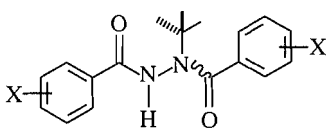

Compound	X	π^a	σ	*L*	LD_{50}, μg/larva
4	H	0.00	0.00	2.06	0.311
17	*m*-Me	0.51	−0.07	3.00	0.159[b]
18	*p*-Me	0.52	−0.17	3.00	0.159[b]
19	*m*-OMe	0.12	0.12	3.98	1.003[b]
20	*p*-OMe	−0.04	−0.27	3.98	—[c]
21	*m*-CN	−0.30	0.56	4.23	—[c]
22	*p*-CN	−0.32	0.66	4.23	—[c]
23	*m*-Br	0.94	0.39	3.83	0.246
24	*p*-Br	1.02	0.23	3.83	0.120
25	*m*-NO_2	0.11	0.71	3.44	—[c]
26	*p*-NO_2	0.24	0.78	3.44	—[c]
27	*m*-Cl	0.76	0.37	3.52	0.124
28	*p*-Cl	0.78	0.23	3.52	0.158
29	*m*-F	0.13	0.34	2.65	0.222
30	*p*-F	0.15	0.06	2.65	0.293
31	*p*-Et	1.02[a]	−0.15	4.11	—[d]

[a]π values of substituted phenoxyacetic acid except *p*-Et which is of substituted benzene.

[b]From probit analysis.

[c]Type 2 (LD_{50}) bioassay data not available for these compounds, but Type 1 assay indicates no biological activity at 10 ppm.

[d]LD_{50} value not determined, but active in Type 1 assay at 10 ppm (Table 1).

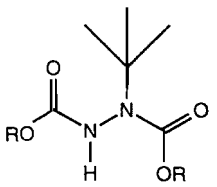

8, R=Me
9, R=Et
10, R=Ph
11, R=PhCH$_2$

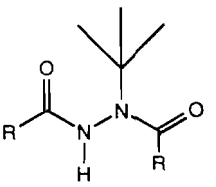

12, R=c-C$_6$H$_{11}$-
13, R=PhCH$_2$-
14, R= 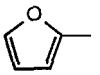
15, R= 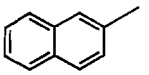
16, R=n-C$_6$H$_{13}$O- 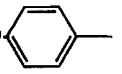

immediately clear that replacement of the hydrazine by a planar *E*-alkene (**5**), or a nonplanar 90° S—S linkage (**6**) led to loss of biological activity. Replacement of the *tert*-butyl group on the hydrazine by a hydrogen gave an inactive compound **7**, suggesting that the bulky *tert*-butyl group is critical to the activity. This is in agreement with observations of Hsu who found that the hydrazine class of compounds is active against Lepidopteran larvae as long as the *tert*-butyl group is present (17). An increase or decrease in the bulkiness of the substituent replacing the *tert*-butyl group led to diminishing activity. The next set of compounds, **8–11**, was designed to probe the effect of replacing the amide function with a carbamate function. It is clear that such modification leads to loss of activity. Exchanging the phenyl rings in **4** with cyclohexyl (**12**) or benzyl (**13**) groups also lead to inactive compounds. Loss of activity was also observed when the phenyl rings were replaced by furanyl (**14**) moieties and attenuated activity was observed for the naphthyl (**15**) analogue. Substitution in the phenyl ring can also cause significant change in biological activity. For example, a *p*-hexanoxy (**16**) or a *p*-methoxy (**20**) substituent in the phenyl ring gave inactive compounds at 10 ppm concentration. On the other hand, the *m*-methoxy compound **19** is active. We undertook therefore a quantitative structure–activity relationship (QSAR) study of derivatives of active prototype **4** according to the method of Hansch et al. (18).

Quantitative structure–activity relationship (QSAR) study

Compounds **17–31**, in which the phenyl rings of the parent compound **4** were substituted at the *meta* or the *para* positions, were compared. Most of these compounds were found to be active in either Type 1 (feeding) or Type 2 (LD_{50}) bioassays. The LD_{50} values of the active compounds were determined using sixth instar larvae by a dosage response study of their mortality and are summarized in Table 2.

For a series of structurally closely related compounds, such as the present series in which only the substituents in the phenyl rings are changed, the correlation between the chemical structures and their biological activities could be governed by a number of factors. The first factor is the probability of a compound reaching the site of action within a given time interval. Hansch suggested that this was related to the partition coefficient (*P*) of the compound between an aqueous phase and an organic phase. For substituted aromatic compounds, Hansch has developed a comparative substituent constant π, which is a free-energy-related constant and is a measure of the free energy change resulting from moving a derivative from one phase to another. In Table 2, the π values were the ones derived from the partition coefficients of substituted phenoxyacetic acids between water and octanol in which

$$\pi = \log (P_x/P_H)$$

for a substituent X replacing hydrogen (H). Since it is expected that a molecule outside a cell will have to make many partitions between "aqueous" phases and a variety of different "organic" phases to reach the site of action inside the cell, the optimum probability would not necessarily be a simple function of π but, to a first approximation, of π and π^2 (or even higher order). Another influence of a substituent on the properties of an aromatic system is measured by the Hammett σ constant. The σ constants have been well established and are also listed in Table 2. Some attempts have been made to develop parameters to take into account the steric effect of a substituent. Verloop et al. have selected five dimensions for each substituent and developed a computer program using van der Waals radii, standard bond angles and lengths, and "reasonable" conformations to define the space requirements of a substituents (20). The five dimensions are labelled *L*, *B*1, *B*2, *B*3, and *B*4. The length parameter, *L*, is defined as the length of the substituent along the axis of the bond between the first atom of the substituents and the parent molecule. The four width parameters *B*1–*B*4, are determined by the distance at their maximum point perpendicular to this attachment bond axis and each other. *B*1 is the smallest and *B*4 the largest width. In effect, these parameters define a box around the substituent. Since most of the substituents in Table 2 are spherical, only the *L* parameters are used for the QSAR study. Based on the data compiled in Table 2, multiple linear regression analysis (20) was used to generate the coefficients in eq. [1] Table 3). The physical parameters of the substituents are the independent variables of the regression and the biological activity is the dependent variable. As one can see, the regression analysis gave good correlation coefficient (*R*) or R^2 and low standard deviation (*s*). This is not unexpected in a multivariate analysis. To find out which of the parameters are important to the biological activity, 14 ([2]–[15], Table 3) were generated based on different combinations of the parameters. Equations [6], [13], and [15] all have high *R* square and low *s* values. Removing the σ parameter (eq. [[15]) and the π^2 parameter (eq. [13]) led to eq. [6] with the correlation coefficient still quite significant (R^2 = 0.931).

Can. J. Chem. Downloaded from www.nrcresearchpress.com by 65.111.164.53 on 09/08/12
For personal use only.

Can. J. Chem. Downloaded from www.nrcresearchpress.com by 65.111.164.53 on 09/08/12
For personal use only.

Table 3. Regression equations for biological activity against the spruce budworm by substituted **4**.

Equation	LD_{50} =	R^2	s
[1]	$(-1.416)\pi + 0.561\pi^2 + (-0.26)\sigma + 0.485L - 0.745$	0.971	0.06
[2]	$(-0.356)\pi + 0.455$	0.257	0.24
[3]	$(-0.308)\pi^2 + 0.393$	0.205	0.249
[4]	$(-0.113)\sigma + 0.297$	0.007	0.278
[5]	$0.109L + (-0.069)$	0.068	0.269
[6]	$(-0.885)\pi + 0.464L + (-0.771)$	0.931	0.078
[7]	$(-0.762)\pi^2 + 0.419L + (-0.781)$	0.77	0.143
[8]	$(-0.82)\pi + 0.464\pi^2 + 0.512$	0.284	0.252
[9]	$(-0.398)\pi + 0.2\sigma + 0.446$	0.275	0.254
[10]	$(-0.367)\pi^2 + 0.244\sigma + 0.379$	0.229	0.262
[11]	$(-0.345)\sigma + 0.157L - 0.17$	0.119	0.28
[12]	$(-0.751)\pi + 0.37\pi^2 + 0.119\sigma + 0.495$	0.29	0.271
[13]	$(-0.873)\pi + (-0.13)\sigma + 0.477L - 0.799$	0.938	0.08
[14]	$(-0.765)\pi^2 + 0.014\sigma + 0.418L - 0.779$	0.77	0.155
[15]	$(-1.243)\pi + 0.361\pi^2 + 0.461L - 0.718$	0.947	0.074

However, removing the π parameter (eqs. [10], [11], and [14]) or the L parameter (eqs. [8], [9], [10], and [12]) greatly lowers the correlation coefficient. The results of the Hansch analysis suggest therefore that the biological activity correlates mainly with π value (lipophilic character) and L value (steric effect). Furthermore, in eq. [6], the π parameter has a negative coefficient, which means that as π value increases, activity increases. Similarly, a positive coefficient for L indicates that as the substituent increases in size, the activity decreases. This may account for the inactivity of compounds **16** and **31**. The inactivity of compounds **20**, **21**, and **22** is then due to the negative π values of these substituents. Finally, compounds **25** and **26** are inactive, possibly because of a combination of low π and high L values.

Molecular mechanics calculations

We previously reported (11) the crystal structure of compound **4**. There are two molecules (labelled A and B) in the asymmetric unit. In terms of the crystal structure, two features are of importance. The first is that while the two amide functions adopt the expected planar structure, the amide bearing the N-H has the *s-cis* conformation, whereas the amide bearing the N-*tert*-butyl group has the *s-trans* conformation. Clearly, the steric bulk of the *tert*-butyl group causes the phenyl group to be directed away. The second important feature is that the N—N bond adopts a *gauche* conformation with a dihedral angle (ϕ) of –71.8° in molecule A and –58.1° in B. The *gauche* conformation is the expected conformation for hydrazine compounds.

Since it has been suggested that the biological activity of **4** is due to its mimicry of ecdysone, we have performed calculations to fit the crystal structure of **4** on a minimized model of ecdysone using MMX. There have been a number of structure–activity relationship studies on ecdysone and its derivatives (21). Most of the studies conclude that there are three important regions, X, Y and Z, of ecdysone involved in binding interactions with the receptor (Fig. 1). The A ring fits into a pocket at the receptor site and important binding interactions take place on the β face (the X region). Particularly strong

Fig. 1. The three binding regions of ecdysone (**3**): X, Y, and Z.

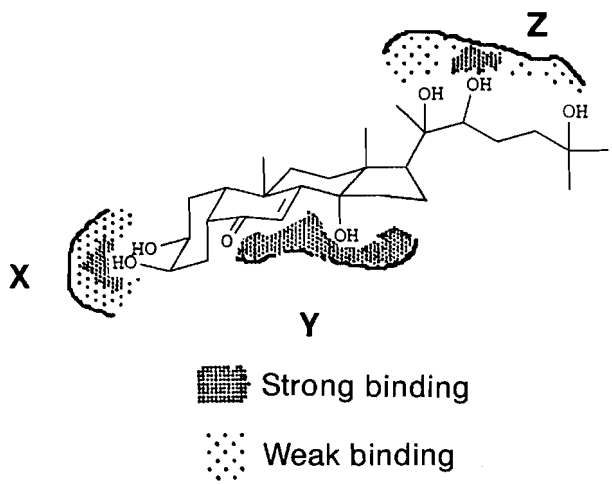

binding occurs at the Y region encompassing the 6-keto-7-ene and the 14-α-OH group in the α face. The Z region is the side chain with specific binding for the 22-OH group but less defined interaction in the other part of the side chain. Because of the difficulty of performing minimization on the side chain of ecdysone, we have performed the calculation on the model **32** (Fig. 2). Our proposal is that atoms 1, 2, 3, 4, and 5 of **4** may mimic atoms 1′, 2′, 3′, 4′ and 5′ of **32**, the strongly binding Y region of ecdysone. The energy-minimized structure of **32** was first obtained using MMX bond angles and bond length data. Certain atoms of the crystal structure of **4** (using A) were then superimposed on the minimized model **32** using the 'compare' function of the program. In the first calculation (Fig. 2), only atoms 1, 2, 3, and 5 were fitted to the corresponding atoms in **32**. It is clear that the relative average deviation of atoms in the best fit was relatively high. In the next three calculations, the *tert*-butyl carbon 4 was included. This lowered the value of average deviation of the atoms significantly. These results suggest that compound **4** can indeed mimic the strongly binding Y region of ecdysone, and that the

Fig. 2. Fitting calculations of the crystal structure **4** and ecdysone model **32** using MMX

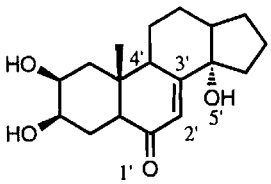

32

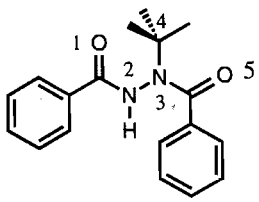

4

Trial	Atoms	Average deviation of atoms in Å
1	1-1', 2-2', 3-3', 5-5'	0.765
2	1-1', 2-2', 3-3', 4-4', 5-5'	0.745
3	1-1', 2-2', 3-3', 4-4'	0.454
4	2-2', 3-3', 4-4', 5-5'	0.085

tert-butyl group is important in fixing the conformation of **4** into the best fit in the binding region. In such a fit, the aromatic rings in **4** replace rings A and D of ecdysone. Large substituents (high *L* value) on the aromatic ring presumably interfere with the binding and thus lower the biological activity.

Conclusions

Our QSAR studies show that the biological activity of the hydrazine class of compounds can be modulated by substituents on the aromatic rings. Substituents with high π value and small *L* value lead to increase in biological activity. Molecular mechanics calculations using MMX indicate that the *tert*-butyl group is critical in locking the hydrazine **4** into an energy minimum conformation that can best fit into the strong binding Y region of ecdysone.

Acknowledgement

We thank the Natural Sciences and Engineering Research Council of Canada for financial support of this research. We also thank Dr. Larry Calhoun, Dr. Peter Penner, and Ms Heather Finlay for assistance.

References

1. D.M. Schmitt, D.G. Grimble, and J.L. Searcy. Managing the spruce budworm in Eastern North America. USDA Agriculture Handbook 620, 1984.
2. A Retnakaran, H. Lauzon, and P. Fast. Entomol. Exp. Appl. **34**, 233 (1983).
3. J. Van Rie, W.H. McGauphey, D.E. Johnson, B.D. Barnett, and H. Van Mellaert. Science, **247**, 72 (1990); C. Anderson. Nature, **355**, 661 (1992).
4. A.W. Thomas, G.M. Strunz, M. Chiasson, and T.H. Chan. Entomol. Exp. Appl. **62**, 37 (1992).
5. S.V. Ley, A.A. Denholm, and A. Wood. Nat. Prod. Rep. **10**, 109 (1993).
6. C.C. Chang and K. Nakanishi. J. Chem. Soc. Chem. Commun. 605 (1983).
7. E. Van der Eycken, A. Debruyn, J. Van der Eycken, P. Callant, and M. Vandewalle. Tetrahedron, **42**, 5385 (1986); J.K. Whitesell and D.E. Allen. J. Am. Chem. Soc. **110**, 3585 (1988); B.H. Kim, P.B. Jacobs, R.L. Elliott, and D.P. Curran. Tetrahedron, **44**, 3078 (1988).
8. A.K. Mohammad-Ali, T.H. Chan, A.W. Thomas, B. Jewett, and G.M. Strunz. Can. J. Chem. **72**, 2137 (1994).
9. J.A. Hoffman (*Editor*). Progress in ecdysone research. Biomedical Press, Elsevier/North Holland, Amsterdam. 1980.
10. K.D. Wing. Science, **241**, 467 (1988); K.D. Wing, R.A. Slawecki, and G.R. Carlson. Science, **241**, 470 (1988).
11. T.H. Chan, A. Ali, J.F. Britten, A.W. Thomas, G.M. Strunz, and A. Salonius. Can. J. Chem. **68**, 1178 (1990).
12. G.T. Harvey. Can Entomol. **106**, 353 (1974).
13. A.W. Thomas. Entomol. Exp. Appl. **52**, 205 (1989).
14. B.R. Funke. Bull. Entomol. Soc. Am. **29**, 41 (1983).
15. A.W. Thomas. Entomol. Exp. Appl. **43**, 251 (1987).
16. SAS Institute Inc. 1990. SAS/STAT User's Guide, Version 6, Volume 2. SAS Institute Inc., Cary, North Carolina.
17. A.C.T. Hsu. *In* Synthesis and chemistry of agrochemicals II, *Edited by* D.R. Baker, J.G. Fenyes, and W.K. Moberg. ACS Symp. Ser. **443**, 478 (1991).
18. C. Hansch, R.M. Muir, T. Fujita, P.P. Maloney, and C.F. Geiger. J. Am. Chem. Soc. **85**, 2817 (1963); C. Hansch and T. Fujita. J. Am. Chem. Soc. **86**, 1616 (1964); A. Leo and C. Hansch. J. Org. Chem. **36**, 1539 (1971).
19. A. Verloop, W. Hoogenstraaten, and J. Tipker. *In* Drug design. Vol. VII. *Edited by* E.J. Ariens. Academic Press, New York. 1976. p. 165; A. Verloop and J. Tipker. Pestic. Sci. **7**, 379 (1976).
20. C. Danile and F.S. Wood. Fitting equations to data. Wiley, New York. 1971.
21. C.F. Cohen, S.R. Dutky, W.E. Robbins, N.N. Serban, T.J. Shortino, J.A. Svoboda, and M.J. Thompson. Lipids, **10**, 615 (1975); F. Sorm. *In* Insect hormones and bioanalogues. *Edited by* K. Slama, M. Romanuk, and F. Sorm. Springer-Verlag, New York. 1974. pp. 318–320; D.H.S. Horn. The ecdysones in naturally occurring insecticides. Marcel Dekker, New York. 1971. pp. 333–459; J.A. Thomson, F.P. Imary, and D.H.S. Horn. Aust. J. Exp. Biol. Med. Sci. **48**, 321 (1970).

Can. J. Chem. Downloaded from www.nrcresearchpress.com by 65.111.164.53 on 09/08/12
For personal use only.

Reaction of γ-nonanolactone with deuterobromic acid

Alessandro Granata, Françoise Sauriol, and Arthur S. Perlin

Can. J. Chem. Downloaded from www.nrcresearchpress.com by 65.111.164.53 on 09/08/12
For personal use only.

Abstract: Series of isomeric monohaloalkanoic acids may be prepared from γ- or δ-alkanoic lactones by reaction with hydrogen halides. For example, γ-nonanolactone in 48% hydrogen bromide under reflux affords a 1:1.5:1.7:2.2:2.4 mixture of 4-, 5-, 6-, 7-, and 8-bromononanoic acids. In an examination of possible ways whereby such products are formed, it has been found that the use of 48% *deuterium* bromide leads to the introduction of up to 14 atoms of the isotope per bromoacid. According to ^{1}H, ^{2}H, and ^{13}C nuclear magnetic resonance observations, however, the major components of the isomer mixture contain 8–10 atoms of deuterium confined mainly to carbons 4–8, i.e., close to full deuteration of each of the carbons. This indicates that a prominent mechanism governing the formation of the bromoacid mixture involves repeated elimination and addition of HBr (^{2}HBr) along a strictly limited segment of the carbon chain. Initiated at the C-4 bridge of the lactone and characterized, hypothetically, by a succession of carbocation intermediates, the halogenation reactions appear to include a repetitive migration of transient alkene functions from C-4 through C-8, and an accompanying series of "zipperlike" hydride (deuteride) shifts in the inverse direction.

Key words: deuterohaloalkanoic acids, carbocation rearrangements.

Résumé : On a préparé une série d'acides monohaloalcanoïques à partir d'acides alcanoïques γ- ou δ-lactones, par réaction avec des halogénures d'acide. Par exemple, la γ-nonalactone soumise à un reflux dans de l'acide bromhydrique à 48% fournit un mélange 1 : 1,5 : 1,7 : 2,2 : 2,4 des acides 4-, 5-, 6-, 7- ou 8-bromononanoïques. Dans une évaluation des diverses voies permettant la formation de ces produits, on a trouvé que l'utilisation de DBr à 48% conduit à l'introduction d'un maximum de 14 atomes de l'isotope par molécule d'acide bromhydrique. Toutefois, en se basant sur les spectres RMN du ^{1}H, ^{2}H et ^{13}C, les composants majeurs du mélange d'isomère contiennent de 8 à 10 atomes de deutérium confinés principalement aux carbones 4–8, c'est-à-dire une deutération pratiquement complète de chacun de ces carbones. Ce résultat indique que le mécanisme prédominant dans la formation du mélange des acides bromés implique des éliminations et additions successives de HBr (^{2}HBr) sur une section strictement limitée de la chaîne carbonée. Initiées au pont C-4 de la lactone et caractérisées d'une façon hypothétique par une succession d'intermédiaires carbocationiques, les réactions d'halogénation semblent inclure un migration répétée des fonctions alcènes transitoires de C-4 à C-8 et une série de transferts d'hydrure (deutérure) comme une «fermeture éclair» en direction inverse.

Mots clés : acides deutérohaloalcanoïques, transpositions carbocationiques.

[Traduit par la rédaction]

Introduction

The motive for this report was an unexpected result obtained (1) on reexamining the classical Kiliani reduction of sugar lactones by hydriodic acid. It was found that the reaction of 57% hydriodic acid with aldono-1,4-lactones having from 5 to 8 carbon atoms gave not only the corresponding γ-alkanolactones anticipated, but also a variety of monoiodoalkanoic acids, which had not been reported earlier. These acids were probably secondary products formed from the alkanolactones in the reaction mixture, because when the pure C_5 to C_8 alkanolactones themselves were reacted with hydriodic acid, the same acids were produced. As well, higher homologs of the monoiodoacids were obtained (2) with lactones in which the chain lengths ranged through C_{18}. Then, by using 48% hydrobromic acid and 37% hydrochloric acid, in place of the hydriodic acid, analogous groups of monobromo and monochloro acids, respectively, were prepared (2).

In effect, our initial interest in the reducing properties of hydriodic acid on sugars and derivatives has been expanded to include unexpectedly complex reactions of aliphatic lactones with hydrogen halides.

An unusual feature of these latter reactions is the fact that the lactones having from 6 to 12 carbon atoms yield mixtures of monohalo acids in which each position, from C-4 to the penultimate carbon atom, is halogenated (1, 2). For example, in equilibrated reactions of ~4 h with 48% hydrobromic acid, γ-hexanolactone affords a 1:3.2 mixture of 4- and 5-bromohexanoic acids, whereas the C_{12} homolog gives a mixture of 4-, 5-, 6-, 7-, 8-, 9-, 10-, and 11-bromododecanoic acids in a ratio of 1:1.4:1.7:1.5:1.9:1.9:2.6:2.2. By contrast, the C_{14} and C_{16} lactones are restricted to the formation of only the 4- and

Received September 26, 1994.

A. Granata, F. Sauriol, and A.S. Perlin.[1] Department of Chemistry, McGill University, Montreal, QC H3A 2A7, Canada.

[1] Author to whom correspondence may be addressed. Telephone: (514) 393-6188. Fax: (514) 398-3797.

Can. J. Chem. Downloaded from www.nrcresearchpress.com by 65.111.164.53 on 09/08/12
For personal use only.

5-monobromo acids, in a ratio of 1:0.1, and the C_{18} lactone undergoes ring opening with virtually no accompanying isomerization, to give 4-bromooctadecanoic acid. Analogous results have been obtained in parallel reactions with 57% hydriodic acid (1, 2).

Overall, these reactions offer a previously unrecognized route to a large number of monohalo-*n*-alkanoic acids, very few of which have been described elsewhere, although their synthetic usefulness will be qualified by the ease with which individual components of the mixtures can be isolated. Of course, there is also a potential for converting the acids into equally novel hydroxy, amino, etc., alkanoic acids, and for the preparation of other series of new compounds from appropriate branched-alkyl and alicyclic lactones.

The fact that so many positional isomers can be created during these reactions, regiospecifically for sites between the lactone bridge and an often-remote penultimate carbon atom, and yet strongly dependent upon chain length, appears to have little precedence in aliphatic chemistry. As a supplement to our earlier comments on these relatively unique observations (1, 2), we offer here some new proposals as to how characteristics of this kind arise.

Results and discussion

Formation of positional isomers of bromononanoic acid in hydrobromic and deuterobromic acid

In each instance, the 4-bromo isomer likely arises through a nucleophilic displacement accompanied by opening of the γ-lactone ring (**1** → **2**). The introduction of halogen at higher positions requires other routes, and we assume that these involve carbocation intermediates. For example, if the formation of a C-4 carbocation (**3**) were to be followed by a transfer of the charge to C-5 via a 1,2-hydride shift (**3** → **4**) and also to higher positions by a succession of 1,2-shifts (or, perhaps, 1,3-, 1,4-, etc. shifts) then the 5-bromoacid (**5**), 6-bromo isomer, etc. would appear in admixture. Alternatively, a thermal loss of HBr from **2**, to give a 4-alkenoic acid (**6**), and then hydrobromination (**6** → **4** → **5**), could also afford the 5-bromoacid (as well as **2**) and, by an analogous sequence of steps, a 5-alkenoic acid (**7**) and a 6-bromoalkanoic acid (**8**). That is, one pathway entails the stepwise migration of positive charge from C-4 to, in most instances, the penultimate carbon, whereas the other amounts to a progression of alkene rearrangements along the same segment of the carboxylic acid chain.

Another way in which bromine may be introduced at several different positions is suggested by the fact (1, 2) that γ and δ-*n*-alkanolactones are converted by HBr (or HI) into equivalent mixtures of isomeric haloacids (e.g., γ- and δ-undecanolactones; see Table 3, ref. 1). Rearrangement of a γ-lactone (**1**) into a δ-lactone (**9**) via intermediates **3** and **4** would give a 5-bromoacid (**5**), and larger-ring lactones, assumed to be generated fleetingly at the elevated temperature of these reactions, also would be rapidly converted into correspondingly higher-numbered halogenated acids. In this context, it is worth noting that the presence of a few percent of δ-lactone among the reaction products of its γ-analog is implied by the observation of appropriate, minor, ^{13}CO signals (e.g., at δ 176 in Fig. 5; see later).

Evidence presented here shows that the addition of HBr to a succession of alkene intermediates (e.g., **6** → **5**, **7** → **8**, etc.) is a prominent event in the formation of the bromoalkanoic

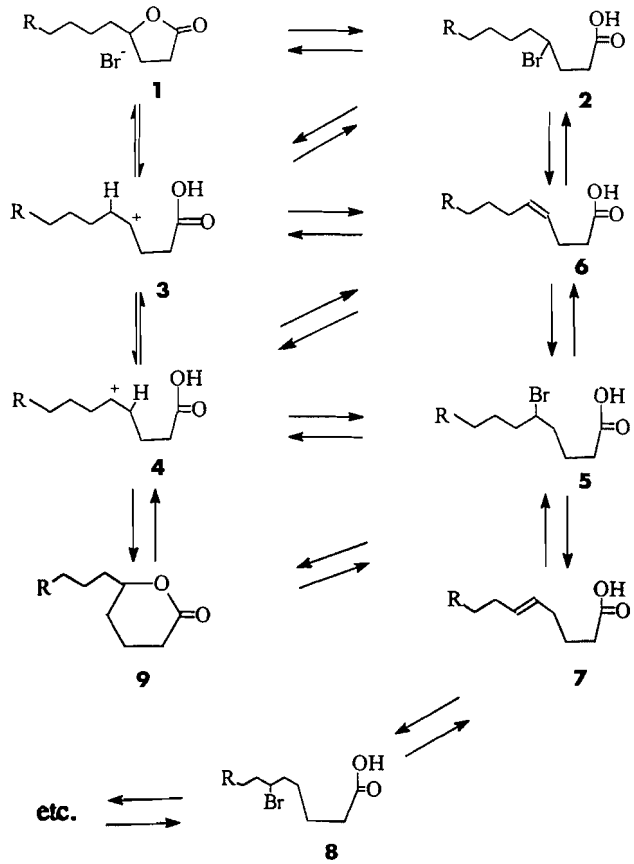

acids. It was obtained by examining the reaction of deuterobromic acid with γ-nonanolactone (**1**, R = CH_3), as a representative of the series. Earlier, we reported (2) that this C_9 lactone, in 48% HBr under reflux for 4 h, gave an equilibrium mixture of 4-, 5-, -6-, 7-, and 8-bromononanoic acids in a ratio of 1:1.5:1.7:2.2:2.4, based on the integrated signals of the Br-substituted carbons. If, in the present study, the latter were to be deuterated, their integrals might be unreliable. Consequently, signals of the carboxyl ^{13}C nuclei (see Fig. 1A) were selected instead, as in our examination (2) of iodoalkanoic acid mixtures for which the methinyl ^{13}C peaks were found unsuitable. Based on evidence (2) that the chemical shifts of the ^{13}CO signals increase in sequence with the position of the bromine atom, the values represented by Fig. 1B amount to a ratio of 1:1.5:1.8:2.6:2.7, i.e., in good agreement with that estimated for the methinyl carbons.

In contrast to the group of signals shown in Fig. 1B, the corresponding spectral region (see Fig. 1C) for the products of a 4 h reaction between γ-nonanolactone and ^{2}HBr shows that the deuterated reagent failed to bring about equilibration of the bromoacid mixture. Rather, the 4-bromo isomer was major, and although the 5-, 6-, 7-, and 8-isomers were present, their proportions decreased relative to the 4-isomer in the ratio of 1:0.74:0.66:0.50:0.54. It is worth noting, for comparative purposes, that the 4-bromoacid was preponderant also (see Fig. 1A) in HBr at only 1 h. By prolonging the reaction time with ^{2}HBr to 18 h, the composition of the product mixture (see Fig. 1D) became 1:1.1:1.4:2.6:3.3, a value similar to that already given for equilibration in hydrobromic acid. However, less of the lactone survived the reaction in the deuterated medium, as

Can. J. Chem. Downloaded from www.nrcresearchpress.com by 65.111.164.53 on 09/08/12
For personal use only.

Fig. 1. The carboxyl ^{13}C nmr signals (at 67.8 MHz) of mixtures of monobromononanoic acids formed in reactions of γ-nonanolactone with 48% hydrobromic acid under reflux (A) for 1 h and (B) for 4 h, and with 47% deuterobromic acid under reflux (C) for 4 h and (D) for 18 h. The numbered signals are those assigned to the individual isomers in which a bromine atom is attached to, for example, carbon-4 (4) or carbon-8 (8); signal L is due to the C=O group of the lactone. (The δ scale for C and D is arbitrarily expanded (× 2.7) relative to that for A and B.)

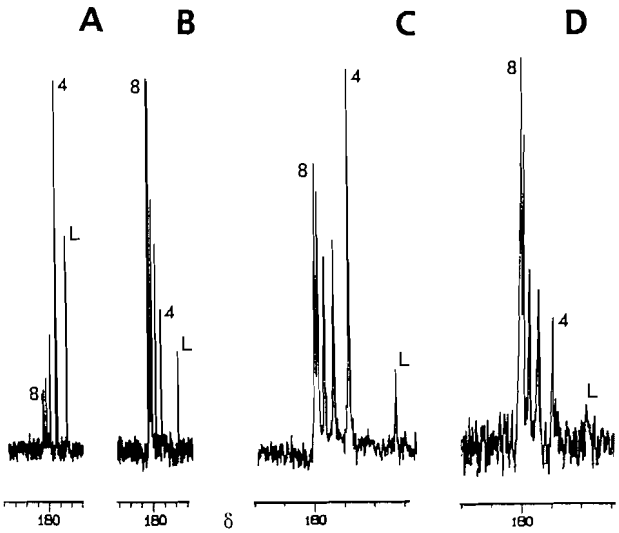

Fig. 2. High-mass regions of the chemically induced (CI) mass spectrum (NH_3 induction) of the mixture of deuterated monobromononanoic acids formed in the reaction of γ-nonanolactone with 47% deuterobromic acid under reflux for 18 h. Inset, above: corresponding response in the molecular ion region for the mixture of acids produced from the lactone in 48% hydrobromic acid.

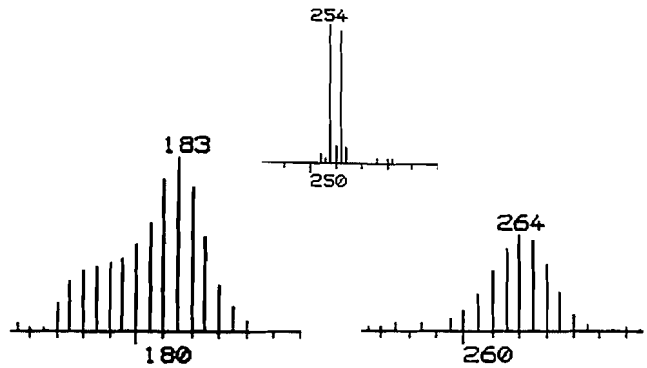

seen from a relatively far weaker ^{13}CO signal at δ 177.6 in Fig. 1D than in Fig. 1B. In the latter, the signal accounts for about 8% of the total carbonyl content (as compared with a lactone content of 12% based on ^1H integrals). By also considering the low relative intensities for lactone peaks ^1H-4 (Fig. 3A) and ^2H-4 (Fig. 3B) at δ 4.47, it is clear that the deuterated 18 h reaction mixture contained only a few percent of γ-nonanolactone.

Consistent with the slower rate of reaction in ^2HBr, and an attendant kinetic isotope effect, is the fact that the products proved to be highly deuterated. As seen from the molecular ion region of the mass spectrum of the 18 h reaction product (Fig. 2; using NH_3 as the chemical ionization reagent), the major MNH_4 ions of *m/z* 263–265 correspond to a combination of species containing ^{79}Br and 9–11 atoms of ^2H, and ^{81}Br and 7–9 atoms of ^2H. (Representing the MNH_4 ions of the nondeuterated bromononanoic acids are the inset peaks of Fig. 2 at *m/z* 254 and 256.) Slightly higher or lower levels of deuteration are represented by the lesser peaks that range from *m/z* 259 to 268. As expected, a similar distribution of peaks is found among fragments of lower mass, such as represented by the cluster about *m/z* 183 arising from the loss of bromine. The "tailing" of this group of peaks is likely due to thermal losses of hydrogen and deuterium from some of the ions.

Distribution of deuterium within the bromoacids

Information about the distribution of isotope within the individual deuterobromoacids in the mixture was obtained by ^1H and ^2H nmr spectroscopy. Major ^1H signals were found for only the H-2,2′, H-3,3′, and CH_3 protons (Fig. 3A). The latter were accounted for by three components: a tall singlet (δ 1.66), produced by the strongly deshielded CH_3 group adjacent to deuterated C-8 of the 8-bromo isomer (in place of a doublet in the spectrum of the nondeuterated compound (see Fig. 3C); a mixture of signals (δ 0.98) attributable to CH_3 groups deshielded slightly by a Br atom on C-7, and showing the effects of partial deuteration nearby; and a cluster of peaks (δ 0.85) due to the CH_3 groups of the other bromoacids. The corresponding resonances for the unlabelled product mixture are to be found in Fig. 3C.

A number of minor signals in Fig. 3A were identified with the aid of a RELAY pulse sequence. These included a group of peaks centered at δ 4.0 due to (proceeding upfield) H-8, -4, -5, -6, and -7, of the individual bromoacids, and a multiplet at δ 2.6 due to H-2,2′ of the 4-bromoacid. A small proportion of undeuterated γ-nonanolactone accounts for a weak multiplet at γ 4.45. The origin of the complex signal at δ 1.3 is the group of methylenic protons that, in the absence of the isotope (see Fig. 3C), produce a far stronger response in this region, as well as methylenic protons of residual lactone.

Complementary to the ^1H data was the ^2H nmr spectrum (see Fig. 3B). For example, the high relative intensity of the group of ^2H peaks around δ 4.0, when compared with that of the corresponding, minor, peaks in Fig. 3A, shows that the halogen-bearing carbons were almost fully deuterated. Similarly, it is evident that the majority of the isotope had been introduced at positions other than C-2, C-3, and CH_3: according to the integrated ^2H spectrum, the latter three locations accounted for only about 15% of the overall deuteration process. In view of the mass spectral evidence that the major molecular species among the monobromononanoic acids contain 8–10 ^2H atoms, most of the methylenic carbons in positions 4 to 8 must have been *doubly* deuterated. As almost full deuteration had taken place at methinyl C-8 of the 8-bromoacid, we assume that isomer would have been full deuterated as well as C-4 to C-8, inclusive, for a total of nine ^2H atoms (as in **10**). Therefore, constituting about one-third of the mixed product, it could substantially account for the major parent ions *m/z* 263 (^{79}Br) and *m/z* 265 (^{81}Br). Similarly for the 7-bromo isomer, which

$CH_3CDBrCD_2CD_2CD_2CD_2CH_2CH_2COOH$

10

$CH_3CH_2CD_2CD_2CD_2CDBrCH_2CH_2COOH$

12

$CH_3CD_2CDBrCD_2CD_2CD_2CH_2CH_2COOH$

11

$CH_2DCD_2CD_2CDBrCD_2CD_2CH_2CH_2COOH$

13

$CH_2DCD_2CDBrCD_2CD_2CD_2CH_2CH_2COOH$

14

Fig. 3. The (A) 500 MHz ^1H and (B) 76.7 MHz ^2H nmr spectra of the mixture of deuterated monobromononanoic acids formed in the reaction of γ-nonanolactone with 47% deuterobromic acid under reflux for 18 h (solvent, C^2HCl_3 and $CHCl_3$, respectively). (C) The 270 MHz ^1H nmr spectrum of the corresponding, nondeuterated, mixture obtained from a 4 h reaction with 48% hydrobromic acid. The subscript numbers refer to the positions of the bromine atom on individual isomers in the mixture.

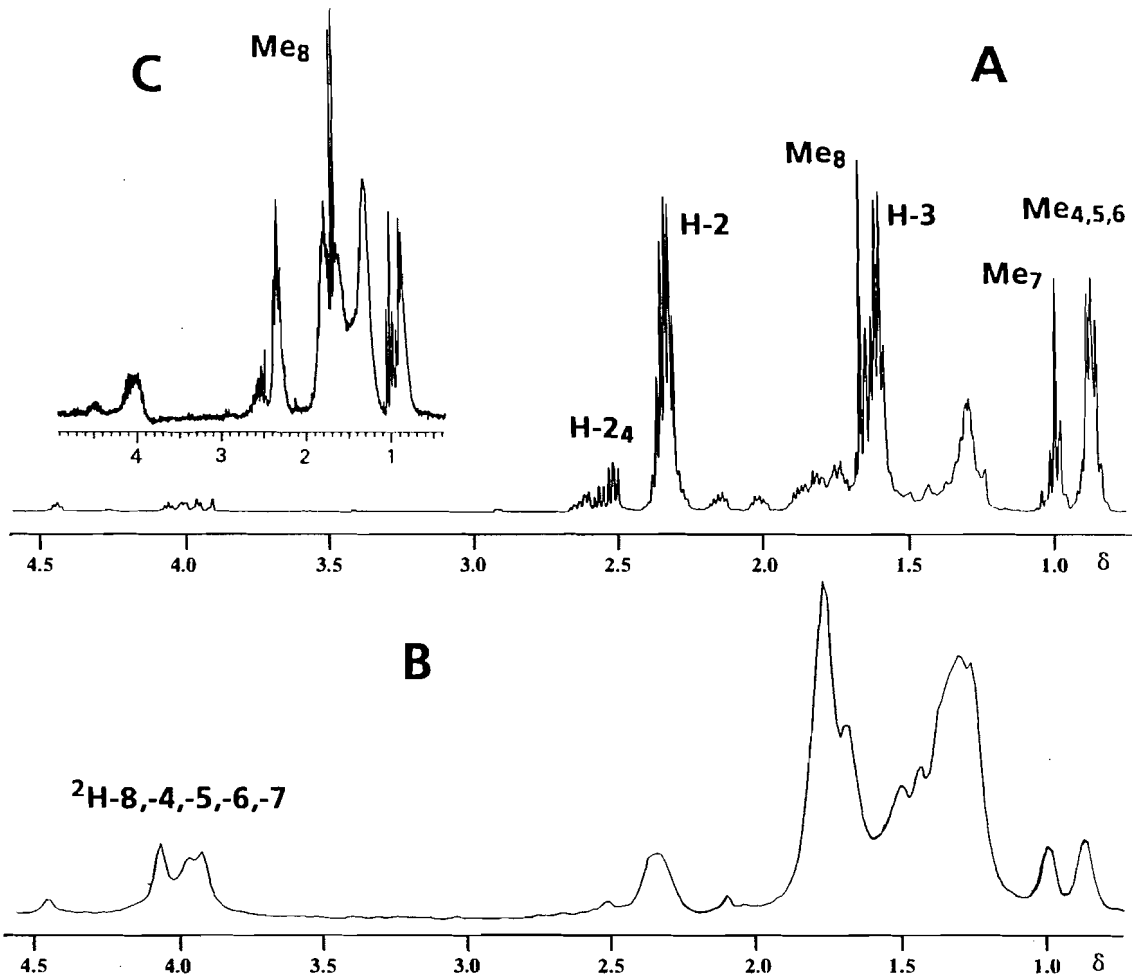

Can. J. Chem. Downloaded from www.nrcresearchpress.com by 65.111.164.53 on 09/08/12
For personal use only.

Modes of deuterium incorporation

These findings raise the possibility that, although there is a constraint under which bromine atoms are introduced sequentially from C-4 towards C-8 and become most heavily populated at that position, there operates simultaneously a stepwise introduction of ^2HBr in the opposite direction. Ultimately, therefore, all protons between C-4 and C-8 could be removed through the elimination of HBr (e.g., **5** → **6**), as equilibration of the mixture of bromoalkanoic acids takes place.

Another possibility may be considered by contrasting the present deuteration pattern with one that occurs (3) during an acid-catalysed (deuterosulfuric acid) conversion of oleic acid into γ-octadecanolactone. In that reaction, most of the isotope incorporated becomes distributed relatively uniformly over the chain segment from C-7 to C-17, presumably through a succession of rearrangements of the alkene group, followed by deuteration at each new site created. However, the methylenic carbons were mainly (if not all) *mono*deuterated. Although the

Table 1. ^{13}C chemical shifts for the monobromononanoic acids produced in the reaction between γ-nonanolactone and HBr.

Carbon no.	Position of bromine atom					Nonanoic acid
	4	5	6	7	8	
1	179.11	179.61	179.92	180.13	180.23	180.71
2	30.93	33.18	33.76	33.86	32.01	34.10
3	33.49	21.96	26.87	24.31	24.36	24.63
4	56.79	38.63	29.50 (+3.5)[b]	28.23	28.41	29.19
5	38.95	57.41	38.01	27.37	27.07	29.09
6	26.95	39.04[a]	57.65	40.85	26.29	29.04
7	31.95	27.81	38.56 (−3.5)	60.08	38.29 (−3.5)	31.78
8	23.60[a]	23.60[a]	20.61	28.68 (−4)	51.55	22.60
9	13.70	13.80	13.28	11.90	22.31	13.98

[a]Signal unaccounted for; calculated value is listed.
[b]This, and other values in parentheses, is the difference between the calculated and observed value in excess of ±2 ppm.

Can. J. Chem. Downloaded from www.nrcresearchpress.com by 65.111.164.53 on 09/08/12
For personal use only.

therefore, all protons between C-4 and C-8 could be removed through the elimination of HBr (e.g., **5** → **6**), as equilibration of the mixture of bromoalkanoic acids takes place.

Another possibility may be considered by contrasting the present deuteration pattern with one that occurs (3) during an acid-catalysed (deuterosulfuric acid) conversion of oleic acid into γ-octadecanolactone. In that reaction, most of the isotope incorporated becomes distributed relatively uniformly over the chain segment from C-7 to C-17, presumably through a succession of rearrangements of the alkene group, followed by deuteration at each new site created. However, the methylenic carbons were mainly (if not all) *mono*deuterated. Although the C_{18} alkene intermediates envisaged are analogous to such hypothetical alkenoic acids as **6** and **7**, they can appear only when the reaction sequence proceeds towards the methyl terminus (C-18), and not be recreated by a reversal of the process. We have surmised (3) that when protonation (deuteration) occurs along the carbon chain between C-7 and C-17, the positive charge generated is transferred by a succession of 1,2-hydride shifts analogous to **4** → **3** (a "zipperlike" mechanism) to reach C-4, where the overall reaction is terminated by closure of the γ-octadecanolactone ring. Hence, *double* deuteration of methylenic carbons did not take place. In the present instance, if a "zipper" were to transfer charge between, e.g., C-8 and C-4 and lead to re-formation of γ-nonanolactone, a repetition of the bromination sequence (**1** → **2** → **3**, etc.) should occur. That is, this could serve to introduce a *second* ^2H atom on carbons 4–8, as an alternative, or in addition, to a reversal of the alkene rearrangement sequence.

Although 1,2-hydride shifts in succession would appear to help accommodate the chemical changes observed, a migration of hydrogen atoms within the carbonium ions also might take place over greater distances, i.e., by means of 1,3-, 1,4-, etc. shifts. This type of alternative was proposed to account for small proportions (<1%) of 1,3-, 1,4-, etc. diols formed in the solvolysis of 1-octene oxide (4). Nevertheless, such shifts are likely to be rare in acyclic systems (5), because of the proximity requirement for orbital overlap, in contrast to their prominence in alicyclic systems that offer suitable geometry (e.g., see ref. 6).

The fact that the deuteration process, as well as the halogenation reaction, is largely contained within the confines of the C-4 to C-8 segment of the nonanoic acid chain (and, for halogenation, between C-4 and the penultimate carbon of other alkanoic acid moieties) is taken as further evidence that a carbocation-, rather than a radical-mediated type of mechanism is involved here. That the methyl group is relatively inert conforms analogously, to behaviour expected on the basis of Saytzeff's rule. Also noteworthy is the fact that both the C-2 and C-3 methylenic groups exhibited so little involvement in the reactions. This is in contrast to free radical halogenation (7) in which C-3 can be far more readily substituted than C-2, or to enol-mediated reactions (see, e.g., ref. 8) in which C-2 but not C-3 is halogenated. If, in the present instance, C-2 is strongly deactivated because of its proximity to an electronic contribution from the carboxyl group, then a substantially smaller influence on the halogenation of C-3 would be expected. Yet, only under limited circumstances, in reactions of C_4 lactones, has the formation of a 3-haloalkanoic acid been observed (1). Hence, 3-iodobutyric acid was produced from D-erythronic-1,4-lactone or γ-butyrolactone with 57% HI under reflux, although probably in both instances via 2-butenoic acid as an intermediate. It also was obtained under the same conditions from β-butyrolactone as the direct product of ring-opening displacement. However, when provision was made for a halogen atom on C-3 to undergo rearrangement along a more extended carbon chain, as with β-valerolactone, then the initial substitution product, i.e., 3-iodopentanoic acid, was detected only as an intermediate during its transformation into 4-iodopentanoic acid.

Similarly, evidence of an unexpectedly limited participation of the C-3 methylenic group in these reactions is found in its low level of deuteration, which is approximately equal to that of C-2. That is, assuming carbonium ion **3** to be a valid intermediate, the probability that **6** is formed by a loss of one H-5 is no greater than that a loss of one H-3 would give the

Fig. 4. The 125 MHz ^{13}C nmr spectral region of the methyl groups of the deuterated monobromononanoic acids represented by Figs. 3A and 3B. The numbers refer to the positions of the bromine atom on individual isomers in the mixture, and the arrows indicate the chemical shift positions for the methyl groups of the nondeuterated compounds.

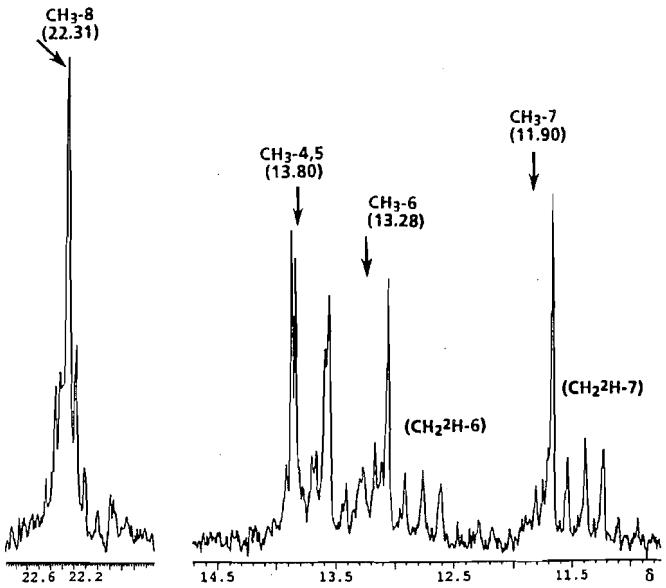

corresponding Δ^3 alkenoic acid. Deuterium could then be introduced on C-3 as readily as on C-5 whereas, in fact, only the latter becomes heavily labelled.

Conceivably, the carboxyl group also exerts a substantial effect on C-4 and beyond in the reactions of higher members of the γ- (and δ-) lactone series, because halogenation is not restricted to the initial location of the lactone bridge. Rather, the introduction of halogen atoms (bromine, chlorine, iodine) seems to be oriented away from the carboxyl terminus, as each position from C-4 (true also for δ-lactone (1, 2)) to the penultimate carbon becomes substituted. The outcome, overall, is the formation of a mixture of the maximally allowed number of isomeric haloalkanoic acids at equilibrium, commensurate (1, 2) with an overall increase in entropy.

^{13}C nuclear magnetic resonance spectra of the monobromononanoic acids

In accord with the foregoing information, by far the strongest signals in the ^{13}C nmr spectrum were those of the nondeuterated C-2, C-3, and CH_3 groups. Signals of the latter exhibited some noteworthy features due to isotope shifts and ^{13}C–^2H coupling. According to data determined for the unlabelled compounds (Table 1) the $^{13}CH_3$ peaks of the 4- and 5-bromo isomers overlap at δ 13.8, whereas those of the 6-, 7-, and 8-isomers resonate at δ 13.2, δ 11.9, and δ 22.3, respectively (see Fig. 4). Some of the corresponding signals of the deuterated bromoacids (Fig. 4) are found to have undergone upfield shifts of about 0.25 ppm, as expected for β-deuterium-isotope shifts by two deuterons (see, e.g., ref. 7). It is possible that the pair of signals centered at δ 13.85 is attributable to the CH_3 groups of those species of the 4- and 5-bromides containing intact penultimate CH_2 groups, and that the pair centered at δ 13.60 represent $CH_3C^2H_2$ structures. Alternatively, the downfield peaks could be due to a CH_3CH_2 structure in most of the 4-bromo molecules (as in **12**), and the upfield pair to a $CH_3C^2H_2$ structure in most molecules of the 5-isomer. Analogously, as the peaks of the 6- and 7-isomers are located ~0.25 ppm upfield, they also represent molecules terminated by a $CH_3C^2H_2$ grouping. As noted earlier, however, the ^1H nmr spectrum (Fig. 3A) suggests that a minor proportion of the 7-bromide molecules contain one or two protons on C-8; no corresponding ^{13}C signal is detected in Fig. 4. Also unaccounted for is the fact that the chemical shift of the $^{13}CH_3$ group in the 8-bromo isomer is found to be unaltered by the presence of the neighboring methinyl deuteron on C-8 (for a similar observation, see ref. 9).

Two triplets ($J \sim 20$ Hz) centered at δ 12.85 and δ 11.40, respectively (Fig. 4), indicate that at least a portion of the deuterium contained in methyl groups (Fig. 3B) is accounted for as $CH_2{}^2H$ in the 6- and 7-bromo isomers. As this is in accord with an α-isotope effect of a single deuteron, causing these triplets to be located 0.23–0.24 ppm upfield, the molecules represented could contain a methyl-terminal grouping of $CH_2{}^2HC^2H_2$, and at least 10 atoms of deuterium, as in **13** and **14**.

The methyl signal assignments were arrived at as part of a fuller analysis of the ^{13}C spectrum of the mixture of bromononanoic acids than made earlier (2). Presented in Table 1, the overall data are based mainly on the following considerations: (*a*) signals of the individual isomers were selected according to their integrated intensities, i.e., the strongest were taken to be those of the 8-isomer, decreasing through 7-, etc., to the weakest as those of the 4-bromide; (*b*) the chemical shifts of C-2 to C-9 were calculated for each isomer relative to the ^{13}C parameters for *n*-nonanoic acid, by assuming that the substituent effects introduced by a bromine atom (10, 11) are (in ppm): α, +28; β, +10; and γ, −3. In most instances, the agreement between the calculated and found ^{13}C chemical shifts was within ±2 ppm.

A final comment (in response to questions raised by one of the referees) is concerned with how suitable nmr spectra may be for the analysis of product composition carried out here, and this applies equally to all of the earlier analyses (1, 2). That is, the samples examined were "crude" residues, extracted from reaction mixtures that had been subjected, ostensibly, to drastic conditions. Although one might have anticipated evidence of substantial degradation and (or) by-product formation, in fact such possibilities are found to occur to an insignificant extent. This is seen from the ^{13}C nmr spectrum of the nondeuterated product described here (see Fig. 5). It shows that virtually all signals of meaningful size may be accounted for by the mixture of the lactone remaining and the five monobromo acids (the latter being identified individually through the assignments proposed in Table 1). This evidence for the absence of other than trace proportions of contaminants is representative of the results obtained consistently throughout the lactone series (1, 2) Accordingly, we conclude that the ^{13}C spectra are sufficiently free of interference as to give reliable product composition data.

Experimental

Nuclear magnetic resonance spectra were recorded with a Varian Unity 500 spectrometer operating at 500 MHz for ^1H,

Can. J. Chem. Downloaded from www.nrcresearchpress.com by 65.111.164.53 on 09/08/12
For personal use only.

Fig. 5. The 125 MHz ^{13}C nmr spectrum of the mixture of monobromononanoic acids formed in the reaction of γ-nonanolactone with 48% hydrobromic acid under reflux for 18 h (solvent, C^2HCl_3). The carbonyl signals in the region of δ 180 are analogous to those exhibited in Fig. 1B, the signal at δ 81.1 is that of C-4 of the lactone remaining, whereas the group of five between δ 60.0 and 51.5 are the $H^{13}CBr$ resonances of the 7-, 6-, 5-, 4-, and 8-bromo derivatives, respectively. Table 1 gives parameters for methylenic and methyl carbons of the individual bromo-acids, and the corresponding signals are displayed on an expanded scale in the partial spectrum (inset).

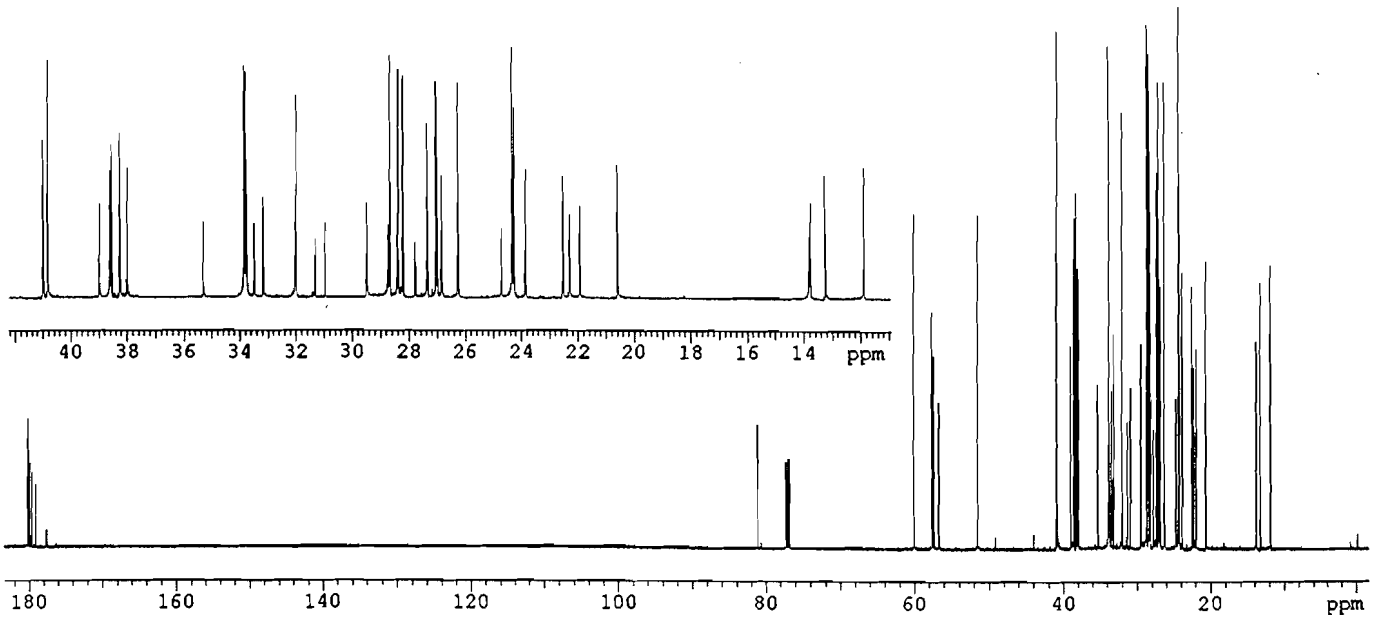

Can. J. Chem. Downloaded from www.nrcresearchpress.com by 65.111.164.53 on 09/08/12
For personal use only.

76.7 MHz for ^2H, and 125.7 MHz for ^{13}C, and (or) a Jeol CPF-270 spectrometer operating at 270 MHz for ^1H and 67.8 MHz for ^{13}C. The solvent was $CDCl_3$, and chemical shifts are given with respect to TMS. Mass spectra were recorded with a double-focusing Kratos MS25RFA mass spectrometer. Chemical ionization mass spectra were obtained with ammonia as the ionization reagent. Hydrobromic acid (48%) and deuterobromic acid (47%, >99.0% ^2H), as well as γ-nonanolactone, were obtained from Aldrich Chemical Co.

Estimation of product ratio

The ^{13}C nmr spectra were used to estimate ratios of the isomeric haloacids produced, based on the relative intensities of the resonances of the individual carbonyl carbons. These data were obtained at 67.8 MHz with a pulse angle of 40°, pulse delay of 0.80 s, and acquisition time of 1.0 s (no allowance was made for possible variations in nOe values among the ^{13}CO nuclei). Individual peak assignments were based on analyses of data obtained earlier (2) and known additivity relationships (e.g., see refs. 10, 11).

Reaction of γ-nonanolactone with HBr

A solution of the lactone (0.33 g, 2.11 mM) in HBr (48%, 5 mL) was heated under reflux for 4 h, and then cooled to room temperature. Saturated aqueous NaCl (5 mL) was added, followed by dichloromethane (50 mL). The organic layer was separated, washed with NaCl solution (2 × 5 mL), dried over anhydrous $MgSO_4$, and concentrated. A light brown oil was obtained, 0.53 g (93%), that according to ^1H and ^{13}C nmr spectra (see Figs. 3C and 1B, and Table 1) consisted of a mixture of five monobromononanoic acids, together with 8–12% of the lactone. Other preparations of these products were made with reflux periods of 1 h and 18 h, respectively (see, e.g., Fig. 1A for ^{13}C data).

Reaction of γ-nonanolactone with ^2HBr

A solution of the lactone (0.16 g, 1.0 mM) in ^2HBr (47%) was heated under reflux for 18 h, followed by work-up as above. A light brown oil was obtained, 0.25 g (~100% yield), that according to ^2H and ^{13}C nmr spectra (see Figs. 3B and 1D) and mass spectra (see Fig. 2) consisted of a mixture of five deuterated monobromononanoic acids, together with <5% of the lactone. Another preparation of these products was made with a reflux period of 4 h (see Fig. 1C for ^{13}C data).

Acknowledgements

We express our thanks to the Natural Sciences and Engineering Research Council of Canada for valuable support.

References

1. Z. Liu, A. Granata, X. Shen, and A.S. Perlin. Can. J. Chem. **70**, 2081 (1992).
2. A. Granata and A.S. Perlin. Can. J. Chem. **71**, 864 (1993).
3. A. Granata, F. Sauriol, and A.S. Perlin. Can. J. Chem. **72**, 1684 (1994).
4. A.C. Cope, L.J. Fleckenstein, S. Noon, and H.E. Petree. J. Am. Chem. Soc. **85**, 3752 (1963).
5. J.L. Fry and G.J. Karabatsos. *In* Carbonium ions. Vol. II. *Edited by* G.A. Olah and P. von R. Schleyer. Wiley, New York. 1972. pp. 555–557.

6. A.C. Cope and D.M. Gale. J. Am. Chem. Soc. **85**, 3747 (1963).
7. F. Minisci, G.P. Gardini, and F. Bertini. Can. J. Chem. **48**, 544 (1970).
8. R.P. Bell and K. Yates. J. Chem. Soc. 1927 (1962).
9. F.W. Wehrli and T. Wirthlin. Interpretation of carbon-13 NMR spectra. Heyden, London. 1978. pp. 107–110.
10. J.B. Stothers. Carbon-13 NMR spectroscopy. Academic, New York. 1972. pp. 128–137.
11. F.W. Wehrli, A.P. Marchand, and S. Wehrli. Interpretation of carbon-13 NMR spectra. 2nd ed. Heyden, London. 1983.

Can. J. Chem. Downloaded from www.nrcresearchpress.com by 65.111.164.53 on 09/08/12
For personal use only.

Dicyclohexylethyleneglycol, -diethyleneglycol, -triethyleneglycol, and related monosubstituted cyclohexanes. Conformational analysis using low-temperature ^{13}C and ^{1}H NMR spectroscopy

G.W. Buchanan, A. Moghimi, V.M. Reynolds, and K. Bourque

Abstract: Two conformations of each of the title molecules have been detected by 100 MHz ^{13}C NMR at 210 K. For the dicyclohexyl systems, the conformations are related via a single ring inversion. In each case the equatorial–axial conformer is 4.7 ± 0.4 kJ/mol less stable than the diequatorially substituted form in CD_2Cl_2 solution. For monosubstituted models, the conformational free energy ($-\Delta G°$) values of the -O-CH_2-CH_2-OCH_3, -OCH_2-CH_2-O-CH_2-CH_3, and -O-CH_2-CH_2-O-CH-$(CH_3)_2$ groups have been determined to be 5.4, 6.1, and 6.1 ± 0.2 kJ/mol, respectively. In methanol, the latter equilibria are slightly more biased towards the axially substituted conformers.

Key words: substituted ethylene glycols, conformational equilibria.

Résumé : On a détecté les deux conformations de chacune des molécules mentionnées dans le titre par RMN du ^{13}C, à 100 MHz, à 210 K. Pour les systèmes dicyclohexyles, les conformations sont reliées par le biais d'une seule inversion de cycle. Dans chaque cas, en solution dans le CD_2Cl_2, le conformère équatorial–axial est 4,7 ± 0,4 kJ/mol moins stable que le diéquatorial. Pour les modèles monosubstitués, on a déterminé que les valeurs des énergies libres conformationnelles ($-\Delta G°$) des groupes -O-CH_2-CH_2-O-CH_3, -O-CH_2-CH_2-O-CH_2-CH_3 et -O-CH_2-CH_2-O-$CH(CH_3)_2$ sont respectivement de 5,4, 6,1 et 6,1 ± 0,2 kJ/mol. Dans le méthanol, les derniers équilibres sont légèrement plus biaisés en faveur des conformères substitués d'une façon axiale.

Mots clés : éthylèneglycols substitués, équilibres conformationnelles.

[Traduit par la rédaction]

Introduction

Conformational equilibria in *cis-syn-cis*- and *cis-anti-cis*-dicyclohexano-12-crown-4-ethers (**1** and **2** below) as well as their 18-crown-6 and 24-crown-8 analogs are amenable to examination via ^{13}C NMR spectroscopy at low temperature (1–4). Generally, the detected processes are cyclohexane ring inversions, and conformational free energy differences ($-\Delta G°$) are small (i.e., <1.5 kJ/mol) due to the *cis*-1,2-disposition of the oxygenated substituents.

The dicyclohexanoethyleneglycol system **3** is a structural constituent of **1** and **2**, while the diethylene and triethyleneglycol congeners **4** and **5** are constituents of the 18-crown-6 and 24-crown-8 moieties, respectively. As such, it is of interest to determine if **3**, **4**, and **5** possess any conformational equilibria detectable by NMR at low temperature.

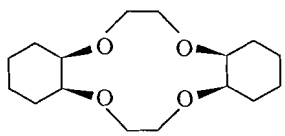

1

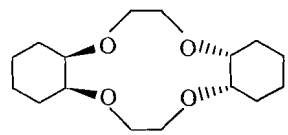

2

Results and discussion

The 100.6 MHz ^{13}C NMR spectrum of **3** at 300 K in CD_2Cl_2 is shown in Fig. 1*a*. The observation of five resonances is consistent with a situation in which all conformational interconversions are rapid on the NMR time scale. Assignments for the cyclohexyl carbons are straightforward and follow from the well-established effects of equatorial OR groups on ^{13}C chemical shifts (2). As the temperature is lowered, resonances for all carbons except C1′ show extensive broadening and finally separate into doublets of relative intensity of ca. 30:1 at 210 K as depicted in Fig. 1*b*. These integrated intensity measure-

Received September 30, 1994.

G.W. Buchanan,[1] **A. Moghimi, V.M. Reynolds, and K. Bourque.** Ottawa–Carleton Chemistry Institute, Department of Chemistry, Carleton University, 1125 Colonel By Drive, Ottawa, ON K1S 5B6, Canada.

[1] Author to whom correspondence may be addressed. Telephone: (613) 788-3840. Fax: (613) 788-3749.

Can. J. Chem. Downloaded from www.nrcresearchpress.com by 65.111.164.53 on 09/08/12
For personal use only.

Table 1. ^{13}C NMR chemical shifts (δ_C from TMS ∓ 0.1).[a]

	3	3ea[b]	3ee	4	4ea[b]	4ee	5	5ea[b]	5ee
C1	78.1	72.9	77.8	78.0	73.6	78.4	78.2	73.2	77.9
C2, 6	32.7	28.9	31.8	32.4	28.8	31.7	32.7	28.8	31.8
C3, 5	24.6	19.9	24.2	24.4	19.9	24.3	24.6	19.9	24.2
C4	26.3	25.5	25.1	26.0	26.3	25.9	26.3	25.5	25.1
C1′	68.0	N.O.[c]	66.7	67.2	67.2	67.1	67.5	N.O.[c]	66.3
C2′				71.1	70.8	70.9	71.0	N.O.[c]	69.9
C3′							71.4	N.O.[c]	70.3

[a]0.1 M in CD_2Cl_2 solution at 300 K; data for **3ea**, **3ee**, **4ea**, **4ee**, **5ea**, and **5ee** obtained at 210 K.

[b]Shifts given are for the axially substituted ring. Resonances for the equatorially substituted ring overlap with those of the ee conformer.

[c]Not observed.

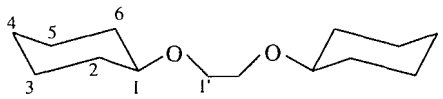

3

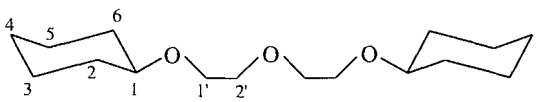

4

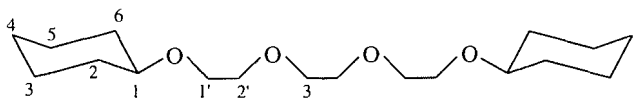

5

ments were made under conditions in which T_1 differences should be minimal, namely with 30° pulses and 5 s delays between pulses. All ^{13}C chemical shift data are summarized in Table 1.

Two possibilities exist for conformational interconversion in **3**, the first being single cyclohexane ring inversion (process I) below, or the second, a less likely double inversion as shown in process II. In the absence of peak overlap, if process I occurred, the minor conformer would be expected to exhibit 10 lines, whereas if process I is present, the symmetrical minor conformer would show only 5 ^{13}C signals.

From Fig. 1*b*, it appears that only four additional lines are evident at 210 K. Hence one is faced with two possible interpretations of the spectral findings. The first is that the minor conformer must be the symmetrical **3aa** form, since only four additional resonances are detected at low temperature. The second possibility is that the minor conformer is **3ea**, with the cyclohexyl ^{13}C resonances for the equatorially substituted ring having essentially the same chemical shifts as those of the favoured conformer **3ee**.

If process II was operative, it would suggest that there must be an unusual interaction between the two terminal cyclohexane rings that either destabilizes the expected minor conformer **3ea** or stabilizes the **3aa** conformation. Such an interaction would clearly decrease as the length of the interconnecting chain increases. Hence, for the diethyleneglycol derivative **4** and the triethyleneglycol derivative **5** one would expect to observe less of the **aa** conformers. In fact, however, the low-temperature ^{13}C intensities for the major and minor conformers of **4** and **5** are essentially identical to those for **3**, indicating that the two cyclohexane rings invert independently of each other and no such unusual stabilization of the **aa** forms is present. Hence we must conclude that the minor conformations in **3**, **4**, and **5** are the **ea** forms in accord with fundamental conformational theory.

With respect to the actual value of the conformational equi-

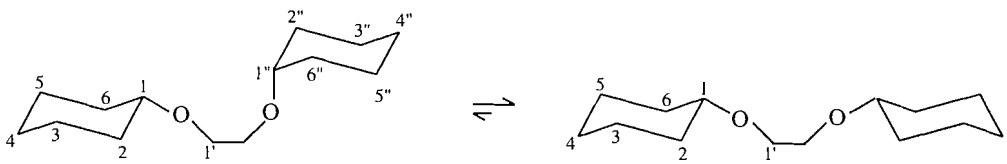

3ea Process I **3ee**

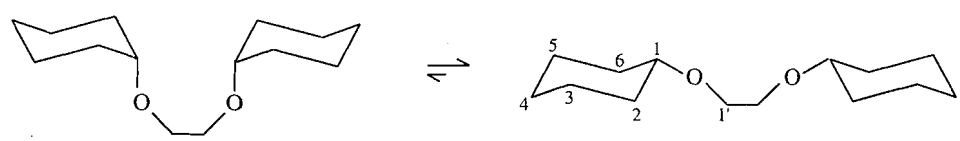

3aa Process II **3ee**

Can. J. Chem. Downloaded from www.nrcresearchpress.com by 65.111.164.53 on 09/08/12
For personal use only.

Fig. 1. (*a*) 100.6 MHz ^{13}C NMR spectrum of **3** at 300 K. (*b*) 100.6 MHz ^{13}C NMR spectrum of **3** at 210 K. C1″ etc. denotes resonance for the C1 site of the axially substituted ring of the **ea** conformer.

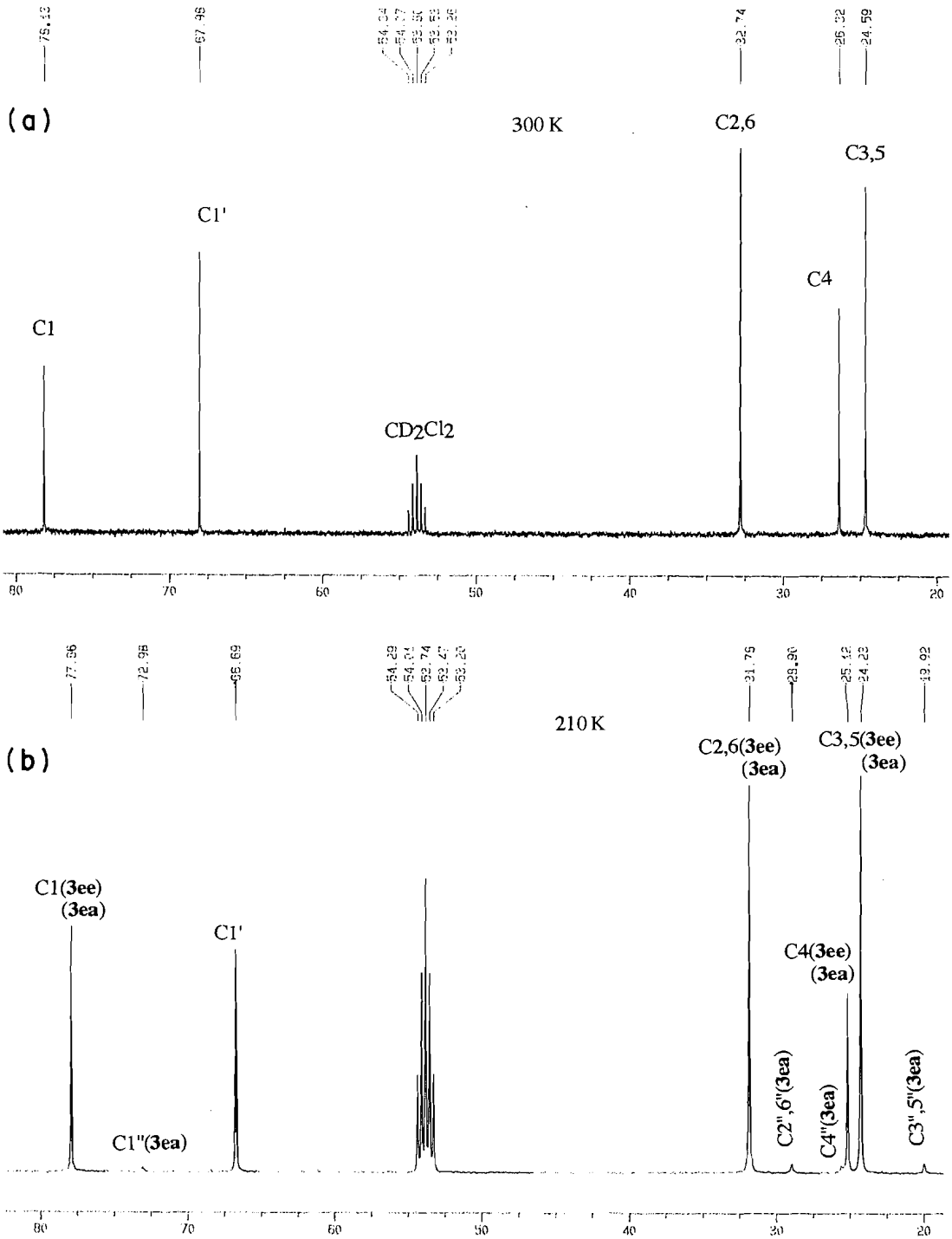

librium constants K, there are two potentially troublesome aspects of employing ^{13}C NMR for quantitative determination. First of all, variable spin lattice relaxation times (T_1) between corresponding carbons of the two conformers could influence the reliability of the results. The potential nonequivalence of the ^1H–^{13}C nuclear Overhauser enhancements (nOe) may also be a factor. Normally, one can circumvent the latter problem by recording spectra under nOe-suppressed conditions using gated decoupling methods. In the present work, however, the intensities of the resonances corresponding to the minor conformers are so low that these cannot be detected in a reasonable time period at low temperature using nOe-suppressed methods.

Hence it is desirable to measure the K values by ^1H NMR if possible, since ^1H T_1's are relatively short and there is no nOe enhancement. In the case of **3**, this was attempted. It was

Can. J. Chem. Downloaded from www.nrcresearchpress.com by 65.111.164.53 on 09/08/12
For personal use only.

Can. J. Chem. Downloaded from www.nrcresearchpress.com by 65.111.164.53 on 09/08/12
For personal use only.

Fig. 2. 400.1 MHz ^{1}H NMR spectra of **3**-d_4 at 300 K and 210 K.

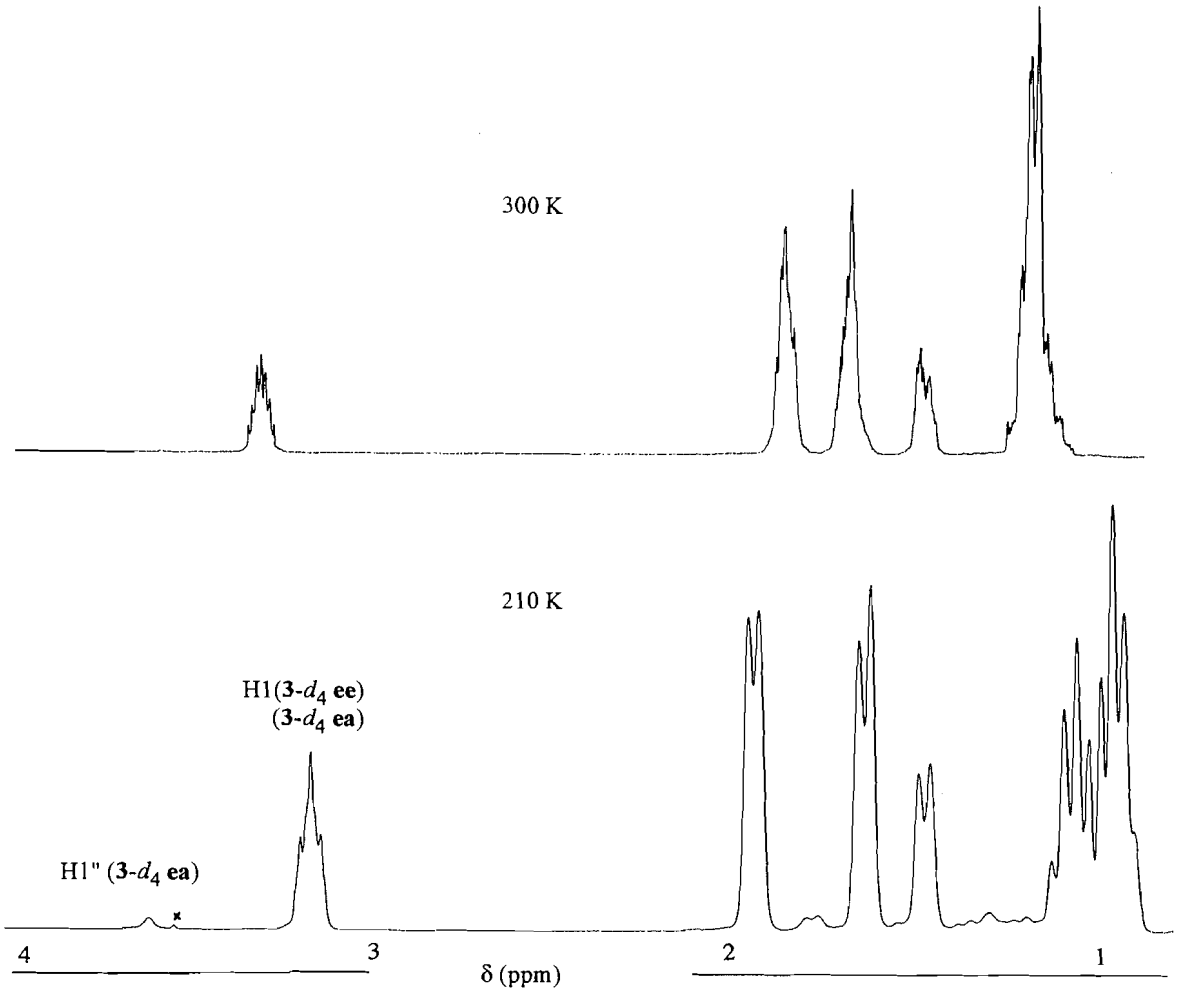

found, however, that the methine proton signal of the minor conformer overlapped with that of the protons at position 1′ at low temperature. Hence synthesis of the d_4 derivative of **3**, depicted below, was undertaken.

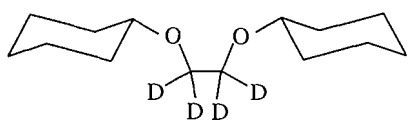

3-d_4

Results on this material (Fig. 2) yield relative intensities for the H1 proton resonances in the two conformations that are identical to those obtained by the ^{13}C NMR method, within error limits. Conformation **3ee**, with the axial methine protons, is favoured. The axial H1 proton is 0.42 ppm more shielded than its equatorial counterpart in the axially substituted ring of the minor conformer **3ea**. The enhanced vicinal coupling for the axial proton is evident from the overall line width of the more shielded signal.

Regarding the numerical value of the conformational equilibrium constant K, one must take into account the fact that the major conformation **3ee** is symmetrical, while **3ea**, the minor one, is not. Hence, although the relative peak intensities at 210 K are ca. 30, the actual value of the equilibrium constant will be essentially one half that. Using a value of 15 for this equilibrium constant at a temperature of 210 K, and employing the equation $-\Delta G^\circ = RT \ln K$, one obtains a value of 4.7 $\mp$ 0.4 kJ/mol for the free energy difference between **3ee** and **3ea**. The uncertainty of 0.4 kJ/mol is obtained from the standard deviation in the K values for 10 determinations. Within error limits, the same values are found for **4** and **5**.

The conformational interchanges in the mono-, di-, and triethyleneglycol portions of **3**, **4**, and **5**, respectively, have substantially lower barriers to interconversion than the cyclohexane ring reversals, and hence individual *gauche* and *trans* glycol conformers remain averaged on the NMR time scale at these temperatures. A recent theoretical study of preferred conformers in substituted ethyleneglycols indicates a slight preference for the *trans* conformation about the central O-C-C-O bond (5).

These $-\Delta G^\circ$ values are substantially larger than that of the $-OCH_3$ group, where a value of 3.1 kJ/mol has been determined, in CF_2Cl_2 at 180 K (6). No such data, however, have been reported for $-O-CH_2-CH_2-OR$ functionalities bonded to cyclohexane. Based on the present results for **3–5**, however, we anticipate $-\Delta G^\circ$ values for $-O-CH_2-CH_2-OR$ groups, measured in the same solvent as **3–5** (i.e., CD_2Cl_2) to be in excess of 4.7 kJ/mol, since there will be no symmetry differences

Can. J. Chem. Downloaded from www.nrcresearchpress.com by 65.111.164.53 on 09/08/12
For personal use only.

Table 2. ^{13}C chemical shifts for **6–8** (δ_C from TMS ∓ 0.1).[a]

	6[b]	**6a**[c]	**6e**[c]	**7**[b]	**7a**[c]	**7e**[c]	**8**	**8a**[c]	**8e**[c]
C1	78.1	73.9	78.6	78.1	73.9	78.6	78.2	72.9	77.7
	79.1[d]	74.7[d]	79.5[d]	79.1[d]	75.0[d]	79.8[d]	79.0[d]	74.8[d]	79.7[d]
				77.3[e]	73.6[e]	78.5[e]			
C2, 6	32.7	29.7	32.5	32.7	29.6	32.5	32.7	28.7	31.6
	33.2[d]	30.2[d]	33.1[d]	33.2[d]	30.3[d]	33.3[d]	33.1[d]	30.4[d]	33.2[c]
				32.4[e]	N.O.	32.5[e]			
C3, 5	24.5	20.6	25.0	24.6	20.6	24.9	24.6	19.8	24.1
	25.1[d]	21.2[d]	25.5[d]	25.1[d]	21.4[d]	25.7[d]	25.2[d]	21.3[d]	25.7[d]
				24.3[e]	20.9[e]	25.3[e]			
C4	26.3	26.3	25.9	26.3	26.3	25.9	26.3	25.4	25.0
	26.9[d]	26.9[d]	26.5[d]	26.9[d]	27.1[d]	26.7[d]	26.8[d]	27.0[d]	26.6[d]
				26.5[e]	26.7[e]	26.2[e]			
C1′	67.4	N.O.	67.1	67.6	N.O.	67.2	67.9[f]	N.O.	66.5
	68.1[d]	N.O.	67.8[d]	68.3[d]	N.O.	68.1[d]	68.8[d]	N.O.	68.6[d]
				67.4[e]	N.O.	66.9[e]			
C2′	72.8	N.O.	72.3	70.7	N.O.	70.7	68.2[f]	N.O.	67.0
	73.1[d]	N.O.	72.7[d]	71.3[d]	71.4[d]	71.2[d]	69.0[d]	N.O.	68.9[d]
				70.5[e]	N.O.	70.3[e]			
C3′	58.9	N.O.	59.2	66.8	N.O.	66.8	72.1	N.O.	71.1
	59.1[d]	N.O.	58.9[d]	67.5[d]	N.O.	67.5[d]	73.9[d]	N.O.	73.0[d]
				66.5[e]	N.O.	66.7[e]			
C4′				15.4	N.O.	15.6	22.3	N.O.	21.1
				15.5[d]	N.O.	15.6[d]	22.1[d]	N.O.	22.2[d]
				15.6[e]	N.O.	15.9[e]			

[a]0.1 M in CD_2Cl_2 unless otherwise indicated.
[b]At 300 K.
[c]At 210 K.
[d]0.1 M in CD_3OD.
[e]0.1 M in CS_2.
[f]Assignments may be interchanged.

between conformers of the monosubstituted cyclohexyl systems and hence no significant entropy differences between major and minor conformers. To examine such equilibria, we have undertaken the study of materials **6**, **7**, and **8** depicted below, initially in CD_2Cl_2, but subsequently also in CH_3OD. For **7**, one ^{13}C NMR measurement in CS_2 was also carried out for comparison.

^{13}C chemical shifts for **6–8** are presented in Table 2. Distinction between the resonances for C1′ and C3′ of **7** was made on the basis of COSY and HETCOR experiments. Due to peak overlap at low temperature, ^1H NMR cannot be employed to determine the conformational equilibrium constants in these materials. The integrated intensities for the cyclohexyl carbons of the individual conformers at 210 K can be used, however, for this purpose. In CD_2Cl_2 the K values for **6**, **7**, and **8** are 22.6 ∓ 2.4, 33.5 ∓ 3.8, and 32.6 ∓ 2.1, respectively. These translate into $-\Delta G°$ values of 5.4 ∓ 0.2, 6.1 ∓ 0.2, and 6.1 ∓ 0.2 kJ/mol for **6**, **7**, and **8**, respectively.

Hence it is clear that the -O-CH_2-CH_2-OR groups of **6**, **7**, and **8** are all substantially larger than the -O-CH_3 function, and that **7** and **8** possess essentially equal populations of their respective axial conformers.

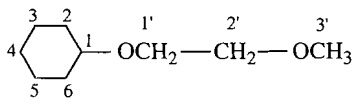

6

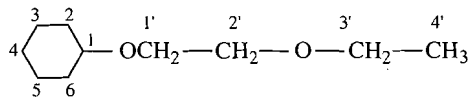

7

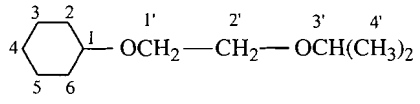

8

These findings also support the interpretation of a single ring inversion as the observed process in **3–5**. Since either of the cyclohexane rings of **3–5** can invert to form the **ea** conformer, this means that the **ea** conformers have an additional entropy of mixing of R ln 2. At 210 K, this translates into a

Can. J. Chem. Downloaded from www.nrcresearchpress.com by 65.111.164.53 on 09/08/12
For personal use only.

$T\Delta S$ term of 1.2 kJ/mol. This, combined with the $-\Delta G°$ value of 4.7 kJ/mol observed for each of **3–5** in CD_2Cl_2 solution, leads to the prediction of $-\Delta G°$ values of 5.9 kJ/mol for an $-OCH_2-CH_2-OR$ moiety, in reasonable agreement with the results obtained for **6–8**.

There appear to be rather few examples in the literature where equilibria of this type involving two cyclohexyl rings have been examined. One recent case (7), however, involves the ditelluride shown below, in which evidence is presented for a single ring inversion, and the $-\Delta G°$ value is ca. 4.2 kJ/mol in $CDCl_3$ solution.

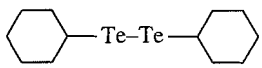

There are significant solvent influences on the conformational preferences of **6–8**. In 0.1 M methanol-*d*, the $-\Delta G°$ values decrease to 4.1, 4.2, and 4.5 ± 0.2 kJ/mol for **6**, **7**, and **8**, respectively, while in CS_2, the value for **7** is 4.6 ± 0.2 kJ/mol. For polar substituents capable of hydrogen bonding with the solvent, one would expect that methanol would lead to an increase in the preference for the equatorial conformer, in contrast to what is observed in these cases. The situation for **6–8** is made more complicated, however, by the presence of the relatively long substituent chain of atoms with two oxygen donor sites for hydrogen bonding.

(i) Spectra

^{13}C NMR spectra with ^1H noise decoupling were recorded at 100.6 MHz using a Bruker AMX-400 instrument. Samples were 0.1 M in CD_2CI_2 contained in 5 mm o.d. tubes. A 30° (4 μs) observe pulse was used routinely, with a 5 s delay period between the pulses. Sweep widths were typically 10 kHz with 16K data points. A line broadening of 3 Hz was introduced during processing. Spectra normally represent 4000 accumulations.

The ^1H spectra were recorded at 400.1 MHz using the same instrument. Normal sweep widths were 4 kHz. Pulse widths were 5 μs (45°) with 1 s pulse interval and 32K data points.

(ii) Materials

Dicyclohexanoethyleneglycol (1,2-dicyclohexoxyethane), **3**, was prepared by hydrogenation of the commercially available 1,2-diphenoxyethane (Aldrich Chemical Company). To 40 mL of absolute ethanol containing 100 mg rhodium-on-alumina catalyst, was added 1,2-diphenoxyethane (2.0 g, 9.3 mmol). Hydrogenation was carried out using an American Instrument Co. 50 000 psi maximum high-pressure apparatus at a pressure of 600 psi (1 psi = 6.9 kPa) and a temperature of 40°C for 20 h. The catalyst was removed by filtration to yield 2.0 g (95%) of **3**, bp 90–91°C at 0.3 Torr (1 Torr = 133.3 Pa) pressure, $n_D^{20} = 1.4699$. Anal. calcd. for $C_{14}H_{26}O_2$: C 74.28, H 11.58; found: C 74.48; H 11.49.

The d_4 derivative of **3** was synthesized starting with the commercially available ethyleneglycol-d_4 (C/D/N isotopes Inc). This was subsequently converted to its ditosylate, via reaction with tosyl chloride in anhydrous pyridine at −5°C. The ditosylate was recrystallized from ethanol to a mp of 124–126°C.

Synthesis of 1,2-diphenoxy-d_4-ethane was accomplished using the following method. Phenol (2.2 g, 20 mmol) was dissolved in 200 mL of anhydrous acetonitrile. To this solution was added 10.0 g of powdered anhydrous potassium carbonate and the solution was stirred vigorously. Subsequently, ethyleneglycol-d_4-ditosylate (2.2 g, 5.8 mmol) dissolved in a minimum volume of acetonitrile was added dropwise with stirring and the mixture was refluxed for 10 days. Following dilution with 0.1 M NaOH (300 mL), the mixture was extracted with CH_2Cl_2 (3 × 100 mL) and the organic layers dried over magnesium sulfate. Solvent removal afforded a white solid, which was recrystallized from ethanol to yield 1,2-diphenoxy-d_4-ethane (1.5 g, 97%), mp 97–98°C.

Hydrogenation to yield **3**-d_4 was carried out as described for the nondeuterated case.

Dicyclohexanodiethyleneglycol (1,5-dicyclohexoxy-3-oxapentane), **4**, was prepared via catalytic hydrogenation of 1,5-diphenoxy-3-oxapentane. The latter material was prepared as follows. A 200 mL round-bottom flask was charged with phenol (3.76 g, 0.04 mol), anhydrous THF (100 mL), and a 57% suspension of sodium hydride (0.84 g, 0.02 mol). This mixture was stirred for 15 min at room temperature. Subsequently, 1,5-dichloro-3-oxapentane (Aldrich Chemical Co.) (1.43 g, 0.01 mol) was added with stirring and the mixture was refluxed for 3 days. Upon cooling, the mixture was filtered and the solvent removed by evaporation at reduced pressure. The residue was dissolved in 100 mL of CH_2Cl_2 and treated with 5% NaOH (3 × 50 mL). The yellowish crude product was purified by column chromatography on silica gel (grade 60, 230–400 mesh) using CH_2Cl_2 as eluent, to yield 2.06 g (80% yield) of 1,5-diphenoxy-3-oxapentane, mp 65–66°C (lit. (8) mp 66°C).

For the hydrogenation, 1,5-diphenoxy-3-oxapentane (1.29 g, 5.0 mmol) was dissolved in 40 mL of methanol. Acetic acid (0.5 mL) and rhodium-on-alumina catalyst (0.3 g) were added to the solution and hydrogenation was performed at 40°C using a pressure of 600 psi for 8 h. Following filtration, the solvent was removed at reduced pressure and the crude product was dissolved in 100 mL of CH_2Cl_2 and washed with saturated NaCl (2 × 10 mL) and water (20 mL). After drying over sodium sulfate and solvent removal, the resultant oil was purified by column chromatography to yield 1.2 g (88%) of 1,5-dicyclohexoxy-3-oxapentane **4**. Anal. calcd. for $C_{16}H_{30}O_3$: C 71.07, H 11.18; found: C 70.39, H 10.87.

1,8-Dicyclohexoxy-3,6-dioxaoctane, **5**, was prepared by hydrogenation of the diphenyl precursor. The latter molecule, 1,8-diphenoxy-3,6-dioxaoctane, was prepared as follows. Phenol (4.0 g, 0.04 mol) was dissolved in 250 mL of anhydrous acetonitrile and powdered potassium carbonate (8.0 g) was added. Subsequently, 1,2-bis(2-chloroethoxy)ethane (Aldrich) (2.7 g, 0.015 mol) dissolved in 50 mL of anhydrous acetonitrile was added dropwise with stirring and the reaction mixture was refluxed for 12 days. Following dilution with 0.1 M NaOH (400 mL), the organic product was extracted with CH_2Cl_2 (3 × 150 mL) and dried over magnesium sulfate. The brown oil resulting from solvent removal was purified by flash chromatography using a 1:1 mixture of ethyl acetate and dichloromethane to give a white solid. Recrystallization from ethanol afforded 1,8-diphenoxy-3,6-dioxaoctane, mp 42–43°C, in 87% yield.

Hydrogenation was carried out by methods analogous to those used for **3** and **4** to give **5** in 90% yield. Purification was accomplished via bulb-to-bulb distillation at an oven temper-

ature of 150°C and 0.3 Torr pressure to yield **5** as a colourless oil, $n_D^{20} = 1.4693$. Anal. calcd. for $C_{18}H_{34}O_4$: C 68.75, H 10.89; found: C 68.56, H 11.01.

Compound **6** was prepared according to the following procedure. Phenol (5.0 g, 0.053 mol) was dissolved in 200 mL of anhydrous acetonitrile. Powdered potassium carbonate (10.0 g, 0.072 mol) was added and the solution was stirred for 15 min. To this was added 2-bromoethyl methyl ether (5.0 g, 0.036 mol) dropwise with stirring and the mixture was refluxed with stirring for 2 days. After cooling, the mixture was filtered and the solvent removed in vacuo. The crude product was vacuum distilled to give 1.4 g (26%) of 1-methyl-4-phenylethylene glycol. Hydrogenation to **6** was carried out via methods analogous to those for **3**, **4**, and **5**. After vacuum distillation the yield of **6** was 90%. This material, $n_D^{20} = 1.4423$, was characterized by high-resolution mass spectrometry, *m/z*: 158.13128 for $C_9H_{18}O_2$.

The precursor to **7**, namely, 1-ethyl-4-phenylethylene glycol, was prepared as described above for the 1-methyl analog, with the exception that 2-bromoethylethyl ether was employed. Catalytic hydrogenation to **7** was accomplished in 95% yield, giving **7**, $n_D^{20} = 1.4738$, high-resolution ms, *m/z*: 172.14357 for $C_{10}H_{20}O_2$.

The precursor to **8**, namely, 1-isopropyl-4-phenyl ethylene glycol, was synthesized via the following method. NaH (2.4 g, 0.1 mol) was added slowly to reagent grade isopropanol (150 mL) and the mixture was stirred for 10 min. To this stirred mixture was added β-bromophenetole (10.0 g, 0.05 mol) and the mixture was refluxed for 2 days. The mixture was diluted with 500 mL of distilled water and extracted with CH_2Cl_2 (3 × 100 mL). The organic extracts were dried over magnesium sulfate and the solvent was removed in vacuo. The crude product was subsequently hydrogenated via methods analogous to those used for **6** and **7** to yield crude **8**. Following column chromatography on silica gel using 1:10 ether:hexane as solvent, pure **8**, $n_D^{20} = 1.4495$, was obtained in 70% overall yield. Anal. calcd. for $C_{11}H_{22}O_2$: C 70.92, H 11.90; found: C 71.02, H 11.65.

Acknowledgments

We are particularly grateful for the insightful comments of a referee and to the Natural Sciences and Engineering Research Council of Canada for continued financial support.

References

1. G.W. Buchanan, R.A. Kirby, and K. Bourque. Can. J. Chem. **67**, 449 (1989).
2. G.W. Buchanan, K. Bourque, J.W. Bovenkamp, A. Rodrigue, and R.A.B. Bannard. Tetrahedron Lett. **25**, 3963 (1984).
3. G.W. Buchanan, K. Bourque, J.W. Bovenkamp, and A. Rodrigue. Can. J. Chem. **63**, 2847 (1985).
4. G.W. Buchanan, Y. Lear, and C. Bensimon. Can. J. Chem. **70**, 1688 (1992).
5. M.A. Murcko and R.A. DiPaola. J. Am. Chem. Soc. **114**, 10010 (1992).
6. H.-J. Schneider and V. Hoppen. Tetrahedron Lett. **15**, 579 (1974).
7. H. Duddeck and A. Biallas. Magn. Reson. Chem. **32**, 303 (1994).
8. Chem. Abstr. **72**, 100 270t (1970).

Can. J. Chem. Downloaded from www.nrcresearchpress.com by 65.111.164.53 on 09/08/12
For personal use only.

Long range antiferromagnetic exchange in dinuclear copper(II) complexes containing 1,4-dicyanamidobenzene dianion bridging ligands

Linnus L. Cheruiyot, Laurence K. Thompson, J.E. Greedan, Guo Liu, and Robert J. Crutchley

Can. J. Chem. Downloaded from www.nrcresearchpress.com by 65.111.164.53 on 09/08/12
For personal use only.

Abstract: Six Cu(II) dimers, $[\{Cu(dien)\}_2(\mu\text{-dicyd})][CF_3SO_3]_2$ (**1**), $[\{Cu(dien)\}_2(\mu\text{-Me}_2\text{dicyd})][CF_3SO_3]_2$ (**2**), $[\{Cu(dien)\}_2(\mu\text{-Cl}_2\text{dicyd})][CF_3SO_3]_2$ (**3**), $[\{Cu(L)\}_2(\mu\text{-dicyd})]$ (**4**), $[\{Cu(L)\}_2(\mu\text{-Me}_2\text{dicyd})]$ (**5**), and $[\{Cu(L)\}_2(\mu\text{-Cl}_2\text{dicyd})]$ (**6**), where dicyd^{2-}, Me$_2$dicyd^{2-} and Cl$_2$dicyd^{2-} are unsubstituted, 2,5-dimethyl- and 2,5-dichloro-1,4-dicyanamidobenzene dianions, respectively, dien is diethylenetriamine, and L^- = 1,3-bis(2-pyridylimino)isoindolinato, have been synthesized and characterized by elemental analysis, IR, UV–vis, and EPR spectroscopy, and magnetic studies. Temperature-dependent magnetic susceptibility measurements of the complexes **1**–**6** from 5 to 300 K are reported. The data for **2**, **3**, **5**, and **6** have been fitted to a dimer model with a modified Bleaney–Bowers expression which derived antiferromagnetic exchange constants $-J$ = 10.6, 4.5, 5.2, and 3.0 cm^{-1}, respectively (where the Hamiltonian is of the form $\mathcal{H} = -2J\boldsymbol{S}_a\cdot\boldsymbol{S}_b$). For **4**, an approach to a maximum in χ_m with decreasing temperature gave an estimated $-J < 3.5$ cm^{-1}. Only complex **1** showed Curie–Weiss behavior. This is far weaker antiferromagnetic exchange compared to that observed for dinuclear Ru(III) complexes incorporating the dicyd^{2-} bridging ligands (J. Am. Chem Soc. **114**, 5130 (1992)) and is attributed to a symmetry and energy mismatch between Cu(II) σ^* magnetic orbitals and the π_{nb} molecular orbitals of the bridging ligand which are important for superexchange.

Key words: superexchange, copper dimer, dicyanamidobenzene.

Résumé : On a préparé six dimères du Cu(II), $[\{Cu(dien)\}_2(\mu\text{-dicyd})][CF_3SO_3]_2$ (**1**), $[\{Cu(dien)\}_2(\mu\text{-Me}_2\text{dicyd})][CF_3SO_3]_2$ (**2**), $[\{Cu(dien)\}_2(\mu\text{-Cl}_2\text{dicyd})][CF_3SO_3]_2$ (**3**), $[\{Cu(L)\}_2(\mu\text{-dicyd})]$ (**4**), $[\{Cu(L)\}_2(\mu\text{-Me}_2\text{dicyd})]$ (**5**), et $[\{Cu(L)\}_2(\mu\text{Cl}_2\text{dicyd})]$ (**6**) (dans lesquels dicyd^{2-}, Me$_2$dicyd^{2-} et Cl$_2$dicyd^{2-} sont respectivement les dianions non substitué, 2,5-diméthyl- et 2,5-dichloro-1,4-dicyanamidobenzènes, dien est la diéthylènetriamine et L^- = 1,3-bis(2-pyridylimino)isoindolinato) et on les a caractérisés par analyse élémentaire, spectroscopies IR, UV-visible et RPE ainsi que par des études magnétiques. Opérant à des températures variant de 5 à 300 K, on a mesuré la susceptibilité magnétique des six complexes (**1** à **6**); elle varie avec la température. On a ajusté les données des composés **2**, **3**, **5** et **6** pour un modèle dimère avec une expression de Bleaney–Bowers modifiée et on en a extrait leurs constantes respectives d'échange antiferromagnétique $-J$ = 10,6, 4,5, 5,2, et 3,0 cm^{-1} (dans lesquelles l'Hamiltonien est de la forme $\mathcal{H} = -2J\boldsymbol{S}_a\cdot\boldsymbol{S}_b$). Pour le composé **4**, une approche d'un maximum dans le valeur de χ_m avec une diminution de la température conduit à une valeur de $J < 3{,}5$ cm^{-1}. Le complexe **1** est le seul à présenter un comportement Curie–Weiss. Ceci correspond à un échange antiferromagnétique beaucoup plus faible que celui observé avec les complexes dinucléaires du Ru(III) contenant des coordinats dicyd^{2-} agissant comme ponts (J. Am. Chem. Soc. **114**, 5130 (1992)) et ce comportement est attribué à une symétrie et à une mauvaise adaptation entre les orbitales magnétiques σ^* du Cu(II) et les orbitales moléculaires π_{nb} du coordinat assurant le pont qui sont importantes pour le superéchange.

Mots clés : superéchange, dimère du cuivre, dicyanamidobenzène.

[Traduit par la rédaction]

Received November 2, 1994.

L.L. Cheruiyot and R.J. Crutchley.[1] Ottawa–Carleton Chemistry Institute, Carleton University, Ottawa, ON K1S 5B6, Canada.
L.K. Thompson. Department of Chemistry, Memorial University of Newfoundland, St. John's, NF A1B 3X7, Canada.
J.E. Greedan and G. Liu. The Institute for Materials Research, McMaster University, Hamilton, ON L8S 4M1, Canada.

[1] To whom correspondence may be addressed. Telephone: (613) 788-3848. Fax: (613) 788-3749, e-mail: rcrutch@ccs.carleton.ca

Can. J. Chem. Downloaded from www.nrcresearchpress.com by 65.111.164.53 on 09/08/12
For personal use only.

Introduction

The purposeful synthesis of novel magnetic or electronic solid state materials composed in part of metal ions requires a fundamental understanding of electron exchange processes at the molecular level. When the metal ions are not in direct contact, coupling is most effectively achieved by the superexchange mechanism in which the molecular orbitals of a bridging ligand provide a pathway for metal–metal interaction (1). Optimization of superexchange requires that metal orbitals be of the correct symmetry and energy to overlap strongly with a continuous and common molecular orbital of the bridging ligand (2).

We are exploring the coordination chemistry of the cyanamide anion group and in particular the properties of dinuclear complexes which incorporate the bridging ligand 1,4-dicyanamidebenzene dianion dicyd^{2-} and its substituted derivatives.

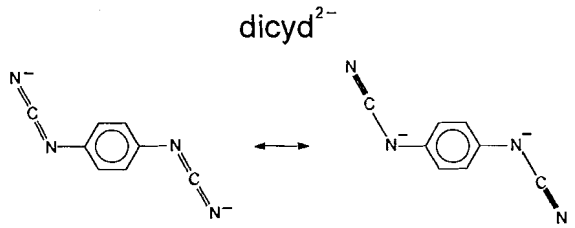

The dicyd^{2-} ligand has proven itself to be a remarkably effective medium for antiferromagnetic superexchange coupling in $[\{(NH_3)_5Ru\}_2(\mu\text{-dicyd})]^{4+}$ complexes despite the fact that the Ru(III) ions are separated by approximately 13 Å (3). Magnetic exchange coupling constants $-J$ for the complexes ranged from 96 to $\geq$ 400 cm^{-1} (where $\mathcal{H} = -2JS_a \cdot S_b$) and were suggested to arise from a continuous and energetically favorable π interaction between the magnetic πd orbitals of the Ru(III) ions and the π HOMO of the dicyd^{2-} ligand. The magnetic properties of these complexes have recently been shown to be solvent dependent (4). In strong donor solvents, antiferromagnetic exchange is dramatically weakened because of a donor–acceptor interaction between the solvent lone pairs and the hydrogens of the ammine ligands bound to Ru(III). This weakens the interaction of the Ru(III) ions with the cyanamide moieties of the bridging ligand which effectively decouples the Ru(III) ions from the superexchange pathway. In addition, the mixed-valence complexes also showed a similar solvent dependence of metal–metal coupling (4, 5).

In this study, Cu(II) dinuclear complexes have been prepared in which the Cu(II) ions are bridged by 1,4-dicyanamidobenzene dianion derivatives. A comparison between the temperature-dependent magnetic susceptibility of these complexes and their Ru(III) analogues explores the effect of the nature of the metal magnetic orbitals on the magnitude of antiferromagnetic superexchange via the dicyd^{2-} bridging ligand.

Experimental

Physical measurements

Ultraviolet–visible absorption spectra were taken on a Cary 5 spectrophotometer. The IR spectra of samples in KBr discs were obtained with a Perkin-Elmer 1600 series FTIR spectrophotometer. Temperature-dependent magnetic susceptibility measurements were performed on a Quantum Design S.Q.U.I.D. magnetometer from 5 to 300 K in a 1.0 T field. C,H, and N elemental analyses were performed by Canadian Microanalytical Services Ltd. The %Cu was determined by atomic absorption spectroscopy with a Perkin-Elmer 600 spectrophotometer. The reported average %Cu and standard deviation are the result of three determinations. The experimental setup used to perform the cyclic voltammetry experiments has already been described (6). The ferricenium/ferrocene couple with E^0 = 400 mV vs. NHE (7) was used as an internal calibrator. EPR spectra were recorded with a Bruker ESP 300 X-band spectrometer at 295 and 77 K.

Materials

All chemicals and solvents were reagent grade or better. $Cu(CF_3SO_3)_2 \cdot nH_2O$, was prepared by digesting copper metal turnings in triflic acid (Aldrich). The protonated ligand 1,4-bis(pyridylimino)isoindoline (LH) (8), the complexes Cu(L)X (X = Br$^-$ and $CF_3SO_3^-$) (9), and $[Cu(dien)(NO_3)][NO_3]$ (10) were prepared by literature methods. The syntheses of the 1,4-dicyanamidebenzene derivatives (dicydH$_2$), their tetraphenylarsonium salts ($[AsPh_4]_2$[dicyd]) (3, 11), 2,3-dichlorophenylcyanamide (2,3-Cl$_2$pcydH), and its thallium salt [T1][2,3-Cl$_2$pcyd] (12), have already been described.

Cu(II) dimer syntheses

*Preparation of $[\{Cu(dien)\}_2(\mu\text{-dicyd})][CF_3SO_3]_2$, **1***

To a solution of $Cu(CF_3SO_3)_2$ (1.15 g) and dicydH$_2$ (0.19 g) in 2-methoxyethanol was added, under an argon atmosphere, the ligand dien (0.23 g) and triethylamine (1 mL). After stirring for 4 h, the volume of the green solution was reduced to 20 mL. The concentrated reaction solution was then filtered and the filtrate placed in a freezer (–16°C) overnight, precipitating the brown microcrystalline product. The crude product was recrystallized by slow evaporation of a solution of the complex in methanol. Yield: 0.50 g (27%). Anal. calcd. for $C_{18}H_{30}N_{10}O_6F_6S_2Cu_2$: C 27.44, H 3.81, N 17.77, Cu 16.17; found: C 27.53, H 3.77, N 17.74, Cu 16.01 ± 0.22.

*Preparation of $[\{Cu(dien)\}_2(\mu\text{-}Me_2dicyd)][CF_3SO_3]_2$, **2***

The same procedure as above was followed with $Cu(CF_3SO_3)_2$ (1.04 g) and Me$_2$dicydH$_2$ (0.20 g). The crude product was recrystallized in 2-methoxyethanol by slow evaporation. Yield: 0.52 g (29%). Anal. calcd. for $C_{20}H_{34}N_{10}O_6F_6S_2Cu_2$: C 29.45, H 4.17, N 17.17, Cu, 15.58; found: C 29.38, H 3.99, H 3.99, N 16.80, Cu 15.53 ± 0.11.

*Preparation of $[\{Cu(dien)\}_2(\mu\text{-}Cl_2dicyd)][CF_3SO_3]_2$, **3***

Under an argon atmosphere $Cu(CF_3SO_3)_2$ (1.0 g) and $[AsPh_4]_2$[Cl$_2$dicyd] (1.06 g) were dissolved in acetone (100 mL). The ligand dien (0.23 g) was then added. Almost immediately, the pale green product began to precipitate from solution. After 1 h, the product was filtered off, and recrystallized from methanol by slow evaporation. Yield: 0.44 g (24%). Anal. calcd. for $C_{18}H_{28}N_{10}O_6F_6S_2Cu_2$: C 25.23, H 3.25, N 16.38, Cu 14.84; found: C 25.33, H 3.33, N 15.99, Cu 14.66 ± 0.15.

*Preparation of $[\{Cu(L)\}_2(\mu\text{-}Cl_2dicyd)]$, **6***

Degassed 1-methyl-2-pyrrolidinone (100 mL) was transferred under argon to a reaction flask containing Cu(L)(CF_3SO_3) (0.62 g) and Cl$_2$dicydH$_2$ (0.14 g). Triethylamine (0.73 g) was

Can. J. Chem. Downloaded from www.nrcresearchpress.com by 65.111.164.53 on 09/08/12
For personal use only.

then added and the solution allowed to stir for 4 h. The now green solution was filtered and the product forced out of the filtrate by the addition of water (150 mL). The resultant green precipitate was collected by filtration and washed with copious quantities of water, acetone, and finally ether. The crude product was recrystallized twice from hot 1,2-dichlorobenzene and dried in vacuo at 110°C. Yield: 0.26 g (45%). Anal. calcd. for $C_{44}H_{26}N_{14}Cl_2Cu_2$: C 55.70, H 2.76, N 20.67, Cu 13.38, found: C 55.06, H 2.78, N 20.29, Cu 13.27 ± 0.10.

Preparation of [{Cu(L)}$_2$(μ-Me$_2$dicyd)]·(1/6)(1,2-dichlorobenzene), 5

This complex was prepared in a similar manner to the Cl_2dicyd analogue except that Cu(L)Br(1.0 g) was used instead of Cu(L)(CF_3SO_3). Yield: 0.55 g (56%). Anal. calcd for $C_{47}H_{32.6}H_{14}Cl_{0.3}Cu_2$: C 60.56, H 3.50, N 21.03, Cl 1.27, Cu 13.62; found: C 59.19, H 3.43, N 21.04, Cl 1.00, Cu 13.55 ± 0.18.

Preparation of [{Cu(L)}$_2$(μ-dicyd)]·(1/6)(1,2-dichlorobenzene), 4

This complex was prepared in a similar manner to the Cl_2dicyd analogue. Yield: 0.41 g (42%). Anal. calcd. for $C_{45}H_{28.6}N_{14}Cl_{0.3}Cu_2$: C 59.76, H 3.17, N 21.69, Cu 14.05; found: C 58.50, H 3.26, N 21.95, Cu 14.31 ± 0.12.

Recrystallization of the above two complexes from 1,2-dichlorobenzene resulted in a persistent solvent impurity despite drying in a vacuum at 110°C.

Mononuclear complex syntheses

Preparation of [{Cu(dien)(2,3-Cl$_2$pcyd)][NO$_3$], 7

[Cu(dien)(NO_3)][NO_3] (0.50 g) and [Tl][2,3-Cl_2pcyd] (0.67 g) were placed in methanol and the mixture refluxed for 5 h. The blue–green reaction mixture was cooled overnight at −15°C then filtered. The filtrate was then concentrated to 30 mL and the product forced out of solution by the addition of ether. Recrystallization from 1:1 methanol/ether at −15°C, gave blue–green needles. Yield: 0.43 g (60%). Anal. calcd. for $C_{11}H_{16}N_6O_3Cl_2Cu$: C 31.87, H 3.86, N 20.26; found: C 31.75, H 3.78, N 19.88.

Preparation of [{Cu(L)(2,3-Cl$_2$pcyd)], 8

[Cu(L)(CF_3SO_3)] (0.50 g) and [Tl][2,3-Cl_2pcyd)] (0.44 g) were placed in 2-methoxyethanol and the mixture refluxed for 2 h. The hot deep green–yellow solution was filtered and the filtrate reduced to 20 mL. Cooling the solution precipitated the crude yellow product. Recrystallization by ether diffusion into 1,2-dichloroethane solution gave pale yellow needles. Yield: 0.32 g (52%). Anal. calcd. for $C_{25}H_{15}N_7Cl_2Cu$: C 54.80, H 2.74, N 17.90; found: C 54.25, H 2.73, N 17.71.

Results

Synthesis

The Cu(dien) dication complexes **1**, **2**, and **3** were prepared from the reaction of the respective 1,4-dicyanamidobenzene dianion ligand with dien and Cu(CF_3-CO_3)$_2$ in 2-methoxyethanol or acetone. These compounds have moderate solubility in polar solvents and various attempts to grow X-ray quality crystals gave microcrystalline powders.

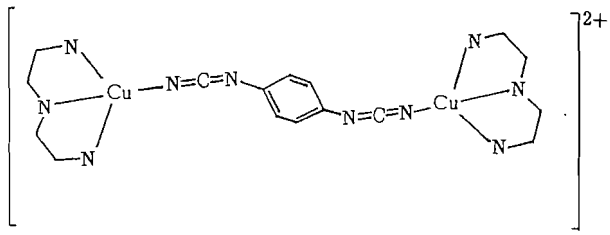

1

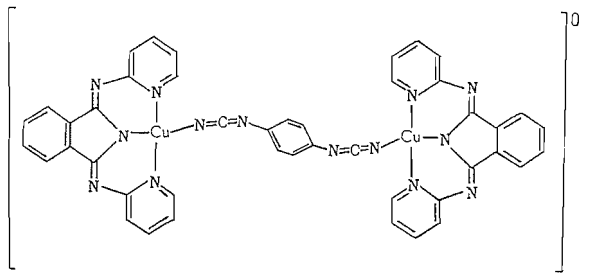

4

Table 1. Electronic absorption and infrared spectroscopic data of the dinuclear copper(II) complexes.

Complex	LMCT[a]	*d–d*[a]	ν(NCN)[b]
1[c]	435 (3.02)	631 (2.83)	2155
2[c]	455 (3.06)	622 (2.85)	2157
3[c]	452 (3.03)	637 (2.75)	2169
4[d]		690 (2.48)	2110
5[d]		689 (2.62)	2108
6[d]		692 (2.53)	2123
7[c]	403 (2.89)	610 (2.35)	2176
8[d]		693 (2.35)	2145

[a]Data in nm (log ε M^{-1} cm^{-1}).
[b]In cm^{-1}, KBr disc, all bands were sharp and intense.
[c]In methanol.
[d]In dichloroethane.

The neutral complexes **4**, **5**, and **6** were prepared by reacting a solution of Cu(L)X, (where X = CF_3SO_3 or Br), in 1-methyl-2-pyrrolidinone with 1,4-dicyanamidebenzene. In the presence of triethylamine, the coordinated dicydH_2 ligand deprotonates and this results in the precipitation of the neutral dinuclear complex. Recrystallization of these complexes gave only powders. The elemental analyses of all the complexes are consistent with their proposed stoichiometry while evidence that dicyd^{2-} is coordinated and bridges two Cu(II) ions can be found through an examination of the copper complexes' visible electronic absorption and IR spectroscopies, electrochemistry, and magnetochemistry. There are numerous crystal structures which show that a phenylcyanamide ligand coordinates to a metal ion by its nitrile nitrogen (3, 13, 14).

Electronic and infrared spectroscopy

Visible electronic absorption data and their assignments for the dinuclear copper complexes have been compiled in Table 1 and a spectrum of the complex [{Cu(dien)}$_2$(μ-dicyd)]$^{2+}$ in methanol is shown in Fig. 1. The two bands seen at wavelengths less than 400 nm are associated with the dicyd^{2-} ligand. There are two main bands in the visible spectra of the

Can. J. Chem. Downloaded from www.nrcresearchpress.com by 65.111.164.53 on 09/08/12
For personal use only.

Fig. 1. Visible absorption spectrum of $[\{Cu(dien)\}_2(\mu\text{-}Cl_2\text{-dicyd})][CF_3SO_3]_2$, 3, 2.27×10^{-4} M in methanol.

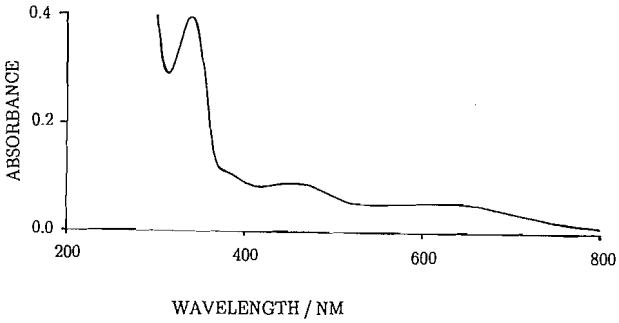

copper dien complexes. The high-energy band has been assigned to a $\pi \rightarrow \sigma^*$ LMCT transition of the Cu(II)-cyanamide chromophore while the lower energy band has the assignment metal-centered *d–d* transition, in analogy to the similar visible spectra of $[Cu(2,2'\text{-bipyridine})_2(\text{phenylcyanamide})]^+$ complexes (13). For the copper 1,3-bis-(pyridylimino)isoindolinato complexes, an intense ligand $\pi \rightarrow \pi^*$ transition obscures the LMCT transition arising from the Cu(II)-cyanamide chromophore so that only the low-energy *d–d* band can be resolved. Predictably the energy of the *d–d* band shifts to lower energies as the π donor properties of the $dicyd^{2-}$ bridging ligand increases (13). In addition, the higher energy of the *d–d* band in the Cu(dien) complexes compared to Cu(L) complexes likely reflects a greater compression to a more planar geometry in the Cu(dien) complexes (15).

The IR spectra of the tetraphenylarsonium salts of $dicyd^{2-}$, Me_2dicyd^{2-}, and Cl_2dicyd^{2-} show a strong single band assigned to ν(NCN) at 2089, 2093, and 2100 cm^{-1}, respectively (11). Upon coordination to Cu(II), ν(NCN) shifts to higher energies (Table 1) in a manner which seems largely dependent on the charge of the complex. Crystallographic and IR studies have shown that inequivalent cyanamide groups result in multiple ν(NCN) bands (3, 13). The observation of only one sharp ν(NCN) band in the IR spectra of the dinuclear copper complexes leads to the conclusion that both cyanamide groups of a respective bridging ligand are in equivalent coordination environments.

Cyclic voltammetry

Electrochemical data of the free $dicyd^{2-}$ ligands and copper complexes are given in Table 2. Representative cyclic voltammograms of the complexes **2** and **5** are shown in Figs. 2 and 3, respectively. The free $dicyd^{2-}$ ligands are easily oxidized,

$$dicyd^{2-} \overset{-e^-}{\rightleftharpoons} dicyd^{-} \overset{-e^-}{\rightleftharpoons} dicyd^{0}$$

and show two redox couples whose potential depends largely on the nature of the substituents on the phenyl ring (16). The $dicyd^{0/-}$ couples for the three derivatives show good reversibility in both 2-methoxyethanol and dichloroethane, having equivalent anodic and cathodic currents and peak-to-peak separations of 60 mV independent of scan rate (50 to 500 mV/s). On the other hand, the $dicyd^{-/2-}$ couples show evidence of irreversibility with peak-to-peak separations >100 mV.

The cyclic voltammograms of the dinuclear copper complexes (Figs. 2 and 3) were complicated by the complete irreversibility of the Cu(II/I) couple and the increased irreversibility of the $dicyd^{-/2-}$ couple when coordinated to two Cu(II) ions. The Cu(L) complexes **4**, **5**, and **6** were the best behaved showing well-defined ligand and copper waves (Fig. 3). A cyclic voltammogram of the precursor complex, $Cu(L)(CF_3SO_3)$ in dichloroethane showed only the Cu(II/I) cathodic wave at –0.82 V vs. NHE in the range of +0.8 V to –1.0 V. The complexes **4**, **5**, and **6** each showed a similar irreversible Cu(II/I) couple at approximately –0.7 V vs. NHE. The $dicyd^{0/-}$ couple for these copper complexes showed little change in potential compared to the corresponding free ligand couple; however, the $dicyd^{-/2-}$ couple was shifted anodically by approximately 300 mV and indicates the preference of Cu(II) ions for the dianion bridging ligand. This was further supported by our failed attempts to observe spectroelectro-

Table 2. Electrochemical data of free 1,4-dicyanamidobenzene dianion derivatives and copper(II) complexes.[a]

	$L^{0/-}$		$L^{-/2-}$		Cu(II/I)	
Species	MET	DCE	MET	DCE	MET	DCE
$dicyd^{2-}$	0.260	0.128	–0.147	–0.529		
Me_2dicyd^{2-}	0.209	0.030	–0.285	–0.598		
Cl_2dicyd^{2-}	0.505	0.365	0.045	–0.363		
1	0.255		[id]			
2	0.205		[id]			
3	0.492		[id]			
4		0.098		–0.227[p]		–0.691[i]
5		–0.008		–0.343[p]		–0.693[i]
6		0.310		–0.066[p]		–0.610[i]
7					–0.665[i]	
8						–0.931[i]

[a]All potentials are in volts versus NHE. Cyclic voltammetry was performed in 2-methoxyethanol (MET) or in dichloroethane (DCE) (0.1 M TBAH) at T = 25°C.
[i]Irreversible cathodic wave only.
[p]Partially reversible.
[id]Ill-defined irreversible reduction couple.

Fig. 2. Cyclic voltammogram of $[\{Cu(dien)\}_2(\mu\text{-}Me_2\text{-dicyd})][CF_3SO_3]_2$, 2, in 2-methoxyethanol.

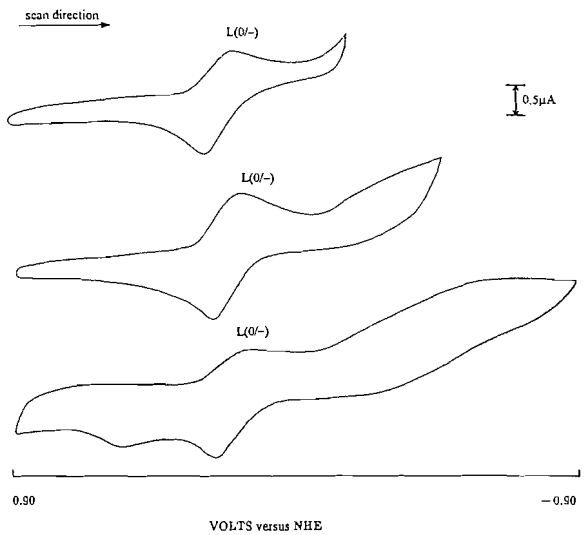

Can. J. Chem. Downloaded from www.nrcresearchpress.com by 65.111.164.53 on 09/08/12
For personal use only.

Fig. 3. Cyclic voltammogram of [{Cu(L)}$_2$(μ-Me$_2$dicyd)], 5, in dichloroethane.

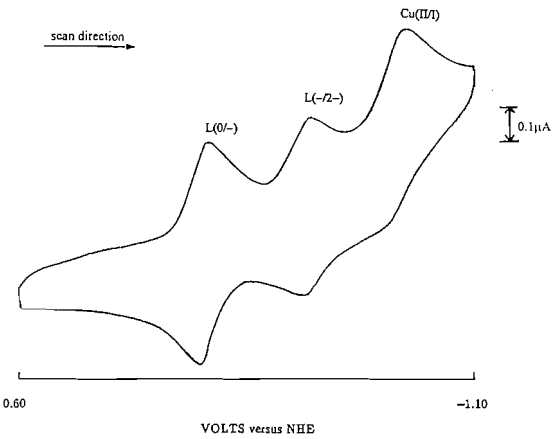

chemically the one electron oxidation product of the dinuclear copper complexes due to its rapid decomposition upon formation. The cyclic voltammograms of the Cu(dien) complexes **1** and **3** are represented by the voltammogram of **2** in Fig. 2. Only the Dicyd$^{0/-}$ couple is well defined while the dicyd$^{-/2-}$ and Cu(II/I) waves are so broadened that an exact determination of peak potential is difficult.

Magnetic susceptibility

Magnetic susceptibility measurements were made over the temperature range 5–300 K. For the complexes **2**, **3**, **4**, **5**, and **6** the variations in χ_m with temperature are consistent with weak intramolecular antiferromagnetic exchange and the data were fitted with a Bleaney–Bowers expression (17)

$$[1] \quad \chi_m = (2Ng^2\beta^2/3kT)[1 + (1/3)\exp(-2J/kT)]^{-1} + \text{TIP}$$

where g is the powder average g value, J is the antiferromagnetic exchange constant, and TIP is a correction for any temperature-independent or Van Vleck paramagnetism which is usually present in Cu(II) systems. These fitting parameters have been placed in Table 3. Figure 4 shows the data and fitting for the most strongly coupled complex, [{Cu(dien)}$_2$(μ-Me$_2$dicyd)][CF$_3$SO$_3$]$_2$ **2**. For complex **4**, the approach to a maximum in χ_m was insufficient to permit a successful analysis and so only an upper limit ($-J < 3.5$ cm^{-1}) is given. Complex **1** was the only system to show Curie–Weiss behavior in the temperature range covered.

Two of the complexes reported in Table 3 possess anomalously large χ_{TIP} values, namely, those for complexes **3** and **6**, for which susceptibilities on the order of 10^{-2} emu mol^{-1} are found. Typically, for Cu(II) complexes in distorted 6-fold or 5-fold coordination, χ_{TIP} values range up to 10^{-4} emu mol^{-1} per Cu(II) ion so values for a dimeric species could attain the values found for complexes **2**, **4**, and **5**. Possible explanations for **3** and **6** might include the presence of an impurity phase which contributes a high χ_{TIP} or that the values are intrinsic to the materials in question and arise by some unusual mechanism. Evidence against the impurity option comes from an analysis of the "high temperature" data, 60–300 K, using just a Curie–Weiss plus χ_{TIP} function for the fitting. The results for complexes **3** and **6**, respectively, are $C = 0.476$ emu K mol^{-1}, $\theta = -8.1$ K, $\chi_{TIP} = 6.8 \times 10^{-3}$ emu mol^{-1} and $C = 0.438$ emu K mol^{-1}, $\theta = -10.6$ K, $\chi_{TIP} = 1.54 \times 10^{-2}$ emu mol^{-1}. The values of the Curie constants are quite consistent with the ESR g-factor data for both compounds, $g_{av} = 3.26\ C^{1/2}$ giving $g_{av} = 2.10$–2.20. One would not expect such close agreement with the presence of a significant impurity concentration which would introduce a large error into the sample mass used to derive C from the data.

One must then consider the possibility that the observed values are intrinsic. There is no simple explanation for this. Factors which might contribute to a large χ_{TIP} include a highly distorted, low-symmetry Cu(II) site which could lead to small energy denominators in the second-order Van Vleck terms. There is evidence from the optical spectral results of such a low-symmetry environment. It is worth noting that both complexes **3** and **6** contain the same bridging ligand, the Cl$_2$dicyd^{2-}.

Table 3. Summary of parameters which gave the best fit of magnetic susceptibility using eq. [1] for the Cu(II) dimers.

Complex	$-J$(cm^{-1})	g_{av}	χ_{TIP} (emu mol)$^{-1}$
2	10.63	2.06	8.81×10^{-4}
3	4.50	2.09	1.43×10^{-2}
4	<3.5		1.95×10^{-4}
5	5.20	1.99	1.18×10^{-3}
6	3.00	2.04	3.19×10^{-2}

Fig. 4. Experimental (*) and modelled (—) temperature dependences of the molar magnetic susceptibility of [{Cu(dien)}$_2$(Me$_2$dicyd)][CF$_3$SO$_3$]$_2$, 2.

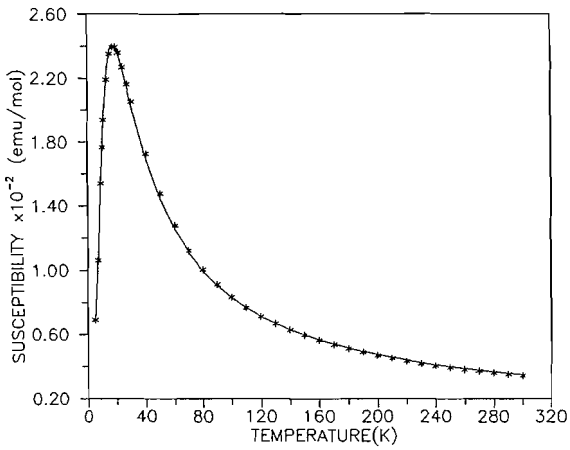

EPR spectroscopy

The X-band EPR spectra of polycrystalline, undoped, powdered samples of the dinuclear copper complexes were obtained at 295 and 77 K. The spectra appeared largely independent of temperature and except for complex **1** showed only

[2] The loss of Cu(II) hyperfine in the powder EPR spectra has been observed in other weakly coupled Cu(II) dimers and has been ascribed to intermolecular exchange broadening (18).

Can. J. Chem. Downloaded from www.nrcresearchpress.com by 65.111.164.53 on 09/08/12
For personal use only.

Table 4. EPR data of the Cu(II) monomer and dimer complexes.

Complex	DMF/powder[a]	$g_\parallel$	$g_\perp$	g_{av}	$A_{av}(\times 10^4\ cm^{-1})$
1	Powder	2.23	2.05		
	DMF			2.07	50.8
2	Powder	2.23	2.07		
	DMF			2.07	55.2
3	Powder	2.24	2.07		
	DMF			2.08	41.7
4	Powder	2.23	2.09		
5	Powder	2.21	2.08		
6	Powder	2.20	2.07		
7	Powder			2.07	
	DMF			2.13	80.6
8	Powder	2.10	2.07		

[a]DMF solutions at 295 K; powder at 77 K.

two main features corresponding to the triplet $\Delta M_s = \pm 1$ transitions associated with an axial **g** tensor.[2] Estimates of the g values at 77 K are given in Table 4. For complex **1**, no resonance was observed at 295 or 77 K. The room temperature and 77 K EPR spectra of the complexes **1**, **2**, and **3** in degassed DMF solution are very similar and representative spectra of $[\{Cu(dien)\}_2(\mu\text{-}Cl_2dicyd)]^{2+}$, **3**, are given in Fig. 5 and the data compiled in Table 4. In the presence of oxygen, these complexes decomposed in DMF solutions forming radical anion $dicyd^{-\cdot}$ and gave monomer Cu(II) EPR spectra. Complex **3** showed the greatest resistance to oxidation but even under rigorously oxygen-free conditions, a weak radical anion $dicyd^{-\cdot}$ absorption can still be seen in Fig. 5A in approximately the same position as DPPH. Seven copper hyperfine lines are expected for an exchange-coupled Cu(II) dimer. Five are clearly observed in Fig. 5A with the other two lost because of the poor resolution of spectrum. The estimated average copper hyperfine splitting $A_{av} = 41.7 \times 10^{-4}\ cm^{-1}$ is approximately one-half that of the monomer complex, $[Cu(dien)(2,3\text{-}Cl_2pcyd)][CF_3SO_3]$, **8**, for which $A_{av} = 80.6 \times 10^{-4}\ cm^{-1}$, as expected for an exchange-coupled system (17, 19). Similar results are seen in the solution EPR spectra of delocalized Cu(II)–Cu(I) mixed-valence dimers.[3] The A_{av} for complexes **1** and **2** (Table 4) are somewhat larger and this may be due to significant decomposition of the complex as evidence by the magnitude of the radical anion $dicyd^{-\cdot}$ absorption in these spectra. At 77 K (Fig. 5*B*), the copper hyperfine is lost and only a single broad resonance is observed. Only a weak radical $dicyd^{-\cdot}$ resonance was observed for the complexes **4**, **5**, and **6** in DMF at 295 at 77 K.

Other solvents were tried in an attempt to improve the resolution of the exchange-coupled spectra of complexes **1**, **2** and **3**. Dimethyl sulfoxide gave the same results as DMF solutions; however, acetonitrile and methanol:ethanol solutions gave spectra that were characteristic of monomer Cu(II) complexes. Complex decomposition could explain the monomer Cu(II) EPR spectra but the cyclic voltammetry in 2-methoxyethanol is consistent with an intact Cu(II) dimer. We speculate that solvent perturbations are decoupling Cu(II) ions in much the same manner as that observed for Ru(III) ions in $[\{(NH)_5Ru\}_2(\mu\text{-}Me_2dicyd)]^{4+}$ (4).

[3] It is possible that the partially unresolved seven-line spectrum in Fig. 5 is due to some radical charge delocalization over both copper centers, independent of any antiferromagnetic coupling as occurs in Cu(II,I) mixed-valence complexes (20). However, the observation of solid state antiferromagnetic coupling and the improved resolution of the seven-line spectrum and decreased radical $dicyd^{-\cdot}$ signal with exclusion of oxygen would seem to make this possibility unlikely for the complexes of this study.

Fig. 5. DMF solution EPR spectra of $[\{Cu(dien)\}_2(\mu\text{-}Cl_2dicyd)][CF_3SO_3]_2$ at (*a*) 295 K and (*b*) 77 K.

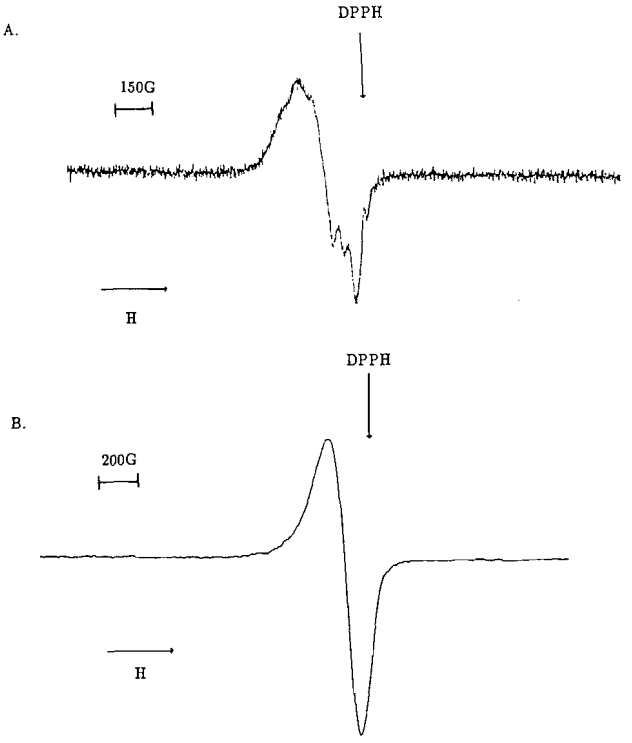

Discussion

Comparison of Cu(II) and Ru(III) dimers

It is clear from this study of the magnetic properties of Cu(II) dimers that considerable attenuation of antiferromagnetic superexchange (reduction of $-J$ by a factor of at least 40 for the Cu(II) dimers) has occurred relative to their pentaammineruthenium(III) analogues, $[\{(NH)_5Ru\}_2(\mu\text{-dicyd})]^{4+}$ (3). The application of theory gives a qualitative understanding of the origin of this difference. From perturbation theory (21, 22),

$$[2] \quad 2J = K - 2H_{ab}^2/J_{aa}\text{-}J_{ab}$$

where the ferromagnetic term K is the energy required to pair electron spins, H_{ab} is the electron exchange integral, and the difference between Coulomb repulsion integrals J_{aa} and J_{ab} represents the energy required to place both spins on the same atom. The ferromagnetic term K is expected to be small (3) and will probably not differ significantly between Ru(III) and Cu(II) dimers. The difference in energy between Coulomb

Can. J. Chem. Downloaded from www.nrcresearchpress.com by 65.111.164.53 on 09/08/12
For personal use only.

repulsion integrals J_{aa} and J_{ab} can be estimated from the difference in Ru(III/II) or Cu(II/I) PES orbital binding energies. In this way, $J_{aa} - J_{ab}$ was estimated to be 2.6 eV for the dinuclear Ru(III) complexes (3) and 1.7 eV for the dinuclear Cu(II) complexes (23). It therefore seems clear that the major contributor to the relative difference between Ru(III) and Cu(II) antiferromagnetic exchange is the magnitude of the electron exchange integral H_{ab}.

The magnitude of H_{ab} is governed by the interaction of the metal magnetic orbitals with the superexchange pathway provided by the dicyd^{2-} bridging ligand. The relative symmetry and energy of the metal orbitals compared to those of the bridging ligand therefore become determining factors. For the Ru(III) dimers, the non-bonding HOMO and SHOMO of dicyd^{2-} are of π symmetry and both can mediate antiferromagnetic superexchange between Ru(III) πd magnetic orbitals (3). For the Cu(II) dimers, the EPR powder spectra (Table 4) and the energy of the solution *d–d* band (Table 1) are consistent with a tetragonally distorted coordination sphere and a Cu(II) $d_{x^2-y^2}$ magnetic orbital of σ^* symmetry. It is only the low symmetry of the Cu(II) coordination sphere which allows for partial mixing of σ and π symmetry orbitals and results in the observation of a formally forbidden $\pi \rightarrow \sigma^*$ LMCT band (Fig. 1, Table 1) and antiferromagnetic superexchange (Figs. 4 and 5) via the π_{nb} orbitals of dicyd^{2-} in the Cu(II) dimers. Nevertheless, this mixing of σ and π orbitals is far from optimal and must decrease H_{ab} in eq [2].

The energy separation (ΔE) between Cu(II) magnetic orbitals and the π_{nb} orbitals of dicyd^{2-} should be small to maximize H_{ab}. A measure of this difference in energy is given by

$$[3] \quad \Delta E = E_{op} - \chi$$

where E_{op} is the energy of the $\pi \rightarrow \sigma^*$ LMCT band maximum and χ is a correction to compensate for the change in inner and outer coordination sphere configurations resulting from a transition into an excited vibrational level. An estimate of $\chi = 1.24$ eV was derived from the intervalence transition energy observed for $Cu^{II}Cu^{I}L(ClO_4)$, where L is a macrocyclic ligand, in acetone solution (24). Thus, for complex **2**, ΔE is calculated to be 1.48 eV. This is considerably greater than the value of 0.48 eV calculated (3) for the Ru(III) analogue $[\{(NH)_5Ru\}_2(\mu\text{-}Me_2Dicyd)]^{4+}$ and can be expected to result in far less mixing of Cu(II) *d* orbitals with the π_{nb} orbitals of the dicyd^{2-} bridging ligand. This may well be the dominant factor that explains the attenuation of antiferromagnetic superexchange in the Cu(II) dimers.

Cu(II) dimer antiferromagnetic exchange constants

No clear trend in *J* is observed in Table 3 except that the complexes incorporating Me_2dicyd^{2-} appear to have the largest antiferromagnetic *J*. Ru(III) dimers show the same dependence (3) and this is probably due to the small ΔE between metal orbitals and π molecular orbitals of Me_2dicyd^{2-}. The solid state magnetic measurements showed that only complex **1** followed Curie–Weiss behavior (Table 3). This seems inconsistent with the solution EPR study which for **1** gave an exchange-coupled spectrum (Table 4). A possible explanation is that crystal packing forces may distort the Cu(II) coordination spheres of **1** sufficiently to decouple the Cu(II) ions from superexchange via dicyd^{2-}.

Summary

A comparison between Ru(III) and Cu(II) dimers emphasizes the importance of the nature of the metal–cyanamide interaction to long-range superexchange via the dicyd^{2-} bridging ligand. For the Cu(II) dimers, a mismatch in symmetry and energy between its σ^* magnetic orbitals and the π_{nb} orbitals of dicyd^{2-} significantly attenuates antiferromagnetic superexchange when compared to their Ru(III) analogues. This study compliments the recent observation that outersphere perturbations of the Ru(III)–cyanamide bond in $[\{(NH_3)_5Ru\}_2(\mu\text{-}Me_2dicyd)]^{4+}$ can "tune" the magnitude of antiferromagnetic superexchange (4).

Acknowledgements

R.J.C. would like to thank the Natural Sciences and Engineering Research Council of Canada (NSERC) for financial support and a University Research Fellowship. J.E.G. and L.K.T. also thank NSERC for financial support. L.L.C. thanks the Canadian Bureau for International Education for a Commonwealth Scholarship. Preliminary EPR studies were performed by Dr. Keith Preston.

References

1. H.A. Kramers. Physica, **1**, 182 (1934).
2. O. Kahn. *In* Magneto–structural correlations in exchange coupled systems. *Edited by* R.D. Willet, D. Gatteshi, and O. Kahn. Reidel, Dordrecht, Holland. 1985. p. 37.
3. M.A.S. Aquino, F.L. Lee, E.J. Gabe, C. Bensimon, J.E. Greedan, and R.J. Crutchley. J. Am. Chem. Soc. **114**, 5130 (1992).
4. M.L. Naklicki and R.J. Crutchley. J. Am. Chem. Soc. **116**, 6045 (1994).
5. M.L. Naklicki and R.J. Crutchley. Inorg. Chim. Acta, **225**, 123 (1994).
6. D.R. McDonald and R.J. Crutchley. Inorg. Chem. **33**, 1899 (1994).
7. R.R. Gagne, C.A. Koval, and G.C. Lisensky. Inorg. Chem. **19**, 2855 (1980).
8. W.O. Siegl. J. Heterocycl. Chem. **18**, 1613 (1981).
9. R.R. Gagne, W.A. Maritt, D.N. Marks, and W.O. Siegl. Inorg. Chem. **20**, 3260 (1981).
10. M. Krestl, R. Allmann, G. Mandussakis, C. Bolos, and G. Nikolov. Inorg. Chim. Acta, **175**, 255 (1990).
11. M.A.S. Aquino. Ph.D. Thesis, Carleton University. Ottawa, Ont., Canada. 1991.
12. R.J. Crutchley and M.L. Naklick. Inorg. Chem. **28**, 1955 (1989).
13. R.J. Crutchley, R. Hynes, and E.J. Gabe. Inorg. Chem. **29**, 4921 (1990).
14. (a) R.J. Crutchley, K. McCaw, F.L. Lee, and E.J. Gabe. Inorg. Chem. **29**, 2576 (1990); (b) R.J. Letcher, W. Zhang, C. Bensimon, and R.J. Crutchley. Inorg. Chim. Acta, **210**, 183 (1993); (*c*) W. Zhang, C. Bensimon, and R.J. Crutchley. Inorg. Chem. **32**, 5808 (1993); (*d*) M.L. Brader, E.W. Ainscough, E.N. Baker, and A.M. Brodie, Polyhedron, **8**, 2219 (1989).
15. A.B.P. Lever. Inorganic electronic spectroscopy. 2nd ed. Elsevier Publishing Co., Amsterdam. 1984. p. 569.

16. A. Aumuller and S. Hunig. Justus Liebigs Ann. Chem. 142 (1986); 165 (1986).
17. R.L. Carlin. Magnetochemistry. Springer-Verlag, Berlin. 1986.
18. S.K. Mandal, L.K. Thompson, M.J. Newlands, E.J. Gabe, and F.L. Lee. Inorg. Chem. **29**, 3556 (1990).
19. A. Bencini and D. Gatteschi. EPR of exchange coupled systems. Springer-Verlag, Berlin. 1990.
20. (*a*) R.C. Long and D.N. Hendrickson. J. Am. Chem. Soc. **105**, 1513 (1983); (*b*) S. Mandal, L.K. Thompson, M.J. Newlands, and E.J. Gabe. Inorg. Chem. **28**, 3707 (1989).
21. J.P. Hay, J.C. Thibeault, and R.J. Hoffmann. J. Am. Chem. Soc. **97**, 4884 (1975).
22. P. Bertrand. Chem. Phys. Lett. **113**, 104 (1985).
23. T. Mori, H. Inokuchi, A. Kobayashi, R. Kato, and H. Kobayashi. Synth. Met. **27**, B237 (1988).
24. R.R. Gagne, C.A. Koval, T.J. Smith, and M.C. Cimolino. J. Am. Chem. Soc. **101**, 4571 (1979).

Can. J. Chem. Downloaded from www.nrcresearchpress.com by 65.111.164.53 on 09/08/12
For personal use only.

Étude par CNDO/2 des mouvements de rotation des unités moléculaires constituant le squelette des polymères du type : PEK, PEEK et PEEKK

S. Verot et P. Battesti

Can. J. Chem. Downloaded from www.nrcresearchpress.com by 65.111.164.53 on 09/08/12
For personal use only.

Résumé : Cette étude a pour objectif une analyse conformationnelle d'unités moléculaires telles que le diphényl éther (DPE) et la diphényl cétone (DPC) constitutives du squelette de polymères tels que PEK, PEEK et le PEEKK, par des calculs semi empiriques en CNDO/2. Deux types de modélisations ont été réalisés : une première série de calculs a été effectuée sans prendre en compte les interactions électroniques et de zones d'impénétrabilité de van der Waals et une deuxième en considérant ces diverses interactions. La conformation d'énergie minimale absolue pour le diphényl éther correspond à la position définie par les angles de torsion $(\theta_1,\theta_2) = (30°,150°)$ avec et sans interaction, et à la position $(\theta_1,\theta_2) = (90°,90°)$ pour la diphényl cétone sans prendre en compte les interactions. Dans les régions sous vitreuses et à contrainte stérique égale au sein d'une chaîne de PEK, PEEK ou PEEKK, on peut stipuler que l'unité moléculaire DPE sera sensiblement plus facilement mise en mouvement que l'unité DPC.

Mots clés : analyse conformationnelle, diphényl éther, diphényl cétone, CNDO/2, barrières de rotation.

Abstract: Diphenyl ether (DPE) and diphenyl ketone (DPK) are the molecular constituents of polymers such as PEK, poly(ether–ketone); PEEK, poly(ether–ether–ketone), and PEEKK, poly(ether–ether–ketone–ketone). A conformational analysis of DPE and DPK is examined by means of semiempirical calculations using CNDO/2 (Complete Neglect of Differential Overlap). The modelization is first run disregarding electronic interactions and steric effects, then introducing them in the calculations. We found that the absolute minimum energy conformer has torsional angles $(\theta_1,\theta_2) = (30°,150°)$ for the DPE (with and without interactions) and $(\theta_1,\theta_2) = (90°,90°)$ for the DPK (without interactions). Considering the polymer chains of PEK, PEEK, and PEEKK, the motion of DPE is expected to be easier than that of DPK in regions of local motions and for equivalent steric effects.

Key words: conformational analysis, diphenyl ether, diphenyl ketone, CNDO/2, rotational barriers.

Introduction

Cette recherche est sous-tendue par une motivation essentielle : l'analyse structurale d'unités moléculaires telles que le diphényl éther (DPE) et la diphényl cétone (DPC), qui constituent le squelette d'unités monomères de divers polymères aromatiques à chaînes linéaires tels que le PEK poly(ether ketone), le PEEK poly(ether ether ketone) et le PEEKK poly(ether ether ketone ketone) (figure 1) employés comme matrices thermoplastiques des matériaux composites technologiquement de pointe.

Depuis plus d'un demi siècle, les études structurales du DPE et de la DPC ont fait l'objet d'un nombre considérable de publications. Plusieurs géométries spatiales ont été envisagées, étudiées et analysées par diverses méthodes théoriques et expérimentales.

Nous jugeons inutile de rappeler, depuis l'origine, tous les travaux publiés sur les différentes approches du problème. Cependant, nous pouvons signaler que les auteurs admettaient, jusque dans les années 1980, quatre modèles principaux

Fig. 1. Unités moléculaires des différents polymères.

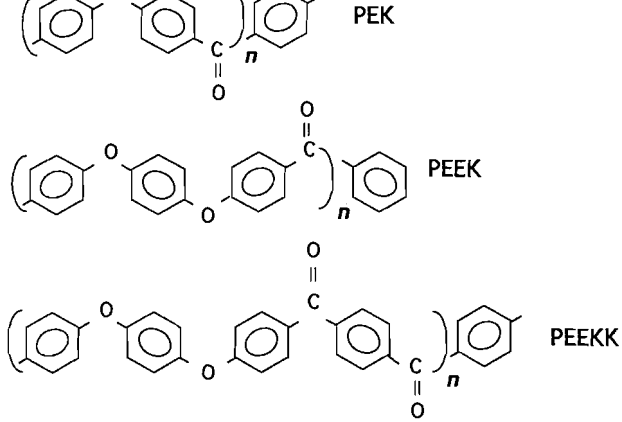

Reçu le 15 juillet 1994. Révision reçue le 2 février 1995.

S. Verot et P. Battesti.[1] Laboratoire des matériaux composites, École Supérieure d'Ingénieurs de Chambéry (ESIGEC), Université de Savoie, Campus Scientifique de Savoie Technolac, 73376 Le Bourget du Lac Cedex, France.

1. Auteur correspondant. Téléphone : 19 33 79 75 87 81. Fax : 19 33 79 75 87 72.

Can. J. Chem. Downloaded from www.nrcresearchpress.com by 65.111.164.53 on 09/08/12
For personal use only.

Fig. 2. Les différents modèles conformationnels envisagés pour les unités moléculaires Ph-X-Ph.

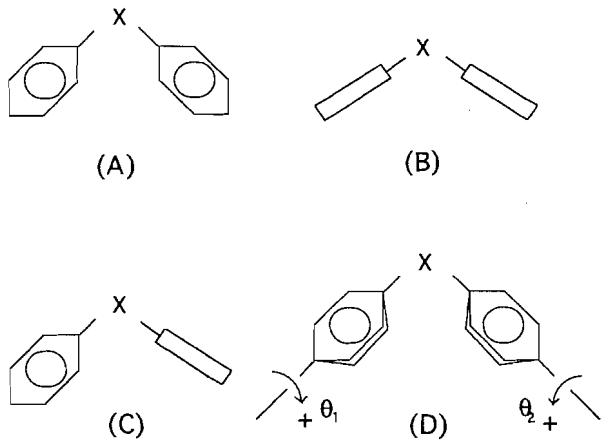

A, B, C et D (figure 2) pour représenter de façon simple les unités moléculaires envisagées dans le titre. Les angles de torsion des deux noyaux aromatiques sont désignés par (θ_1,θ_2) et les noyaux aromatiques par (ϕ_1,ϕ_2).

Pour le premier modèle A $(\theta_1,\theta_2) = (0°,0°)$ (1) à structure rigide, la molécules est entièrement plane présentant une contrainte stérique maximale entre les deux hydrogènes 2 et 2′ situés en position *ortho* par rapport à l'atome (ou au groupe d'atomes) X. Cette forme A est stériquement impossible à la température ambiante.

En ce qui concerne le modèle B $(\theta_1,\theta_2) = (90°,90°)$ (2) à structure rigide, les plans des deux noyaux benzéniques sont perpendiculaires au plan formé par CXC. Dans cette structure, la gêne stérique est réduite entre les quatre hydrogènes 2, 2′, 6 et 6′ situés en *ortho* par rapport à X.

Pour le modèle C $(\theta_1,\theta_2) = (0°,90°)$ (3) également à structure rigide appelé «structure de Morino», l'un des phényles se trouve dans le plan CXC et l'autre est perpendiculaire à ce plan.

La quatrième conformation D (4–13), plus attrayante, est un modèle dans lequel chacun des deux noyaux benzéniques peut pivoter d'un angle variable par rapport au plan défini par CXC. Cette structure mobile peut, selon le sens de rotation des phényles, adopter successivement les géométries des trois modèles A, B et C.

À partir des années 60 (4, 5), les résultats de ces approches, à quelques exceptions, indiquent une nette préférence pour une conformation stable hélicoïdale de type D : l'un des deux noyaux a subit une rotation positive et l'autre négative par rapport au plan CXC. La valeur absolue de ces angles (θ_1,θ_2) de torsion est, selon les auteurs, située dans une plage angulaire allant de 25° à 50° suivant la nature de X. Le fait le plus marquant qui ressort de ces publications est le manque d'homogénéité dans les conclusions qui en ont été tirées.

Tout récemment, certaines approches en mécanique quantique et moléculaire ont été révisées et affinées (14–18 et références citées). Si une relative cohérence apparaît maintenant dans les conclusions, il faut signaler que les divers auteurs se bornent toujours à n'envisager que certains mouvements bien particuliers des noyaux benzéniques, dans chaque cas : DPE et DPC.

Fig. 3. Directions des axes et sens de rotation des noyaux aromatiques.

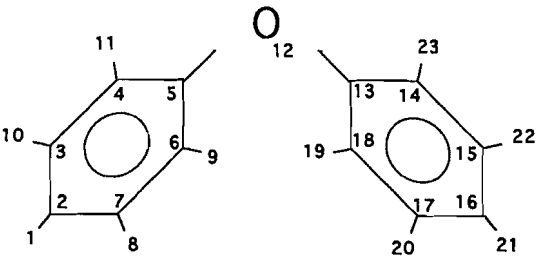

Nous nous proposons donc d'effectuer, à partir du modèle D, l'étude systématique des diverses conformations possibles que sont susceptibles d'adopter, sous certaines conditions, les deux unités moléculaires DPE et DPC, sachant que les modèles A, B et C peuvent être des géométries issues de la mobilité moléculaire de la structure D.

Moyens utilisés et mode opératoire pour la mise en oeuvre des calculs

Notre étude repose essentiellement sur des calculs de mécanique quantique CNDO/2 (19), CNDO/2 avec interactions et ab initio (méthodologie d'Hartree–Fock) dans la base minimum STO-3G. La numérotation des atomes présentée sur la figure 3 est celle que nous avons utilisée pour effectuer nos calculs.

En ce qui concerne la méthode CNDO/2 avec interactions, nous avons utilisé un artefact géométrique (figure 4) qui nous permet de modéliser la couronne électronique du noyau aromatique. Pour cela, nous avons modifié la position de l'hydrogène H_{19} afin que la distance C_{13}—H_{19} soit au maximum de 1.80 Å permettant ainsi de simuler la demi épaisseur (zone d'impénétrabilité de van der Waals) de cette couronne. Si nous tenons compte de la zone d'impénétrabilité de van der Waals de la couronne électronique des noyaux benzéniques, il existe des contraintes stériques et électrostatiques entre une couronne et l'hydrogène aromatique situé en vis-à-vis et parfois entre deux couronnes.

L'ensemble des calculs ont été réalisés à partir d'une station de travail numérique (VT 420) connectée à un VAX 6000-410.

Par ailleurs, signalons que dans des conditions normales, les valeurs des distances interatomiques et celles des angles de valence utilisées par divers auteurs pour les unités moléculaires DPE et DPC sont souvent disparates. Par exemple, pour le diphényl éther, les distances interatomiques d(C—O) s'échelonnent de 1.28 Å (11) à 1.42 Å (12) et les angles de valence COC varient de 115° (13) à 126° (12). En ce qui concerne la diphényl cétone, les distances d(C—C(O)) vont de 1.42 Å (12) à 1.54 Å (10) et les angles de valences CC(O)C se situent entre 120° (10) et 126° (12).

Afin d'éviter de choisir les unes ou les autres valeurs, nous avons effectué nos propres calculs par optimisation à partir de la conformation D avec une méthode ab initio dans la base STO-3G. Les principaux résultats obtenus par cette méthode pour les distances interatomiques sont d(C—X) : 1.40 Å lorsque X = O et 1.42 Å pour X = CO, et pour l'angle de valence CXC on trouve 117° quel que soit X. Ces valeurs sont utilisées pour effectuer nos calculs en CNDO/2 et CNDO/2 avec interactions.

Fig. 4. Simulation de la couronne électronique.

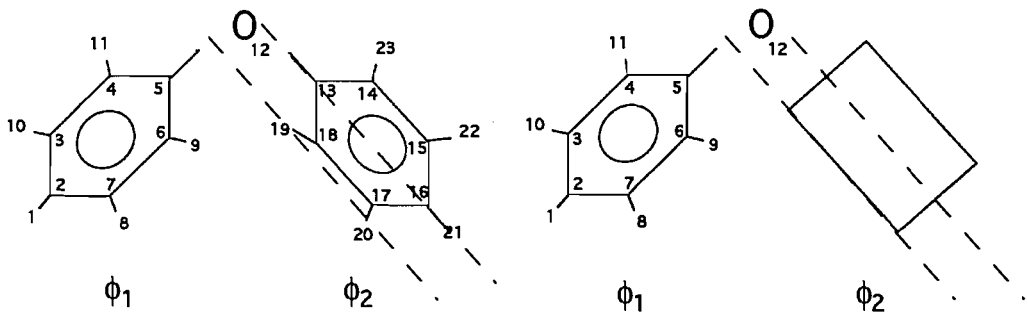

Tableau 1. Paramètres structuraux utilisés dans les calculs en CNDO/2.

Distances interatomiques en angstrom		Angles de valence en degré		
(C—C) aromatique	1,39	(C-C-C)aromatique		120
C—H	1,08	(H-C-C)aromatique		120
C=O	1,23	C-C(O)-C	C-C-C	117
C—C(O)	1,42		O=C-C	121,5
C—O	1,40	C-O-C		117

Pour plus de clarté, nous présentons dans le tableau 1 toutes les distances interatomiques et tous les angles de valence utiles pour effectuer les calculs des unités moléculaires DPE et DPC.

Malgré les nombreuses études, dont ont fait l'objet ces géométries moléculaires, des incohérences demeurent dans la littérature en ce qui concerne la direction des axes autour desquels la giration des phényles se produit et le sens de rotation de ces noyaux benzéniques. Un autre problème essentiel demeure : les noyaux benzéniques pivotent-ils simultanément dans le même sens ou en sens contraire, ou tournent-ils alternativement? En effet, un phényle peut être fixe pendant que l'autre tourne ou inversement.

Pour mener à bien les calculs, nous indiquons les conventions (figure 2 et figure 3) que nous avons utilisées concernant le sens de rotation des noyaux aromatiques ainsi que la direction des axes autour desquels ils pivotent : rotation positive pour les deux phényles ϕ_1 et ϕ_2 lorsqu'ils tournent dans le sens des aiguilles d'une montre avec pour direction des axes respectivement celle de $C_2C_5O_{12}$ et $O_{12}C_{13}C_{16}$.

Pour connaître l'énergie totale de chaque conformation, en prenant en compte toutes les rotations possibles des unités moléculaires, nous avons effectué un nombre important de modélisations. Elles ont été conduites en imprimant une rotation par pas de 10° au phényle ϕ_1, et pour chaque pas, on a fait subir au noyau ϕ_2 une rotation complète de 360° autour de son axe.

Résultats et discussions

Les molécules de DPE et DPC étant symétriques, les tableaux contenant les variations de θ_1 et θ_2 de 0° à 360° peuvent être réduits à un quart en ne présentant les variations des angles de torsion que de 0° à 180°.

Nous devons signaler que les résultats obtenus pour les géométries d'énergie minimale de la DPE et la DPC sont respectivement, selon nos conventions de signe, de : (θ_1,θ_2) = (30°,150°) et (θ_1,θ_2) = (90°,90°). Les conformations d'énergie minimale pour la DPE et la DPC sont d'après Chen et al. (17) celles dont les angles de torsion sont respectivement (θ_1,θ_2) = (30°,30°) et (θ_1,θ_2) = (90°,90°). Nous précisons que notre conformation pour le DPE est parfaitement identique à celle de Chen mais définie selon nos conventions par (θ_1,θ_2) = (30°,−30°) ou (θ_1,θ_2) = 30°,150°). Néanmoins, les barrières d'énergie maximum de rotation qu'ils proposent (61 kcal/mol pour le DPE et 67 kcal/mol pour la DPC) sont nettement inférieures à nos valeurs (419 kcal/mol pour le DPE et 369 kcal/mol pour la DPC). Cependant, nos angles de torsion totaux $(|\theta_1| + |\theta_2|)$ sont assimilables à ceux proposés par Kendrick (18) : 77° pour le DPE et 52.4° pour la DPC, ces valeurs étant déterminées par des calculs ab initio.

Le diphényl éther (DPE)

Le tableau 2 présente la carte des énergies relatives pour toutes les conformations possibles du diphényl éther. La conformation d'énergie minimale «absolue» correspond à la structure D_1 la plus stable avec (θ_1,θ_2) = (30°,150°). Les positions équivalentes sont décalées de 180°.

À partir du tableau 2, nous pouvons proposer et suivre les différents types de mouvements que peuvent subir les phényles à partir d'une position de départ quelconque. En effet, les noyaux aromatiques peuvent effectuer des rotations simultanées ou alternées.

1. Rotations simultanées

Lorsque les deux noyaux subissent une rotation simultanée à partir de positions quelconques, deux types de mouvements sont possibles : (*i*) soit les deux phényles ϕ_1 et ϕ_2 tournent en sens inverse (rotation en engrenage) : rotations simultanées positives (ou négatives) selon nos conventions; (*ii*) soit ils tournent dans le même sens (rotation corrélée) : rotations simultanées, l'une positive l'autre négative selon nos conventions.

Pour imprimer une rotation inversée à ϕ_1 et ϕ_2, les angles de torsion respectifs, θ_1 et θ_2, sont simultanément incrémentés positivement (ou négativement) par pas de 10°, à partir de n'importe quelle position de départ. Pour suivre ce mouvement sur le tableau 2, il faut se déplacer sur une droite de pente

Can. J. Chem. Downloaded from www.nrcresearchpress.com by 65.111.164.53 on 09/08/12
For personal use only.

Tableau 2. Energies relatives en kcal/mol pour les différentes conformations du DPE calculées par CNDO/2.

	E_{rel} (kcal/mol)																		
θ1 \ θ2	0	10	20	30	40	50	60	70	80	90	100	110	120	130	140	150	160	170	180
0	419	229	77	22	5	1	0	0	0	0	0	0	0	1	5	22	77	229	419
10	229	360	184	60	17	4	0	0	0	0	0	0	0	0	1	6	25	83	229
20	77	184	232	116	38	10	2	0	0	0	0	0	0	0	0	1	6	28	77
30	22	60	116	117	58	19	5	1	0	0	0	0	0	0	0	0	1	6	22
40	5	17	38	58	47	23	8	2	1	1	1	1	1	0	0	0	0	1	5
50	1	4	10	19	23	16	7	3	1	1	1	1	1	1	0	0	0	0	1
60	0	0	2	5	8	7	5	3	1	1	1	1	1	1	1	0	0	0	0
70	0	0	0	1	2	3	3	2	1	1	1	1	1	1	1	0	0	0	0
80	0	0	0	0	1	1	1	1	1	1	1	1	1	1	1	0	0	0	0
90	0	0	0	0	1	1	1	1	1	1	1	1	1	1	1	0	0	0	0
100	0	0	0	0	1	1	1	1	1	1	1	1	1	1	1	0	0	0	0
110	0	0	0	0	1	1	1	1	1	1	1	2	3	3	2	1	0	0	0
120	0	0	0	0	1	1	1	1	1	1	1	3	5	7	8	5	2	0	0
130	1	0	0	0	0	1	1	1	1	1	1	3	7	16	23	19	10	4	1
140	5	1	0	0	0	0	1	1	1	1	1	2	8	23	47	58	38	17	5
150	22	6	1	0	0	0	0	0	0	0	0	1	5	19	58	117	116	60	22
160	77	25	6	1	0	0	0	0	0	0	0	0	2	10	38	116	232	184	77
170	229	83	28	6	1	0	0	0	0	0	0	0	0	4	17	60	184	360	229
180	419	229	77	22	5	1	0	0	0	0	0	0	0	1	5	22	77	229	419

négative (avec θ_1 en ordonnées et θ_2 en abscisses). Cette mobilité moléculaire est reconnue par divers auteurs (10) comme étant la plus logique et la plus facile.

Une droite particulière de ce type est la diagonale de pente négative (θ_1,θ_2) dont les bornes extrêmes sont (0°,0°) et (180°,180°). Nous avons représenté dans ce cas à partir du tableau 2, la courbe d'énergie relative «E_{rel} (kcal/mol) sans interaction» en fonction des variations des angles de torsion (figure 5).

Nous constatons sur cette courbe, la présence d'un minimum «relatif» d'énergie situé à (θ_1,θ_2) = (90°,90°).

Dans le programme CNDO/2 classique que l'on utilise, les interactions électrostatiques (de couronne électronique) et surtout les zones d'impénétrabilité de van der Waals du noyau aromatique (la demi épaisseur du phényle est en moyenne de 1,80 Å) (20, 21) ne sont prises que très partiellement en compte. Nous avons donc réalisé de nouvelles modélisations à l'aide d'un programme CNDO/2 avec interactions.

Nous pouvons à nouveau proposer comme droite particulière la diagonale (θ_1,θ_2) dont les bornes extrêmes sont (0°,0°) et (180°,180°). Nous représentons (figure 5) à partir du tableau 3 la courbe d'énergie relative «E_{rel} (kcal/mol) avec interactions» en fonction des variations des angles de torsion. Afin de faciliter la comparaison des cas sans et avec interactions, nous avons superposé les deux courbes précédentes sur ce même graphe.

Nous pouvons constater sur la courbe d'énergie «E_{rel} (kcal/mol) avec interactions» l'absence de minima d'énergie relative ainsi qu'une augmentation de la hauteur des barrières énergétiques dans certaines plages angulaires.

Dans le cas où, selon nos conventions, les deux phényles tournent dans le même sens il faut, pour effectuer ces mouvements, incrémenter simultanément θ_1 positivement et θ_2 négativement (ou inversement), à partir de n'importe quelle conformation initiale. Pour visualiser cette mobilité moléculaire, il faut se déplacer sur une droite de pente positive. Nous pouvons proposer comme droite particulière (tableau 2), la diagonale (θ_1,θ_2) bornée par (0°,180°) et (180°,0°) sur laquelle on observe deux minima «absolus» d'énergie situés respectivement à (θ_1,θ_2) = (30°,150°) et (150°,30°). Son profil d'énergie relative peut être tracé à partir de ce tableau «E_{rel} (kcal/mol) sans interaction» en fonction des variations des angles de torsion (figure 6).

Si nous voulons prendre en compte les différentes interactions (tableau 3), la même diagonale possède les mêmes minima «absolus» d'énergie que dans le cas précédent avec un profil énergétique différent représenté par la figure 6 : «E_{rel} (kcal/mol) avec interactions» en fonction des variations des angles de torsion.

2. Rotations alternées

Lorsque les phényles ne subissent pas de rotation simultanée, l'un des noyaux peut se situer dans une position fixe quelconque pendant que l'autre décrit 360° autour de son axe.

Deux types de cheminements sont possibles : (*i*) soit ϕ_1 est bloqué et ϕ_2 subit une rotation de 360°; (*ii*) soit ϕ_1 décrit une rotation de 360° et ϕ_2 est bloqué.

Pour le premier, le mouvement est représenté sur le tableau 2 par une horizontale énergétique, alors que pour le second, le mouvement est défini par une verticale. Nous devons faire remarquer que ces mobilités moléculaires sont énergétiquement identiques lorsque la molécule est symétrique (noyaux non diversement substitués).

Pour exploiter de manière plus approfondie les résultats du tableau 2, nous pouvons envisager certains mouvements moléculaires particuliers à partir de probabilités conformationnelles stables :

Hypothèse 1 : cas de molécules de diphényl éther isolées : À basse température, et en supposant l'angle de valence COC

Can. J. Chem. Downloaded from www.nrcresearchpress.com by 65.111.164.53 on 09/08/12
For personal use only.

Can. J. Chem. Downloaded from www.nrcresearchpress.com by 65.111.164.53 on 09/08/12
For personal use only.

Tableau 3. Énergies relatives en kcal/mol pour les différentes conformations du DPE calculées avec CNDO/2 avec interactions.

	E_{rel} (kcal/mol)																		
θ1 \ θ2	0	10	20	30	40	50	60	70	80	90	100	110	120	130	140	150	160	170	180
0	419	229	77	22	5	1	0	48	137	206	137	48	0	1	5	22	77	229	419
10	229	360	184	60	17	4	0	3	52	137	182	109	32	0	1	6	26	83	229
20	77	184	232	116	38	10	2	0	3	46	109	123	54	12	0	1	6	26	77
30	22	69	116	117	58	19	5	1	0	0	32	64	60	23	0	0	1	6	22
40	5	17	38	58	47	23	8	2	1	1	1	11	23	14	0	0	0	1	5
50	1	4	10	19	23	16	7	3	1	1	1	1	1	1	14	23	12	0	1
60	0	0	2	5	8	7	49	57	19	1	1	1	1	1	23	60	64	32	0
70	48	3	0	1	2	3	57	123	109	41	1	1	1	1	11	64	123	109	48
80	137	52	3	0	1	1	19	109	195	146	48	1	1	1	1	32	109	182	137
90	206	137	46	0	1	1	1	41	146	226	146	41	1	1	1	0	46	137	206
100	137	182	109	32	1	1	1	1	48	146	195	109	19	1	1	0	3	52	137
110	48	109	123	64	11	1	1	1	1	41	109	123	57	3	2	1	0	3	48
120	0	32	64	60	23	1	1	1	1	1	19	57	49	7	8	5	2	0	0
130	1	0	12	23	14	1	1	1	1	1	1	3	7	16	23	19	10	4	1
140	5	1	0	0	0	14	23	11	1	1	1	2	8	23	47	58	38	17	5
150	22	6	1	0	0	23	60	64	32	0	0	1	5	19	58	117	116	60	22
160	77	26	6	1	0	12	64	123	109	46	3	0	2	10	38	116	232	184	77
170	229	83	26	6	1	0	32	109	182	137	52	3	0	4	17	60	184	360	229
180	419	229	77	22	5	1	0	48	137	206	137	48	0	1	5	22	77	229	419

Fig. 5. Variation de l'énergie relative en fonction de l'angle de torsion θ_1 suivant la diagonale (θ_1,θ_2) allant de (0°,0°) à (180°,180°) pour le DPE avec CNDO/2 et CNDO/2 avec interactions.

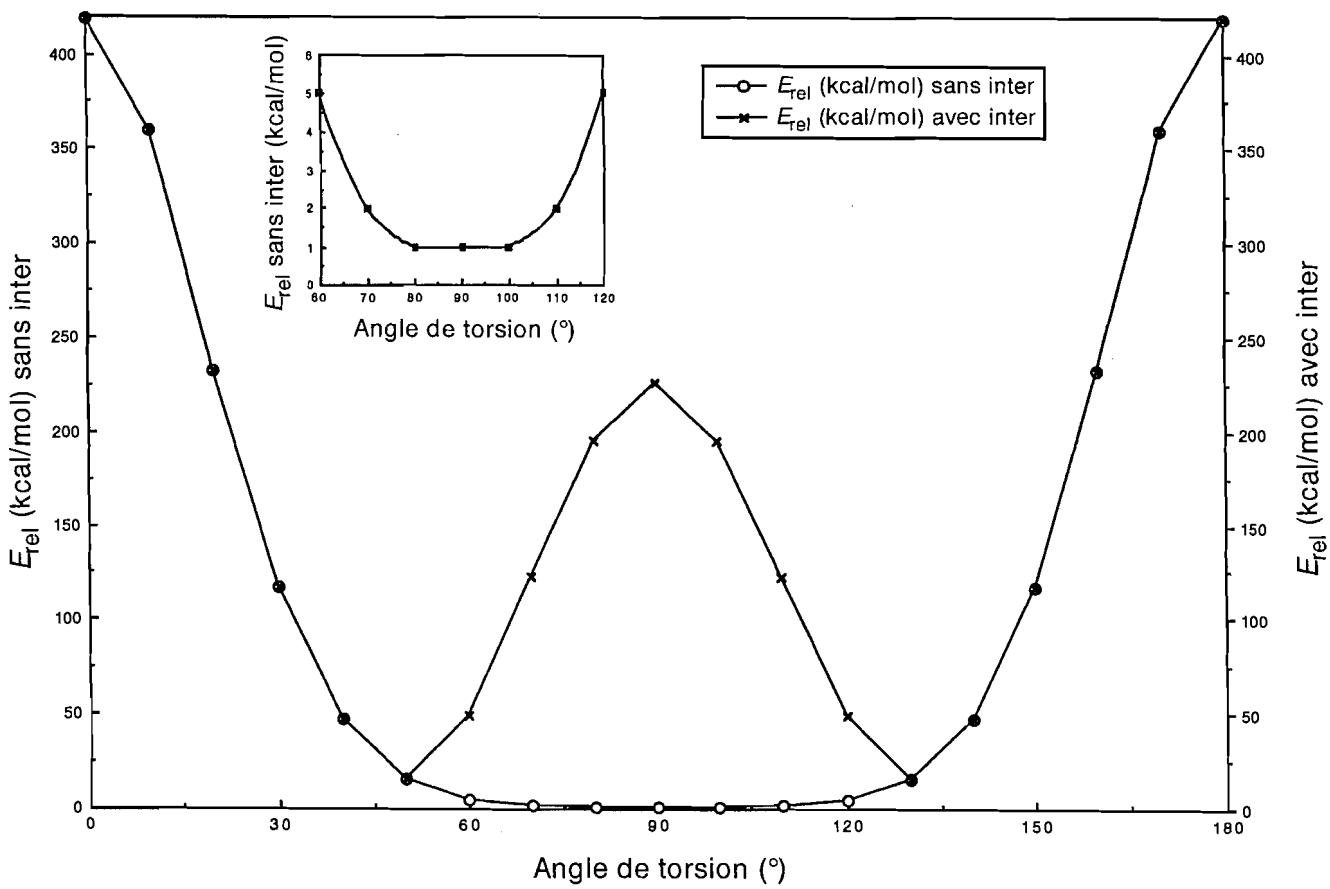

Fig. 6. Variation de l'énergie relative en fonction de l'angle de torsion θ_1, suivant la diagonale (θ_1,θ_2) allant de (0°,180°) à (180°,0°) pour le DPE avec CNDO/2 et CNDO/2 avec interactions.

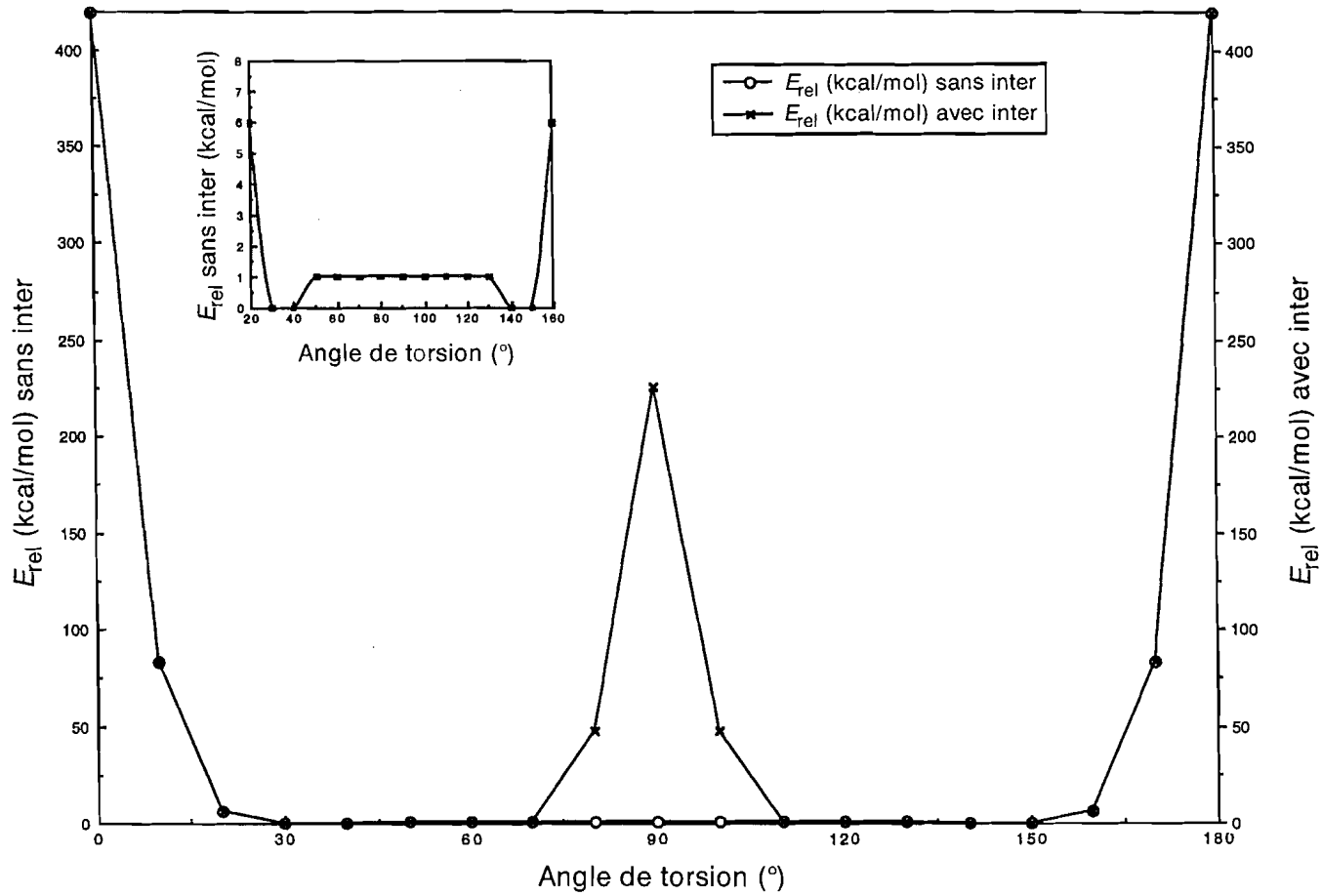

constant au cours du mouvement, la probabilité est maximale pour que cette molécule soit dans la conformation hélicoïdale D_1 la plus stable (30°,150°). Nous sommes en mesure d'étudier tous les mouvements possibles, dans les quatre directions citées précédemment, à partir de cette position en considérant une barrière d'énergie maximale de 14 kcal/mol qui est la valeur approximative du saut énergétique rendant compte de la relaxation sous vitreuse d'un polymère du type PEEK (nous avons choisit cette valeur moyenne à partir de celles proposées par Chen et al. (17) qui indiquent 21 kcal/mol obtenus en spectrométrie mécanique et 10 kcal/mol mesurées en spectrométrie diélectrique). Ces valeurs sont le reflet d'un mouvement local restreint à une ou deux unités moléculaires.

Dans le cas où l'on ne prend pas en compte les interactions, à partir de la structure stable D_1, (θ_1,θ_2) = (30°,150°), la mobilité conrotatoire (les phényles ϕ_1 et ϕ_2 pivotent dans le même sens) suit une droite de pente positive. Le mouvement se limite à un balancement des noyaux compris entre (θ_1,θ_2) = (20°,160°) et (160°,20°). Le coût énergétique ne dépasse pas 6 kcal/mol.

À partir de la géométrie stable D_1, la mobilité disrotatoire (les noyaux ϕ_1 et ϕ_2 pivotent en sens inverse) suit une droite de pente négative. Les rotations simultanées des deux noyaux aromatiques sont définies par les segments de droites (θ_1,θ_2) dont les bornes sont respectivement (0°,120°) et (60°,180°) puis (60°,0°) et (180°,120°). La plage angulaire de torsion de chaque noyau est totale (soit 360°) et le coût énergétique est proche de 1 kcal/mol.

La conformation stable D_1 peut aussi évaluer en suivant l'horizontale (θ_1 est fixé à 30° alors que θ_2 varie). Le balancement angulaire de ϕ_2 est compris entre 60° et 170° pour θ_2. L'énergie nécessaire est encore proche de 6 kcal/mol.

D_1 peut enfin évoluer suivant la verticale (θ_1 variant alors que θ_2 est fixé à 150° (ou −30°)). Le mouvement se réduit aussi à une oscillation de ϕ_1 avec θ_1 compris entre 10° et 120°. L'énergie mise en jeu est au maximum de 6 kcal/mol.

Cependant, si l'on envisage la possibilité d'une pulsation de la molécule animée par une élévation modérée de température (ouverture progressive, mais limitée, de l'angle de valence COC au cours du mouvement) l'amplitude des balancements des noyaux est susceptible d'augmenter tout au plus de la valeur d'un pas de 10° pour θ_1 et θ_2. En effet, au delà l'énergie à mettre en œuvre serait trop importante pour compter ce mouvement dans la zone de la relaxation sous vitreuse d'un polymère.

Lorsque l'on prend en compte les diverses interactions (tableau 3), la conformation la plus stable est toujours D_1 : (θ_1,θ_2) = (30°,150°).

À partir de ce tableau, nous pouvons décrire les différents mouvements possibles de cette conformation D_1 dans les quatre directions définies précédemment :

1. Suivant la droite de pente négative : le cheminement

Can. J. Chem. Downloaded from www.nrcresearchpress.com by 65.111.164.53 on 09/08/12
For personal use only.

Can. J. Chem. Downloaded from www.nrcresearchpress.com by 65.111.164.53 on 09/08/12
For personal use only.

géométrique possible a lieu suivant les segments de droite $(\theta_1,\theta_2) = (0°,120°)$, $(60°,180°)$ puis $(60°,0°)$, $(180°,120°)$ tout comme précédemment pour le cas où la zone d'impénétrabilité n'était pas prise en compte. Cependant, dans cette nouvelle approche, la différence vient du coût énergétique; il faut maintenant 3 kcal/mol au lieu de 1 kcal/mol.

2. Suivant la droite de pente positive : le mouvement possible est un battement des noyaux ϕ_1 et ϕ_2 avec (θ_1,θ_2) décrivant de $(20°,160°)$ à $(70°,110°)$. Nous pouvons remarquer que celui-ci est très largement réduit par rapport au cas où l'on ne prenait pas en compte les interactions électrostatiques et les zones d'impénétrabilité de van der Waals.

3. Suivant l'horizontale avec $\theta_1 = 30°$: le mouvement possible est un balancement du phényle ϕ_2 avec θ_2 s'étendant de 140° à 170°. À nouveau, l'amplitude angulaire de l'oscillation est réduite par rapport au cas où l'on ne tenait pas compte des interactions.

4. Suivant la verticale avec $\theta_2 = 150°$: le mouvement se réduit à une rotation du phényle ϕ_1 avec θ_1 allant de 10° à 40°. Dans ce cas également, la plage angulaire est réduite.

Hypothèse 2 : cas d'agrégats de molécules de diphényl éther : Nous considérons tout d'abord le cas sans interaction. Ici, les molécules sont susceptibles de présenter un grand nombre de géométries originelles. En effet, en plus des conformations indiquées précédemment, il n'est pas vérifié que les géométries des molécules associées soient rigoureusement les mêmes que celles des molécules isolées et des minima «relatifs» peuvent être observés pour des conformations sensiblement différentes. Dans un agrégat, les molécules subissent certainement les influences de leurs voisines.

En particulier, il est impossible d'exclure au départ, par exemple, des molécules de géométrie de type C : $(\theta_1,\theta_2) = (0°,90°)$. Cette conformation est susceptible d'évoluer dans les quatre directions, si elle le peut, en adoptant diverses géométries. La principale évolution est définie par les segments de droite de pente négative dont les bornes sont $(0°,90°)$, $(90°,180°)$ et $(90°,0°)$, $(180°,90°)$. Le coût énergétique pour décrire ce parcours est, en effet, inférieur à 1 kcal/mol. Dans ce cas, bien que la molécule ne passe par aucune conformation d'énergie minimale «absolue», nous pouvons constater qu'il s'agit de la seule mobilité moléculaire qui ne nécessite pas d'énergie sachant que la déformation structurale existait au départ.

Nous pouvons penser que d'une manière générale, la molécule va plutôt choisir des chemins nécessitant des barrières d'énergie moindre plutôt que décrire une diagonale passant par des minima «absolus» qui obligent la molécule à franchir des barrières d'énergie très importante. Donc, il n'est pas inconcevable d'envisager que la conformation la plus stable D_1, $(\theta_1,\theta_2) = (30°,150°)$ se modifie continuellement en suivant un cheminement en ligne brisée. En effet, la mobilité moléculaire peut suivre un parcours d'énergie faible et modifier son cheminement à l'abord d'un obstacle énergétique. Les divers changements de direction permettent à la molécule de suivre un parcours sinueux ne nécessitant aucun saut énergétique. Nous pouvons systématiquement appliquer ce principe à partir d'une structure conformationnelle quelconque.

Nous remarquons que si nous nous situons dans les «vallées» du tableau 3, c'est à dire, pour des valeurs d'énergie de 0 à 1 kcal/mol, ce sont les mouvements de type engrenage (suivant les droites de pente négative) qui nécessitent un moindre coût énergétique.

Nous constatons d'une façon générale que lorsque nous prenons en compte certaines interactions, le nombre de géométries possibles est fortement réduit ainsi que l'amplitude des battements des noyaux. En conclusion, les mouvements de la molécule sont beaucoup plus restreints et sûrement plus proches de la réalité.

Pour une représentation plus claire des barrières énergétiques, nous avons tracé une courbe 3D en fonction des deux angles de torsion θ_1 et θ_2 ainsi que de l'énergie relative de la molécule en kcal/mol, respectivement, dans le cas sans et avec interactions (figures 7 et 8).

La diphényl cétone (DPC)

Nous suivons exactement le même processus de calculs que pour le diphényl éther, en débutant par des modélisations ne prenant pas en compte les diverses interactions.

Il existe de même quatre types de mouvements possibles suivant les directions envisagées précédemment.

Nous avons représenté (figure 9) d'après le tableau 4, la variation de l'énergie relative en fonction des angles de torsion suivant la diagonale (θ_1,θ_2) de pente négative allant de $(0°,0°)$ à $(180°,180°)$ par «E_{rel} (kcal/mol) sans interaction».

Nous constatons sur cette courbe la présence d'un minimum «absolu» d'énergie situé à $(90°,90°)$.

Nous avons effectué une nouvelle modélisation en tenant compte des différentes interactions électroniques et de zones d'impénétrabilité de van der Waals.

Il est possible de proposer aussi comme droite particulière la diagonale (θ_1,θ_2) dont les bornes extrêmes sont $(0°,0°)$ et $(180°,180°)$. À partir du tableau 5, nous représentons la courbe d'énergie relative dont le profil est donné sur la figure 9 : «E_{rel} (kcal/mol) avec interactions» en fonction des angles de torsion.

Nous constatons dans ce cas, la disparition du minimum «absolu» d'énergie relative préalablement situé à $(90°,90°)$. En effet, lorsque les zones d'impénétrabilité de van der Waals sont prises en compte, cette position devient un maximum d'énergie. Nous pouvons remarquer également une augmentation importante des hauteurs des barrières énergétiques dans certaines plages angulaires, lorsque l'on considère les divers types d'interactions.

Nous avons également représenté à partir du tableau 4 (sans prendre en compte les interactions) la variation de l'énergie relative (figure 10) en fonction des angles de torsion suivant la diagonale (θ_1,θ_2) de pente positive allant de $(0°,180°)$ à $(180°,0°)$ par «E_{rel} (kcal/mol) sans interaction». Nous constatons sur cette courbe, la présence d'un minimum «absolu» d'énergie situé aussi à $(\theta_1,\theta_2) = (90°,90°)$.

Dans le cas où nous prenons en compte les interactions, nous pouvons considérer sur le tableau 5 la même diagonale (θ_1,θ_2) dont les bornes extrêmes sont $(180°,0°)$ et $(0°,180°)$. Nous pouvons représenter la courbe d'énergie dont le profil est donné par la figure 10 : «E_{rel} (kcal/mol) avec interactions» en fonction des variations des angles de torsion.

Sur cette courbe, nous constatons la disparition du minimum «absolu» d'énergie préalablement situé à $(\theta_1,\theta_2) = (90°,90°)$, ainsi qu'une forte augmentation de la hauteur des barrières énergétiques dans certaines plages angulaires. Néanmoins, il existe un minimum d'énergie correspondant à la géométrie $(70°,110°)$.

Fig. 7. Représentation tridimensionnelle des énergies relatives du DPE calculées avec CNDO/2.

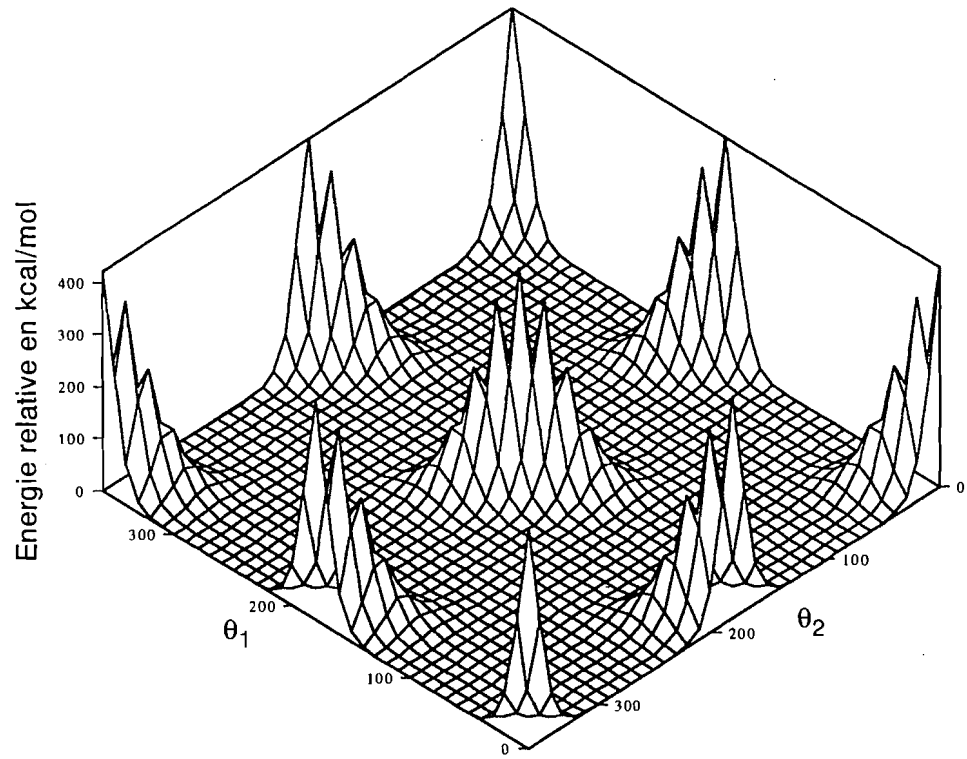

Fig. 8. Représentation tridimensionnelle des énergies relatives du DPE calculées avec CNDO/2 avec interactions.

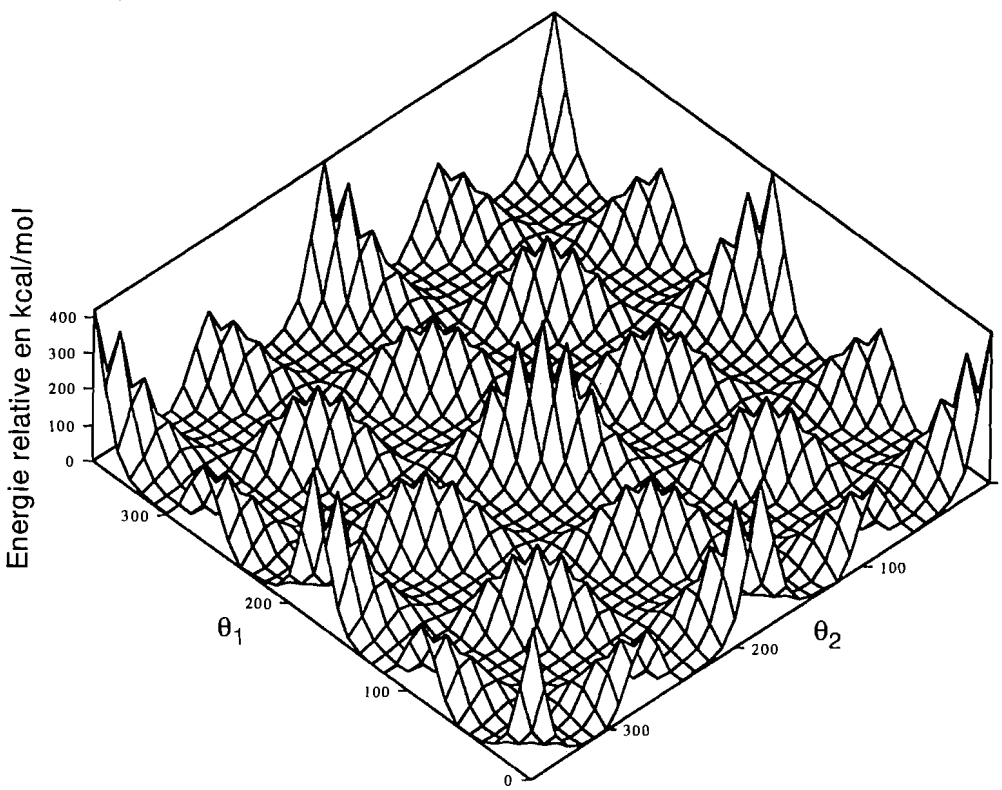

Comme dans le cas du diphényl éther, nous pouvons faire les hypothèses à environnements différents, c'est à dire, d'une molécule isolée et d'un agrégat de molécules.

À basse température, la probabilité pour que la molécule isolée se trouve dans la conformation la plus stable, type B (90°,90°), est maximale. Nous pouvons alors décrire les différents types de mouvements possibles à partir de cette position dans les quatre axes choisis.

Sans considérer les interactions, d'après le tableau 4, suivant la droite de pente négative : le mouvement possible pos-

Can. J. Chem. Downloaded from www.nrcresearchpress.com by 65.111.164.53 on 09/08/12
For personal use only.

Tableau 4. Énergies relatives en kcal/mol pour les différentes conformations de la DPC calculées avec CNDO/2.

	E_{rel} (kcal/mol)																		
θ1 \ θ2	0	10	20	30	40	50	60	70	80	90	100	110	120	130	140	150	160	170	180
0	369	213	77	26	10	6	5	5	5	5	5	5	5	6	10	26	77	213	369
10	231	318	171	61	21	8	5	5	4	4	4	5	5	6	7	11	29	83	231
20	77	171	209	109	40	14	6	4	4	4	4	4	5	5	6	7	12	29	77
30	26	61	109	108	56	21	8	4	3	3	3	4	4	5	5	6	7	11	26
40	10	21	40	56	46	23	9	4	2	2	3	3	4	4	5	5	6	7	10
50	6	8	14	21	23	16	8	4	2	2	2	2	3	4	4	5	5	6	6
60	5	5	6	8	9	8	5	3	1	1	1	2	2	3	4	4	5	5	5
70	5	5	4	4	4	4	3	1	1	0	1	1	2	2	3	4	4	5	5
80	5	4	4	3	2	2	1	1	0	0	0	1	1	2	3	3	4	4	5
90	5	4	4	3	2	2	1	1	0	0	0	0	1	2	2	3	4	4	5
100	5	4	4	3	3	2	1	1	0	0	0	1	1	2	2	3	4	4	5
110	5	5	4	4	3	2	2	1	1	0	1	0	3	4	4	4	4	5	5
120	5	5	5	4	4	3	2	2	1	1	1	3	5	8	9	8	6	5	5
130	6	6	5	5	4	4	3	2	2	2	2	4	8	16	23	21	14	8	6
140	10	7	6	5	4	4	4	3	3	2	2	4	9	23	46	56	40	21	10
150	26	11	7	6	5	5	4	4	3	3	3	4	8	21	56	108	109	61	26
160	77	29	12	7	5	5	5	4	4	4	4	4	6	14	40	109	209	171	77
170	213	83	29	11	6	6	5	5	4	4	4	5	5	8	21	61	171	318	213
180	369	213	77	26	10	6	5	5	5	5	5	5	5	6	10	26	77	213	369

Tableau 5. Énergies relatives en kcal/mol pour les différentes conformations de la DPC calculées avec CNDO/2 avec interactions.

	E_{rel} (kcal/mol)																		
θ1 \ θ2	0	10	20	30	40	50	60	70	80	90	100	110	120	130	140	150	160	170	180
0	369	213	77	26	10	6	5	62	144	204	144	62	5	6	10	26	77	213	369
10	213	318	171	61	21	8	5	22	67	143	182	118	47	6	7	11	29	83	213
20	77	171	209	109	40	14	6	4	23	62	115	128	77	28	6	7	12	29	77
30	26	61	109	108	56	21	8	4	3	3	47	47	70	37	5	6	7	11	26
40	10	21	40	56	46	23	9	4	2	2	3	31	40	28	5	5	6	7	10
50	6	8	14	21	23	16	8	4	2	2	2	2	3	4	28	37	28	6	6
60	5	5	6	8	9	8	80	85	57	1	1	2	2	3	40	70	77	47	5
70	62	22	4	4	4	4	85	146	136	76	1	1	2	2	31	47	128	118	62
80	144	67	23	3	2	2	57	136	210	170	83	1	1	2	3	47	115	182	144
90	204	143	62	3	2	2	1	76	170	238	170	76	1	2	2	3	62	143	204
100	144	182	115	47	3	2	1	1	83	170	210	136	57	2	2	3	23	67	144
110	62	118	128	47	31	2	2	1	1	76	136	146	85	4	4	4	4	22	62
120	5	47	77	70	40	3	2	2	1	1	57	85	80	8	9	8	6	5	5
130	6	6	28	37	28	4	3	2	2	2	2	4	8	16	23	21	14	8	6
140	10	7	6	5	5	28	40	31	3	2	2	4	9	23	46	56	40	21	10
150	26	11	7	6	5	37	70	47	47	3	3	4	8	21	56	108	109	61	26
160	77	29	12	7	6	28	77	128	115	62	23	4	6	14	40	109	209	171	77
170	213	83	29	11	7	6	47	118	182	143	67	22	5	8	21	61	171	318	213
180	369	213	77	26	10	6	5	62	144	204	144	62	5	6	10	26	77	213	369

sède une plage angulaire allant de (60°,60°) à (120°,120°). Nous pouvons remarquer que l'amplitude du battement dans ce cas est nettement moins importante que celle que possédait le diphényl éther sans interaction.

1. Suivant la droite de pente positive : le mouvement est réduit à un balancement entre les positions (20°,160°) et (160°,20°). Nous constatons également dans ce cas, que l'amplitude est moindre par rapport à celle observée pour le diphényl éther sans interaction. Le coût énergétique est ici de 12 kcal/mol alors qu'il ne dépassait pas les 6 kcal/mol pour le diphényl éther pour une plage angulaire identique.

2. Suivant l'horizontale : la DPC peut décrire entièrement la droite (θ_1,θ_2) allant de (90°,0°) à (90°,180°); ce mouvement nécessite une énergie maximum de 5 kcal/mol. Dans le cas du

Can. J. Chem. Downloaded from www.nrcresearchpress.com by 65.111.164.53 on 09/08/12
For personal use only.

Fig. 9. Variation de l'énergie relative en fonction de l'angle de torsion θ_1 suivant la diagonale (θ_1,θ_2) allant de (0°,0°) à (180°,180°) pour la DPC avec CNDO/2 et CNDO/2 avec interactions.

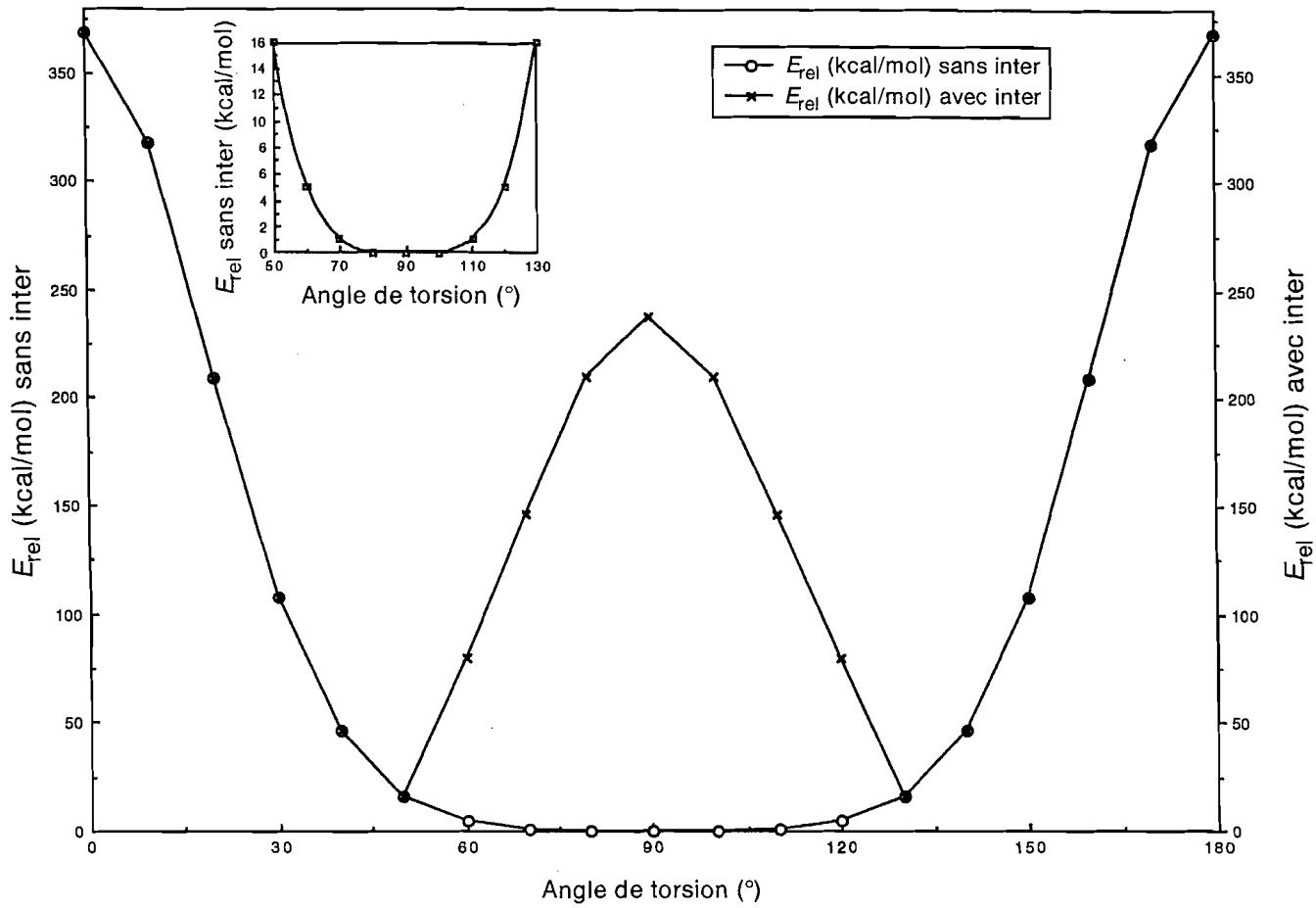

diphényl éther, le cheminement suivant l'horizontale nécessitait un coût énergétique de 1 kcal/mol.

3. Suivant la verticale : la DPC peut décrire entièrement la droite, avec une énergie de 5 kcal/mol (identique au cheminement horizontal car la molécule est symétrique). Le diphényl éther avait décrit lui aussi complètement la droite (θ_1,θ_2) allant de (0°,90°) à (180°,90°) pour un apport énergétique de 1 kcal/mol seulement.

Dans le cas d'un agrégat de molécules, nous pouvons considérer des mouvements suivant d'autres droites nécessitant un coût énergétique moindre ou équivalent même si la molécule ne passe pas par des positions d'énergie minimale absolue.

En ce qui concerne les segments de droites de pente négative, nous pouvons envisager les diagonales (0°,70°); (0°,80°); (0°,90°) et les diagonales équivalentes : réciproquement (0°,110°); (0°,100°); (0°,90°) pour une barrière de rotation de 5 kcal/mol.

En comparant le tableau 4 (la DPC sans interaction) et le tableau 5 (la DPC avec interactions), nous pouvons remarquer que lorsque les diverses interactions sont prises en compte : (i) aucun mouvement complet n'est probable suivant une horizontale ou une verticale. Seuls des mouvements ayant une plage angulaire réduite sont possibles. (ii) De même, aucun mouvement complet n'est envisageable suivant une droite de pente positive. La molécule ne peut effectuer que des oscillations avec des battements angulaires faibles. (iii) La description d'un mouvement suivant une droite de pente négative n'est possible que suivant deux droites distinctes alors que lorsque les interactions ne sont pas prises en compte, on peut envisager près d'une dizaine de droites. (iv) Il existe une augmentation de la hauteur des barrières énergétiques pour certaines plages angulaires.

Il nous a paru intéressant d'analyser par comparaison les différents résultats obtenus sur les diverses modélisations du DPE et de la DPC en prenant en compte les diverses interactions : à partir du tableau 3 et du tableau 5, nous pouvons constater que :

1. Suivant les horizontales et les verticales, les mouvements des deux molécules ne sont probables que pour des amplitudes angulaires très faibles.

2. Suivant les droites de pente positive, les balancements de la diphényl cétone sont plus réduits que ceux observés pour le diphényl éther.

3. Pour le diphényl éther, un mouvement peut être observé suivant trois droites de pente négative alors que pour la diphényl cétone, un tel mouvement ne peut être considéré que suivant deux droites.

Conclusion

En ce qui concerne les modélisations moléculaires du diphényl éther et de la diphényl cétone, sans tenir compte des inter-

Can. J. Chem. Downloaded from www.nrcresearchpress.com by 65.111.164.53 on 09/08/12
For personal use only.

Fig. 10. Variation de l'énergie relative en fonction de l'angle de torsion θ_1 suivant la diagonale (θ_1,θ_2) allant de (0°,180°) à (180°,0°) pour la DPC avec CNDO/2 et CNDO/2 avec interactions.

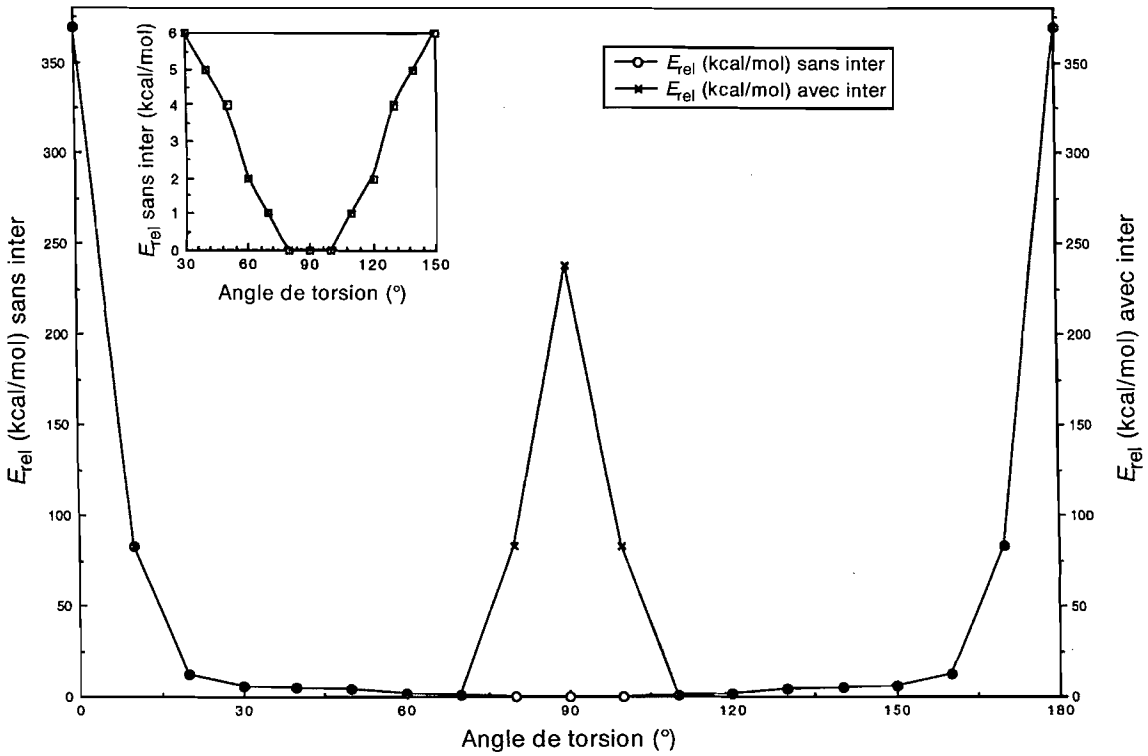

Tableau 6. Tableau récapitulatif des différents balancements possibles pour la géométrie la plus stable du DPE.

Conformation d'énergie minimale	Balancement possible suivant une droite de pente positive	Balancement possible suivant une droite de pente négative	Balancement possible suivant l'horizontale	Balancement possible suivant verticale	Coût énergétique en kcal/mol
		Sans interactions			
	De (20°,160°) à (160°,20°)				6
D_1(30°,150°)		De (0°,120°) à (60°,180°) et de (60°,0°) à (180°,120°)			1
			De (30°,60°) à (30°,170°)		6
				De (10°,150°) à (120°,150°)	6
		Avec interactions			
	De (20°,160°) à (70°,110°)				6
D_1(30°,150°)		De (0°,120°) à (60°,180°) et de (60°,0°) à (180°,120°)			3
			De (30°,140°) à (30°,170°)		6
				De (10°,150°) à (40°,150°)	6

Can. J. Chem. Downloaded from www.nrcresearchpress.com by 65.111.164.53 on 09/08/12
For personal use only.

actions électroniques et des zones d'impénétrabilité de van der Waals, un grand nombre de mouvements est envisageable mais la mobilité de la DPC est plus contrainte que celle du DPE.

Lorsque ces modélisations sont reconduites en prenant en compte les différentes interactions possibles, le nombre de mouvements probables de la DPC et du DPE est très fortement réduit ainsi que les plages angulaires. La diphényl cétone est toujours plus difficilement mobile que le diphényl éther.

Si l'on se trouve dans un liquide pur, on est en mesure de penser que la plupart des molécules ont des difficultés à se mettre en mouvement et que les mobilités, si elles existent, sont certainement dispersées.

Cependant, on peut penser qu'une molécule isolée suivra, en partant de sa conformation la plus stable, le chemin le plus favorable énergétiquement dans l'une des quatre directions possibles. Elle devra modifier sa structure conformationnelle à l'approche d'une barrière énergétique et suivra ainsi un cheminement sinueux énergétiquement faible. En conclusion, dans les zones sous vitreuses et à contrainte stérique égale au sein d'une chaîne de PEK, PEEK ou PEEKK, on peut stipuler que l'unité moléculaire DPE sera sensiblement plus facilement mise en mouvement que l'unité DPC.

Remerciements

Nous tenons à remercier l'ITODYS (Institut de Topologie et de Dynamique des Systèmes) pour nous avoir permis d'accéder à certains programmes de mécanique quantique et moléculaire.

Références bibliographiques

1. L.E. Sutton et G.C. Hampton. Trans. Faraday Soc. **31**, 945 (1935).
2. C.P. Smyth et W.S. Walls. J. Am. Chem. Soc. **54**, 3230 (1935).
3. K. Higasi et S. Uyeo. Bull. Chem. Soc. Jpn. **14**, 87 (1939).
4. R.J.W. Lefèvre, A. Sundaram et K.M.S. Sundaram. Bull. Chem. Soc. Jpn. **35**, 690 (1962).
5. R.J.W. Lefèvre et J.D. Saxby. J. Chem. Soc. B, 1167 (1966).
6. J. Boon et E.P. Magré. Makromol. Chem. **126**, 130 (1969).
7. C. Garrigou-Lagrange, M. Horak, R.K. Khanna et E.R. Lippincott. Collect. Czech. Chem. Commun. **35**, 3230 (1970).
8. V. Galasso, G. De Alti et A. Bigotto. Tetrahedron, **27**, 6151 (1967).
9. Y.G. Smeyers et A. Hernandez-Laguna. J. Chim. Phys. **1**, 75 (1978).
10. J.N. Hay et D.J. Kemmish. Polym. Commun. **30**, 77 (1989).
11. G. Llabrès, M. Baiwir, K. Christiaens et J.L. Piette. Can. J. Chem. **57**, 2967 (1967).
12. J.H.S. Green. Spectrochim. Acta, Part A: **24A**, 1627 (1968).
13. I.A. Bogdanov et M.F. Vuks. Vestn. Leningr. Univ. 20 Serv. Fiz. Chim. **3**, 46 (1965).
14. T. Schaefer, G.H. Penner, C. Takenchi et P. Tseki. Can. J. Chem. **66**, 1647 (1988).
15. R.J. Abraham et I.S. Haworth. J. Chem. Soc. Perkin Trans. 2, 1429 (1988).
16. R.J. Abraham et I.S. Haworth. Polymer, **32**, 121 (1991).
17. C.L. Chen, J.L. Chang et A.C. Su. Macromolecules, **25**, 1941 (1992).
18. J. Kendrick. J. Chem. Soc. Faraday Trans. **86**, 3995 (1990).
19. J.A. Pople et D.L. Beveridge. Approximate molecular orbital theory. McGraw Hill, New York. 1970.
20. L. Pauling. *Dans* La nature de la liaison chimique et la structure des molécules et des cristaux. Presses Universitaires de France, Paris. 1949. p. 192.
21. A. Dunand. Thèse : Faculté des Sciences de l'Université de Genève, Département de Chimie Organique, n° 1778, 1977.

Can. J. Chem. Downloaded from www.nrcresearchpress.com by 65.111.164.53 on 09/08/12
For personal use only.

Some physicochemical characteristics of molten salts derived from trimethylsulfonium bromide

M. Ma and K.E. Johnson

Abstract: Ambient temperature melts were derived from trimethylsulfonium bromide (TMSuBr) and $AlBr_3$, $AlCl_3$, or HBr. The aluminum halide melts have low-wavelength UV cutoffs and single-band ^1H NMR spectra. In the TMSuBr–HBr system, the formation of HBr_2^- and likely existence of $H_2Br_3^-$ are indicated by ^1H NMR and IR spectra. Conductivity and viscosity data indicate stronger $TMSu^+$–anion interactions than those between substituted imidazolium and halide anions. A Grotthus mechanism may operate for conduction in TMSuBr:HBr melts.

Key words: ambiant temperature melts, trimethylsulfonium–anion itneractions, Grotthus mechanism.

Résumé : À la température ambiante, des mélanges de bromure de triméthylsulfonium (TMSuBr) et de $AlBr_3$, $AlCl_3$ ou HBr existent à l'état fondu. Les mélanges fondus d'halogénures d'aluminium absorbent complètement à de basses longueurs d'onde dans l'UV alors que leurs spectres RMN du ^1H ne présentent qu'une bande. Dans le système TMSuBr–HBR, les spectres IR et de RMN du ^1H indiquent qu'il y a formation de HBr_2^- et possiblement de $H_2Br_3^-$. Les données de conductivité et de viscosité indiquent que les interactions $TMSu^+$–anion sont plus fortes que celles entre les imidazolium substitués et les anions halogénures. Dans les sels fondus de TMSuBr:HBr, il est possible qu'un mécanisme de Grotthus soit en opération.

Mots clés : mélanges fondus à la température ambiante, interactions triméthylsulfonium–anion, mécanisme de Grotthus.

[Traduit par la rédaction]

Introduction

Although a variety of organic salts can be mixed with the appropriate aluminum halide to produce haloaluminate melts that are liquid at or below ambient temperature, most work in the field has involved two systems: $AlCl_3$:1-butylpyridinium chloride ($AlCl_3$:BPC) (1) and $AlCl_3$:1-ethyl-3-methyl-*1H*-imidazolium chloride ($AlCl_3$:ImCl) (2). Liquids are obtained for $AlCl_3$ mole fractions ranging from 0.37 to 0.67 for the former and from 0.33 to 0.67 for the latter. Potentiometry suggests (3, 4) that acid–base properties of these melts are governed by tetrachloroaluminate dissociation with $K_{eq} \cong 10^{-17}$ at 40°C. Some formation of $Al_3Cl_{10}^-$ may be important at high (>64 mol%) $AlCl_3$ mole fractions (5, 6). The anion–cation interactions that take place in ambient temperature melts have been studied by NMR spectroscopy (7–9). In basic melts the organic cations interact strongly with halide ions, apparently through hydrogen bond formation; in particular, all three Im^+ ring protons interact (10–13) with Cl^-. In acidic melts (excess $AlCl_3$ over Cl^-) little interaction seems to occur (7–9).

Received August 26, 1994.

M. Ma[1] and K.E. Johnson.[2] Department of Chemistry, University of Regina, Regina, SK S4S 0A2, Canada.

[1] Department of Chemistry, University of Alberta, Edmonton, AB T6G 2G2, Canada.

[2] Author to whom correspndence may be addressed. Telephone: (306) 585-4012. Fax: (306) 585-4894.

Both $AlCl_3$:BPC and $AlCl_3$:ImCl melts do provide wide acidity ranges and electrochemical windows but take considerable time and work to obtain pure. In this context Jones and Blomgren (14) found that a 2:1 $AlCl_3$:trimethylsulfonium chloride (TMSuCl) mixture remained liquid to −50°C and had useful electrochemical stability and electrical conductivity. However, TMSuCl is difficult to prepare and the system was not exploited. TMSuBr, on the other hand, is commercially available and should (like TMSuCl) provide a haloaluminate melt with a high-energy UV cutoff (no unsaturation!) and simple solvent NMR (one methyl signal). We therefore evaluated the $AlBr_3$:TMSuBr and $AlCl_3$:TMSuBr solvent systems.

Furthermore, we followed up recently (15) on the discovery (16) that $ImHCl_2$ is also liquid at ambient temperatures and usable as a proton source in $AlCl_3$:ImCl melts by studying the HCl:ImCl system over the HCl mole fraction range of 0.31 to 0.67 (15). It transpires that the controlling equilibrium in this system is

$$[1] \quad H_2Cl_3^- + Cl^- \Leftrightarrow 2HCl_2^-$$

with $K_{eq} \cong 218$ at 297 K (15, 17). It was appropriate, therefore, to examine the TMSuBr:HBr system in a search for the formation of HBr_2^- and $H_2Br_3^-$ in particular: evidence for the formation of $X(HX)_n^-$ where X = Cl, Br dates from 1909 (18) and extensive discussions of HX_2^- and HXY^- species (19) and systems with strong hydrogen bonding (20) are available.

Can. J. Chem. Downloaded from www.nrcresearchpress.com by 65.111.164.53 on 09/08/12
For personal use only.

Can. J. Chem. Downloaded from www.nrcresearchpress.com by 65.111.164.53 on 09/08/12
For personal use only.

Experimental

Materials and melt preparation

Trimethylsulfonium bromide (TMSuBr, Eastman, 99%) was twice recrystallized from anhydrous ethanol (Aldrich) and dried *in vacuo* at ~40°C for 3 days. Anhydrous hydrogen bromide was used as received from Matheson. Anhydrous hydrogen chloride, prepared from concentrated sulfuric and hydrochloric acids (Fisher ACS), was kept free of moisture with a gas trap at −78°C, two sulfuric acid wash bottles, and a magnesium perchlorate column. 1-Ethyl-3-methyl-*1H*-imidazolium chloride was provided by J.L.E. Campbell (15). Anhydrous aluminum chloride (Fluka, >99%) was purified by vacuum sublimation at ~210°C through a fine-porosity Pyrex frit. About 1% by weight of NaCl (BDH, ACS) and a piece of Al wire (Aldrich, 99.999%) were added prior to the sublimation to form a molten $NaAlCl_4$ layer to extract ionic impurities. Two or three sublimations produced colorless $AlCl_3$ crystals, which were ground and sealed in glass ampoules awaiting use. Anhydrous aluminum bromide (Fluka, >98%) was vacuum sublimed (× 3) at ~130°C. The purified crystals were colorless.

$AlCl_3$:ImCl (2:1), $AlCl_3$:TMSuBr (2:1), and $AlBr_3$:TMSuBr (2:1) acidic melts were prepared by adding the aluminum halide slowly to the second salt with continuous stirring. The three melts were colorless, pale yellow turning yellow in days, and colorless turning pale yellow in days, respectively. Reactions with TMSuBr were much less exothermic than that with ImCl.

$TMSuHBr_2$ was prepared at room temperature by passing HBr through a needle (26 or 22 G) over weighed amounts of TMSuBr crystals in a 10 mL serum bottle or in a 30 mL Barnes dropping bottle fitted with a septum. The speed of the reaction depended on the HBr pressure, being very slow at 1 atm (101.3 kPa). Consequently, melts of composition $TMSuBr(HBr)_n$ ($1.00 < n < 1.15$) were prepared by applying HBr at a little higher than 1 atm for several minutes and then pumping HBr out of the melts until the required mole ratio, as indicated by gravimetry, was achieved. Melts with $1.15 < n_{HBr} < 1.40$ were prepared directly. All melts were pale yellow. They were transferred to the drybox ready for physical measurements. For melts with $n_{HBr} > 1.25$, the HBr partial pressures above them were quite high so that the melts had to be transferred to appropriate measuring bottles through cannulation using a cannula of Teflon tubing and a syringe. For NMR measurements only, melts with $n_{HBr} > 1.40$ were prepared in situ in NMR tubes with rubber septa secured by Parafilm, and n values were determined gravimetrically. Small needles (26 G) were required to eliminate leaks.

Physical measurements

Densities of $AlCl_3$:TMSuBr and $AlBr_3$:TMSuBr melts were measured at 25°C with either 5 mL or 10 mL volumetric flasks that had been calibrated with distilled water at 25 ± 0.2°C. Densities of $TMSuBr(HBr)_n$ ($1.00 < n < 1.40$) were measured at 25°C using 2.5 mL dilatometric tubes calibrated with distilled water. A reference mark was etched midway up the 2.5 mm bore stem. Once melts were loaded to the mark they were capped with septa to minimize HBr loss.

Viscosities of melts were measured using Cannon–Fenske viscometers (sizes 50, 100, 150, and 300) that had been calibrated with aqueous glycerol (Fisher ACS) solutions (21, 22). A paraffin oil bath with a submerged heater and an Omega 871 digital thermometer were used in temperature control. Viscometers were calibrated by an overlapping technique: distilled water was the primary standard (sizes 50 and 100), 50% aqueous glycerol (sizes 50, 100, and 150) and 85% aqueous glycerol (sizes 150 and 300) the secondary standards. The densities of 50% and 85% glycerol were measured with a 10 mL dilatometer and their viscosities agreed with Sheely's (21) table. Before each measurement the viscometer loaded with melt was immersed in the bath for 10 min; the melt was then drawn (or forced) up by vacuum (or pressure) to 5–10 mm above the upper mark. A minimum flow time of 120 s was required. To minimize HBr loss from TMSuBr(HBr) melts, the ends of the viscometer were capped with rubber septa and connected with Teflon tubing to equalize pressures.

Conductances of $AlBr_3$:TMSuBr and $AlCl_3$:TmSuBr were measured with an Orion model 160 conductivity meter with an Orion 016010 conductance cell that has four glassy carbon electrodes and a temperature sensor. The conductances were frequency independent and the cell constant was 0.609 cm^{-1} (confirmed with 0.1 demal aqueous KCl). Melts were contained in a small glass cylinder and two O-rings were mounted between the cell and the cylinder to get an airtight seal. Conductances of $TMSuBr(HBr)_n$ melts were measured with a YSI model 31 conductivity bridge (Yellow Springs) at 1 kHz. This cell was made by attaching two Pt electrodes on opposite sides of a glass block attached to a glass tube bearing the separated leads; the tube in turn was placed in a melt container drawn from a 50 mL buret fragment, and tube and container were sealed by a nut with Teflon and silicone rubber bushings. The cell was calibrated at 25 ± 0.2°C with 0.1 demal aqueous KCl (23) and the cell constant was 2.26 cm^{-1} ± 1%. The container was immersed in an oil bath such that the melt surface was 3 cm below the oil surface.

Melting points were determined visually by immersing an NMR tube filled with melt in a well-stirred water bath and monitoring the temperature with a digital thermometer. No sharp phase change was observed for these melts, so melting points were taken as the temperatures at which most melt in the NMR tube was melted in a short period (about 10 min).

All of the melts supercooled and, to have an idea of how low the temperature of their supercooling states could go, freezing points were also determined visually with the same NMR tube immersed either in an ice–water bath or in a Dewar bottle filled with acetone and cooled with Dry Ice. Freezing points were less reproducible than melting points and could vary up to 5°C. Therefore, these freezing and melting points can only be taken as a practical guide.

^1H *NMR* spectra were obtained with a Bruker AC-200 NMR spectrometer. 3-(Trimethylsilyl)-1-propanesulfonic acid, sodium salt (Thompson–Packard) dissolved in dimethyl sulfoxide-d_6 was sealed into melting point capillaries and then inserted into 5 mm NMR tubes as an external standard (at 0.49 ppm vs. TMS in $CDCl_3$). NMR tubes were filled with melt in the drybox, capped, and sealed with Parafilm before transfer to the spectrometer.

UV–visible spectra were measured with a Hewlett–Packard model 8452A diode array spectrophotometer.

Infrared spectra of $TMSuBr(HBr)_n$ were recorded with a Perkin–Elmer model 1600 FT-IR spectrophotometer. One or two drops of melt were sandwiched between the two films cut off from a polyethylene sampling bag that, in turn, was placed

Can. J. Chem. Downloaded from www.nrcresearchpress.com by 65.111.164.53 on 09/08/12
For personal use only.

Table 1. Physical properties of melts at 25°C.

Acid	Base	Ratio	ρ (g cm^{-3})	V_M (mL mol^{-1})	κ (mS cm^{-1})	η (cP)	T_m (°C)	T_f (°C)	Ref.
$AlCl_3$	EPBr	2	1.52	299	8.43	22.5	−40		24
$AlCl_3$	ImCl	2	1.39	297	14.7	13.5		−90	25
$AlCl_3$	TMSuCl	2	1.40	271	5.5	39.3	−5	−50	14
$AlCl_3$	TMSuBr	2	1.59	266	4.21	54.9	5	−45	
$AlBr_3$	EPBr	2	2.20	328		~50			26
$AlBr_3$	ImBr	2	2.22	326	5.6	31		−100	27
$AlBr_3$	TMSuBr	2	2.40	288	1.44	138	37	−5	
$AlBr_3$	TMSuBr	2	2.38	290	2.59	50			
HBr	TMSuBr	1.00	1.74	137	34	20.5	27	10	
HBr	TMSuBr	1.15	1.76	142	43	15.3	25	2	
HBr	TMSuBr	1.24	1.77	145	48	12.4	22	0	
HBr	TMSuBr	1.32	1.78	148	54	10.2	20	−3	
HBr	TMSuBr	1.38	1.79	150	56	8.3	18	−10	

[a]EP ≡ 1-ethylpyridinium.
[b]At 50°C.
V_M is an average molar volume.

between two KBr windows: the film thickness was adjusted by gently pressing the upper window (17).

Cyclic voltammograms were obtained with a BAS model 100A electrochemical analyzer (Bioanalytical Systems) and recorded with a Hewlett–Packard 7475A plotter. A glassy carbon disk (0.071 cm^2) served as working electrode, a coiled Al wire (Aldrich, 99.999%) as counter electrode, and an Al wire, immersed in the 2:1 AlX_3:TMSuBr melt in a compartment separated by a fine porosity glass frit, served as reference electrode.

Elemental analyses were performed on a Perkin–Elmer model 2400 CHN analyzer.

Weighing and material transfers involving AlX_3, TMSuBr, and their mixtures were performed in a drybox under a purified nitrogen atmosphere. Stored materials in the drybox were capped, sealed with Parafilm, and wrapped with Al foil.

Results and discussion

Recrystallized and dried TMSuBr gave satisfactory C and H analyses and, moreover, showed little deterioration after exposure to the laboratory atmosphere (purified salt: C = 22.71%, H = 5.74%, H/C = 3.01; exposed salt: C = 23.19%, H = 5.87%, H/C = 3.02; theoretical: C = 22.94%, H= 5.77%, H/C = 3.00). The reactions of TMSuBr with aluminum halides are much less exothermic than those of ImCl. These two factors favor the preparation and use of TMSuBr derivatives over those of ImCl.

$AlCl_3$:TMSuBr and $AlBr_3$:TMSuBr are liquid at ambient temperature only for AlX_3:TMSuBr mole ratios close to 2:1. They show a range >40°C between freezing and melting temperatures. For the HBr:TMSuBr systems, liquids are found for HBr:TMSuBr ratios >1.00 and the melting and freezing temperatures differ by ~20°C.

Density (ρ), viscosity (η), and conductance (κ) data for the melts studied are compared with literature values for other ambient temperature melts in Table 1. The specific conductance (κ, mS cm^{-1}) of 2:1 $AlBr_3$:TMSuBr showed a linear dependence on temperature (t, °C) over the range 25–60°C, viz.

[2] $\kappa = 0.303 + 0.0455t$ (corr. coeff. 0.9998)

Fig. 1. Cyclic voltammograms of (*a*) 2:1 $AlBr_3$:TMSuBr and (*b*) 2:1 $AlCl_3$:TMSuBr melts at a glassy carbon electrode at 24°C. Scan rate = 100 mV/s.

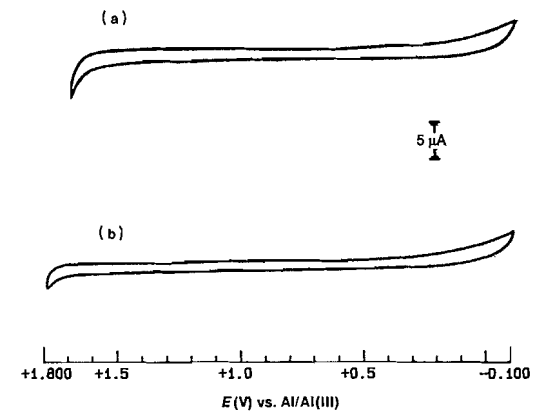

Melts derived from trimethylsulfonium and aluminum halides were the least conducting and most viscous among those listed, suggesting a stronger cation–anion interaction than in the other acidic chloroaluminates. The n:1 HBr:TMSuBr melts possess viscosities similar to that of 2:1 $AlCl_3$:ImCl but conductances up to 4 times greater. Within the n:1 HBr:TMSuBr system the viscosity variation is more extreme (notice that by $n > 1.24$ we have the most fluid of the systems quoted). Comparing 2:1 $AlBr_3$:TMSuBr and 1:1 HBr:TMSuBr we see that a change from $Al_2Br_7^-$ to HBr_2^- brings about a 7-fold viscosity decrease but a 24-fold conductance increase. This viscosity change may be ascribed to ion size but the conductance change suggests that a Grotthus mechanism of Br^- exchange may be facilitating conduction in a manner similar to that suggested for molten polyiodides by Stegemann et al. (28).

[3] $[Br–H–Br]^- + HBr \Leftrightarrow Br–H + [Br–H–Br]^-$

The electrochemical windows for 2:1 TMSuBr:$AlCl_3$ and TMSuBr:$AlBr_3$ melts are 1.9 and 1.8 V, respectively ($Al_2Br_7^-$ is easier to oxidize than $Al_2Br_6Cl^-$) (Fig. 1). The UV–visible

Can. J. Chem. Downloaded from www.nrcresearchpress.com by 65.111.164.53 on 09/08/12
For personal use only.

Fig. 2. UV–visible spectra of (*a*) 2:1 $AlCl_3$:TMSuBr, (*b*) 2:1 $AlBr_3$:TMSuBr, and (*c*) 2:1 $AlCl_3$:ImCl with 0.1 cm quartz cell at 23°C (air reference).

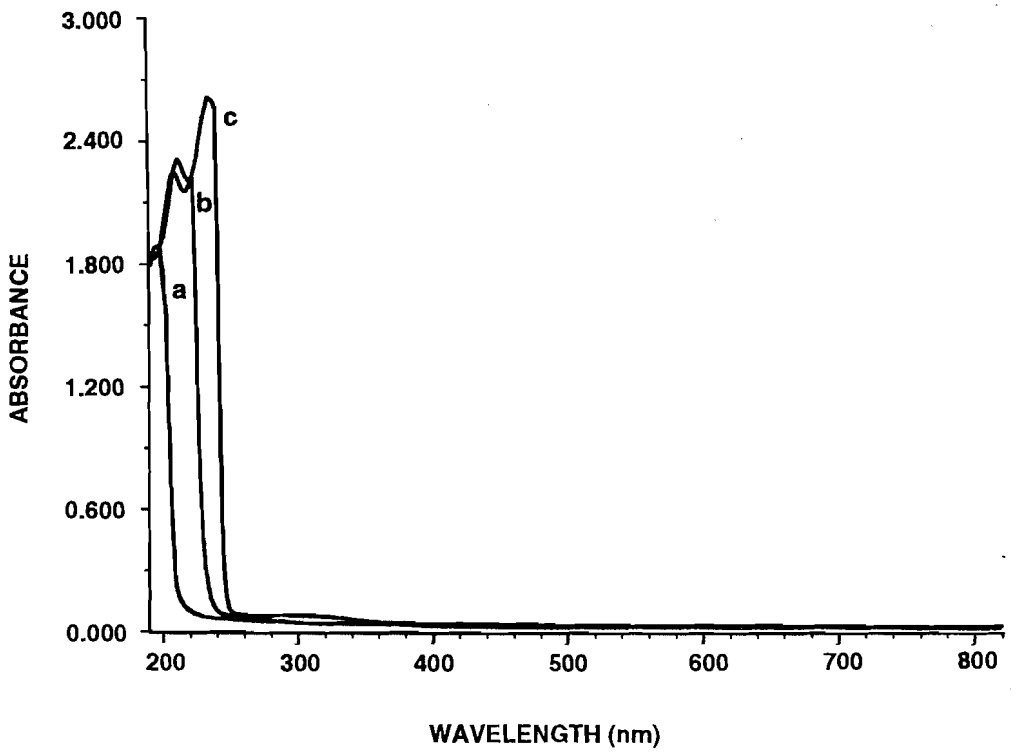

Fig. 3. ^1H NMR spectra of (*a*) 2.0:1 (*b*) 1.4:1, and (*c*) 1.0:1 HBr:TMSuBr melts at 24°C.

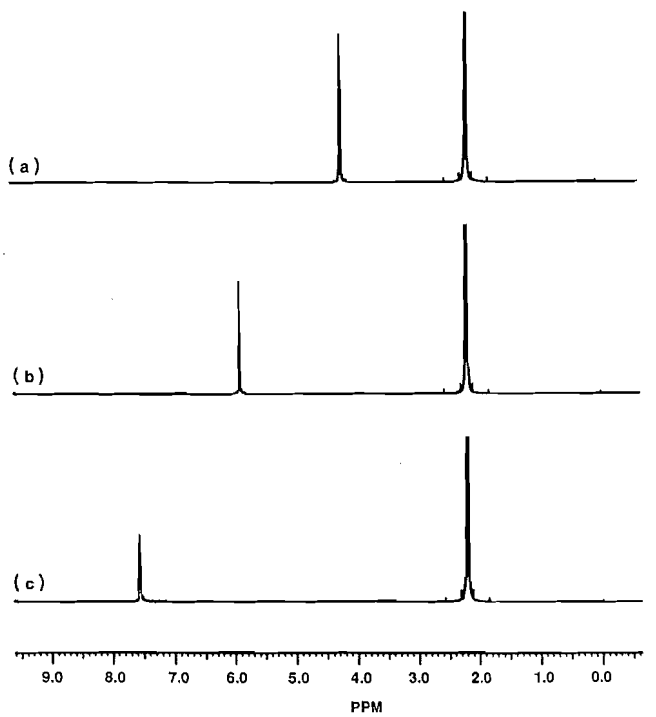

spectra of 2:1 $AlCl_3$:ImCl, $AlBr_3$:TMSuBr and $AlCl_3$:TMSuBr, obtained with a 1 mm cell show UV cutoffs (absorbance = 1) of 242, 228, and 210 nm, respectively (Fig. 2). Thus, bands such as the B band of benzene (λ_{max} = 256 nm) should be completely viewable in the 2:1 AlX_3:TMSuBr (where X is Cl or Br) melts (30).

Fig. 4. ^1H chemical shift vs. HBr:TMSuBr ratio in melts.

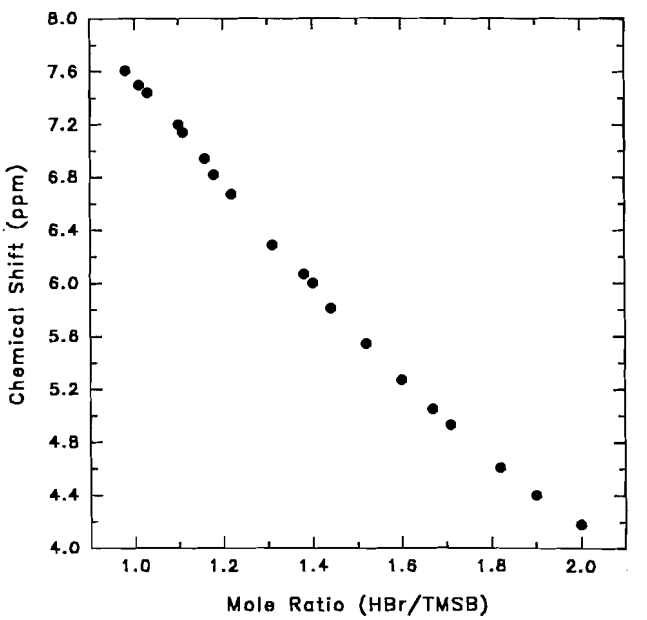

The ^1H NMR spectra of 2:1 AlX_3:TMSuBr melts show the simple $TMSu^+$ methyl proton band. This means that a greater scope for studying ^1H-containing solutes exists in TMSuBr-based melts than in $AlCl_3$:ImCl systems (five distinct solvent bands). Typical ^1H NMR spectra of HBr:TMSuBr melts (Fig. 3) consist of a larger singlet at ~2.18 ppm, attributable to the methyl protons of $TMSu^+$ and a singlet at lower field arising

Can. J. Chem. Downloaded from www.nrcresearchpress.com by 65.111.164.53 on 09/08/12
For personal use only.

Fig. 5. IR spectrum of 1:1 HBr:TMSuBr melt at 23°C.

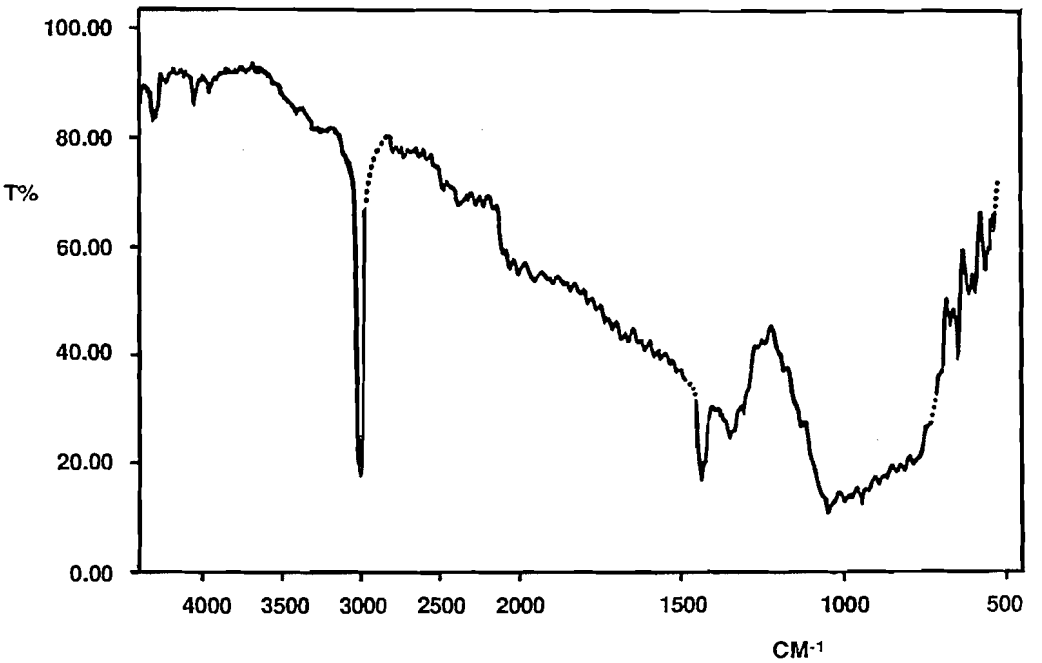

from the added HBr. Since the ^1H signal in $CHCl_2CHCl_2$ occurs at −2.73 ppm vs. TMS for HBr and at 10.2 ppm for HBr_2^- (29) we conclude that the HBr_2^- formation reaction is not complete in the 1:1 mixture with a shift of 8.1 ppm vs. TMS (or 7.60 ppm vs. the external standard). This situation is not found in ImCl:HCl melts (15, 16). As the HBr:TMSuBr mole ratio is increased, the $TMSu^+$ signal is unchanged but the lower field signal intensifies and shifts upfield, reaching 4.18 ppm at a ratio of 2:1 (Fig. 4). This type of behavior *is* observed for HCl:ImCl melts and is readily explained in terms of $H_2Cl_3^-$ formation (15). We suggest that the $H_2Br_3^-$ formation reaction may be occurring at higher HBr concentrations in the HBr:TMSuBr system.

Figure 5 depicts the IR spectrum of 1:1 HBr:TMSuBr. The sharp bands at 3000 and 1435 cm^{-1} can be assigned to the methyl C–H stretching and bending vibrations (14) while the broad bands at 1350 cm^{-1} and 780–1050 cm^{-1} can be assigned by comparison with the spectrum of tetrabutylammonium hydrogen dibromide to ν_2, the degenerate bending mode, and combinations of ν_3 and ν_1, the antisymmetric and symmetric stretching modes, of HBr_2^- (31, 32). The broad absorption between 1500 and 2200 cm^{-1} and the weak band at 2500 cm^{-1} are not found for $(R_4N)(HBr_2)$ (31) or TMSuCl (14) and therefore, must be due to HBr or $H_2Br_3^-$. Comparison with spectral data for $H_2Cl_3^-$ (17), which has a broad absorption centred about 2000 cm^{-1}, and HBr gas (33) with absorption at 2650 cm^{-1} leads to the assignment of the 1500–2200 cm^{-1} band(s) to $H_2Br_3^-$ and the weak 2500 cm^{-1} band to HBr.

The overall implication of the NMR and IR data is that stepwise $Br(HBr)_n^-$ formation proceeds less readily than stepwise $Cl(HCl)_n^-$ formation. Thus, ostensibly stoichiometric TMSuHBr$_2$ contains detectable quantities of $H_2Br_3^-$ and HBr while HBr_2^- and $H_2Br_3^-$ require significant HBr pressure for their formation and endurance. In ImCl:HCl systems, by contrast, HCl is *not* found in solution over the composition range studied (17, 34).

In conclusion, TMSuBr readily forms salts with aluminum halides that are liquid at ambient temperature in the more Lewis acidic composition range and, although somewhat viscous, are promising solvents in terms of their spectroscopic and electrochemical windows. Intuitively, one would wonder about the photostability of bromide melts. Reaction of TMSuBr with HBr can produce HBr_2^- and $H_2Br_3^-$ ions, but less readily than ImCl + HCl yield the chloride species. TMSuHBr$_2$ could be used as an HBr source, but it likely includes Br^-, H_2Br_3, and free HBr as well as HBr_2^-.

References

1. J. Robinson and R.A. Osteryoung. J. Am. Chem. Soc. **101**, 323 (1979).
2. J.S. Wilkes, J.A. Levisky, R.A. Wilson, and C.L. Hussey. Inorg. Chem. **21**, 1263 (1982).
3. Z.J. Karpinski and R.A. Osteryoung. Inorg. Chem. **24**, 2259 (1985).
4. C.L. Hussey, T.B. Scheffler, J.S. Wilkes, and A.A. Fannin, Jr. J. Electrochem. Soc. **133**, 1389 (1986).
5. J. Matsumoto and K. Ichikawa. J. Am. Chem. Soc. **106**, 4316 (1984).
6. L. Heerman and W. D'Oliesleger. Inorg. Chem. **24**, 4704 (1985).
7. J.S. Wilkes, J.S. Frye, and G.F. Reynolds. Inorg. Chem. **22**, 3870 (1983).
8. A.A. Fannin, Jr., L.A. King, J.A. Levisky, and J.S. Wilkes. J. Phys. Chem. **88**, 2609 (1984).
9. J.S. Wilkes, C.L. Hussey, and J.R. Sanders. Polyhedron, **5**, 1567 (1986).
10. A.K. Abdul-Sada, A.M. Greenway, P.B. Hitchcock, T.J. Mohammed, K.R. Seddon, and J.A. Zora. Chem. Commun. 1753 (1986).
11. C.J. Dymek, Jr., D.A. Grossie, A.V. Fretini, and W.W. Adams. J. Mol. Struct. **213**, 25 (1989).

12. S. Tait and R.A. Osteryoung. Inorg. Chem. **23**, 4352 (1984).
13. A.G. Avent, P.A. Chaloner, M.P. Day, K.R. Seddon, and T. Welton. Proc. Int. Symp. Molten Salts, 7th, *Edited by* C.L. Hussey, S.N. Flengas, J.S. Wilkes, and Y. Ito. Electrochemical Society, Pennington, N.J. **98** (1989).
14. S.D. Jones and G.E. Blomgren, Proc. Int. Symp. Molten Salts, 7th, *Edited by* C.L. Hussey, S.N. Flengas, J.S. Wilkes, and Y. Ito. Electrochemical Society, Pennington, N.J. **273** (1989).
15. J.L.E. Campbell and K.E. Johnson. Inorg. Chem. **32**, 3809 (1993).
16. T.A. Zawodzinski, Jr. and R.A. Osteryoung. Inorg. Chem. **27**, 4383 (1988).
17. J.L.E. Campbell, K.E. Johnson, and J.R. Torkelson. Inorg. Chem. **33**, 3340 1994).
18. F. Kaufler and E. Kunz. Ber. Dtsch. Chem. Ges. **42**, 2482 (1909).
19. D.G. Tuck. Prog. Inorg. Chem. **9**, 161 (1968).
20. J. Emsley. Chem. Soc. Rev. **9**, 91 (1980).
21. M.L. Sheely. Ind. Eng. Chem. **24**, 1060 (1932).
22. J.B. Segur and H.E. Oberstar. Ind. Eng. Chem. **43**, 2117 (1951).
23. G. Jones and B.C. Bradshaw. J. Am. Chem. Soc. **55**, 1780 (1933).
24. R.A. Carpio. L.A. King, R.E. Lindstrom, J.C. Nardi, and C.L. Hussey. J. Electrochem. Soc. **126**, 1644 (1979).
25. A.A. Fannin, Jr., D.A. Floreani, L.A. King, J.S. Landers, B.J. Piersma, D.J. Stech, R.L. Vaughn, J.S. Wilkes, and J.L. Williams. J. Phys. Chem. **88**, 2614 (1984).
26. J. Robinson, R.C. Bugle, H.L. Chum, D. Koran, and R.A. Osteryoung. J. Am. Chem. Soc. **101**, 3776 (1979).
27. J.R. Sanders, E.H. Ward, and C.L. Hussey. J. Electrochem. Soc. **133**, 325 (1986).
28. H. Stegemann, A. Rohde, A. Reiche, A. Schnittke, and H. Fullbier. Electrochim. Acta, **37**, 379 (1992).
29. F.Y. Fujiwara and J.S. Martin. J. Chem. Phys. **56**, 4091 (1972).
30. M. Ma and K.E. Johsnon. J. Am. Chem. Soc. **117**, 1508 (1995).
31. J.C. Evans and G.Y-S. Lo. J. Phys. Chem. **71**, 3942 (1967).
32. J.C. Evans and G. Y.-S. Lo. J. Phys. Chem. **73**, 448 (1969).
33. D.E. Gray (*Editor*). American Institute of Physics Handbook. McGraw–Hill, New York. 1972.
34. J.L.E. Campbell. Ph.D. Thesis, University of Regina (1994).

Can. J. Chem. Downloaded from www.nrcresearchpress.com by 65.111.164.53 on 09/08/12
For personal use only.

Ouverture sélective d'époxydes styréniques substitués à l'aide d'azoture de lithium en présence de β-cyclodextrine

Alain Guy, Joël Doussot, Agnès Dallamaggiore et Robert Garreau

Résumé : L'ouverture régio et énantiosélective d'époxydes styréniques substitués racémiques par l'azoture de lithium en présence de β-cyclodextrine est décrite. Le contrôle de la régiosélectivité de la réaction dépend du caractère hydrophobe du substrat qui impose un degré de pénétration plus ou moins important à l'intérieur de la cavité et favorise l'ouverture en β. L'énantiosélectivité observée au cours de la réaction de dédoublement cinétique de l'époxyde racémique est due pour sa part aux interactions non covalentes entre la partie supérieure de la cyclodextrine et la fonction époxyde.

Mots clés : β-cyclodextrine, complexes d'inclusion, contrôle de la régio et stéréosélectivité, chimie en milieu aqueux.

Abstract: Regio- and enantioselective opening of substituted styrenic epoxides by lithium azide in presence of β-cyclodextrin is described. The regioselectivity of the reaction is related to the hydrophobicity of the substrate, which governs its penetration inside the cavity of the cyclodextrin and is favorable to the β opening of the epoxide. The enantioselectivity observed during the kinetic resolution of the racemic epoxide is mainly dependent on the non-covalent interactions between the upper rim of the cyclodextrin and the epoxide.

Key words: β-cyclodextrin, inclusion complexes, regio- and stereocontrol, chemistry in aqueous medium.

Can. J. Chem. Downloaded from www.nrcresearchpress.com by 65.111.164.53 on 09/08/12
For personal use only.

Introduction

La synthèse de β-aminophényléthanols chiraux est un domaine de recherche extrêmement actif en pharmacochimie compte tenu des différences d'activités remarquables observées pour les différents stéréoisomères (1). Parmi les méthodes d'accès à ces β-aminoalcools l'ouverture des époxydes par les réactifs azotés est une méthode avantageuse sur le plan industriel car elle permet d'intégrer dans le produit attendu la majorité des atomes présents dans les différents partenaires de la réaction. Comparée à l'ouverture des époxydes aliphatiques celle des époxydes styréniques pose toutefois un problème de régiosélectivité car une attaque nucléophile se fera sur le carbone benzylique qui est le plus électrophile pour conduire au produit d'ouverture α (2). Seules quelques exceptions permettent d'inverser la régiosélectivité en faveur de l'isomère β (3). L'utilisation des phénomèmes d'association intermoléculaires pour contrôler la sélectivité des réactions est particulièrement étudiée ces dernières années (4). Depuis les travaux de Breslow et Campbell (5) l'utilisation de cyclodextrines comme «microréacteurs» dans le contrôle de la régiosélectivité a été souvent étudiée dans des réactions aussi diverses que l'halogénation, la carboxylation, la formylation, la dihalométhylation et l'allylation de composés aromatiques (6). Dans un article récent nous avons montré que l'ouverture de l'oxyde de styrène dans la β-cyclodextrine (β CD) conduit majoritairement au régioisomère β, contrairement à l'ouverture observée dans l'eau en l'absence de cyclodextrine (7).

Reçu le 27 octobre 1994.

A. Guy,[1] J. Doussot, A. Dallamaggiore et R. Garreau. Conservatoire national des arts et métiers (Laboratoire de chimie organique), 292, rue Saint-Martin, 75141 Paris Cedex 03, France.

1 Auteur correspondant. Téléphone et Fax : (1) 40.27.20.13.

Résultats et discussion

Ouverture régiosélective en β d'époxydes styréniques substitués

Dans ce présent travail nous avons étudié l'influence de la substitution en *para* du noyau aromatique sur la régiosélectivité de l'attaque nucléophile au niveau du carbone homobenzylique. De nombreux auteurs ont montré que l'interaction entre la cavité hydrophobe de la cyclodextrine et le substrat aromatique dépend fortement de la nature de la substitution du noyau aromatique. Dans une étude récente Sanemasa et al. ont montré dans le cas de la β-cyclodextrine que l'association des différents halogénobenzènes suivait l'ordre : I > Br > Cl > H > F (8) qui correspond bien à la variation du caractère hydrophobe du noyau aromatique; cette même séquence se répète pour les *p*-dihalogénobenzènes (9). Notre présente étude a été effectuée sur une série d'époxydes substitués en *para* par des halogènes ou par des groupements alkyles. Tous ces époxydes **1***b–g* ont été obtenus à partir des benzaldéhydes correspondants selon la méthode de Corey et Chaykowsky (10). Leur ouverture a été réalisée par l'azoture de lithium en milieu aqueux soit en absence ou soit en présence de deux équivalents de β-cyclodextrine (figure 1). L'influence de la cyclodextrine s'exerce de deux façons et ceci quelle que soit la nature du substituant (tableau 1). Tout d'abord la régiosélec-

Tableau 1. Ouverture régio et stéréosélective des époxides **1***a*–**1***g* par par LiN_3.

Substrats **1**	Conditions expérimentales β CD/**1** (équiv.)	Durée (h)	Temp. (°C)	Résultats[a] **1**[b] Rdt. (%)	**2**[b] Rdt. (%)	**3** Rdt. (%)	**3** e.e.[c] (%)	Sélect. β (%)
	—	17	20	7	85	8	—	8,5
1*a*	2	17	20	28	36	36	78	50
	5	80	8	34	27	39	74	59
	—	18	20	10,5	86,5	3	—	3,5
1*b*	2	18	20	58	30	12	60	28,5
	2	144	4	77	17	6	66	26
	—	17	20	60,5	37,5	2	—	5
1*c*	2	48	20	70	14	16	28	53,5
	2,5	168	3	55,5	16,5	28	35	63
	5	168	3	62,5	15	22,5	47	60
	—	96	20	76	23	1	—	4
1*d*	2	17	20	75	3	25	10	90
	2,5	162	2	74	5	21	30	80,5
	—	170	20	14	86	0	—	0
1*e*	2	40	20	16,5	51,5	32	38,5	38,5
	2	168	2	80	10,5	9,5	52	47,5
	—	72	20	20	80	0	—	0
1*f*	2	69	20	56	27	17	32	38,5
	2	207	2	56	11	33	60	75
	—	96	20	11	89	0	—	0
1*g*	2	116	20	68	25	7	33	22
	2	258	2	84	11	5	30,5	31

[a]Déterminé par dosage rmn ^1H.

[b]Les e.e. de **1** et **2** sont déterminés par CLHP chirale et varient de 5 à 10%.

[c]Configuration *R* identique pour toute la série, déduite de la comparaison à l'ester de Mosher (12) dérivé du composé *R*(–) **3***a* (7).

Fig. 1. Ouverture des époxides styréniques par l'azoture de lithium.

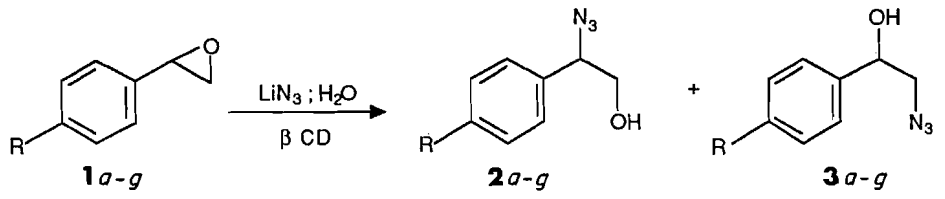

1*a-g* **2***a-g* (Régioisomère α) **3***a-g* (Régioisomère β)

1-3	R	**1-3**	R
a	H	*e*	Me
b	F	*f*	Et
c	Cl	*g*	iPr
d	Br		

Can. J. Chem. Downloaded from www.nrcresearchpress.com by 65.111.164.53 on 09/08/12
For personal use only.

Can. J. Chem. Downloaded from www.nrcresearchpress.com by 65.111.164.53 on 09/08/12
For personal use only.

tivité de l'attaque est inversée par rapport à une réaction sans cyclodextrine. L'ouverture des époxydes par LiN_3 en milieu aqueux fournit les 2-aryl-2-azidoéthanols **2***b–g* avec des régiosélectivités $\alpha > 95\%$ tandis qu'une réaction effectuée sur l'époxyde inclus dans la cyclodextrine inverse la régiosélectivité en conduisant par exemple dans le cas du *p*-bromophényloxirane **1***d* au 2-azido-1-(4-bromo-phényl)-éthanol **3***d* avec une régiosélectivité β de 90%. Aucun effet catalytique n'est observé au cours de cette réaction qui est plus rapide en l'absence de β-cyclodextrine. Cette augmentation des temps de réaction semble due à des problèmes d'insolubilité des complexes en milieu aqueux liés à la nature des époxydes de départ. En présence de β-cyclodextrine l'ouverture peut se produire soit à l'extérieur de celle-ci et conduire uniquement au régioisomère α ou soit à l'intérieur en privilégiant cette fois une ouverture en β. Le principal facteur responsable de ce renversement de régiosélectivité semble être le degré d'enfoncement du noyau aromatique à l'intérieur de la cyclodextrine qui conduit à une ouverture en β grâce à un effet microscopique de solvant inhérent au caractère hydrophobe de la cavité. Lorsque le substrat est inclus moins profondément dans cette cavité, l'attaque de l'époxyde se déroule d'une part dans un environnement bien plus polaire et d'autre part est soumise à une assistance électrophile des hydroxyles secondaires ce qui est favorable à une ouverture en α (figure 2). Ce phénomème s'observe d'une façon concordante en comparant l'évolution parallèle de la régiosélectivité de l'attaque en β des oxiranes substitués par les halogènes aux valeurs des contantes d'associations décrites par Sanemasa pour une substitution identique du noyau aromatique.

Dédoublement cinétique au cours de l'ouverture des époxydes

L'étude de l'induction asymétrique obtenue au cours de l'ouverture nucléophile des époxydes conforte l'hypothèse avancée pour expliquer les variations observées sur la régiosélectivité. Il est connu que l'induction asymétrique résultant de la présence des cyclodextrines est due à une participation préférentielle des hydroxyles secondaires de la partie supérieure plutôt qu'à celle des hydroxyles primaires de la partie inférieure (11). Dans le cas de l'ouverture des époxydes la participation de ces hydroxyles secondaires à une catalyse électrophile est fort probable, compte tenu du mécanisme d'ouverture. Le modèle proposé pour rendre compte de la régiosélectivité observée, pour lequel les époxydes présentant le caractère hydrophobe le plus faible se rapprochent de la partie supérieure de la cyclodextrine, est en accord avec la variation de l'énantiosélectivité obtenue : l'excès énantiomérique (e.e.) atteint 66% en énantiomère de configuration *R* pour l'isomère *para*-fluoré β **3***b* et seulement 30% pour le composé *para*-bromé **3***d* (tableau 1). Des phénomènes de dynamique moléculaire difficile à mettre en évidence jouent aussi probablement un rôle déterminant au cours du contrôle de la sélectivité des réactions. L'inclusion d'un substrat dans la cyclodextrine est un phénomène d'échange rapide et l'examen de l'influence de la température montre que l'abaissement de celle-ci produit un effet important sur l'excès énantiométrique comme le montre les résultats obtenus à partir des époxydes **1***d* et **2***g* qui présentent le caractère hydrophobe le plus important et sont donc à priori les moins rapides à s'échanger. L'encombrement stérique du substituant et donc du noyau aromatique qui va de pair avec l'augmentation du caractère hydrophobe défavorise ces phénomèmes d'échange et permet ainsi une amélioration du contrôle de la régiosélectivité.

Fig. 2. Influence de la substitution sur la sélectivité de l'ouverture dans la β CD.

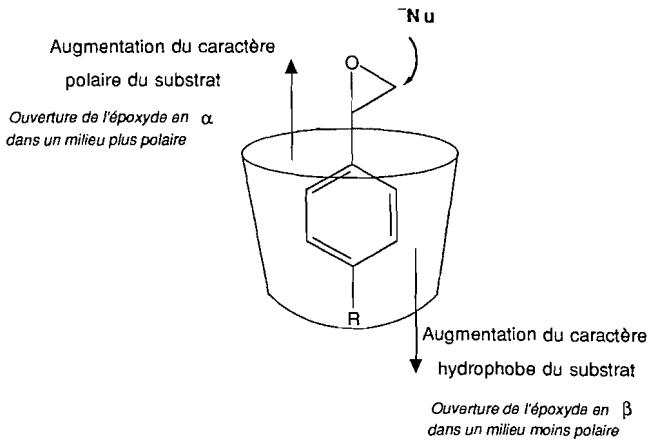

Conclusion

Nous avons montré qu'en présence de β CD l'ouverture en milieu aqueux par l'azoture de lithium d'époxydes styréniques *para*-substitués se fait préférentiellement en position β. Cette régiosélectivité de la réaction dépend du caractère hydrophobe du substrat car il est responsable du degré de pénétration plus ou moins important à l'intérieur de la cavité de la β CD où s'effectue l'ouverture en β.

Le dédoublement cinétique observé au cours de l'ouverture de ces époxydes racémiques est dû pour sa part aux interactions non covalentes entre la partie supérieure de la β et la fonction époxyde ce qui explique que les e.e. les plus élevés sont obtenus cette fois avec les substrats les moins hydrophobes.

Partie expérimentale

Les points de fusion déterminés à l'aide d'un appareil Büchi «méthode Dr Tottoli» ne sont pas corrigés. Les spectres d'absorption ir ont été obtenus avec un spectrophotomètre Philips PU 7916, les produits étants déposés sur des pastilles de KBr. Les spectres de rmn ont été obtenus avec un spectromètre Bruker AC 200 (200 MHz pour le proton et 50 MHz pour le ^{13}C), les échantillons étant dissous dans $CDCl_3$. Les analyses de chromatographie liquide haute performance (CLHP) ont été effectuées à l'aide d'un appareil Waters 590, associé à un détecteur UV Varian de type Vari-chrom. Les basses températures ont été maintenues grâce à un cryostat Fryka-kältetechnik KP 250 avec agitateur magnétique monobloc incorporé. Les microanalyses ont été assurées par les laboratoires Wolff (92583 Clichy Cedex, France).

Synthèses des 2-azido-2-aryléthanols 2 de références

Mode opératoire : L'époxyde **1** (1 mmol) et l'azoture de lithium (1,2 mmol; 0,0588 g) sont mis en suspension dans 10 mL d'eau et agités à la température du laboratoire. La réaction est suivie en chromatographie sur couche mince (ccm) à l'aide de

Can. J. Chem. Downloaded from www.nrcresearchpress.com by 65.111.164.53 on 09/08/12
For personal use only.

l'éluant : heptane/acétate d'éthyle 70/30 (en volume). Les produits sont révélés par pulvérisation d'acide phosphomolybdique : 20% en poids dans l'éthanol. Une moyenne de 80 h est nécessaire pour qu'elle soit complète. Le mélange est extrait deux fois avec 15 mL de dichlorométhane. Les phases organiques regroupées sont séchées sur sulfate de magnésium et évaporées. Le brut est purifié sur colonne de silice 70–230 mesh avec le même éluant que la ccm.

2-Azido-2-phényléthanol **2**a
Régiosélectivité α 96,5%; Rdt. isolé 60%; R_f 0,33; les autres caractéristiques sont conformes à la littérature (13).

2-Azido-2-(4-fluoro-phényl)-éthanol **2**b
Régiosélectivité α 96,5%; Rdt. isolé 65%; R_f 0,43; ir, $\lambda_{max.}$: 3350 (OH), 2100 (N_3); rmn ^{1}H, δ : 2,94 (s large, 1H, OH), 3,58 (m, 2H, partie AB d'un système ABX), 4,48 (dd, 1H, J = 8,1 et 3,9 Hz), 6,90–7,17 (m, 4H arom.); rmn ^{13}C, δ : 66,2 (C1), 66,9 (C2), 115,5–115,9, 128,7–128,9, 132,0–132,1, 160,1–165,0 (C_6H_4). Anal. calc. pour $C_8H_8N_3FO$: C 53,03, H 4,45, N 23,19; tr. : C 52,97, H 4,38, N 23,27.

2-Azido-2-(4-chloro-phényl)-éthanol **2**c
Régiosélectivité α 95%; Rdt. isolé 63%; R_f 0,26; F 60°C; ir, $\lambda_{max.}$: 3350 (OH), 2100 (N_3); rmn ^{1}H, δ : 2,50 (s large, 1H, OH), 3,71 (m, 2H, partie AB d'un système ABX), 4,65 (dd, 1H, J = 7,2 et 5,4 Hz), 7,25–7,39 (m, 4H arom.); rmn ^{13}C, δ : 66,2 (C1), 67,0 (C2), 128,4, 129,0, 134,4, 134,7 (C_6H_4). Anal. calc. pour $C_8H_8N_3ClO$: C 48,62, H 4,08, N 21,26; tr. : C 48,57, H 4,02, N 21,38.

2-Azido-2-(4-bromo-phényl)-éthanol **2**d
Régiosélectivité α 96%; Rdt. isolé 64%; R_f 0,23; F 72°C; ir, $\lambda_{max.}$: 3400 (OH), 2100 (N_3); rmn ^{1}H, δ : 2,17 (s large, 1H, OH), 3,71 (m, 2H, partie AB d'un système ABX), 4,65 (dd, 1H, J = 7,1 et 5,3 Hz), 7,20–7,51 (m, 4H arom.); rmn ^{13}C, δ : 66,2 (C1), 67,0 (C2), 122,6, 128,7, 131,9, 135,2, (C_6H_4). Anal. calc. pour $C_8H_8N_3BrO$: C 39,69, H 3,33, N 17,35; tr. : C 39,65, H 3,29, N 17,41.

2-Azido-2-(4-méthyl-phényl)-éthanol **2**e
Régiosélectivité α 100%; Rdt. isolé 69%; R_f 0,33; les autres caractéristiques sont conformes à la littérature (4*d*).

2-Azido-2-(4-éthyl-phényl)-éthanol **2**f
Régiosélectivité α 100%; Rdt. isolé 60%; R_f 0,48; ir, $\lambda_{max.}$: 3400 (OH), 2100 (N_3); rmn ^{1}H, δ : 1,25 (t, 3H, J = 7,6 Hz), 2,39 (s large, 1H, OH), 2,67 (q, 2H, J = 7,6 Hz), 3,73 (d, 2H, J = 6,4 Hz), 4,65 (t, 1H, J = 6,4 Hz), 7,25 (s, 4H arom.); rmn ^{13}C, δ : 15,3 (CH_3), 28,4 (CH_2), 66,3 (C1), 67,6 (C2), 127,0, 128,3, 133,3, 144,7 (C_6H_4). Anal. calc. pour $C_{10}H_{13}N_3O$: C 62,80, H 6,85, N 21,97; tr. : C 62,78, H 6,83, N 22,01.

2-Azido-2-(4-isopropyl-phényl)-éthanol **2**g
Régiosélectivité α 100%; Rdt. isolé 60%; R_f 0,37; ir, $\nu_{max.}$: 3400 (OH), 2100 (N_3); rmn ^{1}H, δ : 1,26 (d, 6H, J = 6,9 Hz), 2,37 (s large, 1H, OH), 2,92 (hept., 1H, J = 6,9 Hz), 3,73 (d, 2H, J = 6,4 Hz), 4,65 (t, 1H, J = 6,4 Hz), 7,26 (s, 4H arom.); rmn ^{13}C, δ : 27,3 (CH_3), 33,7 (CH), 66,3 (C1), 67,6 (C2), 126,9, 127,0, 133,4, 149,3 (C_6H_4). Anal. calc. pour $C_{11}H_{15}N_3O$: C 64,36, H 7,36, N 20,47; tr. : C 64,39, H 7,35, N 20.52.

Synthèses des 2-azido-1-aryléthanols 3 de références
Le mode opératoire est calqué sur celui de notre précédente publication (4*d*). La seule différence intervient dans le choix du solvant : HMPA pur est remplacé par un mélange 50/50 HMPA/THF sec. On opère à partir de 1 mmol d'époxyde **1**.

2-azido-1-phényléthanol **3**a
Régiosélectivité β 100%; Rdt. isolé 60%; R_f 0,40; les autres caractéristiques sont conformes à la littérature (13).

2-Azido-1-(4-fluoro-phényl)-éthanol **3**b
Régiosélectivité β 86%; Rdt. isolé 55%; R_f 0,51; ir, $\lambda_{max.}$: 3400 (OH), 2100 (N_3); rmn ^{1}H, δ : 3,15 (s large, 1H, OH), 3,38 (m, 2H, partie AB d'un système ABX), 4,80 (dd, 1H, J = 7 et 4,8 Hz), 6,98–7,34 (m, 4H arom.); rmn ^{13}C, δ : 57,8 (C2), 72,5 (C1), 114,9–115,9, 127,4–128,7, 136,2–136,3, 160,0–164,9 (C_6H_4). Anal. calc. pour $C_8H_8N_3FO$: C 53,03, H 4,45, N 23,19; tr. : C 52,95, H 4,34, N 23,29.

2-Azido-1-(4-chloro-phényl)-éthanol **3**c
Régiosélectivité β 98%; Rdt. isolé 68%; R_f 0,39; ir, $\lambda_{max.}$: 3400 (OH), 2100 (N_3); rmn ^{1}H, δ : 3,20 (s large, 1H, OH), 3,39 (m, 2H, partie AB d'un système ABX), 4,84 (dd, 1H, J = 7,0 et 4,8 Hz), 7,30 (s, 4H arom.); rmn ^{13}C, δ : 57,8 (C2), 72,5 (C1), 127,2, 128,6, 133,7, 139,2 (C_6H_4). Anal. calc. pour $C_8H_8N_3ClO$: C 48,62, H 4,08, N 21,26; tr. : C 48,55, H 4,01, N 21,39.

2-Azido-1-(4-bromo-phényl)-éthanol **3**d
Régiosélectivité β 100%; Rdt. isolé 70%; R_f 0,36; ir, $\lambda_{max.}$: 3400 (OH), 2100 (N_3); rmn ^{1}H, δ : 2,56 (s large, 1H, OH), 3,37 (m, 2H, partie AB d'un système ABX), 4,79 (dd, 1H, J = 7,2 et 4,5 Hz), 7,10–7,47 (m, 4H arom.); rmn ^{13}C, δ : 57,9 (C2), 72,8 (C1), 125,9, 127,7, 138,9, 143,7 (C_6H_4). Anal. calc. pour $C_8H_8N_3BrO$: C 39,69, H 3,33, N 17,35; tr. : C 39,66, H 3,31, N 17,39.

2-Azido-1-(4-méthyl-phényl)-éthanol **3**e
Régiosélectivité β 88%; Rdt. isolé 56%; R_f 0,41; les autres caractéristiques sont conformes à la littérature (4*d*).

2-Azido-1-(4-éthyl-phényl)-éthanol **3**f
Régiosélectivité β 84%; Rdt. isolé 44%; R_f 0,56; ir, $\lambda_{max.}$: 3400 (OH), 2100 (N_3); rmn ^{1}H, δ : 1,20 (t, 3H, J = 7,7 Hz), 2,60 (q, 2H, J = 7,7 Hz), 3,39 (m, 2H, partie AB d'un système ABX), 4,10 (s large, 1H, OH), 4,81 (dd, 1H, J = 7,8 Hz et 4,2 Hz), 7,17–7,25 (m, 4H arom.); rmn ^{13}C, δ : 15,2 (CH_3), 28,3 (CH_2), 57,9 (C2), 72,8 (C1), 125,7, 125,9, 133,8, 143,7 (C_6H_4). Anal. calc. pour $C_{10}H_{13}N_3O$: C 62,80, H 6,85, N 21,97; tr. : C 62,77, H 6,81, N 22,03.

2-Azido-1-(4-isopropyl-phényl)-éthanol **3**g
Régiosélectivité β 81%; Rdt. isolé 55%; R_f 0,47; ir, $\lambda_{max.}$: 3400 (OH), 2100 (N_3); rmn ^{1}H, δ : 1,22 (d, 6H, J = 7 Hz), 2,89 (hept., 1H, J = 7 Hz), 3,42 (m, 2H, partie AB d'un système ABX), 3,69 (s large, 1H, OH), 4,82 (dd, 1H, J = 7,9 et 4,1 Hz), 7,16–7,31 (m, 4H arom.); rmn ^{13}C, δ : 23,8 (CH_3), 33,7 (CH), 57,8 (C2), 72,9 (C1), 125,8, 126,4, 138,5, 148,6 (C_6H_4). Anal. calc. pour $C_{11}H_{15}N_3O$: C 64,36, H 7,36, N 20,47; tr. : C 64,40, H 7,34, N 20,50.

Ouverture des époxydes 1 par LiN_3 en présence de β CD
Mode opératoire : Une suspension de β CD (le nombre de moles est indiqué dans le tableau 1) et d'époxyde **1** (1 mmol) dans 10 mL d'eau est vigoureusement agitée 2 h à la température ambiante avant d'être refroidie à l'aide d'un cryostat. L'azoture de lithium (1,5 mmol) est alors ajouté en une seule fois. L'évolution de la réaction est suivie par analyse CLHP dans les conditions suivantes : colonne Hypersil Si 60 (granulométrie 5 μm, longueur 15 cm, diamètre 4,6 mm), détecteur UV : $\lambda = 260$ nm, phase éluante : heptane/acétate d'éthyle 90/10, débit 1 mL min^{-1}. La réaction est interrompue en versant la suspension sur un mélange de 50 mL de DMSO et 30 mL d'eau glacée. Les produits sont extraits à l'éther (3 fois 20 mL). Les phases organiques regroupées sont lavées avec une solution saturée de chlorure de sodium, séchées sur sulfate de magnésium et évaporées pour donner un brut qui est chromatographié sur colonne de silice à l'aide du mélange éluant heptane/acétate d'éthyle 70/30. L'e.e. du composé **3** est déterminé après dérivation avec l'acide (*S*)-(−)-α-méthoxy-α-(trifluorométhyl)-phénylacétique (12), ceux de **1** et **2** par analyse CLHP sur une colonne Chiralpack AD de Daicel. Le tableau 1 regroupe les différents résultats.

Bibliographie

1. R.R. Ruffolo. Tetrahedron Rep. 303, **47**(48), 9953 (1991).
2. J. Gorzinski-Smith. Synthesis, 629 (1984).
3. (*a*) Y. Hu, M. Uno, A. Harada et S. Takahashi. Chem. Lett. 797 (1990); (*b*) Bull. Soc. Chem. Jpn. **64**, 1884 (1991); (*c*) A. Guy, T. Dubuffet et J. Doussot. Synlett, 403 (1991); (*d*) A. Guy, J. Doussot, C. Ferroud, R. Garreau et A. Godefroy-Falguières. Synthesis, 821 (1992); (*e*) J. Iqbal et A. Pandey. Tetrahedron Lett. 575 (1990); (*f*) J. Yamada, M. Yumoto et Y. Yamamoto. Tetrahedron Lett. 4255 (1989).
4. (*a*) G. Wenz. Angew. Chem. Int. Ed. Engl. **33**, 803 (1994); (*b*) K. Takahashi et K. Hattori. J. Inclusion Phenom. Mol. Recognit. Chem. **17**, 1, (1994).
5. R. Breslow et P. Campbell. J. Am. Chem. Soc. **91**, 3085 (1969).
6. M. Komiyama et H. Hirai. J. Am. Chem. Soc. **106**, 174 (1984).
7. A. Guy, J. Doussot, R. Garreau et A. Godefroy-Falguières. Tetrahedron: Asymmetry, **3**, 247 (1992).
8. I. Sanemasa, Y. Wu, Y. Koide, M. Shigenaga, K. Ishibashi et T. Deguchi. Bull. Soc. Chem. Jpn. **66**, 1424 (1993).
9. T. Takuma, T. Deguchi et I. Sanemasa. Bull. Soc. Chem. Jpn. **64**, 480 (1991).
10. E.J. Corey et M.J. Chaykowsky. J. Am. Chem. Soc. **87**, 1353 (1965).
11. (*a*) R.L. VanEtten, J.F. Sebastian, G.A. Clowes et M.L. Bender. J. Am. Chem. Soc. **89**, 3242 (1967); **89**, 3253 (1967); (*b*) C. Van Hooidonk et J.C.A.E. Breebart-Hansen. Recl. Trav. Chim. Pays-Bas, **89**, 289 (1970).
12. J.A. Dale, D.L. Dull et H.S. Mosher. J. Org. Chem. **34**, 2543 (1969).
13. E. Foelsche, A. Hickel, H. Hönig et P. Seufer-Wasserthal. J. Org. Chem. **55**, 1749 (1990).

Can. J. Chem. Downloaded from www.nrcresearchpress.com by 65.111.164.53 on 09/08/12
For personal use only.

A solid-state ^{13}C NMR and theoretical investigation of carbonyl and thiocarbonyl carbon chemical shift tensors

Christopher W. Kirby, Michael D. Lumsden, and Roderick E. Wasylishen

Can. J. Chem. Downloaded from www.nrcresearchpress.com by 65.111.164.53 on 09/08/12
For personal use only.

Abstract: The carbon chemical shift tensors of the carbonyl and thiocarbonyl groups of acetamide, thioacetamide, thioacetanilide, 4′-methoxyacetanilide, and 4′-methoxythioacetanilide have been experimentally determined using dipolar – chemical shift solid-state ^{13}C NMR spectroscopy. The magnitudes of the three principal components of the carbon chemical shift tensors are found to exhibit marked variations between the carbonyl and thiocarbonyl functionalities. However, in contrast to the conclusions of an earlier comparative investigation involving benzophenone and thiobenzophenone, the orientations of the principal axis systems of these chemical shift tensors are found to be similar. These experimental results represent the first complete characterizations of the carbon chemical shift tensor in organic thiocarbonyls. The results of our ab initio GIAO and LORG calculations of carbon chemical shielding tensors in formaldehyde, thioformaldehyde, formamide, and thioformamide as well as in acetamide and thioacetamide are in qualitative agreement with experiment. The findings of the present investigation provide conclusive evidence that the well-known isotropic deshielding of the carbon nucleus in the C=S group relative to C=O is primarily attributable to the decreased energy associated with the $\sigma \leftrightarrow \pi^*$ excitation within the thiocarbonyl fragment. This result is in contrast with the conventional interpretation that the deshielding originates from a red shift in the C=S HOMO–LUMO $n \rightarrow \pi^*$ transition.

Key words: chemical shift tensors, solid-state ^{13}C NMR, carbonyls, thiocarbonyls, ab initio calculations.

Résumé : Utilisant les déplacements chimiques dipolaires de la spectroscopie RMN du ^{13}C à l'état solide, on a déterminé expérimentalement les tenseurs des déplacements chimiques du carbone des groupes carbonyle et thiocarbonyle des acétamide, thioacétamide, thioacétanilide, 4′-méthoxyacétanilide et 4′-méthoxythioacétanilide. On a trouvé que les amplitudes des trois principales composantes des tenseurs des déplacements chimiques du carbone présentent des variations importantes entre les fonctions carbonyles et thiocarbonyles. Toutefois, en opposition avec les conclusions tirées à partir d'une étude comparative antérieure impliquant la benzophénone et la thiobenzophénone, on a trouvé que les orientations des principaux axes de référence de ces tenseurs des désplacements chimiques sont semblables. Ces résultats expérimentaux représentent les premières caractérisations complètes du tenseur du déplacement chimique des thiocarbonyles organiques. Les résultats de nos calculs ab initio GIAO et LORG des tenseurs d'écran chimique du carbone dans les formaldéhyde, thioformaldéhyde, formamide, thioformamide ainsi qu'acétamide et thioacétamide sont en accord qualitatif avec les résultats expérimentaux. Les observations faites dans le présent travail fournissent des bases concluantes qui permettent d'attribuer le déblindage bien connu du noyau du carbone dans le groupe C=S par rapport au C=O à une diminution de l'énergie associée à une excitation $\sigma \leftrightarrow \pi^*$ dans le fragment thiocarbonyle. Ce résultat est en opposition avec l'interprétation conventionnelle qui attribue le déblindage à une déplacement vers le rouge de la transition $n \rightarrow \pi^*$ HO–BV du C=S.

Mots clés : tenseurs des déplacements chimiques, RMN du ^{13}C à l'état solide, carbonyles, thiocarbonyles, calculs ab initio.

[Traduit par la rédaction]

Introduction

The carbonyl carbon chemical shift (CS) tensor has been well characterized with a vast amount of experimental data available for numerous organic and organometallic carbonyls (1). Unfortunately, a comparatively small amount of data exists for thiocarbonyl carbon CS tensors. In fact, to the best of our knowledge, there are only five reports pertaining to the CS tensors of compounds containing C=S (2). Furthermore, only one of these studies involved an organic thiocarbonyl compound (2*b*). In that study, the thiocarbonyl carbon CS tensor of thiobenzophenone was compared with the carbonyl carbon CS tensor in benzophenone using solid-state ^{13}C NMR spectroscopy of powdered samples. Although large differences in the magnitudes of the three principal components of the carbon CS tensors were observed, information concerning the orien-

Received November 25, 1994.

C.W. Kirby, M.D. Lumsden, and R.E. Wasylishen.[1]
Department of Chemistry, Dalhousie University, Halifax, NS B3H 4J3, Canada.

[1] Author to whom correspondence may be addressed. Telephone: (902) 494-2564. Fax: (902) 494-1310. E-mail: RODW@AC.DAL.CA

Can. J. Chem. Downloaded from www.nrcresearchpress.com by 65.111.164.53 on 09/08/12
For personal use only.

tation of these tensors in the molecular frame, which would aid in understanding the observed variations, was unavailable from such powder studies. In an earlier ^{13}C single-crystal NMR investigation of benzophenone (3), it was concluded that the least shielded component lies perpendicular to the carbonyl bond and in the C-C(O)-C plane while the component of intermediate shielding lies parallel with the carbonyl bond. The most shielded direction was associated with the normal to the aforementioned plane. Qualitatively, such an orientation is invariably observed for the carbonyl fragment (4, 5). Consequently, based on the observed differences in the magnitudes of the three principal components of the carbon CS tensors in benzophenone and thiobenzophenone as well as simple electronic structure arguments, it was proposed that the two in-plane principal components exchange orientation in thiobenzophenone with respect to benzophenone. The most shielded direction was predicted to lie perpendicular to the C-C(S)-C plane.

The primary objective of this study was to perform a complete investigation of the carbonyl and, for the first time, thiocarbonyl carbon CS tensors of some simple amides and thioamides using dipolar – chemical shift solid-state ^{13}C NMR spectroscopy (6). This has been performed with two main goals in mind. First, to experimentally characterize the orientation of the thiocarbonyl carbon CS tensor principal axis system (PAS) in thioamides and to compare the results with that in the amides. Secondly, such information then permits a concrete analysis of the origin of the well-known large deshieldings observed for the isotropic carbon CS in the C=S group relative to the C=O fragment. Such deshieldings were previously observed in both solution (7) and the earlier solid-state NMR studies (2) and have also been theoretically calculated (8). The solid-state NMR results have been augmented with ab initio GIAO and LORG carbon chemical shielding tensor calculations involving several small carbonyl- and thiocarbonyl-containing molecules.

Theoretical background

Nuclear magnetic shielding is an orientation-dependent interaction that can be described by a second-rank Cartesian tensor (9–11). The chemical shielding tensor can be quantified by three principal components and three angles that specify the orientation of the tensor principal axis system (PAS). The PAS is a reference frame in which the tensor is diagonal. The NMR spectrum of an isolated spin-½ nucleus in a static powder sample consists of a particular pattern known as a powder pattern (12). The powder pattern is observed because all possible orientations of the molecule are present in the applied magnetic field. In practice, one measures chemical shifts in NMR spectra. The three principal components of the CS tensor (the diagonal elements in the PAS), δ_{11}, δ_{22}, and δ_{33}, are directly available from the powder pattern line shape. The isotropic CS, δ_{iso}, observed in high-resolution NMR studies, is the average of the three principal components. The span of the CS tensor, Ω, is defined as $\delta_{11} - \delta_{33}$ and provides a measure of the anisotropic or orientation-dependent nature of the chemical shielding interaction (13). Another informative parameter is the skew, κ, which is given by $3(\delta_{22} - \delta_{iso})/\Omega$ (13).

As mentioned, the three principal components of the CS tensor are readily available from the powder pattern line shape. However, to determine the orientation of the principal components of the CS tensor in the molecular reference frame requires further experimentation. One technique of relevance to the present work involves introducing a second spin (X) in the vicinity of the $I = ½$ nucleus (A) such that the two spins are dipolar coupled (6). Such a spin system can be described as an isolated spin-pair (AX). The powder pattern for nucleus A will then consist of $2S + 1$ sub-spectra, where S is the spin of nucleus X. The magnitude of the dipolar splittings observed at the positions of each of the three principal components of the CS tensor for nucleus A depends upon the relative orientation of the A spin CS tensor and the AX dipolar interaction. Since the orientation of the dipolar interaction is fixed in the molecular reference frame with the unique axis directed along the internuclear vector, information on the orientation of the A spin CS tensor in the molecule can be obtained from the dipolar splittings. The magnitudes of the dipolar splittings, $\Delta\nu_{ii}$, at each of the three principal components of the CS tensor are given by (12, 14)

$$[1] \quad \Delta\nu_{11} = R_{eff}(1 - 3\sin^2\beta\cos^2\alpha)$$

$$[2] \quad \Delta\nu_{22} = R_{eff}(1 - 3\sin^2\beta\sin^2\alpha)$$

$$[3] \quad \Delta\nu_{33} = R_{eff}(1 - 3\cos^2\beta)$$

where α and β are the polar angles defining the relative orientations of the dipolar and CS tensors (Fig. 1) and

$$[4] \quad R_{eff} = R_{AX} - \frac{\Delta J}{3}$$

$$[5] \quad R_{AX} = \frac{\mu_0}{4\pi}\frac{\gamma_A\gamma_X}{r_{AX}^3}\frac{\hbar}{2\pi}$$

In the above equations, R_{eff} is the effective dipolar coupling constant, R_{AX} is the direct dipolar coupling constant, and ΔJ is the anisotropy in the AX indirect spin–spin (J) coupling. R_{AX} can be calculated provided the AX internuclear separation, r_{AX}, is available (cf. eq. [5]). Note that eqs. [1]–[3] are only strictly valid in the "high-field" limit such that the magnitude of the CS interaction is much greater than the AX dipolar interaction. Under conditions where this requirement is not satisfied and depending upon the relative orientations of these two interactions, asymmetric dipolar splittings may result (14, 15) (cf. Fig. 2 vide infra). Also, since the J coupling involving carbon and nitrogen has previously been found to be small (16), the anisotropy in the J couplings is anticipated to be negligibly small and has not been considered in the present investigation (i.e., $R_{eff} = R_{AX}$).

It is important to indicate that although chemical *shifts*, δ, are measured from NMR spectra, this quantity actually refers to a difference in chemical *shielding*, σ, between the nucleus of interest in a given molecule and in some standard reference compound. Absolute chemical shieldings are reported relative to the bare nucleus (σ = 0 ppm). Consequently, to compare experimental chemical shifts with the theoretical calculations of chemical shielding, the absolute chemical shielding of the nucleus in the reference compound must be known. The refer-

Fig. 1. The orientation of the dipolar vector, r_{AX}, with respect to the chemical shift tensor is defined by the polar angles, α and β.

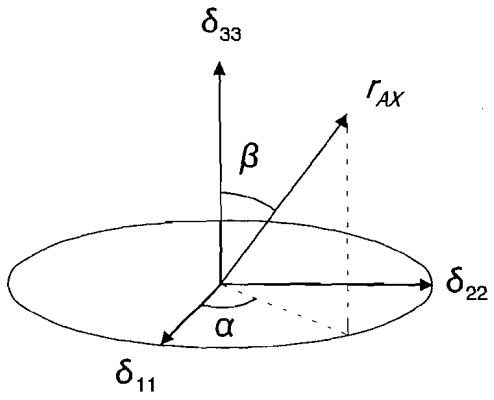

ence compound used in ^{13}C NMR spectroscopy is tetramethylsilane in which the absolute carbon chemical shielding is 186.0 ppm (17). The convention used for designating the three principal components of the CS tensor is $\delta_{11} \geq \delta_{22} \geq \delta_{33}$ where δ_{11} and δ_{33} are the least shielded and most shielded components, respectively (i.e., $\sigma_{11} \leq \sigma_{22} \leq \sigma_{33}$).

Experimental

Preparation of amides

The 10% labelled acetamide-^{13}C(CO) was prepared by adding a mixture of 250 mg (3 mmol) of acetyl chloride-^{13}C(CO) and 2.25 g (29 mmol) of acetyl chloride to 10 g (86 mmol) of concentrated aqueous ammonia at −4°C (18). The solvent was then allowed to evaporate and the acetamide was separated from the ammonium chloride by dissolving the acetamide in hot ethyl acetate, filtering the hot mixture, and allowing it to cool. The 10% labelled acetamide-^{13}C(CO) was collected by filtration after the ethyl acetate had cooled to room temperature.

Acetanilide-^{15}N,^{13}C(CO) and 4′-methoxyacetanilide-^{13}C-(CO) were prepared according to the procedure outlined in ref. 19 with the exception that *p*-anisidine was used in the synthesis of the latter compound.

Preparation of thioamides

The amides above were converted to the corresponding thioamides using Lawesson's reagent (LR) (20). The 10% labelled thioacetamide-^{13}C(CS) was prepared by addition of 1.1 g (2.7 mmol) of LR to 0.32 g (5.4 mmol) of 10% labelled acetamide-^{13}C(CO) in THF which was predried over calcium hydride. The solvent was allowed to evaporate under a stream of nitrogen gas (thioacetamide appeared to decompose under reduced pressure) and the mixture was separated on a silica gel column (12:1 dichloromethane:diethyl ether). Thioacetanilide-^{15}N,^{13}C(CS) and 4′-methoxythioacetanilide-^{13}C(CS) were prepared in an analogous fashion except that the solvent was evaporated under vacuum.

Solid-state NMR spectroscopy

The ^{13}C solid-state NMR spectra were acquired at 50.3 MHz on a Bruker MSL-200 spectrometer (B_0 = 4.7 T) and at 100.6 MHz on a Bruker AMX-400 spectrometer (B_0 = 9.4 T). For the MSL, samples were packed into 7 mm o.d. zirconium oxide rotors. For the AMX, 4 mm o.d. zirconium oxide rotors were used. Cross polarization (CP) under the Hartmann–Hahn matching condition (21) was used to increase the sensitivity of the spectra with typical CP contact times between 5 and 6 ms. Proton 90° pulse widths of 3.5 μs at 4.7 T and 5.7 μs at 9.4 T were employed. High-power ^1H decoupling was used during the acquisition of all spectra. The recycle delay time used for 4′-methoxyacetanilide-^{13}C(CO) and 4′-methoxythioacetanilide-^{13}C(CS) was 10 s. Typical recycle delay times of 30–60 s were used for the remaining compounds. Carbon chemical shifts were referenced to tetramethylsilane by setting the high-frequency carbon signal of adamantane to 38.56 ppm (CH_2).

Calculations

Calculations of the carbonyl or thiocarbonyl carbon chemical shielding tensors of formaldehyde, thioformaldehyde, formamide, thioformamide, and thioacetamide were carried out on an IBM RS6000/580 workstation using a direct version of the TEXAS 90 ab initio program package (22), which implements the GIAO (**G**auge-**I**ncluding **A**tomic **O**rbitals) method (23). A Dunning TZP basis set augmented with 2 sets of polarization functions on all atoms was employed. The geometries of formamide and thioformamide used in these calculations were optimized using GAUSSIAN 92 (24) and a 6-311G** basis set. Experimental geometries were used for the remaining molecules (25). The carbonyl or thiocarbonyl carbon chemical shielding tensors of acetamide and thioacetamide have also been calculated using a Silicon Graphics Indigo^2 XL workstation employing the Localized Orbital/Local Origin (LORG) method (26, 27) and a 6-311 + G(3*d*, 2*p*) basis set. The prerequisite SCF wave functions for the LORG calculations were generated using GAUSSIAN 92 (24).

Calculations of ^{13}C NMR powder pattern line shapes were performed on a 486 personal computer with a FORTRAN-77 program that incorporates the POWDER routine (28). The approach employed here for analyzing the ^{13}C solid-state NMR spectra has been to first use the dipolar-splitting-ratio technique (14) to obtain initial guesses for the polar angles α and β. Consequently, this set of solutions was reduced by considering characteristic values for the carbonyl carbon–nitrogen dipolar coupling in amides (15, 19) and thioamides in conjunction with local symmetry considerations. The corresponding values for α, β, and R_{eff} were then optimized by maximizing the agreement between the experimental and calculated dipolar – chemical shift NMR spectra. To emphasize this agreement in the regions of the shoulders and discontinuities of the powder patterns, these comparisons were performed by examining both the first and second derivatives of the static powder pattern line shapes (29).

Results and discussion

(a) Characterization of the carbon CS tensors

(i) Results for 4′-methoxyacetanilide-^{13}C(CO) and 4′-methoxythioacetanilide-^{13}C(CS)

The experimental ^{13}C NMR spectra obtained for a static powder sample of 4′-methoxyacetanilide at external magnetic field strengths of 4.7 and 9.4 T are presented in Fig. 2. Also shown are the calculated spectra that have been found to best fit the experimental data. The calculated spectra were obtained using

Can. J. Chem. Downloaded from www.nrcresearchpress.com by 65.111.164.53 on 09/08/12
For personal use only.

Can. J. Chem. Downloaded from www.nrcresearchpress.com by 65.111.164.53 on 09/08/12
For personal use only.

Fig. 2. Experimental and calculated ^{13}C NMR spectra for a static powder sample of 4′-methoxyacetanilide-^{13}C(CO) at external magnetic field strengths of 4.7 and 9.4 T, as indicated. The parameters used to calculate the powder patterns are summarized in Table 1.

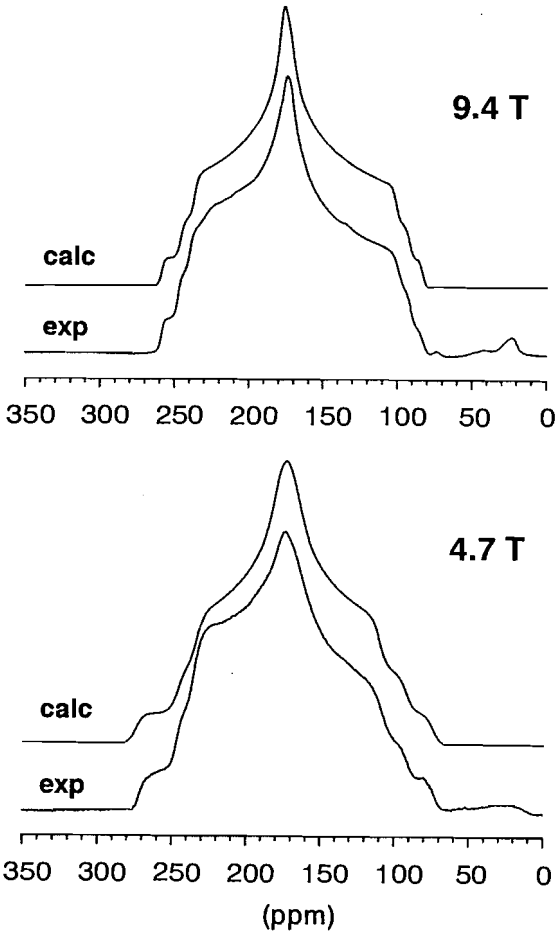

the following parameters (see Table 1): $\delta_{11} = 246 \pm 2$ ppm, $\delta_{22} = 177 \pm 2$ ppm, $\delta_{33} = 92 \pm 2$ pm, $\alpha = 29 \pm 3°$, $\beta = 90 \pm 2°$, $R_{eff} = 895 \pm 40$ Hz. The spectral simulations are in very good agreement with the experimental spectra at both external magnetic field strengths employed in this study. It is worth noting that the spectra obtained at the two magnetic field strengths exhibit significant differences from one another. In particular, notice the large asymmetry observed in the dipolar splittings for the δ_{11} region of the spectrum at 4.7 T. At 9.4 T, this asymmetry is significantly attenuated and is qualitatively due to the increased magnitude of the carbon CS tensor with respect to the ^{13}C–^{14}N dipolar interaction at the larger external field strength (14, 15). Also, as expected, the carbonyl carbon CS tensor of 4′-methoxyacetanilide is the same, within experimental error, as that obtained earlier for acetanilide (cf. Table 1) (19). Finally, given the fact that the dipolar interaction is axially symmetric about the dipolar vector axis and considering the local mirror plane defined by the O=C—N fragment, values of $\alpha = 29°$ and $\beta = 90°$ are consistent with two possible orientations of the CS tensor PAS in the molecular reference frame (cf. Fig. 3). Assuming the molecular geometry within the amide plane of 4′-methoxyacetanilide to be the same as that in acetanilide (30), these correspond to orientations of the

Fig. 3. The two possible orientations of the carbonyl carbon CS tensor PAS for 4′-methoxyacetanilide consistent with the results of the analysis of the dipolar – chemical shift NMR spectra. For orientation (*b*), δ_{11} makes an angle of approximately 30° with respect to the C=O bond axis. The most shielded direction is perpendicular to the plane of the page for both orientations.

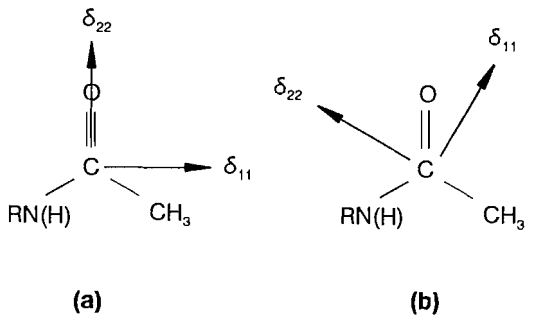

PAS such that (*a*) the two in-plane components, δ_{11} and δ_{22}, lie approximately perpendicular and parallel to the C=O bond axis, respectively, or (*b*) these components lie at angles of approximately 30° and 60°, respectively, with respect to this axis. As already mentioned, it is well established that the former of these two orientations is invariably observed for the carbonyl fragment (4, 5).

In Fig. 4, ^{13}C NMR spectra obtained at 9.4 T for static powder samples of 4′-methoxythioacetanilide (upper) and 4′-methoxyacetanilide (lower) are displayed on the same chemical shift scale for ease of comparison. Immediately apparent are the marked variations present in the magnitudes of each of the three CS tensor principal components; both the least shielded and intermediately shielded components are significantly more deshielded in the thioamide species while the most shielded component is notably more shielded. These variations lead to an overall increase of approximately 125 ppm in the span of the thioamide CS tensor. However, despite these significant differences, the magnitudes of the dipolar splittings, $\Delta\nu_{ii}$, exhibit striking similarities, which immediately suggests analogous orientations of the carbon CS tensor PAS in these two compounds. It should be emphasized that the possibility of an exchange in orientation of the two in-plane CS tensor components, as speculated for the benzophenone/thiobenzophenone system (2*b*), is readily rejected based on the relative magnitudes of the dipolar splittings, $\Delta\nu_{11}$ and $\Delta\nu_{22}$, extracted from the dipolar – chemical shift powder pattern observed for the thioamide. Such an exchange would result in larger dipolar splittings in the δ_{22} region of the powder pattern compared with the δ_{11} region, contrary to the experimentally observed result. The parameters used to calculate the ^{13}C NMR powder spectra of 4′-methoxythioacetanilide at both applied fields employed in this study are summarized in Table 1. The fact that $\beta = 90°$ indicates that the most shielded component, δ_{33}, lies normal to the S=C—N mirror plane. Although there exists a twofold ambiguity in defining the directions of the two in-plane tensor components, if one considers the symmetry of the electronic framework of the thiocarbonyl fragment as well as the results of ab initio MO carbon chemical shielding tensor calculations for several simple thioamides (vide infra), only the solution for which the intermediately shielded component is directed close to the C=S bond direction is reasonable.

Can. J. Chem. Downloaded from www.nrcresearchpress.com by 65.111.164.53 on 09/08/12
For personal use only.

Table 1. Principal components and orientations of the C=O and C=S carbon CS tensors in several amides and thioamides.[a]

Compound	δ_{iso} (ppm)	δ_{11} (ppm)	δ_{22} (ppm)	δ_{33} (ppm)	α (°)	β (°)	R_{eff} (Hz)	Ω (ppm)
4′-Methoxyacetanilide-^{13}C(CO)	171.3[b]	246	177	92	29	90	895	154
4′-Methoxythioacetanilide-^{13}C(CS)	205.5[b]	343	211	62	29	90	925	281
Acetanilide-^{15}N,^{13}C(CO)[c]	171.5[b]	248	175	90	30	90	1230	158
Thioacetanilide-^{15}N,^{13}C(CS)	202	341	205	61	30	90	1257	280
Acetamide-^{13}C(CO)	176.9[b]	243	202	86	38	90	888	157
Thioacetamide-^{13}C(CS)	206	330	228	61	30	90	950	269
Benzophenone-^{13}C(CO)[d]	200	272	229	99	—	—	—	173
Thiobenzophenone-^{13}C(CS)[d]	236	384	275	49	—	—	—	335

[a]The errors associated with the data obtained in the present investigation are as follows: δ_{ii} ±2 ppm, α ±3°, β ±2°, and R ±40 Hz unless otherwise indicated in the text.

[b]Obtained from CP/MAS solid-state NMR spectra.

[c]From ref. 19.

[d]From ref. 2. Note that the chemical shifts reported in this study were with respect to liquid CS_2. These chemical shifts have been converted to the TMS scale using an isotropic shift for CS_2 of 192.8 ppm with respect to TMS.

Fig. 4. Experimental ^{13}C NMR spectra obtained at 9.4 T for static powder samples of 4′-methoxyacetanilide-^{13}C(CO) (lower) and 4′-methoxythioacetanilide-^{13}C(CS) (upper). Features apparent in the experimental spectra in the region 10–80 ppm are due to carbon-13 nuclei present in natural abundance.

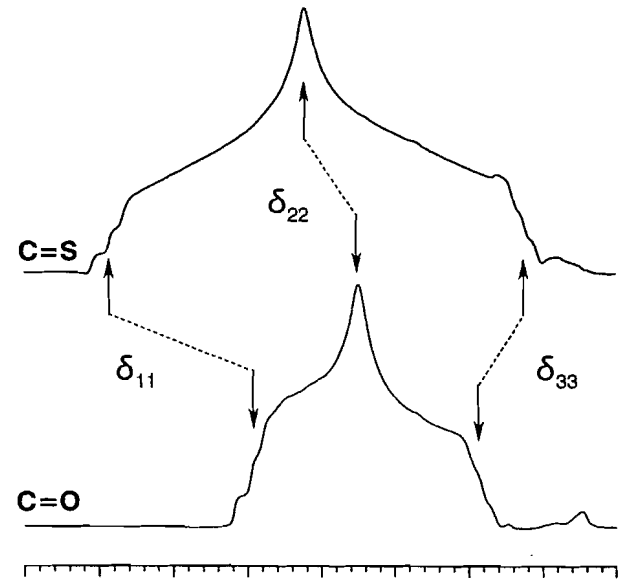

(ii) Results for thioacetanilide-^{15}N,^{13}C(CS)

Carbon-13 NMR spectra for static powder samples of thioacetanilide-^{15}N,^{13}C(CS) have been obtained and analyzed at external magnetic field strengths of 4.7 and 9.4 T, the results of which are summarized in Table 1. These findings can be compared with those of an earlier investigation involving acetanilide-^{15}N,^{13}C(CO) (cf. Table 1) (19). As anticipated, the three principal components of the carbon CS tensor show trends analogous to those observed for the methoxy-substituted species, with the least shielded component displaying the largest sensitivity to sulfur substitution. Analysis of the ^{15}N–^{13}C dipolar splittings observed for thioacetanilide-^{15}N,^{13}C(CS) indicates a similar orientation of the CS tensor PAS to that observed in acetanilide-^{15}N,^{13}C(CO) (19). Despite the aforementioned ambiguity inherent in assigning this orientation to the molecular reference frame, it is quite clear for reasons previously outlined that the CS tensor PAS is oriented such that the most shielded direction is normal to the S=C—N plane while δ_{22} lies within this plane near the thiocarbonyl bond axis. Unfortunately, the absence of structural data for this system precludes a more quantitative analysis of this tensor orientation in the molecular reference frame.

Upon examination of the isotropic region of the ^{13}C CP/MAS spectrum of thioacetanilide-^{15}N,^{13}C(CS) obtained at 4.7 T, a rather peculiar line shape was observed (cf. Fig. 5*a*). The spectrum suggests the presence of at least two crystallographically nonequivalent molecules in the unit cell of thioacetanilide. This conclusion has been verified by a preliminary X-ray structural analysis (T.S. Cameron, unpublished results); unfortunately, the exact number of distinct sites could not be defined due to the poor diffracting characteristics of the thioacetanilide crystals. Also apparent from the spectrum in Fig. 5*a* is the fact that the low-frequency peak has an integrated area approximately three times that of the high-frequency peak, suggesting the presence of unresolved peaks. A ^{13}C CP/MAS spectrum was also obtained at 9.4 T and is displayed in Fig. 5*b*. Clearly, the spectrum obtained at the higher field suggests that there actually exist four crystallographically nonequivalent molecules in the unit cell. We wish to emphasize, however, that given the small range of isotropic chemical shifts observed, 204.1–201.9 ppm, differences in the individual principal components of the carbon CS tensors for the unique sites are expected to be negligibly small and hence have not been considered in analyzing the NMR spectra obtained for a static powder sample of thioacetanilide-^{15}N,^{13}C(CS).

(iii) Results for acetamide and thioacetamide

The results of the analysis of the ^{13}C NMR spectra obtained

Can. J. Chem. Downloaded from www.nrcresearchpress.com by 65.111.164.53 on 09/08/12
For personal use only.

for static powder samples of 10% labelled acetamide-^{13}C(CO) and thioacetamide-^{13}C(CS) at 4.7 and 9.4 T are summarized in Table 1. As for the previous two amide/thioamide pairs investigated here, each of the three CS tensor components shows a significant sensitivity to sulfur substitution with both δ_{11} and δ_{22} more deshielded and δ_{33} more shielded in the thiocarbonyl fragment. As well, the least shielded component once again shows the greatest sensitivity, shifting some 87 ppm to higher frequency in the thioamide. The orientations of the carbon CS tensor PAS in these two compounds are qualitatively analogous in that the intermediately shielded component lies near the carbonyl or thiocarbonyl bond and the most shielded direction is normal to the amide/thioamide plane. Once again, a switch in orientation of the two in-plane components, δ_{11} and δ_{22}, would contradict the results of the present investigation. Based on an O=C—N bond angle of 122.3° in acetamide, obtained from an earlier low-temperature neutron diffraction study (31), δ_{22} is calculated to lie 6° off the carbonyl bond axis but on the opposite side compared with the other amides and thioamides considered here. A low-temperature neutron diffraction study has also been carried out for thioacetamide, indicating two crystallographically nonequivalent molecules in the unit cell (25*b*).[2] The two distinct molecules were found to possess slightly different geometries about the thiocarbonyl carbon atom, with one environment planar and the other slightly pyramidal (25*b*). CP/MAS carbon NMR spectra obtained for thioacetamide presumably reflect the presence of these distinct sites; instead of observing a simple asymmetric doublet (32) as for the majority of the amides investigated here, additional fine structure was evident. However, it should be noted that no evidence for these independent sites was apparent in the NMR spectra obtained for static powder samples of thioacetamide. Using the S=C—N bond angle observed for the planar site, 122.7°, yields the result that the intermediately shielded component lies 3° off the C=S bond axis but on the opposite side as in acetamide. The results for the orientations of the carbon CS tensor PAS in these two compounds are illustrated in Fig. 6. It should be mentioned that the errors in the orientation of the CS tensor PAS in thioacetamide are somewhat larger than in the remaining compounds investigated here due to an extensive overlap of the low-frequency end of the thiocarbonyl powder pattern with the methyl region of the spectrum arising from naturally abundant ^{13}C nuclei (1.1% natural abundance).

It is interesting to examine the changes observed in the three principal components of the CS tensors upon comparing the acetamides to the acetanilides. Although the spans of these CS tensors do not exhibit dramatic variations, significant increases are evident in the skew of the acetamide tensors; this is predominantly attributable to sizeable deshieldings of the intermediately shielded component in the acetamides relative to the corresponding acetanilides. Although the complex task of definitively tracing the origins of such deshieldings is not directly feasible, it is worth mentioning that intermolecular influences on the carbon CS tensors will undoubtedly show a

[2] Note that the unit cell of thioacetamide contains two crystallographically nonequivalent molecules in the unit cell. The geometry of the molecule possessing a S=C—N mirror plane was employed in the carbon chemical shielding calculation for thioacetamide.

Fig. 5. CP/MAS ^{13}C NMR spectra of thioacetanilide-^{15}N,^{13}C(CS) obtained at 50.3 MHz (*a*) and 100.6 MHz (*b*). The MAS frequencies employed were 2707 and 5500 Hz for (*a*) and (*b*), respectively.

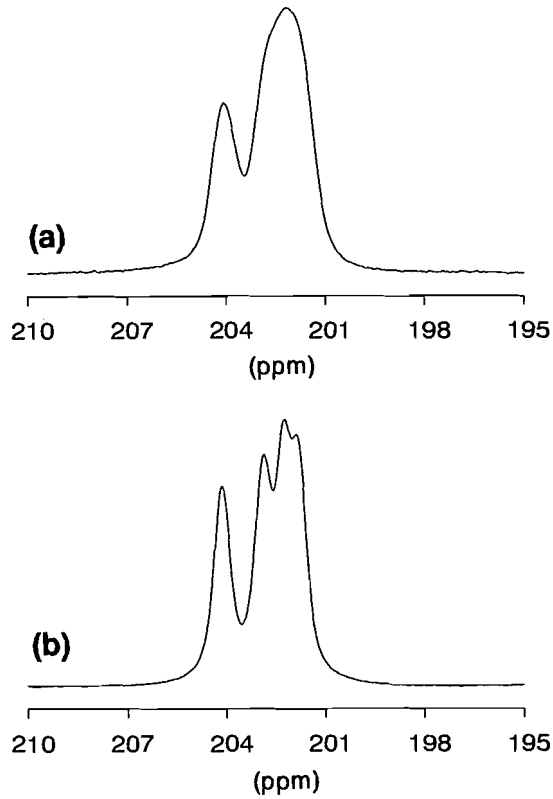

Fig. 6. Experimental results for the orientation of the carbon CS tensor PAS in acetamide (*a*) and thioacetamide (*b*). The angle between δ_{22} and the carbonyl/thiocarbonyl bond axis is 6° and 3° for acetamide and thioacetamide, respectively. The most shielded direction is perpendicular to the plane of the page for both compounds.

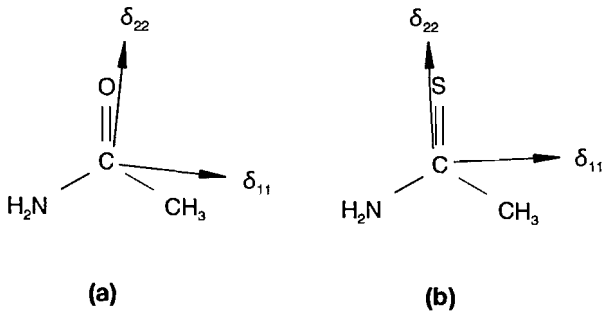

wide variation between the primary and secondary amides/thioamides. For example, in both acetamide and thioacetamide, the group 16 atom is involved in two asymmetric hydrogen bonds with neighbouring molecules (25*b*, 31), unlike the case for acetanilide where a single intermolecular hydrogen bond exists (30). Previous experimental and theoretical work has suggested the component of the carbonyl carbon CS tensor most sensitive to hydrogen bonding to be the component lying nearest the carbonyl bond axis, the intermediately shielded component, δ_{22} (19, 33). This component has been observed to become more deshielded with increasing

Can. J. Chem. Downloaded from www.nrcresearchpress.com by 65.111.164.53 on 09/08/12
For personal use only.

hydrogen bond strength. Consequently, differences in the hydrogen bonding networks may partially account for the observed deshielding of δ_{22} in acetamide relative to the acetanilides. Despite the fact that N-H·····S=C hydrogen bonds are expected to be weaker than N-H·····O=C bonding, the fact that thioacetamide and the thioacetanilides also display this trend is consistent with this argument and provides further support for our conclusion that the intermediately shielded component lies nearest the thiocarbonyl bond axis.

(b) Carbon chemical shielding tensor calculations

The results of the ab initio MO carbon chemical shielding tensor calculations using the GIAO method for formaldehyde, thioformaldehyde, formamide, thioformamide, as well as acetamide and thioacetamide are presented in Table 2. Examination of the magnitudes of the carbon chemical shielding tensor components for each of the three pairs of molecules indicates analogous trends to those observed experimentally, although the calculated shielding differences are somewhat larger than observed. In each case both the least shielded and intermediately shielded components are calculated to be more deshielded in the thiocarbonyl compounds while the most shielded components are predicted to be more shielded in these species. The fact that σ_{11} displays the greatest sensitivity to sulfur substitution in each case is also in agreement with the experimental findings. More importantly for the purposes of the present investigation, for each of the six molecules theoretically examined, the orientation of the carbon chemical shielding tensor PAS is calculated such that σ_{33} is oriented normal to the O=C—N or S=C—N plane and σ_{22} lies within this plane parallel to or nearest the carbonyl/thiocarbonyl bond axis. These results provide further conclusive evidence that the orientations of the carbon CS tensor PAS within the carbonyl and thiocarbonyl fragments are qualitatively the same and that the two in-plane components, σ_{11} and σ_{22}, do not switch orientation within these groups.

In Table 3, the results of the carbon chemical shielding tensor calculations for acetamide and thioacetamide have been converted to chemical shift values in order to facilitate a direct comparison between the experimental and theoretical results. The calculations are reasonably successful in predicting the orientations of the tensors as well as in reproducing the magnitudes of the δ_{22} and δ_{33} components. However, the agreement in the least shielded components is much less satisfactory, particularly in thioacetamide. It is interesting that the calculated isotropic chemical shift in acetamide is the same as the experimental value despite the deviations in the tensor components. This result emphasizes the significance of including the tensor principal components and not just the isotropic value when reporting the results of shielding tensor computations. Finally, improving the agreement between the experimental and theoretical results could undoubtedly be achieved by incorporating the effects of intermolecular interactions into the calculations. Furthermore, electron correlation has previously been found to be significant for the carbon shielding within the carbonyl fragment (34). In light of the nature of the electronic structure of thiocarbonyls relative to carbonyls, this argument is anticipated to also hold true for the C=S group.

(c) Discussion

According to the theory of Ramsey (35), the small induced magnetic fields that are the basis of the chemical shielding interaction originate from two distinct modes of induced electronic motion in the presence of an external magnetic field. These motions give rise to the diamagnetic and paramagnetic contributions to the total chemical shielding experienced by a nucleus. The diamagnetic shielding contribution is positive and yields an increase in shielding. Qualitatively, diamagnetic shielding is dominated by the core electrons of an atom. Consequently, it shows little variation with the orientation of a molecule in an external magnetic field and, for a given nucleus, is relatively insensitive to the nature of the molecular system under investigation. On the other hand, the paramagnetic shielding interaction, which is generally negative and gives rise to decreased shieldings, is highly orientation dependent with the magnitude of paramagnetic shielding in a particular direction being sensitive to induced electronic currents in a plane perpendicular to this direction (36). Qualitatively, such

Table 2. Calculated carbon chemical shielding tensors within the carbonyl or thiocarbonyl fragment for several small model compounds.[a]

Compound	σ_{11} (ppm)	σ_{22} (ppm)	σ_{33} (ppm)	σ_{iso} (ppm)	ϕ^b (°)
Formaldehyde	−111	−13	122	−1	0
Thioformaldehyde	−273	−109	173	−70	0
Formamide	−69	53	116	33	−6
Thioformamide	−211	−10	149	−24	0
Acetamide[c]	−101	14	113	9	+2
Thioacetamide	−241	−46	145	−47	+5

[a]The calculations were performed using the GIAO method and a Dunning TZP basis set.

[b]ϕ is the angle between σ_{22} and the carbonyl or thiocarbonyl bond axis. Positive angles refer to the side of the bond that corresponds to the direction towards the nitrogen atom. In all cases, the most shielded direction is calculated to be perpendicular to the O=C—N or S=C—N plane.

[c]From ref. 19.

Table 3. Comparison of the calculated and experimental carbonyl/thiocarbonyl carbon CS tensors in acetamide and thioacetamide[a]

Compound		δ_{11} (ppm)	δ_{22} (ppm)	δ_{33} (ppm)	δ_{iso} (ppm)	ϕ^b (°)
Acetamide	Calcd.[c]	287	172	73	177	+2
	Expt.	243	202	86	177	−6
Thioacetamide	Calcd.	427	232	41	233	+5
	Expt.	330	228	61	206	+3

[a]The calculated chemical shielding tensor principal components have been converted to chemical shift values using the absolute carbon chemical shielding in TMS, 186.0 ppm (17).

[b]ϕ is the angle between δ_{22} and the carbonyl or thiocarbonyl bond axis. Positive angles refer to the side of the bond that corresponds to the direction towards the nitrogen atom. In all cases, the most shielded direction is calculated to be perpendicular to the O=C—N or S=C—N plane.

[c]From ref. 19.

Can. J. Chem. Downloaded from www.nrcresearchpress.com by 65.111.164.53 on 09/08/12
For personal use only.

electronic motion can be envisioned as arising from perturbations to the ground-state electronic structure of a molecule due to the presence of an external magnetic field. More specifically, the external field induces a mixing of certain excited electronic states with the ground state of a molecule provided that the mixed states are related via a rotation of electronic charge (i.e., the mixing is driven by the orbital angular momentum of the relevant electronic states). For further information, the reader is referred to an early article by Jameson and Gutowsky, which provides a "multiplication table" showing the effects of the orbital angular momentum operators on the various *p* atomic orbitals (37). Consequently, the paramagnetic shielding contribution to the total chemical shielding tensor is intricately related to both the local symmetry and structure of the electronic framework of a molecule in the vicinity of the shielded nucleus. It is precisely the nature of these relationships that gives rise to the anisotropic behaviour of paramagnetic shielding as well as its dominance in dictating the range of chemical shifts observed within a particular molecular fragment. Therefore, to understand the orientation dependence of the carbon CS within the carbonyl and thiocarbonyl groups as well as the observed differences between these groups, it is most important to consider variations within the paramagnetic shielding term. Crucial to the following discussions is the fact that paramagnetic shielding is not only sensitive to the molecular wave functions for the relevant mixed electronic states but is also weighted by the inverse energy separation between these states and the ground state (i.e., $\sigma_p \propto 1/\Delta E$). As well, the contributions of the relevant electrons to the paramagnetic shielding term are further weighted according to the inverse cube of their separation from the shielded nucleus (35).

As indicated, the orientation of the carbon CS tensor PAS within the carbonyl fragment is well established (4, 5). In agreement with the experimental results obtained here, the most shielded direction is invariably found to lie normal to the plane comprising the carbonyl group. Therefore, symmetry dictates that the paramagnetic shielding in this direction must originate from high-energy $\sigma \leftrightarrow \sigma^*$ excitations. The least shielded component, δ_{11}, lies within the aforementioned plane and approximately perpendicular to the carbonyl bond axis and is thus influenced by $\sigma \leftrightarrow \pi^*$ as well as $\pi \leftrightarrow \sigma^*$ transitions. Finally, the intermediately shielded component, δ_{22}, also consistently lies within this plane but approximately collinear with the carbonyl bond axis. Based on symmetry considerations, $n \leftrightarrow \pi^*$ excitations contribute to the paramagnetic shielding in this direction. Furthermore, $\sigma \leftrightarrow \pi^*$ and $\pi \leftrightarrow \sigma^*$ transitions involving the C-C and C-N σ-bonds can also influence the paramagnetic shielding along the C=O bond axis. Before discussing the results obtained for the thioamides, it is important to mention that, in general, a rationalization of a tensor orientation based exclusively upon energy differences between the contributing excited states is not justifiable; the orientation of the carbonyl carbon CS tensor illustrates this point. Clearly, based solely on energy considerations, one would anticipate the least shielded direction (δ_{11}) to be along the CO bond as the $n \leftrightarrow \pi^*$ excitation is the HOMO–LUMO transition within the carbonyl fragment. The fact that the CO bond axis corresponds to the intermediately shielded direction must primarily be a manifestation of the distance dependence of the paramagnetic shielding term. More specifically, the lone pair MO involved in the $n \leftrightarrow \pi^*$ transition is essentially localized on the oxygen atom. Consequently, although favoured based on energy considerations, this influence is undoubtedly offset by an attenuation of the paramagnetic shielding along the carbonyl bond axis due to the r^{-3} dependence, resulting in this axis being the intermediately shielded direction.

The fact that both the experimental and theoretical results indicate analogous orientations of the carbon CS tensor PAS within the carbonyl and thiocarbonyl groups immediately indicates that the thiocarbonyl tensor orientation can be understood using electronic transition symmetry arguments as for the carbonyl fragment. An interesting finding of the present investigation is that both of the in-plane CS tensor components, δ_{11} and δ_{22}, are more deshielded in the thioamides than in the amides. Although the origin(s) of this deshielding cannot be traced with certainty from these results, it is worth emphasizing that both δ_{11} and δ_{22} are sensitive to the relative accessibility of the π^* MO given that the in-plane paramagnetic shielding is controlled by out-of-plane excitations. Consequently, the anticipated stabilization of the π-antibonding MO within the thioamides relative to the amides (2*e*) must contribute, at least in part, to the observed in-plane deshielding. The result that the in-plane CS tensor component sensitive to the HOMO–LUMO $n \leftrightarrow \pi^*$ transition, δ_{22}, exhibits an apparent smaller sensitivity to sulfur substitution than that of the in-plane perpendicular component, δ_{11}, is not readily rationalized based exclusively on energy considerations. Once again, the distance dependence of the paramagnetic shielding term must, at least in part, be responsible for this result. Clearly, the fact that the in-plane perpendicular component is influenced by transitions involving MOs that possess a relatively large amount of carbon-2*p* AO character must also contribute to the relative sensitivities of the two in-plane CS tensor components. Finally, it is interesting that the component perpendicular to the amide/thioamide plane is more shielded in the thioamides than in the amides. However, given the multitude of plausible factors that could be influencing this trend, a definitive explanation unfortunately remains elusive.

In an effort to gain further information concerning the origins of the observed CS within the amides and thioamides, ab initio LORG carbon chemical shielding tensor calculations have been performed for acetamide and thioacetamide. Although both the GIAO and LORG approaches employ distributed gauge origins in order to attenuate the well-known gauge dependence of chemical shielding calculations, the latter method has the advantage that these origins are incorporated within localized MOs of the molecule under investigation. Consequently, the chemical shielding tensor within this formalism is constructed as a series of localized bond contributions, which facilitates a physical understanding of the computed tensors. The calculated LORG tensor components of acetamide and thioacetamide are provided in Table 4 and are found to be very similar to the results of the GIAO calculations (cf. Table 2). The calculated σ_{ii} have also been decomposed in Table 4 according to the contributions of the relevant valence MOs. The results predict that the least shielded components in these species are indeed dominated by the carbonyl/thiocarbonyl σ and π MOs (i.e., $\sigma \leftrightarrow \pi^*$ and $\pi \leftrightarrow \sigma^*$) and that the major contributor to the deshielding of δ_{11} in the thioamides relative to the amides involves the C-S σ-bond. As well, the major contributions to the paramagnetic

Table 4. Decomposition of the principal components of the carbon chemical shielding tensors in acetamide and thioacetamide, σ_{ii}, according to the contributions of the relevant valence localized MOs.[a]

	Acetamide[b]				Thioacetamide[c]		
	σ_{11}	σ_{22}	σ_{33}		σ_{11}	σ_{22}	σ_{33}
C-O σ	−161	13	−33	C-S σ	−252	13	−11
C-O π	−45	20	3	C-S π	−80	15	1
O l.p.	−34	47	−12	S l.p.	−27	27	−10
C-N	−13	−95	−14	C-N	−8	−78	−9
C-C	−42	−120	−20	C-C	−68	−124	−5
Other	201	147	193	Other	198	110	189
Total	−94	12	117	Total	−237	−37	155

[a]The calculations have been performed using the LORG method and a 6-311+G(3*d*, 2*p*) basis set.

[b]The results for the orientation of the chemical shielding tensor PAS in acetamide are analogous to the GIAO results (cf. Table 2). The angle ϕ is calculated to be +4°.

[c]The results for the orientation of the chemical shielding tensor PAS in thioacetamide are analogous to the GIAO results (cf. Table 2). The angle ϕ is calculated to be +8°.

shielding along the carbonyl/thiocarbonyl bond axis are associated with the C-C and C-N σ-bonds whereas the lone pair (l.p.) MOs of oxygen and sulfur make a shielding contribution in this direction. It should be mentioned that similar findings were previously reported by Schindler and Kutzelnigg from an IGLO calculation on formaldehyde (38). However, it is interesting that the lone pair MOs are predicted to make the largest contribution to the decreased shielding observed for δ_{22} in thioacetamide relative to acetamide. Finally, the calculations indicate that both the C-S and C-C σ-bonds are the primary sources of the shielding observed normal to the thioamide plane in thioacetamide relative to acetamide.

In light of the experimental findings for the thioamide CS tensors obtained here, the common interpretation of the decreased isotropic chemical shielding in the thiocarbonyl group relative to the carbonyl group in terms of decreased $n \rightarrow \pi^*$ energies (see, for example, ref. 39) must be revoked; it appears a decrease in energy of $\sigma \rightarrow \pi^*$ transitions is the predominant cause of this deshielding. This result is illustrative of the dangers inherent in the familiar practice of deriving relationships between HOMO–LUMO excitation energies and *isotropic* chemical shifts and emphasizes the sensitivity of paramagnetic shielding to factors other than energy differences. Clearly, regardless of the strength of HOMO–LUMO excitation energy and isotropic CS correlations, projecting such findings to rationalize isotropic chemical shift differences is completely unsubstantiated in the absence of information concerning trends in the individual CS tensor components as well as the orientation of these components in the molecular frame.

In closing, some comments concerning the results of the benzophenone/thiobenzophenone investigation (2*b*) are in order. The three principal components of the carbonyl/thiocarbonyl carbon CS tensors measured for these compounds are provided in Table 1. The tensor components show analogous trends to those observed within the amides and thioamides investigated here. It appears that the conclusion of this paper that the two in-plane tensor components exchange orientation was based on the assumption that the CS tensor components lying along the C=O and C=S bonds should be inversely proportional to the $n \rightarrow \pi^*$ excitation energies within these compounds (26 800 cm^{-1} in benzophenone and 16 400 cm^{-1} for thiobenzophenone) (2*b*). Since δ_{22} was known to lie along the C=O bond in benzophenone (3), such a correlation is most closely observed with δ_{11} oriented along the C=S bond in thiobenzophenone. However, based on the results of the present investigation and the discussion in the preceding paragraph, such an assumption is clearly not valid.

Conclusions

The orientations of the carbonyl/thiocarbonyl carbon CS tensors within a series of amides and thioamides have been experimentally characterized using ^{13}C dipolar – chemical shift NMR and are found to be analogous. These findings are supported by the results of ab initio GIAO and LORG carbon chemical shielding tensor calculations. The results of this investigation identify the least shielded component, δ_{11}, to be primarily responsible for the deshielding of the isotropic chemical shift observed within the thiocarbonyl group relative to the carbonyl group. The fact that this component lies approximately perpendicular to the C=S bond and is governed by $\sigma \leftrightarrow \pi^*$ as well as $\pi \leftrightarrow \sigma^*$ excitations dispels the popular belief that this deshielding originates from energy shifts associated with the HOMO–LUMO $n \leftrightarrow \pi^*$ transition. Finally, the present study provides some insight into the complexity of the paramagnetic shielding term and its sensitivity to a multitude of structural factors and, furthermore, exemplifies the need to exercise extreme caution in correlating trends in chemical shifts with any one of these parameters.

Acknowledgements

We wish to thank the Natural Sciences and Engineering Research Council of Canada (NSERC) for financial assistance in the form of equipment and operating grants (R.E.W.) and a postgraduate scholarship (M.D.L.). We would like to thank Dr. J. Stuart Grossert for some advice on the synthesis of thioamides, Mr. Jaime Martell for help in using the IBM RS6000/580 workstation, and Prof. W.P. Power for access to his workstation in order to perform the LORG calculations. As well, Dr. Klaus Eichele and Dr. Gang Wu are acknowledged for

Can. J. Chem. Downloaded from www.nrcresearchpress.com by 65.111.164.53 on 09/08/12
For personal use only.

obtaining some of the solid-state ^{13}C NMR spectra and for helpful discussions. All solid-state NMR spectra were obtained at the Atlantic Region Magnetic Resonance Centre, which is also supported by NSERC.

References

1. (*a*) T.M. Duncan. *In* A compilation of chemical shift anisotropies. The Farragut Press, Chicago. 1990; (*b*) J. Phys. Chem. Ref. Data, **16**, 125 (1987).
2. (*a*) A. Pines, W-K. Rhim, and J.S. Waugh. J. Chem. Phys. **54**, 5438 (1971); (*b*) J. Kempf, H.W. Spiess, U. Haeberlen, and H. Zimmermann. Chem. Phys. **4**, 269 (1974); (*c*) A.J. Beeler, A.M. Orendt, D.M. Grant, P.W. Cutts, J. Michl, K.W. Zilm, J.W. Downing, J.C. Facelli, M.S. Schindler, and W. Kutzelnigg. J. Am. Chem. Soc. **106**, 7672 (1984); (*d*) R.M. Dickson, M.S. McKinnon, J.F. Britten, and R.E. Wasylishen. Can. J. Chem. **65**, 941 (1987); (*e*) Y. Huang, D.F.R. Gilson, I.S. Butler, and F.G. Morin. Inorg. Chem. **31**, 322 (1992).
3. J. Kempf, H.W. Spiess, U. Haeberlen, and H. Zimmermann. Chem. Phys. Lett. **17**, 39 (1972).
4. H.W. Spiess. *In* NMR basic principles and progress. Vol. 15. *Edited by* P. Diehl, E. Fluck, and R. Kosfeld. Springer-Verlag, Berlin. 1978. pp. 167–168.
5. W.S. Veeman. Prog. NMR Spectrosc. **16**, 193 (1984).
6. W.P. Power and R.E. Wasylishen. Annu. Rep. NMR Spectrosc. **23**, 1 (1991).
7. G.C. Levy, R.L. Lichter, and G.L. Nelson. *In* Carbon-13 nuclear magnetic resonance for organic chemists. John Wiley & Sons, New York. 1980. Chap. 5. p. 164.
8. J. Jokisaari, P. Lazzeretti, and P. Pyykkö. Chem. Phys. **123**, 339 (1988).
9. M. Mehring. *In* principles of high-resolution NMR in solids. 2nd ed. Springer-Verlag, Berlin. 1983.
10. U. Haeberlen. *In* Advances in magnetic resonance. Supplement I. *Edited by* J.S. Waugh. Academic Press, New York. 1976.
11. F.A.L. Anet and D.J. O'Leary. Concepts Magn. Reson. **3**, 193 (1991).
12. R.E. Wasylishen, R.D. Curtis, K. Eichele, M.D. Lumsden, G.H. Penner, W.P. Power, and G. Wu. NATO ASI Ser. C: **386**, 297 (1993).
13. J. Mason. Solid State Nucl. Magn. Reson. **2**, 285 (1993).
14. K. Eichele and R.E. Wasylishen. J. Magn. Reson. Ser. A, **106**, 46 (1994).
15. K. Eichele, M.D. Lumsden, and R.E. Wasylishen. J. Phys. Chem. **97**, 8909 (1993).
16. R.L. Lichter, P.R. Srinivasan, A.B. Smith, R.K. Dieter, C.T. Denny, and J.M. Schulman. J. Chem. Soc. Chem. Commun. 366 (1977).
17. (*a*) W.T. Raynes, R. McVay, and S.J. Wright. J. Chem. Soc. Faraday Trans. 2, **85**, 759 (1989); (*b*) A.K. Jameson and C.J. Jameson. Chem. Phys. Lett. **134**, 461 (1987).
18. L. Claison. Chem. Ber. **31**, 2344 (1898).
19. M.D. Lumsden, R.E. Wasylishen, K. Eichele, M. Schindler, G.H. Penner, W.P. Power, and R.D. Curtis. J. Am. Chem. Soc. **116**, 1403 (1994).
20. B. Yde, N.M. Yousif, U. Pedersen, I. Thomsen, and S.O. Lawesson. Tetrahedron, **40**, 2047 (1984).
21. (*a*) S.R. Hartmann and E.L. Hahn. Phys. Rev. **128**, 2042 (1962); (*b*) A. Pines, M.G. Gibby, and J.S. Waugh. J. Chem. Phys. **56**, 1776 (1972); **59**, 569 (1973).
22. K. Wolinski, J.F. Hinton, and P. Pulay. J. Am. Chem. Soc. **112**, 8251 (1990).
23. R. Ditchfield. Mol. Phys. **27**, 789 (1974).
24. M.J. Frisch, G.W. Trucks, M. Head-Gordon, P.M.W. Gill, M.W. Wong, J.B. Foresman, B.G. Johnson, H.B. Schlegel, M.A. Robb, E.S. Replogle, R. Gomperts, J.L. Andres, K. Raghavachari, J.S. Binkley, C. Gonzalez, R.L. Martin, D.J. Fox, D.J. DeFrees, J. Baker, J.J.P. Stewart, and J.A. Pople. GAUSSIAN 92. Revision D.2. Gaussian, Inc., Pittsburgh. 1992.
25. (*a*) D.J. Clouthier and D.A. Ramsay. Annu. Rev. Phys. Chem. **34**, 31 (1983); (*b*) G.A. Jeffrey, J.R. Ruble, and J.H. Yates. J. Am. Chem. Soc. **106**, 1571 (1984).
26. (*a*) T.D. Bouman and Aa. E. Hansen. Int. J. Quantum Chem., Quantum Chem. Symp. **23**, 381 (1989); (*b*) Aa. E. Hansen and T.D. Bouman. J. Chem. Phys. **82**, 5035 (1985).
27. T.D. Bouman and Aa. E. Hansen. RPAC molecular properties package. Version 9.0. 1992.
28. D.W. Alderman, M.S. Solum, and D.M. Grant. J. Chem. Phys. **84**, 3717 (1986).
29. T.G. Oas, G.P. Drobny, and F.W. Dahlquist. J. Magn. Reson. **78**, 408 (1988).
30. H.J. Wasserman, R.R. Ryan, and S.P. Layne. Acta Crystallogr. Sect. C: Cryst. Struct. Commun. **C41**, 783 (1985).
31. G.A. Jeffrey, J.R. Ruble, R.K. McMullan, D.J. DeFrees, J.S. Binkley, and J.A. Pople. Acta Crystallogr. Sect. B: Struct. Crystallogr. Cryst. Chem. **B36**, 2292 (1980).
32. R.K. Harris and A.C. Olivieri. Prog. NMR Spectrosc. **24**, 435 (1992).
33. N. Asakawa, S. Kuroki, H. Kurosu, I. Ando, A. Shoji, and T. Ozaki. J. Am. Chem. Soc. **114**, 3261 (1992).
34. J. Gauss. J. Chem. Phys. **99**, 3629 (1993).
35. N.F. Ramsey. Phys. Rev. **78**, 699 (1950).
36. (*a*) J.B. Grutzner. *In* Recent advances in organic NMR spectroscopy. *Edited by* J.B. Lambert and R. Rittner. Norell Press, Landisville, N.J. 1987. pp. 17–42; (*b*) J. Mason. Adv. Inorg. Chem. Radiochem. **18**, 197 (1976); **22**, 199 (1979).
37. C.J. Jameson and H.S. Gutowsky. J. Chem. Phys. **40**, 1714 (1964).
38. M. Schindler and W. Kutzelnigg. J. Chem. Phys. **76**, 1919 (1982).
39. (*a*) G.B. Savitsky, K. Namikawa, and G. Zweifel. J. Phys. Chem. **69**, 3105 (1965); (*b*) R.T.C. Brownlee and M. Sadek. Magn. Reson. Chem. **24**, 821 (1986); (*c*) G. Barbarella, A. Bongini, and S. Rossini. J. Org. Chem. **53**, 5140 (1988).

Can. J. Chem. Downloaded from www.nrcresearchpress.com by 65.111.164.53 on 09/08/12
For personal use only.

Reaction of methylphthalimidoketene with benzylidene- and cinnamylidene-anilines: structure and configuration of the products

Arya K. Mukerjee, Gangadhar J. Sanjayan, and Krishnan Ravikumar

Abstract: Methylphthalimidoketene reacts with cinnamylideneanilines to give tetrahydrooxazin-6-ones exclusively, whereas with benzylideneaniline it also forms β-lactam. Configurations are based on X-ray studies.

Key words: β-lactam, tetrahydro-1,3-oxazin-5-ones, ketene–imine reactions, cycloaddition of methylphthalimidoketene, 3-phthaloylamino-3-methylazetidin-2-one.

Résumé : Le méthylphtalimidocétène réagit avec les cinnamylidèneanilines pour conduire exclusivement aux tétrahydrooxazin-6-ones alors que, avec la benzylidène aniline, il forme aussi une β-lactone. Les configurations sont basées sur des études par diffraction des rayons X.

Mots clés : β-lactames, tétrahydro-1,3-oxazin-5-ones, réactions cétène–imine, cycloaddition du méthylphtalimidocétène, 3-phtaloylamino-3-méthylazétidin-2-one.

[Traduit par la rédaction]

β-Lactams **3**, generally known as azetidin-2-ones, have emerged as important synthons (1, 2), and interest in 3-aminoazetidin-2-ones (3) continues unabated. The first useful synthesis of **3** ($Ar^1 = Ar^2 = Ph$; $R^1 = H_2N$; $R^2 = H$) was achieved by the triethylamine-mediated reaction of phthaloylglycyl chloride (**1***a*) with benzylideneaniline (**2***a*) followed by hydrazinolysis of the resultant 3-phthaloylamino compound **3***a* (4). The similar annulation of **1***a* with cinnamylidene-4-anisidine (**2***b*) afforded (*Z*)-azetidin-2-one **3***b* (5). In continuation of our studies (6) on dehydropeptides carrying a 3-aminoazetidin-2-one ring, we investigated the reaction of phthaloylalaninyl chloride (**1***b*) (for a preliminary report see ref. 7) with imines **2***a, b, c*, with a view to incorporating an alaninyl moiety in the target azetidin-2-ones; the outcome of this attempt is presented in this article.

Results were found to be dependent on the type of reactants and on the reaction conditions. For instance, addition of **1***b* to a solution of benzylideneaniline (**2***a*) containing triethylamine led to the formation of (±)(*E*)-1,4-diphenyl-3-methyl-3-phthaloylaminoazetidin-2-one (**3***c*) and (±)-3,4-diphenyl-5-methyl-5-phthaloylamino-2-(1-phthaloylaminoethylidene)tetrahydro-1,3-oxazin-6-one (**4***a*). Yields of **4***a* improved considerably on increasing the amounts of **1***b* and triethylamine. On the other hand, addition of triethylamine to an equimolar mixture of **1***b* and **2***a* in methylene chloride furnished only azetidin-2-one **3***c*. The triethylamine-mediated reaction of **1***b*, unlike that of **1***a*, with cinnamylideneanilines **2***b, c* gave the corresponding 4-styryl-tetrahydro-1,3-oxazin-6-ones **4***b*, **4***c* exclusively, the formation of **3***d* not being discernible.

The reaction affording oxazinones **4***a, b, c* could be best explained by the intermediacy of ketene **5**. On the other hand, azetidin-2-ones **3***a–c* could be obtained by the cyclodehydrohalogenation of the iminium salt **8**, besides following the ketene route (Scheme 1). It should be mentioned that 2:1 addition in the ketene–imine reaction was reported only in a limited number of cases (8–10), but the precise structural requirements for the reactants have not been established.

Fig. 1. X-ray structure of compound **3***c*.

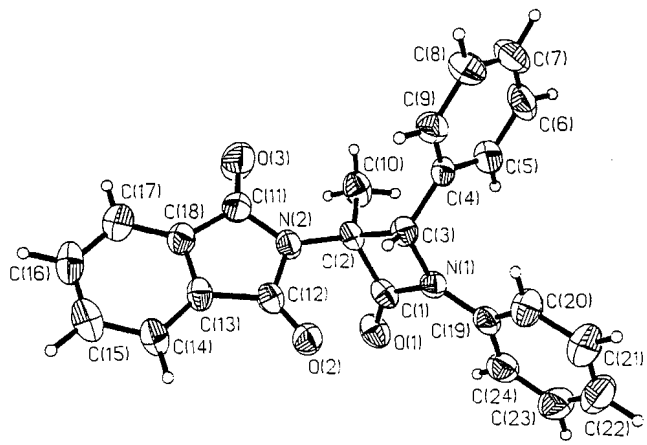

Received October 3, 1994.

A.K. Mukerjee[1] **and G.J. Sanjayan.** Chemistry Department, Faculty of Science, Banaras Hindu University, Varanasi-221005, India.

K. Ravikumar. Laboratory of Crystallography, Indian Institute of Chemical Technology, Hyderabad-500007, India.

[1] Author to whom correspondence may be addressed.

Can. J. Chem. Downloaded from www.nrcresearchpress.com by 65.111.164.53 on 09/08/12
For personal use only.

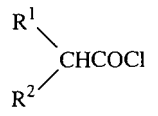

1

a; R^1 = phthalimido, R^2 = H
b; R^1 = phthalimido, R^2 = Me

$Ar^2CH{=}NAr^1$

2

a; $Ar^1 = Ar^2$ = Ph
b; Ar^1 = 4-$MeOC_6H_4$, Ar^2 = PhCH=CH
c; Ar^1 = Ph, Ar^2 = PhCH=CH

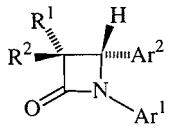

3

a; $Ar^1 = Ar^2$ = Ph, R^1 = H, R^2 phthalimido
b; Ar^1 = 4-$MeOC_6H_4$, Ar^2 = PhCH=CH, R^1 = phthalimido, R^2 = H
c; $Ar^1 = Ar^2$ = Ph, R^1 = Me, R^2 = phthalimido
d; Ar^1 = Ph or 4-$MeOC_6H_4$, Ar^2 = PhCH=CH, R^1 = phthalimido, R^2 = Me

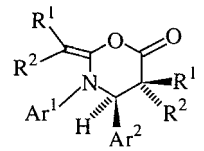

4

a; $Ar^1 = Ar^2$ = Ph, R^1 = Me, R^2 phthalimido
b; Ar^1 = 4-$MeOC_6H_4$, Ar^2 = PhCH=CH, R^1 = Me, R^2 = phthalimido,
c; Ar^1 = Ph, Ar^2 = PhCH=CH, R^1 = Me, R^2 = phthalimido

Scheme 1

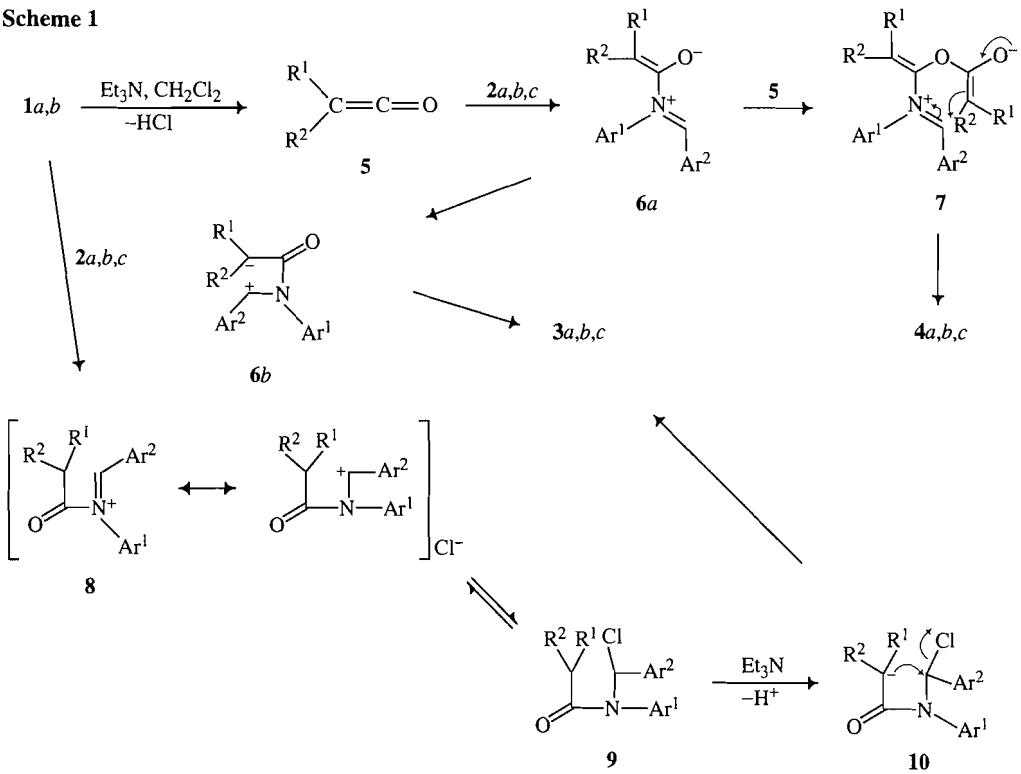

Products were characterized by spectral data and elemental analyses, and their stereochemistry was based on ^{1}H NMR spectra. Also, the configurations of **3***c* and **4***a* were confirmed by X-ray studies. Oxazinones **4***a, b, c* afforded (±)-3-(*N*-aryl, *N*-phthaloylalaninyl)amino-3-aryl-2-methyl-2-phthaloylaminopropionic acids **11***a, b, c* on saponification (Scheme 2). The acid derivative **11***a* underwent cyclization to **4***a* when treated with tosyl chloride in the presence of triethylamine.

The present finding indicates the possibility of synthesizing tetrahydrooxazinones and (or) azetidin-2-ones starting from *N,N*-diprotected alanine. The compounds reported herein are potentially important as intermediates in the synthesis of peptides and other amino acid related products.

Experimental

Melting points were determined by a Toshniwal melting point apparatus. IR spectra were recorded on a Perkin–Elmer 783 spectrophotometer and ^{1}H NMR spectra, using TMS as an internal reference, were recorded on a JEOL FX 90Q instrument. Mass spectra were recorded on a VG Micromass

Can. J. Chem. Downloaded from www.nrcresearchpress.com by 65.111.164.53 on 09/08/12
For personal use only.

Scheme 2

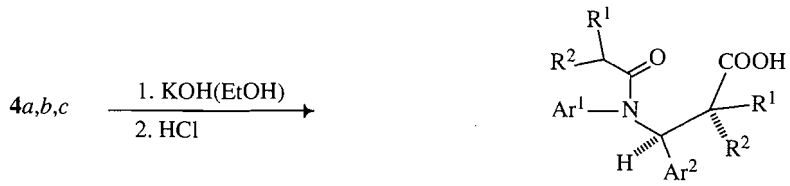

11

a; $Ar^1 = Ar^2 = Ph$, $R^1 = Me$, R^2 phthalimido
b; $Ar^1 = 4\text{-}MeOC_6H_4$, $Ar^2 = PhCH{=}CH$, $R^1 = Me$, R^2 = phthalimido,
c; $Ar^1 = Ph$, $Ar^2 = PhCH{=}CH$, $R^1 = Me$, R^2 = phthalimido

Fig. 2. X-ray structure of compound **4***a*.

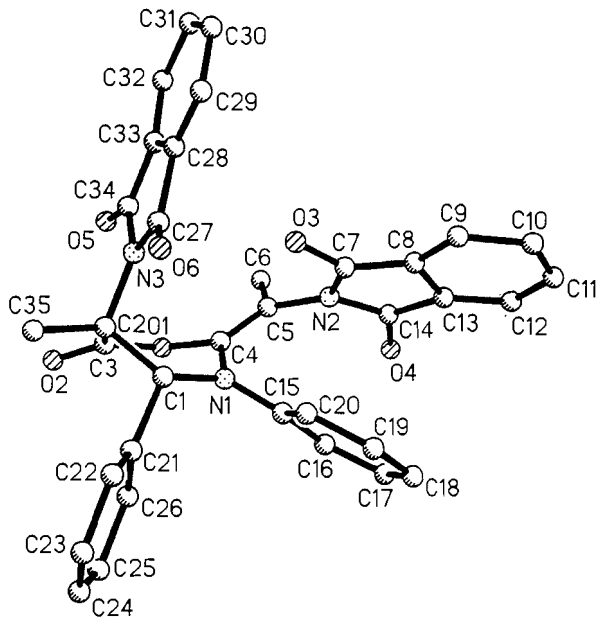

70-70H and (or) a Finnigan-Mat 1020 instrument using a direct inlet system at 70 eV.

Reaction of (±)phthaloylalaninyl chloride (1*b*) with benzylideneaniline (2*a*): formation of 3*c* and 4*a* (7)

Method A

To a cold solution of **2***a* (1.81 g, 0.01 mol) and triethylamine (1.31 g; 1.8 mL; 0.013 mol) in dry methylene chloride (20 mL) was slowly added a solution of **1***b* (2.37 g; 0.01 mol) in dry methylene chloride (20 mL). The reaction mixture was stored overnight at room temperature, concentrated to dryness under vacuum, and the pasty residue obtained was repeatedly washed with cold ethanol, filtered, and recrystallized from ethyl acetate – chloroform (1:1) to give pure **3***c*; yield, 1.72 g (45%); mp 263°C; ν_{max} (Nujol): 1780 (CO, phthalimide), 1750 (CO, β-lactam), 1710 (CO, phthalimide) cm^{-1}; δ ($CDCl_3$): 1.60 (s, 3H, CH_3), 5.45 (s, 1H, C4-H), 7.10–7.90 (m, 14H, ArH) ppm. Anal. calcd. for $C_{24}H_{18}N_2O_3$: C 75.39, H 4.71, N 7.32%; found: C 75.25, H 4.58, N 7.44%.

The ethanolic filtrate and washings were combined and concentrated to dryness under reduced pressure and the residue was triturated with cold ethanol to give yellow crystals of **4***a*. The crude product was recrystallized from chloroform–benzene (1:1); yield, 0.8 g (14%); mp 164°C; ν_{max} (Nujol): 1780 (CO, phthalimide), 1730 (CO, oxazinone), 1680 (C=C) cm^{-1}; δ ($CDCl_3$): 1.52 (s, 3H, C5-CH_3), 2.1 (s, 3H, $CH_3C{=}C$), 6.90–7.90 (m, 19H, C4-H and ArH) ppm. Anal. calcd. for $C_{35}H_{25}N_3O_6$: C 72.04, H 4.28, N 7.20%; found: C 72.02, H 4.36, N 7.46%.

The X-ray data for compounds **3***c* and **4***a* have been deposited as supplementary data.[2]

Method B

This method was similar to Method A with the difference that **1***b*, **2***a*, and triethylamine were taken in the mole ratio 2:1:2.6. Yields of **3***c* and **4***a* were 20 and 46%, respectively.

Method C

To an equimolar mixture of **1**b and **2**a in methylene chloride (30 mL/g of **1**b), cooled in an ice-bath, a solution of triethylamine (1.3 mol/mol of **1**b) in methylene chloride (10 mL/mol of the base) was slowly added. On completion of the reaction, it was worked up as before. In this method azetidin-2-one **3**c was the only product; yield, 62%.

Reaction of (±)phthaloylalaninyl chloride (1*b*) with cinnamylideneanilines 2*b*, *c*. Formation of tetrahydrooxazinones 4*b*, *c*

General procedure

This was the same as outlined in Method B. The crude products were recrystallized from chloroform–ethanol (1:1) to give yellow crystals.

Compound **4**b: Yield, 86%, mp 257°C; ν_{max} (KBr): 1793 (CO, phthalimide), 1716 (CO, oxazinone), 1678 (C=C) cm^{-1}; δ ($CDCl_3$): 1.70 (s, 3H, C5-CH_3), 1.95 (s, 3H, $CH_3C{=}C$), 3.25 (s, 3H, OCH_3), 5.75 (d, 1H, J = 6.50 Hz, C4-H), 6.10–7.70 (m,

[2] These data, as well as tables of atomic coordinates, bond lengths and angles, and anisotropic and isotropic displacement coefficients, can be purchased from: The Depository of Unpublished Data, Document Delivery, CISTI, National Research Council Canada, Ottawa ON K1A 0S2, Canada.

This material, excluding the anisotropic displacement coefficients, has also been deposited with the Cambridge Crystallographic Data Centre, and can be obtained on request from The Director, Cambridge Crystallographic Data Centre, University Chemical Laboratory, 12 Union Road, Cambridge, CB2 1EZ, U.K.

Can. J. Chem. Downloaded from www.nrcresearchpress.com by 65.111.164.53 on 09/08/12
For personal use only.

19H, C*H*=C*H*Ph and ArH) ppm. M^+ = 639; Anal. calcd. for $C_{38}H_{29}N_3O_7 \cdot 1.5\ H_2O$: C 68.46, H 4.80, N 6.30%; found: C 68.54, H 4.52, N 6.26%.

Compound **4**c: Yield, 90%; mp 268°C; ν_{max} (KBr): 1795 (CO, phthalimide), 1718 (CO, oxazinone), 1674 (C=C) cm^{-1}; δ ($CDCl_3$): 1.76 (s, 3H, C5-CH_3), 2.08 (s, 3H, CH_3C=C), 6.04 (d, 1H, J = 7.5 Hz, C4-H), 6.36–7.80 (m, 20H, C*H*=C*H*Ph and ArH) ppm. M^+ = 609; Anal. calcd. for $C_{35}H_{25}N_3O_3 \cdot H_2O$: 70.81, H 4.62, N 6.69%; found: C 70.70, H 4.99, N 6.39%.

Hydrolysis of tetrahydrooxazinones 4*a*, *b*, *c*. Formation of acids 11*a*, *b*, *c*

General procedure

To a solution of potassium hydroxide (1.2 mol) in 95% ethanol (20 mL/g of **4**) was added **4** (1.0 mol); a brown colour developed that soon disappeared. The reaction mixture was stirred for 10 min in an ice bath. The solvent was removed under reduced pressure, and the pasty substance obtained was dissolved in the minimum amount of water and filtered. The filtrate was acidified with concentrated HCl with cooling, to give a solid that was collected, washed with water, and recrystallized from aqueous ethanol.

Compound **11**a: Yield, 85%; mp 135–137°C; ν_{max} (KBr): 3420, 3200 (OH), 1714 (CO, acid) cm^{-1}; δ ($CDCl_3$): 1.10 (d, 3H, J = 8.0 Hz, C*H*$_3$-CH), 1.70 (s, 3H, CH_3CCOOH), 6.30–7.90 (m, 21H, one exchangeable with D_2O, CH_3CH, Ar^1CH, OH, and ArH) ppm. Anal. calcd. for $C_{35}H_{27}N_3O_7 \cdot 0.5\ H_2O$: C 68.85, H 4.59, N 6.88%; found: C 68.49, H 4.86, N 6.72%.

Compound **11**b: Yield, 84%; mp 150–151°C; ν_{max} (KBr): 3414, 3227 (OH), 1722 (CO, acid), 1639 (CO, amide), 1618 (C=C) cm^{-1}; δ ($CDCl_3$): 1.15 (d, 3H, J = 9.0 Hz, C*H*$_3$CH), 1.75 (s, 3H, CH_3CCOOH), 3.75 (s, 3H, OCH_3), 6.35–8.20 (m, 22H, CH_3CH, C*H*=C*H*, OH, and ArH) ppm. Due to precipitation, the D_2O exchange could not be recorded. Anal. calcd. for $C_{38}H_{31}N_3O_8 \cdot 2\ H_2O$: C 65.80, H 5.05, N 6.06%; found: C 65.42, H 5.0, N 5.66%.

Compound **11**c: Yield, 80%; mp 140–142°C; ν_{max} (KBr): 3481, 3220 (OH), 1722 (CO, acid), 1649 (CO, amide), 1639 (C=C) cm^{-1}; δ ($CDCl_3$): 1.15 (br, d, 3H, C*H*$_3$CH), 1.73 (s, CH_3CCOOH), 6.40–7.70 (m, 23H, CH_3CH, C*H*=C*H*, OH, and ArH) ppm. Due to precipitation, the D_2O exchange could not be recorded. Anal. calcd. for $C_{37}H_{29}N_3O_7$: C 70.81, H 4.62, N 6.69%; found: C 70.55, H 4.75, N 6.59%.

Cyclocondensation of 11*a*. Formation of 4*a*

To a stirred solution of the carboxylic acid (**11***a*, 0.2 g; 0.00033 mol) and triethylamine (0.073 g; 0.1 mL; 0.0072 mol) in dry methylene chloride (10 mL) was added tosyl chloride (0.06 g; 0.00033 mol) at 5–10°C; stirring was continued for 10 min, when an intense colour developed. The reaction mixture was concentrated to dryness and treated with benzene (10 mL); the precipitated triethylamine hydrochloride was filtered and washed with benzene (10 mL). The filtrate and washings were combined and heated under reflux for 30 min. The solvent was removed under reduced pressure and compound **4***a* was separated by preparative TLC (silica gel/ethyl acetate). It was recrystallized from chloroform–benzene (1:1); yield, 0.05 g (26%); mp 264°C. It was identical with the product described above.

Acknowledgement

We sincerely thank the Council of Scientific and Industrial Research (New Delhi) for the award of a Senior Research Fellowship to one of us (G.J.S.).

References

1. A.K. Mukerjee and A.K. Singh. Tetrahedron, **34**, 1731 (1978).
2. M.S. Manhas, D.R. Wagle, J. Chiang, and A.K. Bose. Heterocycles, **27**, 1755 (1988).
3. F.H. van der Steen and G. van Koten. Tetrahedron, **47**, 7503 (1991).
4. J.C. Sheehan and J.J. Ryan. J. Am. Chem. Soc. **73**, 1204 (1951).
5. A.K. Bose, J.F. Womelsdorf, L. Krishnan, Z. Urbanczyk-Lipkiowska, D.C. Shelly, and M.S. Manhas. Tetrahedron, **47**, 5379 (1991).
6. A.K. Mukerjee and G.J. Sanjayan. J. Chem. Res. (S), 280 (1993).
7. P. Kumar and A.K. Mukerjee. Indian J. Chem. **20B**, 420 (1981).
8. J.C. Martin, K.C. Brannock, R.D. Burpitt, P.G. Gott, V.A. Hoyle, Jr. J. Org. Chem. **36**, 2211 (1971).
9. M. Furukawa, T. Okawara, Y. Noguchi, and Y. Terawaki. Chem. Pharm. Bull. **27**, 2795 (1979).
10. E. Schaumann, H. Behr, and G. Adiwidjaya. Liebigs Ann. Chem. 1322 (1979).

Can. J. Chem. Downloaded from www.nrcresearchpress.com by 65.111.164.53 on 09/08/12
For personal use only.

1994 Polanyi Award Lecture Concept of active electrons in chemistry[1]

Sigeru Huzinaga

Abstract: The notion of division between active and dormant electrons has been well received and widely used in the chemists' way of thinking. The core–valence separation in atoms is the best-known example. This paper describes a theoretical and computational method called the model potential method, which deals only with active electrons in molecular and solid state calculations. The method is capable of reaching computational accuracy of testing the validity of the separation of active and dormant electrons in individual cases.

Key words: separability of electrons, model potential method, valence orbitals, relativistic effects.

Résumé : La notion de division entre les électrons actifs et dormants est bien accueillie et largement utilisée dans la façon de penser des chimistes. L'exemple le plus connu est la séparation de la valence centrale des atomes. Ce travail décrit une méthode de calculs théoriques, appelée méthode du potentiel modèle, qui ne traite que des électrons actifs dans les calculs moléculaires et de l'état solide. La méthode peut atteindre une précision permettant, dans des cas individuels, de vérifier la validité de la séparation des électrons actifs et dormants.

Mots clés : séparabilité des électrons, méthode du potentiel modèle, orbitales de valence, effets relativistiques.

[Traduit par la rédaction]

1. Introduction

The idea of dividing electrons in atoms into valence electrons and core electrons has been popular among chemists and physicists. The very existence of the periodic table attests to the validity of the notion that the valence electrons determine most of the chemical properties of atoms and molecules and the core electrons are inactive and dormant, just shielding the nuclei and providing an effective potential for the valence electrons.

At the same time, however, we are also intrigued and fascinated by remarkable differences in the chemistry and the physics among atoms with the same number of valence electrons, for instance, among C, Si, and Ge. Is this simply because the effective potentials are different for the valence electrons of the individual atoms? Or, something else is involved?

It would certainly be a worthwhile enterprise to mold the idea of the valence–core separation into a computational scheme in such a way that the validity and the limitations of valence–core language could be tested in precise numerical fashion. Then our interpretative power would be solidified and enhanced in organizing and categorizing a wide variety of chemical and physical observations. At the same time, of course, we expect to be able to economize the computational cost by reducing the number of electrons to be treated explicitly, if so justified.

Since the early days of quantum mechanics, many theoretical formulations have been advanced in which only valence electrons are treated explicitly. "This is not an easy task, although formally one may write the essential equations rather trivially," as Krauss and Stevens (1) stated in their comprehensive review article on the subject. Once Van Vleck and Sherman (2) called the difficulty "the nightmare of the inner core." One of the purposes of the present paper is to address the question: why has this been no easy task?

My own effort to develop a sound theoretical framework for the valence–core separation was first reported in 1971 (3). On the basis of the theoretical framework, the first paper of our model potential method was presented in 1974 (4). Since then, various extensions and improvements have been made. A formal description of the mathematical structure of the method, including some new developments, was published in 1991 (5). In the present paper some cardinal points of what we call the model potential method are explained in a less formal way so that the method may have some appeal to a wider readership than just to specialists in the field.

First of all, we must remind ourselves that electrons are *not* distinguishable: we can not put a tag on an individual electron. All we can do is to rely on the concept of the electron

Received December 12, 1994.

S. Huzinaga.[2] Department of Chemistry, University of Alberta, Edmonton, AB T6G 2G2, Canada.

[1] This is an invited review article based on the 1994 Polanyi Award Lecture presented by Professor Huzinaga at the annual conference of the Canadian Society for Chemistry in Winnipeg, June 1994.

[2] Telephone: (403) 492-5309. Fax: (403) 492-8231.

Can. J. Chem. Downloaded from www.nrcresearchpress.com by 65.111.164.53 on 09/08/12
For personal use only.

Can. J. Chem. Downloaded from www.nrcresearchpress.com by 65.111.164.53 on 09/08/12
For personal use only.

orbital to divide electrons into a certain set of groups. Secondly, we should be aware of the fact that the core–valence separation is an approximate concept. It follows then that the wavefunction we are dealing with will be an approximate one.

The total wavefunction including both the core and the valence electrons may be written as

$$\Phi = A_{SL}(\Phi_{core}\Phi_{valence})$$

[1] $$\Phi_{core} \equiv \Phi_{core}(1, 2, \ldots, n_c)$$

$$\Phi_{valence} \equiv \Phi_{valence}(n_c + 1, \ldots, n_c + n_v)$$

Φ_{core} and $\Phi_{valence}$ are assumed to be already antisymmetrized according to the Pauli principle. The Slater-type antisymmetrizer A_{SL} takes care of permutations between the core electrons and the valence electrons.

Our mandate is to build a theoretical method to obtain $\Phi_{valence}$ in eq. [1] without explicitly including Φ_{core} in the wavefunction. It means that the antisymmetrizer A_{SL} that ensures the Pauli exclusion between the core and the valence electrons is no longer available. Therefore, we have somehow to incorporate the effect of the Pauli principle into the theory without treating the core electrons explicitly. This is the gist of the matter and the source of Van Vleck's nightmare. The effect may be incorporated into either (*a*) the valence wavefunction $\Phi_{valence}$ in the form of orthogonality constraints, or (*b*) a modified form of the Hamiltonian for the valence electrons.

In general, the exact wavefunction cannot be factored in the form of eq. [1] but a class of approximate wavefunctions may be, as discussed by McWeeny (6). The simplest and most useful example is the Hartree–Fock (HF) wavefunction. At this level, Höjer and Chung (7) laid a firm theoretical foundation for our model potential method.[3] Applying their discussion to a simple example of a closed-shell atom, Be, we shall describe the essential features of the method.

The concept of core and valence electrons is but an example of the general idea of separating physically and (or) chemically active electrons from those inactive and dormant in molecular systems. Lone-pair electrons, π and σ electrons of conjugated hydrocarbons, frontier electrons, and functional groups in organic compounds are other examples. The solid state also presents a variety of phenomena that are supposed to be understood in terms of localized active electrons.

The separation of active and dormant electrons in chemical and physical systems is a wide subject and has been studied by many authors in recent years. This review article is far from comprehensive. Even within our model potential method, there have been numerous contributions from many friends and colleagues. I shall acknowledge them at the end of the paper.

2. Hartree–Fock method for valence electrons in the frozen core approximation

The all-electron HF wavefunction for Be $[1s^2 2s^2, {}^1S]$ is

[2] $$\Phi(1, 2, 3, 4) = A_{SL}[\varphi_{1s}(1)\alpha(1)\varphi_{1s}(2)\beta(2)\varphi_{2s} \times (3)\alpha(3)\varphi_{2s}(4)\beta(4)]$$

[3] The term "model potential" may not have been a good choice. See ref. 8.

The total Hamiltonian in atomic units is

[3] $$\hat{H} = \sum_{i=1}^{4} \hat{h}(i) + \sum_{i>j} \frac{1}{r_{ij}}, \qquad \hat{h}(i) = -\frac{1}{2}\Delta_i - \frac{Z}{r_i}$$

The total energy

$$E = \langle\Phi|\hat{H}|\Phi\rangle \equiv E[\varphi_{1s}, \varphi_{2s}]$$

may be regarded as a functional of φ_{1s} and φ_{2s}. Applying the variational principle to E under the orthonormal constraints for φ_{1s} and φ_{2s},

[4] $$\langle\varphi_{1s}|\varphi_{1s}\rangle = \langle\varphi_{2s}|\varphi_{2s}\rangle = 1, \ \langle\varphi_{1s}|\varphi_{2s}\rangle = \langle\varphi_{2s}|\varphi_{1s}\rangle = 0$$

we obtain the HF equations for the determination of φ_{1s} and φ_{2s},

$$\hat{F}|\varphi_{ns}\rangle = \varepsilon_{ns}|\varphi_{ns}\rangle, \qquad n = 1, 2$$

[5] $$\hat{F} = -\frac{1}{2}\Delta - \frac{Z}{r} + (2\hat{J}_{1s} - \hat{K}_{1s}) + (2\hat{J}_{2s} - \hat{K}_{2s})$$

where

[6] $$\hat{J}_{ns}f(r) = \int \frac{\varphi_{ns}(r')\varphi_{ns}(r')}{|r - r'|}\,dr' \cdot f(r)$$

[7] $$\hat{K}_{ns}f(r) = \int \frac{\varphi_{ns}(r')f(r')}{|r - r'|}\,dr' \cdot \varphi_{ns}(r)$$

$f(r)$ being an arbitrary spatial function. Because the core orbital φ_{1s} and the valence orbital φ_{2s} are eigenfunctions of the same Fock operator $\hat{F}$, they are mutually orthogonal.

Suppose we have solved the HF equations for Be and have obtained the solutions φ_{1s}, ε_{1s}, and φ_{2s}, ε_{2s}. Now, we start all over again with eqs. [2] and [3], but this time φ_{1s} is given and fixed (frozen) and only φ_{2s} is subjected to variation under the constraints,

[8] $$\langle\varphi_{1s}|\varphi_{2s}\rangle = \langle\varphi_{2s}|\varphi_{1s}\rangle = 0, \qquad \langle\varphi_{2s}|\varphi_{2s}\rangle = 1$$

The HF equation for φ_{2s} will be found to be

[9] $$\hat{F}'|\varphi_{2s}\rangle = \varepsilon_{2s}|\varphi_{2s}\rangle$$

[10] $$\hat{F}' = -\frac{1}{2}\Delta - \frac{Z}{r} + (2\hat{J}_{1s} - \hat{K}_{1s}) + (2\hat{J}_{2s} - \hat{K}_{2s}) - 2\varepsilon_{1s}|\varphi_{1s}\rangle\langle\varphi_{1s}|$$

Now, we deal with only the two valence electrons in Be. The wavefunction is

[11] $$\Phi(1,2) = A_{SL}[\varphi_{2s}(1)\alpha(1)\varphi_{2s}(2)\beta(2)]$$

We introduce a modified Hamiltonian (compare with eq. [3]),

[12] $$\hat{H}' = \hat{h}'_1 + \hat{h}'_2 + \frac{1}{r_{12}}$$

[13] $$\hat{h}'_i = -\frac{1}{2}\Delta_i - \frac{Z}{r_i} + (2\hat{J}_{1s} - \hat{K}_{1s}) - 2\varepsilon_{1s}|\varphi_{1s}\rangle\langle\varphi_{1s}|$$

The operators $(2\hat{J}_{1s} - \hat{K}_{1s})$ and $-2\varepsilon_{1s}|\varphi_{1s}\rangle\langle\varphi_{1s}|$ are to be

constructed with the frozen core orbital φ_{1s} and the orbital energy ε_{1s}.

If we derive a new HF equation from $\Phi(1,2)$ and $\hat{H}'$ with the normalization constraint $\langle\varphi_{2s}|\varphi_{2s}\rangle = 1$ but *without* the orthogonality constraint $\langle\varphi_{1s}|\varphi_{2s}\rangle = \langle\varphi_{2s}|\varphi_{1s}\rangle = 0$, we arrive at the same Fock operator in eqs. [9] and [10].

Let us recapitulate what we have achieved so far. We introduce a modified total Hamiltonian [12] for the two valence electrons in Be using the knowledge of $\{\varphi_{1s}, \varepsilon_{1s}\}$. We write the wavefunction as

$$\Phi(1,2) = A_{SL}[\varphi_v(1)\alpha(1)\varphi_v(2)\beta(2)]$$

and work out the HF equation for φ_v *without* paying any attention to the orthogonality of φ_v to the frozen core orbital φ_{1s}. Then we obtain the HF equation for φ_v as

$$[14] \qquad \hat{F}'|\varphi_v\rangle = \varepsilon_v|\varphi_v\rangle$$

where $\hat{F}'$ is identical with $\hat{F}'$ in eq. [10].

To go on toward our model potential method, let us examine the modified one-electron Hamiltonian [13] more carefully. The term $2\hat{J}_{1s}$ represents a Coulombic potential due to the charge cloud $|\varphi_{1s}|^2$ as seen in eq. [6]. Once φ_{1s} is given, $2\hat{J}_{1s}$ can be integrated to be a spherically symmetric local potential function,

$$[15] \qquad 2\hat{J}_{1s} = 2\int \frac{|\varphi_{1s}(r')|^2}{|r-r'|}\,dr' \equiv V_{Coul}(r)$$

The term $\hat{K}_{1s}$ is a quantum mechanical exchange operator and, being a genuine integral operator, it may be replaced *only approximately* by a local function of r. This is one of the pivotal points around which our model potential method have evolved. The last term in eq. [13],

$$[16] \qquad -2\varepsilon_{1s}|\varphi_{1s}\rangle\langle\varphi_{1s}|$$

is to prevent the valence orbital φ_v from collapsing onto the $1s$ core region. It may also be regarded as an energy shift operator in the HF equation [9]. From eqs. [5] and [10],

$$[17] \qquad \hat{F}' = \hat{F} - 2\varepsilon_{1s}|\varphi_{1s}\rangle\langle\varphi_{1s}|$$

Therefore,

$$[18] \qquad \hat{F}'|\varphi_{1s}\rangle = (\varepsilon_{1s} - 2\varepsilon_{1s})|\varphi_{1s}\rangle = -\varepsilon_{1s}|\varphi_{1s}\rangle$$

$$[19] \qquad \hat{F}'|\varphi_{2s}\rangle = \varepsilon_{2s}|\varphi_{2s}\rangle$$

Hence the energy level of the lowest eigenfunction φ_{1s} of the original HF equation [5] is shifted upward by the amount $2|\varepsilon_{1s}|$ by the operator [16], and $\{\varphi_{2s}, \varepsilon_{2s}\}$ becomes the lowest eigensolution of the modified HF equation [14].

The only difference between the energy level spectrum of eq. [14] and that of eq. [5] is the position of the energy level of the eigenfunction φ_{1s}. All other eigensolutions are unchanged in the transition from eq. [5] to eq. [14]. It is also to be noted that all the nodal structures of eigenfunctions of eq. [5] are perfectly preserved in eq. [14].

3. Hartree–Fock method for valence electrons in the model potential approximation

First let us generalize the one-electron Hamiltonian [13] to the case of Z_c core electrons:

$$[20] \qquad \begin{aligned}\hat{h}' &= -\frac{1}{2}\Delta - \frac{Z}{r} + \sum_c (2\hat{J}_c - \hat{K}_c) - \sum_c 2\varepsilon_c|\varphi_c\rangle\langle\varphi_c| \\ &= -\frac{1}{2}\Delta - \frac{(Z-Z_c)}{r} + \hat{V}_{core} + \hat{\sigma}\end{aligned}$$

where

$$[21] \qquad \hat{V}_{core} = \hat{V}_{Coul} + \hat{V}_{exch}$$

$$[22] \qquad \hat{V}_{Coul} = -\frac{Z_c}{r} + 2\sum_c \hat{J}_c$$

$$[23] \qquad \hat{V}_{exch} = -\sum_c \hat{K}_c$$

$$[24] \qquad \hat{\sigma} = -\sum_c 2\varepsilon_c|\varphi_c\rangle\langle\varphi_c|$$

It is assumed that the core orbitals and the orbital energies $\{\varphi_c, \varepsilon_c\}$ have been obtained from the all-electron HF calculation, which has also produced the valence orbitals and the orbital energies $\{\varphi_v, \varepsilon_v\}$.

The Hamiltonian $\hat{h}'$ in eq. [20] is certainly a one-electron operator but the evaluation of the expectation values involves computation of so-called two-electron energy integrals because of $\hat{J}_c$ and $\hat{K}_c$ in $\hat{V}_{core}$, This is *not* a welcome feature because we are actually interested in economizing the molecular calculation by dealing only with valence electrons from the constituent atoms. It is desirable to replace $\hat{V}_{core}$ with something more economical computationally. How to approximate and replace $\hat{V}_{core}$ is the central issue of the model potential method. A challenge here is the non-local character of the exchange operators $\{\hat{K}_c\}$.

Another important point in the development of the model potential method is the inclusion of relativistic effects. We have been motivated to develop the valence-electron-only method because the all-electron molecular calculation of systems that contain heavy atoms is often very expensive. Relativistic effects are significant in the core region of heavy atoms and they often influence the chemistry and phsics of the valence electrons. We should also notice that there is a distinct advantage in dealing with the relativistic effect at the level of the valence electron approximation. It is because valence electrons are still essentially non-relativistic even under the spilled-out influence of relativistic core electrons.

There are several types that have been developed within our model potential method. Before proceeding to describe them, however, we would like to equip ourselves with the rudimental knowledge of the relativistic treatment of electrons in the Cowan–Griffin–Wood–Boring theory and also with a mathematical tool that has turned out to be convenient for handling both exchange operators and relativistic operators.

Can. J. Chem. Downloaded from www.nrcresearchpress.com by 65.111.164.53 on 09/08/12
For personal use only.

Can. J. Chem. Downloaded from www.nrcresearchpress.com by 65.111.164.53 on 09/08/12
For personal use only.

3.1 Spectral representation of operators

Suppose that $\hat{\Omega}$ is an operator in quantum mechanics and Φ and Ψ are two wavefunctions. We shall consider the following integral,

$$[25] \qquad I = \langle \Phi | \hat{\Omega} | \Psi \rangle$$

If we expand Φ and Ψ by a complete orthonormal basis function set $\{\psi_i\}$,

$$[26] \qquad \langle \Phi | = \sum_i \langle \Phi | \psi_i \rangle \langle \psi_i |$$

$$[27] \qquad | \Psi \rangle = \sum_i | \psi_j \rangle \langle \psi_j | \Psi \rangle$$

then

$$[28] \qquad I = \sum_i \sum_j \langle \Phi | \psi_i \rangle \langle \psi_i | \hat{\Omega} | \psi_j \rangle \langle \psi_j | \Psi \rangle = \langle \Phi | \hat{P} \hat{\Omega} \hat{P} | \Psi \rangle$$

where

$$[29] \qquad \hat{P} = \sum_i | \psi_i \rangle \langle \psi_i |$$

is a projection operator: $\hat{P}^2 = \hat{P}$. Comparing eqs. [25] and [28], we call

$$[30] \qquad \hat{P} \hat{\Omega} \hat{P} = \sum_i \sum_j | \psi_i \rangle \langle \psi_i | \hat{\Omega} | \psi_j \rangle \langle \psi_j |$$

a spectral representation of an operator $\hat{\Omega}$. If $\hat{P}\hat{\Omega}\hat{P}$ has some computational advantage over the original operator $\hat{\Omega}$, the representation becomes a useful mathematical tool. This is the case in the model potential approach to handle $\hat{V}_{\text{core}}$ in eq. [21].

If the integrals $\{\langle \psi_i | \hat{\Omega} | \psi_j \rangle\}$ happen to be negligibly small outside a certain finite range of $\{i\}$, a finite expansion approximation becomes acceptable. Expecting such situations, we shall use a finite basis function set $\{\chi_p\}$ to represent a certain class of operators. In the Roothaan–Hartree–Fock equations such finite *non-orthogonal* basis function sets are used to represent the Hartree–Fock integro-differential equations.

For the present purpose, we limit ourselves to the case where $\hat{\Omega}$ is the one-electron operator and Φ, Ψ, $\{\psi_i\}$, and $\{\chi_p\}$ are all one-electron functions. We also assume that $\{\chi_p\}$ is an n-membered finite non-orthogonal basis function set with a real symmetric overlap matrix,

$$[31] \qquad S_{pq} = \langle \chi_p | \chi_q \rangle = S_{qp}, \qquad p, q = 1, 2, \ldots, n$$

Then, from $\{\chi_p\}$ we can construct a finite orthonormal basis function set $\{\psi_i\}$,

$$[32] \qquad \psi_i = \sum_p \chi_p (S^{-1/2})_{pi}, \qquad i = 1, 2, \ldots, n$$

Let us assume that the integral I in eq. [28] may be computed quite accurately by the finite set $\{\psi_i\}$. Then, in terms of $\{\chi_p\}$,

$$[33] \qquad \hat{P} = \sum_{pq} | \chi_p \rangle (S^{-1})_{pq} \langle \chi_q |$$

and

$$[34] \qquad \begin{aligned} \hat{P} \hat{\Omega} \hat{P} &= \sum_{pq} \sum_{rs} | \chi_p \rangle (S^{-1})_{pq} \langle \chi_q | \hat{\Omega} | \chi_r \rangle (S^{-1})_{rs} \langle \chi_s | \\ &= \sum_{pq} | \chi_p \rangle (S^{-1} \hat{\Omega} S^{-1})_{pq} \langle \chi_q | \end{aligned}$$

Here, it is to be noted that the representation is approximate,

$$\hat{\Omega} \sim \hat{P} \hat{\Omega} \hat{P}$$

3.2 Cowan–Griffin and Wood–Boring formalisms for atoms

There is no counterpart in relativistic quantum mechanics for the many-electron system corresponding to the non-relativistic many-electron Schrödinger equation. We start with the Dirac equations (9) for one electron in a central potential field $V(r)$,

$$[35] \qquad F_k = \left(\frac{\alpha}{2}\right) \frac{1}{1 + (\alpha^2/4)(\varepsilon_k - V)} \left(\frac{\mathrm{d}}{\mathrm{d}r} + \frac{k}{r}\right) G_k$$

$$[36] \qquad G_k = \frac{-2}{\alpha(\varepsilon_k - V)} \left(\frac{\mathrm{d}}{\mathrm{d}r} - \frac{k}{r}\right) F_k$$

where ε_k is the eigenvalue (less the rest energy of the electron) and the quantum number k is related to l and j according to

$$[37] \qquad \begin{aligned} k &= 1 && \text{for } j = l - \tfrac{1}{2} \\ k &= -(l+1) && \text{for } j = l - \tfrac{1}{2} \end{aligned}$$

The Rydberg atomic units are used. $G_k(r)$ is called the large-component and $F_k(r)$ the small-component radial function. Substituting F_k from eq. [35] into eq. [36], we have

$$[38] \qquad \left[-\frac{\mathrm{d}^2}{\mathrm{d}r^2} + \frac{k(k+1)}{r^2} + V(r) + H_{\text{MV}} + H_{\text{D}} + H_{\text{SO}}\right] G_k = \varepsilon_k G_k$$

where

$$[39] \qquad H_{\text{MV}} = -\frac{\alpha^2}{4}(\varepsilon_k - V)^2$$

$$[40] \qquad H_{\text{D}} = -\frac{\alpha^2}{4} B_k \frac{\mathrm{d}V}{\mathrm{d}r} \left(\frac{\mathrm{d}}{\mathrm{d}r} - \frac{1}{r}\right)$$

$$[41] \qquad H_{\text{SO}} = -\frac{\alpha^2}{4} B_k \left(\frac{k+1}{r}\right) \frac{\mathrm{d}V}{\mathrm{d}r}$$

$$[42] \qquad B_k = \left[1 + \frac{\alpha^2}{4}(\varepsilon_k - V)\right]^{-1}$$

H_{MV} is called the mass-velocity term, H_{D} the Darwin term, H_{SO} the spin-orbit interaction term. α is the fine-structure constant. This is essentially the Wood–Boring equation (10).

For a single electron in a central potential field $V(r)$, eq. [38] is still exact. If we solve eq. [38] accurately for G_k, then F_k can be obtained from eq. [40], and they constitute the accurate solution.

Can. J. Chem. Downloaded from www.nrcresearchpress.com by 65.111.164.53 on 09/08/12
For personal use only.

Now we take several steps to transform eq. [38] to a modified form of the Hartree–Fock equations for a many-electron atom. First, we disregard the small component F_k. Second, the spin-orbit term H_{SO} is dropped. Consequently, l can be used instead of k in the equation, because $k(k+1) = l(l+1)$ for both $k = l$ and $k = -(l+1)$. Third, we replace $V(r)$ with the standard potential energy operator in the Fock operator,

$$[43] \qquad V(r) \rightarrow \hat{V} = -\frac{2Z}{r} + \sum_i (a_i \hat{J}_i - b_i \hat{K}_i)$$

The first term is the nuclear attraction (in Rydberg units) and $\hat{J}_i$ and $\hat{K}_i$ are defined with the occupied orbitals $\{G_{nl}\}$. Note that the principal quantum number n is supplied. The constants $\{a_i, b_i\}$ specify the electronic state of the atoms. $\hat{V}$ in eq. [43] is a non-local operator because of the exchange operators $\{\hat{K}_i\}$, and it is not convenient to use in H_{MV} and H_D. Therefore we introduce a local potential approximation of $\hat{V}$,

$$\hat{V} \rightarrow V_{nl}(r)$$

The local potential depends on the quantum numbers of the operand orbital G_{nl}. The resulting equations are

$$[44] \qquad \left[-\frac{d^2}{dr^2} + \frac{l(l+1)}{r^2} + \hat{V} + H_{MV} + H_D \right] G_{nl} = \varepsilon_{nl} G_{nl}$$

where

$$[45] \qquad H_{MV} = -\frac{\alpha^2}{4} (\varepsilon_{nl} - V_{nl}(r))^2$$

$$[46] \qquad H_D = -\frac{\alpha^2}{4} B_{nl} \frac{dV_{nl}(r)}{dr} \left(\frac{d}{dr} - \frac{1}{r} \right)$$

$$[47] \qquad B_{nl} = \left[1 + \frac{\alpha^2}{4} (\varepsilon_{nl} - V_{nl}(r)) \right]^{-1}$$

If we also replace $\hat{V}$ in eq. [44] with the local potential approximation $V_{nl}(r)$, and further replace the differential operator H_D with the local potential

$$[48] \qquad V_{D,nl}(r) = -\frac{\alpha^2}{4} B_{nl} \frac{dV_{nl}}{dr} \left(\frac{1}{G_{nl}} \frac{dG_{nl}}{dr} - \frac{1}{r} \right)$$

we have the Cowan–Griffin equation. The equation is discussed in detal by Cowan and Griffin (11) and by Wood and Boring (10). The solutions $\{G_{nl}\}$ are numerically given at mesh points of the numerical integration of the equation and so are $\{V_{nl}(r)\}$.

We shall now describe four versions of our model potential method. The classification is just for the clarity of describing various developments that have happened over the past 20 years within the method, and as such there is no hierarchic implication.

3.2.1 Version 0

This is little more than a historical record. In the originally proposed form of the method (4), the whole $\hat{V}_{core}$ in eq. [21] is expressed as a local spherical function of r in the form,

$$[49] \qquad \hat{V}_{core} \approx V_{mp}(r) = \frac{1}{r} \left[\sum_I A_I \exp(-\alpha_I r^2) \right]$$

This is the origin of the term "model potential," which probably has survived too long in view of many later developments in the method. The model potential (mp) parameters $\{A_I, \alpha_I\}$ were optimized through a series of atomic HF calculations for the valence electrons using the one-electron Hamiltonian [20] in such a way that the orbital energies and the radial orbital functions $\{\varepsilon_v^{mp}, R_v^{mp}\}$ will be as close as possible to those of the reference all-electron calculation, $\{\varepsilon_v^{ref}, R_v^{ref}\}$. At this stage, the process of optimization was not automated. The model potentials determined in this way were used in several molecular calculations with moderate success. The implementation of the model potential method into a molecular program was originally made by Gropen and we have profited immensely from the work since then.

3.2.2 Version 1

This is a result of the joint work of many people. In this version $\hat{V}_{core}$ is given the form,

$$[50] \qquad \hat{V}_{core} \approx V_{mp}(r) = \frac{1}{r} \left[\sum_I A_I \exp(-\alpha_I r^2) + \sum_J B_J r \exp(-\beta_J r^2) \right]$$

The parameters $\{A_I, \alpha_I; B_J, \beta_J\}$ are optimized through a series of atomic HF calculations by minimizing the following quantity,

$$[51] \qquad \Delta = \sum_v \omega_v |\varepsilon_v^{ref} - \varepsilon_v^{mp}| + \sum_v \sum_k W_v \times [r_k R_v^{ref}(r_k) - r_k R_v^{mp}(r_k)]^2$$

where ε_v and $R_v(r)$ are the orbital energy and the radial function of the v-th valence orbital, and ω_v and W_v are appropriately chosen weight factors. Values of $rR(r)$ are computed at properly chosen discrete points $\{r_k\}$. Minimization of Δ as the function of $\{A_I, \alpha_I; B_J, \beta_J\}$ is computationally automated. This improvement was made by Sakai (12) and proved to be a substantial step toward the extensive preparation of the parameters in the method.

This fitting procedure between $\{\varepsilon_v^{ref}, R_v^{ref}\}$ and $\{\varepsilon_v^{mp}, R_v^{mp}\}$ may be used conveniently to incorporate the relativistic effects at the level of Cowan–Griffin approximation into the model potential method, which was implemented by Klobukowski. As explained in eqs. [44] through [48], we may solve the Cowan–Griffin equations as the reference. $(G_{nl}(r) \rightarrow R_{nl}(r))$. Then we obtain $\{\varepsilon_v^{ref}, \varphi_v^{ref}\}$ as well as $\{\varepsilon_c, \varphi_c\}$, and they then are used in Δ of eq. [51] for the determination of $\{A_I, \alpha_I; B_J, \beta_J\}$, and also for the shift operator $\hat{\sigma}$ in eq. [24].

Actually, the shift operator $\hat{\sigma}$ is also parametrized as

$$[52] \qquad \hat{\sigma}' = -\sum f_c \varepsilon_c |\varphi_c\rangle\langle\varphi_c|$$

Can. J. Chem. Downloaded from www.nrcresearchpress.com by 65.111.164.53 on 09/08/12
For personal use only.

In this version, $f_c = 2$ is the chosen value for the majority of atoms, which is referred to as the hard-core value. For some heavy atoms, the soft-core value of $f_c \cong 1.0$ is chosen for better agreement between results of the model potential calculation and those of the reference all-electron calculation for molecules. The reduction of the value of f_c from the theoretical (hard-core) value ($f_c = 2$) is to compensate for the inadequacy of small basis sets adopted in molecular calculations for economic reasons. There are two types of Version 1. One is the non-relativistic (NR) version and another is the quasi-relativistic (QR) version based on the Cowan–Griffin approximation. This version of the model potential method has been extensively developed by Sakai, Klobukowski, Miyoshi, and others (12), and implemented in a couple of major molecular programs. In principle, the implementation of the model potential method is not difficult because changes are required only in the form of the one-electron Hamiltonian.

3.2.3 Version 2

Andzelm et al. (13) initiated the use of the technique of spectral representation of operators in our model potential method. First, the technique was applied only to the tail part of the exchange operator $\hat{V}_{\text{exch}}$ in eq. [23] but now is applied to the whole $\hat{V}_{\text{exch}}$. The present version has been extensively developed, mainly by Seijo and Barandiarán et al. (14), and called the ab initio model potential (AIMP) method.

In the AIMP method, $\hat{V}_{\text{Coul}}$ in eq. [22] is expressed as

$$[53] \qquad \hat{V}_{\text{Coul}} \cong V_{\text{Coul,mp}}(r) = \frac{1}{r}\sum_k A_k \exp(-\alpha_k r^2)$$

where the parameters $\{A_k, \alpha_k\}$ are determined through least-squares fitting to the $\hat{V}_{\text{Coul}}$ calculated with eq. [22] using the frozen core orbitals $\{\varphi_c\}$ and tabulated numerically. Choice of the number of terms in the expansion [53] is a matter of computational convenience. Otherwise $\{A_k, \alpha_k\}$ are completely determined, once $\{\varphi_c\}$ are given. They are *not* adjustable parameters of the method.

The exchange operator $\hat{V}_{\text{exch}}$ is now expressed in the spectral representation by using an appropriate projection operator $\hat{P}$ as given in eq. [33],

$$[54] \qquad \hat{V}_{\text{exch}} \rightarrow \hat{P}\hat{V}_{\text{exch}}\hat{P}$$

To include the quasi-relativistic (QR) effects at the level of the Cowan–Griffin approximation, we use the following one-electron Hamiltonian in place of $\hat{h}'$ in eq. [20],

$$[55] \qquad \hat{h}'_{\text{qr}} = -\frac{1}{2}\Delta - \frac{(Z - Z_c)}{r} + \hat{V}_{\text{core,qr}} + \hat{\sigma}$$

where

$$[56] \qquad \hat{V}_{\text{core,qr}} = \hat{V}_{\text{Coul}} + \hat{V}_{\text{exch}} + \hat{V}_{\text{MV}} + \hat{V}_{\text{D}}$$

At this point, we need to be more explicit about the quantum number specification of the expansion basis functions in eq. [33],

$$\{|\chi_p\rangle\} \rightarrow \{|alm\rangle\}$$

And now,

$$[57] \qquad \hat{P} = \sum_{a,b}\sum_{l}\sum_{m=-l}^{+l} |alm\rangle (S^{-1})_{l,ab} \langle blm|$$

$$(S)_{l,ab} = \langle alm|blm\rangle$$

The operators, $H_{\text{MV}} + H_{\text{D}}$, in eq. [44] depend on nl. Assuming that the valence shell contains only one valence orbital for each symmetry l ($l = s, p, d, \ldots$), we use the following form for $\hat{V}_{\text{MV}} + \hat{V}_{\text{D}}$ in eq. [56],

$$[58] \qquad \hat{V}_{\text{MV}} + \hat{V}_{\text{D}} = \hat{P}\left[\sum_{l\in v} \hat{O}_l (H_{\text{MV},l} + H_{\text{D},l})\hat{O}_l\right]\hat{P}$$

where

$$[59] \qquad \hat{O}_l = \sum_{m=-l}^{+l} |lm\rangle\langle lm|$$

Seijo and Barandiarán call the above formalism the CG-AIMP approximation. They also discuss the approximation based on the Wood–Boring equation [38], including the effect of the spin-orbit interaction.[4] This is called the WB-AIMP approximation.

3.2.4 Version 3

This version has been developed mainly by Katsuki (15). Here the Coulomb potential $\hat{V}_{\text{Coul}}$ is also expressed in the spectral representation,

$$[60] \qquad \hat{V}_{\text{Coul}} \rightarrow \hat{P}\hat{V}_{\text{Coul}}\hat{P}$$

Thus the least-squares fitting in eq. [53] is eliminated. In this method, therefore, once the judicious choice of the expansion basis function set is made, there will be no other parameters in the method.

For atoms where the frozen core electron charge distribution is spherically symmetric, the analytic expression [53] for $\hat{V}_{\text{Coul}}$ would probably be more convenient and accurate than the spectral representation. There are, however, cases where the dormant frozen core may be nonspherical. Often the chemical properties of a functional group are supposed to be governed by a few electrons. For example, the donor characteristics of ammonia may be understood in terms of its lone pair electrons and the rest of the molecule may be regarded as a nonspherical frozen core region. Another example is the planer ethylene as a system of two active electrons (π electrons) and the dormant σ-skeleton core. In such cases it is cumbersome to generalize the analytical expansion [53] to a nonspherical spatial function and it seems more expedient to use the spectral representation technique (15). This strategy has been adopted in Version 3, and applied to a couple of cases. The results of the preliminary applications are encouraging.

The handling of the relativistic effects is very similar to that of the CG-AIMP method, differing only in the technical detail.

[4] To be published.

Can. J. Chem. Downloaded from www.nrcresearchpress.com by 65.111.164.53 on 09/08/12
For personal use only.

4. The nodal structure of valence orbitals

There are various approximate methods in which only the valence electrons are treated explicitly. There is one distinct feature in our model potential method that separates the method from the rest of valence-electron-only methods.

In our method, the nodal structure of valence orbitals in atoms is preserved. The degree of the preservation depends on the flexibility of the basis set to expand the valence orbitals in the Roothaan–Hartree–Fock approximation. If the set is flexible enough, the nodal structure will be reproduced perfectly. This should be obvious from the discussion of the energy shift operator in Sect. 2.

It has been often debated whether or not the valence orbitals in the valence-electron-only method should keep the inner nodal structure existing in the corresponding all-electron method. It is known that reduction of the size of basis set is far more effective in reducing the cost of computation than reduction of the number of electrons to be treated explicitly. Therefore, it is argued that only by smoothing out the inner nodes of the valence orbitals will a substantial saving of the computational cost be achieved. On the other hand, our method enjoys a theoretical transparency that the use of the same basis set employed in the all-electron calculation will reproduce exactly the same valence orbitals and the same orbital energies, granted, at the expense of economy.

We shall discuss some other aspects of the issue by using the hydrogen atom as a simple example. The Schrödinger equation (in atomic units) is

$$[62]\qquad \hat{H}|\varphi_n\rangle = E_n|\varphi_n\rangle, \qquad n = 1, 2, \ldots$$

$$\hat{H} = -\frac{1}{2}\Delta - \frac{1}{r}$$

$$\varphi_1 \equiv \varphi_{1s} = (4\pi)^{-1/2}R_{1s}(r), \qquad E = -1/2$$

$$[63]\qquad \varphi_2 \equiv \varphi_{2s} = (4\pi)^{-1/2}R_{2s}(r), \qquad E_2 = -1/8$$

$$R_{1s}(r) = 2\exp(-r)$$

$$R_{2s}(r) = 2^{-1/2}\left(1 - \frac{r}{2}\right)\exp\left(-\frac{r}{2}\right)$$

We define an energy shift operator to shift the position of the $1s$ energy level,

$$[64]\qquad \hat{\sigma} = \Delta E|\varphi_1\rangle\langle\varphi_1|$$

and add it to the original Hamiltonian [63],

$$[65]\qquad \hat{H} \rightarrow \hat{H}' = \hat{H} + \hat{\sigma} = \hat{H} + \Delta E|\varphi_1\rangle\langle\varphi_1|$$

Then we have

$$\hat{H}'|\varphi_1\rangle = (E_1 + \Delta E)|\varphi_1\rangle$$

$$\hat{H}'|\varphi_2\rangle = E_2|\varphi_2\rangle$$

Note here that $\langle\varphi_1|\varphi_2\rangle = 0$. If we choose $\Delta E = -2E_1 = 1.0$, as in eq. [16],

$$\hat{H}'|\varphi_1\rangle = (+1/2)|\varphi_1\rangle$$

$$\hat{H}'|\varphi_2\rangle = (-1/8)|\varphi_2\rangle$$

Thus, with $\hat{H}'$, the *exact* $2s$ orbital φ_2 is obtained as the *lowest* s eigensolution of the equation,

$$[66]\qquad \hat{H}'|\varphi\rangle = E|\varphi\rangle$$

because the originally lowest energy level of φ_1 is shifted to the position far above the E_2 level, as a matter of fact, in the positive energy continuum. This is an example of unwelcome intruder eigensolutions in the higher region of the energy spectrum of a modified one-electron equation such as eq. [66]. A very similar situation is expected to rise in our modified HF equation [14] or in its generalization. In the Roothaan–Hartree–Fock approximation, these intruder orbitals will be embedded in the so-called virtual orbital space and they should never accommodate electrons in them in the configuration calculation or in the perturbation calculation.

To return to the problem of the nodal structure of valence orbitals, we shall further use the case of the hydrogen atom. This time we choose the amount of the energy shift ΔE as $\Delta E = (E_2 - E_1)$,

$$[67]\qquad \hat{H}' = -\frac{1}{2}\Delta - \frac{1}{r} + (E_2 - E_1)|\varphi_1\rangle\langle\varphi_1|$$

In the eigenvalue spectrum of the above Hamiltonian, the $1s$ level is brought up to the position of the $2s$ level and now they are degenerate. Therefore, any linear combination of φ_1 and φ_2,

$$[68]\qquad \psi = c_1\varphi_1 + c_2\varphi_2$$

also belongs to the eigenvalue E_2:

$$[69]\qquad \left[-\frac{1}{2}\Delta - \frac{1}{r} + (E_2 - E_1)|\varphi_1\rangle\langle\varphi_1|\right]|\psi\rangle = E_2|\psi\rangle$$

From the explicit forms of φ_1 and φ_2 given before, it is seen that we can make the function ψ *nodeless* by choosing c_1 and c_2 properly. The effect of the shift operator on ψ may be formally expressed in the form of a local potential $U(r)$,

$$(E_2 - E_1)|\varphi_1\rangle\langle\varphi_1|\psi\rangle = U(r)|\psi\rangle$$

or

$$[70]\qquad U(r) = \frac{c_1(E_2 - E_1)\varphi_1}{\psi} = \frac{c_1(E_2 - E_1)\varphi_1}{c_1\varphi_1 + c_2\varphi_2}$$

As long as ψ has no zeros except at $r = \infty$ and 0, $U(r)$ can be obtained from eq. [70] for arbitrary values of c_1 and c_2. It is important to note, however, that the energy eigenvalues and eigenfunctions other than E_2 and ψ will be arbitrarily disturbed. A more general approach to obtain $U(r)$ would be to solve the following equation in terms of $U(r)$ with the appropriately chosen nodeless function ψ,

$$[71]\qquad \left[-\frac{1}{2}\Delta - \frac{1}{r} + U(r)\right]|\psi\rangle = E_2|\psi\rangle$$

$$[72]\qquad U(r) = E_2\frac{\left(-\frac{1}{2}\Delta - \frac{1}{r}\right)\psi}{\psi}$$

Can. J. Chem. Downloaded from www.nrcresearchpress.com by 65.111.164.53 on 09/08/12
For personal use only.

This is the essence of the method used by Kahn et al. (16). With the special choice of the form of ψ as a linear combination of φ_1 and φ_2, eq. [72] takes the same form as eq. [70]. However, the choice is not limited to this form and can be made such that the outer portion of ψ resembles as closely as possible that of the original φ_2. Here again, however, other eigensolutions will be disturbed, because the influence of $U(r)$ is not selective as that of the shift operator.

5. The molecular Hamiltonian

The basic idea is that the active electrons in a molecule consist of valence electrons of the constituent atoms and the molecular core is the sum of the spherical atomic cores. As indicated in the Introduction and especially in the discussion of Version 3, the definition of the active and dormant electrons can be much wider. The following form of the molecular Hamiltonian is general enough to accommodate wider definitions of the active and dormant electrons in molecular and solid state systems.

All the Hamiltonian in the present chapter are the Schrödinger Hamiltonian (in atomic units). Quasi-relativistic effects are included in the form of the effective operators at this level.

The total Hamiltonian for the atom is

$$[73] \quad \hat{H}_{\mathrm{mp}} = \sum_{i=1}^{n} \hat{h}_{\mathrm{mp}}(i) + \sum_{i>j} \frac{1}{r_{ij}}$$

$$[74] \quad \hat{h}_{\mathrm{mp}}(i) = -\frac{1}{2}\Delta_i - \frac{(Z - Z_c)}{r_i} + \hat{V}_{\mathrm{mp}}(i) + \hat{\sigma}(i)$$

The total Hamiltonian for the molecule is

$$[75] \quad \hat{H}_{\mathrm{mp}} = \sum_{i=1}^{n} \hat{h}_{\mathrm{mp}}(i) + \sum_{i>j} \frac{1}{r_{ij}} + \sum_{I>J} \frac{(Z_I - Z_{I,c})(Z_J - Z_{J,c})}{R_{IJ}}$$

$$[76] \quad \hat{h}_{\mathrm{mp}}(i) = -\frac{1}{2}\Delta_i + \sum_{I=1}^{N} \left[-\frac{(Z_I - Z_{I,c})}{r_{Ii}} + \hat{V}_{I,\mathrm{mp}}(i) + \hat{\sigma}(i) \right]$$

In the above molecular total Hamiltonian, it is assumed that the nuclear charge Z_I of the I-th atom is perfectly shielded by the $Z_{I,c}$ core electrons. If the molecular core is not defined as the sum of the spherical atomic cores, it is necessary to use some other appropriate formulas (5).

The operator $\hat{V}_{\mathrm{mp}}$ is the model potential approximation of the core operator $\hat{V}_{\mathrm{core}}$ in eq. [21] in the non-relativistic approximation or $\hat{V}_{\mathrm{core,qr}}$ in eq. [56] in the quasi-relativistic approximation:

$$[77] \quad (\mathrm{NR}): \quad \hat{V}_{\mathrm{core}} = \hat{V}_{\mathrm{Coul}} + \hat{V}_{\mathrm{exch}}$$

$$[78] \quad (\mathrm{QR}): \quad \hat{V}_{\mathrm{core,qr}} = \hat{V}_{\mathrm{Coul}} + \hat{V}_{\mathrm{exch}} + \hat{V}_{\mathrm{MV}} + \hat{V}_{\mathrm{D}}$$

The following is a summary of the explicit expressions for $\hat{V}_{\mathrm{mp}}$ in the three versions.

5.1 Version 1

$$[79] \quad (\mathrm{NR}): \quad \hat{V}_{\mathrm{mp}} = \frac{1}{r}\left[\sum_I A_I \exp(-\alpha_I r^2) + \sum_J B_J r \exp(-\beta_J r^2) \right]$$

(QR): same as above

$$[80] \quad \hat{\sigma} = -\sum f_c \varepsilon_c |\varphi_c\rangle\langle\varphi_c|$$

5.2 Version 2

$$[81] \quad (\mathrm{NR}): \quad \hat{V}_{\mathrm{mp}} = \sum_k A_k \frac{\exp(-\alpha_k r^2)}{r} + \hat{P}\hat{V}_{\mathrm{exch}}\hat{P}$$

$$[82] \quad (\mathrm{QR}): \quad \hat{V}_{\mathrm{mp}} = \sum_k A_k \frac{\exp(-\alpha_k r^2)}{r} + \hat{P}\hat{V}_{\mathrm{exch}}\hat{P} + \hat{V}_{\mathrm{MV}} + \hat{V}_{\mathrm{D}}$$

Note here that the relativistic operators $\hat{V}_{\mathrm{MV}}$ and $\hat{V}_{\mathrm{D}}$ are already processed by the projection operators as shown in eq. [58].

$$[83] \quad \hat{\sigma} = -\sum 2\varepsilon_c |\varphi_c\rangle\langle\varphi_c|$$

5.3 Version 3

$$[84] \quad (\mathrm{NR}): \quad \hat{V}_{\mathrm{mp}} = \hat{P}(\hat{V}_{\mathrm{Coul}} + \hat{V}_{\mathrm{exch}})\hat{P}$$

$$[85] \quad (\mathrm{QR}): \quad \hat{V}_{\mathrm{mp}} = \hat{P}(\hat{V}_{\mathrm{Coul}} + \hat{V}_{\mathrm{exch}})\hat{P} + \hat{V}_{\mathrm{MV}} + \hat{V}_{\mathrm{D}}$$
$$\hat{\sigma} = -\sum 2\varepsilon_c |\varphi_c\rangle\langle\varphi_c|$$

Note that this version may conveniently be applied to the case where the core region is nonspherical (15).

6. Applications

Various versions of the model potential method have been applied to many molecular systems. Through these applications, the atomic parameters $\{A_I, \alpha_I; B_J, \beta_J\}$ and f_c in Version 1 have been determined for a majority of atoms in the periodic table, and along with them adequate Gaussian basis sets for the Roothaan expansion of the valence orbitals have been established. A very gratifying feature of Version 1 is that the quasi-relativistic effects are incorporated into $\{A_I, \alpha_I; B_J, \beta_J\}$ and hence the QR calculation is no more expensive than the corresponding NR calculation. To choose the basis set, a near-Hartree–Fock all-electron calculation is used as the reference. We believe that a good valence-electron-only calculation with a fairly large basis set is better than an all-electron calculation with a small basis set.

In Version 2, the AIMP method of Seijo and Barandiarán, the non-relativistic Hamiltonian is completely specified by the knowledge of the frozen core orbitals and the orbital energies. If the basis set for $\hat{P}$ is judiciously chosen and the expansion basis set for the valence orbitals is the same as that of the reference all-electron Hartree–Fock calculation, the result of the calculation should be the same as that of

Can. J. Chem. Downloaded from www.nrcresearchpress.com by 65.111.164.53 on 09/08/12
For personal use only.

the all-electron Hartree–Fock calculation in the frozen core approximation with the assumption that the core electrons completely shield the nuclear charges. This is true also with Version 3. This is a unique feature not found in any other available effective core methods with nodeless valence orbitals.

It is known that reduction of the size of basis set is much more effective than reduction of the number of electrons explicitly treated when it comes to economizing the computational cost. Our model potential method requires expansion basis sets flexible enough to produce proper inner nodes of the valence orbitals. Therefore one may not expect a very drastic cut in the computational cost. The saving seems to be in the range from 90 to 40% of the cost of the all-electron calculation. However, there are cases where the all-electron calculation is next to impossible. For example, the quasi-relativistic all-electron molecular calculation would be extremely difficult, if not impossible, but our model potential method can be used with confidence and at a reasonable cost. Other such examples may be found in the solid state and in surface phenomena where some sort of localization of electrons must already be assumed in the "all-electron" treatment. Our model potential method is inherently well equipped to handle such localizations.

The following is a very cursory and uneven review of the applications of the model potential method, primarily because I have made only a nominal contribution there. It excludes the works in which the reference all-electron results are used for comparison, through which the dependability of the method is tested and confirmed.

6.1 Version 1

A number of molecular clusters including Pd_4 Pt_4, Pd_4H, and Pt_4H were studied at both the NR and QR level of approximation. The electron affinity of various hexafluoride molecules MF_6 (M = Cr, Mo, W, Au) were studied by the Hartree–Fock calculation and also by the post-Hartree–Fock calculation at the level of singly and doubly excited CI (SDCI) (17). The effects of relativity and the electron correlation were carefully assessed.

This version of the model potential method has been applied actively to the study of various surface phenomena including the study of the CO molecule coadsorbed with *K* on metallic Cu and Ag surfaces. The actual sizes to which the model potential method was applied are $Cu_{12}K_2CO$ and $Ag_{12}K_2CO$ (18).

Inclusion of the electron correlation effect has also been practiced with considerable success in this version. To cite one example, multireference singly and doubly excited CI (MRSDCI) calculations were performed on the NaI molecule (19).

6.2 Version 2

This version, the AIMP method of Seijo and Barandiarán, was applied to study the equilibrium geometry of alkaline earth dihalides MX_2 (M = Mg, Ca, Sr, Ba: X = F, Cl, Br, I) (20), the hydrides XH_2, XH_4 (X = Si, Ge, Sn, Pb), and also the oxides XO (X = Ge, Sn, Pb). These are mostly without the reference all-electron calculation and emphasis was placed on the comparison between the NR-AIMP and the QR-AIMP to gauge the relativistic effect.

Barandiarán and Seijo (21, 22) developed an interesting variation of their AIMP method called the ab initio environment model potential (AIEMP) method. Similar developments have been made also in Version 1 and Version 3. Since the development clearly indicates the applicability of the model potential method to a wider class of phenomena, we shall describe the essential point of the AIEMP method as an illustration.

The method applies to the crystalline system with an impurity as formed by a cluster, that is, a group of nuclei and active electrons that are responsible for the local properties of the crystal associated with the impurity, and groups of nuclei and dormant electrons that are essentially unperturbed and act as the environment for the cluster. Then, we may adopt the following wavefunction as an approximation to describe the crystalline system:

$$[86] \qquad \Phi = A_{SL}(\Phi_{clus}\Phi_{env})$$

which is an obvious variation of Φ in eq. [1]. Φ_{clus} may be a closed-shell, an open-shell, or even a multiconfiguration wavefunction. Φ_{env} may be a product of atomic wavefunctions representing the ions $e, f, \ldots, s$ located on lattice sites outside of the cluster,

$$[87] \qquad \Phi_{env} = \Phi_e\Phi_f \cdots \Phi_s$$

Suppose that $\{\varphi_{clus}\}$ are the orbitals in Φ_{clus}, $\{\varphi_e\}$ in Φ_e, $\{\varphi_f\}$ in Φ_f, and so on. The orthogonalities among these orbital sets are imposed,

$$\{\varphi_{clus}\}\perp\{\varphi_e\}, \qquad \{\varphi_{clus}\}\perp\{\varphi_f\}, \qquad \{\varphi_e\}\perp\{\varphi_f\}, \text{ etc.}$$

Therefore, the trade-mark projection operator in the model potential method for the ion *e*,

$$[88] \qquad \hat{o}_e = -\sum_k 2\varepsilon_{e,k}|\varphi_{e,k}\rangle\langle\varphi_{e,k}|$$

contains all the occupied orbitals of the ion *e*, $\{\varphi_e\}$.

The AIEMP method has been applied to (*a*) the $CuCl_6^{5-}$ cluster embedded in an NaCl lattice (21), (*b*) the $(CrF_8)^{q-}$ lattice ($q = 7$ for the Cr^+ defect and $q = 5$ for the Cr^{3+} defect) in fluorite (23), (*c*) the CrF_6^{3-} cluster in the K_2NaGaF_6 lattice (24), and (*d*) the $(CuO_6)^{10-}$ and $(AgO_6)^{10-}$ clusters in the MgO, CaO, and SrO family of hosts (25).

6.3 Version 3

In 1985 Katsuki already entertained the idea of the environment potential (26). Therefore it is only natural for him to adopt the technique of spectral representation to treat a nonspherical environment, that is, active electrons interacting with a nonspherical core region of dormant electrons. So far, the method has been applied to the interaction between three ammonia molecules (26), and also to the molecules CH_3COOH, CH_3CH_2COOH, and $CH_3CH_2CH_2COOH$, where the functional group COOH is treated as a system with 6 frozen electrons and then progressively with 10, 12, and 18 frozen electrons (27).

7. Concluding remarks

We posed two questions in the Introduction. First, to account

for the differences among atoms with the same number of valence electrons, the carefully crafted effective Hamiltonian is required, and it has been shown that it can be done in our model potential method. Second, do we still have Van Vleck's nightmare? Perhaps no for the atomic inner core, but still yes for the general problem of the localization of electrons in quantum mechanics (28). One manifestation of the problem in our model potential method is the intruder orbitals in virtual orbital space as mentioned in Sect. 4. Care should be taken in performing the CI or the perturbational calculation with our model potential method (29).

The method has been developed to a satisfactory level of sophistication and accuracy. There is, however, one aspect of the method to be supplemented in the near future. In the nonrelativistic formulation, knowledge of the frozen, dormant electrons is sufficient for constructing the effective Hamiltonian for the active electrons. However, in the relativistic formulation based on the Cowan–Griffin–Wood–Boring approximation, knowledge of the valence electrons is also necessary in the reference atomic calculation. This necessity will be removed if we develop the model potential version of the Fock–Dirac relativistic method.

Acknowledgments

I would like to express my sincere gratitude to all of my friends and colleagues who have contributed to the development of the present work. The order of acknowledging their names is more or less chronological: D. McWilliams, A.A. Cantu, V. Bonifacic, O. Gropen, U. Wahlgren, G. Höjer, J. Chung, S. Katsuki, M. Klobukowski, J. Andzelm, E. Radzio, Y. Sakai, H. Tatewaki, L. Seijo, Z. Barandiarán, and E. Miyoshi.

References

1. M. Krauss and W.J. Stevens. Annu. Rev. Phys. Chem. **35**, 357 (1984).
2. J.H. Van Vleck and A. Sherman. Rev. Mod. Phys. **7**, 167 (1935).
3. S. Huzinaga and A.A. Cantu. J. Chem. Phys. **55**, 5543 (1971); S. Huzinaga, D. McWilliams, and A.A. Cantu. Adv. Quantum Chem. **7**, 187 (1973).
4. V. Bonifacic and S. Huzinaga. J. Chem. Phys. **60**, 2779 (1974).
5. S. Huzingaga. J. Mol. Structure (Theochem), **234**, 51 (1991).
6. R. McWeeny. Proc. R. Soc. London A: **253**, 242 (1959).
7. G. Höjer and J. Chung. Int. J. Quantum Chem. **14**, 623 (1978).
8. P. Durand and Jean-Paul Malrieu. Adv. Chem. **67**, 321 (1987).
9. L.I. Schiff. Quantum mechanics. 3rd ed. McGraw–Hill, New York. 1968. Chap. 13, pp. 481–484.
10. J.H. Wood and A.M. Boring. Phys. Rev. B: Condens. Matter, **18**, 2710 (1978).
11. R.D. Cowan and D.C. Griffin. J. Opt. Soc. Am. **66**, 1010 (1976).
12. Y. Sakai. J. Chem. Phys. **75**, 1303 (1981); Y. Sakai and S. Huzinaga. J. Chem. Phys. **76**, 2537 (1982); **76**, 2552 (1982); Y. Sakai, E. Miyoshi, M. Klobukowski, and S. Huzinaga. J. Comput. Chem. **8**, 226 (1987); **8**, 264 (1987); E. Miyoshi and Y. Sakai. J. Comput. Chem **9**, 719 (1988).
13. J. Andzelm, E. Radzio, Z. Barandiarán, and L. Seijo. J. Chem. Phys. **83**, 4565 (1985).
14. S. Huzinaga, L. Seijo, Z. Barandiarán, and M. Klobukowski. J. Chem. Phys. **86**, 2132 (1987); L. Seijo, Z. Barandiarán, and S. Huzinaga. J. Chem. Phys. **91**, 7011 (1989); Z. Barandiarán, L. Seijo, and S. Huzinaga. J. Chem. Phys. **93**, 5843 (1990).
15. S. Katsuki and S. Huzinaga. Chem. Phys. Lett. **152**, 203 (1988).
16. L.R. Kahn, P. Baybutt, and D.G. Truhlar. J. Chem. Phys. **65**, 3826 (1976).
17. Y. Sakai and E. Miyoshi. J. Chem. Phys. **87**, 2885 (1987); E. Miyoshi and Y. Sakai. J. Chem. Phys. **89**, 7363 (1988).
18. E. Miyoshi, Y. Sakai, and S. Katsuki. Surf. Sci. **242**, 531 (1991).
19. Y. Sakai, E. Miyoshi, and T. Anno. Can. J. Chem. **70**, 309 (1992).
20. L. Seijo, Z. Barandiarán, and S. Huzinaga. J. Chem. Phys. **94**, 3762 (1991).
21. Z. Barandiarán and L. Seijo. J. Chem. Phys. **89**, 5739 (1988).
22. Z. Barandiarán and L. Seijo. Stud. Phys. Theor. Chem. **77(B)**, 436 (1992).
23. L. Seijo and Z. Barandiarán. J. Chem. Phys. **94**, 8158 (1991).
24. L. Seijo, Z. Barandiarán, and L.G.M. Petterson. J. Chem. Phys. **98**, 4041 (1933).
25. J.L. Pascual, L. Seijo, and Z. Barandiarán. J. Chem. Phys. **98**, 9715 (1993).
26. S. Katsuki. Can. J. Chem. **70**, 285 (1992).
27. S. Katsuki. J. Chem. Phys. **98**, 496 (1993).
28. W.H. Adams. Electron delocalization in the theory of intermolecular and intergroup interactions; cause, effect, prevention. To appear in the successor volume to Conceptual Trends in Quantum Chemistry. *Edited by* J.L. Calais and E. Kryachko.
29. M. Klobukowski. Chem. Phys. Lett. **172**, 361 (1990); L. Seijo, Z. Barandiarán, and S. Huzinaga. Chem. Phys. Lett. **192**, 217 (1992).

Can. J. Chem. Downloaded from www.nrcresearchpress.com by 65.111.164.53 on 09/08/12
For personal use only.

The heterogeneity of two Canadian kraft lignins

R.W. Thring and S.L. Griffin

Abstract: Two kraft lignins, one precipitated with carbon dioxide and the other with sulphuric acid, have been fractionated into three distinct fractions by sequential extraction using organic solvents of increasing hydrogen-bonding capacity. The lignins and fractions were comparatively characterized in terms of yield, methoxyl group content, molecular weight distribution, and ^{13}C NMR spectroscopy. For a given lignin, the fractions showed differences in yield, composition, and chemical structure. A significant portion (21%) of the carbon dioxide precipitated kraft lignin is composed of ethyl acetate soluble material of low molecular weight. This fraction, which is richer in guaiacyl moieties than the other fractions, is virtually absent in the sulphuric acid precipitated kraft lignin. The occurrence of "tails" in the high molecular weight fraction, especially from the carbon dioxide precipitated kraft lignin, suggests the presence of material of very high molecular weight. Data from ^{13}C NMR spectroscopy does little to elucidate the nature or origin of the material causing these tails.

Key words: kraft lignins, heterogeneity, fractionation, characterization.

Résumé : On a précipité deux lignines kraft, l'une par du dioxyde de carbone et l'autre par de l'acide sulfurique, et, utilisant des solvants organiques de capacité croissante à former des liaisons hydrogènes, on les a séparées en fractions distinctes par des extractions séquentielles. On a effectué une caractérisation comparative des lignines et des fractions en fonction des rendements, des contenus en groupes méthoxyles, des distributions des poids moléculaires et de la spectroscopie RMN du ^{13}C. Pour une lignine donnée, les fractions présentent des différences dans les rendements, les compositions et la structure chimique. Une fraction importante (21%) de la lignine kraft obtenue par précipitation avec du dioxyde de carbone est formée de matériel de bas poids moléculaire, soluble dans l'acétate d'éthyle. Cette fraction, qui est plus riche en portions guaïacyles que les autres fractions, est pratiquement absente de la lignine kraft obtenue par précipitation à l'acide sulfurique. La présence de traînées dans la fraction de poids moléculaire élevé, en particulier celle de la lignine kraft obtenue par précipitation avec du dioxyde de carbone, suggère la présence de matériel de poids moléculaire très élevé. Les données de la RMN du ^{13}C n'apportent que peu de lumière sur la nature ou l'origine du produit provoquant ces traînées.

Mots clés : lignines kraft, hétérogénéité, fractionnement, caractérisation.

[Traduit par la rédaction]

Introduction

The economic viability of any pulping process would be greatly improved if a high-value application were developed for lignin, the major by-product from such facilities. It is therefore of considerable interest to elucidate the composition, structure, and properties of commercially produced lignins if one or more high-value applications are to be developed from these materials.

The importance of heterogeneity of lignins and their subsequent performance has been demonstrated in the past (1). Chemical heterogeneity affects the chemical reactivities in modification reactions as well as the accessibility of the lignins to solvents. As a consequence, the former will dictate the performance properties of these modified technical lignins. It is therefore imperative that a better understanding of the heterogeneity of lignin and the methodology to eliminate the deleterious components be attained so as to achieve a major improvement of lignins as chemical raw materials.

A number of investigations have been conducted into the elucidation of the physical and chemical structural heterogeneity of lignin by fractionation. As early as 1962, Wada et al. (2) fractionated this lignin from kraft waste liquor into 10 fractions by acid precipitation, by varying the pH of the solution with sodium carbonate, carbon dioxide, and hydrochloric acid. Lin and Detroit (1) studied the heterogeneity of lignin by fractionating sulphite and kraft lignins into five and six fractions, respectively, using ultrafiltration.

More recently, Kringstad et al. (3) used gel permeation chromatography to fractionate a pine kraft lignin. The method, based upon the initial production of silylated lignin derivatives followed by gel permeation chromatography as eluent, was deemed convenient and rapid by the authors. However, small quantities of samples, typically less than 1 g, were obtained by this technique. Hatakeyama et al. (4) fractionated kraft lignin by successive precipitation with water from a dioxane solution. Recently, increasing interest has been shown in the use of

Received October 5, 1994.

R.W. Thring[1] **and S.L. Griffin.** Department of Chemical Engineering, University of New Brunswick, P.O. Box 4400, Fredericton, NB E3B 5A3, Canada.

[1] Author to whom correspondence may be addressed. Telephone: (506) 453-4520. Fax: (506) 453-3591.

Can. J. Chem. Downloaded from www.nrcresearchpress.com by 65.111.164.53 on 09/08/12
For personal use only.

Can. J. Chem. Downloaded from www.nrcresearchpress.com by 65.111.164.53 on 09/08/12
For personal use only.

organic solvents in lignin fractionation (5, 6). This may be due to the fact that bulk (kg) quantities of lignin can be fractionated rather effectively by sequential extraction with organic solvents of increasing hydrogen-bonding capability. This approach is based on the work of Schuerch (7), who discovered that the solvation power of a solvent for lignin was a function of both the cohesive energy density and hydrogen-bonding capacity of the solvent. In other words, organic solvents of weak or moderate hydrogen-bonding capacity will solubilize low molecular weight fragments of lignins.

The present paper describes the fractionation of two Canadian kraft lignins by successive extraction with organic solvents of increasing hydrogen-bonding capacity. The starting lignins and their fractions are compared in terms of their yield, molecular weight distribution, functional group analysis, and ^{13}C NMR spectroscopy.

Experimental

Materials

Both kraft lignins were donated by the research group of Professor P. Watkinson (University of British Columbia), involved in conducting research on the use of lignin as a lime kiln fuel (8). One kraft lignin was isolated from a mostly spruce wood furnish at Irving Pulp and Paper Company (New Brunswick, Canada). This lignin was precipitated from strong black liquor using pure carbon dioxide and recovered on a 200 mesh belt filter with some water washing. Since the acid used for precipitation was carbon dioxide, this lignin will be designated as CPKL (carbon dioxide precipitated kraft lignin). The other kraft lignin was extracted from a wood furnish of 45% lodgepole pine, 50% spruce, and 5% Douglas fir at Canfor's Intercontinental Mill in Prince George (British Columbia, Canada). It was acid precipitated from strong (~50% solids) oxidized black liquor using 9.5 N sulphuric acid. This lignin will be designated at SPKL (sulphuric acid precipitated kraft lignin).

Ethyl acetate (ACS Reagent Grade) was purchased from Mallinckrodt Inc., Paris, Kentucky, U.S.A. Methanol (ACS Reagent Grade) was obtained from Anachemia, Montreal, Canada. Hildebrand solubility parameters (σ/MPa$^{1/2}$) for these solvents are 18.6 and 29.6, respectively. Ethyl acetate has a moderate hydrogen-bonding capacity but that of methanol is strong.

Analytical methods

Methoxy group determination

The methoxyl content was quantified using the TAPPI method T209-WD-79 (9).

Fractionation scheme

Each lignin was subjected to the fractionation sequence depicted in Fig. 1. Fractionation was carried out at room temperature using an ultrasonic water bath to facilitate both the penetration of the solvent into the lignin residue and dissolution of the soluble portion of the lignin.

The method may be described as follows. Approximately 50 g (dry basis) of lignin and 200 mL of ethyl acetate were added to a 500 mL extraction flask. The contents were then agitated by ultrasound for 10 min. After allowing the mixture to stand so that any suspended particles could settle out, the supernatant was decanted into a 1 L volumetric flask. The same procedure was repeated three to four times, after which it was considered that most of the solvent-soluble lignin was dissolved and separated from the lignin residue (i.e., the supernatant was very light coloured after the last extraction). The ethyl acetate insolubles were dried for 15 min using a rotary evaporator under reduced pressure.

Fig. 1. Scheme for the fractionation of kraft lignins.

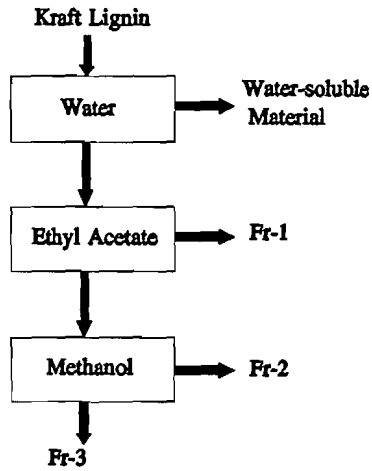

Methanol was then used in the sequence. In this case, removal of the soluble material was deemed complete after three extractions. The remaining residue in the extraction flask, after evaporation of the remaining methanol, constituted the third fraction.

The combined extracts for each of the first two fractions were evaporated under reduced pressure and the residue was dried to constant weight within 100 mg. To ensure complete removal of the solvent, all three residues were kept in a desiccator under vacuum for 2 days. Each fraction was then stored in bottles under a nitrogen blanket in the dark until further use.

All fractions from both kraft lignins were free-running powders and light brown in colour.

The fractionation method described above was rather time consuming but very reproducible, with a high degree of recovery of the solvents.

High-pressure solvent elution chromatography (HPSEC)

A Waters liquid chromatograph connected to an on-line computer via a Waters Maxima NEC 80486 data system was used. Three stainless steel columns in series (3 cm length; 7.5 mm i.d.), packed with ultrastyragel columns (Polymer Laboratories, U.K.) of pore size 10^4, 500, and 100 Å, and a UV detector set at 277 nm were used. A single-piston reciprocating pump maintained a constant flow rate through the system. Operating conditions were as follows: eluent, degassed THF (purged with N_2); temperature, 25°C; injection volume, 100 μL; flow rate, 1 mL/min.

A relative calibration curve was obtained using monodisperse polystyrene standards (Polymer Laboratories). A third-order polynomial of the form $y = ax^3 + bx^2 + cx + d$ best describes the relation between the log of the actual molecular weights of polystyrene standards (y) and their retention times (x). The following coefficients were calculated: $a = 0.0021$, b

Can. J. Chem. Downloaded from www.nrcresearchpress.com by 65.111.164.53 on 09/08/12
For personal use only.

Table 1. Fractionation yields and methoxyl group content of kraft lignins and fractions.

	CPKL		SPKL	
Fraction	Yield[a] (%)	Methoxy content (%)	Yield[a] (%)	Methoxy content (%)
1	21	14.1	5	12.0
2	33	15.4	48	14.8
3	46	19.4	47	13.2
Original lignin	100	13.0	100	12.5

[a]Yields were determined on 50 g samples; losses, calculated by difference, amounted to less than 1% (initial sample) for both lignins.

= 0.0283, $c = -1.279$, $d = 20.64$. These gave a fit with a correlation coefficient of 0.99. The size exclusion volume (V_0) for the column system was 6.4.

^{13}C NMR

Both kraft lignins and their fractions were acetylated and analyzed using a Brüker 400 WD spectrometer. Samples were prepared by dissolving ca. 800 mg of lignin in 2 g of DMSO-d_6 at room temperature and placing the solution in 10 mm i.d. glass tubes. In some cases, particularly for the high molecular weight samples, a little heating (~40°C) was required to completely dissolve the acetylated lignin. The instrument was set in proton inverse-gated decoupled mode, with a scan delay of 2 s. All samples were run at a temperature of 50°C.

Results and discussion

Yields

The objective was to determine whether there were significant differences in the fractional yields from each kraft lignin, as a function of the type of lignin. The method of fractionation is based on a previous study on the selective fractionation of a glycol lignin (10). It was found that at the conditions employed, ethyl acetate preferentially solubilized the low molecular weight portion of lignin. Methanol, on the other hand, extracted both low and medium molecular weight material. From Table 1, it is seen that both kraft lignins are heterogeneous in terms of fractional yields. The extraction procedure solubilized an identical quantity of 54% from each lignin. However, Fr-1 represents 21% of CPKL but only 5% is solubilized from SPKL. In both lignins, the methanol solubles are high but are more significant in SPKL (48 versus 33%, respectively).

Thus, both lignins contain comparable quantities of insoluble material not solubilized by the solvent extraction procedure utilized here. However, the CPKL is composed of almost 75% more ethyl acetate solubles but 31% less methanol solubles than the SPKL.

Methoxy content

Analytical determinations of the content of methoxyl groups were carried out for both lignins and their fractions. As shown in the second column of Table 1, the content of methoxyl groups is highest at 19.4% in Fr-3 for CPKL, and, for SPKL, it is highest in Fr-2 (14.8%). This suggests that these fractions

Fig. 2. HPSEC chromatograms of acetylated SPKL lignin and its fractions (calibration based on polystyrene standards).

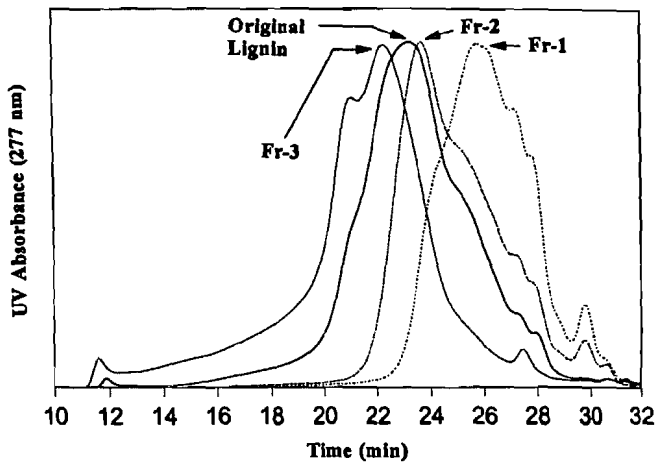

are the richest in structures consisting of syringyl units. On the other hand, the low molecular weight material, Fr-1, has the lowest methoxyl group content in both lignins, indicative of the high guaiacyl character in this fraction. It should, however, be noted that Fr-1 is almost completely absent in SPKL. Also, it is interesting to observe that both starting kraft lignins have methoxyl group contents of 13%. Clearly, the extraction procedure is more selective in fractionating CPKL than SPKL according to methoxyl group functionality.

HPSEC

As seen in Figs. 2 and 3, both kraft lignins yield three fractions of increasing molecular weight when subjected to sequential solvent extraction. A number of important observations can be made about the chromatograms of the two lignins and corresponding fractions. Both starting lignins exhibit similar distribution patterns, with large peaks whose maxima correspond to about 4500 g/mol (polystyrene weight equivalent). Therefore, this suggests that both lignins contain significant amounts of medium and high molecular weight material. The chromatograms of Fr-1 for both lignins are well separated from the medium and high molecular weight fractions. In both lignins, Fr-3 exhibits a tail of very high molecular weight material. This is much more pronounced for Fr-3 from CPKL. The origin or nature of the material causing this tail is not known at this time. It should be noted that this tail is not present in the chromatograms of the starting lignins. Mörck et al. (5, 11) also observed a tail in HPSEC chromatograms of acetylated softwood kraft lignins. The existence of a tail in a chromatogram will strongly affect the value of M_w, the weight-average molecular weight.

The weight- and number-average molecular weight (relative values of polystyrene) and polydispersity are all shown in Table 2. M_w and M_n values of the CPKL lignin and its fractions are discernibly higher than those of SPKL and its corresponding fractions. However, CPKL lignin contains a higher proportion of low molecular weight material than SPKL as demonstrated by the higher content of ethyl acetate soluble material in the former lignin. A steady increase can be seen in both molecular weight and polydispersity from Fr-1 to Fr-3 in both lignins, suggesting that Fr-1 from either lignin is composed of structures of essentially similar low molecular

Can. J. Chem. Downloaded from www.nrcresearchpress.com by 65.111.164.53 on 09/08/12
For personal use only.

Fig. 3. HPSEC chromatograms of acetylated CPKL lignin and its fractions (calibration based on polystyrene standards).

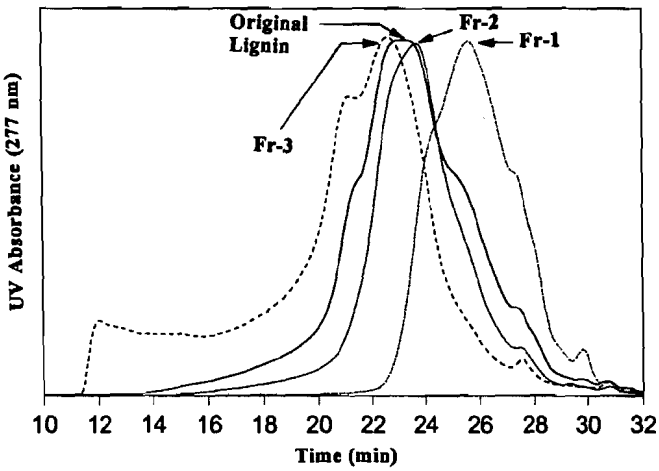

Table 2. Molecular weight averages (polystyrene standards) and polydispersity of kraft lignins and fractions.[a]

	CPKL			SPKL		
Fraction	M_w	M_n	d	M_w	M_n	d
1	1 316	648	1.9	1 280	562	2.3
2	14 037	1960	7.2	4 134	884	4.7
3	93 388	4615	20.2	67 603	4239	18.1
Original lignin	29 668	1594	18.6	21 845	1917	11.4

[a] M_w = apparent weight-average molecular weight; M_n = apparent number-average molecular weight; d = polydispersity (M_w/M_n).

weight. The high polydispersity of Fr-3 from both lignins is a reflection of the presence of a mixture of medium and high molecular weight structures. As seen in Fig. 2 and 3, the occurrence of "tails" in the chromatograms of Fr-3 is indicative of very high molecular weight material, which will strongly dictate the calculated M_w and M_n and, therefore, the polydispersity of this fraction.

^{13}C NMR

The spectra of both kraft lignins and their corresponding fractions are shown in Figs. 4 and 5. Assignments of important signals can be found in previous reports (5, 6, 12). The carboxylic signal at 172 ppm is barely perceptible in both starting lignins but is more significant in the fractions, particularly in Fr-1 and Fr-2 for SPKL. Signals at 170 and 168 ppm are attributed to aliphatic and phenolic hydroxyl groups, respectively. A coarse estimate of the relative abundance of these groups is possible in routine NMR analysis from the intensities of the signals because of the similarity in spin-lattice relaxation times of the various acetyl carbonyl carbon atoms (13). As seen in both lignins and fractions, the intensity of the signal of phenolic hydroxyl groups is higher, suggesting that there are more phenolic than aliphatic hydroxyl groups in all cases. This is to be expected since it is known that hydrolysis of lignin during alkaline pulping increases the phenolic hydroxyl groups in lignin (14). From all the spectra it is not obvious whether the aliphatic hydroxyl groups are primary or secondary. Broad peaks can be observed in some of the spectra, particularly in the aromatic region. Since each sample was run overnight, it is probable that some of them, especially the high molecular weight fractions (Fr-3) from each lignin, were not completely dissolved in DMSO-d_6. However, all the lignin samples should be soluble in this solvent since each was acetylated for 2 days in a 50/50 mixture of acetic anhydride and pyridine at room temperature. It is possible, however, that Fr-3 is composed of material whose molecular weight is just too high to be rendered soluble. The decrease in intensity of the signal at 149 ppm (guaiacyl) and the corresponding increase in intensity of the signal at 152 ppm (syringyl) from Fr-1 to Fr-3 suggests the trend form guaiacyl to syringyl moieties with increasing fraction number. The aromatic region (103–148 ppm) is difficult to interpret due to the presence of broad signals, especially in the high molecular weight fractions from both kraft lignins. Thus, no further interpretation of the signals in this region will be attempted in the present study. The almost complete absence of signals in the 85–64 ppm region (aliphatic carbons) in the starting lignins and fractions is indicative of extensive cleavage of interunit linkages (-C-C- and -C-O-C-) as well as those of the side chains of lignin during kraft pulping.

The intensity of signals in the 34–14 ppm region (methine, methylene, and methyl carbons) in the spectra of both kraft lignins reveals the presence of saturated hydrocarbon structures. These signals arise from the formation of new bonds due to condensation reactions. As suggested by Gierer et al. (15), these reactions involve intermediate coniferyl alcohol structures generated after initial cleavage of phenolic β-aryl ether bonds, and may introduce conjugated double bonds as well as saturated hydrocarbon structures to the side chains in lignin. Thus, the nature of the spectra in both lignins and corresponding fractions indicates that these saturated hydrocarbon structures are roughly the same in each set of fractions, except for Fr-1 in both series. In Fr-1 from both lignins, the distribution of the signals in the aliphatic region strongly suggests the dominance of structures containing saturated hydrocarbon side chains. Therefore it can be concluded that CPKL contains a significant amount (21%) of low molecular weight material composed of saturated aliphatic residues. As seen previously, this Fr-1 is virtually absent in SPKL.

Conclusions

Fractionation of both kraft lignins according to solubility is feasible and yields fractions of increasing molecular weight. Fractions of low molecular weight have narrow molecular weight distributions, while the high molecular weight fractions have broad distributions. For the same solvent, the magnitude of the difference between the yields in each lignin decreases with increasing molecular weight. The molecular weight distribution patterns show that the solvent sequence used is more selective for fractionating carbon dioxide precipitated lignin than sulphuric acid precipitated lignin. The low molecular weight fractions (Fr-1) from both lignins are composed of material of essentially the same molecular weight, as reflected by their low polydispersity. Low molecular weight material (EtAc soluble) is virtually absent in the sulphuric acid precipitated kraft lignin, whereas the carbon dioxide precipitated kraft lignin is composed of 21 wt% of this fraction. Also,

Can. J. Chem. Downloaded from www.nrcresearchpress.com by 65.111.164.53 on 09/08/12
For personal use only.

Fig. 4. ^{13}C NMR spectra of acetylated SPKL lignin and its fractions: solvent, DMSO-d_6.

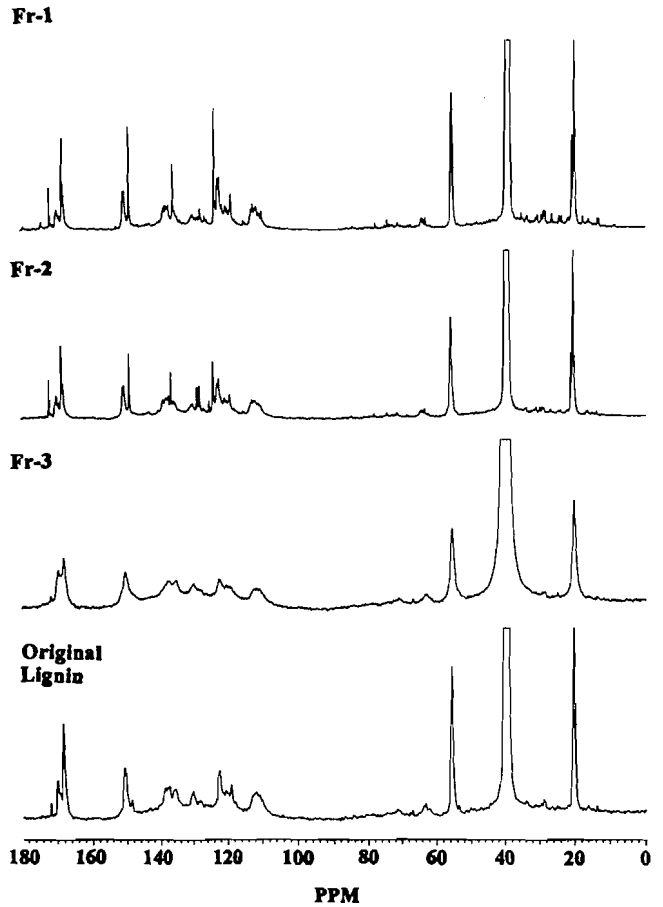

Fig. 5. ^{13}C NMR spectra of acetylated CPKL lignin and its fractions: solvent, DMSO-d_6.

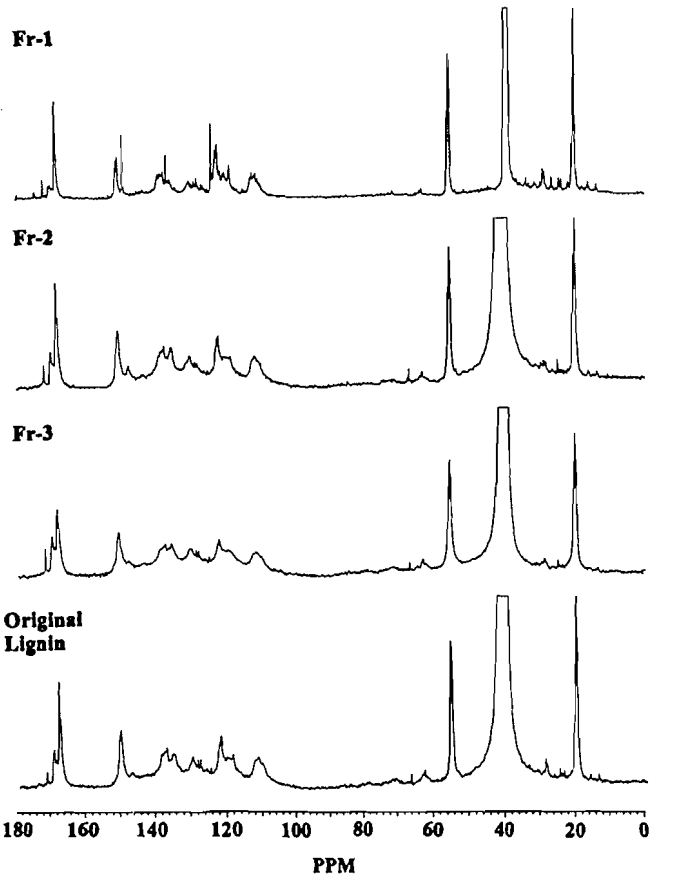

characterization of both lignins and their fractions by methoxyl group determination and ^{13}C NMR spectroscopy confirms the chemical differences existing not only between the lignins, but particularly between Fr-1 and the other fractions. For both lignins, the data indicates the low molecular weight fraction (Fr-1) is richest in guaiacyl moieties, whilst Fr-3 has the highest syringyl character. The low molecular weight fraction is essentially composed of residues containing saturated aliphatic side-chain structures that were selectively extracted from the kraft lignins. The results demonstrate the inhomogeneity of both lignins. More importantly, the data suggest that a little less than 50% of either lignin may be inaccessible to solubilization by many common solvents or to modification reactions.

Therefore, the two technical lignins examined in this study exhibit significant heterogeneity with respect to both molecular dispersity and structural variation.

Acknowledgements

We would like to thank Professor P. Watkinson of the University of British Columbia for supplying samples of both kraft lignins. Useful discussions on kraft lignin recovery with V. Uloth, Senior Research Engineer of the Pulp and Paper Research Institute of Canada, were deeply appreciated. Also, we would like to express our sincere gratitude to the Natural Sciences and Engineering Research Council of Canada for financial support.

References

1. S.Y. Lin and W.J. Detroit. Ekman–Days V. 1981. Int. Symp. Wood Pulping Chem. Stockholm. Vol. IV, pp. 44–40.
2. S. Wada, T. Iwamida, R. Iizima, and K. Yabe. Kobunshi Kagaku, **19**, 699 (1962).
3. K.P. Kringstad, P. Mansson, and R. Mörck. Ekman–Days V. 1981. Int. Symp. Wood Pulping Chem. Stockholm. Vol. V, pp. 91–93.
4. H. Hatakeyama, K. Iwashita, G. Meshitsuka, and J. Nakano. Mokuzai Gakkaishi, **21**, 618 (1975).
5. R. Mörck, H. Yoshida, K.P. Kringstad, and H. Hatakeyama. Holzforschung. (Supp.), **40**, 51 (1986).
6. R.W. Thring, E. Chornet, J. Bouchard, P.F. Vidal, and R.P. Overend. Ind. Eng. Chem. Res. **29**, 232 (1991).
7. C. Schuerch. J. Am. Chem. Soc. **74**, 5061 (1952).
8. B. Richardson, A.P. Watkinson, and P.V. Barr. TAPPI J. 133 (1990).
9. B. Browning. *In* Methods of wood chemistry, Vol. 2. John Wiley & Sons, New York. 1967. Chap. 29, pp. 653–672.
10. R.W. Thring, E. Chornet, and R.P. Overend. Can. J. Chem. Eng. **71**, 116 (1993).

11. R. Mörck, A. Reimann, and K.P. Kringstad. Holzforschung, **42**, 111 (1988).
12. C. Lapierre, J.Y. Lallemand, and B. Monties. Holzforschung, **36**, 275 (1982).
13. R. Mörck and K.P. Kringstad. Holzforschung. **39**, 109 (1985).
14. J. Gierer, B. Lenz, I. Noren, and S. Soderberg. TAPPI J. **47**, 233 (1964).
15. J. Gierer, F. Imsgard, and I. Petterson. J. Appl. Polym. Sci.: Appl. Polym. Symp. **28**, 1195 (1976).

Can. J. Chem. Downloaded from www.nrcresearchpress.com by 65.111.164.53 on 09/08/12
For personal use only.

Preparation and properties of rhodium(I) and iridium(I) diolefin complexes of heterodifunctional phosphorus–imine chelating ligands and a related iminophosphine. ^{103}Rh NMR parameters of the rhodium complexes obtained via indirect two-dimensional ^{31}P, ^{103}Rh{^{1}H} NMR spectroscopy

David J. Law, Glen Bigam, and Ronald G. Cavell

Abstract: Treatment of $[M(cod)Cl]_2$ (M = Rh, Ir) with iminophosphoranophosphine ligands of the type $Ph_2PQP(Ph_2)$=$NSiMe_3$ (Q = CH_2, CH_2CH_2, 1,2-C_6H_4) afforded the new metallacycles $[(cod)\overline{MPPh_2QPPh_2N}]$ through elimination of Me_3SiCl, ultimately "anchoring" the ligand to the metal through a metal–nitrogen σ bond. The phosphine functionality completes the chelate. Cationic complexes of the type $[M(cod)L_2]^+PF_6^-$ (M = Rh or Ir; L_2 = Ph_2PQPPh_2NR where Q = CH_2, $CH(CH_3)$, 1,2-C_6H_4, and R = *p*-C_6F_4CN, $C_6H_2F(NO_2)_2$, and $C_6H_3(NO_2)_2$ or L = Ph_2PN=C(H)Ph) were readily prepared by treating $[M(cod)Cl]_2$ with L_2 and KPF_6. The detection and chemical shift determination of the insensitive ^{103}Rh nucleus was easily accomplished via ^{31}P detected indirect two-dimensional ^{31}P, ^{103}Rh{^{1}H} NMR spectroscopy. The ^{103}Rh, ^{1}H, and ^{31}P NMR data are discussed.

Key words: rhodium, iridium, phosphoranimine, iminophosphine, Rh NMR.

Résumé : La traitement des $[M(cod)Cl]_2$ (M = Rh, Ir) avec des coordinats iminophosphoranophosphines du type $Ph_2PQP(Ph_2)$=$NSiMe_3$ (Q = CH_2, CH_2CH_2, 1,4-C_6H_4) conduit à de nouveaux métallacycles $[(cod)\overline{MPPh_2QPPh_2N}]$ par une élimination de Me_3SiCl qui « ancre » éventuellement le coordinat au métal par le biais d'une liaison σ métal–azote. Le chélate est complété par la fonctionnalité de la phosphine. On peut facilement préparer les complexes cationiques du type $[M(cod)L_2]^+PF_6^-$ (M = Rh ou Ir; L_2 = Ph_2PQPPh_2NR dans lesquels Q = CH_2, $CH(CH_3)$, 1,2-C_6H_4 et R = *p*-C_6F_4CN, $C_6H_2F(NO_2)_2$ et $C_6H_3(NO_2)_2$ ou L = Ph_2PN=C(H)Ph) en faisant réagir du $[M(cod)Cl]_2$ avec du L_2 et du KPF_6. On peut facilement détecter et déterminer le déplacement chimique du noyau ^{103}Rh insensible en faisant appel à la spectroscopie RMN bidimensionnelle ^{31}P, ^{103}Rh{^{1}H} qui permet de détecter le ^{31}P d'une façon indirecte. On discute des données RMN du ^{103}Rh, du ^{1}H et du ^{31}P.

Mots clés : rhodium, iridium, phosphoranimine, iminophosphine, RMN du Rh.

[Traduit par la rédaction]

Introduction

Previous work from our laboratories described the synthesis of novel rhodium(I) (**11**) (1, 2) and iridium(I) (**26**) (2) metallacycles $[(cod)\overline{M\text{-}N{=}P(Ph)_2CH_2P(Ph)_2}]$ utilizing the heterobifunctional iminophosphoranophosphine ligand $Ph_2PCH_2P(Ph)_2$=$NSiMe_3$. Elimination of Me_3SiCl during reaction of this ligand with 1,5-cyclooctadiene rhodium(I) or iridium(I) chloride dimers formed rhodium– or iridium–nitrogen σ bonds and produced a strongly bonded phosphine chelate. There are only a few examples of related P–N chelates in which the nitrogen forms a σ bond with rhodium (3–8). In our laboratories we recently developed an extensive series of heterobifunctional iminophosphoranophosphines with firmly attached substituents on the nitrogen (such as fluoroaromatics

Received March 16, 1994. Revision received February 3, 1995.

D.J. Law, G. Bigam, and R.G. Cavell.[1] Department of Chemistry, University of Alberta, Edmonton, AB T6G 2G2, Canada.

[1] Author to whom correspondence may be addressed. Telephone: (403) 492-5310. Fax: (403) 492-8231. E-mail: rcavell@gpu.srv.ualberta.ca

Can. J. Chem. Downloaded from www.nrcresearchpress.com by 65.111.164.53 on 09/08/12
For personal use only.

Can. J. Chem. Downloaded from www.nrcresearchpress.com by 65.111.164.53 on 09/08/12
For personal use only.

Scheme 1

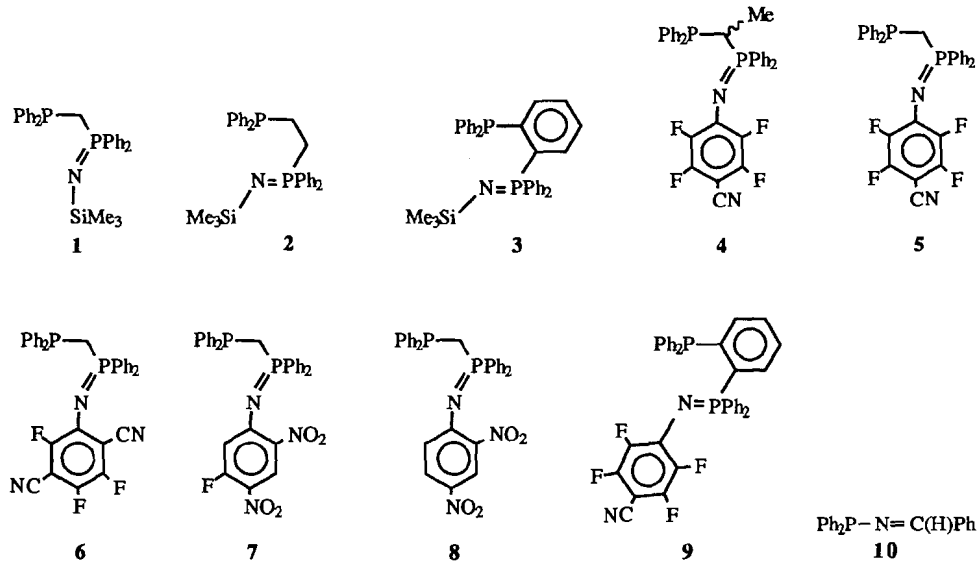

Scheme 2

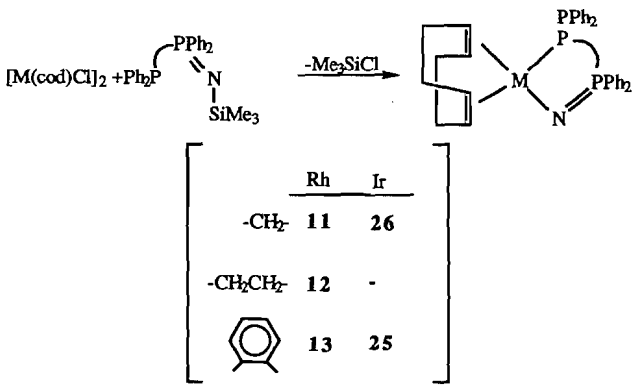

obtained from Me_3SiF elimination from activated fluoroaromatics (1, 2, 9–11)) and these ligands were found to be strong bidentate chelators. Each ligand is similar in that it possesses one hard (N) and one soft (P) donor site but the structure, basicity, and "bite" differences conferred by the backbone variety produce complexes of differing conformation and properties. To investigate the chemistry of these ligands we have now examined a series of complexes in which several examples of our heterobifunctional ligands are coordinated to rhodium(I) and iridium(I) centers. The analogous Rh(I) and Ir(I) metallacycles formed by elimination of Me_3SiCl from the parent iminophosphoranophosphine(1, 2) are also included in the comparison.

Mononuclear cationic rhodium and iridium diene–diphosphine complexes have been extensively studied since the report by Schrock and Osborn (12) that treatment of dimeric diene complexes of rhodium(I) or iridium(I), $[M(diene)Cl]_2$ (M = Rh or Ir) with a phosphine ligand L and a non-coordinating counterion X^- ($X = BF_4^-$, ClO_4^-, PF_6^-), gave cationic four-coordinate complexes of the type $[M(diene)(L)_2]^+X^-$. Complexes of this type have been made with monodentate chelating and chiral phosphines and, in many cases, these complexes have been found to be effective catalyst precursors for homogeneous hydrogenation at ambient temperature and pressure (13–16). Pyridyl phosphines have also been widely used as chelating and bridging ligands for a variety of transition metals including rhodium (17–20). Also widely known are rhodium complexes derived from chelating phosphine–amine bidentate ligands (21–35). There are, however, only a few examples of rhodium complexes containing chelating ligands with both a phosphine and an imine donor site (36–39). There are no examples of cationic rhodium(I) or iridium(I) complexes of phosphoranimine-phosphine heterodifunctional ligands such as those described herein, although the work of Imhoff et al. (40–43) provides several examples of cationic complexes containing doubly oxidized iminophosphorane ligands acting as bidentate ligands to Ir and Rh through the nitrogen atoms or through one nitrogen and one carbon atom.

Although ^{103}Rh NMR spectra have been obtained by various techniques for some time now, as described in two major reviews (44, 45), the method of obtaining rhodium chemical shifts via indirect 2D techniques has only recently been described and only a few examples of an indirect ^{31}P, $^{103}Rh\{^1H\}$ NMR spectrum have been reported (46–48).

Results and discussion

Rhodium and iridium cyclometallaphosphoran-iminatophosphines

We have previously shown (1) that the presence of a reactive Me_3Si—N bond in a ligand such as **1** (Scheme 1) presents the possibility of σ-bond formation by reaction with a metal halide *via* elimination of trimethylsilylhalide to form **11** and **26** (Scheme 2). This is further demonstrated in the present work by ligands **2** (2) and **3** (11), which reacted in a similar manner with $[Rh(cod)Cl]_2$ or $[Ir(cod)Cl]_2$ with elimination of Me_3SiCl to give metallacycles **12**, **13**, and **25** in good yields (Scheme 2). It is interesting to note that the reaction with the ligand **3** containing a 1,2-substituted benzene backbone required extensive refluxing in dichloromethane to obtain the complexes **13** and **25**, whereas reactions with ligands **1** and **2** were facile at room temperature. This pattern of reactivity is related to the mechanism of Me_3SiCl elimination, which probably requires the imine nitrogen of the ligand to act as a

Can. J. Chem. Downloaded from www.nrcresearchpress.com by 65.111.164.53 on 09/08/12
For personal use only.

Scheme 3

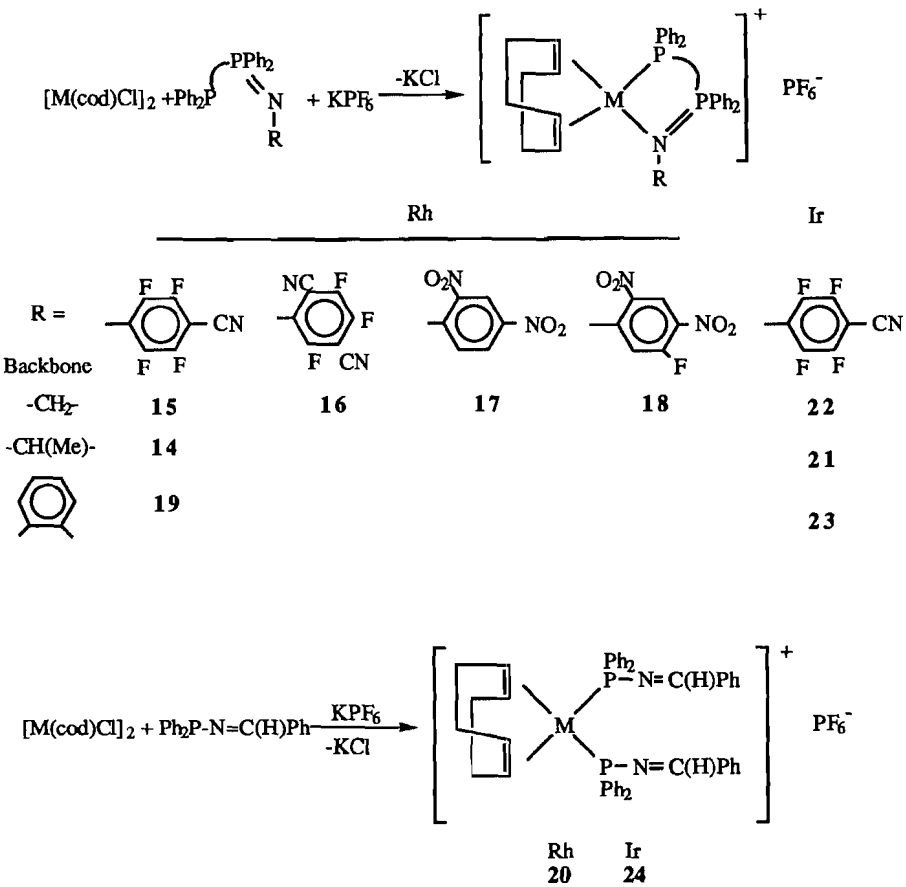

nucleophile on a metal center. The electron-withdrawing or delocalization effects of the aromatic ligand backbone in **3** reduce the nucleophilicity of the imine nitrogen, which is reflected in lower reactivity for M—Cl bond substitution. The compounds are red-orange microcrystalline solids, soluble in most common organic solvents. Contrary to our preliminary observations (1, 2), these types of compound are now known to decompose slowly in air over relatively long periods of time. Little visual indication of the reaction with air is observed; for example there is almost no visible color change. When the complexes are stored under argon there is no evidence for decomposition, indicating that the complexes are thermally and structurally stable.

The rhodium complexes **12** and **13** exhibit sharp doublets of doublets in their phosphorus-31 NMR spectra, with $^{1}J_{P^{III}Rh}$ and $^{2}J_{P^{V}Rh}$ couplings of the order of 155 and 4 Hz, respectively (Tables 1 and 2). The large coupling to Rh is diagnostic of the formation of a direct Rh—P bond, and the smaller Rh–P coupling and the preservation of $^{2}J_{PP}$ is indicative of the maintenance of the backbone structure. The observed $^{2}J_{P^{V}Rh}$ coupling was smaller than would have been predicted from previous observations for complexes derived from the analogous $Ph_2AsCH_2CH_2P(Ph_2)$=$NSiMe_3$ ligand (2) but the values compare directly to those observed for the complexes of phosphoramine–phosphine ligands, complexes **16**, **17**, and **18**. The spectrum of the iridium complex **25** exhibits two sharp doublets demonstrating the presence of coupled P(III) and P(V) nuclei in the backbone in accord with our formulation.

Trends in the $J_{P^{III}P^{V}}$ coupling constants can be discerned in all the values reported for phosphoraniminephosphine and phosphoraniminatophosphine complexes (Tables 1 and 2). Interestingly, comparison of the $J_{P^{III}P^{V}}$ coupling values for the "free" ligands with the J_{PP} values in complexed ligands indicated that only the ligands containing a 1,2-benzene backbone (**3** and **9**) show an increase in $^{3}J_{P^{III}P^{V}}$ values upon coordination when forming compounds **13**, **19**, **23**, and **25**. Each of the ligands **4**–**8** with a single carbon backbone shows a typical decrease in $^{2}J_{PP}$ of about 20 Hz upon coordination regardless of the substituent on the imine nitrogen. An exception is the chelation of rhodium(I) by ligand **1** to form complex **11** wherein the decrease in $^{2}J_{P^{III}P^{V}}$ is 13 Hz. The ethane backbone ligand **2** shows a larger decrease of 34 Hz in $^{3}J_{P^{III}P^{V}}$ upon the formation of the analogous Rh—N σ-bonded complex **12**. The behavior noted for the 1,2-benzene backbone ligands might be due to the restricted flexibility of this backbone and the strong possibility of some electron delocalization within the metallacycle supported by the aromatic ring.

Rhodium and iridium diolefin cyclometallaphosphoraniminephosphines

Rhodium and iridium chloride 1,5-cyclooctadiene (cod) dimers, $[Rh(cod)Cl]_2$ and $[Ir(cod)Cl]_2$, react cleanly with the ligands **4**–**10** (Scheme 1) in the presence of potassium hexafluorophosphate to give new cationic cyclometallaphosphoraniminephosphine hexafluorophosphate salts **14**–**20** (Rh) and **21**–**24** (Ir) in good yields (Scheme 3). These are the first

Can. J. Chem. Downloaded from www.nrcresearchpress.com by 65.111.164.53 on 09/08/12
For personal use only.

Table 1. Phosphorus-31 and rhodium-103 NMR spectroscopic data for rhodium complexes.

Compound	δ, Rh ppm	δ, P^{III} ppm	$^1J_{PRh}$, Hz	δ, P^V ppm	$^2J_{PRh}$, Hz	J_{PP}
11	152.4	33.0	158.6	52.2	7.5	44.1
12	259.3	21.7	157.4	34.7	3.9	14.9
13	207.9	25.4	155.7	28.8	4.1	31.1
14	244.0	31.9	152.7	53.4	—	41.8
15	233.8	24.2	153.7	51.3	—	33.0
16	264.5	22.9	153.7	51.6	4.5	33.0
17	264.0	23.0	152.9	51.0	3.6	33.0
18	253.3	23.9	153.9	49.4	4.9	32.1
19	504.7	19.3	154.2	30.6	—	25.2
20	−274.4	71.6	158.8	—	—	—
27[a]	−71.3	26.4	143.4	—	—	—

[a]Complex **27** is $[(cod)Rh(PPh_3)_2]^+PF_6^-$.

Table 2. Phosphorus-31 NMR spectroscopic data for iridium complexes.

Compound	δ, P^{III} ppm	δ, P^V ppm	J_{PP}
26	20.1	61.2	35.0
25	11.0	26.2	27.0
21	19.0	62.0	34.9
22	12.6	61.6	27.2
23	6.0	30.4	23.2
24	59.4	—	—

examples of phosphoraniminophosphine ligands in P–N chelates with cationic rhodium(I) and iridium(I) centers. The compounds are microcrystalline solids that are stable over several days in air, monomeric in solution, and only sparingly soluble in common organic solvents. Dichloromethane gives optimum solubility. It was noted that small amounts of decomposition occurred in air after several months, although the compounds appeared to be indefinitely stable under an argon atmosphere.

The phosphorus-31 NMR spectra of the rhodium complexes **14–19** (Tables 1 and 2) exhibit two sharp doublets of doublets readily attributable to the P(III) phosphine and P(V) phosphoranimine moieties, respectively. The P(III) signals show typically large $^1J_{RhP}$ coupling constant values in the order of 152–154 Hz, confirming the binding of P^{III} to Rh, and the P(V) signals occasionally showed small resolved $^2J_{RhP}$ coupling of 3.6–4.9 Hz (complexes **16**, **17**, **18**), again confirming the assigned structure. The spectra of the iridium complexes **21-23** also show the two sharp doublets that are due to the phosphorus(III) and phosphorus(V) centers coupled to each other. The spectra of the rhodium and iridium complexes of the diphenylphosphino–benzylimine ligand **10**, complexes **20** and **24**, showed one signal, with **20** also exhibiting the doublet typical of $^1J_{RhP}$ of 158.8 Hz. All the above compounds showed resonances for the PF_6^- counterion in their ^{31}P NMR spectra with the typical shift value of −144.3 ppm and $^1J_{PF}$ of 711 Hz.

For some years, coordination shifts have been of interest as a means of deducing the nature of metal–ligand interactions in metal–phosphine complexes, particularly where there is a chelate-ring contribution (49). The ^{31}P NMR chemical shifts of the free ligands **1-10** are presented in Table 3 along with observed

Fig. 1. Two-dimensional ^{103}Rh, ^{31}P NMR spectrum of **17** obtained by reverse 2D ^{31}P, $^{103}Rh\{^1H\}$ spectroscopy. $F_1[\delta(Rh)]$ is plotted vertically and $F_2[\delta(P)]$ horizontally. The coupling shown by $F_1[\delta(Rh)]$ is $^2J_{PP}$.

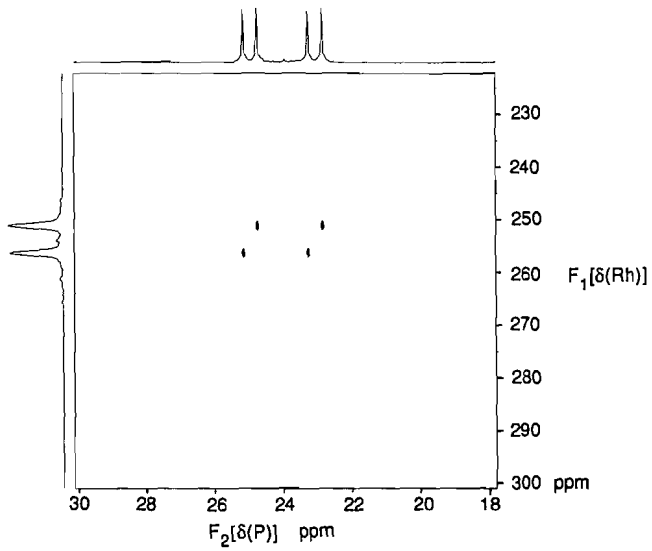

coordination shifts Δ for the present set of complexes. The rhodium and iridium phosphoraniminephosphine complexes **14–18**, **21**, and **22** follow similar patterns of Δ values, whereas the 1,2-benzene backbone phosphoraniminephosphine complexes **19** and **23** show significantly deviant Δ values, which we attribute to the formation of a six-membered metallocycle capable of extensive electron delocalization.

The coordination shifts ΔP^V of the P(V) moiety for complexes **11**, **12**, **13**, **25**, and **26** do not support an extension of our previous interpretation (1, 2). The previously reported (1, 2) complexes **11** and **26** showed marked deshielding of the phosphoraniminato phosphorus (ΔP^V = 52.3 and 62.3 ppm, respectively), which was attributed to the presence of an M—N σ bond. A similar effect was noted for the six-membered cyclometallaphosphoraniminatoarsines

$[(cod)\overline{M\text{-}N{=}P(Ph_2)CH_2CH_2AsPh_2}]$

(ΔP^V; M = Rh, 55.45, M = Ir, 62.2 ppm) (2) and this parallel

Can. J. Chem. Downloaded from www.nrcresearchpress.com by 65.111.164.53 on 09/08/12
For personal use only.

Table 3. Phosphorus-31 NMR spectroscopic data for ligands, and coordination shifts (Δ) for Rh and Ir complexes.

			Coordination shifts (ppm)					
	Chemical shift (ppm)		Rhodium			Iridium		
Ligand	δP(III)	δP(V)	Complex	ΔP(III)	ΔP(V)	Complex	ΔP(III)	ΔP(V)
1	−27.4	−1.1	**11**	60.4	52.3	**26**	47.5	62.3
2	−11.8	3.3	**12**	33.5	31.4			
3	−14.5	1.3	**13**	39.9	27.5	**25**	25.5	24.9
4	−14.0	22.0	**14**	45.9	31.4	**21**	33.0	40.0
5	−30.0	12.9	**15**	54.2	38.4	**22**	42.6	29.7
6	−30.6	11.5	**16**	53.5	40.1			
7	−29.6	10.1	**17**	52.6	40.9			
8	−30.1	11.5	**18**	54.0	37.9			
9	−14.8	11.9	**19**	34.1	18.7	**23**	20.8	18.5
10	+49.6		**20**	22.0		**24**	9.8	

suggested that the effect was due to the formation of the M—N σ bond and was also relatively independent of ring size. The ring-size effect, however, seems to be obscured by the simultaneous introduction of As as the coordinating trivalent center. Metallacycles in which the backbone length is increased (e.g., **2** and **3**) whilst maintaining phosphorus coordination show a marked decrease in the P^V coordination shift to 31.4 and 27.5 ppm, respectively, for **2** and **3**, implying a pronounced reduction in this coordination shift with increasing ring size. The Ir metallacycle with the 1,2-phenyl backbone ligand (**25**) also shows a much smaller P^V coordination shift (24.9 ppm). All of the complexes formed from substituted imine and P^{III} donors in the present limited series show very similar coordination shifts and thus no correlation with substituent or backbone is discernable. The reason for the large shifts in certain of the metallacycles is not fully resolved at this time. It does appear, however, that large ΔP^V values in these and other analogous complexes is not a consistent diagnostic of an M—N σ-bond formation as previously suggested (1, 2).

The ^1H NMR resonances of the cod olefinic protons are of interest as they reflect the heterodifunctionality of the ligands by their *trans*-influence and hence their relative shielding or deshielding effect on the coordinated olefin. The complexes **12–23** in general exhibit two distinct ^1H NMR resonances for the cod olefinic proton signals, a high-field set δ 2.9–4.3 ppm and a low-field set δ 4.1–5.9 ppm. Related cationic rhodium complexes (43) show that the cod olefin ^1H signals *trans* to the σ-bound N of phosphoranimine ligands occur in the range δ 2.9–3.8 ppm. Thus the *trans* influence of the phosphoranimine moiety appears to have a shielding effect on the *trans* related olefin signals. With this as a basis, we can assign the high-field olefin resonances of **12–23** to the cod moiety *trans* to phosphorus and the low-field resonances to those *trans* to nitrogen. These qualitative observations also indicate that there is little difference in the *trans* influence of nitrogen-coordinated phosphoranimine to a nitrogen σ-bonded phosphoranimine ligand in these complexes.

Rhodium-103 NMR measurements

The rhodium-103 NMR chemical shifts, reported relative to $\Xi(^{103}Rh) = 3.16$ MHz,[2] for the reported rhodium imine and iminato complexes are given in Table 1. The rhodium-103 chemical shift of the well-known rhodium complex $[(cod)Rh(PPh_3)_2]^+PF_6^-$ is also included for comparison. The ^{103}Rh chemical shift is readily obtained from knowledge of the J_{Rh-P} coupling constant, obtained from the ^{31}P NMR spectrum and by application of recently developed indirect two-dimensional NMR techniques (46–48). An example of a typical spectrum obtained by this technique is given in Fig. 1. The chemical shifts of the majority of the chelated complexes fall in the range of +152.38–+264.48 ppm with the only exceptions being the 1,2-benzene backbone phosphoraniminephosphine complex, **19**, which exhibits a starkly contrasting shift of +504.71. From previously reported ^{103}Rh NMR data (45–48, 51) it is clear that large ranges of chemical shift can be expected. Compared to similar diphosphine complexes such as $[Rh(nbd)dppe]^+ClO_4^-$, $\delta(^{103}Rh) = -390$ ppm, the shifts for the present series of complexes are significantly downfield by the order of 600 ppm. Also of interest are the apparent ΔR contributions within the present series of compounds, which behave oppositely to previously reported systems wherein an upfield shift of $\delta(^{103}Rh)$ is associated with expansion of the ring from five to six members. For example, **11**, containing a five-membered ring, lies to lower field of the six-membered ring systems **12** and **13**; **14-18**, also five-membered ring systems, lie downfield of the analog, **19**, which contains a six-membered ring. It is predictable that strong σ donation by the imine nitrogen to rhodium will make a significant increase in the ligand field splitting of these related compounds and may account for the different NMR behavior exhibited by these complexes relative to the homofunctional bis(phosphine) complexes. However, previous observations have suggested that large upfield shifts for $\delta(^{103}Rh)$ are seen with increasingly strong σ-donor ligands, and not downfield shifts as occur in the present cases. It is, however, unclear how the coordination sphere about rhodium affects the ^{103}Rh chemical shift, but we suggest that chelate ring size and ligand basicity play an important role. It is clear

[2] The Rh NMR shifts are given relative to the absolute frequency standard of 3.16 MHz in the field where TMS protons resonate at 100 MHz (50).

Can. J. Chem. Downloaded from www.nrcresearchpress.com by 65.111.164.53 on 09/08/12
For personal use only.

that more ^{103}Rh NMR data for different types of compounds must be correlated before the factors influencing ^{103}Rh chemical shifts can be extracted and understood.

Experimental section

All experimental manipulations were performed under an atmosphere of dry argon. Solvents were dried and distilled prior to use. $[Rh(cod)Cl]_2$ and $[Ir(cod)Cl]_2$ were prepared by standard procedures (52). The ligands **1–10** were prepared as described elsewhere (1, 2, 9–11).

^{1}H and ^{31}P NMR spectra were obtained on a Bruker WH400 instrument (operating at 400.13 and 161.97 MHz, respectively) using $SiMe_4$ and 85% H_3PO_4 as external standards. In all spectroscopic studies CD_2Cl_2 was used as both solvent and internal lock. Positive shifts lie downfield of the standard in all cases.

Inverse 2D ^{31}P and ^{103}Rh{^{1}H} NMR spectra were obtained on a Bruker WH-200 spectrometer using a 10 mm ^{1}H/^{31}P/^{2}H/^{103}Rh probe, built in our own laboratories, a second PTS 160 synthesizer (ϕ90), BSV-3 heteronuclear decoupler with broadband 1-65 MHz pulse amplifier for ^{103}Rh excitation, and a BVT 1000 temperature controller (±0.5°C). Samples were dissolved in 0.7 cm^3 of CD_2Cl_2 in 5 mm tubes. Pulse lengths were $\tau_{90}(^{31}P) = 15.5$ μs, $\tau_{90}(^{103}Rh) = 87$ μs.

[1] $90°(^{31}P)–1/2\ J(PRh)–90°(Rh)–t_1/2–180°(P)–t_1/2–90°(Rh)–AQ(^{31}P)$

The pulse sequence employed (eq. [1]) uses no 180°(Rh) pulses thus mitigating resonance offset effects caused by the long τ_{90}(Rh) and the large chemical shift range of this nucleus.

The value of J(PRh) and the ^{31}P window were first obtained from a routine ^{31}P{^{1}H} NMR spectrum. A guess of the ^{103}Rh frequency (approximately 6.124 MHz) was then made and a 2D survey spectrum (^{103}Rh sweep width = 50 000 Hz) taken, using an acquisition time of 1 s ($16t_1$ increments).

This process was repeated until the sweep width could be narrowed to 500 Hz. At this stage a complete 2D spectrum can be obtained with high resolution on both axes. After zero filling, the 256 × 1K matrix was transformed and the projections plotted. The F_2 projection is the ^{31}P spectrum with P–Rh coupling. The F_1 projection is the ^{103}Rh spectrum with P–P coupling, a consequence of the chosen pulse sequence. The accuracy of the $\delta(^{103}Rh)$ obtained is ±0.3 ppm.

Synthesis of [Rh(cod)(ligand)]$^+$PF$_6^-$ complexes. General method

The ligand (0.8 mmol) was added to a mixture of $[Rh(cod)Cl]_2$ (0.2 g, 0.4 mmol) and KPF_6 (0.2 g, 1.0 mmol) in dichloromethane (30 cm^3) and water (20 cm^3). The mixture was stirred vigorously at room temperature for up to 2 h. The dichloromethane layer was then removed and washed with water to remove excess KPF_6. The dichloromethane layer was decanted once more and the volume reduced to about 5 cm^3 under reduced pressure. Addition of hexane to the solution precipitated the complexes as microcrystalline orange-brown powders, which were filtered and dried *in vacuo*.

$[Ir(cod)(ligand)]^+PF_6^-$ complexes were obtained by an identical method to the above using $[Ir(cod)Cl]_2$ as the metal source.

*(i) [Rh(cod)(Ph$_2$PCH(Me)P(Ph)$_2$=NC$_6$F$_4$CN)]$^+$ PF$_6^-$ (**14**)*

Treatment with $(Ph_2PCH(Me)P(Ph_2)=NC_6F_4CN)$ (11) (0.46 g, 0.8 mmol) gave **14** as a fine orange microcrystalline powder (0.690 g, 93%); mp 168–180°C (dec.) ^{1}H NMR (CD_2Cl_2) δ: 7.1–8.3 (m, 20H, phenyl), 5.3 (m br, 1H, cod olefinic), 4.4 (m br, 1H, cod olefinic), 3.9 (ddq, 1H, $^3J_{HH}$ 7.2, $^2J_{P^VH}$ 12.2, $^2J_{P^{III}H}$ 22.2 Hz), 3.3 (m. br, 2H, cod olefinic), 1.7–2.7 (m, 8H, cod alkyl), 1.35 (ddd, 3H, $^3J_{HH}$ 7.2, $^3J_{P^VH}$ 10.4, $^3J_{P^{III}H}$ 18.0 Hz). ^{31}P NMR (CD_2Cl_2) δ: 53.4 (d, 1P^V, $^2J_{PP}$ 41.8 Hz), 31.92 (dd, 1P^{III} $^2J_{PP}$, 41.8, $^1J_{PRh}$ 152.7 Hz), −144.3 (PF_6^-) (sept, 1P, $^1J_{PF}$ 710.8 Hz). MS (FAB): (100%) 796.4, [M]$^+$. Anal. calcd. for $C_{41}H_{34}F_{10}N_2PRh$: C 52.3, H 3.8, N 3.0; found: C 51.7, H 3.9, N 2.8%.

The complexes **15–24** were obtained similarly.

*(ii) [Rh(cod)(Ph$_2$PCH$_2$P(Ph$_2$)=NC$_6$F$_4$CN]$^+$ PF$_6^-$ (**15**)*

Treatment with $Ph_2PCH_2P(Ph_2)=NC_6F_4CN$ (2) (0.46 g, 0.8 mmol) gave **15** as a fine orange powder (0.606 g, 81.5%); mp 156–160°C (dec.). ^{1}H NMR (CD_2Cl_2) δ: 7.6 (m, 20H, phenyl), 3.5 (d, 2H, $^1J_{PH}$ 9.25 Hz), 3.3 (s br, 4H, olefinic), 2.2 (m, 8H, cod). ^{31}P NMR (CD_2Cl_2) δ: 51.3 (d, 1P^V, $^2J_{PP}$ 33 Hz), 24.2 (dd, 1P^{III}, $^2J_{PP}$ 33, $^1J_{PRh}$ 153.7 Hz), −144.3 (PF_6^-) (sept, 1P, $^1J_{PF}$ 710.9 Hz). MS (FAB): (100%) 783 [M]$^+$. Anal. calcd. for $C_{40}H_{34}F_{10}N_2P_3Rh{\cdot}CH_2Cl_2$: C 48.5, H 3.5, N 2.8; found: C 48.6, H 3.5, N 2.8%.

*(iii) [Rh(cod)(Ph$_2$PCH$_2$P(Ph$_2$)=NC$_6$F$_3$(CN)$_2$]$^+$ PF$_6^-$ (**16**)*

Treatment with $Ph_2PCH_2P(Ph_2)=NC_6F_3(CN)_2$ (9) (0.46 g, 0.8 mmol) gave **16** as an orange-brown microcrystalline powder (0.427 g, 57%); mp 214°C (dec.). ^{1}H NMR (CD_2Cl_2) δ: 7.1–8.0 (m, 20H, phenyl), 5.3 (m, 2H, cod olefinic), 4.3 (m, 2H, cod olefinic), 3.7 (m, 2H, PCH_2P), 1.9–2.8 (m, 8H, cod alkyl). ^{31}P NMR (CD_2Cl_2) δ: 51.6 (dd, 1P^V, $^2J_{PP}$ 33, $^2J_{PRh}$ 4.5 Hz), 22.9 (dd, 1P^{III}, $^2J_{PP}$ 33, $^1J_{PRh}$ 153.7 Hz), −144.3 (PF_6^-) (sept, 1P, $^1J_{PF}$ 711.1 Hz). MS (FAB): (49%) 790.2 [M]$^+$. Anal. calcd. for $C_{41}H_{34}F_9N_3P_3Rh$: C 49.5, H 3.5, N 4.1; found: C 49.8, H 3.3, N 4.3%.

*(iv) [Rh(cod)(Ph$_2$PCH$_2$P(Ph$_2$)=NC$_6$H$_2$F(NO$_2$)$_2$)]$^+$ PF$_6^-$ (**17**)*

Treatment with $Ph_2PCH_2P(Ph_2)=NC_6H_2F(NO_2)_2$ (9) (0.46 g, 0.8 mmol) gave **17** as an orange-red microcrystalline powder (0.517 g, 67%); mp 180°C (dec.). ^{1}H NMR (CD_2Cl_2) δ: 8.5 (dd, 1H, $^4J_{HF}$ 7.5, $^5J_{HP}$ 1.4 Hz), 7.1–8.0 (m, 20H, phenyl), 6.8 (dd, 1H, $^3J_{HF}$ 11.0, $^3J_{HP}$ 2.0 Hz), 5.5 (m, 1H, cod olefinic), 4.2 (m, 1H, cod olefinic), 3.7 (m, 2H, PCH_2P), 3.4 (m, 1H, cod olefinic), 3.2 (m, 1H, cod olefinic) 1.8–2.9 (m, 8H, cod alkyl). ^{31}P NMR (CD_2Cl_2) δ: 51.0 (dd, 1P^V, $^2J_{PP}$ 32.1, $^2J_{PRh}$ 3.6 Hz), 23.0 (dd, 1P, $^2J_{PP}$ 32.1, $^1J_{PRh}$ 152.9 Hz), −144.3 (PF_6^-) (sept, 1P, $^1J_{PF}$ 712.2 Hz). MS (FAB): (13.6%) 794 [M]$^+$. Anal. calcd. for $C_{39}H_{36}F_7N_3O_4P_3Rh{\cdot}CH_2Cl_2$: C 46.8; H 3.7; N 4.1; found: C 45.3, H 3.8, N 4.0%.

*(v) [Rh(cod)(Ph$_2$PCH$_2$P(Ph$_2$)=NC$_6$H$_3$(NO$_2$)$_2$)]$^+$ PF$_6^-$ (**18**)*

Treatment with $Ph_2PCH_2P(Ph_2)=NC_6H_3(NO_2)_2$ (9) (0.455 g, 0.8 mmol) gave **18** as a fine yellow-brown powder (0.51 g, 69%); mp 180°C (dec.). ^{1}H NMR (CD_2Cl_2) δ: 7.05–8.05 (m, 23H, phenyl), 5.2 (m, 1H, olefinic cod), 4.1 (m, 1H, olefinic cod), 3.85 (m, 1H, cod olefinic), 3.4 (m, 2H, PCH_2P), 3.2 (m, 2H, cod olefinic), 1.8–2.8 (m, 8H, cod alkyl). ^{31}P NMR (CD_2Cl_2) δ: 49.4 (dd, 1P^V, $^2J_{PP}$ 33.0, $^2J_{PRh}$ 4.9 Hz), 23.9 (dd, 1P^{III}, $^2J_{PP}$ 33.0, $^1J_{PRh}$ 153.9 Hz), −144.3 (PF_6^-) (sept, 1P, $^1J_{PF}$ 711.1 Hz). MS (FAB): (26%) 776.2 [M]$^+$. Anal. calcd. for

Can. J. Chem. Downloaded from www.nrcresearchpress.com by 65.111.164.53 on 09/08/12
For personal use only.

$C_{39}H_{36}F_6N_3O_4P_3Rh$: C 50.7, H 4.0, N 4.5; found: C 50.8, H 3.8, N 4.8%.

*(vi) [Rh(cod)($Ph_2PC_6H_4P(Ph_2)$=NC_6F_4CN)]$^+$ PF_6^- (**19**)*
Treatment with $Ph_2PC_6H_4P(Ph_2)$=NC_6F_4CN (**11**) (0.507 g, 0.8 mmol) gave **19** as a fine yellow powder (0.775 g, 98%); mp 250°C (dec.). ^{1}H NMR (CD_2Cl_2) δ: 7.8 (m, 4H, aromatic), 7.4 (m, 20H, phenyl), 4.8 (s br, 2H, olefinic cod), 3.2 (s br, 2H, olefinic cod), 2.1 (m, 8H, alkyl cod). ^{31}P NMR (CD_2Cl_2). δ: 30.6 (d, 1P^V, $^3J_{PP}$ 25.2 Hz), 19.3 (dd, 1P^{III}, $^3J_{PP}$ 25.2, $^1J_{PRh}$ 154.2 Hz), −144 (PF_6^-) (sept, 1P, $^1J_{PF}$ 711.2 Hz). MS (FAB): (100%) 845 [M]$^+$. Anal. calcd. for $C_{45}H_{36}F_{10}N_2P_2Rh{\cdot}CH_2Cl_2$: C 51.0, H 3.6, N 2.7; found: C 51.3, H 3.5, N 2.6%.

*(vii) [Rh(cod)(Ph_2P-N=CHPh)$_2$]$^+PF_6^-$ (**20**)*
Treatment with Ph_2P-N=CHPh (**11**) (0.46 g, 1.6 mmol) gave **20** as a fine orange-brown powder (0.49 g, 60%); mp 154–156°C (dec.). ^{1}H NMR (CD_2Cl_2) δ: 8.0 (d, 2H, $^2J_{PH}$ 29.6 Hz, N=CH), 7.2–7.7 (m, 30H, phenyl), 4.9 (s br, 4H, olefinic cod), 2.45 (m, 8H, alkyl cod). ^{31}P NMR (CD_2Cl_2) δ: 71.54 (d, 2P, $^1J_{PRh}$ 158.8 Hz), −144.2 (PF_6^-) (sept, 1P, $^1J_{PF}$ 710.5 Hz). MS (FAB): (2.2%) 789 [M]$^+$, (32%) 290 [$Ph_2PNCHPh$]$^+$. Anal. calcd. for $C_{46}H_{44}F_6N_2P_3Rh{\cdot}CH_2Cl_2$: C 55.3, H 4.5, N 2.7; found: C 55.2, H 4.6, N 2.7%.

*(viii) [Ir(cod)($Ph_2PCH(Me)P(Ph_2)$=NC_6F_4CN)]$^+$ PF_6^- (**21**)*
Treatment with $Ph_2PCH(Me)P(Ph_2)$=NC_6F_4CN (**11**) (0.35 g, 0.6 mmol) gave **21** as fine orange microcrystals, (0.474 g, 77%); mp 195–220°C (dec.). ^{1}H NMR (CD_2Cl_2) δ: 7.1–8.1 (m, 20H, phenyl), 5.0 (m, 1H, cod olefinic), 4.05 (m, 1H, cod olefinic), 3.9 (ddq, 1H, $^3J_{HH}$ 7.2, $^2J_{PV_H}$ 12.2, $^2J_{PIII_H}$ 22.2 Hz), 2.9 (m, 2H, cod olefinic), 1.7–2.6 (m, 8H, cod alkyl), 1.4 (ddd, $^3J_{HH}$ 7.2, $^3J_{PV_H}$ 10.4, $^3J_{PIII_H}$ 18.0 Hz). ^{31}P NMR (CD_2Cl_2) δ: 62.0 (d, 1P^{III}, $^2J_{PP}$ 34.9 Hz), 19.0 (d, 1P^V, $^2J_{PP}$ 34.9 Hz), −144.3 (PF_6^-) (sept, $^1J_{PF}$ 711.0 Hz). MS (FAB): (73%) 886 [M]$^+$. Anal. calcd. for $C_{41}H_{36}F_{10}IrN_2P_3{\cdot}1/2\ CH_2Cl_2$: C 46.9, H 3.6, N 2.6; found: C 46.2, H 3.3, N 2.5%.

*(ix) [Ir(cod)($Ph_2PCH_2P(Ph_2)$=NC_6F_4CN)]$^+$ PF_6^- (**22**)*
Treatment with $Ph_2PCH_2P(Ph_2)$=NC_6F_4CN (**2**) (0.34 g, 0.59 mmol) gave **22** as an orange microcrystalline powder (0.506 g, 84%); mp 170–185°C (dec.). ^{1}H NMR (CD_2Cl_2) δ: 7.3–7.8 (m, 20H, phenyl), 4.6 (m, 2H, cod olefinic), 3.56 (dd, 2H, $^2J_{PV_H}$ 8.2, $^2J_{PIII_H}$ 9.8 Hz), 3.0 (m, 2H, cod olefinic), 1.8–2.4 (m, 8H, cod alkyl). ^{31}P NMR (CD_2Cl_2) δ: 61.6 (d, 1P^V, $^2J_{PP}$ 27.2 Hz), 12.6 (d, 1P^{III}, $^2J_{PP}$ 27.2 Hz), −144.4 (PF_6^-) (sept, 1P, $^1J_{PF}$ 711.0 Hz). MS (FAB): (55.9%) 873 [M]$^+$, (15%) 572 [$Ph_2PCH_2P(Ph_2)$=NC_6F_4CN]$^+$. Anal. calcd. for $C_{40}H_{34}F_{10}N_2P_3Ir{\cdot}CH_2Cl_2$: C 44.5, H 3.3, N 2.5; found: C 44.5, H 3.3, N 2.5%.

*(x) [Ir(cod)($Ph_2PC_6H_4P(Ph_2)$=NC_6F_4CN)]$^+$ PF_6^- (**23**)*
Treatment with $Ph_2PC_6H_4P(Ph_2)$=NC_6F_4CN (**11**) (0.38 g, 0.6 mmol) gave **23** as a red-orange microcrystalline solid (0.55 g, 85.5%); mp 200–240°C (dec.). ^{1}H NMR (CD_2Cl_2) δ: 7.3–7.9 (m, 24H, phenyl), 4.5 (m, 2H, cod olefinic), 2.9 (m, 2H, cod olefinic), 1.6–2.3 (m, 8H, cod alkyl). ^{31}P NMR (CD_2Cl_2) δ: 30.4 (d, 1P^V, $^3J_{PP}$ 23.2 Hz), 6.0 (d, 1P^{III}, $^3J_{PP}$ 23.2 Hz), −144.4 (PF_6^-) (sept, 1P, $^1J_{PF}$ 710.0 Hz). MS (FAB): (100%) 936 [M]$^+$. Anal. calcd. for $C_{45}H_{36}F_{10}N_2P_3Ir{\cdot}CH_2Cl_2$: C 47.4, H 3.3, N 2.4; found: C 47.8, H 3.2, N 2.5%.

*(xi) [(Ir(cod)(Ph_2P-N=CHPh)$_2$]$^+$ PF_6^- (**24**)*
Treatment with Ph_2P-N=CHPh(**11**) (0.347 g, 1.2 mmol) gave (**24**) as a red-brown microcrystalline solid (0.18 g, 29%); mp 160–168°C (dec.). ^{1}H NMR (CD_2Cl_2) δ: 8.1 (d, 2H, $^3J_{PH}$ 30.4 Hz), 7.1–7.8 (m, 20H, phenyl), 4.6 (m br, 4H, cod olefinic), 2.2 (m, 8H, cod alkyl). ^{31}P NMR (CD_2Cl_2) δ: 59.4 (s, 2P), −144.2 (PF_6^-) (sept, 1P, $^1J_{PF}$ 711.3 Hz). MS (FAB): (92%) 878.7 [M]$^+$. Anal. calcd. for $C_{46}H_{44}F_6N_2P_3Ir{\cdot}CH_2Cl_2$: C 50.9, H 4.1, N 2.5; found: C 49.8, H 4.1, N 2.6%.

Synthesis of metallacycles

*(i) [(cod)RhP$Ph_2CH_2CH_2P(Ph_2)$=N] (**12**)*
A solution of [Rh(cod)Cl]$_2$ (0.1 g, 0.2 mmol) and **2** (10) (0.2 g, 0.4 mmol) in dichloromethane (40 cm^3) was stirred for 6 h at room temperature. The solvent was then removed under reduced pressure and the resultant residue recrystallized from dichloromethane–hexane to give **12** as a fine yellow microcrystalline powder. The product was filtered and dried *in vacuo* (0.157 g, 83%); mp 147°C (dec.). ^{1}H NMR (CD_2Cl_2) δ: 7.2–8.1 (m, 20H, phenyl), 5.6 (m br, 2H, cod olefinic), 2.9 (m br, 2H, cod olefinic), 1.9–2.7 (m, overlapping, 12H, alkyl). ^{31}P NMR (CD_2Cl_2) δ: 21.65 (dd, 1P^V, $^3J_{PP}$ 14.9, $^1J_{PRh}$ 157.4 Hz), 34.66 (dd, 1P,^{III} $^3J_{PP}$ 14.9, $^2J_{PRh}$ 3.9 Hz). MS (FAB): (85%) 103 [Rh]$^+$, (47%) 517 [RhP$Ph_2CH_2CH_2P(Ph_2)$=N]$^+$, (39%) 213 [Rh(cod)]$^+$. Anal. calcd. for $C_{34}H_{36}NP_2Rh{\cdot}CH_2Cl_2$: C 59.3, H 5.4, N 2.0; found: C 60.6, H 6.3, N 1.7%.

*(ii) [(cod)RhP$Ph_2C_6H_4P(Ph_2)$=N] (**13**)*
A solution of [Rh(cod)Cl]$_2$ (0.1 g, 0.2 mmol) and **3** (11) (0.233 g, 0.4 mmol) in dichloromethane (40 cm^3) was refluxed for 6 h. The solvent was then removed under reduced pressure and the resulting solid precipitated from a dichloromethane solution by addition of hexane, giving **13** as a fine orange powder (0.15 g, 56%); mp 174–176°C. ^{1}H NMR (CD_2Cl_2) δ: 7.2–7.7 (m, 24H, aromatic), 5.8 (m, 2H, cod olefinic), 2.9 (m, 2H, cod olefinic), 2.0–2.6 (m, 8H, cod alkyl). ^{31}P NMR (CD_2Cl_2) δ: 28.8 (dd, 1P^V, $^3J_{PP}$ 31.1, $^2J_{PRh}$ 4.1 Hz), 25.36 (dd, 1P^{III}, $^3J_{PP}$ 31.1, $^1J_{PRh}$ 155.7 Hz). MS (FAB): (100%) 460 [$Ph_2PC_6H_4P(Ph_2)$=N]$^+$, (4.9%) 672 [M]$^+$. Anal. calcd. for $C_{38}H_{36}NP_2Rh{\cdot}CH_2Cl_2$: C 59.7, H 4.9, N 1.7; found: C 59.4, H 4.9, N 1.7%.

*(iii) [(cod)IrP$Ph_2C_6H_4P(Ph_2)$=N] (**25**)*
A solution of [Ir(cod)Cl]$_2$ (0.2 g, 0.3 mmol) and **3** (11) (0.32 g, 0.6 mmol) in dichloromethane (40 cm^3) was refluxed for 6 h. The solvent was removed under reduced pressure and the resultant residue recrystallized from dichloromethane-hexane to give **25** as bright golden crystals (0.4 g, 88%). ^{1}H NMR (CD_2Cl_2) δ: 7.1–7.8 (m, 24H, aromatic), 5.9 (m, 2H, cod olefinic), 5.6 (m, 2H, cod olefinic), 1.8–2.4 (m, 8H, cod alkyl). ^{31}P NMR (CD_2Cl_2) δ: 26.2 (d, 1P^V, $^3J_{PP}$ 27.0 Hz), 11.0 (d, 1P^{III}, $^3J_{PP}$ 27.0 Hz). M.S. (FAB): (67%) 762 [M]$^+$, (29%) 460 [$Ph_2PC_6H_4P(Ph_2)$=N]$^+$. Anal. calcd. for $C_{38}H_{36}NP_2Ir{\cdot}2CH_2Cl_2$: C 51.7, H 4.3, N 1.5; found: C 51.7, H 4.3, N 2.1%.

Acknowledgements

We thank the Natural Sciences and Engineering Research Council of Canada and Ligands Inc. of Calgary, Alberta, for financial support of this work.

Can. J. Chem. Downloaded from www.nrcresearchpress.com by 65.111.164.53 on 09/08/12
For personal use only.

References

1. K.V. Katti and R.G. Cavell. Organometallics, **7**, 2236 (1988).
2. K.V. Katti and R.G. Cavell. Organometallics, **8**, 2147 (1989).
3. M.J. Menu, G. Crocco, M. Dartiguenave, Y. Dartiguenave, and G. Bertrand. Organometallics, **7**, 2231 (1988).
4. T.G. Schenck, J.M. Downes, C.R.C. Milne, P.B. MacKenzie, H. Boucher, J. Whelan, and B. Bosnich. Inorg. Chem. **24**, 2334 (1985).
5. J. Erbe and W. Beck. Chem. Ber. **116**, 3867 (1983).
6. D.H.M.W. Thewissen, H.P.M.M. Ambrosius, H.L.M. Van Gaal, and J.J. Steggerda. J. Organomet. Chem. **192**, 101 (1980).
7. M.D. Fryzuk and C.D. Montgomery. Coord. Chem. Rev. **95**, 1 (1989).
8. M.D. Fryzuk. Can. J. Chem. **70**, 2839 (1993).
9. K.V. Katti, B.D. Santarsiero, A.A. Pinkerton, and R.G. Cavell. Inorg. Chem. **32**, 5919 (1993).
10. K.V. Katti, R.J. Batchelor, F.W.B. Einstein, and R.G. Cavell. Inorg. Chem. **29**, 808 (1990).
11. R. W. Reed. Ph. D. Thesis, University of Alberta, 1992.
12. R.R. Schrock and J.A. Osborn. J. Am. Chem. Soc. **93**, 2397 (1971).
13. R.R. Schrock and J.A. Osborn. J. Am. Chem. Soc. **98**, 2134 (1976).
14. R.H. Crabtree, H. Felkin, and G.E. Morris. J. Organomet. Chem. **141**, 205 (1977).
15. J. Halpern. Phosphorus Sulfur, **18**, 307 (1983).
16. J.M. Brown. Angew. Chem. Int. Ed. Engl. **26**, 190 (1987).
17. G.R. Newkome. Chem. Rev. **93**, 2067 (1993).
18. M. Alvarez, N. Lugan, and R. Mathieu. J. Chem. Soc. Dalton Trans. 2755 (1994).
19. A. Hessler, J. Fischer, S. Kucken, and O. Stelzer. Chem. Ber. **127**, 481 (1994).
20. Y. Xie, C.-L. Lee, Y. Yang, S.J. Rettig, and B.R. James. Can. J. Chem. **70**, 751 (1992).
21. M.P. Anderson, B.M. Mattson, and L.H. Pignolet. Inorg. Chem. **22**, 2644 (1983).
22. H. Wang, A.L. Casalnuovo, B.L. Johnson, A.M. Mueting, and L.H. Pignolet. Inorg. Chem. **27**, 325 (1988).
23. K.N. Gavrilov, A.T. Teleshev, and E.E. Nifantyev. J. Organomet. Chem. **461**, 233 (1993).
24. H. Werner, A. Hampp, and B. Windmüller. J. Organomet. Chem. **435**, 169 (1992).
25. C. Bianchini, A. Meli, M. Peruzzini, F. Vizza, and P. Frediani. Organometallics, **9**, 1146 (1990).
26. M.K. Cooper, P.A. Duckworth, T.W. Hambley, G.J. Organ, K. Henrick, M. McPartlin, and A. Parekh. J. Chem. Soc. Dalton Trans. 1067 (1989).
27. M.M.T. Khan, V.V.S. Reddy, and H.C. Baja. Inorg. Chim. Acta, **130**, 163 (1987).
28. M.M.T. Khan and B. Swamy. Inorg. Chem. **26**, 178 (1987).
29. P. Brun, P. Vierling, and J.G. Reiss. Inorg. Chem. **26**, 1451 (1987).
30. N.C. Payne and D.C. Stephan. Inorg. Chem. **21**, 182 (1982).
31. D. Bondoux, B.F. Mentzen, and I. Tkatchenko. Inorg. Chem. **20**, 839 (1981).
32. B.A. Boyce, A. Carroy, J.-M. Lehn, and D. Parker. J. Chem. Soc. Chem. Commun. 1546 (1984).
33. Z.M. Michalska. 5th Int. Symp. on Homogeneous and Heterogeneous Catalysis, UNV Scientific Press, The Netherlands. 1986. p. 527.
34. D.M. Roundhill, R.A. Bechtold, and S.G.N. Roundhill. Inorg. Chem. **19**, 284 (1980).
35. M.C. Bonnet, B. Stitou, and I. Tkatchenko. J. Organomet. Chem. **279**, C1 (1985).
36. T. Chivers, K. McGregor, and M. Parvez. Inorg. Chem. **32**, 5119 (1993).
37. C.A. Ghilardi, S. Midollini, S. Moneti, A. Orlandini, and G. Scapacci. J. Chem. Soc. Dalton Trans. 3371 (1992).
38. P. Barbaro, C. Bianchini, F. Laschi, S. Midollini, S. Moneti, G. Scapacci, and P. Zanello. Inorg. Chem. **33**, 1622 (1994).
39. H. Brunner and H. Weber. Chem. Ber. **118**, 3380 (1985).
40. P. Imhoff and C.J. Elsevier. J. Organomet. Chem. **361**, C61 (1989).
41. P. Imhoff, R.V. Asselt, C.J. Elsevier, K. Vrieze, K. Goubitz, K.F.V. Malssen, and C.H. Stam. Phosphorus, Sulphur Silicon, **47**, 401 (1990).
42. P. Imhoff, S.C.A. Nefkens, C.J. Elsevier, K. Goubitz, and C.H. Stan. Organometallics, **10**, 1421 (1991).
43. P. Imhoff, R.V. Asselt, C.J. Elsevier, M.C. Zoutberg, and C.H. Stan. Inorg. Chim. Acta, **184**, 73 (1991).
44. B.E. Mann. *In* NMR of newly accessible nuclei. *Edited by* P. Laszlo. Academic Press, London. 1983. pp. 301–318.
45. B.E. Mann. *In* Transition metal nuclear magnetic resonance. *Edited by* P.S. Pregosin. Elsevier, Amsterdam. 1991. pp. 177–215.
46. C.J. Elsevier, J.M. Ernsting, and W.G.J. deLange. J. Chem. Soc. Chem. Commun. 585 (1989).
47. B.R. Bender, M. Koller, D. Nanz, and W. von Philipsborn. J. Am. Chem. Soc. **115**, 5889 (1993).
48. J.M. Ernsting, C.J. Elsevier, W.G.J. de Lange, and K. Timmer. Magn. Reson. Chem. **29**, S118 (1991).
49. P.E. Garrou. Chem. Rev. **81**, 229 (1981).
50. R.G. Kydd and R.J. Goodfellow. *In* NMR and the Periodic Table. *Edited by* R.K. Harris and B.E. Mann. Academic Press, London. 1978.
51. B. Bonnaire, D. Davoust, and N. Platzer. Org. Magn. Reson. **22**, 80 (1984).
52. J. Chatt and L.M. Venanzi. J. Chem. Soc. 4735 (1957).

Isolation and structures of the uprolides. I. Thirteen new cytotoxic cembranolides from the Caribbean gorgonian *Eunicea mammosa*[1]

Abimael D. Rodríguez, Ivette C. Piña, Javier J. Soto, Dalila R. Rojas, and Charles L. Barnes

Abstract: Thirteen new cembranolide diterpenoids, uprolides **3–15**, have been isolated from the Caribbean gorgonian *Eunicea mammosa* collected off the West coast of Puerto Rico. Several known metabolites, such as eupalmerin acetate (**1**) and eupalmerin (**2**), were also isolated from the same organism. The structures of the new compounds, which also showed modest in vitro cytotoxic activity, were assigned on the basis of extensive nuclear magnetic resonance analysis, chemical correlation studies, and by comparison with analogous spectral data from known cembranolide diterpenoids. One structure (**3**) was confirmed by X-ray diffraction analysis.

Key words: uprolides, *Eunicea mammosa*, cytotoxicity, Caribbean, gorgonian.

Résumé : On a insolé 13 nouveaux diterpénoïdes de la famille du cembranolide, les uprolides **3–15**, à partir d'*Eunicea mammosa* gorgone des Caraïbes récoltés près de la côte ouest de Porto Rico. À partir des mêmes organismes, on a aussi isolé plusieurs métabolites connus, comme l'acétate d'eupalmérine (**1**) et l'eupalmérine (**2**). Les structures des nouveaux composés, qui présentent aussi une faible activité cytotoxique in vitro, ont été attribuées en se basant sur des analyses poussées de RMN, sur des études de corrélation chimique et par comparaison avec des données spectrales analogues obtenues à partir de diterpénoïdes cembranolides connus. La structure **3** a été confirmée par diffraction des rayons X.

Mots clés : uprolides, *Eunicea mammosa*, cytotoxicité, Caraïbes, gorgonidé.

[Traduit par la rédaction]

Introduction

Although many secondary metabolites isolated from coelenterates have been reported to possess very exciting pharmacological properties, the number of research articles describing new natural products from gorgonians and soft corals appears to be declining. However, despite their paucity, new structures continue to emerge. Invariably, diterpenes continue to represent the major group of compounds isolated from both soft corals and gorgonians (1). The success of gorgonians against predation and against overgrowth by competing organisms may be at least in part due to the secretion of defense substances (2). These substances include diterpenoids related to cembrene, a diterpene with a 14-membered ring. Specimens of *Eunicea mammosa* and *Eunicea succinea*, two common Caribbean gorgonian species, have yielded throughout the last three decades many highly functionalized biologically active cembranolides depending upon their geographical origin (3–20). Recent investigations of the cytotoxic constituents of the Caribbean gorgonian octocoral *E. mammosa* in this laboratory have resulted in the isolation of eight new cembranoid diterpenes that were identified by interpretation of spectral data and chemical interconversions (21–24). Continuing to examine *E. mammosa* extracts from Puerto Rico, we have now isolated and report here on 13 new cembranolide diterpenes, which can be considered as the first examples of naturally occurring cembranolides isolated from a Caribbean gorgonian depicting unsaturation at position C-6 or C-8. The new cembranolide diterpenoids, named collectively as the uprolides,[6] were identified by spectroscopic methods and chemical interconversions, and one structure has been confirmed by X-ray diffraction analysis. These metabolites, which showed moder-

Received January 20, 1995.

A.D. Rodríguez,[2] **I.C. Piña,**[3] **J.J. Soto,**[4] **and D.R. Rojas.**[5] Department of Chemistry, P.O. Box 23346, U.P.R. Station, University of Puerto Rico, Río Piedras, Puerto Rico 00931-3346.
C.L. Barnes. Department of Chemistry, 123 Chemistry Building, University of Missouri–Columbia, Columbia, MO 65211, U.S.A.

[1] Presented at the 35th Annual Meeting of the American Society of Pharmacognosy, Halifax, Nova Scotia, Canada, July 31 – August 4, 1994.

[2] Author to whom correspondence may be addressed. Telephone: (809) 764-0000, ext. 4799. Fax: (809) 751-0625. E-mail: A_Rodriguez@UPR1.UPR.CLU.EDU

[3] Graduate student sponsored by the Minority Research Center of Excellence Program of the University of Puerto Rico.

[4] Undergraduate student sponsored by the NIH–MBRS Program of the University of Puerto Rico, Río Piedras Campus.

[5] Undergraduate student sponsored by the FIPI Program of the University of Puerto Rico, Río Piedras Campus.

[6] Uprolide is an acronym of University of Puerto Rico.

Can. J. Chem. Downloaded from www.nrcresearchpress.com by 65.111.164.53 on 09/08/12
For personal use only.

ate cytotoxic action against several animal and human tumor cell lines, could be envisioned as functionalized structural congeners of eupalmerin acetate (**1**) and eupalmerin (**2**), two well-known γ-cembranolides isolated earlier from specimens of the gorgonian collected near Puerto Rican waters (21–24). The specimens of *E. mammosa* were collected off the West coast of Puerto Rico near Mona Island and were frozen after collection and then freeze-dried prior to extraction with 1:1 MeOH–EtOAc. From the hexane and $CHCl_3$ extracts, diterpenes **3–15** were isolated by conventional chromatographic procedures (see Experimental).

Results and discussion

The composition $C_{22}H_{32}O_6$ for the new terpenoid uprolide-A acetate (**3**) derives from high-resolution fabms and ^{13}C nmr

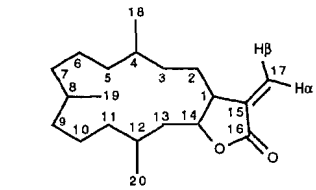

γ-CEMBRANOLIDE SKELETON

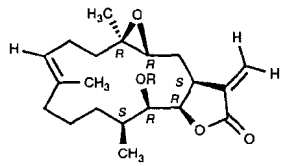

1 R = Ac
2 R = H

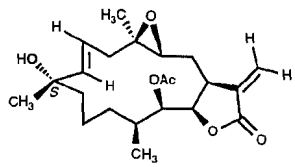

3

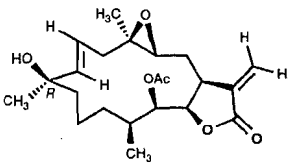

4

data. The latter, obtained in $CDCl_3$, revealed 22 resonances for 4 CH_3, 6 CH_2, 7 CH, and 5 C. Three of the seven methine carbons were sp^3 at a heteroatom, two were sp^3 not connected to a heteroatom, and two were olefinic. One of the methylene carbons was sp^2 and two of the quaternary carbon atoms were those of ester C=O functionalities. This suggests a tricyclic diterpene all three cycles of which are accounted for by an epoxidized cembranolide, as in the case of eupalmerin acetate (**1**). Uprolide-A acetate (**3**) shows an ultraviolet absorption maximum at 212 nm (ε 25 300) suggesting the existence of an α-methylene-γ-butyrolactone ring. The infrared spectrum inferred the presence of a hydroxyl (3550 cm^{-1}), a conjugated carbonyl (1766 cm^{-1}), and isolated ester (1733 cm^{-1}) moieties. The ^1H nmr spectrum (300 MHz; $CDCl_3$) shows the signals of four olefinic protons (δ 6.10 (1H, d, J = 3.3 Hz), 5.45 (1H, d, J = 15.6 Hz), 5.39 (1H, m), and 5.29 (1H, d, J = 3.3 Hz)), the presence of three 3H singlets at δ 1.89, 1.35, and 1.27 indicating an acetate ester group and methyl groups in an *E*-trisubstituted epoxide and tertiary carbinol, respectively, while a 3H doublet at δ 0.85 (J = 6.9 Hz) indicated a methyl group bonded to a tertiary carbon atom. In addition, the ^1H nmr spectrum shows three separate methine protons on carbon atoms bearing oxygen at δ 5.11 (1H, d, J = 10.2 Hz), 4.80 (1H, d, J = 8.1 Hz), and 2.93 (1H, dd, J = 3.6, 10.2 Hz). The proton networks were determined by H–H COSY and decoupling difference spectra, and the connectivity of each network through the quaternary carbons was deduced by INEPT and NOESY spectra, which led to the structure **3** for uprolide-A acetate. The *E* configuration of the Δ^6 olefin was suspected from the high-field chemical shift value (δ 73.7) of the allylic C-8 resonance line (25), the presence of a strong sharp infrared band at 968 cm^{-1}, the absence of nOe between the ethylenic protons H-6 and H-7, and the coupling constant observed for the partially overlapped doublet centered at δ 5.45 (J = 15.6 Hz) ascribed to H-7. The relative configurations at C-1, C-3, C-4, C-12, C-13, and C-14, all common stereochemistry elements present in eupalmerin acetate (**1**), were established from the ^1H and ^{13}C nmr data, H–H COSY, NOESY, and the similarity of the J values involving protons at these sites to those observed for **1** (22). At this point the only major structural feature that remained to be determined was the stereochemical orientation of the C-8 methyl substituent. Although there were a few intense nOe responses to the Me-19 protons in the NOESY spectrum of **3**, none gave reliable information about the stereochemical identity at C-8. Fortunately, compound **3** could be crystallized in a form suitable for X-ray diffraction analysis, which established the relative configuration at C-8 and confirmed the rest of our structural assignments (Fig. 1). Since the absolute configuration of eupalmerin acetate (**1**) has been established (11) and compounds **1** and **3** have identical relative configuration at all common chiral centers, we can safely assume that they also have the same absolute configuration. Since the C-1,3,4,12,13,14 constellation has been correlated by X-ray diffraction analysis with the remaining chiral center at C-8, the absolute stereochemistry at that center must be *S*.

The high-resolution ei mass spectrum of compound **4**, obtained as a uv-active colorless oil, gave major ions at *m/z* 374.20624 for $C_{22}H_{30}O_5$ and *m/z* 332.19765 for $C_{20}H_{28}O_4$, which reflect fragmentations of $[M - H_2O]^+$ and $[M - AcOH]^+$, respectively, from the actual molecular composition of $C_{22}H_{32}O_6$. This homogeneous compound also showed a hydroxyl absorption at 3552 cm^{-1} and two ester carbonyl absorptions at 1770 and 1740 cm^{-1} in its infrared spectrum. The ^1H and ^{13}C nmr spectra of compound **4** showed a striking similarity to those of uprolide-A acetate (**3**) (see Tables 1 and 4). These similarities, together with the fact that **3** and **4** possess identical molecular formulae, suggested a close structural relationship between these compounds. A detailed comparison of their ^1H and ^{13}C nmr spectra revealed that the few differences observed were in fact consistent with a change in relative stereochemical orientation of the Me-19 group at C-8. The change at C-8 from *S* in **3** to *R* in **4** was clearly indicated by the ^{13}C nmr chemical shift difference of the Me-19 groups (δ 25.6 in **3** vs. 30.1 in **4**) and the signal at δ 18.9 associated with the nearby C-10 methylene in **3**, which appears shifted upfield to 17.1 ppm in **4**. The ^1H and ^{13}C nmr data for **4**, along with the analysis of J values, H–H COSY, NOESY, and a heteronuclear chemical shift correlation with broad-band decoupling (CSCMBB) experiment showed that all common stereochemistry elements remaining were un-changed. Compound **4** was therefore named 8-epi-uprolide-A acetate.

Compound **5**, which was named uprolide-B, was isolated as a uv-active (λ_{max} 212 nm) oily substance that analyzed for $C_{20}H_{30}O_5$ by combined high-resolution fabms and ^{13}C nmr methods. The compound showed ir spectral characteristics consistent with the presence of an epoxide ring (1268 and 822 cm^{-1}) and of an ester carbonyl functionality (1755 cm^{-1}). A very intense broad absorption near 3405 cm^{-1} suggested the presence of more than one hydroxyl functionality. The ^1H nmr

Can. J. Chem. Downloaded from www.nrcresearchpress.com by 65.111.164.53 on 09/08/12
For personal use only.

Can. J. Chem. Downloaded from www.nrcresearchpress.com by 65.111.164.53 on 09/08/12
For personal use only.

Table 1. ^{1}H NMR (300 MHz) spectral data of the uprolides **3–7** ($CDCl_3$, TMS).[a]

H	**3** δ, mult, *J* (Hz), intgrtn	**4** δ, mult, *J* (Hz), intgrtn	**5** δ, mult, *J* (Hz), intgrtn	**6** δ, mult, *J* (Hz), intgrtn	**7** δ, mult, *J* (Hz), intgrtn
H_1	3.10, m, 1H	3.11, m, 1H	3.20, m, 1H	3.09, m, 1H	3.09, m, 1H
H_2 (α)	2.00, m, 1H	2.02, br t, 12.3, 1H	2.20, m, 1H	2.16, m, 1H	2.03, m, 1H
(β)	1.72, m, 1H	1.70, m, 1H	1.90, m, 1H	1.74, m, 1H	1.71, m, 1H
H_3	2.93, dd, 3.6, 10.2, 1H	3.06, dd, 3.0, 10.5, 1H	3.00, dd, 3.0, 10.8, 1H	2.93, dd, 3.9, 10.8, 1H	2.92, dd, 3.0, 10.5, 1H
H_5 (α)	2.48, ddd, 7.5, 8.1, 19.8, 2H	2.68, br d, 15.0, 1H	2.55, dd, 4.8, 14.7, 1H	2.68, dd, 3.9, 14.7, 1H	2.68, dd, 3.9, 14.7, 1H
(β)	—	2.37, dd, 9.6, 15.0, 1H	2.46, dd, 9.6, 14.7, 1H	2.44, dd, 9.0, 14.7, 1H	2.41, dd, 9.9, 14.7, 1H
H_6	5.39, m, 1H	5.43, m, 1H	5.33, ddd, 4.8, 9.6, 15.9, 1H	5.44, m, 1H	5.38, m, 1H
H_7	5.45, d, 15.6, 1H	5.36, d, 15.6, 1H	5.56, d, 15.9, 1H	5.48, d, 1H	5.62, d, 15.6, 1H
H_9 (α)	1.63, m, 1H	1.52, m, 1H	1.35, m, 1H	1.55, m, 1H	1.42, m, 1H
(β)	0.91, m, 1H	1.03, m, 1H	0.91, m, 1H	0.95, m, 1H	0.86, m, 1H
H_{10} (α)	1.67, m, 1H	1.73, m, 1H	1.63, m, 1H	1.68, m, 1H	1.86, m, 1H
(β)	1.28, m, 1H	1.14, m, 1H	1.25, m, 1H	1.17, m, 1H	1.61, m, 1H
H_{11} (α)	1.55, m, 1H	1.70, m, 1H	1.55, m, 1H	1.53, m, 1H	1.54, m, 1H
(β)	1.44, m, 1H	1.47, m, 1H	1.18, m, 1H	1.53, m, 1H	1.54, m, 1H
H_{12}	2.16, m, 1H	2.18, m, 1H	2.01, m, 1H	2.20, m, 1H	2.18, m, 1H
H_{13}	5.11, d, 10.2, 1H	5.16, d, 10.5, 1H	3.65, d, 10.2, 1H	5.13, d, 10.5, 1H	5.12, d, 10.5, 1H
H_{14}	4.80, d, 8.1, 1H	4.75, d, 8.1, 1H	4.80, d, 8.2, 1H	4.77, d, 8.1, 1H	4.75, d, 7.8, 1H
H_{17} (α)	6.10, d, 3.3, 1H	6.09, d, 3.0, 1H	5.98, d, 3.1, 1H	6.11, d, 3.3, 1H	6.11, d, 3.0, 1H
(β)	5.29, d, 3.3, 1H	5.30, d, 3.0, 1H	5.43, d, 3.1, 1H	5.31, d, 3.3, 1H	5.30, d, 3.0, 1H
Me_{18}	1.35, s, 3H	1.33, s, 3H	1.27, s, 3H	1.34, s, 3H	1.34, s, 3H
Me_{19}	1.27, s, 3H	1.26, s, 3H	1.39, s, 3H	1.35, s, 3H	1.50, s, 3H
Me_{20}	0.85, d, 6.9, 3H	0.86, d, 6.9, 3H	1.03, d, 6.9, 3H	0.87, d, 6.9, 3H	0.86, d, 6.9, 3H
Me_{22}	1.89, s, 3H	1.88 s, 3H	—	1.90, s, 3H	1.89, s, 3H
Me_{24}	—	—	—	—	1.96, s, 3H

[a]Assignments were aided by H–H COSY, H–C COSY, spin splitting patterns, and comparison of *J* values.

Fig. 1. 3D structure for uprolide-A acetate (**3**) obtained by X-ray diffraction analysis with atomic labeling. Small circles represent hydrogen atoms.

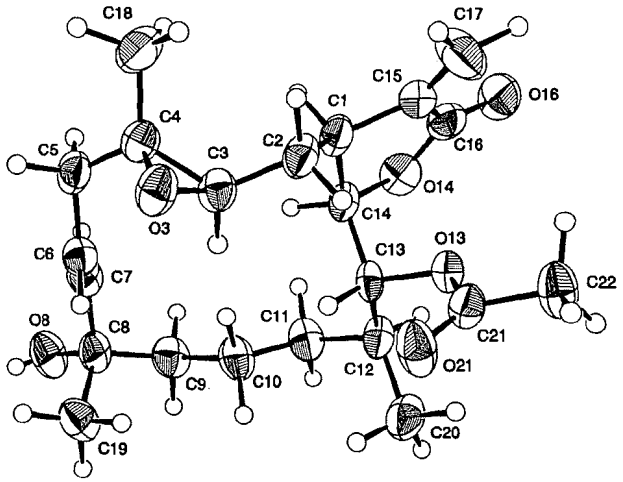

spectrum of uprolide-B (Table 1) showed two sharp 1H doublets at δ 5.98 (*J* = 3.1 Hz) and 5.43 (*J* = 3.1 Hz), suggesting the presence of a γ-lactone conjugated to an exomethylene group, and two multiplets at δ 5.56 (1H, d, *J* = 15.9 Hz) and 5.33 (1H, ddd, *J* = 4.8, 9.6, 15.9 Hz), due, respectively, to a 1,2-disubstituted olefin. Moreover, two doublets centered near δ 4.80 (1H, *J* = 8.2 Hz) and 3.65 (1H, *J* = 10.2 Hz), and one doublet of doublets at δ 3.00 (1H, *J* = 3.0 and 10.8 Hz), could be attributed to methine protons on carbon atoms bearing oxygen (H-14, H-13, and H-3, respectively). The two 3H singlets at δ 1.39 and 1.27 have been ascribed to the methyl groups placed, respectively, at C-8 and C-4, while the doublet at δ 1.03 (*J* = 6.9 Hz), integrating as 3H, is ascribable to the methyl group attached to C-12. The ^{13}C nmr spectrum of uprolide-B exhibited 20 signals separated by APT into 4 quaternary carbons (C-4, C-8, C-15, and C-16), 7 CH groups (C-1, C-3, C-6, C-7, C-12, C-13, and C-14), 6 methylenes (C-2, C-5, C-9, C-10, C-11, and C-17), and 3 Me groups (C-18, C-19, and C-20), 1 ester carbonyl (δ 172.8 (s)), 5 oxygenated carbons (δ 86.2 (s), 79.6 (d), 72.5 (d), 62.8 (s), and 59.1 (d)), and 4 olefinic (δ 140.8 (s), 139.6 (d), 127.5 (d), and 117.0 (t)) carbons. By use of a H–H correlation COSY experiment the chain of coupling between protons H-12 through H-14 and H-1 through H-3, including the terminal methylene protons H-17αβ, could be established. Comparison of the ^{1}H and ^{13}C nmr spectra of uprolide-B (**5**) and eupalmerin (**2**) (23) revealed that these compounds share many common structural features and that all common stereochemistry elements (C-1, C-3, C-4, C-12, C-13, and C-14) remain unchanged. Likewise, comparison of the nmr spectra of uprolides **3** and **5** (including COSY and NOESY) also revealed many common structural features (i.e., same relative configuration at C-8), which suggested that the major differences between these compounds were associated mainly with the stereochemical orientation of the Δ^6 olefin. In the spectrum of uprolide-A acetate (**3**) the olefinic protons H-6 and H-7 nearly

Table 2. ^{1}H NMR (300 MHz) spectral data of the uprolides **8–12** ($CDCl_3$, TMS).[a]

H	**8** δ, mult, *J* (Hz), intgrtn	**9** δ, mult, *J* (Hz), intgrtn	**10** δ, mult, *J* (Hz), intgrtn	**11** δ, mult, *J* (Hz), intgrtn	**12** δ, mult, *J* (Hz), intgrtn
H_1	3.08, m, 1H	3.09, m, 1H	3.10, m, 1H	3.16, m, 1H	3.26, m, 1H
H_2 (α)	2.27, m, 1H	2.02, m, 1H	2.03, m, 1H	2.32, m, 1H	2.05, m, 1H
(β)	1.85, m, 1H	1.75, m, 1H	1.72, m, 1H	1.83, m, 1H	1.75, m, 1H
H_3	3.03, dd, 3.6, 10.5, 1H	3.02, dd, 3.6, 10.2, 1H	3.00, dd, 3.3, 10.5, 1H	2.82, dd, 4.8, 9.0, 1H	2.94, dd, 5.4, 8.7, 1H
H_5 (α)	2.63, dd, 3.9, 15.0, 1H	2.61, dd, 4.0, 15.0, 1H	2.67, dd, 3.3, 15.0, 1H	2.01, m, 1H	2.20, m, 1H
(β)	2.38, dd, 8.7, 15.0, 1H	2.37, dd, 8.5, 15.0, 1H	2.36, dd, 10.5, 15.0, 1H	1.20, m, 1H	1.67, m, 1H
H_6 (α)	5.33, ddd, 3.9, 8.7, 12.6, 1H	5.37, m, 1H	5.39, m, 1H	1.98, m, 1H	1.90, m, 1H
(β)	—	—	—	1.37, m, 1H	1.24, m, 1H
H_7	5.28, d, 12.0, 1H	5.28, d, 11.4, 1H	5.20, d, 11.4, 1H	4.36, br t, 3.9, 1H	4.24, dd, 3.3, 9.9, 1H
H_9 (α)	1.18, m, 1H	1.49, m, 1H	1.32, m, 1H	2.29, m, 1H	2.15, m, 1H
(β)	1.45, m, 1H	1.12, m, 1H	1.04, m, 1H	1.46, m, 1H	1.05, m, 1H
H_{10} (α)	1.92, m, 1H	1.94, m, 1H	2.50, m, 1H	1.61, m, 1H	1.60, m, 1H
(β)	1.12, m, 1H	1.16, m, 1H	1.04, m, 1H	1.10, m, 1H	1.01, m, 1H
H_{11} (α)	1.45, m, 1H	1.49, m, 1H	2.18, m, 1H	1.59, m, 1H	1.63, m, 1H
(β)	1.45, m, 1H	1.23, m, 1H	1.49, m, 1H	1.59, m, 1H	1.63, m, 1H
H_{12}	1.97, m, 1H	2.16, m, 1H	2.16, m, 1H	1.87, m, 1H	2.21, m, 1H
H_{13}	3.80, br d, 9.9, 1H	5.15, d, 10.5, 1H	5.17, d, 10.5, 1H	3.69, br d, 8.4, 1H	5.13, d, 10.8, 1H
H_{14}	4.66, d, 8.4, 1H	4.74, d, 8.1, 1H	4.74, d, 8.1, 1H	4.71, d, 8.1, 1H	4.83, d, 8.4, 1H
H_{17} (α)	6.13, d, 3.3, 1H	6.10, d, 3.6, 1H	6.10, d, 3.0, 1H	6.12, d, 3.3, 1H	6.12, d, 3.3, 1H
(β)	5.38, d, 3.3, 1H	5.31, d, 3.6, 1H	5.30, d, 3.0, 1H	5.38, d, 3.3, 1H	5.31, d, 3.3, 1H
Me_{18}	1.37, s, 3H	1.34, s, 3H	1.34, s, 3H	1.32, s, 3H	1.33, s, 3H
H_{19} (α)	1.35, s, 3H	1.35, s, 3H	1.52, s, 3H	5.05, br s, 1H	5.17, br s, 1H
(β)	—	—	—	5.03, br s, 1H	5.11, br s, 1H
Me_{20}	1.05, d, 6.9, 3H	0.86, d, 6.9, 3H	0.85, d, 7.2, 3H	1.03, d, 6.6, 3H	0.89, d, 6.9, 3H
Me_{22}	—	1.89, s, 3H	1.89, s, 3H	—	1.92, s, 3H
Me_{24}	—	—	2.07, s, 3H	—	—

[a]Assignments were aided by H–H COSY, H–C COSY, spin splitting patterns, and comparison of *J* values.

overlap at δ 5.42, whereas the spectrum of uprolide-B (**5**) contains an olefinic signal at δ 5.33 (1H, ddd, $J = 4.8, 9.6, 15.9$ Hz) for H-6 and another at δ 5.56 (1H, d, $J = 15.9$ Hz) ascribable to H-7. Although the large coupling constant (15.9 Hz) observed in **5** for the Δ^6 olefinic protons suggests a *trans* configuration, the strong downfield shift experienced by the C-8 resonance (δ 86.2 in **5** vs. 73.7 in **3**) clearly indicates a change in stereochemical orientation about the ethylenic double bond. *trans* Ethylenic coupling constants (12–24 Hz) are always larger than *cis* ethylenic coupling constants (3–18 Hz) in any vinyl compound or for a pair of 1,2-disubstituted ethylenes (26). However, the literature contains a large amount of scattered data for coupling in olefinic systems that show that the two ranges often overlap (27). Because bond order or bond length, valence angles, and hybridization of the olefinic carbon atoms may also constitute factors determining the magnitude of the olefinic coupling constant, it is unlikely that, at the present state of knowledge, the magnitude of *J* in structure **5** (and that of its acetylated derivatives **6** and **7**), could be directly applied to the solution of their structures. The almost identical coupling constant values of $J_{6,7} \cong 15.7$ Hz observed for **3** and **5** clearly show that the assignment of *trans* and *cis* stereochemistry at Δ^6 in this series is not a simple task and that one must carefully examine other evidence available before the correct geometry can be established. On the other hand, the *E* and *Z* geometry of the Δ^6 double bonds in **3** and **5**, respectively, is clearly shown by the ^{13}C nmr chemical shift difference of the Me-19 groups (δ 25.6 vs. 19.3), the C-8 carbons (δ 73.7 vs. 86.2), and the signal at δ 42.2 associated with the C-9 methylene in **3**, which appears shifted upfield to 38.4 in **5**. Thus an empirical relationship appears to exist between the C-19 methyl, the C-8, and the nearby C-9 methylene carbon chemical shifts with the *E-Z* configuration of the Δ^6 olefin in the uprolide series. The *Z* geometry of the ethylenic double bond in **5** was also supported by a strong nOe between the olefinic protons H-6 and H-7 (absent in **3**) and the absence of a strong band near 968 cm^{-1} in the infrared spectrum that is present in **3**. The present analysis confirms the structure proposed for uprolide-B, including all the stereochemical assignments.

The low-resolution fab mass spectrum and the ^{1}H and ^{13}C nmr data of **6** were consistent with the molecular formula $C_{22}H_{32}O_6$. The infrared band at 3380 cm^{-1} suggested the presence of a hydroxyl group and two strong bands at 1764 and 1740 cm^{-1} could be assigned to ester carbonyl groups. The uv spectrum indicated the presence of the same chromophore observed in all the previous compounds: λ_{max} = 214 nm (ε 9825). Comparison of the ^{1}H and ^{13}C nmr spectra of **6** with those of uprolide-B (**5**) revealed only a few differences, all of which were consistent with the replacement of the hydroxyl group at C-13 in **5** with an acetoxy group in **6**. For instance, in the ^{1}H nmr spectrum of uprolide-B the H-13 proton resonates at δ 3.65 (1H, d, $J = 10.2$ Hz), whereas the spectrum of **6** contained the H-13 signal at δ 5.13 (1H, d, $J = 10.5$ Hz), Also, the presence in the nmr spectra of an acetate signal (δ 1.90 (3H, s);

Can. J. Chem. Downloaded from www.nrcresearchpress.com by 65.111.164.53 on 09/08/12
For personal use only.

Can. J. Chem. Downloaded from www.nrcresearchpress.com by 65.111.164.53 on 09/08/12
For personal use only.

Table 3. ^{1}H NMR (300 MHz) spectral data of the uprolides **13–15** ($CDCl_3$, TMS).[a]

H	**13** δ, mult, *J* (Hz), intgrtn	**14** δ, mult, *J* (Hz), intgrtn	**15** δ, mult, *J* (Hz), intgrtn
H_1	3.21, m, 1H	3.20, m, 1H	3.27, m, 1H
H_2 (α)	2.09, m, 1H	2.07, m, 1H	2.11, m, 1H
(β)	1.73 m, 1H	1.74, m, 1H	1.74, m, 1H
H_3	2.86, dd, 5.4, 8.7, 1H	2.89, dd, 5.1, 9.3, 1H	2.96, dd, 4.8, 9.6, 1H
H_5 (α)	2.03, m, 1H	2.03, m, 1H	1.89, m, 1H
(β)	0.97, m, 1H	1.12, m, 1H	1.43, m, 1H
H_6 (α)	1.79, m, 1H	2.01, m, 1H	1.84, m, 1H
(β)	1.40, m, 1H	1.30, m, 1H	1.39, m, 1H
H_7	5.05, m, 1H	4.25, br s, 1H	5.25, br t, 4.8, 1H
H_9 (α)	2.15, m, 1H	2.32, m, 1H	2.34, m, 1H
(β)	1.78, m, 1H	1.48, m, 1H	1.72, m, 1H
H_{10} (α)	1.68, m, 1H	1.64, m, 1H	1.67, m, 1H
(β)	0.98, m, 1H	1.05, m, 1H	1.15, m, 1H
H_{11} (α)	1.64, m, 1H	1.64, m, 1H	1.55, m, 1H
(β)	1.64, m, 1H	1.64, m, 1H	1.55, m, 1H
H_{12}	2.19, m, 1H	2.20, m, 1H	2.19, m, 1H
H_{13}	5.14, d, 10.2, 1H	5.12, d, 10.8, 1H	5.16, d, 10.2, 1H
H_{14}	4.85, d, 8.1, 1H	4.81, d, 8.1, 1H	4.99, d, 8.1, 1H
H_{17} (α)	6.12, d, 3.3, 1H	6.11, d, 3.3, 1H	6.11, d, 3.3, 1H
(β)	5.31, d, 3.3, 1H	5.31, d, 3.3, 1H	5.30, d, 3.3, 1H
Me_{18}	1.32, s, 3H	1.31, s, 3H	1.31, s, 3H
H_{19} (α)	5.05, br s, 1H	5.10, br s, 1H	5.01, br s, 1H
(β)	5.05, br s, 1H	5.00, br s, 1H	4.98, br s, 1H
Me_{20}	0.88, d, 6.9, 3H	0.88, d, 6.9, 3H	0.88, d, 6.9, 3H
Me_{22}	1.92, s, 3H	1.91, s, 3H	1.92, s, 3H
Me_{24}	2.04, s, 3H	—	2.10, s, 3H

[a]Assignments were aided by H–H COSY, H–C COSY, spin splitting patterns, and comparison of *J* values.

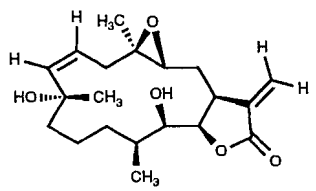

5

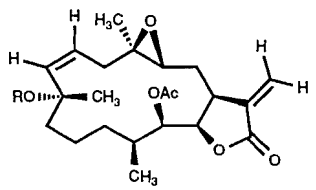

6 R = H
7 R = Ac

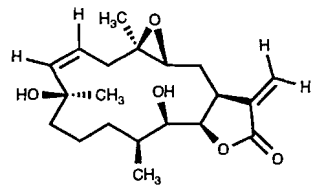

8

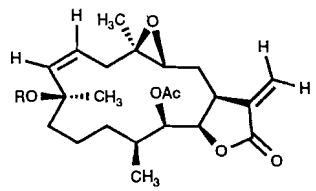

9 R = H
10 R = Ac

169.9 (s) or 169.6 (s)) also supported structure **6** for uprolide-B acetate. These spectral features suggested a close similarity between **6** and uprolide-B (**5**).

The ^{1}H nmr spectrum of **7** was almost identical with that of uprolide-B acetate (**6**), with the exception that it contained an extra acetate signal at δ 1.96 (3H, s) and that the signal for Me-19 had shifted from δ 1.35 in **6** to δ 1.50 in compound **7**. The high-resolution ei mass spectrum showed its highest ion peak at *m/z* 392.22073 for $C_{22}H_{32}O_6$, which reflects the loss of one molecule of ketene from the actual molecular composition of $C_{24}H_{34}O_7$, followed by major ions at *m/z* 374.20849 for $C_{22}H_{30}O_5$, *m/z* 332.19698 for $C_{20}H_{28}O_4$, and *m/z* 314.18701 for $C_{20}H_{26}O_3$. The latter ion peaks reflect fragmentations of $[M - AcOH]^+$, $[M - AcOH - C_2H_2O]^+$, and $[M - 2AcOH]^+$, respectively. The ^{13}C nmr spectrum in $CDCl_3$, which also showed a striking resemblance to that of uprolide-B acetate (**6**), exhibited signals for 24 carbon atoms suggesting a diterpene diacetate: 3 were carbonyls (δ 170.0, 169.8, and 169.6) and 5 were methyl carbons (δ 22.4, 20.9, 20.8, 18.3, and 15.9). These spectral features suggested that **7**, named uprolide-B diacetate, had a close similarity to both uprolide-B (**5**) and uprolide-B acetate (**6**). That the stereochemistry at the Δ^6 double bond and chiral center C-8 was identical for the uprolides **5**, **6**, and **7** could be shown by the similarity of the ^{13}C nmr chemical shift values involving these sites (see Table 4).

The ir, uv, high-resolution fabms, and the ^{1}H and ^{13}C nmr data of **8**, **9**, and **10** clearly indicated that they too belonged to the uprolide-B diterpene class. These metabolites exhibited nmr spectra that were virtually superimposable on those of uprolides **5**, **6**, and **7**, respectively, except that the ^{13}C nmr signals for the Me-19 group consistently showed a downfield shift to 24–25 ppm that argued for the net inversion of their stereochemical orientation at C-8. The near identical upfield shift to

Can. J. Chem. Downloaded from www.nrcresearchpress.com by 65.111.164.53 on 09/08/12
For personal use only.

Table 4. ^{13}C NMR spectral data of the uprolides **3–7** (75 MHz; $CDCl_3$).[a]

C	**3** δ (mult)	**4** δ (mult)	**5** δ (mult)	**6** δ (mult)	**7** δ (mult)
1	40.6 (d)	40.7 (d)	41.3 (d)	40.6 (d)	40.6 (d)
2	25.7 (t)	25.5 (t)	27.3 (t)	25.6 (t)	25.6 (t)
3	57.2 (d)	57.0 (d)	59.1 (d)	57.1 (d)	57.0 (d)
4	60.9 (s)	61.0 (s)	62.8 (s)	60.9 (s)	60.8 (s)
5	39.5 (t)	38.5 (t)	39.9 (t)	39.2 (t)	39.1 (t)
6	124.1 (d)	122.6 (d)	127.5 (d)	127.6 (d)	125.4 (d)
7	140.6 (d)	140.7 (d)	139.6 (d)	137.2 (d)	137.1 (d)
8	73.7 (s)	73.6 (s)	86.2 (s)	85.7 (s)	83.7 (s)
9	42.2 (t)	41.6 (t)	38.4 (t)	37.0 (t)	39.3 (t)
10	18.9 (t)	17.1 (t)	19.1 (t)	18.0 (t)	17.6 (t)
11	33.1 (t)	32.8 (t)	33.9 (t)	33.0 (t)	32.8 (t)
12	32.9 (d)	32.7 (d)	35.2 (d)	32.8 (d)	32.7 (d)
13	73.1 (d)	73.0 (d)	72.5 (d)	72.9 (d)	72.9 (d)
14	77.2 (d)	77.1 (d)	79.6 (d)	77.1 (d)	77.2 (d)
15	138.2 (s)	138.2 (s)	140.8 (s)	138.2 (s)	138.1 (s)
16	169.7 (s)[b]	169.7 (s)[b]	172.8 (s)	169.6 (s)[b]	169.6 (s)[b]
17	116.8 (t)	116.7 (t)	117.0 (t)	116.8 (t)	116.8 (t)
18	18.2 (q)	18.4 (q)	18.5 (q)	18.3 (q)	18.3 (q)
19	25.6 (q)	30.1 (q)	19.3 (q)	19.1 (q)	20.8 (q)
20	15.9 (q)	15.9 (q)	16.7 (q)	15.9 (q)	15.9 (q)
21	169.9 (s)[b]	169.7 (s)[b]	—	169.9 (s)[b]	169.8 (s)[b]
22	20.9 (q)	20.9 (q)	—	20.9 (q)	20.9 (q)
23	—	—	—	—	170.0 (s)
24	—	—	—	—	22.4 (q)

[a]Multiplicities were obtained by an Attached Proton Test (APT) experiment. Assignments were made on the basis of heteronuclear chemical shift correlation methods, carbon atom multiplicities, and chemical shift values. The δ values are in parts per million and are referenced to $CDCl_3$ (77.0 ppm).

[b]Values with identical superscripts in each column may be interchanged.

19–20 ppm experienced by the Me-19 group in uprolides **5**, **6**, and **7** is in line with the opposite stereochemistry at C-8 shown for these compounds. Moreover, the 8*R* configuration depicted in **8**, **9**, and **10** is also consistent with the ^{13}C nmr chemical shift values in $CDCl_3$ solution observed for C-10 (16–17 ppm) that consistently appear shifted downfield to 18–19 ppm in uprolides **5**, **6**, and **7**. These trends, which were observed consistently in those cembranolides belonging to the uprolide-A series (i.e., **3** and **4**), where the Δ^6 olefin has the *E* configuration, may constitute an invaluable method for the assignment of relative stereochemistry at C-8 in the uprolide diterpene series. Interestingly, *Z*-olefins **8–10**, in addition to having ^{13}C nmr chemical shift values for C-8 in the expected range (82–84 ppm; see Table 5), have the usual J_{cis} values (11–12 Hz). This observation suggests that the relative stereochemistry of the substituents at C-8 in the uprolide B series may in fact constitute yet another factor in determining the large coupling constant observed for the *Z*-olefinic protons in uprolides **5–7**. The present analysis confirms the structure proposed for 8-epi-uprolide-B (**8**), 8-epi-uprolide-B acetate (**9**), and 8-epi-uprolide-B diacetate (**10**), including their complete stereochemical assignments. The rigorous assignments of the ^1H and ^{13}C nmr spectra of uprolides **8**, **9**, and **10** (Tables 2 and 5) were established by application of several 2D-nmr techniques that included H–H COSY, CSCMBB, and NOESY experiments.

Uprolide-C (**11**) had the molecular formula $C_{20}H_{30}O_5$, *m/z* 357.22510, $[M + Li]^+$, and showed a uv absorption at λ_{max} 212 nm (ε 9800) and infrared absorptions at ν 3433, 1740, 1643, and 1274 cm^{-1}, typical for an alcohol, a γ-lactone, an olefin, and one epoxy group. The ^{13}C nmr spectrum (Table 5) exhibited 20 signals divided by APT into 4 quaternary carbons, 6 methine carbons, 8 methylenes, and 2 methyl groups. The ^1H nmr spectrum (Table 2) contained a proton signal at δ 2.82 (dd, J = 4.8, 9.0 Hz), which could be assigned to an α-epoxy proton, and showed additional signals at δ 6.12 (1H, d, J = 3.3 Hz) and 5.38 (1H, d, J = 3.3 Hz) due to a pair of terminal methylene protons. In addition, the spectrum of uprolide-C showed signals at δ 5.05 (1H, br s) and 5.03 (1H, br s) due to a second pair of terminal methylene protons, some key signals at δ 4.71 (1H, d, J = 8.1 Hz), 4.36 (1H, br t, J = 3.9 Hz), and 3.69 (1H, br d, J = 8.4 Hz), and two methyl signals: one a singlet at δ 1.32 (3H) and one a doublet at δ 1.03 (3H, J = 6.6 Hz). Comparison of the ^1H and ^{13}C nmr spectra of **11** with those of **5** and **8** suggested for **11** the same substituted cembranolide ring as in compounds **5** and **8** and, in addition, suggested that the usual Δ^6 olefin in the latter compounds had now shifted to an exocyclic position and that the C-8 hydroxyl group is now located at C-7 in uprolide-C (**11**). The COSY experiment established the following correlations: H-20 to H-12; H-12 to H-11 and H-13; H-13 to H-14; H-14 to H-1; H-1 to H-2αβ and H-17αβ; H-2αβ to H-3; H-5αβ to H-6αβ; H-6αβ to H-7; and H-7 to H-19αβ. These connec-

Can. J. Chem. Downloaded from www.nrcresearchpress.com by 65.111.164.53 on 09/08/12
For personal use only.

Table 5. ^{13}C NMR spectral data of the uprolides **8–12** (75 MHz; $CDCl_3$).[a]

C	**8** δ (mult)	**9** δ (mult)	**10** δ (mult)	**11**[c] δ (mult)	**12** δ (mult)
1	40.2 (d)	40.6 (d)	40.7 (d)	40.3 (d)	40.5 (d)
2	26.8 (t)	25.7 (t)	25.6 (t)	26.8 (t)	27.0 (t)
3	57.7 (d)	57.1 (d)	57.1 (d)	59.6 (d)	59.7 (d)
4	61.2 (s)	60.8 (s)	60.9 (s)	61.0 (s)	60.6 (s)
5	39.4 (t)	39.5 (t)	38.9 (t)	31.4 (t)	34.9 (t)
6	124.3 (d)	124.5 (d)	123.4 (d)	27.9 (t)	27.7 (t)
7	136.2 (d)	136.1 (d)	137.5 (d)	85.9 (d)	89.8 (d)
8	84.3 (s)	84.1 (s)	82.4 (s)	145.4 (s)	145.4 (s)
9	38.6 (t)	38.5 (t)	39.0 (t)	34.1 (t)	29.9 (t)
10	17.0 (t)	17.3 (t)	16.8 (t)	24.2 (t)	24.8 (t)
11	32.7 (t)	33.1 (t)	32.7 (t)	32.9 (t)	32.7 (t)
12	34.4 (d)	32.9 (d)	32.8 (d)	34.7 (d)	32.7 (d)
13	72.4 (d)	73.2 (d)	73.1 (d)	72.9 (d)	73.6 (d)
14	77.8 (d)	77.3 (d)	77.1 (d)	78.2 (d)	77.2 (d)
15	138.0 (s)	138.2 (s)	138.2 (s)	138.0 (s)	138.5 (s)
16	170.7 (s)	169.7 (s)[b]	169.6 (s)[b]	170.5 (s)	169.4 (s)[b]
17	118.0 (t)	116.9 (t)	116.8 (t)	118.6 (t)	117.3 (t)
18	18.3 (q)	18.3 (q)	18.4 (q)	16.9 (q)	16.4 (q)
19	24.3 (q)	24.0 (q)	25.3 (q)	112.6 (t)	118.0 (t)
20	16.1 (q)	16.0 (q)	16.0 (q)	16.0 (q)	15.9 (q)
21	—	169.8 (s)[b]	169.8 (s)[b]	—	170.0 (s)[b]
22	—	20.9 (q)	20.9 (q)	—	20.9 (q)
23	—	—	169.9 (s)	—	—
24	—	—	22.3 (q)	—	—

[a]Multiplicities were obtained by an Attached Proton Test (APT) experiment. Assignments were made on the basis of heteronuclear chemical shift correlation methods, carbon atom multiplicities, and chemical shift values. The δ values are in parts per million and are referenced to $CDCl_3$ (77.0 ppm).

[b]Values with identical superscripts in each column may be interchanged.

[c]Due to poor solubility this sample was run in a mixture of $CDCl_3/CD_3OD$.

tions established the C-11 to C-3 (including C-17) and C-5 to C-7 (including C-19) segments of the molecule, leaving unconnected the C-3 to C-5 and C-7 to C-9 bonds in a manner consistent with the proposed structure for uprolide-C. The relative stereochemistry shown at C-7 is based on the ^{13}C nmr chemical shift difference of the C-7 carbon (δ 85.9), which appears shifted upfield to 70–73 ppm when the C-7 hydroxyl group is in the β configuration (28–30). Moreover, because uprolide-C is sparingly soluble in $CHCl_3$, we argue that the two hydroxyl groups of diol **11** must be oriented in opposite directions with respect to the cembrane skeleton (i.e., *trans*). Examination of a Dreiding model of uprolide-C (**11**) reveals that when the two hydroxyl groups lie on opposite faces of the cembrane ring, **11** can adopt a stable conformation allowing favorable hydrogen-bonding interactions between them that could reduce its solubility in $CHCl_3$. Interestingly, an attempt to acetylate uprolide-C with pyridine – acetic anhydride at 25°C did not produce the expected diacetate (i.e., **13**). Instead, diol **11** was found to be unstable under these conditions, yielding exclusively uprolide-A acetate (**3**).

The structure of uprolide-C acetate (**12**) could readily be assigned by comparison of its ^1H and ^{13}C nmr data with those of uprolide-C (**11**). The multiplicities of all ^1H nmr resonances in these two compounds were nearly identical as were the chemical shifts, except for one acetate methyl signal in the

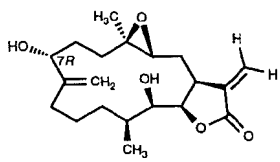

11

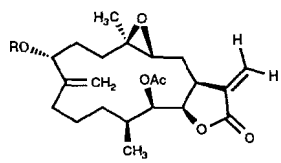

12 R = H
13 R = Ac

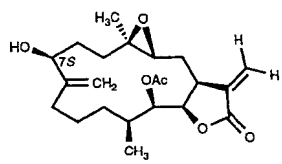

14

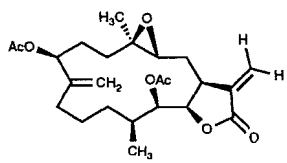

15

spectrum of **12** and a downfield shift for H-13 consistent with replacing the C-13 hydroxyl group of **11** with an acetoxy group in **12**. Compound **12**, which was readily soluble in $CHCl_3$, can be assigned the same stereochemical orientation at C-7 as found for uprolide-C since, as in **11**, the C-7 nmr resonance appears more downfield (δ 89.8) than those found in the next set of compounds (i.e., **14** and **15**) (28–30). These data, combined with the ir, uv, ms, and 2D-nmr spectra, support the structure assigned to uprolide-C acetate (**12**).

The ^1H nmr spectrum of uprolide-C diacetate (**13**) was vir-

Can. J. Chem. Downloaded from www.nrcresearchpress.com by 65.111.164.53 on 09/08/12
For personal use only.

Table 6. ^{13}C NMR spectral data of the uprolides **13–15** (75 MHz; $CDCl_3$).[a]

C	**13** δ (mult)	**14** δ (mult)	**15** δ (mult)
1	40.6 (d)	40.6 (d)	40.3 (d)
2	26.9 (t)	27.0 (t)	26.8 (t)
3	59.7 (d)	59.5 (d)	59.2 (d)
4	60.4 (s)	60.8 (s)	60.1 (s)
5	34.5 (t)	31.0 (t)	27.0 (t)
6	30.1 (t)	29.5 (t)	31.5 (t)
7	78.1 (d)	73.3 (d)	73.1 (d)
8	144.6 (s)	149.5 (s)	144.7 (s)
9	30.7 (t)	33.4 (t)	33.5 (t)
10	24.7 (t)	24.2 (t)	23.2 (t)
11	32.7 (t)	33.2 (t)	32.5 (t)
12	32.7 (d)	32.9 (d)	32.7 (d)
13	73.6 (d)	73.5 (d)	73.2 (d)
14	77.1 (d)	77.3 (d)	77.3 (d)
15	138.4 (s)	138.5 (s)	138.5 (s)
16	169.4 (s)[b]	169.4 (s)[b]	169.6 (s)[b]
17	117.2 (t)	117.2 (t)	117.0 (t)
18	16.3 (q)	16.8 (q)	17.3 (q)
19	117.2 (t)	111.2 (t)	112.6 (t)
20	15.9 (q)	16.1 (q)	16.1 (q)
21	169.9 (s)[b]	169.9 (s)[b]	170.0 (s)[b]
22	20.8 (q)	20.8 (q)	20.8 (q)
23	169.9 (s)	—	170.4 (s)
24	21.2 (q)	—	21.0 (q)

[a]Multiplicities were obtained by an Attached Proton Test (APT) experiment. Assignments were made on the basis of heteronuclear chemical shift correlation methods, carbon atom multiplicities and chemical shift values. The δ values are in parts per million and are referenced to $CDCl_3$ (77.0 ppm).

[b]Values with identical superscripts in each column may be interchanged.

tually superimposable on that of **12** except that it contained one more acetate methyl signal at δ 2.04 (3H, s). The strong upfield shift experienced by C-7 and the downfield shift observed for H-7 in the ^{13}C and ^{1}H nmr spectra, respectively, confirmed that the new acetate group is at position 7. Structure **13** was thus inferred, and this was adequately substantiated by results of ir, uv, high-resolution fabms, H–H COSY, CSCMBB, and NOESY experiments that provided ^{1}H and ^{13}C nmr resonance assignments and skeletal connectivity evidence.

The high-resolution fabms established a molecular formula of $C_{22}H_{32}O_6$ for cembranolide **14**, indicating that it was an isomer of uprolide-C acetate (**12**). Like **12**, compound **14** showed ir absorptions (3493, 1775, and 1741 cm^{-1}) that indicated the presence of a hydroxyl and diester functionalities. Comparison of the ^{1}H and ^{13}C nmr spectra of **14** with those of uprolide-C acetate (**12**) confirmed the structural similarity of these compounds and revealed the presence of one structural feature unique to **14**. The identity and location of the substituents around the cembranolide ring system as well as the unsaturation profile were assumed to be intact in **14** on the basis of similar ir, ms, uv, and 1D- and 2D-nmr data (compare signals of related H's and C's in Tables 3 and 6). The major differences observed, however, were associated with a change in **14** in its relative configuration at C-7. A broad signal at δ 4.25 (1H, br s), assigned to an allylic β-hydroxyl proton (H-7), was correlated in the ^{13}C nmr spectrum to a carbon resonance at δ 73.3 (C-7). Thus, the stereochemistry at C-7 in **14** is based on the chemical shift difference of the C-7 carbon resonance, which appears shifted downfield to δ 89.8 in **12** (28–30). These data suggested that 7-epi-uprolide-C acetate (**14**) contained an allylic β-hydroxyl group at C-7.

Although no molecular ion peak was detected in the high-resolution ei mass spectrum of 7-epi-uprolide-C diacetate (**15**), analysis of the major ion peaks and ^{13}C nmr data revealed the actual molecular composition to be $C_{24}H_{34}O_7$. Therefore, **15** was shown to be an isomer of uprolide-C diacetate (**13**). The high-resolution mass spectrum exhibited $[M - C_2H_2O]^+$, $[M - AcOH]^+$, $[M - AcOH - C_2H_2O]^+$, and $[M - 2AcOH]^+$ peaks at *m/z* 392.21976, 374.21395, 332.19826, and 314.18851, respectively, under a variety of conditions. H–H COSY experiments, and comparison of overall ^{1}H and ^{13}C nmr data revealed similarities between **13** and **15**, and showed that the same partial structures are also present in this compound. However, there were several significant differences in the spectral data that indicated that **15** was the C-7 epimer of uprolide-C diacetate (**13**). Thus, the stereochemistry at position 7 in **15** is based on the chemical shift difference of the C-7 carbon (δ 73.1), which appears shifted downfield to δ 78.1 in epimer **13**. Also, the structure of compound **15** was correlated chemically with that of **14** upon acetylation of the latter with a mixture of pyridine – acetic anhydride for 12 h at 25°C. The acetylation of **14** to give 7-epi-uprolide-C diacetate (**15**) proceeded normally without rearrangement to either **3**, **4**, **6**, or **9**.

Like most structural congeners of eupalmerin acetate (**1**), the uprolides also showed modest cytotoxic activity (in vitro testing). The inhibitory activities of the uprolides A–C against several human tumor cell lines are depicted in Table 7.

Conclusions

Conclusions regarding the spectral analyses of the uprolides were strongly supported by the simultaneous isolation, from the same source, of 13 closely related compounds. The structure of model compound uprolide-A acetate (**3**) was determined by spectral and crystallographic methods. The nmr and other spectral data for the other uprolides were highly analogous with comparable data from **3**. Moreover, an empirical relationship appears to exist in the uprolide-A and -B series between the ^{13}C nmr chemical shift values of C-19, C-8, C-9, and C-10 with the *E-Z* configuration of the Δ^6 olefin. Also, there seems to be an empirical relationship between the ^{13}C nmr chemical shift values of C-19 and C-10 and the relative configuration at C-8. The relative configuration at C-8 in the uprolide-B series could also be a factor in determining the magnitude of the Δ^6 olefinic coupling constant. These efforts provide a partial data base that can be employed in the structure elucidation of new cembranolide analogues.

Table 7. In vitro inhibitory activity of the uprolides against several human tumor cell lines.

	Cell Line				
Compound	MCF-7 ED_{50} (μg/mL)	HCT 116 ED_{50} (μg/mL)	CCRF-CEM ED_{50} (μg/mL)	SK5-MEL ED_{50} (μg/mL)	A 549 ED_{50} (μg/mL)
3	—	—	—	3.5	5.5
4	20.5	16.5	4.1	—	—
7	21.5	29.5	4.8	—	—
9	—	—	—	4.7	7.8
10	—	—	—	8.0	6.5
13	21.5	22.5	2.8	—	—
14	—	—	—	2.7	10.2
15	—	—	—	5.7	8.2

Can. J. Chem. Downloaded from www.nrcresearchpress.com by 65.111.164.53 on 09/08/12
For personal use only.

Experimental

Collection and extraction of *E. mammosa*

The Caribbean gorgonian *E. mammosa* was collected by hand in November 1992 from Mona Island, Puerto Rico, using SCUBA at 15–20 m. The gorgonian was freeze-dried upon arrival and kept frozen until extraction. The dried animal (1.30 kg) was blended with MeOH:EtOAc (1:1) (3 × 2 L) and after filtration the crude extract was evaporated under vacuum to yield a residue (162.25 g) that was partitioned between hexane and H_2O and then between $CHCl_3$ and H_2O. The hexane extract was concentrated in vacuo to yield 94.45 g of a dark-green oily residue. This residue was dissolved in 1 L of toluene and, after filtration through a mixture of sand and Celite, the resulting filtrate was concentrated in vacuo. The residue obtained (49.78 g) was fractionated by size exclusion chromatography on a Bio-Beads SX-2 column using toluene as eluent. The combined terpenoid-rich fractions (tlc-guided) were concentrated to a yellow-orange oil (39.02 g) that was chromatographed over a silica gel column (850 g) with 10% EtOAc in hexane. The less polar fractions consisted of a complex mixture of unidentified sesquiterpenes, sterols, and fatty acid derivatives (17.2 g) and the following known cembranolide diterpenes: eupalmerin acetate (**1**) (2.00 g), eupalmerin (**2**) (2.33 g), pseudoplexauric acid methyl ester (0.47 g), euniolide (6.02 g), (−)-eunicenone (0.65 g), 14-deoxycrassin (1.03 g), eupalmerone (1.12 g), and the known cembranoid diterpene (7*E*, 11*E*)-(1*S*, 3*R*, 4*R*)-3,4; 15,17-diepoxycembra-7,11-diene (0.83 g) (21–24, 31). The more polar portion of the lipids was fractionated roughly into fractions A through O on the basis of the tlc analyses. Repeated column chromatography of fraction O (3.40 g) on silica gel (100 g) with 10% EtOAc in hexane gave four fractions. Purification of fraction II (287 mg) by hplc (Zorbax C-8 ODS silica gel with 35% H_2O in MeOH) afforded 13.1 mg of 8-epi-uprolide-B acetate (**9**). Fraction III (1.38 g) was purified by hplc (Partisil 10 silica gel using 10% isopropanol in hexane) to give pure uprolide-B acetate (**6**) (9.1 mg) and uprolide-C acetate (**12**) (15.9 mg). Fraction IV (1.04 g) was purified by reversed-phase column chromatography with ODS silica gel using a 80:20 mixture of MeOH–H_2O to give pure 8-epi-uprolide-B (**8**) (11.3 mg), followed by a mixture that, after subsequent separation by hplc (Partisil 10 silica gel with 15% isopropanol in hexane), afforded uprolide-B (**5**) (53.7 mg) and uprolide-C (**11**) (33.3 mg).

After filtration and concentration, the $CHCl_3$ extract yielded 39.16 g of a dark-orange oily residue. This residue was dissolved in toluene and then was fractionated by size exclusion chromatography on a Bio-Beads SX-2 column using toluene as eluent. The combined terpenoid-rich fraction (36.06 g) was chromatographed over a silica gel column (850 g) with 20% EtOAc in hexane and separated into seven major fractions on the basis of tlc analyses. Repeated column chromatography of fraction 7 (2.86 g) on silica gel (100 g) with 40% EtOAc in hexane gave fractions I through IX. Fraction III (340 mg) was subsequently purified by hplc (Zorbax C-8 ODS silica gel with MeOH–H_2O (55:45)) to give pure uprolide-B diacetate (**7**) (23 mg), 8-epi-uprolide-B diacetate (**10**) (24 mg), uprolide-C diacetate (**13**) (35 mg), and a fraction that was subsequently purified by hplc (Partisil 10 silica gel with 10% isopropanol in hexane) to yield pure 7-epi-uprolide-C diacetate (**15**) (34 mg) and eupalmerin (**2**) (23 mg). Fraction VII (270 mg) was purified by hplc (Partisil 10 silica gel with 13% isopropanol in hexane), yielding 36 mg of 8-epi-uprolide-A acetate (**4**). Fraction V (208 mg) was also purified by hplc (Zorbax C-8 ODS silica gel with MeOH–H_2O (60:40)), yielding some more 8-epi-uprolide-B acetate (**9**) (11 mg). Fraction IX (575 mg) was chromatographed by hplc (Partisil 10 silica gel with 25% isopropanol in hexane) to give pure uprolide-A acetate (**3**) (110 mg) and 7-epi-uprolide-C acetate (**14**) (55 mg).

Uprolide-A acetate (3): White crystalline solid: mp 210.0–211.0°C; $[\alpha]_D^{25}$ +29.23 (*c* 4.63, $CHCl_3$); ir (neat): 3550, 2970, 2954, 2918, 2889, 1766, 1733, 1385, 1253, 1116, 982, 968, 939 cm^{-1}; uv λ_{max} (MeOH): 212 nm (ε 25 300); ^1H nmr (300 MHz, $CDCl_3$) see Table 1; ^{13}C nmr (75 MHz, $CDCl_3$) see Table 4; hrfabms *m/z* $[M + H]^+$ (rel. %): 393.22750 (100%) ($C_{22}H_{33}O_6$ requires 393.22779).

8-Epi-uprolide-A acetate (4): Colorless oil; $[\alpha]_D^{25}$ +12.03 (*c* 9.12, $CHCl_3$); ir (neat): 3552, 2984, 2911, 2888, 1770, 1740, 1456, 1370, 1261, 1228, 1099, 1028, 981, 968 cm^{-1}; uv λ_{max} (MeOH): 208 nm (ε 23 400); ^1H nmr (300 MHz, $CDCl_3$) see Table 1; ^{13}C nmr (75 MHz, $CDCl_3$) see Table 4; hreims *m/z* $[M - H_2O]^+$ (rel. %): 374.20620 (0.25%) ($C_{22}H_{30}O_5$ requires 374.20940), 332(1.2), 309(1.3), 271(1.4), 249(4.0), 196(5.8), 111(34.9), 81(13.6).

Can. J. Chem. Downloaded from www.nrcresearchpress.com by 65.111.164.53 on 09/08/12
For personal use only.

Uprolide-B (5): Colorless oil: $[\alpha]_D^{25}$ −22.3 (*c* 5.4, MeOH); ir (neat): 3405, 2955, 2873, 1755, 1463, 1268, 1117, 1051, 984, 822, 754 cm^{-1}; uv λ_{max} (MeOH): 212 nm (ϵ 22 800); ^1H nmr (300 MHz, $CDCl_3$) see Table 1; ^{13}C nmr (75 MHz, $CDCl_3$) see Table 4; hrfabms *m/z* $[M + Na]^+$ (rel. %): 373.19930 (100%) ($C_{20}H_{30}O_5Na$ requires 373.19917).

Uprolide-B acetate (6): Colorless oil: $[\alpha]_D^{25}$ +30.0 (*c* 4.9, $CHCl_3$); ir (neat): 3380, 2939, 2875, 1764, 1740, 1457, 1380, 1231, 1027 cm^{-1}; uv λ_{max} (MeOH): 214 nm (ϵ 9825); ^1H nmr (300 MHz, $CDCl_3$) see Table 1; ^{13}C-nmr (75 MHz, $CDCl_3$) see Table 4; lrfabms *m/z* $[M + Na]^+$ (rel. %): 415(5.0%) ($C_{22}H_{32}O_6Na$ requires 415), 397 (4.8), 387(5.2), 355 (6.3), 325(19.0), 281(27.3), 207(51.0), 154(37.0), 147(100), 136(66).

Uprolide-B diacetate (7): Colorless semisolid: $[\alpha]_D^{25}$ +9.3 (*c* 2.7, $CHCl_3$); ir (neat): 2989, 2874, 1776, 1738, 1371, 1261, 1238, 1096, 1027 cm^{-1}; uv λ_{max} (MeOH): 210 nm (ϵ 7800); ^1H nmr (300 MHz, $CDCl_3$) see Table 1; ^{13}C nmr (75 MHz, $CDCl_3$) see Table 4; hreims *m/z* $[M - C_2H_2O]^+$ (rel. %): 392.22073 (17.7%) ($C_{22}H_{32}O_6$ requires 392.21996), 374(19.1), 332(10.3), 314(13.3), 257(13.5), 177(16.1), 159(19.1), 93(100), 79(64.5).

8-Epi-uprolide-B (8): Colorless oil: $[\alpha]_D^{25}$ −17.70 (*c* 2.26, $CHCl_3$); ir (neat): 3388, 2961, 2934, 2877, 1755, 1667, 1346, 1262, 1114, 1048, 981, 802, 756 cm^{-1}; uv λ_{max} (MeOH): 216 nm (ϵ 19 280); ^1H nmr (300 MHz, $CDCl_3$) see Table 2; ^{13}C nmr (75 MHz, $CDCl_3$) see Table 5; hrfabms *m/z* $[M + Na]^+$ (rel. %): 373.19840 (100%) ($C_{20}H_{30}O_5Na$ requires 373.19917).

8-Epi-uprolide-B acetate (9): Colorless oil: $[\alpha]_D^{25}$ −33.0 (*c* 7.8, $CHCl_3$); ir (neat): 3392, 2955, 2930, 2872, 2855, 1747, 1661, 1455, 1374, 1284, 1148, 1027, 992, 884, 815, 756 cm^{-1}; uv λ_{max} (MeOH): 212 nm (ϵ 18 355); ^1H nmr (300 MHz, $CDCl_3$) see Table 2; ^{13}C nmr (75 MHz, $CDCl_3$) see Table 5; hrfabms *m/z* $[M + Na]^+$ (rel. %): 415.21160 (100%) ($C_{22}H_{32}O_6Na$ requires 415.20973).

8-Epi-uprolide-B diacetate (10): Colorless oil: $[\alpha]_D^{25}$ −5.2 (*c* 5.6, $CHCl_3$); ir (neat): 2963, 2938, 2878, 1775, 1741, 1480, 1371, 1260, 1233, 1108, 1029, 982 cm^{-1}; uv λ_{max} (MeOH): 210 nm (ϵ 9300); ^1H nmr (300 MHz, $CDCl_3$) see Table 2; ^{13}C nmr (75 MHz, $CDCl_3$) see Table 5; hrfabms *m/z* $[M + Na]^+$ (rel. %): 457.22090 (100%) ($C_{24}H_{34}O_7Na$ requires 457.22029).

Uprolide-C (11): Colorless oil: $[\alpha]_D^{25}$ −11.38 (*c* 1.93, MeOH); ir (neat): 3433, 2962, 2933, 2864, 1740, 1666, 1643, 1274, 1168, 1115, 1079 cm^{-1}; uv λ_{max} (MeOH): 212 nm (ϵ 9800); ^1H nmr (300 MHz, $CDCl_3$) see Table 2; ^{13}C nmr (75 MHz, $CDCl_3$/CD_3OD) see Table 5; hrfabms *m/z* $[M + Li]^+$ (rel. %): 357.22510 (100%) ($C_{20}H_{30}O_5Li$ requires 357.22544).

Uprolide-C acetate (12): Colorless oil: $[\alpha]_D^{25}$ +7.22 (*c* 7.0, $CHCl_3$); ir (neat): 3405, 2964, 2920, 2870, 1765, 1741, 1667, 1373, 1260, 1234, 1095, 1028 cm^{-1}; uv λ_{max} ($CHCl_3$): 242 nm (ϵ 3536); ^1H nmr (300 MHz, $CDCl_3$) see Table 2; ^{13}C nmr (75 MHz, $CDCl_3$) see Table 5; lrfabms *m/z* $[M + Na]^+$ (rel. %): 415 (2.0%) ($C_{22}H_{32}O_6Na$ requires 415), 397(2.8), 383(3.2), 355(6.1), 281(25.0), 221(32.5), 207(44.0), 147(100), 133(25.5).

Uprolide-C diacetate (13): Colorless semisolid: $[\alpha]_D^{25}$ +7.22 (*c* 7.1, $CHCl_3$); ir (neat): 2962, 2928, 2873, 1771, 1738, 1372, 1260, 1239, 1095, 1023, 920, 863, 800 cm^{-1}; uv λ_{max} ($CHCl_3$): 244 nm (ϵ 200); ^1H nmr (300 MHz, $CDCl_3$) see Table 3; ^{13}C nmr (75 MHz, $CDCl_3$) see Table 6; hrfabms *m/z* $[M + H]^+$ (rel. %): 435.23790 (100%) ($C_{24}H_{35}O_7$ requires 435.23835).

7-Epi-uprolide-C acetate (14): Colorless oil: $[\alpha]_D^{25}$ +19.02 (*c* 5.1, $CHCl_3$); ir (neat): 3493, 2945, 2871, 1775, 1741, 1372, 1259, 1233, 1096, 1030, 754 cm^{-1}; uv λ_{max} (MeOH): 212 nm (ϵ 9800); ^1H nmr (300 MHz, $CDCl_3$) see Table 3; ^{13}C nmr (75 MHz, $CDCl_3$) see Table 6; hrfabms *m/z* $[M + Na]^+$ (rel. %): 415.20810 (100%) ($C_{22}H_{32}O_6Na$ requires 415.20973).

7-Epi-uprolide-C diacetate (15): Colorless semisolid: $[\alpha]_D^{25}$ +17.51 (*c* 8.3, $CHCl_3$); ir (neat): 2979, 2950, 2875, 1779, 1742, 1372, 1237, 1101, 1029 cm^{-1}; uv λ_{max} (MeOH): 208 nm (ϵ 10 500); ^1H nmr (300 MHz, $CDCl_3$) see Table 3; ^{13}C nmr (75 MHz, $CDCl_3$) see Table 6; hreims *m/z* $[M - C_2H_2O]^+$ (rel. %): 392.21976 (5.1%) ($C_{22}H_{32}O_6$ requires 392.21996), 374(9.5), 332(11.5), 314(14.2), 286(5.7), 179(22.5), 159(28.2), 93(98.0), 55(100).

Acetylation of uprolide-C (11)

A solution of uprolide-C (5 mg, 0.014 mmol) in a mixture of acetic anhydride (2.0 mL) and pyridine (1.0 mL) was stirred at 25°C for 14 h. Excess reagents were removed by rotaevaporation and, after concentration and storage in vacuo, we obtained 8 mg of a homogeneous compound whose retention time (by tlc) and nmr spectra (^1H and ^{13}C) conclusively identified it as uprolide-A acetate (**3**).

Acetylation of 7-epi-uprolide-C acetate (14)

A solution of 7-epi-uprolide-C acetate (12 mg, 0.031 mmol) in a mixture of acetic anhydride (3.0 mL) and pyridine (1.0 mL) was stirred at 25°C for 12 h. Excess reagents were removed by rotaevaporation and the residue obtained was chromatographed over a short column of silica gel (80:20 hexane–EtOAc). After concentration in vacuo 13 mg of pure 7-epi-uprolide-C diacetate (**15**) were obtained.

X-ray diffraction study of uprolide-A acetate (3)[7]

X-ray diffraction data were collected on an Enraf–Nonius CAD4 diffractometer using CuKα radiation (λ = 1.540 56 Å). The structure was solved by direct methods and completed by successive Fourier calculations. The structure was refined by full-matrix least-squares methods, with anisotropic thermal parameters for all non-H atoms. Following initial refinement, H atoms were located from a difference Fourier map. HO8 was refined with a fixed isotropic thermal parameter and all remaining H atoms were included in the final model at calculated positions, riding on the connected atoms. All calculations were performed with the NRCVAX program package (32). Details of the X-ray experiment, crystal data, data collection, reduction, and refinement are given in Table 8 and the atomic parameters are given in Table 9.

Acknowledgments

The assistance of Mr. Anthony Sostre in specimen collection

[7] Atomic coordinates and other material required for X-ray structure validation may be purchased from: The Depository of Unpublished Data, Document Delivery, CISTI, National Research Council Canada, Ottawa, Canada K1A 0S2.

Tables of atomic coordinates and of bond lengths and angles have also been deposited with the Cambridge Crystallographic Data Centre, and can be obtained on request from the Director, Cambridge Crystallographic Data Centre, University Chemical Laboratory, 12 Union Road, Cambridge, CB2 1EZ, U.K.

Structure factor amplitudes are no longer being deposited and may be obtained directly from the author.

Can. J. Chem. Downloaded from www.nrcresearchpress.com by 65.111.164.53 on 09/08/12
For personal use only.

Table 8. Crystal data, structure determination, and refinement data for uprolide-A acetate (**3**).

Formula	$C_{22}H_{32}O_6$
M(amu)	392.49
Space group	$P2_12_12_1$
a(Å)	9.6120(10)
b(Å)	10.9922(4)
c(Å)	21.0044(9)
U(Å^3)	2219.3(3)
Z	4
D_c(g cm^{-3})	1.175
μ(cm^{-1})	0.65
F(000)	848
Crystal size (mm)	0.05 × 0.05 × 0.40
Radiation CuKα, graphite monochromator	λ = 1.540 56 Å
Diffractometer	Enraf–Nonius CAD4
Orienting reflections, range	25, 30° < θ < 40°
Temperature (°C)	22 ± 1
Scan method	ω–2θ
Data collection range	2.0° < 2θ < 130°
No. data measured	3381
No. of unique data	2530
R_i (data averaging)	0.024
No. of observed data ($I > 1.8\sigma(I)$), N	1848
No. of parameters, P	257
R^a	5.1%
R_w^b	5.2%
S, goodness-of-fit^c	1.34
Max. shift/error, final	0.032
Largest positive peak (e/Å^3)	0.18
Largest negative hole (e/Å^3)	−0.20

$^aR = \Sigma(|F_o| - |F_c|)/\Sigma|F_o|$.
$^bR_w = \{\Sigma w(|F_o| - |F_c|)^2/\Sigma w|F_o|^2\}^{1/2}$; $w = 1/[(\sigma F_o)^2 + 0.0005*F_o^2]$.
$^cS = [\Sigma w(|F_o| - |F_c|)^2/(N - P)]^{1/2}$.

Table 9. Atomic Parameters x, y, z and B_{eq}. ESDs refer to the last digit printed.

	x	y	z	B_{eq}
O3	0.5699(4)	0.8960(3)	0.08762(14)	4.3(2)
O8	0.6363(4)	1.3910(3)	0.2573(2)	5.0(2)
O13	0.0213(3)	0.9872(2)	0.11049(12)	3.03(13)
O14	0.0680(4)	1.1923(3)	0.03969(14)	4.1(2)
O16	−0.0791(4)	1.1531(3)	−0.0400(2)	5.4(2)
O21	0.1098(4)	0.8329(3)	0.1679(2)	5.0(2)
C1	0.2459(5)	1.0469(4)	0.0197(2)	3.6(2)
C2	0.3311(5)	0.9388(4)	0.0418(2)	3.7(2)
C3	0.4540(5)	0.9790(4)	0.0802(2)	3.5(2)
C4	0.5923(5)	1.0103(4)	0.0539(2)	3.5(2)
C5	0.6851(5)	1.1008(4)	0.0882(2)	3.8(2)
C6	0.6440(5)	1.1315(4)	0.1555(2)	3.6(2)
C7	0.6131(6)	1.2410(4)	0.1755(2)	3.6(2)
C8	0.5631(6)	1.2801(4)	0.2404(2)	3.6(2)
C9	0.4096(6)	1.3194(4)	0.2363(2)	4.1(2)
C10	0.3085(6)	1.2178(4)	0.2211(2)	4.0(2)
C11	0.1681(6)	1.2621(4)	0.1975(2)	4.0(2)
C12	0.0639(5)	1.1602(4)	0.1797(2)	3.7(2)
C13	0.1293(5)	1.0716(3)	0.1315(2)	2.9(2)
C14	0.1850(5)	1.1313(4)	0.0717(2)	3.0(2)
C15	0.1197(6)	1.0226(4)	−0.0206(2)	3.9(2)
C16	0.0222(6)	1.1255(5)	−0.0104(2)	4.1(3)
C17	0.0906(7)	0.9311(5)	−0.0588(2)	6.2(3)
C18	0.6245(6)	0.9937(5)	−0.0156(2)	5.0(3)
C19	0.5848(6)	1.1854(4)	0.2924(2)	4.5(2)
C20	0.0104(6)	1.0907(4)	0.2380(2)	4.9(3)
C21	0.0221(5)	0.8721(4)	0.1318(2)	3.5(2)
C22	−0.0954(6)	0.8011(4)	0.1052(2)	4.7(3)

B_{eq} is the mean of the principal axes of the thermal ellipsoid.

is gratefully acknowledged. We extend our sincere appreciation to the crew of the R/V Isla Magueyes for their assistance during a trip to Mona Island, Puerto Rico, and to Dr. Louis R. Barrows from the University of Utah Center for Drug Discovery for cytotoxicity assays on human cells. The hreims, hrfabms, and lrfabms spectral determinations were performed by the Midwest Center for Mass Spectrometry, a National Science Foundation Regional Facility (Grant No. CHE8211164). This study was supported in part by the National Science Foundation EPSCoR Program (Grant No. R118610677), the NIH-MBRS Program (Grant No. S06RR08102-17), the NSF-MRCE Program (Grant No. R11-8802961), and the University of Puerto Rico FIPI Program.

References

1. D.J. Faulkner. Nat Prod. Rep. **11**, 355 (1994), and previous papers in this series.
2. L.S. Ciereszko. Laporan — Lambaga Penelitian Hasil Hulan (Marine Research in Indonesia), **17**, 113 (1977).
3. L.S. Ciereszko, D.H. Sifford, and A.J. Weinheimer. Ann. N.Y. Acad. Sci. **90**, 917 (1960).
4. L.S. Ciereszko, P.H. Odense, and R.W. Schmidt. Ann. N.Y. Acad. Sci. **90**, 920 (1960).
5. L.S. Ciereszko. Trans. N.Y. Acad. Sci. **24**, 502 (1962).
6. A.J. Weinheimer, F.J. Schmitz, and L.S. Ciereszko. *In* Drugs Sea, Trans. Symp. *Edited by* H.D. Freudenthal. Marine Technology Society, Washington, D.C. 1968. p. 135.
7. A.J. Weinheimer, R.E. Middlebrook, J.O. Bledsoe, Jr., W.E. Marsico, and T.K.B. Karns. J. Chem. Soc. Chem. Commun. 384 (1968).
8. M.B. Hossain, A.F. Nicholas, and D. Van der Helm. J. Chem. Soc. Chem. Commun. 385 (1968).
9. A.J. Weinheimer, W.W. Youngblood, P.H. Washecheck, T.K.B. Karns, and L.S. Ciereszko. Tetrahedron Lett. 497 (1970).
10. L.S. Ciereszko and T.K.B. Karns. *In* Biology and geology of coral reef. *Edited by* O.A. Jones and R. Endean. Academic Press, New York. 1973. p. 183.
11. S.E. Ealick, D. Van der Helm, and A.J. Weinheimer. Acta Crystallogr. Sect. B: Struct. Crystallogr. Cryst. Chem. **B31**, 1618 (1975).
12. D. Van der Helm, E.L. Enwall, A.J. Weinheimer, T.K.B. Karns, and L.S. Ciereszko. Acta Crystallogr. Sect. B: Struct. Crystallogr. Cryst. Chem. **B32**, 1558 (1976).
13. W. Fenical. *In* Marine natural products chemistry, chemical and biological perspectives. Vol II. *Edited by* P.J. Scheuer. Academic Press, New York. 1978. p. 173.

14. B. Tursch, J.C. Braekman, D. Daloze, and M. Kaisin. *In* Marine natural products chemistry, chemical and biological perspectives. Vol II. *Edited by* P.J. Scheuer. Academic Press, New York. 1978. p. 247.
15. A.J. Weinheimer, C.W.J. Chang, and J.A. Matson. Fortschr. Chem. Org. Naturst. **36**, 285 (1979).
16. C.Y. Chang, L.S. Ciereszko, M.B. Hossain, and D. Van der Helm. Acta Crystallogr. Sect. B: Struct. Crystallogr. Cryst. Chem. **B36**, 731 (1980).
17. A.J. Weinheimer, J.A. Matson, M. Poling, and D. Van der Helm. Acta Crystallogr. Sect. B: Struct. Crystallogr. Cryst. Chem. **B38**, 580 (1982).
18. Y. Gopichand, L.S. Ciereszko, F.J. Schmitz, D. Switzner, A. Rahman, M.B. Hossain, and D. Van der Helm. J. Nat. Prod. **47**, 607 (1984).
19. P.K.S. Gupta, M.B. Hossain, and D. Van der Helm. Acta Crystallogr. Sect. C: Cryst. Struct. Commun. **C42**, 434 (1986).
20. A.D. Rodríguez and H. Dhasmana. J. Nat. Prod. **56**, 564 (1993).
21. J.J. Morales, J.R. Espina, and A.D. Rodríguez. Tetrahedron, **46**, 5889 (1990).
22. L.A. Fontán, W.Y. Yoshida, and A.D. Rodríguez. J. Org. Chem. **55**, 4956 (1990).
23. L.A. Fontán and A.D. Rodríguez. J. Nat. Prod. **54**, 298 (1991).
24. A.D. Rodríguez, Y. Li, H. Dhasmana, and C.L. Barnes. J. Nat. Prod. **56**, 1101 (1993).
25. M. Kobayashi. Chem. Pharm. Bull. **36**, 488 (1988).
26. R.J. Abraham and P. Loftus. Proton and carbon-13 NMR spectroscopy. Heyden & Son Ltd., Philadelphia. 1980. p. 41.
27. L.M. Jackman and S. Sternhell. Applications of nuclear magnetic resonance spectroscopy in organic chemistry. Vol. 10. 2nd ed. Pergamon Press, New York. 1978. pp. 280–304.
28. M. Kobayashi, K. Kondo, K. Osabe, and H. Mitsuhashi. Chem. Pharm. Bull. **36**, 2331 (1988).
29. M. Kobayashi and K. Osabe. Chem. Pharm. Bull. **37**, 631 (1989).
30. M. Kobayashi and K. Osabe. Chem. Pharm. Bull. **37**, 1192 (1989).
31. A.D. Rodríguez and N. Martínez. Experientia, **49**, 179 (1993).
32. E.J. Gabe, Y. Le Page, J.-P. Charland, F.L. Lee, and P.S. White. J. Appl. Crystallogr. **22**, 348 (1989).

Can. J. Chem. Downloaded from www.nrcresearchpress.com by 65.111.164.53 on 09/08/12
For personal use only.

Taxus canadensis taxanes: structures and stereochemistry[1]

Lolita O. Zamir, Maria E. Nedea, Zhen-Hua Zhou, Sophie Bélair, Gaétan Caron, Françoise Sauriol, Emile Jacqmain, France I. Jean, François-X. Garneau, and Orval Mamer

Abstract: The structures and stereochemistry of 14 taxanes isolated from *Taxus canadensis* have been rigorously established by high-resolution NMR techniques and mass spectrometry. *Taxus canadensis* is the only yew that accumulates 9-dihydro-13-acetylbaccatin III (also called 7,9-deacetylbaccatin VI) as the most abundant taxane. Five 9-dihydrotaxanes derived from the Canadian yew are novel natural products not reported in the needles of other species of yew (**8–11**, **14**, Fig. 1).

Key words: *Taxus canadensis*, Taxaceae, taxanes, 9-dihydro-13-acetylbaccatin III, taxol.

Résumé : Les structures et la stéréochimie de 14 taxanes isolés du *Taxus canadensis* ont été rigoureusement prouvées à l'aide d'expériences à haute résolution de RMN et SM. *Taxus canadensis* est le seul if accumulant la 9-dihydro-13-acétylbaccatine III (aussi appelée 7,9-désacétylbaccatine VI) comme taxane majoritaire. Cinq 9-dihydrotaxanes dérivés de l'if du Canada sont des nouveaux produits naturels qui n'ont pas été découverts dans les aiguilles d'autres ifs (**8–11**, **14**, Fig. 1).

Mots clés : *Taxus canadensis*, Taxaceae, taxanes, 9-dihydro-13-acétylbaccatine III, taxol.

Introduction

Taxol (**1**, Fig. 1), the anticancer drug of the 1990s[3] was originally extracted from the bark of the Pacific yew, *Taxus brevifolia* (2). Two elegant total syntheses of taxol were recently reported (3, 4). Another very important drug, taxotere (which seems to be more active than taxol) (5), was derived by semi-synthesis: the natural product 10-deacetyl baccatin III (which is abundant in *Taxus baccata* (6, 7) and is very similar to the diterpenoid core of taxol) was chemically coupled at C-13 with a synthetic side chain. There are many reported syntheses of the side chain of taxol (8) and various derivatives are being made and tested.

In this publication we have focused on the Canadian yew, which differs from other yews not only in its physical appearance (it is a ramping small evergreen bush very common in Quebec), but also in its composition. *Taxus canadensis* does produce taxol, cephalomannine, and 10-deacetylbaccatin III (**1**, **4**, **5**, Fig. 1), which are common to all yews, as demonstrated by a major work of the National Cancer Institute research group (9). On the other hand, in a preliminary communication (1), we have shown that *T. canadensis* accumulates a taxane that differs from the diterpenoid core of taxol by a hydroxyl group at C-9, instead of a ketone: 9-dihydro-13-acetylbaccatin III (**7**, Fig. 1). This metabolite, which was reported in trace amounts in the bark of *Taxus chinensis* (10), is at least three to five times more abundant than taxol in the needles of *T. canadensis*. The structure that we proposed for this 9-dihydrotaxane, on the basis of NMR and MS data (**7**, Fig. 1), was subsequently confirmed by X-ray (11). This was an interesting finding, since the successful attachment of the taxol side chain by the Abbott group (12) led to in vivo anticancer activity. Further investigations in our laboratory with *T. canadensis* needles enabled us to rigorously characterize 14 taxanes. Five of these taxanes are new natural products that have not been reported in the needles of other yews (**8**, **9**, **10**, **11**, **14**, Fig. 1).

Received September 9, 1994.

L.O. Zamir,[2] M. E. Nedea, Z.-H. Zhou, S. Bélair, and G. Caron. Université du Québec, Institut Armand-Frappier, Centre de recherche en microbiologie appliquée, 531 boul. des Prairies, Laval, QC H7N 4Z3, Canada
F. Sauriol. Department of Chemistry, McGill University, 801 Sherbrooke Street West, Montreal, QC H3A 2K6, Canada.
E. Jacqmain. Jardin Botanique de Montreal, 4101 Sherbrooke Street Est, Montréal, QC H1X 2B2, Canada.
F.I. Jean and F.-X. Garneau. Université du Québec à Chicoutimi, 555 boul. de l'Université, Chicoutimi, QC G7H 2B1, Canada.
O. Mamer. Biomedical Mass Spectrometry Unit, McGill University, 1130 Pine Ave. West, Montreal, QC H3A 1A3, Canada.

[1] Presented in part as a communication (see ref. 1).
[2] Author to whom correspondence may be addressed. Telephone: (514) 687-5010, ext. 4260. Fax: (514) 686-5501.
[3] Taxol was recently approved in the U.S. and Canada for treatment of ovarian cancers.

Results and Discussion

Isolation and purification of taxanes

The discovery of a major taxane, 9-dihydro-13-acetylbaccatin III (**7**, Fig. 1), encouraged us to devise a method whereby this compound and taxol eluted in the same chromatographic fraction and could be easily separated. The choice of solvents and chromatographic techniques enabled us to obtain 9-dihydro-13-acetylbaccatin III at an R_t of 27.34 min, whereas taxol is obtained at R_t = 33.3 min on HPLC. Several steps of reverse-phase HPLC were usually needed to obtain highly pure tax-

Can. J. Chem. Downloaded from www.nrcresearchpress.com by 65.111.164.53 on 09/08/12
For personal use only.

Fig. 1. *Taxus canadensis* metabolites. Metabolites **2**, **3**, **6**, and **12** common to other *Taxus* species have been identified for the first time in *T. canadensis*. Metabolites **7**, **8**, **9**, **10**, **11**, **14** have not been found in the needles of other Taxus species.

(a) 9-Keto-Taxanes

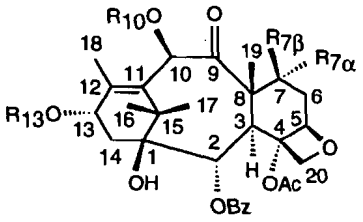

1 Taxol, R_{10}=Ac; $R_{7\beta}$=OH; $R_{7\alpha}$=H; R_{13}=PhCONHCH(Ph)CH(OH)CO

2 10-Deacetyltaxol, R_{10}=$R_{7\alpha}$=H; $R_{7\beta}$=OH; R_{13}=PhCONHCH(Ph)CH(OH)CO

3 7-Epitaxol, R_{10}=Ac; $R_{7\beta}$=H; $R_{7\alpha}$=OH R_{13}=PhCONHCH(Ph)CH(OH)CO

4 Cephalomannine, R_{10}=Ac; $R_{7\beta}$=OH; $R_{7\alpha}$=H; R_{13}=CH_3CH:$C(CH_3)CONHCH(Ph)CH(OH)CO$

5 10-Deacetylbaccatin III, R_{10}=$R_{7\alpha}$=R_{13}=H; $R_{7\beta}$=OH

6 7-Epi-10-Deacetylbaccatin III (10-Deacetyl-baccatin V), R_{10}=$R_{7\beta}$=R_{13}=H; $R_{7\alpha}$=OH

(b) 9-Dihydrotaxanes

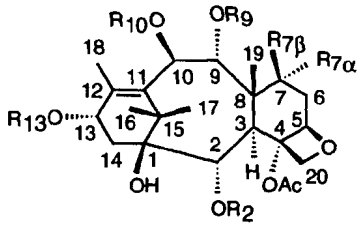

7 9-Dihydro-13-acetylbaccatin III R_2=Bz; $R_{7\beta}$=OH; R_9=$R_{7\alpha}$=H; R_{10}=R_{13}=Ac

8 7,9-Deacetylbaccatin IV R_2=R_{10}=R_{13}=Ac; $R_{7\beta}$=OH; R_9=$R_{7\alpha}$=H

9 10-Hydroxyacetylbaccatin VI R_2=Bz; R_9=R_{13}=Ac $R_{7\beta}$=OAc; $R_{7\alpha}$=H; R_{10}=$COCH_2OH$

10, 11 7-and 7Epi-9,10-Deacetylbaccatin VI R_2=Bz; R_7=β- and α-OH; R_9=R_{10}=H; R_{13}=Ac

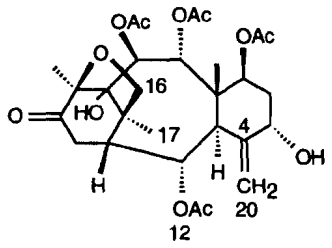

5-Decinnamate taxagifine

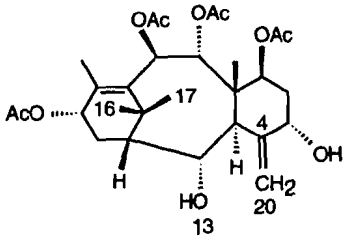

2-Deacetyl-5-Decinnamoyl taxinine J

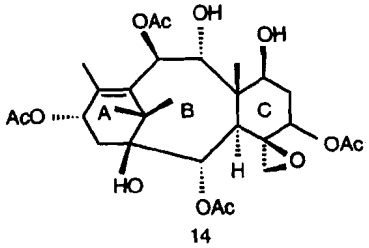

1β-Hydroxy-7, 9-Deacetyl baccatin I

anes. Purity of these taxanes was assessed by the formation of symmetrical peaks under three different gradient systems.

Taxanes isolated from *Taxus canadensis*

The structural characterizations of the taxanes were proven by high-field NMR techniques. High-resolution mass spectrometry confirmed the empirical formulas. Known taxanes were compared to the literature and spiked with standards for which we gratefully acknowledge the assistance of Ms Nancita Lomez and Dr. Kathleen H. Groover (National Cancer Institute, Maryland, U.S.A.). *Taxus canadensis* differs from other species of taxus by the presence of large amounts of the taxane

Can. J. Chem. Downloaded from www.nrcresearchpress.com by 65.111.164.53 on 09/08/12
For personal use only.

Table 1. Proton NMR, carbon NMR, and NOESY analyses of 7-epitaxol (metabolite **3**) isolated from *Taxus canadensis*. The ^{13}C assignments have been extracted from HMQC and HMBC. The stereochemistry was determined by NOESY.

Position	Parts/million	^1H NMR		NMR, δ	NOESY
		Multiplicity	*J*(Hz)		
				ppm	
1	---	---	---	78.93	
2	5.75	d	7.8	75.18	H-20, H-3, Me-17, Me-19
3	3.92	br d	7.3	40.19	H-10, H-2, Me-18, OH-7, Ac-4
4	---	---	---	81.83	
5	4.91	dd	9.3; 3.4	82.51	H-6, H-20, OH-7
6	2.29; 2.23	m	---	35.11	
7	3.693	br dd	10.2; 3.4	75.46	OH-7, H-6, Me-19, H-10
	4.68	d (OH-7)	11.7	---	H-5, H-3, H-7, Ac-4, Me-18
8	---	---	---	57.39	
9	---	---	---	207.38	
10	6.78	s	---	78.00	H-3, Me-18, OH-7
11	---	---	---	133.21	
12	---	---	---	139.43	
13	6.23	br t	8.8	72.07	Me-16
14	2.41	m		35.96	
	2.33			---	
15	---	---	---	42.47	
16	1.19	---	---	25.80	H-14B, H-13
17	1.14	---	---	21.00	Me-19, H-2, H-10
18	1.79	s	---	14.51	H-10, OH-7, H-3
19	1.66	s		15.92	H-7, H-20, H-2, Me-17
20	4.38	s	---	77.44	H-2, H-13, Me-19
NH	6.99	d	9.0		
H-3'	5.81	dd	9.3; 2.4	54.58	Ac-4, H-2', NH, Ph
H-2'	4.80	d	2.4	72.92	Ph, NH, H-3', Ac-4, Me-18
Ac-4	2.50	s		22.41	
Ac-10	2.19	s		20.72	
13(C=O)				172.57	
NH(C=O)				167.19	
Bz-2	8.17			130.20	
Bz-NH-3'	7.72			127.20	

9-dihydro-13-acetylbaccatin III (**7**, Fig. 1). We have therefore chosen to use the nature of the oxygenation at C-9 as the classification criteria.

A. 9-Keto-taxanes

We found taxol (**1**, Fig. 1), cephalomannine (**4**, Fig. 1), and 10-deacetylbaccatin III (**5**, Fig. 1) in *T. canadensis* needles.[4] We identified 10-deacetyltaxol (**2**, Fig. 1), 7-epitaxol (**3**, Fig. 1), and 7-epi-10-deacetylbaccatin III (**6**, Fig. 1) for the first time in the needles of the Canadian yew. These metabolites are known natural products isolated in other taxus species (13). The high-resolution 2D NMR analyses for 7-epitaxol and 7-epi-10-deacetylbaccatin III (**3** and **6**, Fig. 1) are shown in Tables 1 and 2.

B. 9-Dihydrotaxanes (7–14 Fig. 1)

Taxus canadensis is the only species accumulating 9-dihydro-13-acetylbaccatin III (**7**, Fig. 1) in its needles in quantities 3–5 times that of taxol. Structures **7** and **14** were identified subsequently as minor metabolites in the bark of *Taxus chinensis* (10) but were never found in yew needles. The taxane **12** was described in a Chinese publication (14) and compound **13** was also found in *Austrotaxus spicata* (15). The derivatives **8–11** have not been found in other taxus species. We can subdivide this group of 9-dihydrotaxanes into those with an oxetane ring (**7–11**, Fig. 1) and those with a pre-oxetane ring (double bond or C-4 epoxide such as **12–14** (Fig. 1). The initial characterization (1) of the abundant taxane (**7**, Fig. 1) involved 300 MHz NMR analysis and high-resolution mass spectrometry. The structure was confirmed by X-ray analysis (11). The 500 MHz NMR analyses of the new natural products are shown in Tables 3–7. The data for metabolite **7** are included for comparison. Compound **8** is very similar to the major metabolite **7**, the only difference being a substituent at C-2: an acetate replaces the benzoate. Compound **9** has a benzoyl at C-2 and a hydroxyl group on the acetyl at C-10 but otherwise is completely acetylated. Compounds **10** and **11** are stereoisomers differing in the stereochemistry at C-7. These compounds are the least acetylated, having three hydroxyl groups at C-7, C-9, C-10, a benzoyl at C-2, and an acetyl at C-13. The natural co-occurrence of these dihydrotaxanes (**7–11**, Fig. 1) suggests a biosynthetic order of acetylation, the first hydroxyl to be esterified being C-13 (and (or) C-4), followed by the one at C-2, then the other at C-10. The additional 9-dihydrotaxanes shown in Fig. 1 isolated for the first time in *T. canadensis* (1) have pre-oxetane structures on ring C. In compound **12**, ring

[4] We isolated a taxane that we characterized as 1-acetyl-10-deacetylbaccatin III (same structure as **5**, Fig. 1, but with OAc at C-1). The 500 MHz NMR and high-resolution mass spectral data were in agreement with the structure proposed. Unfortunately, we were only able to isolate this compound once!

Can. J. Chem. Downloaded from www.nrcresearchpress.com by 65.111.164.53 on 09/08/12
For personal use only.

Table 2. Proton NMR, carbon NMR, and NOESY analyses of 7-epi-10-deacetylbaccatin III (metabolite **6**) isolated from *Taxus canadensis*. The ^{13}C assignments have been extracted from HMQC and HMBC. The stereochemistry was determined by NOESY.

Position	Parts/million	^1H NMR		^{13}C NMR, δ	NOESY
		Multiplicity	*J*(Hz)	ppm	
1	---	---		---	
2	5.71	d	7.3	75.08	H-3, Me-17, Me-19, H-20B
3	4.05	d	7.3	40.37	H-2, H-10, H-6A/14A, Me-18
4	---	---	---	---	
5	4.94	dd	9.5; 3.7	82.37	H-6B
6A	2.37	m		38.33	
6B	2.23	o			
7	3.66	ddd	11.5; 4.6; 1.7	75.66	H-6A, Me-19
	4.87	d (OH-7)	11.5	---	H-3, H-7
8	---	---	---	---	
9	---	---	---	---	
10	5.49	s	---	78.29	H-3, Me-18
11	---	---	---	---	
12	---	---	---	---	
13	4.86	ot	7.7	67.79	Me-16, Me-18
14	2.34-2.25	m		35.12	
15	---	---	---	---	
16	1.07	---	---	19.37	H-13
17	1.08	---	---	26.37	H-2, Me-19
18	1.98	---	---	15.28	H-3, H-10, H-13
19	1.69			16.45	H-2, H-7, Me-17, H-20B
20A	4.41	d	8.8	77.71	H-2, Me-19, H-20B
20B	4.38	d	8.8		H-2, Me-19, H-20A
Ac	2.37	s		22.29	
Bz-2	---				
C1	---				
C2, 6	8.12	d	8.3	129.82	
C3, 5	7.50	t		128.46	
C4	7.62	t		133.42	

A is altered, with a cyclization containing a hydroxylated methyl (C-16 or C-17) on the double bond, assisted by an oxygenase.

High-resolution NMR analyses of *T. canadensis* taxanes

The detailed ^1H and ^{13}C assignments of all the metabolites reported for the first time in *T. canadensis* are shown in Tables 1–7. The 500 MHz NMR analyses utilized for all the new taxanes will be illustrated on the metabolite **14**, isolated for the first time in *T. canadensis*.

The proton NMR shifts and the COSY spectrum (16) allowed us to assign most of the protons. However, it was not possible to distinguish H-5 from H-7, H-10 from H-13, and H9/H10 coupled together could have reverse assignments. The four methyl groups could be identified by their couplings. The *gem*-dimethyl (Me-16 and Me-17) could be recognized by a small correlation in the COSY spectra. The methyl at position 19 (Me-19) showed a long-range coupling with H-3, and Me-18 with H-13/H-10. Three of the four acetyls of compound **14** could be easily located by the extra deshielding (~0.8–1 ppm) to the geminal proton (-C*H*-OAc) by comparison to an -OH (-C*H*-OH). These positions are H-2, H-10, and H-13. The position of the fourth acetyl was not immediately apparent.

The carbon-13 NMR assignments of the protonated carbons were established using the HMQC technique (*H*eteronuclear *M*ultiple *Q*uantum *C*oherence) (17) (Table 4). The carbon shifts that could not be determined were the quaternary carbons (C-1, C-4, C-8, C-11, C-12, C-15) and C-5, C-7, C-9, C-10, and C-13. Indeed, the signals of the attached protons (H-5/H-7; H-9/H-10; H-10/H-13) either overlap or are not assigned with certainty.

The additional heteronuclear correlation experiment HMBC (*H*etero *M*ultiple *B*ound *C*orrelation) (18) was therefore crucial for unambiguous assignment of all the carbons. The two-dimensional ^1H–^{13}C correlations for the four methyls are shown in Fig. 2*a*. The protons Me-16 and Me-17 are both correlated to C-15, C-11, and C-1. The protons Me-19 show coupling to C-8, C-9, C-7, and C-3 while methyl-18 correlates to C-13, C-11, and C-12. The HMBC experiment has also enabled us to corroborate the presence of the acetyls at C-10, C-13, and C-2. Indeed, in Fig. 2*b* we note that H-2, H-10, and H-13 are coupled to carbonyl groups. Surprisingly, we also note the most shielded proton (compared to H-13, H-10, H-2, H-9, H-7): a triplet at 4.2 ppm is correlated also to a carbonyl ester carbon (170 ppm). This triplet is also correlated to C-20, C-4, and C-3, confirming that it is indeed H-5. The higher chemical shift observed for H-5 on the acetylated C-5 position can be rationalized by the presence of an α-epoxide. The H-2 proton (Fig. 2*b*) also shows connectivities to six other carbons describing the total environment of that proton. These are C-1, C-14, C-15, C-3, C-4, and C-8 (the quaternary carbons that have not been assigned in HMQC are underlined). Among these quaternary carbons, C-15 and C-1 are assigned by analyzing the correlations of Me-16 and -17, which are coupled to

Can. J. Chem. Downloaded from www.nrcresearchpress.com by 65.111.164.53 on 09/08/12
For personal use only.

Table 3. Proton NMR analyses of 9-dihydrotaxanes (metabolites (*a*) **7–9**; (*b*) **10**, **11**, **14**.

(a)

Position	7	8	9
2	5.756 (d) J=5.9	5.471 (d) J=5.8	5.868 (d) J=5.9
3	3.05	2.91 (d)	3.159 (d)
5	4.954 (d) J=8.3	4.953 (d) J=8.7	4.959 (d) J=9.3
6A	2.55	2.53 (m)	2.487 (dt) J=8.3; 8.3; 15.1
6B	1.9	1.92 (o.m)	1.890 (o.m)
7	4.44 (o.m)	4.368 (o.m)	5.557 (dd) J=7.8; 9.3
9	4.44 (o.m)	4.383 (o.m)	6.027 (d) J=11.3
10	6.174 (d) J=10.7	6.122 (d) J=10.7	6.397 (d) J=11.3
13	6.163 (t) J=8.0	6.133 (o.m)	6.178 (br t) J=8.3
14A/14B	2.21(o.m)	2.25 (m)/2.00 (m)	2.22-2.19 (m)
16	1.249 (s)	1.233 (s)	1.223 (s)
17	1.676 (s)	1.605 (s)	1.744 (s)
18	1.946	1.911 (d) J=1.0 Hz	2.065 (d)
19	1.818	1.757 (s)	1.601 (s)
20A	4.309 (d) J=8.2	4.493 (d) J=7.8	4.332 (d) J=8.3
20B	4.161 (d) J=8.2	4.223 (d) J=7.8	4.117 (d) J=8.3
11'-A/11'-B	---	---	4.090 (J=16.6),4.027 (J=16.6)
Ac	---	2.159 (s)	2.294 (s)
Ac	2.276 (s)	2.156 (s)	2.202 (s)
Ac	2.190 (s)	2.124(s)	2.114 (s)
Ac	2.139 (s)	2.095 (s)	2.097 (s)
Benzoyl	H-ortho 8.1 ppm (d)	---	H-ortho 8.089 (d)
	H-meta 7.5 ppm (t)	---	H-meta 7.481 (t)
	H-para 7.6 ppm (t)	---	H-para 7.614 (t)

(b)

Position	10	11	14
2	5.828 (d) J=6.3	5.754 (d) J=5.9	5.331 (d) J=3.7
3	3.210 (d) J=5.8	3.058 (d) J=5.9	3.071 (d) J=3.7
5	4.926 (d) J=9.8	4.942 (od) J=7.8	4.202 (t) J=3.1
6A	2.6 (m)	2.54 (m)	2.038 (ddd) J=3.7, 12.0, 15.1
6B	1.8 (m)	1.9 (m)	1.887 (ddd) J=2.9, 4.4, 14.6
7	4.350 (dd) J=7.7, 10.3	4.364 (≈t)	4.253 (dd) J=4.6, 11.7
9	4.542 (d) J=10.3	4.306 (o.m)	4.591 (dd) J=4.4, 10.7
10	4.825 (d) J=10.3	4.924 (o.d) J=10.2	6.035 (d) J=10.7
13	6.182 (br t) J ≈5.8-7.3	6.190 (br t) J=7.3-9.3	6.051 (ddd) J=1.5, 6.6, 9.7
14A/14B	2.2 (o.m)	2.2 (o.m)	2.510 (dd) J=9.7, 14.9/1.864 (dd) J=6.6, 14.7
16	1.305 (s)	1.305 (s)	1.228 (s)
17	1.664 (s)	1.703 (s)	1.527 (s)
18	1.814 (s)	1.838 (d) J=1.0	2.157(d) J=1.5
19	1.58 (s)	1.810 (s)	1.388 (s)
20A	4.314 (d) J=8.3	4.306 (d) J=8.3	3.475 (d) J=5.4
20B	4.160 (d) J=8.3	4.166 (d) J=8.3	2.322 (d) J=5.4
11'-A/11'-B	---	---	---
Ac	2.288 (s)	2.278 (s)	2.184 (s)
Ac	2.183 (s)	2.185 (s)	2.134 (s)
Ac	---	---	2.099 (s)
Ac	---	---	2.051 (s)
OH-1	---	3.769 (s)	1.944 (s)
OH-7	---	3.283 (br s)	4.725 (s)
OH-9	---	4.870 (br d) J=7.2	3.574 (d) J=4.4
OH-10	---	3.193 (br s)	---
Benzoyl		8.078 (d) J=8.3	
		7.470 (t) J=7.7	
		7.600 (t)	

these two carbons, while the C-8 quaternary carbon is unambiguously identified from the Me-19 trace that is coupled to it (Fig. 2*a*). The H-9 proton, coupled to only one olefinic carbon (C-11), is also associated with C-10, C-7, C-8, and C-19, which describes the environment of this proton and confirms its assignment (Fig. 2*b*). The doublet of doublets located at 4.25 ppm is correlated to C-19 ($^3J_{C-H}$). This correlation allows us to definitely assign this proton as H-7. H-7 is also coupled to C-6 and C-5 (Fig. 2*b*). The connectivities in HMBC that enabled us to position the four acetates are shown in Fig. 2*c*.

The stereochemistry of the substituents, as well as the stereospecific assignment of Me-16 and Me-17, have been established using the NOESY experiment (NOE-2D) (19). In taxanes, despite their relative small size, the NOE cross peaks

Can. J. Chem. Downloaded from www.nrcresearchpress.com by 65.111.164.53 on 09/08/12
For personal use only.

Can. J. Chem. Downloaded from www.nrcresearchpress.com by 65.111.164.53 on 09/08/12
For personal use only.

Table 4. ^{13}C NMR analyses of 9-dihydrotaxanes (metabolites **7–14**).

Carbons	7	8	9	10	11	14
1	78.76	---	79.20	78.69	---	76.01
2	73.50	72.78	73.04	73.69	73.39	72.63
3	46.98	46.78	47.08	45.83	46.67	40.21
4	82.01	---	81.78	81.55	---	58.36
5	83.99	84.12	83.54	83.70	83.95	78.19
6	37.96	35.16	34.24	36.91	38.16	33.09
7	74.00	72.51 (or C-9)	71.58	72.26	74.27	69.60
8	45.00	---	46.10	41.54	---	46.52
9	76.85	73.89 (or C-7)	74.50	79.77	78.06	78.36
10	73.26	73.06 (or C-13)	71.87	~72	70.74	74.09
11	134.76	---	133.64	137.29	---	136.13
12	139.82	---	142.84	135.86	---	140.20
13	69.73	69.74 (or C-10)	69.54	69.76	69.86	71.16
14	35.33		34.83	35.11	35.23	38.61
15	43.00		42.79	42.97	---	43.39
16	28.28	27.96	28.12	28.32	28.18	28.43
17	22.57	22.15	21.99	21.89	22.02	22.05
18	14.88	14.68	14.70	14.00	14.68	15.48
19	12.48	12.19	12.37	12.00	12.33	13.54
20	76.56	76.66	76.25	76.55	76.61	49.88
Ac	22.84, 170.45	22.71	22.58, 169.69		22.60	21.70, 169.20
Ac	21.31, 170.23	21.05	20.83, 170.79		21.14	21.21, 169.80
Ac	21.29, 169.32	21.05	21.12, 170.43		---	21.38, 170.1
Ac	---	21.05	20.54, 170.79		---	20.92, 169.80
Benzoyl (CO)	167.04		167.48 (CO)		---	
C-1	128.67		128.75		---	
C-2, 6	130.08		130.21		129.96	
C-3, 5	128.64		128.75		128.61	
C-4	132.72		133.71		133.55	
10'	---	---	172.27			
11'	---	---	60.50			

Table 5. Comparison between ^{13}C chemical shifts for **10** and **11**. Most chemical shifts are similar (within 0.2 ppm) except for the ones shown in this table.

^{13}C	10	11	Difference (11-10)
C-3	45.83	46.67	Δ=0.8
C-6	36.91	38.16	Δ=1.2
C-7	72.26	74.27	Δ=2.0
C-9	79.77	78.06	Δ=1.7

are relatively strong. In these experiments, the NOE interactions are phased in an opposite fashion to the diagonal (negative phase), whereas the cross peaks originating from chemical exchange (OHs) are phased in a positive fashion. For the hydroxy protons we observe strong chemical exchange peaks (negative phase) and small NOE positive signals. In the NOESY tables (Tables 6, 7), only small positive NOEs (marked with an asterisk) are reported for these groups. Figure 3*a* illustrates the most informative NOEs, which rigorously establish the stereochemistry of ring A in compound **14**: we see that Me-16 points towards ring A and we can observe an NOE between Me-16, H-13 and 14A. Figures 3*b* and 3*c* show the most informative NOEs, which prove the stereochemistry of ring B from the β-side (Fig. 3*b*), and the α-side (Fig. 3*c*) of metabolite **14**. From Fig. 3*b*, we can conclude that Me-17, Me-19, H-2, and H-9 are on the β-side of the molecule **14**. On the other hand, in Fig. 3*c*, H-10, H-7, H-3, and Me-18 are on the α-side of compound **14**. The H-20A on the epoxide ring exhibits a small medium NOE with H-14B (α-orientation). The presence of this NOE suggests that the epoxide is β. For H-5, the vicinal coupling constants with its neighboring H-6 protons are small (J = 3 Hz), indicating a pseudo-equatorial orientation. The NOEs observed for H-5 are not very informative, since this proton interacts only with the vicinal H-6 protons and with H-20B. By molecular modelling we can identify two possible conformations for ring C shown in Figs. 3*d* and 3*e*. The twist-boat conformation of ring C (Fig. 3*d*) is characterized by a β-oxirane and an α-H-5. This configuration explains the observed coupling constants, as well as the NOEs (Fig. 3*d*). Indeed, the H-7 exhibits a large diaxial coupling with H-6A (ϕ = 174°) and a smaller coupling with H-6B (ϕ = 67°). The H-5 has two small couplings with H-6A (ϕ = 156°) and H-6B (ϕ = 37°). The H-5 and H-20B are close in space (≈2, 4 Å), explaining the strong NOE observed between these protons. Figure 3*e* represents a different possible conformation for ring C, which can also explain all the vicinal couplings and the NOEs observed. Indeed, in this chair conformation, the axial H-7 proton exhibits large diaxial coupling with H-6A and smaller axial-equatorial coupling with H-6B. The equatorial H-5 proton would show small couplings with the vicinal H-6A/H-6B. This configuration can also explain the observed NOEs and coupling constants. We can therefore conclude that the stereochemistry of H-5 could not be determined. On the other hand, the β-oxirane seems to be suggested by the data.

*Stereoisomers **10** and **11***

The stereoisomers **10** and **11** were first isolated in a 60:40 ratio. They were then separated and purified. The assignments are shown in Tables 3 and 4. The ^1H NMR of both compounds are very similar. The ^{13}C chemical shifts for both compounds appear at similar shifts (within 0.2 ppm), except for the car-

Can. J. Chem. Downloaded from www.nrcresearchpress.com by 65.111.164.53 on 09/08/12
For personal use only.

Fig. 2. Two-dimensional ^{1}H–^{13}C correlations obtained for metabolite **14**. Arrows indicate carbon–hydrogen connectivities. Arrow head indicates location of proton. Figure 2*a* shows the ^{1}H–^{13}C correlations for the four methyls. Figure 2*b* shows the ^{1}H–^{13}C connectivities that confirm the assignment of H-9. Figure 2*c* shows the ^{1}H–^{13}C correlations that led to the positioning of the four acetyls.

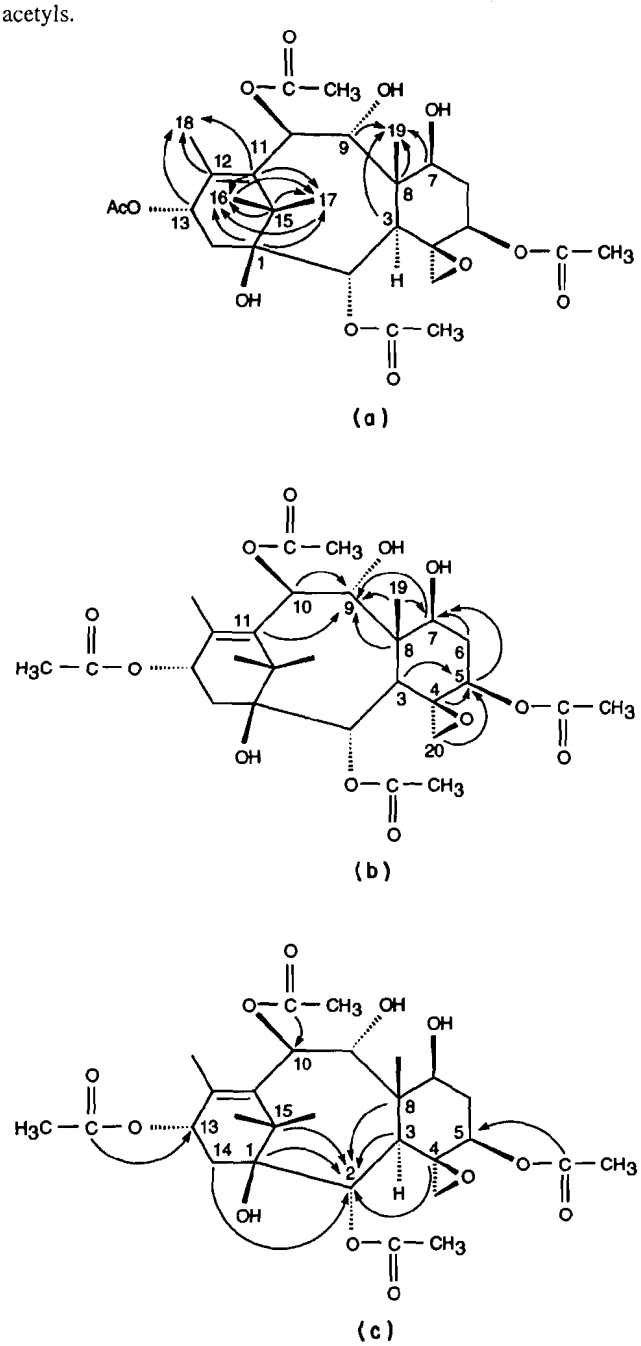

bons C-3, C-6, C-7, and C-9 (Table 5). The carbons showing these shifts are part of ring C (or close to ring C). In addition, the largest difference is at C-7, suggesting that they differ in the stereochemistry of C-7. Due to the similar NOEs we cannot conclusively determine in which stereoisomer the OH at C-7 is β and in which one it is α.

Mass spectra of *T. canadensis* taxanes

In the experimental section, the low-resolution and high-resolution mass spectra of taxanes are reported. The assignments of the different ions are also given. The results confirm our NMR data.

Experimental

High-performance liquid chromatography

Analytical high-performance liquid chromatography (HPLC) was carried out on a Perkin–Elmer instrument with an isocratic and binary LC pump model 250 coupled to a Waters 990 photodiode array detector, a NEC APC IV computer for data processing, and a Waters 990 plotter. HPLC was performed with two ODS-2 reversed phase columns (Whatman) connected in series (4.6 × 500 mm), at a flow rate of 1 mL/min. Sample injections were done manually using a 1.0 mL loop on a Waters UK6 injector. Separation was achieved with a linear gradient beginning with 75% water – 25% acetonitrile and increasing over 50 min to 100% acetonitrile. Semi-preparative HPLC was performed with two ODS-2 MAG-9 semi-preparative columns (Whatman) connected in series (9.4 × 500 mm), at a flow rate of 3 mL/min. The gradient program was the same, but it lasted either 70 min or 120 min. All ultraviolet detectors were set at 227 nm. All samples were filtered (0.45 μm) before injection. Water and acetonitrile were HPLC grade. The purity of all isolated products was checked by analytical HPLC. Semi-preparative HPLC was performed on a Waters Delta Prep 3000 instrument coupled to a Lambda-Max model 481 variable wavelength detector (Waters) and a Perkin–Elmer 024 recorder.

Nuclear magnetic resonance methodology

All the NMR spectra were obtained at room temperature on a UNITY-500 spectrometer operating at 499.843 MHz for proton and at 125.697 MHz for carbon-13. The NMR spectra were obtained on 1–2 mg samples dissolved in 0.3–0.4 mL of deuterated chloroform ($CDCl_3$). The solvent was used as an internal reference (77.0 ppm for ^{13}C and 7.25 ppm for ^{1}H). For the proton spectra, 8–64 transients were recorded with an 8000 Hz spectral window, 45° pulse, 30K data points, and 1.0 s acquisition time. The carbon-13 NMR spectra were obtained with a spectral window of 30 007.5 Hz, using a 40° pulse, and 50 000–70 000 transients were acquired. In cases were the concentration was too weak to obtain a good spectrum, the shifts were extracted from the HMQC experiment. The NOESY experiment (hypercomplex phase mode) was obtained using a mixing time of 0.3 s and a relaxation delay of 1 s. The acquisition was repeated for 16–32 transients, and 256 complex increments were acquired. The data were processed using a Gaussian apodization function. The final data matrix have 2K by 1K points (zero filling was used only in the evolution domain). For all the studies with taxol derivatives, when the diagonal signals are phased positive, the cross peaks resulting from dipolar relaxation (NOE) are phased negative, while the cross peaks originating from chemical exchange (OH) have positive phasing.

The HMQC experiment with a preceding BIRD nulling period was used with hypercomplex phased mode. The recycling delay was set to 1 s, while the nulling period (following the bird pulse) was set to 0.3 s. The acquisition was repeated 8–16 times and 256 fids were acquired. During acquisition of the proton spectra, C-13 broadband waltz decoupling was

Table 6. NOESY observed on the diastereoisomers **10** and **11**. In these experiments, the NOE cross peaks have a reverse phase (positive) relative to the diagonal (negative), whereas the chemical exchange cross peaks (hydroxy groups) are phased like the diagonal peaks. For the hydroxy protons we observed strong chemical exchange peaks (negative phase) and small NOE positive signal. In the table below, only the small positive NOEs are reported for these groups (*).

Proton	**10**	**11**
H-2	H-9 (w), Me-17 (s)	H-9 (s), Me-17 (s), Me-19 (m), H-20B (w)
H-3	H-7 (s), H-14 (m), Me-18 (w)	H-2 (w), H-7 (s), H-10 (w), H-14 (or Ac) (m), Me-18 (m)
H-5	H-6A (s), H-20A (s)	
H-6A	H-6B (s), H-5 (m), H-7 (m)	H-6B (s), H-5 (m), H-7 (m)
H-6B		
H-7	H-3 (m), H-6A (s), H-10 (m)	H-3 (s), H-6A (m), H-10 (s), Me-18 (m), OH-7 (w)
H-9	H-2 (w), Me-17 (s)	H-2 (m), Me-17 (s), Me-19 (m)
H-10	H-7 (m), Me-18 (m)	H-7 (m), Me-18 (m), OH-10 (w), H-3 (w)
H-13	H-14 (m), Me-16 (m), Me-18 (w)	H-14 (m), Me-16 (m), Me-18 (w)
H-14	H-13 (m)	
H-15		
H-16		H-13 (s), Me-17 (s), H-14 (w)
H-17		H-2 (s), H-9 (s), Me-16 (s)
H-18		H-3 (m), H-6A (m), H-7 (m), H-10 (s), H-13 (w), H-14 (w)
H-19		H-2 (s), H-9 (s), OH-9 (m), H20B (s)
H-20A	H-20B (s), Me-17 (m)	H-20B (s), H-5 (m)
H-20B	H-20A (s), Me-19 (m)	H-20A (s), Me-19 (s), H-2 (w)
Bz C-2/6		H-20A (m)
OH-7*		H-7 (m), H-6B (w)
OH-9*		H-9 (m), H-7 (w), Me-19 (m)
OH-10*		H-10 (m), H-14 (w)

Table 7. NOESY observed on metabolite **14** (NOE positive cross peaks).

Proton	NOE observed: s (strong), m (medium), w (weak)
H-2	H-9 (s), Me-17 (s), Me-19 (m), H-3 (w), OH-1 (w)
H-3	H-7 (s), H-14B (s), Me-18 (m), H-2 (w), H10/13 (w), H20A (w)
H-5	H-20B (s), H-6A (m-s), H-6B (m-s), H-9 (w)
H-6A	H-6B (s), H-5 (m), Me-19 (m)
H-6B	- - -
H-7	H-3 (m), H-10/13 (m), H-14B (m), Me-18 (m), H-6A (w), H-6B (w),OH-7 (w)
H-9	H-2 (s), Me-17 (s), OH-9 (w), Me-19 (w)
H-10/H-13	H-7 (s), H-14A (s), Me-16 (s), Me-18 (s), H-3 (w), H-9 (w)
H-13	- - -
H-14A	H-14B (v.s), H-13/10 (s), Me-16 (m)
H-14B/H-6B	H-6A (v.s), H-14A (v.s), H-3 (m), H-7 (m), H-20A (m), H-5 (m)
Me-16	H-10/H-13 (s), Me-17 (s), H-14A (m-w), Me18 (w)
Me-17 (1.51)	H-2 (s), H-9 (s), Me-16 (s)
Me-18 (2.151)	H-10/H-13 (s), H-7 (m), H-3 (m)
Me-19 (1.386)	H-2 (m), H-6A (m), H-9 (m), OH-7 (w)
H-20A	H-20B (v.s), 14B/6B (m-w), 6A (w)
H-20B	H-20A (v.s), H-5 (s)
OH-1*	H-2 (m), Me17 (m), Me16 (w)
OH-7*	H-7 (w), Me-19 (w)
OH-9*	H-9 (m), Me19 (w), H-10/13 (w)

applied. The data were processed with a Gaussian function with zero filling in the evolution domain (^{13}C). The final matrix size was 2K by 1K. The spectral window in the carbon domain was 120–140 ppm, while it was about 7–8 ppm in the proton domain. The HMBC experiment was acquired using similar conditions, but without the null period and without ^{13}C decoupling during acquisition. The τ delay to emphasize long-range coupling was set to 100 ms. Also, the carbon window was set larger to accommodate carbonyl carbons (180–200 ppm) in the carbon domain. The HMBC data were processed using a shifted Gaussian function and were displayed and plotted in an absolute value mode.

Mass spectrometry

Low-resolution xenon fast atom bombardment mass spectra were obtained in glycerol, except as noted, with a VG ZAB-HS instrument operated under the following conditions: resolution, 2000; atom energy, 8 kV at 1 mA beam current; scan range 1200–200 Da at 10 s/decade. The samples were dissolved in 0.2 μL of dimethyl sulfoxide in the stage before addition of 0.5 μL of glycerol. The 10 spectra obtained for each sample were averaged to reduce statistical variations.

High-resolution measurements were made similarly in glycerol–DMSO, at a resolving power of 12 000. The ions of interest were manually peak-matched against glycerol cluster

Can. J. Chem. Downloaded from www.nrcresearchpress.com by 65.111.164.53 on 09/08/12
For personal use only.

Fig. 3. (*a*) NOESY correlations about ring A of **14**; (*b*), (*c*) NOESY correlations establishing stereochemistry of ring B (β-face b, α-face c); (*d*), (*e*) Plausible conformations for ring C and NOESY correlations.

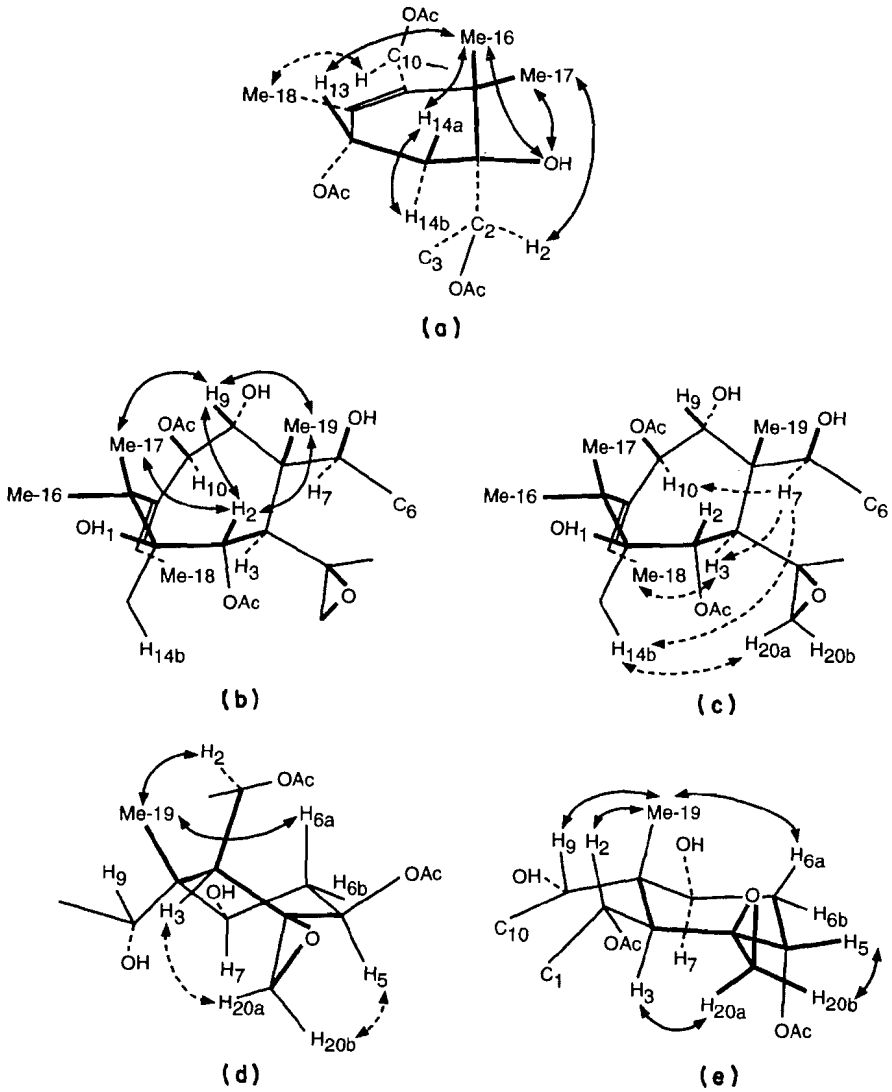

ions of known compositions, closest to the ions being measured.

IR spectroscopy

IR spectra were recorded using a Bruker IFS-48 FTIR spectrophotometer.

Circular dichroism

CD spectra were recorded using a Jasco J-500C spectropolarimeter with a 1.0 cm wide cuvette.

Plant material

Stems and needles of *Taxus canadensis* were collected at two different sites in Quebec. The material was stored at 4°C. When needed, they were dried at room temperature and ground in a blender for extraction.

Extraction, isolation, and purification of taxanes

Dried powdered needles and small branches of *T. canadensis* (480 g) were extracted twice with CH_3OH–CH_2Cl_2 (1:1, v/v, 4.8 L) during 24 h, at room temperature. The combined extracts were filtered and concentrated in vacuum to a dark brown residue. The residue was suspended in water and extracted with hexane to eliminate lipids. The aqueous layer was extracted with CH_2Cl_2 (3 × 300 mL) and the combined extracts were dried, filtered, and evaporated, giving a syrupy residue (18 g). The resulting extract was coated on Celite 545 and fractioned by flash chromatography on a silica gel column (150 g, 5 × 30 cm). The mixture was eluted with CH_2Cl_2–$CH_3COOC_2H_5$ (85:15) and then with a 5% step gradient starting with hexane–acetone (65:35) and ending with 100% acetone. Fractions eluted with hexane–acetone (65:35) contained taxol **1**, 7-epitaxol **3**, cephalomannine **4**, 9-dihydro-13-acetylbaccatin III **7**, 10-hydroxyacetylbaccatin VI **9**, 5-decinnamate taxagifine **12**, 2-deacetyl-5-decinnamoyl taxinine J **13**, and 1β-hydroxy-7,9-deacetylbaccatin I **14**. Further elution of the mixture with hexane–acetone (60:40) afforded mainly 10-deacetylbaccatin III **5**, and small amounts of 10-deacetyl taxol

Can. J. Chem. Downloaded from www.nrcresearchpress.com by 65.111.164.53 on 09/08/12
For personal use only.

Can. J. Chem. Downloaded from www.nrcresearchpress.com by 65.111.164.53 on 09/08/12
For personal use only.

2, 10-deacetylbaccatin V **6**, 7,9-deacetylbaccatin IV **8**, and 7,9,10-deacetylbaccatin VI **10** and **11**. For each peak, acetonitrile was removed by evaporation under vacuum and the remaining aqueous solution was lyophilized to yield white amorphous solids. The different taxanes were purified by repetitive HPLC runs, using gradient and isocratic conditions. The very pure taxanes were analyzed by high-resolution NMR and mass spectrometry.

9-Keto-taxanes (1–6, Fig. 1)

The 9-keto-taxanes were purified by repetitive HPLC runs. The preliminary purifications of compounds **1–6** involved semi-preparative HPLC with a gradient over 70 min of CH_3CN:H_2O (25:75) to 100% CH_3CN. The retention times under those conditions are the following: compound **1**, R_t = 36.2 min; **2** (same gradient but over 100 min), R_t = 44.5 min; **3**, R_t = 39.1 min; **4**, R_t = 34.5 min; **5** (same gradient but over 120 min), R_t = 24.2 min; **6** (same gradient but over 120 min), R_t = 34.5 min. These compounds were further purified by analytical HPLC with the same gradient, but over 50 min. The retention times and the overall yields of the pure taxanes are as follows: **1**, R_t = 33.29 min (0.016%); **2**, R_t = 29.15 min (0.0008%); **3**, R_t = 36.75 min (0.0013%); **4**, R_t = 32.43 min (0.002%); **5**, R_t = 19.68 min (0.015%); **6**, R_t = 25.15 min (0.0006%).

The NMR of **1–6** were identical to literature values (13). In addition, their structures were confirmed by high-resolution mass spectrometry: **1** (taxol) MH^+: 854.33850; $C_{47}H_{52}NO_{14}$ requires 854.33878; **2** (10-deacetyltaxol) MH^+: 812.32791; $C_{45}H_{50}NO_{13}$ requires 812.32821; **3** (7-epitaxol) MH^+: 854.33850; $C_{47}H_{52}NO_{14}$ requires 854.33878; **4** (cephalomannine) MH^+: 832.35435; $C_{45}H_{54}NO_{14}$ requires 832.35443; **5** (10-deacetylbaccatin III) MH^+: 545.23871: $C_{29}H_{37}O_{10}$ requires 545.23867; **6** (10-deacetylbaccatin V) M + H^+ − $2H_2O$: 509.21758; $C_{29}H_{33}NO_8$ requires 509.21754; MH^+ − H_2O − HOAc: 449.19620; $C_{27}H_{29}NO_6$ requires 449.19641.

9-Dihydrotaxanes (7 – 14)

The purifications for all these taxanes involved (*i*) a semi-preparative HPLC with a gradient of acetonitrile (25–100%) in water over times specified for individual taxane followed when necessary by an isocratic run and (*ii*) analytical HPLC. The 500 MHz ^1H and ^{13}C NMR analyses and NOESY experiments for these 9-dihydrotaxanes are reported in Tables 3–7. The chemical structures of these metabolites were confirmed by mass spectrometry and low- and high-resolution data.

9-Dihydrotaxane **7**: IR (film) ν_{max}: 1743, 1714, 1371, 1245, 1179, 1111, 1053, 1018, 970 cm^{-1}; UV λ_{max} (CH_3OH): 228 nm (ϵ = 19 200); $[\alpha]_D^{22}$ −24.1 (c = 1.01, $CHCl_3$); [Θ] from CD (CH_3OH): +18.9 deg M^{-1} cm^{-1} at λ_{max} 252 nm and −8.6 deg M^{-1} cm^{-1} at λ_{min} 293 nm; MH^+: 631.27567; $C_{33}H_{43}O_{12}$ requires 631.27545. The retention time of **7** in semi-preparative HPLC with a gradient over 70 min, R_t: 39.10 min; analytical HPLC R_t: 27.34 min. The overall yield of **7** is 0.04%. Acetylation of metabolite **7** led to baccatin VI (9). The acetylation procedure is the following: 1 mg of **7** in dry pyridine (60 μL) was mixed with 90 μL acetic anhydride and stirred at room temperature overnight. Following removal of the pyridine, the acetylated product was purified by semi-preparative HPLC. Analyses of the NMRs of **7** and its acetylated derivative (1) established that metabolite **7** has hydroxyls at C-7 and C-9. In addition, the mass spectral data (low and high resolution) confirmed the structure of acetylated metabolite **7**: *m/z*: 715 (49.7%) MH^+: 715.29679; $C_{37}H_{47}O_{14}$ requires 715.29658); 697 (38.0%) ($MH^+ - H_2O$; 655 (90.8%) (MH^+ − AcOH); 637 (24.8%) (655−H_2O or 697−AcOH); 595 (60.7%) (655−AcOH); 535 (40.8%) (595 – AcOH).

9-Dihydrotaxane **8**: IR (film) ν_{max}: 1733, 1436, 1370, 1234, 1043, 1053, 1018, cm^{-1}; UV λ_{max} (CH_3OH): 217 nm (ϵ = 7400); $[\alpha]_D^{22}$ +24.05 (c = 1.83, $CHCl_3$); [Θ] from CD (CH_3OH): +32.9 deg M^{-1} cm^{-1} at ν_{max} 245 nm; *m/z*: 569 (35.9%) MH^+: 569.25989; $C_{28}H_{41}O_{12}$ requires 569.25980); 551 (29.6%) ($MH^+ - H_2O$); 509 (100%) (MH^+−AcOH), 491 (38.1%) (509−H_2O); 449 (37.3%) (509−AcOH); 431 (15.1%) (491−AcOH or 449 – H_2O). The retention time of **8** in semi-preparative HPLC with a gradient over 120 min, R_t = 20.5 min; isocratic CH_3CN:H_2O (26:74), R_t = 27.9 min; analytical HPLC R_t: 18.9 min. The overall yield of **8** was 0.0006%.

9-Dihydrotaxane **9**: IR (film) ν_{max}: 1734, 1374, 1245, 1099, 1052, 1027, 983, 803, cm^{-1}; UV λ_{max} (CH_3OH): 229 nm (ϵ = 13 653); [Θ] from CD (CH_3OH): 94.2 deg M^{-1} cm^{-1} at λ_{max} 290 nm; *m/z*: 753 (15.1%) (M + Na^+: 753.27357; $C_{37}H_{46}O_{15}Na$ requires 753.27344); 731 (5.7%) (MH^+); 713 (3.1%) ($MH^+ - H_2O$). The retention time of **9** in semi-preparative HPLC with a gradient over 70 min, R_t = 37 min; analytical HPLC isocratic CH_3CN:H_2O (42:58), R_t = 47.9 min. The overall yield of **9** is 0.0006%.

*9-Dihydrotaxanes **10** and **11***: UV λ_{max} (CH_3OH): 228 nm (ϵ = 12 600). The high-resolution NMR data of the two stereoisomers corresponding to **10** and **11** are shown in Tables 3–6. The stereochemistry of C-7 in both stereoisomers **10** and **11** could not be rigorously proven by NOESY experiments. The low- and high-resolution mass spectral data were identical for both. The Exact Mass for each compound was 589.26471: $C_{31}H_{41}O_{11}$ requires 589.26488. Both metabolites form a sodium adduct found *m/z* 611 and peaks corresponding to $MH^+ - H_2O$ at *m/z* 571. The retention time of **10** in semi-preparative HPLC with a gradient over 120 min, R_t = 30.3 min; isocratic CH_3CN:H_2O (28:72), R_t = 54.5 min. The retention time of **11** in semi-preparative HPLC with a gradient over 70 min, R_t = 25.5 min. In analytical HPLC isocratic compounds **10** and **11**, R_t = 23.85 min. The overall yield of **10** is 0.002% and of **11** is 0.0008%.

The detailed NMR analyses of **12** and **13** are shown in Tables 3 and 4. Since **12** and **13** are not new natural products, their structures were confirmed by rigorous NMR analyses, comparison with the literature, and low-resolution mass spectrometry. Metabolite **12** showed a weak (M+ H^+) peak at *m/z* 567 (7.2%), a prominent M+ H^+ − H_2O peak at *m/z* 549 (92.6%), and a sodium adduct at *m/z* 589 (M + Na^+); other peaks were at *m/z* 489 (549 – AcOH) (67.0%); 531 (549−H_2O) (6.1%); 429 (489 – AcOH) (29.5%); 507 (M+ H^+−AcOH) (18.7%); 467 (507 – AcOH) (25.8%). Metabolite **13** showed a sodium adduct at *m/z* 559 (14%) and a prominent peak at *m/z* 477 (M+ H^+ – AcOH) (68.7%) and at *m/z* 459 (477 – H_2O) (33.7%). The retention time of both **12** and **13** in semi-preparative HPLC with a gradient over 70 min is R_t = 25.5

min. They were separated in analytical HPLC: R_t of **12**: 23.55, and of **13**: 25.48 min. The overall yield of **12** and of **13** is 0.004%.

9-Dihydrotaxane ***14***: IR (film) ν_{max} : 1734, 1436, 1371, 1239, 1022, 979, 962 cm^{-1}; UV λ_{max} (CH_3OH): 220 nm (ϵ = 7500); $[\alpha]_D^{22}$ +65.84 (c = 0.571, $CHCl_3$); [Θ] from CD (CH_3OH): +57.2 deg M^{-1} cm^{-1} at λ_{max} 286 nm; MH^+: 569.25989; $C_{28}H_{41}O_{12}$ requires 569.25980. The fragmentation pattern shows the following peaks: *m/z*: 569 ($M + H^+$) (11.1%); 591 ($M + Na^+$) (12.5%); 551 ($MH^+ - H_2O$) (12.1%); 509 (569 − AcOH) (21.1%); 491 (551 − AcOH) (26.5%); 449 (569 − 2AcOH) (12.6%); 431 (551 − 2AcOH) (11.9%); 389 (MH^+ − 3AcOH) (24.7%); 371 ($MH^+ - H_2O$ − 3AcOH) (10.5%). The retention time of **14** in semi-preparative HPLC with a gradient over 70 min, R_t: 22.5 min; analytical HPLC, R_t: 21.05. The overall yield of **14** is 0.004%.

Acknowledgments

We thank the Natural Sciences and Engineering Research Council of Canada and the Canadian Breast Cancer Research Initiative for support of this work via operating grants to Lolita O. Zamir. La Fondation Armand-Frappier is acknowledged for a fellowship to G.C.

References

1. L.O. Zamir, M.E. Nedea, S. Bélair, F. Sauriol, O. Mamer, E. Jacqmain, F.I. Jean, and F.X. Garneau. Tetrahedron Lett. **33**, 5173 (1992); **33**, 6548 (1992).
2. M.C. Wani, H.L. Taylor, M.E. Wall, P. Coggon, and A.T. McPhail. J. Am. Chem. Soc. **93**, 2325 (1971).
3. R.A. Holton, C. Somoza, H.-B. Kim, F. Liang, R.J. Biediger, P.D. Boatman, M. Shindo, C.C. Smith, S. Kim, H. Nadizadeh, Y. Suzuki, C. Tao, P. Vu, S. Tang, P. Zhang, K.K. Murthi, L.N. Gentile, and J.H. Liu. J. Am. Chem. Soc. **116**, 1597 (1994); R.A. Holton, H.-B. Kim, C. Somoza, F. Liang, R.J. Biediger, P.D. Boatman, M. Shindo, C.C. Smith, S. Kim, H. Nadizadeh, Y. Suzuki, C. Tao, P. Vu, S. Tang, P. Zhang, K.K. Murthi, L.N. Gentile, and J.H. Liu. J. Am. Chem. Soc. **116**, 1599 (1994).
4. K.C. Nicolaou, Z. Yang, J.J. Liu, H. Veno, P.G. Nantermet, R.K. Guy, C.F. Claiborne, J. Renaud, E.A. Couladouros, K. Paulvannan, and E.J. Sorensen. Nature (London), **367**, 630 (1994); K.C. Nicolaou, C.F. Claiborne, P.G. Nantermet, A. Couladouros, and E.J. Sorensen. J. Am. Chem. Soc. **116**, 1531 (1994).
5. M.C. Bissery, D. Guénard, G. Guéritte-Voegelein, and F. Lavelle. Cancer Res. **51**, 4845 (1991).
6. V. Senilh, S. Blechert, M. Colin, D. Guénard, F. Picot, P. Potier, and P. Varenne, J. Nat. Prod. **47**, 131 (1984).
7. J.N. Denis, A.E. Green, D. Guénard, F. Guéritte-Voegelein, L. Mangatal, and P. Potier. J. Am. Chem. Soc. **110**, 5917 (1988).
8. I. Ojima, I. Habus, M. Zhao, M. Zucco, Y.H. Park, C.M. Sun, and T. Brigaud. Tetrahedron, **48**, 6985 (1992); I. Ojima, I. Habus, and M. Zhao. J. Org. Chem. **56**, 1681 (1991); J.-N. Denis, A. Correa, and A.E. Greene. J. Org. Chem. **55**, 1957 (1990).
9. K.M. Witherup, S.A. Look, M.W. Stasko, T.J. Ghiorri, G.M. Muschik, and G.M. Cragg. J. Nat. Prod. **53**, 1249 (1990).
10. S. Zhang, W.M. Chen, and Y.H. Chen. Yaoxue Xuebao, **27**, 268 (1992).
11. G.P. Gunawardana, U. Premachandran, N.S. Burres, D.N. Whittern, R. Henry, S. Spanton, and J.B. McAlpine. J. Nat. Prod. **55**, 1686 (1992).
12. L.L. Klein. Tetrahedron Lett. **34**, 2047 (1993).
13. D.G.I. Kingston, A.A. Molinero, and J.M. Rimoldi. Prog. Chem. Org. Nat. Prod. **61**, 10 (1993).
14. Z.P. Zhang, Z.J. Jia, Z.O. Zhu, Y.X. Cui, J.L. Cheng, and Q.G. Wang. Planta Med. **56**, 293 (1990).
15. L. Ettouati, A. Ahond, O. Convert, D. Laurent, C. Poupat, and P. Potier. Bull. Soc. Chim. Fr. 749 (1988).
16. J. Jeener. Ampère international summer school, Basko Polje, Yugoslavia. 1971; W.P. Ave, E. Bartholdi, and R.R. Ernst. J. Chem. Phys. **64**, 2229 (1975).
17. L.J. Müeller. J. Am. Chem. Soc. **101**, 4481 (1979); A. Bax, R.H. Griffey, and B.L. Hawkins. J. Magn. Reson. **55**, 301 (1983); M.R. Bendall, D.T. Pegg, and D.M. Doddrell. J. Magn. Reson. **52**, 81 (1983).
18. A. Bax and M.F. Summers. J. Am. Chem. Soc. **108**, 2093 (1986).
19. S. Macura and R.R. Ernst. Mol. Phys. **41**, 95 (1980).

Can. J. Chem. Downloaded from www.nrcresearchpress.com by 65.111.164.53 on 09/08/12
For personal use only.

The reactions of $O(^3P)$ with acetonitrile and propionitrile

Suzanne Budge and John M. Roscoe

Abstract: The reactions of $O(^3P)$ with acetonitrile and propionitrile have been studied kinetically in the gas phase as a function of temperature and nitrile concentration. The rate constants obtained experimentally for the consumption of $O(^3P)$ in these reactions, in the units L mol^{-1} s^{-1}, obey the following relations: O + acetonitrile: $\ln k = 20.98 \pm 0.23 - 2100 \pm 200/T$; and O + propionitrile: $\ln k = 21.01 \pm 0.19 - 1900 \pm 200/T$. Mechanisms are discussed in which the reaction is initiated by hydrogen atom abstraction and in which initiation is by addition of $O(^3P)$ to the nitrile, followed by decomposition of the addition complex. The kinetic and analytical results are best explained by the mechanism in which the reactions are initiated by RCN + O → R + OCN. In the case of the reaction with acetonitrile, the absolute rate constant is smaller than the experimental value by a factor of 7 ± 20%, independent of temperature, as a result of secondary reactions.

Key words: kinetics, reactions of $O(^3P)$ with nitriles.

Résumé : On a réalisé une étude cinétique des réactions du $O(^3P)$ dans l'acétonitrile et le propionitrile en phase gazeuse, en fonction de la température et de la concentration en nitrile. Les constantes de vitesse obtenues expérimentalement pour la consommation du $O(^3P)$ dans ces réactions, exprimées en L mol^{-1} s^{-1}, obéissent aux relations suivantes : O + acétonitrile : $\ln k = 20{,}98 \pm 0{,}23 - 2100 \pm 200/T$; et O + propionitrile : $\ln k = 21{,}01 \pm 0{,}19 - 1900 \pm 200/T$. On discute des mécanismes dans lesquels la réaction est initiée soit par l'enlèvement d'un atome d'hydrogène soit par l'addition du $O(^3P)$ sur le nitrile, suivie par une décomposition du complexe d'addition. La meilleure façon d'expliquer les résultats est de faire appel au mécanisme dans lequel les réactions sont initées par : RCN + O → R + OCN. Dans le cas de la réaction avec l'acétonitrile, des réactions secondaires font que la constante absolue de vitesse est plus faible que la valeur expérimentale par un facteur de 7 ± 20%.

Mots clés : cinétique, réactions du $O(^3P)$ dans les nitriles.

[Traduit par la rédaction]

Introduction

Reactions of polar organic compounds with atomic oxygen tend to have unusually small preexponential factors when compared with the corresponding reactions of saturated hydrocarbons (e.g., refs. 1–8). While it is usually accepted that the reactions of $O(^3P)$ with polar organic compounds proceed by hydrogen abstraction, the small preexponential factors have been attributed to the electrophilic nature of $O(^3P)$ (2). It has been postulated that the initial attack is between the oxygen atom and an electron-rich site on the substrate molecule. The resulting collision complex can then either decompose back to reactants or proceed to products via hydrogen atom abstraction. The qualitative picture is that a large proportion of the collision complexes simply decompose to reactants because of unfavourable geometry for chemical reaction, leading to an unusually small preexponential factor.

The effect described above has been observed for organic compounds containing oxygen at the electron-rich site. However, it seemed desirable to study reactions in which an addition complex between $O(^3P)$ and the organic reactant might be able to yield a characteristic decomposition product, permitting detection of a reaction channel other than hydrogen abstraction. The nitriles seemed to represent such a system since one might expect a relatively stable addition complex to form between $O(^3P)$ and the C≡N bond. The resulting complex might then decompose to products containing the CN functional group. It is also possible that hydrogen abstraction from the alkyl group might occur. This would lead to a second channel in which one might expect the initial production of OH followed by its reaction with the excess organic reagent to give water. Analysis of the reaction products for water and for compounds containing the CN group would then allow separation of the reaction into two identifiable channels and the relative importance of these channels could be evaluated as a function of the nature of the aliphatic group.

Examination of the literature reveals only a single study of reactions of $O(^3P)$ with nitriles (9). In that work, the reactions of CH_3CN and CF_3CN with $O(^3P)$ were studied. Rate constants were measured from the loss of $O(^3P)$ in the presence of a large excess of the nitrile using flash photolysis. Four temperatures were used, in the range 383–500 K, at pressures of 100–300 Torr (1 Torr = 133.3 Pa) Evidence from mass spectrometric measurements was consistent with the formation of HCN and H_2CO or NO. The measurement of a very small deuterium isotope effect, which increased in magnitude with

Received November 16, 1994.

S. Budge and J.M. Roscoe.[1] Department of Chemistry, Acadia University, Wolfville, NS B0P 1X0, Canada.

[1] Author to whom correspondence may be addressed. Telephone: (902) 542-2200.

Can. J. Chem. Downloaded from www.nrcresearchpress.com by 65.111.164.53 on 09/08/12
For personal use only.

Can. J. Chem. Downloaded from www.nrcresearchpress.com by 65.111.164.53 on 09/08/12
For personal use only.

increasing temperature, was taken to suggest that the dominant reaction channel did not involve hydrogen abstraction but that at higher temperatures hydrogen abstraction might become more important. We report here the results of kinetic experiments over the temperature range 320–578 K in which the reactions of $O(^3P)$ with acetonitrile and propionitrile were studied to provide information on the nature of the available reaction channels in these systems.

Experimental

The experimental methods used have been outlined in earlier publications from this laboratory (1, 3, 7, 8). The main features will be described here. The reactions were studied in a conventional flow system at a pressure of approximately 1 Torr and linear flow velocities in the cylindrical reaction vessel ranged from 700 to 1100 cm s^{-1}. The substrate entered the reactor through a movable inlet and the $O(^3P)$ concentration was monitored at a fixed point at the downstream end of the reaction vessel. The reaction vessel was heated electrically and the temperature was measured by a calibrated iron–constantan thermocouple located in the tip of the movable inlet. This arrangement also made it possible to verify uniformity of temperature along the axis of the reaction vessel. At the highest temperatures used, the temperature variation was no more than ±2°C over the part of the reaction vessel used for the kinetic measurements and this variation became smaller as the temperature was lowered.

Oxygen atoms were made by titrating $N(^4S)$ atoms, formed in a microwave-powered discharge through N_2, with NO. This procedure avoids interference from O_2, which has been found to alter the mechanism of some reactions of $O(^3P)$ (1). The concentration of $O(^3P)$ was controlled and kept small in the kinetics experiments by passing only a small part of the total N_2 flow through the discharge. The balance of the N_2 was diverted through a bypass around the discharge and mixed with the discharge products upstream from the NO inlet. This arrangement made it possible to attain as much as a 5000-fold excess of the organic reagent to minimize the effects of secondary reactions of $O(^3P)$ with free radical intermediates such as OH. It also provided a suitable range of concentrations of the organic reagent for the kinetic analysis. The concentration of $O(^3P)$ was monitored by observing the NO_2 chemiluminescence produced by addition of a small (a few percent) excess of NO beyond the titration end point. The initial concentration of $O(^3P)$ was obtained from the flow rate of NO at the titration end point in the absence of the organic reagent. The rate constants obtained in this way were independent of the amount of excess NO.

Acetonitrile (Fisher, certified, ACS), propionitrile (Aldrich, 99%), and acetone (Anachemia, toxigraphic, distilled glass) were dried and thoroughly degassed before use and showed no impurities detectable by gas chromatography. A few kinetic experiments were done periodically with acetone, which has been well characterized kinetically under conditions such as those used in this work (2, 8), to verify that the entire apparatus was functioning reliably. Gas chromatographic analysis was done on an 8 ft column packed with Porapak Q, using a thermal conductivity detector because of the need to determine HCN and water. Reaction products were collected for chromatographic analysis by pumping approximately 1% of the gas stream leaving the reaction vessel through the glass sample loop of the gas chromatograph. The sample loop was cooled in liquid nitrogen and, after the sample had been collected for a measured period of time, the loop was isolated, warmed rapidly to room temperature, and its contents injected onto the column. The transfer time between the reaction vessel and the sample loop was long enough to ensure virtually complete consumption of all free radical and atomic species before the sample was collected for analysis.

Two procedures were used to calibrate the gas chromatograph. In the first method, measured flow rates of the analytes were added to the gas stream flowing through the reactor in the absence of $O(^3P)$ and $N(^4S)$. The condensable material was collected in the sample loop in the same manner as described above and was injected into the gas chromatograph for analysis. In the second method, an aliquot of a calibration mixture of known composition was injected into the gas chromatograph for analysis. The mixture contained a known amount of acetonitrile, which was used as an internal standard. This was possible since the experiments with atomic oxygen always had a sufficient excess of acetonitrile that only a negligible amount was consumed by reaction. The results obtained with these methods agreed within the experimental uncertainty of the chromatographic measurements. The latter method was preferred because of its greater convenience and speed in that no trapping in the sample loop was required.

The method of calculating first-order rate constants was altered slightly from that used in our earlier work by using the Guggenheim first-order analysis (10) rather than simply fitting the data to a single exponential decay. This has the advantage of automatically correcting the light intensities for small amounts of stray light, which can be troublesome to measure and can lead to relatively large errors in the NO_2 chemiluminescence measurements at the longer reaction times. Briefly, this analysis requires that the data be divided into two sets containing an equal number of points. Pairs of points in the two sets are separated by a constant time interval. If the atom signals corresponding to the two sets are S_1 and S_2, and the signal decays as a single exponential, it may be shown that

$$\ln(S_1 - S_2) = -kt_1 + \ln[S_0(1 - \exp(-k\Delta t)]$$

Since the signal at "zero time", S_0, and the separation of points in the two data sets, Δt, are both constants, a plot of $\ln(S_1 - S_2)$ against t_1, the time for the set 1 data points, will be linear with slope equal to $-k$, the negative of the first-order rate constant. Some typical Guggenheim plots are found in Fig. 1. These plots typically had linear correlation coefficients of better than 99% and the first-order rate constants calculated from them had standard deviations of less than 5%.

As in some of our earlier work (8, 9), the organic reactants were found to adsorb strongly on the surface of the reaction vessel and desorbed very slowly. The effects of possible heterogeneous reactions of $O(^3P)$ were avoided as in the earlier work by measuring first-order rate constants of $O(^3P)$ removal with several large excesses of the organic reagent. The first-order rate constants were then plotted against the concentration of the organic reagent, giving good straight lines of the form

$$k_{obs} = k_0 + k_R[\text{nitrile}]$$

The intercept presumably reflects the composite of all constant first-order loss routes for $O(^3P)$ and the slope represents

Can. J. Chem. Downloaded from www.nrcresearchpress.com by 65.111.164.53 on 09/08/12
For personal use only.

Fig. 1. Guggenheim plots for first-order rate constants. (○) CH_3CN, 386 K, [O] = 1.91×10^{-8} mol L^{-1}, [CH_3CN] = 4.58×10^{-6} mol L^{-1}; (△) CH_3CN, 521 K, [O] = 6.56×10^{-9} mol L^{-1}, [CH_3CN] = 3.26×10^{-6} mol L^{-1}; (□) C_2H_5CN, 577 K, [O] = 6.70×10^{-9} mol L^{-1}, [C_2H_5CN] = 1.83×10^{-6} mol L^{-1}; (▽) C_2H_5CN, 354 K, [O] = 1.34×10^{-8} mol L^{-1}, [C_2H_5CN] = 3.98×10^{-6} mol L^{-1}

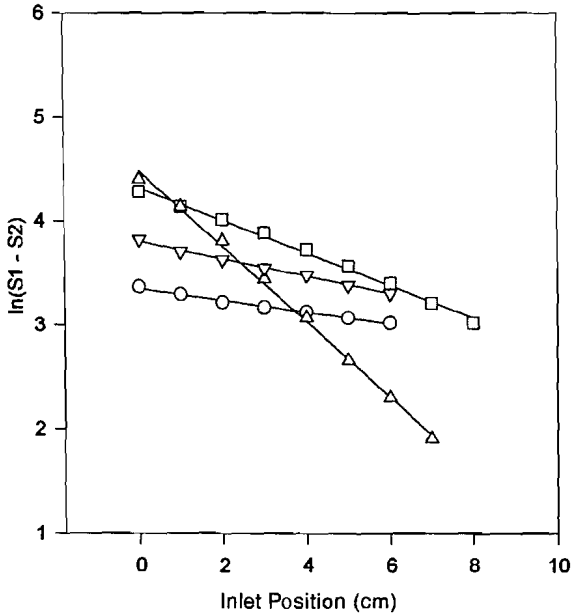

the second-order rate constant for homogeneous loss of $O(^3P)$. Interpretation of the intercepts is difficult, at best, since detailed analysis of the behaviour of a flow system operated in our configuration requires consideration of heterogeneous effects both upstream and downstream from the movable reactant inlet. Such analysis shows that the intercepts of plots such as those in Fig. 2 will be positive if heterogeneous atom loss is greater in the reaction zone than upstream from the reactant inlet, and negative if the reverse is true. Since the region upstream from the reaction zone contains both the surface of the movable reactant inlet and the reactor surface, it has a larger *S/V* than the reaction zone. Consequently, a negative intercept would be expected even for uniform wall conditions along the entire length of the reaction vessel. Some typical plots are found in Fig. 2. The linearity of these plots was not as good as that of the Guggenheim plots, partly because of the limited number of data points that could be obtained. However, in all cases the linear correlation coefficients were greater than 90% and in most cases greater than 98%. The slopes of the plots had standard deviations of less than 10%.

Results

The kinetic data for acetonitrile and propionitrile are summarized in Table 1 and Fig. 3. In both systems, good Arrhenius behaviour was observed within the scatter of the data. Also shown in Fig. 3 for comparison are the results of the flash photolysis experiments of Bonanno et al. (9) for acetonitrile. All three activation energies are within their combined standard deviations, while our Arrhenius preexponential factors are significantly larger than those obtained by Bonanno et al. As discussed later, this is likely to be due to a stoichiometric factor resulting from secondary reactions in our experiments that

Fig. 2. Concentration dependence of pseudo-first-order rate constants. (○) CH_3CN, 386 K; (□) CH_3CN, 521 K; (△) C_2H_5CN, 577 K; (▽) C_2H_5CN, 354 K.

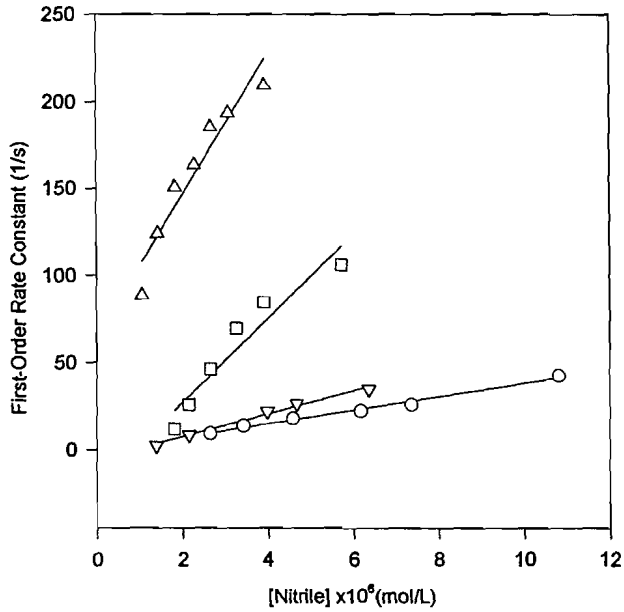

may not have been applicable under the conditions used by Bonanno et al.

The observation of effectively equal activation energies for the reactions of $O(^3P)$ with acetonitrile and propionitrile differs significantly from the behaviour found for the reactions of $O(^3P)$ with alcohols (1, 7) and with ketones (2, 8) in which lengthening and branching of the aliphatic chain significantly reduced the activation energy of the reaction. This lends support to the suggestion by Bonanno et al. that the main channel in the reaction of $O(^3P)$ with acetonitrile is addition to the CN group. On the other hand, the activation energies are comparable to or slightly larger than those for the reactions of $O(^3P)$ with alcohols and ketones while the preexponential factors are comparable to those for the reactions of $O(^3P)$ with ketones (1–8). If the reactions of $O(^3P)$ with nitriles were to proceed by addition, the activation energies would be expected to be much smaller and perhaps negative. If addition is the mode of attack, it seems that the addition complex must undergo a rearrangement requiring a significant activation energy before it decomposes to products.

The two possibilities for the initial mode of attack of $O(^3P)$ on acetonitrile, abstraction and addition, lead to the mechanisms outlined in Table 2. The addition mechanism is based on the reactions suggested by Bonanno et al., initiated by reaction [1*a*], with the inclusion of some additional secondary reactions such as reaction [4] that might be involved. The addition mechanism is invoked by setting A_{1b} equal to zero and A_{1a} equal to 4.38×10^8. The abstraction mechanism is initiated by reaction [1*b*] and is invoked by setting A_{1a} equal to zero and A_{1b} equal to 4.38×10^8. Otherwise, it differs from the addition mechanism only in the absence of reaction [11] for which the necessary OCN intermediate is no longer formed. It will be noted that only one loss route for the OCN radical is included. Hydrogen abstraction from CH_3CN by this radical has been omitted because the available kinetic data (17) for such reactions of OCN suggest that the rate constant would be

Table 1. Summary of kinetic data.

Temperature (K)	Pressure (Torr)	$[O]_0 \times 10^8$ (mol L^{-1})	[Nitrile] $\times 10^6$ (mol L^{-1})	k_{obs} (s^{-1})	$k_R \times 10^{-6}$ (L mol^{-1} s^{-1})
O + acetonitrile					
321	0.97	1.85	2.57	16.3	1.7 ± 0.2
	0.92	1.63	5.35	22.1	k_0 = 13 ± 2
	1.01	1.67	8.82	30.9	r = 0.97
	1.03	1.59	11.8	35.0	
	1.03	1.47	14.6	36.2	
367	1.09	2.65	4.43	13.9	3.6 ± 0.4
	1.07	2.56	4.95	14.5	k_0 = 0 ± 2
	1.11	2.60	5.92	19.2	r = 0.98
	1.12	2.58	6.72	17.0	
	1.09	2.44	7.76	24.1	
	1.11	2.26	11.6	39.1	
386	1.04	2.00	2.65	9.50	3.8 ± 0.2
	1.04	1.97	3.42	13.9	k_0 = 0 ± 1
	1.04	1.91	4.58	17.7	r = 0.99
	1.06	1.87	6.17	22.2	
	1.06	1.81	7.35	25.9	
	1.08	1.68	10.8	42.8	
388	1.04	0.993	3.33	19.5	4.1 ± 0.7
	1.00	0.948	3.60	13.1	k_0 = 3 ± 3
	1.01	0.930	4.69	22.7	r = 0.94
	1.01	0.902	5.83	25.9	
	1.04	0.914	6.47	27.0	
	0.99	0.855	6.59	32.1	
	1.00	0.839	7.99	32.5	
	1.02	0.857	8.02	35.0	
394	1.09	2.19	3.06	1.41	6.3 ± 0.6
	1.09	2.12	4.52	16.0	k_0 = −14 ± 3
	1.08	2.04	5.61	22.6	r = 0.98
	1.08	2.01	6.09	25.4	
	1.12	2.01	7.67	35.6	
	1.12	1.92	9.34	41.5	
417	1.10	4.50	2.75	1.80	12.0 ± 0.7
	1.12	4.50	3.44	13.8	k_0 = −29 ± 2
	1.10	4.33	4.19	20.7	r = 0.99
	1.12	4.35	4.80	29.4	
	1.14	4.27	6.19	44.0	
438	1.13	0.249	2.79	8.98	11.5 ± 0.5
	1.14	0.247	3.37	11.9	k_0 = −25 ± 2
	1.15	0.244	4.28	23.0	r = 0.99
	1.15	0.237	5.28	36.1	
	1.16	0.230	6.80	53.7	
456	1.11	1.54	1.89	4.09	10.8 ± 0.6
	1.12	1.53	2.48	13.8	k_0 = −14 ± 2
	1.12	1.50	3.22	20.6	r = 0.99
	1.12	1.47	3.90	31.5	
	1.13	1.45	4.80	39.7	
	1.13	1.36	6.87	58.7	
478	1.10	0.222	1.70	11.0	12 ± 2
	1.09	0.216	2.48	19.3	k_0 = −5 ± 9
	1.12	0.214	3.69	41.1	r = 0.97
	1.12	0.204	5.26	69.2	
	1.14	0.186	8.66	90.2	

Can. J. Chem. Downloaded from www.nrcresearchpress.com by 65.111.164.53 on 09/08/12
For personal use only.

Table 1 (*continued*).

Temperature (K)	Pressure (Torr)	$[O]_0 \times 10^8$ (mol L^{-1})	[Nitrile] $\times 10^6$ (mol L^{-1})	k_{obs} (s^{-1})	$k_R \times 10^{-6}$ (L mol^{-1} s^{-1})
502	1.14	1.60	1.64	5.04	16 ± 2
	1.13	1.55	2.25	17.6	k_0 = −14 ± 9
	1.15	1.54	3.23	42.7	r = 0.97
	1.15	1.49	4.23	60.9	
	1.16	1.47	4.97	75.4	
	1.16	1.37	7.09	90.1	
521	1.17	0.673	1.81	11.8	24 ± 4
	1.16	0.660	2.15	25.8	k_0 = −21 ± 12
	1.17	0.662	2.66	46.5	r = 0.96
	1.18	0.656	3.26	69.6	
	1.17	0.632	3.91	84.4	
	1.18	0.608	5.72	106	
O + propionitrile					
354	1.04	1.42	1.38	2.5	6.5 ± 0.4
	1.04	1.40	2.15	8.6	k_0 = −5 ± 1
	1.04	1.34	3.98	22.0	r = 1.00
	1.04	1.32	4.67	26.1	
	1.04	1.27	6.35	34.6	
382	1.03	1.24	2.94	49.2	8.6 ± 1.3
	1.06	1.26	3.61	50.8	k_0 = 22 ± 2
	1.04	1.22	4.06	55.8	r = 0.96
	1.04	1.21	4.45	61.9	
	1.04	1.19	4.92	64.7	
404	1.05	0.677	2.90	58.8	9.9 ± 1.5
	1.02	0.648	3.45	72.3	k_0 = 36 ± 4
	1.02	0.643	3.77	77.2	r = 0.95
	1.03	0.637	4.45	81.0	
	1.04	0.634	4.98	86.4	
	1.03	0.617	5.60	93.7	
	1.04	0.617	5.95	89.8	
430	1.01	0.578	1.87	51.1	15 ± 2
	1.03	0.581	2.33	64.7	k_0 = 30 ± 6
	1.00	0.559	2.73	75.5	r = 0.95
	1.02	0.562	3.18	78.4	
	1.02	0.551	3.90	93.9	
	1.02	0.543	4.39	97.1	
	1.01	0.530	4.85	94.1	
461	1.05	0.538	1.22	56.1	17 ± 3
	1.04	0.527	1.63	76.0	k_0 = 47 ± 10
	1.05	0.523	2.23	94.3	r = 0.93
	1.02	0.494	3.13	112	
	1.06	0.499	4.13	119	
	1.05	0.486	4.63	119	
464	1.11	0.228	1.20	29.6	25 ± 1
	1.10	0.223	1.61	45.9	k_0 = 2 ± 2
	1.11	0.223	1.96	50.0	r = 1.00
	1.11	0.220	2.41	60.6	
	1.12	0.218	3.08	80.9	
	1.12	0.211	4.30	109	
477	1.09	0.886	2.11	72.6	20 ± 5
	1.09	0.868	2.81	98.3	k_0 = 35 ± 7
	1.10	0.868	3.14	92.3	r = 0.93
	1.09	0.848	3.57	111	
	1.10	0.845	4.02	111	

Can. J. Chem. Downloaded from www.nrcresearchpress.com by 65.111.164.53 on 09/08/12
For personal use only.

Table 1 (*concluded*).

Temperature (K)	Pressure (Torr)	$[O]_0 \times 10^8$ (mol L^{-1})	[Nitrile] $\times 10^6$ (mol L^{-1})	k_{obs} (s^{-1})	$k_R \times 10^{-6}$ (L mol^{-1} s^{-1})
496	1.15	0.972	1.27	59.2	38 ± 3
	1.15	0.963	1.59	70.5	k_0 = 13 ± 6
	1.15	0.956	1.84	85.2	r = 0.99
	1.15	0.947	2.22	104	
	1.15	0.928	2.90	133	
	1.16	0.911	3.82	154	
522	1.12	0.751	1.07	64.4	45 ± 2
	1.13	0.756	1.12	21.0	k_0 = 15 ± 4
	1.12	0.739	1.58	83.3	r = 1.00
	1.10	0.705	2.52	133	
	1.12	0.696	3.48	170	
534	1.13	1.29	1.00	52.7	34 ± 3
	1.10	1.23	1.54	76.9	k_0 = 25 ± 8
	1.09	1.19	2.42	118	r = 0.99
	1.12	1.19	3.28	136	
	1.10	1.12	4.32	166	
552	1.14	1.20	1.13	69.8	40 ± 3
	1.13	1.18	1.40	85.2	k_0 = 34 ± 9
	1.12	1.15	1.75	111	r = 0.98
	1.13	1.14	2.30	136	
	1.13	1.12	2.94	146	
	1.13	1.10	3.52	179	
	1.13	1.08	4.09	188	
577	1.17	0.668	1.07	88.6	41 ± 6
	1.19	0.672	1.42	124	k_0 = 65 ± 14
	1.20	0.670	1.83	151	r = 0.96
	1.20	0.660	2.28	164	
	1.20	0.652	2.67	186	
	1.21	0.649	3.08	193	
	1.21	0.631	3.93	210	

Can. J. Chem. Downloaded from www.nrcresearchpress.com by 65.111.164.53 on 09/08/12
For personal use only.

Fig. 3. Arrhenius plots for reactions of $O(^3P)$ with nitriles. (○) CH_3CN, this work; (□) CH_3CN, data of ref. 9; (△) C_2H_5CN, this work.

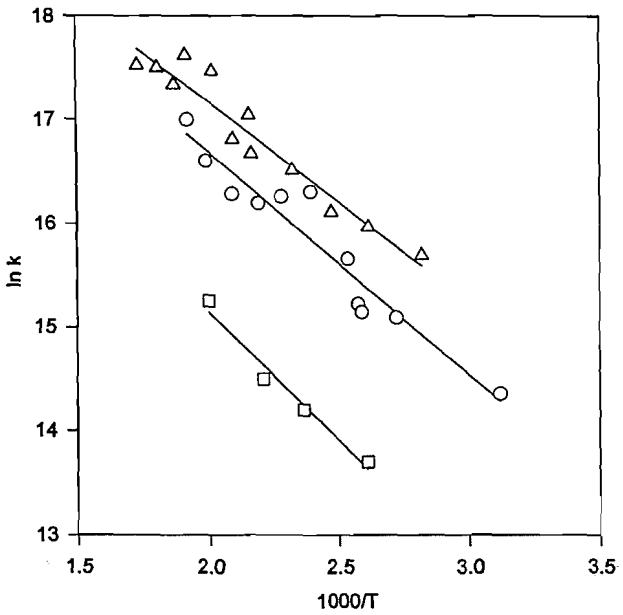

too small to enable it to compete effectively with reaction [11]. Addition of OCN to CH_3CN has also been omitted for the same reason. Also given in these tables are the kinetic parameters for the reactions that have been reported in the literature. In only two cases are direct measurements of these parameters not available and in both cases reasonable estimates can be made.

It should be possible to test these mechanisms by product analysis. The most obvious difference between them is the production of NO in only the addition mechanism. However, the two mechanisms also differ in their sources of OH and HCN and should lead to different relative yields of HCN and H_2O. We must rely largely on analytical data for the yields of these latter products since we were unable to analyse reliably for NO. This results from its incomplete trapping at liquid nitrogen temperature. Moreover, the necessity to use a thermal conductivity detector for H_2O and HCN resulted in comparatively poor sensitivity for H_2CO. While formaldehyde was well resolved from the other possible reaction products in chromatograms of standard mixtures, the detection sensitivity was too poor to detect it in the yields that would have been produced under our reaction conditions.

Yields of reaction products were measured with [nitrile]/$[O(^3P)]$ ratios in the range 5–30. These ratios are some 10–100

Table 2. Summary of the reaction mechanism for $O + CH_3CN$.

Reaction	*A*-factor ($L\ mol^{-1}\ s^{-1}$)	Activation energy ($kJ\ mol^{-1}$)	Reference
[1*a*] $O + CH_3CN \rightarrow CH_3 + OCN$	4.38×10^8	20	9
[1*b*] $O + CH_3CN \rightarrow OH + CH_2CN$	4.38×10^8	20	9
[2] $O + OH \rightarrow O_2 + H$	1.21×10^{10}	−0.93	11
[3] $O + CH_3CN \rightarrow CH_2O + CN$	8.43×10^{10}	0	[a]
[4] $O + CH_2O \rightarrow OH + HCO$	1.76×10^{10}	12.8	12
[5] $O + CH_3 \rightarrow CH_2O + H$	8.43×10^{10}	0	11
[6] $OH + CH_3CN \rightarrow H_2O + CH_2CN$	3.78×10^8	8.56	13
[7] $H + CH_3CN \rightarrow CH_3 + HCN$	2.04×10^9	33	14
[8] $CN + CH_3CN \rightarrow HCN + CH_2CN$	3.89×10^{10}	9.89	15
[9] $CH_3 + CH_3CN \rightarrow CH_4 + CH_2CN$	1.0×10^7	0	[b]
[10] $O + HCO + OH + CO$	3.01×10^{10}	0	11
[11] $O + OCN \rightarrow CO + NO$	1.00×10^{10}	0	17

[a]No direct value available. Assumed to be the same as reaction [5].
[b]Upper limit. This value is given for 1000 K in ref. 16.

times smaller than those used in the kinetic measurements, but this was necessary in order to produce large enough quantities of reaction products for analysis in a reasonable length of time. Both H_2O and HCN were found in the products of the reaction of atomic oxygen with acetonitrile and the results are summarized in Table 3. The yields of HCN were generally more reproducible than those of H_2O. The yields of H_2O were roughly five times as large as the yields of HCN and this ratio showed no systematic variation with temperature and [nitrile]/[$O(^3P)$] ratio within the scatter of the data. The yields of HCN amounted to some 5–15% of the oxygen atom consumption, increasing somewhat with increasing temperature. The yields of water ranged from about 30% of the oxygen atom consumption at 304 K to about 50% at 552 K. In all these measurements, strong adsorption of acetronitrile was evident, as easily measurable peaks were obtained for acetonitrile in chromatograms of material collected in the traps a considerable time after the acetonitrile flow had been turned off. To minimize the effects of adsorbed acetonitrile on the chromatographic analysis, a blank was run as the first measurement each day before the actonitrile had been turned on. Product yields were then measured for systematically increasing flow rates of acetonitrile. The observation of yields of water that were larger than those of HCN was unexpected in view of the failure of Bonanno et al. to find a primary deuterium kinetic isotope effect. On the surface, the implication of the significant water yields could be that the reaction was initiated to a significant degree by hydrogen abstraction and that the OH formed in this way was producing the water found in the product analysis. On the other hand, the reaction of OH with acetonitrile has been studied (13) and is evidently too slow to be able to produce the amount of water found in our experiments.

Theoretical product yields were calculated for comparison with the measured yields by numerical integration of the set of differential equations for the system of reactions summarized in Table 2, using the kinetic parameters given in that table. The calculations used the LSODE subroutine for stiff systems of differential equations, included in a computer program that we have used in other work (18). Both the abstraction- and addition-initiated mechanisms predicted yields of water that were roughly two orders of magnitude smaller than the measured values. The yields of HCN were predicted to be some five to ten times the measured yields. The calculated yields of HCN could be made comparable to the experimentally measured yields if the rate constant for the reaction

[3] $O + CH_2CN \rightarrow CH_2O + CN$

was decreased by factor of 10 from the estimate given in Table 2. However, the yield of water was unaffected. The only reaction that had a significant impact on the yield of water was

[6] $OH + CH_3CN \rightarrow H_2O + CH_2CN$

but the rate parameters for this reaction were measured by direct experiment (13) and the increase in the rate constant for this reaction that would be required to make the water yield agree with our experiments was far greater than would be permitted by reasonable uncertainty limits for the directly measured kinetic parameters. Finally, the rates of consumption of atomic oxygen calculated from either the addition or the abstraction mechanism were very much greater than those measured in our experiments. It seemed clear that the extent of secondary reactions consuming $O(^3P)$ was seriously overestimated by the mechanism outlined in Table 2.

A plausible solution to the difficulties outlined above was suggested by the strong adsorption of acetonitrile on the walls of the reaction vessel, referred to earlier. If one estimates the number of collisions of OH radicals, present in concentrations of the magnitude predicted by the kinetic model, with the walls of our reaction vessel during the time period used for collecting the products for chromatographic analysis, the measured yields of water would be obtained if many of these collisions led to heterogeneous production of water. This seems reasonable since the CN group is likely to be closest to the glass surface so that the CH_3 groups would be exposed to the OH radicals striking the surface. When a heterogeneous first-order reaction of OH with CH_3CN adsorbed on the walls of the reactor, producing water, is inserted in the model, with a rate constant estimated from the collision frequency with the walls of the reaction vessel, the calculated yields of water and HCN predicted by the addition mechanism were brought into good

Can. J. Chem. Downloaded from www.nrcresearchpress.com by 65.111.164.53 on 09/08/12
For personal use only.

Can. J. Chem. Downloaded from www.nrcresearchpress.com by 65.111.164.53 on 09/08/12
For personal use only.

Table 3. Summary of product analysis for O + CH_3CN.

Temperature (K)	$[CH_3CN]/[O]$	$[HCN]/[O]$		$[H_2O]/[O]$	
		Measured	Calculated	Measured	Calculated
552	10.8	0.067	0.069	0.45	0.34
508	8.0	0.040	0.051	0.53	0.37
508	9.6	0.047	0.056	0.50	0.36
508	17.0	0.076	0.075	—	—
508	18.2	0.083	0.083	—	—
439	8.3	0.086	0.098	0.24	0.38
439	15.6	0.12	0.12	0.39	0.34
439	20.1	0.14	0.13	—	—
375	13.0	0.034	0.033	0.23	0.23
375	14.9	0.039	0.039	—	—
375	21.7	0.046	0.048	0.20	0.35
375	37.1	0.061	0.073	0.27	0.32
304	24.4	0.042	0.055	0.36	0.35
304	31.4	0.058	0.069	—	—

Fig. 4. Comparison of kinetic data for CH_3CN obtained experimentally and with the four potential reaction mechanisms. (○) Experimental data, this work; (□) experiments of ref. 9; (----) calculated for initiation by addition with wall reactions; (·····) calculated for initiation by addition without wall reactions; (-·-·) calculated for initiation by abstraction with wall reactions; (-···-) calculated for initiation by abstraction without wall reactions.

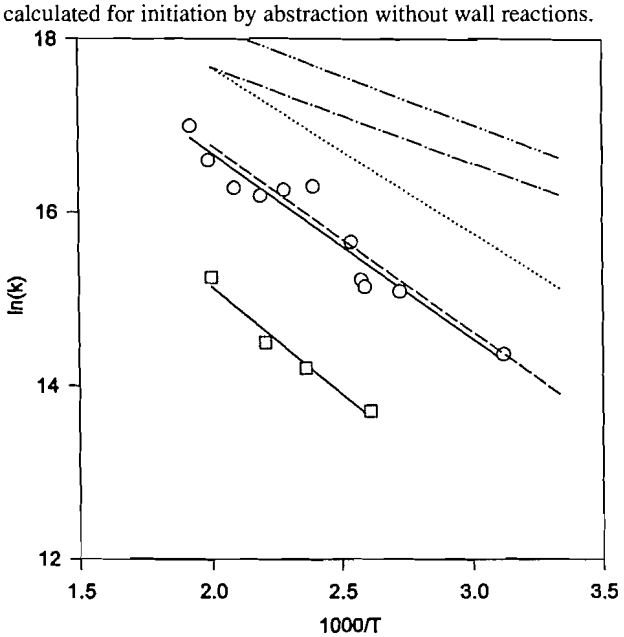

agreement with the measured yields. The quality of the agreement with experiment did not change as the rate constant for the heterogeneous reaction was substantially reduced. As few as 0.5% of the collisions of OH with the walls were required to provide acceptable agreement with the experimental results. The abstraction mechanism still did not provide good agreement with the experimental yields. Inclusion to a comparable extent of the analogous heterogeneous reactions of the other reaction intermediates such as H and CH_2CN had no discernable effect on the calculated yields of HCN or H_2O. The extent of agreement with the measured yields of HCN the H_2O is indicated in Table 3. The fundamental significance of these results is somewhat limited because of the intrinsic variability of surface conditions in such experiments. Indeed, variations in surface conditions are likely to be responsible for much of the scatter in the product analysis. The main value of these results is in confirming that heterogeneous reactions are a plausible explanation of the behaviour observed experimentally.

Perhaps the most convincing evidence in support of the mechanism initiated by reaction [1*a*], addition of $O(^3P)$ to CH_3CN, is found in the data summarized in Fig. 4. These data, both experimental and calculated from the mechanism, are based on the rate of loss of $O(^3P)$ at much larger [nitrile]/$[O(^3P)]$ ratios than those used to measure the product yields. In that figure are presented (*i*) the experimental kinetic data from ref. 9, (*ii*) our experimental kinetic data, and the rate constants calculated from the rates of $O(^3P)$ consumption calculated theoretically from the models for (*iii*) abstraction without wall reactions, (*iv*) abstraction with wall reactions, (*v*) addition without wall reactions, and (*vi*) addition with wall reactions. It is clear that the only model that provides agreement with our experimental data is the model initiated by reaction [1*a*], the addition channel. In that case, use of the kinetic parameters reported by Bonanno et al. (9) leads to virtually exact agreement with our kinetic measurements over the entire temperature range covered by our experiments. On that basis, we estimate that a stoichiometric factor of (1/7) ± 20% should be applied to our experimental rate constants, since these are approximately seven times as large as those calculated from the Arrhenius temperature dependence of ref. 9.

The results obtained for the reaction of $O(^3P)$ with propionitrile were similar to those for acetonitrile. The yield of HCN was again some 5–15% of the consumption of atomic oxygen. The yields of water were somewhat larger, up to an amount approximately equivalent to the consumption of atomic oxygen. However, very few kinetic data are available for the relevant secondary reactions so it is not clear to what extent heterogeneous reactions are responsible for the increased water yields. Nevertheless, the similarity of the kinetic behav-

iour of the reactions of atomic oxygen with acetonitrile and propionitrile suggests that both reactions occur by similar mechanisms involving initiation by addition of $O(^3P)$ to the CN bond, followed by decomposition of the addition complex to give intermediates that lead to the final products.

Acknowledgement

This work was supported by an operating grant from the Natural Sciences and Engineering Research Council of Canada.

References

1. C.M. Owens and J.M. Roscoe. Can. J. Chem. **54**, 984 (1976).
2. J.H. Lee and R.B. Timmons. Int. J. Chem. Kinet. **9**, 133 (1977).
3. A.L. Ayub and J.M. Roscoe. Can. J. Chem. **57**, 1269 (1979).
4. H.H. Grotheer and Th. Just. Chem. Phys. Lett. **78**, 71 (1981).
5. D.G. Keil, T. Tanzawa, E.G. Skolnik, R.B. Klemm, and J.V. Michael. J. Chem. Phys. **75**, 2693 (1981).
6. R.L. Failes, D.L. Singleton, G. Paraskevopoulos, and R.S. Irwin. Int. J. Chem. Kinet. **14**, 371 (1982).
7. J.M. Roscoe. Can. J. Chem. **61**, 2716 (1983).
8. J.M. Roscoe. Can. J. Chem. **64**, 1458 (1986).
9. R.J. Bonanno, R.B. Timmons, L.J. Stief, and R.B. Klemm. J. Chem. Phys. **66**, 92 (1977).
10. D.P. Shoemaker, C.W. Garland, and J.W. Nibeler. Experiments in physical chemistry. 5th ed. McGraw-Hill, New York. 1989. pp. 289–290.
11. D.L. Baulch, C.J. Cobos, R.A. Cox, C. Esser, P. Frank, Th. Just, J.A. Kerr, M.J. Pilling, J. Troe, R.W. Walker, and J. Warnatz. J. Phys. Chem. Ref. Data, **21**, 411 (1992).
12. R.B. Klemm, E.G. Skolnik, and J.V. Michael. J. Chem. Phys. **72**, 1256 (1980).
13. M.J. Kurylo and G.L. Knable. J. Phys. Chem. **88**, 3305 (1984).
14. J.W.S. Jamieson, G.R. Brown, and J.S. Tanner. Can. J. Chem. **48**, 3619 (1970).
15. S. Zabarnick and M.C. Lin. Chem. Phys. **134**, 185 (1989).
16. E. Metcalfe, D. Booth, H. McAndrew, and W.D. Wooley. Fire Mater. **7**, 185 (1983).
17. F. Westley, D.H. Frizzell, J.T. Herron, R.F. Hampson, and W.G. Maillard. NIST Standard Reference Database 17, Ver. 5.0. 1993.
18. M.J. MacDonald and J.M. Roscoe. J. Photochem. Photobiol. A: **57**, 441 (1991).

Can. J. Chem. Downloaded from www.nrcresearchpress.com by 65.111.164.53 on 09/08/12
For personal use only.

Synthesis of 5-substituted pyrrole-2-carboxaldehydes. Part I. Generation of formal 5-lithiopyrrole-2-carboxaldehyde equivalents by bromine–lithium exchange of 2-bromo-6-(diisopropylamino)-1-azafulvene derivatives[1]

Sylvie L. Berthiaume, Brian L. Bray, Petr Hess, Yanzhou Liu, Michael L. Maddox, Joseph M. Muchowski, and Markus E. Scheller

Abstract: The first known lithiated 1-azafulvene derivatives, e.g., **8** and **13***a*, were generated by a low-temperature bromine–lithium exchange procedure with *tert*-butyllithium. These lithio species show substantial stability at ≤–90°C because, at these temperatures, the sterically demanding 6-diisopropylamino moiety, unlike the dimethylamino group, completely inhibits nucleophilic addition to C-6. At higher temperatures, the addition of *tert*-butyllithium to C-6 is significant and it can become the dominant process. The lithio species **8** is a useful formal equivalent of 5-lithiopyrrole-2-carboxaldehyde since, on reaction with electrophilic reagents and subsequent hydrolysis, a wide variety of regiochemically pure 5-substituted pyrrole-2-carboxaldehydes is formed. The 6-dialkylamino-1-azafulvenes described herein exist predominantly or exclusively as the *syn* conformer in solution at room temperature. This conformational preference is confirmed by a significance NOE effect between H-4 and H-6 in the parent diisopropylamino compound **3***f*. The origin of the *syn* conformational preference stems from a substantial contribution of the charge-separated form **16** to the ground state structure of these compounds, a phenomenon that is strongly supported by variable temperature NMR measurements on 2-bromo-6-diisopropylamino-1-azafulvene (**3***c*).

Key words: 2-bromo-6-diisopropylamino-1-azafulvenes, stereochemistry, lithiation, pyrrole-2-carboxaldehydes.

Résumé : On a préparé les premiers dérivés 1-azafulvène lithiés connus, **8** et **13***a*, par une méthode d'échange du brome et du lithium, à basse température, utilisant du *tert*-butyllithium. Ces espèces lithiées présentent une stabilité importante à des températures ≤ –90°C parce que, à ces températures, la portion 6-diisopropylamino, qui possède une demande stérique importante par rapport à celle du groupe diméthylamino, inhibe complètement l'addition nucléophile en C-6. À des températures plus élevées, l'addition du *tert*-butyllithium en C-6 devient importante et, dans quelques cas, elle peut devenir prédominante. L'espèce lithiée **8** est un équivalent formel utile du 5-lithiopyrrole-2-carboxaldéhyde puisque, par réaction avec des réactifs électrophiles et hydrolyse subséquente, il y a formation d'une grande variété de pyrrole-2-carboxaldéhydes substitués en position 5 régiochimiquement purs. En solution, à la température ambiante, les 6-dialkylamino-1-azafulvènes décrits dans le présent travail existent exclusivement ou d'une façon prédominante comme conformères *syn*. Cette préférence conformationnelle est confirmée par un EON important entre les H-4 et H-6 du composé parent diisopropylamino **3***f*. La préférence conformationnelle *syn* provient d'une contribution

Received December 12, 1994.

This paper is dedicated to Professor Charles W. Jefford, University of Geneva, on the occasion of his 65th birthday.

S. L. Berthiaume, B.L. Bray,[2] Petr Hess,[3] Y. Liu, M.L. Maddox, J.M. Muchowski,[4] and M.E. Scheller.[5] Syntex Research, Institute of Organic Chemistry, 3401 Hillview Avenue, Palo Alto, CA 94304, U.S.A.

[1] Contribution No. 903 from Syntex Institute of Organic Chemistry.
[2] Syntex Research Postdoctorate Fellow, 1987–1989.
[3] Syntex Research Postdoctorate Fellow, 1987–1988.
[4] Author to whom correspondence may be addressed. Telephone: (415) 855-5050.
[5] Syntex Research Postdoctorate Fellow, 1985–1986.

Can. J. Chem. Downloaded from www.nrcresearchpress.com by 65.111.164.53 on 09/08/12
For personal use only.

substantielle de la forme **16**, ayant une séparation de charge, à la structure de l'état fondamental; il s'agit d'un phénomène qui est fortement supporté par des mesures de RMN à température variable sur le 2-bromo-6-diisopropylamino-1-azafulvène (**3***c*).

Mots clés : 2-bromo-6-diisopropylamino-1-azafulvènes, stéréochimie, lithiation, pyrrole-2-carboxaldéhyde.

[Traduit par la rédaction]

Can. J. Chem. Downloaded from www.nrcresearchpress.com by 65.111.164.53 on 09/08/12
For personal use only.

Introduction

Substituted pyrrole-2-carboxaldehydes are synthetic intermediates of much importance (1–5). The most generally useful synthesis of these compounds is by the Vilsmeier–Haack formylation of the appropriate 2-substituted pyrrole (6). This process is, however, associated with the inconvenience of requiring the separate preparation of each 2-substituted pyrrole, and has the limitation that a deactivating substituent (at C-2) gives rise to a mixture in which the 4-formylated compound (kinetic product) is a significant or even the major component (1, 4, 6). We have devised two complementary routes to 5-substituted pyrrole-2-carboxaldehydes based on the generation of 5-lithiopyrrole-2-carboxaldehyde equivalents of a nature such that there is no need for pyrrole N-protection.[6] One of these involves the lithiation of the easily prepared 6-(dimethylamino)-1-azafulvene dimer and its 3-bromo derivative (8). The other concerns the bromine–lithium exchange of the stable monomeric 2-bromo-6-(diisopropylamino)-1-azafulvenes. Herein are found the full details of the latter process as well as information on the synthesis and some of the properties of such azafulvenes (for preliminary communications, see ref. (9)).

The first 2-halo-6-(dialkylamino)-1-azafulvenes were prepared by von Dobeneck and co-workers (10) by reaction of 3,4-dialkyl-3-pyrrolin-2-ones with the Vilsmeier–Haack reagents derived from DMF and $POCl_3$ or $POBr_3$ followed by basification under mild conditions. Such compounds have also been obtained by the sodium hydride deprotonation of the di- and tribromination products of the ternary iminium perchlorates derived from pyrrole-2-carboxaldehyde (11). von Dobeneck and co-workers (10) showed that these azafulvenes were particularly susceptible to nucleophilic addition at C-6, undergoing a variety of addition elimination reactions[7] including hydrolysis to the corresponding aldehydes. We recognized that if this proclivity for nucleophilic addition could be reduced, halogen–lithium exchange at C-2 would produce a lithiated 1-azafulvene functionally equivalent to a 5-lithiopyrrole-2-carboxaldehyde derivative.

Results and discussion

Synthesis of the azafulvenes

2-Bromo-6-dimethylamino-1-azafulvene (**3***a*, Scheme 1) was the first azafulvene unsubstituted at C-3,4 that we prepared. This compound was obtained by deprotonation (10, 11) of the iminium salt **2***a* with aqueous sodium hydrogen carbonate. When prepared by this route, compound **3***a* was always contaminated with a small amount of the 2-chloro compound **3***b*, which stemmed from the hydrogen chloride induced bromine–chlorine exchange during the formation of **2***a* by the Vilsmeier–Haack reaction on 2-bromopyrrole (**1***a*).[8] The halogen exchange problem was solved (13) by conversion of the iminium salts **2***d,e* into the covalent Strecker-type nitriles (**4**), which underwent highly regioselective bromination at C-5 at –70°C with *N*-bromosuccinimide. These bromo compounds (**5**) were converted into the 2-bromoazafulvenes **3***c* and the 6-methyl compound **3***e* by sequential treatment with aqueous hydrochloric acid and sodium hydroxide, a process that proceeds via the iminium salts **2** (not isolated).

The azafulvenes **3***c* and **3***d* could also be generated, in modest yields, by heating the carboxaldehydes **6***a* and **6***c* with excess diisopropylamine. This condensation was expected based on the observation of Kira et al. (14) that 4- and 5-nitropyrrole-2-carboxaldehydes were converted into the corresponding stable azafulvenes with unhindered secondary amines in ethanol at room temperature.

As expected (see below), the brominated 6-diisopropylamino-1-azafulvenes **3***c* and **3***d* showed pronounced resistance to nucleophilic attack at C-6. Thus, complete hydrolysis of **3***c* to the carboxaldehyde **6***a* with excess sodium hydroxide (6 equiv.) in aqueous methanol at room temperature required 5 h (13)[9] whereas the 6-dimethylamino compound **3***a* already reacted at 0°C. The significant stability of **3***c* suggested that the parent compound itself ought to be isolable. Indeed, deprotonation of the iminium salt **2***e* with triethylamine at room temperature efficiently generated **3***f*, which, though sensitive to hydrolysis, is indefinitely stable in the absence of water and, in contrast to the 6-dimethylamino congener, shows no tendency whatsoever to dimerize (15).

Bromine–lithium exchange of the bromoazafulvenes

Reaction of 2-bromo-6-dimethylamino-1-azafulvene (**3***a*) with 2 equivalents of *tert*-butyllithium in THF at –78°C and subsequent quenching of the reaction mixture with water or other electrophilic reagents gave variable amounts of the highly unstable amine **7***a* (Scheme 2). In no case were products derived from the 2-lithiated azafulvene observed. In contrast, bromine–lithium exchange of the 6-diisopropylamine compound **3***c* under the same conditions, followed by reaction

[6] The generation of C-lithiopyrroles by halogen–lithium exchange of N-unsubstituted halogenopyrroles has been accomplished at least twice (7). In contrast, 2-bromo-1*H*-pyrrole is not C-lithiated even with excess *t*-BuLi in THF. J.M. Muchowski and R. Naef. Unpublished data.

[7] For a review on the synthesis and properties of this general class of compounds see ref. 12.

[8] The extent of this exchange, which must occur by protonation of **2***a* at C-4, is dependent on the length of time that this salt remains in contact with the reaction medium. Thus hydrolysis to the aldehyde immediately upon consumption of **1***a* gave a 95:5 mixture of aldehydes **6***a* and **6***b* whereas hydrolysis after 24 h gave a 1:1 mixture of **6***a* and **6***b*.

[9] It was previously erroneously reported (13) that the hydrolysis of **3***a* (compound **5***a* in ref. 13) required 5 h at room temperature. The hydrolysis conditions given are actually those for the conversion of **3***c* to the aldehyde **6***a* (i.e., **5***b* to **6***a* in ref. 13, p. 1307).

Scheme 1

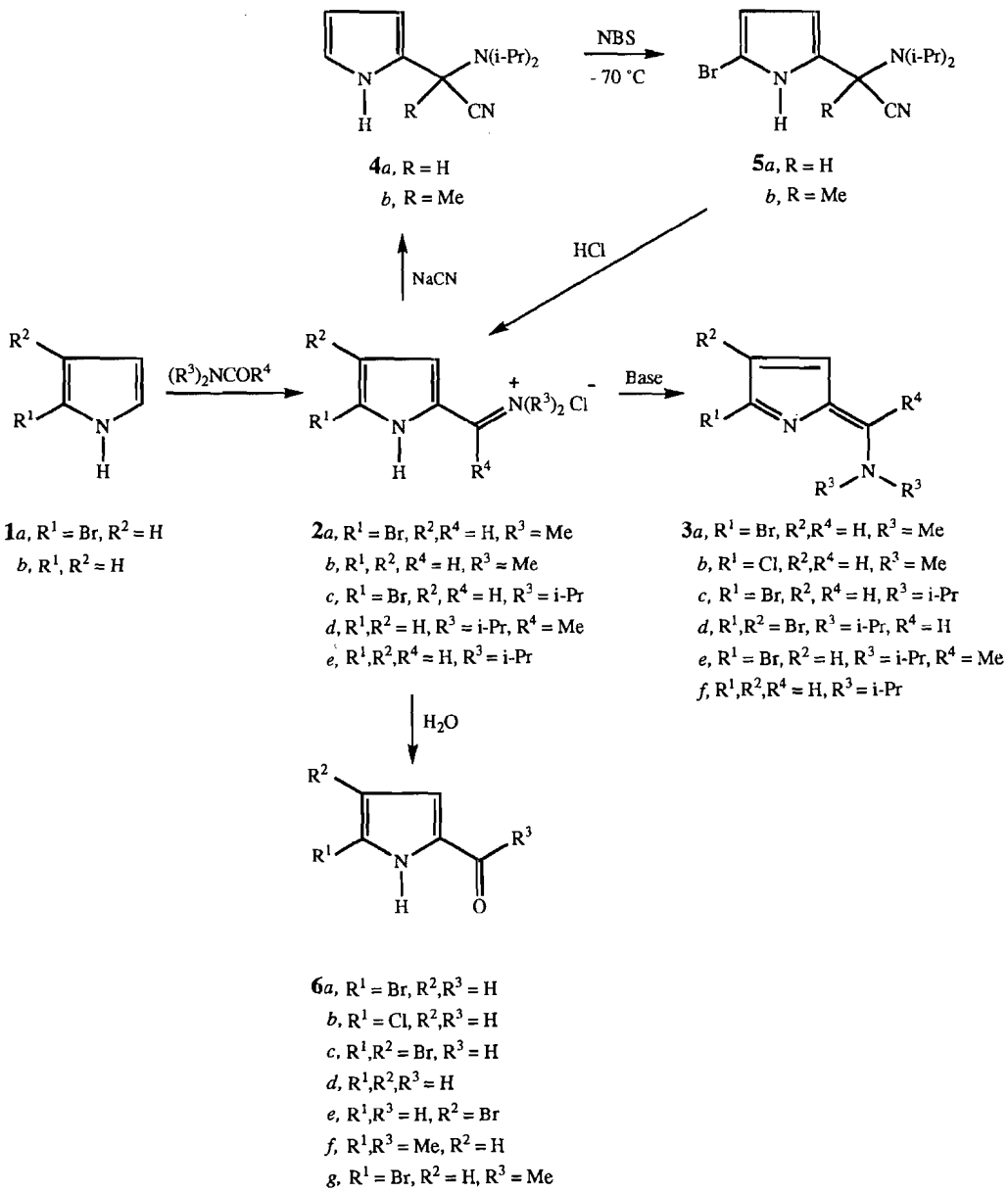

4*a*, R = H
b, R = Me

5*a*, R = H
b, R = Me

1*a*, R^1 = Br, R^2 = H
b, R^1, R^2 = H

2*a*, R^1 = Br, R^2,R^4 = H, R^3 = Me
b, R^1, R^2, R^4 = H, R^3 = Me
c, R^1 = Br, R^2, R^4 = H, R^3 = i-Pr
d, R^1,R^2 = H, R^3 = i-Pr, R^4 = Me
e, R^1,R^2,R^4 = H, R^3 = i-Pr

3*a*, R^1 = Br, R^2,R^4 = H, R^3 = Me
b, R^1 = Cl, R^2,R^4 = H, R^3 = Me
c, R^1 = Br, R^2, R^4 = H, R^3 = i-Pr
d, R^1,R^2 = Br, R^3 = i-Pr, R^4 = H
e, R^1 = Br, R^2 = H, R^3 = i-Pr, R^4 = Me
f, R^1,R^2,R^4 = H, R^3 = i-Pr

6*a*, R^1 = Br, R^2,R^3 = H
b, R^1 = Cl, R^2,R^3 = H
c, R^1,R^2 = Br, R^3 = H
d, R^1,R^2,R^3 = H
e, R^1,R^3 = H, R^2 = Br
f, R^1,R^3 = Me, R^2 = H
g, R^1 = Br, R^2 = H, R^3 = Me

with methyl iodide and aqueous sodium acetate hydrolysis in the same pot, gave 5-methylpyrrole-2-carboxaldehyde (**10***a*) in 61% yield after column chromatography (Expt. 3, Table 1). Obviously, the bulky nitrogen substituents had significantly suppressed nucleophilic addition to C-6, permitting the generation of the 2-lithioazafulvene **8** (Scheme 2). The lithio species thus generated was reacted with a series of electrophilic reagents, giving rise to the corresponding 5-substituted pyrrole-2-carboxaldehydes **10** (Scheme 1), in most cases in modest yields (Table 1). It was noted that the product mixture from each of these reactions contained significant amounts of an unstable substance determined to be the alcohol **11**, the hydrolysis product of **7***b*. These results demonstrated that addition of *tert*-butyllithium to **3***c* was still occurring at –78°C. When the bromine–lithium exchange was conducted at –105°C, compound **11** was only a minor component (<10%) of the reaction mixture, and the protonolysis–hydrolysis product, pyrrole-2-carboxaldehyde (**6***d*), was isolated in 90% yield (Expt. 2). It is absolutely necessary that the THF used in all of these lithium–bromine exchange reactions be freshly distilled from sodium benzophenone ketyl to remove any inhibitor of peroxide formation and (or) peroxides themselves. If this is not done, neither the exchange nor the addition process takes place (e.g., with undistilled 99.9% THF containing butylated hydroxytoluene). This is consistent with both processes occurring by a mechanism involving electron transfer.) In contrast, at –10°C, addition product **11** was obtained in 97% yield (Expt. 1). The lithioazafulvene **8**, when generated at –105°C, reacted with a broad spectrum of electrophilic reagents, producing the expected 5-substituted pyrrole-2-carboxaldehydes **10**, usually in considerably better yields than when the lithiation was effected at –78°C (Table 1). *n*-Butyl iodide and triisopropylsilyl chloride both gave the anticipated products but only when HMPA (2 equiv.) was used. Benzaldehyde and cyclohexanone also reacted in the expected sense, but because the primary products are quite unstable, they were reduced in the

Can. J. Chem. Downloaded from www.nrcresearchpress.com by 65.111.164.53 on 09/08/12
For personal use only.

Table 1. Lithiation of 2-bromo-6-diisopropylamino-1-azafulvene. Generation of 5-substituted pyrrole-2-carboxaldehydes and related compounds.

Expt. no.	Lithiation temp., °C	EX	Hydrolysis conditions (h)[a]	CC solvent hex:EtOAc[b]	Product(s)	Yields,[c] %	Cryst. solvent	Melting point, °C
1	–10	H_2O	A (15)		**11**	97[d]		Oil
2	–105	H_2O	A (15)	5:1	**6***d*, **11**	90, <10		
3	–78	MeI	A (15)	5:1	**10***a*	61	Hexane–ether	66–67[e]
4	–105	MeI	A (15)	5:1 to 4:1	**10***a*	80		
5	–105	*n*-BuI[f]	B (2)	5:1[g]	**10***b*	62	Pentane	41–43
6	–105	TipsCl[f]	B (1)	7:1	**10***c*	69	MeOH	107–108
7	–78	MeSSMe	A (120)	5:1 to 4:1	**10***d*	48	Hexane–ether	103–104[h]
8	–105	MeSSMe	A (120)	5:1 to 4:1	**10***d*	67		
9	–78	PhSSPh	A (15)	5:1	**10***e*	57	Hexane–ether	96–97
10	–105	PhSSPh	A (15)	4:1	**10***e*	60		
11	–78	DMF	A (15)	5:1 to 3:1	**10***f*	31	Hexane	121–122[i]
12	–90	DMF	A (0.7)	4:1	**10***f*, **6***b*	63, 10		
13	–78	$ClCO_2Et$	A (15)	4:1	**10***g*	36	Hexane–ether	73–74[j]
14	–105	$ClCO_2Et$	B (0.7)	4:1	**10***g*	31–41		
15	–78	PhCOCl	A (15)	5:1	**10***h*	31	Hexane–ether	118–119
16	–105	PhCOCl	A (15)	5:1	**10***h*	70		
17	–105	PhCHO	C (1)	40:1	**12***a*	60		Oil
18	–78	$(CH_2)_5CO$	C (1)	40:1	**12***b*	37		Oil
19	–105	$(CH_2)_5(CO)$	C (15)	40:1	**12***b*	39		

[a]A = 5 equiv. of NaOAc in H_2O, one-pot reaction, reflux; B = 5 equiv. of NaOAc in MeOH–H_2O after removal of THF, r.t.; C = 2–3 parts $NaBH_4$ (by wt.) in i-PrOH, reflux.
[b]Column chromatography on silica gel unless indicated otherwise.
[c]Yield of chromatographyically pure material unless indicated otherwise.
[d]Yield of crude product pure by tlc.
[e]Literature (17) mp 68°C.
[f]HMPA (2 equiv.) added.
[g]Column chromatography on Act II netural alummina.
[h]Literature (4) mp 105–106°C.
[i]Literature (1) mp 121–122°C.
[j]Literature (18) mp 75°C.

same pot to the 2,5-disubstituted pyrroles **12***a* and **12***b* with sodium borohydride in boiling 2-propanol (16). It should be noted that –105°C is probably an unnecessarily low temperature for the efficient formation of the lithioazafulvene **8**, since a –90°C reaction with DMF gave rise to pyrrole-2,5-dicarboxaldehyde in over 60% yield (Expt. 12).

The primary product in the reaction of **8** with electrophilic reagents is the azafulvene **9**, the presence of which is readily established by ^1H NMR spectroscopy. The susceptibility of these compounds to hydrolysis varies greatly. For example, with aqueous sodium acetate in a two-phase system (reflux) the hydrolysis of the 2-methyl compound **9***a* is complete in 15 h (Expt. 3) whereas the 2-methylthio compound **9***d* requires 5 days (Expt. 7). The hydrolyses are considerably faster in homogeneous solution, e.g., the conversion of the 2-butyl compound **9***b* to **10***b* is complete in 2 h at room temperature in aqueous methanolic sodium acetate (Expt. 5).

It was of interest to examine 2,3-dibromo-6-isopropylamino-1-azafulvene (**3***d*) as a progenitor of 3,4-disubstituted pyrrole-2-carboxaldehydes. To be synthetically valuable this would require a highly selective exchange of one of the bromine atoms in **3***d* for lithium. Indeed, lithiation of this compound with a *tert*-butyllithium at –105°C followed by quenching with water and hydrolysis, gave a >65:1 mixture of the aldehydes **6***a* and **6***e*. When the lithiation was effected at –78°C, this ratio decreased to ca. 20:1. Lithiation of **3***d* at –105°C, followed by aging the solution of **13***a*,*b* at –78°C and then sequentially quenching with methyl iodide and hydrolysis, gave an 18:1 mixture of the methylated aldehydes **14***a* and **14***b* (Scheme 3) from which pure 3-methyl-5-bromopyrrole-2-carboxaldehyde (**14***a*) could be obtained by crystallization. Elimination of the hydrolysis step permitted the isolation of the azafulvene **13***c* in about 60% yield. Alternatively, if the mixture of azafulvenes **13***c* and **13***d*, generated as described above, was sequentially lithiated, reacted with DMF, and hydrolyzed, 3-methylpyrrole-2,5-dicarboxaldehyde (**15**) could be isolated from the product mixture by column chromatography in about 30% yield (unoptimized). Thus, the dibromoazafulvene **3***d* would appear to have potential utility as a 4,5-dilithiopyrrole-2-carboxaldehyde equivalent although it is clear that optimization of the second lithiation would be necessary to make the process more synthetically attractive.

To date, our efforts to extend the scope of the 2-lithiated-1-azafulvene process to the synthesis of 5-substituted 2-acylpyrroles in general have met with failure. Firstly, reaction of 2-bromo-6-methyl-6-diisopropylamino-1-azafulvene (**3***e*, Scheme 1) with *tert*-butyllithium at –105°C, followed by quenching with methyl iodide and hydrolysis, gave a complex

Can. J. Chem. Downloaded from www.nrcresearchpress.com by 65.111.164.53 on 09/08/12
For personal use only.

Can. J. Chem. Downloaded from www.nrcresearchpress.com by 65.111.164.53 on 09/08/12
For personal use only.

Scheme 2

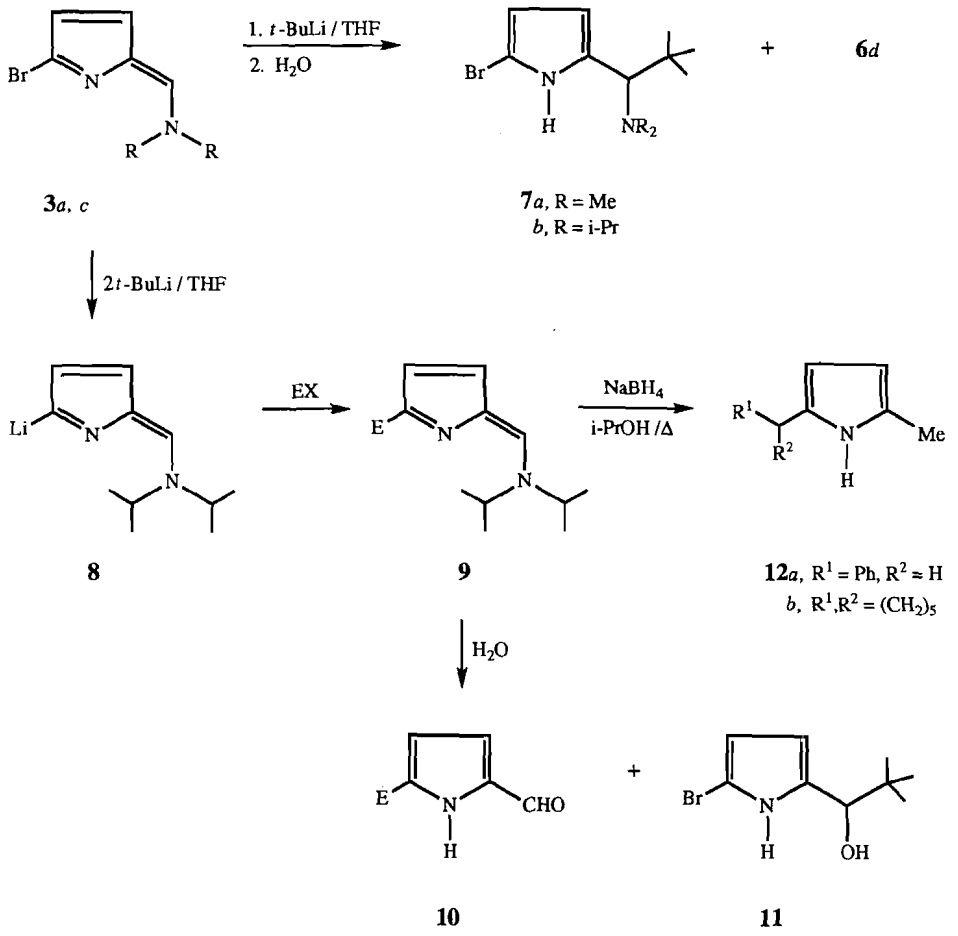

mixture that contained little, if any, 5-methyl-2-acetylpyrrole (**6***f*). Small amounts of 5-bromo-2-acetylpyrrole (**6***g*) and the corresponding N-methyl derivative, that is, the hydrolysis and N^1-methylation–hydrolysis products, respectively, of **3***e*, were the only pure compounds isolated from the mixture. Secondly, the generation of the 6-phenyl analog of **3***e* could not be achieved because the Vilsmeier–Haack reaction of pyrrole with the iminium salt derived from *N,N*-diisopropylbenzamide and oxalyl chloride did not produce the required product.

Some properties of 6-dialkylamino-1-azafulvenes

The stable monomeric 6-dialkylamino-1-azafulvenes comprise two types. The most widely studied class consists of those congeners that are push–pull stabilized (10, 11, 13, 14) and contain one to three electron-attracting substituents at C-2,4. Compounds **3***a–e* are examples of this type. The second type, which so far consists of a single member (**3***f*), owes its stability as a monomer entirely to the presence of the sterically demanding N-6 substituents. In the absence of push–pull stabilization, the size of these substituents is crucial since azafulvenes with less bulky N-6 substituents spontaneously dimerize at room temperature (15). These monomers can, however, be generated in situ at low temperature where they have an appreciable half-life, by deprotonation of the corresponding iminium salts (19).

The 6-dialkylamino-1-azafulvenes obviously are basic, but only weakly so. For example, the pK_a of **2***c*, the conjugate acid of **3***c*, was found to be ~6.7 in 50% aqueous methanol. The pK_a of **2***e* could not be measured under these conditions because of its facile conversion into pyrrole-2-carboxaldehyde (**6***d*). These azafulvenes undergo [6 + 2] cycloaddition reactions at N-1 and C-6 with a variety of dipolarophiles (11, 20) and also are alkylated at N-1 with methyl iodide (11, 21).

Perhaps one of the more notable properties of these azafulvenes is that in solution they exist predominantly, if not exclusively, as one conformer,[10] and in this conformer the dialkylamino group is *syn* to the azafulvene nitrogen atom. This conformation was unequivocally established for compound **3***f* by NMR spectroscopic methods. Thus, the methine protons of the two isopropyl groups are found at δ 3.83 and 6.61 (Fig. 1*a*). The low-field absorption indubitably corresponds to the methine hydrogen of the isopropyl group that is proximal to the azafulvene nitrogen atom by which it is

[10] Most of the azafulvenes described herein contain a minor amount (10–20%) of another component the NMR spectrum of which is consistent with that expected for the *anti* conformer (see also ref. 11). There is no doubt that we are dealing with conformers since the ratio of the two species is solvent dependent. For example, **3***c* is an 85:15 *syn–anti* mixture in $CDCl_3$ and $C_2D_2Cl_4$ but exists as the pure *syn* species in DMSO-d_6, C_6D_6, and C_7D_8. Furthermore, saturation of either of the singlets corresponding to H-6 of the *syn* and *anti* conformers of **3***c* (δ 7.09 and 7.79) results in a strong diminution of the intensity of the other, indicating that the two species are exchanging at room temperature.

Scheme 3

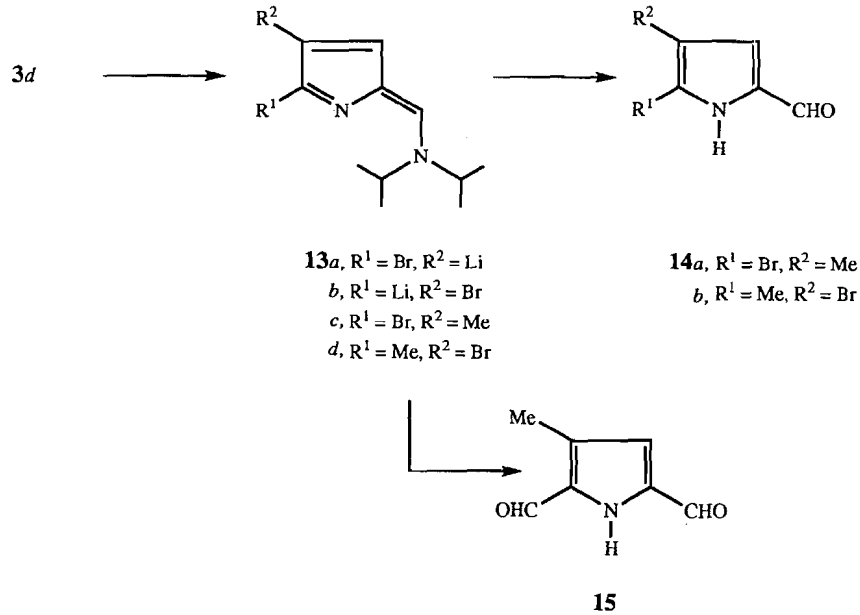

Fig. 1. (*a*) Chemical shifts and coupling constants of **3***f* in $CDCl_3$. The isopropyl methyl doublets appear at δ 1.34 and 1.37. (*b*). Chemical shifts and coupling constants of **2***e* in $CDCl_3$ taken from ref. 1. (*c*). NOE differences for **3***f* in DMSO-d_6.

(a)

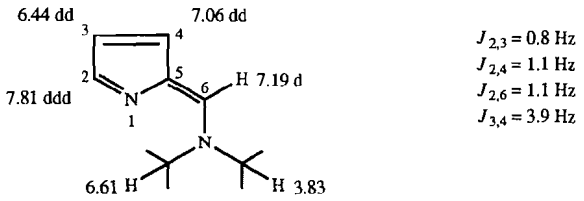

(b)

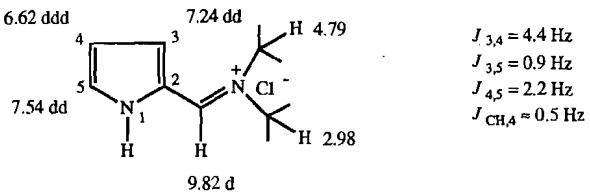

(c)

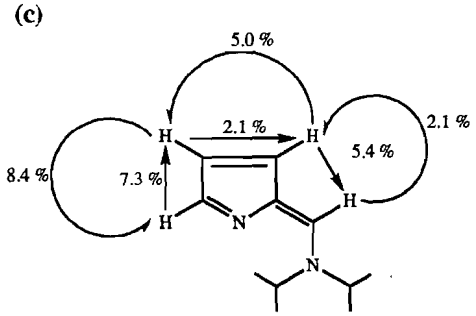

strongly deshielded. This deshielding is considerably greater than that found in **2***e*, the iminium salt precursor of **3***f* (Fig. 1*b*). In addition to the large chemical shift difference of the isopropyl methine hydrogens, H-6 is long-range coupled to H-1 by 1.1 Hz. (The connectivity in **3***f* was established by COSY and decoupling experiments.) This long-range coupling is analogous to that observed for most pyrrole-2-carboxaldehydes (22) for which the *syn* conformer predominates at room temperature. In contrast, in the iminium salt **2***e* the proton of the iminium carbon is weakly coupled to H-4, indicative of the *anti* conformation (23). Also noteworthy in the ^{1}H NMR spectrum of **3***f* is the small value of $J_{2,3}$ (0.8 Hz) as compared to $J_{4,5}$ (2.2 Hz) in the iminium salt **2***e*. This coupling constant is nearly identical to that reported (0.86 Hz) for $J_{2,3}$ in 6,6-diphenyl-1-azafulvene by Hafner and Pfeiffer (24). The most definitive evidence for the *syn* conformer in **3***f* is derived from NOE difference measurements, which show a 2–5% NOE between H-4 and H-6 (Fig. 1C)! The NOE difference measurements also confirmed the connectivity sequence of the hydrogens bonded to the sp^2 carbon as established by the COSY and decoupling experiments.

What is the reason for the preponderance of the *syn* conformer in 6-dialkylamino-1-azafulvenes? We suggest that the charge-separated form **16** (Scheme 4) must make a substantial contribution to the ground state structure of these compounds and the consequent electrostatic attraction between the two nitrogen atoms causes the *syn* form to be favored. Variable temperature NMR experiments on the 2-bromo compound **3***c* support this contention. Compound **3***c* exists as an 85:15 mixture of *syn* and *anti* conformers in dideuterated 1,1,2,2-tetrachloroethane (also in $CDCl_3$) as indicated by major and minor absorptions for H-6 at δ 7.02 and 7.79. The isopropyl methine hydrogens for the *syn* conformer are found at δ 3.82 and 6.37 and at δ 3.82 and 4.62 for the *anti* conformer. The doublets for the isopropyl methyl groups of the *anti* conformer are obscured by those for the *syn* conformer centered at δ 1.33. On warming, the isopropyl doublets coalesced to a clean doublet at about 353 K, but the absorptions for H-6 had only broad-

Can. J. Chem. Downloaded from www.nrcresearchpress.com by 65.111.164.53 on 09/08/12
For personal use only.

Can. J. Chem. Downloaded from www.nrcresearchpress.com by 65.111.164.53 on 09/08/12
For personal use only.

Scheme 4

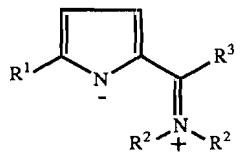

16

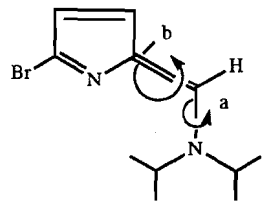

3*c*

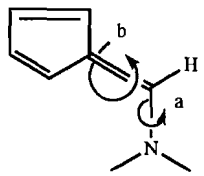

17

ened. These latter absorptions had broadened further but were still showing no signs of coalescing at 383 K at which temperature the HD salt of **3***c* formed by dehydrohalogenation of the solvent. Although coalescence of the signals for H-6 could not be achieved (*syn* conformer exclusively in DMSO-d_6 or toluene d_8) it is clear that the higher and lower energy dynamic processes in **3***c* correspond to rotation around bonds "b" and "a" (Scheme 4) analogous to that found in 6-dimethylaminofulvene (**17**, Scheme 4; see ref. 25). Although the rotational barrier about the isopropyl groups is clearly the lower energy process, the existence of this barrier is still consistent with a substantial contribution of the charge-separated form **16** to the ground state structure of **3***c*. In contrast, the 6-methyl analog **3***e* of **3***c* shows a singlet at δ 2.71 for the 6-methyl group, a single doublet for the four isopropyl methyls, and a very broad (δ 4.2–5.4) absorption for the two isopropyl methine hydrogens. This indicates that the coalesence temperature for rotation about the C-6—N bond is at or near ambient temperature and that the charge-separated form contributes much less to the ground state structure in this case.

Conclusions

2-Bromo-6-diisopropylamino-1-azafulvene (**3***c*) undergoes bromine–lithium exchange with *tert*-butyllithium at ≤90°C, and the lithium species **8** obtained thereby on reaction with electrophilic reagents and subsequent hydrolysis provides a wide variety of 5-substituted pyrrole-2-carboxaldehydes.

6-Dialkylamino-1-azafulvenes exist predominantly or exclusively in the *syn* conformer in solution at room temperature. This conformer is favored over the *anti* conformer because the charge-separated form **16** contributes substantially to the ground state structure of these molecules. These phenomena are supported by both ambient and variable temperature NMR experiments.

Experimental section

The melting points were determined in a Mel-Temp II melting point apparatus and are not corrected. The infrared spectra were measured with a Nicolet 5 PC FT infrared spectrophotometer. The ^{1}H NMR spectra were measured with a Bruker WM 300 or a Bruker AM 500 NMR spectrometer in $CDCl_3$ (unless specified otherwise) and are expressed as parts per million (δ) from internal tetramethylsilane. When exchangeable protons were present, the data are given for D_2O exchanged spectra. Those NMR spectra not found in the experimental section can be obtained from the Depository of Unpublished Data.[11] The low-resolution mass spectra were obtained with a MAT CH-7 or a MAT 1125 mass spectrometer while the high-resolution mass spectrum was measured on a Finnigan MAT 311A mass spectrometer.

The terms "worked up in the usual manner" or "the usual work-up" signify that the extract was dried over anhydrous magnesium or sodium sulfate and evaporated in vacuo.

N,N-Diisopropyl 2-bromopyrrole-5-formiminium chloride (2*c*)

To a solution of pure 2-bromo-6-diisopropylamino-1-azafulvene (**3***c*) (0.50 g, 1.94 mmol) in ether (25 mL) at 0°C, prepared by one of the methods described below, was added a freshly prepared 0.23 M solution of HCl gas in ether (8.5 mL, 1.96 mmol). The precipitated solid was collected by filtration and dried in vacuo (0.50 g, 88% yield). It was analytically pure and had mp 200–201°C; pK_a (1:1 MeOH–H_2O) = 6.67 ± 0.08; IR (KBr): 3440, 1634 cm^{-1}; NMR (300) δ: 1.53 (d, 6H, J = 6.66 Hz, NCH*Me*$_2$), 1.60 (d, 6H, J = 6.71 Hz, NCH*Me*$_2$), 4.18 (sept, 1H, J = 6.71 Hz, NC*H*Me$_2$), 4.74 (sept, 1H, J = 6.66 Hz, NC*H*Me$_2$), 6.57 (d, 1H, $J_{3,4}$ = 4.44 Hz, H-3), 7.20 (d, 1H, $J_{3,4}$ = 4.44 Hz, H-4), 9.76 (s, 1H, CH=N). Anal. calcd. for $C_{11}H_{18}BrClN_2$: C 44.99, H 6.17, N 9.54, found: C 44.96, H 6.15, N 9.51.

2-Bromo-6-dimethylamino-1-azafulvene (3*a*) by deprotonation of the iminium salt 2*a*

Oxalyl chloride (2.1 mL, 3.06 g, 24.1 mmol) was carefully added dropwise at room temperature (vigorous exotherm) to a stirred solution of dry DMF (1.57 mL, 1.48 g, 20.3 mmol) in dry dichloromethane (40 mL). After 25 min at room temperature, the solvent was evaporated in vacuo with protection from moisture and the very hygroscopic white solid was dried in vacuo for 20 min. A solution of 2-bromopyrrole (1*a*) (prepared from 20 mmol of pyrrole (26)) in dry dichloromethane (20 mL) was slowly added to the above solid at 0°C. When the addition was complete, the solution was left to reach room temperature and 25 min thereafter 0.5 M $NaHCO_3$ solution was added. The organic phase was separated, combined with a dichloromethane extract of the aqueous phase, and the extract was washed sequentially with 10% aqueous NaOH, 0.5 M $NaHCO_3$, and saturated NaCl solutions. After the usual work-up the crude product was crystallized from hexane–ethyl acetate to give 3*a* as a solid (3.25 g, 81%) with mp 101–103°C; IR (CCl_4): 1640 cm^{-1}; NMR (300) δ: 3.30 (s, 3H, NMe), 3.75 (s, 3H, NMe), 6.32 (d, 1H, J = 3.8 Hz, H-3), 6.90 (d, 1H, J = 3.8 Hz, H-4), 6.98 (s, H-6). The NMR spectrum also showed absorptions for the *anti* conformer (17%) at δ 6.42 (d), 7.04

[11] These spectra can be purchased from: The Depository of Unpublished Data, Document Delivery, CISTI, National Research Council Canada, Ottawa, Canada ON K1A 0S2.

Can. J. Chem. Downloaded from www.nrcresearchpress.com by 65.111.164.53 on 09/08/12
For personal use only.

(d), 7.68 (s) and for the chloro compound **3***b* (8%) at δ 6.15 (d), 6.96 (s). Anal. calcd. for 0.92 $C_7H_9BrN_2$·0.08 $C_7H_9ClN_2$: C 42.76, H 4.61, N 14.25; found: C 42.58, 42.38; H 4.63, 4.58; N 13.92, 14.08.

2-Bromo-6-diisopropylamino-1-azafulvene (3*c*) from the bromoaldehyde 6*a* and diisopropylamine

A solution of the aldehyde **6***a* (18) (7.28 g, 41.8 mmol) and diisopropylamine (15.2 mL, 11.7 g, 116 mmol) in ethanol (150 mL) was heated at reflux temperature for 20 h. The solution was evaporated to dryness in vacuo and the residue was dissolved in ether and extracted with ice-cold 1 M HCl solution. The usual work-up of the ether phase gave recovered **6***a* (2.40 g). The ice-cold acidic phase was made alkaline with ice-cold 10% aqueous NaOH solution and the product was extracted into ether. The usual work-up gave the azafulvene **3***c* as a solid (5.64 g, 52% yield; 78% based on recovered **6***a*), mp 108–112°C. Recrystallization of this material from hexane–ether gave pure **3***c*, mp 110.5–112°C, identical in all respects to a specimen synthesized via the brominated Strecker-type nitrile **5***a* (13).

2,3-Dibromo-6-diisopropylamino-1-azafulvene (3*d*) from the dibromoaldehyde 6*c* and diisopropylamine

A solution of the dibromo aldehyde **6***a* (18) (2.00 g, 7.9 mmol) in diisopropylamine (100 mL) containing suspended 4A molecular sieves (large excess) was heated at reflux temperature for 38 h. The mixture was cooled to room temperature, filtered, and the filtrate was evaporated in vacuo. The residue was worked up as described for **3***c* except that 0.5 M HCl was used. This procedure gave the starting material (0.29 g) and crude **3***d* (2.3 g, mp 131–133°C). One crystallization from pentane–ether gave the pure compound (2.00 g, 75% yield), mp 135–137°C; IR ($CHCl_3$): 1618 cm^{-1}; NMR (500) δ: 1.32 (d, 6H, J = 6.7 Hz, NCH*Me*$_2$), 1.36 (d, 6H, J = 6.7 Hz, NCH*Me*$_2$), 3.85 (sept, 1H, J = 6.7 Hz, N*CH*Me$_2$), 6.33 (sept, 1H, J = 6.7 Hz, N*CH*Me$_2$), 6.72 (s, 1H, H-3), 7.00 (s, 1H, H-6). The NMR spectrum also showed peaks for the *anti* conformer (20%) at 1.36 (d), 1.38 (d), 3.87 (sept), 4.56 (sept), 7.08 (s), and 7.72 (s). Anal. calcd. for $C_{11}H_{15}Br_2N_2$: C 39.43, H 4.51, N 8.36; found: C 39.28, H 4.78, N 8.27.

2-Bromo-6-methyl-6-diisopropylamino-1-azafulvene (3*e*) via Strecker-type nitrile 5*b*. Hydrolysis of 3*e* to 5-bromo-2-acetylpyrrole 6*g*

Phosphorus oxychloride (5.9 g, 38.5 mmol) and dry *N,N*-diisopropylacetamide (5.0 g, 35 mmol) were combined and the solution was left at room temperature for 6 h by which time the contents of the flask had solidified. A solution of pyrrole (2.3 g, 35 mmol) in dry dichloromethane (50 mL) was added and the resulting solution was left at room temperature for 10 h. The solvent was removed in vacuo to give the crude Vilsmeier–Haack product in quantitative yield. This salt (**2***d*) was dissolved in dry MeCN (250 mL) and solid NaCN (25 g, 500 mmol) was added. The resulting mixture was stirred at room temperature for 8 h and about 75% of the solvent was removed in vacuo. The slurry so obtained poured into water (250 mL) and the product was extracted into ether. The extract was washed with saturated NaCl solution and then dried over anhydrous potassium carbonate. The ether solution of **4***b* was decolorized with activated charcoal, filtered, and evaporated in vacuo to give a solid (4.5 g) that was crystallized from hexane–ethyl acetate to give pure **4***b* (2.3 g, 34% yield), mp 86–88°C; IR (KBr): 3337, 2217 cm^{-1}; NMR (300) δ: 1.16 (d, 6H, J = 6.9 Hz, NCH*Me*$_2$), 1.28 (d, 6H, J = 6.9 Hz, NCH*Me*$_2$), 1.86 (s, 3H, 6-Me), 3.20 (sept, 2H, J = 6.9 Hz, N*CH*Me$_2$), 6.13 (t, 1H, H-4), 6.32 (dd, 1H, $J_{3,4}$ = 3.5 Hz, $J_{3,5}$ = 1.5 Hz, H-3), 6.75 (dd, 1H, $J_{3,5}$ = 1.5 Hz, $J_{4,5}$ = 2.8 Hz, H-5). Anal. calcd. for $C_{13}H_{21}N_3$: C 71.19, H 9.65, N 19.16, found: C 71.20, H 9.63, N 19.30.

N-Bromosuccinimide (0.203 g, 1.14 mmol) was added to a stirred solution of **4***b* (0.250 g, 1.14 mmol) in dry THF (25 mL) at –78°C. The solution was stirred at –78°C for 3 h, left to reach room temperature, and then evaporated in vacuo. The residue (**5***b*) was dissolved in MeOH (10 mL), 10 wt.% NaOH (3 mL) was added, and the solution was left at room temperature for 10 min and poured into water. This solution was brought to pH 2 with 1 M HCl and then the reaction mixture was worked up as described for the synthesis of **3***c* to give the azafulvene **3***e* as an oil (0.210 g, 68% yield) that solidified on standing. This compound is chromatographically unstable and could not be recrystallized. It had a purity of ca.95% by NMR spectroscopy; the only contaminant was 5-bromo-2-acetylpyrrole (**6***g*). This sample of **3***e* was used as such for the bromine–lithium exchange experiment; NMR (300) δ: 1.44 (d, 12 H, J = 6.9 Hz, NCH*Me*$_2$), 2.71 (s, 3H, 6-Me), 4.2–5.4 (v br, 2H, N*CH*Me$_2$), 6.32 (d, 1H, J = 3.9 Hz, H-3), 7.02 (d, 1H, J = 3.9 Hz, H-4); MS (EI) *m/z*: 272 (8), 270 (8), 229 (35), 227 (38), 189 (61), 187 (63), 174 (87), 172 (100), 146 (21), 144 (22), 86 (42), 44 (73). The identity of this material was further established by hydrolysis to **6***g*.

A sample of the azafulvene **3***e* (0.110 g, 0.41 mmol) was passed through a column of Act II neutral alumina using hexane – ethyl acetate (2:1) as the eluting solvent. Compound **6***g*, a solid (0.070 g, 92% yield, mp 100–101°C), was obtained that on recrystallization from hexane–ethyl acetate had mp 105–106°C; IR (KBr): 3432, 3345, 1646 cm^{-1}; NMR (300) δ: 2.40 (s, 3H, COMe), 6.24 (d, 1H, J = 3.9 Hz, H-4), 6.81 (d, 1H, J = 3.9 Hz, H-3). Anal. calcd. for C_6H_6BrNO: C 38.32, H 3.21, N 7.44; found: C 38.40, H 3.20, N 7.43.

6-Diisopropylamino-1-azafulvene 3*f* by deprotonation of the iminium salt 2*e*

Triethylamine (1.49 g, 14.7 mmol) was added to a solution of the iminium salt **2***e* (13) (2.10 g, 9.80 mmol) in dichloromethane (50 mL) at room temperature. After 10 min the solution was washed with saturated NaCl solution, dried over anhydrous potassium carbonate, and then the solvent was removed in vacuo. The oil thus obtained (1.37 g, 78% yield) crystallized on standing. One crystallization of this material from hexane–ether gave analytically pure **3***f* (1.05 g, 60% yield), mp 63–65°C; IR (KBr): 1615 cm^{-1}. For the NMR spectrum in $CDCl_3$ see Fig. 1*a*; for other solvents see supplementary data.[11] Anal. calcd. for $C_{11}H_{18}N_2$: C 74.11, H 10.17, N 15.71; found: C 74.21, H 10.45, N 16.01.

Generation of 2-lithio-6-diisopropylamino-1-azafulvene (8) and reaction electrophilic reagents

(a) Formation of 8 in THF solution

A solution of 1.7 M *tert*-butyllithium in pentane (2.4 mL, 4.08 mmol) was added dropwise to a stirred solution of **3***c* (0.499 g,

Can. J. Chem. Downloaded from www.nrcresearchpress.com by 65.111.164.53 on 09/08/12
For personal use only.

1.94 mmol) in dry THF (30 mL, freshly distilled from sodium benzophenone ketyl) cooled to –105°C under an inert atmosphere at a rate such that the internal temperature did not exceed –100°C. The solution thus obtained was stirred at –105°C for 15 min; then the electrophilic reagent (1.2–3 equiv.) was added and the reaction temperature was raised to –78°C where it was maintained for 15 min. The temperature was then left to rise to 0°C and the reaction mixture was worked up by one of the methods described below.

(b) Formation of ***8*** *in THF solution containing HMPA*

A solution of **8** in THF prepared at –105°C as described above was warmed to –78°C and after 15 min HMPA (2 equiv.) dissolved in dry THF (1.5 mL/mmol HMPA) was added. After a further 15 min at –78°C the electrophilic reagent was added. The remainder of the procedure was identical to that described above.

Conversion of the 2-substituted-6-diisopropylamino-1-azafulvenes (9) to 5-substituted pyrrole-2-carboxaldehydes 10 or 5-alkyl-2-methylpyrroles (12)

(a) Procedure A

A solution of sodium acetate (5 equiv.) in water (1 mL/mmol) was added to the azafulvene solution prepared as in (a) above and the mixture was heated at reflux temperature for the time period indicated in Table 1. The mixture was poured into water and extracted with ether. The ether extract was washed with saturated NaCl solution and then worked up in the usual manner. The crude product was then purified by column chromatography (see Table 1) and then, if appropriate, the product was recrystallized from a suitable solvent system (Table 1).

Alternatively, for compounds **10***b* and **10***g* the aqueous sodium acetate solution was first brought to pH 2 with 1 M HCl (to remove small amounts of unhydrolyzed azafulvene) and then the usual work-up was followed.

(b) Procedure B

The azafulvene solution obtained as in (*a*) or (*b*) above was concentrated in vacuo. The residue was dissolved in methanol (5 mL/mmol azafulvene) and a solution of sodium acetate (5 equiv.) in water (0.5 mL/mmol) was added. The mixture was stirred at room temperature for the time period indicated in Table 1 and then it was poured into saturated NaCl solution. The remainder of the work-up followed that described in procedure A.

(c) Procedure C

To the THF solution of the azafulvene obtained as in (a) above was added 2-propanol (50 mL/mmol azafulvene) and sodium borohydride (2–3 parts by weight) and the solution was treated at reflux temperature for 15 h. The reaction mixture was poured into saturated aqueous ammonium chloride solution and extracted with ether. The remainder of the work-up was the same as that described in procedure A. The crude product was purified by column chromatography on silica gel using hexane – ethyl acetate (40:1) to elute the 5-alkyl-2-methylpyrrole derivatives.

*5-*n*-Butylpyrrole-2-carboxaldehyde (**10**b):* IR (neat): 3260, 1645 cm^{-1}; NMR (300) δ: 0.93 (t, 3H, J = 7.3 Hz, Me), 1.38 (sext, 2H, ΣJ = 7.5 Hz, Me$CH_2$$CH_2$$CH_2$), 1.65 (m, 2H, Me$CH_2$$CH_2$$CH_2$), 2.69 (t, 2H, J = 7.7 Hz, Me$CH_2$$CH_2$$CH_2$), 6.08 (d, 1H, J = 3.8 Hz, H-4), 6.91 (d, 1H, J = 3.8 Hz, H-3), 9.34 (s, 1H, CHO). Anal. calcd. for $C_9H_{13}NO$: C 71.49, H 8.66, N 9.26; found: C 71.65, H 8.85, N 9.41.

*5-Triisopropylsilylpyrrole-2-carboxaldehyde (**10**c):* IR (KBr): 3250, 1657 cm^{-1}; NMR (300) δ: 1.09 (d, 18H, J = 7.1 Hz, Me_2CH), 1.31 (sept, 3H, J = 7.1 Hz, $Me_2$$CH$), 6.52 (d, 1H, J = 3.7 Hz, H-4), 7.02 (d, 1H, J = 3.7 Hz, H-3), 9.52 (s, 1H, CHO). Anal. calcd. for $C_{14}H_{25}NOSi$: C 66.87, H 10.02, N 5.57; found: C 66.86, H 10.04, N 5.52.

*5-Phenylthiopyrrole-2-carboxaldehyde (**10**e):* IR ($CHCl_3$): 3436, 3236, 1650 cm^{-1}; NMR (300) δ: 6.50 (d, 1H, J = 3.9 Hz, H-4), 6.97 (d, 1H, J = 3.9 Hz, H-3), 7.21–7.32 (m, 5H, Ph), 9.45 (s, 1H, CHO). Anal. calcd. for $C_{11}H_9NOS$: C 65.00, H 4.46, N 6.89; found: C 64.84, H 4.51, N 6.82.

*5-Benzoylpyrrole-2-carboxaldehyde (**10**h):* IR ($CHCl_3$): 3430, 1668, 1635 cm^{-1}; NMR (30) δ: 6.91 (d, 1H, J = 4.1 Hz, H-4 or H-3), 7.01 (d, 1H, J = 4.1 Hz, H-3 or H-4), 7.49–7.61 (m, 2H, H-3′,5′), 7.62–7.65 (m, 1H, H-4′), 7.92–7.95 (m, 2H, H-2′, 6′), 9.77 (s, 1H, CHO). Anal. calcd. for $C_{12}H_9NO_2$: C 72.35, H 4.55, N 7.03; found: C 72.28, H 4.55, N 7.02.

*5-Benzyl-2-methylpyrrole (**12**a):* IR (CCl_4): 3475, 3390 cm^{-1}; ^{1}H NMR (300) δ: 2.19 (s, 3H, Me), 3.91 (s, 2H, CH_2), 5.78 (m, 1H, H-3), 5.84 (d, 1H, J = 3.7 Hz, H-4), 7.20–7.32 (m, 5H, Ph); ^{13}C NMR δ: 13.003 (Me), 34.235 (CH_2), 105.812 (C-3 or C-4), 106.572 (C-4 or C-3), 126.329 (C-4′), 126.982 (C-2 or C-5), 128.5735 (C-2′,6′ or C-3′, 5′), 128.6757 (C-3′,5′ or C-2′,6′), 129.259 (C-5 or C-2), 139.885 (C-2′).

*5-Cyclohexyl-2-methylpyrrole (**12**b):* IR (CCl_4): 3485, 3335 cm^{-1}; NMR (300) δ: 1.18–1.42 (m, 5H), 1.68–1.82 (m, 3H), 1.95–1.99 (m, 2H), 2.24 (s, 3H, Me), 2.51 (m, 1H, H-1′), 5.76 (s, 2H, H-3,4); MS (EI) *m/z*: 163 (M^+, 64), 148 (25), 134 (32), 121 (55), 120 (100), 108 (37), 107 (52), 106 (49), 95 (44), 94 (62), 82 (39), 81 (56), 80 (61), 79 (42), 53 (47), 44 (38), 42 (46), 41 (48).

Monolithiation of 2,3-dibromo-6-diisopropylamino-1-azafulvene (3*d*) and reaction with methyl iodide

*(a) Synthesis of 2-bromo-3-methyl-6-diisopropylamino-1-azafulvene (**13**c)*

tert-Butyllithium in pentane (5.0 mL of a 1.4 M solution; 7.0 mmol) was added to a stirred solution of **3***d* (1.12 g, 3.34 mmol) in dry THF (75 mL) maintained at –105°C in an inert atmosphere. The solution was stirred for 15 min at –105°C, warmed to –78°C, stirred 15 min at this temperature, and then methyl iodide (0.62 mL, 1.42 g, 10.0 mmol) was added. The cooling bath was removed and after 1 h the solution was poured into ice-cold 0.1 M HCl. The aqueous phase was washed with ether and then made alkaline with ice-cold 10 wt.% NaOH solution. The product was extracted into ether, the extract was washed with saturated NaCl solution and dried over anhydrous potassium carbonate, and the solvent was removed in vacuo. The residue was subjected to column chromatographic separation on Act II neutral alumina using hexane – ethyl acetate (4:1) to elute the azafulvene **13***c* as a solid. Crystallization of this material from hexane gave pure **13***c* (0.575 g, 63.5%), mp 84–86°C. IR (KBr): 1618 cm^{-1}. The NMR spectrum ($CDCl_3$) indicates that the azafulvene is a 7:3 mixture of *syn* and *anti* conformers; δ (syn): 1.29 (d, J = 6.7 Hz, Me_2CH), 1.33 (d, J = 6.7 Hz, Me_2CH), 2.06 (s, 3-Me), 3.78

(sept, J = 6.7 Hz, Me_2CH), 6.32 (sept, J = 6.7 Hz, Me_2CH), 6.67 (s, H-4), 6.87 (s, H-6); δ (*anti*): 2.11 (s, 3-Me), 4.58 (sept, Me_2CH), 6.82 (s, H-4), 7.63 (s, H-6). Anal. calcd. for $C_{12}H_{19}BrN_2$: C 53.14, H 7.06, N 10.33; found: C 53.33, H 7.19, N 10.01.

*(b) Synthesis of 5-bromo-4-methylpyrrole-2-carboxaldehyde (**14***a*)*

A solution of the azafulvene **13***c* was prepared as in (a) above and the THF was removed in vacuo. The residue (from a 2.40 mmol reaction) was dissolved in methanol (20 mL) and 20 wt.% aqueous NaOH (8 mL) and the solution was left at room temperature for 60 h. The reaction mixture was poured into saturated NaCl solution and the solution was made acidic (pH 2) with 1 M HCl. The products were extracted into dichloromethane and after the usual work-up the solid mixture of **14***a* and **14***b* was purified by column chromatography on Act II neutral alumina using hexane – ethyl acetate (3:1) to coelute the 18:1 **14***a*:**14***b* mixture as a solid (0.385 g, 85% yield) from which **14***a* was obtained pure by crystallization from hexane – ethyl acetate, mp 124–125°C. NMR (300) δ: 2.07 (d, 3H, J = 0.6 Hz, 4-Me), 6.78 (q, 1H, J = 0.6 Hz, H-3), 9.30 (s, 1H, CHO). Anal. calcd. for C_6H_6BrNO: C 38.32, H 3.21, N 7.45; found: C 38.41, H 3.19, N 7.49.

Sequential lithiation of 3*d* and synthesis of 3-methylpyrrole-2,5-dicarboxaldehyde 15

The azafulvene **3***d* (0.645 g, 1.93 mmol) was lithiated as described in (*a*) above. Methyl iodide (0.13 mL, 0.296 g, 2.09 mmol) was added to the THF–pentane solution (40 mL THF) at –78°C. After 10 min, the solution was warmed to 0°C and after 30 min it was cooled back down to –105°C. A 1.7 M solution of *tert*-butyllithium in pentane (2.49 mL, 4.23 mmol) was added to the stirred solution. After 10 min the solution was warmed to –78°C and 20 min later a solution of DMF (0.30 mL, 0.283 g, 3.87 mmol) in dry THF (1 mL) was added. After 10 min the cooling bath was removed and after a further 45 min water (0.5 mL) was added and the solution was concentrated in vacuo. The residue was dissolved in methanol (20 mL) and 10 wt.% sodium hydroxide (8 mL) and after 30 min at room temperature the reaction mixture was poured into a mixture of ice and 1 M HCl. The products were extracted into dichloromethane, the extract was washed with saturated NaCl solution, and after the usual work-up the residue was subjected to flash column chromatographic separation on silica gel using hexane – ethyl acetate (3:1) to elute the crystalline (0.075 g, 28% yield) dialdehyde **13***c*. **13***c* had mp 80–81°C after crystallization from ether–hexane; IR (KBr): 3426, 1682, 1661 cm^{-1}; NMR (300) δ: 2.43 (s, 3H, 3-Me), 6.79 (s, 1H, H-4), 9.71 (s, 1H, CHO), 9.90 (s, 1H, CHO); MS (EI) *m/z*: 137 (M^+, 100), 136 (44), 108 (17), 80 (22), 53 (28). This substance contained 0.075 H_2O as determined by integration of the NMR signal for water at δ 1.78. Anal. calcd. for $C_7H_7NO_2 \cdot 0.075\ H_2O$: C 60.73, H 5.15, N 10.12; found: C 60.73, H 5.16, N 10.12.

References

1. W.A.M. Davies, A.R. Pinder, and I.G. Morris. Tetrahedron, **18**, 405 (1962).
2. V.H. Rawal, R.J. Jones, and M.P. Cava. J. Org. Chem. **52**, 19 (1987).
3. F-P. Montforts and V.M. Schwartz. Liebigs Ann. Chim. 2301 (1985), and refs. therein.
4. T.M. Cresp and M.V. Sargent. J. Chem. Soc. Perkin Trans. 1, 2961 (1973).
5. J.M. Calzada Badia. Spanish Patent 456,334 (1975); Chem. Abstr. **89**, 179850 q (1978); D.E. Butler, U.S. Patent 4,638,006 (1987).
6. H.J. Anderson and C.E. Loader. *In* Pyrroles. Part one. The synthesis and the physical and chemical aspects of the pyrrole ring. *Edited by* R.A. Jones. John Wiley & Sons, New York. 1990. pp. 452–465.
7. M. Farnier and P. Fournari. J. Heterocycl. Chem. **12**, 373 (1975); R.J. Sundberg and B.C. Pearce. J. Org. Chem. **50**, 425 (1985).
8. J.M. Muchowski and P. Hess. Tetrahedron Lett. **29**, 777 (1988); **29**, 3215 (1988).
9. B.L. Bray, P. Hess, J.M. Muchowski, and M.E. Scheller. Helv. Chim. Acta, **71**, 2053 (1988);
10. F. Schnierle, H. Reinhard, N. Dieter, E. Lippacher, and H. von Dobeneck. Liebigs Ann. Chem. **715**, 90 (1968); H. von Dobeneck and T. Messerschmitt. Liebigs Ann. Chem. **751**, 32 (1971). H. von Dobeneck. T. Messerschmitt, E. Brunner, and U. Wunderer. Liebigs Ann. Chem. **751**, 40 (1971).
11. P.E. Sonnet, J.L. Flippen, and R.D. Gilardi. J. Heterocycl. Chem. **11**, 811 (1974).
12. P. Sammes. *In* Pyrroles. Part one. The synthesis and the physical and chemical aspects of the pyrrole ring. *Edited by* R.A. Jones. John Wiley & Sons, New York. 1990. pp. 549–728.
13. B.L. Bray and J.M. Muchowski. Can. J. Chem. **68**, 1305 (1990).
14. M.A. Kira, H.A. Shoeb, and M.I. Korkor. Egypt. J. Chem. **15**, 609 (1972).
15. W. Herz and J. Brasch. J. Org. Chem. **23**, 711 (1958); H.R. Henzel. Chem. Ber. **99**, 868 (1966).
16. R. Greenhouse, C. Ramirez, and J.M. Muchowski. J. Org. Chem. **50**, 2961 (1985).
17. S. Gronowitz, A.B. Hoernfeldt, B. Gestblom, and R.A. Hoffman. J. Org. Chem. **26**, 2615 (1962).
18. H.J. Anderson and S. Lee, Can. J. Chem. **43**, 409 (1965).
19. J.M. Muchowski and M.E. Scheller. Synth. Commun. **17**, 863 (1987); Tetrahedron Lett. **28**, 3453 (1987).
20. M. Watanabe, T. Kobayashi, S. Kajigaeshi, and S. Kanemasa. Chem. Lett. 607 (1975); S. Mori, M. Watanabe, S. Kajigaeshi, and S. Kanemasa. Heterocycles, **4**, 957 (1976).
21. H. von Dobeneck and F. Schnierle. Tetrahedron Lett. 5327 (1966).
22. R.A. Jones and G.P. Bean. *In* The chemistry of pyrroles. Academic Press, London. 1977. pp. 286–289 and 474–475.
23. B.L. Bray and J.M. Muchowski. J. Org. Chem. **53**, 6115 (1988).
24. K. Hafner and K. Pfeiffer. Tetrahedron Lett. 4311 (1968).
25. J.H. Crabtree and D.J. Bertelli. J. Am. Chem. Soc. **89**, 5384 (1967).
26. H.M. Gilow and D.E. Burton. J. Org. Chem. **46**, 221 (1981).

Can. J. Chem. Downloaded from www.nrcresearchpress.com by 65.111.164.53 on 09/08/12
For personal use only.

Synthesis and characterization of various unsubstituted and mono-N-substituted tetraazamacrocycles

I. Meunier, A.K. Mishra, B. Hanquet, P. Cocolios, and R. Guilard

Abstract: Syntheses of tetraazamacrocycles have been carried out by using *p*-toluenesulfonyl chloride as protective group. The [14(ane) N4] and [15(ane) N4] were also obtained by the template synthesis. Mono-N-functionalization of tetraazamacrocycles was accomplished by reaction of a fivefold excess of the free macrocycles with 1 equivalent of a suitable alkylating or arylating reagent. The key point of the synthesis lies in the use of an excess of the macrocycle over the substituting reactants to reduce the formation of polysubstituted derivatives, and in the easy separation of the excess of unreacted macrocycle. All the products were characterized on the basis of spectral studies (^{1}H and ^{13}C NMR, including 2D NMR and NOE difference studies) and mass spectrometry.

Key words: tetraazamacrocycles, improved synthesis, protective group, N-tosylation, template synthesis, NOE difference spectroscopy.

Résumé : La synthèse de tétraazamacrocycles a été réalisée en utilisant le chlorure de *p*-toluène sulfonyle comme réactif de protection. Les [14(ane) N4] et [15(ane) N4] ont également été préparés par la voie «template». La monofonctionnalisation sur l'un des atomes d'azote des tétraazamacrocycles a été effectuée en faisant réagir un excès (5 fois) de macrocycle avec 1 équivalent du ligand alkylant ou arylant adapté. Le point crucial de la synthèse réside dans l'utilisation de l'excès de macrocycle par rapport au réactif de substitution afin de réduire la formation de dérivés polysubstitués, ainsi que dans la facilité de séparation de l'excès de macrocycle inchangé qui peut être recyclé. L'ensemble des produits a été caractérisé par des études spectroscopiques (RMN ^{1}H et ^{13}C à une et deux dimensions, étude par différence d'effet Overhauser) et par spectrométrie de masse.

Mots clés : tétraazamacrocycles, amélioration de synthèse, groupe protecteur, N-tosylation, synthèse «template», spectroscopie de différence d'effet Overhauser.

[Traduit par la rédaction]

Introduction

The interest in polyazamacrocycles, compared to simple aliphatic linear polyamines, conjugated aromatic ligands, or porphyrins, as ligands for metal ions has considerably increased during the past decade. Attention has been particularly drawn to the structure and the properties of metal complexes useful in therapy or those able to coordinate reversibly or activate small molecules. Our interest is mostly oriented towards cobalt and iron metal complexes, which can be good models for metal–dioxygen binding.

The polyazamacrocycles show some advantages over the other ligands in their ability to form stable complexes, their good behavior towards oxidation, and their solubility in aqueous media without any addition of hydrophilic groups. However, simple and cheap syntheses, applicable to industrial processes, are not described in the literature.

These polyazamacrocycles have been shown generally to produce strong ligand field, but they cannot always completely wrap up the majority of transition metal ions. To obtain more insight into their ability to coordinate such ions, it is interesting either to modify the ring size or to append coordinating groups to the periphery of the macrocycle. These groups may coordinate the central metal (see **A** below) and thus increase the ligating ability of the macrocycle towards axially coordinated small molecules, preventing further reaction of the complex. For example, compounds having a pendant pyridine (**B**) or carboxylic (**C**) group as a side chain could be suitable ligands for such purposes:

Several synthetic procedures (1) have already been described in the literature for the synthesis of different sizes of both free and N-monofunctionalized tetraazamacrocycles. Among them, the family of N-monofunctionalized tetraazamacrocyclic [14 (ane) N4] compounds has been well studied (2–9) and their corresponding transition metal complexes have been synthesized (10–18) and characterized. However, these starting tetraazamacrocycles were not obtained with high yields (8% overall yield for cyclam) and

Received July 20, 1994. Revision received February 23, 1995.

I. Meunier, A.K. Mishra, B. Hanquet, and R. Guilard.[1] Laboratoire de synthèse et d'électrosynthèse organométalliques, Unité de recherche associée 1685, Faculté des sciences «Gabriel», 6, boulevard Gabriel, F21100 Dijon, France.
P. Cocolios. L'Air Liquide S.A., Centre de recherche Claude-Delorme B.P. 126, F78350 Jouy-en-Josas, France.

[1] Author to whom correspondence may be addressed. Telephone: (011-33)-80-39-61-11. Fax: (011-33)-80-39-61-17.

Can. J. Chem. Downloaded from www.nrcresearchpress.com by 65.111.164.53 on 09/08/12
For personal use only.

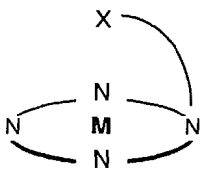

(A)

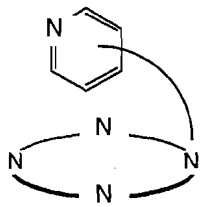

(B)

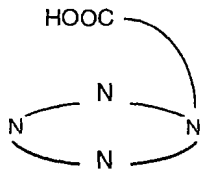

(C)

their spectroscopic properties have not been fully investigated.

To increase the yields of free ligands and to get access to new N-substituted macrocycles, we report here an *improved* synthesis of 1,4,7,10-tetraazacyclododecane (or cyclen) **1***a*, 1,4,8,11-tetraazacyclotetradecane (or cyclam) **2***a*, and 1,5,9,13-tetraazacyclohexadecane **3***a* based on the so-called "template synthesis" and by use of tosyl protective groups. Among the synthesized ligands the following are reported here *for the first time*: 1,4,7,10-tetraazacyclododecanes **1***b*–**1***d*, 1,4,8,11-tetraazacyclotetradecanes **2***d*–**2***f*, and 1,5,9,13-tetraazacyclohexadecanes **3***b*–**3***c*.

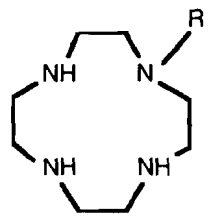

[12 (ane) N4]

1*a*, R = H
1*b*, R = CH_2-CO_2H
1*c*, R = $(CH_2)_2$-CO_2H
1*d*, R = CH_2-*m*Py

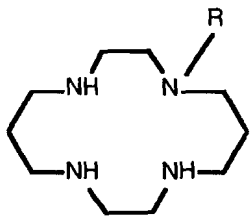

[14 (ane) N4]

2*a*, R = H
2*b*, R = CH_2-CO_2H
2*c*, R = $(CH_2)_2$-CO_2H
2*d*, R = CH_2-*m*Py
2*e*, R = CH_2-*o*Py
2*f*, R = $(CH_2)_2$-*o*Py

In this paper we also report ^1H and ^{13}H NMR data for the above ligands with particular emphasis on the three pyridine derivatives **2***d*, **2***e*, and **2***f*.

Results

(a) Synthesis of unsubstituted tetraazamacrocycles

Cyclam, or 1,4,8,11-tetraazacyclotetradecane **2***a*, was synthesized using the kinetic template effect (2). In this approach, the geometric arrangement of macrocycles within the coordination sphere of a metal ion provides constraints that control the final product obtained by reaction of precursors with the metal

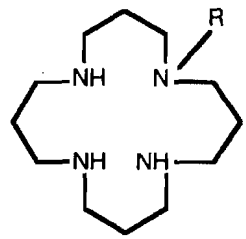

[16 (ane) N4]

3*a*, R = H
3*b*, R = CH_2-CO_2H
3*c*, R = $(CH_2)_2$-CO_2H

ion. Instead of the reported reduction of the diimine with hydrogen under pressure (20% yield) or with $NaBH_4$ (40% yield) (3), reduction with Raney alloy in sodium hydroxide solution (19) increased the yield of **2***a* after demetallation with NaCN, up to 67% (see Scheme 1).

This scheme is a very simple one-pot synthesis. Large quantities of cyclam (about 50 g) may be isolated in a 2-day work-up procedure. The final product is obtained in an acid-free form and can be used easily in the complexation step. However, to avoid the use of large quantities of cyanide ions during the demetallation process, we investigated another synthesis approach.

The tosyl approach includes the protection of the four nitrogen atoms in order to prevent the formation of polymerization products. Cyclen or 1,4,7,11-tetraazacyclododecane (20–22) **1***a*, 1,4,8,11-tetraazacyclotetradecane **2***a*, and 1,5,9,13-tetraazacyclohexadecane (23) **3***a*, have been synthesized according to Scheme 2, using tosyl moieties (24–28). This condensation step in performed in DMF giving a tetratosylated derivative, which is further cleaved at 100°C in concentrated sulfuric acid.

The tosyl approach, although it has some advantages for industrial application, includes a challenging step, i.e., the cleavage of the tosyl groups, and requires careful crystallization of the free macrocycle.

(b) Synthesis of mono-N-substituted tetraazamacrocycles

Carboxylic acid side chain

The unequivocal synthesis of mono-N-functionalized derivatives involves several synthetic steps including the protection (29–31) of some nitrogen atoms. These procedures can be convenient methods of synthesis but are not general, especially when a functional group is present on the side chain.

The substitution can also be done by condensation of the alkylating reagent with the free macrocycle. The tetraazamac-

Can. J. Chem. Downloaded from www.nrcresearchpress.com by 65.111.164.53 on 09/08/12
For personal use only.

Scheme 1. Synthesis of cyclam by improved template synthesis.

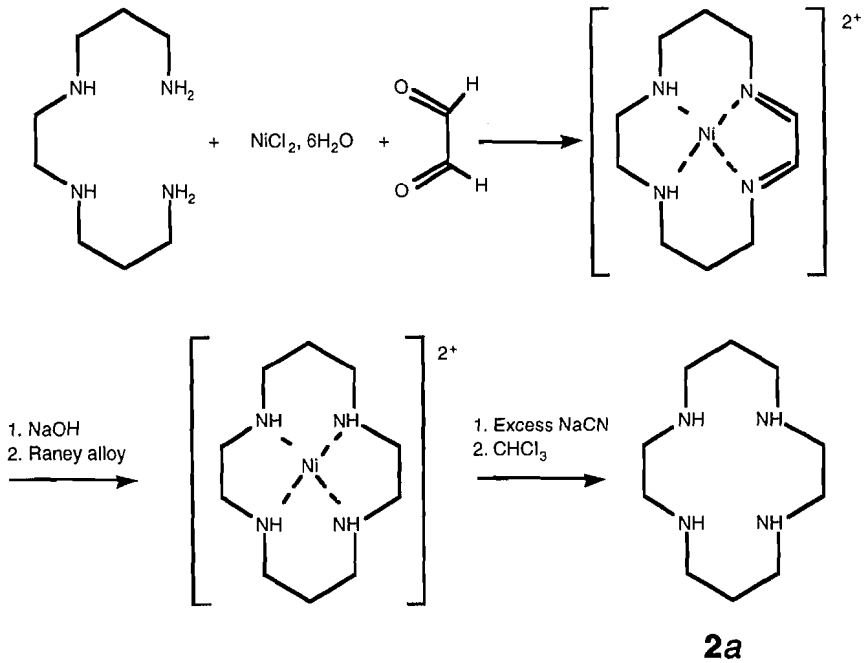

2a

Scheme 2. Synthesis of free tetraazamacrocycles by condensation of tosylated precursors.

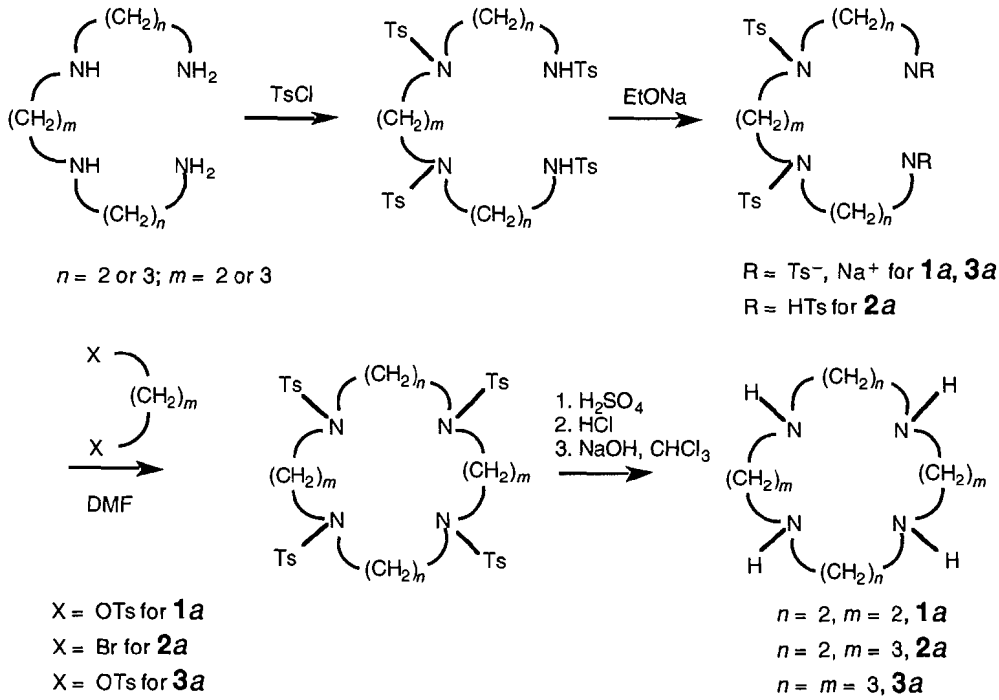

rocycles bearing a carboxylic group are obtained in high yields by reaction of a fivefold excess of the macrocycle and 1 equivalent of halogen-substituted alkyl carboxylic acid in ethanol with LiOH as base. In the presence of a large excess of macrocycle, the *mono-N*-alkylated derivative is the major product of the reaction, together with unreacted derivative recovered (about 90–95% of pure macrocycle) at the end of the synthesis. After refluxing the mixture, extraction, and protonation with concentrated HCl, the tetramines **1***b*, **1***c*, **3***b*, and **3***c* are obtained in good yields (56–78%) as new macrocycles.

Pyridinic side chain

The macrocycles bearing a pyridyl group as a side chain on one of the nitrogen atoms have been synthesized by reaction of a fivefold excess of the free macrocycle and 1 equivalent of the chloromethyl or chloroethylpyridine in DMF at 110°C while stirring for few hours (32). After cooling the reaction mixture at 10°C, the excess of unreacted macrocycle is recovered (about 90–95% of the pure macrocycle after partial removal of DMF). Mono-N-substituted derivatives (**1***d*, **2***d*, **2***e*, **2***f*) are obtained as chlorhydrates with yields in the range of 40–80%.

Can. J. Chem. Downloaded from www.nrcresearchpress.com by 65.111.164.53 on 09/08/12
For personal use only.

Can. J. Chem. Downloaded from www.nrcresearchpress.com by 65.111.164.53 on 09/08/12
For personal use only.

(c) NMR analysis

All the products were characterized on the basis of their spectral data, which are summarized in the experimental section. Three of them (**2***d*, **2***e*, and **2***f*) have been studied in detail by one- and two-dimensional ^1H and ^{13}C NMR spectroscopy (NOE difference and homo and heteronuclear correlation spectra). All the spectra of the final products were recorded in acidic D_2O in order to protonate the four nitrogen atoms. The ^1H and ^{13}C NMR spectral data of these derivatives are given in Table 1 with numbering used in the text.

Knowledge of the spectroscopic data of the free bases in solution is essential to study the further complexation reaction and the axial ligand coordination reactions as well as to determine the pK_a values of the ligands. However, because the peak assignments and the spectral interpretation were not possible on the basis of one-dimensional ^1H and ^{13}C NMR spectroscopy, NOE difference and homo and heteronuclear correlation spectroscopy of compounds **2***d*, **2***e*, and **2***f* were performed.

Study of the N-(2-pyridylmethyl), 2e, and N-(3-pyridylmethyl), 2d, derivatives

On the basis of the one-dimensional ^1H NMR spectrum of the *N*-(2-pyridylmethyl) cyclam **2***e* (not reproduced) it is easy to assign the methylene protons of the pyridinic chain. The ^1H–^1H correlation (COSY) spectrum (see Fig. 1) only concerns the aliphatic region: the two and three methylene moieties are clearly identified. The final attribution is given by the NOE difference experiments. The spectrum obtained after presaturation of peak K (see Fig. 2, spectrum *b*) is compared to the normal 1D spectrum (spectrum *a*). The observed enhancements are given on the formula. Other NOE experiments led to complete information.

The NOE data are summarized in Table 2 where we differentiate the presaturated peak and the signals showing an Overhauser effect. These results allow to assign all the protons of the macrocycle (see Table 1).

The proton-decoupled ^{13}C-1D spectrum only permits us to assign the peak at position 15 due to its important deshielding. The other signals and, more specifically, the cyclic methylene protons give signals between 20 and 53 ppm. Thus it appears necessary to record the ^{13}C–^1H heteronuclear correlation spectrum to totally assign the ^{13}C spectrum.

Coupling of each carbon–proton system appears as a correlation spot. It has to be noted that only short couplings ($^1J_{C-H}$) are observed and quaternary carbon atoms do not give rise to any correlation. Each carbon atom in the aliphatic region is coupled to two isochronous protons, leading to only one correlation spot. The assignments of each carbon atom are given in Table 1.

A similar study has been performed for compound **2***d*. The ^1H and ^{13}C NMR parameters are listed in Table 1.

Study of the N-(2-pyridylethyl) cyclam, 2f

In acidic D_2O solution compound **2***f* exhibits (see Fig. 3, spectrum *a*) a very crowded region (18 protons) between 3.2 and 3.5 ppm. To solve the problem of the chemical shift assignments, a *J*-resolved spectrum has been recorded. On the *F*2 projection (see Fig. 3, spectrum *c*) the different methylenic protons are well separated, making it possible to explain the COSY spectrum (not reproduced). Most of the resonances were attributed on the basis of the previous studies. Different NOE difference experiments were performed, giving the enhancements shown in Table 3.

The simulated spectrum obtained from the chemical shifts and the coupling constants (see Fig. 3, spectrum *b*) is in good accordance with the experimental spectrum.

Comparisons between the pyridinic derivatives 2d, 2e, and 2f

The proton NMR spectra of the three pyridinic derivatives are very similar. By comparison with the cyclam, the methylene protons α to the N-substituted atom show a slight upfield shift (up to 0.3 ppm). All the other protons are deshielded by 0.1–0.3 ppm. The most important feature to be pointed out is the wrap-up of the ethyl-pyridinic arm in compound **2f**, promising a coordination ability.

The carbon-13 chemical shifts are all upfield-shifted except for C14 (α to the nitrogen atom). The largest shift variations (about 10 ppm) are observed for C9 and C10, indicating a significant overlap of the appending group.

Conclusion

Two different syntheses, namely, the template effect or the use of tosyl derivatives of the free bases, for the preparation of cyclen, cyclam, and 1,5,9,11-tetraazacyclohexadecane have been improved in order to produce these compounds on a large scale. New mono-N-substituted macrocycles have been synthesized in high yields. The most promising target molecules in the cyclam series, for complexation by cobalt and reactivity of the complexes with dioxygen, have been fully characterized by using a combination of several NMR techniques.

This study also demonstrates the ability of pendant arms to overlap the cavity of the macrocycle and the possible use of such monosubstituted derivatives to lead to pentacoordinating ligands exhibiting hydrophobic pockets. These ligands may thus be suitable to mimic molecules of biological relevance.

Experimental part

Elemental analyses were obtained from the Service Central d'Analyse du C.N.R.S.

The NMR spectra were recorded on a Bruker WM400 NMR spectrometer operating at 400.13 MHz for ^1H and at 100.64 MHz for ^{13}C. The samples were prepared as acidic D_2O (or $CDCl_3$) solutions containing TMSP (or TMS) as internal reference. The chemical shifts (δ) are given in parts per million (ppm) and the coupling constants (*J*) in hertz (Hz). The multiplicities (m) are noted s: singlet, d: doublet, t: triplet, quint: quintet. Proton spectra were recorded using a 4 kHz spectra width and 32K data points, giving a final resolution of 0.2 Hz (for ^{13}C: 16 kHz, 32K, 1 Hz). The 1D and 2D spectra were recorded using the standard Bruker library programs. Homonuclear COSY consisted of a 256 × 2K data matrix (16 scans, 5 s saturation time for residual water suppression), giving a 3 Hz final resolution in both dimensions. For heteronuclear COSY a 128 × 4K matrix was acquired (128 scans, 1.5 s recovery time). The *F*1 and *F*2 resolutions were, respectively, 8 and 7 Hz. NOE difference spectra were recorded with 3 s of relaxation time and 2 s of presaturation time using two control frequencies.

The mass spectra were performed on the Kratos Concept IS

Table 1. ^{1}H and ^{13}C NMR data of the *N*-(3-pyridylmethyl) cyclam **2***d*, the *N*-(2-pyridylmethyl) cyclam **2***e*, and the *N*-(2-pyridylethyl) cyclam **2***f*.

	Proton				Carbon	
	No.	δ (ppm)	*m/i*	*J* (Hz)	No.	δ (ppm)
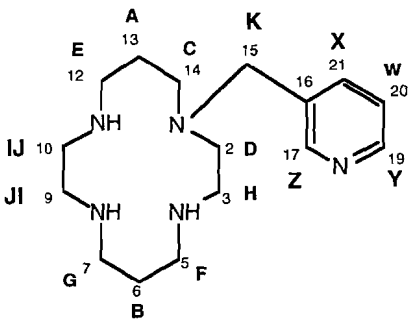 **2***d*	13	2.08	q/2	J_{12-13} = 6.8	6	21.74
	6	2.24	q/2	J_{5-6} = 7.0	13	23.22
	14	2.96	t/2		9–10	40.76–41.34
	2	3.20	t/2	J_{2-3} = 6.7	3	43.27
	12	3.30	t/2		7	43.91
	5	3.33	t/2		5	44.37
	7	3.39	t/2		12	44.78
	3	3.52	t/2		2	49.01
	9–10	3.61	s/4		14	51.22
	15	4.25	s/2		15	56.06
	20	8.09	t/1	J_{20-21} = 7.8	20	130.01
	21	8.70	d/1		16	136.78
	19	8.77	d/1		19	143.62
	17	8.92	s/1		17	144.37
					21	150.96
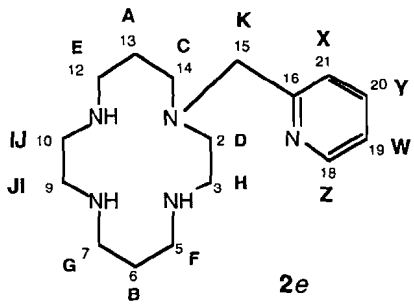 **2***e*	13	1.99	q/2	J_{12-13} = 7.3	6	22.00
	6	2.31	q/2	J_{5-6} = 7.4	13	24.48
	14	2.70	t/2		9–10	41.11–41.52
	2	2.98	t/2	J_{2-3} = 5.8	7	44.12
	12	3.26	t/2		5	44.60
	5	3.32	t/2		3	45.15
	7	3.38	t/2		12	45.33
	3	3.44	t/2		2	50.43
	9–10	3.57	s/4		14	52.78
	15	4.13	s/2		15	57.61
	19	7.99	t/1	J_{18-19} = 7.1	19	128.86
	21	8.05	d/1	J_{20-21} = 7.9	21	130.19
	20	8.55	td/1	J_{18-20} = 1.1	18	143.82
	18	8.75	dd/1		20	149.85
					16	154.41
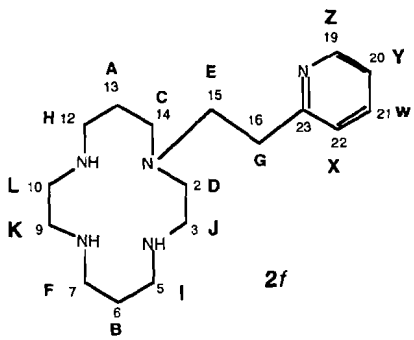 **2***f*	13	2.04	q/2	J_{12-13} = 7.1	6	22.23
	6	2.16	q/2	J_{5-6} = 7.5	13	22.79
	14	3.02	t/2		15	29.13
	2	3.18	t/2	J_{2-3} = 6.3	9	41.76
	15	3.24	t/2	J_{15-16} = 7.3	10	42.83
	7	3.30	t/2		7	44.41
	16	3.32	t/2		5	44.59
	12	3.33	t/2		3–12	44.84
	5	3.37	t/2		2	49.23
	3	3.41	t/2		14	50.84
	9	3.44	t/2	J_{9-10} = 6.1	16	52.68
	10	3.52	t/2		20	127.84
	21	7.90	t/1	J_{20-21} = 7.3	22	129.93
	22	7.95	d/1		19	143.72
	20	8.50	t/1		21	149.49
	19	8.65	d/1	J_{19-20} = 6.8	23	154.89

at CSMUB (Centre de Spectroscopie Moléculaire de l'Université de Bourgogne) using DCI or EI mode. Peak positions are given in *m/z* and relative abundance as a percentage.

1,4,7,10-Tetraazacyclododecane (cyclen), 1*a*

The compound **1***a* is obtained in four steps, according to the following procedure.

Step 1: 1,4,7,10-tetratosyl-1,4,7,10-tetraazadecane

To a stirred solution of triethylenetetramine (14.6 g; 0.1 mol) and sodium hydroxide (16 g; 0.4 mol) in water (108 mL), *p*-toluenesulfonyl chloride (76.2 g; 0.4 mol) in 400 mL of ether is added dropwise. The mixture is left at room temperature under stirring for 1 h. The white precipitate is filtered off and washed in hot methanol (60 g; yield 78.6%).

Can. J. Chem. Downloaded from www.nrcresearchpress.com by 65.111.164.53 on 09/08/12
For personal use only.

Fig. 1. COSY map of the *N*-(2-pyridylmethyl) derivative **2***e* in D_2O at pH 1.74.

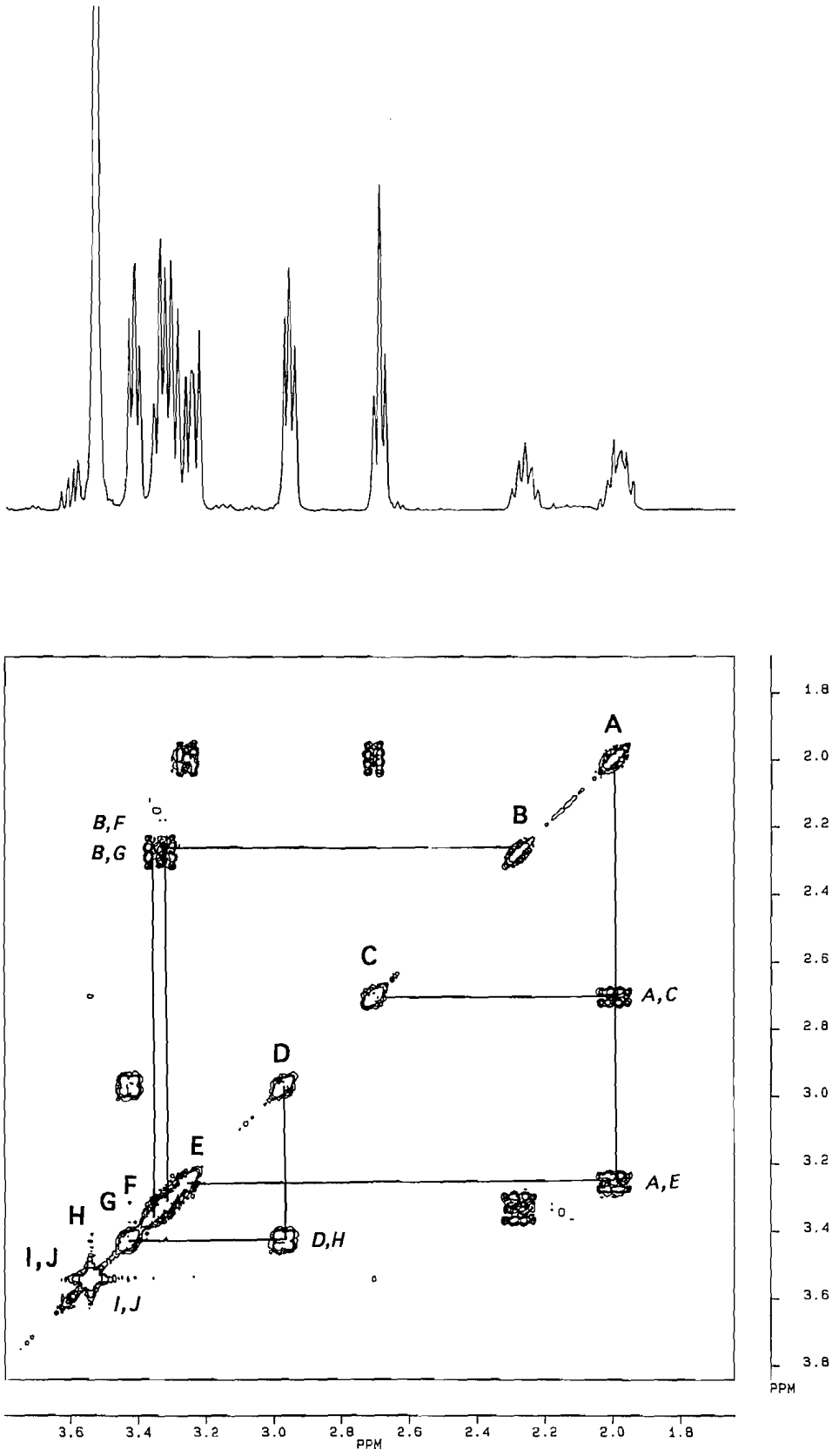

Can. J. Chem. Downloaded from www.nrcresearchpress.com by 65.111.164.53 on 09/08/12
For personal use only.

Fig. 2. (*a*) Normal proton spectrum and (*b*) NOE difference spectrum of the *N*-2(2-pyridylmethyl) derivative **2***a* in D_2O at pH 1.74.

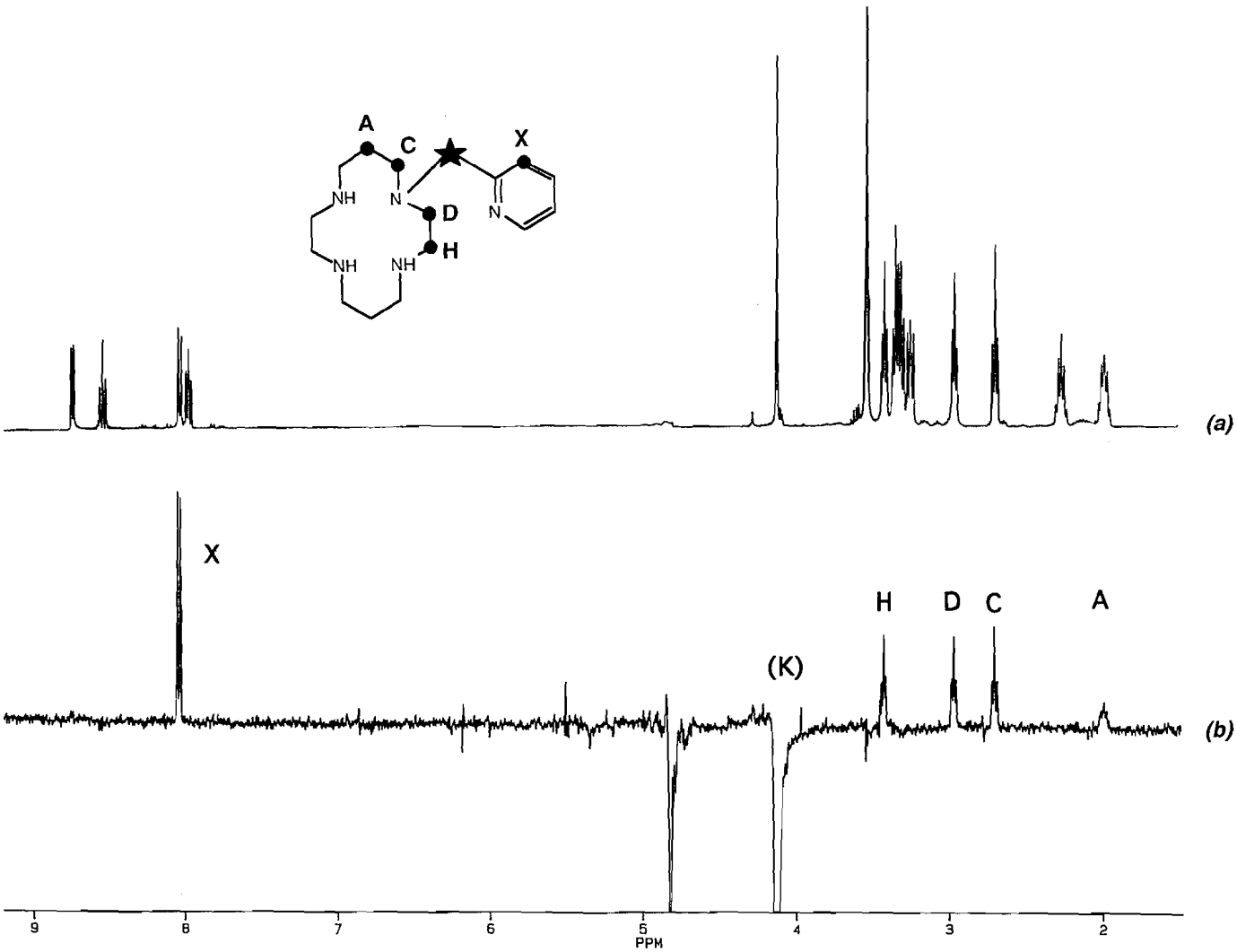

Step 2: disodium salt of 1,4,7,10-tetratosyl-1,4,7,10-tetraazadecane

A suspension of 10 g of 1,4,7,10-tetratosyl-1,4,7,10-tetraazadecane in boiling ethanol (50 mL) is reacted with 2 equivalents of sodium ethoxide. After dissolution, the mixture is refluxed for 30 min after which time the desired product precipitates. The product is filtered and dried under vacuum (yield 100%).

Step 3: 1,4,7,10-tetratosyl-1,4,7,10-tetraazacyclododecane

To a heated mixture (110–120°C) of the sodium salt of 1,4,7,10-tetratosyl-1,4,7,10-tetraazadecane (0.021 mol) in 200 mL of DMF is added, over a period of 2 h, a solution of ditosylated ethylene glycol (14.3 g; 0.038 mol) in 200 mL of DMF. The reaction mixture is maintained at 110°C with stirring. After 24 h, the solvent is evaporated to one tenth of the original volume. The resulting mixture is poured over cold water (800 mL). The white solid that precipitates is filtered and dried at 30–40°C under vacuum (12.2 g; yield 74%).

Step 4: 1,4,7,10-tetraazacyclododecane (cyclen, 1a)

Tetratosylated cyclen (12.0 g; 0.015 mol) is treated in 96% sulfuric acid (50 mL) at 110°C for 72 h. The resulting brown solution is brought to 5°C and 175 mL of ethanol, followed by 148 mL of ether, are slowly added. The brown precipitate is filtered, washed with ethanol and ether, and dried under vacuum for 6 h. It is then dissolved in 150 mL of water and the pH is brought to 12 by addition of 2 M NaOH. The resulting solution is then extracted with chloroform (6 × 130 mL). The organic phase is dried over $MgSO_4$, filtered, and evaporated to yield a white solid. Recrystallization from THF affords cyclen (mp 110–112°C; 1.4 g; yield 54%). ^1H NMR δ ($CDCl_3$): 2.12 (s, 4H, NH), 2.67 (s, 16H, CH_2). ^{13}C NMR δ ($CDCl_3$): 46 (CH_2). MS *m/z* (EI): 173 [M + 1] (100%). Anal. calcd. for $C_8H_{20}N_4$: C 57.78, H 11.70, N 32.52; found: C 57.55, H 11.4, N 32.9.

1,4,8,11-tetraazacyclotetradecane (cyclam), 2*a*, (template synthesis)

1,5,8,12-Tetraazadodecane (15 g; 0.086 mol) obtained as described in the literature is placed in 348 mL of distilled water and nickel chloride hexahydrate (20.4 g; 0.086 mol) is added. The resulting violet solution is cooled at 6°C, and 14.4 mL of 40% aqueous glyoxal solution is added dropwise. The reaction mixture is kept at room temperature under stir-

Can. J. Chem. Downloaded from www.nrcresearchpress.com by 65.111.164.53 on 09/08/12
For personal use only.

Can. J. Chem. Downloaded from www.nrcresearchpress.com by 65.111.164.53 on 09/08/12
For personal use only.

Fig. 3. (*a*) Normal proton spectrum, (*b*) simulated proton spectrum, and (*c*) *F*2 projection of the *J*-resolved map of the *N*-(2-pyridylethyl) derivative **2***f* in D_2O at pH 1.74.

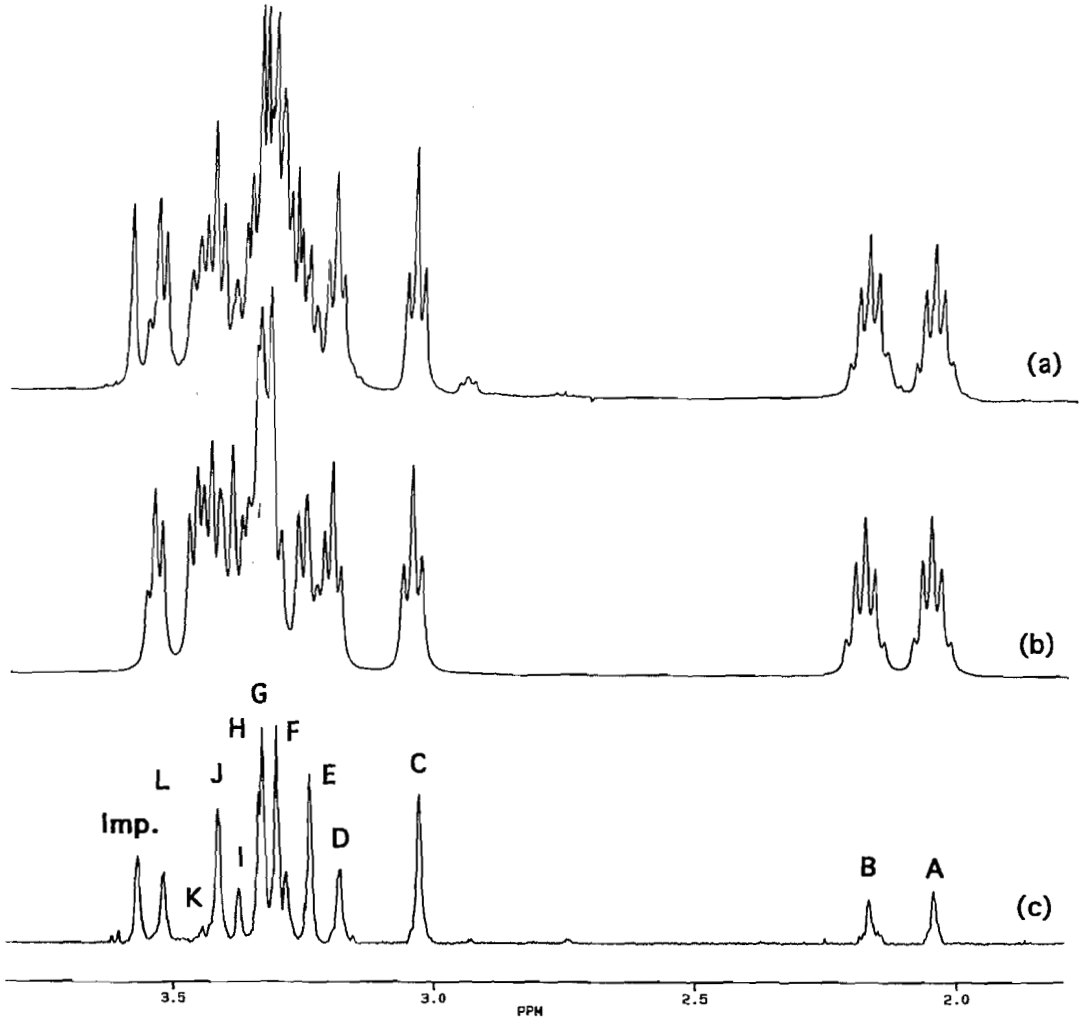

Table 2. NOE difference data obtained for the *N*-(2-pyridylmethyl) cyclam, **2***e*.

Presaturated peak	Peaks showing an Overhauser effect	Structural formula
K	A C D H X	
(IJ)	A B E G	
H	B C D	

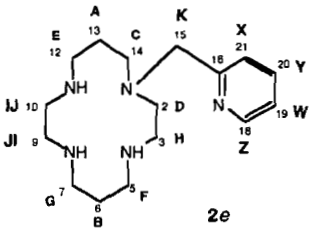

2*e*

ring for 12 h. A 2 M NaOH solution (384 mL) is added quickly, followed by fractional addition of Raney alloy (19.2 g). The stirring is maintained for 2 h. The solution is then filtered over Celite to remove the Raney alloy. Sodium cyanide (28.8 g) is added to the resulting brown solution, which is refluxed for 2 h. The remaining solid is filtered off and the filtrate is extracted with chloroform (8 × 100 mL). Extracts are combined and dried over $MgSO_4$, then filtered and the solvent evaporated. The crude product is crystallized from THF and dried under vacuum (mp 187–188°C; 11.5 g,

Table 3. NOE difference data obtained for the *N*-(2-pyridylethyl) cyclam, **2***f*.

Presaturated peak	Peaks showing an Overhauser effect	Structural formula
B	F G I J K	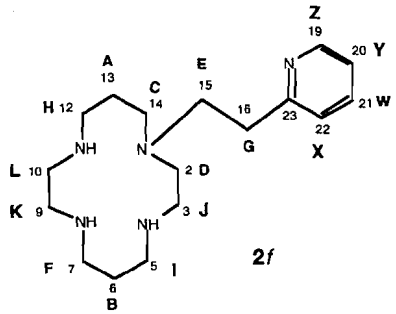
C	A J G	
D	A C J	
G	B C X	
J	B C D	

2*f*

yield 67%). ^{1}H NMR d (D_2O): 2.18 (quint, 4H, CH_2-CH_2-CH_2), 3.27 (t, 8H, NH-CH_2-CH_2-CH_2), 3.51 (s, 8H, NH-CH_2-CH_2-NH). ^{13}C NMR d (D_2O): 30.12 (CH_2-CH_2-CH_2), 49.89, 50.93 (2 NH-CH_2). MS *m/z* (EI): 201 [M + 1] (100%). Anal. calcd. for $C_{10}H_{24}N_4$: C 59.96, H 12.08, N 27.97; found: C 60.1, H 11.9, N 27.3.

1,4,8,11-Tetraazacyclotetradecane (cyclam), 2*a*, (tosyl coupling)

Step 1: 1,5,8,12-tetratosyl-1,5,8,12-tetraazadodecane
To a stirred solution of 1,5,8,12-tetraazadodecane (6.9 g; 0.043 mol) and sodium hydroxide (6.8 g; 0.17 mol) in water (54 mL), *p*-toluenesulfonyl chloride (32.4 g; 0.17 mol) in 420 mL of ether is added dropwise. The mixture is kept at room temperature under stirring for 1 h. The tetratosyl tetramine is isolated as an oily phase separated by decantation. After drying, a white semi-solid is obtained (25 g; yield 74.6%).

Step 2: 1,4,8,11-tetratosyl-1,4,8,11-tetraazacyclotetradecane
To a heated mixture (110–120°C) and anhydrous potassium carbonate (20 g; 0.144 mol) in 1000 mL of DMF, is added dropwise (1 drop every 10 s) a solution of 1,5,8,12-tetratosyl-1,5,8,12-tetraazadodecane (11.65 g; 0.015 mol) and 1,3-dibromopropane (3.03 g; 0.015 mol) mixed in 270 mL of DMF. The reaction mixture is maintained under stirring at 110°C. After 8 h, the reaction mixture is brought to room temperature and the salt present is eliminated by filtration. After concentration to one tenth of the filtrate, the resulting mixture is poured over cold water (1000 mL). The white solid that precipitates is dried at 30–40°C under vacuum (9.6 g; yield 78.3%).

Step 3: 1,4,8,11-tetraazacyclotetradecane, 2a
The tetratosylated derivative (8 g; 0.098 mol) is treated with 96% sulfuric acid (33 mL) at 110°C for 50 h. The resulting brown solution is brought to 5°C and 125 mL of ethanol, followed by 120 mL of ether, are slowly added. The brown precipitate is filtered, washed with ethanol and ether, and dried under vacuum for 6 h. It is then dissolved in 150 mL of water and the pH is brought to 12 by addition of 2 M NaOH. The resulting solution is then extracted with chloroform (6 × 130 mL). The organic phase is dried over $MgSO_4$, filtered, and evaporated to yield a white solid that is recrystallized from THF, giving 0.7 g of free cyclam (yield 35%).

1,5,9,13-Tetraazacyclohexadecane, 3*a*

The compound **3***a* is obtained in a four-step procedure, described as follows.

Step 1: 1,5,9,13-tetratosyl-1,5,9,13-tetraazatridecane
To a stirred solution of tripropylenetetramine (18.8 g; 0.1 mol) and sodium hydroxide (16 g; 0.4 mol) in water (108 mL), *p*-toluenesulfonyl chloride (76.2 g; 0.4 mol) in 400 mL of ether is added dropwise. The mixture is kept at room temperature under stirring. The white precipitate is filtered and washed by hot methanol (62.5 g; yield 77.6%).

Step 2: disodium salt of 1,5,9,13-tetratosyl-1,5,9,13-tetraazatridecane
A suspension of 16 g of 1,5,9,13-tetratosyl-1,5,9,13-tetraazatridecane in boiling ethanol (70 mL) is reacted with 2 equivalents of sodium ethoxide. After dissolution the mixture is refluxed for 30 min after which time the desired product precipitates. It is filtered and dried under vacuum (yield 100%).

Step 3: 1,5,9,13-tetratosyl-1,5,9,13-tetraazacyclohexadecane
To a heated mixture (110–120°C) of the sodium salt of the 1,5,9,13-tetratosyl-1,5,9,13-tetraazatridecane (16.9 g; 0.02 mol) in 200 mL of DMF is added, over a period of 2 h, a solution of *O*,*O*′-ditosyl-1,3-propanediol (11.5 g; 0.03 mol) in 200 mL of DMF. The reaction mixture is maintained under stirring at 110°C. After 24 h, the solvent is evaporated to one tenth of the original volume. The resulting mixture is poured over cold water (800 mL). The white solid that precipitates is filtered and dried at 30–40°C under vacuum (yield 63%).

Step 4: 1,5,9,13-tetraazacyclohexadecane, 3a
The tetratosylated derivative (0.015 mol) is treated in 96% sulfuric acid (50 mL) at 110°C for 72 h. The resulting brown solution is brought to 5°C and 175 mL of ethanol, followed by 148 mL of ether, are slowly added. The brown precipitate is filtered, washed with ethanol and ether, and dried under vacuum for 6 h. It is then dissolved in 150 mL of water and the pH is brought to 12 by addition of sodium hydroxide (2 mol/L).

Can. J. Chem. Downloaded from www.nrcresearchpress.com by 65.111.164.53 on 09/08/12
For personal use only.

Can. J. Chem. Downloaded from www.nrcresearchpress.com by 65.111.164.53 on 09/08/12
For personal use only.

The resulting solution is then extracted with chloroform (6 × 130 mL). The organic phase is dried over $MgSO_4$, filtered, and evaporated to yield a white solid that is recrystallized from THF (yield 71%). ^{1}H NMR d ($CDCl_3$): 1.68 (q, 8H, CH_2-*CH_2*-CH_2), 2.67 (t, 16H, NH-CH_2), 1.83 (s, 4H, NH). ^{13}C NMR d ($CDCl_3$): 28.8 (CH_2-*CH_2*-CH_2); 47.7 (NH-*CH_2*). MS *m/z* (EI): 228 [M + 1] (100%). Anal. calcd. for $C_{12}H_{28}N_4$: C 63.11, H 12.36, N 24.53; found: C 63.0, H 11.79, N 24.2.

1-(2-Acetic acid)-1,4,7,10-tetraazacyclododecane, 1*b*

Cyclen (10 g; 0.058 mol) is dissolved in 150 mL of ethanol and 30 mL of cold water (5°C) containing 0.84 g (0.02 mol) of lithium hydroxide. After complete dissolution a mixture of bromoacetic acid (1.53 g; 0.011 mol) in 80 mL of water is added slowly. The reaction mixture is then refluxed for 6 h after which time the solvent is evaporated. The product is taken up in water and the pH adjusted to 12.5 by addition of a NaOH solution. The solution is extracted several times with chloroform to remove the excess of cyclen. The aqueous phase is concentrated and cooled to 0°C. Cold ethanol (100 mL) is added and the solution kept at 5°C for 3 h. The precipitate is filtered off and the filtrate is treated with 37% HCl at 220°C. The turbid solution obtained is kept at 5°C for 4 h. During this period a white solid separates out and is filtered, washed with ethanol and acetone, and dried under vacuum to give 3.1 g of the 1-(2-acetic acid)-1,4,7,10-tetraazacyclododecane in its protonated form (yield 74%). ^{1}H NMR d (D_2O): 3.44, 3.64, 3.71, 3.79 (t, 16H, NH-*CH_2*), 3.90 (s, 2H, *CH_2*-CO_2H). ^{13}C NMR d (D_2O): 44.66, 45.55, 45.81, 51.83, 56.04, 177.25. MS *m/z* (EI): 58 [(CH_2CO_2H) 2 H]$^+$ (9.7%), 212 [M 2 H_2O]$^+$ (21%), 231 [M + H]$^+$ (5.3%). Anal. calcd. for $C_{10}H_{22}N_4O_2 \cdot 4HCl \cdot 2H_2O$: C 29.14, H 7.34, N 13.59, Cl 34.40; found: C 28.9, H 7.0, N 13.4, Cl 31.55.

1-(2-Carboxyethyl)-1,4,7,10-tetraazacyclododecane, 1*c*

The *N*-(2-carboxyethyl)-1,4,7,10-tetraazacyclododecane is synthesized following the same method as previously described using 1.68 g of bromopropionic acid (0.011 mol) and 10 g (0.058 mol) of cyclen (yield 72%). ^{1}H NMR d (D_2O): 3.20, 3.09, 3.28 (t, 12H), 3.40–3.70 (m, 8H). ^{13}C NMR d (D_2O): 33.0, 45.2, 45.79, 47.25, 47.34, 51.89, 179.11. MS *m/z* (EI): 73 [$(CH_2)_2CO_2H$)]$^+$ (74%), 173 [M 2 [$(CH_2)_2CO_2H$] + 2H] (12.5%), 245 [M + H]$^+$ (3.2%).

1-(2-Acetic acid)-1,4,8,11-tetraazacyclotetradecane, 2*b*

Compound **2*b*** is obtained in the same way as **1*b***, starting from cyclam (20.0 g; 0.1 mol), lithium hydroxide (1.68 g; 0.04 mol), and 2-bromoacetic acid (2.78 g; 0.02 mol) in 77% yield. ^{1}H NMR d (D_2O): 1.93 (quint, 2H, CH_2-*CH_2*-CH_2), 2.03 (quint, 2H, CH_2-*CH_2*-CH_2), 2.86 (t, 2H), 2.93 (t, 2H), 3.13 (t, 2H), 3.19 (t, 4H), 3.25 (t, 2H), 3.27 (t, 2H), 3.34 (t, 2H), 3.47 (s, 2H, *CH_2*-CO_2H). ^{13}C NMR d (D_2O): 22.97, 23.61, 42.17, 43.41, 44.23, 45.30, 45.56, 46.09, 52.14, 54.31, 56.98, 175.89. Anal. calcd. for $C_{12}H_{26}O_2N_4 \cdot 3HCl \cdot 2H_2O$: C 35.70, H 8.24, N 13.88, Cl 26.34; found: C 35.1, H 8.2, N 13.4, Cl 25.2.

3-(1,4,8,11-Tetraazacyclotetradec-1-yl) propionic acid, 2*c*

Following the same procedure as above, compound **2*c*** is obtained from cyclam (20 g; 0.1 mol) and 3-iodopropionic acid (3.98 g; 0.02 mol) in 65% yield. ^{1}H NMR d (D_2O): 2.09 (quint, 2H, CH_2-*CH_2*-CH_2), 2.13 (quint, 2H, CH_2-*CH_2*-CH_2), 2.83 (t, 2H), 3.23 (t, 2H), 3.31 (t, 4H), 3.33 (t, 4H), 3.42 (t, 2H), 3.46–3.57 (m, 6H). ^{13}C NMR d (D_2O): 20.97, 21.44, 31.57, 40.23, 40.37, 40.56, 43.74, 43.86, 44.32, 48.08, 50.10, 53.13, 176.57. Anal. calcd. for $C_{13}H_{28}O_2N_4 \cdot 4HCl \cdot 2H_2O$: C 34.37, H 7.99, O 14.09, N 12.33, Cl 31.22; found: C 34.3, H 8.1, O 15.1, N 13, Cl 32.0.

2-(1,5,9,13-Tetraazacyclohexadec-1-yl) acetic acid, 3*b*

Compound **3*b*** is synthesized following the same method as previously described for **1*b*** using bromoacetic acid and 1,5,9,13-tetraazacyclohexadecane (yield 62%). ^{1}H NMR d: 2.05 (2q, 4H, CH_2-*CH_2*-CH_2), 2.10 (2q, 4H, CH_2-*CH_2*-CH_2), 3.32 (m, 12H, N-*CH_2*-CH_2), 3.45 (t, 4H, N-*CH_2*-CH_2), 3.90 (s, 2H, *CH_2*-CO_2H). ^{13}C NMR d: 20.61, 21.18, 42.75, 43.02, 43.57, 51.56, 58.47, 170.81. Anal. calcd. for $C_{14}H_{30}O_2N_4 \cdot 5HCl \cdot 3H_2O$: C 32.17, H 7.91, N 10.72, Cl 33.91; found: C 32.8, H 8.1, N 10.1, Cl 32.7.

1-(2-Carboxyethyl)-1,5,9,13-tetraazacyclohexadecane, 3*c*

N-(2-Carboxyethyl)-1,5,9,13-tetraazacyclohexadecane is synthesized following the same method as previously described for **1*b*** using bromopropionic acid and 1,5,9,13-tetraazacyclohexadecane (yield 68%). ^{1}H NMR d: 2.06 (q 4H, CH_2-*CH_2*-CH_2), 2.10 (q, 4H, CH_2-*CH_2*-CH_2), 2.86 (t, 2H, N-*CH_2*-CH_2-CO_2H), 3.32 (t, 12H, N-*CH_2*-CH_2), 3.45 (t, 4H, N-*CH_2*-CH_2), 3.54 (t, 2H, *CH_2*-CO_2H). ^{13}C NMR: 20.18, 21.05, 31.58, 42.59, 42.93, 43.51, 50.30, 53.54, 176.35.

1-(2-Pyridylmethyl)-1,4,8,11-tetraazacyclotetradecane, 2*e*

Cyclam (5.0 g; 0.025 mol) is dissolved in 125 mL of DMF at 110–120°C and 2-chloromethylpyridine-hydrochloride (0.82 g; 0.005 mol) in 5 mL of DMF is slowly added. The stirring is maintained at this temperature for 2 h, after which time the reaction mixture is left for 12 h at 5°C. The precipitate is filtered off to remove excess of cyclam and the filtrate is concentrated by evaporation. The obtained oily product is taken up in 20 mL of water and the pH is adjusted to 11.5 by addition of NaOH. The solution is extracted with chloroform and the organic phase is dried over $MgSO_4$, filtered, and evaporated. The orange oily product is treated with ether to precipitate the remaining cyclam, which is then eliminated by filtration. The filtrate is evaporated and the residue (1.2 g) is taken up in 10 mL of ethanol, 37% HCl is added at 220°C, and the mixture is left for 12 h. The white solid is filtered, washed with ether, and dried under vacuum (yield 74%). MS *m/z* (EI): 93[CH_2(*o*-Py) + H]$^+$ (100%), 199[M 2 [CH_2(*o*-Py)]]$^+$ (88.4%), 292[M + H]$^+$ (52.7%). Anal. calcd. for $C_{16}H_{29}N_5 \cdot 4HCl \cdot 5H_2O$: C 36.44, H 8.22, N 13.28, Cl 26.89; found: C 36.3, H 8.0, N 13.0, Cl 27.1.

1-(3-Pyridylmethyl)-1,4,7,10-tetraazacyclododecane, 1*d*

N-(3-Pyridylmethyl)-1,4,7,10-tetraazacyclododecane is prepared following the same method as described for the preparation of *N*-(2-pyridylmethyl)-1,4,8,11-tetraazacyclotetradecane (yield 60%). ^{1}H NMR d (D_2O): 2.93 (t, 4H, *CH_2*-CH_2), 3.00 (t, 4H, *CH_2*-CH_2), 3.22 (t, 4H, *CH_2*-CH_2), 3.31 (t, 4H, *CH_2*-CH_2), 4.13 (s, 2H, *CH_2*-*m*-Py), 8.11 (t, 1H, *m*-Py), 8.66 (d, 1H, *m*-Py), 8.88 (s, 1H, *m*-Py). ^{13}C NMR d ($CDCl_3$): 46.12, 46.73, 48.08, 52.05, 57.55, 124.03, 134.93, 137.15, 149.21, 150.88. MS *m/z* (EI): 93 [CH_2 (*o*-Py) + H]$^+$ (100%), 171 [M 2 [CH_2(*o*-Py)]$^+$ (19.7%), 264 [M + H]$^+$ (51.4%). Anal. calcd. for

$C_{14}H_{25}N_5$: C 63.84, H 9.57, N 26.59; found: C 63.7, H 9.6, N 26.0.

1-(3-Pyridylmethyl)-1,4,8,11-tetraazacyclotetradecane, 2*d*

N-(3-Pyridylmethyl)-1,4,8,11-tetraazacyclotetradecane is prepared as described above using 3-chloromethyl pyridine and 1,4,8,11-tetraazacyclotetradecane (yield 80%). MS *m/z* (EI): 94 $[CH_2(m\text{-Py}) + 2H]^+$ (100%), 199 $[M\ 2\ [CH_2(m\text{-Py})]]^+$ (1.5%), 292 $[M + H]^+$ (19.8%). Anal. calcd. for $C_{16}H_{29}N_5 \cdot 4.8HCl \cdot 2.2H_2O$: C 37.95, H 7.55, N 13.84, Cl 33.68, found: C 37.6, H 7.2, N 13.1, Cl 33.5.

1-(2(-2-Pyridyl)ethyl)-1,4,8,11-tetraazacyclotetradecane, 2*f*

N-(2(-2-Pyridyl)ethyl)-1,4,8,11-tetraazacyclotetradecane is prepared as described above by using 5 g (0.025 mol) of cyclam and 0.89 g (0.005 mol) of 2-(2-chloroethyl) pyridine in DMF (yield 40%). MS *m/z* (EI): 106 $[(CH_2)_2(o\text{-Py})]^+$ (83.7%), 201 $[M\ 2\ [(CH_2)_2(o\text{-Py}) + 2H]^+$ (17%), 306 $[M + H]^+$ (18.4%). Anal. calcd. for $C_{17}H_{31}N_5 \cdot 5HCl \cdot 3H_2O$: C 37.65, H 7.55, N 12.92, Cl 32.78; found: C 37.8, H 8.3, N 12.9, Cl 33.0.

References

1. J.S. Bradshaw, K.E. Krakowiak, and R.M. Izattg. *In* Aza-crown macrocycles. Wiley Interscience, New York. 1993.
2. E.K. Barefield, F. Wagner, and K.D. Hodges. Inorg. Chem. **15**, 1370 (1976).
3. E.K. Barefield, F. Wagner, A.W. Herliger, and A.R. Dahl. Inorg. Synth. **16**, 220 (1976).
4. J.E. Richman and T.J. Atkins. J. Am. Chem. Soc. **96**, 2268 (1974).
5. T.A. Kaden. Top. Curr. Chem. **121**, 157 (1984).
6. M. Studer and T.A. Kaden. Helv. Chim. Acta, **69**, 2081 (1986).
7. J.S. Bradshaw, K.E. Krakowiak, R.M. Izatt, and D.J. Zamecka-Krakowiak. Tetrahedron Lett. **31**, 1077 (1990).
8. I. Tabushi, Y. Tanigushi, and H. Kato. Tetrahedron Lett. **12**, 1049 (1977).
9. E. Kimura, M. Shionoya, M. Okamoto, and H. Nada. J. Am. Chem. Soc. **110**, 3679 (1988).
10. A. Bakac and J.H. Espenson. Inorg. Chem. **26**, 4353 (1987).
11. A. Bakac and J.H. Espenson. J. Am. Chem. Soc. **112**, 2273 (1990).
12. E. Asato, S. Kida, and I. Murase. Inorg. Chem. **28**, 800 (1989).
13. E.K. Barefield and F. Wagner. Inorg. Chem. **12**, 2435 (1973).
14. H. Harada, M. Kodera, G. Vuckovic, N. Matsumoto, and S. Kida. Inorg. Chem. **30**, 1190 (1991).
15. G.H. Robinson, W.T. Pennington, B. Lee, M.F. Self, and D.C. Hrncir. Inorg. Chem. **30**, 809 (1991).
16. E. Kimura, T. Koike, K. Uenishi, M. Hediger, M. Kuramoto, S. Joko, Y. Arai, M. Kodama, and Y. Iitaka. Inorg. Chem. **26**, 2975 (1987).
17. N. Shinohara, K. Ishii, and M. Hirose. J. Chem. Soc. Chem. Commun. 700 (1990).
18. E. Kimura. Pure Appl. Chem. **61**, 823 (1989).
19. B. Staskun and T. Van Es. J. Chem. Soc. (C), 531 (1966).
20. T.J. Atkins, J.E. Richman, and W.F. Oettle. Org. Synth. **58**, 86 (1978).
21. B. Boisselier-Cocolios, R. Guilard, L. Taurin, and C. Jean. Demande de brevet européen n° 396 435 publiée le 7 nov 1990, extension AU, CA, JP, US, ZA.
22. R. Guilard, I. Meunier, C. Jean, and B. Boisselier-Cocolios. Brevet français n° 8 914 719 du 10 janvier 1992, extension AU, CA, EP, JP, US, ZA.
23. W.L. Smith and K.N. Raymond. Inorg. Synth. **20**, 109 (1980).
24. W. Wehner and F. Vögtle. ChED. Chem.: Exp. Didakt. **1**, 77 (1975).
25. W.L. Smith, J.D. Ekstrand, and K.N. Raymond. J. Am. Chem. Soc. **100**, 3539 (1978).
26. F. Chavez and A.D. Sherry. J. Org. Chem. **54**, 2990 (1989).
27. D.D. Watkins, D.P. Riley, J.A. Stone, and D.H. Busch. Inorg. Chem. **15**, 387 (1976).
28. E.R. Nelson, M. Maienthal, L.A. Lane, and A.A. Benderly. J. Am. Chem. Soc. **79**, 3467 (1957).
29. H. Bernard, J.J. Yaouanc, J.C. Clément, H. des Abbayes, and H. Handel. Tetrahedron Lett. **32**, 639 (1991).
30. P.L. Anelli, M. Murru, F. Uggeri, and M. Virtuani. J. Chem. Soc. Chem. Commun. 1317 (1991).
31. A. Filali, J.-J. Yaouanc, and H. Handel. Angew. Chem. Int. Ed. Engl. **30**, 560 (1991).
32. H. Handel and H. Chaumeil. Brevet, demande d'extension aux Pays Européens enregistré le 7 avr 1998, AT, BE, CH, DE, ES, FR, GB, GR, IT, LI, LU, NL, SE, n° 88 400 839.2.

Can. J. Chem. Downloaded from www.nrcresearchpress.com by 65.111.164.53 on 09/08/12
For personal use only.

Model potential in spectral representation form. Its fidelity to the frozen-core operator and comparison with other model potentials[1]

Shinichi Katsuki

Can. J. Chem. Downloaded from www.nrcresearchpress.com by 65.111.164.53 on 09/08/12
For personal use only.

Abstract: The model potential, in which the Coulomb and exchange core operators are converted to the matrix elements by use of the spectral representation technique, should be equivalent to the frozen-core operator, if the basis set of the spectral representation is complete. Its fidelity to the frozen-core operator is examined in this paper through a thorough study of basis set convergence in both the spectral space and the atomic orbital space, along with comparison with the Sakai–Huzinaga and the Huzinaga–Seijo–Barandiaran–Klobukowski model potentials. The RHF molecular calculations on N_2, P_2, As_2, Sb_2, PN, and AsN show that the present model potential can approximate, with reliable accuracy, the results obtained from the frozen-core calculations.

Key words: model potential, spectral representation, molecular orbital calculation, electronic structure.

Résumé : Le potentiel modèle, dans lequel les opérateurs centraux de Coulomb et d'échange sont transformés en éléments matriciels par le biais de la représentation spectrale, devrait être équivalent à l'opérateur central fixe si l'ensemble de base de la représentation spectrale est complet. Dans ce travail, on examine sa fidélité par rapport à l'opérateur central fixe par le biais d'une étude de la convergence de l'ensemble de base dans l'espace spectral ainsi que dans l'espace de l'orbitale atomique et aussi par une comparaison avec le potentiel du modèle de Sakai–Huzinaga et avec le potentiel du modèle de Huzinaga–Seijo–Barandiaran–Klobukowski. Des calculs moléculaires RHF sur les N_2, P_2, As_2, Sb_2, PN et AsN montrent que le potentiel modèle proposé peut fournir une approximation fiable et précise des résultats obtenus à l'aide de calculs effectués par la méthode de l'opérateur central fixe.

Mots clés : potentiel modèle, représentation spectrale, calculs d'orbitales moléculaires, structure électronique.

[Traduit par la rédaction]

Introduction

A number of valence-electron methods, known as pseudopotential, effective potential, or model potential, have recently been proposed (1, 2). Their main purpose is to make feasible calculations that would be prohibitively expensive if done at the all-electron level, without loss of accuracy. Among these, the model potential method first introduced by Bonifacic and Huzinaga (3), improved by Sakai and Huzinaga (4) (mp1), and reformulated, based on an ab initio philosophy, by Huzinaga, Seijo, Barandiaran, and Klobukowski (5) (mp2) makes use of valence orbitals showing the correct nodal structure. The model potential discussed in this paper is derived from the Huzinaga model potential (3). In the present model (6–8), the mathematical technique of spectral representation (5, 9) is used to replace not only the exchange (5, 10) but also the Coulomb interaction between the core electrons and the valence electrons with a model potential V_{mp3}. As a result, the present model potential (mp3), which is the third version of the Huzinaga model potential (3), invokes no adjustable and (or) fitting parameters. Therefore, once the core orbitals of the constituent atoms are obtained and basis sets for the spectral representation are chosen, the model potentials in the spectral representation form can be prepared without parameters. Thus, anyone can obtain a model potential suitable to particular requirements, such as a model potential for an atom in a neutral state, or a model potential for an atom in an ionic state embedded in a crystal, etc., if and only if the orbitals to be frozen have already been obtained.

The quality of the model potential should be evaluated by its fidelity to the frozen-core operator. The closer a model potential approximates frozen-core results, the more useful it is. In this paper we examine the fidelity of the present model potential to the frozen-core operator by a thorough study of basis set convergence in both the spectral space and the atomic orbital space, along with comparison with mp1 and mp2.

Received August 9, 1994. Revision received February 10, 1995.

S. Katsuki.[2] Department of Applied Physics, Faculty of Engineering, Kyushu University Ropponmatsu, 4-2-1 Ropponmatsu, Fukuoka, 810 Japan.

[1] This paper was presented at the "Quantum Chemistry" Satellite Symposium of the 77th Canadian Society for Chemistry Conference and Exhibition held in Winnipeg from May 29 to June 2, 1994.

[2] Telephone: 092-771-4161, ext. 275. Fax: 092-724-0790. E-mail: a70370a@kyu-cc.cc.kyushu-u.ac.jp

Can. J. Chem. Downloaded from www.nrcresearchpress.com by 65.111.164.53 on 09/08/12
For personal use only.

Method

According to the Hartree–Fock approximation, the eigenfunction is expressed in terms of molecular orbitals ψ_i which satisfy the Hartree–Fock equation

$$[1] \qquad F\psi_i = \epsilon_i\psi_i$$

with the Fock operator F (in the case of a closed-shell electron configuration)

$$[2] \qquad F = -\frac{1}{2}\Delta - \sum_A \frac{Z_A}{r_A} + \sum_j (2J_j - K_j)$$

where

$$[3] \qquad J_j f(1) = \int d\nu_2 \psi_j^*(2)\psi_j(2)\frac{1}{r_{12}} f(1)$$

$$[4] \qquad K_j f(1) = \int d\nu_2 \psi_j^*(2) f(2)\frac{1}{r_{12}} \psi_j(1)$$

Under the frozen-core approximation, the Fock operator [2] may be rewritten as follows by introducing a complete set $\{\chi\}$, which is not necessarily an orthogonal set

$$[5] \qquad F = -\frac{1}{2}\Delta - \sum_A \frac{Z_A - Z_A^c}{r_A} + \sum_j^{val}(2J_j - K_j) + \sum_A V_{mp3}^A$$

where

$$[6] \qquad V_{mp3}^A = \Omega^A\left[-\frac{Z_A^c}{r_A} + \sum_j^{core}(2J_j^A - K_j^A)\right]\Omega^A + P^A$$

$$[7] \qquad \Omega^A = \sum_{ab}|\chi_a^A\rangle(S^A)_{ab}^{-1}\langle\chi_b^A|$$

$$[8] \qquad S_{ab}^A = \langle\chi_a^A|\chi_b^A\rangle$$

$$[9] \qquad P^A = -\sum_j^{core} 2\epsilon_j^A|\phi_j^A\rangle\langle\phi_j^A|$$

and Z_A, Z_A^c, ϵ_j^A, ϕ_j^A represent the atomic number, the number of core electrons, the core-orbital energies, and core orbitals belonging to the atom A, respectively. The projection operator P^A is added in eq. [6] to guarantee the Fock equation [1] being solved in the functional space excluding the core-function space. The operator.

$$[10] \qquad \Omega O\Omega = \Sigma_{abcd}|\chi_a\rangle(S^{-1})_{ab}\langle\chi_b|O|\chi_c\rangle(S^{-1})_{cd}\langle\chi_d|$$

is called the spectral representation of operator O. V_{mp3}^A (eq. [6]) may be called the model potential in spectral representation form. We designate it the mp3 model potential, because it is the third version of the Huzinaga model potential. The energy of the valence electrons E_v in this case is calculated as

$$[11] \qquad E_v = \sum_j^{val}\left\{\epsilon_j + \langle\psi_j|-\frac{1}{2}\Delta - \sum_A\left(\frac{Z_A - Z_A^c}{r_A} + V_{mp3}^A\right)|\psi_j\rangle\right\} + \sum_{AB}\frac{(Z_A - Z_A^c)(Z_B - Z_B^c)}{R_{AB}}$$

Fidelity of the model potential in the spectral representation

The procedure to obtain the model potential by spectral representation is straightforward; this property is one of the merits the mp3 has over the other model potentials. However, the most important property that a model potential should have is fidelity to the frozen-core operator; the valence-electron method with the model potential should faithfully approximate the results obtained from the frozen-core calculation. Equation [5] could produce the same results as those obtained by the frozen-core approximation, if a complete set $\{\chi\}$ were used. However, $\{\chi\}$ is always an incomplete set. Therefore, we evaluated the fidelity of the mp3 by using limited basis sets.

We calculated the spectroscopic constants of N_2, P_2, and As_2 using common valence-orbital basis sets in the frozen-core calculations and in the mp3 calculations using several $\{\chi\}$, and compared the results obtained from these two calculations. The results are presented in Tables 1*a* through 1*c*. The results obtained from the all-electron calculations are also listed in Tables 1*a*–1*c*. A comparison of the results confirms that the frozen-core approximation is valid.

We used two valence-orbital basis functions for nitrogen (Table 1*a*). The first one was the well-tempered Gaussian-type orbital (wtgto) of Huzinaga et al. composed of (14*s*9*p*) primitive Gaussian-type orbitals (pgto) and contracted as (10,10,1111/51111) according to their suggestion (11). The second one was the (10*s*7*p*) pgto set taken from Huzinaga's book (12) and contracted as (7111/4111). The results obtained by the mp3 method agree very well with the values obtained from the frozen-core calculation and the all-electron calculation. Because the frozen-core orbital of nitrogen is the only 1*s* orbital localized tightly around the nucleus, the results listed in Table 1*a* are very similar each other.

We used two valence-orbital basis sets for phosphorus (Table 1*b*): the wtgto composed of (14*s*9*p*) pgto and contracted as (13,13,13,111/88111) according to the suggestion of Huzinaga et al. (11) and the basis set of (11*s*8*p*) pgto contracted as (53111/5111) (12). The equilibrium bond distances R and the stretching frequencies ν obtained by the mp3 agree well with the frozen-core and all-electron results. The dissociation energies obtained by the mp3 method, however, deviate slightly from the values obtained from the frozen-core and the all-electron calculations. If we use a larger wtgto (13) as the spectral representation basis function, we get better results, as seen in the fourth and the eighth rows of Table 1*b*.

The following should be noted here. The all-electron calculation predicts that the P_2 molecule is unbounded by 0.60 or 0.66 eV and addition of the *d* polarization function is required (5, 11). However, we do not perform here the molecular calculation using the basis set augmented with the *d* polarization function, because the purpose of this paper is to examine the fidelity of the mp3 and not to obtain the realistic dissociation energy.

As the wtgto for arsenic (Table 1*c*) was too large to perform the all-electron calculation, we used only one basis function: (11*s*8*p*3*d*) pgto contracted as (43211/4211/3) (12), and four basis sets for the spectral representation: (11*s*8*p*3*d*) (12), (20*s*14*p*9*d*) (13), (26*s*20*p*14*d*) (14), and (30*s*23*p*17*d*) (15). The values of R and ν are slightly dependent on the basis sets for the spectral representation, but the value of D is severely

Can. J. Chem. Downloaded from www.nrcresearchpress.com by 65.111.164.53 on 09/08/12
For personal use only.

Table 1*a*. Spectroscopic constants of N_2 obtained by the all-electron calculations (ae), the frozen-core calculations (fc), and the mp3 calculations.

Valence orbitals	Core orbitals	$\{\chi\}^a$	R(au)	$\nu(cm^{-1})$	D(eV)	Method
(10,10,1111/51111)[b]			2.050	2590	2.93	ae
(10,10,1111/51111)	(14*s*9*p*)[b]		2.046	2588	2.85	fc
(10,10,1111/51111)	(14*s*9*p*)	(14*s*9*p*)	2.052	2595	2.97	mp3
(7111/4111)[c]			2.048	2649	2.88	ae
(7111/4111)	(73/43)[c]		2.047	2648	2.88	fc
(7111/4111)	(73/43)	(10*s*7*p*)[c]	2.047	2681	3.01	mp3
(7111/4111)	(73/43)	(14*s*9*p*)[b]	2.049	2651	2.92	mp3

[a]Cf. eq. [7] in the text.
[b]Reference 11.
[c]Reference 12.

Table 1*b*. Spectroscopic constants of P_2 obtained by the all-electron calculation calculations (ae), the frozen-core calculations (fc), and the mp3 calculations.

Valence orbitals	Core orbitals	$\{\chi\}^a$	R(au)	$\nu(cm^{-1})$	D(eV)	Method
(13,13,13,111/88111)[b]			3.667	796.5	−0.60	ae
(13,13,13,111/88111)[b]	(16*s*11*p*)[b]		3.671	794.9	−0.61	fc
(13,13,13,111/88111)	(16*s*11*p*)	(16*s*11*p*)	3.695	779.1	−0.49	mp3
(13,13,13,111/88111)	(16*s*11*p*)	(23*s*16*p*)[d]	3.671	800.6	−0.59	mp3
(53111/5111)[c]			3.669	794.6	−0.66	ae
(53111/5111)	(533/53)[c]		3.670	793.2	−0.65	fc
(53111/5111)	(533/53)	(11*s*8*p*)[c]	3.662	795.5	−0.32	mp3
(53111/5111)	(533/53)	(23*s*16*p*)	3.669	798.8	−0.63	mp3

[a]Cf. eq. [7] in the text.
[b]Reference 11.
[c]Reference 12.
[d]Reference 13.

Table 1*c*. Spectroscopic constants of As_2 obtained by the all-electron calculation (ae), the frozen-core calculation (fc), and the mp3 calculations.

Valence orbitals	Core orbitals	$\{\chi\}^a$	R(au)	$\nu(cm^{-1})$	D(eV)	Method
(43211/4211/3)[b]			3.995	451	−0.69	ae
(43211/4211/3)	(4322/422/3)[b]		4.041	448	−0.87	fc
(43211/4211/3)	(4322/422/3)	(11*s*8*p*3*d*)[b]	3.890	456	+0.78	mp3
(43211/4211/3)	(4322/422/3)	(20*s*14*p*9*d*)[c]	4.065	461	+0.13	mp3
(43211/4211/3)	(4322/422/3)	(26*s*20*p*14*d*)[d]	4.009	464	−0.34	mp3
(43211/4211/3)	(4322/422/3)	(30*s*23*p*17*d*)[e]	4.047	449	−0.80	mp3

[a]Cf. eq. [7] in the text.
[b]Reference 12.
[c]Reference 13.
[d]Reference 14.
[e]Reference 15.

dependent on them. We will discuss this point in more detail in the last section. Table 1*c* indicates that a better basis set for the spectral representation can produce better results.

Our results indicate that if we use the proper basis functions for spectral representation, the mp3 can approximate, with a high degree of fidelity, the results obtained from frozen-core calculations.

Reduction of sizes of basis sets and comparison with other model potentials

We used the same basis sets for the mp3 calculations, the frozen-core calculations, and the all-electron calculations, because we wished to examine the fidelity of the mp3 to the

Can. J. Chem. Downloaded from www.nrcresearchpress.com by 65.111.164.53 on 09/08/12
For personal use only.

frozen-core operator. The reason the model potential methods are widely used is that they have made it feasible at reasonable expense to calculate the electronic structures of large molecules. The most important single factor for economizing molecular calculations is the reduction in the sizes of the valence-orbital basis sets. We attempt to determine if the sizes of the valence-orbital basis sets used in the mp3 can be reduced without degrading the quality of the results, comparing the results with those obtained from the frozen-core calculation and those by the other two model potentials mp1 and mp2.

There are three generations of the Huzinaga model potential family including the present model potential mp3. They are designated in this paper as mp1, mp2, and mp3, respectively. The model potential mp1 has the following form:

$$[12] \quad V_{\mathrm{mp1}} = -\frac{Z - Z^{\mathrm{c}}}{r}\sum_{\mathrm{I}} A_{\mathrm{I}} r^{\nu_{\mathrm{I}}} \exp(-\varsigma_{\mathrm{I}} r) - \sum_i^{\mathrm{core}} F_i \epsilon_i |\phi_i\rangle\langle\phi_i|$$

where Z, Z^{c}, ϵ_i, and $|\phi_i\rangle$ represent the atomic number, the number of core electrons, the core-orbital energies, and the core orbitals, respectively, and ν_{I} is allowed to take values 0 and 1. The factors F_i are usually taken to be equal to 2. The model potential parameters, A_{I} and ς_{I}, are adjustable parameters and determined from minimization of the differences between the reference valence-orbital shapes and energies and those generated from the model potential eigenvalue problem with these parameters (4). The basis sets for the valence orbitals obtained by the mp1 are rather small and economical.

The local core Coulomb operator $V_{\mathrm{mp2}}^{\mathrm{core}}$ of the model potential mp2 (5)

$$[13] \quad V_{\mathrm{mp2}} = V_{\mathrm{mp2}}^{\mathrm{core}} + V_{\mathrm{mp2}}^{\mathrm{exch}} - \sum_i^{\mathrm{core}} 2\epsilon_i |\phi_i\rangle\langle\phi_i|$$

is well tailored to the following model function

$$[14] \quad V_{\mathrm{mp2}}^{\mathrm{core}} = \sum_{\mathrm{I}} A_{\mathrm{I}} r^{\mathrm{vI}} \left[\frac{\exp(-\zeta_I r^2)}{r}\right]$$

where the parameters A_{I} and ζ_I are determined through least-squares fitting to the core Coulomb potential calculated with use of core orbitals obtained from the all-electron calculation. The spectral representation (cf. eq. [10]) is used for the nonlocal exchange potential $V_{\mathrm{mp2}}^{\mathrm{exch}}$. Once the atomic model potential V_{mp2} is obtained, the valence basis set is optimized by minimization of the valence self-consistent-field energy using the standard all-electron calculation.

The present model potential mp3 is defined by eq. [6]. If the fitting for the Coulomb potential $V_{\mathrm{mp2}}^{\mathrm{Coul}}$ of the mp2 is perfect and the spectral-representation basis sets $\{\chi\}$ for the exchange potential $V_{\mathrm{mp2}}^{\mathrm{exch}}$ of the mp2 and for the model potential $V_{\mathrm{mp3}}^{\mathrm{A}}$ of the mp3 are complete, then the mp2 and mp3 have the same effect on the valence orbitals. Therefore, the valence-orbital basis sets obtained by the mp2 may be suitable basis sets for the mp3 calculations. We used the valence-orbital basis sets obtained by the mp2 for the present calculations.

Tables 2*a*, 2*b*, 2*c*, and 2*d* present the results obtained from the calculations using the mp3 with the valence basis sets obtained by the mp2 (5) for N_2, P_2, As_2, and Sb_2, respectively. The results obtained from the frozen-core calculations and the calculations using the mp2 and mp1 are also included in Tables 2*a* through 2*d* for comparison.

Comparison of the results obtained by the mp2 and mp1 methods with those obtained by the frozen-core calculations suggest that the fitting of the Coulomb potential $V_{\mathrm{mp2}}^{\mathrm{Coul}}$ of the mp2 is excellent and that the mp1 can produce remarkable results in spite of the smaller and more economical sizes of the valence-orbital basis sets. (The mp1 for antimony (Table 2*d*) includes the quasi-relativistic effects, and the results in the last row are, therefore, a little different from the other values, which were obtained without relativistic effects.) From the numerical values listed in Tables 2*a* through 2*d*, we see that if we use the better basis sets for the spectral representation $\{\chi\}$ we get better results, and that the results obtained by the mp3 methods are comparable with those obtained by the mp2 and the mp1 methods, which have already been recognized as reliable model potentials in the quantum chemistry community.

To test the balance of different cores, we tried calculations on PN and AsN and listed the results in Tables 2*e* and 2*f*. The agreement between the results obtained by mp3 and by the frozen-core method is excellent.

Discussion and conclusions

We have seen in the preceding sections that the equilibrium bond distances and the stretching frequencies (i.e., the curvature and minimum of the potential curve) are slightly dependent on the basis sets for the spectral representation $\{\chi\}$, but the dissociation energies are dependent on $\{\chi\}$. We will elucidate this basis set dependence in more detail by using As_2 as a typical example. The results obtained by using the same basis set for the valence and core orbitals and several different basis sets $\{\chi\}$ for the spectral representation are tabulated in Table 3. In the first row of the table, the results obtained by the frozen-core calculation are listed once more for comparison. The dissociation energy obtained using the (26*s*20*p*14*d*) wtgto of Huzinaga and Klobukowski (14) deviates from the frozen-core value as shown in the second row. The even-tempered gto basis function (etgto) of Clementi et al. (15) shows good dissociation energy as listed in the third row. While the results obtained by using the hybrid basis function between the *sp* orbitals of the etgto (30*s*23*p*) and the *d* orbital of the wtgto (14*d*) (listed in the fourth row) is almost the same as the values listed in the second row, the dissociation energy obtained with the hybrid basis function between the *sp* orbitals of the wtgto (26*s*20*p*) and the *d* orbital of the etgto (17*d*) (listed in the fifth row) is very close to the value obtained by the frozen-core calculation. To reinforce the wtgto, we augmented its *d* orbital with three more exponents: 6602.447, 2902.7472, and 0.10425203, which are used in the *sp* orbitals of the wtgto. The dissociation energy obtained by the use of this augmented basis set (26*s*20*p*17*d*) is very good. The results listed in the last row of Table 3 are obtained with the wtgto augmented to the *d*-orbital pgto with one exponent of the value 0.10425203. Therefore, the wtgto (26*s*20*p*14*d*) becomes a good basis set for the spectral representation, if its *d*-orbital pgto is augmented with one exponent of the value 0.10425203. It should be noted that the present study may be used to determine whether the basis sets are complete. It should also be noted

Table 2*a*. Spectroscopic constants of N_2 obtained by the frozen-core calculation (fc) and the three model potentials (mp1, mp2, mp3).

Valence orbitals	Core orbitals	$\{\chi\}^a$	R(au)	ν(cm^{-1})	D(eV)	Method
(41/311)[b]	(14*s*9*p*)[c]		2.061	2588	2.89	fc
(41/311)	(14*s*9*p*)	(14*s*9*p*)	2.063	2594	2.69	mp3[d]
(41/311)			2.062	2566	2.70	mp2[b]
(211/211)[e]			2.051[f]	2471[f]	2.73[f]	mp1[g]

[a]Cf. eq. [7] in the text.
[b]Cf. ref. 5 and see the text.
[c]Reference 11.
[d]Present srmp calculation.
[e]Y. Sakai and E. Miyoshi. Model Potential Basis set Data Base (MPBDB) at the Computer Center of the Institute for Molecular Science in Japan.
[f]Calculated with the use of the computer program JAMOL3 (16).
[g]Calculated with the use of the computer program JAMOL3 (16) and see the text.

Table 2*b*. Spectroscopic constants of P_2 obtained by the frozen-core calculation (fc) and the three model potentials (mp1, mp2, mp3).

Valence orbitals	Core orbitals	$\{\chi\}^a$	R(au)	ν(cm^{-1})	D(eV)	Method
(61/411)[b]	(16*s*11*p*)[c]		3.678	793.4	−0.80	fc
(61/411)	(16*s*11*p*)	(16*s*11*p*)	3.703	774.3	−0.68	mp3[d]
(61/411)	(16*s*11*p*)	(23*s*16*p*)[e]	3.678	799.5	−0.78	mp3[d]
(61/411)			3.676	786.	−0.94	mp2[b]
(211/211)[f]			3.646[g]	831.8[g]	−0.50[g]	mp1[h]

[a]Cf. eq. [7] in the text.
[b]Cf. ref. 5 and see the text.
[c]Reference 11.
[d]Present srmp calculation.
[e]Reference 13.
[f]Y. Sakai and E. Miyoshi. Model Potential Basis set Data Base (MPBDB) at the Computer Center of the Institute for Molecular Science in Japan.
[g]Calculated with the use of computer program JAMOL3 (16).
[h]See the text.

Table 2*c*. Spectroscopic constants of As_2 obtained by the frozen-core calculation (fc) and the three model potentials (mp1, mp2, mp3).

Valence orbitals	Core orbitals	$\{\chi\}^a$	R(au)	ν(cm^{-1})	D(eV)	Method
(711/511)[b]	(20*s*14*p*9*d*)[c]		4.022	452	−1.06	fc
(711/511)	(20*s*14*p*9*d*)	(20*s*14*p*9*d*)	4.046	464	−0.30	mp3[d]
(711/511)	(20*s*14*p*9*d*)	(26*s*20*p*14*d*)[e]	3.991	467	−0.48	mp3[d]
(711/511)	(20*s*14*p*9*d*)	(30*s*23*p*17*d*)[f]	4.031	450	−0.98	mp3[d]
(711/511)			4.035	449	−1.05	mp2[b]
(311/311)[g]			4.005[h]	464[h]	−0.80[h]	mp1[i]

[a]Cf. eq. [7] in the text.
[b]Cf. ref. 5 and see the text.
[c]Reference 14.
[d]Present srmp calculation.
[e]Reference 13.
[f]Reference 15.
[g]Y. Sakai and E. Miyoshi. Model Potential Basis set Data Base (MPBDB) at the Computer Center of the Institute for Molecular Science in Japan.
[h]Calculated with the use of computer program JAMOL3 (16)
[i]See the text.

Can. J. Chem. Downloaded from www.nrcresearchpress.com by 65.111.164.53 on 09/08/12
For personal use only.

Table 2d. Spectroscopic constants of Sb_2 obtained by the frozen-core calculation (fc) and the three model potentials (mp1, mp2, mp3).

Valence orbitals	Core orbitals	$\{\chi\}^a$	R(au)	ν(cm^{-1})	D(eV)	Method
(911/7111)[b]	(28*s*23*p*17*d*)[c]		4.793	288	−1.51	fc
(911/7111)	(28*s*23*p*17*d*)	(28*s*23*p*17*d*)	4.783	293	−0.77	mp3[d]
(911/7111)	(28*s*23*p*17*d*)	(33*s*26*p*20*d*)[e]	4.807	286	−1.41	mp3[d]
(911/7111)			4.813	285	−1.64	mp2[h]
(411/311)[f]			4.635[g]	297[g]	−0.39[g]	mp1[h]

[a]Cf. eq. [7] in the text.
[b]Cf. ref. 5 and see the text.
[c]Reference 14.
[d]Present srmp calculation.
[e]Reference 15.
[f]Y. Sakai and E. Miyoshi. Model Potential Basis set Data Base (MPBDB) at the Computer Center of the Institute for Molecular Science in Japan.
[g]Calculated with the use of computer program JAMOL3 (16).
[h]See the text.

Table 2e. Spectroscopic constants of PN obtained by the frozen-core calculation (fc) and the mp3 calculation.

R(au)	ν(cm^{-1})	D(eV)	Method
2.840	1471	0.719	fc
2.840	1492	0.694	mp3

Basis functions, for valence orbitals: P (61/411)

Table 2f. Spectroscopic constants of AsN obtained by the frozen-core calculation (fc) and the mp3 calculation.

R(au)	ν(cm^{-1})	D(eV)	Method
3.047	1212	1.74	fc
3.067	1191	1.66	mp3

Basis functions, for valence orbitals: As (711/5111) N (41/311); for core orbitals: As (20*s*14*p*9*d*) N (14*s*9*p*); for spectral representations: As (30*s*23*p*17*d*) N (14*s*9*p*).

that the total atomic energies of the arsenic atom calculated with the use of the original wtgto (26*s*20*p*14*d*) and the two augmented basis sets (26*s*20*p*17*d*) and (26*s*20*p*15*d*) are the same to within 12 digits. Therefore it may be said that the wtgto (26*s*20*p*14*d*) works quite well as the atomic basis set.

We conclude that the mp3 model potential is a reliable one and stable in the sense that the better basis set for spectral representation produces results closer to the frozen-core results. As far as the curvature and minimal point of the potential energy are concerned, the same basis set as the all-electron valence orbital may be enough for spectral representation. However, if reliable values of the molecular valence electron energy relative to the atomic valence electron energies are desired, the wtgto or the etgto should be used.

We would like to emphasize that the procedure for obtaining the mp3 model potential is straightforward, and anyone who has the Hartree–Fock program for the one- and two-electron integral calculations can obtain it. Once the mp3 model potential is obtained and stored in the computer file, it can be economically incorporated in the molecular orbital calculations, because the necessary calculations are the overlap integrals between the basis functions of the valence orbitals and those of the spectral representation. As the calculation needed

Table 3. Spectroscopic constants of As_2 obtained by the mp3 calculations with various basis sets for spectral representations $\{\chi\}$.

Valence orbitals	Core orbitals	$\{\chi\}^a$	R(au)	ν(cm^{-1})	D(eV)
(43211/4211/3)	(4322/422/3)		4.041	448	−0.87
(43211/4211/3)	(4322/422/3)	(26*s*20*p*14*d*)[b]	4.009	464	−0.34
(43211/4211/3)	(4322/422/3)	(30*s*23*p*17*d*)[c]	4.047	449	−0.80
(43211/4211/3)	(4322/422/3)	(30*s*23*p*14*d*)[d]	4.023	465	−0.34
(43211/4211/3)	(4322/422/3)	(26*s*20*p*17*d*)[d]	4.033	448	−0.85
(43211/4211/3)	(4322/422/3)	(26*s*20*p*17*d*)[e]	4.043	451	−0.75
(43211/4211/3)	(4322/422/3)	(26*s*20*p*15*d*)[e]	4.044	451	−0.75

[a]Cf. eq. [7] in the text.
[b]Reference 14.
[c]Reference 15.
[d]The hybrid basis function; see text.
[e]The augumented basis function; see text.

Can. J. Chem. Downloaded from www.nrcresearchpress.com by 65.111.164.53 on 09/08/12
For personal use only.

is only the overlap calculation, the mp3 model potential may be a correct fit for the energy gradient method.

We are presently calculating the ionization potentials and the electron affinities of copper clusters, and the electronic structures of the *F*-centers in the magnesium oxide crystal. We hope to present these in near future.

Acknowledgements

The author would like to express his cordial thanks to Professor Huzinaga of the University of Alberta. Without his suggestions and continuing interest, this paper would have never been written. The author also would like to thank Professor Sakai of Kyushu University for giving him the data on the mp1 model potential and the basis sets used here, and for her stimulating discussions. The author also would like to thank Professor Miyoshi of Kyushu University for helpful discussion. The numerical calculations were done using the IBM RISC system/6000 model 320 and 220 computing facility. The present work was supported in part by a Grant-in-Aid for Scientific Research In Priority Areas by the Ministry of Education, Science and Culture.

References

1. R.N. Dixon and I.L. Robertson. Theor. Chem. (London), **3**, 100 (1978).
2. S. Huzinaga, M. Klobukoski, and Y. Sakai. J. Phys. Chem. **88**, 4880 (1984).
3. V. Bonifacic and S. Huzinaga. J. Chem. Phys. **60**, 2779 (1974).
4. Y. Sakai and S. Huzinaga. J. Chem. Phys. **76**, 2552 (1982).
5. S. Huzinaga, L. Seijo, Z. Barandiaran, and M. Klobukowski. J. Chem. Phys. **86**, 2132 (1987).
6. S. Huzinaga, S. Katsuki, and O. Matsuoka. J. Math. Chem. **10**, 25 (1992).
7. S. Katsuki. Can. J. Chem. **70**, 285 (1992).
8. S. Katsuki. J. Chem. Phys. **98**, 496 (1993).
9. R.N. Dixon and I.L. Robertson. Mol. Phys. **37**, 1223 (1979).
10. S.C. Leasure, T.P. Martin, and G.G. Balint-Kurti. J. Chem. Phys. **80**, 1186 (1984).
11. S. Huzinaga, M. Klobukowski, and H. Tatewaki. Can. J. Chem. **63**, 1812 (1985).
12. J. Andzelm, M. Klobukowski, E. Radzio-Andzelm, Y. Sakai, and H. Tatewaki. *In* Gaussian basis sets for molecular calculations. *Edited by* S. Huzinaga. Elsevier, Amsterdam. 1984.
13. S. Huzinaga, B. Miguel, and M. Klobukowski. Tech. Rep. of Univ. of Alberta (1993).
14. S. Huzinaga and M. Klobukowski. Tech. Rep. of Univ. of Alberta (1991).
15. E. Clementi et al. Modern techniques in computational chemistry. MOTECC-89 (1989).
16. H. Kashiwagi, T. Takada, E. Miyoshi, S. Obara, and F. Sasaki. JAMOL3: A program package for SCF-MO calculations.

Can. J. Chem. Downloaded from www.nrcresearchpress.com by 65.111.164.53 on 09/08/12
For personal use only.

Solvent effect on the conformational behavior of substituted spiro[4.5]decanes and spiro[5.5]undecanes[1]

S. Sağ Erdem, T. Varnali, V. Aviyente, and M.F. Ruiz-Lopez

Can. J. Chem. Downloaded from www.nrcresearchpress.com by 65.111.164.53 on 09/08/12
For personal use only.

Abstract: We studied the relatively complex polar systems 6-substituted-1,4-dioxospiro[4.5]decanes and 7-substituted-1,5-dioxospiro[5.5]undecanes with substituents X = CH_3, F, Cl, CN, OH, OCH_3, and NO_2. Solvent effects on the equilibrium have been analysed by means of a Self-Consistent-Reaction-Field model and the PM3 method. Complete geometry optimizations have been carried out for all the structures in the gas phase and in solution. For some substituents, a set of rotamers have been separately optimized. The discussion of the results is focussed on the effects arising from structural aspects and from steric and electrostatic interactions on the axial/equatorial relative stability. The role played by multipole moment is considered. In general, good agreement with available experimental data and with previous theoretical studies has been obtained. Though the use of semiempirical methods and simple solvent models prevents us from reaching definitive conclusions, this approach seems to be very useful in predicting the main role of solute–solvent interactions in conformational equilibria of complex systems for which ab initio calculations cannot be performed.

Key words: conformational equilibria, spiro decanes and undecanes, cavity model, SCRF, solvent effect, PM3 calculations.

Résumé : On a étudié les systèmes polaires relativement complexes des 1,4-dioxospiro[4.5]décanes substitués en position 6 et des 1,5-dioxospiro[5.5]undécanes substitués en 7 portant chacun des substituants X = CH_3, F, Cl, CN, OH, OCH_3, et NO_2. On a analysé les effets de solvants sur les équilibre en se basant sur le modèle d'un champ réactionnel autocohérent et par la méthode PM3. On a effectué une optimisation complète de la géométrie de toutes les structures en phase gazeuse et en solution. Pour quelques-uns des substituants, on a aussi optimisé un ensemble de rotamères séparément. La discussion des résultats est orientée vers les effets provoqués par des aspects structuraux et des interactions stériques et électrostatiques sur les stabilités relatives axiales/équatoriales. On a considéré le rôle joué par le moment dipolaire. D'une façon générale, on a obtenu de bons accords entre les données expérimentales disponibles et les résultats de calculs théoriques antérieure. Même si l'utilisation de méthodes semiempiriques et de modèles simples pour les solvants nous empêchent de donner des conclusions définitives, il semble que cette approche soit utile pour prédire le rôle principal des interactions soluté–solvant dans les équilibres conformationnels de systèmes complexes pour lesquels il n'est pas possible d'effectuer des calculs ab initio.

Mots clés : équilibre conformationnel, spiro décanes et undécanes, modèle de cavité, SCRF, effet de solvant, calculs PM3.

[Traduit par la rédaction]

Introduction

Experimental data on conformational equilibria are quite useful in improving the understanding of intramolecular interactions and ultimately in allowing prediction of the most stable structure of complex systems (1–7). Conformational equilibria of 1,1,2 trisubstituted cyclohexanes have been studied (6) and the experimental ΔG values give direct information on the most stable conformations. In particular, 1-(OR), 1-(OR′), 2-(R″) derivatives have atracted much attention because they are suitable for investigating different interactions. Zefirov and co-workers (3, 4) showed that 2-substituted propylene ketals usually prefer the axial orientation but this preference decreases as the polarity of the solvent increases. Ethylene ketals behave in almost the opposite direction except for OH and OCH_3 derivatives. Some experimental results are given in Table 1. Wolff et al. studied similar compounds experimen-

Received December 19, 1994.

S. Sağ Erdem, T. Varnali,[2] and V. Aviyente. Chemistry Department, Boğaziçi University, Bebek 80815, Istanbul, Turkey. **M.F. Ruiz-Lopez.** Laboratire de chimie théorique, Université de nancy, BP 239, 54506 Vandoeuvre-les-Nancy, France.

[1] Taken in part from the Ph.D. thesis of S. Sağ Erdem to be submitted to Boğaziçi University Chemistry Department.

[2] Author to whom correspondence may be addressed.

Table 1. Experimental total axial conformer percentages for 2-substituted cyclohexanone ketal derivatives in CCl_4 and CD_3CN.

	Propylene ketals		Ethylene ketals	
X	% ax in CCl_4	% ax in CD_3CN	% ax in CCl_4	% ax in CD_3CN
F	70.5, 65.7(4)[a]	64.8, 59.0(4)	31.5(4)	38.9(4)
Cl	56.2(4), 57.1(3)	38.1(4), 37.5(3)	19.6(4), 28.4(3)	21.6(4), 30.4(3)
CN	82.91(16)[b]	—	40(16)[b]	—
CH_3	—	—	—	—
NO_2	7.28(15)	—	3.6(15)	—
OCH_3	72.4(4)	61.9, 78.1(4)	46.1(3)	42.2(3)
OH	76.5, 64.7(3)	—	52.9(3)	38.2(3)

[a]Reference numbers are in parentheses.
[b]Studied in $CDCl_3$.

tally and compared their results with molecular mechanic calculations (7). Other molecular mechanics results are available for these compounds (5).

Molecular mechanics has been widely used and represents an interesting approach to dealing with conformational problems in large systems (5, 7). Its main limitation is due to the rather poor description of electronic effects, in particular in those cases in which there are lone pairs. On the other hand, ab initio computations are too expensive for large molecules, which are in general the most interesting ones for the experimentalists. Hence, semiempirical methods appear as an intermediate approach. Though quantitative molecular properties are not always obtained with these methods, their trend in a chemical family, or their modification through an external perturbation, is, in general, correctly reproduced. Moreover, a common problem to tackle in conformational equilibrium analysis is the effect of electrostatic solute–solvent interactions. The possibility offered by continuum models to include this perturbation in the solute's Hamiltonian has allowed quantum chemistry to study chemical processes in solution. In previous papers (8), we used a self-consistent reaction field (SCRF) model to study solvent effects on some conformational problems.

In the present work, we extend the methodology to the case of 2-substituted cyclohexanone ethylene and propylene ketal derivatives. The substituents considered are F, Cl, CN, CH_3, OH, OCH_3, and NO_2.

Methodology

We used the PM3 method (9) and the MOPAC (10) and GEOMOS (11) program packages. We carried out the solvated molecule computations using a continuum model of the solvent that has previously been described (12, 13) and implemented in GEOMOS. The electrostatic and the induction energies are assumed to be responsible for the main variations of the ΔG of the conformational equilibrium in solution and are the only terms considered here. Other terms such as the dispersion term or the cavitation term might be important in the conformational equilibria but these terms remain almost constant in the different conformations of this work. An ellipsoidal cavity shape has been employed. Full geometry optimizations have been carried out.

Fig. 1. *syn* and *anti* orientations of 2-substituted cyclohexanone propylene ketal derivatives. X = F, Cl, CN, CH_3, OH, NO_2, OCH_3.

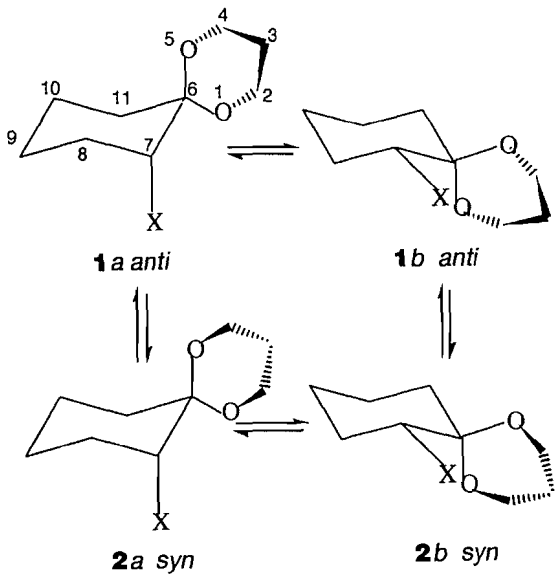

Results

Structures

Combining the two chair forms of cyclohexane and the two chair forms of dioxane, four different conformers, represented in Fig. 1, are obtained.

Conformations of the cyclohexane and puckered dioxolane rings are represented in Fig. 2. For *anti* conformers **1***a* and **1***b*, the dioxolane fragment is positioned away from the substituent whereas for *syn* conformers **2***a* and **2***b* it is extended towards the substituent.

We scanned the rotation around the C5—O1 and C5—O4 bonds at 5° intervals from 95° to 140°. The most stable form of dioxolane ring was then used as the starting geometry for substituted molecules (it corresponds to about 15°–20° deviation from planarity).

We fully optimized the geometries and calculated the energies of the four most probable conformers in Figs. 1 and 2 for

Can. J. Chem. Downloaded from www.nrcresearchpress.com by 65.111.164.53 on 09/08/12
For personal use only.

Can. J. Chem. Downloaded from www.nrcresearchpress.com by 65.111.164.53 on 09/08/12
For personal use only.

Fig. 2. *syn* and *anti* orientations of 2-substituted cyclohexanone ethylene ketal derivatives. X = F, Cl, CN, CH_3, OH, NO_2, OCH_3.

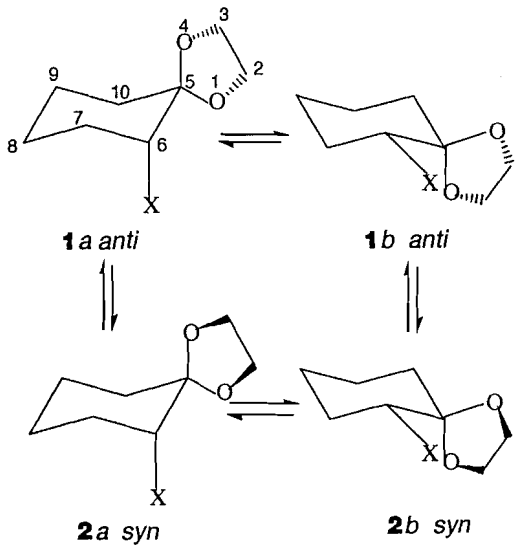

Fig. 3. Illustration of the exocyclic angles of cyclohexane, α and β.

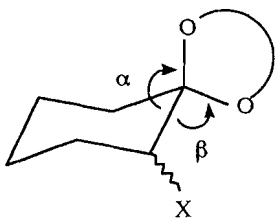

each substituent. Minima were further checked by force calculations.

Angles around the quaternary carbon are those that are subjected to change with varying conformation (*syn* vs. *anti* and axial vs. equatorial). The *syn* vs. *anti* conformations are manifestations of the dihedral angles in the ketal ring and are accompanied by alterations of the exocyclic angles of cyclohexane, α and β, in Fig. 3.

The general trend observed is such that the α and β angles are larger for equatorial conformations than are their analogues for axial conformations and they are also larger for *syn* conformations that are their analogues for *anti* conformations. Comparison of α to β in axial and equatorial conformations indicates a slightly twisted ketal ring for equatorial conformations. In addition, for the OH, OCH_3, and NO_2 substituents, we also computed the potential energy corresponding to the rotation around the bond between the cyclohexane ring and the first atom of the substituent, since several rotamers having close energies may exist. The results are given for the rotamer of lowest energy (unless otherwise indicated). Complete data for potential energy surfaces are available from the authors upon request.

Careful analysis of geometrical parameters for the optimized structures shows thay they are, in general, not much affected by the solvent.

Table 2. Computed total, E_{total}, and relative energies, ΔE (kcal/mol); dipole moments, μ (debye); total axial conformer percentages for 2-substituted cyclohexanone propylene ketals in the gas phase.

X		E_{total}	ΔE_{total}	μ	% ax
F	1*a*	−53 646.802	0.46	2.76	37.83
	2*a*	−53 646.453	0.81	2.16	
	1*b*	−53 647.262	0.00	3.16	
	2*b*	−53 646.275	0.99	0.19	
Cl	1*a*	−50 797.973	0.00	2.58	68.84
	2*a*	−50 797.569	0.40	2.06	
	1*b*	−50 797.673	0.30	2.95	
	2*b*	−50 796.426	1.55	0.14	
CN	1*a*	−49 940.837	0.31	4.28	48.28
	2*a*	−49 940.542	0.60	3.49	
	1*b*	−49 941.144	0.00	4.81	
	2*b*	−49 939.166	1.98	1.74	
CH_3	1*a*	−47 296.177	0.75	1.72	53.05
	2*a*	−47 296.930	0.00	1.77	
	1*b*	−47 296.608	0.32	1.76	
	2*b*	−47 296.573	0.36	1.62	
NO_2	1*a*	−60 709.226	0.56	5.34	35.11
	2*a*	−60 708.672	1.11	4.20	
	1*b*	−60 709.783	0.00	5.82	
	2*b*	−60 707.538	2.26	4.93	
OCH_3	1*a*	−54 058.068	0.81	2.81	90.25
	2*a*	−54 058.879	0.00	0.87	
	1*b*	−54 057.460	1.42	2.66	
	2*b*	−54 056.963	1.92	1.50	
OH	1*a*	−50 621.791	1.07	3.15	45.74
	2*a*	−50 622.660	0.79	0.95	
	1*b*	−50 622.794	0.00	3.08	
	2*b*	−50 621.741	1.05	1.32	

Relative energies

We present the computed total and relative energies and the corresponding dipole moments for the gas phase in Tables 2 and 3. Total axial-conformer percentages, computed using a Boltzmann distribution for the four conformers, are also summarized. Table 2 shows that for propylene ketals, F, CN, NO_2, and OH prefer the equatorial orientation but Cl, CH_3, and OCH_3 prefer the axial orientation in the gas phase. In contrast, all ethylene ketal derivatives except OCH_3 prefer the equatorial orientation.

Solvent effects on conformational equilibria have been evaluated in a nonpolar solvent (CCl_4, ε = 2.24) and a polar solvent (CD_3CN, ε = 37.50) where ε represents the dielectric constant of the solvent. The results for the solvation energies and the relative energies in solution are given in Tables 4 and 5.

The common trend for all the propylene ketals studied (except for the methyl derivative, which is not quite sensitive to the medium) is that as the dielectric constant of the medium increases, the computed axial percentage decreases. This is in agreement with the experimental data in Table 1. The total % axial trends for ethylene ketal derivatives (Table 5) are also in

Can. J. Chem. Downloaded from www.nrcresearchpress.com by 65.111.164.53 on 09/08/12
For personal use only.

Table 3. Computed total, E_{total}, and relative energies, ΔE (kcal/mol); dipole moments, μ (debye); and total axial conformer percentages for 2-substituted cyclohexanone ethylene ketals in the gas phase.

X		E_{total}	ΔE_{total}	μ	% ax
F	1*a*	−50 200.850	1.21	2.25	14.65
	2*a*	−50 200.882	1.18	2.02	
	1*b*	−50 201.749	0.32	1.99	
	2*b*	−50 202.064	0.00	0.76	
Cl	1*a*	−47 352.111	0.29	2.04	40.85
	2*a*	−47 352.009	0.39	1.84	
	1*b*	−47 352.149	0.25	1.75	
	2*b*	−47 352.396	0.00	0.72	
CN	1*a*	−46 495.025	0.77	3.91	22.74
	2*a*	−46 495.048	0.75	3.62	
	1*b*	−46 495.795	0.00	3.30	
	2*b*	−46 495.750	0.05	2.87	
CH_3	1*a*	−43 850.818	0.63	0.90	31.32
	2*a*	−43 850.983	0.47	0.95	
	1*b*	−43 851.299	0.15	0.83	
	2*b*	−43 851.449	0.00	0.84	
NO_2	1*a*	−57 263.360	0.72	4.72	36.96
	2*a*	−57 263.570	0.51	4.40	
	1*b*	−57 264.075	0.00	4.60	
	2*b*	−57 263.245	0.83	3.59	
OCH_3	1*a*	−50 612.681	0.29	1.82	57.19
	2*a*	−50 612.969	0.00	0.66	
	1*b*	−50 612.280	0.67	1.77	
	2*b*	−50 612.902	0.07	1.08	
OH	1*a*	−47 176.226	1.18	2.18	16.06
	2*a*	−47 176.533	0.88	1.16	
	1*b*	−47 177.380	0.03	2.08	
	2*b*	−47 177.409	0.00	1.48	

parallel with experimental data in Table 1 except for the OH derivative. For ethylene ketal derivatives, calculations for F-, Cl-, CN-, and OH-substituted molecules show that the amount of axial orientation increases with increase in polarity of the solvent. On the other hand, CH_3, OCH_3, and NO_2 derivatives show a trend in the opposite direction.

Discussion

Gas phase

Propylene ketals

On the basis of steric effects only, one could expect the axial conformation to be the most stable since the dioxane moiety and the substituent are closer when the latter occupies the equatorial position. The dependence of preference for the axial or the equatorial position on the nature of the substituent indicates that other important factors have to be considered. Our results (Table 2) show that at the PM3 level the equatorial *anti* conformation, **1***b*, is preferred for the F, CN, OH, and NO_2 derivatives whereas the axial conformation, *anti* or *syn*, is preferred by the CH_3 and OCH_3 and by the Cl derivatives, respectively.

Table 4. Solvation energies, E_{solv} (kcal/mol), ΔE_{total} (kcal/mol), and total axial conformer percentages of 2-substituted cyclohexanone propylene ketals.

		CCl_4[a] (ε = 2.24)			CD_3CN (ε = 37.5)		
		E_{solv}	ΔE_{total}	% ax	E_{solv}	ΔE_{total}	% ax
F	1*a*	−0.989	0.65	32.11	−2.341	0.90	23.23
	2*a*	−0.882	1.10		−2.086	1.51	
	1*b*	−1.177	0.00		−2.782	0.00	
	2*b*	−0.453	1.71		−1.047	2.72	
Cl	1*a*	−0.647	0.00	64.18	−1.529	0.07	56.21
	2*a*	−0.616	0.44		−1.487	0.52	
	1*b*	−0.798	0.15		−1.900	0.00	
	2*b*	−0.364	1.83		−0.859	2.29	
CN	1*a*	−5.026	0.51	39.88	−7.517	1.17	18.35
	2*a*	−4.968	0.87		−7.473	1.51	
	1*b*	−5.232	0.00		−8.380	0.00	
	2*b*	−2.912	4.30		−4.242	6.12	
CH_3	1*a*	−0.369	0.81	53.58	−0.877	0.87	54.92
	2*a*	−0.421	0.00		−0.997	0.00	
	1*b*	−0.395	0.35		−0.922	0.40	
	2*b*	−0.399	0.38		−0.932	0.42	
NO_2	1*a*	−1.913	1.26	12.37	−6.434	2.15	2.85
	2*a*	−2.004	2.41		−5.876	3.96	
	1*b*	−3.303	0.00		−8.721	0.00	
	2*b*	−2.763	2.79		−7.626	3.34	
OCH_3	1*a*	−0.218	0.55	87.36	−2.064	0.14	81.32
	2*a*	−0.661	0.00		−0.684	0.00	
	1*b*	−0.288	1.09		−1.517	0.59	
	2*b*	−0.087	1.96		−0.593	2.01	
OH	1*a*	−0.765	0.99	35.11	−2.580	0.88	26.02
	2*a*	−0.826	0.65		−1.948	1.23	
	1*b*	−0.682	0.00		−2.389	0.00	
	2*b*	−0.210	1.53		−1.250	2.19	

[a]The CN derivative has been calculated in $CDCl_3$ (ε = 4.81).

Fig. 4. Net atomic charges in 2-nitro cyclohexanone propylene ketal in the gas phase and in acetonitrile (values in parentheses).

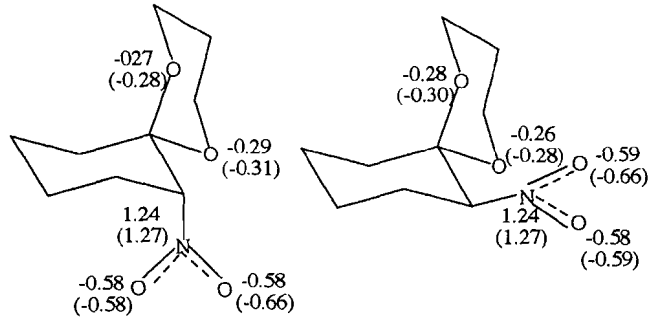

Electrostatic interactions between the substituent and the oxygens of the dioxane moiety may be responsible for the equatorial preference of CN, and NO_2 (Fig. 4). The fluorine derivative is observed to behave in the opposite direction to that of the other halogen derivative as it usually is in equilibration with other fluorocyclohexane derivatives. Interpretations

Can. J. Chem. Downloaded from www.nrcresearchpress.com by 65.111.164.53 on 09/08/12
For personal use only.

Table 5. Solvation energies, E_{solv} (kcal/mol), ΔE_{total} (kcal/mol), and total axial conformer percentages of 2-substituted cyclohexanone ethylene ketals.

		CCl_4[a] (ε = 2.24)			CD_3CN (ε = 37.5)		
		E_{solv}	ΔE_{total}	% ax	E_{solv}	ΔE_{total}	% ax
F	**1***a*	−1.045	0.77	23.23	−2.121	0.55	35.34
	2*a*	−1.029	0.76		−2.467	0.54	
	1*b*	−0.914	0.03		−1.821	0.00	
	2*b*	−0.602	0.00		−1.184	0.43	
Cl	**1***a*	−0.657	0.13	46.47	−1.571	0.05	51.37
	2*a*	−0.747	0.14		−1.683	0.04	
	1*b*	−0.646	0.10		−1.580	0.00	
	2*b*	−0.499	0.00		−1.172	0.16	
CN	**1***a*	−5.141	0.58	71.62	−8.094	0.71	89.97
	2*a*	−5.695	0.00		−8.778	0.00	
	1*b*	−4.517	0.43		−6.853	1.18	
	2*b*	−3.295	1.70		−4.828	3.25	
CH_3	**1***a*	−0.474	0.90	25.58	−0.713	0.97	23.84
	2*a*	−0.633	0.58		−0.888	0.63	
	1*b*	−0.737	0.16		−1.042	0.16	
	2*b*	−0.742	0.00		−1.048	0.00	
NO_2	**1***a*	−3.387	0.89	29.60	−7.917	0.97	24.21
	2*a*	−3.182	0.88		−7.444	1.24	
	1*b*	−3.559	0.00		−8.176	0.00	
	2*b*	−2.970	1.42		−6.712	2.29	
OCH_3	**1***a*	−0.826	0.24	52.68	−1.712	0.37	42.28
	2*a*	−0.714	0.07		−1.513	0.35	
	1*b*	−0.921	0.55		−2.134	0.42	
	2*b*	−0.749	0.00		−1.932	0.00	
OH	**1***a*	−1.313	1.02	18.51	−2.982	0.85	22.03
	2*a*	−1.128	0.90		−2.541	1.98	
	1*b*	−1.177	0.00		−2.676	0.00	
	2*b*	−1.018	0.13		−2.296	0.35	

[a]The CN derivative has been calculated in $CDCl_3$ (ε = 4.81).

based on the small size of fluorine and (or) lone-pair interactions (14) have been given. Finally, for the hydroxyl substituent, the equatorial preference may be explained through weak hydrogen bond interactions since in the equatorial conformation the optimized geometry shows that the hydrogen atom of the hydroxyl is pointing towards one of the oxygens in the dioxane ring with an O—H distance of 2.48 Å.

In general, for the propylene ketal derivatives considered, *anti* conformations are more favorable than *syn* conformations. The preference for the axial or equatorial conformations to be *anti* depends basically on the balance between steric effects and the electrostatic repulsive forces between the dipole moments situated at the dioxane ring and CX bond. This is illustrated for the **1***b* and **2***b* propylene ketal conformers in Fig. 5. The dipoles are more or less parallel in the *anti* conformation, leading to a destabilizing electrostatic interaction. From the results in Table 2 one may conclude that steric effects are the main factors in determining the *syn* or *anti* conformation for the equatorial conformers since, in all cases, **1***b* is substantially more stable than **2***b*. However, for the axial

Fig. 5. Newman projection through C6—O5 bond for propylene ketal derivative. (Arrows show the direction of dipoles).

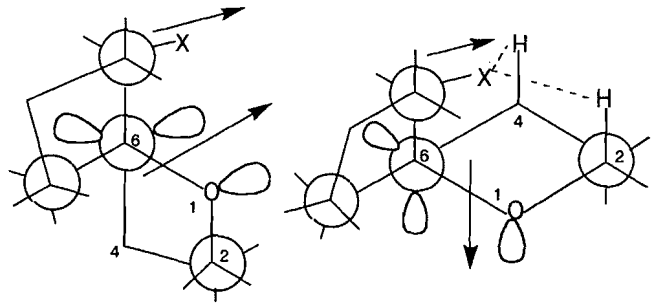

1*b anti*
larger μ

2*b syn*
smaller μ

conformers, where the steric interactions between the substituent and the dioxane ring are less important, electrostatic effects play a role that is probably at the origin of the larger stability of **2***a* with respect to **1***a*, predicted for the OH and OCH_3 derivatives.

In a similar way, energy change through rotation of the substituent may be interpreted in general as due to steric and electronic interactions between the substituent and the dioxane ring. For NO_2, we found that there is only one minimum for a geometry in which the H-C-N plane and the NO_2 group are nearly coplanar and only one maximum at an O-N-C-H dihedral angle of 90°. The barrier to rotation varies from 2 kcal/mol (for **1***b* and **2***b*) to 4.2 kcal/mol (for **1***a*). In the case of OH, the computed potential energy is represented in Fig. 6. The absolute minimum is also a coplanar structure in which the H-C-O-H angle is close to 180°. The energy barriers are 3.5 kcal/mol (**1***a* and **2***b*) and 4.5 kcal/mol (**1***b* and **2***a*). Local minima have been also found for angles close to 300° and 60° for all four conformations. The energy differences between the rotamers are not very large (about 1.5 kcal/mol). Finally, for OCH_3, we found two rotamers for each conformation at H-C-O-C angles 174° and −16°, 180° and −5°, 174° and −21°, and 150° and 9° for **1***a*, **2***a*, **1***b*, and **2***b*, respectively. The absolute minima correspond to H-C-O-C ~180° in the case of **1***a*, **2***a*, and **1***b* and 9° in the case of **2***b*. Here, the energy differences between rotamers are smaller than the results for the OH derivative.

Ethylene ketals

When the substituent is in the axial position, **2***a-syn* is generally the preferred conformer except for the Cl derivative (Table 3). Similarly, when the substituent is in the equatorial position, conformer **2***b-syn* is generally preferred except for CN and NO_2. The fact that in most of them **2***a* and **2***b* exhibit smaller dipole moments than **1***a* and **1***b* indicates, contrary to the propylene ketals, the predominance of electrostatic forces between the dipole moments situated at the dioxolane ring and the C—X bond over the steric interactions shown in Fig. 5. For CN and NO_2 derivatives, electrostatic forces between the substituents and the oxygens of the dioxalane fragment dominate because these equatorial substituents interact with negatively charged ring oxygens (Fig. 4). In addition, the dipole moment of **2***b* is smaller than that of **1***b*, which is a favorable situation in terms of electrostatic interactions in the gas phase. Therefore, all the other ethylene ketals except CN and NO_2 prefer **2***b* over **1***b*. The rotamer studies for the poten-

Fig. 6. Potential scans of four conformers from PM3 calculations of 2-hydroxy propylene ketal.

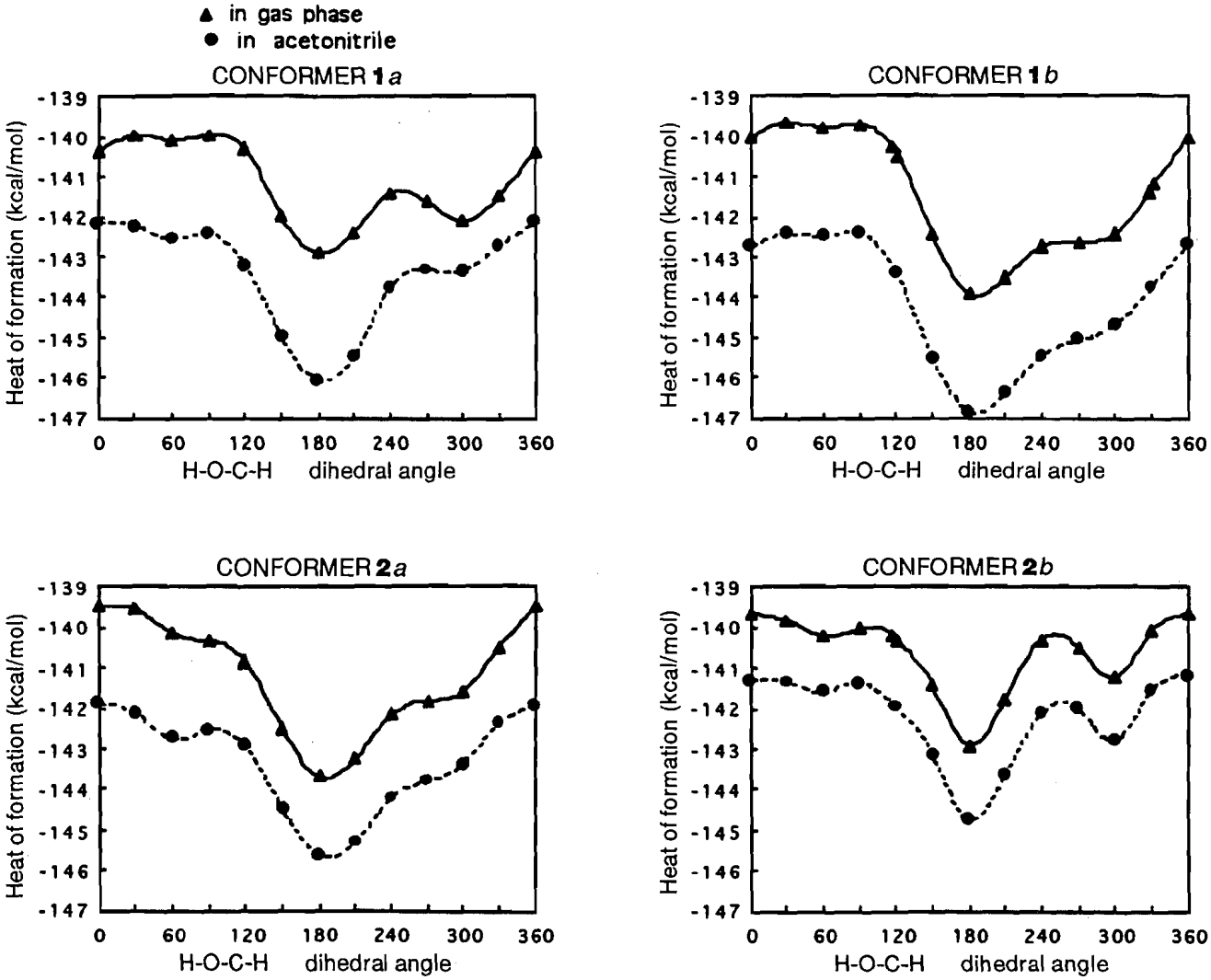

tial curve of the NO_2 derivative show features similar to its propylene ketal analogue: only one minimum around 180° and one maximum around 90°, the dihedral angles showing a flat surface near the minimum. The potential curves of OH and OCH_3 showed a very similar rotational profile to that of the propylene ketals. The absolute minima of these molecules appear around the 180° dihedral angle for **1***a*, **2***a*, **1***b*, and **2***b* except for OCH_3 **1***b* and **2***b*, which are 169° and 166°, respectively.

Finally, when we compare the propylene and ethylene ketal systems, the most striking difference is that, in general, conformer **2***b* is destabilized in propylene ketals whereas it is the most favorable conformer in ethylene ketals and, usually, the least polar conformer in both systems. This indicates the predominance of electronic interactions over steric ones in ethylene ketals since in **2***b* there are also unfavorable X—H repulsions as shown in Fig. 5 for propylene ketals. In this system, such repulsions are not very effective because the five-membered dioxolane ring is more flattened than the six-membered dioxane ring that allows hydrogens to stay further away from the substituent. These repulsions are dominant in propylene ketals. This interpretation is confirmed by potential scans around the C—OMe bond of methoxy derivatives where the rotational barrier for **2***b* at a dihedral angle of 240° is about 9 kcal in propylene ketal but only 6 kcal in ethylene ketal. A common feature of both systems is the stability of conformer **1***b*-*anti* over the others for the CN and NO_2 derivatives despite the fact that this preference is contrary to the behavior of other derivatives in ethylene ketals.

Solution

The generally most stable *anti* structures for propylene ketals, **1***a* and **1***b*, have the highest solvation energy for the equatorial conformer **1***b* (Table 4). Only for the OH and OCH_3 derivative is the solvation energy of **1***a* in acetonitrile greater than that for **1***b*. In the gas phase, the *syn* structure is preferred in the axial conformation for these molecules. In polar solvents, however, the *anti* structure is expected to be more stable.

The electrostatic solvation energy is in general larger for the most polar conformations although there are some exceptions that are due to the fact that multipole contributions are substantial in many cases. The molecules considered may be

Can. J. Chem. Downloaded from www.nrcresearchpress.com by 65.111.164.53 on 09/08/12
For personal use only.

Can. J. Chem. Downloaded from www.nrcresearchpress.com by 65.111.164.53 on 09/08/12
For personal use only.

divided into three categories according to the effect that the solvent has on their relative conformational energies.

The first group corresponds to those systems in which the substituent X has a dipole moment contribution parallel to the CX bond (F, Cl, CN, NO_2). In that case, *anti* equatorial conformations **1***b* have always the largest total dipole moment since the CX dipole adds to the dioxane ring dipole. The solvent stabilizes these conformations to a larger extent so that in a medium polar solvent, such as acetonitrile, they become the most stable.

The OH- and OCH_3-substituted molecules represent another group of derivatives. Here, the situation is different since the oxygen lone pairs of the substituent contribute to the CX dipole moment so that its direction is not parallel to the CX bond. Besides, they may have several stable rotamers with close energies, the stability of which may be substantially modified through the effect of the environment. The total dipole moment is obviously quite dependent on the rotation angle. However, the rotamer study in acetonitrile showed that the location of the minima does not change upon rotation around C—X in these molecules. The dipole moment values of the most stable rotamer for the **1***a* and **1***b* conformers are close and larger than those for the **2***a* and **2***b* conformers (Table 2). Therefore, the solvation energies of **1***a* and **1***b* are also larger than those for the other conformations.

Finally, the CH_3 derivative may be considered. Since in this case the CX dipole is small, the total molecular dipole moment does not change much (Table 2) with conformation and the solvent effect on the conformational equilibrium is small.

For the ethylene ketals, the molecules can be categorized in two groups. The first group consists of F, Cl, CN, and OH derivatives. In these molecules, the content of axially oriented molecules starts to increase as the solvent polarity increases in our calculations. This tendency to axial orientation is expected on the basis of solute–solvent electrostatic interactions since **1***a* and **2***a* conformers, having larger dipole moments than **1***b* and **2***b* conformers, are stabilized more in polar solvents than an equatorially oriented substituent. Note in Table 5 that **1***b*, whose dipole moment is close to those of **1***a* and **2***a*, is more stable than **2***b* in acetonitrile for F and Cl derivatives. The CH_3-, NO_2-, and OCH_3-substituted ethylene ketals fall in the second category. In these molecules, the tendency to equatorial position increases as the dielectric constant of the solvent increases. As expected, for CH_3 the magnitude of the tendency is small. As pointed out above, comparison with available experimental data shows that the predicted solvent effects are in general correct, except for the OH derivative. Though it is difficult to elucidate the origin of this disagreement without performing more accurate computations one can imagine that specific interactions can play a role in this case and should stabilize the axial conformation in solvents like acetonitrile.

Conclusion

Semiempirical PM3 calculations on conformational equilibria of 2-substituted cyclohexanone ketal derivatives showed that these conformational equilibria are strongly solvent dependent. Without exception, in all of the propylene ketal derivatives studied, the polar solvent stabilizes the equatorial substituent. Therefore, preference to equatorial orientation increases as the polarity of solvent increases. We showed that the equatorial orientation that would be stabilized by the polar solvent should be **1***b* due to its large dipole moment. For ethylene ketal derivatives, calculations of F-, Cl-, CN-, and OH-substituted molecules showed that the content of the axial orientation increases with increase in the polarity of the solvent. On the other hand, CH_3, OCH_3, and NO_2 derivatives show a trend in the opposite direction. The predicted solvent effects are in fairly good agreement with available experimental data except in 2-hydroxy cyclohexanone ethylene ketal for which specific interactions with the solvent are probably important. Hence, the SCRF-PM3 method appears to be a suitable approach to analysing conformational equilibria in solutions of polar molecules of large size.

Acknowledgement

This work was supported by TUBITAK–CNRS cooperation, Project No 1 (1993), and by the Boğaziçi University Research Funds (grant No 89EB0559).

References

1. E.L. Eliel, N.L. Allinger, S.J. Angyal, and G.A. Morrison. Conformational analysis. Interscience, New York. 1965.
2. R.J. Abraham and E. Bretschneider. Internal rotation in molecules. *Edited by* W.J. Orville-Thomas. J. Wiley & Sons, London. 1974. p. 568.
3. I.G.M. Mursakulov, M. Guseinov, N.K. Kasumov, N.S. Zefirov, V.V. Samoshin, and E.G. Chalenko. Tetrahedron, **38**, 2213 (1982).
4. I.G. Mursakulov, V.V. Samoshin, R.V. Binnatov, N.K. Kasumov, M.I. Povolotskii, and N.S. Zefirov. Zh. Org. Khim. **19**, 2527 (1983).
5. T. Varnali. J. Mol. Struct. **268**, 181 (1992).
6. I.G. Mursakulov, E.A. Ramazanov, M.M. Guseinov, N.S. Zefirov, and V.V. Samoshin. Tetrahedron, **36**, 1885 (1980).
7. J.J. Wolff, G. Frenking, and K. Harms. Chem. Ber. **124**, 551 (1991).
8. (*a*) T. Varnali, V. Aviyente, B. Terryn, and M.F. Ruiz-Lopez. J. Mol. Struct. (Theochem), **280**, 169 (1993); (*b*) G. Apaydin, T. Varnali, V. Aviyente, and M.F. Ruiz-Lopez. J. Mol. Struct. (Theochem), **287**, 185 (1993).
9. J.J.P. Stewart. J. Comput. Chem. **10**, 209 (1989).
10. J.J.P. Stewart. MOPAC, QCPE Program 455, Bloomington, Ind. 1990.
11. D. Rinaldi, P.E. Hoggan, and A. Cartier. GEOMOS, QCPE Program 584, Bloomington, Ind., 1989.
12. J.L. Rivail, B. Terryn, D. Rinaldi, and M.F. Ruiz-Lopez. NATO ASI Ser. C: **339**, 79 (1991).
13. D. Rinaldi, M.F. Ruiz-Lopez, and J.L. Rivail. J. Chem. Phys. **78**, 834 (1982).
14. O. Eisenstein, N.T. Anh, Y. Jean, A. Devaquet, J. Cantacuzene, and L. Salem. Tetrahedron, **30**, 1717 (1974).
15. T. Varnali. Ph.D. Thesis, Boğaziçi. University, Istanbul, 1986.
16. T. Varnali, H. Özbal, and E. Çetin. Turk. J. Chem. **6**, 177 (1992).

Density Functional calculations for some hydrogen-bonded systems. Influence of a dielectric surrounding

Y. Jeanvoine, F. Bohr, and M.F. Ruiz-López

Abstract: We present Density Functional calculations for hydrogen-bonded systems with small, medium, and large association energies, in a vacuum and in a dielectric environment. The results are in reasonably good agreement with accurate ab initio results and available experimental data. They confirm that DFT is very promising for modeling liquid state properties.

Key words: hydrogen bond, Density Functional, cooperative effect, liquid state.

Résumé : Une série de systèmes liés par des liaisons hydrogène plus ou moins fortes a été étudiée à l'aide des calculs de type «Fonctionnelle de la densité» en phase gazeuse et dans un environnement diélectrique. Les résultats sont en bon accord avec ceux obtenus par des calculs ab initio poussés et avec les données expérimentales disponibles. Ils confirment que la théorie de la fonctionnelle de la densité est très prometteuse pour l'étude des propriétés de l'état liquide.

Mots clés : liaison hydrogène, fonctionnelle de la densité, effet coopératif, état liquide.

Can. J. Chem. Downloaded from www.nrcresearchpress.com by 65.111.164.53 on 09/08/12
For personal use only.

1. Introduction

Among the most interesting approaches to studying the liquid state and chemical processes in solution, mixed Molecular Mechanics – Density Functional Theory (DFT) methods are very promising (1). Formally, DFT can be easily coupled with liquid simulations although the aptness of current DFT exchange-correlation potentials to correctly describe intermolecular interactions remains to be tested. The Gordon–Kim method (2) or other approximate related approaches (3, 4) can be envisaged, although a rigorous treatment requires solving the Kohn–Sham equations (5) for a supermolecule or cluster. Hydrogen-bonded systems are particularly important and some work has already been reported, for instance, for water (6*a*, 6*b*) and ammonia (6*c*) dimers.

With the aim of studying a larger interaction energy range, we have considered here slightly bonded complexes, such as $(H_2S)_2$ and $(HCl)_2$, as well as systems in which proton transfer is partially carried out, such as $FH\cdots NH_3$. The intermediate dimers $(HF)_2$ and $(HCN)_2$ have been also studied.

Since cooperative interactions in the liquid state are important, we have also investigated the influence of a dielectric surrounding on the water–dimer structure. This system has been chosen because of the large number of studies that have been devoted to liquid properties of water. In particular, recent ab initio results have shown that the properties of the water dimer in liquid water are substantially modified through electrostatic interactions (7).

Received November 7, 1994.

Y. Jeanvoine, F. Bohr,[1] and M.F. Ruiz-López.[2] Laboratoire de chimie théorique, Unité de recherche associée n° 510 du Centre national de la recherche scientifique, Université Henri Poincaré, Nancy I, BP 239, 54506 Vandoeuvre-lès-Nancy, France.

[1] Present address: Laboratoire de chimie physique, Université de Reims, Faculté des sciences, Moulin de la Housse, BP 347, 51062 Reims Cedex France. Telephone: (33) 26 05 32 33.

[2] Author to whom correspondence may be addressed. Telephone: (33) 83 91 25 27. Fax: (33) 83 91 25 30. E-mail: ruiz@lctn.u-nancy.fr

2. Computations

Computations were carried out using the deMon program (8). Atomic orbital basis sets are (8) (41/1) for H, (7111/411/1) for C, N, O, and F, (7321/621/1) for Cl, and (7321/621/1) for S. Auxiliary basis sets used for density integrals are H(4;4), C(4,4;4,4), N(4,4;4,4), O(4,4;4,4), F(4,4;4,4), Cl(5,4;5,4), and S(5,4;5,4) (8).[3] The total energy is computed using numerical integration for the exchange-correlation contribution on a FINE grid (8), as proposed and described in ref. 6*a*. Results using the VWN local potential (9*a*) and the gradient-corrected BP potential (9*b*) are compared.[4] Gradient corrections are included self-consistently.

To evaluate the effect of a dielectric surrounding on the properties of hydrogen-bonded complexes, we used the SCRF approach (10), which has recently been implemented (10*a*) in deMon. In this method, the solute is assumed to be placed into a cavity created in a infinite dielectric and polarizable continuum. The charge distribution of the solute polarizes the continuum, which in turn creates an electric field inside the cavity. The total electrostatic free energy change corresponding to the electrostatic solvation process is given by the expression

$$[1] \qquad \Delta F = -1/2\, E_{int}$$

[3] For details on basis sets, see program deMon (7), ref. 6*a*, and Sim et al. (8).

[4] BP potential refers to Becke's correction for exchange combined with Perdew's correlation correction. PP potential refers to Perdew's correction for both exchange and correlation.

where E_{int} is the interaction energy, which in our approach is written:

$$[2] \qquad E_{int} = \sum_{\substack{l=0,\infty \\ m=-l,+l}} \sum_{\substack{l'=0,\infty \\ m'=-l',+l'}} f^{lm,l'm'} \langle M^{lm} \rangle \langle M^{l'm'} \rangle$$

The quantities M^{lm} are the components of the spherical multipole moments of the solute molecule. The factors $f^{lm,l'm'}$ depend only on the dielectric permittivity of the continuum and on the cavity shape, and are computed from the continuity conditions at the cavity surface boundary. Analytical expressions are obtained for constant cavity surfaces such as the sphere or the ellipsoid but they may be computed numerically for any cavity shape (10*b*, *c*). The reaction field polarizes the electronic distribution of the solute. To account for this polarization, the Kohn–Sham equations are solved iteratively by minimizing the intrinsic energy of the solute plus the free energy of solvation.

In this work, we employed an ellipsoidal cavity shape that appears to be a good approximation for the systems studied and allows geometry optimization with analytical algorithms (10*d*). The volume is constrained to be equal to the average molecular volume in the liquid, which can be evaluated from the volume limited by the van der Waals surface. The axes of the cavity are related to the axes of inertia of a solid of uniform density limited by the van der Waals surface. More details on cavity definition can be found in previous papers (7, 10).

3. Results and discussion

In Table 1, we have summarized the results for the series of hydrogen-bonded complexes considered. Available experimental and ab initio results are also included. To compare the theoretical binding energies to the experimental data, the values gathered in Table 1 do not include zero-point energy (ZPE) contributions. Part of the difference between theory and experiment can then be associated with the way the experimental data have been corrected for ZPE, although this effect is expected to be small. Besides, our theoretical calculations have not been corrected to account for BSSE so that our association energies are probably overestimated. However, on the basis of previous works, BSSE corrections are not expected to be very large. For instance, Frisch et al. (15) evaluated BSSE for the water dimer using the counterpoise method. Obviously, the correction depends on the basis set used but for a medium size basis set, such as the 6-31 + G**, it is of the order of 0.14 kcal mol^{-1} at the RHF level and 0.04 kcal mol^{-1} at the MP2 level. DFT computations for the water dimer by Sim et al. (6*a*) predicted a counterpoise correction of 0.4 kcal mol^{-1} using basis set and exchange-correlation potentials close to those used here. Hence, in our results, the same order of magnitude is expected.

A scheme representation of the optimized structures is given in Fig. 1 (structures 1–5).

The distances d_{AB} and d_{AH}, and the angle θ, i.e., the HAB angle for the A—H···B complexes, are given in Table 1. Other geometrical parameters can be obtained from the authors but it must be pointed out that, in all cases, the symmetry of the most stable conformation predicted by our computations (at the VWN or BP levels) is in agreement with that obtained with the best ab initio calculations reported to date (see the figure).

As previously shown (6*a*), the local density approach (here

Fig. 1. Structures obtained at the BP level for energy minima (left) and saddle points (right) of some hydrogen bonded systems. 1: $(H_2S)_2$; 2: $(HCl)_2$; 3: $(HFl)_2$; 4: $(HCN)_2$; 5: $FH\cdots NH_3$; 6: bifurcated $(H_2S)_2$; 7: cyclic $(HCl)_2$; 8: cyclic $(HFl)_2$.

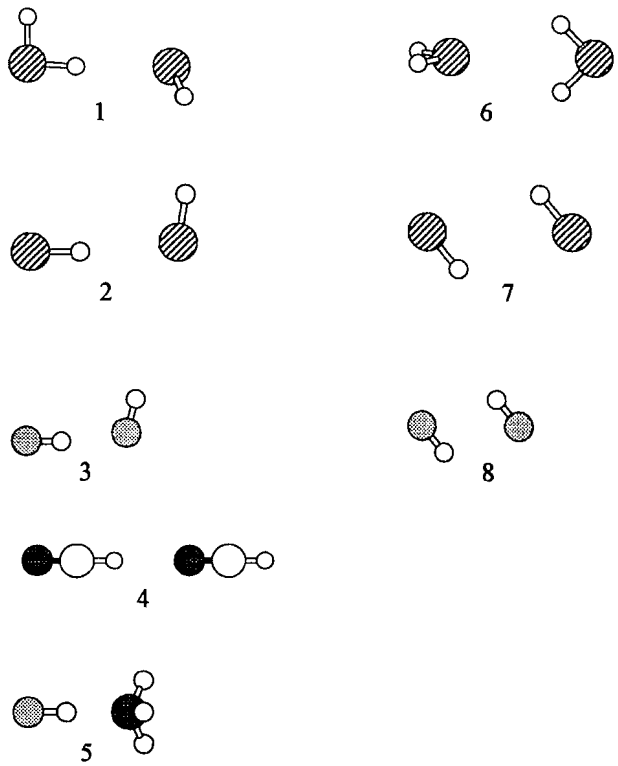

the VWN results) substantially overestimates the association energy through hydrogen-bond interaction. The dimer formation energy is too large, especially for $(HCl)_2$ where the VWN is twice the experimental value. Gradient-corrected computations (BP) lead to substantially better agreement with ab initio results and experimental data. The agreement is very good for $(HF)_2$ and $(HCl)_2$ and appears to be fairly good for $FH\cdots NH_3$ and $(HCN)_2$ (note that, in the latter, correlation energy was not included in the ab initio calculation so that the BP result is probably more reliable). In the case of $(H_2S)_2$, the BP association energy is in better agreement with experiment than the ab initio result, probably because of the relatively simple basis set used in the latter calculation.

The local density approach predicts too short intermolecular distances in all cases. On the other hand, the AH bonds are lengthened too much through hydrogen-bond formation, as compared to ab initio predictions. It appears that proton transfer is substantially overestimated, as shown also by the charge transfer values. Note, however, that values of Δq cannot be compared directly to ab initio data since the former are obtained using Mulliken Population Analysis while the latter are computed through Natural Population Analysis. Geometrical parameters obtained at the BP level are again in much better agreement with ab initio and experimental values.

Therefore, in DFT studies of hydrogen-bonded complexes, density gradient corrections in the exchange-correlation potentials must be included in order to get reliable results. It is important to point out that BP gives reasonably good results even for weakly bonded complexes, such as $(HCl)_2$ or $(H_2S)_2$. We have not carried out a systematic study with other

Can. J. Chem. Downloaded from www.nrcresearchpress.com by 65.111.164.53 on 09/08/12
For personal use only.

Can. J. Chem. Downloaded from www.nrcresearchpress.com by 65.111.164.53 on 09/08/12
For personal use only.

Table 1. Computed vs. experimental results for A—H····B hydrogen-bonded systems. Δ is the increase of the AH bond length in the complex with respect to the monomer, θ is the HAB angle, Δq is the charge transfer, as computed from a Mulliken population analysis, and ΔE is the association energy (without ZPE corrections). Units are angstrom, degrees, and kcal mol^{-1} (1 kcal mol^{-1} = 4.187 kJ mol^{-1}).

System		d_{AB}	d_{AH}	(Δ)	θ	Δq	ΔE
$(H_2S)_2$	VWN[a]	3.826	1.378	(0.017)	1.5	0.042	−4.7
	BP[a]	4.090	1.367	(0.009)	2.0	0.023	−1.5
	Ab initio[b]	4.16	1.361	(0.004)	3.2		−2.3
	Exp[c]						−1.7
$(HCl)_2$	VWN[a]	3.543	1.316	(0.018)	2.4	0.056	−4.7
	BP[a]	3.876	1.303	(0.008)	3.8	0.026	−1.5
	Ab initio[d]	3.838	1.269	(0.000)	11.3		−2.3
	Ab initio[e]	3.860	1.271		3.7	0.008	−2.1
	Exp[f]	3.80					−2.3
$(HF)_2$	VWN[a]	2.553	0.953	(0.016)	7.7	0.048	−9.3
	BP[a]	2.694	0.947	(0.010)	5.6	0.030	−4.9
	PP[a]	2.692	0.953	(0.012)	5.6	0.036	−6.6
	Ab initio[g]	2.759	0.923	(0.006)	5.5		−5.0
	Ab initio[e]	2.769	0.932		9.5	0.010	−5.0
	Exp[h]	2.72			10 ± 6		−4.9
$(HCN)_2$	VWN[a]	3.099	1.095	(0.015)	0.0	0.039	−7.0
	BP[a]	3.305	1.084	(0.008)	0.0	0.022	−3.8
	PP[a]	3.302	1.082	(0.008)	0.0	0.022	−5.1
	Ab initio[i]	3.31			0.0		−5.0
	Exp[j]	3.29			0.0		
$FH\cdots NH_3$	VWN[a]	2.530	1.000	(0.063)	0.0	0.085	−21.8
	BP[a]	2.604	0.989	(0.052)	0.0	0.068	−15.3
	PP[a]	2.630	0.989	(0.048)	0.0	0.061	−16.7
	Ab initio[k]	2.756	0.930		0.0		−12.8
	Ab initio[e]	2.633	0.963		0.0	0.057	−14.6
	Exp[l]	2.66					

[a]This work.
[b]MP2/6-21G(2*d*), ref. 11.
[c]Reference 11.
[d]MP2/+VP[s](2*d*)[s], see ref. 12. Optimization was carried out at the RHF level. The basis set is a modified 6-31G** basis with other diffuse and polarization functions.
[e]MP2(full)/6–31+G**, ref. 13; charge transfer from Natural Population Analysis.
[f]Reference 14 (zero point center-of-mass separation of the monomers).
[g]MP2/6-311++G(2*d*, 2*p*), ref. 15.
[h]Reference 16.
[i](5*s*, 3*p*/3*s*) + polarization, values corrected for BSSE, see ref. 17.
[j]Reference 18.
[k]MP2/6-31+G(2*d*, 2*p*)//6-31G(*d*), ref. 19.
[l]Reference 20.

exchange-correlation functionals but we recomputed the $(HF)_2$, $(HCN)_2$, and $FH\cdots NH_3$ complexes using the PP functional (9*a*). d_{AB} distances very close to BP results are obtained but larger association energies are predicted, as has also been pointed out in the water dimer study (6*a*).

Some other systems have been considered. A bifurcated structure of $(H_2S)_2$ (structure 6 in Fig. 1) has been optimized. The energy of this structure is 0.88 kcal mol^{-1} higher than the global minimum in Table 1. This compares well with the semiempirical value of 1.2 kcal mol^{-1} obtained in previous work (21). Vibrational frequency computations predict, however, that this is not a local minimum but a saddle point. Experimental data in the gas phase cannot clearly determine whether the trans-linear water dimer-like structure or the bifurcated one is the most stable (22). We have also considered a cyclic $(HX)_2$ structure with C_{2h} symmetry for X = Cl, F (structures 7 and 8 in the figure), which is in fact a transition structure for the exchange of the donor and acceptor molecules in the noncyclic dimers. We predict these structures to lie 1.36 kcal mol^{-1} (for F) and 0.69 kcal mol^{-1} (for Cl) over the most stable ones in Table 1. These values are in very good agreement with MP2/6-31+G**//6-31+G** results (13), which led to 1.28 kcal mol^{-1} and 0.53 kcal mol^{-1}, respectively.

Table 2. Computed properties for the water molecule and water dimer in liquid water: ab initio vs. Density Functional (BP) calculations. Atom numbering in the water dimer is the following: $H_1O_1H_2 \cdots O_2H_3H_4$. Geometry in Å and degrees, dipole moment in Debye, association and solvation energies in kcal mol^{-1}. Bond orders are computed as proposed by Mayer (23). Cavity volumes employed in this work are 36.98 $Å^3$ for water and 73.73 $Å^3$ for the water dimer.

	Vacuum		Increments in liquid water	
	MP2[a]	BP	MP2[a]	BP
Water molecule				
Geometry				
OH	0.957	0.974	0.003	0.003
HOH	104.4	104.7	−0.3	−0.6
OH bond order	0.977	0.960	−0.041	−0.022
μ	2.063	2.097	0.319	0.312
Free energy of solvation			−5.52	−6.52
Water dimer				
Geometry				
O_1H_1	0.957	0.973	0.004	0.006
O_1H_2	0.964	0.986	0.005	0.006
$O_2H_{3,4}$	0.958	0.974	0.005	0.006
O_1O_2	2.912	2.876	0.010	0.063
Bond orders				
O_1H_1	0.973	0.969	−0.049	−0.031
O_1H_2	0.918	0.908	−0.047	−0.020
O_2H_2	0.013	0.061	+0.034	+0.016
$O_2H_{3,4}$	0.960	0.942	−0.043	−0.027
Charge transfer	0.0023	0.0313	0.0082	0.0071
μ	2.848	2.950	0.419	0.352
Association energy	−5.45	−3.97	−1.90	−1.22
Free energy of solvation			−12.95	−12.55

[a]MP2/6-311G++(2*d*, 2*p*) calculations (7).

To investigate hydrogen-bond formation in the liquid phase, we considered the water dimer immersed in a polarizable dielectric continuum. The SCRF model described above was employed to evaluate the electrostatic medium effect on the dimer structure. We chose this system because of its physical importance and the availability of ab initio results (7). The latter have shown that cooperative interactions with the surroundings tend to enhance the hydrogen-bond strength and the study of this fundamental property is suitable for testing DFT calculations in liquid-phase chemical problems.

Comparison between BP and MP2 calculations for the water monomer and the water dimer is made in Table 2. Note that MP2 results are those reported in ref. 7 and refer to MP2/6-311G++(2*d*, 2*p*) computations. Since the DFT basis set is less extended, comparison must be made with some caution. For instance, in a vacuum, the O—H bond lengths predicted by the BP calculations are larger (by about 0.02 Å) than the MP2 results whereas the O—O distance in the water dimer is substantially shorter (by 0.036 Å). Nevertheless, our DFT results for the water molecule and water dimer are close to other DFT values reported in the literature (6). They are also comparable to ab initio calculations with smaller basis sets. Thus, MP2/6-31++G* predicts an O—H bond length of 0.971 Å for the water monomer and an O—O bond length of 2.895 Å in the water dimer (see ref. 15 for a detailed analysis of the basis set dependence of the water molecule and water dimer structures).

Qualitatively, the solvent effects predicted by the MP2 and BP computations are in good agreement. The absolute values are substantially different for some properties, but this is due in part to the fact that the description of the hydrogen bond in a vacuum presents some discrepancies, as already described (*6a*). For instance, the intermolecular O_2H_2 bond order is rather large in DFT calculations.

When the water molecule is placed in a dielectric medium, the O—H bonds are lengthened (by 0.003 Å at the MP2 or BP levels) and weakened and the molecule is substantially polarized. The solvation energy is slightly larger in BP calculations. It is interesting to compare these perturbations on the water molecule with those produced by the formation of an isolated water dimer. In this case, the O—H length of the donating bond is substantially increased (by 0.007 Å at the MP2 and 0.012 Å at the BP level) whereas the other O—H bond lengths change slightly. The perturbation due to specific interactions is larger than the electrostatic effect, which is probably due to neglect of charge-transfer interactions in the continuum model.

Let us now consider the electrostatic effect on the water dimer. Going from the gas phase to the liquid, the hydrogen bond is strengthened. This is illustrated by the decrease of the O_1H_2 bond order and the increase of the O_2H_2 bond order (for

Can. J. Chem. Downloaded from www.nrcresearchpress.com by 65.111.164.53 on 09/08/12
For personal use only.

atom numbering, see Table 2). In spite of that, the O_1—O_2 bond length increases when electrostatic interactions with the medium are considered. The increase is especially large in the BP computations. Due to the flatness of the potential energy surface, the electrostatic effect on the intermolecular parameters is quite sensitive to the computational scheme (7) and the large differences obtained between MP2 and BP calculations are not surprising. Note that, for the same reason, the intermolecular parameters may depend on the cavity shape although the ellipsoidal cavities used here fit the molecular shape well and are, in any case, almost equivalent in the MP2 and BP computations.

The implicit hydrogen bonds of the external hydrogen atoms with other molecules in the liquid (see O_1H_1, $O_2H_{3,4}$ bond lengths and bond orders) are strengthened. The increase in charge transfer through the effect of the bulk liquid is noticeable. Moreover, the absolute value of the association energy is greater in the liquid. It must be pointed out that, in the liquid, the association energies represent the difference between the free energy of solvation of the dimer and the monomers and, strictly speaking, they are not true association energies. The internal energy may be estimated as proposed in ref. 7. This would lead to a still larger stabilization of the hydrogen bond in the dielectric medium.

From these results, one sees that DFT calculations predict a cooperative effect between long-range electrostatic interactions and hydrogen-bond formation, which is in reasonably good agreement with the ab initio results. However, as pointed out above, specific interactions in water are only qualitatively reproduced by the continuum model and a more sophisticated liquid model should be employed to obtain accurate properties in water solution. This can be done by means of various approaches. The simplest one would consist of the study of a cluster of water molecules immersed in a continuum. However, the number of energy minima increases with the number of water molecules and a statistical treatment may be necessary. On the other hand, Monte Carlo or molecular dynamics simulations of a quantum system in a classic liquid can now be carried out with several mixed DFT/MM potentials (1). These techniques represent a substantial improvement in the modeling of molecular liquids but they remain expensive and we do not envisage employing them here.

4. Conclusions

In this paper, several hydrogen-bonded systems with quite different association energies have been studied at the DFT level with non-local exchange-correlation corrections to the total energy. The effect of a dielectric continuum on the structure of the water dimer has been examined and cooperative interactions have been discussed. The results agree fairly well with previous ab initio calculations and experimental measurements. Though it is not easy from these preliminary results to give definitive conclusions on the performance of approximate DFT methods in investigating the liquid state, in particular when hydrogen bonds are present, the approach appears to be very promising.

Acknowledgment

The authors thank D.R. Salahub and H. Chermette for providing them with the program deMon and for helpful discussions.

References

1. (*a*) R.V. Stanton, D.V. Hartsough, and K.N. Merz, Jr. J. Phys. Chem. **97**, 11868 (1993); (*b*) D. Wei and D.R. Salahub. Chem. Phys. Lett. **224**, 291 (1994); (*c*) I. Tuñón, M.T.C. Martins-Costa, C. Millot, M.F. Ruiz-López, and J.L. Rivail. J. Comput. Chem. Submitted.
2. R.G. Gordon and Y.S. Kim. J. Chem. Phys. **56**, 3122 (1972).
3. Y.S. Kim and R.G. Gordon. J. Chem. Phys. **61**, 1 (1974); E. Radzio-Andzelm. Int. J. Quantum Chem. **20**, 601 (1981); R.A. Harris. J. Chem. Phys. **81**, 2403 (1984); M.A. Spackman. J. Chem. Phys. **85**, 6587 (1986); R.A. Harris. Chem. Phys. Lett. **33**, 495 (1975); T.A. Wesolowski and A. Warshel. J. Phys. Chem. **97**, 8050 (1993).
4. W. Yang. Phys. Rev. Lett. **66**, 1438 (1991).
5. W. Kohn and L.J. Sham. Phys. Rev. A, **140**, 1133 (1965).
6. (*a*) F. Sim, A. St-Amant, I. Papai, and D.R. Salahub. J. Am. Chem. Soc. **114**, 4391 (1992); (*b*) K. Laasonen, M. Parrinello, R. Car, C. Lee, and D. Vanderbilt. Chem. Phys. Lett. **207**, 208 (1993); (*c*) T. Zhu and W. Yang. Int. J. Quantum Chem. **49**, 613 (1994).
7. J. Bertrán, M.F. Ruiz-López, D. Rinaldi, and J.L. Rivail. Theor. Chim. Acta, **84**, 181 (1992).
8. A. St-Amant and D.R. Salahub. Chem. Phys. Lett. **169**, 387 (1990); D.R. Salahub, R. Fournier, P. Mlynarski, I. Papai, A. St-Amant, and J. Ushio. *In* Theory and applications of density functional approaches to chemistry. *Edited by* J. Labanowski and J. Andzelm. Springer Verlag, Berlin. 1991. F. Sim, D.R. Salahub, S. Chin, and M. Dupuis. J. Chem. Phys. **95**, 4317 (1990).
9. (*a*) S.H. Vosko, L. Wilk, and M. Nusair. Can. J. Phys. **58**, 1200 (1980); (*b*) A.D. Becke. Phys. Rev. A: Gen. Phys. **38**, 3098 (1988); J.P. Perdew. Phys. Rev. B: Condens. Matter, **33**, 8822 (1986); (Erratum) **34**, 7406 (1986).
10. (*a*) M.F. Ruiz-López, F. Bohr, M.T. Martins-Costa, and D. Rinaldi. Chem. Phys. Lett. **221**, 109 (1994); (*b*) J.L. Rivail, D. Rinaldi, and M.F. Ruiz-Lopez. NATO ASI Ser. C, **339**, 79 (1991); (*c*) V. Dillet, D. Rinaldi, J.G. Angyán, and J.L. Rivail. Chem. Phys. Lett. **202**, 18 (1993); (*d*) D. Rinaldi, J.L. Rivail, and N. Rguini. J. Comput. Chem. **13**, 675 (1962).
11. E.L. Woodbridge, T.L. Tso, M.P. McGrath, W.J. Hehre, and E.K.C. Lee. J. Chem. Phys. **85**, 6991 (1986).
12. Z. Latajka and S. Scheiner. Chem. Phys. **122**, 413 (1988).
13. D. Heidrich, N.J.R.v.E. Hommes, and P.v.R. Schleyer. J. Comput. Chem. **14**, 1149 (1993).
14. N. Ohashi and A.S. Pine. J. Chem. Phys. **81**, 73 (1984); A.S. Pine and B.J. Howard. J. Chem. Phys. **84**, 590 (1986).
15. M.J. Frisch, J.E. Del Bene, J.S. Binkley, and H.F. Schaefer III. J. Chem. Phys. **84**, 2279 (1986).
16. B.J. Howar, T.R. Dyke, and W. Klemperer. J. Chem. Phys. **81**, 5417 (1984); A.E. Barton and B.J. Howard. Faraday Discuss. Chem. Soc. **73**, 45 (1982).
17. K. Somasundran, R.D. Amos, and N.C. Handy. Theor. Chim. Acta, **69**, 491 (1986).
18. L.W. Buxton, E.J. Campbell, and W.H. Flygare. Chem. Phys. **56**, 399 (1981).
19. J.E. Del Bene. J. Comput. Chem. **10**, 603 (1989).
20. G.L. Johnson and L. Andrews. J. Am. Chem. Soc. **104**, 3043 (1982).

Can. J. Chem. Downloaded from www.nrcresearchpress.com by 65.111.164.53 on 09/08/12
For personal use only.

21. K. Jug and G. Geudtner. J. Comput. Chem. **14**, 639 (1993).
22. T.R. Dyke, K.M. Mack, and J.S. Muenter. J. Chem. Phys. **66**, 498 (1977).
23. I. Mayer. Chem. Phys. Lett. **97**, 270 (1983); **117**, 396 (1985); Int. J. Quantum Chem. **29**, 73 (1986).

Can. J. Chem. Downloaded from www.nrcresearchpress.com by 65.111.164.53 on 09/08/12
For personal use only.

Studies on the interaction of selenite and selenium with sulfur donors. Part 3. Sulfite

Sheila Ball and John Milne

Can. J. Chem. Downloaded from www.nrcresearchpress.com by 65.111.164.53 on 09/08/12
For personal use only.

Abstract: Elemental selenium dissolves in sulfite solution to form selenosulfate ion: $Se + SO_3^{2-} = SeSO_3^{2-}$. The formation constants for this equilibrium at temperatures from 0 to 35°C are reported for the first time. The isomeric thioselenate anion, $SSeO_3^{2-}$, is not, however, produced by the reaction of sulfur with selenite nor is the selenoselenate ion, $Se_2O_3^{2-}$, formed from selenium and selenite. Selenotrithionate is formed rapidly from the reaction of selenous acid with sulfite and hydrogen sulfite according to: $HSeO_3^- + 3\ HSO_3^- = Se(SO_3)_2^{2-} + SO_4^{2-} + 2\ H_2O$. Two isomers of the selenotrithionate ion are observed by Se-77 NMR and Raman spectroscopy, one with O-bonded Se, $Se(OSO_2)_2^{2-}$, and the other with S-bonded Se, $Se(SO_3)_2^{2-}$. Both isomers are formed in reactions with hydrogen sulfite but only the O-bonded isomer is formed in sulfite solutions at ambient temperatures. The Raman and Se-77 NMR spectra of the various sulfur–selenium anions formed are given and the parallel with the reactions of selenous acid and thiols is discussed.

Key words: selenium, sulfite, selenosulfate, selenotrithionate, Se-77 NMR, Raman spectroscopy, equilibria, aqueous solutions.

Résumé : Le sélénium élémentaire se dissout dans une solution de sulfite pour former l'ion sélénosulfate : $Se + SO_3^{2-} = SeSO_3^{2-}$. On a déterminé pour la première fois les constantes de formation pour cet équilibre, à des températures allant de 0 à 35°C. Toutefois, l'ion isomère thiosélénate, $SSeO_3^{2-}$, n'est pas produit par la réaction du soufre avec le sélénite; l'ion sélénosélénate, $Se_2O_3^{2-}$, ne se forme pas non plus à partir du sélénium et du sélénite. Le sélénotrithionate se forme rapidement par la réaction de l'acide séléneux avec le sulfite et le sulfite d'hydrogène, suivant l'équation : $HSeO_3^- + 3\ HSO_3^- = Se(SO_3)_2^{2-} + SO_4^{2-} + 2\ H_2O$. On a observé deux isomères de l'ion sélénotrithionate par RMN du ^{77}Se et par spectroscopie Raman; l'un comporte un O lié au Se, $Se(OSO_2)_2^{2-}$, et l'autre comporte un S lié au Se, $Se(SO_3)_2^{2-}$. Les deux isomères se forment au cours de réactions avec le sulfite d'hydrogène; toutefois, à la température ambiante, en solutions dans le sulfite, il ne se forme que l'isomère comportant une liaison O. On rapporte les spectres RMN du ^{77}Se des divers anions soufre–sélénium obtenus et on discute du parallèle qui existe avec les réactions de l'acide séléneux et des thiols.

Mots clés : sélénium, sulfite, sélénosulfate, sélénotrithionate, RMN du ^{77}Se, spectroscopie Raman, équilibre, solutions aqueuses.

[Traduit par la rédaction]

Introduction

Our knowledge of the chemistry of the oxosulfur anions that exist is well developed and for the common oxidation states parallel selenium species are known (1). The stepwise substitution of sulfur by selenium in polyoxosulfur anions has been little studied. For thiosulfate, for instance, two isomers are possible. Early work showed that elemental selenium could be taken up by sulfite, indicating that selenosulfate, $SeSO_3^{2-}$ (2), was stable, but the formation of thioselenate, $SSeO_3^{2-}$, from sulfur and selenite, has been controversial (3–5). Substitution of sulfur by selenium in the trithionate ion gives two possible isomers. In the selenotrithionate anion, $SeS_2O_6^{2-}$, selenium lies in the central position of a three-chalcogen chain (6). The second isomer has not been observed. In the selenium disulfur dichlorides, however, both isomers, ClSeSSCl and ClSSeSCl, are known (7). Other species related to selenotrithionate but with more Se atoms, $Se_nS_2O_6^{2-}(n = 2,3,4)$, have been detected by electrophoretic methods (8) but no isomers amongst these species have been observed. The synthesis of potassium diselenotetrathionate by the oxidation of selenosulfate has been reported (9, 10). Probably the most easily prepared selenopolythionate is selenopentathionate, $SeS_4O_6^{2-}$ (11). The crystal structure of the barium salt shows selenium in the central position of a five-chalcogen chain (12).

None of these selenothionates have been characterized by Raman and Se-77 NMR spectroscopy and, for this reason, it was of interest to use these methods to study the formation and structural nature of the simpler species, selenosulfate and selenotrithionate. The formation of selenotrithionate from selenous acid and sulfite may parallel the formation of bis(thio)selenides according to (13)

Received January 30, 1995.

S. Ball and J. Milne.[1] Ottawa–Carleton Chemistry Institute, Department of Chemistry, University of Ottawa, Ottawa, ON K1N 6N5, Canada.

[1] Author to whom correspondence may be addressed. Telephone: (613) 562-5800, ext. 6054. Fax: (613) 562-5170.

Can. J. Chem. Downloaded from www.nrcresearchpress.com by 65.111.164.53 on 09/08/12
For personal use only.

[1] $SeO_2 + 4\,RSH = RSSeSR + RSSR$

and, in view of our understanding of the mechanism of this reaction for alkyl thiols (14) and 2-mercaptoethanol (15), extension of this work to sulfite was of interest.

Experimental section

Materials

Sulfur (BDH;>99%) and freshly ground vitreous selenium (BDH;>99.5%) were used directly. Selenium dioxide (Aldrich) was analyzed before use by potentiometric titration with standard NaOH. Sodium (Sigma) and potassium metabisulfite (BDH) were used directly. These salts showed no evidence of any oxidation to sulfate. Sulfite salts, on the other hand, were often contaminated with sulfate. Sodium sulfite (BDH), which was free flowing, contained no sulfate but sodium sulfite from other suppliers contained varying amounts of sulfate. The contamination was associated with clumping of the salt, probably as a result of bottling while still moist. Wet sulfites are subject to air oxidation. None of the potassium sulfite from various suppliers was free of sulfate and it was found preferable to make up potassium sulfite solutions by neutralization of potassium metabisulfite with potassium hydroxide in oxygen-free water. The criterion of purity for the sulfites was the absence of the 453 cm^{-1} band of sulfate in the Raman spectrum. The strong sulfate band at 980 cm^{-1} is a poor measure of the presence of sulfate since it is coincident with a strong sulfite band. Ammonium sulfate (BDH), sodium thiosulfate (BDH), barium chloride dihydrate (BDH), and sulfur dioxide (Air Products) were used directly. Distilled water, purged of oxygen by passage of nitrogen, was used throughout.

Preparations

Potassium trithionate was prepared by standard methods (16). Saturated sulfur dioxide solution (10.64 g/100 mL = 1.6 M (17)) was prepared by passing sulfur dioxide through water at 20°C via a sintered inlet for 1 h. Potassium selenosulfate was prepared by dissolving 24 g of analyzed K_2SO_3 (82.4%) and 5.9 g $BaCl_2 2H_2O$ in 10 mL water, removing the $BaSO_4$ by filtration, and then saturating with Se (3.1 g) over 2 h at ca 60°C, filtering through a glass fibre filter paper to remove any excess Se, and leaving standing at 0°C, protected from oxygen, overnight. The colourless solution produces white crystals, which analyze as $K_2SeSO_3 \cdot 3.5H_2O$ (obsd. %Se: 26.4; calcd. %Se: 26.3). Care must be taken that no residual Se is present since this acts as seed crystal for the decomposition to sulfite (reverse of reaction [2]). The product was stable if stored dry in the dark at ambient temperatures. The salt has kinetic stability when dissolved in water but does produce elemental selenium on standing. Immediate precipitation of selenium normally occurs upon addition of hydrochloric acid but with good mixing a 1.29 M solution of selenosulfate did not produce elemental selenium until the acid concentration reached 0.29 M at ambient temperature. Potassium selenotrithionate was prepared by exploiting the stoichiometry of the sulfite/selenium dioxide reaction discussed below. A solution of 4.44 g of selenium dioxide was prepared in 10 mL of water and another solution of 8.89 g potassium metabisulfite ($K_2S_2O_5$) and 6.32 g potassium sulfite was made up in 85 mL of water with mild heating. The solutions were cooled and mixed with efficient stirring. A barium chloride solution (9.8 g $BaCl_2 \cdot 2H_2O$ in 20.0 mL of water) was then added to precipitate sulfate and the solution was filtered. The yellow coloured supernatant was left to cool at 0°C and produced pale yellow crystals. Both the crystals and the yellow supernatant produced red selenium over a period of hours even when protected from light and stored at −10°C. The crystals analyzed as $K_2SeS_2O_6$ (obsd. %Se: 23.5; calcd. %Se: 24.9 %) and gave an X-ray powder diffraction pattern consistent with the unit cell dimensions reported earlier (6).

Methods

Selenium analysis was done by gravimetry (18). Formation constants for selenosulfate were determined by saturation of the sulfite solution with a known mass of selenium over a 2 h period. This time period was shown to be sufficient for complete saturation. The remaining selenium was filtered and weighed and the amount of selenium dissolved was determined by difference. Temperature control was within ±0.2°C.

Raman spectra were measured with a Jobin–Yvon Ramanor HG.2S monochromator in conjunction with a PAR/Hamamatsu photon-counting system. The spectra were excited with the krypton ion line at 15 454 cm^{-1}. Quantitative spectra were measured at ambient temperature (23°C) and normalized against 1.0 M perchloric acid for which the 910 cm^{-1} band was taken to have an intensity of 6.45 cm^2 (19). The spectra were taken at fixed slit width (1600 μm), which gave a resolution of 5–7 cm^{-1}. The molar scattering intensity for the 1150 cm^{-1} band of SO_2 was determined from the spectrum of a solution saturated with SO_2 at 20°C (1.6 M (17)) ($I^{1150}(SO_2) = 5.5 \pm 0.2$ cm^2 M^{-1}). The molar scattering intensity for the 980 cm^{-1} band of the sulfate ion was determined for 0.5, 1, and 2 M $(NH_4)_2SO_4$ solutions and found to be 6.7 ± 0.4 cm^2 M^{-1}. Deconvolution of overlapped peaks was done assuming Lorentzian line shapes.

Se-77 NMR spectra were determined using a Bruker AMX 500 spectrometer operating at 95.47 MHz. A 30° tip angle was used with 0.3 s acquisition time and no pulse delay. Probe temperature was 21°C. Samples were contained in 10 mm o.d. precision NMR tubes. Chemical shifts were determined by sample replacement and using saturated selenous acid as the standard (20). All chemical shifts are given on the dimethylselenide scale ($\delta(Me_2Se) = \delta(H_2SeO_3) + 1300$ ppm (20)).

Results and discussion

Selenosulfate formation constant

Sulfite and selenosulfate are in equilibrium according to

[2] $SO_3^{2-}(aq) + Se(s) \overset{K}{=} SeSO_3^{2-}$

The values of K at various temperatures are given in Table 1. Our result at 20°C, $K = 0.43 \pm 0.01$, lies in the range of values previously reported for ambient temperature (21), $K = 0.33 - 1.0$. The results given in Table 1 show that the solubility of selenium in sulfite solution increases with temperature, as reported previously (22). A plot of ln K against $1/T$ for the data in Table 1 gives $\Delta H = 18.1 \pm 0.6$ kJ mol^{-1}. This value, the standard free energy change calculated from the equilibrium constant at 25°C, and the entropy change from the Gibbs–

Can. J. Chem. Downloaded from www.nrcresearchpress.com by 65.111.164.53 on 09/08/12
For personal use only.

Table 1. Selenium solubility in 1.0 M Na_2SO_3 at various temperatures and selenosulfate formation constants, K.

T (°C)	c(Se) (mol L^{-1})	K
0	0.203	0.255
13	0.268	0.366
20	0.300	0.430
20	0.300	0.430
20	0.306	0.440
25	0.340	0.515
35	0.379	0.610

Table 2. $\Delta G°$, $\Delta H°$ and $\Delta S°$ for $SeSO_3^{2-}$ formation.

Anion	$SeSO_3^{2-}$	$S_2O_3^{2-}$[a]	$SeSC_2H_4OH^-$
$\Delta G°$ (kJ mol^{-1})	1.60±0.03	−3.5	2.8±0.4
$\Delta H°$ (kJ mol^{-1})	18.1±0.6	20	46±1[b]
$\Delta S°$ (J $K^{-1}mol^{-1}$)	56±1	77.8	144±2[b]

[a]Reference 23.
[b]Recalculated from data in ref. 24

Helmholtz equation are listed in Table 2 along with comparable data for $HOC_2H_4SSe^-$ and thiosulfate formation. The thiosulfate formation constant at 25°C, calculated from $\Delta G°$, is 14.2, significantly greater than that for selenosulfate. The enthalpies of chalcogenosulfate formation for sulfur and selenium are comparable and the difference in formation constant is largely determined by the more favourable entropy change for the thiosulfate. The enthalpy of formation of the SeS bond in $SeSC_2H_4OH^-(aq)$ is less favourable than that in the selenosulfate, which parallels the greater bond strength of the S(VI)–selenium linkage compared to that of the S(II)–selenium linkage. The more favourable entropy change for $SeSC_2H_4OH^-$ compared to $SeSO_3^{2-}$ is a result of decreased solvation effects in the mononegative ion compared to the dinegative ion as well as the less symmetric nature of the selenomercaptide.

No evidence for the formation of selenoselenate, $SeSeO_3^{2-}$, by the reaction of SeO_3^{2-} with Se in water was found by gravimetry.

Spectroscopy

The Se-77 NMR spectrum of a 1.0 M sodium sulfite solution saturated with elemental selenium gives a single resonance at 646.3 ppm with a half-height linewidth of 6.3 Hz (Table 3), which is assigned to the selenosulfate ion. The Raman spectrum of this solution is given in Fig. 1 (Trace A) along with spectra of a 1.0 M sodium sulfite (Trace B) and solid potassium selenosulfate (Trace C). In addition to strong bands due to sulfite ion at 480, 620, and 965 cm^{-1}, trace A shows bands at 310, 530, 645, 995, and 1120 cm^{-1}. These bands parallel those observed for solid K_2SeSO_3 (Trace C) and are assigned to the $SeSO_3^{2-}$ ion. From the normalized molar peak intensity of the sulfite band at 965 cm^{-1} in Trace B ($I^{968}(SO_3^{2-}) = 4.4\ cm^2\ M^{-1}$) and the normalized peak intensity measured of the deconvoluted envelope at 965 cm^{-1} in the selenosulfate solution (Trace A), the sulfite concentration is found to be 0.66 M and K for equilibrium [2] is estimated to be 0.52, in reasonable agree-

Table 3. Se-77 NMR chemical shifts for selenosulfate and selenotrithionate solutions.

Solution	Chemical shifts[a] (ppm)	Origin
1.0 M Na_2SO_3 saturated with Se	646.3	$SeSO_3^{2-}$
0.91 M $Na_2S_2O_5$, 0.46 M SeO_2 (mixed at 5 °C)	881.2(0.9) 958.9(0.1) 1191.7(1.0)	$Se(SO_3)_2^{2-}$ $O_2SOSeSO_3^{2-}$ $Se(OSO_2)_2^{2-}$
0.80 M Na_2SO_3, 0.80 M SeO_2 (mixed at 5°C)	1191.2(0.5) 1315.2(1.0)	$Se(OSO_2)_2^{2-}$ $HSeO_3^-$
0.80 M Na_2SO_3, 0.80 M SeO_2 (mixed at 25° C)	880(trace) 1191.0(0.56) 1315.3(1.0)	$Se(SO_3)_2^{2-}$ $Se(OSO_2)_2^{2-}$ $HSeO_3^-$
0.80 M Na_2SO_3, 0.80 M SeO_2 (5 min. at 80°C)	880.6(0.06) 1191.0(0.56) 1314.9(1.0)	$Se(SO_3)_2^{2-}$ $Se(OSO_2)_2^{2-}$ $HSeO_3^-$
0.80 M Na_2SO_3, 0.80 M SeO_2 (refluxed for 0.5 h; Se° present)	880.5(0.25) 962.5(0.08) 1190.9(0.06) 1303.4(1.0)	$Se(SO_3)_2^{2-}$ $O_2SOSeSO_3^{2-}$ $Se(OSO_2)_2^{2-}$ $HSeO_3^-$
0.80 M Na_2SO_3, 0.40 M SeO_2 (mixed at 5°C)	1190.9(0.9) 1296.8(1.0)	$Se(OSO_2)_2^{2-}$ $HSeO_3^-/SeO_3^{2-}$
1.82 M Na_2SO_3, 0.45 M SeO_2 (mixed at 5°C)	1190.9(1.25) 1283.6(1.0)	$Se(OSO_2)_2^{2-}$ $HSeO_3^-/SeO_3^{2-}$

[a]$\delta(Me_2Se) = 0$ ppm; relative signal height in parenthesis.

Fig. 1. Raman spectra of a 1.0 M solution of Na_2SO_3 saturated with Se (Trace A), 1.0 M Na_2SO_3 (Trace B), and solid $K_2SeSO_3 \cdot 3H_2O$ (Trace C).

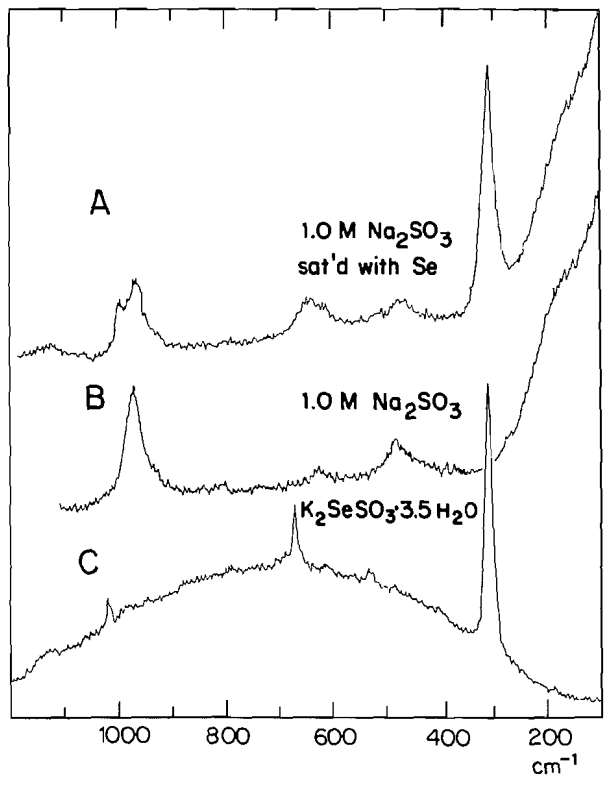

Table 4. Raman spectra of $SeSO_3^{2-}$ and related ions.

$SeSO_3^{2-a}$	K_2SeSO_3 3.5H_2O	$S_2O_3^{2-b}$	$BrSO_3^{-c}$	Assignment
310(10,p)	309(10)	450(10)	280	ν(XS)(A_1)[d]
—	—	340(1)	290	δ(XSO)(E)[d]
530(0)	530(0)	540(0)	540	$\delta_a(E)$
645(2,p)	669(1)	670(2)	625	$\delta_s(A_1)$
995(1,p)	1015(0)	1000(2)	1042	ν_s(SO)(A_1)
1120(0,br)	1130(0,br)	1125(1,br)	1250	ν_a(SO)(E)

[a]1.0 M Na_2SO_3 solution saturated with Se (Fig. 1, Trace A).
[b]1.0 M $Na_2S_2O_3$.
[c]Reference 25.
[d]X = Se, S, Br.

ment with that determined from gravimetry at ambient temperature. The frequencies of the normal modes of the selenosulfate ion in solid and solution are listed along with those of some symmetry-related ions in Table 4. Except for the selenium–sulfur stretching mode, the frequencies of the $SeSO_3^{2-}$ and $S_2O_3^{2-}$ are very similar. Judging from the frequency of the δ(BrSO) mode in the $BrSO_3^-$ ion, the related deformation for selenosulfate ion is masked by the strong band at 310 cm^{-1}.

Selenoselenate and thioselenate

Elemental selenium undergoes no reaction in 1.0 M Na_2SeO_3 as demonstrated by gravimetry, Se-77 NMR, and Raman spectroscopy, which confirms Rathke's observations (2). The reported solubility and evidence for the formation of $Se_2O_3^{2-}$ (4) may be accounted for by the disproportionation of selenium in basic solution according to the reaction (26),

[3] $$(2n + 1)\ Se + 6\ OH^- = 2\ Se_n^{2-} + SeO_3^{2-} + 3\ H_2O$$

Similarly, no evidence was found for the formation of thioselenate, $SSeO_3^{2-}$, from sulfur and hydrogen selenite or selenite. The Raman spectrum of a 1.0 M $NaHSeO_3$ solution containing sulfur, which was heated at 110°C in an ampoule for 72 h, showed only bands due to hydrogen selenite ion (810 and 370 cm^{-1}). Heating for longer periods of time (7 days) produced bands corresponding to the formation of $S_2O_3^{2-}$ (450 and 1000 cm^{-1}) and SO_4^{2-} (980 cm^{-1}). With even longer heating the thiosulfate peaks disappeared and only sulfate was observed. These changes were accompanied by precipitation of red Se on the surface of the sulfur and the solution remained colourless, which indicates that hydrogen selenite oxidizes sulfur and disproportionation of sulfur at the pH of a 1.0 M sodium hydrogen selenite solution (pH 5) does not occur. Similarly sulfur does not dissolve in 1.0 M Na_2SeO_3 over a period of days at ambient temperature. It has been claimed that thioselenate formation is optimal after 30 min reflux of a selenite–sulfur solution (4, 5). We found no change in the Raman spectrum after such treatment. After heating for 1 day at 115°C in a sealed ampoule only traces of elemental selenium were observed and the Raman spectrum showed only bands for selenite ion. After 9 days heating selenite was still present but the characteristic sulfate band at 980 cm^{-1} was apparent and elemental selenium was present. In earlier preparative work on thioselenate salts (4, 5) excess hydroxide was used and the results may be accounted for by the disproportionation of sulfur in basic solution to give thiosulfate and polysulfides (27).

[4] $$(2n + 2)\ S + 6\ OH^- = S_2O_3^{2-} + 2\ S_n^{2-} + 3\ H_2O$$

In this earlier work no protective measures against air oxidation were taken and this may also account for some of the results.

Reaction of selenite and sulfite

The addition of sulfur dioxide to a strongly acidic solution of selenite immediately produces a yellow solution that rapidly precipitates elemental selenium. This is the basis of the gravimetric analysis for selenite (18). The addition of hydrogen sulfite to selenite produces an immediate yellow coloration but selenium precipitation does not take place for several hours. With sulfite, the selenite solution is initially colourless, turns yellow over a period of hours, and does not yield selenium for several days. Paper electrophoresis studies of the sulfite–selenite solutions have shown that a range of selenopolythionates are formed (8). The Raman spectrum of a solution 0.91 M in $Na_2S_2O_5$ and 0.46 M in SeO_2 (4:1 S(IV)/Se(IV)), which was prepared at –10°C and the spectrum recorded immediately, is given in Fig. 2. No peaks due to HSO_3^- or $S_2O_5^{2-}$ (28) or selenite species (29) are observed. The characteristic strong peaks due to SO_2 and SO_4^{2-} appear at 1151 and 980 cm^{-1}, respectively. Using the molar scattering intensities for SO_2(5.5±0.3 $cm^2\ M^{-1}$) and SO_4^{2-}(6.7±0.4 $cm^2\ M^{-1}$) and the normalized intensities for these bands in this spectrum, the concentrations both of SO_2 and SO_4^{2-} may be estimated to be 0.5 M. This is consistent with the reaction

[5] $$4\ HSO_3^- + H_2SeO_3 = Se(SO_3)_2^{2-} + SO_2 + SO_4^{2-} + 3\ H_2O$$

At 3:1 S(IV)/Se(IV) stoichiometry, no peak corresponding to SO_2 formation is observed and addition of an amount of barium chloride equimolar to H_2SeO_3 caused the 980 cm^{-1} peak to disappear, confirming the stoichiometry of reaction [5]. This 3:1 S(IV)/Se(IV) stoichiometry was proposed earlier to account for the rapid and exothermic reaction of hydrogen sulfite and hydrogen selenite (30) and the appearance of sulfate in the electrophoresis of such solutions (8). The Se-77 NMR spectrum of a 0.91 M $Na_2S_2O_5$ and 0.46 M SeO_2 solution, listed in Table 3, gives two strong signals at 1191.7(1.0) and 881.2(0.9) ppm and a very weak signal at 958.9(0.1) ppm (intensities in parentheses). These three signals must arise from isomers of the selenotrithionate ion, $O_3SSeSO_3^{2-}$,

Can. J. Chem. Downloaded from www.nrcresearchpress.com by 65.111.164.53 on 09/08/12
For personal use only.

Can. J. Chem. Downloaded from www.nrcresearchpress.com by 65.111.164.53 on 09/08/12
For personal use only.

Fig. 2. Raman spectrum of a solution of 0.91 M $Na_2S_2O_5$ and 0.46 M SeO_2.

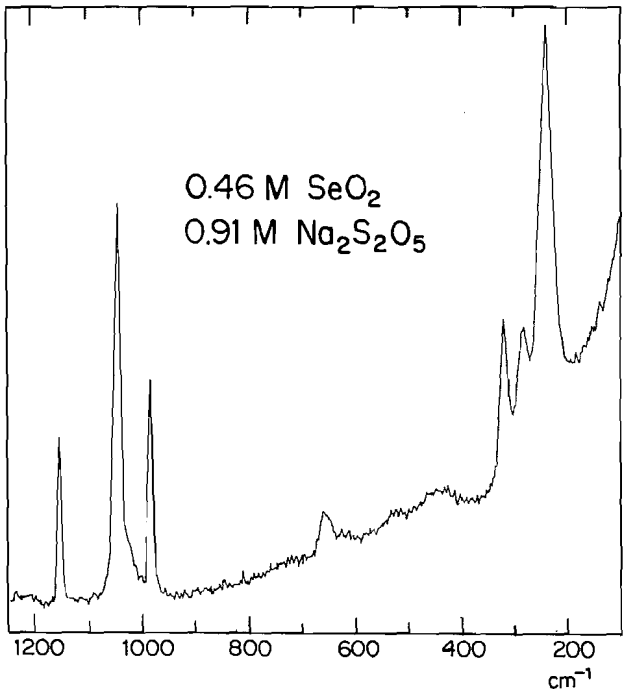

Fig. 3. Raman spectrum of solid $K_2Se(SO_3)_2$ and $K_2S_3O_6$.

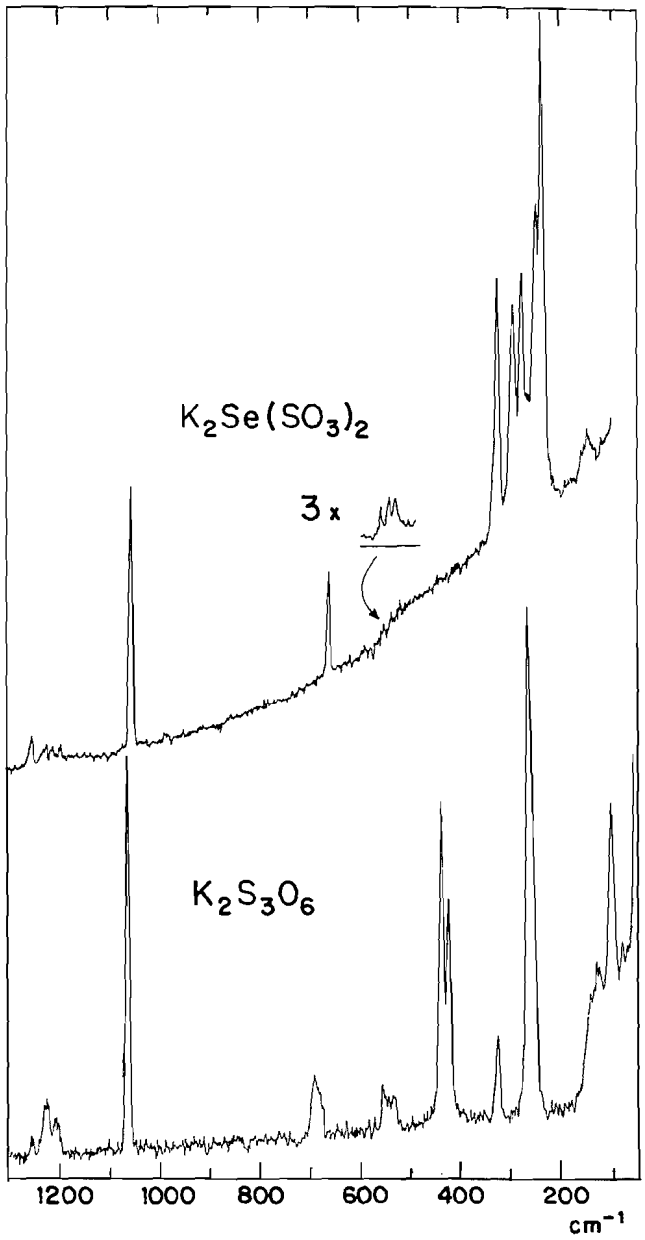

$O_2SOSeSO_3^{2-}$, and $O_2SOSeOSO_2^{2-}$. In general, the more electronegative the group attached, the less shielded the Se-77 signal (31), and the three signals may be assigned to -OSeO-, -OSeS-, and -SSeS- species in order of decreasing shift. The signal for the -SSeS- species at 881.2 ppm lies some 200 ppm above the normal range for the -SSeS- group in RSSeSR compounds (600–700 ppm)(32) but the high value is expected since the attached sulfur atoms (S(VI)) are the most electronegative bound to Se(II), studied until now. There are no examples of NMR shifts for Se(II) bound to two oxygens. Selenenic acids and their esters represent the closest models and the Se-77 NMR shift range for these is 1053–1269 ppm (33), which brackets the signal observed at 1191.7 ppm. The weak signal at 958.9 ppm is intermediate between the two strong signals for -OSeO- and -SSeS-, as expected for a -OSeS- group.

No evidence for the formation of higher selenopolythionates, which were observed by paper electrophoresis (8), was found in the NMR or Raman spectra. The chromatographic work was done with more dilute solutions (c(Se(IV)) = 0.10 M) than our work (c(Se(IV)) = 0.46 M) and the duration of the experiments was over weeks compared to hours. These differences in conditions as well as the presence of buffer in the chromatographic work could account for the observation of other selenopolythionates in the earlier work (8).

Selenotrithionates are difficult to prepare and decompose to give a red selenium coloration even when stored dry and protected from light. Preparation from selenium acetylacetonate (34) has been used but involves the preparation of the Se(II) starting material. Other methods (10, 35) result in the precipitation of large amounts of elemental selenium and are unreliable, no doubt due to kinetic factors. We have found that dropwise addition of a solution of potassium hydrogen sulfite and potassium sulfite in 2:1 mole ratio to one of selenous acid in 3:1 S(IV)/Se(IV) mole ratio at 0°C produces no elemental selenium, and addition of the stoichiometric amount of barium chloride, to precipitate the sulfate produced, gives a solution from which potassium selenotrithionate is readily crystallized. The Raman spectrum of this product and that of crystalline potassium trithionate are given in Fig. 3. Except for the pair of bands at 276 and 293 cm^{-1} in the spectrum of the selenium anion and the pair at 423 and 437 cm^{-1} in that of the trithionate anion, the spectra are very similar. The crystal structures of potassium trithionate (36) and selenotrithionate (6) show the anions to possess -SSS- and -SSeS- chains. This indicates that these pairs of bands in each case are associated with modes involving the central trichalcogen chain and represent the symmetric and asymmetric -SSeS- (-SSS-) stretching modes. In each case the bands lie slightly below those for the comparable seleno-(SeS-) and thio-sulfate (SS-) stretching modes given in Table 4, further strengthening this assignment. The

Table 5. Raman spectra of $Se(SO_3)_2^{2-}$ and $S(SO_3)_2^{2-}$ in solid and solution.[a]

$K_2Se(SO_3)_2$ solid	$K_2S(SO_3)_2$ solid	$Se(SO_3)_2^{2-}$ (0.36 M)	$S(SO_3)_2^{2-}$ (0.48 M)	Assignments $O_3SChSO_3^{2-}$ (Ch = S, Se)
—	77(0)	—	—	
—	100(5)	—	—	
148(1)	125(1,br)	—	—	
182(0)	—	—	—	
236(10)	254(5,sh)	236(10,br,p)	263(6,br,p)	δ(SChS)
249(6)	263(10)			
276(5)	—	285(4,[b] p)	—	ν(SeS)
293(4)	—			
326(5)	327(2)	320(3,p)	—	δ(ChSO)
—	422(5)	—	412(3,p)	ν(SS)
—	438(7)	—	426(4,p)	
528(0)	530(0)			
540(0)	543(0)	530(0,br)	540(0,br)	$\delta_a(SO_3)$
556(0)	556(0)			
661(2)	691(1,br)	640(0,[b] br,p)	673(1,br,p)	$\delta_s(SO_3)$
—	—	653(0,[b] p)	—	[c]
1052(5)	1061(8)	1030(2,sh,p)	1053(10,p)	$\nu_s(SO_3)$
—	—	1044(5,p)	—	[d]
1193(0)	1208(0)			
1210(0)	1227(1)	1205(0,br,p)		
1228(0)		1233(0,p)	1233(0,br,p)	$\nu_a(SO_3)$
1252(1)	1256(0)	1245(0,p)		

[a]Scanned to 1300 cm^{-1}; p, polarized, br, broad, sh, shoulder
[b]Variable intensity with degree of reaction.
[c]ν(SeO) for $Se(OSO_2)_2^{2-}$.
[d]$\nu_s(SO_2)$ for $Se(OSO_2)_2^{2-}$.

bands for each compound and those for their aqueous solutions are listed in Table 5. The Raman spectrum of the aqueous solution of the selenotrithionate anion made up from disulfite and selenium dioxide at room temperature is complicated by the presence of both the S- and O- bonded isomers. However, a preliminary assignment based upon the frequencies of similar modes in other sulfur oxoanions (37) may be made for the $S(SO_3)_2^{2-}$ and $Se(SO_3)_2^{2-}$ anions and this is given in Table 5. The Raman spectrum for the aqueous solution of the $Se(SO_3)_2^{2-}$ given Fig. 2 shows predominantly bands due to the O-bonded isomer but solutions made up at room temperature also exhibit bands due to the S-bonded isomer. The bands listed for an aqueous solution of selenotrithionate ion in Table 5 arise from both isomers and the assignment is more tentative in this case. It is noteworthy that all of the Raman bands observed, for which accurate intensity measurements can be made, are polarized. This suggests that for the trithionate ion, and very likely for the S-bonded selenotrithionate ion also, the symmetry adopted in solution is C_1 ($\Gamma = 21A$), for which all of the modes are polarized, and not the other possible symmetries, C_{2v} ($\Gamma = 7A_1 + 4A_2 + 6B_1 + 4B_2$), C_s ($\Gamma = 13A' + 8A''$), or C_2 ($\Gamma = 11A + 10B$), for which a smaller proportion of the modes is totally symmetric.

It was not possible to record the spectrum of the S-bonded isomer alone. Solutions made up from $K_2Se(SO_3)_2$ continually produced elemental selenium, even after filtration, which interfered with measurement of the Raman spectrum. The difference in the Raman spectra of the O- and S-bonded selenotrithionate ions is clearer for less acidic solutions where reactants may be mixed at room temperature and conversion to the S-bonded ion is slower. The Raman spectra of 0.375 M selenotrithionate solutions made up from sodium sulfite, sodium disulfite, and selenium dioxide in 1:1:1 mole ratio are given in Fig. 4. The spectrum in trace A was taken immediately upon mixing, when the solution was colourless, and that in Trace B after 6 days at room temperature, when the solution had become yellow but no sign of Se^0 was observed. The two spectra are presented under the same conditions of normalization and the band intensities are, therefore, directly comparable as shown by the identical scattering intensities for the 980 cm^{-1} band of the sulfate ion in the two traces. A small peak at 450 cm^{-1}, due to the E deformation mode of sulfate ion (ν_2), is also observed in the spectra. On standing over several days the SO stretch at 1044 cm^{-1} has fallen in intensity and a new peak at 1030 cm^{-1} has appeared, the peaks at 653, 320, and 236 cm^{-1} have decreased while that at 285 cm^{-1} has grown stronger. A peak at 285 cm^{-1} arises from the SeS modes of the S-bonded anion, which forms with time at the expense of the O-bonded isomer. The new peak at 1030 cm^{-1} must also arise from the S-bonded species while the peak at 655 cm^{-1}, which lies in the region expected for SeO single bond stretching (620 cm^{-1} for H_2SeO_3 and 600 cm^{-1} for $HSeO_3^-$ ion (37)), falls in intensity as expected for a band belonging to the O-bonded isomer.

Various stoichiometric ratios of Na_2SO_3 to SeO_2 were studied by Se-77 NMR (Table 3) and Raman (Fig. 5) spectros-

Can. J. Chem. Downloaded from www.nrcresearchpress.com by 65.111.164.53 on 09/08/12
For personal use only.

Can. J. Chem. Downloaded from www.nrcresearchpress.com by 65.111.164.53 on 09/08/12
For personal use only.

Fig. 4. Raman spectra of 0.375 M solutions of selenotrithionate ion made up from a 1:1:1 stoichiometric ratio of Na_2SO_3, $Na_2S_2O_5$, and SeO_2. Trace A is the spectrum taken immediately after preparation of the solution and Trace B, after 6 days.

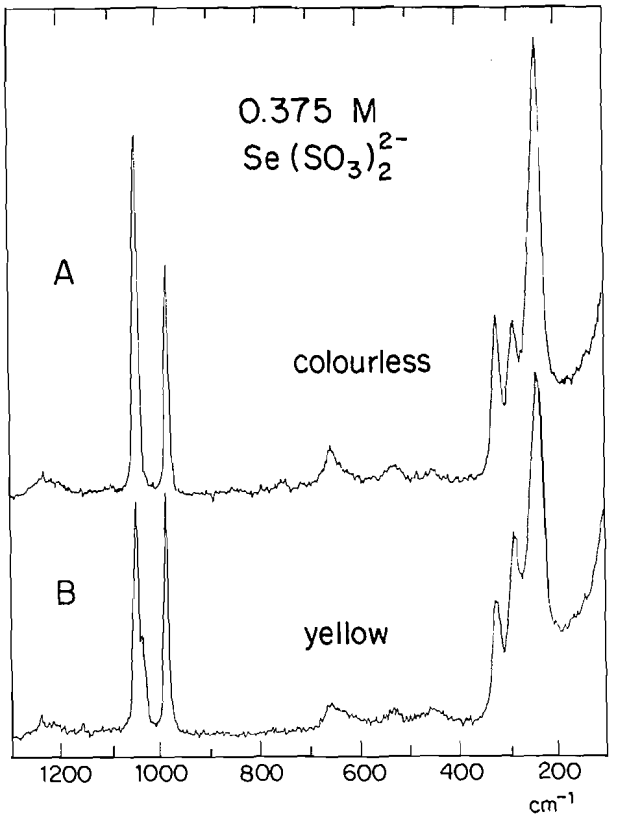

copy. A solution of 0.80 M Na_2SO_3 and 0.80 M SeO_2, mixed at 5°C and run immediately, gave an Se-77 NMR spectrum that consisted of two signals, at 1315.2 ppm from $HSeO_3^-$ (20), and 1191.2 ppm from O-bonded selenotrithionate, with intensity ratio 2 to 1, respectively. The same solution, made up at ambient temperature, showed that a small trace of S-bonded selenotrithionate was formed (Table 3). The Raman spectrum, which is given in Fig. 5, shows a normalized peak intensity for sulfate ion corresponding to a concentration of 0.26 M. No characteristic peak for the HSO_3^- ion at 1030 cm^{-1} (28) is observed although $HSeO_3^-$ is present as shown by the peak at 860 cm^{-1} (37). These observations are consistent with the formation of the O-bonded selenotrithionate according to the reaction:

$$[6] \quad HSeO_3^- + HSO_3^- = 1/3\ Se(OSO_2)_2^{2-} + 1/3\ SO_4^{2-} + 2/3\ HSeO_3^- + 2/3\ H_2O$$

Heating of this solution for 5 min at 80°C produced a trace amount of S-bonded selenotrithionate, shown by the NMR signal at 880.6 ppm, and heating over a period of 0.5 h at 100°C resulted in signals at 1190.9, 962.5, and 880.5 ppm due to the three selenotrithionate isomers, in addition to the $HSeO_3^-$ signal at 1303.4 ppm. Some red Se was present in this solution. The Se-77 NMR chemical shifts, for solutions with larger sulfite to selenium dioxide stoichiometric ratios are also given in Table 3. This increase in stoichiometric ratio gives generally more basic solutions and this is reflected in the selenite chemical shifts which decrease as the ratio increases, as expected ($\delta(HSeO_3^-)$ = 1313.9 ppm; δ (SeO_3^{2-}) = 1272.6 ppm (20)). As the ratio increases, the amount of O-bonded isomer sele-

Fig. 5. Raman spectra of solutions of Na_2SO_3 and SeO_2. Trace A: 0.80 M Na_2SO_3 and 0.80 M SeO_2, Trace B: 1.60 M Na_2SO_3 and 0.80 M SeO_2, Trace C: 1.71 M Na_2SO_3 and 0.57 M SeO_2, Trace D: 1.82 M Na_2SO_3 and 0.46 M SeO_2.

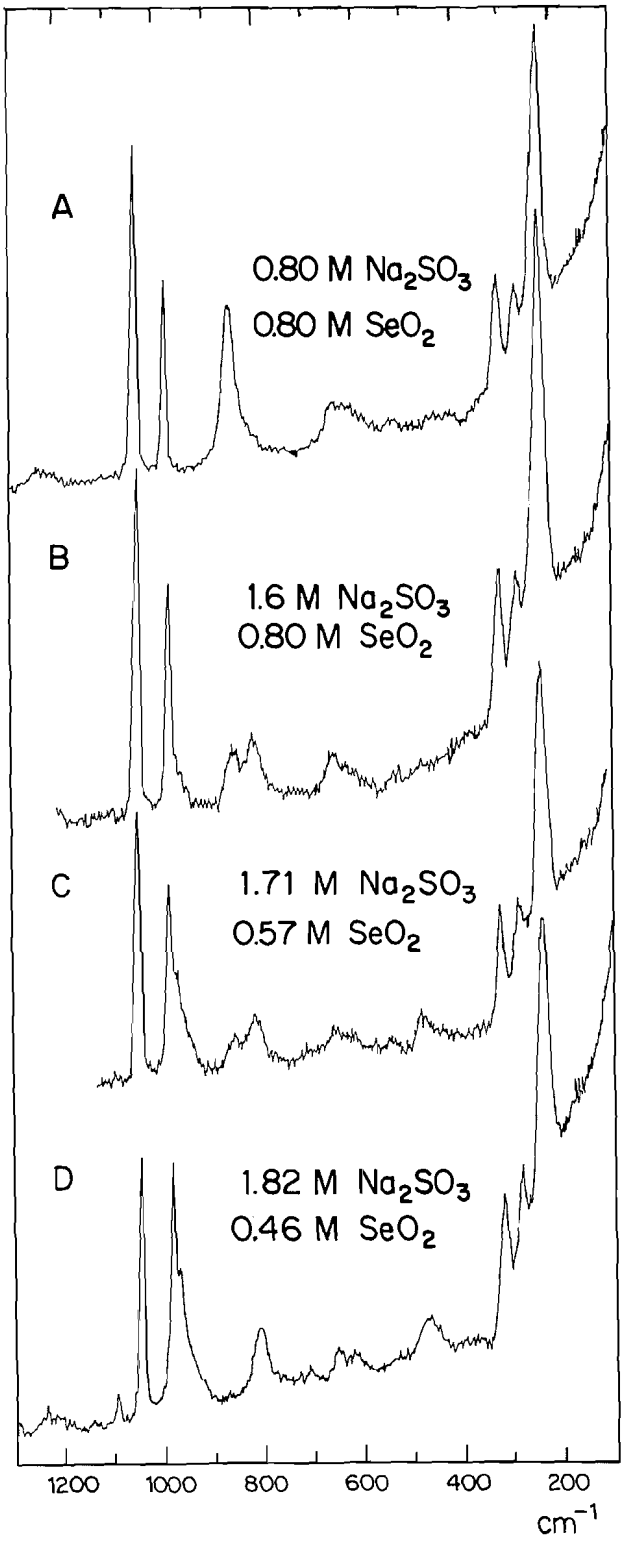

Can. J. Chem. Downloaded from www.nrcresearchpress.com by 65.111.164.53 on 09/08/12
For personal use only.

notrithionate increases but selenite is always present in excess of that expected if the reaction were complete. Selenotrithionate to selenite concentration ratios of 1:2, 2:1, and 1:0 are expected for sulfite to selenous acid stoichiometric ratios of 1:1 (reaction [6]), 2:1, and 4:1 but the observed concentration ratios are 1:2, 0.9:1, and 1.25:1, indicating that selenotrithionate formation is less complete in more basic solutions. Similar conclusions may be drawn from the Raman spectra for these stoichiometries shown in Fig. 5. All of these spectra show the 980 cm^{-1} band for the sulfate ion as well as the characteristic bands for the selenotrithionate. As the stoichiometric ratio of sulfite to selenium dioxide increases, the sulfite peak at 970 cm^{-1} grows in relative strength and, because of the increasing basicity of the solutions, hydrogen selenite (860 cm^{-1}(37)) concentration decreases while selenite (810 cm^{-1}(37)) concentration increases. In addition, the peak at 655 cm^{-1} is present in all spectra, indicating the presence of the O-bonded selenotrithionate ion. The apparent slight increase in relative intensity of the 285 cm^{-1} band is due to the strong shoulder from sulfite ion, which lies on the broad low-frequency wing of the exciting line and extends from 320 to 110 cm^{-1} (Fig. 1, trace B). Inasmuch as the NMR spectra do not show the presence of the S-bonded selenotrithionate ion, this peak must also arise in part from the O-bonded isomer. No sulfite ion is present in the solution with 1:1 stoichiometry (Trace A, Fig. 5; $c_{Se} = 0.80$ M) and quantitative Raman spectroscopy gives a sulfate concentration of 0.25 M, which supports the stoichiometry for reaction [6]. As in the case of the NMR experiments, however, the Raman spectra show that as the solutions become more basic as a result of increasing sulfite concentration, the formation of selenotrithionate is less complete. For instance, at 2:1 sulfite to selenous acid stoichiometry (Trace B, Fig. 5; $c_{Se} = 0.80$ M) deconvolution of the sulfate and sulfite peaks near 980 cm^{-1} permits calculation of the normalized peak intensities for these anions and calculation of a sulfate concentration of 0.32 M, which is less than the 0.53 M, calculated for this stoichiometry, assuming the reaction goes to completion. It should be noted that the Raman spectrum of the solution with 4:1 sulfite to selenous acid stoichiometry (Trace D, Fig. 5; $c_{Se} = 0.46$ M) exhibits a peak at 1097 cm^{-1} due to dithionate ion (37). This suggests that selenotrithionate decomposes in the presence of excess sulfite in a similar way to that observed for bis(thio)selenides in the presence of a stoichiometric excess of thiolate (15, 38).

[7] $Se(OSO_2)_2^{2-} + SO_3^{2-} = S_2O_6^{2-} + SeSO_3^{2-}$

Further work will be necessary to confirm this.

Conclusions

In a parallel reaction to that of sulfur and sulfite to produce thiosulfate, elemental selenium dissolves in sulfite solution to produce selenosulfate. The isomer, thioselenate, is not, however, produced by reaction of sulfur and selenite. Generally for isomers such as these, the stable compound is the one in which the most electronegative elements are in terminal positions and the most electropositive share their valence electrons with the terminal ligands. However, selenosulfate is exceptional, since the least metallic element, sulfur, is central and the most metallic is terminal. Certainly this stereochemistry is contrary to that expected from Pauling's scale of electronegativity, where sulfur is more electronegative than selenium (S:2.58, Se:2.55 (39)) but it should be noted that others have found the electronegativities of S and Se to be reversed (Sanderson scale; S:2.66, Se:2.76; Allred–Rochow; S:2.44, Se:2.48 (39)). On the other hand, Se(VI) is more strongly oxidizing than S(VI) and selenosulfate is expected to be more stable than thioselenate on this basis.

Hydrogen sulfite reacts with selenous acid quantitatively, according to 3:1 SO_3^{2-}/H_2SeO_3 stoichiometry, to give selenotrithionate. The O-bonded isomer is formed first and this converts slowly to the S-bonded isomer. The mechanism is probably parallel to that established for the reaction of thiolates and selenous acid (13–15) but for thiolates 4:1 stoichiometry is observed.

[8] $RSH + H_2SeO_3 = RSSeO_2H + H_2O$

[9] $RSH + RSSeO_2H \longrightarrow (RS)_2SeO + H_2O$

[10] $(RS)_2SeO \longrightarrow RSSeOSR$

[11] $RSH + RSSeOSR \longrightarrow (RS)_2Se + RSOH$

[12] $RSH + RSOH \longrightarrow RSSR + H_2O$

The fourth mole of thiolate is consumed in reaction with sulfenate which is displaced when the selenium dithiolate is formed. In the case of sulfite, when selenotrithionate is formed the displaced group is sulfate ion and a fourth mole of sulfite is not used. The reaction then requires 3:1 and not 4:1 stoichiometry. Drawing from the proposed mechanism for the thiolate reaction with selenous acid (14, 15), the mechanism would be

[13] $HSO_3^- + H_2SeO_3 = HSeSO_5^- + H_2O$

[14] $HSeSO_5^- + HSO_3^- \longrightarrow OSe(OSO_2)_2^{2-} + H_2O$

[15] $OSe(OSO_2)_2^{2-} + HSO_3^- \longrightarrow Se(OSO_2)_2^{2-} + H^+ + SO_4^{2-}$

[16] $Se(OSO_2)_2^{2-} \longrightarrow Se(SO_3)_2^{2-}$

We observed no spectroscopic evidence for the Se(IV) products of steps [13] and [14] and conclude that reactions [13],[14], and [15] are rapid on the time scale of solution preparation and reaction [16] is slow. Step [15] requires, in addition to nucleophilic attack on Se(IV) by hydrogen sulfite, the transfer of oxygen from Se to S, which is different from the analogous step for thiolates where oxygen insertion into the SeS bond occurs.

Several examples of sulfite ion binding, through either oxygen or sulfur to a Lewis acid centre (Co^{3+}(40); H^+(28*a*); SO_2(41)), are known. In this work we have observed for the first time linkage isomerism in binding to Se(II). Although the selenotrithionates are undergoing slow decomposition, it is clear that the O-bonded isomer, $Se(OSO_2)_2^{2-}$, is favoured in basic solution and is the first species formed. Isomerization may take place intramolecularly, parallel to the isomerization of nitrito Co(III) complexes (42), but the evidence suggests that conversion to the S-bonded isomer is promoted by acid conditions. Further work, particularly kinetic studies,

will be necessary to complete our understanding of these reductions.

Acknowledgements

Raj Capoor is thanked for measuring the NMR spectra. The Natural Sciences and Engineering Research Council of Canada is thanked for financial support. Students of the 4th year laboratory and B.A. Morrow are thanked for the sample of potassium trithionate.

References

1. K.W. Bagnall. Selenium, tellurium and polonium. *In* Comprehensive inorganic chemistry. *Edited by* J.C. Bailar, H.J. Emeleus, R.S. Nyholm, and A.F. Trotman-Dickenson. Pergamon, Oxford. 1973.
2. B. Rathke. J. prakt. Chem. **95**, 2 (1865).
3. J. Milbauer. Photogr. Korresp. **65**, 11 (1929).
4. O.M. Baram and M.P. Soldatov. Zh. Neorg. Khim. **2**, 1289 (1957).
5. A. Kozhakova, E.A. Butekov, M.I. Bakeev, and A.K. Shokanov. Russ. J. Inorg. Chem. **11**, 953 (1966).
6. A.S. Foust and V. Janickis. Inorg. Chem. **19**, 1063 (1980).
7. J.B. Milne. Can. J. Chem. **70**, 693 (1992).
8. E. Blasius and G. Schonhard. J. Chromatogr. **28**, 385 (1967).
9. I.V. Yanitskii and V.I. Zelionkaite. J. Inorg. Chem. USSR, **6**, 222 (1957).
10. I.V. Yanitsky and V. I. Zelenkaite. J. Gen. Chem. USSR, **25**, 805 (1955).
11. O. Foss. *In* Inorg. Synth. Vol. IV. *Edited by* J.C. Bailar. McGraw–Hill, New York. 1953. p. 88.
12. O. Foss and O. Tjomsland. Acta Chem. Scand. **8**, 1701 (1954).
13. H.E. Ganther. Biochemistry, **7**, 2898 (1968).
14. J.L. Kice, T.W.S. Lee, and S. Pan. J. Am. Chem. Soc. **102**, 4448 (1980).
15. W. Amaratunga and J. Milne. Can. J. Chem. **72**, 2506 (1994).
16. F. Feher. *In* Handbook of preparative inorganic chemistry. *Edited by* G. Brauer. Academic Press, New York. 1963. p. 398.
17. W.F. Linke. Solubilities of inorganic and metal organic compounds. 4th ed. Am. Chem. Soc., Washington, D.C. 1965. p. 1407.
18. A.I. Vogel. Quantitative inorganic analysis. 3rd ed. Longman, London. 1972, p. 508.
19. J. Milne and P. Lahaie. Inorg. Chem. **24**, 840 (1985).
20. J. Milne. Magn. Reson. Chem. **31**, 652 (1993).
21. (*a*) A. Lumière, L. Lumière, A. Seyewetz. Bull. Soc. Fr. Photogr. Cinematogr. **16**, 321 (1929); (*b*) A. Seyewetz. Rev. Fr. Photogr. Cinematogr. **10**, 368 (1929).
22. A. Seywetz. Rev. Fr. Photogr. Cinematogr. **11**, 332 (1930).
23. R.C. Weast (*Editor*) Handbook of chemistry and physics. 50th ed. The Chemical Rubber Publishing Co., Cleveland, Ohio. 1969. p. D70.
24. W. Amaratunga, O. Chaudry, and J. Milne. Can. J. Chem. **72**, 1165 (1994).
25. S. Noel, P. Dhamelincourt, and G. Palavit. C. R. Seances Acad. Sci. Ser. C: **278**, 569 (1974).
26. A.A. Kudryavtsev. The chemistry and technology of selenium and tellurium. *Translated by* E.M. Elkin. Collet's Ltd., London. 1974. p. 36.
27. P. Pascal. Nouveau traite de chimie minerale. Vol. XIII. Masson, Paris. 1960. p. 914.
28. (*a*) R.E. Connick, T.M. Tan, and E. von Deuster. Inorg. Chem. **21**, 103 (1982); (*b*) A.W. Herlinger and T.V. Long. Inorg. Chem. **8**, 2661 (1969); (*c*) A. Simon and K. Waldmann. Z. Anorg. Allg. Chem. **284**, 36 (1956).
29. J. Milne. Can. J. Chem. **65**, 316 (1987).
30. F. Foerster and E. Haufe. Z. Anorg. Allg. Chem. **177**, 17 (1929).
31. H. Nakatsuji, T. Higashioji, and M. Sugimoto. Bull. Chem. Soc. Jpn. **66**, 3235 (1993).
32. D.L. Rabenstein and K.-S. Tan. Magn. Reson. Chem. **26**, 1079 (1988)
33. H.J. Reich and C.P. Jasperse. J. Org. Chem. **53**, 2389 (1988), and references therein.
34. O. Foss and O.H. Mörch. Acta Chem. Scand. **8**, 1169 (1954).
35. O. Foss. Acta Chem. Scand. **3**, 435 (1949), and references therein.
36. J.M. Stewart and J.T. Szymanski, Acta Crystallogr. Sect. B: Struct. Crystallogr. Cryst. Chem. **B35**, 1967 (1979).
37. H. Siebert. Anwendungen der Schwingungsspektroskopie in der Anorganischen Chemie. Springer, Berlin. 1966.
38. J.L. Kice and H. Slebocka-Tilk. J. Am. Chem. Soc. **104**, 7123 (1982).
39. J.E. Huheey. Inorganic chemistry. Principles of structure and reactivity. 3rd ed. Harper and Row, Cambridge, Mass. 1983. p. 146.
40. A.C. Dash, A.A. El-Awady, and G.M. Harris. Inorg. Chem. **20**, 3160 (1981).
41. S.J. David and B.S. Ault. Inorg. Chem. **23**, 1211 (1984).
42. R.G. Wilkins and M.J.G. Williams. *In* Modern coordination chemistry. *Edited by* J. Lewis and R.G. Wilkins. Interscience, New York. 1960. p. 214.

Can. J. Chem. Downloaded from www.nrcresearchpress.com by 65.111.164.53 on 09/08/12
For personal use only.

Calorimetric investigations of aqueous amino acid and dipeptide systems from 288.15 to 328.15 K

Andrew W. Hakin, Michelle M. Duke, Lori L. Groft, Jocelyn L. Marty, and Matthew L. Rushfeldt

Abstract: Densities and heat capacities have been measured for aqueous solutions of L-asparagine, L-glutamine, glycylglycine, glycyl-L-valine, glycyl-L-asparagine, and glycyl-DL-leucine at 288.15, 298.15, 313.15, and 328.15 K. These data have been used to calculate apparent molar volumes, $V_{2,\phi}$, and apparent molar heat capacities, $C_{p,2,\phi}$, which in turn have been used to obtain standard state volumes, $\overline{V}^0_2$, and heat capacities, $\overline{C}^0_{p,2}$. The semi-empirical modelling procedures of Helgeson, Kirkham, and Flowers have been used to subdivide the calculated standard state volume and heat capacity data into solvation and nonsolvation contributions. The nonsolvation components of the standard state properties are used in group additivity analyses. These analyses yield structural contributions to standard state volumes and heat capacities for the $CH(NH_2)CO_2H$, CH_2, OH, COOH, CH, $CONH_2$, and CONH groups. The temperature dependences of these contributions are discussed. Some comments are reported concerning the practicality of using the thermodynamic properties of aqueous amino acid and peptide systems as the basis for modelling standard state thermodynamic properties of aqueous protein systems.

Key words: heat capacities, densities, volumes, amino acids, peptides, group additivity.

Résumé : On a mesuré les densités et les capacités calorifiques de solutions aqueuses de L-asparagine, L-glutamine, L-glycylgycine, glycyl-L-valine, glycyl-L-asparagine et glycyl-DL-leucine à 288,15, 298,15, 313,15 et 328,15 K. On a utilisé ces données pour calculer les volumes molaires apparents, $V_{2,\phi}$, ainsi que les capacités calorifiques molaires apparents, $C_{p,2,\phi}$, qui ont été à leur tour utilisés pour obtenir les volumes et les capacités calorifiques dans les états standard, $\overline{V}^0_2$ et $\overline{C}^0_{p,2}$. On a utilisé les méthodes de modélisations semi-empiriques de Helgeson, Kirkham et Flowers pour subdiviser les données calculées pour le volume et capacité calorifique dans l'état standard en contributions de solvatation et de non solvatation. On a utilisé les composantes de non solvatation des propriétés de l'état standard dans des analyses d'additivité de groupe. Ces analyses fournissent des contributions structurales aux volumes et aux capacités calorifiques standard des groupes $CH(NH_2)CO_2H$, CH_2, OH, COOH, CH, $CONH_2$ et CONH. On discute des variations de ces contributions avec la température. On rapporte quelques commentaires relatifs au caractère pratique de l'utilisation des propriétés thermodynamiques des systèmes aqueux d'acides aminés et de peptides pour la modélisation des propriétés thermodynamiques standard des systèmes aqueux de protéines.

Mots clés : capacités calorifiques, densités, volumes, acides aminés, peptides, additivité de groupes.

[Traduit par la rédaction]

Introduction

The investigation of the thermodynamic properties of aqueous amino acid and simple aqueous peptide systems continues to attract our attention (1–3), and that of several other authors (4–6). Most recently, we proposed a group additivity scheme that may be used to estimate standard state volumes and heat capacities for aqueous amino acid systems in the temperature range 288.15–328.15 K at ambient pressure (3). One aim of this research is to assess the feasibility of using amino acid systems as potential building blocks for estimating the properties of aqueous protein systems at elevated temperatures and pressures. There are many uses for such data, but one area that is currently of great interest is the investigation of microbial life forms that can exist at temperatures in excess of 100°C and at elevated pressures. These organisms are very important commercially. For example, thermophilic *Pyrococcus furiosus* is used to obtain thermostable DNA polymerases, which are utilized in the technique of DNA amplification (7).

One problem associated with using amino acids in additivity-type schemes is the inherent charge associated with such systems in solution, the zwitterionic form of the amino acid species almost invariably being the major component in nonbuffered aqueous systems. Our analyses overcome this prob-

Received September 8, 1994.[1]

A.W. Hakin,[2] M.M. Duke, L.L. Groft, J.L. Marty, and M.L. Rushfeldt. Department of Chemistry, University of Lethbridge, 4401 University Drive, Lethbridge, AB T1K 3M4, Canada.

[1] Revision received March 15, 1995.

[2] Author to whom correspondence may be addressed. Telephone: (403) 329-2083. Fax: (403) 329-2057.

Can. J. Chem. Downloaded from www.nrcresearchpress.com by 65.111.164.53 on 09/08/12
For personal use only.

Can. J. Chem. Downloaded from www.nrcresearchpress.com by 65.111.164.53 on 09/08/12
For personal use only.

lem by utilizing a semi-empirical modeling procedure proposed by Helgeson, Kirkham, and Flowers (HKF) (8) to access only the structural components of the standard state properties of interest. It is these calculated structural contributions to standard state properties that are used as input into our group additivity analyses.

To advance our previous additivity analyses (3) from simple amino acid systems to peptide systems necessitates that we obtain group contributions to standard state volumes and heat capacities for the peptide group, CONH. The current paper addresses this problem by utilizing standard state volume and heat capacity data for aqueous solutions of the amino acids L-asparagine L-glutamine, and the dipeptides glycylglycine (glygly), glycyl-L-valine (glyval), glycyl-L-asparagine (glyasn), and glycyl-DL-leucine (glyleu). These data have been used to obtain peptide group contributions to the structural components of standard state volumes and heat capacities over the temperature range 288.15–328.15 K at ambient pressure. The predictive powers of our analyses are investigated by comparing literature values for standard state volumes and heat capacities for several N-terminal glycyl dipeptide systems (9) at 298.15 K with those that can be estimated from our additivity analyses.

Experimental

L-Asparagine (99+%), L-glutamine (99+%), and glygly (99.5 +%) were obtained from Sigma Chemicals Limited whilst glyval, glyasn, and glyleu were obtained from ICN Biochemicals Inc. All compounds were purified by repeated recrystallization from water + ethanol. The purified chemicals were dried and stored over phosphorus pentoxide in a vacuum oven set at 50°C. Characterization of these systems was performed using a Brüker 250 MHz NMR instrument in which D_2O was used as an internal standard. The recorded NMR spectra were in excellent agreement with those reported in the literature (10).

All solutions used in our investigations were prepared by weight on the molality concentration scale using bi-distilled, degassed water. The unbuffered solutions were stored in sealable 125 mL Nalgene bottles.

The densities of our solutions were measured relative to water with a Sodev O2D vibrating tube, flow densitometer (11). This instrument has a thermal stability of ±0.001°C and routinely measures densities with part per million precision. Volumetric heat capacities were measured relative to water using a Picker flow microcalorimeter (12). Small residual heat leaks in our calorimeter were corrected for by a calorimetric heat loss correction factor, or f factor (13). This factor was evaluated as $f = 0.997 \pm 0.003$ at 298.15 K using standard solutions of sodium chloride in water. For our calorimetric system f is assumed to be a constant that is independent of temperature.

Details of the densitometer, the flow microcalorimeter, and procedures used in their calibration have been described previously (1, 2, 14).

Results and discussion

Experimentally determined data, namely, relative densities $(\rho-\rho_1^0)$ and heat capacity ratios $[c_p\rho/(c_{p,1}^0\rho_1^0) - 1]$, for L-glutamine, L-asparagine, glygly, glyval, glyasn, and glyleu are reported in Tables 1–6. These tables also contain apparent molar volumes and heat capacities that were calculated from the experimental data using eqs. [1] and [2], respectively.

$$[1] \qquad V_{2,\phi} = \left[\frac{M}{\rho}\right] - \left[\frac{\rho-\rho_1^0}{m\rho\rho_1^0}\right]$$

$$[2] \qquad C_{p,2,\phi} = Mc_p + \frac{(c_p - c_{p,1}^0)}{m}$$

In these equations M represents the molar mass of the solute, m is the molality of the solution, c_p and $c_{p,1}^0$ are the specific heat capacities of the solution and of pure water, and ρ and ρ_1^0 are the densities of the solution and of pure water. The densities and heat capacities of pure water, used in our calculations, are those reported by Kell (15, 16). Standard state volumes and heat capacities for the six systems investigated were calculated at each temperature by fitting equations of the general form described by eq. [3] to our calculated apparent molar volume and apparent molar heat capacity data. Weighted linear regression analyses were utilized.

$$[3] \qquad Y_{2,\phi} = Y_{2,\phi}^0 + S_Y m$$

In eq. [3] Y represents the extensive thermodynamic property of interest, $Y_{2,\phi}^0$ is the value of $Y_{2,\phi}$ at infinite dilution (i.e., the standard state property $\overline{Y}_2^0$), and S_Y is the experimental slope. The weights used in these calculations were calculated as the reciprocals of the squares of the uncertainties in the apparent molar volumes and heat capacities (1, 17). Calculated uncertainties are contained in parentheses in Tables 1–6. Calculated standard state volumes and heat capacities are reported, and compared to available literature data (5, 9, 18–26),[3] in Table 7.

The temperature dependences of apparent molar volumes of aqueous solutions of L-glutamine and L-asparagine have been previously investigated by Kharakoz (20). Good agreement is shown between the two sets of data for the L-glutamine system; however, agreement is not so good for the L-asparagine system. The values reported in ref. 20 for this system appear to be consistently lower than ours. In trying to explain this apparent discrepancy, we note that Kharakoz reports averaged apparent molar volumes obtained at concentrations of 3 mg mL^{-1} (approximately 0.023 mol kg^{-1}). This concentration does not strictly apply to infinitely dilute solutions.

The reported standard state volume at 298.15 K for glygly is in very good agreement with the results reported by Mishra and Ahluwalia (19) and Jolicoeur and Boileau (18); however, the result reported by Cabani and co-workers (23) appears to be too high. Our standard state data for this system are in very good agreement with the averaged apparent molar volumes reported as a function of temperature in a recent paper by Chalikian et al. (5).

The standard state volume data at 288.15 K, reported in Table 7 for glyleu, glyval, and glyasn, are in good agreement with data obtained by Hedwig.[3] Hedwig has also obtained standard state volume data at 298.15, 303.15, and 308.15 K for glyval and at 303.15 and 308.15 K for glyasn.[3] These data closely follow the temperature dependence trends we observe in our own standard state volume data.

[3] Also, G.R. Hedwig, personal communication.

Can. J. Chem. Downloaded from www.nrcresearchpress.com by 65.111.164.53 on 09/08/12
For personal use only.

Table 1. Relative densities, $(\rho - \rho_1^0)$, apparent molar volumes, $V_{2,\phi}$, heat capacity ratios, $[c_p\rho/(c_{p,1}^0\rho_1^0) - 1]$, and apparent molar heat capacities, $C_{p,2,\phi}$, of aqueous solutions of L-asparagine at 288.15, 298.15, 313.15, and 328.15 K.[a]

m (mol kg^{-1})	$(\rho - \rho_1^0)$ (g cm^{-3})	$V_{2,\phi}$ (cm^3 mol^{-1})	$10^3\left(\frac{c_p\rho}{c_{p,1}^0\rho_1^0}-1\right)$	$C_{p,2,\phi}$ (J K^{-1} mol^{-1})
288.15 K				
0.1512	8.314×10^{-3}	76.52 (0.03)	−7.762	103.3 (0.5)
0.1135	6.265×10^{-3}	76.47 (0.04)	−5.886	101.6 (0.6)
0.1026	5.672×10^{-3}	76.41 (0.05)	−5.339	100.7 (0.7)
0.08944	4.952×10^{-3}	76.40 (0.06)	−4.671	100.1 (0.8)
0.06611	3.668×10^{-3}	76.38 (0.08)	−3.438	101.4 (1.1)
0.05095	2.831×10^{-3}	76.35 (0.10)	−2.664	100.3 (1.4)
0.02786	1.549×10^{-3}	76.43 (0.18)	−1.439	103.7 (2.5)
0.02505	1.394×10^{-3}	76.39 (0.20)	−1.322	98.8 (2.8)
0.03493	1.944×10^{-3}	76.34 (0.14)	−1.873	94.9 (2.0)
0.01375	7.67×10^{-4}	76.30 (0.36)	−0.720	100.3 (5.1)
298.15 K				
0.1512	8.123×10^{-3}	77.84 (0.03)	−6.926	131.3 (0.5)
0.1135	6.124×10^{-3}	77.77 (0.04)	−5.274	128.2 (0.6)
0.1026	5.540×10^{-3}	77.75 (0.05)	−4.784	128.1 (0.7)
0.08944	4.834×10^{-3}	77.76 (0.06)	−4.163	128.8 (0.8)
0.06611	3.581×10^{-3}	77.73 (0.08)	−3.127	125.7 (1.1)
0.05095	2.764×10^{-3}	77.71 (0.10)	−2.383	128.2 (1.4)
0.02786	1.516×10^{-3}	77.65 (0.18)	−1.312	126.9 (2.5)
0.02505	1.364×10^{-3}	77.63 (0.20)	−1.188	125.4 (2.8)
0.03493	1.899×10^{-3}	77.69 (0.14)	−1.655	125.8 (2.0)
0.01375	7.49×10^{-4}	77.69 (0.37)	−0.655	124.9 (5.1)
313.15 K				
0.1512	7.926×10^{-3}	79.28 (0.03)	−6.038	160.4 (0.5)
0.1135	5.971×10^{-3}	79.26 (0.04)	−4.482	162.7 (0.6)
0.1026	5.407×10^{-3}	79.18 (0.05)	−4.125	159.4 (0.7)
0.08944	4.719×10^{-3}	79.19 (0.06)	−3.582	160.3 (0.8)
0.06611	3.494×10^{-3}	79.19 (0.08)	−2.604	163.4 (1.1)
0.05095	2.697×10^{-3}	79.17 (0.10)	−2.068	158.5 (1.4)
0.02786	1.476×10^{-3}	79.23 (0.18)	−1.124	160.0 (2.5)
0.02505	1.323×10^{-3}	79.41 (0.20)	−1.025	158.5 (2.8)
0.03493	1.850×10^{-3}	79.20 (0.15)	−1.393	161.9 (2.0)
0.01375	7.30×10^{-4}	79.21 (0.37)	−0.551	161.4 (5.1)
0.1743	9.094×10^{-3}	79.44 (0.03)	—	—
0.1510	7.870×10^{-3}	79.59 (0.03)	—	—
0.1052	5.521×10^{-3}	79.40 (0.05)	—	—
0.06813	3.594×10^{-3}	79.28 (0.07)	—	—
0.04603	2.435×10^{-3}	79.21 (0.11)	—	—
0.03103	1.642×10^{-3}	79.26 (0.16)	—	—
0.01761	9.32×10^{-4}	79.32 (0.29)	—	—
328.15 K				
0.1512	7.794×10^{-3}	80.34 (0.03)	−5.329	182.6 (0.5)
0.1135	5.866×10^{-3}	80.38 (0.05)	−4.066	180.7 (0.6)
0.1026	5.316×10^{-3}	80.26 (0.05)	−3.619	182.6 (0.7)
0.08944	4.638×10^{-3}	80.29 (0.06)	—	—
0.06611	3.419×10^{-3}	80.53 (0.08)	−2.406	179.4 (1.1)
0.05095	2.642×10^{-3}	80.46 (0.10)	−1.813	182.7 (1.4)
0.02786	1.475×10^{-3}	79.45 (0.18)	−0.982	180.3 (2.5)
0.02505	1.276×10^{-3}	81.48 (0.21)	−0.938	179.5 (2.8)
0.03493	1.805×10^{-3}	80.72 (0.15)	−1.210	188.0 (2.0)
0.01375	7.10×10^{-4}	80.82 (0.37)	−0.474	189.2 (5.1)

[a]Estimated uncertainties for $V_{2,\phi}$ and $C_{p,2,\phi}$ appear in parentheses.

Table 2. Relative densities, $(\rho - \rho_1^0)$, apparent molar volumes, $V_{2,\phi}$, heat capacity ratios, $[c_p\rho/(c_{p,1}^0\rho_1^0) - 1]$, and apparent molar heat capacities, $C_{p,2,\phi}$, of aqueous solutions of L-glutamine at 288.15, 298.15, 313.15, and 328.15 K.[a]

m (mol kg^{-1})	$(\rho - \rho_1^0)$ (g cm^{-3})	$V_{2,\phi}$ (cm^3 mol^{-1})	$10^3\left(\frac{c_p\rho}{c_{p,1}^0\rho_1^0}-1\right)$	$C_{p,2,\phi}$ (J K^{-1} mol^{-1})
288.15 K				
0.1256	6.599×10^{-3}	93.00 (0.04)	−7.148	148.4 (0.6)
0.07657	4.079×10^{-3}	92.48 (0.07)	−4.413	144.6 (0.9)
0.04393	2.327×10^{-3}	92.99 (0.11)	−2.508	149.7 (1.6)
0.02905	1.541×10^{-3}	93.00 (0.17)	−1.702	143.9 (2.4)
0.02139	1.163×10^{-3}	91.71 (0.23)	−1.269	135.6 (3.2)
0.009515	5.13×10^{-4}	92.21 (0.52)	−0.594	125.1 (7.4)
0.005580	2.89×10^{-4}	94.37 (0.90)	−0.362	123.1 (12.6)
0.1380	7.225×10^{-3}	93.15 (0.04)	−7.831	149.7 (0.5)
298.15 K				
0.1256	6.453×10^{-3}	94.00 (0.04)	−6.385	177.4 (0.6)
0.07657	3.977×10^{-3}	93.96 (0.07)	−3.944	175.7 (0.9)
0.04393	2.288×10^{-3}	93.97 (0.11)	−2.253	177.0 (1.6)
0.02905	1.518×10^{-3}	93.87 (0.17)	−1.487	178.4 (2.4)
0.02139	1.118×10^{-3}	93.92 (0.23)	−1.125	173.2 (3.3)
0.009515	4.93×10^{-4}	94.41 (0.52)	−0.490	176.3 (7.4)
0.005580	2.93×10^{-4}	93.70 (0.90)	−0.280	185.5 (12.6)
0.1380	7.116×10^{-3}	94.04 (0.04)	−6.980	178.2 (0.5)
313.15 K				
0.1256	6.331×10^{-3}	95.48 (0.04)	−5.585	208.4 (0.6)
0.07657	3.880×10^{-3}	95.43 (0.07)	−3.395	209.6 (0.9)
0.04393	2.235×10^{-3}	96.39 (0.11)	−1.970	207.9 (1.6)
0.02905	1.491×10^{-3}	95.04 (0.18)	−1.314	205.1 (2.4)
0.02139	1.094×10^{-3}	95.26 (0.24)	—	—
0.009515	4.84×10^{-4}	95.56 (0.53)	−0.439	203.7 (7.4)
0.005580	2.84×10^{-4}	95.59 (0.91)	—	—
0.1380	6.922×10^{-3}	95.67 (0.04)	−6.096	210.2 (0.5)
328.15 K				
0.01089	5.55×10^{-4}	95.76 (0.47)	−0.431	229.6 (6.4)
0.02324	1.178×10^{-3}	95.98 (0.22)	−0.862	240.7 (3.0)
0.04065	2.034×10^{-3}	96.58 (0.13)	−1.582	235.3 (1.7)
0.06159	3.101×10^{-3}	96.14 (0.08)	−2.330	237.7 (1.1)
0.08174	4.091×10^{-3}	96.36 (0.06)	−3.108	237.5 (0.9)
0.08983	4.511×10^{-3}	96.15 (0.06)	−3.507	232.2 (0.8)
0.1117	5.598×10^{-3}	96.15 (0.05)	−4.232	236.8 (0.6)
0.1146	5.745×10^{-3}	96.09 (0.05)	−4.374	235.2 (0.6)
0.1216	6.065×10^{-3}	96.34 (0.04)	−4.595	237.8 (0.6)
0.1256	6.268×10^{-3}	96.29 (0.04)	−4.692	239.3 (0.6)
0.07657	3.826×10^{-3}	96.46 (0.07)	−2.816	243.2 (0.9)
0.04393	2.197×10^{-3}	96.58 (0.11)	−1.653	240.6 (1.6)
0.02905	1.472×10^{-3}	95.98 (0.18)	−1.100	237.4 (2.4)
0.02139	1.077×10^{-3}	96.37 (0.24)	−0.761	248.7 (3.3)
0.009515	4.74×10^{-4}	96.90 (0.54)	−0.375	234.9 (7.4)
0.005580	2.73×10^{-4}	97.98 (0.92)	−0.229	232.5 (12.6)
0.1380	6.861×10^{-3}	96.42 (0.04)	−5.239	237.1 (0.5)

[a]Estimated uncertainties for $V_{2,\phi}$ and $C_{p,2,\phi}$ appear in parentheses.

Can. J. Chem. Downloaded from www.nrcresearchpress.com by 65.111.164.53 on 09/08/12
For personal use only.

Table 3. Relative densities, $(\rho - \rho_1^0)$, apparent molar volumes, $V_{2,\phi}$, heat capacity ratios, $[c_p^0\rho/(c_{p,1}\rho_1^0) - 1]$, and apparent molar heat capacities, $C_{p,2,\phi}$, of aqueous solutions of glycylglycine at 288.15, 298.15, 313.15, and 328.15 K.[a]

m (mol kg^{-1})	$(\rho - \rho_1^0)$ (g cm^{-3})	$V_{2,\phi}$ (cm^3 mol^{-1})	$10^3\left(\frac{c_p\rho}{c_{p,1}^0\rho_1^0} - 1\right)$	$C_{p,2,\phi}$ (J K^{-1} mol^{-1})
288.15 K				
0.01031	5.87×10^{-4}	75.16 (0.49)	−0.613	66.0 (6.8)
0.01802	1.024×10^{-3}	75.25 (0.28)	−1.066	67.6 (3.9)
0.03365	1.895×10^{-3}	75.69 (0.15)	−1.978	70.8 (2.1)
0.06590	3.724×10^{-3}	75.35 (0.08)	−3.784	74.3 (1.1)
0.08453	4.769×10^{-3}	75.35 (0.06)	−4.853	74.1 (0.8)
0.1127	6.325×10^{-3}	75.51 (0.04)	−6.409	76.5 (0.6)
0.1465	8.199×10^{-3}	75.54 (0.03)	−8.235	78.8 (0.5)
0.1702	9.498×10^{-3}	75.61 (0.03)	−9.568	78.6 (0.4)
298.15 K				
0.01031	5.81×10^{-4}	75.76 (0.49)	−0.553	92.3 (6.8)
0.01802	1.000×10^{-3}	76.59 (0.28)	−0.928	104.4 (3.9)
0.03365	1.868×10^{-3}	76.52 (0.15)	−1.750	101.7 (2.1)
0.06590	3.654×10^{-3}	76.45 (0.08)	−3.363	104.9 (1.1)
0.08453	4.680×10^{-3}	76.45 (0.06)	−4.289	105.9 (0.8)
0.1127	6.211×10^{-3}	76.58 (0.04)	−5.673	107.5 (0.6)
0.1465	8.051×10^{-3}	76.60 (0.03)	−7.342	108.1 (0.5)
0.1702	9.319×10^{-3}	76.72 (0.03)	−8.504	108.8 (0.4)
313.15 K				
0.01031	5.71×10^{-4}	76.93 (0.49)	−0.455	134.9 (6.8)
0.01802	9.96×10^{-4}	76.94 (0.28)	−0.789	136.3 (3.9)
0.03365	1.825×10^{-3}	77.91 (0.15)	−1.489	137.2 (2.1)
0.06590	3.580×10^{-3}	77.69 (0.08)	−2.853	140.9 (1.1)
0.08453	4.583×10^{-3}	77.73 (0.06)	−3.645	141.5 (0.8)
0.1127	6.078×10^{-3}	77.88 (0.05)	−4.804	143.7 (0.6)
0.1465	7.881×10^{-3}	77.89 (0.03)	−6.189	144.9 (0.5)
0.1702	9.134×10^{-3}	77.93 (0.03)	−7.199	144.6 (0.4)
328.15 K				
0.01802	9.85×10^{-4}	77.69 (0.29)	—	—
0.03365	1.830×10^{-3}	77.93 (0.15)	−1.203	171.9 (2.1)
0.06590	3.551×10^{-3}	78.27 (0.08)	−2.355	173.0 (1.1)
0.08453	4.550×10^{-3}	78.27 (0.06)	−3.002	173.6 (0.8)
0.1127	6.038×10^{-3}	78.40 (0.05)	−4.110	169.8 (0.6)
0.1465	7.835×10^{-3}	78.39 (0.04)	−5.284	170.9 (0.5)
0.1702	9.050×10^{-3}	78.59 (0.03)	−6.136	171.7 (0.4)

[a]Estimated uncertainties for $V_{2,\phi}$ and $C_{p,2,\phi}$ appear in parentheses.

Literature data for the standard state heat capacities of the systems investigated in this paper are limited to 298.15 K. For glygly, our value of 102.6 ± 0.9 J K^{-1} mol^{-1} is in good agreement with the value of 100.8 ± 0.3 J K^{-1} mol^{-1} reported by Reading and Hedwig (9) and the value of 99.3 ± 1.0 J K^{-1} mol^{-1} reported by Bhat and Ahluwalia (26). For L-glutamine, our standard state heat capacity at 298.15 K is in apparent disagreement with the value obtained, using a Picker flow microcalorimeter, reported by Jolicoeur et al. (25). We have repeated this experiment several times with new samples of L-glutamine and remain unable to explain this discrepancy. Our value of 123.9 J K^{-1} mol^{-1} for L-asparagine agrees well with the value reported by Jolicoeur et al. (25) and would appear to confirm that the earlier value reported by Huffman and Bersook (22) is too high. There is reasonable agreement between the standard state heat capacities for glyleu and glyval reported by Bhat and Alhuwalia (26) and those reported in Table 7. The standard state heat capacity for glyasn at 298.15 K (188.1 J K^{-1} mol^{-1}) reported by Reading and Hedwig (9) is in excellent agreement with our reported value of 189.8 J K^{-1} mol^{-1}.

Table 4. Relative densities, $(\rho - \rho_1^0)$, apparent molar volumes, $V_{2,\phi}$, heat capacity ratios, $[c_p^0\rho/(c_{p,1}\rho_1^0) - 1]$, and apparent molar heat capacities, $C_{p,2,\phi}$, of aqueous solutions of glycyl-L-valine at 288.15, 298.15, 313.15, and 328.15 K.[a]

m (mol kg^{-1})	$(\rho - \rho_1^0)$ (g cm^{-3})	$V_{2,\phi}$ (cm^3 mol^{-1})	$10^3\left(\frac{c_p\rho}{c_{p,1}^0\rho_1^0} - 1\right)$	$C_{p,2,\phi}$ (J K^{-1} mol^{-1})
288.15 K				
0.04099	2.182×10^{-3}	121.01 (0.12)	−1.594	343.0 (1.7)
0.05120	2.710×10^{-3}	121.01 (0.10)	−2.004	341.8 (1.4)
0.05889	3.111×10^{-3}	121.01 (0.09)	−2.251	345.7 (1.2)
0.06856	3.622×10^{-3}	121.00 (0.07)	−2.579	347.8 (1.0)
0.08682	4.570×10^{-3}	121.07 (0.06)	−3.275	347.3 (0.8)
0.1064	5.577×10^{-3}	121.16 (0.05)	−4.055	345.6 (0.7)
0.1256	6.572×10^{-3}	121.41 (0.04)	−4.736	347.0 (0.6)
298.15 K				
0.04099	2.128×10^{-3}	122.22 (0.12)	−1.351	371.3 (1.7)
0.05120	2.647×10^{-3}	122.40 (0.10)	−1.690	371.7 (1.4)
0.05889	3.040×10^{-3}	122.42 (0.09)	−1.975	369.4 (1.2)
0.06856	4.459×10^{-3}	122.47 (0.07)	−2.243	372.9 (1.0)
0.08682	4.459×10^{-3}	122.51 (0.06)	−2.850	372.3 (0.8)
0.1064	5.447×10^{-3}	122.55 (0.05)	−3.468	373.1 (0.7)
0.1256	6.411×10^{-3}	122.58 (0.04)	−4.074	373.6 (0.6)
313.15 K				
0.02026	1.044×10^{-3}	123.12 (0.25)	−1.162	386.3 (3.5)
0.04099	2.062×10^{-3}	124.21 (0.12)	−0.602	396.3 (1.7)
0.05120	2.572×10^{-3}	124.22 (0.10)	−1.409	399.6 (1.4)
0.05889	2.958×10^{-3}	124.17 (0.09)	−1.648	397.4 (1.2)
0.06856	3.444×10^{-3}	124.12 (0.07)	−1.820	403.1 (1.0)
0.08682	4.335×10^{-3}	124.30 (0.06)	−2.366	400.6 (0.8)
0.1064	5.303×10^{-3}	124.27 (0.05)	−2.968	397.5 (0.7)
0.1256	6.236×10^{-3}	124.35 (0.04)	−3.397	401.1 (0.6)
328.15 K				
0.04099	2.037×10^{-3}	125.32 (0.13)	—	—
0.05120	2.587×10^{-3}	125.21 (0.10)	−1.235	415.0 (1.4)
0.05889	2.921×10^{-3}	125.31 (0.09)	—	—
0.06856	3.402×10^{-3}	125.29 (0.08)	−1.694	412.4 (1.0)
0.08682	4.286×10^{-3}	125.38 (0.06)	−1.966	421.4 (0.8)
0.10639	5.205×10^{-3}	125.71 (0.05)	—	—
0.12559	6.111×10^{-3}	125.87 (0.04)	−2.914	420.6 (0.6)
0.05889	2.922×10^{-3}	125.28 (0.09)	−1.413	415.6 (1.2)
0.06856	3.390×10^{-3}	125.41 (0.08)	−1.670	414.6 (1.0)
0.08682	4.267×10^{-3}	125.61 (0.06)	−2.102	415.7 (0.8)
0.1064	5.221×10^{-3}	125.55 (0.05)	−2.642	412.7 (0.7)

[a]Estimated uncertainties for $V_{2,\phi}$ and $C_{p,2,\phi}$ appear in parentheses.

Group additivity analyses

The volume and heat capacity data reported in this paper substantially augment the data base of volumetric and thermo-

Can. J. Chem. Downloaded from www.nrcresearchpress.com by 65.111.164.53 on 09/08/12
For personal use only.

Table 5. Relative densities, $(\rho - \rho_1^0)$, apparent molar volumes, $V_{2,\phi}$, heat capacity ratios, $[c_p^0\rho/(c_{p,1}\rho_1^0) - 1]$, and apparent molar heat capacities, $C_{p,2,\phi}$, of aqueous solutions of glycyl-L-asparagine at 288.15, 298.15, 313.15, and 328.15 K.[a]

m (mol kg^{-1})	$(\rho - \rho_1^0)$ (g cm^{-3})	$V_{2,\phi}$ (cm^3 mol^{-1})	$10^3\left(\frac{c_p\rho}{c_{p,1}^0\rho_1^0} - 1\right)$	$C_{p,2,\phi}$ (J K^{-1} mol^{-1})
288.15 K				
0.02368	1.902×10^{-3}	108.68 (0.21)	−1.810	134.7 (3.0)
0.03712	2.963×10^{-3}	109.06 (0.14)	−2.734	147.6 (1.9)
0.05301	4.226×10^{-3}	109.01 (0.10)	−3.877	149.0 (1.3)
0.08866	7.041×10^{-3}	109.02 (0.06)	−6.507	146.8 (0.8)
0.10714	8.448×10^{-3}	109.43 (0.05)	−7.667	155.6 (0.7)
0.14743	1.116×10^{-2}	109.75 (0.03)	−10.369	161.6 (0.5)
0.07529	5.974×10^{-3}	109.20 (0.07)	−5.437	152.9 (0.9)
298.15 K				
0.02368	1.866×10^{-3}	110.25 (0.21)	−1.520	191.5 (3.0)
0.03712	2.920×10^{-3}	110.28 (0.14)	−2.349	195.0 (1.9)
0.05301	4.160×10^{-3}	110.31 (0.10)	−3.330	196.6 (1.3)
0.08866	6.851×10^{-3}	111.24 (0.06)	−5.497	202.9 (0.8)
0.10714	8.241×10^{-3}	111.44 (0.05)	−6.629	203.7 (0.7)
0.07529	5.855×10^{-3}	110.85 (0.07)	−4.703	199.6 (0.9)
313.15 K				
0.01202	9.28×10^{-4}	112.08 (0.25)	−0.684	227.5 (5.8)
0.02368	1.822×10^{-3}	112.29 (0.09)	−1.307	235.1 (3.0)
0.03712	2.835×10^{-3}	112.75 (0.06)	−1.985	243.8 (1.9)
0.05301	4.050×10^{-3}	112.59 (0.03)	−4.748	242.3 (1.3)
0.08866	6.732×10^{-3}	112.77 (0.03)	−2.833	242.9 (0.8)
0.1071	8.114×10^{-3}	112.81 (0.03)	−5.720	242.7 (0.7)
0.1474	1.109×10^{-2}	113.00 (0.02)	−7.815	244.1 (0.5)
0.07529	5.730×10^{-3}	112.70 (0.02)	−3.972	245.6 (0.9)
328.15 K				
0.01520	1.153×10^{-3}	113.66 (0.34)	−0.736	266.4 (4.6)
0.05142	3.885×10^{-3}	113.70 (0.10)	−2.392	273.7 (1.4)
0.06677	5.040×10^{-3}	113.66 (0.08)	−3.157	269.2 (1.1)
0.08932	6.709×10^{-3}	113.84 (0.06)	−4.220	270.4 (0.8)
0.1130	8.458×10^{-3}	113.93 (0.05)	−5.300	271.0 (0.6)
0.1264	9.453×10^{-3}	113.82 (0.04)	−6.049	266.8 (0.6)
0.1005	7.529×10^{-3}	113.94 (0.05)	−4.415	284.5 (0.7)

[a]Estimated uncertainties for $V_{2,\phi}$ and $C_{p,2,\phi}$ appear in parentheses.

Table 6. Relative densities, $(\rho - \rho_1^0)$, apparent molar volumes, $V_{2,\phi}$, heat capacity ratios, $[c_p^0\rho/(c_{p,1}\rho_1^0) - 1]$, and apparent molar heat capacities, $C_{p,2,\phi}$, of aqueous solutions of glycyl-DL-leucine at 288.15, 298.15, 313.15, and 328.15 K.[a]

m (mol kg^{-1})	$(\rho - \rho_1^0)$ (g cm^{-3})	$V_{2,\phi}$ (cm^3 mol^{-1})	$10^3\left(\frac{c_p\rho}{c_{p,1}^0\rho_1^0} - 1\right)$	$C_{p,2,\phi}$ (J K^{-1} mol^{-1})
288.15 K				
0.01119	5.65×10^{-4}	137.76 (0.45)	−0.401	426.3 (6.3)
0.04463	2.217×10^{-3}	138.32 (0.11)	−1.535	434.1 (1.6)
0.05924	2.939×10^{-3}	138.28 (0.09)	−2.093	429.7 (1.2)
0.07800	3.856×10^{-3}	138.34 (0.07)	−2.632	436.3 (0.9)
0.09534	4.702×10^{-3}	138.34 (0.05)	−3.216	436.0 (0.7)
0.06751	3.344×10^{-3}	138.31 (0.08)	−2.342	432.4 (1.1)
0.02381	1.186×10^{-3}	138.33 (0.21)	−0.842	430.5 (3.0)
298.15 K				
0.01119	5.50×10^{-4}	139.24 (0.45)	−0.372	441.4 (6.3)
0.04463	2.154×10^{-3}	139.92 (0.11)	−1.326	458.5 (1.6)
0.05924	2.860×10^{-3}	139.82 (0.09)	−1.712	461.2 (1.2)
0.07800	3.749×10^{-3}	139.91 (0.06)	−2.258	461.1 (0.9)
0.09534	4.566×10^{-3}	139.97 (0.05)	−2.742	461.8 (0.7)
0.06751	3.247×10^{-3}	139.94 (0.07)	−1.939	462.3 (1.0)
0.02381	1.158×10^{-3}	139.61 (0.21)	−0.654	467.4 (3.0)
313.15 K				
0.01119	5.22×10^{-4}	142.22 (0.45)	−0.286	483.0 (6.3)
0.04463	2.087×10^{-3}	141.91 (0.11)	−1.123	482.9 (1.6)
0.05924	2.767×10^{-3}	141.87 (0.09)	−1.439	486.2 (1.2)
0.07800	3.629×10^{-3}	141.93 (0.07)	−1.827	489.8 (0.9)
0.09534	4.418×10^{-3}	142.00 (0.05)	−2.191	491.7 (0.7)
0.06751	3.147×10^{-3}	141.90 (0.08)	−1.514	494.0 (1.1)
0.02381	1.120×10^{-3}	141.75 (0.21)	—	—
328.15 K				
0.04463	2.042×10^{-3}	143.55 (0.12)	−0.880	509.0 (1.6)
0.05924	2.705×10^{-3}	143.58 (0.09)	−1.214	505.7 (1.2)
0.07800	3.544×10^{-3}	143.69 (0.07)	−1.647	503.3 (0.9)
0.09534	4.295×10^{-3}	143.96 (0.05)	−2.116	499.7 (0.7)
0.06751	3.062×10^{-3}	143.86 (0.08)	−1.403	505.4 (1.1)
0.02381	1.09×10^{-3}	143.70 (0.21)	−0.476	508.7 (3.0)

[a]Estimated uncertainties for $V_{2,\phi}$ and $C_{p,2,\phi}$ appear in parentheses.

chemical properties of aqueous amino acid systems that we are constructing (1–3). This data base provides the framework on which we have constructed group additivity analyses that allow for the estimation of standard state volume and heat capacity data for aqueous amino acid and peptide systems in the temperature range 288.15–328.15 K. More specifically, the data reported in this paper allow for the calculation of the temperature dependences of peptide group contributions to structural components of standard state volumes and heat capacities.

Group contribution schemes, which may provide a means of modelling the thermodynamic properties of aqueous protein systems, have been previously investigated by several authors (27, 28). However, these authors do not usually consider using thermodynamic data for amino acids as the bases of their analyses, the major problem discouraging them from this route being the inherent charge of the zwitterionic species in aqueous solution. We avoided this obstacle by subdividing our standard state volume and heat capacity data into solvation and structural contributions. We subsequently used only the structural contributions in our group analyses schemes. This subdivision of the extensive thermodynamic standard state properties is represented by eq. [4];

$$[4] \qquad \overline{Y}_2^0 = \overline{Y}_s^0 + \overline{Y}_e^0$$

where subscripts s and e define the structural and solvation contributions to the standard state property, respectively. The solvation contributions of the standard state properties may be calculated using reported effective Born coefficients and parameters calculated using the temperature and pressure

Table 7. Comparison of calculated $\overline{V}_2^0$ and $\overline{C}_{p,2}^0$ data with literature data.

T (K)	$\overline{V}_2^0$ (cm^3 mol^{-1})	S_V (cm^3 mol^{-2} kg)	$\overline{C}_{p,2}^0$ (J K^{-1} mol^{-1})	S_{Cp} (J K^{-1} mol^{-2} kg)
L-Asparagine				
288.15	76.28 ± 0.03 (76.0[d])	1.55 ± 0.22	97.6 ± 1.2	35.9 ± 9.9
298.15	77.63 ± 0.01 (77.2,[d] 77.52,[h] 77.56,[b] 77.18[i])	1.35 ± 0.11	123.9 ± 1.0 (125,[i] 160[f])	46.1 ± 9.9
313.15	79.07 ± 0.10 (78.8[d])	2.14 ± 0.70	161.1 ± 1.3	6.8 ± 8.5
328.15	80.48 ± 0.20 (79.5[d])	−1.09 ± 1.72	181.3 ± 1.9	5.9 ± 15.5
L-Glutamine				
288.15	92.29 ± 0.29 (92.3[d])	5.90 ± 2.39	141.3 ± 2.9	59.3 ± 23.5
298.15	93.90 ± 0.05 (93.8,[d] 93.61,[b] 94.36[i])	0.89 ± 0.38	174.2 ± 1.2 (184,[e] 187[i])	28.3 ± 9.9
313.15	95.14 ± 0.13 (94.9[d])	3.48 ± 1.37	206.9 ± 1.9	19.8 ± 15.6
328.15	96.25 ± 0.15 (96.3[d])	0.33 ± 1.37	238.5 ± 2.6	−10.2 ± 23.5
Glycylglycine				
288.15	75.25 ± 0.08	2.06 ± 0.59	70.3 ± 1.1	51.9 ± 7.9
298.15	76.29 ± 0.07 (76.27,[a] 76.23,[b] 76.60,[g] 76.2[k])	2.37 ± 0.47	102.6 ± 0.9 (100.8,[c] 105.0[a], 99.3[j])	37.4 ± 6.5
313.15	77.59 ± 0.10 (77.6[k])	2.04 ± 0.74	138.5 ± 1.2	39.1 ± 8.3
328.15	77.96 ± 0.11 (76.0,[d] 78.0[k])	3.51 ± 0.77	172.5 ± 2.1	−7.7 ± 14.7
Glycyl-L-valine				
288.15	120.89 ± 0.05 (121.02±0.06[l])	2.10 ± 0.46 (1.5 ± 0.6[l])	343.7 ± 2.2	26.6 ± 21.7
298.15	122.25 ± 0.05 (122.34±0.04,[l] 121.99 ± 0.02[b])	2.70 ± 0.51 (2.6 ± 4,[l] 1.7 ± 0.424[b])	369.5 ± 1.1 (352.6 ± 5.3[j])	32.9 ± 11.4
313.15	124.06 ± 0.07	2.24 ± 0.69	397.3 ± 3.3	25.4 ± 32.6
328.15	124.81 ± 0.11	8.08 ± 1.12	408.8 ± 3.8	75.2 ± 35.4
Glycyl-L-asparagine				
288.15	108.50 ± 0.16 (108.45 ± 0.05[l])	8.37 ± 1.32 (0.6 ± 0.4[l])	137.9 ± 3.9	158.8 ± 33.4
298.15	109.54 ± 0.19 (110.11 ± 0.03[c])	18.00 ± 2.1 (3.3 ± 0.2[c])	189.8 ± 1.4 (188.1 ± 0.4[c])	134.0 ± 16.2 (69 ± 3[c])
313.15	112.39 ± 0.06	4.08 ± 0.53	241.8 ± 2.0	15.43 ± 17.1
328.15	113.64 ± 0.16	2.02 ± 1.51	269.0 ± 14.7	57.5 ± 152.8
Glycyl-L-leucine				
288.15	138.23 ± 0.07 (138.15 ± 0.05[l])	1.23 ± 0.92 (0.6 ± 0.4[l])	426.89 ± 3.2	97.4 ± 41.1
298.15	139.69 ± 0.10 (139.62 ± ± 0.02[c])	2.94 ± 1.3 (2.1 ± 0.2[c])	459.6 ± 3.5 (473.3 ± 0.8[j])	24.7 ± 45.2
313.15	141.72 ± 0.05	2.86 ± 0.61	480.9 ± 5.7	120.9 ± 72.9
328.15	143.25 ± 0.20	7.01 ± 2.56	516.00 ± 1.5	−167.1 ± 18.9

[a]Reference 18.
[b]Reference 19.
[c]Reference 9.
[d]Reference 20.
[e]Reference 21.
[f]Reference 22.
[g]Reference 23.
[h]Reference 24.
[i]Reference 25.
[j]Reference 26.
[k]Reference 5.
[l]See footnote 3.

Can. J. Chem. Downloaded from www.nrcresearchpress.com by 65.111.164.53 on 09/08/12
For personal use only.

Can. J. Chem. Downloaded from www.nrcresearchpress.com by 65.111.164.53 on 09/08/12
For personal use only.

dependences of the dielectric constant of the solvent (3, 29). Effective Born coefficients, for the dipeptide systems used in our analyses, were calculated from estimated standard state entropies using the relationship described in ref. 29. Standard state entropies for the dipeptides were estimated using a group additivity type scheme. This method of analysis is based upon the HKF semi-empirical modelling procedures (8, 29, 30), and we reported details of our calculations in previous publications (1–3).

The format of our additivity analyses may be represented by the general equation

$$[5] \qquad \overline{Y}^0_s = \sum_i n_i \overline{Y}^0_i$$

where n_i represents the number of times each structural group appears in a given molecule and $\overline{Y}^0_i$ represents the extensive thermodynamic group contribution to the structural component of the standard state property of interest. Our analyses yield estimates of the contributions made by the $CHNH_2COOH$, OH, COOH, CH_2, CH, $CONH_2$, and CONH groups. Equation [5] may therefore be written in the form:

$$[6] \qquad \overline{Y}^0_s = n_{CH(NH_2)COOH}\overline{Y}^0_{CH(NH_2)COOH} + n_{CH_2}\overline{Y}^0_{CH_2} + n_{OH}\overline{Y}^0_{OH} + n_{COOH}\overline{Y}^0_{COOH} + n_{CH}\overline{Y}^0_{CH} + n_{CONH_2}\overline{Y}^0_{CONH_2} + n_{CONH}\overline{Y}^0_{CONH}$$

In addition, contributions from H atoms and methyl groups may be obtained by the use of two simplifying assumptions (31–33), eqs. [7] and [8].

$$[7] \qquad \overline{Y}^0_{CH_3} = 1.5\ \overline{Y}^0_{CH_2}$$

$$[8] \qquad \overline{Y}^0_H = 0.5\ \overline{Y}^0_{CH_2}$$

Estimates of structural contributions, $\overline{Y}^0_i$, were obtained from eq. [6] using conventional multiple regression fitting procedures. Calculated group contributions to structural standard state volumes and heat capacities are contained in Table 8 together with their calculated standard errors. Experimental standard state properties are compared to our group analyses calculated values in Table 9. In general, standard state volumes appear to be slightly better represented than standard state heat capacities by our group additivity approach. An explanation for this behaviour is explored in a discussion of our calculated structural group contributions.

The addition of the six systems investigated in this paper to our input data base for the group additivity analyses significantly adds to the numbers of degrees of freedom of the analyses. Accordingly, we have been able to expand the number of structural groups for which we solve at any one time and hence overcome some of the structural approximations we were forced to make in our previous analyses (3).

The current additivity analyses do not significantly alter previously reported (3) trends in the temperature dependences of the structural components of standard state volumes and heat capacities for the $CH(NH_2)CO_2H$, CH_2, OH, and COOH groups. It is interesting to note, however, that our analyses predict that the apolar CH and CH_2 (hence CH_3 and H) group contributions dominate the magnitude of standard state heat capacities. By comparison, the contributions made by polar groups to standard state heat capacities are small.

Table 8. Calculated group contributions of structural components of standard state volumes and heat capacities at 288.15, 298.15, 313.15, and 328.15 K.

Structural group	$\overline{V}^0_s$ ($cm^3\ mol^{-1}$)	$\overline{C}^0_{p,s}$ ($J\ K^{-1}\ mol^{-1}$)
***T* = 288.15 K**		
$CH(NH_2)COOH$	34.80 ± 0.42	−14.6 ± 9.0
CH_2	15.58 ± 0.23	75.4 ± 5.1
OH	8.77 ± 0.50	9.1 ± 10.9
COOH	20.85 ± 0.47	3.8 ± 10.2
CONH	15.37 ± 0.36	−40.5 ± 7.8
CH	7.53 ± 0.64	72.6 ± 13.7
$CONH_2$	24.73 ± 0.41	3.6 ± 8.8
***T* = 298.15 K**		
$CH(NH_2)COOH$	35.49 ± 0.42	2.1 ± 9.9
CH_2	15.70 ± 0.24	76.2 ± 5.6
OH	8.84 ± 0.51	14.7 ± 11.9
COOH	21.68 ± 0.48	17.3 ± 11.2
CONH	15.48 ± 0.36	−23.0 ± 8.5
CH	7.33 ± 0.64	62.9 ± 15.1
$CONH_2$	25.10 ± 0.41	16.1 ± 9.7
***T* = 313.15 K**		
$CH(NH_2)COOH$	35.93 ± 0.43	24.7 ± 12.0
CH_2	15.83 ± 0.24	71.0 ± 6.8
OH	9.13 ± 0.51	20.1 ± 14.5
COOH	22.30 ± 0.48	31.3 ± 13.7
CONH	16.26 ± 0.37	−3.3 ± 10.4
CH	7.37 ± 0.65	67.4 ± 18.3
$CONH_2$	25.87 ± 0.42	35.2 ± 11.8
***T* = 328.15 K**		
$CH(NH_2)COOH$	36.14 ± 0.44	37.3 ± 9.3
CH_2	16.01 ± 0.25	74.3 ± 5.2
OH	9.14 ± 0.53	25.6 ± 11.3
COOH	22.85 ± 0.50	43.6 ± 10.6
CONH	16.08 ± 0.38	6.5 ± 8.1
CH	7.44 ± 0.66	50.7 ± 14.2
$CONH_2$	26.51 ± 0.43	38.5 ± 9.1

In brief, the group contributions to structural components of standard state heat capacities of apolar species are seen to decrease with increasing temperature whilst the group contributions of polar species increase with increasing temperature. These trends are indicative of the respective hydrophobic or hydrophilic character of the species under discussion.

The temperature dependences of group contributions to structural components of standard state volumes yield less definitive conclusions. The differences between group contributions reported in this paper and those we reported previously (3) are not unexpected given the manner in which we have expanded our additivity analyses to look at an increased number of functional groups. Trends in group contributions for the $CH(NH_2)CO_2H$, OH, and COOH groups follow the expected behavior of polar groups, i.e., increases in the vol-

Table 9. A comparison of experimental standard state volume and heat capacity data with calculated standard state data for the set of aqueous amino acid and dipeptide systems that were used as the input data base to our group additivity analyses.

(*a*) Standard state volumes (cm^3 mol^{-1})

	T = 288.15 (K)		T = 298.15 K		T = 313.15 (K)		T = 328.15 (K)	
System	Expt.	Calcd.	Expt.	Calcd.	Expt.	Calcd.	Expt.	Calcd.
L-Alanine[a]	59.67	58.89	60.47	59.78	61.14	60.47	61.53	61.02
L-Serine[a]	59.70	60.14	60.66	61.06	61.63	61.98	62.22	62.48
L-Threonine[a]	76.18	75.73	76.90	76.51	77.93	77.58	78.52	78.26
L-Valine[b]	90.08	89.90	90.80	90.76	91.67	91.71	92.57	92.61
L-Leucine[b]	106.81	105.84	107.73	106.84	109.00	107.95	110.18	109.05
L-Glutamic acid[c]	88.52	88.79	90.06	90.59	91.62	92.07	92.84	93.40
L-Aspartic acid[c]	72.84	72.56	74.77	74.23	75.98	75.53	77.18	76.61
L-Isoleucine[b]	104.90	105.89	105.76	106.89	107.04	108.01	108.09	109.11
Glycine[a]	42.48	43.23	43.26	43.99	44.01	44.54	44.51	44.91
Asparagine	76.28	76.46	77.63	77.66	79.07	79.12	80.48	80.28
Glutamine	92.29	92.31	93.90	93.64	95.13	95.26	96.25	96.62
Diglycine	75.25	74.84	76.29	75.86	77.59	77.38	77.96	77.81
Glyasn	108.50	108.30	109.54	109.77	112.39	112.21	113.64	113.47
Glyval	120.89	121.91	122.25	123.04	124.06	124.99	124.81	125.99
Glyleu	138.23	137.82	139.69	139.09	141.72	141.19	143.25	142.40

(*b*) Standard state heat capacities (J K^{-1} mol^{-1})

	T = 288.15 (K)		T = 298.15 K		T = 313.15 (K)		T = 328.15 (K)	
System	Expt.	Calcd.	Expt.	Calcd.	Expt.	Calcd.	Expt.	Calcd.
L-Alanine[a]	126.3	108.6	141.2	126.8	153.7	142.0	166.5	160.2
L-Serine[a]	89.0	83.8	114.1	107.2	140.0	130.7	157.9	152.9
L-Threonine[a]	192.8	198.0	205.3	212.2	228.5	237.8	240.2	245.2
L-Valine[b]	294.4	295.8	305.8	305.5	316.3	317.5	325.2	324.0
L-Leucine[b]	388.1	376.3	397.5	386.9	406.8	394.0	411.9	404.1
L-Glutamic acid[c]	152.3	167.8	180.6	200.2	202.3	227.6	239.7	261.0
L-Aspartic acid[c]	98.8	83.3	134.4	114.8	172.3	147.0	197.7	176.4
L-Isoleucine[b]	372.9	377.1	383.8	387.7	392.8	394.8	399.5	405.0
Glycine[a]	15.2	32.0	37.6	49.3	57.8	69.7	76.8	84.5
Asparagine	97.6	83.3	123.9	113.8	161.1	151.1	181.3	171.6
Glutamine	141.3	162.6	174.2	194.0	206.9	226.2	238.5	250.3
Diglycine	70.3	76.4	102.6	112.2	138.5	147.5	172.5	176.1
Glyasn	137.9	130.9	189.8	180.1	241.8	232.4	269.0	266.9
Glyval	342.3	345.7	369.5	374.1	397.3	401.3	408.8	421.9
Glyleu	426.9	425.8	459.6	455.1	480.9	477.3	516.0	501.5

[a]Experimental data from ref. 1.
[b]Experimental data from ref. 2.
[c]Experimental data from ref. 3.

ume contributions with increasing temperature. However, the CH_2 group exhibits a very small increase in its standard state volume contribution as a function of temperature that would appear to be in conflict with the apolar nature of the species.

Structural group contributions of the CH group to standard state volumes are predicted to be virtually temperature independent, and in this respect follow the trends shown by the CH_2 group. Contributions to the standard state heat capacities by CH generally decrease with increasing temperature as one would expect of an apolar group. Our $\overline{C}^0_{p\mathrm{CH}}$ value of 62.9 J K^{-1} mol^{-1} at 298.15 K is in good agreement with the value of 65 J K^{-1} mol^{-1} reported in ref. 27. By comparison, the value of 23 J K^{-1} mol^{-1}, obtained from an analysis of standard state heat capacities of compounds of the type H-$(CH_2)_n$-X by Nichols, Skold, Spink, Suurskuusk, and Wadsö (28), would appear to be low.

Increases in structural contributions to standard state volumes and heat capacities of the $CONH_2$ group as a function of

Can. J. Chem. Downloaded from www.nrcresearchpress.com by 65.111.164.53 on 09/08/12
For personal use only.

Table 10. A comparison of literature standard state volume and heat capacity data for several glycyl dipeptides at 298.15 K with those that may be calculated using estimates of solvation contributions to standard properties and the structural group contributions to standard state properties contained in Table 8.

Solute	$\overline{V}^0_2$ (lit.)[a] (cm^3 mol^{-1})	$\overline{V}^0_2$ (calcd.) (cm^3 mol^{-1})	$\overline{C}^0_{p,2}$ (lit.)[a] (J K^{-1} mol^{-1})	$\overline{C}^0_{p,2}$ (calcd.) (J K^{-1} mol^{-1})
Glycyl-DL-alanine	92.37	91.84	219.7	192.2
Glycyl-DL-serine	92.93	93.16	161.2	173.5
Glycyl-DL-threonine	108.50	108.51	251.0	276.9

[a]Standard state volume and heat capacity data obtained from ref. 9.

Can. J. Chem. Downloaded from www.nrcresearchpress.com by 65.111.164.53 on 09/08/12
For personal use only.

temperature follow the expected trends of a polar group. Mishra and Ahluwalia (19) report $\overline{V}^0_{CONH_2} = 38.9$ cm^3 mol^{-1} at 298.15 K using an additivity analysis based on compounds of the general form $CH_3(CH_2)_nCONH_2$. This value is much higher than our predicted value of 25.10 cm^3 mol^{-1}.

Our group additivity analysis of heat capacity data indicates that structural components to standard state heat capacities for the peptide group increase with increasing temperature. This behavior chimes well with the known hydrophilic character of the group. Several authors have reported CONH group contributions for standard state heat capacities at 298.15 K and ambient pressure and there appears to be considerable disagreement regarding a recommended value. Nichols, Skold, Spink, Suurskuusk, and Wadsö (28) report a value of -61 J K^{-1} mol^{-1} calculated from heat capacity data for simple amide systems. Cabani et al. (34) give an approximate value of 0 J K^{-1} mol^{-1} calculated from heat capacity data for cyclo mono- and dipeptide systems, and a value of 2 J K^{-1} mol^{-1} may be calculated from the homopeptide heat capacity data reported by Makhatadze and Privalov (35). In a recent investigation, Hedwig, Reading, and Lilley (27) report values, depending upon which form of additivity scheme was utilized, of -7.5 and -13 J K^{-1} mol^{-1}. Our calculated value of -23.0 ± 8.5 J K^{-1} mol^{-1} falls between these reported values.

Structural contributions to standard state volumes of the peptide group, calculated from our data base of standard state volume data, are predicted to increase with increasing temperature. As noted for the heat capacities of the peptide group, this behavior is indicative of hydrophilic character. There are already several estimations in the literature of the standard state volume contribution of the peptide group at 298.15 K. Mishra and Ahluwalia (19) report values of 20.5 ± 0.3, 19.3, 35.8, and 16 ± 1 cm^3 mol^{-1} from the analyses of standard state volume data for *N*-acetylamino acids, alkyl ureas, alkyl amides, and amino acids and dipeptides, respectively. Accepting that the methylene group contribution to standard state volumes is approximately 16 cm^3 mol^{-1} at 298.15 K, then a value of $\overline{V}^0_{CONH} = 22$ cm^3 mol^{-1} may be obtained from Jolicoeur and Boileau's (18) value for $\overline{V}^0_{CH_2CONH}$, which is calculated from standard state volume data for low molecular weight peptide systems. Our value of $\overline{V}^0_{CONH} = 15.48 \pm 0.36$ cm^3 mol^{-1} agrees very well with the amino acid dipeptide-derived value reported in ref. 19.

In comparing our group standard state data to those obtained by other authors, we remind the reader that our group contributions represent only structural contributions. Our analyses do not provide for the calculation of group solvation contributions to standard state volumes and heat capacities.

We conclude from our survey of available group additivity data that any values of group contributions to standard state volumes and heat capacities are extremely sensitive to the data set used as input to an additivity scheme. In addition, although the HKF analysis we have used in this paper goes some way towards accounting for the solvation characteristics of the investigated amino acids and peptides, it may well be that this contribution is underestimated in the low temperature and pressure region that we have studied. The charging of these species is known to have a large effect on standard state heat capacities.

The predictive powers of our group additivity analyses can be partially demonstrated by using the group contributions contained in Table 8 to calculate standard state volumes and heat capacities for several aqueous dipeptide systems for which literature data are available at 298.15 K (9). Solvation contributions to the standard state properties were calculated in the manner described earlier. The results of these calculations are contained in Table 10.

The agreement between the literature and our calculated standard state properties is promising, especially for standard state volumes, given that at best the results of group additivity analyses should be viewed as approximations.

There are several areas that require further examination before it would be feasible to apply simple additivity schemes, of the type described in this paper, to the calculation of standard state properties for aqueous protein systems. It is clear from our work that additivity schemes are often unable to differentiate between structural isomers. For example, the calculated structural components to standard state volumes and heat capacities of L-leucine and L-isoleucine are identical. In effect, the difference in structure between these two amino acids has been averaged out by our additivity analyses. A previous investigation (27) indicated a problem when using an additivity approach to obtain standard state volumes for dipeptide systems in which one switches the amino acid residue at the N-terminus, e.g., glycylalanine and alanylglycine. Simple group additivity analyses cannot distinguish between these two structures and it is likely that one should expand any analyses to account for the way in which a given molecule orients itself in the solvent. The correlations between side-chain group contributions to standard state heat capacities and solvent-accessible surface area of amino acid side chains reported by Jolicoeur et al. (25) would appear to support this expectation.

We recently began to investigate the orientations of dipeptide molecules, of the type described above, in water using the commercial modeling software package Hyperchem. It is hoped that these investigations will lead to a greater understanding of the dynamics of aqueous peptide systems. This in turn should lead us to enhanced additivity analyses and closer to our goal of estimating key thermodynamic properties for aqueous protein systems.

Acknowledgments

The authors are very grateful to Dr. Gavin Hedwig of Massey University, Palmerston North, New Zealand, for an advanced copy of the temperature dependences of standard state volumes for the aqueous dipeptide systems: glyleu, glyval, and glyasn. A.W.H. is grateful to the Natural Sciences and Engineering Research Council of Canada (NSERC) for operating support and to the University of Lethbridge for equipment funding. L.L.G. and M.L.R. are grateful to NSERC for the award of Undergraduate Student Research Awards.

References

1. A.W. Hakin, M.M. Duke, S.A. Klassen, R.M. McKay, and K.E. Preuss. Can. J. Chem. **72**, 362 (1994).
2. M.M. Duke, A.W. Hakin, R.M. McKay, and K.E. Preuss. Can. J. Chem. **72**, 1489 (1994).
3. A.W. Hakin, M.M. Duke, J.L. Marty, and K.E. Preuss. J. Chem. Soc. Faraday Trans. **90**, 2027 (1994).
4. G.R. Hedwig. J. Chem. Soc. Faraday Trans. **89**, 2761 (1993).
5. T.V. Chalikian, A.P. Sarvazyan, T. Funck, and K.J. Breslauer. Bioploymers, **34**, 541 (1994).
6. G.R. Hedwig and H. Høiland. Biophys. Chem. **49**, 175 (1994).
7. R.M. Kelly, J.A. Baross, and M.W.W. Adams. Chem. Br. **30**, 555 (1994).
8. H.C. Helgeson, D.H. Kirkham, and G.C. Flowers. Am. J. Sci. **281**, 1249 (1981).
9. J.F. Reading and G.R. Hedwig. J. Solution Chem. **18**, 159 (1989).
10. C.J. Pouchert and J.R. Campbell. The Aldrich Library of NMR Spectra. Vol. III. Aldrich Chemical Co. Inc., Wisconsin. 1974.
11. P. Picker, E. Tremblay, and C. Jolicoeur. J. Solution Chem. **3**, 377 (1974).
12. P. Picker, P.-A. Leduc, P.R. Philip, and J.E. Desnoyers. J. Chem. Thermodyn. **3**, 631 (1971).
13. J.E. Desnoyers, C. DeVisser, G. Perron, and P. Picker. J. Solution Chem. **5**, 605 (1976).
14. A.W. Hakin, S.A.M. Mudrack, and C.L. Beswick. Can. J. Chem. **71**, 925 (1993).
15. G.S. Kell. J. Chem. Eng. Data, **12**, 66, (1967).
16. G.S. Kell. *In* Water — A comprehensive treatise. Vol. I. *Edited by* F. Franks. Plenum Press, New York. 1972. pp. 363–412.
17. G.R. Hedwig. J. Solution Chem. **17**, 383 (1988).
18. C. Jolicoeur and J. Boileau. Can. J. Chem. **56**, 2707 (1978).
19. A.K. Mishra and J.C. Ahluwalia. J. Phys. Chem. **88**, 86 (1984).
20. D.P. Kharakoz. Biophys. Chem. **34**, 115 (1989).
21. J.O. Hutchins, A.G. Cole, R.A. Robie, and J. Stout. J. Biol. Chem. **238**, 2407 (1963).
22. H.M. Huffman and H. Bersook. J. Am. Chem. Soc. **54**, 4297 (1932).
23. S. Cabani, G. Conti, E. Matteoli, and M.R. Tiné. J. Chem. Soc. Faraday Trans. 1, **77**, 2385 (1981).
24. G.R. Hedwig. J. Chem. Thermodyn. **23**, 123 (1991).
25. C. Jolicoeur, B. Riedl, D. Desrochers, L.L. Lemelin, R. Zamojska, and O. Enea. J. Solution Chem. **15**, 109 (1986).
26. R. Bhat and J.C. Ahluwalia. J. Phys. Chem. **89**, 1099 (1985).
27. G.R. Hedwig, J.F. Reading, and T.H. Lilley. J. Chem. Soc. Faraday Trans. **87**, 1751 (1991).
28. N. Nichols, R. Skold, C. Spink, J. Suurskuusk, and I. Wadsö. J. Chem. Thermodyn. **8**, 1081 (1976).
29. E.L. Shock and H.C. Helgeson. Geochim. Cosmochim. Acta, **54**, 915 (1990).
30. E.L. Shock. Geochim. Cosmochim. Acta, **56**, 3481 (1992).
31. J.J. Spitzer, S.K. Suri, and R.H. Wood. J. Solution Chem. **14**, 571 (1985).
32. S.K. Suri and R.H. Wood. J. Solution Chem. **15**, 705 (1986).
33. M.J. Blandamer, J. Burgess, M.R. Cottrell, and A.W. Hakin. J. Chem. Soc. Faraday Trans. 1, **83**, 3039 (1987).
34. S. Cabani, G. Conti, and E. Matteoli. Bioploymers, **16**, 465 (1977).
35. G.I. Makhatadze and P.L. Privalov. J. Mol. Biol. **213**, 375 (1990).

Can. J. Chem. Downloaded from www.nrcresearchpress.com by 65.111.164.53 on 09/08/12
For personal use only.

Evidence for reversible dissociative adsorption in the reaction of molecular chlorine with gallium arsenide

Kin-Chung Wong and Elmer A. Ogryzlo

Abstract: The reaction of molecular chlorine with the (100) face of a gallium arsenide crystal has been studied at pressures of Cl_2 between 0.10 and 9.0 Torr and in the temperature range from 90 to 110°C. In contrast to an earlier report, the etch rate was found to be half order with respect to Cl_2. The similarity of these results to those obtained for the reaction of molecular chlorine and bromine with silicon points to a mechanism in which the gaseous halogen molecule is first physisorbed on the semiconductor surface and then dissociates into chemisorbed atoms. The data indicate that both steps occur reversibly at higher pressures, where the composite half-order rate constant can be represented by the Arrhenius equation:

$k_{1/2} = 10^{13.6\pm2.6}$ μm min^{-1} Torr$^{-1/2}$ $e^{-(100\pm19\text{ kJ mol}^{-1}/RT)}$

At low pressures the first-order rate constant is given by the equation:

$k_1 = 10^{10.4\pm2.3}$ μm min^{-1} Torr^{-1} $e^{-(76\pm16\text{ kJ mol}^{-1}/RT)}$

Key words: etching, gallium arsenide, molecular chlorine, kinetics.

Résumé : On a étudié la réaction du chlore moléculaire avec la face (100) d'un cristal d'arséniure de gallium à des pressions de chlore allant de 0,10 à 9,0 Torr et à des températures allant de 90 à 110°C. En opposition avec un rapport antérieur, on a trouvé que la vitesse de gravage est d'ordre une demie par rapport au chlore. La similarité de ces résultats avec ceux obtenus lors de la réaction du chlore et du brome moléculaires avec le silicium suggère un mécanisme dans lequel la molécule d'halogène gazeux subit dans un premier temps une adsorption physique sur la surface du semiconducteur et qu'elle se dissocie par la suite en atomes chimisorbés. Les données indiquent que, à des pressions plus élevées, les deux étapes se produisent d'une façon réversible alors que la constante de vitesse composée d'ordre une demie peut être représentée par l'équation d'Arrhenius :

$k_{1/2} = 10^{13.6\pm2.6}$ μm min^{-1} Torr$^{-1/2}$ $e^{-(100\pm19\text{ kJ mol}^{-1}/RT)}$

À de faibles pressions, la constante de vitesse du premier ordre est donnée par l'équation suivante :

$k_1 = 10^{10.4\pm2.3}$ μm min^{-1} Torr^{-1} $e^{-(76\pm16\text{ kJ mol}^{-1}/RT)}$

Mots clés : gravage, arséniure de gallium, chlore moléculaire.

[Traduit par la rédaction]

Introduction

Etching of gallium arsenide (GaAs) by halogen atoms and molecules is commonly used in the fabrication of microelectronic circuits based on this semicondutor. However, the mechanisms of these reactions and the rate constants for the elementary steps in the processes remain largely poorly characterized. In 1988 Ha et al. (1) reported a kinetics study of the etching of GaAs by molecular chlorine in which they found that the etch rate was not a linear function of the chlorine pressure. From the form of the pressure dependence that they observed, they concluded that the etch rate reached a plateau at high pressures because of the "saturation" of sites for reaction on the surface. Such an interpretation of the nonlinear kinetics was reinforced by similar earlier observations and interpretations in the reactions of Br_2 (2) and Cl_2 (3) with silicon. However, more recently it has been shown that neither of these latter reactions reaches a plateau at high pressures, and that at high pressures they both simply remain half order with respect to the partial pressure of the molecular halogen (4, 5). Furthermore, the reaction of GaAs with Br_2 (6), I_2 (7), and ICl (8) have all been found to be consistent with half-order kinetics. We therefore decided to reinvestigate the GaAs–Cl_2 reaction to see if any systematic errors occurred in the earlier work that prevented this reaction from being recognized as half order.

Received August 25, 1994.

K.C. Wong and E.A. Ogryzlo.[1] Department of Chemistry, The University of British Columbia, Vancouver, BC V6T 1Z1, Canada.

[1] Author to whom correspondence may be addressed. Telephone: (604) 822-2474. Fax: (604) 822-2847. E-mail: ogryzlo@Chem.ubc.ca

Can. J. Chem. Downloaded from www.nrcresearchpress.com by 65.111.164.53 on 09/08/12
For personal use only.

Can. J. Chem. Downloaded from www.nrcresearchpress.com by 65.111.164.53 on 09/08/12
For personal use only.

Experimental

Single crystal GaAs (100) chips were cut from a 7.5 cm diameter and 0.5 mm thick wafer supplied by Crystar (nee Johnson Matthey, nee Cominco). They were patterned with silicon nitride stripes, which were 20 μm wide and 20 μm apart, aligned either along the $\langle 0\bar{1}\bar{1}\rangle$ or the $\langle 01\bar{1}\rangle$. direction. Chips were generally rectangular and had a surface area of about 0.04 cm^2.

Matheson High Purity chlorine with a quoted purity of 99.99% was used without further purification. The Cl_2 was passed over the GaAs samples at a flow rate that was at least 5000 times that consumed by reaction. This avoided any dilution of reactant stream by the gaseous products and also prevented the formation of any reactant concentration gradient above the GaAs surface. A rotary vacuum pump was used to back a liquid-nitrogen-cooled trap, which functioned as a cryogenic pump for the Cl_2. A control valve located upstream from the reactor (the flow controller) was used to change the pressure over the substrate by increasing the flow rate of chlorine into the system. A second control valve (the exhaust throttle) located between the reactor and the cryostatic pump could be used to change the evacuation speed. In the present study, the pressure was regulated only by adjusting the flow controller setting. This ensured that the residence time of the gas over the etching sample was relatively constant at all pressures. This is in contrast to the manner in which the pressure was changed in the earlier work (1). In that study, the pressure was changed by adjusting the throttle valve. This meant that the total gas flow through the system was not changed and therefore the residence time of the gas over the sample increased with increasing pressure. Under these circumstances, the reaction became increasingly diffusion controlled at high pressures because the products were not swept away as quickly as they might be if the pressure were increased by increasing the total gas flow rather than by throttling the flow. It is quite probable that the small but significant differences between the data obtained in this work and the earlier study can be attributed to this simple difference in flow control techniques.

Before the etching experiment, the GaAs sample was immersed in 38% concentrated hydrochloric acid for 30 s to remove any native oxide layer on the surface and then it was mounted with a glass spring on a thermally oxidized silicon block that acted as a heat sink. The temperature of the GaAs chip was measured with a thermocouple embedded in the silicon block and the pressure of $Cl_{2(g)}$ was measured with an MKS baratron pressure gauge.

Etch rates were measured in situ by laser interferometry (1, 3). Temperatures and pressures were chosen so that the etch rates were between 0.05 and 2.0 μm min^{-1} because these were most easily measured by our monitoring method.

Results and discussion

The reaction of Cl_2 with GaAs(100) was studied at 90, 100, and 110°C to determine the activation energy and the order of the reaction with respect to Cl_2. The pressure dependence of the etch rate (ER) is shown in Fig. 1. It can be seen that although the relationship is not linear, the etch rate continues to increase as the pressure of the Cl_2 increases and no obvious saturation of the reaction rate is observed in this pressure range.

Fig. 1. The GaAs(100) etch rate as a function of the pressure of Cl_2 at 90 (○), 100 (△), and 110°C (□).

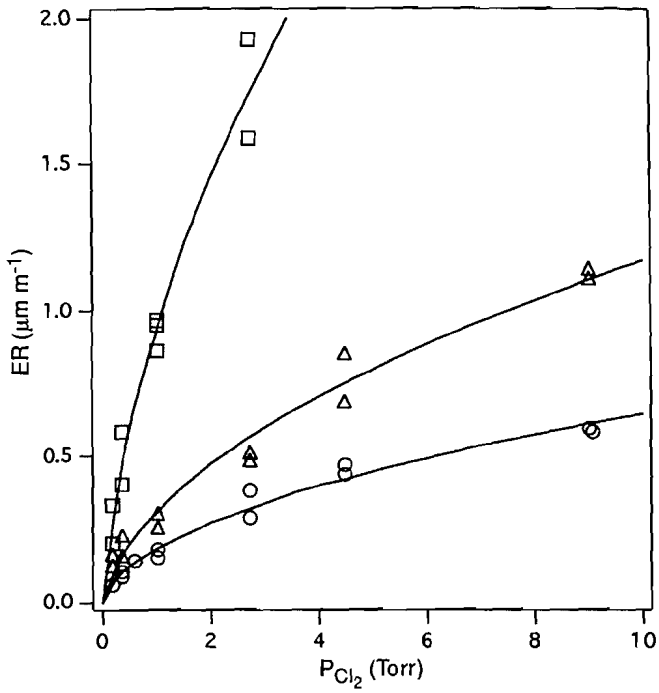

To determine the order of the reaction with respect to Cl_2 pressure, ln (ER) was plotted against ln (P_{Cl_2}). For the data shown in Fig. 1, straight lines with slopes between 0.5 and 0.7 were obtained, suggesting a half-order dependence on the Cl_2 pressure over the entire pressure range for which data were obtained. A plot of etch rate against $\sqrt{P_{Cl_2}}$ is presented in Fig. 2. As in the silicon etching experiments (4, 5), the "least-squares" lines through these points have small negative y-intercepts and the magnitudes of these intercepts show a systematic increase with increasing temperature.

Such behavior is consistent with the "reversible dissociative adsorption" mechanism proposed earlier (4, 5). In this mechanism, the Cl_2 molecule first dissociatively adsorbs on the GaAs surface to form two chemisorbed chlorine atoms ($Cl_{(ads)}$) as represented by eqs. [1,-1]. In the second step (eq. [2]), this $Cl_{(ads)}$ species reacts with the surface to form reaction products or some intermediates that yield such products in a subsequent non-rate-controlling process.

$$[1,-1] \quad Cl_{2(g)} \underset{k_{-1}}{\overset{k_1}{\rightleftharpoons}} 2Cl_{(ads)}$$

$$[2] \quad Cl_{(ads)} + GaAs \xrightarrow{k_2} \text{product}$$

The rate law for such a reaction mechanism was derived previously (4). Once a steady state is established, the rate law takes the form:

$$[3] \quad ER = \frac{k_2^2}{4k_{-1}}\sqrt{1 + \frac{16k_1k_{-1}}{k_2^2}P_{Cl_2}} - \frac{k_2^2}{4k_{-1}}$$

Can. J. Chem. Downloaded from www.nrcresearchpress.com by 65.111.164.53 on 09/08/12
For personal use only.

Fig. 2. A plot of the etch rate versus $\sqrt{P_{Cl_2}}$ at 90 (○), 100 (△), and 110°C (□).

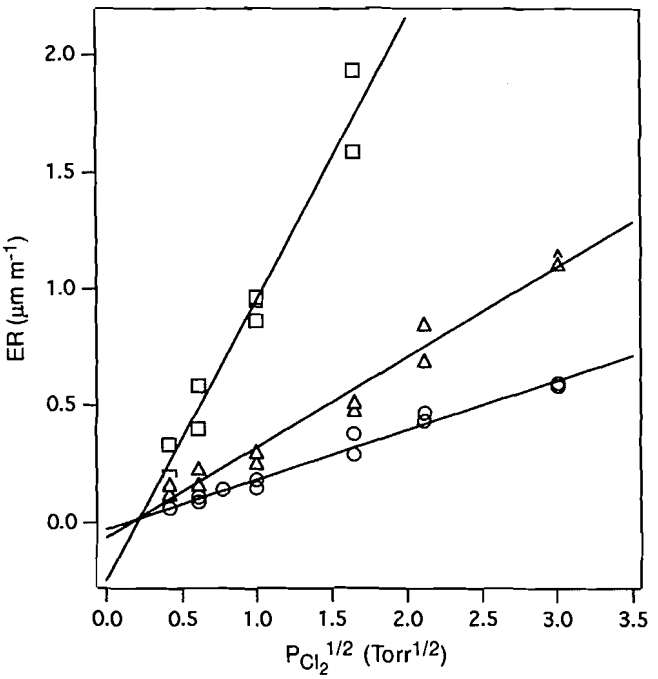

At low pressure, eq. [3] reduces to

$$[4] \qquad \mathrm{ER} = 2k_1 P_{Cl_2}$$

i.e., reaction [1] is rate controlling and so the etch rate exhibits a first-order dependence on P_{Cl_2}. On the other hand, at high pressures, eq. [3] reduces to

$$[5] \qquad \mathrm{ER} = k_2\sqrt{\frac{k_1}{k_{-1}}}\sqrt{P_{Cl_2}} - \frac{k_2^2}{4k_{-1}}$$

i.e., the reaction approaches half-order kinetics with respect to Cl_2 because reaction [2] now becomes rate controlling and an equilibrium concentration of $Cl_{(ads)}$ is maintained by reactions [1,-1]. We will refer to $(k_2\sqrt{k_1/k_{-1}})$ as the "composite half-order rate constant" and abbreviate it as $k_{1/2}$.

According to eq. [5], in the high-pressure regime, the plot of ER versus $\sqrt{P_{Cl_2}}$ will result in a straight line with a negative y-intercept. This is consistent with the data shown in Fig. 2 where the slopes and intercepts are equal to $(k_2\sqrt{k_1/k_{-1}})$ and $(-k_2^2/4k_{-1})$, respectively, and the first-order rate constant k_1 can subsequently be determined from the relationship:

$$[6] \qquad k_1 = \frac{-\text{slope}^2}{4 \times y\text{-intercept}}$$

The rate constants calculated in this way are presented in Table 1. Assuming that both k_1 and $k_{1/2}$ exhibit an Arrhenius temperature dependence, i.e.,

$$k = Ae^{-E_a/RT}$$

where A is a temperature-independent pre-exponential factor, E_a is the activation energy, R is the gas constant, and T is the temperature in Kelvin; E_a and A for k_1 and $k_{1/2}$ can be determined by plotting ln (k) versus $1/T$. Such plots are shown in Fig. 3, and the following expressions for k_1 and $k_{1/2}$ are obtained:

Table 1. Experimental values of the first- and the half-order rate constants.

Temperature (°C)	k_1 (μm min^{-1} Torr^{-1})	$k_{1/2}$ (μm min^{-1} Torr$^{-1/2}$)
90	0.40 ± 0.23	0.21 ± 0.01
100	0.60 ± 0.41	0.39 ± 0.02
110	1.47 ± 0.75	1.20 ± 0.09

Fig. 3. An Arrhenius plot for k_1 (open circle) and $k_2\sqrt{k_1/k_{-1}}$ (closed circle).

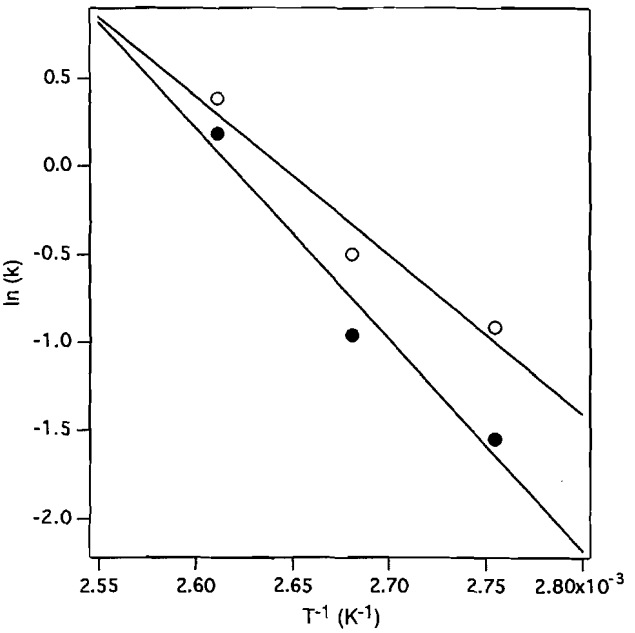

$$[7] \qquad k_1 = 10^{10.4\pm2.3}\,\mu\mathrm{m\ min^{-1}\ Torr^{-1}}\ e^{-(76\pm16\ \mathrm{kJ\ mol^{-1}}/RT)}$$

$$[8] \qquad k_{1/2} = 10^{13.6\pm2.6}\,\mu\mathrm{m\ min^{-1}\ Torr^{-1/2}}\ e^{-(100\pm19\ \mathrm{kJ\ mol^{-1}}/RT)}$$

The activation energy for k_1 (i.e., for the dissociative adsorption) is 76 kJ mol^{-1}. This is 166.6 kJ mol^{-1} below the bond dissociative energy of Cl_2. Although it represents a large reduction in the dissociation energy, the value is not unreasonable. The potential energy curve for the reaction is shown schematically in Fig. 4. The dissociative adsorption of $Cl_{2(g)}$ on the GaAs surface to form 2 $Cl_{(ads)}$ is represented by movement over the first energy barrier of 76 kJ mol^{-1} on the left-hand side of the diagram. Although $Cl_{(ads)}$ must lie below the first transition state, its position in the figure is undetermined and it is therefore represented by a dotted line on the diagram. This $Cl_{(ads)}$ species then reacts to yield reaction products through a second transition state. Though the

Can. J. Chem. Downloaded from www.nrcresearchpress.com by 65.111.164.53 on 09/08/12
For personal use only.

Fig. 4. Potential energy curve for the rate-determining steps in the etching of gallium arsenide by molecular chlorine gas.

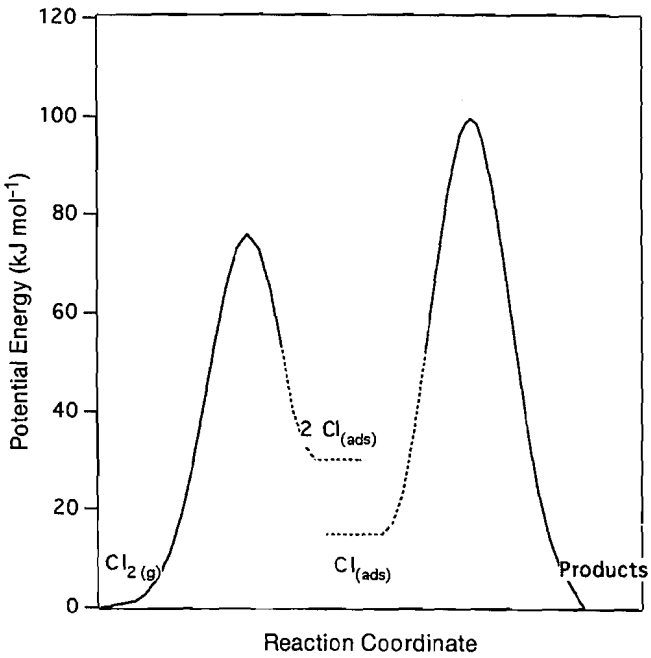

activation energy for the second step is also undetermined, the energy of the second transition state relative to the initial reactants is 100 kJ mol^{-1}.

As in the case of the reaction of silicon with halogen molecules, the pre-exponential factor in eq. [7] is several orders of magnitude larger than the collision frequency. The collision frequency for Cl_2 molecules on a surface under our experimental condition is 2.17×10^{24} collision m^{-2} s^{-1} $Torr^{-1}$, which, expressed in the same units as the etch rate, equals 6000 μm min^{-1} $Torr^{-1}$. However, the experimental pre-exponential factor is $10^{10.4}$, i.e., 2.5×10^{10} μm min^{-1}, which is more than 6 orders of magnitude larger than the collision frequency. Such "large" pre-exponential factors have also been observed in silicon etching by Br_2 and Cl_2 (3, 4). They have been rationalized by proposing the occurrence of a reversible physisorption step (with a zero or very small activation energy) prior to the dissociative chemisorption. The experimental rate constant (k_1) then represents a composite rate constant that can have a pre-exponential factor not directly related to the Cl_2 collision frequency. Such a reaction sequence is illustrated in eq. [9],

$$[9] \qquad Cl_{2(g)} \rightleftharpoons Cl_{2(ads)} \rightleftharpoons 2Cl_{(ads)}$$

Although the above mechanism can provide a rationalization of the observed half-order kinetics, alternative mechanisms have been considered (4). In these mechanisms, the Cl_2 molecule is thermally dissociated into gas phase Cl atoms either through collisions with other molecules in the gas phase or by collisions with the walls of the reaction vessel. Provided the gas phase atom concentration is in equilibrium with molecular chlorine, this mechanism is equally capable of explaining the change from first- to half-order kinetics. However, using thermodynamic data for this equilibrium at 100°C (9), the degree of dissociation of Cl_2 is found to be only 1.48×10^{-11}%. Under a Cl_2 partial pressure of 2.0 Torr, the number of Cl_2 molecules flowing past the sample is 4.69×10^{19} molecule s^{-1}, and so, if an equilibrium concentration of atoms is formed, there will be 1.39×10^7 Cl atom passing over the GaAs per second. Assuming that all the Cl atoms react with GaAs with zero activation energy, the predicated etch rate would be 9.41×10^{-9} μm min^{-1}. This is only 2.35×10^{-6}% of the observed etch rate (0.40 μm min^{-1}). The above analysis shows that the thermal dissociation of Cl_2 in the gas phase is insufficient to explain the observed kinetics, even if we disregard the need for the occurrence of a back reaction, and the unlikelihood that the dissociation can be made to occur rapidly enough in the short heated region immediately before the gas strikes the GaAs surface.

It is probably worth noting that, because of the limited pressure and temperature range of our current experiments, our results can be fitted equally well to the "surface site saturation mechanism" originally proposed for this reaction (1). The significance of our experiments lies in the fact that the original data in ref. 1 could not be fitted to the "dissociative absorption mechanism," and hence presented a conundrum because every other etching reaction by diatomic molecules that we have studied could be fitted to this mechanism. The experiments described in this paper simply indicate that the kinetic behavior of this system does indeed resemble that observed for other such etching reactions, and hence this reaction does not necessarily occur by another mechanism.

Conclusions

A reinvestigation of the reaction of Cl_2 with GaAs suggests that the nonlinear dependence of the etch rate on the Cl_2 pressure is probably not due to the occurrence of a plateau in the etch rate at high pressures, but is the result of a change in the order of the reaction from first order to half order as the pressure is increased. The first- and the half-order rate constants were determined and can be represented in the form of the following Arrhenius equations:

$$k_1 = 10^{10.4 \pm 2.3} \text{ μm min}^{-1} \text{ Torr}^{-1} \, e^{-(76 \pm 16 \text{ kJ mol}^{-1}/RT)}$$

$$k_{1/2} = 10^{13.6 \pm 2.6} \text{ μm min}^{-1} \text{ Torr}^{-1/2} \, e^{-(100 \pm 19 \text{ kJ mol}^{-1}/RT)}$$

This behavior can be explained by a reversible dissociative adsorption mechanism in which the gaseous molecules are first physisorbed on the semiconductor surface, then dissociate into chemisorbed atoms, and finally react with the surface to yield gaseous products.

Acknowledgements

GaAs wafers were generously supplied by Brian Lent of Crystar, Victoria, B.C. The research was partially financed by a grant from the Natural Sciences and Engineering Research Council of Canada.

References

1. J.H. Ha, E.A. Ogryzlo, and S. Polyhronopoulos. J. Chem. Phys. **89**, 2844 (1988).
2. L.L. Sveshnikova, S.M. Repinskii, and A.B. Posadov. Poverkhnost, **8**, 134 (1982).

3. E.A. Ogryzlo, D.L. Flamm, D.E. Ibbotson, and J.A. Mucha. J. Appl. Phys. **64**, 6510 (1988).
4. Z.H. Walker and E.A. Ogryzlo. J. Chem. Soc. Faraday Trans. **87**, 45 (1991).
5. Z.H. Walker and E.A. Ogryzlo. J. Appl. Phys. **69**, 548 (1991).
6. I.M. Salusbury and E.A. Ogryzlo. Int. J. Chem. Kinet. **23**, 529 (1991).
7. K.C. Wong and E.A. Ogryzlo. J. Vac. Sci. Technol. B:**10**, 668 (1992).
8. L. Hahn, K.-C. Wong, and E.A. Ogryzlo. J. Electrochem. Soc. **140**, 226 (1993).
9. A.F. Trotman-Dickenson, (Editor). Comprehensive inorganic chemistry. Vol. 2. Pergamon Press, 1973. p. 1144.

Can. J. Chem. Downloaded from www.nrcresearchpress.com by 65.111.164.53 on 09/08/12
For personal use only.

COMMUNICATION

A new synthesis of lactones from tertiary alkenylcarbinols by cobalt-catalyzed photocarbonylation under ambient conditions

Yuan L. Chow, Yu-Jin Huang, and Veljko Dragojlovic

Abstract: In the presence of a Co catalyst, tertiary vinyl-, propenyl-, and allylcarbinols were chelatively cycloadded to carbon monoxide to produce lactones by xanthone-sensitized photoreaction in tetrahydrofuran, under CO at 1 atmosphere and at room temperature. At lower temperatures the isomerization of alkenylcarbinols was suppressed and lactones were obtained with improved selectivity. The photoprocess was facilitated by addition of pyridine or hydrogen and retarded in presence of amines or phosphines. Mechanistic interpretations for the process and the accompanying effects are discussed.

Key words: chelative carbonylation, photocarbonylation, carbonylation of olefins, lactones synthesis from alkenylalcohols.

Résumé : En solution dans le tétrahydrofurane, à la température ambiante, sous 1 atmosphère de CO en présence de catalyseurs de Co, les carbinols tertiaires contenant des chaînes vinyle, propényle et allyle donnent, par une photoréaction sensibilisée par la xanthone, une cycloaddition chélatante conduisant à des lactones. À des températures inférieures, l'isomérisation des alcénylcarbinols est supprimée et les lactones sont obtenues avec une sélectivité accrue. Le photoprocessus est facilité par l'addition de pyridine ou d'hydrogène et il est retardé en présence d'amines ou des phosphines. On discute du mécanisme de ces processus et des effets qui les accompagnent.

Mots clés : carbonylation chélatante, photocarbonylation, carbonylation des oléfines, synthèses de lactones à partir d'alcools alcéniques.

[Traduit par la rédaction]

The carbonylation of olefins catalyzed by transition metal carbonyls is a major homogeneous catalytic reaction of industrial importance and occurs typically either under high temperature (140–170°C) and pressure (100–200 atm; 1 atm = 101.3 kPa) or aided by redox cycles of a noble metal (Pt or Rh) under more moderate conditions (1). We have established that olefins incorporate CO and an alcohol in the presence of cobalt catalysts promoted by ketone sensitization at 1 atmosphere CO and room temperature (2). An application of this mild photocarbonylation to insert CO into the termini of alkenylcarbinols would be facilitated by preferential sizes of ring formation and by the ready availability of starting alkenylcarbinols. The alcohols **1**, **4**, and **7** (Scheme 1) were prepared from appropriate ketones and vinyl-, propenyl-, or allylmagnesium halides according to standard procedures.

A solution of **1** (2 mmol), bisacetylacetonylcobalt(II) [$Co(acac)_2$] (0.1 mmol), pyridine (ca. 0.4 mmol), and xanthone (0.2 mmol) in THF (20 mL) was irradiated in a Pyrex Hanovia-type irradiator equipped with a 450-W medium-pressure mercury lamp (PC 451.050) under slow purging of CO and H_2 (9:1) to give about 95% conversion in 10–15 h. At intervals, the photolysate was withdrawn for GC analysis. At the end of irradiation, water was added to the reaction mixture and products were extracted with ether and chromatographed to afford 76–80% of γ-lactones **2** and small amounts of the γ-lactols **3**. The latter were identified by GC–MS. The presence of either pyridine or hydrogen, but not necessarily both, increased the rate of conversion and the yields were comparable to those obtained with photocarbonylation without pyridine or hydrogen. Also, the presence of hydrogen in the purging gas increased the yield

Received November 18, 1994.

Y.L. Chow,[1] Y.J. Huang, and V. Dragojlovic. Department of Chemistry, Simon Fraser University, Burnaby, BC V5A 1S6, Canada.

[1] Author to whom correspondence may be addressed. Telephone: (604) 291-3352. Fax: (604) 291-3765. E-mail: ychow@sfu.ca

Can. J. Chem. Downloaded from www.nrcresearchpress.com by 65.111.164.53 on 09/08/12
For personal use only.

Can. J. Chem. Downloaded from www.nrcresearchpress.com by 65.111.164.53 on 09/08/12
For personal use only.

Scheme 1.

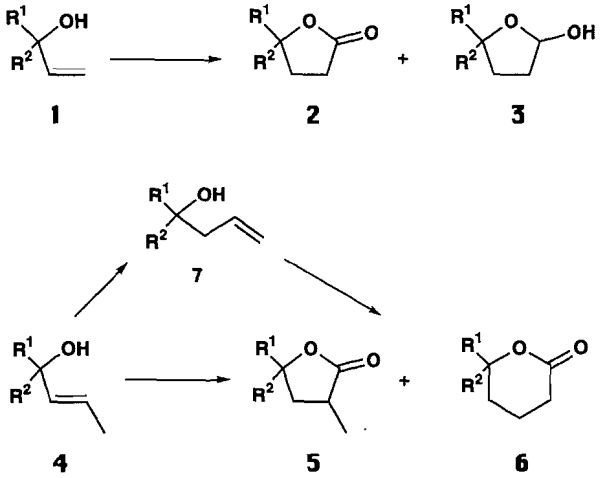

of lactols slightly. In contrast, attempted photocarbonylation of 2-propenol and 2-butenol gave a complex mixture arising from disproportionation and other reactions. 1-Phenyl-2-propenol gave propiophenone (74%) and a trace of the expected 4-phenylbutyrolactone (3%).

Photocarbonylation of geminal propenylcarbinols **4** gave not only γ-lactones **5** but also minor amounts of δ-lactones **6** (Table 1). The latter are produced from rearranged olefin **7** as evidenced by other experimental data (vide infra). The effect of temperature on the photocarbonylation of ***4a*** was significant, giving the ratio of lactones ***5a/6a*** as 2/1, 71/29, and 89/11 at 17, 11, and 0–2°C, respectively. The results indicate that the isomerization of **4** to the corresponding allylcarbinols **7** was suppressed at lower temperatures. The migration of a double bond during cobalt-catalyzed carbonylation is known (2, 3). Indeed, in separate experiments conducted under the same conditions, allylcarbinols **7** gave the mixture of lactones **5** and **6** in which the δ-lactones **6** predominated (Table 1). While the presence of pyridine increased the rate and the yields of photocarbonylation, *N,N,N′,N′*-tetramethyl-1,3-propyldiamine, 4,4′-dipyridine, 4-dimethylaminopyridine, or tributylphosphine retarded the rate and decreased the yield. Addition of phosphines also increased yields of the corresponding lactols **3**.[2]

Previous reports have established that the photosensitized reduction of cobalt salts with triplet-excited ketones under CO atmosphere in methanol or THF gives a 16-valence electron species $HCo(CO)_3$ or $Co(CO)_3^-$, which is most likely the species entering into the carbonylation sequence **8–11** (Scheme 2) (4, 5). This cobalt species was also proposed in thermal carbonylation processes, with supporting evidence (6, 7). A catalytic photochemical mechanism is proposed in Scheme 2 as the basis for the discussion, although the sensitization step may be also required in steps other than the excitation of $Co(CO)_4^-$.

Phosphines and amines retard the reaction rate through quenching triplet-excited ketones by electron transfer (8, 9), and 4,4′-bipyridine does the same, most likely by energy transfer mechanisms. These observations confirm that triplet sensitization is required to drive the catalytic cycle. The isomerization of propenylcarbinol **4** to the corresponding allylcarbinol **7** is a thermal process, which can be accounted for by reversible addition and nonspecific elimination of $HCo(CO)_3$ (2, 3). The process accounts for the isomerization of 2-propenol and 2-butenol to the corresponding aldehydes. While the reaction sensitized by triplet ketone is simple and facile, the use of substrates and ligands that interact with excited ketones could pose complications and further modifications may be necessary. However, the photoprocess offers

Table 1. Preparation of lactones.

Starting material	R^1, R^2	Products (yield,[a] %)	
1*a*	CH_3, CH_3	**2***a*(53)	**3***a*[b]
1*b*	CH_3, *n*-Bu	**2***b*(80)	**3***b*[b]
1*c*	$-(CH_2)_4-$	**2***c*(80)	**3***c*[b]
1*d*	$-(CH_2)_5-$	**2***d*(78)	**3***d*[b]
1*e*	$-(CH_2)_6-$	**2***e*(76)	**3***e*[b]
4*a*	CH_3,CH_3	**5***a*(42)	**6***a*(21)
4*b*	$-(CH_2)_4-$	**5***b*(39)	**6***b*(5)
4*c*	$-(CH_2)_5-$	**5***c*(47)	**6***c*(6)
4*d*	$-(CH_2)_6-$	**5***d*(56)	**6***d*(8)
7*a*	CH_3,CH_3	**5***e* and **6***a*(42)[c]	
7*b*	$-(CH_2)_4-$	**5***b*(18)	**6***b*(46)
7*c*	$-(CH_2)_5-$	**5***c*(17)	**6***c*(57)
7*e*	CH_3, Ph	**5***e* and **6***e*(49)[d]	

[a]Isolated % yield based on olefins.
[b]Minor products observed by GC and identified by GC-MS.
[c]**6***b* and **5***b* are isolated as 2:1 mixture as determined by GC analysis.
[d]**6***e* and **5***e* are isolated as 3:1 mixture as determined by GC analysis.

Scheme 2.

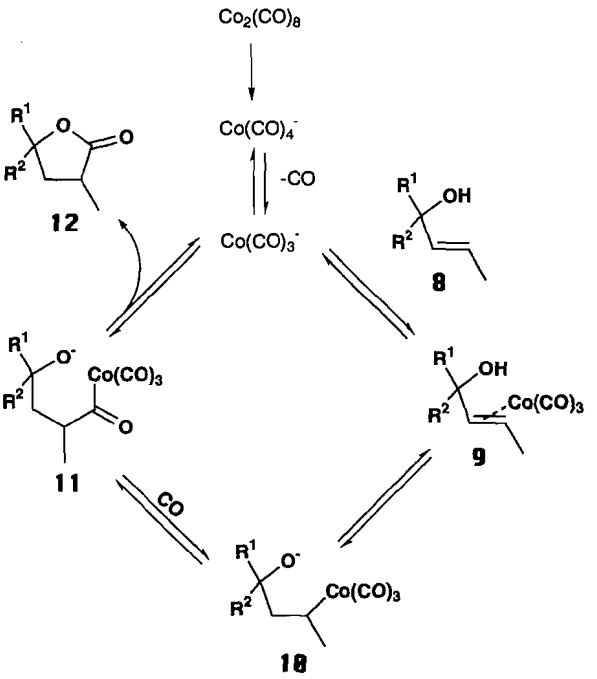

[2] IR, NMR, and MS data for compounds **2**, **5**, and **6** are available as supplementary material and can be purchased from: The Depository of Unpublished Data, Document Delivery, CISTI, National Research Council Canada, Ottawa, ON K1A 0S2, Canada.

control of temperature, which can suppress isomerization and improve regioselectivity. Further improvement of the process is under study.

References

1. (*a*) I. Wender and P. Pino. Organic synthesis via metal carbonyls. Vols. 1 and 2. Wiley–Interscience, New York. 1968 and 1977; (*b*) J. Falbe. Carbon monoxide in organic synthesis. Springer Verlag, West Berlin. 1970; (*c*) New synthesis with carbon monoxide. Springer Verlag, West Berlin. 1980; (*d*) G.W. Parshall. Homogeneous Catalysis. John Wiley, New York. 1980. Chap. 5; (*e*) J. Mol. Catal. **4**, 243 (1978); (*f*) H. Alper. Adv. Organometal. Chem. **19**, 183 (1981); (*g*) Rev. Pure Appl. Chem. **60**, 35 (1988); (*h*) I. J. B. Lin and H. Alper. J. Chem. Soc. Chem. Commun. 248 (1989).
2. (*a*) Y.T. Tao, T.J. Chow, J.T. Lin, C.C. Lin, M.T. Chien, C.C. Lin, Y.L. Chow, and G.E. Bueno-Core. J. Chem. Soc. Perkin Trans. 1, 2509 (1989); (*b*) Y.T. Tao, W.L. Yeh, C.L. Tu, and Y.L. Chow. J. Mol. Catal. **67**, 105 (1991).
3. C.P. Casey and C.R. Cyr. J. Am. Chem. Soc. **95**, 2240 (1973).
4. J.T. Lin, S.Y. Wang, S. K. Yeh, and Y. L. Chow. J. Organomet. Chem. **359**, C17 (1989).
5. M.J. Mirbach, M.F. Mirbach, A. Saus, N. Topasavoglou, and T.N. Phu. J. Am. Chem. Soc. **103**, 7590 (1981); **103** 7594 (1981).
6. (*a*) R.F. Heck and D.S. Breslow. J. Am. Chem. Soc. **85**, 2779 (1963); (*b*) J. Am. Chem. Soc. **83**, 4023 (1961).
7. F. Ungvary and A. Wojcicki. J. Am. Chem. Soc. **109**, 6848 (1987).
8. B. Marciniak and Y.L. Chow. J. Photochem. **32**, 165 (1986).
9. S.G. Cohen, A. Parola, and G.H. Parsons, Jr. Chem. Rev. **73**, 141 (1973).

Can. J. Chem. Downloaded from www.nrcresearchpress.com by 65.111.164.53 on 09/08/12
For personal use only.

8790

The 1994 Alcan Award Lecture Density functional theory as a practical tool in studies of organometallic energetics and kinetics. Beating the heavy metal blues with DFT[1]

Tom Ziegler

Abstract: An evaluation is given of approximate density functional theory as a practical tool in studies on organometallic energetics and kinetics. The evaluation covers electronic excitations and ionizations, electron capture, conformational changes, molecular vibrations, and bond energies, as well as reaction profiles.

Key words: density functional theory, energetics, kinetics, organometallic, catalysis.

Résumé : On présente une évaluation de la théorie de la densité fonctionnelle comme un outil pratique dans l'étude des énergétiques et des cinétiques des organométalliques. L'évaluation comprend les excitations et les ionisations électroniques, la capture électronique, les changements conformationnels, les vibrations moléculaires et les énergies de liaison ainsi que les profils réactionnels.

Mots clés : théorie de la densité fonctionnelle, énergétique, cinétique, organométallique, catalyse.

[Traduit par la rédaction]

1. Introduction

Molecular energetics covers a variety of properties, **1**, encompassing electronic excitations and ionizations, electron capture, conformational changes, molecular vibrations, and bond breakings, as well as the flipping of an electronic spin. Most of these properties are important at one time or another in studies involving organometallic thermochemistry and kinetics. It is thus necessary in theoretical studies on organometallic energetics to make use of computational methods that are able to treat all the properties in **1** accurately, or at least on an "equal footing."

Traditionally most theoretical studies have been carried out by *ab initio* Hartree–Fock (HF) methods or post-HF extensions in which electron correlation is included. We shall here discuss an alternative approach based on approximate Density Functional Theory (DFT) (1), which over the past decade has emerged as a tangible and versatile computational method. It has been employed successfully to obtain thermochemical data (2, 3) ; molecular structures (4, 5) ; force fields and frequencies (6); assignments of NMR (7), photoelectron (8), UV (9), and ESR (10) spectra; and transition state structures, as well as activation barriers (11); dipole moments (12); and other one-electron properties. Thus, approximate DFT is now applied to many problems previously covered exclusively by *ab initio* Hartree–Fock (HF) and post-HF methods. The recently acquired popularity of approximate DFT stems in large measure from its computational expedience, which makes it amenable even to large-size molecules. More important, perhaps, is the fact that expectation values derived from approximate DFT in most cases are better in line with experiment than results obtained from HF calculations and standard post-HF methods. This is, in particular, the case for systems involving transition metals. An analysis of why approximate DFT affords more reliable results than HF has recently been published by Cook and Karplus (13*a*) as well as Tschinke and Ziegler (13*b*). A recent analysis of DFT has been given by van Leeuwen (14).

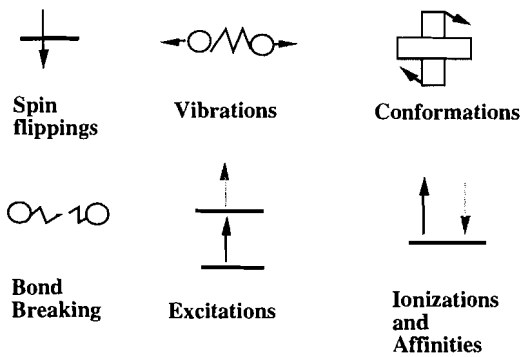

1

We shall in the present account evaluate DFT as a practical tool in studies of organometallic energetics and kinetics.

Received December 7, 1994.

T. Ziegler.[2] Department of Chemistry, University of Calgary, Calgary, AB T2N 1N4, Canada.

[1] This is an invited review article based on the 1994 Alcan Award Lecture delivered by Professor Ziegler at the annual conference of the Canadian Society for Chemistry in Winnipeg, Manitoba, in June 1994.

[2] Telephone: (403) 220-5368. Fax: (403) 220-9488. E-mail: Ziegler@zinc.chem.ucalgary.ca.

Can. J. Chem. Downloaded from www.nrcresearchpress.com by 80.90.12.36 on 09/08/12
For personal use only.

Can. J. Chem. Downloaded from www.nrcresearchpress.com by 80.90.12.36 on 09/08/12
For personal use only.

2. General theory and practical implementations

An electron will try to maximize the attraction from the nuclei and minimize the repulsion from the other electrons, **2a**, as it moves around in the molecular framework. This is done by creating an exclusion area or "no-fly zone" around each electron, **2b**, into which no other electron can penetrate. The exclusion zone is referred to as the exchange and correlation hole, and it is the way in which this hole is modeled that distinguishes one electronic theory from another (14, 15).

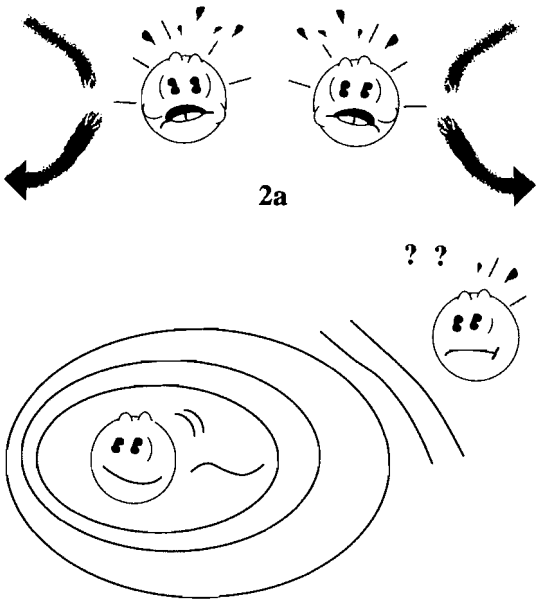

2a

2b

The first generation of DFT-based methods took their hole from the homogeneous electron gas. The Hartree–Fock–Slater method (HFS) (16) treats only exchange whereas the local density approximation (LDA) (17) takes into account both exchange and correlation. The HFS and LDA schemes are often referred to as the local methods. The second generation of DFT based theories acknowledges the fact that the density in molecules is far from homogeneous by introducing correction terms based on electron density gradients. These theories (LDA/NL) due to Langreth and Mehl (18*a*), Becke (18*b*), and Perdew (18*c*) are referred to as nonlocal. Nonlocal corrections are essential for a quantitative estimate of bond energies (18*e–k*) as well as metal–ligand bond distances (4*b*). They are also of importance for other properties (11*e*, 18*l*). Both LDA and LDA/NL suffer from the fact that they allow an electron to interact with itself to some degree. A number of authors have recently suggested ways in which the "self-interaction" error can be eliminated in a computationally efficient way (18*m*, *n*). These new methods form the vanguard for the third generation of DFT-based schemes.

A practical DFT-based calculation is in many ways similar to a traditional HF treatment in that the final outcome is a set of molecular orbitals. These functions are referred to as Kohn–Sham (KS) orbitals (1*a*) and are often expanded in terms of a basis set as in the traditional linear combination of atomic orbital (LCAO) approach of traditional methods.

In the earliest implementation of DFT applied to molecular problems, Johnson (19) used scattered-plane waves (20) as a basis, and the exchange–correlation energy was that of the LDA method. This SW-Xα method assumed in addition that the Coulomb potential is spherical around each atom, the muffin-tin approximation. This approximation is well suited for solids for which the SW-Xα method originally was developed. However, it is less appropriate in molecules where the potential around each atom might be far from spherical. The SW-Xα method is computationally expedient compared to standard ab initio techniques and has been used with considerable success (9) to elucidate the electronic structure in complexes and clusters of transition metals. However, the use of the muffin-tin approximation precludes accurate calculations of total energies. The method has for this reason not been successful (21) in studies involving molecular structures and bond energies.

The first implementations of self-consistent DFT, without recourse to the muffin-tin approximations, are due to Ellis and Painter (22) (DVM), Baerends et al. (23) (ADF),[3] Sambe and Felton (24), Dunlap et al. (25) (LCGT-LDA), as well as Gunnarson et al. (26) (LCMTO). Other implementations (27–30)[4] and refinements have also appeared more recently.

A unique approach in which the KS-orbitals are found directly without basis sets has lately been taken by Becke (31).[5] This approach, which seems promising, was first applied to diatomic molecules and more recently to polyatomics.

The use of plane waves as basis functions has received renewed interest in connection with the recent pioneering work by Car and Parrinello (CP) (32*a*). These authors were able to study molecular dynamics from first principles by evaluating the required forces "on the go" from DFT calculations. The method is best suited for plane-wave basis sets. Blöchl and co-workers (32*b*) eliminated some of the drawbacks of plane waves by introducing projector-augmented plane waves (CP-LAPW). The CP-LAPW method has great potential in studies of organometallic kinetics.

The various SCF schemes based on DFT are attractive alternatives to conventional *ab initio* methods in studies on large-size molecules since the computational effort increases as n^3 with the number of electrons, n, as opposed to between n^4 and n^7 for post-HF methods of similar accuracy. The scope of density-functional-based methods has further been enhanced to include pseudo-potentials (33) and relativistic effects (34), as well as energy gradients of use in geometry optimization (4, 35) and analytical second derivatives (32*d–g*) with respect to nuclear displacements. The existing program packages, ADF (23), DeMon, DMOL (35*f*),[4] DGAUSS (30*b*), GAUSSIAN/DFT (32*c*), and CADPAC (32*d*), are now nearly as user friendly as their *ab initio* counterparts although much work remains to be done.

3. A validation of approximate density functional theory

Our contribution to the development of practical DFT-based methods has focused on schemes that would enable a full

[3] The ADF program is available from Molecular Simulation and E.J. Baerends.

[4] DGauss available from CRAY; DMol available from Biosym. DMon was developed by Salahub et al. at the University of Montreal, Canada. NUMOL was developed by Becke at Queens University, Kingston, Canada

[5] The program outlined in refs. 31*d*, *e* is called NUMOL.

Table 1. First metal–carbonyl dissociation energy[a] in a number of metal carbonyls.

Molecule	LSD[b]	LSD/NL[b]	Expt.
$Cr(CO)_6$	276	193	192/155
$Mo(CO)_6$	226	166	170
$W(CO)_6$	249(202)[c]	183(162)[c]	192
$Fe(CO)_5$	263	192	176
$Ni(CO)_4$	192	121	104

[a]All energies in kJ/mol.

[b]References 18*i*, *j*.

[c]Numbers in parentheses for $W(CO)_6$ are nonrelativistic results, all other energies include relativistic effects.

study of an elementary reaction step in organometallic chemistry and homogeneous catalysis. We have as a prerequisite explored how well approximate DFT evaluates the structure and energetics of organometallics, and developed algorithms that would make the calculation of these properties tractable. We shall in the following provide an account of the results obtained from these efforts.

Bond energy calculations

The generation of a coordinatively unsaturated 16-electron reactive species (catalyst) by dissociation of an 18-electron saturated (and unreactive) complex, **3**, is a recurring theme in homogeneous catalysis. Table 1 affords calculated values for such a process involving the first CO dissociation in a number of binary metal carbonyls.

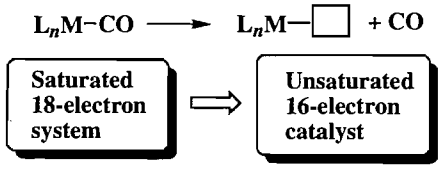

3

It follows from Table 1 that the first generation of DFT methods based on LDA overestimate the M—CO bond energies considerably. The overbinding is typical for LDA (1*c*), and it appeared for a while as if approximate DFT would be of limited use in studies of organometallic thermochemistry.

This situation was changed by the development of gradient-based corrections due to Becke (18*b*), Perdew (18*c*), and others. Thus, adding the nonlocal exchange (18*b*) and correlation (18*c*) corrections to the LDA energy expressions, LDA/NL, improves considerably the agreement between theory and experiment. In fact, the agreement is now so good that LDA/NL actually might be useful as a predictive tool, Table 1. This is important since reliable metal–ligand bond energies are difficult to obtain experimentally.

The results in Table 1 include relativistic effects for all three members of the chromium triad although these only are important for the heavier 5*d* congener tungsten. The importance of relativistic effects for the heavier 5*d* element is underlined by including the calculated nonrelativistic W—CO bond energy in parentheses. It follows from the comparison between the two sets of W—CO bond energies that relativity strengthens the W—CO bond to the point where it is stronger than the Mo—CO linkage. Thus relativity is responsible for the V-shaped trend in the M—CO bond energies within the chromium triad with a minimum at the 4*d* element molybdenium. We have found a similar V-shaped trend in the series $M(CO)_5$ (M = Fe, Ru, Os) (18*j*); $M(CO)_4$ (M = Ni, Pd, Pt) (18*j*); $M(PH_3)_2X$ (M = Ni, Pd, Pt; X = O_2, C_2H_2, C_2H_4) (36*a*); $M(PH_3)_4X^+$ (M = Co, Rh, Ir; X = O_2, C_2H_2, C_2H_4) (36*b*); $M(PH_3)_4C_2H_4$ (M = Fe, Ru, Os (36*a*); and $M(CO)_5H_2$ (M = Cr, Ru, Os) (36*c*).

The relativistic stabilization of the M—X bond, where X is a π^* or σ^* acceptor, is a result of a relativistic destabilization of the metal 5*d* orbitals that increases the back-donation to the ligand X. The 5*d* levels are destabilized as relativity contracts the core orbitals and reduces the effective nuclear charge (36*d*,*e*). Our calculations confirmed and rationalized the experimental observation according to which the dissociation of a π-acceptor ligand often is most facile within a homologous series for the 4*d* member of a triad.

The most important steps in a catalytic cycle, after the coordinatively unsaturated 16-electronic species, **3**, has been generated, involve the formation and dissociation of metal–carbon or metal–hydrogen σ-bonds. The relative strength of these bonds is further delicately balanced and this balance has important implications for the type of elementary reaction steps that are possible in homogeneous catalysis.

Thus, CO will readily insert into a M—CH_3 bond, eq. [1*a*], whereas the corresponding insertion into a M—H linkage basically is unknown, eq. [1*b*].

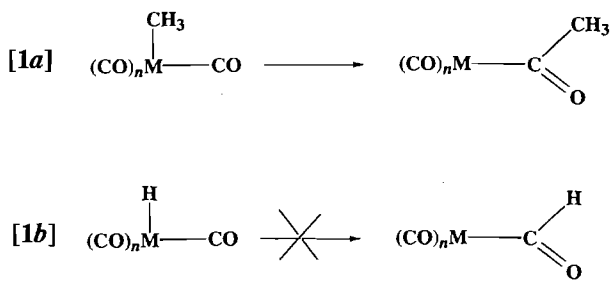

Also, the H_2 molecule is known to add oxidatively to several metal fragments, eq. [2*a*], whereas the corresponding oxidative addition of the H–alkyl bond, eq. [2*b*], is more difficult and the alkyl–alkyl bond addition is virtually unknown, eq. [2*c*].

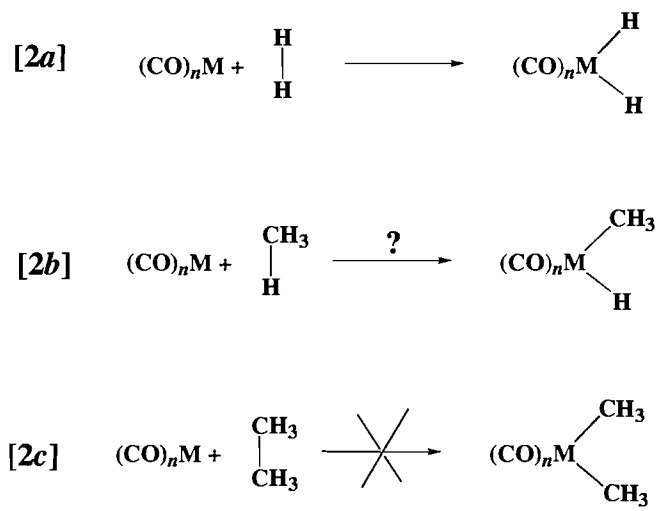

Oxidative addition and CO insertion are typical for late to middle transition metals and the trends in eqs. [1 and 2] have

Can. J. Chem. Downloaded from www.nrcresearchpress.com by 80.90.12.36 on 09/08/12
For personal use only.

Can. J. Chem. Downloaded from www.nrcresearchpress.com by 80.90.12.36 on 09/08/12
For personal use only.

Table 2. Calculated[a] and experimental[b] σ-bond energies.

Bond	LDA	LDA/NL	Expt.
$(CO)_5Mn—H$	324	288	284 ± 4
$(CO)_5Mn—CH_3$	322	207	192 ± 11
$(CO)_4Co—H$	332	282	280 ± 4
$(CO)_4Co—CH_3$	287	197	—
$(CO)_5Mn—Mn(CO)_5$	—	174	171
$(CO)_4Co—Co(CO)_4$	—	148	61–88

[a]References 37 and 39.
[b]Reference 40.

been explained by assuming that the M—H bond is stronger than the M–alkyl bond for these metals.

It is clear that the approximate DFT methods must be able to account for the important differences between M—H and M—CH_3 bond energies in order to be of use in studies of organometallic energetics. Table 2 compares calculated M—R (R = CH_3, H) bond energies with the experimental data available for late to middle transition metals. It follows from Table 2 that LDA/NL is able to reproduce the experimental $(CO)_3Mn—H$, $(CO)_5Mn—CH_3$, and $(CO)_4Co—H$ bond energies well and to predict the Mn—H bond to be stronger than the Mn—CH_3 linkage. Unfortunately, reliable experimental (37–39) bond energies for both M—H and M–alkyl with respect to the same metal are only available for a few systems, which makes a more extensive comparison between experiment and theory (40) impossible.

However, we present in Fig. 1 a systematic theoretical study of M—R (R = H, CH_3) bond energies for late, middle, and early transition metals as well as *f*-block elements. The figure provides in addition the trends in the M—R bond energies within a triad of metals. The study presented in Fig. 1 is based on an older and less accurate second-generation functional (18*e*,*f*, 41*b*) than that used to generate the data in Table 1 (40). Thus, the Mn—R and Co—R bond energies differ slightly from those in Fig. 1. However, the trends should be accurate.

It follows from Fig. 1 that the M—R bond increases in strength as we descend a triad of transition metals. Further, for the late to middle transition metals the M—H bond is stronger than the M—CH_3 linkage. On the other hand, for early transition metals and *f*-block elements the two bonds are quite similar in strength. The trend can be rationalized by observing that the occupied C—H bond orbitals suffer a destabilizing interaction with occupied *d*-orbitals for the electron-rich late to middle transition metals. A similar repulsive interaction is not present in the metal hydrides. On the other hand, for the early transition metals and *f*-block elements the destabilization of the M—CH_3 bond disapears since the *d*-orbitals on the metal center are empty. Thus, the M—H and M—CH_3 bonds become similar in energy.

It seems at the present time that the LDA method augmented with nonlocal exchange and correlation corrections (LDA/NL) represents the most efficient and accurate method for the evaluation of bond energies within the density functional framework. Calculations on metal carbonyls (18*i*,*j*), binuclear metal complexes (40, 41*g*), and alkyl and hydride complexes (18*e*,*h*), as well as complexes containing M—L bonds for a number of different ligands (18*h*), have shown that LDA/NL affords metal–ligand and metal–metal bond energies of nearly chemical accuracy (±5 kcal mol^{-1}).

Molecular structures

The full optimization of molecular structures has been carried out routinely by *ab initio* methods since the algorithm of analytical energy gradients was developed in the early 1970s. *Ab initio* methods at the Hartree–Fock level usually yield satisfactory equilibrium structures for main group molecules (42). More accurate electron-correlation calculations can also be carried out to improve the agreement between theory and experiment as long as the size of the molecule under investigation remains reasonably small. The size of systems that can be handled by such calculations has been constantly increasing for the past two decades due to the fast development of computer technology and improved software.

The reasonable performance of the Hartree–Fock method on main group molecules seems not to be transferable to transition-metal complexes (43). Thus, a discrepancy of 0.1 Å between HF results and experimental findings is not uncommon for metal–ligand and metal–metal bonds. Faegri et al. (44*a*) have pointed out that such discrepancies most likely are due to the inherent shortcomings of the HF method rather than basis set limitations. Thus post-HF methods are essentially necessary in the study of transition metal compounds. It is, however, unlikely that *ab initio* methods beyond the Hartree–Fock level can be applied routinely to larger systems involving transition-metal complexes in the foreseeable future.

Density functional theory (DFT) has been widely applied to the investigations of systems involving transition metal complexes, and it has proven to be a very successful alternative to the computationally more demanding post-HF *ab initio* methods (1). Geometry optimizations by LDA and LDA/NL are now feasible due to the successful implementation of analytical energy gradients (4, 5, 35). The agreement between experimental geometries and structures optimized by DFT is, in general, good (4, 5, 35). For main group molecules, LDA/NL overestimates bond distances by 0.01 Å (35*g*) and angles deviate by 1°. The third-generation functionals by Becke (18*m*) reduce the error in bond distances to 0.005 Å (35*g*).

The superiority of DFT-based methods over the HF scheme is most striking in the prediction of metal–ligand bond lengths, as shown in Table 3. The M—L bond distances optimized by the LDA method are 0.02–0.05 Å shorter than the experimental values for the molecules listed in Table 3. On the other hand, *ab initio* calculations at the HF level yield bond distances that are too long by 0.05–0.2 Å. The only exception is the HF calculation on C_5H_5NiNO, where the the Ni—N bond distance was found to be too short by 0.2 Å, most likely due to the minimal STO-3G basis sets employed in the calculations. It is important to note that the HF method in the case of $Fe(CO)_5$ provides a distorted geometry for $Fe(CO)_5$ with the Fe—C_{ax} bond much longer than the Fe—C_{eq} distance, whereas experiment and LDA find the two Fe—CO distances to be about equal, Table 3.

The LDA method systematically underestimates (4*b*, 45) metal–ligand bond distances, and the same trend (4*b*) is found in connection with calculations based on other first-generation DFT schemes. Fortunately, the deficiencies of the local methods are seen largely to be eliminated by the nonlocal correction to exchange and correlation. Thus, the LDA/NL metal–ligand bond distances (4*b*) in Table 3 are within 0.01 Å of experiment. It is gratifying that the LDA/NL method not only

Fig. 1. Calculated M—H and M—CH_3 bond energies.

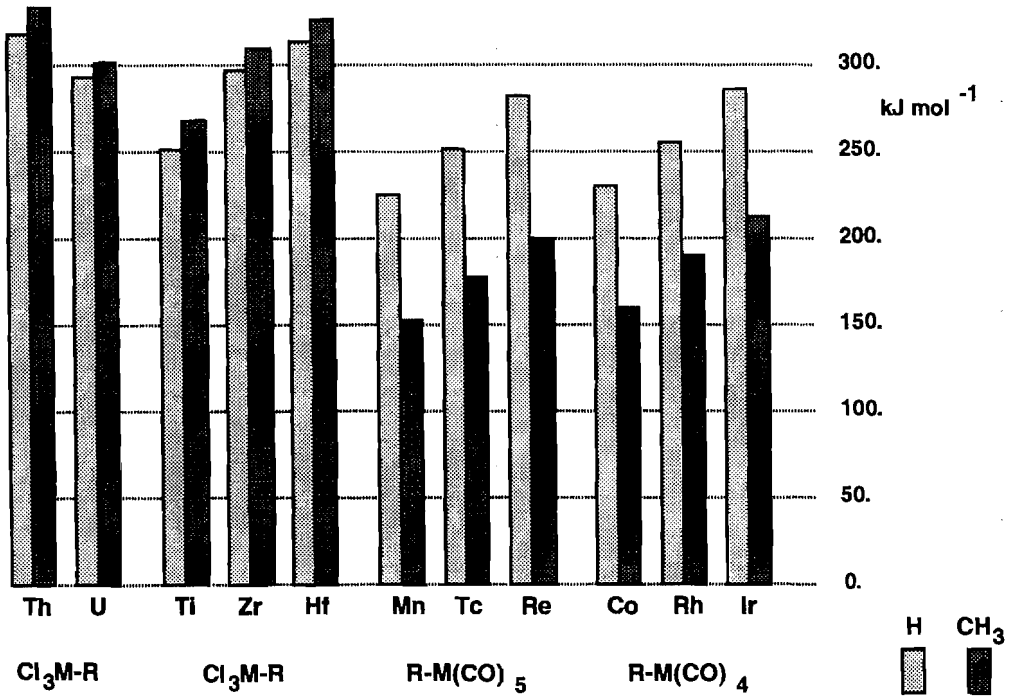

Table 3. Structures of transition-metal complexes optimized by different methods.[a]

Molecule	Bond(Å)	LDA	LDA/NL	HF	Expt.
C_5H_5NiNO	Ni—N	1.592	1.620	1.424	1.626
$Ni(CO)_4$	Ni—C	1.794	1.841	1.921	1.838
$Fe(CO)_5$	Fe—C_{ax}	1.774	1.817	2.047	1.807
	Fe—Ceq	1.798	1.814	1.874	1.827
$Fe(C_5H_5)_2$	Fe—Cp	1.60	1.648	1.88	1.65
$Cr(CO)_6$	Cr—C	1.868	1.909	~2.00	1.914
MnO_4^-	Mn—O	1.603	1.631		1.63

[a]Reference to original data in ref. 4*b*.

Table 4. Calculated and experimental bond lengths (Å) for $M(CO)_6$.

	$Cr(CO)_6$		$Mo(CO)_6$		$W(CO)_6$	
Method	M—C	C—O	M—C	C—O	M—C	C—O
LDA	1.866	1.145	2.035	1.144	2.060	1.144
LDA/NL	1.910	1.153	2.077	1.152	2.116	1.154
LDA/NL + QR	1.910	1.153	2.076	1.153	2.049	1.155
MP2[a]	1.883	1.168	2.066	1.164	2.054	1.166
CCSD(T)[b]	1.939	1.178				
Exp	1.918	1.141	2.063	1.145	2.058	1.148

[a]Reference 44*b*.
[b]References 44*c*,*d*.

affords better bond energies, Table 1, but also more accurate geometrical parameters.

Table 4 displays M—CO and C—O distances for the three hexacarbonyls $M(CO)_6$ (M = Cr, Mo, W) determined by various computational methods as well as by X-ray diffraction. We note that LDA/NL improves the LDA M—CO estimates for M = Cr and Mo whereas the W—CO distance calculated by LDA/NL is too long. However, a much better agreement with experiment is obtained for the W—CO distance by including relativistic effects in the LDA/NL+QR scheme, Table 4. Thus, relativity is essential for an accurate estimate of geometries since it might result in metal–ligand bond contractions of 0.10 Å (18*i*–*k*).

Also included are estimates of the M—CO bond distances calculated by the simplest post-HF method, MP2 (44*b*), with

Can. J. Chem. Downloaded from www.nrcresearchpress.com by 80.90.12.36 on 09/08/12
For personal use only.

Table 5. Decomposition of the first carbonyl dissociation energy (FCDE)[a] for $W(CO)_6$ at the non-relativistic (NL-SCF) and relativistic (NL-SCF + QR) levels.

	E_{steric}	$E_{donation}$	$E_{back\text{-}donation}$	E_{prep}	FCDE[b]
NL-SCF	−39.5	29.2	44.2	−0.3[c]	34.2[c]
NL-SCF + QR	−35.0	19.6	60.1	−1.0	43.7

[a]Energies in kcal/mol.

[b]Total bond energy is given as FCDE = $E_{steric} + E_{donation} + E_{back\text{-}donation} + E_{prep}$.

[c]The geometry used in the ETS calculations is the one obtained at NL-SCF + QR level in both cases. The NL-SCF bond energy is increased by 4.6 kcal/mol at the NL-SCF geometry.

Can. J. Chem. Downloaded from www.nrcresearchpress.com by 80.90.12.36 on 09/08/12
For personal use only.

relativistic effects included. We note that the MP2 results are in line with experiment for the 4*d* and 5*d* elements whereas the Cr—CO distance is too short. For 3*d* elements, high-level and rather expensive methods such as the coupled cluster scheme CCSD(T) are required in order to obtain good geometries (44*d*). It should be noted that the CCSD(T) scheme also provides accurate estimates of the M—CO dissociation energies (44*d*).

Energy differences of isomers and conformers.

There have been a number of DFT-based studies on the relative stability of isomers and conformers. These include the relative energies of eclipsed and staggered conformations in $Fe(C_5H_5)_2$ and C_2H_6 (45), as well as a number of binuclear metal complexes (41*g*, 46, 47). Conformational energy differences seem (45) to be well represented even by the first generation of DFT methods such as LDA and HFS. The energetics for different coordination modes of ligands complexed to transition metals have been studied for phosphaalkene (48*a*), F_2 and H_2 (48*b*), alkenes and alkynes (48*c*,d), BH_4^- (48*e*), O_2 (48*d*), X_2, CX_2 (X = O, S, Se, Te) (48*f*,*g*), carbocycles (48*i*), thio- and selenoethers (48*j*,*k*), and carbenes (48*l*–*n*), as well as H (48*h*). A special energy decomposition scheme, the extended transition state method (ETS), has been devised (30,41*d*,48*c*,49) that breaks down the coordination energy of a ligand into steric and electronic factors. The ETS scheme makes it possible to explain interaction energies as well as conformational preference of a ligand in terms of well-established chemical concepts. As examples, the decomposition analysis is able to provide estimates of the respective contributions from the σ π and δ components in binuclear metal complexes (41*g*, 47, 48*j*) with multiple bonds, **4a**; the relative importance of donation and back-donation in transition metal complexes of unsaturated ligands (48, 49) such as olefins, **4b**, or carbonyls; the contributions (48*h*) to the protonation energy, **4c**, from the pure electrostatic interaction between the proton and the metal fragment, as well as the charge rearrangement following the formation of the protonated complex.

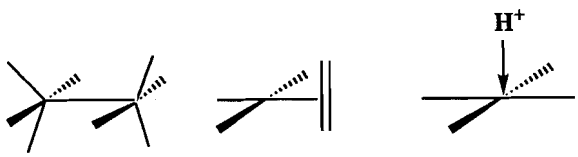

4a **4b** **4c**

An illustrative example of how ETS is used is given in Table 5 where the first carbonyl dissociation energy (FCDE) of $W(CO)_6$ is decomposed as

[3] $FCDE = E_{steric} + E_{donation} + E_{back\text{-}donation} + E_{prep}$

for both the nonrelativistic (LDA/NL) and relativistic (LDA/NL+QR) case. In eq. [3] E_{steric} represents the steric interaction energy (destabilizing) between CO and $W(CO)_5$ whereas $E_{donation}$ represents the stabilizing CO to $W(CO)_5$ charge donation and $E_{back\text{-}donation}$ the corresponding stabilizing $W(CO)_5$ to CO back-donation. Finally, E_{prep} represents the energy required to distort CO and $W(CO)_5$ to the geometries they have in the combined $W(CO)_6$ complex. The ETS analysis in Table 5 clearly indicates that relativity enhances the back-donation contribution, $E_{back\text{-}donation}$, and decreases the donation energy term, $E_{donation}$. The reason for this was explained previously in the section on bond energy calculations. Further, back-donation is seen to be more important than donation for the W—CO bond strength.

The HF method represents conformational energies of saturated systems, such as rotation barriers in alkanes, quite well. It is not likely that LDA or LDA/NL will afford substantially different results for this type of systems. However, examples are known among transition-metal complexes for which HF- and DFT-based methods differ. Thus, HF (50*a*) finds $HCo(CO)_4$ of C_{2v} symmetry, with hydrogen in an equatorial position, to be more stable than the experimentally observed C_{3v} structure where hydrogen is in the axial position. On the other hand, LDA (50*b*) finds the C_{3v} structure to be the more stable conformation.

A very recent (40) conformational study based on DFT involves $Co_2(CO)_8$ with the two structures **5a** and **5b**. The study finds **5a** with bridging carbonyls to be 22 kJ/mol more stable than **5b** with an unsupported cobalt-cobalt bond. Conformation **5a** is found to be the more stable in the gas phase and the solid state whereas **5b** is prevalent in solution.

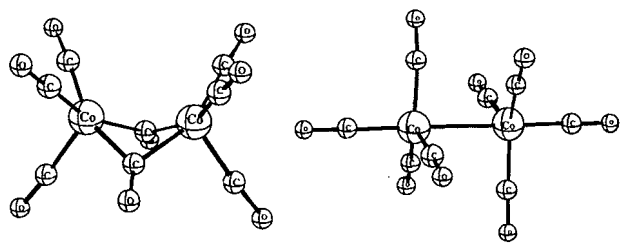

5a **5b**

Electronic excitation energies and excited states

We shall in the following sections discuss calculations on energy differences associated with the processes of (*a*) excitation from one electronic state to another; (*b*) ionization; (*c*) electron attachment. The change in energy ΔE associated with these processes can be written as

Table 6. Excitation energies (eV).

	HFS	LDA	LDA/NL	Expt.
CO ($5\sigma \rightarrow 2\pi$)	5.37	6.12	6.18	6.3
CS ($5\sigma \rightarrow 2\pi$)	2.87	3.42	3.48	3.42
O_2 ($^3\Sigma g \rightarrow {}^1\Delta g$)	1.34	1.04	0.82	0.98

Reference to original data given in ref. 51.

Fig. 2. Comparative estimates of the first excitation energy of the CO molecule from HFS and LDA calculations. The energy of the triplet states is the reference level for the HFS and LDA energies.

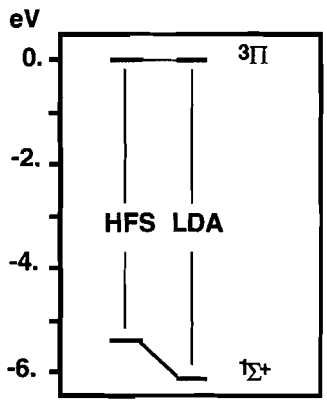

$$[4] \quad \Delta E = \Delta E_k + \Delta E_{ne} + \Delta E_{ee} + \Delta E_x + \Delta E_c$$

The first three terms in eq. [4] represent the change in kinetic, electron–nuclear attraction, and electron–electron repulsion energies, respectively, whereas the last two terms represent the change in exchange and correlation energies, respectively.

In our assessment of the HFS, LDA, and LDA/NL methods, we shall consider as our first case the energy ΔE required to promote CO or CS from the $^1\Sigma$ ground state to the first excited triplet state $^3\Pi$. The HFS method differs from LDA in that ΔE_c in eq. [4] is neglected ($\Delta E_c = 0$). The contribution from ΔE_c to ΔE should, however, be positive, as $^1\Sigma$ has one additional pair of electrons with opposite spins compared to $^3\Pi$, and thus[6] $E(^1\Sigma)$ has a larger negative contribution from E_c than $E(^3\Pi)$. Thus, we expect that ΔE from a HFS calculation (51) should be smaller than ΔE calculated by the LDA method, as indicated in Fig. 2. This expectation is borne out by our numerical calculations, Table 6. In fact, for CO and CS the excitation energies calculated by the HFS method are too small compared to experiment, whereas the larger ΔE values due to the LDA method are more in line with experimental excitation energies, Table 6.

Also considered in Table 6 is the energy ΔE required to promote O_2 from its $^3\Sigma_g$ ground state to the first excited state $^1\Delta_g$. For this process, the term ΔE_c in the expression of eq. [4] should be negative, since $^1\Delta_g$, compared to $^3\Sigma_g$, has one additional pair of electrons with opposite spins. Neglecting the contribution to ΔE from ΔE_c, as is done in the HFS method, must now lead to too large an excitation energy, Table 6, whereas LDA in which correlation between electrons of different spins is taken into account provides a smaller value for ΔE (since ΔE_c is negative), more in line with the experimental excitation energy, Table 6. It is finally seen that nonlocal corrections give rise to a small improvement in the calculated excitation energies.

The local DFT scheme (16) has been used extensively to calculate excitation energies, and many of the applications have been reviewed (9). An indication of the high accuracy usually obtained by approximate DFT methods is given in Table 7. This table presents calculation (52*a*) on the three first excited states in tetrahedral d^0 oxo complexes MnO_4^-, CrO_4^{2-}, and VO_4^{3-}. A special method has been developed by Ziegler et al. (52*b*) to resolve multiplets in electronic configurations by DFT.

In particular, the electronic spectrum of MnO_4^- has served as an acid test for new theoretical methods, and post-HF schemes failed for a long time to calculate the excitation energies of MnO_4^- with near quantitative accuracy. It is only recently, nearly 20 years after the DFT results, that post-HF methods have become available (53*b*,*c*) that can deal accurately with the excited states of transition-metal complexes such as MnO_4^-. Buijse and Baerends (54) recently analyzed the error sources in HF calculations on MnO_4^-. A more recent DFT study looked at the electronic spectrum of iron(III) porphines (53*a*).

It has often been stated that DFT applies only to ground state properties. This is not the case, either from a formal (53*d*) or a practical (52*b*) point of view. In fact, the first chemical applications (19) of DFT all dealt with excitation energies of metal complexes. DFT can be used to evaluate molecular properties of excited states in much the same way it treats ground state properties. As an example involving geometries, we display in Fig. 3 the harmonic potential energy surface along the totally symmetric Mn—O stretch in the case of the three first excited states corresponding to the $t_1 \rightarrow 2e$, Fig. 3*a*, $4t_2 \rightarrow 2e$, Fig. 3*b*, and $t_1 \rightarrow 5t_2$, Fig. 3c, transitions. All transitions are from nonbonding oxygen lone pairs (t_1 and $4t_2$) to antibonding metal *d*-orbitals ($2e$ and $5t_2$). We note a substantial elongation of the Mn—O bond from the ground state equilibrium distance, indicated by an arrow, at R(Mn—O) = 1.632 Å. It should be possible to use DFT to calculate excited state properties in much the same way as expectation values for the ground state, and studies on this subject are likely to appear in the near future.

Ionization potentials

Photoelectron spectroscopy (PES) emerged in the early 70s as a new and exciting technique with direct bearing on molecular orbital energies. It is thus not surprising that PES has served as a testing ground for new and increasingly sophisticated theoretical methods including DFT-based schemes. In fact, one of the first successful applications of the HFS method in chemistry involved the assignment of photoelectron spectra. The early work based on the SW-Xα method has been reviewed by Case (9).

We shall now consider the energy ΔE required to remove an electron from a molecule. In the corresponding expression of

[6] We base our rationalization of the trend in ΔE_c on the assumptions that the correlation energy in atoms and molecules is roughly proportional to the number of opposite-spin electron pairs.

Can. J. Chem. Downloaded from www.nrcresearchpress.com by 80.90.12.36 on 09/08/12
For personal use only.

Can. J. Chem. Downloaded from www.nrcresearchpress.com by 80.90.12.36 on 09/08/12
For personal use only.

Fig. 3. Harmonic potential energy surface for the first three excited states of permanganate along the a_1 mode corresponding to the Mn—O stretch. The calculated ground state Mn—O distance at 1.632 Å is indicated by arrow. (*a*) $t_1 \rightarrow 2e$; (*b*) $4t_2 \rightarrow 2e$; (*c*) $t_1 \rightarrow 5t_2$.

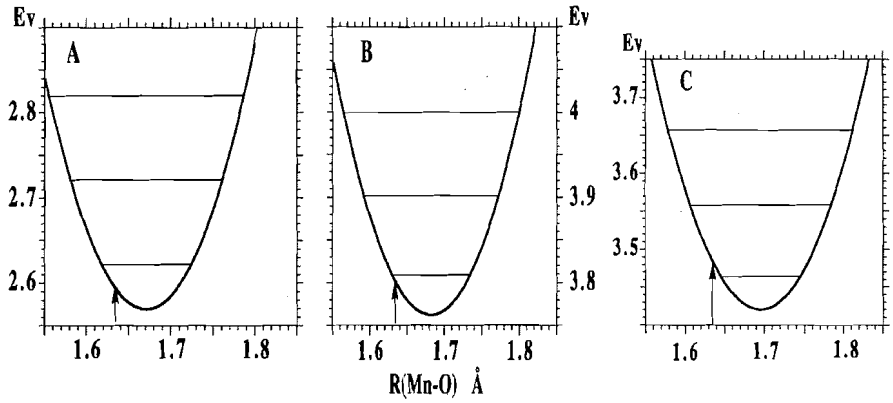

Table 7. Singlet excitation[a] energies for tetrahedral d^0 oxo complexes in eV.

	MnO_4^-		CrO_4^{2-}		VO_4^{3-}	
Transition	E_S^{cal}	E_s^{exp}	E_S^{cal}	E_s^{exp}	E_S^{cal}	E_s^{exp}
$t_1 \rightarrow 2e$	2.48	2.27	3.30	3.32	4.51	4.58
$4t_2 \rightarrow 2e$	3.96	3.47	4.58	4.53	5.71	5.58
$t_1 \rightarrow 5t_2$	4.15	3.99	4.90	4.86	6.15	6.15

[a]Original data from ref. 52*a*. [b]Calculated values based on the HFS method.

Fig. 4. Comparative estimates of the first ionization energy of the CO molecule by HFS and LDA calculations. The energy of the ion is the reference level for the HFS and LDA energies.

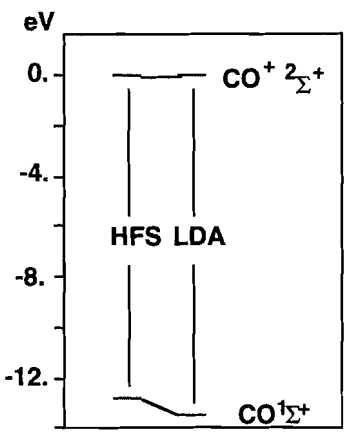

eq. [4], the contribution from ΔE_c to ΔE will be positive for the molecules considered here, since the neutral molecule has one additional pair of electrons with opposite spins compared to the ion. As indicated in Fig. 4, we must thus expect HFS ($\Delta E_c = 0$) to provide smaller ionization energies than LDA ($\Delta E_c > 0$).

It follows from Table 8, where we compare the first two ionization energies for a number of molecules calculated by the two methods with experimental values, that HFS provides too small ionization energies, whereas the larger LDA values are more in line with experiment. However, as shown in Table 8,

Table 8. Ionization energies (eV).

	HFS	LDA	LDA/NL	Expt.[a]
N_2	14.60	16.95	16.81	16.98
	16.6	16.95	16.81	16.98
CO	12.81	13.50	13.85	14.01
	16.71	17.17	17.01	16.53
F_2	14.78	15.02	15.34	15.70
	18.08	18.35	18.58	18.98
H_2O	12.03	12.55	12.59	12.62
	13.95	14.46	14.60	14.75
NH_3	10.06	10.62	10.76	10.88
	15.59	15.98	16.37	16.0
CH_4	13.18	13.61	14.01	14.35
	21.20	21.50	22.00	23.00
C_2H_4	10.14	10.60	10.56	10.51
	11.84	12.22	12.75	12.85

The first and second ionization energies of each molecule are presented in the given order. All ionization energies are vertical ionization energies; all values presented are from ΔSCF calculations.

[a]Original data in ref. 51.

the correlation correction to the HFS method, while of the right sign, is not large enough to align LDA ionization energies with experiment, leaving some room — and need — for further improvement of the HFS method. This improvement is accomplished by the LDA/NL scheme. The non local corrections are seen to supply a small but significant improvement for all the molecules. A more detailed analysis of how

Can. J. Chem. Downloaded from www.nrcresearchpress.com by 80.90.12.36 on 09/08/12
For personal use only.

Fig. 5. Schematic representation for the energy of the quadruple-bonded binuclear complex M_2L_{2n} in its ground state and first three ion states, corresponding to ionization out of the σ, π, and δ bonding orbitals, as a function of the metal–metal bond distance R_{MM}. Schematic representation of the three first PE bands *A*, *B* and *C* with their vibrational shapes.

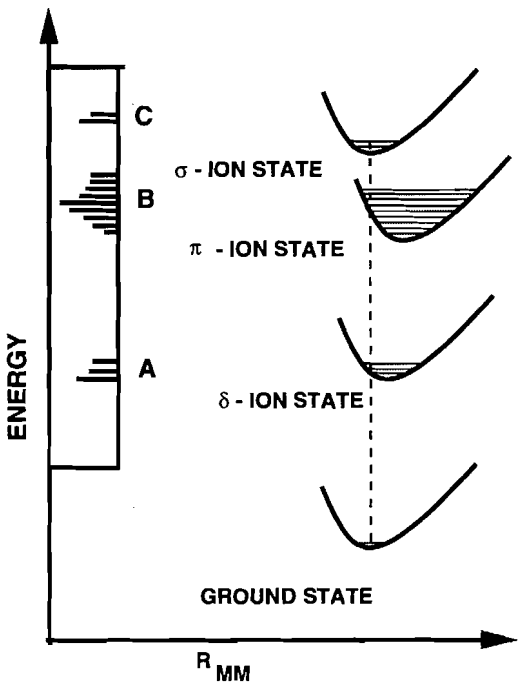

Table 9. Ionization potentials (eV) for transition metal complexes.

ML_n	HFS	Expt.
$Ni(CO)_4$	9.3	8.9
	10.3	9.8
$Cr(CO)_6$	8.9	8.4
	10.3	13.4
$Fe(CO)_5$	9.0	8.6
	10.2	9.9
RuO_4	11.9	12.1
	12.9	12.9
Cp_2Fe	6.7	6.9
	6.7	7.2

nonlocal corrections improve on the calculated ionization potentials is given elsewhere (51).

There have been several recent applications of approximate DFT to photoelectron spectroscopy, including some in which relativistic effects have been taken into account (46, 47, 48*g*). In Table 9 we present HFS calculations on the first two ionization potentials for a number of organometallics. The agreement with experiment is in general quite good. An extensive investigation combining the calculation of bond distances and PE spectra involves the binuclear complexes $M_2(O_2CR)_4$ and $M_2Cl_4(PR_3)_4$ (M = Cr, Mo, W) with a quadruple metal–metal bond (47*b*). Their PE spectra, see Fig. 5, reveal three bands (*A*, *B*, *C*) corresponding to an ionization out of the δ, π, and σ, metal–metal bonding orbitals with the *B* band being considerably broader than either *A* or *C*. The assignment of *A*, *B*, and *C* has been controversial. Approximate DFT calculations (47*b*) assign *A*, *B*, and *C* to δ, π, and σ, respectively. The potential energy surfaces in Fig. 5 were, in addition, able to explain the broad feature of *B* in terms of a large change in the the R_{MM} equilibrium distance for the π ion state.

It is to be expected that the more accurate LDA/NL scheme will replace the HFS method in calculation of ionization potentials. It would be interesting to carry out a systematic evaluation of how well LDA/NL is able to calculate ionization potential and PES spectra for transition-metal complexes. However, such a study has not yet been carried out.

Electron affinities

The adiabatic electron affinity (EA_{ad}) of a molecule represents the decrease in energy of the molecular system when a single electron is added. It is, in general, a difficult property to obtain from experimental as well as computational techniques. The most accurate experimental estimates of electron affinities are obtained by laser photo-ionization of negatively charged systems. However, this technique is limited to anions that can be studied in the gas phase. It is still not routine to measure electron affinities accurately, and values obtained by alternative techniques often differ considerably even for relatively simple molecules.

Electron affinities also offer a considerable challenge from the computational point of view. In the first place, one must be able to describe accurately the difference in geometry between the neutral molecule M and the corresponding anion M^-. The computational method must in addition be able to account quantitatively for the difference in electron correlation energy between M and M^-. This difference is in most cases substantial due to the change in the number of electron pairs. Finally, the basis set employed must be flexible enough to describe M as well as M^- with a somewhat more diffuse charge distribution. It is thus not surprising that accurate electron affinities are available only for a very limited number of molecules.

We compare in Table 10 calculated EA_{ad} values with experiment for a number of small well-studied molecules. The comparison includes (55) HFS and LDA, as well as LDA with nonlocal exchange corrections (LDA/NL). Also included are results (56) based on HF, configuration interaction with all single and doubles (RCISD), as well as the equation of motion approach (EOM) (57). Several experimental EA_{ad} values have been published for each of the molecules in Table 10, covering quite a range. The experimental data selected represent what currently are considered to represent the best estimates. Flexible basis sets are crucial in theoretical evaluations of EA_{ad} and all calculations were carried out with extensive basis sets.

It follows from Table 10 that HF and HFS, in which correlation between electrons of different spins is absent, underestimate EA_{ad}. This is understandable as the lack of correlation is more crucial (destabilizing) for the negative ions A^- than for the neutral species. This is because A^- has one more pair of electrons than A. Thus the exclusion of correlation will underestimate the energy gap between A and A^-. The explicit inclusion of electron correlation greatly improves the theoretical

Table 10. Adiabatic electron affinities (eV). Comparisons between theoretical and experimental values.

Molecule	HF	CISD[a]	EOM[a]	HFS[b]	LDA[b]	LDA/NL[b]	Expt.
CN	2.93	3.70	4.15	2.78	3.25	3.51	3.82 3.1
BO	1.41	2.35	2.97	1.25	1.96	2.33	2.2
OCN	2.28	3.21	—	2.83	3.19	3.35	3.6
N_3	0.89	2.15	—	2.12	2.50	2.65	2.7
NO_2	1.51	2.00		1.02	1.43	1.90	2.32

[a]Reference 56.
[b]Reference 55.

Table 11. Vibrational frequencies for $Ni(CO)_4$.

Mode				LDA[a]	LDA/NL[b]	HF[c]	LDA*[d,e]	Expt.
A_1	C-O	s-stretch	ν_1	2142	2112	2351	2153	2154
	Ni-C	s-stretch	ν_2	433	363	277	369	371
E	Ni-C-O	bend	ν_3	488	447	493	465	380?
	C-Ni-C	bend	ν_4	43	27i	43	59	62
F_2	C-O	a-stretch	ν_5	2073	2039	2262	2085	2092
	Ni-C-O	bend	ν_6	483	445	493	460	459
	Ni-C	a-stretch	ν_7	476	419	377	428	423
	C-Ni-C	bend	ν_8	78	35	93	67	79
F_1	Ni-C-O	bend	ν_9	292	251	326	279	300

[a]LDA optimized geometery.
[b]LDA/NL optimized geometry.
[c]HF calculations from ref. 58*d*.
[d]LDA calculations based on the experimental geometry taken from ref. 58*f*.
[e]Calculations from ref. 58*e*.

results both in the case of the *ab initio* methods (CISD, EOM) and in the case of the DFT-based LDA scheme. The addition of nonlocal exchange correction to LDA (LDA/NL) is seen to bring the theoretical results further in line with experiment. It seems clear that approximate DFT calculations on EA_{ad} require the inclusion of both electron correlation and nonlocal correction. However, at that level of approximate DFT the calculated results are comparable in quality to *ab initio* values based on extensive configuration interaction (CISD and EOM). Approximate DFT has also been used to calculate atomic electron affinities.

Molecular force fields

The construction of molecular harmonic force fields from experimental data (based on infrared and Raman spectroscopy) has benefited considerably over the past decade from new developments in computational chemistry. Thus, Pulay (58*a*) with his force method, in which force fields and vibrational frequencies are evaluated from a numerical differentiation of analytical energy gradient calculated by *ab initio* methods, has been able to study a number of small molecules. The studies by Pulay have more recently been augmented by investigations in which the second derivatives of the total energy with respect to nuclear displacements were calculated analytically (42).

Calculations of frequencies and force fields on the Hartree–Fock level of theory are now carried out almost routinely (42) although the basis sets employed in calculations on larger size molecules are often somewhat restricted to cut down on the computational cost. The HF frequencies differ considerably from experimental estimates and it is general practice to scale the calculated force constants in order to obtain good agreement with experiment (58*b*). Alternatively, one might improve the fit with experiment by resorting to post-HF calculations. However, frequencies and force-field calculations in which correlated *ab initio* methods have been employed are still restricted to small-size molecules and the evaluation of first, and in particular, second derivatives of the energy by such methods is rather demanding.

The recent implementation of energy derivatives (4, 5, 35) within the DFT framework makes it now manageable (6, 59) to evaluate frequencies from a numerical differentiation of the energy gradients in the spirit of Pulay's force method or directly from analytical second derivatives of the energy with respect to nuclear displacements (32*c–g*). Frequencies have also been calculated by Margl et al. (32*b*) from dynamic Car–Parrinello (32*a*) calculations. It is the general conclusion (6, 32*e,f*, 58*c,f*, 59) that frequencies calculated by LDA/NL and third-generation functionals (18*m*, 59) are of the same quality as post-HF second-order Møller–Plesset results (MP2) for main group molecules.

For transition-metal complexes, DFT seems at the moment to be the only practical scheme by which one can obtain accurate force fields (6*b,d*, 58*e*, 60). Table 11 displays the harmonic frequencies for $Ni(CO)_4$ calculated by several methods and compared to experimental estimates. The HF frequencies (58*d*) evaluated at the experimental geometry for $Ni(CO)_4$ are as usual overestimated, and scaling factors (58*b*) would have

Can. J. Chem. Downloaded from www.nrcresearchpress.com by 80.90.12.36 on 09/08/12
For personal use only.

Table 12. Calculated force constants for benzene (Bz), cyclopentadienyl (Cp) anion, $Fe(Cp)_2$, LiCp, $Cr(Bz)_2$, and $Cr(Bz)(CO)_3$.

Compound	C—C stretch (mdyn/Å)	C—H stretch (mdyn/Å)	M–ring stretch (mdyn/Å)	M–ring tilt (mdyn/rad)
Bz[b]	6.952 (6.578)[a]	5.200 (5.176)	—	—
Cp[-][c]	5.857	5.242	—	—
Bz_2Cr[d]	5.956	5.201	3.119	1.225
$BzCr(CO)_3$[d]	6.306	5.362	2.300	1.037
$(Cp)_2Fe$[c]	5.548 (5.565)	5.410	3.243 (3.15)	1.354
LiCp[c]	5.768	5.373	1.084	0.480

[a]Experimental values in parentheses.
[b]Reference 6*c*.
[c]Reference 6*b*.
[d]Reference 60.

to be applied in order to reproduce experiment. The LDA and LDA/NL schemes afford a much better fit to experiment, especially in the case of the C—O stretching frequencies, although deviations as large as 60 cm^{-1} still remain.

The remaining deviations could be due to differences between optimized and observed geometries or the inability of LDA and LDA/NL to evaluate force constants accurately. This point has been examined (58*e*) by calculating the LDA frequencies at the experimental geometry with the appropriate correction terms due to non-zero forces (58*g*) included. The results are shown under the heading LDA*. It follows from Table 11 that the LDA* frequencies are in excellent agreement with experiment. Thus, more accurate force-field calculations by DFT methods will depend on the development of functionals that can reproduce geometrical parameters with even higher accuracy than LDA/NL.

A promising related application of DFT is the evaluation of molecular mechanics (MM) force fields for transition-metal complexes. MM force fields are usually developed from experimental data. However, the available empirical imput is too limited in the area of organometallic chemistry for the construction of accurate force fields. Thus, the only alternative seems to be a generation of force constants from quantum mechanical calculations based on DFT.

Table 12 affords a few key force constants from two recent LDA studies on benzene (Bz) (6*c*), the cyclopentadienyl (Cp) anion (6*b*), $Fe(Cp)_2$ (6*b*), LiCp (6*b*), $Cr(Bz)_2$ (60), and $Cr(Bz)(CO)_3$ (60). The table reveals how the force constants for the C—H and, in particular, C—C stretches are changed as Bz and Cp are coordinated to a metal center. Also shown are the variations in the skeletal force constants for the M–ring stretch and M–ring tilt. The calculated force constants are in good agreement with the few experimental estimates, and might form the basis for constructing a MM force field.

Reaction profiles for elementary organic reaction steps

One of the most fundamental tasks of theoretical chemistry is undoubtedly to provide a perspective on reaction mechanisms through a determination of transition state structures and reaction profiles. The application of DFT to reaction profiles involving main group elements was pioneered by Fan and Ziegler (11*a*,*e*), and a number of applications in the field of organic chemistry have since appeared (11*b*–*d*, 61). The experience to date is that LDA/NL affords much better estimates of activation energies than either HF or MP2 (11*b*–*d*). For transition states in which bond making is involved, LDA/NL and MP4 provide energy barriers of similar accuracy (11*b*–*d*), with the LDA/NL estimate being too low and the MP4 barrier too high. The deviations are typically in the range of 1–5 kcal/mol. An example is given in Fig. 6 where the cyclization of butadiene to cyclobutene has been considered by both *ab initio* and DFT techniques (61*c*). There are indications (61*d*) that the third generation of functionals (18*m*) improve the agreement with experiment compared to LDA/NL.

It should also be mentioned that DFT makes it possible to follow a reaction path by the so-called intrinsic reaction coordinate (IRC) method due to Fukui (61*e*). This scheme traces the reaction path by a steepest descend in terms of energy from the transition state towards the product(s) and reactant(s). Deng has pioneered the application of IRC within the DFT framework (11*b*–*d*, 61*c*).

Fig. 6. Schematic potential energy surface for the cyclication of *cis*-butadiene to cyclo-butene calculated by different methods.

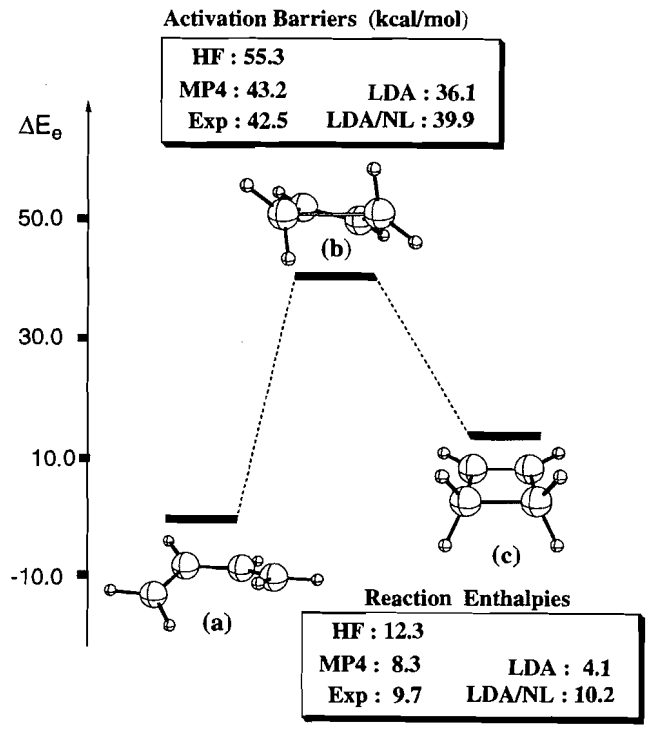

Can. J. Chem. Downloaded from www.nrcresearchpress.com by 80.90.12.36 on 09/08/12
For personal use only.

Can. J. Chem. Downloaded from www.nrcresearchpress.com by 80.90.12.36 on 09/08/12
For personal use only.

Scheme 1.

Hydroformylation Mechanism

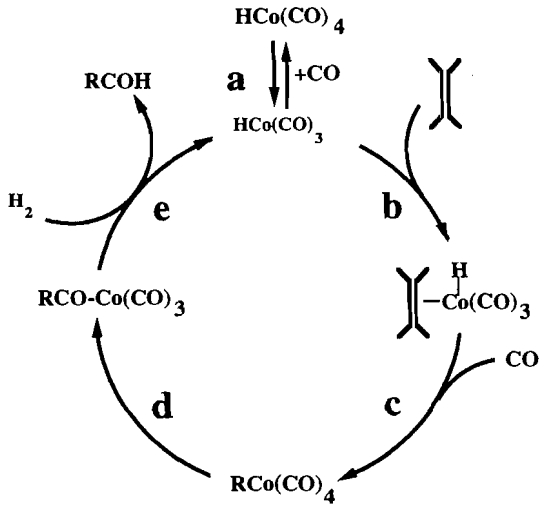

Heck and Breslow, 1962

4. Applications of approximate density functional theory to elementary reaction steps in organometallic chemistry

We have in the previous sections documented that DFT-based methods are able to provide information on bond energies and molecular geometries of reasonable accuracy. We shall in the ensuing section provide a single illustration of how the same methods can be used to trace energy profiles for elementary reaction steps involving organometallic compounds. Reference will, in addition, be given to a number of recent DFT-based studies on organometallic kinetics.

Hydroformylation

We shall use the hydroformylation process of Scheme 1 to illustrate how DFT is applied in studies of organometallic reaction steps. The hydroformylation process according to the mechanism by Heck and Breslow (62) was the first complete catalytic cycle investigated by a DFT-based method. We shall in the following give a more detailed account of the steps **a** (63*a*), **b** (63*b*), **c**–**d** (64), and **e** (65) of Scheme 1.

Insertion of ethylene into the cobalt–hydrogen bond

The first step in the catalytic hydroformylation process is the insertion of ethylene into the cobalt–hydrogen bond, **b** of Scheme 1. Experimental findings suggest that the migration of a hydride to a coordinated olefin group is very facile. In fact, the hydride–olefin insertion reaction has, with a few exceptions, rarely been directly observed. As a consequence, metal complexes containing both hydride and olefin are scarce and it has only in a few cases been possible to study the insertion process by experimental techniques.

We have studied (63*b*) the insertion process, **6a** → **6b**. The energy profile for the reaction is given in Fig. 7. We find the reaction to have a very small activation barrier, $\Delta E^{\neq}$, of only 6 kJ/mol and a modest reaction enthalpy of −8 kJ/mol. The

Fig. 7. Energy profile for the step **6a** → **6b**. The energy zero point refers to structure **6b.**

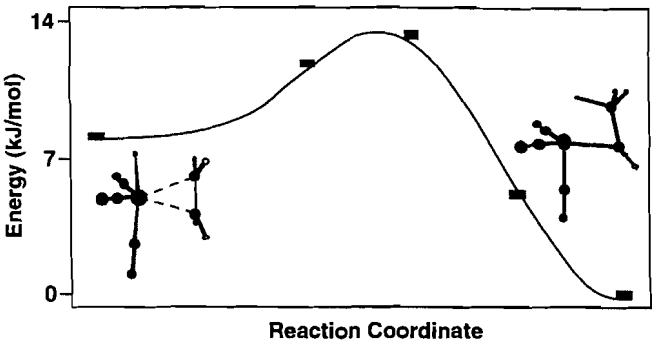

product of the reaction is an ethyl complex, **6b**, with a pronounced agostic interaction between the metal center and hydrogen. The ethyl complex, **6b**, has a short metal–hydrogen distance of 1.62 Å. This distance is only 0.12 Å longer than the Co—H bond distance in the parent complex **6a**. The bond length of the agostic hydrogen with the corresponding carbon atom of the ethyl ligand is, on the other hand, substantially elongated with R(H—C) = 1.21 Å, in comparison to a normal ethyl C—H bond length of 1.11 Å. The C—C bond distance in the ethyl group is 1.45 Å, which is somewhat longer than the corresponding value in the parent structure **6a** (1.37 Å), but it is still substantially shorter than the C—C bond length of an undistorted ethyl group (1.53 Å). Also the bond angle Co-C_{et}-C_{et} is, with 74°, considerably smaller than the expected value of about 109° for a normal ethyl ligand. The optimized molecular parameters of structure **6b** clearly indicate that the π-bond character of the initial ethylene ligand has been retained to a large extent. This is also underlined by the small calculated energy difference of 8 kJ/mol between the parent structure **6a** and complex **6b**. The modest activation barrier found in this study stems from the fact that the hydrogen atom is close to cobalt throughout the migration reaction.

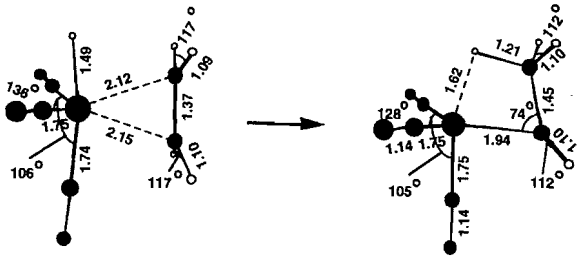

6a **6b**

Migratory insertion of alkyl into the Co—CO bond

The next important elementary reaction step in the hydroformylation cycle, **d** of Scheme 1, is the migratory insertion of an alkyl group into the metal–carbonyl bond.

[5] $RCo(CO)_4 \rightarrow RC(O)Co(CO)_3$

We have modeled this step with R = CH_3. The process in eq. [5] could in principle proceed by an insertion of a CO into the Co—CH_3 bond of **7a**, producing the coordinatively unsaturated complex, **7b**, with the acyl group in an axial position. Alternatively, the methyl group might migrate to a *cis*-carbo-

Can. J. Chem. Downloaded from www.nrcresearchpress.com by 80.90.12.36 on 09/08/12
For personal use only.

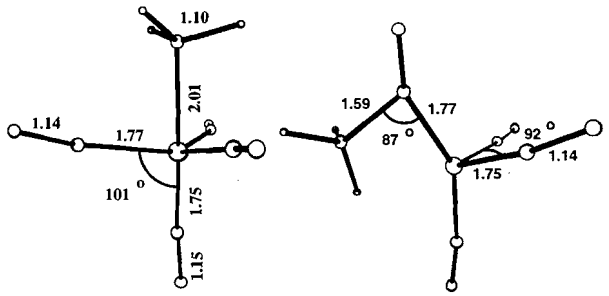

7a **7b**

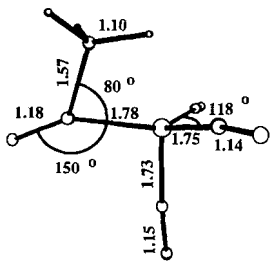

7c

nyl, thus affording the complex **7c** with the acyl group in an equatorial position.

We find (64), perhaps not surprisingly, that the energy profile for the CO insertion, **7a** → **7b**, into the Co—CH_3 bond has a prohibitively high activation barrier of 200 kJ/mol, Fig. 8. The CO insertion can, as a consequence, not be a viable mechanism for the process in eq. [5]. The migration of CH_3 to the *cis*-CO ligand, **7a** → **7c**, was on the other hand calculated (64) to have an endothermicity, ΔH, of 71 kJ/mol and a very modest activation barrier, $\Delta E^{\neq}$, of only 9 kJ/mol for the reverse reaction **7c** → **7a**, Fig. 9. Thus the CH_3 migration, **7a** → **7c**, seems to be favored as the mechanism for the process in eq. [5].

The calculated reaction enthalpy and activation barrier for **7a** → **7c** compare well with an earlier study (66) on the CH_3 to CO migration in $CH_3Mn(CO)_5$, where we found ΔH to be 75 kJ/mol and $\Delta E^{\neq}$ 11 kJ/mol. Our findings are also in agreement with a recent kinetic study by Roe (67), who found the rate constant of the methyl back-migration of $CH_3C(O)Co(CO)_3$ to be considerably larger than the rate constant for the corresponding forward reaction. The structures in Fig. 9 illustrate nicely how the methyl group can slide almost parallel along the *cis* C—Co bond onto the *cis* carbonyl carbon, while the remaining $Co(CO)_3$ framework stays almost unchanged. The 10 kJ/mol calculated for $\Delta E^{\neq}$ in the present study is an upper bound to the actual value, and we can thus conclude that the methyl migration, **7a** → **7c**, should proceed with a rather modest activation barrier.

H_2-induced aldehyde elimination

The last step in the catalytic cycle of the hydroformylation process, **e** of Scheme 1, is the reaction of the acyl intermediate with H_2, which results in the formation of the desired aldehyde molecule and the regeneration of the catalyst $HCo(CO)_3$.

There are several possible routes by which the aldehyde product can be formed from the acyl intermediate. Heck and

Fig. 8. Reaction profile for the CO insertion process.

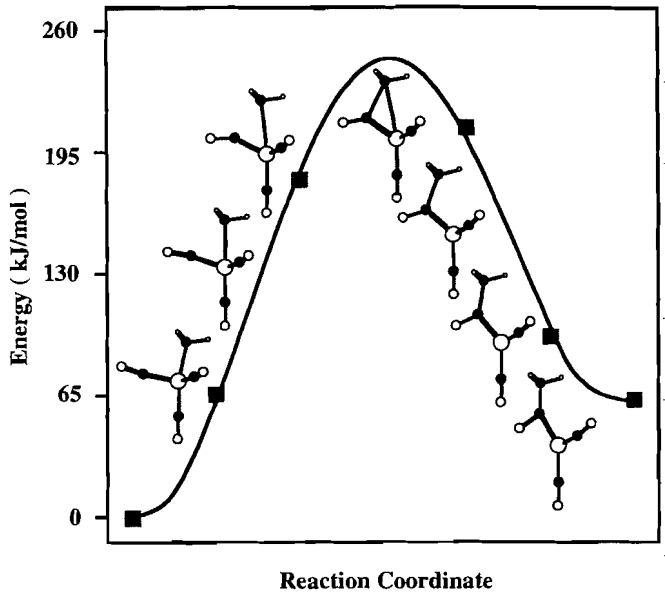

Fig. 9. Reaction profile for the methyl migration process.

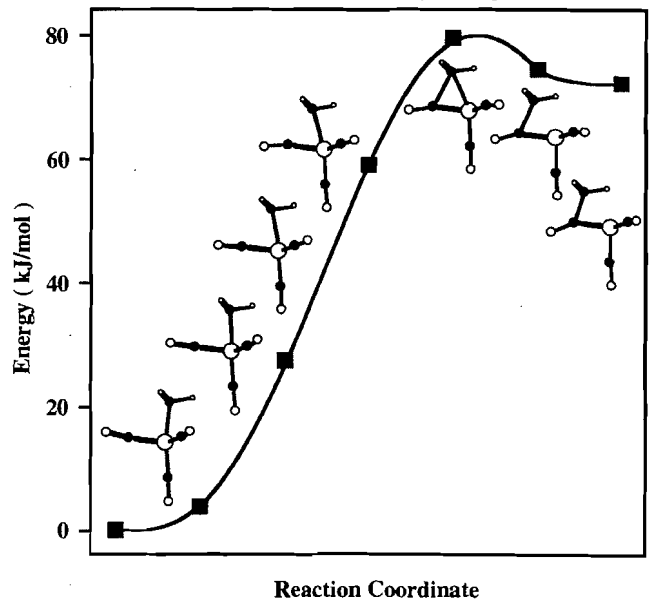

Breslow (62) proposed a mechanism in which the coordinatively unsaturated acyl complex undergoes first an oxidative addition of H_2, affording a dihydro acyl compound, eq. [6], followed by an irreversible reductive elimination of an aldehyde molecule, eq. [7].

[6] $R(O)CCo(CO)_3 + H_2 \rightarrow R(O)CCo(CO)_3(H)_2$

[7] $R(O)CCo(CO)_3(H)_2 \rightarrow RCHO + HCo(CO)_3$

This type of process has been inferred for numerous catalytic and stoichiometric systems; as a consequence these reactions have been studied extensively by experimental as well as theoretical techniques. However, in the case of the cobalt-based hydroformylation process it has not been established

Can. J. Chem. Downloaded from www.nrcresearchpress.com by 80.90.12.36 on 09/08/12
For personal use only.

that the product formation proceeds in fact via the oxidative addition – reductive elimination mechanism.

For electron-poor systems such as early-transition-metal complexes the hydrogenolysis of the M—C bond proceeds via a mechanism in which an incoming H_2 molecule initially forms an η^2 adduct with the metal complex, followed by the concerted cleavage of the hydrogen bond and the formation of an H—M and H—C bond by way of a four-center intermediary structure such as illustrated by **8**.

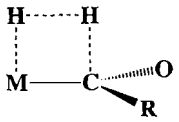

8

This reaction mode thus omits the oxidative addition – reductive elimination mechanism. Such a process could also be envisioned for the cobalt system studied here and has been speculated upon by earlier workers (68).

In this section we will concentrate our efforts on the study of those cobalt complexes that can result from an interaction of the acyl intermediates with an incoming H_2 molecule. Furthermore, attention will be given to the oxidative addition process of H_2 to the metal fragment as well as to the hydrogenolysis reaction through a four-center intermediary structure (vide ante).

The two most stable products from the interaction between an acyl complex and H_2 are the dihydrogen complexes **9a** and **9b** with H_2 in the equatorial position. Both represent energy minima on the energy surface and **9b** is about 19 kJ/mol above **9a** in energy.

It is suggested in the mechanism by Heck and Breslow (62) that H_2 adds oxidatively to the unsaturated acyl complex to form a dihydride, **9c**. The dihydride complex of configuration **9c** was found to be 25 kJ/mol higher in energy than the η^2 adduct **9a**. Thus the H_2 complex is more stable than the product of the oxidative addition.

We display in Fig. 10 the energy profile for the oxidative addition reaction **9a** → **9c**. We find an activation energy ΔE^* of 77 kJ/mol. This value is markedly larger than the activation energies determined theoretically for the oxidative addition of H_2 to transition-metal complexes containing phosphine ligands. This can be attributed to the stabilization of the η^2–H_2 adduct by the π-acceptor CO ligands. The energy curve modeled in Fig. 10 ascends steeply during the early stages of the reaction, indicating that the activation energy arises largely from the initial elongation of the H—H bond distance.

The fact that the oxidative addition process, **9a** → **9c**, exhibits a sizable activation barrier led us to consider an alternative mechanism for the last product-forming step, **e** of Scheme 1, in the hydroformylation cycle. The alternative mechanism considers that one hydrogen atom of the η^2–H_2 complex shifts directly towards the acyl group, thereby forming an aldehyde molecule and regenerating the catalyst $HCo(CO)_3$. This type of reaction mechanism, in which a direct oxidative addition of H_2 is avoided, has, to our knowledge, never been investigated theoretically for the cobalt-based hydroformylation process.

The approximate profile for the reaction **10a** →**10b** → **10c** is given in Fig. 11. The first part of the profile connecting **10a** and **10b** was obtained by changing the internal coordinates of

Fig. 10. Energy profile for the oxidative addition of H_2 according to eq. [6].

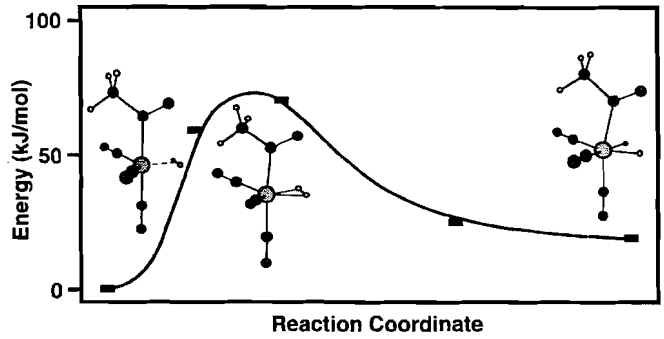

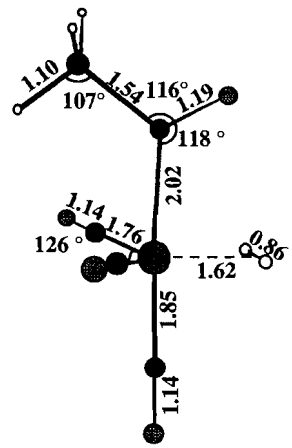

9a

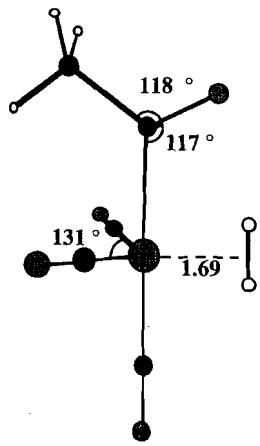

9b

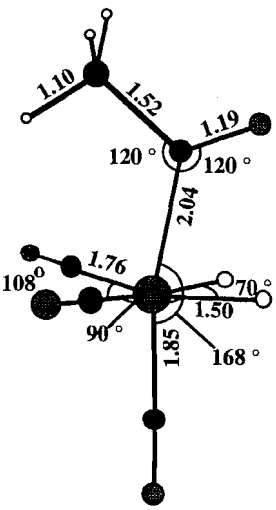

9c

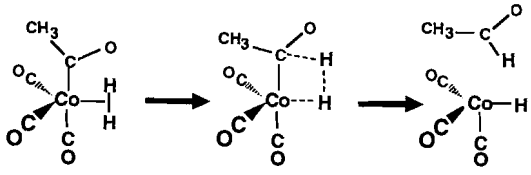

10a **10b** **10c**

Fig. 11. Energy profile for the reaction **10a** → **10b** → **10c**.

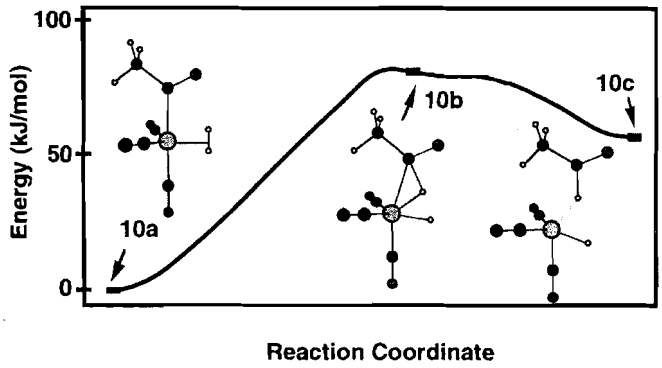

10a into those of **10b** in a linear and stepwise fashion. A total of six steps was used in the transit. We find the reaction to proceed with a minimal activation barrier, Fig. 11. The activation energy for the first part, **10a** → **10b**, is therefore essentially equivalent to the reaction enthalpy ΔE for the reaction **10a** → **10b**, which was calculated to be 83 kJ/mol (vide ante). We also traced the energy surface for the reaction **10b** → **10c**. The step **10b** → **10c,** which as already mentioned is exothermic with a reaction enthalpy of $\Delta E = -26$ kJ/mol, is seen to have a negligible activation energy. Finally, the system **10c** is lowered in energy by 69 kJ/mol as the adduct **10c** breaks up into acetaldehyde and $HCo(CO)_3$ in its ground state conformation.

Dissociation of CO from $HCo(CO)_4$ to form the catalyst $HCo(CO)_3$

The initial key step, **a** of Scheme 1, in the hydroformylation process is represented by the dissociation of a CO ligand from $HCo(CO)_4$. The dissociation process results in the formation of the catalytically active species $HCo(CO)_3$, eq. [8].

[8] $HCo(CO)_4 \rightarrow HCo(CO)_3 + CO$

The dissociation is assumed to take place prior to, or in concert with, the complexation of an olefin leading to the olefinic π-complex $HCo(CO)_3(\eta^2$-olefin), step **b** of Scheme 1. The coordinatively unsaturated 16-electron species, $HCo(CO)_3$, has been identified by matrix isolation techniques (69), but its structure is unknown. We have explored (63) possible structures for $HCo(CO)_3$.

The pre-catalyst $HCo(CO)_4$ has a TBP ground state conformation with the hydride in an axial position. Dissociation of either an equatorial or axial CO ligand from $HCo(CO)_4$ will thus give rise to **11a** and **11b**, respectively.

Both **1a** and **1b** constitute in our calculations local minima on the singlet surface of $HCo(CO)_3$. We calculate $HCo(CO)_3$ with the butterfly shape (**11a**) to be 35 kJ/mol lower in energy than the trigonal-shaped $HCo(CO)_3$ species, **11b**. The equatorial ($HCo(CO)_4 \rightarrow$ **11a**) and axial ($HCo(CO)_4 \rightarrow$ **11b**) CO dissociation energies were found to be 169 and 207 kJ/mol, respectively. Some experimental evidence for the existence of $HCo(CO)_3$ in different configurations was given in a recent publication by Sweany (70), who inferred, based on results from the photolysis of $HCo(CO)_4$ in an argon matrix, that $HCo(CO)_3$ forms two isomers consistent with the structures **11a** and **11b**.

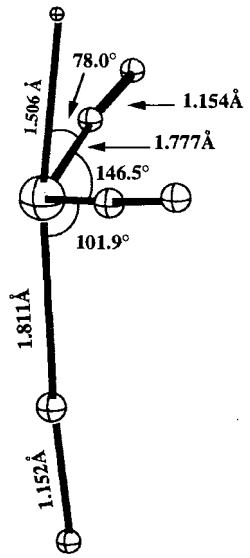

11a

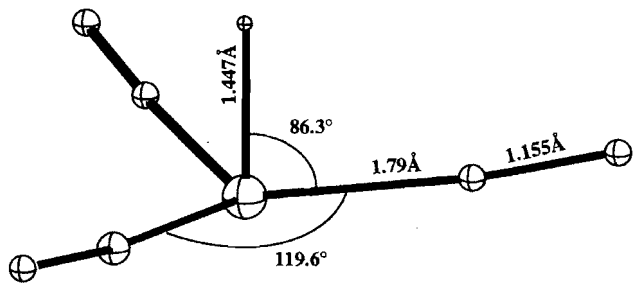

11b

Concluding remarks on hydroformylation study

The DFT calculations indicate that the last product-forming step, **e** of Scheme 1, in which aldehyde elimination is induced, has the highest activation energy with $\Delta H^{\neq} \sim 80$–90 kJ/mol. Step **d** was calculated to have a similar activation energy of $\Delta H^{\neq} \sim 70$–80 kJ/mol. The insertion of olefin into the Co—H bond, steps **b–c**, was on the other hand estimated to have a negligible activation energy of $\Delta H^{\neq} \sim 10$–20 kJ/mol. We finally determined that the formation of the active catalyst $HCo(CO)_3$ from $HCo(CO)_4$ by CO dissociation, step **a**, requires 169 kJ/mol.

Other DFT studies on elementary reaction steps

Other studies on organometallic reactions include oxidative addition of H_2 to $Co(CO)_4$ (65) as well as H_2 and CH_4 to CpML (L = CO, PH_3; M = Rh, Ir) (71) and CH_3Cl (72) to Pd, polymerization of organosilanes (73), halogen abstraction by metal carbonyl anions (74), and insertion of aldehydes into the Co—H bond (75).

A large number of studies have been concerned with the role of four-center transition states and intermediates(76*a*,*b*). They include the metathetical ($2\sigma+2\sigma$) exchange reactions between Cp_2MR (M = Lu, Sc; R = H, CH_3) and H_2,

Can. J. Chem. Downloaded from www.nrcresearchpress.com by 80.90.12.36 on 09/08/12
For personal use only.

Table 13. The development of DFT as a practical tool in chemical research

Year		References
1966	First chemical application of DFT using the muffin-tin approximation	19
	UV spectra and photoelectron spectroscopy	
1973–1976	First implementations of DFT without use of muffin-tin approximation	22,23
	UV spectra and photoelectron spectroscopy	24
1977	The implementation of accurate algorithms for total energy calculations	25,26
	Geometries, bond energies, vibrational spectra	30
1983–1988	The introduction of nonlocal density functionals	18*a–c*
	Accurate bond energies and geometries	
1985	The development of first principle molecular dynamics methods	32*a,b*
1988	Implementation of analytical energy gradients	4,5
	Automated geometry optimization	35
1989	Force field calculations based on analytical energy gradients	6,59
	Accurate vibrational spectra for large molecules	
1990	The determination of transition state structures	11*a*
1990	The Divide and Conquer method by Yang	80
1993	Accurate calculations of NMR and ESR parameters	7*d*,79
		7*a–c,e*
1994	Analytical second derivatives	32*c–g*

CH_4,C_2H_4, or C_2H_2 (76*c–e*), and the (2π+2π) additions of olefin to metal carbenes (76*f*) or acetylenes to metal carbynes (76*g*), as well as the (2σ+2π) addition of C—H and O—H links to M—O multiple bonds [76*h,i*).

Most recently investigations have been carried out on ethylene dimerization (77) as well as on olefin polymerization by Brinzinger–Kaminsky-type metallocene catalysts (78).

5. Concluding remarks. A personal and historical perspective on the application of density functional in chemistry

Johnson (19) was the first to apply a density-functional-based method to chemical problems, Table 13. In his approach use was made of the muffin-tin approximation with spherical potentials around each atom (20). This approximation precluded calculations of geometries and bond energies. The muffin-tin approximation was eliminated in subsequent approaches put forward by Ellis and Painter (22), Baerends et al. (23), and Sambe and Felton (24). A further step forward was taken when Ziegler and Rauk (30), Dunlap et al. (25), and Jones and co-workers (26) introduced methods that allowed total energies to be calculated accurately within the DFT framework, Table 13.

By 1977 the way had been paved in principle for DFT-based studies of molecular energetic and dynamics, and some promising applications did appear shortly after (25, 26, 30, 48*c*, 41*a*, 41*d*). However, from a theoretical and practical point of view, several hurdles had to be overcome.

From a theoretical point of view, all calculations were based on the first generation of local approximations such as HFS (16) or LDA (17). These methods provided reasonable frequencies and geometries (1*d*) but overestimated bond energies by as much as 100%. The energy problem was overcome by the introduction of nonlocal corrections (LDA/NL) due to Langreth and Mehl (18*a*), Becke (18*b*), and Perdew (18*c*), as well as others. Thus, Becke demonstrated in a number of seminal papers (18*b*, 31*c–e*), in which he combined the nonlocal corrections with his unique NUMOL[5] program, that LDA/NL affords bond energies for main-group molecules of nearly chemical accuracy (±5 kcal/mol). Similar promising results based on LDA/NL were obtained for structures (4*b*) and bond energies (18*j*, 40) of transition-metal complexes.

From a practical point of view, the early implementations (20, 25, 26) in which total energies could be calculated lacked automated features for geometry optimizations. Thus structure determinations were carried out from a laborious and manual tracing of the potential energy surface. This was changed by the introduction of analytical energy gradients (4, 5, 35) that also made it possible to calculate force constants (6, 59). Force constants can now also be calculated directly by analytical second-order energy derivatives (32*c–g*).

DFT is now a well-established method after a bumpy and exhilarating path through the 1970s and 1980s. Many of its previous opponents have become lukewarm practitioners or even staunch supporters, and it has been incorporated into a number of major program packages such as ADF (23, 29*c*), DeMon (30*e*), DMOL (35*f*, 30*d*), DGAUSS (30*b,c*), GAUSSIAN/DFT (32*c*), and CADPAC (32*d*).

Much still has to be done in terms of improving the existing functionals (18*m,n*). Applications to excited states have to be explored (52, 53*d,e*), further and new applications to properties such as NMR shifts (7) and ESR (79) hyperfine tensor are emerging. Other new developments are the first-principle molecular dynamics method by Car and Parrinello (32*a*), which has the potential to introduce temperature into the description of molecular behavior, and the divide and conquer scheme by Yang (80), which allows one to describe large systems, as well as several recent inclusions of solvation effects (81) into the DFT formalism.

All of the new methods are bound to benefit organometallic chemistry to the same degree as the development of DFT over the past decade, and it is this author's expectation that DFT will become as indispensable a research tool in chemistry as any of the major spectroscopic techniques.

Can. J. Chem. Downloaded from www.nrcresearchpress.com by 80.90.12.36 on 09/08/12
For personal use only.

Can. J. Chem. Downloaded from www.nrcresearchpress.com by 80.90.12.36 on 09/08/12
For personal use only.

Acknowledgment

I would like to thank my inorganic colleagues, Professors T. Chivers and M. Boorman at the University of Calgary, for their support and encouragement. Also a thanks to former students: Dr. L. Versluis, Dr. V. Tschinke, Dr. L. Fan, and E. Folga, as well as present students H. Jacobsen, A. Berces, L. Deng, G. Schreckenbach, and T.K. Woo and research associates Dr. J. Li, Dr. R. Dickson, Dr. J. Lohrenz, and D. Swerhone. Finally a special thanks to Professors A.D. Becke (Queens University) and E.J. Baerends (Free University of Amsterdam) as well as to the Natural Sciences and Engineering Research Council of Canada (NSERC) for support.

References

1. (*a*) W. Kohn and L.J. Sham. Phys. Rev. [Sect.] A, **140**, 1133 (1965); (*b*) R.G. Parr and W. Yang. Density-functional theory of atoms and molecules. Oxford University Press, New York. 1989; (*c*) E.S. Kryachko and E.V. Ludena. Density functional theory of many-electron systems; Kluwer Press, Dordrecht. 1991; (*d*) T. Ziegler. Chem. Rev. **91**, 651 (1991).
2. A.D. Becke. Int. J. Quantum Chem. **S23**, 599 (1989).
3. T. Ziegler. V. Tschinke, L. Versluis, E.J. Baerends, and W. Ravenek. Polyhedron, **7**, 1625 (1988).
4. (*a*) L. Versluis and T. Ziegler. J. Chem. Phys. **88**, 322 (1988); (*b*) L. Fan and T. Ziegler. J. Chem. Phys. **95**, 7401 (1991).
5. R. Fournier, J. Andzelm, and D.R. Salahub. J. Chem. Phys. **90**, 6371 (1989).
6. (*a*) L. Fan, L. Versluis, T. Ziegler. E.J. Baerends, and W. Ravenek. Int. J. Quantum Chem. **S22**, 173 (1988); (*b*) A. Berces. T. Ziegler, and L. Fan. J. Phys. Chem. **98**, 1584 (1994); (*c*) A. Berces and T. Ziegler, J. Chem. Phys. **98**, 4793 (1993); (*d*) L. Fan and T. Ziegler. J. Chem. Phys. **96**, 9005 (1992).
7. (*a*) W. Bieger, G. Seifert, H. Eschrig, and G. Grossman. Chem. Phys. Lett. **115**, 275 (1985); (*b*) D.A. Freier, R.F. Fenske, and Y. Xiao-Zeng, J. Chem. Phys. **83**, 3526 (1985); (*c*) V.G. Malkin and Z. Zhidomirov. Zh. Strukt. Khim. **29**, 32 (1988); (*d*) V.G. Malkin, O.L. Malkina, and D.R. Salahub. Chem. Phys. Lett. **204**, 80 (1993); (*e*) G. Schreckenbach and T. Ziegler. J. Phys. Chem. **99**, 606 (1995).
8. A.J. van der Est, P.B. Barker, E.E. Burnell, C.A. de Lange, and J.G. Snijders. Mol. Phys. **56**, 1 (1985).
9. D.A. Case. Annu. Rev. Phys. Chem. **33**, 151 (1982).
10. (*a*) L. Noodleman and J.G. Norman. J. Chem. Phys. **70**, 4903 (1979); (*b*) L. Noodleman. J. Chem. Phys. **74**, 5737 (1981); (*c*) L. Noodleman and E.J. Baerends. J. Am. Chem. Soc. **106**, 2316 (1984); (*d*) L. Noodleman, J.G. Norman, J.H. Osborne, A. Aizman, and D.A. Case. J. Am. Chem. Soc. **107**, 3418 (1985).
11. (*a*) L. Fan and T. Ziegler. J. Chem. Phys. **92**, 3645 (1990); (*b*) L. Deng and T. Ziegler. Int. J. Quant. Chem. **52**, 731 (1994); (*c*) J. Chem. Phys. **99**, 3823 (1993); (*d*) L. Deng, V. Branchadell, and T. Ziegler. J. Am. Chem. Soc. **116**, 10645 (1994); (*e*) L. Fan and T. Ziegler. J. Am. Chem. Soc. **114**, 10890 (1992).
12. M. Trsic, T. Ziegler, and W.G. Laidlaw. Chem. Phys. **15**, 383 (1976).
13. (*a*) M. Cook and M. Karplus. J. Phys. Chem. **91**, 31 (1987); (*b*) V. Tschinke and T. Ziegler. J. Chem. Phys. **93**, 8051 (1990).
14. E. van Leeuwen. Ph.D. Thesis, Free University, Amsterdam, The Netherlands. 1994.
15. A.D. Becke. J. Chem. Phys. **88**, 1053 (1988).
16. J.C. Slater. Adv. Quantum Chem. **6**, 1 (1972).
17. (*a*) O. Gunnarsson and L. Lundquist. Phys. Rev. B: Condens. Matter, **10**, 1319 (1974); (*b*) Phys. Rev. B: Condens. Matter, **13**, 4274 (1976); (*c*) O. Gunnarsson, M. Johnson, and I. Lundquist. Phys. Rev. B: Condens. Matter, **20**, 3136 (1979); (*d*) U. von Barth and L. Hedin. Phys. Rev. A: Gen. Phys. **20**, 1693 (1979).
18. (*a*) D.C. Langreth and M.J. Mehl. Phys. Rev. B: Condens. Matter, **28**, 1809, (1983); (*b*) A.D. Becke. Phys. Rev. A: Gen. Phys. **33**, 2786 (1988); (*c*) J.P. Perdew. Phys. Rev. B: Condens. Matter, **33**, 8822 (1986). Also see the erratum, Phys. Rev. B: Condens. Matter, **34**, 7046 (1986); (*d*) V. Tschinke and T. Ziegler, Can. J. Chem. **67**, 460 (1988); (*e*) T. Ziegler, V. Tschinke, and A.D. Becke. J. Am. Chem. Soc. **109**, 1351 (1987); (*f*) T. Ziegler, W. Cheng, E.J. Baerends, and W. Ravenek. Inorg. Chem. **27**, 3458 (1988); (*g*) T. Ziegler, V. Tschinke, L. Fan, and A.D. Becke. J. Am. Chem. Soc. **111**, 9177 (1989); (*h*) T. Ziegler, V. Tschenke, L. Versluis, E.J. Baerends, and W. Ravenek. Polyhedron, **7**, 1625 (1988); (*i*) J. Li, G. Schreckenbach, and T. Ziegler. J. Phys. Chem. **98**, 4838 (1994); (*j*) J. Am. Chem. Soc. **117**, 486 (1995); (*k*) A.D. Becke. Int. J. Quantum Chem. **S23**, 599 (1989); (*l*) L. Fan and T. Ziegler. J. Chem. Phys. **94**, 6057 (1991); (*m*) A.D. Becke. J. Chem. Phys. **98**, 1372 (1993); (*n*) R. van Leeuwen and E.J. Baerends. Phys. Rev. A: Gen. Phys. **49**, 2421 (1994).
19. K.H. Johnson. J. Chem. Phys. **45**, 3085 (1966).
20. J. Korringa. Physica. (Amsterdam), **13**, 392 (1947).
21. D.R. Salahub, R.P. Messmer, and K.H. Johnson. Mol. Phys. **31**, 521 (1975).
22. D.E. Ellis and G.S. Painter. Phys. Rev. B: Condens. Matter, **2**, 2887 (1970).
23. E.J. Baerends, D.E. Ellis, and P. Ros. Chem. Phys. **2**, 41 (1973).
24. H. Sambe and R.H. Felton. J. Chem. Phys. **62**, 1122 (1975).
25. B.I. Dunlap, J.W.D. Connolly, and J.F. Sabin. J. Chem. Phys. **71**, 3396 (1977).
26. O. Gunnarson, J. Harris, and R.O. Jones. Phys. Rev. **15**, 3027 (1977).
27. (*a*) B. Delley and D.E. Ellis. J. Chem. Phys. **76**, 1949 (1982); (*b*) G.L. Gutsev and A.A. Levin. Chem. Phys. **51**, 459 (1980); (*c*) W. Bieger, G. Seifert, and G. Grossmann. Z. Chem. **24**, 156 (1984); (*d*) F.W. Kutzler and G.S. Painter. Phys. Rev. B: Condens. Matter, **37**, 285 (1988); (*e*) M.A. Pederson. Phys. Rev. B: Condens. Matter, **38**, 3825 (1988).
28. (*a*) W. Ravenek. *In* Algorithms and applications on vector and parallel computers. *Edited by* H.J.J. Riele, Th. J. Dekker, and H.A. van de Vorst. Elsevier, Amsterdam. 1987; (*b*) *In* Scientific computing on supercomputers. *Edited by* J. de Vreese and P.E. van Camp. Plenum, New York. 1988.
29. (*a*) E. Wimmer, A. Freeman, C.-L. Fu, S.-H. Cao, B. Delley. ACS Symp. Ser. **353**, 49 (1987); (*b*) J. Andzelm, E. Wimmer, and D.R. Salahub. ACS Symp. Ser. **394**, 229 (1989).
30. T. Ziegler and A. Rauk. Theor. Chim. Acta, **46**, 1 (1977).
31. (*a*) A.D. Becke. J. Chem. Phys. **76**, 6037 (1982); (*b*) J. Chem. Phys. **78**, 4787 (1983); (*c*) A.D. Becke and R.M. Dickson. J. Chem. Phys. **89**, 2993 (1988); (*d*) A.D. Becke. Int. J. Quantum Chem. Quantum Chem. Symp. **23**, 599 (1989); (*e*) A.D. Becke and R.M. Dickson, J. Chem. Phys. **92**, 3610 (1990).
32. (*a*) R. Car and M. Parrinello. Phys. Rev. Lett. **55**, 2471 (1985); (*b*) P. Margl, K. Schwarz, and P.E. Blöchl. J. Chem. Phys. **100**, 8194 (1994); (*c*) B.G. Johnson, C.A. Gonzales, P.M.W. Gill, and J.A. Pople. Chem. Phys. Lett. **221**, 100 (1994); (*d*) N.C. Handy, D.J. Tozer, C.W. Murray, G.J. Laming, and R.D. Amos. Isr. J. Chem. **33**, 331 (1993); (*e*) A. Komornicki and G. Frizgerald. J. Chem. Phys. **98**, 1398 (1993); (*f*) B.G. Johnson and M.J. Fisch. J. Chem. Phys. **100**, 7429 (1994); (*g*) A. Berces, R.M. Dickson, L. Fan, H. Jacobsen, D. Swerhone, and T. Ziegler. Comput. Phys. Commun. In press.
33. (*a*) J.G. Snijders and E.J. Baerends. Mol. Phys. **33**, 1651 (1977); (*b*) J. Andzelm, E. Radzio, and D.R. Salahub. J. Chem. Phys. **83**, 4573 (1985); (*c*) W. Ravenek. Ph.D. Thesis, Nijmegen. 1983; (*d*) W. Ravenek and E.J. Baerends. J. Chem. Phys. **81**, 865 (1984).

Can. J. Chem. Downloaded from www.nrcresearchpress.com by 80.90.12.36 on 09/08/12
For personal use only.

34. (*a*) J.G. Snijders and E.J. Baerends. Mol. Phys. **36**, 1789 (1978); (*b*) J.G. Snijders, E.J. Baerends, and P. Ros. Mol. Phys. **38**, 1909 (1979); (*c*) H. Gollisch and L. Fritsche. Phys. Status Solidi B: **86**, 145 (1978); (*d*) D.D. Koelling and P.N. Harmon. J. Phys. C: Solid State Phys. **10**, 3107 (1977); (*e*) D.E. Ellis and A. Rosen. Z. Phys. A: At. Nucl. **283**, 3 (1977); (*f*) C.Y. Yang and S. Rabii. Phys. Rev. A: Gen. Phys. **12**, 362 (1977).
35. (*a*) C. Satoko. Chem. Phys. Lett. **83**, 111 (1981); (*b*) F.W. Averill and G.S. Painter. Phys. Rev. B: Condens. Matter, **32**, 2141 (1985); (*c*) C. Satoko. Phys. Rev. **30**, 1754 (1984); (*d*) J. Harris, R.O. Jones, and J.E. Mueller. J. Chem. Phys. **75**, 3904 (1981); (*e*) L. Martins, J. Buttet, and R. Carr. Phys. Rev. Lett. **53**, 655 (1984); (*f*) B. Delley. J. Chem. Phys. **92**, 508 (1990); (*g*) B.G. Johnson, P.M.W. Gill, and J.A. Pople. J. Chem. Phys. **98**, 5612 (1993).
36 (*a*) J. Li, G. Schreckenbach, and T. Ziegler. Inorg. Chem. In press; (*b*) T. Ziegler. Inorg. Chem. **24**, 1547 (1985); (*c*) J. Li and T. Ziegler. Organometallics, **14**, 214 (1995); (*d*) W.H.E. Schwarz, E.M. van Wezenbeek, E.J. Baerends, and J.G. Snijders. J. Phys. B: At. Mol. Opt. Phys. **22**, 1515 (1989); (*e*) J.-P. Desclaux. Int. J. Quantum Chem. **6**, 28 (1972).
37. J.A. Conner, M.T. ZafaraniMoatter, J. Bickerton, N.I. Saied, S. Suradi, R. Carson, G.A. Altackhin, and H.A. Skinner. Organometallics, **1**, 1166 (1982).
38. J.W. Bruno, H.A. Stecher, L.R. Mors, D.C. Sonnenberg, and T.J. Marks. J. Am. Chem. Soc. **108**, 7275 (1986).
39. F. Ungvary. Organomet. Chem. **36**, 363 (1972).
40 E. Folga and T. Ziegler. J. Am. Chem. Soc. **115**, 5169 (1993).
41. (*a*) T. Ziegler, J.G. Snijders and E.J. Baerends. J. Chem. Phys. **74**, 5737 (1981); (*b*) T. Ziegler, V. Tschinke, E.J. Baerends, J.G. Snijders, and W. Ravenek. J. Phys. Chem. **93**, 3050 (1989); (*c*) T. Ziegler. NATO Adv. Study Inst. Ser., Ser. B: **87**, 421 (1981); (*d*) NATO ASI Ser., Ser. C: **176**, 189 (1986); (*e*) T. Ziegler, J.G. Snijders, and E.J. Baerends. ACS Symp. Ser. **395**, 322 (1989); (*f*) T. Ziegler and V. Tschinke. ACS Symp. Ser. **428**, 75 (1990); (*g*) T. Ziegler, V. Tschinke, and A. Becke. Polyhedron, **6**, 685 (1987).
42. W.J. Hehre, L. Radom, P.v.R. Schleyer, and J.A. Pople. Ab initio molecular theory. John Wiley & Sons, New York. 1986.
43. (*a*) K. Faegri, Jr. and J. Almlöf. Chem. Phys. Lett. **107**, 121 (1984); (*b*) H.P. Lüthi, P.E.M. Siegbahn, and J. Almlöf. J. Phys. Chem. **89**, 2156 (1985); (*c*) H.P. Lüthi, J.H. Ammeter, J. Almlöf, and K. Faegri, Jr. J. Chem. Phys. **77**, 2002 (1982); (*d*) J. Almlöf, K. Faegri, Jr. B.E.R. Schilling, and H.P. Lüthi, Chem. Phys. Lett. **106**, 266 (1984).
44. (*a*) K. Faegri, Jr. and J. Almlöf. Chem. Phys. Lett. **107**, 121 (1984); (*b*) A.W. Ehlers and G. Frenking. J. Am. Chem. Soc. **116**, 1514 (1994); (*c*) L.A. Barnes, M. Rosi, and C.W. Bauschlicher, Jr. J. Chem. Phys. **94**, 2031 (1991); (*d*) L.A. Barnes, B. Liu and R. Lindh. J. Chem. Phys. **98**, 3978 (1993).
45. J. Labanowski and J. Andzelm (*Editors*). Density functional methods in chemistry. Springer-Verlag, Heidelberg. 1991.
46. T. Ziegler. J. Am. Chem. Soc. **105**, 7543 (1983).
47. (*a*) T. Ziegler. J. Am. Chem. Soc. **106**, 5901 (1984); (*b*) **107**, 4453 (1985).
48. (*a*) Th.A. van der Knaap, F. Bickelhaupt, J.G. Kraaykamp, G. van Koten, J.C.P. Bernards, H.T. Edzes, W.S. Weeman, E. de Boer, and E.J. Baerends. Organometallics, **3**, 1804 (1984); (*b*) F.M. Bickelhaupt, E.J. Baerends, and W. Ravenek. Inorg. Chem. **29**, 350 (1990); (*c*) T. Ziegler and A. Rauk. Inorg. Chem. **18**, 1558 (1979); (*d*) T. Ziegler. Inorg. Chem. **24**, 1547 (1985); (*e*) A.P. Hitchcock, N.G. Hao, N.H. Werstiuk, M.G. McGlinchey, and T. Ziegler. Inorg. Chem. **21**, 793 (1982); (*f*) T. Ziegler. Inorg. Chem. **25**, 2723 (1986); (*g*) R.L. DeKock, E.J. Baerends, and R. Hengelmolen. Organometallics, **3**, 289 (1984); (*h*) T. Ziegler. Organometallics, **4**, 675 (1985); (*i*) C. Famiglietti, E.J. Baerends. Chem. Phys. **62**, 407 (1981); (*j*) H. Jacobsen, H.B. Kraatz, T. Ziegler, and P.M. Boorman, J. Am. Chem. Soc. **114**, 7851 (1992); (*k*) H.B. Kraatz, H. Jacobsen, T. Ziegler, and P.M. Boorman. Organometallics, **12**, 76 (1993); (*l*) H. Jacobsen, G. Schreckenbach, and T. Ziegler. J. Phys. Chem. **98**, 11406 (1994); (*m*) H. Jacobsen and T. Ziegler. Organometallics, **14**, 224 (1995); (*n*) Inorg. Chem. In press; (*o*) A. Rosa and E.J. Baerends. Inorg. Chem. **32**, 5637 (1993).
49. (*a*) T. Ziegler and A. Rauk. Inorg. Chem. **18**, 1755 (1979); (*b*) T. Ziegler. NATO ASI Ser. Ser. C: **378**, 367 (1992).
50. (*a*) D. Antolovic and E.R. Davidson. J. Chem. Phys. **88**, 4967 (1988); (*b*) L. Versluis and T. Ziegler. J. Am. Chem. Soc. **111**, 2018 (1989).
51. V. Tschinke and T. Ziegler. Theor. Chim. Acta, **81**, 65 (1991).
52. (*a*) T. Ziegler, A. Rauk, and E.J. Baerends. Chem. Phys. **16**, 290 (1976); (*b*) Theor. Chim. Acta, **43**, 261 (1977).
53. (*a*) D.H. Jones, A.S. Hinman, and T. Ziegler. Inorg. Chem. **32**, 2092 (1993); (*b*) S. Jitsuhiro, H. Nakai, M. Hada, and H. Nakatsuji. J. Chem. Phys. **101**, 1029 (1994); (*c*) B.O. Roos, K. Anderson, and M.P. Pulscher. Chem. Phys. Lett. **192**, 5 (1992); (*d*) L.N. Oliveira, E.K.V. Gross, and W. Kohn. Phys. Rev. A: Gen. Phys. **37**, 2809 (1988); (*e*) C Daul. Int. J. Quantum Chem. **52**, 867 (1994).
54. M. Buijse and E.J. Baerends. J. Chem. Phys. **93**, 4129 (1990).
55. (*a*) T. Ziegler and G.L. Gutsev. J. Comput. Chem. **13**, 70 (1992); (*b*) G.L. Gutsev and T. Ziegler. Inorg. Chem. **31**, 1909 (1992); (*c*) J. Phys. Chem. **91**, 7220 (1991).
56. J. Baker, R.H. Nobes, and L. Radom, J. Comput. Chem. **3**, 349 (1986).
57. T.T. Chen, W.D. Smith, and J. Simons. Chem. Phys. Lett. **26**, 296 (1974).
58. (*a*) P. Pulay. Mol. Phys. **17**, 197 (1967); (*b*) G. Fogarasi, X. Zhou, P.W. Taylor, and P. Pulay. J. Am. Chem. Soc. **114**, 8191 (1992); (*c*) G. Rauhut and P. Pulay. J. Phys. Chem. In press; (*d*) P. Carsky and A. Dedieu. Chem. Phys. **103**, 265 (1986); (*e*) A. Berces and T. Ziegler. J. Phys. Chem. **98**, 13 233 (1994); (*f*) P.J. Stephens, F.J. Devlin, C.F. Chabalowski, and M.J. Frisch. J. Phys. Chem. **98**, 11623 (1994); (*g*) W.D. Allen and A. Csaszar. J. Chem. Phys. **98**, 2983 (1993).
59. A. St-Amant, R. Fournier, and D.R. Salahub. Int. J. Quantum Chem. **S23** (1989).
60. A. Berces and T. Ziegler. J. Phys. Chem. **98**, 13233 (1994).
61. (*a*) R.V. Stanton and K. Merz. J. Chem. Phys. **100**, 434 (1994); (*b*) C. Sosa, J. Andzelm, C. Lee, J.F. Blake, B.L. Chenard, and T.W. Butler, Int. J. Quantum Chem. **49**, 511 (1994); (*c*) L. Deng and T. Ziegler. J. Phys. Chem. **99**, 612 9 (1995); (*d*) O. Wiest, K.A. Black, and K.N. Houk. J. Am. Chem. Soc. **116**, 10336 (1994); (*e*) K. Fukui. J. Phys. Chem. **74**, 4161 (1970).
62. R.F. Heck and D.S. Breslow. J. Am. Chem. Soc. **83**, 4023 (1961).
63. (*a*) T. Ziegler, L. Cavallo, and T. Ziegler. Organometallics, **12**, 3586 (1993); (*b*) L. Versluis, T. Ziegler, and L. Fan. Inorg. Chem. **29**, 5340 (1990).
64. L. Versluis and T. Ziegler. J. Am. Chem. Soc. **111**, 2018 (1989).
65. L. Versluis and T. Ziegler. Organometallics, **9**, 2985 (1990).
66. T. Ziegler, L. Versluis, and V. Tschinke. J. Am. Chem. Soc. **108**, 612 (1986).
67. D.C. Roe. Organometallics, **6**, 942 (1987).
68. (*a*) H.H. Brintzinger. J. Organomet. Chem. **171**, 337 (1979); (*b*) M. Orchin and W. Rupilius. Catal. Rev. **6**, 85 (1972).
69. P. Wermer, B.S. Ault, and M. Orchin. J. Organomet. Chem. **162**, 189 (1978).
70 R.L. Sweany, Organometallics, **8**, 175 (1989).
71. T. Ziegler, V. Tschinke, L. Fan, and A.D. Becke. J. Am. Chem. Soc. **111**, 9177 (1990).
72. M. Bickelhaupt and T. Ziegler. Organometallics, **14**, 2288 (1995).

73. (*a*) J.F. Harrod, V. Tschinke, and T. Ziegler. Organometallics, **9**, 897 (1990); (*b*) T. Ziegler and E. Folga. J. Organomet. Chem. **478**, 57 (1994).
74. A.P. Masters, T.S. Soerensen, and T. Ziegler. Organometallics, **8**, 1088 (1989).
75. L. Versluis and T. Ziegler. J. Am. Chem. Soc. **112**, 6163 (1990).
76. (*a*) E. Folga, T.K. Woo, and T. Ziegler. *In* Theoretical aspects of homogeneous catalysis. *Edited by* P.W.N.M. van Leeuwen. Kluwer Academic Publishers, Amsterdam. 1995. pp. 115–165; (*b*) E. Folga. Ph.D. Thesis, Calgary 1993; (*c*) E. Folga and T. Ziegler. Can. J. Chem. **70**, 333 (1992); (*d*) E. Folga, A. Berces, and T. Ziegler. J. Am. Chem. Soc. **115**, 636 (1993); (*e*) E. Folga, T. Ziegler, and L. Fan. New. J. Chem. **15**, 741 (1991); (*f*) E. Folga and T. Ziegler. Organometallics, **12**, 325 (1993); (*g*) T.K. Woo, E. Folga, and T. Ziegler. Organometallics, **12**, 1289 (1993); (*h*) T. Ziegler. and J. Li. Organometallics, **14**, 214 (1995); (*i*) L. Deng and T. Ziegler. Organometallics. In press.
77. L. Fan, A. Krzywicki, A. Somogyvari, and T. Ziegler. Inorg. Chem. **33**, 5287 (1994).
78. (*a*) T. Woo, L. Fan, and T. Ziegler. Organometallics, **13**, 432 (1994); (*b*) Organometallics, **13**, 2252 (1994); (*c*) Springer 1995, accepted; (*d*) L. Fan, D. Harrison, L. Deng, T.K. Woo, D. Swerhone, and T. Ziegler. J. Can. Chem. Submitted; (*e*) L. Fan, D. Harrison, T.K. Woo, and T. Ziegler. Organometallics. In press.
79. L.A. Eriksson, J. Wang, and R.J. Boyd. Chem. Phys. Lett. **211**, 88 (1993).
80. W. Yang. Phys. Rev. A: Gen. Phys. **44**, 7823 (1991).
81. (*a*) J.L. Chen, L. Noodleman, and D. Bashford. J. Phys. Chem. **98**, 11059 (1994); (*b*) M.F. Ruiz-Lopez, F. Bohr, and M.T.C. Martins-Costa. Chem. Phys. Lett **221**, 109 (1994).

Can. J. Chem. Downloaded from www.nrcresearchpress.com by 80.90.12.36 on 09/08/12
For personal use only.

Photochemical nucleophile–olefin combination, aromatic substitution (photo-NOCAS) reaction. Part 9: methanol–2,6-dimethyl-1,6-heptadiene, and 1,4-dicyanobenzene[1]

Dennis A. Connor, Donald R. Arnold, Pradip K. Bakshi, and T. Stanley Cameron

Can. J. Chem. Downloaded from www.nrcresearchpress.com by 65.111.164.53 on 09/08/12
For personal use only.

Abstract: The photochemical nucleophile–olefin combination, aromatic substitution (photo-NOCAS) reaction of methanol, 2,6-dimethyl-1,6-heptadiene, and 1,4-dicyanobenzene yields three distinct types of 1:1:1 adducts: an acyclic product, 4-(1-methoxymethyl-1,5-dimethyl-5-hexenyl)benzonitrile (**8**, 5%); a *cis–trans* pair of cyclohexanes, 4-(3-methoxymethyl-1,3-dimethylcyclohexyl)benzonitrile (**9** *cis* (12%) and **9** *trans* (11%)); and a *cis–trans* pair of cycloheptanes, 4-(4-methoxy-1,4-dimethylcycloheptyl)benzonitrile (**10** *cis* (12%) and **10** *trans* (10%)). Variation in the concentration of the nucleophile, methanol, and codonor, biphenyl, affects the product ratio and it has been possible to establish the mechanisms for the formation of these products. The acyclic product is formed by a typical photo-NOCAS reaction, that is, addition (*anti*-Markovnikov) across one of the heptadiene double bonds. The cyclohexane products are formed following 1,6-*endo* cyclization of the intermediate β-alkoxy radical. And the cycloheptane products result from 1,7-*endo,endo* cyclization of the initially formed 2,6-dimethyl-1,6-heptadiene radical cation. Comparison of the relative rates of these cyclization processes can be made with those of the next smaller homolog, 2,5-dimethyl-1,5-hexadiene.

Key words: photochemistry, photoinduced electron transfer, radical ions, radicals, cyclization.

Résumé : La réaction de substitution aromatique par combinaison photochimique nucléophile–oléfine (photo-NOCAS) du méthanol avec le 2,6-diméthylhepta-1,6-diène et le 1,4-dicyanobenzène conduit à trois types distincts d'adduits 1 : 1 : 1 : un produit acyclique, le 4-(1-méthoxyméthyl-1,5-diméthylhex-5-ényl)benzonitrile (**8**, 5%); une paire de cyclohexanes *cis–trans*, les 4-(3-méthoxyméthyl-1,3-diméthylcyclohexyl)benzonitriles (**9** *cis* (12%) and **9** *trans* (11%)) et une paire de cycloheptanes *cis–trans* les 4-(4-méthoxy-1,4-diméthylcycloheptyl)benzonitriles (**10** *cis* (12%) and **10** *trans* (10%)). Des variations dans la concentration du nucléophile, du méthanol et du co-donneur, le biphényle, affectent les concentrations relatives des produits et il a été possible d'établir les mécanisme de formation de ces produits. Le produit acyclique se forme par une réaction photo-NOCAS typique, à savoir une addition (*anti*-Markovnikov) sur les doubles liaisons de l'heptadiène. Les produits cyclohexaniques se forment par une cyclisation 1,6-*endo* du radical intermédiaire β-alkoxy. Et les produits du cycloheptane résultent d'une cyclisation 1,7-*endo,endo* du cation radical 2,6-diméthylhepta-1,6-diène qui se forme initialement. On peut faire une comparaison des vitesses relatives de ces divers processus de cyclisation avec celles observées pour l'homologue inférieur immédiat, le 2,5-diméthylhexa-1,5-diène.

Mots clés : transfert électronique photoinduit, ions radicaux, radicaux, cyclisation.

[Traduit par la rédaction]

Introduction

Part 6 of this series on the photo-NOCAS reaction reported the formation of acyclic and cyclic 1:1:1 (methanol, 2,5-dimethyl-1,5-hexadiene (**2**), and 1,4-dicyanobenzene (**1**)) adducts (reactions [1] and [2]) (1*a*). The ratio of acyclic (**3**) to cyclic (**6**) products was dependent upon the concentration of methanol and biphenyl (**5**), serving as a codonor. The mechanism proposed to account for these results is summarized in Scheme 1. This study has now been extended to the next higher homolog, 2,6-dimethyl-1,6-heptadiene (**7**), with these objectives: to increase our understanding of radical cation reaction dynamics, and to further define the scope and synthetic utility of this reaction. We were particularly interested in the possibility of a 1,7-*endo,endo* cyclization of the 2,6-dimethyl-1,6-heptadiene radical cation ($\mathbf{7}^{+\cdot}$); there are few general methods for the synthesis of medium-sized rings.

Received January 18, 1995.

D.A. Connor, D.R. Arnold,[2] P.K. Bakshi, and T.S. Cameron.[2] Department of Chemistry, Dalhousie University Halifax, NS B3H 4J3, Canada.

[1] This is also Part 36 of the series Radical Ions in Photochemistry; see refs. 1 and 2 for preceding parts of these series.

[2] Authors to whom correspondence may be addressed. Telephone: (902) 494-3714. Fax: (902) 494-1310. E-mail: arnold@ac.dal.ca

Can. J. Chem. Downloaded from www.nrcresearchpress.com by 65.111.164.53 on 09/08/12
For personal use only.

Reaction [1] (1*a*)

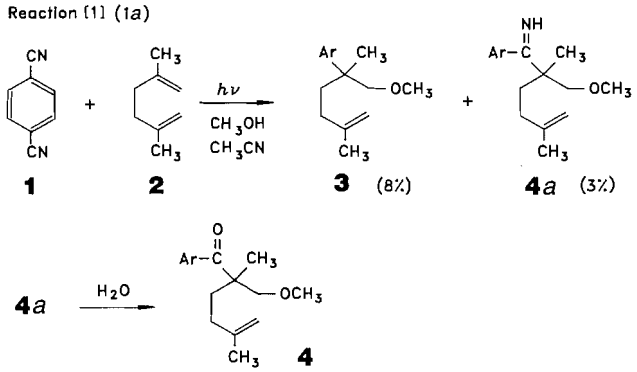

Reaction [2] (1*a*)

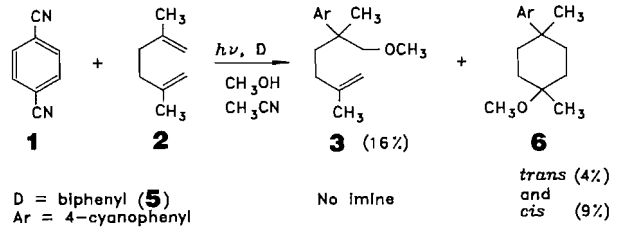

D = biphenyl (**5**)
Ar = 4-cyanophenyl

No imine

Organic reactions that induce cyclization have attracted considerable attention; the scope and limitations of this process involving the more common intermediates, closed-shell ions and neutral radicals, have been defined. We have Baldwin's "rules" for the cyclization of carbocations and carbanions and we have the generalizations of Beckwith and Ingold for cyclization of radical intermediates (3, 4). Much less is known regarding the cyclization of radical cations and radical anions (5–8). Some cyclizations of radical cations involving the formation of a new oxygen–carbon bond are known (5). Examples of the cyclization of 1,5-hexadienes have been reported (1*a*, 6, 7). Recently, the cyclization of enol silyl ethers into pendant double bonds has been demonstrated (8). There is no reason to doubt that these cyclization reactions of radical ions will be as important as those involving ions and radicals.

Results

A solution of 1,4-dicyanobenzene (**1**) (0.1 M), biphenyl (**5**) (0.1 M), and 2,6-dimethyl-1,6-heptadiene (**7**) (0.1 M), in acetonitrile–methanol (3:1), was irradiated through Pyrex with a medium-pressure mercury vapour lamp (reaction [3]). Progress of the reaction was followed by capillary column gas chromatography with either a flame ionization (gc/fid) or a mass selective (gc/ms) detector. Five products were formed with molar mass corresponding to 1:1:1 (methanol:2,6-dimethyl-1,6-heptadiene:1,4-dicyanobenzene–HCN) adducts. Biphenyl (**5**) was largely recovered. Products were isolated by medium-pressure liquid chromatography (mplc) on silica gel.

Reaction [3]

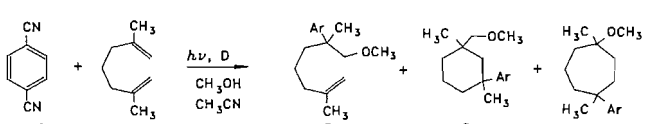

D = biphenyl (**5**)
Ar = 4-cyanophenyl

(5%)

cis (12%) *trans* (11%)

cis (12%) *trans* (10%)

Scheme 1.

Mechanism for formation of photo–NOCAS products.

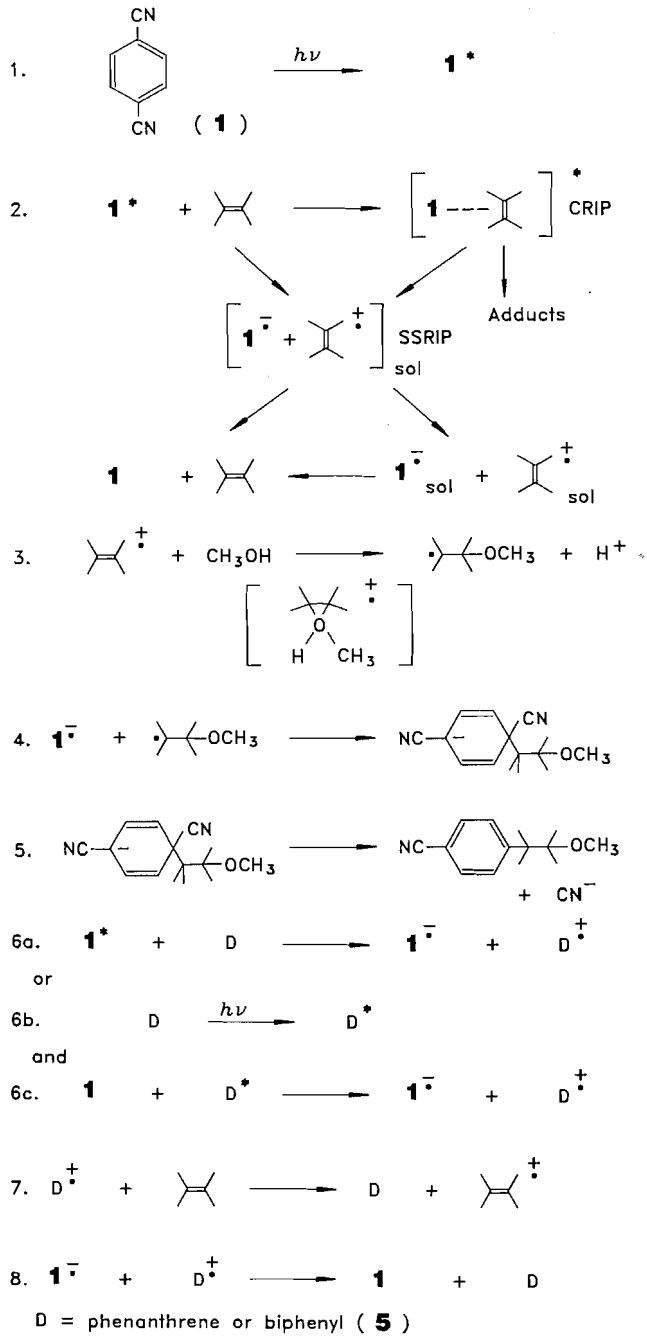

D = phenanthrene or biphenyl (**5**)

One of the five photo-NOCAS adducts, 4-(1-methoxymethyl-1,5-dimethyl-5-hexenyl)benzonitrile (**8**, (5%)) involves only one of the double bonds of the diene and is therefore analogous to a simple mono-alkene adduct. The other four products involve cyclization of the diene: a *cis–trans* pair of cyclohexanes, 4-(3-methoxymethyl-1,3-dimethylcyclohexyl)-benzonitrile (**9** *cis* (12%) and **9** *trans* (11%)); and a *cis–trans* pair of cycloheptanes, 4-(4-methoxy-1,4-dimethylcycloheptyl)benzonitrile (**10** *cis* (12%) and **10** *trans* (10%)). The combined yield of photo-NOCAS adducts was 50% at ca. 50% conversion.

Can. J. Chem. Downloaded from www.nrcresearchpress.com by 65.111.164.53 on 09/08/12
For personal use only.

Fig. 1. The dependence of the product ratio ((**10** *cis* + **10** *trans*) / (**8** + **9** *cis* + **9** *trans*)) on the concentration of methanol.

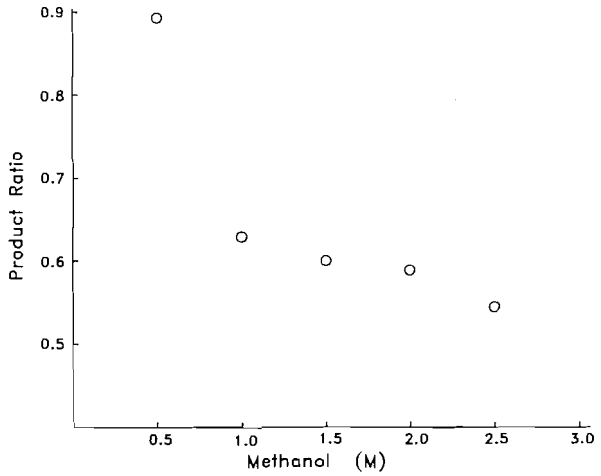

Table 1. The dependence of the product ratio ((**10** *cis* + **10** *trans*) / (**8** + **9** *cis* + **9** *trans*)) on the concentration of methanol.

[CH3OH] (M)	Product ratio
0.5	0.894 (0.034)[a]
1.0	0.630 (0.015)
1.5	0.600 (0.009)
2.0	0.589 (0.024)
2.5	0.545 (0.009)

[a]Population standard deviation.

Structures were established largely on the basis of ^{1}H and ^{13}C nmr spectra. The structures of **9** *cis* and 4-(*cis*-4-methoxy-1,4-dimethylcycloheptyl)benzoic acid (**10a** *cis*), obtained upon mild hydrolysis of **10** *cis*, were determined by X-ray diffraction analysis on single crystals.[3]

The product ratios were dependent upon the concentration of methanol and biphenyl (**5**). Small-scale irradiations were carried out in Pyrex tubes (5 mm) under conditions similar to those used for the preparative scale reaction described above. The concentrations of the reactants, other than methanol, were kept the same as in the preparative scale reaction. The concentration of methanol was varied, 0.50–3.0 M. The ratio of products was determined from the corresponding peak heights in the gas chromatogram (gc/fid, Table 1 and Fig. 1). An increase in methanol concentration caused an increase in the yield of the acyclic (**8**) and cyclohexane products (**9** *cis* and *trans*) relative to the cycloheptanes (**10** *cis* and *trans*).

Similarly, small-scale irradiations were carried out with variation in the concentration of biphenyl (**5**) (0–0.1 M) while the concentrations of the other reactants were maintained the same as in the preparative scale reaction (acetonitrile–methanol (3:1), ca. 6 M methanol). When no biphenyl was present, neither the cyclohexanes (**9** *cis* and *trans*) nor the cycloheptanes (**10** *cis* and *trans*) were produced in detectable (gc/fid) quantities. As the concentration of biphenyl (**5**) was increased, the yield of the cycloheptanes (**10** *cis* and *trans*) increased relative to the other photo-NOCAS products (Table 2 and Fig. 2).

Fig. 2. The dependence of the product ratio ((**10** *cis* + **10** *trans*) / (**8** + **9** *cis* + **9** *trans*)) on the concentration of biphenyl (**5**).

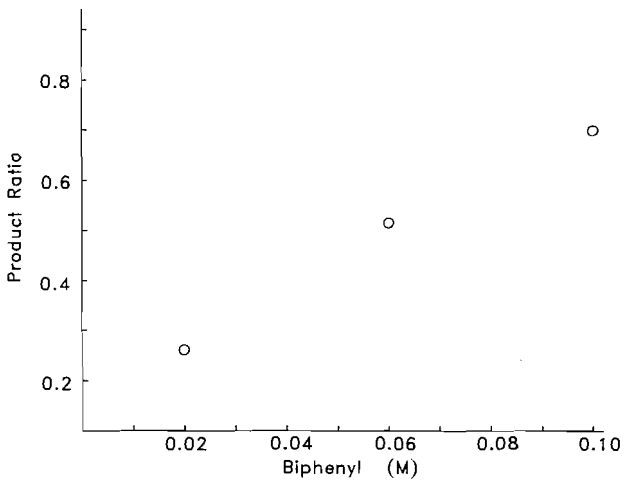

Table 2. The dependence of the product ratio ((**10** *cis* + **10** *trans*) / (**8** + **9** *cis* + **9** *trans*)) on the concentration of biphenyl (**5**).

[CH3OH] (M)	Product ratio
0.02	0.261 (0.003)[a]
0.06	0.518 (0.003)
0.10	0.704 (0.017)

[a]Population standard deviation.

Structural assignments

The connectivity of all of the products was readily established from the infrared, the mass, and the ^{1}H and ^{13}C nmr spectra. Determining the stereochemistry of the cyclohexanes (**9**) and cycloheptanes (**10**) afforded a more formidable challenge and was ultimately achieved by X-ray diffraction analysis on single crystals. The *cis*-cyclohexane product (**9** *cis*) is a crystalline compound and an X-ray analysis established the structure (Fig. 3). The *cis*-cycloheptane product (**10** *cis*), a colourless liquid, was hydrolysed to the crystalline carboxylic acid, 4-(*cis*-4-methoxy-1,4-dimethylcycloheptyl)benzoic acid (**10***a* *cis*) and an X-ray analysis was carried out on this derivative (Fig. 4). The ^{1}H nmr spectra of the nitrile (**10** *cis*) and the carboxylic acid (**10***a* *cis*) are almost identical; the X-ray analysis on the crystalline derivative provides firm evidence for the structure of the initial product (**10** *cis*).

The structure of the acyclic adduct (**8**) was easily established. The ^{1}H nmr spectrum has two weakly coupled signals in the vinyl proton region, similar to those seen in the starting diene (**7**), which integrate for one proton each. Distinctive signals in the aromatic region for the *para*-substituted phenyl ring, a sharp singlet at relatively low field assigned to the methoxy methyl group, and two higher-field singlets for the

[3] These data may be purchased from: The Depository of Unpublished Data, Document Delivery, CISTI, National Research Council Canada, Ottawa, Canada K1A 0S2.

Details of data collection, structure analysis and refinement, and tables of interatomic distances and bond angles have also been deposited with the Cambridge Crystallographic Data Centre and may be obtained on request from the Director, Cambridge Crystallographic Data Centre, University Chemical Laboratory, 12 Union Road, Cambridge, CB2 1EZ, U.K.

Fig. 3. X-ray crystallographic structure of 4-(3-methoxymethyl-1,3-dimethylcyclohexyl)benzonitrile (**9** *cis*).

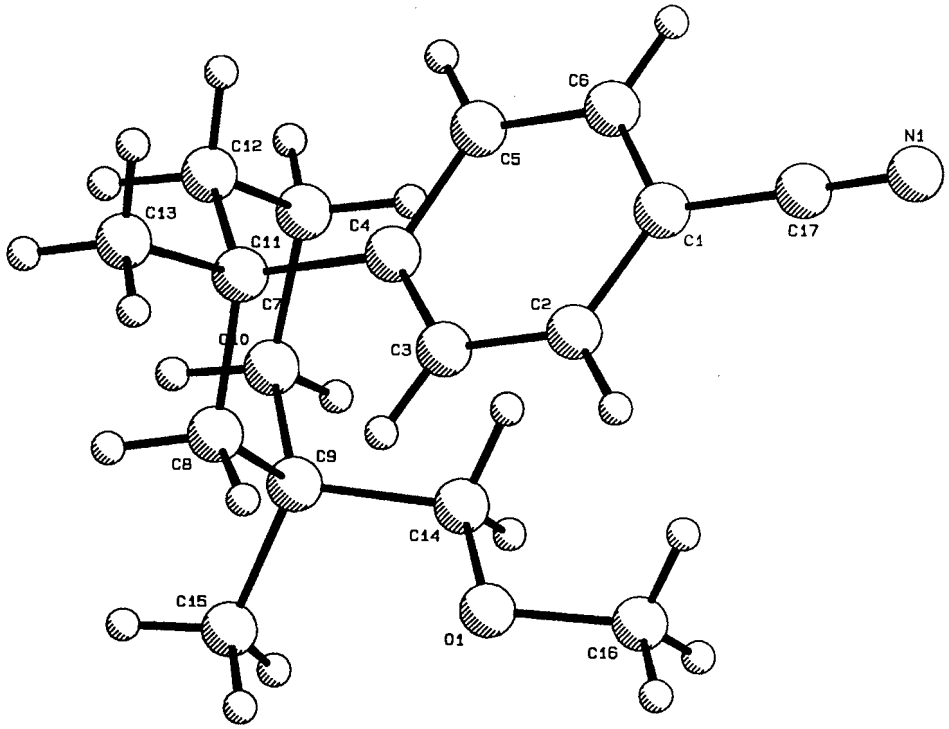

Can. J. Chem. Downloaded from www.nrcresearchpress.com by 65.111.164.53 on 09/08/12
For personal use only.

other methyl groups, show that this is a 1:1:1 adduct. The relatively high-frequency AB quartet is evidence for the methylene bearing a methoxy group and a stereogenic quaternary carbon. The remaining three signals in the aliphatic region integrate for two protons each. Of these, the signal at highest frequency, a slightly broadened triplet, is assigned to the allylic methylene (C-4). The other two signals are complex second-order patterns as expected for adjacent methylene groups in an asymmetric environment.

Two-dimensional nmr (COSY) confirms that the triplet splitting of the allylic methylene is the result of coupling to the protons at lowest frequency (bonded to C-3), and that the allylic protons are also weakly coupled to one of the vinyl protons. The C-3 methylene is also coupled to the other methylene, which is not further coupled, and is therefore assigned to C-2, i.e., the methylene adjacent to the quaternary stereogenic carbon.

This assigned structure is consistent with the number, multiplicity, and chemical shift of the signals in the ^{13}C nmr spectrum of **8**.

The *cis* cyclohexane (**9** *cis*) is a crystalline compound and an X-ray diffraction analysis of a single crystal firmly established the structure. The mass spectral fragmentation pattern, and the ^{1}H and the ^{13}C nmr spectra of **9** *trans* are very similar to those of **9** *cis*; clearly, these compounds are diastereomers.

The ^{1}H nmr spectra of both **9** *cis* and *trans* have the expected AA′XX′ pattern in the aromatic region indicative of a *para*-substituted phenyl ring. Both spectra have a low-field (ca. 3 ppm) three-proton singlet consistent with a methoxy methyl group, and two higher-field singlets for the uncoupled methyl groups. There are no signals in the vinyl proton region of the spectrum of either isomer. These observations indicate that both products, **9** *cis* and **9** *trans*, are 1:1:1 adducts of methanol, the diene, and 1,4-dicyanobenzene, which have cyclized in such a way that the aliphatic methyl groups are on quaternary centres. The spectra of both of these compounds have AB quartets for two protons, slightly upfield of the methoxy methyl signals. This is good evidence that the methoxy group is bonded to what was a terminal methylene carbon of a former double bond and that the vicinal olefinic carbon has become quaternary. The upfield shift of this AB quartet of **9** *cis*, relative to that of **9** *trans*, is consistent with the *cis* stereochemistry evident from the X-ray data. This upfield shift indicates that the methoxy-substituted methylene is in the shielding cone of the phenyl ring. A similar upfield shift is seen in the signal due to the methoxy methyl group of **9** *cis*.

The *cis* cyclohexane (**9** *cis*) has ^{1}H nmr spectral evidence for another isolated diastereotopic methylene group (C-2); the sharp doublets (J = 14 Hz) at 2.30 and 1.29 ppm are assigned to the equatorial and axial protons, respectively. The mutual and exclusive coupling of these protons was confirmed by the COSY experiment. The difference in chemical shift between these geminal protons is expected for a conformationally constrained cyclohexane.

Signals were assigned for the other six aliphatic protons, aided by the results of the COSY experiment. The axial proton on the central carbon (C-5) of this group of methylenes would be expected to have three relatively large couplings. Geminal couplings and axial–axial couplings are larger than axial–equatorial and equatorial–equatorial couplings. This expectation assumes that all the large couplings are observable and the coupled protons are not coincident. The two-proton multiplet at 1.44 ppm is the only one that has more than one correlation (COSY). One of these protons must be the axial C-5 proton. The broad doublet (J = 13 Hz) for one proton (2.25 ppm) must be one of the equatorial protons, and the single-proton signal at

Can. J. Chem. Downloaded from www.nrcresearchpress.com by 65.111.164.53 on 09/08/12
For personal use only.

Fig. 4. X-ray crystallographic structure of 4-(4-methoxy-1,4-dimethylcycloheptyl)benzoic acid (**10***a cis*).

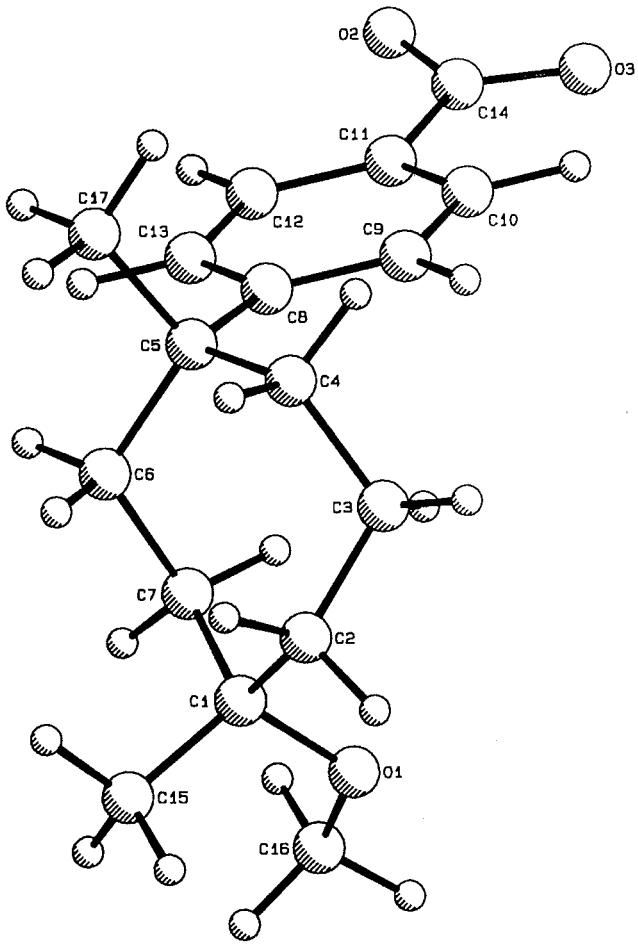

1.18 ppm must be another axial proton because it has two large and one small couplings. In view of the fact that this signal (1.18 ppm) has only one correlation, which is to the proton assigned to the central axial position (1.44 ppm), the other (geminal) coupling must be to the proton at the same shift position (1.44 ppm). This might represent either of the methylenes C-4 or C-6. The alternate methylene must have proton signals coincident at 1.6 ppm since that signal shows only one correlation, which is to the signal at 1.44 ppm. The broad doublet (2.25 ppm) must be the C-5 equatorial proton. It seems likely that the coincident methylene protons (1.6 ppm) are at C-6. At that position it is possible that only the axial proton is in the aromatic deshielding region and (or) only the equatorial proton is in the shielding cone. These affects could counteract the normal deshielding of equatorial protons relative to axial protons such that these geminal protons have coincident chemical shifts.

The ^{1}H nmr spectrum of the *trans* cyclohexane (**9** *trans*) shows less dispersion of the signals due to the aliphatic protons than does the diastereomer and a complete assignment would be speculative; however, the spectrum does have several features, in addition to those mentioned above, which are consistent with the assigned regio- and stereochemistry. The spectrum has two relatively low-field doublets (2.31 and 2.09 ppm) as does **9** *cis*. One of these doublets is probably due to the equatorial proton on C-2, between the quaternary ring positions, and the other is due to an equatorial proton on the other side of the ring (C-5). Neither doublet is sharp; perhaps some four-bond coupling is operative on the proton on the isolated ring position in this isomer. Both doublets are coupled to protons at higher field (1.6 and 1.3 ppm, respectively) as shown by COSY and C–H heterocorrelation data.

The high-field singlet (0.31 ppm) is evidence for a methyl group in the shielding cone of the aryl ring. This indicates that this molecule is in a conformation where the aryl ring and this shielded methyl group are in a 1,3-diaxial relationship. This conclusion is reasonable, the aryl group is known, from the X-ray diffraction data, to be axial in the *cis* isomer and this conformation has been shown, by molecular mechanics calculations, to be preferred when phenyl and methyl groups are geminal on a cyclohexane ring (9).

The infrared, the mass, and the ^{1}H and ^{13}C nmr spectra of **10** *cis* and **10** *trans* are very similar; clearly, these two compounds are diastereomers. The ^{1}H nmr spectra of these compounds were not as well dispersed as they were for the isomeric cyclohexanes. The spectra of both show the AA′XX′ pattern in the aromatic proton region for the *para*-substituted phenyl ring. Both spectra have relatively low-field singlets, attributable to the methoxy methyl groups, and both have a pair of singlets for the aliphatic methyl groups. The signals due to the other aliphatic methylene groups were poorly dispersed and further analysis was not feasible. The assigned structures were consistent with the number, the coupling pattern, and the chemical shifts of all of the peaks in the ^{13}C nmr spectra for both isomers (**10** *cis* and **10** *trans*). The distinction between these two isomers rests firmly upon the X-ray analysis of **10***a cis*.

Discussion

These results provide insight into the behaviour of the unusual intermediates involved and further evidence of the potential synthetic utility of the photo-NOCAS reaction. Three different reaction pathways produce the acyclic adduct (**8**), the *cis–trans* pair of cyclohexanes (**9** *cis* and *trans*), and the *cis–trans* pair of cycloheptanes (**10** *cis* and *trans*). The sequence of events that produces the acyclic adduct is analogous to the general mechanism originally proposed for the reaction with mono alkenes (Scheme 1); formation of the cyclic products requires a more complex mechanism.

The acyclic adduct (**8**) is the *anti*-Markovnikov addition product. Step 1 of the proposed mechanism (Scheme 1) involves excitation of the 1,4-dicyanobenzene (**1**) to the first electronically excited singlet state (^1L_b). This state has a long enough lifetime (9.74 ns (10)) to allow rapid bimolecular reaction. The oxidation potential of 2,6-dimethyl-1,6-heptadiene (**7**) is low enough (2.6 V (sce)) to allow exothermic electron transfer; the ΔG_{ET}, calculated from the Weller equation, is -2.8 kJ mol^{-1} (11). This photo-induced single electron transfer occurs within the solvent cage, forming a solvent-separated radical ion pair (SSRIP) (step 2). Reaction of the radical cation $\mathbf{7}^{+\cdot}$ with methanol, within the methanol-solvent cage, leads to formation of the β-alkoxy radical (step 3). Rapid coupling of this radical with the geminate radical anion ($\mathbf{1}^{-\cdot}$) at the *ipso* position (step 4), before solvent separation or cyclization, leads on to the acyclic product (**8**).

As expected, methanol attacks the less hindered carbon of

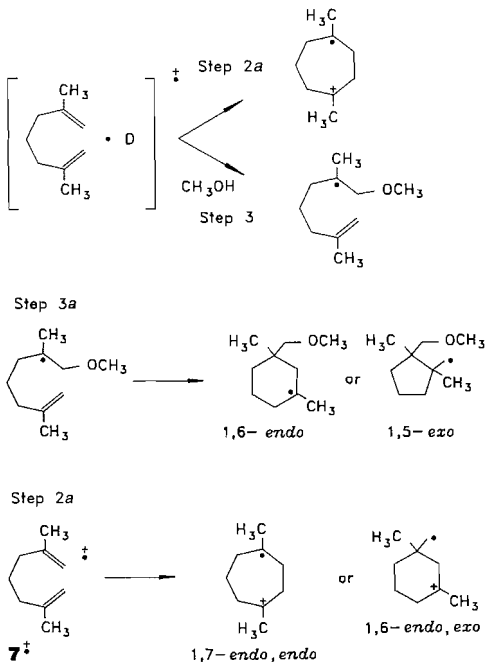

the alkene radical cation to produce the more heavily substituted (more stable) tertiary radical. The Markovnikov addition product was not detected. This is consistent with the results of the photo-NOCAS reaction involving 2-methylpropene, a similarly substituted mono-alkene (1*d*,*e*). In general, the Markovnikov adduct is a minor product when the olefinic carbons are secondary and tertiary; the reaction is regioselective when the olefinic carbons are primary and tertiary, as in this diene (**7**). The first-formed intermediate is a bridged distonic radical cation (Scheme 1, step 3). Deprotonation of the distonic radical cation, from the oxygen, forms the alternative β-alkoxy radicals, which are not bridged, in a ratio dependent upon relative stability.

The acyclic adduct (**8**) might react further at the remaining double bond; the oxidation potential of **8** is not significantly higher than that of **7**. However, under the conditions used for this reaction (reaction [3]), carried out to ca. 50% conversion, 2:1:2 adducts were not observed (gc/ms).

The efficiency of the reaction is greatly increased upon the addition of biphenyl (**5**). Biphenyl (**5**) serves as a codonor. This increase in efficiency has been attributed to a greater ratio for the rate of separation of the SSRIP [$\mathbf{1}^{-\cdot} - \mathbf{5}^{+\cdot}$] (step 6*a*) divided by the rate of back electron transfer (step 8) for this pair than for the SSRIP [$\mathbf{1}^{-\cdot} - \mathbf{7}^{+\cdot}$] (1). The free, completely solvated, biphenyl radical cation ($\mathbf{5}^{+\cdot}$) then oxidizes the diene to the radical cation $\mathbf{7}^{+\cdot}$ (step 7). Under these conditions, the radical cation $\mathbf{7}^{+\cdot}$ is generated completely separated from the radical anion $\mathbf{1}^{-\cdot}$. Reaction of the radical cation $\mathbf{7}^{+\cdot}$ with methanol leads to the β-alkoxy radical, which now has time to cyclize (step 3*a*).

Formation of the cyclohexanes (**9** *cis* and *trans*) is attributed to a 1,6-*endo* cyclization of the intermediate β-alkoxy radical (step 3*a*). The resulting tertiary radical then couples with the radical anion of 1,4-dicyanobenzene ($\mathbf{1}^{-\cdot}$) (step 4) followed by rearomatization by loss of cyanide ion (step 5) of the general mechanism.

An alternate route to the cyclohexanes would involve 1,6-*endo,exo* cyclization of the radical cation of the diene ($\mathbf{7}^{+\cdot}$) (step 2*a*). The resulting cyclic, distonic radical cation would be expected to have high positive charge density on the tertiary position while the spin density would be largely associated with the primary centre. This follows from the relative stability of the radical and cationic centres; the oxidation potential of a tertiary radical is significantly lower that of a primary radical (12). This intermediate would lead to products in which the methoxy and cyanophenyl groups are interchanged with respect to the observed products.

Cyclization of the intermediate β-methoxy radical (step 3*a*) is expected to proceed 1,6-*endo*, rather than the alternative 1,5-*exo*, based upon Beckwith's work with 5-hexenyl radicals bearing different substitution patterns. For the unsubstituted 5-hexenyl radical the rate ratio, 1,6-*endo*/1,5-*exo* cyclization, is 1:50, in favour of 1,5-*exo* closure. For the 1,1,5-trimethyl-hex-5-enyl radical, 1,6-*endo* cyclization is 100 times faster than 1,5-*exo* cyclization (13). The reversal is observed upon substitution at the 5-position alone; however, cyclization becomes regioselective only when both the 5- and 1-positions are substituted.

There is a slight preference for formation of the *cis* cyclohexane (**9** *cis*) over the *trans* isomer (**9** *trans*). This product ratio must be determined at the time of coupling between the cyclized radical and the 1,4-dicyanobenzene radical anion ($\mathbf{1}^{-\cdot}$) (step 4). The intermediate methylcyclohexyl radical, in a *pseudo*-chair conformation, is substituted at the 3-position by methyl and methoxy methyl groups. The *A* values for the methyl (1.74) and methoxy methyl (1.72) groups, *in nonpolar solvent*, are essentially identical (14). Molecular mechanics calculations on cyclohexane bearing geminal methyl and methoxy methyl groups indicate a slight (0.13 kJ mol) preference for the axial methoxy methyl conformer.[4] However, in polar hydrogen-bonding solvents the effective size of the methoxy methyl group may be larger. Coupling of the methylcyclohexyl radical with the radical anion ($\mathbf{1}^{-\cdot}$) will take place preferentially on the side leading to equatorial aryl substitution; the axial directing effect of an α-methyl group is not as great as the equatorial directing effect of the axial methyl, or methoxy methyl, group at the 3-position (15). The rates of equatorial attack on the two conformations of the radical should be almost the same. The fact that the *cis* product dominates may indicate that, under these reaction conditions (polar hydrogen-bonding solvent), the conformer with the axial methyl is preferred (slightly) over the axial methoxymethylene in the methylcyclohexyl radical.

The initially formed chair conformer of either diastereomer will convert to an axial aryl conformer; the 1-phenyl-1,3,3-trimethylcyclohexane molecule has a preference (14 kJ mol^{-1}, calculated) for the chair conformer having the axial phenyl group (9). These force field calculations also show that the twist-boat conformer is less stable than the chair conformer, and that the axial phenyl ring is rotated to avoid the axial methyl group. This fits well with the observations of the upfield shift in the ^{1}H nmr signals for the axial methyl group in the *trans* isomer (**9** *trans*) and for the axial methylene of the methoxy methyl group in the *cis* isomer (**9** *cis*).

The cycloheptane products (**10** *cis* and *trans*) are the result

[4] Molecular mechanics calculations used the PCMODEL (PCM4) software from Serena Software, Bloomington, IN 47402-3076, U.S.A.

Can. J. Chem. Downloaded from www.nrcresearchpress.com by 65.111.164.53 on 09/08/12
For personal use only.

Can. J. Chem. Downloaded from www.nrcresearchpress.com by 65.111.164.53 on 09/08/12
For personal use only.

of 1,7-*endo,endo* cyclization of the radical cation of the diene ($7^{+\cdot}$) (step 2*a*). This mode of cyclization is the least hindered of the alternatives and the only option that leaves the reactive centres, both the radical and the carbocation, at tertiary positions. The *cis* and *trans* products, (**10** *cis*) and (**10** *trans*), are formed by steps 3, 4, and 5 of the general mechanism (Scheme 1). Again, there is a slight preference for the formation of the *cis* isomer (**10** *cis*). This stereochemistry is determined at the aromatic substitution step (step 4), as in the case of the cyclohexanes described above, but the analysis of the conformations of the cycloheptyl radical and the diastereofacial selectivity for the radical coupling step are less well established with the cycloheptyl ring system.

The effect of variation in methanol and biphenyl (5) concentration.

The results of variation in the concentration of methanol are shown in Table 1 and Fig. 1; lowering the concentration of methanol results in an increase in the yield of the cycloheptanes (**10** *cis* and *trans*) relative to the cyclohexanes (**9** *cis* and *trans*) and acyclic (**8**) products. Following the initial formation of the solvated diene radical cation ($7^{+\cdot}$) (step 7), 1,7-*endo, endo* cyclization leading ultimately to the cycloheptanes (step 2*a*) is in direct competition with reaction with methanol (step 3) leading to the acyclic and cyclohexane products. The observed variation in product ratio is consistent with this proposed mechanism. These results are similar to those observed with the homolog, 2,5-dimethyl-1,5-hexadiene (**2**) (1*a*). In that case also, lowering the concentration of methanol favoured radical cation cyclization and increased the relative yield of the radical cation cyclized product (**6**) (reaction [2]). No quantitative conclusions regarding the rates of cyclization and attack by methanol can be made in either of these cases. It seems likely that cyclization of the radical cation $7^{+\cdot}$ is reversible. Calculations show the acyclic radical cation of 2,5-dimethyl-1,5-hexadiene ($2^{+\cdot}$) is 10 kJ mol^{-1} more stable than the 1,6-*endo,endo* cyclized distonic radical cation (16). The kinetic expressions are further complicated by the interaction of the radical cations, acyclic and cyclic, with biphenyl (**5**).

The variation in biphenyl (**5**) concentration also has an effect on the product ratio. In addition to the initial role of biphenyl (**5**), generating the radical cation $7^{+\cdot}$ remote from the radical anion $1^{-\cdot}$, further increase in the biphenyl concentration produces relatively more cycloheptanes (Table 2 and Fig. 2). Again, analogous results were observed for the reaction of 2,5-dimethyl-1,5-hexadiene (**2**) (reaction [1]) (1*a*). These results support the hypothesis that there is a complex formed between the radical cation of the diene (or alkene) and biphenyl (**5**). The complexing biphenyl could have a shielding (steric) effect. Furthermore, biphenyl has a lower oxidation potential than the diene and therefore most of the spin and charge density resides on the biphenyl (**5**). The complexed alkene radical cation may be deactivated toward nucleophilic attack for electronic as well as steric reasons. This complex might also facilitate the cyclization process (step 2*a*) by favouring a conformation of the diene that brings the double bonds closer together.

The fact that the electron transfer from the alkene to the biphenyl is, in many cases, endothermic has been cause for previous consideration of the existence of a complex (1, 17). Some support for this hypothesis is the observation of a radical cation complex of benzene and ethylene as well as the observation of dimeric complexes involving aromatic radical cation (18, 19).

Experimental

General information

The ^1H and ^{13}C nmr spectra were recorded on Bruker AC 250F (Quattro Probe) and AMX 400 (wide bore) spectrometers. Spectra are reported in parts per million (ppm) relative to tetramethylsilane. The infrared spectra were produced on a Nicolet 205 Fourier transform infrared spectrometer. The samples were thin liquid films on sodium chloride plates unless otherwise noted. The peaks are reported in wavenumbers (cm^{-1}) calibrated with the absorption of polystyrene at 1601.4 cm^{-1}. The mass spectra were taken with a Hewlett–Packard 5970 series quadrupole mass selective detector. Mass-to-charge ratios are listed with the relative intensities in parentheses. Exact Mass determinations were obtained on a ZAB-E mass spectrometer. Elemental analyses were carried out by Canadian Microanalytical Services Limited, Delta, B.C.

Gas chromatography, for analyses of reaction mixtures, was done on a Hewlett–Packard 5890 chromatograph fitted with a DB-1701 fused silica WCOT column (30 m × 0.25 mm) and a flame ionization detector (gc/fid) or on a Hewlett–Packard 5890 with a 5% phenyl methyl silicone fused silica WCOT column (25 m × 0.20 mm) and a Hewlett–Packard 5970 mass selective detector (gc/ms).

Purification of 2,6-dimethyl-1,6-heptadiene (**7**) and the volatile products, for elemental analysis, by preparative gas chromatography was done on a Varian Aerograph 90-P gas chromatograph (prep-gc). Medium-pressure liquid column chromatography (mplc) was done on thin-layer grade silica gel, without binder (Merck, 60 PF_{254}). The chromatographic columns were 2.5 cm × 1 m and were eluted with a hexanes – ethyl acetate solvent gradient under helium pressure (10 psi; 1 psi = 6.9 kPa). The eluent was monitored by a uv–visible spectrophotometer. The fraction size was 10 mL.

Materials

Acetonitrile (Fisher, ACS grade) was distilled over sodium hydride and then over phosphorus pentoxide. It was then passed through a column of basic alumina, refluxed over calcium hydride in a nitrogen-purged apparatus for 24 h, and distilled. The purified acetonitrile was stored over 3Å molecular sieve. Distilled methanol was also stored over 3Å molecular sieve.

The tetrahydrofuran was dried and purified by refluxing over phosphorus pentoxide, distillation, refluxing over sodium until added benzophenone caused a persistent blue colour (the radical anion), and a final distillation from sodium.

The Zn dust was activated by stirring several minutes in hydrochloric acid (2 M) followed by consecutive washing with water, ethanol, acetone, and diethyl ether, after which it was oven-dried.

Purification of 1,4-dicyanobenzene (**1**) (Aldrich) was accomplished by treatment with activated charcoal (Norite) followed by filtration and recrystallization from ethanol (95%). Biphenyl (**5**) was recrystallized from methanol.

Preparation of 2,6-dimethyl-1,6-heptadiene (7)

2,6-Dimethyl-1,6-heptadiene (**7**) was synthesized by a two-

Can. J. Chem. Downloaded from www.nrcresearchpress.com by 65.111.164.53 on 09/08/12
For personal use only.

step procedure. 2,6-Heptanedione was made by a previously reported method from diketene and formalin in 20% yield (20). The diene (**7**) was made from this diketone in 22% yield by a method using $Zn–CH_2Br_2–TiCl_4$ as described by Lombardo (21).

Diketene (100 g) (Aldrich) was added to formaldehyde (50 g, 37% aqueous solution with 10–15% methanol as stabilizer) and distilled water (240 mL). This mixture was heated and stirred in a round-bottom flask equipped with a condenser. When the temperature reached 50°C the heat was removed and ice-water was occasionally used to keep the temperature from rising much above 50°C. When the exothermic reaction subsided, heat was again applied to keep the mixture warm (50°C) overnight. Sodium chloride (80 g) was added to the reaction mixture, which was stirred for 1 h. The organic product was extracted into benzene. The combined extract was washed with brine, dried over magnesium sulphate (anhydrous), and the solvent was evaporated. The resulting yellow liquid was purified by vacuum distillation on a silvered, vacuum-jacked column (40 cm × 1.5 cm) with a variable-take-off head. The crude mixture gave a clear, colourless product that distilled at 89°C (7 Torr; 1 Torr = 133.3 Pa) and usually crystallized.

Activated zinc metal dust (21 g) and dry tetrahydrofuran (200 mL) were put in an oven-dried flask with dibromomethane (7.0 mL) and cooled to −40°C. Titanium tetrachloride (8.1 mL) was added over about 20 min. The mixture was stirred at 5°C under a nitrogen atmosphere for 3 days. The flask was cooled in an ice-water bath and dichloromethane (35 mL) was added. 2,6-Heptanedione (4.2 g) was added, over 15–20 min, by syringe. The mixture was allowed to come to room temperature. It was stirred occasionally over 4 h. Distilled pentane (210 mL) and a slurry of sodium bicarbonate (105 g) in water (55 mL) were added. After effervescence, the organic layer was poured off and the remainder shaken with more pentane. The combined pentane solution was shaken with a mixture of sodium sulphate (70 g) and sodium bicarbonate (15 g). The solution was filtered and distilled. The distillate was purified by column chromatography using silica (70–230 mesh) with dichloromethane as eluent. The diene **7** was purified by prep-gc (40% SE-30, 100°C) to give a clear, colourless volatile oil (1.7 g). The ^{1}H nmr spectrum was similar to that reported (22).

2,6-Dimethyl-1,6-heptadiene (**7**): ^{1}H nmr (250.13 MHz, $CDCl_3$) δ_{TMS}: 4.70 (s, 2H, vinyl), 4.68 (s, 2H, vinyl), 2.01 (t, 4H, $^3J_{3-4}$ = 7.4 Hz, C-3 and C-5), 1.72 (s, 6H, 2 methyls), 1.57 (quintet, 2H, $^3J_{4-3}$ = 7.4 Hz, C-4); ^{13}C nmr (62.9 MHz, $CDCl_3$) δ_{TMS}: 145.94 (tertiary vinyl), 109.85 (primary vinyl), 37.40 (C-3 and C-5), 25.58 (C-4), 22.41 (methyls).

Formation of the methanol, 2,6-dimethyl-1,6-heptadiene (7), 1,4-dicyanobenzene (1) photo-NOCAS adducts 8, 9 *cis* and *trans*, and 10 *cis* and *trans*: reaction [3]

A solution of 1,4-dicyanobenzene (**1**) (0.10 M) and biphenyl (**5**) (0.10 M) in acetonitrile–methanol (3:1 by volume) was purged by nitrogen ebullition for 3 min in Pyrex tubes (2 cm i.d.) and the tubes were sealed with Teflon-lined caps. 2,6-Dimethyl-1,6-heptadiene was then injected into the solution through the cap to make the alkene concentration 0.10 M. Solutions were irradiated with a 1-kW, medium-pressure mercury vapour lamp (Canadian General Electric) in a Pyrex jacket with water cooling. The tubes were arranged around the jacket in a water-bath kept at 10°C. Progress of the reaction was followed by gc/fid. The solvent was removed by distillation at atmospheric pressure. Five 1:1:1 adducts were detected (gc/ms). The photolysate was separated by column chromatography (mplc) using hexanes–ethyl acetate as the solvent system. Of the isolated products: **8**, **9** *trans*, and **10** *cis* and *trans* were colourless oils; **9** *cis* was a solid. The combined yield was 49%. The yield was based on the amount of 1,4-dicyanobenzene (**1**) consumed (44%). The yields of the individual products are based on the integrated peaks in the gas chromatogram (gc/fid) of the photolysate.

4-(1-Methoxymethyl-1,5-dimethyl-5-hexenyl)benzonitrile (**8**): yield: 5%; infrared (Nicolet 205) ν: 3074(w), 2969(s), 2938(s), 2875(s), 2831(m), 2227(s), 1649(w), 1607(m), 1507(w), 1459(m), 1452(m), 1407(w), 1390(w), 1374(w), 1198(w), 1109(s), 888(m), 838(m); ^{1}H nmr (250.13 MHz, $CDCl_3$) δ_{TMS}: 7.60 (dt, 2H, aryl hydrogens adjacent to nitrile), 7.44 (dt, 2H, aryl hydrogens adjacent to alkyl group), 4.67 (s, 1H, terminal vinyl H), 4.59 (s, 1H, terminal vinyl H), 3.49 (d, 1H, ^2J = 9.0 Hz, H on methoxy-substituted carbon), 3.36 (d, 1H, ^2J = 9.0 Hz, H on methoxy-substituted carbon), 3.29 (s, 3H, methoxy), 1.93 (t, 2H, $^3J_{3-4} = {}^2J$ = 7.3 Hz, allylic methylene C-4), 1.50–1.76 (multiplet, 2H, H's at C-2), 1.61 (s, 3H, allylic Me), 1.35 (s, 3H, methyl on C-1), 1.00–1.33 (multiplet, 2H, H's on C-3); ^{13}C nmr (62.9 MHz, $CDCl_3$, multiplicities by DEPT) δ_{TMS}: 152.04 (s, 4′ aryl C), 145.35 (s, substituted end of double bond), 131.89 (d, 2′ and 6′ aryl C), 127.80 (d, 3′ and 5′ aryl C), 119.15 (s, cyano C), 110.19 (t, unsubstituted end of double bond), 109.63 (s, 1′(cyano-substituted) aryl C), 81.24 (t, methoxy-substituted C), 59.36 (q, methoxy), 42.79 (s, benzylic C-1), 38.55 (t, C-2 methylene), 38.07 (C-4 methylene), 22.58 (q, benzylic methyl) 22.20 (q, allylic methyl), 21.54 (t, C-3 methylene); ms *m/z* (% rel. abund.): 257(6), 169(11), 156(35), 143(11), 142(13), 130(44), 129(12), 116(23), 115(11), 69(13), 55(13), 45(100), 43(10), 41(27). Exact Mass calcd. for $C_{17}H_{23}NO$: 257.1780; found: 257.1780.

*4-(*cis*-3-Methoxymethyl-1,3-dimethylcyclohexyl)benzonitrile* (**9** cis): yield: 12%; mp 56–57°C; infrared (Nicolet 205) ν: 2952(s), 2927(s), 2894(s), 2869(s), 2826(m), 2813(m), 2227(s), 1606(m), 1505(m), 1477(m), 1467(m), 1453(m), 1195(w), 1187(w), 1110(s), 961(w), 837(m); ^{1}H nmr (250.13 MHz, $CDCl_3$) δ_{TMS}: 7.58 (dd, 2H, aryl H next to cyano), 7.52 (dd, 2H, aryl H next to alkyl substituent), 2.83 (s, 3H, methoxy), 2.43 and 2.51 (AB quartet, 2H, J_{gem} = 8.9 Hz, methylene next to methoxy), 2.30 (d, 1H, $^2J_{2ax-2eq}$ = 14.2 Hz, eq H on C-2), 2.25 (d, 1H, $^2J_{5ax-5eq}$ = 13.0 Hz, eq H on C-5), 1.5–1.65 (m, 2H, hydrogens on C-6), 1.44 (m, 2H, ax H on C-5 and eq H on C-4), 1.29 (d, 1H, $^2J_{2ax-2eq}$ = 14.3 Hz, ax H on C-2), 1.18 (m, 1H (seen as ddd 10 Hz, 8 Hz, 4 Hz in 400 MHz), ax H on C-4), 1.14 (s, 3H, methyl on C-1), 0.94 (s, 3H, methyl on C-3); ^{13}C nmr (62.9 MHz, $CDCl_3$, multiplicities by DEPT) δ_{TMS}: 154.93 (s), 131.71 (d), 126.72 (d), 199.24 (s), 108.88 (s), 78.65 (t), 58.38 (q), 45.82 (t), 38.32 (s), 36.02 (t), 35.60 (t), 35.19 (q+s), 28.10 (q), 19.26 (t); ms *m/z* (% rel. abund.): 257(14), 212(45), 211(51), 196(28), 156(57), 143(25), 142(25), 130(100), 116(39), 81(23), 69(22), 68(26), 55(28), 45(68), 41(50). Anal. calcd. for $C_{17}H_{23}NO$: C 79.33, H 9.01, N 5.44; found: C 79.13, H 8.85, N 5.24; X-ray data: see supplementary material $C_{17}H_{23}NO$.[3]

Can. J. Chem. Downloaded from www.nrcresearchpress.com by 65.111.164.53 on 09/08/12
For personal use only.

*4-(*trans-*3-Methoxymethyl-1, 3-dimethylcyclohexyl)benzonitrile (**9** trans)*: yield: 11%; infrared (Nicolet 205) ν: 2928(s), 2866(s), 2827(s), 2227(s), 1606(m), 1505(m), 1461(m), 1196(m), 1189(w), 1178(w), 1111(s), 1083(m), 838(s); ^{1}H nmr (250.13 MHz, $CDCl_3$) δ_{TMS}: 7.59 (d, 2H, one half of AA′BB′, aryl hydrogens adjacent to cyano group), 7.49 (d, 2H, the other half of the AA′BB′, aryl hydrogens adjacent to alkyl substituent), 3.33 (s, 3H, methoxy), 2.98 and 3.01 (AB quartet, 2H, J_{gem} = 8.9 Hz, methylene next to methoxy), 2.31 (dq, 1H, 14.0 Hz, 3.2 Hz, eq H), 2.09 (dt, 1H, 14.2 Hz, 2 Hz, eq H), 1.6 (m, 3H), 1.3 (m, 3H), 1.12 (s, 3H, methyl on C-1), 0.31 (s, 3H, methyl on C-3 in aromatic shielding cone); ^{13}C nmr (62.9 MHz, $CDCl_3$, multiplicities by DEPT) δ_{TMS}: 154.96 (s, alkyl-substituted aryl), 131.90 (d, aryl C's adjacent to cyano substituent), 126.83 (d, aryl C's adjacent to alkyl substituent), 119.21 (s, cyano), 108.93 (s, cyano-substituted aryl), 84.71 (t, methoxy-substituted C), 59.31 (q, methoxy), 45.87 (t, C-2), 38.04 (s), 36.04 (q, benzylic methyl), 36.04 (t), 35.74 (s), 34.22 (t), 22.65 (q, methyl on C-3 in shielding cone), 18.69 (t); ms *m/z* (% rel. abund.): 257(3), 212(37), 211(55), 196(25), 156(50), 143(23), 142(22), 130(100), 116(37), 81(23), 69(19), 68(25), 55(27), 45(76), 41(51). Anal. calcd. for $C_{17}H_{23}NO$: C 79.33, H 9.01, N 5.44; found: C 78.99, H 8.86, N 5.32.

*4-(*cis-*4-Methoxy-1,4-dimethylcycloheptyl)benzonitrile (**10** cis)*: yield: 12%; infrared (Nicolet 205) ν: 2964(s), 2929(s), 2869(m), 2227(s), 1606(m), 1505(m), 1471(m), 1376(w), 1126(m), 1085(m), 1072(s), 834(m), 569(m); ^{1}H nmr (250.13 MHz, $CDCl_3$) δ_{TMS}: 7.59 (d, 2H, aryl hydrogens next to cyano), 7.46 (d, 2H, aryl hydrogens next to alkyl), 3.11 (s, 3H, methoxy), 2.10–2.24 (m, 2H), 1.86–1.94 (m, 1H), 1.6 (m, 2H), 1.5 (m, 4H), 1.4 (m, 1H), 1.23 (s, 3H), 1.16 (s, 3H); ^{13}C nmr (62.9 MHz, $CDCl_3$, multiplicities by DEPT) δ_{TMS}: 156.42 (s), 131.94 (d), 126.76 (d), 119.05 (s), 109.17 (s), 76.39 (s), 48.58 (q), 41.54 (s), 41.29 (t), 41.07 (t), 33.05 (t), 32.85 (t), 31.11 (q), 25.37 (q), 19.33 (t); ms *m/z* (% rel. abund.): 257(7), 116(14), 99(20), 85(100), 72(17), 55(15), 43(15), 42(12), 41(15). Exact Mass calcd. for $C_{17}H_{23}NO$: 257.1780; found: 257.1780.

Preparation of 4-(*cis*-4-methoxy-1,4-dimethylcycloheptyl)benzoic acid (10*a cis*)

A small sample of 4-(*cis*-4-methoxy-1,4-dimethylcycloheptyl)benzonitrile (**10** *cis*) (44.5 mg) in aqueous sodium hydroxide (4.0 mL, 10%) was stirred and heated, at the boiling point, until the oily photo-NOCAS product dissolved; the solution turned slightly yellow. This mixture was cooled and extracted with dichloromethane. The aqueous layer was acidified with hydrochloric acid (conc.), and extracted with benzene. Evaporation of the solvent left a colourless viscous oil (35 mg). Ammonia gas was bubbled into a benzene solution of this oil and a solid precipitated. The solvent was evaporated to dryness, the residue was redissolved in benzene, and crystals (**10***a cis*) for X-ray analysis, grew upon cooling.

*4-(*cis-*4-Methoxy-1,4-dimethylcycloheptyl)benzoic acid (**10a** cis)*: mp 117–120°C; infrared (Nicolet 205) ν: 2961(s), 2937(s), 2926(s), 2905(s), 2871(s), 1718(s), 1688(vs), 1610(m), 1417(m), 1284(s), 1248(m), 1122(m), 1070(m); ^{1}H nmr (250.13 MHz, $CDCl_3$) δ_{TMS}: 8.03 (d, 2H, aryl hydrogens next to carbonyl), 7.47 (d, 2H, aryl hydrogens next to alkyl), 3.12 (s, 3H, methoxy), 2.10–2.35 (m, 2H), 1.86–1.94 (m, 1H), 1.35–1.65 (m, 7H), 1.25 (s, 3H), 1.16 (s, 3H); ^{13}C nmr (62.9 MHz, $CDCl_3$, proton decoupled) δ_{TMS}: 171.56, 157.12, 130.17 (d), 126.48, 126.21 (d), 76.92, 48.66 (q), 41.55 (t), 41.51, 41.16, 33.25, 32.86 (t), 31.44, 25.45, 19.47; mass spectral data by Finnigan 4500 with programmed solids probe (70 eV) *m/z* (% rel. abund.): 276.3(11.4), 261.3(2.8), 215(2.7), 149.1(5.2), 99.1(23.5), 85.1(100); X-ray data: see supplementary material; $C_{17}H_{24}O_3$.[3]

*4-(*trans-*4-Methoxy-1,4-dimethylcycloheptyl)benzonitrile (**10** trans)*: yield: 10%; infrared (Nicolet 205) ν: 2964(s), 2929(s), 2868(m), 2825(w), 2227(s), 1606(m), 1505(m), 1473(m), 1459(m), 1376(w), 1368(w), 1117(m), 1085(s), 1072(s), 835(m), 665(w); ^{1}H nmr (250.13 MHz, $CDCl_3$) δ_{TMS}: 7.60 (d, 2H, aryl hydrogens next to cyano), 7.45 (d, 2H, aryl hydrogens next to alkyl), 3.19 (s, 3H, methoxy), 1.7–2.0 (m, 7H), 1.4 (m, 2H), 1.23 (ddd, 1H, 14.7 Hz, 9.3 Hz, 1.3 Hz), 1.21 (s, 3H), 1.05 (s, 3H); ^{13}C nmr (62.9 MHz, $CDCl_3$) δ_{TMS}: 156.28 (s), 131.98 (d), 126.87 (d), 119.00 (s), 109.17 (s), 76.28 (s), 48.68 (q), 41.70 (t), 41.69 (s), 41.63 (t), 32.69 (t), 32.34 (q), 31.50 (t), 25.47 (q), 19.16 (t); ms *m/z* (% rel. abund.): 257(6), 116(13), 99(18), 85(100), 72(20), 55(20), 43(18), 42(12), 41(19). Exact Mass calcd. for $C_{17}H_{23}NO$: 257.1780; found: 257.1780.

Acknowledgements

This work was supported by a grant from the Natural Sciences and Engineering Research Council of Canada. We thank Dr. D.L. Hooper at the Atlantic Regional Magnetic Resonance Centre at Dalhousie University for the high-field NMR spectra and for help in the preparation of the manuscript. Exact mass measurements were carried out by Mr. D. Embree at the Institute for Marine Biosciences, Halifax.

References

1. (*a*) D.R. Arnold, K.A. McManus, and X. Du. Can. J. Chem. **72**, 415 (1994); (*b*) D.R. Arnold and X. Du. Can. J. Chem. **72**, 403 (1994); (*c*) K.A. McManus and D.R. Arnold. Can. J. Chem. **72**, 2291 (1994); (*d*) R.M. Borg, D.R. Arnold, and T.S. Cameron. Can. J. Chem. **62**, 1785 (1984); (*e*) D.R. Arnold and M.S. Snow. Can. J. Chem. **66**, 3012 (1988).
2. (*a*) D.R. Arnold, X. Du, and H.J.P. de Lijser. Can. J. Chem. **73**, 522 (1995); (*b*) D.R. Arnold, X. Du, and J. Chen. Can. J. Chem. **73**, 307 (1995); (*c*) A.L. Perrott and D.R. Arnold. Can J. Chem. **70**, 272 (1992).
3. J.E. Baldwin. J. Chem. Soc. Chem. Commun. 734 (1976); 738 (1976).
4. A.L.J. Beckwith and K.U. Ingold. Rearrangements in ground and excited states. Vol. 1. *Edited by* P. de Mayo. Academic Press, Toronto. 1980.
5. (*a*) P.G. Gassman and K.J. Bottorff. J. Am. Chem. Soc. **109**, 7547 (1987); (*b*) K. Mizuno, T. Tamai, T. Nishiyama, K. Tani, M. Sawasaki, and Y. Otsuji. Angew. Chem. Int. Ed. Engl. **33**, 2113 (1994).
6. F. Williams and Q.X. Guo. J. Am. Chem. Soc. **111**, 4133 (1989).
7. T. Miyashi, A. Konno, and Y. Takahashi. J. Am. Chem. Soc. **110**, 3676 (1988).
8. A. Heidbreder and J. Mattay. Tetrahedron Lett. **33**, 1973 (1992).
9. (*a*) N.L. Allinger and M.T. Tribble. Tetrahedron Lett. 3259 (1971); (*b*) D.J. Hodgson, U. Rychlewska, E.L. Eliel, M. Manoharan, D.E. Knox, and E.M. Olefirowicz. J. Org. Chem. **50**, 4838 (1985).

10. D.R. Arnold and A.J. Maroulis. J. Am. Chem. Soc. **98**, 5931 (1976).
11. (*a*) D. Rehm and A. Weller. Isr. J. Chem. **8**, 259 (1970); (*b*) D. Rehm and A. Weller. Ber. Bunsen-ges. Phys. Chem. **73**, 834 (1968).
12. (*a*) D.D.M. Wayner, D.J. McPhee, and D. Griller. J. Am. Chem. Soc. **110**, 132 (1988); (*b*) D.D.M. Wayner and D. Griller. *In* From atoms to polymers. *Edited by* J.F. Liebman and A. Greenberg. V.C.H. Publishers, Inc. 1989. Chap. 3.
13. A.L.J. Beckwith, I.A. Blair, and G. Phillipou. Tetrahedron Lett. **38**, 2251 (1974).
14. W. Kitching, H. Olszowy, and W. Adcock. Org. Magn. Reson. **15**, 230 (1981).
15. W. Damm, B. Giese, J. Hartung, T. Hasskerl, K.N. Houk, O. Huter, and H. Zipse. J. Am. Chem. Soc. **114**, 4067 (1992).
16. T. Tsuji, T. Miura, K. Sugiura, Y. Matsumoto, and S. Nishida. J. Am. Chem. Soc. **115**, 482 (1993).
17. T. Majima, C. Pac, and H. Sakurai. Chem. Lett. 1133 (1979).
18. T. Bally, K. Roth, and R. Straub. J. Am. Chem. Soc. **110**, 1639 (1988).
19. (*a*) A. Terahara, H. Ohys-Nishiguchi, N. Hirota, and A. Oku. J. Phys Chem. **90**, 1564 (1986); (*b*) O.W. Howarth and G.K. Fraenkel. J. Chem. Phys. **52**, 6258 (1970).
20. R.A. Micheli, Z.G. Hajos, N. Cohen, D.R. Parrish, L.A. Portland, W. Sciamanna, M.A. Scott, and P.A. Wehrli. J. Org. Chem. **40**, 675 (1975).
21. (*a*) L. Lombardo. Org. Synth. **65**, 81 (1987); (*b*) Tetrahedron Lett. **23**, 4293 (1982).
22. B. Irrgang and H. Mayr. Tetrahedron, **47**, 219 (1991).

Can. J. Chem. Downloaded from www.nrcresearchpress.com by 65.111.164.53 on 09/08/12
For personal use only.

Metal ion – biomolecule interactions. Part 16.[1] C(2)-H isotopic exchange in Co(III)-coordinated imidazoles

Erwin Buncel, Fan Yang, Robert Y. Moir, and Ikenna Onyido

Abstract: Transition-metal-bound imidazoles are suitable models for evaluating the roles of metal ions in biomolecules having the imidazole moiety and similar heterocyclic residues as part of their structure. Such studies provide useful insights into metal–biomolecule interactions in biological systems, especially when the lability of the metal–ligand bond is substantially reduced, such that the identity of the metal–ligand complex is preserved during the course of the reaction under investigation. The present paper reports on a kinetic study of tritium exchange from the C(2) position of the imidazole moiety in the substitution-inert complex cations $[Co(NH_3)_5[2\text{-}^3H]\text{-imidazole}]^{3+}$ (**1**) and $[Co(NH_3)_5\text{-1-methyl-}[2\text{-}^3H]\text{-imidazole}]^{3+}$ (**2**). Rate–pH profiles have been determined in aqueous solution at 60°C. Both substrates are believed to react through rate-determining attack of hydroxide ion (k^{M+} pathway) at C(2)-T. Dissection of the kinetic data reveals an additional pathway for **1** consequent upon deprotonation of its pyrrole-like N-H(T) to yield **3**, which is then attacked by hydroxide at C(2) (k^M pathway). The ratio $k^{M+}/k^M = 10^3$ that is obtained is in accord with the expected reduced reactivity of **3**. Comparison of the present data with those reported for a variety of heterocyclic substrates shows that the order of reactivity, protonated ≫ metal ion coordinated ≫ neutral form of substrates, prevails. The superiority of the proton over metal ions in catalyzing isotopic hydrogen exchange is attributed to its larger ground state acidifying effect coupled with the greater transition state stabilization it affords, relative to metal ions. The exchange reaction of **3** via the k^M pathway is the first example of a reactive anionic species in which the negative charge is located α to the exchanging C-H.

Key words: tritium exchange, cobalt (III)-coordinated imidazoles.

Résumé : Les imidazoles liés à des métaux de transition sont des modèles appropriés pour évaluer les rôles des ions métalliques dans des biomolécules dont une partie de la structure contient de l'imidazole ou des résidus hétérocycliques semblables. De telles études fournissent des données utiles sur les interactions métal–biomolécule des systèmes biologiques, en particulier lorsque la labilité du complexe métal–coordinat est grandement réduite alors que l'identité du complexe métal–coordinat est préservée durant la réaction étudiée. Dans ce travail on rapporte les données obtenues au cours d'une étude cinétique de l'échange du tritium de la position C(2) de la portion imidazole lors de substitutions des cations complexes inertes $[Co(NH_3)_5\{2\text{-}^3H\}\text{-imidazole}]^{3+}$ (**1**) et $[Co(NH_3)_5\text{-1-méthyl-}\{2\text{-}^3H\}\text{-imidazole}]^{3+}$ (**2**). On a déterminé les profils vitesse–pH en solutions aqueuses à 60°C. On croit que les deux substrats réagissent par le biais d'une attaque de la position C(2)-T par l'ion hydroxyde (voie k^{M+}) qui détermine la vitesse de la réaction. La dissection des données cinétiques révèle l'existence d'une autre voie réactionnelle du composé **1** qui suit la déprotonation de son N-H(T), qui ressemble à un pyrrole, en composé **3** qui est alors attaqué par l'hydroxyde en position C(2) (voie k^M). Le rapport $k^{M+}/k^M = 10^3$ qui est obtenu est en accord avec la réactivité réduite attendue pour le composé **3**. Une comparaison des données obtenues ici avec celles rapportées pour une variété de substrats hétérocycliques montre que l'ordre de réactivité, protoné ≫ ion métallique coordiné ≫ forme neutre des substrats, prévaut. On attribue la supériorité du proton sur les ions métalliques dans la catalyse de l'échange des isotopes de l'hydrogène à son effet plus prononcé d'acidification de l'état fondamental couplé à la stabilisation plus grande de l'état qu'il lui fournit par rapport aux ions métalliques. La réaction d'échange du composé **3** par le biais d'une voie k^M est le premier exemple d'une espèce anionique réactive dans laquelle la charge négative est située en alpha de la liaison C-H qui s'échange.

Mots clés : échange du tritium, imidazoles coordinés au cobalt(III).

[Traduit par la rédaction]

Received January 17, 1995.

E. Buncel,[2] F. Yang, and R.Y. Moir. Department of Chemistry, Queen's University, Kingston, ON K7L 3N6, Canada.
I. Onyido. Department of Chemistry, University of Agriculture, Makurdi, Nigeria.

[1] Part 15: see ref. 1*b*.
[2] Author to whom correspondence may be addressed. Telephone: (613) 545-2616. Fax: (613) 545-6669.

Can. J. Chem. Downloaded from www.nrcresearchpress.com by 80.90.12.36 on 09/08/12
For personal use only.

Can. J. Chem. Downloaded from www.nrcresearchpress.com by 80.90.12.36 on 09/08/12
For personal use only.

Introduction

Considerable interest has been devoted to the study of isotopic hydrogen exchange in imidazole and similar five-membered heterocycles and their derivatives (1–4), which are key constituents of many naturally occurring biologically important molecules whose roles are important to life processes (5, 6). As the heteroaromatic component of histidine, imidazole functions to bind metal ions to protons (7). The utility of isotopic hydrogen exchange from the C(2) position of imidazole as a diagnostic tool in biological system has been successfully exploited in the identification of site specificity in the binding of histidine residues of β-lactamase II and superoxide dismutase with metal ions (8).

Studies of metal ion effects on isotopic hydrogen exchange in these ligands and their derivatives, including purines, have been undertaken with the aim of evaluating the role of metal ions in biological systems (9–11). Two approaches are available in these studies. The first consists in the direct introduction of metal ions as their soluble salts into reaction media containing the ligand. A common problem with this method lies in the fact that, in most cases, the metal ions involved, e.g., $CH_3Hg(II)$, Ag(I), Pb(II), Co(II), Zn(II), etc., form *kinetically labile* complexes in solution (12), leading to unknown dissociation equilibria and uncertain stoichiometries, with attendant kinetic complications and ambiguities in evaluating rate data. A new strategy that we have adopted in the present paper involves the synthesis, isolation, and study of the exchange rates of labelled *substitution inert* complexes (12). This approach overcomes the pitfalls pointed out above and is preferred because it ensures that the identity of the reacting species is established under optimized experimental conditions. Both these approaches have been combined in the general Scheme 1. In this scheme the metal-coordinated species can be considered as formed through addition of salts, or alternatively, as in the present work, isotopic exchange is studied on the isolated complexes.

We report herein a kinetic investigation of the detritiation of the *substitution inert* complex cations $[Co(NH_3)_5[2\text{-}^3H]\text{-imidazole}]^{3+}$, **1**, and $[Co(NH_3)_5\text{-1-methyl-}\{2\text{-}^3H\]\text{-imidazole}]^{3+}$, **2**. There is general interest in cobalt (III) complexes of imidazole derivatives because of the role this metal has in vitamin B_{12} and related compounds (13).

A number of studies in the literature compare reactivity towards hydron exchange at C(2) of free and Co(III)-coordinated imidazoles. Thus imidazole undergoes C(2) deuteration at 50°C and pH 10–11 with $t_{1/2}$ = 119 min (2*b*). Coordination to Co(III) as in **1** reduces reactivity of the ligand to the extent that no exchange occurs at 44°C under basic or acidic conditions (14). Similarly, 1-methylimidazole undergoes deuteration in D_2O at the same position with $t_{1/2}$ = 42 min at pH 10–11 and 50°C (2*b*), and $t_{1/2}$ = 99 min and 5 days at pH 8.1 and 5.0, respectively, at 44°C (14). When the imidazole ligand is coordinated to Co(III) as in **4**, deuterium exchange at room temperature and pH 12 occurs with the substantially different $t_{1/2}$ of 16 h (15). These data point to the apparent inhibitory effect of Co(III) coordinated at N(3), relative to the proton, towards C(2)-H exchange in the imidazoles. Similar effects by other metals ions have been reported in our earlier work (9) and by other workers (10, 11) for other imidazole-containing systems.

The present paper reports on the detritiation rates of **1** and **2**

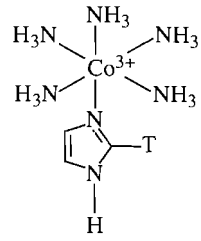

1

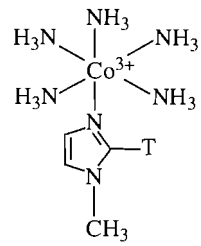

2

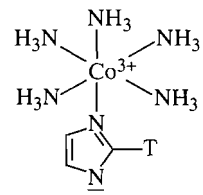

3

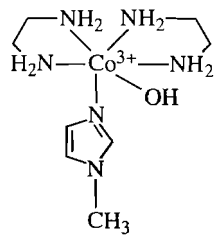

4

Scheme 1.

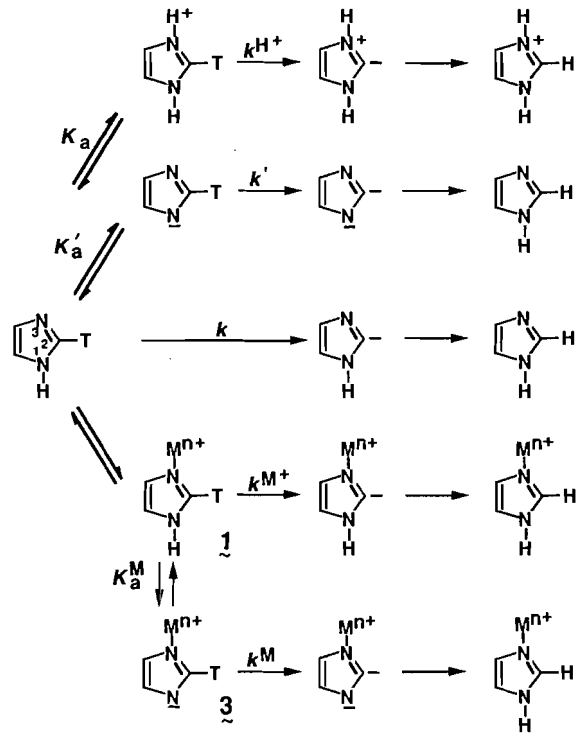

under experimental conditions corresponding to work reported in our previous paper (9), thus enabling comparison of reactivity in these systems. As well, the data presented herein provide a firm basis for the comparison of proton activation versus metal ion activation.

Kinetic and thermodynamic rationales for the inferior activating capability of metal ions relative to the proton are discussed in relation to Scheme 1 in which structures **1** and **3** are shown in abbreviated form. Surprisingly, dissection of the rate data for **1** provides kinetic evidence for the exchange of the imidazolide ion, **3**, resulting from N-H deprotonation of **1**.

Can. J. Chem. Downloaded from www.nrcresearchpress.com by 80.90.12.36 on 09/08/12
For personal use only.

This is the first reported instance of hydroxide ion attack on an imidazolide ion bearing negative charge adjacent to the exchange site. Comparison with rate data for detritiation of anionic forms of purine derivatives (at N(1) or N(3)) (16*a*) affords an indication of the magnitude of electrostatic influences on reactivity in these systems, noting that in the purines N-H ionization takes place in the ring annelated onto the imidazole ring where C-H exchange occurs, whereas in imidazoles the effect of N-H deprotonation on exchange is expected to be much greater.

Results and discussion

Rate profiles, mechanism, and identity of reacting species

The observed first-order rate constants, k_{obs}, measured for the detritiation of $[Co(NH_3)_5\{2\text{-}^3H\}\text{-imidazole}]^{3+}$ (**1**) and $[Co(NH_3)_5\text{-1-methyl-}\{2\text{-}^3H\}\text{-imidazole}]^{3+}$ (**2**) in aqueous buffer solutions at 60°C are listed in Table 1 and shown graphically in Figs 1 and 2 in the forms of rate–pH profile over the pH range 7.7–10.5 for **1** and a plot of k_{obs} vs. $[OH^-]$ for **2**.

The mechanism of detritiation of imidazole-type compounds as shown in Scheme 1 is believed to involve rate-limiting attack of hydroxide ion on either the N(3)-protonated (k^{H+} pathway) or the neutral forms (k pathway) of the substrate (1*a*, 3, 4, 16). In the former case, the reaction proceeds through an ylide intermediate. Neutral forms of the substrate are by far less reactive than their protonated counterparts, rate constants for the reaction of the latter species being 10^7–10^9 times greater than for the former in purines where data are available. It is reasonable to suppose that rate differences of a similar magnitude also exist in imidazole and related heterocycles. At high pH the pyrrole-type N-H in these substrates can undergo deprotonation and the resulting species may in principle also be reactive (k' pathway). Note that this pathway has been observed in purines where deprotonation occurs in the other ring, at N(1) as in Scheme 2, but not in imidazoles. Rate–pH profiles of various descriptions have been reported and these provide information regarding the identity of reacting species as well as the presence of any derived but unreactive species (16).

The simplest kinetic scenario for isotopic exchange in these heterocycles is presented by model compounds such as 1,3-dimethylimidazolium (2*d*) and 1,3-dimethylbenzimidazolium (16*d*) ions in which N-alkylation at N(1) and N(3) prevents proton transfer processes that occur at the heteroatoms in acidic and basic media. Such compounds obey a simple second-order rate expression, as in the present case for complex **2**. Thus complex **2** obeys eq. [1], as is shown by the linear plot in Fig. 2. The second-order rate constant for hydroxide ion attack on **2** is obtained as the slope of the plot in Fig. 2, $k^{M+} = 1.47 \times 10^{-1}$ m^{-1} s^{-1}, $r = 0.997$, at 60°C.

$$[1] \quad k_{obs} = k^{M+}[OH^-]$$

Comparing **1** and **2**, the only structural difference between the two complexes is in the methylation state at N(1) and any difference in the rate profiles of the two substrates can reasonably be accounted for by consideration of N-H deprotonation in **1**. Scheme 1 provides a composite picture for the reaction of **1** and two mechanisms are discernable. In the first mechanism, termed *Mechanism I*, hydroxide ion attack on **1** is the only significant pathway to generate products; thus $k^M = 0$ and **3** forms a reservoir of unreactive substrate. The relevant rate expression for this mechanism, derived according to standard procedures, is given by eq. [2] in which k^{M+} is the second-order rate constant for hydroxide ion attack on the complex, while K_w (= 9.64×10^{-14}) (17) and K_a^M are the ionization constants for water and N(1)-H of **1**, respectively.

$$[2] \quad k_{obs} = \frac{k^{M+}K_w}{K_a^M + [H^+]}$$

The second mechanism (*Mechanism II*) confers kinetic activity on both substrate forms in solution, hence k^{M+} and k^M have finite values, although it is reasonable to expect that the condition $k^{M+} > k^M$ holds. Equation [3] is the appropriate rate equation for this mechanism, k^M being the second-order rate constant for hydroxide ion attack on **3**, the anionic form of **1**.

Table 1. Detritiation first-order rate constants (k_{obs}) for **1** and **2** in aqueous buffers at 60°C.

	$10^6 k_{obs}$ (s^{-1})	
pH (at 60°C)	**1**	**2**
7.77	4.66	
8.30	7.34	27.0
8.89	9.67	37.9
9.49	13.4	78.0
9.96	13.0	155
10.46	14.9	

Fig. 1. Rate–pH profile for the detritiation of $[Co(NH_3)_5\{2\text{-}^3H\}\text{imidazole}]^{3+}$, **1**, in aqueous buffers at 60°C. The solid line represents the theoretical profile calculated from eq. [3] using the values in the text.

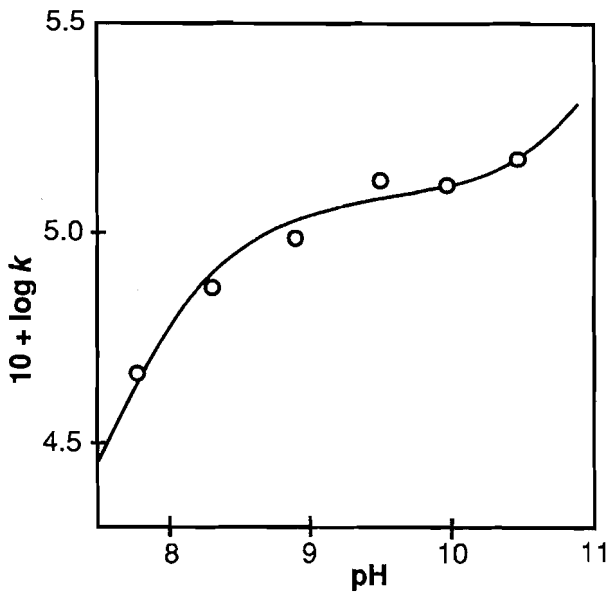

Can. J. Chem. Downloaded from www.nrcresearchpress.com by 80.90.12.36 on 09/08/12
For personal use only.

Fig. 2. Plot of k_{obs} vs. $[OH^-]$ according to eq. [1] for the detritiation of $[Co(NH_3)_5$-1-methyl{2-^{3}H}imidazole$]^{3+}$, **2**, in aqueous buffers at 60°C.

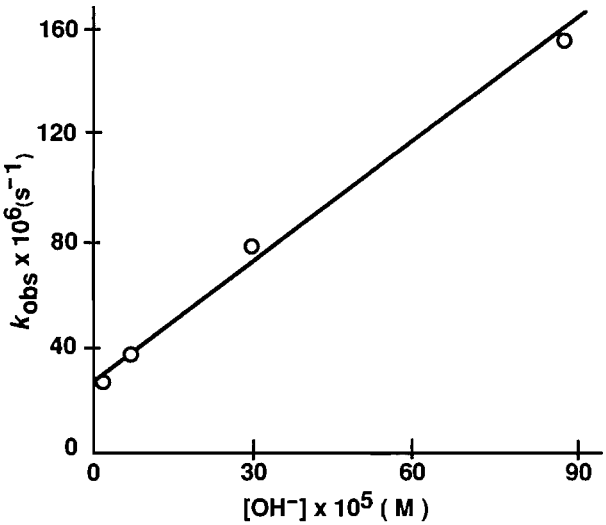

Scheme 2.

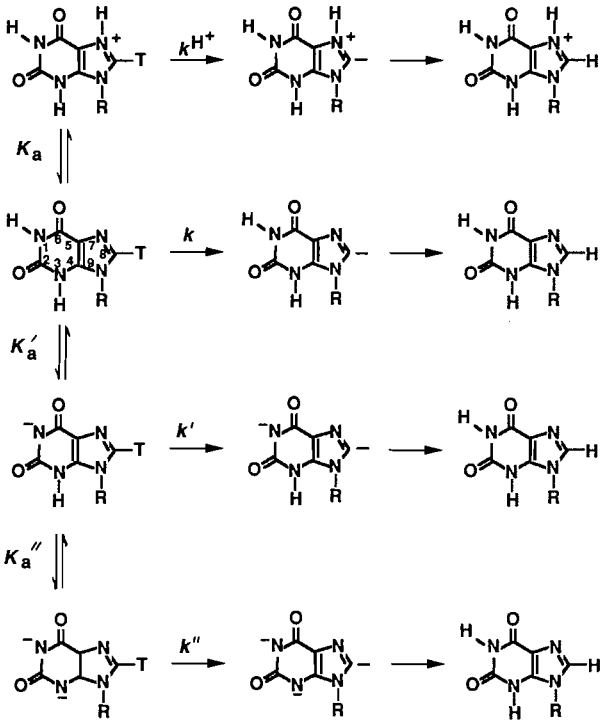

$$[3]\quad k_{obs} = \frac{k^{M+}K_w + k^M K_a{}^M[OH^-]}{K_a{}^M + [H^+]}$$

In consideration of the two mechanisms, I and II, an important clue lies in the nature of the rate–pH profiles that are predicted by eqs. [2] and [3]. Rate–pH profiles have in the past been found diagnostic of mechanism in isotopic exchange studies of imidazole and purine compounds in the presence of metal ions (16). Thus eq. [2] corresponding to Mechanism I predicts an initial increase in rate at low pH to be followed by a plateau at high pH. On the other hand, for eq. [3], which corresponds to Mechanism II, no pH-independent region is expected, rather a curve with an inflection point is predicted, with an increase in k_{obs} in the high pH region (>10).

Table 2. Rate and equilibrium data obtained by nonlinear least-squares treatment of kinetic data for **1**.

Mechanism	$pK_a{}^{M}$[a,b]	k^{M+} (M^{-1} s^{-1})[a]	k^M (M^{-1} s^{-1})[a]	s.d.[c]
I	8.09	1.10		0.127
II	8.00	1.24	1.21×10^{-3}	0.046

[a]These quantities are defined in the text.
[b]Values are obtained as adjustable constants in the nonlinear least-squares treatment.
[c]Standard deviation from calculated curve.

Kinetic data for **1** in Table 1 have been subjected to nonlinear least-squares treatment for both mechanisms. The results are given in Table 2, along with $pK_a{}^M$ values obtained as adjustable constants by logarithmic fitting. *The superiority of Mechanism II over Mechanism I is clearly evident* from the magnitude of the standard deviation obtained by assuming either mechanism.

Figure 1 shows that the curve calculated according to eq. [3] fits the experimental data well in the sense that an initial sharp rise in rate in the low-pH region is followed by a region of moderate increase in rate, with an inflection point apparent in the curve, and is followed by a more rapid increase in rate at pH > 10. Experimental points could not be obtained at pH ≥ 11 due to instability of **1** in strongly basic solutions. However, it is noted that if one chooses to remove the experimental point at pH 10.5, the fit of the data according to eq. [3] (i.e., nonlinear least-squares treatment) is essentially as good as when the point is incorporated and the resulting curve passes above the omitted point. The increase in rate in the high-pH region on the basis of Mechanism II is readily seen, on inspection of eq. [3], as resulting from the second term in the equation, which accords the contribution from the k^M-containing term to the ionized form of the substrate, **3**. In the present case N(1)-H in **1** is relatively acidic with a calculated $pK_a{}^M$ value at 60°C of 8.00 (the measured value is 10.0 at 25°C (8)). Hence even at the lowest pH studied a significant proportion of the substrate (36%) exists as **3**. At pH 10.5 an overwhelming proportion (99.6%) is in its N(1)-deprotonated form. Thus as long as k^M holds a finite value, an increase in rate in the high-pH region is predicted.

Therefore we have here clear evidence of titrium exchange from an anionic species in which the negative charge is located α to the exchanging position, the first reported instance of such a process. The ratio $k^{M+}/k^M = 10^3$ shows overwhelming preference for the former pathway and indicates the magnitude of the unfavourable electrostatic interaction resulting from approach of hydroxide ion to the exchange site. Hitherto, such information was available only in purines where the negative charge is located *outside* the imidazole ring (vide infra).

In concluding this section it is appropriate to comment on the magnitude of the acidifying effect of Co(III) in this system. First we can compare the pK_a value for N(I)-H ionization in **1** with that in neutral imidazole, for which pK_a values have been given as 10.0 and 14.2, respectively (18, 6*b*). This acidi-

Table 3. Comparison of rate and equilibrium data for detritiation of a variety of heterocycles.[a]

Substrate	pK_a	pK_a'	pK_a''	k^{H+} (M^{-1} s^{-1})	k^{M+} (M^{-1} s^{-1})	k^{M} (M^{-1} s^{-1})	k(M^{-1} s^{-1})	k'(M^{-1} s^{-1})	k''(M^{-1} s^{-1})	Ref.
Imidazole	7.12	14.2		6.0×10^3						6*b*
1-Methylimidazole	7.20			1.0×10^4						1*a*
Benzimidazole	5.53	13.2		6.2×10^4						30
1-Methylbenzimidazole	5.55			2.0×10^5						30
$[Co(NH_3)_5ImH]^{3+}$, **1**		10.0(8.0)[b]			1.24, Co(III)[b,c]	1.2×10^{-3}				This work
$[Co(NH_3)_5^{-1}$-MeIm$)^{3+}$, **2**					0.15, Co(III)[c]	Co(III)[b,c]				This work
Histidine	6.05	9.12[d]		6.1×10^3			49			31
1-Methylhistidine	6.58	8.60[d]		1.0×10^4	1.3×10^{-2}, Pd(II)		1.0×10^2			1
Guanosine	2.20	9.25[d]	12.33	3.1×10^6	$\leq 1 \times 10^{-1}$ MeHg(II)		6.05			21*c*
1-Methylguanosine				5.3×10^6	1.4×10^4, Cu(II)		2.51×10^{-3}			21*c*
Inosine	1.50	8.96	12.36	1.6×10^7			16.8			21*c*
1-Methylinosine				1.8×10^7	2.1×10^4, Cu(II)		1.9×10^{-2}			21*c*
Adenine	4.12	9.83[d]		3.0×10^4	4.0×10^2, Ag(I)					16*a*
Adenosine	3.50	12.5[d]		6.7×10^4[f]			1.92×10^{-2}			21*b*
5′-Adenosine monophosphate	3.80	5.65		8.6×10^6	8.2×10^3, Cu(II)		7.3×10^2	4.0×10^{-3}		4*d*
3′-Adenosine monophosphate	3.65	5.65		1.7×10^5	1.3×10^3, Ag(I)		3.2×10^2	1.0×10^{-2}		4*d*
9-Propylpurine	2.5[e]			1.0×10^6[f]			1.07×10^{-2}			21*a*
9-Butylpurine	2.8[e]			2.8×10^5[f]			2.54×10^{-3}			21*a*
6-Mercaptopurine	<2	8.67[d,e]		3.2×10^6			77			25
6-Mercaptopurine riboside				3.7×10^6			1.6×10^3	2.74×10^{-3}		25
Theobromine	0.3	11.0		3.8×10^6			6.34×10^{-2}	1.95×10^{-3}		16*a*
Xanthine	1.2	7.5		6.0×10^5			92			16*a*
Xanthosine	2.0	5.58	9.87	3.6×10^6			2.1×10^4	0.58	6.06×10^{-4}	16*a*
Paraxanthine	0.5	8.6		5.5×10^6			98.4	$\sim 5 \times 10^{-4}$		16*a*
Hypoxanthine	1.79	8.91	12.67				1.3			4*c*
Theophylline	0.7	8.5		1.1×10^6						16*a*
Caffeine	0.5			2.5×10^6			2.72×10^{-2}			16*a*

[a]The quantities given in this table are defined in the text; p*K* values are at 25°C while kinetic data are at 85°C, except when stated otherwise.
[b]Value obtained from nonlinear least-squares treatment of kinetic data for **1** at 60°C. (pK_a^M, see Scheme 1).
[c]Kinetic data at 60°C.
[d]Refers to the dissociation of the exocyclic $-NH_2$ or -SH function.
[e]Calculated from kinetic data at 85°C by application of the Perrin equation (see ref. 32).
[f]Calculated from original data.

fying effect can be ascribed to a highly effective charge withdrawal by Co(III), thus stabilizing the deprotonated form. Considering next proton loss at C(2), the stabilizing effect of Co(III) will be greater than for N(1)-H ionization since this effect attenuates with distance (18). The *kinetic acidity* enhancement is expected to be less than thermodynamic acidity enhancement, but one could well expect a 10^3–10^4 enhancement of kinetic acidity in **1** relative to imidazole in C(2)-H abstraction.

Since we have previously found (19), for detritiation of imidazole at C(2), $k = 1.28 \times 10^{-2}$ M^{-1} s^{-1} at 85°C, which can be corrected to 60°C as $k = 1.15 \times 10^{-3}$ M^{-1} s^{-1}, then using E_a = 20.2 kcal/mol (2*d*) and the presently determined value k^{M+} = 1.24 M^{-1} s^{-1} (Table 2), we obtain the rate ratio $k^{M+}/k \approx 1 \times 10^3$. Though N(1)-deprotonated imidazole is unreactive in isotopic exchange (11*a*, 19) (i.e., k' in Scheme 1 not measurable), it is feasible that the acidifying effect of Co(III), as in **3**, has brought this kinetic process into a measurable range, thus accounting for our conclusion that Mechanism II in Scheme 1 is operating, with $k^{M+}/k^{M} \approx 10^3$. Further discussion of the acidifying effect of various metal ions at N(3)/N(7), in imidazoles and purines, is given in a later section.

Proton activation versus metal ion activation

Table 3 summarizes rate and equilibrium data for a number of heterocycles for subsequent discussion. For compounds containing the imidazole moiety, including **1**–**3**, rate constants are as defined in Scheme 1 while K_a and K_a' refer to ionization constants for N(3) and N(2). For purines k' and k'' refer to second-order rate constants for hydroxide ion attack on the N(1) mono-anionic and N(1), N(3) dianionic species while K_a' and K_a'' are the corresponding acid ionization constants and K_a is the ionization constant for N(7), see Scheme 2; other quantities for the purines retain the same significance as for imidazoles.

Previous studies (11, 16, 20) involving purines and related substrates have shown that, where no kinetic complications arise from the existence of zwitterionic forms of the substrate in solution, the conjugate acid of the substrate reacts 10^7–10^9 times faster than the neutral substrate. This can be illustrated

Can. J. Chem. Downloaded from www.nrcresearchpress.com by 80.90.12.36 on 09/08/12
For personal use only.

Scheme 3

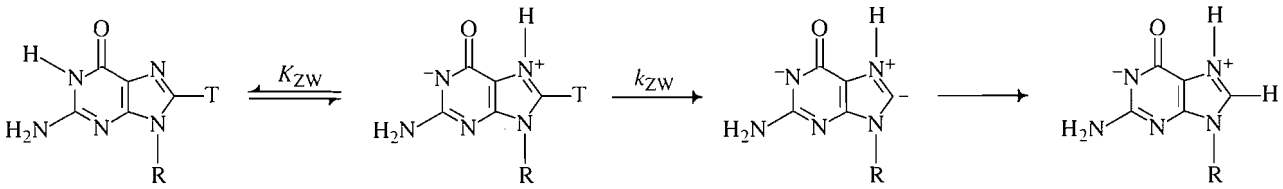

by considering the ratios k^{H+}/k, the proton-activating factor (16*b*, *c*) obtainable from Table 3 for 9-alkylpurines, adenosine, caffeine, and theobromine (not shown in Table 3). Values of k for the reactions of the neutral forms of imidazole, 1-methylimidazole, and benzimidazole are not available, but it is reasonable to expect k^{H+}/k ratios of similar magnitude. The rest of the substrates in Table 3, including histidine (4*e*) and 1-methylhistidine (9), give rise to zwitterionic forms in solution. It has been shown (9, 21*c*) that for such substrates k is a composite function according to eq. [4], where k_0 is the rate constant

$$[4] \quad k = k_0 + k_{zw}K_{zw}$$

for hydroxide ion attack on the "neutral" molecule, k_{zw} is the rate constant for attack on the zwitterionic form, and K_{zw} is the equilibrium constant for zwitterion formation. Guanosine affords a good example of such substrates and the relationship between k_{zw} and K_{zw} is shown in Scheme 3. This latter group of substrates are not good models for the reaction of neutral forms because k_{zw} is of the same magnitude as k^{H+}, giving rise to exaggerated k values (eq. [4]).

The kinetic superiority of protonated substrates over their neutral counterparts arises from the location of the positive charge at N(3)/N(7) in the protonated forms, a position α to the exchange site. In principle, placement of multiple charges at N(3)/N(7) of imidazoles or purines through coordination with multiply charged metal ions should produce accelerations of greater magnitude than those induced by the proton, such that $k^{M+} > k^{H+}$. Hence k^{H+}/k^{M+} ratios should be less than 1 but, in practice, metal-coordinated substrates have exhibited reactivity far smaller in magnitude than their protonated analogues, reported k^{H+}/k^{M+} values being of the order of 10^2–10^5. The values of this ratio for several heterocycles and different metal ions are listed in Table 4. Combination of the rate data for imidazole and 1-methylimidazole (1) with the present results for **1** and **2** provides estimates of k^{H+}/k^{M+} values of ca. 8×10^2 and 1×10^4 for imidazole and 1-methylimidazole, respectively, after correction for temperature differences in the two studies. This provides a quantitative indication of the kinetic effect of Co(III) relative to the proton in these processes. To date, there has been only one reported case of acceleration of isotopic hydrogen exchange in heterocycles due to coordination by a metal ion, of equal magnitude to or exceeding that induced by protonation (1*b*).

Metal-ion-coordinated species versus neutral species

In Table 4 is evaluated also the activating influence of metal ions, the so-called metal-activating factor (16*b*), expressed as the ratio k^{M+}/k. This quantity has been obtained either directly from rate data reported for the relevant species or as an estimate by taking the ratio $(k^{H+}/k)/(k^{H+}/k^{M+})$. The picture that emerges is one in which metal-coordinated species are 10^3–10^6 times more reactive than the neutral substrates, even though the former are themselves less reactive than the protonated forms. The following hierarchy of reactivity therefore emerges: protonated ≫ metal-ion-coordinated ≫ neutral species.

We have already examined (9) the disparity in behaviour between protonated and metal-coordinated forms of substrates in these systems and concluded that it results from a difference in the magnitude of positive charge located on N(3) or N(7) α to the exchange site, based on a simple electrostatic model proposed by Norris, Buncel, and Taylor some years ago (22). Thus the fractional charge at N(3) of imidazoles (or N(7) of purines and similar substrates) is much higher with the proton or the methyl cation (a good model for the proton on electrostatic grounds) than with metal ions. The C(2)/C(8) proton is substantially acidified through N(3)/N(7) protonation as is evident from the estimated pK_a values listed in Table 5. Deprotonation of C(2)-H/C(8)-H from the conjugate acid of the substrate produces an ylide intermediate that is stabilized by charge delocalization. The transition state for C(2)-H/C(8)-H deprotonation is believed to be product-like (4*b*); hence it will benefit substantially from resonance stabilization of the ylide and this would result in appreciable rate enhancement when compared with the unprotonated substrate. Both of these ground-state and transition-state effects are absent in the neutral molecule. We have here a clear case of thermodynamic and kinetic factors reinforcing each other to produce relatively facile C(2)/C(8) proton transfer in the protonated species.

When the proton is replaced by a metal ion, the positively charged centre is effectively removed from N(3)/N(7) and is located on the metal itself; hence the acidifying effect of the metal is far less than that of the proton. The pK_a values of C(2)-H in Table 5 are in this direction. As well, Rowan et al. (14) reported ^{1}H nmr chemical shift differences (Δδ) of 1 and 0.5 ppm for C(2)-H of imidazole upon protonation and coordination to Co(III), respectively. Also consistent with the above hypothesis is the observed (23) decrease in electron density in coordinated heterocycles induced by the following electrophiles according to the order: H^+ > Co(III) > Rh(III). Furthermore, the pK_a values of −1.7, 7.3, and 1.7 measured for the acid–base equilibrium of eq. [5] for M = H^+, Cu(II), and Co(III), respectively (10, 24), indicate that (*i*) these metal ions are poorer Lewis acids than the proton, and (*ii*) the polarizing power of the proton is by far greater than of the metals. Taken together, it is manifestly clear that C(2)-H/C(8)-H is more acidic in the protonated substrate than in the metal-ion-coordinated form.

$$[5] \quad M(H_2O)_n^{z+} \rightleftharpoons M(H_2O)_{n-1}(OH^-)^{(z-1)+} + H^+$$

Can. J. Chem. Downloaded from www.nrcresearchpress.com by 80.90.12.36 on 09/08/12
For personal use only.

Can. J. Chem. Downloaded from www.nrcresearchpress.com by 80.90.12.36 on 09/08/12
For personal use only.

Table 4. Comparison of kinetic effect of protonation versus metal-ion coordination in detritiation of several heterocycles.

Heterocycle	Metal ion	k^{H+}/k^{M+}	k^{M+}/k	Ref.
Imidazole	Co(III)	$\geq 8 \times 10^2$	$\sim 1 \times 10^3$	This work
1-Methylimidazole	Co(III)	$\geq 1 \times 10^4$	$\sim 1 \times 10^3$	This work
1-Methylhistidine	Pd(II)	2.5×10^5		10
	$CH_3Hg(II)$	$\geq 1 \times 10^3$		1
1-Methylinosine	Cu(II)	8.2×10^2	1.1×10^6	11*b*
	Ag(I)	4.5×10^4	2.1×10^6	11*b*
1-Methylguanosine	Cu(II)	3.8×10^2	5.6×10^6	11*b*
5′-Adenosine monophosphate	Cu(II)	1.1×10^3		4*a*
3′-Adenosine monophosphate	Ag(I)	1.3×10^2		4*a*

Table 5. Comparison of C(2)-H acidity in different heterocycles.

Heterocycle	pK_a of C(2)–H
Imidazole	32.5[a]
1,3-Dimethylbenzimidazolium ion	19–20[b]
3-Benzylthiazolium ion	16–18[c]
3-Benzyl-4,5-dimethylthiazolium ion	18–20[c]
$[Co(NH_3)_5$imidazole$]^{3+}$, **1**	23–25[d]
$[Co(NH_3)_5$-1-methylimidazole$]^{3+}$, **2**	24–26[d]

[a]Reference 18*b*.
[b]Estimated in ref. 16*d* from kinetic data obtained at 85°C.
[c]Estimated (3*b*) from kinetic data obtained at 30°C.
[d]Estimated from kinetic data obtained in this work at 60°C by assuming that reprotonation of the carbenoid intermediates is diffusion controlled.

Superimposed on the inferior acidifying capability of the metal ion relative to the proton is the loss of resonance stabilization by the carbenoid intermediate derived from the metal-coordinated species. This intermediate is stabilized solely by the inductive effect provided by the metal through M^{n+}—N σ-bond polarization. Conceivably, this effect will be much less than the resonance stabilization afforded the ylide intermediate, with the consequence that the transition state for formation of the metal-coordinated carbenoid species will be less stabilized than the corresponding transition state for ylide formation, leading to rate reduction in the former process. On both thermodynamic and kinetic grounds, therefore, the protonated species is favoured over its metal-ion-coordinated counterpart.

There are indications, however, that π-type metal–ligand back-bonding may be important in these systems (20)[3], though a full discussion of the scope and magnitude of such an effect is not warranted at this stage. Systematic variation of transition metal ions coordinated to N(3)/N(7) to produce a range of *substitution-inert* complexes will aid such discussion. Such experiments are being planned.

Isotopic exchange in anionic species

Anionic forms of imidazole and benzimidazole produced through N(1)-H deprotonation at high pH have not previously been observed to show kinetic activity (11*a*, 16*a*, 19). The same situation is observed with purine itself in which the N(9)-H deprotonated form is unreactive (21*a*). This has been attributed to the proximity of the negative charge on N(1)/N(9) to the exchange site, with the effect that the approaching hydroxide ion experiences unfavourable electrostatic interactions (destabilization of the dianionic intermediate and of the transition state leading up to it). In principle, therefore, development of negative charge at a site remote from the exchanging C(2)-H/C(8)-H should result in less inhibiting electrostatic interactions, with the possibility of observing anionic species with measurable kinetic activity. Purine-type molecules, with ionizable N-H groups at N(1) or N(3), sites that are well removed from the exchanging C(8)-H, meet this requirement.

Jones and co-workers have reported rate constants (k') for exchange reactions of anionic species derived from theobromine (16*a*), paraxanthine (16*a*), 6-mercaptopurine riboside (25), and xanthosine (16*a*) (Table 3). Values of k' obtained, though small (10^{-4}–10^{-3} M^{-1} s^{-1}), are not drastically different from those of k (10^{-3}–10^{-2} M^{-1} s^{-1}), emphasizing the fact that electrostatic interactions become less important with increased distance, as expected. The anionic form of 6-mercaptopurine riboside, in which the negative charge resides on the exocyclic sulfur atom, has reactivity comparable to that of theobromine. Values of k and k' for xanthosine appear to be unusually high and it is interesting to note that this substrate exchanges also in its dianionic form, via the k'' pathway.

Complex **3** with its negative charge located on N(1), α to the exchange site, shows a reactivity that is comparable to that of N(1)-deprotonated theobromine. This reflects a balance between the destabilizing electrostatic effect of the negative charge on N(1) and the evidently larger acidifying/stabilizing effect of Co(III) in **3**. A good model with which to compare the behaviour of **3** would be the anionic form of 3-methylimidazolium ion, for which, however, no data are available.

Reactivity of imidazole/1-methylimidazole versus 1/2

In our previous studies (1*a*, 9) we observed increased reactivity consequent upon methyl or benzo substitution of the imidazole nucleus. These reactivity differences could not be explained on the basis of linear free energy considerations (3*a*, 16) in which the pK_a for N(3) or N(7) protonation in imidazoles or purines would reflect the magnitude of fractional charge on C(2) and thus provide a measure of C(2)-H acidity. Thus, in the pairs imidazole/1-methylimidazole,

[3] E. Buncel and H.A. Joly. Unpublished work.

Can. J. Chem. Downloaded from www.nrcresearchpress.com by 80.90.12.36 on 09/08/12
For personal use only.

benzimidazole1/1-methylbenzimidazole, and histidine/1-methylhistidine, the N-methylated substrate reacts ca. 2–3 times faster than its unmethylated analogue, in spite of their identical pK_a's. We explained (1*a*, 9) this unusual reactivity sequence in terms of frontier and perturbational molecular orbital theory (FMO and PMO theory, respectively), in which N-methylation effects greater stabilization energy difference in the intermediate state than in the reactant state such that $\delta SE^I > \delta SE^R$. Comparing the substrate pair **1/2** with the imidazole/1-methylimidazole pair, it is noted that the reactivity sequence observed in the latter is reversed in the former. Thus, while k_{Me}/k_H is ca. 2 in the imidazole/1-methylimidazole pair, the same ratio is 0.13 in **1/2**. The rate constant k_{Me}/k_H ratio for the imidazole/1-methylimidazole pair actually refers to their protonated forms; hence replacing the proton in that reactant pair with Co(III) in **1/2** has reversed the observed reactivity pattern.

The effect of Co(III) on the magnitude of the k_{Me}/k_H ratios probably reflects the influence of *d*-orbital interactions in the systems involving transition metal ions that are absent when the electrophile coordinated at N(3) is the proton. It is to be noted that the present results can be accommodated by the inductive effect of the N(1)-CH_3 in the transition state, which is destabilizing on the incipient negative charge at C(2). Clearly more work is needed in order to understand more fully the effects of different transition metal ions on k_{Me}/k_H ratios.

Conclusions

The results discussed herein permit us to draw the following conclusions:

1. The effect of N(3) protonation on C(2)-H exchange in imidazoles is far greater than the effect of Co(III) coordination at the same site, as in **1** and **2**, which in turn, is activating for C(2)-H deprotonation relative to the neutral substrates. Thus the order of reactivity is protonated ≫ metal coordinated ≫ neutral forms of the substrate.

2. When the substrate is capable of existing as a zwitterion in solution, the value of the second-order rate constant for reaction of the neutral form, *k*, is exaggerated through contribution from k_{zw}, the kinetic constant for reaction of the zwitterionic form; the latter quantity is of the same magnitude as the rate constant for the proton-catalyzed pathway, k^{H+}.

3. The superiority of protonation over metal-ion coordination in facilitating the exchange process has both thermodynamic and kinetic components. Thus the acidifying effect of the proton and the stabilization of the transition state of reactions in which it is present at N(3)/N(7) are both greater than the corresponding effects of metal ions.

4. Deprotonation of **1** produces **3** in solution, which, in turn, has been found to undergo exchange at C(2), thus furnishing the first reported example of C(2)-H exchange occurring at a position α to N(1) bearing negative charge. Both acidifying and rate-enhancing effects of Co(III) override the destabilizing influence of the negative charge, to produce rates comparable to those in anionic forms of purines where the negative charge is remote from the exchange site.

5. The observed reactivity relationship in which N(1)-CH_3 is rate enhancing relative to N(1)-H is reversed on coordination by Co(III), pointing to the more complex situation represented by replacement of a proton by a transition metal ion in these processes.

Experimental section

Preparation of complexes

$[Co(NH_3)_5imidazole](ClO_4)$ and $[Co(NH_3)_5$-1-methylimidazole$](ClO_4)$ were prepared according to literature procedures (14, 26, 27) and their identities and purity checked by comparing their uv–visible and ^1H nmr spectroscopic characteristics with published data (26–29).

Tritiation of complexes

Tritiated water (20 μL, 1 Ci/mL) was added via a syringe to $[Co(NH_3)_5imidazole](ClO_4)$ (17.4 mg) placed in a heavy-walled glass ampoule. The glass ampoule was stoppered with a rubber septum, its contents frozen in liquid N_2, and the ampoule evacuated. It was then sealed, and suspended in an oil-bath at 75°C for 48 h, following which it was removed and allowed to equilibrate to room temperature. The ampoule was then opened and its contents pipetted into a 25 mL pear-shaped flask to which 1 mL of distilled water was added to exchange labile tritium. The solvent was removed by lyophilization. Aliquots of 1 mL of water were added successively and lyophilized until the activity of the lyophilized water became negligible. A stock solution of **1** was then prepared by dissolving a known amount in 0.8 mL of freshly distilled DMSO in a test tube, which was stoppered and stored in a refrigerator.

The same procedure was adopted for $[Co(NH_3)_5$-1-methylimidazole$](ClO_4)_3$ except that 15 mg of the complex was used and that the tritriation was carried out in an oil bath at 60°C for 30 h.

Hydrogen–deuterium exchange experiments

Preparation of NaOD solutions

Sodium metal, purified by refluxing freshly cut sodium metal for 1.5 h in pure xylene, was dissolved in small portions in 50 mL of D_2O in a dry box previously flushed with dry N_2. The resulting NaOD was standardized with HCl and diluted as appropriate for the deuterium exchange experiments.

2. C(2)-H exchange measurement by nmr

The diamagnetic nature of Co(III) complexes makes it possible to optimize reaction conditions for detritiation experiments by following the rates of deuteriation of the exchangeable proton using ^1H nmr spectroscopy, which was done using a Bruker HX-60 or AC-F200 spectrometer. Typically, a sample of the substrate (ca. 15 mg) was dissolved in D_2O and the pH adjusted to the required value with NaOD in a dry box. An aliquot was then pipetted into an nmr tube and kept at constant temperature. At various intervals, the ^1H nmr spectrum of the sample was recorded with integration of peak areas. The fraction of the exchanging H left at a given time was calculated by reference to a nonexchanging peak, in this case the C(4)-H or C(5)-H, which are unreactive under the experimental conditions. The result was expressed as per cent exchange.

It was found from these ^1H nmr studies that the detritiation experiments could be conveniently carried out within the pH range 7.7–10.5 at a temperature of 60°C. At lower pH the exchange rate was very slow, while the complexes decomposed at higher pH and higher temperatures.

Can. J. Chem. Downloaded from www.nrcresearchpress.com by 80.90.12.36 on 09/08/12
For personal use only.

Preparation of buffer solutions

Sodium borate – hydrochloric acid and sodium carbonate – sodium bicarbonate buffers (32) were prepared for the kinetic measurements at the pH range of the study.

Kinetic study of tritium exchange

The rates of detritiation of **1** and **2** were measured by determining changes in radioactivity of the reaction mixtures with time (t_n). The substrate solution (20 μL) was in each case pipetted into 20 mL of buffer solution contained in a 50 mL round-bottom flask. The reaction mixture was equilibrated for no less than 30 min at 60°C and then shaken thoroughly. Aliquots of 1 mL were withdrawn at known times (t_0, ... t_n) using an Eppendorf automatic pipette and transferred to a 50 mL round-bottom flask containing 0.1 g NaCl. The flask was quickly frozen with liquid N_2 and the time recorded. The flask was then attached to a freeze-drying apparatus and water was removed by lyophilization. An aliquot of 0.1 mL of the lyophilized water was pipetted into a scintillation vial containing 4 mL of Beckman HP Ready-solv and assayed for tritium (C_t) on a Beckman LS5801 liquid scintillation counter. All kinetic samples were treated similarly. The infinity count (C_∞) was taken by assaying 0.1 mL of the initial reaction mixture in 4 mL of the liquid scintillator.

The first-order rate constants, k_{obs}, for C(2)–T exchange of **1** and **2** in aqueous buffers were obtained from the slopes of the plots of log ($C_\infty - C_t$) vs. time. All such plots yielded good straight lines for 75% exchange or more.

Acknowledgements

Financial support of this research by the Natural Sciences and Engineering Research Council of Canada in the form of an operating grant to E.B. and partial travel support by the University of Agriculture, Makurdi, to I.O. are gratefully acknowledged.

References

1. (*a*) E. Buncel, H.A. Joly, and D.C. Yee. Can. J. Chem. **67**, 1426 (1989); (*b*) E. Buncel, O. Clement, and I. Onyido. J. Am. Chem. Soc. **116**, 2679 (1994).
2. (*a*) J.D. Vaughan, Z. Mughrabi, and E.C. Wu. J. Org. Chem. **35**, 1141 (1970); (*b*) Y. Takeuchi, K.L. Kirk, and L.A. Cohen. J. Org. Chem. **43**, 3570 (1978); (*c*) Y. Takeuchi, H.J.C. Yeh, K.L. Kirk, and L.A. Cohen. J. Org. Chem. **43**, 3565 (1978); (*d*) J.L. Wong and J.H. Keck. Jr. J. Org. Chem. **39**, 2398 (1974).
3. (*a*) M.W. Washabaugh and W.P. Jencks. J. Am. Chem. Soc. **111**, 674 (1989); **111**, 683 (1989); (*b*) D.S. Kemp and J.T. O'Brien. J. Am. Chem. Soc. **92**, 2554 (1970); (*c*) R. Breslow. Ann. N.Y. Acad. Sci. **98**, 445 (1962).
4. (*a*) J.A. Elvidge, J.R. Jones, R. Salih, M. Shandala, and S.E. Taylor. J. Chem. Res. (M), 2373 (1980); (*b*) J.A. Elvidge, J.R. Jones, C. O'Brien, E.A. Evans, and H.C. Sheppard. Adv. Heterocycl. Chem. **16**, 1 (1974); (*c*) J. Chem. Soc. Perkin Trans. 2, 174 (1974); (*d*) J.R. Jones and S.E. Taylor. J. Chem. Soc. Perkin Trans. **2**, 441 (1980); (*e*) J.A. Elvidge, J.R. Jones, R. Salih, M. Shandala, and S.E. Taylor. J. Chem. Soc. Perkin Trans. 2, 447 (1980).
5. A. Fersht. Enzyme structure and mechanisms. Freeman, New York. 1985.
6. (*a*) C.A. Matuszak and A.J. Matuszak. J. Chem. Educ. **53**, 281 (1976); (*b*) R.J. Sundberg and R.B. Martin. Chem. Rev. **74**, 471 (1974); (*c*) M.N. Hughes. The inorganic chemistry of biological processes. Wiley, London. 1982. pp. 15, 139.
7. A.E. Martell and R.M. Smith (*Editors*). Critical stability constants. Plenum, New York. 1982.
8. (*a*) G.S. Baldwin, S.G. Waley, and E.P. Abraham. Biochem. J. **179**, 459 (1979); (*b*) A.E.G. Cass, H.A.O. Hill, J.V. Bannister, and W.H. Bannister. Biochem. J. **183**, 127 (1979).
9. E. Buncel, H.A. Joly, and J.R. Jones. Can. J. Chem. **64**, 1240 (1986).
10. B. Noszal, V. Scheller-Krattiger, and R.B. Martin. J. Am. Chem. Soc. **104**, 1078 (1982).
11. (*a*) D.H. Buisson, J.R. Jones, and S.E. Taylor. J. Chem. Soc. Chem. Commun. 856 (1975); (*b*) J.R. Jones and S.E. Taylor. J. Chem. Soc. Perkin Trans. 2, 1773 (1979).
12. F.A. Cotton and G. Wilkinson. Advanced inorganic chemistry. 5th ed. Wiley Interscience, New York. 1988. pp. 1283–1334.
13. T. Toraya and S. Fukui. Metalloproteins: chemical properties and biological effects. *Edited by* S. Otsuka and T. Yamanaka. Elsevier, Amsterdam. 1988. pp. 267–274.
14. N.S. Rowan, C.B. Storm, and R. Rowan III. J. Inorg. Biochem. **15**, 59 (1981).
15. N.R. Brodsky, N.M. Nguyen, N.S. Rowan, C.B. Storm, R.J. Butcher, and E. Sinn. Inorg. Chem. **23**, 891 (1984).
16. (*a*) J.R. Jones and S.E. Taylor. J. Chem. Soc. Perkin Trans. 2, 1253 (1979); (*b*) Chem. Soc. Rev. **10**, 329 (1981); (*c*) R. Stewart and R. Srinivasan. Acc. Chem. Res. **11**, 271 (1978); (*d*) J.A. Elvidge, J.R. Jones, C. O'Brien, E.A. Evans, and J.C. Turner. J. Chem. Soc. Perkin Trans. 2, 432 (1973).
17. H.L. Clever. J. Chem. Educ. **45**, 231 (1968).
18. (*a*) J.A. Winter, D. Caruso, and R.E. Shepherd. Inorg. Chem. **27**, 1086 (1988); (*b*) M.F. Hoq, C.R. Johnson, S. Paden, and R.E. Shepherd. Inorg. Chem. **22**, 2693 (1983).
19. H.A. Joly. Ph.D. Thesis, Queen's University, 1987.
20. E. Buncel, H.A. Joly, J.R. Jones, and I. Onyido. Synthesis and applications of isotopically labelled compounds. *Edited by* T.A. Baillie and J.R. Jones. Elsevier, Amsterdam. 1989. p. 219.
21. (*a*) J.A. Elvidge, J.R. Jones, C. O'Brien, E.A. Evans, and H.C. Sheppard. J. Chem. Soc. Perkin Trans. 2, 1889 (1973); (*b*) J. Chem. Soc. Perkin Trans. 2, 2138 (1973); (*c*) J.R. Jones and S.E. Taylor. J. Chem. Soc. Perkin Trans. 2, 1587 (1979).
22. A.R. Norris, E. Buncel, and S.E. Taylor. J. Inorg. Biochem. **16**, 279 (1982).
23. (*a*) D.K. Lavallee, M.D. Baughman, and M.N. Phillips. J. Am. Chem. Soc. **99**, 718 (1977); (*b*) D.K. Lavallee and E.B. Fleisher. J. Am. Chem. Soc. **94**, 2583 (1972).
24. R.B. Martin. J. Am. Chem. Soc. **89**, 2502 (1967).
25. J.A. Elvidge, J.R. Jones, and R. Salih. J. Chem. Soc. Perkin Trans. 2, 1590 (1979).
26. J.M. Harrowfield, V. Norris, and A.M. Sargeson. J. Am. Chem. Soc. **98**, 7282 (1979).
27. W.W. Henderson, R.E. Shepherd, and J. Abola. Inorg. Chem. **25**, 3157 (1986).
28. C.R. Johnson, W.W. Henderson, and R.E. Shepherd. Inorg. Chem. **23**, 2754 (1984).
29. C.B. Storm, A.H. Turner, and N.S. Rowan. Inorg. Chem. **24**, 1269 (1985).
30. (*a*) R.A. Olofson, W.R. Thompson, and J.S. Michelman. J. Am. Chem. Soc. **86**, 1865 (1964); (*b*) A. Noordam, L. Maat, and H.C. Beyerman. Recl. Trav. Chim. Pays-Bas, **97**, 293 (1978).
31. A. Yokoyama, H. Aibz, and H. Tanaka. Bull. Chem. Soc. Jpn. **47**, 112 (1974).
32. D.D. Perrin. Aust. J. Chem. **17**, 484 (1964).

Calculation of surface tension of salt solutions: effective polarizability of solvated ions

Robert A. Stairs

Abstract: The Onsager–Samaras version of Wagner's theory of surface tension of solutions of 1:1 salts has been modified to include ion-induced dipole terms in the image potential. Effective solvated ionic polarizabilities are used, which are large and negative owing to local dielectric saturation around the ions. The modified theory agrees with the order of magnitude of the variation among various alkali halides (e.g., $\Delta\sigma$ for 0.1 molar aqueous KI is about 70% of the corresponding value for KCl). Polarizabilities were estimated from Hasted's dielectric decrements.

Key words: surface tension, salt solutions, symmetric electrolytes, effective polarizability, theory.

Résumé : On a modifié la version de la théorie de Wagner, elaborée par Onsager et Samaras, de la tension superficielle des solutions des sels 1 : 1, par l'addition à l'expression pour l'énergie potentielle due à l'image d'un terme représentant l'énergie charge/dipolaire. On a employé des polarisabilités effectives qui sont grandes et négatives, à cause de la saturation diélectrique près de l'ion solvaté. La théorie ainsi modifiée est en accord approximatif avec la variation entre divers sels. (Par exemple, l'élévation de la tension superficielle de l'eau dans une solution 0,1 molaire par le IK est de 70% de celle par le CIK.) On a estimé les polarisabilités à partir des décroissements diéléctriques de Hasted.

Motsclés : tension superficielle, solutions de sels, électrolytes symétriques, polarisabilité effective, théorie.

[Traduit par la rédaction]

Can. J. Chem. Downloaded from www.nrcresearchpress.com by 80.90.12.36 on 09/08/12
For personal use only.

Simple salts, when dissolved in a molecular solvent, raise the surface tension, σ, by small amounts (in contrast with surface-active agents, which may depress the surface tension substantially at very low concentrations). The magnitude of the increase depends upon the charge and size of the ions and on the nature of the solvent.

The functional form of the dependence of $\Delta\sigma$ ($= \sigma - \sigma_0$) on concentration is very uncertain, especially the approach to zero concentration. Most data (1) for aqueous solutions are at concentrations above 0.1 mol L^{-1}. Other properties of strong electrolyte solutions, such as equivalent conductivity and the logarithm of the activity coefficient, which are explained by the Debye–Hückel theory or theories based on it, are represented by equations having a leading term in the square root of c. It would not be surprising if surface tension was similar in this respect:

$$[1] \quad \Delta\sigma = A_0\sqrt{c} + Bc$$

The leading constants, corresponding to A_0, for the other properties depend only on charge type and on εT to a negative power. To see whether this was the case with surface tension also, data for half a dozen alkali halides in five solvents were fitted (2) to equations of the above form, and the values of A_0 were then fitted to an equation of the form:

$$[2] \quad A_0 = a + b/\varepsilon T$$

with $a = -2.4 \times 10^{-6}$ J $m^{-1/2}$ $mol^{-1/2}$ and $b = 1.83 \times 10^7$ J $m^{-1/2}$ $mol^{-1/2}$ K^{-1}. The coefficient of determination (a statistic that is unity for a perfect fit and zero for uncorrelated data) was only 0.64.

Theories

Published theories fall into three groups: (*i*) direct calculations (typified by those of Oka (3) and Ariyama (4)) of the work of separation at a surface originally in the interior of the solution to make two new surfaces; (*ii*) calculations of the depletion ("negative adsorption") of electrolyte in a surface layer, followed by use of the Gibbs adsorption equation (see below); (*iii*) calculations starting from a radial distribution for the ions, and proceeding by statistical-mechanical methods (5, 6). The main theories in the second group are (a) those of Wagner (7) and Onsager and Samaras (8) ("WOS"), modified by later authors (9, 10), and (b) that of Péres Masiá and co-workers (11, 12).

Binary mixtures of nonelectrolytes exhibit surface tensions that are lower than the values calculated with an assumption of additivity on a molar basis, i.e., :

$$[3] \quad \sigma < \sigma_1 x_1 + \sigma_2 x_2$$

where σ represents the surface tension of the solution, σ_i is

Received November 21, 1994.

R.A. Stairs.[1] Department of Chemistry, Trent University, Peterborough, ON K9J 7B8, Canada.

[1] Telephone: (705)748-1201. Fax: (705)748-1625. E- mail: rstairs@trentu.ca

Can. J. Chem. Downloaded from www.nrcresearchpress.com by 80.90.12.36 on 09/08/12
For personal use only.

the surface tension of pure component **i** and x_i is its mole fraction. The reason for this is that the surface tension, which is the same as the surface free energy, is reduced by an excess of the component with the lower surface free energy appearing in the surface layer. Gibbs showed how to relate the surface excess ("adsorption") of one component to the decrease in the surface tension, through the Gibbs Adsorption Equation (13), a form of which is eq. [4]:

$$[4] \quad d\sigma/d\ln a_2 = -RT\Gamma_2$$

Here σ is as defined above, a_2 is the activity of component **2**, R is the gas constant, T the absolute temperature, and Γ_2 is the surface excess of component **2**. The definition of Γ_2 is somewhat dependent on the placing of an arbitrary plane that marks the geometrical surface (the real surface being actually a somewhat diffuse region). Gibbs showed that for dilute binary solutions it is always possible to place this plane so that the surface excess is equal to the integral of the local excess of component **2** (the solute) from the arbitrary plane into the body of the solution, to infinity, eq. [5]:

$$[5] \quad \Gamma = \int_0^\infty [c(x) - c(\infty)]\,dx$$

where x is the distance from the surface into the solution, and $c(x)$ and $c(\infty)$ are the concentrations at x and ∞ ("bulk").

Where the solute is a strong electrolyte, each of the ions interacts with the surface, independently of the others in the limit of extreme dilution. By treating the surface as a plane that divides space into two regions, one the solvent, with electric permittivity ε, and the other the gas or vapour, with a permittivity essentially equal to the permittivity of free space, ε_o, it may be shown (14) that an ion of charge ze will be subject to a repulsive force equal to that which would be exerted by a charge of magnitude $ze(\varepsilon - \varepsilon_0)/(\varepsilon + \varepsilon_0)$ at the place where the image of the ion would be were the surface a mirror, with the permittivity everywhere equal to ε. This results in the ion having an x-dependent contribution to its potential energy, given by eq. [6],

$$[6] \quad W = fe^2/16\pi\varepsilon x$$

where $f = (\varepsilon - \varepsilon_0)/(\varepsilon + \varepsilon_0)$, the ratio of the image charge to the real charge. The extra factor 4 in the denominator arises because, in the integration of the force to obtain the potential energy, one must take account of the motion of the image as the ion is moved.

The dependence of concentration on distance from the surface is then obtained as $c(x) = c(\infty)\exp(-W/kT)$, where k is Boltzmann's constant. WOS show that this leads to Γ's being negative and infinite. At any finite concentration of electrolyte, however, the range of the Coulombic force of repulsion (the "image force") should be limited by the effect of the ionic atmosphere, being attenuated by the Debye–Hückel factor $\exp(-\kappa r)$. The radial coordinate r causes intractable mathematical complications; it was replaced by Wagner by a new coordinate parallel to x, and by Onsager and Samaras by $2x$ (because the distance from the image to the real ion is $2x$). The Debye–Hückel reciprocal length κ is not constant in the region of the solution where the concentration is not uniform. Onsager and Samaras argue that the value corresponding to the bulk concentration may be used without serious error. With these simplifications, they obtain a dependence of concentration on distance from the surface of the form shown in Fig. 1 (redrawn from part of Onsager and Samaras's Fig. 2). The area between the curve and the horizontal line at $c(\infty)$ is the quantity $-\Gamma$. Treatment of the liquid as a continuous dielectric should break down within molecular distances from the geometrical surface. Fortunately this is just the region that is essentially salt free. Integration of the Gibbs equation then gives $\sigma(a)$ or $\sigma(c)$.

Fig. 1. Distribution of an ionic solute near the solution surface. The bulk concentration is 1.000 mmol L^{-1}. The local concentration is plotted as a function of the distance from the surface, x; the quantity $-\Gamma$, which is the depletion (negative adsorption) of the solute, is the area between the curve and the horizontal line at c = 1 mmol L^{-1}. It is equivalent to total exclusion of solute from a surface layer about 0.8 nm thick. (Recalculated after Onsager and Samaras's Fig. 2 (8).)

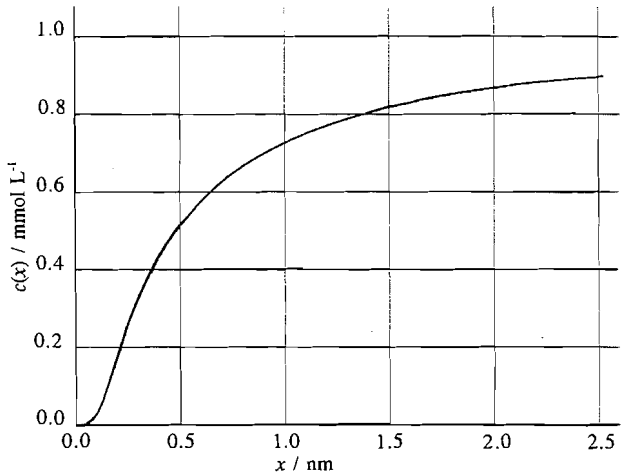

Pérez Masiá and co-workers (11, 12) begin by calculating the Born solvation energy of the ions, and then the loss of solvation due to truncation of the solvation sphere by the surface. They then proceed to calculate $c(x)$ and $-\Gamma$ essentially as WOS, except that they explicitly calculate the effect of the difference in the solvation of the cation and anion. Any difference in the degree of repulsion from the surface creates an electrical double layer; this gives rise to an additional effect that they calculate through the Lippman–Helmholtz equation:

$$[7] \quad \left(\frac{\partial\sigma}{\partial E}\right)_{T,p,n} = -\left(\frac{\partial Q}{\partial A}\right)_{T,p,n} = -q$$

where E is the surface potential, and q is the surface charge density, defined by the middle term. The subscripts indicate that the derivatives are at constant temperature, pressure and composition. This additional effect (which would lead to a decrease in surface tension) is small when the ions have equal and opposite charges. It was neglected by WOS, and is neglected in **this work**.

All of these theories predict concentration dependence that is either linear for strong electrolytes or slightly concave towards the concentration axis. The curvature arises from two sources: (*a*) at higher concentrations from ion pairing (e.g.,

Can. J. Chem. Downloaded from www.nrcresearchpress.com by 80.90.12.36 on 09/08/12
For personal use only.

Oka (*3b*): he includes a factor α for the degree of dissociation) or from the activity coefficient (e.g., WOS) and (*b*) at low concentrations from a term proportional to $-c\ln(c)$ (WOS and successors). Nichols and Pratt (15) show that in their application of the WOS approach to interfacial tension between two liquids the leading term may have the form either $-c\ln(c)$ or $c^{1/2}$, depending on the difference in the degree of repulsion from the surface between the anion and the cation, especially if the salt shows some solubility in both liquids. Unfortunately the effect is so small that these two forms of dependence on c are experimentally indistinguishable.

In reviewing these various theories from the point of view of an engineer seeking smoothed or estimated values, Horvath (16) concludes that for lower concentrations (below about 0.1 mol L^{-1}), WOS best represents the data. (He prefers Schmutzer (5), Buff–Stillinger (6), or Molyneux (17) at higher concentrations, although their derivations are also for very dilute solutions.) The chief problem seems to be that WOS underestimate the effect of ionic size. Onsager and Samaras themselves also say that they slightly underestimate the magnitude of the main effect (8).

Calculations

Onsager and Samaras, in calculating the "image" force, treat the ions as having no properties except charge and size, but, without elaborating, they mention the possibility of including polarizability. M.J. Sienko, in about 1953, suggested in conversation[2] that we should explore the addition of polarizability to see whether it might account for ionic size effects more realistically. The calculation seemed too difficult, and, except for a rough order-of-magnitude estimate, we were unable to pursue the problem at that time. The present paper is the belated fruit of Sienko's suggestion.

To allow for the size of the ions, WOS modify the potential energy of the ion by introducing the Debye–Hückel distance of closest approach, a, and arrive at the form (their eq. 19):

$$[8]\quad W(x) = \left(\frac{\exp(\kappa a)}{1+\kappa a}\right)\left(\frac{fz^2e^2}{16\pi\varepsilon x}\right)\exp(-2\kappa x)$$

(where x is the distance from the surface, a and κ are the Debye–Hückel distance of closest approach and ionic-atmosphere parameter, ε is the permittivity, z is the charge number, e is the elementary charge, and we have here restored the omitted f, the ratio of the image to the real charge: $(\varepsilon-\varepsilon_0)/(\varepsilon+\varepsilon_0)$).

We now add a term, the sum of two identical terms, for the potential energy W_μ due to the force (*i*) between the image charge and the induced dipole at the real ion and (*ii*) between the image of the induced dipole and the real charge. To obtain this term, consider the local field, E, which is (in one dimension) the derivative of the potential due to the image:

$$[9]\quad E = \frac{d\phi}{dx} = \frac{d}{dx}(W(x)/ze)$$

The induced dipole moment, μ, is equal to the product of the local field and the polarizability α. The force on the dipole is given by the product of the dipole moment and the derivative of the field:

$$[10]\quad F_\mu = \frac{dE}{dx}\alpha E = \alpha\frac{d^2\phi}{dx^2}\frac{d\phi}{dx}$$

and the potential energy W_μ due to this force is:

$$[11]\quad W_\mu = -\alpha\int\frac{d\phi}{dx}\frac{d^2\phi}{dx^2}dx = -\alpha\int\frac{d\phi}{dx}d\left(\frac{d\phi}{dx}\right) = -\frac{\alpha}{2}\left(\frac{d\phi}{dx}\right)^2$$

(The constant of integration is taken to be zero, the force and the potential energy both being zero at great distance.)

By itself, this term, which is attractive if α is positive, causes the potential energy of an ion at the surface to be large and negative, so the area Γ again becomes infinite and positive. Since the effective polarizability of a solvated ion is always negative, however (see below), the area remains finite and negative. A term representing the (induced) dipole–dipole potential was originally added. Since the range of the corresponding force is short, it serves only to reduce further the concentration very close to the surface, from which the solute is nearly totally excluded by the other forces. Its effect is therefore negligible.

The final form of the potential function is now:

$$[12]\quad W(u) = \frac{\exp(\kappa_0 a c^{1/2})}{1+\kappa_0 a c^{1/2}}F_1(u)c^{1/2} - 2\left\{\frac{\exp(\kappa_0 a c^{1/2})}{1+\kappa_0 a c^{1/2}}\right\}^2 F_2(u)c^2\alpha$$

where $u = 2\kappa x = 2\kappa_0 c^{1/2}x$ (writing κ_0 for $\kappa/c^{1/2}$), and

$$[13]\quad F_1 = \frac{fz^2e^2\kappa_0\exp(-u)}{2\varepsilon u}$$

$$F_2 = \left\{\frac{2\kappa_0(1+u)F_1(u)}{zeu}\right\}^2$$

Then the concentration as a function of distance from the surface:

$$[14]\quad c(u) = c(\infty)\exp\left(\frac{-W(u)}{kT}\right)$$

is used to obtain the adsorption:

$$[15]\quad -\Gamma = \int_0^\infty (c(\infty)-c(u))dx = 2\kappa\int_0^\infty (c(\infty)-c(u))du$$

followed by integration of the Gibbs equation, eq. [4], to obtain $\Delta\sigma(c)$. Corrections for the activity coefficient were made following Onsager and Samaras (8). They state that the effect of the added term linear in ionic strength to the extended Debye–Hückel equation makes little difference. By the use of Davies's approximation (18) to the extended Debye–Hückel equation for aqueous solutions at 25°C:

$$[16]\quad -\log_{10} f_\pm = \frac{z^2}{2}\left(\frac{1}{1+I^{-1/2}} - 0.3I\right)$$

[2] M.J. Sienko, private communication, 1953.

Can. J. Chem. Downloaded from www.nrcresearchpress.com by 80.90.12.36 on 09/08/12
For personal use only.

where I is the ionic strength in mol/L, we found that it does indeed make a difference at concentrations above 0.1 mol L^{-1} for 1:1 electrolytes; presumably it is even more important with ions of higher charge.

Polarizability

We have not yet discussed the choice of the values for the polarizabilities of the solvated ions. Hasted, Ritson, and Collie (19) have considered this problem and have made (very difficult!) measurements of the effect of dissolved salts on the permittivity of water, in the limit of low frequency, expressing the results in the form:

$$[17] \quad \varepsilon = \varepsilon_s + \delta c$$

The factor δ is called the "dielectric decrement," for the effect of the ions is to strongly orient the solvent molecules in their vicinity, much reducing their freedom to respond to an applied field, and so decreasing ε below the solvent value, ε_s. The measurements were made at concentrations from 0.5 molar upwards and extrapolated to zero concentration. The authors make a somewhat arbitrary division of the observed values between cation and anion, and report for univalent ions: H^+ −17, Li^+ −11, Na^+ −8, K^+ −8, Rb^+ −7, F^- −5, Cl^- −3, I^- −7, and OH^- −13 (all ±0.5) L mol^{-1}. The relative magnitudes accord more or less with expectation, those for the cations diminishing as the radius increases, a trend that seems to be followed also by fluoride and chloride. Iodide seems to be anomalous. That H^+ and OH^- show the largest effects in their respective series is not surprising, considering their unusually large mobilities in water and their special structural relation to that solvent.

To translate the dielectric decrement into effective polarizability, we use the mixing rule for a dilute suspension of spheres of permittivity ε_1 in a medium of permittivity ε_s, eq. [18] (20):

$$[18] \quad \varepsilon = \varepsilon_m + 1.5\phi_2(\varepsilon_1 - \varepsilon_m)$$

(Here ϕ_2 is the volume fraction of the suspended spheres.) Writing the volume fraction ϕ_2 in terms of the molar concentration c, and noting that one mole of a symmetrical electrolyte contains two moles of particles (eq. [19]),

$$[19] \quad \phi_2 = 2Lvc$$

(v is the volume of a sphere and L is Avogadro's constant), we obtain eq. [20]:

$$[20] \quad \varepsilon = \varepsilon_m + 3Lv(\varepsilon_1 - \varepsilon_m)c$$

Bleaney and Bleaney (21) express the polarizability of such a suspended sphere by eq. [21]:

$$[21] \quad \alpha = \frac{3}{4\pi} \frac{\varepsilon_m(\varepsilon_1 - \varepsilon_m)v}{(\varepsilon_1 + 2\varepsilon_m}$$

Eliminating the volume of the spheres between eqs. [20] and [21], we obtain eq. [22]:

$$[22] \quad \varepsilon = \varepsilon_m + 4\pi L \frac{(\varepsilon_1 + \varepsilon_m)}{\varepsilon_m} \alpha c$$

which, by comparison with the Hasted equation (eq. [17]), allows us to write:

$$[23] \quad \bar{\alpha} = \frac{1}{4\pi L} \frac{\varepsilon_m}{(\varepsilon_1 + 2\varepsilon_m)} \bar{\delta} = G\bar{\delta}$$

The bars are added to indicate that the properties δ and α refer to averages of the properties of the two ionic species. The numerical value of the proportionality constant G is 6.52×10^{-26} mol in aqueous solutions at 25°C, taking $\varepsilon_m = 78.304\ \varepsilon_0$ and assuming $\varepsilon_1 = 2\varepsilon_0$, close to the "optical" value. (The Hasted values of δ are in L mol^{-1}, and should be expressed in m^3 mol^{-1} to obtain polarizabilities in m^3. The value for a salt is the average, not the sum, of the ionic values.)

Results and discussion

The calculated values of $\Delta\sigma$ ($= \sigma - \sigma_0$) for concentrations from 0.0004 to 0.100 molar for uni-univalent electrolytes with mean effective ionic polarizabilities from zero to −2.0 nm^3 are listed in Table 1. For $\alpha = 0$ they are in close (though not exact) agreement with those calculated by Onsager and Samaras (8). Figure 2 shows the results of this work plotted as $\Delta\sigma/c$ vs. $\log_{10}c$. The lowest curve is for $\alpha = 0$. A few of Onsager and Samaras's calculated values are shown: their simplest calculation, ignoring the activity coefficient and the size of the ions, as squares, and their full calculation as crosses. The small differences are due to slightly different values of the fundamental constants used, slightly different values (22)[3] for ε and (following Bravina (23) the restoration of the factor $(\varepsilon - \varepsilon_0)/(\varepsilon + \varepsilon_0)$ in the magnitude of the image charge, which WOS omit. The circles represent very careful measurements by Long and Nutting (24) on KCl solutions. As noted above, they are somewhat higher than the calculated values, except at the lowest concentrations, where Long and Nutting suggest that they may not have quite eliminated the Jones and Ray effect (25).[4] The upper curves represent the results of this work with α varied, plotted in the same fashion. Values of $-\alpha$ used were 0.5, 1.0, 1.5, and 2.0 nm^3. (cf. argon: $\alpha = 0.00166$ pm^3.) The value of $-\alpha$ required to reproduce the experimental results for KCl is greater than 2 nm^3. The additional effect, $\sigma(\alpha) - \sigma(0)$ at $c = 0.100$ mol L^{1-} is closely proportional to $(-\alpha)^{1/2}$. The value $-\alpha = 0.36$ nm^3 corresponds to $\delta = -5.5$ L mol^{-1} for KCl (Hasted (20), p. 140).

It appears that the present theory using these effective polarizabilities is able to predict only very approximately the effect of ion size differences on surface tension for 1:1 salts, as represented by the alkali halides. There also remain some puzzles, the chief of which is the behaviour of strong acids. The Hasted dielectric decrement value for HCl is −10 L mol^{-1}, which translates to an effective polarizability of −1.3

[3] For temperatures other than 298 K, quadratically smoothed values were used.

[4] The Jones–Ray effect consists of an apparent depression of the surface tension of salt solutions at very low concentrations, as measured by the method of capillary rise. Langmuir's explanation of the effect as due to the electrical double layer at the glass–solution interface (26) has been generally accepted.

Can. J. Chem. Downloaded from www.nrcresearchpress.com by 80.90.12.36 on 09/08/12
For personal use only.

Table 1. Surface tension increment divided by concentration of solutions of 1:1 salts in water, for various values of polarizability, $\alpha(nm^3)$.

		$(\Delta\sigma/c)/(\mu N\ m^2\ mol^{-1})$				
c(mol L^{-1})	log(c)	α: 0	−0.5	−1.0	−1.5	−2.0
0.000 40	−3.4	3.6138	3.7900	3.8688	3.9271	3.9748
0.000 63	−3.2	3.4233	3.6000	3.6789	3.7373	3.7853
0.001 00	−3.0	3.2345	3.4117	3.4909	3.5496	3.5975
0.001 58	−2.8	3.0477	3.2256	3.3051	3.3638	3.4119
0.002 51	−2.6	2.8633	3.0420	3.1218	3.1808	3.2290
0/003 96	−2.4	2.6816	2.8613	2.9414	3.0006	3.0490
0.006 31	−2.2	2.5032	2.6840	2.7645	2.8240	2.8726
0.010 00	−2.0	2.3286	2.5108	2.5917	2.6513	2.7001
0.015 85	−1.8	2.1585	2.3421	2.4234	2.4834	2.5322
0.025 12	−1.6	1.9937	2.1788	2.2604	2.3204	2.3694
0.039 81	−1.4	1.8349	2.0215	2.1035	2.1635	2.2123
0.063 10	−1.2	1.6831	1.8712	1.9531	2.0129	2.0614
0.100 00	−1.0	1.5393	1.7284	1.8100	1.8694	1.9173
0.158 49	−0.8	1.4045	1.5940	1.6747	1.7331	1.7802
0.251 19	−0.6	1.2797	1.4683	1.5477	1.6048	1.6505
0.398 11	−0.4	1.1657	1.3519	1.4291	1.4840	1.5279
0.630 96	−0.2	1.6034	1.2447	1.3188	1.3713	1.4129
1.000 00	0.0	0.9732	1.1468	1.2168	1.2658	1.3044

Temperature 298.15 K, dielectric constant 78.304.

Fig. 2. Surface tension divided by concentration for solutions of 1:1 electrolytes in water at 25°C, plotted against log(c/mol L^{-1}). The curves are calculated (this work) for values of the mean polarizability of the solvated ions (from the lowest curve upwards): α = 0, −0.5, −1.0, −1.5, −2.0 nm^3. The plotted points are (○) experimental (KCl, Long and Nutting (24)); (+) Onsager and Samara's simplest calculation; (□) Onsager and Samara's full calculation (8).

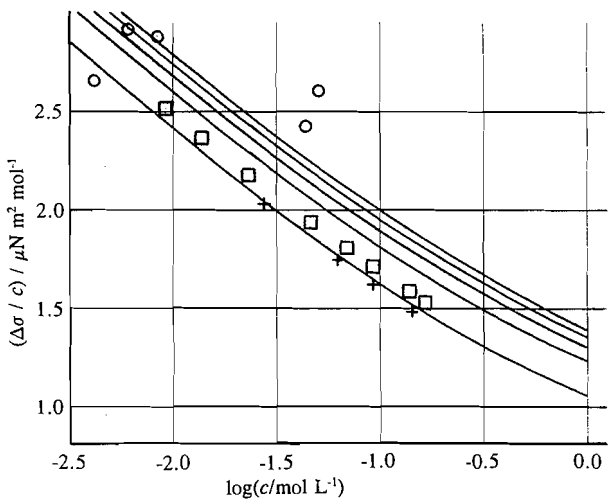

nm^3, and predicts a surface tension increment higher than for any of these salts. Experimental values are much lower, in fact slightly negative (1). Some structural or other special effect arising in the surface from the close relation of the hydronium ion to water must be operating. Among the alkali halides, Hasted's values of δ do not correlate very well with other properties that would be expected to show similar trends with changes in ionic radii (e.g., entropies of solvation, viscosity B coefficients). The value of δ for KI is more negative (−8) than that for KCl (−5), but measured surface tension increments[1i] are nearly 30% smaller.

The effects of variation of temperature, and of independent variation of the temperature, the permittivity, and the ionic charge (symmetric electrolytes only) were explored. The nature of the solvent might be expected to appear, given the electrostatic basis of the calculation, as proportionality to the permittivity to some negative power. Available data (27) do not give this much support. Good data for nonaqueous solvents are hard to find. Part (*a*) of Table 2 lists calculated values of the relative increment of surface tension for 1:1 salts at several concentrations and at several temperatures. Part (*b*) of the same table lists the results of similar calculations, but with the relative permittivity ("dielectric constant," $D = \varepsilon/\varepsilon_0$) fixed at the value appropriate to 298 K. In Part (*c*) the temperature is fixed at 298 K, with the dielectric constant varied from 60 to 100. The last column of Table 2(*b*) lists the values of the slopes of plots of the calculated values as log($\Delta v/c$) vs. log (T). The temperature effect appears to work mainly indirectly, through the temperature dependence of the permittivity, the factor RT in the Gibbs equation and the Boltzmann factor exp(-W/kT) having contrary effects. The slopes in Table 2(*b*) show the near-cancellation of the direct temperature effects. Part (*c*) of Table 2 shows the result of varying the dielectric constant while keeping T constant. The last column, analogous to that in Part (*a*), shows that the effect depends approximately on D^{-1}, in the range explored.

The dependence on charge type is curious. I naïvely expected dependence on the charge as z or z^2, and proportionality to the number of ions of each kind. This would lead to the effects of, e.g., LiCl, $BaCl_2$, and $MgSO_4$ being in the ratios 1:2:2 (if proportional to z) or 1:3:4 (if z^2). In

Can. J. Chem. Downloaded from www.nrcresearchpress.com by 80.90.12.36 on 09/08/12
For personal use only.

Table 2. Surface tension increment divided by concentration ($\Delta\sigma/c$) in $\mu N\ m^2\ mol^{-1}$ (identical with dyne cm^{-1}/mol L^{-1}), calculated for solutions of 1:1 electrolytes in water (polarizability neglected).

(*a*) Effect of temperature.

		$\Delta\sigma/c$				
c(mol L^{-1})	log(c)	T (K): 273.15	278.15	288.15	298.15	303.15
0.0001	−4.0	3.7308	3.8186	4.0012	4.1930	4.2923
0.0010	−3.0	2.8833	2.9502	3.0891	3.2345	3.3097
0.0100	−2.0	2.0812	2.1285	2.2264	2.3286	2.3813
0.1000	−1.0	1.3800	1.4106	1.4737	1.5393	1.5730
1.0000	0.0	0.8730	0.8922	0.9320	0.9732	0.9944
	D[a]	87.742	85.766	81.947	78.304	76.548

[a]Dielectric constant (= $\varepsilon/\varepsilon_0$) from Parsons (22) (smoothed).

(*b*) Effect of temperature with dielectric constant fixed at 78.304.

		$\Delta\sigma/c$				
log(c/M)	T(K): 273.15	278.15	288.15	298.15	303.15	Slope[a]
−4.0	4.2648	4.2501	4.2212	4.1930	4.1792	−0.195
−3.0	3.2675	3.2609	3.2477	3.2345	3.2279	−0.117
−2.0	2.3300	2.3300	2.3295	2.3286	2.3280	−0.009
−1.0	1.5233	1.5268	1.5333	1.5393	1.5421	0.117
0.0	0.9612	0.9637	0.9685	0.9732	0.9755	0.142

[a]Slope of a plot of log($\Delta\sigma/c$) *vs.* log(T).

(*c*) Effect of dielectric constant at fixed temperature, 298.15 K.

		$\Delta\sigma/c$				
log(c/M)	D: 60	70	80	90	100	Slope[a]
−4.0	5.7150	4.7814	4.0885	3.5559	3.1350	−1.1853
−3.0	4.3160	3.6567	3.1589	2.7709	2.4608	−1.0161
−2.0	3.0166	2.6009	2.2793	2.0235	1.8155	−1.0104
−1.0	1.9292	1.6955	1.5107	1.3607	1.2364	−0.8879
0.0	1.2197	1.0700	0.9557	0.8650	0.7909	−0.8466

[a]Slope of plot of log($\Delta\sigma/c$) *vs.* log(D).

aqueous solution at concentrations above 1 mol L^{-1} they are actually (28) in the ratios 1:1.8:1.3, which suggest a dependence on $z^{1/2}$, approximately, not obviously predicted by any current theory. The effect of ionic charge calculated here is surprising, in that it is strongly concentration dependent (see Table 3). At 1 mol L^{-1} the ratio of the surface tension increments predicted for 2:2 to 1:1 salts is about 1.9, which may be compared to the experimental value of about 1.3 cited above. At 0.0001 mol L^{-1} the ratio is nearly 5. The reason for this strange behaviour relates to the two influences of z on the results: at the lowest concentrations the repulsive force is of long range and depends on z^2, while at higher concentration the range of the force is limited by the ionic atmosphere, so the thickness of the layer of solution depleted in solute decreases as z increases. Thus the effect of increasing z is to increase $-\Gamma$ at low concentrations, but

Table 3. Surface tension increment divided by concentration, calculated for solutions of symmetric electrolytes in water: effect of ionic charge.

	$\Delta\sigma/c$		
log(c/M)	$\lvert z\rvert$: 1	2	3
−4.0	4.1930	20.0778	44.5752
−3.0	3.2345	13.4571	26.4473
−2.0	2.3286	7.9712	13.2374
−1.0	1.5393	4.0431	5.1603
0.0	0.9732	1.8622	1.6056

Temperature 298.15 K, dielectric constant 78.304, polarizability zero.

ultimately to decrease it at high concentrations. Note the behaviour of $\Delta\sigma/c$ for $z = 2$ and 3 in Table 3.

In conclusion, it should be pointed out that comparison of these and other theoretical calculations of surface tension of electrolyte solutions with experiment is difficult owing to the paucity of data for sufficiently dilute solutions. The present theory and all the other theories cited here were derived using assumptions that are most appropriate at very low concentrations, while the data mostly refer to concentrations much above 0.1 molar. Trustworthy data for nonaqueous systems in any concentration range are especially rare.

Acknowledgements

The author acknowledges with gratitude the hospitality and opportunity for fruitful discussion afforded by Professor A. D. Buckingham and other members of the Department of Chemistry at Cambridge University and early assistance with programming by Carol-Ann Lugtigheid. Thanks are also due to K. B. Oldham for kindly reading and commenting on an early draft of the manuscript. The work was supported by Trent University with funds provided by the Natural Sciences and Engineering Research Council of Canada.

References

1. (*a*) International critical tables. Vol. IV. McGraw–Hill, New York and London. 1928. pp. 463 ff; (*b*) Landolt–Börnstein, 1927; 5th ed. Springer-Verlag, Berlin. *Edited by* W.A. Roth and K. Scheel. 1927; 6th ed. *Edited by* K. Schäfer and E. Max. Springer-Verlag, Berlin. 1956; (*c*) W.D. Harkins and H.M. McLaughlin. J. Am. Chem. Soc. **47**, 2083 (1925); (*d*) F. DeBlock. Bull. Sci. Acad. R. Belg. **11**, 333 (1925); (*e*) P.P. Kosakevich, Z. Phys. Chem. (Leipzig), **133**, 1 (1928); (*f*) H. Falkenhagen and E. Schmutzer. Naturwissenschaften, **42**, 92 (1955); (*g*) C. Salceanu. C.R. Hebd. Seances Acad. Sci. **253**, 862 (1961); (*h*) Tsv. Tonchev and G. Popov. Nauchni Tr. Vissh. Pedagog. Inst. Plovdiv, Mat. Fiz. Khim. Biol. **8**, 93 (1970); (*i*) K. Johannson and J.C. Erikson. J. Colloid Interface Sci. **49**, 469 (1979).
2. R.A. Stairs, W.T. Rispin, and R.C. Makhija. Can. J. Chem. **48**, 2755 (1970).
3. S. Oka. Proc. Physico-Math. Soc. Jpn. (*a*) **14**, 233 (1932); **14**, 527 (1932); **14**, 649 (1932); (*b*) **15**, 407 (1933).
4. K. Ariyama. Bull. Chem. Soc. Jpn. **11**, 687 (1936); **12**, 32 (1937).
5. E. Schmutzer. Z. Phys. Chem. (Leipzig), **204**, 131 (1956).
6. F.P. Buff and F.H. Stillinger, Jr. J. Chem. Phys. **25**, 312 (1956).
7. C. Wagner. Phys. Z. **25**, 474 (1924).
8. L. Onsager and N.N.T. Samaras. J. Chem. Phys. **2**, 529 (1934).
9. V.E. Bravina. Zh. Eksp. Teor. Fiz. **33**, 1065 (1957); Dokl. Akad. Nauk SSSR, **120**, 381 (1958); 120, 815 (1958).
10. T.L. Croxton and D.A. McQuarrie. Mol. Phys. **42**, 141 (1981); T.L. Croxton, D.A. McQuarrie, G.N. Patey, G.M. Torrie, and J.P. Valleau. Can. J. Chem. **59**, 1998 (1981); T.L. Croxton and D.A. McQuarrie. J. Phys. Chem. **87**, 3407 (1983).
11. A. Pérez Masiá. An. R. Soc. Esp. Fis. Quim. Ser. A: **50**, 5 (1954); **54B**, 629 (1958).
12. Kl. Schäfer, A. Pérez Masiá, and H. Jüntgen. Z. Elektrochem. **59**, 425 (1955).
13. J.W. Gibbs. *Reprinted in* The collected works of J. Willard Gibbs. Yale U. Press, New Haven, Conn. 1948.
14. R.K. Wangsness. Electromagnetic fields. Wiley, New York. 1979. p. 204.
15. A.L. Nichols and L.H. Pratt. J. Chem. Phys. **80**, 6225 (1984).
16. A.L. Horvath. Handbook of aqueous electrolyte solutions. Ellis Horwood, Chichester. 1985.
17. F. Molyneux. Aust. Chem. Eng. **14**, 13 (1973).
18. C.W. Davies. Ion association. Butterworths, London. 1962. p 41.
19. J.B. Hasted, D.M. Ritson, and C.H. Collie. J. Chem. Phys. **16**, 1 (1948).
20. J.B. Hasted. Aqueous dielectrics. Chapman and Hall, London. 1973. p. 146, eq. 6.26.
21. B.I. Bleaney and B. Bleaney. Electricity and magnetism. 3rd ed. Oxford University Press, 1976. pp. 44 ff.
22. R. Parsons (*Editor*). Handbook of electrochemical constants. Butterworths, London. 1959. p. 8.
23. V.E. Bravina. Dokl. Akad. Nauk SSSR, **120**, 815 (1958).
24. F.A. Long and G.C. Nutting. J. Am. Chem. Soc. **64**, 2476 (1942).
25. G. Jones and W.A. Ray. J. Am. Chem. Soc. **59**, 187 (1937).
26. I. Langmuir. Science, **88**, 450 (1938).
27. P.P. Kosakevich. Z. Phys. Chem. (Leipzig), **136**, 195 (1928).
28. C.J. West and C. Hull (*Editors*). International critical tables. Vol. IV. McGraw–Hill, New York and London. 463 ff (1928); J. Timmermans. Physico-chemical constants of binary systems. Vol. 3. Interscience, New York. 1960. pp. 302 ff.

Can. J. Chem. Downloaded from www.nrcresearchpress.com by 80.90.12.36 on 09/08/12
For personal use only.

Aqueous nonelectrolyte solutions. Part XIII. Ice and hydrate freezing points of aqueous ethylene oxide solutions and the formula of congruent ethylene oxide hydrate

David N. Glew and Norman S. Rath

Abstract: Ice freezing temperatures and hydrate formation temperatures have been measured by the dynamic cooling method for aqueous ethylene oxide (EO) solutions containing from 0 to 95 mol% EO. The ice and the congruent hydrate freezing temperatures exhibited standard errors on a single measurement of 0.004°C and 0.013°C, respectively. The ice–hydrate eutectic temperature was observed at –2.107°C with standard error 0.001°C and composition 1.991 mol% EO with standard error 0.008 mol% EO. The congruent hydrate was found to freeze at 11.083°C with standard error 0.002°C and composition 12.64 mol% EO with standard error 0.02 mol% EO. The formula of the congruent hydrate was EO·6.91H_2O with standard error 0.013 mol water/mol EO. Only a single hydrate was found over the whole composition range down to –26°C: the shoulder of the hydrate freezing curve above 40 mol% EO resulted from the high activity coefficients to dilute water in concentrated EO solutions. Equations and best values for the ice freezing temperatures and the hydrate formation temperatures together with their standard errors were evaluated by the method of least squares.

Key words: clathrate hydrate of ethylene oxide, freezing of water – ethylene oxide, ethylene oxide hydrate.

Résumé : Faisant appel à la méthode de refroidissement dynamique sur des solutions aqueuses d'oxyde d'éthylène (OE) contenant de 0 à 95% d'OE, on a mesuré les températures de congélation de la glace et de formation d'hydrate. Sur une seule mesure, les températures de congélation et de formation congruente d'hydrate ont présentés des erreurs standards qui sont respectivement de 0,004°C et 0,013°C. On a observé la température eutectique glace–hydrate à –2,107°C, avec une erreur standard de 0,001°C; la composition est alors de 1,991 mol% d'OE, avec une arreur standard de 0,008 mol% d'OE. On a trouvé que le point de congélation de l'hydrate congruent est 11,083°C avec une erreur standard de 0,002°C et une composition de 12,64 mol% d'OE, avec une erreur standard de 0,02 mol% d'OE. La formule de l'hydrate congruent est OE·6,91H_2O avec une erreur standard de 0,013 mol d'eau par mol d'OE. On n'a trouvé qu'un seul hydrate sur l'ensemble des compositions, jusqu'à –26,0°C : l'épaulement observé dans la courbe de congélation de l'hydrate, au-dessus de 40% d'OE, est le résultat de coefficients d'activité élevés de l'eau dans des solutions concentrées en OE. On a fait appel à la méthode des moindres carrés pour évaluer les équations, les meilleures valeurs des températures de congélation et de formation d'hydrate ainsi que leurs erreurs standards.

Mots clés : clathrate hydrate d'oxyde d'éthylène, congélation d'eau – oxyde d'éthylène, hydrate d'oxyde d'éthylène.

[Traduit par la rédaction]

Introduction

As a part of earlier studies on aqueous nonelectrolyte solutions and gas hydrates (1–17), the water – ethylene oxide (EO) system was of particular interest to us because the liquids water and EO (*i*) exhibited a complete range of liquid miscibility, and (*ii*) thus provided homogeneous solutions, which on cooling precipitated solid EO hydrate.

Received June 30, 1994.

D.N. Glew[1] **and N.S. Rath.** Exploratory Research Laboratory, Dow Chemical Canada Inc., Sarnia, ON N7T 7M1, Canada

[1] Retired; author to whom correspondence may be addressed at 536 Highbury Park, Sarnia, ON N7V 2J9, Canada. Telephone: (519) 337-3136.

The complete miscibility made it possible to measure directly the volumetric properties (11), the proton magnetic resonance chemical shifts (11), and the enthalpy of mixing (17) for aqueous EO solutions over the whole range of composition: these solution properties showed the variation of the water – hydrogen bond interactions from the extensively and strongly bonded water-rich solutions to the weakly bonded solutions of dilute water in aprotic EO (11, 17).

The complete miscibility also permitted direct measurement of the temperature for hydrate formation from solution over nearly the whole composition range, enabling a direct and accurate determination of the formula for the congruent EO hydrate.

The freezing point curve for EO hydrate had been measured

Can. J. Chem. Downloaded from www.nrcresearchpress.com by 80.90.12.36 on 09/08/12
For personal use only.

on two earlier occasions (1, 2). In consideration of the lesser purity of the liquid EO and of the equipment used at the earlier time, we decided (*i*) to remeasure the freezing point curve for EO hydrate with improved precision over a wider range of solution composition and temperature, and (*ii*) to measure for the first time the freezing point curve for the EO deuterohydrate.

Work with the deuterium oxide solutions of EO will be reported later.

A comprehensive review of the clathrate hydrates, including much work on the EO hydrate, up to 1973 has been given Davidson (18).

Experimental

Materials

Briefly, all materials were as described earlier (11). EO was selected from the production of Dow Chemical Canada, Limited; analysis for water, aldehydes, and nonvolatiles showed that the total of these impurities was less than 80 parts per million by weight.

Water was triply distilled and had a specific conductivity of less than 4×10^{-7} ohm^{-1} at room temperature, about 25°C.

Apparatus and procedure

The construction, testing, and the method of use of the freezing point cell have already been described (8). The data for the ice freezing points of the water solutions of EO were reported in part, and analysed in a different manner, earlier (11).

The experimental runs, e.g., denoted R125, were numbered consecutively in the order in which they were performed: after measurements with the water solutions were complete, runs were made with the deuterium oxide solutions. The later runs with the higher run numbers were usually found to be slightly more reliable, because of the small improvements of technique that inevitably evolved with increased experience of operation.

For data comparison and later statistical analysis the measurements using the water solutions were divided into three chronological sets: the early runs R106–R462 were defined as Set 1, R463–R584 were Set 2, and the later runs R585–R833 Set 3.

Calibration of thermocouple of freezing point cell

The thermocouple of the freezing point cell was calibrated against a standardized (IPTS-48) platinum resistance thermometer in a thermostat bath at more than 200 temperatures between +15 and –25°C (11). Calibrations were made (*i*) initially, (*ii*) in the middle of, and (*iii*) at the end of the runs with the water solutions, and (*iv*) at the end of the runs with the deuterium oxide solutions. Over this 4-year period the electrical signal of the thermocouple indicated no significant deviation or drift from the initial calibrations. The standard error on a single temperature determination, due only to electrical instrumental effects, (*i*) was 0.0035°C between –6.5 and +6.5°C, (*ii*), was 0.0070°C between –13 and –6.5°C and between 6.5 and 13.0°C, and (*iii*) was 0.014°C between –26 and –13°C and between 13 and 15°C. These estimates give the minimum values for the standard error on any single temperature determination.

The original experimental temperatures were measured on the International Practical Temperature Scale of 1948 (IPTS-48): these measurements were converted to the International Temperature Scale of 1990 (ITS-90), using the approximate differences in Table 4 given by Goldberg and Weir (19). The conversion had a root-mean-squared bias of less than 0.0004°C over the range –25 to +15°C, almost an order of magnitude smaller than our most precise measurements. All temperatures and equations are reported in units of degree Celsius (ITS-90).

Measurement of temperature for freezing of ice

The freezing of ice from water and dilute EO solutions generally exhibited much larger supercoolings (~0.4–0.7°C) than those found for the formation of hydrate (~0.005–0.1°C) from the same solutions. Consequently, the preselected cooling temperature differentials applied to the freezing point cell for freezing ice could not be reduced to less than ~0.4°C, and so the resulting observed temperature for the freezing of ice was invariably biased below its true equilibrium value. Table 1 lists the ice freezing temperatures corrected for bias.

Measurement of temperature for formation of eutectic

Measurement of the eutectic temperature was made directly, both from solutions initially freezing ice and those initially forming hydrate, using a final small cooling differential of ~0.1°C. The 15 eutectic temperatures found in Set 3 are listed in Table 1.

The earlier direct measurements of the eutectic temperature in Set 2 used a larger final cooling differential of ~0.4°C.

Measurement of temperature for formation of hydrate

With the development of the cooling technique of the freezing point cell, the preselected temperature differential applied to the freezing point cell was reduced from 1.7°C, used initially in Set 1, to 0.1°C, used later in Set 3. Consequently, the observed solution supercooling was reduced and the resulting temperature of formation of hydrate was found to be slightly increased, and thus nearer to its true equilibrium value. All temperatures for the formation of hydrate listed in Table 2 were extrapolated from two or more measurements to zero supercooling (8).

After the temperature of hydrate formation had been measured, the result was plotted against solution composition on a large-scale graph so that the continuity and smoothness of the temperature envelope of adjacent measurements could immediately be assessed. Any measurement that showed an obvious large deviation was repeated and replaced by an acceptable replicate measurement or measurements. Obvious deviations usually exhibited a negative bias of the measured temperature below that of the adjacent smooth envelope. This indicated experimentally that the temperature of formation of hydrate listed in Table 2, as determined by our dynamic cooling method, would usually contain an associated negative bias relative to its true equilibrium value. Support for the same negative bias was found in later least-squares regression analyses, where the few observed outliers usually exhibited negative temperature deviations below their model estimates.

Results and discussion

Measurements of freezing of ice

Table 1 lists the corrected temperature for freezing of ice for measurements of aqueous solutions containing between zero and 2.0003 mol% EO. The first column of the table shows the R-number of the run, the second column the solution composition, and the third the corrected temperature for the freezing of

Can. J. Chem. Downloaded from www.nrcresearchpress.com by 80.90.12.36 on 09/08/12
For personal use only.

Can. J. Chem. Downloaded from www.nrcresearchpress.com by 80.90.12.36 on 09/08/12
For personal use only.

Table 1. (ITS-90) Variation of temperature for freezing of ice with composition and the eutectic temperature.

Run no. R	EO mf (mol%)	T_{FI} (deg C)	Run no. R	EO mf mol%	T_{FI} (deg C)	Eutectic (deg C)
109	0.0000	0.003	600	1.0105	−1.062	
594	0.0000	0.009	601	1.2513	−1.319	
596	0.0000	0.009	127	1.2749	−1.342	
692	0.0000	−0.007	499	1.4332	−1.510	
693	0.0000	−0.004	602	1.5042	−1.592	
694	0.0000	−0.007	603	1.7502	−1.856	
695	0.0000	−0.004	125	1.7644	−1.879	
696	0.0000	−0.007	650	1.8510	−1.975	
697	0.0000	−0.005	649	1.8750	−2.002	
698	0.0000	−0.002	653	1.8998	−2.021	
699	0.0000	−0.002	484	1.9002	−2.025	
700	0.0000	−0.000	651	1.9004	−2.034	
701	0.0000	−0.002	652	1.9059	−2.032	
702	0.0000	0.000	654	1.9260	−2.053	
707	0.0000	−0.001	605	1.9498	−2.071	−2.107
708	0.0000	−0.000	607	1.9565	−2.084	−2.109
709	0.0000	−0.001	483	1.9629	−2.091	
710	0.0000	0.002	606	1.9629		−2.107
712	0.0000	0.001	655	1.9695	−2.099	−2.106
713	0.0000	0.003	480	1.9705	−2.100	
721	0.0000	0.003	608	1.9717	−2.100	−2.107
731	0.0000	−0.001	609	1.9718		−2.107
740	0.0000	−0.002	482	1.9786	−2.117	
750	0.0000	0.008	610	1.9814	−2.117	−2.107
760	0.0000	−0.000	612	1.9881		−2.107
773	0.0000	0.002	611	1.9991		−2.107
783	0.0000	0.006	481	1.9996	−2.135	
804	0.0000	−0.002	657	1.9997	−2.140	−2.106
597	0.2542	−0.267	661	1.9999	−2.132	−2.113
131	0.2619	−0.273	656	2.0003	−2.142	
132	0.2619	−0.273	662	2.0003	−2.129	−2.109
598	0.5040	−0.523	660	2.0251		−2.106
108	0.5171	−0.542	668	2.0880		−2.106
599	0.7465	−0.777	679	2.3499		−2.113
129	0.7592	−0.790	426	3.0039		−2.110
106	0.9851	−1.043				

ice from that solution. The 28 calibrations, for freezing ice from pure water, showed a bias of −0.0126°C with an estimated standard error of 0.0042°C for a single freezing point determination. The 35 measurements, for freezing ice from EO solutions, comprised the following: 24 from Set 3+2 with bias −0.0129 and standard error 0.0044°C, and 11 from Set 1+2 with bias −0.0297 and standard error 0.0041°C. The large bias of −0.0297°C for Set 1+2 resulted from the large cooling differential of about 1.7°C initially used for those earlier measurements.

The temperature for freezing of ice, T_{FI}, from aqueous EO is best represented by the three-parameter equation

$$[1]\quad T_{FI} = \underset{(0.0008)}{0.0000} - \underset{(0.0034)}{1.0327}\,C - \underset{(0.00173)}{0.01727}\,C^2$$

whereas T_{FI} is in degree Celsius and C is the solution concentration of EO in mol% EO. Least-squares estimates of the standard error on the parameters are shown in parentheses and the standard error on a single ice freezing point determination was 0.0043°C with 58 degrees of freedom.

Measurement of formation of eutectic

The eutectic temperature −2.107°C, with estimated standard error 0.0006°C, was the mean of the 15+1 measurements of Set 3+2 listed in Table 1, with initial solution compositions between 1.9498 and 3.0039 mol% EO. The standard error for a single eutectic temperature determination was 0.0023°C, which corresponded with the minimum error 0.0035°C from thermocouple calibration.

Thirteen earlier direct measurements of the eutectic temperature in Set 2 had given a mean value −2.134°C, with bias −0.027°C below the best value from Set 3+2, and with a standard error 0.0036°C on a single determination: the larger negative bias resulted from the earlier use in Set 2 of larger final cooling temperature differentials.

The eutectic composition 1.991 mol% EO, with standard

Table 2. (ITS-90) Variation of temperature for formation of hydrate with composition.

Run no. R	EO mf (mol%)	T_{FH} (deg C)	Run no. R	EO mf (mol%)	T_{FH} (deg C)	Run no. R	EO mf (mol%)	T_{FH} (deg C)
607	1.9565	−2.354	724	3.0098	2.429	751	4.3993	6.056
606	1.9629	−2.315	725	3.0503	2.573	752	4.4003	6.068
608	1.9717	−2.285	726	3.0999	2.736	753	4.5005	6.267
609	1.9718	−2.278	727	3.1503	2.906	754	4.6005	6.457
610	1.9814	−2.208	728	3.2003	3.076	755	4.7002	6.640
612	1.9881	−2.156	729	3.2494	3.213	756	4.8004	6.820
611	1.9991	−2.119	730	3.3000	3.374	554	4.8538	6.884
657	1.9997	−2.128	732	3.3505	3.530	757	4.8995	6.996
661	1.9999	−2.119	733	3.3998	3.658	553	4.9508	7.053
662	2.0003	−2.107	734	3.4500	3.797	758	5.0003	7.175
604	2.0020	−2.074	735	3.5003	3.929	555	5.0505	7.210
659	2.0146	−2.053	736	3.5499	4.081	759	5.1005	7.322
663	2.0248	−1.978	615	3.5993	4.214	500	5.1101	7.295
664	2.0369	−1.911	639	3.5994	4.245	761	5.2001	7.446
665	2.0502	−1.797	620	3.5996	4.224	762	5.2994	7.593
666	2.0631	−1.742	629	3.5996	4.222	763	5.4005	7.716
667	2.0752	−1.669	622	3.5997	4.186	764	5.5001	7.867
668	2.0880	−1.623	632	3.5998	4.227	765	5.5994	7.988
669	2.0998	−1.544	643	3.5998	4.198	766	5.7004	8.105
670	2.1250	−1.396	638	3.5999	4.227	501	5.7544	8.183
671	2.1498	−1.267	641	3.5999	4.189	767	5.8004	8.248
672	2.1751	−1.131	616	3.6000	4.224	768	5.9002	8.350
673	2.1997	−1.007	621	3.6000	4.230	769	5.9995	8.472
674	2.2247	−0.858	636	3.6000	4.221	772	6.1000	8.577
675	2.2500	−0.774	637	3.6000	4.227	770	6.1005	8.554
676	2.2752	−0.645	640	3.6000	4.237	771	6.2001	8.687
677	2.3001	−0.494	617	3.6001	4.262	502	6.2566	8.749
678	2.3252	−0.384	625	3.6001	4.215	774	6.3004	8.774
679	2.3499	−0.271	631	3.6001	4.191	775	6.4000	8.869
680	2.3751	−0.126	633	3.6001	4.230	776	6.5001	8.966
681	2.3997	0.003	642	3.6001	4.236	777	6.6004	9.054
682	2.4253	0.126	618	3.6002	4.211	778	6.7001	9.152
683	2.4500	0.214	623	3.6002	4.230	503	6.7499	9.224
684	2.4748	0.336	626	3.6002	4.230	782	6.7995	9.245
685	2.5001	0.473	634	3.6002	4.230	779	6.8002	9.258
686	2.5253	0.574	635	3.6002	4.222	780	6.9002	9.335
687	2.5503	0.674	644	3.6002	4.198	781	7.0002	9.414
688	2.5753	0.757	628	3.6004	4.214	784	7.0995	9.502
689	2.6000	0.856	737	3.6004	4.221	785	7.2000	9.576
690	2.6248	0.952	614	3.6006	4.217	504	7.2425	9.604
691	2.6502	1.047	613	3.6012	4.219	786	7.3003	9.658
703	2.6750	1.176	738	3.6496	4.356	787	7.3993	9.727
704	2.7001	1.265	739	3.7002	4.489	790	7.5001	9.786
705	2.7254	1.357	741	3.7497	4.621	788	7.5006	9.772
706	2.7500	1.481	592	3.7992	4.756	789	7.5998	9.859
714	2.7748	1.586	742	3.7998	4.761	791	7.6988	9.913
715	2.8004	1.708	590	3.8011	4.752	505	7.7497	9.961
716	2.8248	1.814	743	3.8494	4.887	793	7.7994	9.964
717	2.8501	1.900	744	3.8999	5.019	797	7.7995	9.953
718	2.8751	1.979	745	3.9494	5.135	798	7.8000	9.966
719	2.9000	2.067	746	3.9994	5.230	805	7.8002	9.977
720	2.9251	2.143	747	4.1000	5.442	794	7.9004	10.033
722	2.9502	2.244	748	4.1995	5.664	795	7.9998	10.091
723	2.9752	2.330	749	4.3003	5.866	796	8.0996	10.147

Can. J. Chem. Downloaded from www.nrcresearchpress.com by 80.90.12.36 on 09/08/12
For personal use only.

Table 2. (*continued*)

Run no. R	EO mf (mol%)	T_{FH} (deg C)	Run no. R	EO mf (mol%)	T_{FH} (deg C)	Run no. R	EO mf (mol%)	T_{FH} (deg C)
806	8.1001	10.135	514	12.0027	11.089	257	17.5028	10.632
802	8.2006	10.189	545	12.2525	11.084	258	17.9916	10.566
506	8.2470	10.218	549	12.2537	11.083	259	18.4953	10.455
803	8.3003	10.237	536	12.2558	11.064	260	19.0054	10.395
807	8.3993	10.284	249	12.2892	11.057	261	19.5044	10.290
507	8.4993	10.344	228	12.5007	11.095	584	20.0027	10.183
808	8.5008	10.341	515	12.5064	11.096	262	20.0308	10.202
809	8.5998	10.392	252	12.5947	11.075	263	20.5056	10.142
810	8.6992	10.433	593	12.6800	11.061	265	21.4855	9.917
541	8.7459	10.471	535	12.7436	11.065	266	22.0220	9.846
812	8.8002	10.471	246	12.7517	11.068	267	22.4882	9.772
811	8.8006	10.464	546	12.7544	11.100	268	22.9949	9.678
813	8.9008	10.508	550	12.7557	11.083	269	23.5116	9.586
817	8.9982	10.554	251	12.8777	11.076	270	24.0116	9.486
814	8.9990	10.533	248	13.0032	11.077	271	24.5049	9.422
821	8.9992	10.533	227	13.0211	11.063	273	25.5211	9.257
822	9.0001	10.545	226	13.0395	11.076	274	26.0160	9.199
819	9.0002	10.534	225	13.0404	11.095	275	26.4900	9.116
508	9.0033	10.547	551	13.0418	11.084	276	27.0054	9.038
815	9.0991	10.580	516	13.0449	11.096	277	27.5018	8.939
816	9.1998	10.607	250	13.1262	11.067	278	27.9916	8.885
540	9.2449	10.635	552	13.2476	11.070	279	28.4992	8.819
818	9.3002	10.639	534	13.2543	11.071	280	29.0032	8.750
820	9.4000	10.662	547	13.2557	11.090	281	29.5942	8.653
509	9.4983	10.717	253	13.3995	11.056	282	30.0050	8.555
823	9.4984	10.676	229	13.5017	11.072	283	30.4924	8.517
825	9.5001	10.683	517	13.5052	11.084	284	30.9919	8.453
831	9.5005	10.685	245	13.7503	11.051	285	31.5022	8.355
826	9.5997	10.703	533	13.7525	11.039	286	32.1243	8.290
830	9.5997	10.709	548	13.7538	11.060	287	32.5041	8.233
824	9.6008	10.711	232	13.9834	11.013	288	33.0063	8.159
827	9.6989	10.747	518	14.0048	11.045	289	33.5456	8.109
828	9.6999	10.741	243	14.2344	11.001	290	34.0057	8.061
539	9.7524	10.780	544	14.2436	11.026	291	34.5036	7.983
829	9.8001	10.771	530	14.2470	11.002	292	35.0024	7.952
832	9.9007	10.796	233	14.4982	11.017	293	35.5080	7.855
833	10.0005	10.810	519	14.5006	11.014	294	35.9937	7.826
510	10.0006	10.831	241	14.7451	10.977	295	36.4986	7.747
538	10.2515	10.888	529	14.7500	10.985	296	36.9993	7.682
236	10.4967	10.912	520	14.9980	10.964	297	37.4942	7.654
511	10.4985	10.933	235	15.0032	10.947	298	38.0003	7.611
238	10.7385	10.952	239	15.2401	10.919	299	38.4941	7.561
542	10.7460	10.978	528	15.2496	10.926	300	39.0057	7.528
537	10.7560	10.938	237	15.5000	10.886	301	39.4968	7.488
512	10.9991	10.995	521	15.5043	10.906	302	40.0007	7.450
234	11.0018	10.988	527	15.7462	10.856	303	40.5579	7.381
240	11.2432	11.026	254	16.0023	10.847	304	41.0041	7.311
532	11.2536	11.022	522	16.0033	10.838	305	41.5619	7.246
231	11.4894	11.013	526	16.2523	10.817	306	42.0127	7.222
513	11.4982	11.053	255	16.5026	10.773	307	42.5091	7.170
242	11.7449	11.044	523	16.5057	10.780	308	43.0021	7.121
543	11.7451	11.077	525	16.7553	10.748	309	43.7439	7.047
531	11.7502	11.046	256	16.9966	10.685	310	44.0328	7.029
230	12.0009	11.082	524	17.0048	10.704	311	44.4900	6.997

Can. J. Chem. Downloaded from www.nrcresearchpress.com by 80.90.12.36 on 09/08/12
For personal use only.

Table 2. (*concluded*)

Run no. R	EO mf (mol%)	T_{FH} (deg C)	Run no. R	EO mf (mol%)	T_{FH} (deg C)	Run no. R	EO mf (mol%)	T_{FH} (deg C)
312	45.0078	6.926	360	65.5021	4.810	413	80.5008	0.296
313	45.4918	6.887	361	65.9979	4.763	414	80.9997	−0.011
314	46.0062	6.857	362	66.5017	4.641	415	81.2954	−0.200
315	46.4980	6.815	368	67.0018	4.561	416	82.0007	−0.658
316	47.0051	6.730	369	67.4986	4.474	417	82.0013	−0.640
317	47.5236	6.689	370	68.0012	4.399	419	83.0025	−1.347
318	48.0192	6.669	371	68.5045	4.280	420	83.5024	−1.763
319	48.5008	6.640	586	68.9958	4.236	423	84.0016	−2.153
320	49.0045	6.580	585	68.9994	4.225	422	84.0016	−2.131
321	49.5023	6.523	587	69.0008	4.237	421	84.0041	−2.191
323	49.9978	6.513	372	69.0016	4.202	424	84.5008	−2.574
326	49.9986	6.503	373	69.5003	4.083	427	84.9991	−3.020
327	49.9993	6.486	374	69.9968	3.985	428	85.4996	−3.480
325	50.0012	6.491	375	70.5038	3.885	429	85.9983	−4.026
322	50.0021	6.477	376	71.0151	3.741	430	86.5010	−4.593
324	50.0036	6.478	377	71.5010	3.639	431	87.0015	−5.172
328	50.4995	6.473	378	72.1979	3.444	432	87.5017	−5.839
329	51.0023	6.401	379	72.6300	3.353	433	87.9996	−6.545
330	51.5072	6.351	380	73.0010	3.250	434	88.4998	−7.254
331	52.0028	6.312	381	73.5027	3.132	435	89.0007	−8.037
332	52.5020	6.276	382	73.9999	2.969	436	89.5007	−8.915
333	52.9942	6.253	383	74.4945	2.819	437	90.0009	−9.903
334	53.4959	6.181	384	74.9993	2.610	438	90.5016	−10.839
341	54.5067	6.084	385	75.4969	2.512	439	91.0001	−11.911
342	55.5027	5.985	386	75.9955	2.302	440	91.5005	−13.075
339	55.9995	5.927	387	76.5138	2.127	441	92.0011	−14.465
340	56.4944	5.909	388	77.0007	1.986	461	92.2475	−15.009
343	57.0667	5.849	389	77.5011	1.772	442	92.4997	−15.983
344	57.5076	5.795	401	78.0013	1.519	460	92.7507	−16.731
345	58.0058	5.747	390	78.0023	1.545	433	93.0011	−17.381
346	58.5005	5.705	400	78.5002	1.292	459	93.2496	−18.118
347	59.0041	5.623	391	78.5037	1.303	444	93.5011	−19.044
348	59.5037	5.593	392	79.0031	1.075	458	93.7503	−20.126
349	59.9999	5.528	398	79.5004	0.843	445	94.0014	−20.959
350	60.4965	5.470	393	79.5028	0.846	457	94.2503	−22.115
351	61.0061	5.418	405	79.9980	0.526	446	94.5008	−22.994
352	61.5051	5.382	412	79.9994	0.610	451	94.7492	−24.321
353	62.0067	5.313	394	79.9994	0.616	450	94.7497	−24.390
354	62.5014	5.237	409	79.9998	0.550	448	94.7498	−24.265
355	63.0050	5.176	410	80.0003	0.585	454	94.7499	−24.708
356	63.4949	5.110	411	80.0004	0.531	449	94.7502	−24.611
357	63.9941	5.031	404	80.0011	0.545	452	94.7507	−24.251
358	64.5031	4.955	406	80.0014	0.525	453	94.7510	−24.238
359	64.9966	4.910	407	80.0017	0.524	447	94.9994	−24.958
591	65.4995	4.831	408	80.0021	0.622	456	95.0001	−25.775
588	65.5006	4.821	402	80.0025	0.570			

error 0.0076 mol% EO, was estimated from the observed eutectic temperature together with the intersections of the curves for the freezing of ice and for the formation of hydrate. The ice–hydrate intersection estimate for the eutectic temperature was −2.130°C, with bias −0.023°C below the best observed value from Set 3+2: this negative bias arose from the combined biases both for the freezing of ice and for the formation of hydrate.

Since it was found experimentally that the direct eutectic temperature measurements of Set 3+2 had minimum bias, the bias of the temperature for formation of hydrate in Set 3 was at least −0.023°C at 1.991 mol% EO. This bias is to be compared with that −0.106°C found for eight replicates of Set 2 relative to Set 3 at 2.0488–2.0603 mol% EO.

Measurement of formation of hydrate

Table 2 lists the measurements of the temperature for formation of EO hydrate from aqueous solutions containing between 1.9565 and 95.0001 mol% EO. The first column of the table

Can. J. Chem. Downloaded from www.nrcresearchpress.com by 80.90.12.36 on 09/08/12
For personal use only.

Can. J. Chem. Downloaded from www.nrcresearchpress.com by 80.90.12.36 on 09/08/12
For personal use only.

Fig. 1. Freezing point curve of EO hydrate.
Y-axis: Temperature for formation of hydrate /deg C.
X-axis: Ethylene oxide fraction /mol%.

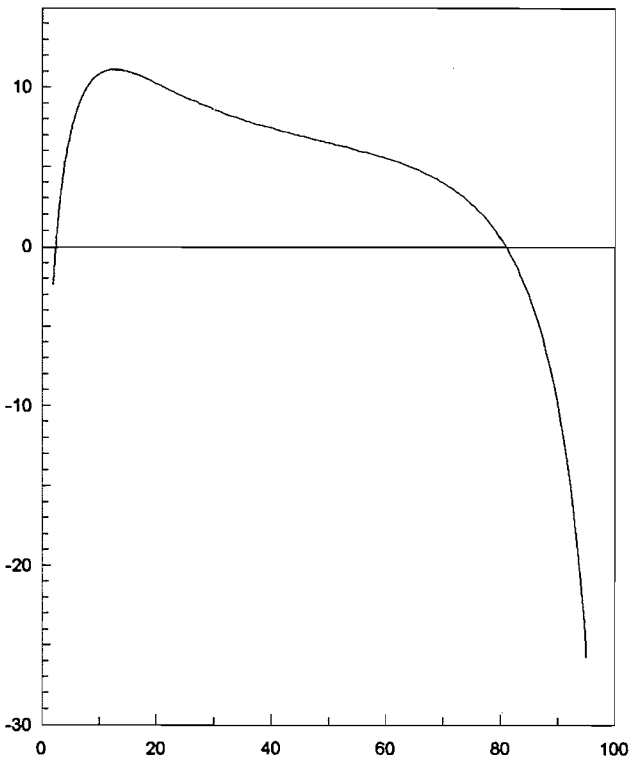

shows the R-number of the run, the second column the solution composition, and the third the temperature for formation of hydrate from that solution. The precision of the measurements justifies four decimal places for the mol% EO in solution, and three places for the temperature of hydrate formation in °C. Figure 1 provides a line plot of these measurements showing the envelope of the temperature for formation of hydrate with solution composition: this envelope is commonly known as the hydrate "freezing point" curve.

Initial data analyses indicated that our early hydrate measurements up to run R224 in Set 1 were incomplete and of lower reliability so they were excluded from Table 2.

Preliminary and separate regression analyses indicated that the measurements of Set 1 and of Set 2 in the congruent region were of equal precision despite the fact that they were made at times more than 1 year apart. These measurements were subsequently analysed together with those of Set 3 as the single combined Set 1+2+3 and were found to give a proper estimate of error in the congruent region between compositions 8.3993 and 20.5056 mol% EO.

Set 1 contained almost all of the measurements in the EO-rich region with compositions between 20.0308 and 95.0001 mol% EO: a few replicate determinations, made later as a check in Set 3, were found to be in good agreement with those of Set 1. Subsequent regression analyses used the combined measurements as a single Set 1+3.

In the water-rich region, for solutions containing less than 10 mol% EO, comparison of the hydrate measurements of Set 2 with those of Set 3 showed that the earlier measurements of Set 2 became systematically more biased and unreliable as the solution was diluted below 5 mol% EO and as the hydrate formation temperature moved towards the eutectic temperature. As a result the measurements in Set 2 for solutions containing less than 3.6019 mol% EO were evaluated as unreliable and were excluded from Table 2.

The water-rich region was defined by the measurements of only Set 3 between 1.9565 and 3.6012 mol% EO, by the combined measurements of Set 3 and Set 2 between 3.6496 and 10.0005 mol% EO, and by the combined measurements of Set 2 and Set 1 between 10.0006 and 12.5947 mol% EO.

Apparently, in those runs of Set 2 that were rejected, the large impressed cooling jacket temperature differential, of 1.7°C below that of the stirred test solution, for example, was the main cause for the large mean bias –0.106°C of hydrate formation temperature for the eight replicate solutions containing 2.0488–2.0603 mol% EO: the internal variability of these replicates gave an estimated standard error of 0.033°C for a single measurement, indicating their internal precision. The bias of these Set 2 measurements relative to Set 3 was discovered experimentally by checking with repeat measurements in Set 3 using reduced impressed cooling differentials of ~0.1°C. The large observed bias in Set 2 was shown to be clearly related to three factors: (*i*) the large cooling temperature differential applied to the freezing point cell, (*ii*) the large local slope of the hydrate formation temperature envelope, and (*iii*) the large change of solution composition caused by the formation of a relatively small amount of hydrate. The slow rate of energy release, derived from the slow rate of formation of hydrate from these incongruent water-rich solutions (15, 16), was inadequate to balance the large impressed cooling energy loss.

The hydrate measurements of Set 3, in the same water-rich region, still include a negative bias –0.023°C of hydrate formation temperature similar to, but much smaller than, that found for Set 2.

The final measurements included in Table 2 and shown in Fig. 1 exhibited a smooth and continuous envelope for all compositions, without discontinuities of value or of slope: this experimental continuity proved the existence of only one type of EO hydrate over the whole range of solution composition.

The later statistical analyses of the data in Table 2 involved taking a significant number (e.g., 24–112) of adjacent measurements around a predefined solution composition and making a local least-squares regression analysis of the hydrate formation temperature as a polynomial function of the solution composition. The order of the polynomial equations tested ranged from first up to sixth power of composition. This gave consecutive representative equations that (*i*) under-fitted the data, (*ii*) best-fitted the data, and (*iii*) over-fitted the data. The best-fit and over-fit equations gave unbiased estimates of the local standard error of a single temperature measurement for formation of hydrate. The best-fit and over-fit residuals were invariably random and reconfirmed the continuity of the measurements over the whole solution composition range.

Estimates of temperature for formation of hydrate with composition

The eutectic point is listed in the first row of Table 3. Estimates of the EO hydrate formation temperature with composition are listed in Table 3 and were defined by the 34 best-fit regression analyses at the solution compositions shown in column one. Estimates of the temperature for formation of hydrate T_{FH}, its standard error SE T_{FH}, the standard error on a

Table 3. (ITS-90) Estimates of temperature for formation of hydrate with composition: value, slope, and errors.

Solution composition (mol% EO)	Temperature for formation of hydrate T_{FH} (deg C)	Standard error on T_{FH} SE T_{FH} (deg C)	Standard error on a single measurement SE T_{obs} (deg C)	Slope of T_{FH} envelope (°C/mol%)	Standard error of slope (°C/mol%)	Number of data – number of parameters
1.991	−2.107	0.0006	0.002	—	—	16–1
2.00	−2.110	0.0028	0.016	5.849	0.0723	30–3
3.00	2.404	0.0018	0.017	3.456	0.0097	90–6
3.60	4.221	0.0031	0.017	—	—	29–1
3.60	4.225	0.0018	0.018	2.700	0.0100	92–6
4.00	5.218	0.0017	0.017	2.305	0.0074	97–6
5.00	7.140	0.0013	0.014	1.575	0.0043	109–6
6.00	8.464	0.0015	0.013	1.113	0.0031	70–5
7.00	9.418	0.0016	0.010	0.812	0.0023	39–3
8.00	10.091	0.0015	0.011	0.554	0.0041	53–4
9.00	10.539	0.0015	0.011	0.350	0.0043	53–4
10.00	10.822	0.0018	0.012	0.227	0.0021	45–3
11.00	10.992	0.0017	0.013	0.123	0.0038	56–4
12.50	11.082	0.0020	0.014	0.007	0.0043	52–4
12.644	11.083	0.0018	0.013	0.000	0.0012	112–5
14.00	11.037	0.0018	0.013	−0.067	0.0029	57–4
16.00	10.840	0.0020	0.012	−0.124	0.0027	36–4
18.00	10.549	0.0021	0.013	−0.163	0.0025	39–5
20.00	10.206	0.0021	0.013	−0.178	0.0025	39–5
22.00	9.860	0.0023	0.016	−0.176	0.0010	50–5
25.00	9.345	0.0023	0.016	−0.167	0.0010	50–5
30.00	8.587	0.0024	0.016	−0.145	0.0010	41–5
35.00	7.934	0.0017	0.014	−0.118	0.0006	64–6
40.00	7.400	0.0017	0.013	−0.099	0.0006	64–6
45.00	6.936	0.0017	0.013	−0.090	0.0006	64–6
50.00	6.491	0.0058	0.014	—	—	6–1
50.00	6.492	0.0016	0.013	−0.089	0.0006	64–6
55.00	6.041	0.0016	0.013	−0.095	0.0006	64–6
60.00	5.536	0.0016	0.013	−0.111	0.0007	64–6
65.00	4.902	0.0016	0.013	−0.147	0.0007	64–6
70.00	3.990	0.0027	0.019	−0.217	0.0012	48–5
75.00	2.661	0.0030	0.024	−0.325	0.0012	63–5
80.00	0.564	0.0116	0.039	—	—	11–1
80.00	0.560	0.0038	0.029	−0.544	0.0031	58–7
85.00	−3.020	0.0029	0.016	−0.938	0.0047	29–7
90.00	−9.844	0.0140	0.071	−1.932	0.0124	26–5
92.50	−15.840	0.0168	0.126	−2.995	0.0239	56–6
94.75	−24.398	0.0711	0.188	—	—	7–1
95.00	−25.513	0.0399	0.196	−4.902	0.2237	24–4

single hydrate measurement SE T_{obs}, the slope of the T_{FH} envelope and its standard error are listed, respectively, in columns two to six. In column seven the two numbers separated by a dash indicate the number of measurements and the number of parameters used in the best representative polynomial model.

The results for four sets of replicate measurements at the compositions 3.60, 50.0, 80.0, and 94.75 mol% EO are included in Table 3 to provide a comparison of the standard error on a single determination with those estimates from the regressions.

The errors of hydrate measurements were greatest at the lowest temperatures using the most EO-rich (water-dilute) solutions, as seen in the final row of Table 3. Column four shows the progressive decrease of error with the increase both of hydrate formation temperature and of water content of the solution, down to a minimum error at 7.0 mol% EO. Below 7.0 mol% EO the errors of measurement again increase with the decrease both of hydrate temperature and of EO content of the solution. Over the wide range of solution composition 6.0–60.0 mol% EO, the standard error on a single hydrate temperature determination was 0.015°C, and was sensibly constant.

The congruent temperature 11.083°C, with estimated standard error 0.0018°C, was determined from the maximum of the hydrate formation curve representing 112 measurements with solution compositions between 8.3993 and 20.5056 mol% EO. The temperature for formation of hydrate, T_{FH}, was best represented by the five-parameter equation

Can. J. Chem. Downloaded from www.nrcresearchpress.com by 80.90.12.36 on 09/08/12
For personal use only.

$$[2]\quad T_{FH} = \underset{(0.0018)}{11.083} + \underset{(0.0012)}{0.0000D} - \underset{(0.00026)}{0.02919D^2} + \underset{(0.000085)}{0.002739D^3} - \underset{(0.000011)}{0.000137D^4}$$

where T_{FH} is in °C and D = (mol% EO –12.644) = (C–12.644) mol% EO. Least-squares estimates of the standard error on the parameters are shown in parentheses and the standard error on a single hydrate temperature determination was 0.013 °C with 107 degrees of freedom, in excellent agreement with the estimates from the smaller adjacent local regressions.

The congruent composition 12.644 mol% EO, with estimated standard error 0.021 mol% EO, was determined as the composition for zero slope of eq. [2], and the standard error from the error on that slope. The formula found for the congruent EO hydrate was $EO{\cdot}6.91H_2O$ with an estimated standard error 0.013 mol water/mol EO.

The congruent hydrate comprises $6.66EO{\cdot}46H_2O$ per unit cell, with EO molecules occupying mainly the six tetrakaidecahedral sites and filling at least one third of the two dodecahedral sites (8, 9, 10).

These estimates of the congruent hydrate freezing temperature and composition and their standard errors are in general agreement with, and supersede all of our earlier estimates (8, 10, 15, 18).

The slope of the hydrate formation curve in the EO-rich region is negative and passes through a narrow minimum at about 20 mol% EO and through a wide maximum at about 50 mol% EO. The small absolute values of the negative slopes between 14.0 and 60.0 mol% EO reflect (*i*) a high enthalpy change for crystallization of EO hydrate from solution (20), together with (*ii*) positive and high Raoult-law activity coefficients for water in these EO-rich solutions (21, 22).

Comparison with earlier work

A similar numerical evaluation by us of seven hydrate measurements from Maass and Boomer (1) indicated a congruent hydrate freezing at 10.72°C with standard error 0.08°C, consistent with their error estimate 0.20°C on a single determination. This congruent hydrate freezing temperature was significantly lower by –0.36°C (–4.7 their standard errors) than that of our work. The lower hydrate temperatures observed probably resulted from the use of relatively larger cooling jacket energy fluxes in that earlier work (1). The congruent composition found was 13.28 mol% EO with standard error 1.22 mol% EO, which gave a hydrate formula $EO{\cdot}6.53H_2O$ with standard error 0.69 mol water/mol EO. This congruent composition with its large standard error was not significantly different from our present value. The hydrate formula indicated was near to the mean of the formula limits, $EO{\cdot}5H_2O$ and $EO{\cdot}8H_2O$, given by the authors (1). An earlier assessment of these measurements (1) by von Stackelberg and Meuthen (4) had suggested a hydrate formula $EO{\cdot}6.5H_2O$ with an error 0.5 mol water/mol EO.

The EO hydrate temperatures reported by Mazzucchelli and Armenante (2) were significantly higher by 0.88°C (59 standard errors) than those found in our work, and indicated a large standard error of 0.76°C on a single hydrate temperature determination. The paucity of measurements in the congruent region together with their low accuracy precluded any reliable evaluation of the congruent hydrate properties from that work (2).

The ice freezing temperatures given by Mazzucchelli and Armenante (2) were significantly higher by 0.25°C (59 standard errors) than those observed in our work. Their reported eutectic temperature and composition were, respectively, significantly lower by –0.12°C (–53 standard errors) and significantly higher by 0.29 mol% EO (45 standard errors) than those observed in our work.

Acknowledgment

This work was supported in part by grants under the National Research Council of Canada, Industrial Research Assistance Program, for 1964, 1965, and 1966.

References

1. O. Maass and E.H. Boomer. J. Am. Chem. Soc. **44**, 1709 (1922).
2. A. Mazzucchelli and R. Armenante. Gazz. Chim. Ital. **52**, 344 (1922).
3. D.N. Glew and E.A. Moelwyn-Hughes. Discuss Faraday Soc. **15**, 150 (1953).
4. M. von Stackelberg and B. Meuthen. Z. Elektrochem. **62**, 130 (1958).
5. D.N. Glew. Can. J. Chem. **38**, 208 (1960).
6. D.N. Glew. Nature, **195**, 698 (1962).
7. D.N. Glew. J. Phys. Chem. **66**, 605 (1962).
8. D.N. Glew and N.S. Rath. J. Sci. Instrum. **42**, 665 (1965).
9. R.K. McMullan and G.A. Jeffrey. J. Chem. Phys. **42**, 2725 (1965).
10. D.N. Glew and N.S. Rath. J. Chem. Phys. **44**, 1710 (1966).
11. D.N. Glew, H.D. Mak, and N.S. Rath. Can. J. Chem. **45** 3059 (1967).
12. J.A. McIntyre and D.R. Petersen. J. Chem. Phys. **47**, 3850 (1967).
13. D.N. Glew, H.D. Mak, and N.S. Rath. Chem. Commun. 264 (1968).
14. D.N. Glew, H.D. Mak, and N.S. Rath. *In* Hydrogen-bonded solvent systems. *Edited by* A.K. Covington and P. Jones. Taylor and Francis, London. 1968. pp. 195–210.
15. D.N. Glew and M.L. Haggett. Can. J. Chem. **46**, 3857 (1968).
16. D.N. Glew and M.L. Haggett. Can. J. Chem. **46**, 3867 (1968).
17. D.N. Glew and Harry Watts. Can. J. Chem. **49**, 1830 (1971).
18. D.W. Davidson. *In* Water: a comprehensive treatise. Vol. 2. *Edited by* F. Franks. Plenum Press, New York. 1973. pp. 115–234.
19. R.N. Goldberg and R.D. Weir. Pure Appl. Chem. **10**, 1545 (1992).
20. D.N. Glew. Trans. Faraday Soc. **61**, 30 (1965).
21. K.F. Coles and F. Popper. Ind. Eng. Chem. **42**, 1434 (1950).
22. K.E. MacCormack and J.H.B. Chenier. Ind. Eng. Chem. **47**, 1454 (1955).

Can. J. Chem. Downloaded from www.nrcresearchpress.com by 80.90.12.36 on 09/08/12
For personal use only.

Synthesis and structural characterization of barium complexes containing the bulky amino-siloxide hybrid ligand $^{-}OSi(^{t}Bu)_2((CH_2)_3NMe_2)$

Pengcheng Shao, David J. Berg, and Gordon W. Bushnell

Abstract: The bulky amino-siloxide hybrid ligand $^{-}OSi(^{t}Bu)_2((CH_2)_3NMe_2)$ allows isolation of dinuclear, hydrocarbon-soluble barium complexes. The structures of two mono(ligand) complexes, $\{Ba[OSi(^{t}Bu)_2((CH_2)_3NMe_2)][N(SiMe_3)_2]\}_2$ (**1**) and $\{Ba[OSi(^{t}Bu)_2((CH_2)_3NMe_2)][N(SiMe_3)_2][THF]\}_2$ (**3**), have been determined by X-ray diffraction (crystal data: **1**, monoclinic, *C*2/*c*, $a = 20.451(4)$ Å, $b = 14.277(3)$ Å, $c = 22.258(5)$ Å, $\beta = 101.14(2)°$, $V = 6376.1(2)$ Å^3, $Z = 4$ (dimers), $R = 0.069$, $R_w = 0.100$; **3**, monoclinic, $P2_1/c$, $a = 11.025(4)$ Å, $b = 22.414(3)$ Å, $c = 13.925(2)$ Å, $\beta = 104.05(2)°$, $V = 3338.0(1)$ Å^3, $Z = 2$ (dimers), $R = 0.090$, $R_w = 0.117$). Complex **1** is stable towards ligand redistribution in d_6-benzene or d_8-toluene, but in d_8-THF both **1** and **3** exist in equilibrium with the ligand redistribution products $Ba[N(SiMe_3)_2]_2[THF]_2$ and $Ba[OSi(^{t}Bu)_2((CH_2)_3NMe_2)]_2$ (**2**). Complex **2** was prepared independently and appears to exist as a monomer–dimer equilibrium in d_6-benzene solution. Complexes **1**–**3** do not sublime when heated under high vacuum (200°C, 10^{-4} Torr).

Key words: siloxide, barium, synthesis, structure, bis(trimethylsilyl)amide.

Résumé : Le coordinat hybride amino-siloxyde volumineux $^{-}OSi(^{t}Bu)_2((CH_2)_3NMe_2)$ permet d'isoler les complexes dinucléaires du baryum solubles dans les hydrocarbures. Faisant appel à la diffraction des rayons X, on a déterminé la structure de deux complexes monocoordinés, $\{Ba[OSi(^{t}Bu)_2((CH_2)_3NMe_2)][N(SiMe_3)_2]\}_2$ (**1**) et $\{Ba[OSi(^{t}Bu)_2((CH_2)_3NMe_2)][N(SiMe_3)_2][THF]\}_2$ (**3**) (données cristallographiques : **1**, monoclinique, *C*2/c, $a = 20{,}451(4)$, $b = 14{,}277(3)$ et $c = 22{,}258(5)$ Å, $\beta = 101{,}14(2)°$, $V = 6376{,}1(2)$ Å^3, $Z = 4$ (dimères), $R = 0{,}069$ et $R_w = 0{,}100$; **3**, monoclinique, $P2_1/c$, $a = 11{,}025(4)$, $b = 22{,}414(3)$ et $c = 13{,}925(2)$ Å, $\beta = 104{,}05(2)°$, $V = 3338{,}0(1)$ Å^3, $Z = 2$ (dimères), $R = 0{,}090$, $R_w = 0{,}117$). Le complexe **1** est stable par rapport à une redistribution des coordinats dans du d_6-benzène ou du d_8-toluène; toutefois, dans du d_8-THF, les composés **1** et **3** subissent tous les deux une redistribution de coordinats conduisant aux produits $Ba[N(SiMe_3)_2]_2[THF]_2$ et $Ba[OSi(^{t}Bu)_2((CH_2)_3NMe_2)]_2$. On a préparé le complexe **2** d'une manière indépendante et, en solution dans le d_6-benzène, il semble exister sous la forme d'un équilibre monomère–dimère. Les complexe **1**–**3** ne se subliment pas lorsqu'on les chauffe sous vide poussé (200°C, 10^{-4} Torr).

Mots clés : siloxyde, baryum, synthèse, structure, bis(triméthylsilyl)amide.

Introduction

The current interest in high T_c mixed metal oxide superconductors (1) has led to intense investigation of metal alkoxides as potential precursors to these materials (2). As a result, the design of soluble alkoxide complexes suitable for the sol–gel process is now possible (3). However, the preparation of high volatility alkoxides for use in the growth of thin-film superconductors remains problematic, particularly for large electropositive metals such as barium. Several approaches to this problem have been investigated, including the use of fluorinated or bulky alkoxides (4). Recently, we reported that the use of a bulky siloxide containing a pendant amine donor (**I**) leads to monomeric yttrium and lanthanide complexes of enhanced solubility and volatility (5). Herrmann et al. have reported a similar strategy using bulky alkoxides incorporating amine or ether donors (6).

I 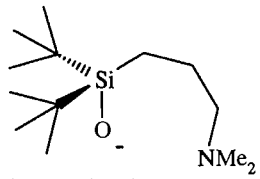

In this contribution we report the extension of this approach to barium complexes. The larger size of barium makes it much more difficult to achieve coordinative saturation than for yttrium or the lanthanides (ionic radii in six coordination: Ba^{2+} 1.35, La^{3+} 1.032, and Y^{3+} 0.900 Å) (7). In addition, the 2+ oxidation state limits the number of anionic ligands per barium to two in a neutral complex, so that ligand bulk becomes partic-

Received February 23, 1995.

P. Shao, D.J. Berg,[1] and G.W. Bushnell. Department of Chemistry, University of Victoria, P.O. Box 3055, Victoria, BC V8W 3P6, Canada.

[1] Author to whom correspondence may be addressed. Telephone: (604) 721-7161. Fax: (604) 721-7147. E-mail: DJBERG@UVVM.UVIC.CA

Can. J. Chem. Downloaded from www.nrcresearchpress.com by 80.90.12.36 on 09/08/12
For personal use only.

Can. J. Chem. Downloaded from www.nrcresearchpress.com by 80.90.12.36 on 09/08/12
For personal use only.

Table 1. NMR chemical shift data in d_6-benzene.

Assignment	**1**	**2**[a]	**3**[b]	$Ba[N(SiMe_3)_2]_2[THF]_2$
^{1}H				
α-CH_2 THF			3.54	3.49
CH_2N	2.10	2.22, 2.39	2.15	
NMe_2	1.98	2.16, 2.27	1.98	
$CH_2CH_2CH_2$	1.41	1.74, 1.83	1.49	
β-CH_2 THF			1.35	1.32
CMe_3	1.10	1.20, 1.29	1.15	
CH_2Si	0.47	0.70[c]	0.57	
$SiMe_3$	0.30		0.36	0.33
^{13}C{^{1}H}				
α-CH_2 THF			68.19	68.48
CH_2N	61.14	63.84, 65.75	61.69	
NMe_2	45.95	45.28, 46.10	45.81	
CMe_3	30.12	30.13, 30.01	30.20	
β-CH_2 THF			25.47	25.24
$CH_2CH_2CH_2$	24.10	23.96, 25.20	24.18	
CMe_3	21.81	21.84, 22.11	21.89	
CH_2Si	9.55	14.31, 12.79	10.61	
$SiMe_3$	6.20		6.14	5.50
^{29}Si{^{1}H}				
SiO	−0.13	−1.95, −4.70	0.03	
$SiMe_3$	−18.01		−18.04	−18.99

[a]Resonances due to the major component (60%) are listed first and those of the minor component (40%) are listed second.
[b]Trace **2** and $Ba[N(SiMe_3)_2]_2[THF]_2$ are always present.
[c]Obscured by the major component.

Table 2. NMR chemical shift data in d_8-THF.

Assignment	**1** or **3**[a]	**2**	$Ba[N(SiMe_3)_2]_2[THF]_2$
^{1}H			
CH_2N	2.11[b]	2.14[b]	
NMe_2	2.10	2.12	
$CH_2CH_2CH_2$	1.55	1.58	
CMe_3	0.91	0.95	
CH_2Si	0.36	0.40	
$SiMe_3$	−0.09		−0.05
^{13}C{^{1}H}			
CH_2N	65.95	65.96	
NMe_2	46.04	46.07	
CMe_3	29.86	30.05	
$CH_2CH_2CH_2$	25.33[c]	[c]	
CMe_3	22.26	22.42	
CH_2Si	12.17	12.43	
$SiMe_3$	5.83		5.68

[a]contains ca. 10% **2** and $Ba[N(SiMe_3)_2]_2$ as minor components.
[b]partially obscured by NMe_2.
[c]obscured by d_8-THF.

ularly important. The combination of ligand bulk and an additional amine donor site should make **I** an attractive ligand for generating barium complexes of low nuclearity.

Experimental section

General procedures

All manipulations were carried out under an argon atmosphere, with the rigorous exclusion of oxygen and water, using standard glovebox (Braun MB150-GII) or Schlenk techniques. Tetrahydrofuran (THF), hexane, and toluene were dried by distillation from sodium benzophenone ketyl under argon immediately prior to use. $Ba[N(SiMe_3)_2]_2[THF]_2$ (8) and $HOSi(^tBu)_2((CH_2)_3NMe_2)$ (5) were prepared according to literature methods.

^{1}H, ^{13}C, and ^{29}Si NMR spectra were recorded on a Bruker WM-250 MHz or a Bruker AMX-360 MHz spectrometer. Spectra were recorded in C_6D_6, C_7D_8, or C_4D_8O solvent, previously distilled from sodium under argon, using 5 mm tubes fitted with a Teflon valve (Brunfeldt). ^{29}Si spectra were recorded using an INEPT pulse sequence. ^{1}H and ^{13}C NMR spectra were referenced to residual solvent resonances while ^{29}Si NMR were referenced to external TMS. NMR data for compounds **1–3** are collected in Tables 1 and 2. Melting points were recorded using a Reichert hot stage and are not corrected. Elemental analyses were performed by Canadian Microanalytical, Delta, B.C.

$\{Ba[OSi(^tBu)_2((CH_2)_3NMe_2)][N(SiMe_3)_2]\}_2$ (1)

A solution of $HOSi(^tBu)_2((CH_2)_3NMe_2)$ (0.514 g, 2.09 mmol) in 25 mL of toluene was added dropwise over 15 min to a stirred solution of $Ba[N(SiMe_3)_2]_2[THF]_2$ (1.259 g, 2.09

Can. J. Chem. Downloaded from www.nrcresearchpress.com by 80.90.12.36 on 09/08/12
For personal use only.

Table 3. Summary of crystallographic data for **1** and **3**.

	1	**3**
Empirical formula	$C_{38}H_{96}Ba_2N_4O_2Si_6$	$C_{46}H_{112}Ba_2N_4O_4Si_6$
fw	1082.4	1228.6
Cryst. system	Monoclinic	Monoclinic
Space group	*C*2/*c* (No. 15)	$P2_1/c$ (No. 14)
a (Å)	20.451(4)	11.025(4)
b (Å)	14.277(3)	22.414(3)
c (Å)	22.258(5)	13.925(2)
α (deg)	90	90
β (deg)	101.14(2)	104.05(2)
γ (deg)	90	90
V (Å^3)	6376.1(2)	3338.0(1)
Z	4 (dimers)	2 (dimers)
ρ (calcd.) (g cm^{-3})	1.130	1.222
μ (cm^{-1})	13.65	13.13
Radiation, λ (Å)	Mo Kα, 0.70932	Mo Kα, 0.70932
T	Ambient	Ambient
$2\theta_{max}$ (deg)	45	45
No. of obsd. reflcns.	4158	4330
No. of unique reflcns.	2484	1995
R^a	0.069	0.090
$R_w{}^b$	0.100	0.117

$^aR = \Sigma(|F_o| - |F_c|) / \Sigma|F_o|$.
$^bR_w = [\Sigma w(|F_o| - |F_c|)^2 / \Sigma w(|F_o|)^2]^{1/2}$.

mmol) in 25 mL of toluene in the glovebox. After an additional 30 min of stirring, the solvent was removed by rotary evaporation and the white powder redissolved in a minimum of hexane. Cooling at −30°C afforded colourless crystals of **1**. Yield: 0.74 g (66%); mp 143–145°C. Anal. calcd. for $C_{38}H_{96}Ba_2N_4O_2Si_6$: C 42.09, H 8.92, N 5.17%; found: C 41.32, H 8.61, N 4.98%.

$Ba[OSi(^tBu)_2((CH_2)_3NMe_2)]_2$ (2)

Compound **2** was prepared using a procedure analogous to that described above for **1** except that a 2:1 ratio of silanol to silylamide was employed. The product **2** was isolated as a colourless oil of extremely high hexane solubility. We were unable to obtain satisfactory elemental data on this compound, presumably because of the presence of trace impurities. The low volatility of this compound did not allow purification by distillation because significant decomposition occurred during heating. Similarly, attempts to obtain mass spectroscopic data for **2** led to extensive fragmentation under chemical ionization conditions and the compound is not compatible with other techniques due to reaction with the common matrix solvents employed. Despite these difficulties, the extremely clean NMR spectra obtained in d_8-THF (see Tables 1, 2, and the discussion section) indicate that **2** is of reasonably high purity and that the impurities that affect the elemental data are minor in nature. Nevertheless, the formulation of **2**, while consistent with the data we were been able to obtain, must remain tentative in the absence of adequate analytical or mass spectroscopic data.

$[Ba[OSi(^tBu)_2((CH_2)_3NMe_2)][N(SiMe_3)_2][THF]]_2$ (3)

Compound **3** was isolated directly from the reaction mother liquors using the same procedure as given for **1** but with hexane rather than toluene as solvent. Yield: 82%; mp. 94–95°C. A satisfactory elemental analysis could not be obtained due to the tendency of **3** to lose THF. Despite prolonged vacuum drying, the analytical data were consistently low in carbon and hydrogen and high in nitrogen, consistent with loss of weakly coordinated THF. A typical analysis is as follows: calcd. for $C_{46}H_{112}Ba_2N_4O_4Si_6$: C 44.97, H 9.19, N 4.56%. found: C 42.86, H 8.36, N 4.65%.

X-ray crystallographic studies

Crystallographic data for **1** and **3** are summarized in Table 3. Crystals of **1** (0.4 × 0.4 × 0.4 mm) and **3** (0.37 × 0.74 × 0.22 mm) were loaded into glass capillaries in the glove box and subsequently flame sealed. The crystals were transferred to a Nonius CAD4F diffractometer equipped with Mo Kα radiation. The unit cell of **1** was refined using 24 reflections in the 2θ range of 17°–35° while that of **3** was refined using 25 reflections in the 2θ range of 21°–36°. Experimental densities were not obtained because of the air sensitivity of both compounds. Three standard reflections, measured periodically during data collection (for **1**: 0,6,0; 12,0,0; 0,0,8 and for **3**: 3,0,0; 0,8,0; 0,0,4), showed no significant decline in intensity during data collection. Intensity measurements were collected over one quarter of the sphere for both **1** and **3**. After the usual data reduction procedures, including an absorption correction according to a measured PSI scan, the structures were solved by direct methods (NRC Solver) (9). The refinements minimized $\Sigma w((|F_o|-|F_c|)^2)$ and proceeded normally using SHELX76 (10). Criteria for inclusion of reflections were $I > 2.5\sigma(I)$ and $I > 4\sigma(I)$ for **1** and **3**, respectively. The weighting scheme was determined by counting statistics using $w = 1/(\sigma^2(F) + 0.001F^2)$. Convergence was satisfactory for both compounds: max shift/esd = 0.069 for **1**, and 0.045 for **3**. A total of 235

Can. J. Chem. Downloaded from www.nrcresearchpress.com by 80.90.12.36 on 09/08/12
For personal use only.

Fig. 1. ORTEP drawing of **1**.

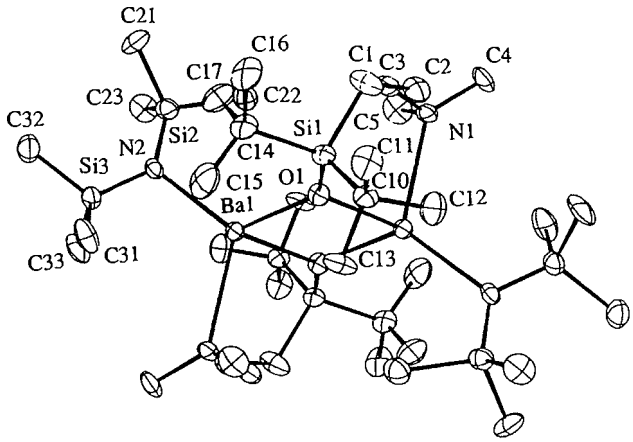

parameters (26 atoms × 9 parameters per atom + scale) were refined for **1**. For **3**, 280 parameters (31 atoms × 9 parameters per atom + scale) were refined in two blocks. No intermolecular contacts shorter than 3.5 Å were observed in either structure. The structural perspective plots were drawn using ORTEP (11). Complete tables of bond distances and angles (Tables S1, S3, S4) and anisotropic temperature parameters Tables S2, S5) have been deposited as supplementary material.[2]

Results and discussion

Reaction of $Ba[N(SiMe_3)_2]_2[THF]_2$ with 1 or 2 equivalents of $HOSi(^tBu)_2((CH_2)_3NMe_2)$ proceeded smoothly in toluene to yield the mono- (**1**) or bis(siloxide) (**2**) complexes (eqs. [1] and [2]). Complex **1** was isolated as a crystalline, solvent-free dimer (*vide infra*) while **2** was obtained as an oil of extremely high hexane solubility.

$$[1]\quad 2\,Ba[N(SiMe_3)_2]_2[THF]_2 + 2\,HOSi(^tBu)_2((CH_2)_3NMe_2) \rightarrow \{Ba[OSi(^tBu)_2((CH_2)_3NMe_2)][N(SiMe_3)_2]\}_2 + 2\,HN(SiMe_3)_2 + 4\,THF \qquad (1)$$

$$[2]\quad Ba[N(SiMe_3)_2]_2[THF]_2 + 2\,HOSi(^tBu)_2((CH_2)_3NMe_2) \rightarrow Ba[OSi(^tBu)_2((CH_2)_3NMe_2)]_2 + 2\,HN(SiMe_3)_2 + 2\,THF \qquad (2)$$

An X-ray diffraction study of **1** was carried out in order to shed light on its molecular structure. The structure of **1** is shown in Fig. 1, atomic coordinates are given in Table 4, and selected bond lengths and angles are collected in Table 5. Complex **1** crystallizes as a centrosymmetric dimer containing bridging siloxide ligands. The geometry at barium is distorted tetrahedral with one terminal silylamide and one dimethylamino group completing the coordination sphere. As expected, the bridging Ba—O(siloxide) distances in **1** (2.602(11) and 2.645(12) Å) are considerably longer than the terminal Y—O(siloxide) distances in $Y[OSi(^tBu)_2((CH_2)_3NMe_2)]_3$ (**4**) (5) even after correction for metal ionic radius and coordination number (C.N.) (predicts ca. 2.53 Å) (7).[3] The Ba—N(amine) distance of 2.94(2) Å is significantly shorter than that in **4** (predicts ca. 3.03 Å)[3] suggesting that **1** is less sterically crowded than **4**.

The bis(siloxide) complex **2** gives a single set of ^1H NMR resonances for the $OSi(^tBu)_2((CH_2)_3NMe_2)$ ligands in d_8-THF solution between −80 and +80°C (Table 2). However, in d_6-benzene two sets of resonances are observed in ca. 3:2 ratio at room temperature (Table 1). These observations are consistent with the existence of a monomer–dimer equilibrium in benzene solution and cleavage to a monomeric species in THF (eq. [3]). The variable temperature NMR data do not allow us to determine whether the predominant species at room temperature is the monomer or the dimer because the ratio changes little throughout the accessible temperature range. Furthermore, we cannot be certain whether or not the NMe_2 arms are coordinated or how many THF molecules bind to the monomer in d_8-THF solution. This is because the exchange of free and coordinated Lewis bases is generally rapid for barium compounds and, as a result, fluxional behaviour is usually observed even at −80°C. The structures depicted in eq [3] are reasonable given the apparent tendency of barium to be 4-coordinate in complexes containing the $OSi(^tBu)_2((CH_2)_3NMe_2)$ ligand, as evidenced by the solid state structures of **1** and **3** (discussed below).

[3]

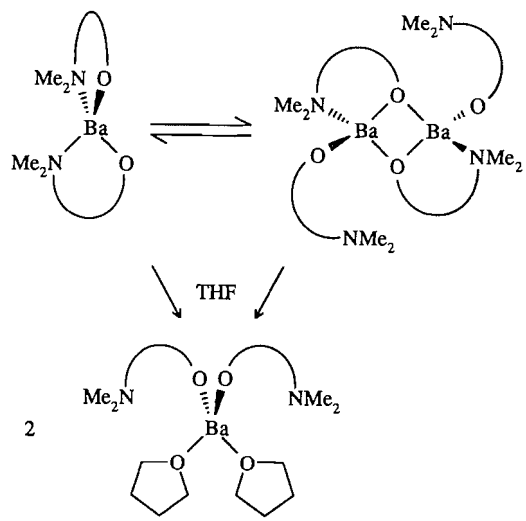

During the preparation of **1**, we noticed that the ^1H NMR spectrum of the crude powder differed from that of the recrystallized product. This was attributed to the presence of residual THF (from $Ba[N(SiMe_3)_2]_2[THF]_2$). Crystals of a THF adduct $\{Ba[OSi(^tBu)_2((CH_2)_3NMe_2)][N(SiMe_3)_2][THF]\}_2$ (**3**) were subsequently isolated directly from the reaction mother liquors. Recrystallization of **3** from hexane afforded pure **1**. The crystal structure of **3** is shown in Fig. 2, while selected distances and angles and atomic coordinates are given in Tables 5 and 6, respectively. The structure of **3** is similar to that of **1** with the important difference that one THF molecule

[2] Copies of material on deposit may be purchased from: The Depository of Unpublished Data, Document Delivery, CISTI, National Research Council Canada, Ottawa, Canada K1A 0S2.

Tables S1, S3, and S4 have also been deposited with the Cambridge Crystallographic Data Centre, and can be obtained on request from The Director, Cambridge Crystallographic Data Centre, University Chemical Laboratory, 12 Union Road, Cambridge, CB2 1EZ, U.K.

[3] The required correction is ca. +0.43 Å based on ionic radii of 1.27 Å for Ba^{2+} (C.N. 4) and 0.84 Å for Y^{3+} (C.N. 5) extrapolated from the data given in ref. 7.

Can. J. Chem. Downloaded from www.nrcresearchpress.com by 80.90.12.36 on 09/08/12
For personal use only.

Table 4. Fractional atomic coordinates[a] and equivalent isotropic temperature[b] factors for **1** (estimated standard deviations in parentheses).

Atom	*x/a*	*y/b*	*z/c*	U_{eq}
Ba(1)	21463(6)	22756(8)	7578(5)	435(4)
Si(1)	3796(3)	3661(4)	794(2)	48(2)
Si(2)	1018(3)	4166(4)	1156(3)	61(2)
Si(3)	1213(3)	2481(4)	1972(3)	61(2)
O(1)	3189(5)	3022(8)	435(5)	45(4)
N(1)	2550(9)	4704(12)	−1054(8)	71(8)
N(2)	1350(7)	3130(10)	1381(6)	49(6)
C(1)	380(1)	487(2)	45(1)	75(9)
C(2)	357(1)	495(2)	−26(1)	78(10)
C(3)	279(1)	500(2)	−39(1)	69(9)
C(4)	277(1)	540(2)	−151(1)	102(12)
C(5)	177(1)	477(2)	−116(1)	104(13)
C(10)	464(1)	309(1)	76(1)	57(8)
C(11)	525(1)	356(2)	118(1)	88(10)
C(12)	474(1)	309(2)	9(1)	84(10)
C(13)	466(1)	204(2)	96(1)	97(13)
C(14)	369(1)	388(2)	163(1)	68(9)
C(15)	377(2)	296(2)	202(1)	120(15)
C(16)	418(1)	473(2)	194(1)	104(12)
C(17)	297(1)	433(2)	163(1)	98(12)
C(21)	125(1)	515(2)	174(1)	102(12)
C(22)	132(1)	451(2)	41(1)	81(11)
C(23)	6(1)	417(2)	95(1)	96(11)
C(31)	54(1)	156(2)	171(1)	98(12)
C(32)	101(1)	317(2)	265(1)	95(11)
C(33)	201(1)	180(2)	232(1)	91(11)

[a]Coordinates × 10^n where n = 5 for Ba, 4 for Si, O, and N, and 3 for C. Temperature parameters × 10^n where n = 4 for Ba, and 3 for Si, O, N, and C.

[b]U_{eq} = the equivalent isotropic temperature parameter = $1/3\ \Sigma_i\Sigma_j U_{ij} a_i^* a_j^* (a_i \cdot a_j)$. $T = \exp(-8\pi^2 U_{iso} \sin^2\theta/\lambda^2)$.

has displaced the dimethylamino arm from each Ba center (the closest Ba···NMe_2 contact is 6.19 Å between Ba(1) and N(1)). The Ba(1)—O(2) (THF) distance of 2.78(2) Å is significantly shorter than the Ba(1)—N(1)′ (amine) distance of 2.94(2) Å in **1**. Nevertheless, the THF ligands in **3** are readily lost under vacuum, implying that THF is not a significantly better donor than the dimethylamino groups in these complexes. Presumably the tendency for amine dissociation, which was also observed with $Y[OSi(^tBu)_2((CH_2)_3NMe_2)]_3$ (5), could be decreased by using shorter chain lengths so that 5- and 6-membered chelate rings are formed rather than the 7-membered rings formed with **I**.[4]

While this work was in progress Hanusa and co-workers reported the structural characterization of (clox)Ca-$[N(SiMe_3)_2][THF]_3$ (clox = $OCPh_6(CH_6C_6H_4$-Cl-4) (12), which is, to our knowledge, the only other mixed alkoxide-amide complex of a group-2 metal. The Ca—$N(SiMe_3)_2$ distance of 2.353(5) Å is only marginally longer than those found

[4] The choice of chain length was in part dictated by synthetic practicalities (2-chloroethylamines do not form Grignards while 3-chloropropylamines do) but we are currently investigating alternate synthetic routes to the 1- and 2-C chain (5- and 6-membered chelate ring) ligands.

Table 5. Selected distances (Å) and angles (deg) for **1** and **3**.[a,b]

1		**3**	
Distances			
Ba(1)—O(1)	2.602(11)	Ba(1)—O(1)	2.603(14)
Ba(1)—O(1)′	2.645(12)	Ba(1)—O(1)′	2.596(14)
Ba(1)—N(1)′	2.94(2)	Ba(1)—O(2)	2.78(2)
Ba(1)—N(2)	2.630(14)	Ba(1)—N(2)	2.58(2)
Si(1)—O(1)	1.618(11)	Si(1)—O(1)	1.637(14)
Si(2)—N(2)	1.662(15)	Si(2)—N(2)	1.65(2)
Si(3)—N(2)	1.672(14)	Si(3)—N(2)	1.71(2)
Angles			
O(1)-Ba(1)-O(1)′	82.0(3)	O(1)-Ba(1)-O(1)′	84.0(6)
O(1)-Ba(1)-N(1)′	107.5(3)	O(1)-Ba(1)-O(2)	109.8(7)
O(1)-Ba(1)-N(2)	125.3(4)	O(1)-Ba(1)-N(2)	113.5(5)
N(1)′-Ba(1)-O(1)′	94.5(3)	O(2)-Ba(1)-O(1)′	121.1(7)
N(1)′-Ba(1)-N(2)	117.1(4)	O(2)-Ba(1)-N(2)	115.6(9)
N(2)-Ba(1)-O(1)′	122.4(3)	N(2)-Ba(1)-O(1)′	109.7(7)
Ba(1)-N(2)-Si(2)	120.8(7)	Ba(1)-N(2)-Si(2)	116.9(10)
Ba(1)-N(2)-Si(3)	111.8(7)	Ba(1)-N(2)-Si(3)	117.0(10)
Ba(1)-O(1)-Si(1)	133.2(6)	Ba(1)-O(1)-Si(1)	130.8(8)
Ba(1)-O(1)′-Si(1)′	128.2(5)	Ba(1)-O(1)′-Si(1)′	130.8(8)
Ba(1)-O(1)-Ba(1)′	98.0(3)	Ba(1)-O(1)-Ba(1)′	96.0(7)
Si(2)-N(2)-Si(3)	127.4(9)	Si(2)-N(2)-Si(3)	126.0(12)

[a]Estimated standard deviation in parentheses.

[b]Prime denotes symmetry (inversion) related atom.

in **1** and **3** (2.630(14) and 2.58(2) Å, respectively) after applying a correction of +0.33 Å to account for differences in metal ionic radius and coordination number.[5] Similarly the Ba(1)—O(2) (THF) distance in **3** (2.78(2) Å) falls within the range of Ca—O(THF) distances observed for (clox)Ca-$[N(SiMe_3)_2][THF]_3$ (2.398(5)–2.460(5) Å) after application of this correction factor.

Complexes **1** and **3** exhibit the same NMR spectra as one another in d_8-THF solution but these spectra differ markedly from those obtained in d_6-benzene. In d_8-THF, the *same two sets* of silylamide and siloxide resonances are observed in the ^1H, ^{13}C, and ^{29}Si NMR spectra of either **1** or **3** (Table 2), indicating that the *same species* is present in solution for both compounds. Close inspection of the ^{29}Si and ^1H NMR chemical shifts also indicated the presence of Ba[N-$(SiMe_3)_2]_2[THF]_2$ and **2** as the minor components (ca. 10%). This was confirmed by the disappearance of signals due to **2** upon addition of a fivefold excess of free Ba[N-$(SiMe_2)_2]_2[THF]_2$ (Fig. 3). Thus, in THF solution, ligand redistribution *is* occurring although the equilibrium lies well on the side of intact **3** (eq. [4]).

In d_6-benzene (or d_8-toluene) **1** and **3** exist as distinct compounds, as is clearly evident from the observation of different NMR spectra. Variable temperature NMR spectra of **3** from −80 to +80°C shows a single set of siloxide resonances that is consistent with either complete dissociation of dimeric **3** into monomers *or* rapid exchange of free and coordinated NMe_2 arms in a dimeric structure similar to that observed in the solid

[5] Based on extrapolated ionic radii of 1.27 and 0.94 Å for Ba^{2+} in 4-coordination and Ca^{2+} in 5-coordination, respectively (ref. 7).

Can. J. Chem. Downloaded from www.nrcresearchpress.com by 80.90.12.36 on 09/08/12
For personal use only.

Fig. 2. ORTEP drawing of **3**.

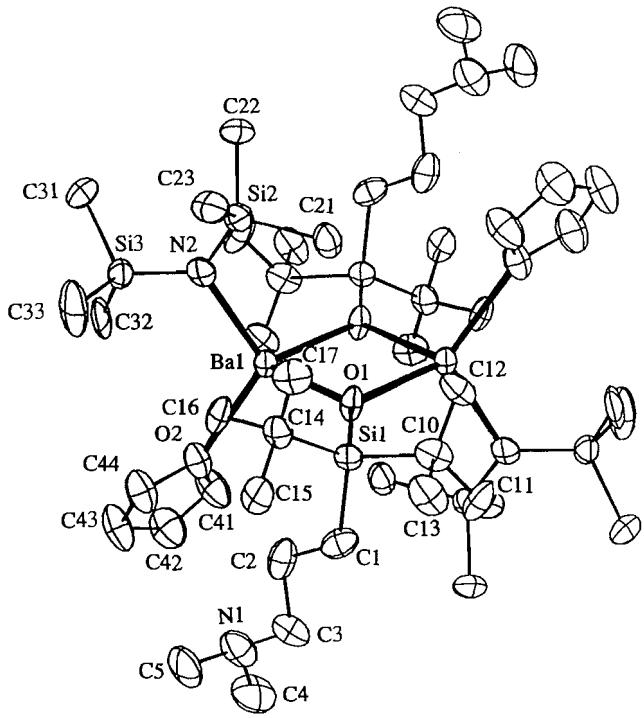

Fig. 3. $^{29}Si\{^1H\}$ NMR spectrum of (*a*) pure **3** in d_8-THF; (*b*) after addition of excess $Ba[N(SiMe_3)_2]_2[THF]_2$. Assignments: A, $Ba[OSi(^tBu)_2((CH_2)_3NMe_2)][N(SiMe_3)_2]$; B, $Ba[OSi(^tBu)_2((CH_2)_3NMe_2)]_2$; C, $Ba[N(SiMe_3)_2]_2$; D, $Ba[OSi^tBu_2(CH_2)_3NMe_2][N(SiMe_3)_2]$.

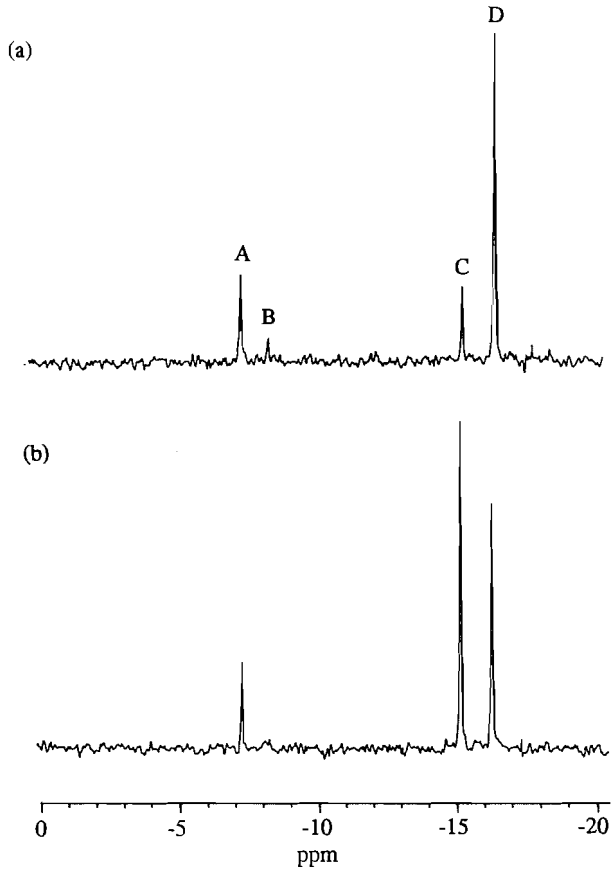

Table 6. Fractional atomic coordinates[a] and equivalent isotropic temperature[b] factors for **3** (estimated standard deviations in parentheses).

Atom	*x/a*	*y/b*	*z/c*	U_{eq}
Ba(1)	21463(6)	22756(8)	7578(5)	435(4)
Ba(1)	49546(13)	91396(5)	677(10)	530(5)
Si(1)	4636(5)	10082(4)	2327(4)	62(3)
Si(2)	1625(7)	9004(4)	-1077(6)	76(3)
Si(3)	2933(8)	7824(4)	-672(6)	80(3)
O(1)	469(1)	1005(1)	117(1)	6(1)
O(2)	686(2)	841(1)	112(1)	9(1)
N(1)	886(3)	890(1)	403(2)	12(1)
N(2)	289(2)	859(1)	-68(1)	7(1)
C(1)	620(2)	999(2)	323(2)	9(1)
C(2)	680(3)	941(2)	324(2)	10(2)
C(3)	818(3)	945(2)	400(3)	11(2)
C(4)	1015(3)	901(2)	430(4)	18(3)
C(5)	843(4)	847(2)	466(3)	16(2)
C(10)	417(3)	1087(1)	262(2)	8(1)
C(11)	382(4)	1094(2)	364(3)	15(2)
C(12)	315(3)	1112(1)	181(2)	9(1)
C(13)	534(3)	1130(1)	272(2)	11(2)
C(14)	343(3)	950(1)	259(2)	8(1)
C(15)	373(4)	941(2)	376(2)	12(2)
C(16)	370(4)	891(1)	210(2)	10(2)
C(17)	215(3)	971(2)	221(2)	9(1)
C(21)	211(3)	982(1)	-87(2)	9(1)
C(22)	83(3)	895(1)	-249(2)	10(1)
C(23)	37(3)	887(2)	-39(2)	11(2)
C(31)	176(3)	746(1)	-177(2)	10(1)
C(32)	460(3)	754(2)	-68(3)	15(2)
C(33)	260(4)	751(2)	47(3)	16(2)
C(41)	812(3)	852(2)	102(4)	15(2)
C(42)	889(3)	803(2)	146(3)	13(2)
C(43)	799(5)	764(2)	188(3)	17(3)
C(44)	681(3)	794(1)	183(2)	10(1)

[a]Coordinates × 10^n where n = 5 for Ba, 4 for Si, and 3 for O, N, and C. Temperature parameters × 10^n where n = 4 for Ba, 3 for Si, and 2 for O, N, and C.

[b]U_{eq} = the equivalent isotropic temperature parameter = $1/3\ \Sigma_i\Sigma_j U_{ij} a_i^* a_j^* (a_i \cdot a_j)$. $T = \exp(-8\pi^2 U_{iso} \sin^2\theta/\lambda^2)$.

state (Fig. 2). We favour the latter explanation because rapid exchange of free and coordinated NMe_2 groups has previously been observed in $Y[OSi(^tBu)_2((CH_2)_3NMe_2)]_3$ (5). Complex **1** also shows a single set of resonances for the siloxide ligand over the same temperature range. This observation is consistent with either a monomeric or dimeric structure but we favour the dimeric structure because the large barium ion is unlikely to prefer 3-coordination in solution when 4-coordination is easily accommodated, without any unusual distortions, in the solid state structure.

Complexes **1** and **3** do not appear to undergo ligand redistribution as readily in benzene or toluene as they do in THF. There is no evidence for the presence of **2** or $Ba[N(SiMe_3)_2]_2$ in solutions of **1** in toluene or benzene throughout the −80 to +80°C range. Trace (<5%) amounts of **2** and $Ba[N(SiMe_3)_2]_2$ are just detectable in the NMR spectra of **3**. The presence of

some ligand redistribution in the case of **3** is probably attributable to the presence of THF in this compound.

It is possible that ligand redistribution occurs more readily in d_8-THF solution because THF is required to stabilize $Ba[N(SiMe_3)_2]_2$ (i.e., to favour the right-hand side of eq. [4]). The solution behaviour of **1** is more reminiscent of $Cp^*CaI(THF)_2$ (13) than $(clox)Ca[N(SiMe_3)_2][THF]_3$ since the former undergoes ligand redistribution in THF while the latter does so in toluene. It appears from these results that the susceptibility to ligand redistribution cannot be predicted reliably from the type of ancillary ligation (e.g., Cp* versus alkoxide) but depends, as might be expected, on the subtle interplay between steric and electronic factors for *all species* involved in the redistribution process (such as those in eq. [4]).

[4] $\{Ba[OSi(^tBu)_2((CH_2)_3NMe_2)][N(SiMe_3)_2][THF]\}_2$
(3)

$$\rightleftharpoons Ba[N(SiMe_3)_2]_2[THF]_2 + Ba[OSi(^tBu)_2((CH_2)_3NMe_2)]_2$$
(2)

While complexes **1**–**3** are soluble in hydrocarbons, they are not volatile at 10^{-4} Torr (1 Torr = 133.3 Pa) and undergo decomposition during prolonged heating at 200°C. Consistent with this observation, none of these complexes gives molecular ions in the mass spectrum (EI or CI). Attempts are currently underway to modify the amino–siloxide ligand described in this work with the goal of achieving increased volatility and greater stability towards ligand redistribution for the mono(ligand) derivatives.

Acknowledgements

We thank Mrs. C. Greenwood for assistance in recording the NMR spectra and Dr. Becky Chak for help with the X-ray structural studies. This research was supported by the Natural Sciences and Engineering Research Council of Canada and a University of Victoria Internal Research Grant (to D.J.B.).

References

1. (*a*) M.K. Wu, J.R. Ashburn, C.J. Thorng, P.H. Hor, R.L. Meng, L. Gao, Z.J. Huang, Y.Q. Wang, and C.W. Chu. Phys. Rev. Lett. **58**, 908 (1987); (*b*) J.K. Burdett, and G.V. Kulkarni. ACS Adv. Chem. Ser. **226**, 323 (1990); (*c*) Z.Z. Sheng and A.M. Hermann. Nature, **27**, 138 (1988).
2. D.C. Bradley. Chem. Rev. **89**, 1317 (1989).
3. (*a*) L.G. Hubert-Pfalzgraf. New J. Chem. **11**, 663 (1987); (*b*) D.R. Ulrich. *In* Transformations of organometallics into common and exotic materials. *Edited by* R.M. Laine. Martinus Nijhoff, Dordrecht. 1988. pp. 261–278; (*c*) pp. 261-288; (*d*) S. Hirano, T. Hayashi, M. Miura, and H. Tomanaga. Bull. Chem. Soc. Jpn. **62**, 888 (1989); (*e*) S.C. Goel, K.S. Kramer, P.C. Gibbons, and W.E. Buhro. Inorg. Chem. **28**, 3619 (1989); (*f*) C. Sanchez and J. Livage. New J. Chem. **14**, 513 (1990); (*g*) N.N. Sauer, E. Garcia, K.V. Salazar, R.R. Ryan, and J.A. Martin. J. Am. Chem. Soc. **112**, 1524 (1990).
4. (*a*) K.G. Caulton, and L.G. Hubert-Pfalzgraf. Chem. Rev. **90**, 969 (1990); (*b*) D.C. Bradley, H. Chudzynska, M.E. Hammond, M.B. Hursthouse, M. Motevalli, and W. Rouwen. Polyhedron, **11**, 375 (1992); (*c*) K. Timmer, C.I.M.A. Spee, and H.A. Meinema. *In* Metal–organic chemical vapor deposition of electronic ceramics. Mater. Res. Soc. Symp. Proc. Fall 1993. Meeting. Materials Research Society, Pittsburgh, Pa. 1994.
5. P. Shao, D.J. Berg, and G.W. Bushnell. Inorg. Chem. **33**, 3452 (1994).
6. W.A. Herrmann, R. Anwander, and M. Denk. Chem. Ber. **125**, 2399 (1992).
7. R.D. Shannon. Acta Crystallogr. Sect. A: Cryst. Phys. Diffr. Theor. Gen. Crystallogr. **A32**, 751 (1976).
8. B.A. Vaarstra, J.C. Huffman, W.E. Streib, and K.G. Caulton. Inorg. Chem. **30**, 121 (1991).
9. A. Larson, F. Lee, Y. Page, M. Webster, J. Charland, and E.J. Gabe. NRC Solver: a program for crystal structure determination. National Research Council of Canada, Chemistry Division, Ottawa. 1985.
10. G.M. Sheldrick. SHELX76, Programs for crystal structure determination. Cambridge University, U.K. 1976.
11. C.K. Johnson. ORTEPII. Oak Ridge National Laboratory, Oak Ridge, Tenn. 1976.
12. K.F. Tesh, D.J. Burkey, and T.P. Hanusa. J. Am. Chem. Soc. **116**, 2409 (1994).
13. M.J. McCormick, S.C. Sockwell, C.E.H. Davies, T.P. Hanusa, and J.C. Huffman. Organometallics, **8**, 2044 (1989).

Can. J. Chem. Downloaded from www.nrcresearchpress.com by 80.90.12.36 on 09/08/12
For personal use only.

The influence of surfactants on the electrocatalytic hydrogenation of organic compounds in micellar, emulsified, and hydroorganic solutions at Raney nickel electrodes[1]

Philippe Chambrion, Laurence Roger, Jean Lessard, Valérie Béraud, Josée Mailhot, and Marc Thomalla

Abstract: The electrocatalytic hydrogenation (ECH) of limonene (**1**) and carvone (**4**) at a Raney nickel cathode was studied both in hydroorganic medium (methanol–water) and aqueous micellar and emulsified solutions. In methanol–water, the ECH of **1** stopped at *p*-menthene (**2**) and proceeded with low current efficiencies (18–24%). In micellar solutions containing a cationic surfactant (CTAB), the ECH of **1** was more efficient, giving *p*-menthane (**3**) as the main product with current efficiencies up to 30%. The pH of the solution (hydroorganic and micellar) had little influence. With anionic (SDS) and nonionic (Brij 35) surfactants, some *p*-menthane (**3**) was formed but the conversion rate and current efficiency were much lower. The ECH of carvone (**4**) was slightly less efficient in methanol–water than in micellar and emulsified solutions. The saturated alcohols neocarvomenthol (**8**), carvomenthol (**9**), isocarvomenthol (**10**), and neoisocarvomenthol (**11**) were the main products with current efficiencies of 75% (hydroorganic medium) to 90% (micellar solutions). The effect of surfactant concentration and pH on the efficiency and stereochemistry of the ECH of carvone (**4**) was also studied.

Key words: electrocatalytic hydrogenation, limonene, carvone, Raney nickel, micellar medium.

Résumé : L'hydrogénation électrocatalytique (HEC) du limonène (**1**) et de la carvone (**4**) sur cathodes de nickel de Raney a été étudiée et en milieu hydroorganique (méthanol–eau) et en milieu aqueux micellaire et émulsionné. Dans le méthanol–eau, l'HEC de **1** s'arrête au *p*-menthène (**2**) avec de faibles efficacités de courant (18–24%). En milieu micellaire avec un surfactant cationique (CTAB), l'HEC de **1** est plus efficace : formation de *p*-menthane (**3**) comme produit principal avec des efficacités de courant de 30%. Le pH de la solution (hydroorganique et micellaire) a peu d'influence. La formation de *p*-menthane (**3**) est observée aussi avec des surfactants anioniques (SDS) et non-ioniques (Brij 35) mais avec des rendements, taux de conversion et efficacités de courant beaucoup plus faibles. L'HEC de la carvone (**4**) est un peu moins efficace en milieu méthanol–eau qu'en milieu micellaire et émulsionné. Les alcools saturés, néocarvomenthol (**8**), carvomenthol (**9**), isocarvomenthol (**10**) et neoisocarvomenthol (**11**) sont obtenus très majoritairement avec des efficacités de courant allant de 75% (milieu hydroorganique) à 90% (milieu micellaire). On a aussi étudié l'influence de la concentration du surfactant et du pH sur l'efficacité et la stéréochimie de l'HEC de la carvone (**4**).

Mots clés : hydrogénation électrocatalytique, limonène, carvone, nickel de Raney, milieu micellaire.

Introduction

The electrocatalytic hydrogenation (ECH) of unsaturated organic substrates in hydroorganic solutions at a Raney nickel cathode has significant advantages over the chemical catalytic hydrogenation (2): (*i*) the chemisorbed hydrogen is generated in situ at low overpotential (reaction [1]) and its concentration may be controlled by monitoring the current density; (*ii*) the kinetic barrier related to the low hydrogen solubility and its dissociative adsorption is bypassed (3); and, as a consequence, (*iii*) the hydrogenation can be carried out at relatively low pressures and temperatures with few or no side reactions. However, the competing hydrogen evolution reaction (HER) (reactions [2]) can drastically lower the current efficiency of ECH and in the worst cases can even prevent the hydrogenation of the organic compound (reactions [3] – [5]). On highly porous

Received January 2, 1995.

P. Chambrion, L. Roger, and J. Lessard.[2] Laboratoire d'électrochimie, Université de Sherbrooke, Sherbrooke, QC J1K 2R1, Canada
V. Béraud, J. Mailhot, and M. Thomalla.[2] Laboratoire d'électrochimie organique, Unité de recherche associée du Centre national de la recherche scientifique n° 467, Université Claude Bernard – Lyon I, 43, Boulevard du 11 novembre 1918, 69622 Villeurbanne Cédex, France.

[1] Part IX in the series "Electrocatalytic hydrogenation of organic compounds." For part VIII, see ref. 1.
[2] Authors to whom correspondence may be addressed. For J. Lessard, telephone: (819) 821-7088. Fax: (819) 821-8107.

Can. J. Chem. Downloaded from www.nrcresearchpress.com by 65.111.164.53 on 09/08/12
For personal use only.

Can. J. Chem. Downloaded from www.nrcresearchpress.com by 65.111.164.53 on 09/08/12
For personal use only.

Raney nickel electrodes and in basic medium (1 M KOH), the HER was shown to occur through a Vomer (eq. [1]) – Herovsky (eq. [2]) mechanism both in aqueous (4) and in aqueous–methanolic (5) solutions. Furthermore, in the presence of an ECH reaction, the Heyrovsky reaction is the rate-limiting step of the HER, which implies that the surface coverage by adsorbed hydrogen increases with the potential (6). The relative rates of hydrogenation (reactions [3]–[5]) and hydrogen evolution (reactions [2]) depend on several parameters among which, for a given electrode, the strength of the bond to be hydrogenated and the local concentration of the organic substrate adsorbed on the catalyst are particularly important (2).

[1] $H_3O^+ (H_2O) + e^- \rightarrow H_{ads} + H_2O(OH^-)$ (Volmer step)

[2] $2H_{ads} \rightarrow H_2$ (Tafel step)

or

$H_{ads} + H_3O^+ (H_2O) + e^- \rightarrow H_2 + H_2O(OH^-)$
(Heyrovsky step)

[3] $Y = Z \rightarrow Y = Z_{ads}$

[4] $Y = Z_{ads} + 2H_{ads} \rightarrow \rightarrow YH - ZH_{ads}$

[5] $YH - ZH_{ads} \rightarrow YH - ZH$

Electrochemical reactions can take place in aqueous electrolytes in the presence of surfactants in either heterogeneous (emulsions) or homogeneous (micelles, microemulsions) solutions (7). Micelle formation and especially surfactant adsorption strongly influence the electrochemical processes by changing formal potentials, local reactant concentrations, and (or) activation parameters (7–9) as in the well-known micellar catalysis and inhibition phenomena (10, 11). The substrate–micelle association can lead to chemo- and regioselectivity in thermal and photochemical reactions (10–13). Chemical heterogeneous catalytic hydrogenation of unsaturated organic substrates has been performed in direct and reversed micellar and microemulsified systems with modification of both the activity of the catalyst and the selectivity of the reaction (14–16). Surfactants can also enhance the rate of homogeneous hydrogenation (17) and they have recently been used in asymmetric hydrogenation reactions (18).

For these reasons, we have studied the influence of cationic (cetyltrimethylammonium salts), anionic (sodium dodecylsulfate), and nonionic (Brij 35) surfactants on the ECH of limonene (**1**), *p*-menthene (**2**), and carvone (**4**) (Fig. 1) in emulsified and micellar solutions and compared the results obtained in these systems with those observed in hydroorganic solutions with limonene (**1**) and carvone (**4**). The chemo-, regio-, and stereoselectivity of ECH was also investigated.

Experimental

Reagents

Commercially available compounds were used as received: D-limonene (98%) from Eastman Kodak, (+)-*p*-menthene (99%) from Fluka, (–)-carvone (98%) and cetyltrimethylammonium bromide (CTAB) (99%) from Jansen Chemica, polyoxyethylene-23-dodecanol (Brij 35) (purum) from Aldrich, sodium dodecylsulfate (SDS) and 25% aqueous solution of cetyltrimethylammonium chloride (purum) from Fluka. Methanol, ethanol, and water were distilled before use.

Fig. 1. Structure of substrates and reactions products.

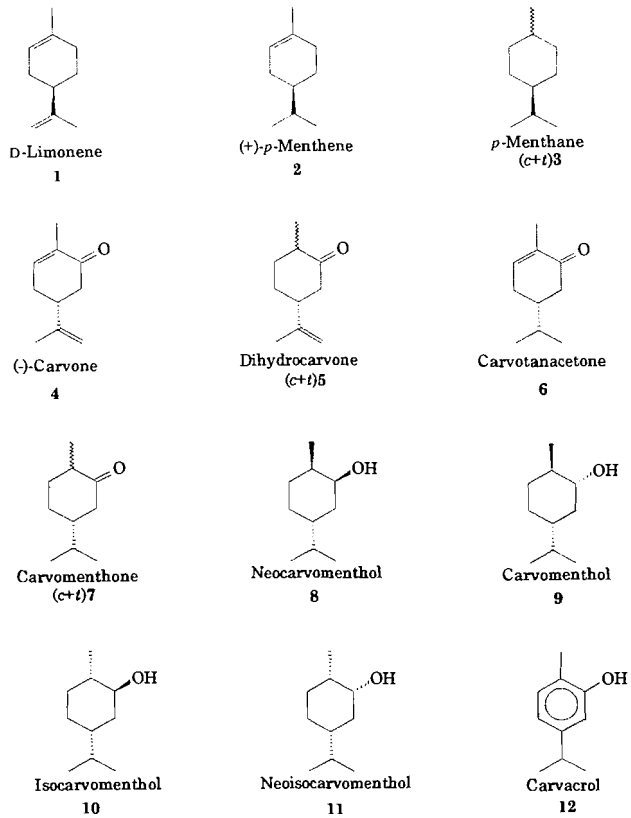

Electrolyses

The electrochemical apparatus, the cell, the preparation of Raney Ni electrodes, and the electrolysis procedure were previously described (2). Some experiments, especially the ECH of carvone, were performed on a Tacussel PRT-100 potentiostat with a Tacussel IG5-LN integrator in the auxiliary circuit. As previously indicated (2), the percentage of alloy deposited on the cathode was calculated by the relation 100 $m_1/(m_1 + m_2)$ where m_1 and m_2 are, respectively, the mass in grams of alloy and electroplated Ni. This percentage varied between 50 and 65% and the corresponding amount of Raney Ni catalyst (after leaching of the 50/50 Ni–Al alloy) on the 4 × 3 cm^2 cathode varied between 0.6 and 0.9 g. The electrolysis conditions are indicated in the tables (footnotes *a*). In galvanostatic experiments, the cathodic potential changed with the pH (unbuffered conditions). Otherwise it was constant and varied between –0.6 (acidic solutions) and –1.1 V (basic solutions) vs. SCE. These potential values were those used in potentiostatic electrolyses in acidic and basic solutions, respectively. All the electrolyses were carried out at 30°C (temperature higher than that of the Kraft point for the different surfactants).

The catholyte composition is indicated in the tables (footnotes). The aqueous buffers used are described in the Handbook of Chemistry and Physics (19). The pH was measured either with a glass electrode or with Merck non-bleeding pH

Table 1. ECH of limonene (**1**) and *p*-methanene (**2**) at Raney Ni cathodes[a]

Entry	Substrate	Solution[b]	pH[c]	Recovered substrate (%)	Yield		Current efficiency (%)	Material balance (%)
					2	**3**		
1	Limonene	Hydroorganic	4–3.6	28	62	<1	18	90
2	Limonene	Hydroorganic (+H_3BO_3)	5–4	5	88	<4	24	97
3	Limonene	Hydroorganic	13–14	27	66	—	19	93
4	*p*-Menthene	Hydroorganic	3–2	92	—	—	0	92
5	Limonene	Emulsified	2	89	—	—	0	89
6	Limonene	Micellar	2–2.3	3	9	57	30	69
7	Limonene	Micellar	3–11	10	29	33	29	72
8	Limonene	Micellar	11.8–12	4	44	25	27	73
9	*p*-Menthene	Micellar	2.2–2	39	—	61	18	100

[a]Constant current electrolyses (J = 3.3 mA cm^{-2}) at 30°C on 10 mmol of **1** (76 mM solution) and on 3.9 mmol of **2** (30 mM solution), Q = 7 F mol^{-1} (except in entries 6 (8 F mol^{-1}) and 7 (6.5 F mol^{-1}).

[b]Hydroorganic: 0.2 M NaCl, ethanol–water (85:15 v/v) (entry 2: +H_3BO_3 0.2 M); micellar: 5.5 × 10^{-2} M CTAB, 0.2 M NaCl, water; emulsified: 3.6 mmol of **1** (36 mM) in aqueous buffer without surfactant.

[c]Unbuffered solutions (except in entry 5). The first and second figures correspond to the pH at the beginning and at the end of electrolysis, respectively. The initial pH was adjusted with dilute HCl or NaOH solutions (except in entry 7).

[d]Determined by vpc and based on the initial amount of substrate.

indicator strips (see ref. 20 on pH measurements in micellar systems). To favor the proton transfer from the anodic to the cathodic compartment through the cation exchange Nafion-324 (E.I. du Pont de Nemours & Co) membrane, the anolyte consisted of a solution (in the same solvent as the one used for the catholyte) of a mineral acid (H_2SO_4) or HCl) at higher concentrations than those in the catholyte, without any other additive (supporting electrolyte, surfactant, etc.). The concentration of the acid in the anolyte (from 0.1 M to 4 M) was a function of the medium (homogeneous or micellar solutions). The buffering effect of such a device was only partial, as shown by the pH variation during the electrolyses in unbuffered solutions (especially in the presence of surfactants).

Products

For the ECH of limonene (**1**) and *p*-menthene (**2**) in homogeneous solutions, the work-up procedure was the same as that reported in ref. 2. With micellar solutions, the surfactant was removed by filtration on Merck 60 silica gel, then the usual work-up procedure was followed, or the cathodic solution was saturated with NaCl and then continuously extracted by ether. The products were identified by comparison (IR, ^{1}H NMR, mass spectra) with authentic samples (*p*-menthene, see above, *cis* and *trans* paramenthane from Wiley Organics (98% and 99%)). The yields were determined by vapor phase chromatography (vpc) as described in ref. 2, using nonane (99%) (Aldrich) or 2-decyne (Fluka) as internal standard.

In the experiments with carvone (**4**) in hydroorganic solutions, before the usual work-up, methanol was removed from the cathodic solution by distillation at atmospheric pressure. For micellar solutions, the surfactant was removed by filtration on silica gel or continuous with ether (see above). The crude product was separated by flash chromatography on silica gel (0.03–0.075 mm) and preparative vpc, and the products were identified by comparison of their spectral characteristics (IR, ^{1}H and ^{13}C NMR, mass spectra) with those of commercially available authentic samples (dihydrocarvone (**5**) (98%) from Jansen Chemica, carvacrol (**12**) (98%) from Aldrich Chemicals) or with literature data (21–27). Yields were determined by vpc on semi-capillary (15 m, 1 μm) or capillary (30 m, 0.25 μm) polar DBwax columns (J and W) (Varian 3300 chromatograph equipped with thermal conductivity or flame ionization detectors) using pentadecane (99+%, Aldrich) as internal standard. Product distribution (yields and mass balance) during the electrolyses on limonene and carvone was determined by vpc with aliquots (0.5 or 1 mL) extracted with ether after addition of a saturated NaCl solution (1 or 2 mL).

Results and discussion

ECH of limonene (1) and *p*-menthene (2)

In ethanol–water, the ECH of limonene (**1**) stopped at *p*-menthene (**2**) (Table 1, entries 1 and 3), even in the presence of boric acid (entry 2), which is known to increase the ECH efficiency (2). Current efficiencies were low (18–24%), which indicates that competing hydrogen evolution (reaction [2]) was important. In the same conditions, ECH of *p*-menthene (**2**) did not occur (entry 4). The pH of the solution has no influence: the conversion rate, chemical yield, and current efficiency at the end of the electrolysis (entries 1 and 3) and the relative percentages of **1** and **2** during the electrolysis (Fig. 2, curves 1 and 2) were similar in acidic and basic media. However, the variation of these relative percentages with the quantity of electricity depends on the amount of Raney Ni on the cathode: with 60% of Raney Ni alloy on the precursory electrode (see Experimental), the ECH was more efficient (Fig. 2, curves 3 and 4) than with 50% of alloy (curves 1 and 2).

In cationic micelles, namely cetyltrimethylammonium bromide (CTAB, 5.5 × 10^{-2} M), ECH was more efficient than in hydroorganic solutions. Indeed, the ECH of limonene (**1**) gave a mixture of *p*-menthene (**2**) and *p*-menthane (**3**) and the current efficiencies were higher in the micellar solutions (compare entries 6–8 (micellar solution) with entries 1–3 (hydroorganic solution) of Table 1 and curves 3–6 (micellar solution) with curves 1 and 2 (hydroorganic solution) of Fig.

Can. J. Chem. Downloaded from www.nrcresearchpress.com by 65.111.164.53 on 09/08/12
For personal use only.

Can. J. Chem. Downloaded from www.nrcresearchpress.com by 65.111.164.53 on 09/08/12
For personal use only.

Fig. 2. Variation of the relative percentage of limonene (**1**) and *p*-menthene (**2**) with the charge of the ECH of **1** in hydroorganic solution. Electrolysis conditions: $J = 3.3$ mA cm^{-2}, 30°C, 10 mmol of **1** (76 mM solution), EtOH–H_2O 85:15 (v/v), NaCl 0.2 M. Curves 1 and 2: 50% Raney Ni alloy, ○ pH 4–3.6 and ● pH 13–14. Curves 3 and 4: 60% Raney Ni alloy, pH 10.

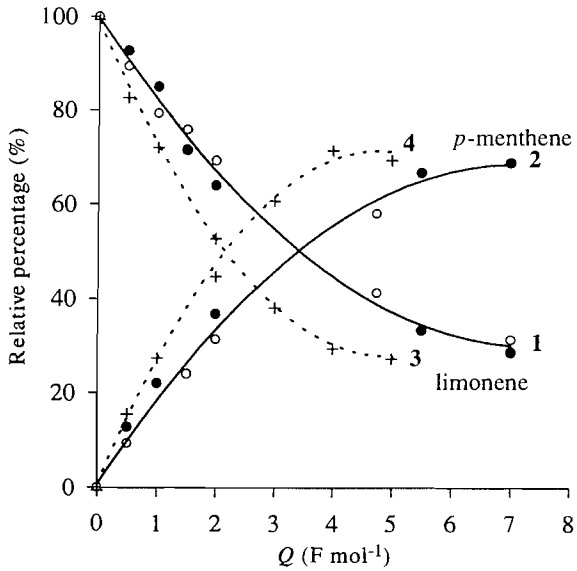

Fig. 3. Variation of the relative percentage of limonene (**1**) and *p*-menthene (**2**) + *p*-menthane (**3**) with the charge during the ECH of **1** in hydroorganic and micellar solutions. Electrolysis conditions: $J = 3.3$ mA cm^{-2}, 30°C, 76 mM solution of **1**. Curves 1 (**1**) and 2 (**2**): hydroorganic solution (EtOH–H_2O 85:15 (v/v), NaCl 0.2 M). Curves 3–6: cationic micellar solution (CTAB 5.5 × 10^{-2} M, NaCl 0.2 M); curves 3 (**1**) and 4 (**2** + **3**): pH 2; curves 5 (**1**) and 6 (**2** + **3**): pH 12.

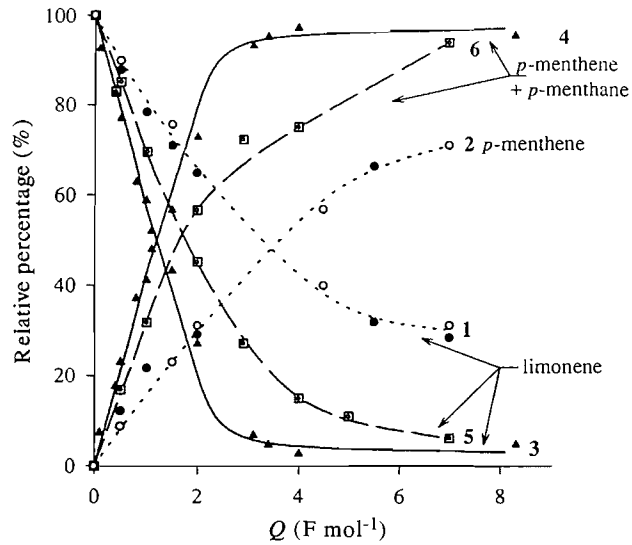

3). The ECH of **1** was more efficient in acidic medium with a 57% yield of **3** and a current efficiency of 30% (entry 6) than in basic medium (25% yield of **3**, 27% current efficiency (entry 8)). In acidic medium, **3** was converted quantitatively to **3** with an 18% current efficiency (entry 9). The percentage of precursory alloy on the precursory electrode was higher in entry 6 (55%) than in entry 8 (51%), so this contributes slightly, as well, to the higher yield of **3** in entry 6.

The higher efficiency of ECH in cationic micelles can result from an increase in the rate of reaction [4] or from a decrease in the rate of reaction [2] or both. Maoka and Enyo (28, 29) previously found that the adsorption of thiourea retarded the Tafel step (reaction [2]) of the HER on a palladium electrode. Moreover, they found that the adsorption of tetrabutylammonium hydroxide accelerated the Tafel step but slowed down the Volmer step (reaction [1]) (28, 29). If CTAB has a similar influence on the HER at Raney nickel electrodes, the amount of chemisorbed hydrogen would be less in micellar solution and both the HER and ECH should be disfavoured. Recently Vittori and co-workers (30) studied the influence of different surfactants (CTAB, SDS, Brij) on the HER on Ni cathodes. Even at the higher concentrations used (1.4–8 mM), the adsorption of surfactants had only a slight effect on the HER (the formal rate constant for the overall process was decreased by a factor of 3 in the presence of surfactant, and variations of the transfer coefficient were small (except with SDS)) (30). Considering the above results from the literature, a decrease in the rate of reaction [2] should play a minor role on the influence of surfactants on ECH. So the increase in the efficiency of ECH in micellar solutions would be due to an increase in the rate of hydrogenation (reaction [4]).

Rate enhancement of bimolecular processes in micellar solutions is mainly a consequence of high reactant concentrations in the micellar volume (pseudophase); solvent effects and changes in activation parameters are often less important (10–13, 31), The same is true for catalytic hydrogenation in direct and reversed micellar and microemulsified systems: the main effects result from an increase in local reactant concentrations on the catalyst (15, 16). Then, in ECH, a similar trend[3] would lead to higher concentrations of adsorbed organic substrate (eq. [3]) in micellar solutions and to an increase of the rate of hydrogenation (reaction [4]).

In an aqueous emulsion, in the absence of surfactant, the ECH of limonene (**1**) did not occur (Table 1, entry 5). That means there was no (or very little) substrate adsorption on the catalyst. The different mechanisms of charge and *mass transfer* for the electrochemical conversion of an organic depolarizer emulsified in an aqueous electrolyte have been described by Wendt and co-workers in several basic papers (32–36). They have shown that wetting of the electrode by the dispersed organic phase (direct contact between organic droplets and the electrode) is not operative, especially when the density of the organic phase is lower than that of the aqueous phase (this is the case for organic liquids like limonene and *p*-menthene). Under such conditions, diffusion of the organic substrate to the electrode (and its subsequent adsorption) is limited by its solubility in the aqueous electrolyte. Owing to the low solubility of limonene (**1**) in water, the amount adsorbed on the cathode was too small to allow its hydrogenation in aqueous emulsions.

In emulsions containing surfactant and in micellar solutions, the efficiency of the ECH of limonene (**1**) (i.e., competition between reactions [2] and [4]) was strongly dependent

[3] In the ECH of carvone (**4**), solvent effects, if they occur at all (see below), are not important.

Can. J. Chem. Downloaded from www.nrcresearchpress.com by 65.111.164.53 on 09/08/12
For personal use only.

Fig. 4. Variation of the current efficiency (curve 3) and of the relative percentage of limonene (**1**) (curve 1) and *p*-menthene (**2**) + *p*-menthane (**3**) (curve 2) with the concentration of surfactant (logarithmic scale) during the ECH of **1**. Electrolysis conditions: $J = 3.3$ mA cm^{-2} (–0.9 to –1 V vs. SCE), 30°C, pH 10 (buffer), NaCl 0.1 M, 18 mM (emulsions) or 35 mM (homogeneous micelles) solutions of **1**, $Q = 5$ F mol^{-1}.

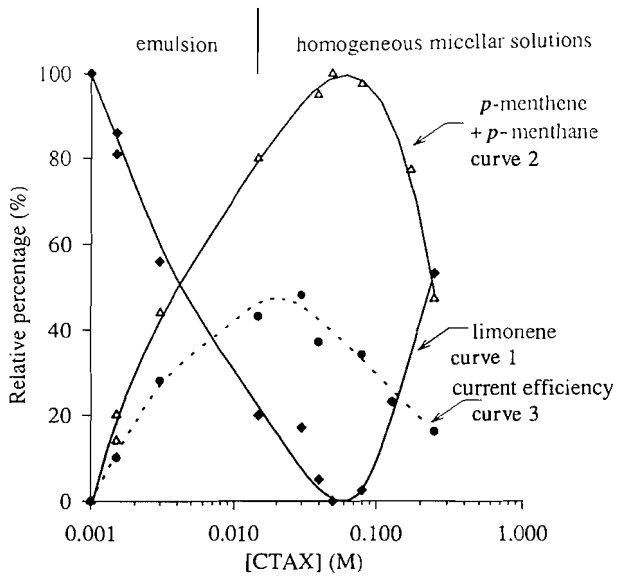

on the cationic surfactant concentration. The conversion of **1**, the amount of *p*-menthene (**2**) and *p*-menthane (**3**) formed, and the current efficiency first increased with the cetyltrimethylammonium salt concentration, then reached a maximum for surfactant concentrations between 2.5×10^{-2} and 5.5×10^{-2} M, and finally decreased (Fig. 4). In these experiments, the surfactant concentration was always higher than the critical micellar concentration (CMS $\sim 9 \times 10^{-4}$ M).

The presence of a surfactant can enhance the substrate adsorption in two ways: (*i*) by increasing the substrate solubility in the whole bulk; (*ii*) by the formation, on the cathode, of a hydrophobic adsorbed surfactant layer in which the substrate can be incorporated (Figs. 5*a* and 5*b*). In the first way, the solubility of the organic substrate increases with the number (and the size) of micelles, i.e., with the surfactant concentration. At lower concentrations of surfactant, limonene (**1**) remained partially emulsified. At concentrations of CTAX (X = Br or Cl) higher than 2.5×10^{-2} M, **1** was entirely soluble in the micelles and maximum efficiency for the ECH was then obtained. For still higher surfactant concentrations, dilution of **1** in the micellar pseudophase (the whole micelles in the electrolyte bulk) lowered its adsorption on the cathode and therefore did lower the efficiency of hydrogenation (Fig. 4). It must be noticed that the higher efficiency of ECH in micelles compared to hydroorganic solutions does not result from a solubility effect because the amounts of limonene in micellar solutions were lower than those in EtOH–H_2O (see caption of Fig. 4 and footnote *a* of Table 1). The second way to enhance substrate adsorption has been shown to be operative in heterogeneous catalytic hydrogenation of unsaturated fatty acids (16). Surfactant adsorption (especially of the cationic ones) can be important even for low concentrations (below CMC). For instance, ac impedance measurements of double layer capacity of a Ni electrode indicate that there is adsorption of Brij 35 and CTAB at concentrations of 10^{-5} and 10^{-4} M, respectively (30). The importance of the hydrophobic adsorbed CTAX layer on the ECH of limonene (**1**) is shown by the extent of hydrogenation, which is the molar fraction of *p*-menthane (**3**) in the hydrogenated products (mol of **3**/(mol of **2** + mol of **3**). This ratio was the highest (0.8) for the lowest CTAX concentration and decreased as the surfactant concentration increased (Fig. 6). This can be interpreted as a competition between the hydrogenation of **1** to **2** and the hydrogenation of **2** to **3**. As in catalytic hydrogenation over different catalysts (37, 38*a*, 39), the hydrogenation by ECH of the trisubstituted endocylic carbon–carbon double bond (in **1** and in **2**) is more difficult than that of the exocyclic disubstituted one (in **1**). However, the relative rates of ECH of **1** and **2** depend also on the relative amounts of **1** and **2** adsorbed on the catalyst. The CTAX concentration influences the relative amounts of adsorbed **1** and **2** in two ways: in controlling the thickness of adsorbed surfactant layer and in controlling the solubility of the compounds in the bulk solution. Both the thickness of the surfactant layer and the solubility of **1** and **2** increase as the CTAX concentration increases. At the beginning of the electrolysis, the concentration of limonene (**1**) in the bulk solution is high (for an emulsion, this corresponds to saturation). As a result, an increase of surfactant concentration leads to an increase of limonene adsorption but to a decrease of *p*-menthene (**2**) adsorption because the low concentration of **2** in the bulk solution favours its desorption. Moreover, the partition coefficient P between octanol and water is smaller for **2** than for limonene (**1**) (log P(octanol / H_2O) = 4.4 and 4.7, respectively (40)). Thus, for low CTAX concentrations, *p*-menthene (**2**) would desorb slowly and remain on the surface long enough to be hydrogenated to *p*-menthane (**3**) (mol of **3**/(mol of **2** + mol of **3**) closer to 1). As the surfactant concentration and thus the solubility of **2** increases, less remains adsorbed on the electrode long enough to be hydrogenated and the ratio (mol of **3**/(mol of **2** + mol of **3**)) decreases. This is clearly seen from the product distribution in the ECH of **1** at the "optimum" CTAB concentration (Fig. 7): very little *p*-menthane (**3**) was formed at the beginning of the electrolysis; the hydrogenation of **2** became important only after about 70% of **1** had been hydrogenated, which corresponds to a **2**/**1** ratio close to **2** (after a charge corresponding to 2 F mol^{-1}).

Changing the counterion of the cetyltrimethylammonium salt (from Br^- to Cl^-) had little influence on the conversion rate and current efficiency of the ECH of limonene (**1**) and had no influence on the molar fraction of *p*-menthane (**3**) (Table 2). On the other hand, the *nature of the surfactant* did strongly influence the hydrogenation. Changing the surfactant (2% by weight, 10^{-2}–10^{-1} M) from CTAB to SDS or Brij 35 lead to a significant decrease of substrate conversion, lower current efficiencies, and low yields of **3**: compare entries 3 and 4 of Table 3 (respectively, 57 and 67% of recovered **1**, 14 and 11% current efficiency, 8 and 6% yield of **3**) with entry 1 (3% of recovered **1**, 30% current efficiency, 57% yield of **3**). Even at a low cationic surfactant concentration (entry 2, Table 3) that gave a poor conversion rate (19%) and a poor current efficiency (13%), **3** did represent 80% of the hydrogenated products, i.e., a much higher proportion than the 18–19% obtained in the presence of SDS or Brij 35. This is in agreement with numerous literature results (41): cationic surfactants have a

Fig. 5. Solubilization equilibria and substrate diffusion to the electrode in (*a*) emulsified and (*b*) micellar solutions. S: substrate; : surfactant; X^-: counterion. See ref. 36 for emulsions (*a*).

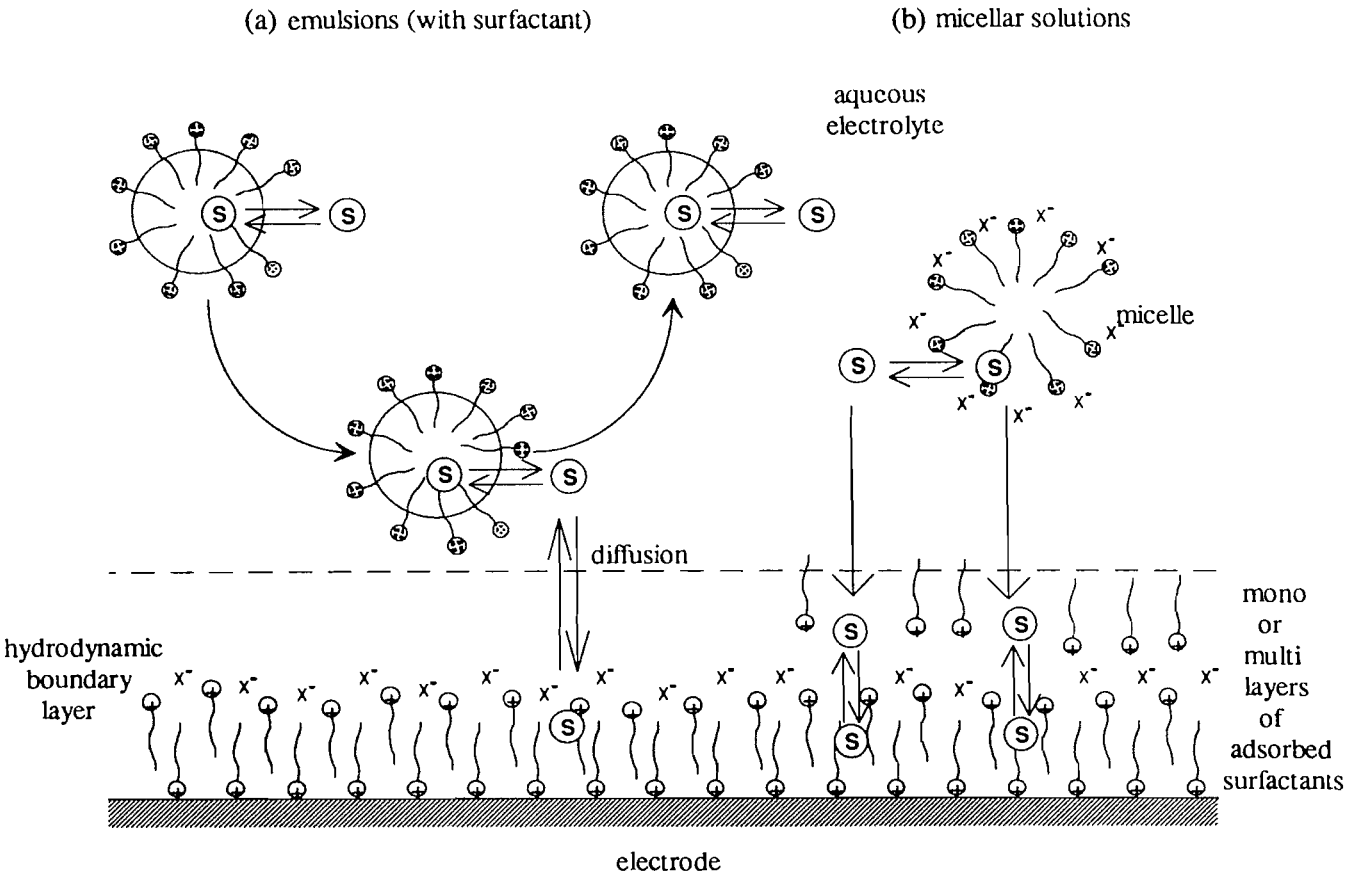

Fig. 6. Molar fraction of *p*-menthane (**3**) (mol of **3**/mol of **2** + mol of **3**) as a function of the concentration of CTAX (logarithmic scale) in the ECH of limonene (**1**). Electrolysis conditions: same as in Fig. 5 (see caption): o, [**1**] = 18 mM (emulsions); ●, [**1**] = 35 mM (homogeneous micelles).

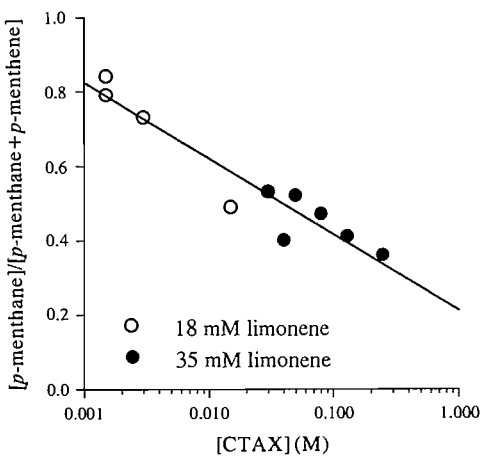

stronger influence than anionic and nonionic surfactants.

Concerning the *stereochemistry* of the ECH of limonene (**1**) (and *p*-menthene (**2**)), the *trans* isomer of *p*-menthane (**3**) was predominant in cationic micellar solutions, the *cis/trans* ratio varying between 0.59 and 0.85 (see Table 3 and Fig. 8). There

Fig. 7. Variation of the relative percentage of limonene (**1**) (●), *p*-menthene (**2**) (▲), and *p*-menthane (**3**) (□) with the charge during the ECH of **1**. Electrolysis conditions: $J = 3.3$ mA cm^{-2}, 30°C, pH 1.7–2.3, CTAB 5.5×10^{-2} M, NaCl 0.2 M, [**1**] = 76 mM.

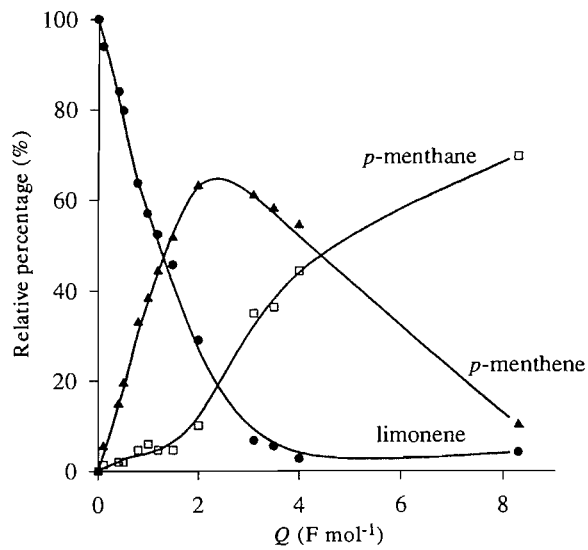

was a small concentration effect in the case of CTAX, as shown in Fig. 8. The *cis/trans* ratio reached a maximum value (0.85) for a CTAX concentration corresponding to the highest

Can. J. Chem. Downloaded from www.nrcresearchpress.com by 65.111.164.53 on 09/08/12
For personal use only.

Can. J. Chem. Downloaded from www.nrcresearchpress.com by 65.111.164.53 on 09/08/12
For personal use only.

Table 2. ECH of limonene (**1**) in CTAB and CTAC micellar solutions.[a]

Entry	Surfactant[b]	[1][c] / [CTAX]	Recovered **1** (%)	Molar fraction of **3**	Current efficiency (%)
1	CTAB	0.65	0	0.52	32
2	CTAB	1.3	6	0.53	32
3	CTAC	0.63	17	0.53	48
4	CTAC	1.18	20	0.49	43

[a] J = 3.3 mA cm^{-2} (E_c = −0.9 to −1 V vs. SCE), 30°C, 5 F mol^{-1}, pH 10.
[b] Cetyltrimethylammonium bromide (CTAB) or chloride (CTAC) 0.015–0.055 M.
[c] [Limonene] = 0.018–0.036 M.

Table 3. Influence of the nature of the surfactant on the ECH of limonene (**1**) in micellar solutions.[a]

Entry	Surfactant[b]	pH[c]	Recovered (**1**) (%)	Yield of products (%)[d] **2**	Yield of products (%)[d] **3** (*c*/*t*)	Current efficiency (%)
1	CTAB	2–2.3	3	9	57 (0.85)	30
2	CTAC[e]	10[f]	81	4	16 (0.61)	13
3	SDS	2.8–2.2	57	34	8	14
4	Brij 35	2.4–2.7	67	27	6	11

[a] Electrolysis conditions: see footnote *a* of Table 1: Q = 7 F mol^{-1} (entry 2: Q = 5 F mol^{-1}).
[b] 2% by weight: 5 × 10^{-2} M CTAB; 7 × 10^{-2} M SDS; 10^{-2} M Brij 35. CTA = $C_{16}H_{33}N(CH_3)_3$, X^- = Br^-, Cl^-, SDS = $C_{12}H_{25}OSO_3^-$ Na^+; Brij 35 = $C_{12}H_{25}(OCH_2CH_2)_{23}OH$.
[c] See footnote *c* of Table 1.
[d] See footnote *d* of Table 1.
[e] [CTAC] = 1.5 × 10^{-3} M.
[f] Buffered solutions.

ECH efficiency (compare Figs. 8 and 4).

ECH of (–)-carvone (4)

In methanol–water solutions, the ECH of carvone (**4**) gave *cis* and *trans* dihydrocarvone (**5**), carvomenthone (**7**),[4] and the four diastereoisomeric saturated alcohols **8**–**11** (Fig. 1). Carvotanacetone (**6**) was detected (≤1%) under basic conditions (pH 12) only. Small amounts (2–6%) of carvacrol (**12**) were also observed (Table 4). This aromatic product results from hydrogenation–dehydrogenation and (or) isomerization reactions. No unsaturated alcohol (carveol or dihydrocarveol) was detected by vpc during the electrolyses using authentic samples. Thus the electrohydrogenation of the conjugated carbon–carbon double bond was faster than that of the carbonyl groups, as in the catalytic hydrogenation of carvone (**4**) over Raney nickel (42), and in accordance with the fact that the energy barrier for the hydrogenation of a carbon–carbon double bond on nickel (14.2 kJ mol^{-1}) is lower than the barrier for the hydrogenation of a carbonyl group (44.7 kJ mol^{-1}) (42).

The following points can be drawn from the study of the product distribution during the progress of the electrohydrogenation of carvone (**4**) *in methanol–water* at pH 2 and 12 (Fig. 9). *Firstly*, the fact that the saturated alcohols **8** and **9** were formed at the beginning of the electrolysis (after a charge corresponding to 1 F mol^{-1}, see Figs. 9*a* and 9*b*) shows that the complete electrohydrogenation of **4** is easier than that of limonene (**1**), as a consequence of the presence of the polar carbonyl group. This cannot be due to a classical electroreduction (electronation–protonation (EP)) process since the controlled-potential electrohydrogenations of Table 4 were carried out at a much less negative potential (–0.6 to –1 V vs. SCE) than that required to electronate an α,β-unsaturated car-

Fig. 8. Variation of the *c*-**3**/*t*-**3** ratio with the surfactant concentration (logarithmic scale) for the ECH of limonene (**1**). Electrolysis conditions: same as in Fig. 5 (see caption). Concentration of **1**: ○, 18 mM; ●, 35 mM; △, 76 mM.

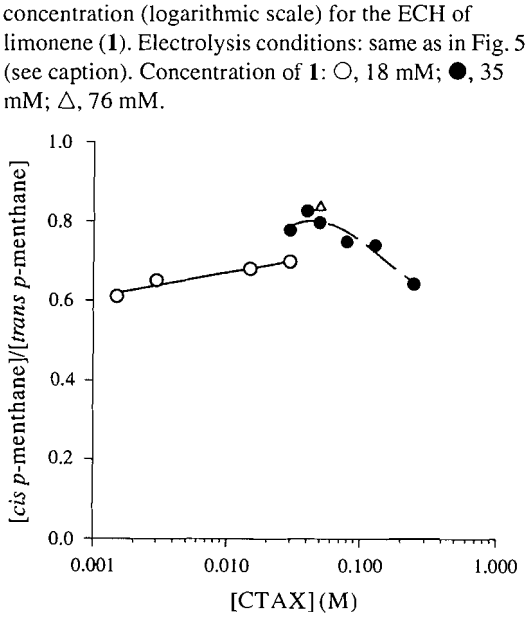

[4] The *cis* and *trans* isomers of **7** were not separated by vpc.

Table 4. ECH of (–)-carvone (**4**) at a Raney Ni cathode in different media.[a]

Entry	Solution[b]	pH[c]	Q (F mol^{-1})	Recovered **4** (%)	Yields of products (%)[d] Ketones **5**, **6**, **7**[e]	Alcohols **8**–**11**[e]	Carvacrol **12**	Current efficiency (%)	Material balance (%)
1	Hydroorganic	2	6	4	16	44	—	57	75
2	Hydroorganic	9–7	4.6	2	21	42	4	74	69
3	Hydroorganic	5–7	4.9	0	26	45	6	76	86
4	Hydroorganic	5–7	5.4	1	24	59	2	75	86
5	Hydroorganic	12	3.9	11	33	26	—	67	75
6	Emulsified	2	6	8	25	61	1,2	77	95
7	Emulsified + CTAB	2	6	0	4	84	5	86	93
8	Micellar	2	6	3	25	62	1	78	95
9	Micellar	5–9	4.6	5	15	66	5	93	91
10	Micellar	5–9	4.4	19	5	67	1	99	92

[a]Constant potential electrolyese (–0.65 ± 0.5 V vs. SCE in entries 1, 6, 7, and 8; –1 ± 0.05 V in entries 2–5, 8–10) at 30°C.
[b]Hydroorganic: MeOH–H_2O (50:50 v/v) + NaCl 0.1 M + **4** 31.9 mM; emulsified: carvone 15.9 mM in aqueous buffer without (entry 6) or with CTAB 8.2×10^{-5} (entry 7); micellar: CTAB 5.5×10^{-2} M, aqueous buffer (entry 8) or water + 0.1 M NaCl (entries 9, 10).
[c]Buffered solutions except in entries 2, 3, 4, 9, and 10 where pH values at the beginning and at the end of the electrolysis are given.
[d]Determined by vpc and based on the initial amount of **4**.
[e]See Fig. 1 for the structures.

bonyl group (e.g., –1.5 V vs. SCE in neutral and alkaline solution) (43). Moreover, the electroreduction (EP) of **4** is known to give coupling products (44) and none were detected in the electrolyses of Table 4. *Secondly*, the fact that (*i*) up to a 70% conversion of **4**, dihydrocarvone (**5**), and carvomenthone (**7**) still represented more than 50% of the hydrogenated products, (*ii*) that the amount of **5** remained higher than that of **7**, and (*iii*) that no carvotanacetone (**6**) was formed indicates that the electrohydrogenation did proceed according to the sequence of Scheme 1. This is in agreement with the results of catalytic hydrogenation in which a carbon–carbon double bond conjugated to a carbonyl is hydrogenated in preference to an isolated double bond (38). *Thirdly*, the pH of the medium had little influence on the conversion rate, the product yields and distribution, and the current efficiency (see Fig. 9 and Table 4, entries 1–5). The small variations observed could be attributed to differences in the percentage of Raney nickel on the electrode (e.g., 54 and 46% of Raney alloy in the precursory electrode in entry 1 (pH 2) and entry 5 (pH 12), respectively) as in the case of limonene (**1**). The absence of carvotanacetone (**6**) is surprising considering the fact that the catalytic hydrogenation of (+)-carvone over Raney Ni under neutral and acidic conditions was reported to give a mixture of ketones where **6** is always the major product (42). Yet **6** was not detected in alkaline solutions (42). This suggests that in the electrohydrogenations, even at pH 2, the pH at the electrode surface might be alkaline as a consequence of continuous production of hydroxide ions (or consumption of protons) (reactions [1]).

Concerning the *stereochemistry* of the electrohydrogenation of **4** *in methanol–water*, the pH had some effect on the relative proportion of isomers with the methyl and isopropyl (or isopropylidene) groups *trans* and isomers with these two substituents *cis*. Indeed, the *trans*-dihydrocarvone (*t*-**5**)/*cis*-dihydrocarvone (*c*-**5**) ratio was 2.2 at pH 2 and 4.4 at pH 12 and the ratio of alcohols **8** + **9** (resulting from the electrohydrogenation of *t*-**5**) over alcohols **10** + 11 (coming from the electrohy-

Fig. 9. Relative percentage of carvone (**4**) and the hydrogenation products during its ECH in hydroorganic solution. Electrolysis conditions: [**4**] = 31.9 mM, CH_3OH–H_2O 50:50 (v/v), NaCl 0.1 M, 30°C. (*a*) pH 2, E = –0.65 ±0.05 V vs. SCE; (*b*) pH 12, E = –1.0 ±0.05 V. ●, **4**; ○, dihydrocarvone (**5**); ■, carvomenthone (**7**); □, saturated alcohols (**8** + **9** + **10** + **11**); ▼, carvotanacetone (**6**).

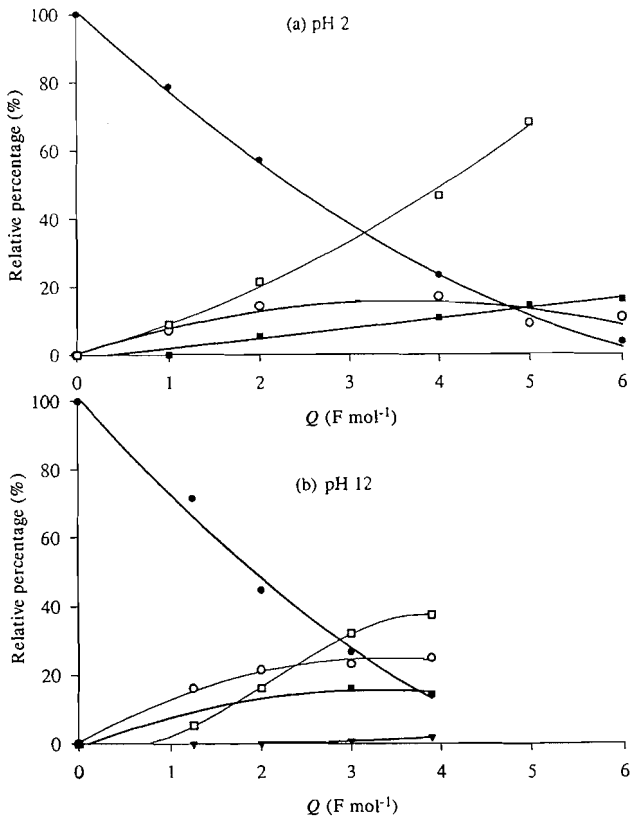

Can. J. Chem. Downloaded from www.nrcresearchpress.com by 65.111.164.53 on 09/08/12
For personal use only.

Table 5. Distribution of the saturated alcohols obtained by ECH of carvone (**4**) in the different conditions studied.[a]

Entry[b]	Solution[c]	pH[d]	Q (F mol^{-1})	Relative percentage of alcohols				
				8	**9 (8/9)**	**10**	**11 (10/11)**	**8 + 9/10 + 11**
1	Hydroorganic	2	6	42	20 (2.1)	10	28 (0.36)	1.6
2	Hydroorganic	9–7	4.6	47	10 (4.7)	17	26 (0.65)	1.3
3	Hydroorganic	5–7	4.9	44	15 (2.9)	14	27 (0.52)	1.4
4	Hydroorganic	5–7	5.4	49	11 (4.5)	14	26 (0.54)	1.5
5	Hydroorganic	12	3.9	60	8 (7.5)	12	20 (0.60)	2.1
6	Emulsified	2	6	36	16	15	33	1.1
7	Emulsified + CTAB	2	6	40	18	17	25	1.4
8	Micellar	2	6	40	12	22	26	1.1
9	Micellar	5–9	4.6	59	23	9	9	4.6
10	Micellar	5–9	4.4	54	20	8	18	2.8

[a,c,d]See, respectively, footnotes *a*, *b*, and *c* of Table 4.
[b]Same experiments as in Table 4.

Scheme 1.

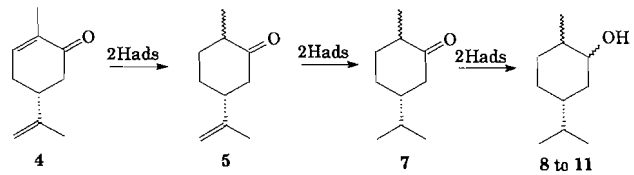

drogenation of *c*-**5**) was 1.6 at pH 2 (Table 5, entry 1) and 2.1 at pH 12 (Table 5, entry 5). Both the *t*-**5**/*c*-**5** and the **8** + **9/10** + **11** ratios were constant during the electrolysis. The *trans*/*cis* ratio is thus larger than 1, as in catalytic hydrogenation of **4** over Raney nickel in EtOH–H_2O (94/6) at 20°C and atmospheric pressure, e.g., *t*-**5**/*c*-**5** = 3.5 at pH 4.5, 2.2 at pH 7, 2.5 at pH 11 (42). As previously indicated by Godunova et al. (42), the adsorption of the conjugated double bond of carvone (**4**) on the catalyst would be less hindered for the formation of *trans* **5**. So the *trans* isomer is kinetically favored. It is also the more stable isomer with the two alkyl substituents in the equatorial orientation. The stereochemistry of the reduction of the carbonyl group of *trans* and *cis* dihydrocarvones (*t*-**5** and *c*-**5**) and carvomenthones (*t*-**7** and *c*-**7**) is given by the ratios of alcohol **8**/alcohol **9** and alcohol **10**/alcohol **11**, respectively. These ratios (and the relative proportions of alcohols **8**, **9**, **10**, and **11**) were constant throughout the electrolyses. As shown in Table 5, entries 1–5, the relative proportions of alcohols **10** and **11** did not change significantly with the pH whereas the percentage of the major isomer, alcohol **8**, increased and that of alcohol **9** decreased as the pH was increased. The relative proportions of the four alcohols **8**–**11** at pH **12**, respectively 60, 8, 12, and 20% (entry 5), are close to those obtained in catalytic hydrogenation over Raney nickel at pH 11, respectively 64, 12, 8, and 16% (42). As discussed before by Godunova et al. (42), alcohol **8** predominates over alcohol **9** because the approach of *trans* carvomenthone (*t*-**7**) to the catalyst leading to the formation of neocarvomenthol (**8**) is less hindered than the approach giving the isomeric carvomenthol (**9**). For similar reasons, the hydrogenation of *cis* carvomenthone (*c*-**7**) gives predominantly neoisocarvomenthol (**11**) (42). One explanation for an increase of the **8/9** ratio from 2.1 at pH 2 to 7.5 at pH 12 could be the slow hydrogenation of the enolate at pH 12.[5] Epimerization of alcohol **9** to alcohol **8** (through dehydrogenation–hydrogenation) is very unlikely since **8** with the hydroxy group axial should be less stable than **9** with the hydroxy group equatorial (38*c*).

In aqueous emulsions without any surfactant, the ECH of (–)-carvone (**4**) proceeded with a current efficiency (77%), conversion rate (92%), and yield of ketones (25%) and alcohols (61%) (Table 4, entry 6) similar to those observed in hydroorganic solutions (Table 4, entries 1–5). Under these conditions, limonene (**1**) was not electrohydrogenated (see above) and the greater facility of electrohydrogenation of **4** can be attributed to its higher solubility in water.

In emulsified or micellar solutions containing a cationic surfactant (CTAB), the electrohydrogenation of carvone (**4**) was more efficient than in hydroorganic or emulsified solutions with higher current efficiencies (78–99%) and a greater extent of hydrogenation (61–84% of alcohols) (Table 4, entries 7–10). The effect of surfactant is less pronounced than with limonene (**1**) as a consequence of the more facile hydrogenation of **4**. Moreover, with **4**, the maximum effect was observed at a much lower surfactant concentration (8.2×10^{-5} M, see Table 6, entry 6, and Fig. 10) than with **1** ($\sim 10^{-3}$ M, see Fig. 6). The molar fraction of alcohols (**8** + **9** + **10** + **11**)/(all hydrogenated products)) is a measure of the extent of hydrogenation of **4**. It is clear from Fig. 10 and Table 6 that the largest extent of hydrogenation was obtained with a CTAB concentration (8×10^{-5} M) lower than the CMC ($\sim 9 \times 10^{-4}$ M). *Therefore there were no micelles in the solution and the effect of surfactant on the reaction can only result from the formation of an hydrophobic layer on the cathode* (Fig. 5*a*). The association between the hydrophobic layer of adsorbed CTAB and the organic compounds enhances their adsorption and subsequently favours their hydrogenation. The importance of a hydrophobic layer on the efficiency of ECH reactions has been recently shown by Pintauro and Boutha (45): the ECH of aromatic compounds was achieved using *very high* concentrations (up to 2.5 M) of hydrotopic tetraethylammonium salts that cannot give micelles but only adsorption on the electrode. The variations of the ECH efficiency of **4** with

[5] As suggested by a referee.

Can. J. Chem. Downloaded from www.nrcresearchpress.com by 65.111.164.53 on 09/08/12
For personal use only.

Table 6. ECH[a] of carvone (**4**) over a Ni Raney cathode in emulsified and micellar solution: influence of CTAB concentration.[a]

Entry	[CTAB] (M)	Recovered **4** (%)	Yields of products (%)[b] Ketones **5** + **6**	Carvomenthone **7**	Alcohols **8** + **9** + **10** + **11**	Carvacrol **12**	Current efficiency (%)	Material balance[b] (%)
1	0.274	14	9	33	22	3	50	89
2	0.164	9	5	41	33	—	64	95
3	0.054	—	—	32	54	—	78	91
4	0.013	—	—	22	64	—	78	89
5	0.0027[c]	11	1	5	66	3	70	87
6	8.2×10^{-5}[c]	—	—	4	84	5	87	93
7	2.7×10^{-5}[c]	—	—	12	72	1	80	85
8	0[c]	8	3	22	61	1	77	95

[a]Constant potential electrolyses (−0.6 to −0.7 V vs. ECS), pH 2, 30°C, Q = 6 F mol^{-1}, [carvone] = 15.9 mM.
[b]Determined by vpc an based on the initial amount of **4**. See Fig. 1 for the structures.
[c]Emulsion.

Fig. 10. Molar fraction of saturated alcohols **8**–**11** (alcohols **8** + **11**/totality of hydrogenated products) in the ECH of carvone (**4**) at different surfactant (CTAB) concentrations. Electrolysis conditions: E = −0.65 ±0.05 V vs. SCE, Q = 6 F mol^{-1}, pH 2, 30°C, 0.1 M NaCl, 15.9 mM solution of **4** (□, hydroorganic solution: CH_3OH–H_2O (50:50 v/v), 31.9 mM solution of **4**).

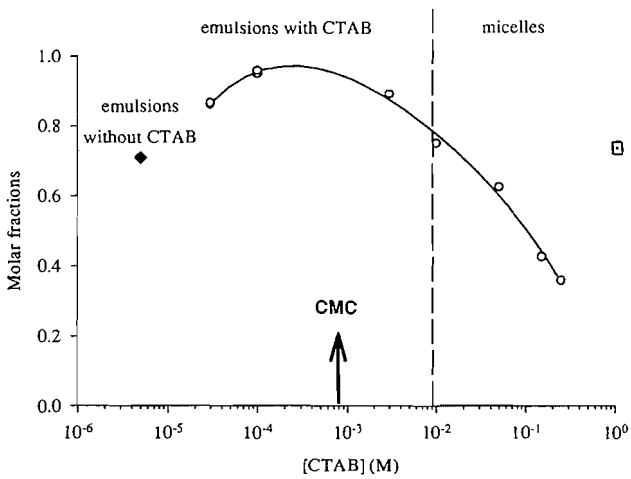

the CTAB concentration (Fig. 10) can thus be interpreted as follows. At concentrations of CTAB lower than 8×10^{-5} M, the hydrophobic layer is thinner than at the 8×10^{-5} M concentration and therefore the adsorption of **4** was less important and the ECH less efficient (Fig. 10 and Table 6, entries 6 and 7). At concentrations of CTAB higher than the CMC and as the concentration of surfactant increases, the adsorption of **4** on the catalyst was less important than at the CMC and gradually decreased because of the dilution of **4** in the micellar pseudophase (as in the case of limonene (**1**)). This resulted in a lowering of the efficiency (extent of hydrogenation) of the ECH of **4** as measured by the molar fraction of the alcohols **8**–**11** (see Fig. 10 and entries 5 to 1 of Table 6) because of a decrease in the rate of hydrogenation (eqs. [3]–[5]) competing with hydrogen evolution (eq. [2]). At the highest CTAB concentration (0.274 M, entry 1), the extent of hydrogenation was much lower than that in hydroorganic solutions as shown in Fig. 10 (point ⊡ corresponds to the molar fraction in hydroorganic solutions).

The *regiochemistry* of the ECH of carvone (**4**) in micellar solutions[6] differs from that in hydroorganic solutions. As already pointed out, in hydroorganic solutions, carvotanacetone (**6**) was barely detected so the electrohydrogenation proceeded as in Scheme 1: hydrogenation of the conjugated double bond (**4** → dihydrocarvone (**5**)) followed by hydrogenation of the isopropylidene group (**5** → carvomenthone (**7**)), then hydrogenation of the carbonyl group. In micellar solutions, carvotanacetone (**6**) was formed and could be the major unsaturated ketone at the beginning of the electrolysis (see Fig. 11). Thus, the CTAB hydrophobic layer on the electrode must orient the adsorption of carvone (**4**) through the isopropylidene chain so it can be hydrogenated before or at the same time as the conjugated double bond. On the other hand, the adsorption of CTAB has little or no influence on the *stereochemistry* of the ECH of **4**.[7] Indeed, the relative proportions of alcohols **9**–**11** were nearly the same for a similar pH of the solution, in the absence (hydroorganic solution, emulsion) and in the presence of CTAB (emulsified and micellar solution) as can be seen from Table 5.

Contrary to what was observed with limonene (**1**), the association of carvone (**4**) with the hydrophobic layer does not depend on the surfactant. Indeed, as shown in Table 7, the efficiency of the ECH of **4** (yield of alcohols, current efficiency) was the same in emulsions containing a surfactant at concentrations below the CMC whether the surfactant was cationic (CTAB, entry 1), anionic (SDS, entry 2) or nonionic (Brij 35, entry 3). Moreover, the isomeric distribution of alcohols was the same with the three surfactants.

Conclusion

In emulsified and micellar solutions, the presence of hydrophobic layer formed by surfactant adsorption on the cathode surface increases the efficiency and the extent of ECH of unsaturated

[6] It was not possible to take representative samples during the electrolysis of emulsions and therefore to follow the sequence of formation of the products as the electrolysis proceeded.
[7] The relative proportions of the *cis* (*c*-**7**) and *trans* (*t*-**7**) carvomenthones are not taken into account because of the *cis* ↔ *trans* isomerization.

Can. J. Chem. Downloaded from www.nrcresearchpress.com by 65.111.164.53 on 09/08/12
For personal use only.

Table 7. ECH of carvone (**4**) at a Raney Ni cathode in emulsions: influence o the nature of the surfactant.

Entry	Surfactant	Concentration (M)	Recovered **4** (%)	Yield of products (%)[b]					Distribution of alcohols (%)				Current efficiency (%)	Material balance (%)
				5	**6**	**7**	**8** + **9** + **10** + **11**	**12**	**8**	**9**	**10**	**11**		
1	CTAB	8.2×10^{-5}	0	0	0	4	84	5	40	19	16	25	87	93
2	SDS	11×10^{-5}	0	0	0	4	85	6	41	19	15	25	87	94
3	Brij 35	3×10^{-5}	0	0	0	8	79	~0.5	39	18	15	28	84	89

[a]Constant potential electrolyses (−0.6 to −0.65 V vs. SCE), pH 2, 30°C, Q = 6 F mol^{-1}, [carvone] = 15.9 mM.
[b]By vpc and based on the initial amount of **4**. See Fig. 1 for the structures.

Fig. 11. Variation of the relative percentage of ketones **5**–**7** with the charge during the ECH of carvone (**4**) in micellar (CTAB) solution: ●, dihydrocarvone (**5**), ■, carvotanacetone (**6**), ○, carvomenthone (**7**). Electrolysis conditions: E = −0.65 ±0.05 vs. SCE, pH 2, 30°C, 0.1 M NaCl, Q = 6 F mol^{-1}, 15.9 mM solution of **4**.

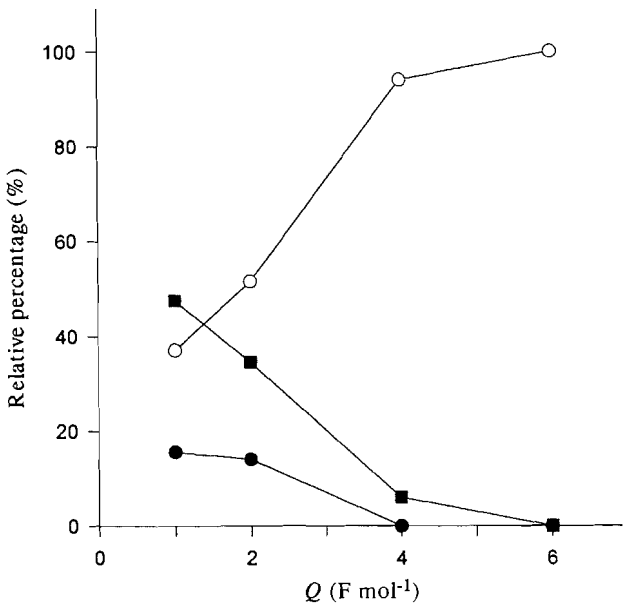

organic compounds. This results from an increase of the local substrate concentration on the catalyst. For each substrate, the maximum effects are obtained at a given surfactant concentration range. With carvone (**4**), quasi-quantitative formation of alcohols was obtained for surfactant concentrations below the CMC whatever the nature of surfactant. On the contrary, with limonene (**1**), the best results were obtained with a cationic surfactant (CTAB) and at concentrations 20 to 50 times the CMC. Nevertheless, even using the best conditions, the hydrogenation of **1** was not complete and mixtures of *p*-menthene (**2**) and *p*-menthane (**3**) were obtained. In methanol–water, the ECH of limonene (**1**) was less efficient than in micellar medium and stopped at *p*-menthene (**2**) with low current efficiencies whatever the pH of the solution, whereas the ECH of carvone (**4**) was slightly less efficient than in micellar and emulsified solutions. Both the ease of hydrogenation of the conjugated double bond of **4** and its higher solubility in water (and in methanol–water) can account for the different behaviour of **4** and **1**. With **1**, micelles are needed to increase its solubility and allow adsorption on the electrode surface. In the case of carvone (**4**), the regiochemistry of ECH, hence the orientation of the adsorption on the electrode surface, was influenced by the presence of a hydrophobic layer of CTAB. With the two substrates and for the three surfactants studied, the surfactant had no noticeable influence on the stereochemistry of ECH.

Acknowledgements

We gratefully acknowledge the financial support from the Ministère des Relations Internationales du Québec and the Ministère des Affaires Étrangères de France (coopération franco–québécoise), the Fonds pour la Formation des Chercheurs et l'Aide à la Recherche (FCAR) du Québec, the Natural Sciences and Engineering Research Council of Canada, the Centre National de la Recherche Scientifique (CNRS) de France and the Ministère de l'Enseignement Supérieur et de la Recherche de France.

References

1. B. Mahdavi, P. Chambrion, J. Binette, E. Martel, and J. Lessard. Can. J. Chem. **73**, 846 (1995).
2. D. Robin, M. Comtois, A. Martel, L. Lemieux, A. Kam Cheong, G. Belot, and J. Lessard. Can. J. Chem. **68**, 1218 (1990), and refs. cited.
3. M. Enyo. *In* Comprehensive treatise of electrochemistry. Vol. 7. *Edited by* B.E. Conway, J. O'M. Bockris, E. Yeager, S.U.M. Khan, and R.E. White. Plenum Press, New York. 1983. pp. 241–298.
4. A. Lasia. *In* Current topics in electrochemistry. Vol. 2. Research Trends, Trivandrum, India. 1993. pp. 240–252. and refs. cited.
5. A. Kam Cheong, A. Lasia, and J. Lessard. J. Electrochem. Soc. **140**, 2721 (1993).
6. A. Kam Cheong, A. Lasia, and J. Lessard. J. Electrochem. Soc. **141**, 975 (1994).
7. M. Thomalla. *In* Electrochemistry in colloids and dispersions. *Edited by* R.A. Mackay and J. Texter. VCH, New York. 1992. pp. 273–280, and refs. cited.
8. G.L. McIntire. Am. Lab. (Fairfield, Conn.), **18**, 173 (1986); An. Chem. **21**, 257 (1990), and refs. cited.
9. T.C. Franklin and S. Mathew. *In* Surfactants in solution. Vol. 10. *Edited by* K.L. Mittal. Plenum Press, New York. 1989. pp. 267–286, and refs. cited.
10. J.H. Fendler. Membrane mimetic chemistry. John Wiley and Sons, New York. 1982. pp. 293–491, and refs. cited.
11. C.A. Bunton and G. Savelli. Adv. Phys. Org. Chem. **22**, 213 (1986), and refs. cited.
12. J.K. Sutter and C.N. Sukenic. J. Org. Chem. **49**, 1295 (1984).

Can. J. Chem. Downloaded from www.nrcresearchpress.com by 65.111.164.53 on 09/08/12
For personal use only.

13. N.J. Turro, G.S. Cox, and M.A. Paczkowski. Top. Curr. Chem. **129**, 57 (1985), and refs. cited.
14. M. Boutonnet, J. Kizling, R. Touronde, G. Maire, and P. Stenius. Appl. Catal. **20**, 163 (1986).
15. J.B. Nagy, I. Bodart-Ravet, and E.G. Derouane. Faraday Discuss. Chem. Soc. **87**, 189 (1989).
16. N. Toshima and T. Kakahashi. Chem. Lett. 573 (1988).
17. R.G. Nuzzo, S.L. Haynie, M.E. Wilson, and G.M. Whitesides. J. Org. Chem. **46**, 2861 (1981).
18. G. Oehme, E. Paetzold, and R. Selke. J. Mol. Catal. **71**, L1 (1992).
19. R.C. Weast (*Editor*). Handbook of chemistry and physics. 64th ed. CRC Press, Boca Raton, Fla. 1984. D-150.
20. A. Berthod and C. Saliba. Analusis, **13**, 437 (1985).
21. Y.R. Naves. Helv. Chim. Acta, **47**, 1617 (1964).
22. W. Hückel and P. Heinzelmann. Justus Liebigs Ann. Chem. **687**, 82 (1965).
23. S.H. Shroeter and E.L. Eliel. J. Org. Chem. **30**, 1 (1965).
24. J. Firl, G. Kresze, T. Bosch, and V. Arndt. Justus Liebigs Ann. Chem. **1978**, 87 (1978).
25. D. Dauzonne, N. Goasdone, and N. Platzer. Org. Magn. Reson. **17**, 18 (1981).
26. H. Hamada. Bull. Chem. Soc. Jpn. **61**, 869 (1988).
27. M. Decouzon. J.F. Gal. S. Geribaldi, M. Rouillard, and J.M. Sturka. Org. Mass Spectrom. **25**, 312 (1990).
28. T. Maoka and M. Enyo. Surface Technol. **9**, 147 (1979).
29. T. Maoka and M. Enyo. Electrochim. Acta, **26**, 607 (1981); **26**, 615 (1981).
30. R. Menini, P.K. Wrona, H. Ménard, and O. Vittori. Can. J. Chem. **70**, 2948 (1992).
31. D. Lardet and M. Thomalla. Bull. Soc. Chim. Fr. 524 (1988).
32. R. Dworak and H. Wendt. Ber. Bunsen-ges. Phys. Chem. **81**, 728 (1977).
33. R. Dworak, H. Feess, and H. Wendt. AICE Symp. Ser. **185**, 38 (1979).
34. H. Feess and H. Wendt. J. Chem. Technol. Biotechnol. **30**, 297 (1980).
35. H. Feess and H. Wendt. Ber. Bunsen-ges. Phys. Chem. **85**, 914 (1981).
36. H. Feess and H. Wendt. *In* Techniques of electroorganic synthesis. Part III. *Edited by* N.L. Weinberg and B. Tilak. John Wiley and Sons, New York. 1982. pp. 81–177.
37. A.F. Thomas and Y. Bessière. Nat. Prod. Rep. **6**, 291 (1989), and refs cited.
38. R.L. Augustine. Catalytic hydrogenation. Marcel Dekker Inc., New York. 1965. (*a*) p. 58; (*b*) p. 61; (*c*) p. 86.
39. F. Zymalkowski. Katalytische Hydrierungen in Organisch Chemischen Laboratorium. Ferdinand Enke Verlag, Stuttgart. 1965. p. 76.
40. A. Leo, C. Hansch, and D. Elkins. Chem. Rev. **71**, 525 (1971).
41. C. Mousty and G. Mousset. *In* Electrochemistry in colloids and dispersions. *Edited by* R.A. Mackay and J. Texter. VCH, New York. 1992. p. 291; J.F. Rusling, N. Hu, H. Zhang, D.H. Howe, C.L. Miaw, and E.C. Couture. *In* Electrochemistry in colloids and dispersions. *Edited by* R.A. Mackay and J. Texter. VCH, New York. 1992. p. 303. T.C. Franklin, J. Darlington, R. Nnodimele, and R.C. Duty. *In* Electrochemistry in colloids and dispersions. *Edited by* R.A. Mackay and J. Texter. VCH, New York. 1992. p. 319.
42. L.F. Godunova, E.I. Klabunovskii, A.A. Balandin, E.A. Oger, and I.A. Rubtsov. Izv. Akad. Nauk SSSR, Ser. Khim. **7**, 1593 (1968).
43. M.M. Baizer, *In* Organic electrochemistry. *Edited by* H. Lund and M.M. Baizer. Marcel Dekker Inc., New York. 1991. p. 451.
44. J. Grimshaw and J. Trocha-Grimshaw. J. Chem. Soc. Perkin Trans. 1, 2584 (1973).
45. P.N. Pintauro and J.R. Boutha. J. Appl. Electrochem. **21**, 799 (1991).

Can. J. Chem. Downloaded from www.nrcresearchpress.com by 65.111.164.53 on 09/08/12
For personal use only.

Experimental and theoretical assessments of the substituent and medium dependence of the internal rotational potentials in benzyl fluoride. 3,5-Difluorobenzyl fluoride and 4-fluorobenzyl fluoride

Ted Schaefer, Robert W. Schurko, Rudy Sebastian, and Frank E. Hruska

Can. J. Chem. Downloaded from www.nrcresearchpress.com by 80.90.12.36 on 09/08/12
For personal use only.

Abstract: The ^1H, ^{19}F, and ^{13}C {H} nuclear magnetic resonance spectra at 300 K of 4-fluoro- and 3,5-difluorobenzyl fluoride, dissolved in CS_2–C_6D_{12} and acetone-d_6, are fully analyzed. Spin–spin coupling constants over four, five, and six formal bonds are used to derive expectation values of $\sin^2\theta$ and $\sin^2\phi$ and the apparent twofold internal rotational potentials; $\phi(\theta)$ is the angle by which the α C—F (C—H) bond twists out of the ring plane. The conformation of lowest energy has $\phi = 0°$ for the 3,5-difluoro compound in the polar and nonpolar solutions, whereas it has $\phi = 90°$ for the 4-fluoro derivative. The magnitudes of the potentials lie between 2 and 4 kJ/mol, that is, comparable to thermal energies. These data are compared with previous results for the parent compound and its 3,5-dichloro derivative. Geometry-optimized molecular orbital computations, including some correlation-gradient procedures, for benzyl fluoride and the two fluoro derivatives have $\phi = 90°$ for the conformations of highest energy of the free molecules. However, geometry-optimized SCFRF calculations of the solvent perturbations of the potential (dipole terms are insufficient) are in semiquantitative agreement with experiment in the sense that both solvents are predicted to destabilize the conformation with $\phi = 0°$. For example, the predominant twofold component in the computed (6-31G*) potential is 3.4 (free), −0.7 (CS_2), and −3.3 (acetone-d_6) kJ/mol for benzyl fluoride, a negative number indicating $\phi = 90°$ for the stable conformer; the experimental values are −0.8(2) (CS_2) and −2.7(2) (acetone-d_6) kJ/mol. The agreement between experiment and theory is of a similar quality for the fluoro derivatives. The stabilization of the conformer with $\phi = 90°$ for the 4-fluoro derivative is tentatively attributed to hyperconjugative electron acceptance by the α C—F bond, enhanced by the π-electron donor at the *para* position. A number of coupling constants are discussed in terms of the possible mechanisms of their transmission. Future experiments are indicated.

Key words: ^1H, ^{19}F, ^{13}C NMR of 4-fluorobenzyl fluoride and 3,5-difluorobenzyl fluoride; MO calculations and internal rotational potentials in benzyl fluoride, 3,5-difluorobenzyl fluoride, and 4-fluorobenzyl fluoride; solvent effects and experimental and theoretical approaches to internal rotational potentials in 3,5-difluorobenzyl fluoride and 4-fluorobenzyl fluoride.

Résumé : On a déterminé les spectres résonance magnétique nucléaire du ^1H, du ^{19}F et du $^{13}C\{H\}$ des fluorures des 4-fluoro- et 3,5-difluorobenzyles, à 300 K, en solution dans l'acétone-d_6 et dans le mélange CS_2–C_6D_{12} et on a analysé les spectres obtenus. On a utilisé les constantes de couplage spin–spin à travers quatre, cinq et six liaisons formelles pour calculer les valeurs attendues de $\sin^2\theta$ et $\sin^2\phi$ ainsi que les potentiels binaires apparents à la rotation interne; $\phi(\theta)$ est l'angle de déplacement de la liaison C—F (C—H) α par rapport au plan du noyau. Pour la conformation de plus base énergie du composé 3,5-difluoré en solutions dans des solvants polaires et non polaires $\phi = 0°$ alors que, pour le dérivé 4-fluoré, cette valeur est égale à 90°. Les amplitudes des potentiels se situent entre 2 et 4 kJ/mol; cette valeur est comparable à celle des énergies thermiques. On a comparé ces données avec les résultats rapportés antérieurement pour le composé fondamental et son dérivé 3,5-dichloré. Des calculs d'orbitales moléculaires avec optimisation de la géométrie, comprenant quelques méthodes de gradient de corrélation, ont été effectués sur le fluorure de benzyle et ses deux dérivés fluorés; elles conduisent

Received February 22, 1995.

T. Schaefer,[1] R.W. Schurko, R. Sebastian, and F.E. Hruska. Department of Chemistry, University of Manitoba, Winnipeg, MB R3T 2N2, Canada.

[1] Author to whom correspondence may be addressed. Telephone: (204) 474-9335. Fax: (204) 275-0905.

à des valeurs de $\phi = 90°$ pour les conformations de plus haute énergie des molécules libres. Toutefois, des calculs SCFRF optimisés pour la géométrie des perturbations du potentiel par les solvants (les moments dipolaires sont insuffisants) sont en accord semiquantitatif avec les valeurs expérimentales, c'est-à-dire que les calculs permettent de prédire que les deux solvants déstabilisent la conformation pour laquelle $\phi = 0°$. Par exemple, pour le fluorure de benzyle, la composante binaire prédominante du potentiel calculé (6-31G*) est de 3,4 (libre), −0,7 (CS_2) et −3,3 (acétone-d_6) kJ/mol alors qu'une valeur négative indique que $\phi = 90°$ pour le conformère stable; les valeurs expérimentales sont de −0,8(2) (CS_2) et −2,7(2) (acétone-d_6) kJ/mol. L'accord entre les valeurs expérimentales et calculées est d'une qualité semblable pour les dérivés fluorés. Pour le dérivé 4-fluoré, on attribue la stabilisation du conformère pour lequel $\phi = 90°$ à une par une acceptation d'électron de la liaison C—F α par hyperconjugaison aidée par le donneur-π présent en position *para*. On discute d'un certain nombre de constantes de couplage en fonction de mécanismes possibles pour leur transmission. On indique l'orientation de futures expériences.

Mots clés : RMN du ^1H, RMN du ^{13}C, RMN du ^{19}F du fluorure de 4-fluorobenzyle et de 3,5-difluorobenzyle; calculs d'OM et potentiels à la rotation interne dans les fluorures de benzyle, de 4-fluorobenzyle et de 3,5-difluorobenzyle; effets de solvant et approches expérimentales et théoriques aux potentiels à la rotation interne dans les fluorures de 4-fluorobenzyle et de 3,5-difluorobenzyle.

[Traduit par la rédaction]

Introduction

The phase of the internal rotational potential in benzyl fluoride, **1**, small and of the order of thermal energies at ambient temperatures, is determined by the presence or absence of intermolecular forces (1–6). Molecular orbital studies (refs. 1 and 6, and see below) imply that *A* is the conformation near which the potential[2] has a minimum, that the latter is dominated by a twofold term in the angle, ϕ, and, therefore, that *B* is the conformation of highest energy. The twofold term is computed to have a magnitude near 3 kJ/mol so that, at ordinary temperatures, all angles ϕ are significantly represented in an ensemble; a discussion in terms of discrete conformations (the so-called rotational isomeric state model) would be bootless.

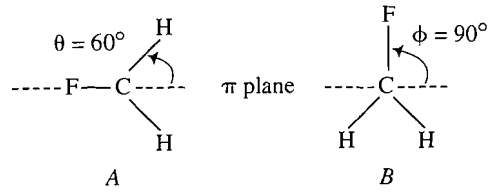

A *B*

In solution, long-range nuclear spin–spin coupling constants (1, 7), as well as residual dipolar coupling constants[3] for nematic solutions (2), imply that the phase of the internal potential is shifted by 90°: *B* now lies at the minimum. For example, the apparent twofold barrier is 3.2(2) kJ/mol in the polar CD_3CN solution and sinks to 0.7(2) kJ/mol in the nonpolar C_6D_{12} solution (1). It is therefore plausible that experiment will find *A* to correspond to a potential minimum for the gas phase of benzyl fluoride. Such a definitive experiment has not been done (but see ref. 11); it cannot be done by the use of small spin–spin coupling constants, for obvious reasons.

Not only intermolecular force fields, but also ring substituents, can alter the phase of the internal potential in benzyl fluoride. The long-range coupling constants between ring protons and the protons or ^{19}F nuclei in the side chain show that the conformer analogous to *A* is now most stable for 3,5-dichlorobenzyl fluoride in solvents of various polarities (12). Just as for the parent compound, however, the polar solvents act to favor a phase shift of the potential minimum towards the perpendicular *B*. It seems possible that the proper combination of substituents and solvent will lead to a vanishing internal rotational potential.

This report has two aims. First, the solvent dependence of internal barriers in 3,5-difluorobenzyl fluoride, **2**, and 4-fluorobenzyl fluoride, **3**, is to be determined from a number of long-range coupling constants involving ^1H, ^{13}C, and ^{19}F nuclei. It is anticipated, and confirmed, that **2** behaves similarly to 3,5-dichlorobenzyl fluoride, **4**, *A* being the conformer with a lower energy than that of *B*. By way of contrast, the π-electron donor, fluorine, is predicted (6) to favor the perpendicular conformer, *B*; this prediction is also confirmed.

The second aim is to compute the solvent effect on the internal rotational potential by means of ab initio continuum methods (13–15). In particular, the model of Rivail and co-workers (13) is employed. The model uses an ellipsoidal cavity for the solute molecule and a multipole expansion (up to $l = 6$, $l = 1$ corresponding to the dipole term) for the solute charge density. As computed dipole moments for the various conformers of **2** and **3** demonstrate, for example, truncation at $l = 1$ is unsuitable. Use of the basis 6-31 G*, geometries being optimized, yields qualitative agreement with experiment for **1**–**3**, based on comparisons of expectation values of $\sin^2 \phi$.

Experimental

Compounds **2** and **3** were prepared by fluorination of the corresponding alcohols (Aldrich) with morpholinosulfur trifluoride (morph-DAST) in the standard way (16). Dilute solutions of **2** and **3** in CS_2–C_6D_{12}–C_6F_6–TMS and in acetone-d_6–C_6F_6–

[2] The computed potentials are spectroscopic potentials, not activation energies; the spin–spin coupling constants, discussed below, sample the spectroscopic potential and are determined by its shape over the whole range of ϕ or, equivalently, θ.

[3] A recent investigation (8) of the other benzyl halides finds that an increase in the height of the potential, located at *B*, is caused by more polar liquid crystal solvents. The same conclusion was reached for benzyl chloride on the basis of spin–spin coupling constants for isotropic solvents (9). In the gas phase these heavier halides are also nonplanar, according to low-resolution microwave studies (10). So far, no definitive spectroscopic studies are available for benzyl fluoride as a vapor.

Can. J. Chem. Downloaded from www.nrcresearchpress.com by 80.90.12.36 on 09/08/12
For personal use only.

Table 1. The ^1H nmr and ^{19}F nmr spectral parameters for 3,5-difluorobenzyl fluoride, **2**, in CS_2–C_6D_{12} and acetone-d_6 solutions at 300 K.

	Solvent			Solvent	
Parameter	CS_2–C_6D_{12}[a]	Acetone-d_6	Parameter	CS_2–C_6D_{12}[a]	Acetone-d_6[b]
$\nu(CH_2)$[c]	1 584.813[e]	1 641.446	$^4J(H, CH_2)$	−0.713	−0.661
$\nu_2 = \nu_6$[c]	2 039.128	2 120.665	$^6J(H, CH_2)$	−0.533	−0.496
ν_4[c]	2 002.425	2 102.956	$^5J(F, CH_2)$	(−)0.240	(−)0.155
$\nu_3 = \nu_5$[d]	15 010.742	15 167.789	$^4J(H, CH_2F)$	−1.108	−1.344
$\nu(F)$[d]	−14 734.271	−13 828.884(2)	$^6J(H, CH_2F)$	−0.934	−1.161
$^2J(H, F)$	47.077	47.043	$^5J(F, F)$	(+)0.585	(+)0.219
$^3J_{23} = {}^3J_{56}$	8.609	9.086[f]	Calcd. transitions	768	768
$^3J_{34} = {}^3J_{45}$	8.760	9.240			
$^4J_{24} = {}^4J_{46}$	2.350	2.372	Assigned	510	515
$^4J_{26}$	1.370	1.327	Peaks observed	376	398
$^4J_{35}$	7.142	6.954	Largest difference	0.014	0.016
$^5J_{25} = {}^5J_{36}$	−0.954	−0.929	Root-mean-square deviation	0.006	0.007

[a]For a 5.0 mol% solution in CS_2 containing also 10 mol% of C_6D_{12}, 0.5 mol% of TMS, and 0.25 mol% of C_6F_6.
[b]For a 5.0 mol% solution in acetone-d_6 containing also 0.5 mol% of TMS and 0.25 mol% of C_6F_6.
[c]In Hz to high frequency of internal TMS at 300.13493 MHz.
[d]In Hz relative to internal C_6F_6 at 282.362 64 MHz, a negative number indicating increased screening.
[e]Except where otherwise noted, the standard deviations in all parameters were $\leq 10^{-3}$ Hz.
[f]The marked solvent dependence of $^nJ(H, F)$ within the phenyl group for a variety of fluorobenzene derivatives is well documented (32–34, 44); more polar solvents increase $^5J(H, F)$ algebraically, that is, a negative $^5J(H, F)$, for example, becomes smaller in magnitude (35, 36).

TMS (see Tables 1 and 2 for details) were filtered into 5 mm o.d. nmr sample tubes, degassed by at least four freeze–pump–thaw cycles, and were then flame-sealed under vacuum, taking care to produce reasonably symmetric tops.

The ^1H, ^{19}F, and proton-decoupled ^{13}C nmr spectra were acquired on a Bruker AM 300 spectrometer at 300 K. Intensive shimming, employing the TMS and C_6F_6 free induction decays, eventually yielded peak widths as low as 0.025 Hz in some instances. For ^1H and ^{19}F spectra, 32 decays, with acquisition times of 41 s, were coadded, followed by zero-filling to twice or four times the original data table. Digital resolution was 0.004 to 0.006 Hz/point. The ^{13}C nmr spectra resulted from the transformation of between 200 and 2500 decays, using acquisition times of 10–12 and digital resolution of 0.01 to 0.02 Hz/point. Resolution enhancements, normally 0.6 GB and −0.1 LB, were also imposed on the final data.

Spectral analyses used the program NUMARIT (17), the latter having been reworked extensively by R. Sebastian.

The ^1H and ^{19}F nmr spectra of **2** and **3** arise from AA′B M_2R_2X and AA′BB′M_2RX spin systems, respectively. Because of perturbations of ^{19}F chemical shifts by ^{13}C nuclei, the spectra arising from ^{13}C-2 and ^{13}C-3 in **2** were analyzed as arising from ABMX spin systems, under conditions of proton decoupling. First-order spectra were obtained for the other ^{13}C nuclei in **2** and for those in **3**.

Molecular orbital computations in **1**–**3** used the program GAUSSIAN 92 (18). Internal rotational potentials were obtained by fixing the angle ϕ in *B* at values of 0°, 30°, 45°, 60°, 75°, and 90° and optimizing the values of the other angles and bond lengths, with the constraint, however, that the phenyl moiety remained planar. Various basis sets[4] were employed in the HF SCF procedures. In addition, correlation-gradient computations, MP2/6-31G* and MP2/6-31G**, were also done for the free molecules. The calculations of solvent perturbations[5] of the internal rotational potentials used the program SCRF PAC (15), utilizing the full multipole expansion, that is, up to $l = 6$. Again, geometries were optimized as for the free molecules, now using the 6-31G* basis set.

[4] Explanations of the various split-valence basis functions, their notation, and references to them, and of the MP2 method of approximating electron correlation, can be found in ref. 19.

[5] A recent comprehensive discussion of methods based on continuous distribution of the solvent is given by Tomasi and Persico (20).

Can. J. Chem. Downloaded from www.nrcresearchpress.com by 80.90.12.36 on 09/08/12
For personal use only.

Table 2. The ^{1}H nmr and ^{19}F nmr spectral parameters CS_2–C_6D_{12} and acetone-d_6 solutions of 4-fluorobenzyl fluoride, **3**, at 300 K.

	Solvent			Solvent	
Parameter	CS_2-C_6D_{12}[a]	Acetone-d_6[b]	Parameter	CS_2–C_6D_{12}[a]	Acetone-d_6[b]
$\nu(CH_2)$[c]	1 566.022[e]	1 616.338	^4J(H, CH_2)	−0.580	−0.532
$\nu_2 = \nu_6$[c]	2 179.956	2 246.545	^5J(H, CH_2)	0.296	0.288
$\nu_3 = \nu_5$[c]	2 091.491	2 153.131	^6J(F, CH_2)	0.778	0.667
ν(F)[d]	−12 081.612	−11 389.771	^4J(H, CH_2F)	−1.786	−2.053
ν_4[d]	14 069.253	14 035.023	^5J(H, CH_2F)	1.055	1.118
^2J(H, F)	47.987	48.015	^6J(F, F)	4.919	5.591
$^3J_{23} = {}^3J_{56}$	8.475	8.511	Calcd. transitions	768	768
$^3J_{34} = {}^3J_{45}$	8.439	8.955	Assigned	656	640
$^4J_{24} = {}^4J_{46}$	5.253	5.407	Peaks observed	388	423
$^4J_{26}$	2.722	2.786	Largest difference	0.017	0.026
$^4J_{35}$	2.318	2.339			
$^5J_{25} = {}^5J_{36}$	0.405	0.410	Root-mean-square deviations	0.006	0.007

[a]For a 5.0 mol% solution in CS_2 containing also 10.0 mol% C_6D_{12}, 0.5 mol% TMS, and 0.25 mol C_6F_6.
[b]For a 5.0 mol% solution in acetone-d_6 containing also 0.5 mol% TMS and 0.25 mol% C_6F_6.
[c]In Hz at 300.134 93 MHz to high frequency of internal TMS.
[d]In Hz at 282.362 64 MHz to high (positive sign) frequency of internal C_6F_6.
[e]The standard deviations were all ≤0.001 Hz.

Table 3. The $^{13}C\{^1H\}$ nmr spectral parameters for solutions[a] in CS_2–C_6D_{12} and acetone-d_6 of 3,5-difluorobenzyl fluoride at 300 K.

	Solvent			Solvent			Solvent				
Parameter	CS_2-C_6D_{12}	Acetone-d_6	Parameter	CS_2–C_6D_{12}	Acetone-d_6	Parameter	C-α	C-1	C-2	C-3	C-4
ν_α	6 214.68[b,c]	6 307.08	^2J(C-4, F)	25.13	25.67	Calcd. transitions[d]	24	24	36[e]	32	24
ν_1	10 620.05	10 720.45	^3J(C-1m F)	8.94	9.27	Assigned transitions	6	8	12	8	8
$\nu_2 = \nu_6$	8 225.68	8 343.62	^3J(C-2, F)	7.23	7.01	Peaks observed	6	6	12	8	6
$\nu_3 = \nu_5$	12 325.36	12 373.98	^3J(C-3, F)	12.51	12.96	Largest difference	0.011	0.033	0.007	0.027	0.010
ν_4	7 808.91	7 868.78	^4J(C-α, F)	2.28	2.26	Root-mean-square					
^1J(C-α, F)	−173.45	−166.88	^4J(C-3, F)	(−)0.21(2)	(−)0.33	deviation	0.010	0.026	0.007	0.024	0.007
^1J(C-3, F)	−250.13(2)	−246.96	^5J(C-2, F)	3.29	3.46						
^2J(C-1, F)	18.83(2)	18.18	^5J(C-4, 5)	1.80	2.13(2)						
^2J(C-2, F)	22.60	22.52(2)									

[a]For the samples in Table 1.
[b]In Hz at 75.468 92 MHz to high frequency of internal TMS.
[c]Unless otherwise noted, the standard deviations were ≤10^{-2} Hz.
[d]For the CS_2–C_6D_{12} solution; similar numbers occur for the acetone-d_6 solution.
[e]A two-bond isotope shift on fluorine, $^2\Delta(^{13}C/^{12}C)$, relative to $^4\Delta$, gave $^2\Delta - {}^4\Delta$ as 5.951(6) Hz for the CS_2–C_6D_{12}, 6.01(2) Hz for the acetone-d_6, solution, entirely similar to values (39–43) for other aromatics. The C-2 spectra corresponded to the X parts of ABRX spin systems (increased screening of F-3 by C-2).

The SAS nonlinear regression procedure, NLIN (21), gave fits of the internal potentials to functions of the form

$$V(\phi) = \Sigma_n V_n \sin^2 (n\phi/2)$$

where n indicated the foldedness of the contributing term. Expectation values of $\sin^2\phi$ and $\sin^2\theta$ were calculated at 300 K with the software known as MAPLE V (22). INDO MO FPT (23) computations of the conformational dependencies of spin–spin coupling constants utilized the geometries obtained by MP2/6-31G** approaches for **1** and by MP2/6-31G* methods for **2** and **3**. The ensuing numbers were fit to various functions of θ and φ, as desired, with the SAS programs, to confirm previous assessment (7, 24, 25) of their angular dependence.

Results and discussion

Spectral data

Tables 1–4 present the ^{1}H, ^{19}F, and ^{13}C nmr spectral parameters for the 3,5-difluoro, 2, and 4-fluoro, 3, derivatives of benzyl fluoride. An example of a typical ^{1}H nmr spectrum is displayed in Fig. 1, showing the methylene proton spectrum of 3 in acetone-d_6 solution.

Experimental values of $\langle\sin^2\phi\rangle$ and $\langle\sin^2\theta\rangle$

There is little doubt that ^6J(H, CH_2) and ^6J(H, CH_2F) are proportional to $\sin^2\theta$ and $\sin^2\phi$, respectively (1), the proportionality constants between these quantities being the $^6J_{90}$ values, either for θ or φ. These coupling constants arise from σ, π

Can. J. Chem. Downloaded from www.nrcresearchpress.com by 80.90.12.36 on 09/08/12
For personal use only.

Can. J. Chem. Downloaded from www.nrcresearchpress.com by 80.90.12.36 on 09/08/12
For personal use only.

Table 4. The $^{13}C\{H\}$ nmr spectral parameters for 4-fluorobenzyl fluoride, **3**, in CS_2–C_6D_{12} and acetone-d_6 solution[a] at 300 K.

	Solvent			Solvent	
Parameter	CS_2–C_6D_{12}	Acetone-d_6	Parameter	CS_2–C_6D_{12}	Acetone-d_6
ν_α	6 131.95[b,c]	6 368.35	^2J(C-3, F)	21.56	21.76
ν_1	9 854.94(2)	10 091.20	^3J(C-2, F_α)	5.58	5.46
$\nu_2 = \nu_6$	9 609.72	9 883.37	^3J(C-2, F)	8.16	8.50
$\nu_3 = \nu_5$	8 569.02	8 764.18	^4J(C-3, F)	(−)1.27	(−)1.71
ν_4	12 153.82	12 359.97	^4J(C-1, F)	3.37(4)	3.12
^1J(C-α, F)	−170.04	−163.67	^5J(C-α, F)	0.77(5)	0.89
^1J(C-3, F)	−248.34	−245.14	^5J(C-4, F)	3.10	3.47
^2J(C-1, F)	18.05(4)	17.41			

[a]For the samples described in Table 1.
[b]In Hz at 75.468 92 MHz to high frequency of internal TMS.
[c]All spectra were analyzed as arising from AMX spin systems; the standard deviations in the parameters were all $\leq 10^{-2}$ Hz, except as noted. The root-mean-square deviations ranged from 0.000 to 0.04 Hz; the latter value occurred for C-1 in the CS_2–C_6D_{12} solution due to a noisy signal.

Fig. 1. Half the ^1H nmr spectrum at 300 MHz and 300 K of the methylene protons of 4-fluorobenzyl fluoride as a 5.0 mol% solution in CS_2–C_6D_{12} is shown. The computed spectrum assumes the spectral parameters in Table 2 and a linewidth of 0.03 Hz. The experimental spectrum displays relatively minor imperfect shimming characteristics, usually more prevalent in this solvent than in acetone-d_6.

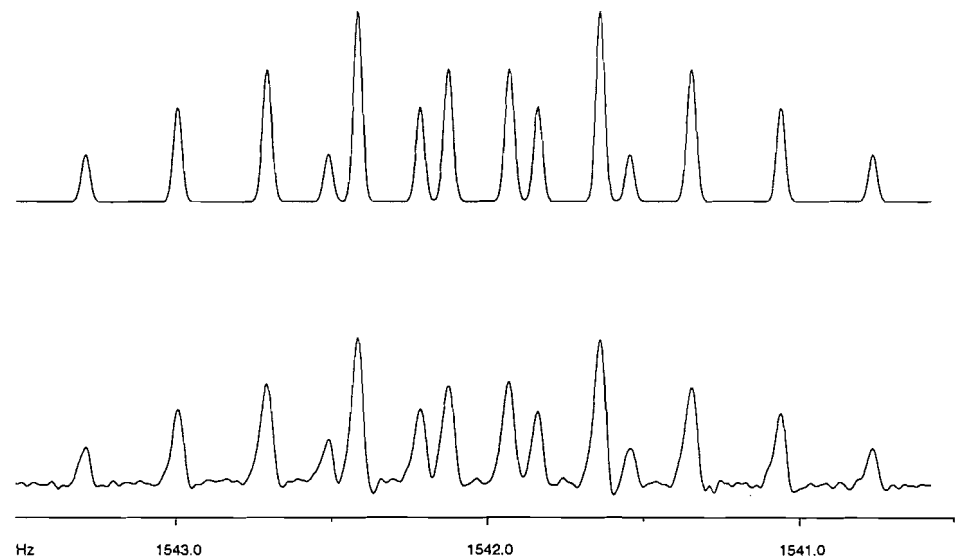

electron mechanisms and can be thought of as being proportional to the product of the hyperfine interaction parameter, Q_{CH}^H, with either Q_{CCH}^H or Q_{CCH}^F: the latter two are positive, the former is negative.[6] To a good approximation (see some computed molecular structures below and ref. 12), one may therefore write that $\langle \sin^2\phi \rangle = 1.5 - 2.0 \langle \sin^2\theta \rangle$, angular brackets indicating expectation values. A change in the internal rotational potential, caused by a change in the solvent, entails a change in the expectation values. On the assumption that the $^6J_{90}$ values are solvent-independent, one then has enough equations to establish these values, as well as the expectation values in each solvent. This calculation was done for benzyl fluoride (1) with the results summarized in Table 5. The values of $\langle \sin^2\phi \rangle$ are greater than 0.5 in both solutions (a value of 0.5 corresponds to a vanishing barrier) and hence the minimum in the potential occurs at $\phi = 90°$, defining the perpendicular conformer. The apparent twofold barrier, V_2, derived from a hindered rotor model (26, 27) or from a classical averaging procedure, increases in the more polar solvent.

Turning to the 3,5-dichloro derivative, **4**, the substituents shift the phase of the potential so that its minimum occurs at $\phi = 0°$ (12), but the polar solvent again *tends* to stabilize the perpendicular conformer and therefore *lowers* the height of the potential for the range of solvents used for **4** (12); two examples are given in Table 5. Note that the $^6J_{90}$ values for ^6J(H,

[6] Thus, a spin polarization mechanism ensures that a certain spin state of a proton at the *para* position favors a spin state of the same sign for the electron in the π-type orbital on the *para* carbon atom. By definition, this situation is described by $Q_{CH}^H < 0$.

Table 5. Experimental solvent dependence of the internal rotational potentials in benzyl fluoride and some of its derivatives.

	$C_6H_5CH_2F$ (**1**)		3,5-di Cl (**4**)		3,5-di F (**2**)		4-F (**3**)	
Parameter	CS_2–C_6D_{12}	Acetone-d_6[b]	CS_2–C_6D_{12}	Acetone-d_6[c]	CS_2–C_6D_{12}	Acetone-d_6	CS_2–C_6D_{12}	Acetone-d_6
^6J(H, CH_2)	−0.452(2)	−0.408(2)	−0.534(1)	−0.499(1)	−0.533(1)	−0.496(1)	—	—
$^6J_{90}$(H, CH_2)	−0.941(4)		−0.934(2)		−0.910(2)		—	
^6J(H, CH_2F)	−1.539(2)	−1.800(2)	−1.038(1)	−1.256(1)	−0.934(1)	−1.161(1)	0.778(1)[d]	0.667(1)[d]
$^6J_{90}$(H, CH_2F)	−2.855(4)		−2.909(2)		−2.832(2)		1.66(9)[d]	
^5J(C-4, F)	2.76(1)	3.11(1)	—	—	1.80(1)	2.13(2)	3.10(1)	3.47(1)
$^5J_{50}$(C-4, F)	5.03(10)		—		5.32(15)		5.20(2)	
^4J(H, CH_2)	−0.610(1)	−0.560(2)	−0.705(1)	−0.608(1)	−0.713(1)	−0.661(1)	−0.580(1)	−0.532(1)
$^4J_{90}$(H, CH_2)	−1.28(1)		−1.23(1)		−1.22(1)		−1.28(1)[e]	
$\langle\sin^2\theta\rangle$	0.481	0.435	0.572	0.534	0.585	0.545	0.453	0.416
$\langle\sin^2\phi\rangle$	0.539	0.631	0.357[g]	0.432[g]	0.330[g]	0.410[g]	0.594	0.668
V_2(kJ/mol)[f]	−0.8(2)	−2.6(2)	3.0(2)	1.4(2)	3.8(2)	1.9(2)	−1.9(2)	−3.6(2)

[a]2.3 mol% in CS_2 containing also 10 mol% of C_6D_{12}, 0.5 mol% of TMS, and 0.25 mol% of C_6F_6.
[b]2.8 mol% in acetone-d_6 containing also 0.5 mol% of TMS and 0.25 mol% of C_6F_6 (1).
[c]5.0 mol% and as for **1** (12).
[d]These are values for ^6J(F, CH_2F).
[e]Assumed to be the value for **1** and used to derive $\langle\sin^2\theta\rangle$.
[f]Assuming a purely twofold barrier. A negative sign means that the minimum in the potential occurs in the perpendicular conformer, *B*, for $\phi = 90°$.
[g]The minimum in the potential occurs at $\phi = 0°$.

CH_2) and ^6J(H, CH_2F) differ by only about 1% from those derived for benzyl fluoride. For **4** it was demonstrated (12) that ^4J(H, CH_2) could be treated in the same way as ^6J(H, CH_2) and that $^4J_{90}$ was −1.23(1) Hz. Application of this procedure to the parent compound gives $^4J_{90}$ as 1.28(1) Hz, in reasonable agreement with the magnitude for **4**.

The spectral data for the 3,5-difluoro derivative, **2**, confirm the phase shift in the internal rotational potential found for **4**. Furthermore, the decrease in $\langle\sin^2\phi\rangle$ and the concomitant increase in $\langle\sin^2\theta\rangle$ relative to **4** implies a greater stabilization of the in-plane conformer by the fluorine than by the chlorine substituents. The simplest plausible reason for this result is that the more electronegative fluorine substituents are more effective in their polarization of *ortho* C—H bonds, thereby causing a larger attractive C^--H^+ ··· $^-$F-$^+$C interaction with the C—F bond in the side chain. Again, $^4J_{90}$ for ^4J(H, CH_2) in **2** is −1.22(1) Hz, assuming the behaviour displayed by **4** (Table 5). This result, apparently satisfactory, is important for the 4-fluoro derivative, **3**, where ^{6}plain8J(H, VH_2) and ^6J(H, CH_2F) are not present.

In this connection, an examination and interpretation of ^5J(C-4, F) for benzyl fluoride in a range of solvents (1) concluded that it is also a σ, π parameter and, as such, proportional to $\sin^2\phi$. A $^5J_{90}$ of 5.03(10) Hz was deduced, compatible with the number (4) for a model compound. Use of $\langle\sin^2\phi\rangle$ for **2** and the values of ^5J(C-4, F) in Table 3, yields $^5J_{90}$ as 5.32(15), implying a reasonably minor perturbation by the *meta* fluorine substituents.

A comparison of the $^{4,5,6}J_{50}$ values in Table 5 for **1**, **2**, and **4** suggests that such numbers do not vary by more than a few percent and that they form a reliably consistent set. Hence a subset may well be applicable to 4-fluorobenzyl fluoride, **3**.

For **3** it is sensible to take $^4J_{90}$(H, CH_2) as that for the parent compound; the substituent is relatively remote from the coupling pathway. The values of $\langle\sin^2\phi\rangle$ and $\langle\sin^2\theta\rangle$ that follow from this assumption are found in Table 5. The $^5J_{90}$ (C-4, F) then follows as 5.20(2) Hz, suggesting[7] a minor perturbation of the σ, π parameter by the fluorine atom attached to C-4 (the π electron spin density in the $2p\pi$ orbital at C-4 is not altered appreciably or, if it is, a compensating change occurs at the fluorine atom in the CH_2F group).

Note that the 4-fluoro substituent, a π-electron donor, stabilizes the perpendicular conformer in both solvents relative to the parent compound. The stabilization makes sense if it is accepted that the α-CF bond is a hyperconjugative π-electron acceptor, as previously postulated on the basis of ^{19}F nmr chemical shifts in **1** and some of its *para* derivatives (6). The present results in Table 5 represent the first experimental assessment of the energy involved in such a hyperconjugative interaction. It amounts to 1.0 ± 0.4 kJ/mol for **3** in both CS_2 and acetone-d_6 solution (the errors in the apparent V_2 values in Table 5 are quoted as twice the formal errors). It is apparent that the present methods, based on ^4J(H, CH_2) and ^5J(C-4, F), should allow similar assessments for a range of 4-X-benzyl fluoride derivatives.

Other long-range coupling constants

The many other long-range coupling constants in Tables 1–4 are only partially understood. As an extreme example, consider ^5J(F, CH_2) in **2**; the magnitudes are 0.24 and 0.16 Hz in CS_2 and acetone-d_6 solutions, respectively (Table 1). It is known that, in the 3,5-difluoro derivatives of toluene, ethylbenzene, and isopropylbenzene (29), ^5J(F, CH_2) can be positive or negative, depending on the orientation of the C—H bonds with respect to the benzene plane: it is given by $^5J = 0.08 - 2.43\langle\sin^2\theta\rangle + 1.68\langle\sin^2(\theta/2)\rangle$ and reproduces the magnitudes and signs correctly. If the coefficient of $\langle\sin^2\theta\rangle$ is reduced by a factor of 0.94/1.20, for well-documented reasons (1, 30, 31), then ^5J(F, CH_2) for **2** is predicted to be −0.20 and

[7] Indeed, in 4-fluorotoluene, ^5J(C-4, H) is not very strongly perturbed by the fluorine attached to C-4 (28).

Can. J. Chem. Downloaded from www.nrcresearchpress.com by 80.90.12.36 on 09/08/12
For personal use only.

Table 6. Theoretical internal rotational potentials in kJ/mol for benzyl fluoride, **1**, 3,5-difluorobenzyl fluoride, **2**, and 4-fluorobenzyl fluoride, **3**.

Molecule	Basis[a]	V_2	V_4	V_6	V_8	$-E_{min}$[f]
1	6-31G*	3.38	−0.61	0.07	0.02	368.586 377
	6-31G**	3.69	−0.47	0.07	0.01	368.598 780
	6-311G*	2.86	−0.18	0.12	—	368.662 713
	MP2/6-31G*	3.07[b]	−0.88	−0.08	0.03	369.639 866
	MP2/6-31G**	3.14[c]	−0.73	−0.09	0.01	369.695 547
2	6-31G*	6.84	−0.57	0.08	0.01	566.288 524
	6-31G**	7.16	−0.43	0.08	0.00	566.297 511
	6-311G*	6.23	−0.10	0.14	0.00	566.422 230
	MP2/6-31G*	5.57	−0.91	−0.09	0.03	567.677 043
	MP2/6-31G**	5.44	−0.77	−0.10	0.01	567.716 015
3	6-31G*	2.45	−0.68	0.05	0.02	467.437 253
	6-31G**	2.73	−0.54	0.06	0.01	467.447 907
	6-31G*	1.86	−0.24	0.12	0.00	467.542 287
	MP2/6-31G*	2.62[d]	−0.93	−0.10	0.03	468.658 545
	MP2/6-31G**	2.67[e]	−0.80	−0.11	0.01	468.705 874

[a]Geometry-optimized at intervals of 15° in ϕ (ϕ = 0 corresponds to the conformer in which the C—F bond of the side chain lies in the benzene plane) with the proviso that the atoms of the benzene moiety remain in a plane.

[b]The energy minimum occurs at ϕ = 18.7°, 0.04 kJ/mol lower than at ϕ = 0°.

[c]The minimum energy corresponds to ϕ = 13.5°, 0.01 kJ/mol lower than at ϕ = 0°.

[d]At ϕ = 24.7°, the energy is 0.14 kJ/mol lower than at ϕ = 0°.

[e]The energy is 0.08 kJ/mol lower at ϕ = 21.1° than at ϕ = 0°.

[f]The total lowest computed energy; the fits to $V(\phi) = \Sigma_n V_n \sin^2 (n\phi/2)$ had standard errors near 0.01 kJ/mol.

−0.13 Hz in CS_2 and acetone-d_6 solutions, respectively. The conclusion is very likely, therefore, that these numbers are, in fact, negative, and are so designated (within parentheses) in Table 1.

Similar sign assessments can be made for some other long-range coupling constants in these tables. Such signs are indicated within parentheses in Tables 1–4. We postpone more discussion, which would not further the aims of the present report, until data are available for a number of other derivatives of the parent compound.

The computed barriers

(a) Free molecules

Table 6 presents the internal rotational potentials for benzyl fluoride, **1**, and its 3,5-difluoro, **2**, and 4-fluoro, **3**, derivatives. All basis sets, including the correlation-gradient calculations, yield a dominent twofold component, V_2, of the potential. Yet, V_4 is significant in magnitude and opposite in sign to V_2. Indeed, the magnitude of V_4 is large enough to cause the minimum energy to occur, not at ϕ = 0° (which is indeed the minimum in the potential for **2**), but between 13° and 25° for **1** and **3**. These minima are predicted by the correlation-gradient computations. However, the barrier to ϕ = 0° is very small, amounting to only as much as 0.14 kJ/mol. The HF computations have the in-plane conformer, *A*, at a definite minimum in the potential. Notice that, qualitatively, the computations agree with the conclusions from the coupling constants measured in solution: the *meta* substituents enhance the stability of *A*, the *para* substituent does the opposite. Quantitatively, the discrepancy between theory for the free molecules and experiment in solution is marked: for **1** and **3** there exist phase shifts of 90° in the potential minima and for **2** the magnitudes of the potentials differ by as much as a factor of two. Prior to the description of the computational results about solvent effects, some information of use to molecular spectroscopists is presented.

Figure 2 displays the MP2/6-31G** geometries of benzyl fluoride for the in-plane and perpendicular conformers. The equilibrium bond lengths and angles appear eminently reasonable and should be useful to microwave spectroscopists, for example, in studies of the internal rotational potential, which, it is stressed, is likely of a magnitude particularly suitable to such a method.

It is also of interest that the bond angles at the formally sp^3 carbon atom in the side chain do not deviate substantially from tetrahedral. In *A*, the HCH angle is 108.4°. For an ideal angle, the twist angle, θ, is 60° for the α-CH bonds. The theoretical angle of 108.4° implies a twist angle between 59.5° and 60°, so that the assumption of ideal angles in computing $\langle\sin^2\theta\rangle$ and $\langle\sin^2\phi\rangle$ is rather good.

Another point of interest concerns the lengthening and shortening, respectively, of the C—F and Csp^2—Csp^3 bonds, as the molecule rotates internally from *A* to *B*. The increase in the C—F bond length is consistent with hyperconjugation in *B* (bond, no-bond resonance structures in valence-bond terminology); hyperconjugation should shorten the Csp^2—Csp^3 bond in *B* relative to *A*, as in the resonance structure, *C*.

Can. J. Chem. Downloaded from www.nrcresearchpress.com by 80.90.12.36 on 09/08/12
For personal use only.

Fig. 2. The MP2/6-31G* geometries are displayed for the in-plane and perpendicular conformers of benzyl fluoride, **1**. The bond lengths and angles are as expected on the basis of available data (1, 37). Note that the fluorine substituent reduces the perturbation by a methyl group of the bond angles in the phenyl group. Thus, at the ipso position, a methyl group reduces the bond angle to 118.1° (38). The tetrahedral geometry at the α carbon atom is not severely altered, important for the arguments used in deriving expectation values of conformational angles (see text).

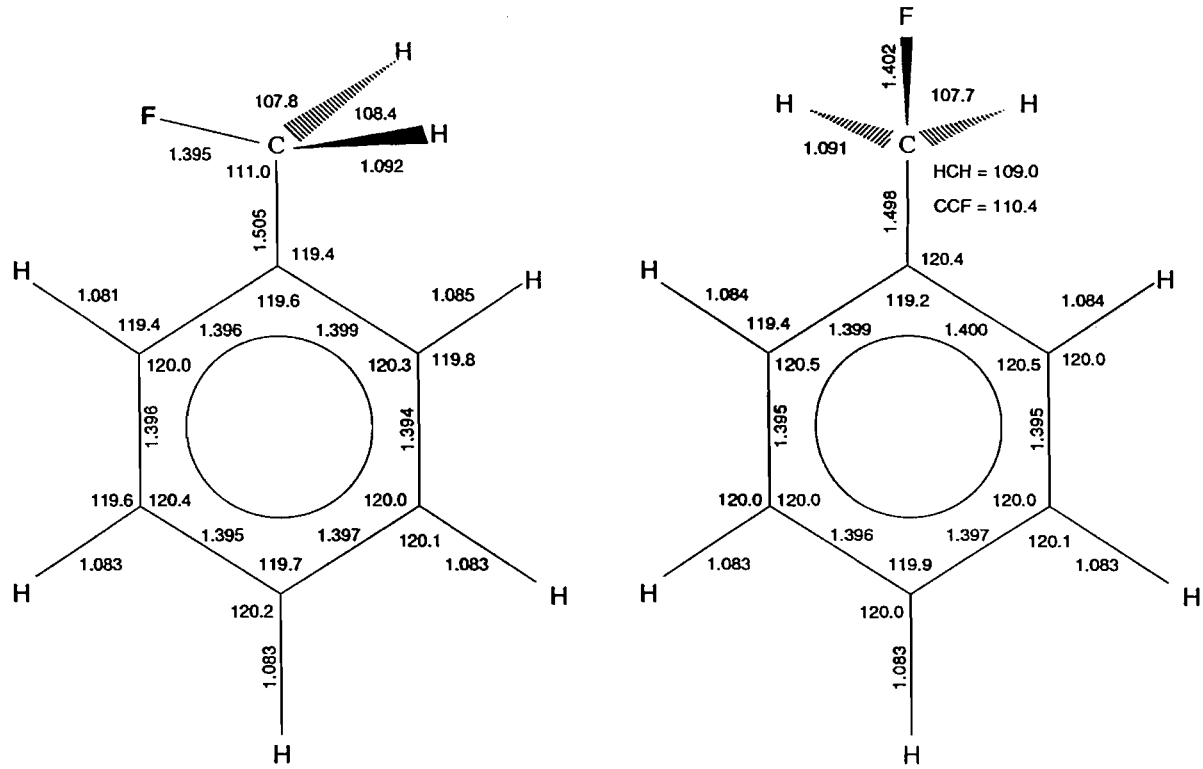

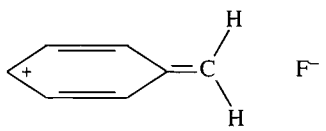

C

(b) Theoretical internal rotational potentials in solution

The potentials for the free molecule and that dissolved in CS_2 and acetone solutions are presented in Table 7. The dielectric constants of the solutions were taken as 2.6 and 20.3; no doubt these are not exact and may be a source of error in the computations. The basis set, 6-31G*, was used and the geometry was optimized at each value of the conformational angle, ϕ. As can be seen from the total energies appearing in Tables 6 and 7, the solvent is calculated to lower the energy of all conformers of benzyl fluoride and its 3,5-difluoro and 4-fluoro derivatives. Furthermore, qualitatively the computed solvent effects agree with experiment in the sense that while, for the free molecule, the minimum in the potential occurs for *A*, the solvent acts to favor *B*: that is, *B may* not be computed to lie at the minimum in the potential, but for each molecule the in-plane conformer is less stable in solution than in the free state.

Comparison of the theoretical and experimental values of $\langle \sin^2\phi \rangle$ in Table 7 suggests that theory, at this level, overestimates the interaction with the polar solvent and perhaps underestimates it for the less polar solution. Whether this disagreement can be attributed to the basis set or to the model is not clear. Note that the dipole term ($l = 1$) for benzyl fluoride itself can contribute significantly to solvent effects (see computed dipole moments in Table 7) but, within the present model, will have a negligible contribution to the solvent perturbations for the two derivatives.

Figure 3 conflates the theoretical and experimental results for benzyl fluoride. It would be of interest to perform solvent-effect calculations using much larger basis sets and also at the post-Hartree–Fock level of theory. Such computations are not feasible with our present resources.

Nevertheless, we take the present computations as a confirmation of our previous nmr experiments, which yielded *B* as the minimum in the internal rotational potential for benzyl fluoride in six solvents and which, on the basis of an extrapolation of a dielectric function, predicted *A* as the minimum in the potential for the free molecule (1).

Further experiments

It is clear that each benzyl fluoride derivative in a particular solvent will have a unique internal rotational potential. At present, some symmetrical 2,6-disubstituted derivatives are under investigation with a view to establishment of solvent effects on the rather larger internal rotational potentials in such molecules. Perturbations of the long-range coupling constants by polar and nonpolar *ortho* substituents are of interest. As the number of reliable coupling constants involving ^1H, ^{13}C, and ^{19}F nuclei in benzyl fluoride derivatives grows, it may well be that additional conformational markers will be found; another aim is to provide theoreticians with a body of data for

Can. J. Chem. Downloaded from www.nrcresearchpress.com by 80.90.12.36 on 09/08/12
For personal use only.

Table 7. Computed internal potentials[a] and dipole moments for free and solvated molecules, together with computed and experimental values of $\langle\sin^2\phi\rangle$ at 300 K.

Molecule	V_2	V_4	V_6	V_8	$\langle\sin^2\phi\rangle$	$\langle\sin^2\phi\rangle$exp	$\mu(0°)^k$	$\mu(90°)^k$
CH_2F^b	3.38	−0.61	0.07	0.02	0.349	—	1.74	2.10
CS_2^c	0.67(3)	−0.48	−0.14	—	0.468	0.539	1.91	2.33
Acetone[d]	−3.26(3)	−0.17	−0.25	0.08	0.653	0.631	2.08	2.62
3,5-diF[e]	6.84	−0.57	0.08	0.01	0.230	—	1.84	1.85
CD_2^f	4.06(1)	−0.46	0.04	0.02	0.319	0.330	2.12	2.11
Acetone[g]	−0.40(1)	−0.33	−0.09	0.07	0.519	0.410	2.49	2.47
4-F[h]	2.45	−0.68	0.05	0.02	0.389	—	1.81	1.82
CS_2^i	−0.44(1)	−0.52	0.01	0.02	0.521	0.594	2.06	2.04
Acetone[j]	−4.61(3)	−0.23	−0.08	—	0.706	0.668	2.29	2.33

[a]Potential components in kJ/mol, standard errors in the fit (intervals of 15° in ϕ) being indicated under V_2; for the free molecule the errors were <0.01 kJ/mol. Geometry-optimized computations used basis 6-31G*.
[b]Lowest energy −368.586 377 au. (ϕ = 0°).
[c]−368.588 772 (ϕ = 30°).
[d]−368.592 201 (ϕ = 90°).
[e]−566.288 524 (ϕ = 0°).
[f]−566.290 886 (ϕ = 0°).
[g]−566.293 279 (ϕ = 90°).
[h]−467.437 253 (ϕ = 0°).
[i]−467.439 869 (ϕ = 45°).
[j]−467.443 586 (ϕ = 90°).
[k]Dipole moment in units of debye at ϕ = 0° and ϕ = 90°.

Can. J. Chem. Downloaded from www.nrcresearchpress.com by 80.90.12.36 on 09/08/12
For personal use only.

Fig. 3. The theoretical 6-31G* potential for the free benzyl fluoride molecule, curve 1, is compared with those computed for its solution in CS_2, curve 2, and acetone, curve 5, as calculated with the SCRF PAC program (15) in which the solvent is treated as a dielectric continuum. The apparent twofold potentials, derived from coupling constants, are shown for CS_2, curve 3, and acetone, curve 4. Part of the disagreement between theory and experiment, of course, may be basis set dependent. As well, the exact dielectric constants of the solutions are unknown. Table 7 summarizes the computations of the solvent perturbations of the internal rotational potential for benzyl fluoride and its 3,5-difluoro and 4-fluoro derivatives.

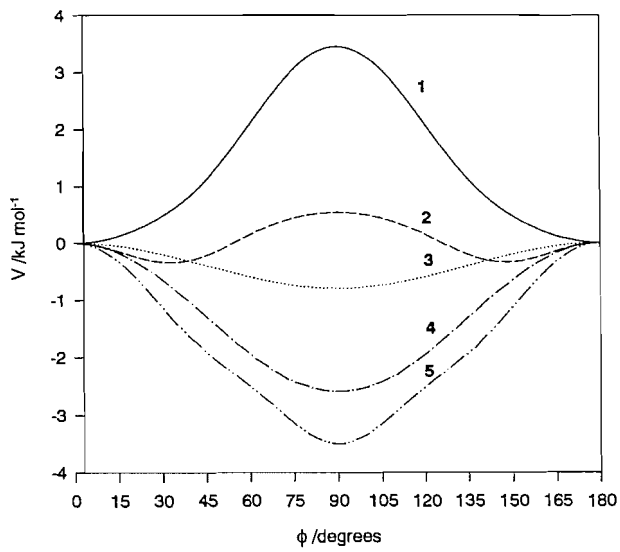

one basic system sufficient to stimulate computational progress. After all, if the complete conformational dependence of J, that is, its value at every value of the defining angle, were known, then high-resolution nmr of "small" molecules would become a powerful method for the characterization of their flexibility in solution.

Acknowledgments

We thank the Natural Sciences and Engineering Research Council of Canada for financial assistance.

References

1. T. Schaefer, C. Beaulieu, R. Sebastian, and G.H. Penner. Can. J. Chem. **68**, 581 (1990).
2. G. Celebre, G. De Luca, M. Longeri, and J.W. Emsley. Mol. Phys. **67**, 239 (1989).
3. R. Dupeyre and C. Béguin. J. Chim. Phys. **78**, 363 (1981).
4. W. Adcock and A.N. Abeywickrema. Aust. J. Chem. **33**, 181 (1980).
5. R.J. Abraham, R.A. Hearmon, M. Traetteberg, and P. Bakken. J. Mol. Struct. **57**, 149 (1979).
6. R.T.C. Brownlee and D.J. Craik. Tetrahedron Lett. **21**, 1681 (1980).
7. T. Schaefer, J. Peeling, and R. Sebastian. Can. J. Chem. **63**, 3219 (1985).
8. G. Celebre, G. De Luca, M. Longeri, and A. Ferrarini. Mol. Phys. **83**, 309 (1994).
9. T. Schaefer, R. Sebastian, and G.H. Penner. Can. J. Chem. **64**, 1372 (1986).
10. S.A. Sorenson and N.S. True. J. Mol. Struct. **263**, 21 (1991).
11. H.-S. Im, E.R. Bernstein, H.V. Secor, and J.I. Seeman. J. Am. Chem. Soc. **113**, 4422 (1991).

12. T. Schaefer, J.R. Mansfield, F.E. Hruska, and R. Sebastian. Can. J. Chem. **70**, 1750 (1992).
13. D. Rinaldi, J.L. Rivail, and N. Rguini. J. Comput. Chem. **13**, 675 (1992).
14. M.F. Ruiz-López, X. Assfeld, J.L. Garcia, J.A. Mayoral, and L. Salvatella. J. Am. Chem. Soc. **115**, 8780 (1993).
15. D. Rinaldi and R.R. Pappalardo. SCRF PAC, A self-consistent reaction field package, Quantum Chemistry Progam Exchange 622. QCPE Bull. **12**, 69 (1992).
16. P. Messina, K. Mange, and W.J. Middleton. J. Fluorine Chem. **42**, 137 (1989).
17. J.S. Martin, A.R. Quirt, and K.E. Worvill. The NMR program library. Daresbury Laboratory, Daresbury, U.K.
18. C.M.J. Frisch, G.W. Trucks, M. Head-Gordon, P.M.W. Gill, M.W. Wong, J.B. Foresman, B.G. Johnson, H.B. Schlegel, M.A. Robb, E.S. Replogle, R. Gomperts, J.L. Andres, K. Raghavachari, J.S. Binkley, C. Gonzalez, R.L. Margin, D.J. Fox, D.J. Defrees, J. Baker, J.J.P. Stewart, and J.A. Pople. GAUSSIAN 92, Revision. Gaussian, Inc., Pittsburg, Pa. 1992.
19. W.J. Hehre, L. Radom, P.v.R. Schleyer, and J.A. Pople. *Ab initio* molecular orbital theory. Wiley and Sons, New York. 1986.
20. J. Tomasi and M. Persico. Chem. Rev. **94**, 2067 (1994).
21. A.A. Ray (*Editor*). SAS users guide: statistics. Statistical Analysis System Institute, Cary, N.C. 1985.
22. MAPLE V Release 2, Waterloo Maple Software, University of Waterloo, Waterloo, Ont. 1981–1983.
23. P.A. Dobosh and N.S. Ostlund. QCPE, **11**, 281 (1975).
24. J.C. Facelli, C.G. Giribet, and R.H. Contreras. Org. Magn. Reson. **19**, 138 (1982).
25. R.H. Contreras and J.C. Facelli. Annu. Rep. NMR Spectrosc. **27**, 255 (1993).
26. P.B. Ayscough, M.S. Brice, and R.E.D. McClung. Mol. Phys. **20**, 41 (1971).
27. W.J.E. Parr and T. Schaefer. Acc. Chem. Res. **13**, 400 (1980).
28. T. Schaefer, J. Peeling, and G.H. Penner. Can. J. Chem. **61**, 2773 (1983).
29. T. Schaefer, C.S. Takeuchi, and S.E. Sveinson. Can. J. Chem. **66**, 1490 (1988).
30. R. Laatikainen and K. Tuppurainen. J. Chem. Soc. Perkin Trans. 2, 121 (1987).
31. T. Schaefer, R. Sebastian, and G.H. Penner. Can. J. Chem. **63**, 2597 (1985).
32. H.M. Hutton, B. Richardson, and T. Schaefer. Can. J. Chem. **45**, 1795 (1967).
33. J.E. Loemker, J.M. Read, Jr., and J.H. Goldstein. Mol. Phys. **13**, 433 (1967).
34. T.F. Page. Mol. Phys. **13**, 523 (1967).
35. T. Schaefer and R. Sebastian. Can. J. Chem. **68**, 1383 (1990).
36. T. Schaefer and C.S. Takeuchi. Can. J. Chem. **68**, 1383 (1990).
37. P. Nosberger, A. Bauder, and Hs. H. Günthard. Chem. Phys. **1**, 418 (1973).
38. A. Domenicano, P. Mazzeo, and A. Vaciago. Tetrahedron Lett. 1029 (1976).
39. V. Wray, L. Ernst, and E. Lustig. J. Magn. Reson. **27**, 1 (1977).
40. L Ernst, R.N. Lincoln, and V. Wray. J. Magn. Reson. **21**, 115 (1976).
41. W.S. Brey, K.H. Ladner, R.E. Block, and W.A. Tallon. J. Magn. Reson. **8**, 406 (1972).
42. P.E. Hansen. Annu. Rep. NMR Spectrosc. **15**, 105 (1983).
43. T. Schaefer, J. Peeling, and G.H. Penner. Can. J. Chem. **64**, 2162 (1986).
44. S. Suntioinen and R. Laatikainen. Magn. Reson. Chem. **30**, 415 (1992).

Can. J. Chem. Downloaded from www.nrcresearchpress.com by 80.90.12.36 on 09/08/12
For personal use only.

Synthesis of nitropolychlorinated dibenzo-*p*-dioxins (NPCDDs) and their photochemical reaction with nucleophiles[1]

Simona G. Merica and Nigel J. Bunce

Abstract: A series of nitropolychlorodibenzo-*p*-dioxins (NPCDDs) was synthesized by condensation between catechols and 2,6-dinitrohalobenzene derivatives. In the presence of sodium ethoxide in anhydrous ethanol, these underwent photochemical S_N2Ar^* substitutions *meta* to the nitro group in high chemical yield and moderate quantum yield. Both ring-opening and chloride replacement reactions were observed. The reactions involved the triplet excited state of the NPCDD, and showed a linear relationship between Φ^{-1} and $[\text{nucleophile}]^{-1}$. Analogous reactions with KCN in methanol showed similar behaviour, but the products could not be isolated.

Key words: photosubstitution, S_N2Ar^*, dibenzo-*p*-dioxins.

Résumé : On a synthétisé une série de nitropolychlorodibenzo-*p*-dioxines (NPCDD) par condensation de catéchols et de dérivés 2,6-dinitrohalobenzènes. En présence d'éthylate de sodium dans l'éthanol anhydre, ces derniers subissent des réactions de substitutions photochimiques S_N2Ar^* en *méta* du groupe nitro; les rendements chimiques sont élevés et les rendements quantiques sont modérés. On a observé des réactions d'ouverture de cycle ainsi que des réactions de remplacement de l'halogénure. Les réactions impliquent l'état triplet excité du NPCDD et elles présentent une relation linéaire entre Φ^{-1} et $[\text{nucléophile}]^{-1}$. Les réactions analogues avec le KCN dans le méthanol présentent un comportement similaire; toutefois, on n'a pas pu isoler les produits.

Mots clés : photosubstitution, S_N2Ar^*, dibenzo-*p*-dioxines.

[Traduit par la rédaction]

Introduction

Polychlorinated dibenzo-*p*-dioxins (PCDDs) are well known as environmental contaminants, but their chemistry is relatively unexplored. Concern about PCDDs in the environment stems from the toxicity of the congeners that are fully chlorinated in the 2, 3, 7, and 8 positions (1–3); their toxicity has been shown to correlate with the efficiency of binding to an intracellular protein known as the Ah receptor, which accommodates them on the basis of size, shape, and lipophilicity (4–6).

In a preliminary paper, we showed that the binding ability of certain nitropolychlorinated dibenzo-*p*-dioxins (NPCDDs) to the Ah receptor is rapidly lost upon photolysis in the presence of hydroxide ion (7). Although no product identification was carried out in this preliminary study, the failure to complex with the Ah receptor implied that photochemical reaction with hydroxide ion had changed the molecular size, shape, or lipophilicity of the NPCDDs. In turn, this suggested that the photochemical reaction products might be less toxic than the starting NPCDDs, and that such a photochemical reaction might be useful for destroying the parent PCDDs.

Fig. 1. Structures of 3-nitroveratrole and 1-nitrodibenzo-*p*-dioxin.

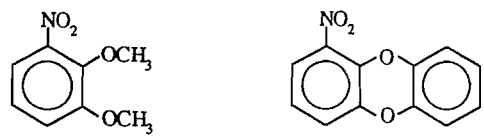

A reasonable hypothesis for an efficient photoreaction between NPCDDs and OH^- is nucleophilic substitution (S_N2Ar^*) *meta* to the nitro group, thereby opening the central ring of the dibenzo-*p*-dioxin system and changing the shape and lipophilicity of the molecule. The dibenzo-*p*-dioxin system contains 16 π-electrons, and so the nitro-substituted moiety of an NPCDD was expected to behave like a nitro-substituted veratrole rather than as a delocalized aromatic system (Fig. 1). Nucleophilic aromatic photosubstitutions have been extensively examined for nearly 40 years, with nitrophenyl ethers being among the most thoroughly studied (8–11). Two major reaction mechanisms have been distinguished: the S_N2Ar^* mechanism involving direct formation of a σ-complex by attack of the nucleophile at a ring position *meta* to NO_2; and an electron transfer reaction that is possible when

Received February 2, 1995.

S.G. Merica and N.J. Bunce.[2] Guelph–Waterloo Centre for Graduate Work in Chemistry. University of Guelph, Guelph, ON N1G 2W1, Canada.

[1] Taken from the M.Sc. thesis of S.G.M.

[2] Author to whom correspondence may be addressed. Telephone: (519) 824-4120, ext. 3962. Fax: (519) 836-9967.

Can. J. Chem. Downloaded from www.nrcresearchpress.com by 65.111.164.53 on 09/08/12
For personal use only.

the "nucleophile" is relatively easily oxidized, and which normally leads to substitution *para* to the nitro group (12–17). In the present work we have explored the feasibility of inducing the S_N2Ar^* reaction between NPCDD congeners and the poorly oxidizable nucleophiles CN^- and EtO^-, with a view to identifying the products and elucidating the reaction mechanisms. Since one of the two ring oxygen atoms of the dibenzo-*p*-dioxin is always *meta* to the nitro group, ring photochemical opening was expected to be facile, with the formation of a dihydroxydiphenyl ether derivative (eq. [1]).

[1] 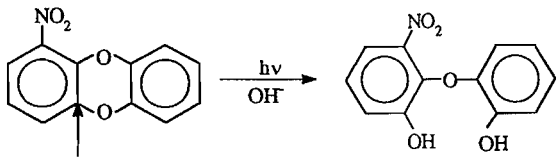

Experimental

Fuming nitric acid, fuming sulphuric acid, and most organic chemicals were obtained from Aldrich. Melting points were measured with a Mel-Temp apparatus using open capillaries. Thin-layer chromatography (TLC) was performed using premade glass plates coated with silica gel GF (Merck), containing a 254 nm fluorescence indicator, with a thickness of 0.25 mm. Flash chromatography on 60–120 mesh silica gel (BDH) or 230–400 mesh silica gel (Merck) was used for purifying reaction products. HPLC analyses were performed on a Waters system: Waters 501 HPLC pump, U6K injector, and model 440 absorbance detector (254 nm) and were recorded using a Hewlett Packard model 3390 A integrator. Analytical separations were performed using a Waters μBondapak C_{18} 3.9 mm × 300 mm column. Preparative separations (samples ≤100 mg) were performed on a Whatman Magnum 9 Partisil ODS-3 C_{18} (reversed phase) 9.4 mm × 250 mm column or an Econosphere C_{18}, 10 mm × 250 mm column. All solvents used were HPLC grade and were filtered through 0.45 μm Nylon 66 membranes to remove microparticulates.

^{1}H NMR spectra were recorded on a 200 MHz Varian Gemini spectrometer or on a Varian Unity 400 MHz NMR spectrometer; samples were dissolved in $CDCl_3$ with TMS as an internal standard. Analytical GC–MS was performed on a Hewlett Packard 5890 Series II gas chromatograph equipped with a J&W DB5 capillary column (0.25 mm i.d., 30 m length, 0.25 μm film thickness), with temperature programming, interfaced to a Hewlett Packard 5971 Series mass selective detector. High-resolution GC–MS employed a Kratos 890 double focussing mass spectrometer. FT-IR analyses were performed on a Nicolet model 205 SX/C FT-IR using NaCl cells; UV–visible spectra were obtained using a Perkin–Elmer Lambda 3 UV–visible spectrometer.

Synthesis of nitropolychlorinated dibenzo-*p*-dioxins and precursors

2,6-Dinitrochlorobenzene was prepared by the procedure of Gunstone and Tucker (18) from 2,6-dinitroaniline (3 g, 16 mmol) in glacial acetic acid (33 mL), which was added dropwise to a stirred solution prepared from concentrated H_2SO_4 (14 mL) and sodium nitrite (1.24 g, 18 mmol), keeping the temperature during the addition below 40°C. The diazonium salt was added dropwise to a suspension of CuCl (3.6 g, 36 mmol) in concentrated HCl (33 mL), and the solution was then heated to 80°C for 30 min, diluted with an equal volume of water, and kept at 0°C overnight. After filtration and air drying, the yellow product was crystallized from benzene – petroleum ether, affording 2.21 g (67%) of pure 2,6-dinitrochlorobenzene, mp 86–87°C (lit. (18) mp: 86–88°C), ^{1}H NMR ($CDCl_3$) δ: 8.01 (d, J = 8.1 Hz, 2H), 7.61 (t, J = 8.1 Hz, 1H).

3,4,5-Trichlorofluorobenzene was prepared in 71% yield by the method of Mahiou and Deinzer (19), involving Schiemann decomposition of the diazonium tetrafluoroborate prepared from 3,4,5-trichloroaniline. After purification by flash chromatography, eluting with 20% dichloromethane in hexane, the product had ^{1}H NMR ($CDCl_3$)δ: 7.16 (d, J = 7.8 Hz, 2H). Similarly prepared was *2,3-dichlorofluorobenzene* (90% yield); after flash chromatography, eluting with 2% dichloromethane in hexane, it had ^{1}H NMR ($CDCl_3$)δ: 7.25 (dd, J = 7.1, 5.4 Hz, 1H), 7.18 (ddd, J = 9.2, 6.7, 3.1 Hz, 1H), 7.08 (ddd, J = 8.0, 6.5, 8.5 Hz, 1H).

3,4,5-Trichloro-2,6-dinitrofluorobenzene was prepared by a modification of the procedure reported by Mahiou and Deinzer (19), which gave a very low yield. In a 50-mL round-bottomed flask equipped with a stir bar and a condenser (connected to a drying tube) were placed 3,4,5-trichlorofluorobenzene (1.0 g, 5.0 mmol), fuming nitric acid (3 mL), and fuming sulphuric acid (3 mL) containing 20% of sulphur trioxide. The mixture was refluxed for 24 h and at every 8 h a new portion of fuming nitric acid (3 mL) was added. After cooling, the reaction mixture was poured onto ice, and the precipitate collected by filtration and dissolved in chloroform. The chloroform layer was washed with water and dried over anhydrous magnesium sulphate. The solvent was removed using the rotary evaporator. The solid was recrystallized from 95% ethanol–water and dried under vacuum to give the product in 88% yield (1.27 g). GC–MS *m/z* (relative intensity): 288(78, M^+), 196(100), 161(85), 126(80). *2,3-Dichloro-4,6-dinitrofluorobenzene* was prepared similarly in 74% yield; after purification by flash chromatography, eluting with 50% dichloromethane in hexane, it had ^{1}H NMR ($CDCl_3$) δ: 8.61 (d, J = 7.0 Hz, 1H).

1,4-Dinitrotetrachlorobenzene was prepared from 1,2,3,5-tetrachlorobenzene by the procedure of Berckmans and Holleman (20): yield, 75% after two recrystallizations from 95% ethanol–water; mp 227–228°C (lit. (19, 20) mp 227–228°C); GC–MS *m/z* (relative intensity): 304(74, M^+), 230(15), 214(65), 177(43), 142(81).

4,5-Dichlorocatechol (21, 22): To an ice-cooled solution (maintained under nitrogen) of catechol (37.5 g, 0.325 mol) in anhydrous ether (150 mL) was added, dropwise, with stirring over a period of 180 min, sulphuryl chloride (58 mL, 97 g, 0.72 mol), which was distilled under nitrogen before reaction. The solution was allowed to warm to room temperature and was evaporated under nitrogen to a volume of ca 75 mL. The crystalline precipitate that formed on standing was collected to afford 4,5-dichlorocatechol (29.5 g, 51%); ^{1}H NMR ($CDCl_3$) δ: 6.98 (s, 2H), 5.56 (s, 2H, 2 × O*H*); GC–MS *m/z* (relative intensity): 178(85, M^+), 149(15), 113(10), 97(66), 85(32).

1-Nitrodibenzo-p-*dioxin* (**1**) was prepared by the procedure of Loudon and McCapra (23). In a 50 mL three-necked, round-bottomed flask, equipped with a stir bar, nitrogen inlet, and a reflux condenser (connected to a bubbler), were placed catechol (0.544 g, 4.9 mmol), potassium carbonate (1.365 g,

Can. J. Chem. Downloaded from www.nrcresearchpress.com by 65.111.164.53 on 09/08/12
For personal use only.

Can. J. Chem. Downloaded from www.nrcresearchpress.com by 65.111.164.53 on 09/08/12
For personal use only.

9.8 mmol), and dried acetone (10 mL). 18-Crown-6 (2.5 g, 9.8 mmol) was added and the mixture was refluxed under nitrogen for 45 min. A solution of 2,6-dinitrochlorobenzene (0.993 g, 4.9 mmol) in dried acetone (10 mL) was then added using a syringe. The reaction mixture was refluxed under nitrogen for an additional 8 h. After cooling, the reaction mixture was poured onto ice, and the yellow precipitate was collected by vacuum filtration and air dried. The product was purified by flash chromatography, eluting with 40% dichloromethane in hexane, affording 1-nitrodibenzo-*p*-dioxin (0.74 g, 66%): mp 126–126.5°C (lit. (23) mp 126°C); IR (CH_2Cl_2): 3058; 1539 and 1358 (NO_2); 1593, 1495, 1477, 1427, 1295, 1262, 1259, 1104, 1070, 1032, 848 cm^{-1}; ^1H NMR ($CDCl_3$) δ: 7.51 (dd, J = 8.0, 1.8 Hz, 1H), 7.07 (dd, J = 7.2, 1.6 Hz, 1H), 6.96 (m, 4H), 6.87 (m, 1H); GC–MS *m/z* (relative intensity): 229(100, M^+), 183(53), 171(6), 155(7), 127(29).

2-Nitrodibenzo-p-*dioxin* (**2**) was obtained in 83% yield by the condensation of catechol with 2,4-dinitrofluorobenzene, using the procedure described above for the preparation of the 1-isomer: mp 140–141°C; IR (CH_2Cl_2): 3058, 2991; 1533 and 1345 (NO_2); 1506, 1490, 1431, 1421, 1297, 1264, 1125, 1101, 1078, 1030, 825 cm^{-1}; ^1H NMR ($CDCl_3$) δ: 7.82 (dd, J = 9.0, 2.8 Hz, 1H), 7.73 (d, J = 2.6 Hz, 1H), 6.96 (m, 4H), 6.86 (m, 1H); GC–MS *m/z* (relative intensity): 229(100, M^+), 183(44), 171(9), 155(3), 127(20).

1,2-Dichloro-3-nitrodibenzo-p-*dioxin* (**3**) was prepared similarly by the base-promoted condensation of catechol (0.414 g, 3.7 mmol) and 2,3-dichloro-4,6-dinitrofluorobenzene (0.95 g, 3.7 mmol) in refluxing acetone in the presence of 18-crown-6 (1.038 g, 7.45 mmol). The product (**3**) was obtained in mixture with 1-chloro-2,4-dinitrodibenzo-*p*-dioxin (**4**). The isomers were separated by silica gel column chromatography, eluting with 40% dichloromethane in hexane. 1,2-Dichloro-3-nitrodibenzo-*p*-dioxin (**3**, 31%) had mp 171–172°C; IR (CCl_4): 2968, 2927; 1561 and 1338 (NO_2); 1541, 1505, 1475, 1453, 1303, 1298, 1261, 1100, 1020, 863, 841 cm^{-1}; ^1H NMR ($CDCl_3$) δ: 7.40 (s, 1H), 7.00 (m, 3H), 6.84 (m, 1H); MS *m/z* (relative intensity): 297(100, M^+), 251(53), 160(40), 108(12). The by-product 1-chloro-2,4-dinitrodibenzo-*p*-dioxin (**4**, 45%) had ^1H NMR ($CDCl_3$) δ: 7.42 (s, 1H), 7.02 (m, 3H), 6.88 (m, 1H); GC–MS *m/z* (relative intensity): 308(100, M^+), 232(12), 216(54), 183(14), 160(20).

2,3,4,7,8-Pentachloro-1-nitrodibenzo-p-*dioxin* (**5**) was prepared similarly by the condensation of 4,5-dichlorocatechol (0.68 g, 3.8 mmol) and 3,4,5-trichloro-2,6-dinitrofluorobenzene (1.1 g, 3.8 mmol) in the presence of potassium carbonate (1.058 g, 7.6 mmol) and 18-crown-6 (1.0 g, 3.8 mmol) in refluxing acetone. After purification by flash chromatography, eluting with 10% dichloromethane in hexane, the product **5** was obtained in 91% yield; mp 238–239°C; IR (CH_2Cl_2): 3020; 1555 and 1306 (NO_2), 1489, 1471, 1440, 1379, 1359, 1110, 995, 890, 859 cm^{-1}; ^1H NMR ($CDCl_3$) δ: 7.17 (s, 1H), 7.07 (s, 1H); GC–MS *m/z* (relative intensity): 399(100, M^+), 353(31), 318(8), 262(22).

1,3,4,7,8-Pentachloro-2-nitrodibenzo-p-*dioxin* (**6**) was prepared by the method of Mahiou and Deinzer (19), in which 4,5-dichlorocatechol (0.836 g, 4.67 mmol) and 1,4-dinitrotetrachlorobenzene (1.0935 g, 4.67 mmol) were condensed in refluxing acetone in the presence of potassium carbonate (1.291 g, 9.34 mmol) and 18-crown-6 (1.23 g, 4.67 mmol). The product was obtained in 80% yield after purification by flash chromatography, eluting with 2% dichloromethane in hexane; mp 206–207°C; IR (CCl_4): 2970, 2934; 1570 and 1302 (NO_2); 1480, 1469, 1433, 1362, 1360, 1060, 984, 868, 832 cm^{-1}; ^1H NMR ($CDCl_3$)δ: 7.15 (s, 1H), 7.13 (s, 1H); GC–MS *m/z* (relative intensity): 399(100, M^+), 353(34), 318(16), 262(31).

Preparative irradiations

Preparative scale irradiations were performed in 25 mm × 195 mm Pyrex tubes, using as the light source a Rayonet model RPR photoreactor, equipped with 16 lamps, having maximum emission at 300 nm. Sodium ethoxide solutions were prepared by dissolving the calculated quantity of metallic sodium in anhydrous ethanol.

1-Nitrodibenzo-p-*dioxin/EtO⁻*

A solution of **1** (22.9 mg 1-NDD in 100 mL ethanol, 1.0 mM) was mixed with 0.1 M NaOEt in ethanol (100 mL) and irradiated in four Pyrex tubes for 2 h. After irradiation, a large amount of water (≈200 mL) was added to the reaction mixture and the aqueous solution was then extracted repeatedly with dichloromethane (20 × 10 mL). The organic extract was dried over $MgSO_4$ and the solvent removed under reduced pressure. HPLC showed a large peak due to the product, along with a small peak from the unreacted starting material. After preparative HPLC, eluting with methanol at a flow rate of 4 mL/min, the product (71%) was analyzed by GC–MS and ^1H NMR, which showed that two isomers were present in 4:1 ratio: 2-ethoxy-6-nitro-2′-hydroxydiphenyl ether **7** and 2-ethoxy-3-nitro-2′-hydroxydiphenyl ether **8**. The minor isomer **8** was the product of a thermal reaction, and was isolated pure, as follows. In a 50 mL round-bottomed flask, equipped with a stir bar and a reflux condenser, a solution of 1-NDD (20 mg, 0.087 mmol) in anhydrous ethanol (10 mL) was combined with a solution of 0.5 M NaOEt (10 mL). The reaction mixture was heated to reflux for 1 h, and the product appearance was monitored on HPLC. After the reaction was complete, a large amount of water was added and the aqueous solution was extracted with dichloromethane (20 × 10 mL). The organic extract was then dried ($MgSO_4$), evaporated to dryness, and a portion of the residue was purified by preparative HPLC. Compound **8**: ^1H NMR ($CDCl_3$) δ: 7.55 (dd, J = 7.4, 2.2 Hz, 1H), 7.12 (m, 4H), 6.97 (m, 2H), 4.27 (q, J = 7.0 Hz, 2H, -OCH_2CH$_3$), 1.65 (s, 1H, -O*H*), 1.39 (t, J = 7.0 Hz, 3H, -OCH$_2$CH_3); GC–MS: RT = 15.60 min, *m/z* (relative intensity): 275(53, M^+), 247(5), 229(100), 199(15), 183(9). HRMS calcd. for $C_{14}H_{13}NO_5$: 275.0794; found: 275.0776. By comparing the ^1H NMR and GC–MS spectra of the isomer mixture with those of the thermal isomer, the following data were deduced for isomer **7**: ^1H NMR ($CDCl_3$) δ: 7.45 (dd, J = 8.0, 1.6 Hz, 1H), 7.28 (m, 3H), 6.65 (m, 3H), 3.98 (q, J = 7.0 Hz, 2H, -OCH_2CH$_3$), 3.78 (s, 1H, -O*H*), 1.21 (t, J = 7.0 Hz, 3H, -OCH$_2$CH_3); GC–MS: RT = 16.26 min, *m/z* (relative intensity): 275(100, M^+), 229(2), 199(2), 183(1), 167(15). HRMS calcd. for $C_{14}H_{13}NO_5$: 275.0794; found: 275.0773.

2-Nitrodibenzo-p-*dioxin/EtO⁻*

A similar procedure afforded a mixture of isomers in 73% yield and a 1:1 ratio. A thermal reaction yielded 2-ethoxy-5-nitro-2′-hydroxy-diphenyl ether (**10**): ^1H NMR ($CDCl_3$) δ:

Can. J. Chem. Downloaded from www.nrcresearchpress.com by 65.111.164.53 on 09/08/12
For personal use only.

8.05 (dd, J = 9.0, 2.8 Hz, 1H), 7.93 (d, J = 2.4 Hz, 1H), 7.02 (m, 3H), 6.90 (m, 1H), 6.83 (dd, J = 6.2, 2.4 Hz, 1H), 5.92 (s, 1H, -O*H*), 4.17 (q, J = 7.0 Hz, 2H, -OCH_2CH$_3$), 1.42 (t, J = 7.0 Hz, 3H, -OCH$_2$CH_3); GC–MS: RT = 16.94 min, *m/z* (relative intensity): 275(100, M^+), 247(9), 230(59), 200(37), 171(8). HRMS calcd. for $C_{14}H_{13}NO_5$: 275.0794; found: 275.0779. By comparing the ^{1}H NMR and GC–MS spectra of the photochemical isomer mixture with those of the thermal isomer, the following data were deduced for 2-ethoxy-4-nitro-2′-hydroxydiphenyl ether (**9**): ^{1}H NMR ($CDCl_3$) δ: 7.82 (m, 3H), 7.02 (m, 3H), 6.86 (m, 1H), 4.17 (q, J = 7.0 Hz, 2H, -OCH_2CH$_3$), 1.62 (bs, 1H, -O*H*), 1.43 (t, J = 7.0 Hz, 2H, -OCH$_2$CH_3); GC–MS: RT = 16.43 min, *m/z* (relative intensity): 275(100, M^+), 247(13), 230(34), 200(21), 183(3), 171(7). HRMS calcd. for $C_{14}H_{13}NO_5$: 275.0794; found: 275.0778.

1,2-Dichloro-3-nitrodibenzo-p-*dioxin/EtO*$^-$

A solution of **3** (10 mg in 33 mL anhydrous ethanol, 1.0 mM) was mixed with a solution of 0.1 M NaOEt (33.5 mL) and divided between two Pyrex tubes (25 mm × 195 mm) which were irradiated for 90 min. After irradiation, the reaction mixture was extracted as described for **1**. The products were 2,3-dichloro-6-ethoxy-4-nitro-2′-hydroxydiphenyl ether **11** and 3,4-dichloro-2-ethoxy-5-nitro-2′-hydroxydiphenyl ether **12**. Isomer **12** was synthesized by thermal reaction of **3** with NaOEt: ^{1}H NMR ($CDCl_3$) δ: 7.33 (s, 1H), 7.11 (dd, J = 6.8, 2.0 Hz, 1H), 7.03 (m, 1H), 6.91 (m, 2H), 4.26 (q, J = 7.0 Hz, 2H, -OCH_2CH$_3$), 3.12 (bs, 1H, -O*H*), 1.43 (t, J = 7.0 Hz, 3H, -OCH$_2$CH_3); GC–MS: RT = 19.19 min, *m/z* (relative intensity): 347(11, M^+ + 4), 345 (66, M^+ + 2), 343(100, M^+), 315(59), 298(31), 268(32), 251(4), 233(7). HRMS calcd. for $C_{14}H_{11}Cl_2NO_5$: 343.0014; found: 343.0014. Spectral comparison allowed the following data to be deduced for isomer **11**: ^{1}H NMR ($CDCl_3$) δ: 7.38 (s, 1H), 7.03 (m, 2H), 6.91 (m, 2H), 3.99 (q, J = 6.6 Hz, 2H, -OCH_2CH$_3$), 2.40 (bs, 1H, -O*H*), 1.25 (t, J = 6.6 Hz, 3H, -OCH$_2$CH_3); GC–MS: RT = 19.06 min, *m/z* (relative intensity): 347(11, M^+ + 4), 345(66, M^+ + 2), 343(100, M^+), 315(17), 298(13), 268(14), 251(6), 233(7). HRMS calcd. for $C_{14}H_{11}Cl_2NO_5$: 343.0014; found: 343.0010.

2,3,4,7,8-Pentachloro-1-nitrodibenzo-p-*dioxin/EtO*$^-$

A solution of 0.1 M NaOEt (100 mL) was added to a 0.4 mM solution (100 mL) of **5** in anhydrous ethanol and the reaction mixture was irradiated at 300 nm for 1 h. A similar work-up procedure as described previously yielded 2,4,7,8-tetrachloro-3-ethoxy-1-nitrodibenzo-*p*-dioxin **13** (12.0 mg, 0.0293 mmol, 73%): ^{1}H NMR ($CDCl_3$)δ: 7.16 (s, 1H), 6.60 (s, 1H), 4.14 (q, J = 7.0 Hz, 2H, -OCH_2CH$_3$), 1.25 (t, J = 7.0 Hz, 3H, -OCH$_2$CH_3); GC–MS: RT = 22.49 min, *m/z* (relative intensity): 413(24, M^+ + 4), 411(52, M^+ + 2), 409(39, M^+), 381(79), 364(12), 307(10), 271(11). HRMS calcd. for $C_{14}H_7Cl_4NO_5$: 408.9078; found: 408.9065.

1,3,4,7,8-Pentachloro-2-nitrodibenzo-p-*dioxin/EtO*$^-$

A solution of 0.1 M NaOEt (50 mL) was combined with a solution of **6** (8.03 mg in 50 mL anhydrous ethanol, 0.4 mM) and the reaction mixture was irradiated in two Pyrex tubes for 1 h. Work-up by the procedure already described afforded 1,3,7,8-tetrachloro-4-ethoxy-2-nitrodibenzo-*p*-dioxin **14** (7.2 mg, 0.0175 mmol, 86%): ^{1}H NMR ($CDCl_3$)δ: 7.15 (s, 1H), 6.63 (s, 1H), 4.08 (q, J = 7.0 Hz, 2H, -OCH_2CH$_3$), 1.32 (t, J = 7.0 Hz, 3H, -OCH$_2$CH_3); GC–MS: RT = 23.06 min, *m/z* (relative intensity): 413(40, M^+ + 4), 411(79, M^+ + 2), 409(61, M^+), 381(79), 350(9), 335(52), 307(13), 271(22). HRMS calcd. for $C_{14}H_7Cl_4NO_5$: 408.9078; found: 408.9069. A thermal reaction was also performed in which **6** (10 mg, 0.025 mmol) was dissolved in a solution of 0.1 M NaOEt (100 mL) and the reaction mixture was refluxed for 1 h. After reaction, a large amount of water (≈200 mL) was added and then the reaction mixture was extracted with dichloromethane (15 × 10 mL). One major product (compound **15**) with molar mass 457 g/mol (a tetrachlorodiethoxyhydroxynitrodiphenyl ether) was obtained (7.96 mg, 0.0174 mmol, 70%); ^{1}H NMR ($CDCl_3$)δ: 7.13 (s, 1H), 6.78 (s, 1H), 4.11 (q, J = 7.04 Hz, 2H, -OCH_2CH$_3$), 4.01 (q, J = 7.04 Hz, 2H, -OCH_2CH$_3$), 1.65 (bs, 1H, -O*H*), 1.30 (t, J = 7.04 Hz, 3H, -OCH$_2$CH_3), 1.26 (t, J = 7.04 Hz, 3H, -OCH$_2$CH_3); GC–MS: RT = 22.61 min, *m/z* (relative intensity): 459(52, M^+ + 4), 457(100, M^+ + 2), 455(84, M^+), 409(51), 381(28), 351(10), 335(12), 308(19). HRMS calcd. for $C_{16}H_{13}Cl_4NO_6$: 454.9497; found: 454.9475. A tetrachloroethoxynitrodibenzo-*p*-dioxin (molar mass 411 g/mol) was also found to be present in trace amounts in the reaction mixture; it had GC–MS: RT = 23.10 min, *m/z* (relative intensity): 413(40, M^+ + 4), 411(79, M^+ + 2), 409(M^+, 61), 381(78), 350(13), 335(43), 307(9), 271(17).

Kinetic irradiations

Analytical scale irradiations were performed in Pyrex tubes using a "merry-go-round" Rayonet model RPR photoreactor, equipped with 16 lamps, having maximum emission at 300 nm. Because of the low solubility of NPCDDs, the solutions were prepared in the concentration range 0.4–1.0 mM, using methanol (for reactions with KCN) or anhydrous ethanol (for reactions with NaOEt) as solvent. To make sure the solid was completely dissolved, the solution was sonicated for at least 5 min. Solutions of 0.1 M nucleophile (NaOEt, KCN) were also prepared. In 18 mm × 150 mm Pyrex tubes, solutions of substrate (2 mL) were combined with solutions of nucleophile (2 mL) to give the final samples, which were sealed with serum caps and irradiated at the ambient temperature. Four samples were analyzed for each NPCDD congener: deaerated sample, aerated sample, dark sample, and sample without nucleophile. The samples were deaerated by bubbling nitrogen in the solution for 2 min. The samples were irradiated and periodically a 50–100 μL aliquot was removed by means of a syringe for HPLC monitoring of reaction progress. The reaction was monitored for substrate loss and product appearance using the external standard method, using hexachlorobenzene (1×10^{-3} M solution) as the external standard.

Yields

Chemical yields were calculated in terms of substrate reacted, using hexachlorobenzene as an external standard (added after irradiation). Standards for quantitation were prepared from the NPCDD congeners previously synthesized and a separate calibration curve was drawn for each.

Quantum yields were determined using the method of Hatchard and Parker (24), using potassium ferrioxalate as actinometer. The actinometer and the test solution (2 mL, prepared as for the determination of chemical yields) were placed into 5 mm i.d. Pyrex tubes, which were then inserted into 25 mm i.d. Pyrex tubes containing the chemical filter

Can. J. Chem. Downloaded from www.nrcresearchpress.com by 65.111.164.53 on 09/08/12
For personal use only.

Table 1. Quantum yields for the disappearance of NPCDDs.

Substrate	Nucleophile (0.1 M)	Solvent	Φ_{313}
1-NDD (**1**)	EtO^-	Ethanol	0.10
	CN^-	Methanol	0.13
2-NDD (**2**)	EtO^-	Ethanol	0.12
	CN^-	Methanol	0.11
1,2,-DCDD-3-NO_2 (**3**)	EtO^-	Ethanol	0.03
	CN^-	Methanol	0.02
1,3,4,7,8-PeCDD-2-NO_2 (**6**)	EtO^-	Ethanol	0.04
	CN^-	Methanol	0.03
2,3,4,7,8-PeCDD-1-NO_2 (**5**)	EtO^-	Ethanol	0.04
	CN^-	Methanol	0.04

solution (25) (0.2 g/L K_2CrO_4–$NiSO_4$, 0.1% NaOH) to isolate radiation at 313 ± 10 nm. These solutions were irradiated in the Rayonet photoreactor, using 300 nm lamps and a "merry-go-round" to ensure equal illumination of all samples. The reaction was monitored for substrate loss by HPLC, using the external standard method. The intensity of the incident radiation near 313 nm was 1.53×10^{-6} mol min^{-1}. The results are presented in Table 1.

Results and discussion

Preparation of NPCDD congeners

Two general methods have been used to prepare NPCDDs: nitration of the parent PCDDs and condensation between a chlorinated catechol and a suitably substituted chlorinated 1,3-dinitrobenzene. Disadvantages of the former method include the extremely low reactivity of the apical (1, 4, 6, and 9) positions compared with the lateral (2, 3, 7, and 8) positions, and lack of regioselectivity when more than one lateral (or apical) position is available. For example, whereas 1,3,6,8-tetrachlorodibenzo-*p*-dioxin (1,3,6,8-TCDD) nitrated smoothly using NH_4NO_3 in trifluoroacetic acid (26), the isomeric 2,3,7,8-TCDD could be nitrated only with reagents such as NO_2BF_4 at elevated temperature (27). The condensation method is more generally applicable, although the possibility of positional isomerism in the products still exists, due to the intervention of a Smiles-like rearrangement at an intermediate stage of the condensation (28), see Scheme 1. In this work, we avoided this complication by using only symmetrical catechol synthons, thereby rendering the Smiles-like rearrangement degenerate. In the presence of base, the conjugate base of the catechol attacks the chlorinated dinitrobenzene *ortho* to both NO_2 groups; the leaving group may be either chloride or, as in the improvement introduced by Mahiou and Deinzer (19), fluoride ion. Attack by the second $-O^-$ of the original catechol leads to cyclization with elimination of one of the NO_2 groups as NO_2^- (although, in the case of the condensation of catechol with 2,3-dichloro-4,6-dinitrofluorobenzene, elimination of Cl^- to give 1-chloro-2,4-dinitrodibenzo-*p*-dioxin **4** competed to a minor extent with elimination of NO_2^- to give 1,2-dichloro-3-nitrodibenzo-*p*-dioxin **3**.

Nucleophilic photosubstitution of NPCDDs

In earlier work on nitrodibenzo-*p*-dioxins, Leoni et al. (29) observed that **2** reacted photochemically with propylamine to give chiefly the isomeric (*N*-propylamino)hydroxynitrodiphenyl ethers **16** and **17** in polar solvents (Scheme 2), while **1** was photochemically inert. In cyclohexane, *N*-(propylamino)-2-nitrophenoxazine, **18**, a minor product in the polar solvent, was the sole product isolated. The quantum yield of the disappearance of 2-NDD gradually fell with the solvent polarity, as did the quantum yield of formation of **16** and **17**, but the quantum yield of formation of product **18** remained practically unchanged. The authors explained this effect by assuming that the interaction of triplet **2** with the amine leads initially to an exciplex, which either dissociates into radical ions affording **16** and **17**, or which forms **18** from the undissociated exciplex. Another possible explanation is that **16** and **17** are S_N2Ar^* products and **18** comes from electron transfer within the exciplex.

NPCDDs absorb with moderate intensity at 300 nm ($\log \epsilon \approx 3$) with shoulders near 360 nm due to the $n\pi^*$ transition centred on the nitro group. We have previously shown that NPCDDs photolyze rapidly at 300 nm in the presence of dilute sodium hydroxide (7). The photolyzates from the NPCDDs failed to bind to the Ah receptor, implying that the photoproducts had changed their shape, presumably by ring opening. An attempt to identify the products was unsuccessful due to their intractability (B. Mahiou, unpublished work). In the present study also, the products obtained using CN^- were intractable, but those from EtO^- were identifiable. Ethoxide was chosen as the nucleophile rather than methoxide because the ^1H NMR pattern of the ethoxy group was more diagnostically useful than that of a singlet methoxy. The semipreparative irradiations were carried out in a Rayonet photoreactor equipped with 300 nm lamps; for the quantum yield determinations, low-pressure mercury lamps were used with a chemical filter (K_2CrO_4–$NiSO_4$, 0.1% NaOH) (25) to isolate radiation near 313 nm.

The photoreactions of **1**, **2**, and **3** with NaOEt all afforded ring-opened products compatible with an S_N2Ar^* reaction. In every case, a competing thermal ring opening also occurred *para* to the nitro group: e.g., Scheme 3. The isomeric ethoxyhydroxydiphenyl ethers obtained in the photochemical reactions could not be separated preparatively, although they were separable by capillary GC, and so it was necessary to deduce the ^1H NMR spectrum of the photoproduct by isolating the thermal product in a separate reaction, and then substracting its spectrum from that of the mixture.

The two pentachlorinated NPCDDs both underwent substi-

Can. J. Chem. Downloaded from www.nrcresearchpress.com by 65.111.164.53 on 09/08/12
For personal use only.

Scheme 1. Smiles rearrangement in the synthesis of NPCDDs.

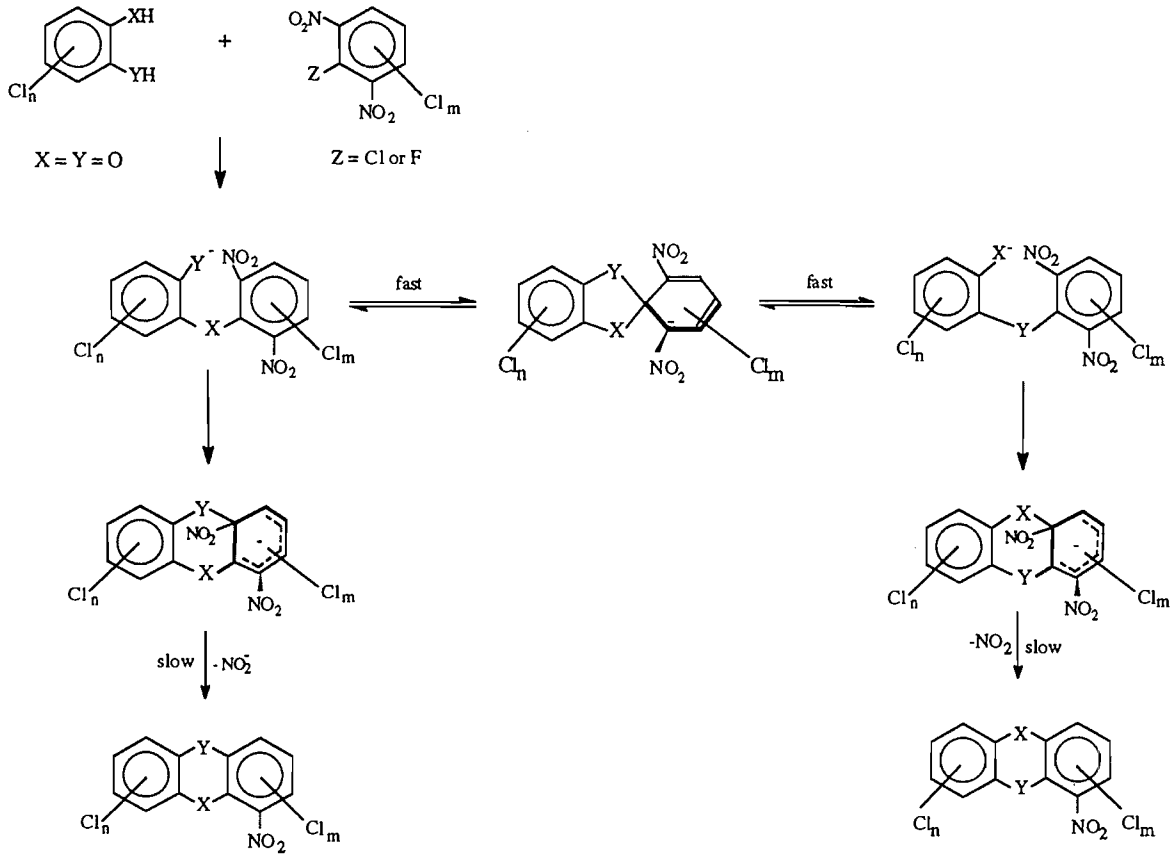

Scheme 2. Photosubstitution reactions of 2-NDD in the presence of primary amines.

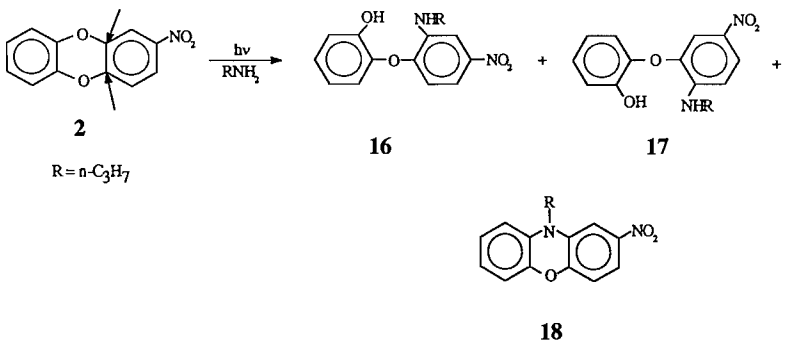

Scheme 3. Substitution reactions of 1-NDD with NaOEt.

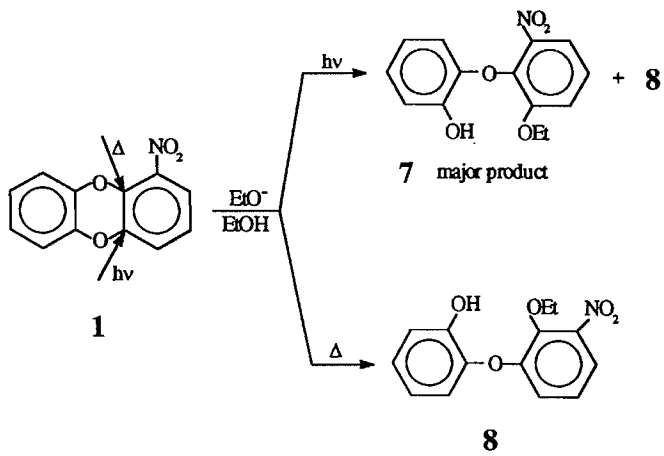

tution with loss of chloride, instead of ring opening. 2,3,4,7,8-Pentachloro-1-nitrodibenzo-*p*-dioxin (**5**) yielded, upon irradiation with NaOEt, a tetrachloroethoxynitrodibenzo-*p*-dioxin, which was presumed to be 2,4,7,8-tetrachloro-3-ethoxy-1-nitrodibenzo-*p*-dioxin, **13**, based on the *meta* activation of the nitro group (eq. [2]). Control experiments showed that compound **5** is stable on irradiation in the absence of the nucleophile. A thermal reaction was detected in the dark sample containing NaOEt, which yielded a tetrachlorodiethoxyhydroxynitrodiphenyl ether. The isomeric 1,3,4,7,8-pentachloro-

[2] 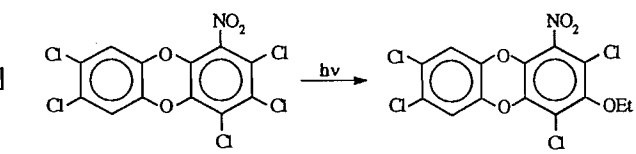

Scheme 4. Substitution reactions of 1,3,4,7,8-PeCDD-2-NO_2 with NaOEt.

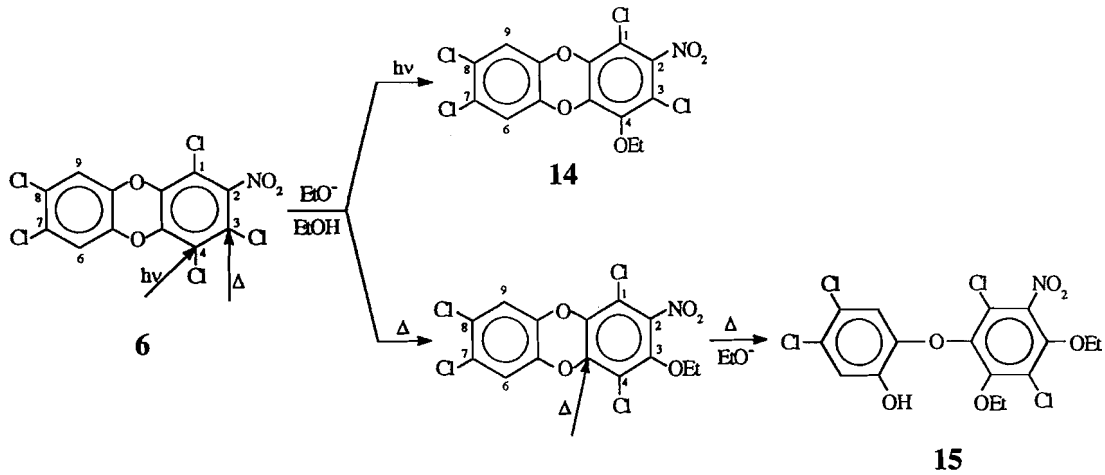

Fig. 2. Pseudo-first-order kinetic plot for the photoethoxidation of 2-nitrodibenzo-*p*-dioxin.

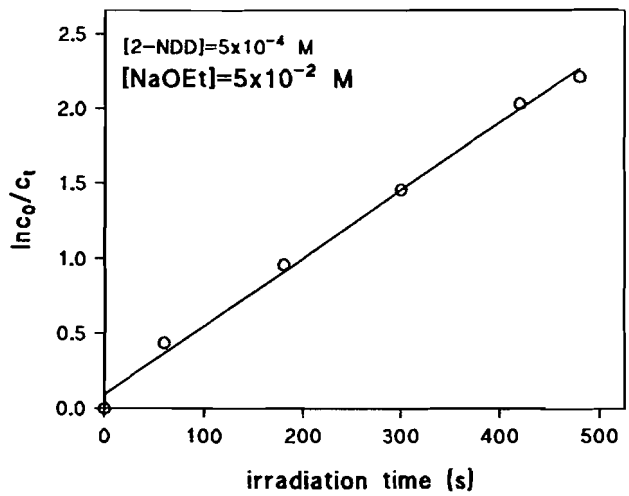

Fig. 3. Stern–Volmer plot for quenching the photoethoxidation of 2-nitrodibenzo-*p*-dioxin by piperylene.

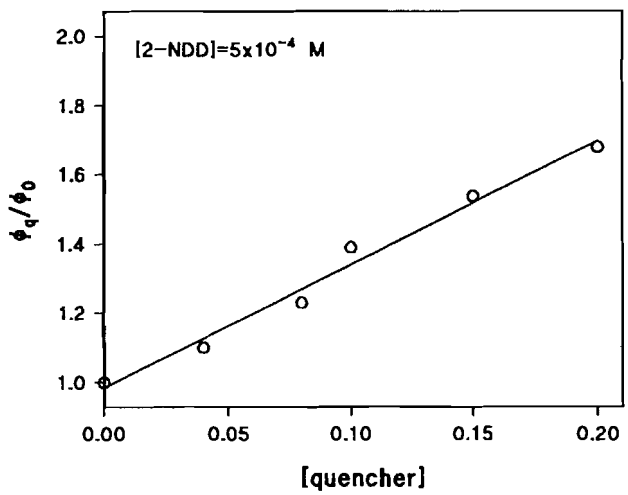

2-nitrodibenzo-*p*-dioxin (1,3,4,7,8-PeCDD-2-NO_2) **6**, when irradiated in the presence of NaOEt, afforded only one product **14**, which was identified as 1,3,7,8-tetrachloro-4-ethoxy-2-nitrodibenzo-*p*-dioxin, resulting from substitution of chlorine *meta* to the nitro group rather than from ring opening (Scheme 4). Control experiments showed that 1,3,4,7,8-PeCDD-2-NO_2 is stable on irradiation in the absence of EtO^- but a slow reaction was detected in the dark sample containing NaOEt.

Scheme 5.

$$ArX \xrightarrow{h\nu} ArX^*$$

$$ArX^* \xrightarrow{k_1} ArX$$

$$ArX^* + Nu^- \xrightarrow{k_2} [ArXNu]^-$$

$$[ArXNu]^- \xrightarrow{k_3} ArX + Nu^-$$

$$[ArXNu]^- \xrightarrow{k_4} ArNu + X^-$$

Reaction mechanism

Because of the low solubilities of the NPCDDs, the photoreactions were all carried out under conditions where little of the initial light intensity was absorbed. Under conditions of constant light intensity, such photoreactions are pseudo first order; experimentally, linear relationships were obtained between ln c_0/c_t (c_0: initial concentration of NPCDD; c_t: NPCDD concentration at time t) and time of irradiation, t, see Fig. 2, for example.

Quenching with piperylene showed that the reactive excited state is of triplet multiplicity, consistent with the NPCDDs, like other nitroaromatic compounds, undergoing intersystem crossing to the lowest triplet state with high efficiency following photoexcitation. Plots of Φ_q/Φ_0 vs. [quencher] (Φ_q: quantum yield of reaction in the presence of quencher and Φ_0 in the absence of quencher) were linear for all substrates, over the concentration range 0–0.2 M piperylene, see Fig. 3 for example.

Scheme 5 shows a reaction pathway consistent with the S_N2Ar^* mechanism. The excited triplet ArX* (assumed to be formed with near maximum efficiency) can undergo radiationless decay to the ground state (rate constant k_1) or interact with the nucleophile Nu^- (rate constant k_2) to give a σ-complex

Can. J. Chem. Downloaded from www.nrcresearchpress.com by 65.111.164.53 on 09/08/12
For personal use only.

Table 2. Kinetic parameters for the irradiation of NPCDDs at varying concentrations of NaOEt (1/consumed concentration vs. 1/[NaOEt]).

Substrate (starting concentration)	Slope	Intercept ($\times 10^{-3}$ M)	Intercept/slope	Regression coefficient
1-NDD (5×10^{-4} M)	34	2.9	86	0.984
2-NDD (5×10^{-4} M)	5.6	2.7	480	0.994
1,2-DCDD-3-NO_2 (5×10^{-4} M)	3.8	2.5	660	0.979
2,3,4,7,8-PeCDD-1-NO_2 (2×10^{-4} M)	18	11	62	0.983
1,3,4,7,8-PeCDD-2-NO_2 (2×10^{-4} M)	49	16	330	0.991

Fig. 4. Double reciprocal plot: conversion^{-1} vs. (nucleophile concentration)$^{-1}$ for the photoethoxidation of 2-nitrodibenzo-*p*-dioxin.

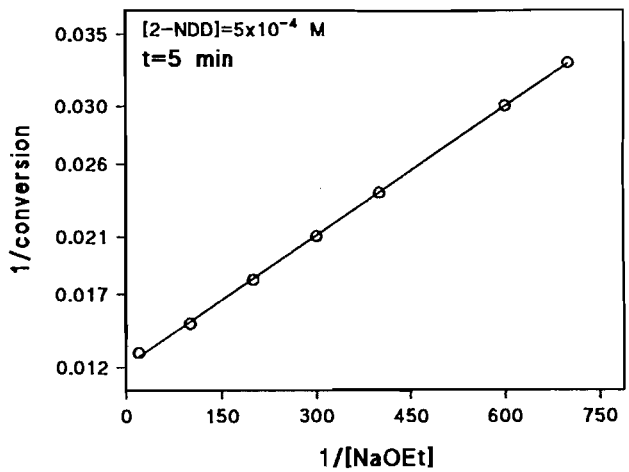

$[ArXNu]^-$, which may then dissociate to ground state reactants (k_3) or afford the substitution products (k_4). Application of the steady-state approximation to Scheme 5 affords eq. 3, consistent with the observed linear relationship between Φ^{-1} and $[Nu]^{-1}$.

$$[3] \quad \Phi^{-1} = (1 + k_3/k_4)(1 + k_1/k_2[Nu^-])$$

The quantum yields for disappearance of the NPCDDs (± 10%) were determined using potassium ferrioxalate actinometry (24) at 313 nm in the presence of 0.1 M nucleophile and are summarized in Table 1. The low quantum yield even at a high concentration of nucleophile means either that the majority of triplets must fail to form σ-complexes, or that the σ-complexes must preferentially revert to reactant rather than proceed to products. The dependence of the reaction quantum yield upon the concentration of nucleophile showed the linear relationship between Φ^{-1} and $[Nu]^{-1}$ characteristic of an S_N2Ar^* reaction. This was seen for all the NPCDDs studied, for both CN^- and EtO^- as the nucleophiles: see Table 2, and Fig. 4. In every case the high value of the parameter intercept/slope $\equiv k_2/k_1$ shows that a high proportion of excited triplets will form σ-complexes whenever [Nu] > 0.01 M and hence that the low overall quantum yield results principally from the inherent tendency of the σ-complex to partition towards reactants rather than products.

The present work had as one objective, to explore whether photochemically induced nucleophilic substitution reactions of NPCDDs might be a technologically viable method for the destruction of PCDDs in an environmental matrix. Such a putative technology might involve nitration of the PCDD followed by photochemical ring opening in the presence of a nucleophile. Our studies show that this idea is not feasible. PCDDs are difficult to nitrate unless they have an open lateral position, yet the congeners of the greatest environmental concern are precisely those that are fully chlorinated in the lateral positions. In addition, nucleophilic ring opening is not universal among the NPCDDs studied; the pentachloro congeners underwent nucleophilic replacement of a *meta* chlorine instead. Finally, the intractability of the products, using a "convenient" nucleophile such as OH^-, means that the nature and toxicity of the products cannot be determined, and so it would be unacceptable to release them into the environment.

In conclusion, the nitrodibenzo-*p*-dioxin congeners studied here behave as typical nitro-substituted ethers such as the 3- and 4-nitroveratroles (8, 17) in their photochemical reaction with the poorly oxidizable nucleophile ethoxide ion. One triplet excited state is involved, and the photochemical kinetics are completely consistent with substitution by the S_N2Ar^* mechanism.

Acknowledgements

We thank the Natural Sciences and Engineering Research Council of Canada for financial support and Mr. H.S. McKinnon for running the HRMS analyses.

References

1. E.S. Johnson. Environ. Health Perspect. **99**, 383 (1993).
2. G.W. Lucier, C.J. Portier, and M.A. Gallo. Environ. Health Perspect. **101**, 36 (1993).
3. S. Safe. Crit. Rev. Toxicol. **21**, 51 (1990).
4. J.P. Whitlock. Chem. Res. Toxicol. **6**, 754 (1993).
5. J.P. Landers and N.J. Bunce. Biochem. J. **267**, 273 (1991).
6. S. Safe. Annu. Rev. Pharmacol. Toxicol. **26**, 371 (1986).
7. N.J. Bunce, G. DiDiodato, and S.H. Safe. Chemosphere, **24**, 433 (1992).
8. J. Cornelisse and E. Havinga. Chem. Rev. **75**, 353 (1975).
9. J. Cornelisse, G.P. de Gunst, and E. Havinga. Adv. Phys. Org. Chem. **11**, 225 (1975).
10. C.A.G.O. Varma, J.J. Taminga, and J. Cornelisse. J. Chem. Soc. Faraday Trans. 2, **78**, 265 (1982).
11. P.H.M. van Zeijl, L.M.J. van Eijk, and C.A.G.O. Varma. J. Photochem. **29**, 415 (1985).
12. J.H. McCain and R.L. Letsinger. J. Am. Chem. Soc. **91**, 6425 (1967).
13. E. Havinga and R.O. de Jongh. Bull. Soc. Chim. Belg. **71**, 803 (1962).
14. K. Mutai and K. Kobayashi. Bull. Chem. Soc. Jpn. **54**, 462 (1981).

Can. J. Chem. Downloaded from www.nrcresearchpress.com by 65.111.164.53 on 09/08/12
For personal use only.

15. K. Mutai, K. Kobayashi, K. Yokoyama, and S. Kanno. Bull. Chem. Soc. Jpn. **55**, 1112 (1982).
16. K. Mutai, R. Nakagaki, and H. Tokada. Bull. Chem. Soc. Jpn. **58**, 2066 (1985).
17. N.J. Bunce and K. Labonte-Stephenson. Can. J. Chem. **67**, 220 (1989).
18. F.D. Gunstone and H.S. Tucker. Org. Synth. Collect. **4**, 160 (1963).
19. B. Mahiou and M.L. Deinzer. J. Labelled Compd. Radiopharm. **31**, 261 (1992).
20. V.S.F. Berckmans and A.F. Holleman. Recl. Trav. Chim. Pays-Bas, **44**, 851 (1925).
21. R. Willstatter and H.E. Muller. Ber. Dtsch. Chem. Ges. **44**, 2182 (1911).
22. A.P. Gray, S.P. Cepa, I.J. Solomon, and O. Aniline. J. Org. Chem. **41**, 2435 (1976).
23. J.D. Loudon and F. McCapra. J. Chem. Soc. 1899 (1959).
24. C.G. Hatchard and C.A. Parker. Proc. R. Soc. London A: **236**, 518 (1956).
25. CRC Handbook of organic photochemistry. Vol. 1. Boca Raton, Fla. 1989. p. 47.
26. J.V. Crivello. J. Org. Chem. **46**, 3056 (1981).
27. J.E. Oliver and J.M. Ruth. Chemosphere, **12**, 1497 (1983).
28. A.P. Gray, S.P. Cepa, and J.S. Cantrell. Tetrahedron Lett. 2873 (1975).
29. M.A. Leoni, G.F. Bettinetti, G. Minoli, and A. Albini. J. Org. Chem. **45**, 2331 (1980).

Can. J. Chem. Downloaded from www.nrcresearchpress.com by 65.111.164.53 on 09/08/12
For personal use only.

Structural studies of organoboron compounds LXIII.[1] Reaction of ketoximes with aldehydes and diphenylborinic acid, and the crystal and molecular structures of two different types of boron chelates and one of the precursor aldehyde adducts

Wolfgang Kliegel, Ulf Riebe, Steven J. Rettig, and James Trotter

Abstract: The diphenylboron chelates of ketoxime adducts to formaldehyde and trichloroacetaldehyde (chloral) have been synthesized. The reactions were carried out as three-component one-pot reactions, and also as two-step reactions for the ketoxime chloral adducts, which were isolated and characterized before reaction with oxybis(diphenylborane) to form the diphenylboron chelates. One of the intermediate adducts and two of the diphenylboron chelates have been characterized by X-ray crystallographic analysis. Crystals of *O*-(2,2,2-trichloro-1-hydroxyethyl)-2-propanonoxime, **8***d*, are monoclinic, $a = 7.010(2)$, $b = 11.832(3)$, $c = 11.684(2)$ Å, $\beta = 90.48(2)°$, $Z = 4$, space group $P2_1/c$; those of 4-isopropylidene-2,2-diphenyl-1,3-dioxa-4-azonia-2-boratacyclopentane, **9***a*, are orthorhombic, $a = 11.098(2)$, $b = 15.364(1)$, $c = 8.715(2)$ Å, $Z = 4$, space group $P2_12_12_1$; and those of 5-trichloromethyl-2-isopropylidene-3,3-diphenyl-1,4-dioxa-2-azonia-3-boratacyclopentane, **10***d*, are monoclinic, $a = 9.164(2)$, $b = 15.304(3)$, $c = 13.859(2)$ Å, $\beta = 105.28(1)°$, $Z = 4$, space group $P2_1/n$. The structures were solved by direct methods and refined by full-matrix least-squares procedures to $R = 0.037$, 0.044, and 0.040 ($R_w = 0.041$, 0.016, and 0.042) for 1082, 1256, and 3062 reflections with $I \geq 3\sigma(F^2)$, respectively. The X-ray analyses show that the products from the reaction between acetonoxime, oxybis(diphenylborane), and formaldehyde or trichloroacetaldehyde, respectively, possess different boron chelate structures. With formaldehyde a COBON chelate ring is obtained and with trichloroacetaldehyde a BOCON chelate ring is formed.

Key words: boron chelates, boron compounds, organboron compounds, crystal structures.

Résumé : On a synthétisé les chélates du diphénylbore des adduits de la cétoxime avec le formaldéhyde et le trichloroacétaldéhyde (chloral). On a fait appel à des réactions unipots à trois composants ainsi qu'à des réactions en deux étapes pour les adduits de la cétoxime du chloral qui ont été isolés et caractérisés avant leur réaction avec l'oxybis(diphénylborane) pour former les chélates du diphénylbore. On a caractérisé un des adduits intermédiaires et deux des chélates du diphénylbore par diffraction des rayons X. Les cristaux du *O*-(2,2,2-trichloro-1-hydroxyéthyl)propan-2-onoxime, **8***d*, sont monocliniques, groupe d'espace $P2_1/c$ avec $a = 7{,}010(2)$, $b = 11{,}832(3)$ et $c = 11{,}684(2)$ Å, $\beta = 90{,}48(2)°$ et $Z = 4$; ceux du 4-isopropylidène-2,2-diphényl-1,3-dioxa-4-azonia-2-boratacyclopentane, **9***a*, sont orthorhombiques, groupe d'espace $P2_12_12_1$ avec $a = 11{,}098(2)$, $b = 15{,}364(1)$ et $c = 8{,}715(2)$ Å, et $Z = 4$ et ceux du 5-trichlorométhyl-2-isopropylidène-3,3-diphényl-1,4-dioxa-2-azonia-3-boratacyclopentane, **10***d*, sont monocliniques, groupe d'espace $P2_1/n$ avec $a = 9{,}164(2)$, $b = 15{,}304(3)$ et $c = 13{,}859(2)$ Å, $\beta = 105{,}28(1)°$ et $Z = 4$. On a résolu les structures par des méthodes directes et on les a affinées par la méthode des moindres carrés jusqu'à des valeurs de R de 0,037, 0,044 et 0,040 ($R_w = 0{,}041$, 0,016 et 0,042) pour respectivement 1082, 1256 et 3062 réflexions avec $I \geq 3\sigma(F^2)$. Les analyses par rayons X montrent que les produits des réactions entre l'acétonoxime, l'oxybis(diphényl)bore et le formaldéhyde (ou le

Received January 13, 1995.

W. Kliegel and U. Riebe. Institut für Pharmazeutische Chemie der Technischen Universität Braunschweig, Beethovenstrasse 55, 38106 Braunschweig, Germany.
S.J. Rettig and J. Trotter.[2] Department of Chemistry, University of British Columbia, 2036 Main Mall, Vancouver, BC V6T 1Z1, Canada.

[1] Previous paper in this series: ref. 27.
[2] Author to whom correspondence may be addressed. Telephone: (604) 822-4865. Fax: (604) 822-2847. E-mail: james_trotter@mtsg.ubc.ca

Can. J. Chem. Downloaded from www.nrcresearchpress.com by 65.111.164.53 on 09/08/12
For personal use only.

trichloroacétaldéhyde) possèdent chacun des structures de chélates du bore différentes. Avec le formaldédyde, on obtient un cycle de chélate COBON alors qu'avec le trichloroacétaldéhyde il se forme un cycle de chélate BOCON.

Mots clés : chélates du bore, composés du bore, composés organobores, structures cristallines.

[Traduit par la rédaction]

Introduction

N-Hydroxydialkylamines form labile adducts with carbonyl compounds that can be trapped as boron chelates (1). Because of the ambident nucleophilic character of the hydroxylamine components the molecular structure of the resulting chelates had to be questioned (2). To provide unambiguous proof, the reaction of *N*-hydroxydimethylamine, **1**, with formaldehyde ($R^1 = R^2 = H$) and a diphenylborinic acid delivering reagent (anhydride or ester) was carried out, as an example. The resulting diphenylboron chelate **4***a* was characterized by an X-ray crystallographic analysis (3).[3] The analogous molecular structure **4***b* resulted when the bulkier carbonyl compound acetone ($R^1 = R^2 = CH_3$) was employed in the chelate-forming reaction (4). These results demonstrate that of the two possible α-hydroxyalkylation intermediates, **2** and **3**, the *N*-oxide **2** is preferred as the bidentate ligand, even if the sterically hindered acetone is applied as the carbonyl component in the chelatization reaction.[4] Likewise ambident, though less basic, nucleophiles are the ketoximes **6**, which can also be α-hydroxyalkylated to give either the *N*-oxides **7**, or the *O,O*-hemiacetal derivatives **8**, as initial adducts. The structure **7** ($R = CCl_3$) has already been ascribed to the crystalline adducts of trichloroacetaldehyde (chloral) to several oximes in a German patent of 1892 (5). Later (1*c*) an analogous formulation **8** (R = H) was suggested for the labile adducts of formaldehyde to acetone- and cyclohexanonoxime, both of which could be trapped as diphenylboron chelates with a postulated BOCON ring structure **10**. This assumption seemed, however, somewhat contradictory considering the analytical results for the diphenylboron chelates **4**, and also those for the similar six-membered boron chelates **12** that are derived from *N*-(β-hydroxyalkyl)oximes (nitrones) **11** (6). Thus, by analogy to the CCOBON ring skeleton of **12**, the five-membered COBON ring structure **9** was most likely that of the diphenylboron chelates of oxime/aldehyde adducts (7).

Because the existing analytical data are unsatisfactory, and not sufficient for structure assignment, we have synthesized the diphenylboron chelates of ketoxime adducts to formaldehyde and trichloroacetaldehyde (chloral). The reactions were carried out as three-component one-pot reactions, and also as two-step reactions for the ketoxime chloral adducts, which were isolated and characterized before reaction with oxybis(diphenylborane) to form the diphenylboron chelates. The elemental analyses, infrared spectra, and ^1H and ^{11}B nmr spectra are consistent with both of the isomeric chelate structures, the COBON ring **9** and the BOCON ring **10**, but offer no means of distinguishing between the two.

Table 1. Selected infrared and nmr data for **8**, **9**, and **10**.

Compound	Infrared (cm^{-1})	^1H nmr (δ, ppm)	^{11}B nmr (δ, ppm)
	(C=N)	(O-CH-O)	
8/10*d*	1653/1671	5.63/5.80	—/9.5
8/10*e*	1659/1688	5.67/5.80	—/8.7
8/10*f*	1647/1651	5.66/5.83	—/9.2
		($N-CH_2-O$)	
9*a*	1676	5.36	12.7
9*b*	1690	5.33	12.7
9*c*	1665	5.40	12.1

	R_2C	R^1
7–10 *a*	Me_2C	H
7–10 *b*	$(CH_2)_4C$	H
7–10 *c*	$(CH_2)_5C$	H
7–10 *d*	Me_2C	CCl_3
7–10 *e*	$(CH_2)_4C$	CCl_3
7–10 *f*	$(CH_2)_5C$	CCl_3

Comparison of the spectral data of the intermediate ketoxime chloral adducts with those of the corresponding diphenylboron chelates shows: (*i*) the disappearance of the hydroxyl group (infrared and ^1H nmr); (*ii*) the characteristic shift of the C=N stretching to higher frequencies in the infrared, indicating the enhanced iminium salt character upon chelate formation (6); and (*iii*) a minor downfield shift of the acetalic methine proton signal (~0.2 ppm), consistent with an increased deshielding of this proton by greater electron withdrawal upon chelation of the Lewis acid diphenylborenium ion (Table 1). Furthermore, the magnetically equivalent methyl groups of the acetone oxime give rise to two signals of distinctly different shift in the diphenylboron chelates of both the formaldehyde and the chloral adducts, showing the incorporation into a rigid ring system that fixes the methyl groups in magnetically inequivalent environments.

For a definitive assignment to the structure **9** or **10** we prepared single crystals of the diphenylboron chelates derived from the acetonoxime adducts of formaldehyde and chloral for X-ray analysis. The isolable acetonoxime-chloral adduct gave high-quality crystals and was also subjected to an X-ray analysis to establish the structure of the initial α-hydroxylation product of the oxime, either **7** or **8**.

[3] Proceeding on the assumption that all boron chelates of this structural type are cyclic *B,N*-betaines with a COBON ring skeleton (**4**), the previously suggested BOCON ring formulation **5** for these chelates (1), based on the α-hydroxyalkylation product **3**, has to be corrected to **4**.

[4] There is no direct proof of the existence of the *N*-oxide forms **2** and **7**, and the rearrangement intermediate **3**. However, (*i*) alkylations at *N*-hydroxydialkylamines generally lead preferably to *N*-oxides, but alkylations at oximes give both *N*-oxides and *O*-alkyls; (*ii*) the 1,2-shift of carbenium ions from N to O in *N*-oxides (e.g., Meisenheimer rearrangement) is well known and should be very easy and fast in an acetal type *N*-oxide; (*iii*) thus 1,2-shift equilibria **2** ⇌ **3** and **7** ⇌ **8** could probably occur as well as the addition/elimination equilibria.

Can. J. Chem. Downloaded from www.nrcresearchpress.com by 65.111.164.53 on 09/08/12
For personal use only.

Can. J. Chem. Downloaded from www.nrcresearchpress.com by 65.111.164.53 on 09/08/12
For personal use only.

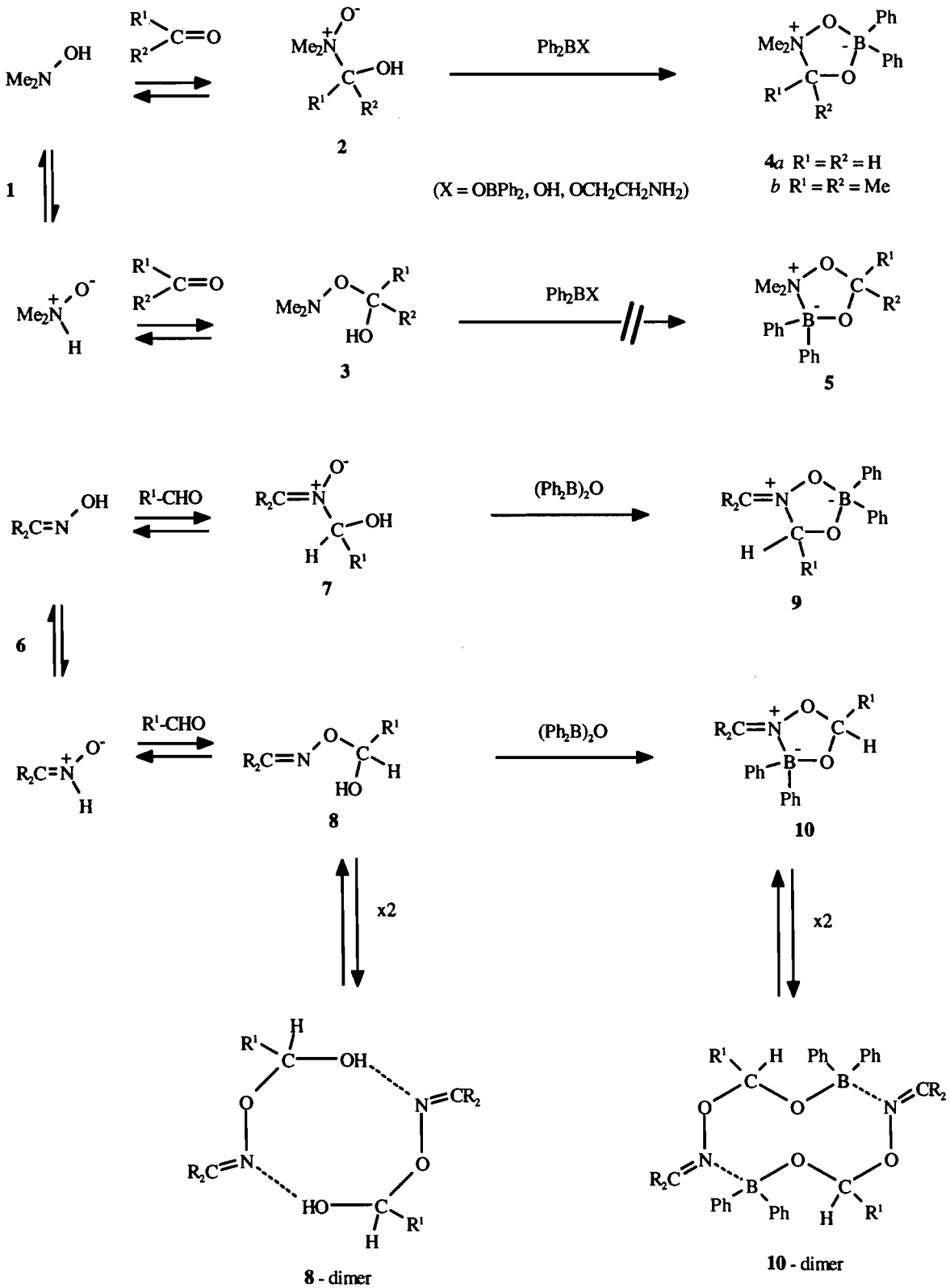

Experimental

O*-(2,2,2-Trichloro-1-hydroxyethyl)-2-propanonoxime, 8*d

Acetonoxime (2.2 g, 30 mmol), chloral hydrate (5.0 g, 30 mmol), and dry Na_2SO_4 (5 g) are refluxed in 40 mL of dichloromethane for 4 h. After filtration and evaporation of the solvent the residue is crystallized from dichloromethane – petroleum ether. Yield: 2.9 g (43%) of colorless crystals; mp 72°C (lit. (5) mp 72°C). Infrared (KBr): 3130 (br, O—H), 1653 (C=N) cm^{-1}; ^1H nmr (90 MHz, $CDCl_3$–TMS),

Can. J. Chem. Downloaded from www.nrcresearchpress.com by 65.111.164.53 on 09/08/12
For personal use only.

δ (ppm): 2.00 (s, 2 CH_3), 5.36 (s, br, O-CH-O), 6.10 (s, br, exchangeable, OH). Anal. calcd. for $C_5H_8Cl_3NO_2$: C 27.24, H 3.66, Cl 48.24, N 6.35; found: C 26.68, H 3.66, Cl 47.44, N 6.13.

Crystals of **8***d*, suitable for an X-ray analysis were obtained by slow crystallization over a period of 5 weeks using the liquid diffusion method (8) with chloroform as solvent and petroleum ether as precipitant at 6–8°C.

O-(2,2,2-Trichloro-1-hydroxyethyl)-cyclopentanonoxime, 8*e*

Cyclopentanonoxime (3.0 g, 30 mmol) is reacted with chloral hydrate (5.0 g, 30 mmol), as described above for **8***d*. Yield: 4.8 g (63%) of colorless crystals; mp 90–91°C (from CH_2Cl_2 – petroleum ether). Infrared (KBr): 3160 (br, O-H), 1659 (C=N) cm^{-1}; ^1H nmr (90 MHz, $CDCl_3$–TMS), δ (ppm): 1.67–1.93 (m, C-CH_2-CH_2-C), 2.33–2.70 (m, N=C(CH_2)$_2$), 5.66 (s, O-CH-O), 5.00–7.00 (s, br, exchangeable, OH). Anal. calcd. for $C_7H_{10}Cl_3NO_2$: C 34.11, H 4.09, Cl 43.14, N 5.68; found: C 33.95, H 4.09, Cl 42.92, N 5.50.

O-(2,2,2-Trichloro-1-hydroxyethyl)-cyclohexanonoxime, 8*f*

Cyclohexanonoxime (3.4 g, 30 mmol) is reacted with chloral hydrate (5.0 g, 30 mmol), as described above for **8***d*. Yield: 5.0 g (61%) of colorless crystals; mp 108–109°C (from CH_2Cl_2 – petroleum ether) (lit. (1*c*): mp 107°C). Infrared (KBr): 3160 (br, O-H), 1647 (C=N) cm^{-1}; ^1H nmr (90 MHz, $CDCl_3$–TMS), δ (ppm): 1.67 (m_c, C-(CH_2)$_3$-C), 2.27 and 2.57 (m and m, N=C(CH_2)$_2$), 5.63 (s, br, O-CH-O), 6.20 (s, br, exchangeable, OH). Anal. calcd. for $C_8H_{12}Cl_3NO_2$: C 36.88, H 4.64, Cl 40.82, N 5.38; found: C 35.89, H 5.12, Cl 40.84, N 4.78.

4-Isopropylidene-2,2-diphenyl-1,3-dioxa-4-azonia-2-boratacyclopentane, 9*a*

Acetonoxime (0.37 g, 5 mmol), oxybis(diphenylborane) (0.87 g, 2.5 mmol), and 1 mL of aqueous formaldehyde solution (35%) are dissolved in 5 mL of ethanol (96%). Crystallization commences while the solution is stirred at room temperature. Yield: 1.09 g (82%) of colorless crystals; mp 145–147°C (from ethanol); 144–145°C (from $CHCl_3$ – petroleum ether) (lit. (1*c*) mp 148–149°C). Infrared (KBr): 1676 (C=N) cm^{-1}; ^1H nmr (90 MHz, $CDCl_3$–TMS), δ (ppm): 1.80 and 2.25 (s and s, N=C(CH_2)$_2$), 5.36 (s, N-CH_2-O), 7.13–7.60 (m, 10 aromatic H); ^{11}B nmr (64.2 MHz, $CDCl_3$–Et_2OBF_3), δ (ppm): 12.7 ($w_{1/2}$ = 190 Hz). Mass spectrum (EI, 70 eV, 400°C); *m/z*: 237 (24%, $M^+ - CH_2O$), 222 (100%, $M^+ - CH_2O - CH_3$), 181 (26%, Ph_2BO), 165 (12%, Ph_2B), 133 (6%), 118 (20%, PhBON), 103 (6%), 77 (52%), 57 (38%). Anal. calcd. for $C_{16}H_{18}BNO_2$: C 71.94, H 6.79, B 4.05, N 5.24; found: C 71.88, H 6.74, B 4.04, N 5.20.

The product gives a blue-colored solution upon addition of diphenylcarbazone in ethanol, indicating the presence of the chelated diphenylborenium ion (9). Crystals suitable for X-ray analysis were obtained by very slow crystallization from $CHCl_3$ – petroleum ether using the liquid diffusion method (8).

4-Cyclopentylidene-2,2-diphenyl-1,3-dioxa-4-azonia-2-boratacyclopentane, 9*b*

Cyclopentanonoxime (0.50 g, 5 mmol), oxybis(diphenylborane) (0.87 g, 2.5 mmol), and 1 mL of aqueous formaldehyde solution (35%) are dissolved in 5 mL of ethanol and heated rapidly to the boiling point. Crystallization commences as the solution is cooled to room temperature. Yield: 1.37 g (93%) of colorless crystals; mp 151–153°C (from ethanol). Infrared (KBr): 1690 (C=N) cm^{-1}; ^1H nmr (90 MHz, $CDCl_3$–TMS), δ (ppm): 1.70–2.00 (m, C-$CH_2$$CH_2$-C), 2.17–2.47 and 2.63–2.97 (m and m, N=C(CH_2)$_2$), 5.33 (s, N-CH_2-O), 7.14–7.66 (m, 10 aromatic H); ^{11}B nmr (64.2 MHz, $CDCl_3$–Et_2OBF_3), δ (ppm) = 12.7 ($w_{1/2}$ = 280 Hz). Anal. calcd. for $C_{18}H_{20}BNO_2$: C 73.74, H 6.88, B 3.69, N 4.78; found: C 73.74, H 6.95, B 3.58, N 4.76. **9***b* gives a blue color reaction with diphenylcarbazone as described for **9***a*.

4-Cyclohexylidene-2,2-diphenyl-1,3-dioxa-4-azonia-2-boratacyclopentane, 9*c*

Cyclohexanonoxime (0.57 g, 5 mmol) is reacted with oxybis(diphenylborane) (0.87 g, 2.5 mmol) and formaldehyde (1 mL 35% aqueous solution) as described above for **9***a*. Yield: 1.05 g (68%) of colorless crystals; mp 134–136°C (from ethanol) (lit. (1*c*) mp 137–138°C). Infrared (KBr): 1665 (C=N) cm^{-1}; ^1H nmr (90 MHz, $CDCl_3$–TMS), δ (ppm): 1.40–1.90 (m, C-(CH_2)$_3$-C), 2.03–2.26 and 2.68–2.93 (m and m, N=C(CH_2)$_2$), 5.40 (s, N-CH_2-O), 7.13–7.65 (m, 10 aromatic H); ^{11}B nmr (64.2 MHz, $CDCl_3$–Et_2OBF_3), δ (ppm): 12.1 ($w_{1/2}$ = 260 Hz). Mass spectrum (EI, 70 eV, 400°C); *m/z*: 237 (24%, $M^+ - CH_2O$), 222 (100%, $M^+ - CH_2O - CH_3$), 181 (26%, Ph_2BO), 165 (12%, Ph_2B), 133 (6%), 118 (20%, PhBON), 103 (6%), 77 (52%), 57 (38%). Anal. calcd. for $C_{19}H_{22}BNO_2$: C 74.29, H 7.22, B 3.52, N 4.56; found: C 74.26, H 7.21, B 3.54, N 4.54. **9***c* gives a blue color reaction with diphenylcarbazone as described for **9***a*.

5-Trichloromethyl-2-isopropylidene-3,3-diphenyl-1,4-dioxa-2-azonia-3-boratacyclopentane, 10*d*

Method A

Acetonoxime (0.37 g, 5 mmol), oxybis(diphenylborane) (0.87 g, 2.5 mmol), and chloral hydrate (0.81 g, 5 mmol) are dissolved in 5 mL of ethanol and heated rapidly to the boiling point. The solvent is removed in vacuo, and the residue taken up in chloroform. Crystallization is induced by addition of petroleum ether. Yield: 1.41 g (73%) of colorless crystals; mp 175–179°C (from $CHCl_3$ – petroleum ether).

Method B

8*d* (0.55 g, 2.5 mmol) and oxybis(diphenylborane) (0.44 g, 1.25 mmol) are each dissolved separately in 2.5 mL of ethanol. The solutions are mixed under stirring at room temperature. After 1 h of stirring, the microcrystalline precipitate is filtered off, and recrystallized from ethanol. Yield: 0.39 g (41%); mp 175–177°C (from ethanol). Infrared (KBr): 1671 (C=N) cm^{-1}; the spectra of the materials obtained from methods A and B are identical; ^1H nmr (90 MHz, $CDCl_3$–TMS), δ (ppm): 1.90 and 2.31 (s and s, N=C(CH_2)$_2$), 5.80 (s, O-CH-O), 7.23–7.56 (m, 10 aromatic H); ^{11}B nmr (64.2 MHz, $CDCl_3$–Et_2OBF_3), δ (ppm): 9.5 ($w_{1/2}$ = 300 Hz). Mass spectrum (EI, 70 eV, 110°C), *m/z*: 308/306 (98%/100%, $M^+ - C_6H_5$), 264 (2%, $M^+ - C_6H_5 - (CH_3)_2C$), 222 (5%, $Ph_2BONCCH_3$), 165 (30%, Ph_2B), 105 (15%, PhBOH), 77 (16%), 57 (86%); (DCI, NH_3, pos. mode); *m/z*: 786 (4%, 2 M + NH_4), 401 (100%, M + NH_4), 384 (41%, M + H), 306 (18%,

Can. J. Chem. Downloaded from www.nrcresearchpress.com by 65.111.164.53 on 09/08/12
For personal use only.

M − C_6H_5), 238 (44%, $Ph_2BN(OH)C(CH_3)_2$), 199 (22%), 182 (43%, Ph_2BOH), 121 (10%), 91 (12%), 74 (51%), 58 (19%). The experimental isotope pattern of the molecular ion (M + H)$^+$ is in excellent agreement with that calculated for **10***d*. Anal. calcd. for $C_{17}H_{17}BCl_3NO_2$: C 53.11, H 4.46, B 2.81, Cl 27.66, N 3.64; found: C 53.11, H 4.47, B 2.78, Cl 27.62, N 3.61. **10***d* gives a blue color reaction with diphenylcarbazone as described for **9***a*. Crystals suitable for X-ray analysis were obtained by slow crystallization (3 days) from $CHCl_3$ – petroleum ether using the liquid diffusion method (8).

5-Trichloromethyl-2-cyclopentylidene-3,3-diphenyl-1,4-dioxa-2-azonia-3-boratacyclopentane, 10*e*

8*e* (0.62 g, 2.5 mmol) and oxybis(diphenylborane) (0.44 g, 1.25 mmol) are reacted as described above for **10***d* (method B). Yield: 0.48 g (47%) of colorless crystals; mp 158–159°C (from ethanol). Infrared (KBr): 1688 (C=N) cm^{-1}; ^{1}H nmr (90 MHz, $CDCl_3$–TMS), δ (ppm): 1.60–2.00 (m, C-CH_2CH_2-C), 2.00–2.70 and 2.70–3.00 (m and m, N=C$(CH_2)_2$), 5.80 (s, O-CH-O), 7.16–7.60 (m, 10 aromatic H); ^{11}B nmr (64.2 MHz, $CDCl_3$–Et_2OBF_3), δ (ppm): 8.7 ($w_{1/2}$ = 300 Hz). Anal. calcd. for $C_{19}H_{19}BCl_3NO_2$: C 55.59, H 4.66, B 2.63, Cl 25.91, N 3.41; found: C 55.63, H 4.82, B 2.85, Cl 25.31, N 3.27. **10***e* gives a blue color reaction with diphenylcarbazone as described for **9***a*.

5-Trichloromethyl-2-cyclohexylidene-3,3-diphenyl-1,4-dioxa-2-azonia-3-boratacyclopentane, 10*f*

Method A

Cyclohexanonoxime (0.37 g, 5 mmol), oxybis(diphenylborane) (0.87 g, 2.5 mmol), and chloral hydrate (0.81 g, 5 mmol) are reacted as described for **10***d* (method A). Yield: 1.27 g (60%) of colorless crystals; mp 158–159°C (from $CHCl_3$ – petroleum ether).

Method B

8*f* (1.30 g, 5 mmol) and oxybis(diphenylborane) (0.87 g, 2.5 mmol) are reacted as described above for **10***d* (method B). Yield: 1.45 g (68%); mp 157–158°C (from ethanol). Infrared (KBr): 1651 (C=N) cm^{-1}; the spectra of the materials obtained from methods A and B are identical; ^{1}H nmr (90 MHz, $CDCl_3$–TMS), δ (ppm): 1.20 and 3.10 (m, -$(CH_2)_5$-), 5.83 (s, O-CH-O), 7.20–7.60 (m, 10 aromatic H); ^{11}B nmr (64.2 MHz, $CDCl_3$–Et_2OBF_3), δ (ppm): 9.2 ($w_{1/2}$ = 280 Hz). Anal. calcd. for $C_{20}H_{21}BCl_3NO_2$: C 56.58, H 4.99, B 2.55, Cl 25.05, N 3.30; found: C 56.86, H 5.05, B 2.80, Cl 24.36, N 3.09. **10***f* gives a blue color reaction with diphenylcarbazone as described for **9***a*.

X-ray crystallographic analyses of 8*d*, 9*a*, and 10*d*

Crystallographic data appear in Table 2. The final unit-cell parameters were obtained by least squares on the setting angles for 25 reflections with 2θ = 27.6°–35.9° for **8***d*, 70.2°–91.0° for **9***a*, and 35.0°–41.7° for **10***d*. The intensities of three standard reflections, measured every 200 reflections throughout the data collections, showed only small random fluctuations for **8***d* and **9***a*, and decayed linearly by 2.7% for **10***d*. The data were processed,[5] corrected for Lorentz and polarization effects, decay (for **10***d*), and absorption (empirical, based on azimuthal scans for three reflections).

The structures were solved by direct methods, the coordinates of the non-hydrogen atoms being determined from an *E*-map or from subsequent difference Fourier syntheses. Non-hydrogen atoms were refined with anisotropic thermal parameters. The hydrogen atoms of **8***d* and **10***d* were refined with isotropic thermal parameters and those of **9***a* were fixed in idealized positions (C—H = 0.98 Å, B_H = 1.2 $B_{\text{bonded atom}}$). Corrections for secondary extinction were applied for **8***d* and **9***a*, the final values of the extinction coefficients being 1.2(3) × 10^{-6} and 7.7(2) × 10^{-6}, respectively. Neutral atom scattering factors for all atoms (10*a*) and anomalous dispersion corrections for the non-hydrogen atoms (10*b*) were taken from the *International tables for X-ray crystallography*. A parallel refinement of the mirror-image structure of **9***a* gave slightly higher residuals, the *R* and R_w factor ratios both being 1.002. Final atomic coordinates and equivalent isotropic thermal parameters, bond lengths, bond angles, and intra-annular torsion angles appear in Tables 3–6, respectively. Stereoviews of the **8***d*, **9***a*, and **10***d* molecules are shown in Figs. 1–3, respectively. Hydrogen atom parameters, anisotropic thermal parameters, torsion angles, intermolecular contacts, and least-squares planes have been deposited as supplementary material.[6] Measured and calculated structure factor amplitudes are available from the authors.

Results and discussion

The X-ray analyses show that the products from the reaction between acetonoxime **6** (R = Me), oxybis(diphenylborane), and formaldehyde or trichloroacetaldehyde, respectively, possess essentially different boron chelate structures. The diphenylboron chelate of the formaldehyde adduct to acetonoxime has the molecular structure **9***a* (Fig. 2), corresponding to the reaction products of *N*-hydroxydialkylamines with carbonyl compounds and diphenylborinic acid, **4**. The COBON ring skeleton that can also be assigned to the other ketoxime derivatives, **9***b* and *c*, demonstrates that α-hydroxymethylated oximes react in the *N*-oxide (nitrone) form **7** preferentially as bidentate ligands, similar to the *N*-oxide form of α-hydroxyalkylated hydroxylamines, **2**. Thus the five-membered che-

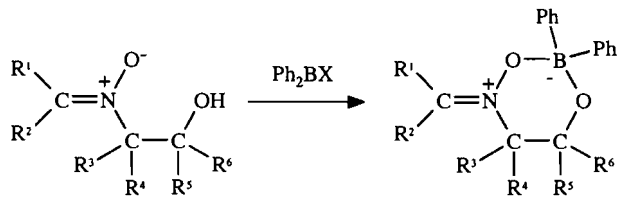

11 **12**

[5] teXsan: Crystal structure analysis package. Molecular Structure Corp., The Woodlands, Tex. 1985 and 1992.

[6] Supplementary material mentioned in the text may be purchased from the Depository of Unpublished Data, Document Delivery, CISTI, National Research Council of Canada, Ottawa, Canada K1A 0S2.

Tables of hydrogen atom coordinates and bond lengths and angles involving hydrogen atoms have also been deposited with the Cambridge Crystallographic Data Centre and can be obtained on request from The Director, Cambridge Crystallographic Data Centre, University Chemical Laboratory, 12 Union Road, Cambridge CB2 1EZ, U.K.

Can. J. Chem. Downloaded from www.nrcresearchpress.com by 65.111.164.53 on 09/08/12
For personal use only.

Table 2. Crystallographic data.[a]

Compound	**8***d*	**9***a*	**10***d*
Formula	$C_5H_8Cl_3NO_2$	$C_{16}H_{18}BNO_2$	$C_{17}H_{17}BCl_3NO_2$
fw	220.48	267.13	384.50
Crystal system	Monoclinic	Orthorhombic	Monoclinic
Space group	$P2_1/c$	$P2_12_12_1$	$P2_1/n$
a, Å	7.010(2)	11.098(2)	9.164(2)
b, Å	11.832(2)	15.364(1)	15.304(3)
c, Å	11.684(2)	8.715(2)	13.859(2)
β,°	90.48(2)	90	105.28(1)
V, Å^3	969.0(3)	1486.1(4)	1875.0(5)
Z	4	4	4
ρ_{calc}, g cm^{-3}	1.511	1.194	1.362
F(000)	448	568	792
Radiation	Mo-K_α	Cu-K_α	Mo-K_α
μ, cm^{-1}	8.99	6.13	4.97
Crystal size , mm	0.25 × 0.30 × 0.35	0.25 × 0.30 × 0.35	0.30 × 0.30 × 0.35
Transmission factors	0.96–1.00	0.93–1.00	0.94–1.00
Scan type	ω–2θ	ω–2θ	ω–2θ
Scan range, deg in ω	1.21 + 0.35 tan θ	1.10 + 0.20 tan θ	1.15 + 0.35 tan θ
Scan speed, deg min^{-1}	32	32	16
Data collected	$+h, +k, \pm l$	$+h, +k, +l$	$+h, +k, \pm l$
$2\theta_{max}$, deg	55	155	65
Crystal decay, %	Negligible	Negligible	2.7
Total reflections	2533	1844	7335
Unique reflections	2345	1844	6965
R_{merge}	0.040	—	0.018
No. with $I \geq 3\sigma(I)$	1082	1256	3062
No. of variables	133	182	285
R	0.037	0.044	0.040
R_w	0.041	0.016	0.042
gof	1.85	3.48	2.86
Max Δ/σ (final cycle)	0.009	0.0002	0.02
Residual density e Å^{-3}	−0.21 to 0.22	−0.12 to 0.15	−0.26 to 0.25

[a]Temperature 294 K, Rigaku AFC6S diffractometer, Mo-K_α (λ = 0.71069 Å) or Cu-K_α (λ = 1.54178 Å) radiation, graphite monochromator, takeoff angle 6.0°, aperture 6.0 × 6.0 mm at a distance of 285 mm from the crystal, stationary background counts at each end of the scan (scan/background time ratio 2:1, up to 8 rescans), $\sigma^2(F^2) = [S^2(C + 4B)]/Lp^2$ (S = scan rate, C = scan count, B = normalized background count) (*no* fudge factors (pI^2) used, which accounts for the slightly high gof values), function minimized $\Sigma w(|F_o|-|F_c|)^2$ where $w = 4F_o^2/\sigma^2(F_o^2)$, $R = \Sigma||F_o|-|F_c||/\Sigma|F_o|$, $R_w = (\Sigma w(|F_o|-|F_c|)^2/\Sigma w|F_o|^2)^{1/2}$, and gof = $[\Sigma w(|F_o|-|F_c|)^2/(m-n)]^{1/2}$. Values given for R, R_w, and gof are based on those reflections with $I \geq 3\sigma(F^2)$.

Fig. 1. Stereoview of **8***d*; 33% probability thermal ellipsoids are shown for the non-hydrogen atoms.

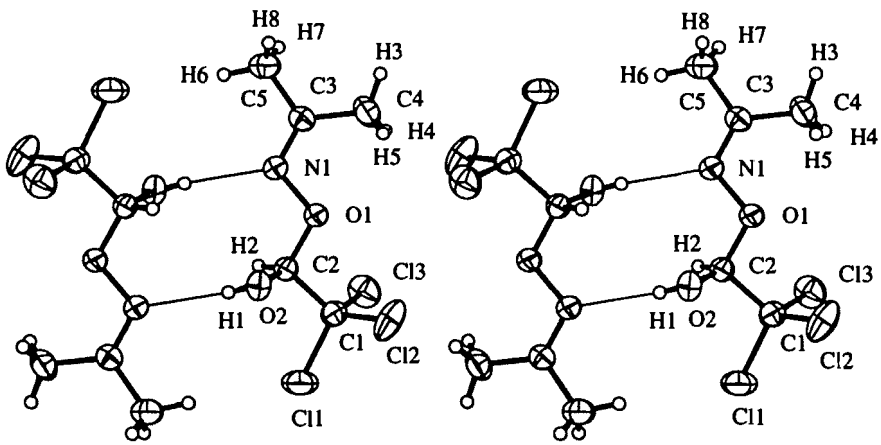

Fig. 2. Stereoview of the **9***a* molecule; 33% probability thermal ellipsoids are shown for the non-hydrogen atoms.

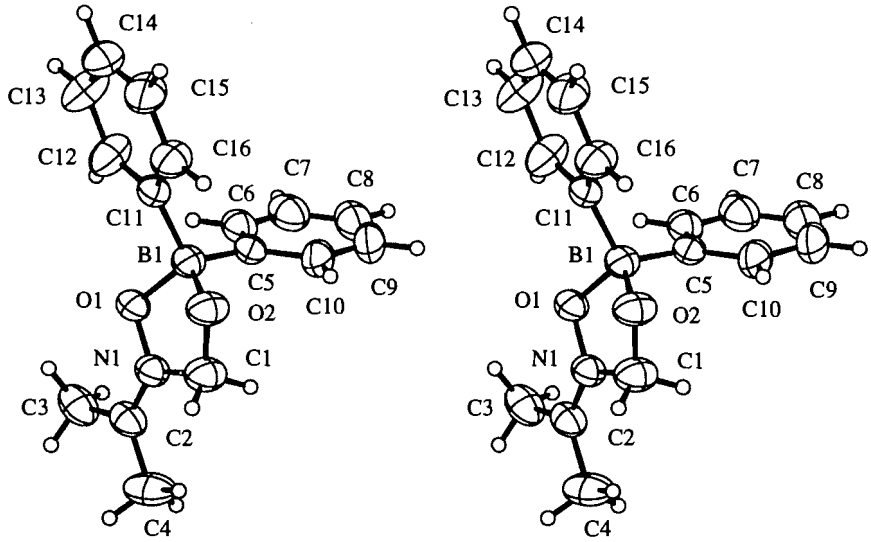

Fig. 3. Stereoview of the **10***d* molecule; 33% probability thermal ellipsoids are shown for the non-hydrogen atoms.

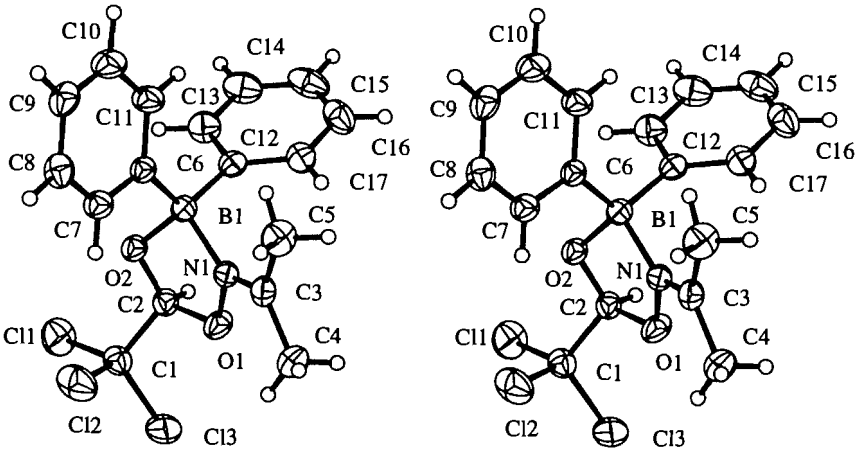

lates **9** are in accord with the six-membered diphenylboron chelates **12**, derived from the *N*-(β-hydroxyalkyl)nitrones **11** (6). As expected (11), the C=N absorption band in the infrared spectra of five-membered COBON species **9** (1665–1690 cm^{-1}) is found at higher frequencies than the analogous six-membered CCOBON ring compounds **12**. The highest frequency of 1690 cm^{-1} is found in the spectrum of **9***b*, the C=N vibration of which is influenced by the ring strain of the two five-membered rings fused at the C=N double bond.

The ^1H nmr signals of the *N,O*-acetalic methylene group in **9** (5.33–5.40 ppm) appear in the same region as the comparable signal of **4***a* (5.25 ppm) (3), as do the ^{11}B nmr signals of **9** (12.1–12.7 ppm) compared to those of **4***a* (11.1 ppm) (3).

No molecular ion signal was detected in the EI mass spectrum of **9***a*. The highest mass fragment, characterized by the (thermolytic?) loss of formaldehyde, corresponds to the monomeric (alkylideniminoxy)-diarylboranes observed in the mass spectra of the BONBON dimers, $(R_2C{=}NOBPh_2)_2$ (12).

In contrast to the O-B-O diphenylboron chelate of *N*-hydroxymethylated acetoxime (**9***a*), the chelate of the acetonoxime chloral adduct has an isomeric BOCON ring structure, **10***d*, formed by O-B-N coordination (Fig. 3). In this case the α-hydroxyalkoximine **8** (and not the α-hydroxyalkylamine *N*-oxide **7**) serves as a bidentate ligand for the chelate formation. Further support for **8** as an intermediate comes from the reaction of the preformed crystalline acetonoxime chloral adduct **8***d* with oxybis(diphenylborane), which gives a boron chelate identical to the product from the three-component reaction.

The X-ray analysis of the acetonoxime chloral adduct confirms the molecular structure **8***d* (Fig. 1), indicating a preferred α-hydroxyalklation at the oxime oxygen atom by the strongly electrophilic trichloroacetaldehyde as the alkylating agent, similar to the favored *O*-acylation of oximes (13). In the crystal, **8***d* does not form an intramolecular hydrogen bond, but is stabilized as a centrosymmetric, twofold O—H···N bonded dimer (Fig. 1).[7]

Interestingly, in a mass spectroscopic experiment employing chemical ionization of **10***d* conducted to verify a molecu-

Can. J. Chem. Downloaded from www.nrcresearchpress.com by 65.111.164.53 on 09/08/12
For personal use only.

Can. J. Chem. Downloaded from www.nrcresearchpress.com by 65.111.164.53 on 09/08/12
For personal use only.

Table 3. Final atomic coordinates (fractional) and B_{eq} (Å^2)[a]

Atom	x	y	x	B_{eq}
8*d*				
Cl(1)	0.6621(2)	0.17494(9)	0.45314(10)	7.41(6)
Cl(2)	0.2562(2)	0.15295(8)	0.42051(10)	7.82(7)
Cl(3)	0.41998(15)	0.15500(9)	0.64698(9)	6.34(6)
O(1)	0.2399(3)	0.3623(2)	0.5585(2)	4.4(1)
O(2)	0.4381(4)	0.3876(2)	0.4061(2)	4.6(1)
N(1)	0.2412(4)	0.4711(2)	0.6105(2)	3.9(1)
C(1)	0.4362(5)	0.2106(3)	0.5078(3)	4.4(2)
C(2)	0.4207(5)	0.3402(3)	0.5129(3)	3.8(1)
C(3)	0.0860(5)	0.4888(3)	0.6636(3)	3.9(1)
C(4)	−0.0753(6)	0.4080(4)	0.6692(5)	5.6(2)
C(5)	0.0692(8)	0.5999(4)	0.7222(5)	5.8(2)
9*a*				
O(1)	0.4147(2)	0.48959(13)	0.3885(2)	5.7(1)
O(2)	0.2877(2)	0.42579(14)	0.2074(3)	6.8(1)
N(1)	0.3504(3)	0.5528(2)	0.3166(3)	5.4(1)
C(1)	0.2766(4)	0.5146(2)	0.1882(5)	7.4(2)
C(2)	0.3568(3)	0.6330(2)	0.3551(5)	6.2(2)
C(3)	0.4362(4)	0.6584(2)	0.4834(5)	7.7(2)
C(4)	0.2857(4)	0.6988(2)	0.2744(6)	9.1(3)
C(5)	0.5164(4)	0.4161(2)	0.1575(4)	5.5(2)
C(6)	0.6338(4)	0.4294(2)	0.2032(5)	6.5(2)
C(7)	0.7299(4)	0.4304(3)	0.1045(6)	8.0(3)
C(8)	0.7111(6)	0.4176(3)	−0.0473(6)	9.4(3)
C(9)	0.5993(7)	0.4039(3)	−0.1009(5)	9.8(3)
C(10)	0.4996(4)	0.4042(3)	0.0012(5)	7.7(2)
C(11)	0.4127(3)	0.3228(2)	0.3779(4)	5.1(2)
C(12)	0.4904(4)	0.3124(3)	0.4963(5)	8.1(3)
C(13)	0.5034(4)	0.2335(3)	0.5741(6)	9.6(3)
C(14)	0.4340(5)	0.1632(3)	0.5331(6)	8.5(3)
C(15)	0.3576(5)	0.1720(2)	0.4188(5)	8.6(3)
C(16)	0.3454(4)	0.2507(2)	0.3402(5)	7.2(2)
B(1)	0.4074(4)	0.4097(2)	0.2789(4)	5.3(2)
10*d*				
Cl(1)	0.16735(9)	0.16916(5)	0.57374(5)	6.59(4)
Cl(2)	0.27102(8)	0.08791(5)	0.41653(7)	6.86(4)
Cl(3)	−0.04695(8)	0.09024(4)	0.40657(6)	6.03(3)
O(1)	0.0597(2)	0.21841(11)	0.28317(11)	4.67(7)
O(2)	0.23675(15)	0.28343(9)	0.41064(10)	3.46(6)
N(1)	0.1509(2)	0.26953(11)	0.23863(12)	3.35(7)
C(1)	0.1254(2)	0.1494(2)	0.4444(2)	4.1(1)
C(2)	0.1060(2)	0.23704(14)	0.3894(2)	3.50(8)
C(3)	0.1432(2)	0.24986(14)	0.1478(2)	3.80(9)
C(4)	0.0500(4)	0.1758(2)	0.0955(2)	5.6(1)
C(5)	0.2299(4)	0.3043(2)	0.0925(2)	5.5(1)
C(6)	0.4125(2)	0.35322(13)	0.32070(14)	3.12(8)
C(7)	0.5097(2)	0.2832(2)	0.3260(2)	3.9(1)
C(8)	0.6611(3)	0.2941(2)	0.3281(2)	4.5(1)
C(9)	0.7187(3)	0.3769(2)	0.3264(2)	4.7(1)
C(10)	0.6260(3)	0.4476(2)	0.3207(2)	5.2(1)
C(11)	0.4736(3)	0.4360(2)	0.3174(2)	4.4(1)
C(12)	0.1372(2)	0.42596(13)	0.3145(2)	3.49(8)
C(13)	0.1482(3)	0.4753(2)	0.4007(2)	5.0(1)
C(14)	0.0654(4)	0.5518(2)	0.3990(3)	5.9(1)
C(15)	−0.0287(3)	0.5804(2)	0.3119(3)	6.1(1)
C(16)	−0.0423(3)	0.5343(2)	0.2255(3)	5.6(1)
C(17)	0.0402(3)	0.4575(2)	0.2276(2)	4.3(1)
B(1)	0.2395(3)	0.3395(2)	0.3224(2)	3.25(9)

[a] $B_{eq} = (8/3)\pi^2\Sigma\Sigma U_{ij}a_i^*a_j^*(\mathbf{a}_i\cdot\mathbf{a}_j)$

lar mass (not detectable in the EI experiment), a dimer[8] was observed in addition to the molecular ion, although in low relative abundance. This dimer might have the structure "**10**-dimer" which could be formed directly from the 10-membered hydrogen-bridged "**8**-dimer" found in the crystal of **8*d*** by replacement of the ring hydrogen atoms by diphenylboron moieties.

The reaction of chloral hydrate, $Cl_3C\text{-}CH(OH)_2$, with the ketoximes and the subsequent chelatization with diphenylborinic acid is analogous to the reaction of phenylboronic acid, $Ph\text{-}B(OH)_2$, with acetonoxime and diphenylborinic acid, resulting in the BOBON heterocycle **13** (16), which is a boron analog to the BOCON ring type **10**. In both cases a strongly electrophilic alkylation/acylation agent attacks the oxime oxygen atom, followed by the stabilizing chelate formation with diphenylborinic acid using the oxime nitrogen atom as one of the ligands. A nitrogen analog (azalog) of **10** is exemplified by

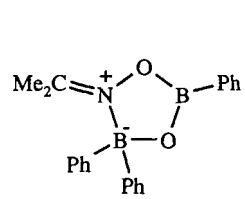

13

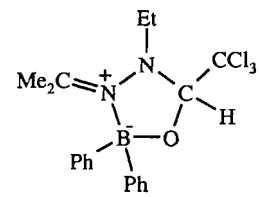

14

the diphenylboron chelate **14**, obtained by the reaction of an acetone hydrazone derivative with chloral and a diphenylborinic acid ester (17). Both structures, of **13** (16) and of **14** (17), were established by X-ray crystallographic analyses, and thus confirm the analogy to **10**.

The five-membered COBON ring of **9*a*** has an envelope conformation with a slightly distorted O(1)-N(1)-C(1)-O(2)

[7] In solution an equilibrium between **8**-dimer and **8** can be supposed. A possible ring tautomer of the open-chain oxime form **8** could not be detected by ^1H nmr spectroscopy in $CDCl_3$ solutions:

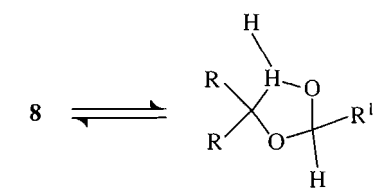

This type of 1,4,2-dioxazolidine ring system is found within various molecules reported in the literature, *N*-unsubstituted (14) as well as *N*-substituted (15).

[8] It is not yet clear whether the dimer was produced in the mass spectrometer, or whether it was a contaminant of the sample used for the experiment.

Can. J. Chem. Downloaded from www.nrcresearchpress.com by 65.111.164.53 on 09/08/12
For personal use only.

Table 4. Bond lengths (Å) with estimated standard deviations.

Atoms	Distance	Atoms	Distance
8*d*			
Cl(1)—C(1)	1.763(3)	O(2)—C(2)	1.374(4)
Cl(2)—C(1)	1.754(4)	N(1)—C(3)	1.274(4)
Cl(3)—C(1)	1.759(4)	C(1)—C(2)	1.539(5)
O(1)—N(1)	1.424(3)	C(3)—C(4)	1.483(5)
O(1)—C(2)	1.403(4)	C(3)—C(5)	1.487(5)
9*a*			
O(1)—N(1)	1.358(3)	C(6)—C(7)	1.370(5)
O(1)—B(1)	1.558(4)	C(7)—C(8)	1.354(6)
O(2)—C(1)	1.380(4)	C(8)—C(9)	1.343(7)
O(2)—B(1)	1.489(5)	C(9)—C(10)	1.420(7)
N(1)—C(1)	1.506(4)	C(11)—C(12)	1.354(5)
N(1)—C(2)	1.279(4)	C(11)—C(16)	1.376(4)
C(2)—C(3)	1.476(6)	C(11)—B(1)	1.590(5)
C(2)—C(4)	1.463(6)	C(12)—C(13)	1.397(5)
C(5)—C(6)	1.378(5)	C(13)—C(14)	1.374(6)
C(5)—C(10)	1.387(5)	C(14)—C(15)	1.315(6)
C(5)—B(1)	1.610(5)	C(15)—C(16)	1.396(5)
10*d*			
Cl(1)—C(1)	1.757(2)	C(6)—C(11)	1.391(3)
Cl(2)—C(1)	1.757(2)	C(6)—B(1)	1.606(3)
Cl(3)—C(1)	1.776(2)	C(7)—C(8)	1.390(3)
O(1)—N(1)	1.401(2)	C(8)—C(9)	1.376(3)
O(1)—C(2)	1.450(2)	C(9)—C(10)	1.365(4)
O(2)—C(2)	1.357(2)	C(10)—C(11)	1.396(3)
O(2)—B(1)	1.500(3)	C(12)—C(13)	1.394(3)
N(1)—C(3)	1.278(3)	C(12)—C(17)	1.382(3)
N(1)—B(1)	1.631(3)	C(12)—B(1)	1.608(3)
C(1)—C(2)	1.530(3)	C(13)—C(14)	1.391(4)
C(3)—C(4)	1.488(4)	C(14)—C(15)	1.358(4)
C(3)—C(5)	1.495(4)	C(15)—C(16)	1.367(4)
C(6)—C(7)	1.383(3)	C(16)—C(17)	1.395(3)

Table 5. Bond angles (deg) with estimated standard deviations.

Atoms	Angle	Atoms	Angle
8*d*			
N(1)-O(1)-C(2)	109.1(2)	Cl(3)-C(1)-C(2)	109.3(2)
O(1)-N(1)-C(3)	110.8(2)	O(1)-C(2)-O(2)	110.8(3)
Cl(1)-C(1)-Cl(2)	109.9(2)	O(1)-C(2)-C(1)	105.3(3)
Cl(1)-C(1)-Cl(3)	108.1(2)	O(2)-C(2)-C(1)	111.4(3)
Cl(1)-C(1)-C(2)	108.4(2)	N(1)-C(3)-C(4)	124.7(3)
Cl(2)-C(1)-Cl(3)	109.9(2)	N(1)-C(3)-C(5)	116.2(3)
Cl(2)-C(1)-C(2)	111.1(2)	C(4)-C(3)-C(5)	119.1(4)
9*a*			
N(1)-O(1)-B(1)	104.7(2)	C(5)-C(10)-C(9)	120.7(5)
C(1)-O(2)-B(1)	107.2(3)	C(12)-C(11)-C(16)	115.7(3)
O(1)-N(1)-C(1)	110.5(2)	C(12)-C(11)-B(1)	122.4(3)
O(1)-N(1)-C(2)	122.6(3)	C(16)-C(11)-B(1)	121.7(3)
C(1)-N(1)-C(2)	126.9(3)	C(11)-C(12)-C(13)	122.6(4)
O(2)-C(1)-N(1)	104.3(3)	C(12)-C(13)-C(14)	119.9(5)
N(1)-C(2)-C(3)	119.1(4)	C(13)-C(14)-C(15)	118.5(4)
N(1)-C(2)-C(4)	120.6(4)	C(14)-C(15)-C(16)	121.6(4)
C(3)-C(2)-C(4)	120.2(3)	C(11)-C(16)-C(15)	121.8(4)
C(6)-C(5)-C(10)	115.5(4)	O(1)-B(1)-O(2)	99.9(3)
C(6)-C(5)-B(1)	122.0(3)	O(1)-B(1)-C(5)	108.4(3)
C(10)-C(5)-B(1)	122.4(4)	O(1)-B(1)-C(11)	109.1(3)
C(5)-C(6)-C(7)	123.8(4)	O(2)-B(1)-C(5)	112.7(3)
C(6)-C(7)-C(8)	119.5(5)	O(2)-B(1)-C(11)	113.6(3)
C(7)-C(8)-C(9)	120.3(5)	C(5)-B(1)-C(11)	112.3(3)
C(8)-C(9)-C(10)	120.1(5)		
10*d*			
N(1)-O(1)-C(2)	106.8(1)	C(6)-C(7)-C(8)	122.2(2)
C(2)-O(2)-B(1)	109.1(1)	C(7)-C(8)-C(9)	119.7(2)
O(1)-N(1)-C(3)	114.7(2)	C(8)-C(9)-C(10)	119.7(2)
O(1)-N(1)-B(1)	107.2(1)	C(9)-C(10)-C(11)	120.2(2)
C(3)-N(1)-B(1)	138.1(2)	C(6)-C(11)-C(10)	121.4(2)
Cl(1)-C(1)-Cl(2)	110.0(1)	C(13)-C(12)-C(17)	116.2(2)
Cl(1)-C(1)-Cl(3)	109.1(1)	C(13)-C(12)-B(1)	118.6(2)
Cl(1)-C(1)-C(2)	108.8(2)	C(17)-C(12)-B(1)	125.1(2)
Cl(2)-C(1)-Cl(3)	109.3(1)	C(12)-C(13)-C(14)	121.7(3)
Cl(2)-C(1)-C(2)	110.8(2)	C(13)-C(14)-C(15)	120.1(3)
Cl(3)-C(1)-C(2)	108.8(1)	C(14)-C(15)-C(16)	120.2(3)
O(1)-C(2)-O(2)	109.1(2)	C(15)-C(16)-C(17)	119.5(3)
O(1)-C(2)-C(1)	107.3(2)	C(12)-C(17)-C(16)	122.2(3)
O(2)-C(2)-C(1)	111.8(2)	O(2)-B(1)-N(1)	95.3(1)
N(1)-C(3)-C(4)	122.3(2)	O(2)-B(1)-C(6)	108.4(2)
N(1)-C(3)-C(5)	118.4(2)	O(2)-B(1)-C(12)	113.0(2)
C(4)-C(3)-C(5)	119.3(2)	N(1)-B(1)-C(6)	112.6(2)
C(7)-C(6)-C(11)	116.7(2)	N(1)-B(1)-C(12)	108.7(2)
C(7)-C(6)-B(1)	121.5(2)	C(6)-B(1)-C(12)	116.9(2)
C(11)-C(6)-B(1)	121.8(2)		

plane (maximum deviation from the mean plane is 0.081(4) Å) with the B(1) atom on the flap, displaced 0.521(4) Å from the ONCO mean plane. The 4-isopropylidene moiety is nearly coplanar with the envelope mean plane (ONCO), the dihedral angle between normals to the mean planes being 4.7°. The C=N bond length (1.279(4) Å) is not significantly different from that reported for acetonoxime (1.29(3) Å) (18), and is close to the value observed for an acetonoximato complex of gadolinium (1.26(2) Å) (19). The N—O bond length of **9***a* (1.358(3) Å) is equal to that of the above-mentioned Gd complex (1.36(2) Å) (19). The C=N and N—O distances both lie within the general ranges reported for oximes (20). The most striking differences between the COBON rings of **9***a* and the related diphenylboron chelate **4***a* (3) involve the N—O bond, which is shorter in **9***a* than in **4***a* by 0.051(6) Å, and the endocyclic C-N-O angle, which is 5.5(5)° wider in **9***a* (C(1)-N(1)-O(1) = 110.5(2)°) than in **4***a* (105.0(4)°). This is to be expected on the basis of the hybridization differences between the ring nitrogen atoms (sp^2 in **9***a* vs. sp^3 in **4***a*). As in **4***a* there is a conspicuous difference between the two O—B bonds in **9***a*. The B(1)—O(1) bond involving the azomethine *N*-oxide oxygen atom is longer by 0.069(6) Å than the B(1)—O(2) bond involving the alcoholate oxygen atom originating from the carbonyl oxygen. This difference in the nucleophilic character of the ligand oxygen atoms is a general phenomenon in compounds containing both *N*-oxide and alcoholate or phenolate groups within the same boron chelate molecule (21). The C(1)—O(2) bond in **9***a* (1.380(4) Å), derived from the inserted

Can. J. Chem. Downloaded from www.nrcresearchpress.com by 65.111.164.53 on 09/08/12
For personal use only.

Table 6. Intra-annular torsion angles (deg) with estimated standard deviations.

Atoms	Angle
9*a*	
B(1)-O(1)-N(1)-C(1)	13.8(4)
O(1)-N(1)-C(1)-O(2)	9.3(4)
N(1)-C(1)-O(2)-B(1)	−29.7(4)
C(1)-O(2)-B(1)-O(1)	37.1(4)
O(2)-B(1)-O(1)-N(1)	−30.0(3)
10*d*	
B(1)-N(1)-O(1)-C(2)	−11.5(2)
N(1)-O(1)-C(2)-O(2)	−11.3(2)
O(1)-C(2)-O(2)-B(1)	31.7(2)
C(2)-O(2)-B(1)-N(1)	−34.7(2)
O(2)-B(1)-N(1)-O(1)	27.1(2)

formaldehyde, is, like that in **4***a* (3) and related boron chelates of formaldehyde adducts (22) and the acetone adduct **4***b* (4), shorter than the C—O bonds found in other boron chelates with hydroxyalkyl ligands that have normal C—O single bond distances (21). The B—C(phenyl) bond lengths in **9***a* are in good agreement with those observed in other five- to eight-membered chelates of the type "Ph_2BO_2" (21) and display a typical difference of 0.020(7) Å between the B—C bonds involving the (pseudo)equatorial and the (pseudo)axial phenyl groups, the axial B—C bonds being longer as a rule (21). The mean B—C distance of 1.600 Å is typical for B—C(phenyl) bonds involving tetrahedrally coordinated sp^3-boron atoms in this type of compound. The boron coordination is distorted tetrahedral, with a narrow O-B-O angle of 99.9(3)° within the chelate ring.

The five-membered BOCON ring of **10***d* also has a distorted envelope conformation; the OCON moiety is planar within 0.083(2) Å with B(1) displaced 0.530(2) Å from the OCON mean plane. The 4-isopropylidene grouping (planar to within 0.058(4) Å) is nearly coplanar with the OCON fragment of the chelate ring, the angle between normals to the mean planes being 18.6°. The positioning of the two *B*-phenyl groups above and below the mean BOCON ring plane is not distinctly axial or equatorial, and in this case the two B—C(phenyl) distances are equal within experimental error. The coordinative N(1)—B(1) bond in **10***d* (1.631(3) Å) is significantly shorter than the corresponding N—B bond in the BOBON ring of **13** (1.665(4) Å) (16), indicative of a higher basicity of the oxime nitrogen atom in **10***d* and (or) a decreased Lewis- acidity of the diphenylboryloxy moiety in **13**. In the hydrazone derivative **14** (17) the N—B bond is even shorter (1.603 Å). The difference of about 0.03 Å between the N—B coordinative bonds of **10***d* and **14** reflects the basicity difference between the oxime and hydrazone moieties. A N—B distance similar to that in **10***d* has been reported for the five-membered diphenylboron chelate of 2-hydroxymethylpyridine: 1.642 Å (23), in which the coordinative donor bond involves the (sp^2) pyridine nitrogen atom and forms a ring of the same size as that in **10***d*. The C(2)—O(2) bond in **10***d*, derived from the C=O bond of the inserted chloral, is even shorter (1.357(2) Å) than the comparable C—O bond in the COBON ring of **9***a* (see above). A similar shortening of the C—O single bond of the inserted chloral is observed in compound **14** (17). For crystalline chloral hydrate the C—O bond distances are reported as 1.44 and 1.52 Å (X-ray) (24), and more reliably as 1.386(1) and 1.387(1) Å (neutron data) (25). The C(2)—O(1) bond in **10***d*, originating from the oxime oxygen alkylated by chloral, is 0.093(3) Å longer than the C(2)—O(2) bond derived from the chloral C=O function.

The acetonoxime moieties in both compounds, the COBON chelate **9***a* and the BOCON chelate **10***d*, have nearly equal dimensions except for the N—O bond distance, which is shorter in **9***a* (1.358(3) Å) than in **10***d* (1.401(2) Å). This reflects the main difference between the two ligands involved, the *N*-oxide (nitrone) intermediate **7** introducing the short N—O bond in the case of **9***a*, and the *O*-hydroxyalkylated intermediate **8** inserting the longer N—O bond in the case of **10***d*.

Comparing the intermediate **8***d* with the diphenylboron chelate **10***d*, it can be seen that there is no change in the dimensions of the isopropylidene moiety. The C=N double bond is of nearly equal length in both compounds, as are the C—C bonds and angles. The most notable differences occur at the N(1)-O(1)-C(2) section. The N—O bond of **8***d* (1.423(3) Å) is shortened to 1.401(2) Å in **10***d*, whereas the C—O bond is lengthened from 1.403(4) Å in **8***d* to 1.449(2) Å in **10***d*. In addition, the replacement of the proton at O(2) of the ligand **8***d* by the diphenylborenium ion (Ph_2B^+) to give the chelate **10***d* causes a shortening of the C(2)—O(2) bond from 1.374(4) to 1.357(2) Å. As expected, there are no structural changes in the tetrahedral arrangement of the trichloromethyl substituent going from the ligand to the chelate.

In the crystal, two molecules of **8***d* are linked by O—H···N hydrogen bonds (O(2)—H(1)···N(1)$(1-x, 1-y, 1-z)$, H···N = 2.10(4) Å, O···N = 2.810(4) Å, O—H···N = 172(4)°) to form centrosymmetric dimeric units ("**8**-dimer"). A similar dimeric associate was reported for the benzamidoxime chloral adduct, a stable *O*-hemiacetal with O—H···N hydrogen bonds having O···N = 2.775 Å (26). Molecules of **9***a* are separated by normal van der Waals interactions, the shortest intermolecular distance between non-hydrogen atoms being O(1)···C(1) = 3.367(5) Å. Molecules of **10***d* are linked by weak C—H···O interactions in the solid state (C(4)—H(2)···O(2)$(-1/2 + x, 1/2 - y, -1/2 + z)$, H···O = 2.49(4) Å, C···O = 3.364(4) Å, C—H···O = 158(3)°).

To the best of our knowledge, **8***d* is the first structurally characterized *O*-(α-hydroxyalkyl)oxime in the literature.The compounds **9***a* and **10***d*, described in this work, are the first structurally defined examples of boron chelates of the types **9** and **10**.

Acknowledgments

We thank the Natural Sciences and Engineering Research Council of Canada and the Fonds der Chemischen Industrie, Frankfurt am Main, for financial support. We are grateful to the Chemische Institute der Technischen Universität Braunschweig for running the ^{11}B nmr and mass spectra.

[9] The only related chloral *O*-hemiacetal crystallographically studied, the benzamidoxime chloral adduct (26), is a functional carboxylic acid derivative.

References

1. (*a*) G. Zinner, W. Ritter, and W. Kliegel. Pharmazie, **20**, 291 (1965); (*b*) G. Zinner and W. Kliegel. Arch. Pharm. Ber. Dtsch. Pharm. Ges. **299**, 166 (1966); (*c*) Chem. Ber. **99**, 895 (1966); (*d*) G. Zinner and R. Moll. Chem. Ber. **99**, 1292 (1966); (*e*) G. Zinner and E. Düerkop. Arch. Pharm. Ber. Dtsch. Pharm. Ges. **301**, 776 (1968).
2. (*a*) W. Kliegel. Z. Chem. **9**, 112 (1969); (*b*) G. Zinner, D. Moderhack, and W. Kliegel. Chem. Ber. **102**, 2536 (1969).
3. S.J. Rettig, J. Trotter, and W. Kliegel. Can. J. Chem. **52**, 2531 (1974).
4. W. Kliegel, H.-W. Motzkus, S.J. Rettig, and J. Trotter. Can. J. Chem. **62**, 838 (1984).
5. F. von Heyden Nachfolger. D.R.P. 66877 (20/5/1892); Chem. Zentralbl. **64**, I, 1000 (1893).
6. (*a*) W. Kliegel. Tetrahedron Lett. 223 (1969); (*b*) W. Kliegel and H. Becker. Chem. Ber. **110**, 2067 (1977); (*c*) Chem. Ber. **110**, 2090 (1977); (d) W. Kliegel, B. Enders, and H. Becker. Liebigs Ann. Chem. 1712 (1982); (*e*) Chem. Ber. **116**, 27 (1983).
7. W. Kliegel. Organomet. Chem. Rev. Sect. A: **8**, 153 (1972).
8. P.G. Jones. Chem. Br. **17**, 222 (1981).
9. (*a*) R. Neu. Z. Anal. Chem. **176**, 334 (1960); (*b*) B. Friese and F. Umland. Anal. Chim. Acta, **96**, 303 (1978).
10. (*a*) International tables for X-ray crystallography. Vol. IV. Kynoch Press, Birmingham, U.K. (present distributor Kluwer Academic Publishers, Boston, Mass. 1974. pp. 99–102; (*b*) International tables for crystallography. Vol. C. Kluwer Academic Publishers, Boston, Mass. 1992. pp. 200–206.
11. (*a*) D.H. Williams and I. Fleming. Spectroscopic methods in organic chemistry. McGraw–Hill, London. 1973. p. 60; (*b*) M. Hesse, H. Meier, and B. Zeeh. Spectroskopische methoden in der organischen chemie. Georg Thieme Verlag, Stuttgart. 1984. p. 69.
12. W. Kliegel, G. Lubkowitz, U. Riebe, S.J. Rettig, and J. Trotter. Can. J. Chem. **72**, 1735 (1994), and references cited therein.
13. (*a*) P. A. S. Smith. The chemistry of open-chain organic nitrogen compounds. Vol. II. New York. 1966. p. 29; (*b*) H. Metzger. *In* Houben-Weyl Methoden der organische Chemie. Bd. X/4. Stuttgart. 1968. p. 180; (*c*) B. Unterhalt. *In* Methodicum Chimicum. Bd. 6. Stuttgart. 1974. p. 413; (*d*) *In* Houben-Weyl Methoden der organische Chemie. Bd. E 14 b. Stuttgart. 1990. p. 386.
14. G. Eikelmann, W. Heimberger, G. Nonnenmacher, and W.M. Weigert. Liebigs Ann. Chem. **759**, 183 (1972).
15. (*a*) G. Zinner and B. Geister. Chem. Ztg. **96**, 693 (1972); (*b*) G. Zinner and H. Blass. Angew. Chem. Int. Ed. Engl. 16, 882 (1977); (*c*) J. Varwig and R. Mews. Angew. Chem. Int. Ed. Engl. **16**, 646 (1977); (*d*) F. De Sarlo and A. Brandi. J. Chem. Res. Synop. 122 (1980); (*e*) D.P. Del'tsova, N.P. Gambaryan, and E.P. Lur'e. Izv. Akad. Nauk SSSR, Ser. Khim. 1788 (1979); Chem. Abstr. **92**, 6475e (1980); (*f*) W.Y. Lam and D.D. DesMarteau. J. Am. Chem. Soc. **104**, 4034 (1982).
16. W. Kliegel, D. Nanninga, S.J. Rettig, and J. Trotter. Can. J. Chem. **61**, 2329 (1983).
17. Z.A. Bredikhina, L.F. Chertanova, A.A. Gazikasheva, N.G. Gazetdinova, and O.A. Erastov. Izv. Akad. Nauk SSSR, Ser. Khim. 178 (1991); Bull. Acad. Sci USSR, Div. Chem. Sci. 161 (1991).
18. T.K. Bierlein and E.C. Lingafelter. Acta Crystallogr. **4**, 450 (1951).
19. Z. Wu, X. Zhou, W. Zhang, Z. Xu, X. Tou, and X. Huang. J. Chem. Soc. Chem. Commun. 813 (1994).
20. S.J. Rettig and J. Trotter. Can. J. Chem. **53**, 765 (1975).
21. E. Ebeling, W. Kliegel, S.J. Rettig, and J. Trotter. Can. J. Chem. **67**, 933 (1989), and references therein.
22. W. Kliegel, S.J. Rettig, and J. Trotter. Can. J. Chem. **66**, 377 (1988).
23. N. Farfan, D. Castillo, P. Joseph-Nathan, R. Contreras, and L.V. Szentpály. J. Chem. Soc. Perkin Trans. 2, 527 (1992).
24. K. Ogawa. Bull. Chem. Soc. Jpn. **36**, 610 (1963).
25. G.M. Brown and H.A. Levy. Cryst. Struct. Commun. **2**, 107 (1973).
26. G.B. Carpenter and R.M. Srivastava. Acta Crystallogr. Sect. C: Cryst. Struct. Commun. **C43**, 695 (1987).
27. W. Kliegel, H. Amt, H. Becker, U. Lauterbach, G. Lubkowitz, S.J. Rettig, and J. Trotter. Can. J. Chem. **74**, 2118 (1994).

Can. J. Chem. Downloaded from www.nrcresearchpress.com by 65.111.164.53 on 09/08/12
For personal use only.

Electrocatalytic hydrogenation of conjugated enones on nickel boride, nickel, and Raney nickel electrodes[1]

Behzad Mahdavi, Philippe Chambrion, Julie Binette, Eric Martel, and Jean Lessard

Abstract: The selectivity of the electrocatalytic hydrogenation (ECH) of conjugated enones to the corresponding carbonyl compounds has been investigated in aqueous methanol under constant current at nickel boride, fractal nickel, and Raney nickel electrodes made of pressed powders. The influence of various parameters (water percentage, pH, concentration of substrate, and current density) on the selectivity of the carbon–carbon double bond hydrogenation was studied with cyclohex-2-en-1-one at nickel boride electrodes. Under given electrolysis conditions, fractal nickel electrodes were found to give the highest selectivity. The selectivity of the ECH of a variety of conjugated enones at fractal nickel electrodes was determined under electrolysis conditions that gave the best selectivity with cyclohexenone at nickel boride electrodes.

Key words: electrocatalytic hydrogenation, α,β-unsaturated ketones, selective hydrogenation, nickel based cathodes.

Résumé : Nous avons fait l'étude de la sélectivité de l'hydrogénation électrocatalytique (HEC) d'énones conjuguées en cétones saturées correspondantes dans le methanol–eau à courant constant sur des électrodes de borure de nickel, nickel fractal et nickel de Raney fabriquées par pressage de poudres. L'influence de divers paramètres (le pourcentage d'eau, le pH, la concentration du substrat et la densité du courant) sur la sélectivité a été étudiée avec la cyclohex-2-én-1-one sur électrodes de borure de nickel. Sous des conditions d'électrolyse données, la sélectivité s'est averée la plus élevée avec les électrodes de nickel fractal et celles-ci ont été utilisées pour une étude de la sélectivité de l'HEC de diverses cétones conjugées sous les conditions d'électrolyse ayant donné la meilleure sélectivité dans le cas de la cyclohexénone.

Mots clés : hydrogénation électrocatalytique, cétones α,β-éthyléniques, hydrogénation sélective, cathodes à base de nickel.

Introduction

Electrocatalytic hydrogenation (ECH) of unsaturated organic molecules in aqueous or mixed aqueous-organic media has been carried out since the beginning of the century.[3] The mechanism is described by reactions [1]–[4] where M represents the metallic surface, (H)M chemisorbed hydrogen, and (Y=Z)M the adsorbed organic substrate. The first step is the electroreduction of water (or hydronium ions) with the formation of adsorbed hydrogen on the electrode surface (Volmer reaction [1]), followed by reaction of the adsorbed substrate (Y=Z)M with chemisorbed hydrogen (reaction [3]). There is a competition between hydrogenation (reaction [3]) and the desorption of hydrogen by an electrochemical (Heyrovsky reaction [5]) and (or) chemical (Tafel reaction [6]) pathway. Since, in the ECH of organic substances, the sole processes occurring are hydrogenation and hydrogen evolution (1, 9), the current efficiency is a measure of the competition between the two reactions.

[1] $2H_2O(H_3O^+) + 2e^- + M \rightarrow 2\,(H)M + 2OH^-(H_2O)$

[2] $Y{=}Z + M \rightarrow (Y{=}Z)M$

[3] $(Y{=}Z)M + 2(H)M \rightarrow (YH{-}ZH)M$

[4] $(YH{-}ZH)M \rightarrow YH{-}ZH + M$

[5] $(H)M + H_2O + e^- \rightarrow H_2 + M + OH^-$

[6] $(H)M + (H)M \rightarrow H_2 + M$

This competition depends on a number of factors such as the substrate, the electrode, and reaction conditions (1, 3, 7). The hydrogenation steps (reactions [2], [3], and [4]) are the same

Received November 28, 1994.

B. Mahdavi, P. Chambrion, J. Binette, E. Martel, and J. Lessard.[2] Centre de recherche en électrochimie et électrocatalyse, Département de chimie, Université de Sherbrooke, Sherbrooke, QC J1K 2R1, Canada.

[1] Part VIII in the series Electrocatalytic hydrogenation of organic compounds. For parts IV–VIII, see refs. 1–4.

[2] Author to whom correspondence may be addressed. Telephone: (819) 821-7091. Fax: (819) 821-8017.

[3] A short review on the ECH of organic compounds from 1906 can be found in refs. 1 and 8. For some more recent works, see refs. 2–7 and references therein.

Can. J. Chem. Downloaded from www.nrcresearchpress.com by 80.90.12.36 on 09/08/12
For personal use only.

Can. J. Chem. Downloaded from www.nrcresearchpress.com by 80.90.12.36 on 09/08/12
For personal use only.

as in catalytic hydrogenation and this was recently shown experimentally by Anantharaman and Pintauro (7) who were able to describe the rate of ECH of glucose to sorbitol from the chemical catalytic hydrogenation rate equation.

ECH presents several advantages over catalytic hydrogenation. *Firstly* ECH uses the very mild conditions (room temperature and atmospheric pressure) normally employed in electrochemical synthesis, mainly because there is no mass transport of poorly soluble molecular hydrogen and because the kinetic barrier for its dissociation is bypassed (1). In fact, the chemisorbed hydrogen is produced in situ, at the surface of the catalyst. Furthermore, its generation can be controlled by adjusting the current density, which makes the reaction easier to handle and may also increase the reaction selectivity (1, 7, 9). Thus, ECH is expected to be more selective than catalytic hydrogenation. *Secondly*, in some cases, the adsorption of poisons can be diminished or even prevented by cathodic polarization of the catalyst (1). When compared to electrohydrogenation by the electronation–protonation (EP) process, ECH has the advantage of requiring less energy. Indeed, the formation of chemisorbed hydrogen by reduction of water on a low hydrogen overvoltage cathode requires a less negative potential than the electronation of most functional groups of organic chemistry (with the exception of the nitro group family). Furthermore, the formation, for instance, of dimerization products in the electrohydrogenation of carbonyl compounds may be avoided since reactive intermediates such as radical anions and radicals are not produced (3, 9). However, an advantage of the EP process is the possibility of controlling the product selectivity by potentiostatic reduction.

This paper reports the results of a study of the ECH of various conjugated enones in aqueous methanol at nickel boride, fractal nickel, and Raney nickel electrodes made of pressed powders. First, we describe the influence of different electrolysis conditions (water percentage, pH, concentration of substrate, and current efficiency) on the selectivity, and of the ECH of cyclohex-2-en-1-one at nickel boride electrodes. Then, we compare fractal nickel and Raney nickel electrodes with nickel boride electrodes under given electrolysis conditions. Finally, the ECH of some conjugated enones was investigated at fractal nickel electrodes under electrolysis conditions giving the best selectivity with cyclohexenone at nickel boride electrodes.

Experimental

The electrolyses were carried out with a 410 potentiostatic controller, 640 digital coulometer, and 2830 digital multimeter (Electrosynthesis Company). A two-compartment glass H-cell (volume of each compartment 25 mL) having a Nafion-324 (E.I. du Pont de Nemours & CO) membrane (1.8 cm^2) as separator was used. The counter electrode was a glassy carbon plate (≈12 cm^2). The substrate was dissolved in a stock solution (25 mL) of sodium chloride (0.1 M) and boric acid (0.1 M) in methanol–water (v/v) by stirring the solution in the cathodic compartment. The anodic compartment was filled with the above stock solution (25 mL). The cathodic compartment was deaerated (N_2). The cathode and the counter electrode were immersed and electrolysis was performed at constant current. The catholyte was stirred magnetically. The apparent pH was measured with a Sargent Welch 6000 pH meter and a Cole Parmer glass electrode that was calibrated in aqueous buffer. Aliquots (0.2 mL) from the catholyte were extracted with ether after the addition of a saturated NaCl solution (1 mL) and were analyzed by vpc. The products were identified by comparison of retention times with those of authentic samples. They were identified also by GC–MS and by IR and ^1H and ^{13}C NMR spectroscopy after extraction with ether and, when needed, thick-layer chromatographic separation (Merck Silica Gel 60 F_{254}, layer tickness: 250 μm). The mass balance was determined by weighing the isolated crude product after extraction and thorough rinsing (CH_3OH, then ether) of the electrode. Some cyclohexanone and cyclohexanol (less than 8% altogether in the worse cases) were lost upon solvent removal. With the other less volatile substrates, the material balance was close to 100% in all cases. There was no organic product in the anolyte after completion of the electrolysis, according to vpc analysis.

P-1 nickel boride (Ni_2B) was obtained as a powder (average particle size of 0.5 μm and specific surface area of 9 $m^2\ g^{-1}$ (5)) by reduction of nickel acetate with $NaBH_4$ in aqueous NaOH (10). The filamentary nickel powder (particle size of 2.2–2.8 μm and specific surface area of 0.68 $m^2\ g^{-1}$) was purchased from Inco (type 255 nickel powder) and consisted of spiky (fractal characteristics) spheres. The Raney nickel alloy (Ni–Al 50:50 w/w) powder (particle size of 45–125 μm) was purchased from BDH. The specific surface area of the spongy Raney nickel (RaNi) particles (average diameter <40 μm) after leaching in aqueous NaOH is of the order of 65 $m^2\ g^{-1}$ (11). The electrodes were obtained by pressing the powders at p = 800 MPa at room temperature. The pressed Raney alloy powder was leached in 10% NaOH for 3 h at 50°C to afford the RaNi electrodes. The geometric area of the electrodes was 2π cm2 considering that both faces of the disc were used.

Results and discussion

Electrocatalytic hydrogenation of cyclohex-2-en-1-one on nickel boride electrodes

The electrocatalytic hydrogenation (ECH) of cyclohex-2-en-1-one to cyclohexanone has been already studied under different experimental conditions on various electrodes: Pd(0) microparticles in poly(pyrrole-viologen) film (6), Raney nickel powder on a nickel plate (9), palladium and platinum deposited on carbon powder (9), and Ni(0) microparticles electrodeposited in Nafion films (12). In all cases, the ECH of cyclohex-2-en-1-one produced cyclohexanone and cyclohexanol as major products. The presence of cyclohex-2-en-1-ol was hardly or not detected in the reaction mixture (9, 12). We studied the influence of the proportion of water, the pH of the solution, the substrate concentration, and the current density on the selectivity of the ECH of the carbon–carbon double bond of cyclohexenone in methanol–water solutions under constant current conditions. The hydrogenated products observed were cyclohexanone and cyclohexanol, as expected. No other product was detected by vpc analysis. The material balance was determined by weighing the reaction product after extraction with ether and solvent removal, and in some cases small amounts (≤8%) of material were lost by evaporation. The selectivity was evaluated by the ratio of the yield of cyclohexanone to the conversion rate. The efficiency of the electrohydrogenation was evaluated from the conversion rate and the

Can. J. Chem. Downloaded from www.nrcresearchpress.com by 80.90.12.36 on 09/08/12
For personal use only.

Table 1. ECH of cyclohex-2-en-1-one at nickel boride electrodes:[a] effect of water percentage, pH, concentration of substrate, and current density.[b]

Entry	MeOH–H_2O (v/v)	pH_i–pH_f[c]	J[d] (mA dm^{-2})	C (mM)	Conversion[e] (%)	Selectivity[f] (%)	Current efficiency (%)
1	50/50	5.3–8.6	250	16	66–68[g]	74–74[g]	83–84[g]
2	20/80	5.3–8.6	250	16	60	80	71
3	95/5	5.3–8.5	250	16	64	78	78
4	50/50	1.7–4.6[h]	250	16	75	74	95
5	50/50	5.3–8.9	250	32	77	76	96
6	50/50	5.3–9.3	250	48	80	75	100
7	50/50	5.3–8.6	125	16	77	91	84
8	50/50	5.3–8.6	83	16	82	98	83
9	50/50	5.3–8.6	50	16	84	98	86
10	50/50	1.7–5.5[h]	50	48	95–100[g]	>99	95–100[g]

[a]The electrodes were prepared by pressing the Ni_2B powder at p = 800 MPa.

[b]Electrolysis conditions: MeOH–H_2O (v/v); 0.1 M NaCl; 0.1 M H_3BO_3; room temperature; charge passed = 2 moles of electrons per mole of cyclohex-2-en-1-one.

[c]pH_i = pH at the begining of the electrolysis, pH_f = pH at the end. The pH meter was calibrated using buffers in aqueous solutions.

[d]Based on the geometric area.

[e]The conversion rate and yield of products were determined by vpc analysis. The yields are based on converted cyclohex-2-en-1-one (material balance 92–100%).

[f]Selectivity = (yield of cyclohexanone/conversion) × 100.

[g]Range obtained from two different electrolyses.

[h]HCl was added at the begining of the electrolysis.

current efficiency. The charge passed corresponded to two moles of electrons per mole of substrate, the charge required for complete hydrogenation of the carbon–carbon double bond of the substrate. The results obtained under the different electrolysis conditions are summarized in Table 1. As shown in entry 1, different pressed nickel boride powder electrodes gave very reproducible results as in the case of the ECH of phenanthrene (5). Changing the proportion of water from 5 to 80% (entries 1–3) had little effect on the selectivity, which varied from 74–80%. The effect on the conversion rate (64–68%) and the current efficiency (71–84%) was also not very important. Kam Cheong et al. (3) likewise observed that the relative proportion of water had little effect on the efficiency of the ECH of cyclohexanone on RaNi electrodes. A methanol–water ratio of 50/50 was chosen because this ratio permits a range of organic substrates and supporting electrolytes to dissolve easily.

As seen from Table 1 by comparing entry 4 (pH 1.7–4.6) with entry 1 (pH 5.3–8.6), the ECH of cyclohexenone was more efficient (higher conversion rate and current efficiency) under the more acidic conditions but the pH of the medium had no effect on the selectivity (74% in both entries).[4] Osa and al. (9) reported that there was no well-defined correlation between the pK_a of the proton source and the efficiency and selectivity of the ECH of cyclohexenone at Raney Ni, Pt/C, and Pd/C electrodes.

The effect of increasing the cyclohexenone concentration from 16 to 48 mM is shown in entries 1, 5, and 6 of Table 1. The efficiency of the process increases upon increasing the concentration of the substrate due to an increase of the hydrogenation step (reaction [4]) (see Scheme 1). A current efficiency of 100% was obtained for a 48 mM solution (entry 6). At this concentration, under the conditions used, all the chemisorbed hydrogens did react with the adsorbed substrate and there was no formation of gaseous hydrogen by the Heyrovsky and (or) Tafel reactions (reactions [5] and [6]). As expected, the cyclohexenone concentration had no effect on the selectivity of the hydrogenation (74–76%).

Scheme 1. Competition between hydrogenation and desorption of hydrogen.

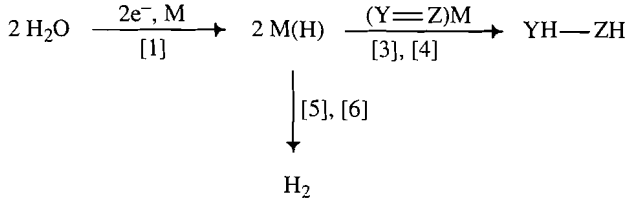

The effect of current density on the efficiency and on the selectivity of the ECH of cyclohex-2-en-1-one is shown in entries 1 and 7–9 of Table 1. The conversion rate increases from 67% (entry 1) to 84% (entry 9) as the current density decreases from 250 to 50 mA dm^{-2} (geometric area), which shows that a decrease of current density favors hydrogenation over hydrogen evolution (Scheme 1). Assuming that the mechanism of the HER in methanol–water at pH 5.3–8.3 on nickel boride electrodes is the same as in aqueous alkaline solutions, that is, a Volmer–Heyrovsky mechanism (reactions [1] and [5]) (14, 15), the competition between hydrogenation and hydrogen evolution (Scheme 1) becomes a competition between a chemical process (reactions [2]–[4]) and an electrochemical process (reaction [5]) (Scheme 1). The increase in

[4] Apparent pH values of 10 or higher during the electrolysis had to be avoided to prevent the formation of 3-methoxycyclohexanone (9, 13).

Table 2. Effect of the electrode material and the charge passed on the ECH of cyclohex-2-en-1-one[a]

		Conversion[c,d] (%)		Selectivity[d,e] (%)		Current efficiency[d] (%)	
Entry	Electrode[b]	2 F mol^{-1}	4 F mol^{-1}	2 F mol^{-1}	4 F mol^{-1}	2 F mol^{-1}	4 F mol^{-1}
1	Ni_2B	68	91	74	46	84	71
2	Ni	62	90	86	78	71	55
3	RaNi	79	95	20	9	143	91
4	RaNi (catalytic hydrogenation)[f]	73	85	48	50		
5	RaNi[g]	77	93	57	34	110	77

[a]Electrolysis conditions: 16 mM solution of cyclohex-2-en-1-one; MeOH–H_2O (50/50, v/v); 0.1 M NaCl; 0.1 M H_3BO_3; pH = 5.3–9.3; room temperature; J = 250 mA dm^{-2}.

[b]The electrodes were prepared by pressing the powder at p = 800 MPa.

[c]See footnote *e* of Table 1.

[d]The values were obtained at a charge of 80 coulombs (2 F mol^{-1}) and 160 coulombs (4 F mol^{-1}).

[e]See footnote *f* of Table 1.

[f]The catalytic hydrogenation was carried out under the same conditions as those of ECH except that no potential was applied to the electrode (open circuit). The values were obtained after periods of time corresponding to the consumption of 2 moles (90 min) and 4 moles (180 min) of electrons per mole of cyclohex-2-en-1-one, respectively, in the ECH experiments.

[g]The electrode used in the catalytic hydrogenation experiment (entry 4) was washed with MeOH–H_2O (50:50, v/v) and used in the ECH experiment of entry 5.

the ECH efficiency upon decreasing the current density would then result from a decrease in the rate of the electrochemical reaction. It is noteworthy that the current efficiency remained the same (83–86%) as the current density was decreased by a factor of five (compare entries 1 and 7–9). In other examples of ECH reported in the literature (1, 2, 16), a decrease of current density was generally associated with an increase of current efficiency and of conversion rate. But in the ECH of cyclohexenone, a decrease in current density is associated with an increase in conversion rate and a decrease in the extent of further hydrogenation of cyclohexanone to cyclohexanol (increase in selectivity). This can be explained by the fact that the chemisorbed hydrogen would be more active at higher current densities (at more negative potentials), which would translate into a faster hydrogenation of the cyclohexanone molecules generated at the surface of the electrode by the hydrogenation of cyclohexenone. At lower current densities, the hydrogenation of cyclohexanone would become slow enough to allow its diffusion to the bulk solution before being hydrogenated. The results of entries 1–9 of Table 1 discussed above allowed us to choose the optimum conditions: MeOH–H_2O = 50/50, pH = 1.7–5.5, J = 50 mA dm^{-2} (geometric area), substrate concentration = 48 mM (see entry 10). Under these conditions, a selectivity of 100% and an efficiency close to 100% were obtained for the formation of cyclohexanone (entry 10). Before the present systematic study, the ECH of cyclohexenone had been studied on various electrodes but under different electrolysis conditions (6, 9, 12). The differences observed in the efficiency and selectivity were attributed solely to the performance of the electrode (catalytic) material (6). A true and meaningful comparison of various electrode materials must be carried out under specific electrolysis conditions.

Table 2 summarizes the results of a study of the effect of the electrode material (nickel boride (Ni_2B), fractal nickel (Ni), and Raney nickel (RaNi)) and the charge passed (80 C (2 F mol^{-1}) and 160 C (4 F mol^{-1}) corresponding to the theoretical charge for hydrogenation to cyclohexanone and to cyclohexanol, respectively) on the ECH of cyclohex-2-en-1-one under electrolysis conditions corresponding to those of entry 1 of Table 1: MeOH–H_2O = 50/50, pH = 5.3–8.6, J = 250 mA dm^{-2} (geometric area), substrate concentration = 16 mM. Both the selectivity and the efficiency were found to depend on the electrocatalyst and the charge. As expected, the current efficiency decreased with the charge for the three types of electrode materials (see entries 1, 2, 3, and 5). Indeed, as the charge increases, the concentration of cyclohexenone decreases, and hydrogen evolution becomes more and more important (Scheme 1) (1, 3) since cyclohexanone is more difficult to hydrogenate than cyclohexenone and cyclohexanol is not reducible. As a result, the current efficiency decreases. The current efficiencies higher than 100% in entries 3 and 5 reflect the fact that chemisorbed hydrogen generated during leaching of the Raney alloy was present on the electrode at the beginning of the electrolysis (1). The results of catalytic hydrogenation of cyclohexenone on a freshly leached RaNi electrode (Table 2, entry 4) show that the amount of chemisorbed hydrogen present after leaching corresponds to more than 0.63 mmole of molecular hydrogen[5] since there was still some chemisorbed hydrogen left, as shown by the current efficiency of 110% after a charge of 2 F mol^{-1} when the same electrode as that used in the catalytic hydrogenation experiment (entry 4) was reused for the ECH experiment of entry 5. There was no active chemisorbed hydrogen present on the Ni_2B and Ni electrodes before the electrolysis: no hydrogenation of cyclohexenone was observed in open circuit experiments. The decrease of selectivity as the charge increases is due to the decrease in concentration of cyclohexenone and the

[5] Similar quantities of active chemisorbed hydrogen were found for RaNi electrodes consisting of RaNi particles embedded in a nickel matrix: 0.48–0.66 mmol when the precursory electrodes contained about 0.7 g of precursory alloy (57–59% of alloy in the nickel matrix) (1).

Can. J. Chem. Downloaded from www.nrcresearchpress.com by 80.90.12.36 on 09/08/12
For personal use only.

Can. J. Chem. Downloaded from www.nrcresearchpress.com by 80.90.12.36 on 09/08/12
For personal use only.

increase in the amount of cyclohexanone formed; as a result, a point is reached where the rate of hydrogenation of cyclohexanone becomes equal to that of hydrogenation of cyclohexenone. The selectivity was also greatly dependent on the type of catalytic electrode, increasing from 20% (2 F mol^{-1}) and 9% (4 F mol^{-1}) with the RaNi electrodes (entry 3) to 74 and 46%, respectively, with the Ni2B electrodes (entry 1) and to 86 and 78% with the fractal Ni electrodes (entry 2). This is the order of decreasing activity (apparent activity) of these three electrodes for the ECH of phenanthrene in ethylene glycol–water at 80°C, fractal Ni being much less active than the two other electrodes (5).[6] It is reasonable to assume that the order of activity would be the same for the ECH of cyclohexenone in methanol–water at room temperature and the most active RaNi electrodes then gave the lowest selectivity for the hydrogenation of the carbon–carbon double bond, as expected. A RaNi electrode that had been used in an open circuit experiment (the catalytic hydrogenation experiment of entry 4) gave higher selectivities (57% (2 F mol^{-1}) and 34% (4 F mol^{-1}), entry 5) than a freshly prepared RaNi electrode (20 and 9%, respectively, entry 3) for the ECH of cyclohexenone. This results from the deactivation of RaNi in the catalytic hydrogenation experiment and confirms the conclusion reached above by comparing the selectivities of the three electrode materials; that is, the selectivity reflects the activity. In the catalytic hydrogenation experiment in which only the chemisorbed hydrogen produced during the leaching process was used (entry 4), the selectivity was the same after 90 min (48%) and 180 min (50%) since the conversion merely increased (from 73–83%, respectively) over the last 90 min due to a decrease in both the amount of chemisorbed hydrogen and in the substrate concentration. For similar conversion rates, the selectivity obtained with a freshly prepared RaNi electrode was lower in the ECH experiment (20% after 2 F mol^{-1}, entry 3) than in the catalytic hydrogenation experiment (48–50%, entry 4). Thus polarized RaNi (entry 3) would be more active than nonpolarized RaNi (entry 4). As already pointed out, in the ECH reactions, the selectivity decreases as the electrolysis proceeds due to mass transfer phenomena related to changes in the relative concentrations of cyclohexenone and cyclohexanone. The decrease in selectivity in increasing the charge from 2 to 4 F mol^{-1} was the most pronounced with the freshly leached RaNi (most active) electrode (55% decrease, entry 3), was of the same order of magnitude for the deactivated RaNi electrode (38% decrease, entry 5) and the Ni_2B electrode (40% decrease, entry 1), and was by far the smallest for the least active fractal Ni electrode (9% decrease, entry 2). This shows that fractal Ni is the best electrocatalytic material for the selective electrohydrogenation of the carbon–carbon double bond of cyclohexenone.

Electrocatalytic hydrogenation of various conjugated enones at fractal nickel electrodes

The fact that fractal nickel can be used as a catalytic material for the selective ECH of a carbon–carbon double bond conjugated to a keto group is very interesting because it is not an expensive material. The ECH of some conjugated enones has been investigated at fractal Ni electrodes under conditions that gave the highest selectivity with cyclohexenone at Ni_2B electrodes (see Table 1, entry 10). The results are reported in Table 3. Comparison was made both at a given charge of 2 F mol^{-1} (the theorical charge for hydrogenation the α,β carbon–carbon double bond) and at conversion rates of the order of 80–93%.

At a given charge of 2 F mol^{-1}, only the carbon–carbon double bond of the conjugated enones was electrohydrogenated, as shown by selectivities higher than 99% in entries 1, 2, 4, 6, 10, 12, and 14 of Table 3. Then, the efficiency of the ECH process evaluated from the conversion rate and the current efficiency, which both depend on the ratio of the rate of hydrogenation to the rate of hydrogen desorption (Scheme 1), the latter being constant under given conditions, reflects the ease of hydrogenation of the α,β carbon–carbon double bond. From the conversion rates and current efficiencies of entry 1 (93–95%), entry 2 (48–51%), entry 4 (42–43%), and entry 6 (33%), the rate of hydrogenation of the double bond decreases in the order cyclohexenone > isophorone ≥ 2,4,4-trimethylcyclohex-2-en-1-one > verbenone. This can be attributed to an increase in steric interactions, making the adsorption of the substrate on the catalytic surface more difficult (17), and, as a result, the transfer of adsorbed hydrogens to the double bond is also more difficult. The lower efficiency of the ECH of the carbon–carbon double bond of β-ionone (28–36%, entry 10) when compared to *trans*-4-phenylbut-3-en-2-one (23–36%, entry 14) must also be due mainly to larger steric interactions with β-ionone although the adsorption of the phenyl ring of phenylbutenone probably has some influence as well. The slightly less efficient ECH of the double bond of 2,4,4-trimethylcyclohex-2-en-1-one (42–43%, entry 4) when compared to isophorone (48–51%, entry 2) most probably reflects the fact that the *gem*-dimethyl group is closer to the double bond in the former (stronger steric interactions), rather than the effect of the position of the methyl group on the double bond (β and α position in trimethylcyclohexanone and isophorone, respectively). Acetylcyclohexene with a trisubstituted endocyclic double bond is more difficult to hydrogenate (69–73% efficiency, entry 8) than cyclohexenone with a disubstituted double bond (93–95% efficiency), as expected again from steric effects. In the case of carvone (entry 12), there was extensive hydrogenation of the isopropylidene group, as shown by product distribution and yields after 4 F mol^{-1}: 5-isopropyl-2-methylcyclohex-2-ene-1-one (carvotanacetone), 12%; 3-isopropyl-6-methylcyclohexanone (carvomenthone), 55%; 3-isopropylidene-6-methylcyclohexanone (dihydrocarvone), 8%. This corresponds, for the hydrogenation of the conjugated double bond only (2 F mol^{-1}), to a conversion of 65% and a current efficiency of 65%. Thus the efficiency of the hydrogenation of the conjugated double bond of carvone and carvotanacetone is similar to that of acetylcyclohexene (entry 8), as expected from the fact that the conjugated double bond is trisubstituted in both cases. Being equatorial, the isopropylidene group of carvone and the isopropyl group of carvotanacetone have little effect on the adsorption of the molecule and the hydrogenation of the conjugated double bond.

The results of ECH of the enones of Table 3 on fractal nickel electrodes at high substrate conversion (≥80%, see entries 1, 3, 5, 7, 9, 11, 13, and 15) show that high selectivities (96–100%) for the hydrogenation of the conjugated carbon–carbon double bond were obtained in all cases. The lower selectivities

[6] The intrinsic or true activity of the electrode material for the ECH of phenanthrene was found to be the same for RaNi and Ni_2B but lower for fractal Ni (5).

Table 3. ECH of conjugated enones on fractal nickel electrodes[a]

Entry	Substrate	Charge (F mol^{-1})	Conversion[b] (%)	Selectivity[c] (%)	Current efficiency (%)
1	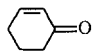	2	93–95	>99	93–95
2	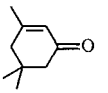	2	48–51	>99	48–51
3		6	88–93	>99	29–31
4	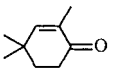	2	42–43	>99	42–43
5		6	80	96	28
6	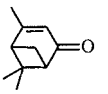	2	33	>99	33
7		6	80	98	27
8	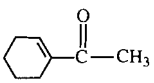	2	69–75	>99	69–75
9		4	92	98	46
10	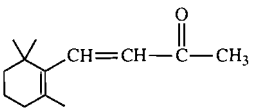	2	28–36	>99	28–36
11		6.25	89	99	28
12	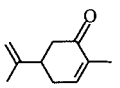	4[d]	65	>99[e]	65
13		15	93	>99[e]	25
14	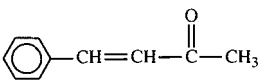	2	73–76	>99	73–76
15		2.25	87	>99	70
16	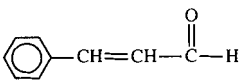	2	69	56	97
17		4	100	51	75

[a]Electrolysis conditions: 48 mM solution of substrate; MeOH–H_2O (50/50, v/v); 0.1 M NaCl; 0.1 M H_3BO_3; pH = 1.7–5.5; room temperature; fractal nickel pressed powder electrodes (p = 800 MPa); J = 50 mA dm^{-2}.

[b]See footnote *e* of Table 1.

[c]Selectivity = (yield of α,β-dihydroketone/conversion rate) × 100.

[d]Data after a charge corresponding to 4 F mol^{-1} are given because there was extensive hydrogenation of the isopropylidene group (2 F mol^{-1}, 67%).

[e]Selectivity = ((yield of dihydrocarvone + yield of carvomenthone)/(100 – (yield of carvone + yield of carvotanacetone)) × 100.

observed with 2,4,4-trimethylcyclohex-2-ene-1-one (96% at 80% conversion) and β-ionone (98% at 80% conversion) reflect once more the fact the double bond is more hindered relative to the carbonyl group than in the other enones. The ECH of the conjugated double bond was much less selective in *trans*-cinnamaldehyde (entries 16 and 17: selectivities of 56 and 51% for conversion rates of 69 and 100%, respectively) than in *trans*-phenylbutenone (100% selectivity at 87% conversion in entry 15), in agreement with the fact that the carbonyl group of an aldehyde is less hindered and more reactive than that of a ketone. Aldehydes have indeed been shown to be hydrogenated more readily than ketones in both catalytic (18) and electrocatalytic (3) hydrogenations.

Conclusion

We have shown that, in the ECH of cyclohex-2-en-1-one at nickel boride electrodes, the selectivity of the carbon–carbon double bond hydrogenation can be increased to 100% by decreasing the current density, and the efficiency can be increased to 100%, also by both increasing the concentration of the substrate and decreasing the current density. The selectivities were quite low with the more active Raney nickel electrodes. Fractal nickel electrodes were found to give higher selectivities than nickel boride electrodes under given conditions and were shown to be quite useful for the selective ECH of the conjugated carbon–carbon double bond of a variety of enones.

Acknowledgements

Financial support from the Natural Sciences and Engineering Research Council of Canada, the Fonds pour la formation de chercheurs et l'aide à la recherche (FCAR) du Québec, and the Ministère de l'Energie et des Ressources du Québec is gratefully acknowledged.

Can. J. Chem. Downloaded from www.nrcresearchpress.com by 80.90.12.36 on 09/08/12
For personal use only.

References

1. D. Robin, M. Comtois, A. Martel, R. Lemieux, A. Kam Cheong, G. Belot, and J. Lessard. Can. J. Chem. **68**, 1218 (1990).
2. B. Mahdavi, J.-M. Chapuzet, and J. Lessard. Electrochim. Acta, **38**, 1377 (1993).
3. A. Kam Cheong, Y. Bolduc, and J. Lessard. Can. J. Chem. **71**, 1850 (1993).
4. J. Lessard, G. Belot, Y. Couture, S. Desjardins, and C. Roy. Int. J. Hydrogen Energy, **18**, 681 (1993).
5. B. Mahdavi, P. Los, M.-J. Lessard, and J. Lessard. Can. J. Chem. **72**, 2268 (1994).
6. L. Coche, B. Ehui, D. Limosin, and J.- C. Moutet. J. Org. Chem. **55**, 5905 (1990).
7. V. Anantharaman and P. N. Pintauro. J. Electrochem. Soc. **141**, 2729 (1994).
8. A. Cyr, P. Huot, G. Belot, and J. Lessard. Electrochim. Acta, **35**, 147 (1990).
9. T. Osa, T. Matsue, A. Yokozawa, and T. Yamada. Denki Kagaku, **54**, 484 (1986).
10. C.A. Brown. J. Org. Chem. **35**, 1900 (1970).
11. J.-P. Candy, P. Fouilloux, M. Keddam, and H. Takenouti. Electrochim. Acta, **27**, 1585 (1982).
12. T. Yamada, T. Osa, and T. Matsue. Chem. Lett. 1611 (1987).
13. P. Chamberlain and G.H. Whitham. J. Chem. Soc. 1131 (1969).
14. P. Los and A. Lasia. J. Electroanal. Chem. **333**, 115 (1992).
15. A. Kam Cheong, A. Lasia, and J. Lessard. J. Electrochem. Soc. **140**, 2721 (1993).
16. K. Amouzegar and O. Savadogo. Electrochim. Acta, **39**, 557 (1994).
17. F. Bossanyi, C.A. Hassani, H. Ménard, and J. Lessard. Can. J. Chem. **67**, 365 (1989).
18. R.L. Augustine. Catalytic hydrogenation. Marcel Dekker Inc., New York. 1965. Chaps. 3 and 4.

Can. J. Chem. Downloaded from www.nrcresearchpress.com by 80.90.12.36 on 09/08/12
For personal use only.

The crystal structure of 2-(4-bromophenyl)-4-(2-fluoroethyl)-5,6-dihydro-4*H*-1,3,4-oxadiazine hydrochloride, an octopaminergic insecticide/miticide

Mark A. Dekeyser, W. Ashley Harrison, Nicholas J. Taylor, and Roger G.H. Downer

Abstract: The crystal structure of 2-(4-bromophenyl)-4-(2-fluoroethyl)-5,6-dihydro-4*H*-1,3,4-oxadiazine hydrochloride, a new octopamine agonist, has been established by Patterson and Fourier methods and refined to a final *R* value of 0.0293 for 2123 absorption-corrected observed data. The crystals are monoclinic, a = 14.336(3), b = 12.649(3), c = 6.989(1) Å, β = 93.48(1)°, and the space group is $P2_1/c$. Its structural similarities with the crystal structure of the invertebrate neurotransmitter, octopamine, are described and support the hypothesis that the pesticidal properties of dihydrooxadiazines are, at least partially, due to perturbation of octopaminergic systems.

Key words: dihydrooxadiazine, octopamine agonist.

Résumé : Utilisant les méthodes de Patterson et de Fourier, on a déterminé la structure cristalline du chlorhydrate de 2-(4-bromophényl)-4-(2-fluoroéthyl)-5,6-dihydro-4*H*-1,3,4-oxadiazine, une nouvelle octopamine agoniste, et on l'a affinée jusqu'à des valeurs finales de R = 0,0293 pour 2123 absorptions corrigées à partir des données observées. Les cristaux appartiennent au group d'espace monoclinique $P2_1/c$ avec a = 14,336(3), b = 12,649(3), c = 6,989(1) Å, β = 93,48 (1)°. On décrit ses ressemblances structurelles avec la structure cristalline du neurotransmetteur des invertébrés, octopamine, qui confirment l'hypothèse à savoir que les propriétés pesticides des dihydrooxadiazines sont, au moins partiellement, dues à une perturbation du système octopaminergique.

Mots clés : dihydrooxadiazine, octopamine agoniste.

[Traduit par la rédaction]

Introduction

One biorational approach in the development of safer and more selective pesticides is to select targets that are vital and specific to pest species, thereby minimizing toxicity to nontarget organisms (1). In this regard, much attention has been directed at the octopaminergic system as a valid target in the search for novel pesticides (2, 3). Octopamine **1** is one of the most abundant and studied biogenic amines in the insect nervous system (4, 5). Octopamine functions as a neurotransmitter, neurohormone, and neuromodulator, regulating several vital physiological functions in insects and mites, including

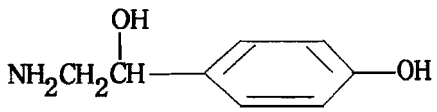

1

feeding, locomotion, and reproduction (6, 7). Compounds that stimulate octopaminergic systems in insects and mites have the potential to cause physiological, behavioral, and lethal effects that often are highly compatible with integrated pest management (IPM) systems. The octopamine receptor has been recognized as a useful target since the discovery of the insecticidal and miticidal properties of formamidines, which function as octopamine agonists by stimulating cyclic adenosine monophosphate (cyclic AMP) (8–10). Two formamidines, chlordimeform **2** and amitraz **3**, are commercial pesticides (11). Pesticidal activity has been also associated with the imidazoline (12) and oxazoline (13) classes of octopamine agonists.

Recently, dihydrooxadiazines were identified (14, 15) as novel octopaminergic insecticides. They were shown to be octopamine agonists in the two-spotted spider mite, *Tetranychus urticae* (16), and in the American cockroach,

Received February 7, 1995.

M.A. Dekeyser[1] **and W.A. Harrison.** Research Laboratories, Uniroyal Chemical Ltd., P.O. Box 1120, Guelph, ON N1H 6N3, Canada.
N.J. Taylor. Chemistry Department, University of Waterloo, Waterloo, ON N2L 3G1, Canada.
R.G.H. Downer. Biology Department, University of Waterloo, Waterloo, ON N2L 3G1, Canada.

[1] Author to whom correspondence may be addressed. Telephone: (519) 822-3790. Fax: (519) 821-1956.

Can. J. Chem. Downloaded from www.nrcresearchpress.com by 80.90.12.36 on 09/08/12
For personal use only.

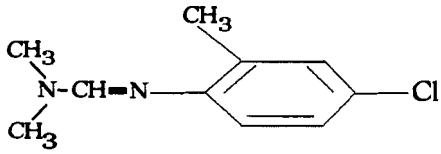

2

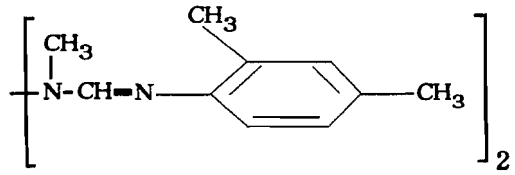

3

Periplaneta americana (17). 2-(4-Bromophenyl)-4-(2-fluoroethyl)-5,6-dihydro-4*H*-1,3,4-oxadiazine hydrochloride **4** was reported to mimic the action of octopamine in stimulating the production of cyclic AMP (16, 17). Furthermore, the compound was found to be extremely potent at controlling eggs of the two-spotted spider mite, *T. urticae*, and the tobacco budworm, *Helicoverpa virescens* (15).

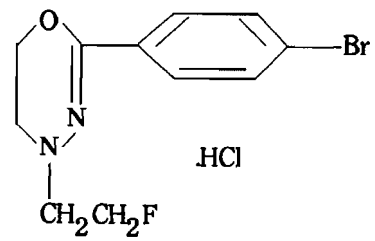

4

The significant activity reported for **4** is encouraging with regard to its possible use as a new octopamine agonist for control of insect and mite pests. From the chemistry point of view, it is interesting to speculate why **4** should behave as an octopamine agonist when the two compounds, **1** and **4**, do not obviously resemble one another. Through molecular modelling studies, structural similarities between dihydrooxadiazines and octopamine have been shown (14). To validate the molecular modelling studies, we required a precise structure of a highly active dihydrooxadiazine compound. In this study, we determined the crystal structure of **4** and compared this structure to the crystal structure of **1**.

Experimental

(4-Bromophenyl)-4-(2-fluoroethyl)-5,6-dihydro-4*H*-1,3,4-oxadiazine hydrochloride **4** was synthesized according to the procedure of Dekeyser et al. (18). It was recrystallized from methanol to give colorless needles with mp 163°C. A crystal of dimensions 0.08 × 0.16 × 0.72 mm was mounted on a glass fibre. Data were collected at 180 K on a Nicolet LT2 equipped R3m/V diffractometer using Mo $K\alpha$ radiation (λ = 0.71073 Å). Twenty-five reflections (22° < 2θ < 32°) were used in the unit cell refinement. An ω scan data collection (4° < 2θ < 56°) of $hk \pm l$ reflections yielded 3056 unique data of which 2123 with $F_o > 4\sigma(F_o)$ were considered observed and were used in the structure solution and refinement. Two standard reflections, monitored every 100 measurements, exhibited only statistical fluctuations. Background measurements were made at the beginning and end of each scan for a total of half the scan time. Crystal data are as follows:

$C_{11}H_{13}BrClFN_2O$ MW 323.6 g mol^{-1}

Monoclinic, $P2_1/c$ (no. 14), a = 14.336(3), b = 12.649(3), c = 6.989(1) Å, β = 93.48(1)°, V = 1265.1(4) Å^3 (180 K), Z = 4, d_c = 1.699 g cm^{-3}, μ = 34.58 cm^{-1} (face-indexed absorption correction, transmission factors 0.5348–0.7734).

Data reduction, structure solution, and refinement were carried out using Siemens SHELXTL PLUS software on a VAX 3100. The structure was solved by Patterson and Fourier techniques and refined by full-matrix least-squares methods. All hydrogen atoms were located by difference Fourier synthesis but were included in the refinement riding in calculated positions, except H(4), which was fixed in the found location. Hydrogen atom isotopic thermal parameters were refined. The final refinement, on 168 parameters, based on observed wF's, was weighted with $w^{-1} = \sigma^2(F)$ and gave residuals R = 0.0293, wR = 0.0263 with S = 1.32 where $R = \Sigma||F_o| - |F_c||/\Sigma F_o$, $wR = [\Sigma w(|F_o| - |F_c|)^2/\Sigma(wF_o^2)]^{1/2}$, and $S = [\Sigma w(|F_o| - |F_c|)^2/(N_{obs} - N_{var})]^{1/2}$. The largest final cycle shift/error was 0.005 and the most significant features of a final difference map were a hole of −0.40 e/Å^3 and a peak of 0.34 e/Å^3. An extinction correction of the form $F^* = F[1 + 0.002\ X\ F^2/\sin 2\theta]$, X variable, gave X = 0.00012(1).

The X-ray conformations of octopamine **1** and dihydrooxadiazine **4** were superimposed using the HyperChem® Release 4 and ChemPlus™ package[2] running on a 80486 33 MHz IBM-compatible personal computer. Superimpositions were done using the RMS Fit module of ChemPlus to find the best fit for the two structures by overlaying three pairs of atoms in the two structures. The atoms chosen for this fit procedure were the first and fourth carbon atoms in the phenyl rings and the corresponding nitrogen atom of each structure.

Results and discussion

The final atomic coordinates[3] and equivalent isotropic temperature factors for the non-hydrogen atoms are listed in Table 1 and a view of the crystal structure, showing the atom-numbering scheme, is presented in Fig. 1. Bond distances and bond angles are given in Tables 2 and 3, respectively.

The racemic dihydrooxadiazine hydrochloride **4** crystals contained four molecules, two pairs of enantiomers, in the

[2] HyperChem® and ChemPlus™ programs, Hypercube, Inc., 419 Phillip Street, Waterloo, ON, N2L 3X2, Canada.

[3] Lists of the atomic coordinates, bond lengths and angles, torsion angles, and anisotropic thermal parameters may be purchased from: The Depository of Unpublished Data, Document Delivery, CISTI, National Research Council Canada, Ottawa ON K1A 0S2, Canada.

Tables of atomic coordinates and bond lengths and angles have also been deposited with the Cambridge Crystallographic Data Centre, and can be obtained on request from The Director, Cambridge Crystallographic Data Centre, University Chemical Laboratory, 12 Union Road, Cambridge, CB2 1EZ, U.K.

Structure factor amplitudes are no longer being deposited and may be obtained directly from the author.

Can. J. Chem. Downloaded from www.nrcresearchpress.com by 80.90.12.36 on 09/08/12
For personal use only.

Can. J. Chem. Downloaded from www.nrcresearchpress.com by 80.90.12.36 on 09/08/12
For personal use only.

Table 1. Atomic coordinates ($\times 10^4$) and equivalent isotropic displacement coefficients ($Å^2 \times 10^3$) for **4**.

Atom	*x*	*y*	*z*	U_{eq}[a]
O(1)	6963(1)	2039(2)	3715(3)	28.5(7)
C(2)	7701(2)	1388(3)	3829(4)	19.9(9)
N(3)	7741(2)	408(2)	3374(3)	20.0(8)
N(4)	6857(2)	−90(2)	2762(3)	19.3(8)
C(5)	6019(2)	477(2)	3395(5)	23(1)
C(6)	6120(2)	1599(2)	2797(5)	27(1)
C(7)	8574(2)	1922(2)	4559(4)	19.5(9)
C(8)	9355(2)	1320(3)	5138(4)	25(1)
C(9)	10188(2)	1809(2)	5705(4)	25(1)
C(10)	10229(2)	2901(3)	5691(4)	23(1)
C(11)	9452(2)	3508(3)	5183(4)	27(1)
C(12)	8624(2)	3018(2)	4596(4)	22(1)
C(13)	6946(2)	−1209(2)	3417(5)	24(1)
C(14)	6114(2)	−1882(3)	2769(5)	30(1)
F(15)	5385(1)	−1726(1)	3967(3)	37.4(7)
Br(16)	11393.3(2)	3593.3(3)	6296.2(5)	31.4(1)
Cl(17)	6501.4(6)	−163.0(7)	−1489(1)	30.5(3)

[a] U_{eq} = 1/3 of the trace of the orthogonalized U_{ij} tensor.

Table 2. Bond lengths (Å) for **4**.

Bond	Length	Bond	Length
O(1)—C(2)	1.339(4)	O(1)—C(6)	1.445(4)
C(2)—N(3)	1.282(4)	C(2)—C(7)	1.485(4)
N(3)—N(4)	1.455(3)	N(4)—C(5)	1.489(4)
N(4)—C(13)	1.490(4)	C(5)—C(6)	1.490(4)
C(7)—C(8)	1.393(4)	C(7)—C(12)	1.388(4)
C(8)—C(9)	1.382(4)	C(9)—C(10)	1.383(4)
C(10)—C(11)	1.381(4)	C(10)—Br(16)	1.909(3)
C(11)—C(12)	1.380(4)	C(13)—C(14)	1.513(4)
C(14)—F(15)	1.392(4)	N(4)—H(4)	0.96
H(4)—Cl(17)	2.03	N(4)—Cl(17)	2.985(3)

crystallographic unit cell, which is centrosymmetric. The analysis shows that the dihydrooxadiazine ring adopts a half-chair conformation. Figure 2 illustrates the puckering of the dihydrooxadiazine ring. Atoms C(6), O(1), C(2), N(3), and N(4) define a plane (plane 1), whereas C(5) lies 0.685 Å below this plane. A similar conformation of a dihydrooxadiazine ring was reported for the crystal structure of (*E*)-6-(bromomethylene)-5,6-dihydro-4,4-dimethyl-2-phenyl-4*H*-1,3,4-oxadiazinium bromide (19).

The phenyl ring is planar, with the bromine atom located just above this plane. The phenyl ring and the dihydrooxadiazine ring are almost coplanar. The phenyl ring plane is twisted 12.9° from plane 1 of the dihydrooxadiazine ring. In the study of the above oxadiazinium compound, it was found that the phenyl ring was twisted by 20° (19). This twist angle is also typical of biphenyl compounds without *ortho* substituents (20). The fluoroethyl chain lies extended from and nearly coplanar with the dihydrooxadiazine ring. The fluorine atom lies below plane 1 of the dihydrooxadiazine ring. The hydrogen and chlorine atoms of the salt portion both lie above the dihydrooxadiazine ring.

Fig. 1. Molecular structure of dihydrooxadiazine **4** and its atomic numbering scheme with thermal ellipsoids at the 50% probability level. (Hydrogen atoms are shown with arbitrary size for clarity.)

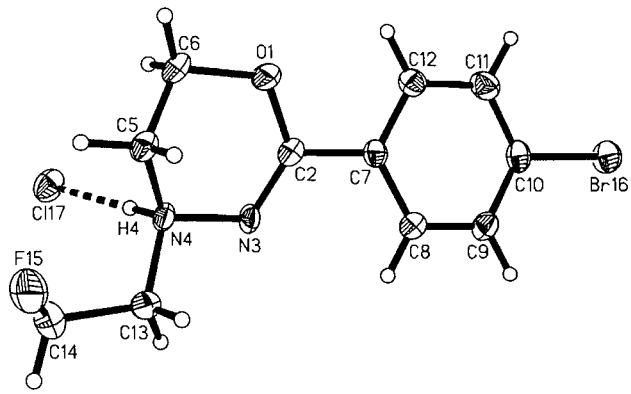

Fig. 2. Half-chair conformation of the dihydrooxadiazine ring.

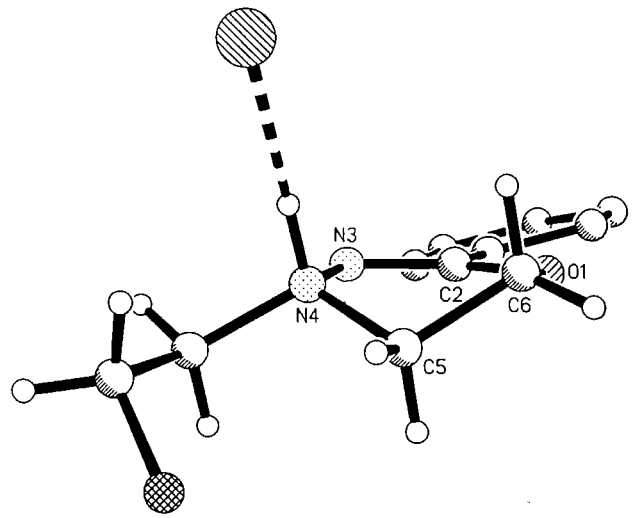

Most of the bond distances (Table 2) are close to accepted values (21–24) with the exception of the hydrogen–chlorine bond, which, at 2.03 Å, is somewhat shorter than the more typical 2.30–2.40 Å. There are no untoward intramolecular contacts, the shortest being F(15) – H(5y) at 2.54 Å. There are also no untoward intermolecular contacts, the shortest being 2.52 Å between H(6y) and the fluorine atom of an adjacent molecule.

In view of the proposed octopamine agonist activity of **4**, it was decided to compare its crystal structure with that of octopamine. In 1977, the crystal structure of octopamine hydrochloride was determined by Paxton and Hamor (25). For comparison purposes, a computer-generated perspective drawing of the final X-ray model of octopamine hydrochloride **1** superimposed on dihydrooxadiazine **4** is shown in Fig. 3. The most obvious difference, apart from the larger size of the dihydrooxadiazine molecule, is the orientation of the phenyl rings. A comparison of the dihedral angles of five corresponding atoms shows that the phenyl ring in **4** is rotated 62.8° from

Table 3. Bond angles (deg) for **4**.

Bonds	Angle	Bonds	Angle
C(2)—O(1)—C(6)	115.2(2)	O(1)—C(2)—N(3)	128.8(3)
O(1)—C(2)—C(7)	112.8(3)	N(3)—C(2)—C(7)	118.4(3)
C(2)—N(3)—N(4)	116.1(2)	N(3)—N(4)—C(5)	114.1(2)
N(3)—N(4)—C(13)	105.3(2)	C(5)—N(4)—C(13)	114.9(2)
N(4)—C(5)—C(6)	106.4(2)	O(1)—C(6)—C(5)	109.6(2)
C(2)—C(7)—C(8)	119.8(3)	C(2)—C(7)—C(12)	120.1(3)
C(8)—C(7)—C(12)	120.1(3)	C(7)—C(8)—C(9)	120.3(3)
C(8)—C(9)—C(10)	118.8(3)	C(9)—C(10)—C(11)	121.6(3)
C(9)—C(10)—Br(16)	119.6(2)	C(11)—C(10)—Br(16)	118.8(2)
C(10)—C(11)—C(12)	119.5(3)	C(7)—C(12)—C(11)	119.8(3)
N(4)—C(13)—C(14)	113.1(2)	C(13)—C(14)—F(15)	110.3(3)

Can. J. Chem. Downloaded from www.nrcresearchpress.com by 80.90.12.36 on 09/08/12
For personal use only.

Fig. 3. Superimposed computer-generated structure of octopamine **1** (light) and dihydrooxadiazine **4** (dark). (Hydrogen and chlorine atoms have been omitted for clarity.)

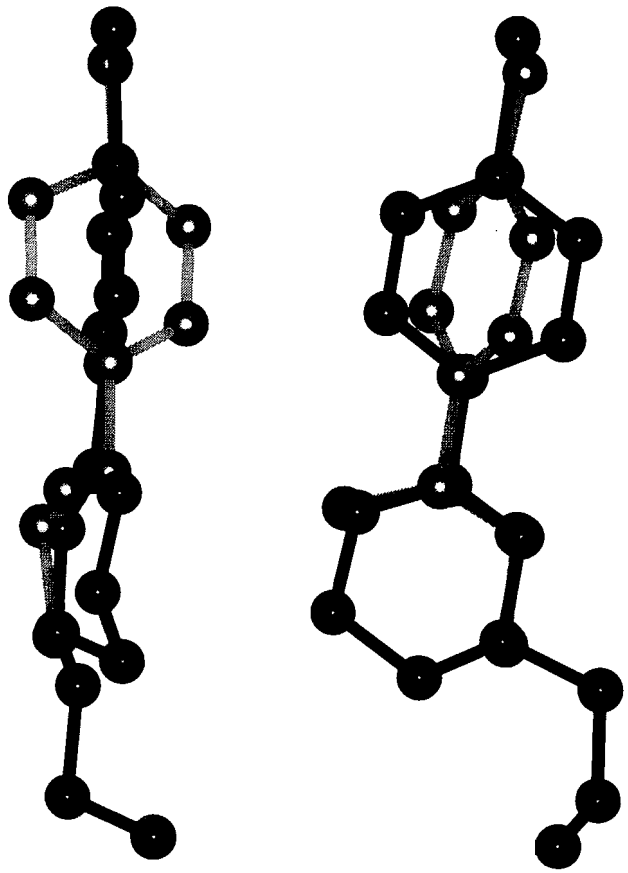

that in **1**. Variations in the dihedral angles of similar compounds have been rationalized in terms of the effects of crystal packing on molecular conformations (20).

Superimposition of **1** and **4** revealed structural and conformational similarities that might account for the agonistic activity of **4**. As shown in Fig. 3, when the amino nitrogen and the first and fourth carbon atoms in the phenyl ring of each molecule are overlaid, C(2)-N(3)-N(4) oxadiazine ring atoms of **4** can occupy space similar to the ethylamino group of octopamine **1**. The RMS deviation of the superimposition of **4** and **1** based on these atoms was 0.1 Å. The two functionalities deemed to be essential to octopaminergic pesticidal action (14), a phenyl ring and a suitably situated amino group, appear to be conserved in **4**. A similar comparison between the octopaminergic pesticide, chlordimeform **2**, and octopamine **1** also resulted in identification of common structural features (26). Therefore, in spite of the extra steric volume, dihydrooxadiazine **4** appears to be structurally and conformationally analogous to octopamine **1**.

In conclusion, we have studied the crystal structure of one pesticidally active example of a new class of conformationally restricted octopamine agonists. We have established the structure of **4** unequivocally by X-ray crystallography and shown that it closely overlays the X-ray structure of octopamine hydrochloride **1**. The conformational constraint and the extra steric volume introduced by the dihydrooxadiazine ring allow the overlay of the presumed essential functionality of octopamine **1** with the dihydrooxadiazine **4**. This evidence supports the proposal that dihydrooxadiazine **4** exerts its insecticidal and miticidal activity through an interaction with octapamine receptors. Our results suggest that certain structural requirements are important for the rational design of octopaminergic pesticides. Further studies to evaluate structure–activity relationships in dihydrooxadiazines are in progress.

References

1. M.W. Goosey. Pestic. Sci. **34**, 313 (1992).
2. V.W. Hertel, H. Agricola, and H. Penzlin. Biol. Rundsch. **27**, 307 (1989).
3. R.G.H. Downer. *In* Cockroaches as models for neurobiology: applications in biomedical research. Vol. 2. *Edited by* I. Huber, E.P. Masler, and B.R. Rao. CRC Press, Boca Raton, Fla. 1990. pp. 103–124.
4. R.G.H. Downer. *In* Neurotox '88: molecular basis of drug and pesticide action. *Edited by* G.G. Lunt. Excerpta Medica, Amsterdam. 1988. pp. 255–265.
5. T.C. Sparks, J.R. Skomp, J. Babcock, and C. Geng. Arch. Insect Biochem. Physiol. **25**, 1 (1994).
6. P.D. Evans. *In* Comprehensive insect physiology, biochemistry, and pharmacology. Vol. 11. *Edited by* G.A. Kerkut and L.I. Gilbert. Pergamon Press, Oxford. 1985. pp. 499–530.
7. I. Orchard and A.B. Lange. ACS Symp. Ser. **356**, 136 (1987).
8. R.G.H. Downer, J.W.D. Gole, and G.L. Orr. Pestic. Sci. **16**, 472 (1985).
9. P.D. Evans and J.D. Gee. Nature, **287**, 60 (1980).
10. S.M.M. Ismail and F. Matsumura. Pestic. Biochem. Physiol. **39**, 219 (1989).

11. G.W. Ware. The pesticide book. Thomson Publications, Fresno, Calif. 1989.
12. J.A. Nathanson. Proc. Natl. Acad. Sci. U.S.A. **82**, 599 (1985).
13. K.R. Jennings, D.G. Kuhn, C.F. Kukel, S.H. Trotto, and W.K. Whitney. Pestic. Biochem. Physiol. **30**, 190 (1988).
14. M.A. Dekeyser, W.A. Harrison, P.T. McDonald, and R.G.H. Downer. Pestic. Sci. **38**, 309 (1993).
15. M.A. Dekeyser, P.T. McDonald, G.W. Angle, Jr., and R.G.H. Downer. J. Agric. Food Chem. **41**, 1329 (1993).
16. S.M.M. Ismail, M.A. Dekeyser, and R.G.H. Downer. Pestic. Biochem. Physiol. **47**, 1 (1993).
17. M.A. Dekeyser. Ph.D. Dissertation, University of Waterloo, 1994.
18. M.A. Dekeyser, D.S. Mitchell, and R.G.H. Downer. J. Agric. Food Chem. **42**, 1783 (1994).
19. D.M. Thompson, I.D. Brindle, and M.F. Richardson. Can. J. Chem. **57**, 3157 (1979).
20. C.P. Brock and R.P. Minton. J. Am. Chem. Soc. **111**, 4586 (1989).
21. International tables for X-ray crystallography. Vol. C. The Kynoch Press, Birmingham, England. 1992.
22. F. Garbassi and L. Giarda. Acta Crystallogr. B29, 1190 (1973).
23. A. Prakash, C. Calvo, A.M. Cameron, and J. Warkentin. J. Cryst. Mol. Struct. 3, 71 (1973).
24. C.S. Huber. Acta Crystallogr. Sect. B: Struct. Crystallogr. Cryst. Chem. **B29**, 1046 (1973).
25. K. Paxton and T.A. Hamor. Acta Crystallogr. Sect. B: Struct. Crystallogr. Cryst. Chem. **B33**, 2143 (1977).
26. C. Tosi, L. Barino, and R. Scrodamaglia. Theochem, **15**, 241 (1984).

Can. J. Chem. Downloaded from www.nrcresearchpress.com by 80.90.12.36 on 09/08/12
For personal use only.

Electrochemistry of polyoxometalates immobilized in ion exchange polymer films

Kasem K. Kasem and Franklin A. Schultz

Abstract: The polyoxometalate ions $PMo_{12}O_{40}^{3-}$, $PW_{12}O_{40}^{3-}$, and $SiW_{12}O_{40}^{4-}$ are incorporated in polymeric ruthenium(II)(vinyl)bipyridine (poly-Ru(vbpy)$_3^{2+}$) films from aqueous and dioxane–water electrolytes. Despite their large mass the ions exist as freely diffusing species that compensate for up to 30% of the charge in poly-Ru(vbpy)$_3^{2+}$. An investigation of the effect of environmental conditions on electrochemical behavior reveals that the first two one-electron reduction waves of $SiW_{12}O_{40}^{4-}$ coalesce into a single two-electron reaction and those of $PW_{12}O_{40}^{3-}$ shift significantly in potential upon a change from pure aqueous to 50(v/v)% dioxane/water solvent. The observation is attributed to destabilization of the one-electron reaction products as the solvent is enriched is dioxane. Incorporation of polyoxometalates in protonated poly(vinyl)pyridine and poly-Ru(vbpy)$_3^{2+}$ films from dioxane–water solvent results in differences in electrochemical behavior. Polyoxometalate anions incorporated in poly-Ru(vbpy)$_3^{2+}$ films catalyze the electrochemical reduction of hydrogen ion.

Key words: polyoxometalate, electrochemistry, poly-Ru(vbpy)$_3^{2+}$, electrocatalysis, immobilization.

Résumé : On a incorporé les ions polyoxométallates $PMo_{12}O_{40}^{3-}$, $PW_{12}O_{40}^{3-}$ et $SiW_{12}O_{40}^{4-}$ dans des films polymériques de ruthénium(II)(vinyl)bipyridine (poly-Ru(vbpy)$_3^{3+}$) à partir d'électrolytes en solutions dans l'eau ou dans un mélange eau–dioxane. Malgré leurs masses importantes, les ions existent sous la forme d'espèces qui diffusent librement et ils peuvent compenser électrostatiquement jusqu'à 30% de la charge du poly-Ru(vbpy)$_3^{3+}$. Une étude de l'effet des conditions environnementales sur le comportement électrochimique révèle que le potentiel des deux premières vagues de réduction du $SiW_{12}O_{40}^{4-}$ par un électron est fortement modifié lorsqu'on passe de l'eau pure à un mélange de solvants formé à 50% (v/v) de dioxane/eau. On attribue ces observations à la déstabilisation des produits de réduction par un électron lorsqu'on enrichit le solvant en dioxane. L'incorporation de polyoxométallates dans des films de poly(vinyl)pyridine ou de poly-Ru(vbpy)$_3^{3+}$ protonés à partir de solvants mixtes dioxane–eau provoque des différences dans le comportement électrochimique. Les anions polyoxométallates incorporés dans les films de poly-Ru(vbpy)$_3^{3+}$ catalysent la réduction électrochimique de l'ion hydrogène.

Mots clés : polyoxométallate, électrochimie, poly-Ru(vbpy)$_3^{3+}$, électrocatalyse, immobilisation.

[Traduit par la rédaction]

Introduction

Polyoxometalates are soluble polymeric oxides formed by hydrolysis of the early transition elements (1–4). They have been widely studied as catalysts of thermal (5–7) and photochemical (8–10) reactions and as models for catalytic reactions at metal oxide surfaces (11). Although the electrochemistry of polyoxometalates has been investigated for several decades (12–25), exploitation of their catalytic properties in electrochemical reactions has begun only recently. Polyoxometalates should be excellent electrocatalysts because of their chemical stability and capacity to undergo multielectron charge transfer reactions. Several recent investigations have illustrated the electrocatalytic properties of polyoxometalates and of related metal oxide aggregates (26–31).

One means of enhancing the properties of electrocatalytic reagents is by entrapping them in chemically modified layers on electrode surfaces (32). Although widely used in applications based on its electron transfer properties (33), polymeric tris(4-vinyl-4′-methyl-2,2′-bipyridine)ruthenium(II), poly-Ru(vbpy)$_3^{2+}$, is a useful ion exchange polymer (34) because of its chemical stability, wide electrochemical window, and ability to be used in aqueous and non-aqueous solvents. In this publication we describe incorporation of three heteropolyoxometalate Keggin anions, $PMo_{12}O_{40}^{3-}$, (PMo_{12}), $PW_{12}O_{40}^{3-}$, (PW_{12}), and $SiW_{12}O_{40}^{4-}$ (SiW_{12}) in poly-Ru(vbpy)$_3^{2+}$ films. The present work compares the electrochemistry of these heteropolyanions in poly-Ru(vbpy)$_3^{2+}$ with that observed in homogeneous solution and in other polymeric matrices (28, 35–37) and reports on their ability to electrocatalytically reduce hydrogen ion under such conditions.

Received July 4, 1994.[1]

K.K. Kasem.[2] Department of Biological and Physical Sciences, Indiana University at Kokomo, Kokomo, IN 46904-9003, U.S.A.
F.A. Schultz. Department of Chemistry, Indiana University – Purdue University at Indianapolis Indianapolis, IN 46202-3274, U.S.A.

[1] Revision received April 5, 1995.
[2] Author to whom correspondence may be addressed. Telephone: (317) 455-9245. Fax: (317) 455-9276.

Can. J. Chem. Downloaded from www.nrcresearchpress.com by 80.90.12.36 on 09/08/12
For personal use only.

Table 1. Influence of immersion time and experimental conditions on quantity and electrochemical properties of $SiW_{12}O_{40}^{4-}$ incorporated in poly-Ru(vbpy)films.

Immersion conditions[a]	Γ_{Si}(mol cm^{-2})	Γ_{Si}/Γ_{Ru}	D_{app}(cm^2 s^{-1})
15 min, 5 mM $SiW_{12}O_{40}^{4-}$	1.0×10^{-10}	0.022	1.6×10^{-8}
1 h, 5 mM $SiW_{12}O_{40}^{4-}$	0.7×10^{-10}	0.016	2.6×10^{-8}
2 h, 10 mM $SiW_{12}O_{40}^{4-}$	2.1×10^{-10}	0.046	2.2×10^{-9}
4 days, 10 mM $SiW_{12}O_{40}^{4-}$	7.1×10^{-10}	0.156	1.3×10^{-9}

[a]0.5 M H_2SO_4, 50% dioxane/water, $\Gamma_{Ru} = 4.6 \times 10^{-9}$ mol cm^{-2}.

Experimental section

Material and methods

The $PMo_{12}O_{40}^{3-}$, $PW_{12}O_{40}^{3-}$, and $SiW_{12}O_{40}^{4-}$ ions were obtained commercially as phosphomolybdic (Aldrich), phosphotungstic (Fluka), and tungstosilicic (Fluka) acid, respectively, and used as received. The monomeric reagent, $Ru(vbpy)_3^{2+}$, was prepared from $RuCl_3$ and 4-vinyl-4′-methyl-2,2′-bipyridine (vbpy) following the procedure of Denisevich et al. (33) and isolated as the hexafluorophosphate salt. The vbpy ligand was prepared by the method of Abruna et al. (38) and characterized by ^{1}H NMR spectroscopy. Poly(4-vinyl) pyridine (PVP) was obtained from Scientific Polymer Products. Films of poly-$Ru(vbpy)_3^{2+}$ were prepared as described in ref. 34 by cycling the potential of a glassy carbon (GC) disk electrode (0.071 cm^2 surface area, Bioanalytical Systems) between −0.9 and −1.9 V vs. Ag/AgCl in an acetonitrile solution containing 1–2 mM $[Ru(vbpy)_3](PF_6)_2$ plus 0.1 M tetra-*n*-butylammonium hexafluorophosphate. Scans were carried out at a sweep rate of 200 mV s^{-1} for a period of ca. 8 min, which resulted in electrodes with surface coverages of (4–9) $\times 10^{-9}$ moles Ru per cm^2. Films of PVP on GC electrodes were prepared and cross-linked with 1,12-dibromododecane as described in ref. 35.

Heteropolyanions were incorporated in the ion polymer films by soaking modified electrodes for 2–24 h in aqueous or 50(v/v)% dioxane/water solutions containing 0.5 M H_2SO_4 and 0.01 M heteropolyacid. The electrodes then were rinsed thoroughly and transferred to reactant-free electrolyte where their electrochemical response was examined. The electrode surface coverage, Γ, of the anions was determined by integrating the area under voltammetric *i–E* curves using equipment and procedures described previously (34). The apparent diffusion coefficient of ions in the film, D_{app}, was determined from the slope of i–$t^{-1/2}$ transients of potential step electrolysis experiments (33). Formal potentials were determined as the average of cathodic and anodic peak potentials in cyclic voltammetry experiments. The number of electrons transferred in each electrode reaction was evaluated from the magnitude of the voltammetric response and, in bulk solution experiments, from the separation between reverse and forward peak potentials. Electrode potentials are reported relative to a Ag/AgCl reference electrode whose potential is −45 mV vs. the saturated calomel electrode.

Results and discussion

Incorporation of heteropolyanions in Poly-$Ru(vbpy)_3^{2+}$

The $PMo_{12}O_{40}^{3-}$, $PW_{12}O_{40}^{3-}$, and $SiW_{12}O_{40}^{4-}$ ions are incorporated in poly-$Ru(vbpy)_3^{2+}$ films by immersing modified electrodes in aqueous or 50(v/v)% dioxane/water solutions of these reagents. Figure 1*A* shows the result of soaking a 4.6×10^{-9} mol cm^{-2} poly-$Ru(vbpy)_3^{2+}$ film for 2 h in a 0.5 M H_2SO_4 dioxane–water solution containing 10 mM $SiW_{12}O_{40}^{4-}$ and then transferring the electrode to reactant-free electrolyte. The waves observed near −0.45 and −0.60 V are due to reduction and reoxidation of $SiW_{12}O_{40}^{4-}$. The small broad feature at −0.05 to −0.2 V is a component of the voltammetric background of poly-$Ru(vbpy)_3^{2+}$-covered GC electrodes. It is observed before and after loading of the polymer films with heteropolyanions. A fraction of the electroactive material initially retained by the film is lost upon repeated voltammetric cycling of the SiW_{12} redox waves, but after a period of several minutes a steady-state concentration of reactant is achieved within the film (Fig. 1*B*). This material exhibits the symmetrical wave shape, small peak potential separation and linear peak current vs. sweep rate response (Fig. 1*C*) that is characteristic of a surface-confined species. The behavior is similar to that exhibited by anionic transition metal complexes confined within poly-$Ru(vbpy)_3^{2+}$ films (34).

Table 1 illustrates the effect of varying the immersion time and conditions on the amount of $SiW_{12}O_{40}^{4-}$ incorporated in the film. The quantity of material incorporated increases with immersion time; at longer times a limiting steady-state coverage is reached. SiW_{12} exhibits the largest limiting coverage of the three heteropolyanions. The value of $G_{Si}/G_{Ru} = 0.156$ corresponds to electrostatic compensation of 30% of the Ru^{2+} charge sites in the film. PMo_{12} and PW_{12} exhibit lower limiting coverages of G_P/G_{Ru} equal to 0.074 (11%) and 0.09 (13%), respectively. At these lower than saturation coverages, the larger incorporation of $SiW_{12}O_{40}^{4-}$ is consistent with greater electrostatic interaction between the Ru^{2+} sites and the tetranegative SiW_{12} ion compared with trinegative PW_{12} and PMo_{12}. The foregoing results demonstrate that high molecular mass polyoxometalate ions can be incorporated in $Ru(vbpy)_3^{2+}$ films. This result is of interest because of the ability of $Ru(vbpy)_3^{2+}$ films to exclude reagents on the basis of molecular size (39). However, the 5.6 Å hydrodynamic radius of the Keggin ions (12) is not much larger than that of transition metal cyanides (e.g., $r = 4.6$ Å for $Fe(CN)_6^{3-}$ (40)), which are readily incorporated in such films, and is significantly smaller than that of reagents such as $Ru(bpy)_3^{2+}$ ($r = 6.9$ Å (41)), which are excluded. Therefore, incorporation of Keggin ions in poly-$Ru(vbpy)_3^{2+}$ is dimensionally feasible.

However, when so incorporated, the polyoxometalates exhibit apparent diffusion coefficients that are 2 to 3 orders of magnitude smaller than their bulk solution values of ca. 10^{-6} cm^2 s^{-1} (Table 1). The magnitude of D_{app} decreases as the

Can. J. Chem. Downloaded from www.nrcresearchpress.com by 80.90.12.36 on 09/08/12
For personal use only.

Can. J. Chem. Downloaded from www.nrcresearchpress.com by 80.90.12.36 on 09/08/12
For personal use only.

Fig. 1. (*A*) Cyclic voltammetric traces at 200 mV s^{-1} following immersion of poly-Ru(vbpy)$_3^{2+}$ electrode in 10 mM $SiW_{12}O_{40}^{4-}$ + 0.5 M H_2SO_4 (50% dioxane/water) for 2 h, rinsing, and transfer to reactant-free electrolyte. The shaded area represents the decrease in current between the 2nd and 20th cycles. (*B*) Decrease in current of the first cathodic peak with number of cycles at 200 mV s^{-1}. (C) Variation of the first cathodic peak current with sweep rate.

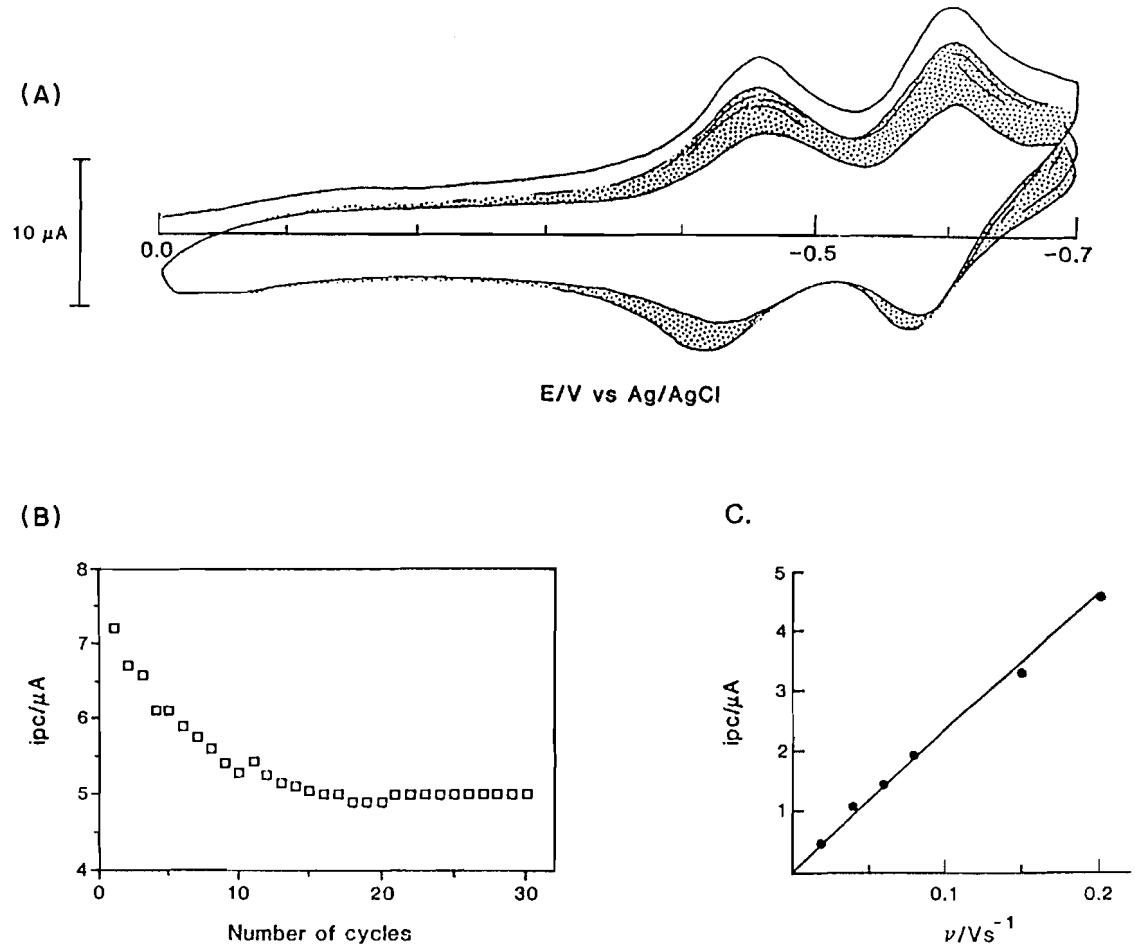

Table 2. Formal potentials and electron stoichiometries of polyoxometalate ions in homogeneous solution and in polymer films of poly-Ru(vbpy)and polyvinylpyridine.[a]

Ion		Homogeneous solution		Poly-Ru(vbpy)$_3^{2+}$	PVP
		Aqueous	Dioxane–water	Dioxane–water	Dioxane–water
$PMo_{12}O_{40}^{3-}$	E_1^{0-} (n_1)		0.37 (2)	0.41 (2)	0.38 (2)
	E_2^{0-} (n_2)		0.25 (2)	0.28 (2)	0.21 (2)
	E_3^{0-} (n_3)		−0.02 (2)	0.04 (4)	0.00 (4)
	E_4^{0-} (n_4)		−0.16 (2)		
	E_5^{0-} (n_5)		−0.25 (2)		−0.22 (2)
$SiW_{12}O_{40}^{4-}$	E_1^{0-} (n_1)	−0.19 (1)			−0.24 (1)
	E_2^{0-} (n_2)	−0.43 (1)	−0.43 (2)	−0.46 (2)	−0.45 (1)
	E_3^{0-} (n_3)	−0.60 (2)	−0.58 (2)	−0.59 (2)	−0.61 (2)
$PW_{12}O_{40}^{3-}$	E_1^{0-} (n_1)	−0.01 (1)	−0.24 (1)	−0.20 [b]	[c]
	E_2^{0-} (n_2)	−0.28 (1)	−0.42 (1)	−0.42 [b]	[c]
	E_3^{0-} (n_3)	−0.61 (2)	−0.56 (2)	−0.60 [b]	−0.60[b]

[a]Recorded in solutions containing 0.5 M H_2SO_4 at a sweep rate of 20 mV s^{-1} unless otherwise noted.
E^{0-} is the formal potential in V vs. Ag/AgCl and n the number of electrons transferred in the electrode reaction.
[b]200 mV s^{-1}.
[c]Overlapping waves at −0.2 to −0.5 V.

Can. J. Chem. Downloaded from www.nrcresearchpress.com by 80.90.12.36 on 09/08/12
For personal use only.

Fig. 2. Cyclic voltammetric traces of $PMo_{12}O_{40}^{3-}$. (*A*) At a bare GC electrode in 50% dioxane/water containing 0.5 M H_2SO_4 (1 mM PM_{12}, sweep rate = 100 mV s^{-1}). (B) After incorporation in poly-Ru(vbpy)$_3^{2+}$from the same electrolyte ($\Gamma_{PMo12} = 4.4 \times 10^{-10}$ mol cm^{-2}, sweep rate = 5, 20, 40, 60, 80, 100, and 150 mV s^{-1} for traces 1–7, respectively). (*C*) After incorporation in PVP from the same electrolyte ($\Gamma_{PMo12} = 1.4 \times 10^{-10}$ mol cm^{-2}, sweep rate = 150 mV s^{-1}).

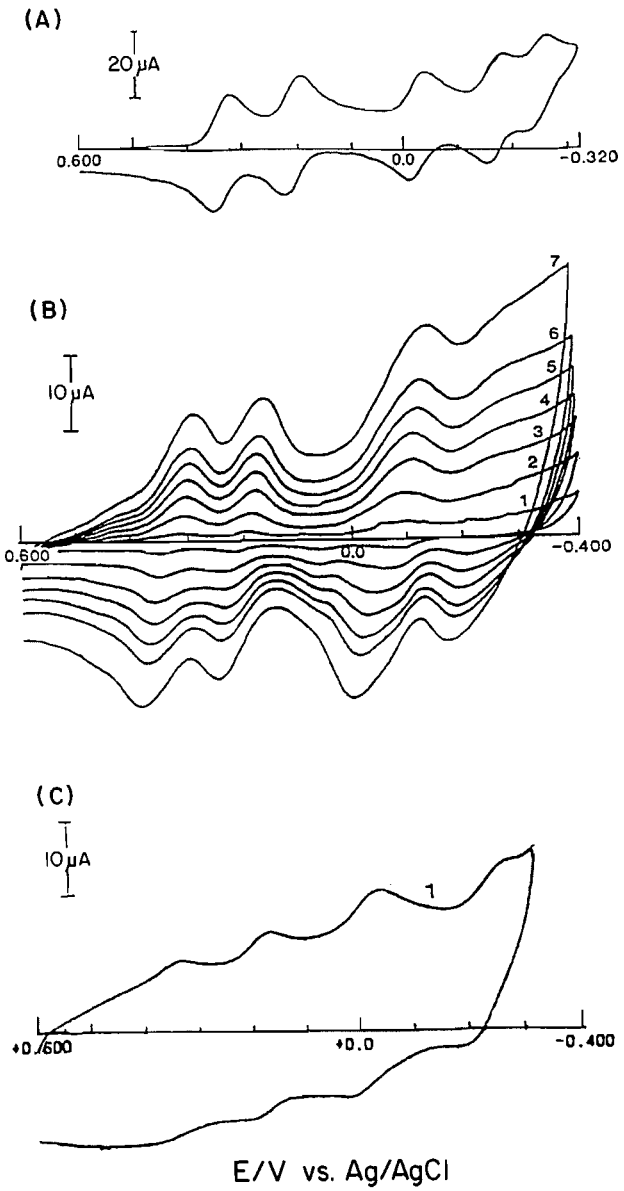

loading of the film increases. The behavior may be due to single-file diffusion or to electrostatically induced constriction of the film as the concentration of electroactive ion increases. The effect is observed for transition metal anions incorporated in poly-Ru(vbpy)$_3^{2+}$ (34).

Effect of solution and polymer environment on redox properties

The electrochemical response of polyoxometalates is influenced by solvent and other solution variables (8, 22–24). Since changes in electrochemical response may alter potential electrocatalytic ability, we have characterized the extent to which redox potentials and the number of electrons transferred in the first two to three redox waves of PMo_{12}, SiW_{12}, and PW_{12} are altered by changing from aqueous to dioxane–water solvent and by incorporation in different ion-exchange polymer films.

Figure 2 shows the cyclic voltammetric response of $PMo_{12}O_{40}^{3-}$ at a bare GC electrode in dioxane–water solution containing 0.5 M H_2SO_4 and after incorporation in a poly-Ru(vbpy)$_3^{2+}$and PVP films from the same medium. The homogeneous solution response of PMo_{12} agrees with the previously reported behavior of this compound (15, 18–20) and consists of a series of chemically reversible two-electron reductions, which occur at +0.37, +0.25 , −0.02, −0.16, and −0.25 V vs. Ag/AgCl. Figures 2*B* and 2*C* and Table 2 show that some changes in PMo_{12} electrochemistry occur after incorporation in poly-Ru(vbpy)$_3^{2+}$ and PVP. Specifically, the third and fourth reductions merge into a single composite wave that is approximately twice as large as the first two, and the fifth wave becomes broad and poorly defined in poly-Ru(vbpy)$_3^{2+}$ (Fig. 2*B*). On the other hand, Fig. 2*C* shows that, whereas the merging of the third and the fourth reduction waves occurs also in PVP, the fifth wave can be identified at $E^{0'} \approx -0.220$ V. Calculation of the charge involved in the reduction process by integrating the area under the reduction waves indicated that ca. four electrons are involved in the third wave in poly-Ru(vbpy)$_3^{2+}$ and PVP, which is twice the value for the first and the second reduction waves (Fig. 2*B* and *C*). Thus, incorporation of PMo_{12} in either PVP or poly-Ru(vbpy)$_3^{2+}$ results in the merging of the third and the fourth waves into a single four-electron reduction.

Figures 3*A* and 3*B* compare the bulk solution electrochemical behavior of SiW_{12} in dioxane–water and water containing 0.5 M H_2SO_4. The voltammetric trace in Fig. 3*B* shows two one-electron reactions followed by a two-electron transfer, which is typical of the behavior exhibited by this ion in aqueous electrolytes (12, 15, 16, 22, 23). The response differs from that of Fig. 3*A*, where two two-electron transfers are observed in dioxane–water. The electron stoichiometry of these waves is established from the magnitudes of the peak currents and the peak potential separations ($\Delta E_p = 35$–50 mV), which are consistent with electron transfer accompanied by a small amount of uncompensated solution resistance or slow electrode kinetics. Coalescence of two one-electron reductions into a single two-electron step has been observed in nonaqueous solvents (8) and in aqueous media containing high concentrations of hydrogen ion (22). Solvent studies (24) show that E_1^{0-} for $SiW_{12}O_{40}^{4-}$ shifts in the negative direction by several hundred millivolts upon a change from aqueous to non-aqueous solvent. The results are consistent with destabilization of the one-electron reduction product of $SiW_{12}O_{40}^{4-}$ by a change from aqueous to non-aqueous conditions. However, molecular details of the process are unclear at this time.

Realization that the electrochemistry of $SiW_{12}O_{40}^{4-}$ is sensitive to its environment prompted an examination of its reactivity following incorporation in ion polymer films. Figure 3*C* shows the result of incorporating SiW_{12} in poly-Ru(vbpy)$_3^{2+}$ from dioxane–water. The response is similar to that in the homogeneous mixed solvent solution. Incorporation of $SiW_{12}O_{40}^{4-}$ into a PVP film from dioxane–water, however,produces a change in the electrochemical response to one

Can. J. Chem. Downloaded from www.nrcresearchpress.com by 80.90.12.36 on 09/08/12
For personal use only.

Fig. 3. Cyclic voltammetric traces of $SiW_{12}O_{40}^{4-}$. (*A*) At a bare GC electrode in 50% dioxane/water containing 0.5 M H_2SO_4 (1 mM SiW_{12}, sweep rate = 200 mV s^{-1}); (*B*) At a bare GC electrode in aqueous 0.5 M H_2SO_4 (5 mM SiW_{12}, sweep rate = 200 mV s^{-1}); (*C*) Incorporated in poly-$Ru(vbpy)_3^{2+}$ in dioxane–water containing 0.5 M H_2SO_4 ($\Gamma_{SiW_{12}} = 2.1 \times 10^{-10}$ mol cm^{-2}, sweep rate = 200 mV s^{-1}); (*D*) Incorporated in PVP in dioxane–water containing 0.5 M H_2SO_4 ($\Gamma_{SiW_{12}} = 4.2 \times 10^{-10}$ mol cm^{-2}, sweep rate = 50 mV s^{-1}).

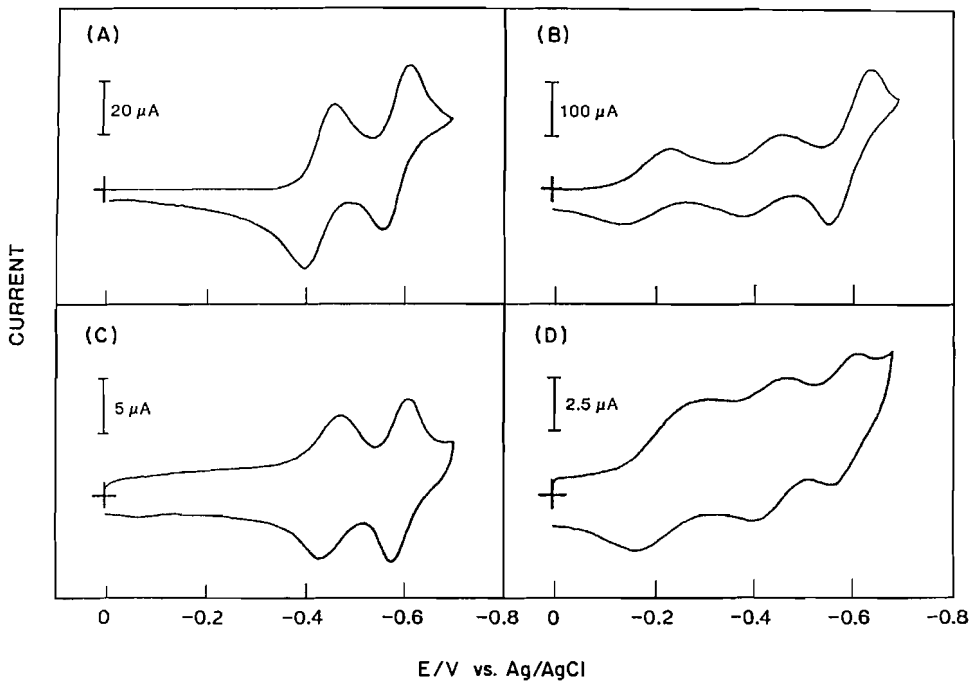

Fig. 4. Cyclic voltammetric traces of $PW_{12}O_{40}^{3-}$. (*A*) At a bare GC electrode in dioxane–water containing 0.5 M H_2SO_4 (1 mM PW_{12}, sweep rate = 100 mV s^{-1}); (*B*) At a bare electrode in aqueous 0.5 M H_2SO_4 (1 mM PW_{12}, sweep rate = 40 mV s^{-1}); (*C*) Incorporated in poly-$Ru(vbpy)_3^{2+}$ in dioxane–water containing 0.5 M H_2SO_4 ($\Gamma_{PW12} = 2.7 \times 10^{-10}$ mol cm^{-2}, sweep rate = 200 mV s^{-1}); (*D*) Incorporated in PVP in dioxane–water containing 0.5 M H_2SO_4 ($\Gamma_{PW_{12}} = 2.4 \times 10^{-10}$ mol cm^{-2}, sweep rate = 100 mV s^{-1}).

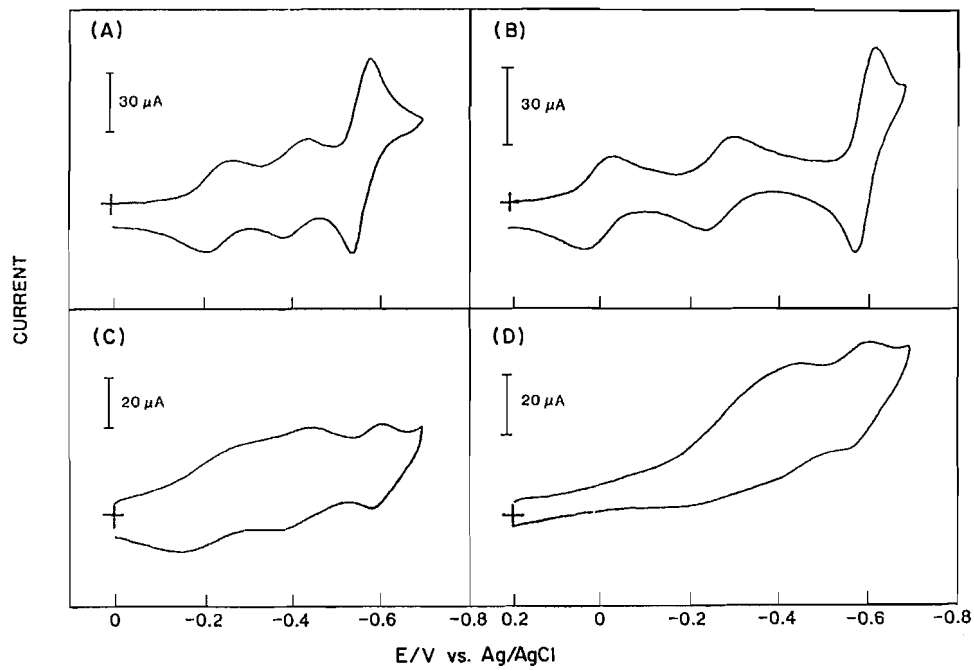

Can. J. Chem. Downloaded from www.nrcresearchpress.com by 80.90.12.36 on 09/08/12
For personal use only.

that is more like that in aqueous medium (Fig. 3*D*). The behavior suggests that the solvent environment accessible to $SiW_{12}O_{40}^{4-}$ in PVP under these conditions more closely approximates an aqueous solution.

Figure 4 and Table 2 illustrate the effects of solvent composition and of polymer film incorporation on electrochemical reduction of $PW_{12}O_{40}^{3-}$. In this case, the change from an aqueous (Fig. 4*B*) to a mixed solvent (Fig. 4*A*) shifts both E_1^{0-} and E_2^{0-} in the negative direction. Since, the one-electron electrode reactions do not combine into a single two-electron transfer, two one-electron and one two-electron waves are observed in dioxane–water. PW_{12} does not exhibit well-defined electrochemistry following incorporation in poly-$Ru(vbpy)_3^{2+}$ (Fig. 4*C*) and PVP (Fig. 4*D*). However, the response is sufficient to determine approximate formal potentials (Table 2), which do not differ significantly from bulk solution values.

The results of the foregoing experiments indicate that changes in solution conditions and polymer environment influence the electrochemical behavior of all three polyoxometalates. The nature of the change depends on the transition metal heteroatom. For the heteropolytungstates, changes occur primarily in the first two one-electron reactions of SiW_{12} and PW_{12}. However, for PMo_{12} the first two waves are relatively unaffected, and changes in response occur in subsequent redox processes.

Electrocatalytic reduction of hydrogen ion

In mixed dioxane–water with acidic electrolyte, heteropolyanions incorporated in poly-$Ru(vbpy)_3^{2+}$ show no evidence of catalytic activity towards hydrogen reduction. Thus catalytic studies were performed in aqueous 0.5 M H_2SO_4; $PMo_{12}O_{40}^{3-}$ is not stable indefinitely under these conditions. However, as the electrocatalytic behavior of PMo_{12} is similar to that of PW_{12} and SiW_{12}, we assume that the species produced by reduction of PMo_{12} or its decomposition products are similar to those derived from the other polyoxoanions.

Figure 5 illustrates the electrocatalytic reduction of H^+ in 0.5 M H_2SO_4 initiated by reduction of PMo_{12}, PW_{12}, and SiW_{12} incorporated in poly-$Ru(vbpy)_3^{2+}$. In this experiment the electrode was cycled between 0 and −1.2 V five times over a period of 1.5 before the observed catalytic response was recorded. After this time the characteristic redox waves of the polyoxoanions are no longer observable, indicating that the initial electrode products have undergone subsequent chemical reaction. However, the species produced in these reactions are catalytically active as illustrated by the solid traces in Fig. 5. Furthermore, this response is unchanged by continued scanning at 200 mV s^{-1} for a period of 1.5 h, indicating that the electrocatalysts are stable and that they have prolonged activity.

Figure 5 shows that significant hydrogen ion reduction commences at −0.5 to −0.7 V. At this potential the initial PW_{12} and SiW_{12} reactants are reduced by four electrons and PMo_{12} by ≥ eight electrons. Thus, as observed previously in studies of hydrogen ion reduction at surfaces modified with electrodeposited derivatives of polyoxometalates (27, 42, 43), it appears that several electrons must be added to each polyoxoanion unit to produce a catalytically active species. The composition of the catalytically active substances described in the present work is not known. However, XPS analysis of reduced poly-

Fig. 5. Catalytic reduction of hydrogen ion initiated by reduction of polyoxometalates ions incorporated in poly-$Ru(vbpy)_3^{2+}$ films. Aqueous 0.5 M H_2SO_4, sweep rate = 100 mV s^{-1}. In each panel trace 1 was recorded at a bare GC electrode, trace 2 at GC electrode modified with (3–6) × 10^{-9} mol cm^{-2} poly-$Ru(vbpy)_3^{2+}$ and trace 3 at a poly-$Ru(vbpy)_3^{2+}$-modified electrode containing (*A*) 0.5 × 10^{-10} mol cm^{-2}; (*B*) 2.8 × 10^{-10} mol cm^{-2}; (*C*) 2.7 × 10^{-10} mol cm^{-2} of the indicated polyoxometalate. The indicated current scale is applicable in all three experiments.

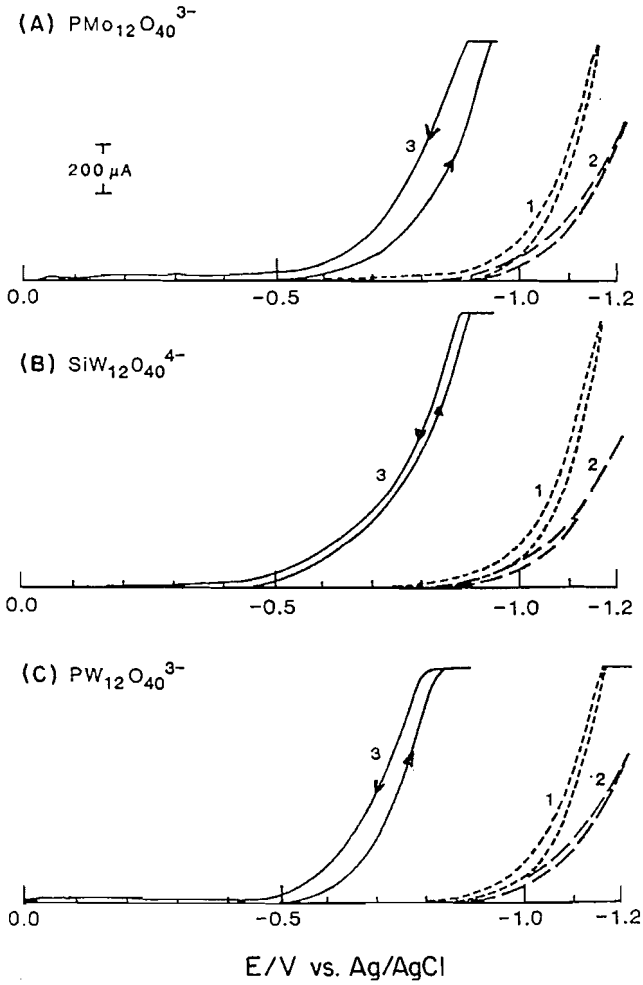

tungstate ions[3] indicates the presence of W(VI), -(V), and -(IV) oxidation states. Thus, we believe the observed catalytic activities arise from stable, mixed-valence species of heteropolyanions , whose reduction at potentials more negative than ca. −0.5 V catalyzes the reduction of H^+.

Acknowledgment

Acknowledgment is made to the Donors of the Petroleum Research Fund, administered by the American Chemical Society (Grant No. 22211-AC3,5 to F.A.S.), for partial support of this research.

[3] K.K. Kasem, unpublished results.

References

1. M.T. Pope. Heteropoly and isopoly oxometalates. Springer-Verlag, New York. 1983.
2. V.M. Day and W.G. Klemperer. Science, **228**, 533 (1985).
3. T.J.R. Weakley. Struct. Bonding (Berlin), **18**, 131 (1974).
4. Y. Jeannin and M. Fournier. Pure Appl. Chem. **59**, 1529 (1987).
5. (a) L. Eberson. J. Am. Chem. Soc. **105**, 3192 (1983); (*b*) D. Mansuy, J.F. Battioni, D.K. Lyon, and R.G. Finke. J. Am. Chem. Soc. **113**, 7222 (1991); (*c*) R. Amadelli, G. Varani, A. Maldotti, and V. Carassiti. J. Mol. Catal. **59**, L9–L14 (1990); (*d*) M.D. Navalikhina, I.L. Malkina, and V.I. Garanin. Neftekhimiya, **30**, 26 (1990).
6. K. Nomiya, M. Miwa, and Y. Sugaya. Polyhedron, **3**, 607 (1984).
7. K. Piepgrass and M.T. Pope. J. Am. Chem. Soc. **111**, 753 (1989).
8. M.A. Fox, R. Cardona, and E. Gaillard. J. Am. Chem. Soc. **109**, 6347 (1987).
9. K. Nomiya, T. Miyazaki, K. Maeda, and M. Miwa. Inorg. Chim. Acta, **127**, 65 (1987).
10. R.F. Renneke and C.L. Hill. J. Am. Chem. Soc. **110**, 5461 (1988).
11. R.K. Grasselli. J. Chem. Educ. **63**, 215 (1986).
12. M.T. Pope and G.M. Varga. Inorg. Chem. **5**, 1249 (1966).
13. M.T. Pope and E. Papaconstantinou. Inorg. Chem. **6**, 1147 (1967).
14. E. Papaconstantinou and M.T. Pope. Inorg. Chem. **6**, 1152 (1966).
15. P. Souchay. Rev. Polarogr. **14**, 270 (1967).
16. G. Herve. Ann. Chim. **6**, 219 (1971).
17. G.A. Tsigdinos and C.J. Hallada. J. Less-Common Metals, **36**, 79 (1974).
18. N. Tanaka, K. Unoura, and E. Itabashi. Inorg. Chem. **21**, 1662 (1982).
19. K. Unoura and N. Tanaka. Inorg. Chem. **22**, 2963 (1983).
20. E. Itabashi. Bull. Chem. Soc. Jpn. **60**, 1333 (1987).
21. B. Keita, T. Lucas, and L. Nadjo. J. Electroanal. Chem. **208**, 343 (1986).
22. B. Keita and L. Nadjo. J. Electroanal. Chem. **217**, 287 (1987).
23. B. Keita and L. Nadjo. J. Electroanal. Chem. **227**, 77 (1987).
24. B. Keita, D. Bouaziz, and L. Nadjo. J. Electrochem. Soc. **135**, 87 (1988).
25. J.E. Toth and F.C. Anson. J. Electroanal. Chem. **256**, 361 (1988).
26. K. Unoura, A. Iwashita, E. Itabashi, and N. Tanaka. Bull. Chem. Soc. Jpn. **57**, 597 (1984).
27. B. Keita and L. Nadjo. J. Electroanal. Chem. **191**, 441 (1985).
28. B. Keita and L. Nadjo. J. Electroanal. Chem. **243**, 481 (1988).
29. P.J. Kulesza and L.R. Faulkner. J. Am. Chem. Soc. **110**, 4905 (1988).
30. J.E. Toth and F.C. Anson. J. Am. Chem. Soc. **111**, 2444 (1989).
31. K.-K. Shiu and F.C. Anson. J. Electroanal. Chem. **309**, 115 (1991).
32. R.W. Murray. *In* Electroanalytical chemistry. Vol. 13. Edited by A.J. Bard. Marcel Dekker, New York. 1984. pp. 191–368.
33. P. Denisevich, H.D. Abru–a, C.R. Leidner, T.J. Meyer, and R.W. Murray. Inorg. Chem. **21**, 2153 (1982).
34. K.K. Kasem and F.A. Schultz. J. Inorg. Organomet. Polymers, **4**, 377(1994).
35. B. Keita and L. Nadjo. J. Electroanal. Chem. **240**, 325 (1988).
36. G. Bidan, E.M. Genies, and M. Lapkowski. J. Chem. Soc. Chem. Commun. 533 (1988).
37. G. Bidan, E.M. Genies, and M. Lapkowski. J. Electroanal. Chem. **251**, 297 (1988).
38. H.D. Abruna, A.I. Breikss, and D.B. Collum. Inorg. Chem. **24**, 987 (1985).
39. T. Ikeda, R. Schmehl, P. Denisevich, K. Willman, and R.W. Murray. J. Am. Chem. Soc. **104**, 2683 (1982).
40. B.I. Swanson and R. Ryan. Inorg. Chem. **12**, 283 (1973).
41. M.S. Chan and A.C. Wahl. J. Phys. Chem. **82**, 2543 (1978).
42. B. Keita, L. Nadjo, and J.P. Haeussler. J. Electroanal. Chem. **230**, 85 (1987).
43. B. Keita and L. Nadjo. J. Electroanal. Chem. **247**, 157 (1988).

Can. J. Chem. Downloaded from www.nrcresearchpress.com by 80.90.12.36 on 09/08/12
For personal use only.

Synthesis and photoisomerization of provitamin D analog with 11β,19-oxide bridge

Rafał R. Siciński

Abstract: Triol diester **1** was converted into the B-ring 5,7-diene **6** representing the first example of the provitamin D analog where the 10β angular methyl group is connected to ring C by a C11/C19 ether linkage. Ultraviolet light irradiation of **6** resulted in the formation of stereoisomeric 9β,10α-compound **8***a*. The structure of the photoproduct was established by analysis of vicinal ^1H–^1H coupling constants and by molecular mechanics.

Key words: 11β,19-oxido steroids, lumisterol analog, 5,7-androstadienes, electrocyclic reactions, photochemistry.

Résumé : On a transformé le diester du triol **1** en un cycle B 5,7-diène **6** représentant le premier exemple d'un analogue de la provitamine D dans lequel le méthyle angulaire 10β est relié au cycle C par un lien éther en C11/C19. L'irradiation ultraviolette du composé **6** conduit à la formation du stéréoisomère 9β,10α **8***a*. On a établi la structure du produit photochimique par l'analyse des constantes de couplage vicinal ^1H–^1H et par la mécanique moléculaire.

Mots clés : 11β,19-oxido stéroides, analogue du lumistérol, 5,7-androstadienes, réactions électrocycliques, photochimie.

[Traduit par la rédaction]

Introduction

Vitamin D_3 (cholecalciferol) is formed biogenetically in the skin (1), by irradiation of 7-dehydrocholesterol (provitamin D_3) to previtamin D_3, followed by a thermal isomerization (Fig. 1). An analogous route has commonly been used for the chemical synthesis of vitamin D_3 as well as of its metabolites and analogs (2, 3). Photochemical and thermal conversions of previtamins D have proved to be an interesting area of organic chemistry. It is well established that the cisoid previtamin D triene, that produced by an ultraviolet light-induced opening of the B-ring 5,7-diene, can undergo a photochemical *Z*/*E* isomerization into tachysterol, as well as an electrocyclic ring closure to the starting provitamin D and lumisterol (4, 5). The sequence of these reversible photoisomerizations was determined in 1955 by Velluz et al. (6) for the D_2 series. Previtamin D can also be thermally equilibrated with the thermodynamically more stable vitamin D; higher temperatures (>100°C) cause an irreversible electrocyclization of the previtamin triene system and result in the formation of pyro- and isopyrocalciferols (4).

It was proposed (7) that the kind of products formed in photochemical and thermal processes of previtamin D_3 can be predicted from the corresponding ground-state conformations of the latter. Thus, various reaction pathways were proposed for antarafacial, sigmatropic 1,7-hydrogen shifts occurring in the thermal previtamin–vitamin equilibration. It was postulated (8, 9) that hydrogen migration involves the s-*cis*, s-*cis* (*cZc*) conformation of the previtamin triene moiety (Fig. 2) twisted in a right- or left-handed sense (*P* and *M* chirality); the absence of such a preference was also suggested (10). Studies on the photochemistry of previtamins D led to a conclusion that the most stable, planar s-*trans*, s-*cis* conformation (*tZc*) of the triene is responsible for the formation of tachysterols, whereas right- and left-handed helical *cZc* conformations are precursors of lumisterols and provitamins D, respectively (11). Analogously, it was also suggested that the latter *P* and *M* conformations were involved in the pyrolysis of previtamins D to the respective cyclized compounds, i.e., pyro- and isopyrocalciferols.

Force-field calculations carried out by Dauben and Funhoff (12) on a previtamin D analog showed that interconversion of the two *cZc* forms via the *tZc* conformation seems possible at room temperatures. On the contrary, the calculated rotational barriers (ca. 29 and 34 kcal/mol) of direct interconversion of the *cZc* forms passing through a planar transition state led to the conclusion that such processes are not feasible.

It was, therefore, of interest to synthesize the previtamin D analog with a "frozen" *cZc* geometry and examine its photochemical isomerization. We chose easily accessible compounds possessing the 11β,19-oxide bridge. The ether linkage between C-19 and the C-ring carbon seemed to be a reasonable choice since it was established (13, 14) that an alkoxy

Received January 27, 1995.

R.R. Siciński.[1] Department of Chemistry, University of Warsaw, 02-093 Warszawa, Pasteura 1, Poland.

[1] Telephone: 22-02-11, ext. 292. Fax: 22-59-96. E-mail: rasici@chem.uw.edu.pl

Can. J. Chem. Downloaded from www.nrcresearchpress.com by 80.90.12.36 on 09/08/12
For personal use only.

Can. J. Chem. Downloaded from www.nrcresearchpress.com by 80.90.12.36 on 09/08/12
For personal use only.

Fig. 1. Scheme of established photochemical and thermal isomerizations within the vitamin D_2 and D_3 series.

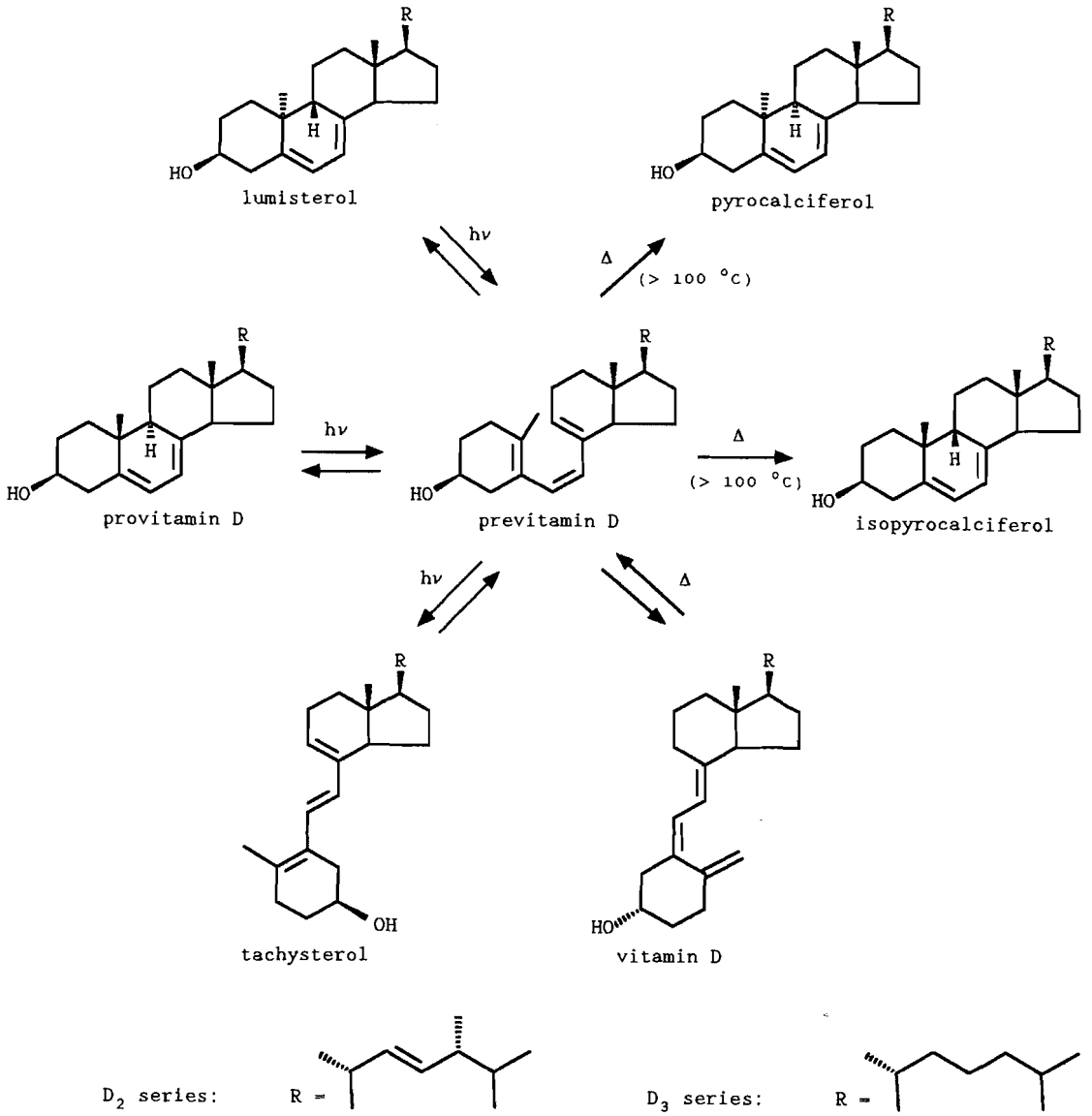

substituent at C-19 in the previtamin D molecule does not influence the course of the photochemical opening of the B-ring diene moiety. It is well known that the nature of the side chain in the previtamin D system does not play any significant role in its photochemical and thermal processes. Therefore, in the present work, the triol diester **1** (Fig. 3) was used as a starting material; its synthesis from androstenolone acetate was reported previously (15).

Results

The synthetic sequence involved first a transformation of **1** into diepoxide **3** using the approach described by Kaufman and co-workers (16, 17). Epoxidation of the olefin **1** with *m*-chloroperbenzoic acid in dichloromethane gave a mixture of the α- and β-epoxides **2***a,b* in 74% yield. The products, easily distinguishable by ^{1}H NMR, were separated by column chromatography on silica. Predominant formation of the β-epoxide **2***b* results from an interaction between the peracid molecule and the 19-OH group. Reaction of **2***b* with lead tetraacetate and iodine in boiling cyclohexane afforded, in addition to the expected diepoxy compound **3** (41% yield), a number of minor, unidentified products. The β-epoxide moiety present in the oxidized compound **2***b* plays an important role by (*i*) protecting the double bond (19-hydroxy-5-ene steroids are known to undergo an oxidative fragmentation upon conditions of the lead tetraacetate reaction), (*ii*) increasing the internuclear distances between the C-19 oxy radical and the relevant A-ring δ-carbon atoms, with the result that the corresponding axial hydrogens at C-2 and C-4 are less likely to be abstracted (17). The next synthetic step involved the regeneration of the C(5)—C(6) double bond. Reduction of the diepoxide **3** with tungsten chlorides of low valency (18) gave the expected 5,6-unsaturated compound **4** in high yield (88%).

Another set of experiments was aimed at the introduction of an additional C(7)—C(8) double bond into the olefin **4**. At first, this was accomplished by the traditional method of allylic bromination–dehydrobromination (19). Thus, the reaction of **4** with 1,3-dibromo-5,5-dimethylhydantoin in refluxing benzene–hexane afforded two allylic bromides **5***a* and **5***b*

Fig. 2. Conformers of previtamin D and the corresponding isomers that originate from them (ref. 11).

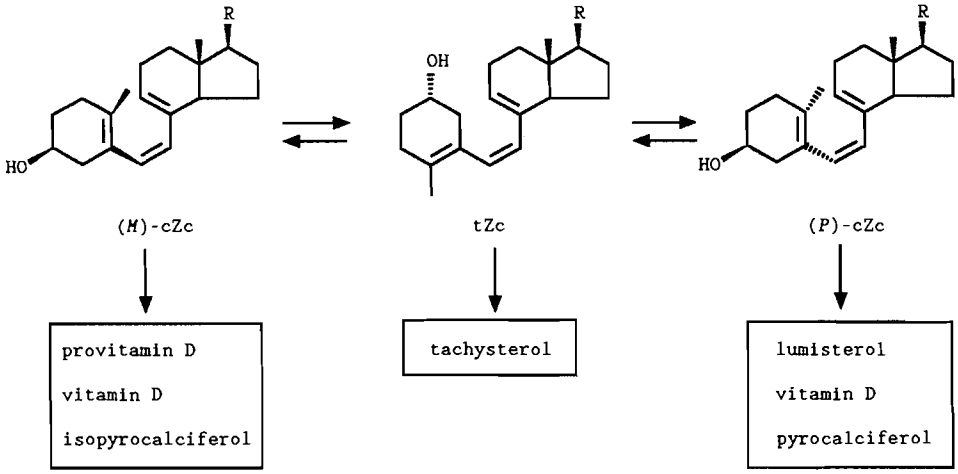

Fig. 3. Chemical structures of starting triol diester **1** and the synthesized compounds.

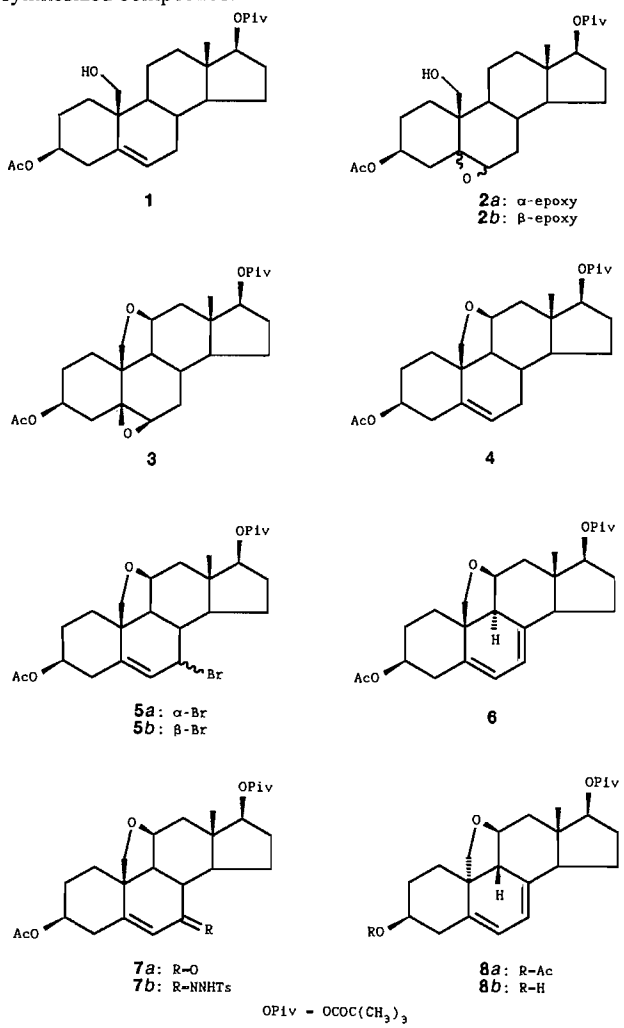

in a 3:1 ratio. Due to the instability of the latter, only the major isomer **5***a* could be obtained in the analytically pure form (62% yield). However, a careful analysis of the ^{1}H NMR spectrum of the crude mixture of bromides **5***a*,*b* allowed assignment of the resonances derived from the minor epimer **5***b*. The large diaxial coupling constant found for its allylic proton at C-7 (δ 4.50, dt, J = 10.0, 1.5 Hz) clearly established the equatorial 7β-orientation of the bromine atom. A comparison of the optical rotation values of the main bromination product ($[\alpha]_D^{24}$ −208.1) and the starting olefin **4** ($[\alpha]_D^{24}$ +10.9) supported the presence of the 7α-bromine substituent in **5***a*; literature data indicate that 7α-substituted-5-ene steroids are considerably more levorotatory than their parent 7-unsubstituted olefins, whereas the 7β-epimers are usually more dextrogyratory (20). The dehydrobromination of **5a** to give the desired 5,7-diene **6** in a good yield turned out to be difficult; this indicates that the 11β,19-oxide bridge affects the process. A treatment of **5***a* with s-collidine or trimethyl phosphite in refluxing xylene, successfully employed in the synthesis of some provitamins D, failed to give the expected elimination product. However, the fluoride ion-promoted dehydrobromination (21) of **5***a* afforded 5,7-diene **6** in an 84% yield; when the crude mixture of bromides **5***a*,*b* was used, the overall yield of the reaction sequence **4** → **5** → **6** amounted to 70%. The UV spectrum of **6** does not differ essentially from those of steroidal 19-unsubstituted- (22) or 19-alkoxy-5,7-dienes (23), the corresponding absorption maxima being shifted (5–6 nm) to smaller wavelengths. Understandably, the multiplet of the homoallylic 11α-H in the ^{1}H NMR spectrum of diene **6** was significantly more deshielded (Δδ 0.22) than an analogous signal in the spectrum of olefin **4**.

The high yield of the bromination–dehydrobromination procedure was somewhat surprising in view of the fact that the synthesis of 19-functionalized provitamins D from 5,6-unsaturated steroids usually employs another pathway, that involving allylic oxidation to 7-oxo compounds and reduction of their tosylhydrazone derivatives (23, 24). It was therefore interesting to examine also the latter alternative route leading to the ring-B diene **6**. However, the first step of the attempted synthesis, i.e., the direct conversion of **4** into the 7-oxo compound **7***a*, failed because the starting olefin was highly deactivated toward allylic oxidation. Using a reactive chromium trioxide–pyridine reagent (25), even under forcing conditions and long reaction times, the oxidation was incomplete and

Can. J. Chem. Downloaded from www.nrcresearchpress.com by 80.90.12.36 on 09/08/12
For personal use only.

Can. J. Chem. Downloaded from www.nrcresearchpress.com by 80.90.12.36 on 09/08/12
For personal use only.

afforded a complex mixture of products. However, the desired α,β-unsaturated ketone **7***a* was efficiently prepared (71% overall yield from **4**) by an oxidation of the allylic bromides **5***a*,*b* with bis(tetrabutylammonium) dichromate in methylene chloride (26). The UV spectrum of the enone **7***a* exhibited a maximum at 238.0 nm (ε 9700) indicating, in comparison with the spectra of other 19-alkoxy enones (23), a weak blue shift (ca. 4 nm) and a decreased ε value. Reaction of the conjugated ketone **7***a* with *p*-toluenesulfonyl hydrazide yielded quantitatively a tosylhydrazone **7***b*. Subsequent modified Bamford–Stevens reaction of **7***b* afforded the ring-B diene **6** in a 67% yield. Thus, the overall yield of **6** synthesized by the path **4** → **5** → **7***a* → **7***b* → **6** was considerably lower (48%) than the previously investigated customary procedure.

Ultraviolet irradiation of **6** was carried out in benzene–ether (1:4) solution at 0°C, and the concomitant reaction was monitored by TLC and analytical HPLC. It was found previously for the 10β-methyl analog and for various nonbridged 19-substituted compounds that 10 min were sufficient to achieve photoequilibrium (14). However, with the diene **6**, even after 20 min of irradiation, more than 60% of the starting material was still present in the reaction mixture. A slow buildup of a more polar product was observed and, in addition, a number of other minor ultraviolet-detectable compounds were formed. It was established that further irradiation did not offer an increasing proportion of the main product but, on the contrary, it resulted in the more complex HPLC profile with no major product present. Unreacted substrate **6** and the slightly impure main photoproduct (ca. 12% yield based on recovered **6**) were isolated from the reaction mixture by column chromatography on silica. Final HPLC purification provided the analytically pure compound. The "lumisterol-like" 5,7-diene 9β,10α-structure has been assigned to this main photoisomer **8***a* and its 3β-hydroxy derivative **8***b*, prepared for a further characterization purpose, on the basis of spectral data and molecular mechanics calculations.

A molecular ion peak at *m*/*z* 428 found in the mass spectrum of **8***a* indicated that the structure is isomeric to that of **6**. The line shape of the UV absorption of **8***a* closely resembles that of lumisterol$_2$ (22*a*), with the corresponding absorption maxima at 267.0 and 275.5 nm; the latter, as in the case of an analogous pair, **6** and ergosterol, are blue-shifted by ca. 6 nm. In the ^{1}H NMR spectrum of the isolated photoproduct **8***a*, the presence of two ring-olefinic signals at δ 5.66 (m) and 5.80 (d, J = 5.4 Hz) supported the $\Delta^{5,7}$-unsaturation whereas the single-proton signals at δ 3.64, 4.05, and 4.34 indicated an intact 11,19-oxide bridge. The latter signal, ascribed to the methine proton at C-11, as well as the multiplet of the methine proton at C-3 were particularly informative because an analysis of their coupling constants was helpful in establishing the configuration at C-9 and C-10. Thus, the signal of the methine 3α-proton at δ 5.07 was deshielded by ca. 0.3 ppm in **8***a* when compared to the analogous signal of the 9α,10β-compound **6**; a similar effect was observed in the case of the corresponding lumisteryl$_2$ acetate – ergosteryl acetate pair (22b). Moreover, the halfwidth of the 3α-H multiplet (8 Hz) in compound **8***a* indicated an equatorial orientation of the proton and, therefore, the *cis* A/B-ring system. The signal of 11α-H, differing considerably from the multiplet patterns of the analogous protons in the spectra of other 11β,19-oxides **3**–**7**, indicated an axial position of the proton concerned; the latter could result from the *cis* B/C-ring junction. To support these conclusions and to get some information on the conformations of the pentacyclic compounds synthesized, molecular mechanics calculations were employed. Molecular modeling was performed using the MM+ molecular mechanics algorithm (an enhanced version of MM2).[2] Force-field calculations were carried out for the starting provitamin analog **6** ("pro"), the 9,10-seco structure **9** (in the *M*-helical conformation), and other cyclized B-ring 5,7-dienes differing in configurations at C-9 and C-10, i.e., structures **8***a*, **10**, and **11** representing lumisterol ("lumi"), pyrocalciferol ("pyro"), and isopyrocalciferol ("isopyro") analogs, respectively (Fig. 4). The estimated values of steric energies and other conformational properties of the isomeric compounds concerned are given in Table 1.

Fig. 4. Previtamin D analog **9** (in the left-handed helical conformation) and ring-B closed compounds of the pyro- and isopyrocalciferol structure.

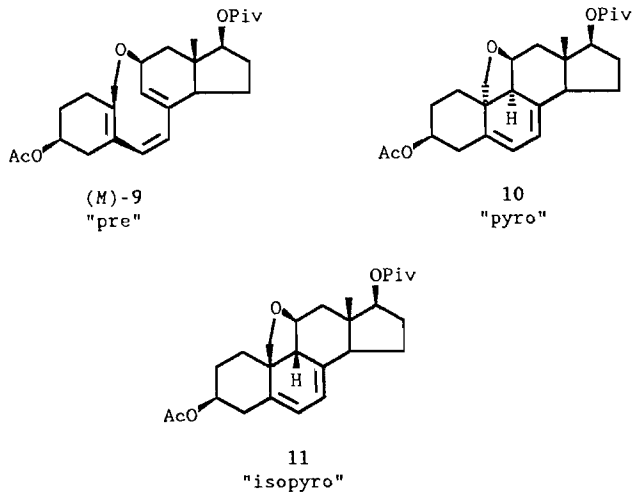

According to the force-field calculations, the chair conformation of the A ring (with the exception of **9**) and the half-chair conformation of the D ring are energetically favorable for all of the compounds examined. Energy-minimized structures were utilized in order to establish the orientation of 3α-H and to calculate the respective dihedral angles between 11α-H and the vicinal protons at the neighboring carbon atoms C-9 and C-12. These torsional angles were used, in turn, to calculate the expected ^{1}H–^{1}H coupling constants. Analysis of the vicinal coupling constants for compounds **6**, **8***a*, **10**, and **11** was aided by Altona's modified Karplus relationship (27), which takes into account the electronegativities of the substituents. The experimental coupling constants for the methine protons at C-11 (dt, J = 8.0, 10.1 Hz) and C-9 (br d, J = 10 Hz) in the isolated photoproduct **8***a* provide a best match with the calculated values for the "lumi" 9β,10α-structure. Of the remaining isomeric structures only **10** ("pyro"), with the 3α-H in equatorial position, could be considered but the calculated coupling constants of its 11α-proton differ considerably from the experimental values.

[2] The calculations of optimized geometries and strain energies were carried out using the algorithm from the MM+ HyperChem™ (release 4.0) software package (*Autodesk, Inc.*, 1994). MM+ is an all-atom force field based on the MM2 functional form.

Can. J. Chem. Downloaded from www.nrcresearchpress.com by 80.90.12.36 on 09/08/12
For personal use only.

Table 1. Calculated properties of the isomeric structures **6**, **8***a*, and **9**–**11**.

Structure	Configuration at C-9 and C-10	Steric energy (kcal/mol)[a]	Ring conformation[b,c] A	C	Position of 3α-H[d]	Torsion angle (deg)[b] H-C11-C9-H	H-C11-C12-H	Calculated coupling constant (Hz) $J_{11\alpha,9}$[e]	$J_{11\alpha,12\alpha}$[f]	$J_{11\alpha,12\beta}$[f]
6	9α,10β						−49.1[g]	3.4	3.3	3.0
"pro"	9*S*,10*S*	44.01	ch	ch	ax	45.8	66.4[h]			
8*a*	9β,10α						39.0[g]	10.1	7.3	9.0
"lumi"	9*R*,10*R*	55.69	ch	t-b	eq	163.5	154.9[h]			
(*M*)-**9**							−56.5[g]			
"pre"		84.66	h-ch	ch	ax	−45.1	59.4[h]			
10	9α,10α						31.9[g]	8.0	8.2	7.3
"pyro"	9*S*,10*R*	62.75	ch	b	eq	−21.1	144.6[h]			
11	9β,10β						35.1[g]	10.3	7.8	8.2
"isopyro"	9*R*,10*S*	63.41	ch	t-b	ax	178.5	149.9[h]			

[a] The energies calculated by the MM+ force-field method.
[b] Determined for the energy-minimized structures.
[c] Ring D has a half-chair conformation in all cases; abbreviatons: b, boat; ch, chair; h-ch, half-chair; t-b, twist-boat.
[d] Axial (ax) or equatorial (eq) orientation of the 3α-proton determined for the energy-minimized structures.
[e] Values calculated from Altona's modified Karplus equation using parameter set E (ref. 27).
[f] Values calculated from Altona's modified Karplus equation using parameter set D (ref. 27).
[g] Dihedral angle between 11α-H and 12α-H.
[h] Dihedral angle between 11α-H and 12β-H.

Fig. 5. Possible photochemical interconversion of the diene **6** into 9β,10α-diastereoisomer **8***a* (energy-minimized structures; top to bottom: **6**, (*M*)-**9** and **8***a*).

Discussion

Considering previtamin analog **9** as an obvious initial product of the photoinduced ring opening of diene **6**, the subsequent photochemical cyclization of its hexatriene system should occur by a conrotatory process leading to **8***a* or back to **6**, if the requirements of retention of orbital symmetry are met (28). The energy-minimized conformations for **6**, **8***a*, and **9** are represented in Fig. 5. It can be expected that the primary conformation of **9** formed from **6** is that with the 19-CH_2 group above the plane of the C ring; therefore, the following reverse electrocyclization reaction yielding the starting 9α,10β-structure **6** ("pro") should be more feasible than the alternative process providing the "lumi" 9β,10α-isomer **8***a*. The latter would require an interconversion of the highly strained molecule **9** from its left- to right-handed conformation passing through an extremely crowded transition state. Taking into account previous results of our studies (13, 14) on the photochemistry of 19-alkoxy 5,7-dienes, it is reasonable to assume that the photoinduced ring opening of diene **6** can be the preferred photoreaction. The high proportion of unreacted **6** during the irradiation would, consequently, indicate that the photoequilibrium between **6** and energetically unfavorable **9** is shifted to the diene side.

In spite of the fact that the symmetry-allowed photochemical conrotatory electrocyclization of the *M*-triene system in **9**

Can. J. Chem. Downloaded from www.nrcresearchpress.com by 80.90.12.36 on 09/08/12
For personal use only.

to the lumisterol analog **8***a* seems unlikely, in view of the geometrical restraints involved, the formation of such a cyclic product observed in the present work leaves open the question of whether the possibility of a direct interconversion between both helical (*M*)- and (*P*)-*cZc* conformers of previtamin D analogs (or their $\pi \rightarrow \pi^*$ excited forms) can be excluded.

Experimental

General procedures

Proton magnetic resonance spectra (^{1}H NMR) were recorded on a Bruker AM-500 spectrometer using $CDCl_3$ as a solvent and Me_4Si (δ 0.00) as an internal standard. Ultraviolet spectra (UV) were taken on a Beckman Acta M VI apparatus (solutions in 96% ethanol). Infrared spectra (IR) of KBr pellets were recorded on a Zeiss UR-20 spectrometer. Mass spectra (MS) were determined with a AMD-604 instrument at 70 eV. High-resolution data (HRMS) were obtained by peak matching. Optical rotations were measured in chloroform using a Perkin–Elmer 241 automatic polarimeter at 24°C.

Thin-layer chromatography (TLC) was carried out on precoated aluminum silica sheets from Merck (R_f values are given for the benzene–ethyl acetate 8:2 solvent system), column chromatography on silica gel Macherey–Nagel (100–200 mesh), and high-pressure liquid chromatography (HPLC) on a Zorbax-Sil 6.2 mm × 25 cm column (R_V values are given for the hexane–ethyl acetate 85:15 solvent system). Melting points were measured on a Köfler type (Boetius) hot stage apparatus and are cited without corrections.

*5α,6-Oxido-5α- and 5β,6-oxido-5β-androstan-3β,17β,19-triol 3-acetate 17-trimethylacetate (***2**a *and* **2**b*)*

Triol diester **1** (15) (10 g, 23.1 mmol) in dichloromethane (100 mL) was treated with 3-chloroperoxybenzoic acid (80–85%, 6.0 g; added in portions). The temperature of the reaction mixture was maintained below 25°C. After addition of all reagent the mixture was allowed to stand at room temperature with occasional shaking. When the reaction reached completion (about 1 h), the aromatic acids were removed by extraction with 5% NaOH, and the organic layer was washed with water and dried (Na_2SO_4). The solvent was evaporated to give a colorless solid residue, which was repeatedly crystallized from acetone to obtain 6.1 g of pure 5β,6-oxide **2***b*. The mother liquor was chromatographed on silica gel column. Elution with benzene–ether (95:5) gave an additional 1.1 g of crystalline **2***b* (total yield 7.2 g, 69%). Further elution with benzene-ether (93:7) afforded an isomeric 5α,6-oxide **2***a*, which was crystallized from acetone–hexane (yield 0.52 g, 5%).

2*a*: mp 193–197°C; $[\alpha]_D^{24}$ −58.2 (*c* 0.9); TLC, R_f 0.28; IR ν_{max}: 1040, 1169, 1252, 1734, 3430 (br) cm^{-1}; ^{1}H NMR δ: 0.80 (3H, s, 18-H3), 1.18 (9H, s, CO-*t*Bu), 2.02 (3H, s, OAc), 3.02 (1H, d, *J* = 3.9 Hz, 6β-H), 3.86–4.06 (2H, m, 19-H2; after D_2O 3.91 and 4.00 (1H and 1H, each d, *J* = 11.6 Hz)), 4.53 (1H, dd, *J* = 9.2, 7.4 Hz, 17α-H), 4.99 (1H, tt, *J* = 11.5, 5.2 Hz, 3α-H). Anal. calcd. for $C_{26}H_{40}O_6$: C 69.61, H 8.99; found: C 69.70, H 9.10.

2*b*: mp 161–163°C; $[\alpha]_D^{24}$ −4.8 (*c* 1.3); TLC, R_f 0.43; IR ν_{max}: 1045, 1169, 1260, 1728, 3525 cm^{-1}; ^{1}H NMR δ: 0.85 (3H, s, 18-H3), 1.19 (9H, s, CO-*t*Bu), 2.04 (3H, s, OAc), 3.07 (1H, d, *J* = 2.1 Hz, 6α-H), 3.50–3.65 (1H, m, one of 19-H2; after D_2O 3.57 (d, J = 11.7 Hz)), 4.20 (1H, br d, *J* ≈ 12 Hz, one of 19-H2; after D_2O d, *J* = 11.7 Hz), 4.55 (1H, dd, *J* = 9.1, 7.4 Hz, 17α-H), 4.83 (1H, m, *w*/2 = 26 Hz, 3α-H). Anal. calcd. for $C_{26}H_{40}O_6$: C 69.61, H 8.99; found: C 69.68, H 9.11.

*5β,6:11β,19-Dioxido-5β-androstan-3β,17β,19-triol 3-acetate 17-trimethylacetate (***3***)*

A suspension of lead tetraacetate (39.9 g, 90 mmol; dried over KOH) and calcium carbonate (40 g) in cyclohexane (1100 mL, distilled from P_2O_5) was refluxed with vigorous stirring for 1 h (heating with a 1000 W lamp). Epoxide **2***b* (4.9 g, 11 mmol) was then added and stirring continued while iodine (12.7 g, 50 mmol) was added in portions during 15 min. After the substrate vanished on TLC (about 1 h) the mixture was filtered off and the filtrate was washed with dilute Na_2SO_3, water, dried (Na_2SO_4), and evaporated. The oily residue was chromatographed on a silica gel column. Elution with benzene–ether (95:5) afforded a solid material (2.4 g) that was repeatedly crystallized from acetone–hexane; the first and second crop of crystals gave analytically pure diepoxide **3** (1.2 g). Chromatography of the mother liquor on silica and subsequent crystallization from hexane afforded an additional 0.8 g of **3** (total yield 2.0 g, 41%): mp 186–190°C; $[\alpha]_D^{24}$ +13.1 (*c* 1.0); TLC, R_f 0.47; IR ν_{max}: 1042, 1172, 1249, 1734 cm^{-1}; ^{1}H NMR δ: 0.94 (3H, s, 18-H3), 1.18 (9H, s, CO-*t*Bu), 2.03 (3H, s, OAc), 3.24 (1H, d, *J* = 2.8 Hz, 6α-H), 3.73 (1H, d, *J* = 8.4 Hz, one of 19-H2), 4.06 (1H, br t, *J* = 3.6 Hz, 11α-H), 4.08 (1H, dd, *J* = 8.4, 0.9 Hz, one of 19-H2), 4.58 (1H, dd, *J* = 9.1, 7.9 Hz, 17α-H), 4.79 (1H, m, *w*/2 = 28 Hz, 3α-H). Anal. calcd. for $C_{26}H_{38}O_6$: C 69.93, H 8.58; found: C 69.86, H 8.62.

*11β,19-Oxido-5-androsten-3β,17β,19-triol 3-acetate 17-trimethylacetate (***4***)*

Tungsten (VI) chloride (6.0 g, 15 mmol) in freshly distilled THF (42 mL) was cooled to −62°C and a solution of *n*-BuLi (18 mL, 20% in hexane) was added with stirring. The mixture was allowed to warm up to room temperature within 20 min and a solution of diepoxide **3** (1.1 g, 2.5 mmol) in THF (20 mL) was then added. The reaction mixture was left for 30 min at ambient temperature; the liquid phase was then decanted from a semisolid violet residue, concentrated to a small volume under vacuum, and diluted with chloroform. The semisolid residue was dissolved in 5% KOH (500 mL) and extracted with chloroform. The combined chloroform solutions were washed with water, dried (Na_2SO_4), and evaporated. The crude product was purified on a silica gel column and it was eluted with benzene–ether (96:4). Crystallization from acetone–hexane afforded pure compound **4** (0.93 g, 88%): mp 180–183°C; $[\alpha]_D^{24}$ +10.9° (*c* 0.9); TLC, R_f 0.59; IR ν_{max}: 1039, 1168, 1247, 1665 (w), 1734 cm^{-1}; ^{1}H NMR δ: 0.97 (3H, s, 18-H3), 1.20 (9H, s, CO-*t*Bu), 2.03 (3H, s, OAc), 3.73 (1H, dd, *J* = 8.2, 1.6 Hz, one of 19-H2), 3.96 (1H, d, *J* = 8.2 Hz, one of 19-H2), 4.27 (1H, dt, *J* = 1.8, 3.8 Hz, 11α-H), 4.61 (1H, dd, *J* = 9.3, 7.8 Hz, 17α-H), 4.65 (1H, tt, *J* = 11.4, 4.6 Hz, 3α-H), 5.61 (1H, dt, *J* = 6.3, 1.6 Hz, 6-H). Anal. calcd. for $C_{26}H_{38}O_5$: C 72.53, H 8.90; found: C 72.76, H 8.82.

*7α-Bromo- and 7β-bromo-11β,19-oxido-5-androsten-3β,17β,19-triol 3-acetate 17-trimethylacetate (***5***a and* **5**b*)*

A mixture of olefin **4** (215 mg, 0.5 mmol) and $NaHCO_3$ (200 mg) in benzene-hexane (1:1, 10 mL) was heated under reflux, and the hot solution was treated with 1,3-dibromo-5,5-dimethylhydantoin (86 mg, 0.3 mmol). The mixture was refluxed for

Can. J. Chem. Downloaded from www.nrcresearchpress.com by 80.90.12.36 on 09/08/12
For personal use only.

10 min, and an additional portion of dibromantine (23 mg, 0.08 mmol) was added. The reflux was continued for an additional 10 min until no **4** was detected on TLC. The cooled reaction mixture was filtered and the filtrate dried under reduced pressure. The residue consisted of two main products **5***a* and **5***b* (R_f values 0.62 and 0.51, respectively) in a 3:1 ratio. Analysis of the ^{1}H NMR spectrum of the material allowed us to assign the following resonances (not overlapped by those derived from the prevailing **5***a*; see below) for the minor isomer **5***b*: δ: 1.02 (s, 18-H3), 3.79 (dd, J = 8.2, 1.5 Hz, one of 19-H2), 3.94 (d, J = 8.2 Hz, one of 19-H2), 4.30 (m, $w/2$ = 12 Hz, 11α-H), 4.50 (dt, J = 10.0, 1.5 Hz, 7α-H), 5.81 (m, $w/2$ = 4 Hz, 6-H).

The crude mixture of bromides could be used for subsequent reactions without further purification. For analytical purposes, the predominant epimer **5***a* was obtained in a pure form after column chromatography on silica. Elution with benzene–ether (98:2) afforded a crystalline compound. Recrystallization from acetone–hexane gave **5***a* (158 mg, 62%): mp 194–198°C; $[\alpha]_D^{24}$ −208.1° (*c* 0.9); TLC, R_f 0.62; IR ν_{max}: 1042, 1166, 1255, 1655 (w), 1732 cm^{-1}; ^{1}H NMR δ: 0.99 (3H, s, 18-H3), 1.20 (9H, s, CO-*t*Bu), 2.03 (3H, s, OAc), 3.72 (1H, dd, J = 8.3, 1.4 Hz, one of 19-H2), 3.97 (1H, d, J = 8.3 Hz, one of 19-H2), 4.35 (1H, m, $w/2$ = 11 Hz, 11α-H), 4.56 (1H, m, $w/2$ = 12 Hz, 7β-H), 4.66 (1H, dd, J = 9.0, 7.9 Hz, 17α-H), 4.73 (1H, tt, J = 11.3, 4.7 Hz, 3α-H), 5.87 (1H, dd, J = 5.9, 1.7 Hz, 6-H). Anal. calcd. for $C_{26}H_{37}O_5Br$: C 61.29, H 7.32; found: C 61.26, H 7.52.

11β,19-Oxido-7-oxo-5-androsten-3β,17β,19-triol 3-acetate 17-trimethylacetate (7a)

(*a*) A solution of bromide **5***a* (127 mg, 0.25 mmol) and bis(tetrabutylammonium) dichromate (1.75 g, 2.5 mmol) in dry chloroform (8 mL) was heated under reflux for 4 h. The reaction mixture was cooled and applied to a silica gel column. Elution with benzene–ether (95:5) yielded a yellowish residue that was crystallized from acetone–hexane to give pure enone **7***a* (92 mg, 83%): mp 197–200°C; $[\alpha]_D^{24}$ −3.5 (*c* 0.9); TLC, R_f 0.37; UV (EtOH) λ_{max}: 238.0 nm (ε 9700); IR ν_{max}: 1043, 1169, 1248, 1633 (w), 1694, 1732 cm^{-1}; ^{1}H NMR δ: 0.99 (3H, s, 18-H3), 1.19 (9H, s, CO-*t*Bu), 2.05 (3H, s, OAc), 4.03 (1H, dd, J = 8.6, 1.4 Hz, one of 19-H2), 4.06 (1H, d, J = 8.6 Hz, one of 19-H2), 4.38 (1H, dt, J = 2.0, 3.6 Hz, 11α-H), 4.62 (1H, dd, J = 9.3, 7.5 Hz, 17α-H), 4.75 (1H, tt, J = 11.3, 4.6 Hz, 3α-H), 5.79 (1H, d, J = 1.6 Hz, 6-H). Anal. calcd. for $C_{26}H_{36}O_6$: C 70.24, H 8.16; found: C 70.26, H 8.00.

An analogous reaction of the crude mixture of bromides **5***a* and **5***b* (obtained from the bromination of **4**) afforded also the crystalline enone **7***a* (71% overall yield from **4**).

(*b*) Olefin **4** (69 mg, 0.16 mmol) in dry CH_2Cl_2 (1 mL) was added to a solution of CrO_3–(pyridine)$_2$ complex, prepared from CrO_3 (390 mg, 3.9 mmol) and pyridine (0.63 mL, 7.8 mmol) in CH_2Cl_2 (1 mL), and the mixture was allowed to react for several days at room temperature with constant stirring. TLC control of the reaction indicated that a complex mixture of products was formed with traces of **7***a* only.

11β,19-Oxido-5,7-androstadien-3β,17β,19-triol 3-acetate 17-trimethylacetate (6)

A. Dehydrobromination of the allylic bromides **5**a *and* **5**b: (*a*) Bromide **5**a (41 mg, 0.08 mmol) was dissolved in a solution of tetrabutylammonium fluoride (0.8 mL, 1 M in THF) containing s-collidine (5 μL). The mixture was stirred at room temperature for 2 h. The solution was diluted with ether, washed with water, cold 5% HCl, and saturated $NaHCO_3$, and then dried with Na_2SO_4. Concentration in vacuo yielded a residue that was chromatographed on a silica gel column. The column was eluted with benzene–ether (98:2) yielding pure crystalline diene **6** (29 mg, 84%): mp 169–171°C (from acetone–hexane); $[\alpha]_D^{24}$ +133.5° (c 0.4); HPLC, R_V 31 mL; TLC, R_f 0.57; UV (EtOH) λ_{max}: 257.5 nm (sh, ε 8100), 265.5 (10 800), 276.0 (10 900), 287.0 (5900); IR ($CHCl_3$) ν_{max}: 1037, 1172, 1259, 1620 (w), 1675 (w), 1728 cm^{-1}; ^{1}H NMR δ: 0.76 (3H, s, 18-H3), 1.19 (9H, s, CO-tBu), 2.04 (3H, s, OAc), 3.63 (1H, dd, J = 8.0, 1.3 Hz, one of 19-H2), 3.93 (1H, d, J = 8.0 Hz, one of 19-H2), 4.49 (1H, m, $w/2$ = 12 Hz, 11α-H), 4.70–4.78 (2H, m, 3α- and 17α-H), 5.52 (1H, m, $w/2$ = 10 Hz, 7-H), 5.69 (1H, dd, J = 5.7, 2.4 Hz, 6-H). Anal. calcd. for $C_{26}H_{36}O_5$: C 72.87, H 8.47; found: C 72.96, H 8.51.

The reaction of the crude mixture of bromides **5***a* and **5***b*, obtained from the bromination of **4**, carried out in an analogous manner (except that catalytic amount of Bu_4NBr was added) afforded also the crystalline diene **6** (70% overall yield from **4**). The compound gave a single peak on HPLC and was judged to be 99% pure.

(*b*) A solution of bromide **5***a* (10 mg) in anhydrous *p*-xylene (2 mL) containing s-collidine (70 μL) was heated at reflux for 30 h under nitrogen. TLC of the reaction mixture showed the presence of unreacted **5***a* (more than 50%) and traces of the desired diene **6** accompanied by other by-products.

(*c*) A solution of bromide **5***a* (10 mg) in anhydrous *p*-xylene (3 mL) containing trimethyl phosphite (100 μL) was refluxed for 7 h; only unchanged starting material was shown on TLC.

B. Reduction of the tosylhydrazone 7b: A solution of enone **7***a* (89 mg, 0.2 mmol) and *p*-toluenesulfonyl hydrazide (93 mg, 0.5 mmol) in benzene (2 mL) was heated at 65°C for 10 h. The mixture was cooled, diluted with benzene–ether (1:1, 20 mL), and washed thoroughly with 5% HCl. The organic phase was washed with saturated $NaHCO_3$ and water, dried (Na_2SO_4), and evaporated to dryness under vacuo to yield a solid residue (122 mg) that was sufficiently pure (TLC and NMR) to be used for the next step without any further purification.

Tosylhydrazone **7***b*: TLC, R_f 0.32; IR ν_{max}: 819, 1041, 1172, 1246, 1603 (w), 1641 (w), 1731, 3230 cm^{-1}; ^{1}H NMR δ: 0.96 (3H, s, 18-H3), 1.20 (9H, s, CO-*t*Bu), 2.05 (3H, s, OAc), 2.44 (3H, s, Ar-CH_3), 3.82 (1H, dd, J = 8.5, 1.3 Hz, one of 19-H2), 3.97 (1H, d, J = 8.5 Hz, one of 19-H2), 4.26 (1H, m, $w/2$ = 10 Hz, 11α-H), 4.60 (1H, dd, J = 9.0, 8.0 Hz, 17α-H), 4.65 (1H, tt, J = 11.3, 4.6 Hz, 3α-H), 6.07 (1H, d, J = 1.4 Hz, 6-H), 7.32 (2H, br d, J = 8.3 Hz, Ar-H), 7.52 (1H, m, $w/2$ = 9 Hz, NH), 7.84 (2H, d, J = 8.3 Hz, Ar-H).

Lithium hydride (36 mg, 4.5 mmol) was added to a solution of the crude tosylhydrazone **7***b* (110 mg, 0.18 mmol) in dry toluene (4.5 mL) and the mixture was heated under reflux for 1.5 h. An additional portion of lithium hydride (16 mg, 2 mmol) was added and the reflux was continued for 30 min. Fast filtration of the cooled reaction mixture into ice-cold 2% H_2SO_4, followed by washing of the organic layer with saturated $NaHCO_3$ and water, drying (Na_2SO_4), and concentration under vacuo, yielded a residue that was chromatographed on a silica gel column. Elution with benzene–ether (98:2) afforded a crys-

talline material (62 mg), which after recrystallization from acetone–hexane gave an analytically pure diene **6** (52 mg, 67%).

11β,19-Oxido-9β,10α-androsta-5,7-dien-3β,17β,19-triol 3-acetate 17-trimethylacetate (8a) and 3β-hydroxy derivative 8b

A solution of diene **6** (30 mg) in benzene–ether (1:4, 350 mL) was cooled to 0°C and degassed by an argon purge for 40 min. The mixture was irradiated for 20 min through a water-cooled (0°C) quartz inner well with a 350 W Hanau S 81 lamp. Solvents were evaporated and the residue was chromatographed on a silica gel column. Elution with benzene–ether (98:2) provided the unreacted **6** (19 mg). Further elution with the same solvent gave a complex mixture of compounds. Slightly impure compound **8a** (1.3 mg, 12% based on recovered substrate **6**) was then eluted with benzene–ether (97:3). The identical irradiation experiments and chromatographical separations were repeated twice and all fractions containing **8a** were combined. Subsequent high-pressure liquid chromatography afforded analytically pure diene **8*a*** (2.0 mg): HPLC, R_V 54 mL; TLC, R_f 0.48; UV (EtOH) λ_{max}: 267.0 nm (ϵ 7000), 275.5 (6700), 288.0 (sh, 4200); ^{1}H NMR δ: 0.92 (3H, s, 18-H3), 1.20 (9H, s, CO-tBu), 2.06 (3H, s, OAc), 2.93 (1H, br d, J = 10 Hz, 9β-H), 3.64 (1H, dd, J = 7.9, 2.0 Hz, one of 19-H_2), 4.05 (1H, d, J = 7.9 Hz, one of 19-H_2), 4.34 (1H, dt, J = 8.0, 10.1 Hz, 11α-H), 4.89 (1H, dd, J = 9.0, 7.8 Hz, 17α-H), 5.07 (1H, m, w/2 = 8 Hz, 3α-H), 5.66 (1H, m, w/2 = 11 Hz, 7-H), 5.80 (1H, d, J = 5.4 Hz, 6-H); MS, *m/z* (rel. intensity): 428 (M^+, 13), 368 (14), 366 (27), 57 (100); HRMS calcd. for $C_{26}H_{36}O_5$: 428.2563; found: 428.2559.

Saponification of the diene **8*a*** (1 mg) was carried out in 5% methanolic NaOH (1 mL) at 40°C for 20 min. Conventional work-up afforded the 3-hydroxy derivative **8*b*** (0.9 mg): TLC, R_f 0.28; UV (EtOH) λ_{max}: 267.0 and 276.0 nm ($\epsilon \sim 7000$); ^{1}H NMR δ: 0.92 (3H, s, 18-H3), 1.20 (9H, s, CO-*t*Bu), 2.96 (1H, br d, J = 10 Hz, 9β-H), 3.64 (1H, dd, J = 7.8, 2.0 Hz, one of 19-H2), 4.03 (1H, d, J = 7.8 Hz, one of 19-H2), 4.13 (1H, m, *w*/2 = 12 Hz, 3α-H), 4.34 (1H, dt, J = 8.0, 9.8 Hz, 11α-H), 4.88 (1H, dd, J = 9.0, 7.8 Hz, 17α-H), 5.68 (1H, m, *w*/2 = 11 Hz, 7-H), 5.91 (1H, d, J = 5.4 Hz, 6-H).

References

1. (*a*) R.P. Esvelt, H.K. Schnoes, and H.F. DeLuca. Arch. Biochem. Biophys. **188**, 282 (1978); (*b*) M.F. Holick, J.A. MacLaughlin, and S.H. Doppelt. Science, **211**, 590 (1981); (*c*) T.L. Clemens. J. Clin. Immunol. **9**, 183 (1986).
2. P.E. Georghiou. Chem. Soc. Rev. **6**, 83 (1977).
3. H.F. DeLuca, H.E. Paaren, and H.K. Schnoes. Top. Curr. Chem. **83**, 1 (1979).
4. G.M. Sanders, J. Pot, and E. Havinga. Fortschr. Chem. Org. Naturst. **27**, 129 (1969).
5. E. Havinga. Experientia, **29**, 1181 (1973).
6. L. Velluz, G. Amiard, and B. Goffinet. Bull. Soc. Chim. Fr. 1341 (1955).
7. (*a*) W.G. Dauben, J. Rabinowitz, N.D. Vietmeyer, and P. Wendschuh. J. Am. Chem. Soc. **94**, 4285 (1972); (*b*) H.J.C. Jacobs and E. Havinga. Adv. Photochem. **11**, 305 (1979).
8. M. Sheves, E. Berman, Y. Mazur, and Z.V.I. Zaretskii. J. Am. Chem. Soc. **101**, 1882 (1979).
9. R.M. Moriarty and H.E. Paaren. Tetrahedron Lett. **21**, 2389 (1980).
10. M. Akhtar and G.J. Gibbons. J. Chem. Soc. 5964 (1963).
11. K. Pfoertner. Helv. Chim. Acta, **55**, 937 (1972).
12. W.G. Dauben and D.J.H. Funhoff. J. Org. Chem. **53**, 5070 (1988).
13. W.J. Rodewald and R.R. Siciński. Pol. J. Chem. **57**, 1267 (1983).
14. R.R. Siciński. Acta Chim. Hung. **129**, 191 (1992).
15. W.J. Rodewald, J.R. Jaszczyński, and R.R. Siciński. Pol. J. Chem. **52**, 501 (1978).
16. (*a*) R.R. Fraser, M. Kaufman, P. Morand, and G. Govil. Can. J. Chem. **47**, 403 (1969); (*b*) P. Morand and M. Kaufman. Can. J. Chem. **49**, 3185 (1971).
17. M. Kaufman, P. Morand, and S.A. Samad. J. Org. Chem. **37**, 1067 (1972).
18. K.B. Sharpless, M.A. Umbreit, M.T. Nieh, and T.C. Flood. J. Am. Chem. Soc. **94**, 6538 (1972).
19. F. Hunziker and F.X. Müllner. Helv. Chim. Acta, **41**, 70 (1958).
20. (*a*) L.F. Fieser and M. Fieser. *In* Steroids. Reinhold, New York. 1959. pp. 158–161; (*b*) P. Morand and A. Van Tongerloo. Steroids, **21**, 65 (1973).
21. M.P. Rappoldt, J. Hoogendoorn, and L.F. Pauli. *In* Vitamin D. Chemical biological and clinical endocrinology of calcium metabolism. Walter de Gruyter and Co., Berlin. 1982. p. 1133.
22. (*a*) W.H.C. Shaw, J.P. Jefferies, and T.E. Holt. Analyst, **82**, 2 (1957); (*b*) K. Tsukida, K. Akutsu, and M. Ito. J. Nutr. Sci. Vitaminol. **22**, 7 (1976).
23. J.J. Jaszczyński, R.R. Siciński, and W.J. Rodewald. Pol. J. Chem. **58**, 711 (1984).
24. (*a*) R.M. Moriarty, H. Paaren, and J. Gilmore. J. Chem. Soc. Chem. Commun. 927 (1974); (*b*) R.M. Moriarty and H.E. Paaren. J. Org. Chem. **46**, 970 (1981).
25. W.G. Dauben, M. Lorber, and D.S. Fullerton. J. Org. Chem. **34**, 3587 (1969).
26. F. Rolla and D. Landini. Chem. Ind. 213 (1979).
27. C.A.G. Haasnoot, F.A.A.M. de Leeuw, and C. Altona. Tetrahedron Lett. **36**, 2783 (1980).
28. R.B. Woodward and R. Hoffmann. *In* The conservation of orbital symmetry. Verlag Chemie, Academic Press, Weinheim. 1970. pp. 38–64.

Can. J. Chem. Downloaded from www.nrcresearchpress.com by 80.90.12.36 on 09/08/12
For personal use only.

Fragmentation of 2-(dialkylamino)ethyl phosphate derivatives. Mechanism change as a function of substituents at phosphorus

Andre Pienaar and Tomasz A. Modro

Abstract: The products and the first-order rate constants for the fragmentation of six phosphonic diesters (**2**) and two phosphonic monester chlorides (**3**), all containing the 2-(dialkylaminoethyl) group as one of the ester functions, have been determined. On the basis of different reaction products, different rates of decomposition, and different activation parameters, a new mechanism for the fragmentation of ester chlorides (**3**) is proposed: fragmentation involving release of the chloride ion and the formation of the 1,1-dialkylaziridinium ion and metaphosphonate as the reactive intermediates.

Key words: fragmentation of phosphates and phosphorochloridates, "metaphosphate" mechanism of phosphates, activation entropy in mechanistic change, 2-(dialkylamino)ethylphosphates.

Résumé : On a déterminé la nature des produits et les constantes de vitesse du premier ordre des fragmentations de six diesters (**2**) et de deux chlorures monoestérifiés (**3**) de l'acide phosphonique qui contenaient tous le groupe 2-(dialkylaminoéthyle) comme l'une des fonctions esters. Sur la base des produits des réactions, des diverses vitesses de décomposition et des paramètres d'activation, on propose un nouveau mécanisme pour la fragmentation des chlorures monoestérifiés **3**: fragmentation impliquant la libération de l'ion chlorure avec formation de l'ion 1,1-dialkylaziridinium et du métaphosphonate comme intermédiaires réactifs.

Mots clés : fragmentation des phosphates et phosphorochloridates, mécanisme «métaphosphate» des phosphates, entropie d'activation dans les changements de mécanisme, 2-(dialkylamino)éthylphosphates.

[Traduit par la rédaction]

Can. J. Chem. Downloaded from www.nrcresearchpress.com by 80.90.12.36 on 09/08/12
For personal use only.

Alkyl 2-(dialkylamino)ethyl esters of phosphorus acids **1** are interesting substrates because they undergo spontaneous structural changes, often under very mild conditions. Transformations of systems **1** can proceed in two directions (Scheme 1): bimolecular dealkylation leading to a final zwitterionic product (pathway (a)), and (or) the unimolecular fragmentation resulting in the final formation of a piperazinium phosphate salt (pathway (b)). The mechanisms of those reactions are well understood (1–4), and the isomerization to a zwitterionic species found application as a route to phospholipid analogues (5). Convincing kinetic evidence for pathway (b) was given by Benschop et al. (1), who studied the decomposition of two phosphonic derivatives: isopropyl 2-(dimethylamino)ethylmethylphosphonate, Me-P(O)(OPr^i)($OCH_2CH_2NMe_2$), **2a**, and 2-(dimethylamino)ethylmethylphosphonofluoridate, Me-P(O)($OCH_2CH_2NMe_2$)F. Both substrates gave the same *N,N,N′,N′*-tetramethylpiperazinium ion according to first-order kinetics, but the fluoro derivative was found ca. 800 times more reactive than **2***a* ($\log k_{rel} = 2.92$). The difference in the rate was explained by the basicity difference of the leaving groups (methylphosphonofluoridate anion vs. isopropyl methylphosphonate anion). The difference in the acidities of the respective conjugate acids is, however, only $\Delta pK_a = 1.15$, conspicuously low to explain the observed relative rates. For example, the rates of the base-promoted elimination of 1-halo-2-phenylethanes decrease with the decrease of the nucleofugality of a halide ion ($\log (k_I/k_F) = 4.42$) (6), but the acidities of the corresponding acids HX span a range of ΔpK_a of ca. 13. Since the rates faster than predicted from the Bronsted plot of pK_a (leaving group) often indicate change in the reaction mechanism (7), and since we observed earlier (8) that 2-arylethyl phosphorochloridate systems decompose easily via a "metaphosphate" mechanism (9), we decided to reinvestigate the mechanism of the fragmentation of 2-(dialkylamino)ethyl alkylphosphonic derivatives with variable substituents at phosphorus.

Received February 24, 1995.

A. Pienaar and T. A. Modro.[1] Centre for Heteroatom Chemistry, Department of Chemistry, University of Pretoria, Pretoria 0002, South Africa.

[1] Author to whom correspondence may be addressed.

Results and discussion

Six alkyl 2-(dialkylamino)ethyl alkylphosphonic diesters **2***a*–**2***f*, and two 2-(dialkylamino)ethyl alkylphosphonochloridates **3***a*, **3***b*, were prepared (Scheme 2), and the products and the rates of their fragmentation were determined. Preparation of substrates **3** proved difficult, and will be discussed in a separate report. Once synthesized, chloridates **3** were found highly

Can. J. Chem. Downloaded from www.nrcresearchpress.com by 80.90.12.36 on 09/08/12
For personal use only.

Scheme 1.

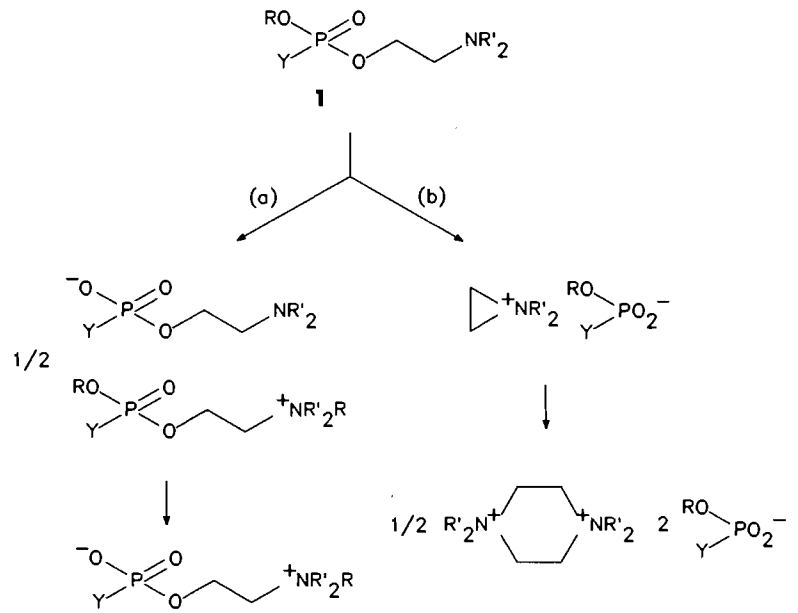

Scheme 2. Substrates used for fragmentation studies.

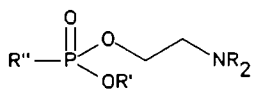

2

	R	R'	R''
a	Me	Pr^i	Me
b	Me	Et	Et
c	Me	Me	Me
d	Me	Et	Me
e	Et	Me	Me
f	Et	Et	Et

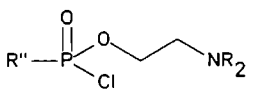

3

	R	R''
a	Et	Me
b	Et	Et

unstable, and had to be used without purification, immediately after their preparation. The rates of the fragmentation of esters **2** were measured under the same conditions as described in the literature for **2***a* (1), that is, in DMSO-d_6 at 60°C. The products were identified by NMR (^{1}H and ^{31}P) spectroscopy, and in all cases were in full agreement with the reaction shown in Scheme 1, pathway (b). Concentration changes were monitored by ^{1}H NMR spectroscopy, in most cases following the increase in intensity of the piperazinium ion signal at $\delta_H = 3.4$. Phosphonochloridates **3** were found to be remarkably stable in DMSO solutions (no change in the ^{1}H NMR spectrum after 56 h at 60°C). The nature of that stabilizing solvent effect is currently being studied in our laboratory, but the fragmentation of substrates **3** could easily be determined in $CDCl_3$ or CD_3CN solutions. For the kinetic studies, the *N,N*-diethylaminoethyl derivatives **3***a* and **3***b* were used, since the *N,N*-dimethylaminoethyl analogues decomposed so quickly that it was not possible to prepare pure samples of the substrates.

Table 1. Kinetic data on the fragmentation of phosphonic diesters **2** and phosphonochloridates **3** at 60°C.

Substrate	Solvent	$10^7 \times k_1$ (s^{-1})	k_{rel}
2*a*	DMSO-d_6	0.82[a]	1.0
2*b*	DMSO-d_6	1.02	1.2
2*c*	DMSO-d_6	6.83	8.3
	$CDCl_3$	1.03	1.3
	CD_3CN	5.00	6.1
2*d*	DMSO-d_6	2.00	2.4
2*e*	DMSO-d_6	5.17	6.3
2*f*	DMSO-d_6	8.33	10.2
3*a*	$CDCl_3$	31.7	38.7
	CD_3CN	70.0	85.4
3*b*	$CDCl_3$	55.0	67.1

[a]Literature (1) $k_1 = 1.35 \times 10^{-7}$ s^{-1}.

Fragmentations of all substrates followed first-order kinetics, and the rate data are given in Table 1. The diesters **2** react with similar rates, the variations of k_{rel} values not exceeding a factor of 10. Reactivity variations do not seem to follow any particular trend, with perhaps the exception of the case when k(**2***c*) > k(**2***d*) > k(**2***a*), following the expected order of the effect of an alkyl ester group on the acidity of the phosphate group (9). Since the relative acidities of phosphates and phosphonates in DMSO are not known, any correlations with the pK_a values for aqueous solutions have to be, however, treated with caution. We think that small reactivity differences observed for diesters **2** result mostly from the entropic factors, associated with the conformational changes required for the closure of the aziridinium ring in the rate-determinig step of the fragmentation, and we believe that all diesters **2** decompose according to a common mechanism. As for a reaction in which two ions are formed from a neutral substrate in a slow step, the fragmentation is expected to be sensitive to the polar-

Scheme 3.

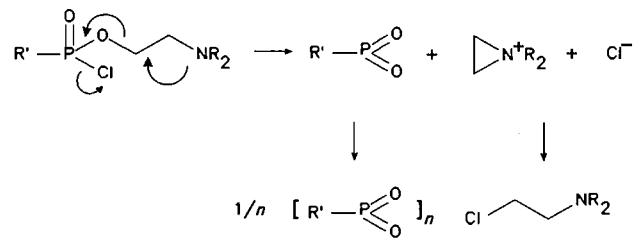

Scheme 4.

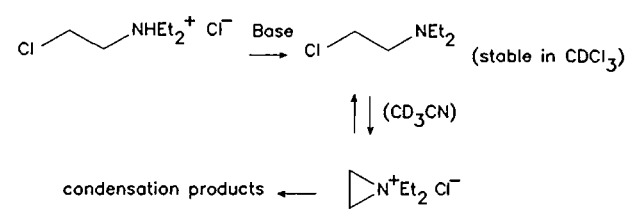

ity of the solvent (10). Table 1 shows that the rate of fragmentation of **2***c* decreases with the decrease in the polarity of the medium.

Phosphonic monoester monochlorides **3** show fragmentation behavior significantly different from that observed for diesters **2**. Although the rates were measured in a less polar solvent than DMSO, the reactions were in all cases much faster, giving (after accounting for a solvent effect) the approximate relative reactivity $k_3/k_2 \geq 50$. The difference in the reactivity itself is not sufficient evidence for a mechanistic change; we have found, however, that the fragmentation of **3** leads to different products that cannot be explained by the mechanism presented in Scheme 1, pathway (b). In both cases the piperazinium ion was absent in the reaction product, and the sole non-phosphorus product observed in $CDCl_3$ was diethyl (2-chloroethyl)amine, unambigously identified by comparison with and addition of the authentic material. The same product was formed in CD_3CN solution, but in that solvent it slowly changed to a mixture of polycondensation products (*vide infra*). As far as the phosphorus-containing products are concerned, the ^{31}P and ^{1}H NMR spectra were also different from those obtained for the diesters: instead of single signals of the corresponding phosphonic monoester monoanion, the spectra showed formation of large number of structurally similar products.

We propose therefore that the fragmentation of substrates **3** follows a different mechanistic pattern, that is, it involves departure of the chloride ion and the release of the aziridinium ion, together with a metaphosphonate species (Scheme 3). In that sense, decomposition of substrates **3** has a close analogy in the previously reported (8) fragmentation of the (2-arylethyl)phosphorochloridates, where the 2-aryl group provided the "internal nucleophile" that aided the cleavage of the phosphate P—O bond, with a simultaneous release of a good leaving group present at phosphorus (Cl^-). The released chloride ion can then compete with the unreacted substrate in the opening of the aziridinium ion, yielding the dialkyl (2-chloroethyl)amine product. We tested the stability of that amine in a given solvent by releasing it from the commercial hydrochloride salt and recording the ^{1}H NMR spectra of the solution as a function of time. In $CDCl_3$ the free amine was found to be perfectly stable, giving rise to the same spectrum as that observed for the fragmentation product of **3**. In CD_3CN the amine was slowly converted into the *N,N*-diethylaziridinium ion (δ_H 2.20), which, after reaching a maximum, slowly gave way to a mixture of products resulting from self-condensation of the aziridinium species (11) (Scheme 4).

The reaction shown in Scheme 3 represents another example of a facile fragmentation of an organophosphorus substrate proceeding with the extrusion of a "metaphosphate" species. Since the transition state for the proposed fragmentation

Table 2. Activation parameters for the unimolecular fragmentation of phosphonic and phosphoric esters.

Substrate (solvent)	$\Delta G^{\ddagger}$ (kJ mol^{-1})	$\Delta H^{\ddagger}$ (kJ mol^{-1})	$\Delta S^{\ddagger}$ (J mol^{-1} K^{-1})
2*c*			
(CD_3CN)	122.4	85.4	−111
3*a*			
(CD_3CN)	117.3	49.3	−204
1*a*[a]			
(EtOH)		86.0	−76
(H_2O)		93.7	−28
4[b]			
(none)	125.1	114.4	−32

[a]Taken from ref. 2.
[b]Calculated from rate data given in ref. 12.

involves the cleavage of two bonds, and the formation of two bonds (as opposed to the cleavage of one bond and the formation of one bond in the "classical" mechanism), the activation parameters, and the entropy term in particular, should be significantly different for those two types of fragmentation. In their study on the hydrolysis of alkyl chlorosulfates, Buncel and Millington (12) pointed out that the mechanistic change from the "classical" displacement to the fragmentation of the leaving group to SO_3 and Cl^- should strongly affect the activation entropy. The direction of the change is difficult to predict, as the increased solvation of the species being formed in the transition state should lead to a more negative $\Delta S^{\ddagger}$, while the gain in the degrees of freedom might result in the increase of the entropic term. We have determined activation parameters for one phosphonic diester (**2***c*) and one phosphonochloridate (**3***a*); acetonitrile-d_3 was found to be the best solvent in which the rates could be conveniently measured for both substrates. The results, together with those reported for an analogous fragmentation of the triester, dimethyl 2-(dimethylamino)ethyl phosphate (**1***a*, R = R′ = Me; Y = OMe) (2), and for a similar reaction of diethyl 2-(ethylmercapto)ethyl thionophosphate $(EtO)_2P(S)OCH_2CH_2SEt$, **4** (13), are given in Table 2. It is clear that the behavior of the phosphonochloridate is qualitatively different from that of the other substrates, in full agreement with the hypothesis of a different ("metaphosphate") mechanism of its fragmentation. Although the activation energies obtained for **2***c* and **3***a* are very similar, fragmentation of **3***a* is characterized by a much lower $\Delta H^{\ddagger}$ value, and by a much more negative value of $\Delta S^{\ddagger}$. According to the accepted mechanism for the fragmentation of diesters **2**, and the proposed mechanism for the fragmentation of chlorides **3**, the respective activated complexes can be represented

Can. J. Chem. Downloaded from www.nrcresearchpress.com by 80.90.12.36 on 09/08/12
For personal use only.

Can. J. Chem. Downloaded from www.nrcresearchpress.com by 80.90.12.36 on 09/08/12
For personal use only.

Scheme 5.

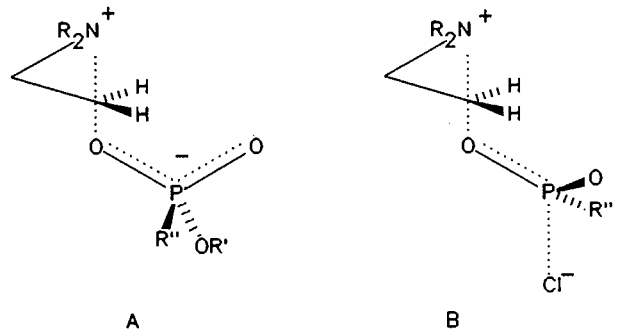

A B

by structures A and B, given in Scheme 5. As far as the enthalpy of activation is concerned, the major difference is that, in B, cleavage of a relatively weak bond (P—Cl) is compensated by the formation of a strong (phosphoryl) bond in the incipient metaphosphonate. Our results show that such a difference is reflected by a ca. 40% reduction of the $\Delta H^{\neq}$ value. The enthalpy gain is, however, almost completely counterbalanced by the further, strong decrease in the entropy of activation. As illustrated in Scheme 5, the difference in the $\Delta S^{\neq}$ indicates a much more rigorous geometry of the transition state B, dictated presumably by the stereoelectronic requirements of the whole N···C···O···P···Cl system in which two bonds are being cleaved and two are being formed in a more or less concerted fashion. We previously also obtained highly negative entropies of activation ($\Delta S^{\neq} < -100$ J mol^{-1} K^{-1}) for another type of fragmentation of an organophosphorus substrate, thermal decomposition of dialkyl 2-acyloxyalkyl-phosphonates, which also involves extrusion of a metaphosphate species and requires transfer of the alkyl group from the phosphate function to the carbonyl oxygen (14).

In conclusion, we believe that substrates of the type **3** represent yet another example of the organophosphorus system in which a "metaphosphate" unit is incorporated into the molecular framework, and can be released via a fragmentation under mild conditions.

Experimental section

NMR spectra were recorded on a Bruker AC300 spectrometer at a probe temperature of 30°C. Chemical shift values are given relative to $SiMe_4$ (^{1}H and ^{13}C) or 85% H_3PO_4 (^{31}P). Coupling constants are given in Hz. Chloroform-*d*, acetonitrile-d_3, and DMSO-d_3 (all Uvasol, Merck) were dried over molecular sieves (Merck, 0.4 nm). Kinetic studies were performed in a thermoregulated water bath fitted with a Gallenkamp Thermostirrer. Micro distillations were carried out using a Buchi GKR-50 glass tube oven. Diethyl 2-chloroethylammonium chloride (Aldrich) was dried azeotropically with benzene, kept under high vacuum, and pulverized before use.

2-(Dialkylamino)ethyl alkyl alkylphosphonates **2** were prepared from the corresponding alkyl alkylphosphonochloridates and the corresponding 2-(dialkylamino)ethanol as described in the general procedure below. The details of the preparation of substrates **3** (alkyl alkylphosphonochloridates) will be described elsewhere.[2]

[2] A. Pienaar and T.A. Modro. In preparation.

Preparation of ***2****. General procedure*

A mixture of 2-(dialkylamino)ethanol (5.7 mmol) and triethylamine (6.3 mmol) in ether (2 mL) was added dropwise to a stirred solution of the alkyl alkylphosphonochloridate (5.7 mmol) in ether (10 mL) at −15°C. The precipitate formed was filtered off and dissolved in chloroform (20 mL), anhydrous potassium carbonate (6.6 mmol) was added, and the mixture was stirred overnight. After filtration and evaporation of the solvent, crude **2** was purified by bulb-to-bulb (b-t-b) distillation. The distilled products were spectroscopically pure (single signal in the ^{31}P NMR spectrum) and they were identified by ^{1}H and ^{13}C NMR spectroscopy in $CDCl_3$, as well as by heteronuclear 2D (^{13}C, ^{1}H) NMR spectra (correlating signals are indicated below by matching superscripts at the δ_H and δ_C values).

2a (36%): distilled b-t-b (at 70°C/0.3 Torr; 1 Torr = 133.3 Pa); δ_P: 30.6; δ_H: 1.28^x (6H, d, J_{HH} 6.2), 1.44^y (3H, d, J_{HP} 17.5), 2.24^z (6H, s), 2.54^w (2H, t, J_{HH} 5.9), 4.05^v (2H, m), 4.66^u (1H, m); δ_C: 11.9^y (dq, J_{CP} 144.9, J_{CH} 128.1), 23.9^x (dq, J_{CP} 4.1, J_{CH} 126.7), 45.6^z (q, J_{CH} 133.2), 59.2^w (dt, J_{CP} 6.4, J_{CH} 131.3), 62.8^v (dt, J_{CP} 6.3, J_{CH} 146.1), 70.15^u (dd, J_{CP} 6.3, J_{CH} 146.3).

2b (22%): distilled b-t-b (at 75°C/0.3 Torr); δ_P: 34.8; δ_H: 1.12^x (3H, dt, J_{HP} 20.0, J_{HH} 7.7), 1.29^y (3H, t, J_{HH} 7.0), 1.73^z (2H, dq, J_{HP} 18.3, J_{HH} 7.7), 2.24^w (6H, s), 2.55^v (2H, t, J_{HH} 5.9), 4.07^u (4H, m); δ_C: 6.53^x (dq, J_{CP} 6.4, J_{CH} 129.3), 16.4^y (dq, J_{CP} 6.4, J_{CH} 127.1), 18.8^z (dt, J_{CP} 143.1, J_{CH} 126.7), 45.7^w (q, J_{CH} 133.2), 59.4^v (dt, J_{CP} 6.4, J_{CH} 132.8), 61.6^u (dt, J_{CP} 6.4, J_{CH} 146.6), 63.1^u (dt, J_{CP} 6.4, J_{CH} 146.3).

2c (33%): distilled b-t-b (at 60°C/0.5 Torr); δ_P: 33.1; δ_H: 1.46^x (3H, d, J_{HP} 17.4), 2,24^y (6H, s), 2.54^z (2H, t, J_{HH} 5.7), 3.69^w (3H, d, J_{HP} 11.3), 4.08^v (2H, m); δ_C: 10.5^x (dq, J_{CP} 144.8, J_{CH} 128.4), 45.6^y (q, J_{CH} 133.1), 52.0^z (dq, J_{CP} 6.3, J_{CH} 147.3), 59.3^w (dt, J_{CP} 5.8, J_{CH} 131.7), 63.1^v (dt, J_{CP} 15.5, J_{CH} 147.4).

2d (72%): distilled b-t-b (at 65°C/0.5 Torr); δ_P: 31.7; δ_H: 1.29^x (3H, t, J_{HH} 7.1), 1.46^y (3H, d, J_{HP} 17.6), 2.24^z (6H, s), 2.54^w (2H, t, J_{HH} 5.9), 4.07^v (4H, m); δ_C: 10.8^y (dq, J_{CP} 144.8, J_{CH} 128.4), 15.9^x (dq, J_{CP} 5.7, J_{CH} 126.5), 45.2^z (q, J_{CH} 133.0), 58.9^w (dt, J_{CP} 6.0, J_{CH} 133.7), 61.0^v (dt, J_{CP} 6.0, J_{CH} 147.0), 62.6^v (dt, J_{CP} 6.1, J_{CH} 145.1).

2e (6%): bp 87°C/0.9 Torr; δ_P: 32.8; δ_H: 0.99^x (6H, t, J_{HH} 7.2), 1.44^y (3H, d, J_{HP} 17.5), 2.54^z (4H, q, J_{HH} 7.1), 2.68^w (2H, t, J_{HH} 6.3), 3.68^v (3H, d, J_{HP} 11.1), 4.03^u (2H, m); δ_C: 10.5^y (dq, J_{CP} 144.6, J_{CH} 128.5), 11.6^x (q, J_{CH} 125.4), 47.5^z (t, J_{CH} 132.6), 52.0^v (dq, J_{CP} 6.3, J_{CH} 144.2), 52.8^w (dt, J_{CP} 6.2, J_{CH} 134.6), 63.6^u (dt, J_{CP} 6.4, J_{CH} 147.2).

2f (39%): distilled b-t-b (at 75°C/0.2 Torr); δ_P: 34.6; δ_H: 1.00^x (6H, t, J_{HH} 7.1), 1.12^y (3H, dt, J_{HP} 20.0, J_{HH} 7.7), 1.28^z (3H, t, J_{HH} 7.1), 1.73^v (2H, dq, J_{HP} 18.3, J_{HH} 7.7), 2.56^w (4H, q, J_{HH} 7.1), 2.70^u (2H, t, J_{HH} 6.4), 4.07^t (4H, m); δ_C 6.31^y (q, J_{CH}130.0), 11.6^x (q, J_{CH} 125.4), 16.2^z dq, J_{CP} 5.9, J_{CH} 126.9), 18.6^v (dt, J_{CP} 142.7, J_{CH} 126.8), 47.4^w (t, J_{CH} 132.8), 52.7^u (dt, J_{CP} 6.3, J_{CH} 133.0), 61.3^t (dt, J_{CP} 6.4, J_{CH} 148.5), 63.3^t (dt, J_{CP} 6.5, J_{CH} 149.7).

2-(Dialkylamino)ethyl alkylphosphonochloridates ***3***: were prepared from the corresponding diesters (**3***a* from **2***e* and **3***b*

Can. J. Chem. Downloaded from www.nrcresearchpress.com by 80.90.12.36 on 09/08/12
For personal use only.

from **2***f*) and $SOCl_2$ by modification of the literature procedure (15). The products were prepared immediately before further use since they decomposed slowly and could not be purified by distillation or chromatography. They were, however, found to be formed as spectroscopically pure materials (single signal in the ^{31}P NMR spectra), and were identified by ^{1}H NMR spectroscopy.

3a (87%): δ_P: 43.3; δ_H: 1.41 (6H, t, J_{HH} 7.3), 2.10 (3H, d, J_{HP} 17.5), 3.21 (4H, m), 3.41 (2H, m), 4.67 (2H, m).

3b (86%): δ_P: 49.7; δ_H: 1.27 (3H, dt, J_{HP} 25.4, J_{HH} 7.7), 1.40 (6H, t, J_{HH} 7.3), 2.25 (2H, dq, J_{HP} 17.2, J_{HH} 7.6), 3.21 (4H, m), 3.41 (4H, m), 4.66 (2H, m).

Product studies

Decomposition of substrates **2** was followed in DMSO-d_6 by ^{1}H NMR spectroscopy and the products (alkyl alkylphosphonate ion and *N,N,N′,N′*-tetraalkylpiperazinium ion) were easily identified by comparison with literature data (1). In the fragmentation of substrates **3**, followed in $CDCl_3$, the piperazinium ion was absent, and diethyl 2-chloroethylamine formed was identified by its characteristic ^{1}H NMR spectrum, and by the addition of the authentic material.

N,N,N′,N′-*Tetramethylpiperazinium ion*: δ_H (DMSO-d_6): 3.37 (12H, s), 3.95 (8H, s).

N,N,N′,N′-*Tetraethylpiperazinium ion*: δ_H (DMSO-d_6): 1.21 (12H, t, J_{HH} 7.1), 3.01 (8H, q, J_{HH} 7.1), 3.82 (8H, br s).

Diethyl (2-chloroethyl)amine: δ_H ($CDCl_3$): 1.34 (6H, t, J_{HH} 7.2), 3.10 (4H, q, J_{HH} 7.3), 3.28 (2H, t, J_{HH} 6.9), 3.91 (2H, t, J_{HH} 6.9).

Kinetic measurements

A sample of the substrate (30 mg) was dissolved in the appropriate solvent (0.5 mL) in an NMR tube, and the tube was sealed and incubated in a thermoregulated water bath. The ^{1}H NMR spectrum of the solution was recorded periodically, and the reaction progress was determined from the integrated areas of selected signals for the substrate and (or) the product. Good first-order linear plots were obtained (r^2 = 0.996).

Stability of diethyl (2-chloroethyl)amine in solution

Samples of diethyl (2-chloroethyl)ammonium chloride (0.101 g, 0.59 mmol) were dissolved in $CDCl_3$ and in CD_3CN (2 mL each), and anhydrous K_2CO_3 (0.082 g, 0.59 mmol) was added to each solution. The mixtures were stirred at room temperature, and the ^{1}H NMR spectra of the solutions were periodically recorded. The spectrum of the $CDCl_3$ solution was identical to that of the pure free base (*vide supra*), and did not change over the period of 6 days. The spectrum of the CD_3CN solution was initially identical to that obtained in $CDCl_3$ (with a small change in the chemical shift values), but after 1 day a signal at δ_H 2.20 (ring protons in 1,1-diethylaziridinium ion) started to appear. The signal increased in intensity, together with new signals appearing in the range of δ_H 1.2–3.4; 4 days later the aziridinium signal, after passing through a maximum, had disappeared, and the spectrum showed only a large number of signals in the range of δ_H values 1.2–3.4.

References

1. H.P Benschop, G.R. Van Den Berg, and G.W. Kraay. Recl. Trav. Chim. Pays-Bas, **89**, 1025 (1970).
2. P.A. Manninen. Acta Chem. Scand. Ser. B: **32**, 269 (1978).
3. S.Cocks, K.R. Koch, and T.A. Modro. J. Org. Chem. **51**, 265 (1986).
4. T.A. Modro and C.M. Moorhoff. J. Phys. Org. Chem. **2**, 263 (1989).
5. C.J. Lacey and L.M. Loew. J. Org. Chem. **48**, 5214 (1983).
6. W.H. Saunders. Acc. Chem. Res. **9**, 19 (1976).
7. N.S. Isaacs. Physical organic chemistry. Longman Scientific, New York. 1987. Chap. 11.1.10.
8. S. Cocks and T.A. Modro. Tetrahedron Lett. **26**, 945 (1985).
9. D.E.C. Corbridge. Phosphorus. An outline of its chemistry, biochemistry and technology. 4th ed. Elsevier, Amsterdam. 1990. p. 502.
10. C. Reichardt. Solvent effects in organic chemistry. Verlag Chemie, Weinheim. 1979. Chap. 5.
11. O.C. Dermer and G.E. Ham. Ethyleneimine and other aziridines. Academic Press, New York. 1969.
12. E. Buncel and J.P. Millington. Can. J. Chem. **43**, 556 (1965).
13. T.R. Fukuto and R.L. Metcalf. J. Am. Chem. Soc. **76**, 5103 (1954).
14. C.P. de Jongh, T.A. Modro, and A.M. Modro. Heteroat. Chem. **4**, 503 (1993).
15. L. Maier. Phosphorus, Sulfur, Silicon, **47**, 465 (1990).

Molecular mechanics calculations on the complexes between analogues of Hoechst 33258 and d(CGCGAATTCGCG)$_2$: influence of bulky group substitution on base pair preference of DNA minor groove binders

Ding-Kwo Chang, Shu-Fang Cheng, and Ting-Lin Chien

Abstract: Molecular mechanics calculations were performed on the three structures of the complexes formed by the derivatives of Hoechst 33258 and dodecameric DNA duplex d(CGCGAATTCGCG)$_2$. Formation and docking energies of these complexes were compared. It was found that the CG site that is 3′ to the central AATT region can be tolerated by the drugs. This is probably due to the presence of the bulky piperazine ring and, more pronouncedly, by alkylated analogues of the drug that prefer the wider minor groove formed by the GC base pair region of B-DNA. The argument of bulkiness of the piperazine moiety as the origin of enhancement of GC affinity is supported by detailed structural analysis of the intermolecular interface and widening of the DNA minor groove at the binding site. Implications of the results are discussed.

Key words: minor groove binder, docking energy, sequence specificity.

Résumé : On a effectué des calculs de mécanique moléculaire sur les trois structures des complexes qui se forment à partir des dérivés du Hoechst 33258 et du duplexe dodécamérique de l'ADN, d(CGCGAATTCGCG)$_2$. On a comparé les énergies de formation et de jonction de ces complexes. On a trouvé que le site CG, qui se trouve à 3′ de la région centrale AATT, peut être toléré par les drogues et que cette propriété est probablement due à la présence du volumineux noyau pipérazine et, d'une façon plus prononcée, par les analogues alkylés de la drogue qui préfèrent la rainure mineure plus large qui est formée par la région B-ADN de la paire des bases GC. L'argument de la grosseur de la portion pipérazine comme origine du rehaussement de l'affinité GC est en accord avec l'étude structurale détaillée de l'interface intermoléculaire et de l'élargissement de la rainure mineure de l'ADN au niveau du site de liaison. On discute des implications de ces résultats.

Mots clés : liaison de la rainure mineure, énergie de jonction, spécificité de la séquence.

[Traduit par la rédaction]

Introduction

DNA molecules are targets for many anti-viral, anti-bacterial, and anti-cancer antibiotics (1, 2). DNA may be irreversibly modified as in strand cleavage (3) and interstrand cross-linking (4). Alternatively, DNA may interact reversibly with the drugs through intercalation (5), groove binding (6), or charge–charge interaction (7). One of the central issues in the design of DNA-interacting drugs is sequence specificity of DNA by the drugs. In this aspect, groove binders appear to be of advantage since one can extend the number of base pairs spanned by the groove binder, as desired, in a systematic way, to increase the degree of differentiation by increasing the number of base pair sequences for recognition. In the B-DNA structure the minor groove is deep and narrow; a deep electronegative potential well (8) exists that is well suited to a positively charged ligand whose size closely fits the minor groove. This is the case for netropsin and distamycin, which are known to bind strongly to the minor groove of the B-DNA double-stranded helix in the A,T-rich region, which is notably narrower than the GC-rich region (9). Computational study has shown that both van der Waals (vdW) and electrostatic forces, including hydrogen bonding, contribute comparably to the binding stability (enthalpy) of netropsin complexed to B-DNA oligomers containing the AATT sequence (10).

Attempts were made to switch the sequence specificity from AT to GC by replacing pyrrole with an imidazole ring in netropsin analogues. This approach is based on avoiding steric clash between the hydrogen atom on the pyrrole ring and the amino group of guanine and replacing it with a hydrogen bond between the imidazole nitrogen atom and the guanine amino group. Although these "lexitropsins" (11, 12) exhibited a substantial increase in GC recognition, no clear rejection of the

Received December 15, 1994.

D.-K. Chang,[1] S.-F. Cheng, and T.-L. Chien. Institute of Chemistry, Academia Sinica, Taipei, Taiwan, Republic of China.

[1] Author to whom correspondence may be addressed. Fax: 886-2-783-1237.

Can. J. Chem. Downloaded from www.nrcresearchpress.com by 80.90.12.36 on 09/08/12
For personal use only.

Can. J. Chem. Downloaded from www.nrcresearchpress.com by 80.90.12.36 on 09/08/12
For personal use only.

AT base pair was observed and in a number of cases AT-rich sequences were still preferred.

Hoechst 33258 is a synthetic compound that shows anthelmintic (13) and topoisomerase-inhibiting (14) activities. Several studies have shown that the drug binds preferentially to the AT-rich region of double-stranded DNA with a minimum of four consecutive AT base pairs (6). It was found that there were two different modes of the Hoechst 33258 binding to DNA, with binding affinity differing by two orders of magnitude. X-ray crystallographical studies on the complex of Hoechst 33258:d(CGCGAATTCGCG)$_2$ showed the central AATT as binding site (15) at low temperature (16) while ATTC emerged as a possible binding site at room temperature (17). The ATTC mode was also reported for Hoechst 33258 binding to a DNA dodecamer containing central ATAT (18). The AATT binding site is consistent with footprinting (19) and NMR (20) results. The one base shift from GC of the AATT binding site to ATTC was rationalized by the bulky piperazine ring (which fits better the wider groove at the GC pair) and the hydrogen-bond-acceptor N atom connecting the ring to the benzimidazole group (which forms a hydrogen bond with the amino proton of guanine N2). The bulky group could be used as a potential discriminator against the AT base pair, in addition to a hydrogen-bond acceptor such as the nitrogen atom in the imidazole ring that favors the GC base pair.

Energy computation in association with molecular modeling has been increasingly employed to gain insight into the mechanism of the interaction between biopolymers and ligands (21). In particular, it affords an analysis of intermolecular energy by contributions from vdW, hydrogen bonding, and electrostatic terms. In the following, the results of an energetics computation of Hoechst 33258: d(CGCGAATTCGCG)$_2$ complexes using structures deduced from an X-ray diffraction experiment are reported. For the ATTC mode, only the conformation in which the piperazine ring points toward the groove was considered, as the other orientation, in which the ring points away from the minor groove, would yield a smaller docking energy. In addition, to evaluate the steric interference of the piperazine ring on the stability of drug binding to the AATT site, the piperazine ring was rotated approximately 90 degrees with respect to the orientation derived from X-ray diffraction data mentioned previously (17). To explore the effect of the bulky piperazine ring on GC base pair recognition, methyl and ethyl groups were used to substitute the hydrogen atoms on two carbon atoms *ortho* to the bridge nitrogen on the piperazine ring. The comparison sheds some light on the nature of the minor-groove binding mode of the drugs to DNA and may contribute to the rational design of ligands that recognize the desired DNA sequence.

Methods

The coordinates of the complex were taken from data deposited by Pjura et al. in the protein data bank (17) for the reference structure of computation. The initial structures with AATT and two ATTC binding modes (see below) were obtained by docking the drug at appropriate locations and orientations onto the oligonucleotide, whose coordinates were taken from the same crystal structure. For the initial structures used in minimization, docking of drugs onto the oligonucleotide was tried until the van der Waals energy dropped to a negative value, typically -60 kcal mol^{-1}. Attempts were made to use different docked complex structures in each of the three binding modes to examine the effect of varying the starting structures. To minimize the end effect, six atoms at the two ends of the oligonucleotide were fixed in space: C2, C4, C6 of cytosine[1] and C4, C6, C8 of guanine[12]. The Discover program from Biosym Technologies Inc. (San Diego, California, U.S.A) and the AMBER (22) force field were used to compute the energy and to minimize the structure using 15 000 steps of the steepest descent method followed by 500 steps of the conjugate gradient method. In all computations the complex systems were minimized until the root-mean-square (RMS) gradient was 0.15 kcal mol^{-1} Å^{-1} or less. A distance-dependent dielectric constant (i.e., ϵ is numerically equal to the interactomic distance in Å) was employed in the computation. Twenty-one sodium ions were added to neutralize the complex system. These counterions were placed at least 4.5 Å from the two nearest phosphorus atoms. Polarization was not taken into account in considering intermolecular interaction energy as its contribution is relatively small and effectively the same for complexes in the present study. The energy of the system can be expressed as follows.

$$E = E_{\text{bond}} + E_{\text{theta}} + E_{\text{phi}} + E_{\text{imp}} + E_{\text{elect}} + E_{\text{hb}} + E_{\text{vdW}}$$

where E_{bond}, E_{theta}, E_{phi}, E_{imp}, E_{elec}, E_{hb}, and E_{vdW} represent the energies of the chemical bond, angle, dihedral angle, improper angle, Coulombic electrostatic, hydrogen bond (H-bond), and van der Waals (vdW) interactions, respectively; 6–12 Leonard–Jones and 10–12 potential functions were used for vdW and hydrogen bond energies, respectively. The final calculated energies were not dependent on the initial docking positions, indicating that a structure corresponding to the local energy minimum is obtained using appropriately docked initial structures for minimization.

In the evaluation of components of intermolecular interaction energy, only vdW and electrostatic terms are reported. Intermolecular docking energy was calculated using the docking module of the Biosym program. Hydrogen bond energy is included in the electrostatic energy. Only enthalpy is considered; entropy is neglected because it requires a more accurate model of the solvent molecules to take account of the hydrophobic effect as water molecules are expelled from the minor groove into the surrounding bulk solvent upon complex formation. Furthermore, only the relative binding energy is relevant in the present study.

Results

The schematic structures of Hoechst 33258 as well as its derivatives and some of the atomic numbering schemes are presented in Fig. 1. Figures 2(*a*), 2(*b*), and 2(*c*) show the starting structures of Hoechst 33258 complexed to d(CGCGAATTCGCG)$_2$ at the AATT site and two piperazine orientations at the ATTC site, respectively. Table 1 shows the intermolecular interaction energy for the three binding modes of Hoechst 33258 and its methyl and ethyl derivatives complexed to the oligomeric helical duplex. Some of the representative intermolecular distances are summarized in Table 2. Detailed stereo views of these three complexes after energy minimization are presented in Fig. 3. Figure 4 indicates the width of the

Fig. 1. Schematic structure of Hoechst 33258, its derivatives, and the atomic numbering scheme.

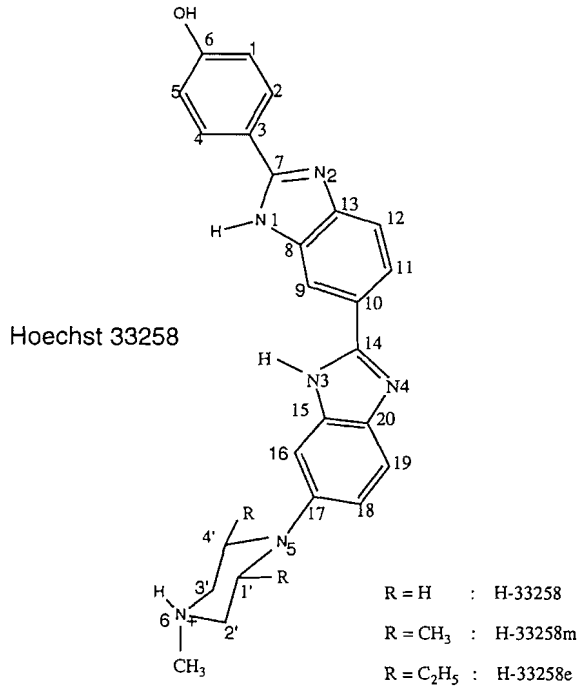

minor groove as measured from the shortest distance between O4′ and O4′ and P and P on the two opposite strands.

It is also found that the effect of varying the starting complex structures on the final structures and energies is minimal. The conclusions drawn are independent of the starting structures.

Discussion

The results of the computation on the AATT-b mode, in which the orientation of the piperazine moiety is parallel to the floor of the minor groove, are not shown. This is because, after energy minimization, the orientation of drug reverted to the AATT-a mode. For the methyl and ethyl analogues, the phenomenon is more pronounced, presumably due to the bulkiness of the drugs that reduced the binding affinity and stability of the complexes. From Table 1, it can be seen that both vdW and electrostatic components are smaller for the two ATTC binding modes for Hoechst 33258. The difference is significantly smaller for the methyl and ethyl analogues.

The effect of bulky group substitution on the intermolecular distance can be inferred from Table 2 for some representative atom pairs. Since substitution on the piperazine group occurs at one end of the drug analogues, the effect is expected to be more visible at the minor groove of the region T8–C9 and G16–A17 where the piperazine is attached to the oligonucleotide. Thus the distances between C4′ of the drug and N3 of A17 (or N2 of G16) and between C4′ of the drug and O2 of T8 (or O2 of C9) are smaller for H-33258 than for its methylated or ethylated derivatives in the AATT-a mode (or both ATTC modes). This can be visualized from the stereo diagrams of Fig. 3. In the AATT mode, the penetration of both substituted derivatives into the minor groove is not as deep as Hoechst 33258 in the piperazine portion of the drug while the difference is not as significant in the other part of the drug. In both ATTC modes, the effect of methyl and ethyl substitution is not as pronounced as in the AATT mode, which presumably is the result of the larger width of the minor groove at the GC base pair. Figures 4 indicate that the width of the minor groove at

Fig. 2. Starting structures of Hoechst 33258 complexed to d(CGCGAATTCGCG)$_2$ in AATT-a mode (*a*), ATTC-a mode (*b*), and ATTC-b mode (*c*), respectively. The piperazine rings of the drugs are perpendicular and parallel to the floor of the DNA minor groove for modes a and b, respectively.

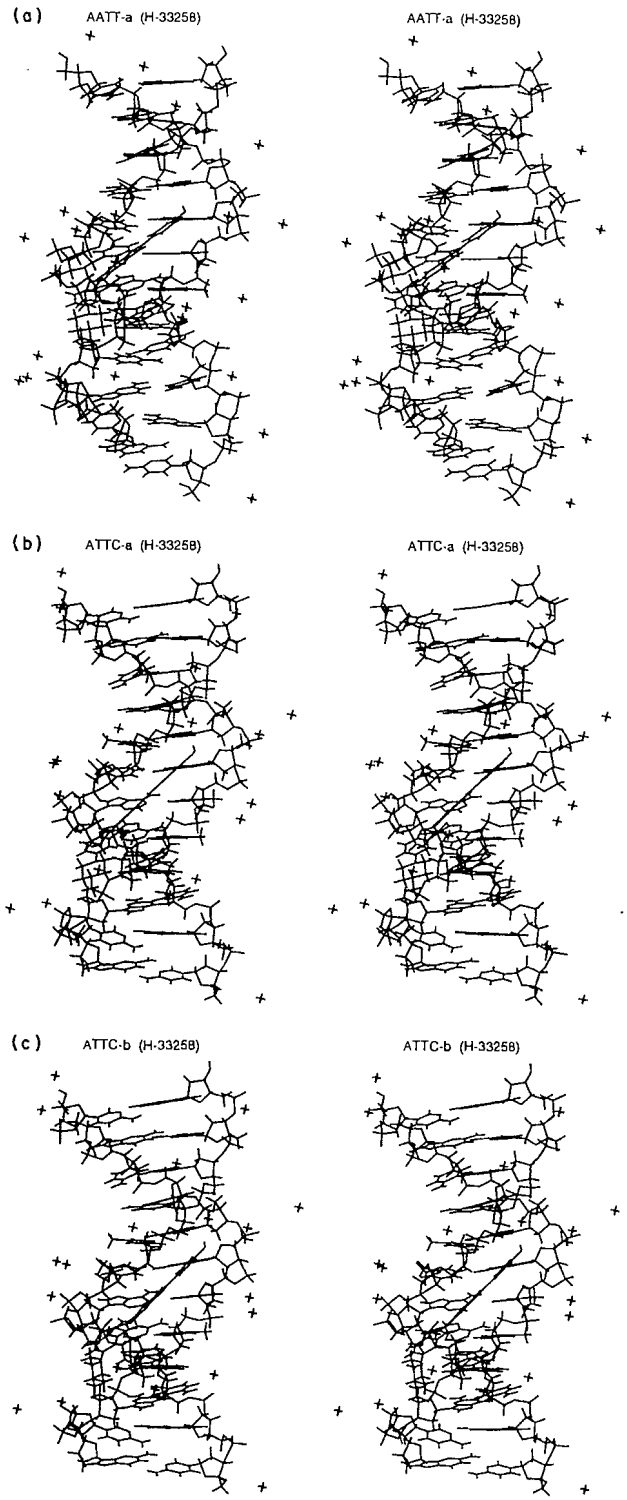

Can. J. Chem. Downloaded from www.nrcresearchpress.com by 80.90.12.36 on 09/08/12
For personal use only.

Fig. 3. Central region of the final stereo diagrams of H-33258 (*a*), H-33258m (*b*), and H-33258e (*c*) complexed to d(CGCGAATTCGCG)$_2$ in AATT-a mode after energy minimization. Dotted lines extending from N (or O) of the oligonucleotide to the N atom of the drugs are used to indicate the close interaction of the complexes; numbers are in angstrom units.

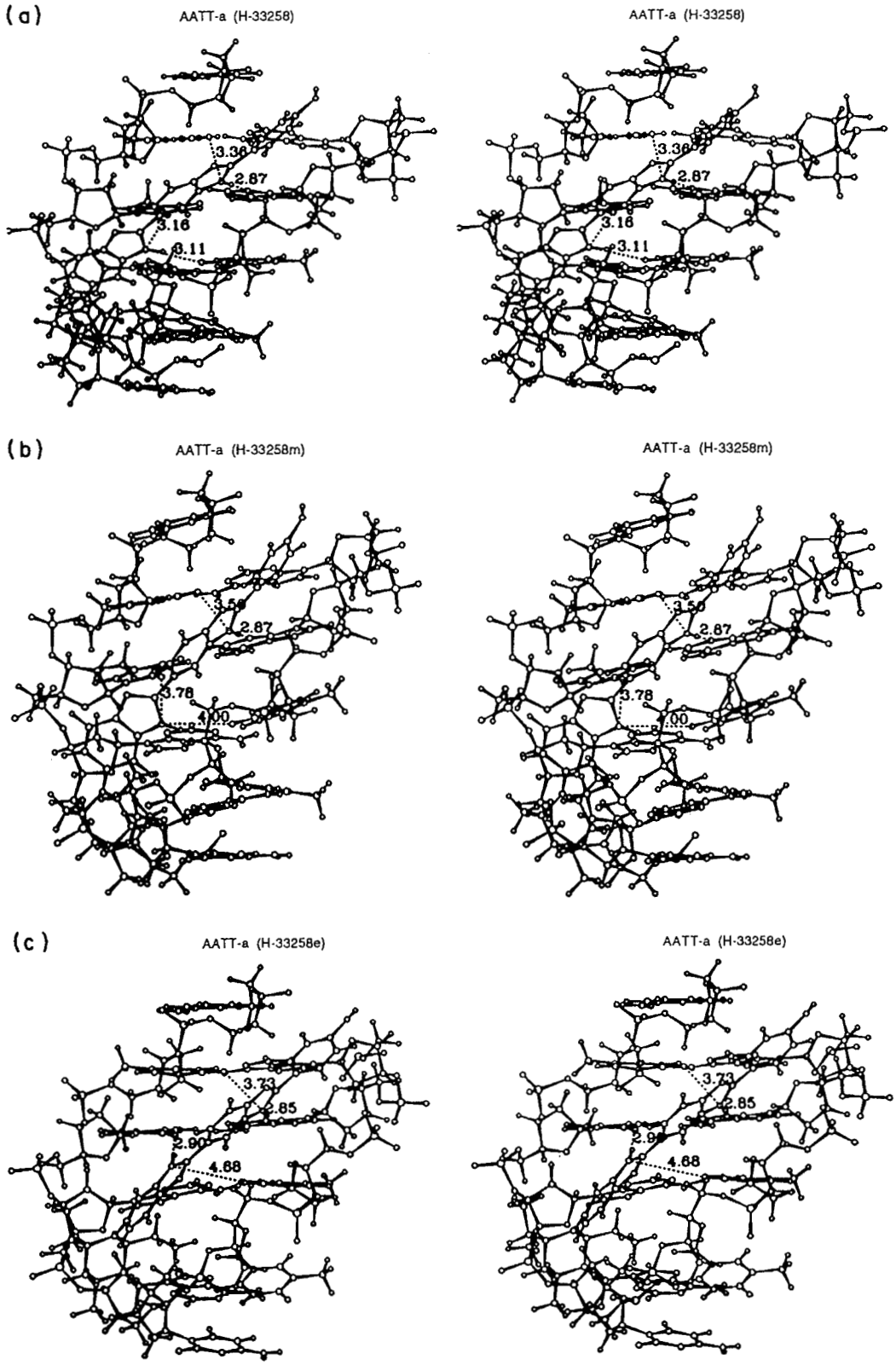

Can. J. Chem. Downloaded from www.nrcresearchpress.com by 80.90.12.36 on 09/08/12
For personal use only.

Can. J. Chem. Downloaded from www.nrcresearchpress.com by 80.90.12.36 on 09/08/12
For personal use only.

Fig. 4. Minor groove width of AATT-a (*a*), ATTC-a (*b*), and ATTC-b (*c*) as measured by the shortest distances between O4′ and O4′ less 2.8 Å and between P and P less 5.8 Å on the two opposite strands. The numbers of oxygen and phosphorus are shown along the horizontal axis. The C1–G24 end of the helix is on the left, and the G12–C13 end is on the right. Arrows indicate the position on the backbone of the DNA duplex where methyl or ethyl substitution occurs. The structure of the oligonucleotide double helix alone was obtained utilizing water molecules to solvate the molecule and neutralizing counterions; a dielectric constant of unity was used in this particular calculation.

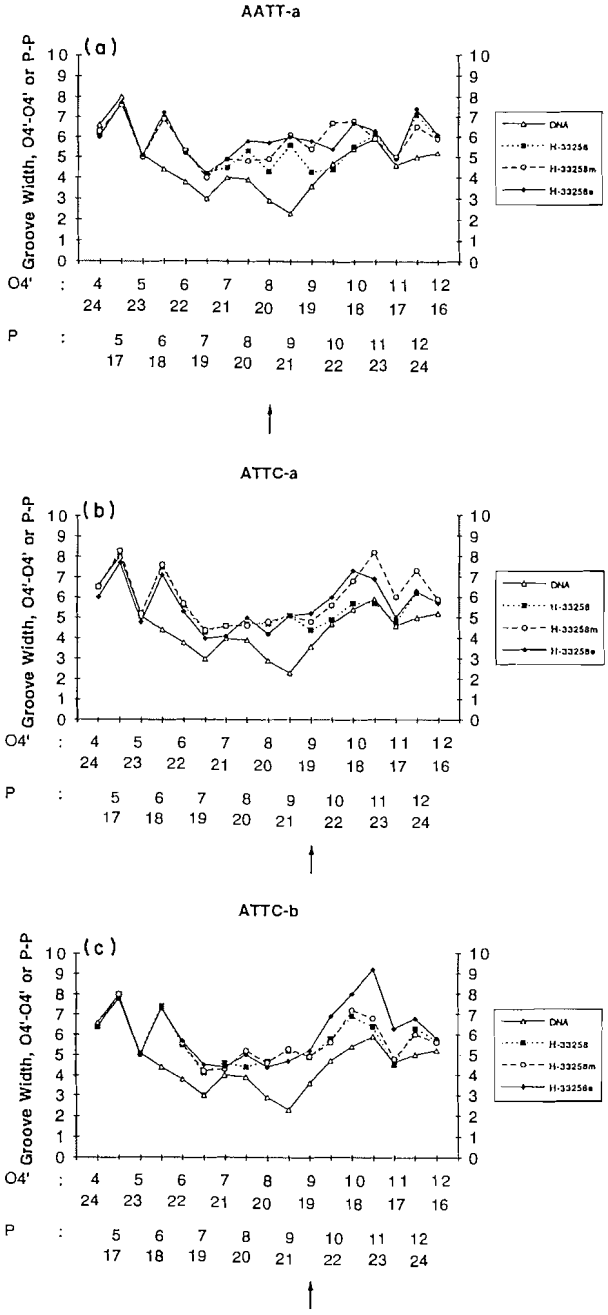

the binding site is substantially increased by the insertion of drug into the groove and the extent of widening is larger for complexes containing methyl or ethyl substituents. Clearly, the latter effect is the result of the substituted piperazine ring. The effect is also manifested in the distance between the drugs and atoms of DNA at the floor of minor groove. For example, the distance of G16 N2 to C4′ of Hoechst 33258 is considerably shorter than that of G16 N2 to C4′ of methyl- or ethyl-Hoechst 33258, in particular in the ATTC-a mode. It is noteworthy in examining the components of docking energy for the complexes in Table 2, that both components are reduced in the case of the methylated or ethylated drug, a phenomenon that correlates with an increase in the distance between the drug and DNA.

Comparison of the distortion energy of DNA and drug upon complex formation reveals that deformation of the drugs is substantially smaller than that of DNA for the three drug complexes in the three different binding modes. In view of the large variation of DNA distortion energy, it is perhaps more reliable to use only the docking energy in evaluating the affinity of drug to DNA. From the docking energy shown in Table 1, it is clear that the difference among the three binding modes is insignificant for methyl or ethyl analogues. This can be rationalized by the deeper electronegative potential well for the minor groove of the A,T-rich stretch of B-DNA, so that electrostatic energy is larger for the AATT site. In the case of methylated and ethylated Hoechst 33258, the difference in the electrostatic term is by and large offset by the vdW term. Notably, due to the bulkiness of the piperazine group the drug does not penetrate as deeply into the groove for the complex in which the piperazine ring is parallel to the floor of the minor groove (cf. ATTC-a and ATTC-b in Table 1). Consequently, both vdW and electrostatic terms are smaller. The difference is significant as the bifurcate hydrogen bond between each of the peptidyl hydrogens of netropsin and N3 of adenine or O2 of thymine amount to 3 kcal mol^{-1}.[2] The effect of introducing methyl or ethyl groups into the piperazine ring of the drug can also be observed in Figs. 4, where the width of the minor groove of the DNA duplex was measured. The widening of the minor groove at the point of substitution is evident. From the energetic and geometric consequences presented here, it is clear that introduction of a bulky moiety into the minor groove binder can be used to reduce AATT specificity while ATTC specificity is enhanced. It may be possible to combine the present approach, taking advantage of local differences in geometry of the minor groove, with the substitution of an aromatic or aliphatic heterocyclic group such as imidazole replacing the pyrrole ring to switch recognition from AT to GC. It is also clear that the potential hydrogen bond between the piperazine nitrogen and the guanine amino hydrogen does not play a dominant role in shifting the binding site to GC since the electrostatic energy is smaller for a complex in the ATTC binding mode than in the AATT mode and the decrease in the vdW term of interaction energy is greater in the AATT than in the ATTC mode when a methyl or ethyl group is introduced into the piperazine ring. Table 1 also shows that the complexes of methylated and ethylated drugs are more stable in the ATTC-b mode than in the ATTC-a mode.

According to computational (21 and footnote 2), spectroscopic (23), and thermodynamic (24) data on several systems involving minor groove interaction, the binding energy for the GC-rich region as binding site is invariably smaller than for

[2] D.-K. Chang and T.-L. Chien, unpublished results.

Table 1. Intermolecular interaction energy for the three binding modes for Hoechst 33258 and its methyl and ethyl derivatives complexed to the d(CGCGAATTCGCG)$_2$ helical duplex.

		Docking energy (kcal mol^{-1})		
Drug[a]	DNA	VdW	Elect	Total
	AATT-a	−53.7	−75.0	−128.7
H-33258	ATTC-a	−52.9	−67.9	−120.8
	ATTC-b	−52.5	−72.1	−124.6
	AATT-a	−50.9	−70.6	−121.5
H-33258m	ATTC-a	−50.2	−60.3	−110.5
	ATTC-b	−54.3	−67.6	−121.9
	AATT-a	−45.6	−70.9	−116.5
H-33258e	ATTC-a	−50.5	−62.5	−113.0
	ATTC-b	−52.9	−63.4	−116.3

Drug[a]	DNA	Docking (kcal mol^{-1})	DNA[b] (kcal mol^{-1})	Drug[b] (kcal mol^{-1})	Total (kcal mol^{-1})
	AATT-a	−128.7	0.0	0.0	−128.7
H-33258	ATTC-a	−120.8	19.5	−0.1	−101.4
	ATTC-b	−124.6	26.7	−0.2	−98.1
	AATT-a	−121.5	0.0	0.0	−121.5
H-33258m	ATTC-a	−110.5	5.5	−2.0	−107.0
	ATTC-b	−121.9	3.8	−0.7	−118.8
	AATT-a	−116.5	0.0	0.0	−116.5
H-33258e	ATTC-a	−113.0	8.3	0.5	−104.2
	ATTC-b	−116.3	9.9	−2.4	−108.8

[a]H-33258, Hoechst 33258; H-33258m, methylated Hoechst 33258; H-33258e, ethylated Hoechst 33258.

[b]The values are relative to the reference AATT-a.

the AT-rich region. For example, netropsin has a higher binding affinity than the analogues, which are shown to be less AT specific (24). This is probably due to the deep electronegative potential for the narrow B-DNA minor groove formed by the AT cluster and to the fact that the amino group in the guanine base reduces the electrostatic potential of the minor groove. The design of a DNA sequence-specific minor-groove binding drug is made more complicated by the fact that DNA is not rigid, i.e., it possesses a local degree of freedom so that a small adjustment in atomic position is easily achieved to facilitate ligand binding (25). Thus, it was noted that the difference in the vdW term is small for netropsin binding to the AATT site relative to the GGCC site.[2] This can be explained by the observation that there is a small change in propeller twist for the guanine amino group to avoid steric clash with the hydrogen atom of the pyrrole ring of netropsin (25). The replacement of pyrrole by imidazole ring, so that the extra nitrogen can form a favorable hydrogen bond with the guanine amino group to enhance GC preference, is partially offset by the shallower electrostatic potential in the minor groove of the GC base pair. In the present study, bulky groups were used to render one portion of the drug more favorable to the GC site or less AT-preferable. The basis for this change is the fact that the GC base pair provides a wider minor groove, which better accommodates the bulkier substituent groups so that penetration of the drug containing bulky substituents is deeper, as shown in Table 1. Our results also demonstrate the correlation between vdW and electrostatic interaction energies. The bulky groups can be introduced into molecular chains consisting of charged groups, aromatic rings, and peptidyl linkers, as well as hydrocarbon spacers. The importance of length of the latter has been reported by Greenidge et al. (26).

Conclusion

Using the molecular mechanics method, the energy of various structures of Hoechst 33258 complexed with d(CGCGAATTCGCG)$_2$ was computed and compared. It was found that the bulky piperazine ring reduced AT specificity considerably owing to steric hindrance of substituted derivatives by the narrow minor groove in the AT-rich region of B-DNA. While Hoechst 33258 exhibits some tolerance for the GC base pair, docking energy for the methyl and ethyl analogues is essentially the same for the three binding modes studied in the present study. Van der Waals interaction can thus be utilized to aid in the design of sequence recognition of minor groove binders for B-DNA. The importance of the vdW term in determining AT/GC preference lies, apparently, more in the exclu-

Can. J. Chem. Downloaded from www.nrcresearchpress.com by 80.90.12.36 on 09/08/12
For personal use only.

Table 2. Representative distances (Å) between Hoechst 33258 analogues and DNA.

Drug	DNA		H-33258	H-33258m	H-33258e
AATT-a					
N1	A6	N3	2.87	2.87	2.85
N1	T20	O2	3.36	3.50	3.73
N3	T7	O2	3.11	4.00	4.68
N3	T19	O2	3.16	3.78	2.90
C5	A5	N3	3.84	3.96	3.90
C5	C21	O2	3.80	4.05	3.58
C9	T7	O2	3.65	4.00	3.98
C9	T19	O2	3.51	3.62	3.77
C4′	T8	O2	3.56	5.19	5.32
C4′	A17	N3	3.68	3.89	4.49
ATTC-a					
N1	T7	O2	2.84	2.84	3.44
N1	T19	O2	3.16	3.24	2.84
N3	T8	O2	2.92	2.89	4.57
N3	A18	N3	3.63	4.14	3.91
C5	A6	N3	3.33	3.34	3.54
C5	T20	O2	3.28	3.29	3.25
C9	T8	O2	3.40	2.54	3.59
C9	A18	C2	4.07	4.00	4.23
C4′	C9	O2	3.86	4.62	5.18
C4′	G16	N2	3.50	3.99	4.12
ATTC-b					
N1	T7	O2	2.84	2.88	2.84
N1	T19	O2	3.19	3.33	3.31
N3	T8	O2	2.89	3.16	2.91
N3	A18	N3	4.26	4.05	4.23
C5	A6	N3	3.39	3.56	3.56
C5	T20	O2	3.62	3.36	3.34
C9	T8	O2	3.33	3.05	3.21
C9	A18	C2	4.05	3.78	3.80
C4′	C9	O2	5.23	6.02	5.73
C4′	G16	N2	4.35	4.56	4.44

sion of bulky heterocycles by the side wall of the minor groove of the AT-rich segment than in the steric clash involving single atomic contact at the bottom of the minor groove.

Acknowledgement

Financial support from the National Science Council of the Republic of China (NSC81-0208-M-001-533) and the Academia Sinica of the Republic of China is greatly appreciated.

References

1. L.H. Hurley. J. Med. Chem. **32**, 2027 (1989).
2. C. Chagas and B. Pullman (*Editors*). Molecular mechanisms of carcinogenic and antitumor activity. Academic Press, New York. 1987.
3. J. Stubbe and J.W. Kozarich. Chem. Rev. **87**, 1107 (1987).
4. L.H. Hurley and D.R. Needham-Van Devanter. Acc. Chem. Res. **19**, 230 (1986).
5. W.D. Wilson and R.L. Jones. Adv. Pharmacol. Chemother. **18**, 177 (1981).
6. C. Zimmer and U. Wahnert. Prog. Biophys. Mol. Biol. **47**, 31 (1986).
7. G.S. Manning. Q. Rev. Biophys. **11**, 179 (1986).
8. A. Pullman and B. Pullman. Q. Rev. Biophys. **14**, 289 (1981).
9. R.E. Klevit, D.E. Wemmer, and B.R. Reid. Biochemistry, **25**, 3296 (1986).
10. K. Zakrzewska, R. Lavery, and B. Pullman. J. Biomol. Struct. Dyn. **4**, 833 (1986).
11. M.L. Kopka, C. Yoon, D. Goodsell, P. Pjura, and R.E. Dickerson. Proc. Natl. Acad. Sci. U.S.A. **82**, 1376 (1985).
12. M. Lee, K. Krowicki, J.A. Hartley, R.T. Pon, and J.W. Lown. J. Am. Chem. Soc. **110**, 3641 (1988).
13. G. Lämmler and W. Raether. International Congress on Tropical Medicine and Malaria, Tehran, Iran, 1968. Vol. 23, pp. 39–43.
14. M.M. McHugh, J.M. Woynaroski, R.D. Sigmund, and T.A. Beerman. Biochem. Pharmacol. **38**, 2323 (1989).
15. M.K. Teng, M. Usman, C.A. Frederick, and A.H.-J. Wang. Nucleic Acids Res. **16**, 2671 (1989).
16. J.R. Quintana, A.A. Lipanov, and R.E. Dickerson. Biochemistry, **30**, 10294 (1991).
17. P.E. Pjura, K. Grzeskowiak, and R.E. Dickerson. J. Mol. Biol. **197**, 257 (1987).
18. M.A.A.F. Carrondo, M. Coll, J. Aymami, A.H.-J. Wang, G.A. v.d. Marel, J.H. van Boom, and A. Rich. Biochemistry, **28**, 7849 (1989).
19. K.D. Harshman and P.B. Dervan. Nucleic Acids Res. **13**, 4825 (1985).
20. M.S. Searl and K.J. Embrey. Nucleic Acids Res. **18**, 3753 (1990).
21. F. Gago, C.A. Reynolds, and W.G. Richards. Mol. Pharmacol. **35**, 232 (1989).
22. S.J. Weiner, P.A. Kollman, D.A. Case, U.C. Singh, C. Ghio, G. Alagona, S. Profeta, Jr., and P. Weiner. J. Am. Chem. Soc. **106**, 765 (1984).
23. S. Kumar, T. Joseph, M.P. Singh, Y. Bathini, and J.W. Lown. J. Biomol. Struct. Dyn. **9**, 853 (1992).
24. G. Burckhardt, G. Luck, C. Zimmer, J. Störl, K. Krowicki, and J.W. Lown. Biochem. Biophys. Acta, **1009**, 11 (1989).
25. B.H. Geierstanger, T.J. Dwyer, Y. Bathini, J.W. Lown, and D.E. Wemmer. J. Am. Chem. Soc. **115**, 4474 D.E. (1993).
26. P.A. Greenidge, T.C. Jenkins, and S. Neidle. Mol. Pharmacol. **43**, 982 (1993).

Can. J. Chem. Downloaded from www.nrcresearchpress.com by 80.90.12.36 on 09/08/12
For personal use only.

Internal return in the photochemistry of ring-substituted 1-(1-naphthyl)ethyl esters of phenylacetic acid

J.M. Kim and J.A. Pincock

Can. J. Chem. Downloaded from www.nrcresearchpress.com by 80.90.12.36 on 09/08/12
For personal use only.

Abstract: The photochemistry in methanol of the esters **12***a–d* has been studied in order to determine the importance of internal return of both ion pair and radical pair intermediates. The efficiency of internal return, determined by monitoring ^{18}O exchange between the alcohol and carbonyl oxygens, was shown to be substituent dependent, varying from approximately 10% for the 4,7-dimethoxy substrate to nearly 50% for the 4-cyano case. The corresponding ground state solvolysis reactions gave about 10% internal return and, within experimental error, were substituent independent. Internal return was also examined by racemization of the chiral center in **12***a* and **12***d*. In summary, these combined results reveal that internal return probably occurs mainly through a contact (not solvent-separated) radical pair. More important, internal return has little effect on previously calculated electron transfer rate constants for converting the radical pair to the ion pair. Therefore, the previously reported Marcus' correlations are valid.

Key words: photochemistry of benzylic esters, internal return, photosolvolysis, electron transfer, radical pairs.

Résumé : Afin d'évaluer l'importance du retour interne de la paire d'ions et de la paire de radicaux intermédiaires, on a étudié la photochimie des esters **12***a–d* dans le méthanol. On a montré que l'efficacité du retour interne, tel que déterminé par une évaluation de l'échange du ^{18}O entre les oxygènes de l'alcool et du carbonyle, dépend de la nature du substituant et qu'il varie d'approximativement 10% pour le substrat 4,7-diméthoxylé à pratiquement 50% dans le cas du dérivé 4-cyano. Les réactions de solvolyse à l'état fondamental conduisent à environ 10% de retour interne et, dans les limites des erreurs expérimentales, elles ne dépendent pas de la nature des substituants. On a aussi étudié le retour interne par un examen de la racémisation du centre chiral des composés **12***a* et **12***d*. En résumé, les résultats combinés révèlent que le retour interne se produit principalement par le biais d'une paire de radicaux en contact (non séparés par le solvant). Il est très important de noter que le retour interne ne provoque que de faibles effets sur les constantes de vitesse de transfert d'électron calculées antérieurement pour la conversion de la paire de radicaux en paire d'ions. On peut en conclure que les corrélations rapportées antérieurement par Marcus sont valides.

Mots clés : photochimie, esters benzyliques, retour interne, photosolvolyse, transfert d'électron, paires de radicaux.

[Traduit par la rédaction]

Introduction

Recently, we reported detailed (1–3) studies on the photochemistry in methanol of arylmethyl esters, **1**, of aliphatic carboxylic acids. The observed products and the resulting mechanism are shown in Scheme 1. The major products from these reactions are arylmethyl ethers, **2**, along with the corresponding carboxylic acid, **3**, resulting from photosolvolysis, and coupling products, **4**, **5**, and **6**, resulting from loss of CO_2.

The products **2** and **3** are clearly derived from the ion pair whereas the products **4**, **5**, and **6** are derived from the radical pair. Product yields as a function of the variation of Ar (substituent effects (1, 3), and phenyl (3) versus 1-naphthyl (1)) and R (CH_3, 1°, 2°, 3°, benzyl) (2, 3) are rationalized by a pathway dominated by homolytic cleavage of the acyl oxygen – arylmethyl carbon bond in the excited singlet state ($k_R^S \gg k_I^S$ in Scheme 1). This excited state process is followed by ground state competition between electron transfer (k_{ET}) that converts the radical pair to the ion pair, decarboxylation (k_{CO_2}) of the acyloxy radical, and diffusional escape (k_D) of the radical pair from the solvent cage. Values of k_{ET} range from $\sim 10^7$ s^{-1} to 6×10^{10} s^{-1} and were shown (1, 3) to follow Marcus' theory in both the normal and inverted regions. Values of k_{CO_2} range from $\sim 10^9$ s^{-1} for $R = CH_3$ up to 11×10^9 s^{-1} for $R = C(CH_3)_3$.

A concern during the development of this mechanistic scheme was the possibility that internal return could be an important pathway. There are two possible internal return pathways: internal return to the ground state of the ester by collapse of the radical pair with rate constant k_{IR}^R in Scheme 1 and the corresponding internal return of the ion pair, k_{IR}^I.

Qualitatively, examination of Scheme 1 reveals two very different possibilities. In the first case, $k_R^S \gg k_I^S$; i.e., only

Received February 21, 1995.

J.M. Kim and J.A. Pincock.[1] Department of Chemistry, Dalhousie University, Halifax, NS B3H 4J3, Canada.

[1] Author to whom correspondence may be addressed. Telephone: (902) 494-3305. Fax: (902) 494-1310.

Scheme 1. General mechanism for the photoreactivity of arylmethyl esters in methanol.

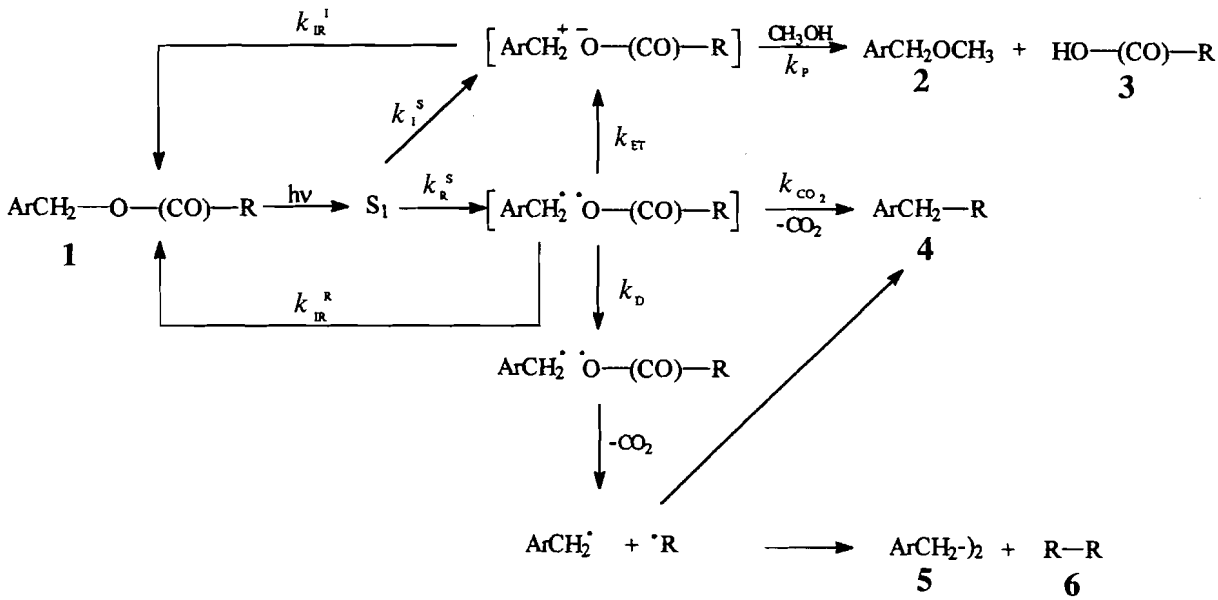

homolytic cleavage of the excited singlet state occurs. Therefore, internal return of the radical pair only decreases the efficiency of product formation and does not alter the partitioning of the radical pair to products. Product yield ratios will still be a reliable measure of k_{ET}, k_{CO_2}, and k_D. On the other hand, internal return of the ion pair will selectively reduce the yield of the ether **2**. Therefore, the value of k_{ET}, determined from that yield, will be lower than the correct value. If the efficiency of this internal return is substituent dependent then the previously reported variation of k_{ET} as a function of substituents is also in error. The correlation with Marcus' theory might then also be incorrect.

The second possibility, from Scheme 1, is that k_R^S and k_I^S are competitive, i.e., both homolytic and heterolytic cleavage of the excited singlet state occur. In this case, either radical pair or ion pair internal return will alter the product distribution. The mechanistic scheme and kinetic analysis are now quite complicated and obtaining reliable values of k_{ET} and k_{CO_2} will be difficult. These kinetic possibilities will be quantified in more detail later in the Discussion section of this paper.

Internal return is a well-established process in ground state solvolysis reactions and has been studied for a number of benzylic benzoates (4). For instance, solvolysis of **7** in 70:30 (v:v) acetone:water at 60°C revealed, by ^{18}O equilibrium between alkyl and carbonyl oxygens, that the rate of internal return is

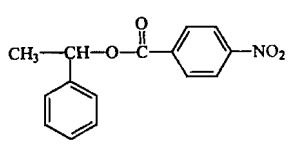

7

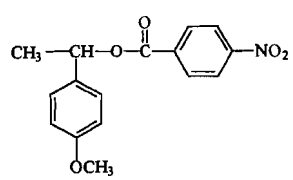

8

76% that of the rate of solvolysis but that racemization is negligible. In contrast, for the more reactive 4-methoxy substrate, **8**, the rate of internal return is 57% that of solvolysis but, in this case, 70% of the internal return results in racemization. These effects are also solvent dependent. In 90:10 (v:v) acetone:water, a solvent of lower ionizing power, the rate of internal return for **8** is now 2.5 times as fast as solvolysis but only 45% of the internal return results in racemization. Detailed trapping studies by azide ion led to the conclusion that, for both substrates, internal return is from the contact ion pair and not the solvent-separated ion pair. Clearly, from these results, the extent of molecular motion in the contact ion pair is dependent on both solvent ionizing power and the stability of the benzylic cation.

Four papers on internal return for excited state benzylic cleavage reactions of esters have also been published and these will be briefly summarized.

Photolysis (5, 6) of **9** in 50% (v/v) methanol:water to 75% conversion resulted in recovered **9** that was 64% equilibrated by ^{18}O scrambling but with no loss of optical activity. In trifluoroethanol, photolysis to 85% conversion gave 100% equilibration and 19% racemization. The authors concluded that the ^{18}O scrambling in methanol is probably by a concerted migration of the benzylic cation from the alcohol oxygen to the carbonyl oxygen so that racemization is prevented. In trifluoroethanol, some ^{18}O equilibration is by an ion pair intermediate that also allows racemization. The radical pair was not invoked as an intermediate since the decarboxylation rate constant of the acyloxy radical at $\sim 10^9$ s^{-1} was stated to be too large to allow internal return.

As reported by Givens et al. (7, 8), photolysis of **10** in dioxane to 50% conversion resulted in recovered ester that was 35% equilibrated by ^{18}O labelling. No racemization was observed. In this non-nucleophilic solvent, no photosolvolysis is possible and only hydrocarbon dimers analogous to **4**, **5**, and **6** are formed. Clearly only radical pair intermediates are important in this case. In the same paper, photolysis of **11** in methanol to 53% conversion was reported to give neither ^{18}O equilibration nor *trans* to *cis* isomerization. In contrast, the product, 1,2-diphenylcyclopropane, was formed as a mixture of *trans* and *cis* isomers. No photosolvolysis products were detected so radical pair intermediates were the only ones considered. Based on these results, Givens et al. also proposed that ^{18}O equilibration

Can. J. Chem. Downloaded from www.nrcresearchpress.com by 80.90.12.36 on 09/08/12
For personal use only.

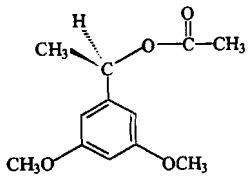

9

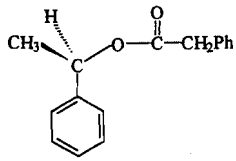

10

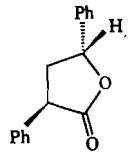

11

occurs by a concerted migration that prevents stereochemical isomerization. For **11**, the concerted migration is geometrically impossible so that even ^{18}O equilibration stops.

To simplify the discussion that follows, no distinction will be made between a "concerted" (5, 7, 8) pathway for ^{18}O exchange and a pathway involving a contact radical pair, which would presumably also allow exchange but not have enough rotational freedom to allow racemization. An experimental distinction between these two mechanistic pathways is probably not currently possible.

On the basis of these results, which are fragmentary but, nevertheless, do show that internal return is competitive with reaction, a systematic study of internal return in photochemical reactions of benzylic esters as a function of substituents seemed necessary.

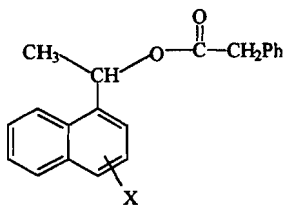

12*a*, X=H
12*b*, X=4-OCH_3
12*c*, X=4,7-Di-OCH_3
12*d*, X=4-CN

We report here results for the photochemistry in methanol of four esters, **12*a–d***. These were chosen to allow a simultaneous study of both ^{18}O equilibration and racemization. As with our previous studies (1, 3), the substituents were chosen so that that the incipient 1-naphthylethyl radicals span a range of oxidation potentials that includes both the normal and inverted regions of the Marcus' correlation for the electron transfer rates that convert the radical pair to the ion pair. For comparison, ground state solvolysis results for **12b** and **12c** are also reported.

Results

Syntheses of esters 12*a–d*

Four substituted 1-(1-naphthyl)ethyl phenylacetates, **12*a–d***, were synthesized from the corresponding alcohols. The alcohols were prepared by reaction of the aldehydes with either methyllithium or methyl magnesium iodide. Details are given in the experimental section. The 4,7-dimethoxy alcohol is quite unstable and difficult to isolate and purify. By ^1H NMR, the major products of its decomposition are probably two diastereomeric dimers, $ArCH(CH_3)—O—CH(CH_3)Ar$, although no molecular ion corresponding to these dimers was detected by mass spectrometry. Fragmentation to the arylethyl cation, the observed base peak, is presumably too facile. The dimer assignment was made on the basis of the absence of an OH stretch in the IR spectrum and the similarity between the NMR spectra of these mixtures and the alcohol itself.

Syntheses of ^{18}O enriched esters 12*a–d*

The preparation of the labelled esters followed the same procedure as above except that the precursor aldehydes were first equilibrated in ~10% ^{18}O water (Aldrich) – dioxane. The total amount of ^{18}O incorporated is shown in Table 1 as the 0% conversion values. These were calculated using a computer program[2] that corrects the experimentally measured M, M + 1, and M + 2 peak intensities in the mass spectrum for the natural abundance of all isotopes of the molecular formula. The synthetic procedure should specifically enrich the alkyl oxygen of the ester with ^{18}O. Some initial experiments were attempted to see if this premise could be confirmed by mass spectrometry. The unsubstituted ester ($M^{+\cdot}$ = 290) has a fragment ion at m/z = 172 ($C_{12}H_{12}O$) corresponding to the alcohol of the ester and containing only the oxygen where the excess ^{18}O was expected. However, the ^{18}O content of this oxygen was only about 50% of the total. As demonstrated below, this ^{18}O equilibration is occurring in the mass spectrometer after formation of the radical cation. A detailed study of the fragmentations–rearrangements occurring in the mass spectra of these esters is in progress.[3]

Because of this difficulty, the esters were reduced with $LiAlH_4$ to substituted 1-(1-naphthyl)ethanols and 2-phenylethanol. Each alcohol now contains only one oxygen of the ester, the former the alcohol oxygen and the latter the carbonyl oxygen. The ^{18}O content of these alcohols was then measured, without prior separation, by GC–MS using selected ion monitoring of the M, M + 1, and M + 2 peaks for each. For each sample, two injections were made and five mass spectra were taken across the GC peak. These values, given again as 0% conversion, are in Table 1 for both the alkyl oxygen, the carbonyl oxygen, and the sum of the two. This independently determined sum agrees very well with the value for the ester before hydride reduction and confirms that the synthetic esters are selectively ^{18}O enriched at the alcohol oxygen.

Syntheses of optically active esters 12*a* and 12*d*

These optically active esters were prepared from the corresponding alcohols as before. The alcohols were prepared by reduction of 1-acetonaphthones with (+)-DIP-chloride. By analogy with literature results (9) for 2-acetonaphthone, acetophenone, and 4-cyanoacetophenone, these reductions should give the *R* enantiomer with high enantiomeric excess (96–98%). Initially, we attempted to determine the enantiomeric excess of the alcohols by ^1H NMR using the chiral shift reagent, $Eu(hfc)_3$. This worked well for the unsubstituted case, which gave good resolution of the methyl signal and some of the aromatic hydrogens. The enantiomeric excess was greater than 98% since signals for the other enantiomer could be easily

[2] J.S. Grossert, Department of Chemistry, Dalhousie University.
[3] J.S. Grossert, B. Yhard, J.A. Pincock, and J.M. Curtis. To be published.

Can. J. Chem. Downloaded from www.nrcresearchpress.com by 80.90.12.36 on 09/08/12
For personal use only.

Can. J. Chem. Downloaded from www.nrcresearchpress.com by 80.90.12.36 on 09/08/12
For personal use only.

Table 1. Conversion (%) and ^{18}O exchange (%) in the photolyses of esters **12***a–d*.

Esters **12**	Conversion %	Amount of ^{18}O,[a] -O-	Amount of ^{18}O,[b] -CO-	Sum of ^{18}O in both[c]	Difference of ^{18}O[d]	^{18}O excess,[e] %	^{18}O exchange,[f] %
a: X = H	0	9.12 (±0.03)	0.22 (±0.00)	9.34 (±0.03) [9.13][g]	8.90 (±0.03)	95.3 (±0.4)	0
	44	7.07 (±0.07)	1.36 (±0.02)	4.83 (±0.07)	5.71 (±0.07)	67.7 (±1.0)	29.0 (±1.1)
	59	6.84 (±0.02)	1.57 (±0.04)	8.41 (±0.04)	5.27 (±0.04)	62.7 (±0.60)	34.2 (±0.7)
b: X = 4-OCH_3	0	5.22 (±0.04)	0.26 (±0.01)	5.48 (±0.04) [5.73][g]	4.96 (±0.04)	90.5 (±1.0)	0
	43	4.22 (±0.14)	0.61 (±0.01)	4.83 (±0.14)	3.61 (±0.14)	74.7 (±3.7)	17.5 (±3.9)
	65	3.86 (±0.03)	0.79 (±0.01)	4.65 (±0.03)	3.07 (±0.03)	66.0 (±0.8)	27.1 (±1.3)
c: X = 4,7-$(OCH_3)_2$	0	8.38 (±0.20)	0.22 (±0.01)	8.60 (±0.20) [8.60][g]	8.16 (±0.20)	94.9 (±3.1)	0
	65	7.96 (±0.25)	0.64 (±0.02)	8.60 (±0.25)	7.32 (±0.25)	85.1 (±3.8)	10.3 (±4.9)
	88	7.98 (±0.30)	0.62 (±0.02)	8.60 (±0.30)	7.36 (±0.30)	85.6 (±4.6)	9.3 (±5.6)
d: X = 4-CN	0	9.11 (±0.43)	0.22 (±0.01)	9.33 (±0.43) [9.01][g]	8.89 (±0.43)	95.3 (±6.4)	0
	60	4.40 (±0.32)	1.73 (±0.02)	6.13 (±0.33)	2.67 (±0.33)	43.6 (±5.8)	54.2 (±8.6)
	68	3.33 (±0.43)	1.78 (±0.02)	5.11 (±0.43)	1.55 (±0.43)	30.3 (±8.8)	68.2 (±10.9)

[a]-O- is alcohol oxygen of ester.
[b]-CO- is carbonyl oxygen of ester.
[c]Sum of -O- and -CO-.
[d]Difference of ^{18}O in -O- and -CO-.
[e]Difference divided by sum, i.e., *d*/*c*.
[f]See text.
[g]These values are the total ^{18}O content of the ester as determined by mass spectrometry before reduction to the individual alcohols.

detected after addition of only 4% of the racemic alcohol to the enantiomerically enriched material. Unfortunately, samples of the alcohol obtained after hydride reduction of the optically active ester gave very broadened ^1H NMR signals and poor resolution of the protons of the individual enantiomers. The 4-cyano alcohol also gave unresolved signals in the ^1H NMR.

Because of these difficulties, optical activities were used to measure photochemical racemization. Values for the esters, at 0% conversion, are given in Table 2.

Table 2. Specific rotation of esters **12***a* and **12***d*.

Esters **12**	Conversion %	Specific rotation $[\alpha]_D^{28}$ ($CDCl_3$)	Enantiomeric excess, %
a: X = H	0	4.4	100
	44	3.9	89
	51	4.2	95
d: X = 4-CN	0	4.3	100
	52	3.3	77
	67	3.4	79

Photolyses of esters 12*a–d* in methanol

The esters were photolyzed in nitrogen-purged methanol using a Pyrex-filtered 200 W medium-pressure Hanovia mercury lamp. For preparative runs the irradiations were continued until more than 90% of the starting material (as determined by HPLC) was consumed. The photoproducts were then separated and their structures determined by spec-

Table 3. Yield (%) of products in the photolyses of esters **12***a–d*.

Esters **12**	Ether **13**	Coupled product, **14**	Dimer[a] **15**	log k_{ET}[b]
a: X = H	58	27	Trace[c]	10.4 (10.4)
b: X = 4-OCH_3	64	38	Trace[c]	10.1 (10.2)
c: X = 4,7-$(OCH_3)_2$	36[d]	28[d]	36[d]	9.5 (9.5)
d: X = 4-CN	25	82	Trace[c]	8.8 (8.8)

[a]Twice the molar yield.

[b]Calculated from eq. [2]. Values in parentheses are for the corresponding 1-naphthylmethyl esters.

[c]Less than 2%.

[d]These values were determined by the areas of the peaks on the HPLC trace assuming equal instrument response for each by UV absorbance at 280 nm.

troscopic methods using ^1H and ^{13}C NMR and GC–MS. As shown in eq. [1],

[1] $$\underset{\mathbf{12}a\text{–}d}{ArCH(CH_3)—O—(CO)CH_2Ph} \xrightarrow[CH_3OH]{h\nu} \underset{\mathbf{13}a\text{–}d}{ArCH(CH_3)OCH_3} + \underset{\mathbf{14}a\text{–}d}{ArCH(CH_3)CH_2PH} + \underset{\mathbf{15}c}{[ArCH(CH_3)]_2}$$

the major products are the ether **13** and the in-cage coupling product **14**. For the 4,7-dimethoxy ester, a significant yield of the out-of-cage dimer **15** was also obtained. For quantitative runs, the esters were only irradiated to about 50% conversion and the yields of the products then obtained by calibrated HPLC. Values for these yields are given in Table 3.

Photolyses of alcohol oxygen ^{18}O-enriched esters

In these experiments, the esters were photolyzed to between 43 and 88% conversion. After evaporation of the methanol, the reaction mixture, dissolved in dichloromethane, was extracted with 5% aqueous NaOH to remove phenylacetic acid, and the neutral reaction mixture containing photoproducts and unreacted ester was then reduced in ether with $LiAlH_4$. The resulting alcohols were then analyzed by GC–MS for ^{18}O content. The values are given in Table 1. For the 4,7-dimethoxy ester, **12c**, the reduction product, 1-(4,7-dimethoxy-1-naphthyl)ethanol, did not have an observable molecular ion by GC–MS. The signal at highest mass corresponded to loss of water and, therefore, also to loss of the ^{18}O. Because of this facile fragmentation, the ^{18}O content of this alcohol could not be determined and the values reported are assumed to be the difference between the total ^{18}O and that measured for the ^{18}O content of the carbonyl oxygen.

The definition of ^{18}O exchange in Table 1 requires some explanation. Since this process of ^{18}O exchange is a two-site exchange, -O- to -CO-, it can be treated in the same way as a racemization process between two enantiomers. This method of reporting the results for ^{18}O exchange is recommended in order to avoid the ambiguities in interpreting some of the values in the literature. Even before photolysis, there is some ^{18}O isotope in the -CO- oxygen from natural abundance and, consequently, the sample does not have an ^{18}O excess of 100% in the alcohol oxygen. In the enantiomeric case, the sum of the two forms is always 100% but in these ^{18}O exchange experiments most of the ester molecules are not isotopically enriched and have two ^{16}O isotopes. The sum of the two ^{18}O sites is therefore much less than 100%. "^{18}O excess" in the alcohol oxygen site in Table 1 is therefore reported as the difference between the two sites over the sum. If there is internal return, this value will decrease asymptotically, with percent conversion, toward 0%. "^{18}O exchange" in Table 1 is the measure of this equilibration. Thus, it is evaluated by the difference between ^{18}O excess at a given percent conversion divided by the original ^{18}O excess at 0% conversion. This value will increase asymptotically towards 100%. The data are summarized in Table 4 as the ratio of ^{18}O exchange to % conversion.

Table 4. Ratio of ^{18}O exchange to % conversion for the photochemical and thermal reactions of the esters **12**.

Esters **12**	Photochemical	Thermal
a: X = H	0.66 ± 0.02 0.58 ± 0.01	—
b: X = 4-OCH_3	0.41 ± 0.09 0.42 ± 0.02	0.24 ± 0.10 0.19 ± 0.04
c: X = 4,7-$(OCH_3)_2$	0.15 ± 0.07 0.11 ± 0.07	0.22 ± 0.09
d: X = 4-CN	0.90 ± 0.14 1.00 ± 0.16	—

Ground state solvolyses of esters 12 in methanol

These experiments were used to assess the importance of internal return in ground state solvolysis reactions where only ion pair intermediates are possible. The ester was dissolved in methanol and left to react at room temperature until the ester was 50% consumed. Work-up, $LiAlH_4$ reduction, and GC–MS analysis as described above gave the results shown in Table 5 and summarized, along with those for photochemical ^{18}O exchange, in Table 4. Only the esters, **12***b* and **12***c*, with electron-donating groups reacted rapidly enough for these experiments to be possible. The unsubstituted compound, **12***a*, had not measurably reacted even on heating in methanol in a sealed tube for 7 days at 125°C.

Can. J. Chem. Downloaded from www.nrcresearchpress.com by 80.90.12.36 on 09/08/12
For personal use only.

Table 5. Conversion (%) and ^{18}O-exchange (%) in the ground state solvolyses of esters **12b** and **12c**.

Esters **12**	Conversion %	Amount of ^{18}O,[a] -O-	Amount of ^{18}O,[b] -CO-	Sum of ^{18}O in both[c]	Difference of ^{18}O[d]	^{18}O excess,[e] %	^{18}O exchange,[f] %
b: X = 4-OCH_3	0	5.22 (±0.04)	0.26 (±0.01)	5.48 (±0.04)	4.96 (±0.04)	90.5 (±1.0)	0
	41	4.98 (±0.17)	0.51 (±0.01)	5.49 (±0.17)	4.47 (±0.17)	81.4 (±3.90)	10.1 (±4.0)
	43	5.05 (±0.06)	0.46 (±0.01)	5.51 (±0.06)	4.59 (±0.06)	83.3 (±1.4)	8.00 (±1.74)
c: X = 4,7-$(OCH_3)_2$	0	8.31 (±0.22)	0.24 (±0.01)	8.55 (±0.22)	8.07 (±0.22)	94.4 (±3.5)	0
	45	7.91 (±0.21)	0.64 (±0.02)	8.55 (±0.21)	7.27 (±0.21)	85.0 (±2.4)	10.0 (±4.3)

[a]-O- is alcohol oxygen of ester.
[b]-CO- is carbonyl oxygen of ester.
[c]Sum of -O- and -CO-.
[d]Difference of ^{18}O in -O- and -CO-.
[e]Difference divided by sum, i.e., *d*/*c*.
[f]See text.

Photolyses of optically active esters, 12*a* and 12*d*, in methanol

The same procedure for photolysis as described above was used. The esters were re-isolated by column chromatography and the optical activity determined by polarimetry. The values are given in Table 2.

Discussion

Product yields

The products from the photolysis in methanol of the esters, **12**, (eq. [1] and Table 3) will be discussed first. If the general mechanism for the photolysis of arylmethyl esters (Scheme 1) is correct, then the rate constant of a reaction pathway, either k_{ET} or k_{CO_2}, can be obtained from the ratio of products, eq. [2], where k_{ET}^0 is the electron transfer rate constant calculated with the assumption of no internal return, i.e., that both k_{IR}^I and k_{IR}^R are negligibly small.

[2] [Yield of ether **13**]/[Yield of **14** + **15**] = $[P_I]/[P_R]$

$$= k_{ET}^0/(k_{CO_2} + k_D)$$

The coupled product and the dimer are obtained from the decarboxylation pathway and the ether is obtained from the ion pair intermediate after the electron transfer from 1-(1-naphthyl)ethyl radical to phenylacetyloxy radical. The rate constant (4.6×10^9 s^{-1}) of decarboxylation for the phenylacetyloxy radical, from the previous work of Hilborn and Pincock (2), can be used as a "radical clock" to calculate k_{ET} from the product yields. The ratio of product yields and the calculated rate constants of electron transfer from eq. [2] are shown in Table 3. There is very good agreement between the values of k_{ET} obtained from the esters examined here and the previously reported values for the 1-naphthylmethyl esters (1). The rate of electron transfer is slow for the electron-withdrawing cyano group, passes through a maximum for the unsubstituted case, and then decreases again for the strongly electron-donating 4,7-dimethoxy case. This observation reinforces our previous conclusion that these rate constants for electron transfer follow Marcus' theory in both the normal and the inverted regions.

However, as mentioned in the Introduction, the general mechanism in Scheme 1 includes a pathway for internal return from the intermediate ion pair and (or) radical pair. If internal return processes are important and also vary significantly as a function of the substituents on the aromatic ring, then the calculated values of k_{ET} reported here and previously would be incorrect.

Internal return in the photolyses of 1-(1-naphthyl)ethyl esters by ^{18}O exchange

In each case, the labelled ester, in two separate runs, was photolysed to different percent conversions. As described in the Results, the unreacted ester was then reduced with lithium aluminum hydride and the ^{18}O content of the resulting alcohols determined by GC–MS (Tables 1 and 4). The results from these analyses clearly indicate that internal return is dependent on the substituents on the naphthalene ring, electron-withdrawing substituents increasing the efficiency of exchange. The ratio of ^{18}O exchange to % conversion varies from a low of 0.13 for the 4,7-dimethoxy substituted ester to a high of 0.95 for the 4-cyano one.

There are two possible pathways for this ^{18}O exchange in the photolysis. According to Scheme 1, the internal return can occur from the radical pair (k_{IR}^R) and (or) the ion pair intermediate (k_{IR}^I). Results from ground state solvolysis reactions can be used to assess the importance of ion pair internal return.

Internal return in the ground state solvolyses of 1-(1-naphthyl)ethyl esters by ^{18}O exchange

Because the ground state solvolysis mechanism includes only the ion pair intermediate, a comparison of the results for the ground state solvolysis with those for the photolysis was instructive. The assumption used in this analysis is that the ion pairs generated in the thermal and photochemical reactions would have comparable efficiencies of internal return. The

Can. J. Chem. Downloaded from www.nrcresearchpress.com by 80.90.12.36 on 09/08/12
For personal use only.

Can. J. Chem. Downloaded from www.nrcresearchpress.com by 80.90.12.36 on 09/08/12
For personal use only.

only compounds examined for solvolysis in the ground state were 1-(4-methoxy-1-naphthyl)ethyl phenylacetate, **12***b*, and 1-(4,7-dimethoxy-1-naphthyl)ethyl phenylacetate, **12***c*. For 1-(1-naphthyl)ethyl phenylacetate, **12***a*, thermal solvolysis was tried but the rate of solvolysis was too slow. This observation can be easily explained by an estimate of the time required for solvolysis of the unsubstituted compound compared to that for the 4-methoxy case. A Hammett value of ρ^+ of greater than -5 for the S_N1 solvolysis of benzyl tosylates with electron-donating substituents (10) along with a σ^+ value of -0.78 for the 4-methoxy substituent (11) give a calculated difference in reactivity between the unsubstituted and the 4-methoxy ester of approximately four orders of magnitude. In the methanol solvolysis of the 4-methoxy ester, the time for ~50% conversion was 8 days; the time for the unsubstituted one would be approximately 80 000 days.

The same procedure and work-up as for the photolysis was carried out for the solvolysis reactions in the ground state. The results for **12***b* and **12***c* are shown in Table 5 and are also included in Table 4 as the ratio of ^{18}O exchange to % conversion.

In contrast to the results for the photolysis reactions, the ^{18}O exchange in the ground state solvolysis is, within experimental error, substituent independent, at least for the limited range of compounds studied. When the results from the photolysis and the solvolysis in the ground state are compared, internal return is seen to be mostly from the ion pair intermediate for 1-(4,7-dimethoxy-1-naphthyl)ethyl phenylacetate, **12***c*. In both the excited state and the ground state reactions, internal return is a minor pathway. In contrast, for 1-(4-methoxy-1-naphthyl)ethyl phenylacetate, **12***a*, the efficiency of internal return from the ion pair in the ground state is only about 50% of the total internal return in the excited state reaction. The other 50% of internal return in the photolysis is, therefore, probably by internal return from the radical pair or by the concerted migration. These results can perhaps be extended to the other esters, **12***c* and **12***d*. If internal return for the ion pair is relatively substituent independent, then the larger amounts of internal return observed in the photochemical reactions for the other cases do not reflect internal return in the ion pair. As mentioned in the Introduction, only internal return from the ion pair intermediate will change the calculated values of k_{ET}. Other pathways for internal return only decrease the quantum yield of product formation.

Internal return by racemization

Internal return by racemization was only studied for the 4-cyano and the unsubstituted esters, **12***a* and **12***d*. The results are shown in Table 2. For the 4-methoxy and 4,7-dimethoxy substrates, **12***b* and **12***c*, respectively, internal return by ^{18}O exchange has already been shown to be inefficient. Because the molecular motions required for internal return by ^{18}O exchange are always less than those required for racemization, the former process is always more efficient than the latter. Therefore, racemization results for **12***b* and **12***c* are unnecessary.

The results show that photolyses of the chiral esters to about 50% conversion result in recovered ester with about 20% racemization for the 4-cyano case, **12***d*, and between 5 and 10% for the unsubstituted case, **12***a*. For these same compounds, at the same percent conversion, ^{18}O exchange can be estimated at about 50% and 30%, respectively. These results imply that the intermediate(s) leading to internal return are not completely solvent separated since the racemization is less efficient than the ^{18}O exchange. The contact radical pair or the concerted process are the most likely possibilities.

Kinetic analysis of the effect of internal return on the determination of k_{ET} values

The quantitative effect of internal return on the calculated value of k_{ET} can be determined by a kinetic analysis using the steady state approximation for the ion pair and radical pair intermediates. Scheme 1 shows the possible pathways for the kinetic analysis. Equations [3] and [4] represent the rate of product formation from the intermediate ion pair and radical pair, respectively. The integrated ratio of these two equations gives the ratio of the two products from the two intermediates, $[P_I]/[P_R]$. Application of the steady state approximation for both the ion pair and the radical pair leads to eq. [5] where $\Sigma k = (k_D + k_{CO_2} + k_{ET} + k_{IR}{}^R)$ represents all the possible processes of the radical pair.

$$[3] \quad dP_I/dt = k_P[IP]$$

$$[4] \quad dP_R/dt = (k_{CO_2} + k_D)[RP]$$

$$[5] \quad [P_I]/[P_R] = \{k_{ET}/\Sigma k + k_I{}^S/k_R{}^S\}\{k_P/(k_P + k_{IR}{}^I)\}/\{k_{CO_2} + k_D)/\Sigma k\}$$

The three terms in braces in eq. [5] can be easily visualized. The first term in the numerator represents the sum of the efficiencies for formation of the ion pair from both the radical pair ($k_{ET}/\Sigma k$) and the excited singlet state ($k_I{}^S/k_R{}^S$), respectively. The second term in the numerator corrects for the possibility of internal return for that ion pair. The denominator ($\{(k_{CO_2} + k_D)/\Sigma k\}$) represents the efficiency of the radical pair proceeding to products. Simplification of this equation shows its generality.

First, if the excited singlet state only reacts to give the radical pair by homolytic cleavage because $k_R{}^S \gg k_I{}^S$ and if there is no internal return from the ion pair because $k_P \gg k_{IR}{}^I$, then eq. [5] becomes eq. [2]. Second, if internal return is occuring so that k_P and $k_{IR}{}^I$ are competitive, then eq. [6] results.

$$[6] \quad [P_I]/[P_R] = \{k_{ET}/(k_{CO_2} + k_D)\}\{k_P/(k_P + k_{IR}{}^I)\}$$

These two equations can be used to assess the effect that internal return from the ion pair has on the calculated k_{ET} values. Dividing eq. [6] by eq. [2] and rearranging gives eq. [7].

$$[7] \quad k_{ET} = k_{ET}{}^0(1 + k_{IR}{}^I/k_P)$$

The calculated k_{ET} values can now be directly related to the efficiency of internal return: ^{18}O exchange/% conversion = $k_{IR}{}^I/k_P = 0.1$, $k_{ET} = 1.1k_{ET}{}^0$; $k_{IR}{}^I/k_P = 1.0$, $k_{ET} = 2k_{ET}{}^0$; $k_{IR}{}^I/k_P = 10$, $k_{ET} = 11k_{ET}{}^0$.

From the results reported above, the highest efficiency of internal return occurs for the 4-cyano ester, **12***d*, with the ratio of ^{18}O exchange to % conversion of 0.95. Therefore, the maximum deviation possible for the previously calculated k_{ET} values from the correct ones is a factor of two. Moreover, the ground state solvolyses results suggest that most of the internal return is not from the ion pair. Therefore, the difference is probably much less than this maximum possible factor of two.

Finally, the Marcus' plots we reported previously (1, 3) are

Can. J. Chem. Downloaded from www.nrcresearchpress.com by 80.90.12.36 on 09/08/12
For personal use only.

plots of log k_{ET} versus the oxidation potential of the arylmethyl radical. The rate constants span two powers of 10. On this logarithmic scale, a difference of a factor of two, the maximum possible error for a calculated rate of electron transfer, would not significantly alter the observed correlations.

Experimental

General procedures

^1H and ^{13}C NMR spectra were obtained on an AC 250 F NMR spectrometer. Chloroform-*d* ($CDCl_3$) containing tetramethylsilane (TMS) as an internal standard was used as the solvent. Chemical shifts are reported in parts per million (ppm). Multiplicities are abbreviated as follows: s = singlet, d = doublet, dd = doublet of doublets, t = triplet, q = quartet, and m = multiplet. Infrared spectra were obtained on a Nicolet 205 FTIR spectrometer and frequencies are reported in wavenumbers (cm^{-1}). GC–MS analyses were done on a Hewlett Packard 5890 A GC 5970 with a mass selective detector. The column used was a 25 m × 0.2 mm 5% phenylmethyl silicone on fused silica with a film thickness of 0.25 μm. The carrier gas was helium. The temperature program used was 45°C (2.6 min), 45–250°C (10.25 min), and 250°C (17.15 min). Masses are reported in units of mass over charge (m/z). Intensities are reported as a percent of the base peak intensity. The molecular ion is indicated by $M^{+\cdot}$. HPLC analyses were obtained with a Waters 6000 solvent delivery system and a Waters U6K injector under isocratic conditions with a flow rate of 2 mL/min using a Brownlee Lab Spheri-10 10 μm reverse-phase column (25 × 0.46 cm) with a Waters Model 450 variable wavelength detector. UV detection for monitoring the reactions was at 280 nm. Silica gel on polyester plates from Sigma were used for thin-layer chromatography (TLC). Silica gel 60 Å (70–230 mesh), purchased from the Aldrich Chemical Co., was used for column chromatography. Mass spectra were done by Dr. J. H. Kim, Dalhousie University, on a CEC 21–104 mass spectrometer run at 70 eV using a glass direct introduction probe and a source temperature of 110–120°C. Optical activities of chiral compounds were measured using a Perkin–Elmer 141 polarimeter at 589 nm (the sodium D line) at the National Research Council Laboratory, Halifax, Nova Scotia. Combustion analyses were carried out by Canadian Microanalytical Service Ltd., Delta, B.C., Canada.

The following compounds were purchased from the Aldrich Chemical Company: 1-acetonaphthone, 1-methoxynaphthalene, methyl iodide, methyllithium, phenylacetyl chloride, 10% $H_2{}^{18}O$, (+)-Dip-chloride, $Eu(hfc)_3$, and $AlCl_3$. The preparation of the substituted 1-naphthaldehydes has been described previously (1).

Syntheses of the 1-(1-naphthyl)ethanols

The alcohols required for the corresponding esters were synthesized by the following methods.

1-(1-Naphthyl)ethanol

To a suspension of magnesium metal (7.68 mmol, 20% excess) in anhydrous ether (3 mL) was added dropwise methyl iodide (7.68 mmol, 20% excess) in ether (3 mL). Then 1-naphthaldehyde (6.40 mmol) in ether (5 mL) was added and the reaction mixture stirred for 3 h at room temperature under nitrogen. Saturated aqueous ammonium chloride (25 mL) was then added and the mixture was extracted with ether (2 × 25 mL) and dried with anhydrous magnesium sulfate. Column chromatography, using silica gel and a mixed eluent of ethyl acetate and hexane (10:90), gave a colourless oil (0.94 g, 85% yield); ^1H NMR ($CDCl_3$) δ: 8.14–8.10 (m, 1H), 7.90–7.86 (m, 1H), 7.78 (d, 1H, J = 8.1 Hz), 7.68 (d, 1H, J = 7.0 Hz), 7.56–7.45 (m, 3H), 5.68 (q, 1H, J = 6.6 Hz), 1.96 (s, 1H, exchangeable), 1.68 (d, 3H, J = 6.6 Hz); ^{13}C NMR ($CDCl_3$) δ: 141.5(C), 133.8 (C), 130.3 (C), 128.9 (CH), 127.9 (CH), 126.0 (CH), 125.6 (CH), 125.6 (CH), 123.2 (CH), 122.1 (CH), 67.0 (CH-O), 24.4 (CH_3).

(R)-(+)-1-(1-Naphthyl)ethanol

(*R*)-(+)-1-(1-Naphthyl)ethanol was prepared using the method of Singh (12). In a 3-necked flask, (+)-*B*-chlorodiisopinocampheylborane ((+)-DIP-chloride) (10.8 mmol, 10% excess) was dissolved in tetrahydrofuran (10 mL). Then, 1-acetonaphthone (9.87 mmol) in tetrahydrofuran (5 mL) was added dropwise and the solution was stirred at 0°C for 5 h under nitrogen. After another 5 h at room temperature, the solvent was removed under reduced pressure to give a brown oil. α-Pinene, liberated during the reaction, was collected in a cold trap by a vacuum pumping (~0.3 Torr, 15 h (1 Torr = 133.3 Pa)). The residue was dissolved in ether (50 mL) and diethanolamine (21.7 mmol) was added. The mixture was stirred for 2 h, filtered, and the solid washed with pentane (2 × 20 mL). The combined filtrate was concentrated to give the crude product. Column chromatography on silica gel gave a colourless oil (7.68 mol, 78% yield) with over 96% enantiomeric excess. The ^1H NMR of the purified alcohol was identical to that of racemic 1-(1-naphthyl)ethanol. The enantiomeric excess was determined by ^1H NMR analyses using the chiral shift reagent ($Eu(hfc)_3$).

1-(4-Methoxy-1-naphthyl)ethanol

In a 3-necked flask, 4-methoxy-1-naphthaldehyde (2.69 mmol) was stirred in tetrahydrofuran (5 mL) under nitrogen. Methyllithium (3.50 mmol, 30% excess) was added dropwise. The reaction mixture was then stirred at room temperature for 5 h. After adding 5% sodium bicarbonate (25 mL), the mixture was extracted with ether (2 × 25 mL). The organic layer was then washed with water (2 × 25 mL) and dried over anhydrous magnesium sulfate. The crude alcohol was a yellowish oil (2.13 mmol, 79.2% yield): ^1H NMR ($CDCl_3$) δ: 8.31–8.21 (m, 1H), 7.98–7.90 (m, 1H), 7.49–7.36 (m, 3H), 6.65 (d, 1H, J = 7.9 Hz), 5.42 (q, 1H, J = 6.6 Hz), 3.89 (s, 3H), 2.97 (s, 1H, exchangeable), 1.58 (d, 3H, J = 6.6 Hz); ^{13}C NMR ($CDCl_3$) δ: 155.0 (C), 132.0 (C), 131.7 (C), 126.2 (CH), 126.0 (C), 124.9 (CH), 124.1 (CH), 123.7 (CH), 122.6 (CH), 103.4 (CH), 71.7 (CH-O), 55.5 (OCH_3), 24.1 (CH_3).

1-(4,7-Dimethoxy-1-naphthyl)ethanol

This compound was prepared from the aldehyde using the same procedure as described previously for 1-(4-methoxy-1-naphthyl)ethanol. The resulting alcohol was a yellowish oil that could not be purified using column chromatography due to its instability on silica gel; IR (neat): 3400 (O-H), 2960, 2940, 2805, 1625, 1591, 1455, 1430, 1223, 1094, 1034 (C-O), 815 cm^{-1}; ^1H NMR ($CDCl_3$) δ: 8.18 (d, 1H, J = 9.9 Hz), 7.39 (d, 1H, J = 9.9 Hz), 7.36 (s, 1H), 7.08 (dd, 1H, J = 9.6 Hz, 3.0 Hz), 6.55 (d, 1H, J = 9.0 Hz), 5.38 (q, 1H, J = 6.6 Hz), 3.89 (s,

Can. J. Chem. Downloaded from www.nrcresearchpress.com by 80.90.12.36 on 09/08/12
For personal use only.

3H), 3.83 (s, 3H), 2.47 (s, 1H, exchangeable), 1.56 (d, 3H, $J = 6.6$ Hz).

1-(4-Cyano-1-naphthyl)ethanol
This compound was prepared from 4-cyano-1-naphthaldehyde using the same method as that for 1-(1-naphthyl)ethanol (92% yield). The alcohol was chromatographed using a mixed solvent of ethyl acetate and hexane (25:75) as an eluent to give pale yellow crystals: mp 109–110°C; ^{1}H NMR ($CDCl_3$) δ: 8.19 (m, 1H), 8.08 (m, 1H), 7.85 (d, 1H, $J = 7.6$ Hz), 7.75 (d, 1H, 7.6 Hz), 7.68–7.57 (m, 2H), 5.67 (q, 1H, $J = 6.0$ Hz), 2.52 (s, 1H, exchangeable), 1.63 (d, 1H, $J = 6.6$ Hz); ^{13}C NMR ($CDCl_3$) δ: 147.9 (C), 132.6 (C), 132.6 (CH), 129.7 (C), 128.1 (CH), 127.6 (CH), 126.0 (CH), 123.7 (CH), 121.2 (CH), 118.0 (CN), 109.5 (*C*-CN), 66.7 (C-OH), 24.8 (CH_3).

4-Cyano-1-acetonaphthone
Following the method of Jacobs *et al.* (13), acylation of 1-bromonaphthalene using acetyl chloride and aluminum chloride in carbon disulfide gave 4-bromo-1-acetonaphthone (75% yield). The bromide was converted to the nitrile (85% yield) according to the method of Friedman and Shechter (14) using CuCN in dimethyl formamide. Vacuum distillation of the crude ketone gave a yellow solid: bp 150°C at 0.3 Torr (lit.(14) bp 165–175°C at 2–4 Torr); ^{1}H NMR ($CDCl_3$) δ: 8.75–8.64 (m, 1H), 8.27–8.20 (m, 1H), 7.68 (dd, 2H, $J = 21.0$ Hz, 8.8 Hz), 7.60–7.54 (m, 2H), 2.67 (s, 3H).

(R)-(+)-1-(4-Cyano-1-naphthyl)ethanol
The same procedure as described previously for the preparation of (*R*)-(+)-1-(1-naphthyl)ethanol was used for the preparation of (*R*)-(+)-1-(4-cyano-1-naphthyl)ethanol. The ^{1}H NMR of the purified alcohol (65% yield) was identical to that found for 1-(4-cyano-1-naphthyl)ethanol.

General method for the preparation of esters 12*a–d*
To a solution of the corresponding alcohol (7.4 mmol) in benzene (20 mL) was added a solution of phenylacetyl chloride (8.2 mmol, 10% excess) and pyridine (1 mL) in benzene (10 mL). The solution was stirred at room temperature overnight. Water (20 mL) was added to this solution, then the separated organic layer was washed with 10% hydrochloric acid, 5% sodium hydroxide, and water. The organic layer was dried with anhydrous magnesium sulfate and the solvent was evaporated under reduced pressure to give the crude esters. The esters were chromatographed on silica gel with a mixed solvent of ethyl acetate and hexane as an eluent.

1-(1-Naphthyl)ethyl phenylacetate, ***12a***: Colourless oil; IR(neat): 3140–2950 (C-H), 1737 (C=O), 1257, 1237, 1158, 1069, 799 cm^{-1}; ^{1}H NMR ($CDCl_3$) δ: 8.29–8.25 (m, 1H), 8.05–8.01 (m, 1H), 7.97 (d, 1H, $J = 8.1$ Hz), 7.75 (d, 1H, $J = 7.0$ Hz), 7.71–7.58 (m, 3H), 7.54–7.46 (m, 5H), 6.94 (q, 1H, $J = 6.5$ Hz), 3.89 (s, 2H), 1.90 (d, 3H, $J = 6.5$ Hz); ^{13}C NMR ($CDCl_3$) δ: 170.9 (C=O), 137.4 (C), 134.1 (C), 133.9 (C), 130.3 (C), 129.4 (CH), 129.0 (CH), 128.7 (CH), 128.5 (CH), 127.2 (CH), 126.4 (CH), 125.7 (CH), 125.4 (CH), 123.3 (CH), 123.3 (CH), 70.1 (CH-O), 41.8 (CH_2Ph), 21.8 (CH_3); MS: 290 (M^+, 29), 156 (13), 155(100), 154 (15), 153 (25), 152 (10), 91 (20). Exact Mass calcd. for $C_{20}H_{18}O_2$: 290.131; found: 290.131. Anal. calcd. for $C_{20}H_{18}O_2$: C 82.73, H 6.25; found: C 82.73, H 6.37.

1-(4-Methoxy-1-naphthyl)ethyl phenylacetate, ***12b***: Colourless oil; IR (neat): 3072–2936 (C-H), 1735 (C=O), 1586, 1294, 1245, 1195, 1096 cm^{-1}; ^{1}H NMR ($CDCl_3$) δ: 8.36–8.32 (m, 1H), 8.00–7.96 (m, 1H), 7.54–7.48 (m, 2H), 7.44 (d, 1H, $J = 7.9$ Hz), 7.36–7.26 (m, 5H), 6.77 (d, 1H, $J = 8.1$ Hz), 6.60 (q, 1H, $J = 6.6$ Hz), 4.00 (s, 3H), 3.68 (s, 2H), 1.70 (d, 3H, $J = 6.6$ Hz); ^{13}C NMR ($CDCl_3$) δ: 171.1 (C=O), 155.6 (*C*-OCH_3), 134.3 (C), 131.6 (C), 129.5 (CH), 129.1 (C), 128.7 (CH), 127.2 (CH), 127.0 (CH), 126.0 (C), 125.2 (CH), 124.1 (CH), 123.3 (CH), 122.9 (CH), 103.2 (CH), 70.3 (CH-O), 55.6 (OCH_3), 41.9 (CH_2Ph), 21.5 (CH_3); MS: 320 (M^+, 25), 186 (15), 185 (100), 184 (15), 169 (11), 141 (16), 136 (10), 115 (13), 92 (10), 91 (58), 65 (11). Exact Mass calcd. for $C_{21}H_{20}O_3$: 320.141; found: 320.141. Anal. calcd. for $C_{21}H_{20}O_3$: C 78.73, H 6.29; found: C 78.34, H 6.22.

1-(4,7-Dimethoxy-1-naphthyl)ethyl phenylacetate, ***12c***: Yellowish oil; ^{1}H NMR ($CDCl_3$) δ: 8.26 (d, 1H, $J = 9.2$ Hz), 7.46 (d, 1H, $J = 8.1$ Hz), 7.34–7.26 (m, 5H), 7.18 (s, 1H), 7.16 (d, 1H, $J = 9.2$ Hz), 6.66 (d, 1H, $J = 8.1$ Hz), 6.61 (q, 1H, 6.6 Hz), 3.98 (s, 3H, OCH_3), 3.79 (s, 3H, OCH_3), 3.69 (s, 2H, $PhCH_2$), 1.74 (d, 3H, $J = 6.6$ Hz); ^{13}C NMR ($CDCl_3$) δ: 171.3 (C=O), 158.4 (*C*-OCH_3), 155.8 (*C*-OCH_3), 134.1 (C), 133.2 (C), 129.4 (CH), 128.6 (CH), 127.5 (C), 127.3 (CH), 124.9 (CH), 124.5 (CH), 120.9 (C), 117.2 (CH), 102.1 (CH), 101.3 (CH), 70.0 (C-O), 55.5 (OCH_3), 55.2 (OCH_3), 41.8 (CH_2Ph), 20.5 (CH_3); MS: 350 (M^+, 26), 217 (12), 216 (13), 215 (78), 214 (10), 136 (31), 92 (21), 91 (100), 65 (13). Exact Mass calcd. for $C_{22}H_{22}O_4$: 350.152; found: 350.154. This ester was quite unstable and satisfactory elemental analysis could not be obtained.

1-(4-Cyano-1-naphthyl)ethyl phenylacetate, ***12d***: Colourless oil; IR (neat): 3075–2895 (C-H), 2224 (CN), 1739 (C=O), 1585, 1497, 1217, 1191, 1059 cm^{-1}; ^{1}H NMR ($CDCl_3$) δ: 8.27 (dd, 1H, $J = 7.9$ Hz, $J = 1.2$ Hz), 8.08 (dd, 1H, $J = 7.8$ Hz, $J = 1.1$ Hz), 7.82 (d, 1H, $J = 7.6$ Hz), 7.72–7.58 (m, 2H), 7.44 (d, 1H, $J = 7.6$ Hz), 7.37–7.26 (m, 5H), 6.63 (q, 1H, $J = 6.7$ Hz), 3.72 (s, 2H), 1.67 (d, 3H, $J = 6.7$ Hz); ^{13}C NMR ($CDCl_3$) δ: 170.6 (C=O), 143.7 (C), 133.6 (C), 132.6 (C), 132.3 (CH), 129.7 (C), 129.3 (CH), 128.7 (CH), 128.4 (CH), 127.9(CH), 127.3 (CH), 126.1(CH), 123.7(CH), 121.9 (CH), 117.8 (CN), 110.3 (*C*-CN), 69.4 (C-O), 41.7 (CH_2Ph), 21.9 (CH_3); MS: 315 (M^+, 24), 181 (13), 180 (100), 178 (11), 153 (19), 152 (12), 91 (41), 65 (11). Exact Mass calcd. for $C_{21}H_{17}NO_2$: 315.126; found: 315.126. Anal. calcd. for $C_{21}H_{17}NO_2$: C 79.97, H 5.44; found: C 79.51, H 5.57.

Preparative photolyses
For each photolysis, 300–400 mg of the ester was dissolved in 420 mL of sodium-distilled methanol. The solution, in an immersion well, was purged with nitrogen for 15 min before and during the irradiation. A Pyrex-filtered 200 W medium-pressure Hanovia mercury lamp was used as the light source. The progress of the reaction was monitored by HPLC using a mixed solvent of methanol and doubly distilled water (90:10). Irradiation was stopped when more than 90% of the ester was consumed. The solution was then concentrated under reduced pressure to ~10 mL, and water (20 mL) was added. The aqueous solution was extracted with dichloromethane (3×25 mL). The dichloromethane layer was washed with 5% sodium hydroxide (2 × 25 mL) and evaporated under reduced pressure

to give the photoproduct mixture. The aqueous alkaline layer was acidified with concentrated hydrochloric acid and extracted with dichloromethane (2 × 25 mL). Evaporation of the solvent gave phenylacetic acid.

Characterization of the photoproducts

The photoproducts were isolated by column chromatography and identified by ^1H and ^{13}C NMR and GC–MS.

1-(1-Naphthyl)ethyl methyl ethers, ***13***

X = H, ***13a***: ^1H NMR ($CDCl_3$) δ: 8.25–8.20 (m, 1H), 7.94–7.88 (m, 1H), 7.82 (d, 1H, J = 8.1 Hz), 7.58 (d, 1H, J = 10.7 Hz), 7.63–7.49 (m, 3H), 5.10 (q, 1H, J = 6.6 Hz), 3.36 (s, 3H), 1.66 (d, 3H, J = 6.4 Hz); ^{13}C NMR ($CDCl_3$) δ: 139.1 (C), 134.0 (C), 130.9 (C), 129.0 (CH), 127.9 (CH), 126.1 (CH), 125.9 (CH), 125.6 (CH), 125.5 (CH), 123.4 (CH); GC–MS, R_t = 11.0 min, 186 ($M^{+\cdot}$, 15), 172 (12), 171 (100), 156 (12), 155 (28), 153 (15), 152 (12), 128 (47), 127 (29), 63 (10).

X = 4-OCH$_3$, ***13b***: ^1H NMR ($CDCl_3$) δ: 8.32 (d, 1H, J = 9.5 Hz), 8.14 (d, 1H, J = 9.5 Hz), 7.52–7.45 (m, 2H), 7.43 (d, 1H, J = 8.3 Hz), 6.77 (d, 1H, J = 8.3 Hz), 4.96 (q, 1H, J = 7.7 Hz), 3.94 (s, 3H), 3.29 (s, 3H), 1.60 (d, 3H, J = 7.7 Hz); GC–MS, R_t = 12.6 min, 216 ($M^{+\cdot}$, 16), 202 (14), 201 (100), 186 (25), 185 (50), 141 (22), 115 (39).

X = 4-CN, ***13d***: ^1H NMR ($CDCl_3$) δ: 8.43–8.07 (m, 2H), 7.94 (d, 1H, J = 7.2 Hz), 7.83–7.60 (m, 1H), 7.62 (d, 1H, J = 7.2 Hz), 7.34–7.15 (m, 1H), 5.10 (q, 1H, J = 6.6 Hz), 3.32 (s, 3H), 1.57 (d, 3H, J = 7.2 Hz); GC–MS, R_t = 13.3 min, 211 ($M^{+\cdot}$, 16), 197 (12), 196 (100), 180 (15), 153 (25), 152 (15).

2-(1-Naphthyl)-1-phenylpropanes, ***14***

X = H, ***14a***: ^1H NMR ($CDCl_3$) δ: 8.19 (d, 1H, J = 8.1 Hz), 7.88 (dd, 1H, J = 7.3 Hz, 2.0 Hz), 7.74 (dd, 1H, J = 7.0 Hz, 2.3 Hz), 7.57–7.43 (m, 4H), 7.32–7.20 (m, 5H), 3.95–3.84 (m, 1H), 3.21 (dd, 1H, J = 13.4 Hz, 4.9 Hz), 2.85 (dd, 1H, J = 13.4, 9.3 Hz), 1.36 (d, 3H, 6.9 Hz); GC–MS, R_t = 15.0 min, 246 ($M^{+\cdot}$, 10), 156 (13), 155 (100), 153 (21), 152 (11), 128 (10), 115 (10), 91 (12), 65 (10).

X = 4-OCH$_3$, ***14b***: ^1H NMR ($CDCl_3$) δ: 8.51–8.37 (m, 1H), 8.26–8.12 (m, 1H), 7.68–7.49 (m, 3H), 7.44–7.09 (m, 5H), 6.84 (d, 1H, J = 10.0 Hz), 4.06 (s, 3H), 3.36–3.19 (m, 1H), 3.04–2.80 (m, 2H), 1.42 (d, 3H, J = 7.5 Hz); GC–MS, R_t = 16.8 min, 276 ($M^{+\cdot}$, 25), 262 (21), 261 (100), 245 (14), 202 (10), 91 (20).

X = 4,7-Di-OCH$_3$, ***14c***: ^1H NMR ($CDCl_3$) δ: 8.27 (d, 1H, J = 9.2 Hz), 7.39–7.14 (m, 8H), 6.70 (d, 1H, J = 8.1 Hz), 3.99 (s, 3H), 3.95 (s, 3H), 3.78-3.64 (m, 1H), 3.19 (dd, 1H, J = 13.3 and 4.9 Hz), 2.82 (dd, 1H, J = 13.3 and 9.2 Hz), 1.36 (d, 3H, J = 6.9 Hz); GC–MS, R_t = 21.6 min, 306 ($M^{+\cdot}$, 7), 216 (15), 215 (100), 200 (6), 184 (8), 91 (8).

X = 4-CN, ***14d***: ^1H NMR ($CDCl_3$) δ: 8.44–8.16 (m, 2H), 7.88 (d, 1H, J = 6.6 Hz), 7.79–7.54 (m, 2H), 7.45 (d, 1H, J = 6.6 Hz), 7.35–7.11 (m, 5H), 4.20–3.77 (m, 1H), 3.22–2.86 (m, 2H), 1.40 (d, 3H, J = 6.6 Hz); GC–MS, R_t = 20.1 min, 271 ($M^{+\cdot}$, 29), 181 (13), 180 (100), 153 (15), 152 (10), 91 (30).

Quantitative photolyses

The procedure for the quantitative photolysis was the same as that for the preparative photolysis. However, less than 50% of the starting material was converted into the products. The amount of the esters used for these analyses was 100–200 mg. A standard solution of each photoproduct was prepared using products that were previously isolated from the preparative photolysis. The photolysis samples and standards were analyzed by HPLC and the areas under the peaks of the photolysis samples were compared with those of the standards.

Method of ^{18}O isotope exchange

As an ^{18}O isotope source, ~10% ^{18}O-enriched water (Aldrich) was used. The following procedure is for the preparation of labelled 4-methoxy-1-naphthaldehyde.

In a 3-necked flask, the aldehyde (8.06 mmol) was dissolved in dioxane (10 mL), which had been purified by passing through a neutral alumina column. ^{18}O-labelled water (1.0 g, 55 mmol) was then added. The progress of ^{18}O isotope incorporation was monitored by GC–MS. The solvent was then evaporated under reduced pressure and dichloromethane (20 mL) was added. This solution was dried over anhydrous magnesium sulfate. The ^{18}O-labelled aldehyde was then purified (6.72 mmol, 83.3% yield) by chromatography on silica gel.

Preparation of ^{18}O-labelled esters

The ^{18}O-labelled aldehydes were used to prepare the esters by the same procedure as for the unlabelled esters.

Photolyses of ^{18}O-labelled esters and analytical determination of ^{18}O exchange

The ^{18}O exchange between the alcohol oxygen and the carbonyl oxygens of the esters was determined by analyzing the amount of ^{18}O incorporated in each oxygen. The labelled esters were photolyzed until ~50% of the starting material was converted into photoproducts. The same work-up procedure as that for preparative photolysis was done to obtain the photoproduct mixture. This mixture, containing the unreacted ester, was dissolved in anhydrous diethyl ether (10 mL) and excess lithium aluminum hydride was added. The mixture was then stirred at room temperature for 2 h. Saturated aqueous ether was then added dropwise to destroy any unreacted lithium aluminum hydride. The mixture was then filtered to remove the precipitate of lithium and aluminum hydroxides. The ether filtrate was washed with water and dried over anhydrous magnesium sulfate.

The ether layer was analyzed by GC–MS. The retention times of the two alcohols, substituted 1-(1-naphthyl)ethanol and 2-phenylethanol, were obtained using the standard GC–MS method. More accurate values of peak intensities were then obtained using "Selected Ion Monitoring (SIM)." The peaks corresponding to the two alcohols were analyzed and the amount of ^{18}O isotope was determined by the intensities of the ($M^{+\cdot}$, M + 1, M + 2) ions, taking five scans across the chromatographic peak. The numbers obtained from the GC–MS results were corrected to those reported here using a program that corrects for the natural abundance of all isotopes of the molecular formula.

Can. J. Chem. Downloaded from www.nrcresearchpress.com by 80.90.12.36 on 09/08/12
For personal use only.

Photolyses of optically active esters and determination of optical activities of the unreacted esters

Optically active ester (200–300 mg) was dissolved in 420 mL of sodium-distilled methanol and photolyzed until ~50% of starting material was consumed. The solution was concentrated and the carboxylic acid produced was separated by using simple extraction with 5% sodium hydroxide. The unreacted ester was isolated using column chromatography. The optical activity of these samples was measured using a Perkin–Elmer 141 polarimeter at 589 nm at room temperature. The average value from three readings is reported in Table 2.

Acknowledgements

This research was supported by a grant from the Natural Sciences and Engineering Research Council of Canada. J. M. Kim thanks the Dalhousie University Faculty of Graduate Studies for a fellowship. We thank G. Fallows and B. Ngai for some preliminary experiments and Professor J. S. Grossert for assistance with the mass spectrometry and for helpful discussions.

References

1. D.P. DeCosta and J.A. Pincock. J. Am. Chem. Soc. **115**, 2180 (1993).
2. J.W. Hilborn and J.A. Pincock. J. Am. Chem. Soc. **113**, 2683 (1991).
3. J.W. Hilborn, E. MacKnight, J.A. Pincock, and P.J. Wedge. J. Am. Chem. Soc. **116**, 3337 (1994).
4. H.L. Goering, R.G. Briody, and G. Sandrock. J. Am. Chem. Soc. **92**, 7401 (1970).
5. D.A. Jaeger. J. Am. Chem. Soc. **97**, 902 (1975).
6. D.A. Jaeger and G.H. Angelos. Tetrahedron Lett. **22**, 803 (1981).
7. R.S. Givens and B. Matuszewski. J. Am. Chem. Soc. **97**, 5619 (1975).
8. R.S. Givens, B. Matuszewski, N. Levi, and D. Leung. J. Am. Chem. Soc. **99**, 1896 (1977).
9. H.C. Brown and P.V. Ramachandran. Acc. Chem. Res. **25**, 16 (1992).
10. M. Fujio, M. Goto, T. Susuki, I. Akasaka, M. Mishima, and Y. Tsuno. Bull. Chem. Soc. Jpn. **63**, 1146 (1990).
11. S.L. Murov, I. Carmichael, and G.L. Hug. Handbook of photochemistry. 2nd ed. Marcel Dekker, New York. 1993. p. 347.
12. V.K. Singh. Synthesis, 605 (1992).
13. T.L. Jacobs, S. Winstein, J.W. Ralls, and J.H. Robson. J. Org. Chem. **11**, 21 (1946).
14. L. Friedman and H. Shechter. J. Org. Chem. **26**, 2522, (1961).

Can. J. Chem. Downloaded from www.nrcresearchpress.com by 80.90.12.36 on 09/08/12
For personal use only.

Excess molar volumes and excess viscosities of ternary mixtures (2-butanol + 1-chlorobutane + 1-butylamine) and (2-methyl-2-propanol + 1-chlorobutane + 1-butylamine) at 298.15 K

M. Domínguez, A. Camacho, M.C. López, F.M. Royo, and J.S. Urieta

Can. J. Chem. Downloaded from www.nrcresearchpress.com by 80.90.12.36 on 09/08/12
For personal use only.

Abstract: Excess molar volumes and excess viscosities, at 298.15 K, of the ternary mixtures (2-butanol + 1-chlorobutane + 1-butylamine) and (2-methyl-2-propanol + 1-chlorobutane + 1-butylamine) and of the binary mixtures (2-butanol + 1-butylamine), (2-methyl-2-propanol + 1-butylamine), and (1-chlorobutane + 1-butylamine) have been measured. The ternary excess properties were fitted to the polynomial equation of Cibulka. The experimental results were also compared with those predicted by the empirical equations of Redlich–Kister, Tsao–Smith, Kohler, and Colinet.

Key words: binary and ternary mixtures, excess properties, 2-butanol, 2-methyl-2-propanol, 1-chlorobutane, 1-butylamine.

Résumé : Opérant à 298,15 K, on a mesuré les volumes molaires en excès et les viscosités en excès des mélanges ternaires (butan-2-ol + 1-chlorobutane + 1-butylamine) et (2-méthylpropan-2-ol + 1-chlorobutane + 1-butylamine) et des mélanges binaires (butan-2-ol + 1-butylamine), (2-méthylpropan-2-ol + 1-butylamine) et (1-chlorobutane + 1-butylamine). On a ajusté les propriétés ternaires en excès à l'aide de l'équation binaire de Cibulka. On a aussi comparé les résultats expérimentaux à ceux prédits par les équations empiriques de Redlich–Kister, Tsao–Smith, Kohler et Colinet.

Mots clés : mélanges binaires et ternaires, propriétés en excès, butan-2-ol, 2-méthylbutan-2-ol, 1-chlorobutane, 1-butylamine.

[Traduit par la rédaction]

Introduction

In previous papers we reported the determination of some excess thermodynamic properties of several binary mixtures containing either isomers of butanol or a haloalkane (1–7). In this work, in addition to the binary mixtures, the V^E and η^E of ternary mixtures have been measured at the temperature 298.15 K in order to study the interactions between the OH, NH_2, and Cl groups.

Experimental section

Materials

The liquids used, 2-butanol (better than 99.5 mol%), 2-methyl-2-propanol (better than 99.5 mol%), 1-chlorobutane (better than 99.0 mol%), and 1-butylamine (better than 99.0 mol%), were obtained from Aldrich. The purity of the chemicals was checked not only by comparing the measured densities and viscosities with those reported in the literature but also by gas chromatography using a semicapillary methyl silicone column (o.d. 530 μm) and a flame-ionization detector. Analysis showed that the major peak area exceeds 99.8%. No further purification was considered necessary. The butanols were dried over activated molecular sieve, type 0.3 nm from Merck. Table 1 shows the experimental values of density and viscosity for the pure components at 298.15 K compared with those found in the literature.

Methods

Densities, ρ, of the pure components and the binary and ternary mixtures were determined with an Anton Paar DMA-58 vibrating tube densimeter, calibrated with deionized doubly distilled water and dry air. The uncertainty for the density measurements was $\pm 1 \times 10^{-5}$ g cm^{-3}.

Viscosities, η, of the pure components and the binary and ternary mixtures were determined by using an Ubbelhode

Received December 12, 1994.

M. Domínguez, A. Camacho, M.C. López, F.M. Royo, and J.S. Urieta.[1] Departamento de Química Orgánica — Química Física, Facultad de Ciencias, Sección de Químicas, Universidad de Zaragoza, Ciudad universitaria, Zaragoza 50009, Spain.

[1] Author to whom correspondence may be addressed.

Can. J. Chem. Downloaded from www.nrcresearchpress.com by 80.90.12.36 on 09/08/12
For personal use only.

Table 1. Densities, ρ, and viscosities, η, of pure components at 298.15 K, and comparison with literature data.

	ρ (g cm^{-3})		η (cP)	
Component	This work	Literature	This work	Literature
2-Butanol	0.80239	0.80241 (8)	3.0804	2.9980 (8)
2-Methyl-2-propanol	0.78063	0.78120 (8)	4.4638	4.4380 (8)
1-Chlorobutane	0.88085	0.88085 (8)	0.4273	0.4260 (8)
1-Butylamine	0.73225	0.73300 (9)	0.4690	0.4700 (9)

Table 2. Coefficients A_p of eq. [1] and standard deviations (σ).

		A_0	A_1	A_2	A_3	σ
2-Butanol(1)	$^5V^E$	1.6390	−0.5502	0.3739	−0.6305	0.0036
+ 1-chlorobutane(2)	$^6\eta^E$	−4.1005	−2.8481	−2.5205	−1.5759	0.0110
2-Methyl-2-propanol(1)	$^5V^E$	2.7877	0.0395	1.0048	−0.3763	0.0045
+ 1-chlorobutane(2)	$^6\eta^E$	−6.9587	−5.9243	−6.2925	−4.1917	0.0190
2-Butanol(1)	V^E	−2.8500	0.1378	0.5102	0.2631	0.0027
+ 1-butylamine(3)	η^E	−3.1867	−2.1026	−1.4678	−0.7384	0.0061
2-Methyl-2-propanol(1)	V^E	−2.2708	−0.1113	0.0547	0.2332	0.0042
+ 1-butylamine(3)	η^E	−5.6661	−3.8529	−3.2408	−2.1003	0.0100
1-Chlorobutane(2)	V^E	1.0457	0.1288	0.0773	−0.0024	0.0024
+ 1-butylamine(3)	η^E	−0.0889	−0.0014	−0.0237	0.0220	0.0005

viscosimeter with a Schott-Geräte automatic measuring unit model AVS-440, for which the accuracy of the flow time measurement is ±0.01 s. Details of calibrations and procedures can be found in an earlier paper (3).

The compositions (mole fraction) of binary and ternary blends were determined directly by using a Mettler H20T balance. The uncertainty of the weighing was ±0.01 mg.

Results and discussion

The experimental results for the excess molar volumes and the excess viscosities of the binary mixtures (2-butanol + 1-butylamine), (2-methyl-2-propanol + 1-butylamine), and (1-chlorobutane + 1-butylamine) were fitted to a Redlich–Kister-type equation:

$$[1]\quad Y^E(x_i, x_j)/(\text{cm}^3\ \text{mol}^{-1}) = x_i x_j \sum_{p=0}^{p} A_p (x_i - x_j)^p$$

where $Y^E = V^E$ or η^E, x_i denotes the mole fraction of component i of an i,j mixture with $x_j = 1 - x_i$, and A_p are adjustable parameters by the unweighted least-squares method. In previous papers we determined the V^E and η^E of (alkanol + 1-chlorobutane) mixtures (5, 6). The coefficients A_p and the standard deviations are given in Table 2.

The excess molar volume and excess viscosity data for the binary mixtures are plotted in Figs. 1 and 2.

The excess molar volumes and excess viscosities for the ternary mixtures were fitted to the polynomial equation proposed by Cibulka (10):

$$[2]\quad Y^E_{123} = Y^E_{12} + Y^E_{13} + Y^E_{23} + x_1x_2x_3(B_1 + B_2x_1 + B_3x_2)$$

where Y^E_{ij} is the contribution to the excess property for the binary system i,j given by eq. [1]. The B_i parameters were calculated by the least-squares method. Table 3 presents the values of the B_i coefficients of eq. [2] and the corresponding standard deviations, σ, for the ternary systems. Curves of constant V^E_{123} and η^E_{123} for the ternary systems have been plotted in Figs. 3 and 4.

Also V^E and η^E for the ternary systems have been calculated using the empirical equations proposed by Redlich–Kister, Tsao–Smith, Kohler, and Colinet, which take only the binary contributions into account.

Redlich and Kister (11) proposed an expression to determine any excess property of a ternary mixture:

$$[3]\quad Y^E_{123} = x_1x_2\sum_{\nu=0}^{r}(Av)_{12}(x_1 - x_2)^\nu + x_1x_3\sum_{\nu=0}^{r}(Av)_{13}(x_1 - x_3)^\nu + x_2x_3\sum_{\nu=0}^{r}(Av)_{23}(x_2 - x_3)^\nu$$

where x_i is the mole fraction of component i, and $(Av)_{ij}$ are adjustable coefficients for the binary mixture i,j obtained by the least-squares method.

Tsao and Smith (12) proposed an equation for predicting the excess properties of a ternary mixture:

$$[4]\quad Y^E_{123} = x_2(1 - x_1)^{-1}Y^E_{12} + x_3(1 - x_1)^{-1}Y^E_{13} + (1 - x_1)Y^E_{23}$$

Can. J. Chem. Downloaded from www.nrcresearchpress.com by 80.90.12.36 on 09/08/12
For personal use only.

Fig. 1. Excess molar volumes V^E of binary mixtures at 298.15 K; 2-butanol + 1-butylamine (△), 2-methyl-2-propanol + 1-butylamine (□), and 1-chlorobutane + 1-butylamine (▲).

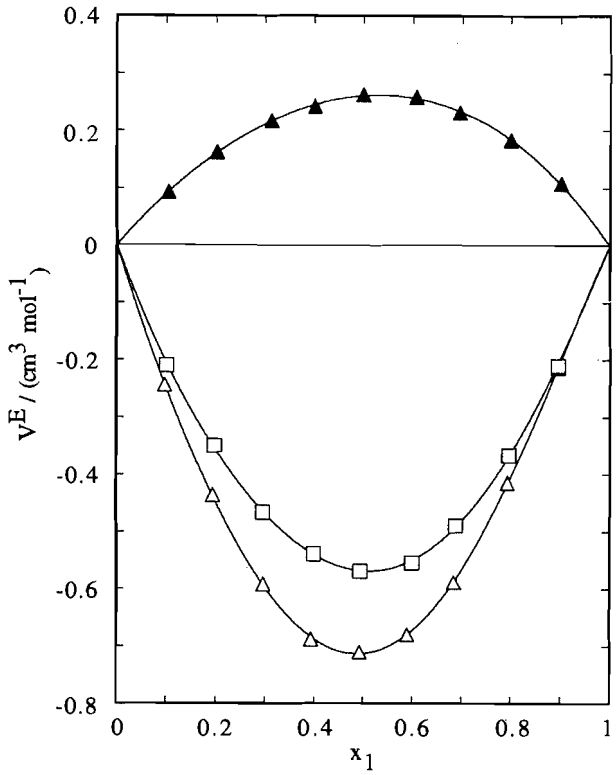

Fig. 2. Excess viscosities η^E of binary mixtures at 298.15 K; 2-butanol + 1-butylamine (△), 2-methyl-2-propanol + 1-butylamine (□), and 1-chlorobutane + 1-butylamine (▲).

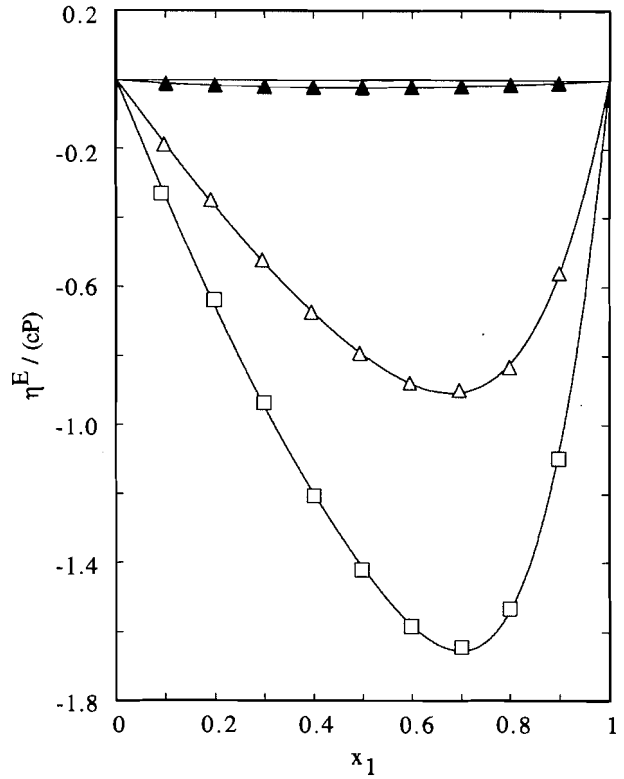

in which x_i is the mole fraction of component i, and Y_{ij}^E refers to the excess properties for the binary mixtures at compositions (x_i^0, x_j^0) such that $x_i^0 = x_1$ for the 1,2 and 1,3 binary systems and $x_j^0 = x_2/(x_2 + x_3)$ for the 2,3 binary system.

Kohler (13) proposed an equation for the excess properties of mixing of a ternary solution:

$$[5] \quad Y_{123}^E = (x_1 + x_2)^2 Y_{12}^E + (x_1 + x_3)^2 Y_{13}^E + (x_2 + x_3)^2 Y_{23}^E$$

in which x_i is the mole fraction of component i, and Y_{ij}^E refers to the excess property of the binary mixtures at a composition (x_i^0, x_j^0) such that $x_i^0 = 1 - x_j^0 = x_i/(x_i + x_j)$.

Coliner (14) established a slightly more complex relationship for expressing the thermodynamic excess properties of multicomponent systems:

$$[6a] \quad Y_{1,2\ldots n}^E = 0.5 \sum_{i=1}^{n-1} \sum_{j>1}^{n} x_i (1 - x_j)^{-1} (Y_{ij}^E)_{xj}$$

in which x_i is the mole fraction of component i, and Y_{ij}^E are calculated from the binary data at constant mole fraction x_j. This equation, although perfectly symmetrical, requires the addition of the thermodynamic properties at six different binary compositions for a ternary solution. In this way the following equation is obtained:

$$[6b] \quad Y_{123}^E = 0.5 \left[\frac{x_2}{1 - x_1} Y_{12}^E(x_1, 1 - x_1) + \frac{x_1}{1 - x_2} Y_{12}^E(1 - x_2, x_2) + \frac{x_3}{1 - x_1} Y_{13}^E(x_1, 1 - x_1) + \frac{x_1}{1 - x_3} Y_{13}^E(1 - x_3, x_3) + \frac{x_3}{1 - x_2} Y_{23}^E(x_2, 1 - x_2) + \frac{x_2}{1 - x_3} Y_{23}^E(1 - x_3, x_3) \right]$$

Table 4 presents the values of standard deviations, σ, of eqs. [3], [4], [5] and [6*b*] for the ternary systems.

The results of V^E for binary mixtures (2-butanol + 1-butylamine) and (2-methyl-2-propanol + 1-butylamine) are negative over the entire composition range, whereas for the system (1-chlorobutane + 1-butylamine) the V^E are positive over the entire composition range. The experimental ternary excess volumes are negative over the whole composition range except for mixtures with a high mole fraction of chlorinated compound for which V_{123}^E shows positive values. The diagrams showing the excess properties for the ternary systems (Figs. 3*a*, 3*b* and 4*a*, 4*b*) have the same shape, although the more negative values appear for the ternary system with 2-methyl-2-propanol.

In view of the results included in Tables 3 and 4 it can be observed that only the V^E obtained by applying the Cibulka equation fit the experimental values. The equations of Redlich–Kister (11), Tsao–Smith (12), Kohler (13), and Colinet (14) (which take only binary contributions into ac-

Table 3. Coefficients B_i for Cibulka equation [2] and standard deviations, σ, in estimating excess molar volumes V^E (cm^3 mol^{-1}) and excess viscosities η^E (cP) for ternary mixtures at 298.15 K.

Ternary mixture		B_1	B_2	B_3	σ
2-Butanol(1) + 1-chlorobutane(2)	V^E	−2.2617	−3.9224	−12.7209	0.009 11
+ 1-butylamine(3)	η^E	1.2833	10.2115	0.5880	0.015 09
2-Methyl-2-propanol(1)	V^E	−0.8242	−10.2172	−14.7702	0.012 46
+ 1-chlorobutane(2) + 1-butylamine(3)	η^E	2.0750	22.2768	0.2318	0.016 64

Can. J. Chem. Downloaded from www.nrcresearchpress.com by 80.90.12.36 on 09/08/12
For personal use only.

Fig. 3. Curves of constant V^E_{123} (cm^3 mol^{-1}) of ternary systems: (*a*) 2-butanol(1) + 1-chlorobutane(2) + 1-butylamine(3); (*b*) 2-methyl-2-propanol(1) + 1-chlorobutane(2) + 1-butylamine(3).

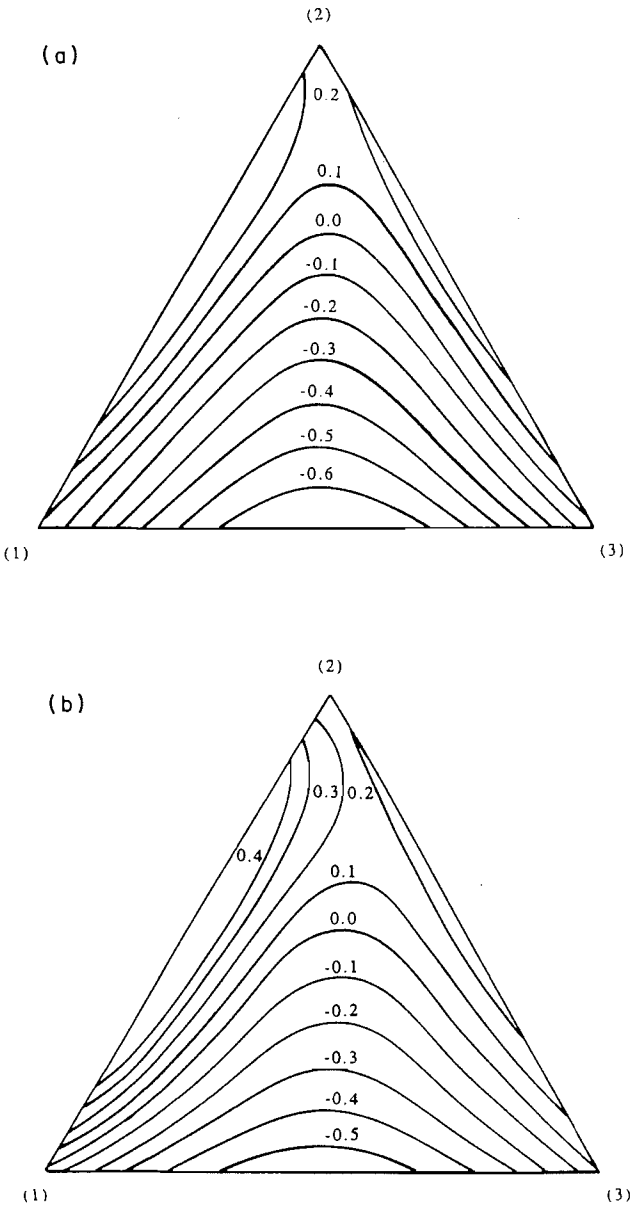

Fig. 4. Curves of constant η^E_{123} (centipoise) of ternary systems: (*a*) 2-butanol(1) + 1-chlorobutane(2) + 1-butylamine(3); (*b*) 2-methyl-2-propanol(1) + 1-chlorobutane(2) + 1-butylamine(3).

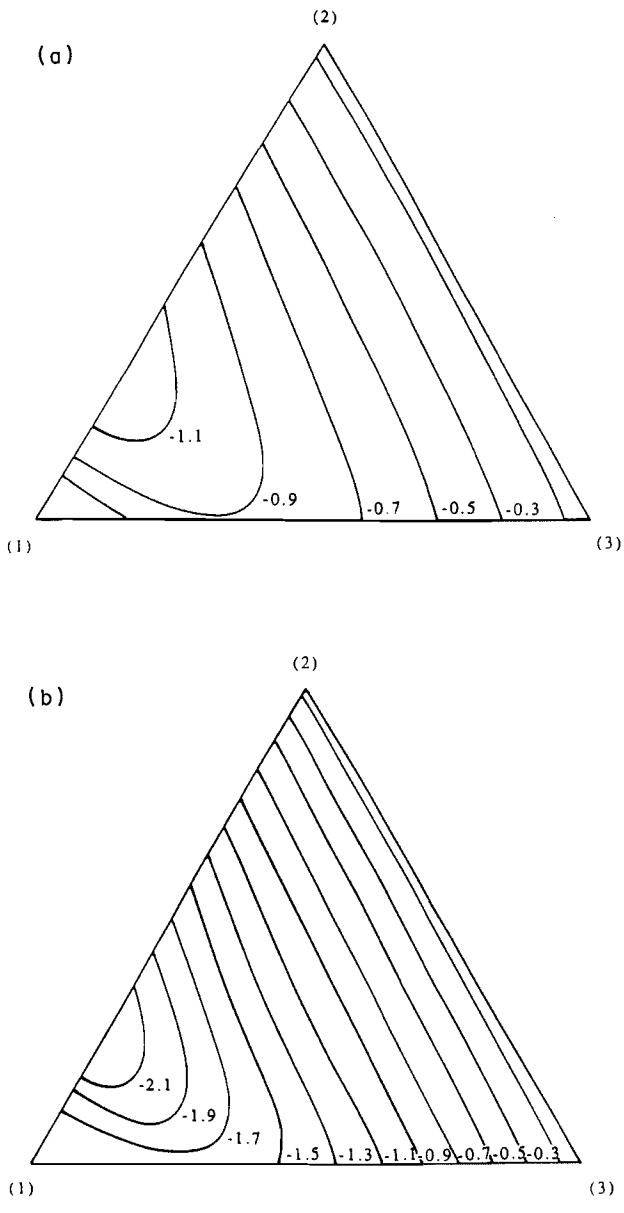

Table 4. Standard deviations, σ, of eqs. [3], [4], [5], and [6*b*] in estimating excess molar volumes V^E (cm^3 mol^{-1}) and excess viscosities η^E (cP) for ternary mixtures at 298.15 K.

Ternary system		σ			
		Eq. [3] Redlich–Kister	Eq. [4] Tsao–Smith	Eq. [5] Kohler	Eq. [6*b*] Colinet
2-Butanol(1) + 1-chlorobutane(2)	V^E	0.168 15	0.224 34	0.176 78	0.177 59
+ 1-butylamine(3)	η^E	0.108 08	0.014 47	0.147 71	0.135 41
2-Methyl-2-propanol(1) + 1-chlorobutane(2)	V^E	0.198 91	0.245 80	0.205 22	0.206 50
+ 1-butylamine(3)	η^E	0.212 67	0.033 39	0.304 71	0.278 79

Can. J. Chem. Downloaded from www.nrcresearchpress.com by 80.90.12.36 on 09/08/12
For personal use only.

count) predict V^E values that are quite different from the experimental ones for the ternary mixtures (2-butanol + 1-chlorobutane + 1-butylamine) and (2-methyl-2-propanol + 1-chlorobutane + 1-butylamine); consequently the existence of strong interactions between OH–Cl–NH_2 groups in the ternary systems under study could be deduced. On the other hand, both the Cibulka equation and that of Tsao–Smith lead to good agreement with experimental values of η^E, as can be seen in Tables 3 and 4. These results tally with those reported by M.J. Souza et al. (15).

Knowing that V^E is the result of a sum of several effects, chemical, structural, and physical, these values would represent the breaking of the associated species formed through hydrogen bonds (namely, cyclic and noncyclic multimers in alkanols and noncyclic trimers in the amine (16)), and the subsequent formation of bonds of the same type between OH and NH_2 groups, processes that will yield a greater packing of molecules and therefore a negative excess volume for the mixture (alkanol + 1-butylamine). On the contrary, if a nonassociated compound (such as a chlorinated derivative) is added to the alkanols or the amine, the forceful association of these compounds is broken in such a way that an increase in disorder takes place, making the excess volume values positive. This same argument can be applicable to the V^E of ternary mixtures. Thus, the smaller the ratio of the chlorinated derivative, the more negative V^E will be, and in the reverse manner, an increase in the amount of 1-chlorobutane will be accompanied by a destruction of hydrogen bonds and a rise in excess volume that will become positive in the zone corresponding to a high mole fraction of chlorinated compound and low mole fractions for the other two components. On the other hand, the V^E values obtained for the ternary system with 2-butanol (secondary alkanol) are more negative than those obtained with 2-methyl-2-propanol (tertiary alkanol). This can be justified by means of structural effects. In fact, the ratio of cyclic multimers is larger in 2-methyl-2-propanol than in 2-butanol (17). Moreover, according to electrical information (18), the conversion from linear multimers to cyclic structures (with lower dipole moments) is more extensive for 2-methyl-2-propanol than for the other isomers of butanol. This could explain the volumetric behaviour of mixtures containing 2-methyl-2-propanol, assuming that linear structures occupy a smaller volume than the cyclic ones. Thus, the highest V^E values are expected for those systems in which 2-methyl-2-propanol is included.

The η^E obtained for the binary systems (alkanol + 1-butylamine) and (1-chlorobutane + 1-butylamine) are negative over the whole composition range; these results agree with those provided by Ramanjaneyulu et al. (19) for mixtures of (1-butylamine + cyclic hydrocarbons). The η^E obtained for the ternary systems studied are negative throughout, as well.

A negative excess viscosity indicates a greater facility to flow for the real mixture with respect to the ideal behaviour. This occurs when interactions between the molecules are stronger for the pure compounds than for their mixtures. In our case, the experimental results would suggest that interaction between different functional groups is weaker than that existing between identical groups (OH–OH and NH_2–NH_2). η^E is very close to zero for the mixture (1-chlorobutane + 1-butylamine). This would be caused by the interactions Cl–NH_2 (20), which would compensate for the breaking of hydrogen bonds in the amine. A remarkable asymmetrical distribution can be observed in the ternary mixtures. This distribution could be explained by the character of 1-chlorobutane as a breaker of structures, namely, of the hydrogen bonds of alcoholic and aminic components. The more negative η^E shown by 2-methyl-2-propanol might be a consequence of the greater facility for breaking of its multimers compared to that of mixtures containing 2-butanol.

References

1. J. Pardo, V. Rodríguez, M.C. López, F.M. Royo, and J.S. Urieta. J. Chem. Thermodyn. **17**, 371 (1985).
2. C. Lafuente, J. Pardo, V. Rodríguez, F.M. Royo, and J.S. Urieta. J. Chem. Eng. Data, **38**, 554 (1993).
3. D. Blasco, C. Lafuente, J. Santafé, F.M. Royo, and J.S. Urieta. Thermochim. Acta, **55**, 230 (1993).
4. P. Pérez, M. Gracia, and C. Gutiérrez Losa. J. Chem. Thermodyn. **17**, 1067 (1985).
5. H. Artigas, J. Santafé, M.C. López, F.M. Royo, and J.S. Urieta. J. Chem. Thermodyn. **25**, 1 (1993).
6. H. Artigas. Doctoral Thesis, Universidad de Zaragoza, España. 1995.
7. P. Cea, C. Lafuente, H. Artigas, F.M. Royo, and J.S. Urieta. Can. J. Chem. **72**, 1921 (1994).
8. J.A. Riddick, N.B. Bunger, and T. Sakano. Organic solvents. 4th ed. Wiley–Interscience, New York. 1986.
9. F. Davolio, C.R. de Schaefer, M.F. Ruiz Holgado, and M. Katz. J. Solution Chem. **19**, 1085 (1990).
10. I. Cibulka. Collect. Czech. Chem. Commun. **47**, 1414 (1982).
11. O. Redlich and A.T. Kister. Ind. Eng. Chem. **40**, 345 (1948).
12. C.C. Tsao and J.M. Smith. Chem. Eng. Prog. Symp. Ser. **49**, 107 (1953).
13. F. Kohler. Monatsh. Chem. **91**, 738 (1960).

14. C. Colinet. Thesis, University of Grenoble, France. 1967.
15. M.J. Souza, E. Jiménez, J.L. Legido, J. Fernández, E. Pérez Martell, and M.I. Paz Andrade. J. Chem. Thermodyn. **24**, 119 (1992).
16. J.C. Schug and W.E. Chang. J. Phys. Chem. **75**, 938 (1971).
17. R.H. Stokes. Chem. Soc. Rev. **11**, 257 (1982).
18. C.J.F. Böttcher. Theory of electric polarization. Elsevier, Amsterdam. 1973. p. 277.
19. K. Ramanjaneyulu, A.C. Chandrasekhar, P. Venkateswarlu, and A. Kirshnaiah. Phys. Chem. Liq. **16**, 217 (1987).
20. L. Inés Acevedo and M. Katz. J. Solution Chem. **19**, 1041 (1990).

Can. J. Chem. Downloaded from www.nrcresearchpress.com by 80.90.12.36 on 09/08/12
For personal use only.

Cyclometallation of bis(diphenylphosphino)methane ligands on a binuclear ruthenium(0) carbonyl complex

Hameed A. Mirza, Jagadese J. Vittal, and Richard J. Puddephatt

Abstract: The first example of simple orthometallation of a bis(diphenylphosphino)methane ligand at a binuclear centre is reported. Both dppm ligands of the binuclear ruthenium(0) complex $[Ru_2(CO)_5(\mu\text{-dppm})_2]$, **1**, are orthometallated when the complex is heated in benzene solution to yield the unusual complex $[Ru_2(CO)_4(Ph_2PCH_2PPhC_6H_4)_2]$, **2**. The structure of **2** was determined crystallographically (monoclinic, $P2_1/n$, a = 21.349(4), b = 12.209(5), c = 22.457(5) Å, β = 104.34(2)°, Z = 4, R, R_w = 0.0658, 0.0561) and the unusual cyclometallated complex was also characterized spectroscopically. The cyclometallation occurs in such a way that each ligand gives rise to two fused five-membered rings, RuRuPCP and RuRuPCC, fused at the Ru—Ru and Ru—P bonds.

Key words: ruthenium, bis(diphenylphosphino)methane, metallation.

Résumé : On rapporte le préparation du premier exemple d'une orthométallation simple d'un coordinat bis(diphénylphosphino)méthane à un centre binucléaire. Il se produit une orthométallation des deux coordinats dppm du complexe binucléaire du ruthénium(0) $[Ru_2(CO)_5(\mu\text{-dppm})_2]$, **1**, lorsqu'on chauffe le complexe en solution dans le benzène et il y a formation du complexe inhabituel $[Ru_2(CO)_4(Ph_2PCH_2PPhC_6H_4)_2]$, **2**. On a en déterminé la structure par diffraction des rayons X (monoclinique, $P2_1/n$, a = 21,349(4), b = 12,209(5) et c = 22,457(5) Å, β = 104,34(2)°, Z = 4, R = 0,0658 et R_w = 0,0561) et on a aussi caractérisé le complexe inhabituel cyclométallé par spectroscopie. La cyclométallation se produit d'une telle façon que chaque coordinate donne lieu à deux cycles condensés à cinq chaînons, RuRuPCP et RuRuPCC, condensés au niveau des liaisons Ru—Ru et Ru—P.

Mots clés : ruthénium, bis(diphénylphosphino)méthane, métallation.

[Traduit par la rédaction]

Introduction

Diphosphine ligands such as bis(diphenylphosphino)methane, dppm, are well known to stabilize and maintain the integrity of the metallic frameworks in binuclear or cluster complexes during chemical transformations (1). However, under forcing conditions, these ligands can be involved in C—P and (or) C—H bond cleavage reactions, thus forming phosphido (1, 2) and cyclometallated (3–5) complexes, respectively. Phosphido complexes may be formed by cleavage of either P—CH_2 or P—Ph bonds and cyclometallated complexes by activation of a C—H bond of either the CH_2 group or a phenyl group of a dppm ligand (1–5). Cyclometallation by activation of an *ortho* C—H bond of a phenyl substituent of a phenylphosphorus group constitutes an important example of orthometallation, a reaction that is very useful in metal–carbon bond-forming reactions with applications in both organometallic and organic synthesis (6). There are many examples of orthometallation of monodentate tertiary phosphine ligands such as PPh_3 (6, 7), but a much smaller number with diphosphine ligands (3–5, 8).

Because orthometallation of an arylphosphine at a mononuclear centre generates a strained four-membered MPCC ring, **A**, the reactions may be less favourable than in binuclear or cluster complexes where the stable five-membered rings, **B**, are found, for example, in the products of orthometallation of triphenylphosphine on binuclear rhodium complexes (6, 7). An excellent example of a reaction in which rearrangement of a mononuclear to binuclear complex occurs is found in the thermolysis of the mononuclear platinum complex [Pt(OH)(Me)(dppe)], dppe = $Ph_2PCH_2CH_2PPh_2$, to give the binuclear complex $[Pt_2(Ph_2PCH_2CH_2PPhC_6H_4)_2]$, containing the favourable five-membered MMPCC ring in **C** (8). Similar reactions with dppm are not known. There appears to be only one example of simple orthometallation of a dppm ligand, which occurs in the thermolysis of $[Os_3(CO)_{10}(dppm)]$ to give $[Os_3(CO)_8(\mu\text{-H})(Ph_2PCH_2PPhC_6H_4)]$ containing the functional group **D** (3). It is likely that similar reactions occur in other cluster complexes of dppm but the metal hydride formed combines with a phenyl substituent to eliminate benzene and so yield orthometallated phosphido ligands (4). For example, thermolysis of $[Ru_3(CO)_{10}(dppm)]$ gives binuclear and trinuclear complexes containing the functional groups **E** and **F**,

Received August 10, 1994.

This article is dedicated to Professor William A.G. Graham on the occasion of his 65th birthday.

H.A. Mirza, J.J. Vittal, and R.J. Puddephatt.[1] Department of Chemistry, University of Western Ontario, London, ON N6A 5B7, Canada.

[1]Author to whom correspondence may be addressed. Telephone: (519) 679-2111, ext. 6336. Fax: (519) 661-3022. E-mail: rpuddeph@uwovax

Can. J. Chem. Downloaded from www.nrcresearchpress.com by 80.90.12.36 on 09/08/12
For personal use only.

Can. J. Chem. Downloaded from www.nrcresearchpress.com by 80.90.12.36 on 09/08/12
For personal use only.

Fig. 1. A view of the structure of complex **2**. H-atoms are not shown.

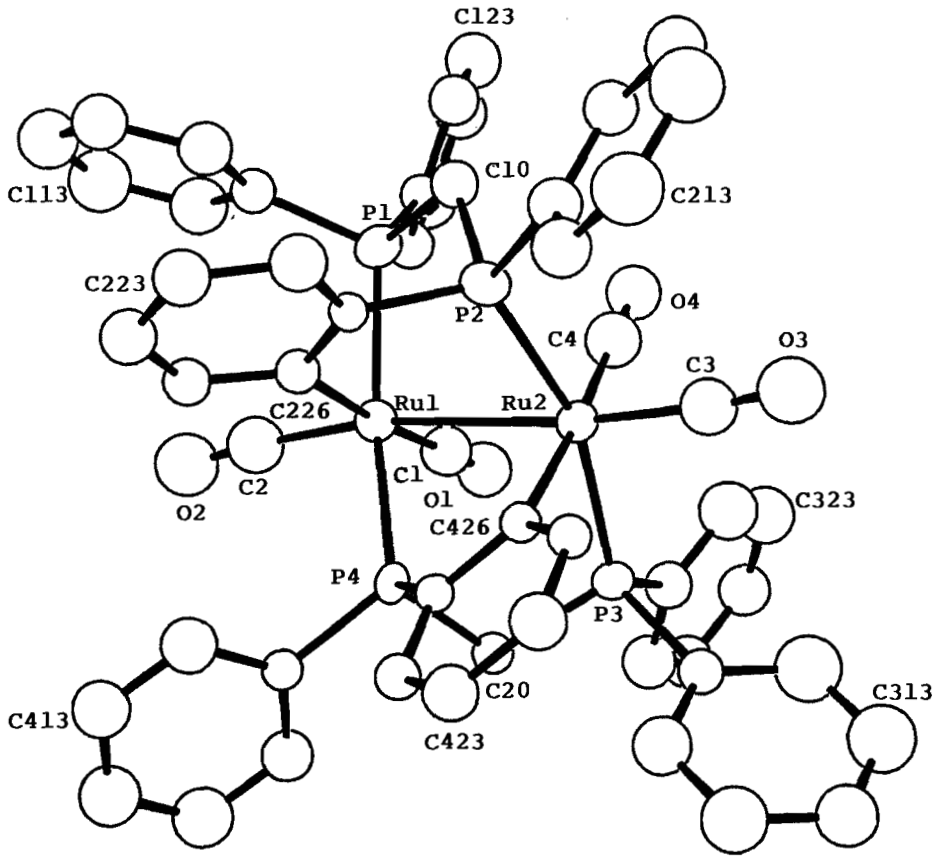

respectively (4). Although a very large number of binuclear dppm complexes have been studied, there appear to be no reported examples of simple orthometallation reactions at a binuclear centre (1–4). Instead, P—CH_2, P—Ph, or P_2CH—H bond activation reactions occur either alone in or in combination with orthometallation (1–4).

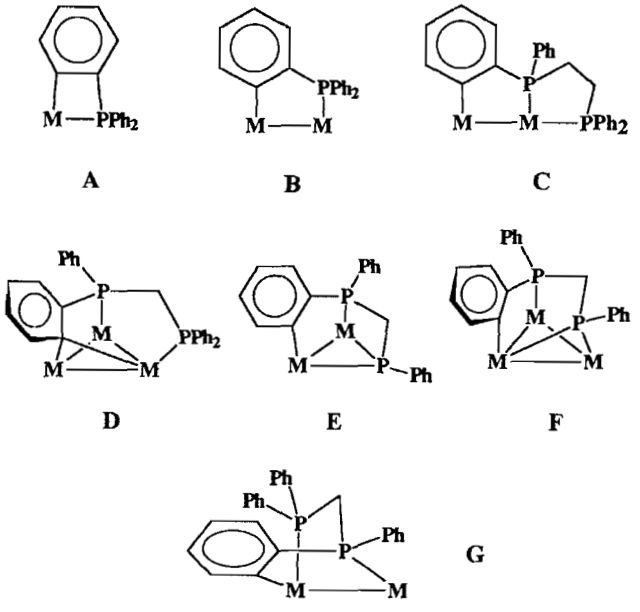

This article reports the first example of simple orthometallation of a dppm ($Ph_2PCH_2PPh_2$) ligand at a binuclear centre to give the functional grouping **G**. In fact, both dppm ligands of the binuclear ruthenium(0) complex $[Ru_2(CO)_5(\mu\text{-dppm})_2]$, **1**, are orthometallated. The functional group **G** has recently been reported in two tetraruthenium clusters prepared, in each case as a component of a very complex mixture of products, by reaction of $[Ru_3(CO)_{10}(\mu\text{-dppm})]$ with the alkyne $MeO_2CC{\equiv}CCO_2Me$ and with benzyl bromide (6).

Results

Synthesis of the cyclometallated complex

When a solution of $[Ru_2(CO)_5(\mu\text{-dppm})_2]$, **1**, was heated under reflux in benzene under a nitrogen atmosphere for a period of 3 days, a dark orange-brown solution was obtained, from which the yellow crystalline product $[Ru_2(CO)_4(Ph_2PCH_2PPhC_6H_4)_2]$, **2**, was isolated in 45% yield. A possible reaction stoichiometry is shown in eq. [1], although it is not possible to identify the gaseous products under the experimental conditions used.

[1] $[Ru_2(CO)_5(dppm)_2]$

$$\rightarrow [Ru_2(CO)_4(Ph_2PCH_2PPhC_6H_4)_2] + CO + H_2$$

The same product is obtained when the reaction is carried out in the presence of one molar equivalent of $PhC{\equiv}CPh$ but the reaction is then appreciably faster, being complete in 20 h

Can. J. Chem. Downloaded from www.nrcresearchpress.com by 80.90.12.36 on 09/08/12
For personal use only.

Table 1. Crystal data and experimental details for complex **2**.

Compound, formula weight	$C_{58}H_{50}Br_4O_4P_4Ru_2$, 1456.68
Crystal system, space group	Monoclinic, $P2_1/n$
Cell dimensions	a = 21.349(4) Å
	b = 12.209(5) Å
	c = 22.457(5) Å
	β = 104.34(2)°
Temperature	295 K
Cell volume (Å^3), Z	5671(3), 4
Density, g cm^{-3} calcd.	1.706
Diffractometer, monochromator	Enraf–Nonius CAD4F; graphite
Radiation, wavelength (Å)	MoKα, 0.71073
Absorption coeff. (cm^{-1})	19.8
No. of observ., variables	2489($I \geq 2.5\sigma(I)$), 266
Final model; R and R_w	0.0658, 0.0561

$R = \Sigma(||F_o| - |F_c||)/\Sigma|F_o|$; $R_w = [\Sigma\sqrt{w}(||F_o| - |F_c||)^2/\Sigma\sqrt{w}|F_o|]$.

in refluxing benzene. The role of the PhC≡CPh in this reaction is not clear; it does not appear to act as a hydrogen acceptor since analysis of the reaction mixture does not indicate the presence of stilbene among the products. The alkyne was added in an attempt to trap possible intermediates but no alkyne incorporation into the diruthenium unit was detected.

The structure of complex 2

The complex **2** was characterized by an X-ray structure determination. A view of the molecular structure is given in Fig. 1. Crystal data, selected positional parameters, and bond distances and angles are in Tables 1–3.

Each ruthenium centre has approximately octahedral stereochemistry, with bonds to two *cis* carbonyl ligands, two *trans* phosphine donors, the neighbouring ruthenium atom, and the orthometallated phenyl substituent of a diphosphine ligand. The Ru—Ru distance at 2.933(2) Å is within the bonding range (9) and is slightly longer than in the parent complex $[Ru_2(CO)_4(\mu\text{-}CO)(\mu\text{-}dppm)_2]$, **1**, which has Ru—Ru = 2.903(2) Å (10), while significantly shorter than in $[Ru_2(CO)_4(\mu\text{-}C_2H_2CO)(\mu\text{-}dppm)_2]$ with Ru—Ru = 2.988(1) Å (10). As expected for octahedral coordination, the atoms Ru(1)C(1)C(2)C(226)Ru(2) and Ru(2)C(3)C(4)C(426)Ru(1) are each approximately coplanar with only the carbonyl carbon atoms *trans* to the metal–metal bond lying more than 0.1 Å from the corresponding least-squares plane (C(2) by 0.32(2) and C(3) by 0.24(2) Å). The dihedral angle between the above two planes is 50.7(6)°, which clearly indicates a very significant twist. This large twist is clearly necessary to allow the orthometallated phenyl group on P(2) to bind to Ru(1), thus giving

Table 2. Selected atomic positional and thermal parameters for **2**.

Atom	x	y	z	B_{iso}
Ru(1)	0.11230(8)	0.14513(15)	0.83186(8)	2.45(10)
Ru(2)	−0.01274(8)	0.23396(14)	0.76416(8)	2.40(10)
P(1)	0.0969(3)	−0.0186(5)	0.7739(3)	2.8(3)
P(2)	−0.0316(3)	0.0532(5)	0.7854(3)	2.7(3)
P(3)	0.0292(3)	0.4140(5)	0.7750(3)	2.5(3)
P(4)	0.0926(3)	0.2952(4)	0.8884(3)	2.2(3)
C(10)	0.0106(8)	−0.0445(15)	0.7461(8)	3.1(5)

Table 2 (*concluded*).

Atom	x	y	z	B_{iso}
C(20)	0.0939(8)	0.4247(15)	0.8481(8)	2.4(5)
O(1)	0.1732(7)	0.2794(12)	0.7459(6)	4.9(4)
O(2)	0.2440(8)	0.1001(13)	0.9136(7)	6.1(4)
O(3)	−0.1501(7)	0.2882(12)	0.6947(7)	5.5(4)
O(4)	0.0313(6)	0.1673(11)	0.6489(6)	4.5(4)
C(1)	0.1491(10)	0.2286(18)	0.7775(9)	3.9(5)
C(2)	0.1948(11)	0.1130(18)	0.8819(10)	4.8(6)
C(3)	−0.0966(10)	0.2722(18)	0.7213(9)	4.2(5)
C(4)	0.0141(10)	0.1925(18)	0.6933(10)	4.5(6)
C(111)	0.1320(7)	−0.1378(10)	0.8190(6)	2.9(5)
C(112)	0.1988(7)	−0.1494(10)	0.8292(6)	4.9(6)
C(113)	0.2315(7)	−0.2270(10)	0.8711(6)	5.9(6)
C(114)	0.1973(7)	−0.2930(10)	0.9029(6)	5.1(6)
C(115)	0.1305(7)	−0.2814(10)	0.8927(6)	4.2(5)
C(116)	0.0978(7)	−0.2038(10)	0.8507(6)	3.9(5)
C(121)	0.1293(5)	−0.0382(10)	0.7066(6)	2.7(5)
C(122)	0.1000(5)	−0.1143(10)	0.6621(6)	3.9(5)
C(123)	0.1284(5)	−0.1402(10)	0.6142(6)	5.0(6)
C(124)	0.1861(5)	−0.0899(10)	0.6109(6)	4.6(6)
C(125)	0.2154(5)	−0.0137(10)	0.6554(6)	4.7(6)
C(126)	0.1869(5)	0.0122(10)	0.7033(6)	3.8(5)
C(211)	−0.1157(7)	0.0078(10)	0.7625(5)	3.5(5)
C(212)	−0.1574(7)	0.0374(10)	0.7988(5)	4.0(5)
C(213)	−0.2229(7)	0.0108(10)	0.7800(5)	5.5(6)
C(214)	−0.2467(7)	−0.0453(10)	0.7250(5)	5.9(6)
C(215)	−0.2051(7)	−0.0749(10)	0.6886(5)	4.1(5)
C(216)	−0.1396(7)	−0.0483(10)	0.7074(5)	3.6(5)
C(221)	0.0009(9)	0.0080(15)	0.8645(8)	1.9(4)
C(222)	−0.0306(10)	−0.0648(17)	0.8936(9)	3.9(5)
C(223)	0.0038(10)	−0.1071(16)	0.9501(9)	3.8(5)
C(224)	0.0666(10)	−0.0770(17)	0.9739(9)	3.8(5)
C(225)	0.0963(9)	−0.0030(16)	0.9428(9)	2.9(5)
C(226)	0.0642(9)	0.0437(15)	0.8862(9)	2.6(5)
C(311)	−0.0281(7)	0.5233(12)	0.7807(5)	2.7(5)
C(312)	−0.0621(7)	0.5766(12)	0.7276(5)	5.9(6)
C(313)	−0.1068(7)	0.6580(12)	0.7314(5)	6.0(6)
C(314)	−0.1174(7)	0.6862(12)	0.7883(5)	4.7(6)
C(315)	−0.0833(7)	0.6330(12)	0.8414(5)	5.5(6)
C(316)	−0.0386(7)	0.5515(12)	0.8376(5)	4.4(6)
C(321)	0.0664(5)	0.4749(9)	0.7173(7)	3.3(5)
C(322)	0.0472(5)	0.4404(9)	0.6562(7)	5.3(6)
C(323)	0.0756(5)	0.4859(9)	0.6123(7)	5.4(6)
C(324)	0.1233(5)	0.5660(9)	0.6295(7)	4.5(6)
C(325)	0.1425(5)	0.6006(9)	0.6905(7)	4.6(6)
C(326)	0.1141(5)	0.5550(9)	0.7344(7)	4.5(6)
C(411)	0.1481(6)	0.3216(9)	0.9632(7)	2.3(5)
C(412)	0.1516(6)	0.2428(9)	1.0089(7)	4.2(5)
C(413)	0.1930(6)	0.2584(9)	1.0669(7)	4.4(5)
C(414)	0.2309(6)	0.3527(9)	1.0793(7)	5.1(6)
C(415)	0.2274(6)	0.4315(9)	1.0336(7)	5.2(6)
C(416)	0.1860(6)	0.4159(9)	0.9755(7)	3.8(5)
C(421)	0.0130(8)	0.3011(14)	0.9018(8)	1.9(4)
C(422)	0.0023(9)	0.3433(15)	0.9555(8)	2.5(4)
C(423)	−0.0623(9)	0.3600(16)	0.9585(9)	3.5(5)
C(424)	−0.1129(10)	0.3343(16)	0.9097(9)	3.6(5)
C(425)	−0.0992(8)	0.2924(14)	0.8565(8)	2.2(4)
C(426)	−0.0376(8)	0.2761(15)	0.8494(8)	2.1(4)

Can. J. Chem. Downloaded from www.nrcresearchpress.com by 80.90.12.36 on 09/08/12
For personal use only.

Table 3. Selected bond distances (Å) and angles (°) in complex **2**.

Ru(1)—Ru(2)	2.933(2)	Ru(1)—P(1)	2.364(6)
Ru(1)—P(4)	2.327(5)	Ru(2)—P(2)	2.314(6)
Ru(2)—P(3)	2.363(6)	Ru(1)—C(1)	1.90(2)
Ru(1)—C(2)	1.88(2)	Ru(2)—C(3)	1.87(2)
Ru(2)—C(4)	1.89(2)	Ru(1)—C(226)	2.17(2)
Ru(2)—C(426)	2.17(2)	P(1)—C(111)	1.82(1)
P(1)—C(121)	1.82(1)	P(2)—C(211)	1.83(1)
P(2)—C(221)	1.82(2)	P(3)—C(311)	1.84(1)
P(3)—C(321)	1.84(1)	P(4)—C(411)	1.83(1)
P(4)—C(421)	1.80(2)	P(1)—C(10)	1.82(2)
P(2)—C(10)	1.85(2)	P(3)—C(20)	1.87(2)
P(4)—C(20)	1.83(2)	C(1)—O(1)	1.15(2)
C(2)—O(2)	1.13(2)	C(3)—O(3)	1.17(2)
C(4)—O(4)	1.18(2)		
P(1)—Ru(1)—Ru(2)	92.4(1)	P(4)—Ru(1)—Ru(2)	74.2(1)
P(4)—Ru(1)—P(1)	161.3(2)	C(1)—Ru(1)—Ru(2)	86.4(6)
C(1)—Ru(1)—P(1)	97.0(6)	C(1)—Ru(1)—P(4)	95.0(6)
C(2)—Ru(1)—Ru(2)	169.8(7)	C(2)—Ru(1)—P(1)	97.7(7)
C(2)—Ru(1)—P(4)	96.2(7)	C(2)—Ru(1)—C(1)	91.2(9)
C(226)—Ru(1)—Ru(2)	90.3(5)	C(226)—Ru(1)—P(1)	78.8(5)
C(226)—Ru(1)—P(4)	88.1(5)	C(226)—Ru(1)—C(1)	174.6(8)
C(226)—Ru(1)—C(2)	92.8(8)	P(2)—Ru(2)—Ru(1)	73.9(1)
P(3)—Ru(2)—Ru(1)	91.0(1)	P(3)—Ru(2)—P(2)	161.2(2)
C(3)—Ru(2)—Ru(1)	172.6(7)	C(3)—Ru(2)—P(2)	98.7(7)
C(3)—Ru(2)—P(3)	96.4(7)	C(4)—Ru(2)—Ru(1)	84.9(6)
C(4)—Ru(2)—P(2)	91.3(7)	C(4)—Ru(2)—P(3)	98.6(7)
C(4)—Ru(2)—C(3)	94.9(9)	C(426)—Ru(2)—Ru(1)	91.2(5)
C(426)—Ru(2)—P(2)	87.2(5)	C(426)—Ru(2)—P(3)	81.8(5)
C(426)—Ru(2)—C(3)	89.0(8)	C(426)—Ru(2)—C(4)	176.0(8)

rise to two pairs of five-membered rings with the Ru(1)Ru(2) and Ru(2)P(2) bonds common to both, but it does appear to cause strain in the molecule. For example, the angle P(2)Ru(2)Ru(1) = 73.9(1)° and P(2)Ru(2)P(3) = 161.2(2)° are significantly distorted from the ideal octahedral angles. An alternative structure would have the orthometallated phenyl substituent on P(2) bind to Ru(2) but that would give a four-membered RuPCC ring, which would presumably be even more strained. It is interesting to note that both orthometallated phenyl rings are on the same side of the Ru2P4 plane; the molecules therefore have approximate C_2 symmetry and are chiral.

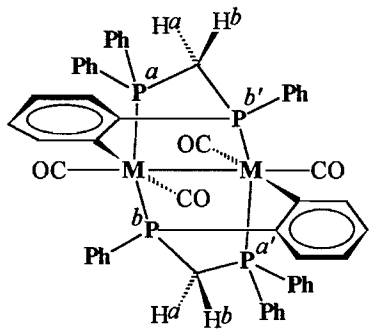

2

Spectroscopic properties of 2

The spectroscopic data for **2** are fully consistent with the crystallographically determined structure. The infrared spectrum contains four bands due to ν(CO) in the region 1989–1912 cm^{-1}, typical for terminal carbonyl groups.

The ^{31}P NMR spectrum in CD_2Cl_2 solution, shown in Fig. 2, exhibits an AA′BB′ pattern, as expected for structure **2**. Note that the nonequivalent phosphorus atoms P^a and P^b are mutually *trans* on the same ruthenium centre and so the coupling $^2J(P^aP^b)$ is expected to be large. Since the molecule **2** contains no plane of symmetry, the dppm methylene protons are expected to be nonequivalent. However, only one resonance, which appeared as an unsymmetrical multiplet at δ = 4.47, was observed (Fig. 2). This is attributed to accidental degeneracy of the chemical shifts of H^a and H^b.

The FAB mass spectrum of **2** contains an envelope of peaks centred at the expected molecular ion peak at *m/z* = 1082 and similar peaks due to the loss of one, two, three, and four carbonyl groups at *m/z* = 1054, 1026, 998, and 968, respectively.

Discussion

The formation of the bis(cyclometallated) complex **2** in good yield by thermolysis of complex **1** is remarkable. In previous studies, thermolysis of binuclear dppm complexes has led to P—C bond cleavage, either alone or along with cyclometallation (2). There are a few precedents in cluster chemistry for cyclometallation of a coordinated dppm ligand (3, 6) but most such reactions also lead to P—C bond cleavage (4). There is obviously a competition between these possible reactions and the formation of **2** represents the first high-yield example of

Can. J. Chem. Downloaded from www.nrcresearchpress.com by 80.90.12.36 on 09/08/12
For personal use only.

Fig. 2. The ^1H (300 MHz, above) and ^{31}P (121.5 MHz, below) nmr spectra of complex **2**. The peak at δ 5.6 in the ^1H nmr spectrum is due to $CHDCl_2$ and that at δ 3.9 is due to an impurity.

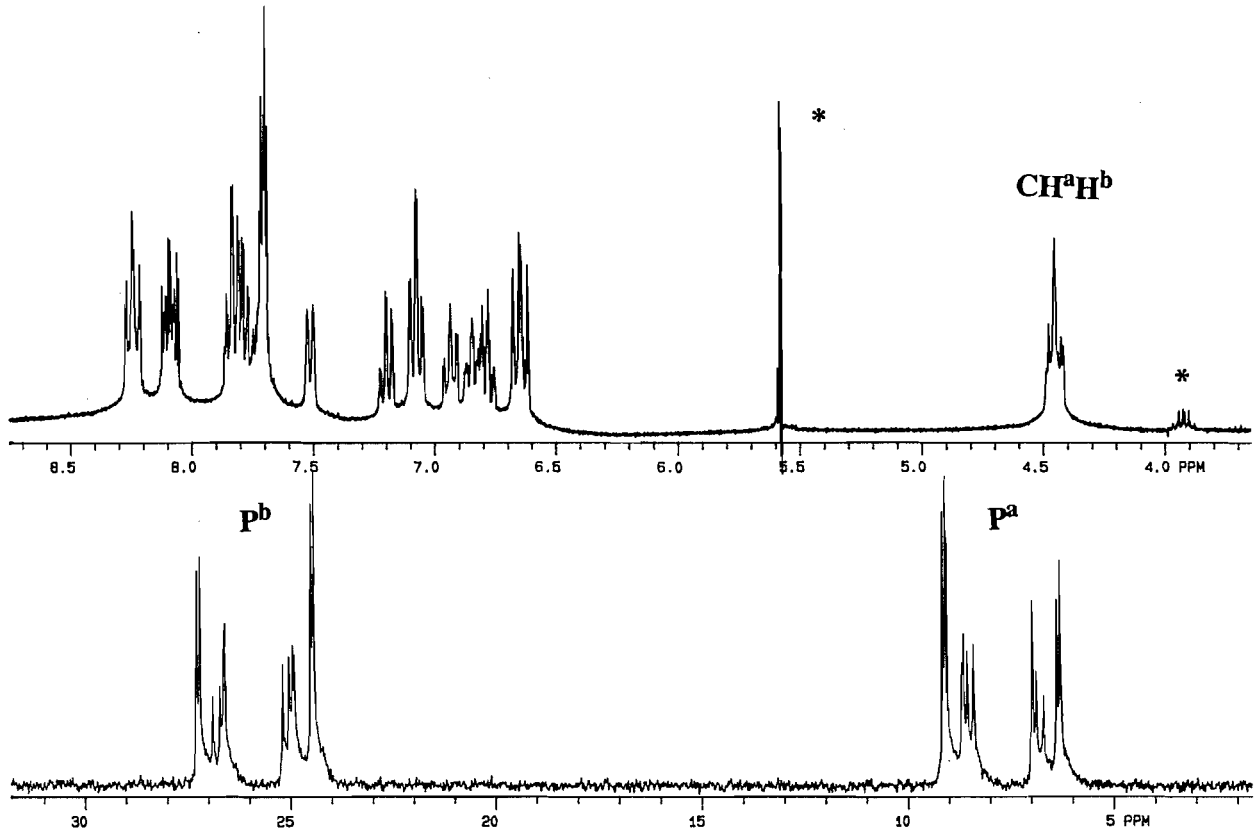

selective orthometallation in competition with P—C bond cleavage (6).

Experimental

Synthesis of $[Ru_2(CO)_4\{Ph_2PCH_2PPh(C_6H_4)\}_2]$, 2

A mixture of $[Ru_2(\mu\text{-}CO)(CO)_4(\mu\text{-}dppm)_2]$ (0.34 g, 0.31 mmol) (10) and PhC≡CPh (0.06 g, 0.34 mmol) was heated under reflux in C_6H_6 (30 mL) for 20 h. The colour of the solution initially changed to deep green, then after 6 h of reflux it became dark orange-brown. The solvent was removed under vacuum, the orange solid product was redissolved in CH_2Cl_2 (4–5 mL), and the solution was layered with EtOH (15 mL). Large yellow crystals of the product **2** formed slowly over a period of 4 weeks. They were separated by filtration, washed with EtOH (5 mL), and dried under vacuum. Yield 45%; mp 220°C (dec.). Anal. (sample isolated from benzene solution) calcd. for $C_{54}H_{42}O_4P_4Ru_2 \cdot 0.5C_6H_6$: C 61.07, H 4.02; found: C 61.27, H 4.25%. IR (Nujol), ν(CO): 1991(vs), 1969(vs), 1933(vs), 1915(vs) cm^{-1}; NMR (CD_2Cl_2), ^1H, δ: 4.47 (m, 4H, CH_2P_2), 6.6–8.4 (m, 38H, Ph and C_6H_4); ^{31}P, δ: 7.7 (m, P^a), 25.9 (m, P^b), assignments of P^a and P^b are arbitrary. Solution gives approximate couplings $^2J(P^aP^b) = 280$ Hz, $^2J(P^aP^{b'}) = 75$ Hz. When the solvent was removed from the initial green solution, the NMR indicated the presence of the complexes **1** and **2** and minor amounts of unidentified compounds; the source of the green colour is therefore unknown.

X-ray structure determination

Pale yellow crystals of $\mathbf{2} \cdot 2C_2H_4Br_2$ were grown from a mixture of $C_2H_4Br_2$, C_2H_5OH, and paraffin oil. Many attempts to grow crystals from other solvent mixtures gave crystals that decayed very rapidly; the use of a high-boiling solvent to reduce problems due to solvent loss from crystals appears necessary and explains the very unusual solvent medium. Crystals decayed rapidly on exposure to air so a suitable crystal for diffraction experiments was cut to a size of 0.27 × 0.24 × 0.15 mm, wedged inside a Lindeman capillary tube along with mother liquor, and the tube was flame sealed at both ends. Photo and automatic indexing routines, followed by least-squares fits of 21 reflections ($22.1° \leq 2\theta \leq 28.5°$) gave cell constants and an orientation matrix (11). The Niggli matrix suggested a monoclinic system having symmetry 2/*m* and this was confirmed from an inspection of equivalent reflections. Intensity data were recorded in ω–2θ scan mode at variable scan speeds (1.03–4.12), chosen to optimize counting statistics within a maximum time per dataum of 60 s. Background measurements were made by extending the scan by 25% on each side. Three standard reflections (200, −103, −10−3) were monitored every 120 min of X-ray exposure time and orientation checks were done for every 300 reflections measured. In total, 8697 reflections were collected in the 2θ range 0°–45° ($-23 \leq h \leq 23$, $-1 \leq k \leq 13$, $-1 \leq l \leq 24$). The crystal did not decay significantly during data collection but diffracted poorly when $2\theta > 40°$. The data were processed using the NRCVAX crystal structure programs (12) running on a

Can. J. Chem. Downloaded from www.nrcresearchpress.com by 80.90.12.36 on 09/08/12
For personal use only.

SUN 3/80 workstation. An empirical absorption correction was applied to the data based upon the ψ scans of four reflections with θ ranging from 3.2 to 14.7 (μ = 7.87 cm^{-1}). The maximum and minimum correction factors were 0.984 and 0.755, respectively. The space group was determined to be $P2_1/n$ from the systematic absences (13) and the correctness of the choice of the space group was confirmed by successful solution and refinement of the structure. The equivalent reflections were averaged (R_{int} = 0.026) leaving 7393 unique reflections, of which only 2489 had $I \geq 2.5\sigma(I)$ due to the weakly diffracting nature of the crystal. The structure was solved using the SHELXS-86 program (14) and subsequent difference Fourier techniques. The final full-matrix least-squares refinements on F were done using the SHELX-76 software (15). Scattering factors for neutral non-hydrogen atoms were taken from the International Tables (13). The phenyl rings were treated as regular hexagons (with C—C distance of 1.395 Å) except for those bonded to Ru atoms. The hydrogen atoms of the dppm ligands and the dibromoethane molecules were placed in the calculated positions (C—H = 0.95 Å) and they were included in the least-squares cycles for the purpose of structure factor calculations only. A common thermal parameter was assigned to all the hydrogen atoms and refined in the least-squares cycles. The thermal parameters of Ru, P, and Br atoms were refined anisotropically. In the final difference Fourier synthesis the electron density fluctuated in the range of 0.86 to -1.0 e $Å^{-3}$; of these, the top two peaks were associated with the Br(3) atom at distances of 1.52 and 0.32 Å. The maximum shift/esd in the final cycle was -0.004. The secondary extinction coefficient was refined to $49(23) \times 10^{-6}$. The crystal data are given in Table 1. More complete positional and thermal parameters, anisotropic thermal parameters, calculated hydrogen atom coordinates, selected weighted least-squares planes, and selected torsion angles have been deposited as supplementary material.[2]

Acknowledgments

We thank the Natural Sciences and Engineering Research Council of Canada for financial support and Dr. N.C. Payne for the use of X-ray facilities.

References

1. R.J. Puddephatt. Chem. Soc. Rev. 99 (1983); B. Chaudret, B. Delavaux, and R. Poilblanc. Coord. Chem. Rev. **85**, 191 (1988); R.J. Puddephatt, LJ. Manojlovic-Muir, and K.W. Muir. Polyhedron, **9**, 2767 (1990).
2. P.E. Garrou. Chem. Rev. **85**, 171 (1985); A.J. Deeming, S.E. Kabir, N.I. Powell, P.A. Bates, and M.B. Hursthouse. J. Chem. Soc. Dalton. Trans. 1529 (1987); H. Jugbluth, G. Suss-Fink, M.A. Pellinghelli, and A. Tiripicchio. Organometallics, **8**, 925 (1989); D.J. Elliott, D.G. Holah, A.N. Hughes, H.A. Mirza, and E. Zawada. J. Chem. Soc. Chem. Commun. 32 (1990); N.M. Doherty, G. Hogarth, S.A.R. Knox, K.A. MacPherson, F. Melchior, and G.A. Orpen. J. Chem. Soc. Chem. Commun. 540 (1986); N.M. Doherty, G. Hogarth, S.A.R. Knox, K.A. MacPherson, F. Melchior, D.A.V. Morton, and G.A. Orpen. Inorg. Chim. Acta, **200**, 257 (1992); I.J.B. Lin, J.S. Lai, L.K. Liu, and Y.S. Wen. J. Organomet. Chem. **399**, 361 (1990); O. Binshawkataly, S.G. Teoh, and H.K. Fun. J. Organomet. Chem. **464**, C29 (1994).
3. J.A. Clucas, D.F. Foster, M.M. Harding, and A.K. Smith. J. Chem. Soc. Chem. Commun. 949 (1984); M.M. Harding, B. Kariuki, A.J. Mathews, A.K. Smith, and P. Braunstein. J. Chem. Soc. Dalton Trans. 33 (1994).
4. N. Lugan, J. Bonnet, and J.A. Ibers. J. Am. Chem. Soc. **107**, 4484 (1985); Organometallics, **7**, 1538 (1988); S.K. Hao, J.I. Song, H. Aghabozorg, and S. Gambarotta. J. Chem. Soc. Chem. Commun. 157 (1994); K.L. Lu, H.J. Chen, P.Y. Lu, S.Y. Li, F.E. Hong, S.M. Peng, and G.H. Lee. Organometallics, **13**, 585 (1994).
5. V.G. Albano, D. Braga, R. Ros, and A. Scrivanti. J. Chem. Soc. Chem. Commun. 866 (1985); F. Neumann, H. Stoeckli-Evans, and G. Suss-Fink. J. Organomet. Chem. **379**, 151 (1989); A.J. Deeming, K.I. Hardcastle, and S.E. Kabir. J. Chem. Soc. Dalton. Trans. 827 (1988); M.I. Bruce, P.A. Humphrey, O.B. Shawkataly, M.R. Snow, and E.R.T. Tiekink. Organometallics, **9**, 2910 (1990).
6. M.I. Bruce. Angew. Chem. Int. Ed. Engl. **16**, 73 (1977); M.I. Bruce, J.R. Hinchliffe, R. Surynt, B.W. Skelton, and A.H. White. J. Organomet. Chem. **469**, 89 (1994); M.I. Bruce, P.A. Humphrey, H. Miyamae, B.W. Skelton, and A.H. White. J. Organomet. Chem. **429**, 187 (1992).
7. A.R. Chakravarty, F.A. Cotton, D.A. Tocher, and J.H. Tocher. Organometallics, **4**, 8 (1985); P. Lahuerta, J. Paya, E. Peris, M.A. Pellinghelli, and A. Tiripicchio. J. Organomet. Chem. **373**, C5 (1989); E.C. Morrison and D.A. Tocher. J. Organomet. Chem. **408**, 105 (1991).
8. D.P. Arnold, M.A. Bennett, M.S. Bilton, and G.B. Robertson. J. Chem. Soc. Chem. Commun. 115 (1982).
9. L.A. Brady, A.F. Dyke, S.E. Garner, S.A.R. Knox, A. Irving, S.M. Nicholls, and A.G. Orpen. J. Chem. Soc. Dalton. Trans. 487 (1993); K.A. Johnson and W.L. Gladfelter. J. Am. Chem. Soc. **113**, 5097 (1991); Organometallics, **8**, 2866 (1989); A.F. Dyke, S.A.R. Knox, P.J. Naish, and G.E. Taylor. J. Chem. Soc. Dalton Trans. 1297 (1982); J.S. Field, R.J. Haines, J. Sundermeyer, and S.F. Woollam. J. Chem. Soc. Dalton. Trans. 3749 (1993).
10. H.A. Mirza, J.J. Vittal, and R.J. Puddephatt. Inorg. Chem. **32**, 1327 (1993); Organometallics. In press.
11. CAD4 diffractometer manual. Enraf–Nonius, Delft, The Netherlands. 1988.
12. E.J. Gabe, Y. Le Page, J.-P. Charland, and F.C. Lee. J. Appl. Crystallogr. **22**, 384 (1989).
13. International tables for X-ray crystallography. Vol. A. D. Reidel Publishing Co., Boston. 1983.
14. G.M. Sheldrick. SHELXS-86. University of Gottingen, Gottingen, Germany. 1986.
15. G.M. Sheldrick. SHELX-76. University of Cambridge, Cambridge, England. 1976.

[2] Supplementary material mentioned in the text can be purchased from: The Depository of Unpublished Data, Document Delivery, CISTI, National Research Council of Canada, Ottawa, ON K1A 0S2, Canada.

Tables of bond lengths and angles and of atomic parameters have also been deposited with the Cambridge Crystallographic Data Centre, and can be obtained on request from The Director, Cambridge Crystallographic Data Centre, University Chemical Laboratory, 12 Union Road, Cambridge, CB2 1EZ, U.K.

Synthesis and crystal structure of the allyl(carborane)nickel complex $[N(PPh_3)_2][Ni(\eta^3\text{-}C_3H_5)(\eta^6\text{-}7,9\text{-}Me_2\text{-}7,9\text{-}C_2B_{10}H_{10})]$

Donald F. Mullica, Eric L. Sappenfield, F. Gordon A. Stone, and Stephen F. Woollam

Can. J. Chem. Downloaded from www.nrcresearchpress.com by 80.90.12.36 on 09/08/12
For personal use only.

Abstract: Treatment of $[Ni_2(\mu\text{-}Br)_2(\eta^3\text{-}C_3H_5)_2]$ with $Na_2[nido\text{-}7,9\text{-}C_2B_{10}H_{12}]$ in THF (tetrahydrofuran) affords the anionic species $[Ni(\eta^3\text{-}C_3H_5)(\eta^6\text{-}7,9\text{-}C_2B_{10}H_{12})]^-$, which was isolated as its $[NEt_4]^+$ salt **8***a*. A similar reaction between $Na_2[nido\text{-}7,9\text{-}Me_2\text{-}7,9\text{-}C_2B_{10}H_{10}]$ and $[Ni_2(\mu\text{-}Br)_2(\eta^3\text{-}C_3H_5)_2]$ in thf gives the anionic species $[Ni(\eta^3\text{-}C_3H_5)(\eta^6\text{-}7,9\text{-}Me_2\text{-}7,9\text{-}C_2B_{10}H_{10})]^-$ isolated as $[N(PPh_3)_2]^+$ (**8***b*) and $[NEt_4]^+$ (**8***c*) salts, respectively. The molecular structure of **8***b* has been established by X-ray diffraction. Crystals are monoclinic, space group $P2_1/c$ (No. 14) with $a = 14.685(3)$ Å, $b = 18.346(2)$ Å, $c = 16.319(1)$ Å, $\beta = 99.93(1)°$, and $Z = 4$. The nickel atom is ligated by the *nido*-7,9-Me_2-7,9-$C_2B_{10}H_{10}$ cage in an η^6 manner, as well as by the allyl group, with the latter adopting an η^3-bonding mode (Ni—C = 2.023(5), 1.939(8), and 1.988(5) Å). The palladium analog **8***d* was similarly prepared from $Na_2[nido\text{-}7,9\text{-}Me_2\text{-}7,9\text{-}C_2B_{10}H_{10}]$ and $[Pd_2(\mu\text{-}Cl)_2(\eta^3\text{-}C_3H_5)_2]$, followed by addition of $[NEt_4]Cl\cdot H_2O$, but in contrast with the nickel species this product was unstable, especially its solutions in air.

Key words: nickel, palladium, allyl complex, carborane.

Résumé : La réaction du $[Ni_2(\mu\text{-}Br)_2(\eta^3\text{-}C_3H_5)_2]$ avec du $Na_2[nido\text{-}7,9\text{-}C_2B_{10}H_{12}]$ dans le tétrahydrofurane (THF) fournit l'espèce anionique $[Ni(\eta^3\text{-}C_3H_5)(\eta^6\text{-}7,9\text{-}C_2B_{10}H_{12})]^-$ qui a été isolée sous la forme de sel de $[NEt_4]^+$ (**8***a*). Une réaction similaire du $[Ni_2(\mu\text{-}Br)_2(\eta^3\text{-}C_3H_5)_2]$ avec du $Na_2[nido\text{-}7,9\text{-}Me_2\text{-}7,9\text{-}C_2B_{10}H_{10}]$ dans le THF fournit l'espèce anionique $[Ni(\eta^3\text{-}C_3H_5)(\eta^6\text{-}7,9\text{-}Me_2\text{-}7,9\text{-}C_2B_{10}H_{10})]^-$ qui a été isolée sous la forme des sels de $[N(PPh_3)_2]^+$ (**8***b*) et de $[NEt_4]^+$ (**8***c*). On a déterminé la structure moléculaire du composé **8***b* par diffraction des rayons X. Les cristaux sont monocliniques, groupe d'espace $P2_1/c$ (No. 14), avec a = 14,685(3), b = 18,346(2) et c = 16,319(1) Å, β = 99,93(1)° et Z = 4. L'atome de nickel et le groupe allyle sont liés à la cage du *nido*-7,9-Me_2-7,9-$C_2B_{10}H_{10}$ d'une façon η^6, alors que le dernier adopte un mode de liaison η^3 (Ni—C = 2,023(5), 1,939(8) et 1,988(5) Å). On a préparé l'analogue du palladium (**8***d*) d'une façon semblable par réaction du $Na_2[nido\text{-}7,9\text{-}Me_2\text{-}7,9\text{-}C_2B_{10}H_{10}]$ et du $[Pd_2(\mu\text{-}Cl)_2(\eta^3\text{-}C_3H_5)_2]$ suivie d'une addition de $[NEt_4]Cl\cdot H_2O$; toutefois, par opposition au comportement des espèces du nickel, celle-ci est instable, particulièrement lorsque ses solutions sont mises en présence d'air.

Mots clés : nickel, palladium, complexe allyle, carborane.

[Traduit par la rédaction]

Introduction

We have recently synthesized the salts $[X][M(\eta^3\text{-}C_3H_5)(\eta^5\text{-}7,8\text{-}Me_2\text{-}7,8\text{-}C_2B_9H_9)]$ (M = Ni, Pd, or Pt, X = NEt_4^+ or $N(PPh_3)_2^+$) (**1**). Protonation ($HBF_4\cdot Et_2O$) of these products releases propylene, and if CO or CNBu^t are present the complexes $[M(L)_2(\eta^5\text{-}7,8\text{-}Me_2\text{-}7,8\text{-}C_2B_9H_9)]$ (**2**, L = CO or CNBu^t) are formed, respectively (1).[2] The allyl(carborane)-molybdenum and -tungsten complexes $[X][M(CO)_2(\eta^3\text{-}C_3H_5)(\eta^5\text{-}7,8\text{-}R_2\text{-}7,8\text{-}C_2B_9H_9)]$ (**3**, M = Mo or W, R = Me or H, X = NEt_4 or $N(PPh_3)_2$) undergo similar protonation reactions in the presence of donor ligands, yielding a variety of neutral species such as $[M(CO)_2(L)_2(\eta^5\text{-}7,8\text{-}Me_2\text{-}7,8\text{-}C_2B_9H_9)]$ (**4**, M = Mo or W, L = CO or PPh_3), $[Mo(CO)(\eta^2\text{-}MeC{\equiv}CMe)_2(\eta^5\text{-}7,8\text{-}Me_2\text{-}$

Received June 23, 1994.

This paper is dedicated to Professor William A.G. Graham on the occasion of his 65th birthday.

D.F. Mullica, E.L. Sappenfield, F. G.A. Stone,[1] and S. F. Woollam. Department of Chemistry, Baylor University, Waco, TX 76798 - 7348, U.S.A.

[1] Author to whom correspondence may be addressed.

[2] In the compounds discussed in this paper [*nido*-7,8-R_2-7,8-$C_2B_9H_9]^{2-}$ and [*nido*-7,9-R_2-7,9-$C_2B_{10}H_{10}]^{2-}$ dianions form *closo*-1,2-dicarba-3- and *closo*-1,6-dicarba-4 metallacarborane structures. Use of this numbering scheme results in a cumbersome and confusing nomenclature for the complexes. As in earlier papers we treat the cages as *nido*-11 and *nido*-12 vertex ligands with numbering as for an icosahedron or a docosahedron, respectively, from which one vertex has been removed.

Can. J. Chem. Downloaded from www.nrcresearchpress.com by 80.90.12.36 on 09/08/12
For personal use only.

7,8-$C_2B_9H_9$)] (**5**), and [Mo(CO)(η^2-$Me_3SiC{\equiv}CH$){η^2,η^5-7,8-Me_2-10-[C(H)=C(H)$SiMe_3$]-7,8-$C_2B_9H_8$}] (**6**) (2). In all these compounds the metal atoms are ligated in a pentahapto manner by the open pentagonal CCBBB face of a *nido*-icosahedral C_2B_9 cage, a bonding mode for this group to transition metals first identified by Hawthorne and co-workers (3*a*).

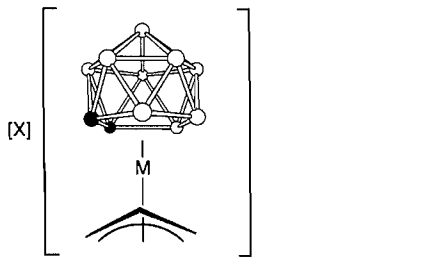

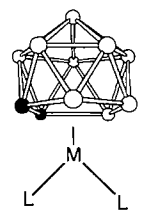

● CMe ○ BH

	M	X
1a	Ni	NEt_4
1b	Ni	$N(PPh_3)_2$
1c	Pd	NEt_4
1d	Pt	NEt_4
1e	Pt	$N(PPh_3)_2$

	M	L
2a	Ni	CO
2b	Ni	$CNBu^t$
2c	Pd	$CNBu^t$
2d	Pt	CO
2e	Pt	$CNBu^t$

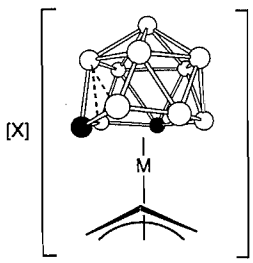

	M	X	●
8a	Ni	NEt_4	CH
8b	Ni	$N(PPh_3)_2$	CMe
8c	Ni	NEt_4	CMe
8d	Pd	NEt_4	CMe

Like [*nido*-7,8-R_2-7,8-$C_2B_9H_9$]$^{2-}$ (R = H or Me), the dianions [*nido*-7,9-R_2-7,9-$C_2B_{10}H_{10}$]$^{2-}$ also coordinate to transition metal centers but in a hexahapto manner (3*b*, 4). This led us to prepare and study the complexes [$N(PPh_3)_2$][$M(CO)_2$(η^3-C_3H_5)(η^6-7,9-Me_2-7,9-$C_2B_{10}H_{10}$)] (**7**, M = Mo or W) (5), which are akin to **3**. The close connection between the salts **3** and **7** suggested that a similar relationship might exist between the anions of the salts **1** and a new series of complex anions of formulation [M(η^3-C_3H_5)(η^6-7,9-R_2-7,9-$C_2B_{10}H_{10}$)]$^-$ (M = Ni, Pd, or Pt; R = Me or H), thus prompting the work described in this paper.

Results and discussion

Treatment of [Ni_2(μ-Br)$_2$(η^3-C_3H_5)$_2$] in THF (tetrahydrofuran) with a solution of Na_2[*nido*-7,9-$C_2B_{10}H_{12}$] in the same solvent gave orange crystals of [NEt_4][Ni(η^3-C_3H_5)(η^6-7,9-$C_2B_{10}H_{12}$)] (**8***a*), after addition of [NEt_4]Cl and column chromatography of the mixture on alumina. A similar procedure employing Na_2[*nido*-7,9-Me_2-7,9-$C_2B_{10}H_{10}$] and [Ni_2(μ-Br)$_2$(η^3-C_3H_5)$_2$], with addition of [$N(PPh_3)_2$]Cl or [NEt_4]Cl yielded, respectively, the salts [X][Ni(η^3-C_3H_5)(η^6-7,9-Me_2-7,9-$C_2B_{10}H_{10}$)] (X = [$N(PPh_3)_2$]$^+$ (**8***b*) and [NEt_4]$^+$ (**8***c*)). The palladium compound [NEt_4][Pd(η^3-C_3H_5)(η^6-7,9-Me_2-7,9-$C_2B_{10}H_{10}$)] (**8***d*) was obtained from the reaction between [Pd_2(μ-Cl)$_2$(η^3-C_3H_5)$_2$] and Na_2[*nido*-7,9-Me_2-7,9-$C_2B_{10}H_{10}$] followed by addition of [NEt_4]Cl. The ^{1}H, ^{13}C{^{1}H}, and ^{11}B{^{1}H} NMR data for these products are listed in Table 1 but discussion is deferred until the results of an X-ray diffraction study on **8***b* are described.

Fig. 1. Molecular structure of the anion of [$N(PPh_3)_2$]-[Ni(η^3-C_3H_5)(η^6-7,9-Me_2-7,9-$C_2H_{10}H_{10}$)] (**8***b*), showing the crystallographic labeling scheme. Thermal ellipsoids are shown at 50% probability level.

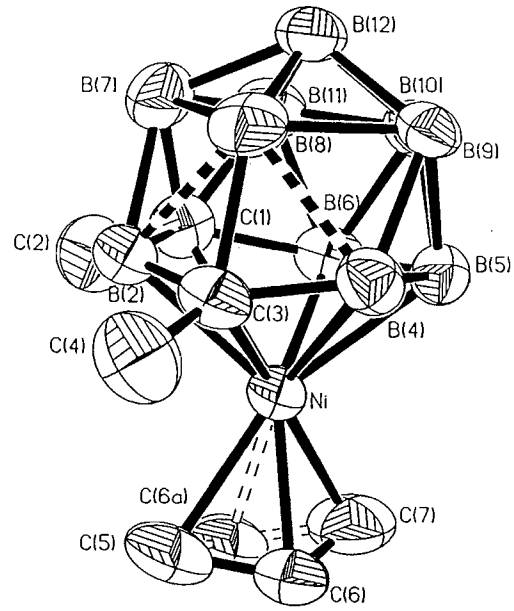

The structure of the anion of **8***b* is shown in Fig. 1 and selected internuclear distances and bond angles are listed in Table 2. The nickel atom is ligated by the allyl group and a *nido*-$C_2B_{10}H_{10}Me_2$ cage. The allyl ligand is coordinated to the nickel atom in the usual trihapto manner, but the central methine carbon atom is disordered occupying, respectively, the C(6) and the C(6*a*) positions 50% of the time. The C(5)—C(6,6*a*) distance (avg. 1.317 Å) is slightly shorter than the C(6,6*a*)—C(7) distance (1.355 Å). The nickel is also coordinated to the *nido*-C_2B_{10} cage in a hexahapto manner. Since the *closo*-4,1,6-NiC_2B_{10} skeleton of **8***b* has 13 vertices, distortions occur within this framework which are not found in 12 vertex systems with *closo*-3,1,2-MC_2B_9 icosahedral structures. Thus the CBCBBB face ligating the nickel atom is distinctly non-planar, as in other complexes containing a MC_2B_{10} cage system (5–8). The non-planarity of the CBCBBB ring in **8***b* results in differences in the contact distances between the metal and cage atoms: Ni—C(1) 2.319(4), Ni—B(2) 2.170(5), Ni—C(3) 2.016(4), Ni—B(4) 2.206(5), Ni—B(5) 2.119(5), Ni—B(6) 2.115(5) Å. The C(3) carbon atom is the cage vertex with the lowest connectivity and has the shortest contact distance to the metal atom. The C(3) atom also displays relatively short distances to B(2) (1.548(6) Å) and B(4) (1.520(7) Å). The B(8) boron atom is the highest

Can. J. Chem. Downloaded from www.nrcresearchpress.com by 80.90.12.36 on 09/08/12
For personal use only.

Table 1. ^{1}H, ^{13}C and ^{11}B NMR data[a] for the new compounds

Compound	$^{1}H(\delta)$[b,c]	$^{13}C(\delta)$[d]	$^{11}B(\delta)$[e]
8*a*	1.32 (t, 12H, NCH_2Me, J_{H-H} = 7), 2.17 (d, 2H, H_a, J_{H-H} = 12), 3.19 to 3.25 (m, 10H, NCH_2Me and H_s), 3.55 (s, br, 2H, CH), 5.10 (tt, 1H, H_c, J_{H-H} = 6, 12)	99.2 (CH), 61.0 (br, cage CH), 55.9 (CH_2), 53.0 (t, NCH_2Me, J_{N-C} = 3), 7.7 (NCH_2Me)	−3.2 (3 B), −8.9 (4 B), −16.4 (1 B), −17.6 (1 B), −18.9 (1 B)
8*b*	1.98 (s, 6H, CMe), 2.03 (d, 2H, H_a, J_{H-H} = 12), 3.23 (d, 2H, H_s, J_{H-H} = 6), 4.90 (tt, 1H, H_c, J_{H-H} = 6, 12), 7.48 to 7.70 (m, 30H, Ph)	133.9 (C^4(Ph)), 132.3 (vt, C^2(Ph), $\{J_{P-C} + J_{P'-C}\}$ = 11), 129.6 (vt, C^3(Ph), $\{J_{P-C} + J_{P'-C}\}$ = 13), 127.4 (d, C^1(Ph), J_{P-C} = 109), 101.3 (CH), 75.0 (br, *C*Me), 56.7 (CH_2), 32.2 (*CMe*)	−1.0 (br, 1 B), −4.4 (1 B), −6.9 (1 B), −10.4 (4 B), −14.2 (3 B)
8*c*[f]	1.37 (tt, 12H, NCH_2Me, J_{H-H} = 2, J_{H-H} = 7), 1.95 (s, 6H, CMe), 1.97 (d, 2H, H_a, J_{H-H} = 12), 3.14 (d, 2H, H_s, J_{H-H} = 6), 3.42 (q, 8H, NCH_2Me, J_{H-H} = 7), 4.89 (tt, 1H, H_c, J_{H-H} = 6, 12)	101.1 (CH), 74.5 (*C*Me), 56.2 (CH_2), 52.8 (t, NCH_2Me, J_{N-C} = 3), 32.3 (*CMe*), 7.51 (NCH_2Me)	2.0 (br, 1 B), −0.8 (1 B), −3.9 (1 B), −6.8 (4 B), −11.0 (3 B)
8*d*	1.29 (tt, 12H, NCH_2Me, J_{N-H} = 2, J_{H-H} = 7), 2.02 (s, br, 2H, CMe), 2.74 (d, 2H, H_a, J_{H-H} = 12), 3.14 to 3.20 (m, 10H, NCH_2Me and H_s), 5.00 (tt, 1H, H_c, J_{H-H} = 5, 12)	[g] 107.8 (CH), 63.0 (br, CH_2), 53.0 (t, NCH_2Me, J_{N-C} = 3), 33.8 (br, *CMe*), 7.8 (NCH_2Me)	10.0 (br, 1 B), 0.1 (1 B), −5.3 (2 B), −8.2 (1 B), −9.5 (2 B), −11.2 (2 B), −22.5 (br, 1 B)

[a]Measured in CD_2Cl_2 at ambient temperatures, unless otherwise stated. Chemical shifts (δ) in ppm, coupling constants (*J*) in Hz. Abbreviations used: s = singlet, d = doublet, m = multiplet, q = quartet, t = triplet, tt = triplet of triplets, vt = virtual triplet, br = broad.

[b]H_a, H_c, and H_s refer to the protons:

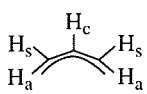

[c]Proton resonances for terminal B-H groups occur as broad unresolved peaks in the range δ ca. −2 to +3.

[d]Hydrogen-1 decoupled. Chemical shifts are positive to high frequency of $SiMe_4$.

[e]Hydrogen-1 decoupled. Chemical shifts are positive to high frequency of $BF_3{\cdot}Et_2O$ (external). Signals ascribed to more than one boron nucleus may result from overlapping peaks, and do not necessarily indicate symmetry equivalence.

[f]Measured in acetone-d_6.

[g]Signals ascribed to the cage carbons were not observed in this spectrum, see text.

connectivity vertex with the longest separations represented in Fig. 1 by dashed lines involving B(2) (2.084(8) Å) and B(4) (1.947(7) Å). This results in two essentially quadrilateral faces about C(3). The bond distances and angles within the carborane cage in **8***b* are similar to those found in other compounds with MC_2B_{10} (M = Ti, Mo, W, Co, Ir, or Pd) cages which have been structurally characterized by X-ray diffraction (5–8). As far as we are aware **8***b* is the first such species containing a nickel atom to be synthesized and structurally characterized.

The NMR data (Table 1) for the complexes **8**, measured at ambient temperatures, indicate the occurrence of dynamic behavior, a common feature for compounds containing a MC_2B_{10} cage framework (3*b*, 4, 5). As established for **8***b* and many related 4,1,6-MC_2B_{10} species in the solid state, the CBCBBB face of the cage ligating the metal atom is non-planar, consequently the CMe vertices are in different environments lying on either side of a mean plane through the four boron atoms in this face. Nevertheless, in the ^{1}H NMR spectra of the complexes **8** the cage CMe vertices give rise to one resonance (e.g., **8***b*, δ 1.98) rather than two, and in the $^{13}C\{^{1}H\}$ spectra only two peaks are observed (e.g., **8***b*, δ 75.0 (*C*Me) and 32.2 (*CMe*)) rather than four. As discussed elsewhere (3*b*, 4), the fluxionality results from the CMe fragments changing their relationship with respect to the metal center via a pathway involving a twofold diamond–square–diamond polytopal rearrangement of the cage. The time-averaged structure has a plane of symmetry, and via this intermediate the cage CMe groups are able to flip synchronously from one side of the mean plane through the four boron atoms to the other.

The ^{1}H and $^{13}C\{^{1}H\}$ NMR spectra of the complexes **8** display diagnostic resonances for the allyl ligands similar to those observed in the corresponding spectra of the species **1** and **7**. Thus in the ^{1}H NMR spectrum of **8***c* three signals occur at δ 1.97 (d, 2H, J_{H-H} = 12 Hz), 3.14 (d, 2H, J_{H-H} = 6 Hz), and 4.89 (tt, 1H, J_{H-H} = 6 and 12 Hz). The doublet signals may be assigned to the protons in the methylene groups of the allyl ligand, while the triplet-of-triplets is due to the methine proton. In the ^{1}H NMR spectrum of **1***a*, with a C_2B_9Ni rather than a $C_2B_{10}Ni$ cage, the corresponding resonances are seen at δ 2.22 (d, 2H, J_{H-H} = 12 Hz), 2.71 (d, 2H, J_{H-H} = 6 Hz), and 4.74 (tt, 1H, J_{H-H} = 6 and 12 Hz) (1*a*). In the $^{13}C\{^{1}H\}$ NMR spectrum of **8***c* resonances for the allyl ligand are at δ 101.1 for the CH nucleus and at δ 56.7 for the CH_2 moieties to be com-

Can. J. Chem. Downloaded from www.nrcresearchpress.com by 80.90.12.36 on 09/08/12
For personal use only.

Table 2. Selected bond distances (Å) and angles (deg) for $[N(PPh_3)_2][Ni(\eta^3\text{-}C_3H_5)(\eta^6\text{-}7,9\text{-}Me_2\text{-}7,9\text{-}C_2B_{10}H_{10})]$ (**8***b*)

Bond	Distance	Bond	Distance	Bond	Distance	Bond	Distance
Ni—C(5)	2.023(5)	Ni—C(6)	1.939(8)	Ni–C(6a)	1.957(8)	Ni–C(7)	1.988(5)
Ni—C(1)	2.319(4)	Ni—B(2)	2.170(5)	Ni–C(3)	2.016(4)	Ni—B(4)	2.206(5)
Ni—B(5)	2.119(5)	Ni—B(6)	2.115(5)	C(5)–C(6)	1.310(9)	C(5)—C(6a)	1.323(9)
C(6)—C(7)	1.354(9)	C(6a)—C(7)	1.351(9)	C(1)–B(2)	1.657(6)	C(1)—B(6)	1.686(7)
C(1)—B(11)	1.680(7)	C(1)—C(2)	1.529(6)	B(2)–C(3)	1.548(6)	B(2)—B(7)	1.821(7)
B(2)···B(8)	2.084(8)	C(3)—B(4)	1.520(7)	C(3)–B(8)	1.742(7)	C(3)—C(4)	1.515(6)
B(4)—B(5)	1.821(7)	B(4)···B(8)	1.947(7)	B(4)–B(9)	1.789(7)	B(5)—B(6)	1.794(7)
B(5)—B(9)	1.771(7)	B(5)—B(10)	1.767(7)	B(6)–B(10)	1.796(8)	B(6)—B(11)	1.778(7)
B(7)—B(8)	1.928(7)	B(7)—B(11)	1.711(8)	B(7)–B(12)	1.734(8)	B(8)–B(9)	1.888(7)
B(8)—B(12)	1.800(7)	B(9)—B(10)	1.735(7)	B(9)–B(12)	1.728(7)	B(10)—B(11)	1.724(7)
B(10)—B(12)	1.783(8)	B(11)—B(12)	1.775(8)				
Bond	**Angle**	**Bond**	**Angle**	**Bond**	**Angle**	**Bond**	**Angle**
C(5)–Ni–C(6)	38.5(3)	C(5)–Ni–C(7)	71.5(2)	C(6)–Ni–C(7)	40.3(3)	C(5)–C(6)–C(7)	123.2(6)
C(5)–C(6a)–C(7)	122.4(6)	B(2)–C(1)–B(6)	116.6(3)	B(2)–C(3)–B(4)	124.7(4)	C(1)–B(2)–C(3)	124.1(4)
C(3)–B(4)–B(5)	116.2(4)	B(4)–B(5)–B(6)	115.7(4)	C(1)–B(6)–B(5)	117.3(4)		

pared with signals for these groups in the spectrum of **1***a* at δ 93.7 and 52.0, respectively.

The palladium complex **8***d* proved to be unstable and microanalytical data were not obtained. Solutions of the compound at room temperature rapidly decomposed to black material presumably palladium metal. However, below ca. −30°C decomposition is slowed. Despite these difficulties the ^1H and $^{13}C\{^1H\}$ NMR spectra were measured and the data obtained (Table 1) are in complete accord with the formulation proposed. As mentioned earlier, protonation of the salts **1** in the presence of substrate molecules affords a variety of products (1) and it was hoped that similar behavior would be shown by the species **8**. Disappointingly this proved not to be so. Treatment of **8***d* with $HBF_4{\cdot}Et_2O$ at −78°C led to the formation of a black intractable solid assumed to be palladium metal. Similar protonation reactions of **8***b* in the presence of CO, $CNBu^t$, PPh_3, $P(OMe)_3$, $Ph_2PCH_2CH_2PPh_2$, $[Co_2(CO)_8]$, cycloocta-1,4-diene, and bicyclo-2,2,2-heptadiene all failed to yield stable products.

Experimental

All solvents were dried over appropriate drying agents before use. Light petroleum refers to that fraction of bp 40–60°C. Chromatography columns ca. 15 cm long and 3 cm in diameter were packed with alumina (Brockmann activity II). All experiments were carried out under nitrogen using Schlenk tube techniques. Spectroscopic equipment used has been described previously (2*a*). The compounds $[Ni_2(\mu\text{-}Br)_2(\eta^3\text{-}C_3H_5)_2]$ (9) and $[Pd_2(\mu\text{-}Cl)_2(\eta^3\text{-}C_3H_5)_2]$ (10) were prepared as previously described.

Synthesis of the allyl(carborane) nickel and palladium complexes $[X][M(\eta^3\text{-}C_3H_5)(\eta^6\text{-}7,9\text{-}R_2\text{-}7,9\text{-}C_2B_{10}H_{10})]$ (M = Ni, R = H or Me, X = NEt_4 or $N(PPh_3)_2$; M = Pd, R = Me, X = NEt_4).

The preparation of complex **8***b* illustrates the general procedure followed. A THF (20 cm^3) solution of 1,2-Me_2-1,2-$C_2B_{10}H_{10}$ (0.50 g, 2.9 mmol) was treated with Na cuttings (ca. 1.0 g, 43.5 mmol) and a trace amount of naphthalene, and the mixture was stirred at room temperature for 2 h. The solution containing $Na_2[nido\text{-}7,9\text{-}Me_2\text{-}7,9\text{-}C_2B_{10}H_{10}]$ so formed (3*b*) was then slowly syringed in to a solution of freshly prepared $[Ni_2(\mu\text{-}Br)_2(\eta^3\text{-}C_3H_5)_2]$ (0.54 g, 1.5 mmol) in THF (10 cm^3) held at −50°C. After stirring the mixture for 1 h, it was warmed to 0°C and stirring was continued for a further 15 h. Solid $[N(PPh_3)_2]Cl$ (1.72 g, 3.0 mmol) was then added and the mixture warmed slowly to room temperature. Volatile materials were removed in vacuo, the residue was extracted with CH_2Cl_2 (15 cm^3) and the extracts were filtered through a Celite pad (ca. 5 cm thick). The volume of the solvent was then reduced in vacuo to ca. 5 cm^3, and the solution chromatographed, eluting with CH_2Cl_2/light petroleum (2:1). An orange eluate was collected from which the solvent was removed in vacuo to give $[N(PPh_3)_2][Ni(\eta^3\text{-}C_3H_5)(\eta^6\text{-}7,9\text{-}Me_2\text{-}7,9\text{-}C_2B_{10}H_{10})]$ (**8***b*) (1.55 g) as an orange powder (64% yield). Analytically pure orange crystals of **8***b* may be obtained by crystallization from CH_2Cl_2/Et_2O/light petroleum (1:1:1). Anal. calcd. for $C_{43}H_{51}B_{10}NNiP_2$: C 63.7, H 6.3, N 1.7; found: C 64.3, H 6.6, N 1.8.

The $[NEt_4]^+$ salt **8***c* was obtained in a similar manner, employing $[NEt_4]Cl{\cdot}H_2O$ in place of $[N(PPh_3)_2]Cl$ (60% yield). Anal. calcd. for $C_{15}H_{41}B_{10}NNi$: C 44.8, H 10.3, N 3.5; found: C 45.3, H 10.8, N 4.2.

Similarly, the complex $[NEt_4][Ni(\eta^3\text{-}C_3H_5)(\eta^5\text{-}7,9\text{-}C_2B_{10}H_{12})]$ (**8***a*) (0.61 g, 54% yield) may be obtained from the reaction of $Na_2[nido\text{-}7,9\text{-}C_2B_{10}H_{12}]$ with a half-molar amount of $[Ni_2(\mu\text{-}Br)_2(\eta^3\text{-}C_3H_5)_2]$ (0.54 g, 1.5 mmol) in THF at −50°C, followed by addition of $[NEt_4]Cl{\cdot}H_2O$. Anal. calcd. for $C_{13}H_{37}B_{10}NNi$: C 41.7, H 10.0, N 3.7; found: C 42.2, H 10.5, N 4.4.

Following a similar procedure, $Na_2[nido\text{-}7,9\text{-}Me_2\text{-}7,9\text{-}C_2B_{10}H_{10}]$ was treated with a half-molar amount of $[Pd_2(\mu\text{-}Cl)_2(\eta^3\text{-}C_3H_5)_2]$ (0.55 g, 1.50 mmol) to afford $[NEt_4][Pd(\eta^3\text{-}C_3H_5)(\eta^6\text{-}7,9\text{-}Me_2\text{-}7,9\text{-}C_2B_{10}H_{10})]$ (**8***d*) (0.45 g, 34% yield) as a bright yellow solid. Compound **8***d* may be crystallized from

Can. J. Chem. Downloaded from www.nrcresearchpress.com by 80.90.12.36 on 09/08/12
For personal use only.

Table 3. Data for crystal structure analysis of compound **8***b*

Formula	$C_{43}H_{51}B_{10}NNiP_2$
fw	810.6
Crystal system	Monoclinic
Space group	$P2_1/c$
a, Å	14.685(3)
b, Å	18.346(2)
c, Å	16.319(1)
β, deg	99.93(1)
V, Å^3	4330.6(10)
Z	4
$D_{(calcd.)}$, g/cm^{-3}	1.24
F(000)	1696
μ(Mo Kα), cm^{-1}	5.53
Temperature, K	292
Diffractometer	Enraf–Nonius CAD4-F
Scan type	ω–2θ
Scan speed, deg/min^{-1}	0.54–5.17
Scan range(ω, deg)	1.15 + 0.34 tan θ
2θ range, deg	3.0–40.0
Observed data ($F \geq 4.0\sigma(F)$)	3387
Refined parameters	524
Radiation (λ, Å)	Mo–K_α (0.71073)
Data–to–parameter ratio	6.5:1
R, *R*′ (R_{all})	0.041, 0.050 (0.056)
R_{int}	0.019
S (goodness-of-fit)	1.35
Residual density (max., min.)/e Å^{-3}	0.36, −0.29

CH_2Cl_2/Et_2O (1:1) but satisfactory microanalytical data were not obtained.

Crystal structure determination and refinement

A clear red single crystal (0.21 × 0.36 × 0.49 mm) of **8***b* was selected for X-ray diffraction analysis on the basis of its optical homogeneity. A conoscopic examination confirmed the biaxial (birefringent) nature and quality of the crystal. Data were collected on an automated diffractometer (*h*: 0 to 14, *k*: 0 to 17, *l*: −15 to 15). A variation of less than 1.3% in the monitored standard reflections (every 2 h of collection time) verified the electronic reliability and crystal stability. All intensity data were corrected for Lorentz and polarization effects after which an empirical absorption correction, based on high-angle ψ scans (minimum, maximum transmission factors = 0.6679, 0.9989), was performed. After elimination of the check reflections and averaging redundant data (R_{int}), 4031 independent reflections remained, of which 3387 were used in the solution. Examination of the resultant data revealed the conditions: *h*0*l*, $l = 2n$ and 0*k*0, $k = 2n$ which are consistent with the space group $P2_1/c$ (No. 14). Crystal data, experimental and statistical summaries, and pertinent refinement parameters are presented in Table 3.

Crystallographic analysis (direct methods) of the data, using the SHELXTL-PC package of programs (11), disclosed the positions of the PNP atoms of the cation and the Ni atom. Subsequent refinement and difference Fourier analysis revealed the location of the remaining non-hydrogen atoms. All non-hydrogen atoms were refined with anisotropic thermal parameters. Boron hydrogen atoms were located by difference Fou-

Table 4. Atomic positional parameters (fractional coordinates, × 10^4) for compound **8***b* with estimated standard deviations in parentheses

Name	*x*	*y*	*z*
Ni	9240(1)	8509(1)	1129(1)
C(5)	10276(3)	7818(3)	989(4)
C(6)[a]	10553(5)	8495(4)	1095(5)
C(6a)[a]	10161(6)	8335(4)	415(5)
C(7)	10167(3)	9050(3)	610(3)
C(1)	7784(3)	8240(2)	392(2)
B(2)	8183(3)	7692(3)	1179(3)
C(3)	8740(3)	7954(2)	2020(3)
B(4)	8786(3)	8739(3)	2323(3)
B(5)	8573(3)	9438(3)	1521(3)
B(6)	8115(3)	9120(3)	493(3)
B(7)	7002(4)	8035(3)	988(3)
B(8)	7620(4)	8210(3)	2113(3)
B(9)	7722(3)	9236(3)	2136(3)
B(10)	7383(3)	9549(3)	1126(3)
B(11)	6949(3)	8849(3)	469(3)
B(12)	6791(3)	8817(3)	1523(3)
C(2)	7715(4)	7881(3)	−463(3)
C(4)	9222(3)	7365(3)	2586(3)
N	6880(2)	3707(2)	−111(2)
P(1)	7788(1)	3674(1)	565(1)
C(11)	7768(3)	4369(2)	1344(2)
C(12)	6942(3)	4691(2)	1430(3)
C(13)	6912(4)	5191(3)	2042(3)
C(14)	7692(4)	5389(3)	2579(3)
C(15)	8517(4)	5077(3)	2500(3)
C(16)	8559(3)	4557(2)	1893(3)
C(21)	7972(3)	2821(2)	1111(2)
C(22)	7686(3)	2729(2)	1871(3)
C(23)	7733(4)	2037(3)	2226(3)
C(24)	8055(3)	1456(2)	1847(3)
C(25)	8341(3)	1553(2)	1099(3)
C(26)	8300(3)	2230(2)	737(3)
C(31)	8765(3)	3857(2)	67(2)
C(32)	8632(3)	4202(2)	−697(3)
C(33)	9393(3)	4380(3)	−1069(3)
C(34)	10260(3)	4205(2)	−674(3)
C(35)	10402(3)	3864(3)	85(3)
C(36)	9648(3)	3679(2)	451(3)
P(2)	5964(1)	3273(1)	−446(1)
C(41)	5077(3)	3455(2)	168(3)
C(42)	5225(4)	3276(3)	1004(3)
C(43)	4612(4)	3478(3)	1505(3)
C(44)	3836(4)	3844(3)	1181(3)
C(45)	3665(4)	4019(3)	357(4)
C(46)	4303(3)	3828(3)	−152(3)
C(51)	6121(3)	2308(2)	−518(2)
C(52)	5619(3)	1796(2)	−184(3)
C(53)	5772(3)	1065(3)	−291(3)
C(54)	6420(3)	834(3)	−727(3)
C(55)	6916(4)	1327(3)	−1076(3)
C(56)	6777(4)	2062(3)	−970(3)
C(61)	5552(3)	3575(2)	−1500(2)
C(62)	4886(3)	3175(2)	−2008(3)
C(63)	4587(3)	3401(3)	−2818(3)
C(64)	4956(3)	4012(3)	−3108(3)
C(65)	5609(3)	4414(3)	−2608(3)
C(66)	5909(3)	4199(3)	−1797(3)

[a]Refined at one-half occupancy.

rier, and the carbon hydrogen atoms were included at geometrically calculated positions (C—H, 0.96 Å). The hydrogen atoms were allowed to ride on their parent carbon or boron atoms with fixed isotropic thermal parameters (U_{iso} = 0.08 and 0.06 Å^2, respectively). The methine carbon atom (C(6) and C(6a)) of the allyl group was disordered and was refined at one-half occupancy for each carbon position. Hydrogen atoms bonded to C(5) and C(7) were also disordered and were placed in calculated positions according to the appropriate adjacent disordered carbon atoms and refined at one-half occupancy. The final cycle of block full-matrix least-squares refinement which included a secondary extinction correction ($g = 1.0(6) \times 10^{-4}$ e^{-2}) yielded final residual indices and a respectable "goodness-of-fit" value. The quantity minimized was $\Sigma w(|F_o| - |F_c|)^2$ and the weighting function was $w = [\sigma^2(F) + 0.0023F^2]^{-1}$. The final electron-density difference synthesis displayed only random fluctuations. Atomic scattering and associated anomalous dispersion correction factors were taken from the usual source (12). Final atoms positional parameters are presented in Table 4. Anisotropic thermal parameters, hydrogen atom parameters, and a complete set of bond lengths and angles are available as supplementary data.[3]

Acknowledgment

We thank the Robert A. Welch Foundation for support (Grants AA-1201 and 0668).

References

1. (*a*) N. Carr, D.F. Mullica, E.L. Sappenfield and F.G.A. Stone. Inorg. Chem. **33**, 1666 (1994); (*b*) K.W. Fallis, D.F. Mullica, E.L. Sappenfield, and F.G.A. Stone. Inorg. Chem. **33**, 4927 (1994).
2. (*a*) S.J. Dossett, S. Li, and F.G.A. Stone. J. Chem. Soc. Dalton Trans. 1585 (1993); (*b*) S. Li and F.G.A. Stone. Polyhedron, **12**, 1689 (1993); (*c*) S.J. Dossett, S. Li, D.F. Mullica, E.L. Sappenfield, and F.G.A. Stone. J. Chem. Soc. Dalton Trans. 3551 (1993).
3. (*a*) M.F. Hawthorne, D.C. Young, T.D. Andrews, D.V. Howe, R.L. Pilling, A.D. Pitts, M. Reintjes, L.F. Warren, and P.A. Wegner. J. Am. Chem. Soc. **90**, 879 (1968); (*b*) D.F. Dustin, G.B. Dunks, and M.F. Hawthorne. J. Am. Chem. Soc. **95**, 1109 (1973).
4. S.J. Crennell, D.D. Devore, S.J.B. Henderson, J.A.K. Howard, and F.G.A. Stone. J. Chem. Soc. Dalton Trans. 1363 (1989).
5. S. Li, D. F. Mullica, E.L. Sappenfield, and F.G.A. Stone. J. Organomet. Chem. **467**, 95 (1994).
6. (*a*) F.Y. Lo, C.E. Strouse, K.P. Callahan, C.B. Knobler, and M.F. Hawthorne. J. Am. Chem. Soc. **97**, 428 (1975); (*b*) M.R. Churchill and B.G. DeBoer. Inorg. Chem. **13**, 1411 (1974).
7. N.W. Alcock, J.G. Taylor and M.G.H. Wallbridge. J. Chem. Soc. Dalton Trans. 1805 (1987).
8. (*a*) N. Carr, M.C. Gimeno and F.G.A. Stone. J. Chem. Soc. Dalton Trans. 2617 (1990); (*b*) S.J. Dossett, D.F. Mullica, E.L. Sappenfield, F.G.A. Stone and M.J. Went. J. Chem. Soc. Dalton Trans. 281 (1993); (*c*) N. Carr, D.F. Mullica, E.L. Sappenfield, and F.G.A. Stone. Organometallics, **12**, 1131 (1993); (*d*) N. Carr, D.F. Mullica, E.L. Sappenfield, F.G.A. Stone, and M. J. Went. Organometallics, **12**, 4350 (1993).
9. E.O. Fischer and G. Bürger. Z. Naturforsch. B: Anorg. Chem. Org. Chem. Biochem. Biophys. Biol. **16**, 77 (1961).
10. Y. Tatsuno, T. Yoshida and S. Otsuka. Inorg. Synth. **28**, 342 (1990).
11. SHELXTL-PC, Siemens Analytical X-Ray Instruments, Madison, Wis. 1989.
12. International tables for X-ray crystallography. Vol. 4. Kynoch Press, Birmingham. 1975.

[3] A complete set of supplementary data may be purchased from the Depository of Unpublished Data, Document Delivery, CISTI, National Research Council Canada, Ottawa, Canada K1A OS2.

Tables of atom parameters and a full listing of bond distances and angles have been deposited with the Cambridge Crystallographic Data Centre, University Chemical Laboratory, 12 Union Road, Cambridge, CB21EZ, U.K.

Can. J. Chem. Downloaded from www.nrcresearchpress.com by 80.90.12.36 on 09/08/12
For personal use only.

A study of a variety of *O,O*-alkylene dithiophosphate derivatives of triphenyl- and diphenylgermane. Crystal structures of $Ph_3Ge[S_2POCMe_2CMe_2O]$, $Ph_3Ge[S_2POCH_2CMe_2CH_2O]$, and $Ph_3Ge[S_2POCH_2CEt_2CH_2O]\cdot C_6H_6$

John E. Drake, Anil G. Mislankar, Raju Ratnani, and Jincai Yang

Abstract: The *O,O*-alkylene dithiophosphate derivatives of triphenyl- and diphenylgermane, $Ph_3Ge[S_2POCMe_2CMe_2O]$, $Ph_3Ge[S_2POCH_2CMe_2CH_2O]$, $Ph_3Ge[S_2POCH_2CEt_2CH_2O]$, $Ph_2Ge[S_2POCMe_2CMe_2O]_2$, $Ph_2Ge[S_2POCH_2CMe_2CH_2O]_2$, and $Ph_2Ge[S_2POCH_2CEt_2CH_2O]_2$, have been prepared and characterized by infrared, Raman, and ^1H, ^{13}C, and ^{31}P NMR spectroscopy, mass spectrometry, and, in three cases, X-ray crystallography. $Ph_3Ge[S_2POCMe_2CMe_2O]$, **1**, crystallizes as monoclinic in the space group $P2_1/a$ (No. 14) with the cell parameters $a = 12.868(5)$ Å, $b = 11.354(4)$ Å, $c = 17.207(4)$ Å, $\beta = 95.42(2)°$, $V = 2502(1)$ Å^3, $Z = 4$, $R = 0.0640$, and $R_w = 0.0585$. $Ph_3Ge[S_2POCH_2CMe_2CH_2O]$, **2**, crystallizes as orthorhombic in the space group *Pbca* (No. 61) with the cell parameters $a = 23.007(4)$ Å, $b = 16.840(4)$ Å, $c = 12.068(3)$ Å, $V = 4657(3)$ Å^3, $Z = 8$, $R = 0.0502$, and $R_w = 0.0329$. $Ph_3Ge[S_2POCH_2CEt_2CH_2O]\cdot C_6H_6$, **3**, crystallizes as monoclinic in the space group *C2/c* (No. 15) with the cell parameters $a = 35.48(2)$ Å, $b = 9.275(5)$ Å, $c = 20.78(1)$ Å, $\beta = 120.93(3)°$ $V = 5866(5)$ Å^3, $Z = 8$, $R = 0.0674$, and $R_w = 0.0562$. As with their methylgermanium analogues, the environment about germanium is essentially that of a distorted tetrahedron, with the terminal sulfur atoms oriented towards germanium rather than away from it, in contrast with analogous noncyclic dithiophosphatogermanes. The substituents on the atoms in both the five- and six-membered rings maintain their nonequivalence in solution, in contrast with tin analogues.

Key words: structure, germanium, diphenyl, triphenyl, cyclic dithiophosphates

Résumé : On a préparé les dérivés. *O,O*-alkylène diphosphates des triphényl- et tétraphénylgermanes, $Ph_3Ge[S_2POCMe_2CMe_2O]$, $Ph_3Ge[S_2POCH_2CMe_2CH_2O]$, $Ph_3Ge[S_2POCH_2CEt_2CH_2O]$, $Ph_2Ge[S_2POCMe_2CMe_2O]_2$, $Ph_2Ge[S_2POCH_2CMe_2CH_2O]_2$ et $Ph_2Ge[S_2POCH_2CEt_2CH_2O]_2$ et on les a caractérisé par spectroscopies infrarouge, Raman et RMN du ^1H, du ^{13}C et du ^{31}P, par spectrométrie de masse et, dans trois cas, par diffraction des rayons X. Le composé $Ph_3Ge[S_2POCMe_2CMe_2O]$, **1**, cristallise dans le groupe monoclinique $P2_1/a$ (No. 14) avec $a = 12,868(5)$, $b = 11,354(4)$ et $c = 17,207(4)$ Å, $\beta = 95,42(2)°$, $V = 2502(1)$ Å, $Z = 4$, $R = 0,0640$, and $R_w = 0,0585$. Le composé $Ph_3Ge[S_2POCH_2CMe_2CH_2O]$, **2**, cristallise dans le groupe orthorhombique *Pbca* (No. 61) avec $a = 23,007(4)$, $b = 16,840(4)$ et $c = 12,068(3)$ Å,

Received September 30, 1994.

This paper is dedicated to Professor William A.G. Graham on the occasion of his 65th birthday.

J.E. Drake,[1] A.G. Mislankar, R. Ratnani,[2] and J. Yang. Department of Chemistry and Biochemistry, University of Windsor, Windsor, ON N9B 3P4, Canada.

[1] Author to whom correspondence may be addressed. Telephone: (519) 253-4232 (Ext. 3551). Fax: (519) 973-7098. E-mail: ak4@uwindsor.ca

[2] Present address: Department of Chemistry, Dayanand College, Ajmer, India.

Can. J. Chem. Downloaded from www.nrcresearchpress.com by 80.90.12.36 on 09/08/12
For personal use only.

$V = 4657(3)$ Å^3, $Z = 8$, $R = 0{,}0502$, and $R_w = 0{,}0329$. Le composé $Ph_3Ge[S_2POCH_2CEt_2CH_2O]\cdot C_6H_6$, **3**, cristallise dans le groupe monoclinique *C2/c* (No. 15) avec $a = 35{,}48(2)$ Å, $b = 9{,}275(5)$ et $c = 20{,}78(1)$ Å, $\beta = 120{,}93(3)°$, $V = 5866(5)$ Å^3, $Z = 8$, $R = 0{,}0674$ et $R_w = 0{,}0562$. Comme dans le cas de leurs analogues méthylgermanium, l'environnement autour du germanium est essentiellement celui d'un tétraèdre déformé dans lequel les atomes de soufre terminaux sont orientés vers le germanium plutôt que dans le sens inverse; ceci fait contraste avec les analogues non cycliques dithiophosphatogermanes. Les substituants sur les atomes des cycles à cinq ainsi qu'à six chaînons maintiennent leur non équivalence en solution, en opposition avec la situation observée avec leurs analogues de l'étain.

Mots clés : structure, germanium, diphényl, triphényl, dithiophosphates cycliques.

[Traduit par la rédaction]

Can. J. Chem. Downloaded from www.nrcresearchpress.com by 80.90.12.36 on 09/08/12
For personal use only.

Introduction

We have demonstrated that *O,O*-dialkyldithiophosphate derivatives of germanium are monodentate with the nonbonding sulfur atom oriented away from germanium (1, 2), the distance of 5.253 (1) Å in $Ph_3Ge[S_2P(OMe)_2]$ being typical (1). This structure is also typical of xanthate derivatives of germanium (3–5). Recently, we reported the synthesis and characterization of a number of cyclic dithiophosphate derivatives of methylgermanes (6) whose NMR spectra showed unusual features that suggested that the solid state structures were maintained in solution, in contrast to what had been observed in general (7–17) and for tin and tellurium analogues in particular (14, 17). Unfortunately, we were only successful in obtaining a crystal structure for one derivative, $Me_2Ge[S_2POCMe_2CMe_2O]_2$, and so had no evidence of the solid state structures of derivatives containing only one dithiophosphate group. Ironically, we have been able to ob-tain the X-ray structures of all three triphenyl(dithiophosphato)germanes, $Ph_3Ge[S_2POCMe_2CMe_2O]$, **1**, $Ph_3Ge[S_2POCH_2CMe_2CH_2O]$, **2**, and $Ph_3Ge[S_2POCH_2CEt_2CH_2O]\cdot C_6H_6$, **3**, but have not been able to get data of sufficient quality to fully solve the structures of any of the diphenylgermanium analogues, **4**–**6**. In all three structures, the second sulfur atom of the dithiophosphate group is oriented toward germanium, rather than away from it as was found for the noncyclic dithiophosphates. However, the Ge--S secondary interactions are much weaker than in tin analogues such as $Ph_2Sn[S_2P(Oi\text{-}Pr)_2]_2$, where the dithiophosphate groups are fully bidentate (18), and are also apparently weaker than those in $Ph_3Sn[S_2POCMe_2CMe_2O]$, even though the dithiophosphate group therein is also anisobidentate (16).

Experimental

Materials

Chlorotriphenyl- and dichlorodiphenylgermane were obtained from Alfa and were used as supplied. Sodium and ammonium salts of *O,O*-alkylene dithiophosphates were prepared in the manner described in the literature and their purity was checked by ^{1}H, ^{13}C, and ^{31}P NMR spectroscopy (19). Benzene, toluene, carbon disulfide, and *n*-hexane were dried and distilled prior to use. All the reactions were carried out in air- and moisture-free conditions to prevent the formation of germanium oxides.

Synthesis of triphenylgermane derivatives of alkylene dithiophosphates

$Ph_3Ge[S_2POCMe_2CMe_2O]$, 1

Typically, the sodium salt of *O,O*-2,3-dimethylbutylene dithiophosphate, $Na[S_2POCMe_2CMe_2O]$ (0.111 g, 0.48 mmol), Ph_3GeCl (0.138 g, 0.40 mmol), and benzene (8 mL) were placed in a reaction vessel attached to a vacuum line and degassed at −196°C. Dry nitrogen was introduced and the mixture was allowed to warm up to ambient temperature and then refluxed for 7 h. The reaction mixture was filtered to separate NaCl and any unreacted salt, after which the solvent was evaporated off in vacuo to yield a pale yellow viscous liquid, which was dissolved in toluene and layered with *n*-hexane. Crystals formed in a matter of days in the refrigerator to give $Ph_3Ge[S_2POCMe_2CMe_2O]$, **1**; pale yellow solid, mp 99–101°C, yield 53%. Peaks corresponding to ^{74}Ge in a typical germanium cluster are seen at *m/z* (relative intensity): 515 ($(M-H)^+$, 1%), 438 ($(M-PhH)^+$, 20%), and 304 ($(M-HS_2POCMe_2CMe_2O)^+$, 100%) with a peak clearly not part of a germanium cluster at 212 ($(H_2S_2POCMe_2CMe_2O)^+$, 15%).

$Ph_3Ge[S_2POCH_2CMe_2CH_2O]$, 2, and

$Ph_3Ge[S_2POCH_2CEt_2CH_2O]$, 3

Similarly, using the salts $Na[S_2POCH_2CMe_2CH_2O]$ or $Na[S_2POCH_2CEt_2CH_2O]$ in slight excess to ensure complete substitution of chlorine, the following were prepared: $Ph_3Ge[S_2POCH_2CMe_2CH_2O]$, **2**; white solid, mp 145–147°C, yield 50%. Anal. calcd. for $C_{23}H_{25}O_4P_2S_4Ge$: C 55.12, H, 5.05; found: C 54.90, H 5.00. Peaks corresponding to ^{74}Ge in a typical germanium cluster are seen at *m/z* (relative intensity): 501 ($(M-H)^+$, 2%), 424 ($(M-PhH)^+$, 8%), and 304 ($(M-HS_2POCH_2CMe_2CH_2O)^+$, 100%) with a peak clearly not part of a germanium cluster at 199 ($(H_2S_2POCH_2CMe_2CH_2O)^+$, 15%). $Ph_3Ge[S_2POCH_2CEt_2CH_2O]$, **3**; white solid; mp 38–40°C, yield 54%. Peaks corresponding to ^{74}Ge in a typical germanium cluster are seen at *m/z* (relative intensity): 529 ($(M-H)^+$, 2%), 452 ($(M-PhH)^+$, 30%), and 304 ($(M-HS_2POCH_2CEt_2CH_2O)^+$,

Can. J. Chem. Downloaded from www.nrcresearchpress.com by 80.90.12.36 on 09/08/12
For personal use only.

100%) with a peak clearly not part of a germanium cluster at 227 ($(H_2S_2POCH_2CMe_2CH_2O)^+$, 30%). In the case of **3**, crystals of X-ray quality were obtained on recrystallization from benzene to yield $Ph_3Ge[S_2POCH_2CEt_2CH_2O]\cdot C_6H_6$.

Synthesis of diphenylgermane derivatives of alkylene dithiophosphates

$Ph_2Ge[S_2POCMe_2CMe_2O]_2$, 4

Typically, $Na[S_2POCMe_2CMe_2O]$ (0.509 g, 2.18 mmol), Ph_2GeCl_2 (0.240 g, 0.68 mmol), and benzene (10 mL) were placed in a Schlenk flask and degassed for *ca.* 30 min at −196°C. The mixture was allowed to gradually warm up to ambient temperature and then stirred for 7 h. The reaction mixture was filtered to separate NaCl and any unreacted salt, after which the solvent was evaporated off in vacuo to yield a white solid of the desired product, $Ph_2Ge[S_2POCMe_2\ CMe_2O]_2$, **4**; mp 174–175°C, yield 65 %. Anal. calcd. for $C_{24}H_{34}O_4P_2S_4Ge$: C 44.44, H 5.28; found: C 43.04, H 5.35. A peak corresponding to ^{74}Ge in a typical germanium cluster that dominates the spectrum is seen at *m/z* (relative intensity): 438 ($(M-HS_2POCMe_2CMe_2O)^+$, 100%).

$Ph_2Ge[S_2POCH_2CMe_2CH_2O]_2$, 5, and
$Ph_2Ge[S_2POCH_2CEt_2CH_2O]_2$, 6

Similarly, using the salts $NaS_2POCH_2CMe_2CH_2O$ or $NaS_2POCH_2CEt_2CH_2O$ in slight excess to ensure complete substitution of chlorine, were prepared: $Ph_2Ge[S_2POCH_2CMe_2CH_2O]_2$, **5**; white solid, mp 68–69°C, yield 62%. A peak corresponding to ^{74}Ge in a typical germanium cluster that dominates the spectrum is seen at *m/z* (relative intensity): 424 ($(M-HS_2POCH_2CMe_2CH_2O)^+$, 100%). $Ph_2Ge[S_2POCH_2CEt_2CH_2O]_2$, **6**; viscous liquid, yield 65%. A peak corresponding to ^{74}Ge in a typical germanium cluster that dominates the spectrum is seen at *m/z* (relative intensity): 452 ($(M-HS_2POCH_2CEt_2CH_2O)^+$, 100%). Unfortunately, despite extensive efforts to grow X-ray quality crystals, none were obtained for compounds **4–6**.

Physical measurements

All solvents were distilled prior to use. The elemental analyses were performed at Guelph Chemical Laboratories, Guelph, Ontario. The infrared spectra were recorded on a Nicolet 5DX FT spectrometer as KBr pellets. The ^1H and ^{13}C NMR spectra were recorded on a Bruker 300 FT NMR spectrometer in $CDCl_3$ solutions using Me_4Si as internal standard. The ^{31}P NMR spectra were recorded on a Bruker 200 FT NMR spectrometer in $CDCl_3$ using H_3PO_4 as external standard. The mass spectra were recorded by LSIMS on a Kratos Profile mass spectrometer. The melting points were determined on a Fisher–Johns apparatus.

X-ray crystallographic analysis

Block-like crystals of $Ph_3Ge[S_2POCMe_2CMe_2O]$, **1**, $Ph_3Ge[S_2POCH_2CMe_2CH_2O]$, **2**, and $Ph_3Ge[S_2POCH_2CEt_2CH_2O]\cdot C_6H_6$, **3**, were sealed in thin-walled glass capillaries and mounted on a Rigaku AFC6S diffractometer, with graphite-monochromated Mo Kα radiation.

Cell constants and an orientation matrix for data collection, obtained from a least-squares refinement using the setting angles of 25 carefully centered reflections in the range $8 < 2\theta < 29°$, corresponded to monoclinic (for **1** and **3**) and orthorhombic (for **5**) cells whose dimensions are given in Table 1. The systematic absences (*h0l*, $h = 2n + 1$; *0k0*, $k = 2n + 1$) for **1**, (*0kl*, $k = 2n + 1$; *h0l*, $l = 2n + 1$; *hk0*, $h = 2n + 1$) for **2**, and (*hkl*, $h + k = 2n + 1$; *h0l*, $l = 2n + 1$) for **3** are observed. Based on packing considerations, statistical analyses of intensity distributions, and the successful solution and refinement of the structure, the space group was determined to be $P2_1/a$ (No. 14), *Pbca* (No. 61), and *C2/c* (No. 15) for **1, 2,** and **3**, respectively.

The data were collected at a temperature of 23 ± 1°C using the ω–2θ scan technique to a maximum 2θ value of 50.0° for **1** and **2**, and 45.0° for **3**. The ω scans of several intense reflections, made prior to data collection, had an average width at half-height of 0.25°, 0.29°, and 0.28° for **1**, **2**, and **3**, respectively, with a takeoff angle of 6.0°. Scans of (1.42 + 0.30 tan θ)° for **1**, (1.00 + 0.30 tan θ)° for **2**, (1.37 + 0.30 tan θ)° for **3** were made at a speed of 16.0°/min (in ω). The weak reflections ($I < 10.0\sigma(I)$) were rescanned (maximum of two rescans) and the counts were accumulated to assure good counting statistics. Stationary background counts were recorded on each side of the reflection. The ratio of peak counting time to background counting time was 2:1. The diameter of the incident beam collimator was 0.5 mm, and the crystal-to-detector distance was 285.0 mm.

Of the 4894 (for **1**), 4626 (for **2**), or 4443 (for **3**) reflections that were collected, 4673 (for **1**), 4626 (for **2**), or 4111 (for **3**) were unique ($R_{int} = 0.097, 0.192, 0.202$) for **1**, **2**, and **3**, respectively. The intensities of three representative reflections that were measured after every 150 reflections remained constant throughout data collection, indicating crystal and electronic stability (no decay correction was applied).

The linear absorption coefficient for Mo Kα is 14.7 (for **1**), 15.5 (for **2**), and 12.4 cm^{-1} (for **3**). An empirical absorption correction, based on azimuthal scans of several reflections, was applied that resulted in transmission factors ranging from 0.82 to 1.00 (for **1**), 0.56 to 1.00 (for **2**), and 0.84 to 1.00 (for **3**). The data were corrected for Lorentz and polarization effects.

The structure was solved by direct methods (for structure solution methods, see ref. 20). The non-hydrogen atoms other than oxygen and carbon atoms were refined anisotropically and the hydrogen atoms were included in their idealized positions with C—H set at 0.95 Å and with isotropic thermal parameters set at 1.2 times that of the carbon atom to which they were attached. The final cycle of full-matrix least-squares refinement[3] was based on 2130 (for **1**), 1532 (for **2**), and 1176 (for **3**) observed reflections ($I > 3.00\sigma(I)$), and 136 (for **1**), 145 (for **2**), and 151 (for **3**) variable parameters, and converged

[3] Least-squares function minimized: $\Sigma w(|F_o| - |F_c|)^2$, where $w = 4F_o^2(F_o^2), \sigma^2(F_o^2) = [S^2(C + R^2B) + pF_o^2)^2]/(Lp)^2$, S = scan rate, c = total integrated peak count, R = ratio of scan time to background counting time, Lp = Lorentz-polarization factor, and $p = p$ factor.

Table 1. Summary of crystal data, intensity collection, and structural refinement for $Ph_3Ge[S_2POCMe_2CMe_2O]$, **1**, $Ph_3Ge[S_2POCH_2CMe_2CH_2O]$, **2**, and $Ph_3Ge[S_2POCH_2CEt_2CH_2O]\cdot C_6H_6$, **3**.

Parameter	$Ph_3Ge[S_2POCMe_2CMe_2O]$ **1**	$Ph_3Ge[S_2POCH_2CMe_2CH_2O]$ **2**	$Ph_3Ge[S_2POCH_2CEt_2CH_2O]\cdot C_6H_6$ **3**
Cell constants			
a (Å)	12.868 (5)	23.007 (4)	35.48 (2)
b (Å)	11.354 (4)	16.840 (4)	9.275 (5)
c (Å)	17.207 (4)	12.068 (3)	20.78 (1)
α (deg)	90.00	90.00	90.00
β (deg)	95.42 (2)	90.00	120.93 (3)
γ (deg)	90.00	90.00	90.00
Cell volume (Å^3)	2502 (1)	4675 (3)	5866 (5)
Space group	$P2_1/a$	$Pbca$	$C2/c$
Mol. wt (g mol^{-1})	515.16	501.13	607.30
Z	4	8	8
ρ_{calcd} (g cm^{-3})	1.37	1.42	1.38
Absorption coefficient μ (cm^{-1})	14.72	15.47	12.67
Transmission factors	0.82–1.00	0.56–1.00	0.77–1.00
Temperature (°C)	23	23	23
Radiation	MoKα 0.71069 Å		
Monochromator	Highly oriented graphite		
Total reflections measured	4894	4616	4111
Unique data used	2130	1531	1176
No. of parameters (NP)	145	136	151
$R = \Sigma\|\|F_o\| - \|F_c\|\|/\Sigma\|F_o\|$	0.0640	0.0502	0.0674
$R_w = [(\Sigma w(\|F_o\| - \|F_c\|)^2/\Sigma wF_o^2)]^{1/2}$	0.0585	0.0329	0.0562
Largest shift/esd, final cycle	0.001	0.0004	0.001
Largest residual electron density (e Å^{-3})	0.72	0.65	1.02
Atom associated with residual density	C(9)	C(15)	C(26)

(largest parameter shift was 0.001 times its esd) with unweighted and weighted agreement factors of $R = \Sigma||F_o| - |F_c||\Sigma|F_o| = 0.0640$ (for **1**), 0.0502 (for **2**), and 0.0674(for **3**) and $R_w = [(\Sigma w(|F_o| - |F_c|)^2/\Sigma wF_o^2)]^{1/2} = 0.0585$ (for **1**), 0.0329 (for **2**), and 0.0562 (for **3**).

The standard deviations of an observation of unit weight[4] were 2.44, 1.70, and 2.12 for **1, 2**, and **3**, respectively . The weighting scheme was based on counting statistics and included a factor ($p = 0.004$, 0.001, and 0.007 for **1, 2**, and **3**, respectively) to downweight the intense reflections. Plots of $\Sigma w(|F_o| - |F_c|)^2$ versus $|F_o|$, reflection order in data collection, sin θ/λ, and various classes of indices showed no unusual trends. The maximum and minimum peaks on the final difference Fourier map corresponded to 0.72 and −0.55 (for **1**), 0.65 and −0.34 (for **2**), and 0.43 and −0.39 e/Å^3 (for **3**).

Neutral-atom scattering factors were taken from Cromer and Waber (21). Anomalous dispersion effects were included in F_c (22); the values for $\Delta f'$ and $\Delta f''$ were those of Cromer (23). All calculations were performed using the TEXSAN (24) crystallographic software package.

The final atomic coordinates and equivalent isotropic thermal parameters for the non-hydrogen atoms are given in Tables 2, 3, and 4, important distances and bond angles in Tables 5 and 6, respectively, and ORTEP diagrams in Figs. 1, 2, and 3. Tables of final thermal parameters of non-hydrogen atoms, final fractional coordinates and thermal parameters of hydrogen atoms, and anisotropic thermal parameters have been deposited.[5]

Results and discussion

Several *O,O*-alkylene dithiophosphate derivatives of triphenyl- and diphenylgermane were prepared in 55–65% yields by the reaction of a slight excess of the sodium or ammonium salt of the appropriate *O,O*-alkylene dithiophosphoric acid with

[4] Standard deviation of an observation of unit weight: $[\Sigma w(|F_o| - |F_c|)^2]/(N_o - N_v)^{1/2}$, where N_o = number of observations and N_v = number of variables.

[5] Copies of material on deposit may be purchased from: The Depository of Unpublished Data, Document Delivery, CISTI, National Research Council Canada, Ottawa, Canada K1A 0S2.

The tables of atomic coordinates have also been deposited with the Cambridge Crystallographic Data Centre, and can be obtained on request from The Director, Cambridge Crystallographic Data Centre, University Chemical Laboratory, 12 Union Road, Cambridge, CB2 1EZ, U.K.

Structure factor amplitudes are no longer being deposited and may be obtained directly from the author.

Can. J. Chem. Downloaded from www.nrcresearchpress.com by 80.90.12.36 on 09/08/12
For personal use only.

Can. J. Chem. Downloaded from www.nrcresearchpress.com by 80.90.12.36 on 09/08/12
For personal use only.

Table 2. Final fractional coordinates and B(eq) for non-hydrogen atoms of $Ph_3Ge[S_2POCMe_2CMe_2O]$, **1**, with standard deviations in parentheses.

Atom	x	y	z	B(eq)
Ge(1)	0.30277(7)	0.06601(9)	0.68202(6)	2.94(4)
S(1)	0.1998(2)	−0.0478(2)	0.7500(1)	4.0(1)
S(2)	0.4007(2)	0.0179(2)	0.8818(2)	4.1(1)
P(1)	0.2744(2)	−0.0692(2)	0.8609(1)	2.9(1)
O(1)	0.1880(4)	−0.0460(5)	0.9213(3)	3.0(3)
O(2)	0.2794(5)	−0.2082(5)	0.8700(3)	3.5(3)
C(1)	0.1376(7)	−0.1580(8)	0.9429(5)	2.9(4)
C(2)	0.2258(8)	−0.2494(8)	0.9380(5)	3.0(4)
C(3)	0.0447(8)	−0.1795(8)	0.8856(6)	3.9(5)
C(4)	0.1061(8)	−0.143(1)	1.0250(5)	4.1(5)
C(5)	0.3053(8)	−0.249(1)	1.0074(6)	4.6(5)
C(6)	0.1862(9)	−0.3731(9)	0.9193(6)	4.8(6)
C(7)	0.4335(4)	−0.0106(6)	0.6637(4)	3.5
C(8)	0.4928(5)	0.0444(5)	0.6104(4)	4.8
C(9)	0.5852(5)	−0.0075(6)	0.5909(4)	5.5
C(10)	0.6181(4)	−0.1144(6)	0.6247(4)	5.1
C(11)	0.5588(5)	−0.1695(5)	0.6780(4)	5.6
C(12)	0.4665(5)	−0.1176(6)	0.6975(4)	4.3
C(13)	0.2164(5)	0.0725(7)	0.5825(3)	3.5
C(14)	0.1757(5)	0.1792(5)	0.5532(4)	4.3
C(15)	0.1154(6)	0.1823(5)	0.4815(4)	5.3
C(16)	0.0959(5)	0.0788(7)	0.4390(3)	5.7
C(17)	0.1366(6)	−0.0279(6)	0.4682(4)	5.4
C(18)	0.1969(5)	−0.0310(5)	0.5400(4)	4.5
C(19)	0.3162(5)	0.2236(4)	0.7252(4)	2.9
C(20)	0.2268(4)	0.2834(6)	0.7431(4)	4.5
C(21)	0.2335(5)	0.4009(6)	0.7666(4)	5.3
C(22)	0.3296(6)	0.4587(5)	0.7722(4)	5.6
C(23)	0.4190(4)	0.3990(6)	0.7543(4)	5.7
C(24)	0.4123(4)	0.2814(6)	0.7308(4)	4.8

Table 3. Final fractional coordinates and B(eq) for non-hydrogen atoms of $Ph_3Ge[S_2POCH_2CMe_2CH_2O]$, **2**, with standard deviations in parentheses.

Atom	x	y	z	B(eq)
Ge(1)	0.39222(5)	0.58558(6)	0.22913(8)	2.80(4)
S(1)	0.4300(1)	0.5512(2)	0.0629(2)	3.5(1)
S(2)	0.3201(1)	0.4168(2)	0.0573(2)	5.6(2)
P(1)	0.3639(1)	0.4934(2)	−0.0231(2)	3.4(1)
O(1)	0.3243(3)	0.5598(4)	−0.0759(5)	3.6(4)
O(2)	0.3993(3)	0.4561(3)	−0.1233(5)	3.6(4)
C(1)	0.3486(5)	0.6125(6)	−0.1608(9)	4.1(6)
C(2)	0.3753(4)	0.5656(5)	−0.2564(8)	3.6(6)
C(3)	0.4212(4)	0.5093(6)	−0.2096(8)	3.8(6)
C(4)	0.4059(5)	0.6224(6)	−0.3369(8)	5.4(7)
C(5)	0.3276(5)	0.5168(7)	−0.318(1)	6.3(8)
C(6)	0.3200(2)	0.6457(3)	0.2132(5)	2.8
C(7)	0.3104(2)	0.6924(4)	0.1195(4)	3.3
C(8)	0.2608(3)	0.7398(3)	0.1127(4)	3.7
C(9)	0.2208(2)	0.7405(3)	0.1996(6)	4.3
C(10)	0.2304(3)	0.6937(4)	0.2932(5)	4.5
C(11)	0.2800(3)	0.6463(3)	0.3000(4)	3.7
C(12)	0.4522(3)	0.6594(3)	0.2827(6)	2.6
C(13)	0.5028(3)	0.6766(4)	0.2238(4)	4.3
C(14)	0.5416(2)	0.7335(4)	0.2638(6)	5.4
C(15)	0.5297(3)	0.7732(3)	0.3627(6)	5.5
C(16)	0.4790(3)	0.7560(4)	0.4216(4)	5.8
C(17)	0.4403(2)	0.6991(4)	0.3816(5)	4.4
C(18)	0.3858(3)	0.4943(3)	0.3287(4)	2.6
C(19)	0.4351(2)	0.4686(4)	0.3857(5)	3.7
C(20)	0.4316(2)	0.4033(4)	0.4566(5)	4.7
C(21)	0.3789(3)	0.3637(3)	0.4704(4)	4.5
C(22)	0.3296(2)	0.3893(4)	0.4134(5)	4.0
C(23)	0.3331(2)	0.4546(4)	0.3425(5)	3.1

chlorotriphenyl- or dichlorodiphenylgermane in benzene in accord with the equations below.

[1] $Ph_3GeCl + MS_2POGO \rightarrow Ph_3Ge[S_2POGO] + MCl$

[2] $Ph_2GeCl_2 + 2MS_2POGO \rightarrow Ph_2Ge[S_2POGO]_2 + 2MCl$

(M = Na or NH_4;G = $-CMe_2CMe_2-$, $-CH_2CMe_2CH_2-$, or $-CH_2CEt_2CH_2-$)

The reactions with dichlorodiphenylgermane took place readily at room temperature under standard Schlenk-tube conditions to yield the $Ph_2Ge[S_2POGO]_2$ derivatives $Ph_2Ge[S_2POCMe_2CMe_2O]_2$, **4**, $Ph_2Ge[S_2POCH_2CMe_2CH_2O]_2$, **5**, and $Ph_2Ge[S_2POCH_2CEt_2CH_2O]_2$, **6**. By contrast, the starting materials showed little or no sign of reaction under the same conditions with chlorotriphenylgermane. However, when these reactants were refluxed for several hours in benzene, similar yields of the $Ph_3Ge[S_2POGO]$ derivatives $Ph_3Ge[S_2POCMe_2CMe_2O]$, **1**, $Ph_3Ge[S_2POCH_2CMe_2CH_2O]$, **2**, and $Ph_3Ge[S_2POCH_2CEt_2CH_2O]$, **3**, were obtained.

All of the compounds **1–6** are stable on exposure to atmospheric oxygen and moisture and in common organic solvents such as benzene, *n*-hexane, toluene, carbon disulfide, and chloroform, the latter being used as the preferred solvent for NMR spectroscopic studies. Samples of **1-6** are stable over a long period, particularly when kept refrigerated, as can be confirmed by the fact that NMR spectra recorded after several months show no changes from the spectra recorded initially. The ^1H NMR spectra confirm that they are 99% pure relative to any hydrogen-containing impurities.

Extensive attempts were made to grow X-ray quality crystals using a variety of solvents or solvent mixtures for **1–6**, but unfortunately crystals of acceptable quality were only obtained for the three triphenyl derivatives, $Ph_3Ge[S_2POCMe_2CMe_2O]$, **1**, $Ph_3Ge[S_2POCH_2CMe_2CH_2O]$, **2**, and $Ph_3Ge[S_2POCH_2CEt_2CH_2O]\cdot C_6H_6$, **3**.

The crystal structure of $Ph_3Ge[S_2POCMe_2CMe_2O]$, 1

Triphenyl(*O,O*-2,3-dimethylbutylene dithiophosphato)ger-

Can. J. Chem. Downloaded from www.nrcresearchpress.com by 80.90.12.36 on 09/08/12
For personal use only.

Table 4. Final fractional coordinates and B(eq) for non-hydrogen atoms of $Ph_3Ge[S_2POCH_2CEt_2CH_2O]\cdot C_6H_6$, **3**, with standard deviations in parentheses.

Atom	x	y	z	B(eq)
Ge(1)	0.32836(7)	0.1651(2)	0.4920(1)	4.19(9)
S(1)	0.3923(2)	0.0643(6)	0.5169(3)	5.9(3)
S(2)	0.3852(2)	0.2381(7)	0.3669(3)	7.8(3)
P(1)	0.4199(2)	0.2007(6)	0.4723(3)	5.0(3)
O(1)	0.4343(4)	0.344(1)	0.5192(6)	5.2(6)
O(2)	0.4650(4)	0.115(1)	0.4971(7)	6.0(7)
C(1)	0.4681(6)	0.335(2)	0.598(1)	6(1)
C(2)	0.5104(6)	0.265(2)	0.610(1)	4(1)
C(3)	0.4988(6)	0.114(2)	0.579(1)	5(1)
C(4)	0.5420(6)	0.240(2)	0.696(1)	6(1)
C(5)	0.5603(7)	0.379(3)	0.741(1)	9(1)
C(6)	0.5311(6)	0.356(2)	0.575(1)	7(1)
C(7)	0.5745(7)	0.301(3)	0.586(1)	9(1)
C(8)	0.3341(4)	0.370(1)	0.5119(8)	6.1
C(9)	0.3387(3)	0.466(2)	0.4648(5)	6.1
C(10)	0.3442(3)	0.613(1)	0.4818(7)	6.1
C(11)	0.3451(4)	0.663(1)	0.5459(8)	6.1
C(12)	0.3405(3)	0.567(2)	0.5929(5)	6.1
C(13)	0.3350(4)	0.420(1)	0.5759(7)	6.1
C(14)	0.3199(5)	0.056(1)	0.5646(7)	5.8
C(15)	0.3530(3)	0.056(1)	0.6401(9)	5.8
C(16)	0.3472(4)	−0.020(1)	0.6923(5)	5.8
C(17)	0.3084(5)	−0.097(1)	0.6689(7)	5.8
C(18)	0.2754(3)	−0.097(1)	0.5934(8)	5.8
C(19)	0.2811(4)	−0.021(1)	0.5412(5)	5.8
C(20)	0.2821(4)	0.120(2)	0.3923(6)	7.1
C(21)	0.2449(5)	0.207(1)	0.3599(8)	7.1
C(22)	0.2082(4)	0.170(1)	0.2911(8)	7.1
C(23)	0.2088(4)	0.044(2)	0.2546(6)	7.1
C(24)	0.2460(5)	−0.044(1)	0.2870(8)	7.1
C(25)	0.2826(4)	−0.006(1)	0.3558(9)	7.1
C(26)	0.4635(7)	0.229(2)	0.202(1)	10.1(7)
C(27)	0.466(1)	0.223(3)	0.278(2)	17(1)
C(28)	0.514(1)	0.235(4)	0.352(2)	18(1)

mane, **1**, crystallizes in the space group $P2_1/a$ and its ORTEP diagram (Fig. 1) illustrates that the immediate environment about germanium is that of a distorted tetrahedron. The C-Ge-C angles range from 107.7(3)° to 115.3(3)° and the S-Ge-C angles from 99.4(2)° to 112.8(2)° so that, although the former have an average value larger, 111(4)°, and the latter an average value smaller, 108(7)°, than the all-tetrahedral angle, the difference is within statistical error. This is similar to the situation reported for $Ph_3Sn[S_2POCMe_2CMe_2O]$ where the C-Sn-C angles ranged from 105.7(4) to 118.9(3)° and those of S-Sn-C from 99.8(3) to 111.5(3)° (16). However, it is in contrast to the situation in $Me_2Ge[S_2POCMe_2CMe_2O]_2$ where the C-Ge-C angle is 121.6(5)° and the average of the S-Ge-C angles is 110.2(5)° (6) but not very different from the situation in the noncyclic germanium analogue, $Ph_3Ge[S_2P(OMe)_2]$, where the C-Ge-C angles ranged from 110.6(2) to 114.4(2)° and those of S-Ge-C from 98.7(1)° to 111.9(1)° (1), or in its tin analogue, $Ph_3Sn[S_2P(OEt)_2]$, which has been described as a

Fig. 1. ORTEP plot of the molecule $Ph_3Ge[S_2POCMe_2CMe_2O]$, **1**. The atoms are drawn with 25% probability ellipsoids. Hydrogen atoms are omitted for clarity.

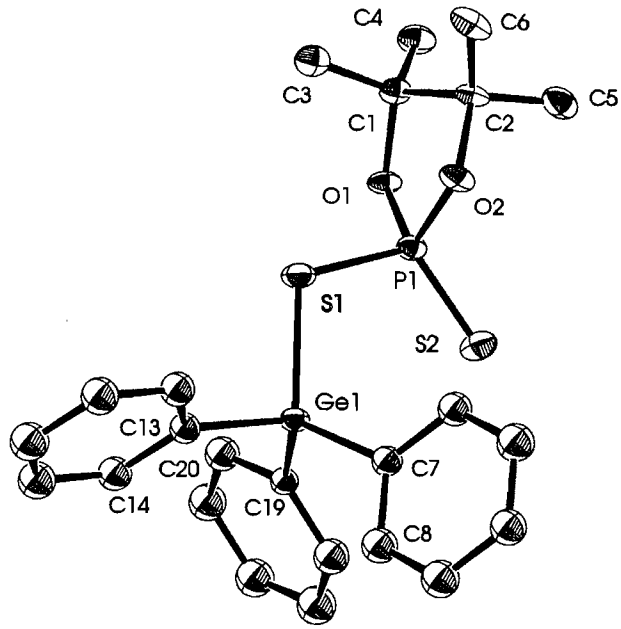

unique, monodentate dithiophosphate derivative (25), in which the C-Sn-C angles ranged from 110.8(1)° to 113.1(1)° and those of S-Sn-C from 100.09(9)° to 114.47(9)°. The smallest S-Ge-C angle in $Ph_3Ge[S_2POCMe_2CMe_2O]$, **1**, involves the carbon atom on the side of the tetrahedron furthest from the dithiophosphate group where there is least steric hindrance, as was observed for $Ph_3Ge[S_2P(OMe)_2]$.

The average Ge—C bond length in **1** of 1.946(10) Å is very similar to that in $Ph_3Ge[S_2P(OMe_2]$ and slightly longer than that in $Me_2Ge[S_2POCMe_2CMe_2O]_2$ where it is 1.915(7) Å (6). The difference is probably associated with the fact that in the latter case there are two dithiophosphate groups rather than one and that methyl groups are present rather than phenyl. Thus the Ge—C bond in $Ph_2Ge[S_2P(OMe)_2]_2$ is shorter, 1.931(2) Å, than in the triphenyl analogue and, in related dithiocarbamates, the methyl derivatives have shorter Ge—C bonds than the phenyl as is demonstrated by those in $Me_2Ge[S_2CNMe_2]_2$, 1.921(7) and 1.910(6) Å, and $Ph_2Ge[S_2CNEt_2]_2$, 1.928(3) Å (26, 27). Ironically, in the methyl series, $Me_3Ge[S_2POGO]$ and $Me_2Ge[S_2POGO]_2$, we were only able to get X-ray quality crystals for $Me_2Ge[S_2POCMe_2CMe_2O]_2$ (1), whereas for the phenyl analogues we solved three structures but all are triphenyl derivatives. The Ge—S bond length of 2.255(3) Å in **1** is similar to those in $Ph_2Ge[S_2P(OMe)_2]_2$, 2.255(4) Å, but shorter than that in $Ph_3Ge[S_2P(OMe)_2]$, 2.285(1) Å, or the average value in $Me_2Ge[S_2POCMe_2CMe_2O]_2$, 2.272(5) Å. The Ge--S distances to the second sulfur atom are very different for the cyclic and noncyclic dithiophosphates, as will be discussed later.

The P—S(Ge) bonds in $Ph_3Ge[S_2POCMe_2CMe_2O]$, **1**, are only slightly longer, 2.068(3) Å, than the P=S bonds,

Table 5. Interatomic distances (Å) in compounds **1–3**, with standard deviations in parentheses.

$Ph_3Ge[S_2POCMe_2CMe_2O]$, **1**		$Ph_3Ge[S_2POCH_2CMe_2CH_2O]$, **2**		$Ph_3Ge[S_2POCH_2CEt_2CH_2O]\cdot C_6H_6$, **3**	
Atoms	Distance	Atoms	Distance	Atoms	Distance
Ge(1)—S(1)	2.255(3)	Ge(1)—S(1)	2.262(3)	Ge(1)—S(1)	2.254(6)
Ge(1)—C(7)	1.946(6)	Ge(1)—C(6)	1.956(5)	Ge(1)—C(8)	1.93(1)
Ge(1)—C(13)	1.953(5)	Ge(1)—C(12)	1.966(5)	Ge(1)—C(14)	1.96(2)
Ge(1)—C(19)	1.939(5)	Ge(1)—C(18)	1.957(5)	Ge(1)—C(20)	1.916(9)
S(1)—P(1)	2.068(3)	S(1)—P(1)	2.084(4)	S(1)—P(1)	2.09(1)
S(2)—P(1)	1.908(4)	S(2)—P(1)	1.901(4)	S(2)—P(1)	1.912(7)
P(1)—O(1)	1.614(6)	P(1)—O(1)	1.576(7)	P(1)—O(1)	1.57(1)
P(1)—O(2)	1.587(6)	P(1)—O(2)	1.587(5)	P(1)—O(2)	1.62(1)
O(1)—C(1)	1.49(1)	O(1)—C(1)	1.47(1)	O(1)—C(1)	1.45(2)
O(2)—C(3)	1.49(1)	O(2)—C(3)	1.46(1)	O(2)—C(3)	1.49(2)
C(1)—C(2)	1.55(1)	C(1)—C(2)	1.53(1)	C(1)—C(2)	1.54(3)
C(1)—C(3)	1.50(1)	C(2)—C(3)	1.53(1)	C(2)—C(3)	1.51(3)
C(1)—C(4)	1.52(1)	C(2)—C(4)	1.53(1)	C(2)—C(4)	1.57(3)
C(2)—C(5)	1.50(1)	C(2)—C(5)	1.56(2)	C(2)—C(6)	1.53(4)
C(2)—C(6)	1.52(1)			C(4)—C(5)	1.53(3)
				C(6)—C(7)	1.53(3)
Ge(1)--S(2)	3.590(3)	Ge(1)--S(2)	3.889(3)	Ge(1)--S(2)	4.082(8)
Ge(1)--O(1)	4.680(6)	Ge(1)--O(1)	4.022(6)	Ge(1)--O(1)	3.87(1)
Ge(1)--O(2)	4.579(6)	Ge(1)--O(2)	4.782(6)	Ge(1)--O(2)	4.82(2)
P(1)--C(3)	3.27(1)	P(1)--H(2)	2.86	P(1)--H(2)	2.81
P(1)--C(4)	3.81(1)	P(1)--H(1)	3.41	P(1)--H(1)	3.39
P(1)--C(5)	3.24(1)	P(1)--H(3)	2.86	P(1)--H(3)	2.87
P(1)--C(6)	3.80(1)	P(1)--H(4)	3.41	P(1)--H(4)	3.45
		P(1)--C(4)	4.47(1)	P(1)--C(4)	4.45(2)
		P(1)--C(5)	3.67(1)	P(1)--C(6)	3.82(2)

1.908(4) Å, and essentially the same as in $Me_2Ge[S_2POCMe_2CMe_2O]_2$. These relatively small differences are typical of all metal dithiophosphates, irrespective of their mode of bonding, and are similar to those reported for $Ph_3Sn[S_2POCMe_2CMe_2O]$ (16) and for the diligands, $[OCMe_2CMe_2OP(S)S]_2$ (28) and $[(i\text{-}PrO)_2P(S)S]_2$ (29). In view of this insensitivity to changes in environment, it is not surprising that the distortion around phosphorus from all tetrahedral angles is similar to that found in $Ph_3Ge[S_2P(OMe)_2]$. The orientation in the five-membered ring system is such that two of the carbon methyl atoms are at an average distance of 3.26(2) Å from the phosphorus atom and the other two are at 3.805(7) Å. A view down the C—C bond of the ring shows that the four methyl groups attached to them are in the staggered configuration expected for the more stable arrangement with the pair at 3.26(2) Å pointing above and below the approximate plane of the distorted ring in an arrangement essentially identical to that observed in $Me_2Ge[S_2POCMe_2CMe_2O]_2$ (6) and $Me_2Te[S_2POCMe_2CMe_2O]_2$ (17).

The crystal structures of $Ph_3Ge[S_2POCH_2CMe_2CH_2O]$, 2, and $Ph_3Ge[S_2POCH_2CEt_2CH_2O]\cdot C_6H_6$, 3

$Ph_3Ge[S_2POCH_2CMe_2CH_2O]$, **2**, crystallizes in the space group *Pbca* and $Ph_3Ge[S_2POCH_2CEt_2CH_2O]\cdot C_6H_6$, **3**, in *C2/c*, and the orientations chosen for their ORTEP diagrams (Figs. 2 and 3) illustrate that, as with **1**, the immediate environment about germanium is that of a distorted tetrahedron. The C-Ge-C angles range from 107.6(2)° to 113.7(3)° for **2** and from 109.4(6)° to 112.7(6)° for **3** to give very similar average values of 111(3)° and 112(2)°, respectively. The S-Ge-C angles range from 100.6(2)° to 111.9(2)° for **2** and 98.2(5)° to 112.1(4)° for **3** with essentially the same average values of 108(7)° and 107(8)°. Thus, as with **1**, the average value of the C-Ge-C angle is larger than the all-tetrahedral angle and that of the S-Ge-C angle is smaller, but the differences are within statistical error. Also, as with **1**, the smallest S-Ge-C angle in **2** and **3** involves the carbon atom on the side of the tetrahedron furthest from the dithiophosphate group where there is least steric hindrance.

The average Ge—C bond lengths in **2** and **3** of 1.960(6) and 1.94 (2) Å, respectively, are similar to that in **1** of 1.946(10) Å. The Ge—S bond lengths of 2.262(3) and 2.254(6) Å in **2** and **3**, respectively, are similar to that in **1** and those in $Ph_2Ge[S_2P(OMe)_2]_2$, but shorter than that in $Ph_3Ge[S_2P(OMe)_2]$, or the average value in $Me_2Ge[S_2POCMe_2CMe_2O]_2$. It has been noted that the Ge—S bond length of 2.272(5) Å in $Me_2Ge[S_2POCMe_2CMe_2O]_2$ is similar to those in $Ph_2Ge[S_2CNEt_2]_2$ and $Me_2Ge[S_2CNMe_2]_2$, where the dithiocarbamate groups are assumed to be anisobidentate, but longer

Can. J. Chem. Downloaded from www.nrcresearchpress.com by 80.90.12.36 on 09/08/12
For personal use only.

Table 6. Bond angles (deg) in compounds **1–3**, with standard deviations in parentheses.

$Ph_3Ge[S_2POCMe_2CMe_2O]$, **1**		$Ph_3Ge[S_2POCH_2CMe_2CH_2O]$, **2**		$Ph_3Ge[S_2POCH_2CEt_2CH_2O]\cdot C_6H_6$, **3**	
Bonds	Angle	Bonds	Angle	Bonds	Angle
S(1)—Ge(1)—C(7)	112.8(2)	S(1)—Ge(1)—C(6)	111.8(2)	S(1)—Ge(1)—C(8)	112.1(4)
S(1)—Ge(1)—C(13)	99.4(2)	S(1)—Ge(1)—C(12)	100.6(2)	S(1)—Ge(1)—C(14)	98.2(5)
S(1)—Ge(1)—C(19)	111.5(2)	S(1)—Ge(1)—C(18)	111.9(2)	S(1)—Ge(1)—C(20)	111.1(5)
C(7)—Ge(1)—C(13)	107.7(3)	C(6)—Ge(1)—C(12)	107.6(2)	C(8)—Ge(1)—C(14)	112.6(7)
C(7)—Ge(1)—C(19)	115.3(3)	C(6)—Ge(1)—C(18)	113.7(3)	C(8)—Ge(1)—C(20)	112.7(6)
C(13)—Ge(1)—C(19)	108.9(3)	C(12)—Ge(1)—C(18)	110.4(3)	C(14)—Ge(1)—C(20)	109.4(6)
Ge(1)—S(1)—P(1)	107.5(1)	Ge(1)—S(1)—P(1)	106.3(1)	Ge(1)—S(1)—P(1)	107.1(3)
S(1)—P(1)—S(2)	115.2(2)	S(1)—P(1)—S(2)	116.7(2)	S(1)—P(1)—S(2)	116.4(3)
S(1)—P(1)—O(1)	106.7(2)	S(1)—P(1)—O(1)	106.9(3)	S(1)—P(1)—O(1)	108.2(7)
S(1)—P(1)—O(2)	102.7(2)	S(1)—P(1)—O(2)	100.9(3)	S(1)—P(1)—O(2)	100.0(6)
S(2)—P(1)—O(1)	114.8(2)	S(2)—P(1)—O(1)	112.4(3)	S(2)—P(1)—O(1)	111.7(6)
S(2)—P(1)—O(2)	118.1(3)	S(2)—P(1)—O(2)	113.1(3)	S(2)—P(1)—O(2)	113.9(7)
O(1)—P(1)—O(2)	97.1(3)	O(1)—P(1)—O(2)	105.6(3)	O(1)—P(1)—O(2)	105.4(7)
P(1)—O(1)—C(1)	111.3(5)	P(1)—O(1)—C(1)	119.5(6)	P(1)—O(1)—C(1)	118(1)
P(1)—O(2)—C(2)	111.8(5)	P(1)—O(2)—C(3)	118.5(5)	P(1)—O(2)—C(3)	117(1)
O(1)—C(1)—C(2)	102.8(7)	O(1)—C(1)—C(2)	111.5(8)	O(1)—C(1)—C(2)	112(1)
O(1)—C(1)—C(3)	108.3(7)				
O(1)—C(1)—C(4)	107.1(7)				
O(2)—C(2)—C(1)	103.2(7)	O(2)—C(3)—C(2)	113.9(8)	O(2)—C(3)—C(2)	111(1)
O(2)—C(2)—C(5)	107.0(8)				
O(2)—C(2)—C(6)	107.1(7)				
C(1)—C(2)—C(5)	113.7(8)	C(1)—C(2)—C(3)	108.7(8)	C(1)—C(2)—C(3)	107(2)
C(1)—C(2)—C(6)	113.5(8)	C(1)—C(2)—C(4)	109.8(8)	C(1)—C(2)—C(4)	108(2)
C(2)—C(1)—C(3)	113.5(8)	C(1)—C(2)—C(5)	110.4(8)	C(1)—C(2)—C(6)	111(2)
C(2)—C(1)—C(4)	113.0(7)	C(3)—C(2)—C(4)	107.7(8)	C(3)—C(2)—C(4)	103(1)
C(3)—C(1)—C(4)	111.4(8)	C(3)—C(2)—C(5)	109.6(8)	C(3)—C(2)—C(6)	114(2)
C(5)—C(2)—C(6)	111.4(8)	C(4)—C(2)—C(5)	110.6(8)	C(4)—C(2)—C(6)	113(2)
				C(2)—C(4)—C(5)	114(2)
				C(2)—C(6)—C(7)	116(2)
S(1)—Ge(1)--S(2)	65.59(2)	S(1)—Ge(1)--S(2)	60.27(8)	S(1)—Ge(1)--S(2)	56.4(2)

than those in $Ph_2Ge[S_2CO(i\text{-}Pr)]_2$, 2.252(3) Å (3), and $Ph_2Ge[S_2P(OMe)_2]_2$, 2.255(4), where the xanthate and noncyclic dithiophosphate ligands are undoubtedly monodentate, because the Ge--S distances to the terminal sulfur atom are 4.754(1) Å in $Ph_2Ge[S_2CO(i\text{-}Pr)]_2$, 5.38(2) Å in $Ph_2Ge[S_2P(OMe)_2]_2$, and 5.253(1) Å in $Ph_3Ge[S_2P(OMe)_2]$. The longer Ge—S bonds in $Me_2Ge[S_2POCMe_2CMe_2O]_2$ and $Ph_2Ge[S_2CNEt_2]_2$ were thus apparently related to the orientation of the second sulfur atom toward, rather than away from, germanium, with Ge--S distances of 3.183(1) Å in $Ph_2Ge[S_2CNEt_2]_2$ and 3.49(3) Å in $Me_2Ge[S_2POCMe_2CMe_2O]_2$. A Ge--S distance of 3.183 (1) Å is considerably shorter than the sum of the van der Waals radii of germanium and sulfur of 3.75 Å (30), whereas one of 3.49(3) Å is relatively long and corresponds to a Pauling partial bond order (17) of only about 0.05. Thus, while the claim of anisobidentate behaviour for the dithiocarbamates appears to be valid, there is some doubt in the case of the cyclic dithiophosphate. For **1, 2**, and **3**, the Ge—S bonds appear to be relatively short and of the same order of magnitude as the clearly monodentate, noncyclic dithiophosphates, but, by contrast, the second sulfur atom is oriented toward, rather than away from, germanium. The Ge--S distances of 3.590(3), 3.889(3), and 4.082(8) Å, respectively, for **1, 2**, and **3,** are considerably less than those in the noncyclic derivatives, but they approach or exceed the sum of the van der Waals radii, and the Pauling partial bond orders are only 0.03, 0.02, and 0.01, for **1, 2**, and **3**, respectively. Thus, in contrast to **1**, where the orientation of the second sulfur atom toward germanium in preference to either of the two oxygen atoms is clear even though the interaction is very weak, for **2** and **3**, with the six-membered ring dithiophosphate, the orientation becomes less defined as the Ge--O distances decrease. This is also demonstrated by the S-Ge-S bite angle, which is 65.59(2)° in **1** but which decreases considerably to 60.27(8)° and 56.4(2)°, respectively, in **2** and **3**.

In the related tin compounds, $Me_2Sn[S_2POCMe_2CMe_2O]_2$ (15) and $Ph_3Sn[S_2POCMe_2CMe_2O]$ (16), the aniso Sn--S distances are shorter, ranging from 3.130(1) to 3.411(3) Å, respectively, in the dimethyl and triphenyl compound, and because of the larger covalent radius of tin these distances correspond to Pauling partial bond orders ranging from 0.19 to 0.10. The S-Sn-S bite angles of 70.68(3)° and 66.8(8)° are consistent with stronger anisobidentate bonding in the dimethyl derivative. By contrast, in the noncyclic dithiophosphate tin derivative, $Ph_2Sn[S_2P(Oi\text{-}Pr)_2]_2$, the dithiophosphate

Can. J. Chem. Downloaded from www.nrcresearchpress.com by 80.90.12.36 on 09/08/12
For personal use only.

Can. J. Chem. Downloaded from www.nrcresearchpress.com by 80.90.12.36 on 09/08/12
For personal use only.

Fig. 2. ORTEP plot of the molecule $Ph_3Ge[S_2POCH_2CMe_2CH_2O]$, **2**. The atoms are drawn with 25% probability ellipsoids. Hydrogen atoms are omitted for clarity.

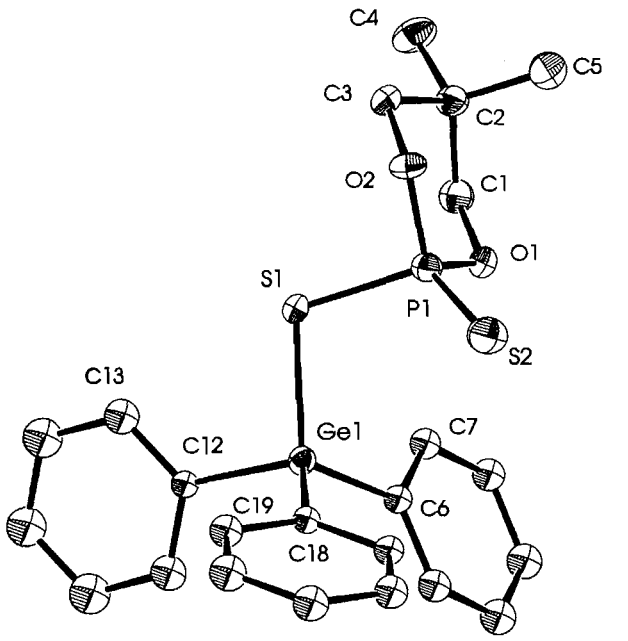

Fig. 3. ORTEP plot of the molecule $Ph_3Ge[S_2POCH_2CEt_2CH_2O]\cdot C_6H_6$, **3**. The atoms are drawn with 25% probability ellipsoids. Hydrogen atoms are omitted for clarity.

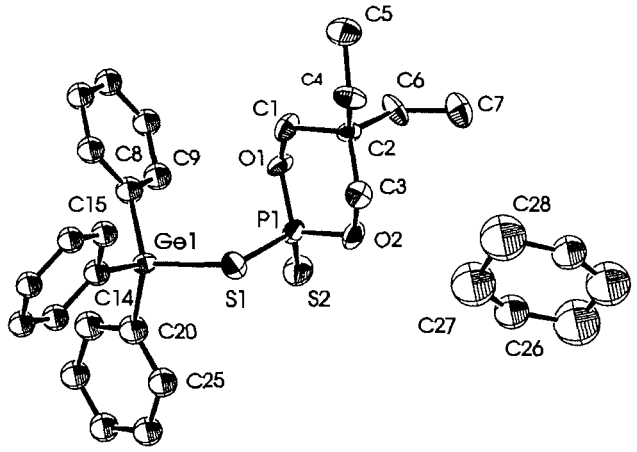

groups are fully bidentate with all four Sn—S bonds covering the range 2.678(1)–2.689(1) Å, with an average partial bond order of 0.55, and with a bite angle of 76.03(3)° (18). Thus, although noncyclic dithiophosphate derivatives of tin are generally bidentate and those of germanium are monodentate, the cyclic dithiophosphates of tin appear to be anisobidentate and those of germanium either weakly anisobidentate or essentially monodentate but still oriented approximately in a similar fashion to the tin analogues.

As with $Ph_3Ge[S_2POCMe_2CMe_2O]$, **1**, the P—S(Ge) bonds in **2** and **3** are slightly longer, 2.084(4) and 2.09(1) Å for **2** and **3**, respectively, than the P═S bonds, 1.901(4) and 1.912 (7) Å for **2** and **3**, respectively, and, as mentioned earlier, essentially the same as in other related cyclic dithiophosphate derivatives. Thus, again it is not surprising that the distortion around phosphorus from all tetrahedral angles is also similar.

Fig. 4. ORTEP plot of a part of the molecule $Ph_3Ge[S_2POCH_2CMe_2CH_2O]$, **2**, emphasizing the chair conformation of the six-membered ring. The atoms are drawn with 25% probability ellipsoids. Hydrogen atoms on the carbon atoms in the ring are included. The carbon atoms of the phenyl ring, except those attached to germanium, are omitted for clarity.

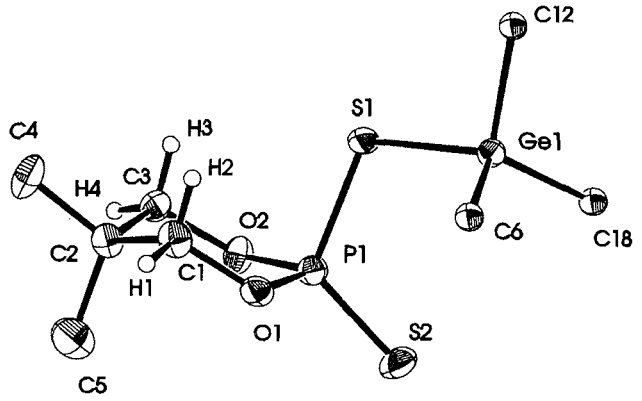

Fig. 5. ORTEP plot of part of the molecule $Ph_3Ge[S_2POCH_2CEt_2CH_2O]\cdot C_6H_6$, **3**, emphasizing the chair conformation of the six-membered ring. The atoms are drawn with 25% probability ellipsoids. Hydrogen atoms on the carbon atoms in the ring are included. The carbon atoms of the phenyl ring, except those attached to germanium, and those of the benzene ring are omitted for clarity.

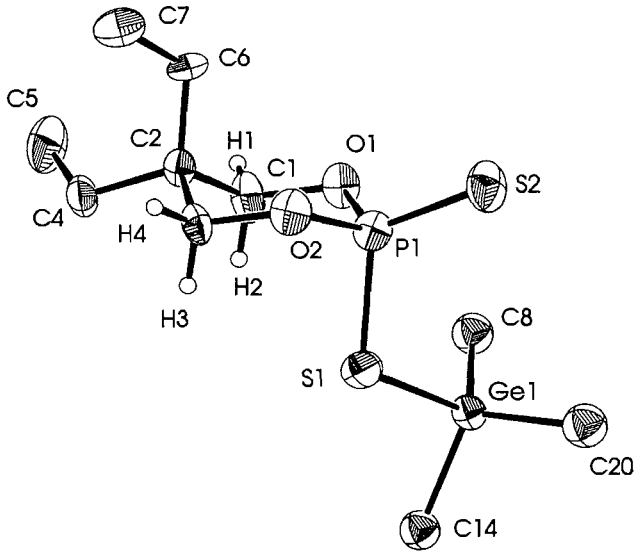

The carbon atoms of the phenyl rings, with the exception of the ones attached to germanium, are omitted from the ORTEP diagrams of $Ph_3Ge[S_2POCH_2CMe_2CH_2O]$, **2**, and $Ph_3Ge[S_2POCH_2CEt_2CH_2O]\cdot C_6H_6$, **3**, in Figs. 4 and 5, respectively, as is the benzene ring in the lattice in the latter case. As a result the figures clearly show that the six-membered ring system is in the chair configuration with one pair of hydrogen atoms being closer to phosphorus, at an average distance of 2.87 Å in **2** and 2.84 Å in **3** for H(2) and H(3), than the second pair at 3.41 Å in **2** and 3.42 Å for in **3** for H(1) and H(4). The methyl

Table 7. Selected features in the vibrational spectra (cm^{-1}) of compounds **1** and **4**.[a,b]

$Ph_3Ge[S_2POCMe_2CMe_2O]$, **1**		$Ph_2Ge[S_2POCMe_2CMe_2O]_2$, **4**		
IR[c]	Raman[d]	IR[c]	Raman[d]	Assignments
1432 ms	[g]	1435 m	1430 (5)	*n*-Phenyl
1131 s	1090 (5)	1134 s	1133 (5)	$\nu[S_2POGO]$ /**PO–C**[e,f]
1095 s	1088 (5)	1086 m	1082 (5)	*q*-Phenyl
1028 s	1027 (15)	1026 m	1023 (30)	$\nu[S_2POGO]$ /**PO—C**[f]
[g]	999 (100)	[g]	999 (100)	*p*-Phenyl
958 sh	[g]	952 s	952 (5)	$\nu[S_2POGO]$ /$\mathbf{PO_2}$[e,f]
917 vs, br	[g]	916 vs, br	[g]	$\nu[S_2POGO]$ /ring[e]
808 s, br	[g]	851 s,	[g]	$\nu[S_2POGO]$ /$\mathbf{PO_2}$[f]
737 s	[g]	738 m	[g]	*f*-Phenyl
701 vs, br	709 (7)	704 vs, br	704 (30)	$\nu[S_2POGO]$ /$\mathbf{PS_2}$/*v*-phenyl[f]
670 sh	658 (21)	664 m	663 (50)	*v*-Phenyl/$\upsilon[S_2POGO]$ /$\mathbf{PS_2}$[f]
574 s	[g]	639 s	[g]	$\nu[S_2POGO]$ /$\mathbf{PS_2}$[f]
461 ms	454 (7)	460 m	462 (10)	*y*-Phenyl
390 ms	393 (10)	432 m	432 (10)	$\nu(Ge–S)_{asym}$
		389 m	380 (25)	$\nu(Ge–S)_{sym}$
338 ms	[g]	331 m	[g]	*t*-Phenyl

[a]Parentheses denote relative intensities in the Raman effect.
[b]s = strong, m = medium, v = very, sh = shoulder, br = broad.
[c]Run as KBr pellets to 400 cm^{-1} and as Nujol mulls below 450 cm^{-1}.
[d]Run neat in a glass capillary.
[e]Correspond to strongest peaks in the IR of the salts at 1138 s, 955 s, 902 vs.
[f]Most probable principal contribution: e.g., /**PO–C**, O–C stretching and /$\mathbf{PS_2}$, P–S stretching.
[g]Not observed.

groups attached to the center carbon atom in the ring are also in unique positions relative to their distances to phosphorus, C(4) in **2** and **3** being at 4.47(1) and 4.45(2) Å, respectively, and C(5) in **2** and C(6) in **3** at 3.67(1) and 3.68(2) Å, respectively.

Infrared and Raman spectra

The assignments of the vibrational spectra of **1** and **4** are given in Table 7 and those of **2, 3, 5**, and **6** in Table 8 because characteristic features of the five- and six-membered ring dithiophosphates are sufficiently different that a collation in one table appeared to be confusing rather than helpful. For all six molecules, distinctive features are observed that are characteristic of a monosubstituted benzene ring and are relatively insensitive to the nature of the substituent (31). In general, for Ph_3GeX and Ph_2GeX_2 species, no specific assignments to Ge—C stretching vibrations are possible (32) but six prominent peaks in the infrared spectra are excellent fingerprints for phenyl groups attached to germanium that in decreasing order of intensity are consistently seen at approximately 737 and 696 cm^{-1}, 460 and 335 cm^{-1}, and 1434 and 1090 cm^{-1}. The relative intensities are consistent and increase as the number of phenyl groups attached to germanium increase. In the Raman effect there is only one very intense feature at approximately 1000 cm^{-1}, which is very weak in the infrared spectrum. Thus a distinct change in relative intensities of these peaks associated with the phenyl groups is indicative of an overlapping feature arising from vibrations within the dithiophosphate groups. The infrared spectra of **1–6**, particularly in the region around 1000 cm^{-1}, also contain distinctive strong bands that are similar, but not identical, to those of the starting salts. These are summarized in the tables and assigned to the motion that is probably contributing most to the fundamental, even though the modes are undoubtedly extensively mixed. The similarity of these characteristic features within the dithiophosphate groups is not surprising in view of the similarity in the structure of $Ph_3Ge[S_2POCH_2CMe_2CH_2O]$ and $Ph_3Ge[S_2POCH_2CEt_2CH_2O]$ and in the similarity of the arrangement of the dithiophosphate groups in $Ph_3Ge[S_2POCMe_2CMe_2O]$ and $Me_2Ge[S_2POCMe_2CMe_2O]_2$ (6). The assignments of the Ge–S stretching vibrations in **1–6** are consistent with the dithiophosphate groups being bonded in similar fashion in all six derivatives.

Nuclear magnetic resonance spectra

The ^1H NMR spectra data for compounds **1–6** are presented in Table 9. The splitting patterns and relative intensities of peaks are consistent with the solid state structures being maintained in solution. The peaks attributable to C_6H_5-Ge are clustered to essentially give identical patterns for all six compounds with the chemical shifts being within the range 7.70–7.38 ppm for the triphenyl derivatives, **1–3**, and 7.91–7.40 ppm for the diphenyl compounds **4–6**. The observation of two peaks in the ^1H NMR spectrum of $Ph_3Ge[S_2POCMe_2CMe_2O]$, **1**, at 1.40 and 1.45 ppm, indicates that the four methyl groups in the dithiophosphate are in two different environments. This is in agreement with the structure of **1**, in which the carbon atoms of one pair of methyl groups are at an average distance of

Can. J. Chem. Downloaded from www.nrcresearchpress.com by 80.90.12.36 on 09/08/12
For personal use only.

Can. J. Chem. Downloaded from www.nrcresearchpress.com by 80.90.12.36 on 09/08/12
For personal use only.

Table 8. Selected features in the vibrational spectra (cm^{-1}) of compounds **2, 3, 5**, and **6**.[a,b]

$Ph_3Ge[S_2POCH_2CMe_2CH_2O]$ **2**		$Ph_2Ge[S_2POCH_2CMe_2CH_2O]_2$ **5**		$Ph_3Ge[S_2POCH_2CEt_2CH_2O]$ **3**		$Ph_2Ge[S_2POCH_2CEt_2CH_2O]_2$ **6**	
IR[c]	Raman[d]	IR[c]	Raman[d]	IR[c]	Raman[d]	IR[c]	Assigments
1428 s	[g]	1431 m	[g]	1429 ms	[g]	1435 m	*n*-Phenyl
1091 s	1090 (5)	1090 m	[g]	1091 s	1088 (5)	1090 sh	*q*-Phenyl
1044 s	[g]	1045 vs	1045 (5)	1068 s	1068 (5)	1067 s	ν[S_2POGO] /**PO–C**[e,f]
1020 sh	1025 (15)	1020 sh	1026 (20)	1021 s	1026 (20)	1020 vs	ν[S_2POGO] /**PO–C**[e,f]
[g]	999 (100)	[g]	999 (100)	[g]	999 (100)	[g]	*p*-Phenyl
995 s	[g]	995 vs	[g]	995 sh	[g]	996 vs	ν[S_2POGO] /ring[e]
960 sh	[g]	963 ms	[g]	934 ms	[g]	935 s	ν[S_2POGO] /**PO_2**[e,f]
800 s, br	[g]	816 s, br	[g]	799 vs, br	[g]	821 s, br	ν[S_2POGO] /**PO_2**[f]
735 vs	[g]	735 m	[g]	737 m	[g]	737 ms	*f*-Phenyl
694 vs	[g]	684 vs, br	[g]	690 s, br	[g]	686 s, br	*v*-Phenyl
670 sh	668 (15)	684 vs, br	685 (30)	690 s, br	685 (30)		ν[S_2POGO] /**PS_2**[f]
501 m	500 (5)	495 s	501 (15)	505 m	505 (5)	501 ms	ν[S_2POGO] /**PS_2**[f]
460 s	[g]	457 m	[g]	460 s	[g]	457 m	*y*-Phenyl
375 s	374 (10)	402 m	407 (20)	388 ms	371 (10)	393s	$\nu(Ge–S)_{asym}$
		362 m	365 (15)		[g]	365 ms	$\nu(Ge–S)_{sym}$
332 s	[g]	330 m	[g]	328 ms		333 ms	*t*-Phenyl

[a]Parentheses denote relative intensities in the Raman effect.
[b]s = strong, m = medium, v = very, sh = shoulder, br = broad.
[c]Run as KBr pellets to 400 cm^{-1} and as Nujol mulls below 450 cm^{-1}.
[d]Run neat in a glass capillary.
[e]Correspond to strongest peaks in the IR of the starting salts for **2** and **5** at 1051 s and 1001 vs and for **3** and **6** at 1071 s, 1021 vs, 1000 vs, and 937 s.
[f]Most probable principal contribution: e.g., /**PO–C**, O–C stretching, /**PS_2**, P–S stretching.
[g]Not observed.

3.26(2) Å from phosphorus and at an average distance of 3.81(2) Å for the second pair. Two peaks are also observed in the ^1H NMR spectrum of $Ph_2Ge[S_2POCMe_2CMe_2O]_2$, **4**, at 1.34 and 1.38 ppm with the appropriate increase in intensity relative to the peaks arising from the phenyl groups. Thus each of the dithiophosphate groups in **4** is maintaining a similar configuration in solution to each other and it is reasonable to assume that the orientation is the same as in the solid state structure of **1**. This is in agreement with the observations for the corresponding methylgermanium derivatives (6) but the maintenance of the nonequivalence in solution is surprising because there have been no reports of such splitting in the ^1H NMR spectra of any other derivatives containing similar cyclic dithiophosphates (7–14). Even the closely related tin compound, $Ph_2Sn[S_2POCMe_2CMe_2O]_2$, displays only one peak in this region at 1.0 ppm (14). Thus the apparent uniqueness of the maintenance of the nonequivalence that we found in the case of $Me_3Ge[S_2POCMe_2CMe_2O]$ and $Me_2Ge[S_2POCMe_2CMe_2O]_2$ (6) is also a feature for these phenyl analogues.

The ^1H NMR spectra of compounds **2, 3, 5**, and **6** all display the same complex pattern arising from the nonequivalence of the hydrogen atoms of the CH_2 groups in the six-membered ring, which is apparent from the X-ray structures of $Ph_3Ge[S_2POCH_2CMe_2CH_2O]$, **2** and $Ph_3Ge[S_2POCH_2CEt_2CH_2O]\cdot C_6H_6$, **3**, as displayed in the ORTEP diagrams in Figs. 4 and 5. The feature is displayed in Fig. 6 for compound **2**, as a representative example. The four CH_2 protons give two sets of multiplets that are as expected for an ABX system, and which appear as two sets of approximate 1:1:1:1 quartets, centered at 4.12 and 3.64 ppm. The multiplet at 4.12 ppm can be analyzed as arising from geminal spin–spin coupling with a value for $J(H_aH_b)$ of 10.8 Hz, with further splitting as a result of coupling with phosphorus to give a value for $J(PH_a)$ of 5.6 Hz. The second multiplet at 3.64 ppm is apparently more clearly split into two doublets because the coupling to phosphorus is much larger with the value of the $J(PH_b)$ coupling constant being 25.0 Hz. The appearance of these two multiplets in the spectra of **3, 5**, and **6** is essentially the same because the values of the chemical shifts and coupling constants are virtually identical in all four compounds, as can be seen from Table 9. Thus the two protons on carbon are nonequivalent, as was observed for the two methyl groups substituted in the corresponding positions in the five-membered rings in **1** and **4**, and the values of the spin–spin coupling constants with phosphorus are different. It is reasonable to assume, by analogy with cyclohexane, that protons H_a (i.e., H(1), H(4)) and H_b (i.e., H(2), H(3)) in Figs. 4 and 5 occupy axial and equatorial positions, respectively, in a chair, rather than boat (6), configuration that is maintained in solution. The values for $J(PH)$ differ because the distance from P to the H_a positions is much larger than that to the H_b positions. Figure 6

Can. J. Chem. Downloaded from www.nrcresearchpress.com by 80.90.12.36 on 09/08/12
For personal use only.

Table 9. ^{1}H and ^{31}P chemical shifts in the NMR spectra of compounds **1–6**.[a,b,c]

Compounds	Ge-C_6H_5	O-CH_2[d]	OC-CH_3/-CCH_n[d]	$OCCCH_2CH_3$[d]	^{31}P[e]
$Ph_3Ge[S_2POCMe_2CMe_2O]$, **1**	7.70–7.38 (15 H, m)		1.45 (6 H, s) 1.40 (6 H, s)		96.66
$Ph_3Ge[S_2POCH_2CMe_2CH_2O]$, **2**	7.71–7.38 (15 H, m)	4.12 (2 H, m) [10.8; 5.6][e] 3.64 (2 H, m) [10.8; 25.0][f]	1.15 (3 H, s) 0.78 (3 H, s)		79.59
$Ph_3Ge[S_2POCH_2CEt_2CH_2O]$, **3**	7.71–7.38 (15 H, m)	4.11 (2 H, m) [10.9; 6.2][e] 3.79 (2 H, m) [11.1; 25.3][f]	1.61 (2 H, q) [7.5] 1.13 (2 H, q) [7.5]	0.79 (3 H, t) [7.5] 0.74 (3 H, t) [7.6]	81.05
$Ph_2Ge[S_2POCMe_2CMe_2O]_2$, **4**	7.91–7.42 (10 H, m)		1.38 (12 H, s) 1.34 (12 H, s)		94.75
$Ph_2Ge[S_2POCH_2CMe_2CH_2O]_2$, **5**	7.83–7.40 (10 H, m)	4.18 (4 H, m) [10.8; 5.2][e] 3.65 (4 H, m) [11.1; 25.9][f]	1.19 (6 H, s) 0.85 (6 H, s)		74.58
$Ph_2Ge[S_2POCH_2CEt_2CH_2O]_2$, **6**	7.83–7.40 (10 H, m)	4.15 (4 H, m) [11.2; 5.5][e] 3.84 (4 H, m) [11.4; 26.2][f]	1.61 (4 H, q) [7.5] 1.14 (4 H, q) [7.6]	0.86 (3 H, t) [7.5] 0.81 (3 H, t) [7.6]	77.80

[a]The spectra were recorded in $CDCl_3$ and reported in ppm from Me_4Si for ^{1}H and from H_3PO_4 for ^{31}P.

[b]Number of protons and multiplicities are in parentheses (s = singlet; t = triplet; q = quartet; m = multiplet).

[c]Coupling constants in Hz shown in square brackets [ ].

[d]Peaks attributable to the corresponding salts are seen in the ^{1}H NMR spectra of $Na[S_2POCMe_2CMe_2O]$ at 1.46 (12 H, s); of $Na[S_2POCH_2CMe_2CH_2O]$ at 4.03 (4 H, d [15.2]) and 1.05 (6 H, s); and of $NH_4[S_2POCH_2CEt_2CH_2O]$ at 4.13 (4 H, d [15.4]), 1.44 (4 H, q [7.6]), and 0.88 (6 H, t [7.6]).

[e]Both $J(H_aH_b)$ and $J(PH_a)$ coupling are observed.

[f]Both $J(H_aH_b)$ and $J(PH_b)$ coupling are observed.

also demonstrates the absence of any unidentified peaks due to hydrogen-containing impurities. The ^{31}P NMR spectra of **2**, **3**, **5**, and **6** all show a single peak unless recorded without hydrogen decoupling when a triplet of triplets is observed. The larger triplet has a coupling constant of 25.0 Hz, as expected for coupling of phosphorus with the two equatorial protons, and the triplet is further split into a triplet from coupling of the phosphorus with the two axial protons with a value of 5.6 Hz for this coupling constant. These observations are essentially identical to those in $Me_3Ge[S_2POCH_2CMe_2CH_2O]$, $Me_3Ge[S_2POCH_2CEt_2CH_2O]$, $Me_2Ge[S_2POCH_2CMe_2CH_2O]_2$, and $Me_2Ge[S_2POCH_2CEt_2CH_2O]_2$ (6) so that, although we were unable to obtain crystal structures for these methyl derivatives, it is reasonable to assume the conformation of the dithiophosphate groups is the same for them. It is worth noting that a typical value for J(PH) in the starting salts and related cyclic dithiophosphate derivatives that do not show the two separate couplings falls between those of these $J(PH_a)$ and $J(PH_b)$ values (8, 9, 12–14), the values for $Me_2Te[S_2POCH_2CMe_2CH_2O]_2$ and $Me_2Te[S_2POCH_2CEt_2CH_2O]_2$ of 15.6 and 15.8 Hz, respectively, being typical (17).

The $^{13}C\{H\}$ NMR spectral data for compounds **1–6** are presented in Table 10. The peaks attributable to C_6H_5-Ge show the same pattern for all six compounds in terms of relative intensities and do not differ to any large degree from compound to compound. All of the other peaks can be readily assigned to the various carbon atoms of the cyclic dithiophosphate groups at positions virtually identical to those found for the corresponding trimethylgermanium and dimethylgermanium analogues and close to, but not identical to, those of the corresponding salts and acids. However, again in contrast to the features in the salts, acids, or other metal derivatives where the observation of single peaks indicates identical or averaged positions, duplicate peaks are observed for compounds **1–6** for all of the atoms attached to the rings. In general, the values of the coupling constants, $J(PCC)$ and $J(PCCC)$, which are included in Table 10, are typical of such groups in a variety of

Can. J. Chem. Downloaded from www.nrcresearchpress.com by 80.90.12.36 on 09/08/12
For personal use only.

Fig. 6. ^{1}H NMR spectrum of $Ph_3Ge[S_2POCH_2CMe_2CH_2O]$, **2.** Peaks due to $CHCl_3$ and H_2O in the solvent, $CDCl_3$, are labelled a and b, respectively.

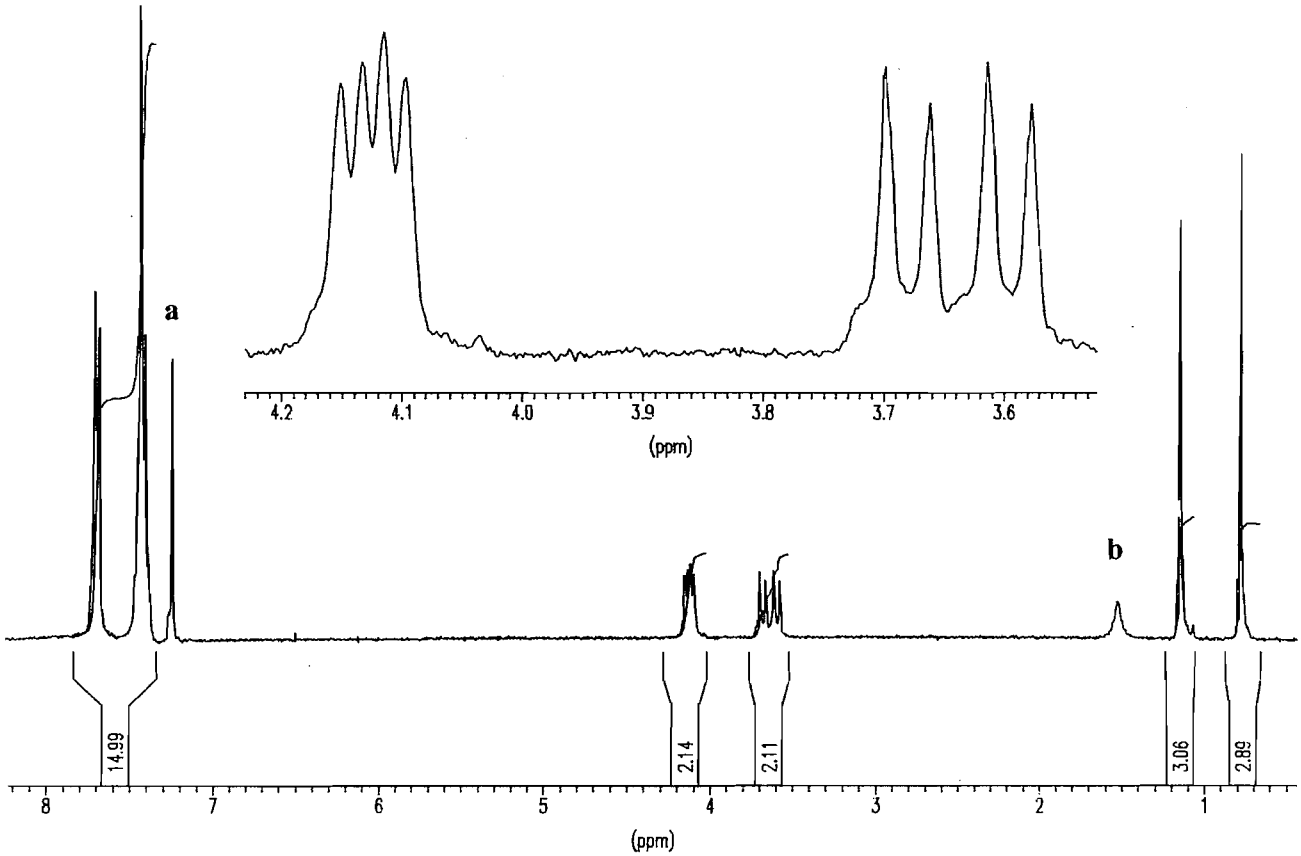

Table 10. ^{13}C NMR chemical shifts for compounds **1–6**.[a,b,c]

Compound	Ge-C_6H_5	O-C[c]	OC-C(ring)[c]	OC-CH_3/-CCH_n[c]	$OCCCH_2$-CH_3[c]
$Ph_3Ge[S_2POCMe_2CMe_2O]$, **1**	135.15 134.16 130.05 128.43	90.10		24.68 [4.5] 24.16 [4.5]	
$Ph_3Ge[S_2POCH_2CMe_2CH_2O]$, **2**	135.04 134.05 130.22 128.41	77.12	32.31 [6.8]	22.33 20.89	
$Ph_3Ge[S_2POCH_2CEt_2CH_2O]$, **3**	135.17 134.04 130.31 128.42	74.51 [8.3]	37.21 [6.8]	23.42 22.41	7.29 6.91
$Ph_2Ge[S_2POCMe_2CMe_2O]_2$, **4**	134.94 133.65 130.63 128.25	90.19		24.47 23.93	
$Ph_2Ge[S_2POCH_2CMe_2CH_2O]_2$, **5**	134.68 133.74 131.43 128.69	77.64 [9.0]	32.32	22.24 20.79	
$Ph_2Ge[S_2POCH_2CEt_2CH_2O]_2$, **6**	134.83 133.86 131.50 128.52	75.01 [9.0]	37.23 [4.5]	23.37 22.32	7.24 6.89

[a]The spectra were recorded in $CDCl_3$ and reported in ppm from Me_4Si.

[b]Values of the coupling constants for the doublets arising from P–C coupling, J(P–C), are given in square brackets [ ].

[c]Peaks attributable to the corresponding salts are seen in $Na[S_2POCMe_2CMe_2O]$ at 90.69 and 24.63 ppm; in $Na[S_2POCH_2CMe_2CH_2O]$ at 77.92 [7.3], 34.55, and 23.20 ppm; and in $NH_4[S_2POCH_2CEt_2CH_2O]$ at 75.29 [7.4], 39.58, 24.91, and 8.79 ppm.

Can. J. Chem. Downloaded from www.nrcresearchpress.com by 80.90.12.36 on 09/08/12
For personal use only.

environments, as is the fact that these couplings are not observed in a consistent manner (8, 9, 12, 14, 17).

The $^{31}P\{H\}$ NMR spectra, which are presented in Table 9 along with the ^{1}H NMR data, show a single peak in all compounds **1–6**, consistent with both dithiophosphate groups in **4–6** being in identical environments. It has been proposed that the difference in the phosphorus chemical shift between a derivative and that of the free acid, ΔP, is an accurate indicator of the mode of binding (33). Thus, downfield shifts in the range ΔP = 8–15 ppm are associated with bidentate ligands, and negligible shifts or even upfield shifts are associated with monodentate linkages. In compounds **1–6** the values of ΔP range from 4.3 ppm downfield in **1** to 2.4 ppm upfield in **3**, and therefore are consistent with monodentate ligands. In other words, the shifts are consistent with the structures in solution apparently remaining the same as the solid state structures of **1–3**, where the ligand is monodentate or weakly anisobidentate because the second sulfur atom is oriented toward rather than away from germanium but at a sufficiently large distance to imply, at best, a weak interaction. The shifts are smaller than those observed for the methyl germanium analogues and considerably smaller than those observed for analogous dimethyltellurium derivatives where ΔP ranged from 11 to 16 ppm downfield (17). Although the dithiophosphate groups had similar orientations in $Me_2Te[S_2POCH_2CMe_2CH_2O]_2$ and $Me_2Te[S_2POCH_2CEt_2CH_2O]_2$, the "nonbonding" Te--S secondary interactions were such as to indicate relatively strong anisobidentate linkages and it was assumed these took on bidentate behaviour in solution by rapid exchange. The similarities in the ^{1}H, ^{13}C, and ^{31}P NMR spectra of **1–6** suggest that the weak anisobidenticity found in the solid state structures of **1–3** is maintained in solution for all six compounds. By contrast, in the tin and tellurium analogues, the dithiophosphate groups undergo exchange in solution to bring about equivalence for all atoms in the groups, presumably by interchanging the bonded and aniso-bonded sulfur positions, which is consistent with the general tendency for dithio ligands to be bidentate when attached to tin and tellurium (34, 35). Germanium is apparently unique in terms of size, affinity to sulfur, or both, so that exchange does not occur and as a result the nonequivalence is maintained in solution.

Acknowledgement

We thank the Natural Sciences and Engineering Research Council of Canada and Imperial Oil Canada for financial support. One of us (J.E.D.) expresses his sincere thanks to the members of the Department of Chemistry of the University of Otago where he spent a short but very productive leave, with particular thanks to Professor Jim Simpson without whose help this paper would not have appeared. One of us (R.R.) thanks Dayanand College, Ajmer, India, for a leave of absence.

References

1. R.K. Chadha, J.E. Drake, and A.B. Sarkar. Inorg. Chem. **24**, 3156 (1985).
2. R.K. Chadha, J.E. Drake, and A.B. Sarkar. Inorg. Chem. **26**, 2885 (1987).
3. J.E. Drake, A.G. Mislankar, and M.L.Y. Wong. Inorg. Chem. **30**, 2174 (1991).
4. J.E. Drake, A.G. Mislankar, and J.Yang. Inorg. Chem. **31**, 5543 (1992).
5. J.E. Drake, A.G. Mislankar, and J.Yang. Inorg. Chim. Acta, **211**, 37 (1993).
6. J.E. Drake, L.N. Khasrou, A.G. Mislankar, and R. Ratnani. Can. J. Chem. **72,** 1830 (1994).
7. R. Ratnani, G. Srivastava, and R.C. Mehrotra. Transition Met. Chem. **17**, 137 (1992).
8. S.K. Pandey, G. Srivastava, and R.C. Mehrotra. Transition Met. Chem. **16**, 252 (1991).
9. R. Ratnani, G. Srivastava, and R.C. Mehrotra. Transition Met. Chem. **16**, 204 (1991).
10. R. Ratnani, G. Srivastava, and R.C. Mehrotra. Phosphorus, Sulfur, Silicon, **48**, 245 (1990).
11. R. Ahmad, G. Srivastava, and R.C. Mehrotra. Inorg. Chim. Acta, **89**, 41 (1984).
12. R. Ratnani, G. Srivastava, and R.C. Mehrotra. Inorg. Chim. Acta, **161**, 253(1989).
13. J.S. Yadav, R.K. Mehrotra, and G. Srivastava. Phosphorus, Sulfur, Silicon, **62**, 169 (1991).
14. R.J. Rao, G. Srivastava, R.C. Mehrotra, B.S. Saraswat, and J. Mason. Polyhedron, **3**, 485 (1984).
15. H. Preut, V-D. Ngo, and F. Huber. Acta Crystallogr. Sect. C: Cryst. Struct. Commun. **C42**, 809 (1986).
16. H. Preut, V-D. Ngo, and F. Huber. Acta Crystallogr. Sect. C: Cryst. Struct. Commun. **C43**, 164 (1987).
17. J.E. Drake, L.N. Khasrou, A.G. Mislankar, and R. Ratnani. Can. J. Chem. **72,** 1328 (1994).
18. K.C. Molloy, M.B. Hossain, D. van der Helm, J.J. Zuckerman, and I. Haiduc. Inorg. Chem. **19**, 2041 (1980).
19. H.P.S. Chauhan, C.P. Bhasin, G. Srivastava, and R.C. Mehrotra. Phosphorus Sulfur, **15**, 99 (1983).
20. (*a*) J.C. Calbrese. Ph.D. Thesis, University of Wisconsin–Madison (1972); (*b*) P.T. Beurskens. DIRDIF: direct methods for difference structures — an automatic procedure for phase extension and refinement of difference structure factors. Technical Report 1984/1; Crystallography Laboratory, Toernooiveld, 6525 Ed Nijmegen, Netherlands.
21. D.T. Cromer and J.T. Waber. International tables for X-ray crystallography. Vol. IV. The Kynoch Press, Birmingham, England. 1974. Table 2.2 A.
22. J.A. Ibers and W.C. Hamilton. Acta Crystallogr. **17**, 781 (1964).
23. D.T. Cromer. International tables for X-ray crystallography. Vol IV. The Kynoch Press, Birmingham, England. 1974. Table 2.3.1.
24. TEXSAN–TEXRAY structure analysis package. Molecular Structure Corp., Woodlands, Tex. 1985.
25. K.C. Molloy, M.B. Hossain, D. van der Helm, J.J. Zuckerman, and I. Haiduc. Inorg. Chem. **18**, 3507 (1979).
26. R.K. Chadha, J.E. Drake, and A.B. Sarkar. Inorg. Chem. **25**, 2201 (1986).
27. R.K. Chadha, J.E. Drake, and A.B. Sarkar. Inorg. Chim. Acta, **143**, 31 (1988).
28. J.S. Yadav, R. Bohra, R.K. Mehrotra, A.K. Rai, and G. Srivastava. Acta Crystallogr. Sect. C: Cryst. Struct. Commun. **C45**, 308 (1989).
29. P.R.H. Alderman, P.G. Owston, and J.M. Rowe. J. Chem. Soc. 668 (1962).
30. A. Bondi. J. Phys. Chem. **68**, 441 (1964).
31. D.H. Wiffen. J. Chem. Soc. 1350 (1956).
32. K.M. Mackay, D.R. Sowerby, and W.C. Young. Spectrochim. Acta, **24A**, 611 (1968).
33. C. Glidewell. Inorg. Chim. Acta, **25**, 159 (1977).
34. K.C. Molloy and J.J. Zuckerman. Acc. Chem. Res. **16**, 386 (1983).
35. I. Haiduc, R.B. King, and M.G. Newton. Chem. Rev. **94**, 301 (1994).

Ruthenium carbonyl complexes of the bridging tetradentate ligands $Ph_4P_2N_4S_2$ and $Ph_4P_2N_4S_2Me^+$

Tristram Chivers, Robert W. Hilts, Masood Parvez, and Dusan Ristic-Petrovic

Can. J. Chem. Downloaded from www.nrcresearchpress.com by 80.90.12.36 on 09/08/12
For personal use only.

Abstract: The reaction of $Ru(CO)_4(C_2H_4)$ or $Ru(CO)_5$ with 1,5-$Ph_4P_2N_4S_2$ in CH_2Cl_2–hexane at 23°C produces the dimer $[Ru(CO)_2(Ph_4P_2N_4S_2)]_2$ (**4**) in 54% and 11% yields, respectively. The treatment of **4** with methyl triflate (1:1 molar ratio) in dichloromethane yields the mono(N-methylated) derivative $[Ru_2(CO)_4(Ph_4P_2N_4S_2)(Ph_4P_2N_4S_2Me)][CF_3SO_3]$ (**5**) or, in a 1:2 molar ratio, the dimethylated derivative $[Ru(CO)_2(Ph_4P_2N_4S_2Me)]_2[CF_3SO_3]_2$, which exists as a ca. equal mixture of two symmetrical isomers on the basis of ^1H and ^{31}P NMR, and IR spectra. The reaction of **4** with two equivalents of Me_3NO in the presence of acetonitrile generates $[Ru(CO)(CH_3CN)(Ph_4P_2N_4S_2)]_2$, which is also formed as a mixture of isomers in a ratio of ca. 2:1 on the basis of ^1H and ^{31}P NMR, and IR spectra. The X-ray structure of **4**·CH_2Cl_2 shows that the $P_2N_4S_2$ ring is bonded to one ruthenium through two (geminal) nitrogen atoms and the remote sulfur atom while the second sulfur atom acts as a bridge to the other ruthenium. The crystals of **4**·CH_2Cl_2 are triclinic, space group $P\bar{1}$ with a = 12.901(1) Å, b = 13.072(1) Å, c = 10.123(1) Å, α = 100.88(1)°, β = 98.90(1)°, γ = 67.50(1)°, V = 1542.4(3) Å^3, and Z = 2. The final R and R_w values were 0.040 and 0.027, respectively. The X-ray structure of **5** reveals that N-methylation does not significantly perturb the bonding between the heterocyclic ligand and ruthenium. The crystals of **5** are triclinic, space group $P\bar{1}$ with a = 12.912(6) Å, b = 13.435(7) Å, c = 9.948(3) Å, α = 105.04(3)°, β = 102.85(3)°, γ = 70.74(4)°, V = 1555(1) Å^3, and Z = 2. The final R and R_w values were 0.063 and 0.071, respectively.

Key words: ruthenium, tetradentate ligand, $P_2N_4S_2$ ring.

Résumé : La réaction du $Ru(CO)_4(C_2H_4)$ ou du $Ru(CO)_5$ avec le 1,5-$Ph_4P_2N_4S_2$, dans le CH_2Cl_2–hexane, à 23°C, fournit le $[Ru(CO)_2Ph_4P_2N_4S_2]_2$ (**4**) avec des rendements respectifs de 54 et de 11%. Le traitement du composé **4** par le triflate de méthyle (rapport molaire de 1 : 1), dans le dichlorométhane, fournit le dérivé mono(*N*-méthylé) $[Ru(CO)_2(Ph_4P_2N_4S_2)(Ph_4P_2N_4S_2Me)][CF_3SO_3]$ (**5**) ou, dans un rapport molaire de 1 : 26, le dérivé diméthylé $[Ru(CO)_2(Ph_4P_2N_4S_2Me)_2][CF_3SO_3]$ qui, sur la base des spectres RMN du ^1H et du ^{31}P et des spectres IR, existe sous la forme d'un mélange approximativement molaire de deux isomères symétriques. La réaction du composé **4** avec deux équivalents de CH_3NO, en présence d'acétonitrile, fournit du $[Ru(CO)(CH_3CN)(Ph_4P_2N_4S_2)]_2$ qui se forme aussi comme un mélange d'isomères dans un rapport approximatif de 2 : 1, sur la base des spectres RMN du ^1H et du ^{31}P et des spectres IR. La structure déterminée par diffraction des rayons X du composé **4**·CH_2Cl_2 montre que le cycle $P_2N_4S_2$ est lié à un ruthénium par le biais de deux atomes d'azote géminaux et de l'atome de soufre éloigné alors que le deuxième atome de soufre agit comme pont pour l'autre ruthénium. Les cristaux de composé **4**·CH_2Cl_2 sont tricliniques, groupe d'espace $P\bar{1}$ avec a = 12,901(1), b = 13,072(1) et c = 10.123(1) Å, α = 100.88(1)°, β = 98.90(1)° et γ = 67.50(1)°, V = 1542.4(3) Å^3 et Z = 2. Les valeurs finales de R et R_w sont respectivement de 0,040 et 0,027. La structure du composé **5**, telle que déterminée par diffraction des rayons X, montre que la *N*-méthylation ne perturbe pas d'une façon significative la liaison entre le coordinat hétérocyclique et le ruthénium. Les cristaux du composé **5** sont tricliniques, groupe d'espace $P\bar{1}$, avec a = 12.912(6), b = 13.435(7) et c = 9.948(3) Å, α = 105.04(3)°, β = 102.85(3)° et γ = 70.74(4)°, V = 1555(1) Å^3 et Z = 2. Les valeurs finales de R et R_w sont respectivement de 0,063 et 0,071.

Mots clés : ruthénium, ligand tétradentate, cycle $P_2N_4S_2$.

[Traduit par la rédaction]

Received May 16, 1994.

This paper is dedicated to Professor William A.G. Graham on the occasion of his 65th birthday.

T. Chivers,[1] R.W. Hilts, and M. Parvez. Department of Chemistry, The University of Calgary, Calgary, AB T2N 1N4, Canada.
D. Ristic-Petrovic. Department of Chemistry, University of Alberta, Edmonton, AB T6G 2G2, Canada.

[1] Author to whom correspondence may be addressed. Telephone: 403-220-5741. Fax: 403-289-9488. E-mail: chivers@acs.ucalgary.ca.

Can. J. Chem. Downloaded from www.nrcresearchpress.com by 80.90.12.36 on 09/08/12
For personal use only.

Introduction

Weak, cross-ring S—S bonds are a common feature of π-electron-rich S—N heterocycles (1). These transannular linkages are the result of intramolecular π*(NSN)–π*(NSN) interactions, which have S—S σ-bonding character (2). The most intriguing example of this unusual functionality is provided by S_4N_4. However, the reactions of this inorganic heterocycle with metal carbonyls produce insoluble complexes that are difficult to characterize, e.g., $(S_5N_5)Mo(CO)$ (3), $(S_4N_4)Fe(CO)$ (4), and $S_4N_4Co_2(CO)_2$ (4, 5). With zerovalent complexes of the platinum group metals, S_4N_4 fragments to give complexes containing MSNSN rings (M = Pt, Pd, Ni) (6–8). By contrast, the integrity of the $P_2N_4S_2$ ring is retained in oxidative-addition reactions of **1** (or its tetraalkyl derivatives) with Pt(0) and Pd(0) complexes. The metal–ligand bonding in the η^2-S,S′ complexes **2** so formed involves primarily back donation from the metal to the σ*(S—S) orbital (LUMO) of **1** with a smaller contribution provided by donation from the σ(S—S) orbital (HOMO) of **1** to the metal (*9a*). The coordinatively saturated P(V) "spectator" nuclei in **1** serve as an informative NMR probe of fluxional behavior in metal complexes such as the centrosymmetric dimers **3** formed upon loss of PPh_3 from **2** (*9b*, 10).

The structures of **2, 3**, and η^1-N complexes of **1** with Pt(II) (11) indicate that the $P_2N_4S_2$ ring readily adapts its bonding mode to suit the electronic requirements of the metal centre. To further test this proposition, and in view of the paucity of information about complexes of S–N ligands with metals of the iron triad (12, 13), we have investigated the reactions of **1** with Ru(0) and Fe(0) complexes. In a preliminary communication we described the preparation and brief details of the structure of the unusual ruthenium dimer $[Ru(CO)_2(Ph_4P_2N_4S_2)]_2$ (**4**) (14). In this article we report investigations of both the ligand and metal-centered reactivities of 4. In addition to a discussion of the effect of metal coordination on the structural parameters of the $P_2N_4S_2$ ligand, the spectroscopic characterization and structure of the mono(N-methylated) derivative $[Ru_2(CO)_4(Ph_4P_2N_4S_2)(Ph_4P_2N_4S_2Me)][CF_3SO_3]$ are depicted. The NMR characterization of the dimethylated derivative $[Ru(CO)_2(Ph_4P_2N_4S_2Me)]_2[CF_3SO_3]_2$ and $[Ru(CO)(MeCN)(Ph_4P_2N_4S_2)]_2$, both of which are formed as a mixture of isomers, is also described.

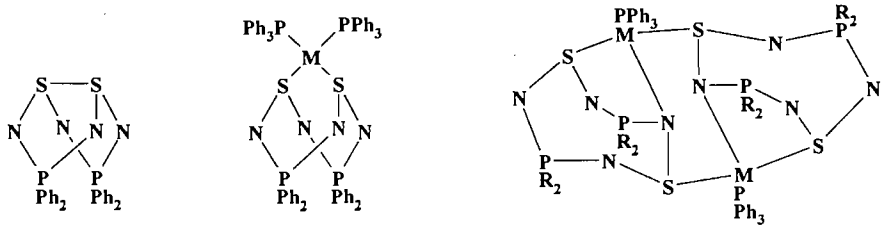

1 **2** (M = Pt, Pd) **3** (M = Pt, Pd)

Experimental

All manipulations were conducted under an atmosphere of prepurified nitrogen or argon by using vacuum line techniques. Diethyl ether, toluene, and hexanes were dried and freshly distilled from sodium benzophenone ketyl while dichloromethane was dried and distilled over CaH_2. Oxygen was removed from the solvents via three freeze–thaw–pump cycles under argon. Anhydrous trimethylamine N-oxide was prepared by subliming $Me_3NO{\cdot}2H_2O$ at 70°C under reduced pressure (ca. 0.1 Torr (1 Torr = 133.3 Pa)). The compound $Ru(CO)_4(C_2H_4)$ was prepared by a modified literature method[3] and 1,5-$Ph_4P_2N_4S_2$ was synthesized as previously described (16). Methyl triflate, trimethylamine oxide dihydrate, and triruthenium dodecacarbonyl (all from Aldrich) were used as received. Ethylene (Matheson Gas) was used directly from the cylinder. Elemental analyses were performed by the microanalytical services within the chemistry departments of the University of Calgary and the University of Alberta.

Infrared spectra were recorded in dichloromethane (0.1 mm thick NaCl solution cells) on a Nicolet MX1 FTIR spectrometer. ^{31}P NMR spectra were recorded at either 161.98 MHz by using a Bruker AM-400 spectrometer in dichloromethane with an external D_2O lock signal or at 81.0 MHz in deuterated dichloromethane by using a Bruker AM-200 spectrometer. ^1H and ^{13}C NMR spectra were recorded in CD_2Cl_2 solution either at 300.1 and 75.5 MHz, respectively, on a Bruker AM-300 instrument or at 200.1 and 50.3 MHz, respectively, on the Bruker AM-200 instrument. ^{31}P chemical shifts are given in ppm relative to 85% H_3PO_4 while ^1H and ^{13}C chemical shifts (ppm) are reported relative to $Si(CH_3)_4$. Fast atom bombardment (FAB) mass spectra were obtained on a Kratos MS9 spectrometer in a cleland matrix. The ^{31}P NMR data for compounds **4–7** are gathered in Table 1. All other data relating to the characterization of these new compounds are provided below with the synthetic procedures.

Preparation of $[Ru(CO)_2(Ph_4P_2N_4S_2)]_2$, 4

A colorless solution of $Ru(CO)_4(CH_2{=}CH_2)$ (0.148 g, 0.61 mmol) in deoxygenated hexane (30 mL) was transferred by cannula, over 15 min, to a stirred colorless solution of 1,5-$Ph_4P_2N_4S_2$ (0.299 g, 0.61 mmol) in dichloromethane (80 mL) under a nitrogen atmosphere at 23°C. Stirring was continued for 16 h at room temperature, during which time a yellow solution was formed. The solvent was removed under vacuum to give a yellow-brown product, which was washed with diethyl ether (2 × 10 mL) and vacuum dried for 2 h. Slow diffusion of hexane (10 mL) into a dichloromethane solution (10 mL) of the

[2] This complex may be a mixture of products since nitrosylation yields $(NO)_2CoSSNS$ (5).

[3] Hydrocarbon solutions of $Ru(CO)_4(C_2H_4)$ were prepared by a slight modification of the published procedure (see refs. 15*a* and 15*b*) involving external photolysis ($\lambda \geq 370$ nm) of $Ru_3(CO)_{12}$ under 2 atm (1 atm = 101.3 kPa) of ethylene (J. Takats and K. Hofmann. Private communication).

Can. J. Chem. Downloaded from www.nrcresearchpress.com by 80.90.12.36 on 09/08/12
For personal use only.

Table 1. $^{31}P\{^1H\}$ NMR parameters for **4**, **5**, **6***a*/*b*, and **7***a*/*b*.[a]

Compound[b]	δP_A[c,d]	δP_B[c,d]	δP_C[c,d]	δP_d[c,d]	J(P–P)[e]
4	64.0(s)	64.0(s)	64.0(s)	64.0(s)	
5	69.3(dd)	63.0(d)	64.9(dd)	64.4(d)	6 (P_AP_B) 8 (P_AP_C) 3 (P_CP_D)
6*a*	64.6(d)	70.1(d)	70.1(d)	64.6(d)	5
6*b*	69.3(s)	65.8(s)	65.8(s)	69.3(s)	
7*a*	63.2(d)	60.0(d)	60.0(d)	63.2(d)	5
7*b*	62.4(s)	60.4(s)	60.4(s)	62.4(s)	

[a]See Scheme 1 for structural drawings of **4**, **5**, **6***a*/*b*, **7***a*/*b*.

[b]In CH_2Cl_2 at 23°C.

[c]The assignments of spin labels for inequivalent P atoms in **5** are shown in Scheme 1. The assignments of the ^{31}P NMR resonances for **7***a* and **7***b* are arbitrary. All four resonances in isomers **6***a* and **7***a* exhibit 5 Hz coupling.

[d]Chemical shifts are quoted in ppm relative to 85% H_3PO_4. Abbreviations used: (s) singlet; (d) doublet; (dd) doublet of doublets.

[e]In Hz.

product afforded bright yellow crystals of **4** (0.213 g, 0.164 mmol, 53%). IR (CH_2Cl_2 solution, cm^{-1}): 2040(s), 1986(s). ^1H NMR (23°C, 200 MHz, CD_2Cl_2): 7.15–7.80 (m, C_6H_5). ^{13}C NMR (23°C, 75.5 MHz, CD_2Cl_2): 127.82–135.19 (m, C_6H_5), 193.69 (s, *C*O). FAB MS (^{102}Ru, *m/z* (%)): 1297 (92, $M + H^+$), 1269 (36, $M - CO + H^+$), 1241 (44, $M - 2CO + H^+$), 1213 (34, $M - 3CO + H^+$), 1185 ($M - 4CO + H^+$). Anal. calcd. for $C_{52}H_{40}N_8O_4P_4Ru_2S_4$: C 48.21, H 3.11, N 8.65, S 9.90, found: C 48.09, H 3.25, N 8.53, S 9.79.

Preparation of $[Ru_2(CO)_4(Ph_4P_2N_4S_2)(Ph_4P_2N_4S_2Me)][SO_3CF_3]$, 5

Methyl trifluoromethanesulfonate (10 μL, 0.092 mmol) in dichloromethane (20 mL) was added dropwise by cannula, over 30 min, to a rapidly stirred yellow-orange solution of $[Ru(CO)_2(Ph_4P_2N_4S_2)]_2$ (0.119 g, 0.092 mmol) in dichloromethane (25 mL) at 23°C. During the addition, the solution gradually changed color from yellow-orange to yellow. After the addition, the yellow mixture was stirred for 1 h and then the solvent volume was reduced to ca. 5 mL under vacuum. Diethyl ether (20 mL) was carefully layered on top of the concentrated orange solution and the resulting bilayer was placed in the freezer (−18°C). Yellow crystals of **5**·CH_2Cl_2 (0.098 g, 0.063 mmol) were obtained after 12 h at −18°C. Yield: 69%. IR (CH_2Cl_2 solution, cm^{-1}): 2069(s), 2052(s), 2013(s), 1996(s,br). ^1H NMR (23°C, 200 MHz, CD_2Cl_2): 6.93–7.90 (m, 40H, C_6H_5), 3.45 (d, ^3J(PH) = 9 Hz, 3H, NCH_3). ^{13}C NMR (23°C, 50.3 MHz, CD_2Cl_2): 136.38–128.16 (m, C_6H_5), 38.80 (d, ^2J(PC) = 6 Hz, NCH_3). Anal. calcd. for $C_{55}H_{45}Cl_2N_8O_7F_3P_4S_5Ru_2$: C 42.78, H 2.94, N 7.26, found: C 42.93, H 2.50, N 6.85.

Preparation of $[Ru(CO)_2(Ph_4P_2N_4S_2Me)]_2[SO_3CF_3]_2$, 6

A colorless solution of methyl trifluoromethanesulfonate (8.3 μL, 0.073 mmol) in dichloromethane (20 mL) was added dropwise by cannula over 10 min to a rapidly stirred yellow solution of $[Ru_2(CO)_4(Ph_4P_2N_4S_2)(Ph_4P_2N_4S_2Me)][SO_3CF_3]$ (0.107 g, 0.073 mmol) in dichloromethane (15 mL) at 23°C. The resulting yellow mixture was stirred for 1 h and then th e solvent was removed under vacuum. Recrystallization of the yellow residue from a 1:1 mixture of dichloromethane – diethyl ether (10 mL) at 23°C afforded yellow crystals of $[Ru(CO)_2$-$(Ph_4P_2N_4S_2Me)]_2[CF_3SO_3]_2$ (**6**) (0.111 g, 0.068 mmol, 93%). IR (cm^{-1}, CH_2Cl_2 solution): 2072(s), 2025(s). The ^1H and ^{31}P NMR spectra (see Table 1) indicate that the product **6** is a ca. 1:1 mixture of isomers. ^1H NMR (23°C, 200.1 MHz, 23°): 7.04–7.76 (m, 40H, C_6H_5), 3.49 (d, ^3J(PH) = 9 Hz, 3H, NCH_3), 3.45 (d, ^3J(PH) = 9 Hz, 3H, NCH_3). Anal. calcd. for $C_{56}H_{46}N_8O_{10}F_6P_4S_6Ru_2$: C 41.43, H 2.86, N 6.90; found: C 41.40, H 2.56, N 6.92.

The isomeric mixture **6** was also obtained in yields of 70–90% by the reaction of $[Ru(CO)_2(Ph_4P_2N_4S_2)]_2$ with two molar equivalents of methyl trifluoromethanesulfonate in dichloromethane at 23°C.

Preparation of $[Ru(CO)(NCMe)(Ph_4P_2N_4S_2)]_2$, 7

A colorless solution of sublimed Me_3NO (0.023 g, 0.308 mmol) in dichloromethane (30 mL) was added dropwise over 30 min by cannula to a rapidly stirred yellow-orange solution of $[Ru(CO)_2(Ph_4P_2N_4S_2)]_2$ (0.200 g, 0.154 mmol) and a large excess of acetonitrile (3.93 g, 96 mmol) in dichloromethane (20 mL) at 23°C. The resulting yellow mixture was stirred for 1 h and the solvent was removed under vacuum. The yellow residue was dissolved in 2 mL of dichloromethane and then 2 mL of diethyl ether were carefully added to this solution by syringe. Yellow crystals of $[Ru(CO)(NCMe)(Ph_4P_2N_4S_2)]_2$·$\frac{1}{2}CH_2Cl_2$ (**7**) (0.120 g, 0.088 mmol, 57%) formed after 5 days at room temperature. IR (cm^{-1}, CH_2Cl_2 solution): 1953(s, br). The ^1H and ^{31}P NMR spectra (see Table 1) indicate that the product **7** is a ca. 2:1 mixture of isomers. ^1H NMR (23°C, 200.1 MHz, CD_2Cl_2): 7.10–8.01 (m, C_6H_5), 5.32 (s, CH_2Cl_2), 1.75 (s, $NCCH_3$), 1.67 (s, $NCCH_3$). The integrated area of the resonance at 1.75 was ca. twice that of the resonance at 1.67. Anal. calcd. for $C_{54.5}H_{47}O_2N_{10}P_4Ru_2ClS_4$: C 47.99, H 3.47, N 10.27; found: C 47.75, H 3.75, N 9.76.

X-ray analyses

Yellow crystals of **4** and **5** suitable for study by X-ray diffraction were grown by the slow diffusion of diethyl ether into

Can. J. Chem. Downloaded from www.nrcresearchpress.com by 80.90.12.36 on 09/08/12
For personal use only.

Table 2. Crystallographic data for $[Ru(CO)_2(Ph_4P_2N_4S_2)]\cdot CH_2Cl_2$ (**4**·CH_2Cl_2) and $[Ru_2(CO)_4(Ph_4P_2N_4S_2)(Ph_4P_2N_4S_2Me)][CF_3SO_3]$, **5**.

	5	**4**·CH_2Cl_2
Formula	$C_{28}H_{23}O_5S_3N_4P_2F_3Ru$	$C_{27}H_{22}O_2N_4S_2P_2RuCl_2$
fw	811.71	732.54
Crystal color/habit	Yellow, block	Yellow, plate
Crystal dimensions, mm	0.30 × 0.20 × 0.12	0.50 × 0.40 × 0.10
Crystal system	Triclinic	Triclinic
Space group	$P\bar{1}$ (No. 2)	$P\bar{1}$ (No. 2)
a (Å)	12.912(6)	12.901(1)
b (Å)	13.435(7)	13.072(1)
c (Å)	9.948(3)	10.123(1)
α (deg)	105.04(3)	100.88(1)
β (deg)	102.85(3)	98.90(1)
γ (deg)	70.74(4)	67.50(1)
V (Å^3)	1555(1)	1542.4(3)
Z	2	2
Radiation	MoK_α (λ = 0.71069 Å)	MoK_α (λ = 0.71069 Å)
μ (cm^{-1})	0.873 mm^{-1}	0.952 mm^{-1}
Temperature	200(1) K	296(1) K
Diffractometer	Rigaku AFC6S	Rigaku AFC6S
Scan type	ω–2θ	ω–2θ
D_{calc}, g cm^{-3}	1.733	1.577
No. of reflections	5772	5717
No. of observations ($I > 3.00\ \sigma(I)$)	3095	3713
Reflection/parameter ratio	7.33	10.26
No. of variables	422	362
Residuals: R; R_w	0.063; 0.071	0.040; 0.027

dichloromethane solutions of the complexes. Crystal data, details of the data collection, and structure refinements for **4** and **5** are summarized in Table 2. Accurate cell dimensions and crystal orientation matrices were determined on a Rigaku AFC6S diffractometer by a least-squares fit of the setting angles of 25 reflections. Data were corrected for Lorentz, polarization, and empirical absorption effects (17).

The structures of **4** and **5** were solved by the heavy-atom method. Refinement of the structures was by full-matrix least-squares calculations, initially with isotropic and finally with anisotropic temperature factors for the non-hydrogen atoms. The phenyl groups were allowed to refine as regular hexagons; one of the phenyl groups in **5** was found to be disordered over two sites with unequal site occupancy factors that were allowed to refine. The structure of **5** contains half an anion of CF_3SO_3, which lies close to a special position and is disordered with fluorine atoms distributed over four sites. A molecule of cocrystallized dichloromethane was located in the unit cell of **4**. The structure for **4** refined to $R = 0.040$; $R_w = 0.027$ while **5** converged to $R = 0.063$; $R_w = 0.071$. Scattering factors were those of Cromer and Waber (18) and Stewart, Davidson, and Simpson (19) and allowance was made for anomalous dispersion (20). Fractional atomic coordinates and isotropic temperature factors for **4** and **5** are given in Tables 3 and 4. Sup-plementary experimental details, hydrogen atom parameters, anisotropic thermal parameters, and complete tables of bond lengths, bond angles, and torsion angles have been deposited.[4]

Results and discussion

Synthesis of $[Ru(CO)_2(Ph_4P_2N_4S_2)]_2$, 4

As part of a study of the displacement of an η^2-alkene by the bidentate (η^2-S,S′) ligand **1** (9) we chose $Ru(CO)_4(C_2H_4)$,[3] which contains an exceptionally labile C_2H_4 ligand, as a source of ruthenium(0). The addition of a hexane solution of $Ru(CO)_4(C_2H_4)$ (pressurized with ca. 2 atm of ethylene) to a solution of **1** in dichloromethane produced a yellow solid that, on the basis of elemental analyses and the FAB mass spectrum, was identified as the dimer $[Ru(CO)_2(Ph_4P_2N_4S_2)]_2$. The yield was 53%. Thus the ring system **1** has replaced both the ethylene ligand and two CO groups (eq. [1]). Compound **4** can be obtained in much lower yield from the reaction of **1** with $Ru(CO)_5$ under similar conditions. Surprisingly, however, the tetraalkyl derivatives of **1** do not add oxidatively to $Ru(CO)_4(C_2H_4)$ even at 70°C in toluene.

$$[1]\quad Ru(CO)_4(C_2H_4) + Ph_4P_2N_4S_2 \xrightarrow[-2CO]{-C_2H_4} \tfrac{1}{2}[Ru(CO)_2(Ph_4P_2N_4S_2)]_2 \qquad \mathbf{4}$$

[4] Copies of the supplementary material may be purchased from: The Depository of Unpublished Data, Document Delivery, CISTI, National Research Council Canada, Ottawa, Canada K1A 0S2.

Tables of atomic parameters, bond lengths and angles, and supplementary experimental details have also been deposited with the Cambridge Crystallographic Data Centre, and can be obtained on request from The Director, Cambridge Crystallographic Data Centre, University Chemical Laboratory, 12 Union road, Cambridge, CB2 1EZ, U.K.

Can. J. Chem. Downloaded from www.nrcresearchpress.com by 80.90.12.36 on 09/08/12
For personal use only.

Table 3. Atomic coordinates and equivalent isotropic thermal parameters for non-H atoms of $[Ru(CO)_2(Ph_4P_2N_4S_2)]_2$, **4**.

Atom	*x*	*y*	*z*	B_{eq}
Ru(1)	0.45493(4)	0.05725(4)	0.82529(5)	2.57(1)
Cl(1)	0.9453(3)	0.3620(3)	0.6479(3)	17.3(1)
Cl(2)	1.1107(3)	0.3088(4)	0.4828(4)	20.2(2)
S(1)	0.4042(1)	0.2482(1)	0.7819(1)	3.23(4)
S(2)	0.5003(1)	0.1210(1)	1.1040(1)	2.54(3)
P(1)	0.2871(1)	0.2740(1)	1.0011(2)	2.87(4)
P(2)	0.6090(1)	0.1931(1)	0.9351(2)	2.89(4)
O(1)	0.6020(4)	−0.0559(4)	0.5957(4)	5.6(1)
O(2)	0.2539(4)	0.0326(4)	0.6464(4)	6.1(1)
N(1)	0.3752(3)	0.1430(3)	1.0073(4)	2.4(1)
N(2)	0.2896(3)	0.3159(4)	0.8629(4)	3.3(1)
N(3)	0.5071(4)	0.2882(4)	0.8673(4)	3.4(1)
N(4)	0.5814(3)	0.0897(3)	0.9735(4)	2.4(1)
C(1)	0.5467(5)	−0.0115(5)	0.6816(6)	3.6(2)
C(2)	0.3299(5)	0.0421(5)	0.7125(5)	3.5(2)
C(3)	0.1465(4)	0.2799(5)	1.0073(6)	3.1(1)
C(4)	0.1155(5)	0.1915(6)	0.9415(7)	5.0(2)
C(5)	0.0038(6)	0.1988(6)	0.9369(7)	6.0(2)
C(6)	−0.0735(6)	0.2919(7)	0.9970(8)	5.6(2)
C(7)	−0.0447(6)	0.3789(6)	1.0644(8)	6.3(2)
C(8)	0.0673(6)	0.3716(5)	1.0676(7)	5.1(2)
C(9)	0.3159(5)	0.3606(5)	1.1518(6)	3.2(1)
C(10)	0.3111(6)	0.3380(5)	1.2787(7)	4.7(2)
C(11)	0.3408(7)	0.4002(7)	1.3934(7)	6.7(3)
C(12)	0.3738(7)	0.4855(8)	1.3827(9)	7.9(3)
C(13)	0.3803(7)	0.5082(6)	1.2593(9)	7.1(3)
C(14)	0.3502(5)	0.4462(5)	1.1437(7)	4.7(2)
C(15)	0.6698(4)	0.2581(5)	1.0817(5)	2.8(1)
C(16)	0.6362(5)	0.3734(5)	1.1102(6)	3.8(2)
C(17)	0.6857(6)	0.4227(5)	1.2213(7)	4.8(2)
C(18)	0.7579(6)	0.3577(6)	1.3055(6)	5.0(2)
C(19)	0.8013(5)	0.2442(6)	1.2822(6)	4.9(2)
C(20)	0.7629(5)	0.1935(5)	1.1693(6)	4.0(2)
C(21)	0.7184(5)	0.1194(5)	0.8235(5)	3.3(2)
C(22)	0.7281(6)	0.1662(5)	0.7179(7)	5.4(2)
C(23)	0.8142(7)	0.1113(7)	0.6350(7)	6.6(3)
C(24)	0.8883(7)	0.0082(8)	0.6519(8)	6.9(3)
C(25)	0.8814(6)	−0.0412(6)	0.7530(8)	6.6(2)
C(26)	0.7962(5)	0.0137(6)	0.8405(6)	5.1(2)
C(27)	1.0695(8)	0.3602(12)	0.6244(10)	17.4(5)

$B_{eq} = \frac{8}{3}\pi^2(U_{11}(aa^*)^2 + U_{22}(bb^*)^2 + U_{33}(cc^*)^2 + 2U_{12}aa^*bb^* \cos\gamma + 2U_{13}aa^*cc^* \cos\beta + 2U_{23}bb^*cc^* \cos\alpha)$

The mode of attachment of the inorganic heterocycle to the metal center in **4** is of interest. The ^{31}P NMR spectrum of **4** in CH_2Cl_2 exhibits a singlet at 63.9 ppm implying that the $P_2N_4S_2$ ring is coordinated symmetrically to ruthenium and that the S–S cross-ring interaction has been cleaved (*9b*). The IR spectrum of **4** in CH_2Cl_2 shows only two bands in the carbonyl region at 2040 and 1986 cm^{-1} (cf. ν(CO) 2048 and 1978 cm^{-1} for RuI_2(*trans*-bis-piperidine)(*cis*-dicarbonyl)) (21), suggesting that **4** contains two equivalent *cis*-$Ru(CO)_2$ units related by a centre of symmetry. An X-ray structure determination of **4** (vide infra) showed it to consist of a centrosymmetric dimer in which each $P_2N_4S_2$ ring is η^3-N,N′,S bonded to one ruthenium and bridged through the other sulfur atom (μ,η^1-S′) to the second ruthenium atom (see Scheme 1).

In an attempt to determine if coordination complexes of iron with the $P_2N_4S_2$ ring resemble those of ruthenium, the reaction of **1** in THF at 23°C with $Fe(CO)_5$ in the presence of Me_3NO was investigated. This reaction produced a complex mixture of phosphorus-containing products (δ ^{31}P in the range 10–35 ppm) in addition to a singlet at 66 ppm, which may correspond to the iron analogue of **4**. It was not possible to isolate a pure sample of this product.

X-Ray structure of $[Ru(CO)_2(Ph_4P_2N_4S_2)]_2$, 4

The coordination geometry of the $P_2N_4S_2$ ring in **4** was estab-

Can. J. Chem. Downloaded from www.nrcresearchpress.com by 80.90.12.36 on 09/08/12
For personal use only.

Table 4. Atomic coordinates ($\times 10^4$) and equivalent isotropic thermal parameters ($\times 10^3$ Å^2) for non-H atoms of $[Ru_2(CO)_4(Ph_4P_2N_4S_2Me)(Ph_4P_2N_4S_2)][CF_3SO_3]$, **5**.

Atom	*x*	*y*	*z*	s.o.f.[a]	U_{eq}[b]
Ru	102(1)	−535(1)	−2018(1)		27(1)
S(1)	−991(2)	312(2)	−3964(3)		34(1)
S(2)	1027(2)	−1199(2)	74(3)		29(1)
P(1)	−2562(2)	377(2)	−2305(3)		37(2)
P(2)	−218(2)	1901(2)	−1996(3)		33(1)
O(1)	−149(8)	−2748(7)	−3498(9)		46(4)
O(2)	2342(8)	−1194(9)	−2973(11)		70(4)
N(1)	−1433(7)	130(7)	−1140(9)		29(3)
N(2)	−2257(8)	334(9)	−3856(11)		47(4)
N(3)	−939(8)	1567(8)	−3506(11)		46(4)
N(4)	40(7)	1065(7)	−890(10)		32(3)
C(1)	−44(10)	−1918(10)	−2984(12)		40(4)
C(2)	1466(10)	−904(9)	−2649(12)		40(4)
C(3)	−3179(22)	463(24)	−4999(26)	0.500	68(5)
C(4)	−3519(6)	1612(6)	−1647(8)		41(4)
C(5)	−3862(6)	2460(6)	−2361(8)		67(4)
C(6)	−4570(6)	3447(6)	−1802(8)		97(4)
C(7)	−4936(6)	3585(6)	−529(8)		83(4)
C(8)	−4593(6)	2736(6)	184(8)		97(5)
C(9)	−3884(6)	1750(6)	−375(8)		64(4)
C(10)	−3221(8)	−666(7)	−2528(10)	0.720(5)	34(4)
C(11)	−2602(8)	−1696(7)	−2317(10)	0.720(5)	61(5)
C(12)	−3097(8)	−2529(7)	−2708(10)	0.720(5)	90(5)
C(13)	−4211(8)	−2330(7)	−3310(10)	0.720(5)	116(5)
C(14)	−4830(8)	−1300(7)	−3521(10)	0.720(5)	87(5)
C(15)	−4335(8)	−467(7)	−3130(10)	0.720(5)	87(5)
C(10b)	−3634(22)	−316(24)	−2760(28)	0.280(5)	107(5)
C(11b)	−3516(22)	−1100(24)	−3994(28)	0.280(5)	103(5)
C(12b)	−3859(22)	−2013(24)	−4164(28)	0.280(5)	84(5)
C(13b)	−4319(22)	−2142(24)	−3100(28)	0.280(5)	96(5)
C(14b)	−4437(22)	−1358(24)	−1866(28)	0.280(5)	104(5)
C(15b)	−4094(22)	−445(24)	−1696(28)	0.280(5)	85(5)
C(16)	−880(5)	3240(5)	−1178(7)		34(4)
C(17)	−409(5)	3678(5)	154(7)		52(4)
C(18)	−936(5)	4715(5)	830(7)		64(5)
C(19)	−1933(5)	5312(5)	174(7)		67(5)
C(20)	−2404(5)	4874(5)	−1159(7)		72(5)
C(21)	−1877(5)	3838(5)	−1835(7)		58(4)
C(22)	1122(6)	1907(6)	−2202(7)		37(4)
C(23)	2090(6)	1427(6)	−1372(7)		49(4)
C(24)	3114(6)	1471(6)	−1553(7)		65(5)
C(25)	3170(6)	1995(6)	−2565(7)		66(5)
C(26)	2202(6)	2475(6)	−3395(7)		74(4)
C(27)	1178(6)	2431(6)	−3214(7)		57(4)
S(3)	5835(8)	4413(8)	4664(10)	0.500	77(4)
O(3)	5709(24)	5176(23)	5936(29)	0.500	109(5)
O(4)	4972(23)	4973(22)	3766(27)	0.500	108(5)
O(5)	6216(24)	3233(23)	4753(29)	0.500	115(5)
C(28)	7183(27)	4179(27)	3478(36)	0.500	91(5)
F(1)	7235(11)	3877(12)	2718(13)	0.375	21(4)
F(2)	7792(21)	4297(22)	4848(25)	0.375	91(5)
F(3)	6848(23)	5402(23)	3817(29)	0.375	107(5)
F(4)	8451(14)	4962(12)	5299(17)	0.375	38(4)

[a]Site occupancy factors.
[b]$U_{eq} = (U_{11} + U_{22} + U_{33})/3$.

Can. J. Chem. Downloaded from www.nrcresearchpress.com by 80.90.12.36 on 09/08/12
For personal use only.

Scheme 1. Formation of $[Ru_2(CO)_4(Ph_4P_2N_4S_2Me)(Ph_4P_2N_4S_2)]^+$ and the *cis* and *trans* isomers of $[Ru(CO)_2(Ph_4P_2N_4S_2Me)]_2^{2+}$ and $[Ru(CO)(NCMe)(Ph_4P_2N_4S_2)]_2$, (*i*) $MeSO_3CF_3$, (*ii*) $2MeSO_3CF_3$, (*iii*) $2Me_3NO/CH_3CN$. The cationic species **5**, **6***a*, and **6***b* are isolated as $SO_3CF_3^-$ salts.

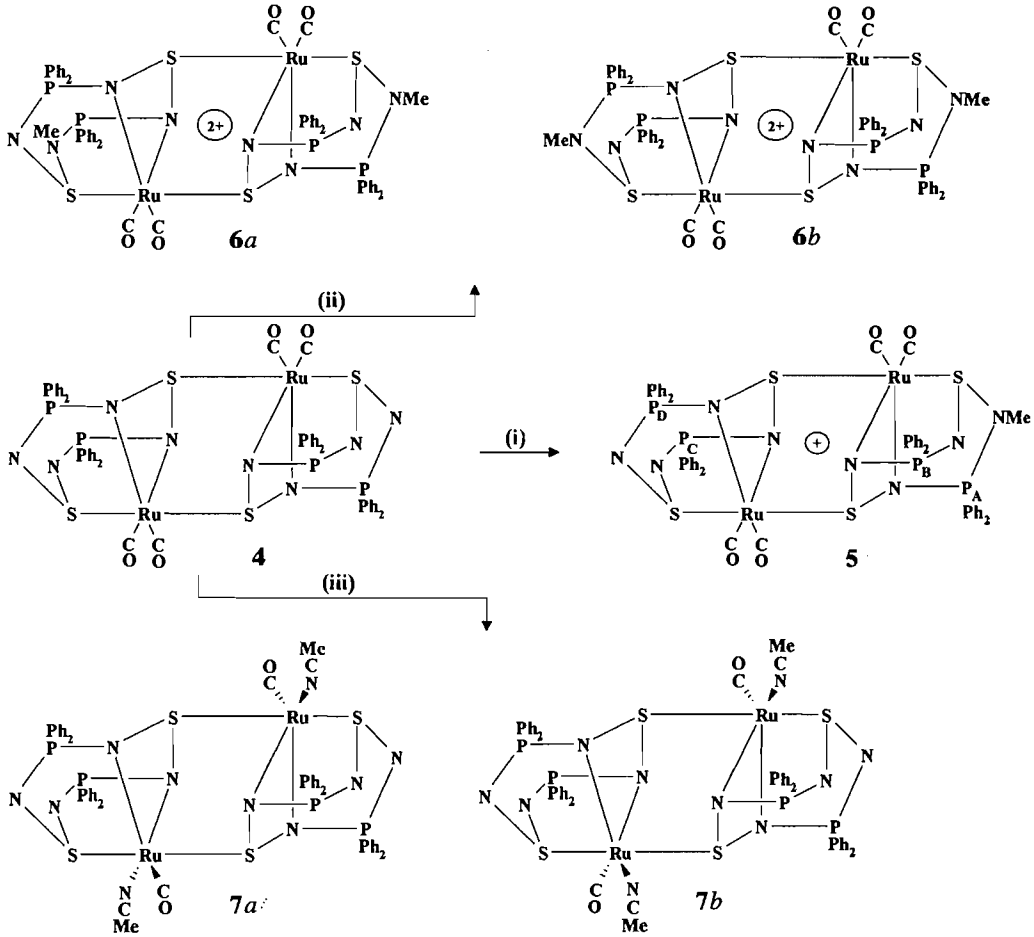

lished by an X-ray structural investigation of $4 \cdot CH_2Cl_2$. An ORTEP drawing of **4** with the atomic numbering scheme is illustrated in Fig. 1 and selected bond lengths and bond angles are summarized in Table 5. The complex **4** is a centrosymmetric dimer in which the $P_2N_4S_2$ ring adopts a tetradentate bonding mode in which it is attached to one ruthenium through two (geminal) nitrogens and the remote sulfur and serves as a bridge via the second sulfur atom to the other ruthenium. It is of particular interest to note that precisely the same bonding mode, i.e., η^3-S,N,N′-μ,η^1-S′, was invoked to explain the fluxional behavior of the dimeric Pt and Pd complexes of the type **3** (10).

In the preliminary communication the distorted octahedral geometry about Ru in **4** was discussed, but the implications of the structural parameters of the heterocyclic ligand were not addressed. The S—N bond lengths involving the three-coordinate nitrogen atoms N(1) and N(4) are 1.705(4) and 1.704(4) Å, respectively, while those containing the two coordinate nitrogens N(2) and N(3) are 1.656(4) and 1.670(4) Å, respectively (cf. *d*(S—N) = 1.584(2) and 1.596(3) Å in **1**) (22). There is also a pronounced inequality in the P—N bond distances for the two- and three-coordinate nitrogens. The former are significantly shorter (1.593(4) and 1.605(4) Å) than the latter (1.648(4) and 1.661(4) Å). These trends in the S—N and P—N bond lengths suggest that the $P_2N_4S_2$ ligand in **4** can be represented approximately by the valence bond structure shown in Fig. 2, i.e., reaction (a) involves an oxidative addition of **1** to the ruthenium(0) complex. We note that the dianion $Ph_4P_2N_4S_2^{2-}$ has been prepared recently as dilithium, disodium, or dipotassium derivatives by the reduction of **1** with Superhydride M[Et_3BH] (M = Li (23), Na, K[5]), but the structures of these alkali metal derivatives are unknown.

Methylation of $[Ru(CO)_2(Ph_4P_2N_4S_2)]_2$

The inorganic heterocycle **1** is readily N-methylated by methyl triflate with the retention of the cross-ring S—S bond (24). N,N′-Dimethylated dications $Ph_4P_2N_4S_2Me_2^{2+}$ can also be generated and exist in solution as a mixture of a symmetrical and an unsymmetrical isomer on the basis of ^{31}P NMR spectra (24). To determine the effect of coordination to a metal centre on the electrophilic methylation of the $P_2N_4S_2$ ring we have investigated the reaction of **4** with methyl triflate. The reaction of **4** with one molar equivalent of $MeSO_3CF_3$ proceeds smoothly at 23°C in dichloromethane to give $[Ru_2(CO)_4$-$(Ph_4P_2N_4S_2Me)(Ph_4P_2N_4S_2)][CF_3SO_3]$. The occurrence of mono-N-methylation was readily established by

[5] T. Chivers, X. Gao, and R. Vollmerhaus. Unpublished results.

Can. J. Chem. Downloaded from www.nrcresearchpress.com by 80.90.12.36 on 09/08/12
For personal use only.

Fig. 1. ORTEP diagram (50% probability ellipsoids) for $[Ru(CO)_2(Ph_4P_2N_4S_2)]_2$, 4. For clarity, only the α-carbon atoms of phenyl groups attached to phosphorus are shown. Starred atoms are related to the unstarred atoms by the symmetry operation: $-x+1, -y, -z+2$.

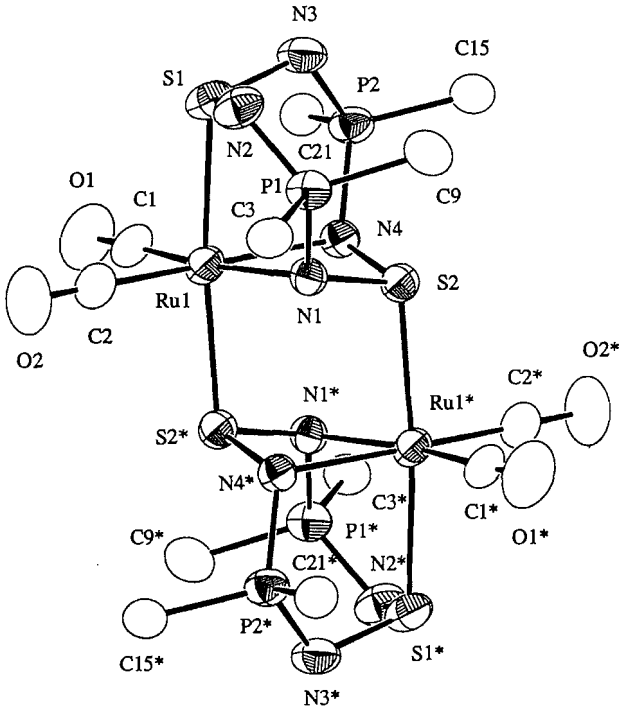

the integrated intensities of the ^1H NMR resonances and the fact that the ^{31}P NMR spectrum exhibits four equally intense resonances (see Fig. 3*a*) suggests that methylation is regiospecific. The X-ray structure of **5**, described below, showed that it is one of the two-coordinate nitrogen atoms in **4** that is methylated. As indicated in Table 1, the ^{31}P NMR chemical shifts of three of the phosphorus atoms in **5** are in the narrow range 63–65 ppm, cf. δ ^{31}P = 64.0 ppm for **4**. The fourth resonance is shifted downfield to 69.3 ppm and is therefore assigned to the phosphorus attached to the methylated nitrogen atom. In addition to the four-bond intraring ^{31}P–^{31}P couplings of ca. 6 Hz for the $Ph_4P_2N_4S_2Me^+$ and ca. 3 Hz for the $Ph_4P_2N_4S_2$ ring in **5** (cf. $^4J(^{31}P–^{31}P)$ = 21 Hz in $[Pt(PPh_3)_2(Ph_4P_2N_4S_2Me)][CF_3SO_3]$) (11), a five-bond coupling of ca. 8 Hz between phosphorus atoms of separate $P_2N_4S_2$ rings is observed.

The complete loss of symmetry upon methylation is also apparent in the IR spectrum of **5**, which shows four distinct carbonyl bands between 1996 and 2069 cm^{-1}. The average value of 2033 cm^{-1} is slightly higher than the average value of 2013 cm^{-1} observed for ν(CO) in **4** consistent with some positive charge delocalization onto the ruthenium atoms.

The treatment of **5** with methyl triflate or of **4** with two molar equivalents of methyl triflate in dichloromethane at 23°C produces the dimethylated derivative $[Ru(CO)_2(Ph_4P_2N_4S_2Me)]_2[CF_3SO_3]$ (**6**). The ^1H NMR spectrum of **6** shows two resonances with approximately equal intensities for N-CH_3 groups while the ^{31}P NMR spectrum (see Fig. 3*b*) consists of a pair of singlets and a pair of mutually coupled doublets (J ~ 5 Hz) with about the same intensity. On the basis of these NMR data, we conclude that **6** consists of an approximately equal mixture of two structural isomers, **6***a* and **6***b*, which are

Fig. 2. Valence bond representation of the $Ph_4P_2N_4S_2^{2-}$ ligand in $[Ru(CO)_2(Ph_4P_2N_4S_2)]_2$.

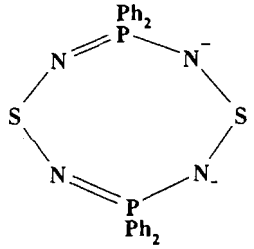

Fig. 3. $^{31}P\{^1H\}$ NMR spectra of (*a*) $[Ru_2(CO)_4(Ph_4P_2N_4S_2Me)(Ph_4P_2N_4S_2)][CF_3SO_3]$ and (*b*) $[Ru(CO)_2(Ph_4P_2N_4S_2Me)]_2[CF_3SO_3]_2$ in CH_2Cl_2.

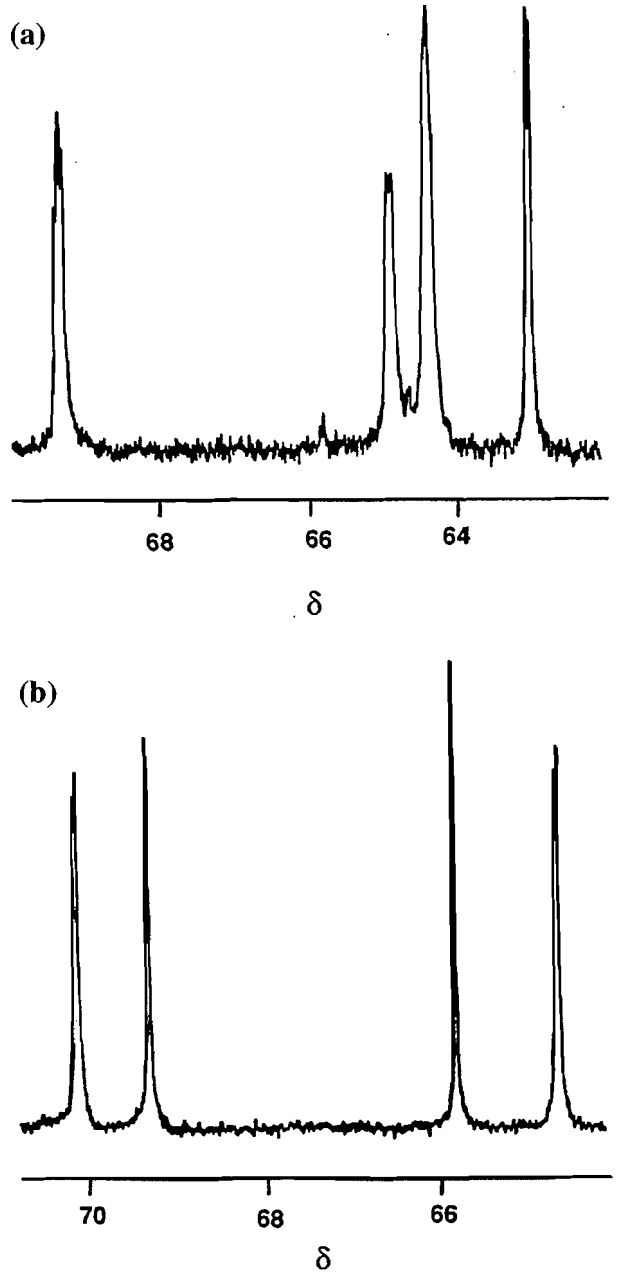

Can. J. Chem. Downloaded from www.nrcresearchpress.com by 80.90.12.36 on 09/08/12
For personal use only.

Table 5. Selected bond lengths (Å) and bond angles (deg) for $[Ru(CO)_2(Ph_4P_2N_4S_2)]$, **4**, and $[Ru_2(CO)_4(Ph_4P_2N_4S_2Me)(Ph_4P_2N_4S_2)][CF_3SO_3]$, **5**.

	4	**5**		**4**	**5**
S(1)—Ru	2.434(2)	2.429(3)	N(1)—P(1)	1.661(4)	1.64(1)
S(2)—Ru	2.397(2)	2.390(3)	N(2)—P(1)	1.605(4)	1.66(1)
N(1)—Ru	2.153(4)	2.165(9)	N(3)—P(2)	1.593(2)	1.62(1)
N(4)—Ru	2.151(4)	2.136(10)	N(4)—P(2)	1.648(4)	1.68(1)
C(1)—Ru	1.884(6)	1.91(1)	C(1)—O(1)	1.134(6)	1.14(2)
C(2)—Ru	1.880(6)	1.87(1)	C(2)—O(2)	1.133(6)	1.16(2)
N(2)—S(1)	1.656(4)	1.65(1)	C(3)—N(2)		1.45(3)
N(3)—S(1)	1.670(4)	1.65(1)			
N(1)—S(2)	1.705(4)	1.71(1)			
N(4)—S(2)	1.704(4)	1.69(1)			
S(2)—Ru—S(1)	172.96(6)	172.9(1)	N(2)—S(1)—Ru	102.2(2)	101.8(4)
N(1)—Ru—S(1)	81.9(1)	83.7(2)	N(3)—S(1)—Ru	104.3(2)	105.4(4)
N(1)—Ru—S(2)	91.2(1)	90.1(2)	N(3)—S(1)—N(2)	107.5(2)	107.2(6)
N(4)—Ru—S(1)	85.9(1)	85.3(3)	N(1)—S(2)—Ru	104.2(2)	102.9(4)
N(4)—Ru—S(2)	90.5(1)	89.6(3)	N(4)—S(2)—Ru	103.2(2)	102.5(4)
N(4)—Ru—N(1)	72.4(1)	72.4(3)	N(1)—S(2)—N(4)	96.4(3)	96.9(6)
C(1)—Ru—S(1)	96.0(2)	92.8(4)	N(2)—P(1)—N(1)	111.7(2)	111.1(5)
C(1)—Ru—S(2)	90.5(2)	91.5(4)	N(4)—P(2)—N(3)	117.0(2)	114.7(5)
C(1)—Ru—N(1)	97.6(2)	99.9(5)	P(1)—N(1)—Ru	115.5(2)	114.8(5)
C(1)—Ru—N(4)	169.9(2)	172.2(5)	P(1)—N(2)—S(1)	116.5(3)	119.1(7)
C(2)—Ru—S(1)	91.6(2)	95.6(4)	C(3)—N(2)—S(1)		124.1(14)
C(2)—Ru—S(2)	91.1(2)	90.0(4)	C(3)—N(2)—P(1)		116.3(14)
C(2)—Ru—N(1)	172.1(2)	171.2(5)	P(2)—N(3)—S(1)	115.4(3)	116.8(6)
C(2)—Ru—N(4)	99.9(2)	98.7(5)	P(2)—N(4)—Ru	108.7(2)	111.1(5)
C(2)—Ru—C(1)	90.1(2)	88.9(6)	O(1)—C(1)—Ru	178.0(60	176.3(13)
			O(2)—C(2)—Ru	178.7(60	174.4(12)

depicted in Scheme 1.[6] In both these isomers methylation occurs at dicoordinate nitrogen atoms of separate $P_2N_4S_2$ rings so that the two methyl groups are related either by a centre inversion (**6***a*) or a C_2 axis (**6***b*) giving rise to two pairs of equivalent phosphorus atoms and equivalent methyl groups for each isomer. By comparison with the ^{31}P NMR chemical shifts for **5**, the resonances at 70.1 and 69.3 ppm for **6***a*/*b* are assigned to the phosphorus atoms closest to the sites of methylation while the resonances at 64.6 and 65.8 ppm are attributed to the other two equivalent phosphorus atoms for each isomer (see Table 1). In one of these isomers the two resonances appear as mutually coupled doublets. However, it is not possible on the basis of the magnitude of the coupling constant (J = 5 Hz) to distinguish between a four-bond and a five-bond coupling between inequivalent phosphorus nuclei as the source of these doublets since the J values for **5** are of a similar size for these two interactions.

X-ray structure of $[Ru_2(CO)_4(Ph_4P_2N_4S_2Me)(Ph_4P_2N_4S_2)][CF_3SO_3]$, 5

The structure of **5** was confirmed by X-ray crystallography and an ORTEP drawing of the $[Ru_2(CO)_4(Ph_4P_2N_4S_2Me)(Ph_4P_2N_4S_2)]^+$ cation is shown in Fig. 4. Selected bond lengths and bond angles are summarized in Table 5. The structure of **5** contains an inversion disorder that places methyl groups with half occupancy at N(2) and N(2)*. This disorder problem, unfortunately, precludes any detailed structural comparisons between **4** and **5**. Nevertheless, the X-ray structure of **5** clearly shows that methylation occurs at a two-coordinate nitrogen atom and that it does not alter the bonding mode between the $P_2N_4S_2$ ring and ruthenium.

Metal-centered reactivity of $[Ru(CO)(NCMe)(Ph_4P_2N_4S_2)]_2$

We have also investigated reactions at the metal center in **4**. The treatment of **4** with PR_3 (R = Me, Ph) in toluene at reflux does not cleave the dimeric structure or result in replacement of CO groups. However, the reaction of **4** with two molar equivalents of trimethylamine-*N*-oxide in the presence of an excess of acetonitrile gives $[Ru(CO)(NCMe)(Ph_4P_2N_4S_2)]_2$ (**7**) as a yellow crystalline solid that, on the basis of ^1H and ^{31}P NMR data, exists as a mixture of isomers in the approximate ratio 2:1. The ^1H NMR spectrum of **7** exhibits two resonances for CH_3CN ligands at 1.75 and 1.67 ppm while the ^{31}P NMR spectrum (see Table 1) consists of a pair of singlets and two mutually coupled doublets. The IR spectrum of **7** contains just one carbonyl band at 1953 cm^{-1} indicative of a symmetrical dimer with one CO group and one acetonitrile ligand on each ruthenium. The shift of ca. 60 cm^{-1} to lower energy compared to the average value of ν(CO) for **4** is attributed to increased back donation from the metal to the

[6] The possibility that dimethylation occurs at the pair of two-coordinate nitrogen atoms of the *same* $P_2N_4S_2$ ring is considered unlikely since it would involve electrophilic attack at a site with a positive charge.

Fig. 4. ORTEP diagram (50% probability ellipsoids) for $[Ru_2(CO)_4(Ph_4P_2N_4S_2Me)(Ph_4P_2N_4S_2)][CF_3SO_3]$, **5**. For clarity, only the α-carbon atoms of phenyl groups attached to phosphorus are shown. Starred atoms are related to the unstarred atoms by the symmetry operation: $-x, -y, -z$.

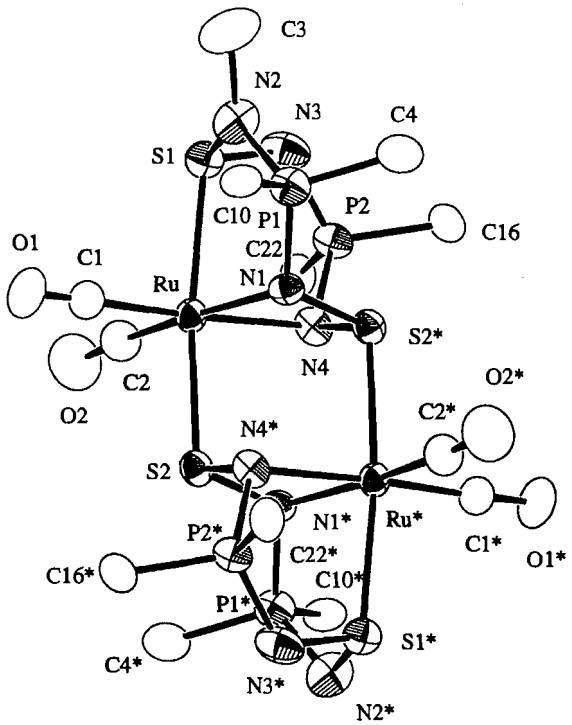

remaining CO ligand as a result of the replacement of one CO by an electron-releasing CH_3CN ligand. The proposed structures of the two isomers *7a* and *7b* are illustrated in Scheme 1. They are distinguished by the relative orientation of the MeCN (or CO) ligands. In *7a* they are related by a centre of inversion and in *7b* by a C_2 axis giving rise to two pairs of equivalent phosphorus atoms for each isomer. A variable temperature ^{31}P NMR study showed that *7a* and *7b* do not interconvert in toluene solution up to 100°C.

Conclusions

The neutral ligand $Ph_4P_2N_4S_2$ undergoes oxidative addition to ruthenium(0) complexes without fragmentation to give a centrosymmetric dimer $[Ru(CO)_2(Ph_4P_2N_4S_2)]_2$ in which the $P_2N_4S_2$ ring adopts an unprecedented tetradentate (η^3-N,N′,S-μ,η^1-S′) bonding mode. The electrophilic monomethylation of $[Ru(CO)_2(Ph_4P_2N_4S_2)]_2$ occurs regiospecifically at a two-coordinate nitrogen atom without disturbing the metal–heterocycle bonding mode and dimethylated derivatives are produced as an approximately equal mixture of structural isomers. The sulfur-bridged structure is stable towards triorganophosphines, but one CO ligand on each ruthenium can be substituted by CH_3CN. The facile generation of an acetonitrile complex provides a potentially useful starting point for future studies of the metal-centered reactivity of these complexes.

Acknowledgements

We thank the Natural Sciences and Engineering Research Council of Canada for financial support. Helpful advice from Professor J. Takats regarding the synthesis of $Ru(CO)_4(C_2H_4)$ is gratefully acknowledged.

References

1. T. Chivers. Chem. Rev. **74**, 341 (1985).
2. R. T. Oakley. Prog. Inorg. Chem. **36**, 299 (1988).
3. K. J. Wynne and W. L. Jolly. J. Inorg. Nucl. Chem. **30**, 2852 (1968).
4. D. A. Brown and F. Frimmel. Chem. Commun. 579 (1971).
5. M. Herberhold, L. Haumaier, and V. Schubert. Inorg. Chim. Acta, **49**, 21 (1981).
6. C. A. Ghilardi, S. Midollini, S. Moneti, and A. Orlandini. J. Organomet. Chem. **286**, 419 (1985).
7. R. Jones, P. F. Kelly, D. J. Williams, and J. D. Woollins. J. Chem. Soc. Chem. Commun. 1325 (1985).
8. T. Chivers, F. Edelmann, U. Behrens, and R. Drews. Inorg. Chim. Acta, **116**, 145 (1986).
9. (*a*) T. Chivers, K. S. Dhathathreyan, and T. Ziegler. J. Chem. Soc. Chem. Commun. 86 (1989); (*b*) T. Chivers, M. Edwards, A. Meetsma, J. C. van de Grampel, and A. van der Lee. Inorg. Chem. **31**, 2156 (1992).
10. T. Chivers, M. Edwards, P. N. Kapoor, A. Meetsma, J. C. van de Grampel, and A. van der Lee. Inorg. Chem. **29**, 3068 (1990).
11. T. Chivers and R. W. Hilts. Inorg. Chem. **31**, 5272 (1992).
12. T. Chivers and F. Edelmann. Polyhedron, **5**, 1661 (1986).
13. P. F. Kelly and J. D. Woollins. Polyhedron, **5**, 607 (1986).
14. T. Chivers, R. W. Hilts, M. Parvez, D. Ristic-Petrovic, and K. Hoffmann. J. Organomet. Chem. **480**, C4 (1994).
15. (*a*) B. F. G. Johnson, J. Lewis, and M. V. Twigg. J. Organomet. **67**, C75 (1974); (*b*) F. W. Grevels, J. G. A. Reuvers, and J. Takats. Inorg. Synth. **24**, 180 (1986).
16. T. Chivers, M. Edwards, M. N. S. Rao, and M. Parvez. Inorg. Chem. **31**, 1861 (1992).
17. A. C. T. North, D. C. Phillips, and F. S. Mathews. Acta Crystallogr. Sect. A: Cryst. Phys. Diffr. Theor. Gen. Crystallogr. **A24**, 351 (1968).
18. D. T. Cromer and J. T. Waber. International tables for X-ray crystallography. Vol. IV. Kynoch Press, Birmingham, England. 1974. Table 2.2A, p. 71.
19. R. F. Stewart, E. R. Davidson, and W. T. Simpson. J. Chem. Phys. **42**, 3175 (1965).
20. D. T. Cromer and D. Liberman. J. Chem. Phys. **53**, 1891 (1970).
21. W. Hieber and P. John. Chem. Ber. **103**, 2161 (1970).
22. N. Burford, T. Chivers, and J. F. Richardson. Inorg. Chem. **22**, 1482 (1983).
23. T. Chivers, M. Cowie, M. Edwards, and R. W. Hilts. Inorg. Chem. **31**, 3349 (1992).
24. T. Chivers, G. Y. Dénès, S. W. Liblong, and J. F. Richardson. Inorg. Chem. **28**, 3683 (1989).

Can. J. Chem. Downloaded from www.nrcresearchpress.com by 80.90.12.36 on 09/08/12
For personal use only.

Aryldiazenido complexes: structure, fluxionality, and properties of the iridium ethylene aryldiazenido complex $[(\eta^5\text{-}C_5Me_5)Ir(C_2H_4)(p\text{-}N_2C_6H_4OMe)][BF_4]$ and a comparison with the analogous nitrosyl complex $[(\eta^5\text{-}C_5Me_5)Ir(C_2H_4)(NO)][BF_4]$

Xiaoqian Yan, Frederick W.B. Einstein, and Derek Sutton

Can. J. Chem. Downloaded from www.nrcresearchpress.com by 80.90.12.36 on 09/08/12
For personal use only.

Abstract: $[Cp^*Ir(C_2H_4)(N_2Ar)][BF_4]$ (**1** $\mathbf{BF_4}$; Ar = *p*-$N_2C_6H_4OMe$) has been synthesized by reacting $[ArN_2][BF_4]$ with $Cp^*Ir(C_2H_4)_2$ at low temperature. An initial electrophilic attack of the incoming diazonium ion at iridium, followed by expulsion of C_2H_4, is postulated to account for the mild reaction conditions that are in sharp contrast to the usual inertness of the bis(ethylene) compound toward ligand substitution. The IR and nitrogen NMR data for **1** $\mathbf{BF_4}$ and its $^{15}N_\alpha$ derivative unambiguously establish that the ArN_2 ligand has the singly bent geometry in this complex in solution. The X-ray crystal structure confirms this for the solid state, and establishes that the plane of the aryldiazenido ligand is approximately perpendicular to the plane defined by the Ir atom and the centers of mass of the Cp* and ethylene ligands. An extended Hückel molecular orbital analysis of the singly bent aryldiazenido ligand has been carried out and satisfactorily accounts for the observed orientation of the ArN_2 ligand. An analysis of the variable-temperature ^1H and ^{13}C NMR of **1** $\mathbf{BF_4}$ indicates that *both* restricted rotation of the C_2H_4 ligand and a conformational isomerization of the aryldiazenido ligand are occurring, and $\Delta G^{\neq}_{270}$ for the ethylene rotation barrier is estimated at $\leq 51.5 \pm 0.4$ kJ mol^{-1}. This is lower than the barrier of $\Delta G^{\neq}_{353} = 68.7 \pm 0.2$ kJ mol^{-1} determined previously for the analogous nitrosyl complex $[Cp^*Ir(C_2H_4)(NO)][BF_4]$ (**2** $\mathbf{BF_4}$) and it is suggested that in these half-sandwich complexes both NO and ArN_2 function as single-faced π-acceptors, and in these circumstances ArN_2 is the better π-acceptor. The ethylene in **1** $\mathbf{BF_4}$ is readily displaced by PPh_3 to give $[Cp^*Ir(PPh_3)(N_2Ar)][BF_4]$ (**3** $\mathbf{BF_4}$). This reacts with $NaBH_4$ to yield $Cp^*IrH(PPh_3)(N_2Ar)$ (**4**) in which the ArN_2 ligand has switched to the doubly bent geometry, on the basis of the $^{15}N_\alpha$ NMR chemical shift data. Attempts to synthesize the corresponding chloro analogue **5** resulted in only the chloride salt of the singly bent ArN_2 cation **3**. For example, reaction of **3** $\mathbf{BF_4}$ with HCl yields the aryldiazene complex $[Cp^*IrCl(PPh_3)(NHNAr)][BF_4]$ (**6**), but deprotonation of this with Et_3N yields **3 Cl**, not **5**. Compound **1** $\mathbf{BF_4}$ crystallized in the space group $P2_1/n$ with $a = 8.5780(10)$ Å, $b = 20.5310(23)$ Å, $c = 12.0310(15)$ Å, $\beta = 93.500(10)°$, and $Z = 4$. The structure was refined to $R_f = 0.0281$ on the basis of 2611 observed reflections with $I_o \geq 2.5\sigma(I_o)$ in the range $2\theta = 0$–$50°$ (Mo-K_α).

Key words: iridium, cyclopentadienyl, aryldiazenido, nitrosyl, ethylene.

Résumé : On a synthétisé le $[Cp^*Ir(C_2H_4)(N_2Ar)][BF_4]$ (**1** $\mathbf{BF_4}$; Ar = *p*-$N_2C_6H_4OMe$) en faisant réagir du $[ArN_2][BF_4]$ avec du $Cp^*Ir(C_2H_4)_2$, à basse température. Pour expliquer les conditions réactionnelles douces qui sont en opposition flagrante avec le manque habituel de réactivité du composé bis(éthylène) vis-à-vis les substitutions du coordinat, on suppose qu'il se produit une attaque initiale de l'ion diazonium au niveau de l'iridium, suivie d'une expulsion du C_2H_4. Les données de l'IR et de la RMN de l'azote pour le composé **1** $\mathbf{BF_4}$ et son dérivé $^{15}N_\alpha$ établissent sans ambiguïté que, en solution, le coordinat ArN_2 de ce complexe possède une géométrie avec un seul repli. La structure cristalline par diffraction des rayons X le confirme à l'état solide et établit que le plan du coordinat aryldiazénido est approximativement perpendiculaire au plan défini par l'atome d'Ir et les centres de masse du Cp* et des coordinats éthylène. Faisant appel à la méthode des orbitales

Received October 28, 1994.
This paper is dedicated to Professor William A.G. Graham on the occasion of his 65th birthday.

X. Yan, F.W.B. Einstein, and D. Sutton.[1] Department of Chemistry, Simon Fraser University, Burnaby, BC V5A 1S6, Canada.

[1] Author to whom correspondence may be addressed. Telephone: (604) 291-4885. Fax: (604) 291-3765. E-mail: sutton@bohr.chem.sfu.ca

moléculaires de Hückel, on a effectué une analyse en profondeur du coordinat aryldiazénido avec un seul repli et elle explique d'une façon satisfaisante l'orientation observée du coordinat ArN_2. Une analyse du composé **1** $\mathbf{BF_4}$ par RMN du ^1H et du ^{13}C à basse température indique qu'il se produit une rotation restreinte du coordinat C_2H_4 en même temps qu'une isomérisation conformationnelle du coordinat aryldiazénido; le $\Delta G^{\neq}_{270}$ pour la barrière à la rotation de l'éthylène est évaluée à $\leq$51,5 $\pm$ 0,4 kJ mol^{-1}. Cette valeur est plus faible que la barrière de $\Delta G^{\neq}_{353}$ 68,7 $\pm$ 0,2 kJ mol^{-1} déterminée antérieurement pour la complexe nitrosyle analogue $[Cp^*Ir(C_2H_4)(NO)][BF_4]$ (**2** $\mathbf{BF_4}$) et on suggère que, dans ces complexes à demi-sandwich, le NO ainsi que le ArN_2 fonctionnent tous les deux comme des accepteurs π à face unique et que, dans ces circonstances, le ArN_2 est un meilleur accepteur π. On peut facilement remplacer l'éthylène du **1** $\mathbf{BF_4}$ par du PPh_3 pour obtenir du $[Cp^*Ir(PPh_3)(N_2Ar)][BF_4]$ (**3** $\mathbf{BF_4}$). Ce dernier réagit avec le $NaBH_4$ pour conduire au $Cp^*IrH(PPh_3)(N_2Ar)$ (**4**) dans lequel, sur la base des données de déplacements chimiques en RMN du $^{15}N_\alpha$, le coordinat ArN_2 est déplacé vers une géométrie à double repli. Des essais de synthèse de l'analogue chloro correspondant **5** n'ont conduit qu'au chlorure du cation ArN_2 à simple repli, **3**. Par exemple, la réaction du composé **3** $\mathbf{BF_4}$ avec du HCl fournit le complexe aryldiazène $[Cp^*IrCl(PPh_3)(NHNAr)][BF_4]$ (**6**), mais la déprotonation de ce composé avec du Et_3N conduit au composé **3 Cl**, et non pas au composé **5**. Le composé **1** $\mathbf{BF_4}$ cristallise dans le groupe d'espace $P2_1/n$ avec a = 8,5780(10), b = 20,5310(23) et c = 12,0310(15) Å, β = 93,500(10)° et Z = 4. On a affiné la structure jusqu'à une valeur de R_f = 0,0281 sur la base de 2611 réflexions observées avec $I_o \geq 2{,}5\sigma(I_o)$ pour 2θ = 0–50° (Mo-K_α).

Mots clés : iridium, aryldiazénido, cyclopentadiényle, nitrosyle, éthylène.

[Traduit par la rédaction]

Introduction

Since the synthesis of $CpMo(CO)_2(N_2Ph)$, the first stable aryldiazenido (ArN_2) complex, in 1964 (1), synthetic, structural, and chemical studies of transition metal aryldiazenido complexes have appeared regularly in the literature (2–4). Historically, this development coincided with renewed interest in transition metal nitrosyl chemistry. There is an evident valence electronic similarity between ArN_2 and NO that is expressed in the structural similarity in the bonding modes of terminally coordinated nitrosyl and aryldiazenido ligands. These are characterized by linear and bent M-N-O, and singly bent and doubly bent M-N-N-Ar structural skeletons, portrayed by the valence structures shown in Scheme 1.

Nitrosyl complexes are numerous (5), and for the majority no exact aryldiazenido analogues are known. Nevertheless, there do exist many pairs of analogous nitrosyl and aryldiazenido complexes, and in several cases these have been used to compare the properties of NO and ArN_2 ligands in similar environments. Of particular interest have been the relative π-accepting abilities. In some studies it has been concluded that NO is a better π-acceptor, whereas in others the reverse has been suggested (6–14).

In this paper, we compare results on a new pair of analogous ArN_2 and NO complexes, namely, the half-sandwich iridium ethylene complexes $[Cp^*Ir(C_2H_4)(p\text{-}N_2C_6H_4OMe)]^+$ (**1**) and $[Cp^*Ir(C_2H_4)(NO)]^+$ (**2**) (where Cp^* = η^5-C_5Me_5). The nitrosyl complex has been described in detail in a previous paper (15), and both compounds were included in an earlier preliminary communication (16). Here we provide full details of the aryldiazenido complex **1** and a triphenylphosphine derivative **3**. We draw attention to three important aspects of **1**. One is the orientation of the plane of the aryldiazenido ligand with respect to the plane of symmetry of the $Cp^*Ir(C_2H_4)$ fragment, for which a theoretical interpretation on the basis of extended Hückel molecular orbital (EHMO) calculations is given. The second is that the aryldiazenido ligand is stereochemically nonrigid, the aryl group undergoing a rapid conformational isomerization by either a rotation or inversion process that interconverts the enantiomers of the cation **1** at room temperature. The third is the relative size of the barriers to rotation of the ethylene ligand in **1** and **2**. These barriers are interpreted to reflect the relative π-acceptor abilities of the aryldiazenido and nitrosyl ligands toward the $Cp^*Ir(C_2H_4)$ fragment.

Scheme 1.

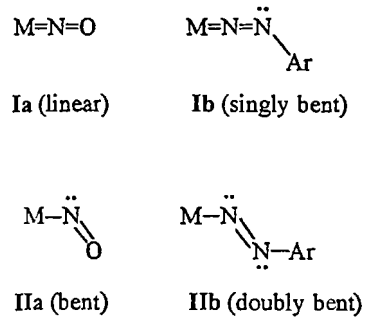

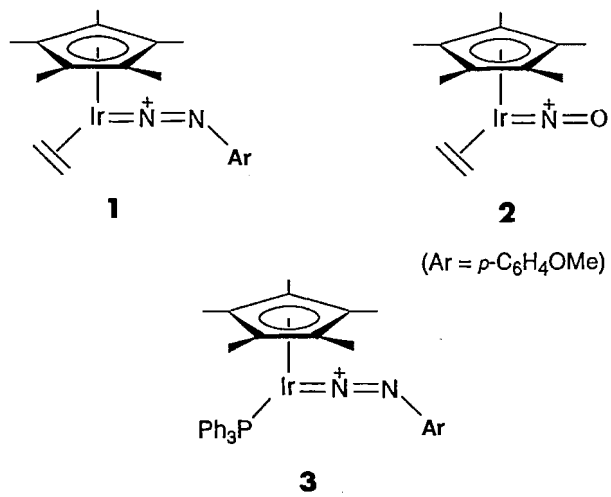

Can. J. Chem. Downloaded from www.nrcresearchpress.com by 80.90.12.36 on 09/08/12
For personal use only.

Can. J. Chem. Downloaded from www.nrcresearchpress.com by 80.90.12.36 on 09/08/12
For personal use only.

Experimental section

General

All solvents were dried and purified by standard methods and were freshly distilled under nitrogen immediately before use. All reactions and manipulations were carried out in a standard Schlenk apparatus. Infrared spectra were measured for solutions in CaF_2 cells by using a Bomem Michelson 120 FTIR instrument. Some of the routine ^1H NMR spectra were recorded at 100 MHz by using a Varian 100-SY spectrometer. Dynamic ^1H NMR, and $^{13}C\{^1H\}$, ^{14}N, and ^{15}N NMR spectra were obtained by M.M. Tracey on a Bruker AMX 400 instrument at operating frequencies of 400.1, 100.6, 28.9, and 40.5 MHz, respectively. Chemical shifts are reported in ppm, downfield positive, relative to tetramethylsilane (TMS) for ^1H and $^{13}C\{^1H\}$ spectra, and relative to $MeNO_2$ for ^{14}N and ^{15}N spectra, respectively. Coupling constants are reported in Hz.

The temperatures of the samples used in the dynamic NMR studies were obtained from the temperature controller of the AMX 400 spectrometer and are accurate to ±1 K. The free energy of activation at the coalescence temperature was calculated from the following equation (17),

$$[1] \quad \Delta G^{\neq} = -RT_c \ln \frac{\pi \Delta \nu h}{\sqrt{2}\, kT_c}$$

$$= aT_c[9.972 + \log (T_c/\Delta\nu)]$$

where $\Delta\nu$ is the chemical shift difference of the coalescing resonances in the absence of exchange, T_c is the coalescence temperature, and R, h, and k have their normal thermodynamic significance. The reduced parameter $a = 1.914 \times 10^{-2}$ kJ mol^{-1} K^{-1}.

Mass spectra were obtained by G. Owen on a Hewlett–Packard model 5985 GC–MS spectrometer equipped with a fast atom bombardment (FAB) probe (xenon source, Phrasor Scientific, Inc., accessory), and utilized samples dispersed or dissolved in sulfolane or *m*-nitrobenzyl alcohol (NOBA). Chemical ionization mass spectra (CIMS) utilized isobutane. The pattern of the envelope of the fragment ions was matched with that simulated by computer for the species in question. The masses are quoted for ^{193}Ir and ^{37}Cl isotopes. Microanalyses were performed by M.-K. Yang of the Microanalytical Laboratory of Simon Fraser University.

Bis(ethylene)pentamethylcyclopentadienyl iridium was synthesized according to the published method (18). *para*-Methoxybenzenediazonium tetrafluoroborate was prepared from *p*-anisidine (Aldrich) and sodium nitrite, and purified by recrystallization from acetone and diethyl ether. The diazonium salt labelled with ^{15}N at the unsubstituted nitrogen (N_α) was prepared by using $Na^{15}NO_2$ (95% ^{15}N, MSD Isotopes).

Computations were performed by using the extended Hückel method. Literature values of H_{ii} were used for nitrogen, carbon, and hydrogen atoms and the off-diagonal elements H_{ij} were evaluated with the weighted H_{ij} formula (19). The bond distances used for NO^+ and HN_2^+ were the same values used in prior calculations (20). The geometric parameters used for the free PhN_2^+ ion were those taken from an X-ray structure determination (21). The NN and NC bond distances used for the bent PhN_2^+ group were averaged from ca. 40 X-ray structurally characterized, singly bent, aryldiazenido complexes in the literature (3).

Preparation of [Cp*Ir(C_2H_4)(*p*-$N_2C_6H_4OMe$)][BF_4] (**1** BF_4) and **1**-$^{15}N_\alpha$ BF_4

$Cp^*Ir(C_2H_4)_2$ (100 mg, 0.26 mmol) was dissolved in acetone (5 mL) in a 100 mL Schlenk tube equipped with a magnetic stir bar. The solution was cooled for 15 min at −78°C, with at least 2/3 the length of the Schlenk tube immersed in the bath. Then [(*p*-$N_2C_6H_4OMe$)][BF_4] or [*p*-$^{15}NNC_6H_4OMe$][BF_4] (18 mg, 0.26 mmol) in acetone (5 mL) was slowly added dropwise by pipet in such a way that the drops of the diazonium salt solution first touched the upper part of the cold Schlenk tube and then slowly flowed down the wall into the reaction mixture. If the diazonium salt solution was added directly to the reaction mixture without allowing it to cool in this way, the result generally was an impure oily product. The reaction mixture was continuously stirred during addition of the diazonium salt solution and then for an additional hour at −78°C. The colour of the reaction solution changed from colourless to yellow, then to orange-red. The reaction was monitored for the disappearance of the ν(NN) IR band at 2253 cm^{-1} for the free diazonium ion. When the reaction was complete, hexane was added slowly until no more solid precipitated. The supernatant solution was removed and the remaining brown solid washed twice with ca. 20 mL of hexane, affording the analytically pure product **1** BF_4 or **1**-$^{15}N_\alpha$ BF_4 almost quantitatively. Recrystallization of the product from acetone–hexane at −10°C gave dark red crystals in greater than 90% yield. More product could be recovered as fine crystals by evaporation of the supernatant solution; mp 150–155°C. IR, ν(NN): 1710 cm^{-1} (KBr), 1724 cm^{-1} (EtOH); $\nu(^{15}NN)$: 1675 cm^{-1} (KBr). ^1H NMR (400 MHz, $CDCl_3$), δ: 2.25 (s, 15H, C_5Me_5), 3.25 (br s, 4H, C_2H_4), 3.91 (s, 3H, OMe), 7.23 (q, 4H, C_6H_4). $^{13}C\{^1H\}$ NMR ($CDCl_3$), δ: 9.61 ($C_5\mathit{Me}_5$), 49.32 (C_2H_4), 56.01 (OMe), 100.89 (C_5Me_5), 111.77, 117.08, 125.21, and 164.09 (C_6H_4). ^{14}N NMR ($MeNO_2$-d_3), δ: −107.0 (br s, N_β), −2.9 (br s, N_α). ^{15}N NMR for **1**-$^{15}N_\alpha$ BF_4 (acetone-d_6), δ: −2.26 (s, N_α). FABMS, *m/z*: 491 (M^+), 463 ($M^+ - C_2H_4$), 433 ($M^+ - C_2H_4 - OMe$), 405 ($M^+ - C_2H_4 - N_2 - OMe$), 354 ($M^+ - N_2C_6H_4OMe - 2H$). Anal. calcd.: C 39.52, H 4.54, N 4.85; found: C 39.11, H 4.53, N 4.84.

X-ray crystal structure determination of [Cp*Ir(C_2H_4)(*p*-$N_2C_6H_4OMe$)][BF_4] (**1** BF_4)

Crystals suitable for X-ray structure analysis were obtained by recrystallization of **1** BF_4 from acetone and diethyl ether at −10°C. After examination by microscopy with polarized light, a large brown single crystal was slowly ground to a sphere and mounted in a capillary tube, the diameter of which was sufficiently close to that of the crystal to keep the crystal motionless. The crystal was then well centered in the X-ray beam of an Enraf–Nonius CAD-4F diffractometer equipped with graphite-monochromatized MoKα radiation. Selected crystallographic and experimental parameters are given in Table 1.

Intensity data were collected at −40 ± 1°C. Three intensity standards were measured every 1.5 h of acquisition time, and showed no significant change in intensity during the data collection. A final unit cell was determined by least-squares procedures from the setting angles of 25 well-centered reflections (with $18° \leq 2\theta \leq 44°$) chosen from a random variety of points in reciprocal space. A monoclinic unit cell was first assumed

Can. J. Chem. Downloaded from www.nrcresearchpress.com by 80.90.12.36 on 09/08/12
For personal use only.

Table 1. Crystallographic data for the structure determination of **1 BF_4**.

Formula	$[Cp^*Ir(C_2H_4)(p\text{-}N_2C_6H_4OMe)][BF_4]$
Crystal system	Monoclinic
space group	$P2_1/n$ (No. 14)[a]
a(Å)	8.5780(10)
b(Å)	20.5310(23)
c(Å)	12.0310(15)
β(deg)	93.500(10)
Z	4
FW	577.22
ρ (g/cm^3)	1.814
μ (MoKα)(cm^{-1})	63.4
Crystal size (mm)	0.30 (∅)
λ (Å)	0.71069
Transmission	0.238–0.253
Min–max 2θ (deg)	0–50
scan type	ω–2θ
Min h, k, l	−10, 0, 0
Max h, k, l	10, 24, 14
R_f[b]	0.0281
R_w[c]	0.0308
GOF	1.10

[a]Alternative setting of $P2_1/c$ (x, y, z; $-x$, $-y$, $-z$; $\frac{1}{2}+x$, $\frac{1}{2}-y$, $\frac{1}{2}+z$; $\frac{1}{2}-x$, $\frac{1}{2}+y$, $\frac{1}{2}-z$).
[b]$R_f = \Sigma(|F_o| - |F_c|)/\Sigma|F_o|$ for observed data.
[c]$R_w = [\Sigma w(|F_o| - |F_c|)^2/\Sigma w|F_o|^2]^{1/2}$ for observed data.

and then proven by investigation of selected symmetry-related reflections from the intensity data file. Lorentz, polarization, and spherical absorption corrections (22, 23) were applied and the intensity data converted into the corresponding structure factor amplitudes and their esd's.

The structure was solved by Patterson and conventional Fourier methods and refined by using full-matrix least-squares procedures. Anisotropic thermal parameters for Ir, F, and O atoms and the C atoms in the methyl groups and ethylene ligand, and isotropic thermal parameters for other atoms, were included in the final refinement. The refinement was considered complete when the maximum shift/esd was <0.01. The positions of hydrogen atoms were generated with d(C—H) = 0.95 Å. A total of 54 atoms and 183 variables against 2611 observations were involved in the final refinement. The quantity minimized by the least-squares program was $\Sigma w(|F_o| - |F_c|)^2$, where w is the unit weight. Inspection of average $\Sigma w\Delta^2$ ordered in the ranges of sin θ/λ, $|F_o|$, and the values of individual indices was near constant. The largest feature in the final difference Fourier map had an electron density 1.2 e^{-1} Å^{-3} and was located 0.9 Å from the Ir atom. Positional parameters and thermal parameters of non-hydrogen atoms are listed in Table 2.[2]

[2] Tables 5 (hydrogen atom coordinates) and 6 (anisotropic thermal parameters) for **1 BF_4** (2 pages) have been deposited. Copies of material on deposit may be purchased from: The Depository of Unpublished Data, Document Delivery, CISTI, National Research Council Canada, Ottawa, Canada K1A 0S2.

Table 5 has also been deposited with the Cambridge Crystallographic Data Centre, and can be obtained on request from The Director, Cambridge Crystallographic Data Centre, University Chemical Laboratory, 12 Union Road, Cambridge, CB2 1EZ, U.K.

Table 2. Positional and thermal parameters for **1 BF_4**.

Atom	x/a	y/b	z/c	B_{iso}
Ir	0.21120(3)	0.11305(2)	0.09575(3)	3.21*[a]
F1	0.1820(8)	0.2909(3)	0.6869(6)	8.5*
F2	0.2383(11)	0.2333(5)	0.5402(6)	13.0*
F3	0.3134(10)	0.2012(4)	0.7052(8)	12.0*
F4	0.0674(10)	0.1970(4)	0.6485(9)	13.8*
O	0.8281(7)	0.0063(3)	0.5538(5)	5.4*
C	0.8732(11)	0.0666(5)	0.6072(7)	5.5*
C10	0.3385(12)	0.1037(5)	−0.0558(8)	5.8*
C20	0.4227(11)	0.1433(5)	0.0196(9)	6.2*
C21	−0.1459(11)	0.0543(5)	0.1378(8)	5.7*
C22	0.0302(13)	0.1366(5)	0.3333(8)	6.5*
C23	0.1984(13)	0.2575(5)	0.2220(10)	6.8*
C24	0.1206(14)	0.2498(5)	−0.0420(9)	6.9*
C25	−0.0923(11)	0.1237(5)	−0.0934(8)	5.8*
B	0.1948(14)	0.2312(6)	0.6445(10)	5.44(23)
N1	0.3172(7)	0.0451(3)	0.1597(5)	4.01(13)
N2	0.3875(8)	−0.0018(3)	0.1962(5)	3.98(13)
C11	−0.0444(8)	0.1124(4)	0.1235(6)	3.53(13)
C12	0.0345(9)	0.1498(4)	0.2096(6)	4.00(15)
C13	0.1094(9)	0.2036(4)	0.1593(7)	4.05(15)
C14	0.0760(9)	0.1999(4)	0.0415(6)	3.97(15)
C15	−0.0197(9)	0.1435(4)	0.0196(6)	3.87(15)
C1	0.5016(8)	0.0049(4)	0.2881(6)	3.49(14)
C2	0.5372(9)	0.0637(4)	0.3401(7)	4.07(15)
C3	0.6476(9)	0.0667(4)	0.4274(7)	4.28(16)
C4	0.7211(9)	0.0100(4)	0.4656(7)	4.00(15)
C5	0.6868(9)	−0.0490(4)	0.4124(7)	4.14(16)
C6	0.5757(9)	−0.0519(4)	0.3242(6)	3.73(14)

[a]Values marked with an asterisk are $B_{eq} = (8\pi^2/3)\,\Sigma_i\Sigma_j U_{ij} a_i^* a_j^* a_i a_j$.

The computing programs used for data reduction and structure solution and refinement were from the NRC VAX crystal structure system (24). The analytical forms of the scattering factors for neutral atoms (including anomalous scattering) were used in the calculations of structure factors (25). All computations were carried out on an in-house Micro VAX-II computer.

Preparation of $[Cp^*Ir(PPh_3)(p\text{-}N_2C_6H_4OMe)][BF_4]$ (3 BF_4) and 3-$^{15}N_\alpha$ BF_4

To an ethanol solution (10 mL) containing equimolar quantities of $Cp^*Ir(C_2H_4)_2$ (30 mg, 0.078 mmol) and PPh_3 (21 mg, 0.080 mmol) was added $[p\text{-}N_2C_6H_4OMe][BF_4]$ or $[p\text{-}^{15}NNC_6H_4OMe][BF_4]$ (17 mg, 0.077 mmol). Following the addition of the diazonium salt, the colourless solution immediately changed to orange-red. The reaction was monitored for the disappearance of ν(NN) at 2253 cm^{-1} for the free diazonium ion. After the solution was stirred for 1 h, the solution was taken to dryness which gave compound **3 BF_4** or **3-$^{15}N_\alpha$ BF_4** quantitatively as an orange-red oil. IR, ν(NN), 1701 cm^{-1} (ethanol), 1710 cm^{-1} (CH_2Cl_2); ν(^{15}NN): 1676 cm^{-1} (ethanol). ^{1}H NMR (100 MHz, acetone-d_6), δ: 2.12 (d, 15H, $J_{P\text{-}Me}$ = 2, Cp*), 3.85 (s, 3H, OMe), 7.06 (q, 4H, AA′BB′ pattern, C_6H_4), 7.20–7.90 (m, 15H, Ph); δ($CDCl_3$): 1.97 (d, 15H, $J_{P\text{-}Me}$ = 2, Cp*), 3.87 (s, 3H, OMe), 6.98 (d, 4H, $J_{H\text{-}H}$ = 1, C_6H_4), 7.40–

Can. J. Chem. Downloaded from www.nrcresearchpress.com by 80.90.12.36 on 09/08/12
For personal use only.

7.52 (m, 15H, Ph). ^{15}N NMR for **3**-$^{15}N_\alpha$ (acetone-d_6), δ: 33.23 (d, $^{15}N\alpha$, $J_{P-^{15}N\alpha} = 7$). FABMS (NOBA, xenon), *m/z*: 725 (M^+), 590 ($M^+ - N_2C_6H_4OMe$). Anal. calcd.: C 51.79, H 4.60, N 3.45; found: C 52.18, H 4.81, N 3.62.

Complex **3** BF_4 or **3**-$^{15}N_\alpha$ BF_4 can also be made quantitatively from the reaction of freshly synthesized **1** BF_4 or **1**-$^{15}N_\alpha$ BF_4 in ethanol solution with solid PPh_3 at room temperature.

Preparation of Cp*IrH(PPh_3)(*p*-$N_2C_6H_4OMe$) (4) and 4-$^{15}N_\alpha$

An excess of $NaBH_4$ (7 mg, 0.2 mmol) was added to an acetone solution (5 mL) of **3** BF_4 or **3**-$^{15}N_\alpha$ BF_4 (42 mg, 0.052 mmol), and the mixture was stirred for 1 h at −10°C. The colour changed from orange-red to peach-red. The solvent was removed by vacuum, excess hexanes (15 mL) were added to the residue, and the mixture was stirred vigorously for 15 min. The peach-red solution was filtered through Celite to remove the insoluble salts ($NaBF_4$ and $NaBH_4$) and then pumped to dryness to give a rose-purple oily product **4** or **4**-$^{15}N_\alpha$ in 89% yield. IR, ν(Ir-H): 2133 br cm^{-1}(hexanes). ^{1}H NMR (100 MHz, acetone-d_6), δ: −15.9 (d, 1H, $J_{P-H} = 33.5$, Ir-H), 1.51 (dd, 15H, $J_{P-H} = 1.8$, $J_{H-H} = 0.7$, Cp*), 3.57 (s, 3H, OMe), 6.58 (d, 4H, $J = 1.7$, C_6H_4), 7.10–7.60 (m, 15H, Ph). ^{15}N NMR for **4**-$^{15}N_\alpha$ (acetone-d_6), δ: 271.89 (s, $^{15}N_\alpha$). CIMS, *m/z*: 590 ([Cp*Ir(PPh_3)]$^+$), 464 ([Cp*Ir(H)($N_2C_6H_4OMe$)]$^+$). Anal. calcd.: C 57.92, H 5.28, N 3.86, found: C 58.12, H 5.43, N 3.89.

Preparation of [Cp*IrCl(PPh_3)(*p*-$NHNC_6H_4OMe$)][BF_4] (6 BF_4) and 6-$^{15}N_\alpha$ BF_4

Method 1

A solution of freshly synthesized **3** BF_4 or **3**-$^{15}N_\alpha$ BF_4 (42 mg, 0.052 mmol) in ethanol (5 mL) was slowly purged by gaseous HCl for 5 min at room temperature with the flask immersed in a cold water bath at ~10°C to absorb the heat released from the solvation of the HCl. The color changed from orange-red to dark green. After stirring for another 5 min the volatiles were pumped off, leaving a dark yellow solid residue. This was then redissolved in a minimum amount of acetone, and an excess of diethyl ether was added slowly with vigorous stirring until no further solid precipitated. The yellow supernatant solution was removed and the remaining yellow solid was washed twice with 20 mL portions of diethyl ether. This gave **6** BF_4·**0.5**Et_2O or **6**-$^{15}N_\alpha$ BF_4·**0.5**Et_2O as a fine yellow powder in 92% yield. IR, ν(NN): 1483 cm^{-1}, ν(^{15}NN): 1460 cm^{-1} (KBr). ^{1}H NMR (100 MHz, acetone-d_6), δ: 1.54 (d, 15H, J_{P-H} = 2.2, Cp*), 3.93 (s, 3H, OMe), 7.05 and 7.40 (d, 4H, AA′BB′ pattern, C_6H_4), 7.52 and 7.58 (s, 15H, Ph), 13.73 (d, 1H, $J_{^{15}N-H}$ = 70); ^{1}H NMR ($CDCl_3$), δ: 1.52 (d, 15H, $J_{P-H} = 2.2$, Cp*), 3.92 (s, 3H, OMe), 6.92 and 7.19 (d, 4H, AA′BB′ pattern, C_6H_4), 7.45 and 7.50 (s, 15H, Ph), 13.01 (d, 1H, $J_{^{15}N-H} = 69$). ^{15}N NMR for **6**-$^{15}N_\alpha$ BF_4 (acetone-d_6), δ: −64.24 (d, $J_{^{15}N-H}$ = 70). FABMS (NOBA, xenon), *m/z*: 761 (M^+), 625 (M^+ − $NHNC_6H_4OMe$), 589 ($M^+ - N_2C_6H_4OMe - Cl$), 511 (M^+ − $NHNC_6H_4OMe - Cl - Ph$). Anal. calcd. for **6** BF_4·**0.5**Et_2O: C 50.20, H 4.89, N 3.16, found: C 50.21, H 4.83, N 3.09.

Method 2

Freshly synthesized **4** or **4**-$^{15}N_\alpha$ (22 mg, 0.031 mmol) in dry CCl_4 (3 mL) was stirred vigorously in the dark at −10°C. After 20 min, under the same conditions, the solvent was pumped off, resulting in a red solid product. This was redissolved in the minimum amount of acetone to give a red solution to which was slowly added 2 drops of HBF_4 – diethyl ether solution, resulting in an immediate brownish precipitate. The supernatant solution was then removed and the remaining dark yellow solid was pumped overnight. ^{1}H NMR spectroscopy of this solid indicated that **6** BF_4 or **6**-$^{15}N_\alpha$ BF_4 was the major product, but was contaminated with variable amounts of Cp*Ir(PPh_3)Cl_2, identified as follows: ^{1}H NMR (100 MHz, acetone-d_6), δ: 1.34 (d, 15H, $J_{P-H} = 2$, Cp*) and 7.35–7.75 (m, 15H, Ph) (18).

Attempts to observe Cp*IrCl(PPh_3)(*p*-$N_2C_6H_4OMe$) (5)

*(a) By deprotonation of [Cp*IrCl(PPh_3)(p-$NHNC_6H_4OMe$)][BF_4] (6 BF_4)*

To a yellow solution of **6** BF_4 (44 mg, 0.052 mmol) in acetone (5 mL) was added 2 drops of NEt_3. The colour immediately changed to red. Diethyl ether (ca. 2 mL) was added carefully to precipitate pale gray $NHEt_3$·BF_4. After filtering, the filtrate was concentrated to 2 mL under vacuum and excess diethyl ether was added slowly until no further solid precipitated. The supernatant was removed and the remaining solid was washed twice with diethyl ether to yield the product as an orange powder. IR and ^{1}H NMR of this solid indicated that it was a mixture of Cp*Ir(PPh_3)Cl_2 (<5% based on the ^{1}H NMR integration) and a major species that had identical IR and ^{1}H NMR features to compound **3** BF_4: (IR, ν(NN): 1711 cm^{-1} (CH_2Cl_2), 1699 cm^{-1} (KBr); ^{1}H NMR (acetone-d_6), δ: 2.12 (d, 15H, $J_{P-H} = 2$, Cp*), 3.85 (s, 3H, OMe), 7.06 (q, 4H, AA′BB′ pattern, C_6H_4), 7.20–7.90 (m, 15H, Ph). Consequently, this major species is assigned as [Cp*Ir(PPh_3)(*p*-$N_2C_6H_4OMe$)]Cl (**3 Cl**).

(b) By exchange of hydride ligand in 4

Freshly synthesized **4** (22 mg, 0.031 mmol) in dry CCl_4 (3 mL) was stirred in the dark at −10°C for 20 min; a longer reaction time resulted in the formation of Cp*Ir(PPh_3)Cl_2 as a major product after the next procedure. The solvent was pumped off to give a red powder. The IR spectrum of this red solid in the range 2300–1600 cm^{-1} showed only a band at 1711 cm^{-1} (in CH_2Cl_2), or at 1717 cm^{-1} (in CCl_4). The ^{1}H NMR spectra of this solid in either $CDCl_3$ or acetone-d_6 clearly showed the expected resonances in the region due to the protons of the Cp* group, OMe group, and the aromatic groups. However, no reproducible resonance patterns could be obtained. Using the ^{15}N-enriched sample **4**-$^{15}N_\alpha$ as the starting material, ^{1}H NMR spectra of the solid in acetone-d_6 showed, in addition to those resonances due to the Cp*, OMe, and the aromatic groups, a weak doublet at δ 13.71 with a coupling constant of 70 Hz assignable to NH, which showed variable intensity for different samples. The ^{15}N NMR spectrum (by using **4**-$^{15}N_\alpha$) in acetone-d_6 showed, however, no signal due to either free or coordinated $ArN^{15}N^+$, but a singlet at −73 ppm assigned to free ^{15}NN. Microanalysis gave 2.77% nitrogen content in this red solid, which was lower than the calculated 3.68% of nitrogen for Cp*Ir(PPh_3)(Cl)(*p*-$N_2C_6H_4OMe$). Attempts to further purify this material failed due to its facile decomposition to give Cp*Ir(PPh_3)Cl_2 as the main isolated

Can. J. Chem. Downloaded from www.nrcresearchpress.com by 80.90.12.36 on 09/08/12
For personal use only.

product. However, protonation of this mixture in solution by HBF_4 – diethyl ether always yielded the compounds $[Cp^*Ir(PPh_3)Cl(p\text{-}NHNC_6H_4OMe)][BF_4]$ (**6** $\mathbf{BF_4}$) and $Cp^*Ir(PPh_3)Cl_2$ as the major products. The relative ratio of these two products produced by the protonation was strongly dependent upon how long the hydrido–chloro exchange reaction had proceeded and the time taken in manipulations in an effort to purify them.

Results

Synthesis and characterization of $[Cp^*Ir(C_2H_4)(p\text{-}N_2C_6H_4OMe)][BF_4]$ (1 $\mathbf{BF_4}$)

The careful, slow addition of a solution of *para*-methoxybenzenediazonium tetrafluoroborate in acetone to a solution of $Cp^*Ir(C_2H_4)_2$ in acetone at −78°C produces the corresponding monoethylene aryldiazenido complex **1** $\mathbf{BF_4}$ in good yield (typically better than 90% after recrystallization). As the reaction proceeds, the mixture first changes from colourless to a transient yellow, and then to orange-red. The final dark-red crystals of **1** $\mathbf{BF_4}$ can be isolated by recrystallization from acetone–hexanes at −10°C. The reaction conditions are rather critical; we have found that a fast addition of the diazonium salt solution to the $Cp^*Ir(C_2H_4)_2$ solution, or a rise in the reaction temperature, often leads to a dark-red reaction mixture. Upon addition of hexanes to this, only a red oily material precipitates. Recrystallization of this red oil from acetone–hexanes at −10°C gave only a low yield of crystals of **1** $\mathbf{BF_4}$, and these were invariably covered with the oily material. Repeating the recrystallization to attempt to obtain crystals free of contamination always resulted instead in more of the red oil. The IR spectrum of a thin film of this on a KBr disc showed (in the range 1600–2300 cm^{-1}) only the absorption at 1710 cm^{-1} due to **1** $\mathbf{BF_4}$. However, the ^1H NMR spectrum in acetone-d_6 showed resonances for **1** $\mathbf{BF_4}$ plus several other small, broad, and featureless signals at δ ca. 1.2–1.8.

Compound **1** $\mathbf{BF_4}$ is very soluble in most common polar solvents, such as acetone, $CHCl_3$, CH_2Cl_2, $MeNO_2$, and MeCN, but is insoluble in nonpolar solvents such as hexanes and diethyl ether. It is stable to air in the solid state; after exposure of the crystals to air at ambient temperature for days, no change in the IR spectrum was observed. However, in solution it has only limited stability. In nonhalogenated solvents it slowly changes from orange-yellow to orange-red over several days, but in halogenated solvents it decomposes rapidly.

1 $\mathbf{BF_4}$ has been characterized by analysis and spectroscopy. Signals due to the parent ion $[Cp^*Ir(C_2H_4)(N_2C_6H_4OMe)]^+$ and the fragments formed by loss of the C_2H_4 ligand and the aryldiazenido ligand are observable in the FABMS spectrum. The IR spectrum displays the expected absorptions for the organic and BF_4 groups and a single absorption at 1724 cm^{-1} (EtOH) that falls within the range generally associated with ν(NN) for a terminally coordinated singly bent aryldiazenido ligand (3). The assignment was confirmed by an isotopic shift of 35 cm^{-1} to lower wavenumber in the $^{15}N_\alpha$-enriched sample. The ^1H NMR spectrum shows all the expected resonances. The aryl group protons occur as a typical AA′BB′ pattern in the aromatic region and singlets at δ 3.91 and 2.25 are assigned to the methyl protons of the OMe and Cp* groups. A broad singlet at δ 3.25 (integral 4H) is assigned to four equivalent protons in the C_2H_4 ligand. The broadness of this peak suggests that the ethylene protons are involved in a dynamic process. Therefore, variable-temperature ^1H and $^{13}C\{H\}$ spectra were obtained and these are reported below. The $^{13}C\{^1H\}$ NMR spectrum of **1** $\mathbf{BF_4}$ is consistent with its ^1H NMR spectrum. At room temperature only a single resonance was observed for C_2H_4, indicating equivalent ethylene carbons. Two broad peaks at δ −2.9 and −107.0 in the ^{14}N NMR spectrum clearly indicate the presence of a singly bent aryldiazenido ligand (3, 26). The downfield signal is assigned to the metal-bound nitrogen (N_α), and this has been confirmed by the ^{15}N NMR of **1**-$^{15}\mathbf{N_\alpha}$ $\mathbf{BF_4}$.

Crystal structure of 1 $\mathbf{BF_4}$

The crystal structure of **1** $\mathbf{BF_4}$ consists of an assembly of an equal number of *R* and *S* enantiomers of the discrete cation $[Cp^*Ir(C_2H_4)(p\text{-}N_2C_6H_4OMe)]^+$ and the anions $[BF_4]^-$ related in the centrosymmetric space group $P2_1/n$. The asymmetric unit is an ion-pair. There are no abnormally short contacts in the crystal.[3] The cation has a half-sandwich structure, and a perspective view together with the numbering scheme is shown in Fig. 1, and important bond lengths and angles are in Table 3.

The Cp* ligand is bonded to the iridium in a typical η^5-coordination mode. The similar bond lengths from the five carbon atoms in the Cp* ring to iridium, from 2.204(8) through 2.238(7) Å, indicate a regular C_{5v} symmetry for the Cp*Ir moiety. Thus, the two different ligands, C_2H_4 and $[p\text{-}N_2C_6H_4OMe]^+$, constituting the "piano stool legs" for this compound, appear to have no measurable differential influence on the coordination geometry of the Cp* ligand.

The ethylene ligand is coordinated in a symmetrical η^2 fashion with Ir—C(10) = 2.190(8) Å and Ir—C(20) = 2.172(9) Å, and is oriented with the C—C bond parallel to the Cp* plane and bisected by the plane defined by Ir, N_α, and the centroid of the Cp* ring. Furthermore, compared to the typical uncoordinated ethylene C═C distance of 1.335(5) Å, the C(10)—C(20) distance of 1.387(16) Å of the ethylene ligand in **1** indicates this bond has been significantly lengthened as a result of coordination. The aryldiazenido ligand clearly has a singly bent geometry, with the Ir-N(1)-N(2) skeleton close to linear and the N(1)-N(2)-C(1) angle about 120°. These values and other related parameters for the aryldiazenido ligand are comparable to those found for $[IrCl(N_2Ph)(PPh_3)_2][BF_4]$ (3), the only other iridium singly bent aryldiazenido complex characterized by X-ray diffraction (Table 4).

The aryldiazenido ligand is essentially planar, which indicates significant π-conjugation throughout the NN, methoxyl, and phenyl ring framework. However, the most striking feature of the aryldiazenido ligand is the orientation of its molecular plane with respect to the rest of the complex. Rather than it being coincident with the local (vertical) plane through Ir and the centroids of the Cp* and ethylene ligands, it is instead approximately perpendicular to it, as indicated by the C-N_β-Ir-Cp*(centroid) torsion angle of 88.4°. A view of the cation **1** down the N(2)-N(1)-Ir axis vividly illustrates this stereochemical arrangement (Fig. 2).

[3] The shortest contacts involve pairs of *p*-methoxyphenyl rings with C—C contacts of approximately 3.65 A across an inversion centre at (1/2, 0, 1/2).

Fig. 1. Structure of the cation $[Cp^*Ir(C_2H_4)(p\text{-}N_2C_6H_4OMe)]^+$ (**1**) showing the atom numbering. Thermal ellipsoids or spheres represent 50% probability enclosures.

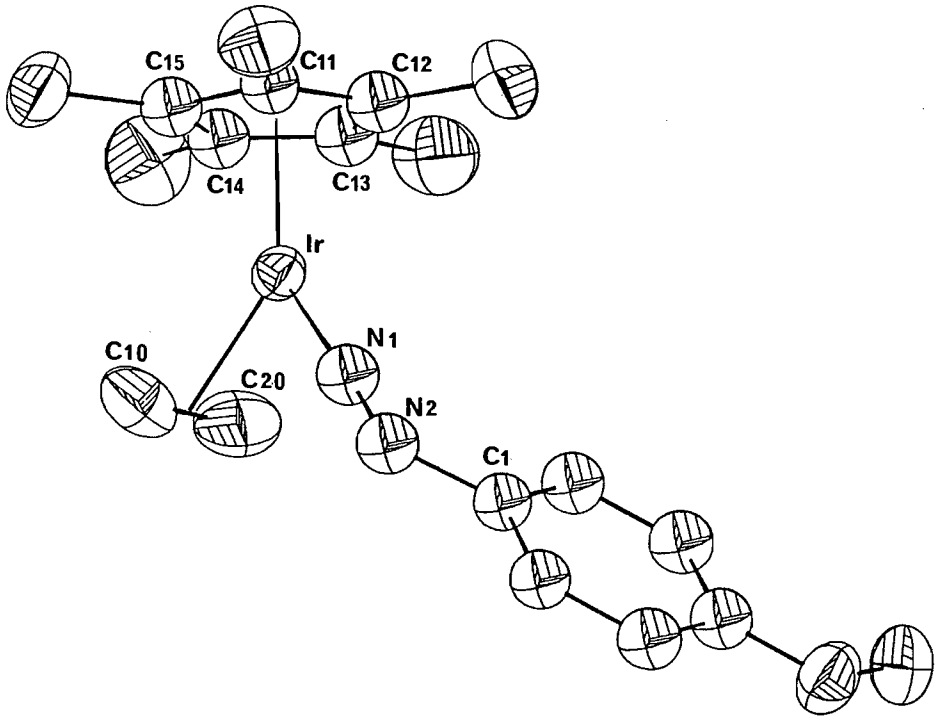

Fig. 2. A view of the cation $[Cp^*Ir(C_2H_4)(p\text{-}N_2C_6H_4OMe)]^+$ (**1**) down the Ir–N axis showing the orientation of the aryldiazenido ligand.

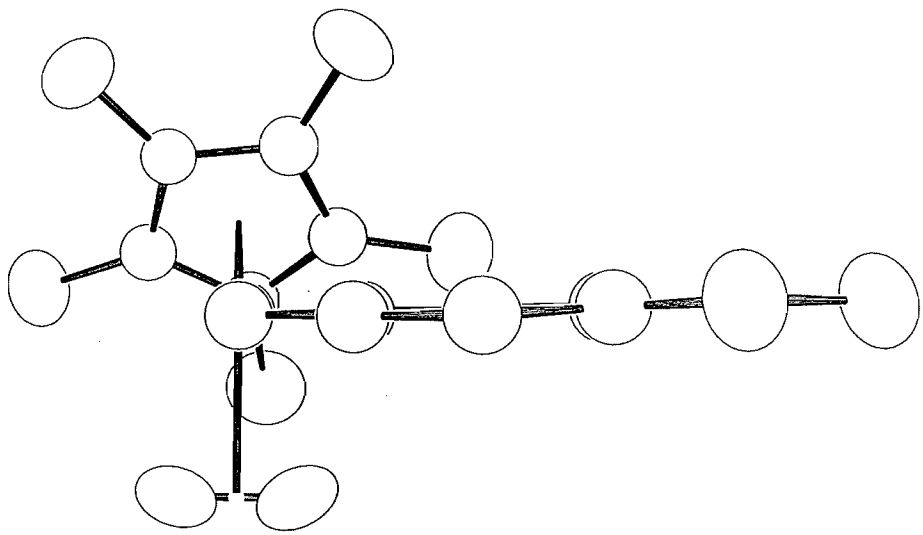

Can. J. Chem. Downloaded from www.nrcresearchpress.com by 80.90.12.36 on 09/08/12
For personal use only.

Geometry and electronic structure of the singly bent aryldiazenido ligand

In an effort to provide a theoretical basis for the observed orientation of the aryldiazenido ligand in the cation **1** the frontier orbitals for the fragments $Cp^*Ir(C_2H_4)$ and PhN_2^+ have been considered. As we will describe in the Discussion, overlap of the appropriate orbitals of these fragments does indeed account satisfactorily for the observed orientation.

There do not appear to be any previously published EHMO calculations for either the free or coordinated PhN_2^+ ion, although EHMO calculations for the free HN_2^+ ion and its complexes as well as for complexes with the MeN_2 ligand have been reported previously (20, 27). However, conclusions derived from these calculations are unlikely to be entirely valid for the *aryl*diazonium ion or the *aryl*diazenido ligand because the lack of cylindrical symmetry in the former, and the effect of π-conjugation of the NN group with the planar phenyl group in both instances, are ignored. The significance of π-conjugation for PhN_2^+ can be determined by a comparison of the calculated relative energies of the valence orbitals of the free ions NO^+, HN_2^+, and PhN_2^+ (Fig. 3). The highest occupied molecular orbital (HOMO) for NO^+ or linear HN_2^+ is a σ-type orbital, but for the free

Can. J. Chem. Downloaded from www.nrcresearchpress.com by 80.90.12.36 on 09/08/12
For personal use only.

Table 3. Selected bond lengths (Å) and inter-bond angles (deg) for **1** BF_4.

(a) Bond lengths

Ir—C(10)	2.190(8)	Ir—C(20)	2.172(9)
N(1)—N(2)	1.205(9)	Ir—N(1)	1.811(7)
N(2)—C(1)	1.438(10)	Ir—C(11)	2.238(7)
C(11)—C(12)	1.427(11)	Ir—C(12)	2.236(8)
C(11)—C(15)	1.430(11)	Ir—C(13)	2.211(8)
C(12)—C(13)	1.431(11)	Ir—C(14)	2.204(8)
C(13)—C(14)	1.431(11)	Ir—C(15)	2.220(8)
C(14)—C(15)	1.434(11)	O—C	1.436(11)
O—C(4)	1.362(10)	C(1)—C(2)	1.384(11)
C(1)—C(6)	1.385(11)	C(2)—C(3)	1.372(11)
C(3)—C(4)	1.389(12)	C(4)—C(5)	1.394(12)
C(5)—C(6)	1.384(11)	C(10)—C(20)	1.387(16)
C(21)—C(11)	1.494(12)	C(22)—C(12)	1.514(12)
C(23)—C(13)	1.518(13)	C(24)—C(14)	1.501(13)
C(25)—C(15)	1.517(11)		

(b) Inter-bond angles

C(10)—Ir—C(20)	37.1(4)	C(10)—Ir—N(1)	91.3(3)
C(20)—Ir—N(1)	89.3(3)	Ir—N(1)—N(2)	176.2(6)
N(1)—N(2)—C(1)	120.4(6)	Ir—C(11)—C(21)	127.3(6)
Ir—C(12)—C(22)	126.8(6)	Ir—C(13)—C(23)	126.0(6)
Ir—C(14)—C(24)	126.8(6)	Ir—C(15)—C(25)	127.0(6)
C(21)—C(11)—C(12)	126.9(7)	C(21)—C(11)—C(15)	125.2(7)
C(12)—C(11)—C(15)	107.8(7)	C(22)—C(12)—C(11)	125.3(8)
C(22)—C(12)—C(13)	126.3(8)	C(23)—C(13)—C(12)	125.2(8)
C(23)—C(13)—C(14)	126.6(8)	C(24)—C(14)—C(13)	125.6(8)
C(24)—C(14)—C(15)	126.5(8)	C(25)—C(15)—C(11)	126.1(7)
C(25)—C(15)—C(14)	125.5(7)	C—O—C(4)	116.8(7)
N(2)—C(1)—C(2)	123.5(7)	N(2)—C(1)—C(6)	116.0(7)
Ir—C(10)—C(20)	70.8(5)	Ir—C(20)—C(10)	72.2(5)
O—C(4)—C(3)	125.1(7)	O—C(4)—C(5)	115.0(7)

Table 4. Bond distances (Å) and angles (deg) for the aryldiazenido ligand in iridium complexes.

Parameters	**1** BF_4	$[IrCl(N_2Ph)(PPh_3)_2][BF_4]$[a]
Ir—N(1)	1.811(7)	1.800(10)
N(1)—N(2)	1.205(9)	1.163(11)
Ir—N(1)—N(2)	176.2(6)	175.8(8)
N(1)—N(2)—C(1)	120.4(6)	126.9(10)

[a]Reference 3.

"linear" PhN_2^+ ion it is a nonbonding orbital of π character. In fact, the filled σ orbital of PhN_2^+ is buried beneath three filled π-type orbitals, one with b_1 symmetry and other two with b_2 symmetry in this C_{2v} system. Interestingly, all these three π orbitals have nonbonding character with respect to the N-N-C linkage and they are energetically located rather higher than the corresponding π orbitals in NO^+ and HN_2^+. Another distinguishing feature is that for NO^+ and HN_2^+ the lowest unoccupied molecular orbitals (LUMO's) are two degenerate π antibonding orbitals, but for PhN_2^+, the corresponding π-type orbitals are nondegenerate (π_x^* and π_y^*); the π_y^* orbital, which is conjugated with the π system of the phenyl ring, lies low, and π_x^*, which is perpendicular to it, lies high. Clearly, the main underlying cause of the differences between the frontier orbitals for NO^+ and HN_2^+ and those of PhN_2^+ is the conjugation of the π-system of the *aryl* group with one directional set of π orbitals of the N_2 group in PhN_2^+ (the orbitals π_y and π_y^* in Fig. 3). Furthermore, energetically the "linear" PhN_2^+ ion seems to be neither a better σ-donor nor a better π-acceptor ligand than NO^+.

However, the linear phenyldiazonium ion is not really what we are interested in, when it comes to considering the frontier orbitals for an aryldiazonium ion acting as a *ligand.* This is because the structure of the cation **1** is typical of the class of "singly bent" aryldiazenido complexes (**Ib**, Scheme 1) in that the ligand is invariably found to be bent, not linear, at N_β with an angle typically near 120° (3). Furthermore, in **1** it is bent in a direction that makes N_α, N_β, and the aryl ring coplanar. Clearly, to use the fragment molecular orbital (FMO) method for singly bent aryldiazenido complexes, the MO's of this *bent* aryldiazenido ligand fragment, rather than the linear one, are needed. Moreover, the singly bent aryldiazenido ligand has NN and NC bond lengths that are different from free ArN_2^+. The effect that this bending at N_β, and lengthening of the NN and NC distances, has on the π, π^*, and σ orbitals is shown sequentially in the middle and right-hand side of Fig. 4 (where the bending is assumed to be in the *xz* plane).

As a result of bending at N_β, the local symmetry of PhN_2^+ drops from C_{2v} to C_s. Consequently, the σ- and π_x-type of

Can. J. Chem. Downloaded from www.nrcresearchpress.com by 80.90.12.36 on 09/08/12
For personal use only.

Fig. 3. The frontier orbitals of NN, NO^+, HNN^+, and $PhNN^+$.

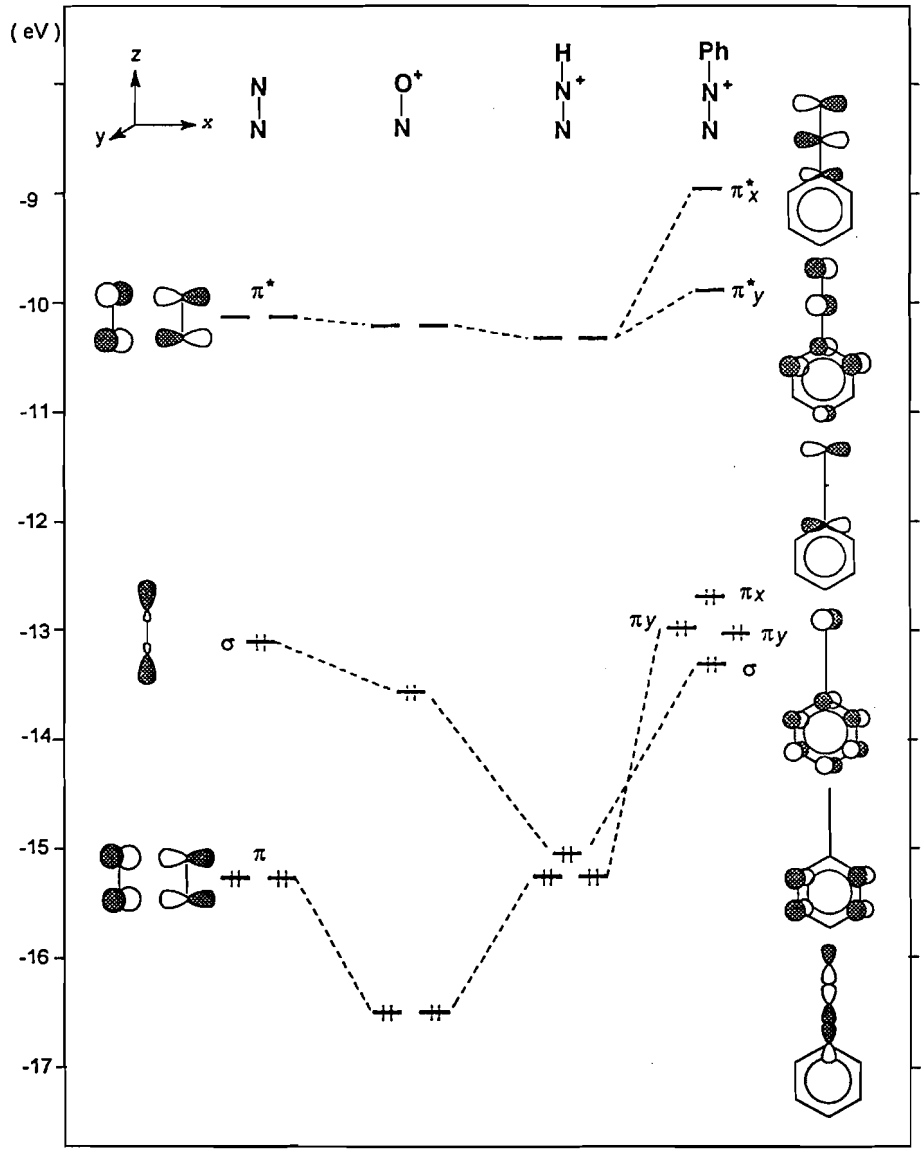

orbitals (π_x and π_x*), which were orthogonal in C_{2v}, are now in principle able to interact with each other. The filled σ and π orbitals are very close to one another in energy in the free PhN_2^+ ion, so a strong mixing of this σ orbital and the π_x orbital would be expected. The resulting higher energy orbital $2a'$ produced by this mixing is an orbital of considerable σ character, and is now the HOMO in the bent PhN_2^+ ion. This contrasts directly with the linear PhN_2^+ ion where the HOMO is a π_y orbital. Interestingly, this $2a'$ orbital is located in the plane and points in a direction slightly *trans* to the phenyl group. The mixing also produces a lower energy orbital, the σ orbital $1a'$, which is primarily bonding between N_β and the ipso C atom. Another notable feature is that the bending decreases the energy of the π_x* orbital dramatically, and indeed this becomes the LUMO $3a'$ in bent PhN_2^+, and is a π-acceptor orbital. Thus, **7** is the formal valence structure for the singly bent PhN_2^+ ligand, and the shape and arrangement of the HOMO **8** and LUMO **9** are together shown in simplified fashion in **10**, and resemble those for a vinylidene ligand **11**, especially inasmuch as the acceptor orbital on the terminal N or C atom is a *p* orbital that lies *in the molecular plane.*

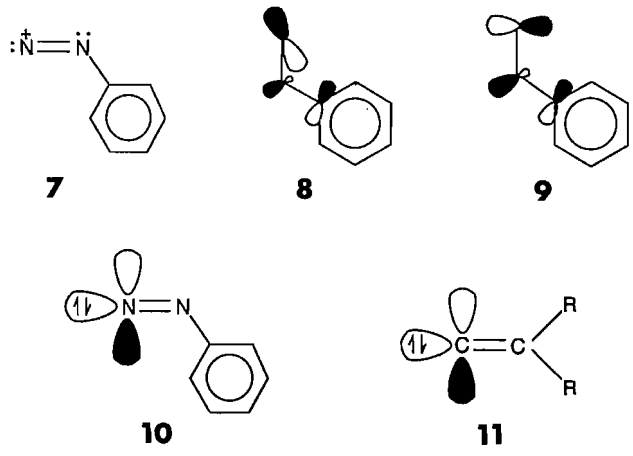

Fig. 4. Effect of NNC bending on the frontier orbitals of $PhNN^+$.

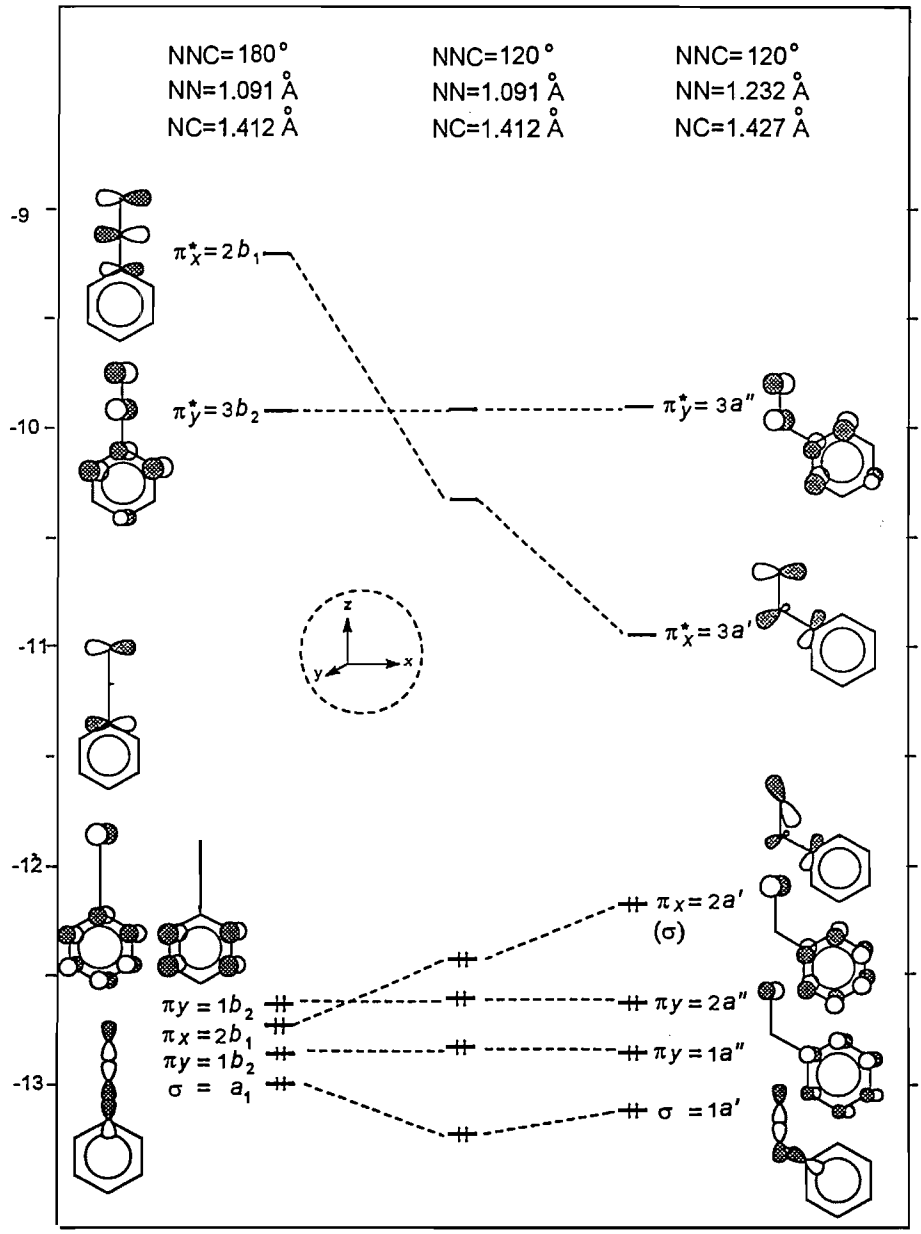

The driving force behind this large energy change of the π_x^* orbital comes mainly from a lessening of the antibonding π interaction between N_α and N_β, and between N_β and the ipso C atom, as a result of the bending at N_β and the longer NN and NC internuclear distances assigned to the bent PhN_2^+ fragment compared with the linear ion. However, the bending and the lengthening have less influence on the energies of the π_y orbitals. This is largely because of the predominantly nonbonding N-N-C character of these π orbitals. Because these occupied $1a''$ and $2a''$ orbitals are of quite high energy, it will be expected that the singly bent PhN_2 ligand will have significant π-basicity, but only in this plane (yz) perpendicular to the molecular plane. Conversely, because the counterpart antibonding orbital π_y^* ($3a'$) is much higher in energy than the LUMO (π_x^*; $3a'$), the bent PhN_2 ligand will be a poor π-acceptor *in this plane yz*. So, as a summary, the bending and bond lengthening have made PhN_2^+ a better σ-donor and a better π-acceptor (but only using the *in-plane* π_x^* orbital), while also possessing some π-donor capacity *perpendicular* to the molecular plane.

From the above analysis, and considering the fact that the d_π orbitals of a transition metal are generally lower in energy than the π^* orbitals of the PhN_2^+ ligand, it is clear that a complex possessing a *linear aryl*diazenido ligand is highly disfavored. This is not only because of the stronger σ-donating ability of the singly bent aryldiazenido ligand, but more importantly because the back-bonding between filled metal d_π orbitals and the empty π^* orbitals is much less favorable for the linear PhN_2^+ ligand than for the singly bent PhN_2^+ ligand. This is clearly consistent with the experimental result that there is not one single structurally characterized example in which the aryldiazenido ligand adopts a linear N-N-Ar arrangement (3).

Can. J. Chem. Downloaded from www.nrcresearchpress.com by 80.90.12.36 on 09/08/12
For personal use only.

Can. J. Chem. Downloaded from www.nrcresearchpress.com by 80.90.12.36 on 09/08/12
For personal use only.

Dynamic NMR spectroscopic study of [Cp*Ir(C_2H_4)(*p*-$N_2C_6H_4OMe$)][BF_4] (**1** BF_4)

The ambient-temperature ^1H NMR spectrum of **1** BF_4 displays a broad singlet at δ 3.25 for the four protons of the ethylene ligand. This indicates that at this temperature a time-averaged signal results. A series of ^1H NMR spectra were measured in acetone-d_6 solution from 22°C to −63°C (Fig. 5(*a*)). As the solution is cooled, the singlet at δ 3.68 broadens, and at the coalescence temperature of −20°C it is very broad and asymmetric. With further decrease in temperature this broad signal retains its asymmetric envelope, but gradually resolves into a complicated multiplet that is sharp at −63°C and unchanged below this temperature. The limiting spectrum and a computer simulation of the ABCD system are shown in Fig. 5(*b*).

A series of variable-temperature $^{13}C\{^1H\}$ NMR spectra in acetone-d_6 were also measured for **1** BF_4. At 21°C, a single broad peak near δ 50 indicates two equivalent ethylene carbons. As the solution is cooled, this signal first collapses into the baseline at 0°C, and then re-emerges as two equal intensity broad peaks. These sharpen on further cooling, and at −64°C the low-limit spectrum with resonances at δ 48.02 and 50.73 is obtained, and this spectrum is unchanged down to −84°C.

Singly and doubly bent aryldiazenido complexes and diazene complexes containing the Cp*Ir(PPh_3) core

Treatment of **1** BF_4 with an equimolar amount of PPh_3 in ethanol at room temperature afforded quantitatively the corresponding triphenylphosphine aryldiazenido complex, [Cp*Ir(PPh_3)(*p*-$N_2C_6H_4OMe$)][BF_4], **3** BF_4.

[2] [Cp*Ir(C_2H_4)(*p*-$N_2C_6H_4OMe$)]$^+$ (**1**) $\xrightarrow{PPh_3}$ [Cp*Ir(PPh_3)(*p*-$N_2C_6H_4OMe$)]$^+$ (**3**) + C_2H_4

Alternatively, a direct reaction of Cp*Ir(C_2H_4)$_2$, in situ, with equimolar amounts of PPh_3 and [*p*-$N_2C_6H_4OMe$][BF_4] also gave **3** BF_4 quantitatively. In both cases it was isolated as an oil that is stable under a nitrogen atmosphere either pure or as solutions in nonhalogenated solvents. It decomposes slowly in halogenated solvents, e.g., $CDCl_3$.

Compound **3** BF_4 has been fully characterized by spectroscopic methods and elemental analysis. The ν(NN) absorption at 1710 cm^{-1} observed in EtOH is lower than that of its ethylene precursor **1** BF_4, which has ν(NN) at 1724 cm^{-1} in the same solvent. This is consistent with the general view that the C_2H_4 ligand is a better π-acid than the PPh_3 ligand. In the ^{15}N and $^{31}P\{^1H\}$ NMR spectra of **3**-$^{15}N_\alpha$ BF_4, ^{15}N–P coupling results in each case in a doublet with $J_{P-^{15}N}$ = 7 Hz. The reaction of compound **3** BF_4 with BH_4^- in acetone at −10°C gives a good yield of the neutral hydrido complex Cp*IrH(PPh_3)(*p*-$N_2C_6H_4OMe$) **4**, which forms peach-red solutions in acetone or hexane and is a beautiful rose-purple colour in the solvent-free state. The formula and spectroscopic properties of **4** indicate that the aryldiazenido ligand is now doubly bent and a $1e^-$ donor (Scheme 2).

A broad IR band at 2133 cm^{-1} that was observed in both **4** and **4**-$^{15}N_\alpha$ is assigned to ν(Ir–H). However, no IR band due to ν(NN) of the doubly bent aryldiazenido ligand could be assigned, even with the aid of the ^{15}N-enriched sample. The proton NMR spectrum in acetone-d_6 showed, in addition to the resonances for the aromatic and the methoxy protons, a sharp doublet at δ −15.9 with $^2J_{P-H}$ = 33.5 Hz integrating for 1H assigned to the hydride, and a well-resolved doublet of doublets (δ 1.51 with J_{P-Me} = 1.8 Hz and J_{H-Me} = 0.7 Hz) in the Cp* methyl region integrating for 15 H.

Scheme 2.

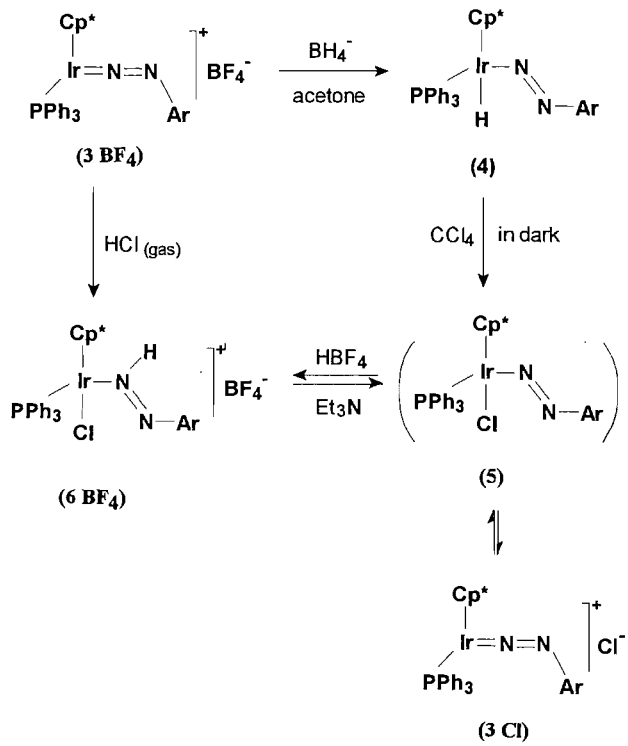

Evidence for a doubly bent aryldiazenido ligand in **4** is unambiguously provided by the ^{15}N NMR spectrum of **4**-$^{15}N_\alpha$. The only resonance is a singlet at δ 271.9, assigned to $^{15}N_\alpha$. This falls within the typical chemical shift range for N_α of a doubly bent aryldiazenido ligand (δ: 200–350 ppm) (3) and can be compared with the values for the corresponding singly bent aryldiazenido ligand in **1**-$^{15}N_\alpha$ and **3**-$^{15}N_\alpha$ (δ −2.26 and 33.2, respectively). No ^{15}N coupling to the hydride or to phosphorus could be observed in the ^1H or ^{15}N NMR spectrum of **4**-$^{15}N_\alpha$.

The aryldiazene complex [Cp*IrCl(PPh_3)(*p*-$NHNC_6H_4OMe$)][BF_4] (**6** BF_4) can be conveniently prepared in high yield from the reaction of **3** BF_4, with HCl gas in ethanol. In the IR spectrum the lower ν(NN) at 1483 cm^{-1} (ν(^{15}NN) 1460 cm^{-1}) is consistent with the presence of a diazene ligand. This has been further substantiated by the ^1H and ^{15}N NMR spectra for **6**-$^{15}N_\alpha$ BF_4. A characteristic doublet (δ 13.73 with $J_{H-^{15}N}$ = 70 Hz in acetone-d_6) observed in the ^1H NMR spectrum, together with a high-field doublet (δ −64.24 with $J_{^{15}N-H}$ = 70 Hz in acetone-d_6) observed in the ^{15}N NMR spectrum, indicates the presence of an aryldiazene ligand. Both the chemical shift and the coupling constant are consistent with analogous data previously established for the η^1-aryldiazene ligand in mononuclear complexes (28–30).

Deprotonation of **6** BF_4 by using triethylamine did not yield the expected compound Cp*IrCl(PPh_3)(*p*-$N_2C_6H_4OMe$) (**5**),

Fig. 5. (*a*) Variable-temperature ^{1}H NMR spectra for the ethylene protons of **1** BF_4. (*b*) Observed and simulated ABCD spectrum at −63°C.

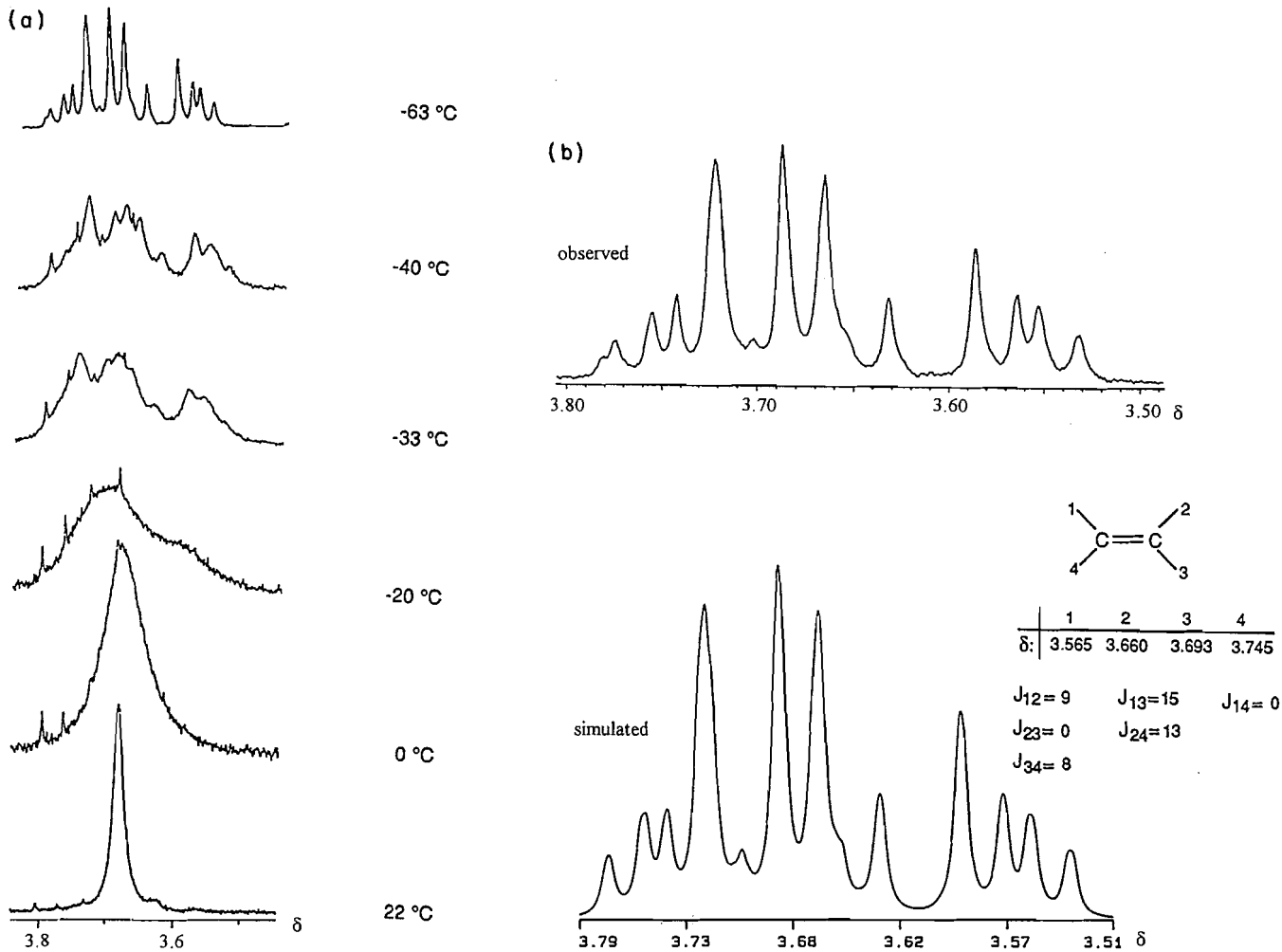

the chloro analogue of the hydride **4**. Instead it produced a mixture of a major product and $Cp^*Ir(PPh_3)Cl_2$ (**31**) (<5%). The major product exhibited IR and ^{1}H NMR spectra identical to **3** BF_4 (except, of course, for BF_4 absorptions), and therefore it is considered that this compound contains the same cation **3**, i.e., $[Cp^*Ir(PPh_3)(p\text{-}N_2C_6H_4OMe)]^+$, but is the chloride salt $[Cp^*Ir(PPh_3)(p\text{-}N_2C_6H_4OMe)]Cl$ (**3 Cl**). In particular, the ν(NN) value of 1711 cm^{-1} in CH_2Cl_2 undoubtedly indicates a singly bent, and not a doubly bent aryldiazenido ligand as required for **3 Cl** but not for **5**. Interestingly, reprotonation of this compound with HBF_4–Et_2O resulted in reformation of the diazene complex $[Cp^*IrCl(PPh_3)(p\text{-}NHNC_6H_4OMe)][BF_4]$ (**6** BF_4) in which the Cl group is again coordinated.

An attempt to obtain $Cp^*IrCl(PPh_3)(p\text{-}N_2C_6H_4OMe)$ (**5**) from hydride **4** by a direct hydrido–chloro exchange reaction using excess CCl_4 also was not successful. The salt $[Cp^*Ir(PPh_3)(p\text{-}N_2C_6H_4OMe)]Cl$ (**3 Cl**), was again produced, as indicated by ν(NN) values (1711 cm^{-1} in CH_2Cl_2 and 1717 cm^{-1} in CCl_4) as well as ^{1}H NMR, together with variable amounts of $Cp^*Ir(PPh_3)Cl_2$. A small amount of $[Cp^*IrCl(PPh_3)(p\text{-}NHNC_6H_4OMe)]Cl$ (**6 Cl**) is also believed to be produced, because a characteristic ^{15}N–H doublet proton signal was invariably observed when using ^{15}N-labelled **4**, although the intensity of this signal varied from preparation to preparation. In situ protonation of the products of this exchange by using HBF_4–OEt_2 always resulted in the production of the aryldiazene complex $[Cp^*IrCl(PPh_3)(p\text{-}NHNC_6H_4OMe)][BF_4]$ (**6** BF_4) and $Cp^*Ir(PPh_3)Cl_2$ as the main products.

Discussion

Mechanism of formation of $[Cp^*Ir(C_2H_4)(p\text{-}N_2C_6H_4OMe)][BF_4]$ (1 BF_4)

The monoethylene aryldiazenido compound **1** BF_4 is readily obtained by the substitution of an ethylene ligand in $Cp^*Ir(C_2H_4)_2$ by the *p*-methoxybenzenediazonium ion at low temperature. $Cp^*Ir(C_2H_4)_2$ appears to be the most inert to substitution among the series of compounds $Cp'ML_2$, (Cp′ = Cp or Cp*; M = Co, Rh, or Ir; L = CO or C_2H_4). Except for the recently reported synthesis of **2** by us (15), direct thermal substitution of an ethylene ligand in $Cp^*Ir(C_2H_4)_2$ to form $Cp^*IrL(C_2H_4)$ is difficult and has rarely been previously reported in the literature (32–35). Attempts by us to obtain $Cp^*IrL(C_2H_4)$ (L = CO or PPh_3) by stirring a hexane solution of $Cp^*Ir(C_2H_4)_2$ saturated with CO gas, or by refluxing $Cp^*Ir(C_2H_4)_2$ with PPh_3 in ethanol for days, were unsuccessful. Obviously, its inertness toward nucleophilic ligand substitution reactions reflects the highly electron-rich metal centre

Can. J. Chem. Downloaded from www.nrcresearchpress.com by 80.90.12.36 on 09/08/12
For personal use only.

Can. J. Chem. Downloaded from www.nrcresearchpress.com by 80.90.12.36 on 09/08/12
For personal use only.

of $Cp^*Ir(C_2H_4)_2$. On the other hand, the observed facile substitution of ethylene by ArN_2^+ or NO^+ indicates that a different mechanism is likely to be involved in these reactions. A mechanism involving an initial *electrophilic* attack by the NO^+ group at the electron-rich metal centre was suggested previously (15), and we postulate a similar mechanism for the reaction with ArN_2^+ (Scheme 3). In this mechanism, the ArN_2^+ ion formally acts as a Lewis acid and an intermediate with a doubly bent aryldiazenido ligand is formed. This intermediate then loses one of the ethylene ligands to give the final singly bent aryldiazenido complex **1**.

Scheme 3.

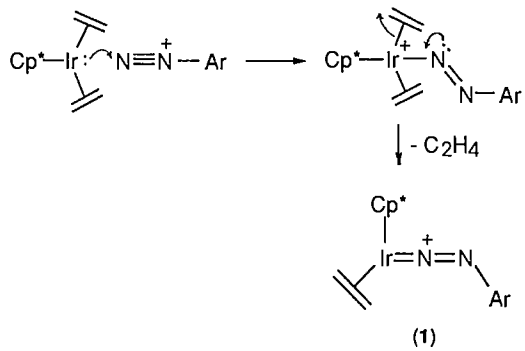

(1)

The singly bent aryldiazenido ligand as a single-faced π-acid and π-base

The valence orbital picture presented in the results section revealed two important electronic features of the singly bent aryldiazenido ligand. First, the HOMO $2a'$ is located at a rather high energy level (ca. −12.4 eV), actually higher than the valence orbital ionization energy of the nitrogen $2p$ orbital (−13.4 eV) used in the calculations. This reflects the antibonding character of this orbital with respect to the NNC skeleton. Thus when we compare the relative energies of the HOMO for singly bent PhN_2^+ at −12.4 eV (Fig. 4) and that of NO^+ at −13.5 eV (Fig. 3), PhN_2^+ should be a better σ-donor. Secondly, the large energy separation of the two π-accepting orbitals π_x^* ($3a'$) and π_y^* ($3a''$) and the relatively high energy of the occupied π_y orbitals $1a''$ and $2a''$ of the singly bent PhN_2^+ ligand indicate the π-bonding ability of this ligand to be highly anisotropic. In the xz plane (which is the ligand plane) it should behave as a strong π-acceptor, whereas in the perpendicular plane yz it should act as a reasonably strong π-donor. The bent PhN_2 ligand may be described as a "single-faced" π-acceptor, and a "single-faced" π-base.

Clearly, because of this anisotropic character, the singly bent aryldiazenido ligand is significantly different from the linear nitrosyl ligand for which the π-system is degenerate. Thus, although as the free ions these ligands are essentially valence isoelectronic and both coordinate through the nitrogen atom, it is misleading to consider them as analogous ligands. Their local symmetry and frontier orbitals are quite different, and they are not isolobal. This distinction must be carefully considered in any attempts to compare the relative π-accepting abilities of these ligands, and such attempts must take into account the symmetry and availability of suitable π-donor orbitals on the metal.

Orientation adopted by the aryldiazenido ligand in the structure of the cation 1

As described in the results section, the aryldiazenido ligand is oriented unsymmetrically. The NN group is coplanar with the aryl plane, but this local molecular plane is approximately parallel with the ethylene C—C axis and perpendicular to the vertical plane defined by the iridium atom and the centroids of the Cp* and ethylene ligands. Because of this, the cation has no molecular symmetry, and is therefore chiral. So, there are equal numbers of *R* and *S* enantiomers in the centrosymmetric crystal structure. These differ only by the direction, to the left or right of the vertical plane, in which the aryldiazenido ligand is bent. Why is this structure adopted, rather than the symmetrical one derived by rotating the aryldiazenido ligand plane through 90° so it is coincident with the vertical plane? An explanation can be found by examining the frontier orbitals of the aryldiazenido ligand and matching them with those for the $Cp^*Ir(C_2H_4)$ fragment.

On the basis of structure determinations on members of the family of cobalt group bis(ethylene) complexes, in $Cp^*Ir(C_2H_4)_2$ the ethylene ligand C—C axes lie parallel and the plane of these four carbon atoms is parallel to the plane of the Cp* ligand. The dominant orbital interaction responsible is the overlap of the filled iridium d_{yz} orbital with the empty ethylene π* orbitals. When one of the ethylenes is substituted by the singly bent aryldiazenido ligand to give **1**, the empty $3a'$ π-acceptor orbital, the LUMO **9**, will preferentially align in the same manner as the ethylene orbital it has replaced, as shown in **12**. This leads directly to the observed orientation of the aryldiazenido ligand, and both ligands are competing for electron density in the iridium d_π orbital.

The stronger π-accepting property of the ArN_2 ligand should reduce the degree of π back-bonding to the ethylene ligand in **1**, leading to both a lower barrier to rotation of the ethylene (see below) and an increased susceptibility to substitution by an incoming donor ligand compared with the parent bis(ethylene) complex. In agreement, the ethylene ligand in **1** was found to be easily and quantitatively substituted by triphenylphosphine at room temperature to give **3**. In fact, **3** $\mathbf{BF_4}$ is most conveniently synthesized by reacting the bis(ethylene) complex directly with a mixture of equimolar amounts of the diazonium salt and PPh_3 at room temperature. Presumably **1** is consumed by reaction with PPh_3 as quickly as it is formed as a result of the greater lability of the ethylene ligand. (Note that good yields in the synthesis of **1** itself could not be obtained at room temperature.)

Stereochemical nonrigidity of the singly bent aryldiazenido ligand in 1

The ABCD pattern for the four protons, and two equal intensity carbon signals, observed for the ethylene ligand in the ^1H and $^{13}C\{^1H\}$ NMR spectra of **1** $\mathbf{BF_4}$ at low temperatures ($\leq$ −64°C) also require an unsymmetrical frozen structure for the cation in solution. It seems reasonable to suggest that this structure is probably the same as that adopted in the solid state, and predicted to be the stable structure on the above orbital overlap grounds. The variable-temperature ^1H and $^{13}C\{^1H\}$ NMR spectra clearly show that a fluxional process is occurring, and at the high-temperature limit all of the ethylene protons are equivalent on the NMR time scale, as also are the ethylene carbons. Fluxional behavior of coordinated ethylene in half-sandwich complexes of this kind has been well docu-

Can. J. Chem. Downloaded from www.nrcresearchpress.com by 80.90.12.36 on 09/08/12
For personal use only.

mented to result from hindered rotation about the axis relating the metal to the midpoint of the double bond of the ethylene (18, 36–39). However, for a rapidly rotating ethylene ligand to give a single proton absorption, the cation **1** must at least have mirror symmetry on the NMR time scale. For this to occur, assuming that the frozen-out structure in solution is similar to the solid state structure, the singly bent aryldiazenido ligand must also be involved in a fluxional process, which is related by this mirror symmetry. Therefore, we conclude that at the high-temperature limit both a rotation of the ethylene and a conformational "flipping" of the aryldiazenido ligand (which interconverts the enantiomers) are occurring simultaneously.

If the ethylene rotation were slower than the NMR time scale while the flipping of the aryldiazenido ligand is rapid, then, relative to the ethylene in its equilibrium position, the fragment $Cp^*Ir(N_2Ar)$ would have a time-averaged plane of symmetry and, therefore, the ethylene protons should give a symmetric AA′BB′ pattern, or at least a broad symmetrical envelope of this pattern, at and below the decoalescence temperature. This is not observed. On the other hand, if flipping of the diazenido ligand is slowed first, while rotation of the ethylene is still fast, then the $Cp^*Ir(N_2Ar)$ fragment possesses no element of symmetry so the four protons of the fast-rotating ethylene ligand would again result in an AA′BB′ pattern.

Even at, and below, the coalescence temperature the broad pattern has an unsymmetrical envelope resembling the low-temperature ABCD envelope, and at no temperature is a symmetrical AA′BB′ type of envelope ever evident. Therefore it seems that the two fluxional processes, rotation of the ethylene and flipping of the aryldiazenido ligand, must slow at comparable rates as the temperature is lowered.

It would be of considerable interest to evaluate the barriers for ethylene rotation and aryldiazenido ligand rearrangement in **1**. From the variable-temperature ^1H or ^{13}C NMR spectra it is possible, in principle, to calculate an activation energy; this will correspond to the activation energy for a process that is a combination of the ethylene and ArN_2 ligand rearrangements if they are mechanistically coupled, or to the activation energy for the process with the higher barrier if they are independent. Either way, it provides at least an upper limit of the barrier for each of the ligand rearrangements. The four-spin ABCD pattern for the ethylene protons in the low-limit ^1H NMR spectrum makes such a calculation not trivial. In the case of the ^{13}C NMR spectrum, either rotation of the ethylene or flipping of the ArN_2 ligand *alone* would result in the observed temperature dependence, as also of course would a combination of both processes. The activation barrier at the coalescence temperature is readily calculated from this spectrum to be $\Delta G^{\neq} = 51.5 \pm 0.4$ kJ at $T_c = 270$ K, and while we cannot assign this unambiguously to the barrier for either ethylene rotation or aryldiazenido ligand flipping, we do know from the proton NMR data discussed above that this value must represent an *upper limit* for each of these processes.

The conformational isomerization or flipping of the aryldiazenido ligand can be envisaged to occur either by rotation about the Ir-N-N axis or by an sp^2 inversion of the lone pair on N_β (i.e., a bent–linear–bent change in the geometry of the NNC skeleton). These two mechanisms are illustrated in Scheme 4. To support the case for flipping of the aryldiazenido ligand in **1**, we sought to find an example in which the nonrigidity of the aryldiazenido ligand alone might be observed

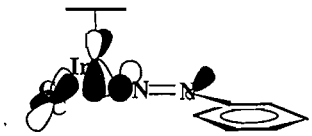

12

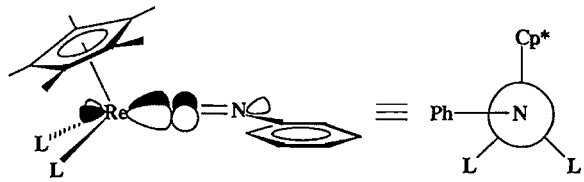

13

directly by NMR, without the complications attending the simultaneously rotating ethylene ligand. As it transpired, such a system had already been synthesized in our laboratory, namely the half-sandwich complex $[Cp^*Re(PMe_3)_2(p\text{-}N_2C_6H_4OMe)][BF_4]$. Subsequently, investigation of the low-temperature $^{31}P\{^1H\}$ NMR spectrum of this complex resulted in two equal intensity resonances that we ascribed to the aryldiazenido ligand, again adopting an unsymmetrical orientation **13** (which is indeed the orientation observed in the X-ray structure of the carbonyl analogue $[Cp^*Re(CO)(PMe_3)(p\text{-}N_2C_6H_4OMe)][BF_4]$), thus making the two PMe_3 ligands (L) inequivalent. Once again, this orientation maximizes the overlap of the π-acceptor orbital **9** with, in this case, the HOMO of the rhenium fragment as illustrated in **13**. At room temperature a time-averaged single $^{31}P\{^1H\}$ resonance occurs, attributable to the fast conformational isomerization of the ArN_2^+ ligand interconverting the enantiomers. The activation barrier $\Delta G^{\neq}$ obtained from the temperature dependence of the spectrum was 37.0 ± 0.6 kJ mol^{-1} at 190 K; the barriers for several related rhenium aryldiazenido complexes were also measured (40).

A comparison of the ethylene rotation barriers of complexes 1 and 2

From the above discussion $\Delta G^{\neq}$ for ethylene rotation in **1** must be no more than 51.5 ± 0.4 kJ mol^{-1} at 270 K. This value is at least 17 kJ lower than the barrier for the nitrosyl compound **2** for which a value of 68.7 ± 0.2 kJ mol^{-1} at 353 K was obtained (15). The crystal structures of **1** and **2** show no close contacts to the ethylene ligand in either case. Consequently, steric influences, if there are any, are expected to be similar for both complexes, so the different rotation barriers of the ethylene ligand in **1** and **2** are likely to directly reflect differences in the binding of the ethylene ligand to the fragments $Cp^*Ir(NO)^+$ and $Cp^*Ir(N_2Ar)^+$ in the ground and activated states. According to the Dewar–Chatt–Duncanson scheme (41, 42), binding of ethylene to a transition metal atom consists of a σ-bond, formed by overlap of the filled π orbital of the olefin with a metal orbital of the same symmetry, and a π-bond, arising from overlap of the vacant π* orbital of the ethylene with a filled d_π orbital of the metal. The σ component is not of interest here, since it is invariant upon rotation of the ethylene ligand about the metal–ethylene bond axis. However,

Can. J. Chem. Downloaded from www.nrcresearchpress.com by 80.90.12.36 on 09/08/12
For personal use only.

Scheme 4. Possible mechanisms for the conformational isomerization of the ArN_2 ligand: (*a*) rotation about IrNN axis; (*b*) sp^2 inversion at N_β.

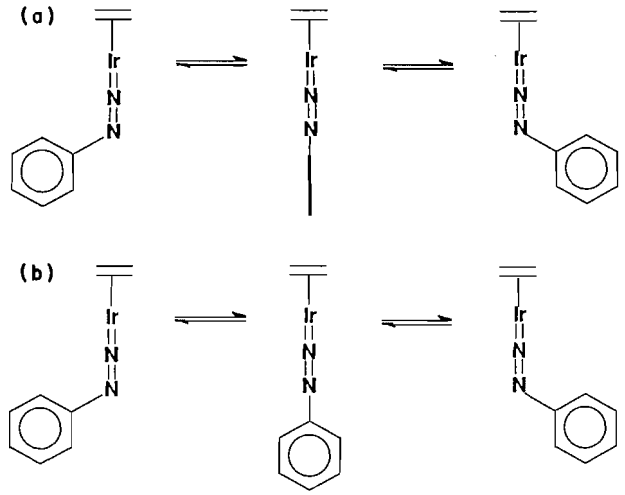

the relative strength of the π-bonding component for **1** and **2** will greatly influence the rotation barrier.

As indicated previously, in the ground state, the primary π interaction for the ArN_2 complex **1** is as illustrated in **12**, and analogously for the NO complex **2**. In effect, there exists a competition for the electrons in the metal d_π orbital between the ethylene and the ancillary ligand, NO or ArN_2. The stronger the π-acidity of this ligand situated "*trans*" to the ethylene, the more electron density will be pulled toward to this ligand from the metal centre and the less electron density will be available for the back-bonding to the ethylene. Consequently, there will be a smaller π component of the metal–ethylene bond and a higher ground state energy. In the activated state for ethylene rotation, the ethylene is rotated by 90° and its π-system is now orthogonal to that of the metal d_π HOMO and lies in its nodal plane so that the π-bond is effectively broken. To a first approximation, therefore, the barrier to ethylene rotation should be lowest for the complex with the ancillary ligand that has the greatest demand for the electrons in the iridium d_π HOMO. The observed barrier is lowest for the aryldiazenido complex **1**; in order words, the π-acidity of the singly bent aryldiazenido ligand in **1** seems to be stronger than that of the linear nitrosyl ligand in **2** for this pair of complexes. Further, in both cases the barrier is very much lower than that for $Cp^*Ir(C_2H_4)_2$ itself, for which there is no coalescence of the C_2H_4 proton resonances up to 110°C, indicating that the ethylene rotation barrier in this compound is in excess of 80 kJ mol^{-1} (15, 18). This can be attributed to the fact that in $Cp^*Ir(C_2H_4)_2$ only a weak π-acid ligand C_2H_4 occupies the position "*trans*" to the ethylene in question, so the π-bond is stronger and the ground state is significantly stabilized compared with those of either **1** or **2**.

The relative π-acidity of linear nitrosyl and singly bent aryldiazenido ligands

To seek an explanation for the evidently greater π-acidity of ArN_2 over NO in these particular two complexes **1** and **2** it is worth returning to the results of the EHMO calculations. It has been pointed out earlier in the Discussion that there is a fundamental difference between the singly bent ArN_2 ligand and the linear NO ligand in regard to their intrinsic π-bonding capabilities. The ArN_2 ligand is a π-acceptor only in the molecular plane and is a π-base in the perpendicular plane. It can be described as having "single-faced" π-accepting and π-donating ability. By virtue of its degenerate π-system, the linear NO ligand, by way of contrast, possesses isotropic or cyclindrical π back-bonding ability. Therefore any attempted comparison of the relative π-acidities displayed by these two ligands has to be undertaken with care. In situations where the metal can provide mutually perpendicular d_π orbitals of identical or relatively similar energies, back-bonding to the NO ligand will probably be more effective than to the singly bent ArN_2 ligand simply because the latter can only accept effectively by using the LUMO situated in its molecular plane. In other words, the NO group can back-bond in both planes, whereas the single-faced ArN_2 ligand can only do so in one plane. In fact, in the other plane it acts as a weak π-donor.

But now consider a situation in which the metal is restricted to π-bonding in only one plane. This might arise if the metal has only a single filled d_π orbital or has a low-symmetry environment that removes the degeneracy of the d_π orbitals and leaves only one *d*-orbital effective in back-bonding. Under such circumstances the NO group is also reduced to effectively π-bonding in only one preferred plane (i.e., it is forced to be single-faced), and now its π-accepting ability, compared with that of ArN_2, can be assessed by considering the calculated relative energies of the relevant π-acceptor orbitals in each case. These are shown in Figs. 3 and 4. For the NO ligand the energy of the π* orbital is −10.5 eV while for the singly bent PhN_2 ligand the energy of the 3*a*′ orbital is somewhat lower, −11.0 eV. Thus when both NO and ArN_2 are acting as single-faced π-acceptors it is entirely possible, and indeed likely, that the aryldiazenido ligand could function as the better π-acceptor.

This, we think, is exactly the situation that pertains to complexes **1** and **2**, where the ArN_2 *and NO* ligands are essentially limited to π-bonding with only one iridium d_π orbital, d_{yz}, and thus *both* are forced to function as single-faced π-acceptors with the result that ArN_2 is the better π-acceptor of the two.

Properties and reactions of $Cp^*Ir(PPh_3)(p\text{-}N_2C_6H_4OMe)][BF_4]$ (3 BF_4)

The reactions of the ethylene aryldiazenido complex **1** are complicated by the presence of several sites of possible attack, as was demonstrated previously for the nitrosyl **2** (15). These include the metal, the ethylene ligand, and the ArN_2 group. Some of these reactions have been reported briefly elsewhere. When the ethylene is replaced by PPh_3 to give **3**, many reactions can be better controlled. Most interestingly, preliminary results reported here indicate this to be a rare system in which to observe both singly bent (3*e*-donor) and doubly bent (1*e*-donor) aryldiazenido ligands in readily accessible and stable complexes and to study their interconversion.

The replacement of the ethylene in **1** by PPh_3 to give **3** results in a lowering of ν(NN) of the ArN_2 ligand. PPh_3 is considered to be a better σ-donor than ethylene as a result of its higher lying HOMO and should on this account weaken the Ir—N_α σ-bond and strengthen the N—N bond. This is contrary to the observed trend in ν(NN). Considering now the π interaction, PPh_3 is generally considered to be a poorer π-acceptor than C_2H_4, so there should be more electron density

Can. J. Chem. Downloaded from www.nrcresearchpress.com by 80.90.12.36 on 09/08/12
For personal use only.

at the metal center available for back-bonding to the antibonding π^* orbitals of the ArN_2 ligand in the phosphine complex **3** than in **1**, and this satisfactorily accounts for the lower ν(NN) value of **3**. The lower field ^{15}N NMR chemical shift for N_α in **3** compared to **1** also indicates greater anisotropy of the π electron density at the N_α position in **3**, which is also consistent with the view that greater π electron density is back-bonded to the ArN_2 ligand from the metal center in **3**.

The reaction of **3** $\mathbf{BF_4}$ with borohydride results in the delivery of a hydrido ligand at the metal and a corresponding rearrangement of the aryldiazenido ligand from a singly bent 3*e* donor to a doubly bent 1*e* donor to give **4**. This type of complex, in which a hydrido ligand coexists with a doubly bent aryldiazenido ligand, is not common. The only other examples of which we are aware are those reported by Haymore and Ibers (43). These are the complexes $MH(CO)_2(PPh_3)_2(N_2Ph)$ (M = Os, Ru), and they were prepared by a very different method, the deprotonation of the corresponding aryldiazene complexes $[MH(CO)_2(PPh_3)_2(NHNPh)]^+$. Haymore and Ibers were unsuccessful in an attempt to obtain these compounds through a reaction of the corresponding five-coordinated singly bent aryldiazenido compounds $[M(CO)_2(PPh_3)_2(N_2Ph)]^+$ with BH_4^-, apparently because the reducing conditions destroyed the aryldiazenido ligand. Therefore, it is significant that we have been able to achieve a similar reaction in high yield in the present system. In another situation we found that borohydride reacts with the singly bent aryldiazenido complex $[CpRe(CO)_2(N_2Ar)]^+$ to give the aryldiazene complex $CpRe(CO)_2(NHNAr)$ (44). The mechanism of this reaction has not been established, so it is not known whether attack may first occur at the metal to give a similar hydrido complex with a doubly bent aryldiazenido ligand, followed by proton migration to N_α. In this context, the observation of a related aryldiazene complex such as **6** in this study becomes important.

Complex **4** is relatively stable either in the solvent-free state or in halogen-free solvents, and so it has been fully characterized. Although no X-ray structure is available, the formulation of this complex is well supported by the spectroscopic data. The hydrido ligand is observed in the ^1H NMR in the expected region and is coupled to the phosphorus of the PPh_3 with an appropriate coupling constant. The best evidence for proposing a doubly bent aryldiazenido ligand is the ^{15}N NMR spectrum of $^{15}N_\alpha$-labeled **4**. The only resonance observed is a singlet at δ 271.9, which must be assigned to N_α, and this falls appropriately within the range established for N_α in other doubly bent aryldiazenido complexes that have been measured, ca. δ 200–350 (3). This large upfield shift has been attributed to the presence of a lone pair of electrons on N_α in the doubly bent structure. A general trend in deshielding of N_α is observed along the series of complexes from **1** (δ −2.26) through **3** (δ 33.2) to **4**. No observable ^{15}N coupling to either the hydride or the phosphorus was evident for **4**. The absence of $^{15}N_\alpha$–H coupling was also noted by Haymore and Ibers for their complexes (43). However, ^{31}P–^{15}N coupling was observed in the ^{15}N NMR spectrum of the singly bent aryldiazenido cation **3**-$^{15}N_\alpha$, so it appears that this coupling is very sensitive to the geometry of the ArN_2 ligand and perhaps the relative disposition of it and the PPh_3 and hydrido ligands.

This simple transformation of the singly bent aryldiazenido ligand to a doubly bent one to incorporate an additional ligand at the metal has, to our knowledge, rarely been observed before (43). However, there are several established examples in which such a transformation effectively occurs, but is accompanied by protonation of the doubly bent aryldiazenido ligand thus formed so that an aryldiazene complex is the actual product. In some cases this can then be deprotonated to give the doubly bent aryldiazenido complex (43). The reaction of **3** with HCl provides a further example of aryldiazene formation in this way, resulting in **6**. However, an attempt to deprotonate this complex by using Et_3N did not yield **5**, the chloro analog of the hydrido complex **6**, but was accompanied by dissociation of the chloride and reversion of the aryldiazenido ligand to the singly bent form, resulting in reformation of the cation **3** as the chloride salt. This serves to underline how sensitive to the nature of the added ligand is the doubly bent – singly bent interrelationship. We shall show in a subsequent article how this relationship can be controlled by the use of added ligands with appropriate σ- or π-donor or -acceptor properties.

Conclusion

In this paper we have presented and discussed in detail several important features of the new half-sandwich iridium ethylene aryldiazenido complex $[Cp^*Ir(C_2H_4)(N_2Ar)]^+$ (**1**), including the orientation of the aryldiazenido ligand, the mechanism of synthesis, the fluxional behavior of the ethylene and aryldiazenido ligands, and the π-accepting ability of the latter relative to nitrosyl in this type of complex. Complex **1** does, by virtue of the substitutional lability of the ethylene ligand, provide a convenient entry to other members of this hitherto unstudied class of half-sandwich iridium aryldiazenido complexes, and we have reported preliminary studies of the PPh_3 derivative, including the transformation of the 3*e*-donor, singly bent aryldiazenido ligand into the 1*e*-donor, doubly bent form. In subsequent papers on this system we shall detail further examples of this substitution chemistry, and the structural variety of the aryldiazenido complexes so obtained.

Acknowledgments

This work was supported by the Natural Sciences and Engineering Research Council of Canada by means of research, equipment, and infrastructure grants to F.W.B.E. and D.S. Johnson Matthey & Co are thanked for a generous loan of iridium trichloride.

References

1. R.B. King and M.B. Bisnette. J. Am. Chem. Soc. **86**, 5694 (1964).
2. S. Sutton. Chem. Soc. Rev. **4**, 443 (1975).
3. B.F.G. Johnson, B.L. Haymore, and J.R. Dilworth. *In* Comprehensive coordination chemistry. Vol. 2. *Edited by* G. Wilkinson, R.D. Gillard, and J.A. McCleverty. Pergamon Press, Oxford. 1987. p. 130.
4. D. Sutton. Chem. Rev. **93**, 995 (1993).
5. G.B. Richter-Addo and P. Legzdins. Metal nitrosyls. Oxford University Press, New York. 1992.
6. M. Cowie, B.L. Haymore, and J.A. Ibers. Inorg. Chem. **14**, 2617 (1975).
7. D.R. Fisher and D. Sutton. Can. J. Chem. **51**, 1697 (1973).
8. B.L. Haymore and J.A. Ibers. J. Am. Chem. Soc. **95**, 3052 (1973).

9. W.E. Carroll, F.A. Deeney, and F.J. Lalor. J. Organomet. Chem. **198**, 189 (1980).
10. W.E. Carroll and F.J. Lalor. J. Organomet. Chem. **54**, C37 (1973).
11. W.E. Carroll, F.A. Deeney, and F.J. Lalor. J. Chem. Soc. Dalton Trans. 1430 (1974).
12. W.E. Carroll and F.J. Lalor. J. Chem. Soc. Dalton Trans. 1754 (1973).
13. W.E. Carroll, M.E. Deane, and F.J. Lalor. J. Chem. Soc. Dalton. Trans. 1837 (1974).
14. N.G. Connelly and Z. Demidowicz. J. Organomet. Chem. **73**, C31 (1974).
15. R.J. Batchelor, F.W.B. Einstein, N.D. Lowe, B.A. Palm, X. Yan, and D. Sutton. Organometallics, **13**, 2041 (1994).
16. F.W.B. Einstein, X. Yan, and D. Sutton. J. Chem. Soc. Chem. Commun. 1466 (1990).
17. W.A. Thomas. Annu. Rev. NMR Spectrosc. **1**, 43 (1968).
18. K. Moseley, J.W. Kang, and P.M. Maitlis. J. Chem. Soc. 2875 (1970).
19. R. Hoffmann. J. Chem. Phys. **39**, 1397 (1963).
20. D.L. DuBois and R. Hoffmann. Nouv. J. Chim. **1**, 479 (1977).
21. C. Romming. Acta. Chem. Scand. **17**, 1444 (1963).
22. H.P. Weber. Acta Crystallogr. Sect. B: Struct. Crystallogr. Cryst. Chem. **B25**, 1174 (1969).
23. A.C. Larson. *In* Crystallographic computing. *Edited by* F.R. Ahmed. Munksgaard, Copenhagen. 1970. p. 293.
24. E.J. Gabe, A.C. Larson, F.Y. Lee, and Y. LePage. NRC VAX crystal structure system. National Research Council, Ottawa, Canada. 1984.
25. International tables for X-ray crystallography. Vol IV. Kynoch Press, Birmingham, England. 1974.
26. A.H. Klahn and D. Sutton. Organometallics, **8**, 198 (1989).
27. E. Moller and K.A. Jorgensen. Acta. Chem. Scand. **45**, 68 (1991).
28. C.F. Barrientos-Penna, A.H. Klahn-Oliva, and D. Sutton. Organometallics, **4**, 367 (1985).
29. G.W. Parshall. J. Am. Chem. Soc. **89**, 1822 (1967).
30. B.L. Haymore and J.A. Ibers. J. Am. Chem. Soc. **97**, 5369 (1975).
31. J.W. Kang, K. Moseley, and P.M. Maitlis. J. Am. Chem. Soc. **91**, 5970 (1969).
32. M. Brookhart and E. Hauptman. J. Am. Chem. Soc. **114**, 4437 (1992).
33. J. Ruiz, P.O. Bentz, B.E. Mann, C.M. Spencer, B. Taylor, and P.M. Maitlis. J. Chem. Soc. Dalton Trans. 2709 (1987).
34. P.B. Hitchcock, M.J. Maah, and J.F. Nixon. J. Chem. Soc. Chem. Commun. 737 (1986).
35. H. Werner. Angew. Chem. Int. Ed. Engl. **22**, 927 (1983).
36. R. Cramer. J. Am. Chem. Soc. **86**, 217 (1964).
37. R. Cramer. J. Am. Chem. Soc. **89**, 5377 (1967).
38. R. Cramer, J.B. Kline, and J.D. Roberts. J. Am. Chem. Soc. **91**, 2519 (1969).
39. M. Mlekuz, P. Bougeard, B.G. Sayer, M.J. McGlinchey, C.A. Rodger, M.R. Churchill, J.W. Ziller, S.-K. Kang, and T.A. Albright. Organometallics, **5**, 656 (1986).
40. A. Cusanelli, R.J. Batchelor, F.W.B. Einstein, and D. Sutton. Organometallics, **13**, 5096 (1994).
41. M.J.S. Dewar. Bull. Soc. Chim. Fr. **18**, C71 (1951).
42. J. Chatt and L.A. Duncanson. J. Chem. Soc. 2939 (1953).
43. B.L. Haymore and J.A. Ibers. Inorg. Chem. **14**, 2784 (1975).
44. C.F. Barrientos-Penna, F.W.B. Einstein, T. Jones, and D. Sutton. Inorg. Chem. **21**, 2578 (1982).

Can. J. Chem. Downloaded from www.nrcresearchpress.com by 80.90.12.36 on 09/08/12
For personal use only.

Synthesis and structure of titanium diolate complexes derived from $CpTiCl_3$

Yujin Huang and Douglas W. Stephan

Abstract: The compounds $[Cl_2CpTi]_2(OCH_2CH_2CH_2O)$ **1**, $[Cl_2CpTi]_2(OCH_2CMe_2CH_2O)$ **2**, and $[Cl_2CpTi]_2$-$(OCHMeCH_2CHMeO)$ **3** were prepared from the reactions of $CpTiCl_3$ and the bis-trimethylsilyl ethers of the diols. Alternatively, these species could be made from the reactions of the diol, imidazole, and $CpTiCl_3$ employing the appropriate stoichiometry. In the presence of excess diol, loss of CpH is observed. In the case of 1,3-propanediol the species $[TiCl(HOCH_2CH_2CH_2O)(OCH_2CH_2CH_2O)]_2$ **4** was isolated. Recrystallization of **4** from THF led to the isolation of $[TiCl_2(OCH_2CH_2CH_2O)(THF)]_{2.5}$, albeit in very low yield. This chemistry is described and the implications are considered. Compounds **1**, **3**, **4**, and **5** were characterized crystallographically; the parameters are summarized as follows: **1**: *C2/c* (No. 15), $a = 12.587(2)$ Å, $b = 9.632(2)$ Å, $c = 15.824(3)$ Å, $\beta = 107.88(1)°$, $V = 1811.3(5)$ Å^3, $Z = 4$; **3**: *C2/c* (No. 15), $a = 12.855(2)$ Å, $b = 10.772(2)$ Å, $c = 15.665(2)$ Å, $\beta = 109.26(1)°$, $V = 2047.7(5)$ Å^3, $Z = 4$; **4**: $P2_1/n$ (No. 14), $a = 8.911(3)$ Å, $b = 7.821(2)$ Å, $c = 13.986(2)$ Å, $\beta = 102.56(2)°$, $V = 951.3(3)$ Å^3, $Z = 2$; **5**: $P2_1/n$ (No. 14), $a = 8.693(3)$ Å, $b = 9.286(2)$ Å, $c = 13.411(2)$ Å, $\beta = 101.18(2)°$, $V = 1062.1(4)$ Å^3, $Z = 2$.

Key words: titanium alkoxides, structure, synthesis.

Résumé : On a préparé les composés $[Cl_2CpTi]_2(OCH_2CH_2CH_2O)$ (**1**), $[Cl_2CpTi]_2(OCH_2CMe_2CH_2O)$ (**2**) et $[Cl_2CpTi]_2(OCHMeCH_2CHMeO)$ (**3**) par réaction du $CpTiCl_3$ avec les bis-triméthylsilyloxydes des diols. On peut aussi les préparer par les réactions des diols, de l'imidazole et du $CpTiCl_3$ en utilisant la stoechiométrie appropriée. En présence d'un excès de diol, on observe une perte de CpH. Dans le cas du propane-1,3-diol, on a isolé le $[TiCl(HOCH_2CH_2CH_2O)(OCH_2CH_2CH_2O)]_2$ (**4**). La recristallisation du composé **4** dans du THF permet d'isoler le $[TiCl_2(OCH_2CH_2CH_2O)(THF)]_2$ (**5**) avec un très faible rendement. On décrit la chimie et on en considère les implications. On a caractérisé les composés **1**, **3**, **4** et **5** par cristallographie; on peut résumer les paramètres comme suit : **1** : *C2/c* (No.15), $a = 12{,}587(2)$ Å, $b = 9{,}632(2)$ Å, $c = 15{,}824(3)$ Å, $\beta = 107{,}88(1)°$, $V = 1811{,}3(5)$ Å^3, $Z = 4$; **3** : *C2/c* (No.15), $a = 12{,}855(2)$ Å, $b = 10{,}772(2)$ Å, $c = 15{,}665(2)$ Å, $\beta = 109{,}26(1)°$, $V = 2047{,}7(5)$ Å^3, $Z = 4$; **4** : $P2_1/n$ (No.14), $a = 8{,}911(3)$ Å, $b = 7.821(2)$ Å, $c = 13{,}986(2)$ Å, $\beta = 102{,}56(2)°$, $V = 951{,}3(3)$ Å^3, $Z = 2$; **5** : $P2_1/n$ (No.14), $a = 8{,}693(3)$ Å, $b = 9{,}286(2)$ Å, $c = 13{,}411(2)$ Å, $\beta = 101{,}18(2)°$, $V = 1062{,}1(4)$ Å^3, $Z = 2$.

Mots clés : alcoolates de titane, structure, synthèse.

[Traduit par la rédaction]

Introduction

As part of our ongoing study of the chemistry of chalcogenide derivatives of the early metals we have described macrocyclic alkoxide and thiolate complex of Zr and Ti metallocenes (1). More recently, we focused attention on chalcogenide derivatives of monocyclopentadienyl-titanium(IV). We previously described the Lewis acidity of CpTi-thiolate derivatives such as $CpTi(SCH_2CH_2CH_2S)Cl$ and $CpTi(SCH_2CH_2)_2S)Cl$ (2). Further complex anions of the form $[CpTi(SCH_2CH_2CH_2S)_2]^-$ were shown to be precursors to heterobimetallic complexes and polymers (3) while radical reaction mechanisms were shown to be operative in reactions affording Ti—S bonds (4). More recently, we have shown that related thiolate complexes can mediate the stoichiometric synthesis of organo-sulfur compounds (5). In initiating extensions of this chemistry to oxygen-containing systems, we examined reactions aimed at the syntheses of simple alkoxide derivatives of CpTi(IV). In this paper, we describe the syntheses and structures of dimeric products in which diolates link two $CpTiCl_2$ fragments. In the presence of excess diol, loss of cyclopentadienyl rings is observed, affording dimeric titanium alkoxide complexes. These products have also been structurally characterized and the implications of this chemistry are considered.

Received September 27, 1994.

This paper is dedicated to Professor William A.G. Graham on the occasion of his 65th birthday.

Y. Huang and D.W. Stephan.[1] Department of Chemistry and Biochemistry, University of Windsor, Windsor, ON N9B 3P4, Canada.

[1] Author to whom correspondence may be addressed. Telephone: (519) 253-4232 x3537. Fax: (519) 973-7098. E-mail: Stephan@UWindsor.ca

Experimental section

General data

All preparations were done under an atmosphere of dry, O_2-free N_2 employing either Schlenk line techniques or a Vacuum Atmospheres Inert atmosphere glove box equipped with a catalyst column and an atmosphere circulation system. Solvents were reagent grade, distilled from the appropriate drying agents

Can. J. Chem. Downloaded from www.nrcresearchpress.com by 80.90.12.36 on 09/08/12
For personal use only.

Can. J. Chem. Downloaded from www.nrcresearchpress.com by 80.90.12.36 on 09/08/12
For personal use only.

under N_2 and degassed by the freeze–thaw method at least three times prior to use. ^1H and $^{13}C\{^1H\}$ NMR spectra were recorded on Bruker AC-300 spectrometers operating at 300 and 75 MHz, respectively. Trace amounts of protonated solvents were used as references and chemical shifts are reported relative to $SiMe_4$. Assignments of the ^1H and ^{13}C NMR resonances and determination of coupling constant values were based on a series of homonuclear decoupling experiments. Combustion analyses were performed by Galbraith Laboratories Inc., Knoxville, Tenn., and Schwarzkopf Laboratories, Woodside, N.Y. $CpTiCl_3$ was purchased from the Strem Chemical Co.

Synthesis of $[Cl_2CpTi]_2(OCH_2CH_2CH_2O)$ 1, $[Cl_2CpTi]_2(OCH_2CMe_2CH_2O)$ 2, and $[Cl_2CpTi]_2(OCHMeCH_2CHMeO)$, 3

These compounds were prepared in similar manners, thus only one preparation is described for each method. (*i*) A mixture of $CpTiCl_3$ (660 mg, 3.0 mmol) and $Me_3SiOCH_2CH_2CH_2OSiMe_3$ (333 mg, 1.50 mmol) in 15 mL THF was stirred for 36 h. The solvent was removed in vacuo, and the residue was washed with 2 × 5 mL pentane and dried. (Yield 90%.) The yellow crystals of **1** were obtained from recrystallization in CH_2Cl_2. (*ii*) Imidazole was added to a stirred 3 mL THF solution of $CpTiCl_3$ (110 mg, 0.5 mmol) and $HOCH_2CH_2CH_2OH$ (45 mg, 0.6 mmol). (34 mg, 0.5 mmol). The reaction mixture was stirred for 1 h, and white solid was formed. The mixture was filtered and solid was washed with 2 × 2 mL THF. The solutions were combined, and solvent was removed in vacuo. After washing with 2 × 2 mL pentane, **1** was obtained in 75% yield. **1**: ^1H NMR ($CDCl_3$, 25°C) δ: 1.97 (q, 2H, $J_{(H-H)}$ = 5.7 Hz), 4.87 (t, 4H, $J_{(H-H)}$ = 5.7 Hz), 6.77 (s, 10H). $^{13}C\{^1H\}$ NMR ($CDCl_3$, 25°C) δ: 35.81, 90.19, 120.06. Anal. calcd. for $C_{13}H_{16}Cl_2O_2Ti_2$: C 42.09, H 4.35; found: C 41.89, H 4.13.

2: Reaction time for method (*i*): 72 h. Recrystallized from THF–pentane. Yield: 65%; ^1H NMR ($CDCl_3$, 25°C) δ: 0.94 (s, 6H), 4.55 (s, 4H), 6.76 (s, 10H). $^{13}C\{^1H\}$ NMR ($CDCl_3$, 25°C) δ: 21.13, 43.05, 89.37, 120.08. Anal. calcd. for $C_{15}H_{20}Cl_2O_2Ti_2$: C 45.16, H: 5.05; found: C 45.00, H 4.95.

3: Yield: 72%; ^1H NMR ($CDCl_3$, 25°C) δ: 1.40 (d, 6H, $|J_{(H-H)}|$ = 6.6 Hz), 1.70 (d, t, 1H, $|J_{(H-H)}|$ = 7.5 Hz, $|J_{(H-H)}|$ = 5.1 Hz), 1.90 (d, t, 1H, $|J_{(H-H)}|$ = 7.5 Hz, $|J_{(H-H)}|$ = 6.6 Hz), 5.28 (m, 2H), 6.77 (s, 10H). $^{13}C\{^1H\}$ NMR ($CDCl_3$, 25°C) δ: 24.19, 48.97, 87.30, 119.68. Anal. calcd. for $C_{15}H_{20}Cl_2O_2Ti_2$: C 45.16, H 5.05; found: C 44.88, H 4.80.

Synthesis of $[TiCl(HOCH_2CH_2CH_2O)(OCH_2CH_2CH_2O)]_2$ 4 and isolation of $[TiCl_2(OCH_2CH_2CH_2O)(THF)]_2$ 5

Imidazole (968 mg, 1 mmol) was added to a stirred 3 mL THF solution of $CpTiCl_3$ (110 mg, 0.5 mmol) and $HOCH_2CH_2CH_2OH$ (45 mg, 0.6 mmol). The reaction was stirred overnight. The compounds **1** and **4** were obtained in 31 and 30% yield (by ^1H NMR). Yellow crystals of **2** were obtained by crystallization from CH_2Cl_2 while subsequent addition of pentane to the mother liquor afforded **4**. Recrystallization of **4** from THF–hexane afforded 4 and a very low yield (less than 1%) of **5**. **4**: ^1H NMR ($CDCl_3$, 25°C) δ: 1.95 (m, 4H), 2.15 (m, 4H), 4.06(m, 2H), 4.17 (m, 2H), 4.24 (m, 2H), 4.32 (m, 4H), 4.45 (m, 4H), 4.60 (br, 2H). $^{13}C\{^1H\}$ NMR ($CDCl_3$, 25°C) δ: 31.57, 35.84, 63.90, 69.77, 74.34, 74.93. Anal. calcd. for $C_{12}H_{26}Cl_2O_8Ti_2$: C 31.00, H 5.64; found: C 30.84, H 5.34.

X-ray data collection and reduction

X-ray quality crystals were obtained directly from the preparations as described above. The crystals were manipulated and mounted in capillaries in a glove box, thus maintaining a dry, O_2-free environment for each crystal. Diffraction experiments were performed on a Rigaku AFC6 diffractometer equipped with graphite-monochromatized Mo Kα radiation. The initial orientation matrices were obtained from 20 machine-centered reflections selected by an automated peak search routine. These data were used to determine the crystal systems. Automated Laue system check routines around each axis were consistent with the crystal systems reported in Table 1. Ultimately, 25 reflections ($20° < 2\theta < 25°$) were used to obtain the final lattice parameters and the orientation matrices. Machine parameters, crystal data, and data collection parameters are summarized in Table 1. The observed extinctions were consistent with the space groups given in Table 1. The data sets were collected in four shells ($4.5° < 2\theta < 50.0°$) and three standard reflections were recorded every 197 reflections. The intensities of the standards showed no statistically significant change over the duration of the data collection. The data were processed using the TEXSAN crystal solution package operating on a VAX workstation 3520 or employing the TEXSAN package operating on an SGI mainframe computer with remote X-terminals. The reflections with $F_o^2 > 3\sigma(F_o^2)$ were used in the refinement. Empirical absorption corrections were applied to the data sets based on ψ-scan data.

Structure solution and refinement

Non-hydrogen atomic scattering factors were taken from the literature tabulations (6, 7). The Ti atom positions were determined using either the SHELX-86 or MITHRIL direct methods routines. In each case, the remaining non-hydrogen atoms were located from successive difference Fourier map calculations. The refinements were carried out by using full-matrix least-squares techniques on F, minimizing the function $\omega(|F_o| - |F_c|)^2$ where the weight ω is defined as $4F_o^2/2\sigma(F_o^2)$ and F_o and F_c are the observed and calculated structure factor amplitudes. In the final cycles of refinement all Ti, Cl, O, and C atoms were refined anisotropically and, with the exception of C8 in **3**, were assigned anisotropic thermal parameters. Hydrogen atom positions were calculated and allowed to ride on the carbon to which they are bonded, assuming a C—H bond length of 0.95 Å. In the case of **4** the proton associated with O4 and Cl1 was located in the difference. Hydrogen atom temperature factors were fixed at 1.10 times the isotropic temperature factor of the carbon atom to which they are bonded. In all cases the hydrogen atom contributions were calculated, but not refined. The following data have been deposited as supplementary material: positional parameters, thermal parameters, selected bond distances and angles, hydrogen atom parameters, and values of 10 F_o and 10 F_c.[2] The final values of R and R_w are given in Table 1. The maximum Δ/σ on any of the parame-

[2] Tables of crystallographic data, positional, thermal, and hydrogen atom parameters, and selected bond distances and angles (19 pages) have been deposited. Copies of the material on deposit may be purchased from: The Depository of Unpublished Data, Document Delivery, CISTI, National Research Council Canada, Ottawa, Canada K1A 0S2.

Tables of crystallographic data, atomic parameters, and bond distances and angles have also been deposited with the Cambridge Crystallographic Data Centre, and can be obtained on request from The Director, Cambridge Crystallographic Data Centre, University Chemical Laboratory, 12 Union Road, Cambridge, CB2 1EZ, U.K.

Can. J. Chem. Downloaded from www.nrcresearchpress.com by 80.90.12.36 on 09/08/12
For personal use only.

Table 1. Crystallographic parameters.

	1	3	4	5
Formula	$C_{13}H_{16}Cl_4O_2Ti_2$	$C_{15}H_{20}Cl_2O_2Ti_2$	$C_6H_{13}Cl_2O_4Ti_2$	$C_{14}H_{28}Cl_4O_2Ti_2$
Crystal color, form	Orange blocks	Orange blocks	Yellow blocks	Yellow blocks
a (Å)	12.587(2)	12.855(2)	8.911(3)	8.693(3)
b (Å)	9.632(2)	10.772(2)	7.821(2)	9.286(2)
c (Å)	15.824(3)	15.665(2)	13.986(2)	13.411(2)
β (deg)	107.88(1)	109.26(1)	102.56(2)	101.18(2)
Crystal system	Monoclinic	Monoclinic	Monoclinic	Triclinic
Space group	*C2/c* (No. 15)	*C2/c* (No. 15)	$P2_1/n$ (No. 14)	$P2_1/n$ (No. 14)
Vol (Å^3)	1811.3(5)	2047.7(5)	951.3(3)	1062.1(4)
D_{calcd} (g cm^{-3})	1.62	1.41	1.62	1.66
Z	4	4	2	2
Crystal dimensions (mm)	0.31 × 0.35 × 0.25	0.20 × 0.30 × 0.45	0.23 × 0.28 × 0.44	0.42 × 0.27 × 0.28
Absorption coeff. μ (cm^{-1})	14.70	10.53	11.54	12.81
Radiation, λ (Å)	Mo Kα (0.71069)	Mo Kα (0.71069)	Mo Kα (0.71069)	Mo Ka (0.71069)
Temp (°C)	24	24	24	24
Scan speed, °/min	8.0 (θ/2θ) (1–3 scans)	8.0 (θ/2θ) (1–3 scans)	8.0 (θ/2θ) (1–3 scans)	16.0 (θ/2θ) (1–3 scans)
Scan range (deg)	1.0 below $Kα_1$ 1.0 above Ka_2	1.0 below Ka_1 1.0 above Ka_2	1.0 below Ka_1 1.0 above Ka_2	1.0 below Ka_1 1.0 above Ka_2
Background/scan ratio	0.5	0.5	0.5	
Data collected	1698	1905	1810	1994
2θ range (deg)	4.5–50.0	4.5–50.0	4.5–50.0	4.5–50.0
Index range	$hk \pm l$	$hk \pm l$	$hk \pm l$	$hk \pm l$
Data $F_o^2 > 3\sigma(F_o^2)$	751	1244	1160	1140
variables	96	105	109	118
R (%)	5.42	5.22	5.03	5.32
R_w (%)	4.56	4.83	4.98	4.43
Largest Δ/σ	0.07	0.05	0.002	0.01
Goodness of fit	2.15	2.94	2.52	2.32

$R = \Sigma||F_o| - |F_c||/\Sigma|F_o|$; $R_w = [\Sigma(|F_o| - |F_c|)^2/\Sigma|F_o|^2]^{0.5}$.

ters in the final cycles of the refinement are also given in Table 1. The residual electron densities were of no chemical significance. Positional parameters and selected bond distances and angles are reported in Tables 2 and 3.

Results

Synthesis

The reaction of two equivalents of $CpTiCl_3$ with $Me_3SiOCH_2CH_2CH_2OSiMe_3$ proceeds slowly over a 3 day period to yield Me_3SiCl and the Ti product **1**. ^1H NMR data for **1** showed resonances at 6.77, 4.87, and 1.97 attributable to the cyclopentadienyl and methylene protons, respectively. $^{13}C\{^1H\}$ NMR data, as well as the integration of the ^1H NMR spectrum, were consistent with the formulation of **1** as $[Cl_2CpTi]_2(OCH_2CH_2CH_2O)$. This formulation was subsequently confirmed by a crystallographic study (*vide infra*). Alternatively, **1** is also formed via the reaction of $CpTiCl_3$ with the diol in the presence of imidazole. Separation from the imidazoleHCl is readily achieved via filtration and extraction of **1** into a small volume of THF, while subsequent recrystallization from CH_2Cl_2 afforded **1** in a crystalline form. Employing analogous procedures and the appropriate diols or disilyl ethers, the compounds $[Cl_2CpTi]_2(OCH_2CMe_2CH_2O)$ **2** and $[Cl_2CpTi]_2$(*rac*-$OCHMeCH_2CHMeO$) **3** were also prepared.

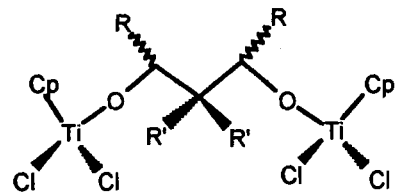

1, R = R' = H; 2, R = H, R' = Me; 3, R = Me, R' = H

In the case of **3** this formulation was also confirmed crystallographically (*vide infra*). In a recent report we demonstrated that substitution reactions involving $CpTiCl_3$, thiol, and imidazole proceed through a radical mechanism involving a Ti(III)–imidazole complex intermediate (4). The formation of **1–3** from the diol–imidazole reactions may also proceed through this intermediate. Similar dimeric products are known to be formed from Ti(III) precursors (eq. [1]) as described by Caulton and co-workers (8, 9) as well as Coutts et al. (10).

[1] $2/n\,[CpTiCl_2]_n + 2R_2CO \longrightarrow CpTiCl_2(OCR_2CR_2O)TiCpCl_2$

6

Can. J. Chem. Downloaded from www.nrcresearchpress.com by 80.90.12.36 on 09/08/12
For personal use only.

Table 2. Positional parameters.

Atom	*x*	*y*	*z*
	Compound **1**		
Ti(1)	0.7185(1)	0.0830(2)	0.3575(1)
Cl(1)	0.7039(2)	0.0216(3)	0.2161(2)
Cl(2)	0.8950(2)	0.1723(3)	0.4074(2)
O(1)	0.6295(5)	0.2253(6)	0.3396(4)
C(1)	0.721(3)	−0.156(1)	0.392(2)
C(2)	0.783(1)	−0.091(2)	0.465(2)
C(3)	0.716(2)	−0.007(2)	0.492(1)
C(4)	0.613(2)	−0.015(2)	0.440(2)
C(5)	0.612(2)	−0.103(3)	0.375(1)
C(6)	0.5325(8)	0.304(1)	0.3345(7)
C(7)	1/2	0.386(2)	1/4
	Compound **3**		
Ti(1)	0.22553(9)	0.0015(1)	0.32662(7)
Cl(1)	0.3977(1)	−0.0807(2)	0.3616(1)
Cl(2)	0.1865(1)	0.0518(2)	0.1785(1)
O(1)	0.1389(3)	−0.1264(4)	0.3188(3)
C(1)	0.201(1)	0.0720(7)	0.4577(6)
C(2)	0.1198(6)	0.1234(9)	0.3873(7)
C(3)	0.1691(9)	0.2031(7)	0.3452(5)
C(4)	0.2793(8)	0.1999(8)	0.3891(8)
C(5)	0.2991(8)	0.120(1)	0.4579(6)
C(6)	0.0532(5)	−0.2006(5)	0.3337(4)
C(7)	0.1038(5)	−0.2798(6)	0.4178(5)
C(8)	0	−0.2747(7)	1/4
	Compound **4**		
Ti(1)	0.9113(1)	0.0665(1)	0.08523(7)
Cl(1)	1.0554(2)	0.3256(2)	0.1090(1)
O(1)	0.8953(4)	0.0478(4)	−0.0603(2)
O(2)	0.7261(5)	0.1677(6)	0.0621(3)
O(3)	0.9370(5)	0.0054(5)	0.2117(3)
O(4)	0.8074(4)	−0.1847(5)	0.0581(3)
C(1)	0.7574(6)	0.0796(9)	−0.1331(4)
C(2)	0.6740(8)	0.234(1)	−0.1109(5)
C(3)	0.6168(7)	0.228(1)	−0.0203(5)
C(4)	0.9365(8)	−0.1333(8)	0.2750(4)
C(5)	0.9201(8)	−0.3000(9)	0.2215(5)
C(6)	0.7912(8)	−0.3050(9)	0.1336(5)
	Compound **5**		
Ti(1)	0.0835(2)	0.1553(1)	0.4875(1)
Cl(1)	0.0506(2)	0.2423(2)	0.6445(1)
Cl(2)	0.3460(2)	0.2247(2)	0.5229(2)
O(1)	−0.1209(5)	0.0521(5)	0.4574(3)
O(2)	−0.0076(6)	0.3039(5)	0.4190(4)
O(3)	0.1397(6)	0.0752(5)	0.3498(4)
C(1)	−0.2620(8)	0.1112(8)	0.3976(6)
C(2)	−0.2812(8)	0.2678(9)	0.4190(6)
C(3)	−0.160(1)	0.3608(8)	0.3831(7)
C(4)	0.043(1)	0.0950(8)	0.2504(6)
C(5)	0.141(1)	0.054(1)	0.1735(6)
C(6)	0.254(1)	−0.049(1)	0.2270(8)
C(7)	0.278(1)	−0.008(1)	0.3382(6)

Reactions performed with a 1:1 ratio of Ti and propanediol were expected to yield either monometallic chelate or macrocyclic dimeric complexes analogous to the pinacolate complexes, $CpTiCl(OCMe_2CMe_2O)$ **7** and $[CpTiCl(OCMe_2CMe_2O)]_2$ **8**, reported by Caulton and co-workers (11). Certainly, in the case of the related reactions of diols with Cp_2ZrCl_2 in the presence of base, dimeric macrocyclic products are derived (1). In the present case, monitoring of the reactions by ^1H NMR spectroscopy revealed resonances attributable to **1** and to a second CpTi derivative that exhibited a resonance at 6.24 ppm, suggesting the formation of macrocyclic species similar to **7**. However, this latter species could not be isolated as it appears to be unstable, degrading to several products. ^1H NMR data suggested the liberation of free CpH. This was confirmed via GC–MS of the reaction mixture.

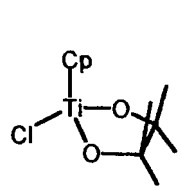

7

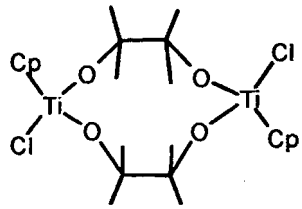

8

Upon removal of the solvent and recrystallization of the residue from CH_2Cl_2–pentane, the product **4** was isolated in crystalline form. ^1H NMR data and subsequent X-ray diffraction data were consistent with the formulation of **4** as $[TiCl(HOCH_2CH_2CH_2O)(OCH_2CH_2CH_2O)]_2$ (*vide infra*). When compound **4** was recrystallized from THF–hexane, a small amount (less than 1%) of a second species was also obtained. The isolation of only a few crystals of **5** precluded characterization by spectroscopic methods, although X-ray methods permitted the identification of **5** as $[TiCl_2(OCH_2CH_2CH_2O)(THF)]_2$ (*vide infra*).

Structural studies

Crystallographic studies of **1** and **3** confirmed both the formulation and the similarity of the structures (Figs. 1, 2). In both cases, crystallographically imposed twofold symmetry relates the two halves of the molecule and dictates an orientation in which the cyclopentadienyl rings on symmetry-related Ti atoms are approximately orthogonal. In the case of **3**, this imposed symmetry also dictates identical configurations for the two chiral carbons of the diolate ligand. As the space group is centrosymmetric, the X-ray data confirm the co-crystallization of the *R,R* and *S,S* diastereomers. In addition, the methyl groups occupy equatorial positions relative to the six-membered chelate ring. This orientation minimizes steric interactions between the cyclopentadienyl ring and the methyl group. The Ti—O distances in **1** and **3** are 1.733(6) and 1.750(4) Å, respectively (Table 3). While the latter distance is identical to that found in **6**, these are significantly shorter than the Ti—O distance seen in $Cp_2TiCl(OEt)$ (1.855(2) Å) (8). This is consistent with the greater Lewis acidity of the Ti center upon replacement of a cyclopentadienyl ligand with chloride. The slightly longer Ti—O bond length observed in **3** compared to that in **1** is consistent with the greater steric demands of the 2,4-pentanediolate ligand. The Ti-O-C angles of 158.7(6)° and 158.1(4)° in **1** and **3**, respectively, compare with an angle

Can. J. Chem. Downloaded from www.nrcresearchpress.com by 80.90.12.36 on 09/08/12
For personal use only.

Fig. 1. ORTEP drawing of **1**, 30% thermal ellipsoids are shown, hydrogen atoms are omitted for clarity.

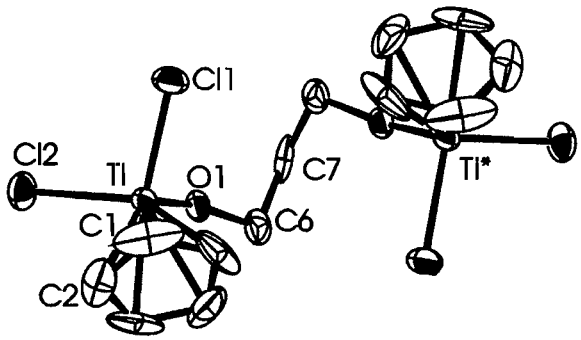

Fig. 2. ORTEP drawing of **3**, 30% thermal ellipsoids are shown, hydrogen atoms are omitted for clarity.

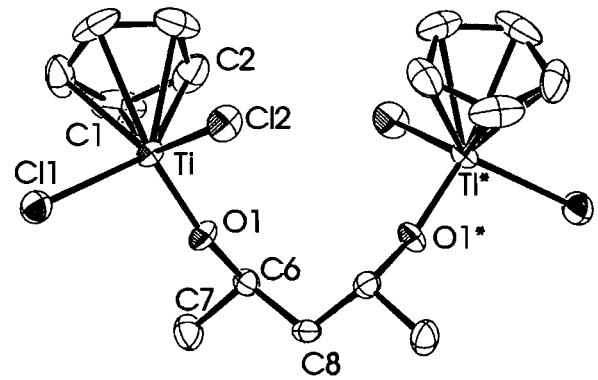

of 166.2(2)° found in **6**. The short Ti—O distances and the obtuse Ti-O-C angles observed in Ti-alkoxide derivatives have been rationalized in term of strong Ti—O π-bonding. Ti—Cl distances range from 2.267(3) to 2.276(2) Å in **1** and **3**, similar to those found in other CpTi(IV)-chloride derivatives.

The structure of **4** was confirmed by an X-ray crystallographic study (Fig. 3). These data show that the compound is a dimeric species in which alkoxide oxygen atoms from each of two diolate ligands bridge the metal centers. The nonbridging end of each diolate ligand occupies the position *trans* to a bridging alkoxide oxygen atom. One more diol ligand chelates to each of the Ti centers. One of the oxygen atoms of these chelates is protonated yielding propanol-olate ligands. The alkoxide ends of these ligands also adopt a position *trans* to a bridging alkoxide oxygen while the alcoholic end occupies an axial position *trans* to a chloride atom. The Ti centers are thus best described as pseudo-octahedral, sharing the edge containing the bridging oxygen atoms. Bite angles for the diol chelates are typical for six-membered rings (89.4(2)°, 83.7(2)°). The Ti—O distances clearly reflect three different oxygen coordination modes. As expected, the bridging alkoxide T—O bond lengths are significantly longer (2.014(3), 2.037(3) Å) than the terminal Ti—O distances (1.795(4) Å, 1.798(4) Å). These terminal and bridging Ti-O distances certainly fall in the range of those seen in related Ti-alkoxide derivatives, among them $Ti_2(DIPT)_3(ONBn_2)_2$, $Ti_3(DIPT)_3(OiPr)_2Br_4$, and $[Ti(DIPT)(OiPr)Br]_4$ (12). The coordinated alcohol moiety results in a Ti—O4 distance that is longer again (2.169(4) Å), consistent with the presence of the proton. The Ti—Cl distance of 2.384(2) Å in **4** is longer than the Ti—Cl distances seen in either **1** or **3**. As the Cl in **4** is axial to the O_4 equatorial plane, π-donation from oxygen to Ti reduces similar π-donation from Cl and thus accounts for the longer Ti—Cl bond. In addition, lengthening of the Ti—Cl bond may be attributed to hydrogen bonding between the alcoholic proton and the Cl (H...Cl 2.06 Å).

The crystallographic characterization of **5** (Fig. 4) revealed a structure similar to that seen for **4**. Two Ti centers are bridged by two alkoxide oxygen atoms while the second oxygen of these diolate ligands binds to the respective Ti atoms in positions *trans* to the bridging oxygens. The pseudo-octahedral coordination spheres of the Ti centers are completed by two *cis* chloride atoms and a molecule of THF. The terminal Ti—O distance in **5** (1.759(5) Å) is slightly shorter than that

Table 3. Selected bond distances and angles.

Compound 1

Atom	Atom	Distance		Atom	Atom	Distance
Ti(1)	Cl(1)	2.267(3)		O(1)	C(6)	1.41(1)
Ti(1)	Cl(2)	2.270(3)		Ti(1)	O(1)	1.733(6)
Ti(1)	C(1)	2.37(1)		Ti(1)	C(2)	2.35(1)
Ti(1)	C(3)	2.31(1)		Ti(1)	C(4)	2.32(1)
Ti(1)	C(5)	2.29(1)				

Atom	Atom	Atom	Angle	Atom	Atom	Atom	Angle
Cl(1)	Ti(1)	Cl(2)	102.6(1)	Cl(1)	Ti(1)	O(1)	101.0(2)
Ti(1)	O(1)	C(6)	158.7(6)	Cl(2)	Ti(1)	O(1)	105.2(2)

Compound 3

Atom	Atom	Distance		Atom	Atom	Distance
Ti(1)	Cl(1)	2.276(2)		O(1)	C(6)	1.442(6)
Ti(1)	Cl(2)	2.273(2)		Ti(1)	O(1)	1.750(4)
Ti(1)	C(1)	2.306(7)		Ti(1)	C(2)	2.308(7)
Ti(1)	C(3)	2.338(7)		Ti(1)	C(4)	2.358(7)
Ti(1)	C(5)	2.336(7)				

Atom	Atom	Atom	Angle	Atom	Atom	Atom	Angle
Cl(1)	Ti(1)	Cl(2)	102.02(8)	Cl(1)	Ti(1)	O(1)	104.9(1)
Ti(1)	O(1)	C(6)	158.1(4)	Cl(2)	Ti(1)	O(1)	101.3(1)

Compound 4

Atom	Atom	Distance		Atom	Atom	Distance
Ti(1)	Cl(1)	2.384(2)		Ti(1)	O(1)	2.014(3)
Ti(1)	O(1)	2.037(3)		Ti(1)	O(2)	1.795(4)
Ti(1)	O(3)	1.798(4)		Ti(1)	O(4)	2.169(4)
O(1)	C(1)	1.437(6)		O(2)	C(3)	1.417(7)
O(3)	C(4)	1.401(6)		O(4)	C(6)	1.446(7)

Atom	Atom	Atom	Angle	Atom	Atom	Atom	Angle
Cl(1)	Ti(1)	O(1)	96.9(1)	Cl(1)	Ti(1)	O(1)	87.0(1)
Cl(1)	Ti(1)	O(2)	5.5(2)	Cl(1)	Ti(1)	O(3)	98.0(1)
Cl(1)	Ti(1)	O(4)	172.2(1)	O(1)	Ti(1)	O(1)	70.8(2)
O(1)	Ti(1)	O(2)	89.4(2)	O(1)	Ti(1)	O(3)	160.2(2)
O(1)	Ti(1)	O(4)	79.8(1)	O(1)	Ti(1)	O(2)	160.3(2)
O(1)	Ti(1)	O(3)	96.9(2)	O(1)	Ti(1)	O(4)	85.3(1)
O(2)	Ti(1)	O(3)	102.1(2)	O(2)	Ti(1)	O(4)	91.6(2)
O(3)	Ti(1)	O(4)	83.7(2)	Ti(1)	O(1)	Ti(1)	109.2(2)

Table 3 (*concluded*).

Compound 5

Atom	Atom	Distance		Atom	Atom	Distance
Ti(1)	Cl(1)	2.325(2)		Ti(1)	Cl(2)	2.330(2)
Ti(1)	O(1)	1.990(5)		Ti(1)	O(1)	2.066(5)
Ti(1)	O(2)	1.759(5)		Ti(1)	O(3)	2.133(5)
O(1)	C(1)	1.438(8)		O(2)	C(3)	1.421(8)
O(3)	C(4)	1.445(8)		O(3)	C(7)	1.459(9)
Atom	Atom	Atom	Angle	Atom	Atom	Atom	Angle
Cl(1)	Ti(1)	Cl(2)	90.38(9)	Cl(1)	Ti(1)	O(1)	95.1(1)
Cl(1)	Ti(1)	O(1)	92.2(1)	Cl(1)	Ti(1)	O(2)	94.5(2)
Cl(1)	Ti(1)	O(3)	173.9(2)	Cl(2)	Ti(1)	O(1)	167.2(2)
Cl(2)	Ti(1)	O(1)	96.0(1)	Cl(2)	Ti(1)	O(2)	102.3(2)
Cl(2)	Ti(1)	O(3)	83.9(1)	O(1)	Ti(1)	O(1)	72.3(2)
O(1)	Ti(1)	O(2)	88.8(2)	O(1)	Ti(1)	O(3)	90.1(2)
O(1)	Ti(1)	O(2)	160.4(2)	O(1)	Ti(1)	O(3)	86.5(2)
O(2)	Ti(1)	O(3)	88.7(2)	Ti(1)	O(1)	Ti(1)	107.7(2)
Ti(1)	O(1)	C(1)	124.1(4)	Ti(1)	O(1)	C(1)	127.8(4)
Ti(1)	O(2)	C(3)	139.8(5)	Ti(1)	O(3)	C(4)	124.3(4)
Ti(1)	O(3)	C(7)	127.4(5)				

Fig. 3. ORTEP drawing of **4**, 30% thermal ellipsoids are shown, hydrogen atoms are omitted for clarity.

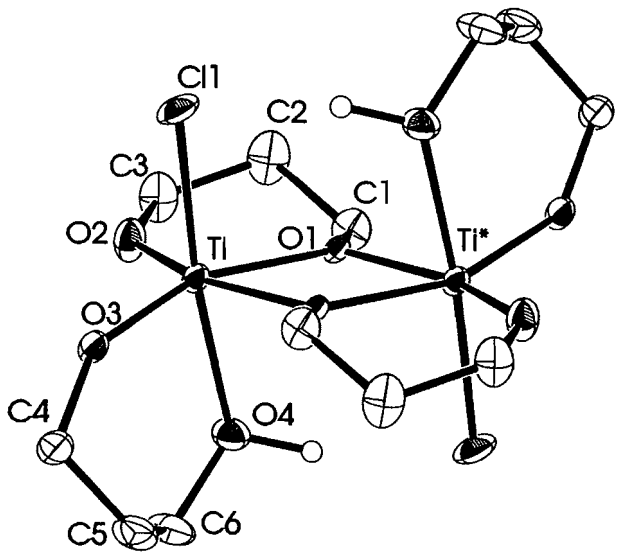

seen in **4** due to the presence of additional oxygen donors in **4** that diminish the Lewis acidity of the Ti center. This is also reflected in the shorter Ti—Cl distances in **5** (2.325(2), 2.330(2) Å). The Ti—O distance for the coordinated THF is 2.133(5) Å, which is slightly shorter than the Ti—O distance seen for the coordinated alcohol of **4**. This is as expected based on basicity trends.

The Ti_2O_2 cores of both **4** and **5** are planar. In the case of **4**, the Ti—O distances are similar, while in **5** the bridging Ti—O distances of 1.990(5) and 2.066(5) Å indicate a distinct asymmetry in the bridge. The Ti...Ti distances of 3.302(2) and 3.275(3) Å in **4** and **5**, respectively, compare with the Ti..Ti distance of 3.348(3) Å found in $[Ti(OiPr)_2(PhCH_2NHCO_2$-

Fig. 4. ORTEP drawing of **5**, 30% thermal ellipsoids are shown, hydrogen atoms are omitted for clarity.

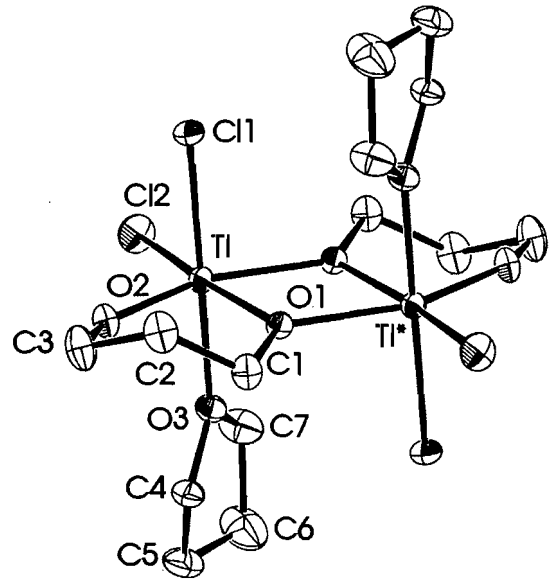

$CHCHO(CONHCH_2Ph)]_2$ (13). The Ti-O-Ti′ and O-Ti-O′ angles in **4** (109.2(2)°, 70.8(2)°) are similar to those seen in **5** (107.7(2)°, 72.3(2)°).These perturbations in the core angles are consistent with the fluctuations in the bridging Ti—O distances and are attributed to the differing acidities of the Ti centers.

Discussion

Caulton and co-workers (8, 9, 11) have studied the formation of **6** from the reaction of **7** and $CpTiCl_3$ and suggest that destabilizing steric interactions between the methyl substituents of the pinacolate and the cyclopentadienyl ring are the driving force for the reaction. Similarly, we suggest that a mononuclear diolate species **9** (Scheme 1) is formed initially in the present reactions and that ligand redistribution reactions in the presence of $CpTiCl_3$ yield the products **1–3**. Such redistributions may be favored by the stabilizing influence of Ti–O p-bonding. Such interactions are maximized via the formation of the bimetallic products since chelation to a single Ti atom restricts the Ti-O-C angle and thus the degree of π-donation. We further suggest that coordination of excess diol affords the intermediate **10** (Scheme 1). The π-donor ability of the oxygen atoms competes with the cyclopentadienyl ring for metal *d*-orbitals and thus facilitates the loss of CpH and the formation of **4**. Although no direct evidence has been obtained for the proposed intermediates, the known species **7** and the established ability of Ti three-legged piano stool complexes to bind additional donor ligands are consistent with these propositions (2).

Ligand redistribution reactions also account for the formation of **5** upon recrystallization of **4** from THF. However, the isolation of only a very few crystals of **5** suggests an equilibrium between **4**, **5**, and other as yet uncharacterized Ti species, in which **4** is the dominant species in solution. A fuller understanding of this solution behaviour and of titanium alkoxide complexes in general requires further study.

Can. J. Chem. Downloaded from www.nrcresearchpress.com by 80.90.12.36 on 09/08/12
For personal use only.

Scheme 1.

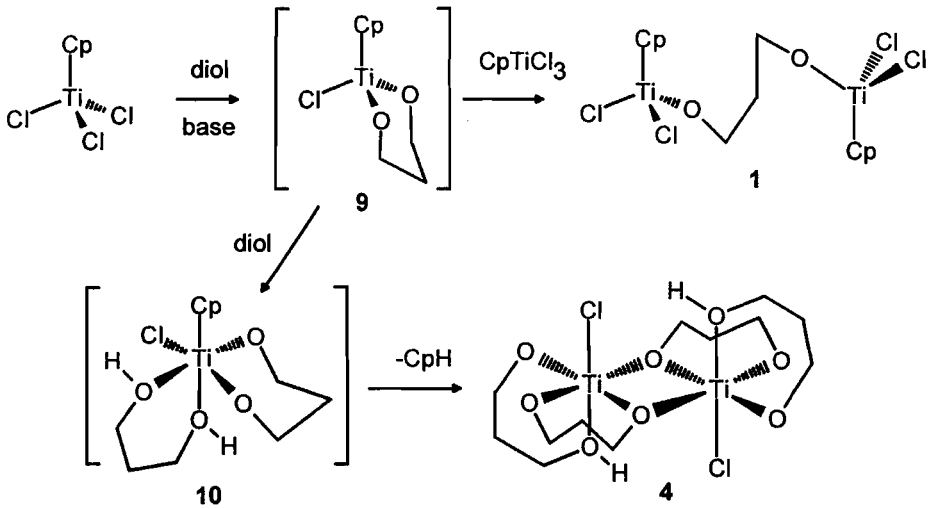

Acknowledgements

Support from the Petroleum Research Fund administered by the American Chemical Society and the Natural Sciences and Engineering Research Council of Canada is acknowledged.

References

1. (*a*) D.W. Stephan. Organometallics, **9**, 2718 (1990); (*b*) T.T. Nadasdi and D.W. Stephan. Organometallics, **11**, 116 (1992).
2. T.T. Nadasdi, Y. Huang, and D.W. Stephan. Inorg. Chem. **32**, 347 (1993).
3. T.T. Nadasdi and D.W. Stephan. Inorg. Chem. **33**, 1532 (1994).
4. T.T. Nadasdi and D.W. Stephan. Inorg. Chem. **32**, 5933 (1993).
5. T.T. Nadasdi, Y. Huang, and D.W. Stephan. J. Am. Chem. Soc. **116**, 5483 (1994).
6. D.T. Cromer and J.B. Mann. Acta Crystallogr. Sect. A: Cryst. Phys. Theor. Gen. Crystallogr. **A24**, 324 (1968).
7. D.T. Cromer and J.B. Mann. Acta Crystallogr. Sect. A: Cryst. Phys. Theor. Gen. Crystallogr. **A24**, 390 (1968).
8. J.C. Huffman, K.G. Moloy, J.A. Marsella, and K.G. Caulton. J.Am. Chem. Soc. **102**, 3009 (1980).
9. J.A. Marsella, K.G. Moloy, and K.G. Caulton. J. Organomet. Chem. **201**, 389 (1980).
10. R.S.P. Coutts, P.C. Wailes, and R.L. Martin. J. Organomet. Chem. **50**, 145 (1973).
11. J.C. Huffman, K.G. Moloy, and K.G. Caulton. Inorg. Chem. **27**, 2190 (1988).
12. S.F. Pedersen, J.C. Dewan, R.R. Eckman, and K.B. Sharpless. J. Am. Chem. Soc. **109**, 1279 (1987).
13. I.D. Williams, S.F. Pedersen, K.B. Sharpless, and S.J. Lippard. J. Am. Chem. Soc. **106**, 6430 (1984).

Can. J. Chem. Downloaded from www.nrcresearchpress.com by 80.90.12.36 on 09/08/12
For personal use only.

The chemical bonding topology of ternary and quaternary transition metal nitrides containing low-coordinate metal atoms

R.B. King

Can. J. Chem. Downloaded from www.nrcresearchpress.com by 80.90.12.36 on 09/08/12
For personal use only.

Abstract: Solid state ternary and quaternary metal nitrides containing a transition metal and one or two very electropositive metals such as alkali and (or) alkaline earth metals exhibit a number of structures containing low-coordinate transition metals in the transition metal – nitrogen subnetwork. Transition metal – nitrogen double and even triple bonds are found in these structures involving $d\pi \rightarrow p\pi$ bonding from a filled transition metal *d* orbital to an otherwise empty nitrogen *p* orbital. Such multiply bonded nitrogen atoms function as strong field ligands in contrast to amido ligands such as $(Me_3Si)_2N^-$, which generally function as weak field ligands in transition metal chemistry. The transition metal environment in these ternary nitrides can be modelled by "banana bonds" from the polyhedron using the atomic orbitals required for both the σ- and π-bonding to the nitride ligands, e.g., the trigonal prism for the trigonal planar derivatives $M^{III}N_3^{6-}$ (M = V, Cr, Mn, Fe) with three M=N double bonds as well as $Fe^{II}N_2^{4-}$ in $Li_4Fe^{II}N_2$ with two Fe≡N triple bonds and the planar square for the discrete linear $Co^{I}N_2^{5-}$ in $LiSr_2CoN_2$. Reasonable electron counts are also obtained for the anionic metal–nitrogen networks in Ca_2FeN_2, $Sr_2LiFe_2N_3$, $Ba_2LiFe_2N_3$, Li_3FeN_2, CaNiN, $Li_3Sr_3Ni_4N_4$, BaNiN, and $Ba_8Ni_6N_7$.

Key words: chemical bonding, topology, nitrides, transition metals.

Résumé : Les nitrures métalliques ternaires et quaternaires à l'état solide contenant un métal de transition et un ou deux métaux très électropositifs, comme les métaux alcalins et (ou) alcalino-terreux, présentent un certain nombre de structures comportant des métaux de transition de basse coordination dans le sous-réseau azote – métal de transition. On a trouvé des liaisons doubles, et même triples, entre l'azote et le métal de transition dans ces structures impliquant une liaison $d\pi \rightarrow p\pi$ formée à partir d'une orbitale *d* remplie du métal de transition et une orbitale *p* par ailleurs vide de l'azote. De tels atomes d'azote à liaisons multiples agissent comme des coordinats à champ fort par opposition aux coordinats amido, tel que $(Me_3Si)_2N^-$, qui agissent généralement comme des coordinats de champ faible dans la chimie des métaux de transition. On peut faire un modèle de l'environnement du métal de transition de ces nitrures ternaires à l'aide de «liaisons bananes» à partir du polyèdre, en utilisant les orbitales atomiques requises pour les liaisons à la fois σ et π des coordinats nitrures, c'est-à-dire le prisme trigonal des dérivés plans trigonaux $M^{III}N_3^{6-}$ (M = V, Cr, Mn et Fe) avec des trois liaisons M=N ainsi que $Fe^{II}N_2^{4-}$ du $Li_4Fe^{II}N_2$ comportant deux Fe≡N et le plan carré du $Co^{I}N_2^{5-}$ du $LiSr_2CoN_2$. On peut aussi faire un compte raisonnable des électrons des réseaux anioniques métal–azote du Ca_2FeN_2, $Sr_2LiFe_2N_3$, $Ba_2LiFe_2N_3$, Li_3FeN_2, CaNiN, $Li_3Sr_3Ni_4N_4$, BaNiN et $Ba_8Ni_6N_7$.

Mots clés : liaisons chimiques, topologie, nitrures, métaux de transition.

[Traduit par la rédaction]

Introduction

A significant development in solid state inorganic chemistry during the past decade has been the discovery of a number of ternary and quaternary transition metal nitrides containing a low-coordinate transition metal and one or two very electropositive metals such as alkali and (or) alkaline earth metals (1). The nitrogen atoms in these metal nitrides function as relatively strong field π-acceptor terminal or bridging ligands leading to apparent multiple transition metal – nitrogen bonding as well as to low transition metal coordination numbers and spin states in the transition metal – nitrogen subnetwork. Interesting structures in recently characterized ternary transition metal nitrides include the discrete trigonal planar MN_3^{6-} ions (M = V, Cr, Mn, Fe) (2) as well as infinite $[NiN_{2/2}^{2-}]_\infty$ chains in AeNiN (Ae = Ca, Ba) (3).

In previous papers the author has discussed the chemical bonding topology in transition metal polyphosphides (4),

Received August 19, 1994.

This paper is dedicated to Professor William A. G. Graham on the occasion of his 65th birthday.

R. B. King.[1] Department of Chemistry, University of Georgia, Athens, GA 30602, U.S.A.

[1] Telephone: 706-542-1901. Fax: 706-542-9454. E-mail: rbking@sunchem.chem.uga.edu

Can. J. Chem. Downloaded from www.nrcresearchpress.com by 80.90.12.36 on 09/08/12
For personal use only.

superconducting transition metal borides and silicides (5), and superconducting alloys (5). This paper extends these methods to solid state ternary and quaternary transition metal nitrides with particular emphasis on compounds exhibiting unusual structural features. Hughbanks and co-workers have also studied some of the ternary transition metal nitrides using various computational methods including both extended Hückel (2) and *ab initio* (3) methods. The topology-based ideas outlined in this paper serve to relate the structures of the solid state ternary transition metal nitrides to molecular species exhibiting analogous metal electronic configurations and coordination environments.

Background

The ternary and quaternary transition metal nitrides of interest in this work (Table 1) contain an electropositive metal (most commonly an alkaline earth metal), the transition metal, and nitrogen. Complete ionization of the electropositive metal to the typical stable cation, e.g., Ae^{2+} in the case of the bivalent alkaline earth metals (Ae), leads to an anionic transition metal – nitrogen subnetwork, which can consist of either discrete ions, such as MN_3^{6-} in Ae_3MN_3, or infinite polymers, such as the $[NiN_{2/2}^{2-}]_\infty$ chains in AeNiN. The environments of the transition metal and nitrogen atoms in these anionic transition metal – nitrogen subnetworks can now be considered.

A. The metal environment

The atomic orbitals of the transition metals in the metal nitrides are used not only for the usual σ-bonding but also for π-bonding to the nitride nitrogen atoms as noted above. However, the π-bonding in metal nitrides can alternatively be represented by equivalent bent σ-bonds or "banana" bonds (Fig. 1) using hybrid metal orbitals from the same set of metal atomic orbitals required for the total σ + π bonding similar to methods used by Messmer (6) for other transition metal compounds. These methods, which are based on generalized valence bond theory, have been supported by computational studies using the generalized valence bond (GVB) method (7–11). Use of the "bent bond" model for the transition metal – nitrogen bonds in the metal nitrides allows the strong π-bonding in metal nitrides to be included in the transition metal coordination polyhedra without the explicit need to separate σ- and π-bonding. This is similar to considering the boron atoms in diborane as using four sp^3 hybrids for the bonds to hydrogen in the bent bond equivalent of the conventional σ+π C=C double bond of ethylene (Fig. 1) (12).

The bent bond model is particularly informative in the case of the trigonal planar derivatives MN_3^{6-} (M = V, Cr, Mn, Fe), which become trigonal prisms if bent bonding is used to describe both the σ- and π-bonding (Fig. 2). The trigonal planar MN_3^{6-} can be considered to use $sp^2(x,y)$ hybridization with no node through the N_3 plane for the σ-bonding and $pd^2(z,xz,yz)$ hybridization for the π-bonding. However, the sum of these six atomic orbitals, namely $sp^3d^2(xz,yz)$, is exactly the set of six atomic orbitals required for trigonal prismatic six-coordination rather than the more familiar set of six atomic orbitals, namely $sp^3d^2(z^2, x^2 - y^2)$, required for octahedral six-coordination. Treatment of MN_3^{6-} as a trigonal prismatic complex in this manner allows the simple angular overlap model (13, 14) to be used to estimate the *d* orbital splittings for such purposes as predicting magnetic properties and Jahn–Teller distortions (2). Similarly, the bent bond model of linear $Co^{I}N_2^{5-}$ considers it as a square planar complex (Fig. 2) with the d^8 metal electronic configuration so common in square planar complexes of transition metals such as M^{I} (M = Co, Rh, Ir), Ni^{II} (M = Ni, Pd, Pt), Au^{III}, etc. The linear $Co^{I}N_2^{5-}$ can be considered to use $sp(x)$ hybridization for the σ-bonding and $pd(y, x^2 - y^2)$ hybridization for the π-bonding.

The electron counting of the central transition metal atom in ternary metal nitrides is of interest. The accessible *spd* valence orbital manifold of most transition metals consists of nine orbitals (sp^3d^5) and has spherical (isotropic) geometry extending equally in all three dimensions, where the geometry of an orbital manifold relates to contours of $\Sigma\psi^2$ over all orbitals in the manifold. Filling this accessible spherical *spd* manifold with electrons from either the central metal atom or its surrounding ligands results in the familiar 18-electron configuration of the next rare gas (15). This is the favored electron count for a transition metal bonding in all three dimensions, such as metals with tetrahedral, octahedral, or trigonal prismatic coordination.

A specific feature of the chemical bonding in some systems containing the late transition and early post-transition metals observed by Nyholm (16) as early as 1961 is the shifting of one or two of the outer *p* orbitals to such high energies that they no longer participate in the chemical bonding and the accessible *spd* valence orbital manifold is no longer spherical (isotropic). If one *p* orbital is so shifted to become antibonding, then the accessible *spd* orbital manifold contains only eight orbitals (sp^2d^5) and has the geometry of a torus or doughnut (Fig. 3). The "missing" *p* orbital is responsible for the hole in the doughnut. This toroidal sp^2d^5 manifold can bond only in the two dimensions of the plane of the ring of the torus. Filling this sp^2d^5 manifold of eight orbitals with electrons leads to the 16-electron configuration found in square planar complexes of the d^8 transition metals such as Co(I), Rh(I), Ir(I), Ni(II), Pd(II), Pt(II), and Au(III). The locations of the four ligands in these square planar complexes can be considered to be points on the surface of the torus corresponding to the sp^2d^5 manifold. The toroidal sp^2d^5 manifold can also lead to trigonal planar and pentagonal planar coordination for three- and five-coordinate complexes, respectively. The *x*, *y*, and *z* axes for a toroidal sp^2d^5 manifold are conventionally chosen so that the missing *p* orbital is the p_z orbital.

In some structures containing the late transition and post-transition metals, two of the outer *p* orbitals are raised to antibonding energy levels. This leaves only one *p* orbital in the accessible *spd* orbital manifold, which now contains seven orbitals (spd^5) and has cylindrical geometry extending in one axial dimension much further than in the remaining two dimensions (Fig. 3). Filling this seven-orbital spd^5 manifold with electrons leads to the 14-electron configuration found in two-coordinate linear complexes of d^{10} metals such as Ni(0), Pt(0), Cu(I), Ag(I), Au(I), Hg(II), and Tl(III).

B. The nitrogen environment

Examples of tetrahedral sp^3-hybridized, planar sp^2-hybridized, or linear *sp*-hybridized nitrogen atoms are found in the ternary transition metal nitrides (Fig. 4). A tetrahedral sp^3-hybridized nitrogen uses all of its valence orbitals for σ-bonding and thus is incapable of forming metal–nitrogen multiple

Can. J. Chem. Downloaded from www.nrcresearchpress.com by 80.90.12.36 on 09/08/12
For personal use only.

Table 1. The ternary metal nitrides discussed in this paper.

Formula	Color	Anion	M—N, Å	M—M, Å	Reference
Ba_3MoN_4	Yellow	$Mo^{VI}N_4^{6-}$	1.87 × 4	—	20
Li_6MoN_4	Sand	$Mo^{VI}N_4^{6-}$	1.88 × 4	—	19
Ca_3VN_3	Brown	$V^{III}N_3^{6-}$	1.82 × 3	—	21
Ca_3CrN_3	Burgundy	$Cr^{III}N_3^{6-}$	1.77,1.77,1.86	—	22
Ca_3MnN_3	Violet	$Mn^{III}N_3^{6-}$	1.79,1.79,1.80	—	23
Sr_3MnN_3	Black-gray	$Mn^{III}N_3^{6-}$	1.74 × 3	—	24
Ba_3MnN_3	Black-gray	$Mn^{III}N_3^{6-}$	1.74 × 3	—	24
Ca_6FeN_5	Yellow	$Fe^{III}N_3^{6-}$	1.77 × 3	—	26
Ba_3FeN_3		$Fe^{III}N_3^{6-}$	1.73 × 3	—	25
Li_4FeN_2	Metallic	$Fe^{II}N_2^{4-}$	1.86 × 2	—	29
Sr_2FeN_2		$Fe^{II}N_2^{4-}$	1.85 × 2	—	30
$LiSr_2CoN_2$	Black-gray	$Co^{I}N_2^{5-}$	1.81 × 2	—	28
Ca_2FeN_2		$[Fe^{II}NN_{2/2}]_2^{8-}$	1.88,1.89,1.94	2.41	30
$Sr_2LiFe_2N_3$	Black	$\{[Fe^{II}N_{3/2}]_2^{5-}\}_\infty$	1.87,1.91,1.92	2.42,2.62	32
Li_3FeN_2	Black	$[Fe^{III}N_{4/2}^{3-}]_\infty$	1.96 × 4	2.40 × 2	33
CaNiN	Black	$[Ni^{I}N_{2/2}^{2-}]_\infty$	1.79 × 2	3.58	34
$Li_3Sr_3Ni_4N_4$	Black	$[Ni^{I}N_{2/2}^{2.25-}]_\infty$	1.78 × 2	—	35
BaNiN		$[Ni^{I}N_{2/2}^{2-}]_\infty$	1.79–1.83	2.42	36
$Ba_8Ni_6N_7$	Red-brown	$[Ni^{I}N_{2/2}^{2.17-}]_\infty$	1.76–1.81	2.57	37

Fig. 1. Equivalent σ + π and "bent" bond models for the multiple metal–nitrogen bonding in metal nitrides and their comparison with standard models for ethylene and diborane. For convenience the σ-bonds drawn in Figs. 1, 2, and 5 include only those parts of the atomic orbitals in which the signs of the wave function are the same, rather than the complete orbital.

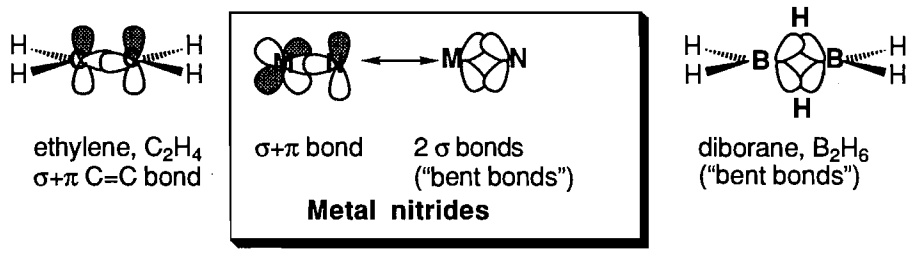

Fig. 2. The relationship of trigonal prismatic "bent bonds" to the metal–nitrogen multiple bonding in $M^{III}N_3^{3-}$ (M = V, Cr, Mn, Fe) and square planar "bent bonds" to the metal–nitrogen multiple bonding in $Co^{I}N_2^{5-}$.

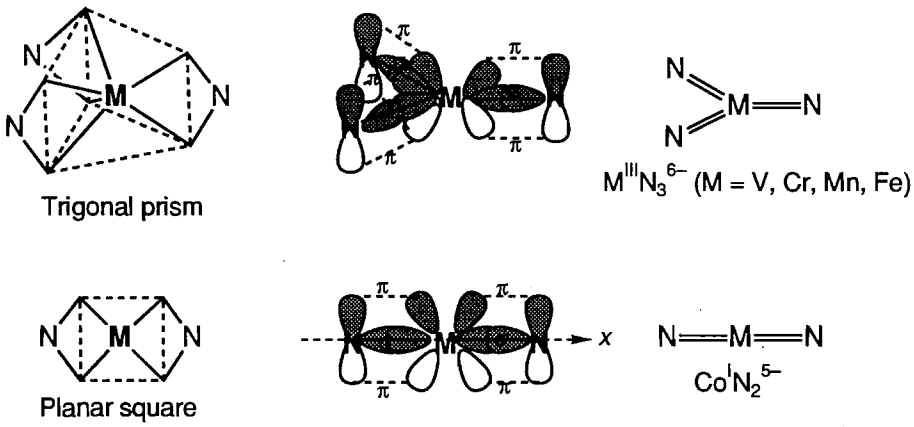

bonds. For this reason tetrahedral sp^3-hybridized nitrogen atoms are not generally favorable in low-coordinate transition metal nitrides in which metal–nitrogen multiple bonding plays a major role. In addition, a neutral terminal sp^3 nitrogen atom singly bonded to a transition metal has three lone pairs and a relatively high –2 formal charge (Fig. 4), also an unfavorable feature, so that this type of sp^3 nitrogen atom is not found in any of the metal nitrides discussed in this paper. A bridging tetrahedral sp^3 nitrogen atom forming single bonds with two transition metals retains two lone pairs and has a –1 formal

Fig. 3. Toroidal sp^2d^5 and cylindrical spd^5 manifolds showing square planar coordination for the toroidal manifold.

Toroidal sp^2d^5 manifold (Square Planar)

Cylindrical spd^5 manifold (Linear)

Fig. 4. The types of nitrogen atoms in the transition metal–nitrogen subnetworks of metal nitrides. Note that all of these types of nitrogen atoms have the favored electron octet.

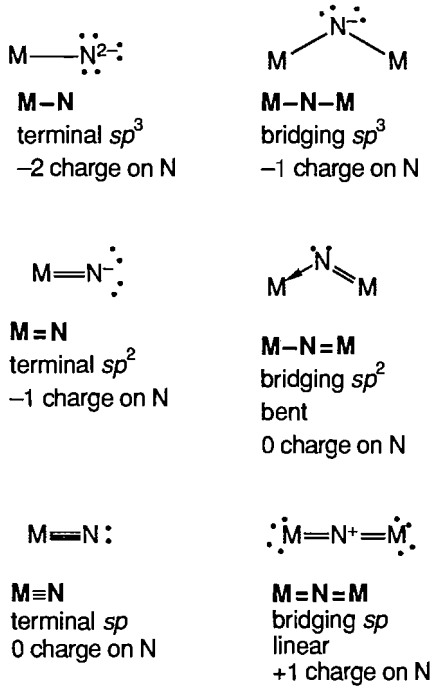

charge (Fig. 4). The polymeric anion $[Fe^{III}N_{4/2}^{3-}]_\infty$ found in Li_3FeN_2 is the only species discussed in this paper that has a bridging sp^3 nitrogen atom; this is also the only species discussed in this paper in which the transition metal is bonded to *four* nitrogen atoms rather than only two or three nitrogen atoms. A *neutral* bridging sp^3 nitrogen atom is a formal donor of zero electrons to one of the metals and a single electron donor to the other metal.

The nitrogen atoms in the ternary transition metal nitrides in which the transition metal is bonded to only two or three nitrogen atoms may either be considered as planar sp^2-hybridized or linear *sp*-hybridized, with the former situation being more common. The empty *p* orbital in an sp^2-hybridized nitrogen participates in $d\pi \rightarrow p\pi$ back bonding with a transition metal *d* orbital of suitable symmetry so that such a nitrogen atom can complete its octet by forming a transition metal M=N double bond (Fig. 5). A terminal sp^2 nitrogen atom forming one such double bond ($\sigma + \pi$) to a transition metal has two lone pairs and a formal –1 charge (Fig. 4). The σ component of the double bond formed by such a terminal sp^2 nitrogen atom considered formally as a neutral ligand makes it a net one-electron

Fig. 5. The atomic orbitals forming the σ-bonding and π-bonding (i.e., $d\pi \rightarrow p\pi$) components of the transition metal–nitrogen multiple bond in metal nitrides and related compounds.

donor to the transition metal. A bridging (μ_2) sp^2 nitrogen atom forms a double bond ($\sigma + \pi$) with one of the transition metals and a single bond (σ only) with the other transition metal leaving only one lone pair and leading to formal neutrality (Fig. 4). A *neutral* μ_2-bridging nitrogen atom thus acts as a formal one-electron donor to the transition metal to which it is doubly bonded and a formal two-electron donor to the other transition metal to which it is formally only singly bonded. Such planar nitrogen atoms (sp^2 hybridized) can be considered as halogen atoms for which the favored octet is attained by accepting two electrons from a metal *d* orbital of π symmetry into the empty *p* orbital perpendicular to the plane. The $d\pi$–$p\pi$ bond does not affect the electron count because both electrons originate from the metal.

A linear nitrogen atom (*sp* hybridized) with two empty orthogonal *p* orbitals can also be either terminal or bridging (Fig. 4). Two electron pairs from filled transition metal *d* orbitals of suitable symmetry overlap with these empty nitrogen *p* orbitals to form the π components of metal – nitrogen multiple bonds. Terminal *sp*-hybridized nitrogen atoms form M≡N triple bonds whereas bridging (μ_2) *sp*-hybridized nitrogen atoms form M=N double bonds in both directions leading to an M=N=M structural unit similar to CO_2 or allene ($H_2C{=}C{=}CH_2$). Note that the formal charge on an *sp*-hybridized nitrogen atom is +1 higher than the formal charge on a similar type of sp^2-hybridized nitrogen atom. For this reason *sp* nitrogen atoms are likely to form weaker, and thus longer, bonds to transition metals than do sp^2 nitrogen atoms. This may explain why the Fe≡N distance in the linear ion FeN_2^{4-}, which is best formulated with Fe≡N triple bonds, is longer (1.86 Å) than the Co=N distance (1.81 Å) in the likewise linear ion CoN_2^{5-}, which is best formulated with Co=N double bonds. Note also that for the purpose of calculating the metal electron configuration in metal nitride structures a *neutral* doubly bonded terminal nitrogen atom serves as a one-electron donor and a *neutral* triply bonded terminal nitrogen atom serves as a three-electron donor.

Ternary metal nitrides containing isolated mononuclear anions

A. Tetrahedral MN_4^{n-} derivatives

A variety of ternary metal nitrides with isolated tetrahedral MN_4^{n-} anions are known. These include $Li_7M^VN_4$ (M = V (17), Nb (17), Ta (17), Mn (18)), $Li_6M^{VI}N_4$ (M = Mo, W) (19), and $Ba_3M^{VI}N_4$ (M = Mo, W) (20) that contain the tetrahedral $M^VN_4^{7-}$ and $M^{VI}N_4^{6-}$ anions, which are isoelectronic and isostructural with the corresponding well-known tetraoxometallates $M^VO_4^{3-}$ and $M^{VI}O_4^{2-}$. These tetrahedral tetranitridometallates present no new interesting questions of

Can. J. Chem. Downloaded from www.nrcresearchpress.com by 80.90.12.36 on 09/08/12
For personal use only.

Fig. 6. The *d*-orbital splittings and electron occupancies for the MN_3^{6-} derivatives.

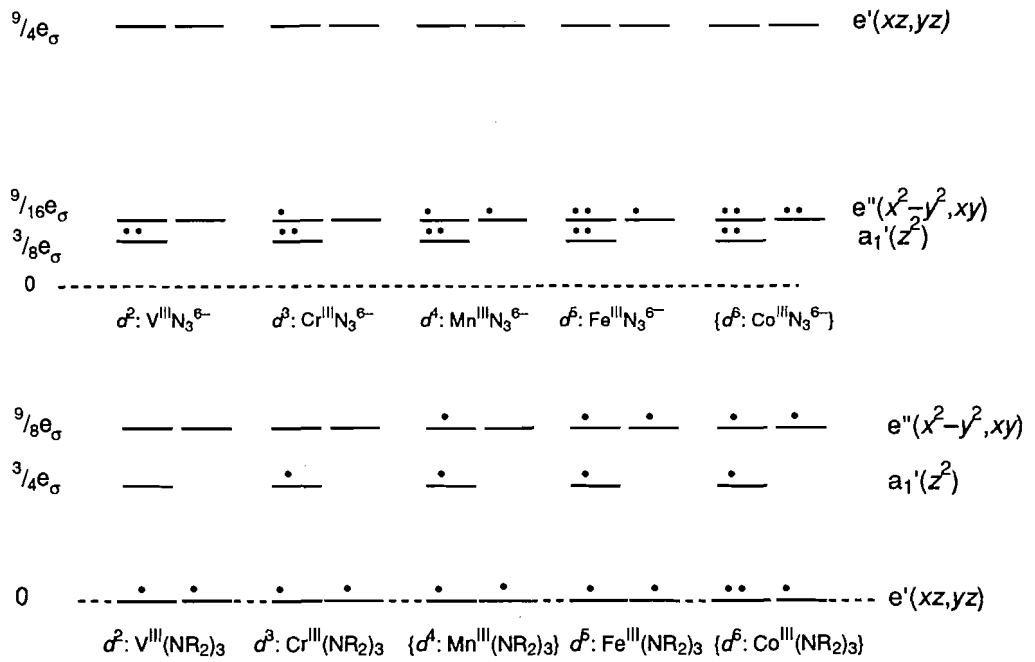

structure and bonding not found in the corresponding tetraoxometallates and thus will not be discussed further in this paper.

B. Trigonal planar MN_3^{6-} derivatives

The trigonal planar anions $M^{III}N_3^{6-}$ (M = V, Cr, Mn, Fe) are found in the compounds Ca_3VN_3 (21), Ca_3CrN_3 (22), Ca_3MnN_3 (23), Sr_3MnN_3 (24), Ba_3MnN_3 (24), Ba_3FeN_3 (25), and Ca_6FeN_5 (= $[NCa_3^{3+}]_2[FeN_3]^{6-}$) (26). The metal–nitrogen π-bonding in these anions is so strong that they can be treated as trigonal prismatic complexes as discussed above (see Fig. 2). Figure 6 shows the *d*-orbital splittings and electron occupancies in these complexes as obtained using the simple angular overlap model with the bond angles 45° above and below the σ_h symmetry plane of the trigonal prism. The general pattern of *d*-orbital splittings is the same as those arising from the extended Hückel calculations of Yee and Hughbanks (2) except for the reversal of the e′ and e″ *d* orbitals.

The orbital splittings and electron occupancies indicated in Fig. 6 suggest the following points:

VN_3^{6-}: This is predicted to be diamagnetic in accord with experimental observations on Ca_3VN_3 (21).

CrN_3^{6-}: Trigonal prismatic Cr(III) has only one unpaired electron in contrast to three unpaired electrons for the much more common octahedral Cr(III). In this connection the magnetic moment of Ca_3CrN_3 was found (22) to be 1.86 μ_B, which is close to the spin only value of $\sqrt{3}$ = 1.73 μ_B for one unpaired electron. In addition, the single electron in the e″ orbital suggests the possibility of a Jahn–Teller distortion from D_{3h} to C_{2v} symmetry (2) consistent with the observed (14) N—Cr—N bond angles in Ca_3CrN_3 of 112.6°, 112.6°, and 134.9° rather than the ideal 120° for D_{3h} symmetry.

MnN_3^{6-}: The half-filled e″ level suggests the absence of Jahn–Teller distortion and two unpaired electrons in MnN_3^{6-}. Ideal D_{3h} symmetry with N—Mn—N angles of 120° is found (24) in Sr_3MnN_3 and Ba_3MnN_3 but not in Ca_3MnN_3 with N—Mn—N angles (23) of 114.7°, 114.7°, and 130.6°.

FeN_3^{6-}: The single hole in the e″ level suggests the possibility of a Jahn–Teller distortion, which is not found experimentally in either Ba_3FeN_3 (25) or $[Ca_3N]_2[FeN_3]$ (26). Information on the magnetic properties of any of the FeN_3^{6-} derivatives does not seem to be available.

CoN_3^{6-}: Ternary metal nitrides containing the CoN_3^{6-} ion have not yet been prepared. The CoN_3^{6-} ion is predicted to be diamagnetic with ideal D_{3h} symmetry and should be favored because of the closed-shell d^6 configuration of the cobalt leading to the favored 18-electron rare gas configuration by the following electron-counting scheme:

Neutral Co atom:	9 electrons
3 Neutral nitrogen ligands: 3 × 1 =	3 electrons
–6 Charge on anion:	6 electrons
Total electronic configuration of cobalt:	*18 electrons*

However, the synthesis of CoN_3^{6-} derivatives may be complicated by the reducing conditions of the high-temperature reactions used to prepare ternary metal nitrides so that Co(I) derivatives, such as $LiSr_2CoN_2$, are formed instead of Co(III) derivatives.

These properties of the trinitridometallates, $M^{III}N_3^{6-}$, relate to the nitride anion, N^{3-}, functioning as a strong field ligand. Exhaustive silylation of the $M^{III}N_3^{6-}$ anions with Me_3SiCl can *formally* lead to the known trigonal planar $[(Me_3Si)_2N]_3M^{III}$ according to the following equation[2]:

[2] In practice, the $[(Me_3Si)_2N]_3M$ derivatives are not prepared by this method but instead by reactions of $(Me_3Si)_2NM$ (M = Li, Na) with transition metal halides.

Can. J. Chem. Downloaded from www.nrcresearchpress.com by 80.90.12.36 on 09/08/12
For personal use only.

Table 2. Metal–nitrogen bond lengths in analogous $[(Me_3Si)_2N]_3M^{III}$ and MN_3^{6-} derivatives

	M = V	M = Cr	M = Fe
M—N length in $[(Me_3Si)_2N]_3M^{III}$, Å	1.910(5)	1.903(6)	1.917(4)
M=N length in $M^{III}N_3^{6-}$, Å	1.81–1.83	1.766(7)	1.770(15)

[1] $MN_3^{6-} + 6\,Me_3SiCl \rightarrow [(Me_3Si)_2N]_3M + 6\,Cl^-$

The $(Me_3Si)_2N^-$ ligands in these $[(Me_3Si)_2N]_3M^{III}$ derivatives (27) function as weak-field ligands forming essentially M—N single bonds in contrast to the N^{3-} ligands in MN_3^{6-} derivatives, which form essentially M=N double bonds. This difference in bond order can be demonstrated by consistently longer metal–nitrogen bond lengths in $[(Me_3Si)_2N]_3M^{III}$ than in the corresponding $M^{III}N_3^{6-}$ derivative (Table 2). The low-field nature of the $(Me_3Si)_2N^-$ ligand leading to high spin complexes is supported by the observed magnetic moments (27) of 3.72 and 5.94 μ_B for the Cr(III) and Fe(III) derivatives, respectively, corresponding to three and five unpaired electrons, respectively.

C. Linear MN_2^{n-} derivatives

1. CoN_2^{5-}

The cobalt–nitrogen bonds in the linear $Co^IN_2^{5-}$ ion (28) in $LiSr_2CoN_2$ can be regarded as Co=N double bonds. Using the bent bond model, the cobalt atom can either be considered as tetrahedral, using sp^3 hybrid orbitals if the two Co—N π-bonds are perpendicular as in allene, or square planar, using $sp^2d(x^2-y^2)$ hybrid orbitals if the two Co—N π-bonds are collinear. The cobalt atom has the typical 16- electron configuration for a square planar d^8 atom determined as follows:

Neutral cobalt atom:	9 electrons
2 Nitrogen ligands: 2 × 1 =	2 electrons
−5 Charge on ion:	5 electrons
Total cobalt valence electrons:	*16 electrons*

This electron counting suggests that the π-bonds from the central cobalt atom to the two nitrogen atoms in $Co^IN_2^{5-}$ are collinear rather than perpendicular, in accord with square planar cobalt hybridization.

(2) FeN_2^{4-}

The linear $Fe^{II}N_2^{4-}$ ion in Li_4FeN_2 (29) and Sr_2FeN_2 (30) has two fewer electrons than the linear $Co^IN_2^{5-}$ ion in $LiSr_2CoN_2$ discussed above. This difference in apparent electron count can be rationalized by considering the iron–nitrogen bonds in $Fe^{II}N_2^{4-}$ to be Fe≡N triple bonds. A *neutral* triply bonded nitrogen atom, (Fig. 4) can be considered to be a three-electron donor in contrast to a neutral doubly bonded nitrogen atom, which, as noted above, functions as a one-electron donor. Using the bent bond model (Fig. 7) the iron coordination can be considered to be trigonal prismatic. The iron atom in FeN_2^{4-} then has the favored 18-electron noble gas configuration by the following electron-counting scheme:

Neutral iron atom:	8 electrons
2 Neutral triply bonded N atoms: 2 × 3 =	6 electrons
−4 Charge on anion:	4 electrons
Total iron valence electrons:	*18 electrons*

The iron–nitrogen triple bonds in FeN_2^{4-} have the same components ($\sigma + 2\perp\pi$) and use the same metal orbitals as the iron–ring triple bonds in ferrocene.

Polynuclear nitridoferrates

A number of polynuclear nitridoferrates (for a brief summary of the types of nitridoferrates see ref. 31) are known in which pairs of iron atoms within bonding distance (typically ~2.4 Å) are bridged by nitride nitrogen atoms. These include the dinuclear (30) $[Fe^{II}_2(\mu\text{-}N)_2N_2]^{8-}$ in Ca_2FeN_2, polymeric (32) $\{[Fe^{II}_2(\mu\text{-}N)_2(\mu\text{-}N)_{2/2}]^{5-}\}_\infty$ in $Sr_2LiFe_2N_3$ and $Ba_2LiFe_2N_3$, and polymeric (33) $[Fe^{III}N_{4/2}^{3-}]_\infty$ in Li_3FeN_2. The iron(II) derivatives (Fig. 8) exhibit distorted trigonal planar FeN_3 coordination whereas the iron(III) derivative (Fig. 9) exhibits tetrahedral FeN_4 coordination. The μ_2-bridging nitride nitrogens, if considered as neutral ligands, can be considered as donors of one electron to one iron atom and two electrons to the second iron atom for a total of three electrons. The direction of the formal one-electron donation from neutral nitrogen to an iron atom is indicated in Fig. 8 by a double bond with the second component of the double bond representing Fe→N $d\pi \rightarrow p\pi^*$ back-donation, which does not affect the formal electron count as noted above. The direction of the formal two-electron donation from neutral nitrogen to an iron atom is indicated in Fig. 8 by an arrow corresponding to donation of a nitrogen lone pair.

A. Iron(II) derivatives (Fig. 8)

The iron atoms in both types of iron(II) derivatives, namely the dinuclear (30) $[Fe^{II}_2(\mu\text{-}N)_2N_2]^{8-}$ anion in Ca_2FeN_2 and the polymeric (32) $\{[Fe^{II}_2(\mu\text{-}N)_2(\mu\text{-}N)_{2/2}]^{5-}\}_\infty$ anion in $Sr_2LiFe_2N_3$ and $Ba_2LiFe_2N_3$, can be considered to have the favored 18-electron configuration if iron–iron bonding is considered. Such iron–iron bonding can be interpreted to be double bonding within an Fe_2N_2 quadrilateral in accord with the short intraquadrilateral iron–iron distances of ~2.4 Å and single bonding between Fe_2N_2 quadrilaterals in the polymeric $\{[Fe^{II}_2(\mu\text{-}N)_2(\mu\text{-}N)_{2/2}]^{5-}\}_\infty$ in accord with the longer interquadrilateral iron–iron distances of 2.6 Å (Fig. 8). The polymeric $\{[Fe^{II}_2(\mu\text{-}N)_2(\mu\text{-}N)_{2/2}]^{5-}\}_\infty$ thus contains infinite chains of alternating single and double iron–iron bonds and might be expected to exhibit one-dimensional conductivity despite the 18-electron configuration of the iron atoms. The magnetic properties of the iron(II) nitride derivatives have not yet been reported.

Can. J. Chem. Downloaded from www.nrcresearchpress.com by 80.90.12.36 on 09/08/12
For personal use only.

Fig. 7. The relationship of trigonal prismatic bent bonds to the metal–nitrogen triple bonding in $Fe^{II}N_2^{4-}$.

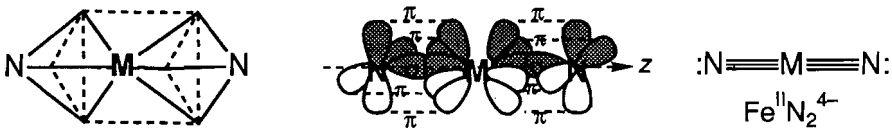

Fig. 8. A schematic representation of the structures of the nitridoferrates(II) showing the distorted trigonal FeN_3 coordination, the distribution of the nitrogen valence electrons, and the iron-iron bonding. The iron–iron distances are labeled in Å.

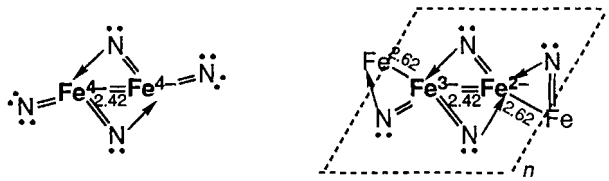

Fig. 9. A portion of the chain of iron atoms in the $[Fe^{III}N_{4/2}]^{3-}$ anion of Li_3FeN_2 showing the tetrahedral FeN_4 unit and two Fe=Fe double bonds from each iron atom. The iron–iron distances are labeled in Å.

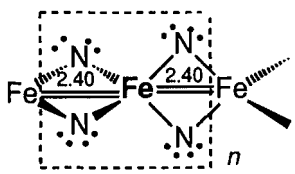

The following electron-counting scheme gives all of the iron atoms in the dinuclear $[Fe^{II}_2(\mu\text{-}N)_2N_2]^{8-}$ anion in Ca_2FeN_2 the normally favored 18-electron configuration:

Neutral iron atom:	8 electrons
Bridging nitride ligand: $^2/_2 \times 3 =$	3 electrons
Terminal nitride ligand: $1 \times 1 =$	1 electrons
–4 Charge on anion per iron atom:	4 electrons
Fe=Fe double bond:	2 electrons
Total iron valence electrons:	*18 electrons*

In this model, each iron atom can be regarded as forming four σ-bonds in an $FeN_3(Fe)$ unit with $sp^2(x,y)d(x^2-y^2)$ distorted square planar hybridization leaving a $p(z)$ orbital for the π component of the Fe=Fe double bond. A pair of d orbitals, $d^2(xz, yz)$ also remains to form the indicated π components of the Fe=N double bonds to the nitride ligands.

A similar-electron counting scheme can be used for the polynuclear (32) $[Fe^{II}_2(\mu\text{-}N)_2(\mu\text{-}N)_{2/2}]^{5-}$ anion in $Sr_2LiFe_2N_3$ and $Ba_2LiFe_2N_3$ as follows (labeling the iron atoms as in Fig. 8):

	"Left" Fe	"Right" Fe
Neutral iron atom:	8 electrons	8 electrons
Intraunit bridging N ligands: $^2/_2 \times 3 =$	3 electrons	3 electrons
Intraunit bridging N ligands:	1 electrons	2 electrons
Negative charge:	3 electrons	2 electrons
Intraquadrilateral Fe=Fe double bond:	2 electrons	2 electrons
Interquadrilateral Fe—Fe single bond:	1 electron	1 electron
Total iron valence electrons:	*18 electrons*	*18 electrons*

In this model each iron atom can be regarded as forming five approximately coplanar σ-bonds in an $FeN_3(Fe_2)$ unit with $sp^2(x,y)d^2(x^2-y^2, xy)$ distorted pentagonal planar hybridization leaving a $p(z)$ orbital for the π component of the Fe=Fe double bond. A pair of d orbitals, $d^2(xz, yz)$, also remains to form the indicated π components of the Fe=N double bonds to the nitride ligands.

B. The iron(III) derivative Li_3FeN_2

The structure of Li_3FeN_2 has been shown to contain infinite chains of $[Fe^{III}N_{4/2}^{3-}]_\infty$ tetrahedra with each iron atom within a short bonding distance to the two adjacent iron atoms in the chain (Fig. 9) (33). The iron–iron bond distances of 2.40 Å are similar to those found in the iron(II) derivatives (30, 32) $[Fe^{II}_2(\mu\text{-}N)_2N_2]^{8-}$ and $\{[Fe^{II}_2(\mu\text{-}N)_2(\mu\text{-}N)_{2/2}]^{5-}\}_\infty$ suggestive of iron-iron double bonds to the two adjacent iron atoms. The magnetic moment of Li_3FeN_2 is 1.71 μ_B, suggesting a single unpaired electron corresponding to low-spin iron(III). The iron atoms in the $[Fe^{III}N_{4/2}^{3-}]_\infty$ anion have 17-electron configurations by the following electron-counting scheme, considering the iron–iron bonds as Fe=Fe double bonds:

Neutral iron atom:	8 electrons
Bridging nitride ligand: $^4/_2 \times 1 =$	2 electrons
Two Fe=Fe double bond: $2 \times 2 =$	4 electrons
–3 Charge per iron atom:	3 electrons
Total iron valence electrons	*17 electrons*

This 17-electron configuration in $[Fe^{III}N_{4/2}^{3-}]_\infty$ is reasonable for a low-spin iron(III) complex (e.g., $Fe^{III}(CN)_6^{3-}$). In addition, note the following about this formulation of $[Fe^{III}N_{4/2}^{3-}]_\infty$ in Li_3FeN_2:

1. This is the only ternary transition metal nitride discussed in detail in this paper in which the nitride nitrogens are formu-

Can. J. Chem. Downloaded from www.nrcresearchpress.com by 80.90.12.36 on 09/08/12
For personal use only.

Can. J. Chem. Downloaded from www.nrcresearchpress.com by 80.90.12.36 on 09/08/12
For personal use only.

lated with tetrahedral sp^3 hybridization with two lone pairs and no multiple bonding rather than with either planar sp^2 hybridization, one lone pair and one π-bond, or linear sp hybridization, no lone pairs and two π-bonds (Fig. 4). However, $[Fe^{III}N_{4/2}^{3-}]_\infty$ in Li_3FeN_2 is also the only species discussed in this paper in which each transition metal is bonded to four nitrogen atoms rather than to only two or three nitrogen atoms. The metal atoms in tetrahedral MN_4 units are much less susceptible to forming additional π-bonds to the nitrogen atoms than the metal atoms in either trigonal MN_3 units or linear MN_2 units so that tetrahedral MN_4 units are more likely to contain sp^3 tetrahedral nitrogens with no π-bonding capability than are sp^2 planar nitrogens or sp linear nitrogens with π-bonding capabilities. Note also that the Fe—N bond lengths of 1.96 Å in Li_3FeN_2 are the longest M—N bond lengths in any of the ternary metal nitrides discussed in this paper (Table 1) in accord with the absence of Fe—N π-bonding in Li_3FeN_2.

2. In this model, each iron atom can be regarded as forming six σ-bonds with $sp^3d^2(z^2,xy)$ octahedral hybridization in an $FeN_4(Fe_2)$ unit, leaving a pair of d orbitals, $d^2(xz,yz)$, for the indicated π components of the Fe═Fe double bonds. The total set of eight orbitals involved in the $6\sigma + 2\pi$ bonds, namely $sp^3d^4(z^2,xy,xz,yz)$, corresponds to a D_{2d} dodecahedron (bisdisphenoid) in which one of the interlocking disphenoids (distorted tetrahedra) is the FeN_4 iron–nitrogen bond network and the other disphenoid is the $Fe(═Fe)_2$ iron–iron double bond network using the bent bond model.

Infinite chains in nitridonickelates

A number of ternary nickel nitrides are known that are constructed from infinite $[Ni^{I}N_{2/2}^{2-}]_\infty$ chains containing formally nickel(I). Such chains are of two types (Fig. 10): (*a*) linear $[Ni^{I}N_{2/2}^{2-}]_\infty$ chains, such as those found in CaNiN (34) and $Li_3Sr_3Ni_4N_4$ (35), in which all of the Ni—N—Ni angles are close to 180°; (*b*) bent $[Ni^{I}N_{2/2}^{2-}]_\infty$ chains, such as those found in BaNiN (36) and $Ba_8Ni_6N_7$ (37), in which every third nitrogen atom has a kink of about 90°, leading to helical structures. In the compounds with linear $[Ni^{I}N_{2/2}^{2-}]_\infty$ chains all of the Ni...Ni distances are too long for metal–metal bonding (e.g., 3.58 Å in CaNiN) whereas in the compounds with kinked $[Ni^{I}N_{2/2}^{2-}]_\infty$ chains some of the Ni—Ni distances are close enough for bonding, e.g., 2.42 Å for BaNiN and 2.57 Å for $Ba_8Ni_6N_7$. In $Ba_8Ni_6N_7$ the nickel atoms are of three different types present in equal quantities: Ni(1) forms one bond with Ni(3) of length 2.57 Å whereas Ni(2) is not within bonding distance of any other nickel atom.

Simple electron counting in these nitridonickelates is consistent with these observations. Each nickel atom forms linear N═Ni═N units that, by using the bent bond approach outlined above, can be based on either square planar hybridization as in the discrete $Co^{I}N_2^{5-}$ ion discussed above or tetrahedral hybridization. Either type of hybridization might appear to be reasonable since the observed nickel(I) formal oxidation state in $[Ni^{I}N_{2/2}^{2-}]_\infty$ is intermediate between nickel(0), which forms tetrahedral complexes such as $Ni(CO)_4$, and nickel(II), which most often forms square planar complexes. If the $[Ni^{I}N_{2/2}^{2-}]_\infty$ chain is linear, then all five valence electrons of each nitrogen atom are bonded to nickel atoms so that a neutral nitrogen atom of this type can be regarded as a donor of two electrons to one nickel atom and three electrons to the other nickel atom,

Fig. 10. Linear and bent $[Ni^{I}N_{2/2}^{2-}]_\infty$ chains in ternary nickel nitrides.

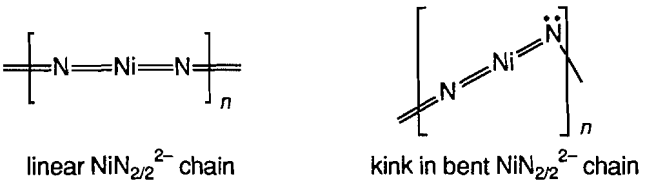

linear $NiN_{2/2}^{2-}$ chain kink in bent $NiN_{2/2}^{2-}$ chain

i.e., a *neutral* $N_{2/2}$ unit of this type is a five-electron donor. This leads to the following electron-counting scheme for a $Ni^{I}N_{2/2}^{2-}$ unit in a *linear* $[Ni^{I}N_{2/2}^{2-}]_\infty$ chain:

Neutral nickel atom:	10 electrons
$^2/_2$ Linear bridging nitrogen atoms: $^2/_2 \times 5 =$	5 electrons
−2 Charge:	2 electrons
Total nickel valence electrons	*17 electrons*

The 17 valence electrons observed for this formal Ni(I) derivative are intermediate between the 18 valence electrons found in tetrahedral Ni(0) and the 16 valence electrons found in square planar Ni(II).

A similar electron-counting scheme can be derived for an $Ni^{I}N_{2/2}^{2-}$ unit in which one of the two nitrogen atoms has a Ni—N—Ni bond angle of ~90° rather than ~180° (i.e., the "kink" nitrogen atom). The "kink" nitrogen atom has a lone pair and thus can use only three of its five valence electrons for bonding to nickel, similar to the bridging nitrogen atoms in the binuclear and polynuclear ternary iron nitrides discussed above. This leads to the following electron-counting scheme for a $Ni^{I}N_{2/2}^{2-}$ unit located at a kink in the chain:

Neutral nickel atom:	10 electrons
$^1/_2$ Linear nitrogen atom: $^1/_2 \times 5 =$	$2^1/_2$ electrons
$^1/_2$ Kink nitrogen atom: $^1/_2 \times 3 =$	$1^1/_2$ electrons
−2 Charge:	2 electrons
Total nickel valence electrons:	*17 electrons*

Thus a nickel atom at a kink in a bent $[Ni^{I}N_{2/2}^{2-}]_\infty$ chain has an effective 16-electron configuration typical for a square planar nickel atom, so that the kink has the effect of averaging out 15- and 17-electron configurations of the two Ni(I) atoms flanking the kink, to give each of these nickel atoms effectively the favored 16-electron configuration for a square planar nickel atom. The Ni—Ni bonded distance between these nickel atoms then represents the typical bonding interaction between pairs of square planar 16-electron metal atoms. This electron-counting scheme for BaNiN is consistent with the observed 1.73 μ_B magnetic moment for each *trimeric* Ni_3N_3 unit in BaNiN, in which one-third of the nitrogen atoms are kink nitrogen atoms so that two of the three nickel atoms are effectively diamagnetic, leaving one unpaired spin for the Ni(I) atom in each Ni_3N_3 unit not bonded to a kink nitrogen atom.

References

1. N.E. Brese and M. O'Keeffe. Struct. Bonding (Berlin), **79**, 307 (1992).

2. K.A. Yee and T. Hughbanks. Inorg. Chem. **31**, 1921 (1992).
3. M.T. Green and T. Hughbanks. Inorg. Chem. **32**, 5611 (1993).
4. R.B. King. Inorg. Chem. **28**, 3048 (1989).
5. R.B. King. Inorg. Chem. **29**, 2164 (1990).
6. R.P. Messmer. Chem. Phys. Lett. **132**, 161 (1986).
7. C.H. Patterson and R.P. Messmer. J. Am. Chem. Soc. **112**, 4138 (1990).
8. R.P. Messmer. J. Am. Chem. Soc. **113**, 433 (1991).
9. P.A. Schultz and R.P. Messmer. J. Am. Chem. Soc. **115**, 10925 (1993).
10. P.A. Schultz and R.P. Messmer. J. Am. Chem. Soc. **115**, 10938 (1993).
11. P.A. Schultz and R.P. Messmer. J. Am. Chem. Soc. **115**, 10943 (1993).
12. W.N. Lipscomb. Boron hydrides. Benjamin, New York. 1963. pp. 34–35; *In* Boron hydride chemistry. *Edited by* E.L. Muetterties. Academic Press, New York. 1975. pp. 39–78.
13. K.F. Purcell and J.C. Kotz. An introduction to inorganic chemistry. Saunders, Philadelphia. 1980. pp 314 ff.
14. J.K. Burdett. Molecular shapes. Wiley, New York. 1980. Chap. 2.
15. F.A. Cotton and G. Wilkinson. Advanced inorganic chemistry. 5th ed Wiley–Interscience, New York. 1988. Sect. 2–1.
16. R.S. Nyholm. Proc. Chem. Soc. 273 (1961).
17. R. Juza, W. Gieren, and J. Haug. Z. Anorg. Allgem. Chem. **300**, 61 (1959).
18. R. Juza, E. Anschutz, and H. Puff. Angew. Chem. **71**, 161 (1959).
19. A. Gudat, S. Haag, R. Kniep, and A. Rabenau. Z. Naturforsch. B: Chem. Sci. **45**, 111 (1990).
20. A. Gudat, P. Höhn, R. Kniep, and A. Rabenau. Z. Naturforsch. B: Chem. Sci. **46**, 566 (1991).
21. D.A. Vennos and F.J. DiSalvo. J. Solid State Chem. **98**, 318 (1992).
22. D.A. Vennos, M.E. Badding, and F.J. DiSalvo. Inorg. Chem. **29**, 4059 (1990).
23. A. Tennstedt, C. Röhr, and R. Kniep. Z. Naturforsch. B: Chem. Sci. **48**, 1831 (1993).
24. A. Tennstedt, C. Röhr, and R. Kniep. Z. Naturforsch. B: Chem. Sci. **48**, 794 (1993).
25. N. Jansen, H. Spiering, P. Gütlich, D. Stahl, R. Kniep, V. Eyert, J. Kübler, and P.C. Schmidt. Angew. Chem. Int. Ed. Engl. **31**, 1624 (1992).
26. G. Cordier, P. Höhn, R. Kniep, and A. Rabenau. Z. Anorg. Allgem. Chem. **591**, 58 (1990).
27. P.G. Eller, D.C. Bradley, M.B. Hursthouse, and D.W. Meek. Coord. Chem. Rev. **24**, 1 (1977).
28. P. Höhn and R. Kniep. Z. Naturforsch. B: Chem. Sci. **47**, 434 (1992).
29. A. Gudat, R. Kniep, and A. Rabenau. Angew. Chem. Int. Ed. Engl. **30**, 199 (1991).
30. P. Höhn and R. Kniep. Z. Naturforsch. B: Chem. Sci. **47**, 477 (1992).
31. A. Gudat, S. Haag, P. Höhn, R. Kniep, W. Milius, and A. Rabenau. J. Alloys Compd. **177**, L17 (1991).
32. P. Höhn, S. Haag, W. Milius, and R. Kniep. Angew. Chem. Int. Ed., **30**, 831 (1991).
33. A. Gudat, R. Kniep, A. Rabenau, W. Bronger, and U. Ruschewitz. J. Less-Common Met. **161**, 31 (1990).
34. M.Y. Chern and F.J. DiSalvo. J. Solid State Chem. **88**, 459 (1990).
35. A. Gudat, R. Kniep, and A. Rabenau. Z. Anorg. Allgem. Chem. **597**, 61 (1991).
36. A. Gudat, S. Haag, R. Kniep, and A. Rabenau. J. Less-Common Met. **159**, L29 (1990).
37. A. Gudat, W. Milius, S. Haag, R. Kniep, and A. Rabenau. J. Less-Common Met. **168**, 305 (1991).

Can. J. Chem. Downloaded from www.nrcresearchpress.com by 80.90.12.36 on 09/08/12
For personal use only.

Effect of a hydrophobic amino acid at position ($i - 1$) on the stability of β-turns in hydrophilic pentapeptides as studied by NMR and molecular mechanics

Xiaohong Liu, Serafin Fraga, Albin Otter, Paul G. Scott, and George Kotovych

Abstract: A detailed NMR study of the peptide NAc-FDEKA-NH_2 in aqueous and in CD_3OH/H_2O solutions as well as the *N*-acetylpentapeptide amides YDEKA, VDEKA, GDEKA, and the protected tetrapeptide NAc-DEKA-NH_2 in methanolic solutions indicates the importance of the first amino acid (at $i - 1$) on stabilizing the type I β-turn. The data illustrate the hydrophobic stabilization of this turn, which is present in FDEKA, YDEKA, and VDEKA. For GDEKA and DEKA, the NMR data indicate that this turn is not present. Molecular mechanics calculations support this conclusion and indicate that for FDEKA and GDEKA the type I β-turn is distorted in both the vacuum and the solvated structures. For the solvated structures, the $C_\alpha(i)$–$C_\alpha(i + 3)$ distance is 4.87 Å for FDEKA and 6.00 Å for GDEKA, which are to be compared with the value of 4.64 Å for an ideal type I β-turn, i.e., the distortion is far greater in GDEKA than in FDEKA. The calculations can be interpreted to indicate the presence of two major conformations in solution.

Key words: β-turns, FDEKA, pentapeptide.

Résumé : Une étude détaillée par RMN du peptide NAc-FDEKA-NH_2 en solution aqueuse et en solution dans le CD_3OH/H_2O et des *N*-acétylpentapeptide amides YDEKA, VDEKA, GDEKA et du tétrapeptide protégé en solution dans le méthanol met en évidence l'importance du premier acide aminé (à $i - 1$) dans la stabilisation de l'hélice du type I-β. Les données illustrent la stabilisation hydrophobique de cette hélice qui est présente dans les peptides FDEKA, YDEKA et VDEKA. Les donnéees de la RMN relatives aux peptides GDEKA et DEKA ne révèlent pas la présence de cette hélice. Cette conclusion est confirmée par les calculs de mécanique moléculaire qui révèlent que cette hélice de type I-β est déformée dans les structures sous vide et dans les structures solvatées des peptides FDEKA et GDEKA. Dans le cas des structures solvatées, la distance $C_\alpha(i)$–$C_\alpha(i + 3)$ est de 4,87 Å pour le peptide FDEKA et de 6,00 Å pour le peptide GDEKA. Ces données comparées à la valeur de 4,64 Å pour une hélice idéale de type I-β montrent que la distorsion est nettement plus accentuée dans le peptide GDEKA que dans le FDEKA. On peut interpréter ces calculs comme étant une indication de la présence de deux conformations principales en solution.

Mots clés : hélices du type β, FDEKA, pentapeptide.

[Traduit par la rédaction]

Introduction

In the process of studying the α-1 chain N-telopeptide of type II collagen with sequence pEMAGGFDEKAGGAQLGVMQ-NH_2 using two-dimensional NMR techniques, a fused βγ-turn between F^6 and A^{10} was observed (1). This turn was stabilized by three hydrogen bonds and a salt bridge between the side-chain end groups of E^8 and K^9. The first five amino acids were extended with a much higher degree of conformational freedom whereas the two Gly residues following the βγ-turn were found to be highly flexible, leaving the spatial position of the second half of the molecule relative to the fused βγ-turn undefined. In view of our continuing interest in the role of salt bridges and hydrogen bonding in the stabilization of β-turns (2), we decided to further investigate the nature of this fused βγ-turn by carrying out a detailed NMR study of NAc-Phe-Asp-Glu-Lys-Ala-NH_2 (NAc-FDEKA-NH_2) in aqueous and in CD_3OH/H_2O (60/40 v/v %) solutions. In addition, the objective was to study the effect of varying the first amino acid ($i - 1$) on the nature of this βγ-turn. Consequently, the protected pentapeptides YDEKA, VDEKA, and GDEKA were synthesized and studied, as well as the protected tetrapeptide

Received August 2, 1994.

This paper is dedicated to Professor William A.G. Graham on the occasion of his 65th birthday.

X. Liu, S. Fraga, A. Otter, and G. Kotovych.[1] Department of Chemistry, University of Alberta, Edmonton, AB T6G 2G2, Canada.
P.G. Scott. Department of Oral Biology, University of Alberta, Edmonton, AB T6G 2G2, Canada.

[1] Author to whom correspondence may be addressed. Telephone: (403) 492-5477. FAX: (403) 492-8231.

Can. J. Chem. Downloaded from www.nrcresearchpress.com by 80.90.12.36 on 09/08/12
For personal use only.

Can. J. Chem. Downloaded from www.nrcresearchpress.com by 80.90.12.36 on 09/08/12
For personal use only.

DEKA. This study is especially important because of the current ongoing interest in the factors favoring formation and stabilization of secondary structures at an early stage in the folding process, as discussed in recent reviews (3, 4).

There has been much interest in the folding of short linear peptides. A pentapeptide Tyr-Pro-Gly-Asp-Val has been shown, by using NMR data (5), to form a high population (about 50%) of type II β-turn in water at 278 K. The four residues involved in the turn begin with Tyr, and proline is at the $i + 1$ position of the β-turn. Nanosecond time scale folding dynamics of this pentapeptide in water were also carried out (6) over a period of 2 ns, and the calculations are in partial agreement with the experimental data. Some transient conformations were predicted that were not necessarily the same as the ensemble-averaged, equilibrium structures observed in the experiments. We have studied side-chain salt-bridge stabilization of type I β-turns by analyzing the NOE data of the following 13 hydrophilic protected tetrapeptides: DEKS, NEKS, EEKS, DDKS, DQKS, NQKS, DERS, NERS, EERS, DDRS, NDRS, DQRS, and DKES (2). In addition, based on the statistical predictions of Wilmot and Thornton (7), the peptides NPDM, NSDM, and NDDS were also studied. The results indicated that only DEKS, DERS, and NEKS exhibited a type I β-turn. These results could be reconciled by classifying β-turns into two classes, namely, those that are intrinsically stable because of local steric interactions and hydrogen bonding, and those that depend on long-range interactions (2). Molecular mechanics calculations by Thornton and Fraga on DEKS (8) and DERS (9) confirmed that the type I β-turn is stabilized by a salt bridge between the side chains of E and K and E and R, respectively.

The present study on the protected pentapeptides focuses on hydrophobic stabilization of β-turns arising from the amino acid at the $(i - 1)$ position of the turn. Molecular mechanics calculations are applied in conjunction with the nuclear Overhauser effect data to further study the factors that stabilize this β-turn.

Materials and methods

Materials and sample preparation

The pentapeptides FDEKA, YDEKA, GDEKA, and the tetrapeptide DEKA were synthesized as the *N*-acetyl amides. They were synthesized on an LKB Biolynx 4175 solid-phase peptide synthesizer using 9-fluorenyl-methoxycarbonyl/amino acid derivatives (Pharmacia (Canada) Ltd., Baie d'Urfe, Quebec). Protected VDEKA was from the Alberta Peptide Institute, University of Alberta. All peptides were purified by reversed-phase high-performance liquid chromatography on a Vydac TP218 column (The Separations Group, Hesperia, California). The peptides were judged to be pure on the basis of amino acid analysis and the NMR spectra.

The NMR samples were prepared by dissolving the solid peptide in 280 μL of deionized H_2O. The pH was then adjusted by adding small aliquots of diluted NaOH or HCl, followed by adding the rest of the solvent, namely 420 μL of CD_3OH (from Merck, Sharpe and Dohme) to make the solvent a 60/40 (v/v) CD_3OH/H_2O mixture. Before the NMR experiments, the samples were degassed by bubbling with argon. In addition, FDEKA was studied in 85% H_2O, 15% D_2O solutions at both pH 3.4 and 5.5. For FDEKA the CD_3OH/H_2O solutions were also prepared at both of these pH values. The other peptides, namely YDEKA, VDEKA, GDEKA, and DEKA, were prepared at pH values between 5.1 and 5.7 and were studied in 60/40 CD_3OH/H_2O solutions. The sample concentrations ranged from 5 to 7 mM. The exact concentrations and pH values are presented in Table 1.

NMR spectroscopy

All NMR experiments were carried out on the Varian UNITY 500 spectrometer using a proton-selective 5 mm probe or a triple resonance probe capable of pulsed field gradients. The 90° pulse length was checked at the beginning of every NMR session and the temperature was always controlled to ±0.1°C. For data collection and processing, VNMR software (versions 3.1 and 3.2) was used on SUN Sparc 4/330 and Sparc 4/470 workstations, respectively. Two-dimensional (2D) spectra were acquired nonspinning whereas for one-dimensional experiments the spinner was turned on. For the mixed solvent studies, all chemical shifts were measured relative to the undeuterated fraction of the methyl group of CD_3OH at 3.30 ppm. For FDEKA in H_2O solutions, the chemical shifts are reported in ppm relative to the H_2O signal at 4.80 ppm.

The temperature coefficients for the NH proton chemical shifts were determined from one-dimensional spectra. For example, in the case of GDEKA, experiments were carried out at five temperatures (0, 5, 10, 15, 20°C). All the NH shifts exhibit a linear dependence on temperature. In the case of YDEKA, six temperatures were recorded and analyzed. For FDEKA, shifts were measured at three temperatures as the data were in agreement with the YDEKA data, as expected.

The two-dimensional NMR experiments (10) were carried out in the hypercomplex, phase-sensitive mode (States–Haberkorn–Ruben method) (11) following procedures described previously (1). The decoupler and transmitter offsets were always set equal, a sweep width of 5000 Hz was used in both dimensions, and typically 4K data points in t_2 and 300 or 512 experiments were acquired in t_1. The HOHAHA (TOCSY) experiments (12) were carried out using the basic pulse sequence proposed by Bax and Davis (13) using a 70 ms MLEV-17 spin-lock. The nuclear Overhauser enhancement spectroscopy (NOESY) (14, 15) was carried out with the 90°–t_1–90°–mix–90°–FID pulse sequence with typical mixing times being 400 ms. Solvent suppression was achieved by presaturation during a 1.5 s relaxation delay. For TOCSY and NOESY experiments, the compensation for the first-point distortion caused by analog filters (16) was achieved by reducing the first point of each FID and each $t1$-interferogram by empirically determined values. For data processing, a Gaussian weighting function or a shifted (90°) sine-bell was used in both dimensions.

Molecular mechanics calculations

The calculations for the pentapeptides FDEKA and GDEKA were performed on an IBM RISC System/6000 Powerstation, using the software package maPSI[2]. (Complete details of the main component of this package are given in the work of Coghlan and Fraga (17) and additional information

[2] Software package maPSI. Protein Software Inc., Box 60499, University of Alberta Postal Outlet, Edmonton, AB T6G 2S7, Canada.

Can. J. Chem. Downloaded from www.nrcresearchpress.com by 80.90.12.36 on 09/08/12
For personal use only.

Table 1. ^{1}H chemical shifts, coupling constants, and NH temperature coefficients[a] of the peptides studied.

(*a*) *N*-Acetyl-FDEKA-NH_2 in aqueous solution at pH 3.4.[b]

	NH	H_α[c]	H_β[c]	H_γ[c]	Other H	$J_{NH-\alpha}$	NH temp. coeff.
NAc		1.80					
F	8.21	4.35	2.91,2.84	—	δ:7.09	6.4	7.7
					ε:7.13		
					ξ:7.18		
D	8.35	4.41	2.66,2.48	—	—	7.5	7.5
E	8.07	4.08	1.93,1.80	2.26,2.26	—	6.7	6.0
K	8.17	4.10	1.65,1.65	1.26,1.26	δ:1.50,1.50	6.7	6.7
					ε:2.84,2.84		
A	8.11	4.08	1.21	—	—	5.8	7.1
NH_2	7.45						6.4
	6.93						5.7

(*b*) *N*-Acetyl-FDEKA-NH_2 in aqueous solution at pH 5.5.[b]

	NH	H_α	H_β	H_γ	Other H	$J_{NH-\alpha}$	NH temp. coeff.
NAc		1.78					
F	8.20	4.37	2.93,2.83	—	δ:7.09	6.9	6.8
					ε:7.13		
					ξ:7.18		
D	8.22	4.37	2.50,2.47	—	—	7.2	5.6
E	8.31	3.98	1.90,1.80	2.15,2.08	—	5.8	4.8
K	8.22	4.08	1.65,1.65	1.35,1.35	δ:1.50,1.50	7.2	4.9
					ε:2.82,2.82		
A	7.93	4.06	1.22	—	—	6.0	4.7
NH_2	7.37						5.0
	6.94						5.5

(*c*) *N*-Acetyl-FDEKA-NH_2 in CD_3OH/H_2O (60/40 v%) at pH 3.4.[d]

	NH	H_α	H_β	H_γ	Other H	$J_{NH-\alpha}$	NH temp. coeff.
NAc		1.94					
F	8.35	4.48	3.07,2.93	—	δ:7.24	6.5	6.0
					ε:7.29		
					ξ:7.24		
D	8.52	4.56	2.85,2.66	—	—	7.5	5.9
E	8.21	4.22	2.10,1.96	2.41,2.41	—	6.5	4.5
K	8.17	4.25	1.83,1.75	1.43,1.43	δ:1.67,1.67	7.0	4.1
					ε:2.97,2.97		
A	8.06	4.24	1.36	—	—	6.5	3.9
NH_2	7.51						
	7.06						

(*d*) *N*-Acetyl-FDEKA-NH_2 in CD_3OH/H_2O (60/40 v%) at pH 5.5.[d]

	NH	H_α	H_β	H_γ	Other H	$J_{NH-\alpha}$	NH temp. coeff.
NAc		1.93					
F	8.36	4.52	2.08,2.91	—	δ:7.22	7.5	6.3
					ε:7.29		
					ξ:7.22		
D	8.32	4.55	2.71,2.58	—	—	7.0	6.0
E	8.62	4.11	2.10,2.00	2.36,2.36	—	4.7	3.8
K	8.33	4.19	1.82,1.82	1.45,1.45	δ:1.68,1.68	7.0	3.1
					ε:2.97,2.97		
A	7.90	4.21	1.38	—	—	6.7	2.3
NH_2	7.51	7.06					

Table 1 (*concluded*).

(*e*) *N*-Acetyl-YDEKA-NH_2 in CD_3OH/H_2O (60/40 v%) at pH 5.1.[e]

	NH	H_α	H_β	H_γ	Other H	$J_{NH-\alpha}$[f]	NH temp. coeff.
NAc		1.95					
Y	8.34	4.43	2,95,2.84	—	δ:7.22 ε:7.29 ξ:7.22	7.0	6.5
D	8.37	4.52	2.67,2.53	—	—	7.0	5.3
E	8.63	4.10	2.00,2.00	2.32,2.32	—	5.0	4.3
K	8.35	4.18	1.82,1.82	1.56,1.56	δ:1.42,1.42 ε:2.97,2.97	6.0	3.4
A	7.93	4.18	1.36	—	—	6.5	2.1
NH_2	7.41 7.15						

(*f*) *N*-Acetyl-VDEKA-NH_2 in CD_3OH/H_2O (60/40 v%) at pH 5.5.[g]

	NH	H_α	H_β	H_γ	Other H	$J_{NH-\alpha}$	NH temp. coeff.
NAc		2.02					
V	8.28	4.04	2.00	0.92,0.90	—	7.5	6.6
D	8.51	4.60	2.76,2.58	—	—	7.0	7.1
E	8.82	4.14	2.08,2.00	2.30,2.24		5.5	4.0
K	8.44	4.21	1.84,1.84	1.46,1.46	δ:1.68,1.68 ε:2.98,2.98 εNH_3: 7.82	7.0	3.8
A	7.94	4.20	1.41	—	—	6.5	2.6
NH_2	7.40 7.19						3.8 7.3

(*g*) *N*-Acetyl-GDEKA-NH_2 in CD_3OH/H_2O (60/40 v%) at pH 5.7.[h]

	NH	H_α	H_β	H_γ	Other H	$J_{NH-\alpha}$	NH temp. coeff.
NAc		2.04					
G	8.51	3.92,3.92	—	—	—	6.0/5.5	5.7
D	8.47	4.59	2.69,2.61	—	—	6.5	3.6
E	8.89	4.16	2.04,1.97	2.31,2.26	—	4.5	5.6
K	8.36	4.23	1.82,1.82	1.44,1.44	δ:1.67,1.67 ε:2.98,2.98	7.0	4.3
A	8.05	4.21	1.40	—	—	6.5	4.1
NH_2	7.50 7.17						4.4 6.3

(*h*) *N*-Acetyl-DEKA-NH_2 in CD_3OH/H_2O (60/40 v%) at pH 5.6.[i]

	NH	H_α	H_β	H_γ	Other H	$J_{NH-\alpha}$	NH temp. coeff.
NAc		2.00					
D	8.38	4.55	2.70,2.55	—	—	7.0	7.0
E	9.03	4.16	2.31,2.24	2.07,1.98		5.0	4.5
K	8.41	4.21	1.84,1.84	1.44,1.44	δ:1.68,1.68 ε:2.98,2.98 NH_3: 7.79	7.5	4.0
A	7.97	4.20	1.40	—	—	6.0	3.3
NH_2	7.44 7.19						4.1 7.0

[a]Chemical shifts are reported in ppm relative to the H_2O signal at 4.80 ppm in aqueous solution and to the methyl group of CD_3OH at 3.30 ppm in CD_3OH/H_2O solution. Coupling constants are measured in hertz. The temperature coefficients of the amide protons are listed in ppb/°C.

[b]The data were recorded in H_2O (15 v% D_2O) at a concentration of 5 mM and the temperature was 10.0 ± 0.1°C.

[c]Pairs of geminal protons x (x = β, γ, δ, ε) are not assigned stereospecifically. When two distinct lines were observed, the larger chemical shift was arbitrarily assigned to x and the smaller to x′.

[d]The data were recorded in CD_3OH/H_2O (60/40 v%) at a concentration of 5 mM and the temperature was 10.0 ± 0.1°C.

[e]The data were recorded in CD_3OH/H_2O (60/40 v%) at a concentration of 6 mM. The pH was 5.1 and the temperature 0.0 ± 0.1°C.

[f]Coupling constants were measured at 5°C from a one-dimensional spectrum.

[g]The data were recorded in CD_3OH/H_2O (60/40 v%) at a concentration of 5 mM. The pH was 5.5 and the temperature 0.0 ± 0.1°C.

[h]The data were recorded in CD_3OH/H_2O (60/40 v%) at a concentration of 5 mM. The pH was 5.7 and the temperature 0.0 ± 0.1°C.

[i]The data were recorded in CD_3OH/H_2O (60/40 v%) at a concentration of 7 mM. The pH was 5.6 and the temperature 0.0 ± 0.1°C.

Can. J. Chem. Downloaded from www.nrcresearchpress.com by 80.90.12.36 on 09/08/12
For personal use only.

Can. J. Chem. Downloaded from www.nrcresearchpress.com by 80.90.12.36 on 09/08/12
For personal use only.

on its use for the study of the solvation of peptidic chains may be found in the more recent work mentioned above (8, 9).)

The peptides were constructed from the crystallographic structures (with the angles ϕ, χ_1, and ψ rezeroed according to the IUPAC convention) of the corresponding amino acids, with the dihedral angle constraint that the pair EK would form a β-I turn in DEKA. All the remaining dihedral angles were optimized during the construction process. After the construction was completed, the N and C termini of the peptidic chains were protected with the groups H_3C-COO- and -HN-CH_3, respectively, in order to simulate the experimental conditions. To simulate the conditions at neutral pH, the residues D, E, and K were used in charged form (i.e., with ionized carboxyl groups in the side chains of D and E and with a protonated amino group in the side chain of K).

The peptidic chains obtained above were then fully optimized, under a minimum energy criterion, by variation of all the dihedral angles ϕ, ψ, and χ_1 until convergence (to $\pm 2°$) was obtained for all those angles.

Next, a solvation process was performed, using the optimized peptidic chains. This process was carried out as follows. Twenty points, on a sphere centered at the geometric center of the peptidic chain and with an appropriate radius, are chosen as starting points for the approach of the water molecules to the peptide, in an attempt to eliminate any directional bias. A water molecule is placed at the first of these positions and the interaction energy, and its gradient, between the water molecule and the peptide are calculated. The water molecule is then allowed to move a controlled distance along the path of steepest descent. This step-by-step approach of the water towards the peptide is continued until a minimum energy is reached, that is, until a stable molecular association peptide–water has been formed. The process is repeated for all the remaining starting points, thus obtaining the interaction energies of the corresponding molecular associations. The most stable of those associations is selected and a water molecule, with the relative position as in that association, is added to the peptidic chain: that is, the three atoms of the water molecule are incorporated into the list of atoms of the peptide, as part of the side chain of the residue to which the water molecule is closest in that molecular association. The complete procedure is now repeated with a second water molecule, interacting now with the peptidic chain that already contains the first water molecule. At the end of this step, the second water molecule is also incorporated into the peptidic chain. The calculation is continued until the desired number of water molecules have been added to the peptide.

In the present calculation seven water molecules were added, on the basis that the peptide consists of five residues and the two protecting groups, and therefore each component was given the chance of being solvated. With the approach adopted here, a larger number of water molecules would, in all probability, not change appreciably the present results because the freedom of the chain for conformational changes would be highly restricted.

This procedure represents a model by which one attempts to simulate the solvation of the peptide, the rationale being that the water molecules added may be considered to represent the first solvation shell, closely attached to the residues. Variations of this procedure have been used, with success, in the study of the environmental effects on the conformation of peptides in solution (8, 9). In this regard it should be mentioned that the calculations, in the present as well as in previous work, have been performed for the molecules in vacuum, without any consideration of dielectric constant.

Finally, the solvated structures thus prepared are then reoptimized, to the same convergence limit ($\pm 2°$).

Results

NMR spectroscopy

The resonance assignments of all five peptides are based on TOCSY experiments and sequential NOEs of the type $H_\alpha(i)$–NH(i + 1) and NH(i)–NH(i + 1) (18). The coupling constants NH–H_α were accurately measured in the one-dimensional spectra. The assigned resonances are presented in Table 1 together with the coupling constants and the temperature dependence of the NH proton shifts. The NH/NH section of the NOESY spectrum is depicted in Fig. 1 for FDEKA in 60% CD_3OH/40% H_2O solution. The fingerprint region (H_α/NH) of the same experiment is shown in Fig. 2. The chemical shift data for FDEKA in H_2O solutions at both pH values, as well as for the CD_3OH/H_2O solutions, are presented in Fig. 3. Finally, the amino acid sequences of the five peptides together with the observed sequential and medium-range NOEs are presented in Fig. 4. The thickness of the lines indicates qualitatively the relative magnitudes of the NOEs. For FDEKA, volumes of cross peaks were calculated relative to the ββ′ NOE for F as 1000 and then the NOEs were classified as strong (~200), medium (≤100), weak (≤50), and very weak (≤20). The data for FDEKA are presented in Table 2. For GDEKA, there is no internal standard for the integrals, hence only relative magnitudes are presented in Fig. 4.

Molecular mechanics

The results of the calculations produce three structures for each peptide: the β-I conformation, the structure optimized in vacuum, and the conformation stabilized by solvation. For the peptidic structures alone, the order of stability is vacuum structure more stable than solvated structure, which is, in turn, more stable than the β-I structure. Figure 5 presents the theoretical structures predicted for the solvated peptides.

These structures were then analyzed and the corresponding results are as follows.

(a) Dihedral angles

The dihedral angles, ϕ and ψ, for the residues E and K are summarized in Table 3, where it can be observed that the β-I turn has been distorted in both the vacuum and the solvated structures. To establish the magnitude of the distortion, use may be made of the criterion proposed by Rose et al. (19), in terms of the distance $C_\alpha(i)$–$C_\alpha(i + 3)$. For the solvated structures, as an example, those distances are 4.87 Å for FDEKA, and 6.00 Å for GDEKA, to be compared with the value 4.64 A for an ideal β-I turn (19); that is, the distortion (in the solvated structures) is far greater in GDEKA than in FDEKA.

(b) Hydrogen bonds and salt bridges

The results for salt bridges (i.e., strong Coulombic interactions) confirm the results above. The distances (again in the

Can. J. Chem. Downloaded from www.nrcresearchpress.com by 80.90.12.36 on 09/08/12
For personal use only.

solvated structures) between the side-chain carboxylic carbon of residue E and the side-chain amino nitrogen of residue K are 5.58 Å in FDEKA and 8.83 Å in GDEKA. That is, there is a much stronger salt bridge in FDEKA than in GDEKA. It should be mentioned that the solvated structure of GDEKA seems to have been stabilized by a salt bridge between the side-chain carboxylic carbon of residue D and the side-chain amine nitrogen of residue K, which are at a distance of 4.94 Å.

The distances between the oxygen of the carboxyl group of residue D and the hydrogen of the amido group of residue A are 5.18 and 3.54 Å, for the vacuum and solvated structures of FDEKA, and 5.81 and 3.89 Å, for the vacuum and solvated structures of GDEKA, respectively. These results, although indicating the absence of a proper H-bond, show a difference between FDEKA and GDEKA, which correlates with the NH temperature-dependent chemical shifts of residues A in both molecules (see Table 1, *d* and *g*).

(c) $d_{NN}(i, i + 1)$ *NOE connectivities*

Because of the dependence of the NOE on the inverse sixth power of the internuclear distance, the NOE connectivities between the amide hydrogens of consecutive residues have been *approximated* in the modeling using eq. [1] (20)

$$[1] \quad d_{NN}(i, i+1) = 10^3 (1.75/R_{i,i+1})^6$$

where $R_{i,i+1}$ denotes the separation between the amide hydrogens of residues i and $i + 1$ and the reference is 1.75 Å for the geminal proton internuclear distance. The corresponding values are presented in Table 2, for the three structures under consideration as well as for a weighted average. The weights used for the evaluation of the averages (3, 63, and 34% for FDEKA and 2, 62, and 36% for GDEKA) have been obtained by a Boltzmann distribution at 298 K. The values are identical for the β-I structures, as they should be, except for the d_{NN} (1,2) connectivity, due to the dependence on the sequence for the optimization of that part of the chain.

Discussion

The NMR data (Fig. 4) on NAc-FDEKA-NH_2 indicate that the fused βγ-turn, observed previously in the 19-amino acid type II N-telopeptide (1), is not present in the pentapeptide, showing the importance of long-range interactions in stabilizing this βγ-turn (2). All five peptides under study (Fig. 4) exhibit strong sequential NOEs, namely ($H_\alpha(i)$–NH), and weaker sequential NH(i)–NH NOEs. In addition, the NOE data for FDEKA, YDEKA, and VDEKA (Fig. 4, Tables 1d–1*f*) indicate that two medium-range NOEs ($H_\alpha(i)$–NH(i + 2)) are observed for these three pentapeptides in CD_3OH/H_2O solutions at pH values above 5.1 where the side chains are ionized. As well, the observation of very small temperature coefficients for the NH proton of A in these three peptides (2.3, 2.1, and 2.6 ppb/°C), respectively, indicates the presence of a hydrogen bond, namely NH(A). . . O═C (D). Consequently, at least three criteria have been met that indicate the high propensity of these peptides to form a type I β-turn in solution (4), namely, (*i*) the NH(i)–NH NOE connectivity between residues 2 and 3 and 3 and 4 of this turn, which are stronger than the NOE from residue 1 to residue 2; (*ii*) the presence of the $H_\alpha(i)$–NH(i + 2) NOE; and (*iii*) the small NH temperature coefficient. The turn involves residues DEKA. In addition, the results indicate that for FDEKA, which was also studied at low pH in CD_3OH/H_2O solutions, a low-field shift of 0.41 ppm is observed for the NH proton of E on increasing the pH from 3.4 to 5.5 (Fig. 3 and Tables 1*c* and 1*d*). This lends further support to the presence of secondary structure for FDEKA in this mixed solvent at high pH. In the case of H_2O solutions (Tables 1*a* and 1*b*, Fig. 3), this shift was only 0.24 ppm and there was no indication of secondary structure in solution at high pH even though there was a lower temperature-dependent coefficient of residue A and a smaller NH–H_α coupling constant of residue E than for the low pH solution.

Fig. 1. The NH/NH region of a 500 MHz phase-sensitive NOESY experiment of NAc-FDEKA-NH_2 in CD_3OH/H_2O (60/40), pH 5.5, 0°C. The mixing time was 400 ms.

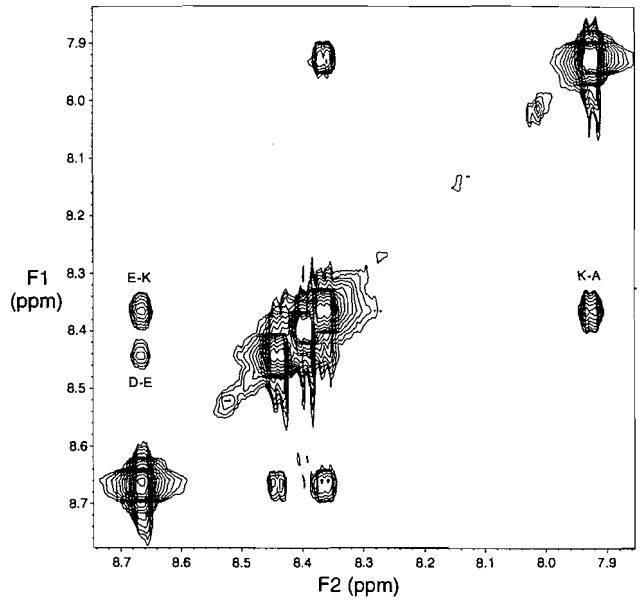

Fig. 2. The H_α/NH region of the same experiment as outlined in Fig. 1. Cross peaks resulting from α(i)–NH(i + 2) interactions are shown in boxes.

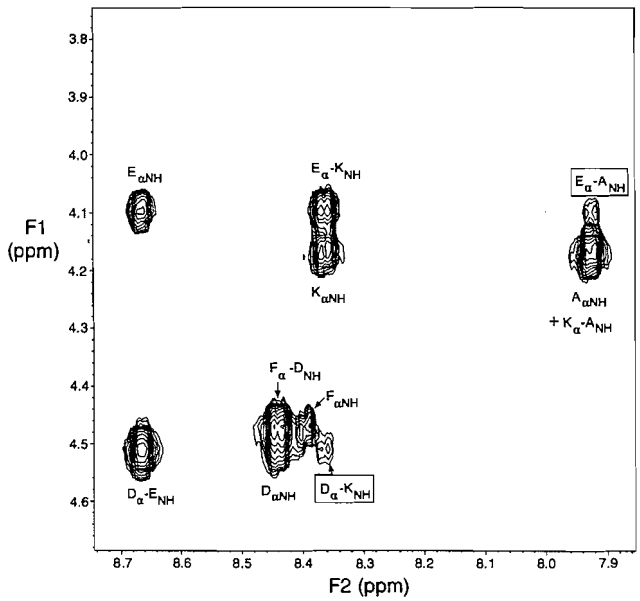

Can. J. Chem. Downloaded from www.nrcresearchpress.com by 80.90.12.36 on 09/08/12
For personal use only.

Table 2. Calculated $d_{NN}(i, i + 1)$ NOE connectivities.[a]

i	FDEKA	GDEKA
	β-I turn structure	
1	87	48
2	259	259
3	116	116
4	157	157
	Vacuum structure	
1	12	4
2	9	10
3	128	214
4	131	151
	Solvated structure	
1	5	5
2	114	4
3	602	486
4	598	516
	Weighted contributions[a]	
1	12	6
2	52 (45)[b]	13
3	289 (86)	315
4	290 (117)	287

[a]See the text for the corresponding Boltzmann weights.

[b]The volumes of the cross peaks were calculated relative to the ββ′ NOE for F as 1000 and are unitless. As discussed in the text, this comparison could not be carried out for GDEKA.

Table 3. Dihedral angles (in degrees) for the residues E and K.

	ϕ_E	ψ_E	ϕ_K	ψ_K
FDEKA				
β-I structure	−60	−30	−90	0
Vacuum structure	63	30	−78	−8
Solvated structure	−106	−11	−133	9
GDEKA				
β-I structure	−60	−30	−90	0
Vacuum structure	−85	−45	80	12
Solvated structure	−126	13	−117	−3

Fig. 3. A comparison of the NAc-FDEKA-NH_2 chemical shifts in different solvents and different pH values.

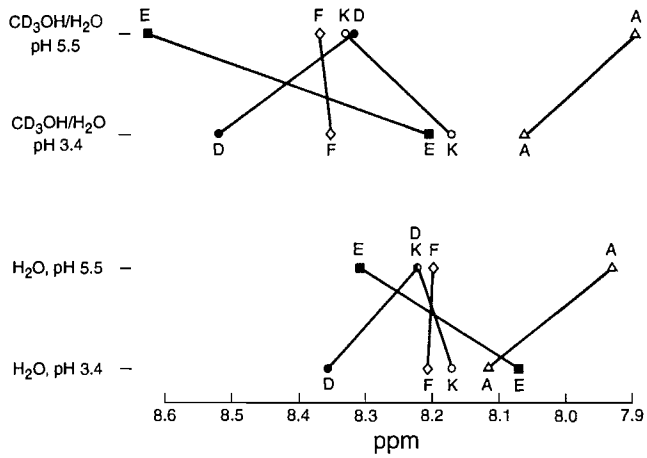

Fig. 4. The amino acid sequences of the five peptides in CD_3OH/H_2O solutions (60/40) at high pH are shown with the observed sequential and medium-range NOEs indicated schematically by solid bars. The temperature coefficients of the amide protons are shown with solid triangles for values below 3.0 ppb/°C. The rectangle indicates vicinal coupling constants of ≤5.5 Hz. The complete coupling constant and NH chemical shift temperature coefficient data are presented in Tables 1*d*–1*h*. The NOEs shown with broken lines may be present but were not observable due to almost identical chemical shifts of the amide protons.

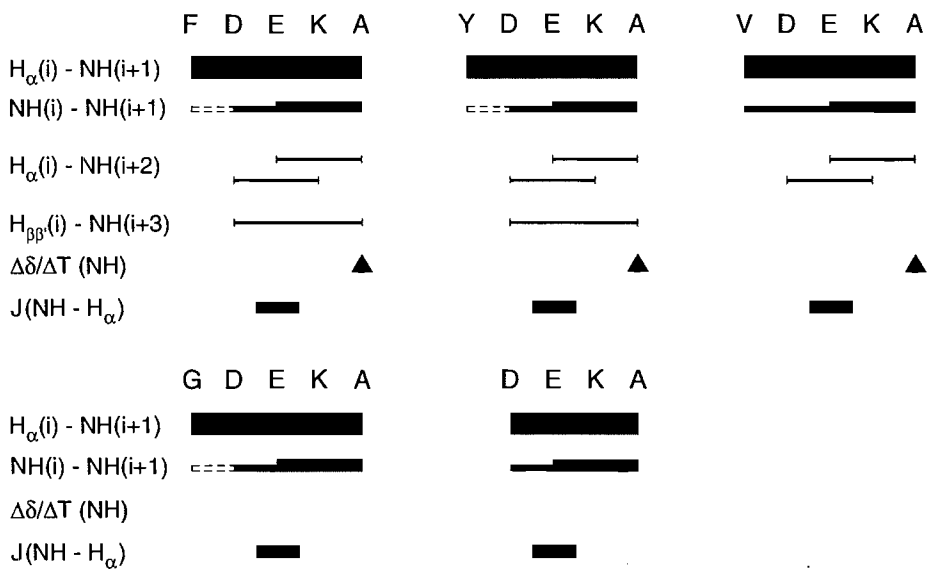

Can. J. Chem. Downloaded from www.nrcresearchpress.com by 80.90.12.36 on 09/08/12
For personal use only.

Fig. 5. Stereoscopic representations (showing only the heavy atoms) of the solvated structures of FDEKA and GDEKA. The symbols ⊕ and ⊖ mark the charged atoms, involved in salt bridges, of the side chains of the residues K and D and E, respectively. The stereo figure was obtained using the program "HyperChem" by inputting the dihedral angles from the modeling as described in the text.

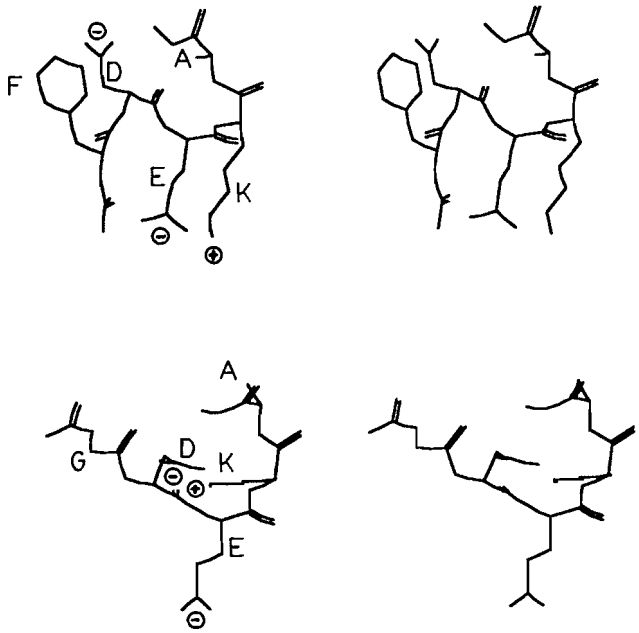

The measured NMR parameters for these short linear peptides are averaged (4, 5) over all conformations present, and this precludes a numerically precise interpretation of the data for FDEKA, YDEKA, and VDEKA. However, a comparison may be made with the data observed for GDEKA and DEKA, where the hydrophobic amino acid at position $(i - 1)$ of the turn was replaced by G in the former peptide or removed completely in the latter peptide. The intensities for the $H_\alpha(i)$–NH$(i + 2)$ NOEs are significantly reduced. The NH temperature coefficient of residue A increases to 4.1 ppb/°C for GDEKA and 3.3 ppb/°C for DEKA, indicating the absence of the hydrogen bond in these two peptides. The conclusion is that these two peptides have at the most only a very weak propensity for forming a type I β-turn.

In view of these experimental data, we tried to understand the role of the hydrophobic $(i - 1)$ amino acid on β-turn formation. This was accomplished by means of the molecular mechanics calculations, which definitely indicate the presence of two predominant conformations in solution. A similar approach was used in the study of β-turn formation in YQNPDGSQA (21).

Comparison of the theoretical and experimental values for the d_{NN} connectivities is very difficult. The experimental results correspond to a measurement for a collection of molecules, in a thermal environment, over a given time interval. As a consequence of the interactions with the environment, those molecules will undergo structural changes, with the result that the experimental results cannot be ascribed to a specific conformation, unless (a) very stable structural motif(s) is/are present. The most appropriate tools for a theoretical study (22) of this problem are the Monte Carlo and Molecular Dynamics techniques, whereby the theoretical description is obtained from the complete history of the simulation, that is, with consideration of all the conformations that have been generated during the simulation. Even so, difficulties in the interpretation of the experimental results may still persist (6).

In the present case, though being aware of those difficulties, the interpretation is attempted in terms of two extreme structures (the β-I conformation and the conformation optimized in vacuum) and an intermediate structure, optimized in the presence of water. It is encouraging that the weighted results (Table 2 and Figs. 4 and 5) are in satisfactory agreement with the experimental observations, with very similar results for both FDEKA and GDEKA. On the basis of this comparison one could say that the experimental results may be described in terms of just two conformations: a somewhat extended conformation (~65%) and a distorted β-I conformation (~35%). One should add that the present results are in line with expectations from previous work, with (8, 9) or without (23) consideration of the solvent.

Acknowledgements

The authors gratefully acknowledge the assistance of Mrs. Gerdy H.M. Aarts in measuring some of the spectra, Dr. Jan Sejbal for valuable discussions, and thank the Alberta Heritage Foundation for Medical Research, the Natural Sciences and Engineering Research Council of Canada, the Medical Research Council, and the University of Alberta for financial assistance.

References

1. A. Otter, P.G. Scott, and G. Kotovych. Biopolymers, **33**, 1443 (1993).
2. X. Liu, P.G. Scott, A. Otter, and G. Kotovych. Biopolymers, **32**, 119 (1992).
3. H.J. Dyson and P.E. Wright. Current Opinion Struct. Biol. **3**, 60 (1993).
4. H.J. Dyson and P.E. Wright. Annu. Rev. Biophys. Biophys. Chem. **20**, 519 (1991).
5. H.J. Dyson, M. Rance, R.A. Houghten, R.A. Lerner, and P.E. Wright. J. Mol. Biol. **201**, 161 (1988).
6. D.J. Tobias, J.E. Mertz, and C.L. Brooks III. Biochemistry, **30**, 6054 (1991).
7. C.M. Wilmot and J.M. Thornton. J. Mol. Biol. **203**, 221 (1988).
8. S.E. Thornton and S. Fraga. Can. J. Chem. **69**, 1636 (1991).
9. S. Fraga and S.E. Thornton. Theor. Chim. Acta, **85**, 61 (1993).
10. R.R. Ernst, G. Bodenhausen, and A. Wokaun. Principles of nuclear magnetic resonance in one and two dimensions. Clarendon Press, Oxford. 1987.
11. D.J. States, R.A. Haberkorn, and D.J. Ruben. J. Magn. Reson. **48**, 286 (1982).
12. L. Braunschweiler and R.R. Ernst. J. Magn. Reson. **53**, 521 (1983).
13. A. Bax and D.G. Davis. J. Magn. Reson. **65**, 355 (1985).
14. J. Jeener, R. Meier, P. Bachmann, and R.R. Ernst. J. Chem. Phys. **71**, 4546 (1979).
15. A. Kumar, R.R. Ernst, and K. Wüthrich. Biochem. Biophys. Res. Commun. **95**, 1 (1980).
16. G. Otting, H. Widmer, G. Wagner, and K. Wüthrich. J. Magn. Reson. **66**, 187 (1986).
17. B. Coghlan and S. Fraga. Computer Phys. Commun. **236**, 391 (1982).

18. K. Wüthrich. NMR of proteins and nucleic acids. Wiley–Interscience, New York. 1986. pp. 126-127.
19. G.D. Rose, L.M. Gierasch, and J.A. Smith. Adv. Protein Chem. **37**, 1 (1985).
20. M.J. Sutcliffe. *In* NMR of macromolecules, a practical approach. *Edited by* G.C.K. Roberts. IRL Press at Oxford University Press, Oxford. 1993 pp. 359–390.
21. F.J. Blanco, M.A. Jiménez, J. Harranz, M. Rico, J. Santoro, and J.L. Nieto. J.Am. Chem. Soc. **115**, 5887 (1993).
22. S. Fraga and J.M.R. Parker. Amino Acids, **7**, 175 (1994).
23. S. Fraga, S. Thornton, and B. Singh. Mol. Struct. (Theochem), **286**, 87 (1993).

Can. J. Chem. Downloaded from www.nrcresearchpress.com by 80.90.12.36 on 09/08/12
For personal use only.

Synthesis of heptamethylindenyl rhodium(III) complexes: molecular structures of $[(\eta^5\text{-}C_9Me_7)RhCl(\mu\text{-}Cl)]_2$ and $[(\eta^5\text{-}C_9Me_7)Rh(PMe_2Ph)Cl_2]$

Ashok K. Kakkar, Graham Stringer, Nicholas J. Taylor, and Todd B. Marder

Abstract: The synthesis of a series of permethylindenyl (Ind*) rhodium(III) complexes, $[(\eta^5\text{-}C_9Me_7)RhCl(\mu\text{-}Cl)]_2$, $[(\eta^5\text{-}C_9Me_7)RhLCl_2]$ (L = PMe_3, PMe_2Ph, PPh_3), and $[(\eta^5\text{-}C_9Me_7)Rh(PMe_3)_2Cl]^+Cl^-$, is reported. The structure of $[(\eta^5\text{-}C_9Me_7)RhCl(\mu\text{-}Cl)]_2$ (**4**) was determined, confirming the dimeric nature of the compound. Ruby red crystals of **4** are monoclinic, space group *C*2/*c*, with four molecules per unit cell of dimensions a = 18.598(5), b = 10.520(3), c = 17.376(3) Å and β = 115.10(2)°. The indenyl rings exhibit minimal distortion from perfect η^5 coordination to the Rh centres. A single crystal X-ray structure determination of $[(\eta^5\text{-}C_9Me_7)Rh(PMe_2Ph)Cl_2]$ (**6**) indicates a more distorted η^5-coordination of the indenyl ligand, with the auxiliary ligand having the greatest *trans* influence, namely, the PMe_2Ph group, being *trans* to the indenyl ring junction C—C bond. Yellow prismatic crystals of **6** are orthorhombic, space group $P2_12_12_1$, with four molecules per unit cell of dimensions a = 8.819(1), b = 15.303(3), c = 17.296(3) Å.

Key words: rhodium, indenyl, permethylindenyl, heptamethylindenyl, phosphine complex, X-ray structure.

Résumé : On a effectué la synthèse d'une série de complexes perméthylindényl(Ind*) rhodium(III), $[(\eta^5\text{-}C_9Me_7)RhCl(\mu\text{-}Cl)]_2$, $[(\eta^5\text{-}C_9Me_7)RhLCl_2]$ (L = PMe_3, PMe_2Ph et PPh_3), et $[(\eta^5\text{-}C_9Me_7)Rh(PMe_3)_2Cl]^+Cl^-$. On a déterminé la structure du composé $[(\eta^5\text{-}C_9Me_7)RhCl(\mu\text{-}Cl)]_2$ (**4**) et confirmé la nature dimère du composé. Les cristaux rubis du composé **4** sont monocliniques, groupe d'espace *C*2/*c*, avec quatre molécules par motif de dimensions a = 18,598(5), b = 10,520(3) et c = 17,376(3) Å et β = 115,10(2)°. Les cycles indényles présentent une distorsion minimale par rapport à une coordination η^5 parfaite avec les centres Rh. Une détermination de structure du $[(\eta^5\text{-}C_9Me_7)Rh(PMe_2Ph)Cl_2]$ (**6**) indique, dans ce cas, qu'il existe une coordination η^5 plus déformée du coordinat indényle avec le coordinat auxiliaire ayant la plus grande influence *trans*, le groupe PMe_2Ph se trouvant *trans* par rapport à la liaison C—C de la jonction avec le cycle indényle. Les cristaux jaunes, prismatiques, du composé **6** sont orthorhombiques, groupe d'espace $P2_12_12_1$, avec quatre molécules par motif de dimensions a = 8,819(1), b = 15,303(3) et c = 17,296(3) Å.

Mots clés : rhodium, indényle, perméthylindényle, heptaméthylindényl, complexe de phosphine, structure par diffraction des rayons X.

[Traduit par la rédaction]

Introduction

The strongly electron-donating pentamethylcyclopentadienyl ligand ($[\eta^5\text{-}C_5Me_5]^-$, Cp*) has received considerable attention in organometallic chemistry, and many useful reagents have been prepared via mono-Cp* halide, Cp^*MX_n, precursors.[3] In contrast, there are few reports (3–10) of metal complexes containing the heptamethylindenyl ligand ($[\eta^5\text{-}C_9Me_7]^-$, Ind*). This may, in part, be due to the lack of experimental details for the synthesis of the ligand in the original communication (3). We recently reported detailed preparative procedures for the synthesis of heptamethylindene, Ind*H, on both the 10 g (9) and 90 g (8) scales. Ind*H is reported to have a pK_a of 27.4 in DMSO compared with values of 20.1 for indene, 26.1 for Cp*H, and 18.0 for cyclopentadiene (11). Thus, Ind* should have donor properties similar to, or even stronger than Cp*, while maintaining the unusually high stoichiometric reactivity (12–14) and catalytic activity (15–17) associated with indenyl metal complexes. For example, kinetic studies (5, 10) on the

Received September 2, 1994.

This paper is dedicated to Professor William A.G. Graham on the occasion of his 65th birthday.

A.K. Kakkar,[1] G. Stringer, N.J. Taylor, and T.B. Marder.[2] Department of Chemistry, University of Waterloo, Waterloo, ON N2L 3G1, Canada.

[1] Present address: Department of Chemistry, McGill University, Montréal, QC H3A 2K6.

[2] Author to whom correspondence may be addressed. Telephone: (519) 888-4582. Fax: (519) 746-0435. E-mail: MARDER@Uwaterloo.ca

[3] For a general review of Cp-type metal halide complexes see ref. 1. For original reports of the synthesis of $[Cp^*RhCl(\mu\text{-}Cl)]_2$ and related studies see, for example, ref. 2.

Can. J. Chem. Downloaded from www.nrcresearchpress.com by 80.90.12.36 on 09/08/12
For personal use only.

Can. J. Chem. Downloaded from www.nrcresearchpress.com by 80.90.12.36 on 09/08/12
For personal use only.

substitution of CO by PR_3 in a series of indenyl ring substituted $[(\eta^5\text{-}C_9H_{7-n}Me_n)Rh(CO)_2]$ complexes indicate that the second-order rate constant for $[(\eta^5\text{-}C_9Me_7)Rh(CO)_2]$ (**1**) is ca. 150 × smaller than that for $[(\eta^5\text{-}C_9H_7)Rh(CO)_2]$ (**2**) but ca. 10^7 larger than that for $[(\eta^5\text{-Cp*})Rh(CO)_2]$ (**3**). The values of ν_{CO} for complexes **1** and **3** are similar, and the average nonbonding *d*-orbital ionization energy (18) for **1** (7.93 eV) is slightly lower than that for **3** (8.12 eV). Interestingly, in the case of the sandwich complexes $[(\eta^5\text{-L})_2M]$ (L = Cp*, Ind*; M = Fe, Cr, Co) PES and electrochemical studies (8) show that the Ind* ligand is a stronger donor than Cp* for M = Fe and Cr, but for M = Co, the first ionization energy was higher for the Ind* compound. It is also worth noting that X-ray crystallographic studies on $[(\eta^5\text{-L})_2Fe]$ (L = Ind, Ind*) (7), and $[(\eta^5\text{-L})Rh(\eta^4\text{-1,5-COD})]$ (L = Ind, Ind*) (*6b*) showed no significant changes in the structural parameters describing metal – indenyl ring bonding upon permethylation.

As part of our continuing study of indenyl complexes, we have begun to examine the synthesis of Ind* complexes that can serve as basic starting materials for subsequent organometallic chemistry. We report herein the synthesis and structure of $[(\eta^5\text{-Ind*})RhCl(\mu\text{-Cl})]_2$ and its reactions with monodentate phosphine ligands.

Results and discussion

Preparation of $[(\eta^5\text{-}C_9Me_7)RhCl(\mu\text{-Cl})]_2$ (4)

Complex **4** was prepared (Scheme 1) by adaptation of the procedure outlined (*2d*, *e*) for the synthesis of $[Cp^*RhCl(\mu\text{-Cl})]_2$ (2). Heptamethylindene and $RhCl_3 \cdot xH_2O$ were heated in refluxing methanol for 24–48 h. Evaporation of the solvent and extraction into toluene gave the dark red compound **4**, which was characterized by elemental analysis, NMR spectroscopy, and by single crystal X-ray diffraction. The solid state structure of **4** is shown in Fig. 1. A summary of the crystallographic data and parameters for data collection is presented in Table 1, and selected bond distances and angles are given in Table 2, together with those reported for $[Cp^*RhCl(\mu\text{-Cl})]_2$ (*2h*). The final atomic coordinates for **4** are given in Table 3. The molecular structure of **4** indicates that the molecule exists as a dimer in the solid state, sitting on a centre of inversion, with two bridging chloride ligands, comparable to $[Cp^*RhCl(\mu\text{-Cl})]_2$. There are, however, differences in the lengths of the metal–chloride bonds in the two compounds. In $[Cp^*RhCl(\mu\text{-Cl})]_2$, the Rh—Cl distances are 2.465(1), 2.452(1), and 2.397(1) Å for the two bridging and one terminal chloride, respectively, whereas the comparable distances for **4** are 2.394(1), 2.499(1), and 2.381(1) Å, respectively. Thus, there is considerably more asymmetry in the bridging system of the Ind* compound. These bond lengths result in nonbonding Rh..Rh′ distances of 3.1791(6) Å for $[Cp^*RhCl(\mu\text{-Cl})]_2$ and 3.612(1) Å for **4**. The yields of **4** were somewhat variable. Occasionally, the preparation of **4** yielded a toluene—insoluble orange-brown solid. It was found, however, that this material reacts with phosphines to yield the same products as does **4.**

Reaction of $[(\eta^5\text{-}C_9Me_7)RhCl(\mu\text{-Cl})]_2$ (4) with phosphines: preparation of $[(\eta^5\text{-}C_9Me_7)RhLCl_2]$ (L = PMe_3 (5), PMe_2Ph (6), PPh_3 (7)

As is the case for the Cp* analogue (1, 2), the bridging Rh—Cl bonds in complex **4** are easily cleaved by tertiary phosphines (Scheme 1) to form monomeric $[\eta^5\text{-Ind*})Rh(PR_3)Cl_2]$ complexes in quantitative yields. These complexes were characterized by elemental analysis, ^1H, $^{13}C\{^1H\}$, $^{31}P\{^1H\}$ NMR spectroscopy for **5–7**, and by a single crystal X-ray structure determination for **6**. The solid state structure of **6** is shown in Fig. 2. A summary of the crystallographic data and parameters for data collection are presented in Table 1, and final atomic coordinates and selected bond lengths and angles for **6** are given in Tables 4 and 5.

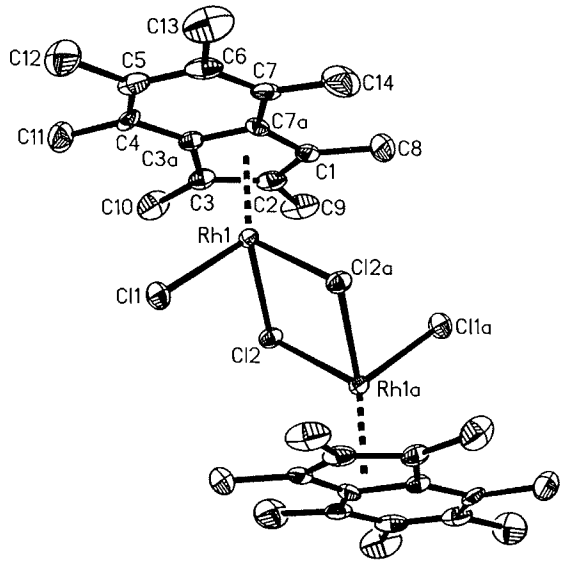

Fig. 1. The ORTEP diagram of the molecular structure of **4**. Hydrogen atoms have been omitted for clarity.

It is well documented (6, 7, 19–23) that all [(η-indenyl)ML_n] complexes show some degree of slip–fold distortion from η^5 *towards* η^3 coordination in the ground state. Structural characterization of many indenyl complexes indicates that the metal to carbon distances M—C_1, M—C_2, M—C_3 are shorter than those to the bridgehead carbons (M—C_{3a}, M—C_{7a}). The degree of distortion in the solid state in these complexes has been discussed (6, 7, 19, 21) in terms of three parameters: (*i*) slip parameter (Δ), which we define as the difference in the average metal to carbon distances of $C_{3a,7a}$ and $C_{1,3}$ ($\Delta = d\{(M\text{—}C_{3a,7a}) - (M\text{—}C_{1,3})\}$); (*ii*) hinge angle (HA), which is the angle between normals to the least-squares planes defined by [C_1, C_2, C_3] and [C_1, C_3, C_{3a}, C_{7a}]; and (iii) fold angle (FA), which is the angle between normals to least-square planes defined by [C_1, C_2, C_3] and [C_{3a}, C_4, C_5, C_6, C_7, C_{7a}]. The values for these parameters range (*6b*, 7, 21) from 0.030 Å (Δ), 2.5° (HA), 4.4° (FA) for "true" η^5 complexes to 0.8 Å (Δ), 28° (FA) for "true" η^3 complexes, with intermediate values of 0.11 – 0.42 Å (Δ), 7–14° (HA), 6–13° (FA) observed for "distorted" complexes in which there is clearly some degree of bonding of the metal to $C_{3a,7a}$. Other geometric parameters have also been used (20, 22) to describe the distortions in indenyl and carboranyl complexes. The critical feature is the soft potential surface for distortions of the indenyl ring system that involve folding of the rings and changes in C—C bond lengths.

The values for the slip–fold parameters for **4** are Δ = 0.087(5) Å; FA = 5.0°, HA = 4.6°. These values imply that

Can. J. Chem. Downloaded from www.nrcresearchpress.com by 80.90.12.36 on 09/08/12
For personal use only.

Scheme 1.

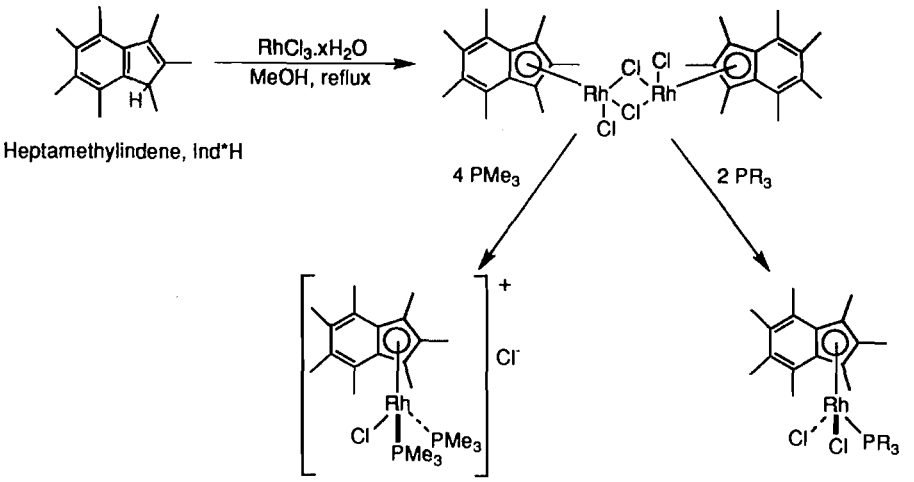

Table 1. X-ray crystal data for compounds $[(\eta^5\text{-}C_9Me_7)RhCl(\mu\text{-}Cl)]_2$ (**4**) and $[Ind^*Rh(PMe_2Ph)Cl_2]$ (**6**).

	4	**6**
Formula	$C_{32}H_{42}Cl_4Rh_2$	$C_{24}H_{32}PCl_2Rh$
FW	774.3	525.34,
Crystal system	Monoclinic	Orthorhombic
a (Å)	18.598(5)	8.819(1),
b (Å)	10.520(3)	15.303(3)
c (Å)	17.376(3)	17.296(3)
β (°)	115.10(2)	—
V (Å^3)	3078.6(13)	2360.7(8)
Z	4	4
ρ_{calc} (g cm^{-3})	1.670	1.478
Space group	*C2/c*	$P2_12_12_1$
Crystal dimensions (mm)	0.110(110, $\bar{1}\bar{1}0$) × 0.070(1$\bar{1}$0, 1$\bar{1}$0) × 0.140($\bar{2}$01, 20$\bar{1}$)	0.32 × 0.50 × 0.54
Temperature (K)	180	200
Radiation	MoKα	MoKα
μ (cm^{-1})	14.40	10.15
Data collection method	ω	ω
Max. 2θ	50.0	60.0
Scan speed (° min^{-1})	2.44–19.53	2.93–29.3
Scan width (°).	1.50	1.20
No. of independent reflections	2733	3879
No. of observed reflections[a]	2113	3546
Range for *h*	0–22	0–12
Range for *k*	0–12	0–21
Range for *l*	–20–18	0–24
Final Δ/σ	0.023	0.150
F(000)	1568	1080
R (%)[b]	2.87	2.27
R_w (%)[c]	2.78	2.47
In the last Δ-map		
the highest peak (e/Å^3)	0.62	0.56
the deepest hole (e/Å^3)	–0.40	–0.34
GOF[d]	1.75	1.95

[a] $F \geq 6\sigma(F)$.
[b] $\Sigma||F_o| - |F_c||/\Sigma|F_o|$.
[c] $[\Sigma w(|F_o| - |F_c|)^2/\Sigma wF_o^2]^{1/2}$.
[d] $[\Sigma w(|F_o| - |F_c|)^2/(N_{obs}\text{-}N_{var})]^{1/2}$.

Table 2. A comparison of selected bond distances and angles for $[(\eta^5\text{-}C_9Me_7)RhCl(\mu\text{-}Cl)]_2$, **4**, and $[Cp^*RhCl(\mu\text{-}Cl)]_2$ (*2h*).

	$[Ind^*RhCl(\mu\text{-}Cl)]_2$	$[Cp^*RhCl(\mu\text{-}Cl)]_2$
Rh.....Rh′	3.612(1)	3.1791(6)
Rh–Cl(1)	2.381(1)	2.3967(11)
Rh–Cl(2)	2.394(1)	2.4522(10)
Rh–Cl(2A)	2.499(1)	2.4649(11)
Rh–C(1)	2.154(5)	—
Rh–C(2)	2.132(5)	—
Rh–C(3)	2.100(4)	—
Rh–C(3A)	2.226(4)	—
Rh–C(7A)	2.201(5)	—
Rh–Cl(2)–Rh′	95.1(1)	98.29(3)
Cl(2)–Rh–Cl(2A)	84.9(1)	81.71(3)

there is very little distortion in this complex. In contrast, the values for the slip–fold parameters for **6** are Δ = 0.154(3) Å; FA = 8.8°, HA = 7.2°, which indicates a distorted η^5 coordination of rhodium to the indenyl ring. Hence, the distortions observed in the d^8-$[(\eta\text{-}C_9H_7)RhL_2]$ complexes also persist for the d^6-$[(\eta\text{-}C_9R_7)RhL_2L']$ systems. Similar findings were reported for d^6-$[(\eta\text{-}C_9H_7)Ir\{P(C_6H_5)_3\}(H)][BF_4]$ for which Δ = 0.185(8) Å (20).

It has been shown (20, 22) that the indenyl ligand exhibits a conformational (i.e., rotational) preference in $[(\eta^5\text{-}C_9R_7)\text{-}ML_2L']$ complexes. The arrangement about the metal centre is such that the ligand with the greatest *trans* influence prefers a position *trans* to the ring junction carbons. For example, in $[(\eta\text{-}C_9H_7)Ir\{P(C_6H_5)_3\}_2(H)][BF_4]$ the hydride ligand, which has a greater *trans* influence than $[P(C_6H_5)_3]$, is *trans* to the C_{3a-7a} bond in the solid state (20). A similar arrangement of ligands is observed in a number of other complexes, including a series of $[(\eta^5\text{-}C_9H_7)Co(\eta^5\text{-}R_2C_2B_9H_9)]$ complexes (22), in which a *cisoid* arrangement of indenyl and carboranyl ligands is preferred. The consequence of having a ligand with a greater *trans* influence *trans* to C_{3a}—C_{7a} is a reduction in the bonding between the metal and $C_{3a,7a}$, which is reflected in increased M—C distances to $C_{3a,7a}$. A more detailed examination of the structure shown in Fig. 2 indicates that the $PPhMe_2$ ligand (which has a higher *trans* influence than chloride) is *trans* to the six-membered ring.

Can. J. Chem. Downloaded from www.nrcresearchpress.com by 80.90.12.36 on 09/08/12
For personal use only.

Table 3. Atomic coordinates ($\times 10^4$) and equivalent isotropic displacement coefficients ($Å^2 \times 1000$) for $[(\eta^5\text{-}C_9Me_7)RhCl(\mu\text{-}Cl)]_2$, (**4**).

	x	y	z	U(eq)[a]
Rh(1)	1007.2(2)	583.3(3)	410.6(2)	15.2(1)
Cl(1)	1396.5(7)	−996(1)	1493.7(7)	26.6(4)
Cl(2)	−147.2(6)	1006(1)	648.6(7)	20.2(4)
C(1)	1154(3)	1748(4)	−532(3)	24(2)
C(2)	1109(3)	2524(4)	118(3)	26(2)
C(3)	1739(2)	2169(4)	936(3)	22(2)
C(3A)	2241(2)	1262(4)	761(3)	19(2)
C(4)	2951(2)	623(4)	1312(3)	21(2)
C(5)	3253(3)	−266(4)	947(3)	28(2)
C(6)	2873(3)	−581(5)	56(3)	28(2)
C(7)	2178(3)	−12(5)	−484(3)	26(2)
C(7A)	1861(2)	958(4)	−134(3)	19(2)
C(8)	589(3)	1854(6)	−1456(3)	39(2)
C(9)	506(3)	3533(5)	−16(4)	41(3)
C(10)	1849(3)	2760(5)	1762(3)	38(2)
C(11)	3325(3)	942(5)	−2245(3)	37(2)
C(12)	4007(3)	−979(6)	1509(4)	46(3)
C(13)	3236(4)	−1588(6)	−292(5)	51(3)
C(14)	1738(3)	−384(6)	−1401(3)	48(3)

[a]Equivalent isotropic U defined as one third of the trace of the orthogonalized U_{ij} tensor.

Fig. 2. The ORTEP diagram of the molecular structure of **6.** Hydrogen atoms have been omitted for clarity.

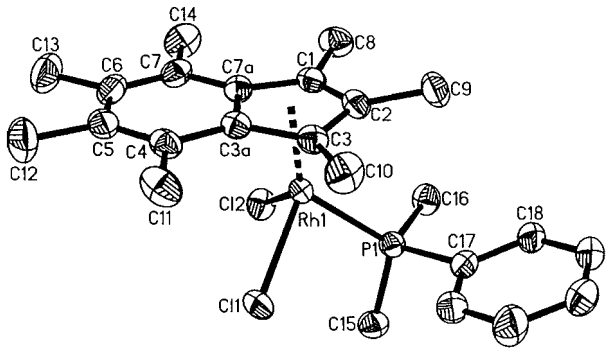

The ring C—C distances in **4** and **6** are shown in Fig. 3. It is clear that the average C_4—C_5, C_6—C_7 distances (1.375(7) Å) is shorter than the C_5—C_6 distance (1.442(7) Å) in **4** by 0.067 Å. The difference between these two distances is less in **6**, at 0.041 Å (1.387(5) Å and 1.428(5) Å for average (C_4—C_5, C_6—C_7) and C_5—C_6 distance, respectively), than in **4**. From these data it can be inferred that there is a more localized diene-like structure for the six-membered ring in **4** than in **6.** This trend is consistent with the slip–fold parameters described above, and comparable to the trends observed in η^5 and η^3 bis(indenyl) metal complexes (7).

Formation of $[(\eta^5\text{-}C_9Me_7)Rh(PMe_3)_2Cl][Cl^-]$ (8)

Treatment of **4** with 4 equivalents of PMe_3 results in the initial formation of an orange solution from which **8** precipitated in a quantitative yield. It was characterized by ^1H, $^{13}C\{^1H\}$, and $^{31}P\{^1H\}$, NMR spectroscopy, and by elemental analysis,

Table 4. Atomic coordinates ($\times 10^4$) and equivalent isotropic displacement coefficients ($Å^2 \times 1000$) for $[Ind^*Rh(PMe_2Ph)Cl_2]$, (**6**)

	x	y	z	U(eq)[a]
Rh(1)	5618.7(2)	8014.5(1)	6928.0(1)	23.83(5)
Cl(1)	5702.6(11)	9245.2(4)	7805.8(5)	36.3(2)
Cl(2)	3175.1(9)	8377.0(6)	6409.2(5)	37.6(2)
P(1)	4288.3(10)	7283.4(5)	7826.5(4)	28.4(2)
C(1)	6361(3)	7184(2)	5994(2)	30.1(8)
C(2)	7230(3)	6989(2)	6667(2)	30.5(8)
C(3)	8017(3)	7764(2)	6905(2)	29.6(7)
C(3A)	7822(3)	8416(2)	6300(2)	27.2(8)
C(4)	8414(3)	9279(2)	6210(2)	33.0(9)
C(5)	7969(4)	9759(2)	5566(2)	38(1)
C(6)	6921(4)	9413(2)	5021(2)	38(1)
C(7)	6323(4)	8585(2)	5094(2)	34.9(9)
C(7A)	6793(3)	8073(2)	5736(2)	28.1(7)
C(8)	5446(5)	6519(3)	5557(2)	44(1)
C(9)	7390(5)	6103(2)	7020(3)	42(1)
C(10)	9085(4)	7786(3)	7577(2)	45(1)
C(11)	9503(4)	9626(2)	6804(3)	45(1)
C(12)	8579(7)	10666(3)	5427(4)	63(2)
C(13)	6462(7)	9992(3)	4344(3)	59(2)
C(14)	5224(5)	8206(3)	4521(3)	51(1)
C(15)	2969(4)	7964(3)	8351(2)	39(1)
C(16)	3122(4)	6429(2)	7419(2)	37(1)
C(17)	5420(4)	6785(2)	8584(2)	31.9(8)
C(18)	5427(5)	5885(2)	8733(2)	38(1)
C(19)	6345(5)	5543(2)	9302(2)	44(1)
C(20)	7269(5)	6081(3)	9721(2)	49(1)
C(21)	7281(5)	6973(3)	9576(2)	53(1)
C(22)	6365(5)	7320(2)	9014(2)	43(1)

[a] Equivalent isotropic U defined as one third of the trace of the orthogonalized U_{ij} tensor.

which indicate that **8** should be formulated as $[(\eta^5\text{-}C_9Me_7)Rh(PMe_3)_2Cl][Cl^-]$. The $^{31}P\{^1H\}$ and $^{13}C\{^1H\}$ NMR spectra showed obvious disparities from those for **5–7**. The chemical shift of the phosphines in **8** is downfield by ~18 ppm from that in **5–7**. Carbons 1, 2, 3, 3a, and 7a also exhibit a downfield shift in the ^{13}C NMR spectrum of **8**. The value of J_{Rh-P} in **8** is 7 Hz smaller than in **5**, presumably reflecting the opposing effects of better donor ligands *vs.* increasing positive charge at rhodium, with the latter being more important.

Conclusion

In conclusion, we have prepared and structurally characterized heptamethylindenyl ($[C_9Me_7^-]$, Ind*) analogues of $[Cp^*RhCl(\mu\text{-}Cl)]_2$ and $[Cp^*Rh(PR_3)Cl_2]$. These complexes are important starting materials in light of the enhanced reactivity of indenyl metal complexes compared with their Cp counterparts.

Experimental section

General procedures

All reactions were carried out under a nitrogen atmosphere in a glove box, except for the synthesis of **4**, which employed

Can. J. Chem. Downloaded from www.nrcresearchpress.com by 80.90.12.36 on 09/08/12
For personal use only.

Table 5. Selected bond distances and angles for [Ind*Rh(PMe_2Ph)Cl_2], (**6**).

Rh(1)—Cl(1)	2.420 (1)	Rh(1)—Cl(2)	2.421 (1)
Rh(1)—P(1)	2.253 (1)	Rh(1)—C(1)	2.160 (3)
Rh(1)—C(2)	2.175 (3)	Rh(1)—C(3)	2.173 (3)
Rh(1)—C(3A)	2.328 (3)	Rh(1)—C(7A)	2.314 (3)
P(1)—C(15)	1.814 (4)	P(1)—C(16)	1.814 (4)
P(1)—C(17)	1.822 (3)	C(1)—C(2)	1.431 (4)
C(1)—C(7A)	1.482 (4)	C(1)—C(8)	1.507 (5)
C(2)—C(3)	1.438 (4)	C(2)—C(9)	1.495 (5)
C(3)—C(3A)	1.456 (4)	C(3)—C(10)	1.503 (5)
C(3A)—C(4)	1.431 (4)	C(3A)—C(7A)	1.439 (4)
C(4)—C(5)	1.392 (5)	C(4)—C(11)	1.510 (5)
C(5)—C(6)	1.428 (5)	C(5)—C(12)	1.511 (6)
C(6)—C(7)	1.382 (5)	C(6)—C(13)	1.525 (6)
C(7)—C(7A)	1.423 (4)	C(7)—C(14)	1.510 (6)
C(17)—C(18)	1.401 (4)	C(17)—C(22)	1.391 (5)
C(18)—C(19)	1.383 (5)	C(19)—C(20)	1.371 (6)
C(20)—C(21)	1.387 (6)	C(21)—C(22)	1.376 (6)

Cl(1)—Rh(1)—Cl(2)	94.7(1)	Cl(1)—Rh(1)—P(1)	88.3(1)
Cl(2)—Rh(1)—P(1)	84.0(1)	Cl(1)—Rh(1)—C(1)	156.6(1)
Cl(2)—Rh(1)—C(1)	97.7(1)	P(1)—Rh(1)—C(1)	112.7(1)
Cl(1)—Rh(1)—C(2)	132.1(1)	Cl(2)—Rh(1)—C(2)	133.1(1)
P(1)—Rh(1)—C(2)	97.6(1)	Cl(1)—Rh(1)—C(2)	38.5(1)
Cl(1)—Rh(1)—C(3)	96.8(1)	Cl(2)—Rh(1)—C(3)	156.9(1)
P(1)—Rh(1)—C(3)	116.3(1)	C(1)—Rh(1)—C(3)	65.2(1)
C(2)—Rh(1)—C(3)	38.6(1)	Cl(1)—Rh(1)—C(3A)	93.5(1)
Cl(2)—Rh(1)—C(3A)	121.8(1)	P(1)—Rh(1)—C(3A)	153.8(1)
C(1)—Rh(1)—C(3A)	63.1(1)	C(2)—Rh(1)—C(3A)	62.3(1)
C(3)—Rh(1)—C(3A)	37.6(1)	Cl(1)—Rh(1)—C(7A)	121.0(1)
Cl(2)—Rh(1)—C(7A)	93.9(1)	P(1)—Rh(1)—C(7A)	150.7(1)
C(1)—Rh(1)—C(7A)	38.5(1)	C(2)—Rh(1)—C(7A)	62.9(1)
C(3)—Rh(1)—C(7A)	62.9(1)	C(3A)—Rh(1)—C(7A)	36.1(1)
Rh(1)—P(1)—C(15)	113.7(1)	Rh(1)—P(1)—C(16)	113.1(1)
C(15)—P(1)—C(16)	103.6(2)	Rh(1)—P(1)—C(17)	114.4(1)
C(15)—P(1)—C(17)	103.9(2)	C(16)—P(1)—C(17)	107.2(2)
Rh(1)—C(1)—C(2)	71.3(2)	Rh(1)—C(1)—C(7A)	76.4(2)
C(2)—C(1)—C(7A)	107.1(3)	Rh(1)—C(1)—C(8)	127.4(2)
C(2)—C(1)—C(8)	124.1(3)	C(7A)—C(1)—C(8)	127.6(3)
Rh(1)—C(2)—C(1)	70.2(2)	Rh(1)—C(2)—C(3)	70.6(2)
C(1)—C(2)—C(3)	109.0(3)	Rh(1)—C(2)—C(9)	129.3(2)
C(1)—C(2)—C(9)	125.0(3)	C(3)—C(2)—C(9)	125.8(3)
Rh(1)—C(3)—C(2)	70.8(2)	Rh(1)—C(3)—C(3A)	77.0(2)
C(2)—C(3)—C(3A)	107.5(3)	Rh(1)—C(3)—C(10)	127.3(2)
C(2)—C(3)—C(10)	123.3(3)	C(3A)—C(3)—C(10)	128.0(3)
Rh(1)—C(3A)—C(3)	65.4(2)	Rh(1)—C(3A)—C(4)	127.3(2)
C(3)—C(3A)—C(4)	131.8(3)	Rh(1)—C(3A)—C(7A)	71.4(2)
C(3)—C(3A)—C(7A)	108.2(3)	C(4)—C(3A)—C(7A)	119.9(3)
C(3A)—C(4)—C(5)	117.9(3)	C(3A)—C(4)—C(11)	119.2(3)
C(5)—C(4)—C(11)	122.9(3)	C(4)—C(5)—C(6)	121.3(3)
C(4)—C(5)—C(12)	120.6(4)	C(6)—C(5)—C(12)	118.1(4)
C(5)—C(6)—C(7)	122.2(3)	C(5)—C(6)—C(13)	117.9(3)
C(7)—C(6)—C(13)	120.0(4)	C(6)—C(7)—C(7A)	117.6(3)
C(6)—C(7)—C(14)	122.9(3)	C(7A)—C(7)—C(14)	119.5(3)
Rh(1)—C(7A)—C(1)	65.1(2)	Rh(1)—C(7A)—C(3A)	72.5(2)
C(1)—C(7A)—C(3A)	107.3(3)	Rh(1)—C(7A)—C(7)	125.7(2)
C(1)—C(7A)—C(7)	131.6(3)	C(3A)—C(7A)—C(7)	121.1(3)
P(1)—C(17)—C(18)	123.1(2)	P(1)—C(17)—C(22)	118.3(2)
C(18)—C(17)—C(22)	118.6(3)	C(17)—C(18)—C(19)	120.3(3)
C(18)—C(19)—C(20)	120.3(3)	C(19)—C(20)—C(21)	120.0(4)
C(20)—C(21)—C(22)	120.2(4)	C(17)—C(22)—C(21)	120.6(3)

Can. J. Chem. Downloaded from www.nrcresearchpress.com by 80.90.12.36 on 09/08/12
For personal use only.

standard Schlenk techniques. THF was dried and distilled from Na–benzophenone, and all deuterated solvents were freeze–pump–thaw degassed and distilled on a vacuum line. $RhCl_3 \cdot 3H_2O$ was obtained from Johnson Matthey Ltd., and the phosphine ligands were obtained from Strem Chemicals and used as received. Heptamethylindene was prepared according to the published procedure (8*a*, 9). ^1H, $^{13}C\{^1H\}$, and $^{31}P\{^1H\}$ NMR spectra were recorded on Bruker AC200 or AM250 spectrometers. ^1H and chemical shifts are reported in ppm relative to external TMS and referenced to $CDCl_3$ residual proton and carbon resonances, respectively; coupling constants are in Hz. Multiplicities are reported as (br) broad, (s) singlet, (d) doublet, (t) triplet, and (m) multiplet. chemical shifts are reported relative to the external standard H_3PO_4.

Preparation of $[(\eta^5\text{-}C_9Me_7)RhCl(\mu\text{-}Cl)]_2$ (4)

A mixture of heptamethylindene (C_9Me_7H, 260 mg, 1.2 mmol) and $RhCl_3 \cdot 3H_2O$ (250 mg, 0.95 mmol) in methanol (15 mL) and water (0.5 mL) was refluxed for 48 h. After removing the volatiles *in vacuo*, the dark red solid was washed with hexane (to remove excess heptamethylindene), and then extracted into toluene. On cooling to –40°C, compound **4** (276 mg, 67% yield) was obtained as a dark red solid. A single, dark ruby, polyhedral crystal suitable for X-ray diffraction was grown by slow evaporation of a $CHCl_3$ solution, which also produced analytically pure material. ^1H NMR ($CDCl_3$, 250 MHz), δ: 1.56 (s, 6H, CH_3), 1.95 (s, 12H, CH_3), 2.04 (s, 12H, CH_3), 2.52 (s, 12H, CH_3). $^{13}C\{^1H\}$ NMR ($CDCl_3$, 63 MHz), δ: 10.2, 13.3, 17.7, 18.4 (s, CH_3), 81.0 (br d, $C_{1,3}$), 95.1 (d, $J_{Rh-C} = 7$ Hz, C_2), 102.5 (d, $J_{Rh-C} = 9$ Hz, $C_{3a,7a}$), 130.4, 143.5 (s, C_{4-7}). Anal. calcd. for $C_{32}H_{42}Rh_2Cl_4$: C 49.64, H 5.47; found: C 49.78, H 5.53.

Preparation of $[(\eta^5\text{-}C_9Me_7)Rh(PMe_3)Cl_2]$ (5)

Compound **4** (32 mg, 0.04 mmol) was reacted with PMe_3 (9 μL, 0.08 mmol) in THF (10 mL) for 24 h. The solvent was removed *in vacuo* and the solid obtained was recrystallized from a THF–hexane mixture at –40°C. Complex **6** (38 mg, 99% yield) was obtained as an orange solid. $^{31}P\{^1H\}$NMR ($CDCl_3$, 81 MHz), δ: 26.7 (d, $J_{Rh-P} = 145$ Hz). ^1H NMR ($CDCl_3$, 200 MHz), δ: 1.58 (d, $J_{P-H} = 12.5$ Hz, 9H, PMe_3), 1.92 (s, 9H, CH_3), 2.16 (s, 6H, CH_3), 2.53 (s, 6H, CH_3). $^{13}C\{^1H\}$ NMR ($CDCl_3$, 50 MHz), δ: 10.2 (s, 1 CH_3), 13.3 (s, 2 CH_3), 15.4 (d, $J_{P-C} = 37$ Hz, PMe_3), 17.5 (br s, 4 CH_3), 82.1 (d, $J_{Rh-C} = 8$ Hz, $C_{1,3}$), 105.3 (s, C_2), 111.2 (d, $J_{Rh-C} = 3$ Hz, $C_{3a,7a}$), 130.2, 140.1 (s, C_{4-7}). Anal. calcd. for $C_{19}H_{30}RhCl_2P$: C 49.27, H 6.53; found: C 49.37, H 6.89.

Preparation of $[(\eta^5\text{-}C_9Me_7)Rh(PMe_2Ph)Cl_2]$ (6)

Compound **4** (35 mg, 0.05 mmol) was reacted with $PPhMe_2$ (13 μL, 0.09 mmol) in THF (10 mL) for 24 h. Following work-up as for **5**, complex **6** (47 mg, 99% yield) was obtained as an orange solid. A single, pale yellow, prismatic crystal suitable for X-ray diffraction was grown by slow evaporation of a THF solution under N_2 in a glove box. Recrystallization of the material from CH_2Cl_2–Et_2O results in the incorporation of CH_2Cl_2 into the complex. $^{31}P\{^1H\}$ NMR ($CDCl_3$, 81 MHz); δ 28.6 (d, $J_{Rh-P} = 149$ Hz). ^1H NMR ($CDCl_3$, 200 MHz), δ: 1.32 (dd, $J_{P-H} = 5.4$ Hz, $J_{Rh-H} = 1.7$ Hz, 3H, CH_3), 1.72 (s, 6H, CH_3), 1.88 (dd, $J_{P-H} = 13$ Hz, $J_{Rh-H} = 0.8$ Hz, 6H, PPhMe_2), 2.21 (d, $J_{P-H} = 2$ Hz, 6H, CH_3), 2.56 (s, 6H, CH_3), 7.46 (m, 3H, P$PhMe_2$), 7.95 (m, 2H, P$PhMe_2$). $^{13}C\{^1H\}$ NMR ($CDCl_3$, 50 MHz), δ: 8.7 (s, 1 CH_3), 13.0 (s, 2 CH_3), 14.4 (d, $J_{P-C} = 39$ Hz, PPhMe_2), 17.5 (br s, 4 CH_3), 82.4 (d, $J = 8$ Hz, $C_{1,3}$), 104.6 (s, C_2), 111.0 (s, $C_{3a,7a}$), 128.2 (d, $J_{P-C} = 10$ Hz, P$PhMe_2$), 131.0 (d, $J_{P-C} = 10$ Hz, P$PhMe_2$), 131.2 (s, P$PhMe_2$), 133.7 (s, P$PhMe_2$), 130.2, 140.4 (s, C_{4-7}). Anal. calcd. for $\{C_{24}H_{32}RhCl_2P\}_4CH_2Cl_2$: C 53.29, H 5.99; found: C 53.34, H 6.10.

Preparation of $[(\eta^5\text{-}C_9Me_7)Rh(PPh_3)Cl_2]$ (7)

Compound **4** (35 mg, 0.05 mmol) was reacted with PPh_3 (24 mg, 0.09 mmol) in THF (10 mL) for 24 h. Following work-up as for **5**, complex **7** (58 mg, 99% yield) was obtained as an orange solid. $^{31}P\{^1H\}$ NMR ($CDCl_3$, 81 MHz), δ: 40.7 (d, $J_{Rh-P} = 157$ Hz). ^1H NMR ($CDCl_3$, 200 MHz), δ: 1.24(dd, $J_{P-H} = 4.6$ Hz, $J_{Rh-H} = 1.4$ Hz, 3H, CH_3), 1.60(s, 6H, CH_3), 2.17 (t, $J_{P-H} = J_{Rh-H} = 1.4$ Hz, 6H, CH_3), 2.56 (s, 6H, CH_3), 7.25 (br s, 9H, P(C_6H_5)$_3$), 7.69 (m, 6H, P(C_6H_5)$_3$). $^{13}C\{^1H\}$ NMR ($CDCl_3$, 50 MHz), δ: 9.22 (s, 1 CH_3), 13.0 (s, 2 CH_3), 17.8 (s, 2 CH_3), 18.0 (s, 2 CH_3), 84.7 (d, $J = 8$ Hz, $C_{1,3}$), 105.6 (d, $J = 7$ Hz, C_2), 109.8 (s, $C_{3a,7a}$), 127.8 (v br s, P(C_6H_5)$_3$), 134.8 (d, $J_{P-C} = 9$ Hz, P(C_6H_5)$_3$), 130.8, 141.4 (s, C_{4-7}). Anal. calcd. for $C_{34}H_{36}RhCl_2P$: C 62.88, H 5.59; found: C 62.89, H 5.49.

Preparation of $[(\eta^5\text{-}C_9Me_7)Rh(PMe_3)_2Cl]^+[Cl^-]$ (8)

Compound **4** (35 mg, 0.05 mmol) was reacted with PMe_3 (21 μL, 0.2 mmol) in THF (10 mL) for 48 h. The resulting precipitate was collected by filtration and dried *in vacuo*. Complex **8** (49 mg, 99% yield) was obtained as a yellow solid. $^{31}P\{^1H\}$ NMR $CDCl_3$, 81 MHz), δ: 8.7 (d, $J_{Rh-P} = 138$ Hz). ^1H NMR ($CDCl_3$, 200 MHz), δ: 1.58 (t, $J = 5.7$ Hz, 18H, PMe_3), 2.10 (t, $J_{P-H} = 2$ Hz, 9H, CH_3), 2.12 (s, 6H, CH_3), 2.49 (s, 6H, CH_3). $^{13}C\{^1H\}$ NMR ($CDCl_3$, 50 MHz), δ: 11.1 (s, 1 CH_3), 13.9 (s, 2 CH_3), 16.3 (m, 2 PMe_3), 17.2 (s, 4 CH_3), 88.9 (s, $C_{1,3}$), 113.4 (s, C_2), 116.4 (s, $C_{3a,7a}$), 129.2, 141.4 (s, C_{4-7}). Anal. calcd. for $C_{22}H_{39}RhCl_2P_2$: C 49.00, H 7.29; found: C 49.12, H 7.40.

A summary of the crystal data for compounds **4** and **6** is given in Table 1. The data were collected on a Nicolet–Siemens R3m/V diffractometer equipped with graphite-monochromated Mo Kα radiation and a Nicolet LT2 low-temperature device. Accurate unit-cell parameters were derived from 25 general reflections well distributed in reciprocal space. Background measurements were made at the beginning and end of each scan for a total time equal to half the scan time. Crystal stability was monitored by measuring two standard reflections every 100 data; only statistical fluctuations (±2%) were observed. Data were corrected for Lorentz and polarization effects and absorption (for **4**, face indexed analytical, transmission factors 0.8558–0.9186; for **6**, ψ-scan, semi-empirical). The structures were solved by Patterson and Fourier techniques, and refined by full-matrix least-squares methods using Siemens SHELXTL PLUS software (24), the function minimized being $\Sigma w(|F_o|-|F_c|)^2$. Difference Fourier synthesis provided the location of all hydrogen atoms, which were included in the refinement with isotropic thermal parameters. A total of 194 and 382 parameters were refined for **4** and **6**, respectively, with data:parameter ratios of 10.9:1 and 9.3:1. During the final cycles of refinement, a weighting scheme of the form $w^{-1} = \sigma^2(F)$ was included. Refinement of the inverse enantiomorph of **6** gave significantly higher R values, $R = 2.55$, $R_w = 2.79\%$. Scattering factors used, including the anom-

Fig. 3. The C—C bond lengths (Å) in Ind* rings of **4** and **6**.

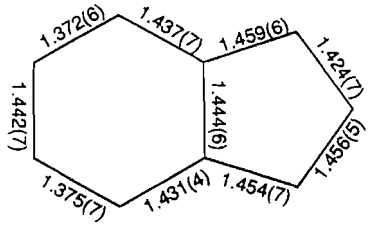

4

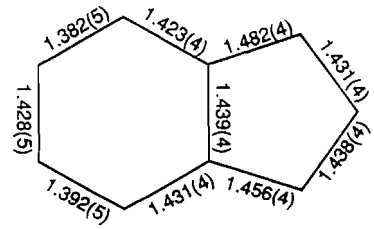

6

alous dispersion corrections for rhodium, were taken from the International Tables, Vol. 4 (25). Details of the crystal structure determination including complete tables of coordinates, bond distances and angles, and anisotropic thermal parameters have been deposited.[4]

Acknowledgments

We thank the Natural Sciences and Engineering Research Council of Canada and Imperial Oil Ltd. for support, Johnson Matthey Ltd. for a loan of rhodium chloride, and Professor William D. Jones (University of Rochester) for helpful discussions.

References

1. R. Poli. Chem. Rev. **91**, 509 (1991).
2. (*a*) J.W. Kang and P.M. Maitlis. J. Am. Chem. Soc. **90**, 3259 (1968); (*b*) J.W. Kang, K. Moseley, and P.M. Maitlis. Chem. Commun. 1304 (1968); (*c*) J. Am. Chem. Soc. **91**, 5970 (1969); (*d*) B.L Booth, R.N. Haszeldine, and M. Hall. J. Chem. Soc. A, 1299 (1969); (*e*) I.R. Lyatifov, G.M. Dzhafarov, and T. Kh. Kurbanov. J. Gen. Chem. USSR, **59**, 1606 (1989); (*f*) C. White, S.J Thompson, and P.M. Maitlis. J. Chem. Soc. Dalton Trans. 1654 (1977); (*g*) P.M. Maitlis. Acc. Chem. Res. **11**, 301 (1978); (*h*) M.R. Churchill, S.A. Julis, and F.J. Rotella. Inorg. Chem. **16**, 1137 (1977).
3. T.K. Miyamoto, M. Tsutsui, and L.-B Chen. Chem. Lett. 729 (1981).
4. M. Tsutsui, L.-B. Chen, D.E. Bergbreiter, and T.K. Miyamoto. J. Am. Chem. Soc. **104**, 855 (1982).
5. M.E. Rerek and F. Basolo. J. Am. Chem. Soc. **106**, 5908 (1984).
6. (*a*) A.K. Kakkar, N.J. Taylor, J.C. Calabrese, W.A. Nugent, D.C. Roe, E.A. Connaway, and T.B. Marder. J. Chem. Soc. Chem. Commun. 990 (1989); (*b*) A.K. Kakkar, S.F Jones, N.J. Taylor, S. Collins, and T.B. Marder. J. Chem. Soc. Chem. Commun. 1454 (1989).
7. S.A. Westcott, A.K. Kakkar, G. Stringer, N.J. Taylor, and T.B. Marder. J. Organomet. Chem. **394**, 777 (1990).
8. D. O'Hare, J.C. Green, T. B. Marder, S Collins, G. Stringer, A.K. Kakkar, N. Kaltsoyannis, A. Kuhn, R. Lewis, C. Menhert, P. Scott, M. Kurmoo, and S. Pugh. Organometallics, **11**, 48 (1992); (*b*) D. O'Hare, V.J. Murphy, and N. Kaltsoyannis. J. Chem. Soc. Dalton Trans. 383 (1993).
9. A.K. Kakkar, Ph.D. Thesis, University of Waterloo, 1990.
10. A.K. Kakkar, N.J Taylor, T.B. Marder, J.K. Shen, N. Hallinan, and F. Basolo. Inorg. Chim. Acta, **198–200**, 219 (1992).
11. F.G. Bordwell and M. Bausch. J. Am. Chem. Soc. **105**, 6188 (1983).
12. (*a*) A.J. Hart-Davis and R. Mawby. J. Chem. Soc. A, 2403 (1969); (*b*) C. White and R. Mawby. Inorg. Chim. Acta, **4,** 261 (1970); (*c*) C. White, R. Mawby, and A.J. Hart-Davis. Inorg. Chim. Acta, **4**, 441 (1970); (*d*) P. Caddy, M. Green, E. O'Brien, L.E. Smart, and P. Woodward. Angew. Chem. Int. Ed. Engl. **16**, 648 (1977); (*e*) H. Eshtiagh-Hosseini and J.F. Nixon. J. Less-Common Met. **61**, 107 (1978); (*f*) P. Caddy, M. Green, E. O'Brien, L.E. Smart, and P.Woodward. J. Chem. Soc. Dalton Trans. 962 (1980); (*g*) M.E. Rerek, L.N. Ji, and F. Basolo. J. Chem. Soc. Chem. Commun. 1208 (1983); (*h*) L.N. Ji, M.E. Rerek, and F. Basolo. Organometallics, **3**, 740 (1984); (*i*) N.N. Turaki, J.M. Huggins, and L. Lebioda. Inorg. Chem. **27**, 424 (1988); (*j*) H. Bang, T.J. Lynch, and F. Basolo. Organometallics, **11**, 40 (1992).
13. (*a*) T.B. Marder and I.D. Williams. J. Chem. Soc. Chem. Commun. 1478 (1987); (*b*) A.K. Kakkar, N.J. Taylor, and T.B. Marder. Organometallics, **8**, 1765 (1989).
14. (*a*) J.M. O'Connor and C.P. Casey. Chem. Rev. **87,** 307 (1987); (b) F. Basolo. Polyhedron, **9**, 1503 (1990).
15. (*a*) P. Caddy, M. Green, L.E. Smart, and N. White. J. Chem. Soc. Chem. Commun. 839 (1978); (*b*) A. Borrini, P. Diversi, G. Ingrosso, A. Lucherini, and G. Serra. J. Mol. Catal. **30**, 181 (1985); (*c*) A. Ceccon, A. Gambaro, S. Santi, and A. Venzo. J. Mol. Catal. **69,** L1 (1991).
16. (*a*) H. Bonneman. Angew. Chem. Int. Ed. Engl. **24,** 248 (1985); (*b*) H. Bonneman and W. Brijoux. *In* Aspects of homogeneous catalysis. Vol. 5. *Edited by* R. Ugo. D. Riedel, Dordrecht, The Netherlands. 1984. p. 75; (*c*) P. Cioni, P. Diversi, G. Ingrosso, A. Lucherini, and P. Ronca. J. Mol. Catal. **40,** 337 (1987).
17. T.B. Marder, D.C. Roe, and D. Milstein. Organometallics, **7**, 1451 (1988).
18. T.M. Frankcom, J.C. Green, A. Nagy, A.K. Kakkar, and T.B. Marder. Organometallics, **12**, 3688 (1993).
19. (*a*) T.B. Marder, J.C. Calabrese, D.C. Roe, and T.H. Tulip. Organometallics, **6,** 2012 (1987); (*b*) R.T. Carl, R.P. Hughes, A.L. Rheingold, T.B. Marder, and N.J. Taylor. Organometallics, **7**, 1613 (1988).
20. J.W. Faller, R.H. Crabtree, and A. Habib. Organometallics, **4**, 929 (1985).
21. R.T. Baker and T.H. Tulip. Organometallics, **5**, 839 (1986).
22. (*a*) D.E. Smith and A.J. Welch. Organometallics, **5**, 760 (1986); (*b*) Z.G. Lewis, D. Reed, and A.J. Welch. J. Chem. Soc. Dalton Trans, 731 (1992).

[4] A complete set of data may be purchased from: The Depository of Unpublished Data, Document Delivery, CISTI, National Research Council Canada, Ottawa, Canada ON K1A 0S2.

Tables of bond lengths and angles and atomic coordinates have also been deposited with the Cambridge Crystallographic Data Centre, and can be obtained on request from The Director, Cambridge Crystallographic Data Centre, University Chemical Laboratory, 12 Union Road, Cambridge, CB2 1EZ, U.K.

Structure factor amplitudes are no longer being deposited and may be obtained directly from the author.

Can. J. Chem. Downloaded from www.nrcresearchpress.com by 80.90.12.36 on 09/08/12
For personal use only.

23. A. Ceccon, C.J. Elsevier, J.M. Ernstang, A. Gambaro, S. Santi, and A. Venzo. Inorg. Chim. Acta, **204**, 15 (1993), and references therein.
24. G.M. Sheldrick. SHELXTL PLUS, Copyright 1990, Siemens Analytical Instruments.
25. International tables for X-ray crystallography. Vol IV. Kynoch Press, Birmingham, England. 1974.

Can. J. Chem. Downloaded from www.nrcresearchpress.com by 80.90.12.36 on 09/08/12
For personal use only.

A density functional study on olefin insertion and hydrogen transfer in the reaction between Cl_2Ti^+–ethyl and ethylene. Possible implications for the stereochemistry and chain termination in olefin polymerization

Liangyou Fan, Daryll Harrison, Liqun Deng, Tom K. Woo, David Swerhone, and Tom Ziegler

Can. J. Chem. Downloaded from www.nrcresearchpress.com by 80.90.12.36 on 09/08/12
For personal use only.

Abstract: Calculations based on density functional theory have been carried out on the reaction between Cl_2Ti^+–ethyl (**1**) and ethylene. In this study **1** was taken as a model for the cationic metallocenes of group-4 elements, which have been developed by Kaminsky and Brintzinger as efficient catalysts for the polymerization of olefins. The ground state structure of **1** has a β-agostic conformation in which a single C_β—H bond is directed towards the metal center. It was assumed that this conformation also serves as a model for the resting state of the growing chain attached to the cationic group-4 metallocenes between insertions. Two paths were considered for the reaction between **1** and ethylene. The first (**2**) has ethylene approaching the agostic C_β—H bond, whereas ethylene in the second approach (**3**) attacks the Ti—C_α link from the side opposite to the C_β—H bond. The front-side attack (**2**) results in a transfer of hydrogen from the β-carbon of ethyl to ethylene and represents a chain-terminating step with an activation energy of 5.3 kcal/mol. It was not possible to locate a path leading to olefin insertion from the front-side attack (**2**). The back-side attack (**3**) resulted readily in insertion with an activation energy of 3.9 kcal/mol. The study made use of full transition state optimization as well as a tracing of the reaction paths by the intrinsic reaction coordinate (IRC) method of Fukui. Previous investigations have all assumed that olefin insertion takes place via a front-side approach (**2**) based on the known stereochemistry of α-olefin polymerization. The present study suggests that insertion takes place by a back-side approach (**3**), and this suggestion is discussed in connection with the known stereochemistry of olefin polymerization.

Key words: Ziegler–Natta, olefin polymerization, density functional.

Résumé : On a effectué des calculs basés sur la théorie de la densité fonctionnelle sur la réaction du Cl_2Ti^+–éthyl (**1**) et l'éthylène. Dans cette étude, on a utilisé le composé **1** comme modèle pour les métallocènes cationiques des éléments du groupe 4 qui ont été développées par Kaminsky et Brintzinger comme des catalyseurs efficaces pour la polymérisation des oléfines. La strucutre de l'état fondamental du composé **1** possède une conformation agostique-β dans laquelle la liaison simple C_β—H est dirigée vers le centre métallique. On a fait l'hypothèse que cette conformation sert aussi de modèle pour l'état au repos de la chaîne qui croît attachée au niveau des métallocènes cationiques du groupe 4 entre les insertions. On a considéré deux voies réactionnelles pour la réaction du composé **1** et l'éthylène. Dans la première (**2**), l'éthylène approche de la liaison C_β—H alors que dans la deuxième approche (**3**), l'éthylène attaque la liaison Ti—C_α à partir de la face opposée à la liaison C_β—H. L'attaque frontale (**2**) provoque un transfert d'hydrogène du carbone β du groupe éthyle de l'éthylène et elle correspond à une étape de terminaison de chaîne avec une énergie d'activation de 5,3 kcal/mol. Il n'a pas été possible de localiser une voie qui pourrait conduire à une insertion de l'oléfine par une attaque frontale (**2**). L'attaque par le côté (**3**) conduit facilement à une insertion avec une énergie d'activation de 3,9 kcal/mol. L'étude a utilisé une optimisation complète de l'état de transition ainsi qu'un tracé des voies réactionnelles par la méthode de la coordonnée réactionnelle intrinsèque de Fukui. En se basant sur la stéréochimie

Received October 7, 1994.

This paper is dedicated to Professor William A.G. Graham on the occasion of his 65th birthday.

L. Fan[1] **and D. Harrison.** Novacor Research & Technology Corporation, 2928-16 Street NE, Calgary, AB T2E 7K7, Canada.
L. Deng, T.K. Woo, D. Swerhone, and T. Ziegler.[1] Department of Chemistry, University of Calgary, Calgary, AB T2N 1N4, Canada.

[1] Authors to whom correspondence may be addressed.

bien connue de la polymérisation des α-oléfines, les études antérieures avaient toujours fait l'hypothèse que l'insertion se fait par une approche frontale (**2**). La présente étude suggère que l'insertion se produit par une approche par l'arrière (**3**) et on discute de cette suggestion en liaison avec la stéréochimie bien connue de la polymérisation des oléfines.

Mots clés : Ziegler–Natta, polymérisation des oléfines, densité fonctionnelle.

[Traduit par la rédaction]

1. Introduction

Metallocene-based systems (**1**) for olefin polymerization have started and will likely continue over the next several years to replace conventional Ziegler–Natta catalyst systems. Metallocene-based products, both conventional and new polymers, are appearing on the market more and more frequently. Metallocene plastics have several unique and desirable properties. Uniformity of the active site in these systems leads to greater uniformity of the polymer microstructure and molecular weight distribution. Additionally, comonomer incorporation with metallocene catalysts is generally uniform throughout the spectrum of molecular weights. Of particular promise have been the cationic metallocenes of group-4 elements first developed by Kaminsky and Brintzinger (1a) as well as by others (1). The cationic catalysts are often generated from neutral dichloro metallocenes of group-4 elements by reaction with a cocatalyst such as methylaluminoxane (MAO) according to eq. [1].

[1]

The polymer is formed in subsequent reactions between olefin and the cationic alkyl species according to eq. [2].

[2] 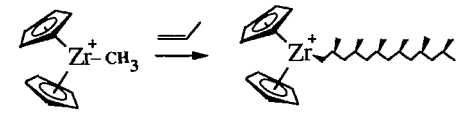

Also, part of the "metallocene revolution" are the half-sandwich constrained geometry catalysts (CGC) as exemplified in recent patent claims of Dow and Exxon (2b,c).

The Cossee–Arlman mechanism (3) is the most widely accepted mechanism for both Ziegler–Natta olefin polymerization and olefin polymerization by Kaminsky-type catalysts. The Cossee–Arlman polymerization mechanism for metallocenes is given in eq. [3].

[3] 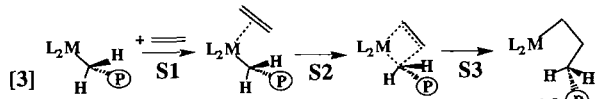

1a Active complex — **1b** π-Complex — **1c** Transition state — **1d** γ-Agostic alkyl product

The active species **1a** possesses a vacant coordination site, and for the group-4 transition metal (Ti, Zr, Hf) catalysts this is the alkylated cationic metallocene. The first step of the process involves the complexation of olefin to form a π complex **1b**. In the second step, the olefin inserts into the metal–carbon bond through a four-membered cyclic transition state, **1c**. The newly formed species, **1d**, possesses a vacant coordination site where the M—C bond was formerly located in **1a**.

The Cossee–Arlman mechanism, although well accepted and understood in a conceptual sense, is not fully understood in a mechanistic sense. For example, the exact nature of the active species and the role of the cocatalyst and (or) counterion is a subject of debate. The current belief is (4) that the active species is a cationic complex such as $[Cp_2ZrR^+]$. Jordan and co-workers (5*a*) detected that the benzyl species, $[Cp_2Zr(CH_2Ph)]^+$, catalyzes ethylene polymerization. The role of the cocatalyst, usually MAO, is even less understood. It is thought that the cocatalyst may act only to generate the active species and remove impurities from the system. On the other hand, it may play a more fundamental role such as assisting in the insertion of each monomer unit or reactivating dormant sites.

Molecular modeling has been used extensively in studies of the steps involved in olefin polymerization. Molecular mechanics simulations have so far focused on the stereoregularity of polyolefins by analyzing the steric repulsion at the assumed transition state, **1c**, for the olefin insertion step in the Cossee mechanism (6, 7). A number of *ab initio* (8), semi-empirical (9), and density functional theory (10) (DFT) methods have been employed in studies of the electronic factors of importance in the Cosse mechanism. The active catalytic species in the electronic studies were assumed to be unsaturated cations, L_2MR^+, where M is a group-4 transition metal and the growing chain R is represented by CH_3, whereas L_2 varies from Cl_2, bis-cyclopentadienyl (Cp), to bridged bis-Cp's. The possible influence of the solvent and the counterion (cocatalyst) was ignored in those calculations.

One of the recurring problems encountered in modeling of the insertion process is associated with a lack of structural information about the active species **1a** of eq. [3]. Thus, little is known about the coordination geometry of the growing chain attached to the L_2M fragment in its resting state between insertions. Calculations on L_2MR^+ systems in which R is either ethyl or propyl have revealed that the most stable structure has a β-agostic conformation, **2a**, in which a single C_β—H bond is directed towards the metal center. Of somewhat higher energy is the γ-agostic species, **2b**. It is the objective of this investigation to look at **2a** as a possible resting state for **1a** with R′ representing the growing chain. A β-agostic conformation has been established by Bercaw and co-workers for $Cp^*2Sc(Et)$ (5*b*,*c*)

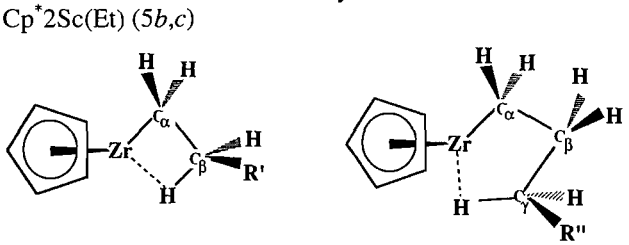

2a **2b**

With **2a** as a model for the resting state of **1a**, one might envision two insertion paths for an approaching olefin. The

Can. J. Chem. Downloaded from www.nrcresearchpress.com by 80.90.12.36 on 09/08/12
For personal use only.

Can. J. Chem. Downloaded from www.nrcresearchpress.com by 80.90.12.36 on 09/08/12
For personal use only.

first, **3a**, involves an approach of olefin towards the Zr—H agostic bond. It will be refered to as the front attack. The second, **3b**, has olefin attacking the Zr—C_α bond, and will be referred to as the back-side attack. We shall investigate both paths in detail.

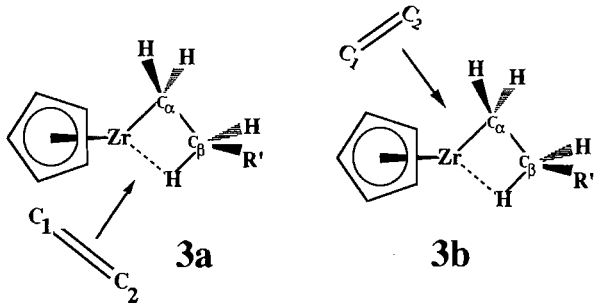

The study will be based on density functional theory (DFT) with the ML_2 moiety modeled by $ZrCl_2^+$ and R' represented by hydrogen. These simplifications allow us to carry out transition state optimizations for the two steps shown in **3a** and **3b**, and to follow the reaction paths by the intrinsic reaction coordinate method of Fukui (11). The IRC method traces the steepest decend paths connecting the transition state with reactants and products. The findings will be compared to the known stereochemistry of the insertion reaction in eq. [3] as well as some of the mechanisms postulated for chain termination of the polymerization process. Many of these issues could not be dealt with in previous quantum mechanical calculations (8–10) on olefin polymerization since the growing chain was modeled with a methyl group where β- and γ-agostic interactions are absent.

2. Computational details

The reported density functional calculations were all carried out by utilizing the program system ADF, developed by Baerends et al. (12, 13) and vectorized by Ravenek (14). The numerical integration procedure applied for the calculations was that of te Velde and co-workers (15). The geometry optimization procedure was based on the method developed by Versluis and Ziegler (16). The electronic configurations of the molecular systems were described by an uncontracted triple-ζ STO basis set (17) for the 3*s*,3*p*,3*d*, 4*s*, and 4*p* valence shells of titanium. Double-ζ STO basis sets (17) were used for carbon (2*s*, 2*p*), hydrogen (1*s*), and chlorine (3*s*, 3*p*). A single 3*d* polarization function was employed for carbon and chlorine whereas a 2*p* function was added to hydrogen. The $1s^22s^22p^6$ configuration on titanium, the $1s^2$ configuration on carbon, as well as the $1s^22s^2$ configuration on chlorine were assigned to the core and treated by the frozen-core approximation (12). A set of auxiliary (18) *s*, *p*, *d*, *f*, and *g* STO functions, centered on all nuclei, was used to fit the molecular density and to present Coulomb and exchange potentials accurately in each SCF cycle. Energy differences were calculated by augmenting the local exchange–correlation energy expression due to Vosko et al. (19) with Becke's nonlocal exchange corrections (20) and Perdew's nonlocal correlation correction (21). The nonlocal corrections were added as a perturbation, NL/P, based on a density obtained from a local calculation. Geometries were optimized without including nonlocal corrections. The application of approximate density functional theory to organometallic chemistry has been reviewed recently (22).

Some of the reactions described in this investigation were studied by the intrinsic reaction coordinate (IRC) method of Fukui (11) in which the transition state is connected to reactant(s) and product(s) by a steepest descend path. The paths can be written as **X**(*s*), where **X** is a nuclear configuration on the path, and |*s*| is the length of the paths from the transition state. Negative values of *s* indicate the direction towards reactant(s), and positive values of *s* the direction towards the product(s). The algorithm used to trace the IRC path was developed by Gonzalez and Schlegel (23). The implementation of the algorithm into the ADF program was carried out by Deng and Ziegler (24). The transition state search was based on the algorithm due to Banerjee et al. (25*a*) in the implementation by Baker (25*b*) and the adaptation for ADF by Fan and Ziegler (25*c*). We expect that the Cl_2Ti^+ fragment is electronically a good model for Cp_2Ti^+. On the other hand, the steric bulk of a Cp ring is not well represented by a chlorine atom.

3. Results and discussion

We shall in the following consider the β-agostic conformation of **2a** as a possible model for the resting state of the polymer attached to the metallocene between insertions. Conformation **2a** can be attacked by an olefin from either the front side, **3a**, or the back side, **3b**, and both approaches will be considered. The species **2a** is in this study represented by $Cl_2Ti^+–C_2H_5$, where the Cp rings have been replaced by chlorine ligands and R' by hydrogen. The β-agostic conformation of $Cl_2Ti^+–C_2H_5$ was optimized without any constraints, and the converged geometry shown in **4a** is virtually of C_s symmetry with a planar Ti-C_α-C_β-$H_{\bar{A}}$ frame. The interaction between the β-hydrogen of the ethyl group and the titanium metal center is visible from the elongated H—C_β bond of 1.16 Å and the Ti—H_β distance of 2.02 Å. The titanium center is tetrahedrally coordinated in **4a** if the β-hydrogen is considered as a normal ligand.

The Ti-C_α-C_β-H_i frame of **4a** can readily move in a plane perpendicular to the Cl_2Ti coordination plane with the normal vector ***x***, **4a**. In fact, another β-agostic structure was found at a C_α-Ti-X angle of 104°, **4b**. The β-agostic interaction in **4b** is even stronger than that in **4a**, which possesses a C_α-Ti-X angle of 33.5°. This is apparent from a longer C—H bond of 1.17 Å and a shorter Ti—H distance of 1.93 Å in **4b** compared to 1.16 and 2.02 Å, respectively, in **4a**. The ClTiCl angle is expanded from 113.8° in **4a** to 125.4° in **4b** due to the deformation from the tetrahedral configuration of the metal center. In terms of energy, **4a** is more stable than **4b** by 1.3 kcal/mol at the LN/P level of theory, most likely due to the distortion of **4b** from a tetrahedral geometry. A calculation of the energy profile leading from **4a** to **4b** reveals a gradual increase in energy. The facile movement of the Ti-C_α-C_β-H frame might provide some flexibility as the incoming olefin approach from the front side,**4a**, and in particular the back side, **4b**.

A detailed description of the two olefin approaches, **3a** and **3b**, is illustrated in Schemes 1 and 2, respectively. For the front-side attack, **3a**, the initial step is the formation of a π-complex, Scheme 1. After the π-complex is formed the process can follow either of the routes A or B. Route A is in accordance with the Cossee mechanism, i.e., olefin insertion is achieved via a four-centered transition state. Route B involves

Can. J. Chem. Downloaded from www.nrcresearchpress.com by 80.90.12.36 on 09/08/12
For personal use only.

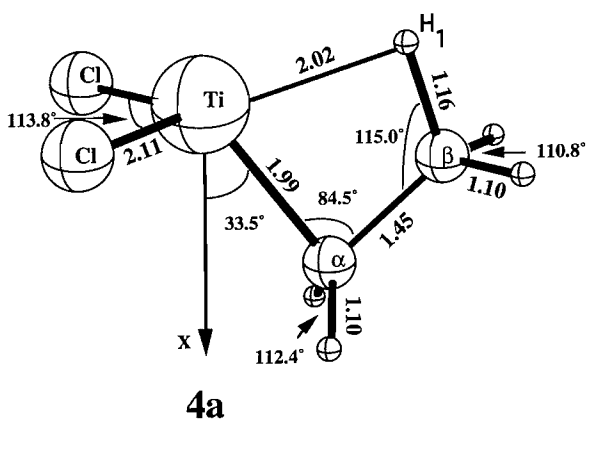

4a

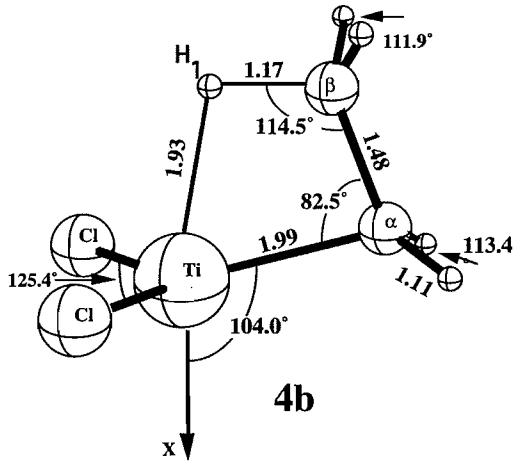

4b

Scheme 1.

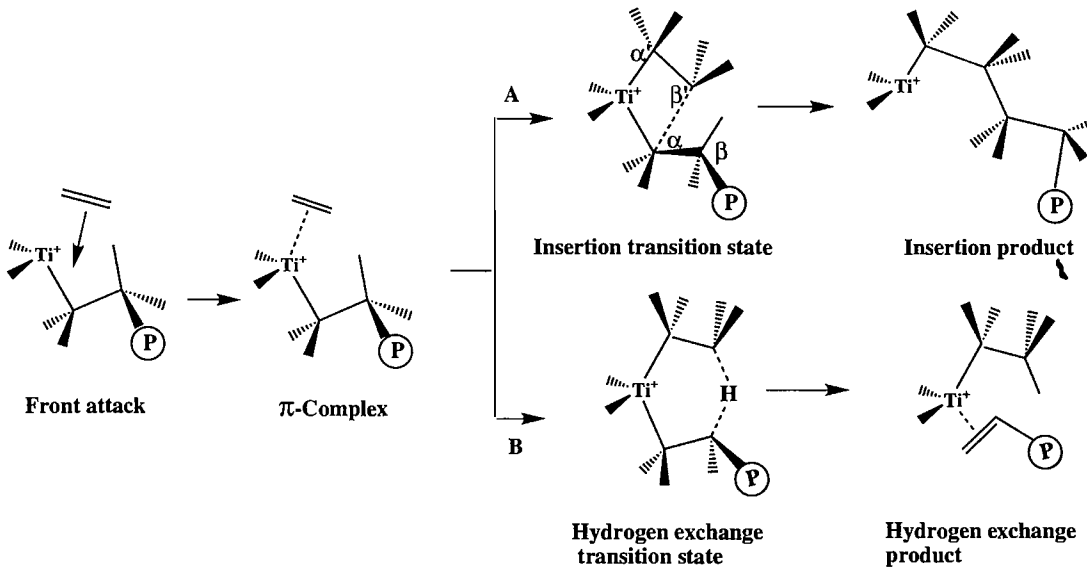

Scheme 2.

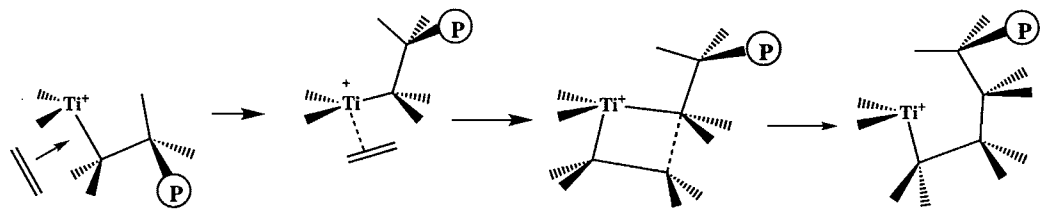

a transfer of the β-hydrogen from the polymer chain to olefin. The process in B can be considered as an olefin-aided chain-termination reaction. The back-side attack, **3b**, is also initiated by the formation of a π-complex, Scheme 2. After that the process proceeds with insertion.

The π-complexes in Schemes 1 and 2 were fully optimized without symmetry constraints. The converged geometries are both virtually of C_s symmetry, with the ethylene carbons and the Ti-C_α-C_β-H frame coplanar. The optimized structures along with most of the parameters are given as **5a** for the π-complex in Scheme 1, and as **5b** for the corresponding complex in Scheme 2.

The ethyl framework in the olefin complex **5a** is very similar to that of **4a**, except that the C_α-Ti-X angle in **5a** is reduced by 10.4° to 23.1°. Thus the Ti-C_α-C_β-H frame has moved to accommodate the approaching olefin. The β-agostic interaction in **5a** is retained as indicated by a Ti—H distance of 1.94 Å and a C—H bond of 1.19 Å. The ethylene is only loosely bonded to the titanium center with TiM-C distances of 2.34 and 2.50 Å, respectively. The C—C bond length in ethylene is

Can. J. Chem. Downloaded from www.nrcresearchpress.com by 80.90.12.36 on 09/08/12
For personal use only.

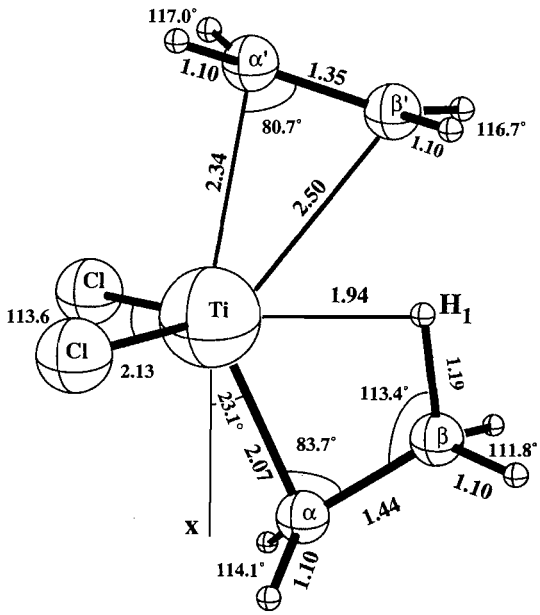

5a

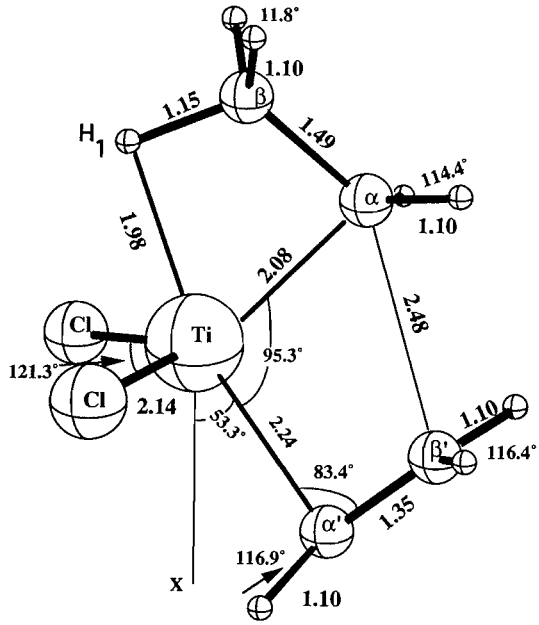

5b

1.35 Å, which is close to the calculated double bond of 1.33 Å for free ethylene.

The π-complex **5b** from the back-side approach of Scheme 2 can be considered as an olefin adduct of **4b**. The ethyl group in **5b** has moved by increasing the C_α-Ti-X angle from 104° in **4b** to 146.6° in **5b**. This is again done to accommodate the incoming olefin. The back donation of electrons from titanium to ethylene is, as expected, weak, judging from the C—C distance of ethylene which is 0.02 Å longer than for free C_2H_4.

The energies of **5a** and **5b** were found to be essentially the same, with **5a** being only 0.5 kcal/mol more stable than **5b**. The coordination of ethylene to **4a**, yielding **5a**, is exothermic by 25.4 kcal/mol. Correspondingly, the coordination of ethylene to **4b**, yielding **5b**, is exothermic by 27.2 kcal/mol. We did not find any barrier for the formation of the π-complex. In solution the formation of the π-complex will require the removal of solvent molecules that will introduce a barrier. Jordan and co-workers (26) determined the structure for a number of group-4 $L_2(E)M^+$–alkyl complexes, **5c**, where E is a donor ligand. They all have a β-agostic interaction and can be viewed as a back-side adduct between **5b** and E.

The initial exploration of the paths in Scheme 1 from the olefin complex **5a** onward were carried out by a linear transit. In the transit, the C_α—$C_{\beta'}$ distance was reduced in steps while all other degrees of freedom were optimized without constraints. The transit gave rise to an energy maximum , and the structure corresponding to the highest energy was used as a starting point in a regular transition state search (25) . The full transition state optimization resulted in the converged structure shown as **6a**. The structure has C_{2v} symmetry and appears from inspection to represent the transition state for the hydrogen exchange reaction of path B in Scheme 1.

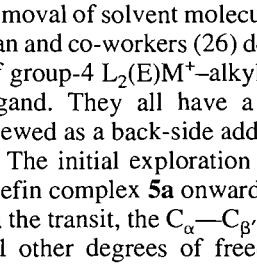

M = Zr,Hf; E = PR_3,$C_4H_{10}O$

5c

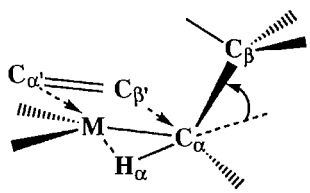

5d

The calculated vibrational spectrum of **6a** revealed a single imaginary frequency of 562i cm^{-1}, thus confirming that this structure represents a transition state. The normal mode related to the imaginary frequency is of b_2 symmetry and corresponds to, respectively, a shortening and an elongation of the two symmetrical H_1—C_β bonds. Thus, the b_2 mode has the characteristics of a reaction coordinate representing the hydride exchange process of path B in Scheme 1. To further verify that **6a** is indeed a transition state of Scheme 1B, we studied the intrinsic reaction coordinate (IRC) path (11, 24) from **6a**. The IRC starts from **6a** in the two directions along the b_2 reaction mode and continues by steepest descend in the energy towards reactants and products. The IRC paths can be written (11) as $\boldsymbol{X}(s)$ where $|s|$ is the length of the path from the transition state, Section 2. A step length of Δs = 0.02 Å was used in the descent. The IRC calculation revealed that **6a** is connected to two symmetrical π-complexes with the structures **5a**, thus confirming that **6a** is the transition state for the hydrogen exchange reaction. In the path from **5a** to **6a** the C_β—H_1 bond is gradually broken while another $C_{\beta'}MH_1$ bond is formed. The change in the two key reaction coordinates along the IRC is shown in Fig. 1. It is clear from this figure that the bond breaking and bond formation take place abruptly in a region close to the transition state, **6a**. The path from **5a** to **6a** gives further rise to a number of alternate increases and decreases in the length of bonds that become equivalent in the transition state **6b**. The IRC calculation revealed that all of these alternate geometrical changes take place gradually along the path. The transition state **6a** is best viewed as an adduct between Cl_2Ti—H and two equivalent olefins.

Can. J. Chem. Downloaded from www.nrcresearchpress.com by 80.90.12.36 on 09/08/12
For personal use only.

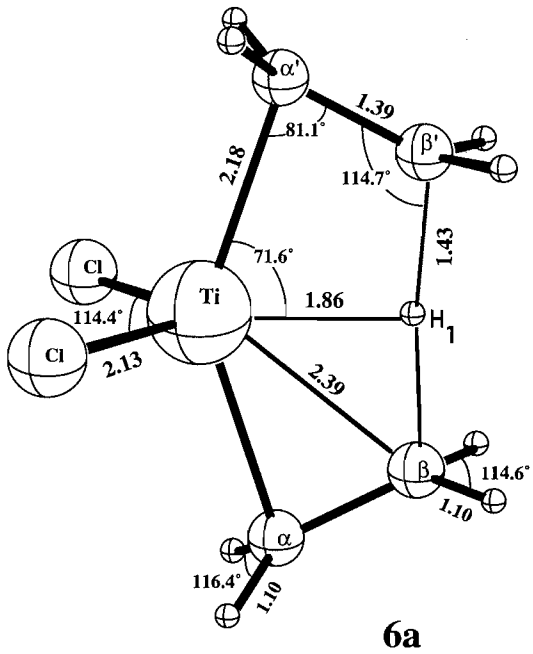

Fig. 1. Change in the $R(C_\beta—H_1)$ and $R(C_{\beta'}MH_1)$ distances along the IRC of the hydrogen exchange process.

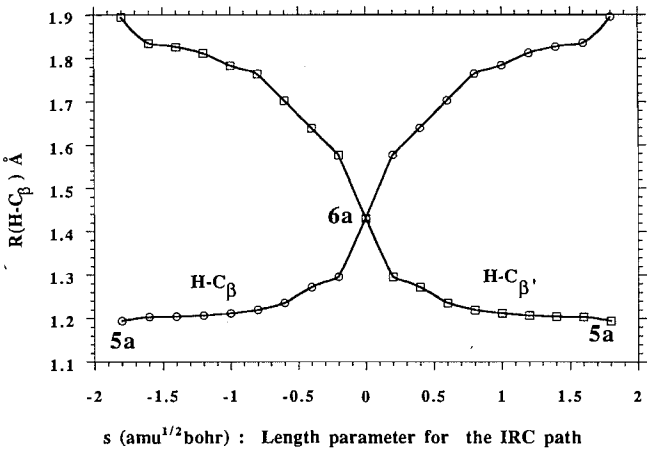

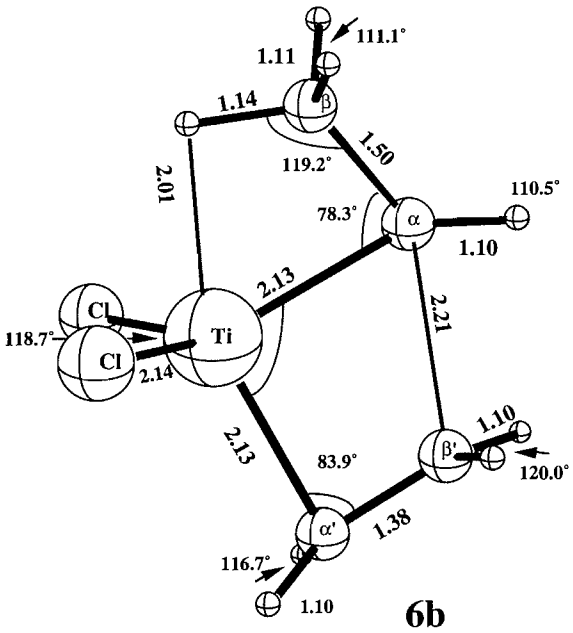

Fig. 2. Energy profile for the hydrogen exchange process along the IRC.

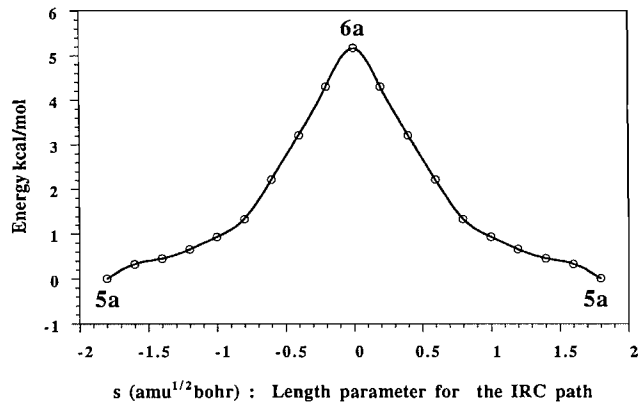

The energy profile for the hydrogen exchange reaction along the IRC path is shown in Fig. 2. The barrier was calculated to be 5.3 kcal/mol at the NL/P level of theory, and it is clear from Fig. 2 that the rise in energy takes place close to the transition state, **6b**, where the stretch in the $C_\beta—H_1$ bond becomes pronounced, Fig. 1.

The linear transit leading from **5a** to the hydrogen exchange transition state **6a** had the Ti-C_α-C_β-H_1 frame coplanar with the incoming ethylene. It is perhaps not surprising that such a coplanar front-side attack will result in hydrogen exchange since the $C_{\beta'}$ atom on ethylene will come into close contact with H_1 before it can interact with C_α on the ethyl group as required for an insertion reaction.

We have attempted several transits in which the C_β atom of the ethyl group was moved out of the C_s plane in **5a** by a rotation around the Ti—C_α axis to ensure a free passage of the $C_{\beta'}$ ethylene atom towards C_α on the ethyl group, **5d**. The rotations were carried out prior to or in concert with the ethylene approach. All of these transits failed to locate a transition state for the insertion along A of Scheme 1. Instead the transits led to hydrogen exchange or high-energy adducts between ethylene and Cl_2Ti^+–C_2H_5, **5d**. The adducts with the C_β atom out of the C_s plane had energies in excess of 15 kcal/mol compared to **5a,** and none of them represented an insertion transition state. We must thus conclude that insertion from a front-side attack along path A in Scheme 1 is highly unlikely or at least unable to compete with hydrogen exchange. Our conclusions will later be reconciled with the available experimental data on the stereochemistry of olefin polymerization catalyzed by cationic metallocenes of group-4 transition metals.

We shall now turn to a discussion of the alternative backside attack of Scheme 2 as a possible route for olefin insertion. A linear transit search for the transition state along the path in Scheme 2 led to a structure that has a planar C_s symmetry. However, a vibrational analysis of this species revealed three normal modes with imaginary frequencies. The symmetric mode with ν = 105 cm^{-1} corresponded to the ethylene insertion, the other two asymmetric modes of 442i cm^{-1} and 198i cm^{-1} were out-of-plane bendings.

Can. J. Chem. Downloaded from www.nrcresearchpress.com by 80.90.12.36 on 09/08/12
For personal use only.

A distortion along the two asymmetric modes resulted in the true transition state **6b**. This species has one single imaginary frequency of ν = 103i cm^{-1} representing the reaction mode, whereas all other modes have real frequencies. The ethylene carbon atom $C_{\beta'}$ is out of the $C_{\alpha'}TiC_{\alpha}$ plane by 17.4° and the ethyl carbon atom C_{β} is out of the $C_{\alpha}TiC_{\alpha'}$ plane by 10.7°. The out-of-plane deformation of the carbon backbone reduces the steric interaction between the otherwise eclipsed hydrogens. The energy difference between **6b** and the C_s structure is 4.8 kcal/mol at the NL/P level of theory. A previous *ab initio* Hartree–Fock (HF) calculation (8*c*) on the $Cl_2TiCH_3^+ + C_2H_4$ insertion process finds a difference of 0.6 kcal/mol between the planar and asymmetric transition states. The out-of-plane deformation is likely more favorable in the planar ethyl insertion with three CH_2 groups eclipsed compared to the planar methyl insertion with only two eclipsed CH_2 groups.

Structure **6b** must be characterized as an early transition state. The Ti-C_α bond about to be broken is only 0.03 Å longer in **6b** than in the π-complex **5b**, and 0.14 Å longer than in the parent ethyl complex, **4b**. At the same time the emerging C_α–$C_{\beta'}$ σ-bond with a distance of 2.21 Å is still far in excess of a single C—C bond length, and has only decreased by 0.26 Å compared to the ethylene adduct **5b**. The β-hydrogen H_1 on ethyl retains its stabilizing interaction with titanium throughout the path from **5b** to **6b**. At the transition state **6b** the C_β—H_1 bond is stretched to 1.14 Å and the Ti—H_1 distance is 2.01 Å. The continuous agostic stabilization from the interaction between the metal center and the C_β—H_1 bond is a distinct feature of the back-side approach. It is in contrast to the front-side attack, **5d**, where the agostic bond between the metal center and the C_β-H_1 linkage has to be broken before the insertion can take place. It is postulated (9*f*) that an α-agostic interaction, **5d**, in this case aids the stability of the transition state.

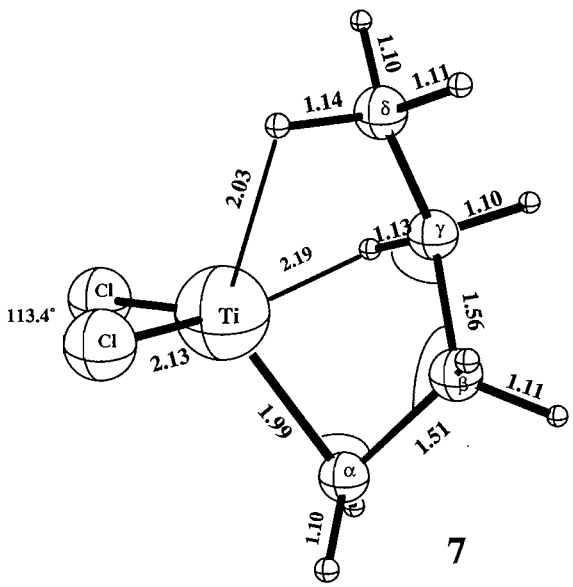

7

A full IRC path calculation from **6b** revealed that this structure is connected by steepest descend to the π-complex, **5b**, as well as the butyl product **7**. Thus, **6b** represents the transition state for the insertion process of Scheme 2. The energy profile obtained by following the IRC from **6b** is shown in Fig. 3. The insertion reaction is exothermic with a reaction enthalpy of 6.1 kcal/mol at the NL/P level of theory. The corresponding activation barrier is determined as 3.9 kcal/mol, Fig. 3. The butyl complex **7** is the kinetic product for the insertion process in Scheme 2. It has a single hydrogen on both the γ and δ carbon interacting with the metal center. The kinetic product **7** might well rearrange to a β-agostic conformation such as **2a**.

Fig. 3. Energy profile for the insertion process **5b** → **6b** → **7** along the IRC.

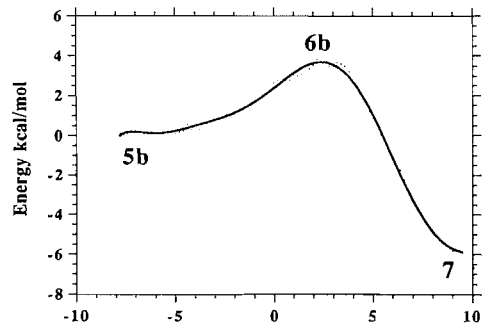

Fig. 4. Change in the $R(C_\alpha—C_{\beta'})$, $R(Ti—C_\alpha)$, and $R(Ti—C_{\alpha'})$ distances for the insertion process **5b** → **6b** → **7** along the IRC.

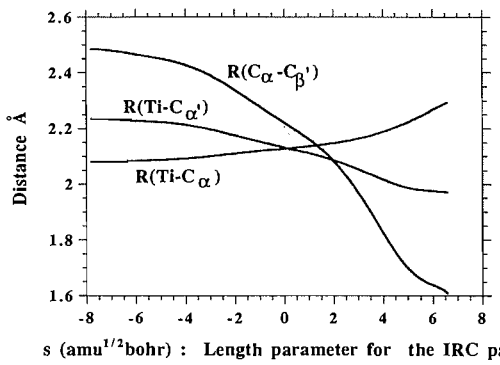

The insertion process of Scheme 2 gives rise to the formation of two bonds, C_α—$C_{\beta'}$ and Ti—$C_{\alpha'}$, whereas the Ti—$C_{\alpha'}$ linkage is broken. Figure 4 displays the change in the length of the three key bonds along the IRC. The graph underlines again that **6b** at $s = 0$ is an early transition state. It is also interesting to note that the two Ti—C bonds are about equidistant at the transition state. The three bonds are further seen to vary linearly in a wide region, $|s| < 4$, around **6b**. The C_α—$C_{\beta'}$ distance has often been used as a reaction coordinate in studies on the insertion process. Figure 4 suggests that this is a reasonable choice given the linear variation of C_α—$C_{\beta'}$ over a long range of the IRC.

4. Concluding remarks

We have carried out DFT-based calculations on the reaction between Cl_2Ti^+–ethyl and ethylene. The Cl_2Ti^+–ethyl species was considered as a model for the cationic group-4 metallocenes used in olefin polymerization (1). The Cl_2Ti^+–ethyl model had a ground state structure, **4a**, with a β-agostic conformation in which a single C_β—H bond is directed towards the metal center, and this conformation was also assumed to represent the resting state of the growing chain attached to the cationic group-4 metallocenes between insertions.

Olefin can approach **4a** in two ways. The first, Scheme 1, leads to an attack on the agostic C_β—H bond whereas the second, Scheme 2, results in an attack of the Ti—C_α link from the side opposite to the C_β—H bond. The present set of calculations found that the front-side attack in Scheme 1 leads to hydrogen exchange, Scheme 1(B), rather than ethylene insertion, Scheme 1(A). On the other hand, the back-side attack of Scheme 2 readily allows for the ethylene insertion.

The isotactic polymerization of propylene has been interpretated in terms of a front-side attack as shown in eq. [4].

[4] 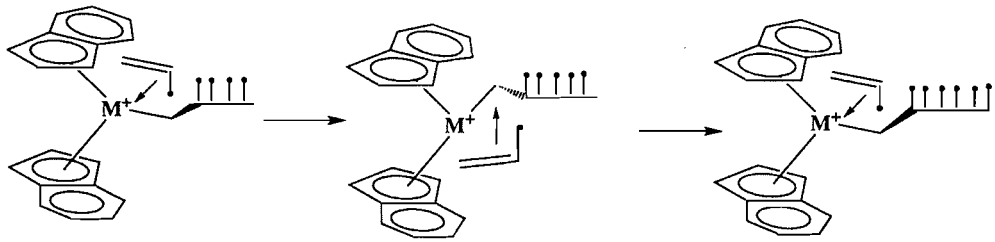

In the front-side attack the chain swings to the side of the incoming olefin following each insertion. Further, propylene will have its methyl group alternating between "up" and "down" in response to the steric demand of the L_2M^+ fragment of C_2 symmetry. However, the isotactic polymerization of propylene by the same L_2M^+ system can also be explained from a back-side approach as illustrated in eq. [5].

[5] 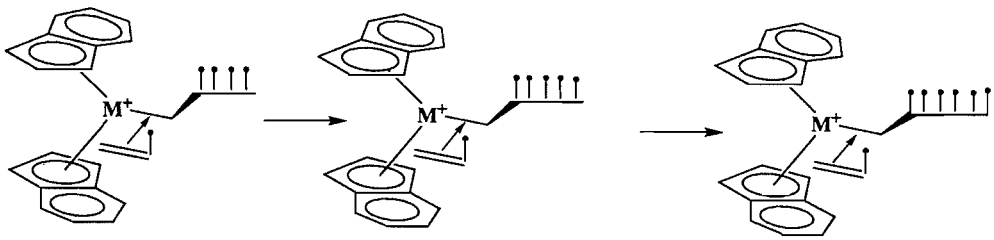

Now the chain remains on one side and propylene is always approaching with the methyl group in the same position.

The syndiotactic propylene polymerization is also readily explained by the front-side approach as shown in eq. [6].

[6] 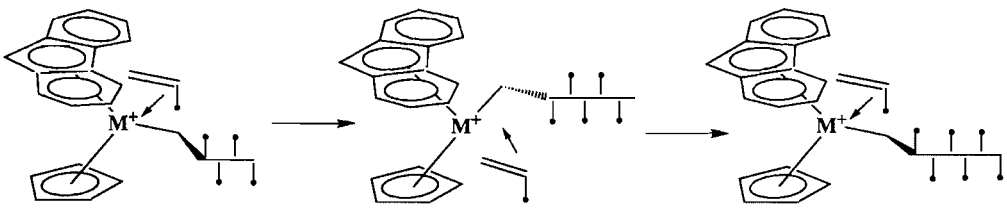

Again, the chain swings to the side of the incoming olefin following each insertion. However, now the methyl group is always in the same (down) position, resulting in a syndiotactic chain growth.

In the corresponding back-side attack of eq. [7], the chain remains on one side and propylene is always approaching with the

[7] 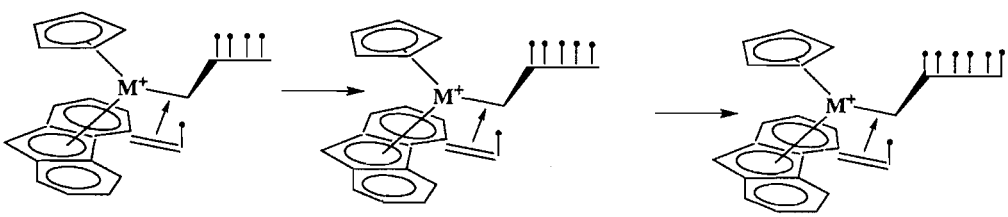

methyl group in the same position if its position is dictated by the steric requirement of the L_2M^+ fragment. Thus, the back-side attack would seemingly not produce the observed syndiotactic chain but instead result in a isotactic polymer.

It might seem that our notion about a preference for back-side insertion leads to predictions, eq. [7], in contradiction with experimental observation. However, it is also possible that the orientation of the methyl group on the incoming propylene is dictated by the chain *rather than* the L_2M^+ fragment. If the former is correct, back-side attack in eq. [7] would lead to syndiotactic polymers. We intend to explore this possibility by a combined DFT and molecular mechanics study in which the steric bulk of the ancillary ligands on the metal as well as the growing chain are taken into account.[2] We intend further to explore the front-side insertion, step A of Scheme 1, in more detail, although it seems that a possible transition state should be of high energy.

[2] J.C.W. Lohrenz, T.K. Woo, L. Fan, and T. Ziegler. Work in progress.

Can. J. Chem. Downloaded from www.nrcresearchpress.com by 80.90.12.36 on 09/08/12
For personal use only.

Can. J. Chem. Downloaded from www.nrcresearchpress.com by 80.90.12.36 on 09/08/12
For personal use only.

This study has also pointed to a facile pathway for chain termination via hydrogen exchange, path B of Scheme 1. Chain terminations have traditionally been associated with β-hydrogen abstraction. However, previous calculations from this group (10b) have shown that β-hydrogen abstraction is a high-energy process requiring more than 100 kJ/mol. We intend to explore further the viability of hydrogen exchange as a chain-terminating mechanism in olefin polymerization. Hydrogen exchange has recently been studied by Brintzinger and co-workers (27).

Acknowledgements

This investigation was supported by the Natural Sciences and Engineering Research Council of Canada (NSERC) as well as the Donors of the Petroleum Research Fund, administered by the American Chemical Society (ACS-PRF no. 27023-AC3).

References

1. (*a*) W. Kaminsky, K. Kulper, H.H Brintzinger, and F.R.W.P. Wild. Angew. Chem. Int. Ed. Engl. **31**, 1347 (1992); (*b*) R.F. Jordan, R.E. LaPoint, N.C. Baenziger, and G.D. Hinch. Organometallics, **9**, 1539 (1990); (*c*) S.L. Borkowsky, R.F. Jordan, and G.D. Hinch. Organometallics, **10**, 1268 (1991); (*d*) G.G. Hlatky, R.R. Eckman, and H.W. Turner. Organometallics, **11**, 1413 (1992); (*e*) J.A. Ewen, M.J. Elder, R.L. Jones, L. Haspeslagh, J.L. Atwood, S.G. Bott, and K. Robinson. Makromol. Chem. Macromol. Symp. **48/48**, 253 (1991); (*f*) A. Zambelli, P. Longo, and A. Grassi. Macromolecules, **22**, 2186 (1989); (*g*) J.J. Eshuis, Y.Y. Tan, A. Meetsma, and J.H. Teuben. Organometallics, **11**, 362 (1992); (*h*) X. Yang, C.L. Stern, and T.J. Marks. J. Am. Chem. Soc. **113**, 3623 (1991); (*i*) A.D. Horton and A.G. Orpen. Organometallics, **10**, 3910 (1991); (*j*) J.J. Eisch, K.R. Caldwell, S. Werner, and C. Krüger. Organometallics, **10**, 3417 (1991); (*k*) W. Kaminsky and R. Steiger. Polyhedron, **7**, 2375 (1988).
2. (*a*) J.C.W. Chien, W.M. Tsai, and M.D. Rausch. J. Am. Chem. Soc. **113**, 8570 (1991); (*b*) J.C. Stevens, F.J. Timmers, D.R. Wilson, G.F. Schmidt, P. Nicklas, R.K. Rosen, G.W. Knight, and S. Lai. European Patent Application EP-416-815-A2, March 13, 1991 (Dow); (*c*) J.A. Canich. PCT Application WO 91/04257, April 4, 1991 (Exxon).
3. (*a*) P. Cossee. J. Catal. **3**, 80 (1964); (*b*) E.J. Arlman and P. Cossee. J. Catal. **3**, 99 (1964).
4. (*a*) P.G. Gassman and M.R. Callstrom. J. Am. Chem. Soc. **109**, 7875 (1987); (*b*) R.F. Jordan, C.S. Bajgur, R. Willett, and B. Scott. J. Am. Chem. Soc. **108**, 7410 (1986).
5. (*a*) Y.W. Alelynuas, R.F. Jordan, S.F. Echols, S.L. Borkowsky, and P.K. Bradley Organometallics, **10**, 1406 (1991); (*b*) B.J. Burger, M.E. Thompson, W.D. Cotter, and J.E. Bercaw. J. Am. Chem. Soc. **112**, 1566 (1990); (*c*) M.E. Thompson, S.M. Buxter, A.R. Bulls, B.J. Burger, M.C. Nolan, B.D. Santarsiero, W.P. Schaefer, and J.E. Bercaw, J. Am. Chem. Soc. **109**, 203 (1987).
6. (*a*) P.Corradini, G. Guerra, M. Vacatello, and V. Villana. Gazz. Chim. Ital. **118**, 173 (1988); (*b*) L. Cavallo, G. Guerra, L. Oliva, M. Vacatello, and P. Corradini. Polym. Commun. **30**, 16 (1989); (*c*) L. Cavallo, P. Corradini, G. Guerra, and M. Vacatello. Polymer, **32**, 1329 (1991); (*d*) L. Cavallo, G. Guerra, M. Vacatello, and P. Corradini. Chirality, **3**, 299 (1991); (*e*) L. Cavallo, G. Guerra, and P. Corradini. Macromolecules, **26**, 260 (1993).
7. (*a*) L.A. Castonguay, and A.K. Rappe. J. Am. Chem. Soc. **114**, 5832 (1992); (*b*) J.R. Hart and A.K. Rappe. J. Am. Chem. Soc. **115**, 6159 (1993).
8. (*a*) O. Novaro, E. Blaisten-Barojas, E. Clementi, G. Giunchi, and M.E. Ruiz-Vizcaya. J. Chem. Phys. **68**, 2337 (1978); (*b*) H. Fuijimoto, T. Yamasaki, H. Mizutani, and N. Koga. J. Am. Chem. Soc. **107**, 6157 (1985); (*c*) H.Kawamura-Kuribayashi, N. Koga, and K. Morokuma J. Am. Chem. Soc. **114**, 2359 (1992); (*d*) J. Am. Chem. Soc. **114**, 8687 (1992); (*e*) N.Koga, T.Yoshida, and K.Morokuma. J. Am. Chem. Soc. **114**, 2359 (1992); (*f*) P.E.M. Siegbahn. Chem. Phys. Lett. **205**, 290 (1993); (*g*) H. Weiss, M. Ehrig, and R. Ahlrichs. J. Am. Chem. Soc. **116**, 4919 (1994); (*h*) E.P. Bierwagen, J.E. Bercaw, and W.A. Goddard III. J. Am. Chem. Soc. **116**, 1481 (1994); (*i*) N. Koga, T. Yoshida, and K. Morokuma. Int. Symp.: 40 years of Ziegler Catalysts. Freiburg, Germany. September 1–3, 1993. In press.
9. (*a*) D.R. Amstrong, P.G. Pekins, and J.J.P. Stewart. J. Chem. Soc. Dalton Trans. 9172 (1972); (*b*) P. Cassoux, F. Crasnifer, and J.-F. Labarre. J. Organomet. Chem. **165**, 303 (1979); (*c*) R.J. McKinney J. Chem. Soc. Chem. Commun. 490 (1980); (*d*) A.C. Balazs and K.H. Johnson. J. Chem. Phys. **77**, 3148 (1982); (*e*) A. Shiga, H. Kawamura, T. Ebara, and T. Sasaki. J. Organomet. Chem. **266**, 95 (1989); (*f*) M.-H. Prosenc, C. Janiak, and H.-H. Brintzinger. Organometallics, **11**, 4036 (1992).
10. (*a*) T.K. Woo, L. Fan, and T. Ziegler. Organometallics, **13**, 432 (1994); (*b*) Organometallics, **13**, 2253 (1994); (*c*) R.J. Meier, van G.H.J. Doremaele, S. Iarlori, and F. Buda. J.Am. Chem. Soc. **116**, 7274 (1994); (*d*) T. K. Woo, L. Fan, and T. Ziegler. Int. Symp.: 40 years of Ziegler Catalysts. Freiburg, Germany. September 1–3, 1993. In press.
11. (*a*) K. Fukui. J. Phys. Chem. **74**, 4161 (1970); (*b*) Acc. Chem. Res. **14**, 363 (1981).
12. E.J. Baerends, D.E. Ellis, and P. Ros. Chem. Phys. **2**, 41 (1973).
13. E.J. Baerends. Ph.D. Thesis, Vrije Universiteit, Amsterdam. 1975.
14. W. Ravenek. *In* Algorithms and applications on vector and parallel computers. *Edited by* H. J. J. te Riele, Th. J. Dekker, and van de H. A.Vorst. Elsevier, Amsterdam 1987.
15. (*a*) P.M. Boerrigter, G. te Velde, and E.J. Baerends. Int. J. Quantum Chem. **33**, 87 (1988); (*b*) G. te Velde and E.J. Baerends. J. Comput. Phys. **99**, 84 (1992).
16. L. Versluis and T. Ziegler. J. Chem. Phys. **88**, 322 (1988).
17. (*a*) G.J. Snijders, E.J. Baerends, and P. Vernooijs. At. Data Nucl. Data Tables, **26**, 483 (1982); (*b*) P. Vernooijs, J.G. Snijders, and E.J. Baerends. Slater type basis functions for the whole periodic system. Internal Report. Free University of Amsterdam, The Netherlands. 1981.
18. J. Krijn and E.J. Baerends. Fit functions in the HFS-method. Internal Report (in Dutch). Free University of Amsterdam, The Netherlands. 1984.
19. S.H. Vosko, L. Wilk, and M. Nusair. Can. J. Phys. **58**, 1200 (1990).
20. A.D. Becke. Phys. Rev. A: Gen. Phys. **38**, 3098 (1988).
21. J.P. Perdew. Phys. Rev. B: Condens. Matter, **33**, 8822 (1986); **34**, 7406 (1986).
22. (*a*) T. Ziegler. Pure Appl. Chem. **63**, 873 (1991); (*b*) T. Ziegler and L. Versluis. Adv. Chem. Ser. **230**, 75 (1992); (*c*) T. Ziegler and T. Tschinke. ACS Symp. Ser. **428**, 277 (1990); (*d*) T. Ziegler, J.G. Snijders, and E.J. Baerends ACS Symp. Ser. **383**, 322 (1989); (*e*) T. Ziegler, V. Tschinke, and L. Versluis. NATO ASI Ser. Ser. **C**: **176**, 189 (1986); (*f*) T. Ziegler. NATO ASI Ser. Ser. **C**: **367**, 357 (1992); (*g*) NATO ASI Ser. Ser. **C**: **378**, 367 (1992); (*h*) T. Ziegler. Chem. Rev. **91**, 651 (1991).
23. C. Gonzalez and H.B. Schlegel. J. Phys. Chem. **94**, 5523 (1990).
24. L. Deng and T. Ziegler. Int. J. Quantum Chem. **52**, 731 (1994).
25. (*a*) A. Banerjee, N. Adams, J. Simons, and R. Shepard. J. Phys. Chem. **89**, 52 (1985); (*b*) J. Baker. J. Comput. Chem. **7**, 385

(1986); (*c*) L. Fan and T. Ziegler. J. Chem. Phys. **92**, 3645 (1990).
26. (*a*) Z. Guo, D.C. Swenson, and R.F. Jordan. Organometallics, **13**, 1424 (1994); (*b*) R.F. Jordan, P.K. Bradleyu, N.C. Baenziger, and R.E. LaPointe. J. Am. Chem. Soc. **112**, 1289 (1990).
27. U. Stehling, J. Diebold, R. Kirsten, W. Röll, H-H. Brintzinger, S. Jüngling, and R. Mülhaupt. Organometallics, **13**, 964 (1994).

Can. J. Chem. Downloaded from www.nrcresearchpress.com by 80.90.12.36 on 09/08/12
For personal use only.

Enantioselective hydrosilation of ketones in the presence of an *S,S*-[1,2-bis(tetrahydroindenyl)ethane]-titanium catalyst

Shixuan Xin and John F. Harrod

Abstract: *S,S*-[1,2-Bis(tetrahydroindenyl)ethane]titanium-based catalysts were used, in conjunction with either diphenyl- or methylphenylsilane, to effect the catalytic hydrosilation of a wide variety of dialkyl ketones. The highest enantioselectivity was observed with *c*-pentylethylketone (70%) and the selectivity was found to be very sensitive to the steric qualities of the alkyl groups, e.g., iPr-Me (15%), iPr-Et (65%), iPr-*n*Pr (60%). Inclusion of a coordinating heteroatom in the alkyl group of the ketone substrate, or carrying out the reaction in a coordinating solvent such as THF, had no significant effect on the rate or selectivity of the reaction.

Key words: hydrosilation, enantioselective catalysis, ketones, *ansa*-metallocenes.

Résumé : On a utilisé des catalyseurs élaborés à partir du *S,S*-[1,2-bis(tétrahydroindényl)éthane]titane, en combinaison avec soit du diphényl- soit du méthylphénylsilane, pour effectuer l'hydrosilation catalytique d'un grand nombre de dialkylcétones. La plus grande énantiosélectivité a été observée avec la *c*-pentyléthylcétone (70%) et on a trouvé que la sélectivité est très sensible aux qualités stériques des groupes alkyles, par exemple, iPr-Me (15%), iPr-Et (65%), iPr-*n*Pr (60%). Si l'on introduit dans le substrat cétonique un hétéroatome pouvant créer une coordination ou si l'on effectue la réaction dans un solvant coordinant comme le THF, on n'observe aucun effet sur la vitesse ou la sélectivité de la réaction.

Mots clés : hydrosilation, catalyse énantiosélective, cétones, métallocènes-*ansa*.

[Traduit par la rédaction]

Introduction

We report here the results of a study of the hydrosilation of a number of prochiral ketones in the presence of a catalyst prepared by reacting *S*-[1,2-bis(tetrahydroindenyl)ethane]titanium(IV) precursors with MeLi, in the presence of organosilane. This study has focused particularly on the reaction of *dialkyl* ketones, for which previously reported asymmetric hydrosilations have only shown very poor enantioselectivities (1, 2). The reaction of primary and secondary organosilanes with simple ketones does not proceed at a measurable rate under ambient conditions in the absence of catalysts.

The susceptibility of hydrosilation to catalysis by coordination complexes has led to extensive study of this class of reaction as a route to chiral products (1). A number of highly enantioselective, chiral, late transition metal complexes have been reported to catalyze hydrosilation of olefinic and carbonyl-containing substrates (3 (reviews for asymmetric hydrosilation), 4). The emergence of chiral early transition metal *ansa*-metallocenes as a class of highly stereospecific catalysts for olefin polymerization has drawn attention to such compounds as potential agents for asymmetric synthesis, both in stoichiometric and catalytic contexts. Group 4 metallocenes have been reported to show activity for hydrosilation of both olefins (5) and ketones (6). A cursory study of the hydrosilation of octan-2-one and acetophenone by triethoxysilane in the presence of several chiral *ansa*-titanocenes gave very discouraging results with respect to enantioselectivity (7). A second report referred to the catalysis of ketone hydrosilation with a catalyst similar to that used in the present work, but no results were described (8).

In the present work we describe results obtained with *S*-[1,2-bis(tetrahydroindenyl)ethane]titanium(IV) catalysts. The catalysts were generated *in situ* by reaction of methyllithium with either the binaphtholate, **1**, or the dichloride, **2**, of S-[1,2-bis(tetrahydroindenyl)ethane]titanium(IV) (9). Although small differences in e/e (enantiomeric excess) were found between the two catalysts, the experiments with **2** confirm that the origin of enantioselectivity is the metal chirality and not the chirality of the ligand. Most the experiments were carried out with **1**, since the preparation and purification of resolved **2** requires several more synthetic steps than **1**.

Results and discussion

The results of a number of hydrosilations of prochiral ketones

Received October 17, 1994.

This paper is dedicated to Professor William A.G. Graham on the occasion of his 65th birthday.

S. Xin and J.F. Harrod.[1] Department of Chemistry, McGill University, Montreal, QC H3A 2K6, Canada.

[1] Author to whom correspondence may be addressed. Telephone: (514) 398-6911. Fax: (514) 398-3797. E-mail: harrod@omc.lan.mcgill.ca

Can. J. Chem. Downloaded from www.nrcresearchpress.com by 80.90.12.36 on 09/08/12
For personal use only.

Can. J. Chem. Downloaded from www.nrcresearchpress.com by 80.90.12.36 on 09/08/12
For personal use only.

by methylphenyl and diphenylsilanes, summarized in Table 1, lead to the following conclusions: (*i*) significant enantioselectivity can be observed for hydrosilation of simple dialkyl ketones with this catalyst, provided the substrate has appropriate steric encumbrance; (*ii*) the catalyst compares favorably with the best phosphine or rhodium catalysts for hydrosilation of dialkyl ketones (10), and much better than previously reported for *ansa*-titanocene catalysts (2, 7); (*iii*) with the present catalyst system, rates become very slow under conditions that give the highest selectivities; (*iv*) the presence of coordinating heteroatoms in the ketone do not inhibit the reaction, but do degrade the enantioselectivity; (*v*) a coordinating solvent (THF) has only a minor influence on enantioselectivity and rate.

To simplify the synthetic requirements of this project, most reactions were carried out with the binaphtholate, **1**, as catalyst precursor. Since it was necessary to establish that the observed enantioselectivity was not due to the influence of the naphtholate ligand, a limited number of test reactions were also carried out with the resolved dichloride, **2**. Although in general the trends in rate and selectivity for the two catalyst precursors were the same, in some cases dramatic differences were observed (e.g., entries 2 and 12). We do not presently have any information that would allow an explanation of this observation. The near quantitative recovery of lithium binaphtholate from the catalyst generation reaction makes any explanation based on the influence of residual binaphtholate implausible. However, since there is no evidence from other studies that significant racemization of the catalyst occurs under the conditions used to generate it in these reactions, it does seem likely that the explanation lies in a difference in the products of the reactions of MeLi with the two precursors.

In addition to the broad conclusions mentioned above, there are other interesting details in these results. In particular, it is evident that the enantioselectivity outcome becomes quite sensitive to small changes in the steric properties of the substrate at the limits of significant catalytic activity. For example, the change from methyl-isopropyl to ethyl-isopropyl ketone causes a dramatic increase in %e/e (entries 5 and 6), as does the change from ethyl-cyclohexyl to ethyl-cyclopentyl (entries 12 and 13). Although we do not have a simple explanation for these particular effects, it is quite clear that the topological constraints in the bisectorial plane of the ligand–metal centre are quite delicate and, if properly accessed, can give significant enantioselection. It may also be concluded that opportunities for fine tuning these constraints exist and could lead to even greater selectivity.

The absence of a significant effect of coordinating solvent, or coordinating atoms on the substrate, clearly shows that the reaction mechanism does not require a free coordination site on the catalyst. It had been hoped that the inclusion of weakly chelating atoms in the substrate would give a more rigid transition state and lead to higher enantioselectivity. The results show that this is clearly not the case.

An important, but puzzling, feature of the results is the reversal of absolute configuration of the product in some cases, with only seemingly minor structural modification in the substrate (entries 3 and 4, 5 and 6, and 11 and 13). With the exception of entry 10, it is the rule that methyl ketones give the *S*(+) products, while those ketones with both alkyl groups larger than methyl give *R*(−). This suggests the existence of two different enantioselective reaction channels. One, favoured by a large steric bias in the ketone, gives rise to *S*(+) stereochemistry, and a second, favoured by large total steric demand, gives rise to *R*(−) stereochemistry. The simultaneous operation of these two channels could be responsible for degradation of the enantioselectivity. The fact that relatively small changes in substrate topology can cause a dramatic switch from one channel to the other suggests that small changes in catalyst topology could well reinforce the effect and give more selectivity.

Rational modification of the catalyst topology is presently precluded by our ignorance of the mechanism(s) of these reactions. The mechanism(s) most probably involves a combination of insertions and σ-bond metatheses of the type:

[1] $\text{Ti-H} + \text{O=CRR}' \longrightarrow \text{Ti-O-CHRR}'$

[2] $\text{Ti-SiR}''_3 + \text{O=CRR}' \longrightarrow \text{Ti-CRR}'(\text{OSiR}''_3)$

[3] $\text{Ti-O-CHRR}' + \text{H-SiR}''_3 \longrightarrow \text{Ti-H} + \text{R}''_3\text{Si-O-CHRR}'$

[4] $\text{Ti-CRR}'(\text{OSiR}''_3) + \text{H-SiR}''_3 \longrightarrow \text{Ti-SiR}''_3 + \text{RR}'\text{HC-O-SiR}''_3$

A third possibility involves activation of a Si—H bond in a silyl ligand towards addition across the C=O bond.

[5] $\text{Ti-SiR}''_2\text{H} + \text{O=CRR}' \longrightarrow \text{Ti-SiR}''_2\text{O-CRR}'\text{H}$

[6] $\text{Ti-SiR}''_2\text{O-CRR}'\text{H} + \text{SiR}''_2\text{H}_2 \longrightarrow \text{Ti-SiR}''_2\text{H} + \text{HSiR}''_2\text{O-CRR}'\text{H}$

Such a mechanism has recently been observed in a rhodium-catalyzed reaction (11). The relatively large distance of the chiral carbon atom from the metal centre in the transition state for such a mechanism would not be expected to lead to strong enantioselection.

At the moment, it is still not clear whether the true catalyst involves Ti(III), or Ti(IV). We recently isolated the Ti(III) hydride dimer, *rac*-{[1,2-bis(tetrahydroindenyl)ethane]titanium(III)H}$_2$, **3**, in high yield from the reaction of *rac*-**2** with MeLi and PhMeSiH_2 (12). However, it cannot be excluded that the isolation of **3** is due to the fact that it is the least soluble species in the reaction mixture, since there is considerable evidence that titanocene(III) species disproportionate into titanocene(II) and titanocene(IV). Further, although less likely than eqs. [1]–[6], the possibility of a cycling between Ti(IV) and Ti(II) by concerted addition of H-Ti(IV)-Si to ketone to generate Ti(II), followed by oxidative addition of Si-H to Ti(II) to regenerate H-Ti(IV)-Si, cannot be excluded.

A final complication is suggested by some preliminary rate studies. The reaction rates are found to be second order in titanium concentration, a fact that can only be explained on the assumption that the rate-determining step involves either a bimetallic complex, or the reaction of two monometallic titanium complexes. In addition, preliminary results suggest there is a very slight decline in enantioselectivity with increasing catalyst concentration (e.g., for the reaction of entry 13 in the table, the e/e was found to drop from 69.0±1.0% to 65.4±1.0% on changing the catalyst concentration from 0.024 to 0.060 M). If this effect is real, then there must be two different pathways, with different dependencies on catalyst concentration. The pathway that is second order in catalyst is both the dominant pathway and the less enantioselective. To produce the observed

Table 1. Results of hydrosilation reactions.

Entry	Substrate	Product	Time (h)	Yield %[e]	%ee	Config[f] (sign)[g]
1[a]			18	89	10(10)[h]	S(+)
1[b]			25	95	4	S(+)
1[d]			80	96	0	—
2			18	93	19(19)	S(+)
2[b]			25	92	5	S(+)
2[c]			18	86	9(10)	S(+)
3	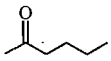	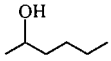	18	92	5(5)	S(+)
4	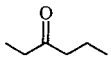	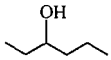	230	97	(11)	R(−)
5			230	82	14(16)	S(+)
5[b]			150	96	18	S(+)
5[c]			80	79	17(16)	S(+)
5[d]			300	95	14	S(+)
6			230	79	64(64)	R(−)
6[b]			230	91	65	R(−)
6[c]			230	85	58(55)	R(−)
7	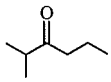	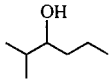	680	63	60(58)	R(−)
8	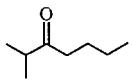	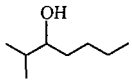	1200	75	(37)	R(−)
9			230	99	27(31)	S(+)
9[b]			150	85	(28)	S(+)
9[c]			230	87	22(27)	S(+)
10			600	88	46(48)	R(−)
10[c]			230	87	40(43)	R(−)
11	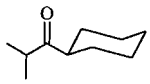	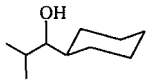	1270	68	(5)	(+)
12	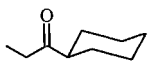	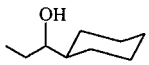	285	96	41(42)	R(−)
12[c]			18	92	8(11)	R(−)
13	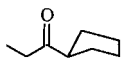	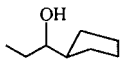	600	94	70(67)	(+)
14	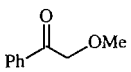	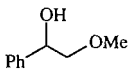	550	84	15(14)	(−)
15			300	91	4(5)	(−)
16	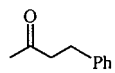	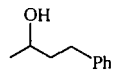	18	95	9(16)	S(+)
16[b]			25	96	11	S(+)
17			No rxn	—	—	—
17[d]			300	90	12	R(+)
18	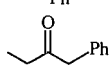		No rxn	—	—	—

[a]Entries 1–18, catalyst system: *S*-(+)-**1**/MeLi/$PhMeSiH_2$ combination with THF solvent.
[b]Catalyst system: *S*-(+)-**1**/MeLi/$PhMeSiH_2$ combination, neat reaction.
[c]Catalyst system: *S*-(−)-**2**/MeLi/$PhMeSiH_2$ combination with THF solvent.
[d]Catalyst system: *S*-(+)-**1**/MeLi/Ph_2SiH_2 combination, neat reaction.
[e]Isolated yield.
[f]Absolute configuration obtained from the ^1H and ^{19}F NMR of MTPA esters of the corresponding alcohols (14).
[g]Optical Rotation was recorded in chloroform solution use sodium D-line(589 nm).
[h]%ee obtained by the integration of ^1H NMR and (^{19}F NMR), and averaging at least two runs for each reaction.

Can. J. Chem. Downloaded from www.nrcresearchpress.com by 80.90.12.36 on 09/08/12
For personal use only.

result, the second pathway, probably first order in catalyst, must have a much higher enantioselectivity.

We are continuing to explore the chemistry of this system, and undertaking a careful kinetic study, in order to resolve these questions. If the mechanism and nature of the two stereoselective channels can be identified, the prospect for the design of more reactive, and more enantioselective, catalysts of this type would be greatly improved.

Experimental

The catalyst precursors, **1** and **2**, were prepared and resolved by methods described in the literature (9). Silanes were prepared by $LiAlH_4$ reduction of the corresponding chlorosilanes, which were purchased fom Hüls America Inc. When unavailable from commercial suppliers, ketones were prepared by oxidation of the corresponding carbinols using standard organic reactions (13).

A typical hydrosilation reaction is as follows (all reactions carried out under inert atmosphere): the catalyst precursor (0.05 mmol) was disolved in 1 mL dry THF (or diethyl ether) in a light-shielded Schlenk tube, and 0.14 mmol MeLi (1.4 M solution in diethyl ether) was added. The mixture was stirred under dry argon until the reaction was complete by ^1H NMR (1 h in THF, or 12 h in ether). Either phenylmethyl- or diphenylsilane (5.0 mmol) was added and the mixture was stirred for 30 min to generate the active catalyst. Ketone (5.0 mmol) was then added and the reaction was followed to completion by ^1H NMR and (or) GLC. The mixture was then diluted with 10 mL of dry ether and cooled to −78°C. A PhMgBr solution in ether (6 mmol) was added dropwise via syringe over 10 min to cleave the alkoxysilane. The reaction was followed to completion by TLC (hexanes–THF) and warmed to 0°C. Cold HCl (5 mL; 2 N) was added to quench the reaction. The organic phase was separated and the aqueous phase was extracted with ether (2 × 5 mL). The combined organic phase was dried over anhydrous sodium sulphate and solvent was carefully removed. The oily residue was distilled under reduced pressure to yield the secondary alcohol with a small amount of silane contamination. The alcohol was then converted to the *R*-(+)-α-methoxy-α-(trifluoromethyl)phenylacetic acid ester by standard procedures (14). The esterification reaction was run using a small excess of the acid chloride (10–15%), and to completion to avoid kinetic resolution effects. The e/e was calculated by integration of both ^1H ($CDCl_3$, 500 MHz) and ^{19}F ($CDCl_3$, 470.48 MHz) NMR spectra.

Can. J. Chem. Downloaded from www.nrcresearchpress.com by 80.90.12.36 on 09/08/12
For personal use only.

Acknowledgements

The authors thank The Natural Sciences and Engineering Research Council (NSERC) of Canada and le Fonds pour la Formation de chercheurs et l'aide à la recherche (FCAR) du Quebec for financial support of this work. We thank Prof. T. H. Chan for useful discussions.

References

1. I. Ojima (*Editor*). Catalytic asymmetric synthesis. VCH Publishers, New York. 1993.
2. S.L. Colletti and R.L. Halterman. Organometallics, **11**, 980 (1992).
3. Reviews for Asymmetric hydrosilation: (*a*) I. Ojima. *In* The chemistry of organic silicon compounds. Part 2. *Edited by* S. Patai and Z. Rappoport. Wiley, New York. 1989. p. 1479; (*b*) I. Ojima, N. Clos, and C. Bastos. Tetrahedron, **45,** 6901 (1989); (*c*) I. Ojima and K. Hirai. *In* Asymmetric synthesis. Vol. 5. *Edited by* J.D. Morrison. Academic Press, Orlando, Fla. 1985. p.103; (*d*) I. Ojima, K. Yamamoto, and M. Kumada. *In* Aspects of homogeneous catalysis. Vol. 3. *Edited by* R. Ugo. Reidel, Dordrecht. 1977. p.185.
4. (*a*) H. Brunner. Synthesis, 645 (1988); (*b*) Top. Stereochem. **18,** 129 (1988); (*c*) G. Consiglio and R.M. Waymouth. Chem. Rev. **89**, 257 (1989); (*d*) R. Noyori and M. Kitamura. *In* Modern synthetic methods. Vol. 5. *Edited by* R. Scheffold. Springer-Verlag, New York. 1989. p.115.
5. (*a*) M.R. Kesti and R.M. Waymouth. Organometallics, **11**, 1095 (1992); (*b*) J.Y. Corey and X.H. Zhu. Organometallics, **11,** 672 (1992); (*c*) T. Takahashi, M. Hasegawa, N. Suzuki, M. Saburi, C.J. Rousset, P.E. Fanwick, and E. Negishi. J. Am. Chem. Soc. **113,** 8564 (1991).
6. T. Nakano and Y. Nagai. Chem. Lett. 481 (1988).
7. R.L. Halterman. Chem. Rev. **92,** 964 (1992).
8. (*a*) C.A. Willoughby and S.L. Buchwald. J. Am. Chem. Soc. **114**, 7562 (1992); (*b*) S.C. Berk, K.A. Kreustina, and S.L. Buchwald. J. Am. Chem. Soc. **113**, 5093 (1991).
9. (*a*) S. Collins, B.A. Kuntz, and Y. Hong. J. Org. Chem. **54**, 4154 (1989); (*b*) S. Collins, B.A. Kuntz, N.J. Taylor, and D.G. Ward, J. Organomet. Chem. **342**, 21 (1988); (*c*) A. Schafer, E. Karl, L. Zsolnai, G. Huttner, and H.H. Brintzinger. J. Organomet. Chem. **328**, 87 (1987); (*d*) F.R.W.P. Wild, L. Zsolnai, G. Huttner, and H.H. Brintzinger. J. Organomet. Chem. **232**, 233 (1982).
10. (*a*) Reference 1, p. 312; (*b*) H.B. Kagan, J.F. Peyronel, and T. Yamagishi. Adv. Chem. Ser. **173**, 50 (1979); (*c*) R.J.P. Corriu and J.J.E. Moreau. J. Organomet. Chem. **85**, 19 (1975); (*d*) R.J.P. Corriu and J.J.E. Moreau. J. Organomet. Chem. **64**, C51 (1974); (*e*) T. Hayashi, K. Yamamoto, and M. Kumada. Tetrahedron Lett. 331 (1974); (*f*) N.C. Payne and D.W. Stephan. Organometallics, **1**, 1390 (1982); (*g*) H. Brunner, R. Becker and G. Riepl. Organometallics, **3**, 1354 (1984); (*h*) H. Brunner, G. Riepl, and H. Weitzer. Angew. Chem. Int. Ed. Engl. **22**, 331 (1983); (*i*) H. Nishiyama, M. Kondo, T. Nakamura, and K. Itoh. Organometallics, **10**, 500 (1991); (*j*) H. Nishiyama, S. Yamaguchi, M. Kondo, and K. Itoh. J. Org. Chem. **57**, 4306 (1992).
11. G. Zhen and T.H. Chan. Organometallics. **14**, 70 (1995).
12. S. Xin and J.F. Harrod. J. Am. Chem. Soc. **116**, 11 563 (1994).
13. Vogel's textbook of organic chemistry. 4th ed. Longman Group Ltd., London. 1978. Chap.III.J. p. 424.
14. (*a*) J.A. Dale and H.S. Mosher. J. Am. Chem Soc. **95**, 512 (1973); (*b*) J.A. Dale, D.L. Dull, and H.S. Mosher, J. Org. Chem. **34**, 2543 (1969); (*c*) G.R. Sullivan, J.A. Dale, and H.S. Mosher. J. Org. Chem. **38**, 2143 (1973); (*d*) S. Yamaguchi. *In* Asymmetric synthesis. Vol. 1. Academic Press, Orlando, Fla. 1983. p. 125.

Reactivity of diosmacycles: complementary syntheses and structure of $[(\mu\text{-}\eta^1,\eta^2\text{-}CHCH_2)Os_2(CO)_8][BF_4]$

R.G. Ball, Gong Y. Kiel, William A. Kiel, Josef Takats, and Friedrich-Wilhelm Grevels

Can. J. Chem. Downloaded from www.nrcresearchpress.com by 80.90.12.36 on 09/08/12
For personal use only.

Abstract: The vinyl-bridged cationic complex, $[(\mu\text{-}CHCH_2)Os_2(CO)_8][BF_4]$ (**3**), is obtained readily and in excellent yield either *via* hydride abstraction from octacarbonyl diosmacyclobutane, $(\mu\text{-}\eta^1,\eta^1\text{-}CH_2CH_2)Os_2(CO)_8$ (**1**), or via protonation of octacarbonyl diosmacyclobutene, $(\mu\text{-}\eta^1,\eta^1\text{-}CHCH)Os_2(CO)_8$ (**2**). It is argued that the ^1H and ^{13}C NMR data of complex **3** are consistent with the traditional view of bonding in μ-alkenyl complexes, involving substantial σ,π donation. The solid state X-ray structure of the complex lends support for this formulation. Complex **3** crystallizes in the orthorhombic space group, $P2_12_12_1$, with a = 12.128(2) Å, b = 14.151(3) Å, c = 9.248(3) Å, V = 1587 Å^3, and Z = 4. The final R and R_w values are 0.032 and 0.038, respectively.

Key words: μ-vinyl, diosmacycles, X-ray structure.

Résumé : On obtient facilement et avec un excellent rendement le complexe cationique comportant un pont vinyle, $[(\mu\text{-}CHCH_2)Os_2(CO)_8][BF_4]$ (**3**), soit par l'enlèvement d'un hydrure du diosmacyclobutane octacarbonyle, $(\mu\text{-}\eta^1,\eta^1\text{-}CH_2CH_2)Os_2(CO)_8$ (**1**), soit par une protonation du diosmacyclobutène octacarbonyle, $(\mu\text{-}\eta^1,\eta^1\text{-}CHCH)Os_2(CO)_8$ (**2**). On insiste sur le fait que les données de la RMN du ^1H et du ^{13}C du complexe **3** sont en accord avec le point de vue traditionnel relatif aux liaisons des complexes μ-alcényles, impliquant un don σ,π important. La structure du complexe à l'état solide, telle que déterminée aux rayons X, supporte ce point de vue. Le complexe **3** cristallise dans le groupe d'espace orthorhombique $P2_12_12_1$, avec a = 12,128(2), b = 14,151(3) et c = 9,248(3) Å, V = 1587 Å^3 et Z = 4. Les valeurs finales de R et R_w sont respectivement 0,032 et 0,038.

Mots clés : μ-vinyle, cycles diosmiques, structure aux rayons X.

[Traduit par la rédaction]

Introduction

The classical method for providing support for proposed mechanisms of homogeneous and heterogeneous catalytic processes and for surface reactions is the synthesis of "model compounds" of the purported intermediates or proposed surface species (1). A prerequisite for the successful isolation and characterization of targeted model compounds is their robustness. Consequently, third-row transition metals, with strong M—L bonds (2), are particularly well suited and have been used extensively for such purposes.

In the annals of the iron triad organometallic chemistry, osmium occupies a unique place (3). Pioneering work by Professor Graham has been instrumental in identifying some of the unique characteristics, with the synthesis of the singly bridged $Os_2(CO)_9$ (4*a*) and the formation of metal chain structures with no bridging ligands, $H_2Os_3(CO)_{12}$ (4*b*) and $ClOs_3(CO)_{12}SnCl_3$ (4*c*). Thus, in hindsight, it may not be totally unexpected that it was osmium which proved to be the first transition metal capable of supporting simple dimetallacyclobutane-type structures, $(\mu\text{-}\eta^1,\eta^1\text{-}CH_2CH_2)Os_2(CO)_8$ (**1**) and substituted derivatives (5), and to provide entry to an extensive series of $M(CO)_4(\eta^2\text{-alkyne})$ complexes of surprising reactivity (6), including facile condensation reactions leading to dimetallacyclobutene, $(\mu\text{-}\eta^1,\eta^1\text{-}CHCH)Os_2(CO)_8$ (**2**), and dimetallacyclopentenone-type products.

Diosmacycles **1** and **2** are attractive candidates as models for the early stages of chemisorption of ethylene and acetylene on metal surfaces (7). Indeed, **1** has been shown to be an excellent model for di-σ-bonded ethylene chemisorbed on Pt(111) at low temperatures (8), while the ready displacement of ethylene from **1** by olefins (9) and alkynes (10) mimics the desorption step, prior to chemical transformation, from surfaces. Once adsorbed, surface ethylene is known to undergo a complex series of transformations (11), the first step being formation of μ-vinyl species. Here we report that complex **1** is capable of supporting chemical transformations; hydride

Received August 27, 1994.

This paper is dedicated to Professor William A.G. Graham on the occasion of his 65th birthday.

R.G. Ball,[1] **G.Y. Kiel, W.A. Kiel, and J. Takats.**[2] Department of Chemistry, University of Alberta, Edmonton, AB T6G 2G2, Canada.
F.-W. Grevels. Max-Planck-Institut für Strahlenchemie, D-45413 Mülheim an der Ruhr, Germany.

[1] Merck, Sharpe & Dohme Research Laboratories, P.O. Box 2000, Rahway, NJ 07065, U.S.A.
[2] Author to whom correspondence may be addressed. Telephone: (403) 492-4944. Fax: (403) 492-8231. E-mail: joe_takats@dept.chem.ualberta.ca

Can. J. Chem. Downloaded from www.nrcresearchpress.com by 80.90.12.36 on 09/08/12
For personal use only.

abstraction leads to $(\mu\text{-}\eta^1,\eta^2\text{-}CHCH_2)Os_2(CO)_8^+$ (**3**), a species also available via protonation of the diosmacyclobutene complex **2**.

Experimental

All manipulations were carried out under an atmosphere of prepurified nitrogen or argon using standard Schlenk technique in conjunction with a double vacuum manifold. Solvents were distilled from appropriate drying agents under nitrogen prior to use (CH_2Cl_2 from P_4O_{10}, hexane from potassium metal, and pentane from CaH_2). Acetone, reagent grade, was dried over molecular sieves. $Ph_3C^+BF_4^-$ (Aldrich) was recrystallized from CH_2Cl_2–hexane, and $HBF_4{\cdot}OEt_2$ (Aldrich) was used as received. The diosmacyclic compounds were prepared by literature methods, $(\mu\text{-}\eta^1,\eta^1\text{-}CH_2CH_2)Os_2(CO)_8$ (**1**) (10*b*) and $(\mu\text{-}\eta^1,\eta^1\text{-}CHCH)Os_2(CO)_8$ (**2**) (6).

Infrared spectra were recorded in CH_3NO_2 solution (0.1 mm path length KBr and CaF_2 cells) on a Nicolet MX-1 FTIR spectrometer. ^1H and ^{13}C NMR spectra were collected on a Bruker WP-400 spectrometer. Elemental analyses were performed by the microanalytical services of the Department of Chemistry, University of Alberta.

Preparation of $[(\mu\text{-}\eta^1,\eta^2\text{-}CHCH_2)Os_2(CO)_8][BF_4]$ (3)

Method A: hydride abstraction from $(\mu\text{-}\eta^1,\eta^1\text{-}CH_2CH_2)Os_2(CO)_8$ (1)

A solution of 0.316 g (0.500 mmol) of **1** in 125 mL of CH_2Cl_2 was cooled to −78°C under nitrogen and 0.182 g (0.550 mmol) of $Ph_3C^+BF_4^-$ was added as a solid to the stirred solution. After warming to room temperature CH_2Cl_2 was removed in vacuo. The residue was extracted with acetone and filtered. Hexanes were added to the filtrate, resulting in a white precipitate. The precipitate was collected, washed with a small amount of CH_2Cl_2, and recrystallized by pentane diffusion into a solution of acetone. This gave **3** (0.330 g, 92%) as off-white crystals that decompose at 220°C. IR (cm^{-1}, CH_3NO_2) ν_{CO}: 2166 w, 2132 s, 2081 vs, 2070 sh, 2045 s. ^1H NMR (δ, CD_3NO_2): 8.56 (dd, J = 9 and 15 Hz, 1H), 5.86 (d, J = 9 Hz, 1H), 3.88 (d, J = 15 Hz, 1H). ^{13}C NMR (δ, CD_3NO_2): 176.3, 172.6, 171.2, 171.1, 170.6, 168.4, 165.7, 164.4, (*CO*); 134.9 (*CH*); 64.8 (CH_2). Anal. calcd. for $C_{10}H_3BF_4O_8Os_2$: C 16.72, H 0.42; found: C 16.64, H 0.42.

Method B: protonation of $(\mu\text{-}\eta^1,\eta^1\text{-}CHCH)Os_2(CO)_8$ (2)

A solution of 0.041 g (0.065 mmol) of **2** was dissolved in 10 mL of CH_2Cl_2 under argon and cooled to −78°C. To this solution was added 8.0 μL (0.065 mmol) of $HBF_4{\cdot}Et_2O$ via syringe. The solution was allowed to warm to room temperature. Solvent was removed in vacuo and the residue recrystallized from acetone–pentane to give off-white crystals of **3** (0.035 g, 75%).

Hydride addition to $[(\mu\text{-}\eta^1,\eta^2\text{-}CHCH_2)Os_2(CO)_8][BF_4]$ (3)

A solution of 0.053 g (0.074 mmol) of **3** in 20 mL of acetone under argon was treated with 0.003 g (0.079 mmol) of $NaBH_4$ at room temperature. After stirring the reaction mixture for 70 min a sample aliquot showed that no **3** remained in solution. Solvent was removed in vacuo and the resulting residue was extracted with the minimum amount of pentane. Cooling the solution gave **1** (0.015 g, 32%) as evidenced by IR and ^1H NMR spectroscopy. It should be noted that in a separate experiment **1** itself was found to react with $NaBH_4$ under the conditions of this procedure, accounting in part for the low isolated yield in the hydride addition reaction.

X-ray crystal structure analysis

A white, needle-shaped, crystal of **3** was mounted in a nonspecific orientation on an Enraf–Nonius CAD4 automated diffractometer. Accurate cell parameters and crystal orientation matrices were obtained from least-squares refinement of the setting angles of 22 reflections in the range $9 < 2\theta < 23°$.[3] Crystal data, details of the data collection, and structure refinements are summarized in Table 1.

The intensity data were collected at room temperature. Two standard reflections were measured every 60 min to check on crystal and electronic stability over the course of data collection; no significant changes were observed. The data were corrected for Lorentz, polarization, and background effects. Absorption effects were corrected also using an empirical correction based on the absorption surface method of Walker and Stuart (12). The maximum and minimum correction coefficients applied to F_o were 1.2221 and 0.6351, respectively.

The structure was solved using the direct method program MULTAN,[4] which gave the positional parameters for the Os atoms. The remaining non-hydrogen atoms were located by the usual combination of least-squares refinement and difference Fourier synthesis.[5] Refinement of atomic parameters was carried out by using full-matrix least-squares technique on F_o, minimizing the function $\Sigma w(|F_o| - |F_c|)^2$. The neutral atomic scattering factors were calculated from the analytical expression for the scattering factor curves (14*a*). The f' and f'' components of anomalous dispersion (14*b*) were included in the calculations for all non-hydrogen atoms. Two of the three H atoms were located in a difference Fourier map and their contributions were included as fixed atoms with fixed isotropic thermal parameters. In the final cycle, all non-hydrogen atoms were refined anisotropically; the final agreement factors were R = 0.032 and R_w = 0.038. The largest shift in any parameter was 0.04 times its estimated standard deviation. The highest peak in the final difference Fourier map was 2.6(3) e Å^{-3} and was located between the two Os atoms. Final atomic positional and equivalent isotropic thermal parameters are given in Table 2, selected bond distances and angles are listed in Table 3. Supplementary X-ray analysis details, anisotropic thermal parameters, derived hydrogen

[3] The diffractometer programs are those supplied by Enraf–Nonius for operating the CAD4F diffractometer, with some local modifications and additions (R.G.B.).

[4] P. Main, L. Lessinger, M.M. Woolfson, G. Germain, and J.P. Declercq. MULTAN 11/82. A system of computer programs for the automatic solution of crystal structures from X-ray diffraction data.

[5] The computer programs used in this analysis include the Enraf–Nonius Structure Determination Package by B.A. Frenz (13) and several locally written or modified programs (R.G.B.).

Can. J. Chem. Downloaded from www.nrcresearchpress.com by 80.90.12.36 on 09/08/12
For personal use only.

Table 1. Summary of crystallographic data for $[(\mu\text{-}\eta^1,\eta^2\text{-}CHCH_2)Os_2(CO)_8][BF_4]$ (3).

Formula	$C_{10}H_3BF_4O_8Os_2$
fw	718.34
Crystal dimensions, mm	0.08 × 0.06 × 0.46
Crystal system	Orthorhombic
Space group	$P2_12_12_1$ (No. 19)
a (Å)	12.128(2)
b (Å)	14.151(3)
c (Å)	9.248(3)
V (Å)	1587
Z	4
D_{calc} (g cm^{-3})	3.006
μ (cm^{-1})	161.00
Temp. (°C)	21
Radiation	MoKα (λ = 0.71073 Å)
Monochromator	Incident beam, graphite crystal
Take-off angle	3.0°
Detector aperture (mm)	2.40 horizontal/4.00 vertical
Crystal-to-detector distance (mm)	105
Scan type	ω–2θ
Scan rate (deg min^{-1})	10.1–1.3
Scan width (deg)	0.68 + 0.35 tan (θ)
Data collection 2θ limit (deg)	55.00°
Data collection index range	*h*, *k*, −*l*
Total no. reflections collected	3945
Number unique reflections	3643
Number with $I > 3\sigma(I)$	2970
Observations: variables ratio	2970:226
R^a	0.032
$R_w{}^b$	0.038
GOF	1.23

$^aR = \Sigma||F_o| - |F_c||/\Sigma F_o$.
$^bR_w = (\Sigma w(|F_o| - |F_c|)^2/\Sigma wF_o^2)^{1/2}$.

atom parameters, and complete tables of bond lengths, bond angles, and torsional angles have been deposited.[6]

Results and discussion

Syntheses

Hydride abstraction from octacarbonyl diosmacyclobutane (**1**) or proton addition to octacarbonyl diosmacyclobutene (**2**) proceed readily and give the cationic μ-vinyl complex, $[(\mu\text{-}\eta^1,\eta^2\text{-}CHCH_2)Os_2(CO)_8][BF_4]$ (**3**) as an off-white air-stable solid in excellent yield (Scheme 1). There are numerous methods available for the preparation of bimetallic μ-alkenyl com-

Scheme 1.

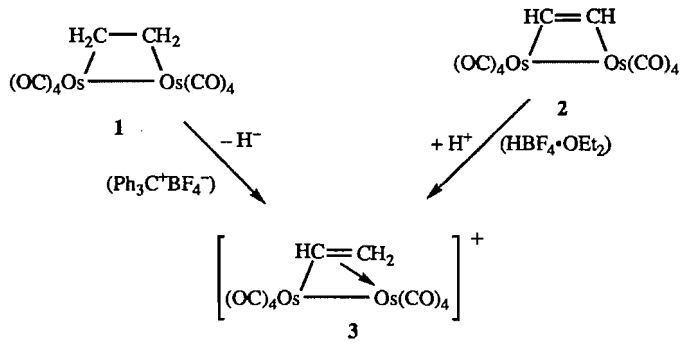

plexes related to **3**. These include insertion of a metal into vinylic C—S (15) or C–halogen (16) bond, protonation of alkyne-bridged bimetallic complexes (17) and dimetallacyclopentenones (18), rearrangement of μ-alkylidyne complexes and their reactions with alkenes (19), β-hydride abstraction from μ-alkylidene complexes (20), and addition of alkynes to transition metal carbonyl hydrides (21). Thus, although the protonation route to **3** is precedented, conversion of **1** is the first documented example of an α-hydride abstraction from a saturated dimetallacyclic species toward μ-alkenyl com-

[6] Copies of the supplementary material may be purchased from: The Depository of Unpublished Data, Document Delivery, CISTI, National Research Council Canada, Ottawa, Canada K1A 0S2.

Tables of positional parameters, bond lengths, and bond angles and X-ray analysis details have also been deposited with the Cambridge Crystallographic Data Centre, and can be obtained on request from The Director, Cambridge Crystallographic Data Centre, University Chemical Laboratory, 12 Union Road, Cambridge, CB2 1EZ, U.K.

Structure factor amplitudes are no longer being deposited and may be obtained directly from the author

Can. J. Chem. Downloaded from www.nrcresearchpress.com by 80.90.12.36 on 09/08/12
For personal use only.

Table 2. Atomic coordinates ($\times 10^3$) and equivalent isotropic thermal parameters ($\times 10^2$) for non-hydrogen atoms of $[(\mu\text{-}\eta^1,\eta^2\text{-}CHCH_2)Os_2(CO)_8][BF_4]$ (**3**).

Atom	*x*	*y*	*z*	*U*, A^2	Atom	*x*	*y*	*z*	*U*, A^2
Os1	−16.12(3)	413.31(3)	625.06(4)	2.818(9)*[a]	O8	−2(1)	162.3(7)	301(1)	8.7(4)*
Os2	34.26(3)	377.89(3)	328.17(5)	3.02(1)*	C1	134(1)	442.6(8)	685(1)	4.1(3)*
F1	752.5(9)	693.8(8)	366(2)	10.5(4)*	C2	−72(1)	466.5(9)	803(1)	4.3(4)*
F2	684.9(8)	838.7(5)	393(1)	7.8(4)*	C3	−168(1)	379.0(8)	568(1)	4.2(3)*
F3	754(1)	763.9(8)	586(1)	14.3(6)*	C4	10(1)	283.2(8)	683(1)	4.1(3)*
F4	595.4(8)	714.9(7)	491(1)	8.5(4)*	C5	188(1)	361.8(8)	387(1)	4.6(4)*
O1	221.1(7)	457.2(7)	723(1)	6.3(3)*	C6	79(1)	406.6(9)	134(1)	4.7(4)*
O2	−105.0(8)	499.2(7)	905(1)	6.5(3)*	C7	−117(1)	407.9(9)	265(1)	4.8(4)*
O3	−253.2(8)	358.1(8)	544(1)	7.1(4)*	C8	14(1)	239.5(8)	305(1)	4.9(4)*
O4	27.2(9)	209.1(6)	709(1)	6.6(3)*	C9	−52(1)	552.6(8)	497(1)	4.6(4)*
O5	276.1(8)	355.2(7)	426(1)	6.3(3)*	C10	39(1)	506.1(7)	434(1)	3.2(3)*
O6	107.1(9)	431(1)	25(1)	8.1(4)*	B	697(1)	752(1)	463(2)	4.9(5)*
O7	−200.2(7)	427.6(8)	228(1)	7.0(4)*					

[a]*Indicates an atom refined anisotropically.

The equivalent isotropic thermal parameter is given by: $U = 1/3\ (U_{11} + U_{22} + U_{33} + 2U_{23} \cos\alpha + 2U_{13} \cos\beta + 2U_{12} \cos\gamma)$.

plexes. The reaction finds analogy in the elegant work of Gladysz and co-workers (22) whereby terminal rhenium-alkylidene complexes $[Re{=}CHR']^+$ (where Re is the $(C_5R_5)Re(NO)L$ fragment, R = H, Me) were generated via α-hydride abstraction from rhenium-bonded hydrocarbyl ligands. No doubt, the strength of the metal–carbon σ-bond, in both instances, is responsible in no small part for the successful outcome of these transformations.

Spectroscopic features and μ-vinyl bonding

Infrared monitoring of the reactions indicated clean conversion to complex **3**. The shift to higher frequencies of the terminal carbonyl-stretching bands compared to the parent complexes (ranges in **1** and **2** are 2122–1967 and 2129–1970 cm^{-1}, respectively) is consistent with the formation of a cationic complex and, consequently, the more electron-deficient nature of the osmium centers in complex **3**.

The ^1H NMR spectrum displays three resonances at 8.56 (dd, J = 9 and 15 Hz), 5.86 (d, J = 9 Hz), and 3.88 (d, J = 15 Hz). The coupling pattern is typical of that observed previously in μ-vinyl complexes, for instance $(\mu\text{-}\eta^1,\eta^2\text{-}CHCH_2)(\mu\text{-}SR)Fe_2(CO)_6$ (15) and $[(\mu\text{-}\eta^1,\eta^2\text{-}CHCH_2)(\mu\text{-}CO)M_2(C_5H_5)_2(CO)_2]^+$ (M = Fe, **4Fe**; Ru, **4Ru**) (18), with *J*(*trans*) > *J* (*cis*) > *J* (*geminal*), the latter small coupling being unobserved in the present case. On this basis the signal at 8.56 ppm is assigned to the vinylic C*H* proton and the other two signals to the methylenic hydrogens *cis* and *trans* to it, respectively. The ^{13}C NMR spectrum shows two signals for the μ-vinyl group at 134.9 and 64.8 ppm, attributable to the vinylic *C*H, and methylenic *C*H_2 carbons, respectively. In addition, there are eight well-resolved terminal carbonyl signals. Corroborating the IR observation, the range of the carbonyl signals, 176.3–164.4 ppm, is at higher field than those of the diosmacyclic parents (**1**, 180.7–169.7 ppm; **2**, 178.4–169.2 ppm). The observation of eight distinct carbonyl signals clearly shows that the molecule is static at room temperature and, since the ^{13}C NMR spectrum is invariant to 90°C, it remains so up to this temperature. Although vinyl group oscillation between two metal centers is well known (23) and renders numerous μ-alkenyl complexes fluxional, the energetics of the process are both substituent (18, 19*a*) and metal dependent (18). In particular, Knox and co-workers have shown that for complexes **4** the onset of vinyl oscillation for the iron complex is around 50°C, whereas the analagous ruthenium complex is static at this temperature (18). Following this trend, the lack of fluxionality of complex **3** is not that surprising.

The bonding in μ-alkenyl complexes has been described in terms of contributions from three VB (valence bond) structures. The early σ,π description **A** (24) has lately been taken over by the dimetallabicyclobutane description (**B**) both on the

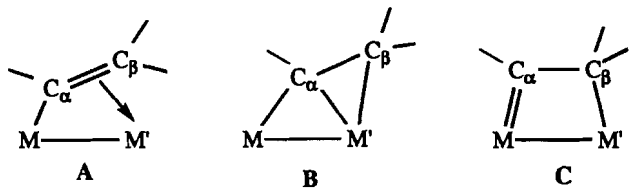

basis of NMR data (18, 19) and structural parameters (25). Indeed the typically low-field ^1H and ^{13}C NMR positions of the $C_\alpha H$ unit argue for substantial μ-carbene character (26). Very convincing examples are provided by the complexes $[(\mu\text{-}\eta^1,\eta^2\text{-}CHCH_2)(\mu\text{-}CO)M_2(C_5H_5)_2(CO)_2]^+$ (M = Fe, **4Fe**; Ru, **4Ru**) prepared by Knox and co-workers (18). The ^1H and ^{13}C chemical shifts are 12.57, 11.22 and 185.8, 163.6 ppm, respectively, and are similar to those of the μ-carbene complex $[(\mu\text{-}C(H)Me)(\mu\text{-}CO)Fe_2(C_5H_5)_2(CO)_2]$ (27): 11.60 ppm μ-C*H*-(Me) and 172.9 ppm, μ-*C*H(Me). Chisholm and co-workers (28) have argued for contribution from VB structure **C** in $(\mu\text{-}\eta^1,\eta^2\text{-}CHCH_2)(\mu\text{-}CH_2NMe)W_2Cl_3(NMe_2)_2(PMe_2Ph)_2$, mostly on the basis of metrical parameters (vide infra), but the pronounced low-field position of the $C_\alpha H$ proton (14.75 ppm) and the high-field shift of one of the methylenic protons (1.75 ppm) were also taken as evidence for this.

Compared to these data, the observed ^1H and ^{13}C chemical shifts of the $C_\alpha H$ unit in complex **3** are at higher field (8.56 and

Can. J. Chem. Downloaded from www.nrcresearchpress.com by 80.90.12.36 on 09/08/12
For personal use only.

134.9 ppm, respectively) and argue for *less* μ-carbene character and consequently more substantial contribution from the σ,π-vinyl-type bonding, a return to the former traditional description. Thus, it appears that reduced back bonding from the electron-deficient $Os(CO)_4^+$ fragment to the bridging vinyl moiety is sufficient to favor form **A** over **B**; form **C** appears not to make significant contribution to the bonding.

It is interesting that the change in bonding is reflected in the chemical behavior of **3**. Normally cationic μ-alkenyl complexes undergo nucleophilic attack, including hydride addition, at the β carbon to generate μ-alkylidene complexes (18, 19*a*, 20*b*, 27). Hydride attack of **3** is dominated by addition to the α-carbon and regeneration of the parent octacarbonyl diosmacyclobutane **1**. It is not immediately obvious why the σ,π-vinyl bonding should lead to preferential C_α attack, especially in view of the existence of $[(\mu\text{-}C(H)Me)Os_2(CO)_8]$ (5*a*), the expected product of C_β attack. Nevertheless, it is interesting to note that whereas hydride addition to **4Fe** proceeds exclusively at the C_β carbon, the ruthenium congener also undergoes minor C_α attack as evidenced by the low-yield formation of the terminal ethylene complex, $[(\mu\text{-}CO)_2Ru_2(C_5H_5)_2(CO)(C_2H_4)]$ (18). Thus, both the chemical and fluxional behavior of complex **3** follow and complete the observed triad trend of Knox on compounds **4Fe** and **4Ru**.

Molecular structure of 3

To obtain precise metrical parameters and to possibly provide quantitative support for the tendency toward σ,π-vinyl bonding, the solid state structure of **3** was determined by single-crystal X-ray analysis. Two views of the cation, with labeling scheme, are shown in Fig. 1, selected bond distances and angles are listed in Table 3.

The figure shows the now classical orientation and bonding of a bridging vinyl unit, σ-bonded to one osmium (Os2) and π-bonded via the double bond to the other osmium (Os1), which carries the formal positive charge. The μ-vinyl moiety is skewed with respect to the Os—Os bond and the two $Os(CO)_4$ fragments are rotated away from eclipsed conformation by an average of 22°. Puckering of the four-membered diosmacyclobutane ring and concomitant twisting of the $Os(CO)_4$ fragments were also observed in complex **1** (8*a*) and its substituted derivatives (5*b*, 9*c*); the respective average values are 27° and 20°. An Os—Os single bond and four carbonyl ligands on each osmium complete the 18-electron requirements of the metals. The Os1—Os2 distance, 2.8569(5) Å, is typical of an Os—Os single bond and compares favorably to 2.845(1) Å, the vinyl-bridged Os—Os bond in $[(\mu\text{-}CHCH_2)(\mu\text{-}H)Os_3(CO)_{12}]$ (29).

As discussed in the previous section, the bonding of the (μ-vinyl)MM′ fragment has been described mainly in terms of two limiting VB canonical structures, σ,π donation (**A**), and localized dimetallabicyclobutane extremes (**B**). Of course, in molecular orbital (MO) parlance there is a continuum between the extremes, akin to the Dewar–Chatt–Duncanson description of metal–olefin bonding. Nevertheless, a measure of the relative importance of the different VB forms obtains on the basis of the metrical parameters. Thus, near-symmetric metal–C_α distances are consistent with form **B** and the μ-carbenoid character of the C_α carbon. It is on this basis that previous iron triad μ-vinyl complexes were assigned this form, in accord with their NMR chemical shift values (vide supra). The

Fig. 1. Two perspective views of the μ-vinyl cation $[(\mu\text{-}\eta^1\text{-}\eta^2\text{-}CHCH_2)Os_2(CO)_8]^+$ showing the atom numbering scheme. Probability ellipsoids are shown at 50% level for non-hydrogen atoms; the latter are drawn as spheres of arbitrary radius.

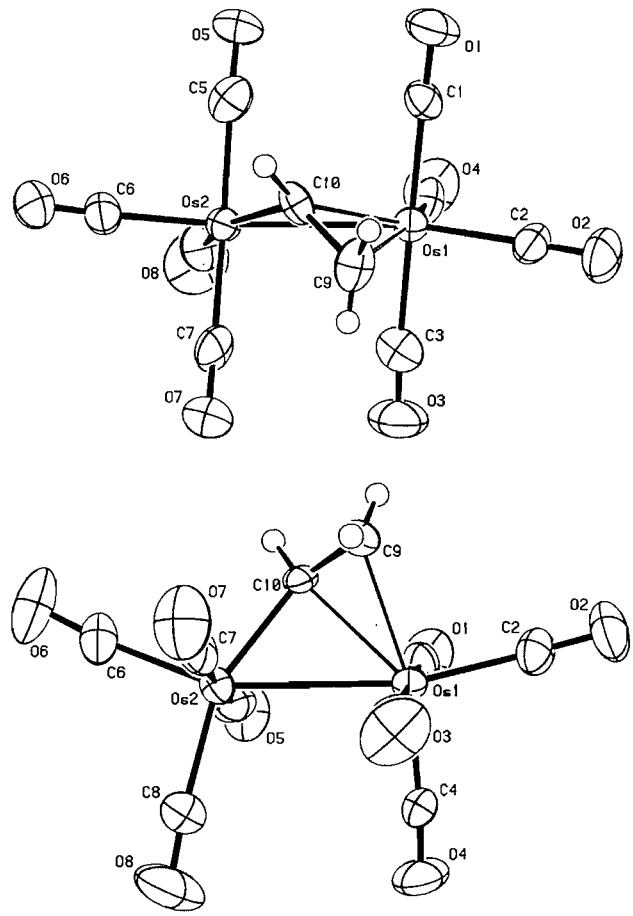

Table 3. Selected bond distances (A) and angles (deg) for $[(\mu\text{-}\eta^1,\eta^2\text{-}CHCH_2)Os_2(CO)_8][BF_4]$ (**3**).

Bond distances					
Os1	Os2	2.8569(5)[a]	Os1	C3	1.98(1)
Os1	C9	2.34(1)	Os1	C4	1.94(1)
Os1	C10	2.30(1)	Os2	C5	1.96(1)
Os2	C10	2.061(9)	Os2	C6	1.92(1)
C9	C10	1.41(2)	Os2	C7	1.97(1)
Os1	C1	1.95(1)	Os2	C8	1.99(1)
Os1	C2	1.93(1)	C≡O (avg.)		1.11(2)

Bond angles							
Os1	C10	Os2	81.6(3)	Os1	C10	C9	73.8(7)
Os1	C9	C10	70.8(6)	Os2	C10	C9	125.9(9)
Os1	Os2	C10	52.8(3)	C9	Os1	C10	35.5(4)
Os2	Os1	C10	45.5(2)	Os2	Os1	C2	164.1(4)
				Os1	Os2	C6	157.2(4)

[a]Numbers in parentheses are estimated standard deviations in the least significant digit.

M,M′—C_α distances in $[(\mu\text{-}CHCH_2)(\mu\text{-}CO)Fe_2(C_5H_5)_2(CO)_2]^+$ (**4Fe**) (25) and $[(\mu\text{-}CHCH_2)(\mu\text{-}H)Os_3(CO)_{10}]$ (29) are 1.980(8) Å for both, and 2.107(3) and 2.273(3) Å, respec-

tively. The nonbridging M′—C_β distance is uniformly longer (2.21(2) Å and 2.362(3) Å), respectively. Clearly, **4Fe** conforms more closely to form **B**. An interesting exception is Chisholm's (μ-$CHCH_2$)(μ-CH_2NMe_2)$W_2Cl_3(NMe)_2(PMe_2Ph)_2$ complex (28) where the difference between M—C_α and M′—C_α distances is pronounced, 2.04(1) versus 2.32(1) Å, with the former the much shorter bond. In addition the M′—C_β distance 2.25(1) Å is shorter than the M′—C_α bond length. The distribution of the metal–carbon distances led to the suggestion of significant contribution from "terminal" metal carbene-type bonding (**C**) in this complex. The relevant M,M′—C_α and M′—C_β distances in complex **3** are Os2—C10 2.061(9) Å, Os1—C10 2.300(10) Å, and Os1—C9 2.340(10) Å, respectively. Although the M—C_α length is short, the other parameters are not in accord with contribution from VB descriptions **C**. If anything, it appears that the σ,π-vinyl structure (**A**) make a more significant contribution to the bonding in **3** than in the related cationic iron complex **4Fe**. The NMR features of the complex also implied this situation. The C—C distance of the coordinated vinyl ligand, C9—C10 is 1.41(2) Å. The lengthening from the free C=C double bond value, 1.34 Å, is expected upon metal coordination. The length of the bond is similar to that found in other μ-vinyl complexes (1.40(2) Å in **4Fe** and 1.42(2) Å in the abovementioned tungsten complex), but shorter than the C—C distance of coordinated ethylene in $Os(CO)_4(\eta^2\text{-}C_2H_4)$ (1.488(24) Å), which has been described as an osmacyclopropane (30). In short, the structural features support significant contribution from VB description **A** to the bonding in complex **3**.

Conclusion

The diosmacyclic complexes **1** and **2** are easily converted to the μ-vinyl cation **3**. The ease of transformations, the stability of the species, and the different behavior of **3** toward hydride addition compared to related iron and ruthenium complexes all are in line with the unique place osmium occupies in the iron triad transition metals.

Acknowledgments

Financial support from The Natural Sciences and Engineering Research Council of Canada and the University of Alberta is gratefully acknowledged. J.T. wishes to thank Bill Graham for "showing the way." Good example generates faithful following, and osmium has also served the author very well for the past several years.

References

1. (*a*) G.W. Parshall and S.D. Ittel. Homogeneous catalysis. 2nd ed. Wiley–Interscience, New York. 1992; (*b*) G.A. Somorjai. Introduction to surface chemistry and catalysis. Wiley–Interscience, New York. 1994. Chap. 7.
2. J.A. Martinho Simões and J.L. Beauchamp. Chem. Rev. **90**, 629 (1990).
3. R.D. Adams and J.P. Selegue. Comprehensive organometallic chemistry. Vol. 4. *Edited by* G. Wilkinson, F.G.A. Stone, and E. Abel. Pergamon Press, London. 1982. Chap. 33.
4. (*a*) J.R. Moss and W.A.G. Graham. J. Chem. Soc. Chem. Commun. 835 (1970); J. Chem. Soc. Dalton Trans. 95 (1977); (*b*) J. Organomet. Chem. **23**, C 47 (1970); Inorg. Chem. **16**, 75 (1977); (*c*) J. Organomet. Chem. **18**, P 24 (1969); J. Chem. Soc. Dalton Trans. 89 (1977).
5. (*a*) K.M. Motyl, J.R. Norton, C.K. Schauer, and O.P. Anderson. J. Am. Chem. Soc. **104**, 7325 (1982); (*b*) M.R. Burke, J. Takats, F.-W. Grevels, and J.G.A. Reuvers. J. Am. Chem. Soc. **105**, 4092 (1983).
6. M.J. Burn, G.-Y. Kiel, F. Seils, J. Takats, and J. Washington. J. Am. Chem. Soc. **111**, 6850 (1989).
7. (*a*) N. Sheppard. Annu. Rev. Phys. Chem. **39**, 589 (1988); (*b*) C.E. Anson, B.T. Keiller, I.A. Oxton, D.B. Powell, and N. Sheppard. J. Chem. Soc. Chem. Commun. 470 (1983).
8. (*a*) O.P. Anderson, B.R. Bender, J.R. Norton, A.C. Larson, and P.J. Vergamini. Organometallics, **10**, 3145 (1991); (*b*) C.E. Anson, B.F.G. Johnson, J. Lewis, D.B. Powell, N. Sheppard, A.K. Battacharyya, B.R. Bender, R.M. Bullock, R.T. Hembre, and J.R. Norton. J. Chem. Soc. Chem. Commun. 703 (1989).
9. (*a*) R.T. Hembre, C.P. Scott, and J.R. Norton. J. Am. Chem. Soc. **109**, 3468 (1987); (*b*) R.T. Hembre, D.L. Ramage, C.P. Scott, and J.R. Norton. Organometallics, **13**, 2995 (1994); (*c*) M.R. Burke. Ph.D. Thesis, University of Alberta (1987).
10. (*a*) M.R. Burke and J. Takats. J. Organomet. Chem. **302**, C25 (1986); (*b*) M.R. Burke, F. Seils, and J. Takats. Organometallics, **13**, 1445 (1994).
11. S.M. Davis, F. Zaera, B.E. Gordon, and G.A. Somorjai. J. Catal. **92**, 240 (1985).
12. N. Walker and D. Stuart. Acta Crystallogr. Sect. A: Found, Crystallogr. **A39**, 158 (1983).
13. B.A. Frenz. Computing in crystallography. Delft University Press, Delft, Holland. 1978. pp. 64–71.
14. International tables for X-ray crystallography. Vol. IV. Kynoch Press, Birmingham, England. 1974. (*a*) Table 2.2B; (*b*) Table 2.3.1.
15. R.B. King, P.M. Treichel, and F.G.A. Stone. J. Am. Chem. Soc. **83**, 3600 (1961).
16. (*a*) C. Krüger, Y.H. Tsay, F.-W. Grevels, and E. Koerner von Gustorf. Isr. J. Chem. **10**, 201 (1972); (*b*) F.-W. Grevels and E. Koerner von Gustorf. Liebigs Ann. Chem. 547 (1975); (*c*) F.-W. Grevels, D. Shulz, E. Koerner von Gustorf, and D. St. P. Bunbury. J. Organomet. Chem. **91**, 341 (1975).
17. (*a*) J.A. Beck, S.A.R. Knox, G.H. Riding, G.E. Taylor, and M.J. Winter. J. Organomet. Chem. **202**, C49 (1980); (*b*) R.S. Dickson, C. Mok, and G.N. Pain. J. Organomet. Chem. **166**, 385 (1979).
18. A.F. Dyke, S.A.R. Knox, M.J. Morris, and P.J. Naish. J. Chem. Soc. Dalton Trans. 1417 (1983).
19. (*a*) C.P. Casey, S.R. Marder, and B.R. Adams. J. Am. Chem. Soc. **107**, 7700 (1985); (*b*) C.P. Casey, M.W. Meszaros, P.J. Fagan, R.K. Bly, and R.E. Colborn. J. Am. Chem. Soc. **108**, 4053 (1986).
20. (*a*) A.F. Dyke, S.A.R. Knox, P.J. Naish, and A.G. Orpen. J. Chem. Soc. Chem. Commun. 441 (1980); (*b*) S.C. Kao, P.P.Y. Lu, and R. Pettit. Organometallics, **1**, 911 (1982).
21. R. Yáñez, J. Ros, and R. Mathieu. J. Organomet. Chem. **414**, 209 (1991), and references therein.
22. (*a*) W.A. Kiel, G.-Y. Lin, A.G. Constable, F.B. McCormick, C.E. Strouse, O. Eisenstein, and J.A. Gladysz. J. Am. Chem. Soc. **104**, 4865 (1982); (*b*) W.A. Kiel, G.-Y. Lin, G.S. Bodner, and J.A. Gladysz. J. Am. Chem. Soc. **105**, 4958 (1983); (*c*) A.T. Patton, C.E. Strouse, C.B. Knobler, and J.A. Gladysz. J. Am. Chem. Soc. **105**, 5804 (1983).
23. J.R. Shapley, S.I. Richter, M. Tachikawa, and J.B. Keister. J. Organomet. Chem. **94**, C43 (1975).
24. A.N. Nesmeyanov, M.I. Rybinskaya, L.V. Rybin, V.S. Kaganovich, and P.V. Petrovskii. J. Organomet. Chem. **31**, 257 (1971).
25. A.G. Orpen. J. Chem. Soc. Dalton Trans. 1427 (1983), and references therein.
26. W.A. Herrmann. Adv. Organomet. Chem. **20**, 159 (1982).
27. C.P. Casey and P.C. Vosejpka. Organometallics, **7**, 934 (1988).

Can. J. Chem. Downloaded from www.nrcresearchpress.com by 80.90.12.36 on 09/08/12
For personal use only.

28. K.J. Ahmed, M.H. Chisholm, K. Folting, and J.C. Huffmann. J. Am. Chem. Soc. **108**, 989 (1986).
29. A.G. Orpen, D. Pippard, G.M. Sheldrick, and K.D. Rouse. Acta Crystallogr. Sect. B: Struct. Crystallogr. Cryst. Chem. **B34**, 2466 (1978).
30. B.R. Bender, J.R. Norton, M.M. Miller, O.P. Anderson, and A.K. Rappé. Organometallics, **11**, 3427 (1992).

Can. J. Chem. Downloaded from www.nrcresearchpress.com by 80.90.12.36 on 09/08/12
For personal use only.

Bidentate and terdentate (P-N-S) complexes of a new thioether azine phosphine *Z,E*-$PPh_2CH_2C(Bu^t)$=N-N=C(Me)$CH_2S(C_6H_4Me$-4) with molybdenum, tungsten, or platinum

Sarath D. Perera, Mustaffa Shamsuddin, and Bernard L. Shaw

Abstract: Treatment of *Z*-$PPh_2CH_2C(Bu^t)$=NNH_2 with 4-methylphenylthiomethyl methyl ketone gave the thioether azine phosphine *Z,E*-$PPh_2CH_2C(Bu^t)$=N-N=C(Me)$CH_2S(C_6H_4Me$-4) **1**, which with H_2O_2 gave the corresponding phosphine oxide **2**. Treatment of **1** with [$Mo(CO)_3(\eta^6$-cht)] or [$W(CO)_3(NCEt)_3$] gave the yellow tricarbonyl complexes *fac*-[$M(CO)_3${$PPh_2CH_2C(Bu^t)$=N-N=C(Me)$CH_2S(C_6H_4Me$-4}] **3a** (Mo) or **3b** (W), respectively. Treatment of **1** with [$Mo(CO)_4$(nbd)] gave the pale yellow tetracarbonylmolbdenum(0) complex [$Mo(CO)_4${$PPh_2CH_2C(Bu^t)$=N-N=C(Me)$CH_2S(C_6H_4Me$-4)}] **4**, in which the ligand **1** is bidentate through P and N. Oxidation of either **3a** or **4** with 1 equivalent of bromine gave the orange neutral seven-coordinate dicarbonylmolybdenum(II) complex [$MoBr_2(CO)_2${$PPh_2CH_2C(Bu^t)$=N-N=C(Me)$CH_2S(C_6H_4Me$-4)}] **5**, whereas the tungsten complex **3b** with 1 equivalent of bromine gave the seven-coordinate tricarbonyltungsten(II) cation [$WBr(CO)_3${$PPh_2CH_2C(Bu^t)$=N-N=C(Me)$CH_2S(C_6H_4Me$-4)}]$^+$ isolated as the PF_6 salt **6**. Treatment of **1** with [$PtCl_2(NCMe)_2$]gave the yellow dichloroplatinum(II) complex [$PtCl_2${$PPh_2CH_2C(Bu^t)$=N-N=C(Me)$CH_2S(C_6H_4Me$-4)}] **7**, in which **1** is bidentate through P and N. When **7** was treated with NH_4PF_6 in methanol it gave the terdentate salt [PtCl{$PPh_2CH_2C(Bu^t)$=N-N=C(Me)$CH_2S(C_6H_4Me$-4)}]PF_6 **8a**. Deprotonation of **7** with NEt_3–NaOH gave the orange neutral chloroplatinum(II) complex [PtCl{PPh_2-$CH_2C(Bu^t)$=N-NC(Me)=CHS(C_6H_4Me-4)}] **9**, containing a terdentate ene-hydrazone phosphine ligand. This neutral complex **9** was reprotonated using HBF_4 to give the BF_4 salt **8b**. Treatment of the phosphine **1** with [$PtMe_2$(cod)] gave the white dimethylplatinum(II) complex [$PtMe_2${$PPh_2CH_2C(Bu^t)$=N-N=C(Me)CH_2-$S(C_6H_4Me$-4)}] **10**, containing the bidentate azine ligand. Treatment of **10** with MeI gave the white platinum(IV) iodide salt *fac*-[$PtMe_3${$PPh_2CH_2C(Bu^t)$=N-N=C(Me)$CH_2S(C_6H_4Me$-4)}]I **11a** in which the azine is terdentate. When **11a** was treated with NH_4PF_6 in MeOH the PF_6 salt **11b** was obtained. Treatment of **10** with picric acid gave the yellow methylplatinum(II) picrate salt [PtMe{$PPh_2CH_2C(Bu^t)$=N-N=C(Me)CH_2-$S(C_6H_4Me$-4)}][$OC_6H_2(NO_2)_3$-2,4,6] **12** and methane. Infrared, ^{31}P–[^1H], ^1H, and some ^{13}C–[^1H] NMR data are given.

Key words: azine phosphine, thioether, metal-carbonyls, platinum.

Résumé : La réaction de la *Z*-PPh_2CH_2C(*tert*-But)=NNH_2 avec la (4-méthylphénylthiométhyl)méthylcétone conduit au thioéther de la phosphine d'azine *Z,E*-PPh_2CH_2C(*tert*-Bu)=N-N=C(Me)$CH_2S(C_6H_4Me$-4), **1**, qui, par réaction avec du H_2O_2, fournit l'oxyde de phosphine correspondant, **2**. Le traitement du composé **1** avec du [$Mo(CO)_3(\eta^6$-cht)] ou [$W(CO)_3(NCEt)_3$] fournit des complexes tricarbonyles jaunes *fac*-[$M(CO)_3${PPh_2CH_2C-(*tert*-Bu)=N-N=C(Me)$CH_2S(C_6H_4Me$-4)}], respectivement **3a** (M = Mo) et **3b** (M = W). Le traitement du composé **1** avec du [$Mo(CO)_4$(nbd)] fournit le complexe jaune pâle tétracarbonylmolybdène(0) [$Mo(CO)_4$-{PPh_2CH_2C(*tert*-Bu)=N-N=C(Me)$CH_2S(C_6H_4Me$-4)}], **4**, dans lequel le coordinat **1** est bidentate par les atomes de P et ce N. L'oxydation soit de **3a** ou de **4** avec un équivalent de brome donne un complexe orange, neutre, heptacoordiné dicarbonylmolybdène(II) [$MoBr_2(CO)_2${PPh_2CH_2C(*tert*-Bu)=N-N=C-(Me)$CH_2S(C_6H_4Me$-4)}], **5**, alors que le complexe de tungstène, **3b**, sous l'action d'un équivalent de brome fournit le cation heptacoordiné tricarbonyltungstène(II), [$WBr(CO)_3${PPh_2CH_2C(*tert*-Bu)=N-N=C-(Me)$CH_2S(C_6H_4Me$-4)}]$^+$, isolé sous la forme de son sel de PF_6, **6**. Le traitement du composé **1** par du [$PtCl_2(NCMe)_2$] donne le complexe jaune de dichloroplatine(II), [$PtCl_2${PPh_2CH_2C(*tert*-Bu)=N-

Received October 5, 1994.

This paper is dedicated to Professor William A.G. Graham on the occasion of his 65th birthday.

S.D. Perera, M. Shamsuddin, and B.L. Shaw.[1] School of Chemistry, The University of Leeds, Leeds LS2 9JT, U.K.

[1] Author to whom correspondence may be addressed. Telephone: 0113-2336401 or 0113-2336400. Fax: 0113-2336565.

Can. J. Chem. Downloaded from www.nrcresearchpress.com by 80.90.12.36 on 09/08/12
For personal use only.

N=C(Me)$CH_2S(C_6H_4Me$-4)}], **7**, dans lequel **1** est bidentate par le biais des atomes de P et de N. Lorsqu'on traite le composé **7** avec du NH_4PF_6 dans le méthanol, il fournit le sel tridentate [PtCl{PPh_2CH_2C(*tert*-Bu)=N-N=C(Me)$CH_2S(C_6H_4Me$-4)}]PF_6, **8a**. La déprotonation du composé **7** à l'aide de NEt_3–NaOH fournit un complexe orange neutre de chloroplatine(II), [PtCl{PPh_2CH_2C(*tert*-Bu)=N-NC(Me)=CHS$(C_6H_4Me$-4)}], **9**, qui contient un coordinat phosphine ène-hydrazone tridentate. On a reprotoné ce complexe neutre **9** à l'aide de HBF_4 pour obtenir le sel de BF_4, **8b**. Le traitement de la phosphine **1** avec du [$PtMe_2$(cod)] fournit le complexe blanc de diméthylplatine(I), [$PtMe_2${PPh_2CH_2C(*tert*-Bu)=N-N=C(Me)-$CH_2S(C_6H_4Me$-4)}], **10**, qui contient un coordinat azine bidentate. Le traitement du composé **10** par du MeI fournit un sel blanc d'iodure de platine(IV), *fac*-$PtMe_3${PPh_2CH_2C(*tert*-Bu)=N-N=C(Me)$CH_2S(C_6H_4Me$-4)}]I, **11a**, dans lequel l'azine est tridentate. Quand on traite le composé **11a** avec du NH_4PF_6 dans le MeOH, il y a formation du sel de PF_6, **11b**. Le traitement du composé **10** avec de l'acide picrique fournit le picrate jaune de méthylplatine(II), [PtMe{PPh_2CH_2C(*tert*-Bu)=N-N=C(Me)$CH_2S(C_6H_4Me$-4)}][$OC_6H_2(NO_2)_3$-2,4,6], **12**, et du méthane. On rapporte les données IR et de RMN du $^{31}P-\{^1H\}$ et du ^1H et quelques données de $^{13}C-\{^1H\}$.

Mots clés : phosphine d'azine, thioéther, métal-carbonyles, platine.

[Traduit par la rédaction]

Introduction

In a previous paper (1) we described the preparation of a new chelating (P-N) ligand *Z*-$PPh_2CH_2C(Bu^t)$=NNH_2 from the phosphino dimethylhydrazone *Z*-$PPh_2CH_2C(Bu^t)$=$NNMe_2$ using a hydrazine exchange reaction. *Z*-$PPh_2CH_2C(Bu^t)$=NNH_2 condenses with aldehydes and ketones {QC(=O)R} to give mixed-azine monophosphines of type *Z,E*-$PPh_2CH_2C(Bu^t)$=N-N=C(Q)R (1–10), where Q = H or Me and R is sterically more demanding than Q. We have studied the coordination chemistry of these azine phosphines, in particular, the promotion of agostic C—H interaction (3) or aryl fluoride coordination (4) with ruthenium(II), and cyclometallation with Ir(I) (5, 6), W(0) (7), and Pt(II) (8). We have also reported the synthesis of an azine diphosphine *Z,Z*-$PPh_2CH_2C(Bu^t)$=N-N=$C(Bu^t)$-CH_2PPh_2 (11), and the ability of it, or its corresponding *E,Z* isomer, to coordinate to group 6 metal carbonyls (11), and also to platinum and palladium (12, 13), either as a bidentate (P-P) or as a terdentate (P-N-P) ligand. We incorporated the thioether functionality into our azine–phosphine system, in order to investigate the coordination chemistry of a potential terdentate (P-N-S) ligand. In this paper we describe the synthesis of a new thioether azine phosphine *Z,E*-$PPh_2CH_2C(Bu^t)$=N-N=C(Me)CH_2-$S(C_6H_4Me$-4) **1** and its complexes with transition metals such as molybdenum, tungsten, or platinum. There are several reports (14–21) on bidentate (P-S) ligands, viz. $Ph_2P(CH_2)_nSR$ (*n* = 1–3, R = H, Me, Et, or Ph) (16–18, 20); *o*-$Ph_2PC_6R_4SMe$ (R = H or F) (14, 15); $PhP(o\text{-}C_6R_4SMe)_2$ (R = H or F) (14, 19); $P(o\text{-}C_6H_4SMe)_3$ (19); and Ph_2PCH_2P(=S)Ph_2 (21); etc. Tertiary phosphine ligands containing both nitrogen and sulfur donor atoms are rare (22, 23); potential terdentate phosphine ligands $PPh_2CH_2CH(NMe_2)(CH_2)_nSMe$ (*n* = 2, 3), derived from α-amino acids, formed bidentate palladium(II) complexes [$PdCl_2${$PPh_2CH_2CH(NMe_2)(CH_2)_nSMe$}], in which sulfur was not coordinated to palladium (23). Very recently, Faller et al. (24) reported the synthesis of the analogous phosphinite ligands $PPh_2OCH_2CH(NMe_2)(CH_2)_nSMe$ (*n* = 1, 2) and their terdentate (P-N-S) complexes of type *fac*-[$M(CO)_3${PPh_2-$OCH_2CH(NMe_2)(CH_2)_nSMe$}] (M = Mo or W).

Results and discussion

Complexes of 1 with molybdenum and tungsten

The phosphino hydrazone *Z*-$PPh_2CH_2C(Bu^t)$=NNH_2 (1) condensed rapidly with 4-methylphenylthiomethyl methyl ketone in ethanol to give the crystalline thioether azine phosphine *Z,E*-$PPh_2CH_2C(Bu^t)$=N-N=C(Me)$CH_2S(C_6H_4Me$-4) **1** in 84% yield. The various reactions of the thioether azine phosphine **1** are summarized in Schemes 1 and 2. Elemental analytical and some mass spectral and carbon-13 NMR data are in the Experimental, IR and phosphorus-31 NMR data are in Table 1, and proton NMR data in Table 2. Carbon-13 spectra were assigned using Attached Proton Tests (APT) and by comparison with published data (2, 7, 11–13). Some satellites due to platinum-195 coupling were not identified because of their low intensities or broadness. The $^{31}P-\{^1H\}$ NMR spectrum of the phosphine **1** in $CDCl_3$ was a singlet at −11.1 ppm. The proton NMR spectrum showed a doublet at 3.22 ppm with ^2J(PH) = 4.2 Hz and singlet at 3.28 ppm for the CH_2P and CH_2S protons, respectively. The azine phosphine **1** was treated with an excess of H_2O_2 to give the corresponding phosphine oxide **2** as a white solid in 88% yield. The phosphine oxide **2** showed a phosphorus-31 resonance at 24.4 ppm and, in the proton NMR spectrum, the CH_2P(=O) protons showed a large coupling to P(V), ^2J(PH) = 15.0 Hz.

We first investigated the coordinating ability of the thioether azine phosphine **1** as a terdentate ligand with Mo(0) and W(0) (Scheme 1). Treatment of **1** with [$Mo(CO)_3(\eta^6$-cht)] (25) (cht = cyclohepta-1,3,5-triene) in benzene solution displaced cyclohepta-1,3,5-triene to give the tricarbonylmolybdenum(0) complex **3a** as yellow needles in 85% yield. The infrared spectrum of this complex showed two strong bands for ν(C≡O) at 1930 and 1810 cm^{-1}, close to literature values observed for zerovalent molybdenum tricarbonyls (26–28). The $^{13}C-\{^1H\}$ NMR spectrum of **3a** showed three doublet resonances for the C≡O ligands in a 1:1:1 ratio. The resonances with small ^2J(PC) values of 8.1 and 10.2 Hz were assigned to the carbonyl carbons *cis* to phosphorus and the resonance with a large ^2J(PC) value of 42.4 Hz was assigned to the carbonyl carbon *trans* to phosphorus (7, 10, 11, 29). Hence, this tricarbonylmolybdenum(0) complex has a *fac* geometry. The observed low δ_C value of 24.9 ppm for the methylene carbon is consistent with the values obtained for methylene carbons in six-membered chelate rings (2, 7, 12, 29). In the proton NMR spectrum, the CH_2P protons were nonequivalent with ^2J(HH) 12.9 and ^2J(PH) 9.0 Hz whereas the CH_2S protons gave a broad peak centred at 3.97 ppm. Interestingly, the *Me*C=N proton resonance appeared as a doublet with a five-bond cou-

Can. J. Chem. Downloaded from www.nrcresearchpress.com by 80.90.12.36 on 09/08/12
For personal use only.

Scheme 1. R = C_6H_4Me-4; (i) H_2O_2; (ii) $[Mo(CO)_3(\eta^6\text{-cht})]$ or $[W(CO)_3(NCEt)_3]$; (iii) $[Mo(CO)_4(nbd)]$; (iv) Br_2; (v) Br_2–NH_4PF_6.

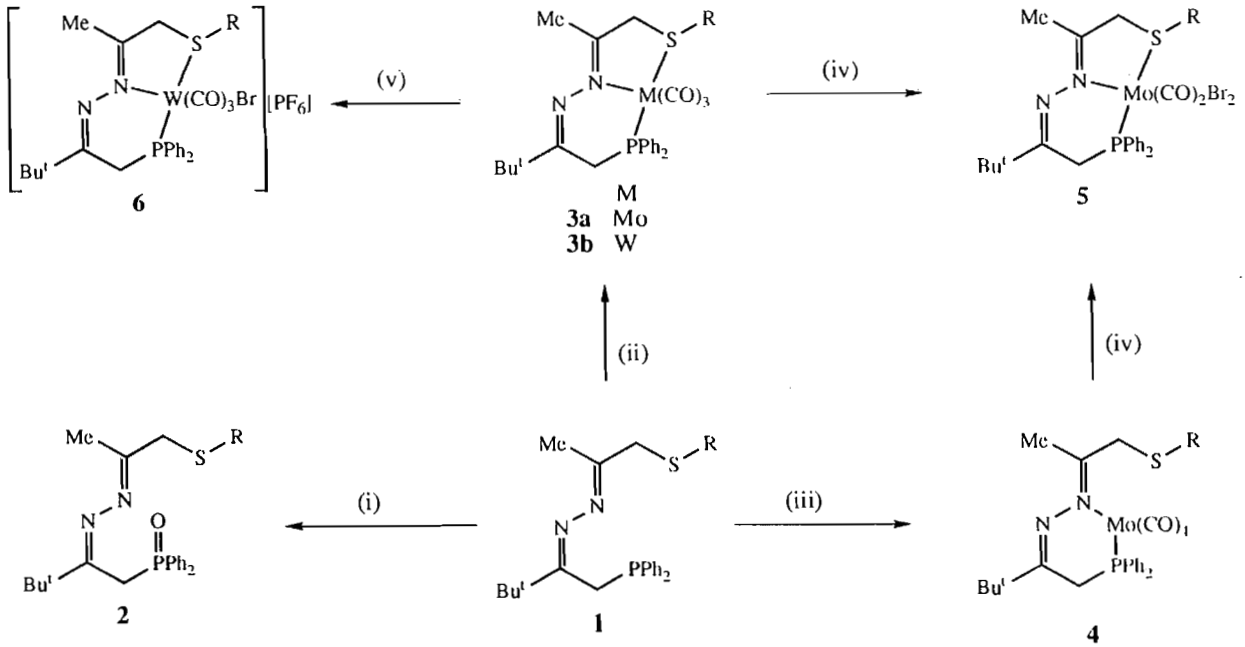

Scheme 2. R = C_6H_4Me-4; (i) $[PtCl_2(NCMe)_2]$; (ii) MeOH–NH_4PF_6; (iii) Et_3N–NaOH; (iv) HBF_4; (v) $[PtMe_2(cod)]$; (vi) excess MeI; (vii) MeOH–NH_4PF_6; (viii) picric acid.

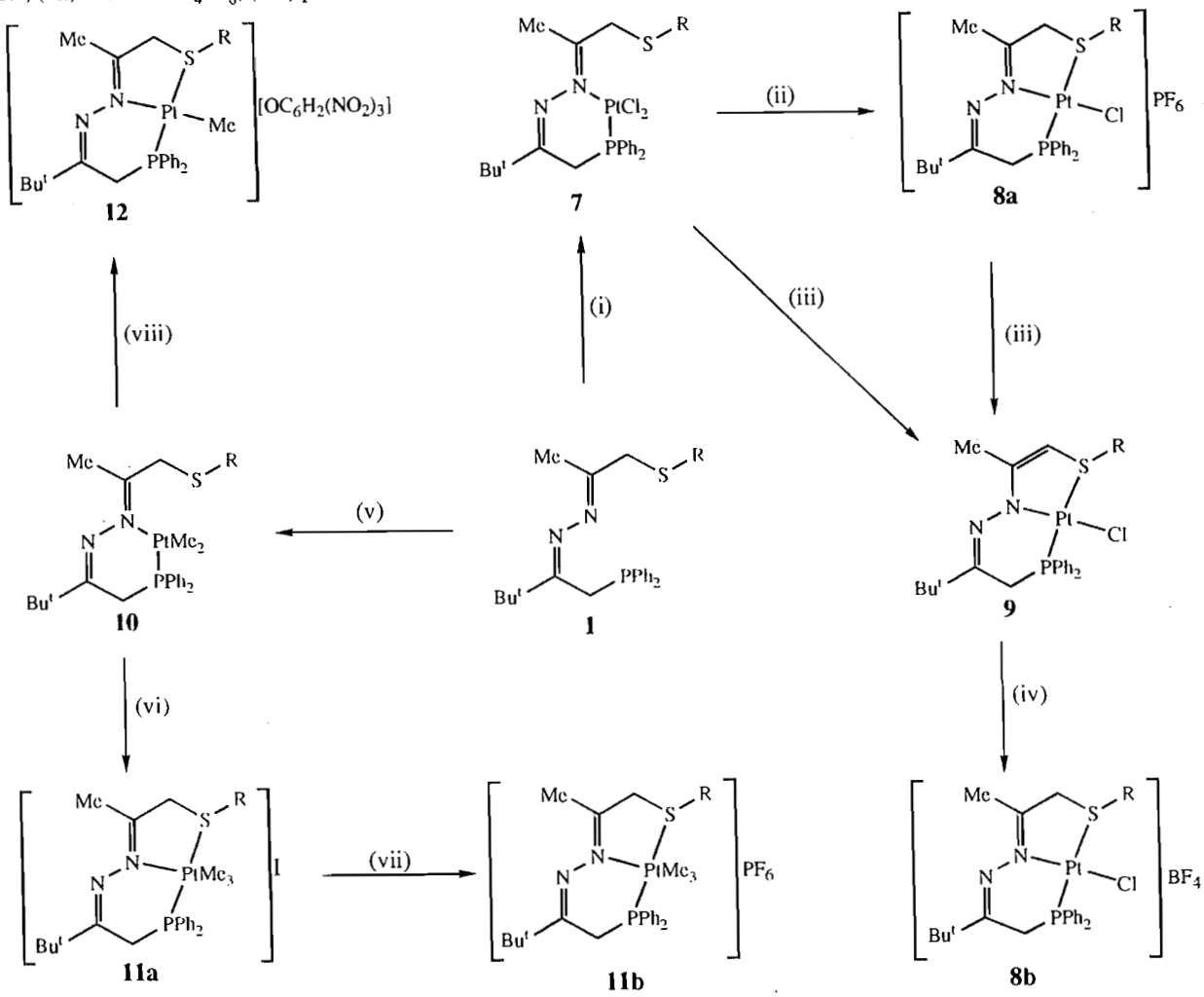

Can. J. Chem. Downloaded from www.nrcresearchpress.com by 80.90.12.36 on 09/08/12
For personal use only.

Can. J. Chem. Downloaded from www.nrcresearchpress.com by 80.90.12.36 on 09/08/12
For personal use only.

Table 1. IR[a] and $^{31}P-\{^1H\}$ NMR[b] data.

Compound	ν(C═N)/cm^{-1}	ν(Pt—Cl)/cm^{-1}	ν(C≡O)[c]/cm^{-1}	δP/ppm	^1J(MP)/Hz
1	1630s	—	—	−11.1	—
2	1630s	—	—	24.4	—
3a	1600m	—	1930s, 1810s	42.3	—
3b	1595w	—	1920s, 1810s	37.7	255
4	1615m	—	2020s, 1900m, 1845m	52.0	—
5	1620m	—	1970s, 1860s	52.5[d]	—
6	1620m	—	2040s, 1965m, 1940m	41.0[d]	—
7	1610m	340w, 290w	—	25.4[d]	4085
8a	1620m	350w	—	43.3	3664
8b	1620m	340w	—	43.8	3674
9	1620m	330w	—	23.3	3776
10	1610s	—	—	36.9[e]	2156
11a	1640m	—	—	15.2	1252
11b	1640m	—	—	13.6	1241
12	1650m	—	—	43.9[e]	4214

[a]As KBr discs.
[b]Recorded at 36.2 MHz, chemical shifts are in ppm relative to 85% H_3PO_4, solvent $CDCl_3$ unless otherwise stated.
[c]In CH_2Cl_2.
[d]In CD_2Cl_2.
[e]In C_6D_6.

pling to phosphorus, ^5J(PH) 2.7 Hz. The mass spectrum gave an intensity profile at *m/z* 642 (for molybdenum-98) for the parent molecular ion and profiles due to successive loss of one, two, and three carbonyl ligands (see experimental section). The corresponding tricarbonyltungsten(0) complex **3b** was prepared in 94% yield by treating **1** with one equivalent of $[W(CO)_3(NCEt)_3]$ (30) in benzene. Details of the preparation and characterizing data are in the experimental section and in Tables 1 and 2.

We anticipated that the azine phosphine **1** could also act as a bidentate ligand through *P* and *N*═CMe nitrogen, giving a six-membered chelate ring, as with other azine phosphine ligands (1–4, 29). To investigate this we treated **1** with $[Mo(CO)_4(nbd)]$ (31) (nbd = norbornadiene) and obtained the hoped-for tetracarbonylmolybdenum(0) complex **4**, which showed a phosphorus-31 chemical shift of 52.0 ppm. The IR bands for ν(C≡O) at 2020, 1900, and 1845 cm^{-1} are similar to other values reported for zerovalent molybdenum tetracarbonyls (1, 11, 29). The mass spectrum gave an intensity profile at *m/z* 670 (for molybdenum-98) for the parent molecular ion and profiles due to successive loss of one, two, three, and four carbonyl ligands. The $^{13}C-\{^1H\}$ NMR data indicated the presence of four carbonyl ligands and a six-membered chelate ring. In the proton NMR spectrum, the resonances due to the CH_2P and CH_2S protons were broad at room temperature (20°C). At −40°C, the $^1H-\{^{31}P\}$ NMR spectrum showed two AB patterns, one at 2.36 and 3.34 ppm with ^2J(HH) 12.5 Hz for the CH_2P protons and the other at 3.81 and 4.37 ppm with ^2J(HH) 12.9 Hz for the CH_2S protons. Probably by −40°C the flexible six-membered chelate ring ceases to be fluxional and the CH_2P methylene hydrogens become pseudo-axial and pseudo-equatorial. Alternatively, at −40°C steric interaction might prevent movement of the CH_2S-*p*-tolyl group past the C≡O ligand in the P-Mo-N plane. In either case the CH_2P hydrogens would be nonequivalent as would the CH_2S hydrogens, which would be diastereotopic. We have observed a similar behaviour for the CH_2P hydrogens in $[W(CO)_4\{PPh_2CH_2C(Bu^t)$═N-N═$CH(C_6H_4F\text{-}2)\}]$, which shows broad resonances at 20°C but an AB pattern at low temperatures (−60°C) (7).

We (1, 11, 32, 33) and many others (34–36) have shown that molybdenum(0) or tungsten(0) carbonyl – tertiary phosphine complexes can be oxidized by halogens to give molybdenum(II) or tungsten(II) species. Treatment of **3a** or **4** in CH_2Cl_2 at 0°C with 1 equivalent of bromine in CCl_4 gave the expected neutral seven-coordinate (37–39) dicarbonylmolybdenum(II) complex **5** as an orange solid in 78% yield. The $^{31}P-\{^1H\}$ NMR spectrum showed a singlet at 52.5 ppm. The IR spectrum showed two strong bands for ν(C≡O) at 1970 and 1860 cm^{-1} that were in good agreement with the values (1975 and 1875 cm^{-1}) observed for the neutral seven-coordinate dicarbonylmolybdenum(II) dibromide $[MoBr_2(CO)_2\{PPh_2CH_2C(Bu^t)$═N-N═$C(Bu^t)CH_2PPh_2\}]$, containing a terdentate (P-N-P) ligand (11). Treatment of the corresponding tricarbonyltungsten(0) complex **3b** with 1 equivalent of bromine followed by NH_4PF_6 in methanol gave the seven-coordinate tricarbonyltungsten(II) salt **6** as yellow microcrystals in 82% yield. As expected, it showed three IR bands at 2040, 1965, and 1940 cm^{-1} for ν(C≡O) (11).

Complexes of 1 with platinum

We also studied the ability of the thioether azine phosphine **1** to act as either bidentate (P-N) or terdentate (P-N-S) ligand with platinum (Scheme 2). Treatment of the phosphine **1** with $[PtCl_2(NCMe)_2]$ (12) gave the bidentate dichloroplatinum(II) complex **7**, containing a six-membered chelate ring. The observed δ_P value of 25.4 ppm with platinum-195 satellites ^1J(PtP) = 4085 Hz, and two IR bands at 340 and 290 cm^{-1} due to ν(Pt–Cl) were indicative of a *cis*-$PtCl_2$ arrangement (2, 40). In the proton NMR spectrum, the resonances due to the CH_2P and CH_2S protons were broad at room temperature, as

Table 2. ^{1}H NMR data.[a]

Compound	δ(Bu^t)	δ(CH_2P)	δ(MeC=N)	δ(C_6H_4Me-4)	Others
1	1.12s	3.22(2H, d, ^2J(PH) 4.2)	1.81s	2.27s	3.28(2H, s, CH_2S)
2	1.17s	3.70(2H, d, ^2J(PH) 15.0)	1.86s	2.29s	3.12(2H, s, CH_2S)
3a	0.96s	2.21(1H, dd, ^2J(PH) 9.0, ^2J(HH) 12.9) 3.53(1H, dd, ^2J(PH) 9.0, ^2J(HH) 12.9)	2.00(d, ^5J(PH) 2.7)	2.32s	3.97(2H, br, CH_2S)
3b	0.95s	2.28(1H, dd, ^2J(PH) 9.9, ^2J(HH) 13.1) 3.65(1H, dd, ^2J(PH) 9.7, ^2J(HH) 13.1)	2.00(dd, ^5J(PH) 3.2, 0.8[b])	2.32s	3.65(1H, m, ^4J(PH) 4.6, ^2J(HH) 14.4, 0.8,[b] CH_2S) 4.25(1H, d, ^2J(HH) 14.4, CH_2S)
4[c]	0.81s	2.36(1H, dd, ^2J(PH) 11.5, ^2J(HH) 12.5) 3.34(1H, dd, ^2J(PH) 11.5, ^2J(HH) 12.5)	1.97(d, ^5J(PH) 2.2)	2.36s	3.81(1H, d, ^2J(HH) 12.9, CH_2S) 4.37(1H, d, ^2J(HH) 12.9, CH_2S)
5	1.40s	3.00(1H, dd, ^2J(PH) 12.6, ^2J(HH) 18.1) 3.97(1H, dd, ^2J(PH) 10.1, ^2J(HH) 18.1)	2.26s	2.51s	3.50(1H, d, ^2J(HH) 18.9, CH_2S) 4.81(1H, d, ^2J(HH) 18.9, CH_2S)
6	1.12s	3.68(1H, dd, ^2J(PH) 4.2, ^2J(HH) 14.9) 3.81(1H, dd, ^2J(PH) 5.6, ^2J(HH) 14.9)	2.48(d, ^5J(PH) 2.0)	2.37s	4.43(1H, dd, ^4J(PH) 1.7, ^2J(HH) 20.7, CH_2S) 5.06(1H, dd, ^4J(PH) 3.1, ^2J(HH) 20.7, CH_2S)
7[c,d]	0.83s	1.88(1H, dd, ^2J(PH) 13.1, ^2J(HH) 13.2) 3.26(1H, dd, ^2J(PH) 14.4, ^2J(HH) 13.2)	2.05(d, ^5J(PH) 1.0, 8.3[e])	2.24s	3.85(1H, d, ^2J(HH) 14.6, CH_2S) 5.09(1H, d, ^2J(HH) 14.6, CH_2S)
8a	0.83s	3.57(2H, d, ^2J(PH) 14, ^3J(PtH) 46)	2.38s	2.35s	4.35(1H, dd, ^4J(PH) 4.6, ^2J(HH) 17.3, CH_2S) 4.56(1H, dd, ^4J(PH) 4.4, ^2J(HH) 17.3, CH_2S)
8b	0.83s	3.66(2H, d, ^2J(PH) 14, ^3J(PtH) 47)	2.37s	2.37s	4.46(1H, dd, ^4J(PH) 5.1, ^2J(HH) 18.1, CH_2S) 4.61(1H, dd, ^4J(PH) 5.1, ^2J(HH) 18.1, CH_2S)
9	0.84s	2.88(2H, d, ^2J(PH) 14, ^3J(PtH) 43)	2.34s	2.29s	4.27(1H, d, ^4J(PH) 5.9, ^3J(PtH) 27.4, =CHS)
10[f]	0.69	2.05(1H, dd, ^2J(PH) 10.7, ^2J(HH) 12.5) 3.14(1H, dd, ^2J(PH) 10.7, ^2J(HH) 12.5)	1.62(d, ^5J(PH) 2.0, 4.8[e])	1.94s	5.27(1H, d, ^2J(HH) 13.7, 7.2,[e] CH_2S) 3.55(1H, dd, ^5J(PH) 2.0, ^2J(HH) 13.7, 5.4,[e] CH_2S) 1.41(3H, d, ^3J(PH) 8.0, ^2J(PtH) 70.8, PtMe) 1.50(3H, d, ^3J(PH) 8.0, ^2J(PtH) 87.4, PtMe)
11a[g]	1.07s	3.79(1H, dd, ^2J(PH) 11.7, ^2J(HH) 14.2) 4.06(1H, dd, ^2J(PH) 13.2, ^2J(HH) 14.2)	2.73(d, ^5J(PH) 1.7)	2.29s	4.56(1H, dd, ^4J(PH) 2.9, ^2J(HH) 15.8, CH_2S) 4.67(1H, d, ^2J(HH) 15.8, ^2J(PtH) 6.5, CH_2S) 0.78(3H, d, ^3J(PH) 7.4, ^2J(PtH) 55.7, PtMe) 0.97(3H, d, ^3J(PH) 6.6, ^2J(PtH) 69.3, PtMe) 1.13(3H, d, ^3J(PH) 7.1, ^3J(PtH) 69.8, PtMe)
11b	1.04s	3.13(1H, dd, ^2J(PH) 12.0, ^2J(HH) 13.8) 3.75(1H, t, ^2J(PH) 13.5, ^2J(HH) 13.8, ^3J(PtH) 12.8)	2.36(d, ^5J(PH) 1.7)	2.29s	4.36(1H, d, ^2J(HH) 15.6, ^3J(PtH) 10.4, CH_2S) 4.56(1H, dd, ^4J(PH) 3.3, ^2J(HH) 15.6, CH_2S)

Can. J. Chem. Downloaded from www.nrcresearchpress.com by 80.90.12.36 on 09/08/12
For personal use only.

Table 2 (*concluded*).

Compound	δ(Bu^t)	δ(CH_2P)	δ(MeC=N)	δ(C_6H_4Me-4)	Others
					0.79(3H, d, ^3J(PH) 8.0, ^2J(PtH) 56.8, PtMe) 0.98(3H, d, ^3J(PH) 6.6, ^2J(PtH) 69.7, PtMe) 1.13(3H, d, ^3J(PH) 7.1, ^2J(PtH) 69.6, PtMe)
12[f]	0.83s	3.59(2H, d, ^2J(PH) 14.2, ^3J(PtH) 47.4)	2.39s	2.25s	4.68(2H, d, ^4J(PH) 4.9, ^3J(PtH) 11.2, CH_2S) 0.32(3H, d, ^3J(PH) 3.9, ^2J(PtH) 75.2, PtMe) 8.81(2H, s, $C_6H_2NO_2$-2,4,6)

[a]Measured at 99.55 MHz in $CDCl_3$, δ values to high frequency of TMS, *J* values in Hz.
[b]$^4J(H–CH_3)$.
[c]Recorded at −40°C.
[d]In CD_2Cl_2.
[e]^4J(PtH).
[f]In C_6D_6.
[g]Recorded at 400 MHz.

observed for the bidentate complex **4** containing a six-membered chelate ring. At −40°C, the $^1H–\{^{31}P\}$ NMR spectrum showed two AB patterns centred at 2.57 and 4.47 ppm for the CH_2P and CH_2S groups, respectively. When this complex was treated with NH_4PF_6 in methanol it yielded the terdentate (P-N-S) complex **8a**, which showed a singlet phosphorus-31 resonance at 43.3 ppm with platinum-195 satellites, ^1J(PtP) = 3664 Hz. The smaller ^1J(PtP) value of 3664 Hz agreed with the other values observed for platinum(II) – tertiary phosphine complexes with phosphorus *trans* to sulfur donors (21, 41). The CH_2S protons were inequivalent (^2J(HH) = 17.3 Hz) and coupled to phosphorus (^4J(PH) ~ 4.5 Hz). The $^{13}C–\{^1H\}$ NMR data were in agreement with the proposed structure. We expected that methylene protons on a carbon adjacent to a C=N bond and to a sulfur group would be activated and could be removed by a base (2, 12). Treatment of the terdentate salt **8a** or the bidentate complex **7** with Et_3N–NaOH gave the hoped-for chloroplatinum(II) complex **9** as an orange solid. This neutral complex **9** showed a phosphorus-31 resonance at 23.3 ppm with a ^1J(PtP) value of 3776 Hz, consistent with a phosphorus atom *trans* to a sulfur donor (21, 41). In the proton NMR spectrum, the =C*H*S proton appeared as a doublet at 4.27 ppm with satellites, ^4J(PH) = 5.9 and ^3J(PtH) = 27.4 Hz, whilst the carbon-13 resonance for the =*C*HS carbon absorbed at 72.5 ppm with ^3J(PC) = 2.1 Hz (12). This neutral terdentate complex **9** was readily reprotonated with an excess of HBF_4 to give the BF_4 salt **8b**, which showed similar NMR properties to **8a**. The cation of **8a** and **8b** showed nonequivalent CH_2S hydrogens but apparently equivalent CH_2P protons; we suggest that the CH_2P hydrogens have accidentally the same chemical shift.

Treatment of the phosphine **1** with $[PtMe_2(cod)]$ (12) (cod = cycloocta-1,5-diene) at ca. 20°C in benzene gave the bidentate dimethylplatinum(II) complex **10**, which has a δ_P value of 36.9 ppm with ^1J(PtP) = 2156 Hz. This small value of ^1J(PtP) value is consistent with phosphorus *trans* to a methyl group (2, 8, 12, 40). The proton NMR spectrum showed two doublets with platinum-195 satellites for the two methyl groups on platinum; the signal at 1.41 ppm with ^2J(PtH) = 70.8 Hz is assigned to the protons of the methyl group *trans* to phosphorus (2, 12, 40) and the other, at 1.50 ppm with ^2J(PtH) = 87.4 Hz, is assigned to the protons of the methyl group *trans* to nitrogen (2, 8, 12, 40). The *Me*C=N proton resonance appeared as a doublet at 1.62 ppm with satellites due to coupling to platinum-195, ^5J(PH) 2.0 and ^4J(PtH) 4.8 Hz. At ca. 25°C the CH_2P and CH_2S protons each give AB patterns in the $^1H–\{^1P\}$ NMR spectrum; possibly steric interaction prevents the CH_2S-*p*-tolyl group from being able to pass a Pt-methyl, or the fluxionality of the six-membered chelate ring has effectively ceased at this temperature; either effect would render both sets of methylene hydrogens nonequivalent, as with compound **4** above. Square planar dichloropalladium or dimethylplatinum compounds of type $[MX_2\{PPh_2CH_2C(Bu^t)=N-N=CHPh\}]$ (M = Pd, X = Cl; M = Pt, X = Me) at 25°C also show CH_2P protons as an AB pattern in the $^1H–\{^{31}P\}$ NMR spectrum, with ^2J(HH) = 13.0 (Pd) or 12.6 (Pt) Hz, respectively (2).

Treatment of the dimethylplatinum(II) complex **10** with MeI gave the *fac*-trimethylplatinum(IV) iodide salt **11a**, with a specific molar conductivity (Λ_m) of 0.134 Ω^{-1} mol^{-1} cm^2 in acetone solution at 20°C, typical for a bi-univalent electrolyte (42). Treatment of **11a** with NH_4PF_6 in methanol gave the corresponding PF_6 salt **11b**. The low ^1J(PtP) values of 1252 and 1241 Hz are similar to other values reported for platinum(IV) – tertiary phosphine complexes (2, 8, 12, 13). In the $^{13}C–\{^1H\}$ NMR spectrum of **11b** the Pt*Me* carbon *trans* to phosphorus appeared as a doublet with a large ^2J(PC) value of 114.8 Hz whilst the methyl carbons *cis* to phosphorus gave two singlets, indicating a *fac*-$PtMe_3$ arrangement. The proton resonance at 0.78(d) ppm with ^3J(PH) 7.4 and ^2J(PtH) 55.7 Hz was assigned to the Pt*Me* group *trans* to phosphorus (2, 12, 13) whilst the two doublets at 0.97 ppm, with ^3J(PH) 6.6 and ^2J(PtH) 69.3 Hz, and 1.13 ppm, with ^3J(PH) 7.1 and ^2J(PtH) 69.8 Hz, were assigned to the two Pt*Me* groups *trans* to nitro-

Can. J. Chem. Downloaded from www.nrcresearchpress.com by 80.90.12.36 on 09/08/12
For personal use only.

Can. J. Chem. Downloaded from www.nrcresearchpress.com by 80.90.12.36 on 09/08/12
For personal use only.

gen (2, 12, 43, 44) or sulfur (45, 46). Protonation of the dimethylplatinum(II) complex **10** with 1 equivalent of picric acid [$HOC_6H_2(NO_2)_3$-2,4,6] gave the methylplatinum(II) picrate salt **12** and methane. The $^{31}P-\{^1H\}$ NMR spectrum showed a singlet at 43.9 ppm with platinum-195 satellites $^1J(PtP)$ = 4214 Hz. The $^1J(PtP)$ value of 4214 Hz is slightly higher than most other values (2800–4100 Hz) (18, 21, 41, 47–53) observed for tertiary phosphine ligands *trans* to sulfur donors, probably due to the presence of the *cis*-methyl group. The presence of a *cis*-alkyl ligand is known to increase $^1J(PtP)$ relative to, say, a halogen ligand (10, 13, 41, 54, 55). In the proton NMR spectrum, the CH_2S protons were coupled to phosphorus ($^4J(PH)$ = 4.9 Hz), indicative of the coordination of sulfur to platinum. Presumably in **12** there is rapid inversion at sulfur on the NMR time scale, causing equivalence of the two sets of CH_2 protons; rapid inversion of sulfur coordinated to platinum is well established (19).

Experimental

All the reactions were carried out in an inert atmosphere of dry nitrogen or dry argon. *tert*-Butyl diphenylphosphinomethyl ketone hydrazone *Z*-$PPh_2CH_2C(Bu^t)$=NNH_2 was prepared as reported in a previous paper (1). 4-Methylphenylthiomethyl methyl ketone was purchased from Maybridge Chemical Co. Ltd. Infrared spectra were recorded using a Perkin–Elmer model 457 grating spectrometer. NMR spectra were recorded using a JEOL FX-90Q spectrometer (operating frequencies for ^1H and ^{31}P of 89.5 and 36.2 MHz, respectively), a JEOL FX-100 spectrometer (operating frequencies for ^1H and ^{31}P of 99.5 and 40.25 MHz, respectively), a Bruker ARX-250 spectrometer (operating frequencies for ^1H, and ^{13}C of 250.13 and 62.9 MHz, respectively), or a Bruker AM-400 spectrometer (operating frequencies for ^1H, ^{31}P, and ^{13}C of 400.13, 161.9, and 100.6 MHz, respectively); ^1H and ^{13}C chemical shifts are relative to tetramethylsilane and ^{31}P shifts are relative to 85% phosphoric acid, coupling constants are in Hz. Electron impact (EI) and fast atom bombardment (FAB) mass spectra were recorded using a VG Autospec with 8 kV acceleration. For metal complexes *m/z* values are quoted for ^{98}Mo, ^{184}W, and ^{195}Pt.

Z,E-{$PPh_2CH_2C(Bu^t)$=N-N=C(Me)$CH_2S(C_6H_4Me$-4) 1

Methylphenylthiomethyl methyl ketone (6.0 cm^3, 6.0 g, 33.3 mmol) was added to a warm solution of *Z*-$PPh_2CH_2C(Bu^t)$=NNH_2 (8.0 g, 26.8 mmol) in ethanol (25 cm^3). The reaction mixture was left to stand at ca. 20°C for 20 h after which it was cooled to −30°C overnight. The required product **1** precipitated out as pale yellow needles. These were filtered off and washed with cold ethanol. Yield 10.5 g, 84%. $^{13}C-\{^1H\}$ NMR (100.6 MHz, $CDCl_3$) δ_C: 169.4 (1C, d, *J*(PC) 5.3, *C*=N), 159.1 (1C, d, *J*(PC) 1.7, *C*=N), 41.6 (1C, s, CH_2S), 39.4 (1C, d, ^3J(PC) 4.3, CMe_3), 28.6 (3C, d, ^4J(PC) 1.5, CMe_3), 28.5 (1C, d, ^1J(PC) 11.0, CH_2P), 20.9 (1C, s, C_6H_4Me-4), and 16.2 (1C, d, ^6J(PC) 3.2, *Me*C=N). *m/z* (EI): 461 (M + 1), 403 (M – Bu^t), and 337 (M-SC_6H_4Me). Anal. calcd. for $C_{28}H_{33}N_2PS$: C 73.0, H 7.2, N 6.1; found: C 72.9, H 7.2, N, 6.1%.

Z,E-Ph_2P(=O)$CH_2C(Bu^t)$=N-N=C(Me)$CH_2S(C_6H_4Me$-4) 2

An excess of hydrogen peroxide (0.2 cm^3, 30% w/v) was added to a solution of the azine phosphine **1** (100 mg, 0.22 mmol) in acetone (4.0 cm^3) at 0°C. The pale yellow solution was left to stand at ca. 20°C for 0.5 h. On the addition of water (2.0 cm^3), the required product **2** precipitated as a white solid. This was filtered off, washed with water, and dried in vacuo over P_2O_5. Yield 92 mg, 88%. *m/z* (EI): 476 (M^+) and 353 (M − SC_6H_4Me). Anal. calcd. for $C_{28}H_{33}N_2OPS$: C 70.6; H, 7.0; N, 5.9; found: C 70.4, H 6.9, N 5.8%.

***fac*-[$Mo(CO)_3${$PPh_2CH_2C(Bu^t)$=N-N=C(Me)CH_2S-(C_6H_4Me-4)}] 3a**

A solution of [$Mo(CO)_3(\eta^6$-cht)] (59 mg, 0.22 mmol) and the azine phosphine **1** (100 mg, 0.22 mmol) in benzene (2.0 cm^3) was put aside for 0.5 h. The required product **3a** precipitated out as yellow needles. These were filtered off, washed with cold methanol, and dried in vacuo. Yield 120 mg, 85%. $^{13}C-\{^1H\}$ NMR (100.6 MHz, CD_2Cl_2) δ_C: 228.1 (1C, d, ^2J(PC) 8.1, C≡O *cis* to P), 224.6 (1C, d, ^2J(PC) 10.2, C≡O *cis* to P), 210.9 (1C, d, ^2J(PC) 42.4, C≡O *trans* to P), 171.3 (1C, s, *C*=N), 162.7 (1C, d, *J*(PC) 4.8, *C*=N), 50.4 (1C, s, CH_2S), 39.4 (1C, d, ^3J(PC) 2.0, CMe_3), 27.6 (3C, s, CMe_3), 24.9 (1C, d, ^1J(PC) 6.4, CH_2P), 21.1 (1C, s, C_6H_4Me-4), and 18.9 (1C, s, *Me*C=N). *m/z* (EI): 642 (M^+), 614 (M-CO), 586 (M − 2CO), and 558 (M − 3CO). Anal. calcd. for $C_{31}H_{33}MoN_2O_3PS$: C 58.1, H 5.2, N 4.4; found: C 57.9, H 5.1, N 4.4%.

***fac*-[$W(CO)_3${$PPh_2CH_2C(Bu^t)$=N-N=C(Me)CH_2S-(C_6H_4Me-4)}] 3b**

A mixture of [$W(CO)_3(NCEt)_3$] (95 mg, 0.22 mmol) and the azine phosphine **1** (100 mg, 0.22 mmol) in benzene (2.0 cm^3) was warmed until a clear yellow solution was obtained. The mixture was then cooled to give the required product as yellow microcrystals. These were filtered, washed with cold methanol, and dried. Yield 150 mg, 94%. *m/z* (EI) 672(M − 2CO) and 644(M − 3CO). Anal. calcd. for $C_{31}H_{33}N_2O_3PSW$: C 51.1, H 4.6, N 3.9; found: C 51.0, H 4.4, N 3.9%.

[$Mo(CO)_4${$PPh_2CH_2C(Bu^t)$=N-N=C(Me)CH_2S-(C_6H_4Me-4)}] 4

A solution of [$Mo(CO)_4$(nbd)] (98 mg, 0.33 mmol) and the azine phosphine **1** (150 mg, 0.33 mmol) in benzene (3.0 cm^3) was put aside at ca. 20°C for 2 h. The reaction mixture was then filtered through Celite and evaporated to dryness. The required product **4** was obtained as a pale yellow solid by recrystallizing the resultant residue from dichloromethane–methanol. Yield 190 mg, 86%. $^{13}C-\{^1H\}$ NMR (100.6 MHz, $CDCl_3$) δ_C: 220.0 (1C, d, ^2J(PC) 6.9, C≡O *cis* to P), 214.7 (1C, d, ^2J(PC) 35.4, C≡O *trans* to P), 208.2 (2C, br, C≡O), 169.5 (1C, s, *C*=N), 167.2 (1C, d, *J*(PC) 4.0, *C*=N), 45.7 (1C, s, CH_2S), 38.9 (1C, d, ^3J(PC) 1.7, CMe_3), 27.4 (3C, s, CMe_3), 25.6 (1C, d, ^1J(PC) 6.5, CH_2P), 21.1 (1C, s, C_6H_4Me-4), and 19.3 (1C, s, *Me*C=N). *m/z* (FAB): 670 (M^+), 642(M − CO), 614 (M − 2CO), 586(M − 3CO), and 558(M − 4CO). Anal. calcd. for $C_{32}H_{33}MoN_2O_4PS{\cdot}0.1\ CH_2Cl_2$: C 56.9, H 4.9, N 4.1; found: C 56.8, H 4.8, N 4.2%.

[$Mo(CO)_2Br_2${$PPh_2CH_2C(Bu^t)$=N-N=C(Me)$CH_2S(C_6$-H_4Me-4)}] 5

(i) From 4

A solution of Br_2 in carbon tetrachloride (0.16 cm^3, 0.751 M,

Can. J. Chem. Downloaded from www.nrcresearchpress.com by 80.90.12.36 on 09/08/12
For personal use only.

0.12 mmol) was added to a solution of the tetracarbonyl complex **4** (80 mg, 0.12 mmol) in dichloromethane (3.0 cm^3) cooled to 0°C. When the effervescence had subsided, the reaction mixture was filtered and evaporated to low volume. The required product **5** precipitated out as orange microcrystals after trituration with methanol. These were filtered off, washed with cold methanol, and dried. Yield 90 mg, 78%.

(ii) From ***3a***

The complex **5** was isolated in 97% yield after treating **3a** with 1 mole equivalent of Br_2 in a similar fashion to that described in method (i).

$[W(CO)_3Br\{PPh_2CH_2C(Bu^t)$=N-N=$C(Me)CH_2S$-$(C_6H_4Me$-4)$\}][PF_6]$ 6

A solution of Br_2 in carbon tetrachloride (0.14 cm^3, 0.751 M, 0.11 mmol) was added to a solution of **3b** (80 mg, 0.11 mmol) in dichloromethane (2.0 cm^3) cooled to 0°C. After the effervescence had subsided, the reaction mixture was filtered and evaporated to dryness. The residue was redissolved in minimum amount of methanol to which a saturated solution of ammonium hexafluorophosphate(V) in methanol (1.0 cm^3) was added. The required product precipitated out as yellow microcrystals. Yield 83.0 mg, 82%.

$\{PtCl_2\{PPh_2CH_2C(Bu^t)$=N-N=$C(Me)CH_2S(C_6H_4Me$-4)$\}]$ 7

$[PtCl_2(NCMe)_2]$ (0.76 g, 2.17 mmol) was added to a solution of the azine phosphine **1** (1.0 g, 2.17 mmol) in dichloromethane (10.0 cm^3). The pale yellow reaction mixture was allowed to stand at ca. 20°C for 0.5 h, after which it was filtered and evaporated to low volume. The dichloroplatinum complex **7** precipitated out as yellow solids after trituration with *n*-hexane. Yield 1.31 g, 83%. Anal. calcd. for $C_{28}H_{33}Cl_2N_2PSPt{\cdot}0.12CH_2Cl_2$: C 45.8, H 4.55, N 3.8, Cl 10.8; found: C 45.5, H 4.3, N 4.0, Cl 10.85%.

$[PtCl\{PPh_2CH_2C(Bu^t)$=N-N=$C(Me)CH_2S(C_6H_4Me$-4$\})PF_6]$ 8a

A suspension of the dichloroplatinum complex **7** (100 mg, 0.14 mmol) in methanol (4.0 cm^3) was heated to reflux for 0.5 h, upon which the starting material had dissolved to give a clear yellow solution. The reaction mixture was then allowed to cool to ca. 20°C, filtered, and the filtrate evaporated. The residue was redissolved in a minimum amount of methanol (10.0 cm^3) to which a saturated solution of ammonium hexafluorophosphate(V) in methanol (1.0 cm^3) was added. The required complex precipitated out as pale yellow microcrystals. Yield 84.0 mg, 73%. $^{13}C-\{^1H\}$ NMR (62.9 MHz, CD_2Cl_2) δ_C: 185.8 (1C, s, *C*=N), 176.2 (1C, s, *C*=N), 50.1 (1C, s,CH_2S), 41.2 (1C, s, CMe_3), 26.9 (3C, s, CMe_3), 21.3 (1C, s, C_6H_4Me-4), 21.2 (1C, s, *Me*C=N), and 20.7 (1C, d, ^1J(PC) 32, CH_2P). *m/z* (FAB): 691(M − PF_6) and 655(M − PF_6 − HCl). Anal. calcd. for $C_{28}H_{33}ClF_6N_2P_2SPt$: C 40.2, H 4.0, Cl 4.25 N 3.35; found: C 40.25, H 4.0, Cl 4.45, N 3.3%.

$[PtCl\{PPh_2CH_2C(Bu^t)$=N-N=$C(Me)CH_2S(C_6H_4Me$-4$)\}BF_6]$ 8b

Tetrafluoroboric acid (2 drops) was added to an orange solution of the chloroplatinum complex **9** (70 mg, 0.10 mmol) in dichloromethane (2.0 cm^3). The resulting yellow solution was then filtered and the filtrate evaporated to low volume. The required product precipitated out as a cream solid after trituration with *n*-hexane. Yield 70 mg, 89%. *m/z* (FAB): 691(M − BF_4) and 655(M − BF_4 − HCl).

$[PtCl\{PPh_2CH_2C(Bu^t)$=N-NC(Me)=CHS$(C_6H_4Me$-4$)\}]$ 9

An excess of triethylamine (0.2 cm^3) was added to a stirred solution of the dichloroplatinum complex **7** (0.3 g, 0.41 mmol) in dichloromethane (5.0 cm^3). After 0.5 h, a 10% sodium hydroxide solution (2.0 cm^3) was added to the dark orange solution. The organic layer was separated, dried over anhydrous magnesium sulphate, and then evaporated to low volume. The required product was obtained as orange microcrystals after trituration of the residue with methanol. Yield 0.2 g, 70%. $^{13}C-\{^1H\}$ NMR (100.6 MHz, $CDCl_3$) δ_C: 174.7 (1C, s, Bu^t*C*=N), 143.8 (1C, s, Me*C*-N), 72.5 (1C, d, ^3J(PC) 2.1, =*C*HS), 40.3 (1C, d, ^3J(PC) 3.7, *C*Me_3), 28.0 (3C, s, CMe_3), 21.2 (1C, s, C_6H_4Me-4), 19.9 (1C, s, *Me*C-N), and 14.9 (1C, d, ^1J(PC) 36.3, CH_2P). *m/z* (FAB): 691(M^+). Anal. calcd. for $C_{28}H_{32}ClN_2PSPt$: C 48.7, H 4.7, Cl 5.1, N 4.1; found: C 49.0, H, 4.7, Cl 5.4, N 4.1%.

$[PtMe_2\{PPh_2CH_2C(Bu^t)$=N-N=$C(Me)CH_2S(C_6H_4Me-4)\}]$ 10

$[PtMe_2(cod)]$ (144 mg, 0.43 mmol) was added to a solution of the azine phosphine **1** (200 mg, 0.43 mmol) in benzene (3.0 cm^3). The reaction mixture was allowed to stand at ca. 20°C for 4 h, after which it was filtered and evaporated to low volume. The dimethylplatinum complex **10** precipitated out as a white solid after trituration with ethanol. This was filtered off and washed with cold ethanol. Yield 190 mg, 64%. $^{13}C-\{^1H\}$ NMR (62.9 MHz, C_6D_6) δ_C: 170.9 (1C, s, *C*=N), 163.9 (1C, d, *J*(PC) 3.8, *C*=N), 42.4 (1C, s, CH_2S), 39.6 (1C, s, CMe_3), 28.1 (3C, s, CMe_3), 24.8 (1C, d, ^1J(PC) 16.3, CH_2P), 21.2 (1C, s, C_6H_4Me-4) 19.0 (1C, s, *Me*C=N), 10.2 (1C, d, ^2J(PC) 113.4, Pt*Me trans* to P), and −20.6 (1C, d, ^2J(PC) 3.8, Pt*Me trans* to N). *m/z* (FAB): 670 (M − CH_4) and 654 (M − $2CH_4$). Anal. calcd. for $C_{30}H_{39}N_2PPtS$: C 52.55, H 5.75, N 4.1; found: C 52.3, H 5.7, N 3.95%.

***fac*-$[PtMe_3\{PPh_2CH_2C(Bu^t)$=N-N=$C(Me)CH_2S$-$(C_6H_4Me-4)\}]$ 11a**

An excess of iodomethane (0.5 cm^3) was added to a solution of the dimethylplatinum complex **10** (60 mg, 0.09 mmol) in benzene (1.5 cm^3). The required product precipitated out as a white microcrystalline solid. Yield 70 mg, 97%. Λ_m (acetone): 0.134 Ω^{-1} mol^{-1} cm^2. *m/z* (FAB): 700 (M − HI), 670 (M − HI − $2CH_3$). Anal. calcd. for $C_{31}H_{42}IN_2PPtS$: C 45.0, H 5.1, N 3.4, I 15.35; found: C 45.05, H 4,9, N 3.1, I 15.5%.

***fac*-$[PtMe_3\{PPh_2CH_2C(Bu^t)$=N-N=$C(Me)CH_2S$-$(C_6H_4Me-4)\}PF_6]$ 11b**

A saturated solution of ammonium hexafluorophosphate(V) (1.0 cm^3) was added to a solution of complex **11a** (40 mg, 0.05 mmol) in methanol (1.5 cm^3). The required product precipitated out as white microcrystals. These were filtered off and washed with cyclohexane. Yield 25 mg, 62%. $^{13}C-\{^1H\}$ NMR (100.6 MHz, $CDCl_3$) δ_C: 176.0 (1C, s, *C*=N), 168.2 (1C, d, *J*(PC) 3.8, *C*=N), 42.9 (1C, s, CH_2S), 39.7 (1C, s, CMe_3), 27.8 (3C, s, CMe_3), 22.2 (1C, d, ^1J(PC) 17.8, CH_2P), 21.1 (1C, s, C_6H_4Me-4), 19.2 (1C, s, *Me*C=N), 10.4 (1C, d,

^2J(PC) 114.8, ^1J(PtC) 525.6, Pt*Me trans* to P), 3.8 (1C, s, ^1J(PtC) 622.4, Pt*Me cis* to P), and −11.6 (1C, s, ^1J(PtC) 622.0, Pt*Me cis* to P). *m/z* (EI): 700 (M − PF_6), 670 (M − PF_6 − $2CH_3$), and 655 (M − PF_6 − $3CH_3$).

[PtMe{$PPh_2CH_2C(Bu^t)$=N-N=C(Me)$CH_2S(C_6H_4Me$-4)}][picrate] 12

Picric acid (20 mg, 0.09 mmol) was added to a solution of the dimethylplatinum complex **10** (60 mg, 0.09 mmol) in benzene (2.0 cm^3). After the gas evolution had subsided, the yellow solution was filtered and evaporated to low volume. The required product precipitated out as yellow microcrystals after trituration with cyclohexane. These were filtered off and dried. Yield 50 mg, 64%. Anal. calcd. for $C_{35}H_{38}N_5O_7PSPt{\cdot}0.65\ C_6H_{12}$: C 49.0, H 4.85, N 7.35; found: C 48.95, H 4.7, N 7.05%.

Acknowledgements

We thank the Sciences and Engineering Research Council for a fellowship (to S.D.P) and for other support, and Johnson Matthey for the generous loan of platinum metal salts. M.S. wishes to thank the Malaysian Government and U.T.M. for a scholarship and leave of absence.

References

1. K.K. Hii, S.D. Perera, B.L. Shaw, and M. Thornton-Pett. J. Chem. Soc. Dalton Trans. 2361 (1992).
2. K.K. Hii, S.D. Perera, B.L. Shaw, and M. Thornton-Pett. J. Chem. Soc. Dalton Trans. 103 (1994), and refs. therein.
3. S.D. Perera and B.L. Shaw. J. Chem. Soc. Chem. Commun. 1201 (1994).
4. S.D. Perera and B.L. Shaw. Inorg. Chim. Acta, **228**, 127 (1995).
5. S.D. Perera and B.L. Shaw. J. Chem. Soc. Chem. Commun. 1203 (1994).
6. S.D. Perera, B.L. Shaw, and M. Thornton-Pett. Inorg. Chim. Acta, **233**, 103 (1995).
7. S.D. Perera and B.L. Shaw. J. Organomet. Chem. **479**, 117 (1994).
8. S.D. Perera and B.L. Shaw. J. Chem. Soc. Dalton Trans. 641 (1995).
9. K.K. Hii, S.D. Perera, and B.L. Shaw. J. Chem. Soc. Dalton Trans. 3589 (1994).
10. K.K. Hii, S.D. Perera, and B.L. Shaw. J. Chem. Soc. Dalton Trans. 625 (1995).
11. S.D. Perera, B.L. Shaw, and M. Thornton-Pett. J. Chem. Soc. Dalton Trans. 1469 (1992).
12. S.D. Perera, B.L. Shaw, and M. Thornton-Pett. J. Chem. Soc. Dalton Trans. 3653 (1993), and refs. therein.
13. S.D. Perera, B.L. Shaw, and M. Thornton-Pett. J. Chem. Soc. Dalton Trans. 3311 (1992).
14. P.G. Eller, J.M. Riker, and D.W. Meek. J. Am. Chem. Soc. **95**, 3540 (1973).
15. G.R. Clark and J.D. Orbell. J. Organomet. Chem. **215**, 121 (1981).
16. D.W. Stephan. Inorg. Chem. **23**, 2207 (1984), and refs. therein.
17. D.G. Dick and D.W. Stephan. Can. J. Chem. **64**, 1870 (1986), and refs. therein.
18. A.D. Zotto, A. Mezzetti, and P. Rigo. Inorg. Chim. Acta, **158**, 151 (1989), and refs. therein.
19. E.W. Abel, J.C. Dormer, D. Ellis, K.G. Orrell, V. Sik, M.B. Hursthouse, and M.A. Mazid. J. Chem. Soc. Dalton Trans. 1073 (1992), and refs. therein.
20. F. Tisato, F. Refosco, G. Bandoli, C. Bolzati, and A. Moresco. J. Chem. Soc. Dalton Trans. 1453 (1994).
21. T.C. Blagborough, R. Davis, and P. Ivison. J. Organomet. Chem. **467**, 85 (1994), and refs. therein.
22. J.H. Griffin and R.M. Kellogg. J. Org. Chem. **50**, 3261 (1985).
23. G. Cross, B.K. Vriesema, G. Boven, R.M. Kellogg, and F. van Bolhuis. J. Organomet. Chem. **370**, 357 (1989).
24. J.W. Faller, N. Zhang, K.J. Chase, W.K. Musker, A.R. Amaro, and C.M. Semko. J. Organomet. Chem. **468**, 175 (1994).
25. M.A. Bennett, L. Pratt, and G. Wilkinson. J. Chem. Soc. 2037 (1961).
26. E.E. Isaacs and W.A.G. Graham. Inorg. Chem. **14**, 2560 (1975).
27. O. Walter, T. Klein, G. Huttner, and L. Zsolnai. J. Organomet. Chem. **458**, 63 (1993).
28. T. Seitz, A. Muth, G. Huttner, T. Klein, O. Walter, M. Fritz, and L. Zsolnai. J. Organomet. Chem. **469**, 155 (1994).
29. S.D. Perera, B.L. Shaw, and M. Thornton-Pett. J. Chem. Soc. Dalton Trans. 713 (1994).
30. G.J. Kubas. Inorg. Chem. **22**, 692 (1983).
31. R.B. King. Organomet. Synth. **1**, 125 (1965).
32. S.D. Perera, B.L. Shaw, and M. Thornton-Pett. J. Organomet. Chem., **428**, 59 (1992).
33. J.R. Moss and B.L. Shaw. J. Chem. Soc. (A), 595 (1970).
34. R. Colton and I.B. Tomkins. Aust. J. Chem. **19**, 1519 (1966).
35. J. Lewis and R. Whyman. J. Chem. Soc. 77 (1967).
36. G. Wilkinson, F.G.A. Stone, and E.W. Abel (*Editors*). Comprehensive organometallic chemistry. Vol. 3. Pergamon, Oxford. 1982. p. 1088 and refs. therein.
37. A. Mawby and G.E. Pringle. J. Inorg. Nucl. Chem. **34**, 517 (1972).
38. M.G.B. Drew and J.D. Wilkins. J. Chem. Soc. Dalton Trans. 557 (1977).
39. A.J. Deeming, M. Karim, and N.I. Powell. J. Chem. Soc. Dalton Trans. 2321 (1990).
40. S.D. Perera, B.L. Shaw, and M. Thornton-Pett. J. Chem. Soc. Dalton Trans. 999 (1992), and refs. therein.
41. W. Henderson, B.K. Nicholson, and R.D.W. Kemmitt. J. Chem. Soc. Dalton Trans. 2489 (1994).
42. W.J. Geary. Coord. Chem. Rev. **7**, 81 (1971).
43. C.M. Anderson, M. Crespo, M.C. Jennings, A.J. Lough, G. Ferguson, and R.J. Puddephatt. Organometallics, **10**, 2672 (1991).
44. M. Crespo, M. Martinez, J. Sales, X. Solans, and M. Font-Bardia. Organometallics, **11**, 1288 (1992).
45. W. Clegg, N. Duran, K.A. Fraser, P. Gonzalez-Durate, J. Sola, and I.C. Taylor. J. Chem. Soc. Dalton Trans. 3453 (1993).
46. K.-T. Aye, J.J. Vittal, and R.J. Puddephatt. J. Chem. Soc. Dalton Trans. 1835 (1993).
47. R. Colton and V. Tedesco. Inorg. Chim. Acta, **202**, 95 (1992).
48. P.S. Jarrett, O.M.N. Dhubhghaill, and P.J. Sadler. J. Chem. Soc. Dalton Trans. 1863 (1993).
49. M. Capdevila, P. Gonzalez-Durate, C. Foces-Foces, F.H. Cano, and M. Martinez-Ripoll. J. Chem. Soc. Dalton Trans. 143 (1990).
50. C. Eaborn, K.J. Odell, and A. Pidcock. J. Organomet. Chem. **170**, 105 (1979).
51. A.R. Sanger. Can. J. Chem. **61**, 2214 (1983).
52. G.K. Anderson and R. Kumar. Inorg. Chem. **23**, 4064 (1984).
53. A.M. Cartner, J. Fawcett, W. Henderson, R.D.W. Kemmitt, P. McKenna, and D.R. Russell. J. Chem. Soc. Dalton Trans. 3735 (1993).
54. J.R. Briggs, C. Crocker, W.S. McDonald, and B.L. Shaw. J. Chem. Soc. Dalton Trans. 457 (1982).
55. F.H. Allen and A. Pidcock. J. Chem. Soc.(A), 2700 (1968).

Can. J. Chem. Downloaded from www.nrcresearchpress.com by 80.90.12.36 on 09/08/12
For personal use only.

On the use of diamond as a pressure calibrant for near-infrared FT–Raman microspectroscopy at high pressures

Ross D. Markwell and Ian S. Butler

Abstract: The pressure-induced shift of the Raman-active t_{2g} phonon mode of the diamond windows in a commercial diamond-anvil cell, located at 1332.5 cm^{-1} at ambient pressure, can be used as an in situ calibrant for near-IR FT–Raman microspectroscopy at high pressures. The measured pressures are considered to be accurate to within ±2 kbar throughout the 4–45 kbar range for which the associated pressure (P, kbar) vs. wavenumber (ν, cm^{-1}) relationship is $P = 6.66\nu - 1335.9$.

Key words: FT–Raman spectroscopy, diamond, high pressures.

Résumé : Le déplacement induit par la pression du mode phonon t_{2g}, actif dans le Raman, des fenêtres de diamant d'une cellule commerciale à enclume de diamant situées à 1332,5 cm^{-1} à la pression ambiante, peut être utilisé comme calibrant in situ pour la microspectroscopie FT–Raman dans le proche IR, à des pressions élevées. On considère que les pressions mesurées sont précises à ±2 kbar sur toute la plage allant de 4 à 45 kbar pour laquelle la relation associée pression (P, kbar vs. nombre d'onde (ν, cm^{-1}) est $P = 6{,}66\nu - 1335{,}9$.

Mots clés : spectroscopie FT–Raman, diamant, pressions élevées.

[Traduit par la rédaction]

Introduction

Diamond-anvil cells for spectroscopic measurements at high pressures are readily available commercially. The majority of these cells are rated for pressures up to ~100 kbar (1 bar = 100 kPa) and can be used for a variety of different applications including infrared, Raman, and UV–visible spectroscopy (1). For many years, there has been considerable interest in determining the effects of high external pressures on the structures and properties of organic, inorganic (1), and even organometallic molecular crystals (for example, see ref. 2). This interest has increased dramatically of late following two remarkable discoveries: (*a*) the room temperature conversion of Buckminsterfullerene (C_{60}) into diamond (3) and (*b*) the possibility of using pressure-tuning vibrational spectroscopy in human cancer diagnosis (4). In the summer of 1991, the National Science Foundation in the United States emphasized the importance of future high-pressure research by launching a special initiative to develop new high-pressure techniques and discover new high-pressure materials (5).

In a conventional high-pressure Raman experiment, employing visible laser excitation, the pressure sensitivity of the R_1 fluorescence band of a tiny ruby chip is used as the internal pressure calibrant (6). Pressure-tuning FT–micro-Raman measurements involving near-IR Nd^{3+}:YAG laser excitation have recently also been successfully undertaken for $Cr(CO)_4$(bipy) (bipy = 2,2′-dipyridyl) (7) and elemental sulfur (8). Unfortunately, the ruby R_1 fluorescence band was too far removed from the 1064.1 nm excitation wavelength to be accessible by the spectrometers and so no direct internal pressure calibration method was available for these studies. It would have been possible to use the standard ruby calibration procedure but this would have necessitated physical removal of the diamond-anvil cell from the FT–Raman spectrometer and subsequent alignment on a visible Raman instrument so that the pressure could be calibrated in the usual way. In fact, in the study of $Cr(CO)_4$(bipy) (7), another pressure calibration method, which is based on the pressure sensitivity of the IR-active e' N–O stretching mode of the NO_3^- ion, was used (9). This N–O stretching mode is a well-known standard for presure-tuning IR measurements. However, for these pressure-tuning near-IR FT–micro-Raman experiments, it was still necessary to have two separate instruments for the pressure calibration and spectroscopic measurements.

Another serious drawback to the new pressure-tuning FT–Raman microspectroscopic technique is the high sample loading required for all but the strongest Raman scatterers if sufficient signal-to-noise ratios are to be achieved within a reasonable time. This drawback limits the number of pressure calibrants that can be used in such experiments. Ideally, the sample cavity of the diamond-anvil cell should be packed only with sample and an external pressure calibration method should be used. With this objective in mind, we decided to investigate the possibility of using the 1332.5 cm^{-1} Raman-active t_{2g} phonon band of the diamond windows in a diamond-

Received December 14, 1994.

This paper is dedicated to Professor William A.G. Graham on the occasion of his 65th birthday.

R.D. Markwell and I.S. Butler.[1] Department of Chemistry, McGill University, 801 Sherbrooke Street West, Montreal, QC H3A 2K6, Canada.

[1] Author to whom correspondence may be addressed. Telephone: (514) 398-6999. Fax: (514) 398-3797. E-mail: butler@omc.lan.mcgill.ca

Can. J. Chem. Downloaded from www.nrcresearchpress.com by 80.90.12.36 on 09/08/12
For personal use only.

Can. J. Chem. Downloaded from www.nrcresearchpress.com by 80.90.12.36 on 09/08/12
For personal use only.

anvil cell as an in situ pressure calibrant. The results of this investigation are presented in this paper.

Experimental

A diamond-anvil cell rated to withstand ~100 kbar pressure was purchased from High Pressure Diamond Optics, Tucson, Arizona, U.S.A. The parallel faces of the two type-II diamonds in the cell were separated by a 12 mm × 12 mm × 240 μm stainless-steel gasket that had been punctured in the center (300 μm diameter round hole). A small crystal chip of $NaNO_3$ (1%) in an NaBr matrix was loaded into the hole with the aid of an optical microscopic. The variation of the position of the NO_3^- calibrant IR peak (1401.3 cm^{-1} at ambient pressure) was measured on a Bruker IFS-48 FT-IR spectrometer coupled to a Bruker A-590 IR microscope equipped with a liquid-N_2-cooled mercury – cadmium telluride detector. Periodic checks were made for pressure gradients within the cell by measuring the spectrum at several points within the gasket hole (a spatial resolution of <10 μm is attainable with this apparatus). No such variation was detected across the sample at the 0.5 cm^{-1} resolution employed. FT–Raman spectra (2.5 cm^{-1} resolution) were recorded on a Bruker IFS-88 FT-IR/FRA-105 Raman module fitted with a Ge proprietary detector and coupled via two 1.0 m photooptic cables to a Nikon Optiphot-II optical microscope equipped with a Nikon 20X super-long-range objective. Near-IR laser radiation (Nd^{3+}:YAG, 1064.1 nm) was directed onto the sample through the objective and collected along the same optical pathway in a 180° backscattering mode. The two faces of the top diamond and the sample were clearly observable with the optical microscope of the Raman instrument and measurements were taken with the objective focused at the internal diamond–sample interface. Pressures in the 1–60 kbar range were applied mechanically to the sample and the measured positions (ν) of the diamond peak (vide infra) were correlated against the pressure (P) determined from the IR calibration procedure.

Results and discussion

The diamond windows in a typical high-pressure spectroscopic anvil cell are extremely strong Raman scatterers and often, because of signal-to-noise considerations, the intense, sharp, triply degenerate (t_{2g}) diamond phonon mode at 1332.5 cm^{-1} is filtered out from the spectra with a holographic notch filter. Under uniaxial pressure, as in the case of the two fixed diamonds in a diamond-anvil cell, the t_{2g} peak loses its degeneracy and splits into a higher energy singlet and a lower energy (unresolved) doublet (10). Raman microspectra of the internal diamond–sample interface in the diamond-anvil cell at different external pressures have shown that there is a linear relationship between the position of the t_{2g} phonon peak and pressure up to ~200 kbar (11). Similar behaviour has been noted for other types of diamond anvils (12) and diamond fragments (13), although the actual mathematical relationships do differ somewhat. It occurred to us that FT-Raman microspectroscopy at the internal diamond–sample interface in a diamond-anvil cell might lead to a suitable in situ calibration method for high-pressure measurements.

The behaviour of the t_{2g} diamond phonon peak up to 60 kbar is quite complicated (Fig. 1). This pressure region was defined

Fig. 1. Effect of increasing pressure (kbar) on the Raman-active diamond t_{2g} phonon band.

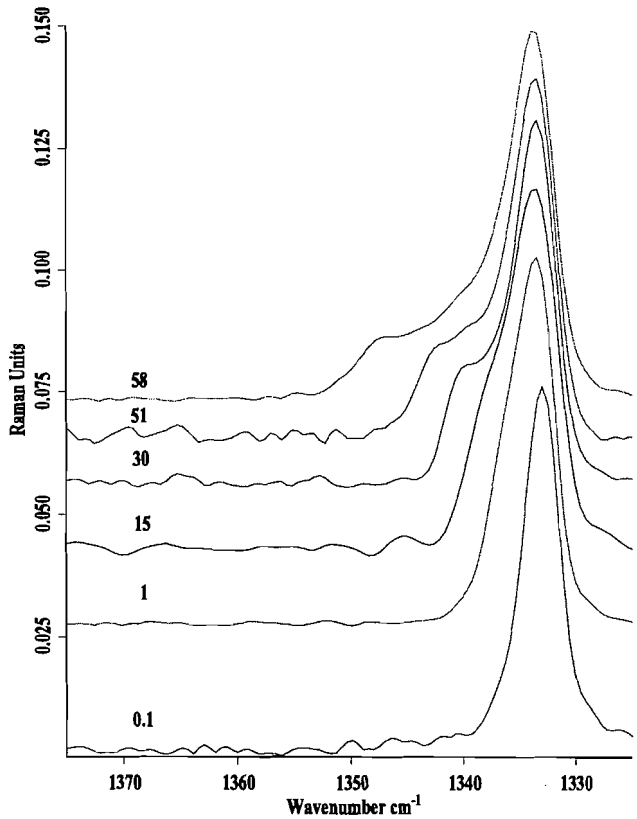

by only a single point in the previous work (11). Although some depth resolution is provided by the optical microscope, particularly after use of the aperturing system in the Bruker Raman attachment, there are always some contributions to the spectrum from regions of the diamond other than the point of focus. The spectra at elevated pressures do not represent a continuum from the unshifted peak of the front diamond surface to the spectra of the interface under high pressure. Hence, there appear to be discrete pressure domains within the diamond anvils, each of which behaves as if it were at a single pressure. The domain at the internal diamond–sample interface is that associated with the pressure experienced by the sample. The higher energy singlet of the t_{2g} diamond phonon peak was the most affected by pressure and this peak is considered to reflect the pressure at the internal diamond–sample interface. Depth profiling studies have supported this assumption.[2] Moreover, since this peak is a singlet (10), it was selected as the calibration peak for the FT–micro-Raman measurements.

Location of the precise position of the singlet within the t_{2g} band envelope proved to be the major difficulty with this calibration procedure. Ideally, a calibration should be executed quickly and unambiguously. Several different approaches were tried in order to overcome this problem. Initially, attempts were made to subtract the spectral contributions due to the lower pressure regions from that of the interfacial spectrum. This procedure afforded a moderately reliable calibra-

[2] R.D. Markwell, I.S. Butler, and C.M. Edwards. Unpublished results.

Can. J. Chem. Downloaded from www.nrcresearchpress.com by 80.90.12.36 on 09/08/12
For personal use only.

Fig. 2. Location of the half-height position of the most shifted component of the Raman-active diamond t_{2g} phonon band at 51 kbar. The minimum of the second derivative (lower spectrum) is chosen as a reflection of the top of the most shifted component (arrow). This frequency is traced to the original spectrum (upper spectrum; offset from 0.05 Raman units for clarity) and the band intensity is divided by 2 to determine the half-height intensity. The point on the band envelope where the half-height intensity intercepts the upper spectrum is the value used in the P vs. ν plot shown in Fig. 3.

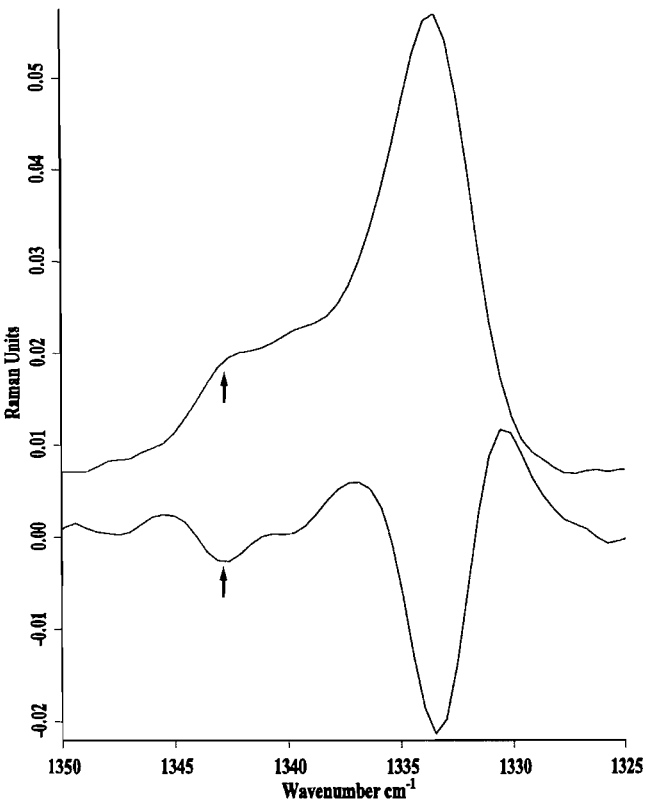

tion, but it suffered from the need for considerable subjective judgement in selecting the band components to be subtracted. Next, a least-squares band-fitting program (Jandel Peakfit 3.11B) was applied to the t_{2g} band envelope at each pressure. This method proved to be the least satisfactory. Quite apart from the time required to acquire and process the spectral data, the loss of degeneracy on application of pressure and the variation of pressure regimes throughout the extent of the anvil precluded precise determination of the number of peaks necessary to fit the data. This approach also required greater signal-to-noise ratios than did the other methods, thus rendering data collection even more time consuming. The most satisfactory calibration procedure, in terms of speed and reproducibility, was to locate the position of the calibration peak from the second derivative spectrum at each pressure.

In using this method it had to be assumed that the width at half height was reasonably constant. The band envelope was essentially free from overlap with neighbouring bands and the good linearity of the wavenumber vs. pressure plot (Fig. 2) demonstrates that the half heights were indeed reasonably constant. In the 4–60 kbar range, this calibration procedure proved to be both precise and much more reliable than were the other methods. Below 4 kbar, the micro-Raman spectra were domi-

Fig. 3. Pressure dependence of the half-height position of the most shifted band of the diamond t_{2g} envelope up to ~60 kbar.

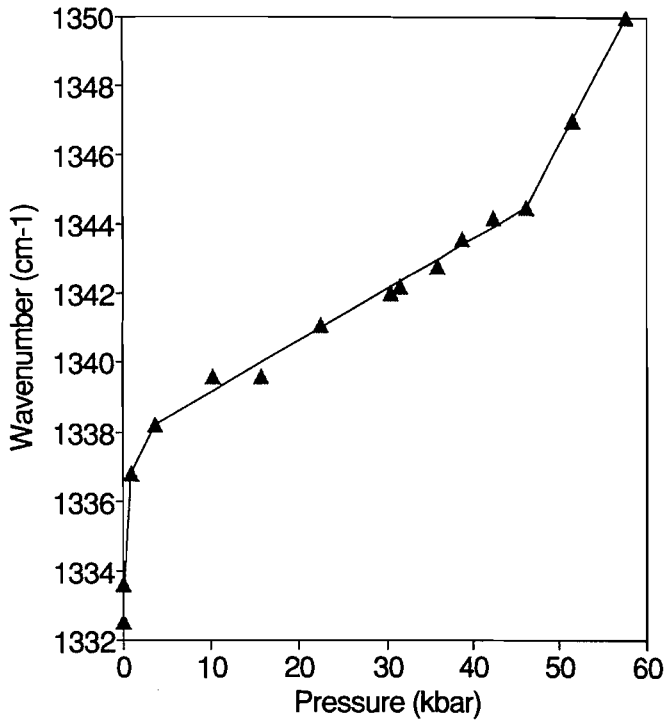

nated by the 1332.5 cm^{-1} peak due to the front face of the diamond window of the anvil. In this pressure range, the 1332.5 cm^{-1} band had to be subtracted first, before processing the data further. This procedure yielded a somewhat less satisfactory calibration, but was only necessary for a limited spectral region.

The diamond phonon peak is reasonably pressure sensitive ($d\nu/dP$ = 0.15 cm^{-1} $kbar^{-1}$) in the 4–60 kbar range and the response is linear up to 45 kbar (Fig. 2). There is a break at 45 kbar and an increase in pressure sensitivity ($d\nu/dP$ = 0.48 cm^{-1} $kbar^{-1}$) from 45 to 60 kbar. Such behaviour would normally indicate a solid-state pressure-induced phase change. However, there was no evidence at all of such a phase change in the earlier studies of diamond fragments under hydrostatic pressure (13) or in diamond anvils (12). The application of pressure in the present case is uniaxial rather than cubic and the data scatter in the previous diamond-anvil experiment (12) appears greater in this region than at higher pressures. The break may also reflect a change in the intensity of the major peak of the spectra. In our work, the behaviour of diamond with respect to pressure was both repoducible and reversible with no evidence of hysteresis.[2] The pressure dependence up to 4 kbar was also linear ($d\nu/dP$ = 0.40 cm^{-1} $kbar^{-1}$) with the phonon peak shifting from 1333.5 to 1334.9 cm^{-1} in this inital applied pressure range. The accuracy of the pressure calibrations in the 4–60 kbar range is estimated to be ±2 kbar.

Despite the need for raw data treatment, our new in situ pressure calibration procedure should find wide applicability in pressure-tuning FT–Raman measurements. However, since the size and shape of the pressure regimes within the anvils may vary from diamond to diamond and may also depend on the cutting process, some caution must be exercised in using the procedure initially. It is probably advisable to calibrate

each diamond anvil individually at the outset. Focusing of the near-IR laser beam directly onto the internal diamond–sample interface is absolutely crucial. For any applications requiring a more detailed pressure analysis, it may be possible to use a more sophisticated peak-fitting routine and (or) principle component analysis to obtain more precise peak positions. The most important benefits of this in situ calibration procedure for pressure-tuning FT–Raman measurements is that a second spectrometer is not required (as is the case for the ruby R_1 fluorescence and IR calibration methods) and the maximum available sample space in the diamond-anvil cell can be used for those materials under investigation.

Acknowledgements

This research project was supported by operating and equipment grants from the following agencies: The Natural Sciences and Engineering Research Council of Canada (NSERC), Energy, Mines and Resources (Canada), and le Fonds pour la formation de chercheurs et l'aide à la recherche (FCAR, Québec). R.D.M. acknowledges the award of an NSERC international postdoctoral fellowship. We thank Professor G.C. Allen for originally asking a question about the possibility of using the diamond phonon peak as a pressure calibrant during a seminar in April 1994 at the University of Bristol, U.K.

References

1. J.R. Ferraro. Vibrational spectroscopy at high external pressures: the diamond anvil cell. Academic Press, Orlando, Fla. 1984, and references therein.
2. (*a*) D.M. Adams, P.W. Ruff, and D.R. Russell. J. Chem. Soc. Faraday Trans. **87**, 1831 (1991); (*b*) N.T. Kawai, I.S. Butler, and D.F.R. Gilson. J. Raman Spectrosc. **23**, 29 (1992), and references therein.
3. M.N. Regueiro, P. Monceau, and J.-L. Hodeau. Nature, **355**, 237 (1992).
4. P.T.T. Wong. NATO Adv. Study Inst. Ser. Ser. C: **406**, 171 (1993), and references therein.
5. R.M. Hazen. The new alchemists: breaking through the barriers of high pressure. Times Books, New York. 1993. p. 5.
6. H.K. Mao, P.M. Bell, J. Shaner, and D. Steinberg. J. Appl. Phys. **49**, 3276 (1978).
7. S.M. Barnett, R.D. Markwell, S.H.R. Brienne, I.S. Butler, D.F.R. Gilson, N.T. Kawai, and A. Vlcek, Jr. J. Raman Spectrosc. **24**, 471 (1993).
8. N.L. Ross. Spectrochim. Acta, **49A**, 681 (1993).
9. D.D. Klug and E. Whalley. Rev. Sci. Instrum. **54**, 1205 (1983).
10. M.H. Grimsditch, E. Anastassakis, and M. Cardona. Phys. Rev. B: Condens. Matter, **B18**, 901 (1978).
11. S.K. Sharma, H.K. Mao, P.M. Bell, and J.A. Xu. J. Raman Spectrosc. **16**, 350 (1985).
12. M. Hanfland and K. Syassan. J. Appl. Phys. **57**, 2752 (1985).
13. E. Whalley, A. Laverge, and P.T.T. Wong. Rev. Sci. Instrum. **47**, 845 (1976).

Can. J. Chem. Downloaded from www.nrcresearchpress.com by 80.90.12.36 on 09/08/12
For personal use only.

Preparations for 1,4,7,11,14,17-hexathiacycloeicosane, 1,4,7-trithiecan-9-ol, 1,11-dioxa-4,8,14,18-tetrathiacycloeicosane, 1-oxa-4,8-dithiacyclodecane, and some complexes of iron, cobalt, nickel, and palladium

C. Robert Lucas, Shuang Liu, and John N. Bridson

Abstract: Preparations are reported for the title ligands (L1–L4, respectively) and for $[Co(L1)][ClO_4]_2$, $[Ni(L1)][ClO_4]_2$, $[\{Pd(\eta^3\text{-}C_3H_5)\}_2(L1)][ClO_4]_2$, $[Co(L2)_2][ClO_4]_2$, $[Ni(L2)_2][ClO_4]_2$, $[Co(L3)][ClO_4]_2$, and $[Ni(L3)_2][ClO_4]_2$. Clarification of earlier reports of L2 and some of its complexes has been achieved by X-ray crystallographic characterization. Crystal data for orthorhombic $[Ni(L1)][ClO_4]_2$: space group $Pna2_1$ (No. 33); $a = 13.270(4)$, $b = 16.564(4)$, $c = 11.348(4)$ Å; $Z = 4$; $R = 0.047$, $R_w = 0.040$ for 1474 reflections. For monoclinic $[Ni(L2)_2][ClO_4]_2$: space group $P2_1/c$ (No. 14); $a = 7.617(3)$, $b = 18.034(3)$, $c = 9.098(2)$ Å, $\beta = 91.58(2)°$; $Z = 2$; $R = 0.046$, $R_w = 0.039$ for 1487 reflections. For tetragonal $[Co(L3)][ClO_4]_2$: space group $I\bar{4}2m$ (No. 121); $a = 13.840(5)$, $c = 14.902(4)$ Å; $Z = 4$; $R = 0.054$, $R_w = 0.058$ for 974 reflections. The new complexes and previously reported $[Fe(L1)][ClO_4]_2$ have been examined by cyclic voltammetry, NMR, ESR, electronic spectroscopy, and magnetic susceptibility measurements. The influence of L2's extra-cyclic hydroxyl, of changes in M—S lengths, and of O for S substitution on structural, magnetic, redox, and spectroscopic properties has been studied.

Key words: X-ray structures, electrochemistry, magnetic phenomena.

Résumé : On rapporte les préparations des coordinats mentionnés dans le titre (L1–L4, respectivement) et des complexes $[Co(L1)][ClO_4]_2$, $[Ni(L1)][ClO_4]_2$, $[\{Pd(\eta^3\text{-}C_3H_5)\}_2(L1)][ClO_4]_2$, $[Co(L2)_2][ClO_4]_2$, $[Ni(L2)_2][ClO_4]_2$, $[Co(L3)][ClO_4]_2$ et $[Ni(L3)_2][ClO_4]_2$. Faisant appel à la diffraction des rayons X, on a obtenu des clarifications de données publiées antérieurement sur le L2 et quelques-uns de ses complexes. Les données cristallographiques pour le $[Ni(L1)][ClO_4]_2$ orthorhombique : groupe d'espace $Pna2_1$ (No. 33), avec $a = 13,270(4)$, $b = 16,564(4)$ et $c = 11,348(4)$ Å, $Z = 4$, $R = 0,047$ et $R_w = 0,040$ pour 1474 réflexions. Pour le $[Ni(L2)_2][ClO_4]_2$ monoclinique : groupe d'espace $P2_1/c$ (No. 14), avec $a = 7,617(3)$, $b = 18,034(3)$ et $c = 9,098(2)$ Å, $\beta = 91,58°$, $Z = 2$, $R = 0,046$ et $R_w = 0,039$ pour 1487 réflexions. Pour le $[Co(L3)][ClO_4]_2$ tétragonal : groupe d'espace $I\bar{4}2m$ (No. 121), avec $a = 13,840(5)$ et $c = 14,902(4)$ Å, $Z = 4$, $R = 0,054$ et $R_w = 0,058$ pour 974 réflexions. On a étudié les nouveaux complexes ainsi que le $[Fe(L1)][ClO_4]_2$ préparé antérieurement par voltampérométrie cyclique, RMN, RPE, spectroscopie électronique et mesures de susceptibilité magnétique. On a étudié l'influence du groupe hydroxyle extracyclique du coordinat L2, des changements dans les longueurs M—S et de la substitution d'un O pour un S sur les propriétés structurales, magnétiques, redox et spectroscopiques.

Mots clés : structures aux rayons X, électrochimie, phénomènes magnétiques.

[Traduit par la rédaction]

Received October 20, 1994.

This paper is dedicated to Professor William. A.G. Graham on the occasion of his 65th birthday.

C.R. Lucas,[1] S. Liu,[2] and J.N. Bridson. Department of Chemistry, Memorial University of Newfoundland, St. John's, NF A1B 3X7, Canada.

[1] Author to whom correspondence may be addressed. Telephone: (709) 737-8118. Fax: (709) 737-3702. E-mail: rlucas@kean.ucs.mun.ca

[2] Present address: Dupont Merck Pharmaceutical Co., Radiopharmaceutical Division, 331 Treble Cove Rd., N. Billerica, MA 01862, U.S.A.

Can. J. Chem. Downloaded from www.nrcresearchpress.com by 80.90.12.36 on 09/08/12
For personal use only.

Can. J. Chem. Downloaded from www.nrcresearchpress.com by 80.90.12.36 on 09/08/12
For personal use only.

Introduction

Crown thioethers have been the subject of considerable research interest for at least 10 years and, in contrast to crown ethers, they bind preferentially but not exclusively to transition metals (1–5). Compared to crown ethers, the sulfur analogues have been shown to exhibit markedly different conformational preferences (5) and to produce complexes with unusual properties (7–10). For example, they stabilize less common oxidation states such as Pd(III), Au(II), or Rh(II) (9, 11, 12), unusual coordination geometries (13, 14), and they have a large nephelauxetic effect (15, 16) that leads to low-spin complexes in coordination geometries or with specific metal ions where low-spin cases are rarely encountered. Likewise, rapid electron exchange kinetics have been measured for these complexes and have been attributed to the unique structural and electronic features of the ligands (17–19).

Many important future applications of chemistry in areas such as materials science, catalysis, communications, and data storage devices will require the ability to adjust properties of existing substances (20). For example, achievement of a liquid crystal mesophase when a metal is added to an otherwise inactive organic molecule (21) and combination of the electrochemical capabilities of an organic system with the photoluminescence of a metal species through coordination can produce an electro-photoswitch device (22). For development of such applications, structure–function relationships at the molecular level and appreciation of the relationship between molecular structure and bulk properties are of importance (23). As part of our continuing interest in the influence of ligand structure on properties of thioether–metal complexes (24–29) we now report property effects caused by introduction of an extra-cyclic functional group, replacement of thioether donors by *trans*-ethers, and increased carbon chain length between donor sites of a macrocyclic ligand. The ligands used in this study are shown in Fig. 1.

Experimental

Commercially available reagents were obtained from the Aldrich Chemical Co. Inc. or from Morton Thiokol Alfa Products Inc. and were used without further purification. Those used for cyclic voltammetry measurements were spectroscopic grade. $[Fe(L1)][ClO_4]_2$ was prepared by the published method (30). Spectroscopic data were obtained by using the following instruments: IR, Mattson Polaris FT; UV–VIS, Cary model 17; ESR, Bruker ESP-300 X-band spectrometer operating at ~9.5 GHz; NMR, General Electric 300-NB. Solution "glasses" for ESR measurements were prepared by plunging sealed capillaries containing $\sim 10^{-4}$ mol/L solutions into liquid nitrogen. Magnetic susceptibility data were obtained at room temperature by the Faraday method. Electrochemical measurements were carried out under a nitrogen atmosphere at room temperature by using a Cypress Systems, Inc., CS-1087 computer-controlled potentiostat. Solution concentrations were 10^{-3} mol/L in complex and 0.1 mol/L in supporting electrolyte (tetraethylammonium perchlorate). Voltammograms were recorded in acetonitrile by using a glassy carbon working electrode that was prepolished with 0.3 μm Al_2O_3, a platinum counter electrode, and an aqueous saturated calomel reference electrode checked periodically relative to a 1.0×10^{-3} mol/L solution of ferrocene in acetonitrile containing 0.1 mol/L tetraethylammonium perchlorate for which the ferrocene/ferrocenium reduction potential was 400 mV. The reference electrode was separated from the bulk of the solution by a porous Vycor tube. Junction potential corrections were not used. Voltages reported versus the normal hydrogen electrode were obtained by adding 244 mV to the potential measured versus SCE. Analyses were performed by Canadian Microanalytical Service Ltd.

Fig. 1. Ligand structures.

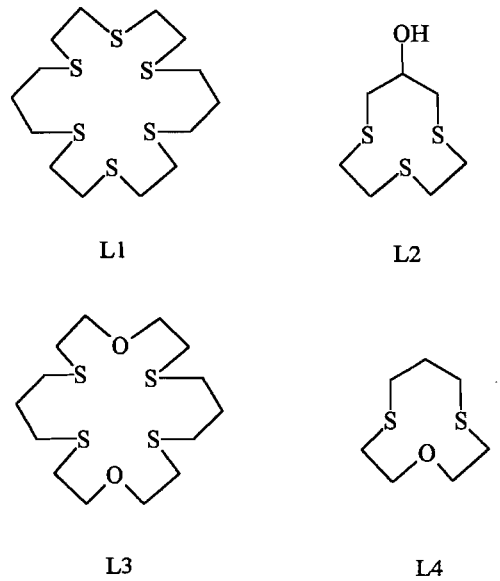

Ligands

(a) 1,4,7,11,14,17-Hexathiacycloeicosane (ligand L1)

The macrocycle was prepared by a modification of the reported method (31). Sodium metal (2.3 g, 0.10 mol) was dissolved in commercial absolute ethanol (600 mL) under a dry nitrogen atmosphere. 2-Mercaptoethyl sulfide (7.7 g, 0.0499 mol) was added cautiously to the solution and the mixture was heated to reflux for 10 min. A solution of 1,3-dibromopropane (10.1 g, 5.08 mL, 0.0500 mol) in commercial absolute ethanol (150 mL) was added dropwise to the refluxing mixture over 3 h. After addition was complete, refluxing was continued for a further hour. Volatiles were removed on a rotary evaporator and the residue was dissolved in $CHCl_3$. This solution was washed with water several times and dried over $CaCl_2$. The dried solution was treated with activated charcoal and, after filtration to remove the charcoal, it was concentrated to 60 mL. To the hot solution was added hot commercial absolute ethanol (75 mL) with vigorous stirring. The solution was filtered while hot and the filtrate was stored at −20°C overnight. The colourless crystals were separated, washed with a little acetone, and dried in air. Yield: 5.8 g (40%); mp 122–124°C. NMR spectrum ($CDCl_3$, ppm from TMS internal standard), ^1H: 2.80 (m, 16H), 2.70 (m, 8H), 1.91 (m, 4H); ^{13}C (proton decoupled): 32.45, 32.25, 30.72, 29.63. Mass spectrum: parent ion, calcd. for $[C_{14}H_{28}S_6]^+$, *m/z*: 388.05138; found, *m/z*: 388.0525.

Can. J. Chem. Downloaded from www.nrcresearchpress.com by 80.90.12.36 on 09/08/12
For personal use only.

(b) 1,4,7-Trithiecan-9-ol (ligand L2)

This macrocycle was prepared in a manner similar to that used to obtain ligand L1 except that 1,3-dichloro-2-propanol (6.45 g, 4.77 mL, 0.0500 mol) was used instead of 1,3-dibromopropane. Yield 4.3 g (41%); mp 87–89°C. NMR spectrum ($CDCl_3$, ppm from TMS internal standard), ^{1}H: 3.87 (m, 1H), 2.07 (br, s, 1H), 2.80 (m, 12H); ^{13}C (proton decoupled): 67.38 ($(CH_2)_2CHOH$), 32.07 ($(CH_2)_2CHOH$), 31.50 ($SCH_2CH_2SCH_2CH_2S$), 31.33 ($SCH_2CH_2SCH_2CH_2S$). Mass spectrum: parent ion, calcd. for $[C_7H_{14}OS_3]^+$, *m/z*: 210 not found; calcd. for $[C_7H_{14}S_3]^+$, *m/z*: 194; found, *m/z*: 194.

(c) 1-Oxa-4,8-dithiacyclodecane (ligand L4)

This preparation was similar to that for L1 except that 2-mercaptoethyl ether was used in place of 2-mercaptoethyl sulfide and that the product was a viscous oil. The oil was chromatographed on silica by using $CHCl_3$ as eluant and the first band was collected. After removal of the solvent under vacuum, the product remained as a clear colourless oil. Yield 1.8 g (20%). NMR spectrum ($CDCl_3$, ppm from TMS internal standard), ^{1}H: 3.75 (m, 4H), 2.93 (m, 4H), 2.74 (m, 4H), 1.96 (quintet, 2H, J = 6.6 Hz); ^{13}C (proton decoupled): 71.45, 32.87, 30.33, 29.94. Mass spectrum: parent iron, calcd. for $[C_7H_{14}OS_2]^+$, *m/z*: 178; found: *m/z*: 178.

(d) 1,11-Dioxa-4,8,14,18-tetrathiacycloeicosane (ligand L3)

Continued elution of the column described in (*c*) eventually removed a second viscous oil. Yield 2.9 g (32%). NMR spectrum ($CDCl_3$, ppm from TMS internal standard), ^{1}H: 3.68 (t, 8H, J = 6.2 Hz), 2.75 (m, 8H), 2.73 (m, 8H), 1.90 (quintet, 4H, J = 7.2 Hz); ^{13}C (proton decoupled): 71.22, 31.68, 31.40, 29.75. Mass spectrum: parent ion, calcd. for $[C_{14}H_{28}O_2S_4]^+$, *m/z*: 356; found, *m/z*: 356.

Complexes

Note: Perchlorate salts are often treacherously explosive (32) and although we have been unable to cause these compounds to detonate from shock or heat we recommend suitable precautions be taken whenever perchlorates are handled.

(a) [Co(L1)][ClO$_4$]$_2$

A solution of L1 (78 mg, 0.20 mmol) in $CHCl_3$ (10 mL) was added to a solution of $Co(ClO_4)_2 \cdot 6H_2O$ (73 mg, 0.20 mmol) in acetonitrile (10 mL). A violet precipitate appeared immediately and was separated by filtration, washed with acetone, and recrystallized from nitromethane by vapour diffusion of diethyl ether to give deep purple crystals. Yield 90 mg (68%). UV–vis (CH_3CN): λ_{max} in nm (ϵ in mol^{-1} L cm^{-1}); 750 (20), 517 (120), 370 (2600). μ_{eff} (22°C) = 1.75 BM. Anal. calcd. for $C_{14}H_{28}Cl_2CoO_8S_6$: C 25.99, H 4.37, S 29.76, Co 9.12; found: C 26.04, H 4.37, S 29.91, Co 9.08.

(b) [Ni(L1)][ClO$_4$]$_2$

Nickel perchlorate hexahydrate (73 mg, 0.20 mmol) was dissolved in nitromethane (15 mL) and a solution of L1 (78 mg, 0.20 mmol) in $CHCl_3$ (8 mL) was added. The solution was filtered and allowed to evaporate slowly until violet crystals formed that were separated by filtration, washed with acetone, and briefly air-dried. These crystals develop a powdery surface upon standing that gives them a purple rather than violet appearance. The nature of this change is associated with the uptake of water and only the violet crystals are suitable for X-ray crystallographic study. Recrystallization from nitromethane by diethyl ether vapour diffusion affords purified violet crystals. Yield 95 mg (74%). UV–vis (CH_3NO_2) (violet crystals): λ_{max} in nm (ϵ in mol^{-1} L cm^{-1}); 775 (30), 530 (50). μ_{eff} (22°C) = 2.83 BM (violet crystals). Anal. calcd. for $C_{14}H_{28}Cl_2NiO_8S_6 \cdot H_2O$ (purple crystals): C 25.31, H 4.55, S 28.96, Ni 8.83; found: C 25.24, H 4.40, S 26.60, Ni 8.14.

(c) [{Pd(η^3-C$_3$H$_5$)}$_2$(L1)][ClO$_4$]$_2$

Solutions of $[Pd(\eta^3\text{-}C_3H_5)Cl]_2$ (74 mg, 0.20 mmol) in acetone (10 mL) and $AgClO_4$ (83 mg, 0.40 mmol) in acetone (10 mL) were mixed and stirred for 10 min. The mixture was filtered and to the filtrate was added a solution of L1 (78 mg, 0.20 mmol) in $CHCl_3$ (10 mL). The solvent was allowed to evaporate slowly and eventually yellow-orange crystals were deposited. Yield 140 mg (79%). NMR spectrum (CD_3CN, ppm from TMS internal standard), ^{1}H: 5.81 (m, 2H), 4.07 (d, 4H, allyl-*syn*, $^3J_{H-H}$ = 6.6 Hz), 3.22 (d, 4H, allyl-*anti*, $^3J_{H-H}$ = 12.0 Hz), 3.15 (m, 6H), 3.00 (m, 10H), 2.88 (m, 4H), 2.45 (m, 4H), 2.30 (m, 2H), 1.55 (m, 2H); ^{13}C (proton decoupled): 109.52 (η^3-CH_2CHCH_2), 65.40 (η^3-CH_2CHCH_2), 37.84, 33.52, 29.50, 27.20. Anal. calcd. for $C_{20}H_{38}Cl_2O_8Pd_2$: C 27.22, H 4.34; found: C 27.30, H 4.45.

(d) [Co(L2)$_2$][ClO$_4$]$_2$·CH$_3$CN

Solutions of $Co(ClO_4)_2 \cdot 6H_2O$ (70 mg, 0.19 mmol) in acetonitrile (5 mL) and L2 (80 mg, 0.38 mmol) in CH_2Cl_2 (5 mL) were mixed and there was an immediate colour change from pink to red. Upon addition of diethyl ether (10 mL) a red precipitate formed that was separated and redissolved in hot acetonitrile (5 mL). Upon cooling and slow evaporation of the solvent, red crystals were deposited that were separated, washed with acetone and then dichloromethane, and dried in air. Yield 89 mg (69%). UV–vis (CH_3CN): λ_{max} in nm (ϵ in mol^{-1} L cm^{-1}); 830 (20), 490 (100), 340 (1000). μ_{eff} (21°C) = 2.71 BM. Anal. calcd. for $C_{16}H_{31}Cl_2CoNO_{10}S_6$: C 26.70, H 4.34, Co 8.19; found: C 26.24, H 4.28, Co 8.90.

(e) [Ni(L2)$_2$][ClO$_4$]$_2$

Preparation of this compound is the same as that for $[Co(L2)_2][ClO_4]_2 \cdot CH_3CN$ in (*e*) except that the final washing of the purple crystalline product was with diethyl ether. Yield 120 mg (93%). UV–vis (CH_3NO_2): λ_{max} in nm (ϵ in mol^{-1} L cm^{-1}); 782 (12), 520 (40). μ_{eff} (20°C) = 2.93 BM. Anal. calcd. for $C_{14}H_{28}Cl_2NiO_{10}S_6$: C 24.79, H 4.16, Ni 8.65; found: C 26.24, H 4.28, Ni 6.51.

(f) [Co(L3)][ClO$_4$]$_2$

To a solution of $Co(ClO_4)_2 \cdot 6H_2O$ (0.18 g, 0.49 mmol) in methanol–nitromethane (3 mL:20 mL) was added a solution of L3 (0.20 g, 0.56 mmol) in nitromethane (5 mL), causing a colour change to red. After filtration, the solution was allowed to evaporate slowly until deep violet needles formed that were collected and washed with small amounts of dichloromethane, nitromethane, and then acetone, and dried in air. Yield 0.22 g (73%). UV–vis (CH_3NO_2): λ_{max} in nm (ϵ in mol^{-1} L cm^{-1}); 780 (25), 540 (100), 370 (500). μ_{eff} (22°C) = 4.37 BM. Anal. calcd. for $C_{14}H_{28}Cl_2CoO_{10}S_4$. C 27.37, H 4.59, S 20.87, Co 9.59; found: C 27.66, H 4.62, S 19.12, Co 8.78.

Can. J. Chem. Downloaded from www.nrcresearchpress.com by 80.90.12.36 on 09/08/12
For personal use only.

(g) [Ni(L3)][ClO$_4$]$_2$

Preparation of [Ni(L3)][ClO$_4$]$_2$ is similar to that for [Co(L3)][ClO$_4$]$_2$ except that the greenish-blue crystalline product was washed with dichloromethane, acetone, and then diethyl ether. Yield 0.20 g (68%). UV–vis (CH_3CN): λ_{max} in nm (ϵ in mol^{-1} L cm^{-1}); 982 (5.9), 596 (4.9), 369 (sh), 328 (40). μ_{eff} (22°C) = 2.98 BM. Anal. calcd. for $C_{14}H_{28}Cl_2NiO_{10}S_4$: C 27.38, H 4.59, S 20.88, Ni 9.56; found: C 27.29, H 4.59, S 18.89, Ni 9.06.

X-ray

A summary of crystallographic data for [Ni(L1)][ClO$_4$]$_2$, [Ni(L2)$_2$][ClO$_4$]$_2$, and [Co(L3)][ClO$_4$]$_2$ is given in Table 1. X-ray diffraction data were collected by using a Rigaku AFC6S diffractometer. All measurements were made with graphite-monochromated Mo Kα radiation and a 2 kW sealed tube generator. Cell constants and an orientation matrix for data collection, obtained from a least-squares refinement of the setting angles of 22 ([Ni(L1)][ClO$_4$]$_2$), 23 ([Ni(L2)$_2$][ClO$_4$]$_2$), or 24 ([Co(L3)][ClO$_4$]$_2$) carefully centred reflections in the range $20.50° < 2\theta < 25.01°$ ([Ni(L1)][ClO$_4$]$_2$), $22.59° < 2\theta < 25.55°$ ([Ni(L2)][ClO$_4$]$_2$), or $30.14° < 2\theta < 37.63°$ ([Co(L3)][ClO$_4$]$_2$) corresponded to an orthorhombic ([Ni(L1)][ClO$_4$]$_2$), a monoclinic ([Ni(L2)$_2$][ClO$_4$]$_2$), or a tetragonal ([Co(L3)][ClO$_4$]$_2$) cell with dimensions as shown in Table 1. The space groups were determined by systematic absences, a statistical analysis of intensity distribution, packing considerations, and the successful solution and refinement of the structures. Of the 2525 ([Ni(L1)][ClO$_4$]$_2$), 2460 ([Ni(L2)$_2$][ClO$_4$]$_2$), or 1437 ([Co-(L3)][ClO$_4$]$_2$) reflections collected, 2515 ([Ni(L1)][ClO$_4$]$_2$), 2285 ([Ni(L2)$_2$][ClO$_4$]$_2$), or 1437 ([Co(L3)][ClO$_4$]$_2$) were unique. The intensities of three representative reflections, measured after every 150 reflections, remained constant for [Ni(L1)][ClO$_4$]$_2$ and [Ni(L2)][ClO$_4$]$_2$ throughout data collection, which indicates crystal and electronic stability. For [Co(L3)][ClO$_4$]$_2$, the intensities of the representative reflections declined by 5.10% and a linear correction factor was applied to account for this phenomenon. The linear absorption coefficient for Mo Kα is 15.2 cm^{-1} ([Ni(L1)][ClO$_4$]$_2$) and [Ni(L2)$_2$][ClO$_4$]$_2$) or 11.2 cm^{-1} ([Co(L3)][ClO$_4$]$_2$). Azimuthal scans of several reflections for [Ni(L1)][ClO$_4$]$_2$ indicated no need for an absorption correction. An empirical absorption correction, based on azimuthal scans of several reflections, was applied for [Ni(L2)$_2$][ClO$_4$]$_2$ and [Co(L3)][ClO$_4$]$_2$, and resulted in transmission factors ranging from 0.88 to 1.00 and 0.87 to 1.00, respectively. The data were corrected for Lorentz and polarization effects. The structures were solved by direct methods (33, 34). Non-hydrogen atoms were all refined anisotropically for [Ni(L1)][ClO$_4$]$_2$ but for [Ni(L2)$_2$][ClO$_4$]$_2$ and [Co(L3)][ClO$_4$]$_2$ some (O(1A), O(1B), C(1A), C(1B), C(2A), C(2B) for [Ni(L2)$_2$][ClO$_4$]$_2$ or O(2), O(2A), O(3), O(3A), O(4), O(4A), O(5), O(5A), O(6), O(7), O(8) for ([Co-(L3)][ClO$_4$]$_2$) were refined isotropically. The final cycle of full-matrix least-squares refinement[3] was based on 1474 ([Ni(L1)][ClO$_4$]$_2$), 1487 ([Ni(L2)$_2$][ClO$_4$]$_2$), or 974 ([Co-(L3)][ClO$_4$]$_2$) observed reflections ($I > 2.00\sigma(I)$) and 279 ([Ni-(L1)][ClO$_4$]$_2$), 149 ([Ni(L2)$_2$][ClO$_4$]$_2$), or 56 ([Co(L3)]-[ClO$_4$]$_2$) variables, and converged with unweighted and weighted agreement factors ($R = \Sigma||F_o| - |F_c||/\Sigma|F_o|$ and $R_w = [(\Sigma w(|F_o| - |F_c|)^2/\Sigma wF_o^2)]^{1/2}$) equal to 0.047 and 0.040 ([Ni(L1)][ClO$_4$]$_2$), 0.046 and 0.039 ([Ni(L2)$_2$][ClO$_4$]$_2$), or 0.054 and 0.058 ([Co(L3)][ClO$_4$]$_2$), respectively. The weighting scheme was based on counting statistics. Neutral atom scattering factors were from the usual source (35). All calculations were performed by using the TEXSAN (36) crystallographic software of Molecular Structure Corporation. A description of the experimental procedure, positional parameters, anisotropic thermal parameters, and a full listing of bond lengths and bond angles are available as supplementary data.[4]

Results and discussion

(a) Ligands

Ligand L1 has been reported previously (31, 37). Our preparation of this substance is similar to the relatively less complicated synthesis described in the earlier of these two reports but involves a slower addition of the final reagent and a more dilute reaction mixture. This raises the yield from 30 to 40% and gives a product with a slightly higher melting point.

Ligand L2 has also been reported previously (38) but was prepared by a different (cesium template) method. The yield from that procedure was somewhat lower than reported herein and the physical characteristics of that product differ significantly from ours. Furthermore, the nickel and cobalt complexes described (38) as having been prepared from that substance have different physical and spectroscopic properties from those of the complexes prepared from our material. Since such ligand preparations tend to give mixtures of "small" (10-membered) and "large" (20-membered) rings (for example L3 and L4) that are difficult to distinguish even by NMR, it is possible that one is the "small" and one the "large" ring. Since our L2 has been used to produce in high yield a crystalline derivative, [Ni(L2)$_2$][ClO$_4$]$_2$, from which an X-ray structure has been obtained that indicates presence of two 10-membered rings (see Fig. 3), we believe the preparations and physical characteristics reported herein for L2 and its complexes are correct.

Synthesis of L3 was described previously by a different method (39). During our preparation of L3, chromatographic purification led to separation of the related "small" ring, $C_7H_{14}OS_2$, in lower yield. The IR and NMR spectroscopic characteristics of this substance are nearly identical to those of the "large" ring, $C_{14}H_{28}O_2S_4$, L3 (See Experimental). The two may, however, be distinguished by their mass spectra, which have appropriate molecular ion peaks, and by their chromatographic retention times, which for the "large" ring is much greater.

[3] Function minimized: $\Sigma w(|F_o| - |F_c|)^2$ where $w = 4F_o^2/\sigma^2(F_o^2)$; $\sigma^2(F_o^2) = [S^2(C + R^2B) + (pF_o^2)^2]/Lp^2$ and S = scan rate; C = total integrated peak count; R = ratio of scan time to background counting time; B = total background count; Lp = Lorentz-polarization factor.

[4] A complete set of data can be purchased from: The Depository of Unpublished Data, Document Delivery, CISTI, National Research Council Canada, Ottawa, ON K1A 0S2, Canada.

The experimental procedure and tables of atomic parameters, bond lengths, and bond angles have also been deposited with the Cambridge Crystallographic Data Centre, University Chemical Laboratory, 12 Union Road, Cambridge, CB2 1EZ, U.K. Structure factor amplitudes are no longer being deposited and may be obtained directly from the author.

Can. J. Chem. Downloaded from www.nrcresearchpress.com by 80.90.12.36 on 09/08/12
For personal use only.

Table 1. Crystallograhic data.[a]

Complex	$[Ni(L1)][ClO_4]_2$	$[Ni(L2)_2][ClO_4]_2$	$[Co(L3)][ClO_4]_2$
Chem. formula	$C_{14}H_{28}Cl_2NiO_8S_6$	$C_{14}H_{28}Cl_2NiO_{10}S_6$	$C_{14}H_{35.2}Cl_2CoO_{13.6}S_4$
fw	646.34	678.34	679.30
Space group	$Pna2_1$ (No. 33)	$P2_1/c$ (No. 14)	$I\bar{4}2m$ (No. 121)
a (Å)	13.270(4)	7.617(3)	13.840(5)
b (Å)	16.564(4)	18.034(3)	
c (Å)	11.348(4)	9.098(2)	14.902(4)
β (deg)		91.58(2)	
T (°C)	24	26	26
μ (cm^{-1})	15.17	15.24	11.24
ρ_{calcd} (g cm^{-3})	1.721	1.803	1.580
V (Å^3)	2494(1)	1249.3(6)	2855(1)
Z	4	2	4
λ (Å)	0.71069	0.71069	0.71069
R^b	0.047	0.046	0.054
$R_w{}^c$	0.040	0.039	0.058

[a]Estimated standard deviations for data in this table and elsewhere in this paper refer to the least significant figure and are given in parentheses.

[b]$R = \Sigma||F_o| - |F_c||/\Sigma|F_o|$.

[c]$R_w = [(\Sigma w(|F_o| - |F_c|)^2/\Sigma w F_o^2)]^{1/2}$.

Fig. 2. Structure of $[Ni(L1)]^{2+}$.

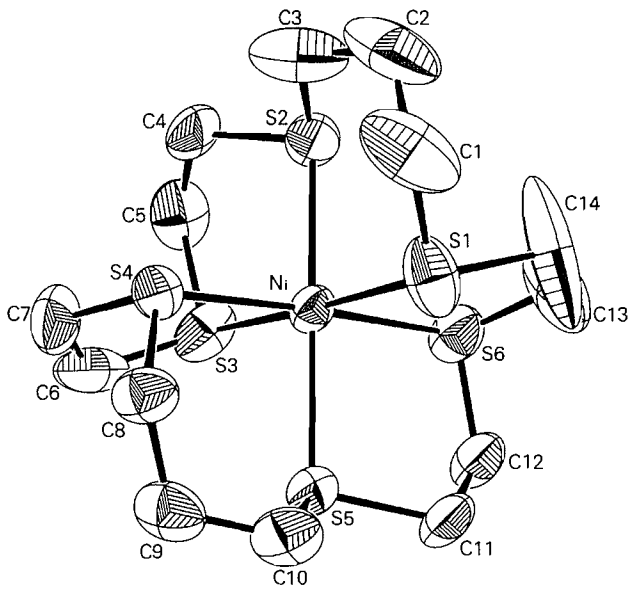

Table 2. Selected bond lengths and angles in $[Ni(L1)][ClO_4]_2$.

Angles (deg)			
S(1)—Ni—S(2)	92.0(2)	S(1)—Ni—S(3)	177.9(2)
S(1)—Ni—S(4)	92.8(1)	S(1)—Ni—S(5)	95.4(1)
S(1)—Ni—S(6)	86.3(1)	S(2)—Ni—S(3)	85.8(1)
S(2)—Ni—S(4)	94.1(1)	S(2)—Ni—S(5)	170.1(1)
S(2)—Ni—S(6)	89.2(1)	S(3)—Ni—S(4)	87.0(1)
S(3)—Ni—S(5)	86.8(1)	S(3)—Ni—S(6)	94.0(2)
S(4)—Ni—S(5)	92.1(1)	S(4)—Ni—S(6)	176.6(2)
Distances (Å)			
Ni—S(1)	2.382(4)	Ni—S(4)	2.393(4)
Ni—S(2)	2.381(4)	Ni—S(5)	2.403(4)
Ni—S(3)	2.376(4)	Ni—S(6)	2.413(4)

(b) Structures

The X-ray structure of $[Ni(L1)]^{2+}$ (Fig. 2) reveals a relatively rare example of an optically active octahedral thioether complex in which the two six-membered chelate rings have *gauche* placement with respect to each other when the octahedron is viewed down the appropriate pseudo-trigonal axis. Normally, such systems adopt a *meso* configuration with the two six-membered chelate rings *anti* as is found in $[Pd(10S3)_2][ClO_4]_2$ (10S3 = 1,4,7-trithiacyclodecane) (40) or the related $[Ni(10N3)_2]^{2+}$ (41) or $[Co(10N3)_2]^{3+}$ (42).

A previous report by Setzer, Grant, and co-workers (39) of a system with similar *gauche* placement of six-membered chelate rings involved $[Fe(10S3)_2][ClO_4]_2$ in which the ligand system is two 10-membered rings instead of one 20-membered ring as for our L1. In their compound, the unit cell contains only one enantiomer whereas in ours there are four cations per unit cell, two of which are the *d* form and two of which are the *l* form so that the sample overall is racemic. Coordination of L1 to produce *gauche* placement of its six-membered chelate rings by use of meridional looping is in contrast to that found for 18S6 (18S6 = 1,4,7,10,13,16-hexathiacyclooctadecane) in $[Ni(18S6)]^{2+}$ in which all loops are facial but is similar to that for 24S6 in $[Ni(24S6)]^{2+}$ (24S6 = 1,5,9,13,17,21-hexathiacyclotetracosane) (43). In $[Ni(L1)]^{2+}$ (L1 = 20S6), there are two meridional loops involving the six-membered chelate rings whereas in $[Ni(18S6)]^{2+}$, which has only five-membered chelate rings, coordination is always facial. In $[Ni(24S6)]^{2+}$, which has all six-membered chelate rings, there are two meridional loops and all others are facial as in our cation. These preferences can be related to ligand dihedral angles that are in turn influenced by intramolecular nonbonding interactions (6). In $[Ni(L1)]^{2+}$,

Can. J. Chem. Downloaded from www.nrcresearchpress.com by 80.90.12.36 on 09/08/12
For personal use only.

Table 3. Positional parameters and equivalent isotropic temperature factors for $[Ni(L1)][ClO_4]_2$.

Atom	x	y	z	B_{eq}[a] (Å^2)
Ni	0.2785(1)	0.1282(1)	0.1997	3.25(6)
Cl(1)	0.5296(3)	0.2372(2)	0.7123(4)	5.2(2)
Cl(2)	0.7966(3)	0.0482(3)	0.1533(4)	5.4(2)
S(1)	0.2112(3)	0.0168(2)	0.3067(4)	5.5(2)
S(2)	0.1682(3)	0.1045(2)	0.0378(4)	5.1(2)
S(3)	0.3419(3)	0.2377(2)	0.0867(3)	5.3(2)
S(4)	0.4126(2)	0.0490(2)	0.1190(3)	3.9(2)
S(5)	0.3832(2)	0.1763(2)	0.3575(3)	4.0(2)
S(6)	0.1484(3)	0.2080(3)	0.2920(4)	5.0(2)
O(1)	0.520(1)	0.300(1)	0.794(1)	11(1)
O(2)	0.6135(8)	0.1978(9)	0.722(2)	16(1)
O(3)	0.516(1)	0.267(1)	0.599(1)	11(1)
O(4)	0.444(1)	0.1864(8)	0.731(1)	9.9(9)
O(5)	0.763(1)	−0.0288(8)	0.168(2)	16(1)
O(6)	0.810(1)	0.085(1)	0.259(1)	12(1)
O(7)	0.8840(8)	0.0550(8)	0.090(1)	10(1)
O(8)	0.7225(9)	0.0880(9)	0.095(2)	12(1)
C(1)	0.182(1)	−0.067(1)	0.218(2)	9(1)
C(2)	0.120(1)	−0.053(1)	0.101(2)	10(1)
C(3)	0.168(2)	−0.003(1)	0.009(2)	9(1)
C(4)	0.243(1)	0.142(1)	−0.082(1)	6(1)
C(5)	0.283(1)	0.225(1)	−0.053(1)	6(1)
C(6)	0.469(1)	0.207(1)	0.062(1)	6(1)
C(7)	0.486(1)	0.119(1)	0.036(1)	6(1)
C(8)	0.496(1)	0.0117(8)	0.232(1)	4.6(7)
C(9)	0.533(1)	0.0664(8)	0.327(1)	5.2(8)
C(10)	0.456(1)	0.0941(9)	0.416(1)	5.2(8)
C(11)	0.291(1)	0.197(1)	0.473(1)	5.7(9)
C(12)	0.206(1)	0.2484(9)	0.419(1)	4.9(7)
C(13)	0.070(1)	0.133(1)	0.350(2)	11(1)
C(14)	0.089(1)	0.051(1)	0.348(3)	14(2)

[a] B_{eq} is the mean of the principal axes of the thermal ellipsoid.

Fig. 3. Structure of $[Ni(L2)_2]^{2+}$.

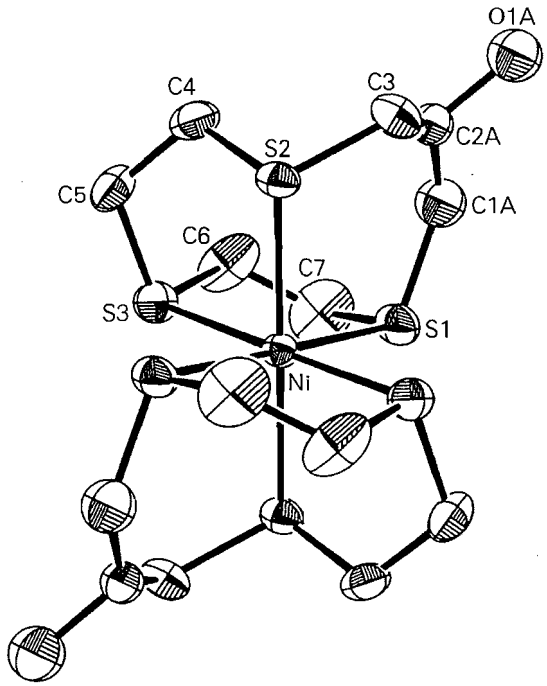

Table 4. Selected bond lengths and angles in $[Ni(L2)_2][ClO_4]_2$.

Angles (deg)			
S(1)—Ni—S(1′)	180.00	S(1)—Ni—S(2)	95.94(6)
S(1)—Ni—S(2′)	84.06(6)	S(1)—Ni—S(3)	88.55(6)
S(1)—Ni—S(3′)	91.45(6)	S(2)—Ni—S(2′)	180.00
S(2)—Ni—S(3)	87.50(6)	S(2)—Ni—S(3′)	92.50(6)
S(3)—Ni—S(3′)	180.00		
Distances (Å)			
Ni—S(1)	2.374(2)	Ni—S(3)	2.400(2)
Ni—S(2)	2.419(2)		

four of the 12 C—S bonds have *anti* placements of their adjacent atoms whereas in $[Ni(18S6)]^{2+}$ all 12 C—S bonds have *gauche* placements and in $[Ni(24S6)]^{2+}$ there are six of 12 C—S bonds with *anti* placements in order to minimize intramolecular repulsions.

The coordination sphere bond lengths and angles in $[Ni(L1)]^{2+}$ (Table 2) indicate nearly regular octahedral coordination. The Ni—S lengths range from 2.376(4) to 2.413(4) Å, which is comparable to the ranges found for $[Ni(9S3)_2]^{2+}$ (2.375(3)–2.400(5) Å) (9S3 = 1,4,7-trithiacyclononane) (44), $[Ni(18S6)]^{2+}$ (2.377(1)–2.397(1) Å), or $[Ni(24S6)]^{2+}$ (2.413(1)–2.443(1) Å) (43) and shorter, presumably due to compression by the cyclic nature of the ligand, than the average (2.43 Å) (1) for octahedral monodentate thioether complexes. Bond angles in the coordination sphere of $[Ni(L1)]^{2+}$ range from 84.8(1)° to 95.4(1)°, which is again comparable to ranges found for $[Ni(9S3)_2]^{2+}$ (88.04(5)°–91.96(5)°), $[Ni(18S6)]^{2+}$ (88.5(1)°–91.3(1)°), and $[Ni(24S6)]^{2+}$ (82.3(4)°–93.9(3)°) with the greatest deviations from ideal values associated with the six-membered chelate rings.

For $[Ni(L2)_2][ClO_4]_2$ (Fig. 3), the Ni—S lengths and coordination sphere bond angles (Table 4) range from 2.374(2) to 2.419(2) Å and from 84.06(6)° to 95.94(6)°, respectively, both of which are very similar to ranges found for $[Ni(L1)]^{2+}$ and for $[Ni(keto\text{-}10S3)_2]^{2+}$ (keto-10S3 = 1,4,7-trithiacyclodecane-9-one) (2.381(3)–2.424(3) Å) (38). As in $[Ni(L1)]^{2+}$, the greatest deviation from ideal angles for $[Ni(L2)]^{2+}$ is associated with the six-membered chelate rings. In $[Ni(L2)_2]^{2+}$ as in $[Ni(keto\text{-}10S3)_2]^{2+}$, the two six-membered chelate rings are *anti* with respect to each other, giving the usual *meso* isomers instead of being *gauche* as in $[Ni(L1)]^{2+}$ and resulting in *d–l* enantiomeric pairs in the unit cell. There is disorder of the L2 ligand rings involving C(1), C(2), O(1), and their associated hydrogens that places the hydroxyl hydrogens pointing into the ring or out of the ring. Occupancy of the two forms (Table 5) in the crystal is close to 50% of each.

For $[Co(L3)][ClO_4]_2$ (Fig. 4), the Co—S lengths are 2.444(2) Å, the Co—O lengths are 2.098(6) Å, and the coordination sphere bond angles range from 80.43(5)° to 99.57(5)° (Table 6). The Co—S bonds are somewhat longer than those

Can. J. Chem. Downloaded from www.nrcresearchpress.com by 80.90.12.36 on 09/08/12
For personal use only.

Table 5. Positional parameters, equivalent isotropic temperature factors, and site occupancies for $[Ni(L2)_2][ClO_4]_2$.

Atom	x	y	z	B_{eq}[a] (Å^2)	Occupancy
Ni	1/2	1/2	0	1.96(4)	1/2
Cl(1)	0.0477(2)	0.8427(1)	0.1051(2)	4.03(9)	
S(1)	0.2247(2)	0.43825(9)	−0.0026(2)	2.97(7)	
S(2)	0.6763(2)	0.38913(9)	−0.0214(2)	2.50(7)	
S(3)	0.4818(2)	0.5032(1)	−0.2637(2)	2.85(7)	
O(1A)	0.355(1)	0.2188(5)	0.057(1)	4.4(2)	0.533
O(1B)	0.331(1)	0.2366(6)	0.138(1)	4.3(3)	0.467
O(2)	0.0108(8)	0.7785(3)	0.1840(6)	8.5(4)	
O(3)	−0.063(1)	0.8991(4)	0.1461(8)	11.9(6)	
O(4)	0.2225(8)	0.8623(4)	0.1296(7)	10.0(5)	
O(5)	0.0181(8)	0.8291(4)	−0.0458(5)	7.6(4)	
C(1A)	0.250(2)	0.3391(8)	−0.014(2)	4.0(3)	0.533
C(1B)	0.247(2)	0.3437(8)	0.069(2)	3.1(3)	0.467
C(2A)	0.389(1)	0.2927(7)	−0.002(1)	2.6(3)	0.533
C(2B)	0.374(2)	0.3137(8)	0.094(2)	3.2(3)	0.467
C(3)	0.5745(8)	0.3077(3)	0.0549(7)	3.4(3)	
C(4)	0.6685(8)	0.3700(4)	−0.2177(7)	3.3(3)	
C(5)	0.6580(8)	0.4403(4)	−0.3089(7)	3.5(3)	
C(6)	0.2880(8)	0.4470(5)	−0.3054(7)	4.8(4)	
C(7)	0.1546(9)	0.4494(5)	−0.1896(8)	5.4(4)	

[a] B_{eq} is the mean of the principal axes of the thermal ellipsoid.

Fig. 4. Structure of $[Co(L3)]^{2+}$.

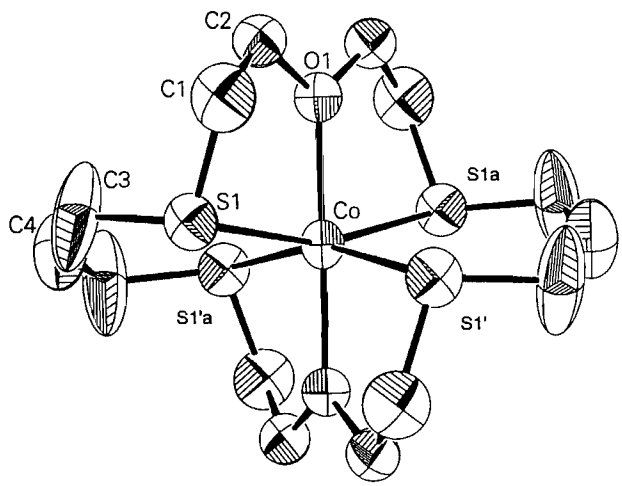

Table 6. Selected bond lengths and angles in $[Co(L3)][ClO_4]_2$.

Angles (deg)			
S(1)—Co—S(1a)	160.9(1)	S(1)—Co—O(1′)	99.57(5)
S(1)—Co—S(1′)	86.7(1)	S(1)—Co—O(1)	80.43(5)
S(1)—Co—S(1a′)	96.5(1)	O(1)—Co—O(1′)	180.00
Distances (Å)			
Co—S	2.444(2)	Co—O	2.098(6)

in $[Co(10S3)_2]^{2+}$, the "small ring" analogue of L3 (45) (2.320(3), 2.257(3), and 2.395(3) Å), which display the expected Jahn–Teller distortion of a low-spin Co(II) species. In the case of $[Co(L3)]^{2+}$, which is high spin (vide infra), such distortion is not apparent. Its Co—S bonds are slightly longer,

Table 7. Positional parameters and equivalent isotropic temperature factors for $[Co(L3)][ClO_4]_2$.

Atom	x	y	z	B_{eq}[a] (Å)
Co	1/2	0	0	4.9(1)
S(1)	0.5294(2)	0.1176(2)	0.1193(1)	6.8(1)
O(1)	0.3484(4)	0	0	5.5(3)
C(1)	0.6509(7)	0.0795(7)	0.1409(5)	9.4(6)
C(2)	0.2925(7)	−0.0508(6)	0.0669(5)	7.0(5)
C(3)	0.538(1)	0.2374(7)	0.0734(7)	18(1)
C(4)	1/2	0.269(1)	0	12(1)
Cl(1)	0.7896(2)	−0.7896	0.8306(2)	9.0(1)
O(2)	0.7268	−0.7046	0.7847	14.4
O(2A)	0.8514	−0.8577	0.8996	8.2
O(3)	0.7314	−0.8717	0.8129	8.8
O(3A)	0.6945	−0.8391	0.8415	4.7
O(4)	0.7984	−0.7631	0.9171	14.3
O(4A)	0.8294	−0.8039	0.7513	13.8
O(5)	0.8745	−0.7883	0.7780	11.4
O(5A)	0.7896	−0.7022	0.8721	10.6
O(6)	0.5602	0.5602	0.2491	20.4
O(7)	0.5023	0.5023	0.2987	28.8
O(8)	0.4869	0.4869	0.1583	20.4

[a] B_{eq} is the mean of the principal axes of the thermal ellipsoid.

and the Co—O distance (2.098(6) Å) is comparable to those in pentagonal bipyramidal $[Co(15O5)(H_2O)_2]Cl_2 \cdot H_2O$ (15O5 = 1,4,7,10,13-pentaoxacyclopentadecane) (46) of 2.076(4) (axial H_2O), 2.166(2), 2.213(2), and 2.172(2) Å. The S-Co-S angles in $[Co(L3)]^{2+}$ of the five-membered (86.7(1)°) and six-membered (96.5(1)°) chelate rings are slightly smaller and slightly larger, respectively, than their counterparts in $[Co(10S3)_2]^{2+}$ of 88.0(1)° or 91.5(1)° (five-membered) and

Can. J. Chem. Downloaded from www.nrcresearchpress.com by 80.90.12.36 on 09/08/12
For personal use only.

94.4(1)° (six-membered). Unlike $[Ni(L1)][ClO_4]_2$, the six-membered chelate rings of $[Co(L3)][ClO_4]_2$ are *anti* with respect to each other but again there are two meridional loops of ligand. The conformations for the 16 C-C-E-C or E-C-C-E (E = O or S) units in these ligands are all *gauche* except for two pairs of *anti* in each, but the location of the *anti* units differs in the two ligands. In L1, they occur about the sulfur that separates the six-membered and the five-membered chelate rings whereas in L3 they occur about the oxygen atoms, which correspond to separators between adjacent five-membered rings. The changed arrangement of the six-membered rings undoubtedly reflects the different intramolecular nonbonded interactions in the S_4O_2 ligand (L3) compared to those in the S_6 ligand (L1) (6).

(c) Magnetic moments

Since early reports of low-spin cobalt(II) (8, 47), it has become increasingly clear from spectroscopic and magnetic data that, especially when cyclic polythioethers are involved, the ability of these ligands to reduce inter-electronic repulsions (see Sect. (*d*)) is adequate to give low-spin complexes as a general rule. A question remains, however, as to how far these ligands take their complexed metals beyond the spin-crossover point. For $[Fe(L1)][ClO_4]_2$, magnetic susceptibility measurements indicate a diamagnetic sample consistent with a low-spin d^6 system (30). Likewise, for $[Co(L1)][ClO_4]_2$, μ_{eff} (22°C) = 1.75 BM indicates a low-spin d^7 system similar in its coordination sphere and magnetic properties to that of $[Co(18S6)]^{2+}$ (8) or $[Co(10S3)_2]^{2+}$ (45). The effective magnetic moment of $[Co(L2)][ClO_4]_2$ at 21°C, on the other hand, is 2.71 BM, which is appropriate for neither low-spin nor high-spin cobalt(II). The electronic spectrum of this complex is subtly different from other species with superficially similar S_6 coordination spheres and can be interpreted to indicate a tetragonal elongation of the coordination sphere (Sect. (*d*)). If this interpretation is correct, it would not be unreasonable to expect that the elongation decreases the ability of the axial thioethers to engage in reduction of spin-pairing energy and, as a consequence, the magnitudes of the ligand field splitting and spin-pairing energies become more nearly equal. This could lead to a spin-crossover situation such as that recently described for Co(II) species with S_2N_3 coordination spheres (48). In the case of $[Co(L2)_2]^{2+}$, application of eq. [1] (48) (in which n_{hs} is the mole fraction of the sample that is high spin, μ_{hs} is 4.8 BM, and μ_{ls} is 1.9 BM) suggests there is approximately 19% of the sample in the high-spin state at 21°C.

$$[1] \qquad n_{hs} = \frac{\mu_{exptl}^2 - \mu_{ls}^2}{\mu_{hs}^2 - \mu_{ls}^2}$$

Further variable-temperature magnetic susceptibility studies of this and related systems are in progress and it is interesting to note that extra-cyclic substituents such as an OH group can be used to "tune" the magnetic properties of this system compared to low-spin $[Co(10S3)_2]^{2+}$ (38). It is also significant that if the axial thioethers in $[Co(L1)]^{2+}$ or $[Co(L2)_2]^{2+}$ are replaced as in $[Co(L3)]^{2+}$ (Fig. 4) by oxygen atoms, which have even less ability to decrease spin-pairing energy, the trend in magnetic moments is continued with the result that the high-spin state is dominant in $[Co(L3)]^{2+}$ at room temperature (μ_{eff} = 4.37 BM at 22°C).

The effective magnetic moments of 2.83 ($[Ni(L1)][ClO_4]_2$), 2.93 ($[Ni(L2)_2][ClO_4]_2$), and 2.98 BM ($[Ni(L3)][ClO_4]_2$) are consistent with the two unpaired electrons expected for octahedral Ni(II) species.

(d) Electronic spectra

As indicated by its magnetic susceptibility, $[Fe(L1)]^{2+}$ is low spin. Low-spin iron(II) in octahedral symmetry is expected to exhibit two spin-allowed *d–d* transitions (49) and both are observed for $[Fe(L1)]^{2+}$. Ligand field parameters (Table 8) are in reasonable agreement with those reported previously for $[Fe(9S3)_2]^{2+}$ (50) and $[Fe(L1)][ClO_4]_2$ (30) and indicate an even greater ligand field for iron than for nickel as well as a greater nephelauxetic effect (vide infra).

Low-spin cobalt(II) would be expected to exhibit Jahn–Teller distortion and among known hexa-thioether Co(II) coordination spheres both tetragonal elongations (47) and compressions (44) have been observed. Electronic spectra of both compressed and elongated species are similar except for their lowest energy band, which represents the $^2A_{1g} \rightarrow {}^2aT_{2g}$ transition and corresponds to Δ_0 (45). For elongated species, this band appears at longer wavelengths (e.g., $[Co(2,5,8\text{-trithianonane})_2]^{2+}$, λ = 950 nm (47)) and as a result the complexes are often brown or red whereas compressed species have bands at shorter wavelengths (e.g., $[Co(9S3)_2]^{2+}$, λ = 750 nm (44, 45)) and are violet or purple. The spectrum of violet $[Co(L1)][ClO_4]_2$ (see Experimental), with its lowest energy band at 750 nm, is more like spectra of compressed hexa-thioether cobalt(II) complexes and it therefore seems likely that it reflects a Jahn–Teller compressed coordination sphere. For red $[Co(L2)_2]^{2+}$, the lowest energy band occurs at 830 nm and suggests a Jahn–Teller elongated coordination sphere. In that respect, this complex is a contrast to $[Co(9S3)_2]^{2+}$, which might be expected to be very similar but which has been shown to have tetragonal compression, is more violet in colour, and has its longest wavelength band at 750 nm (44, 45). For violet $[Co(L3)][ClO_4]_2$, the lowest energy band that was detected is at 780 nm but this is likely not the lowest energy band overall since magnetic studies (vide supra) have shown this compound to be high spin.

The electronic spectra (see Experimental) of violet $[Ni(L1)][ClO_4]_2$ and of purple $[Ni(L2)_2][ClO_4]_2$ in nitromethane are similar to spectra of other nickel species with pseudo-octahedral thioether coordination spheres (43). Of the three *d–d* bands expected, only the first two are observed, while the highest energy band is obscured by a charge transfer band that extends from about 400 nm into the ultraviolet as is usual for such compounds (16, 43). The Racah parameter, *B*, the nephelauxetic ratio, β, and the ligand field parameter, Δ_0, for the compounds reported in this study are given in Table 8 together with those of some related compounds for comparison. The Δ_0 values for $[Ni(L1)][ClO_4]_2$ of 12 900 cm^{-1} and for $[Ni(L2)_2][ClO_4]_2$ of 12 800 cm^{-1} are similar to values found for most six-coordinate thioether systems (Table 8) and slightly larger than those for six-coordinate N-donor species. The *B* values for $[Ni(L1)][ClO_4]_2$ of 670 cm^{-1} and for $[Ni(L2)_2][ClO_4]_2$ of 720 cm^{-1} give nephelauxetic ratios, β = 0.65 ($[Ni(L1)][ClO_4]_2$) and 0.69 ($[Ni(L2)_2][ClO_4]_2$), which are similar to those found for other six-coordinate thioether systems (Table 8) but smaller than for six-coordinate N-donor species. Together these indicate a slightly larger ligand field

Can. J. Chem. Downloaded from www.nrcresearchpress.com by 80.90.12.36 on 09/08/12
For personal use only.

Table 8. Ligand field parameters.

Complex	Δ_0 (cm^{-1})[a]	B (cm^{-1})[b]	β[c]	Ref.
$[Fe(L1)]^{2+}$	19 130	412	0.39	30
$[Fe(L1)]^{2+}$	19 710	341	0.32	
$[Fe(9S3)_2]^{2+}$	20 670	387	0.37	50
$[Fe(9N3)_2]^{2+}$	18 940	575	0.54	50
$[Co(L1)]^{2+}$	13 333			
$[Co(L2)_2]^{2+}$	12 048			
$[Co(L3)]^{2+}$	[d]			
$[Co(ttn)_2]^{2+}$[e]	10 526			47
$[Co(10S3)_2]^{2+}$	13 089			45
$[Co(18S6)]^{2+}$	13 890			47
$[Ni(L1)]^{2+}$	12 900	670	0.65	
$[Ni(L2)_2]^{2+}$	12 800	720	0.69	
$[Ni(L3)]^{2+}$	10 800	1017	0.98	
$[Ni(NH_3)_6]^{2+}$	10 750	986	0.95	43
$[Ni(9N3)_2]^{2+}$	12 500	934	0.90	43
$[Ni(9S3)_2]^{2+}$	12 650	685	0.66	43

[a]Fe: $A_{1g} \rightarrow T_{1g} = \Delta_0 - C$, $A_{1g} \rightarrow T_{2g} = \Delta_0 + 16B - C$, (assume $C = 4B$) (50). Co: (low spin) lowest energy band ($^2A_{1g} \rightarrow {}^2aT_{1g}$) = Δ_0 (45). Ni: lowest energy band ($^3A_{2g} \rightarrow {}^3T_{2g}$) = Δ_0 (45).

[b]Fe: (see *a*). Ni: $B = (2\nu_1^2 + \nu_2^2 - 3\nu_1\nu_2)/(15\nu_2 - 27\nu_1)$ (16).

[c]$\beta = B_{complex}/B_{free\ ion}$; $B_{free\ ion}$(Fe) = 1058, (Ni) = 1038 cm^{-1} (16, 38).

[d]Co: (high spin).

[e]ttn = 2,5,8-trithianonane.

strength and a much larger nephelauxetic effect for the thioethers than for the N-donors. The increased nephelauxetic effect has been noted before and is attributed to π-bonding capabilities of thioether sulfur (10, 16, 51, 52). For greenish-blue $[Ni(L3)][ClO_4]_2$, the effect of changing two thioethers into a pair of *trans*-ether donors as in the L1 or L2 complexes is visually apparent as a change in colour of the complex from purple to greenish-blue. The value of Δ_0 in the L3 complex is decreased to 10 180 cm^{-1} compared to the L1- and L2-containing species, and B has risen sharply to 1017 cm^{-1}, giving β = 0.98. These changes represent quite remarkable decreases in both ligand field strength and nephelauxetic effect. They parallel, however, the changes in ligand field strength observed for Co(II) with the same series of ligands. For Co(II), the magnetic properties show a trend from low spin through spin crossover to high spin through the series, consistent with a steady decrease in ligand field.

(e) Electrochemistry

Cyclic voltammetry of L1, L2, or L3 in CH_3NO_2 reveals irreversible oxidation of the free ligands at potentials $\geq$ +1.45 V vs. NHE. These processes are somewhat solvent dependent and become quasi-reversible in CH_3CN at $E_{1/2} \sim$ +1.56 V vs. NHE. Similar behaviour has been reported recently for 2,5,8-trithia[9]-*o*-benzenophane and was observed previously for other thioethers (53). The ligands show no tendency for reduction in the potential range over which the complexes have been examined.

For $[\{Pd(\eta^3\text{-}C_3H_5)\}_2(L1)][ClO_4]_2$ in acetonitrile, there is no electrochemical activity within the potential range over which the ligand is electrochemically silent. Cyclic voltammetry of $[Co(L1)][ClO_4]_2$, however, in either acetonitrile or nitromethane shows two reversible one-electron transfers at +0.570 V vs. NHE (ΔE_p = 80 mV at scan rates between 50 and 200 mV/s) and −0.355 V vs. NHE (ΔE_p = 90 mV at scan rates between 50 and 200 mV/s). The former is a Co(II)/Co(III) process whereas the latter is Co(II)/Co(I). There is a close comparison between this behaviour and that of $[Co(10S3)_2]^{2+}$ or $[Co(9S3)_2]^{2+}$ under similar conditions (45). The former exhibits reversible waves at +0.41 and −0.45 V vs. NHE whereas the latter has irreversible waves at +0.42 and −0.48 V vs. NHE. Thus, the presence of only one ligand ring compared to two in the coordination sphere or a change in the length of the carbon chain between donor sites has had only a small effect. These changes have resulted in a slight shift towards positive potentials but the general character of these redox processes appears otherwise unaffected. Comparison with the published data for $[Co(18S6)]^{2+}$ (47) is difficult. A dependence of the form of the cyclic voltammetric waves on the identity of the anion has been observed for some thioether complexes (16, 25) and this is also the case for $[Co(L1)]^{2+}$. Since the anion used in the reported study of $[Co(18S6)]^{2+}$ is not the same as in our current study and the reported potentials and wave forms for $[Co(18S6)]^{2+}$ are radically different from those for $[Co(L1)]^{2+}$, this precludes comparison in any meaningful way. For $[Co(L2)_2]^{2+}$, there are two reversible waves in acetonitrile at −0.28 and +0.65 V vs. NHE. Since redox potential is related to the relative size of the stability constants for the reduced and oxidized forms of the couple, the more positive potential values for both waves of the L2 complex compared to its 10S3 analog suggest that introduction of the OH group on the ligand ring to form L2 from 10S3 has resulted in poorer stabilization of Co(III) in the Co(III)/Co(II) and Co(II) in the Co(II)/Co(I) couples of the L2 complex. In other words, extra-cyclic groups may be used to "tune" the redox potentials of these complexes. We previously observed a similar effect in certain Cu(II) complexes (25). For $[Co(L3)][ClO_4]_2$ in nitromethane, there is no response between −0.7 and +0.7 V vs. NHE (and the compound decomposes in CH_3CN). Thus, metal-centred redox does not occur at potentials comparable to those found for other cobalt complexes in this study. This suggests that the electronic environment of cobalt in this complex is significantly different from that of the cobalt atoms in either the L1 or the L2 species, which is consistent with the findings of the magnetic and electronic spectroscopic studies discussed above.

For $[Ni(L1)][ClO_4]_2$ in CH_3CN, there is a quasi-reversible reduction at −351 mV vs. NHE (ΔE_p = 110 mV at scan rates of 50–300 mV/s) and an irreversible oxidation at +1.204 V vs. NHE as well as the ligand-centred process at 1.56 V. The behaviour of $[Ni(L2)_2][ClO_4]_2$ in nitromethane is similar to that of the L1 complex, which is perhaps not too surprising since their spectral characteristics and coordination spheres are similar. These processes are all strongly solvent dependent, becoming completely irreversible in CH_3NO_2 at potentials of −500 mV, +1.54 V, and +1.68 V vs. NHE. The $Ni^{2+/+}$ process at −351 mV vs. NHE may be compared with related processes for $[Ni(9S3)_2]^{2+}$ (quasi-reversible, $E_{1/2}$ = −710 mV vs. NHE) (54) and $[Ni(10S3)_2]^{2+}$ (quasi-reversible, $E_{1/2}$ = −550 mV vs. NHE) (45). Clearly, ligand structure has pronounced influence on the potential of the redox processes but

Can. J. Chem. Downloaded from www.nrcresearchpress.com by 80.90.12.36 on 09/08/12
For personal use only.

the exact details responsible are not yet completely clear. Chain length between coordination sites is by itself not sufficient to explain the effects as was shown in a study of $[Ni(pttd)]^{2+}$ (pttd = 1,12-bis(2-pyridyl)-2,5,8,11-tetrathiadecane) and $[Ni(pttu)]^{2+}$ (pttu = 1,13-bis(2-pyridyl)-2,5,9,12-tetrathiaundecane), which have identical electrochemical characteristics but different chain lengths (16).

That the electronic situation of the Ni atom in $[Ni(L3)]^{2+}$ is quite different from the situations of the Ni atoms in the L1 and L2 complexes is apparent from electronic spectroscopy, as discussed above. This is reflected in the cyclic voltammetry of $[Ni(L3)][ClO_4]_2$, which bears no resemblance to the response of the other two nickel complexes. The ligand is electrochemically silent between −0.80 and +0.94 V vs. NHE. Scans of the complex carried out between −0.5 and +0.9 V vs. NHE also show no response but if the initial potential is set at less than −0.5 V or a scan into that region precedes a scan to +0.9 V, a wave at +0.47 V vs. NHE appears. Under this condition, there is a reduction wave at −0.80 V accompanied by a minor return wave at −0.51 V vs. NHE as well as the major wave at +0.47 V. Thus, metal-centred oxidation is not a favourable process, while reduction is electrochemically irreversible and probably accompanied by substantial structural rearrangement. No attempts have been made to isolate Ni(I) species from this reaction.

(f) NMR and ESR

The proton-decoupled ^{13}C NMR spectrum of $[Fe(L1)][ClO_4]_2$ shows seven lines while the ^1H spectrum is complex (30) but we have found it to be invariant with temperature up to 70°C at least. These observations indicate, as suggested by Grant et al. (30), that the ligand has adopted a conformation leading to the *meso* isomer rather than the enantiomeric forms either singly or in a racemic mixture, both of which would lead to more than seven lines in the spectrum. Furthermore, the behaviour of the ^1H spectrum with temperature suggests the structure is rigid and non-fluxional up to 70°C at least. Thus, in $[Ni(L1)]^{2+}$ and $[Fe(L1)]^{2+}$ two different conformers of the ligand are seen, one of which produces a *d–l* pair of enantiomers and one of which produces the *meso* isomer. It may be, since Fe—S lengths are often shorter than Ni—S in comparable MS_6 coordination spheres (avg. 2.395 Å in $[Ni(10S3)_2]^{2+}$ (45); avg. 2.262 in $[Fe(10S3)_2]^{2+}$ (38)), that increased steric crowding in $[Fe(L1)]^{2+}$ compared to $[Ni(L1)]^{2+}$ causes intramolecular interactions in the ligand that are minimized in the complex in its *meso* form.

The proton-decoupled ^{13}C NMR spectrum of $[\{Pd(\eta^3\text{-}C_3H_5)\}_2(L1)][ClO_4]_2$ consists of six lines (see Experimental), two of which are readily assigned to the central and equivalent terminal carbons of the equivalent η^3-allyl groups. The remaining four lines are due to L1 and show that there are only four distinct carbon environments in the coordinated ring. This suggests that the two (η^3-allyl)Pd fragments are bound symmetrically to the macrocycle and each is bound to three sulfurs separated only by two-carbon bridges. The three-carbon bridges then serve to separate the (η^3-allyl)PdS_3 units. Alternatively, it is possible in view of the behaviour of related (η^3-allyl)Pd thioether complexes (24, 26) that the dinuclear cation could be exhibiting binding site fluxionality involving all six sulfurs that is already rapid at room temperature. Attempts to investigate the latter possibility by variable-temperature NMR studies below room temperature did not provide a definitive answer due to solubility difficulties.

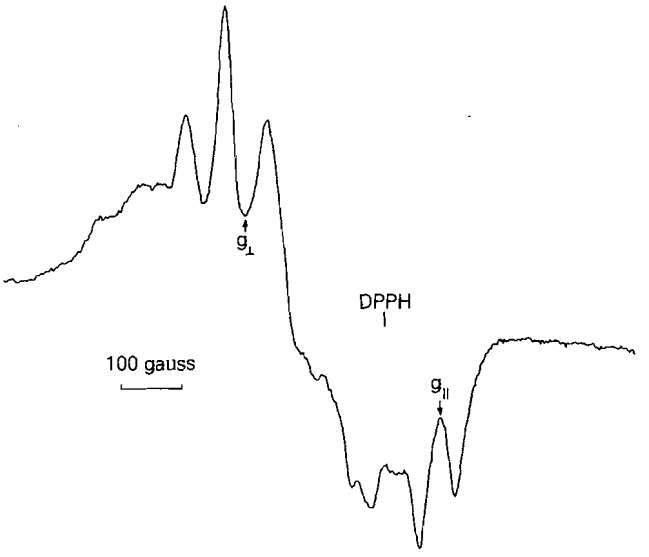

Fig. 5. ESR spectrum at 77 K and 9.60 GHz of $[Co(L2)_2][ClO_4]_2$ in CH_3NO_2 "glass".

The ESR spectrum of a polycrystalline sample of $[Co(L1)][ClO_4]_2$ is invariant with temperature between 77 and 295 K and consists of a single featureless line at $g = 2.13$ with a peak-to-peak width of 292 G. The absence of hyperfine splitting due to ^{59}Co ($I = 7/2$) can be attributed to weak intermolecular exchange interactions found in the crystalline material (47). In CH_3NO_2 solution at room temperature, however, an 8-line isotropic signal ($g_{iso} = 2.106$, $A_{iso} = 38$ G) is detected, confirming the low-spin character of the complex since high-spin species are not expected to exhibit a signal at room temperature (47). At 77 K, the spectrum of a "glass" in CH_3NO_2 is poorly resolved, showing only three distinctly visible lines on the high-field and three more on the low-field branches of the signal. The splitting on these lines is 63 G but no further structural information was extracted from the spectrum.

For $[Co(L2)_2][ClO_4]_2$, the spectrum at 77 K of a CH_3NO_2 "glass" is more clearly resolved (Fig. 5) and resembles that of tetragonally elongated $[Co(10S3)_2]^{2+}$ ($g_\perp = 2.138$ ($A_\perp = 80$ G) and $g_\parallel = 2.067$ ($A_\parallel = 60$ G) (45). Analysis of the spectrum for $[Co(L2)_2]^{2+}$ yields $g_\perp = 2.148$ ($A_\perp = 70$ G) and $g_\parallel = 1.951$ ($A_\parallel = 60$ G) consistent with the tetragonal elongation of the coordination sphere indicated by other physical measurements (see Results and discussion, Sects. (*c*) and (*d*)).

For $[Co(L3)][ClO_4]_2$, no signal is detected in the solid state at room temperature or at 77 K, consistent with the room temperature magnetic moment, $\mu_{eff} = 4.37$ BM, indicating a high-spin complex (47).

Conclusions

Improved preparations for three ligands (L1–L3) have been reported as well as a synthesis for the new ligand L4. Ligand L1 (20S6) differs by only two -CH_2- groups from previously reported 18S6 and comparisons of L1 complexes with published data from 18S6 complexes reveals that the extra -CH_2-

groups have little influence on the properties of the complexes but alter the way in which the ligand loops itself about the central metal. It appears that the choice of meridional or facial looping may be controlled by intramolecular interactions since it is variable with L1 adopting one conformation in $[Ni(L1)]^{2+}$ and another in $[Fe(L1)]^{2+}$, the latter of which is expected to have shorter M—S bonds and therefore greater steric crowding in its coordination sphere. Futhermore, changing to an S_4O_2 donor set in L3 and hence altering the intraligand interactions produces a slightly different looping of the ligand and *anti* placement of the six-membered chelate rings. Confusion in the literature concerning the preparation and properties of L2 and some of its complexes has been corrected and a new macrocyclic ligand (L4) with an S_2O donor set has been prepared. Its separation from the related "large" ring, L3, which is usually also formed in the same reaction, and distinguishing features of L3 and L4 have been described. The use of electronic spectroscopy to distinguish between tetragonally elongated and compressed low-spin Co(II) octahedra has been illustrated and the use of an extra-cyclic functional group and partial substitution of O for S donors to adjust the ligand field, nephelauxetic effect, and hence other dependent properties such as redox potential and magnetic phenomena has been demonstrated.

Acknowledgements

Financial support by the Natural Sciences and Engineering Research Council of Canada and by Memorial University of Newfoundland is gratefully acknowleged. Assistance from Ms. Cheryl Morgan and Mr. David Miller is also acknowledged.

References

1. S.G. Murray and F.R. Hartley. Chem. Rev. **81**, 365 (1981).
2. S.R. Cooper and S.C. Rawle. Struct. Bonding, **72**, 1 (1990).
3. G.H. Robinson. Coord. Chem. Rev. **112**, 227 (1992).
4. A.J. Blake and M. Schröder. Adv. Inorg. Chem. **35**, 1 (1990).
5. G. Reid and M. Schröder. Chem. Soc. Rev. **19**, 239 (1990).
6. R.E.J. Wolf, J.R. Hartman, J.M.E. Storey, B.M. Foxman, and S.R. Cooper. J. Am. Chem. Soc. **109**, 4328 (1987).
7. G.R. Giesbrecht, G.S. Hanan, J.E. Kickham, and S.J. Loeb. Inorg. Chem. **31**, 3286 (1992).
8. J.A.R. Hartman, E.J. Hintsa, and S.R. Cooper. Chem. Commun. 386 (1984).
9. R.J. Angelici. Acc. Chem. Res. **21**, 387 (1988).
10. A.J. Blake, A.J. Holder, T.I. Hyde, and M. Schröder. Chem. Commun. 1433 (1989).
11. A.J. Blake, A.J. Holder, T.I. Hyde, and M. Schröder. Chem. Commun. 987 (1987).
12. A.J. Blake, J.A. Greig, A.J. Holder, T.I. Hyde, A. Taylor, and M. Schröder. Angew. Chem. Int. Ed. Engl. **29**, 197 (1990).
13. A.J. Blake, R.O. Gould, G. Reid, and M. Schröder. Chem. Commun. 974 (1990).
14. C.R. Lucas, S. Liu, M.J. Newlands, J.P. Charland, and E.J. Gabe. Can. J. Chem. **68**, 644 (1990).
15. A.E. Ogilvy, A.E. Skaugset, and T.B. Rauchfuss. Organometallics, **8**, 2739 (1989).
16. B. Adhikary, S. Liu, and C.R. Lucas. Inorg. Chem. **32**, 5957 (1993).
17. M.J. Martin, J.F. Endicott, L.A. Ochrymowycz, and D.B. Rorabacher. Inorg. Chem. **26**, 3012 (1987).
18. M.M. Bernardo, P.V. Robandt, R.R. Schroeder, and D.B. Rorabacher. J. Am. Chem. Soc. **111**, 1224 (1989).
19. A.M.Q. Vande Linde, K.L. Juntunen, O. Mols, M.B. Ksebati, L.A. Ochrymowycz, and D.B. Rorabacher. Inorg. Chem. **30**, 5037 (1991).
20. M.J. Baena, P. Espinet, M.B. Ros, J.L. Serrano, and A. Ezcurra. Angew. Chem. Int. Ed. Engl. **32**, 1203 (1993).
21. D.W. Bruce. J. Chem. Soc. Dalton Trans. 2983 (1993).
22. V. Goulle, A. Harriman, and J.M. Lehn. Chem. Commun. 1034 (1993).
23. C.T. Chen and K.S. Suslick. Coord. Chem. Rev. **128**, 293 (1993).
24. C.R. Lucas and S. Liu. J. Chem. Soc. Dalton Trans. 185 (1994).
25. B. Adhikary and C.R. Lucas. Inorg. Chem. **33**, 1376 (1994).
26. S. Liu, C.R. Lucas, M.J. Newlands, and J.P. Charland. Inorg. Chem. **29**, 4380 (1990).
27. H. Wu and C.R. Lucas. Inorg. Chem. **32**, 526 (1993).
28. C.R. Lucas, S. Liu, and L.K. Thompson. Inorg. Chem. **29**, 85 (1990).
29. S. Liu, C.R. Lucas, R.C. Hynes, and J.P. Charland. Can. J. Chem. **70**, 1773 (1992).
30. G.J. Grant, S.M. Isaac, W.N. Setzer, and D.G. Vanderveer. Inorg. Chem. **32**, 4284 (1993).
31. D.P. Riley and J.D. Oliver. Inorg. Chem. **22**, 3361 (1983).
32. H.-J. Küppers, K. Wieghardt, B. Nuber, J. Weiss, B. Eckhard, and A.X. Trautwein. Inorg. Chem. **26**, 3762 (1987).
33. C.J. Gilmore. J. Appl. Crystallogr. **17**, 42 (1984).
34. P.T. Beurskens. *In* Technical Report 1984/1. Crystallographic Laboratory: Toernooiveld, 6525 Ed. Nijmegen, Netherlands. 1984.
35. International tables for X-ray crystallography. Vol. IV. Kynoch Press, Birmingham, England. 1974. p. 99. Table 2.2B.
36. TEXSAN–TEXRAY Molecular Structure Package. Molecular Structure Corporation, Woodlands, Tex. 1985.
37. J.J.H. Edema, H.T. Stock, J. Buter, R.M. Kellogg, W.J.J. Smeets, A.L. Spek, and F. van Bolhuis. Angew. Chem. Int. Ed. Engl. **32**, 436 (1993).
38. W.N. Setzer, E.L. Cacioppo, Q. Guo, G.J. Grant, D.D. Kim, J.L. Hubbard, and D.G. VanDerveer. Inorg. Chem. **29**, 2672 (1990).
39. H. Singh, M. Kumar, P. Singh, and S. Kumar. Indian J. Chem. **30B**, 237 (1991).
40. G.J. Grant, K.A. Sanders, W.N. Setzer, and D.G. VanDerveer. Inorg. Chem. **30**, 4053 (1991).
41. L.J. Zompa and T.N. Margulis. Inorg. Chim. Acta, **45**, L263 (1980).
42. M.E. Angley, M. Dwyer, S.F. Lincoln, G.H. Searle, R.J. Geul, and F.R. Keene. Inorg. Chim. Acta, **45**, L91 (1980).
43. S.R. Cooper, S.C. Rawle, J.A.R. Hartman, E.J. Hintsa, and G.A. Admans. Inorg. Chem. **27**, 1209 (1988).
44. W.N. Setzer, C.A. Ogle, G.S. Wilson, and R.S. Glass. Inorg. Chem. **22**, 266 (1983).
45. S. Chandrasekhar and A. McAuley. Inorg. Chem. **31**, 480 (1992).
46. N.R. Streltsova, V.K. Belsky, B.M. Bulychev, and O.K. Kireeva. Inorg. Chim. Acta, **189**, 111 (1991).
47. J.A.R. Hartman, E.J. Hintsa, and S.R. Cooper. J. Am. Chem. Soc. **108**, 1208 (1986).
48. A.L. Nivorozhkin, H. Toftlund, and M. Nielsen. J. Chem. Soc. Dalton Trans. 361 (1994).
49. A.B.P. Lever. *In* Inorganic electronic spectroscopy. Elsevier, Amsterdam. 1984.
50. K. Wieghardt, H.J. Küppers, and J. Weiss. Inorg. Chem. **24**, 3067 (1985).
51. C.R. Lucas. Can. J. Chem. **61**, 1096 (1983).
52. C.R. Lucas. Can. J. Chem. **64**, 1758 (1986).

Can. J. Chem. Downloaded from www.nrcresearchpress.com by 80.90.12.36 on 09/08/12
For personal use only.

53. L. Escriche, M.P. Almajano, J. Casabo, F. Teixidor, J. Rius, C. Miravitlles, R. Kivekas, and R. Sillampaa. J. Chem. Soc. Dalton Trans. 2969 (1993).

54. A.J. Blake, R.O. Gould, M.A. Halcrow, A.J. Holder, T.I. Hyde, and M. Schröder. J. Chem. Soc. Dalton Trans. 3427 (1992).

Can. J. Chem. Downloaded from www.nrcresearchpress.com by 80.90.12.36 on 09/08/12
For personal use only.

Synthesis, characterization, and properties of [Cp*M(NO)(η^2-CH_2Ph)-(NCMe)]BF_4 salts (M = Mo, W) and related complexes: the stabilizing influence of benzyl ligands

N.H. Dryden, P. Legzdins, S.F. Sayers, J. Trotter, and V.C. Yee

Can. J. Chem. Downloaded from www.nrcresearchpress.com by 80.90.12.36 on 09/08/12
For personal use only.

Abstract: Treatment of orange solutions of Cp*M(NO)(η^2-CH_2Ph)Cl (M = Mo or W) with an equimolar amount of solid $AgBF_4$ in MeCN affords the salts [Cp*M(NO)(η^2-CH_2Ph)(NCMe)]BF_4 as analytically pure crystals in good yields. Both orange complexes have been subjected to single-crystal X-ray crystallographic analyses in order to establish their molecular geometries and their intramolecular metrical parameters. Both salts consist of discrete organometallic cations and tetrahedral BF_4^- anions, the intramolecular dimensions of the two cationic complexes being essentially the same and resembling those found for related Cp*M(NO)-containing compounds. The isolated [Cp*M(NO)(η^2-CH_2Ph)(NCMe)]$^+$ cations are quite electrophilic, being able to abstract Cl^- from a NaCl IR cell to revert to their chloro precursors. However, treatment of the [Cp*W(NO)(η^2-CH_2Ph)(NCMe)]BF_4 salt with various unsaturated substrates (e.g., diphenylacetylene, 2,3-dimethyl-1,3-butadiene, carbon monoxide, and acetone) in $CDCl_3$ results in no detectable chemical reaction. Lewis bases weaker than Cl^- evidently cannot displace the acetonitrile ligand from the coordination sphere of the metal or induce the benzyl ligand to diminish its hapticity. Such a diminution does occur for the CH_2Ph ligand when the MeCN group in the cationic complexes is replaced by a carboxylate anion to produce neutral Cp'M(NO)(η^1-CH_2Ph)(η^2-O_2CR) complexes. The latter complexes are obtainable by treatment of Cp*M(NO)(η^2-CH_2Ph)Cl with AgO_2CR (R = CH(Et)(Ph)) in CH_2Cl_2 and have been fully characterized by conventional spectroscopic methods.

Key words: organomolybdenum, organotungsten, benzyl, cations.

Résumé : Le traitement des solutions de Cp*M(NO)(η^2-CH_2Ph)Cl (M = Mo ou W) avec une quantité équimolaire de $AgBF_4$ solide dans le MeCN fournit les sels [Cp*M(NO)(η^2-CH_2Ph)(NCMe)]BF_4, sous la forme de cristaux analytiquement purs, avec de bons rendements. Dans le but de déterminer leurs géométries moléculaires et leurs paramètres métriques intramoléculaires, on a soumis les deux complexes oranges à des analyses par diffraction des rayons X par des cristaux uniques. Les deux sels sont formés de cations organométalliques et d'anions BF_4^- individuels; les dimensions intramoléculaires des deux complexes cationiques sont essentiellement les mêmes et elles ressemblent à celles que l'on retrouve dans des composés apparentés contenant du Cp*M(NO). Les cations [Cp*M(NO)(η^2-CH_2Ph)(NCMe)]$^+$ isolés sont assez électrophiles; ils sont capables d'enlever les Cl^- d'une cellule IR en NaCl pour redonner leurs précurseurs chloro. Toutefois, le traitement du sel [Cp*W(NO)(η^2-CH_2Ph)(NCMe)]BF_4 avec divers substrats insaturés (par exemple, le diphénylacétylène, le 2,3-diméthylbuta-1,3-diène, le monoxyde de carbone ou l'acétone) dans du $CDCl_3$ ne conduit pas à des réactions chimiques détectables. Les bases de Lewis plus faibles que le Cl^- ne peuvent évidemment pas déplacer le coordinat acétonitrile de la sphère de coordination du métal ou induire le coordinat benzyle à diminuer son hapticité. Une telle diminution se produit pour le coordinat CH_2Ph lorsque le groupe MeCN des complexes cationiques est remplacé par un anion carboxylate pour conduire à des complexes neutres Cp*M(NO)(η^1-CH_2Ph)(η^2-O_2CR). On peut obtenir ces derniers complexes par le traitement des

Received October 12, 1994.

This paper is dedicated to Professor William A.G. Graham on the occasion of his 65th birthday.

N.H. Dryden, P. Legzdins,[1] S.F. Sayers, J. Trotter,[1] and V.C. Yee. Department of Chemistry, The University of British Columbia, Vancouver, BC V6T 1Z1, Canada.

[1] Authors to whom correspondence may be addressed. Telephone: (604) 822-3266. Fax: (604) 822-2847.

$Cp^*M(NO)(\eta^2\text{-}CH_2Ph)Cl$ avec du AgO_2CR (R = CH(Et)(Ph)), dans le CH_2Cl_2, et on les a totalement caractérisés par des méthodes spectroscopiques conventionnelles.

Mots clés : organomolybdène, organotungstène, benzyle, cations.

[Traduit par la rédaction]

Introduction

The chemistry of coordinatively and (or) electronically unsaturated metal centres continues to be a prime focus of transition-metal organometallic chemistry (1, 2). Our recent efforts in this area have centred principally on the characteristic stoichiometric chemistry of hydrocarbon ligands attached to the 14-valence-electron fragments, $Cp'M(NO)$ (M = Mo, W; Cp′ = $Cp(\eta^5\text{-}C_5H_5)$, $Cp^*(\eta^5\text{-}C_5Me_5)$). In particular, we have expended considerable effort in developing the chemistry of the symmetric 16-electron complexes, $Cp'M(NO)R_2$ (R = alkyl, aryl) (3). Subsequently, we developed methodology to synthesize the asymmetric 16-electron analogues, Cp*M-(NO)(R)R′, (4, 5) and were thus afforded the opportunity to study the comparative reactivity of two different hydrocarbyl ligands attached to the same metal centre (6). In general, the preparation of these hydrocarbyl complexes is non-trivial and presents significant synthetic challenges primarily because of their electronic unsaturation. It was during this work that we discovered the utility of the benzyl group as a hydrocarbyl ligand capable of stabilizing electronically unsaturated metal centres (7). The stabilization arises from the fact that the CH_2Ph ligand can function either as a one- or a three-electron donor to the metal centre when coordinated in an η^1- or an η^2-fashion, respectively, as shown below.

This dual hapticity of the benzyl ligand can, on occasion, permit the metal centre to attain some degree of electronic saturation and consequently diminished reactivity. For instance, the bis(benzyl) complexes, $Cp'M(NO)(CH_2Ph)_2$, are stereochemically nonrigid in solutions and possess the instantaneous 18-valence-electron molecular structures $Cp'M(NO)$-$(\eta^2\text{-}CH_2Ph)(\eta^1\text{-}CH_2Ph)$ that render them less reactive towards air and water than their 16-electron bis(alkyl) analogues, $Cp'M(NO)R_2$ (7*b*). Nevertheless, they can be induced to react just like the bis(alkyl) complexes (8), see eq. [1]. In other words, the stabilization provided by the unique benzyl ligand in these neutral complexes is not so great as to prohibit further reactivity.

It therefore became of interest to us to determine whether benzyl ligands could be utilized similarly to stabilize reactive cationic organometallic complexes, some of which have recently attracted considerable attention as potent Lewis acids (9). In this paper we present the results of our studies in this regard to date. Specifically, we report the extension of our earlier work to encompass the related cationic complexes $[Cp^*M(NO)(\eta^2\text{-}CH_2Ph)(NCMe)]BF_4$. The benzyl ligands in the organometallic cations have the potential to change their coordination modes from η^2 to η^1 (cf. eq.[1]), thereby opening a vacant coordination site and recducing the formal valence-

[1]
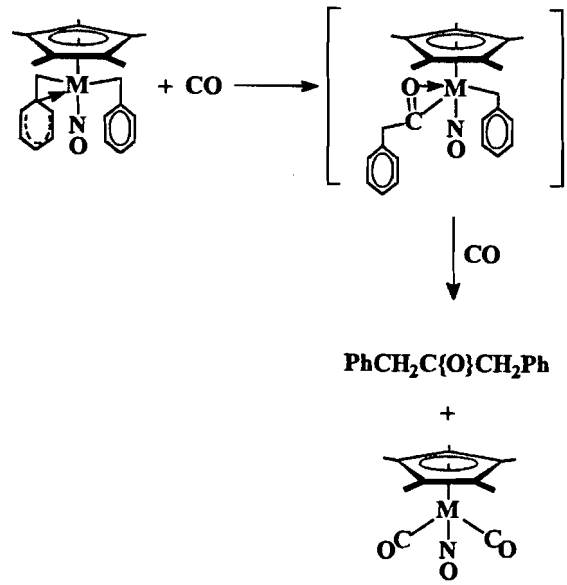

electron configuration at the metal from 18 to 16. During this work we have also demonstrated that just such a hapticity change occurs for the CH_2Ph ligand when the MeCN group in the cationic complexes is replaced by a carboxylate anion to produce neutral $Cp'M(NO)(\eta^1\text{-}CH_2Ph)(\eta^2\text{-}O_2CR)$ complexes.

Experimental

All reactions and subsequent manipulations involving organometallic reagents were performed under anaerobic and anhydrous conditions in an atmosphere of purified dinitrogen or argon. Conventional glovebox and vacuum-line Schlenk techniques were utilized throughout (10). General procedures routinely employed in these laboratories have been described in detail previously (11). $Cp'M(NO)(\eta^2\text{-}CH_2Ph)Cl$ reactants were prepared by the published procedures (7*c*). Infrared and elemental analyses data for all new complexes isolated during this work are collected in Table 1, and their ^1H and ^{13}C NMR data are presented in Table 2.

Preparation of $[Cp^*M(NO)(\eta^2\text{-}CH_2Ph)(NCMe)]BF_4$

The Mo and W complexes were prepared in a similar manner, and the preparation of the W complex is described below as a representative example.

An orange solution of $Cp^*W(NO)(\eta^2\text{-}CH_2Ph)Cl$ (1.4 g, 3.0 mmol) in MeCN (45 mL) was prepared, and its IR spectrum was recorded (AgCl cell, ν_{NO} = 1548 cm^{-1}). Solid $AgBF_4$ (0.58 g, 3.0 mmol) was added to the stirred solution, whereupon the reaction mixture immediately lightened in colour and a flocculent white precipitate formed. The reaction mixture was stirred for 8 h at ambient temperatures to ensure that the reaction was complete, and it was then filtered through a Celite plug (5 × 2 cm) supported on a medium-porosity glass frit. An IR spec-

Can. J. Chem. Downloaded from www.nrcresearchpress.com by 80.90.12.36 on 09/08/12
For personal use only.

Table 1. Infrared and elemental analysis data for the new complexes.

Compound	IR (Nujol (cm^{-1}))		Analysis found (calcd.)		
	ν_{NO}	other	C	H	N
$[Cp^*W(NO)(\eta^2\text{-}CH_2Ph)(NCMe)]BF_4$	1618	2280, 2300[a]	40.16 (40.13)	4.42 (4.43)	4.86 (4.93)
$[Cp^*Mo(NO)(\eta^2\text{-}CH_2Ph)(NCMe)]BF_4$	1638	2282, 2313[a]	47.35 (47.52)	5.25 (5.25)	5.69 (5.84)
$CpMo(NO)(\eta^1\text{-}CH_2Ph)(\eta\text{-}O_2CR)$[b]	1613	1450, 1495[c]	59.35 (59.33)	5.21 (5.20)	3.16 (3.14)
$Cp^*Mo(NO)(\eta^1\text{-}CH_2Ph)(\eta^2\text{-}O_2CR)$[b]	1602	1448, 1510[c]	62.98 (62.91)	6.49 (6.45)	2.70 (2.72)
$Cp^*W(NO)(\eta^1\text{-}CH_2Ph)(\eta^2\text{-}O_2CR)$[b]	1570	1454, 1488[c]	53.62 (53.74)	5.55 (5.51)	2.33 (2.32)

[a]The two bands are ν_{CN} and a combination band ($\nu_{CC} + \delta_{CH}$) of the MeCN ligand (21, 22).
[b]R = CH(Et)(Ph).
[c]These are ν_{CO} bands of the bidentate carboxylate group (23).

Can. J. Chem. Downloaded from www.nrcresearchpress.com by 80.90.12.36 on 09/08/12
For personal use only.

trum of the light orange filtrate in an AgCl cell revealed a ν_{NO} band at 1642 cm^{-1}. The volume of the filtrate was reduced in vacuo to ~8 mL, and Et_2O (30 mL) was then added. The resulting solution was stored at −30°C overnight. The orange crystals that deposited were isolated by removing the supernatant solution via cannula and were then washed with Et_2O (15 mL) to obtain analytically pure $[Cp^*W(NO)(\eta^2\text{-}CH_2Ph)(NCMe)]BF_4$ (1.2 g, 69% yield).

$[Cp^*Mo(NO)(\eta^2\text{-}CH_2Ph)(NCMe)]BF_4$ was prepared in a similar manner and was isolated in 80% yield as an orange crystalline solid. Crystals of both complexes suitable for X-ray crystallographic analyses were selected from the samples prepared as described above.

Treatment of $[Cp^*W(NO)(\eta^2\text{-}CH_2Ph)(NCMe)]BF_4$ with diphenylacetylene, 2,3-dimethyl-1,3-butadiene, and acetone

Typically, $[Cp^*W(NO)(\eta^2\text{-}CH_2Ph)(NCMe)]BF_4$ (50 mg) was mixed in a small vial with approximately 1 equivalent of each reagent. Approximately 600 mg of $CDCl_3$ were added to the vial, and the final solution was transferred to an NMR tube fitted with a Kontes Rotoflow top. ^1H NMR spectra were recorded immediately, and also after warming of the tubes and their contents at 55°C for 3 days. Only signals characteristics of $[Cp^*W(NO)(\eta^2\text{-}CH_2Ph)(NCMe)]BF_4$ and unreacted reagent were present in all spectra recorded.

Treatment of $[Cp^*W(NO)(\eta^2\text{-}CH_2Ph)(NCMe)]BF_4$ with carbon monoxide.

Approximately 50 mg of $[Cp^*W(NO)(\eta^2\text{-}CH_2Ph)(NCMe)]BF_4$ was dissolved in $CDCl_3$ (600 mg) in an NMR tube fitted with a Kontes Rotoflow top. The solution was frozen, and the tube was evacuated before being refilled with CO to a pressure of approximately 2 atm (1 atm = 101.3 kPa). The tube was warmed to room temperature, and the ^1H NMR spectrum of its contents only exhibited signals attributable to the organometallic reactant. The spectrum did not change upon warming the sample to 55°C for 3 days.

Preparation of $Cp'M(NO)(\eta^1\text{-}CH_2Ph)(\eta^2\text{-}O_2CR)$ (R = CH(Et)(Ph))

The three complexes $CpMo(NO)(CH_2Ph)(O_2CR)$, $Cp^*Mo(NO)(CH_2Ph)(O_2CR)$, and $Cp^*W(NO)(CH_2Ph)(O_2CR)$ were prepared in a similar manner. The preparation of the $Cp^*Mo(NO)(CH_2Ph)(O_2CR)$ species is given as a representative example.

To a Schlenk tube containing $Cp^*Mo(NO)(\eta^2\text{-}CH_2Ph)Cl$ (0.41 g, 1.1 mmol) and silver 2-phenylbutyrate (0.29 g, 1.1 mmol) immersed in a water bath at 10°C was added CH_2Cl_2 (40 mL) by syringe. The cooling bath was removed, and the reaction mixture was stirred for 3 h at ambient temperatures. During the course of the reaction, the initial red solution became lighter in colour and a white solid precipitated. The final reaction mixture was filtered through a Celite plug (4 × 2 cm) supported on a medium-porosity frit, and the light orange filtrate was taken in vacuo to a glassy foam. This foam was triturated with hexanes (15 mL) to obtain an orange powder. Toluence was added dropwise to the hexanes suspension of the orange powder until all the solid had dissolved. The saturated solution was placed in a refrigerator (5°C) overnight to induce crystallization fo the desired product. The solid that crystallized from the toluence – hexanes solution was isolated by removing the mother liquor by cannulation and washing the remaining solid with hexanes (10 mL). These operations afforded $Cp^*Mo(NO)(\eta^1\text{-}CH_2Ph)(\eta^2\text{-}O_2CR)$ as large red-orange crystals (0.23 g, 41% yield).

The ^1H NMR spectrum of the product indicated the presence of two diastereomeric pairs of enantiomers (*R,S/S,R* and *R,R/S,S*) in a ~1:1.5 ratio as determined by integration of the proton signals for the Me group of the carboxylate ligands. The supernatant mother liquor was placed in a freezer (−10°C) to induce the crystallization of more product. In this manner an additional 0.21 g (38% yield) of product were obtained (1:1.4 ratio of diastereomeric pairs).

On a similar reaction scale $Cp^*W(NO)(\eta^1\text{-}CH_2Ph)(\eta^2\text{-}O_2CR)$ was isolated as red-orange blocks in two crystallizations (0.26 g, 39% yield, 1:1.4 diastereomeric pair ratio; 0.19 g, 29% yield, 1:1.5 diastereomeric pair ratio) and $CpMo(NO)(\eta^1\text{-}CH_2Ph)(\eta^2\text{-}O_2CR)$ was isolated as orange needles (0.14 g, 29% yield, 1:1 ratio of diastereomeric pairs; second crop crystallized at −25°C: 0.21 g, 42% yield, 1:1.1 ratio of diastereomeric pairs).

X-ray crystallographic analyses of $[Cp^*M(NO)(NCMe)(\eta^2\text{-}CH_2Ph)]BF_4$ (M = Mo, W)

Suitable crystals of the complexes, obtained as described in the preceding paragraphs, were mounted in thin-walled glass capillaries under N_2 and transferrerd to an Enraf–Norius CAD4-F diffractometer (graphite monochromatized Mo*K*α radiation, $\lambda(\alpha_1)$ = 0.70930, $\lambda(\alpha_2)$ = 0.71359 Å). Unit-cell parameters were obtained by least-squares analysis of 2 sin θ/λ values for 25 reflections with θ = 17.6°–20.1° and 21.9°–23.4° for the Mo

Table 2. Mass spectral, ^{1}H and ^{13}C NMR data for the new complexes.

Complex[a]	MS *m/z*[b]	^{1}H NMR δ	^{13}C{1H}NMR[c] δ
[Cp*W(NO)(η^2-CH_2Ph)(NCMe)]BF_4[d]		8.20 (t, 1H, Ar*H*, $^3J_{HH}$ = 7.5 Hz) 7.71 (d, 1H, Ar*H*, $^3J_{HH}$ = 7.5 Hz) 7.55 (t, 1H, Ar*H*, $^3J_{HH}$ = 7.5 Hz) 7.41 (t, 1H, Ar*H*, $^3J_{HH}$ = 7.5 Hz) 6.42 (d, 1H, Ar*H*, $^3J_{HH}$ = 7.5 Hz) 3.47 (d, 1H, CH_AH_B, $^2J_{HH}$ = 6.0 Hz) 2.65 (s, 3H, NCMe) 2.50 (d, 1H, CH_AH_B, $^2J_{HH}$ = 6.0 Hz) 2.10 (s, 15H, Ar*H*, $(C_5(Me)_5)$)	144.54 (C_{arom}) 137.71 (C_{arom}) 132.00 (C_{arom}) 131.42 (C_{arom}) 130.22 (C_{arom}) 112.52 ($C_5(Me)_5$) 111.62 (C_{ipso}) 49.19 (Ph*C*H$_2$) 10.56 (C_5(*Me*)$_5$) 5.96 (NC*Me*)
[Cp*Mo(NO)(η^2-CH_2Ph)(NCMe)]BF_4[d]		7.99 (t, 1H, Ar*H*, $^3J_{HH}$ = 7.2 Hz) 7.65 (d, 1H, Ar*H*, $^3J_{HH}$ = 7.2 Hz) 7.61 (t, 1H, Ar*H*, $^3J_{HH}$ = 7.5 Hz) 7.49 (t, 1H, Ar*H*, $^3J_{HH}$ = 7.5 Hz) 6.38 (d, 1H, Ar*H*, $^3J_{HH}$ = 7.5 Hz) 3.74 (d, 1H, CH_AH_B, $^2J_{HH}$ = 5.0 Hz) 2.48 (s, 3H, NCMe) 2.00 (s, 15H, Ar*H*, $C_5(Me)_5$)	144.05 (C_{arom}) 137.17 (C_{arom}) 136.82 (N*C*Me) 131.94 (C_{arom}) 131.19 (C_{arom}) 130.39 (C_{arom}) 114.61 (C_5Me_5) 114.02 (C_{ipso}) 55.51 (Ph*C*H$_2$) 10.68 (C_5*Me*$_5$) 5.23 (NC*Me*)
CpMo(NO)(η^1-CH_2Ph)(η^2-O_2CR)[e]	447 [P]$^+$	7.05–7.35(m, 9H, Ar*H*) 6.85–6.95 (m, 1H Ar*H*) 5.39, 5.38[f] (2s, 4.5H,[g] C_5H_5) 3.42, 3.39[f] (2d, 1H, PhCH_AH_B, $^2J_{HH}$ = 9.0 Hz) 3.30, 3.29[f] (2t, 1H, C*H*, $^3J_{HH}$ = 7.5 Hz) 3.21, 3.19[f] (2d, 1H, PhCH_AH_B ^2JHH = 9.0 Hz) 2.05[i] (2m, 1H, CHCH_AH_BMe) 1.85[i] (2m, 1H, CHCH_AH_BMe) 0.86, 0.85[f] (2t, 3H, Me, $^3J_{HH}$ = 7.5 Hz)	191.39 (CO_2) 149.92 (C_{ipso}, Bz) 138.18 (C_{ipso}, Ph) 128.71, 127.95, 129.84 129.43, 127.40, 124.02 (C_{arom}) 105.54 (d, C_5H_5) 56.38 (d, *C*H) 50.71, 50.67 (t, Ph*C*H$_2$) 26.35 (t, *C*H$_2$) 12.23 (q, *Me*)
Cp*Mo(NO)(η^1-CH_2Ph)(η^2-O_2CR)[e]	517 [P]$^+$	6.95–7.35 (m, 9H, Ar*H*) 6.80–6.95 (m, 1H Ar*H*) 3.14,[j] 3.08[k] (dd, 1H, C*H*, $^3J_{HH}$ = 7.0, 8.5 Hz) 2.24,[j] 2.22[k] (2d, 1H, PhCH_AH_B $^2J_{HH}$ = 8.6 Hz) 2.00,[j] 1.95[k] (2d, 1H, PhCH_AH_B $^2J_{HH}$ = 8.6 Hz) 1.50–1.95 (4m, CHCH_AH_BMe) 1.64,[j] 1.56[k] (2s, 15H, $C_5(Me)_5$) 0.70,[j] 0.59[k] (2t, 3H, Me, $^3J_{HH}$ = 7.4 Hz)	190.74, 190.50 (CO_2) 148.54, 148.15 (C_{ipso}, Bz) 138.87, 138.64 (C_{ipso}, Ph) 128.48, 128.43, 128.22, 128.18, 128.10, 127.31, 127.04, 126.89, 126.92, 123.44, 123.27 (C_{arom}) 112.93 (C_5Me_5) 56.46 (d, *C*H) 53.17, 53.14 (t, Ph*C*H$_2$) 26.38, 25.78 (t, *C*H$_2$) 12.22, 12.17 (q, *Me*) 9.12, 8.94 (q, C_5*Me*$_5$)

Can. J. Chem. Downloaded from www.nrcresearchpress.com by 80.90.12.36 on 09/08/12
For personal use only.

Table 2 (*concluded*).

Complex[a]	MS *m/z*[b]	^{1}H NMR δ	^{13}C{^{1}H}NMR[c] δ
Cp*W(NO)(η^1-CH_2Ph)(η^2-O_2CR)[e]	603 [P]$^+$	7.00–7.35 (m, 9H, Ar*H*)	190.78, 190.72 (CO_2)
		6.80–6.95 (m, 1H, Ar*H*)	148.32, 148.29 (C_{ipso}, Bz)
		3.09,[j] 3.02[k] (2dd, 1H, C*H*, $^3J_{HH}$ = 7.3, 9.0 Hz)	137.99, 137.61 (C_{ipso},[h] Ph)
		2.12,[j] 2.10[k] (2d, 1H, PhCH_AH_B $^2J_{HH}$ = 10.8 Hz)	128.63, 128.57, 128.47, 128.21, 128.12, 127.59, 127.34 126.82, 126.78, 123.01, 122.99 (C_{arom})
		1.80,[j] 1.76[k] (2d,[l] 1H, PhCH_AH_B $^2J_{HH}$ = 8.6 Hz)	111.58 ($C_5(Me)_5$)56.90, 56.81 (d, *C*H)
		1.45–2.00 (4m, CHCH_AH_BMe)	50.66, 50.57 (t, Ph*C*H_2, $^1J_{WC}$ = 71 Hz)
		1.78,[j] 1.68[k] (2s, 15H, $C_5(Me)_5$)	25.97, 25.34 (t, *C*H_2)
		0.70,[j] 0.58[k] (2t, 3H, Me, $^3J_{HH}$ = 7.5 Hz)	12.09, 12.05 (q, *Me*)
			9.08, 8.91 (q, $C_5(Me)_5$)

[a]Probe temperatures 150°C. No attempts were made to obtain mass spectra of the cationic species.
[b]The *m/z* values are for the highest intensity peak of the calculated isotopic cluster.
[c]Multiplicities of carbon resonances were determined by a gated decoupled pulse sequence.
[d]Spectra recorded in CD_3NO_2.
[e]Spectra recorded in $CDCl_3$.
[f]Spectra contain signals for an equal amount of both diastereomeric pairs of enantiomers.
[g]Intensities of Cp proton signals are lower than expected due to long T_1 values.
[h]Assignment by analogy to the free acid: C_{ipso} = δ 138.38 in $CDCl_3$.
[i]Indistinguishable overlapping signals for both diastereomeric pairs of enantiomers.
[j]Minor diastereomeric pair of enantiomers.
[k]Major diastereomeric pair of enantiomers.
[l]These proton signals were located by resolving them from obscuring resonances of the Cp* rings by use of the HOM2DJ pulse program supplied with the Varian XL-300 NMR spectrometer for homonuclear 2-dimensional *J*-resolved ^{1}H NMR spectroscopy (for example, see ref. 24). The standard parameters supplied for acquisition and processing were used.

and W compounds, respectively. Three standard reflections for the Mo compound showed no significant variation, but those for the W compound had an average decay of 17%, and the data were scaled accordingly. Lorentz, polarization, and absorption corrections were applied (12, 13).[2] The crystallographic data and experimental details are summarized in Table 3.

The Mo and W positions in the isomorphous structures were determined from the Patterson functions, and the full structures were then derived by conventional electron-density methods, and refined full-matrix least-squares methods on *F*, minimizing $\Sigma w(F_o\text{-}F_c)^2$, where $w = 1/\sigma^2(F)$. The F atoms of the BF_4^- anion in the Mo compound were each disordered over two sites (50% occupancies); in the W compound, the F atoms were placed in single sites, but large anisotropic thermal parameters indicate possible disorder. Final cycles were carried out with anisotropic thermal parameters for all heavier atoms, except the disordered F atoms (isotropic); benzyl H atoms were refined, and methyl H atoms were fixed in calculated sites based on difference-map peaks. Final values of $R = 0.050$, 0.038 and $R_w = 0.069$, 0.049 were obtained for the Mo and W complexes, respectively. The largest final difference-map peaks are about 1 e Å^{-3} for the Mo compound (about 1.5 Å from the B atom, suggesting incomplete modeling of the disorder), and 1.7 e Å^{-3} for the W compound (near the W atom).

Scattering factors were from ref. 14. Final positional and isotropic thermal parameters (U_{eq} = 1/3 × trace of diagonalized *U*) are listed in Table 4, and selected interatomic distances and angles are collected in Table 5. Anisotropic thermal parameters, hydrogen parameters, bond lengths and angles, and packing diagrams are provided as supplementary material.[3]

Results and discussion

Preparation and physical properties of the [Cp*M(NO)(η^2-CH_2Ph)(NCMe)]BF_4 salts

These orange organomolybdenum and organotungsten salts are preparable in good yields by chloride abstraction from their alkyl chloride precursors in acetonitrile. The progress of the reactions may be easily monitored by IR spectroscopy, the diminution of the ν_{NO} bands characteristic of the starting

[2] The computer programs used include locally written programs for data processing and locally modified versions of the following: ORFLS, full-matrix least squares, and ORFFE, function and errors, by W.R. Busing, K.O. Martin, and H.A. Levy; FORDAP, Patterson and Fourier syntheses, by A. Zalkin; ORTEPII, illustrations, by C.K. Johnson.

[3] Supplementary material mentioned in the text may be purchased from: The Depository of Unpublished Data, Document Delivery, CISTI, National Research Council Canada, Ottawa, Canada K1A 0S2.

Tables of hydrogen atom parameters, bond lengths, and bond angles as well as the packing diagrams have also been deposited with the Cambridge Crystallographic Data Centre, and can be obtained on request from The Director, Cambridge Crystallographic Data Centre, University Chemical Laboratory, 12 Union Road, Cambridge, CB2 1EZ, U.K.

Structure factor amplitudes are no longer being deposited and may be obtained directly from the author.

Can. J. Chem. Downloaded from www.nrcresearchpress.com by 80.90.12.36 on 09/08/12
For personal use only.

Can. J. Chem. Downloaded from www.nrcresearchpress.com by 80.90.12.36 on 09/08/12
For personal use only.

Table 3. Crystallographic and experimental data for the complexes $[Cp^*M(NO)(\eta^2\text{-}CH_2Ph)(NCMe)]BF_4$, (M = Mo, W).

Parameters	Mo	W
Colour	Orange	Orange
Formula	$C_{19}H_{25}BF_4MoN_2O$	$C_{19}H_{25}BF_4N_2OW$
Formula weight	480.16	568.08
Crystal system	Monoclinic	Monoclinic
Space group	$P2_1/c$	$P2_1/c$
a(Å)	8.518(1)	8.492(1)
b(Å)	17.538(2)	17.452(4)
c(Å)	14.743(1)	14.757(2)
β(deg)	103.40(1)	103.22(1)
V(Å^3)	2142.5(3)	2129.1(7)
Z	4	4
d_{calcd} (Mg/m^{-3})	1.49	1.77
F(000)	976	1104
μ(Mo Kα)(cm^{-1})	6.4	55.8
T(K)	294	294
Crystal dimensions (mm^3)	0.50 × 0.25 × 0.13	0.28 × 0.25 × 0.15
Transmission factors	0.85–0.93	0.33–0.51
Scan type	ω–2θ	ω–2θ
Scan range (deg)	0.70 + 0.35 tan θ	0.65 + 0.35 tan θ
Scan speed (deg/min)	1.4–10	1.3–10
2θ (max)(deg)	55	55
Data collected	$+h, +k, \pm l$	$+h, +k, \pm l$
Unique reflections	4903	4823
Reflections with $I \geq 3\sigma(I)$	3221	3346
No. of variables	277	281
R_F	0.050	0.038
R_wF	0.069	0.049
Goodness of fit	2.18	1.63
Max Δ/σ (final cycle)	0.03	1.3[a]
Residual density (e/Å^3)	−0.9 to +1.0	−1.7 to +1.7

[a] F, thermal parameter.

materials (W, 1584 cm^{-1}; Mo, 1610 cm^{-1}) being accompanied by the growth of new ν_{NO} bands at higher energy (W, 1622 cm^{-1}; Mo, 1647 cm^{-1}) for the cationic products.

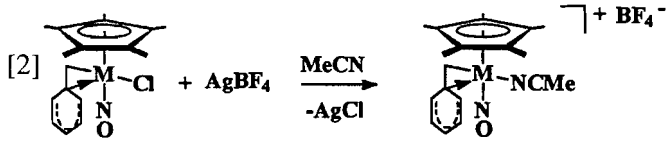

Unlike the related cationic complexes $[Cp^*W(NO)(CH_2CMe_3)(NCMe)_2]BF_4$ (5) and $[Cp^*W(NO)(CH_2SiMe_3)(NCMe)_2]BF_4$ (15), the benzyl-containing cations require only one stabilizing MeCN molecule in the coordination spheres of the metals. This feature reflects the unique ability of the benzyl ligand in its η^2-coordination mode to provide three electrons to the metal centres. Nevertheless, the isolated $[Cp^*M(NO)(\eta^2\text{-}CH_2Ph)(NCMe)]^+$ cations are quite electrophilic, being able to abstract Cl^- from a NaCl IR cell. This process can be detected simply by leaving acetonitrile solutions of the complexes as their BF_4^- salts in NaCl cells and monitoring the progress of the chloride abstraction by IR spectroscopy. This monitoring reveals the complete loss of the ν_{NO} bands for the cationic complexes and the return of the ν_{NO} bands of the starting benzyl chloro species in a matter of minutes at ambient temperatures. The use of AgCl plates in the solution cell allows IR monitoring of reactions [2] without the occurrence of halide abstraction from the cell material.

In preliminary studies we have also established that treatment of the $[Cp^*W(NO)(\eta^2\text{-}CH_2Ph)(MeCN)]BF_4$ salt with various unsaturated substrates (e.g., diphenylacetylene, 2,3-dimethyl-1,3-butadiene, carbon monoxide, and acetone) in $CDCl_3$ results in no detectable chemical reaction. Thus, Lewis bases weaker than Cl^- evidently cannot displace the acetonitrile ligand from the coordination sphere of the metal or induce the benzyl ligand to diminish its hapticity. Our current efforts are thus directed at generating these cations in weakly coordinating solvents such as CH_2Cl_2 and utilizing them in situ.

Solid-state molecular structures of the $[Cp^*M(NO)(\eta^2\text{-}CH_2Ph)(NCMe)]BF_4$ complexes

Solid-state X-ray crystallographic analyses of the cationic molybdenum and tungsten complexes have been performed in order to establish the exact natures of the metal–benzyl linkages present and to compare them with those extant in related neutral benzyl complexes (7). The two complexes are essentially isostructural, and a stereoview of the $[Cp^*W(NO)(\eta^2\text{-}CH_2Ph)(NCMe)]BF_4$ complex is presented in Fig. 1. Both salts

Can. J. Chem. Downloaded from www.nrcresearchpress.com by 80.90.12.36 on 09/08/12
For personal use only.

Table 4. Positional and thermal parameters, with esd's in parentheses, for the complexes $[Cp^*M(NO)(\eta^2\text{-}CH_2Ph)(NCMe)]BF_4$ (M = Mo, W).

	M = Mo				M = W			
Atom	*x*	*y*	*z*	$U_{iso/eq}$ (Å^2 × 10^3)	*x*	*y*	*z*	U_{eq} (Å^2 × 10^3)
M	0.20042(5)	0.53726(2)	0.26551(3)	40	0.20246(3)	0.53535(2)	0.26609(2)	41
O	0.4901(6)	0.4407(3)	0.3307(4)	80	0.4975(8)	0.4395(4)	0.3311(5)	79
N1	0.3769(6)	0.4811(3)	0.2979(3)	52	0.3806(9)	0.4800(4)	0.2997(4)	54
N2	0.3326(5)	0.6393(3)	0.2549(3)	49	0.3298(7)	0.6368(4)	0.2535(4)	45
C1	0.0023(8)	0.4835(4)	0.3329(4)	59	0.0026(11)	0.4838(5)	0.3340(6)	58
C2	0.1349(7)	0.5078(4)	0.4049(4)	52	0.1357(10)	0.5086(5)	0.4062(5)	52
C3	0.1450(7)	0.5886(3)	0.3977(4)	53	0.1490(10)	0.5893(4)	0.3983(5)	52
C4	0.0150(7)	0.6151(4)	0.3244(4)	59	0.0182(10)	0.6140(5)	0.3248(5)	59
C5	−0.0722(7)	0.5509(4)	0.2864(4)	61	−0.0735(10)	0.5509(6)	0.2851(6)	63
C6	−0.0632(11)	0.4040(5)	0.3197(6)	94	−0.0626(14)	0.4040(7)	0.3231(8)	95
C7	0.2381(11)	0.4598(4)	0.4785(5)	80	0.2395(13)	0.4584(5)	0.4791(6)	73
C8	0.2592(10)	0.6403(4)	0.4637(5)	75	0.2637(14)	0.6395(6)	0.4624(6)	76
C9	−0.0234(10)	0.6958(4)	0.2988(6)	85	−0.0194(14)	0.6957(6)	0.2962(7)	85
C10	−0.2317(8)	0.5502(6)	0.2137(6)	96	−0.2276(12)	0.5500(8)	0.2141(8)	97
C11	0.0994(9)	0.4588(4)	0.1521(5)	61	0.1014(13)	0.4562(5)	0.1540(6)	61
C12	0.1612(7)	0.5183(3)	0.1013(4)	52	0.1631(11)	0.5168(5)	0.1024(5)	57
C13	0.3180(8)	0.5147(4)	0.0829(4)	60	0.3233(11)	0.5145(5)	0.0858(5)	56
C14	0.3777(9)	0.5748(4)	0.0440(4)	61	0.3806(11)	0.5736(6)	0.0443(5)	62
C15	0.2856(9)	0.6412(5)	0.0191(4)	64	0.2891(12)	0.6410(6)	0.0206(6)	68
C16	0.1360(9)	0.6473(5)	0.0366(5)	69	0.1367(12)	0.6464(6)	0.0380(6)	70
C17	0.0735(8)	0.5860(4)	0.0798(4)	60	0.0758(10)	0.5846(6)	0.0791(6)	60
C18	0.4004(7)	0.6927(3)	0.2432(4)	51	0.3976(9)	0.6912(5)	0.2421(5)	53
C19	0.4836(10)	0.7628(5)	0.2274(6)	89	0.4822(14)	0.7606(6)	0.2271(7)	93
B	0.2993(10)	0.2659(5)	0.0029(6)	69	0.2974(13)	0.2646(7)	0.0048(8)	67
F1[a]	0.190(2)	0.235(1)	0.045(1)	127(4)	0.1705(13)	0.2322(5)	0.0170(10)	211
F2[a]	0.305(2)	0.332(1)	0.055(1)	127(4)	0.2998(17)	0.3341(5)	0.0268(13)	275
F3[a]	0.436(2)	0.231(1)	0.026(1)	120(4)	0.4173(16)	0.2301(9)	0.0509(11)	297
F4[a]	0.259(2)	0.274(1)	−0.085(1)	176(6)	0.3171(25)	0.2556(11)	−0.0686(8)	312
F1′[a]	0.142(2)	0.230(1)	−0.018(1)	118(4)				
F2′[a]	0.289(2)	0.343(1)	−0.019(1)	141(4)				
F3′[a]	0.372(2)	0.210(1)	0.076(1)	176(6)				
F4′[a]	0.377(2)	0.237(1)	−0.056(1)	162(5)				

[a]Occupancy = 0.5.

Fig. 1. Stereoview of the solid-state molecular structure of $[Cp^*W(NO)(\eta^2\text{-}CH_2Ph)(NCMe)]BF_4$. The molybdenum analogue is isostructural.

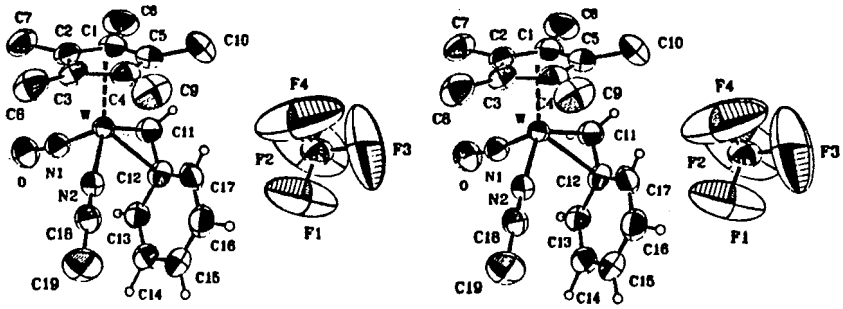

consist of discrete cations and tetrahedral BF_4^- anions, the intramolecular dimensions of the two cationic complexes being essentially the same and resembling those found for related Cp*M(NO)-containing compounds (16). All the metal–ligand bond distances are virtually identical for both congeners (Table 5), an expected feature since the covalent radii of Mo and W are very similar. The Mo and W complexes also contain essentially isostructural M-C_1-C_{ipso} moieties, with similar metal–$C_{methylene}$ (Mo, 2.182 (6) Å; W, 2.175 (8) Å) and metal–C_{ipso} (Mo, 2.389(5) Å; W, 2.383(7) Å) bond lengths.

Can. J. Chem. Downloaded from www.nrcresearchpress.com by 80.90.12.36 on 09/08/12
For personal use only.

Scheme 1.

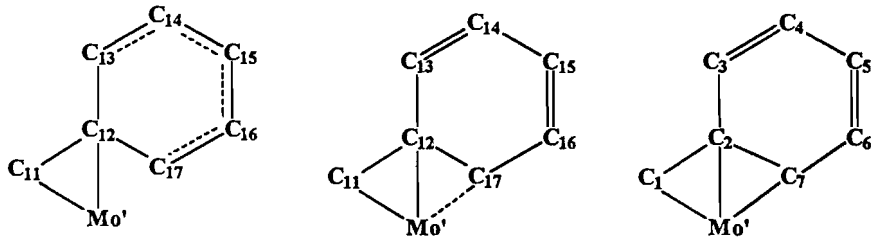

Mo' = Cp*Mo(NO)Cl		Mo' = Cp*Mo(NO)(NCMe)$^+$		Mo' = $CpMo(CO)_2$	
Mo-C_{11}	2.193	Mo-C_{11}	2.182	Mo-C_1	2.269
Mo-C_{12}	2.439	Mo-C_{12}	2.389	Mo-C_2	2.364
Mo-C_{17}	3.004	Mo-C_{17}	2.830	Mo-C_7	2.480
C_{11}-C_{12}	1.460	C_{11}-C_{12}	1.453	C_1-C_2	1.421
C_{12}-C_{13}	1.404	C_{12}-C_{13}	1.424	C_2-C_3	1.432
C_{13}-C_{14}	1.376	C_{13}-C_{14}	1.355	C_3-C_4	1.328
C_{14}-C_{15}	1.375	C_{14}-C_{15}	1.404	C_4-C_5	1.426
C_{15}-C_{16}	1.367	C_{15}-C_{16}	1.362	C_5-C_6	1.361
C_{16}-C_{17}	1.383	C_{16}-C_{17}	1.416	C_6-C_7	1.419
C_{17}-C_{12}	1.392	C_{17}-C_{12}	1.400	C_7-C_2	1.416

Table 5. Selected interatomic distances (Å) and angles (deg) for the complexes [Cp*M(NO)(η^2-CH_2Ph)-(NCMe)]BF_4 (M = Mo, W).

Atoms	M = Mo	M = W
M—No	1.768(5)	1.767(7)
M—NCMe	2.140(5)	2.105(6)
M—CH_2	2.182(6)	2.175(8)
M—C(ar)	2.389(5)	2.383(7)
M—Cp	2.020(3)	2.021(4)
N—O	1.204(6)	1.220(9)
N—CMe	1.134(7)	1.142(9)
CH_2—C(ar)	1.453(9)	1.468(12)
C—C(ar)	1.355–1.424(10)	1.346–1.437(13)
C—C(Cp)	1.394–1.438(9)	1.397–1.448(12)
NC—Me	1.464(9)	1.452(12)
Cp—Me	1.482–1.532(9)	1.478–1.507(12)
N—M—N	93.3(2)	93.5(3)
CH_2—M—C(ar)	36.7(2)	37.2(3)
M—N—O	171.2(4)	173.1(6)
M—N—CMe	175.6(5)	176.7(6)

Interestingly, the bonding in the cationic complexes appears to be slightly different than that extant in the neutral η^2-benzyl complexes. One specific difference to be noted between the neutral and cationic benzyl complexes is in the bond lengths within the aromatic ring. In the neutral complexes, Cp*M(NO)(η^2-CH_2Ph)X (X = Cl, CH_2SiMe_3), the C—C bond lengths within the benzyl ring are indicative of the existence of delocalized π-electron density within the aromatic ring. Conversely, as shown in Scheme 1, alternation of longer and shorter C—C bonds around the phenyl ring in the cations suggests that the π-electrons are slightly more localized in these species. The localization of electron density that occurs in the cationic species is similar to that previously reported for the $CpMo(CO)_2$(η^3-*p*-xylyl) complex (17), though the differences in C—C bond lengths are much more pronounced in the *p*-xylyl complex (Scheme 1). With the existence of these differences, the benzyl ligands in the cationic complexes are intermediate between η^2 and η^3 in character. This conclusion is substantiated by the fact that the smallest metal–C_{ortho} separations for both of the cationic complexes (Mo—C_{ortho} = 2.83 Å, W—C_{ortho} = 2.86 Å) are still much larger than those expected for a normal M—C single-bond length (~2.4 Å)

(18) but less than the 3.004 Å found in authentic metal-η^2-benzyl linkages (Scheme 1).

Preparation and physical properties of the Cp′M(NO)-(CH_2Ph)(O_2CR) complexes (R = CH(Et)(Ph))

In contrast to the halide abstraction effected with a silver salt containing the weakly coordinating BF_4^- anion (eq. [2]), the reactions of the benzyl chloro complexes with a racemic mixture of a chiral silver carboxylate produce neutral carboxylate complexes (eq. [3]) as a mixture of two diastereomeric pairs of enantiomers (*R,S/S,R* and *R,R/S,S*).

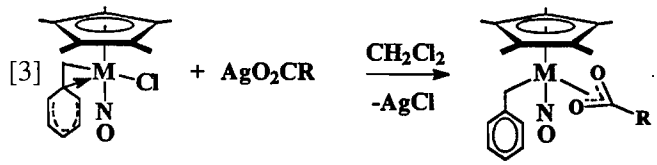

R = CH(Et)(Ph)

It is interesting to note that coordination of the three-electron-donor carboxylate anions causes the benzyl ligands to change their coordination modes from η^2 to η^1. The physical properties of the carboxylate complexes (Tables 1 and 2) are consistent with their possessing the molecular structures shown in eq. [3]. They are thermally stable in solutions, no change in the ^1H NMR spectra of $CDCl_3$ solutions of these complexes being evident after storage at room temperatures for several days. As solids, the complexes can also be transferred and weighed in air with no noticeable decomposition occurring. The slight solubility of the complexes in aliphatic solvents, as well as their ready solubility in aromatic solvents, are features consistent with the formulation of their possessing covalently bonded carboxylate ligands. Finally, the highest *m/z* features in the low-resolution mass spectra of all three complexes may be assigned to the monomeric $[Cp'M(NO)(CH_2Ph)(O_2CR)]^+$ mass ions.

The inherent asymmetry of $Cp'M(NO)(\eta^2\text{-}CH_2Ph)Cl$ and related complexes could make them potentially very useful reagents or catalysts for organic synthesis. However, to realize this synthetic potential, the compounds must be made enantiomerically pure. The reaction of the benzyl chloro complexes with chiral silver carboxylate reagents discussed in the preceding paragraph is one possible means of resolving the racemic mixtures of the starting materials. The utility of the diastereomeric $Cp'M(NO)(\eta^1\text{-}CH_2Ph)(\eta^2\text{-}O_2CR)$ complexes for this purpose is the subject of ongoing research, the initial results of which indicate that resolution of the Cp* complexes may be more easily achieved than that of the Cp complexes. Silver carboxylates are the reagents of choice since optically active carboxylic acids can be readily obtained, either commercially or by established resolution procedures (19), and silver carboxylates are easily prepared from these acids (20).

In summary, this work has afforded new types of benzyl nitrosyl complexes, which demonstrate that even though a dihapto benzyl ligand exerts a more pronounced stabilizing effect at a cationic metal centre than at a neutral one, the electronic stabilization is not so great that its hapticity cannot be reduced from η^2 to η^1 under appropriate experimental conditions. Our studies with these interesting molecules are continuing.

Can. J. Chem. Downloaded from www.nrcresearchpress.com by 80.90.12.36 on 09/08/12
For personal use only.

Acknowledgement

We are grateful to the Natural Sciences and Engineering Research Council of Canada for support of this work in the form of grants to P.L. and J.T. and a postgraduate scholarship to N.H.D.

References

1. J.P. Collman, L.S. Hegedus, J.R. Norton, and R.G. Finke. Principles and applications of organotransition metal chemistry. University Science Books, Mill Valley, Calif. 1987. Chaps. 3 and 14.
2. F.R. Hartley and S. Patai (*Editors*). The chemistry of the metal–carbon bond. Vol. 2. Wiley, New York. 1985.
3. P. Legzdins and J.E. Veltheer. Acc. Chem. Res. **26**, 41 (1993).
4. J.D. Debad, P. Legzdins, R.J. Batchelor, and F.W.B. Einstein. Organometallics, **11**, 6 (1992).
5. J.D. Debad, P. Legzdins, S.J. Rettig, and J.E. Veltheer. Organometallics, **12**, 2714 (1993).
6. J.D. Debad, P. Legzdins, R.J. Batchelor, and F.W.B. Einstein. Organometallics, **12**, 2094 (1993).
7. (*a*) N.H. Dryden, P. Legzdins, E.C. Phillips, J. Trotter, and V.C. Yee. Organometallics, **9**, 882 (1990); (*b*) P. Legzdins, R.H. Jones, E.C. Phillips, V.C. Yee, J. Trotter, and F.W.B. Einstein. Organometallics, **10**, 986 (1991); (*c*) N.H. Dryden, P. Legzdins, J. Trotter, and V.C. Yee. Organometallics, **10**, 2857 (1991).
8. N.H. Dryden, P. Legzdins, P.J. Lundmark, A. Reisen, and F.W.B. Einstein. Organometallics, **12**, 2085 (1993).
9. (*a*) A.S. Guram, Z. Guo, and R.F. Jordan. J. Am. Chem. Soc. **115**, 4902 (1993), and references cited therein; (*b*) X. Yang, C.L. Stern, and T.J. Marks. Angew. Chem. Int. Ed. Engl. **31**, 1375 (1992), and references cited therein; (*c*) T.S. Peng, J. Pu, and J.A. Gladysz. Organometallics, **13**, 929 (1994), and references cited therein.
10. (*a*) D.F. Shriver and M.A. Drezdzon. The manipulation of air-sensitive compounds. 2nd ed. Wiley–Interscience, New York. 1986; (*b*) A.L. Wayda and M.Y. Darensbourg. Experimental organometallic chemistry; a practicum in synthesis and characterization. ACS Symp. Ser. **357**, American Chemical Society, Washington, D.C. 1987.
11. N.H. Dryden, P. Legzdins, S.J. Rettig, and J.E. Veltheer. Organometallics, **11**, 2583 (1992).
12. P. Coppens, L. Leiserowitz, and D. Rabinovich. Acta Crystallogr. **18**, 1035 (1965).
13. W.R. Busing and H.A. Levy. Acta Crystallogr. **22**, 457 (1967).
14. International tables for X-ray crystallography. Vol IV. Kynoch Press, Birmingham, England. 1974. Tables 2.2B and 2.3.1.
15. P. Legzdins, S.J. Rettig, S.F. Sayers. J. Am. Chem. Soc. **116**, 12 105 (1994).
16. N. Brunet, J.D. Debad, P. Legzdins, J. Trotter, J.E. Veltheer, and V.C. Yee. Organometallics, **12**, 4572 (1993), and references cited therein.
17. F.A. Cotton and M.D. LaPrade. J. Am. Chem. Soc. **90**, 5418 (1968).
18. M.D. Curtis, K.B. Shiu, and W.M. Butler. J. Am. Chem. Soc. **108**, 1550 (1986), and references therein.
19. P.A. Levene, L.A. Mikeska, and K. Passoth. J. Biol. Chem. **88**, 27 (1930).
20. C.V. Wilson. Org. React. **9**, 332 (1957).
21. J.B. Milne. Can. J. Chem. **48**, 75 (1970).
22. B.N. Storhoff and C.L. Juntley. Coord. Chem. Rev. **23**, 1 (1977).
23. K. Nakamoto. Infrared and Raman spectra of inorganic and coordination compounds. 4th ed. Wiley, New York. 1986. p. 232.
24. H. Kessler, M. Gehrke, and C. Griesinger. Angew. Chem. Int. Ed. Engl. **27**, 490 (1988), and references cited therein.

Synthesis and structural characterization of an ether-bridged cobalta-bis(dicarbollide): a model for Venus flytrap cluster reagents

David E. Harwell, Juliet Nabakka, Carolyn B. Knobler, and M. Frederick Hawthorne

Abstract: The synthesis of bis-(1-carboranylmethyl) ether was first published in 1963; however, its subsequent complexation with a transition metal was never reported. We now report the complexation of cobalt and the corresponding X-ray structure for the triphenylmethylphosphonium salt of the cobalta-bis(carboranylmethyl) ether. The cobalt complex crystallized in the monoclinic space group $C2/c$ with $a = 21.729(6)$ Å, $b = 9.845(2)$ Å, $c = 35.565(9)$ Å, $\beta = 105.363(9)°$, $V = 7336$ Å^3, and $Z = 8$. Data were collected using CuKα radiation, to a maximum $2\theta = 115°$, giving 4123 unique reflections, and the structure was solved by heavy atom methods. The final discrepancy index was $R = 0.093$, $Rw = 0.100$ for 1919 independent reflections with $I > 3\sigma(I)$. This metala-bis(carboranylalkyl) ether is the first in a new class of Venus flytrap compounds (VFC), containing an ether linkage, to be synthesized as model compounds for the development of reagents suitable for use in the radioimmunodetection and radioimmunotherapy of cancer.

Key words: cobalt, radioimmunodetection, radioimmunotherapy, Venus flytrap.

Résumé : La première synthèse du bis(1-carboranylméthyl)éther a été publié en 1963; toutefois, sa complexation subséquente avec un métal de transition n'a pas encore été rapportée. Dans ce travail, on a réalisé sa complexation avec le cobalt et on rapporte les résultats d'études de diffraction des rayons X sur le sel triphénylméthylphosphonium du cobalta-bis(carboranylméthyl)éther. Les cristaux du complexe de cobalt sont monocliniques, groupe d'espace $C2/c$, avec $a = 21,729(6)$, $b = 9,845(2)$ et $c = 35,565(9)$ Å, $\beta = 105,363(9)°$, $V = 7336$ Å^3 et $Z = 8$. On a obtenu les données (4123 réflexions uniques) en utilisant le rayonnement CuKα, jusqu'à un maximum de $2\theta = 115°$, et on résolu la structure à l'aide de la méthode aux atomes lourds. Les valeurs finales de R et R_w sont respectivement de 0,093 et 0,100 pour 1919 réflexions indépendantes avec $I > 3\sigma(I)$. Ce métala-bis(carboranylalkyl) éther est le premier d'une nouvelle classe de composés dionée gobe mouches, contenant une liaison éther, à être synthétisé comme composé modèle pour le développement de réactifs pouvant être utilisés dans la radioimmunothérapie du cancer.

Mots clés : cobalt, radioimmunodétection, radioimmunothérapie, dionée gobe mouche.

[Traduit par la rédaction]

Introduction

Functionalized Venus flytrap clusters (VFC) have been shown to be useful for binding radiotransition metals to tumor-associated monoclonal antibodies, thus providing conjugates that are clinically useful for radioimmunodiagnosis and radioimmunotherapy (1, 2). Until now the preparation of these compounds has involved tedious reaction schemes culminating in numerous protection and deprotection steps, each step with limited yields. In the past the carboranyl units of the VFC have been linked with alkylene or arylene groups and were derived by direct attachment of the linking group with either the carbon or the boron atoms of the cage (3, 4). This synthetic route has been both challenging and arduous.

Grafstein et al. first reported the synthesis of bis-(1-carboranylmethyl) ether **1** in 1963 (5), and no corresponding metallacarborane derivatives have been previously reported. Compound **1** is easily prepared in high yields, and we subsequently degraded the ether-bridged **1** to the corresponding dianionic species **2**. The salts of **2** are very soluble in tetrahydrofuran and thermally stable, and they may be handled in air for extended periods of time (6, 7).

Results and discussion

Base degradation of **1** with potassium hydroxide in ethanol yielded the corresponding dianionic species **2** in a 67% yield

Received October 21, 1994.

This paper is dedicated to Professor William A.G. Graham on the occasion of his 65th birthday.

D.E. Harwell, J. Nabakka, C.B. Knobler, and M.F. Hawthorne.[1] Department of Chemistry and Biochemistry, University of California at Los Angeles, Los Angeles, CA 90095-1569, U.S.A.

[1] Author to whom correspondence may be addressed. Telephone: (310) 825-7378. Fax: (310) 825-5490. E-mail: mfh@argon.chem.ucla.edu

Can. J. Chem. Downloaded from www.nrcresearchpress.com by 80.90.12.36 on 09/08/12
For personal use only.

Scheme 1. i. (*a*) KOH, EtOH (*b*) Bu_4NBr; ii. NaH/THF; iii. $CoCl_2$; iv. PPh_3MeBr. A similar scheme for the *meso* isomer also exists.

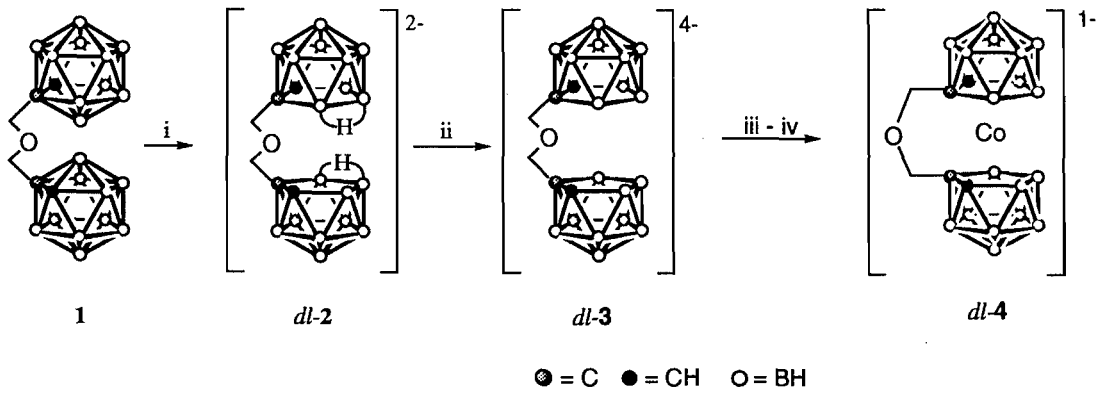

(see Scheme 1). The ^1H NMR spectrum of compound **2** exhibited two sets of peaks for the α-methylene unit of the ether bridge, presumably due to the presence of both *dl* and *meso* isomers. One isomer exhibited a doublet of doublets due to the enantiotopic nature of the α-methylene protons, while the other isomer exhibited only a singlet, indicating the magnetic equivalence of its α-methylene protons. Attempts to separate the isomers by chromatographic methods were unsuccessful and, therefore, resonances due to a specific isomer could not be definitively assigned. The ^{11}B and ^{13}C NMR spectra of **2** were as expected and no spectral differences between the isomers were observed. Treatment of **2** with excess NaH in THF afforded the desired bridged dicarbollide anion **3**. Filtration followed by the addition of anhydrous cobaltous chloride resulted in the cobaltacarborane **4**, which was isolated in 65% yield. *dl* and *meso* isomers are possible, and evidence for both is seen in the ^1H NMR spectra. However, the crystal that was separated from the mixture for X-ray diffraction study contained only the *dl* isomers. The ^{11}B NMR spectrum of **4** exhibited a group of peaks in a 1:1:3:1:1:1:1 ratio consistent with a *commo*-carborane.

Previous studies involving alkylene bridges have indicated an optimal bridge length of four methylene units for metal complexation (3); however, the bite-size of the 2-oxapropylene-bridged VFC, with only three atoms in the linking group, seems to have no such limitation. This is conceivably due to increased flexibility in the linking group afforded by the oxygen in the ether linkage. There is no interaction between the oxygen atom in the bridge and the cobalt atom, as is apparent in the X-ray crystal structure (see Fig. 1). The oxygen does not attain the optimal conformation required for proper molecular overlap and is observed to be 3.14 Å from the cobalt atom, precluding any bonding interaction.

We predict that coordination between the oxygen center and the metal atom will occur in VFC ethers that contain longer bridging units containing more methylene units, thereby enabling the oxygen to obtain such an optimal geometry. Indirect evidence supporting this type of coordination was observed in the case of $[7,7'\text{-}\mu\text{-}TosN(CH_2CH_2\text{-})_2(7,8\text{-}C_2B_9H_{10})_2]^{2-}$. The ligand, which contains a bridging nitrogen, formed complexes with cobalt in higher yields than its corresponding alkylene-linked counterpart. It is suspected that the interaction of the lone pair of electrons on the bridge nitrogen of the ligand provided a favorable chelation effect (3).

The molecular structure of **4** is presented in Fig. 1. Instrument parameters, crystal data, and data collection parameters are summarized in Table 1, while Table 2 lists individual atomic coordinates and their respective thermal parameters. Selected interatomic distances and angles are given in Table 3. Tables containing observed and calculated structure factors, hydrogen atom parameters, and torsion angles have been deposited.[2] The cobalt atom is bound in the η^5-fashion to the five-membered face of each of the two dicarbollide ligands. The distance of the cobalt atom to each mean plane of the dicarbollide cage faces is 1.49 Å, comparable to other cobaltacarboranes (8). Each of the bonding faces of the dicarbollide moieties is planar to within 0.04(1) Å. The two faces are staggered rather than eclipsed. The angle between the normals of these two faces is 6.4°.

The two icosohedra that share the cobalt atom as a common apex in **4** are further linked by a $\text{-}CH_2OCH_2\text{-}$ bridge that spans from C(1) to C(1′). The oxygen atom in the bridge is 3.14 Å away from the cobalt atom, precluding it from any chelation interaction.

A one-electron reduction consistent with Co(III/II) at −1.27 V vs. Ag/AgCl was observed for compound **4**. A plot of $v^{1/2}$ vs. i is linear, indicating electrochemical reversibility for the process.

Experimental

General considerations

Bis-(1-carboranylmethyl) ether was prepared according to literature methods (5, 9). Standard glovebox, Schlenk, and vacuum line techniques were employed for all manipulations of air- and moisture-sensitive compounds.

Reaction solvents were reagent grade and were distilled from appropriate drying agents under nitrogen prior to use. Tetrahydrofuran and toluene were distilled from sodium ben-

2 Supplementary material mentioned in the text may be purchased from: The Depository of Unpublished Data, Document Delivery, CISTI, National Research Council Canada, Ottawa, Canada K1A 0S2.

These data have also been deposited with the Cambridge Crystallographic Data Centre, and can be obtained on request from The Director, Cambridge Crystallographic Data Centre, University Chemical Laboratory, 12 Union Road, Cambridge, CB2 1EZ, U.K.

Can. J. Chem. Downloaded from www.nrcresearchpress.com by 80.90.12.36 on 09/08/12
For personal use only.

Fig. 1. ORTEP representation of *dl*-**4**, showing the numbering scheme. All hydrogens were removed for clarity. Ellipsoids were drawn at the 0.50 probability level.

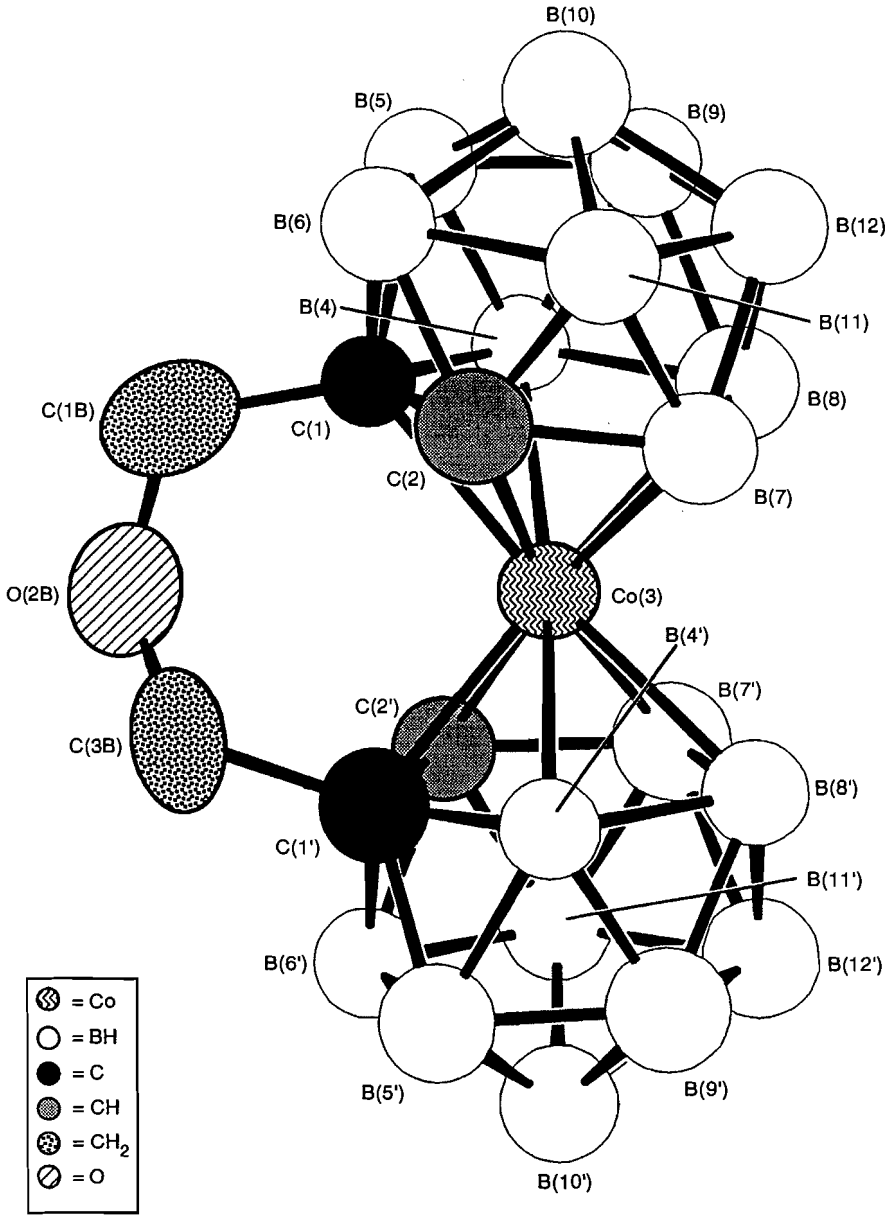

zophenone ketyl; ethyl sulfide was distilled from lithium aluminum hydride. Deuterated solvents were obtained from Cambridge Isotope Laboratories Inc., Knoxville, Tenn. Sodium hydride (Aldrich) was used as received. Cobalt chloride (Cerac) was obtained in argon-filled vessels and was used without further purification. Bis-(1-carboranylmethyl) ether **1** was prepared according to literature methods (5, 9).

Physical measurements

Proton (^{1}H NMR) spectra were obtained on a Brucker AF 200 instrument at 200.133 MHz. Carbon (^{13}C NMR) spectra were obtained on a Brucker AM 400 instrument at 100.625 MHz. Boron (^{11}B NMR) spectra were obtained at 160.46 MHz on a Brucker AM 500 spectrometer. Chemical shifts for ^{1}H and ^{13}C NMR spectra were referenced to $SiMe_4$ (0.00 ppm) and measured with respect to residual protons in deuterated solvents. Chemical shift values for ^{11}B spectra were referenced relative to external $BF_3{\cdot}OEt_2$ (0.00 ppm). Resonances observed upfield of the reference compounds were obtained as Nujol mulls and were recorded on a Nicolet 205 FT-IR instrument. Negative FAB mass spectra were obtained from the UCR Mass Spectrometry Facility at University of California, Riverside. Cyclic voltammetry was performed with a CV-27 cyclic voltammograph from Bioanalytical Systems Inc. All electrochemical measurements were carried out at room temperature under a nitrogen atmosphere with CH_3CN solutions of the complex in 0.1 M Et_4NPF_6 as a supporting electrolyte. Potentials are referenced to a Ag/AgCl electrode. A glassy carbon electrode and a platinum wire were used as the working electrode and the auxiliary electrode, respectively.

Can. J. Chem. Downloaded from www.nrcresearchpress.com by 80.90.12.36 on 09/08/12
For personal use only.

Can. J. Chem. Downloaded from www.nrcresearchpress.com by 80.90.12.36 on 09/08/12
For personal use only.

Table 1. Crystal data and details of data collection and refinement for *dl*-**4**.

Parameter	Value
Formula	$C_{25}H_{42}B_{18}CoOP$
Formula weight	643.12
Temperature (°C)	25
Crystal size (mm)	0.35 × 0.05 × 0.48
normal to faces	100, 001, 010
Appearance	Orange plate
Radiation (graphite monochromator)	CuKα
Wavelength (Å)	1.5418
Space group	*C2/c*
a (Å)	21.729 (6)
b (Å)	9.845 (2)
c (Å)	35.565 (9)
β (Å)	105.363 (9)
V (Å)	7336
Z	8
Density (g cm^{-3}), calcd.	1.30
μ (cm^{-1})	57.9
Scan width, below $K\alpha_1$	1.3
Scan width, above $K\alpha_2$	1.6
Scan rate (deg min^{-1})	3
No. of unique reflections	4123
No. of observed ($I > 3\sigma(I)$) reflections	1919
2θ max (deg)	115
Data collected	$+h, +k, \pm l$
No. of parameters refined	126 + 54 + 38 (3 blocks)
R	0.093
Rw	0.100
GOF	2.64

Preparation of mixture containing [7,7′-μ-1,3-CH_2OCH_2-(7,8-$C_2B_9H_{11}$)$_2$][(C_4H_9)$_4$N]$_2$ and related isomers (2)

To a solution of potassium hydroxide (1.71g, 30.3 mmol) in ethanol (100 mL) was added **1** (1.01g, 3.03 mmol). The solution was heated at reflux overnight and cooled. Dry Ice was added to the solution until no more precipitate was formed. The potassium carbonate was separated by filtration and washed with ethanol (3 × 50 mL). The filtrates were combined and added to a solution of tetrabutylammonium bromide. The solids were filtered out, dried, and recrystallized from hot water to give **2** in 67% yield (1.94 g, 2.04 mmol), mp >245°C. IR (Nujol, cm^{-1}): 2959 (s), 2926 (s), 2854 (s), 2522 (w), 1460 (m), 1377 (m). ^{1}H NMR ($CDCl_3$): 3.52 (dd, 3.2H, α-CH_2 *dl* or *meso*), 3.44 (s, 0.8H, α-CH_2 *dl* or *meso*), 3.19 (m, 16H, NC-H), 1.94 (s, 2H, Cb C-H), 1.62 (m, 16H, NCC-H), 1.42 (m, 16H, NCCC-H) 0.97 (t, 24H, NCCCC-H). ^{13}C NMR (*d*-acetone): 38.4, 59.4, 24.4, 20.3, 13.8. ^{11}B NMR (acetone): −9.3 (d, 2B), −13.9 (d, 1B), −15.6 (d, 1B), −17.3 (d, 2B), −22.0 (d, 1B), −32.4 (d, 1B), −36.5 (d, 1B).

Preparation of mixture containing [1,1′-μ-1,3-CH_2OCH_2-((3)-1,2-$C_2B_9H_{10}$)$_2$Co][(C_6H_5)$_3$$PCH_3$] and related isomers (4)

To a solution of **2** (1.62 g, 2.04 mmol) in THF (100 mL) was added NaH (0.360 g, 15.0 mmol). The reaction mixture was stirred at reflux overnight and then cooled. The solution was filtered through a glass frit. To the solution was added anhydrous cobaltous chloride (0.265 g, 2.04 mmol). The solution gradually changed from blue to brown over a 12 h period. The solution was refluxed overnight, cooled, and filtered to remove cobalt metal and KCl. After removal of the solvent in vacuo, the residue was dissolved in hot water. The resulting aqueous solution was filtered, and the orange solution was added to an aqueous solution of methyltriphenylphosphonium bromide (1.11 g, 3.12 mmol). The aqueous solution was extracted with methylene chloride, dried over magnesium sulfate, and chromatographed (SiO_2) with methylene chloride without separation of isomers; only the *dl*-isomers were observed. The product was crystallized from a CCl_4–pentane solution to give orange platelets of **4** in 65% yield (853 mg, 1.33 mmol), mp 218°C. IR (Nujol, cm^{-1}): 2953 (s), 2924 (s), 2852 (s), 2553 (w), 1459 (m), 1377 (w), 1114 (w). ^{1}H NMR ($CDCl_3$): 7.70 (m, 15H, Ph), 4.02 (m, 4H, α-CH_2), 3.80 (s, 2H, Cb C-H), 2.89 (d, 3H, J_{PH} = 13.0, PCH_3). ^{13}C NMR ($CDCl_3$): 135.5, 133.0, 130.7, 118.4, 73.8, 10.5. ^{11}B NMR (acetone): 5.3 (d, 1B), 1.1 (d, 1B), −5.8 (d, 3B), −7.7 (d, 1B), −15.2 (d, 1B), −16.6 (d, 1B), −18.1 (d, 1B). High-resolution negative-ion mass spectroscopy calculated mass for $C_6H_{24}{}^{10}B_6{}^{11}B_{12}OCo$ *m/e*: 363.30; observed *m/e*: 363.30.

Collection and reduction of X-ray data for *dl*-4·1/2 CCl_4

An orange crystal, obtained from a CCl_4–pentane solution, was mounted on a fiber and placed on a Syntex $P\bar{1}$ diffractometer modified by Professor C.E. Strouse of this department. Unit cell parameters were determined from a least-squares fit of 27 accurately centered reflections (17.1 < 2θ < 40.2°).

Table 2. Positional parameters and U_{eq} for *dl*-**4**.

Atom	*x*	*y*	*z*	U_{eq} or $\langle u^2 \rangle^a$	
Cl(1)	0.0433(7)	0.2363(21)	0.2255(4)	0.132(4)	
Cl(1′)	−0.0551(8)	0.2420(35)	0.2608(7)	0.326(13)	
Cl(2)	0.0675(6)	0.3398(15)	0.2972(4)	0.200(6)	
Cl(3)	0.0000	0.4873(10)	0.2500	0.313(8)	
Co(3)	0.1891(1)	0.7549(2)	0.1332(1)	0.056(1)	
C(1B)	0.1380(8)	0.6461(19)	0.1997(5)	0.110(7)	
O(2B)	0.1279(6)	0.5301(13)	0.1747(4)	0.116(5)	
C(3B)	0.1856(8)	0.4769(16)	0.1667(5)	0.106(7)	
P	0.1254(1)	0.6554(4)	0.4189(1)	0.061(1)	
C(1S)	0.0042(23)	0.3234(26)	0.2610(11)	0.083(10)	*
C(1)	0.1604(5)	0.7712(14)	0.1837(4)	0.049(4)	*
C(2)	0.2355(6)	0.8017(15)	0.1912(4)	0.082(5)	*
B(4)	0.1180(7)	0.8735(16)	0.1472(5)	0.055(5)	*
B(5)	0.1252(8)	0.9160(18)	0.1952(5)	0.073(6)	*
B(6)	0.2004(8)	0.8590(18)	0.2242(5)	0.076(6)	*
B(7)	0.2516(8)	0.9101(18)	0.1584(5)	0.073(6)	*
B(8)	0.1721(8)	0.9659(19)	0.1293(5)	0.083(6)	*
B(9)	0.1348(8)	1.0367(18)	0.1634(5)	0.070(6)	*
B(10)	0.1876(9)	1.0302(21)	0.2093(6)	0.093(7)	*
B(11)	0.2602(8)	0.9564(19)	0.2068(5)	0.075(6)	*
B(12)	0.2182(8)	1.0659(18)	0.1689(5)	0.076(6)	*
C(1′)	0.1921(6)	0.5462(15)	0.1281(4)	0.070(5)	*
C(2′)	0.1287(6)	0.6147(13)	0.0990(4)	0.059(4)	*
B(4′)	0.2581(7)	0.6262(16)	0.1238(5)	0.059(5)	*
B(5′)	0.2377(8)	0.4624(19)	0.1023(5)	0.080(6)	*
B(6′)	0.1532(8)	0.4589(18)	0.0871(5)	0.069(5)	*
B(7′)	0.1471(8)	0.7395(19)	0.0714(5)	0.078(5)	*
B(8′)	0.2354(7)	0.7546(17)	0.0874(4)	0.063(5)	*
B(9′)	0.2632(8)	0.5926(19)	0.0782(5)	0.088(6)	*
B(10′)	0.1974(8)	0.4858(19)	0.0526(5)	0.081(6)	*
B(11′)	0.1264(7)	0.5804(18)	0.0512(5)	0.069(5)	*
B(12′)	0.1968(8)	0.6689(19)	0.0439(5)	0.082(6)	*
C(12)	0.1409(3)	0.8559(9)	0.4748(2)	0.063(4)	*
C(13)	0.1251(3)	0.9261(9)	0.5050(2)	0.076(4)	*
C(14)	0.0721(3)	0.8864(9)	0.5175(2)	0.082(5)	*
C(15)	0.0350(3)	0.7766(9)	0.4998(2)	0.088(5)	*
C(16)	0.0508(3)	0.7064(9)	0.4696(2)	0.073(4)	*
C(11)	0.1038(3)	0.7460(9)	0.4571(2)	0.054(3)	*
C(22)	0.1089(3)	0.3893(9)	0.4383(2)	0.071(4)	*
C(23)	0.0766(3)	0.2654(9)	0.4345(2)	0.076(4)	*
C(24)	0.0209(3)	0.2469(9)	0.4047(2)	0.071(4)	*
C(25)	−0.0027(3)	0.3523(9)	0.3786(2)	0.078(4)	*
C(26)	0.0296(3)	0.4762(9)	0.3824(2)	0.076(4)	*
C(21)	0.0853(3)	0.4947(9)	0.4122(2)	0.051(4)	*
C(32)	0.0751(4)	0.8768(9)	0.3734(2)	0.065(4)	*
C(33)	0.0618(4)	0.9525(9)	0.3390(2)	0.093(5)	*
C(34)	0.0777(4)	0.9013(9)	0.3062(2)	0.094(5)	*
C(35)	0.1068(4)	0.7743(9)	0.3078(2)	0.091(5)	*
C(36)	0.1201(4)	0.6987(9)	0.3422(2)	0.072(4)	*
C(31)	0.1042(4)	0.7499(9)	0.3750(2)	0.054(3)	*

[a]Units of U_{eq} and $\langle u^2 \rangle$ are angstroms squared. Units of each esd, in parentheses, are those of the least significant digit of the corresponding parameter. * Denotes an atom refined isotropically. U_{eq} defined as:
(1/3)[*U*11(*aaa***a**) + *U*22(*bbb***b**) + *U*33(*ccc***c**) + 2*U*12(*aba***b**cosgam) + 2U13(*aca***c**cosbet) + 2U23(*bcb***c**cosalp)]

Can. J. Chem. Downloaded from www.nrcresearchpress.com by 80.90.12.36 on 09/08/12
For personal use only.

Table 3. Selected bond parameters for *dl*-**4**.

Bond	Distance (Å)	Bond	Distance (Å)
Co(3)—C(1)	2.055(12)	Co(3)—C(2)	2.092(15)
Co(3)—B(4)	2.098(15)	Co(3)—B(7)	2.08(2)
Co(3)—B(8)	2.11(2)	C(1)—C(2)	1.61(2)
C(1)—B(4)	1.71(2)	C(1)—B(5)	1.72(2)
B(5)—B(6)	1.78(2)	C(1)—C(1B)	1.49(2)
C(1B)—O(2B)	1.43(2)	O(2B)—C(3B)	1.46(2)
Atoms	**Angle (deg)**	**Atoms**	**Angle (deg)**
C(1)—Co(3)—C(1′)	100.3(5)	Co(3)—C(1)—C(1B)	118.4(10)
C(1)—C(1B)—O(2B)	115.7(14)	C(1B)—O(2B)—C(3B)	114.3(13)

These dimensions and other parameters, including conditions of data collection, are summarized in Table 1. Data were collected on a Syntex $P\bar{1}$ diffractometer modified by Professor C.E. Strouse of this department, at 25°C in the θ–2θ scan mode. Three intense reflections (4 0 2, 2 0 −8, 1 1 −6) were monitored every 97 reflections to check stability. Intensities of these reflections did not decay during the course of the experiment (99.1 h). Of the 4123 unique reflections measured, 1919 were considered to be observed ($I > 3\sigma(I)$) and were used in the subsequent structure analysis. Data were corrected for Lorentz and polarization effects and for secondary extinction and absorption. Programs used in this work include locally modified versions of the following programs: CARESS (Broach, Coppens, Becker, and Blessing), peak profile analysis, Lorentz and polarization corrections; ORFLS (Busing, Martin, and Levy), structure factor calculation and full-matrix least-squares refinement; ABSCOR, absorption correction based on psiscans; SHELX76 (Sheldrick), a crystal structure package; SHELX86 (Sheldrick), a crystal structure solution package; and ORTEP (Johnson).

Solution and refinement of the structure of 4·1/2 CCl_4

Atoms were located by the use of heavy atom methods. All calculations were performed on a VAX 3100 computer in the J.D. McCullough X-ray Crystallography Laboratory. Cl, Co, O, P, and methylene C atoms were refined with anisotropic parameters. All other nonhydrogen atoms were refined with isotropic parameters. Phenyl carbon atoms were included as members of rigid C_6H_5 groups, C—C = 1.395 Å, angles 120°. All phenyl, methyl, and methylene H were included in calculated positions, C—H = 1.0 Å. H on the carborane ligand were included in located positions. H atoms were assigned isotropic displacement values based approximately on the value for the attached atom. Scattering factors for H were obtained from Stewart et al.(10) and for other atoms were taken from The International Tables for X-ray Crystallography (11). The largest peak on a final difference electron density map was 0.23 e $Å^{-3}$. Final position and thermal parameters for nonhydrogen atoms are given in Table 2. The crystal contains 1/2 molecule of CCl_4 per anion. The CCl_4 is located near a 2-fold axis at x = 0, z = 1/4 and is disordered.

Conclusions

The complex **4** described in this report represents the first in a series of ether-bridged and carbon-linked metallacarboranes to be used as model compounds in the development of radiotransition-metal carriers for the antibody-mediated γ-imaging and β-therapy of tumors (1, 2). We are currently in the process of characterizing other metal (Cu, Ni) complexes of **2**. Results of these studies will be published at a later date. We are also developing other ether-linked VFCs that can be readily functionalized and conjugated with monoclonal antibodies.

Acknowledgment

We thank the National Institutes of Health for support of this research under Grant P01 CA43904-05.

References

1. M.F. Hawthorne, A. Varadarajan, C.B. Knobler, and S. Chakrabarti. J. Am. Chem. Soc. **112**, 5365 (1990).
2. R.J. Paxton, B.G. Beatty, M.F. Hawthorne, A. Varadarajan, L.E. Williams, F.L. Curtis, C.B. Knobler, J.D. Beatty, and J.E. Shively. Proc. Natl. Acad. Sci. U.S.A. **88**, 3387 (1991).
3. F.A. Gomez, S.E. Johnson, C.B. Knobler, and M.F. Hawthorne. Inorg. Chem. **31**, 3558 (1992).
4. A. Varadarajan, S.E. Johnson, F.A. Gomez, S. Chakrabarti, C.B. Knobler, and M.F. Hawthorne. J. Am. Chem. Soc. **114**, 9003 (1992).
5. D. Grafstein, J. Bobinski, J. Dvorak, J.E. Paustian, H.F. Smith, S. Karlan, C. Vogel, and M.M. Fein. Inorg. Chem. **2**, 1125 (1963).
6. R.A. Wiesboeck and M.F. Hawthorne. J. Am. Chem. Soc. **86**, 1642 (1964).
7. M.F. Hawthorne, D.C. Young, P.C. Garrett, D.A. Owen, S.G. Schwerin, F.N. Tebbe, and P.A. Wegner. J. Am. Chem. Soc. **90**, 862 (1968).
8. A. Zalkin, T.E. Hopkins, and D.H. Templeton. Inorg. Chem. **6**, 1911 (1967).
9. J.-P. Guermont and I. Marszak. C. Rend. Hebd. Seances Acad. Sci. **235**, 252 (1952).
10. R.F. Stewart, E.R. Davidson, and W.T. Simpson. J. Chem. Phys. **42**, 3175 (1965).
11. International tables for X-ray crystallography. Vol. IV. Kynoch Press, Birmingham, England. 1974.

Can. J. Chem. Downloaded from www.nrcresearchpress.com by 80.90.12.36 on 09/08/12
For personal use only.

Novel binuclear doubly vinyl-bridged iridium complexes formed by olefinic C—H activation

Helmut Werner, Justin Wolf, Angelika Nessel, Arno Fries, Bernd Stempfle, and Oliver Nürnberg

Abstract: Treatment of $[C_5H_5IrX_2]_n$ (**2**: X = Cl; **3**: X = Br) with $CH_2{=}CHtBu$ in the presence of Na_2CO_3–iPrOH gives, besides the bis(olefin) complex $[C_5H_5Ir(CH_2{=}CHtBu)_2]$ (**4**), the doubly vinyl-bridged iridium(II) compound $\{[C_5H_5Ir(\mu\text{-}\eta^1,\eta^2\text{-}CH{=}CHtBu)]_2\}$ (**5**). The related binuclear complex $\{[CH_2(C_5H_4)_2][Ir_2(\mu\text{-}\eta^1,\eta^2\text{-}CH{=}CHtBu)_2]\}$ (**9**) was obtained from $\{[CH_2(C_5H_4)_2][IrBr_2]_2\}_n$ (**8**) and $CH_2{=}CHtBu$–Na_2CO_3 in ethanol and characterized by an X-ray structure analysis (monoclinic, *C2/c* (No. 15), $a = 20.050(8)$, $b = 8.843(1)$, $c = 24.25(1)$ Å, $\beta = 99.53(2)°$, $V = 4241$ Å^3, $Z = 8$, $R = 0.032$, $R_w = 0.041$). Protonation of both **5** and **9** with $HBF_4{\cdot}OEt_2$ yields the BF_4 salts of the unsymmetrical hydridometal cations **10** and **11** in which the vinyl bridges are still intact. The reaction of the binuclear bis(cyclooctene)metal compounds $\{[CH_2(C_5H_4)_2][Rh(C_8H_{14})_2]_2\}$ (**14**) and $\{[CH_2(C_5H_4)_2][Rh(C_8H_{14})_2][Ir(C_8H_{14})_2]\}$ (**17**) with bromine yields almost quantitatively the polymeric (or oligomeric) dibromo derivatives **16** and **18**, which could, however, not be converted to vinyl-bridged complexes by treatment with $CH_2{=}CHtBu$–Na_2CO_3–ROH.

Key words: iridium complexes, C-H activation, bridging vinyl ligands, cationic hydridometal complexes, heterometallic complex.

Résumé : Le traitement du $[C_5H_5IrX_2]_n$ (**2** : X = Cl; **3** : X = Br) avec du $CH_2{=}CHtBu$ en présence de Na_2CO_3–iPrOH conduit, en plus du complexe bis(oléfinique) $[C_5H_5Ir(CH_2{=}CHtBu)_2]$ (**4**), le composé de l'iridium à double pont vinyle $\{[C_5H_5Ir(\mu\text{-}\eta^1,\eta^2\text{-}CH{=}CHtBu)]_2\}$ (**5**). On a obtenu le complexe binucléaire apparenté $\{[CH_2(C_5H_4)_2][Ir_2(\mu\text{-}\eta^1,\eta^2\text{-}CH{=}CHtBu)_2]\}$ (**9**) par réaction du $\{[CH_2(C_5H_4)_2][IrBr_2]_2\}_n$ (**8**) avec du $CH_2{=}CHtBu$–Na_2CO_3 dans l'éthanol et on l'a caractérisé par diffraction des rayons X (monoclinique, groupe d'espace *C2/c* (No. 15), avec $a = 20{,}050(8)$, $b = 8{,}843(1)$, et $c = 24{,}25(1)$ Å, $\beta = 99{,}53(2)°$, $V = 4241$ Å^3, $Z = 8$, $R = 0{,}032$, et $R_w = 0{,}041$). La protonation des composés **5** et **9** par du $HBF_4{\cdot}OEt_2$ conduit aux sels de BF_4 des cations hydridométalliques non symétriques **10** et **11** dans lesquels les ponts vinyles sont encore intacts. La réaction du brome avec les composés binucléaires bis(cyclooctène)métal $\{[CH_2(C_5H_4)_2][Rh(C_8H_{14})_2]_2\}$ (**14**) et $\{[CH_2(C_5H_4)_2][Rh(C_8H_{14})_2][Ir(C_8H_{14})_2]\}$ (**17**) fournit presque quantitativement les dérivés dibromés polymériques (ou oligomériques) **16** et **18** que l'on ne peut malheureusement pas transformé en complexes avec pont vinylique par traitement avec du $CH_2{=}CHtBu$–Na_2CO_3–ROH.

Mots clés : complexes d'iridium, activation du C-H, ponts coordinats vinyliques, complexes cationiques hydridométalliques, complexes hétérométalliques.

[Traduit par la rédaction]

Introduction

In the general context of transition-metal-mediated C-H activation, there has been recent interest in the formation of vinyl-metal complexes from olefinic substrates (1). Bergman and Stoutland originally reported in 1985 (2) that the 16-electron fragment $[(C_5Me_5)Ir(PMe_3)]$, which is generated either on photolysis of $[(C_5Me_5)IrH_2(PMe_3)]$ or thermolysis of $[(C_5Me_5)IrH(C_6H_{11})(PMe_3)]$, reacts with ethene to afford not only the expected olefin derivative $[(C_5Me_5)Ir(C_2H_4)(PMe_3)]$ but also the hydrido(vinyl) complex $[(C_5Me_5)IrH(CH{=}CH_2)(PMe_3)]$. The latter, on heating to ca. 180°C, rearranges to give the thermodynamically more stable isomer $[(C_5Me_5)Ir(C_2H_4)(PMe_3)]$. A clear case in which the stability order $[L_nM(C_2H_4)] > [L_nMH(CH{=}CH_2)]$ is reversed was observed by Graham et al. (3) who found that the iridium compound $[(\eta^2\text{-}HBPf_3)Ir(CO)(C_2H_4)]$ (where $HBPf_3^-$ is the tris(3-(trifluoromethyl)-5-methylpyrazol-1-yl)borato anion) reacts in cyclohexane at 100°C to yield almost quantitatively the isomeric hydrido(vinyl)metal complex. The important role of the formally "innocent" ligands L for the conversion of $M(C_2H_4)$ to $MH(CH{=}CH_2)$ units has also become evident from work in our laboratory on the rearrangement of *trans*-$[IrCl(C_2H_4)$-

Received November 25, 1994.

This paper is dedicated to Professor William A.G. Graham, a pioneer in modern organometallic chemistry and an old friend, on the occasion of his 65th birthday.

H. Werner,[1] **J. Wolf, A. Nessel, A. Fries, B. Stempfle, and O. Nürnberg.** Institut für Anorganische Chemie der Universität, Am Hubland, D-97074 Würzburg, Germany.

[1] Author to whom correspondence may be addressed. Telephone: +49-931-888-5261. Fax: +49-931-888-4605.

Can. J. Chem. Downloaded from www.nrcresearchpress.com by 80.90.12.36 on 09/08/12
For personal use only.

Can. J. Chem. Downloaded from www.nrcresearchpress.com by 80.90.12.36 on 09/08/12
For personal use only.

$(PR_3)_2]$ to $[IrHCl(CH{=}CH_2)(PR_3)_2]$ where the equilibrium between the two isomers is strongly influenced by the nature of the coordinated phosphine (4).

The aim of the present work was to find out whether dihalogenoiridium(III) compounds such as $[C_5H_5IrX_2]_n$ (X = Cl, Br), on treatment with $CH_2{=}CHR$ in the presence of Na_2CO_3–ROH, would afford olefin (possibly hydrido(vinyl)) complexes or, by base-induced fragmentation of the alcohol, would give carbonyl(hydrido)metal derivatives. It was previously shown (5) that $[(mes)OsCl_2]_n$ (mes = 1,3,5-$C_6H_3Me_3$) reacts with ethene and Na_2CO_3–EtOH to form $[(mes)Os(C_2H_4)_2]$ whereas, if C_2H_4 is replaced by $CH_2{=}CHtBu$, the carbonyl(hydrido)methyl complex $[(mes)OsH(CH_3)(CO)]$ is isolated (6). It should furthermore be noted that $[(C_5Me_5)IrCl_2]_2$ behaves similarly to $[(mes)OsCl_2]_n$ and, on treatment with C_2H_4 and Na_2CO_3–EtOH, yields the bis(ethene) derivative $[(C_5Me_5)Ir(C_2H_4)_2]$ (7).

In this paper we describe our investigations on the reactivity of dibromo and dichloro iridium, rhodium, and mixed iridium–rhodium compounds toward $CH_2{=}CHtBu$ and Na_2CO_3–ROH, and in particular the structure and properties of some novel binuclear doubly vinyl-bridged iridium species. Some preliminary results of this work have already been communicated (8).

Results and discussion

In contrast to the behaviour of $[(mes)OsCl_2]_n$ (6), the reaction of $[C_5H_5IrX_2]_n$ (**2**, **3**) with 3,3-dimethyl-1-butene and Na_2CO_3–EtOH does not give a carbonyl(hydrido) complex but leads to a mixture of products in which, besides $[C_5H_5Ir(CH_2{=}CHtBu)_2]$ (**4**), a small amount of the binuclear compound **5** is also present. We note that we observe only one of the two possible isomers of **4**, for which we assume the configuration shown in Scheme 1. Using 2-propanol instead of ethanol, complex **5** (a yellow moderately air-stable solid) is isolated in 30% yield. The proposed structure of **5** is supported by the ^1H as well as the ^{13}C NMR data (for details see experimental section), which unequivocally show the presence of a β-C-substituted vinylic ligand.

A clean reaction occurs between the dibromoiridium(III) species **8** (9) and $CH_2{=}CHtBu$ in the presence of Na_2CO_3–EtOH. Compound **8** as well as the corresponding dichlorometal derivative **7** were prepared from the bis(cyclooctene) complex **6** and bromine or chlorine in hexane–dichloromethane (9:1), respectively. Both compounds **7** and **8** are red air-stable solids and, since they are virtually insoluble in common organic solvents, we assume that they are polymeric (or at least oligomeric) in nature. A structural proposal for **8** is shown in Scheme 2. The reaction of **8** to **9** proceeds in ethanol at 75°C and gives the binuclear product in ca. 60% yield. In contrast to the bis(olefin) complex **6**, the ^1H NMR spectrum of **9** displays four (instead of two) multiplets for the C_5H_4 protons in the intensity ratio of 1:1:1:1, which indicates that there is no plane of symmetry in the molecule passing through the carbon atom of the CH_2 bridging unit and the midpoints of the two five-membered rings. The two doublets of the vinylic protons of **9** appear at δ 9.02 and 2.77 and thus at similar positions as found for **5**. The ^{13}C NMR spectrum of **9** shows, in addition to the signals of the cyclopentadienyl and *tert*-butyl carbon atoms, two resonances at δ 98.7 and 69.6 that according to

Scheme 1.

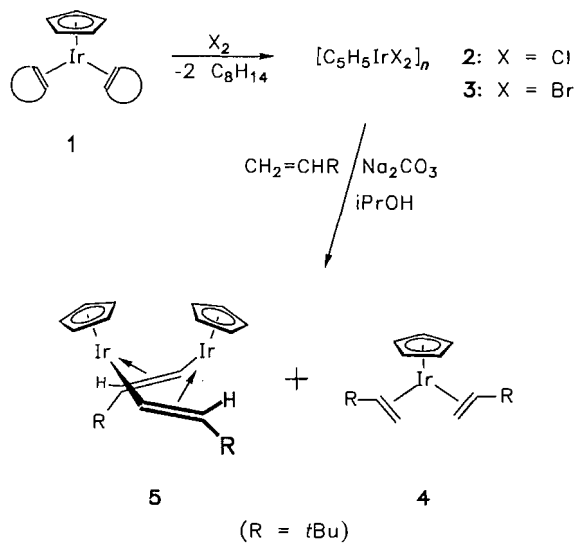

Scheme 2.

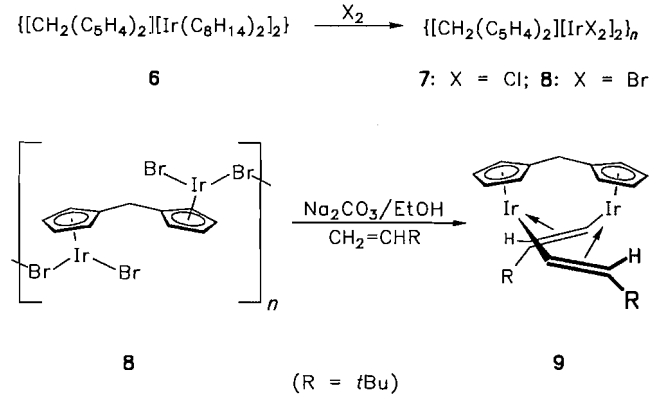

COSY measurements are assigned to the sp^2 C atoms of the vinyl ligands. It should be mentioned that these signals are observed at considerably higher field than in $[C_5H_5IrH(CH{=}CH_2)(C_2H_4)]$ (10), $[C_5H_5IrH(CH{=}CH_2)(CO)]$ (11), and $[(C_5Me_5)IrX(CH{=}CH_2)(PMe_3)]$ (X = H, Br) (2*c*), probably due to the bridging position of the CH=CHR units.

The results of the X-ray structural analysis of compound **9** are shown in Fig. 1. Each vinylic group is coordinated to one metal atom via a σ-bond and to the other via a π-bond and thus behaves as an unsymmetrical bridging ligand. A similar arrangement was found in the binuclear ruthenium complex $\{[C_5H_5(CO)Ru]_2(\mu\text{-}H)(\mu\text{-}CH{=}CHMe)\}$ (12) and the related dirhodium species $\{[(C_9H_6Me)Rh]_2(\mu\text{-}CH{=}CH_2)(\mu\text{-}CMe{=}CHMe)\}$ (13), the latter of which was prepared from $[(C_9H_6Me)Rh(C_2H_4)_2]$ and but-2-yne.

The most noteworthy structural feature of **9** is the Ir—Ir distance of 2.5495(5) Å, which is significantly shorter than an Ir—Ir single bond (2.70–2.75 Å) (14). Although for electronic reasons (both iridium centers are formally in the oxidation state II) such a single bond would be expected, the observed distance is comparable (in fact almost identical) to that of an Ir—Ir double bond (2.55 Å) (15). We assume that the short metal–metal bond length is caused by the strain exerted by the bis(cyclopentadienyl)methane ligand on the rest of the molecule. This strain is reflected in the size of the angle C(17)-

Can. J. Chem. Downloaded from www.nrcresearchpress.com by 80.90.12.36 on 09/08/12
For personal use only.

Table 1. Selected bond distances and angles of **9**.

Bond distances (Å)			
Ir(1)—C(1)	2.098(9)	Ir(2)—C(1)	2.010(9)
Ir(1)—C(2)	2.212(9)	Ir(2)—C(7)	2.137(9)
Ir(1)—C(7)	2.037(9)	Ir(2)—C(8)	2.204(9)
Ir(1)—C(13)	2.16(1)	Ir(2)—C(19)	2.23(1)
Ir(1)—C(14)	2.17(1)	Ir(2)—C(20)	2.16(1)
Ir(1)—C(15)	2.20(1)	Ir(2)—C(21)	2.20(1)
Ir(1)—C(16)	2.23(1)	Ir(2)—C(22)	2.20(1)
Ir(1)—C(17)	2.20(1)	Ir(2)—C(23)	2.25(1)
C(1)—C(2)	1.40(1)	C(7)—C(8)	1.42(1)
C(2)—C(3)	1.55(1)	C(8)—C(9)	1.51(1)
Ir(1)—Ir(2)	2.5495(5)		
Bond angles (deg)			
Ir(1)—C(1)—Ir(2)	76.7(3)	Ir(1)—C(7)—C(8)	126.9(4)
Ir(1)—C(7)—Ir(2)	75.2(3)	Ir(2)—C(1)—C(2)	130.5(4)
Ir(1)—C(1)—C(2)	75.7(4)	Ir(2)—C(7)—C(8)	73.4(3)
Ir(1)—C(2)—C(1)	66.6(3)	Ir(2)—C(8)—C(7)	68.4(3)
Ir(1)—C(2)—C(3)	124.7(4)	Ir(2)—C(8)—C(9)	123.6(4)
C(1)—Ir(1)—C(2)	37.8(4)	C(1)—C(2)—C(3)	124(1)
C(1)—Ir(1)—Ir(2)	50.1(3)	C(7)—C(8)—C(9)	123.1(8)
C(7)—Ir(1)—Ir(2)	54.2(3)	C(1)—Ir(1)—C(7)	83.3(4)
C(1)—Ir(2)—Ir(1)	53.2(3)	C(1)—Ir(2)—C(7)	82.9(4)
C(7)—Ir(2)—Ir(1)	50.6(3)	C(17)—C(18)—C(19)	119.1(9)
C(7)—Ir(2)—C(8)	38.2(3)		

Fig. 1. Molecular structure (SCHAKAL drawing) of compound **9**.

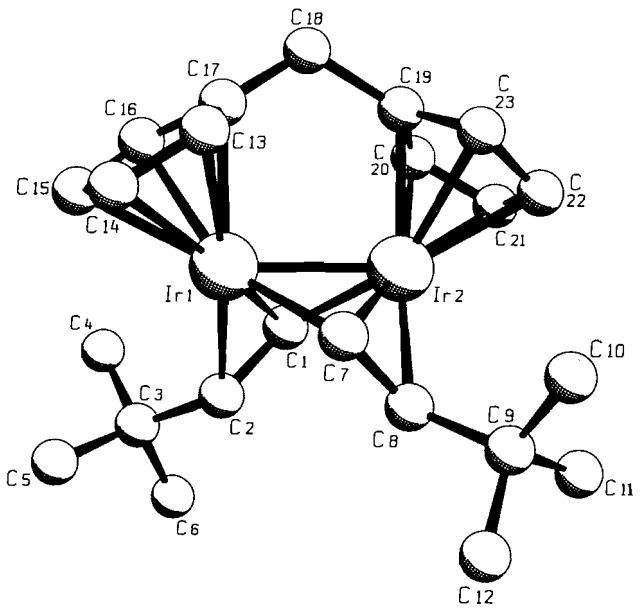

C(18)-C(19) (119.1(9)°), which is about 10° wider than the tetrahedral angle. In the less strained binuclear rhodium complex $\{[CH_2(C_5H_4)_2]Rh_2(CO)_2(\mu\text{-}CO)\}$ (16) and in the analogous mixed-metal Co–Rh compound $\{[CH_2\text{-}(C_5H_4)_2][Rh(CO)][Co(CO)](\mu\text{-}CO)\}$ (17), which in addition to the $[CH_2\text{-}(C_5H_4)_2]^{2-}$ unit contain only one bridging CO ligand, the angle C-CH_2-C is 112.3(4)° and 110.8(3)°, respectively.

While the distances Ir(1)—C(7) and Ir(2)—C(1) (see Table 1) representing the Ir—C σ-bonds correlate quite well with that of the Ir—C(vinyl) bond of $[(C_5Me_5)IrH(CH{=}CH_2)(PMe_3)]$ (2.054(4) Å) (*2c*) and $[IrH(CH{=}CH_2)(acac)(PiPr_3)_2]$ (2.02(1) Å) (18), the bond lengths C(1)—C(2) and C(7)—C(8) are considerably longer than the vinyl C—C distance of the mononuclear iridium compounds. This elongation is certainly due to the π-coordination of the vinylic units. We note that there is an unsymmetrical interaction between the C—C π-bonds and the metal centers, which leads to differences in the Ir—C distances of about 0.12 and 0.07 Å, respectively. A similar effect was observed in vinyl-bridged binuclear ruthenium (12) and trinuclear osmium complexes (19) in which the bond lengths M—C_α are also significantly shorter than M—C_β.

Although the apparent bond strain in the Ir(μ-η^1,η^2-CH=CH*t*Bu)Ir units gives rise to the assumption that the vinyl bridges can be opened by nucleophilic substrates, all attempts to coordinate CO or CNR to one or both of the iridium centers failed. After a solution of **9** in toluene is warmed to 90°C in either a CO atmosphere or the presence of CN*t*Bu, the starting material is recovered almost quantitatively. The inert behaviour of the binuclear iridium complex is remarkable insofar as the related rhodium compound $\{[(C_9H_7)Rh]_2(\mu\text{-}CH{=}CH_2)(\mu\text{-}CMe{=}CHMe)\}$ readily reacts with CO by bridge cleavage to give $[(C_9H_7)Rh(CO)_2]$ and $CH_2{=}CHC(=O)CMe{=}CHMe$ (13).

However, both of the binuclear species **5** and **9** can be protonated by $HBF_4{\cdot}OEt_2$ to form cationic hydridometal derivatives in which the bridging units are still intact. The complexes **10** and **11** (see Scheme 3), which are yellow to orange air-sensitive solids, are isolated in 70–75% yield. For both compounds, correct elemental analyses have been obtained. The ^{1}H NMR spectra of **10** and **11** display, besides the hydride signal at high field, *two* resonances for each of the C*H*= and the =C*H*tBu vinylic protons as well as two resonances for the

Can. J. Chem. Downloaded from www.nrcresearchpress.com by 80.90.12.36 on 09/08/12
For personal use only.

Scheme 3.

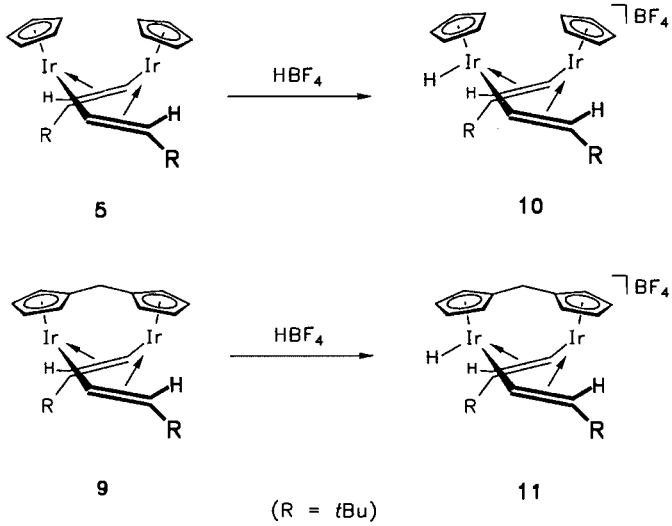

C_5H_5 and four resonances for the C_5H_4 ring protons, which is in agreement with the unsymmetrical structure of the cationic species. Accordingly, also in the ^{13}C NMR spectra of **10** and **11** two signals for each of the *C*H═ and ═*C*H*t*Bu carbons and two signals for the C_5H_5 and *ipso*-*C*(C_5H_4) carbon atoms appear.

With the hope that doubly vinyl-bridged dirhodium and iridium–rhodium compounds analogous in structure to **9** can be obtained via the same route as the diiridium complex, the corresponding dibromometal derivatives were prepared. As outlined in Scheme 4, the crucial initial step is the synthesis of the mono- and binuclear bis(cyclooctene)rhodium compounds **14** and **15**, which are obtained in moderate (**14**) to good (**15**) yield from $[RhCl(C_8H_{14})_2]_2$ and $[C_5H_5CH_2C_5H_4]Na$ (**13**). We note that the formation of *both* mono- and binuclear species containing $[C_5H_5CH_2C_5H_4]^-$ and $[CH_2(C_5H_4)_2]^{2-}$ as ligands from **13** is not unique and has already been observed in the reactions of *trans*-$[RhCl(PhC{\equiv}CPh)(PiPr_3)_2]$ and $[IrCl(C_8H_{14})_2]_2$ with $[C_5H_5CH_2C_5H_4]Na$ (20). The two bis(cyclooctene)rhodium complexes **14** and **15** can be separated by chromatographic techniques and have been characterized both by elemental analysis and NMR spectroscopy.

The synthesis of the mixed-metal compound **17** (Scheme 5) is based on the metalation of the precursor **15** with *n*BuLi at low temperature in hexane followed by treatment of the lithium derivative with $[IrCl(C_8H_{14})_2]_2$ in THF. After chromatographic work-up, the rhodium–iridium complex **17** was isolated in 57% yield. The solid material is thermally remarkably stable and only moderately air-sensitive. In contrast to **14**, in which both C_5H_4 moieties are coordinated to rhodium, an unambiguous assignment of the ring carbon resonances in the ^{13}C NMR spectrum is possible for **17** because those signals which belong to the C_5H_4Rh unit are split into a doublet due to Rh—C coupling.

The reactions of **14** and **17** with bromine proceed almost instantaneously and lead quantitatively to the formation of the dibromometal complexes **16** and **18**. Both are red air-stable solids that, like compound **8**, are insoluble in all common organic solvents. We therefore conclude that they are polymeric in nature, containing bromo bridges between the metal centers. In contrast to **8**, neither **16** nor **18** react with 3,3-dimethylbut-1-ene in the presence of Na_2CO_3–EtOH to give binuclear vinyl-bridged species, and as well, the expected products could not be obtained by using 2-propanol instead of ethanol and NaOH instead of Na_2CO_3 (for comparison, see ref. 21).

Concluding remarks

To the best of our knowledge, compound **9** is the first example of a binuclear iridium complex in which the two iridium centers in the oxidation state II are bridged by three organo groups and in which no terminal ligands such as CO, PR_3, CH_3, or Cl are present. Particularly noteworthy in the synthesis of **9** are the mild conditions for the activation of an olefinic C—H bond in $CH_2{=}CHtBu$ with Na_2CO_3–EtOH, which leads to the formation of a metal-bonded vinylic group. A similar conversion of an olefin $CH_2{=}CHR$ (R = iPr, Ph) to a vinyl ligand CH═CHR in a mononuclear rhenium complex with *t*BuOK as base has recently been described by Peng and Gladysz (22); in that case the positive charge at the metal center presumably supports the cleavage of the C—H bond.

The second remarkable feature of this work is the ease of the protonation that occurs on treatment of **5** and **9** with $HBF_4{\cdot}OEt_2$. The doubly vinyl-bridged compounds thus behave as "metal bases" (23), which is unexpected since no strong donor ligands such as PMe_3 or C_5Me_5 are coordinated to the metal centers. The behaviour of **5** and **9** toward acids is similar to that of the doubly phosphido-bridged complexes $\{[(C_5R_5)M(\mu\text{-}PMe_2)]_2\}$ (M = Co, R = H; M = Rh, R = CH_3) (24) in which the metal is also in the oxidation state II and which equally undergo electrophilic addition reactions without cleavage of the M—M bond.

Experimental

All experiments were carried out under an atmosphere of argon by using standard Schlenk tube techniques. The starting materials $[C_5H_5Ir(C_8H_{14})_2]$ **1** (25), $\{[CH_2(C_5H_4)_2][Ir(C_8H_{14})_2]_2\}$ **6** (9), $\{[CH_2(C_5H_4)_2][IrBr_2]_2\}_n$ **8** (9), $[RhCl(C_8H_{14})_2]_2$ **12** (26), $[C_5H_5CH_2C_5H_4]Na$ **13** (17), and $[IrCl(C_8H_{14})_2]_2$ (27) were prepared as described previously. IR spectra were recorded on a Perkin–Elmer 1420 infrared spectrometer and NMR spectra on a Varian EM 360 L, a Jeol FX 90Q, and Bruker AC 200 and WM 400 instruments. Melting points (dec. temp.) were determined by DTA.

Preparation of $[C_5H_5IrCl_2]_n$ *2*

A solution of **1** (146 mg, 0.31 mmol) in 15 mL of hexane was treated, under continuous stirring, dropwise with a saturated solution of Cl_2 in dichloromethane until the formation of a flocky orange-red precipitate was completed. The solvent was removed, and the precipitate was repeatedly washed with hexane and dried in vacuo. Yield: 83 mg (83%); mp 116°C (dec.). Anal. calcd. for $C_5H_5Cl_2Ir$: C 18.30, H 1.54; found: C 18.63, H 1.64. Due to the low solubility of the orange-red air-stable solid, no reliable NMR spectra could be obtained.

Preparation of $[C_5H_5IrBr_2]_n$ 3

The procedure was analogous to that described for **2**, using **1** and a solution of Br_2 in hexane as starting materials. A dark-red air-stable solid (insoluble in most common organic sol-

Can. J. Chem. Downloaded from www.nrcresearchpress.com by 80.90.12.36 on 09/08/12
For personal use only.

Scheme 4.

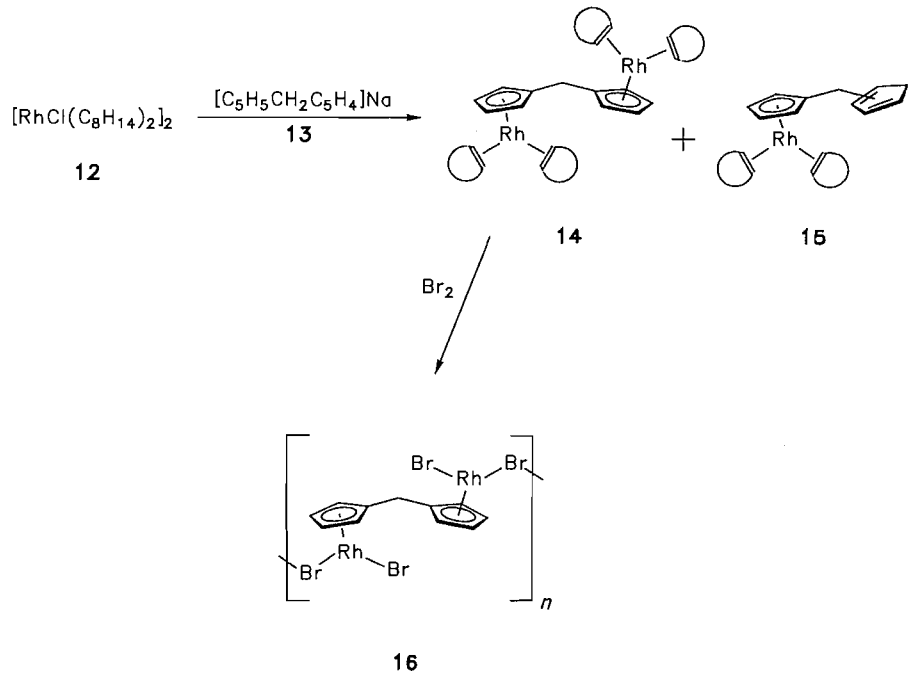

Scheme 5.

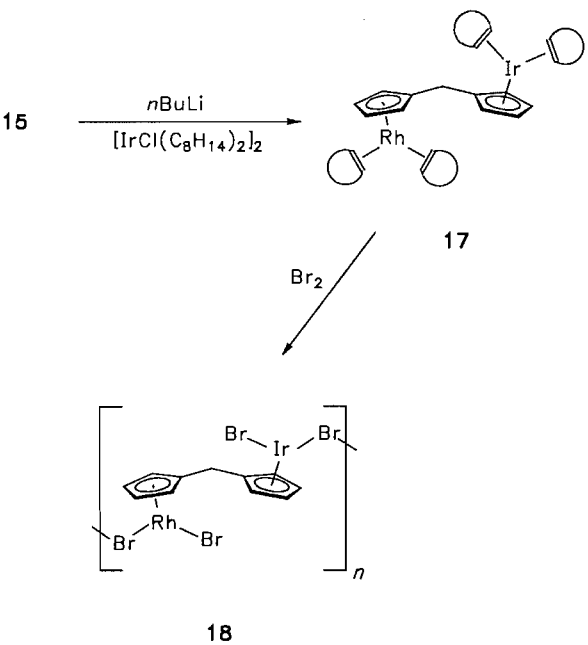

vents) was obtained in about 90% yield. Anal. calcd. for $C_5H_5Br_2Ir$: C 14.40, H 1.21; found: C 14.28, H 1.17.

Preparation of $[C_5H_5Ir(CH_2{=}CHtBu)_2]$ 4 and $\{[C_5H_5Ir(\mu\text{-}\eta^1,\eta^2\text{-}CH{=}CHtBu)]_2\}$ 5

A suspension of **3** (121 mg, 0.15 mmol for $n = 1$) in 10 mL of 2-propanol was treated with $CH_2{=}CHtBu$ (0.4 mL, 3.17 mmol) and excess Na_2CO_3 (ca. 500 mg) and stirred for 3 h at 75°C. After the reaction mixture was cooled to room temperature, the solvent was removed, the residue was extracted with 25 mL of pentane, and the extract was brought to dryness in vacuo. The red-brown oily residue was dissolved in 4 mL of hexane, and the solution was chromatographed on Al_2O_3 (neutral, activity grade V, length of column 20 cm). With hexane, first an orange and then a yellow fraction was eluted. The orange fraction was evaporated in vacuo and the oily residue characterized as **4** by ^1H NMR spectroscopy (see below). The solvent of the yellow fraction was also removed and the residue recrystallized from pentane. After storing at −78°C, yellow moderately air-stable crystals precipitated that were filtered, washed twice with small amounts of pentane (−20°C), and dried. Yield: 30 mg (30%); mp 154°C dec. ^1H NMR (90 MHz, C_6D_6), δ: 8.71 (d, J(HH) = 9.6 Hz, $CH{=}CHtBu$), 5.03 (s, C_5H_5), 2.42 (d, J(HH) = 9.6 Hz, $=CHtBu$), 1.04 (s, CCH_3); ^{13}C NMR (22.5 MHz, C_6D_6), δ: 97.2 (s, $CH{=}CHtBu$), 78.8 (s, C_5H_5), 69.3 (s, $=CHtBu$), 35.2 (s, CCH_3), 31.2 (s, CCH_3). Anal. calcd. for $C_{22}H_{32}Ir_2$: C 38.81, H 4.74; found: C 38.99, H 4.74. ^1H NMR of **4** (60 MHz, C_6D_6), δ: = 4.98 (s, C_5H_5), 2.67 (d J(HH) = 10.6 Hz, H(*cis*) of $CH_2{=}$), 1.56 (d, J(HH) = 8.3 Hz, H(*trans*) of $CH_2{=}$), 0.97 (s, CCH_3), 0.34 (dd, J(HH) = 10.6 and 8.3 Hz, $=CHtBu$).

Preparation of $\{[CH_2(C_5H_4)_2][IrCl_2]_2\}_n$ 7

A solution of **6** (123 mg, 0.13 mmol) in 10 mL of hexane–dichloromethane (9:1) was treated, under continuous stirring, dropwise with a saturated solution of Cl_2 in dichloromethane as described for **2**. An orange-red air-stable solid was obtained. Yield: 73 mg (86%); mp 113°C (dec.). Anal. calcd. for $C_{11}H_{10}Cl_4Ir_2$: C 19.77, H 1.51; found: C 19.89, H 1.68. Due to the low solubility of the compound, no reliable NMR spectra could be obtained.

Preparation of $\{[CH_2(C_5H_4)_2][Ir_2(\mu\text{-}\eta^1,\eta^2\text{-}CH{=}CHtBu)_2]\}$ 9

The procedure was analogous to that described for **5**, using **8** (97 mg, 0.12 mmol for $n = 1$), $CH_2{=}CHtBu$ (0.4 mL, 3.17

Can. J. Chem. Downloaded from www.nrcresearchpress.com by 80.90.12.36 on 09/08/12
For personal use only.

mmol), and Na_2CO_3 (ca. 500 mg) as starting materials and ethanol as solvent. The residue was extracted twice with hexane (10 mL each) and after the solvent was removed a red crystalline solid was obtained. Yield: 49 mg (59%); mp 159°C (dec.). ^{1}H NMR (90 MHz, $CDCl_3$), δ: 9.02 (d, *J*(HH) = 9.8 Hz, C*H*=CH*t*Bu), 5.65, 5.04, 4.10, 3.91 (all m, C_5H_4), 3.90 (m, CH_2), 2.77 (d, *J*(HH) = 9.8 Hz, =C*H*tBu), 1.08 (s, CCH_3); ^{13}C NMR (22.5 MHz, $CDCl_3$), δ: 98.75 (s, *C*H=CH*t*Bu), 95.86 and 95.23 (both s, *ipso*-C of C_5H_4), 85.8, 82.9, 78.85, 77.0 (all s, C_5H_4), 69.7 (s, =*C*H*t*Bu), 34.5 (s, *C*CH_3), 31.4 (s, C*C*H_3), 28.1 (s, *C*H_2). Anal. calcd. for $C_{23}H_{32}Ir_2$: C 39.87, H 4.66; found: C 40.02, H 4.86.

Preparation of $[(C_5H_5)_2Ir_2H(\mu\text{-}\eta^1,\eta^2\text{-}CH{=}CHtBu)_2]BF_4$ 10

A solution of **5** (132 mg, 0.19 mmol) in 5 mL of ether was treated at −78°C with a 54% solution of HBF_4 (26 μL, 0.19 mmol) in ether. While the solution was slowly warmed up to room temperature, a yellow air-sensitive solid precipitated. The solvent was removed, and the precipitate was washed twice with ether (5 mL each) and dried in vacuo. Yield: 106 mg (71%). ^{1}H NMR (400 MHz, CD_3NO_2), δ: 11.02 (d, *J*(HH) = 10.9 Hz, C*H*=CH*t*Bu), 10.67 (d, *J*(HH) = 10.5 Hz, C*H*=CH*t*Bu), 5.99 and 5.92 (both s, C_5H_5), 4.43 (d, *J*(HH) = 10.9 Hz, =C*H*tBu), 3.95 (d, *J*(HH) = 10.5 Hz, =C*H*tBu), 1.11 (s, CCH_3), -21.57 (s, Ir*H*); ^{13}C NMR (100.6 MHz, CD_3NO_2), δ: 103.76 and 102.86 (both s, *C*H=CH*t*Bu), 95.03 and 90.79 (both s, C_5H_5), 85.39 and 84.23 (both s, =*C*H*t*Bu), 39.75 (s, *C*CH_3), 30.12 (s, C*C*H_3). Anal. calcd. for $C_{22}H_{33}BF_4Ir_2$: C 34.37, H 4.33; found: C 35.07, H 4.63.

Preparation of $\{[CH_2(C_5H_4)_2][Ir_2H(\mu\text{-}\eta^1,\eta^2\text{-}CH{=}CHtBu)_2]\}BF_4$ 11

The procedure was analogous to that described for **10**, using **9** (84 mg, 0.12 mmol) and a 54% solution of HBF_4 (16 μL, 0.12 mmol) in ether as starting material. An orange-yellow air-sensitive solid was obtained. Yield: 71 mg (75%); mp 95°C (dec.). ^{1}H NMR (400 MHz, CD_3NO_2), δ: 9.80 (d, *J*(HH) = 10.3 Hz, C*H*=CH*t*Bu), 9.71 (d, *J*(HH) = 11.5 Hz, C*H*=CH*t*Bu), 6.28, 5.80, 5.52, 5.24 (all m, C_5H_4), 4.41 (s, CH_2), 3.37 (d, *J*(HH) = 11.5 Hz, =C*H*tBu), 3.34 (d, *J*(HH) = 10.3 Hz, =C*H*tBu), 0.96 and 0.90 (both s, CCH_3), -16.74 (s, Ir*H*); ^{13}C NMR (100.6 MHz, CD_3NO_2), δ: 110.29 and 108.43 (both s, *C*H=CH*t*Bu), 103.17 and 100.02 (both s, *ipso*-C of C_5H_4), 94.72, 92.57, 85.35, 84.36 (all s, C-2 to C-5 of C_5H_4), 81.90 and 79.95 (both s, =*C*H*t*Bu), 37.47 and 35.23 (both s, *C*CH_3), 30.98 and 30.18 (both s, C*C*H_3), 26.58 (s, *C*H_2). Anal. calcd. for $C_{23}H_{33}BF_4Ir_2$: C 35.38, H 4.26; found: C 35.11, H 4.20.

Preparation of $\{[CH_2(C_5H_4)_2][Rh(C_8H_{14})_2]_2\}$ 14 and $[(C_5H_5CH_2C_5H_4)Rh(C_8H_{14})_2]$ 15

A suspension of **13** (109 mg, 0.66 mmol) in 15 mL of THF was treated at −78°C, under continuous stirring, with a solution of **12** (251 mg, 0.35 mmol) in 10 mL of THF. After the solution was warmed to room temperature, it was stirred for 2 h, then the solvent was removed and the residue was extracted three times with hexane (5 mL each). The combined extracts were concentrated in vacuo to ca. 1 mL and the solution was chromatographed on Al_2O_3 (neutral, activity grade III, length of column 10 cm). With hexane, two yellow fractions were eluted that were brought to dryness in vacuo. From the first fraction, a golden-yellow oil that consisted of the mononuclear complex **15** was isolated. Yield: 174 mg (57%). The second fraction gave a yellow, moderately air-sensitive solid that corresponds to **14**. Yield: 61 mg (24%).

Data for **14**: ^{1}H NMR (200 MHz, C_6D_6), δ: 4.97 (m, H-2 and H-5 of C_5H_4), 4.51 (m, H-3 and H-4 of C_5H_4), 3.49 (s, *C*H_2 of bridge), 2.34 (m, =C*H* of C_8H_{14}), 1.60 and 1.31 (both m, *C*H_2 of C_8H_{14}). Anal. calcd for $C_{43}H_{66}Rh_2$: C 65.47, H 8.43; found: C 65.75, H 8.77.

Data for **15**: ^{1}H NMR (200 MHz, $CDCl_3$), δ: 6.56, 6.40, 6.35, 6.24, 6.14, 5.99 (all m, C*H* of C_5H_5), 4.92 and 4.41 (both vt, *J* = 4.0 Hz, C_5H_4), 3.50 and 3.43 (both m, CH_2 of bridge), 2.85 (m, CH_2 of C_5H_5), 2.30 (m, =C*H* of C_8H_{14}), 1.58 and 1.28 (both m, CH_2 of C_8H_{14}); ^{13}C NMR (50.3 MHz, $CDCl_3$), δ: 148.3 and 146.3 (both s, *ipso*-C of C_5H_5), 135.5, 134.4, 133.1, 128.3, 127.6 (all s, sp^2 C of C_5H_5), 108.3 and 107.4 (both d, *J*(RhC) = 4.0 Hz, *ipso*-C of C_5H_4Rh), 91.00 and 90.05 (both d, *J*(RhC) = 3.7 Hz, C-2 and C-5 of C_5H_4Rh), 88.2 (m, C-3 and C-4 of C_5H_4Rh), 65.1 and 64.2 (both m, =*C*H of C_8H_{14}), 43.6 and 41.9 (both s, *C*H_2 of C_5H_5), 33.4, 33.0, 27.0 (all s, *C*H_2 of C_8H_{14}), 27.05 and 25.3 (both s, *C*H_2 of bridge). Anal. calcd for $C_{27}H_{39}Rh$: C 69.52, H 8.43; found: 70.07, H 8.71.

Preparation of $\{[CH_2(C_5H_4)_2][RhBr_2]_2\}_n$ 16

A solution of **14** (155 mg, 0.20 mmol) in 10 mL of hexane–dichloromethane (9:1) was treated, under continuous stirring, dropwise with a 10% solution of Br_2 in CH_2Cl_2 until the formation of a flocky red precipitate was completed. The work-up procedure was the same as that described for **2**. A red air-stable solid was obtained. Yield: 119 mg (91%); mp 88°C (dec.) Anal. calcd. for $C_{11}H_{10}Br_4Rh_2$: C 19.79, H 1.51; found: C 20.44, H 1.54. Due to the low solubility of the compound, no reliable NMR spectra could be obtained.

Preparation of $\{[CH_2(C_5H_4)_2][Rh(C_8H_{14})_2][Ir(C_8H_{14})_2]\}$ 17

A solution of **15** (173 mg, 0.37 mmol) in 15 mL of hexane was treated, at −78°C, dropwise with a 1.6 M solution (0.23 mL, 0.37 mmol) of *n*BuLi in hexane. After the reaction mixture was warmed to room temperature, it was stirred for 1 h, and then the solvent was removed. The residue was washed twice with hexane and dissolved in 10 mL of THF. The solution was cooled to −78°C and treated with a solution of $[IrCl(C_8H_{14})_2]_2$ (170 mg, 0.19 mmol) in 10 mL of THF. After warming to room temperature, the solution was stirred for 2 h at 25°C and for 1 h at 50°C. It was then brought to room temperature and the solvent was removed. The residue was extracted three times with toluene (5 mL each), the combined extracts were concentrated to ca. 3 mL in vacuo, and the solution was chromatographed on Al_2O_3 (neutral, activity grade V, length of column 15 cm). With ether–hexane (1:5), a yellow fraction was eluted from which a yellow air-stable solid was isolated after removal of the solvent. Yield: 185 mg (57%); mp 203°C (dec.). ^{1}H NMR (400 MHz, C_6D_6), δ: 5.02 (m, H-2 and H-5 of C_5H_4), 4.57 (m, H-3 and H-4 of C_5H_4), 3.63 (s, *C*H_2 of bridge), 2.35 (m, =C*H* of C_8H_{14}), 1.77 and 1.51 (both m, *C*H_2 of C_8H_{14}); ^{13}C NMR (100.6 MHz, C_6D_6), δ: 108.38 (d, *J*(RhC) = 4.1 Hz, *ipso*-C of C_5H_4Rh), 102.69 (s, *ipso*-C of C_5H_4Ir), 91.31 (d, *J*(RhC) = 3.0 Hz, C-2 and C-5 of C_5H_4Rh), 90.69 (s, C-2 and C-5 of C_5H_4Ir), 86.87 (d, *J*(RhC) = 3.7 Hz, C-3 and C-4 of C_5H_4Rh), 86.52 (s, C-3 and C-4 of

Can. J. Chem. Downloaded from www.nrcresearchpress.com by 80.90.12.36 on 09/08/12
For personal use only.

Table 2. Atomic coordinates and thermal parameters of **9**.

Atom	x	y	z	B_{eq}
Ir(1)	0.89688(2)	0.22285(5)	0.64924(2)	2.68(1)
Ir(2)	0.98643(2)	0.16503(5)	0.58892(2)	2.74(1)
C(1)	0.9826(6)	0.078(1)	0.5802(5)	2.8(3)
C(2)	0.8605(6)	−0.003(1)	0.6180(5)	3.9(3)
C(3)	0.7852(5)	−0.052(1)	0.6064(5)	3.4(3)
C(4)	0.7402(6)	0.054(2)	0.5682(7)	5.6(4)
C(5)	0.7590(6)	−0.062(2)	0.6620(6)	7.0(5)
C(6)	0.7843(7)	−0.203(1)	0.5792(8)	7.1(5)
C(7)	0.9867(6)	0.117(1)	0.6753(5)	3.0(3)
C(8)	1.0113(5)	−0.015(1)	0.6517(4)	2.5(2)
C(9)	1.0821(6)	−0.076(1)	0.6699(5)	3.6(3)
C(10)	1.1351(6)	0.044(2)	0.6915(6)	4.7(3)
C(11)	1.1042(6)	−0.161(2)	0.6201(6)	5.4(4)
C(12)	1.0794(7)	−0.190(1)	0.7169(6)	5.3(4)
C(13)	0.9212(7)	0.443(1)	0.6855(5)	4.6(3)
C(14)	0.8695(7)	0.384(1)	0.7092(6)	5.6(3)
C(15)	0.8143(7)	0.368(1)	0.6682(7)	5.7(4)
C(16)	0.8309(7)	0.417(1)	0.6169(6)	5.1(4)
C(17)	0.9000(6)	0.464(1)	0.6271(5)	3.3(3)
C(18)	0.9409(7)	0.519(1)	0.5860(5)	5.1(3)
C(19)	0.9887(6)	0.406(1)	0.5618(5)	3.6(3)
C(20)	0.9706(7)	0.311(1)	0.5164(5)	3.7(3)
C(21)	1.0233(7)	0.215(2)	0.5103(5)	4.9(3)
C(22)	1.0752(8)	0.249(2)	0.5555(6)	5.3(4)
C(23)	1.0536(6)	0.368(1)	0.5871(6)	4.6(3)

C_5H_4Ir), 64.57 and 64.37 (both m, =*C*H of $C_8H_{14}Rh$), 46.20 and 46.12 (both s, =*C*H of $C_8H_{14}Ir$), 33.83, 33.61, 32.86, 26.89, 26.80 (all s, *C*H_2 of C_8H_{14}), 26.50 (s, *C*H_2 of bridge). Anal. calcd. for $C_{43}H_{66}IrRh$: C 58.54, H 7.54; found: C 59.15, H 7.63.

Preparation of $\{[CH_2(C_5H_4)_2][RhBr_2][IrBr_2]\}_n$ 18

The procedure was analogous to that described for **16**, using **17** (141 mg, 0.16 mmol) and a solution of Br_2 in dichloromethane as starting materials. A red air-stable solid was obtained. Yield: 116 mg (96%); mp 114°C (dec.). Anal. calcd. for $C_{11}H_{10}Br_4IrRh$: C 17.45, H 1.33; found: C 17.71, H 1.68. Due to the low solubility of the compound, no reliable NMR spectra could be obtained.

X-ray crystal structure determination of 9

Single crystals were grown from benzene and a crystal of dimensions 0.40×0.35×0.15 mm^3 was used for analysis. Crystal data: monoclinic space group *C*2/*c* (No. 15), $a = 20.050(8)$ Å, $b = 8.843(1)$ Å, $c = 24.25(1)$ Å, $\beta = 99.53(2)°$, $V = 4241$ $Å^3$, $Z = 8$, $d_{calcd} = 2.18$ g cm^{-3}, $d_{exp} = 2.16$ g cm^{-3}. Enraf–Nonius CAD4 diffractometer, Mo-K_α radiation (0.70930 Å), graphite monochromator, zirconium filter (factor 16.55), $T = 293$ K, ω/Θ scan, max. $2\Theta = 40°$; 4458 reflections were measured (only $h + k = 2n$), 4140 independent, 1742 were regarded as being observed ($F_o > 3\sigma(F_o)$); intensity data were corrected for Lorentz and polarization effects, and an empirical absorption correction ($\mu = 62.5$ cm^{-1}, ψ scan method, min. transmission 34%) was applied. The structure was solved by Direct methods (SHELXS86); atomic coordinates (see Table 2) and anisotropic thermal parameters of the non-hydrogen atoms were refined by full-matrix least squares (266 parameters, program packet Enraf–Nonius SDP); hydrogen atoms were calculated for ideal geometry (distance C—H 0.95 Å) and varied according to the riding method. $R = 0.032$, $R_w = 0.041$; reflex/parameter ratio 6.6; residual electron density +0.96/-1.17 $Å^{-3}$. Complete crystallographic data have been deposited as supplementary material.[2]

Acknowledgements

We thank the Deutsche Forschungsgemeinschaft (SFB 347) and the Fonds der Chemischen Industrie for financial support. We also gratefully acknowledge support by Mrs. I. Geiter (experimental assistance), Mrs. A. Burger and Mr. C.P. Kneis (elemental analyses), Mrs. R. Schedl (DTA), Mrs. M.L. Schäfer and Dr. W. Buchner (NMR measurements), and Degussa AG (chemicals).

[2] Crystallographic data and tables of bond distances and angles, least-squares planes, anisotropic displacement parameters, and atomic positional parameters can be purchased from: The Depository of Unpublished Data, Document Delivery, CISTI, National Research Council Canada, Ottawa, ON K1A 0S2, Canada.

These data, with the exception of the anisotropic displacement parameters, have also been deposited with the Cambridge Crystallographic Data Centre, and can be obtained on request from The Director, Cambridge Crystallographic Data Centre, University Chemical Laboratory, 12 Union Road, Cambridge, CB2 1EZ, U.K.

References

1. (*a*) R.G. Bergman. Adv. Chem. **230**, 211 (1992); (*b*) R.N. Perutz. Pure Appl. Chem. **62**, 1103 (1990); (*c*) R.N. Perutz, S.T. Belt, A. McCamley, and M.K. Whittlesey. Pure Appl. Chem. **62**, 1539 (1990); (*d*) T.W. Bell, D.M. Haddleton, A. McCamley, A. Partridge, R.N. Perutz, and H. Willner, J. Am. Chem. Soc. **112**, 9212 (1990); (*e*) A. McCamley, R.N. Perutz, S. Stahl, and H. Werner. Angew. Chem. **101**, 1721 (1989); Angew. Chem. Int. Ed. Engl. **28**, 1690 (1989); (*f*) M.V. Baker, and L.S. Field. J. Am. Chem. Soc. **108**, 7433 (1986); **108**, 7436 (1986).
2. (*a*) P.O. Stoutland, and R.G. Bergman. J. Am. Chem. Soc. **107**, 4581 (1985); (*b*) J. Silvestre, M.J. Calhorda, R. Hoffmann, P.O. Stoutland, and R.G. Bergman. Organometallics, **5**, 1841 (1986); (*c*) J. Am. Chem. Soc. **110**, 5732 (1988).
3. C.K. Ghosh, J.K. Hoyano, R. Krentz, and W.A.G. Graham. J. Am. Chem. Soc. **111**, 5480 (1989).
4. M. Schulz and H. Werner. Organometallics, **11**, 2790 (1992).
5. S. Stahl and H. Werner. Organometallics, **9**, 1876 (1990).
6. S. Stahl and H. Werner. J. Am. Chem. Soc. **113**, 2944 (1991).
7. K. Moseley, J.W. Kang, and P.M. Maitlis. J. Chem. Soc. A, 2875 (1970).
8. A. Nessel, O. Nürnberg, J. Wolf, and H. Werner. Angew. Chem. **103**, 999 (1991); Angew. Chem. Int. Ed. Engl. **30**, 1006 (1991).
9. H. Werner, M. Treiber, A. Nessel, F. Lippert, P. Betz, and C. Krüger. Chem. Ber. **125**, 337 (1992).
10. D.M. Haddleton and R.N. Perutz. J. Chem. Soc. Chem. Commun. 1734 (1986).
11. T.W. Bell, S.-A. Brough, M.G. Partridge, R.N. Perutz, and A.D. Rooney. Organometallics, **12**, 2933 (1993).
12. R.E. Colborn, A.F. Dyke, S.A.R. Knox, K.A. Mead, and P. Woodward. J. Chem. Soc. Dalton Trans. 2099 (1983).
13. P. Caddy, M. Green, L.E. Smart, and N. White. J. Chem. Soc. Chem. Commun. 839 (1978).
14. (*a*) D.M. Heinekey, S.T. Michel, and K.G. Schulte. Organometallics, **8**, 1241 (1989); (*b*) W.D. McGhee and R.G. Bergman. J. Am. Chem. Soc. **110**, 4246 (1988); (*c*) M.D. Rausch, R.G. Gastinger, S.A. Gardner, R.K. Brown, and J.S. Wood. J. Am. Chem. Soc. **99**, 7870 (1977).
15. R.G. Ball, W.A.G. Graham, D.M. Heinekey, J.K. Hoyano, A.D. McMaster, B.M. Mattson, and S.T. Michel. Inorg. Chem. **29**, 2023 (1990).
16. H. Werner, H.J. Scholz, and R. Zolk. Chem. Ber. **118**, 4531 (1985).
17. H. Werner, D. Schneider, and M. Schulz. Chem. Ber. **125**, 1017 (1992).
18. B. Papenfuhs, N. Mahr, and H. Werner. Organometallics, **12**, 4244 (1993).
19. A.D. Clauss, M. Tachikawa, J.R. Shapley, and C.G. Pierpont. Inorg. Chem. **20**, 1528 (1981).
20. D. Schneider and H. Werner. Organometallics, 12, 4420 (1993).
21. U. Wecker, H. Werner, K. Peters, and H.G. von Schnering. Chem. Ber. **127**, 1021 (1994).
22. T.-S. Peng and J.A. Gladysz. Organometallics, **9**, 2884 (1990).
23. (*a*) D.F. Shriver. Acc. Chem. Res. **3**, 231 (1970); (*b*) H. Werner. Angew. Chem. **95**, 932 (1983); Angew. Chem. Int. Ed. Engl. **22**, 927 (1983).
24. (*a*) H. Werner, W. Hofmann, R. Zolk, L.F. Dahl, J. Kocal, and A. Kühn. J. Organomet. Chem. **289**, 173 (1985); (*b*) B. Klingert, and H. Werner. J. Organomet. Chem. **333**, 119 (1987); (*c*) B. Klingert, A.L. Rheingold, and H. Werner. Inorg. Chem. **27**, 1354 (1988).
25. M. Dziallas, A. Höhn, and H. Werner. J. Organomet. Chem. **330**, 207 (1987).
26. A. van der Ent and A.L. Onderdelinden. Inorg. Synth. **14**, 92 (1973).
27. A. L. Onderdelinden and A. van der Ent. Inorg. Chim. Acta, **6**, 420 (1972).

Can. J. Chem. Downloaded from www.nrcresearchpress.com by 80.90.12.36 on 09/08/12
For personal use only.

Alkyne transformations at RhMn centres. Facile conversion between parallel and perpendicular alkyne binding modes and conversions to vinyl groups

Li-Sheng Wang and Martin Cowie

Abstract: The heterobinuclear complex $[RhMn(CO)_4(dppm)_2]$ (**1**) (dppm = $Ph_2PCH_2PPh_2$) reacts with alkynes (RC≡CR; R = CO_2Me (DMAD), CF_3 (HFB)) to yield the alkyne-bridged products $[RhMn(CO)_4(\mu\text{-}RC_2R)(dppm)_2]$ (**3***a*, **3***b*), in which the alkyne binds parallel to the metals. These species lose one carbonyl to yield two isomers in which the bridging alkyne group is either parallel or perpendicular to the Rh–Mn vector (**4** or **5**). Unusually facile interconversion between these two alkyne binding modes occurs. Protonation of the different alkyne-bridged species appears to occur at the metals with subsequent transfer to the alkyne ligand, yielding a series of vinyl complexes. These vinyl complexes are also obtained from the reaction of the hydride-bridged complex $[RhMn(CO)_4(\mu\text{-}H)(dppm)_2][BF_4]$ (**2**) with alkynes. A related vinyl species $[RhMn((CH_3)C{=}CH_2)(CO)_4(dppm)_2][BF_4]$ (**9***a*) is obtained in the reaction of **2** with allene. Also obtained in the allene reaction is the isomeric η^1-allyl complex $[RhMn(\eta^1\text{-}CH_2C(H){=}CH_2)(CO)_4(dppm)_2][BF_4]$ (**9***b*), which converts to **9***a* upon refluxing. The methyl analogues $[RhMnCH_3(CO)_4(dppm)_2][X]$ (X = SO_3CF_3, I) have been characterized and their structural formulations offer support for those of the vinyl species.

Key words: heterobinuclear, alkyne complexes, vinyl complexes.

Résumé : Le complexe hétérobinucléaire $[RhMn(CO)_4(dppm)_2]$ (**1**) (dppm = $Ph_2PCH_2PPh_2$) réagit avec les alcynes (RC≡CR; R = CO_2Me (DMAD), CF_3 (HFB)) pour conduire à des produits avec des ponts alcynes $[RhMn(CO)_4(\mu\text{-}RC_2R)(dppm)_2]$ (**3***a*, **3***b*), dans lesquels l'alcyne se lie d'une façon parallèle avec les métaux. Ces espèces perdent un carbonyle pour donner deux isomères dans lesquels le groupe alcyne agissant comme pont est soit parallèle soit perpendiculaire au vecteur Rh–Mn (**4** or **5**). Il se produit une interconversion inhabituellement facile entre ces deux modes de liaison des alcynes. La protonation de diverses espèces avec ponts alcynes semble se produire au niveau des métaux avec un transfert subséquent vers le coordinat alcyne qui fournit une série de complexes vinyliques. On peut aussi obtenir ces complexes vinyliques par réaction du complexe avec un pont hydrure $[RhMn(CO)_4(\mu\text{-}H)(dppm)_2][BF_4]$ (**2**) avec les alcynes. On obtient une espèce vinylique apparentée $[RhMn((CH_3)C{=}CH_2)(CO)_4(dppm)_2][BF_4]$ (**9***a*) par réaction du composé **2** avec l'allène. Lors de cette réaction, on obtient aussi le complexe η^1-allylique isomère $[RhMn(\eta^1\text{-}CH_2C(H){=}CH_2)(CO)_4(dppm)_2][BF_4]$ (**9***b*), qui se transforme en **9***a* par chauffage au reflux. On a aussi caractérisé les analogues méthylés $[RhMnCH_3(CO)_4(dppm)_2][X]$ (X = SO_3CF_3, I) et leurs formulations structurales offrent un support pour celles des espèces vinyliques.

Mots clés : hétérobinucléaire, complexes alcynes, complexes vinyliques.

[Traduit par la rédaction]

Introduction

The coordination and activation of alkynes at two metal centres and subsequent transformations involving these substrates have attracted considerable attention (see, for example, ref. 1). Our recent interest in such chemistry has been aimed at elucidating the alkyne coordination modes in binuclear systems (2–6) with interest in determining the influence of the different binding modes on the subsequent chemistry. Two types of alkyne transformations, occurring at bimetallic cores, that we have recently been studying involve the conversions to vinyl (7–9) and vinylidene (10–12) ligands. Vinyl complexes can be prepared by the insertion of alkynes into metal–hydrogen bonds — a fundamental process in organometallic chemistry (13), or alternately by protonation of preformed alkyne complexes, or of the tautomeric vinylidene analogues (14).

Our interest in vinyl complexes stems from recent reports in which surface-bound vinyl groups, rather than alkyls, have

Received October 27, 1994.

This paper is dedicated to Professor William A.G. Graham on the occasion of his 65th birthday.

L.-S. Wang and M. Cowie.[1] Department of Chemistry, University of Alberta, Edmonton, AB T6G 2G2, Canada.

[1] Author to whom correspondence may be addressed. Telephone: (403) 492-5581. Fax: (403) 492-8231.

Can. J. Chem. Downloaded from www.nrcresearchpress.com by 80.90.12.36 on 09/08/12
For personal use only.

Can. J. Chem. Downloaded from www.nrcresearchpress.com by 80.90.12.36 on 09/08/12
For personal use only.

been implicated as key species in Fischer–Tropsch synthesis (15). These ideas have been based on the ease of migratory insertions involving vinyl and bridging methylene groups, which occur more readily than for the alkyl analogues (*15b*, 16). The ease of these migratory insertions also suggests applications for vinyl complexes in organic synthesis (17, 18).

In this paper we report alkyne chemistry at adjacent Rh and Mn centres, on the assumption that the tendency of one of these centres (Mn) to maintain a coordinately saturated configuration might lead to subtle differences from analogous species based on dirhodium, diiridium, or rhodium/iridium. In addition, we also report transformations to vinyl complexes based on the conversion of both alkynes and allene.

Experimental section

General procedures

Purified argon and carbon monoxide were obtained from Linde and hydrogen sulfide from Matheson. The 99% carbon-13-enriched carbon monoxide was purchased from Isotec Inc. All gases were used as received. Diethyl ether, hexane, and tetrahydrofuran were dried over Na-benzophenone ketyl, and methylene chloride was dried over P_2O_5. All solvents were distilled under argon before use. The perdeuterated methylene chloride was dried over molecular sieves and deoxygenated by repeated freeze–pump–thaw cycles. The compounds, dimethyl acetylenedicarboxylate (DMAD), tetrafluoroboric acid–diethyl (and dimethyl) etherate, triflic acid, trifluoroacetic acid, and methyl triflate were used as received from Aldrich. Hexafluoro-2-butyne (HFB) was received from PCR Inc., hydrated rhodium trichloride from Johnson Matthey, and $Mn_2(CO)_{10}$ from Strem Chemicals Inc. Compounds $[RhMn(CO)_4(dppm)_2]$ (**1**) (19) and $[RhMn(CO)_4(\mu\text{-}H)(dppm)_2][BF_4]$ (**2**) (20) were prepared by the reported procedures. Reactions were routinely carried out under Schlenk conditions.

All routine NMR experiments were conducted on a Bruker AM-400 spectrometer, whereas the $^{13}C\{^1H\}$ NMR experiments were run on a Bruker AM-200 spectrometer. For all NMR experiments CD_2Cl_2 (except ^2H experiments for which CH_2Cl_2 was used) was used as solvent. IR spectra were recorded on either a Nicolet 7199 Fourier transform interferometer or a Perkin–Elmer 883 spectrophotometer as solids (Nujol mull or CH_2Cl_2 cast) or CH_2Cl_2 solutions. Elemental analyses were performed by the microanalytical service within the department. The spectral data for all compounds are given in Tables 1 and 2. All compounds were moderately air sensitive in solution so were routinely handled under dinitrogen or argon.

Preparation of compounds

*(a) [RhMn(CO)$_3$(μ-DMAD)(μ-CO)(dppm)$_2$] (**3a**).*
To a CH_2Cl_2 solution of $[RhMn(CO)_4(dppm)_2]$ (**1**) (50 mg, 48 μmol in 10 mL under CO) was added 15 μL of DMAD (122 μmol), resulting in an immediate color change from yellow to red. After stirring for 1 h the solvent was reduced to ca. 1 mL by a rapid flow of CO; at that time a red crystalline solid precipitated from solution. The solid was separated from the mother liquor by filtration and was washed with 1 mL of CH_2Cl_2. A red crystalline solid was obtained in 70% yield and was stored under CO. Anal. calcd. for $RhMnP_4O_8C_{60}H_{50}\cdot CH_2Cl_2$: C 57.88, H 4.14, Cl 5.60; found: C 57.79, H 4.16, Cl, 5.66.

*(b) [RhMn(CO)$_3$(μ-HFB)(μ-CO)(dppm)$_2$] (**3b**)*
A CH_2Cl_2 solution of compounds **4***b* and **5***b* (100 mg in 10 mL) was put under CO (10 psi; 1 psi = 6.9 kPa)). The solution was cooled to −78°C and stirred for 1 h. The color of the solution changed to orange from green and an orange solid precipitated out of the solution. Hexane (50 mL) was added to precipitate the solid and the supernatant was removed by canula. The solid was dried by the rapid flow of CO and the solid was stored under CO. The solid was unstable in air toward the loss of CO; therefore the elemental analysis was not attempted.

*(c) [RhMn(CO)$_3$(μ-DMAD)(dppm)$_2$] (**4a**)*
To a THF solution of $[RhMn(CO)_4(dppm)_2]$ (**1**) (50 mg, 48 μmol in 10 mL) was added 8 μL of DMAD (65 μmol). Refluxing for 1 h yielded a black-purple solution. Recrystallization from CH_2Cl_2–hexane gave a black solid in 80% yield. Anal. calcd. for $RhMnP_4O_7C_{49}H_{50}\cdot 0.6\ CH_2Cl_2$: C 59.49, H 4.29, Cl 3.50; found: C 59.15, H 3.76, Cl 3.51. A CH_2Cl_2 solution containing **4***a* could be obtained by dissolving the solid at −78°C.

*(d) [RhMn(CO)$_3$(μ-HFB)(dppm)$_2$] (**4b**)*
Compound **1** (200 mg) was placed in a Schlenk tube (100 mL) and put under vacuum. The tube was filled with hexafluoro-2-butyne and 20 mL of CH_2Cl_2 was added. The solution was stirred for 24 h. Removal of the solvent in vacuo and recrystallization from CH_2Cl_2 (10 mL of Et_2O and 40 mL of hexane) gave a green crystalline solid (80%). Anal. calcd. for $RhMnP_4F_6O_3C_{57}H_{44}$: C 58.36, H 3.75; found: C 57.92, H 3.83. A CH_2Cl_2 solution of **4***b* could be obtained by dissolving the solid at temperatures below 0°C.

*(e) [RhMn(CO)$_3$(μ-η^2:η^2-DMAD)(dppm)$_2$] (**5a**)*
The crystalline solid of compound **4***a* was dissolved in CD_2Cl_2 (5 mg in 0.5 mL) at room temperature. The ^{31}P and ^1H NMR showed the formation of the mixture of compound **5***a* and compound **4***a* in a ratio of about 0.2:1.

*(f) [RhMn(CO)$_3$(μ-η^2:η^2-HFB)(dppm)$_2$] (**5b**)*
The crystalline solid of compound **4***b* was dissolved in CD_2Cl_2 (5 mg in 0.5 mL) at room temperature. After 1 h the ^{31}P and ^1H NMR showed the formation of the mixture of compound **5***b* and compound **4***b* in a ratio of about 0.7:1.

*(g) [RhMn(H)(CO)$_4$(μ-DMAD)(dppm)$_2$][BF$_4$] (**6a**)*
To a CD_2Cl_2 solution of compound **3***a* (3 mg, 2.5 μmol in 0.5 mL, in an NMR tube) at −78°C was added 1 μL of $HBF_4\cdot Et_2O$ (4.8 μmol). The compound was characterized by NMR at −80°C.

*(h) [RhMn(H)(CO)$_4$(μ-HFB)(dppm)$_2$][BF$_4$] (**6b**)*
To a CD_2Cl_2 solution of compound **3***b* (3 mg, 2.5 μmol in 0.5 mL, dissolved at −78°C under 10 psi of CO in an NMR tube) was added 2 μL of $HBF_4\cdot Me_2O$ (16 μmol). The compound was characterized by NMR at −40°C.

*(j) [RhMn(C(COOMe)=CH(COOMe))(CO)$_2$(μ-CO)$_2$(dppm)$_2$][BF$_4$] (**7a**·BF$_4$)*

Method (i): To a CH_2Cl_2 solution of compound **3** (50 mg, 42

Table 1. Spectroscopic data for the compounds.

Compound	IR, cm^{-1} [a]	NMR[a] $\delta(^{31}P\{^1H\})$	NMR[a] $\delta(^1H)$	NMR[a] $\delta(^{13}C)$
$RhMn(CO)_3(\mu\text{-DMAD})(\mu\text{-CO})(dppm)_2$ (**3***a*)	2003(st),[b] 1949(st), 1860(st), 1727(m), 1674(m), 1654(m)	54.7(b),[d] 17.7(dm, $^1J_{RhP}$ = 155 Hz)	4.33(m, 2H, PCH_2P),[d] 3.09(s, 3H, CH_3), 2.93(m, 2H, PCH_2P), 1.65(s, 3H, CH_3)	248.7(dt, $^1J_{RhC}$ = 10 Hz, $^2J_{P(Mn)C}$ = 25 Hz, 1CO)[f], 223.5(t,$^2J_{P(Mn)C}$ = 14 Hz, 1CO), 221.8(t, $^2J_{P(Mn)C}$ = 16 Hz, 1CO), 193.8(dt, $^1J_{RhC}$ = 57 Hz, $^2J_{P(Rh)C}$ = 11 Hz, 1CO)
	1979(m),[c] 1941(vs), 1857(m), 1732(w), 1675(w), 1654(w)			
$RhMn(CO)_3(\mu\text{-HFB})(\mu\text{-CO})(dppm)_2$ (**3***b*)		54.9(b),[e] 13.0(dm, $^1J_{RhP}$ = 144 Hz)	3.98(m, 2H, PCH_2P),[e] 3.14(m, 2H, PCH_2P)	239.5(dt, $^1J_{RhC}$ = 11 Hz, $^2J_{P(Mn)C}$ = 25 Hz, 1CO)[e], 222.3(t,$^2J_{P(Mn)C}$ = 18 Hz, 1CO), 220.8(t, $^2J_{P(Mn)C}$ = 18 Hz, 1CO), 193.5(dt, $^1J_{RhC}$ = 58 Hz, $^2J_{P(Rh)C}$ = 13 Hz, 1CO)
$RhMn(CO)_3(\mu\text{-DMAD})(dppm)_2$ (**4***a*)	1985(st),[b] 1887(st), 1819(vs), 1682(m), 1659(sh)	51.9(m),[d] 19.8(dm, $^1J_{RhP}$ = 124 Hz)	3.75(m, 2H, PCH_2P),[d] 2.93(m, 2H, PCH_2P), 2.65(s, 3H, CH_3), 2.39(s, 3H, CH_3)	239.1(t, $^2J_{P(Mn)C}$ = 32 Hz, 1CO),[d] 232.2(t, $^2J_{P(Mn)C}$ = 16 Hz, 1CO), 189.7(dt, $^1J_{RhC}$ = 58 Hz, $^2J_{P(Rh)C}$ = 15 Hz, 1CO), 175.0(s, 1C, CO_2CH_3), 168.0(s, 1C, CO_2CH_3), 140.9(m, 1C, C=C), 50.3(s, 1C, CH_3), 50.1(s, 1C, CH_3), 22.7(m, 2C,PCH_2P)
	1985(st),[c] 1883(st), 1815(vs), 1672(m), 1652(sh)			
$RhMn(CO)_3(\mu\text{-HFB})(dppm)_2$ (**4***b*)	1997(st),[b] 1987(st), 1896(st), 1827(vs)	46.1(m),[e] 17.3(dm, $^1J_{RhP}$ = 120 Hz)	3.57(b, 2H, PCH_2P),[e] 3.04(m, 2H, PCH_2P)	238.5(t, $^2J_{P(Mn)C}$ = 33 Hz, 1CO),[e] 236.5(t, $^2J_{P(Mn)C}$ = 14 Hz, 1CO), 190.7(dt, $^1J_{RhC}$ = 57 Hz, $^2J_{P(Rh)C}$ = 14 Hz, 1CO)
	2003(st),[c] 1991(sh), 1893(st), 1823(vs)			
$RhMn(CO)_3(\mu\text{-}\eta^2\text{:}\eta^2\text{-DMAD})(dppm)_2$ (**5***a*)		98.9(m),[d] 31.3(dm, $^1J_{RhP}$ = 140 Hz)	3.46(m,4H, PCH_2P),[d] 3.17(s, 6H, CH_3)	242.0(t, $^2J_{P(Mn)C}$ = 48 Hz, 1CO),[d] 225.1(t, $^2J_{P(Mn)C}$ = 38 Hz, 1CO), 194.0(dtt, $^1J_{RhC}$ = 73 Hz, $^2J_{P(Rh)C}$ = 17 Hz,$^2J_{P(Mn)C}$ = 5 Hz, 1CO), 176.0(s, 1C, CO_2CH_3), 51.9(s, 2C, CH_3)
$RhMn(CO)_3(\mu\text{-}\eta^2\text{:}\eta^2\text{-HFB})(dppm)_2$ (**5***b*)		100.0(m),[e] 39.7(dm, $^1J_{RhP}$ = 130 Hz)	3.57(b, 2H, PCH_2P),[e] 2.61(b, 2H, PCH_2P)	243.2(t, $^2J_{P(Mn)C}$ = 46 Hz, 1CO),[d] 225.5(t, $^2J_{P(Mn)C}$ = 44 Hz, 1CO), 192.3(dt, $^1J_{RhC}$ = 73 Hz, $^2J_{P(Rh)C}$ = 15 Hz, 1CO)

Can. J. Chem. Downloaded from www.nrcresearchpress.com by 80.90.12.36 on 09/08/12
For personal use only.

Table 1 (*continued*).

Compound	IR, cm^{-1} [a]	NMR[a] $\delta(^{31}P\{^1H\})$	NMR[a] $\delta(^1H)$	NMR[a] $\delta(^{13}C)$
$[RhMn(H)(CO)_4(\mu\text{-DMAD})(dppm)_2][BF_4]$ (**6***a*)		42.0(m),[h] 18.1(dm, $^1J_{RhP}$ = 104 Hz)	4.11(m,2H, PCH_2P),[h] 3.22(s, 3H, CH_3), 3.17(m, 2H, PCH_2P), 1.90(s, 3H, CH_3), −14.30(dt, $^1J_{RhH}$ = 38 Hz, $^2J_{P(Rh)H}$ = 7 Hz, 1H, hydride)	222.9(b, 1CO),[h] 217.8(b, 1CO), 211.4(b, 1CO), 183.8(db, $^1J_{RhC}$ = 46 Hz, 1CO)
$[RhMn(H)(CO)_4(\mu\text{-HFB})(dppm)_2][BF_4]$ (**6***b*·BF_4)		42.5(b),[e] 15.0(bd, $^1J_{RhP}$ = 98 Hz)	3.87(m,2H, PCH_2P),[e] 3.29(m, 2H, PCH_2P), −12.28(bd, $^1J_{RhH}$ = 34 Hz, 1H, hydride)	222.6(b, 1CO),[e] 221.9(b, 1CO), 211.4(b, 1CO), 183.0(dt, $^1J_{RhC}$ = 45 Hz, $^2J_{P(Rh)C}$ = 10 Hz, 1CO)
$[RhMn(H)(CO)_4(\mu\text{-HFB})(dppm)_2][CO_2CF_3]$ (**6***b*·CO_2CF_3)		42.5(b),[e] 14.9(dm, $^1J_{RhP}$ = 97 Hz)	3.87(m,2H, PCH_2P),[e] 3.28(m, 2H, PCH_2P), −12.29(bd, $^1J_{RhH}$ = 34 Hz, 1H, hydride)	
$[RhMn(CR{=}CHR)(CO)_2(\mu\text{-CO})_2(dppm)_2][BF_4]$ (R = COOMe) (**7***a*·BF_4)	2028(st),[b] 1968(st), 1840(sh), 1813(m), 1706(st), 1585(w)	55.0(m),[e] 23.4(dm, $^1J_{RhP}$ = 127 Hz)	4.38(d, $^3J_{RhCCH}$ = 2 Hz, 1H, C*H*R = CR),[e] 3.13(s, 3H, CH_3), 3.07(s, 3H, CH_3), 3.07(m, 4H, PCH_2P)	243.4(dt,$^1J_{RhC}$ = 29 Hz, $^2J_{P(Mn)C}$ = 8 Hz, 1CO),[e] 235.6(dt, $^1J_{RhC}$ = $^2J_{P(Mn)C}$ = 14 Hz, 1CO), 219.5(t, $^2J_{P(Mn)C}$ = 20 Hz, 1CO), 213.7(t. $^2J_{P(Mn)C}$ = 17 Hz, 1CO)
	2031(st),[c] 1982(st), 1854(m), 1809(m), 1705(st), 1585(w)			
$[RhMn(CR{=}CHR)(CO)_2(\mu\text{-CO})_2(dppm)_2][SO_3CF_3]$ (R = COOMe) (**7***a*·SO_3CF_3)	2028(st),[b] 1972(st), 1848(sh), 1814(m), 1711(st), 1586(w)	55.2(m),[d] 23.3(dm, $^1J_{RhP}$ = 127 Hz)	4.47(d, $^3J_{RhCCH}$ = 2 Hz, 1H, C*H*R=CR),[d] 3.16(s, 3H, CH_3), 3.10(s, 3H, CH_3), 3.10(m, 4H, PCH_2P)	
	2032(st),[c] 1978(st), 1850(m), 1803(m), 1701(st), 1582(w)			

Can. J. Chem. Downloaded from www.nrcresearchpress.com by 80.90.12.36 on 09/08/12
For personal use only.

Table 1 (*continued*).

Compound	IR, cm^{-1} [a]	NMR[a] $\delta(^{31}P\{^1H\})$	NMR[a] $\delta(^1H)$	NMR[a] $\delta(^{13}C)$
$[RhMn(CR{=}CHR)(CO)_2(\mu\text{-}CO)_2(dppm)_2][BF_4]$ (R = CF_3) (**7***b*·BF_4)		54.6(m),[d] 21.9(dm, $^1J_{RhP}$ = 123 Hz)	5.06(q, $^3J_{HCCF}$ = 9 Hz, 1H,C*H*R=CR),[e] 3.17(m, 2H,PCH_2P) 3.11(m, 2H,PCH_2P)	243.8(dt,$^1J_{RhC}$ = 29 Hz, $^2J_{P(Mn)C}$ = 9 Hz, 1CO),[e] 237.8(dt, $^1J_{RhC}$ = 16 Hz, $^2J_{P(Mn)C}$ = 12 Hz, 1CO), 216.9(t, $^2J_{P(Mn)C}$ = 18 Hz, 1CO), 214.8(t. $^2J_{P(Mn)C}$ = 17 Hz, 1CO)
	2031(st),[c] 1989(m), 1850(sh), 1810(m)			
$[RhMn(CO)_3(\mu\text{-}\eta^1{:}\eta^2\text{-}CR{=}CHR)(dppm)_2][BF_4]$ (R = COOMe) (**8***a*·BF_4)		48.1(m),[h] 18.5(dm, $^1J_{RhP}$ = 117 Hz)		238.1(t, $^2J_{P(Mn)C}$ = 12 Hz,1CO),[h] 233.7(t, $^2J_{P(Mn)C}$ = 30 Hz,1CO), 190.0(dt, $^1J_{RhC}$ = 56 Hz, $^2J_{P(Rh)C}$ = 13 Hz,1CO)
$[RhMn(CO)_3(\mu\text{-}\eta^1{:}\eta^2\text{-}CR{=}CHR)(dppm)_2][CO_2CF_3]$ (R = COOMe) (**8***a*·CO_2CF_3)		48.0(m),[h] 18.4(dm, $^1J_{RhP}$ = 118 Hz)	3.12(b, 2H, PCH_2P),[h] 2.85(b, 2H, PCH_2P), 2.34(b, 3H, CH_3), 2.13(b, 3H, CH_3)	
$[RhMn(C(Me){=}CH_2)(CO)_2(\mu\text{-}CO)_2(dppm)_2][SO_3CF_3]$ (**9***a*)	2004(st),[b] 1966(vs), 1810(sh), 1796(vs)	58.2(m),[d] 21.0(dm, $^1J_{RhP}$ = 147 Hz)	4.98(m, 1H, C=CH_2),[d] 4.40(s, 1H, C=CH_2),	247.0(dt, $^1J_{RhC}$ = 20 Hz, $^2J_{P(Mn)C}$ = 11 Hz,1CO),[d] 246.7(dt, $^1J_{RhC}$ = 20 Hz, $^2J_{P(Mn)C}$ = 11 Hz,1CO),
	2018(vs),[c] 1975(st), 1810(sh), 1797(st)		3.14(m, 4H, PCH_2P), 0.91(s, 3H, CH_3)	218.9(t, $^2J_{P(Mn)C}$ = 20 Hz,1CO), 218.0(t, $^2J_{P(Mn)C}$ = 19 Hz,1CO)
$[RhMn(CH_2CH{=}CH_2)(CO)_2(\mu\text{-}CO)_2(dppm)_2][SO_3CF_3]$ (**9***b*)		58.6(m),[c] 26.4(dm, $^1J_{RhP}$ = 146 Hz)	~5.30 (C*H*=CH_2),[e] 3.70(d, 1H, $^3J_{cis}$ = 10 Hz, CH=CH_2), 3.12(2H, m, PCH_2P), 3.06(2H, m, PCH_2P), 2.73(dt, 2H, $^3J_{HCCH}$ = 6 Hz, $^3J_{P(Rh)CH}$ = 8 Hz, $CH_2CH{=}CH_2$), 2.63(d, 1H, $^3J_{trans}$ = 17 Hz, CH=CH_2)	247.7(dt, $^1J_{RhC}$ = 23 Hz, $^2J_{P(Mn)C}$ = 12 Hz, 2CO),[d] 218.5(t, $^2J_{P(Mn)C}$ = 18 Hz,2CO)
$[RhMnMe(CO)_2(\mu\text{-}CO)_2(dppm)_2][SO_3CF_3]$ (**10***a*)	2008(st),[b] 1973(st), 1838(m), 1800(st)	60.0(m),[d] 30.4(dm, $^1J_{RhP}$ = 139 Hz)	3.11(m, 4H, PCH_2P),[d] 0.92(dt, 3H, CH_3, $^2J_{RhH}$ = 2 Hz,	247.2(dt, 2CO, $^1J_{RhC}$ = 22 Hz, $^2J_{P(Mn)C}$ = 13 Hz),[d] 219.0(t, 1CO,
	2016(vs),[c] 1973(st), 1815(sh), 1797(st)		$^3J_{P(Rh)CH}$ = 11 Hz)	$^2J_{P(Mn)C}$ = 19 Hz)

Can. J. Chem. Downloaded from www.nrcresearchpress.com by 80.90.12.36 on 09/08/12
For personal use only.

Table 1 (*concluded*).

Compound	IR, cm^{-1} [a]	NMR[a] $\delta(^{31}P\{^1H\})$	NMR[a] $\delta(^1H)$	NMR[a] $\delta(^{13}C)$
$[RhMnMe(CO)_2(\mu\text{-}CO)_2(dppm)_2][I]$ (**10***b*)	2016(vs),[c] 1974(st), 1820(sh), 1798(vs)	60.1(m),[d] 30.4(dm, $^1J_{RhP}$ = 139 Hz)	3.13(m, 4H, PCH_2P),[d] 0.92(dt, 3H, CH_3, $^2J_{RhH}$ = 2 Hz, $^3J_{P(Rh)CH}$ = 11 Hz)	
$[RhMn(C(O)Me)(CO)_2(\mu\text{-}CO)_2(dppm)_2][SO_3CF_3]$ (**11**)	2008(vs),[b] 1972(st), 1839(m), 1798(st) 1665(m)	58.4(m),[d] 14.9(dm, $^1J_{RhP}$ = 162 Hz)	3.14(m, 4H, PCH_2P),[d] 1.04(s, 3H, CH_3)	251.3(d, 1CO, $^1J_{RhC}$ = 28 Hz),[e] 246.5(dt, $^1J_{RhC}$ = 20 Hz, $^2J_{P(Mn)C}$ = 12 Hz, 1CO), 240.9(dt, $^1J_{RhC}$ = 10 Hz, $^2J_{P(Mn)C}$ = 18 Hz, 1CO), 217.9(t, $^2J_{P(Mn)C}$ = 20 Hz, 1CO), 215.8(t, $^2J_{P(Mn)C}$ = 18 Hz, 1CO)
	2018(vs),[c] 1971(st), 1820(sh), 1797(st) 1655(m)			
$[RhMn(CO)_3(\mu\text{-}H)(\mu\text{-}HFB)(dppm)_2][BF_4]$(**12**)		46.1(b),[j] 13.9(dm, $^1J_{RhP}$ = 90 Hz)	3.81(m, 2H, PCH_2P),[j] −16.98(bd, hydride, $^1J_{RhH}$ = 15 Hz)	232.4(t, $^2J_{P(Mn)C}$ = 29 Hz, 1CO),[j] 228.8(m, 1CO), 184.4(dm, $^1J_{RhC}$ = 58 Hz, 1CO)
$[RhMn(CO)_3(\mu\text{-}H)(\mu\text{-}\eta^2\text{:}\eta^2\text{-}HFB)(dppm)_2][BF_4]$(**13***a*)		82.9(m),[j] 32.0(dm, $^1J_{RhP}$ = 135 Hz)	3.16(m, 2H, PCH_2P),[j] −20.83(dtt, hydride, $^1J_{RhH}$ = 15 Hz, $^2J_{P(Rh)H}$ = 14 Hz, $^2J_{P(Mn)H}$ = 26 Hz)	231.6(t, $^2J_{P(Mn)C}$ = 53 Hz, 1CO),[j] 217.2(m, 1CO), 186.2(dm, $^1J_{RhC}$ = 63 Hz, 1CO)
$[RhMn(CO)_3(\mu\text{-}H)(\mu\text{-}\eta^2\text{:}\eta^2\text{-}HFB)(dppm)_2][CO_2CF_3]$(**13***b*)		82.9(m),[j] 32.0(dm, $^1J_{RhP}$ = 135 Hz)	3.29(m, 2H, PCH_2P),[j] 3.16(m, 2H, PCH_2P), −20.83(dtt, hydride, $^1J_{RhH}$ = 16 Hz, $^2J_{P(Rh)H}$ = 12 Hz, $^2J_{P(Mn)H}$ = 26 Hz)	231.0(t, $^2J_{P(Mn)C}$ = 53 Hz, 1CO),[e] 217.2(m, 1CO), 185.8(dm, $^1J_{RhC}$ = 64 Hz, 1CO)

[a]Abbreviations used IR: w = weak; m = medium; st = strong; vs = very strong. NMR: s = singlet; d = doublet; t = triplet; q = quartet; qui = quintet; m = multiplet; b = broad; or any combination.
[b]Nujol mull.
[c]CH_2Cl_2 solution.
[d]22°C.
[e]−40°C.
[f]−60°C.
[g]−70°C.
[h]−80°C.
[i]−20°C.
[j]0°C

μmol in 10 mL) was added 7.3 μL of $HBF_4 \cdot Et_2O$ (42 μmol), causing an instant color change from red to yellow. After stirring for 1 h the solvent was removed and the residue was recrystallized from CH_2Cl_2–Et_2O. A yellow solid was obtained in 88% yield.

Method (ii): To a CH_2Cl_2 solution of $[RhMn(CO)_4(\mu\text{-}H)(dppm)_2][BF_4]$ (**2**) (50 mg, 44 μmol in 10 mL) was added 5.5 μL of DMAD (44 μmol). After stirring for 3 days the solvent was removed and the residue was recrystallized from CH_2Cl_2–Et_2O. A yellow solid was obtained in 92% yield. Ele-

Can. J. Chem. Downloaded from www.nrcresearchpress.com by 80.90.12.36 on 09/08/12
For personal use only.

Can. J. Chem. Downloaded from www.nrcresearchpress.com by 80.90.12.36 on 09/08/12
For personal use only.

Table 2. ^{19}F NMR data for the compounds.

Compounds	$\delta(^{19}F)^a$
$RhMn(CO)_3(\mu\text{-HFB})(\mu\text{-CO})(dppm)_2$ (**3***b*)	−50.1(q, $^5J_{FF}$ = 17 Hz, 3F),[b] −51.1(q, $^5J_{FF}$ = 17 Hz, 3F)
$RhMn(CO)_3(\mu\text{-HFB})(dppm)_2$ (**4***b*)	−40.8(tq, $^4J_{P(Mn)CCF}$ = 8 Hz, $^5J_{FF}$ = 13 Hz, 3F),[b] −49.0(ttq, $J_{P(Mn)F}$ = 4 Hz, $^4J_{P(Rh)CCF}$ = 6 Hz, $^5J_{FF}$ = 13 Hz, 3F)
$RhMn(CO)_3(\mu\text{-}\eta^2\text{:}\eta^2\text{-HFB})(dppm)_2$ (**5***b*)	−44.8(m)[b]
$[RhMn(H)(CO)_4(\mu\text{-HFB})(dppm)_2][BF_4]$ (**6***b*·BF_4)	−51.1(q, $^5J_{FF}$ = 18 Hz, 3F),[b] −51.8(q, $^5J_{FF}$ = 18 Hz, 3F)
$[RhMn(CR{=}CHR)(CO)_2(\mu\text{-CO})_2(dppm)_2][BF_4]$ (R=CF_3) (**7***b*·BF_4)	−51.1(q, $^5J_{FF}$ = 12 Hz, 3F),[c] −59.1(q, $^5J_{FF}$ = 12 Hz, 3F)
$[RhMn(CO)_3(\mu\text{-H})(\mu\text{-HFB})(dppm)_2][BF_4]$ (**11**)	−45.7(q, $^5J_{FF}$ = 17 Hz, 3F),[d] −55.7(q, $^5J_{FF}$ = 17 Hz, 3F)
$[RhMn(CO)_3(\mu\text{-H})(\mu\text{-}\eta^2\text{:}\eta^2\text{-HFB})(dppm)_2][BF_4]$ (**12***a*)	−45.8(m)[d]

[a]See footnotes on Table 1 for abbreviations.
[b]−40°C.
[c]22°C.
[d]0°C.

mental analysis of the BF_4^- salt was not obtained; that of the $SO_3CF_3^-$ salt (**7a**·SO_3CF_3) is given below.

*(k) [RhMn(C(COOMe)=CH(COOMe))(CO)$_2$(μ-CO)$_2$(dppm)$_2$][SO_3CF_3] (**7a**·SO_3CF_3)*

To a CH_2Cl_2 solution of compound **3** (50 mg, 42 μmol in 10 mL) was added 3.8 μL of CF_3SO_3H (42 μmol), resulting in an immediate color change from red to yellow. After 1 h the solvent was removed and the residue was recrystallized from THF–Et_2O. A yellow solid was obtained in 87% yield. Anal. calcd. for $RhMnSP_4F_3O_{11}C_{61}H_{51}$: C 55.05, H 3.86; found: C 55.48, H 4.54.

*(l) [RhMn(C(CF$_3$)=CH(CF$_3$))(CO)$_2$(μ-CO)$_2$(dppm)$_2$][BF$_4$] (**7b**·BF$_4$)*

To a CH_2Cl_2 solution of compound **3***b* (50 mg, 42 μmol in 10 mL under 10 psi of CO at −78°C) was added 6 μL of $HBF_4{\cdot}Me_2O$ (49 μmol). After stirring for 0.5 h the solution was warmed to room temperature and was stirred for another 0.5 h. The solvent was removed and the residue was recrystallized from CH_2Cl_2–Et_2O. A yellow solid was obtained in 82% yield. Anal. calcd. for $RhMnP_4F_{10}O_4BC_{58}H_{45}$, 0.4 CH_2Cl_2: C 53.01, H 3.46; found: 52.92, H 4.51. The amount of CH_2Cl_2 was established from the ^1H NMR spectrum in d_8-THF.

*(m) [RhMn(CO)$_3$(μ-C(COOMe)=CH(COOMe))(dppm)$_2$][BF$_4$] (**8a**·BF$_4$)*

To a CD_2Cl_2 solution of isomers **4***a* and **5***a* (5 mg, 4 μmol in 0.5 mL in an NMR tube) was added 2 μL of HBF_4Me_2O (16 μmol) at −78°C. The solution turned grey from black. The compound was characterized by NMR experiments at −80°C.

*(n) [RhMn(CO)$_3$(μ-C(COOMe)=CH(COOMe))(dppm)$_2$][CO_2CF_3] (**8a**·CO_2CF_3)*

To a CD_2Cl_2 solution of isomers **4***a* and **5***a* (5 mg, 4 μmol in 0.5 mL in an NMR tube) was added 10 μL of CF_3CO_2H (130 μmol) at −78°C. The solution turned grey from black. The compound was characterized by NMR experiments at −80°C.

*(o) [RhMn(C(Me)=CH$_2$)(CO)$_2$(μ-CO)$_2$(dppm)$_2$][SO_3CF_3] (**9a**)*

Allene (10 mL, ca. 400 μmol) was syringed to a THF solution of $[RhMn(CO)_4(\mu\text{-H})(dppm)_2][SO_3CF_3]$ (**2**) (50 mg, 42 μmol in 10 mL). The solution was refluxed for 6 h and cooled to ambient temperature, resulting in the precipitation of a yellow solid. The supernatant was removed by syringe and the solid was washed with Et_2O. A yellow solid was obtained (yield 64%). Anal. calcd. for $RhMnC_{58}H_{49}O_7F_3P_4S$: C 56.68, H 3.99; found: C 56.39, H 3.99.

*(p) Compound **9** and [RhMn(CH$_2$CH=CH$_2$)(CO)$_2$(μ-CO)$_2$(dppm)$_2$][SO_3CF_3] (**9b**)*

A Schlenk tube containing 50 mg of compound **2** was filled with allene at ca. 1 atm (1 atm = 101.3 kPa) and 5 mL of CH_2Cl_2 was added. The solution was stirred for 4 d. Removal of the solvent and recrystallization from CH_2Cl_2–Et_2O gave a yellow solid (76% yield). NMR characterization showed it to be an approximate 1:1 mix of **9***a* and the η^1-allyl product **9***b*. Refluxing a mixture of **9***a* and **9***b* in THF for 3 h resulted in the transformation of **9***b* to **9***a*.

*(q) [RhMnMe(CO)$_2$(μ-CO)$_2$(dppm)$_2$][SO_3CF_3] (**10b**)*

To a CH_2Cl_2 solution of $[RhMn(CO)_4(dppm)_2]$ (**1**) (100 mg, 96 μmol in 10 mL) was added 15 μL of $CF_3SO_3CH_3$ (133 μmol) and the mixture was stirred for 18 h. Removal of the solvent and recrystallization from CH_2Cl_2–Et_2O gave a yellow compound in 70% yield. Anal. calcd. for $RhMnSP_4F_3O_7C_{56}H_{47}$: C 55.91, H 3.91; found: C 55.58, H 3.80.

*(r) [RhMnMe(CO)$_2$(μ-CO)$_2$(dppm)$_2$] [I] (**10b**)*

To a CH_2Cl_2 solution of $[RhMn(CO)_4(dppm)_2]$ (**1**) (50 mg, 48 μmol in 10 mL) was added 50 μL of CH_3I (80 μmol). The

Can. J. Chem. Downloaded from www.nrcresearchpress.com by 80.90.12.36 on 09/08/12
For personal use only.

solution was stirred for 18 h. Removal of the solvent and recrystallization from CH_2Cl_2–Et_2O gave a yellow compound in 82% yield.

(s) [RhMn(C(O)Me)(CO)$_4$(dppm)$_2$][SO$_3$CF$_3$] (11)
A CH_2Cl_2 solution of [RhMnMe(CO)$_2$(μ-CO)$_2$(dppm)$_2$]-[SO_3CF_3] (**10***a*) (100 mg, 83 μmol in 5 mL) was put under CO (10 psi) and was stirred for 5 weeks. Removal of the solvent and recrystallization from THF–Et_2O gave a yellow solid in 76% yield. Anal. calcd. for $RhMnSP_4F_3O_8C_{57}H_{47}$: C 55.61, H 3.82; found: C 56.25, H 3.95.

(t) [RhMn(CO)$_3$(μ-H)(μ-HFB)(dppm)$_2$][BF$_4$] (12) and [RhMn(CO)$_3$(μ-H)(μ-η^2:η^2-HFB)(dppm)$_2$][BF$_4$] (13a)
[RhMn(CO)$_3$(μ-HFB)(dppm)$_2$] (**4***b*, 5 mg, 4 μmol) was dissolved in 0.5 mL of CD_2Cl_2 at −78°C to which 2 μL of HBF_4·Me_2O (16 μmol) was added. These compounds were formed in ratio of *ca* 0.5:1, respectively, at 0°C and were characterized by NMR experiments.

(u) [RhMn(CO)$_3$(μ-H)(μ-η^2:η^2-HFB)(dppm)$_2$][CO$_2$CF$_3$] (13b)
[RhMn(CO)$_3$(μ-HFB)(dppm)$_2$] (**4***b*, 5 mg, 4 μmol) was dissolved in 0.5 mL of CD_2Cl_2 at −78°C; 25 μL of CF_3CO_2H (16 μmol) was then added. The compound was characterized by NMR experiments at 0°C.

Kinetics for the transformation of 4*b* to 5*b*
The green solid of isomer **4***b* was dissolved in CD_2Cl_2 at −78°C (5 mg in 0.5 mL) in an NMR tube (at this temperature no isomerization occurs) and the temperature of the NMR probe was set to the appropriate running temperature (20, 25, 30, or 35°C (corrected)). A beaker of water was prepared at the same temperature as the probe and the NMR tube was placed in this beaker for 1 min. The use of the bath ensured that the sample warmed to running temperature as soon as possible. The sample was placed into the NMR probe and the ^{19}F NMR spectra were obtained at regular intervals (6 min), starting from the time the sample was immersed into the warm water.

The transformation of **4***b* to **5***b* is a first-order system coming to equilibrium (21), and can be represented as:

$$[1] \quad A \underset{k_{-1}}{\overset{k_1}{\rightleftharpoons}} B$$

in which A and B represent **4***b* and **5***b*, respectively. From this, the expression:

$$[2] \quad -\ln \frac{[B]_e - [B]}{[B]_e - [B]_o} = (k_1 + k_{-1})t$$

can be obtained, where $[B]_o$, [B], and $[B]_e$ are the concentrations of **5***b* at $t = 0$, $t = t$, and $t = \infty$, respectively. Assuming $[B]_o = 0$, eq. [2] simplifies to:

$$[3] \quad -\ln\left(1 - \frac{[B]}{[B]_e}\right) = (k_1 + k_{-1})t$$

The units of concentration used were mole fractions, and $[B]_e$ was obtained after the sample had sat at room temperature for 1 day, and then at the desired temperature for 1.0 h. Plots of $-\ln(1-[B]/[B]_e)$ against t give the slope $k_1 + k_{-1}$. The ratio k_1/k_{-1} equals $[B]_e/(1-[B]_e)$. From $k_1 + k_{-1}$ and k_1/k_{-1} values of k_1 and k_{-1} can be calculated and are given in Table 3. Values of $\Delta H°*$ and $\Delta S°*$ were derived by the application of the transition state theory eq. [4].

Table 3. Forward and reverse rate constants for the reversible conversion of **4***b* to **5***b*.

	Rate constant	
Temperature (°C)	k_1(min^{-1}) × 10^3	k_{-1}(min^{-1}) × 10^3
20	6.63	9.17
25	13.3	19.5
30	26.5	37.3
35	48.2	68.8

$$[4] \quad \ln(k/T) = -\Delta H°*/RT + (23.76 + \Delta S°*/R)$$

Results and discussion

(a) Alkyne species
The reaction of [RhMn(CO)$_4$(dppm)$_2$] (**1**) with dimethyl acetylenedicarboxylate (DMAD) under CO yields the DMAD-bridged product [RhMn(CO)$_4$(μ-DMAD)(dppm)$_2$] (**3***a*), as was observed in the isoelectronic compounds, [RhRe(CO)$_4$(μ-DMAD)(dppm)$_2$] (22), and [RhOs(CO)$_4$(μ-DMAD)(dppm)$_2$]$^+$ (4), and spectral characterization of **3***a* proceeded much as reported for these analogues. Although coordination of the alkyne perpendicular to the Rh–Mn axis was considered in **3***a*, it was ruled out on the basis of the ^1H NMR spectrum. This spectrum showed two separate resonances for the DMAD methyl groups, which are in different environments by virtue of their proximity to either Rh or Mn; a perpendicular arrangement would have only one methyl signal. The $^{13}C\{^1H\}$ NMR spectrum of **3***a* shows a resonance for the terminal carbonyl on Rh at δ 193.8 ($^1J_{Rh-C}$ = 57 Hz), two for the terminal carbonyls on Mn (δ 221.8, 223.5), and one corresponding to a semibridging carbonyl at δ 248.7, showing a weak interaction with Rh($^1J_{Rh-C}$ = 10 Hz). This semibridging interaction is substantiated by the low carbonyl stretch at 1727 cm^{-1} in the IR spectrum. The similarities in the spectroscopic parameters for **3***a* (see Table 1) to those of the Rh/Re and Rh/Os analogues lead to the formulation shown in Scheme 1 (note that in the schemes the dppm groups above and below the plane of the drawing are usually omitted for clarity).

If the reaction of **1** with DMAD is carried out in the absence of CO, a mixture of **3***a* and two new species **4***a* and **5***a* is obtained. Refluxing this mixture in THF yields **4***a* and **5***a* and recrystallization yields only **4***a*, as a black solid. A solution containing only **4***a* can be prepared by dissolving the black solid in CH_2Cl_2 at −78°C. Upon gradually increasing the solution temperature to −40°C compound **5***a* begins to appear, as shown by the $^{31}P\{^1H\}$ NMR spectra. At temperatures between 0° and 20°C an equilibrium mixture of **4***a* and **5***a* is present in an approximate 85:15 molar ratio. Both new

Can. J. Chem. Downloaded from www.nrcresearchpress.com by 80.90.12.36 on 09/08/12
For personal use only.

Scheme 1.

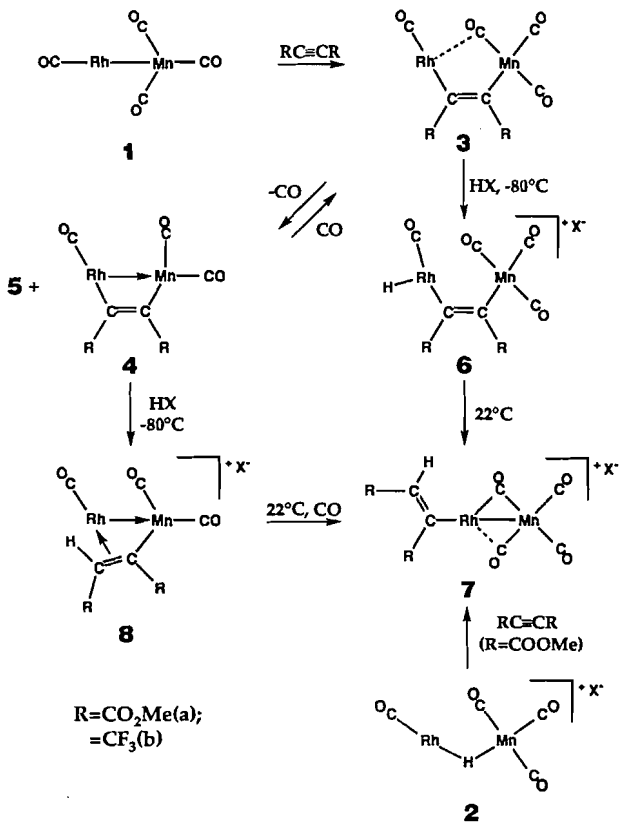

products are isomers of formulation $[RhMn(CO)_3(\mu\text{-}DMAD)(dppm)_2]$, resulting from carbonyl loss from **3***a*. The major isomer (**4***a*) has the structure shown in Scheme 1, and is the species expected based on previous work with the related Rh/Re and Rh/Os systems; in particular the Rh/Os analogue $[RhOs(CO)_3(\mu\text{-}DMAD)(dppm)_2]^+$ was previously characterized by an X-ray structure determination (4). The $^{13}C\{^1H\}$ NMR spectrum of **4***a* shows one carbonyl ligand on Rh and two on Mn, in addition to two singlets for the DMAD-carbonyl groups at δ 175.0 and 168.0, and two signals for the methyl groups at δ 50.3 and 50.1. Only one acetylenic carbon resonance was observed at δ 140.9 as a triplet of triplets, displaying coupling to both sets of ^{31}P nuclei; the other acetylenic resonance was not observed and appears to be obscured by phenyl resonances (non isotopically enriched DMAD was used so the signals due to DMAD are of low intensity). The ^1H NMR spectrum also displays two signals for the DMAD methyl groups consistent with a parallel DMAD coordination in which the two ends of the alkyne are inequivalent by virtue of their proximity to either Rh or Mn. A dative Rh → Mn bond is proposed to give Mn an 18-electron configuration, as was previously suggested for the Rh/Os analogue, in which the metal–metal interaction was supported by the X-ray study. Carbonyl loss from **3** probably occurs by transfer of the semibridging carbonyl to Rh, followed by CO loss from this metal. Concomitant with the transformation of this carbonyl from semibridging, to symmetrically bridging, to terminal on Rh, is a change in the metal–metal bonding, from no bond in **3**, to a conventional Rh—Mn bond in the symmetrically CO-bridged intermediate, to a Rh → Mn dative bond in the last species, as shown below. This shift of electron density from

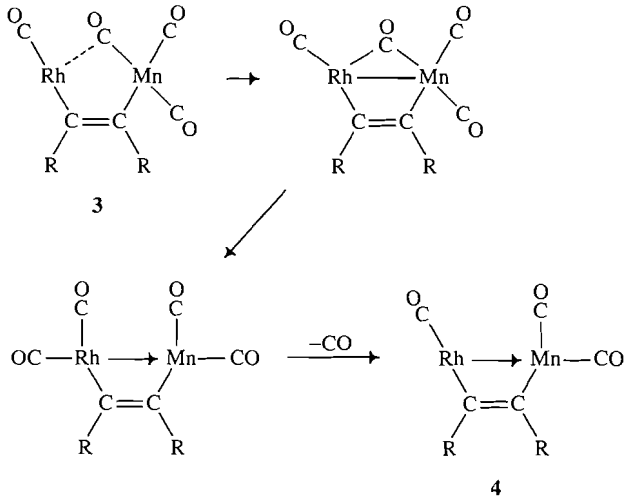

Rh to Mn accompanies the movement of the carbonyl's donor pair from Mn to Rh, and demonstrates how the adjacent metal (Rh) can assist in the labilization of a ligand from normally inert, 18e center (Mn).

The minor isomer **5***a* is proposed to have a perpendicular alkyne binding mode, shown below, as has been previously observed within the Co triad for $[Rh_2(CO)_2(\mu\text{-}\eta^2\text{-}PhC_2Ph)(dppm)_2]$ (23), $[Ir_2(CO)_2(\mu\text{-}\eta^2\text{-}DMAD)(dppm)_2]$ (6), a series of related dicobalt complexes (24–30), as well as other dirhodium (31, 32) and diiridium (33) systems. This proposed structure is based on the spectral data. The $^{31}P\{^1H\}$ NMR spectrum shows an AA′BB′X spin system in which the

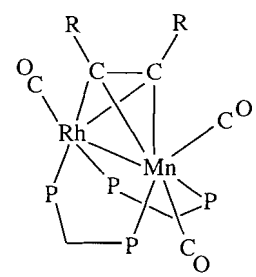

5*a* (R = CO_2Me); **5***b* (R = CF_3)

Mn-bound phosphorus nuclei resonate at δ 98.9; this is 47 ppm downfield from the related signal in **4***a* in which a *trans* arrangement of phosphines is proposed. The resonance for the Rh-bound phosphorus nuclei is also somewhat downfield from that observed in **4***a*. Both Mn-bound carbonyls display unusually high coupling (48 and 38 Hz) to the Mn-bound phosphorus nuclei, compared to values between 10 and 20 Hz when a *trans* diphosphine arrangement is involved, suggesting a geometry in which the CO and phosphines are at an angle other than 90°. Also, unexpectedly, the Rh-bound CO displays weak coupling to the Mn-bound phosphorus nuclei, presumably through the Rh—Mn bond. Only one signal is observed in the $^{13}C\{^1H\}$ NMR spectrum corresponding to the two equivalent DMAD carbonyls (δ 176.0) and another for the two methyl groups. In addition the ^1H NMR spectrum also shows only one resonance for both methyl groups. These data support the perpendicular orientation of the alkyne, which

Can. J. Chem. Downloaded from www.nrcresearchpress.com by 80.90.12.36 on 09/08/12
For personal use only.

would result in both ends of the alkyne being chemically equivalent.

Although the perpendicular coordination mode of the alkyne and the concomitant *cis*-diphosphine arrangement seem clear, the resulting geometry at Mn, regarding the positions of the carbonyls, is still ambiguous.

All routes to **4***a* and **5***a* invariably yield these species in a constant ratio in solution, suggesting an equilibrium between the two. This has been confirmed by spin-saturation transfer experiments at 60°C in which saturation of the signal for the Mn-bound phosphorus nuclei of one isomer results in a substantial intensity decrease (>60%) for the corresponding signal of the other isomer. Although reversible conversion of one alkyne-bridged mode to the other has been reported upon ligand gain or loss (34, 35), we know of only one other study in which such a reversible transformation in alkyne bonding modes occurs with no change in the number of ligands; this conversion from a dimetallacyclobutene structure to the perpendicular binding mode for $[Cp^*(CO)_2Re]_2(\mu\text{-DMAD})$ was induced upon photolysis and was reversed upon heating.[2] However, the facility of this reversible change in alkyne binding mode (**4***a* $\rightleftharpoons$ **5***a*) is unprecedented. A facile interconversion between alkyne bonding modes has been proposed to explain the ease of ligand addition to the coordinatively saturated complex $[Cp_2Rh_2(\mu\text{-CO})(\mu\text{-}\eta^2\text{-}CF_3C_2CF_3)]$, but the other rotamer was not observed (1*k*). At ambient temperature spin-saturation transfer between **4***a* and **5***a* was not observed because at this temperature the exchange rate is too slow.

The reaction of **1** with hexafluoro-2-butyne (HFB) leads to a series of HFB-bridged complexes **3***b*, **4***b*, and **5***b*, exactly analogous to the DMAD-bridged compounds discussed, and are again shown in Scheme 1 (R = CF_3). These products show very similar spectroscopic properties to their DMAD analogues. The major difference lies in the relative proportions of isomers **4** and **5**. Whereas isomer **5***a*, having the perpendicular alkyne bridge, was the minor isomer for DMAD, both isomers **4***b* and **5***b* are present in comparable amounts with HFB. The ^{19}F NMR spectra (see Table 2) conveniently differentiate between the parallel and perpendicular alkyne binding modes, with the parallel isomer **4***b* showing two multiplet resonances for the inequivalent CF_3 groups while **5***b* displays only one multiplet resonance for the chemically equivalent CF_3 groups. Carrying out ^{19}F NMR experiments on **4***b* with selective and broad-band ^{31}P-decoupling shows that the fluorine resonance at δ −40.8 couples to only the Mn-bound phosphorus atoms so is assigned to the CF_3 group adjacent to Mn, whereas the signal at δ −49.0 surprisingly couples to all phosphorus nuclei. In addition, the two CF_3 groups display a mutual coupling of 13 Hz, typical of a *cis* arrangement. The single ^{19}F resonance in **5***b* collapses to a singlet upon decoupling the Rh-bound phosphorus nuclei, but shows no apparent coupling to the Mn-bound ends of the diphosphines, suggesting a stronger binding to Rh. Although the coordinatively unsaturated **4***b* immediately reverts to **3***b* at −40°C under CO, **5***b* remains unreacted at this temperature, consistent with the coordinatively saturated formulation for this species. The electronic effect of substituting DMAD by the better π-accepting HFB group (36) shows up in the greater lability of the fourth carbonyl in **3***b*. Therefore the tetracarbonyl species $[RhMn(CO)_4(\mu\text{-HFB})(dppm)_2]$ (**3***b*) is only observed under CO at −40°C; otherwise the tricarbonyl isomers are the only species observed. In none of the alkyne-bridged species described was a C≡C stretch visible in the IR spectra.

[2] C.P. Casey and R.S. Carino, personal communication.

Fig. 1. ^{19}F NMR spectra (at 376.5 MHz) at 20°C showing the conversion of compound **4***b* to **5***b* over a 90 min period; the spectra were acquired at 6 min intervals.

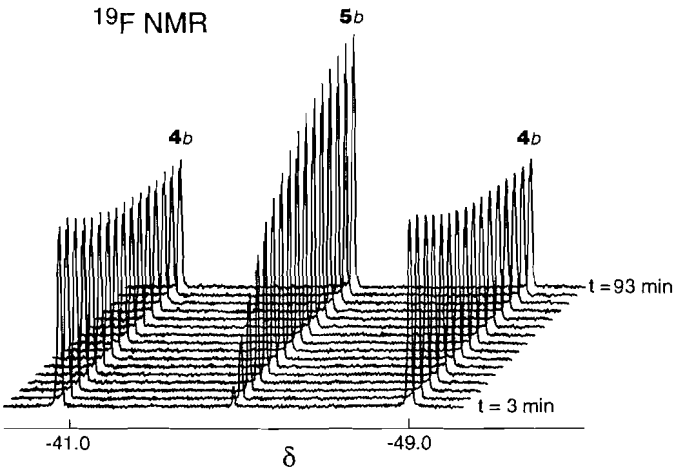

The isomerization of **4***b* to **5***b* is less facile than for the DMAD analogue; whereas conversion of **4***a* to **5***a* was observed at −40°C, that for **4***b* to **5***b* did not occur appreciably until temperatures near 0°C. Even at 60°C, exchange between **4***b* and **5***b* was too slow to be detected by spin-saturation transfer experiments. However, over the temperature range between 20 and 35°C this conversion can be conveniently monitored by ^{19}F NMR. Figure 1 shows the changes in ^{19}F NMR spectra that occur as **4***b* slowly converts to **5***b* at 20°C. For this first-order system coming to equilibrium the forward and reverse rate constants (k_1 and k_{-1}) can be obtained (21), and from the transition-state theory (T = 20, 25, 30, 35°C), values for ΔH^* and ΔS^* for the forward (23.3 kcal mol^{-1}, 2.9 cal K^{-1} mol^{-1}) and reverse (23.6 kcal mol^{-1}, 4.7 cal K^{-1} mol^{-1}) reactions can be obtained. Although the corresponding kinetic study was not carried out for the conversion between the DMAD analogues **4***a* and **5***a*, the more facile conversion at lower temperatures indicates a lower barrier to rotation. This presumably reflects the stronger binding of HFB by virtue of its better π-accepting ability.

(b) Vinyl species

Addition of protic acids to **3***a* at −80°C results in protonation at Rh to yield $[RhMnH(CO)_4(\mu\text{-DMAD})(dppm)_2][X]$ (X = BF_4 (**6***a*)). The hydride resonance at δ −14.3 in the ^1H NMR spectrum displays coupling to Rh of 38 Hz and to the phosphorus nuclei on Rh, confirming its terminal coordination to this metal. All other spectroscopic data (see Table 1), including the observation of two resonances for the DMAD methyl protons, support the structure shown. The observed protonation at only one metal is in contrast to the protonation of the metal–metal bond in the related compound $[Rh_2(CO)_2(\mu\text{-DMAD})(dmpm)_2]$ (dmpm = $Me_2PCH_2PMe_2$) to give a hydride-bridged species (8).

Upon warming, compound **6***a* transforms to the vinyl complex **7***a*. $^{13}C\{^1H\}$ NMR spectra for the BF_4^- salt show four separate carbonyl resonances. The low-field signal, at δ 243.4,

Can. J. Chem. Downloaded from www.nrcresearchpress.com by 80.90.12.36 on 09/08/12
For personal use only.

displays coupling of 29 Hz to Rh and 8 Hz to the Mn-bound phosphines, so is formulated as a bridging carbonyl. The resonance at δ 235.6 displays coupling to Rh and to the Mn-bound phosphines, both of 14 Hz, so is formulated as semibridging, whereas the remaining two carbonyls are terminally bound to Mn, as shown in Scheme 1. It appears that the weaker interaction of the semibridging carbonyl with Rh results from repulsion of this group by a methoxycarbonyl substituent of the terminal vinyl group, with the conventionally bridged carbonyl adjacent to the hydrogen on the β-carbon. Such a proposal presumes that there is no facile rotation about the Rh–vinyl bond. The vinylic proton of **7***a* (X = BF_4 or SO_3CF_3) is observed at ca. δ 4.4 and displays coupling of 2 Hz to Rh, suggesting that the vinyl group is bound to Rh. In any case, with no other ligand bound terminally to Rh, the vinyl group must be terminally bound to this metal. The IR spectra of **7***a* show two terminal-carbonyl stretches, two corresponding to bridged carbonyls, between 1809 and 1854 cm^{-1}, and a strong band due to the ester carbonyl groups and a weak stretch at ca. 1585 due to the C=C bond of the vinyl moiety.

Protonation of the HFB-bridged species **3***b* again parallels that involving the DMAD-bridged analogue, yielding the hydrido intermediate **6***b* at low temperature, which rearranges to the vinyl species **7***b* at ambient temperature. In **7***a* (R = CO_2Me) our spectroscopic data could not differentiate between a *cis* or *trans* arrangement of CO_2Me groups about the vinylic C=C bond, so we assumed a cis arrangement, as normally observed in such migratory insertions (37–41). Having CF_3 substituents we are now able to establish a cis arrangement based on ^{19}F–^{19}F coupling constants. In **7***b* this coupling ($^5J_{F-F}$ = 12 Hz) is typical of a cis arrangement (42-45), and compares well to the values of 17, 13, and 18 Hz observed in **3***b*, **4***b*, and **6***b*, respectively.

Compound **7***a* can also be prepared by the reaction of the hydride-bridged species, $[RhMn(CO)_4(\mu\text{-}H)(dppm)_2][BF_4]$ (**2**) with DMAD, via migratory insertion.

A very similar vinyl product, $[RhMn(C(Me)=CH_2)(CO)_2(\mu\text{-}CO)_2(dppm)_2][SO_3CF_3]$ (**9***a*), containing an isopropenyl group, that is terminally bound to Rh, can be prepared by the insertion of allene ($H_2C=C=CH_2$) into the metal-hydride bond of the above hydride-bridged complex in refluxing THF. A similar transformation was previously observed in a closely related Rh/Os complex and this isopropenyl product was structurally characterized by an X-ray study (46). Compound **9***a* shows four carbonyl resonances in the $^{13}C\{^1H\}$ NMR with two at low field corresponding to bridging groups, displaying 20 Hz coupling to Rh and 11 Hz coupling to the phosphorus nuclei on Mn. On the basis of this coupling pattern and the magnitude of the Rh coupling, these carbonyls are assigned as semibridging. The assignment of two bridging and two terminal carbonyls is also supported by the IR data. In the ^1H NMR spectrum, two separate resonances are observed for the inequivalent vinyl protons of **9***a* and a singlet for the three methyl protons.

Surprisingly, if the reaction of **2** with allene is carried out at room temperature for several days **9***a* is obtained together with another species (**9***b*) in approximately equal proportions. This new species can be shown to be the isomer $[RhMn(CH_2CH=CH_2)(CO)_2(\mu\text{-}CO)_2(dppm)_2][SO_3CF_3]$ containing an η^1-allyl group. The $^{13}P\{^1H\}$ NMR resonances of **9***a* and **9***b* are quite similar, and although the $^{13}C\{^1H\}$ NMR spectrum of **9***b* has only two carbonyl resonances, corresponding to two equivalent semibridging and two equivalent terminal carbonyls, the chemical shifts and coupling constants are similar to those for **9***a*. However, the ^1H NMR spectra of the two isomers are quite distinct, showing four different resonances for the allyl group. The resonance at δ 2.73, corresponding to the two methylene protons adjacent to Rh, shows 8 Hz coupling to the Rh-bound phosphorus nuclei as well as 6 Hz coupling to H^b on the adjacent carbon. The slight broadening of this resonance obscures the expected 2 Hz coupling of these protons to Rh (see, for example, compound **10**). The three olefinic protons resonate at δ 5.30, 3.70, and 2.63, with the low-field signal appearing as a shoulder on the solvent peak (the poor solubility of **9***b* in $CHCl_3$ or THF precluded the use of these solvents). Protons H^b and H^d were shown to be mutually *trans*, based on the 17 Hz coupling between them, and this value can be compared with the 10 Hz coupling between H^b and H^c that is consistent with a *cis* arrangement. Other than the hydrocarbyl ligands, the only substantial difference between **7** and **9** is that, for the latter, two carbonyls are semibridging, instead of one being bridging and the other semibridging. Refluxing a mixture of **9***a* and **9***b* in THF results in the disappearance of **9***b* with a corresponding increase in the concentration of the thermodynamic product **9***a*.

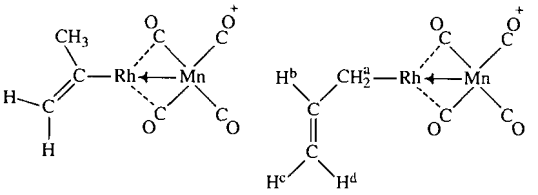

9*a* **9***b*

The formation of both **9***a* and **9***b* from allene and the hydride-bridged compound **2** is presumed to proceed via an allene-hydride intermediate, with allene coordinated at Rh (although this intermediate was not observed). These results support the earlier proposals (47–50) of allene-hydride intermediates being involved in the isomerization of isopropenyl to η^3-allyl groups. In our system this conversion is reversed, with the isopropenyl species being thermodynamically favoured. The stability of the allyl group over the isopropenyl in the previous studies is presumably due to the η^3-binding mode of the former. We assume that this mode is not favoured in our system owing to steric repulsions that would result, involving the dppm phenyl groups above and below the equatorial plane of the metals. That being the case, we propose that when only the η^1-binding mode of an allyl is considered, the isopropenyl isomer is favoured, owing to a stronger metal–carbon bond involving the sp^2 carbon rather than the sp^3 carbon of the η^1-allyl group. In another report involving interconversion between an η^1-allyl and a vinyl group, the vinyl group was again favoured (51).

The prototype in this series, having an organic group (CH_3) σ-bound to Rh, can be prepared either by the addition of methyl triflate to **1**, yielding $[RhMn(CH_3)(CO)_2(\mu\text{-}CO)_2(dppm)_2][SO_3CF_3]$ (**10***a*), or by the addition of MeI to **1** to give the analogous iodide salt, $[RhMn(CH_3)(CO)_2(\mu\text{-}CO)_2(dppm)_2][I]$ (**10***b*). All spectroscopic data (Table 1) support a structure like those proposed for **7** and **9**, with the methyl group terminally bound to Rh, exactly as observed in the Rh/Re analogue, which

Can. J. Chem. Downloaded from www.nrcresearchpress.com by 80.90.12.36 on 09/08/12
For personal use only.

was characterized by an X-ray structure determination (52). The $^{31}P\{^1H\}$ NMR and $^{13}C\{^1H\}$ NMR spectra of **10** are very closely comparable to those of **9***b*, and the ^1H NMR spectrum of **10** shows the expected triplet of doublets for the methyl resonance, displaying 11 Hz coupling to the two Rh-bound phosphorus nuclei and 2 Hz coupling to Rh. This terminal binding of a methyl group to Rh has now been observed in a number of related mixed-metal binuclear systems (9, 52–54), and all display closely comparable spectroscopic parameters, adding further support for our formulation for the closely related isopropenyl (**9***a*) and η^1-allyl (**9***b*) products.

Reaction of **10***a* with CO results in a migratory insertion to give the acyl species $[RhMn(C(O)CH_3)(CO)_2(\mu\text{-}CO)_2(dppm)_2][SO_3CF_3]$ (**11**). The ^1H NMR signal for the methyl group appears as a singlet at δ 1.04 when ^{12}CO is used or as a doublet ($^2J_{CH}$ = 5 Hz) when ^{13}CO is used. In the $^{13}C\{^1H\}$ NMR the acyl carbon appears as a low-field doublet with 28 Hz coupling to Rh. Migratory insertion has resulted in a subtle change in the bridging carbonyls such that one shows stronger coupling to Rh (20 Hz) than the other (10 Hz), suggesting a strong and a weak semibridging interaction. Substitution of the methyl by the poorer donor acyl group means that there is less need for π back donation from Rh. However, it is not clear why the bridging interactions should be asymmetric rather than two identical but weaker semibridging interactions. There appears to be no compelling steric argument, as for the related vinyl species.

The alkyne-bridged tricarbonyl species **4***a* can also be protonated but, in this case, even at −80°C no metal hydride is observed. Instead an unstable species, $[RhMn(CO)_3(\mu\text{-}C(CO_2Me)=C(H)CO_2Me)(dppm)_2][X]$ (**8***a*), containing what is proposed to be a bridging vinyl moiety, is obtained. Unfortunately the presence of paramagnetic impurities, resulting from decomposition of **8***a*, has led to broad resonances and the signal due to the vinylic hydrogen was not observed in the ^1H NMR spectrum. Upon warming, compound **7***a* was obtained (as the tetrafluoroborate salt), together with several unidentified products, some of which are presumably the source of the extra carbonyl needed in the transformation of **8***a* to **7***a*. Whether **8***a* has the structure shown in Scheme 1, or the related structure in which the vinyl moiety is σ-bound to Rh and π-bound to Mn, could not be determined. The interaction of the vinyl π-bond with either Rh or Mn is required to give the metals a 16e or 18e configuration, respectively. An analogous vinyl binding mode was previously proposed in related dirhodium (1*k*, 8, 55) and dimanganese (56) complexes. Compound **8** readily transforms to **7** upon addition of CO.

Although protonation of the species **5***a* having the perpendicularly bound DMAD group could not be followed because of its very low abundance, the protonation of both isomers **4***b* and **5***b*, having parallel and perpendicular HFB groups, respectively, was possible since both are present in comparable amounts. Starting with **4***b*, the addition of $HBF_4\cdot Me_2O$ at −78°C does not result in a reaction until temperatures near 0°C are reached, at which point substantial amounts of **5***b* appear. At 0°C and higher, two hydride-bridged products **12** and **13** are obtained, corresponding to protonation of the Rh—Mn bonds in **4***b* and **5***b*, respectively, as shown in Scheme 2. Compounds **12** and **13** are isomers of $[RhMn(CO)_3(\mu\text{-}H)(\mu\text{-}HFB)(dppm)_2][X]$ having either a parallel (**12**) or perpendicular (**13**) alkyne orientation, as in the respective precursors. The more abundant isomer **13** is assumed to have a perpendicular alkyne orientation based on the similarity of its spectral parameters with those of **5***b*. In particular, **13** shows only one resonance for the CF_3 groups, whereas two resonances are observed in **12** owing to the chemical inequivalence of the two ends of the alkyne. The appropriate selective and broad-band decoupling experiments show that the hydrides in both **12** and **13** couple to Rh($^1J_{RhH}\simeq 15$Hz) and to all four phosphorus nuclei, confirming their bridging assignments. Although both isomers **12** and **13** (as BF_4^- salts) are obtained upon protonation with $HBF_4\cdot Me_2O$, only **13** [$CF_3CO_2^-$] is obtained if trifluoroacetic acid is used. It is not clear what the function of the non-innocent $CF_3CO_2^-$ anion is in this case.

After several hours at ambient temperature both **12** and **13** transform to the vinyl complex **7***b*, together with unidentified species that are presumably the source of the additional carbonyl needed in the transformation of the tricarbonyl precursors to the tetracarbonyl product.

Summary and conclusions

The product resulting from the reaction of either of the activated alkynes, DMAD or HFB, with $[RhMn(CO)_4(dppm)_2]$ is hardly unusual, having the alkyne coordinated parallel to the metal–metal bond, as is frequently observed in dppm-bridged species (1*c*, 2–5, 57). However, the facile loss of CO that occurs from the coordinatively saturated Mn centre is unusual in that it demonstrates two interesting ways in which saturation can be maintained at this centre by virtue of the close proximity of Rh. In one isomer carbonyl loss is accompanied by formation of a dative Rh → Mn bond in which Rh utilizes its filled d_{z^2} orbital for donation to Mn, whereas in the second, rotation of the alkyne to a perpendicular orientation occurs with formation of a conventional metal–metal bond. In this transformation the 2-electron-donor alkyne becomes a 4-electron donor. This system is unique in demonstrating reversible interconversion of the two alkyne bonding modes, which occurs with unprecedented ease; we know of no other system in which both isomers are in equilibrium and are observed simultaneously.

Protonation of all alkyne-bridged products at ambient temperature yields a series of vinyl complexes while at low temperatures observation of metal-hydride intermediates is possible. In the alkyne-bridged complexes without a Rh—Mn bond, protonation appears to occur at Rh, followed by transfer to the alkyne. However, in the Rh—Mn bonded species protonation at the metal–metal bond occurs. Although in this latter case the hydride and alkyne groups are on opposite faces of the dimer, appearing not to be well placed for subsequent migratory insertion, movement of the hydride between the metals to the opposite face of the complex has been shown to be facile (8), so the observed structure appears to present no appreciable barrier to vinyl formation. These vinyl complexes also result from the reaction of the alkyne with the hydride-bridged complex $[RhMn(CO)_4(\mu\text{-}H)(dppm)_2][X]$. This hy-dride species also reacts with allene to give two isomers of $[RhMn(C_3H_5)(CO)_4(dppm)_2][X]$ having either a methyl vinyl (isopropenyl) or an η^1-allyl group σ-bound to Rh; the first results from transfer of the hydride ligand to a terminal carbon of allene while the second is a result of H-transfer to the central carbon. The vinyl species is

Scheme 2.

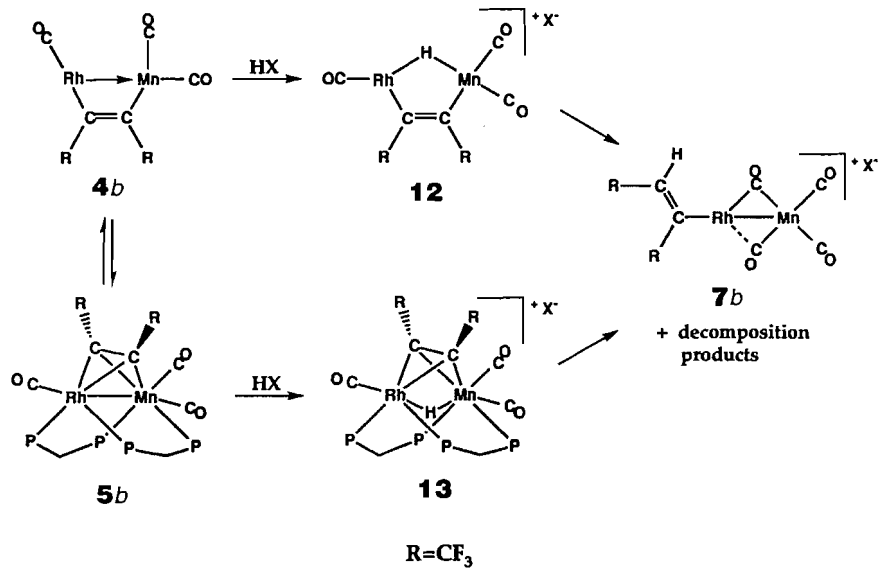

thermodynamically favoured, presumably because of the stronger Rh—C σ-bond involving an sp^2 carbon rather than an sp^3 carbon. This observation of both tautomeric forms resulting from the reaction of allene with a metal hydride is unusual and presents strong support for the involvement of an allene-hydride intermediate in the interconversion between allyl and vinyl complexes.

Acknowledgements

We thank the Natural Sciences and Engineering Research Council of Canada and the University of Alberta for financial support, and Professor C.P. Casey for communicating results prior to their publication.

References

1. (*a*) D.M. Hoffman, R. Hoffmann, and C.R. Fisel. J. Am. Chem. Soc. **104**, 3858 (1982), and references therein; (*b*) R.S. Dickson, B.M. Gatehouse, M.C. Nesbit, and G.N. Pain. J. Organomet. Chem. **215**, 97 (1981); (*c*) K.A. Johnson and W.L. Gladfelter. Organometallics, **11**, 2534 (1992); (*d*) A.F. Dyke, S.A.R. Knox, P.J. Naish, and G.E. Taylor. J. Chem. Soc. Dalton Trans. 1297 (1982); (*e*) S.A.R. Knox. J. Organomet. Chem. **400**, 255 (1990); (*f*) S.A.R. Knox. Pure Appl. Chem. **56**, 81 (1984); (*g*) C.P. Casey, M.W. Meszaros, P.J. Fagan, R.K. Bly, S.R. Marder, and E.A. Austin. J. Am. Chem. Soc. **108**, 4043 (1984); (*h*) C.P. Casey and P.J. Fagan. J. Am. Chem. Soc. **104**, 4950 (1982); (*i*) C.P. Casey and J.D. Audett. Chem. Rev. **86**, 339 (1986), and references therein; (*j*) J. Takats. J. Cluster Sci. **3**, 479 (1992); (*k*) R.S. Dickson. Polyhedron, **10**, 1995 (1991).
2. J.A. Jenkins and M. Cowie. Organometallics, **12**, 2774 (1992).
3. B.A. Vaartstra, J. Xiao, J.A. Jenkins, R. Verhagen, and M. Cowie. Organometallics, **10**, 2708 (1991).
4. R.W. Hilts, R.A. Franchuk, and M. Cowie. Organometallics, **10**, 304 (1991).
5. B.A. Vaartstra and M. Cowie. Organometallics, **8**, 2388 (1989).
6. R. McDonald and M. Cowie. Manuscript in preparation.
7. B.A. Vaartstra and M. Cowie. Organometallics, **9**, 1594 (1990).
8. J.A. Jenkins and M. Cowie. Organometallics, **11**, 2767 (1992), and references therein.
9. B.T. Sterenberg, R.W. Hilts, G. Moro, R. McDonald, and M. Cowie. J. Am. Chem. Soc. **117**, 245 (1995).
10. J. Xiao and M. Cowie. Organometallics, **12**, 463 (1993).
11. F. Antwi-Nsiah and M. Cowie. Manuscript in preparation.
12. L.-S. Wang and M. Cowie. Organometallics. **14**, 2374 (1995).
13. (*a*) S. Otsuka and A. Nakamura. Adv. Organomet. Chem. **14**, 245 (1976); (*b*) A. Nakamura and S. Otsuka. J. Mol. Catal. **1**, 285 (1975/76).
14. M.I. Bruce. Chem. Rev. **91**, 197 (1991), and references therein.
15. (*a*) P.M. Maitlis. Pure Appl. Chem. **61**, 1747 (1989); (*b*) P.M. Maitlis, I.M. Saez, N.J. Meanwell, K. Isobe, A. Nutton, A.V. de Miguel, D.W. Bruce, S. Okeya, P.M. Bailey, D.G. Andrews, P.R. Ashton, and I.R. Johnstone. New J. Chem. **13**, 419 (1989); (*c*) J. Martinez, J.B. Gill, H. Adams, N.A. Bailey, I.M. Saez, G.J. Sunley, and P.M. Maitlis. J. Organomet. Chem. **394**, 583 (1990); (*d*) M.L. Turner, P.K. Byers, H.C. Long, and P.M. Maitlis. J. Am. Chem. Soc. **115**, 4417 (1993).
16. I.M. Saez, N.J. Meanwell, A. Nutton, K. Isobe, A.V. de Miguel, D.W. Bruce, S. Okeya, D.G. Andrews, P.R. Ashton, I.R. Johnstone, and P.M. Maitlis. J. Chem. Soc. Dalton Trans. 1565 (1986).
17. H.E. Selnau and J.S. Merola. J. Am. Chem. Soc. **113**, 4008 (1991), and references therein.
18. M.A. Esteruelas, J. Herrero, and L.A. Oro. Organometallics, **12**, 2377 (1993).
19. D.M. Antonelli and M. Cowie. Organometallics, **9**, 1818 (1990).
20. L.-S. Wang, R. McDonald, and M. Cowie. Inorg. Chem. **33**, 3735 (1994).
21. R.B. Jordan. Reaction mechanisms of inorganic and organometallic systems. Oxford University Press, New York. 1991. Chap. 1.
22. D.M. Antonelli and M. Cowie. Inorg. Chem. **29**, 4039 (1990).
23. D.H. Berry and R. Eisenberg. Organometallics, **6**, 1637 (1987).
24. R.P. Aggarwal, N.G. Connelly, M.C. Crezso, B.J. Dunne, P.J. Hopkins, and A.G. Orpen. J. Chem. Soc. Chem. Commun. 33 (1989).
25. P.H. Bird, A.R. Fraser, and D.N. Hall. Inorg. Chem. **16**, 1923 (1977).
26. W.G. Sly. J. Am. Chem. Soc. **81**, 18 (1959).
27. F.A. Cotton, J.D. Jamerson, and B.R. Stults. J. Am. Chem. Soc. **98**, 1774 (1976).
28. J.-J. Bonnett and R. Mathieu. Inorg. Chem. **17**, 1973 (1978).

Can. J. Chem. Downloaded from www.nrcresearchpress.com by 80.90.12.36 on 09/08/12
For personal use only.

29. C. Bianchini, P. Dapporto, and A. Meli. J. Organomet. Chem. **174**, 205 (1979).
30. N.A. Bailey, M.R. Churchill, R. Hunt, R. Mason, and G. Wilkinson. Proc. Chem. Soc. (London), 401 (1964).
31. M.A. Bennett, R.N. Johnson, G.B. Robertson, T.W. Turney, and P.P. Whimp. J. Am. Chem. Soc. **94**, 6540 (1972).
32. R.S. Dickson, G.N. Pain, and M.F. Mackay. Acta Crystallogr. Sect. B: Struct. Crystallogr. Cryst. Chem. **B35**, 2321 (1979).
33. M. Angoletta, P.L. Bellon, F. Demartin, and M. Sansoni. J. Organomet. Chem. **208**, C12 (1981).
34. R.S. Dickson and G.N. Pain. J. Chem. Soc. Chem. Commun. 277 (1979).
35. M.R. Gagné and J. Takats. Organometallics, **7**, 561 (1988).
36. E.M. Kosower. An introduction to physical organic chemistry. Wiley, New York. 1968. p. 49.
37. N.M. Boag, M. Green, and F.G.A. Stone. J. Chem. Soc. Chem. Commun. 1281 (1980).
38. R.S. Dickson, C. Mok, and G. Pain. J. Organomet. Chem. **166**, 385 (1979).
39. M. Cooke, M. Green, and T.A. Kuc. J. Chem. Soc. A, 1200 (1971).
40. R.D. Kemmitt, B.Y. Kimura, and G.W. Littlecot. J. Chem. Soc. Dalton Trans. 636 (1973), and references therein.
41. E.O. Greaves, C.J.L. Lock, and P.M. Maitlis. Can. J. Chem. **46**, 3879 (1968).
42. J.L. Davidson, M. Green, F.G.A. Stone, and A.J. Welch. J. Chem. Soc. Dalton Trans. 2044 (1976).
43. J.P. Williams and A. Wojcicki. Inorg. Chem. **16**, 3155 (1977), and references therein.
44. M.I. Bruce, R.C.F. Gardner, and F.G.A. Stone. J. Chem. Soc. Dalton Trans. 906 (1979), and references therein.
45. H. Eshtiagh-Hosseini, J.F. Nixon, and J.S. Poland. J. Organomet. Chem. **164**, 107 (1979).
46. B.T. Sterenberg and M. Cowie. Manuscript in preparation.
47. M.D. Fryzuk, L. Huang, N.T. McManus, P. Paglia, S.J. Rettig, and G.S. White. Organometallics, **11**, 2979 (1992).
48. J. Schwartz, D.W. Hart, and B. McGiffert. J. Am. Chem. Soc. **96**, 5613 (1974).
49. J. Wolf and H. Werner. Organometallics, **6**, 1164 (1987).
50. J.S. Merola. Organometallics, **8**, 2975 (1989).
51. A.J. Deeming, B.L. Shaw and R.E. Stainbank. J. Chem. Soc. (A), 374 (1971).
52. D.M. Antonelli and M. Cowie. Organometallics, **10**, 2550 (1991).
53. (*a*) F. Antwi-Nsiah and M. Cowie. Organometallics, **11**, 3157 (1992). (*b*) F. Antwi-Nsiah, O. Oke, and M. Cowie. Manuscript in preparation.
54. T. Graham, F. Van Gastel, and M. Cowie. Manuscript in preparation.
55. Y.N. Al-Obaidi, M. Green, N.D. White, and G.E. Taylor. J. Chem. Soc. Dalton Trans. 319 (1982).
56. F.J. García Alonso, V. Riera, M.A. Ruiz, A. Tiripicchio, and M. Tiripicchio Camellini. Organometallics, **11**, 370 (1992).
57. (*a*) C.-L. Lee, C.T. Hunt, and A.L. Balch. Inorg. Chem. **20**, 2498 (1981); (*b*) J.L. Mague and S.H. DeVries. Inorg. Chem. **21**, 1632 (1982); (*c*) J.T. Mague. Inorg. Chem. **22**, 45 (1983); (*d*) Organometallics, **5**, 918 (1986); (*e*) R.J. Puddephatt and M.A. Thomson. Inorg. Chem. **21**, 725 (1982); (*f*) J.A. Jenkins and M. Cowie. Organometallics, **11**, 2774 (1992), and references therein.

Can. J. Chem. Downloaded from www.nrcresearchpress.com by 80.90.12.36 on 09/08/12
For personal use only.

Electrocatalytic activity of a graphite electrode coated with hexadecachlorophthalocyanatoiron(II) toward sulfide oxidation, and its possible application in electroanalysis

Jiujun Zhang, A.B.P. Lever, and W.J. Pietro

Abstract: A graphite electrode coated with hexadecachlorophthalocyanatoiron(II), $Fe^{II}[Cl_{16}Pc(2-)]$, serves as an electrocatalyst for the oxidation of sulfide ion in basic solutions (pH range: 8–14). The surface electrochemical responses of this catalyst and corresponding electrocatalytic activity are discussed. The sulfide ion concentration dependences of the peak current in cyclic voltammograms are examined to show the possible application of this catalyst-coated electrode in amperometric sulfide sensors.

Key words: phthalocyanine, modified graphite electrode, sulfide oxidation, electroanalysis, electrocatalysis.

Résumé : On peut utiliser une électrode de graphite recouverte d'hexadécachlorophtalocyanatofer(II), $Fe^{II}[Cl_{16}Pc(2-)]$, comme électrocatalyseur pour l'oxydation de l'ion sulfure, en solutions basiques (pH allant de 8 à 14). On discute des réponses électrochimique de surface de ce catalyseur et de l'activité électrocatalytique correspondante. Dans le but de démontrer l'application possible de cette électrode recouverte de catalyseur comme senseur ampérométrique des sulfures, on a examiné les relations qui existent entre la concentration de l'ion sulfure et le courant de pic des voltampérogrammes cycliques.

Mots clés : phtalocyanine, électrode de graphite modifiée, oxydation du sulfure, électroanalyse, électrocatalyse.

[Traduit par la rédaction]

Can. J. Chem. Downloaded from www.nrcresearchpress.com by 80.90.12.36 on 09/08/12
For personal use only.

Introduction

Perhalogenated metallophthalocyanines have been reported to be effective catalysts for the reduction of dioxygen (1, 2). Most recently, we discovered that one of the perhalogenated metallophthalocyanines, hexadecachlorophthalocyanatoiron(II) (abbreviated as $Fe^{II}[Cl_{16}Pc(2-)]$), when it is coated on a graphite electrode (labelled as $Fe^{II}[Cl_{16}Pc(2-)]/C$ in this paper), displays very high activity toward the oxidation of sulfide ion in basic solutions.

The electrocatalytic oxidation of sulfide ion on graphite electrodes modified by metallophthalocyanines such as CoPc and FePc (3), CoTmtppa (Co(II)-N,N′,N″,N‴-tetramethyltetra-3,4-pyridinoporphyrazine) (4),[2] CoTapc (Co(II)-tetraaminophthalocyanine) (5), and CuAc (Cu(II)-alizarin complexone) (6) have been studied extensively. However, of the metallophthalocyanines that we have tested (almost 20 metallophthalocyanines containing Co(II), Fe(II), Mn(II), Ru(II), Cr(II), Cu(II), or Rh(II), and with various substituents), $Fe^{II}[Cl_{16}Pc(2-)]$ proves to form the most stable surface species with very high catalytic activity for sulfide oxidation. As a continuing examination of surface electrocatalysis and its application in electrochemical sensors (1, 4–7), this paper reports the electrocatalytic behaviour of $Fe^{II}[Cl_{16}Pc(2-)]$ toward the oxidation of sulfide ion.

Generally, electrodes used to oxidize sulfide ion are fouled (poisoned) by the elemental sulfur that is then deposited thereon. While deposition also occurs on this electrode, the elemental sulfur can be stripped off by reduction back to sulfide ion and thereby regenerates an electrode that behaves like the pristine electrode.

Received November 30, 1994.

This paper is dedicated to Professor William A.G. Graham on the occasion of his 65th birthday.

J. Zhang, A.B.P. Lever,[1] and W.J. Pietro. Department of Chemistry, York University, North York, ON M3J 1P3, Canada.

[1] Author to whom correspondence may be addressed. Telephone: (416) 736-2100, ext. 22309. Fax: (416) 736-5936. Internet: BLEVER@YORKU.CA

[2] J.J. Zhang, Y.H. Tse, A.B.P. Lever, and W.J. Pietro. Manuscript in preparation.

Experimental section

Chemicals and solutions

Hexadecachlorophthalocyanatoiron(II) was synthesized, purified, and characterized according to the methods described in ref. 1. Sodium sulfide ($Na_2S{\cdot}9H_2O$, BDH Chemicals) was reagent-grade and used without further purification, as were other reagent grade chemicals. The pH (8–14) of the solution was controlled with 0.01 M $NaH_2PO_4/Na_2HPO_4/NaOH$ buffers, which were added to 0.1 M $NaClO_4$ supporting electro-

Can. J. Chem. Downloaded from www.nrcresearchpress.com by 80.90.12.36 on 09/08/12
For personal use only.

lyte. Solutions were deaerated by bubbling with pure argon gas (99.99%). Test solutions of sodium sulfide were prepared from 0.1 M Na_2S stock solution prepared before each experiment, by addition to a previously deaerated supporting electrolyte solution to a desired concentration. Water was purified by double distillation with $KMNO_4$, followed by passage through the Barnstead organic removal cartridge and two Barnstead mixed-resin Ultrapure cartridges.

Electrode preparation

Basal pyrolytic graphite (BPG) electrodes (Union Carbide) were sealed to stainless steel shafts with heat shrinkable polyolefin tubing. The electrodes, mounted with basal planes of the graphite exposed, were polished using 0.5 μm alumina powders, sonicated for 5 min in water, and rinsed with acetone and water before each experiment. The electrode area, 0.17 cm^2, was calibrated using a solution of 1 mM $[Fe(CN)_6]^{3-}$.

The electrode surface was modified by soaking a clean polished electrode in a DMF solution containing 1 mM $Fe^{II}[Cl_{16}Pc(2-)]$ for 15 min; the electrode was then washed and transferred to the test solution to record cyclic voltammetry.

Electrochemical measurements

Cyclic voltammetry was performed using the Pine Instruments RDE3 potentiostat and an X–Y recorder. A conventional three-compartment electrochemical cell with an SCE reference and a Pt counter electrode was used for the electrochemical studies.

Results and discussion

A. Surface electrochemical responses of a graphite electrode coated with $Fe^{II}[Cl_{16}Pc(2-)]$

Cyclic voltammograms (Fig. 1) of a graphite electrode coated with 1.3×10^{-9} mol cm^{-2} of $Fe^{II}[Cl_{16}Pc(2-)]$, recorded in a 0.1 M NaOH + 0.1 M $NaClO_4$ solution, show three redox couples, labelled (I′/I), (II′/II), and (III′/III) to more negative potentials, respectively. Because there is no $Fe^{II}[Cl_{16}Pc(2-)]$ in the test solution, all three waves are attributed to surface responses, which was confirmed by the linear relationships between the peak current and potential scan rate shown by the insert in Fig. 1. These data using basal-plane pyrolytic graphite are of somewhat better quality than those previously described using highly oriented pyrolytic graphite (1), and hence merit further comment. Waves (I′/I), (II′/II) and (III′/III) are the redox processes of couples $Fe^{III}[Cl_{16}Pc(2-)]^+$ /$Fe^{II}[Cl_{16}Pc(2-)]$, $Fe^{II}[Cl_{16}Pc(2-)]$/$Fe^{I}[Cl_{16}Pc(2-)]^-$, and $Fe^{I}[Cl_{16}Pc(2-)]^-$/$Fe^{I}[Cl_{16}Pc(3-)]^{2-}$, respectively, as confirmed in a previous study (1).

The waves for $Fe^{III}[Cl_{16}Pc(2-)]^+$/$Fe^{II}[Cl_{16}Pc(2-)]$ and $Fe^{II}[Cl_{16}Pc(2-)]$/$Fe^{I}[Cl_{16}Pc(2-)]^-$, which are the responses of the metal centre, exhibit much smaller peak currents and area than the wave for the $Fe^{I}[Cl_{16}Pc(2-)]^-$ /$Fe^{I}[Cl_{16}Pc(3-)]^{2-}$ couple, which is a ligand reduction process. This phenomenon was observed in previous studies for a series of metallophthalocyanines (1, 2, 4, 8–10 and footnote 2).

For a one-electron Nernstian response from the reactant confined to the electrode surface, the peak-to-peak potential separation should be zero, and the half-bandwidth should be about 90.6 mV (11). The response of wave (I′/I) (in Fig. 1) with a zero peak-to-peak potential separation and a half-bandwidth of 91 mV is consistent with Nernstian behaviour. However, the responses of wave (II′/II), with a 30 mV peak-to-peak separation and half-bandwidth of 140 mV, and wave (III′/III), with a peak-to-peak separation of 190 mV (scan rate: 100 mV s^{-1}) and half-bandwidths of 55 mV (cathodic) and 120 mV (anodic), deviate from Nernstian behaviour.

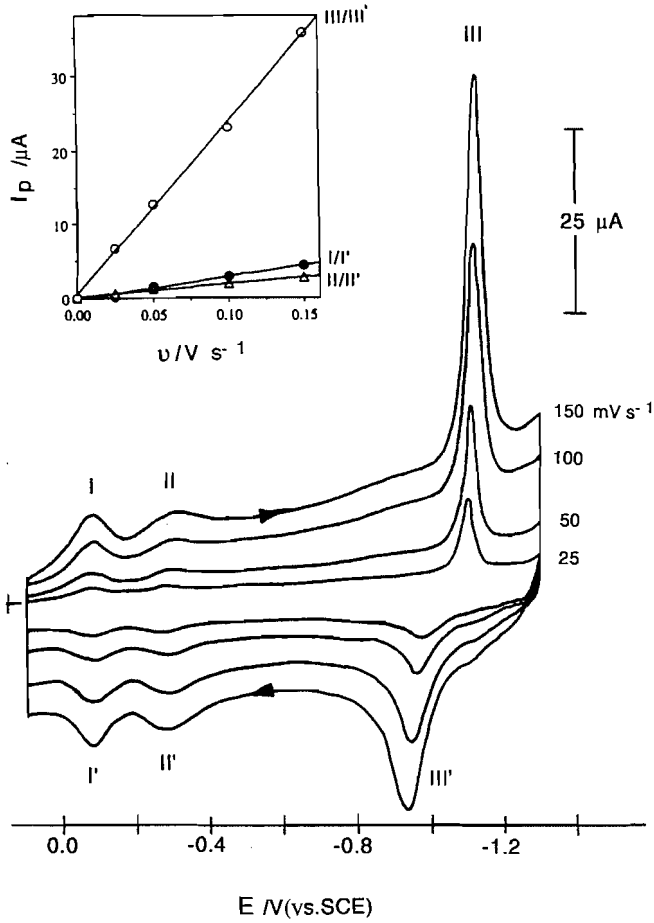

Fig. 1. Cyclic voltammetry of $Fe^{II}[Cl_{16}Pc(2-)]$ (1.3×10^{-9} mol cm^{-2}) coated on a BPG electrode. The freshly polished electrode was first soaked in 1×10^{-3} M $Fe^{II}[Cl_{16}Pc(2-)]$ DMF solution for 15 min, washed, and transferred to pure supporting electrolyte (0.1 M NaOH + 0.1 M $NaClO_4$, pH 13) to record the voltammograms. Equlibrium scan. Potential scan rates as marked in the figure. Insert: Potential scan rate dependence of the average peak current of waves (I′/I), (II′/II), and (III′/III).

By measuring the charge under waves (I′/I) we arrive at a surface concentration of approximately 1.5×10^{-10} mol cm^{-2} (assuming a one-electron process), which corresponds roughly to a monolayer. This suggests that even though the coating is much thicker than a monolayer, only the $Fe^{II}[Cl_{16}Pc(2-)]$ in direct contact with the surface is electrochemically active insofar as the iron centres are concerned.

The charge under wave III is some 10 times greater, suggesting that for this ligand process the entire layer of $Fe^{II}[Cl_{16}Pc(2-)]$ is involved. This is likely interpreted in terms of electronic interactions between adjacent Pc units in the stacked aggregated layer on the electrode surface (1, 2), resulting in rapid electron exchange and hence allowing the entire layer to be oxidized or reduced at the ligand site. Evidently this is not so facile for the metal-centred redox processes. The

Can. J. Chem. Downloaded from www.nrcresearchpress.com by 80.90.12.36 on 09/08/12
For personal use only.

Fig. 2. Cyclic voltammograms for the oxidation of sulfide ion on a BPG electrode: (*A*) a bare electrode in a solution containing 1×10^{-3} M Na_2S; (*B*) a BPG electrode coated by 1.3×10^{-9} mol cm^{-2} of $Fe^{II}[Cl_{16}Pc(2-)]$ in pure supporting electrolyte; and (*C*) a BPG electrode coated by 1.4×10^{-9} mol cm^{-2} of $Fe^{II}[Cl_{16}Pc(2)]$ in the presence of 1×10^{-3} M Na_2S. The supporting electrolyte was 0.1 M $NaClO_4$ + 0.1 M NaOH. First scan. Potential scan rate: 20 mV s^{-1}.

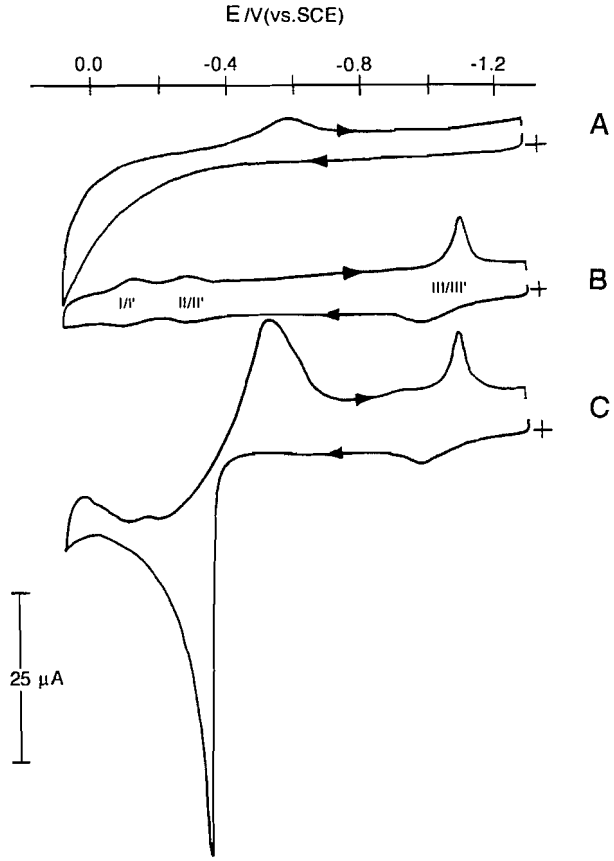

pH dependencies of these waves (average of the anodic and cathodic components) are similar to those previously described (1), i.e., waves (I′/I) and (III′/III) show dependencies of −87 and −68 mV/pH respectively, while waves (II′/II) are essentially pH independent, in agreement with previous literature expectation (10). However, we note that wave III has a potential that becomes pH independent (at −1.12 V) beyond pH 12.0; its oxidation component, wave III′, apparently remains pH dependent in this regime. For further discussion of the pH dependences, see refs. 1 and 2.

B. Electrocatalytic activity of $Fe^{II}[Cl_{16}Pc(2-)]$/C toward the oxidation of sulfide ion

A $Fe^{II}[Cl_{16}Pc(2-)]$ coated graphite electrode displays very strong catalytic activity toward the oxidation of sulfide ion in a basic solution (Fig. 2). On a bare electrode (Fig. 2*A*), in the presence of sulfide ion, the oxidation current that starts at about −0.2 V spreads over a wide potential range. This process corresponds to oxidation from S^{2-} to S^0, which then deposits on the electrode surface (see ref. 6 for more detail). The reduction of the deposited S^0 occurs at about −0.57 V (see reverse wave in Fig. 2*A*). However, when $Fe^{II}[Cl_{16}Pc(2-)]$ is coated on the same electrode, a significant catalytic current for

Fig. 3. Linear sweep voltammetry of a BPG electrode on which 1.2×10^{-9} mol cm^{-2} of $Fe^{II}[Cl_{16}Pc(2-)]$ was coated. (*A*) In 1.2×10^{-3} M Na_2S, potential scanning from −1.3 to 0.1 V; (*B*) the electrode in (*A*) was transferred to a pure supporting electrolyte solution, potential scanning from 0.1 to −1.3 V. The supporting electrolyte was 0.1 M $NaClO_4$ + 0.1 M NaOH. Potential scan rate: 20 mV s^{-1}.

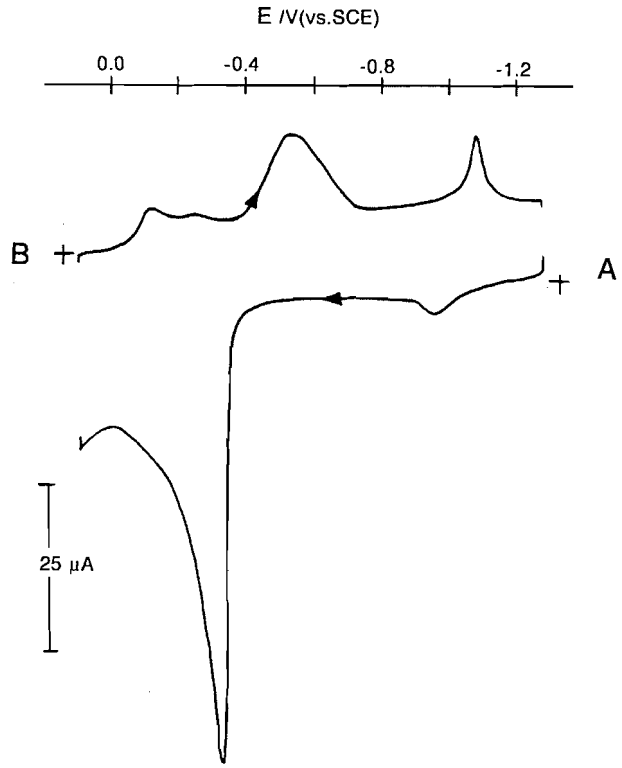

sulfide oxidation starting from −0.4 V can be observed (Fig. 2*C*). The steep rise in oxidation current, maximum at −0.33 V (20 mV s^{-1}), reflects a high catalytic rate. The catalytic oxidation commences near the potential of wave (II′/II) (Fig. 2*B*), which strongly suggests that $Fe^{II}[Cl_{16}Pc(2-)]$ (i.e., in oxidation state (II)) is the active catalyst (see below). A reverse wave near −0.55 V (Fig. 2*C*) indicates that the product of sulfide oxidation can be reduced when the potential is scanned back to the negative range. Since the reduction current rapidly descends to zero current, following (more negative than) the peak, this reverse wave is a surface process, proven by the experiment shown in Fig. 3.

In Fig. 3, linear sweep voltammetry was recorded on a $Fe^{II}[Cl_{16}Pc(2-)]$ coated electrode in a 1.2 mM Na_2S solution from a potential ranging from −1.3 to 0.1 V (Fig. 3*A*). The electrode was then taken out of the sulfide-containing solution, washed, and transferred to a solution containing only supporting electrolyte to record the current–potential curve from 0.1 to −1.3 V (Fig. 3*B*). In curve 3*B*, a surface stripping wave near −0.53 V can be observed. In our previous study of a Cu^{II}–Alizarin complexone coated electrode, a similar stripping wave is assigned to the reduction of electrodeposited S^0 to S^{2-} by a two-electron transfer process (6). The three other peaks near −0.1, −0.27, and −1.1 V in curve 3*B* are the waves I, II, and III, respectively.

To estimate roughly how many electrons are involved in the catalytic oxidation of sulfide ion in Fig. 2*C*, a set of cyclic vol-

Can. J. Chem. Downloaded from www.nrcresearchpress.com by 80.90.12.36 on 09/08/12
For personal use only.

Fig. 4. Cyclic voltammograms of a BPG electrode coated by 1.2×10^{-9} mol cm^{-2} of $Fe^{II}[Cl_{16}Pc(2-)]$ in 1×10^{-3} M Na_2S + 0.1 M $NaClO_4$ + 0.1 M NaOH solution. Potential scan rates as marked in the figure.

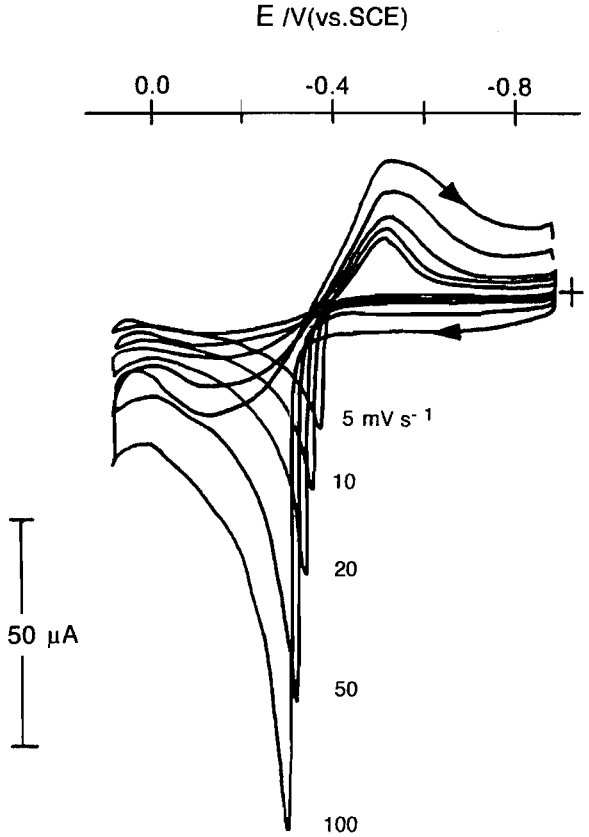

tammograms was obtained at various potential scan rates (Fig. 4). Assuming that the catalytic oxidation is a totally diffusion-controlled process, a combination between the relationships for E_p vs. log v, and I_p vs. $v^{1/2}$ (where E_p is the peak potential of oxidation current, I_p is the peak current, and v is the potential scan rate) allows one to estimate the number of electrons involved in the corresponding process (7). Figure 5 shows these experimental relationships. The linear relationships indicate that the model described by eqs. [1] and [2] fits the electrocatalytic process for sulfide oxidation.

$$[1] \quad E_p = K + (0.03/\alpha n_\alpha) \log v$$

$$[2] \quad I_p = 2.99 \times 10^5 n (\alpha n_\alpha)^{1/2} A C_0 D_0^{1/2} v^{1/2}$$

From the slope of the line in Fig. 5*A*, a value of $\alpha n_\alpha = 0.49$ can be calculated. The slope from Fig. 5*B* can be combined with this value of αn_α, and the assumed value of D_0 (1.7×10^{-5} cm^2 s^{-1}, which is the diffusion coefficient of sulfide ion in the form of HS^-) to obtain the value of the electron number, $n = 2.2$. As expected, we observed a two-electron process of the electrocatalytic oxidation of sulfide ion.

The area under the oxidation wave (Fig. 3*A*) corresponds to 3.3×10^{-9} moles of sulfide ion. The stripping wave near -0.53 V in Fig. 3*B*, which is a reduction of S^0 back to S^{2-} by a two-electron transfer, corresponds to 5.8×10^{-10} moles, which is only 17.5% of the total quantity of sulfide ion involved in the

Fig. 5. (*A*) Peak potential in cyclic voltammograms (Fig. 4) as a function of logarithm of potential scan rate; (*B*) magnitude of the peak current in cyclic voltammograms (Fig. 4) as a function of square root of potential scan rate.

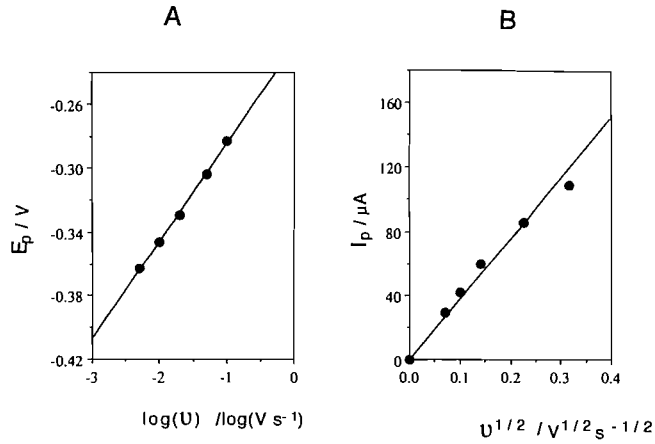

catalytic oxidation. The remaining 82.5% of oxidized sulfide ion is probably in the form of soluble S_x^{2-} in the basic solution, and is not electrochemically detected. The solubility of elemental sulfur in sulfide ion solution will increase with increasing concentration of sulfide; thus at very low concentrations of sulfide ion, a greater proportion of the elemental sulfur remains deposited on the electrode, as indicated by a larger ratio of the stripping current to the oxidation current (data not shown). We must also suppose that, as the potential is scanned through the sulfide oxidation wave, some elemental sulfur is being deposited on the electrode and may partially inhibit the depolarization of the incoming sulfide ion. Thus the current maximum at -0.33 V (20 mV s^{-1}) is probably slightly underestimated.

C. A suggested mechanism for electrocatalytic oxidation of sulfide ion on a $Fe^{II}[Cl_{16}Pc(2-)]$/ C electrode

The electrochemical oxidation of sulfide ion to elemental sulfur has been studied very extensively in the literature (6, 12–22); here we will only deal with the involvement of the surface coating of $Fe^{II}[Cl_{16}Pc(2-)]$ and other aspects will not be explored.

As indicated in Figs. 2*B* and 2*C*, in which the catalytic oxidation commences near the potential of wave (II′/II), the $Fe^{II}[Cl_{16}Pc(2-)]$ species is believed to be the active catalyst that is confined to the electrode surface to undergo the inner-sphere mechanism for sulfide oxidation.

In this inner-sphere mechanism, the first step is formation of a sulfide adduct:

$$[3] \quad Fe^{II}[Cl_{16}Pc(2-)] + HS^- \longleftrightarrow HS^-\text{-}Fe^{II}[Cl_{16}Pc(2-)]$$

followed by electron transfer from bound HS^- to electrode through the catalyst to form, under oxidative polarization by the electrode, the final product:

$$[4] \quad HS^-\text{-}Fe^{II}[Cl_{16}Pc(2-)] + OH^- \longrightarrow Fe^{II}[Cl_{16}Pc(2-)] + S^0 \text{ (and (or) } S_x^{2-}) + H_2O + 2e^-$$

Since the product is the regenerated Fe^{II} species, the process

Fig. 6. Sulfide concentration dependences of peak current in cyclic voltammograms recorded on a BPG electrode on which 9.1×10^{-10} mol cm^{-2} of $Fe^{II}[Cl_{16}Pc(2-)]$ was coated, in three concentration ranges: (*A*) $0–10^{-4}$ M; (*B*) $0–10^{-3}$ M; and (*C*) $0–10^{-2}$ M. The supporting electrolyte was 0.1 M NaOH + 0.1 M $NaClO_4$, pH 13. Potential scan rate: 100 mV s^{-1}.

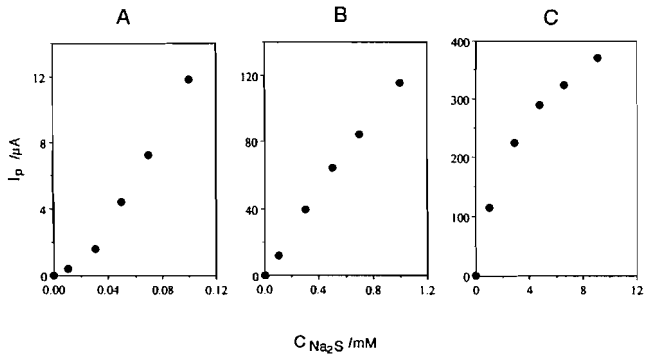

is electrocatalytic. A more detailed assessment of the mechanism would require much more detailed experimental data, which have not yet been obtained.

D. Sulfide concentration dependence of peak current in cyclic voltammograms, and its possible application in sulfide analysis

The dependence of peak current on sulfide ion concentration ($10^{-5}–10^{-2}$ M) in cyclic voltammetric studies recorded at a $Fe^{II}[Cl_{16}Pc(2-)]$/C electrode in basic solution is shown in Fig. 6. Cyclic voltammograms in a solution containing a low sulfide concentration, for example, down to 1×10^{-5} M (not shown here) (0.32 ppm), still show measurable catalytic currents near −0.4 V, indicating that a very low concentration of sulfide could be determined by measuring the peak current. Although the relationship between sulfide ion concentration and peak current, shown in Fig. 6, is not perfectly linear, probably due to the poison effects discussed above, it is reproducible and suitable, after calibration of an electrode, for the purpose of analysis.

The sensitivity for determining sulfide ion using cyclic voltammetry is limited to 1×10^{-5} M (0.32 ppm). The measurable concentration range in aqueous solutions is 1×10^{-5} to 1×10^{-2} M.

D.1 Surface concentration of catalyst

The effect of surface concentration on the electrocatalytic peak current in the cyclic voltammograms was examined briefly in a solution (pH 13) containing 1×10^{-3} M sulfide ion. Below a surface concentration of 0.8×10^{-9} mol cm^{-2} (ca. 5 layers), the peak current is almost proportional to the surface concentration of the catalyst. However, with thicker layers, when the surface concentration exceeds 1.0×10^{-9} mol cm^{-2}, saturation in the peak current can be observed (data not shown). This observation may conflict with our earlier analysis that only the monolayer in contact with the electrode is active insofar as couple (I′/I) is concerned. Possibly the sulfide ions can mediate the redox process occurring at subsequent layers.

D.2 Poisoning of the surface catalyst and recovery therefrom

The S^0 layer deposited upon oxidation (reaction [4]) actually poisons the catalytic activity of the $Fe^{II}[Cl_{16}Pc(2-)]$ surface if the S^0 is not removed. Experiments with a rotating BPG disk electrode coated with $Fe^{II}[Cl_{16}Pc(2-)]$ in a sulfide-containing solution gave very ill-featured current-potential curves. A peaklike diffusion current rather than a plateau was observed, indicating deactivation of the catalyst. However, the catalytic activity of $Fe^{II}[Cl_{16}Pc(2-)]$/C can be recovered if the deposited sulfur layer is stripped at −0.5 V, after which the full catalytic current is retained both in the cyclic voltammogram and current–potential curves using a rotating disk electrode.

Because the coating of sulfur poisons the rotating disk electrode, a more quantative analysis of the kinetics of this electrocatalytic oxidation of sulfide ion was not pursued.

D.3 Long-term stability

The continued cycling of an electrode in a sulfur-containing solution leads to voltammograms that are superimposable over many hours. Coated electrodes that are removed from solution, dried, and stored for several days can then be returned to the same sulfur-containing solution to regenerate an almost identical voltammogram. Longer term studies of stored electrodes are in progress.

D.4 Interference tests

In interference tests, common species such as F^-, Cl^-, Br^-, $[CO_3]^{2-}/[HCO_3]^-$, $[SO_4]^{2-}$, $[SO_3]^{2-}$, $[NO_3]^-$, $[NO_2]^-$, NH_3, H_2O_2, and O_2 show no effect on the catalytic current for sulfide oxidation in pH 13 solution. Common metal ions, which are precipitated in such a basic solution, show no interference with sulfide measurements. However, species such as I^-, SCN^-, and CN^- interfere with the measurements due to strong coordination to the Fe(II) centre in the catalyst blocking the active centre for adduct formation.

Conclusion

A catalyst that is electrocatalytically active toward the oxidation of sulfide ion, $Fe^{II}[Cl_{16}Pc(2-)]$, can be easily coated onto a graphite electrode surface by dipping a freshly polished electrode into a DMF solution of this catalyst.

The active species, $Fe^{II}[Cl_{16}Pc(2-)]$, catalyzes the sulfide ion oxidation in a basic solution through a two-electron transfer process from S^{2-} to S^0, which is then partially deposited on the electrode surface, deactivating the catalyst. However, the active catalyst $Fe^{II}[Cl_{16}Pc(2-)]$/C can easily be recovered, quantitatively, by stripping off the S^0 deposition layer at −0.5 V.

The high stability of $Fe^{II}[Cl_{16}Pc(2-)]$/C and the high reproducibility of catalytic oxidation current in cyclic voltammograms make it feasible to employ this modified electrode for sulfide electroanalysis in basic solutions.

Acknowledgment

We are indebted to the Natural Sciences and Engineering Research Council of Canada for a Strategic Grant supporting this work.

References

1. M.N. Golovin, P. Seymour, K. Jayaraj, Y. Fu, and A.B.P. Lever. Inorg. Chem. **29**, 1719 (1990).

Can. J. Chem. Downloaded from www.nrcresearchpress.com by 80.90.12.36 on 09/08/12
For personal use only.

2. J. Ouyang, K. Shigehara, A. Yamada, and F.C. Anson. J. Electroanal. Chem. **297**, 489 (1991).
3. J.H. Zagal, C. Paez, and S. Barbato. *In* Electrode materials processes for energy conversion storage. Vol. 87-12. *Edited* by S. Srinivasan, S. Wagner, and H. Wrobloba. The Electrochemical Society, Princeton, N.J. 1987. p. 295.
4. Y.H. Tse, P. Janda, and A.B.P. Lever. Anal. Chem. **66**, 384 (1994). US Patent 5,342,490 (1994).
5. Y.H. Tse and A.B.P. Lever. Anal. Chem. **67**, 981 (1995).
6. J.J. Zhang, A.B.P. Lever, and W.J. Pietro. J. Electroanal. Chem. **385**, 191 (1995).
7. J.J. Zhang, A.B.P. Lever, and W.J. Pietro. Inorg. Chem. **33**, 1392 (1993).
8. S. Zecevic, B. Simic-Glavaski, E. Yeager, A.B.P. Lever, and P.C. Minor. J. Electroanal. Chem. **196,** 339 (1985).
9. P. Janda, N. Kobayashi, P.R. Auburn, H. Lam, C.C. Leznoff, and A.B.P. Lever. Can. J. Chem. **67**, 1109 (1989).
10. A.B.P. Lever, E.R. Milaeva, and G. Speier, in Phthalocyanines: properties and applications Vol. 3. Edited by C.C. Leznoff and A.B.P. Lever, VCH, New York. 1993. p. 1.
11. A.J. Bard and L.R. Faulkner. Electrochemical methods, fundamentals and applications. John Wiley & Sons, New York. 1980. Chap. 12.
12. S.I. Zhdanov. *In* Encyclopedia of electrochemistry of the elements. Vol. 4. *Edited by* A.J. Bard. Marcel Dekker, Inc., New York. 1975. Chaps. 4–6.
13. A. Briceno and S. Chander. J. Appl. Electrochem. **20**, 506 (1990).
14. A. Briceno and S. Chander. J. Appl. Electrochem. **20**, 512 (1990).
15. S.A. Shmakov, A.V. Dribinskii, V.A. Rylov, and M.R. Tarasevich. Sov. Electrochem. (Engl. Transl.), **22**, 1285 (1986).
16. L. Edwards, R.I. Holliday, and D. Honey. J. Electroanal. Chem. **297**, 425 (1991).
17. Z. Mao, R.E. White, S. Srinivasan, A.J. Appleby, and B. Dandapani. J. Electrochem. Soc. **137**, 2189 (1990).
18. P.L. Allen and A. Hickling. Trans. Faraday Soc. **53**, 1626 (1957).
19. J.A. Rodriguez. Surf. Sci. **234**, 421 (1990).
20. M. Kazinets and A. Kiriaty. Ultramicroscopy, **14**, 377 (1984).
21. B. Scharifker, J. Mozota, and R. Rugeles. Electrochim. Acta, **29**, 261 (1984).
22. J. Mozota, R. Rugeles, and B. Scharifker. J. Electrochem. Soc. **129**, C142 (1982).

Can. J. Chem. Downloaded from www.nrcresearchpress.com by 80.90.12.36 on 09/08/12
For personal use only.

Extensions of the applicability of the MMX molecular modelling system to determination of barriers to rotation of π-bonded ligands

Joel Polowin, Robert Poe, and Michael C. Baird

Abstract: The commercially available molecular mechanics package PCMODEL, which has been shown to be very useful for determining conformational energy profiles for rotation of σ-bonded ligands, cannot be utilized to determine barriers to rotation of π-bonded ligands because of limitations in the way the π-bonding interactions are defined. This paper describes a partially successful modification of the dihedral driver of PCMODEL that makes possible reasonable calculations of the conformational energy profiles for rotation of the π-bonded arene ligands in the compounds $(\eta^6\text{-arene})Cr(CO)_2(PPh_3)$ (arene = C_6H_6, C_6Me_6) and of the π-bonded ethylene ligands in $[PtCl_3(\eta^2\text{-}CH_2{=}CH_2)]^-$ and $[(\eta^5\text{-}C_5H_5)Re(NO)(PPh_3)(\eta^2\text{-}CH_2{=}CH_2)]^+$. The steric barriers to ethylene rotation in the latter two complexes were found to be small relative to the electronic barriers to ligand rotation.

Key words : molecular mechanics, olefin rotation, conformational energy profile.

Résumé : Le programme de mécanique moléculaire PCMODEL disponible commercialement est très utile pour déterminer les profiles d'énergie conformationnelle des rotations autour des coordinats avec des liaisons σ; toutefois, à cause de ses limitations dans la façon dont les interactions dans les liaisons π y sont définies, on ne peut l'utiliser pour déterminer les barrières à la rotation des coordinats avec des liaisons π. Ce travail décrit un modification conducteur dièdre de PCMODEL qui permet, avec des succès partiels, de faire des calculs raisonnables des profiles d'énergie conformationnelle pour la rotation des coordinats arènes avec des liaisons π dans les composés $(\eta^6\text{-arène})Cr(CO)_2(PPh_3)$ (arène = C_6H_6 et C_6Me_6) et les coordinats éthylène avec des liaisons π dans $[PtCl_3(\eta^2\text{-}CH_2{=}CH_2)]^-$ et $[(\eta^5\text{-}C_5H_5)Re(NO)(PPh_3)(\eta^2\text{-}CH_2{=}CH_2)]^+$. On a trouvé que les barrières stériques à la rotation de l'éthylène dans les deux derniers complexes est faible par rapport aux barrières électroniques à la rotation du coordinat.

Mots clés : mécanismes moléculaires, rotation d'oléfine, profile d'énergie conformationnelle.

[Traduit par la rédaction]

Introduction

Bill Graham joined the Department of Chemistry at the University of Alberta in 1962, and very quickly began making significant contributions to the rapidly developing field of organotransition metal chemistry.[2] One of the earlier contributions by the Graham group, in 1967, involved recognition of possibly the first example of conformational isomerism in an organometallic compound. Compounds of the type $\eta^5\text{-}C_5H_5Fe(CO)_2X$ normally exhibit two bands of comparable intensity in the carbonyl stretching region of the IR, the symmetric and the asymmetric carbonyl stretching modes. In contrast, the solution IR spectra of the compound $\eta^5\text{-}C_5H_5Fe(CO)_2SiMeCl_2$ exhibited doubling of the carbonyl stretching bands, an observation interpreted in terms of population of two rotamers, **A** and **B** (1*a*).

As only a single cyclopentadienyl resonance was observed in the ^1H NMR spectrum, it was concluded that interconversion between **A** and **B** via rotation about the Fe—Si bond is rapid on the NMR time scale.

Since 1967, numerous examples of rotational isomerism in organometallic compounds have been deduced on the basis of IR spectroscopy (1*b–f*), and information concerning the conformational energy profiles has in many cases become avail-

Received September 30, 1994.

This paper is dedicated to Professor William A.G. Graham on the occasion of his 65th birthday, and in memory of the Brunswick House.

J. Polowin, R. Poe, and M.C. Baird.[1] Department of Chemistry, Queen's University, Kingston, ON K7L 3N6, Canada.

[1] Author to whom correspondence may be addressed. Telephone: (613) 545-2616. Fax: 613-545-6669. E-mail bairdmc@qucdn.queensu.ca

[2] Bill Graham made a very significant impact on the development of organometallic chemistry in Canada in particular. During the early 1960s, inorganic chemical research in Canadian universities was carried out almost completely by "imports" from the United Kingdom and, as the first native-born Canadian organometallic chemist to gain an international reputation for his research, Bill served as a much appreciated role model for the many younger Canadians who were beginning their careers at that time.

Can. J. Chem. Downloaded from www.nrcresearchpress.com by 80.90.12.36 on 09/08/12
For personal use only.

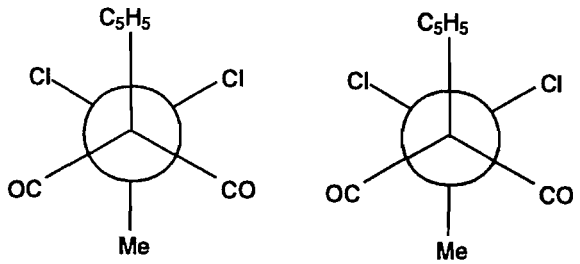

A B

able through variable temperature (VT) NMR spectroscopy (1*e*, 2) and, more recently, via molecular mechanics (MM) calculations (1*e*, 2). We (1*e*, 2*d*), utilizing MMX,[3] and others (2*a*–*c*) have demonstrated that the latter approach has considerable merit. Calculated conformational energy profiles for ligand rotation, for instance, in a variety of flexible organometallic compounds are in very good agreement with relevant experimentally derived information.

Our use of MMX has been limited, however, to determination of barriers to rotation of σ-bonded ligands, which are satisfactorily treated using a normal MM2-based force field (4) (see below). In contrast, while π-ligands are coordinated to metal atoms via otherwise "normal" bonds, MMX does not define force constants for either dihedral angles or bond angles associated with coordination. The dihedral-driver function of PCMODEL requires that the dihedral angle being driven be in the list of dihedral angles used by the program's minimization routines. One of the consequences of this is that one part of a structure cannot be rotated with respect to the rest of the structure unless that part is attached to the main structure with a normal bond. This connection is necessary to create the dihedral angle for the list, and thus calculations of barriers to rotation of π-bonded ligands have heretofore not been possible.

A bonding connection between two atoms is described inside PCMODEL with an integer value that specifies the bond order, i.e., 1, 2, or 3 for single, double, or triple bonding, respectively. Coordination of a π atom to a metal is handled by PCMODEL in much the same way as is a regular bond, the information being stored in the same data array, and the integer 9 being used to describe the bond type. When PCMODEL creates its lists of bond angles and torsional angles for a given molecule, it checks for bonds of type 9 and atoms of type-80 (transition-metal atoms). Bond angles with type 80 atoms at their centres and torsional angles involving bonds of type 9 are excluded from the lists.[4] It is therefore impossible to utilize the dihedral driver to rotate a π-coordinated group with respect to the rest of the structure: none of the dihedral angles between the two parts of the structure are included in the list, since the connections between the parts are made only with type-9 "bonds." This paper describes an algorithm that allows conformational energy profiles to be computed for rotation of simple π-bonded ligands.

Computational methodology

PCMODEL was modified to allow a π-coordinated group to be rotated by defining a new atom type, a dummy atom of atom type number 79. This number is close to the transition-metal type 80, since that type also is treated differently than the other types in many relevant parts of the program; making the two special cases numerically close was found to be advantageous. Similarly, a new bonding type was defined, type 8, for the connections between a dummy atom and its attachments. Again, the numerical similarity between this and the other special case, type 9, expedited modifications.

Bonding type 8 is used for all connections to dummy atoms and only for that purpose. Except when a dummy atom is attached to fewer than two atoms, its location is defined as the centroid of its attachments, i.e., at the arithmetic mean of their (*x*, *y*, *z*) coordinates. A dummy atom is never moved directly by the program, but any time any of its attachments are moved, the position of the dummy is recalculated.

Atom type 79 was defined as having a covalent radius of 0 and a hardness parameter of 0, and the program was otherwise modified so that all bonded and nonbonded interactions between a dummy atom and other atoms are ignored. The routine that makes the lists of bond angles was changed to ignore any angle that included a dummy atom, thus avoiding the usual requirement of PCMODEL that parameters be defined for all of these interactions. The dummy atoms are not in the standard parameter set, and it is desirable not to require a PCMODEL user to use an external parameter file any time a dummy atom is to be used.

The routine that makes the list of torsional angles was changed so that a bond of type 8 would, like a coordination "bond" of type 9, not count as part of a three- or four-membered ring; these small rings are treated specially in the MMX force field. This routine was otherwise not modified, so that regular torsional angles with dummy atoms *would* be included in the list.

When PCMODEL finds a torsional angle for which it does not have appropriate parameters, it uses a default torsional force constant of 0. The routine that checks atom types to try to use generalized parameters, when specific parameters cannot be found, was modified to ensure that any torsional angle that includes a dummy atom would be identified as matching none of the general parameter sets. All torsional angles that include dummy atoms therefore make no contribution to the potential energy of the system, except if one of those angles is used by the dihedral driver. The dihedral-driver function specifies different (and very large) torsional force constants for the specific angle being driven, replacing the usual values.

Thus the dihedral driver now works normally on torsional angles that include dummy atoms, although all other energy functions involving bonding ignore the dummy atoms. Other energy functions, such as charge interactions, were also changed to ignore the dummy atoms, the single exception being the distance-fixing function, which allows the creation of a new bonding-type interaction with user-specified k_s (force constant) and l_0 (bond length) parameters between any pair of atoms regardless of whether or not they are actually con-

[3] Available as PCMODEL from Serena Software, Bloomington, Ind. See ref. 1*e*, 2*d*, and 3. MMX is an extension of the well-known MM2 molecular modelling program (4).

[4] It is possible to specify parameters for a bond angle about a metal atom in an external parameter file, just as for any other kind of bond angle, but this has no effect since the angle itself is ignored by the software. The angle in the model will still be controlled only by steric effects.

Can. J. Chem. Downloaded from www.nrcresearchpress.com by 80.90.12.36 on 09/08/12
For personal use only.

Can. J. Chem. Downloaded from www.nrcresearchpress.com by 80.90.12.36 on 09/08/12
For personal use only.

nected; this is now allowed to work with dummy atoms. It was felt that this could be very useful since, for example, a dummy atom could be set as the centroid of an arene ring and the distance between that centroid and a coordinated metal could be fixed. This would allow the user some control over the distance between the ring and the metal atom without constraining their relative positions and orientations as much as would fixing distances between the metal atom and several of the ring atoms. For space-filling pictures, dummy atoms are drawn as if they have covalent radii of 0.2 Å ; thus they are visible in figures as small spheres amidst the real atoms.

In summary, the properties of a dummy atom as they were defined for this work are as follows. The only potential energy interactions that a dummy atom can have with other atoms are if the user specifies a fixed distance between the dummy and another atom, or if the dummy is one of the defining atoms of a torsional angle that is being operated on by the dihedral driver. A dummy atom has a radius of 0, but is drawn as a small sphere in space-filling pictures. Its location is fixed if it is attached to one atom or not attached at all, and otherwise is defined as the centroid of its attachments.

A limitation of this approach arises from the fact that the algorithm of the energy minimizer assumes that each atom can be moved independently. For each atom in the structure, it determines the gradient of the potential as the sum of the contributions from all of the interactions in which that atom is involved. It then moves the atom a short distance in the direction that it predicts will most rapidly decrease the potential energy of the system. However, the dummy atoms violate the assumption of independent motion because they move whenever one of their attachments moves. If the dummy atom is involved in a fixed-distance or dihedral-driver interaction, its motion changes the potential energy of the system in a way that is not predicted by the usual minimizer. It was expected that this would tend to result in slow minimizations, since the atoms would be moved in directions that lead less directly to the minimum energy configuration. However, tests of the modified program, forcing the rotation of coordinated benzene and ethylene groups in several complexes, indicated that the minimization process was at worst only slightly less efficient with dummy atoms in a dihedral-driver calculation than otherwise.

Results and discussion

We utilized the dihedral driver of PCMODEL to compute the conformational energy profiles for rotation of the arene ligands in the arene complexes (η^6-arene)$Cr(CO)_2(PPh_3)$ (arene = C_6H_6, C_6Me_6), and for ethylene rotation in the olefin complexes $[PtCl_3(\eta^2\text{-}CH_2{=}CH_2)]^-$ and $[(\eta^5\text{-}C_5H_5)Re(NO)(PPh_3)(\eta^2\text{-}CH_2{=}CH_2)]^+$.

(η^6-Arene)$Cr(CO)_2(PPh_3)$

As noted previously (*2d*), Hunter, Schlögl, and co-workers (*2e,f*) observed no decoalescence of the resonances of the coordinated arenes in variable temperature ^{13}C NMR spectra of the compounds (η^6-C_5H_5)$Cr(CO)_2(PPh_3)$ (**1**) and (η^6-C_6Me_6)$Cr(CO)_2(PPh_3)$ (**2**). Minimum energy structures from previous work on these compounds (*2d*), with PCMODEL's aromatic-type carbon atoms and Cr—L distances fixed to the crystal values of (η^6-C_6Et_6)$Cr(CO)_2(PPh_3)$, were modified for both molecules by attaching dummy atoms to each of the arene atoms and the Cr. This placed the dummy atoms of both on the lines between the centroids of the rings alone and the Cr atoms (to be precise, at one seventh of the distances along those lines). The dihedral driver was then used to rotate each ring, using torsional angles defined by one of the ring atoms, the dummy, the Cr, and the P atom.

The calculated barrier to the rotation of the C_6H_6 in **1** was found to be 0.8 kcal/mol regardless of the direction of rotation. The conformational energy profile for arene rotation exhibited, as anticipated, a definite periodicity with minima (and maxima) appearing every 60°. The barrier thus appears to be due to interactions of the benzene hydrogen atoms with the nearest *ortho* hydrogen atoms of the phosphine phenyl rings nearest the benzene, although the origin of such subtle effects is difficult to ascertain with certainty.

In contrast, the barrier to rotation of the C_6Me_6 in **2** was found to depend on the direction of rotation, being 1.9 kcal/mol for (−) rotation, in which the C_6Me_6 slides past the Ph rings in a glancing, face-on manner, and and 3.7 kcal/mol for (+) rotation, which results in edge-on interactions in which the methyl groups collide with the edges of the phenyl rings. Somewhat similar observations were made previously for PPh_3 rotation in **1** and **2** (*2d*). The conformational energy profile again exhibits sixfold maxima and minima, and again the barrier appears to be a result of interactions of the arene methyl groups with the nearby phenyl *ortho* hydrogens.

Unfortunately, no specific experimental results are available for direct comparison. Although Hunter, Schlögl, and coworkers (*2e,f*) reported the lowest temperature used in their study as 158 K, decoalescence was not observed and it was impossible to estimate upper limits to the barriers. However, Gryff-Keller *et al.* (*5a*) found by VT-NMR spectroscopy that the barrier to C_6H_6 rotation in (η^6-C_6H_6)$Cr(CO)_3$ in solution must be less than 0.55 kcal/mol, and Delise *et al.* (*5b*) found that the barrier to C_6H_6 rotation in crystalline (η^6-C_6H_6)$Cr(CO)_3$ is 4.2 ± 0.1 kcal/mol, very close to the barrier to benzene rotation in solid benzene.

Since the MMX force field describes systems that do not interact with their environments, the barriers calculated with PCMODEL are expected to be quite similar to those that would be measured for chemical systems in the gas phase, and reasonably similar to those in solution in a nonpolar solvent. Because of interactions of the arene ring with the phenyl rings in **1**, the barrier to C_6H_6 rotation in this molecule should be slightly greater than that for its rotation in (η^6-C_6H_6)$Cr(CO)_3$, and thus the 0.8 kcal/mol barrier calculated for **1** is in excellent agreement with the experimental results (*5a*).

We find that rotation of the arene rings does not cause the PPh_3 to rotate in the way that the rotation of PPh_3 apparently causes the C_6Me_6 to rotate in **2** (*2d*). Since the phenyl groups are splayed away from the phosphorus atom, they are necessarily forced close to the arene (i.e., within the van der Waals space of the rotating arene ring) in a periodic fashion when the PPh_3 is forced to rotate with the dihedral driver. In contrast, when the arene is forced to rotate, it need not approach a staggered pair of phenyl rings to a significant extent. The effect is rather like a pair of gears, one of which (the PPh_3) is missing most of its teeth. When the latter is made to rotate, the remaining teeth will engage the gear that is whole (the arene) and cause it to rotate, but rotating the whole gear can have little effect on the partial gear.

Can. J. Chem. Downloaded from www.nrcresearchpress.com by 80.90.12.36 on 09/08/12
For personal use only.

$[PtCl_3(\eta^2\text{-}CH_2{=}CH_2)]^-$ (3)

Attempts to build square planar complexes utilizing regular PCMODEL procedures have been found generally to fail because structure optimization routines, which minimize the steric interactions between ligands, invariably result in a tetrahedral structure. Use of two lone-pair "atoms" in the mutually *trans* axial positions[5] was ineffective, presumably because the lone pairs were too small, but use of two hydrogen atoms as "placeholders" in the axial sites[6] did prove effective.

The standard graphical interface of PCMODEL was used to create the model of $[PtCl_3(\eta^2\text{-}CH_2{=}CH_2)]^-$, with the added hydrogen atoms. Initially the ethylene carbon atoms were marked as sp^2-type carbon atoms, but attempted minimizations during dihedral runs failed because of a problem in the π-matrix diagonalization routines.[7] Aromatic-type carbon atoms were therefore used for all further calculations on **3**. The ethylene was coordinated to the platinum with the standard function, the complex was flagged as "square planar," and the metal was designated as uncharged. (The program documentation actually recommends not using charges and, in any case, previous work had indicated that a charge on the metal atom would not significantly affect the results.) All parameters used were the program default values. A dummy atom, the location of which was defined as the centroid of the two ethylene carbon atoms and the platinum atom, was added, and the structure was minimized.

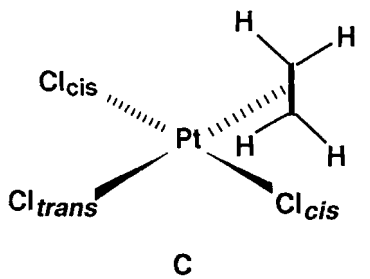

C

As anticipated, the overall structure of the complex was well reproduced, with the C=C axis of the coordinated ethylene being perpendicular to the $PtCl_3$ plane, as in **C**, the Cl_{cis}-Pt-(C_2H_4 centroid)-C torsional angle being 89.8°. The calculated Pt—Cl_{cis} and Pt—Cl_{trans} bond lengths were both found to be 226 pm, in reasonable agreement with neutron diffraction data (230.2, 234.0 pm, respectively) (6), although the subtle electronic weakening of the Pt—Cl_{trans} bond was not, of course, reproduced. The Pt—C distances were calculated to be 268 pm, in poor agreement with the neutron diffraction data (212.8, 213.5 pm), while the Cl_{cis}-Pt-Cl_{trans} and Cl_{cis}-Pt-Cl_{cis} bond angles were found to be 93.9° and 172.2°, respectively, in satisfactory agreement with neutron diffraction data (90.05, 90.43° and 177.65°, respectively).

To obtain the conformational energy profile for ethylene rotation, the olefin was forced to rotate with respect to the $PtCl_3$ plane using the dihedral driver of PCMODEL and working on a C-dummy atom-Pt-Cl_{cis} torsional angle θ. The range of rotation was 1.5 rotations (540°), and the resulting replicated configurations at the beginning and at the end of the run were essentially identical. The resulting conformational energy profile is shown in Fig. 1.

As can be seen, global minima occur at $\theta = \pm 90°$, i.e., the perfectly staggered structure, as expected. Quite unanticipated, however, is the finding that the global maximum occurs not at $\theta = 0°$, where the C=C axis eclipses the $PtCl_3$ plane, but at about $\theta = \pm 35°$, where pairs of hydrogen atoms eclipse the $PtCl_3$ plane. There is actually a local minimum (lying about 0.4 kcal/mol below the global maximum energy) at $\theta = 0°$, apparently corresponding to positions where the pairs of geminal hydrogen atoms straddle the chlorine atoms.[8]

The steric barrier to ethylene rotation in $[PtCl_3(\eta^2\text{-}CH_2{=}CH_2)]^-$ is calculated to be 2.2 kcal/mol using the optimized structural parameters discussed above, while a similar calculation, using fixed, shorter, platinum–ligand bond lengths approximating those reported in the neutron diffraction study (6) gave a somewhat higher barrier of 5.4 kcal/mol. While no experimental data are available for comparison, the free energy of activation for ethylene rotation in the very similar compound $PtCl_2(\eta^2\text{-}CH_2{=}CH_2)$(acac) (acac = acetylacetonate anion) has been found to be 12.5 ± 0.6 kcal/mol (8).[9] This compares well with a theoretical electronic barrier to ethylene rotation of ~15 kcal/mol (9), and it appears that the steric barrier deduced here is small relative to the electronic barrier to ethylene rotation.

$[(\eta^5\text{-}C_5H_5)Re(NO)(PPh_3)(\eta^2\text{-}CH_2{=}CH_2)]^+$ (4)

Gladysz and co-workers (10*a*) used VT-NMR spectroscopy to measure the barrier to the rotation of ethylene in **4**, finding $\Delta G^{\ddagger} = 16.4$ kcal/mol. To carry out the calculations, the structure was built with PCMODEL (bonds being allowed to assume their natural lengths since no crystal structure data were available), and optimized in the usual way (1*e*, 2*d*). No charge was specified for the metal. Only one of the two metal-chiral forms was tested, that with the *S* configuration, but both the *M* and *P* chiralities of PPh_3 (2*d*) were assessed with the C_2H_4 being driven in both directions. Any simulation involving the opposite metal chirality would have been mirror-symmetric with one of the cases that was studied.

A dummy atom was added to the structure, attached to both ethylene C atoms and to the Re. Rotation of the ethylene was then forced, with the dihedral driver operating on a torsional

---

[5] Suggested by Kevin Gilbert, Serena Software.

[6] Suggested by Thomas C. Flood, University of Southern California.

[7] A software bug cause the V_2 force constant applied to the planar ethylene system to sometimes be recalculated as a negative number. As a result, the system would do a half-twist as the two ends of the ethylene suddenly tried to become mutually perpendicular. This problem did not occur when the ethylene atoms were of the aromatic type, since the π calculations were then omitted.

[8] The calculated H—Cl_{cis} distances vary between a maximum of ~307 pm at $\theta = 0, \pm 90°$ and a minimum of ~282 pm at $\theta = \pm 50, 135°$, compared with 297 pm, the sum of the van der Waals radii (7). The calculated C—Cl_{cis} distances vary between a minimum of ~313 pm at $\theta = 0°$ and a maximum of ~340 pm at $\theta = 90°$, compared with 345 pm, the sum of the van der Waals radii (7). While the definitions of van der Waals radii for the hydrogen atoms and for the sp^2-hybridized carbon atoms along the π bond are questionable, it seems clear that H—Cl_{cis} and the C—Cl_{cis} steric interactions are minimal at the global energy minima, and that both contribute at and near the global energy maxima.

[9] The value given was estimated on the basis of an observed coalescence temperature.

Fig. 1. Conformational energy profile for ethylene rotation in $[PtCl_3(\eta^2\text{-}CH_2{=}CH_2)]^-$.

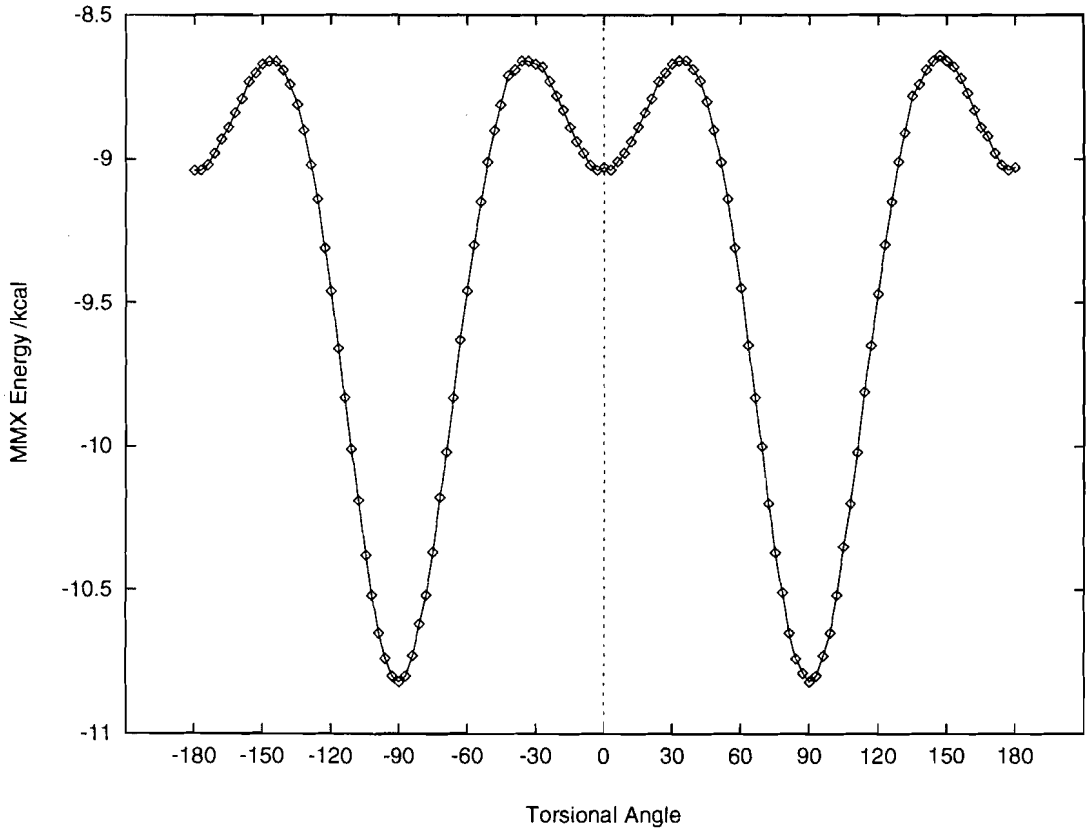

angle defined by one of the ethylene C atoms, the dummy, the Re, and the P atom. Thus dihedral angles of 0° and 180° had the ethylene double bond eclipsing the Re—P bond. The ethylene carbon atoms were marked as aromatic-type carbon atoms, as with $[PtCl_3(\eta^2\text{-}CH_2{=}CH_2)]^-$.

The barriers to the C_2H_4 rotation in **4** were determined as functions of the rotational direction and the phosphine chirality, and energy minima were found for dihedral angles of 110° and −70°, in which the C=C bond lies approximately perpendicular to the Re—P bond, essentially eclipsing the Re—NO bond as in **D**. In all cases, the barriers were found to be ~4.0

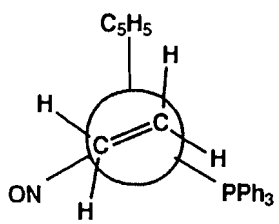

D

kcal/mol, much lower than the experimentally determined value of $\Delta G^{\ddagger}$ for ligand rotation (10). It seems quite unlikely that the explanation lies in a significant difference in entropy between the bottoms and tops of the C_2H_4 rotational barriers for these systems, an argument that has been used to rationalize differences in calculated values of $\Delta H^{\ddagger}$ and experimental values of $\Delta G^{\ddagger}$ for other systems (11).

The most likely reason for the difference is that the orientation of the ethylene ligand is affected strongly by electronic effects, which PCMODEL cannot account for, and indeed, extended Hückel calculations suggest that the most stable orientation of the ethylene group in this complex has the C=C double bond eclipsing the Re—P bond (10*b*). Thus as with the $[PtCl_3(\eta^2\text{-}CH_2{=}CH_2)]^-$ ion, discussed above, it seems likely that the experimentally determined barrier to ethylene rotation reflects dominant electronic rather than steric factors.

Attempts to extend this investigation to complexes of substituted olefins such as $[(\eta^5\text{-}C_5H_5)Re(NO)(PPh_3)(\eta^2\text{-}$*cis*- and *trans*-CHMe=CHMe)]$^+$ (**5**, **6**) (11) failed because of deficiencies in this extension of the functioning of the dihedral driver of PCMODEL. As currently applied, the minimizer halts when, after moving each atom in a direction that should give a lower energy, the total energy of the system increases; this indicates to the minimizer that it has found a minimum energy configuration. However, with a dummy atom included in the definition of a dihedral-driver angle or a fixed-distance atom pair, the computed optimal atom movements may not be truly optimal. This is because, as noted above, movements of dummy atoms resulting from their attachments being moved are not taken into account by the minimizer. As a result, the minimizer is on occasion not merely inefficient; it sometimes stops altogether when the minimization is far from complete because moving the dummy atom makes the energy of the system increase. This happens most often when something like a dihedral-driver series is being performed, because here the torsional angle is being used to push the system past potential barriers. The tendency of the system to oppose forced motion to higher potential energies has the dihedral-driver dummy

Can. J. Chem. Downloaded from www.nrcresearchpress.com by 80.90.12.36 on 09/08/12
For personal use only.

atom moving in directions that lead to much higher total energies, especially because the force constant applied to the dihedral-driver angle is very large.

This problem is most serious when the barrier to the rotation of the ligand is large. With the rotations of the π-coordinated ligands in compounds **1–4**, the barriers are sufficiently small that the minimizer works well. With the more sterically congested **5** and **6**, however, the barriers are sufficiently large that the minimizer often failed. The torsional angle would be changed, the atoms would be moved, the energy would increase immediately, the minimizer would halt, and the torsional angle would be incremented again. Instead of finding the optimal structure for each torsional angle, the coordinated 2-butene ligands kept rotating to increasingly strained configurations until the strain was unrealistically high. This behaviour often occurred after a reasonably anticipated rotational barrier maximum had actually been passed, yielding generally inconsistent results. Attempts to solve the problem failed.

Summary

A useful methodology for utilizing MMX to calculate small steric barriers to rotation of π-bonded ligands has been developed, the barriers calculated for η^6-arene rotation in two chromium(0) complexes being in reasonable agreement with experimentally determined barriers. The finding that calculated steric barriers to η^2-ethylene rotation in two quite different types of olefin complexes are apparently significantly less than the corresponding electronic barriers does not negate the methodology, as comparisons of steric and electronic barriers are generally useful, as is determination of sterically preferred structures.

Acknowledgements

An operating grant from the Natural Sciences and Engineering Research Council of Canada to M.C.B. and an Ontario Graduate Scholarship to J.P. made this research possible. We also thank Dr. Kevin Gilbert for useful advice.

References

1. (*a*) W. Jetz and W.A.G. Graham. J. Am. Chem. Soc. **89**, 2773 (1967); (*b*) J. Dalton. Inorg. Chem. **10**, 1822 (1971); (*c*) Inorg. Chem. **11**, 915 (1972); (*d*) K. Stanley and M.C. Baird. J. Am. Chem. Soc. **97**, 4292 (1975); (*e*) S.C. Mackie and M.C. Baird. Organometallics, **11**, 3712 (1992); (*f*) I.S. Butler and T. Sawai. Inorg. Chem. **12**, 1994 (1973).
2. (*a*) B.K. Blackburn, S.G. Davies, K. H. Sutton, and M. Whittaker. Chem. Soc. Rev. **17**, 147 (1988); (*b*) J.I. Seeman and S. Davies. J. Am. Chem. Soc. **107**, 6522 (1985); (*c*) S. G. Davies, A.E. Derome, and J.P. McNally. J. Am. Chem. Soc. **107**, 6522 (1985); (*d*) J. Polowin, S.C. Mackie, and M.C. Baird. Organometallics, **11**, 3724 (1992); (*e*) G. Hunter, T.J.R. Weakley, and W. Weissensteiner. J. Chem. Soc. Dalton Trans. 1545 (1987); (*f*) J.A. Chudek, G. Hunter, R.L. MacKay, P. Kremminger, K. Schlögl, and W. Weissensteiner. J. Chem. Soc. Dalton Trans. 2001 (1990).
3. J.J. Gajewski, K.E. Gilbert, and J. McKelvy. Adv. Mol. Model. **2**, 65 (1990).
4. U. Burkert, and A.L. Allinger. Molecular mechanics. American Chemical Society, Washington, D.C. 1982.
5. (*a*) A. Gryff-Keller, P. Szczecinski, and H. Koziel. Magn. Reson. Chem. **28**, 25 (1990); (*b*) P. Delise, G. Allegra, E.R. Mognaschi, and A. Chierico. J. Chem. Soc. Faraday Trans. 2, **71**, 207 (1975).
6. R.A. Love, T.F. Koetzle, G.J.B. Williams, L.C. Andrews, and R. Bau. Inorg. Chem. **14**, 2653 (1975).
7. A. Bondi. J. Phys. Chem. **68**, 441 (1964).
8. C.E. Holloway, G. Hulley, B.F.G. Johnson, and J. Lewis. J. Chem. Soc. (A), 53 (1969).
9. P.J. Hay. J. Am. Chem. Soc. **103**, 1390 (1981).
10. (*a*) G.S. Bodner, T.-S. Peng, A.M. Arif, and J.A. Gladysz. Organometallics, **9**, 1191 (1990); (*b*) J. Pu, T.-S. Peng, C.L. Mayne, A.M. Arif, and J.A. Gladysz. Organometallics, **12**, 2686 (1993).
11. J.-H. Li and A.L. Allinger. J. Am. Chem. Soc. **111**, 8566 (1989).

Can. J. Chem. Downloaded from www.nrcresearchpress.com by 80.90.12.36 on 09/08/12
For personal use only.

Routes to dicationic ruthenium(II) nitrile complexes containing chelating diphosphine ligands: X-ray analyses of $Ru(dppb)(MeCN)_4^{2+}2PF_6^-$ (dppb = $Ph_2P(CH_2)_4PPh_2$) and *trans*-$RuCl_2(MeCN)_4$

Deryn E. Fogg, Steven J. Rettig, and Brian R. James

Abstract: Routes to the $Ru(PP)(RCN)_4^{2+}$ $2PF_6^-$ complexes (PP = $Ph_2P(CH_2)_4PPh_2$, dppb; R = Me, Ph) from the Ru(II) precursors $Ru_2Cl_4(PP)_2$ and $RuCl_2(PP)(PPh_3)$ have been established. The X-ray crystal structure of the dppb-MeCN derivative (**3**) is described, and the steric effect of the diphosphine ligand is examined by comparison with the crystal structure of *trans*-$RuCl_2(MeCN)_4$ (**5**), which is also presented. Crystals of **3** are triclinic, a = 13.845(3), b = 14.419(2), c = 12.984(3) Å, α = 108.75(2)°, β = 116.40(1)°, γ = 68.58(1)°, and Z = 2, space group $P\bar{1}$; and those of **5** are orthorhombic, a = 13.058(2), b = 11.790(2), c = 8.562(1) Å, and Z = 4, space group *Pbca*. The structures were solved by the Patterson method and refined by full-matrix least-squares procedures to R = 0.039 and 0.024 (R_w = 0.046 and 0.028) for 9973 and 1131 reflections with $I \geq 3\sigma(I)$, respectively. Crystallographic and infrared data suggest that the nitrile ligands function solely as σ-donors in these ruthenium(II) complexes.

Key words: ruthenium, nitriles, diphosphine ligands.

Résumé : On a déterminé les routes d'accès aux complexes $Ru(PP)(RCN)_4^{2+}$ $2PF_6^-$ (PP = $Ph_2P(CH_2)_4PPh_2$, dppb; R = Me, Ph) à partir des précurseurs du Ru(II) $Ru_2Cl_4(PP)_2$ et $RuCl_2(PP)(PPh_3)$. On décrit la structure cristalline déterminée par diffractions des rayons X du dérivé dppb-MeCN (**3**) et on a examiné l'effet stérique du coordinat diphosphine par comparaison avec la structure cristalline du *trans*-$RuCl_2(MeCN)_4$ (**5**) qui est aussi présentée. Les cristaux du composé **3** sont tricliniques, groupe d'espace $P\bar{1}$, avec a = 13,845(3), b = 14,419(2) et c = 12,984(3) Å, α = 108,75(2)°, β = 116,40(1)°, γ = 68,58(1)° et Z = 2, alors que ceux du composé **5** sont orthorhombiques, groupe d'espace *Pbca*, avec a = 13,058(2), b = 11,790(2) et c = 8,562(1) Å, et Z = 4. On a résolu les structures par la méthode de Patterson et on les a affinées par la méthode des moindes carrés (matrice complète) jusqu'à des valeurs de R = 0,039 et 0,024 (R_w = 0,046 et 0,028) pour respectivement 9973 et 1131 réflexions avec $I \geq 3\sigma(I)$. Les données cristallographiques et d'infrarouge suggèrent que les coordinats nitrile ne fonctionnent que comme des donneurs σ dans ces complexes ruthénium(II).

Mots clés : ruthénium, nitriles, coordinats diphosphine.

[Traduit par la rédaction]

Introduction

Ruthenium(II) complexes with chelating diphosphine ligands have been the focus of considerable recent attention, in large part because of their demonstrated utility in asymmetric hydrogenation of a wide range of substrates (1). To identify the structural features associated with high catalytic and enantioselective ability (2), we have undertaken the preparation of a range of such complexes, in most of which the coordination sphere contains potentially labile nitrile (3) or arene (3, 4) ligands. The monocationic complexes $RuCl(PP)(RCN)_3^+PF_6^-$ (**1**) were of particular interest because of their reported lability regarding loss of nitrile (5, 6), a useful property for a catalyst precursor. Work from this laboratory had originally reported on the PP = dppb, R = Me, *mer* and *fac* species (5), while Shao et al. (6) reported on the PP = binap, R = Ph species during the course of the present studies (binap = 2,2′-bis(diphenylphosphino)-1,1′-binaphthyl); $^{31}P\{^1H\}$ NMR data in solution revealed an "extra" resonance that was assigned to a coordinatively unsaturated species **2**, governed by the equilibrium shown in eq. [1]

Received October 12, 1994.

This paper is dedicated to Professor William A.G. Graham on the occasion of his 65th birthday.

D.E. Fogg, S.J. Rettig, and B.R. James.[1] Department of Chemistry, University of British Columbia, 2036 Main Mall, Vancouver, BC V6T 1Z1, Canada.

[1] Author to whom correspondence may be addressed. Telephone: (604) 822-6645. Fax: (604) 822-2847.

Can. J. Chem. Downloaded from www.nrcresearchpress.com by 80.90.12.36 on 09/08/12
For personal use only.

Can. J. Chem. Downloaded from www.nrcresearchpress.com by 80.90.12.36 on 09/08/12
For personal use only.

[1] $RuCl(PP)(RCN)_3^+ \rightleftharpoons RuCl(PP)(RCN)_2^+ + RCN$
1 **2**

We now report that the "extra" ^{31}P signal, in the case of the dppb system, results from the presence of Ru(dppb)-$(MeCN)_4^{2+}$, which is isolated and structurally characterized as the PF_6 salt **3**; the benzonitrile analogue (**4**) is also isolated, and structural details of **3** are compared with those determined also for *trans*-$RuCl_2(MeCN)_4$ (**5**), a previously known complex (7, 8). It should be noted that the AB quartet assigned to a species of type **2** in the binap work (6) is not due to $Ru(binap)(PhCN)_4^{2+}$ (see below); a ^{31}P singlet is expected for the latter complex (9).

Experimental

Manipulations were carried out under an argon atmosphere using standard Schlenk techniques. Solvents were dried and distilled under nitrogen. Acetonitrile and benzonitrile were obtained from BDH, distilled from CaH_2, and stored under Ar. NH_4PF_6 was used as received from Aldrich. $RuCl_2$-$(dppb)(PPh_3)$ (10), $Ru_2Cl_4(dppb)_2$ (10), and $RuCl_2(C_6H_6)$-(MeCN) (4) were prepared according to published procedures. NMR spectra were recorded at room temperature (r.t.) on a Varian XL300 spectrometer, using the residual proton of the solvent (^1H) or PPh_3 (^{31}P: $CDCl_3$, −5.46 ppm; CD_2Cl_2, −5.64 ppm with respect to 85% external H_3PO_4) as internal standards (s = singlet, sept = septet, m = multiplet). IR spectra (Nujol mulls, KBr plates) were recorded on a Bomem Michelson 100 FT-IR spectrometer (w = weak, m = medium). Elemental analyses were performed by Mr. Peter Borda of this department.

Preparation of $Ru(dppb)(MeCN)_4^{2+}$ $2PF_6^-$, 3

Method a

A mixture of $Ru_2Cl_4(dppb)_2$ (76.1 mg, 0.0635 mmol) and NH_4PF_6 (41.4 mg, 0.254 mmol) in MeCN (5 mL) was stirred for 3 h at r.t. The pale yellow solution was stripped of solvent, the residue redissolved in CH_2Cl_2, and the suspension filtered through Celite. Concentration of the filtrate to ~1 mL and addition of Et_2O precipitated a white crystalline product, which was washed with Et_2O and dried under vacuum (107 mg, 86%). Colourless prisms of **3** were grown from MeCN–Et_2O.

Method b

Addition of MeCN (10 mL) to a mixture of green $RuCl_2(dppb)(PPh_3)$ (140 mg, 0.163 mmol) and NH_4PF_6 (53.4 mg, 0.328 mmol) gave a cloudy yellow solution, which was stirred for 30 min. The solvent was then removed, the residue taken up in CH_2Cl_2, and the mixture filtered through Celite. Concentration of the filtrate and addition of Et_2O gave the product (133 mg, 83%). IR: 2291, 2320 cm^{-1} (w). ^1H NMR (CD_2Cl_2): 7.2–8.0 (m, 20H, Ph), 2.63–2.73 (m, 4H, CH_2), 2.30 (s, 6H, Me), 2.14 (s, 6H, Me), 1.66–1.80 (m, 4H, CH_2). $^{31}P\{^1H\}$ NMR ($CDCl_3$): 39.2 (s), −144.5 (sept, J = 713 Hz, PF_6). $^{31}P\{^1H\}$ (CD_2Cl_2): 38.8 (s), −144.6 (sept, J = 708 Hz). Anal. calcd. for $C_{36}H_{40}F_{12}N_4P_4Ru$: C 44.05, H 4.11, N 5.71; found: C 43.99, H 4.12, N 5.77%.

Preparation of $Ru(dppb)(PhCN)_4^{2+}$ $2PF_6^-$, 4

A solution of $RuCl_2(dppb)(PPh_3)$ (47.4 mg, 0.055 mmol) and NH_4PF_6 (35.7 mg, 0.219 mmol) in a mixture of PhCN (3 mL) and acetone (10 mL) was stirred at r.t. for 24 h, then stripped of solvent. The residue was taken up in CH_2Cl_2 and the mixture filtered through Celite. Concentration of the filtrate and addition of Et_2O gave the product as a white precipitate (42 mg, 63%). IR: ν(C≡N) 2245 cm^{-1} (w). ^1H NMR ($CDCl_3$): 7.3–7.7 (m, 40H, Ph), 2.8–3.0 (m, 4H, CH_2), 1.8–2.0 (m, 4H, CH_2), 1.54 (s, 2H, H_2O). $^{31}P\{^1H\}$ NMR ($CDCl_3$): 37.3 (s), −144.2 (sept, J = 713 Hz, PF_6). Anal. calcd. for $C_{56}H_{48}F_{12}N_4P_4Ru \cdot H_2O$: C 53.89, H 4.04, N 4.49; found: C 54.08, H 4.00, N 4.36%.

Preparation of *trans*-$RuCl_2(MeCN)_4$, 5

The complex was prepared by a reported method (7). IR: ν(C≡N) 2278 cm^{-1} (m). ^1H NMR ($CDCl_3$): 2.51 (s, 12 H, Me), 1.55 (s, 1 H, H_2O). Anal. calcd. for $C_8H_{12}N_4Cl_2Ru \cdot 0.5\ H_2O$: C 27.84, H 3.79, N 16.23, Cl 20.54; Found: C 27.87, H 3.62, N 16.24, Cl 20.75%. Brown prisms of **5** (nonhydrated) suitable for X-ray analysis were serendipitously formed by leaving $RuCl_2(C_6H_6)(MeCN)$ (32 mg, 0.11 mmol) in MeCN–C_6D_6 (~10:1, total volume 0.6 mL) over two weeks at room temperature.

X-ray crystallographic analyses of 3 and 5

Crystallographic data appear in Table 1. The final unit-cell parameters were obtained by least-squares refinement of the setting angles for 25 reflections with 2θ = 39.0°–43.0° for **3** and 47.9°–51.8° for **5**. The intensities of three standard reflections, measured every 200 reflections throughout the data collections, showed only small random fluctuations. The data were processed,[2] corrected for Lorentz and polarization effects, and absorption (empirical, based on azimuthal scans for three reflections).

The structures were solved by conventional heavy atom methods, the coordinates of the heavy atoms being determined from the Patterson function, and those of the remaining non-hydrogen atoms from subsequent Fourier syntheses. The structure analysis of **3** was initiated in the centrosymmetric space group $P\bar{1}$ the basis of the E-statistics and the Patterson function. This choice was confirmed by the subsequent successful solution and refinement of the structure. Complex **5** lies on a crystallographic centre of symmetry. All non-hydrogen atoms were refined with anisotropic thermal parameters. The hydrogen atoms were fixed in idealized positions (C—H = 0.98 Å, B_H = 1.2 $B_{\text{bonded atom}}$). Corrections for secondary extinction were not necessary. Neutral atom scattering factors for all atoms and anomalous dispersion corrections for the non-hydrogen atoms were taken from the International Tables for X-Ray Crystallography (11).

The final atomic coordinates and equivalent isotropic thermal parameters for the non-hydrogen atoms of **3** and **5** are given in Table 2. Selected bond lengths and angles for **3** are given in Table 3; bond lengths and angles for **5** are given in Table 4. Hydrogen atom parameters, anisotropic thermal parameters, complete listing of lengths and angles for **3**, torsion angles, intermolecular contacts, and least-squares planes

[2] TEXSAN/TEXRAY structure analysis package (Version 5.1), Molecular Structure Corp. The Woodlands, Tex. 1985.

Can. J. Chem. Downloaded from www.nrcresearchpress.com by 80.90.12.36 on 09/08/12
For personal use only.

Table 1. Crystallographic data.[a]

Compound	$Ru(dppb)(MeCN)_4^{2+}$ $2PF_6^-$ (**3**)	*t*-$RuCl_2(MeCN)_4$ (**5**)
Formula	$C_{36}H_{40}F_{12}N_4P_4Ru$	$C_8H_{12}Cl_2N_4Ru$
fw	981.68	336.19
Crystal system	Triclinic	Orthorhombic
Space group	$P\bar{1}$ (No. 2)	*Pbca* (No. 61)
a, Å	13.845(3)	13.058(2)
b, Å	14.419(2)	11.790(2)
c, Å	12.984(3)	8.562(1)
α, deg	108.75(2)	90
β, deg	116.40(1)	90
γ, deg	68.58(1)	90
V, Å^3	2121.6(8)	1318.2(6)
Z	2	4
ρ_{calc}, g cm^{-3}	1.537	1.694
F(000)	992	664
μ, cm^{-1}	6.05	15.52
Crystal size, mm	0.20 × 0.40 × 0.40	0.15 × 0.25 × 0.30
Transmission factors (relative)	0.92–1.00	0.87–1.00
Scan type	ω–2θ	ω–2θ
Scan range, deg in ω	1.15 + 0.35 tan θ	1.57 + 0.35 tan θ
Scan speed, deg min^{-1}	32	32
Data collected	$+h, \pm k, \pm l$	$+h, +k, +l$
$2\theta_{max}$, deg	65	60
Crystal decay, %	Negligible	Negligible
Total reflections	15 899	2220
Total unique reflections	15 350	2220
R_{merge}	0.021	—
Reflections with $I \geq 3\sigma(I)$	9973	1131
No. of variables	514	70
R	0.039	0.024
R_w	0.046	0.028
gof	2.55	1.84
Max Δ/σ (final cycle)	0.03	0.003
Residual density e Å^{-3}	−0.51, 0.74 (near Ru)	−0.37, 0.36 (near Ru)

[a]Temperature 294 K, Rigaku AFC6S diffractometer, Mo-K_α radiation (λ = 0.71069 Å), graphite monochromator, takeoff angle 6.0°, aperture 6.0 × 6.0 mm at a distance of 285 mm from the crystal, stationary background counts at each end of the scan (scan/background time ratio 2:1, up to 8 rescans), $\sigma^2(F^2) = [S^2(C + 4B) + (0.01F^2)^2]/Lp^2$ (*S* = scan rate, *C* = scan count, *B* = normalized background count), function minimized $\Sigma w(|F_o|-|F_c|)^2$ where $w = 4F_o^2/\sigma^2(F_o^2)$, $R = \Sigma||F_o|-|F_c||/\Sigma|F_o|$, $R_w = (\Sigma w(|F_o|-|F_c|)^2/\Sigma w|F_o|^2)^{1/2}$, and gof = $[\Sigma w(|F_o|-|F_c|)^2/(m-n)]^{1/2}$. Values given for *R*, R_w, and gof are based on those reflections with $I \geq 3\sigma I$.

are included as supplementary material (Tables S1–S8).[3] Measured and calculated structure factor amplitudes are available from the authors.

Results and discussion

The complex $RuCl(dppb)(MeCN)_3^+PF_6^-$ (**1a**) was synthesized earlier in this laboratory (5) by abstraction of halide from the triply chloro-bridged species $Ru_2Cl_4(dppb)_2$(acetone) (10) using two equivalents of $AgPF_6$. The $^{31}P\{^1H\}$ NMR spectrum in CD_2Cl_2 revealed a principal singlet at δ 41.2 (consistent with *fac*-**1a**), the high-field septet of PF_6^-, and a low-intensity singlet at δ 38.7 (~5% integrated intensity) that was attributed to the five-coordinate species $RuCl(dppb)(MeCN)_2^+$ (**2a**) (5). More detailed studies on the chemistry of **1a** (3) reveal that the less intense singlet is due to the presence of the chlorine-free dication $Ru(dppb)(MeCN)_4^{2+}$ (**3**). A $^{31}P\{^1H\}$ singlet is expected for each of the complexes *fac*-**1a**, **2a**, or **3**, but ^1H NMR data readily distinguish the species. Complex **3**, characterized by X-ray crystallography (see below), shows two methyl singlets in a 1:1 ratio, each integrating 6:20 against the phenyl protons; the singlets correspond to the two acetonitriles *trans* to the P atoms, and to the two mutually *trans* acetonitriles. The associated $^{31}P\{^1H\}$ singlet of **3** corresponds to that incorrectly assigned to **2a** (5).

[3] Supplementary material mentioned in the text may be purchased from: The Depository of Unpublished Data, Document Delivery, CISTI, National Research Council Canada, Ottawa, Canada K1A 0S2

Bond lengths and angles involving hydrogen atoms have also been deposited with the Cambridge Crystallographic Data Centre and can be obtained on request from The Director, Cambridge Crystallographic Data Centre, University Chemical Laboratory, 12 Union Road, Cambridge CB2 1EZ, UK

Fig. 1. Stereoview of the $Ru(dppb)(MeCN)_4^{2+}$ cation in **3**; 33% probability thermal ellipsoids are shown. Hydrogen atoms are omitted for clarity.

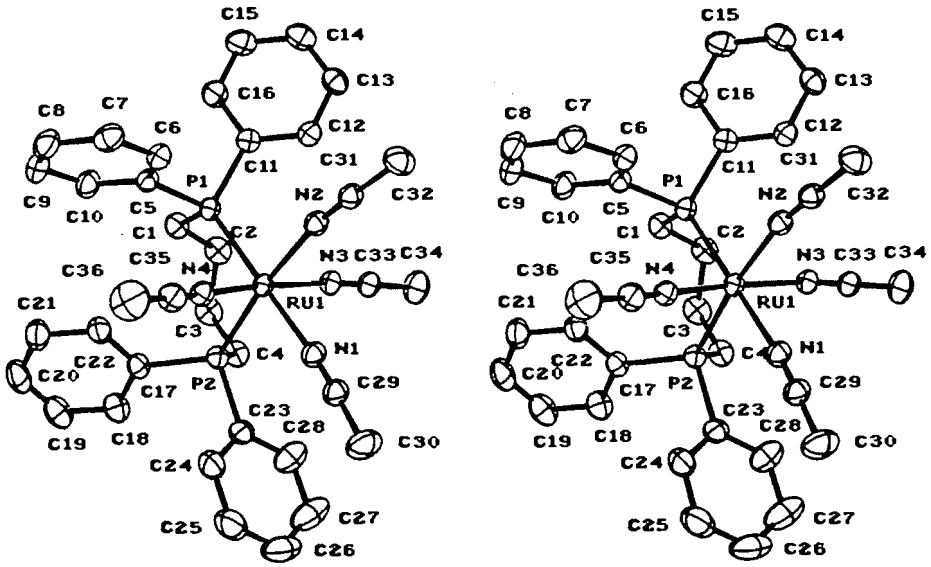

Complex **3** and its PhCN analogue **4** are accessible in quantitative yield by abstraction of halide from $Ru_2Cl_4(dppb)_2$ or $RuCl_2(dppb)(PPh_3)$ in acetonitrile or benzonitrile–acetone solvent, respectively. Treatment with NH_4^+ effects complete removal of chloride via monocationic intermediate **1** (PP = dppb, R = Me or Ph), the reaction being driven by the insolubility of ionic NH_4Cl in MeCN or PhCN–acetone. The mixed phosphine precursors $RuCl_2(PP)(PPh_3)$ are much less air-sensitive than the dimeric $Ru_2Cl_4(PP)_2$ precursors, and in solution they dissociate the monodentate PPh_3. Preliminary results suggest that the corresponding binap-acetonitrile complex is likewise accessible from $RuCl_2(binap)(PPh_3)$, but treatment of this with excess NH_4PF_6 in PhCN yields only a monocation of type **1** (3), removal of the second chloride ligand appears to require use of the stronger halide-abstracting agent Ag^+, perhaps because of an unfavourable steric interaction between the bulky, rigid binap ligand and a coordinated PhCN. Isolation of $Ru(binap)(MeCN)_4^{2+}$ $2BF_4^-$ following treatment of $Ru(binap)(OCOMe)_2$ with aqueous HBF_4 in MeCN was reported by Takaya and co-workers (9) during the course of our work. Analogous complexes with monodentate phosphine and phosphite ligands were obtained by Ashworth and Singleton from the dicationic precursor $Ru(COD)(MeCN)_4^{2+}$ $2PF_6^-$ (12) (COD = 1,5-cyclooctadiene). Rather surprisingly, $AgPF_6$ was apparently required for synthesis of the dication; treatment of polymeric $[RuCl_2(COD)]_x$ with NH_4PF_6 in refluxing MeCN was reported to yield only $RuCl(COD)(MeCN)_3^+PF_6^-$, though whether NH_4PF_6 was used in excess is unclear (12). A practical consequence of facile abstraction of halide from species of type **1** by NH_4^+ is the formation of small amounts of the dication during attempts to synthesize solely **1** from "$RuCl_2$" species (3); such facile abstraction also accounts for the original observation of **3** as a by-product, and led to the incorrect formulation of equilibrium [1] (5). The nitrile chemistry of these systems is in fact intricate, and involves not only species of types **1** and **3** (3), but also $RuCl_2(PP)(RCN)_2$, $Ru_2Cl_4(PP)_2(RCN)$, and $Ru_2Cl_3(PP)_2(RCN)_2^+X^-$ (X = Cl, PF_6) (3). In situ formation of the last-mentioned species (PP = binap, R = Ph, X = Cl) has been shown (3) to be responsible for the AB pattern attributed by Shao et al. to a complex of type **2** (6). A detailed discussion of the complexes accessible, and the pathways relating them, will be reported separately.

Complex **4** gave good elemental analysis for a monohydrate, and the ^1H NMR data were consistent with such a formulation. *trans*-$RuCl_2(MeCN)_4$ (**5**) was made by a reported procedure involving catalyzed H_2-reduction of $RuCl_3 \cdot 3H_2O$ in MeCN (7); our elemental analysis and ^1H NMR data were consistent with a hemi-hydrate formulation, although the crystals used for the X-ray analysis were non-hydrated. These were obtained by a reaction involving displacement of coordinated benzene of $RuCl_2(C_6H_6)(MeCN)$ by MeCN.

The crystal structure of **3** is shown in Fig. 1. Crystallographic analysis of **5**, prepared in the course of related work (4), offers some insight into the structural constraints imposed by the diphosphine ligand in **3**, and an ORTEP representation of **5** is shown in Fig. 2.

The cation within **3** is monomeric, containing chelated dppb in *cis* sites and four N-bound MeCN ligands. Associated with the Ru cation are two essentially octahedral PF_6 counterions (not illustrated); one of the anions has P—F bond lengths in the range 1.566–1.591 Å, while for the other anion the lengths are in the range 1.486–1.564 Å, but the differences likely result from thermal libration; note the significant differences in the thermal parameters of the two anions (Table 2). Within the internuclear distances, there are just two F...H bond lengths <2.5 Å, a criterion that may be used for the existence of a hydrogen bond (13): F(5)—H(12) = 2.39 Å and F(6)—H(35) = 2.36 Å, implying weak hydrogen bonding to a phenyl-H and to a methyl-H of MeCN. Weak H..F interactions involving toluene ring atoms were observed in our earlier work on the $RuCl(\eta^6\text{-toluene})(dppb)^+$ cation (5).

The $Ru(dppb)(MeCN)_4^{2+}$ cation consists of a slightly distorted octahedron, in which the bond angles between the nitrile ligands both in the P-Ru-P plane and projecting above

Can. J. Chem. Downloaded from www.nrcresearchpress.com by 80.90.12.36 on 09/08/12
For personal use only.

Table 2. Final atomic coordinates (fractional) and B_{eq} (Å^2).[a]

Atom	x	y	z	B_{eq}
3				
Ru(1)	0.24350(2)	0.25006(2)	0.19583(2)	2.702(8)
P(1)	0.41507(6)	0.13840(5)	0.27598(6)	2.99(3)
P(2)	0.16990(6)	0.23916(5)	0.32012(6)	3.22(3)
N(1)	0.0887(2)	0.3445(2)	0.1078(2)	3.6(1)
N(2)	0.2944(2)	0.2757(2)	0.0778(2)	3.3(1)
N(3)	0.2884(2)	0.3765(2)	0.3070(2)	3.3(1)
N(4)	0.1821(2)	0.1392(2)	0.0675(2)	3.3(1)
C(1)	0.4518(2)	0.1140(2)	0.4207(2)	3.8(1)
C(2)	0.4433(3)	0.2111(3)	0.5155(2)	4.4(1)
C(3)	0.3440(3)	0.2369(3)	0.5519(2)	4.8(2)
C(4)	0.2318(3)	0.2959(2)	0.4754(2)	4.2(1)
C(5)	0.4262(2)	0.0128(2)	0.1821(2)	3.2(1)
C(6)	0.4110(2)	0.0047(2)	0.0666(2)	3.7(1)
C(7)	0.4071(3)	−0.0865(2)	−0.0118(3)	4.4(1)
C(8)	0.4185(3)	−0.1715(2)	0.0244(3)	5.0(1)
C(9)	0.4362(3)	−0.1658(2)	0.1385(4)	5.6(2)
C(10)	0.4408(3)	−0.0748(2)	0.2173(3)	4.4(1)
C(11)	0.5431(2)	0.1655(2)	0.2965(2)	3.3(1)
C(12)	0.5446(2)	0.2575(2)	0.2855(2)	3.5(1)
C(13)	0.6446(3)	0.2734(2)	0.3026(3)	4.3(1)
C(14)	0.7430(3)	0.1982(3)	0.3315(3)	4.9(2)
C(15)	0.7427(3)	0.1063(3)	0.3420(3)	5.1(2)
C(16)	0.6433(3)	0.0895(2)	0.3243(3)	4.5(1)
C(17)	0.1639(2)	0.1168(2)	0.3275(2)	3.6(1)
C(18)	0.1176(3)	0.1146(3)	0.4027(3)	4.7(2)
C(19)	0.1178(3)	0.0227(3)	0.4142(3)	5.7(2)
C(20)	0.1641(3)	−0.0663(3)	0.3558(4)	5.8(2)
C(21)	0.2084(3)	−0.0659(2)	0.2795(3)	5.3(2)
C(22)	0.2063(3)	0.0266(2)	0.2647(3)	4.2(1)
C(23)	0.0231(3)	0.3104(2)	0.2821(3)	4.0(1)
C(24)	−0.0578(3)	0.2642(3)	0.1959(4)	6.1(2)
C(25)	−0.1698(3)	0.3172(4)	0.1606(5)	8.0(3)
C(26)	−0.2004(4)	0.4183(5)	0.2132(5)	8.5(3)
C(27)	−0.1209(5)	0.4647(4)	0.2947(4)	8.0(3)
C(28)	−0.0091(3)	0.4117(3)	0.3300(3)	6.1(2)
C(29)	0.0036(3)	0.3831(2)	0.0491(3)	3.9(1)
C(30)	−0.1069(3)	0.4304(3)	−0.0270(3)	6.1(2)
C(31)	0.3058(2)	0.2995(2)	0.0096(2)	3.4(1)
C(32)	0.3187(3)	0.3329(3)	−0.0772(3)	4.7(2)
C(33)	0.3034(2)	0.4525(2)	0.3595(2)	3.7(1)
C(34)	0.3229(3)	0.5497(2)	0.4303(3)	5.7(2)
C(35)	0.1450(2)	0.0848(2)	−0.0143(3)	4.2(1)
C(36)	0.1010(4)	0.0124(3)	−0.1191(4)	7.3(2)
P(3)	0.55044(8)	0.44667(7)	0.80767(8)	4.95(4)
F(1)	0.4862(2)	0.5542(2)	0.8609(2)	7.2(1)
F(2)	0.6377(2)	0.4972(2)	0.8130(2)	8.2(2)
F(3)	0.6290(2)	0.4254(2)	0.9338(2)	8.3(1)
F(4)	0.6137(2)	0.3404(2)	0.7541(2)	8.4(1)
F(5)	0.4651(2)	0.3968(2)	0.8054(3)	8.6(1)
F(6)	0.4742(3)	0.4673(2)	0.6796(2)	9.8(2)
P(4)	0.0257(1)	0.2667(1)	0.7013(1)	6.58(6)
F(7)	0.0484(3)	0.3620(3)	0.7954(4)	14.4(3)

Can. J. Chem. Downloaded from www.nrcresearchpress.com by 80.90.12.36 on 09/08/12
For personal use only.

Can. J. Chem. Downloaded from www.nrcresearchpress.com by 80.90.12.36 on 09/08/12
For personal use only.

Table 2 (*concluded*).

Atom	*x*	*y*	*z*	B_{eq}
F(8)	−0.0784(3)	0.2775(3)	0.7226(4)	15.3(3)
F(9)	0.0994(5)	0.2084(4)	0.7969(4)	19.8(4)
F(10)	0.0107(4)	0.1636(3)	0.6156(3)	14.2(3)
F(11)	0.1221(3)	0.2631(3)	0.6705(3)	13.3(3)
F(12)	−0.0471(4)	0.3202(5)	0.5981(5)	22.5(5)
5				
Ru(1)	1/2	1/2	1/2	2.20(1)
Cl(1)	0.34537(6)	0.43138(7)	0.62136(9)	3.26(3)
N(1)	0.5433(2)	0.5680(2)	0.7064(3)	2.5(1)
N(2)	0.5773(2)	0.3594(2)	0.5692(3)	2.6(1)
C(1)	0.5714(2)	0.5955(2)	0.8252(4)	2.8(1)
C(2)	0.6078(3)	0.6291(3)	0.9797(4)	4.4(2)
C(3)	0.6260(2)	0.2903(3)	0.6190(3)	2.9(1)
C(4)	0.6924(3)	0.2022(3)	0.6836(4)	4.0(2)

[a] $B_{eq} = (8/3)\pi^2\Sigma\Sigma U_{ij}a_i^*a_j^*(\mathbf{a}_i \cdot \mathbf{a}_j)$.

Table 3. Selected bond lengths (Å) and angles (deg) for $Ru(dppb)(MeCN)_4^{2+}$ $2PF_6^-$ (**3**).

Bond	Distance	Bond	Distance
Ru(1)—N(1)	2.108(2)	Ru(1)—N(2)	2.120(2)
Ru(1)—N(3)	2.033(2)	Ru(1)—N(4)	2.019(2)
Ru(1)—P(1)	2.3244(9)	Ru(1)—P(2)	2.3259(8)
N(1)—C(29)	1.129(4)	N(2)—C(31)	1.135(3)
N(3)—C(33)	1.126(3)	N(4)—C(35)	1.131(3)
Bonds	**Angle**	**Bonds**	**Angle**
P(1)—Ru(1)—P(2)	93.93(3)	N(1)—Ru(1)—N(2)	83.43(9)
N(1)—Ru(1)—N(3)	88.51(9)	N(1)—Ru(1)—N(4)	83.25(9)
N(2)—Ru(1)—N(3)	87.99 (9)	N(2)—Ru(1)—N(4)	87.44(9)
N(3)—Ru(1)—N(4)	170.98(8)	Ru(1)—N(1)—C(29)	170.3(2)
Ru(1)—N(2)—C(31)	169.5(2)	Ru(1)—N(3)—C(33)	172.2(2)
Ru(1)—N(4)—C(35)	170.9(2)	N(1)—C(29)—C(30)	178.5(3)
N(2)—C(31)—C(32)	178.4(3)	N(3)—C(33)—C(34)	178.2(3)
N(4)—C(35)—C(36)	178.0(3)	C(1)—C(2)—C(3)	114.0(3)
C(2)—C(3)—C(4)	116.8(2)	P(1)—C(1)—C(2)	113.9(2)
P(2)—C(4)—C(3)	118.9(2)		

Table 4. Bond lengths (Å) and angles (deg) for *t*-$RuCl_2(MeCN)_4$ (**5**).

Bond	Distance	Bond	Distance
Ru(1)—Cl(1)	2.4107(8)	Ru(1)—N(1)	2.022(2)
Ru(1)—N(2)	2.029(2)	N(1)—C(1)	1.129(3)
N(2)—C(3)	1.119(3)	C(1)—C(2)	1.460(4)
C(3)—C(4)	1.462(4)		
Bonds	**Angle**	**Bonds**	**Angle**
Cl(1)—Ru(1)—Cl(1)*[a]	180	Cl(1)—Ru(1)—N(1)	89.46(7)
Cl(1)—Ru(1)—N(1)*	90.54(7)	Cl(1)—Ru(1)—N(2)	90.96(7)
Cl(1)—Ru(1)—N(2)*	89.04(7)	N(1)—Ru(1)—N(2)	86.0(1)
N(1)—Ru(1)—N(1)*	180	N(1)—Ru(1)—N(2)*	94.0(1)
N(2)—Ru(1)—N(2)*	180	Ru(1)—N(1)—C(1)	173.0(3)
Ru(1)—N(2)—C(3)	171.8(2)	N(1)—C(1)—C(2)	179.1(3)
N(2)—C(3)—C(4)	178.2(3)		

[a]Asterisk denotes symmetry operation: $1 - x$, $1 - y$, $1 - z$.

Can. J. Chem. Downloaded from www.nrcresearchpress.com by 80.90.12.36 on 09/08/12
For personal use only.

Fig. 2. Perspective view of *trans*-$RuCl_2(MeCN)_4$, **5**; 50% probability thermal ellipsoids are shown for the non-hydrogen atoms.

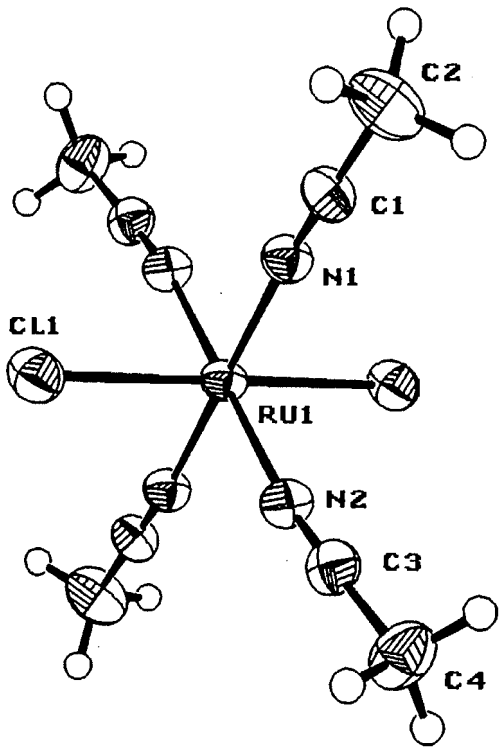

and below it are compressed slightly. Distortions of the coordination sphere in **3** result primarily from intramolecular steric repulsion between the diphosphine ligand and two of the nitrile ligands (the contacts N(1)···C(23) = 3.010 Å, N(4)···C(6) = 3.055 Å, and C(35)···C(6) = 3.199 Å are all at or below the sum of van der Waals radii) as well as the inherent steric constraints of the dppb ligand, and secondarily from the formation of a weak C—H···F hydrogen bond between the nitrile ligand containing N(3) and one of the anions (C(34)—H(35)···F(6), H···F = 2.63 Å, C···F = 3.302 Å, C—H···F = 160°). These factors are responsible for the small but significant deviation from linearity of N(3)-Ru-N(4) angle (171°) relating the mutually *trans* nitrile ligands. The corresponding angle in the related complex $Ru(MeCN)_6^{2+}$ **6**, which is free of the steric constraints imposed by the diphosphine ligand, is 178° (14). All *trans* angles in **5** are exactly linear as a consequence of the crystallographic C_i symmetry. Since the P-Ru-P angle in **3** is obtuse (94°, see Table 3), the opposite N-Ru-N angle is expected to be acute but the actual value of 83° suggests some additional compression arising from the above-mentioned steric factors. The deviation of the *cis* N-Ru-N angles in **5** (86° and 94°, see Table 4) from 90° can only result from intermolecular steric interactions. The Ru-N-C angles in **3** (170°–172°) are similar to those in **5** (172°–173°) while those in both **6** and $Ru(C_6H_6)(MeCN)_3^{2+}$ **7** (15) average 176°. Since the Ru-N-C angles involving the sterically hindered nitrile ligands (those containing N(1) and N(4)) assume the intermediate values (Table 3), it is most likely that the nonlinearity of these angles results from packing forces in both **3** and **5**. The nitrile N-C-C angles in **3**, **5**, and **6** are all ca. 178°.

The high symmetry implied by the appearance of only two methylene multiplets in the ^1H NMR spectrum of **3** (presumably one for the central two CH_2 groups and one for the two P-CH_2 groups) suggests that the two halves of the carbon backbone are related by a twofold axis. Although in the solid state the P-C-C bond angles at C(1) and C(4) differ by nearly 5° (with values of ~114° and 119°, respectively), and the C-C-C angles at C(2) and C(3) by 3° (114° and 117°), flexing of the diphosphine unit in solution must render these differences insignificant. In the solid state structure, the seven-membered chelate ring has an irregular chair conformation and the four phosphine phenyl rings are planar, the geometry of the Ru(dppb) moiety being essentially the same as those within $RuCl(\eta^6$-toluene)$(dppb)^+$ (5) and (DMSO)(dppb)Ru(μ-$Cl)_3$RuCl(dppb), where DMSO is S-bonded dimethyl sulphoxide (10). Based on ^1H NMR data for various $Ph_2P(CH_2)_nPPh_2$ ligands (16), the multiplets at δ ~2.7 and ~1.7 are assigned to the CH_2-P and CH_2-CH_2 protons, respectively.

While the average Ru—N bond distance for the mutually *trans* nitriles in **3** (2.03 Å) is closely comparable to the average values in **5**, **6**, and **7** (2.03, 2.03, and 2.06 Å, respectively), the remaining pair of nitriles exhibits a slight lengthening of these bonds (average 2.12 Å), owing to the strong *trans* influence exerted by the phosphine. Even the shorter Ru—N bonds, however, are slightly longer than ~2.0 Å, the sum of the estimated single covalent radii (17), implying little Ru(II)→N, $d\pi$-$p\pi$ backbonding. Where such backbonding is significant, shorter Ru—N bonds are observed, as, for example, in Ru(II)-N_2 complexes: although the accuracy of crystallographic data for dinitrogen complexes is sometimes low, the more reliable Ru—N bond lengths of 1.822(13) Å (18) and 1.894(9) Å (19) in Ru-porphyrin and -bis(ethylenediamine) species, respectively, are significantly shorter than those in the Ru(II)-nitriles. The C—N bond lengths in the four nitrile complexes range from 1.12 to 1.14 Å, being slightly *shorter* than the value of 1.157 Å calculated for MeCN in the gas phase (20), as commonly observed in both transition metal (21) and main group (22) complexes of nitriles. Shortening of the C—N bond is perhaps evidence against any π-backbonding component to the ligand–metal interaction, as are the positive infrared coordination shifts of ν(C≡N) for N-bonded nitrile complexes generally (21) and for complexes **3**–**5**; see Experimental; cf. values of 2254 and 2231 cm^{-1} for free MeCN and PhCN, respectively. The corresponding data for complexes **6** and **7** are not reported. (Of the two IR bands observed generally in the 2270–2320 cm^{-1} region, the lower energy one is ν(C≡N), while the higher energy one is a combination of ν(C—C) and $\delta(CH_3)$ (21)). Also, while any backbonding from the metal might be expected to be greatest for **5**, in which the metal centre is neutral rather than dicationic, the C—N bond lengths are actually shortest in this complex, although the differences are hardly significant. Thus despite the strong π-donor capacity of low-spin Ru(II) (23), there is no definitive evidence to suggest that the nitrile ligands function as π-acceptors in these Ru(II) species. This view contrasts with that of Ludi and Merbach and co-workers (15, 24, 25) who describe MeCN as a typical π-acceptor that permits strong backbonding from the electron-rich Ru^{2+} ion. In the papers reporting the crystal structures of **6** and **7** (14, 15), the shortening in the Ru—N and C—N bond lengths, which is difficult to reconcile with the π-backbonding model, is not discussed. A smaller downfield ^1H NMR shift of the η^6-C_6H_6 singlet for

$Ru(C_6H_6)(MeCN)_3^{2+}$ (**7**) versus the corresponding tris(aquo) complex was also attributed to π-backbonding to the nitrile (24), but this effect could equally well result from the weaker σ-donor ability of MeCN relative to H_2O. Lower substitutional lability and much higher oxidation potentials of some Ru(II)-nitrile complexes relative to aquo species are certainly, however, readily interpreted in terms of the π-backbonding from Ru(II) to MeCN (24, 25). Clearly, more detailed solution studies on crystallographically characterized Ru(II)-nitrile complexes are needed to unravel the subtleties of the backbonding problem, particularly the effect of the nature and number of ancillary ligands. Coordination shifts of the $\nu(C{\equiv}N)$ of MeCN and PhCN to lower wavenumbers have been observed, for example, within the $Ru(NH_3)_5(RCN)^{2+}$ and related complexes, but this is comparatively rare (particularly for MeCN species), and is usually associated with an enhanced π-donor ability of the metal fragment (26, 27).

Acknowledgements

We thank the Natural Sciences and Engineering Research Council of Canada for financial support, and Johnson Matthey Ltd. and Colonial Metals Inc. for loans of $RuCl_3 \cdot 3H_2O$. D. E. F. thanks the Killam Foundation for a postgraduate fellowship, administered by the University of British Columbia.

References

1. R. Noyori. Science, **248**, 1194 (1990).
2. D.E. Fogg, B.R. James, and M. Kilner. Inorg. Chim. Acta, **222**, 85 (1994).
3. D.E. Fogg. Ph.D. Dissertation, University of British Columbia, Vancouver. 1994.
4. D.E. Fogg and B.R. James. J. Organomet. Chem. **462**, C21 (1993).
5. I.S. Thorburn, S.J. Rettig, and B.R. James. J. Organomet. Chem. **296**, 103 (1985).
6. L. Shao, K. Takeuchi, M. Ikemoto, T. Kawai, M. Ogasawara, H. Takeuchi, H. Kawano, and M. Saburi. J. Organomet. Chem. **435**, 133 (1992).
7. W.E. Newton and J.E. Searles. Inorg. Chim. Acta, **7**, 349 (1973).
8. J.D. Gilbert, D. Rose, and G. Wilkinson. J. Chem. Soc. (A), 2725 (1970).
9. K. Mashima, T. Hino, and H. Takaya. J. Chem. Soc. Dalton Trans. 2099 (1992).
10. A.M. Joshi, I.S. Thorburn, S.J. Rettig, and B.R. James. Inorg. Chim. Acta, **198–200**, 283 (1992).
11. International tables for X-ray crystallography. Vol IV. The Kynoch Press, Birmingham, U.K. (present distributor Kluwer Academic Publishers, Dordrecht, The Netherlands). 1974. pp. 99–102 and 149.
12. T.V. Ashworth and E. Singleton. J. Organomet. Chem. **77**, C31 (1974).
13. J. Emsley. Chem. Soc. Rev. **9**, 91 (1980).
14. W. Luginbühl, A. Ludi, A. Raselli, and H.-B. Bürgi. Acta Crystallogr. Sect. C: Cryst. Struct. Commun. **C45**, 1428 (1989).
15. W. Luginbühl, P. Zbinden, P.A. Pittet, T. Armbruster, H.-B. Bürgi, A.E. Merbach, and A. Ludi. Inorg. Chem. **30**, 2350 (1991).
16. B.R. James and D. Mahajan. Can. J. Chem. **57**, 180 (1979).
17. G.E. Rodgers. Introduction to coordination, solid state, and descriptive inorganic chemistry. McGraw–Hill, New York. 1994. p. 164.
18. M.J. Camenzind, B.R. James, D. Dolphin, J.W. Sparapany, and J.A. Ibers. Inorg. Chem. **27**, 3054 (1988).
19. B.R. Davis and J.A. Ibers. Inorg. Chem. **9**, 2768 (1970).
20. C.C. Costain. J. Chem. Phys. **29**, 864 (1958).
21. H. Endres. *In* Comprehensive coordination chemistry. Vol. 2. *Edited by* G. Wilkinson, R. D. Gillard, and J. A. McCleverty. Pergamon Press, Oxford, U.K. 1987. p. 261.
22. B. Swanson, D.F. Shriver, and J.A. Ibers. Inorg. Chem. **8**, 2182 (1969).
23. D.E. Richardson, D.D. Walker, J.E. Sutton, K.O. Hodgson, and H. Taube. Inorg. Chem. **18**, 2216 (1979).
24. M. Stebler-Röthlisberger and A. Ludi. Polyhedron, **5**, 1217 (1986).
25. I. Rapaport, L. Helm, A.E. Merbach, P. Bernhard, and A. Ludi. Inorg. Chem. **27**, 873 (1988).
26. R.E. Clarke and P.C. Ford. Inorg. Chem. **9**, 227 (1970).
27. B.N. Storhoff and H.C. Lewis, Jr. Coord. Chem. Rev. **23**, 1 (1977).

Can. J. Chem. Downloaded from www.nrcresearchpress.com by 80.90.12.36 on 09/08/12
For personal use only.

Elucidation of the structures of the hydridothiolato complexes $WH(SC_6H_2Pr^i_3\text{-}2,4,6)_3(L)(PMe_2Ph)$, L = PMe_2Ph or pyridine, by NMR and X-ray techniques

Timothy E. Burrow, Alan J. Lough, Robert H. Morris, and Raymond L. Richards

Abstract: Measurement of the T_1 values of the ^{31}P nuclei in the unusual capped trigonal bipyramidal complexes $WH(tipt)_3(PMe_2Ph)_2$ (**1**, tipt = $SC_6H_2Pr^i_3$-2,4,6) and $W(^2H)(tipt)_3(PMe_2Ph)_2$ allows the determination of the phosphorus–hydride distance of 2.2 ± 0.2 Å and the P-W-H angle of about 62 ± 7°. An approximate location of the hydride on an S_2P face is proposed on the basis of steric interactions. The crystal structure of $WH(tipt)_3\text{-}(NC_5H_5)(PMe_2Ph)$ (**2**) is reported; the WS_3NP core consists of a distorted trigonal bipyramidal system with the phosphine and pyridine ligands axial and the thiolate ligands equatorial. The hydride ligand was not located by X-ray diffraction but can be positioned on an open S_2P face at an angle P-W-H of about 65°. The small P-W-H angle results in large $^2J(H,P)$ couplings for **1** and **2**. The ^1H NMR spectrum of complex **2** is assigned by use of NOE and homodecoupling NMR methods. This complex has the same crowded structure in solution as in the crystalline state. The pyridine ligand, which is sandwiched between two tipt aryl groups, is hindered from rotating around the W—N bond.

Key words: molybdenum, tungsten, thiolate, hydride, NMR, NOE.

Résumé : Des mesures des valeurs T_1 des noyaux ^{31}P dans des complexes bipyramidaux trigonaux inhabituels $WH(tipt)_3(PMe_2Ph)_2$ (**1**, tipt = $SC_6H_2Pr^i_3$-2,4,6) et $W(^2H)(tipt)_3(PMe_2Ph)_2$ permettent de déterminer que la distance phosphore–hydrure est égale à 2,2 ± 0,2 Å et que l'angle P-W-H est d'environ 62 ± 7°. En se basant sur les interactions stériques, on propose une location approximative de l'hydrure sur la face S_2P. On a déterminé la structure cristalline du $WH(tipt)_3(NC_5H_5)(PMe_2Ph)$ (**2**); le noyau WS_3NP est un système bipyramidal trigonal déformé dans lequel les coordinats phosphine et pyridine sont axiaux et les coordinats thiolates sont équatoriaux. On n'a pas pu déterminer la position du coordinat hydrure par diffraction des rayons X; on peut toutefois le fixer sur une face ouverte du S_2P, avec un angle P-W-H d'environ 65°. Le petit angle P-W-H conduit à des couplages $^2J(H,P)$ élevés pour les composés **1** et **2**. On a attribué les bandes du spectre RMN du ^1H complexe **2** en faisant appel aux méthodes de l'effet Overhauser nucléaire et de l'homodécouplage RMN. En solution, ce complexe possède la même structure encombrée qu'à l'état solide. Le coordinat pyridine est pris en sandwich entre deux groupes aryles tipt; sa rotation autour de la liaison W–N est empêchée.

Mots clés : molybdène, tungstène, thiolate, hydrure, RMN, EON.

[Traduit par la rédaction]

Introduction

We are studying molybdenum and tungsten complexes that contain hydride and thiolate donor ligands (1, 2) because of their possible relevance to nitrogenase (3, 4) and to the hydrodesulfurization reaction (5, 6).

A difficulty in this work is ascertaining the location of a hydride ligand in such a transition metal compound. In single crystal X-ray diffraction studies, the low electron density of the hydride ligand, next to a heavy metal, makes its location and refinement difficult or impossible. Neutron diffraction analysis gives the most accurate results since it relies on the scattering from the nucleus rather than the electron cloud and the scattering factor for hydrogen is substantial. Unfortunately, there are only a few, heavily used, single crystal neutron diffractometers in the world.

Since the relaxation of a nucleus is dependant on its environment, it can be used to probe the molecular structure of a

Received October 31, 1994.

This paper is dedicated to Professor William A.G. Graham on the occasion of his 65th birthday.

T.E. Burrow, A.J. Lough, and R.H. Morris.[1] Department of Chemistry, University of Toronto, Toronto, ON M5S 1A1, Canada.

R.L. Richards. Nitrogen Fixation Laboratory, University of Sussex, Brighton, BN1 9QR, U.K.

[1] Author to whom correspondence may be addressed. Telephone: (416) 978-6962. Fax: (416) 978-8775. E-mail: rmorris@chem.utoronto.ca

Can. J. Chem. Downloaded from www.nrcresearchpress.com by 80.90.12.36 on 09/08/12
For personal use only.

Can. J. Chem. Downloaded from www.nrcresearchpress.com by 80.90.12.36 on 09/08/12
For personal use only.

Fig. 1. Molecular structure of **1** as determined by single crystal X-ray diffraction; reproduced by permission from ref. 1. The isopropyl groups on the tipt ligands have been omitted for clarity.

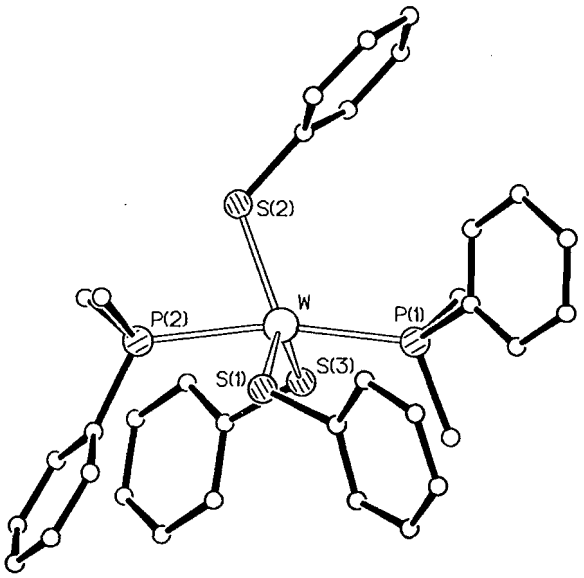

compound. Here we report the use of NOE and T_1 measurements to probe the location of the hydride ligand in $WH(tipt)_3(PMe_2Ph)_2$ (**1**) and $WH(tipt)_3(NC_5H_5)(PMe_2Ph)$ (**2**). The synthesis and crystal structure of **1** have been reported but the hydride ligand was not located (1). Its WS_3P_2 core geometry is distorted trigonal bipyramidal with the thiolate ligands arranged equatorially and the phosphine ligands axial, Fig. 1. The hydride ligand was not located even after repeating the data collection at low temperature. Complex **2** is prepared by substitution of a PMe_2Ph ligand by pyridine in **1** (2). The molecular structure of the molybdenum analogue of **2** has been described recently, but again the hydride position was not certain (7).

Results and discussion

NMR studies of $WH(tipt)_3(PMe_2Ph)_2$

As reported previously (1), the ^{31}P NMR spectrum of **1** has two doublet resonances at −125.2 and −150.5 ppm versus $P(OMe)_3$. These are assigned to atoms P1 and P2, which correspond to P(1) and P(2) of the X-ray-determined structure (Fig. 1) as described below. The coupling $^2J(P1,P2)$ is 100.7 Hz and there are tungsten satellites as reported previously (1). The hydride ligand gives a doublet of doublets resonance in the ^1H NMR spectrum with $^2J(H,P1)$ and $^2J(H,P2)$ of 105 and 8 Hz, respectively; there are also tungsten satellites. These assignments were originally in the reverse order because it was assumed that P2, being pseudo-*trans* to the hydride, would cause the large coupling of 105 Hz; however, we now know that P1, *cis* to the hydride, is associated with this coupling (see below).

The ^1H NMR spectrum also has two doublets belonging to the methyl groups, Me_1, attached to P1, and Me_2 attached to P2, each with a coupling of approximately 8 Hz. The ^1H–^{31}P heteronuclear-correlated two-dimensional NMR spectrum of **1** showed that P1 is coupled to the ^1H nuclei, which resonate at 1.63 ppm (Me_1), and P2 is coupled to the PMe_2Ph resonance at

Fig. 2. Summary of NOE studies of **1**.

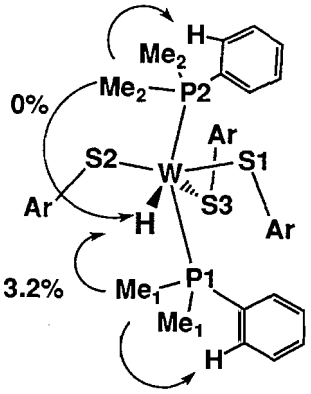

1.69 ppm (Me_2). Low-power irradiation of Me_1 resulted in a 3.2% nuclear Overhauser effect enhancement of the W*H* resonance but irradiation of Me_2 resulted in no enhancement of W*H* (Fig. 2). Thus the hydride ligand is in close proximity to P1. This implies that the hydride ligand has the large *cisoid* coupling of 105 Hz to P1. As Fig. 2 indicates, there are also NOE contacts between neighbouring methyl and *ortho*-phenyl protons in the phosphine ligands.

The hydride location was further refined by calculating the P1–H distance from the difference in relaxation rates of P1 in $W(^1H)(tipt)_3(PMe_2Ph)_2$ and $W(^2H)(tipt)_3(PMe_2Ph)_2$ under identical conditions. The spin-lattice relaxation times of P1, $T_1(P1)$, for the two complexes in toluene-d_8 at −57°C are 0.44 and 0.50 s, respectively, while the $T_1(P2)$ values are identical (Table 1). Since a proton, with its large gyromagnetic ratio, is much more efficient at relaxing nearby nuclei through dipole–dipole relaxation than is a deuteron, the difference in relaxation rates (1/0.44 − 1/0.50) can be used to calculate the H—P internuclear distance. The standard equation for dipole–dipole relaxation, which relates T_1 and distance between dipolar nuclei to the sixth power (8), can be used to calculate the ^1H—^{31}P distance once the correlation time of the molecule, τ_c, is determined. The correlation time was estimated, using the Geirer–Wirtz model of the Stokes–Einstein–Debye equation:

$$[1] \qquad \tau_c = f\frac{V\eta}{kT}$$

where f is the microviscosity factor, V is the volume of the solute, and η is the viscosity of the solute. The volume, V, was calculated from the volume of the unit cell of the crystalline complex, dividing by the number of molecules in the unit cell and correcting for a molecule of benzene in the unit cell. The viscosity of the solvent, η, at 216 K was extrapolated from the values at other temperatures (9). The value for f was estimated as 0.3 from the ratio of solute to solvent volume (Table II in ref. 10). A maximum value of 1.0 was used as an upper limit on τ_c. The internuclear distance was calculated to be between 2.0 and 2.4 Å. Despite the uncertainty in the correlation time, the error in distance (±0.2 Å) becomes acceptably small because the sixth root is taken in calculating the distance.

The best location for the hydride ligand is postulated on the basis of maximizing the distance of the hydride ligand from the sulfur atoms. This was done by using the atomic coordi-

Can. J. Chem. Downloaded from www.nrcresearchpress.com by 80.90.12.36 on 09/08/12
For personal use only.

Table 1. Details of H—P distance calculations from ^{31}P NMR relaxation methods on the complexes $[W(^2H/^1H)(tipt)_3(PMe_2Ph)_2]$.

T_1 for P1 in W(^{1}H) (s):	0.44 ± 0.01	
T_1 for P1 in W(^{2}H) (s):	0.50 ± 0.01	
T_1 for P2 in W(^{1}H) (s):	1.26 ± 0.01	
T_1 for P2 in W(^{2}H) (s):	1.26 ± 0.02	
Rate of relaxation due to hydride ligand (s^{-1}):	0.27	
Volume of unit cell (Å^3):	3154	
Number of molecule per unit cell, Z:	2	
Number of benzene molecules per unit cell:	1	
Volume of molecule:	1547	
T(K):	216	
Viscosity, η (mP):	1.13	
	Minimum	Maximum
Microviscosity factor, f:	0.3	1.0
Correlation time (ps):	170	570
H—P distance (Å):	2.0	2.4

nates from the X-ray crystal structure determination (Fig. 1) and rotating the WH vector around the WP1 vector, keeping a constant distance, d(W—H), of 1.7 Å and a distance from P1 of 2.0 Å. Positions with short distances to carbon or hydrogen atoms were rejected. The best location puts the hydride ligand in the middle of the P1S1S2 face, where S1 and S2 have the aryl groups oriented in the same direction (Fig. 2). These two thiolate ligands define the largest S-W-S angle of 124.7(1)°. This location is similar to that refined for the hydride ligand in the X-ray structure of $WH(SeC_6H_3Pr^i_2\text{-}2,6)_3(PMe_2Ph)_2$ (11).

It is of interest that the approximate H-W-P1 angle is 62 ± 7° (from d(W—H) = 1.70 ± 0.02, d(W—P) = 2.418(3), d(P—H) = 2.2 ± 0.2 Å) and this results in a ^2J(H,P) coupling of 105 Hz while the H-W-P2 angle of approximately 125 ± 5° gives a coupling of only 8 Hz. The complex $MoH(tipt)_3(PMe_2Ph)_2$ must have similar properties because it is virtually isostructural with complex **1** and has a large ^2J(H,P) value of 98 Hz. This could be a general phenomenon for W(IV) and Mo(IV) complexes since the complex $MoH(tp)_2(tipt)(PEtPh_2)$ (tp = NC_5H_4S-2) also has a small H-Mo-P angle of 65 ± 1° and a large ^2J(H,P) coupling of 104 Hz (7). The small size of the ^2J(H,P2) coupling can be explained by considering that 90° H-M-P angles usually give medium-sized negative couplings while 180° angles give large positive couplings. The H-W-P2 angle is between these values so that the coupling may be near to zero. The P1-W-P2 angle is 166.4° and this results in a coupling, ^2J(P,P), of 100.7 Hz.

Structural study of $WH(tipt)_3(NC_5H_5)(PMe_2Ph)$

The molecular structure of $WH(tipt)_3(NC_5H_5)(PMe_2Ph)$ (**2**) is shown in Fig. 3. Atomic coordinates and selected bond distances and angles are given in Tables 2 and 3, respectively. The structure of **2** is very similar to that of $MoH(tipt)_3(NC_5H_5)(PMe_2Ph)$ (Table 3) although the two complexes crystallized in different space groups with the latter containing a crystallographically imposed mirror plane of symmetry (7).

Fig. 3. Molecular structure of **2** as determined by single crystal X-ray diffraction.

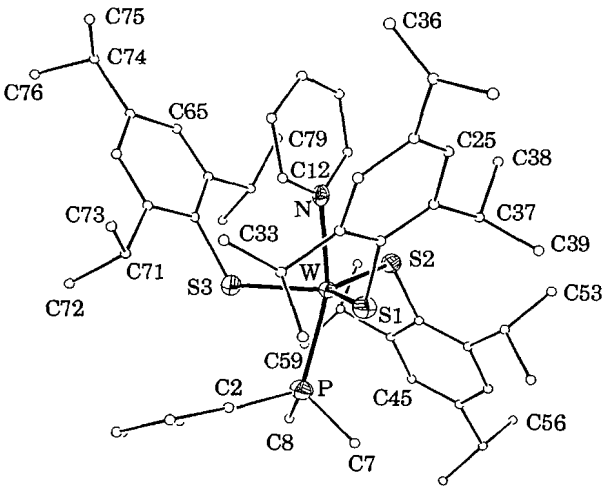

The hydride was not located in the present study nor in the study of the molybdenum complex. The molecule contains a distorted trigonal bipyramidal arrangement of ligands other than the hydride. The thiolate ligands are arranged equatorially to minimize steric repulsion with two arene rings oriented up and the other, down. This arrangement for the bulky thiolate ligands is very common (12). The pyridine ligand is sandwiched between the two "up" aryl rings. The NS_3 grouping defines a fairly regular trigonal pyramid with the N atom at the apex. The P atom does not cap this pyramid symmetrically to form the trigonal bipyramid, but instead has a longer distance to S2 (4.04 Å) than to S1 (3.16) or S3 (3.02 Å); the corresponding angles follow this trend with S2-W-P 116.5(1)°, S1-W-P 84.2(1)°, and S3-W-P 79.2(1)°. It is possible that the hydride is located on the PS1S2 face, which is more open than the PS1S3 face and much more open than the other faces; this would also explain the wide S2-W-P angle. However, the positioning of the hydride on the PS1S3 face, at an angle P-W-H of about 65° is more consistent with the solution NMR data (see below); also the S1-W-S3 angle of 127.8(1)° is the largest of the three S-W-S angles. This is the face proposed to accommodate the hydride in the $MoH(tipt)_3(py)(PMe_2Ph)$ (7).

The MS distances for the complexes $MH(tipt)_3(PMe_2Ph)_2$ and $MH(tipt)_3(py)(PMe_2Ph)$, M = Mo, W, are given in Table 4. The Mo and W analogues are almost isostructural. The covalent radii of tungsten and molybdenum are very similar: 1.38 and 1.37 Å, respectively (13). The Mo—S distances in 31 arene thiolate complexes listed in the Cambridge Structural Database average to a value of 2.408 Å, with a σ of 0.056 (14). There is not a statistically significant number of tungsten thiolate complexes. Therefore the Mo—S and W—S distances in these thiolate hydride complexes are at the short end of this M—S range.

The arene thiolate ligands have both σ and π donor capabilities. The π donation can act to stabilize electron-deficient metal centres. Because of the π bonding, a distortion in the MSR angle is expected; a σ bond would be expected to form the tetrahedral angle of 109°, whereas a π bond would favour a 180° angle. The bond angles observed here are in the range 112–125° and are a compromise of the electronic and steric factors.

Table 2. Final atomic coordinates (fractional $\times 10^4$) with esd in parentheses and B_{eq} for **2**.

Atom	*x*	*y*	*z*	B_{eq}	Atom	*x*	*y*	*z*	B_{eq}
W	7952.1(24)	103.49(20)	9854.22(20)	1.355(13)	C38	8565(9)	2204(7)	8330(6)	4.2(7)
S1	8431.3(17)	−309.8(14)	8837.7(13)	1.99(11)	C39	8046(10)	1271(8)	7503(7)	5.1(7)
S2	7118.5(16)	1222.7(12)	9929 (13)	1.72(10)	C41	6020(6)	1018(5)	9865(6)	1.9(4)
S3	8331.1(17)	−360.6(14)	10895.3(14)	1.95(10)	C42	5636(6)	997(6)	9254(5)	2.0(5)
P	7224.3(16)	−1095.7(14)	9868.2(17)	2.24(11)	C43	4779(7)	860(6)	9212(5)	2.5(5)
N	9042 (5)	884 (4)	9923 (4)	1.60(3)	C44	4294(6)	741(6)	9775(6)	2.6(5)
C1	7870 (7)	−1940 (5)	10074 (6)	3.0(5)	C45	4697(7)	747(6)	10382(5)	2.3(5)
C2	8460 (8)	−2193 (6)	9621 (6)	3.7(6)	C46	5560(7)	898(6)	10441(5)	2.3(5)
C3	8995 (9)	−2810 (7)	9778 (8)	5.0(7)	C51	6097(7)	1129(6)	8609(5)	2.3(5)
C4	8938 (10)	−3160 (7)	10388 (8)	5.9(8)	C52	5839(9)	597(7)	8061(6)	4.0(7)
C6	7820 (9)	−2302 (6)	10678 (6)	4.1(7)	C53	5991(11)	1961(7)	8404(7)	4.9(8)
C5	8366 (10)	−2912 (7)	10835 (8)	5.4(8)	C54	3352(7)	627(7)	9720(6)	3.3(6)
C7	6718 (7)	−1408 (6)	9110 (6)	2.6(5)	C55	2991(7)	49(6)	10178(7)	5.6(7)
C8	6351 (8)	−1163 (7)	10452 (6)	3.8(6)	C56	2913(8)	1390(7)	9808(8)	5.7(8)
C12	9802 (6)	556 (5)	9916 (5)	1.9(4)	C57	5958(7)	950(7)	11122(5)	2.7(5)
C13	10539 (6)	957 (6)	9975 (5)	2.3(5)	C58	5974(9)	1790(7)	11335(6)	3.9(6)
C14	10508 (6)	1754 (6)	10032 (5)	2.7(6)	C59	5519(8)	464(8)	11653(6)	3.8(6)
C15	9754 (6)	2098 (5)	10050 (6)	2.6(6)	C61	9235(6)	61(6)	11284(4)	2.1(4)
C16	9043 (6)	1659 (5)	9989 (5)	2.3(5)	C62	9981(7)	−365(6)	11320(5)	2.2(4)
C21	9332 (6)	167 (6)	8489 (4)	1.9(4)	C63	10646(6)	−63(6)	11652(5)	2.5(5)
C22	10078 (7)	−263 (7)	8439 (5)	3.1(6)	C64	10642(7)	637(6)	11951(5)	2.4(5)
C23	10753 (6)	82 (9)	8104 (5)	3.7(6)	C65	9881(7)	1052(6)	11917(5)	2.2(5)
C24	10700 (8)	819 (9)	7829 (6)	4.3(7)	C66	9194(6)	790(6)	11589(5)	1.7(4)
C25	10002 (8)	1198 (7)	7884 (6)	3.6(6)	C71	10046(8)	−1186(6)	11029(5)	2.7(5)
C26	9262 (8)	898 (6)	8211 (5)	2.8(5)	C72	9956(9)	−1769(7)	11571(7)	4.2(7)
C31	10182 (8)	−1060 (7)	8700 (6)	3.3(6)	C73	10862(9)	−1303(7)	10661(7)	4.5(7)
C32	9823 (10)	−1646 (8)	8206 (6)	4.5(7)	C74	11379(8)	962(6)	12352(6)	3.4(6)
C33	11066 (10)	−1304 (10)	8868 (7)	6.1(9)	C75	12177(8)	985(8)	11933(7)	4.5(7)
C34	11458 (10)	1130 (15)	7450 (8)	10.2(15)	C76	11473(9)	489(7)	12984(7)	4.8(7)
C35	11361 (12)	1099 (12)	6757 (9)	8.8(12)	C77	8380(7)	1241(6)	11621(5)	2.1(4)
C36	12124 (13)	1349 (11)	7826 (10)	9.7(13)	C78	7843(9)	948(7)	12197(6)	4.0(6)
C37	8474 (7)	1351 (7)	8170 (6)	2.9(5)	C79	8521(9)	2108(7)	11660(6)	3.9(6)

Can. J. Chem. Downloaded from www.nrcresearchpress.com by 80.90.12.36 on 09/08/12
For personal use only.

NMR studies of $WH(tipt)_3(py)(PMe_2Ph)$

The hydride resonance of **2** at room temperature is a doublet with tungsten satellites at 9.55 ppm while the proton-coupled ^{31}P NMR spectrum is a doublet with the same large coupling, $^2J(H,P)$, of 102 Hz. This coupling suggests that the hydride is near to the phosphorus atom in **2**, by analogy to the NMR properties of **1**. Indeed, NOE experiments confirm this (see below). This is one piece of evidence that the complex has the same structure in solution as in the solid state; further evidence is presented below.

The proton resonances of **2** at room temperature in the 0–10 ppm region were assigned by use of selective decoupling experiments and NOE and two-dimensional NOESY ^1H experiments. The results are summarized in Table 5 and the labelling of the groups is shown in Fig. 4. Integrations of the peaks are also consistent with the assignments of Table 5. Only the resonance for the *para* proton of the pyridine ligand is observed at room temperature at 500 MHz; the other pyridine peaks are too broad to observe at this temperature. The isopropyl methine region (2.5–4 ppm) shows a pattern of five septets of integration ratio 2:2:2:1:2, which can be explained by the three equatorially arranged triisopropyl benzene thiolate ligands in a "two up – one down" configuration with a mirror plane cutting through the N, P, W, H, and S2 atoms (1, 15). The assignment of the chemical shifts of the *para* isopropyl groups I and III (Table 5) is supported by the ^1H NMR spectrum of the complex $WH(SeC_6H_3Pr^i_2\text{-}2,6)_3(py)(PMe_2Ph)$ (11) which does not have *para* isopropyl groups: the methine region is identical to that of **2** except for the lack of the two septets of groups I and III at 2.96 and 2.66 ppm. One would expect 10 doublets arising from the magnetic inequivalence of the two methyl groups in each isopropyl group of **2**. There are only eight doublets observed (Table 5) because the methyl groups on the (*para*) isopropyl groups I and III are in similar magnetic environments and thus give rise to one doublet each instead of the expected two doublets each. The two doublet resonances for the *para* isopropyl groups are distinctly sharper (smaller line width, greater spin–spin relaxation or T_2) than the other six doublets due to the slower relaxation rates resulting from fewer neighbouring dipolar nuclei in close proximity. The 2D NOESY spectrum was used to establish the assignments of the aromatic ring protons for the tipt and phosphine groups. It is interesting to note that the aryl groups attached to S3 and S1 (Fig. 4) cannot rotate. The aromatic *meta* proton between isopropyl groups IV and III and the one between groups V and III are inequivalent (resonating as doublets at 6.58 and 6.80 ppm, respectively) and couple to each other with $^4J(H,H)$ of 1.7 Hz. Cross peaks in this spectrum rep-

Can. J. Chem. Downloaded from www.nrcresearchpress.com by 80.90.12.36 on 09/08/12
For personal use only.

Table 3. Selected bond distances and angles for complexes $[MH(tipt)_3(py)(PMe_2Ph)]$, M = W (**2**), Mo (**3**) (7) from the X-ray diffraction studies.

2, M = W T = 150 K		**3**, M = Mo T = 293 K	
Bond distances (Å)			
W—N	2.212(7)	Mo—N(5)	2.244(9)
W—P	2.389(2)	Mo—P(4)	2.396(3)
W—S(1)	2.317(3)	Mo—S(2)	2.326(2)
W—S(2)	2.364(2)	Mo—S(1)	2.356(3)
W—S(3)	2.344(3)	Mo—S(2)	2.326(2)[a]
S(1)—C(21)	1.80(1)	S(2)—C(21)	1.810(8)
S(2)—C(41)	1.793(9)	S(1)—C(11)	1.79(1)
S(3)—C(61)	1.80(1)	S(2)—C(21)	1.810(8)[a]
P—C(1)	1.84(1)	P(4)—C(41)	1.82(2)
P—C(7)	1.82(1)	P(4)—C(47)	1.83(1)
P—C(8)	1.83(1)	P(4)—C(47)	1.83(1)[a]
N—C(12)	1.34(1)	N(5)—C(51)	1.34(1)
N—C(16)	1.35(1)	N(5)—C(55)	1.34(1)
Bond angles (deg)			
P—W—N	156.7(2)	P(4)—Mo—N(5)	158.4(2)
N—W—S(1)	89.3(2)	N(5)—Mo—S(2)	89.0(1)
N—W—S(2)	86.1(2)	N(5)—Mo—S(1)	87.2(2)
N—W—S(3)	87.3(2)	N(5)—Mo—S(2)	89.0(1)[a]
P—W—S(1)	84.2(1)	P(4)—Mo—S(2)	81.9(1)
P—W—S(2)	116.49(9)	P(4)—Mo—S(1)	114.4(1)
P—W—S(3)	79.3(1)	P(4)—Mo—S(2)	81.9(1)[a]
S(1)—W—S(2)	119.92(9)	S(2)—Mo—S(1)	115.2(1)
S(1)—W—S(3)	127.77(9)	S(2)—Mo—S(2)[a]	129.6(1)[a]
S(2)—W—S(3)	111.79(9)	S(2)—Mo—S(1)	115.2(1)[a]
W——S(1)—C(21)	118.0(3)	Mo—S(2)—C(21)	118.0(3)
W—S(2)—C(41)	112.4(3)	Mo—S(1)—C(11)	113.3(3)
W—S(1)—C(61)	117.6(3)	Mo—S(2)—C(21)	118.0(3)[a]

[a]From mirror plane of symmetry.

Table 4. Tungsten–sulfur and molybdenum–sulfur bond lengths (Å).

	W	Mo
$MH(tipt)_3(PMe_2Ph)_2$		
M—S	2.314(3)	2.312(3)
M—S	2.311(3)	2.301(3)
M—S	2.352(2)	2.339(3)
$[MH(tipt)_3(py)(PMe_2Ph)]$		
M—S	2.317(3)	2.326(2)
M—S	2.364(2)	2.356(3)
M—S	2.344(3)	2.326(2)

resenting close contacts between the tipt aromatic protons and certain isopropyl groups allowed the assignment of the individual isopropyl methine and methyl resonances. An intergroup contact between the methine protons of isopropyl groups V and II (dotted line in Fig. 4) was another indication that the structure in solution is very similar to the structure in the crystal. The distance between methine hydrogen H57 (on the isopropyl group II of Fig. 4 containing the label C59 in Fig.

Fig. 4. Labelling of the groups of **2**, and important NOE contacts.

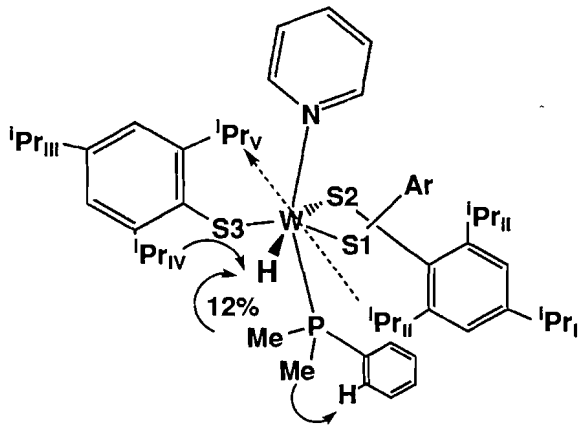

3, which is behind the tungsten atom) and methine hydrogen H77 (on the group V of Fig. 4 with the label C79 in Fig. 3 behind the pyridine ring) is short at 2.58 Å. There is a corresponding set of methine hydrogens related to H57 and H77 on the other groups II and V by the pseudo mirror plane; these are

Can. J. Chem. Downloaded from www.nrcresearchpress.com by 80.90.12.36 on 09/08/12
For personal use only.

Table 5. Assignment of resonances of **2** in C_6D_6. Refer to Fig. 4 for assignment labels. Chemical shifts are in ppm. Couplings, *J*, are in Hz.

		Assignment
tipt methine	**tipt methyl**	
3.98 (sept, 2H, *J* 6.7)	1.52 (d, 6H, *J* 6.6)	Pr^i_{II}; methyl close to
	1.44 (d, 6H, *J* 6.8)	hydride
3.68 (sept, 2H, *J* 6.7)	1.21, (d, 6H, *J* 6.8)	Pr^i_V
	1.14 (d, 6H, *J* 6.7)	
3.20 (sept, 2H, *J* 6.7)	1.33 (d, 6H, *J* 6.8)	Pr^i_{IV}; methine close to
	1.19 (d, 6H, *J* 6.8)	hydride
2.96 (sept, 1H, *J* 7.0)	1.38 (d, 6H, *J* 6.9)	*para* Pr^i_I
2.66 (sept, 2H, *J* 7.0)	1.09 (d, 12H, *J* 7.0)	*para* Pr^i_{III}
tipt aryl		
7.38 (s, 2H)		*meta* to Pr^i_I and Pr^i_{II}
6.80 (d, 2H, *J* 1.7)		*meta* to Pr^i_{III}, Pr^i_{IV}
6.58 (d, 2H, *J* 1.7)		*meta* to Pr^i_{III} and Pr^i_V
Pyridine	**Phosphine**	
9.49 (d, 1H, *J* 5)[a]	7.76 (tm, 2H)	*ortho* H
6.41 (d, 1H, *J* 4)[a]		*ortho* H
6.36 (m, 1H)[a]	7.20 (m, 2H)	*meta* H
5.41 (m, 1H)[a]		*meta* H
6.22 (t, 1H, *J* 7.3)	7.00 (m, 1H)	*para* H
	2.09 (d, 6H, *J* 9.5)	Methyl; close to hydride
Hydride		
9.55 (d, 1H, *J* 102)		WH; *cis* to phosphine

[a]Only observed below 5°C in toluene-d_8 by use of a 500 MHz spectrometer.

H51 and H37, which are separated by 2.30 Å in the crystal. These are the shortest distances between pairs of methine protons. The NOESY spectrum also revealed that the hydride and phosphine methyls are in close proximity, as did the NOED spectra as described below.

The NOESY spectrum did not show the expected cross peak between the *para* and *meta* protons on the pyridine ligand; in fact no *meta* or *para* peaks are visible at room temperature, 500 MHz. The explanation for this became apparent when the variable temperature ^1H spectrum was recorded (shown, in part, in Fig. 5). At −60°C the doublet of the hydride of **2** appears centred at 9.25 ppm and broadens somewhat. It is not known why the hydride resonances shift with temperature. In addition, there is a doublet at 9.48 ppm with a small coupling, ^3J(H,H), of 5 Hz that is assigned to one *ortho* proton of the pyridine ligand. The other *ortho* proton doublet is centred at 6.41 ppm while the *meta* protons are pseudo triplets at 6.36 and 5.41 ppm (Table 5). When the sample is warmed to 5°C these pyridine peaks broaden because of exchange due to pyridine rotation. In a 200 MHz spectrum of **2** at 20°C in C_6D_6, a very broad peak is observed at 5.9 ppm that corresponds to the coalesced lineshape of the *meta* proton resonances. From this information an approximate free-energy barrier to rotation of 14 kcal/mol can be calculated.

Proton NOED spectra of **2** in C_6D_6 at 25°C (Fig. 6) and the knowledge of the proton assignments were used to locate the hydride ligand. Irradiating the methyl resonances of the phosphine at 2.09 ppm, Fig. 6(*d*), caused a 12% enhancement in the hydride resonances as well as an enhancement of the *ortho* phenyl protons of the phosphine at 7.76 ppm. Irradiating the hydride doublet, Fig. 6(*a*), caused a 1% enhancement in the phosphine methyl doublet as well as increases in intensity of the *ortho* phenyl protons of the phosphine, the methine proton of isopropyl group IV at 3.20 ppm, and possibly the methine hydrogens of groups II and V at 3.98 and 3.68 ppm, respectively, as well as the methyl hydrogens of groups II and IV at 1.52, 1.44, and 1.19 ppm. This indicates that the hydride and the phosphine ligand are in close proximity and that the isopropyl groups are positioned predominantly as in the X-ray structure. The observation that irradiating the hydride causes a small enhancement in the phosphine methyl groups (Fig. 6(*a*)) is most likely explained by the fact that relaxation of the hydride is not purely by a dipole–dipole mechanism, see below (16).

The results of irradiation of the tipt aryl resonances at 6.80 (Fig. 6(*b*)) and 6.56 (Fig. 6(*c*)) are consistent with the assignments in Table 5. In (*b*) the peak irradiated consists of the aryl protons of the two "up" tipts (with Pr^iIII and Pr^iIV). This causes enhancement of the methine resonances at 3.20 (Pr^iIV) and 2.66 (Pr^iIII) ppm with the latter showing the greater increase (4%); methyl resonances for groups IV and III are also excited. Irradiation at 6.58 ppm (Fig. 6 (*c*)) excites tipt aryl protons next to groups III and V. The negative enhancement of the *para* pyridine resonance at 6.22 might be due to an error in centering the excitation frequency.

Relaxation measurements on $WH(tipt)_3(py)(PMe_2Ph)$

Unexpectedly the T_1 values of the hydride doublet in the ^1H NMR spectrum of 2 are different; see Tables 6, 7. The lower

Can. J. Chem. Downloaded from www.nrcresearchpress.com by 80.90.12.36 on 09/08/12
For personal use only.

Table 6. Spin lattice relaxation time of **2** in C_6D_6 as a function of spectrometer field (peak 1 is to low field).

B_0(T)	v(MHz)	T(°C)	T_1(peak 1)(s)	T_1(peak 2)(s)
4.7	200	≈25	0.502 ± 0.010	0.448 ± 0.001
7.0	300	25	0.592 ± 0.013	0.532 ± 0.015
9.35	400	25	0.717 ± 0.028	0.615 ± 0.022
11.75	500	25	0.779 ± 0.006	0.643 ± 0.013

Table 7. Spin lattice relaxation times of **2** in toluene-d_8 as a function of temperature at 7 T (300 MHz).

Temperature (K)	Peak 1[a]	Peak 2[a]
209.8	0.64	0.59
247.9	0.51	0.38
276.9	0.52	0.47
298.0[b]	0.59	0.53
313.2	0.69	0.57

[a]Errors ±0.01 s.
[b]In C_6D_6.

frequency peak has a T_1 of 0.72 ± 0.03 s while the other is 0.62 ± 0.02 s at 25°C, 9.4 T. This suggests that another relaxation mechanism than dipole–dipole is important. The minimum T_1 was found to occur between 209 and 220 K at 7.0 T for both resonances.

Könisberger and Sterk (17) state that if there are cross-correlation spectral densities in an AX spin system consisting of two weakly scalar coupled spin 1/2 nuclei with dipole–dipole relaxation, then the two components of each doublet would have different relaxation rates.

The relationship between the T_1 and the spectrometer field was measured, Fig. 7. If the dipole–dipole mechanism were predominant, in the extreme narrowing conditions ($\omega_0\tau_c << 1$), the T_1 should be independent of the field used. If chemical shift anisotropy is predominant, the T_1 should be related to the inverse of the square of the field strength. In the case where the minimum T_1 is near 25°C, the T_1 would also depend upon the inverse of the square of the field. The observed relationship is linear at low field, then levelling off at the higher field. Since the measured minimum T_1 is near −30°C at 7 T, this indicates that chemical shift anisotropy (csa) is the cause of this levelling. Since the contributions of csa and dipolar relaxation are not additive in this case, the effects are difficult to separate.

Conclusions

The measurement of the contribution of the hydride to the relaxation rate of a neighbouring phosphorus in complex **1** allows the $^1H—^{31}P$ distance to be estimated as 2.2 ± 0.2 Å. This allows an unambiguous positioning of the hydride on the S1,S2,P1 face of the distorted trigonal bipyramid of the WS_3P_2 core (Fig. 2). This is the position suggested for the analogous molybdenum complex on the basis of crystallographic considerations (1) and found in the low-temperature single crystal X-ray structure determination of $WH(SeC_6H_3Pr^i2\text{-}2,6)_3(PMe_2\text{-}Ph)_2$ (11).

The geometry suggested for complex **2** is a trigonal bipyramidal WS_3PN core with a hydride capping a triangular S_2P face. NMR studies suggest that the structure in solution is very

Fig. 5. The variable temperature, 500 MHz, ^1H NMR spectra of **2** in toluene-d_8 in the region containing the hydride resonance.

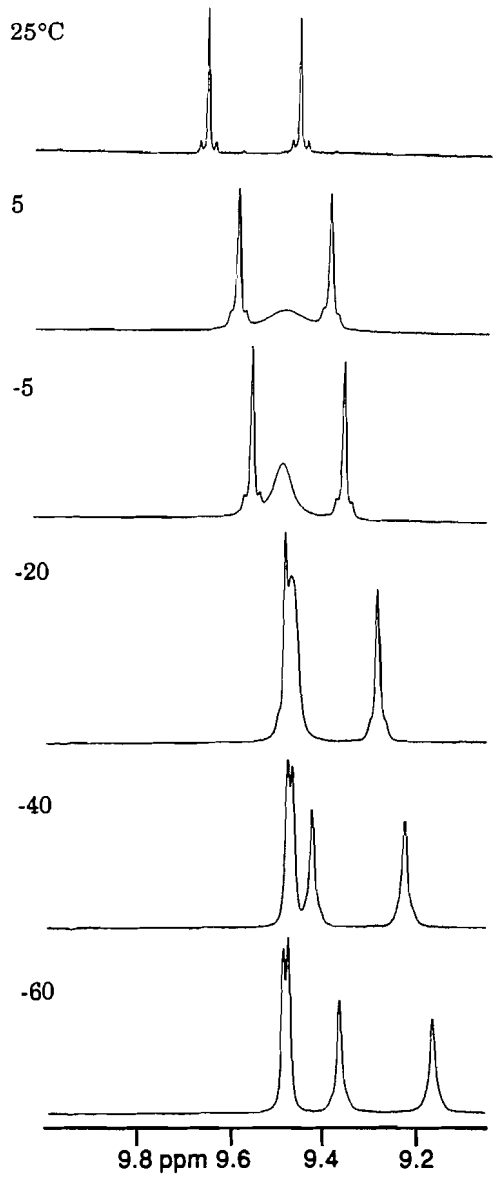

similar to the one determined in the single crystal by X-ray diffraction. Changes in the variable temperature ^1H NMR spectra are explained in terms of restricted rotation of the pyridine ligand, which is observed in the crystal to be sandwiched between two tipt aryl groups. The relaxation rate of the hydride in **2** is determined by contributions from dipolar nuclei and from chemical shift anisotropy of the W—H bond.

A general feature of complexes **1** and **2**, their molybdenum analogues (1, 2), and the complex $MoH(tp)_2(tipt)(PEtPh_2)$ (7) is the large ^2J(H,P) coupling associated with a small P-M-H angle of about 62 ± 7°. The phosphorus–hydride distance is short (≈2 Å) and so ^2J(H,P) might have a through-space component.

Experimental

General

The syntheses of **1** and **2** have been reported previously (1, 2).

NMR samples were prepared under N_2 in 5 mm or 10 mm

Can. J. Chem. Downloaded from www.nrcresearchpress.com by 80.90.12.36 on 09/08/12
For personal use only.

Fig. 6. ^{1}H NOED spectra at 400 MHz of **2** in C_6D_6 at 25°C irradiated at (*a*) the hydride doublet at 9.55 ppm, (*b*) the tipt aryl proton resonance at 6.80 ppm, (*c*) the tipt aryl proton resonance at 6.56 ppm, and (*d*) the phosphine methyl doublet at 2.06 ppm. The singlet at 7.1 ppm in each spectrum is due to the C_6D_6.

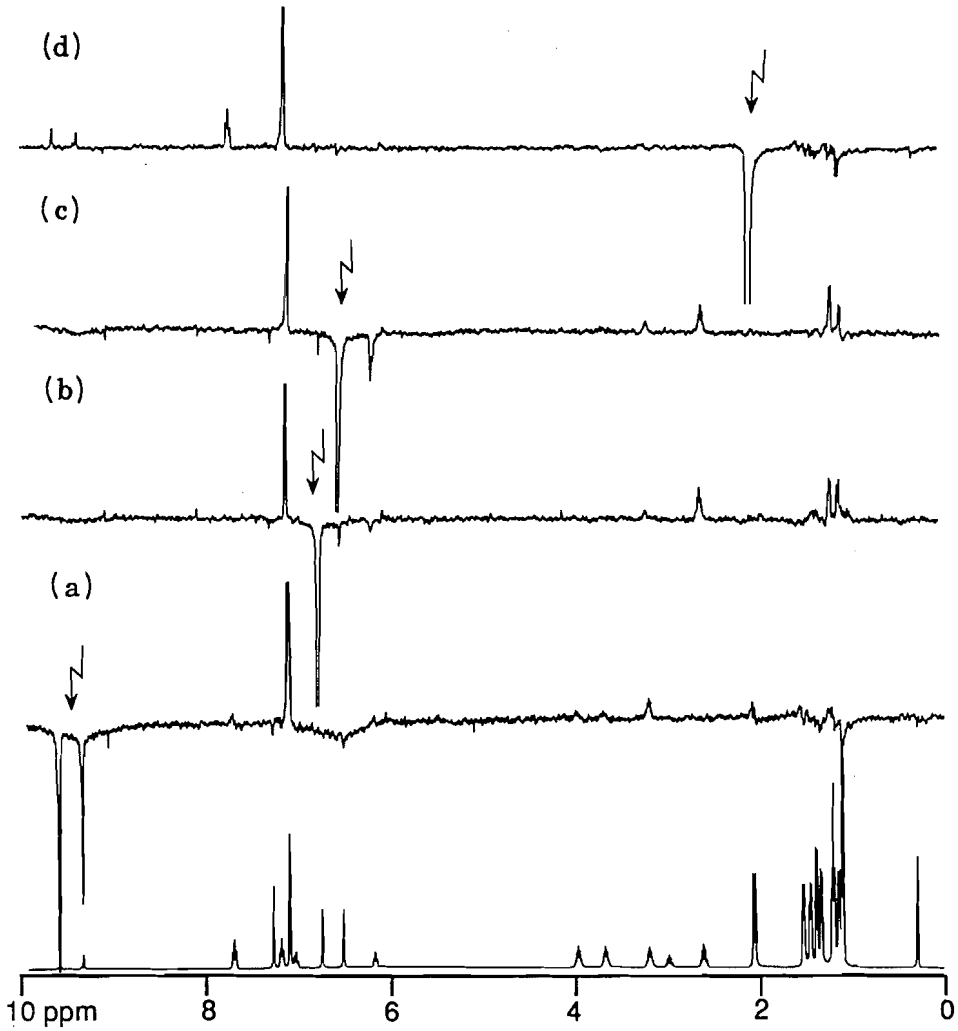

Fig. 7. Plot of T_1 values versus spectrometer field strength for **2** in C_6D_6.

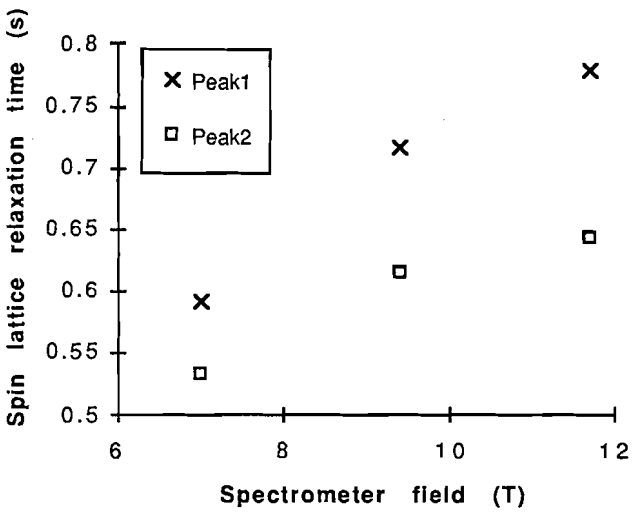

NMR tubes. The spectra were acquired on either a Varian Unity 500 11.8 T machine, a Varian Unity 400 9.4 T machine, a Varian XL-400 9.4 T machine, a Varian Gemini 300 7.0 T machine, a Varian XL-200 4.7 T machine, or a Varian Gemini 200 4.7 T machine. Chemical shifts for ^{31}P were measured internally relative to 1% (v/v) $P(OMe)_3$ in C_6D_6 sealed in coaxial capillaries. ^{31}P NMR are reported as decoupled to ^{1}H unless otherwise indicated. The uncoupled spectra are reported along with significant hydride–phosphorus couplings. ^{1}H chemical shifts are referenced to partially deuterated solvent peaks and are adjusted to the scale of tetramethylsilane (TMS). Deuterated benzene (Cambridge Isotope Laboratories) is the solvent used for proton NMR unless otherwise indicated.

Nuclear Overhauser difference NMR spectroscopy of ***1***

(a) Proton NMR: Data collection was done on a Varian XL-400 using the standard pulse sequence NOEDIF. The sweep width was 5998.8 Hz, the transmitter offset was 800 Hz, $D1$ = 12 s, $D2$ = 50 ms.

Two experiments were conducted. For the first one, $F1$ and

Can. J. Chem. Downloaded from www.nrcresearchpress.com by 80.90.12.36 on 09/08/12
For personal use only.

$F3$ were −1209.5 Hz (corresponding to one half of the doublet of the PMe_2Ph at 1.65 ppm), $F2$ and $F4$ were −1217.3 Hz (corresponding to the other half of the doublet of the PMe_2Ph at 1.65 ppm), OFFRES was 3500 Hz (a blank area of the spectrum downfield). For the second one: $F1$ and $F3$ were −1233.2 Hz (corresponding to one half of the doublet of the PMe_2Ph at 1.70 ppm), $F2$ and $F4$ were −1241.9 Hz (corresponding to the other half of the doublet of the PMe_2Ph at 1.70 ppm), OFFRES was 3500 Hz (a blank area of the spectrum downfield). The irradiation resulted in an asymmetric pattern in the doublet irradiated because only one half of the doublet could be irradiated at one time and so relaxation could occur between the two energy levels.

(b) Phosphorus-31 NMR: Approximately 50 mg of sample was dissolved in about 1 mL of C_6D_6 under N_2 gas.

Data were collected on a Varian XL-400 spectrometer with standard pulse sequences. The hydride resonances were irradiated with low power and a ^{31}P spectrum was acquired. The phosphorus resonances both showed enhancement, the peak at $\delta = -125$ ppm showed 20% enhancement while the peak at −150 ppm showed 15% enhancement.

Heteroscalar correlated two-dimensional NMR spectroscopy of ***1***

The sample (approx. 50 mg) was dissolved in approximately 1 mL C_6D_6 under Ar gas.

Data were collected on a Varian XL-400 using the standard HETCOR pulse sequence assuming a coupling of 11 Hz. Proton NMR was done with a sweep width of 609.3 Hz and transmitter offset of −1400 Hz. Twelve transients were collected, each of 2048 points with 4096 zero points. Phosphorus-31 data collection had a sweep width of 5503.6 Hz with a transmitter offset of −100 Hz.

Measurement of the T_1 values of the phosphorus atoms of ***1***

The T_1 values were measured by use of a Varian Gemini 300 and the standard pulse sequence on a sample of **1** at −57°C in toluene-d_8. The delay was 12 s between pulses and variable delays between the 180° pulse and the 90° observe pulse were 5.45×10^{-3}, 1.65×10^{-2}, 4.94×10^{-2}, 0.148, 0.444, 1.333, 4.000, 12.000 s. Two samples, one of $WH(tipt)_3(PMe_2Ph)_2$ and the other $W^2H(tipt)_3(PMe_2Ph)_2$ (approx. 70% deuterated), were used. The T_1 values for the phosphorus resonances in the partially deuterated sample were used since the resonances for the nondeuterated and deuterated forms could both be measured. The T_1 of the deuterated form (W^2H) was 0.503 ± 0.014 s while the T_1 of the protide form was 0.446 ± 0.011 s.

Crystallization and NMR properties of $WH(tipt)_3(py)(PMe_2Ph)$ (***2***)

The green powder, ca. 100 mg, was dissolved in a minimum amount of hot toluene and then layered with methanol. The mixture was left for 2 weeks at −30°C, producing green crystals. ^1H NMR: (see Table 5). $^{31}P\{^1H\}$ NMR: −118.6 (s; d, $^1J_{PW}$ = 172.3 Hz), $^{31}P\{^1H$ coupled$\}$ NMR: −118.6 (d, $^2J_{PH}$ = 100 Hz; dd, $^2J_{PH}$ = 100 Hz, $^1J_{PW}$ = 172.3 Hz).

Nuclear Overhauser difference NMR spectroscopy of ***2***

The data were collected on a Varian XL-400 using standard pulse sequences. About 50 mg of sample was dissolved in approximately 0.5 mL of C_6D_6.

Homonuclear decoupling NMR spectroscopy of ***2***

The sample, approximately 30 mg, was dissolved in about 1 mL of C_6D_6. Data were acquired on a Varian Gemini-200 with decoupler hardware. The five spectra were recorded with homonuclear decoupler offsets (DO) at −536.4 Hz (2.61 ppm), −461.0 Hz (2.99 ppm), −418.5 Hz (3.20 ppm), −322.5 Hz (3.68 ppm), and −263.2 Hz (3.98 ppm). For all cases the decoupler low power (DLP) was 1800 and DHP was 1.0. The sweep width was 3000.3 Hz for all spectra, with NP of 16 000, PW of 10 ms, and 64 transients were collected.

NOESY NMR spectroscopy of ***2***

Approximately 20 mg of **2** was dissolved in 0.5 mL of toluene-d_8. The sample was run on a 500 MHz (11.8 T) Varian Unity-500 using the standard Varian NOESY pulse sequence. The mixing time was 600 ms.

Single crystal X-ray structure data for $[WH(tipt)_3(py)(PMe_2Ph)]$

Crystal data: $C_{58}H_{86}NPS_3W$, M = 1108.3, orthorhombic, space group $P2_12_12_1$ (no. 19), a = 15.954(5), b = 17.410(3), c = 20.322(4) Å, U = 5644(2) Å^3, Z = 4, D_c = 1.304 g cm^{-3}, T = 150 K, $F(000)$ = 2312, μ(Mo-Kα) = 22.6 cm^{-1}, λ(Mo-Kα) = 0.71069 Å, R = 0.040 for 4205 reflections with $I > 2.5\sigma(I)$.

Data collection: The dark-green crystal had dimensions 0.25 × 0.20 × 0.35 mm. Intensity data were collected on an Enraf–Nonius CAD-4 diffractometer using graphite monochromated Mo-Kα radiation. The ω–2θ scan technique was applied with variable scan speeds. Intensities of three standard reflections measured every 2 h showed less than 1% decay. An empirical absorption correction (18) was applied to the data (max. and min. corrections 1.112 and 0.906).

Structure solution: The coordinates of the W atom were determined from a Patterson map and the positions of the other non-hydrogen atoms were located from successive Fourier and difference Fourier maps. All non-hydrogen atoms were refined with anisotropic thermal parameters by block-diagonal least squares to minimize $\Sigma\omega(F_o - F_c)^2$, where $\omega = (\sigma(F)^2 + 0.005\,F_o^2)^{-1}$. Hydrogen atoms were positioned on geometric grounds (C—H 0.95 Å, U(H) = U(C) + 0.01 Å^2).

All calculations were carried out on an Apollo DN10000 computer using NRCVAX (19), SHELX-76 (20), and SHELXS-86 (21).

Tables: Final atomic coordinates and selected bond distances and angles are listed in Tables 2 and 3, respectively. Complete lists of atomic parameters, thermal parameters, crystal structure information, and bond distances and angles have been deposited as Tables S1–S4.[2]

---

[2] Copies of material on deposit may be purchased from: The Depository of Unpublished Data, Document Delivery, CISTI, National Research Council Canada, Ottawa, Canada K1A 0S2.

With the exception of the thermal parameters, these data have also been deposited with the Cambridge Crystallographic Data Centre, and can be obtained on request from The Director, Cambridge Crystallographic Data Centre, University Chemical Laboratory, 12 Union Road, Cambridge, CB2 1EZ, U.K.

Structure factor amplitudes are no longer being deposited and may be obtained directly from the author.

Acknowledgements

We acknowledge the support of a NATO collaborative research grant (to R.H.M. and R.L.R), operating grants from the Natural Sciences and Engineering Research Council of Canada (NSERC) and Imperial Oil Ltd. (to R.H.M.), and graduate scholarships from NSERC and the University of Toronto (to T.E.B.). We thank Dr Alex Bain and Dr W. Schenk for information on cross-relaxation effects and couplings, respectively. We thank Mr. N. Plavac and Mr. D. Mathers for NMR spectra obtained.

References

1. T.E. Burrow, A. Hills, D.L.Hughes, J.D. Lane, R.H. Morris, and R.L. Richards. J. Chem. Soc. Dalton Trans. 1813 (1991).
2. T.E. Burrow, A.J. Lough, R.H. Morris, A. Hills, D.L. Hughes, J.D. Lane, and R.L. Richards. J. Chem. Soc. Dalton Trans. 2519 (1991).
3. D. Sellmann. Angew. Chem. Int. Ed. Engl. **32**, 64 (1993).
4. R.L. Richards. Chem. Br. 29 (1988).
5. B.C. Wiegand and C.M. Friend. Chem. Rev. (1992).
6. R. Chianelli. Catal. Rev. Sci. Eng. **26**, 361 (1984).
7. D.L. Hughes, N.J. Lazarowych, M.J. Maguire, R.H. Morris, and R.L. Richards. J. Chem. Soc. Dalton Trans. 5 (1995).
8. R.K. Harris. Nuclear magnetic resonance spectroscopy. Longman, Harlow. 1986. p. 88.
9. D.R. Lide (*Editor*). CRC handbook of chemistry and physics. 71st ed. CRC Press Inc., Boca Raton, Fla. 1991.
10. R.T. Boére and R.G. Kidd. Annu. Rep. NMR Spectrosc. **13**, 319 (1982).
11. T.E. Burrow. Ph. D. Thesis, University of Toronto, 1993.
12. P.J. Blower and J.R. Dilworth. Coord. Chem. Rev. **76**, 121 (1987).
13. M. OKeeffe and N.E. Brese. J. Am. Chem. Soc. **113**, 3226 (1991).
14. A.G. Orpen, L. Brammer, F.H. Allen, O. Kennard, and D.G. Watson. J. Chem. Soc. Dalton Trans. S1 (1991).
15. J.S. Murzdek, L. Blum, and R.R. Schrock. Organometallics, **7**, 436 (1988).
16. T.C. Farrar and I.C. Locker. J. Chem. Phys. **87**, 381 (1987).
17. E. Könisberger and H. Sterk. J. Chem. Phys. **83**, 2723 (1985).
18. N. Walker. DIFABS. Empirical absorption correction program, Queen Mary College, London. 1983.
19. P.S. White. The NRCVAX crystal structure system (PC Version), University of North Carolina, 1990.
20. G.M. Sheldrick. SHELX-76, Program for crystal structure determination, University of Cambridge, 1976.
21. G.M. Sheldrick. SHELXS-86, Program for crystal structure determination, University of Gottingen, Federal Republic of Germany, 1986.

Can. J. Chem. Downloaded from www.nrcresearchpress.com by 80.90.12.36 on 09/08/12
For personal use only.

Ruthenium(II) complexes of the thiacyclophane ligands 2,5,8-trithia[9]-*o*-cyclophane (TT[9]OC) and 5-oxa-2,8-dithia[9]-*o*-cyclophane (ODT[9]OC). Structures of $RuCl_2(DMSO)(TT[9]OC)$ and $RuCl_2(PPh_3)(ODT[9]OC)$

Broer de Groot, Hilary A. Jenkins, Stephen J. Loeb, and Shannon L. Murphy

Can. J. Chem, Downloaded from www.nrcresearchpress.com by 80.90.12.36 on 09/08/12
For personal use only.

Abstract: Ruthenium(II) complexes of the thiacyclophane ligands 2,5,8-trithia[9]-*o*-cyclophane (TT[9]OC) and 5-oxa-2,8-dithia[9]-*o*-cyclophane (ODT[9]OC) were synthesized by ligand displacement reactions employing $RuCl_2(DMSO)_4$, $RuCl_2(PPh_3)_3$, and $RuHCl(PPh_3)_3$ as starting materials. X-ray crystal structures of two of these complexes, $RuCl_2(DMSO)(TT[9]OC)$ and $RuCl_2(PPh_3)(ODT[9]OC)$, demonstrate how TT[9]OC and ODT[9]OC bind to Ru(II). $RuCl_2(DMSO)(TT[9]OC)$ crystallized as the DMSO solvate in the orthorhombic space group *Pbca* with $a = 19.590(5)$, $b = 16.849(4)$, $c = 13.149(4)$ Å, $V = 4340(3)$ Å^3, and $Z = 8$. The structure refined to $R = 5.27\%$ and $R_w = 6.27\%$ for 2472 reflections with $F_o^2 > 3\sigma(F_o^2)$. $RuCl_2(PPh_3)$-(ODT[9]OC) crystallized as a $ClCH_2CH_2Cl$ solvate in the monoclinic space group $P2_1/c$ with $a = 7.912(1)$, $b = 22.419(5)$, $c = 18.794(3)$ Å, $\beta = 101.12(1)°$, $V = 3271.2(9)$ Å^3, and $Z = 4$. The structure refined to $R = 4.96\%$ and $R_w = 5.14\%$ for 1800 reflections with $F_o^2 > 3\sigma(F_o^2)$. Both compounds are octahedral with the thiacyclophane ligand bound through three donor atoms in a *facial* coordination mode, *cis* chlorine atoms, and the unique ancillary ligand, DMSO or PPh_3, bound *trans* to the central S or O donor of the macrocycle. The X-ray structures support ^{1}H NMR spectral evidence which shows that the ligands are bound in an "*endo*" mode for L = DMSO and in an "*exo*" mode when L = PPh_3. The reaction of $RuHCl(PPh_3)_3$ with TT[9]OC yields the ruthenium hydride complex $RuHCl(PPh_3)_2(TT[9]OC)$. ^{1}H and ^{31}P NMR spectroscopy are consistent with an octahedral species for which the macrocycle occupies only two coordination sites acting as a bidentate η^2-chelating ligand.

Key words: thioether, macrocycle, hydride, crystal structure.

Résumé : On a synthétisé les complexes du ruthénium contenant des coordinats thiacyclophanes (2,5,8-trithia[9]-*o*-cyclophane, TT[9]OC, et 5-oxa-2,8-dithia[9]-*o*-cyclophane, ODT[9]OC, en soumettant les $RuCl_2(DMSO)_4$, $RuCl_2(PPh_3)_3$ et $RuHCl(PPh_3)_3$ à des réactions de déplacement de coordinats. Les structures cristallines (déterminées par diffraction des rayons X) de deux de ces complexes, $RuCl_2(DMSO)(TT[9]OC)$ et $RuCl_2(PPh_3)(ODT[9]OC)$, démontrent la façon dont le TT[9]OC et le ODT[9]OC se lient au Ru(II). Le $RuCl_2(DMSO)(TT[9]OC)$ cristallise sous une forme solvatée par du DMSO; les cristaux sont orthorhombiques, groupe d'espace *Pbca*, avec $a = 19,590(5)$, $b = 16,849(4)$ et $c = 13,149(4)$ Å, $V = 4340(3)$ Å^3 et $Z = 8$. On a affiné la structure jusqu'à des valeurs de R et R_w de 5,27 et 6,27% respectivement pour 2472 réflexions avec $F_o^2 > 3\sigma(F_o^2)$. Le $RuCl_2(PPh_3)(ODT[9]OC)$ cristallise sous une forme solvatée par du $ClCH_2CH_2Cl$; les cristaux sont monocliniques, groupe d'espace $P2_1/c$, avec $a = 7,912(1)$, $b = 22,419(5)$ et $c = 18,794(3)$ Å, $\beta = 101,12(1)°$, $V = 3271,2(9)$ Å^3 et $Z = 4$. On a affiné la structure jusqu'à des valeurs de R et R_w de 4,96 et 5,14% respectivement pour 1800 réflexions avec $F_o^2 > 3\sigma(F_o^2)$. Les deux composés sont octaédriques avec le coordinat thiacyclophane lié par trois atomes donneurs dans un mode de coordination *facial*; l'atome de chlore est *cis* et le coordinat ancillaire unique, DMSO ou PPh_3, est lié d'une façon *trans* à l'atome donneur central, O ou S, du macrocycle.

Received November 25, 1994.

This paper is dedicated to Professor William A.G. Graham on the occasion of his 65th birthday.

B. de Groot, H.A. Jenkins, S.J. Loeb,[1] and S.L. Murphy. Department of Chemistry and Biochemistry, University of Windsor, Windsor, ON N9B 3P4, Canada.

[1] Author to whom correspondence may be addressed. Telephone: (519) 253-4232 (ext. 3529). Fax: (519) 973-7098. E-mail: LOEB@UWINDSOR.CA

Les données de la diffraction des rayons X sont en accord avec celles de la RMN du ^1H qui montrent que les coordinats sont liés dans un mode *endo* pour L = DMSO et dans un mode *exo* lorsque L = PPh_3. La réaction du $RuHCl(PPh_3)_3$ avec le TT[9]OC fournit l'hydrure complexe du ruthénium, $RuHCl(PPh_3)_2$(TT[9]OC). Les données de la spectroscopie RMN du ^1H et du ^{31}P sont en accord avec l'existence d'une espèce octaédrique dans laquelle le macrocycle occuperait seulement deux sites de coordination et agirait comme un coordinat η^2-chélatant bidentate.

Mots clés : thioéther, macrocycle, hydrure, structure cristalline.

[Traduit par la rédaction]

Can. J. Chem. Downloaded from www.nrcresearchpress.com by 80.90.12.36 on 09/08/12
For personal use only.

Introduction

Until recently, most crown thioether complexes were synthesized for investigations into oxidation state stability and electrochemical properties (1–3). However, investigations by Schröder and co-workers (4), Hill and co-workers (5), and our group (6) have shown that crown thioether complexes of Ru, Rh, and Ir that contain organic ligands such as olefins, σ-vinyl, and thiocarbonyl groups can be prepared. In this regard, Hill (5) showed that the reaction of $[Ru(CH{=}CHR)Cl(CO)(PPh_3)_2]$ with 9S3 (1,4,7-trithiacyclononane) gives $[Ru(CH{=}CHR)(CO)(PPh_3)(9S3)]Cl$ in quantitative yield (*5a*) and Bennett et al. (7) have shown that intramolecular deprotonation, ring opening, and subsequent C—C bond formation occurs when $[Ru(\eta^6\text{-}C_6Me_6)(9S3)][PF_6]_2$ reacts with KO^{t}Bu to yield $[Ru(SCH{=}CH_2)(\eta^6\text{-}C_6Me_5CH_2CH_2CH_2SCH_2CH_2S)]$. This base-induced bond cleavage was found to be irreversible (reprotonation did not occur) and the study suggested that this may limit the extent to which crown thioethers can be attached to electron-rich transition metal centres, and the reaction chemistry they promote or undergo. Ru(II) crown thioether complexes have also been utilized in the modelling of the active sites of the oxidoreductases (8, 9). The influence of the thioether ligand appears to be important in these models, in that there is a tendency to stabilize unusual structures, oxidation states, and species containing NO and N_2H_4.

The thiacyclophane ligands 2,5,8-trithia[9]-*o*-cyclophane (TT[9]OC) and 5-oxa-2,8-dithia[9]-*o*-cyclophane (ODT[9]-OC) also have the potential to bind metal centres as tridentate capping ligands, similar to 9S3, tripodal phosphine, pyrazolylborate, η^5-cyclopentadienyl, or η^6-arene ligands (10–12). In this paper, we describe synthetic routes to the complexes $RuCl_2(X)(L)$ (X = DMSO, PPh_3 and L = TT[9]OC, ODT[9]OC), as well as the hydride complex $RuHCl(PPh_3)_2$(TT[9]OC). NMR spectroscopic characterization of these species is presented along with the X-ray crystal structures of $RuCl_2$(DMSO)(TT[9]OC) and $RuCl_2(PPh_3)$-(ODT[9]OC).

Experimental section

$RuCl_2(PPh_3)_3$ (13), $RuHCl(PPh_3)_3$ (14), TT[9]OC (15), ODT[9]OC (6), and $RuCl_2(DMSO)_4$ (16) were prepared by literature methods. All deuterated solvents were purchased from Aldrich and used as received. All reactions were carried out under an atmosphere of N_2 using standard Schlenk techniques, and all solvents were dried and degassed prior to use. ^1H NMR spectra were recorded at 300.1 MHz on a Bruker AC300 spectrometer locked to the deuterated solvent. $^{31}P\{^1H\}$ NMR spectra were recorded at 81.0 MHz on a Bruker AC200 spectrometer with an external H_3PO_4 reference. Infrared spectra were recorded on a Nicolet 5DX FTIR spectrometer. Elemental analyses were performed by Canadian Microanalytical Services, Delta, British Columbia.

Scheme 1.

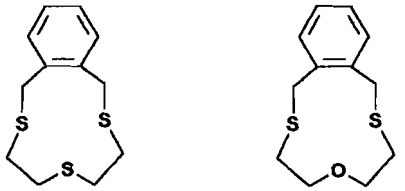

Synthesis of $RuCl_2$(DMSO)(TT[9]OC)

To a yellow solution of $RuCl_2(DMSO)_4$ (330 mg, 0.68 mmol) in $CHCl_3$ (10 mL) was added a colourless solution of TT[9]OC (175 mg, 0.68 mmol) in $CHCl_3$ (5 mL). The clear yellow solution was refluxed for 2 h, producing an orange solution. The solvent was removed and the resulting solid was washed with diethyl ether (2 × 5 mL). The product was recrystallized from DMSO, yielding orange crystals of the complex as the DMSO solvate. Yield 302 mg, 76%. ^1H NMR of the initial reaction product showed the presence of two isomers with an A:B ratio of 1:4. ^1H NMR ($CDCl_3$), isomer A, δ: 7.26–7.16 (m, 4H, aromatic), 4.61 (d, 2H, benzylic, J = 14.1 Hz), 3.81 (d, 2H, benzylic, J = 14.1 Hz), 3.53 (s, 3H, SCH_3), 3.45 (s, 3H, SCH_3), 2.81–2.58 (m, 4H, SCH_2), 2.17–1.68 (m, 4H, SCH_2). Isomer B, δ 7.26–7.16 (m, 4H, aromatic), 4.89 (d, 1H, benzylic, J = 14.0 Hz), 4.78 (d, 1H, benzylic, J = 13.7 Hz), 3.92 (d, 1H, benzylic, J = 14.0 Hz), 3.86 (d, 1H, benzylic, J = 13.7 Hz), 3.38 (s, 3H, SCH_3), 3.29 (s, 3H, SCH_3), 2.81–2.58 (m, 4H, SCH_2), 2.17–1.68 (m, 4H, SCH_2). Anal. calcd. for $C_{16}H_{28}Cl_2O_2RuS_5$: C 32.86, H 4.84; found: C 33.19, H 4.98.

Synthesis of $RuCl_2$(DMSO)(ODT[9]OC)

To a yellow solution of $RuCl_2(DMSO)_4$ (243 mg, 0.52 mmol) in $CHCl_3$ (10 mL) was added a colourless solution of ODT[9]OC (121 mg, 0.52 mmol) in $CHCl_3$ (5 mL). The clear yellow solution was refluxed for 2 h, producing a yellow-orange solution. The solvent was removed and the resulting solid washed with diethyl ether (2 × 5 mL). Yield 219 mg, 89%. ^1H NMR of the initial reaction product showed the presence of two isomers with an A:B ratio of 1:1. ^1H NMR ($CDCl_3$), isomer A, δ: 7.31–7.16 (m, 4H, aromatic), 4.82 (d, 2H, benzylic, J = 14.2 Hz), 4.32–4.19 (m, 4H, OCH_2), 3.85 (d, 2H, benzylic, J = 14.2 Hz), 3.49 (s, 3H, SCH_3), 3.38 (s, 3H, SCH_3), 2.98–2.05 (m, 4H, SCH_2). Isomer B, δ: 7.31–7.16 (m, 4H, aromatic), 4.57 (d, 1H, benzylic, J = 13.9 Hz), 4.56 (d, 1H, benzylic, J = 13.5 Hz), 4.32–4.19 (m, 4H, OCH_2), 4.06 (d, 1H, benzylic, J = 13.9 Hz), 3.85 (d, 1H, benzylic, J =

Can. J. Chem. Downloaded from www.nrcresearchpress.com by 80.90.12.36 on 09/08/12
For personal use only.

13.5 Hz), 3.44 (s, 3H, SCH_3), 3.37 (s, 3H, SCH_3), 2.98–2.05 (m, 4H, SCH_2). Anal. calcd. for $C_{14}H_{22}Cl_2O_2RuS_3$: C 34.28, H 4.53; found: C 34.09, H 4.44.

Synthesis of $RuCl_2(PPh_3)$(TT[9]OC)

To a brown solution of $RuCl_2(PPh_3)_3$ (1.00 g, 1.04 mmol) in CH_2Cl_2 (30 mL) was added a solution of TT[9]OC (267 mg, 1.04 mmol) in CH_2Cl_2 (10 mL). The brown solution was stirred for 12 h, becoming orange. Solvent was removed in vacuo, and the orange oil washed with diethyl ether (4 × 10 mL) to remove excess PPh_3. The product was dried under vacuum, and recrystallized by cooling a concentrated CH_2Cl_2 solution to −20°C for 24 h. Yield 583 mg, 81%. ^1H NMR showed the presence of two isomers with an A:B ratio of 1:1. ^1H NMR ($CDCl_3$), isomer A, δ: 8.09 (m, 3H, PPh_3), 7.91 (m, 3H, PPh_3), 7.66 (m, 3H, PPh_3), 7.44–6.96 (m, 10H, PPh_3, TT[9]OC), 3.30 (d, 2H, benzylic, J = 14.2 Hz), 2.87 (d, 2H, benzylic, J = 14.2 Hz), 3.02–2.49 (m, 4H, SCH_2), 1.97–1.23 (m, 4H, SCH_2). Isomer B, δ: 8.09 (m, 3H, PPh_3), 7.91 (m, 3H, PPh_3), 7.66 (m, 3H, PPh_3), 7.44–6.96 (m, 10H, PPh_3, TT[9]OC), 5.34 (d, 1H, benzylic, J = 14.1 Hz), 5.20 (d, 1H, benzylic, J = 13.1 Hz), 3.88 (d, 1H, benzylic, J = 14.1 Hz, J = 8.0 Hz), 3.74 (d, 1H, benzylic, J = 13.1 Hz), 3.02–2.49 (m, 4H, SCH_2), 1.97–1.23 (m, 4H, SCH_2). $^{31}P\{^1H\}$ NMR (CH_2Cl_2), isomer A, δ: 36.61 (s, PPh_3). Isomer B, δ: 32.06 (s, PPh_3). Anal. calcd. for $C_{30}H_{31}Cl_2PRuS_3$: C 52.16, H 4.53; found: C 51.89, H 4.40.

Synthesis of $RuCl_2(PPh_3)$(ODT[9]OC)

Method 1

To a brown solution of $RuCl_2(PPh_3)_3$ (1.00 g, 1.04 mmol) in CH_2Cl_2 (50 mL) was added a solution of ODT[9]OC (250 mg, 1.04 mmol) in CH_2Cl_2 (10 mL). The mixture was stirred for 3 days, during which time the solution turned orange and an orange precipitate formed. Solvent was removed in vacuo, and the orange residue was washed with toluene (3 × 15 mL) and dried under vacuum. The product was recrystallized by cooling a CH_2Cl_2 solution to −20°C for 24 h. Yield 547 mg, 78%. ^1H NMR ($CDCl_3$), isomer A, δ: 8.09 (m, 9H, PPh_3), 7.74–7.01 (m, 10H, PPh_3 ODT[9]OC), 4.45 (m, 4H, OCH_2), 3.34 (d, 2H, benzylic, J = 13.9 Hz), 2.96 (d, 2H, benzylic, J = 13.9 Hz), 2.92 (m, 2H, SCH_2), 2.80 (m, 4H, SCH_2), 2.51 (m, 2H, SCH_2). $^{31}P\{^1H\}$ NMR (CH_2Cl_2), δ: 56.21 (s, PPh_3). Anal. calcd. for $C_{30}H_{31}Cl_2OPRuS_2$: C 53.40, H 4.64; found: C 53.22, H 4.43.

Method 2

$RuCl_2(PPh_3)_3$ (1.00 g, 1.04 mmol) and ODT[9]OC (250 mg, 1.04 mmol) were stirred together in toluene (50 mL) for 2 days, forming a yellow slurry. The mixture was filtered in air on a Buchner funnel, and washed with toluene (2 × 10 mL). The crude product was then recrystallized by cooling a CH_2Cl_2 solution to −20°C. Yield 510 mg, 73%. ^1H NMR showed the presence of two isomers with an A:B ratio of 1:1. Data for isomer A is given above. ^1H NMR ($CDCl_3$), isomer B, δ: 7.76–7.11 (m, 19H, aromatic), 5.02 (d, 1H, benzylic, J = 13.8 Hz), 4.71 (d, 1H, benzylic, J = 13.2 Hz), 4.28 (m, 4H, OCH_2), 4.00 (d, 1H, benzylic, J = 13.8 Hz), 3.94 (d, 1H, benzylic, J = 13.2 Hz), 2.83 (m, 4H, SCH_2). $^{31}P\{^1H\}$ NMR (CH_2Cl_2), δ: 41.73 (s, PPh_3).

Synthesis of $RuHCl(PPh_3)_2$(TT[9]OC)

$RuHCl(PPh_3)_3$ (200 mg, 0.216 mmol) was suspended in benzene (10 mL) under N_2, and a solution of TT[9]OC (56 mg, 0.216 mmol) in benzene (10 mL) was added via syringe. The $RuHCl(PPh_3)_3$ dissolved, the solution became brown, and an off-white precipitate formed after 15 min. After stirring for 2 h, the solid was filtered on a Schlenk filter, washed with benzene (2 × 3 mL), and dried in vacuo. Yield of pale yellow microcrystals: 85 mg, 43%. IR: ν(Ru–H) 1939 cm^{-1}. ^1H NMR (acetone-d_6), δ: 7.83 (m, 4H, TT[9]OC aromatic), 7.61–7.14 (m, 30H, PPh_3), 4.00 (s, 2H, benzylic), 3.96 (d, 1H, benzylic, J = 13.2 Hz), 3.85 (d, 1H, benzylic, J = 13.2 Hz), 3.24 (m, 2H, SCH_2), 3.02 (m, 2H, SCH_2), 2.88 (m, 2H, SCH_2), −0.01 (td, 1H, SCH_2), −0.39 (td, 1H, SCH_2), −11.69 (dd, 1H, Ru-H, J_{P-H} = 20.2 Hz). $^{31}P\{^1H\}$ NMR (acetone), δ: 53.84 (d, PPh_3, J_{P-P} = 32.7 Hz), 50.37 (d, PPh_3). Anal. calcd. for $C_{48}H_{47}ClP_2RuS_3$: C 62.76, H 5.17; found: C 62.13, H 5.05.

General X-ray crystallography

Diffraction experiments were performed on a four-circle Rigaku AFC6S diffractometer with graphite monochromatized Mo Kα radiation. The unit cell constants and orientation matrices for data collection were obtained from 20 centred reflections (15° < 2θ < 35°). Instrument parameters, crystal data, and data collection parameters are summarized in Table 1. The intensities of three standard reflections were recorded every 150 reflections and showed no statistically significant changes over the duration of the data collections. The intensity data were collected using the ω–2θ scan technique, in four shells (2θ < 30,° 40,° 45,° and 50°). Empirical absorption coefficients were calculated and absorption corrections applied to the data. The data were processed using the TEXSAN software package running on an SGI Challenge XL computer system.[2] Refinements were carried out by using full-matrix least-squares techniques on F by minimizing the function $\Sigma w(|F_o| - |F_o|)^2$, where $w = 1/\sigma^2(F_o)$ and F_o and F_c are the observed and calculated structure factors. Atomic scattering factors (17) and anomalous dispersion terms (18, 19) were taken from the usual sources. Fixed H-atom contributions were included with C—H distances of 0.95 Å and thermal parameters 1.2 times the isotropic thermal parameters of the bonded C atoms. No H atoms were refined, but all values were updated as refinement continued.

X-ray structure determination of $RuCl_2$(DMSO)(TT[9]OC)

Orange crystals of $RuCl_2$(DMSO)(TT[9]OC) suitable for X-ray diffraction were grown by vapour diffusion of diethyl ether into a DMSO solution of the complex. A statistical analysis of intensity distributions and a determination of systematic absences were consistent with the space group *Pbca*. This was confirmed by a successful structure refinement. A total of 4282 reflections were collected and 2472 reflections with $F_o^2 > 3\sigma(F_o^2)$ were used in the refinement. The position of the ruthenium atom was determined using direct methods and the *E*-map with highest figure of merit. The remaining non-hydrogen atoms were located from successive difference Fourier calculations. In the final cycles of refinement, the ruthenium, chlo-

[2] TEXSAN-TEXRAY Structure Analysis Package, Molecular Structure Corp., The Woodlands, Tex. (1985).

Can. J. Chem. Downloaded from www.nrcresearchpress.com by 80.90.12.36 on 09/08/12
For personal use only.

Table 1. Crystal data and details of data collection and refinement for $RuCl_2(DMSO)$-$(TT[9]OC)\cdot DMSO$ and $RuCl_2(PPh_3)(ODT[9]OC)\cdot Cl(CH_2)_2Cl$.

	$RuCl_2(DMSO)(TT[9]OC)$	$RuCl_2(PPh_3)(ODT[9]OC)$
Formula	$C_{16}H_{28}Cl_2O_2RuS_5$	$C_{32}H_{35}Cl_4OPRuS_2$
Crystal colour and form	Orange plate	Yellow prism
Formula weight	584.72	773.6
Crystal system	Orthorhombic	Monoclinic
a(Å)	19.590(5)	7.912(1)
b(Å)	16.849(4)	22.419(5)
c(Å)	13.149(4)	18.794(3)
β(°)	—	101.12(1)
V(Å^3)	4340(3)	3271.2(9)
Space group	*Pbca* (No. 61)	$P2_1/c$ (No. 14)
Z	8	4
Density (g cm^{-3}), calcd.	1.79	1.57
Radiation, λ (Å)	0.7107	0.7107
Absorption coefficient, μ (cm^{-1})	14.64	10.08
Transmission factors	0.585–1.181	0.896–1.000
Temperature (°C)	24	24
Data collected	4282	3459
Number of unique data used	2472	1800
Significance test	$F_o^2 > 3\sigma(F_o^2)$	$F_o^2 > 3\sigma(F_o^2)$
Number of variables	236	211
Secondary extinction coefficient	1.46×10^{-7}	2.00×10^{-7}
Goodness of fit	3.21	1.92
$R(F_o)$, %	5.27	4.96
$R_w(F_o)$, %	6.27	5.14

rine, sulphur, oxygen, and carbon atoms of the complex were assigned anisotropic thermal parameters while the atoms of the DMSO solvent molecule were refined with isotropic thermal parameters. During refinement it became apparent that the DMSO solvent molecule was severely disordered. Repeated Fourier analyses produced a single central sulphur atom with three other major peaks in a triangular arrangement about the centre. Any attempt to model this as overlapping DMSO molecules with separate sulphurs, with or without threefold disorder about the three remaining atoms, resulted in a single central sulphur atom with a relatively large thermal parameter. Since there is no question the molecule of solvation is DMSO and since variations in the disorder model had insignificant effects on the geometric parameters for the complex, the solvent molecule was modelled as a single entity with a flattened geometry and a large thermal parameter for the S-atom. This resulted in $R = 5.27\%$ and $R_w = 6.27\%$ at convergence. A goodness-of-fit calculation resulted in a value of 3.21, and a final difference Fourier map calculation showed a maximum residual of 1.2 e/Å^3 associated with the solvent molecule, S(5). Atomic positional parameters and selected bonding parameters are summarized in Tables 2 and 3. Thermal parameters, hydrogen atom parameters, and a listing of $10|F_o|$ vs. $10|F_c|$ are deposited as supplementary material in Tables S-1, S-2, and S-5.[3]

X-ray structure determination of $RuCl_2(PPh_3)(ODT[9]OC)$

Orange crystals of $RuCl_2(PPh_3)(ODT[9]OC)$ suitable for X-ray diffraction were grown by cooling a dichloroethane solution of the complex to −20°C for 3 days. A statistical analysis of intensity distributions and determination of systematic absences were consistent with the space group $P2_1/c$. This was confirmed by a successful structure refinement. A total of 3459 reflections were collected and 1800 reflections with $F_o^2 > 3\sigma(F_o^2)$ were used in the refinement. Intensities of the standard reflections showed significant decay (18.4%) above $2\theta = 40°$ due to loss of solvent from the crystal lattice; therefore a linear decay correction was applied to the data. The position of the ruthenium atom was determined using direct methods and the E-map with highest figure of merit, and the remaining non-hydrogen atoms were located from successive Fourier calculations. In the final cycles of refinement, the ruthenium, sulphur, oxygen, phosphorous, and chlorine atoms were assigned anisotropic thermal parameters and the carbons isotropic thermal parameters, resulting in $R = 4.96\%$ and $R_w = 5.14\%$. A goodness-of-fit calculation resulted in a value of 1.92, and a final difference Fourier map calculation showed a maximum residual of 0.4 e/Å^3 associated with the solvent molecule, Cl(3). Atomic positional parameters and selected bonding parameters are summarized in Tables 4 and 5. Thermal parameters, hydrogen atom parameters, and a listing of $10|F_o|$ vs. $10|F_c|$ are deposited as supplementary material in Tables S-3, S-4, and S-6.[3]

[3] Supplementary Tables S-1–S-6 may be purchased from: The Depository of Unpublished Data, Document Delivery, CISTI, National Research Council Canada, Ottawa, Canada K1A 0S2.

Tables of nonessential bonding parameters and hydrogen atom parameters have also been deposited with the Cambridge Crystallographic Data Centre, and can be obtained on request from The Director, Cambridge Crystallographic Data Centre, University Chemical Laboratory, 12 Union Road, Cambridge, CB2 1EZ, U.K.

Can. J. Chem. Downloaded from www.nrcresearchpress.com by 80.90.12.36 on 09/08/12
For personal use only.

Table 2. Positional parameters and B(eq) for $RuCl_2$(DMSO)-(TT[9]OC)·DMSO.

Atom	x	y	z	B(eq)
Ru(1)	0.46781(5)	0.12434(5)	0.23187(6)	2.13(4)
Cl(1)	0.4280(2)	−0.0138(2)	0.2428(2)	3.3(1)
Cl(2)	0.4249(2)	0.1492(2)	0.4042(2)	3.4(2)
S(1)	0.4935(2)	0.0860(2)	0.0684(2)	2.4(1)
S(2)	0.3613(2)	0.1679(2)	0.1716(2)	3.1(2)
S(3)	0.5003(1)	0.2549(2)	0.2384(2)	2.6(1)
S(4)	0.5691(2)	0.0749(2)	0.2891(2)	3.5(2)
O(1)	0.6085(4)	0.0197(5)	0.2211(6)	5.2(5)
C(1)	0.5950(7)	0.2578(7)	0.087(1)	3.8(7)
C(2)	0.6576(8)	0.2842(9)	0.121(1)	4.7(8)
C(3)	0.716(1)	0.249(1)	0.089(1)	7(1)
C(4)	0.712(1)	0.186(1)	0.021(1)	7(1)
C(5)	0.6531(8)	0.1555(9)	−0.014(1)	4.7(8)
C(6)	0.5920(8)	0.1920(7)	0.0188(9)	3.7(7)
C(7)	0.5277(6)	0.1598(7)	−0.0173(8)	3.0(6)
C(8)	0.4071(7)	0.0740(7)	0.0156(8)	3.5(6)
C(9)	0.3591(7)	0.1437(7)	0.0358(8)	3.9(7)
C(10)	0.3647(8)	0.2764(7)	0.166(1)	5.2(8)
C(11)	0.4179(6)	0.3057(6)	0.2412(8)	2.9(5)
C(12)	0.5339(6)	0.2989(6)	0.1210(8)	2.8(6)
C(13)	0.5585(8)	0.0257(8)	0.4085(9)	5.9(8)
C(14)	0.6325(7)	0.1456(8)	0.325(1)	5.7(9)
S(5)[a]	0.2465(8)	−0.040(1)	0.246(1)	35(2)
C(15)[a]	0.2525(9)	−0.001(1)	0.158(1)	6(1)
C(16)[a]	0.266(1)	0.023(1)	0.344(1)	11(1)
C(17)[a]	0.240(2)	−0.103(1)	0.266(3)	21(3)

[a]Atoms of the noncoordinated DMSO solvent molecule. See the text for a description of the disorder.

Results and discussion

The ligands TT[9]OC and ODT[9]OC easily displace three molecules of DMSO from $RuCl_2(DMSO)_4$ to produce the octahedral complexes $RuCl_2$(DMSO)(TT[9]OC) and $RuCl_2$(DMSO)(ODT[9]OC) in which the thiacyclophane ligand occupies three coordination sites in a *facial* arrangement. ^{1}H NMR spectra of the initial products indicate that two isomers exist in $CDCl_3$ solution with A:B ratios of 1:4 and 1:1 for $RuCl_2$(DMSO)(TT[9]OC) and $RuCl_2$(DMSO)-(ODT[9]OC), respectively. These isomers exist because there are two possible positions for the unique DMSO ligand: *trans* to the benzylic S-atoms or *trans* to the central donor (S or O) of the thiacyclophane. The two isomers are easily distinguished by their NMR spectra since isomer A contains a mirror plane and is therefore symmetrical while isomer B is asymmetric and the number of resonances observed is doubled.

Recrystallization of $RuCl_2$(DMSO)(TT[9]OC) from DMSO over a 2 week period yields crystals of isomer A as the DMSO adduct and the X-ray structure was determined. The unit cell contains eight molecules of $RuCl_2$(DMSO)(TT[9]OC) and eight molecules of DMSO. A perspective ORTEP drawing of the complex is shown in Fig. 1. $RuCl_2$(DMSO)(TT[9]OC) is six-coordinate with a slightly distorted octahedral geometry at the Ru(II) centre; Cl(1)-Ru-S(3) 174.0(1),° Cl(2)-Ru-S(1) 170.5(1)°, and S(2)-Ru-S(4) 176.8(1)°. TT[9]OC is coordinated *facially*, with Ru—S(benzylic) distances of Ru—S(1) 2.300(3) Å and Ru—S(3) 2.292(3) Å and a Ru—S(2) distance of 2.351(3) Å. The seven-membered chelate ring spans an angle of S(1)-Ru-S(3) 104.1(1)° and the angles at Ru for the five-membered chelate rings are S(1)-Ru-S(2) 88.1(1)° and S(2)-Ru-S(3) 87.6(1)°. The DMSO ligand is sulphur-bound *trans* to the central S(2) atom with a Ru—S(4) distance of

Table 3. Selected bonding parameters for $RuCl_2$(DMSO)-(TT[9]OC)·DMSO.

Distances (Å)			
Ru(1)—Cl(1)	2.459(3)	Ru(1)—Cl2)	2.453(3)
Ru(1)—S(1)	2.300(3)	Ru(1)—S(2)	2.351(3)
Ru(1)—S(3)	2.292(3)	Ru(1)—S(4)	2.279(4)
S(1)—C(7)	1.81(1)	S(1)—C(8)	1.84(1)
S(2)—C(9)	1.83(1)	S(2)—C(10)	1.83(1)
S(3)—C(11)	1.83(1)	S(3)—C(12)	1.83(1)
S(4)—O(1)	1.504(8)	S(4)—C(13)	1.79(1)
S(4)—C(14)	1.79(1)	C(1)—C(2)	1.38(2)
C(1)—C(6)	1.43(2)	C(1)—C(12)	1.45(2)
C(2)—C(3)	1.36(2)	C(3)—C(4)	1.40(2)
C(4)—C(5)	1.35(2)	C(5)—C(6)	1.41(2)
C(6)—C(7)	1.45(2)	C(8)—C(9)	1.53(2)
C(10)—C(11)	1.51(2)		
Angles (°)			
Cl(1)-Ru(1)-Cl(2)	89.9(1)	Cl(1)-Ru(1)-S(1)	81.9(1)
Cl(1)-Ru(1)-S(2)	91.9(1)	Cl(1)-Ru(1)-S(3)	174.0(1)
Cl(1)-Ru(1)-S(4)	84.9(1)	Cl(2)-Ru(1)-S(1)	170.5(1)
Cl(2)-Ru(1)-S(2)	87.3(1)	Cl(2)-Ru(1)-S(3)	84.1(1)
Cl(2)-Ru(1)-S(4)	93.2(1)	S(1)-Ru(1)-S(2)	88.1(1)
S(1)-Ru(1)-S(3)	104.1(1)	S(1)-Ru(1)-S(4)	90.9(1)
S(2)-Ru(1)-S(3)	87.6(1)	S(2)-Ru(1)-S(4)	176.8(1)
S(3)-Ru(1)-S(4)	95.6(1)	Ru(1)-S(1)-C(8)	100.5(4)
Ru(1)-S(1)-C(7)	118.1(4)	C(7)-S(1)-C(8)	100.5(5)
Ru(1)-S(2)-C(9)	106.2(4)	Ru(1)-S(2)-C(10)	107.0(5)
C(9)-S(2)-C(10)	100.8(5)	Ru(1)-S(3)-C(11)	101.9(3)
Ru(1)-S(3)-C(12)	117.1(4)	C(11)-S(3)-C(12)	98.4(5)
Ru(1)-S(4)-O(1)	118.5(4)	Ru(1)-S(4)-C(13)	111.1(5)
Ru(1)-S(4)-C(14)	116.7(5)	O(1)-S(4)-C(13)	107.1(6)
O(1)-S(4)-C(14)	102.3(6)	C(13)-S(4)-C(14)	99.0(7)
C(2)-C(1)-C(6)	119(1)	C(2)-C(1)-C(12)	119(1)
C(6)-C(1)-C(12)	122(1)	C(1)-C(2)-C(3)	121(1)
C(2)-C(3)-C(4)	119(2)	C(3)-C(4)-C(5)	124(2)
C(4)-C(5)-C(6)	118(1)	C(1)-C(6)-C(5)	120(1)
C(1)-C(6)-C(7)	122(1)	C(5)-C(6)-C(7)	118(1)
S(1)-C(7)-C(6)	112.1(8)	S(1)-C(8)-C(9)	114.6(8)
S(2)-C(9)-C(8)	109.1(8)	S(2)-C(10)-C(11)	109.1(8)
S(3)-C(11)C(10)	116.2(8)	S(3)-C(12)-C(1)	111.3(8)

Scheme 2.

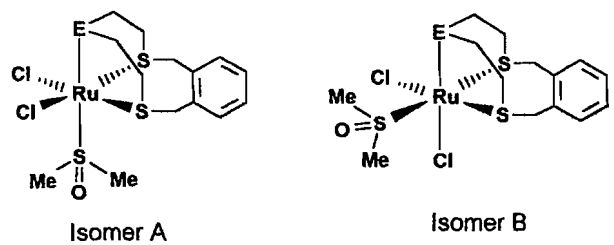

Isomer A Isomer B

Can. J. Chem. Downloaded from www.nrcresearchpress.com by 80.90.12.36 on 09/08/12
For personal use only.

Table 4. Positional parameters and B(eq) for $RuCl_2(PPh_3)$-(ODT[9]OC)·$Cl(CH_2)_2Cl$.

Atom	x	y	z	B(eq)
Ru	0.0938(1)	0.25589(5)	0.67039(6)	1.91(5)
Cl(1)	0.3135(4)	0.2620(2)	0.5965(2)	3.3(2)
Cl(2)	0.2615(5)	0.1836(2)	0.7510(2)	3.1(2)
Cl(3)[a]	0.965(1)	0.0613(3)	0.9347(3)	13.2(5)
Cl(4)[a]	1.384(1)	0.0734(4)	0.9723(5)	20.1(7)
S(1)	−0.0220(5)	0.3353(2)	0.5990(2)	2.5(2)
S(2)	−0.0750(4)	0.2524(2)	0.7564(2)	2.4(1)
P(1)	−0.0434(5)	0.1815(2)	0.6016(2)	1.9(2)
O(1)	0.228(1)	0.3295(4)	0.7392(5)	2.7(4)
C(1)	−0.283(2)	0.3578(6)	0.7348(7)	2.4(3)
C(2)	−0.310(2)	0.3895(7)	0.7965(8)	3.9(3)
C(3)	−0.318(2)	0.4516(7)	0.7945(9)	4.4(4)
C(4)	−0.306(2)	0.4819(7)	0.734(1)	4.7(4)
C(5)	−0.285(2)	0.4528(6)	0.6722(8)	3.6(3)
C(6)	−0.273(2)	0.3892(6)	0.6729(7)	2.5(3)
C(7)	−0.244(2)	0.3597(6)	0.6046(7)	3.2(3)
C(8)	0.102(2)	0.3982(6)	0.6419(7)	3.1(3)
C(9)	0.265(2)	0.3773(6)	0.6953(7)	3.2(3)
C(10)	0.141(2)	0.3497(6)	0.7952(7)	2.7(3)
C(11)	0.057(2)	0.2963(6)	0.8259(7)	2.7(3)
C(12)	−0.282(2)	0.2916(6)	0.7381(7)	2.5(3)
C(13)	−0.207(2)	0.2069(5)	0.5258(6)	1.9(3)
C(14)	−0.378(2)	0.1892(6)	0.5139(7)	3.2(3)
C(15)	−0.497(2)	0.2098(6)	0.4545(8)	4.1(4)
C(16)	−0.446(2)	0.2488(8)	0.4089(7)	4.3(3)
C(17)	−0.278(2)	0.2680(6)	0.4187(7)	3.7(3)
C(18)	−0.157(1)	0.2458(6)	0.4763(6)	2.7(3)
C(19)	0.081(2)	0.1312(5)	0.5529(6)	1.8(3)
C(20)	0.000(2)	0.1034(6)	0.4911(7)	2.7(3)
C(21)	0.091(2)	0.0603(6)	0.4559(8)	3.6(3)
C(22)	0.257(2)	0.0454(6)	0.4866(8)	4.1(4)
C(23)	0.338(2)	0.0724(6)	0.5500(8)	3.8(3)
C(24)	0.249(2)	0.1157(6)	0.5830(7)	2.8(3)
C(25)	−0.148(2)	0.1271(5)	0.6527(7)	2.0(3)
C(26)	−0.072(2)	0.0733(6)	0.6723(7)	2.6(3)
C(27)	−0.138(2)	0.0339(6)	0.7161(8)	3.4(3)
C(28)	−0.280(2)	0.0503(6)	0.7470(8)	3.3(3)
C(29)	−0.356(2)	0.1042(6)	0.7258(7)	3.2(3)
C(30)	−0.293(2)	0.1426(6)	0.6813(7)	2.7(3)
C(31)[a]	1.080(3)	0.105(1)	0.893(1)	8.7(6)
C(32)[a]	1.237(3)	0.128(1)	0.938(1)	8.6(6)

[a]Atoms of the $ClCH_2CH_2Cl$ solvent molecule.

Table 5. Selected bonding parameters for $RuCl_2(PPh_3)$-(ODT[9]OC)·$Cl(CH_2)_2Cl$.

Distances (Å)			
Ru—Cl(1)	2.429(3)	Ru—Cl(2)	2.430(4)
Ru—S(1)	2.310(4)	Ru—S(2)	2.289(3)
Ru—P(1)	2.256(4)	Ru—O(1)	2.234(8)
S(1)—C(7)	1.86(1)	S(10—C(8)	1.82(1)
S(2)—C(11)	1.80(1)	S(2)—C(12)	1.83(1)
P(1)—C(13)	1.82(1)	P(1)—C(1()	1.85(1)
P(1)—C(25)	1.84(1)	O(1)—C(9)	1.42(1)
O(1)—C(10)	1.44(1)	C(1)—C(2)	1.41(2)
C(1)—C(6)	1.38(2)	C(1)—C(12)	1.48(2)
C(2)—C(3)	1.39(2)	C(3)—C(4)	1.34(2)
C(4)—C(5)	1.37(2)	C(5)—C(6)	1.43(2)
C(6)—C(7)	1.50(2)	C(8)—C(9)	1.54(2)
C(10)—C(11)	1.53(2)		
Angles(°)			
Cl(1)-Ru-Cl(2)	91.7(1)	Cl(1)-Ru-S(1)	82.7(1)
Cl(1)-Ru-S(2)	170.2(1)	Cl(1)-Ru-P(1)	91.8(1)
Cl(1)-Ru-O(1)	88.7(3)	Cl(2)-Ru-S(1)	169.7(1)
Cl(2)-Ru-S(2)	81.9(1)	Cl(2)-Ru-P(1)	90.5(1)
Cl(2)-Ru-O(1)	89.5(2)	S(1)-Ru-S(2)	102.5(1)
S(1)-Ru-P(1)	98.3(1)	S(1)-Ru-O(1)	81.8(2)
S(2)-Ru-P(1)	95.6(1)	S(2)-Ru-O(1)	83.9(3)
P(1)-Ru-O(1)	179.5(3)	Ru-S(1)-C(7)	117.8(4)
Ru-S(1)-C(8)	102.8(4)	C(7)-S(1)-C(8)	100.5(6)
Ru-S(2)-C(11)	99.0(4)	Ru-S(2)-C(12)	118.2(4)
C(11)-S(2)-C(12)	104.3(6)	Ru-P(1)-C(13)	114.1(4)
Ru-P(1)-C(19)	119.4(4)	Ru-P(1)-C(25)	113.9(4)
C(13)-P(1)-C(19)	99.8(5)	C(19)-P(1)-C(25)	100.9(6)
C(13)-P(1)-C(25)	106.8(6)	Ru-O(1)-C(9)	110.5(7)
Ru-O(1)-C(10)	114.5(7)	C(9)-O(1)-C(10)	112(1)
C(2)-C(1)-C(6)	119(1)	C(2)-C(1)-C(12)	118(1)
C(6)-C(1)-C(12)	123(1)	C(1)-C(2)-C(3)	120(1)
C(2)-C(3)-C(4)	121(2)	C(3)-C(4)-C(5)	121(2)
C(4)-C(5)-C(6)	119(1)	C(1)-C(6)-C(5)	120(1)
C(1)-C(6)-C(7)	123(1)	C(5)-C(6)-C(7)	117(1)
S(1)-C(7)-C(6)	118.9(8)	S(1)-C(8)-C(9)	111(1)
O(1)-C(9)-C(8)	112(1)	O(1)-C(10)-C(11)	109(1)
S(2)-C(11)-C(10)	112.8(9)	S(2)-C(12)-C(1)	119.2(9)

2.279(4) Å. The two chlorine atoms occupy the two remaining coordination sites: Ru—Cl(1) 2.459(3) Å and Ru—Cl(2) 2.453(4) Å. The Ru—S(benzylic) bond distances are slightly shorter than published Ru—S distances, which range from 2.377 Å for $[Ru(9S3)_2][BPh_4]_2$ (20) to 2.356 Å for $RuCl_2(PPh_3)(9S3)$ (5*c*). This is probably due to the increased flexibility of TT[9]OC compared to 9S3. All other bond distances and angles compare well to those reported. Attempts to isolate a single isomer of $RuCl_2$(DMSO)(ODT[9]OC) by recrystallization from DMSO failed to produce suitable quality crystals.

Both TT[9]OC and ODT[9]OC react slowly with $RuCl_2(PPh_3)_3$ at room temperature, displacing two PPh_3 ligands to yield the coordinatively saturated complexes $RuCl_2(PPh_3)$(TT[9]OC) and $RuCl_2(PPh_3)$(ODT[9]OC). These complexes are soluble in chlorinated solvents, likely due to hydrogen bonding that occurs between the chlorinated solvent, the chloride ligands, and the macrocycle ethylene protons, as observed for the complex $RuCl_2(PPh_3)(9S3)$ (5*b*). They are not, however, soluble in other polar organic solvents such as acetone or acetonitrile, but are soluble in DMSO. Analogous to the complexes with DMSO ligands, those with PPh_3 can exist in two isomeric forms depending on the arrangement of ligands and it was possible to achieve limited control over which isomer was produced by varying the reaction conditions.

$RuCl_2(PPh_3)$(TT[9]OC) was prepared by stirring a CH_2Cl_2 solution of $RuCl_2(PPh_3)_3$ with TT[9]OC for 24 h. This resulted in a moderate, 70%, yield of orange microcrystalline solid after recrystallization from CH_2Cl_2. The ^1H NMR spec-

Can. J. Chem. Downloaded from www.nrcresearchpress.com by 80.90.12.36 on 09/08/12
For personal use only.

Scheme 3.

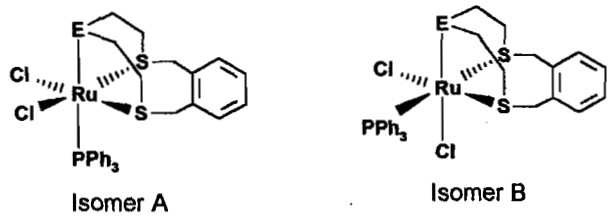

Fig. 1. ORTEP drawing of $RuCl_2(DMSO)(TT[9]OC)$ showing the atom-numbering scheme. Thermal ellipsoids of 30% probability are shown.

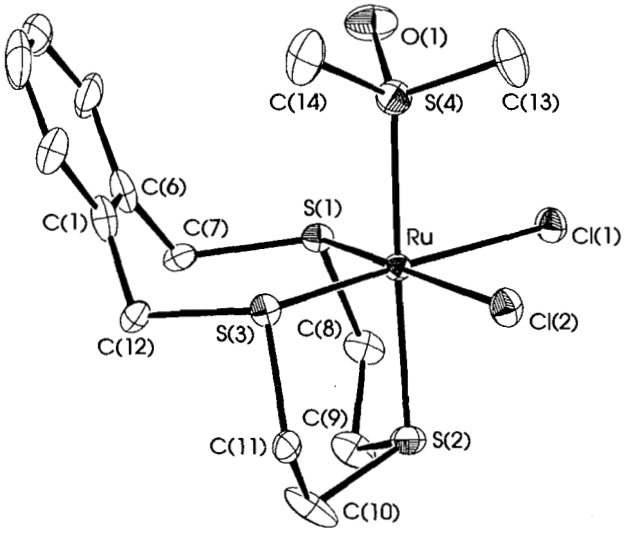

trum showed evidence for both isomers A and B. The $^{31}P\{^1H\}$ NMR spectrum of the mixture shows two resonances at δ 36.61 and 32.06 ppm. Since the PPh_3 ligand is *trans* to sulphur in both isomers, it is not expected that these resonances would be significantly different.

$RuCl_2(PPh_3)(ODT[9]OC)$ is an air-stable, yellow solid obtained in moderate yield by cooling a concentrated CH_2Cl_2 solution of the complex. The ^1H NMR spectrum of $RuCl_2(PPh_3)(ODT[9]OC)$ indicates that only one product is formed when the complex is prepared in CH_2Cl_2. The $^{31}P\{^1H\}$ NMR spectrum of $RuCl_2(PPh_3)(ODT[9]OC)$ shows one resonance at δ 56.21 ppm; the downfield shift compared to $RuCl_2(PPh_3)(TT[9]OC)$ indicates that PPh_3 is *trans* to the oxygen donor of the crown thioether, and this was verified to be isomer A by an X-ray diffraction study (vide infra). The synthesis of $RuCl_2(PPh_3)(ODT[9]OC)$ from toluene results in the formation of two isomers: A in which PPh_3 is *trans* to oxygen, and B, in which PPh_3 is *trans* to sulphur. The ^1H NMR spectrum shows two clearly resolved sets of benzylic resonances for the two isomers and the $^{31}P\{^1H\}$ NMR spectrum shows a second peak at δ 41.73 ppm for isomer B. The mixture of products entirely isomerizes to isomer A after being stirred in chlorinated solvent for 12 h.

Recrystallization of $RuCl_2(PPh_3)(ODT[9]OC)$ from CH_2Cl_2 gave X-ray quality crystals of the complex but these lost solvent in a few hours. Subsequent recrystallization from $Cl(CH_2)_2Cl$ yielded similar crystals and since these lost solvent much more slowly it was possible to obtain an X-ray crystal structure. The unit cell contains four molecules of

Fig. 2. ORTEP drawing of $RuCl_2(PPh_3)(ODT[9]OC)$ showing the atom-numbering scheme. Thermal ellipsoids of 30% probability are shown.

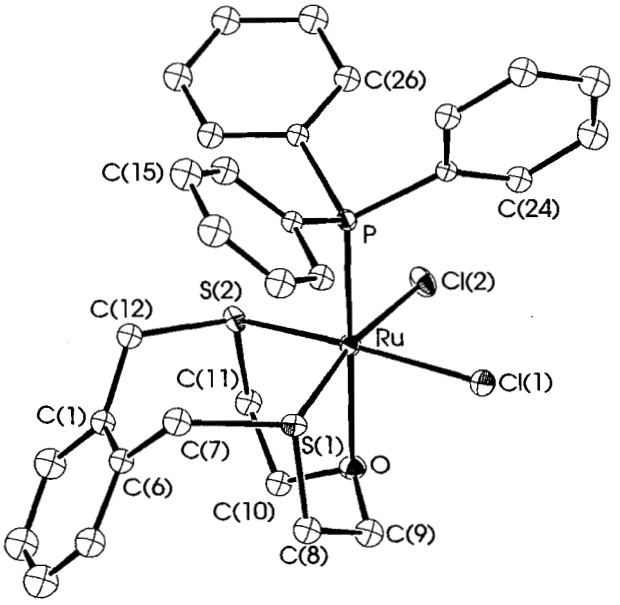

Scheme 4.

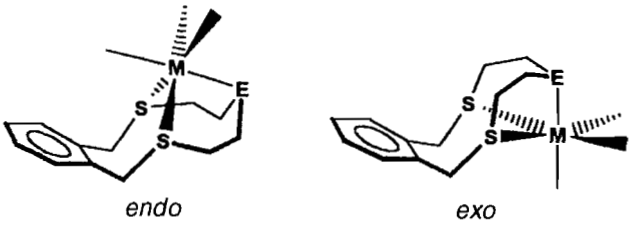

$RuCl_2(PPh_3)(ODT[9]OC)$, isomer A, and four molecules of $Cl(CH_2)_2Cl$. A perspective ORTEP drawing of $RuCl_2(PPh_3)(ODT[9]OC)$ is shown in Fig. 2. $RuCl_2(PPh_3)(ODT[9]OC)$ is six-coordinate with a slightly distorted octahedral geometry at the Ru(II) centre; Cl(1)-Ru-S(2) 170.2(1),° Cl(2)-Ru-S(1) 169.7(1)°, and S(2)-Ru-S(4) 179.5(3)°. ODT[9]OC is coordinated *facially*, with Ru—S(benzylic) distances of Ru—S(1) 2.310(4) Å and Ru—S(2) 2.289(3) Å and a Ru—O distance of 2.234(8) Å. The seven-membered chelate ring spans an angle of S(1)-Ru-S(3) of 102.5(1)°, and the angles at Ru for the five-membered chelate rings are S(1)-Ru-O 81.8(2)° and S(2)-Ru-O 83.9(3).° The PPh_3 ligand is *trans* to the central O-donor atom with a Ru—P distance of 2.256(4) Å. The two chlorine atoms occupy the two remaining coordination sites: Ru—Cl(1) 2.429(3) Å and Ru—Cl(2) 2.430(4) Å. As noted previously for $RuCl_2(DMSO)(TT[9]OC)$, the Ru—S(benzylic) bond distances are slightly shorter than published Ru—S distances; however, all other bond distances and angles compare well to those reported.

It is interesting to compare the structures of $RuCl_2(DMSO)(TT[9]OC)$ and $RuCl_2(PPh_3)(ODT[9]OC)$. Not surprisingly, there are some minor, and to some extent predictable, differences in bonding parameters, attributable to the change from a sulphur to an oxygen donor and the difference between DMSO and PPh_3 as an ancillary ligand. However, there is also a gross structural difference between the bonding

Scheme 5.

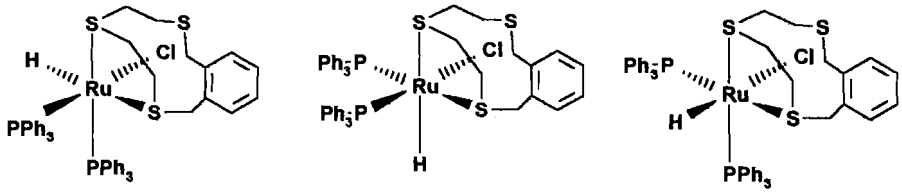

mode for TT[9]OC in $RuCl_2$(DMSO)(TT[9]OC) and ODT[9]OC in $RuCl_2(PPh_3)$(ODT[9]OC).

In every other X-ray structure determined for a complex of the ligand TT[9]OC or ODT[9]OC, the ligand is coordinated in an "*endo*" fashion as observed herein for $RuCl_2$(DMSO)-(TT[9]OC) (6, 21, 22). The structure of $RuCl_2(PPh_3)$-(ODT[9]OC) provides the first example of an "*exo*" coordination mode for this type of ligand. In the more common *endo* mode, the *o*-phenylene moiety is *syn* with respect to the neutral ancillary ligand while in the *exo* mode the *o*-phenylene moiety is *anti* with respect to the neutral ancillary ligand. This can be quantified as a difference in the dihedral angles between the plane defined by the benzylic S atoms, the Ru atom, and the Cl atoms and the plane defined by C(1), C(6), C(7), and C(12) of the thiacyclophane ligand. These dihedral angles are 142.3° and 112.9° for $RuCl_2$(DMSO)(TT[9]OC) and $RuCl_2(PPh_3)$-(ODT[9]OC), respectively. This can be rationalized on steric grounds as the aromatic ring of ODT[9]OC in $RuCl_2(PPh_3)$-(ODT[9]OC) appears to be bent downward away from the PPh_3 group in order to minimize interactions between the two ligands. The benzylic CH_2 groups are then oriented toward the face of one of the aromatic rings of the PPh_3 ligand and this explains the upfield shift of the benzylic protons in the ^1H NMR spectrum, the result of shielding by the phenyl rings of the phosphine ligand. It can also be inferred from ^1H NMR shifts that, in isomer B of this complex, ODT[9]OC is in an *endo* conformation as found previously for Rh(I) and Ir(I) complexes of this ligand.

The A:B isomer distribution formed upon preparation of complexes of the type $RuCl_2(X)(L)$ depends on the nature of X, L, and the conditions used. It appears that the more symmetrical isomer A is the thermodynamic product and can be generated exclusively in various solutions over periods of time varying from a few hours to a few weeks. NMR spectroscopic and X-ray structural evidence provided herein verifies the nature of the bonding and ligand conformation for this isomer.

$RuHCl(PPh_3)_2$(TT[9]OC) was prepared by displacing PPh_3 from $RuHCl(PPh_3)_3$. The product precipitates from a toluene solution as pale yellow microcrystals in 40% yield. Synthesis of $RuHCl(PPh_3)_2$(TT[9]OC) at reduced temperature or under an atmosphere of H_2 does not improve yields. $RuHCl(PPh_3)_2$-(TT[9]OC) is soluble in acetone and chlorinated solvents, and slowly decomposes in the latter. The presence of two sets of benzylic resonances, a pair of doublets at δ 3.96 and 3.85 ppm, and a singlet at δ 4.00 ppm, indicates that the thiacyclophane is bound via an asymmetric η^2-mode to Ru(II), through S(1) and S(2) with S(3) unbound. Two triplets of doublets at approximately δ 0 ppm are due to the ethylene protons of TT[9]OC, which are shielded by the PPh_3 phenyl rings. The ruthenium hydride is observed at δ −11.69 ppm, coupled to two phosphorus atoms, resulting in two doublets with coupling constants of approximately 20 Hz. The $^{31}P\{^1H\}$ NMR spectrum of this complex indicates that two PPh_3 ligands are present, and the P–P coupling of 32.7 Hz is in the range for *cis* phosphorus atoms (23). Thus, spectroscopic characterization indicates that this species contains (*i*) an asymmetrically coordinated thiacyclophane ligand, (*ii*) two PPh_3 ligands with a *cis* orientation, (*iii*) a hydride ligand positioned *cis* to the two phosphines, and (*iv*) a chloride ligand. There are three isomers that could account for these observations although only one is actually present. No solution data are available for unambiguous assignment of structure but it is likely that $RuHCl(PPh_3)$(TT[9]OC) is isomer C since (*i*) the hydride is *trans* to chloride in $RuHCl(PPh_3)_3$, (*ii*) the hydride resonance for RuHCl-(PPh_3)(TT[9]OC) is shifted less than 1 ppm from that found for $RuHCl(PPh_3)_3$, and (*iii*) the PPh_3 resonances are relatively close as would be expected if they are both *trans* to a sulphur atom. Present efforts are focused on obtaining suitable crystals for an X-ray diffraction study to verify this structural assignment.

Heating $RuHCl(PPh_3)_2$(TT[9]OC) in an attempt to displace PPh_3 and form $RuHCl(PPh_3)$(TT[9]OC), in which all three sulphur donors coordinate to the metal centre, was not successful. $RuHCl(PPh_3)_3$ does not react with ODT[9]OC. Since ODT[9]OC requires an S, O chelate, it is presumed the ether O atom is too poor a donor to displace PPh_3. The facile reaction of $RuCl_2(PPh_3)_3$ with crown thioethers or other ligands that substitute for PPh_3 is related to the fact that one PPh_3 ligand is quite labile and in solution $RuCl_2(PPh_3)_3$ readily dissociates to $RuCl_2(PPh_3)_2$. The fact that $RuHCl(PPh_3)_3$ does not undergo a similar facile dissociation of PPh_3 to form $RuHCl(PPh_3)_2$ (24) is consistent with our inability to generate $RuHCl(PPh_3)$-(TT[9]OC) from $RuHCl(PPh_3)_2$(TT[9]OC).

Acknowledgements

We thank the Natural Sciences and Engineering Research Council of Canada for financial support of this research.

References

1. S.R. Cooper. Chem. Res. **21**, 141 (1988).
2. S.R. Cooper and S.C. Rawle. Struct Bonding (Berlin), **72**, 1 (1990).
3. A.J. Blake and M. Schröder. Adv. Inorg. Chem. **35**, 1 (1990).
4. A.J. Blake, M.A. Halcrow, and M. Schröder. J. Chem. Soc. Chem. Commun. 253 (1991).
5. (*a*) J.C. Cannadine, A. Hector, and A.F. Hill. Organometallics, **11**, 2323 (1992); (*b*) A.F. Hill, N.W. Alcock, J.C. Cannadine and G.R. Clark. J. Organomet. Chem. **426**, C40 (1992); (*c*) N.W. Alcock, J.C. Cannadine, G.R. Clark, and A.F. Hill. J. Chem. Soc. Dalton Trans. 1131 (1993).

Can. J. Chem. Downloaded from www.nrcresearchpress.com by 80.90.12.36 on 09/08/12
For personal use only.

6. H.A. Jenkins and S.J. Loeb. Organometallics, **13**, 1840 (1994).
7. M.A. Bennett, L.Y. Goh, and A.C. Willis. J. Chem. Soc. Chem. Commun. 1180 (1992).
8. D. Sellmann, F. Knoch, and C. Wronna. Angew. Chem. Int. Ed. Engl. **27**, 691 (1988), and references therein.
9. D. Sellmann and O. Kappler. Angew. Chem. Int. Ed. Engl. **27**, 689 (1988).
10. (*a*) C. Bianchini, A. Meli, M. Peruzzini, F. Wizza, and F. Zanobini. Coord. Chem. Rev. **120**, 193 (1992), and references therein; (*b*) C. Bianchini, E. Farnetti, M. Graziani, J. Kaspar, and F. Vizza. J. Am. Chem. Soc. **115**, 1753 (1993); (*c*) P. Barbaro, C. Bianchini, A. Meli, M. Peruzzini, A. Vacca, and F. Vizza. Organometallics, **10**, 2227 (1991).
11. (*a*) A.H. Janowicz and R.G. Bergman. J. Am. Chem. Soc. **105**, 3929 (1983); (*b*) J.K. Hoyano, A.D. McMaster, and W.A.G. Graham. J. Am. Chem. Soc. **105**, 7190 (1983); (*c*) W.D. Jones and F.J. Feher. J. Am. Chem. Soc. **108**, 4856 (1986); (*d*) W.D. Jones and F.J. Feher. Acc. Chem. Res. **22**, 91 (1989), and references therein.
12. (*a*) C.K. Ghosh and W.A.G. Graham. J. Am. Chem. Soc. **109**, 4726 (1987); (*b*) J. Am. Chem. Soc. **111**, 375 (1989); (*c*) W.D. Jones and E.T. Hessel. J. Am. Chem. Soc. **114**, 6087 (1992).
13. P.S. Hallman, T.A. Stephenson, and G. Wilkinson. Inorg. Synth. **12**, 237 (1970).
14. P.S. Hallman, B.R. McGarvey, and G. Wilkinson. J. Chem. Soc. (A), 3143 (1968).
15. G.R. Giesbrecht, G.S. Hanan, J.E. Kickham, and S.J. Loeb. Inorg. Chem. **31**, 3286 (1992).
16. B.R. James, E. Ochiai, and G.I. Rempel. Inorg. Nucl. Chem. Lett. **7**, 781 (1971).
17. D.T. Cromer and J.T. Waber. International tables for X-ray crystallography. Vol. IV. Kynoch Press, Birmingham. 1974. Table 2.2A.
18. J.A. Ibers and W.C. Hamilton. Acta Crystallogr. **17**, 781 (1974).
19. D.T. Cromer. International tables for X-ray crystallography. Vol. IV. Kynoch Press, Birmingham. 1974. Table 2.3.1.
20. M.N. Bell, A.J. Blake, M. Schröder, H-J. Küppers, and K. Wieghardt. Angew. Chem. Int. Ed. Engl. **26**, 250 (1987).
21. B. de Groot, H.A. Jenkins, and S.J. Loeb. Inorg. Chem. **31**, 203 (1992).
22. B. de Groot, G.S. Hanan, and S.J. Loeb. Inorg. Chem. **31**, 4644 (1991).
23. J.F. Nixon and A. Pidock. Annu. Rev. NMR Spectrosc. **2**, 245 (1969).
24. P.R. Hoffman and K.G. Caulton. J. Am. Chem. Soc. **97**, 4221 (1975).

Can. J. Chem. Downloaded from www.nrcresearchpress.com by 80.90.12.36 on 09/08/12
For personal use only.

Reaction of $Cp_2(CH_3)Ta{=}CH_2$ with $Ru_3(CO)_{12}$: deoxygenative coupling of carbon monoxide and methylene units to give a heteronuclear cluster-bound 4-cumulene ligand

Grant Proulx, Frederick J. Hollander, and Robert G. Bergman

Abstract: The mechanisms of reactions that deoxygenate carbon monoxide (CO) and convert it into longer-chain hydrocarbons are not well understood. A reaction is reported between an early metal methylidene complex and a late transition metal carbonyl species that results in CO deoxygenation along with coupling of the CO carbon to methylidene groups and other CO carbons. The Schrock tantalum-methylene complex (η^5-C_5H_5)Ta(=CH_2)(CH_3) reacts with the trinuclear metal carbonyl species $Ru_3(CO)_{12}$ to yield the cluster complex $Cp_2(CH_3)Ta(\mu\text{-}O)Ru_3(C_4H_4)(CO)_9$. This material contains a 4-cumulene ligand that bridges the three late-metal centers. Also formed in this reaction is the unstable free tantalum oxo species, (η^5-C_5H_5)Ta(=O)(CH_3). A crystal structure of the $TaRu_3$ cluster is reported along with a proposed mechanism for this unusual carbon–carbon bond-forming reaction.

Key words: deoxygenation, carbon monoxide, alkylidene, coupling, cluster.

Résumé : Les mécanismes des réactions qui permettent de désoxygéner le monoxyde de carbone (CO) pour le transformer en chaînes plus longues d'hydrocarbures ne sont pas bien comprises. On rapporte l'observation d'une réaction impliquant un complexe d'un méthylidène d'un métal du début du tableau avec une espèce carbonylée d'un métal de transition qui provoque une désoxygénation du CO avec le couplage du carbone du CO avec les groupes méthylènes et avec les carbones d'autres CO. Le complexe tantale-méthylène de Schrock (η^5-C_5H_5)Ta(=CH_2)(CH_3) réagit avec l'espèce métal-carbonyl trinucléaire $Ru_3(CO)_{12}$ pour fournir l'agrégat complexe $Cp_2(CH_3)Ta(\mu\text{-}O)Ru_3(C_4H_4)(CO)_9$. Ce matériel comporte un coordinat 4-cumulène qui sert de pont aux trois atomes des métaux de transition. Dans cette réaction, il se forme aussi l'espèce libre d'oxo tantale, (η^5-C_5H_5)Ta(=O)(CH_3). On a déterminé la structure cristalline de l'agrégat $TaRu_3$ et on propose un mécanisme pour cette réaction inhabituelle qui crée des liaisons carbone–carbone.

Mots clés : désoxygénation, monoxyde de carbone, alkylidène, couplage, agrégat.

[Traduit par la rédaction]

The reduction of carbon monoxide and its incorporation into longer-chain hydrocarbons is one of the most intensely studied fields in organotransition metal chemistry. One of the reasons for this is that carbon monoxide offers a potentially inexpensive route to a wide array of useful synthetic fuels and materials (1). A number of homogeneous systems have been found that reduce CO in the presence of H_2 and convert it to methanol (2). Equally interesting are deoxygenation–oligomerization processes, such as the Fischer–Tropsch reaction, that convert CO into longer-chain hydrocarbons by replacement of oxygen with hydrogen and new carbon–carbon bonds (3–5).

One route to understanding such processes is the identification and study of reactions in homogeneous solution that deoxygenate and oligomerize CO. A few homogeneous solution reactions are known in which CO molecules are coupled (6–9) or cleaved (10, 11), but more extensive homogeneous C—C bond-forming processes with this ligand are still rare. We recently reported the stoichiometric reduction and coupling of metal-bound CO in the reactions between Schrock's tantalum alkylidene complex $Cp_2Ta(CH_2)(CH_3)$ (12) (**1**; Cp = η^5-C_5H_5) and various metal carbonyl complexes such as $Co_2(CO)_8$, $Re_2(CO)_{10}$ and $RRe(CO)_5$ (R = alkyl or aryl) (13, 14). In certain steps of the deoxygenation processes, we provided evidence that these reactions proceed through an unstable vinylidene intermediate, which can be trapped in a variety of ways. We have now found that a similar

Received September 12, 1994.

This paper is dedicated to Professor William A.G. Graham on the occasion of his 65th Birthday.

G. Proulx, F.J. Hollander, and R.G. Bergman.[1] Department of Chemistry, University of California, Berkeley, CA 94720, U.S.A.

[1] Author to whom correspondence may be addressed. Telephone (510) 642-2156. Fax (510) 642-7714 (8:30 am – 5:00 pm); (510) 642-8369 (24 h). E-mail: rgberg@violet.berkeley.edu

Can. J. Chem. Downloaded from www.nrcresearchpress.com by 80.90.12.36 on 09/08/12
For personal use only.

reaction between the methylidene complex **1** and a larger cluster, $Ru_3(CO)_{12}$, is capable of deoxygenating several molecules of CO en route to an isolable $TaRu_3$ complex that contains a novel C_4H_4 ligand bridging three metal centers. We report herein the X-ray structure of this novel complex and propose a mechanism for the transformation.

Treatment of a THF slurry of ruthenium dodecacarbonyl ($Ru_3(CO)_{12}$) with two equivalents of the tantalum alkylidene complex $Cp_2Ta(CH_2)(CH_3)$ (**1**) at temperatures greater than 5°C results in the formation of one equivalent of the previously characterized oxo complex, $Cp_2Ta(=O)(CH_3)$ (14) (**2**), and a $TaRu_3$-containing cluster complex, **3** (eq. [1]).[2] Monitoring this reaction by NMR demonstrated that this species was formed in 57% yield (based on ^1H NMR). Recrystallization provided analytically pure **3** as yellow crystals in 32% yield.

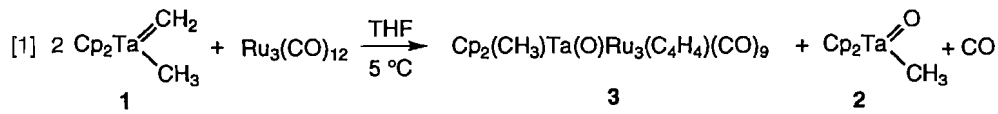

The mass spectrum of **3** showed a parent ion at $[M^+] = 950.8$ *m/z*, and the fragmentation pattern was consistent with a general structural formula of $Cp_2(CH_3)Ta(O)(Ru_3(C_4H_4)(CO)_9$.[3] A C_6D_6 solution of **3** shows a methyl singlet at 0.35 ppm, a singlet for each of two inequivalent cyclopentadienyl groups at 5.10 and 5.17 ppm, and signals for four inequivalent methylene protons. One set of methylene doublets appearing at δ 4.39 and 4.26 ppm are coupled to each other with $^2J_{HH} = 2.6$ Hz while a second set of doublets at δ 2.00 and 1.51 ppm have a coupling constant $^2J_{HH} = 1.3$ Hz. The ^{13}C NMR spectrum with DEPT analysis showed (in addition to the carbonyl resonances) the presence of two methylene carbons and two quaternary carbons and characteristic resonances for the $Cp_2(CH_3)Ta(=O)$ bridging oxo species. Our initial assignment of the species as a triruthenium cluster core, to which are bound a $Cp_2(CH_3)Ta=O$ fragment and a 4-cumulene ($H_2C=C=C=CH_2$) ligand, was based on its similarity to allylic species previously observed in the reactions of **1** with the $Co_2(CO)_8$ and $Fe_2(CO)_9$ clusters. However, there was still some structural ambiguity. For this reason, a single crystal X-ray diffraction analysis was undertaken to confirm our initial hypothesis.[4] An ORTEP diagram of the molecule is shown in Fig. 1, and a blowup of the C_4H_4 ligand with selected distances and angles is shown in Fig. 2. In the solid state, the structure consists of two crystallographically related molecules of **3** and one molecule of benzene in the triclinic unit cell. There are no unusually short contacts between clusters or between clusters and the solvate.

Within the cluster, the $Cp_2(CH_3)Ta=O$ moiety bound to one end of the Ru_3 chain appears to simply fill one of the coordination sites left vacant by loss of a CO ligand at the Ru_1 center, a situation that is superficially similar to that observed in the previously reported $Cp_2(CH_3)Ta=O$-Re(C(=CH_2)Ph)-$(CO)_4$ complex (13). However, the Ta=O-Ru bonding in the two complexes appears to be different. In the Ta=O-Re case, the angle between the three atoms is essentially linear (179°), whereas the Ta=O-Ru angle in **3** is 162.8(2)°. We do not know whether this difference is caused by electronic or steric factors.

Each of the three ruthenium atoms has three apparently normal terminal carbonyl ligands attached to it. These do not seem to have the bridging character that was observed in the $TaFe_2$ allylic cluster structure reported previously, which is not surprising considering the general periodic trends in CO bridging between transition metals (15). There are also two apparent Ru—Ru bonds, from Ru_1 to Ru_2 (2.94 Å) and from Ru_2 to Ru_3 (2.77 Å). The Ru-Ru-Ru angle is 91.3°, indicating that there is no third Ru—Ru bond (the Ru_1 to Ru_3 distance is > 4 Å). The longer Ru_1—Ru_2 interaction may or may not correspond to a full single bond. Distances ranging from 2.64 to 3.16 Å have been found in 140 other ruthenium cluster structures that contain a Ru-Ru-Ru fragment (16, 17). Distances at the higher end of this range (> 3.1 Å) are probably too long to be conventional two-electron covalent bonds and most

---

[2] Preparation of $Cp_2(CH_3)Ta(\mu\text{-}O)Ru(C_4H_4)(CO)$ (**3**): A THF (5 mL) solution of $Cp_2Ta(CH_2)(CH_3)$ (76.2 mg, 0.224 mmol) at 0°C was added dropwise to a rapidly stirring slurry of $Ru_3(CO)_{12}$ (138 mg, 0.217 mmol) in THF (12 mL) at 0°C. The slurry turned a deep red/brown and was stirred for a period of 25 min while slowly warming to room temperature. The slurry was then filtered to remove excess starting $Ru_3(CO)_{12}$. The filtrate was then concentrated in vacuo leaving a brown residue. This residue was extracted with C_6H_6 (ca. 20 mL) and filtered through a 1 in. silylated silica gel plug (Kieselgel 60). The yellow filtrate was then concentrated in vacuo to ca. 5 mL, and a benzene–pentane vapor diffusion recrystallization was performed. The yellow crystals of **3** that formed were isolated (34.1 mg) in 32% yield.

[3] Anal. calcd. for $C_{24}H_{17}O_{10}TaRu_3(0.5\ C_6H_6)$: C 32.80, H 2.04; found: C 32.75, H 2.42. NMR data for $Cp_2(CH_2)Ta(\mu\text{-}O)Ru_3(C_4H_4)(CO)_9$ (**3**): ^1H NMR (400 MHz, C_6D_6) δ: 5.17 (s, 5H, C_5H_5), 5.10 (s, 5H, C_5H_5), 4.39 (d, 1H, $^2J_{HH} = 2.6$ Hz, CH_2), 4.26 (d, 1H, $^2J_{HH} = 2.5$ Hz, CH_2), 2.00 (d, 1H, $^2J_{HH} = 1.3$ Hz, CH_2), 1.51 (d, 1H, $^2J_{HH} = 1.3$ Hz, CH_2), 0.35 (s, 3H, CH_3); $^{13}C\{^1H\}$ NMR (101 MHz, THF-d_8) δ: 208.6 (s, Ru-*C*O), 201.9 (s, Ru-*C*O), 200.3 (s, Ru-*C*O), 199.8 (s, Ru-*C*O), 199.1 (s, Ru-*C*O), 195.3 (s, Ru-*C*O), 190.2 (s, Ru-*C*O), 143.4 (s, H_2CCCCH_2), 112.0 (s, C_5H_5), 111.9 (s, C_5H_5), 85.1 (s, H_2CCCCH_2), 66.7 (s, CH_2), 18.6 (s, CH_2), 15.7 (s, CH_3); MS (FAB) *m/z*: 950.8 (M^+), 922.8 (M^+ − CO), 894.7 (M^+ − 2CO), 866.7 (M^+ − 3CO), 838.7 (M^+ − 4CO), 782.7 (M^+ − 6CO), 500.0 (M^+ − $Ru_2(CO)_7(C_4H_4)$), 472.0 (M^+ − $Ru_2(CO)_8(C_4H_4)$), 444.0 (M^+ − $Ru_2(CO)_9$-(C_4H_4)).

[4] The structure of **3** was solved by Patterson methods and refined via standard least-squares and Fourier techniques. All non-hydrogen atoms were refined anisotropically. Hydrogen atoms were located in difference Fourier maps and allowed to refine with isotropic thermal parameters. A full description of the structure determination is provided as supplementary material (see footnote 7). Crystal data for **3**: $TaRu_3O_{10}C_{27}H_{20}$, triclinic, fw 988.6 amu; space group $P\bar{1}$; $T = -83$°C; $a = 7.6222(9)$ Å; $b = 11.7766(16)$ Å; $c = 16.6829(24)$ Å; $\alpha = 91.143(12)$°, $\beta = 100.011(11)$°, $\gamma = 101.008(11)$°; $V = 1445.4(7)$ Å^3; $Z = 2$; d(calcd.) = 2.27 g cm^{-3}. No. of reflections collected: 5057; no. of unique reflections: 4980. Final residuals for 451 variables refined against the 4112 accepted data (for which $F^2 > 3\sigma > F^2$) were $R = 2.24\%$, $wR = 2.27\%$, and GOF = 1.245. The R value for all 4956 accepted data was 3.35%.

Can. J. Chem. Downloaded from www.nrcresearchpress.com by 80.90.12.36 on 09/08/12
For personal use only.

Fig. 1. Structure of $Cp_2(CH_3)Ta(\mu\text{-}O)Ru_3(C_4H_4)(CO)_9$ (**3**) showing the atom-labeling scheme.

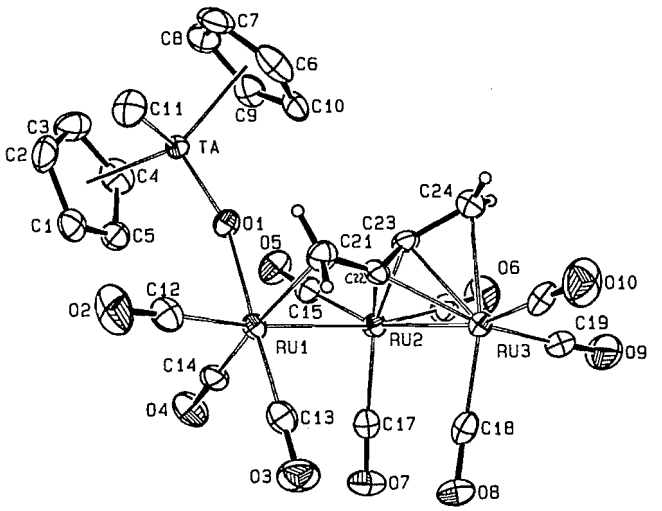

Fig. 2. Expanded view of the $(\mu\text{-}O)Ru(C_4H_4)$ core of **3** showing selected bond distances (Å), bond angles (°) and torsional angles (°) viewed from the Ru_3 plane.

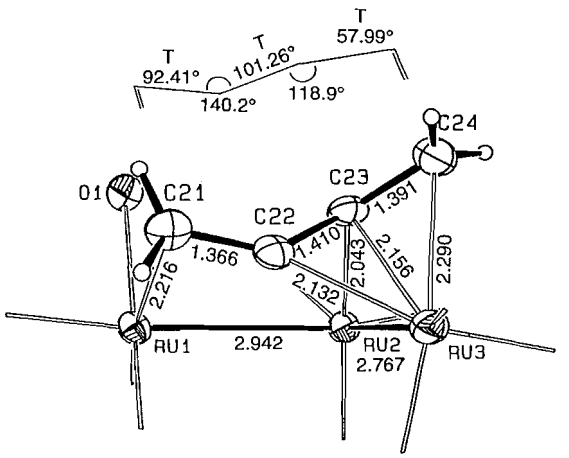

likely represent bridging structures that do not require a large degree of metal–metal interaction. Each Ru center is approximately octahedrally coordinated. The pseudo-octahedron of Ru_1 is tilted about 45° with respect to the pseudo-octahedra of Ru_2 and Ru_3, and the latter are approximately parallel to each other.

There are no apparent systematic differences in the Ru—C distances or Ru—O distances to the carbonyl ligands, so it is unlikely that localized differences in oxidation state are present for the three Ru atoms. The shortest Ru—CO distance (1.853 Å between Ru_1 and C_{13}) is most probably due to the *trans* disposition of this carbonyl to the Ta=O fragment. This is similar to bond lengths observed in previous bridging oxo structures and is not surprising considering the weakly coordinated and weakly electron-accepting oxo species (the Ru_1—O_1 distance is 2.102 Å).

"Above" the Ru_3 plane lies a twisted linear ligand of composition C_4H_4. The hydrogen atoms at each terminus were located and refined. Each carbon atom of the ligand coordinates to at least one Ru atom, and C_{23} bridges the Ru_2—Ru_3 bond. The Ru—C distances vary from 2.04 to 2.29 Å with the longest distance being Ru_3—C_{24}. The C—C distances and angles and C-C-C-C torsion angle are not consistent with any obvious simple organic bonding scheme. The hybridization at C_{21} appears to be essentially sp^2, with a somewhat lengthened C=C double bond, but this atom is also bonded to Ru_1 with a C=C-Ru angle of 82.4° and a C-C-C-Ru torsion angle of 92.4°. The hydrogen atoms are located nearly in the C-C-C plane, with both displaced slightly away from the coordinated Ru.

The bonding at C_{22} and C_{23} is more complex. The C-C-C angle of 140.2° at C_{22} is reasonable for two coordinated *sp*-hybridized carbons, such as those found in complexed alkynes, but the angle at C_{23} (118.9°) is more typical of a relatively undistorted sp^2 carbon. Ru_3 is in the C_{21}-C_{22}-C_{23} plane, but the coordination is more consistent with that of a C=C double bond, with both C_{22} and C_{23} at essentially the same distance from Ru_3 and with the C—C distance lengthened to 1.41 Å. In addition, there is an obvious Ru—C single bond from Ru_2 to C_{23}, but Ru_2 lies out of the plane of C_{21}-C_{22}-C_{23} by 1.81 Å (and out of the C_{22}-C_{23}-C_{24} plane by 1.26 Å).

This is further complicated by a twisting of the C_4 ligand, leading to a C-C-C-C torsion angle of 101.3°. This twist clearly excludes the possibility of an undistorted cumulene structure. Instead, Ru_3 coordinates to three of the carbons in what at first appears to be an allylic-type bonding arrangement with respect to the C_{22}-C_{23}-C_{24} plane. The C_{23}—C_{24} distance of 1.39 Å reflects a typically allylic bond order of approximately 1.5, but the bonding distance to C_{24} is much longer than the distances to C_{22} and C_{23}, making even this interaction highly unsymmetrical. In addition, the hydrogen atom positions on C_{24} are twisted with respect to the C_{21}-C_{22}-C_{23} plane so as to give them more equivalent Ru-C-H angles.

With these unusual positional parameters in mind, a formal bonding scheme is still difficult to formulate. However, a somewhat distorted allylic-type interaction, as shown in Scheme 1, is the simplest formulation of the bonding between C_{22}-C_{23}-C_{24} and the Ru_3 core.[5] With a C_{23}—Ru_2 single bond, the only bonding assignments left are those between C_{21}, C_{22}, and Ru_1. If the 1.366 Å distance between C_{21} and C_{22} is a somewhat lengthened double bond, then one must consider whether there is any significant C_{22}—Ru_1 bonding. This is difficult to say decisively, but we have not found any clear evidence for a Ru—C bonding distance of greater than 2.35 Å. Thus our formulation does not include a bond between these two atoms. Because it seems clear that the sp^2 carbon is in the proper arrangement for it, we postulate a donor coordination from C_{21} to Ru_1.

Complex **3** is the first product that we have been able to isolate from reactions of $Cp_2(CH_3)Ta{=}CH_2$ with a 4*d* metal center as well as the first from reaction with a trimeric metal complex. Although the final product is substantially different from those obtained with other metal carbonyls, the mechanism, at least in its initial stages, may be similar to others in this series. As shown in Scheme 1, we suggest that the reaction is initiated by an overall cycloaddition between the $Ta{=}CH_2$

[5] A referee has cautioned us against attempting to apply simple valence bond theory to clusters. We agree, but the structure in Scheme 1 seems to us a useful way of keeping track of the bonding electrons in this system.

Can. J. Chem. Downloaded from www.nrcresearchpress.com by 80.90.12.36 on 09/08/12
For personal use only.

Scheme 1.

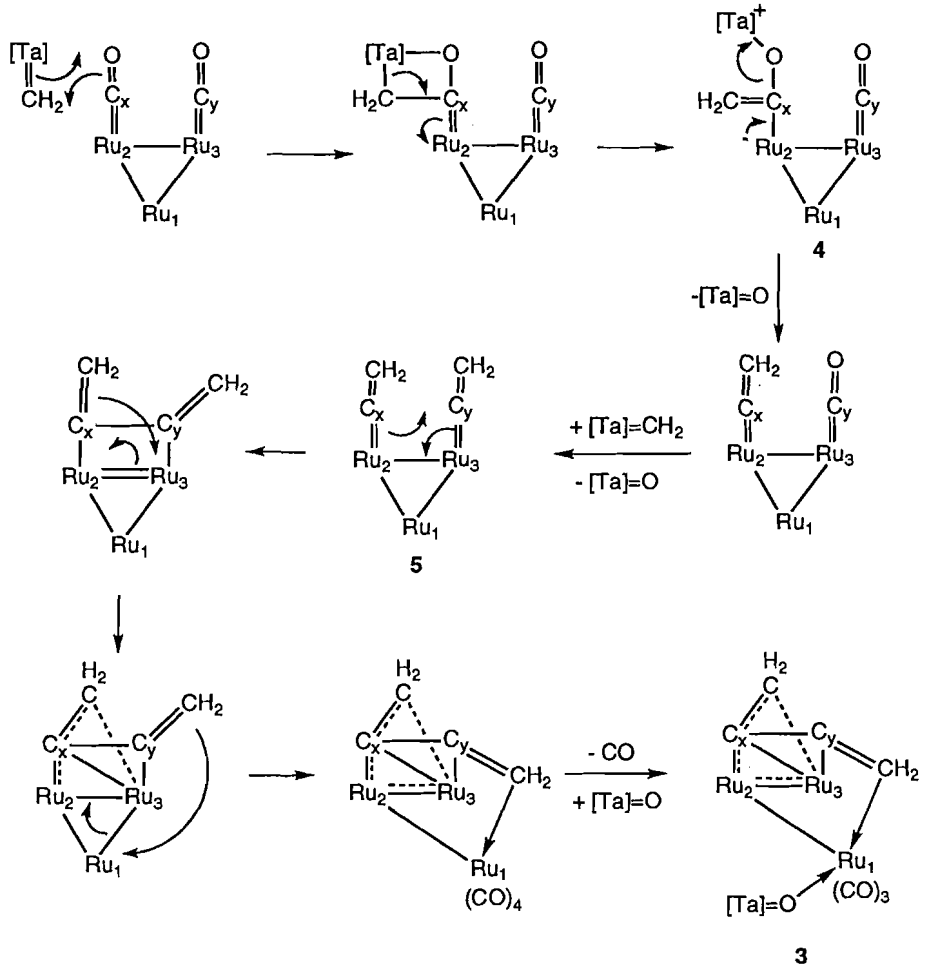

groups from two molecules of **1** and two CO ligands at separate Ru centers, probably through the zwitterionic species **4** similar to the one structurally characterized earlier in the reaction of $Cp_2(CH_3)Ta{=}CH_2$ with $C_3F_7Re(CO)_5$, in which the Ta-C bond is broken.[6] Following this step, two molecules of $Cp_2(CH_3)Ta{=}O$ are extruded to give the bis-vinylidene species **5**. Overall [2+2] cycloaddition of the Ru=C bonds then provides the carbon–carbon bond-forming step necessary to reach a C_4H_4 fragment. We propose this complex then rapidly rearranges, as shown in Scheme 1, to give the final product **3**. During the reaction there must also be loss of CO and addition of one of the $Cp_2(CH_3)Ta(=O)$ fragments to the terminal Ru center, but we do not yet know at which point in the overall transformation this occurs.

In conclusion, these observations constitute a new example of a reaction in homogeneous solution, between early and late transition metal complexes, in which CO molecules are deoxygenated and coupled to one another and to CH_2 ligands. The rapid rate of this reaction appears to be a direct result of the interaction of two electronically different metal centers. It is unclear whether transformations exhibiting related types of cleavage and rearrangement on surfaces proceed by mechanisms similar to those in the reactions described here, but the potential analogies are interesting. We are continuing our investigations in hopes of testing the mechanistic hypotheses engendered by this series of reactions.

[6] G. Proulx and R. G. Bergman, unpublished results.

Material on deposit

The following structural data are provided for complex **3**: tables of crystal and data collection parameters, positional parameters and estimated standard deviations, anisotropic thermal parameters, root-mean-square amplitudes of anisotropic displacement, intramolecular distances, intramolecular angles, and selected torsion angles.[7]

Acknowledgments

We acknowledge the contribution of Dr. Michael J. Hostetler for helpful discussions and some early experiments on the

[7] This supplementary material can be purchased from: The Depository of Unpublished Data, Document Delivery, CISTI, National Research Council Canada, Ottawa, ON K1A 0S2, Canada.

With the exception of the anisotropic thermal parameters, RMS amplitudes of anisotropic displacement, and torsion angles, these data have also been deposited with the Cambridge Crystallographic Data Centre, and can be obtained on request from The Director, Cambridge Crystallographic Data Centre, University Chemical Laboratory, 12 Union Road, Cambridge, CB2 1EZ, U.K.

Can. J. Chem. Downloaded from www.nrcresearchpress.com by 80.90.12.36 on 09/08/12
For personal use only.

reactions of $Cp_2(CH_3)Ta{=}CH_2$ with $Ru_3(CO)_{12}$. We are grateful to the United States National Science Foundation (Grant No. CHE-9113261) for generous financial support of this work. G.P. thanks the United States Department of Education for a predoctoral fellowship.

References

1. M. van der Reit, D. Copperthwaite, R. Hunter, and G.J. Hutchings. J. Chem. Soc. Chem. Commun. 512 (1988).
2. B.D. Dombeck. Adv. Catal. **32**, 325 (1983).
3. J. Falbe. Chemical feedstocks from coal. John Wiley & Sons, New York. 1981.
4. F. Fischer and H. Tropsch. Chem. Ber. **59**, 830 (1926).
5. E.L. Muetterties and J. Stein. Chem. Rev. **79**, 479 (1979).
6. R.E. Cramer, K.T. Higa, S.L. Pruskin, and J.W. Gilje. J. Am. Chem. Soc. **105**, 6749 (1983).
7. E.M. Carnahan and S.J. Lippard. J. Am. Chem. Soc. **114**, 4166 (1992), and references cited.
8. F.A. Cotton. Prog. Inorg. Chem. **21**, 1 (1976).
9. R.V. Anslyn, B.D. Santarsiero, and R.H. Grubbs. Organometallics, **7**, 2137 (1988).
10. J.W. Gilje and R.E. Cramer. Inorg. Chim. Acta, **139**, 177 (1987).
11. D.M. Hamilton, W.S. Willis, and G.D. Stucky, J. Am. Chem. Soc. **103**, 4255 (1981).
12. R.R. Schrock and P.R. Sharp. J. Am. Chem. Soc. **100**, 2389 (1978).
13. G. Proulx and R.G. Bergman. J. Am. Chem. Soc. **115**, 9802 (1993).
14. G. Proulx and R.G. Bergman, Science, **259**, 661 (1993).
15. F.A. Cotton and G. Wilkinson. Advanced inorganic chemistry. John Wiley & Sons, New York. 1988.
16. B.F.G. Johnson, J. Lewis, P.R. Raithby, and G. Süss. J. Chem. Soc. Dalton Trans. 1356 (1979).
17. R. Szostak, C.E. Strouse, and H.D. Kaesz. J. Organomet. Chem. **191**, 243 (1980).

Can. J. Chem. Downloaded from www.nrcresearchpress.com by 80.90.12.36 on 09/08/12
For personal use only.

Dinuclear dihydride complexes of iridium: a study of structure and dynamics

D. Michael Heinekey, David A. Fine, T. Gregory P. Harper, and Suzanne T. Michel

Abstract: Reaction of the neutral dihydride complexes (η-C_5R_5)Ir(L)H_2 (L = P(OPh)$_3$, CO; R = H, Me) with triflic acid (HO_3SCF_3) at ambient temperature or above affords hydrogen and the dimeric hydride bridged species {[(η-C_5R_5)Ir(L)H]$_2$(μ-H)}O_3SCF_3. Deprotonation of the cationic complexes gives the neutral dimers of the form [(η-C_5R_5)Ir(L)H]$_2$. Spectroscopic data are consistent with the presence of only terminal hydride ligands in these complexes. Variable temperature ^{1}H and ^{31}P NMR studies indicate that a rapid dynamic process exchanges the two terminal hydride ligands and that the complexes exist as unequal mixtures of the racemic and meso diastereomers. Synthesis of a lower symmetry derivative, [(η-C_5Me_4Et)Ir(CO)H]$_2$, reveals that a rapid epimerization process occurs that interconverts the two diastereomers. Thermolysis of the carbonyl complex [(η-C_5Me_5)Ir(CO)H]$_2$ affords [(η-C_5Me_5)Ir(CO)]$_2$ and dihydrogen.

Key words: iridium, hydride, bimetallic, dynamics, epimerization.

Résumé : La réaction des complexes neutres dihydrures (η-C_5R_5)Ir(L)H_2(L = P(OPh)$_3$, CO; R = H, Me) avec de l'acide triflique (HO_3SCF_3), à des températures ambiante ou supérieure, fournit les espèces dimériques pontées dihydrures {[η-C_5R_5)Ir(L)H]$_2$(μ-H)}O_3SCF_3. La déprotonation des complexes cationiques fournit les dimères neutres de la forme [(η-C_5R_5)Ir(L)H]$_2$. Pour ces complexes, les données spectroscopiques sont en accord avec la présence uniquement de coordinats hydrures terminaux. Des études de RMN du ^{1}H et du ^{31}P indiquent qu'il existe des processus d'échange dynamiques rapides des deux coordinats hydrures terminaux et que les complexes existent sous la forme de mélanges inégaux de diastéréomères racémiques et méso. La synthèse d'un dérivé de symétrie moindre, [(η-C_5Me_4Et)Ir(CO)H]$_2$, révèle qu'il se produit un processus d'isomérisation rapide qui permet l'interconversion des deux diastéréomères. La thermolyse du complexe [(η-C_5Me_5)Ir(CO)H]$_2$ fournit du [(η-C_5Me_5)Ir(CO)]$_2$ et du dihydrogène.

Mots clés : iridium, hydrure, bimétallique, dynamique, épimérisation.

[Traduit par la rédaction]

Introduction

The reductive elimination of hydrogen from dihydride complexes is a reaction of central importance to organometallic chemistry, and has been studied in great detail in monomeric complexes (1, 2). The corresponding reaction in metal dimers, dinuclear reductive elimination (3–7), has not been conclusively observed and is thought to be unfavorable, based on orbital symmetry considerations (8). The ideal system for studying this problem would be a conformationally flexible metal dimer with a metal–metal single bond and two terminal hydride ligands. Surprisingly, there are relatively few examples of such complexes, since the vast majority of known dinuclear and polynuclear metal hydride complexes contain bridging hydride ligands. The only well-characterized examples of dimers containing only terminal hydride ligands are $H_2Os_2(CO)_8$ (9) and $H_2Os_2(CO)_6(PPh_3)_2$ (10). An iron analog, $H_2Fe_2(CO)_8$, is less well characterized but is thought to have terminal hydride ligands.[2] In all these cases, the putative product of dihydrogen elimination is known to be very unstable.

Attempts to prepare suitable dinuclear complexes have no doubt been hampered by the lack of generally useful synthetic methodology. In this paper, we report the development of a potentially general condensation of monomeric hydride complexes induced by protonation to afford dinuclear complexes in excellent yields. The ultimate products of these procedures are neutral dinuclear iridium dihydride complexes of the form [CpIr(L)H]$_2$(Cp = C_5H_5, L = P(OPh)$_3$; Cp = C_5Me_5 (Cp*), or C_5Me_4Et (Cp′), and L = CO). These complexes have been shown by spectroscopic and structural studies to have terminal hydride ligands. The dimeric complexes in every case have

Received October 28, 1994.

This paper is dedicated to Professor William A.G. Graham on the occasion of his 65th birthday.

D.M. Heinekey,[1] D.A. Fine, T.G.P. Harper, and S.T. Michel. Department of Chemistry Box 351700, University of Washington, Seattle, WA 98195-1700, U.S.A.

[1] Author to whom correspondence may be addressed. Telephone: (206) 543-7522. Fax: (206) 685-8665. E-mail: heinekey@chem.washington.edu

[2] Inferred from the ^{1}H NMR chemical shift value reported for the hydrides: ref. 11.

Can. J. Chem. Downloaded from www.nrcresearchpress.com by 80.90.12.36 on 09/08/12
For personal use only.

Can. J. Chem. Downloaded from www.nrcresearchpress.com by 80.90.12.36 on 09/08/12
For personal use only.

been shown by variable temperature NMR spectroscopy to exist as rapidly equilibrating mixtures of diastereomers.

Preliminary investigations of the thermal chemistry of $[Cp^*Ir(CO)H]_2$ show that there is a very substantial kinetic barrier to elimination of hydrogen and that formation of $[Cp^*Ir(CO)]_2$ occurs very slowly.

Experimental

General procedures

All manipulations were conducted under argon or nitrogen using standard Schlenk and drybox techniques. Argon and nitrogen were deoxygenated and dried by passage through Chemical Dynamics Corp. R3-11 CuO catalyst followed by Mallinckrodt Aquasorb containing P_2O_5. Air-sensitive compounds were manipulated in an MBraun labmaster 130 glove box equipped with integrated dry train loaded with copper catalyst and molecular sieves. Solvents were purified by distillation from Na–K–benzophenone (except CH_2Cl_2 from P_2O_5) under nitrogen. Deuterated NMR solvents (purchased from Cambridge Isotope Laboratories) were degassed, and stored over the following drying agents: CD_2Cl_2, $CDCl_3$ over CaH_2; C_6D_6, THF-d_8 over Na–K–benzophenone. $CDFCl_2$ was prepared according to the reported procedure (12) and stored over CaH_2. Carbon monoxide-^{13}C was purchased from Cambridge Isotope Laboratories and adsorbed on activated charcoal (coconut, 8–12 mesh, EM Science).

$[Cp'IrCl_2]_2$ (Cp′ = η-C_5Me_4Et) was prepared from $[(COD)IrCl]_2$ (COD = 1,5-cyclooctadiene) according to the method reported (13) for $[Cp^*IrCl_2]_2$. $Cp^*Ir(CO)Cl_2$ was prepared with slight modification to the published procedure (14). $CpIr(P(OPh)_3)H_2$ was prepared in a manner analogous to that previously reported (15) for $CpIr(PMe_3)H_2$. Triflic acid (HO_3SCF_3) and 1,8-bis(dimethylamino)naphthalene (Proton Sponge®) were purchased from Aldrich Chemical Co. and used as received.

^1H NMR spectra were recorded on Bruker AC200, WM250, AF300, or WM500 spectrometers and referenced internally to the residual proton resonance of the deuterated solvent or tetramethylsilane (TMS). ^{13}C NMR spectra were collected on the AC200, AF300, and WM500 spectrometers operating at a frequency of 50.32, 75.46, and 125.76 MHz, respectively, and referenced internally to the solvent. ^{31}P NMR spectra were collected on the AC200 and WM500 spectrometers at frequencies of 81.02 and 202.45 MHz, respectively, and referenced externally to 85% H_3PO_4. Variable temperature ^1H NMR measurements were performed using the Bruker B-VT1000 temperature control module with a copper–constantan thermocouple. Temperature calibration was obtained by measurement of the chemical shift difference between the -CH_3 and -OH peaks of pure methanol using the method of Van Geet (16). Temperature calibration below the freezing point of methanol was achieved with a copper–constantan thermocouple inserted in the NMR probe sample chamber. Line shape analysis of variable temperature ^1H NMR spectra was performed using a modified version of the DYNAMAR program (17).

Infrared spectra were recorded on a Perkin–Elmer model 1600 Fourier transform spectrophotometer (2.0 cm^{-1} resolution). Samples were examined as solutions in sealable 0.1 mm path length NaCl cells or as Nujol mulls.

Electron impact mass spectra were obtained using a Kratos Profile HD3 magnetic sector instrument with a direct insertion probe. Data were collected in nominal mode, which rounds off results to the nearest mass unit.

Elemental analyses were performed by Galbraith Laboratories.

$Cp'Ir(CO)Cl_2$

A vessel fitted with a high-vacuum Teflon stopcock was charged with $[Cp'IrCl_2]_2$ (0.62 g, 0.75 mmol). Methylene chloride (10 mL) was vacuum transferred onto the solid. The red-orange solution was subjected to three freeze–pump–thaw cycles, pressurized with CO (2.1 atm; 1 atm = 101.3 kPa), and allowed to stir overnight. The solution was transferred via filter cannula into cold stirring heptane, causing immediate precipitation of the product. The yellow powder was collected by filtration through a medium glass frit, washed with heptane, and dried in a desiccator. Yield 0.61 g (92%). Recrystallization from CH_2Cl_2–Et_2O afforded yellow-olive green crystals. IR (Nujol): 2034 (s, ν_{CO}) cm^{-1}. ^1H NMR ($CDCl_3$) δ: 2.31 (q, J = 7.6 Hz, 2H), 1.95 (s, 6H), 1.90 (s, 6H), 1.19 (t, J = 7.6 Hz, 3H). Anal. calcd. for $C_{12}H_{17}Cl_2IrO$: C 32.73, H 3.89; found: C 32.34, H 3.95.

$Cp^*Ir(CO)H_2$

Methanol (about 20 mL) was added to a Schlenk flask charged with 0.27 g of $Cp^*Ir(CO)Cl_2$ (0.64 mmol) and 0.43 g of Zn dust (6.6 mmol). Glacial acetic acid (1.0 mL) was added and the mixture was immediately subjected to three freeze–pump–thaw cycles. The solution was allowed to stir overnight under argon. An aqueous solution of NaOH saturated with NaCl (approx. 15 mL, argon sparged) was transferred via cannula to the deep purple-red solution and stirred for 20 min. The mixture was extracted with 4 × 10 mL of pentane. The extracts were transferred via cannula onto oven-dried $MgSO_4$ and left to stir for 1 h. The pale gold-colored liquid was transferred via filter cannula to a sublimation apparatus. The $MgSO_4$ was washed with pentane and this liquid was combined with the previous extracts. The solvent was removed in vacuo leaving a mostly white crystalline residue, with some brown material. The air-sensitive product was isolated by sublimation (35°C, dynamic vacuum) into a liquid N_2 cooled Schlenk flask. Low-melting, pale yellow crystals were recovered and stored under argon at −30°C. Yield: 0.23 ± 0.02 g (ca. 100%). IR (Nujol): 2131 (m, ν_{IrH}), 2013 (m), 1990 (s), 1945 (m) cm^{-1}. ^1H NMR (CD_2Cl_2) δ: 2.22 (s, 15H), −16.48 (s, 2H). ^1H NMR (C_6D_6) δ: 1.87 (t, $^4J_{H-H}$ = 0.8 Hz, Cp^*), −15.76 (m, $^4J_{H-H}$ = 0.8 Hz, Ir-H). $^{13}C\{^1H\}$ NMR ($CDFCl_2$) δ: 98.0 (s, $C_5(CH_3)_5$), 11.1 (s, $C_5(CH_3)_5$). $^{13}C\{^1H\}$ NMR (C_6D_6) δ: 97.1 (s, $C_5(CH_3)_5$), 10.6 (s, $C_5(CH_3)_5$). Anal. calcd. for $C_{11}H_{17}IrO$: C 36.96, H 4.79; found: C 36.60, H 4.70.

$Cp^*Ir(^{13}CO)H_2$

Prepared as above for $Cp^*Ir(CO)H_2$. IR (Nujol): 2131 (m, ν_{IrH}), 1964 (sh), 1942 (s), 1900 (m) cm^{-1}. IR (heptane): 2137 (m, ν_{IrH}), 1970 (m), 1950 (s), 1906 (m) cm^{-1}. ^1H NMR (CD_2Cl_2) δ: 2.22 (q, $^4J_{H-H}$ = 0.7 Hz, $^4J_{C-H}$ = 0.6 Hz, Cp^*), −16.49 (d of m, $^4J_{H-H}$ = 0.7 Hz, $^4J_{C-H}$ = 8.7 Hz, Ir-H). In the $^{13}C\{^1H\}$ NMR (CD_2Cl_2) spectrum of the enriched sample, a singlet resonance for the carbonyl ligand was detected at δ 171.5.

Can. J. Chem. Downloaded from www.nrcresearchpress.com by 80.90.12.36 on 09/08/12
For personal use only.

$Cp'Ir(CO)H_2$

Prepared as above for $Cp^*Ir(CO)H_2$. Recovered as an air-sensitive pale yellow oil. ^1H NMR (CD_2Cl_2) δ: 2.46 (q, $J = 7.6$ Hz, 2H), 2.22 (s, 6H), 2.21 (s, 6H), 1.07 (t, $J = 7.6$ Hz, 3H), −16.47 (s, 2H). $^{13}C\{^1H\}$ NMR (CD_2Cl_2) δ: 171.5 (s, CO), 103.9 (s, $C(CH_2CH_3)$), 97.7, 97.6 (s, $C(CH_3)$), 18.8 (s, $C(CH_2CH_3)$), 17.7 (s, $C(CH_2CH_3)$), 11.0, 10.8 (s, $C(CH_3)$).

*$\{[CpIr(P(OPh)_3)H]_2(\mu\text{-}H)\}O_3SCF_3$ (**1**)*

A vessel equipped with a high-vacuum Teflon stopcock was charged with $CpIr(P(OPh)_3)H_2$ (255 mg, 0.448 mmol). Methylene chloride (about 25 mL) was vacuum transferred onto the solid. One-half an equivalent of triflic acid (19.8 μL, 0.224 mmol) was added via syringe. The solution was degassed by three freeze–pump–thaw cycles and kept under vacuum. With the vessel wrapped in foil, the solution was heated to reflux for 15 h in an oil bath at 80°C, during which the solution became deep orange. When the reaction was complete by NMR the solution was transferred via cannula to a Schlenk flask. The solution was concentrated to about 5 mL and heptane (30 mL) added to precipitate the yellow product. The solvent was removed with a filter cannula. The air-stable powder was washed with 2 × 15 mL heptane and dried in vacuo. Yield 262 mg (95%). ^1H NMR (CD_2Cl_2) δ: 7.3–7.2 (m, 30H), 5.01 (d, $J_{P-H} = 2$ Hz, 10H), −18.54 (t, $J_{P-H} = 18.5$ Hz, 3H). ^1H NMR ($CDFCl_2$, 153 K) δ: −17.22 (d, $J = 34$ Hz, Ir-$H_{terminal}$), −19.92 (br t, $J = 19$ Hz, Ir-H_{bridge}). ^{31}P NMR (selective decoupling of aromatic hydrogens, CD_2Cl_2) δ: 79.0 (q, $^2J_{P-H} = 18$ Hz). Anal. calcd. for $C_{47}H_{43}Ir_2O_9P_2SF_3$: C 43.85, H 3.37; found: C 43.96, H 3.23.

*$[CpIr(P(OPh)_3)H]_2$ (**2**)*

The protonated dimer **1** (42 mg, 0.033 mmol) and 1.1 equivalents of lithium diisopropylamide (3.7 mg, 0.034 mmol) were placed in one side of an H-tube reactor. The reactor consisted of two vessels fitted with high-vacuum Teflon stopcocks and joined at a glass frit. THF (20 mL) was vacuum transferred onto the solids. The reactor was wrapped in foil and allowed to stir for 2 h, yielding a clear, bright yellow solution. The solvent was removed in vacuo leaving a pale yellow oil. Heptane was added via vacuum transfer and the solution stirred for 1 h. The solution was filtered through the frit to the other side of the reactor and the heptane removed in vacuo to leave a bright yellow, air-sensitive powder. ^1H NMR (C_6D_6) δ: 7.3–7.0 (m, 30H), 5.00 (d, $J_{P-H} = 2$ Hz, 10H), −16.67 (t, $J_{P-H} = 24$ Hz, 2H). ^1H NMR (THF-d_8) δ: 7.3–7.0 (m, 30H), 4.84 (d, $J_{P-H} = 2$ Hz, 10H), -17.02 (t, $J_{P-H} = 24$ Hz, 2H). $^{31}P\{^1H\}$ NMR (THF-d_8) (300 K) δ: 81.01 (s); (215 K) δ: 86.34 (s), 82.95 (s). Anal. calcd. for $C_{46}H_{42}Ir_2O_6P_2$: C 48.58, H 3.72; found: C 47.92, H 3.82.

*$\{[Cp^*Ir(CO)H]_2(\mu\text{-}H)\}O_3SCF_3$ (**3**)*

A small Schlenk flask was charged with 34 mg of $Cp^*Ir(CO)H_2$ (0.094 mmol). Methylene chloride (2–3 mL) was transferred onto the solids via cannula furnishing a pale yellow solution. With the solution immersed in a CO_2-isopropanol bath, triflic acid (8 μL, 0.09 mmol, 100% stoichiometric excess) was added via syringe. Three freeze–pump–thaw cycles (thaw to −78°C) were performed and the solution stirred for 30 min at −78°C. The flask was then transferred to an ice–NaCl bath and the solution stirred for an additional 30 min, becoming deep yellow. The solvent was removed in vacuo and the yellow-brown residue was washed with three aliquots of cold Et_2O. Residual volatiles were removed under vacuum overnight leaving a light brown, air-sensitive solid. Yield: 26 mg (66%). IR (Nujol): 2111 (w, ν_{Ir-H}), 2020, 1990 (s, ν_{CO}) cm^{-1}. ^1H NMR (CD_2Cl_2) δ: 2.22 (s, 30H), −16.47 (s, 3H). ^1H NMR ($CDFCl_2$, 300 K) δ: 2.23 (s, Cp^*), −16.44 (s, Ir-H); ($CDFCl_2$, 138 K) δ: -15.35 (br s, Ir-$H_{terminal}$), −18.10 (br s, Ir-H_{bridge}). $^{13}C\{^1H\}$ NMR ($CDFCl_2$) δ: 120.1 (q, $J_{C-F} = 317$ Hz, O_3SCF_3), 102.0 (s, C_5Me_5); 10.9 (s, C_5Me_5).

*$\{[Cp^*Ir(^{13}CO)H]_2(\mu\text{-}H)\}O_3SCF_3$ (**3***)*

Prepared using a procedure analogous to that for **3**. ^1H NMR ($CDFCl_2$) δ: 2.23 (s, Cp^*), -16.44 (br s, Ir-H). The linewidth of the hydride resonance is increased by an unresolved coupling to the protons of the Cp^* rings. When a spectrum was collected with homonuclear decoupling of the Cp^* resonance, the hydride resonance was resolved into a triplet ($J_{C-H} = 3.4$ Hz). In the $^{13}C\{^1H\}$ NMR ($CDFCl_2$) a singlet resonance for the carbonyl ligands was observed at δ = 166.9.

*$\{[Cp'Ir(CO)H]_2(\mu\text{-}H)\}O_3SCF_3$ (**5**)*

Prepared as above for **3**. Recovered as yellow-brown oil. ^1H NMR (CD_2Cl_2) δ: 2.48 (q, $J = 7.6$ Hz, 4H), 2.22 (s, 12H), 2.20 (s, 12H), 1.13 (t, $J = 7.6$ Hz, 6H), −16.52 (s, 3H). $^{13}C\{^1H\}$ NMR (CD_2Cl_2) δ: 166.2 (s, CO), 105.7 (s, $C(CH_2CH_3)$), 102.1, 101.4 (s, $C(CH_3)$), 18.7 (s, $C(CH_2CH_3)$), 15.7 (s, $C(CH_2CH_3)$), 10.6, 10.5 (s, $C(CH_3)$).

*$[Cp^*Ir(CO)H]_2$ (**4**)*

Methylene chloride was added via cannula to a Schlenk flask containing 90 mg of **3** (0.10 mmol) and 33 mg of proton sponge (0.15 mmol). The solution was subjected to three freeze–pump–thaw cycles and allowed to stir for 2 h. The solvent was removed under static vacuum leaving a yellow-brown residue. The residue was extracted three times with heptane and the yellow extracts transferred to a clean Schlenk flask via filter cannula. The solution was concentrated in vacuo and storage at −30°C for 16 h afforded yellow crystals. IR (heptane): 2180 (w, ν_{Ir-H}), 1971 (s), 1942 (s) cm^{-1}. ^1H NMR (CD_2Cl_2) δ: 2.13 (s, 30H), −16.30 (s, 2H). ^1H NMR (C_6D_6) δ: 2.04 (s, Cp^*), −15.91 (s, Ir-H). ^1H NMR ($CDFCl_2$, 300 K) δ: −16.2 (s, Ir-H); ($CDFCl_2$, 147 K) δ: −15.89 (s, Ir-H, major species), −19.02 (s, Ir-H, minor species). $^{13}C\{^1H\}$ NMR (CD_2Cl_2): δ 96.82 (s, C_5Me_5), 11.32 (s, C_5Me_5). MS (EI): *m/e* 712 ($[(Cp^*{}^{191}Ir(CO)H)(Cp^*{}^{193}Ir(CO)H)]^+$).

*$[Cp^*Ir(^{13}CO)H]_2$ (**4***)*

Prepared as above for **4**. ^1H NMR ($CDFCl_2$, 300 K) δ: 2.15 (s, Cp^*), −16.22 (br t, $J_{C-H} = 4.5$ Hz, Ir-H). ^1H NMR ($CDFCl_2$, 145 K) δ: −15.89 (d, $J = 7.9$ Hz), −19.04 (t, $J = 6.0$ Hz). $^{13}C\{^1H\}$ NMR (CD_2Cl_2) δ: 176.5 (s, CO), 11.3 (s, C_5Me_5).

*$[Cp'Ir(CO)H]_2$ (**6**)*

Prepared as above for **4**. IR(Nujol): 2202 (w, ν_{Ir-H}), 1968, 1939 (s, ν_{CO}), 1921 (sh) cm^{-1}. ^1H NMR (CD_2Cl_2) δ: 2.46 (q, $J = 7.6$ Hz, 4H), 2.13 (s, 12H), 2.12 (s, 12H), 1.03 (t, $J = 7.6$ Hz, 6H), −16.24 (s, 2H). $^{13}C\{^1H\}$ NMR ($CDFCl_2$) δ: 97.6, 96.8 (s, $C(CH_3)$), 20.0 (s, $C(CH_2CH_3)$), 16.5 (s, $C(CH_2CH_3)$), 11.5, 11.3 (s, $C(CH_3)$). Anal. calcd. for $C_{24}H_{36}Ir_2O_2$: C 38.90, H 4.90; found: C 38.40, H 4.74.

Can. J. Chem. Downloaded from www.nrcresearchpress.com by 80.90.12.36 on 09/08/12
For personal use only.

Structure determination for [Cp'Ir(CO)H]$_2$ (6)

A yellow crystal of dimensions 0.25 × 0.30 × 0.35 mm was mounted in a stream of nitrogen gas at 183 K on an Enraf–Nonius CAD-4 diffractometer using MoKα radiation. Systematic absences were consistent with the monoclinic space group *C2/c*. A total of 2084 independent reflections were collected with $2\theta \leq 50°$, of which 1753 with $I > 3\sigma(I)$ were used in the refinement. The structure was solved by direct methods that gave the location of the Ir atoms. The remaining non-hydrogen atoms were located in difference Fourier maps. The hydrogen atoms were placed at calculated positions. The final R factor was 2.98%.

Crystal data tables, bond lengths and angles, anisotropic displacement coefficients, and hydrogen atom coordinates have been deposited as supplementary material.[3]

*Thermolysis of [Cp*Ir(CO)H]$_2$ (4)*

To an NMR tube fitted with a high-vacuum Teflon stopcock was added 5.0 mg of **4** (7.0 μmol). Degassed benzene-d_6 (about 0.5 mL) was vacuum transferred onto the solids. The NMR tube was sealed under vacuum and placed in an oil bath heated to 100°C and shielded from light.

Results

Synthesis

Reaction of CpIr(P(OPh)$_3$)H$_2$ (Cp = η-C$_5$H$_5$) with one-half equivalent of triflic acid in methylene chloride with subsequent heating affords H$_2$ and the dimeric cation {[CpIr(P(OPh)$_3$)H]$_2$(μ-H)}O$_3$SCF$_3$ (**1**) as shown in Scheme 1 for the analogous Cp'-carbonyl (Cp' = η-C$_5$Me$_4$Et) compounds. Complex **1** can also be prepared by reaction of isolated[4] CpIr(P(OPh)$_3$)H$_3^+$ with CpIr(P(OPh)$_3$)H$_2$.

Deprotonation of **1** is readily carried out by treatment with strong bases such as LDA (lithium diisopropylamide) or sodium bis(trimethylsilyl)amide to afford the neutral species [CpIr(P(OPh)$_3$)H]$_2$ (**2**). The dynamics of this dimeric dihydride as revealed by variable temperature NMR spectroscopy proved to be quite complex, as described below.

By a similar procedure, protonation of Cp*Ir(CO)H$_2$ (Cp* = η-C$_5$Me$_5$) with triflic acid affords the dimeric cation {[Cp*Ir(CO)H]$_2$(μ-H)}O$_3$SCF$_3$ (**3**). Complex **3** is readily deprotonated by relatively mild bases such as triethylamine or 1,8-bis(dimethylamino)naphthalene to afford the neutral dimer [Cp*Ir(CO)H]$_2$ (**4**). The structure and dynamic behaviour of **3** and **4** are similar to those exhibited by the triphenylphosphite complexes **1** and **2**, and are detailed below.

Scheme 1.

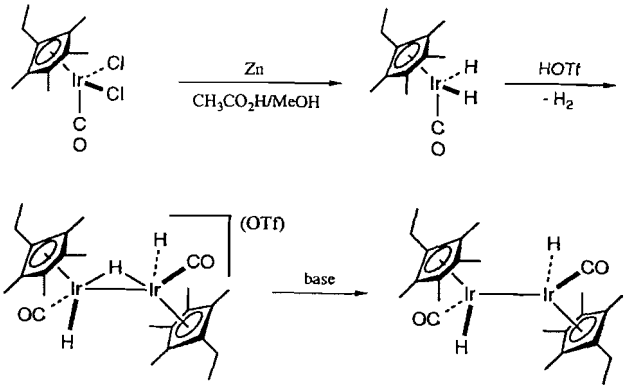

Table 1. Crystallographic data for [Cp'Ir(CO)H]$_2$ (**6**).

$Ir_2C_{24}H_{36}O_2$	fw 740.9
a = 20.262(2) Å	Space group *C2/c*
b = 7.913(2) Å	λ = 0.71073 Å
c = 16.771(3) Å	ρ_{calcd} = 2.077 g/cm^3
β = 117.52(2)°	μ = 112.36 cm^{-1}
V = 2369.7(5) Å^3	Z = 4
$R(F_o)$ = 0.0298	$R_w(F_o)$ = 0.0377

An additional probe of the stereodynamics of these complexes is available in the lower symmetry derivatives prepared with the ethyltetramethylcyclopentadienyl ligand (Cp' = η-C$_5$Me$_4$Et). Thus {[Cp'Ir(CO)H]$_2$(μ-H)}O$_3$SCF$_3$ (**5**) and [Cp'Ir(CO)H]$_2$ (**6**) were prepared from Cp'Ir(CO)H$_2$ by the procedures outlined in Scheme 1.

Structure of [Cp'Ir(CO)H]$_2$ (6)

A summary of the crystallographic data is given in Table 1. An ORTEP diagram is shown in Fig. 1. Atomic coordinates for the non-hydrogen atoms are in Table 2 and selected bond lengths and angles are given in Table 3. The hydride ligands were not located, but a structure with terminal hydride ligands is indicated for **2**, **4**, and **6** based on the observation of terminal Ir–H stretching bands in the infrared spectrum[5] and variable temperature NMR data (see discussion section).

Variable temperature NMR spectroscopy

The ^{1}H NMR spectrum obtained for [CpIr(P(OPh)$_3$)H]$_2$(μ-H)$^+$ in the hydride region at ambient temperature consists of a single triplet resonance with J_{H-P} = 18.5 Hz. At lower temperatures, the signal broadens and ultimately decoalesces to give a doublet resonance at −17.22 ppm (J_{H-P} = 34 Hz) and a poorly resolved triplet at −19.92 ppm (J_{H-P} = 19 Hz) in the intensity ratio 2:1. The limiting spectrum was obtained at 153 K (CDFCl$_2$, 500 MHz). These observations indicate that the ground state structure of **1** has two terminal hydride ligands and one bridging hydride ligand and that a rapid rearrangement process causes site exchange of the terminal and bridging hydride ligands. Lineshape analysis of spectra obtained for

[3] Copies of material on deposit may be purchased from: The Depository of Unpublished Data, Document Delivery, CISTI, National Research Council Canada, Ottawa, Canada K1A 0S2.

The crystal data and tables of bond lengths and angles and H-atom coordinates have also been deposited with the Cambridge Crystallographic Data Centre, and can be obtained on request from The Director, Cambridge Crystallographic Data Centre, University Chemical Laboratory, 12 Union Road, Cambridge, CB2 1EZ, U.K.

Structure factor amplitudes are no longer being deposited and may be obtained directly from the author.

[4] Prepared by addition of HBF$_4$·Et$_2$O to a solution of CpIr(P(OPh)$_3$)H$_2$ in CH$_2$Cl$_2$ (15).

[5] Terminal hydride ligands give rise to IR bands that are sharper, stronger, and at higher energy (2200–1600 cm^{-1}) than the corresponding bands of bridging hydrides (1600–800 cm^{-1}). See, for example, ref. 2, p. 83.

Fig. 1. ORTEP representation of $[Cp'Ir(CO)H]_2$ (**6**). Thermal ellipsoids are shown at 50% probability. Hydrogen atoms are omitted for clarity. Hydride ligands were not located

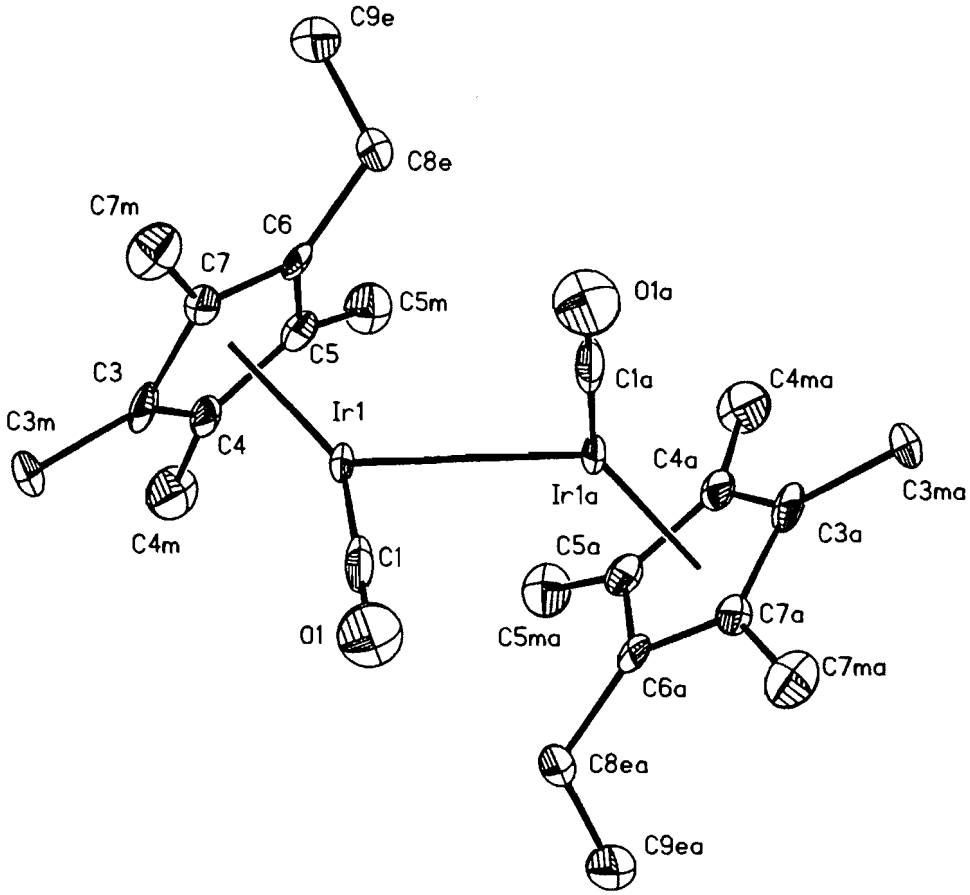

Table 2. Atomic coordinates and isotropic thermal parameters.[a]

Atom	x	y	z	U,[b] Å^2
Ir(1)	3640(1)	9429(3)	19884(2)	157(1)
C(1)	−1483(32)	28936(89)	14965(43)	252(24)
O(1)	−4808(31)	40972(57)	11731(41)	411(24)
C(3)	12572(32)	5623(91)	15562(49)	262(26)
C(3m)	12628(39)	11982(102)	7393(48)	339(30)
C(4)	10236(31)	−10389(78)	17012(45)	232(25)
C(4m)	7182(36)	−24117(90)	10180(50)	376(30)
C(5)	11856(32)	−11588(79)	26356(46)	229(24)
C(5m)	10945(38)	−27234(89)	30781(52)	343(28)
C(6)	15531(27)	3737(87)	30761(40)	193(21)
C(8e)	18955(34)	6889(97)	40798(44)	293(26)
C(9e)	26702(35)	−137(109)	45574(48)	387(29)
C(7)	15915(30)	14400(85)	24341(42)	207(23)
C(7m)	19686(35)	31308(92)	25962(53)	371(29)

[a]Coordinates × 10^5.
[b]Isotropic thermal parameter $U \times 10^4$.

1 in the temperature range 153–210 K gave $\Delta G^{\ddagger}_{298} = 8.8 \pm 0.6$ kcal mol^{-1}, $\Delta H^{\ddagger} = 6.8 \pm 0.2$ kcal mol^{-1}, and $\Delta S^{\ddagger} = -6.8 \pm 1.2$ cal mol^{-1} K^{-1}.

In the case of $[CpIr(P(OPh)_3)H]_2$ (**2**), each metal center is chiral and the complex can in principle exist as a mixture of two diastereomers, which would be expected to give distinct signals in the ^{1}H NMR spectrum. In fact, the ^{1}H NMR spectrum of **2** recorded at ambient temperature (THF-d_8) gives only one resonance in the hydride region at −17.0 ppm (triplet, $J_{H-P} = 24$ Hz) (see Fig. 2). Lowering the observation temperature leads to broadening of this triplet resonance and the appearance of a new, very broad signal at −17.4 ppm. Further cooling causes the new minor resonance to sharpen into a well-resolved triplet ($J_{H-P} = 24$ Hz). At 200 K, the major signal

Can. J. Chem. Downloaded from www.nrcresearchpress.com by 80.90.12.36 on 09/08/12
For personal use only.

Can. J. Chem. Downloaded from www.nrcresearchpress.com by 80.90.12.36 on 09/08/12
For personal use only.

Table 3. Selected bond distances and angles.

(a) **Distances (Å)**			
Ir(1)—C(1)	1.828(7)	C(1)—O(1)	1.146(8)
Ir(1)—Ir(1a)	2.724(1)	C(3)—C(4)	1.411(10)
C(4)—C(5)	1.441(11)	C(5)—C(6)	1.434(9)
C(6)—C(7)	1.394(10)	C(3)—C(7)	1.473(10)
C(3)—C(3m)	1.458(12)	Ir—Cp(1)[a]	1.909
(b) **Bond angles (deg)**			
Ir(1)-C(1)-O(1)	178.5(5)	C(1)-Ir(1)-Ir(1a)	85.5(3)
Cp(1)-Ir(1)-C(1)	137.0	Cp(1)-Ir(1)-Ir(1a)	128.4
(c) **Dihedral angles (deg)**			
Cp(1)-Ir(1)-Ir(1a)-Cp(1a)	122.8	C(1)-Ir(1)-Ir(1a)-C(1a)	64.5

[a]Cp(1) refers to the centroid of the C_5Me_4Et ring on Ir(1).

sharpens into a well-resolved doublet at −16.8 ppm (J_{H-P} = 47 Hz). Integration of the hydride resonance indicates a ratio of the major doublet resonance to the minor triplet resonance of 4.2:1. A similar temperature dependence was noted in the $^{31}P\{^1H\}$ NMR spectra of **2** recorded at various temperatures in that a major and a minor species were observed. The signals coalesced at 288 K. The activation energy for the interconversion was estimated using the method of Shanan-Atidi and Bar-Eli (18). This analysis gives $\Delta G^{\ddagger}_{288} = 13.5 \pm 0.6$ kcal mol^{-1} for the conversion of the major species to the minor species, and $\Delta G^{\ddagger}_{288} = 12.7 \pm 0.5$ kcal mol^{-1} for the reverse reaction.

A second fluxional process is clearly operational in complex **2** and is manifest by the change in the hydride coupling to the two ^{31}P nuclei. At low temperature, the doublet splitting in the major species is consistent with two localized, terminal hydride ligands (the three-bond H–P coupling appears to be approximately zero). At higher temperatures, a dynamic process occurs that interchanges these two hydride ligands, leading to a triplet pattern in the ^1H NMR spectrum, with half the coupling observed in the low-temperature doublet. The hydride exchange in the minor species appears to be more facile and is not frozen out at 200 K. The spectra of the minor species were not sufficiently well resolved for detailed analysis, but analysis of the hydride lineshape for the major species indicates that $\Delta H^{\ddagger} = 10.2 \pm 0.5$ kcal mol^{-1}, $\Delta S^{\ddagger} = -4.4 \pm 2$ cal mol^{-1} K^{-1}, and $\Delta G^{\ddagger}_{288} = 11.5 \pm 1$ kcal mol^{-1}.

The room temperature ^1H NMR spectrum of $[Cp^*Ir(CO)H]_2(\mu\text{-}H)^+$ (**3**) in $CDFCl_2$ exhibits a single sharp resonance in the hydride region at –16.44 ppm. Even at very low temperatures, a static limit ^1H NMR spectrum could not be obtained. At 138 K in $CDFCl_2$ (500 MHz), two broad resonances were observed at −15.3 and −18.1 ppm. Reliable integrals could not be obtained due to the extreme broadness of the resonances. The intensity of the downfield peak is greater and it is assigned by analogy to the spectrum of **1** to the terminal hydride ligands. The peak at −18.1 ppm is attributed to the bridging hydride ligand.

The room temperature ^1H NMR spectrum ($CDFCl_2$, 500 MHz) of $[Cp^*Ir(CO)H]_2$ (**4**) in the hydride region consists of a single resonance at −16.2 ppm. Lowering the temperature to 263 K gives substantial line broadening. At 229 K, a sharp signal at −16.0 ppm and a weak broad peak at −19.2 ppm were observed. The ratio of the two peaks was determined by integration to be 12.3:1. Continued cooling decreases the peak linewidths and shifts the ratio to 2.2:1 at 168 K. All spectral changes with temperature are fully reversible. A van't Hoff plot of ln K_{eq} versus $1/T$ yields the thermodynamic parameters for the interconversion between the two species: $\Delta H° = 1.98 \pm 0.23$ kcal mol^{-1} and $\Delta S° = 13.3 \pm 1.2$ cal mol^{-1} K^{-1}. The activation energy for the interconversion was estimated from the coalescence temperature as outlined above. At the coalescence temperature (240 K) $\Delta G^{\ddagger} = 11.2 \pm 0.6$ kcal mol^{-1} for the conversion of the major species to the minor species, and $\Delta G^{\ddagger} = 10.0 \pm 0.4$ kcal mol^{-1} for the reverse reaction.

To probe for a dynamic process that would exchange the two terminal hydride ligands in **4**, the complex was prepared with ^{13}C labeling in the carbonyl groups, i.e., $[Cp^*Ir(^{13}CO)H]_2$ (**4***). The ^1H NMR spectrum of **4*** exhibits a poorly resolved triplet hydride resonance (J_{C-H} = 4.5 Hz) at room temperature. At 145 K, two resonances are observed as was the case for **4.** The major resonance at −15.89 ppm is a doublet (J_{C-H} = 7.9 Hz), and the minor resonance at −19.04 ppm is a triplet (J_{C-H} = 6.0 Hz).

The variable temperature ^1H NMR spectrum of $[Cp'Ir(CO)H]_2$ (**6**) in the hydride region is similar to that described above for complex **4**. Interconversion between a major and minor species is frozen out at low temperature. In addition, the major species exhibits four distinct methyl resonances, while the minor species shows only two methyl resonances.

Thermolysis of $[Cp^*Ir(CO)H]_2$ (4)

At room temperature, the neutral dihydride dimer (**4**) is thermally stable with respect to loss of H_2 as a solid or in solution. When a solution of **4** in benzene-d_6 is heated to 100°C, $[Cp^*Ir(CO)]_2$ (^1H NMR: δ 1.57) is produced. The reaction is extremely slow, with only ca. 15% conversion after 2 weeks under these conditions. After the initial period in which only $[Cp^*Ir(CO)]_2$ was formed, the appearance of small amounts of monomeric $Cp^*Ir(CO)H_2$ was noted.

Discussion

Synthesis

Protonation of the neutral metal dihydride complex $CpRh(PiPr_3)H_2$ was reported by Werner and Wolf (19) to generate H_2 and a cationic dimeric species, formulated as $[CpRh(PiPr_3)]_2(\mu\text{-}H)_3^+$. In the case of similar iridium complexes, Gilbert and Bergman reported (20) that protonation of $Cp^*Ir(PMe_3)H_2$ affords the monomeric cation $Cp^*Ir(PMe_3)H_3^+$. Hydrogen loss from this cationic species

Can. J. Chem. Downloaded from www.nrcresearchpress.com by 80.90.12.36 on 09/08/12
For personal use only.

Fig. 2. Partial ^{1}H NMR (250 MHz) spectra of $[CpIr(P(OPh)_3)H]_2$ (**2**) in THF-d_8: (*a*) 300 K, (*b*) 257 K, (*c*) 238 K, (*d*) 200 K.

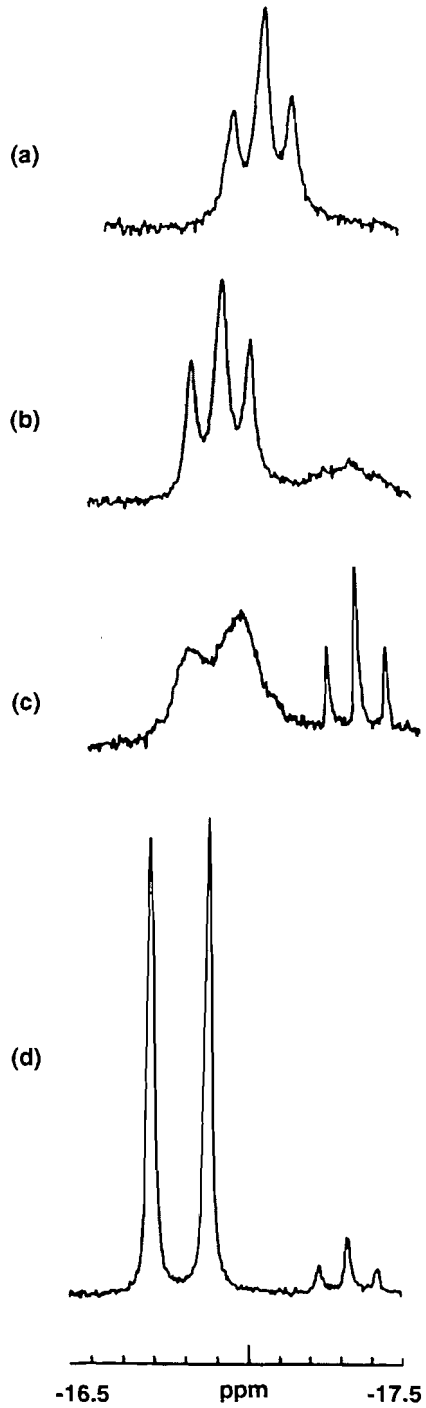

does not occur readily. The dimeric iridium species identified as $[Cp^*Ir(PMe_3)H]_2(\mu\text{-}H)^+$ was prepared (20) by reaction of $[Cp^*Ir]_2(\mu\text{-}H)_3^+$ with PMe_3. We find that protonation of monomeric iridium dihydride complexes such as $CpIr(P(OPh)_3)H_2$ cleanly affords dimeric cations. This reaction also works well for $Cp^*Ir(CO)H_2$. The dimer formation reaction depicted in Scheme 1 proceeds via initial protonation of the neutral dihydrides to afford the cationic trihydride complexes. In the case of L = $P(OPh)_3$ (as well as several other phosphines), this complex is isolable and has been previously reported (15). When L = CO, hydrogen loss is facile, and the monomeric trihydride complex has only been observed at very low temperatures.[6] This condensation methodology is very efficient. When the progress of the reaction between $Cp^*Ir(CO)H_2$ and triflic acid is monitored by ^{1}H NMR spectroscopy, the yield of dimer is quantitative. Isolated yields are somewhat diminished by losses during manipulation. The relative facility with which these various $(\eta\text{-}C_5R_5)Ir(L)H_3^+$ compounds lose H_2 and hence undergo the condensation to dimers (i.e., $Cp^*Ir(CO)H_2$ > $CpIr(P(OPh)_3)H_2 \gg Cp^*Ir(PMe_3)H_2$) correlates well with the decreasing electron density at the metal.

Deprotonation of the carbonyl dimers $[Cp^*Ir(CO)H]_2(\mu\text{-}H)^+$ and $[Cp'Ir(CO)H]_2(\mu\text{-}H)^+$ is readily effected by mild bases such as triethylamine or 1,8-bis(dimethylamino)naphthalene (Proton Sponge®). While quantitative pK_a data have not yet been obtained, it is clear that the phosphite complex $[CpIr(P(OPh)_3)H]_2(\mu\text{-}H)^+$ is a much weaker acid than the cationic carbonyl dimers. A stronger base, such as LDA, is required to carry out the deprotonation in this case. This is consistent with lower electron density at the metal centers in the carbonyl-containing complexes.

The same synthetic path was followed in the preparation of ^{13}C labeled derivatives of the Cp* complexes. Reaction of $[Cp^*IrCl_2]_2$ with ^{13}CO gives $Cp^*Ir(^{13}CO)Cl_2$. Subsequent transformations were carried out as detailed above for the unlabelled analogs.

Structure of $[Cp'Ir(CO)H]_2$ (6)

An X-ray structure determination confirmed the dimeric nature of **6** with an Ir—Ir bond length of 2.724 Å and terminal carbonyl ligands. While the hydride ligands could not be definitively located in the structure determination, the infrared spectrum indicates the presence of terminal hydride and terminal carbonyl ligands. The results of investigations of **2**, **4**, and **6** by variable temperature NMR spectroscopy indicate that the ground state structure has terminal hydrides (see below). Intraligand angles in **6** are similar to those observed (21) in closely related monomeric complexes such as $Cp^*Ir(PMe_3)(H)Cy$, in which, for example, the angle between the Cp* centroid and the phosphine is 131°. The comparable angle in **6** between the Cp′ moiety and the carbonyl group is 137°.

There are few structurally characterized examples of unbridged Ir—Ir single bonds in the literature. Examples include a distance of 2.717 Å reported (22) in 1973 for $Ir_2(NO)_4(PPh_3)_2$ and a distance of 2.839 Å reported (23) for the dication $[Cp^*Ir(CO)_2]_2^{2+}$. A closely related complex with bridging carbonyl ligands and a formal Ir—Ir double bond is $[Cp^*Ir(CO)]_2$, which has an Ir—Ir distance of 2.554 Å (24). Structural characterization of $[Cp^*Os(CO)(\mu\text{-}H)]_2$, a very similar dimeric complex of osmium, indicates that the two hydride ligands are bridging the Os═Os double bond, which has a bond length of 2.677 (25). In $[Cp^*Os(CO)(\mu\text{-}H)]_2$, unlike in $[Cp'Ir(CO)H]_2$ (**6**), the metal atoms, the carbonyl carbons, and the ring centroids all form a plane.

The structural results indicate that **6** has crystallized as the racemic diastereomer (*RR/SS* enantiomeric pair). Solution

[6] D.M. Heinekey and T.G.P. Harper, unpublished results.

Can. J. Chem. Downloaded from www.nrcresearchpress.com by 80.90.12.36 on 09/08/12
For personal use only.

NMR spectroscopy data discussed below show that there is a rapidly established equilibrium between the racemic and meso forms of **6** from which the racemic form crystallizes.

Dynamics

The variable temperature NMR spectroscopy of the trihydride dimers **1**, **3**, and **5** is consistent with the presence of one bridging and two terminal hydride ligands. A rapid dynamic process is operational in these complexes that allows site exchange of the terminal and bridging ligands. In the case of $[CpIr(P(OPh)_3)H]_2(\mu\text{-}H)^+$ (**1**), this process is indicated by the observation of a single triplet resonance (J_{H-P} = 18 Hz) in the hydride region of the ^1H NMR spectrum at room temperature. This observation would also be consistent with a triply bridging structure, as suggested by Werner and Wolf (19) for the related dimeric trihydride complex that results from the reaction of $CpRh(P\textit{i}Pr_3)H_2$ with acid. The observation at low temperature of two distinct hydride resonances in the intensity ratio 2:1 favors the less symmetrical, singly bridged structure. The coupling to ^{31}P is in agreement with this structure, in that the resonance corresponding to one hydride is a triplet, while the more intense signal is a doublet. This same structure was found by Gilbert and Bergman (20) for the closely related trimethylphosphine complex $[Cp^*Ir(PMe_3)H]_2(\mu\text{-}H)^+$. Complex **1** differs from the previously reported PMe_3 complex in having a somewhat lower barrier to the dynamic process that permutes the bridging and terminal hydride ligands. A very similar situation was reported by Werner et al. (26) for the structure of $\{[CH_2(C_5H_4)_2][RhH(P\textit{i}Pr_3)]_2(\mu\text{-}H)\}^+$. In this case, the presence of bridging and terminal hydride ligands was indicated crystallographically, but the bridge–terminal exchange process was too facile to be frozen out by low-temperature NMR spectroscopy.

Qualitatively similar observations were made for $[Cp^*Ir(CO)H]_2(\mu\text{-}H)^+$ (**3**). The structural assignment here is less definitive, since ^{31}P coupling is not available to aid in the differentiation of terminal and bridging hydride ligands. In an attempt to verify that the dynamic behavior of **3** is analogous to that of **1**, we prepared complex **3** with ^{13}C labels in the carbonyl carbon atoms (referred to as **3***). At ambient temperature, the ^1H NMR spectrum for **3*** shows a triplet hydride resonance with J_{H-C} = 3.4 Hz. The expected doublet and triplet H–C couplings in **3*** were not resolvable in the low-temperature spectra.

The structures of complexes **2**, **4**, and **6** are thought to be dihydride dimers with two terminal hydride ligands. This structural hypothesis is based on the observation of terminal Ir–H stretches in the infrared spectra, and on the couplings between the hydride ligands and adjacent spin active nuclei observed in the ^1H NMR spectra. For example, $[CpIr(P(OPh)_3)H]_2$ (**2**) exhibits a triplet signal for the hydride ligands at high temperature, due to coupling to two ^{31}P nuclei. While this observation alone is consistent with the presence of bridging hydrides, variable temperature data show that the hydride resonance (of the major species, see below) simplifies to a doublet at low temperature. This is consistent only with a ground state structure having terminal hydride ligands and a rapid permutation process that causes the hydride ligands to exchange. We propose that this process takes place via an intermediate or transition state with two bridging hydride ligands (see Scheme 2). The observation that the hydride signal of the *minor* species of **2** remains as a triplet in the ^1H NMR down to 200 K is consistent with a ground state structure possessing bridging hydrides (see Fig. 2). We believe, however, that the slight broadening of the triplet resonance at 200 K indicates that the hydrides are indeed terminal and fluxional and that at still lower temperatures the signal would become a doublet.

Scheme 2.

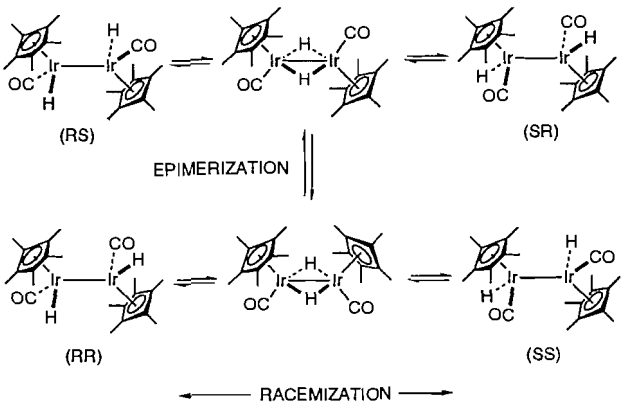

In addition to the dynamic process that causes the permutation of the two hydride ligands, variable temperature NMR (^1H and ^{31}P) observations on complex **2** indicate the presence of two different species. The relative concentrations of these two species vary with temperature, consistent with a rapid reversible equilibrium.

Since both metal centers in dimers such as **2** are chiral, the existence of two diastereomers is possible. The two diastereomers are the racemic form (*RR*/*SS* enantiomeric pair) and the meso structure (*RS* or *SR*). It is proposed that rapid epimerization occurs, causing rapid equilibration of the two diastereomers of **2**. Thermodynamic parameters for the interconversion have been estimated from the lineshapes of the ^1H and ^{31}P NMR spectra. Note that the hydride site exchange process will lead to synchronous inversion of configuration at both Ir centers *without* epimerization.

It should be noted that the suggestion of rapid epimerization of pseudo-octahedral complexes of iridium is somewhat novel. In closely related *monomeric* complexes such as $Cp^*Ir(CO)(H)(\text{-}CH_2CMe_3)$ (27), the diastereotopic methylene protons are distinct in the ^1H NMR spectrum at room temperature, indicating that the metal center is configurationally rigid on the NMR time scale at this temperature. Similar observations have been reported (28) for $Cp^*Ir(PMe_3)(H)(\text{-}CH_2CMe_3)$. The mechanism of the rapid epimerization observed in the dimeric complexes studied here is not clear, but there are obviously large differences in stereochemical nonrigidity between closely related monomeric and dimeric complexes.

Similar observations have been made for $[Cp^*Ir(CO)H]_2$ (**4**). Infrared spectra are only consistent with the presence of terminal carbonyl and terminal hydride ligands. Variable temperature ^1H NMR spectra reveal that two species are present in rapid equilibrium. The incorporation of two ^{13}C labels in the carbonyl groups (designated **4***) allowed the detection of coupling to the hydride ligands. The hydride resonance of **4*** is a poorly resolved triplet ($J_{H-C} \approx$ 4–5 Hz) at room temperature. At lower temperatures, two distinct signals are observed: the major signal is a doublet (J_{H-C} = 7.9 Hz), while the resonance

Can. J. Chem. Downloaded from www.nrcresearchpress.com by 80.90.12.36 on 09/08/12
For personal use only.

due to the minor species remains a triplet (J_{H-C} = 6.0 Hz) at all accessible temperatures. The overall situation for complex **4** is very similar to that of **2**.

To directly verify the stereochemical nonrigidity of the metal centers in these dimers, complex **6** has been prepared in which the Cp^* ligands of **4** have been replaced by η-C_5Me_4Et (Cp′). This ligand provides a convenient probe for stereochemical nonrigidity at the metal centers in that the diastereotopic methylene protons[7] and the diastereotopic methyl groups will be rendered equivalent by a rapid change (on the NMR timescale) of configuration at the metal center. We find that the variable temperature ^{1}H NMR spectrum of **6** at room temperature exhibits a single hydride resonance and only two resonances for the methyl groups attached to the ring carbons. At lower temperatures, two hydride resonances of unequal intensity are observed, similar to the situation observed in complex **4**. The methyl region of the spectrum also exhibits a major and minor set of resonances. The major species has four distinct methyl resonances, consistent with the freezing out of the configuration at the metal centers. This is in accord with the observation of a doublet resonance for the hydride ligands of the major species at low temperature in the ^{1}H NMR spectrum of complex **4***. The minor species of complex **6** exhibits only two methyl resonances at all accessible temperatures, indicating that the metal centers are not configurationally stable. This is again consistent with the observation of a triplet resonance for the hydride ligands of the minor species at all temperatures in the ^{1}H NMR spectrum of complex **4***.

The presence of rotamers with respect to the Ir—Ir bond is an alternative hypothesis that warrants consideration to explain the observation of two rapidly equilibrating species for **2**, **4**, and **6**. In this scenario, the interconversion of the major to minor species involves simple rotation around the Ir—Ir bond and would not alter the configuration at the metal centers. *However*, hydride migration between Ir atoms within a given rotamer would lead to racemization of those metal centers and hence would also render the diastereotopic groups of **6** equivalent. The observation of decoalescence of the resonances of the diastereotopic ring methyl groups in **6** is thus consistent with this hypothesis. We believe, however, that the rotamer hypothesis is unlikely as it requires that only a single diastereomer be present. This would require that the reactions that lead to formation of all the neutral dimers be completely diastereoselective.

Thermolysis of $[Cp^*Ir(CO)H]_2$ (4)

Complex **4** is thermally robust. Prolonged heating to 100°C affords the known (24) carbonyl-bridged, doubly bonded dimer $[Cp^*Ir(CO)]_2$. The apparent large activation energy barrier to elimination of hydrogen is consistent with that expected for a formally symmetry-forbidden, concerted, 1,2-dinuclear reductive elimination reaction. Further studies to elucidate the mechanism of this novel reaction were complicated by secondary chemistry that begins to be significant after about 30% conversion. Specifically, the formation of $Cp^*Ir(CO)H_2$ was noted,[8] indicative of dimer fragmentation. A similar, very slow thermal reaction of a tungsten dihydride dimer to afford H_2 was recently reported by Tilset et al. (29). In this case, a radical chain mechanism was proposed. The stereochemical nonrigidity of the dimeric iridium complexes noted above suggests that a *cis* hydride geometry suitable for 1,2 hydrogen elimination should be accessible. The product doubly bonded dimer $[Cp^*Ir(CO)]_2$ is extremely thermally robust. These observations are consistent with a high kinetic barrier to reductive elimination imposed by orbital symmetry constraints.

[7] We found the diastereotopic methylene protons to be poor probes of stereochemical nonrigidity due to small chemical shift inequivalence and the presence of complicated coupling (ABX_3 spin system). Hence the diastereotopic methyl groups were used exclusively.

[8] $Cp^*Ir(CO)H_2$ has been previously reported (30).

Conclusions

The protonation of monomeric dihydrides of the form $CpIrLH_2$ (Cp = C_5H_5, L = $P(OPh)_3$; Cp = C_5Me_5 or C_5Me_4Et, L = CO) provides a general and efficient route for the generation of the dinuclear complexes (**1**, **3**, **5**). The resulting cationic trihydride dimers each exhibit a single resonance in the hydride region of the ^{1}H NMR spectrum at ambient temperature. Variable temperature ^{1}H NMR spectroscopy reveals that the ground state structure possesses one bridging and two terminal hydride ligands that rapidly exchange at room temperature.

Deprotonation of **1**, **3**, and **5** affords the neutral dihydride dimers (**2**, **4**, and **6**). Variable temperature ^{1}H NMR, IR, and crystallographic analysis indicate that these compounds have terminal hydride and terminal carbonyl ligands, i.e., unsupported Ir—Ir bonds. Very few examples of this structural type have been reported previously. As in **1**, **3**, and **5**, the hydride ligands rapidly permute between Ir centers at room temperature.

Compounds **2**, **4**, and **6** can each achieve two diastereomeric configurations (*RR/SS* or *RS/SR*) due to the presence of two chiral iridium centers per molecule. Although closely related monomeric complexes are configurationally stable on the NMR time scale, these dimers undergo facile epimerization.

Thermolysis of $[Cp^*Ir(CO)H]_2$ (**4**) leads to slow loss of H_2 to afford the doubly bonded dimer $[Cp^*Ir(CO)]_2$. The mechanism of H_2 elimination has yet to be established.

Acknowledgments

We thank the National Science Foundation for support of this research. Partial support was also provided by the Petroleum Research Foundation, administered by the American Chemical Society. We thank Dr. David Barnhart for the crystallographic analysis and Ms. Amber Hinkle for help with variable temperature NMR work.

References

1. J.R. Norton. Acc. Chem. Res. **12**, 139 (1979).
2. J.P. Collman, L.S. Hegedus, J.R. Norton, and R.G. Finke. *In* Principles and applications of organotransition metal chemistry. University Science Books, Mill Valley, Calif. 1987. pp. 322–333.
3. J. Halpern. Inorg. Chim. Acta, **62**, 31 (1982).
4. S.G. Davies, J. Hibberd, S.J. Simpson, and O. Watts. J. Organomet. Chem. **241**, C31 (1983).
5. R.H. Hill and R.J. Puddephatt. Organometallics, **2**, 1472 (1983).
6. R.H. Hill and R.J. Puddephatt. J. Am. Chem. Soc. **105**, 5797 (1983).

7. T.E. Bitterwolf and K.S. Raghuveer. Inorg. Chim. Acta, **172**, 59 (1990).
8. R. Hoffman and G. Trinquier. Organometallics, **3**, 370 (1984).
9. J.R. Moss and W.A.G. Graham. Inorg. Chem. **16**, 75 (1977).
10. J.R. Moss and W.A.G. Graham. J. Chem. Soc. Dalton Trans. 89 (1977).
11. Inferred from the ^{1}H NMR chemical shift value reported for the hydrides: P.J. Krusic, D.J. Jones, and D.C. Roe. Organometallics, **5**, 456 (1986).
12. J.S. Siegel and F.A.L. Anet. J. Org. Chem. **53**, 2629 (1988).
13. H.E. Amouri, M. Gruselle, and G. Jaouen. Synth. React. Inorg. Met.-Org. Chem. **24**, 395 (1994).
14. J.W. Kang and P.M. Maitlis. J. Organomet. Chem. **26**, 393 (1971).
15. D.M. Heinekey, J.M. Millar, T.F. Koetzle, N.G. Payne, and K.W. Zilm. J. Am. Chem. Soc. **112**, 909 (1990).
16. A.L. Van Geet. Anal. Chem. **42**, 679 (1970).
17. J.P. Jesson and P. Meakin. Acc. Chem. Res. **6**, 269 (1973).
18. H. Shanan-Atidi and K.H. Bar-Eli. J. Phys. Chem. **74**, 961 (1970).
19. H. Werner and J. Wolf. Angew. Chem. Int. Ed. Engl. **21**, 296 (1982).
20. T.M. Gilbert and R.G. Bergman. J. Am. Chem. Soc. **107**, 3502 (1985).
21. M.J. Buchanan, J.M. Stryker, and R.G. Bergman. J. Am. Chem. Soc. **108**, 1537 (1986).
22. M. Anoletta, G. Ciani, M. Manassero, and M. Sansoni. J. Chem. Soc. Chem. Commun. 789 (1973).
23. F.W.B. Einstein, R.H. Jones, X. Zhang, X. Yan, R. Negelkerke, and D. Sutton. J. Chem. Soc. Chem. Commun. 1424 (1989).
24. R.G. Ball, W.A.G. Graham, D.M. Heinekey, J.K. Hoyano, A.D. McMaster, B.M. Mattson, and S.T. Michel. Inorg. Chem. **29**, 2023 (1990).
25. J.K. Hoyano and W.A.G. Graham. J. Am. Chem. Soc. **104**, 3722 (1982).
26. H. Werner, M. Treiber, A. Nessel, F. Lippert, P. Betz, and C. Kruger. Chem. Ber. **125**, 337 (1992).
27. W.A.G. Graham and J.K. Hoyano. J. Am. Chem. Soc. **104**, 3723 (1982).
28. R.G. Bergman and A.H. Janowicz. J. Am. Chem. Soc. **105**, 3929 (1983).
29. M. Tilset, K.P.C. Vollhardt, and R. Boese. Organometallics, **13**, 3146 (1994).
30. W.A.G. Graham. J. Organomet. Chem. **300**, 81 (1986).

Can. J. Chem. Downloaded from www.nrcresearchpress.com by 80.90.12.36 on 09/08/12
For personal use only.

Preparation and characterization of a new series of Cr(II) hydroborates

Michel Dionne, Shoukang Hao, and Sandro Gambarotta

Abstract: The synthesis and characterization of a new series of mono-, di-, and trinuclear Cr(II) borohydride compounds is described. The reaction of $CrCl_2$(TMEDA) with two equivalents of $NaBH_4$ afforded the thermally unstable (TMEDA)Cr(BH_4)$_2$ (**1**), which was converted by treatment with pyridine into the octahedral monomeric (Py)$_4$Cr(BH_4)$_2$ (**2**). The reaction proceeds via formation of an intermediate trinuclear complex {[(TMEDA)(Py)Cr(η^2-BH_4)]$_2$[(Py)$_2$Cr(η^2-BH_4)$_2$]}(μ,η^1-BH_4)$_2$ (**3**), which was isolated and characterized by X-ray crystallography. Reaction of **1** and **2** with both CO_2 and RN=C=NR (R = Cy, *i*Pr) afforded hydride insertion and formation of the corresponding diamagnetic lantern-type Cr(II) formate $(HCO_2)_4Cr_2Py_2$ (**4**) and formamidinate compounds [RNC(H)NR]$_2$Cr$_2$(μ-BH)$_4$ (R = Cy (**5***a*), iPr (**5***b*)), respectively, with supershort Cr—Cr quadruple bonds. The structures of **1**, **2**, **3**, and **5***b* were elucidated by X-ray analysis. Crystal data are as follows. **1**: $C_6H_{24}N_2B_2Cr$, monoclinic, *Cc*, a = 8.517(2) Å, b = 15.921(5) Å, c = 9.624(2) Å, β = 115.59(1)°, Z = 4, R = 0.022, R_w = 0.029; **2**: $C_{28}H_{44}N_4B_2O_2Cr$, monoclinic, $P2_1/n$, a = 12.021(1) Å, b = 15.555(1) Å, c = 15.723(1) Å, β = 90.13(2)°, Z = 4, R = 0.074, R_w = 0.086; **3**: $C_{32}H_{76}N_8B_6Cr_3$, monoclinic, $P2_1/n$, a = 8.515(1) Å, b = 14.525(1) Å, c = 18.286(2) Å, β = 91.38(1)°, Z = 2, R = 0.051, R_w = 0.060; **5***b*: $C_{21}H_{49}N_6BCr_2$, monoclinic, *C2/c*, a = 17.000(1) Å, b = 9.033(1) Å, c = 19.160(1) Å, β = 105.579(9)°, Z = 4, R = 0.069, R_w = 0.078.

Key words: divalent chromium, borohydride, Cr—Cr quadruple bond.

Résumé : On décrit la synthèse et la caractérisation d'une série de borohydrures mono-, di- et trinucléaires du Cr(II). La réaction du $CrCl_2$(TMEDA) avec deux équivalents de $NaBH_4$ fournit le (TMEDA)Cr(BH_4)$_2$ (**1**) qui est thermiquement instable et qui, par traitement avec de la pyridine, se transforme en (Py)$_4$Cr(BH_4)$_2$ (**2**). La réaction se produit par le biais de la formation d'un complexe intermédiaire trinucléaire {[(TMEDA)(Py)Cr(η_1-BH_4)]$_2$[(Py)$_2$Cr(η^2-BH_4)$_2$]}(μ,η^1-BH_4)$_2$ (**3**) que l'on a isolé et caractérisé par diffraction des rayons X. Les réactions de composés **1** et **2** avec le CO_2 ou le RN=C=NR (R = Cy ou iPr) conduisent à une insertion d'hydrure et à la formation des composés diamagnétiques correspondants, respectivement le formiate de Cr(II) de type lanterne, $(HCO_2)_4Cr_2Py_2$ (**4**), et les formamidinates, [RNC(H)NR]$_2$Cr$_2$(μ-BH)$_4$ (R = Cy (**5***a*), iPr (**5***b*)), dans lesquels les longueurs des liaisons quadruples Cr—Cr sont extrêmement courtes. On a élucidé les structures des composés **1**, **2**, **3** et **5***b* par diffraction des rayons X. Les données cristallines sont les suivantes: **1**, $C_6H_{24}N_2B_2OCr$, monoclinique, *Cc*, a = 8,517(2), b = 15,921(5) et c = 9,624(2) Å, β = 115,59(1)°, Z = 4, R = 0,022 et R_w = 0,029; **2**, $C_{28}H_{44}N_4B_2O_2Cr$, monoclinique, $P2_1/n$, a = 12,021(1), b = 15,555(1) et c = 15,723(1) Å, β = 90.13(2)°, Z = 4, R = 0,074 et R_w = 0,086; **3**, $C_{32}H_{76}N_8B_6Cr_3$, monoclinique, $P2_1/n$, a = 8,515(1), b = 14,525(1) et c = 18,286(2) Å, β = 91,38(1)°, Z = 2, R = 0,051 et R_w = 0,060; **5***b*, $C_{21}H_{49}N_6BCr_2$, monoclinique, *C2/c*, a = 17,000(1), b = 9,033(1) et c = 19,160(1) Å, β = 105,579(9)°, Z = 4, R = 0,069 et R_w = 0,078.

Mots clés : chrome divalent, borohydrure, liaison quadruple Cr—Cr.

[Traduit par la rédaction]

Introduction

Tetrahydroborate complexes of transition metals are employed not only as versatile precursors for the preparation of transition metal polyhydrides (see, for example, ref. 1) and alkyls (2), but also as important and efficient catalysts for hydrogenation and polymerization reactions (3). For example, tetrahydroborate complexes of group 4, 5, and 6 metals are used in the catalytic hydrorefinement of petroleum sludges and residues to light hydrocarbons and to other useful commodity chemicals freed from asphaltenes, metal impurities, and sulfur (4). In view of these useful applications transition metal, lanthanide and actinide tetrahydroborate complexes have been widely investigated (5–7) and, as a result of the considerable amount of research in this field, only a few transition metal tretrahydroborate complexes remain unexplored. Unfortunately, a large variety of catalytic transformations promoted by these systems has been reported only in the patent literature and therefore knowledge about the chemical behavior of these species remains scarce.

Aside from their importance in industrial processes, tetrahydroborate complexes of transition metals are also popular

Received October 19, 1994.

This paper is dedicated to Professor William A.G. Graham on the occasion of his 65th birthday and in recognition of his accomplishments for the advancement of inorganic chemistry in Canada.

M. Dionne, S. Hao, and S. Gambarotta.[1] Department of Chemistry, University of Ottawa, Ottawa, ON K1N 6N5, Canada.

[1] Author to whom correspondence may be addressed. Telephone: (613) 564-2958. Fax: (613) 564-6793. E-mail: SXGSE@acadvm1.uottawa.ca

Can. J. Chem. Downloaded from www.nrcresearchpress.com by 80.90.12.36 on 09/08/12
For personal use only.

Can. J. Chem. Downloaded from www.nrcresearchpress.com by 80.90.12.36 on 09/08/12
For personal use only.

because of their close relation with transition metal hydrides. As a matter of fact, a common method of preparing polyhydride complexes typically consists of the reaction of transition metal tetrahydroborates with a Lewis base or water (5, 6, 8). In addition, although the mechanisms of reactions catalyzed by transition metal hydroborates have not been completely elucidated, there is evidence that in situ generated polyhydride complexes are likely to be the most important intermediates of the catalytic cycles (9).

Given this background, it is surprising that chromium tetrahydroborates are poorly known, and that only a few very stable species such as $CpCr(BH_4)$ (10), $Cr(BH_4)_2THF_2$ (11), $Cr(BH_4)_2py_2$ (11), and $Cr(BH_4)_2en$ (11) have been reported and formulated on the exclusive basis of their spectroscopic and microanalytical data. Only in the case of $Cr(BH_4)H(dmpe)_2$ (7) has a complete structural analysis been reported. This paucity of the literature is in striking contrast with the great potential offered by these compounds for the preparation of rare chromium hydrides (12).

In this paper we describe the preparation and characterization of a novel series of chromium(II) tetrahydroborates together with a preliminary study of their chemical reactivity. One of the *stimuli* to undertake this study was provided by the variety of possible bonding modes displayed by the BH_4^- anion (5). Since Cr(II) complexes generally display a marked preference for square-planar structures with high-spin electronic configurations (see, for example, ref. 13), we were interested in testing the ability of the tetrahydroborate anion to facilitate the assembly of dimers with a lantern-type structure, where the BH_4^- anion would adopt a three-center chelating bridging bonding mode. To achieve this goal we have decided to use a chelating amine such as TMEDA (TMEDA = *N,N,N',N'*-tetramethylethylenediamine) as supporting ligand. This ligand offers sufficient stabilization for the complex, while at the same time may dissociate to enable dimerization reactions. Chelating amines are also desirable because of their ability to remove BH_3 from the BH_4^- anion, which in the present case should lead to the formation of new Cr(II) hydrides.

Experimental section

All operations were performed under inert atmosphere in a dry-box (Vacuum Atmosphere) or using standard Schlenk techniques. $CrCl_2THF_2$ (14) was prepared according to published procedures. $NaBH_4$, CyN=C=NCy, (iPr)N=C=N(iPr), and $Me_3SiN{=}C{=}NMe_3$ (Aldrich) were purchased and used without further purification. NMR spectra were recorded on a Varian Gemini-200 and a Bruker AMX-500 spectrometer by using vacuum-sealed tubes. Solvents for NMR spectroscopy were dried over the appropriate desiccating agent, vacuum-transferred into ampoules, and stored inside a dry-box. Infrared spectra were recorded on a Mattson 9000 FT-IR instrument from Nujol mulls. Samples for magnetic susceptibility measurements were weighed under inert atmosphere and sealed into calibrated tubes. Magnetic measurements were carried out with a Gouy balance (Johnson Matthey) at room temperature. The magnetic moments were calculated according to standard methods (15), and corrections for underlying diamagnetism (16) were applied to data. Combustion analysis data were obtained with a PE 4000 analyzer.

$Cr(BH_4)_2TMEDA$ (1)

A suspension of $CrCl_2THF_2$ (1.78 g, 6.7 mmol) in THF (100 mL) was stirred at room temperature in the presence of an excess of TMEDA (5 mL, 34.5 mmol). The resulting bright-blue suspension was treated with excess $NaBH_4$ (1.06 g, 26.3 mmol). After stirring for 24 h at room temperature, NaCl and the excess $NaBH_4$ were removed by filtering the boiling solution. The deep-blue filtrate was allowed to cool slowly to room temperature, upon which violet crystals of **1** were formed (0.7 g, 3.5 mmol, 52%). IR (Nujol mull, cm^{-1}) ν: 2380(vs, br), 2230(m), 2120(vs, br), 1455(vs, br), 1405(w), 1375(vs, br), 1295(w), 1285(s), 1230(m), 1200(w), 1175(sh), 1155(s), 1120(vs, br), 1100(sh), 1060(m), 1040(m), 1010(s), 1000(sh), 950(s), 800(s), 770(m), 720(w), 590(w), 510(w, br). Anal. calcd. (found) for $C_6H_{24}N_2B_2Cr$: C 36.36(36.29), H 12.12(12.03), N 14.14(14.09). $\mu_{eff} = 4.8\ \mu_B$.

$Cr(BH_4)_2Py_4$ (2)

A suspension of **1** (1.9 g, 9.6 mmol) in THF (30 mL) was treated with pyridine (3 mL, 38 mmol) at room temperature and boiled for a few minutes until a clear green solution was formed. The solution was allowed to cool slowly to room temperature, upon which very air-sensitive red-orange crystals of **2** separated (1.8 g, 7.5 mmol, 78%). Occasionally formed green prisms of $\{[(TMEDA)(Py)Cr(\eta^1\text{-}BH_4)]_2[(Py)_2Cr(\eta^2\text{-}BH_4)_2]\}$ $(\mu,\eta^1\text{-}BH_4)_2$ (**3**) were eliminated by addition of one extra equivalent of pyridine. IR (Nujol mull, cm^{-1}) ν: 2300(vs, br), 2180(s), 2120(s), 2080(s), 1650(w), 1610(s), 1490(s), 1464(sh), 1450(s, br), 1380(m), 1310(w), 1240(w), 1220(s), 1150(m), 1110(sh), 1080–1040(vs, br), 1015(s), 915(m), 770(s), 705(s), 640(s), 600(w), 510(w, br), 440(s). Anal. calcd. (found) for $C_{20}H_{28}N_4B_2Cr{\cdot}2THF$: C 62.01(61.95), H 8.18(8.16), N 10.33(10.26). $\mu_{eff} = 2.83\ \mu_B$.

$Cr_2(CO_2H)_4Py_2$ (4)

A green solution, obtained by dissolving deep-red crystals of **2** (0.7 g, 2.9 mmol) in THF (100 mL), was saturated with CO_2 (room temperature, 1 atm (101.3 kPa)). The original green color turned red in about 20 min. The resulting solution was concentrated in vacuo and allowed to stand at −30°C overnight, upon which red crystals of **4** separated (0.2 g, 0.7 mmol, 48%). IR (Nujol mull, cm^{-1}) ν: 1620–1580(s, br), 1450(vs, br), 1380–1340(vs, br), 1220(m), 1155(w), 1065(w), 1036(m), 1006(w), 880(w), 770(s), 755(sh), 720(w), 700(s), 620(m), 435(s, br), 404(w). Anal. calcd. (found) for $C_{14}H_{14}N_2O_8Cr_2$: C 38.02(37.99), H 3.19(3.22), N 6.33(6.26). $\mu_{eff} = 0.6\ \mu_B$ per Cr_2 unit.

$Cr_2(CyNCHNCy)_3(BH_4)$ (*5a*)

Solid CyN=C=NCy (2.5 g, 12.1 mmol) was added to a blue suspension of **1** (1.2 g, 6.1 mmol) in THF (100 mL) at room temperature and the color turned dark yellow after a few minutes. The volume of the solution was reduced to ca 10 mL and yellow crystals of ***5a***, along with a small amount of white crystals of $TMEDA(BH_3)_2$, precipitated upon standing at −30°C overnight. Analytically pure yellow crystals of ***5a*** were obtained in low yield after several recrystallizations from THF (0.6 g, 0.8 mmol, 26%). IR (Nujol mull, cm^{-1}) ν: 2410(s), 2360(s), 2220(w), 2062(m, br), 1930(m, br), 1840(w, br), 1578(vs), 1450(vs, br), 1375(s), 1362(s), 1342(s), 1326(s), 1300(m), 1285(s), 1252(m), 1185(m), 1160(sh), 1150(s),

Can. J. Chem. Downloaded from www.nrcresearchpress.com by 80.90.12.36 on 09/08/12
For personal use only.

1120(s), 1102(s), 1086(s), 1080(s), 1048(w), 1020(m), 990(m), 962(w), 886(s), 846(m), 804(m), 782(m), 722(m), 508(s), 484(s), 436(s). ^{1}H NMR (C_6D_6, 200 MHz, 25°C, ppm) δ: 8.6 (s, 2H, C-H formamidine), 8.5 (s, 1H, C-H formamidine), 3.5 (m, 4H, C-H cyclohexyl), 2.65 (m, 2H, C-H cyclohexyl), 2.2–0.8 (series of lines, 34H, cyclohexyl and BH_4). Anal. calcd. (found) for $C_{39}H_{73}N_6BCr_2$: C 63.23(63.17), H 9.93(9.86), N 11.34(11.19).

Cr_2[iPr)NC(H)N(iPr)]$_3$(BH_4) (*5b*)

The addition of neat (iPr)N=C=N(iPr) (2.9 mL, 18.5 mmol) to a blue suspension of **1** (1.83 g, 9.2 mmol) in THF (100 mL) at room temperature formed a dark yellow solution. The resulting solution was concentrated to small volume in vacuum and allowed to stand at −30°C overnight, upon which orange crystals of ***5b***, contaminated by a small amount of colorless needles of $(BH_3)_2$TMEDA, precipitated. Analytically pure ***5b*** was obtained in low yield (less than 10%) after several recrystallizations from THF. IR (Nujol mull, cm^{-1}) ν: 2401(s), 2365(s), 2236(w), 2101(m, br), 1966(w, br), 1583(s, br), 1456(s, br), 1409(m), 1375(s), 1360(s), 1301(s), 1175(s), 1122(s), 1101(s), 1056(w), 1025(m), 953(m), 932(w), 853(w), 816(w), 726(w), 668(w), 649(w), 570(w), 524(s), 486(s), 421(s). ^{1}H NMR (C_6D_6, 400 MHz, 25°C, ppm) δ: 8.53 (s, 2H, C-H formamidine), 8.50 (s, 1H, C-H formamidine), 3.77 (hept, J = 6.5 Hz, 4H, C-H isopropyl), 2.97 (hept, J = 6.5 Hz, 2H, C-H isopropyl), 1.32 (m, 4H, BH_4), 1.21 (d, J = 6.5 Hz, 12H, CH_3 isopropyl), 1.03 (d, J = 6.5 Hz, 12H, CH_3 isopropyl), 0.82 (d, J = 6.5 Hz, 12H, CH_3 isopropyl). Anal. calcd. (found) for $C_{21}H_{49}N_6BCr_2$: C 50.40(50.31), H 9.87(9.81), N 16.79(16.71).

Cr_2[(iPr)NC(H)N(iPr)]$_3$(O_2CH) (*6*)

A yellow solution of ***5b*** in d_6-benzene was saturated with CO_2 (1 atm, room temperature) inside an NMR tube. As the intensity of the signals of the starting material decreased, new peaks were observed. After 2 days the reaction was complete and the spectrum was consistent with the formulation Cr_2(iPr)NC(H)N(iPr)]$_3$(O_2CH). ^{1}H NMR (C_6D_6, 500 MHz, 25°C, ppm) δ: 8.86 (s, 1H, CH formate), 8.65 (s, 2H, CH formamidine), 8.61 (s, 1H, CH formamidine), 3.71 (m, 4H, CH isopropyl), 3.15 (m, 2H, CH isopropyl), 1.31 (d, J = 6.2 Hz, 12H, CH_3 isopropyl), 1.05 (d, J = 6.2 Hz, 12H, CH_3 isopropyl), 0.87 (d, J = 6.2 Hz, CH_3 isopropyl).

Cr_2(CyNCHNCy)$_4$ (*7a*)

A suspension of $Cr_2Cl_2THF_2$ (2.23 g, 8.4 mmol) in THF (100 mL) was stirred at room temperature in the presence of an excess of TMEDA (5 mL, 34.5 mmol). An excess of $NaBH_4$ (1.85 g, 48.7 mmol) was added to the resulting bright-blue suspension. After stirring for 24 h at room temperature, a violet solid was formed. The addition of 1,3-dicyclohexyl carbodiimide (5.0 g, 24.3 mmol) at room temperature immediately produced a yellow suspension. After boiling the mixture for a few minutes, the solvent was evaporated in vacuo. The addition of toluene (40 mL) to the resulting residue produced a yellow solution and a white solid, which was removed by filtration. The filtrate was allowed to stand at −30°C overnight, upon which yellow crystals of **7***a* (0.4 g, 0.86 mmol, 10%) separated. IR (Nujol mull, cm^{-1}) ν: 1662(w), 1596(s, br), 1451(s, br), 1376(s), 1360(s), 1348(s), 1326(s), 1294(s), 1257(s), 1238(w), 1203(w), 1178(w), 1150(s), 1125(s), 1103(s), 1084(s), 1071(s), 1049(w), 1018(m), 986(w), 955(m), 917(w), 889(s), 845(m), 798(m), 729(m), 694(w), 600(w), 550(m), 512(s), 487(s), 465(s), 430(s). ^{1}H NMR (C_6D_6, 200 MHz, 25C°) δ: 8.43 (s, 4H, formamidine), 7.08(pseudo quartet, 4H, toluene), 311(pseudo quintet, 8H, cyclohexyl), 2.10(s, 3H, toluene), 2.07(pseudo d, 16H, cyclohexyl), 1.81(pseudo d, 16H, cyclohexyl), 1.63(pseudo d, 8H, cyclohexyl), 1.30(m, 40H, cyclohexyl). Anal. calcd. (found) for $C_{52}H_{92}N_8Cr_2$·toluene: C 69.10(68.99), H 9.83(9.77), N 10.93(10.85).

Cr_2[(iPr)NC(H)N(iPr)]$_4$ (*7b*)

A suspension of $CrCl_2THF_2$ (2.09 g, 7.8 mmol) in THF (100 mL) was stirred at room temperature in the presence of an excess of TMEDA (5 mL, 34.5 mmol). An excess of $NaBH_4$ (1.91 g, 50.3 mmol) was added to the resulting bright-blue suspension. After stirring for 24 h at room temperature, a violet solid was formed. The addition of 1,3-diisopropylcarbodiimide (5.0 mL, 31.7 mmol) to the resulting suspension at room temperature formed a yellow suspension. The solvent was evaporated in vacuo after boiling for a few minutes. The addition of toluene (30 mL) to the resulting yellow solid produced a yellow solution and a white solid, which was removed by filtration. The filtrate was allowed to stand at −30°C overnight, upon which yellow crystals of **7***b* (0.5 g, 1.8 mmol, 20%) separated. IR (Nujol mull, cm^{-1}) ν: 1598(s, br), 1572(sh), 1458(s, br), 1408(m), 1373(s), 1357(s), 1348(s), 1297(s, br), 1180(s), 1161(s), 1120(s), 1101(s), 1025(s), 952(s), 930(w), 911(w), 873(w), 861(w), 816(m), 800(m), 725(w), 649(w), 551(w), 525(m), 484(s), 446(w), 424(s). ^{1}H NMR (C_6D_6, 200 MHz, 25°C, ppm) δ: 8.42 (s, 4H, CH formamidine), 3.53 (hept, J = 6.6 Hz, 8H, CH isopropyl), 1.20 (d, J = 6.6 Hz, 48H, CH_3 isopropyl). Anal. calcd. (found) for $C_{28}H_{60}N_8Cr_2$: C 54.88(54.81), H 9.87(9.85), N 18.28(18.21).

X-ray crystallography

Data were collected at low T in in the range −157 to −160°C using the ω–2θ scan technique, to a maximum 2θ value of 50.0°, for suitable air-sensitive crystals mounted on glass fibers. Cell constants and orientation matrices were obtained from the least-squares refinement of 25 carefully centered high-angle reflections. The intensities of three representative reflections were measured after every 150 reflections to monitor crystal and instrument stability, showing no significant decay. Data were corrected for Lorentz and polarization effects but not for absorption. The structures were solved by either Patterson or direct methods (11). The non-hydrogen atoms were refined anisotropically. Hydrogen atom positions were located in the difference Fourier maps and refined isotropically in the case of favorable observation/parameter ratio. The final cycle of full-matrix least-squares refinement was based on the number of observed reflections with $I > 2.5\sigma(I)$. Neutral atomic scattering factors were taken from Cromer and Waber (17). Anomalous dispersion effects were included in F_{calc}. All calculations were performed using the TEXSAN software package on a Digital VAX station. Details on data collection and structure refinement are reported in Table 1. Selected bond distances and angles are given in Table 2.

Tables listing atomic positional parameters, temperature

Can. J. Chem. Downloaded from www.nrcresearchpress.com by 80.90.12.36 on 09/08/12
For personal use only.

Table 1. Crystal data and structural analysis results.

Complex	1	2	3	5*b*
Formula	$C_6H_{24}B_2N_2Cr$	$C_{28}H_{44}B_2N_4O_2Cr$	$C_{32}H_{76}N_8B_6Cr_3$	$C_{21}H_{49}N_6BCr_2$
Formula weight	197.88	534.23	793.85	500.46
Crystal system	Monoclinic	Monoclinic	Monoclinic	Monoclinic
Space group	*Cc*	$P2_1/n$	$P2_1/n$	*C*2/*c*
a(Å)	8.517(2)	12.021(1)	8.515(1)	17.000(1)
b(Å)	15.921(5)	15.555(1)	14.525(1)	9.033(1)
c(Å)	9.624	15.723(1)	18.286(2)	19.160(1)
β(deg)	115.59(1)	90.13(2)	91.38(1)	105.579(9)
V(Å^3)	1177.0(5)	2940.1(6)	2261.1(7)	2834.0(9)
Z	4	4	2	4
Radiation (MoKα Å)	0.71069	0.71069	0.71069	0.71069
T(°C)	−160	−143	−150	−30
D_{calcd} (g cm^{-3})	1.117	1.207	1.166	1.173
μ_{calcd} (cm^{-1})	9.02	4.07	7.21	7.65
R, R_w	0.022, 0.029	0.074, 0.086	0.051, 0.060	0.069, 0.078
G.o.F.	1.92	3.10	2.97	3.82

Table 2. Selected bond distances (Å) and angles (deg).

1	2	3	5
Cr1—N1 = 2.128(7)	Cr1—N1 = 2.104(9)	Cr1—N1 = 2.089(3)	Cr1—Cr1a = 1.844(2)
Cr1—N2 = 2.171(7)	Cr1—N2 = 2.128(9)	Cr1—H2 = 2.049(4)	Cr1—N2 = 2.018(5)
Cr1—B1 = 2.44(1)	Cr1—N3 = 2.12(1)	Cr1—H12 = 1.944	Cr1—N3 = 2.021(5)
Cr1—B2 = 2.42(1)	Cr1—N4 = 2.156(9)	Cr1—H32 = 3.20	Cr1—N4 = 2.012(5)
Cr1—H22 = 1.875	Cr1—H37 = 2.33	Cr2—N2 = 2.119(3)	Cr1—H13 = 1.95
Cr1—H21 = 2.081	Cr1—H41 = 1.94	Cr2—N3 = 2.227(3)	B1—H13 = 1.10
Cr1—H18 = 2.094		Cr2—N4 = 2.137(3)	
Cr1—H17 = 1.931		Cr2—H40 = 1.970	
		Cr2—H34 = 2.173	
		B3—H32 = 0.955	
		B3—H34 = 1.051	
N1-Cr1-N2 = 84.30(9)	N1-Cr1-N2 = 89.5(4)	N1-Cr1-N1a = 180.00	N2-Cr1-N3 = 163.5(2)
N1-Cr1-B1 = 94.03	N1-Cr1-N4 = 178.8(4)	H2-Cr1-H12 = 52.12	N2-Cr1-N4 = 94.5(2)
N1-Cr1-B2 = 169.23	N1-Cr1-H37 = 85.4	N1-Cr1-H32 = 99.51	N2-Cr1-H13 = 88.72
H21-Cr1-H22 = 55.18	N1-Cr1-H41 = 90.9	H32-B3-H34 = 115.37	H13-B1-H13 = 125.5
H17-Cr1-H18 = 54.94	H37-Cr1-H41 = 171.7	N2-Cr2-N4 = 172.8(1)	N2-Cr1-Cr1a = 95.7(2)
	Cr1-H37-B1 = 173.9	N2-Cr2-N3 = 92.0(1)	N2-C2-N3 = 121.1(6)
	Cr1-H41-B2 = 159.1	H40-Cr2-N3 = 139.89	C2-N2-C4 = 118.2(6)

factors, torsion angles, bond angles and distances, and hydrogen atom positional parameters associated with complexes **1**, **2**, **3**, and **5***b* have been deposited as supplementary material.[2]

[2] Copies of this material can be purchased from: The Depository of Unpublished Data, Document Delivery, CISTI, National Research Council Canada, Ottawa, Canada K1A 0S2.

Tables of atomic positional parameters, bond angles and distances, and hydrogen atom parameters have also been deposited with the Cambridge Crystallographic Data Centre, and can be obtained on request from The Director, Cambridge Crystallographic Data Centre, University Chemical Laboratory, 12 Union Road, Cambridge, CB2 1EZ, U.K.

Structure factor amplitudes are no longer being deposited and may be obtained directly from the author.

Results and discussion

The reaction of $CrCl_2(THF)_2$ with $NaBH_4$ in THF at room temperature and in the presence of an excess of TMEDA gave the divalent chromium tetrahydroborate complex $Cr(BH_4)_2$(TMEDA) (**1**) in good yield (Scheme 1). Although the reaction was rather straightforward, the purification was somewhat problematic due to the thermal instability of **1**, which prevented normal extraction techniques from being used for its separation from the excess of $NaBH_4$ and NaCl. Complete decomposition of the complex with formation of black tarry material was observed after refluxing for 1 h in THF. The magnetic moment of **1** (μ_{eff} = 4.87 μ_B at room temperature) was as expected for the d^4 electronic configuration of a Cr(II) ion, according to the formulation indicated by analytical data. The infrared spectrum showed the characteristic absorptions of

Scheme 1.

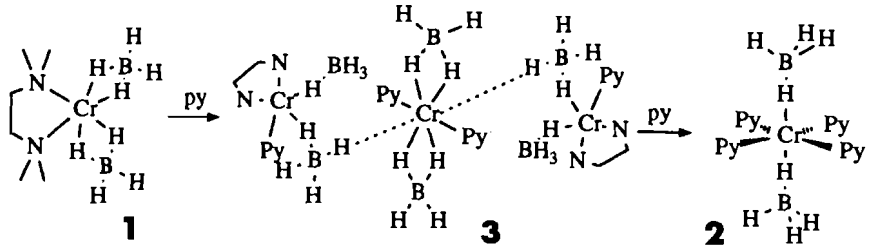

Fig. 1. ORTEP plot of **1**. Thermal ellipsoids are drawn at the 50% probability level.

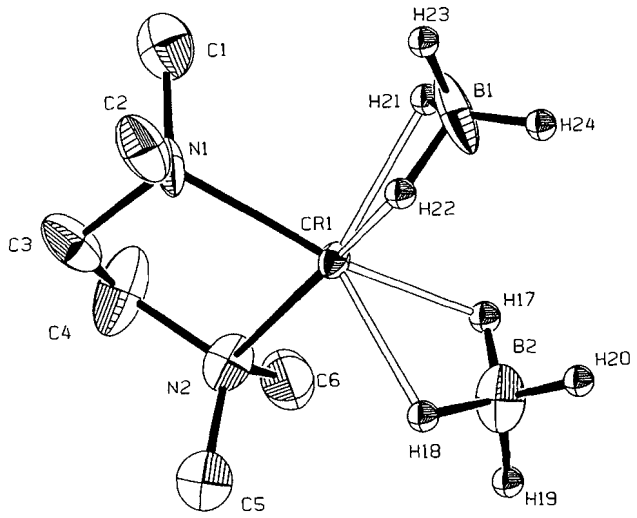

Fig. 2. ORTEP plot of **2**. Thermal ellipsoids are drawn at the 50% probability level.

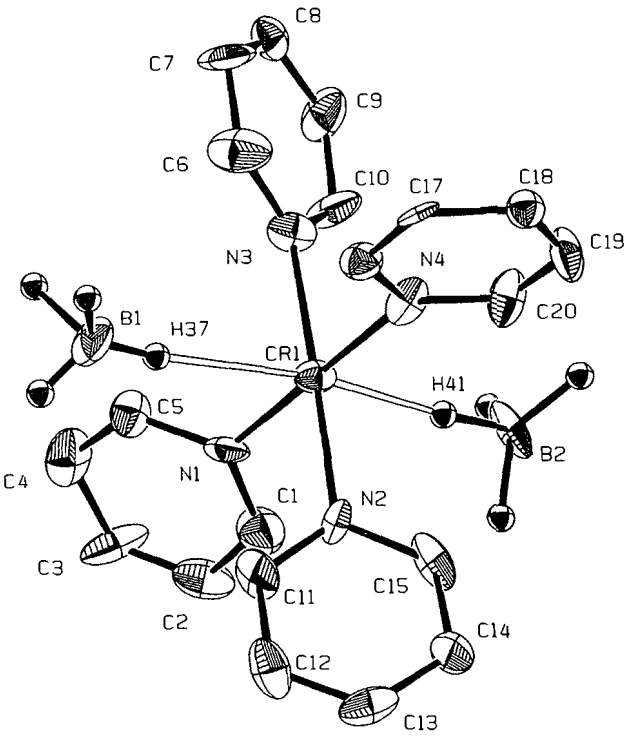

BH_4^- as two very intense and broad resonances at 2380 and 2120 cm^{-1} (terminal boron–hydrogen stretching) and a medium resonance at 2230 cm^{-1} (B–H stretching). These resonances, together with an intense band at 1120 cm^{-1} (BH_2 deformation), are diagnostic of a bidentate bonding mode of the BH_4 group (5). This conclusion is substantiated by the X-ray crystal structure.

Complex **1** is monomeric (Fig. 1) with the chromium atom adopting a distorted pseudo square-planar geometry. The molecular plane centered on chromium is defined by the two nitrogen atoms of TMEDA and the two boron atoms. The coordinated TMEDA shows rather normal bond distances and angles (Cr1—N1 = 2.128(7)Å, Cr—N2 = 2.171(7)Å). As a possible result of the bidentate bonding mode of the BH_4^- groups, the Cr—B distances (Cr1—B1 = 2.44(1)Å, Cr1—B2 = 2.42(1)Å) are rather short compared to those of other Ti and V brohydride complexes (1*d*, *e*, 6). The difference Fourier maps revealed the positions of all the hydrogen atoms. Each of the two BH_4^- tetrahedra points two of the four hydrogen atoms, located above and below the molecular plane, towards the Cr atom (Cr1—H22 = 1.87 Å, Cr1—H17 = 1.93 Å, Cr1—H21 = 2.08 Å, Cr1—H18 = 2.09 Å). The coordination geometry of the boron atom is that of a regular tetrahedron with normal B—H distances (from 0.995 to 1.198 Å) and H-B-H angles. No significant differences were observed between the B—H bond distances of bridging and terminal hydrogens.

Following a trend commonly observed in the chemistry of low-valent early transition metals, the coordinated TMEDA of complex **1** was easily replaced by pyridine, forming different products, depending on the amount of pyridine added. For example, the addition of 2 equivalents of pyridine to an intense blue solution of **1** afforded a light-green solution from which thermally robust brown-red crystals of $Cr(Py)_4(BH_4)_2$ (**2**) were obtained in good yield. While the formula was suggested by analytical results, the IR spectrum showed the resonances characteristic of a BH_4 group bonded in a monodentate fashion. The magnetic moment (μ_{eff} = 2.83 μ_B) was also as expected for a d^4 low-spin electronic configuration of Cr(II), possibly indicating an octahedral structure. Although complex **2** can be conveniently recrystallized from THF, the structure in solution is probably very different since the red crystals dissolved to yield deep-green paramagnetic solutions. Unfortunately, attempts to investigate the structure in solution by both NMR and EPR techniques were unsuccessful because the spectra were uninformative.

Complex **2** is monomeric with the chromium atom placed in the center of a regular octahedron defined by the four nitrogen atoms of the four pyridine molecules (Cr1—N1 = 2.104(9) Å, Cr1—N2 = 2.128(9) Å, Cr1—N3 = 2.12(1) Å, Cr1—N4 = 2.156(9) Å, N1-Cr1-N2 = 89.5(4)°, N1-Cr1-N4 = 180.00°) and two BH_4^- groups placed in *trans* positions with respect to each other (Fig. 2). The positions of the hydrogen atoms were

Can. J. Chem. Downloaded from www.nrcresearchpress.com by 80.90.12.36 on 09/08/12
For personal use only.

Fig. 3. ORTEP plot of **3**. Thermal ellipsoids are drawn at the 50% probability level.

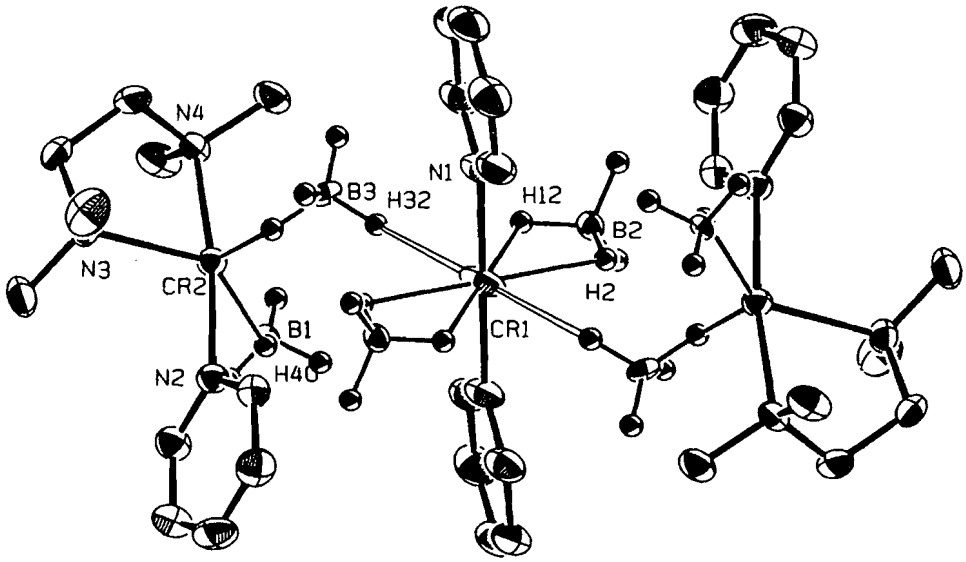

revealed by the difference Fourier maps. Although the data file was not of sufficient quality to refine the hydrogen atom positions, the H atoms were found at their expected positions, forming normal bond distances and angles. The bonding between chromium and the two hydroborate groups is realized through only one bridging hydrogen per each η^1-BH_4 group. The bridging hydrogen atom was found at a rather long distance from the chromium atom (Cr1—H37 = 2.33 Å, Cr1—H41 = 1.94 Å) but close to the boron atom (B1—H37 = 0.98 Å, B2—H41 = 1.16 Å), forming an almost linear Cr-H-B array (H37-Cr1-H41 = 171.7°). Therefore, the bonding of the BH_4^- groups may be considered somewhere between the ionic and the η^1-covalent. The two H atoms of the two BH_4^- groups used for bridging the metal atom are also aligned with the chromium atom, forming an axis perpendicular to the $Cr(Py)_4$ plane (Cr1-H37-B1 = 173.9°). The η^1-bonding mode of the BH_4^- groups is also substantiated by the much longer Cr—B distances (Cr1—B1 = 3.309(9) Å, Cr1—B2 = 3.253(9) Å) compared to complex **1**.

When the reaction of **1** was carried out with a smaller amount of pyridine, the red crystalline mass of **2** was found to be contaminated by a variable amount of bright green crystals of a new compound, **3**. Repeated attempts to make the reaction selective by modifying the amount of pyridine failed and therefore it was not possible to obtain **3** in analytically pure form. Nevertheless, addition of pyridine to the heterogeneous crystalline mass dissolved the green crystals and improved the yield of the red **2**, which could be then isolated in analytically pure form. This indicated that the green **3** might be just an intermediate during the formation of **2**. The green crystals of **3** were sufficiently large and of adequate quality to undertake an X-ray crystal structure determination.

The most interesting feature of the structure is that the unit cell contains two different types of fragments: two $Cr(BH_4)(Py)TMEDA$ units and a central $Cr(BH_4)_2Py_2$ unit that, differently from **2**, contains only two coordinated pyridine moieties rather than four (Fig. 3). The three fragments are loosely connected by bridging hydrogen interactions. The central $Cr(BH_4)_2Py_2$ unit can be regarded as *trans* square planar with the molecular plane bound by the nitrogen of the two pyridine and the two boron atoms (N1-Cr1-N1a = 180.00°, N1-Cr1-B2 = 90.2(1)°, N1-Cr1-B2a = 89.8(1)°, B2-Cr1-B2a = 180.00°). Even in this case it was possible to locate all the H atom positions, thus revealing the bonding of the BH_4^- groups. As indicated by the short Cr—B distances (Cr1—B2 = 2.426(5) Å), the two BH_4^- groups adopt the η^2-bonding mode. The coordination geometry of the Cr atom in the two identical lateral units is that of a distorted trigonal bipyramid with one nitrogen atom of pyridine and one nitrogen atom of TMEDA placed in the axial positions (N2-Cr2-N4 = 172.8(1)°, N2-Cr2-B1 = 87.4(1)°, N2-Cr2-N3 = 92.01(1)°, N3-Cr2-N4 = 82.6(1)°), and two BH_4^- groups and the second nitrogen atom of TMEDA defining the equatorial plane (N4-Cr2-B1 = 93.2(1)°, N4-Cr2-B3 = 92.8(1)°, N3-Cr2-B1 = 136.7(1)°, N3-Cr2-B3 = 106.6(1)°, B1-Cr-B3 = 116.7(1)°). The two BH_4^- groups are placed at remarkably different distances from the chromium atom (Cr2—B1 = 2.488(4) Å, Cr2—B3 = 2.716(4) Å) in spite of the fact that both are placed in two equivalent equatorial positions, as a result of two different monodentate bonding modes. While the first BH_4^- forms a significantly bent Cr-H-B vector (Cr2-H4-B1 = 110.3°), the second BH_4 forms an almost linear array (Cr2-H34-B3 = 178.1°). In addition, one of the hydrogens of the second BH_4^- group points toward the chromium atom of $Py_2Cr(BH_4)_2$, forming a short nonbonding contact (Cr1—H32 = 3.20 Å). Obviously, it is impossible to decide whether these contacts are artifacts of the crystal packing or are weak hydrogen bonds. In any case, it is unlikely that these contacts are able to preserve the trimeric aggregation in solution. The Cr—N distances (Cr—N1 = 2.098(3) Å, Cr2—N2 = 2.119(3) Å, Cr—N3 = 2.227(3) Å, Cr—N4 = 2.137(3) Å) are comparable to those of the other two complexes reported in this work.

The ability of nitrogen donor ligands such as TMEDA and pyridine to stabilize a monomeric "$Cr(BH_4)_2$" moiety is rather remarkable in view of the fact that "$Cr(BH_4)_2THF_2$" exists only below −20°C and rapidly decomposes at room temperature (11). Complexes **1** and **2**, in addition to possessing significantly different geometries from those of the phosphine derivative $Cr(BH_4)H(dmpe)_2$ (18), are chemically rather inert and do not react with a number of substrates such as CO

Can. J. Chem. Downloaded from www.nrcresearchpress.com by 80.90.12.36 on 09/08/12
For personal use only.

Can. J. Chem. Downloaded from www.nrcresearchpress.com by 80.90.12.36 on 09/08/12
For personal use only.

Scheme 2.

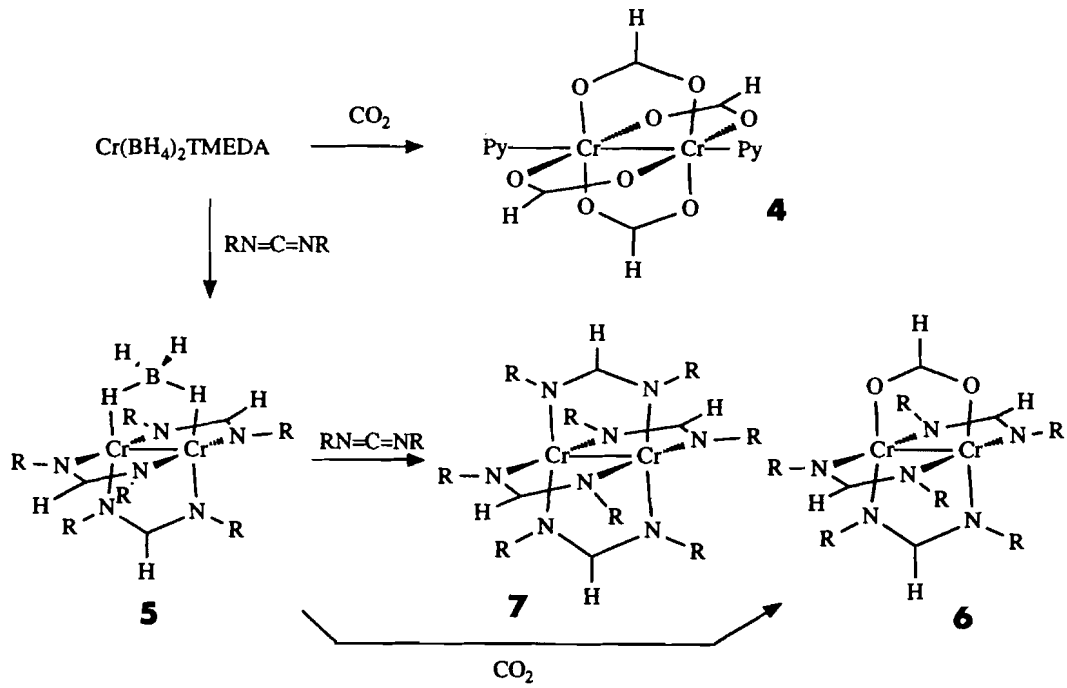

(1 atm, room temperature), $H_2C{=}CH_2$ (1 atm, room temperature), ^{t}BuCCH, or $Me_3SiN{=}C{=}NSiMe_3$. However, complex **1** readily reacted with CO_2 in the presence of pyridine at room temperature to form the paramagnetic $Cr_2(CO_2H)_4Py_2$ (**4**) for which a crystal structure was previously reported (19). It also reacted with other cumulenes such as RN=C=NR (R = Cy, iPr), forming a series of diamagnetic chromium dimers $[RNC(H)NR]_3Cr_2(\mu\text{-}BH_4)$ (**5**) and $[RNC(H)NR]_4Cr_2$ (**7**), depending on the stoichiometry employed (Scheme 2). Reaction of **1** with 3 equivalents of 1,3-dicyclohexylcarbodiimide in THF at room temperature yielded a mixture of $[CyNC(H)NCy]_3Cr_2(\mu\text{-}BH)_4$ (**5***a*) and $(BH_3)_2$TMEDA. The separation of the two components was somewhat problematic due to their rather similar solubility properties. However, it was possible to obtain analytically pure samples, albeit in very poor yield, after several recrystallizations from THF. A very similar behavior was observed with 1,3-diisopropylcarbodiimide. However, in this case not only was the purification of the corresponding $Cr_2[iPr)NC(H)N(iPr)]_3(BH_4)$ (**4***b*) more easily achieved through standard extraction techniques, but also the crystallinity was sufficient to allow an X-ray crystal structure determination.

The structure of the complex showed the typical dimeric arrangement (lantern-type) observed in many other formamidine complexes of several transition metals (20) (Fig. 4). The molecule consists of a Cr_2 unit bridged by three formamidinate groups and one borohydride group, with one pair of *trans*-positioned ligands defining a plane perpendicular to the plane bound by the third formamidine, the Cr_2 unit, and the BH_4^- moiety. Each formamidinate ligand adopts the characteristic three-center chelating geometry where each of the two donor atoms of one ligand molecule binds one of the two metal centers, forming a five-membered ring with the Cr_2 unit. The borohydride also adopts the three-center chelating geometry where boron is connected to each of the two chromium atoms via bridging hydrogens. The coordination geometry of the two

Fig. 4. ORTEP plot of **5***b*. Thermal ellipsoids are drawn at the 50% probability level.

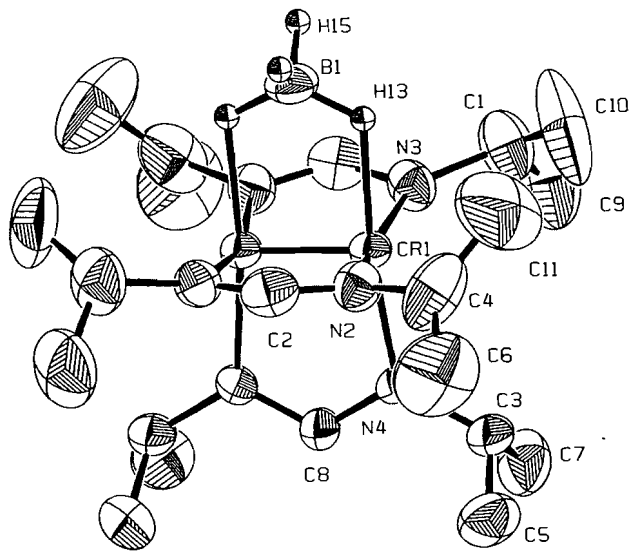

chromium atoms is distorted square planar (N2-Cr1-N3 = 163.5(2)°, N2-Cr1-N4 = 94.5(2)°, N3-Cr1-N4 = 95.1(2)°) with the chromium atoms slightly elevated above the plane defined by the three nitrogen atoms and a hydrogen atom of the $\mu\text{-}BH_4^-$ group (Cr1-Cr1-N angles ranging from 95.7(2)° to 96.5(2)°). The Cr—Cr distance (Cr1—Cr1 = 1.844(2) Å) is among the shortest formed in this type of complex and places **5***b* in the family of the supershort quadruply bonded dichromium species (21). The Cr—N bonding distances are normal (Cr1—N2 = 2.018(5) Å, Cr1—N3 = 2.021(5) Å, Cr1—N4 = 2.012(5) Å) and compare well with those of other monomeric and dimeric Cr(II) complexes reported in this work. The angles subtended at the formamidinic carbon by the nitrogen

Can. J. Chem. Downloaded from www.nrcresearchpress.com by 80.90.12.36 on 09/08/12
For personal use only.

donor atoms (N4-C8-N4 = 121.3(8)°, N2-C2-N3 = 121.1(6)°) are similar to those of the dimeric compound $Cr_2(CyNCHNCy)_4$. The structural features of **1**, **2**, **3**, and **5** compare well with those of other η-BH_4 complexes of different transition metals described in the literature (22).

Both **5***a* and **5***b* are diamagnetic at room temperature and showed well-resolved ^1H NMR spectra. The two resonances expected for the two unequivalent formamidine groups (*cis* and *trans* with respect to the BH_4^- group) were observed at the expected positions. The resonance of the BH_4^- group appeared as a broad multiplet centered at 1.32 ppm in the case of **5***b*, while in the case of **5***a* the resonance was hidden by the resonances of the cyclohexyl groups. Magnetic measurements carried out with a Gouy balance at room temperature were also consistent with the diamagnetism inferred by the NMR data. In fact, no significant variation of chemical shift was observed when NMR spectra in d^8-toluene were recorded at −80°C, thus indicating that these compounds do not possess a significant magnetic anisotropy. This is in contrast to the case of $[(tol)NC(H)N(tol)]_4Cr_2$ (23), which has a comparable Cr—Cr distance. Nevertheless, spectra carried out at variable temperatures above 25°C showed that the two C-H formamidinic signals coalesce, while a very significant signal broadening was observed for all the resonances. Since the coalescence can be reversed by lowering the temperature, so far we are unsure whether this phenomenon is generated by conformational motions or by dissociation equilibria to yield monomeric and paramagnetic units. On the other hand, supershort quadruple bonds are well known to be paradoxically weak in dichromium species (20), unlikely to be able to maintain a dinuclear structure in the absence of bridging interactions and to spontaneously dissociate (24). Therefore, we believe that dissociation equilibria are more likely to be responsible for this behavior in solution. The by-product $(BH_3)_2TMEDA$ was often isolated in variable amounts and characterized by an X-ray crystal structure (20). Its formation suggests that more than one process occurred simultaneously during the insertion reactions.

Further reaction of **5** with CO_2, carried out in deuterated benzene solution, showed during an NMR-tube experiment that the intensities of the original peaks were slowly diminished to yield a new spectrum that accounts very well for a $[(iPr)NC(H)N(iPr)]_3Cr_2(O_2CH)$ (**6**) formulation. The reaction was rather slow at 25°C and it was 48 h before the resonances of the unreacted starting material disappeared from the NMR spectrum. Similarly, reaction of **5** with excess carbodiimide gave the corresponding diamagnetic $[RNC(H)NR]_4Cr_2$ (**7**) dimers.

Acknowledgment

This work was supported by the Natural Sciences and Engineering Research Council of Canada (research and strategic grants).

References

1. (*a*) M.D. Fryzuk, S.J. Rettig, A. Westerhaus, and H.D. Williams. Inorg. Chem. **24**, 4316 (1985); (*b*) M.L. Luetkens, J.C. Huffman, and A.P. Sattelberger. J. Am. Chem. Soc. **107**, 3361 (1985); (*c*) E.E.H. Otto and H.H. Brintzinger. J. Organomet. Chem. **148**, 29 (1978); (*d*) J.E. Gozum and G.S. Girolami. J. Am. Chem. Soc. **113**, 3824 (1991); (*e*) J.E. Gozum, S.R. Wilson, and G.S. Girolami. J. Am. Chem. Soc. **114**, 9483 (1992); (*f*) C.A. Ghilardi, C. Midollini, and A. Orlandini. Inorg. Chem. **21**, 4096 (1982); (*g*) F. Tagusagawa, A. Fumagalli, T.F. Koetzle, S.G. Shore, T. Schmitkons, A.V. Fratini, K.W. Morse, C.-Y. Wei, and R. Bau. J. Am. Chem. Soc. **103**, 5165 (1981).
2. J.A. Jensen, S.R. Wilson, A.J. Schultz, and G.S. Girolami. J. Am. Chem. Soc. **109**, 8094 (1987).
3. (*a*) A.L.J. Raum and D.A. Fraser. British Patent 801 401 (1958); (*b*) D. Apotheker, A.L. Barney, and N. Brodway. U.S. Patent 3 597 367 (1971); (*c*) C.N. Zellner and A. Buerger. German Patent 1 070 148 (1959); (*d*) S.B. Mirviss, H.W Dougherty, and R.W. Looney. U.S. Patent 3 310 547 (1967), (*e*) M. Nakajima, H. Moriyama, A. Kobayashi, T. Saito, and Y. Sasaki. J. Chem. Soc. Chem. Commun. 80 (1975); (*f*) F. McQuillen, P. Abbey, and I. Jardine. J. Chem. Soc. C, 840 (1971); (*g*) R.G. Miller, P.A. Pinke, R.D. Stauffer, H.J. Golden, and D.J. Baker. J. Am. Chem. Soc. **96**, 4211 (1974).
4. W.K.T. Gleim. U.S. Patent 3 796 671 (1972).
5. T.J. Marks and J.R. Kolb. Chem. Rev. **77**, 263 (1977).
6. (*a*) G.E. Toogood and M.G.H. Wallbridge. Adv. Inorg. Chem. Radiochem. **25**, 267 (1982); (*b*) J.A. Jensen and G.S. Girolami. Inorg. Chem. **28**, 2114 (1989).
7. A.R. Barron, J.E. Scott, G. Wilkinson, M. Motevalli, and M.B. Hursthouse. Polyhedron, **5**, 1833 (1986).
8. (*a*) J.P. Collman, L.S. Hegedus, J.R. Norton, and R.G. Finke. Principles and applications of organotransition metal chemistry. University Science, Mill Valley, Calif. 1987; (*b*) G.W. Parshall. Homogeneous catalysis. Wiley, New York. 1979; (*c*) C. Masters. Homogeneous transition-metal catalysis. Chapman and Hall, New York. 1981; (*d*) R.G. Pearson. Chem. Rev. **85**, 41 (1985); (*e*) D.S. Moore and S.D. Robinson. Chem. Soc. Rev. **12**, 415 (1983); (*f*) G. Hlatky and R.H. Crabtree. Coord. Chem. Rev. **65**, 1 (1985).
9. M.L.H. Green and H. Munakata. J. Chem. Soc. A, 269 (1974).
10. J.D. Koola and H.H. Brintzinger. J. Chem. Soc. Chem. Commun. 388 (1976).
11. H. Nöth and M. Seitz. J. Chem. Soc. Chem. Commun. 1004 (1976).
12. (*a*) F.A. Van-Cattledge, S.D. Ittel, and J.P. Jesson. Organometallics, **4**, 18 (1985); (*b*) G.S. Girolami, J.E. Salt, G. Wilkinson, M. Thornton-Pett, and M.B. Hursthouse. J. Am. Chem. Soc. **105**, 5954 (1983); (*c*) R.A. Heintz, B.S. Haggerty, H. Wan, A.L. Rheingold, and K.H. Theopold. Angew. Chem. Int. Ed. Engl. **31**, 1079 (1992).
13. J.J.H. Edema and S. Gambarotta. Commun. Inorg. Chem. **9**, 195 (1991), and refs. cited therein.
14. F.H. Kohler and W.Z. Prossdorf. Z. Naturforsch. B: Anorg. Chem. Org. Chem. **32B**, 1026 (1977).
15. M.B. Mabbs and D.J. Machin. Magnetism and transition metal complexes. Chapman and Hall, London. 1973.
16. G. Foese, C.J. Gorter, and L.J. Smits. Constantes selectionnées diamagnetisme, paramagnetisme, relaxation paramagnetique. Masson, Paris. 1957.
17. D.T. Cromer and J.T. Waber. International Tables for X-ray crystallography. The Kynoch Press, Birmingham, England. 1974.
18. J.A. Jensen, S.R. Wilson, and G.S. Girolami. J. Am. Chem. Soc. **110**, 4977 (1988).
19. F.A. Cotton, M.W. Extine, and G.W. Rice. Inorg. Chem. **17**, 176 (1978).
20. S. Hao, S. Gambarotta, C. Bensimon, and J.J.H. Edema. Inorg. Chim. Acta, **213**, 65 (1993).
21. F.A. Cotton and R.A. Walton. Metal–metal multiple bonds in dinuclear clusters, Struct. Bonding (Berlin), **62**, 1 (1985).
22. (*a*) D.H. Holah, A.N. Hughes, B.C. Hui, and C.T. Khan. Can. J. Chem. **56**, 2552 (1978); (*b*) D.G. Hola, A.N. Hughes, S. Maciaszek, and V.R. Magnuson. J. Chem. Soc. Chem. Com-

mun. 1308, (1983); (*c*) B.E. Green, C.H.L. Kennard, G. Smith, B.D. James, P.C. Healy, and A.H. White. Inorg. Chim. Acta, **81**, 147 (1984); (*d*) T.M. Gilbert, F.J. Hollander, and R.G. Bergman. J. Am. Chem. Soc. **107**, 3508 (1985), (*e*) L.R. Rhodes, L.M. Venanzi, C. Sorato, and A. Albinati. Inorg. Chem. **25**, 3335 (1986); (*f*) J.C. Vites, C. Eigenbrot, and T.P. Fehlner. J. Am. Chem. Soc. **106**, 4633 (1984).

23. F.A. Cotton, H. Chen, L.M. Daniels, and X. Feng. J. Am. Chem. Soc. **114**, 8980 (1992).
24. S. Hao, J.J.H. Edema, S. Gambarotta, and C. Bensimon. Inorg. Chem. **31**, 2676 (1992).

Can. J. Chem. Downloaded from www.nrcresearchpress.com by 80.90.12.36 on 09/08/12
For personal use only.

Activated cycloheptenone dienophiles. A versatile approach to 6,7-fused ring targets[1]

Hsing-Jang Liu, Wen-Lung Yeh, and Eric N.C. Browne

Abstract: Several 2-carbalkoxy-2-cyclohepten-1-ones were prepared and their Diels–Alder characteristics examined in order to develop a facile general approach to the synthesis of cycloheptane ring-containing polycyclic natural products. Substitution pattern on the seven-membered ring was found to greatly affect the Diels–Alder behavior. In addition, some extraordinary facial stereoselectivity was observed.

Key words: Diels–Alder reaction, 2-carbalkoxy-2-cyclohepten-1-ones, 6,7-fused ring system.

Résumé : On a préparé plusieurs 2-carbalcoxycyclohept-2-én-1-ones et, dans le but de développer une approche générale facile à la synthèse de produits naturels polycycliques contenant du cycloheptane, on a examiné leur comportement dans les réactions de Diels–Alder. On a trouvé que le patron de substitution sur le cycle à sept chaînons influence grandement le comportement de Diels–Alder. De plus, on a observé de la stéréosélectivité faciale extraordinaire.

Mots clés : réaction Diels–Alder, 2-carbalcoxycyclohept-2-én-1-ones, système de cycles amalgamés en 6,7.

[Traduit par la rédaction]

Introduction

The rapidly increasing number of natural products possessing a 6,7-fused ring system[4] make attractive synthetic targets because of their structural complexity and interesting biological activity. Few successful synthetic approaches have been directed toward these compounds because general synthetic tools for preparation of systems bearing a seven-membered ring are limited in the literature. One approach that has proven to be useful is homologation by carbocyclic ring expansion. Several methods are available[5] and some are particularly effective for making cycloheptanones with incorporation of specific functionalities. However, the ring expansion approach often suffers from needing multiple steps to accomplish the simple homologation. Of the examples given, the diazoacetate method (2*h*) is particularly useful because it completes the conversion in a single step and in generally high yield.

Over the last two decades, extensive efforts have been directed toward improving the Diels–Alder reactivity of cycloalkenones, resulting in development of two general schemes for enhancement of dienophilicity (3). One approach applies Lewis acid catalysis to increase the rate, as well as the regio- and stereoselectivity of the addition. In the other approach, the rates and yields are improved by placing an additional electron-withdrawing group on either the α- or β-carbon of the dienophilic moiety, as predicted by the Alder rule (4). We have reported on an extensive study of Lewis acid catalyzed Diels–Alder reactions of 2-carbalkoxy-activated cycloalkenones (5). As an example of the two activation approaches mentioned above, the closely related 4,4-dimethyl-2-cyclohexenone is a rather poor dienophile and our preliminary study on its Diels–Alder reaction with isoprene and 1,3-butadiene using boron trifluoride etherate or aluminum chloride as a catalyst was unsuccessful (5*c*). Wenkert and co-workers (6) made this reaction synthetically useful by adding the diene to the solution only after allowing complexation between the dienophile and aluminum chloride. We use an α-carbalkoxy-activated system and discovered that the cycloaddition proceeded smoothly with isoprene in the presence of Lewis acid (5*d*).

In continuation of our research in this field and to find a better synthetic approach to 6,7-fused ring polycyclic natural products, we were interested in the Diels–Alder reaction of various 2-carbalkoxy-2-cycloheptenones. In spite of the apparent utility of the approach suggested by the superior Diels–Alder reactivity of simple cycloheptenone, compared to cyclohexenone and cyclopentenone, there are only three examples of Diels–Alder reactions involving cycloheptenones in the literature (Scheme 1) (6, 7). A study of activated derivatives could provide important and exciting new results, which would significantly broaden the usefulness of the approach. We have undertaken a systematic study of the

Received July 27, 1994.

This paper is dedicated to Professor William A.G. Graham on the occasion of his 65th birthday.

H. J. Liu,[2] W.-L. Yeh, and E.N.C. Browne.[3] Department of Chemistry, The University of Alberta, Edmonton, AB T6G 2G2, Canada.

[1] This report is taken in part from the Ph.D. thesis of W.-L. Yeh, The University of Alberta, 1994.

[2] Author to whom correspondence may be addressed. Telephone: (403) 492-3477. Fax: (403) 492-8231.

[3] Present address: Wyeth-Ayerst Research Inc., 1025 Laurentian Blvd., St. Laurent, QC H4R 1J6, Canada.

[4] For selected examples see refs. 1*a–f*.

[5] For selected examples see refs. 2*a–h*.

Can. J. Chem. Downloaded from www.nrcresearchpress.com by 80.90.12.36 on 09/08/12
For personal use only.

Can. J. Chem. Downloaded from www.nrcresearchpress.com by 80.90.12.36 on 09/08/12
For personal use only.

Scheme 1.

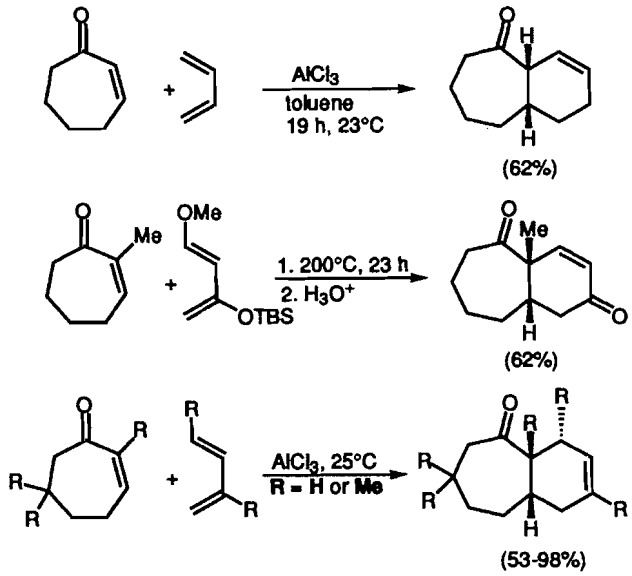

Diels–Alder chracteristics of several 2-carbalkoxy-2-cycloheptenones and preliminary results are described in this report.

Results and discussion

A general two-step approach was used for preparation of various 2-carbalkoxy-2-cycloheptenones. Ring expansion of cyclohexanones with ethyl diazoacetate (2*h*) allowed direct incorporation of the desired β-keto ester system with a high degree of regioselectivity. Phenylselenenylation followed by oxidative elimination was used for insertion of the conjugated double bond (8). The results of these preparations are summarized in Table 1. Bicyclo[2.2.2]octan-2-one **18** (9) was synthesized from 1,3-cyclohexadiene and methyl vinyl ketone via the following operations as shown in Scheme 2: (*i*) Diels–Alder addition, (*ii*) catalytic hydrogenation, (*iii*) Baeyer–Villiger oxidation, (*iv*) hydrolysis, and (*v*) oxidation.

These activated dienophiles are more stable than their six-membered ring analogues and can be purified by flash chromatography without apparent decomposition. Although some enolization was observed by ^{1}H NMR, no polymerization was detected. For example, 2-carbethoxy-2-cycloheptenone (**3**) could be easily purified by flash chromatography, in sharp contrast to 2-carbomethoxy-2-cyclohexenone, which was found to decompose rapidly (5*g*). A variety of temperatures and Lewis acids were explored for the Diels–Alder reaction of enone **3** and isoprene to find the most suitable initial conditions. The results are summarized in Table 2. The experimental procedure for zinc chloride catalyzed reactions was slightly different from those using ferric chloride, boron trifluoride etherate, and tin(IV) chloride. The zinc chloride used in the Diels–Alder reactions was dried carefully by a flame before being dissolved in ether. To the resulting zinc chloride solution was then added an ether solution of the dienophile. After stirring for half an hour, allowing the complex formation, a diene was then added. The procedure for the Diels–Alder reactions catalyzed by the other Lewis acids was straightforward. The Lewis acid was simply added to a solution of dienophile and diene. Zinc chloride required a longer reaction time but gave the best yield of adduct **22**, the regiochemistry of which (from

Scheme 2.

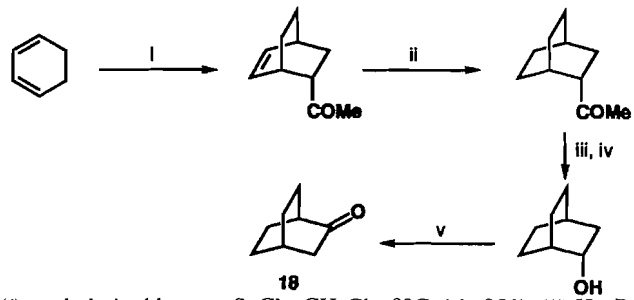

(*i*) methyl vinyl ketone, $SnCl_4$, CH_2Cl_2, 0°C, 1 h, 85%; (*ii*) H_2, Pd/C, EtOAc, 20°C, 5 h, 97%; (*iii*) MCPBA, Na_2HPO_4, CH_2Cl_2, 20°C, 25 h; (*iv*) 1 N NaOH, MeOH, 20°C, 4.5 h, 100% (two steps); (*v*) PCC–Al_2O_3, CH_2Cl_2, 20°C, 2 h, 76%.

Fig. 1.

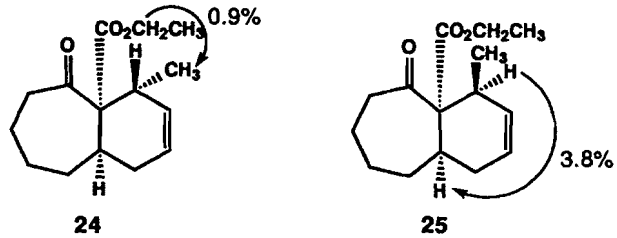

the *para*-rule) was confirmed by the ^{1}H decoupling experiments. Irradiation of the vinylic signal at δ 5.34 resulted in change on the broad doublet at δ 2.33 and the quartet of doublets of doublets at δ 2.65 due to the C-11 methylene protons. Conversely, irradiation of the doublet at δ 2.33 resulted in the change of the vinylic signal. Due to the superiority of zinc chloride in this series, it was used as the catalyst in further investigations of the other cycloheptenone dienophiles.

The results obtained for the zinc chloride catalyzed Diels–Alder reactions of enone **3** with isoprene and other dienes are summarized in Table 3. When one equivalent of zinc chloride catalyst was used, the cycloadditions with 2,3-dimethyl-1,3-butadiene and *trans*-piperylene proceeded faster than with isoprene. However, the rates were generally slower than the rates of similar reactions with six-membered ring analogues. The yields were moderate. The amount of zinc chloride was increased from one equivalent to two equivalents in an attempt to accelerate the reaction, but the results were generally less satisfactory.

The Diels–Alder reaction of enone **3** and *trans*-piperylene catalyzed by zinc chloride did not show any stereoselectivity. A separable 1:1 mixture of ester-*endo* adduct **24** and keto-*endo* adduct **25** was produced in 62% combined yield. The ratio was not changed by employing two equivalents of zinc chloride. The stereochemistry of the epimeric adducts **24** and **25** was deduced on the basis of the results of the NOE experiments summarized in Fig. 1.

Zinc chloride catalyzed Diels–Alder reactions of enone **6** proceeded much less efficiently than those of enone **3**. As shown in Table 4, the required reaction times were doubled or tripled, and the yields were moderate to poor. This could be due to steric hindrance of the germinal dimethyl group, interrupting the access of the diene. Ferric chloride, stannic chloride, and aluminum chloride were also examined as catalysts

Table 1. Preparations of cycloheptanones and 2-cycloheptenones.

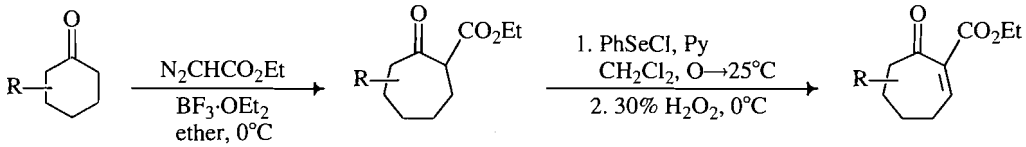

Entry	Starting material	Intermediate product	Time Yield (Keto:Enol)	Dehydrogenation product	Time Yield (Keto:Enol)
1	**1**	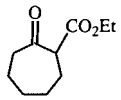 **2**	1 h 74% (3:1)	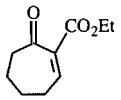 **3**	14.5 h 73% (100:0)
2	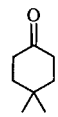 **4**	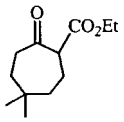 **5**	1 h 86% (95:5)	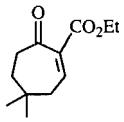 **6**	17 h 90% (90:10)
3	**7**	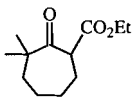 **8**	96 h 87% (100:0)	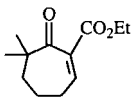 **9**	163 h 15%[a] (100:0)
4	**10**	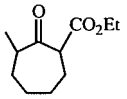 **11**	23 h 84%[b] (100:0)	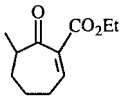 **13**	89 h 71% (2:1)
		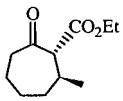 **12**	9% (100:0)	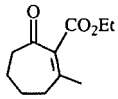 **14**	3% (100:0)
5	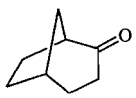 **15**	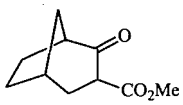 **16**[c]	2.5 h 95% (2:5)	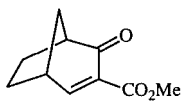 **17**	25 h 31%
6	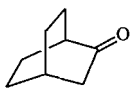 **18**	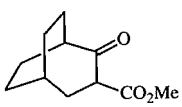 **19**	2 h 67% (5.6)	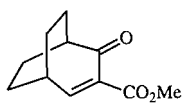 **21**	13 h 70%
		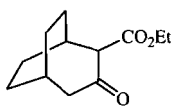 **20**	25% (1:1)	—	—

[a]About 61% of starting keto ester **8** was recovered.

[b]Compounds **11** and **12** were obtained as an inseparable mixture. Compound **11** was a mixture (7:2) of stereoisomers.

[c]Keto ester **16** was obtained by carbomethoxylation of commercial **15** with dimethyl carbonate and sodium hydride in refluxing tetrahydrofuran following the general method used in refs. 5*b* and 5*i*.

Can. J. Chem. Downloaded from www.nrcresearchpress.com by 80.90.12.36 on 09/08/12
For personal use only.

Can. J. Chem. Downloaded from www.nrcresearchpress.com by 80.90.12.36 on 09/08/12
For personal use only.

Table 2. Lewis acid catalyzed Diels–Alder reaction of enone **3** and isoprene.

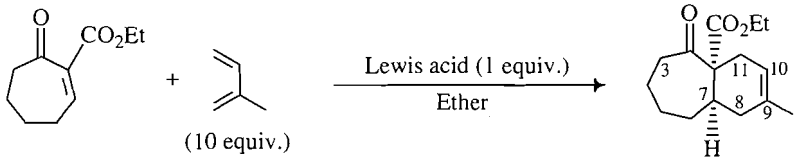

3 **22**

Lewis acid	Temp. (°C)	Time (h)	Yield (%)
$ZnCl_2$	20	73	70
$FeCl_3$	0	1	47
$FeCl_3$	–40	1	47
$FeCl_3$	–78	78	54
$BF_3{\cdot}OEt_2$	20	15	23
$SnCl_4$	0	1	6

Table 3. Zinc chloride catalyzed Diels–Alder reaction of enone **3**.

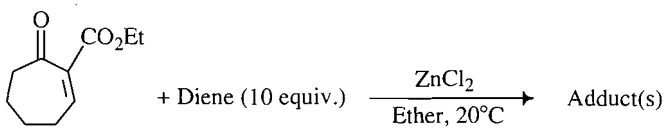

3

Diene	$ZnCl_2$ (equiv.)	Time (h)	Product(s)	Yield (%)
	1	73	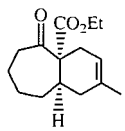	70
	2	47		53
			22	
	1	22	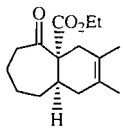	69
	2	23		43
			23	
	1	44	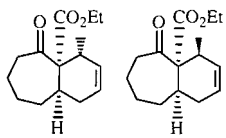	62 (1:1)
	2	42		63 (1:1.1)
			24 **25**	

Table 4. Zinc chloride catalyzed Diels–Alder reaction of enone **6**.

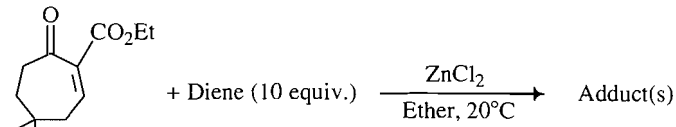

6

Diene	$ZnCl_2$ (equiv.)	Time (h)	Product(s)	Yield (%)
	1	260	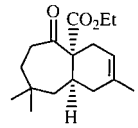	28
	2	68		43
	3	43		39
			26	
	1	69	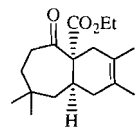	52
	2	46		61
			27	
	1	148	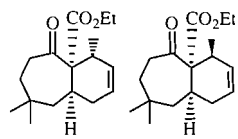	30 (10:1)
	2	94		42 (7:5)
			28 **29**	

in the cycloaddition of **6** with isoprene in an attempt to improve the efficiency of the cycloaddition. However, in every case extensive decomposition was observed.

When one equivalent of zinc chloride was used, the reaction of **6** with isoprene took more than 10 days to give only 28% yield of adduct **26**. By increasing the amount of zinc chloride to two equivalents, the reaction rate was greatly accelerated. Only 68 h were required to give an improved yield of 43%. We attempted to further improve the reaction using three equivalents of zinc chloride. The reaction time was reduced to 43 h but the yield was slightly worse. The regiochemical assignment of the adduct follows from the evidence provided by the ^1H decoupling experiment. Upon irradiation of the broad vinylic singlet at δ 5.33, the pair of broad doublets at δ2.91 and 2.14 due to the protons at C-11 sharpened while the signals for the C-8 protons remained intact.

Better results were obtained for 2,3-dimethyl-1,3-butadiene. When one equivalent of zinc chloride was used, the cycloaddition was complete in 69 h to give cycloadduct **27**, with a melting point of 62–63°C, in 52% yield. When two equivalents of zinc chloride were used, the reaction was complete in 46 h and the yield was improved to 61%. In the cycloaddition of *trans*-piperylene to enone **6**, good stereoselectivity was observed using one equivalent of zinc chloride. A 10:1 mixture of stereoisomers **28** and **29** was produced in 30% yield. The less favored keto-*endo* transition state could be caused by the steric effect of the geminal dimethyl group at C-5. By increasing the amount of zinc chloride to two equivalents, the reaction time was shortened to 94 h and the yield was improved to 42%, but stereoselectivity was sacrificed. Figure 2 depicts the results obtained from the NOE experi-

Can. J. Chem. Downloaded from www.nrcresearchpress.com by 80.90.12.36 on 09/08/12
For personal use only.

Fig. 2.

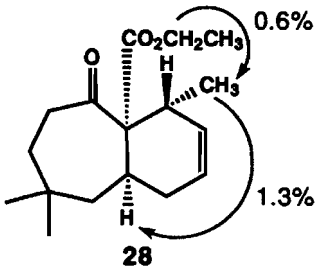

ments carried out on the major isomer **28**. Accordingly, its stereochemistry was determined. The minor isomer **29** could not be isolated in pure form, and its stereochemistry was assigned by inference.

From the cycloadditions of cycloheptenones **3** and **6**, we concluded that two equivalents of zinc chloride typically provided the best results with regard to reaction time and yield. Subsequent reactions with other activated cycloheptenones were carried out using two equivalents of zinc chloride.

Somewhat expectedly, enone **9** was resistant to any Diels–Alder reaction with *trans*-piperylene under zinc chloride catalysis, possibly due to the serious steric hindrance caused by the geminal dimethyl group at C-7. When ferric chloride was used as a catalyst, extensive decomposition occurred.

In the Diels–Alder reactions of enone **13**, some interesting and unexpected phenomena emerged. As shown in Table 5, all the reactions were completed in 1 day and the yields were extraordinarily high. Surprisingly, a high degree of face-selectivity was displayed with preferential addition of the diene from the sterically more hindered methyl side.[6] It appears that the methyl group plays a key role in directing the addition of the diene. The exact cause of this unusual stereoselectivity remains to be determined. Zinc chloride catalyzed Diels–Alder cycloaddition of *trans*-piperylene to enone **13** generated a 1:2 mixture of enones **32** and **33** in a combined yield of 85%. The unusual selectivity favoring keto-*endo* product **33**, in contrast with the previous reactions, and its relation to the inscrutable effect of the C-3 methyl group is unexplained at this time. The stereochemical assignments of adducts **30–33**[7] were again facilitated by the NOE experiments. The results are depicted in Fig. 3.[8]

Fig. 3.

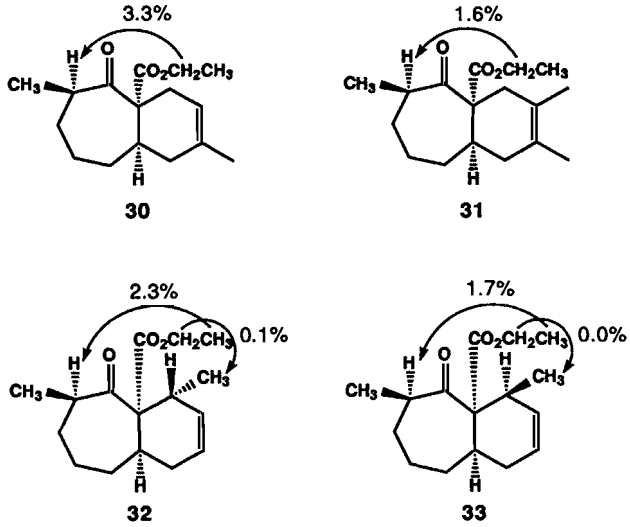

In the additions to **17** complete facial selectivity favoring the addition of the diene from the ethano bridge side, as evident from the NOE experiments on adducts **34–36**[9,10] (Fig. 4), was observed in every case as shown in Table 6. This high selectivity cannot be explained by the steric effect alone. Kobuke and co-workers reported a similar facial stereoselectivity (10). In the Diels–Alder reaction of isodicyclopentadiene and methyl propiolate, the addition occurs completely from the ethano bridge side of isodicyclopentadiene. Two possible explanations are offered. One is a greater steric attraction than steric repulsion by the ethano bridge that stabilizes the *syn* transition state. The other is based on a stereoelectronic effect resulting from a mixing of the unstable σ orbitals of the norbornane skeleton and the π orbitals. This mixing would bias the charge density of the π orbital in space above and below the cyclopentadiene plane and therefore favor the *syn* orientation of an attacking dienophile. However, Gleiter and Paquette (11) later stressed that the σ/π interaction must be carefully evaluated in any rationalization of Diels–Alder stereoselectivity and implies a combined effect with other influences such as van der Waals forces (the first explanation above), induced dipole–dipole interactions, and steric effects. None of these explanations can completely account for the stereoselectivity observed in our case.

Another feature of the reactions of enone **17** is that they proceeded to completion with the shortest reaction time of all the additions examined. The yields were fairly good.

Compared to the facile reactions of **17**, the Diels–Alder reactions of enone **21** were rather sluggish. When the cycloaddition of *trans*-piperylene to enone **21** was performed as usual, using zinc chloride as a catalyst, **21** was still present in large

[6] The possibility that epimerization of the methyl substituent at C-3 in adducts of **13** has occurred is considered highly unlikely. No trace of another product identifiable as a possible C-3 epimer was observed. Examination of Dreiding molecular models indicates that neither of such a pair of epimers should predominate exclusively in an equilibrated mixture and we logically infer that since complete epimerization is not possible and partial epimerization is not detected then no epimerization occurs at C-3 under the applied conditions.

[7] The regiochemistry of adduct **30** was determined by the decoupling experiments. Irradiation of the vinylic signal at δ 5.35 caused simplification of the signals at δ 2.72 and 2.24 (2 × *H*-11) and vice versa.

[8] We believe that the NOE data for **32** and **33** strongly support the assignments as drawn. The enhancement of 0.1% on the C-11 methyl is small but can be contrasted with the enhancement of 0.0% on the isomeric methyl in **33**. This does not, however, constitute absolute proof of the assignments.

[9] The *para* regiochemistry of **34** was confirmed by irradiating the vinylic multiplet at δ 5.52, which simplified the signals at δ 2.57 (H-4).

[10] The bridge stereochemistry of compound **35** is unambiguously defined by the NOE experiment. The NOE evidence strongly supports the assignment of **34** as drawn but the proof is not absolute. The NOE data for compound **36** (5.2% enhancement of the bridge proton) does not prove the stereochemistry and so this structure should not be considered confirmed. We have tentatively drawn it as shown based on analogy with the other two compounds.

Table 5. Zinc chloride catalyzed Diels–Alder reaction of enone **13**.

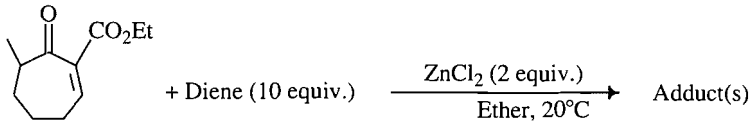

13

Diene	Time (h)	Product(s)	Yield (%)
	24	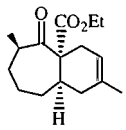 **30**	98
	23	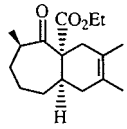 **31**	93 (9:1)
	24	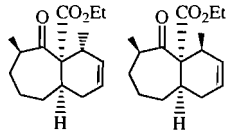 **32** **33**	85 (1:2)

Table 6. Zinc chloride catalyzed Diels–Alder reaction of enone **17**.

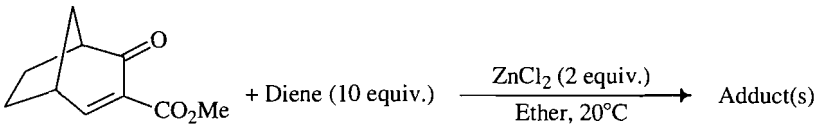

17

Diene	Time (h)	Product(s)	Yield (%)
	7.5	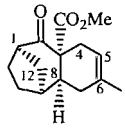 **34**	72
	6	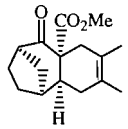 **35**	76
	6	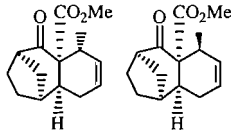 **36** **37**	65 (4:1)

Can. J. Chem. Downloaded from www.nrcresearchpress.com by 80.90.12.36 on 09/08/12
For personal use only.

Table 7. Ferric chloride catalyzed Diels–Alder reaction of enone **21**.

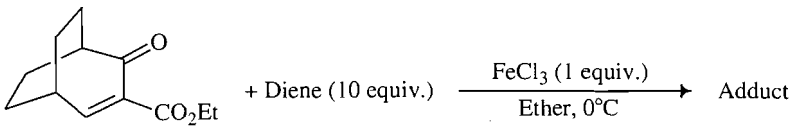

21

Diene	Time (h)	Product(s)	Yield (%)
	19.5	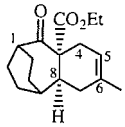 **38**	43
	33	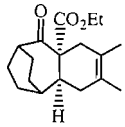 **39**	49
	28	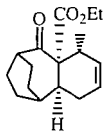 **40**	45

Fig. 4.

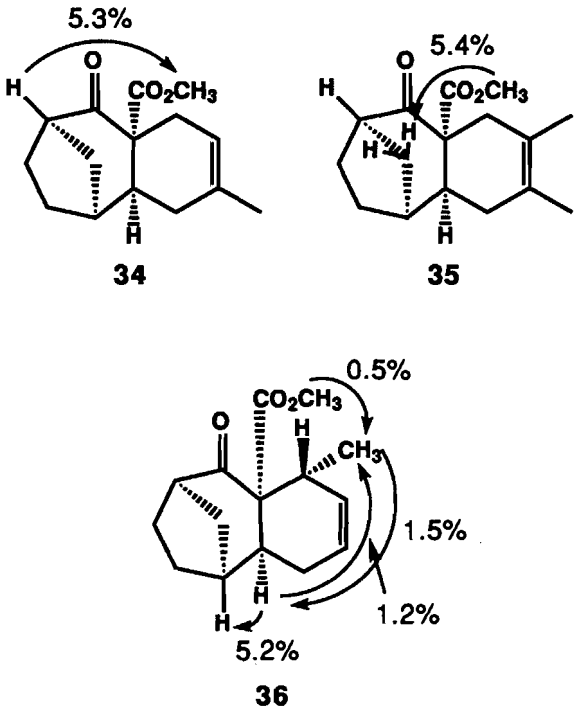

Fig. 5.

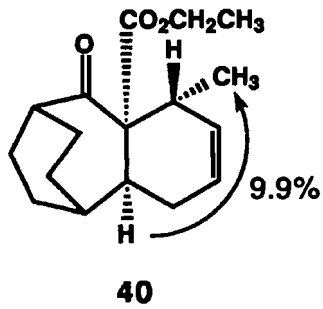

quantity in the reaction medium after prolonged reaction time (272 h), as indicated by TLC analysis. Only by employing ferric chloride as a catalyst did these reactions proceed at reasonable rate and give useful yields of the desired adducts **38**–**40**[11] (Table 7). Complete ester-*endo* selectivity was observed when *trans*-piperylene was added to enone **21** and the cycloadduct **40**, the stereochemistry of which was clearly indicated by the NOE results depicted in Fig. 5, was formed in 45% yield. This selectivity could easily be rationalized by steric hindrance of the ethano bridge in the keto-*endo* transition state.

Conclusion

Lewis acid catalyzed Diels–Alder reaction of 2-carbalkoxy-2-cycloheptenones displayed synthetic promise, interesting

[11] The regiochemistry of **38** was also confirmed by decoupling experiments. When each of the signals at δ 2.38 and 2.55 due to the C-4 methylene protons was irradiated, the broad singlet at δ 5.43 (*H*-5) was sharpened. Conversely, irradiation of the latter signal resulted in simplification of the former signals.

Can. J. Chem. Downloaded from www.nrcresearchpress.com by 80.90.12.36 on 09/08/12
For personal use only.

Can. J. Chem. Downloaded from www.nrcresearchpress.com by 80.90.12.36 on 09/08/12
For personal use only.

stereoselectivity, and unexpectedly high face-selectivity. In most cases the expected stereoselectivity favoring ester-*endo* adducts was exhibited due to sterically disfavored keto-*endo* transition states. In the one exception with favored keto-*endo* adduct, the cycloaddition with enone **13**, the extra methyl group of the dienophile certainly played an important but unclear role in directing the unusual selectivity. Complete facial stereoselectivity was observed in cycloadditions with enones **13** and **17**. Further study is required to explore the reasons for this unusual phenomenon. The substitution pattern on the seven-membered ring also produced large differences in rates and yields of the reactions. As a general trend in the related skeletal series, a monosubstituted enone having diastereotopic faces reacts the fastest and gives the highest yield, followed by the unsubstituted enone that has enantiotopic faces. The disubstituted enone having enantiotopic faces reacts slowly with poor yields. Accordingly for the rate and yield of the corresponding Diels–Alder reactions, the order of **13** (monosubstituted) > **3** (unsubstituted) > **9** (disubstituted) was observed. Similarly, **17** (with diastereotopic faces) was found to be better as a dienophile than **21** (with enantiotopic face). This study on the Diels–Alder chemistry of 2-carbalkoxy-2-cycloheptenones serves as a good basis for the stereoselective synthesis of various polycyclic natural products containing a six-membered ring fused with a seven-membered one.

Experimental

General

Melting points were recorded on a Köfler hot stage apparatus and are uncorrected. Infrared spectra (IR) were recorded using Nicolet 7-199, Nicolet MX-1, or Perkin–Elmer FTIR spectrometers. High-resolution mass spectra (MS) were obtained using a Kratos AEI MS-50 high-resolution mass spectrometer. Elemental analyses were carried out by the microanalytical laboratory of this department. Proton nuclear magnetic resonance spectra (^{1}H NMR) were recorded using Bruker WH-200 (200 MHz) and Bruker WH-400 (400 MHz) spectrometers. Coupling constants are reported to within ± 0.5 Hz. The following abbreviations were used: s = singlet, d = doublet, t = triplet, q = quartet, m = multiplet, br = broad. Carbon-13 nuclear magnetic resonance spectra (^{13}C NMR) were recorded on Bruker WH-200 (50 MHz) and Bruker WH-400 (100 MHz) instruments. Carbon-13 multiplicities were derived from off-resonance or Carr–Purcel–Meiboom–Gill spin echo *J*-modulated experiments (APT or Attached Proton Test). Methylene groups and quaternary carbons appear as signals in-phase with respect to the deuteriochloroform signal while the signals out-of-phase to that of deuteriochloroform are for the methyl and methine groups. Nuclear Overhauser Enhancement (NOE) experiments were determined in the difference mode in which a reference (undecoupled) spectrum was computer-subtracted from the irradiated spectrum after Fourier transformation. Positive enhancements are defined as signals possessing antiphase with respect to the irradiated signal.

Products were purified either by flash chromatography using silica gel 60 (230–400 mesh), distillation using a bulb-to-bulb Kugelrohr apparatus, or by fractional crystallization. All reactions were monitored by analytical thin-layer chromatography (TLC) performed on aluminum-backed plates precoated with silica gel 60 F_{254} as supplied by Merck. The visualization of the chromatograms was performed by dipping in either an ethanol solution of vanillin (5%, w/v) or an aqueous solution of phosphomolybdic acid (3%, w/v). Solvents were removed under reduced pressure on a rotary evaporator. Anhydrous magnesium sulfate was used for drying organic solutions.

General procedure for the ring expansion reactions

Boron trifluoride etherate (15 mmol, 1.5 equiv.) was added to a solution of ketone (10 mmol, 1.0 equiv.) in dry ether (20 mL) at 0°C. A solution of ethyl diazoacetate (15 mmol, 1.5 equiv.) in dry ether (5 mL) was then added over a period of 15 min and the resulting solution was stirred at room temperature under an argon atmosphere. When the reaction completed, it was cooled to 0°C and neutralized with saturated aqueous sodium bicarbonate solution. The resulting mixture was extracted with chloroform (3 × 20 mL). The combined extracts were washed with saturated aqueous sodium chloride solution, dried, and concentrated. Purification by bulb-to-bulb distillation under reduced pressure gave the desired keto ester. Yield and time of each reaction are to be found in Table 1.

Keto esters **2** (12), **5**, **8**, **11**, **12**, **19**, and **20** showed the following spectral data:

2-Carbethoxycycloheptanone (2)

Keto ester **2** was shown by the following spectral data to exist as a mixture of 75% keto form and 25% enol form: IR (CH_2Cl_2, cast): 1742 (C=O, ester), 1707 (C=O, ketone), 1638 (C=O, enol ester) cm^{-1}; ^{1}H NMR (400 MHz, $CDCl_3$) δ: 12.75 (s, 0.25H, =C(O*H*)-), 4.18 (m, 2H, -COOC*H*$_2$CH$_3$), 3.52 (dd, *J* = 10.5, 4 Hz, 0.75H, -COC*H*(COOEt)-), 2.65–1.40 (7 × m, 10H), 1.30 (t, *J* = 7 Hz, 0.75H, -COOCH$_2$C*H*$_3$), 1.26 (t, *J* = 7 Hz, 2.25H, -COOCH$_2$C*H*$_3$); MS *m/z* (M^+) calcd. for $C_{10}H_{16}O_3$: 184.1100; found: 184.1101.

2-Carbethoxy-5,5-dimethylcycloheptanone (5)

Keto ester **5** was shown by the following spectral data to exist as a mixture of 95% keto form and 5% enol form: IR ($CHCl_3$, cast): 1743 (C=O, ester), 1707 (C=O, ketone), 1640 (C=O, enol ester) cm^{-1}; ^{1}H NMR (400 MHz, $CDCl_3$) δ: 12.70 (s, 0.05H, =C(O*H*)-), 4.19 (q, *J* = 7 Hz, 1H, -COOC*H*HCH$_3$), 4.17 (q, *J* = 7 Hz, 1H, -COOCH*H*CH$_3$), 3.51 (t, *J* = 7.5 Hz, 0.95H, -COC*H*(COOEt)-), 2.64 (ddd, *J* = 16.5, 10, 5.5 Hz, 0.95H, -C*H*HCO-), 2.45 (ddd, *J* = 16.5, 6.5, 4 Hz, 0.95H, -CH*H*CO-), 2.35 (m, 0.1H), 1.97 (m, 2H), 1.65–1.55 (m, 3H), 1.38 (m, 1H), 1.26 (t, *J* = 7 Hz, 3H, -COOCH$_2$C*H*$_3$), 0.98 (s, 3H, -C*H*$_3$), 0.93 (s, 3H, -C*H*$_3$); MS *m/z* (M^+) calcd. for $C_{12}H_{20}O_3$: 212.1413; found: 212.1413.

2-Carbethoxy-7,7-dimethylcycloheptanone (8)

Keto ester **8** was shown by the following spectral data to exist completely in the keto form: IR ($CHCl_3$, cast): 1748 (C=O, ester), 1708 (C=O, ketone) cm^{-1}; ^{1}H NMR (400 MHz, $CDCl_3$) δ: 4.14 (q, *J* = 7 Hz, 2H, -COOC*H*$_2$CH$_3$), 3.86 (dd, *J* = 12, 3 Hz, 1H, -COC*H*(COOEt)-), 2.13 (br d, *J* = 14 Hz, 1H), 1.88 (br d, *J* = 14 Hz, 1H), 1.82–1.50 (m, 4H), 1.39 (br dd, *J* = 12, 12 Hz, 1H), 1.22 (t, *J* = 7 Hz, 3H, -COOCH$_2$C*H*$_3$), 1.18 (s, 3H, -C*H*$_3$), 1.14 (m, 1H), 1.10 (s, 3H, -C*H*$_3$); MS *m/z* (M^+) calcd. for $C_{12}H_{20}O_3$: 212.1413; found: 212.1415. Anal. calcd. for $C_{12}H_{20}O_3$: C 67.89%, H 9.50%; found: C 67.60%, H 9.68%.

Can. J. Chem. Downloaded from www.nrcresearchpress.com by 80.90.12.36 on 09/08/12
For personal use only.

*2-Carbethoxy-7-methylcycloheptanone (**11**) and* trans*-2-carbethoxy-3-methylcycloheptanone (**12**)*

Ring expansion of 2-methycyclohexanone gave a 9:1 mixture of regioisomers **11** (existing as a mixture of two stereoisomers in a ratio of 7:2) and **12**. All the isomers were shown to exist completely in the keto form: IR (film): 1743 (C=O, ester), 1709 (C=O, ketone) cm^{-1}; ^1H NMR (200 MHz, $CDCl_3$) δ: 4.15 (m, 2H, -COO*CH*$_2$CH$_3$), 3.67 (dd, *J* = 7.5, 5 Hz, 0.2H, -CO*CH*(COOEt)-), 3.48 (dd, *J* = 12, 4.5 Hz, 0.7H, -CO*CH*(COOEt)-), 3.13 (d, *J* = 10 Hz, 0.1H, -CO*CH*(COOEt)CH(CH$_3$)-), 1.25, 1.23 (2 × t, *J* = 7 Hz, 3H, -COOCH$_2$*CH*$_3$), 1.12 (d, *J* = 6.5 Hz, 2.1H, -*CH*$_3$), 1.11 (d, *J* = 6.5 Hz, 0.6H, -*CH*$_3$), 1.01 (d, *J* = 6.5 Hz, 0.3H, -*CH*$_3$); MS *m/z* (M^+) calcd. for $C_{11}H_{18}O_3$: 198.1256; found: 198.1261. Anal. calcd. for $C_{11}H_{18}O_3$: C 66.64%, H 9.15%; found: C 66.63%, H 9.24%.

*3-Carbethoxybicyclo[3.2.2]nonan-2-one (**19**) and 2-carbethoxybicyclo[3.2.2]nonan-3-one (**20**)*

Ring expansion of bicyclo[2.2.2]octanone gave a 11:4 mixture of regioisomers **19** (keto form:enol form = 5:6) and **20** (keto form:enol form = 1:1): IR ($CHCl_3$, cast): 1744 (C=O, ester), 1704 (C=O, ketone), 1643 (C=O, enol ester), 1610 (-C=C-OH) cm^{-1}; ^1H NMR (400 MHz, $CDCl_3$) δ: 12.72 (s, 0.13H, =C(OH)-), 12.62 (s, 0.4H, =C(O*H*)-), 4.20 (m, 2H, -COO*CH*$_2$CH$_3$), 3.80 (dd, *J* = 12, 8.5 Hz, 0.33H, -CO*CH*(COOEt)-), 3.52 (ddd, *J* = 3, 1, 1 Hz, 0.13H, -CO*CH*(COOEt)-), 1.29 (m, 3H, -COOCH$_2$*CH*$_3$); MS *m/z* (M^+) calcd. for $C_{12}H_{18}O_3$: 210.2156; found: 210.1258. Anal. calcd. for $C_{12}H_{18}O_3$: C 68.56%, H 8.63%; found: C 68.28%, H 8.82%.

(1S,5R*)-3-Carbomethoxybicyclo[3.2.1]octan-2-one (**16**)*

Dimethyl carbonate (4.30 mL, 50.73 mmol) was added to a suspension of sodium hydride (60% dispersion in mineral oil, 1.01 g, 25.37 mmol) in dry tetrahydrofuran (15 mL). The resulting mixture was heated under reflux under an argon atmosphere. A solution of bicyclo[3.2.1]octan-2-one (85%, 1.05 g, 8.455 mmol) in dry tetrahydrofuran (15 mL) was then added. After refluxing for 2.5 h, the solution was cooled, neutralized with 10% acetic acid, and extracted with ether (3 × 30 mL). The combined extracts were washed with saturated aqueous sodium chloride solution, dried, concentrated, and purified by bulb-to-bulb distillation (85°C/1 Torr (= 133.3 Pa)) to give keto ester **16** (1.24 g, 95% yield based on 85% purity of the ketone: keto form:enol form = 2:5) as a colorless oil: IR ($CHCl_3$, cast): 1748 (C=O, ester), 1725 (C=O, ketone), 1655 (C=O, enol ester), 1615 (-C=C-OH) cm^{-1}; ^1H NMR (400 MHz, $CDCl_3$) δ: 11.91 (s, 0.71H, =C(O*H*)-), 3.75 (s, 0.86H, -COO*CH*$_3$), 3.72 (s, 2.14H, -COO*CH*$_3$), 3.47 (dd, *J* = 12, 8 Hz, 0.29H, -CO*CH*(COOCH$_3$)-); MS *m/z* (M^+) calcd. for $C_{10}H_{14}O_3$: 182.0943; found: 182.0949.

Preparation of bicyclo[2.2.2]octanone (18)

A. (1S,4S*,5S*)-5-Acetylbicyclo[2.2.2]oct-2-ene*

To a solution of 1,3-cyclohexadiene (5.02 g, 62.65 mmol) and methyl vinyl ketone (26.1 mL, 313.24 mmol) in dry dichloromethane (40 mL) at 0°C, tin(IV) chloride (7.3 mL, 62.65 mmol) was slowly added. The resulting solution was stirred at 0°C under an argon atmosphere for 1 h. The solution was then neutralized with saturated aqueous sodium bicarbonate solution. The dichloromethane layer was separated and the aqueous layer was extracted with dichloromethane (30 mL). The combined dichloromethane solutions were washed with water, dried, concentrated, and purified by flash chromatography (20% ether in Skelly B) to give the desired adduct (8.0 g, 85% yield) as a colorless oil: IR ($CHCl_3$, cast): 1709 (C=O) cm^{-1}; ^1H NMR (400 MHz, $CDCl_3$) δ: 6.28 (ddd, *J* = 7, 7, 1 Hz, 1H, =C*H*-), 6.10 (ddd, *J* = 7, 7, 0.5 Hz, 1H, =C*H*-), 2.89 (m, 1H), 2.66 (ddd, *J* = 9, 7, 2 Hz, 1H, -C*H*(COCH$_3$)-), 2.60 (m, 1H), 2.10 (s, 3H, C*H*$_3$CO-), 1.65 (m, 2H), 1.60 (m, 1H), 1.49 (m, 1H), 1.32 (m, 1H), 1.25 (m, 1H); MS *m/z* calcd. (M^+) for $C_{10}H_{14}O$: 150.1045; found: 150.1043.

B. 2-Acetylbicyclo[2.2.2]octane

The above enone (7.88 g, 52.46 mmol) was dissolved in ethyl acetate (70 mL), Palladium on carbon (50%, 0.45 g) was added. The mixture was hydrogenated under 20 psi (1 psi = 6.9 kPa) of hydrogen for 5 h using a Parr hydrogenation apparatus. The mixture was then filtered and concentrated to give the title ketone (7.77 g, 97% yield) as a colorless oil: IR (CH_2Cl_2, cast): 1710 (C=O) cm^{-1}; ^1H NMR (200 MHz, $CDCl_3$) δ: 2.63 (ddd, *J* = 10, 6, 2.5 Hz, 1H, -C*H*(COCH$_3$)-), 2.17–1.90 (m, 3H), 2.13 (s, 3H, C*H*$_3$CO-), 1.70–1.35 (m, 9H); MS *m/z* (M^+) calcd. for $C_{10}H_{16}O$: 152.1202; found: 152.1202.

C. Bicyclo[2.2.2]octan-2-ol

To a mixture of the above ketone (4.59 g, 30.15 mmol) and disodium hydrogen phosphate (12.84 g, 90.45 mmol) in dry dichloromethane (50 mL) was added *m*-chloroperoxybenzoic acid (70%, 14.87 g, 60.30 mmol). The resulting solution was stirred at room temperature under an argon atmosphere for 25 h. At the end of this time, the solution was neutralized with saturated sodium bicarbonate solution. The dichloromethane layer was separated and the aqueous layer was extracted with dichloromethane (50 mL). The combined dichloromethane solutions were washed with saturated aqueous sodium sulfite solution, dried, and concentrated. The residue was dissolved in methanol (50 mL). The methanol solution was mixed with 1 N aqueous sodium hydroxide solution (50 mL). After stirring at room temperature for 4.5 h, the solution was acidified with 1 N hydrochloric acid and extracted with dichloromethane (3 × 50 mL). The combined extracts were washed with water, dried, concentrated, and purified by flash chromatography (40–50% ether in Skelly B) to give the alcohol (3.80 g, 100% yield) as a white solid: mp 88–89°C (Skelly B); IR (CH_2Cl_2, cast): 3293 (O-H) cm^{-1}; ^1H NMR (400 MHz, $CDCl_3$) δ: 3.95 (dddd, *J* = 9, 4, 4, 1.5 Hz, 1H, -C*H*(OH)-), 2.01 (dddd, *J* = 14, 9.5, 3, 2.5 Hz, 1H), 1.88 (m, 1H), 1.60 (m, 4H), 1.50–1.30 (m, 7H); MS *m/z* (M^+) calcd. for $C_8H_{14}O$: 126.1045; found: 126.1044.

*D. Bicyclo[2.2.2]octanone (**18**)*

Pyridinium chlorochromate on alumina (0.9 mmol/g, 50.18 g, 45.16 mmol) was added to a solution of the above alcohol (3.80 g, 30.11 mmol) in dry dichloromethane (70 mL) and the resulting mixture was stirred at room temperature under an argon atmosphere for 2 h. The mixture was then filtered through Florisil, concentrated, and purified by flash chromatography (20% ether in Skelly B) to give ketone **18** (2.86 g, 76% yield) as a volatile white solid: IR (CH_2Cl_2, cast): 1727

Can. J. Chem. Downloaded from www.nrcresearchpress.com by 80.90.12.36 on 09/08/12
For personal use only.

(C=O) cm^{-1}; ^1H NMR (200 MHz, $CDCl_3$) δ: 2.24 (br s, 3H), 2.15 (m, 1H), 1.80 (m, 4H), 1.73–1.55 (m, 4H); MS *m/z* (M^+) calcd. for $C_8H_{12}O$: 124.0888; found: 124.0889.

General procedure for phenylselenenylation and oxidative elimination reaction

To a solution of phenylselenenyl chloride (12.0 mmol, 3 equiv.) in dry dichloromethane (20 mL) at 0°C, pyridine (12.0 mmol, 3 equiv.) was slowly added. After stirring at 0°C under an argon atmosphere for 15 min, a solution of keto ester (4.0 mmol, 1 equiv.) in dry dichloromethane (10 mL) was then added. The resulting dark red solution was stirred at room temperature under an argon atmosphere. When the reaction was completed, it was cooled to 0°C. Aqueous 30% hydrogen peroxide (1 mL each addition) was then added at intervals of 10 min until the solution turned colorless (ca. 5–10 times). At the end of this time, the mixture was diluted with water. The dichloromethane layer was separated, washed with saturated aqueous sodium bicarbonate solution, 1 N hydrochloric acid, and saturated aqueous sodium sulfite solution, dried, and concentrated. Purification by either flash chromatography or bulb-to-bulb distillation gave the desired carbalkoxy enone. Yield and time of each transformation are to be found in Table 2.

The keto esters **3**, **6**, **9**, **13**, **14**, **17**, and **21** showed the following spectral data:

*2-Carbethoxy-2-cyclohepten-1-one (**3**)*

Keto ester **3** was shown by the following spectral data to exist completely in the keto form: IR ($CHCl_3$, cast): 1725 (C=O, ester), 1694 (C=O, ketone) cm^{-1}; ^1H NMR (200 MHz, $CDCl_3$) δ: 7.36 (t, *J* = 6 Hz, 1H, -*H*C=CCO-), 4.22 (q, *J* = 7 Hz, 2H, -COOC*H*$_2$CH$_3$), 2.68 (t, *J* = 6.5 Hz, 2H, -C*H*$_2$CO-), 2.49(dt, *J* = 6 Hz, 2H, -C*H*$_2$CH=CCO-), 1.92–1.70 (m, 4H), 1.28 (t, *J* = 7 Hz, 3H, -COOCH$_2$C*H*$_3$); MS *m/z* (M^+) calcd. for $C_{10}H_{14}O_3$: 182.0943; found: 182.0944.

*2-Carbethoxy-5,5-dimethyl-2-cyclohepten-1-one (**6**)*

Keto ester **6** was shown by the following spectral data to exist as a mixture of 90% keto form and 10% enol form: IR ($CHCl_3$, cast): 1728 (C=O, ester), 1690 (C=O, ketone), 1634 (C=O, enol ester) cm^{-1}; ^1H NMR (200 MHz, $CDCl_3$) δ: 13.28 (s, 0.1H, =C(O*H*)-), 7.32 (t, *J* = 7.5 Hz, 0.9H, -*H*C=CCO-), 6.04 (d, *J* = 13.5 Hz, 0.1H, -*H*C=CH-), 5.26 (d, *J* = 13.5 Hz, 0.1H, -HC=C*H*-), 4.25 (q, *J* = 7 Hz, 0.2H, -COOC*H*$_2$CH$_3$), 4.24 (q, *J* = 7 Hz, 1.8H, -COOC*H*$_2$CH$_3$), 2.52 (dd, *J* = 2.5, 2.5 Hz, 1H), 2.51 (d, *J* = 12 Hz, 1H), 2.20 (d, *J* = 7 Hz, 2H), 1.64 (dd, *J* = 2.5, 2.5 Hz, 1H), 1.64 (d, *J* = 12 Hz, 1H), 1.29 (t, *J* = 7 Hz, 3H, -COOCH$_2$C*H*$_3$), 1.03 (s, 6H, 2 × -C*H*$_3$); MS *m/z* (M^+) calcd. for $C_{12}H_{18}O_3$: 210.1256; found: 210.1259.

*2-Carbethoxy-7,7-dimethyl-2-cyclohepten-1-one (**9**)*

Phenylselenenylation – oxidative elimination of keto ester **8** did not proceed to completion; 61% of **8** was recovered. Keto ester **9** was shown by the following spectral data to exist completely in the keto form: IR (CH_2Cl_2, cast): 1722 (C=O, ester), 1695 (C=O, ketone); cm^{-1}; ^1H NMR (400 MHz, $CDCl_3$) δ: 7.16 (t, *J* = 5 Hz, 1H, -*H*C=CCO-), 4.20 (q, *J* = 7 Hz, 2H, -COOC*H*$_2$CH$_3$), 2.42 (ddd, *J* = 6, 6, 6 Hz, 2H, -C*H*$_2$CH=CCO-), 1.71–1.60 (m, 4H), 1.25 (t, *J* = 7 Hz, 3H, -COOCH$_2$C*H*$_3$), 1.18 (s, 6H, 2 × -C*H*$_3$); MS *m/z* (M^+) calcd. for $C_{12}H_{18}O_3$: 210.1256; found: 210.1252.

*2-Carbethoxy-7-methyl-2-cyclohepten-1-one (**13**) and 2-carbethoxy-3-methyl-2-cyclohepten-1-one (**14**)*

Phenylselenenylation – oxidative elimination of the inseparable 9:1 mixture of keto esters **11** and **12** did not proceed to completion; 7% of **12** was recovered. Carbethoxy enones **13** (keto form:enol form = 2:1) and **14** (keto form only) were separated by flash chromatography and obtained in a ratio of 24:1.

13: IR (film): 1724 (br, C=O), 1636 (C=O, enol ester) cm^{-1}; ^1H NMR (200 MHz, $CDCl_3$) δ: 13.46 (s, 0.33H, =C(O*H*)-), 7.32 (dd, *J* = 6, 5.5 Hz, 0.67H, -*H*C=CCO-), 6.22 (ddd, *J* = 12, 2, 2 Hz, 0.33H, -*H*C=CH-), 5.65 (ddd, *J* = 12, 5, 5 Hz, 0.33H, -HC=C*H*-), 4.23 (q, *J* = 7 Hz, 0.67H, -COOC*H*$_2$CH$_3$), 4.21 (q, *J* = 7 Hz, 1.33H, -COOC*H*$_2$CH$_3$), 2.84, 2.46, 2.25, 1.91, 1.75, 1.50 (6 × m, 6.34H), 1.32 (t, *J* = 7 Hz, 1H, -COOCH$_2$C*H*$_3$), 1.27 (t, *J* = 7 Hz, 2H, -COOCH$_2$C*H*$_3$), 1.15 (d, *J* = 6.5 Hz, 3H, -C*H*$_3$); MS *m/z* (M^+) calcd. for $C_{11}H_{16}O_3$: 196.1100; found: 196.1090. Anal. calcd. for $C_{11}H_{16}O_3$: C 67.32%, H 8.22%; found: C 66.84%, H 8.48%.

14: IR (film): 1729 (br, C=O) cm^{-1}; ^1H NMR (200 MHz, $CDCl_3$) δ: 4.24 (q, *J* = 7 Hz, 2H, -COOC*H*$_2$CH$_3$), 2.61 (m, 2H), 2.43 (m, 2H), 2.03 (s, 3H, =C(C*H*$_3$)-), 1.81 (m, 4H), 1.29 (t, *J* = 7 Hz, 3H, 3H, -COOCH$_2$C*H*$_3$); MS *m/z* (M^+) calcd. for $C_{11}H_{16}O_3$: 196.1100; found: 196.1100.

(1S,5R*)-3-Carbomethoxybicyclo[3.2.1]oct-3-en-2-one (**17**)*

Keto ester **17** showed the following spectral data: IR film): 1743 (C=O, ester), 1689 (C=O, ketone) cm^{-1}; ^1H NMR (400 MHz, $CDCl_3$) δ: 8.01 (dd, *J* = 7, 1.5 Hz, 1H, -*H*C=CCO-), 3.78 (s, 3H, -COOC*H*$_3$), 3.04 (m, 2H, -C*H*CO-, =CC*H*-), 2.16 (m, 1H), 2.06 (br d, *J* = 12 Hz, 1H), 2.01 (m, 1H), 1.76 (m, 1H), 1.66 (dddd, *J* = 12, 5, 5, 1.5 Hz, 1H), 1.59 (m, 1H); MS *m/z* (M^+) calcd. for $C_{10}H_{12}O_3$: 180.0787; found: 180.0790.

*3-Carbethoxybicyclo[3.2.2]non-3-en-2-one (**21**)*

Keto ester **21** showed the following spectral data: IR ($CHCl_3$, cast): 1736 (C=O, ester), 1677 (C=O, ketone) cm^{-1}; ^1H NMR (400 MHz, $CDCl_3$) δ: 7.82 (d, *J* = 9.5 Hz, 1H, -*H*C=CCO-), 4.26 (q, *J* = 7 Hz, 2H, -COOC*H*$_2$CH$_3$), 2.90 (m, 2H), 1.82 (m, 4H), 1.67 (m, 4H), 1.32 (t, *J* = 7 Hz, 3H, -COOCH$_2$C*H*$_3$); MS *m/z* (M^+) calcd. for $C_{12}H_{16}O_3$: 208.1099; found: 208.1104. Anal. calcd. for $C_{12}H_{16}O_3$: C 69.21%, H 7.74%; found: C 69.39%, H 7.88%.

General procedure for $ZnCl_2$ catalyzed Diels–Alder reactions

Zinc chloride (1–3 equiv.) was fused in a reaction flask under argon and then dissolved in dry ether (5 mL). A solution of carbalkoxy cycloheptenone (0.3 mmol, 1 equiv.) in dry ether (3 mL) was added. After stirring at room temperature for 30 min, diene (3.0 mmol, 10 equiv.) was added. The resulting mixture was stirred at room temperature until the reaction was complete. Then it was neutralized with saturated aqueous sodium bicarbonate solution. The ether layer was separated and the aqueous layer was extracted with ether (10 mL). The combined ether solutions were washed with saturated aqueous sodium chloride solution, dried, concentrated, and purified by flash chromatography (ether – Skelly B) to give the desired adduct(s). Yields and times of the reactions as well as the

Can. J. Chem. Downloaded from www.nrcresearchpress.com by 80.90.12.36 on 09/08/12
For personal use only.

quantities of zinc chloride relative to carbalkoxy cycloheptenone are shown in Tables 3–6.

General procedure for $FeCl_3$, $AlCl_3$, $SnCl_4$, and $BF_3{\cdot}OEt_2$ catalyzed Diels–Alder reactions

To a solution of carbalkoxy cycloheptenone (0.5 mmol, 1 equiv.) in dry ether (10 mL), diene (5.0 mmol, 10 equiv.) was added. Lewis acid (0.5 mmol, 1 equiv.) was then added and the resulting solution was stirred under argon. When the reaction was complete, it was neutralized with saturated aqueous sodium bicarbonate solution. The ether layer was separated and the aqueous layer was extracted with ether (10 mL). The combined ether solutions were washed with saturated sodium chloride solution, dried, concentrated, and purified by flash chromatography (ether – Skelly B) to give the desired adduct(s). Yields, times, and temperatures of the reactions are shown in Tables 2 and 7.

(1R,7R*)-1-Carbethoxy-9-methylbicyclo[5.4.0]undec-9-en-2-one (**22**)*

IR ($CHCl_3$, cast): 1743 (C=O, ester), 1700 (C=O, ketone) cm^{-1}; ^1H NMR (400 MHz, $CDCl_3$) δ: 5.34 (br s, 1H, *H*-10), 4.16 (q, *J* = 7 Hz, 1H, -COOC*H*HCH$_3$), 4.15 (q, *J* = 7 Hz, 1H, -COOCH*H*CH$_3$), 2.98 (ddd, *J* = 14, 9.5, 3 Hz, 1H, *H*-3), 2.68 (m, 1H, *H*-7), 2.65 (ddq, *J* = 18, 2, 2 Hz, 1H, *H*-11), 2.42 (ddd, *J* = 14, 9, 4 Hz, 1H, *H*-3), 2.33 (br (d, *J* = Hz, 1H, *H*-11), 2.09 (br d, *J* = 18 Hz, 1H, *H*-8), 1.82–1.50 (m, 7H), 1.61 (br s, 3H, 9-CH_3), 1.23 (t, *J* = 7 Hz, 3H, -COOCH$_2$CH_3); ^{13}C NMR APT (50 MHz, $CDCl_3$) δ: 209.72 (p), 171.64 (p), 131.17 (p), 118.46 (a), 61.60 (p), 61.24 (p), 42.67 (p), 36.58 (a), 35.47 (p), 33.12 (p), 29.81 (p), 27.65 (p), 25.27 (p), 23.35 (a), 14.00 (a); MS *m/z* (M^+) calcd. for $C_{15}H_{22}O_3$: 250.1570; found: 250.1568. Anal. calcd. for $C_{15}H_{22}O_3$: C 71.97%, H 8.86%; found: C 71.51%, H 8.65%.

(1R,7R*)-1-Carbethoxy-9,10-dimethylbicyclo[5.4.0]undec-9-en-2-one (**23**)*

IR ($CHCl_3$, cast): 1742 (C=O, ester), 1701 (C=O, ketone) cm^{-1}; ^1H NMR (400 MHz, $CDCl_3$) δ: 4.14 (q, *J* = 7 Hz, 2H, -COOCH_2CH$_3$), 2.96 (ddd, *J* = 14, 10, 3.5 Hz, 1H, *H*-3), 2.64 (m, 1H, *H*-7), 2.56 (br d, *J* = 17.5 Hz, 1H, *H*-11), 2.41 (ddd, *J* = 14, 9, 3Hz, 1H, *H*-3), 2.25 (br d, *J* = 17.5 Hz, 1H, *H*-11), 2.10 (br d, *J* = 17.5 Hz, 1H, *H*-8), 1.82–1.60 (m, 7H), 1.63 (s, 3H, 10-CH_3), 1.56 (s, 3H, 9-CH_3), 1.22 (t, *J* = 7 Hz, 3H, -COOCH$_2$CH_3); ^{13}C NMR APT (50 MHz, $CDCl_3$) δ: 209.94 (p), 199.57 (p), 123.74 (p), 122.76 (p), 62.67 (p), 61.19 (p), 42.71 (p), 37.10 (p), 36.80 (a), 35.53 (p), 33.13 (p), 27.73 (p), 25.34 (p), 18.86 (a), 18.53 (a), 14.01 (a); MS *m/z* (M^+) calcd. for $C_{16}H_{24}O_3$: 264.1726; found: 264.1727. Anal. calcd. for $C_{16}H_{24}O_3$: C 72.69%, H 9.15%; found: C 72.75%, H 9.08%.

(1S,7R*,11R*)-1-Carbethoxy-11-methylbicyclo-[5.4.0]undec-9-en-2-one (**24**)*

IR ($CHCl_3$, cast): 1739 (C=O, ester), 1702 (C=O, ketone) cm^{-1}; ^1H NMR (400 MHz, $CDCl_3$) δ: 5.64 (m, 1H, *H*-10), 5.54 (m, 1H, *H*-9), 4.22 (dq, *J* = 11, 7 Hz, 1H, -COOC*H*HCH$_3$), 4.18 (dq, *J* = 11, 7 Hz, 1H, -COOCH*H*CH$_3$), 2.83 (m, 2H, *H*-3, *H*-11), 2.40 (m, 2H), 2.30 (m, 1H), 1.92 (m, 1H), 1.85–1.67 (m, 4H), 1.42 (m, 2H), 1.27 (t, *J* = 7 Hz, 3H, -COOCH$_2$CH_3), 0.91 (d, *J* = 7 Hz, 3H, 11-CH_3); ^{13}C NMR APT (50 MHz, $CDCl_3$) δ: 206.81 (p), 170.69 (p), 131.65 (a), 123.13 (a), 64.94 (p), 60.79 (p), 43.66 (p), 34.66 (a), 31.87 (a), 31.69 (p), 28.81 (p), 24.91 (p), 23.34 (p), 17.27 (a), 14.05 (a); MS *m/z* (M^+) calcd. for $C_{15}H_{22}O_3$: 250.1570; found: 250.1569.

(1S,7R*,11S*)-1-Carbethoxy-11-methylbicyclo-[5.4.0]undec-9-en-2-one (**25**)*

IR ($CHCl_3$, cast): 1720 (C=O, ester), 1699 (C=O, ketone) cm^{-1}; ^1H NMR (400 MHz, $CDCl_3$) δ: 5.55 (m, 2H, *H*-9, *H*-10), 4.27 (q, *J* = 7 Hz, 1H, -COOC*H*HCH$_3$), 4.26 (q, *J* = 7 Hz, 1H, -COOCH*H*CH$_3$), 2.88 (dddd, *J* = 18.5, 4.5, 4.5, 1.5 Hz, 1H, *H*-3), 2.62 (m, 1H, *H*-11), 2.52 (ddd, *J* = 12, 7.5, 4 Hz, 1H, *H*-7), 2.34 (ddd, *J* = 18.5, 13, 5 Hz, 1H, *H*-3), 1.96 (ddd, *J* = 15, 4, 3 Hz, 1H, *H*-6), 1.90 (m, 2H, 2 × *H*-8), 1.74 (m, 3H), 1.42 (m, 2H), 1.31 (t, *J* = 7 Hz, 3H, -COOCH$_2$CH_3), 1.11 (d, *J* = 7 Hz, 3H, 11-CH_3); ^{13}C NMR APT (50 MHz, $CDCl_3$ δ: 205.95 (p), 172.45 (p), 131.80 (a), 123.05 (a), 123.05 (a), 65.67 (p), 60.97 (p), 44.70 (p), 40.87 (a), 38.52 (a), 32.63 (p), 28.26 (p), 23.96 (p), 23.37 (p), 16.48 (a), 14.12 (a); MS *m/z* (M^+) calcd. for $C_{15}H_{22}O_3$: 250.1570, found: 250.1569. Anal. calcd. for $C_{15}H_{22}O_3$: C 71.97%, H 8.86%; found: C 72.03%, H 9.11%.

(1R,7R*)-1-Carbethoxy-5,5,9-trimethylbicyclo-[5.4.0]undec-9-en-2-one (**26**):* mp 98–99°C (Skelly B); IR ($CHCl_3$, cast): 1733 (C=O, ester), 1694 (C=O, ketone) cm^{-1}; ^1H NMR (400 MHz, $CDCl_3$) δ: 5.33 (br s, 1H, *H*-10), 4.13 (q, *J* = 7 Hz, 2H, -COOCH_2CH$_3$), 3.07 (ddd, *J* = 13, 13, 2 Hz, 1H, *H*-3), 2.91 (m, 2H, *H*-7, *H*-11), 2.31 (ddd, *J* = 13, 8, 2 Hz, 1H, *H*-3), 2.29 (m, 1H, *H*-8), 2.14 (br d, *J* = 18 Hz, 1H, *H*-11), 1.65–1.52 (m, 3H), 1.62 (br s, 3H, 9-CH_3), 1.38 (m, 1H), 1.22 (t, *J* = 7 Hz, 3H, -COOCH$_2$CH_3), 1.16 (m, 1H), 1.12 (s, 3H, 5-CH_3), 0.93 (s, 3H, 5-CH_3); ^{13}C NMR APT (50 MHz, $CDCl_3$) δ: 183.88 (p), 170.98 (p), 130.89 (p), 118.31 (a), 61.32 (2 × p), 46.60 (p), 39.07 (p), 38.16 (p), 37.60 (p), 33.04 (p), 32.83 (a), 31.18 (a), 27.21 (p), 25.50 (a), 23.58 (a), 13.99 (a); MS *m/z* (M^+) calcd. for $C_{17}H_{26}O_3$: 278.1883; found: 278.1885. Anal. calcd. for $C_{17}H_{26}O_3$: C 73.34%, H 9.41%; found: C 73.16%, H 9.20%.

(1R,7R*)-1-Carbethoxy-5,5,9,10-tetramethylbicyclo-[5.4.0]undec-9-en-2-one (**27**):* mp 62–63°C (Skelly B); IR ($CHCl_3$, cast): 1746 (C=O, ester), 1702 (C=O, ketone) cm^{-1}; ^1H NMR (400 MHz, $CDCl_3$) δ: 4.14 (q, *J* = 7 Hz, 1H, -COOC*H*HCH$_3$), 4.13 (q, *J* = 7 Hz, 1H, -COOCH*H*CH$_3$), 3.05 (ddd, *J* = 14, 14, 2 Hz, 1H, *H*-3), 2.86 (m, 1H, *H*-7), 2.73 (br d, *J* = 18 Hz, 1H, *H*-11), 2.29 (m, 2H, *H*-3, *H*-8), 2.10 (br, d, *J* = 18 Hz, 1H, H-11), 1.64 (s, 3H, 10-CH$_3$), 1.60 (m, 2H), 1.57 (br s, 3H, 9-CH_3), 1.51 (dd, *J* = 15.5, 11 Hz, 1H, *H*-6), 1.38 (dd, *J* = 14, 14 Hz, 1H, *H*-4), 1.21 (t, *J* = 7 Hz, 3H, -COOCH$_2$CH_3), 1.12 (dd, *J* = 15, 2.5 Hz, 1H), 1.11 (s, 3H, 5-CH_3), 0.92 (s, 3H, 5-CH_3); ^{13}C NMR APT (50 MHz, $CDCl_3$) δ: 211.35 (p), 171.16 (p), 123.05 (p), 122.66 (p), 62.63 (p), 61.27 (p), 46.71 (p), 39.32 (p), 39.04 (p), 38.15 (p), 33.08 (p), 32.94 (p), 32.79 (a), 31.43 (a), 25.58 (a), 19.05 (a), 18.25 (a), 14.00 (a); MS *m/z* (M^+) calcd. for $C_{18}H_{28}O_3$: 292.2039; found: 292.2040. Anal. calcd. for $C_{18}H_{28}O_3$: C 73.93%, H 9.65%; found: C 73.98%, H 10.05%.

(1S,7S*11R*)-1-Carbethoxy-5,5,11-trimethylbicyclo-[5.4.0]undec-9-en-2-one (**28**)*

IR ($CHCl_3$, cast): 1746 (C=O, ester), 1698 (C=O, ketone)

Can. J. Chem. Downloaded from www.nrcresearchpress.com by 80.90.12.36 on 09/08/12
For personal use only.

cm^{-1}; ^{1}H NMR (400 MHz, $CDCl_3$) δ: 5.62 (m, 1H, *H*-10), 5.55 (m, 1H, *H*-9), 4.16 (q, *J* = 7 Hz, 2H, -COOC*H*$_2$CH$_3$), 3.00 (m, 1H, *H*-11), 2.99 (ddd, *J* = 15, 10.5, 3 Hz, 1H, *H*-3), 2.81 (m, 1H, *H*-7), 2.40 (ddd, *J* = 15, 9.5, 2.5 Hz, 1H, *H*-3), 2.13 (dddddd, *J* = 17.5, 3, 3, 3, 3, 3 Hz, 1H, *H*-8), 1.92 (m, 2H, *H*-6, *H*-8), 1.56–1.28 (m, 3H, 2 × *H*-4, *H*-6), 1.24 (t, *J* = 7 Hz, 3H, -COOCH$_2$C*H*$_3$), 1.11 (d, *J* = 7.5 Hz, 3H, 11-C*H*$_3$), 1.05 (s, 3H, 5-C*H*$_3$), 0.93 (s, 3H, 5-C*H*$_3$); ^{13}C NMR APT (50 MHz, $CDCl_3$) δ: 209.37 (p), 172.16 (p), 131.66 (a), 122.51 (a), 65.54 (p), 61.32 (p), 45.57 (p), 40.06 (p), 35.50 (p), 35.21 (a), 33.58 (a), 33.34 (p), 32.16 (p), 30.98 (a), 28.45 (a), 17.61 (a), 13.97 (a); MS *m/z* (M$^+$) calcd. for $C_{17}H_{26}O_3$: 278.1883; found: 278.1886.

(1R,3R*7R*)-1-Carbethoxy-3,9-dimethylbicyclo-[5.4.0]undec-9-en-2-one* (**30**)

IR ($CHCl_3$, cast): 1735 (C=O, ester), 1697 (C=O, ketone) cm^{-1}; ^{1}H NMR (400 MHz, $CDCl_3$) δ: 5.35 (m, 1H, *H*-10), 4.18 (q, *J* = 7 Hz, 2H, -COOC*H*$_2$CH$_3$), 2.72 (dddd, *J* = 16.5, 3.5, 1.5, 1.5 Hz, 1H, *H*-11), 2.54 (m, 1H, *H*-7), 2.38 (qdd, *J* = 7, 7, 3.5 Hz, 1H, *H*-3), 2.24 (dqd, *J* = 16.5, 2.5, 2.5 Hz, 1H, *H*-11), 2.01 (m, 1H, *H*-8), 1.84 (br d, *J* = 7 Hz, 2H), 1.73 (m, 3H), 1.60 (br s, 3H, 9-C*H*$_3$), 1.55–1.40 (m, 2H), 1.26 (t, *J* = 7 Hz, 3H, -COOCH$_2$C*H*$_3$), 1.22 (d, *J* = 7 Hz, 3H, 3-C*H*$_3$); ^{13}C NMR APT (100 MHz, $CDCl_3$) δ: 210.20 (p), 173.21 (p), 132.21 (p), 118.82 (a), 68.19 (p), 61.11 (p), 48.47 (a), 36.74 (a), 34.06 (p), 33.25 (p), 31.78 (p), 31.73 (p), 24.43 (p), 23.02 (a), 20.79 (a), 14.16 (a); MS *m/z* (M$^+$) calcd. for $C_{16}H_{24}O_3$: 264.1726; found: 264.1725. Anal. calcd. for $C_{16}H_{24}O_3$: C 72.69%, H 9.15%; found: C 72.62%, H 9.45%.

(1R,3R*7R*)-1-Carbethoxy-3,9,10-trimethylbicyclo-[5.4.0]undec-9-en-2-one* (**31**)

IR (CH_2Cl_2, cast): 1736 (C=O, ester), 1697 (C=O, ketone) cm^{-1}; ^{1}H NMR (400 MHz, $CDCl_3$) δ: 4.18 (q, *J* = 7 Hz, 2H, -COOC*H*$_2$CH$_3$), 2.58 (d, *J* = 16 Hz, 1H, *H*-11), 2.51 (ddd, *J* = 16, 5.5, 5.5 Hz, 1H, *H*-8), 2.35 (dqd, *J* = 11, 7, 4 Hz, 1H, *H*-3), 2.21 (dm, *J* = 16 Hz, 1H, *H*-11), 2.00 (m, 1H, *H*-7), 1.85 (br d, *J* = 16 Hz, 1H, *H*-8), 1.83 (m, 1H), 1.72 (m, 3H), 1.63 (s, 3H, 10-C*H*$_3$), 1.55 (m, 1H), 1.54 (s, 3H, 9-C*H*$_3$), 1.44 (m, 1H), 1.26 (t, *J* = 7 Hz, 3H, -COOCH$_2$C*H*$_3$), 1.22 (d, *J* = 7 Hz, 3H, 3-C*H*$_3$); MS *m/z* (M$^+$) calcd. for $C_{17}H_{26}O_3$: 278.1883; found: 278.1882. Anal. calcd. for $C_{17}H_{26}O_3$: C 73.34%, H 9.41%; found: C 72.97%, H 9.58%.

(1S,3R*,7R*,11R*)-1-Carbethoxy-3,11-dimethylbicyclo-[5.4.0]undec-9-en-2-one* (**32**): mp 63–64°C (Skelly B); IR ($CHCl_3$, cast): 1738 (C=O, ester), 1697 (C=O, ketone) cm^{-1}; ^{1}H NMR (400 MHz, $CDCl_3$) δ: 5.65 (m, 1H, H-10), 5.50 (m, 1H, H-9), 4.22 (dq, J = 11, 7 Hz, 1H, -COOCHHCH$_3$), 4.15 (dq, J = 11, 7 Hz, 1H, -COOCHHCH$_3$), 2.93 (m, 1H, H-11), 2.48 (dddd, J = 13.5, 4, 4 Hz, 1H, H-7), 2.40 (m, 1H, H-8), 2.33 (m, 1H, H-3), 1.81 (m, 3H), 1.70 (m, 3H), 1.45 (m, 1H), 1.28 (t, J = 7 Hz, 3H, -COOCH$_2$CH$_3$), 1.26 (d, J = 7 Hz, 3H, 3-CH$_3$), 0.88 (d, J = 7.5 Hz, 3H, 11-CH$_3$); MS m/z (M$^+$) calcd. for $C_{16}H_{24}O_3$: 264.1726; found: 264.1732. Anal. calcd. for $C_{16}H_{24}O_3$: C 72.69%, H 9.15%; found: C 72.46%, H 9.25%.

(1S,3R*,7R*,11S*)-1-Carbethoxy-3,11-dimethylbicyclo-[5.4.0]undec-9-en-2-one* (**33**)

IR (CH_2Cl_2, cast): 1733 (C=O, ester), 1697 (C=O, ketone) cm^{-1}; ^{1}H NMR (400 MHz, $CDCl_3$) δ: 5.57 (br d, *J* = 10 Hz, 1H, *H*-10), 5.51 (m, 1H, *H*-9), 4.30 (dq, *J* = 11, 7 Hz, 1H, -COOC*H*HCH$_3$), 4.24 (dq, *J* = 11, 7 Hz, 1H, -COOCH*H*CH$_3$), 2.62 (m, 1H, *H*-11), 2.52 (ddd, *J* = 15, 9, 4.5 Hz, 1H, *H*-8), 2.25 (dqd, *J* = 11, 7.5, 3 Hz, 1H, *H*-3), 2.00 (m, 1H, *H*-7), 1.92 (m, 2H), 1.73 (m, 2H), 1.63 (m, 1H), 1.40 (m, 2H), 1.32 (t, *J* = 7 Hz, 3H, -COOCH$_2$C*H*$_3$), 1.28 (d, *J* = 7.5 Hz, 3H, 3-C*H*$_3$), 1.14 (d, *J* = 7.5 Hz, 3H, 11-C*H*$_3$); ^{13}C NMR APT (100 MHz, $CDCl_3$) δ: 208.47 (p), 172.69 (p), 132.20 (a), 123.03 (a), 66.10 (p), 60.87 (p), 49.76 (a), 42.51 (a), 39.54 (a), 31.77 (p), 31.59 (p), 27.99 (p), 23.85 (p), 21.71 (a), 16.87 (a), 14.25 (a); MS *m/z* (M$^+$) calcd. for $C_{16}H_{24}O_3$: 264.1726; found: 264.1728. Anal. calcd. for $C_{16}H_{24}O_3$: C 72.69%, H 9.15%; found: C 72.90%, H 9.36%.

(1R,3R*,8S*,9S*)-3-Carbomethoxy-6-methyltricyclo-[7.2.1.0^{3,8}]dodec-5-en-2-one* (**34**)

IR ($CHCl_3$, cast): 1733 (C=O, ester), 1713 (C=O, ketone) cm^{-1}; ^{1}H NMR (400 MHz, $CDCl_3$) δ: 5.52 (m, 1H, *H*-5), 3.68 (s, 3H, -COOC*H*$_3$), 2.85 (dddd, *J* = 7, 7, 2.5, 2.5 Hz, 1H, *H*-8), 2.79 (dd, *J* = 5, 5 Hz, 1H, *H*-1), 2.57 (br dd, *J* = 15, 5.5 Hz, 1H, *H*-4), 2.24–2.11 (m, 3H), 1.92–1.73 (m, 6H), 1.71 (s, 3H, 6-C*H*$_3$), 1.64 (dddd, *J* = 12.5, 5, 5, 2.5 Hz, 1H, *H*-12*syn*); ^{13}C NMR APT (100 MHz, $CDCl_3$) δ: 210.17 (p), 173.99 (p), 136.36 (p), 120.19 (a), 57.80 (p), 52.66 (a), 51.13 (a), 43.33 (a), 42.42 (a), 34.93 (p), 33.14 (p), 31.80 (p), 28.54 (p), 26.85 (p), 23.02 (a); MS *m/z* (M$^+$) calcd. for $C_{15}H_{20}O_3$: 248.1413; found: 248.1412. Anal. calcd. for $C_{15}H_{20}O_3$: C 72.55%, H 8.12%; found: C 72.73%, H 8.41%.

(1R,3R*,8S*,9S*)-3-Carbomethoxy-5,6-dimethyltricyclo-[7.2.1.0^{3,8}]dodec-5-en-2-one* (**35**)

IR (CH_2Cl_2, cast): 1733 (C=O, ester), 1713 (C=O, ketone) cm^{-1}; ^{1}H NMR (400 MHz, $CDCl_3$) δ: 3.68 (s, 3H, -COOC*H*$_3$), 2.74 (m, 2H, *H*-1, *H*-8), 2.42 (d, *J* = 14 Hz, 1H, *H*-4), 2.18 (m, 3H), 1.90–1.72 (m, 6H), 1.70 (s, 3H, 5-C*H*$_3$), 1.66 (s, 3H, 6-C*H*$_3$), 1.62 (dddd, *J* = 12, 4.5, 4.5, 2 Hz, 1H, *H*-12*syn*); MS *m/z* (M$^+$) calcd. for $C_{16}H_{22}O_3$: 262.1569; found: 262.1572. Anal. calcd. for $C_{16}H_{22}O_3$: C 73.25%, H 8.45%; found: C 73.18%, H 8.66%.

(1R,3S*,4R*,8S*,9S*)-3-Carbomethoxy-4-methyltricyclo-[7.2.1.0^{3,8}]dodec-5-en-2-one* (**36**) *and (1R*,3S*,4S*,8S*,9S*)-3-carbomethoxy-4-methyltricyclo-[7.2.1.0^{3,8}]dodec-5-en-2-one* (**37**)

Adducts **36** and **37** were obtained as an inseparable mixture in a ratio of 4:1 (based on ^{1}H NMR integration): IR (film): 1733 (C=O, ester), 1714 (C=O, ketone) cm^{-1}; ^{1}H NMR (400 MHz, $CDCl_3$) δ: 5.91 (m, 0.2H, *H*-5), 5.85 (m, 0.8H, *H*-5), 5.84 (m, 0.2H, *H*-6), 5.74 (ddd, *J* = 9, 5.5, 3 Hz, 0.8H, *H*-6), 3.78 (s, 2.4H, -COOC*H*$_3$), 3.71 (s, 0.6H, -COOC*H*$_3$), 3.17 (dddd, *J* = 12.5, 5.5, 5.5, 3 Hz, 0.8H, *H*-8), 3.07 (qd, *J* = 7, 7 Hz, 0.8H, *H*-4), 2.86 (m, 0.2H), 2.80 (d, *J* = 5, 5 Hz, 0.8H, *H*-1), 2.68 (dd, *J* = 6.5, 4.5 Hz, 0.2H, *H*-4), 2.45 (m, 0.2H), 2.38 (dddd, *J* = 17, 9, 3, 3 Hz, 0.8H, *H*-7), 2.32 (m, 0.2H), 2.21 (m, 1H, *H*-9), 1.97–1.70 (m, 5H), 1.65 (m, 1H), 1.57 (m, 1H), 1.20 (d, *J* = 7 Hz, 0.6H, 4-C*H*$_3$), 0.83 (d, *J* = 7 Hz, 2.4H, 4-C*H*$_3$); MS *m/z* (M$^+$) calcd. for $C_{15}H_{20}O_3$: 248.1413; found: 248.1419. Anal. calcd. for $C_{15}H_{20}O_3$: C 72.55%, H 8.12%; found: C 72.54%, H 8.18%.

Can. J. Chem. Downloaded from www.nrcresearchpress.com by 80.90.12.36 on 09/08/12
For personal use only.

(3R,8S*)-3-Carbethoxy-6-methyltricyclo[7.2.2.0^{3,8}]tridec-5-en-2-one (**38**)*

IR ($CHCl_3$, cast): 1740 (C=O, ester), 1699 (C=O, ketone) cm^{-1}; ^1H NMR (400 MHz, $CDCl_3$) δ: 5.43 (br s, 1H, *H*-5), 4.16 (q, *J* = 7 Hz, 1H, -COOC*H*HCH$_3$), 4.15 (q, *J* = 7 Hz, 1H, -COOCH*H*CH$_3$), 2.82 (ddd, *J* = 6, 6, 2.5 Hz, 1H, *H*-8), 2.64 (br s, 1H, *H*-1), 2.55 (br d, *J* = 18 Hz, 1H, *H*-4), 2.38 (br d, *J* = 18 Hz, 1H, *H*-4), 2.03 (m, 2H), 1.81–1.60 (m, 9H), 1.68 (s, 3H, 6-C*H*$_3$), 1.22 (t, *J* = 7 Hz, 3H, -COOCH$_2$C*H*$_3$); ^{13}C NMR APT (100 MHz, $CDCl_3$) δ: 211.91 (p), 173.60 (p), 134.58 (p), 118.84 (a), 61.39 (p), 60.87 (p), 46.02 (a), 39.51 (a), 37.21 (a), 35.23 (p), 30.40 (p), 25.81 (p), 23.71 (p), 23.26 (a), 21.49 (p), 20.80 (p), 14.14 (a); MS *m/z* (M^+) calcd. for $C_{17}H_{24}O_3$: 276.1726; found: 276.1731.

(3R,8S*)-3-Carbethoxy-5,6-dimethyltricyclo-[7.2.2.0^{3,8}]tridec-5-en-2-one (**39**)*

IR (film): 1738 (C=O, ester), 1702 (C=O, ketone) cm^{-1}; ^1H NMR (400 MHz, $CDCl_3$) δ: 4.18 (dq, *J* = 11,7 Hz, 1H, -COOC*H*HCH$_3$), 4.14 (dq, *J* = 11, 7 Hz, 1H, -COOCH*H*CH$_3$), 2.82 (ddd, *J* = 6.5, 6.5, 3 Hz, 1H, *H*-8), 2.64 (m, 1H, *H*-1), 2.52 (d, *J* = 16 Hz, 1H, *H*-4), 2.25 (d, *J* = 16 Hz, 1H, *H*-4), 2.02 (m, 2H), 1.83–1.50 (m, 9H), 1.68 (s, 3H, 5-C*H*$_3$), 1.65 (s, 3H, 6-C*H*$_3$), 1.23 (t, *J* = 7 Hz, 3H, -COOCH$_2$C*H*$_3$); MS *m/z* (M^+) calcd. for $C_{18}H_{26}O_3$: 290.1882; found: 290.1882.

(3S,4R*,8S*)-3-Carbethoxy-4-methyltricyclo-[7.2.2.0^{3,8}]tridec-5-en-2-one (**40**)*

IR (CH_2Cl_2, cast): 1741 (C=O, ester), 1702 (C=O, ketone) cm^{-1}; ^1H NMR (400 MHz, $CDCl_3$) δ: 5.85 (m, 1H, *H*-5), 5.75 (dd, *J* = 9.5, 5 Hz, 1H, *H*-6), 4.20 (dq, *J* = 11, 7 Hz, 1H, -COOC*H*HCH$_3$), 4.14 (dq, *J* = 11, 7 Hz, 1H, -COOCH*H*CH$_3$), 2.99 (br q, *J* = 7 Hz, 1H, *H*-4), 2.93 (ddd, *J* = 7, 7, 4 Hz, 1H, *H*-8), 2.64 (m, 1H, *H*-1), 2.15 (ddd, *J* = 16, 6, 6 Hz, 1H), 2.05 (br s, 1H), 1.83–1.45 (m, 9H), 1.26 (t, *J* = 7 Hz, 3H, -COOCH$_2$C*H*$_3$), 0.98 (d, *J* = 7 Hz, 3H, 4-C*H*$_3$); ^{13}C NMR APT (100 MHz, $CDCl_3$) δ: 209.92 (p), 172.42 (p), 133.58 (a), 127.30 (a), 65.26 (p), 61.12 (p), 46.08 (a), 41.58 (a), 36.66 (a), 33.69 (a), 28.95 (p), 24.90 (p), 23.74 (p), 21.25 (p), 20.28 (p), 16.17 (a), 14.20 (a); MS *m/z* (M^+) calcd. for $C_{17}H_{24}O_3$: 276.1726; found: 276.1725.

Acknowledgement

We are grateful to the Natural Sciences and Engineering Research Council of Canada and the University of Alberta for financial support.

References

1. (*a*) Mezerein, J. Nyborg and T. La Cour. Nature (London), **257**, 824 (1975). (*b*) Cyathin-A$_3$, W.A. Ayer and H. Taube. Tetrahedron Lett. 1917 (1972). (*c*) Grayanotoxin-II, T. Okuno, N. Hamanaka, H. Miyakoshi, and T. Matsumoto. Tetrahedron **26**, 4765 (1970). (*d*) Aconiline, S.W. Pelletier and Z. Djarmati. J. Am. Chem. Soc. **98**, 2626 (1976). (*e*) Erinacines, H. Kawagishi, A. Shimada, R. Shirai, K. Okamoto, F. Ojima, H. Sakamoto, Y. Ishiguro, and S. Furukawa. Tetrahedron Lett. **35**, 1569 (1994). (*f*) Barekoxide, A. Rudi, and Y. Kashman. J. Nat. Prod. **55**, 1408 (1992).
2. (*a*) Diazoalkanes, E. Mosettig and A. Burger. J. Am. Chem. Soc. **52**, 3456 (1930); E.P. Kohler, M. Tishler, H. Potter, and H.T. Thompson. J. Am. Chem. Soc. **61**, 1057 (1939); D.W. Adamson and J. Kenner. J. Chem. Soc. 181 (1939); J.A. Marshall and J.J. Partiridge. J. Org. Chem. **33**, 4090 (1968); (*b*) Tiffeneau–Demjanov reaction, P.A.S. Smith and D.R. Baer. Org. React. **11**, 157 (1960). (*c*) Decomposition of halohydrin salts, A.J. Sisti. Tetrahedron Lett. 5327 (1967); A.J. Sisti. J. Org. Chem. **33**, 453 (1968); A.J. Sisti and G.M. Rusch. J. Org. Chem. **39**, 1182 (1974). (*d*) Thallium oxidation of exocyclic olefins, D. Farcasiu, P.V.R. Schleyer, and D.B. Ledlie. J. Org. Chem. **38**, 3455 (1973). (e) Rearrangement of sulfur-stabilized ylids, T. Cohen, D. Kuhn, and J.R. Falck. J. Am. Chem. Soc. **97**, 4749 (1975); W.D. Abrahem, M. Bhupath, and T. Cohen. Tetrahedron Lett. **28**, 2203 (1987). (*f*) Rearrangement of β-hydroxy selenides and thallides, D. Labar, J.L. Laboureur, and A. Krief. Tetrahedron Lett. **23**, 983 (1982); J.L. Laboureur and A. Krief. Tetrahedron Lett. **25**, 2713 (1984); A. Krief, J.L. Laboureur, and W. Dumont. Tetrahedron Lett. **28**, 1549 (1987). (*g*) Radical rearrangement, A.L.J. Beckwith, D.M. O'Shea, and S.W. Westwood. J. Am. Chem. Soc. **110**, 2565 (1988); P. Dowd and S.C. Choi. Tetrahedron, **45**, 77 (1989). (*h*) Lewis acid catalyzed diazoacetate, H.J. Liu and S.P. Majumdar. Synth. Commun. **5**, 125 (1975); W.L. Mock and M.E. Hartman. J. Org. Chem. **42**, 459 (1977); J. Org. Chem. **42**, 466 (1977); S.W. Baldwin and N.G. Landmesser. Synth. Commun. **8**, 413 (1978).
3. F. Finguelli, A. Taticchi, and E. Wenkert. Org. Prep. Proced. Int. **22**, 131 (1990).
4. J. Sauer. Angew. Chem. Int. Ed. Engl. **6**, 16 (1967); N.T. Anh, E. Canadell, and O. Eiserstein. Tetrahedron, **34**, 2283 (1978).
5. (*a*) H.J. Liu and E.N.C. Browne. Tetrahedron Lett. 2929 (1977); (*b*) Can. J. Chem. **59**, 601 (1981); (*c*) Can. J. Chem. **65**, 1262 (1987); (*d*) H.J. Liu and E.N.C. Browne, and S.Y. Chew. Can. J. Chem. **66**, 2345 (1988); (*e*) H.J. Liu, S.Y. Chew, and E.N.C. Browne. Tetrahedron Lett. **32**, 2005 (1991); (*f*) H.J. Liu, G. Ulibarri, and E.N.C. Browne. Can. J. Chem. **70**, 1545, (1992); (*g*) H.J. Liu, T.K. Ngooi, and E.N.C. Browne. Can. J. Chem. **66**, 3143 (1988); (*h*) H.J. Liu and T.K. Ngooi. Synth. Commun. **12**, 715 (1982); (*i*) H.J. Liu, S.Y. Chew, E.N.C. Browne, and J.B. Kim. Can. J. Chem. **72**, 1193 (1994); (*j*) H.J. Liu and Y. Han. Tetrahedron Lett. **34**, 423 (1993).
6. F. Fringuelli, F. Pizzo, A. Taticchi, T.D.J. Halls, and E. Wenkert. J. Org. Chem. **47**, 5056 (1982).
7. R.E. Ireland, P.A. Aristoff, and C.F. Hoyng. J. Org. Chem. **44**, 4318 (1979); F. Fringuelli, F. Pizzo, A. Taticchi, and E. Wenkert. Synth. Commun. **9**, 391 (1979); F. Fringuelli, F. Pizzo, A. Taticchi, and E. Wenkert. J. Org. Chem. **48**, 2802 (1983).
8. D. Liotta, C. Barnum, R. Puleo, G. Zima, C. Bayer, and H.S. Kezar. J. Org. Chem. **46**, 2920 (1981); G. Zima and D. Liotta. Synth. Commun. **9**, 697 (1979).
9. G.A. Olah and Q.H. Wu. Synthesis, 407 (1991); R. Mello, M. Fiorentino, C. Fusco, and R. Curci. J. Am. Chem. Soc. **111**, 6749 (1989); V.F. Roche, E.B. Roche, and D.L. Nagel. J. Org. Chem. **47**, 1368 (1982); R.D. Little and S.O. Myong. Tetrahedron Lett. **21**, 3339 (1980); P. Chamberlain and A.E. Rooney. Tetrahedron Lett. 383 (1979); P.A. Verbrugge, J.H. Tielman, P.J. Van der Jagt, and F. Bickelhaupt. Synth. Commun. **7**, 1 (1977); S.A. Monti and G.L. White. J. Org. Chem. **40**, 215 (1975).
10. T. Sugimoto, Y. Kobuke, and J. Furukawa. J. Org. Chem. **41**, 1457 (1976).
11. R. Gleiter and L. Paquette. Acc. Chem. Res. **16**, 328 (1983).
12. W.L. Mock and M.E. Hartman. J. Am. Chem. Soc. **92**, 5767 (1970).

The synthesis of tellurometalates by the reduction of binary telluride melts with potassium in liquid ammonia

Chang-Woo Park, Robert J. Salm, and James A. Ibers

Can. J. Chem. Downloaded from www.nrcresearchpress.com by 80.90.12.36 on 09/08/12
For personal use only.

Abstract: The reduction of binary telluride melts with potassium in liquid ammonia in the presence of 18-Crown-6 or 2,2,2-Crypt has been employed to synthesize and precipitate tellurometalates. The method is more rapid than conventional extraction techniques and, since lower temperatures are involved, potentially unstable fragments are conserved. A melt of nominal composition $CdTe_3$ dissolved with K and 18-Crown-6 in liquid NH_3 affords $[K(18\text{-Crown-6})]_4[Cd_4Te_{12}]$ (**1**) after recrystallization from CH_3CN–Et_2O. Compound **1** crystallizes in the triclinic space group $C_i^1-P\bar{1}$ with one formula unit in a cell of dimensions $a = 12.673(1)$ Å, $b = 13.694(3)$ Å, $c = 14.483(3)$ Å, $\alpha = 117.54(2)°$, $\beta = 96.43(1)°$, and $\gamma = 100.00(1)°$ at 113 K. Full anisotropic refinement of the structure on F_o^2 led to a value of $R_1 = 0.026$ for those 6654 reflections having $F_o^2 > 2\sigma(F_o^2)$. The $[Cd_4Te_{12}]^{4-}$ anion of **1**, which may be formulated as $[Cd_4(Te)_2(Te_2)_2(Te_3)_2]^{4-}$, consists of a rectangular array of four Cd^{2+} centers linked by Te^{2-}, Te_2^{2-}, and Te_3^{2-} ligands. As expected from the solid-state structure, the ^{125}Te NMR spectrum of **1** in CD_3CN shows four resonances at −11, −259, −548, and −1682 ppm. A melt of nominal composition $PbTe_2$ was dissolved with K and 2,2,2-Crypt in liquid NH_3 to afford $[K(2,2,2\text{-Crypt})]_2[Pb_2Te_3]\cdot CH_3CN$ (**2**) after recrystallization from CH_3CN. Compound **2** crystallizes in the triclinic space group C_i^1-P1 with one formula unit in a cell of dimensions $a = 11.105(3)$ Å, $b = 11.748(4)$ Å, $c = 11.922(3)$ Å, $\alpha = 118.78(2)°$, $\beta = 96.52(2)°$, and $\gamma = 91.03(3)°$ at 113 K. Full anisotropic refinement of the structure on F_o^2 led to a value of R_1 of 0.074 for those 11 135 reflections having $F_o^2 > 2\sigma(F_o^2)$. The anion of **2** consists of a triangle of Te^{2-} ligands capped above and below the plane by two Pb^{2+} centers to define a trigonal bipyramid. The ^{125}Te NMR spectrum of **2** in CD_3CN shows one resonance at −928 ppm (J_{Pb-Te}: 1090 Hz).

Key words: tellurometalates, liquid ammonia, synthesis, crystal structure.

Résumé : On a utilisé une réduction de tellurures binaires, à l'état fondu, par du potassium dans de l'ammoniac liquide, en présence de l'éther 18-couronne-6 ou de 2,2,2-Crypt, pour synthétiser et pour précipiter des tellurométallates. La méthode est plus rapide que les techniques conventionnelles d'extraction et, puisque les températures impliquées sont moins élevées, on conserve les fragments qui sont potentiellement instables. Un produit fondu de composition nominale $CdTe_3$ dissous avec du K et de l'éther 18-couronne-6 dans du NH_3 liquide conduit, après recristallisation dans du CH_3CN–Et_2O, au composé $[K(\text{éther 18-couronne-6})]_4[Cd_4Te_{12}]$ (**1**). Les cristaux du composé **1** sont tricliniques, groupe d'espace $C_i^1-P\bar{1}$ avec une formule par unité de dimensions $a = 12{,}673(1)$, $b = 13{,}694(3)$ et $c = 14{,}483(3)$ Å, $\alpha = 117{,}54(2)°$, $\beta = 96{,}43(1)°$ et $\gamma = 100{,}00(1)°$, à 113 K. Un affinement anisotropique complet de la structure sur F_o^2 conduit à une valeur de $R_1 = 0{,}026$ pour les 6654 réflexions pour lesquelles $F_o^2 > 2\sigma(F_o^2)$. L'anion $[Cd_4Te_{12}]^{4-}$ du composé **1** peut être représenté par la formule $[Cd_4(Te)_2(Te_2)_2(Te_3)_2]^{4-}$ et consiste d'un arrangement rectangulaire de quatre centres Cd^{2+} liés par des coordinats Te^{2-}, Te_2^{2-} et Te_3^{2-}. Comme on peut s'y attendre sur la base de la structure à l'état solide, le spectre RMN du ^{125}Te du produit **1**, dans le CD_3CN, présente quatre bandes de résonances à −11, −259, −548 et −1682 ppm. Un produit fondu de composition nominale $PbTe_2$ dissous avec du K et du 2,2,2-Crypt dans du NH_3 liquide conduit, après recristallisation dans du CH_3CN, au composé $[K(2,2,2\text{-Crypt})]_2[Pb_2Te_3]\cdot CH_3CN$ (**2**). Les cristaux du composé **2** sont tricliniques, groupe d'espace C_i^1-P1, avec une formule par unité de dimensions $a = 11{,}105(3)$, $b = 11{,}748(4)$ et $c = 11{,}922(3)$ Å, $\alpha = 118{,}78(2)°$, $\beta = 96{,}52(2)°$ et $\gamma = 91{,}03(3)°$, à 113 K. Un affinement anisotropique complet de la structure sur F_o^2 conduit à une valeur de $R_1 = 0{,}074$ pour les 11 135 réflexions pour lesquelles $F_o^2 > 2\sigma(F_o^2)$. L'anion du composé **2** est formé d'un triangle de coordinats Te^{2-} avec des caps, au-dessus et au-dessous du plan, de deux centres Pb^{2+} qui définissent une bipyramide

Received October 31, 1994.

This paper is dedicated to Professor William A.G. Graham on the occasion of his 65th birthday.

C.-W. Park, R.J. Salm, and J.A. Ibers.[1] Department of Chemistry, Northwestern University, Evanston, IL 60208-3113, U.S.A.

[1] Author to whom correspondence may be addressed. Telephone: (708) 491-5449. Fax: (708) 491-7713. E-mail: ibers@chem.nwu.edu

trigonale. Les spectres RMN du ^{125}Te du composé **2** en solution dans le CD_3CN ne présente qu'une raie de résonance à −928 ppm (J_{Pb-Te} : 1090 Hz).

Mots clés : tellurométallates, ammoniac liquide, synthèse, structure cristalline.

[Traduit par la rédaction]

Introduction

Chalcogenometalates have attracted attention over the past two decades because of their rich chemistry, unusual structures, and their potential role as precursors for technologically important materials (1–3). While most of the studies have centered on the sulfidometalates (4–9), interest in the chemistry of the selenometalates and tellurometalates has developed (10–14).

The number of tellurometalates has increased dramatically in the past few years through the use of synthetic techniques other than that of traditional nonaqueous solution chemistry. These techniques include cathodic dissolution of electrodes composed of metal telluride alloys (15–19), solventothermal sealed-tube reactions (20–29), and the revisiting of the old technique of solvent extraction (30, 31) of metal telluride phases (32–37). Here we report new syntheses and characterization of the previously known tellurometalate anions $[Cd_4Te_{12}]^{4-}$ and $[Pb_2Te_3]^{2-}$. Syntheses were accomplished through the reduction of binary telluride melts in liquid NH_3 in the presence of K and an encapsulating ligand. This method, which has not been previously applied to the synthesis of tellurometalates, is more rapid than conventional solvent extraction techniques and takes place at lower temperatures.

Experimental

Standard Schlenk-line (dry N_2 atmosphere) and glove box (dry Ar atmosphere) techniques were used in the manipulation of the complexes described below. Anhydrous acetonitrile (CH_3CN) and anhydrous diethyl ether (Et_2O) were purchased from the Aldrich Chemical Co., Milwaukee, Wis., distilled under dry N_2 from CaH_2 and Na–benzophenone, respectively, and further purged with dry N_2 before use. Anhydrous NH_3 was purchased from Union Carbide Corp., Linde Div., Hillside, Ill., and used without further purification. Elemental Te (99.999%), Pb (99.999%), and K (99.95%), as well as 18-Crown-6 and 2,2,2-Crypt were purchased from Aldrich Chemical Co., Milwaukee, Wis., elemental Cd (99.999%) was obtained from the Johnson Matthey Co., Ward Hill, Mass. Melts of nominal composition $CdTe_3$ and $PbTe_2$ were prepared by the fusion of stoichiometric amounts of the constituent elements under an inert atmosphere; "$CdTe_3$" is a homogeneous mixture of α-CdTe and Te whereas "$PbTe_2$" is a homogeneous mixture of α-PbTe and Te. These melts were finely ground immediately prior to use. Elemental microanalyses were performed by Oneida Research Services, Whitesboro, N.Y. ^{125}Te NMR data were obtained on samples in DMF/CD_3CN on a Varian Unity + 400 MHz spectrometer equipped with a 10 mm tunable broad-band probe and a deuterium lock. The following conditions were employed: scanning frequency, 126 MHz; delay time, 1 s; pulse width, 14.5 μs; acquisition time, 0.032 s. All ^{125}Te NMR chemical shifts are referenced to the external secondary standard Et_2Te at δ = 380 ppm. The chemical shift scale is based upon Me_2Te at δ = 0.0 ppm.

Syntheses

(a) $[K(18\text{-Crown-6})]_4[Cd_4Te_{12}]$ (1)

18-Crown-6 (528 mg, 2 mmol) and K (80 mg, 2 mmol) were placed in a Schlenk flask. NH_3 (ca. 60 mL) was condensed into the flask at liquid N_2 temperature and the resultant blue solution was stirred for 30 min at −78°C. Finely ground $CdTe_3$ (988 mg, 2 mmol) was then added and the mixture was stirred for 2 d to provide a brown solution. The NH_3 was allowed to evaporate at room temperature and CH_3CN (30 mL) was added to the residual material. The resultant solution was filtered. Et_2O (90 mL) was layered on top of the filtrate to afford, after 5 d, dark red blocks of **1** (yield, 240 mg of crystals, 15.0% based on Cd). Anal. calcd. for $C_{48}H_{96}Cd_4K_4O_{24}Te_{12}$: C 18.05, H 3.03, K 4.90; found: C 18.19, H 2.87, K 4.36. ^{125}Te NMR (DMF/CD_3CN, ppm) δ: −11, −259, −548, −1682 ppm.

(b) $[K(2,2,2\text{-Crypt})]_2[Pb_2Te_3]\cdot CH_3CN$ (2)

2,2,2-Crypt (1506 mg, 4 mmol) and K (160 mg, 4 mmol) were placed in a Schlenk flask. NH_3 (ca. 60 mL) was condensed into the flask at liquid N_2 temperature and the resultant blue solution was stirred for 30 min at −78°C. Finely ground $PbTe_2$ (925 mg, 2 mmol) was then added and the mixture was stirred for 2 d to afford a bright red solution. The NH_3 was allowed to evaporate at room temperature and CH_3CN (30 mL) was added to the residual material. The solution was filtered and the CH_3CN was removed under reduced pressure. The resultant powder was redissolved in CH_3CN (10 mL). The flask was cooled to −20°C to provide, after 3 d, dark red plates of **2** (113 mg of crystals, 6.8% based on Pb). Anal. calcd. for $C_{38}H_{75}K_2N_5O_{12}Pb_2Te_3$: C 27.34, H 4.53, N 4.20, K 4.68; found: C 27.32, H 4.59, N 3.94, K 4.93. ^{125}Te NMR (CD_3CN, ppm) δ: −928 (J_{Pb-Te}: 1090 Hz).

Crystallographic studies

Dark red blocks of **1** or red plates of **2** were placed under degassed Krytox (Dupont) oil and were mounted on glass fibers in a glove bag filled with dry N_2. A fiber with a suitable crystal was transferred to the cold N_2 stream of an Enraf–Nonius CAD4 automatic diffractometer. Intensity data were collected at 113 K with MoKα radiation. The resultant profile data were processed (38) and then were corrected for absorption effects (39). For all structural analyses the SHELXTL–PC graphics programs were employed (40) and the structures were refined on F^2 through the use of the SHELXL–93 least-squares refinement program (41).

(a) $[K(18\text{-Crown-6})]_4[Cd_4Te_{12}]$ (1)

The unit cell of **1** was determined by least-squares refinement of the setting angles of 25 reflections automatically cen-

Can. J. Chem. Downloaded from www.nrcresearchpress.com by 80.90.12.36 on 09/08/12
For personal use only.

Can. J. Chem. Downloaded from www.nrcresearchpress.com by 80.90.12.36 on 09/08/12
For personal use only.

Table 1. Crystallographic details for $[K(18\text{-Crown-6})]_4[Cd_4Te_{12}]$ (**1**) and $[K(2,2,2\text{-Crypt})]_2[Pb_2Te_3]\cdot CH_3CN$ (**2**).

Compound	$[K(18\text{-Crown-6})]_4[Cd_4Te_{12}]$	$[K(2,2,2\text{-Crypt})]_2[Pb_2Te_3]\cdot CH_3CN$
Formula	$C_{48}H_{92}Cd_4K_4O_{24}Te_{12}$	$C_{38}H_{75}K_2N_5O_{12}Pb_2Te_3$
fw	3190.42	1669.41
a, Å	12.673(1)	11.105(3)
b, Å	13.694(3)	11.748(4)
c, Å	14.483(3)	11.922(3)
α, deg	117.54(2)	118.78(2)
β, deg	96.43(1)	96.52(2)
γ, deg	100.00(1)	91.03(3)
V, Å^3	2140.9(7)	1349.8(7)
Z	1	1
Space group	C_i^1–$P\bar{1}$	C_1^1–$P1$
ρ_{calc}, g cm^{-3}	2.475	2.054
μ, cm^{-1}	52.4	80.3
T, K	113	113
R_1[a]	0.0257	0.0736
wR_2[b]	0.0668	0.1531

[a] $R_1 = \Sigma||F_o| - |F_c|| / \Sigma |F_o|$
[b] $wR_2 = \{\Sigma[w(F_o^2 - F_c^2)^2]/\Sigma wF_o^4\}^{1/2}$; $w^{-1} = \sigma^2(F_o^2) + (0.04 \times F_o^2)^2$; $w^{-1} = \sigma^2(F_o^2)$, $F_o^2 < 0$.

tered in the range $19 \leq \theta \leq 20°$. Data were collected for all reflections in the range $2° \leq \theta \leq 25°$. The intensities of six standard reflections, which were measured every 3 h, remained constant throughout the data collection. Crystallographic data are listed in Table 1 and additional details are provided in Table SI.[2]

The triclinic cell did not reduce to indicate higher symmetry. Both the agreement among Friedel pairs and intensity statistics favored the centrosymmetric space group $P\bar{1}$ and the structure was successfully solved and refined in that space group. With one formula unit in the cell, the $[Cd_4Te_{12}]^{4-}$ anion has a crystallographically imposed center of symmetry. The positions of the two Cd, six Te, and two independent K atoms were determined from a direct methods solution (40); the positions of the remaining nonhydrogen atoms were found from successive difference electron density maps. Some disorder of a cation was apparent. The model used to describe this disorder involves two separate conformations of five C atoms and two O atoms in the first cation. The first conformation C(4)-O(3)-C(5)-C(6)-O(4)-C(7)-C(8) has atom O(3) bonded to atom K(1). The second conformation C(4A)-O(3A)-C(5A)-C(6A)-O(4A)-C(7A)-C(8A) has atom O(3A) bonded to K(2) in the other cation. The occupancy of each conformation was refined with the sum of the occupancies of the corresponding atoms in the two conformations fixed at 1.0; the occupancies of the two conformations refine to 0.483(7) and 0.517(7). The locations of atoms C(5) and C(6A), although they correspond to different C atoms in the connectivity of the two groups, could not be distinguished from each other and so were fixed to have the same position and thermal parameters. All hydrogen atom positions were placed at calculated positions and were included in the final refinement. For those reflections having $F_o^2 > 2\sigma(F_o^2)$ the final cycle of least-squares refinement converged to a value of R_1 of 0.026 (6654 observations, 470 parameters). Final nonhydrogen atom positions and equivalent isotropic displacement parameters are listed in Table 2, anisotropic thermal displacement parameters are provided in Table SII, and hydrogen atom positions are listed in Table SIII.[2]

(b) $[K(2,2,2\text{-Crypt})]_2[Pb_2Te_3]\cdot CH_3CN$ (2)

The unit cell of **2** was determined by least-squares refinement of the setting angles of 25 reflections automatically centered in the range $20 \leq \theta \leq 22°$. The resultant cell, which was triclinic, did not reduce. Data were collected for all reflections in the range $2 \leq \theta \leq 30.5°$. The intensities of six standard reflections, which were measured every 3 h, remained constant throughout the data collection. Crystallographic data are listed in Table 1 and additional details are provided in Table SIV.[2]

The distribution of intensities strongly favored the absence of a center of symmetry and thus the apparent space group is $P1$. Among known structures of all types of materials this space group is remarkably rare compared with its centrosymmetric counterpart $P\bar{1}$. Consequently, intensity statistics were ignored and an attempt was made to solve the structure in $P\bar{1}$. The resultant direct-methods solution was interesting. It showed Pb atoms at the apices of a Pb_2Te_3 trigonal bipyramid, but the bipyramid had a crystallographically imposed center of symmetry and thus the equatorial plane consisted of six half-Te atoms. In addition, the solution revealed the positions of two K atoms too close to each other to be encapsulated with 2,2,2-Crypt ligands. Such features suggested that removal of the center of symmetry would lead to a chemically sensible

[2] Copies of material on deposit: crystallographic details (Table SI (**1**), Table SIV (**2**)), thermal displacement parameters (Table SII (**1**), Table SV (**2**)), hydrogen atom positions (Table SIII (**1**), Table SVI (**2**)), bond distances and angles (Table SVII (**1**), Table SVIII (**2**)), may be purchased from: The Depository of Unpublished Data, Document Delivery, CISTI, National Research Council Canada, Ottawa, Canada K1A 0S2.

With the exception of thermal displacement parameters, this material has also been deposited with the Cambridge Crystallographic Data Centre, and can be obtained on request from The Director, Cambridge Crystallographic Data Centre, University Chemical Laboratory, 12 Union Road, Cambridge, CB2 1EZ, U.K.

Can. J. Chem. Downloaded from www.nrcresearchpress.com by 80.90.12.36 on 09/08/12
For personal use only.

Table 2. Atomic positions and equivalent isotropic displacement parameters ($Å^2$) for $[K(18\text{-Crown-6})]_4[Cd_4Te_{12}]$ (**1**).

Atom	*x*	*y*	*z*	*U*(eq)
Cd(1)	0.44432(3)	0.67258(3)	0.14671(3)	0.01833(8)
Cd(2)	0.43635(3)	0.55387(3)	−0.14316(3)	0.01966(9)
Te(1)	0.50706(2)	0.62173(3)	0.30187(3)	0.01880(8)
Te(2)	0.61855(2)	0.70218(3)	0.03976(3)	0.01725(8)
Te(3)	0.29282(2)	0.47132(3)	−0.03436(2)	0.01686(8)
Te(4)	0.33406(2)	0.83780(3)	0.15969(2)	0.01810(8)
Te(5)	0.42828(3)	0.88114(3)	0.01728(3)	0.02477(9)
Te(6)	0.33507(3)	0.70123(3)	−0.18181(3)	0.02715(9)
K(1)	0.24310(9)	0.40361(10)	0.19354(10)	0.0285(3)
O(1)	0.0332(3)	0.3085(3)	0.0596(3)	0.0313(9)
O(2)	0.0844(3)	0.5358(3)	0.2272(3)	0.0338(9)
O(5)	0.3253(4)	0.2638(3)	0.2468(4)	0.0481(13)
O(6)	0.1342(3)	0.1551(3)	0.0897(3)	0.0283(8)
K(2)	0.08164(9)	0.88567(9)	0.52306(8)	0.0193(2)
O(11)	0.1506(3)	0.8421(3)	0.6822(3)	0.0319(9)
O(12)	−0.0565(3)	0.7230(4)	0.5517(4)	0.0441(12)
O(13)	−0.0974(3)	0.7372(3)	0.3660(3)	0.0252(8)
O(14)	0.0111(3)	0.9243(3)	0.3498(2)	0.0186(7)
O(15)	0.2346(3)	0.9819(3)	0.4480(3)	0.0207(7)
O(16)	0.2930(3)	0.9905(3)	0.6415(3)	0.0257(8)
C(1)	−0.0455(5)	0.3743(6)	0.0858(5)	0.046(2)
C(2)	0.0099(5)	0.4962(5)	0.1298(5)	0.039(2)
C(3)	0.1403(5)	0.6511(5)	0.2691(6)	0.047(2)
C(9)	0.2850(5)	0.1437(5)	0.1915(5)	0.0343(13)
C(10)	0.2266(5)	0.1079(5)	0.0817(5)	0.0350(14)
C(11)	0.0724(5)	0.1289(5)	−0.0109(4)	0.0363(14)
C(12)	−0.0161(5)	0.1898(5)	0.0085(4)	0.0359(14)
C(101)	0.3286(4)	0.9561(5)	0.7161(4)	0.0285(12)
C(102)	0.2353(5)	0.9337(5)	0.7647(4)	0.0325(13)
C(103)	0.0640(5)	0.8018(7)	0.7210(6)	0.054(2)
C(104)	−0.0106(5)	0.6966(7)	0.6308(7)	0.067(3)
C(105)	−0.1061(5)	0.6258(6)	0.4519(6)	0.050(2)
C(106)	−0.1719(4)	0.6573(5)	0.3821(5)	0.0341(13)
C(107)	−0.1557(4)	0.7899(4)	0.3197(4)	0.0202(10)
C(108)	−0.0815(4)	0.8378(4)	0.2695(4)	0.0217(10)
C(109)	0.0985(4)	0.9501(4)	0.3039(4)	0.0235(11)
C(110)	0.1963(4)	1.0322(4)	0.3889(4)	0.0225(11)
C(111)	0.3406(4)	1.0481(4)	0.5163(4)	0.0277(12)
C(112)	0.3732(4)	0.9952(5)	0.5815(4)	0.0277(12)
O(3)	0.2434(6)	0.5966(6)	0.3968(5)	0.021(2)
O(4)	0.2785(6)	0.4201(8)	0.4255(6)	0.023(2)
C(4)	0.1891(14)	0.6806(12)	0.4019(14)	0.026(4)
C(6)	0.3503(8)	0.5322(9)	0.4919(8)	0.021(2)
C(7)	0.331(2)	0.3339(14)	0.4198(11)	0.029(4)
C(8)	0.4028(11)	0.3031(10)	0.3373(9)	0.027(3)
C(5)	0.2932(5)	0.6046(5)	0.4899(5)	0.0354(14)
O(3A)	0.2058(9)	0.7243(8)	0.4462(8)	0.027(2)
O(4A)	0.2779(5)	0.4746(7)	0.4120(5)	0.019(2)
C(4A)	0.2327(8)	0.7026(8)	0.3463(8)	0.023(2)
C(5A)	0.1920(8)	0.6283(8)	0.4642(8)	0.025(2)
C(7A)	0.3689(9)	0.4352(8)	0.4311(7)	0.022(2)
C(8A)	0.3415(11)	0.3071(11)	0.3721(11)	0.021(3)
C(6A)	0.2932(5)	0.6046(5)	0.4899(5)	0.0354(14)

Table 3. Atomic positions and equivalent isotropic displacement parameters ($Å^2$) for $[K(2,2,2\text{-Crypt})]_2[Pb_2Te_3]\cdot CH_3CN$ (**2**).

Atom	*x*	*y*	*z*	*U*(eq)
Pb(1)	0.51199(5)	−0.11492(5)	−0.14400(5)	0.0247(2)
Pb(2)	0.48845(5)	0.11526(5)	0.14370(5)	0.0238(2)
Te(1)	0.39119(10)	−0.15736(10)	0.04391(11)	0.0288(3)
Te(2)	0.72793(9)	0.03626(9)	0.04405(9)	0.0186(2)
Te(3)	0.38426(11)	0.12188(13)	−0.09273(13)	0.0349(3)
K(1)	−0.0240(3)	−0.2893(3)	0.3844(3)	0.0163(6)
K(2)	−0.1874(3)	0.3756(3)	0.7139(3)	0.0132(6)
O(1)	0.0853(9)	−0.4967(10)	0.1868(10)	0.022(2)
O(2)	−0.1624(10)	−0.5248(10)	0.2144(10)	0.020(2)
O(3)	0.1065(10)	−0.2842(11)	0.6049(10)	0.026(3)
O(4)	−0.1319(9)	−0.2206(10)	0.6055(10)	0.017(2)
O(5)	0.1067(11)	−0.0735(11)	0.4012(11)	0.028(3)
O(6)	−0.1453(10)	−0.1252(10)	0.3126(10)	0.020(2)
O(7)	−0.3075(10)	0.1338(10)	0.6404(10)	0.019(2)
O(8)	−0.0723(10)	0.2230(9)	0.7942(10)	0.017(2)
O(9)	−0.3060(9)	0.5349(9)	0.9211(9)	0.015(2)
O(10)	−0.0691(9)	0.6091(9)	0.8914(9)	0.014(2)
O(11)	−0.3060(10)	0.4284(10)	0.5232(9)	0.019(2)
O(12)	−0.0708(9)	0.3328(9)	0.5153(9)	0.014(2)
N(1)	0.2409(12)	−0.2864(13)	0.4052(13)	0.026(3)
N(2)	−0.2894(11)	−0.2966(12)	0.3630(11)	0.017(3)
N(3)	−0.4590(12)	0.3526(12)	0.6693(12)	0.016(3)
N(4)	0.0805(11)	0.3984(11)	0.7567(11)	0.015(3)
C(1)	0.276(2)	−0.375(2)	0.280(2)	0.037(5)
C(2)	0.213(2)	−0.505(2)	0.212(2)	0.035(4)
C(3)	0.0168(14)	−0.620(2)	0.138(2)	0.021(3)
C(4)	−0.112(2)	−0.611(2)	0.100(2)	0.021(3)
C(5)	−0.2907(14)	−0.525(2)	0.185(2)	0.024(4)
C(6)	−0.337(2)	−0.4322(14)	0.306(2)	0.019(3)
C(7)	0.283(2)	−0.333(2)	0.494(2)	0.037(4)
C(8)	0.235(2)	−0.264(2)	0.623(2)	0.041(5)
C(9)	0.059(2)	−0.200(2)	0.722(2)	0.026(4)
C(10)	−0.072(2)	−0.239(2)	0.705(2)	0.031(4)
C(11)	−0.264(2)	−0.251(2)	0.5916(14)	0.026(4)
C(12)	−0.325(2)	−0.218(2)	0.491(2)	0.026(4)
C(13)	0.294(2)	−0.153(2)	0.452(2)	0.042(5)
C(14)	0.232(2)	−0.087(2)	0.382(2)	0.035(4)
C(15)	0.047(2)	−0.021(2)	0.329(2)	0.033(4)
C(16)	−0.082(2)	0.000(2)	0.354(2)	0.031(4)
C(17)	−0.271(2)	−0.111(2)	0.314(2)	0.026(4)
C(18)	−0.3337(14)	−0.242(2)	0.279(2)	0.018(3)
C(19)	−0.5011(13)	0.2369(14)	0.675(2)	0.018(3)
C(20)	−0.4365(14)	0.1129(14)	0.596(2)	0.020(3)
C(21)	−0.2769(14)	0.130(2)	0.7583(14)	0.019(3)
C(22)	−0.1423(14)	0.1071(13)	0.769(2)	0.018(3)
C(23)	0.052(2)	0.2012(14)	0.782(2)	0.022(3)
C(24)	0.1208(13)	0.3326(13)	0.8273(13)	0.015(3)
C(25)	−0.496(2)	0.4718(14)	0.7749(14)	0.022(3)
C(26)	−0.4327(13)	0.5061(14)	0.9068(14)	0.018(3)
C(27)	−0.2700(14)	0.6586(13)	0.9380(14)	0.016(3)
C(28)	−0.1372(14)	0.6915(14)	0.9865(14)	0.018(3)
C(29)	0.0557(14)	0.616(2)	0.9392(14)	0.016(3)
C(30)	0.1236(14)	0.5374(14)	0.830(2)	0.016(3)

Can. J. Chem. Downloaded from www.nrcresearchpress.com by 80.90.12.36 on 09/08/12
For personal use only.

Table 3 (*concluded*).

Atom	*x*	*y*	*z*	*U*(eq)
C(31)	−0.497(2)	0.343(2)	0.5456(13)	0.021(3)
C(32)	−0.4337(13)	0.438(2)	0.518(2)	0.020(3)
C(33)	−0.267(2)	0.327(2)	0.4117(14)	0.019(3)
C(34)	−0.1340(14)	0.343(2)	0.4127(14)	0.016(3)
C(35)	0.0570(14)	0.373(2)	0.535(2)	0.020(3)
C(36)	0.1231(14)	0.335(2)	0.6300(14)	0.018(3)
N(5)	0.226(2)	0.223(2)	0.280(2)	0.045(5)
C(37)	0.178(2)	0.146(2)	0.185(2)	0.030(4)
C(38)	0.111(2)	0.048(2)	0.063(2)	0.026(4)

Fig. 1. The $[Cd_4Te_{12}]^{4-}$ anion of **1**. Here and in Fig. 2 the 50% probability ellipsoids are shown.

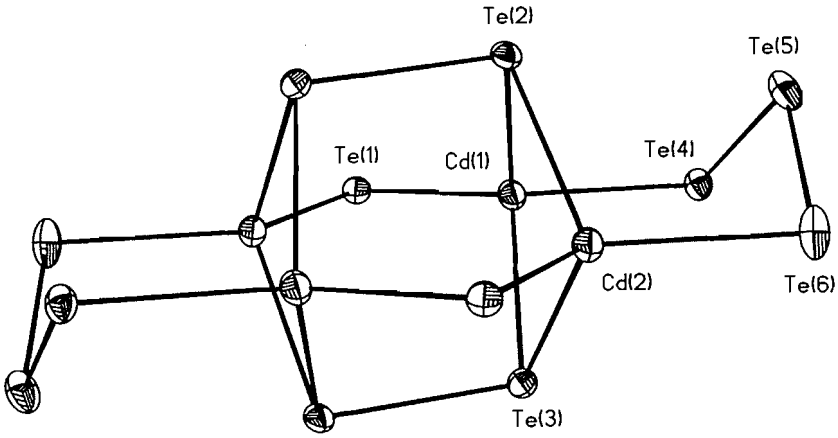

structure. Subsequently, a solution in the non-centrosymmetric space group $P1$ made chemical sense, and successive refinement of this solution revealed not only the positions of the two independent 2,2,2-Crypt ligands but also of one CH_3CN solvent molecule. At the conclusion of a standard anisotropic refinement on F_o^2 of all nonhydrogen atoms, with inclusion of hydrogen atoms at their calculated positions, the values of the agreement indices were $wR_2 = 0.172$ for 12 926 data and 561 parameters and $R_1 = 0.0823$ for 11 135 observations having $F_o^2 > 2\sigma(F_o^2)$. The Flack parameter of 0.372(7) strongly suggested that, while the absolute structure of the major component was correct, there was twinning to the extent of 0.63:0.37. Refinement of a twin led to values of wR_2 of 0.153 and R_1 of 0.0736 and a twinning parameter of 0.376(6). Final nonhydrogen atom positions and equivalent isotropic displacement parameters are listed in Table 3, anisotropic thermal displacement parameters are provided in Table SV, and hydrogen atom positions are listed in Table SVI.[2]

Discussion

The tellurometalates described above were synthesized by dissolving the appropriate binary telluride melt in liquid NH_3 in the presence of K and either 18-Crown-6 or 2,2,2-Crypt. The use of an alkali metal sequestering agent is essential to prevent reversion of the species formed to insoluble materials during the evaporation of the solvent (31). The binary telluride melts were finely ground prior to addition to the K–NH_3 solution to foster rapid dissolution.

Compound **1** is $[K(18\text{-Crown-6})]_4[Cd_4Te_{12}]$. It was obtained as dark red blocks from the reaction of $CdTe_3$ with K and 18-Crown-6 in liquid NH_3, followed by recrystallization from CH_3CN–Et_2O. $CdTe_3$ is a homogeneous mixture of α-CdTe and Te. The corresponding reaction with α-CdTe did not afford **1**. The anion of **1** was previously crystallized as $[Na(15\text{-Crown-5})]_4[Cd_4Te_{12}]\cdot 8DMF$ through a traditional route involving the reaction of Na_2Te_3 with $Cd(OAc)_2\cdot 2H_2O$ in DMF solution in the presence of 15-Crown-5 (42) and as $[NEt_4]_4[Cd_4Te_{12}]$ through a traditional route involving the reaction of K_2Te_2 with CdI_2 in DMF solution in the presence of NEt_4Br (43). The $[Cd_4Te_{12}]^{4-}$ anion may be formulated as $[Cd_4(Te)_2(Te_2)_2(Te_3)_2]^{4-}$ (Fig. 1). The anion has a crystallographically imposed center of symmetry. It contains a rectangular array of tetrahedrally coordinated Cd atoms (formally, Cd^{2+}). The long sides of the rectangle are symmetrically bridged by two Te^{2-} anions and the short sides are linked by two Te_3^{2-} chains. In addition, the four Cd atoms are bridged above and below the rectangular faces by two Te_2^{2-} units. Selected distances found in the present structure are given in Table 4 and a complete listing is given in Table SVII.[2] The metrical details for the anion are very similar to those reported earlier (42, 43). The distances from the Cd atoms to the bridging Te^{2-} species are 2.721(1) and 2.727(1) Å. The distances from the Cd atoms to the Te atoms of the Te_2^{2-} bridges range from 2.911(1) to 2.940(1) Å and the Te—Te distance is 2.773(1) Å. The distances from the Cd atoms to the Te atoms of the Te_3^{2-} chains are 2.796(1) and 2.805(1) Å and the Te—Te distances are 2.727(1) and 2.733(1) Å. The angles about the Cd

Can. J. Chem. Downloaded from www.nrcresearchpress.com by 80.90.12.36 on 09/08/12
For personal use only.

Table 4. Selected bond distances (Å) and angles (deg) for $[K(18\text{-Crown-6})]_4[Cd_4Te_{12}]$ (**1**).

Cd(1)—Te(1)	2.721(1)	K(1)—O(3)	2.907(7)
Cd(1)—Te(2)	2.911(1)	K(1)—O(4)	3.235(8)
Cd(1)—Te(3)	2.917(1)	K(1)—O(4A)	2.801(7)
Cd(1)—Te(4)	2.805(1)	K(1)—O(5)	2.687(4)
Cd(2)—Te(1′)	2.727(1)	K(1)—O(6)	2.986(4)
Cd(2)—Te(2)	2.916(1)	K(2)—O(11)	2.726(4)
Cd(2)—Te(3)	2.940(1)	K(2)—O(12)	2.803(4)
Cd(2)—Te(6)	2.796(1)	K(2)—O(13)	2.724(4)
Te(2)—Te(3′)	2.773(1)	K(2)—O(14)	2.875(3)
Te(4)—Te(5)	2.733(1)	K(2)—O(15)	2.754(3)
Te(5)—Te(6)	2.727(1)	K(2)—O(16)	2.745(4)
K(1)—O(1)	2.800(4)	K(2)—O(3A)	2.814(11)
K(1)—O(2)	2.869(4)		
Te(1)-Cd(1)-Te(2)	113.30(2)	Te(3′)-Te(2)-Cd(2)	95.60(2)
Te(1)-Cd(1)-Te(3)	109.24(2)	Te(5)-Te(4)-Cd(1)	95.38(2)
Te(1)-Cd(1)-Te(4)	128.01(2)	Te(6)-Te(5)-Te(4)	107.67(2)
Te(2)-Cd(1)-Te(4)	103.69(2)	Te(5)-Te(6)-Cd(2)	93.10(2)
Te(2)-Cd(1)-Te(3)	98.60(2)	O(1)-K(1)-O(2)	59.70(12)
Te(3)-Cd(1)-Te(4)	99.48(2)	O(2)-K(1)-O(3)	55.4(2)
Te(1′)-Cd(2)-Te(6)	121.97(2)	O(3)-K(1)-O(4)	52.5(2)
Te(1′)-Cd(2)-Te(2)	113.11(2)	O(4)-K(1)-O(5)	53.3(2)
Te(1′)-Cd(2)-Te(3)	110.98(2)	O(5)-K(1)-O(6)	58.02(11)
Te(2)-Cd(2)-Te(6)	105.11(2)	O(6)-K(1)-O(1)	58.00(11)
Te(2)-Cd(2)-Te(3)	97.97(2)	O(4A)-K(1)-O(5)	66.1(2)
Te(6)-Cd(2)-Te(3)	104.75(2)	O(11)-K(2)-O(12)	60.11(12)
Cd(1)-Te(1)-Cd(2′)	84.44(2)	O(12)-K(2)-O(13)	60.43(12)
Cd(1)-Te(2)-Cd(2)	79.27(2)	O(13)-K(2)-O(14)	60.24(10)
Cd(1)-Te(3)-Cd(2)	78.77(2)	O(14)-K(2)-O(15)	60.08(10)
Te(2′)-Te(3)-Cd(1)	101.95(2)	O(15)-K(2)-O(16)	60.26(10)
Te(2′)-Te(3)-Cd(2)	100.35(2)	O(16)-K(2)-O(11)	61.40(11)
Te(3′)-Te(2)-Cd(1)	97.10(2)		

Primed atoms are related to their unprimed counterparts by the inversion center.

Can. J. Chem. Downloaded from www.nrcresearchpress.com by 80.90.12.36 on 09/08/12
For personal use only.

atoms range from 97.97(2)° to 128.01(2)° to provide distorted tetrahedral geometry about the Cd^{2+} centers. The two $[K(18\text{-Crown-6})]^+$ cations are packed perpendicularly to one another. The two cations are sufficiently close to allow for a disorder in which one of the O atoms (O(3A)) of the first cation coordinates to the atom K(2) of the second cation, as discussed above. The K(2)—O(3A) distance of 2.814(11) Å falls in the range of the other K—O bonds found in the cations (Table 4). The cation distances and angles are normal (Table SVII).

The ^{125}Te NMR spectrum of **1** shows four lines. This strongly suggests that the solid-state structure of the anion of **1** is maintained in solution.

Compound **2** is $[K(2,2,2\text{-Crypt})]_2[Pb_2Te_3]\cdot CH_3CN$. It was obtained as dark red plates from the reaction of a melt of nominal composition $PbTe_2$ with K and 2,2,2-Crypt in liquid NH_3, followed by recrystallization from CH_3CN. The unsolvated compound $[K(2,2,2\text{-Crypt})]_2[Pb_2Te_3]$ was previously synthesized from the dissolution of $KPb_{0.65}Te$ in ethylenediamine in the presence of 2,2,2-Crypt (44). The ^{125}Te NMR spectrum of the **1** (one resonance at −928 ppm, J_{Pb-Te} = 1090 Hz) agrees with that found previously (one resonance at −927.1 ppm, J_{Pb-Te} = 1070 Hz) (45).

The structure of the $[Pb_2Te_3]^{2-}$ anion is shown in Fig. 2. It consists of a triangle of Te^{2-} ligands capped above and below the plane by two Pb^{2+} centers to define a trigonal bipyramid. Selected metrical details for the structure of **2** are given in Table 5 and a complete listing is in Table SVIII.[2] The Pb—Te distances range from 2.954(2) to 3.015(1) Å, the Pb—Pb distance is 3.232(1) Å, and the Te-Pb-Te angles range from 92.21(4)° to 94.33(4)°. These may be compared with the Pb—Te distance of 2.943(2) Å, the Pb—Pb distance of 3.248(3) Å, and the Te-Pb-Te angle of 92.46(4)° in $[K(2,2,2\text{-Crypt})]_2[Pb_2Te_3]$ (44) where the anion has crystallographically imposed 32 symmetry. In the present structure the K(2,2,2-Crypt) anions have their expected structures.

The preparation of $[K(18\text{-Crown-6})]_4[Cd_4Te_{12}]$ (**1**) and $[K(2,2,2\text{-Crypt})]_2[Pb_2Te_3]\cdot CH_3CN$ (**2**) through the reduction of binary telluride melts in liquid NH_3 in the presence of K and an encapsulating ligand appears to be the first use of liquid NH_3 for the preparation of tellurometalates, although liquid NH_3 was used previously in the preparation of Zintl phases (31). The method is more rapid than conventional extraction techniques and, since the reaction is carried out at a lower temperature, potentially unstable fragments are conserved. Indeed, with the use of this technique we recently isolated the very unstable $[GaTe_3]^{3-}$ and $[In_3Te_7]^{5-}$ anions (46).

Can. J. Chem. Downloaded from www.nrcresearchpress.com by 80.90.12.36 on 09/08/12
For personal use only.

Table 5. Selected bond distances (Å) and angles (deg) for $[K(2,2,2\text{-Crypt})]_2[Pb_2Te_3]\cdot CH_3CN$ (**2**).

Pb(1)—Te(1)	2.967(1)	K(1)—O(6)	2.77(1)
Pb(1)—Te(2)	2.954(2)	K(1)—N(1)	2.92(1)
Pb(1)—Te(3)	2.971(2)	K(1)—N(2)	2.93(1)
Pb(1)—Pb(2)	3.232(1)	K(2)—O(7)	2.80(1)
Pb(2)—Te(1)	2.959(2)	K(2)—O(8)	2.69(1)
Pb(2)—Te(2)	3.015(1)	K(2)—O(9)	2.78(1)
Pb(2)—Te(3)	2.961(2)	K(2)—O(10)	2.72(1)
K(1)—O(1)	2.86(1)	K(2)—O(11)	2.83(1)
K(1)—O(2)	2.81(1)	K(2)—O(12)	2.67(1)
K(1)—O(3)	2.83(1)	K(2)—N(3)	2.99(1)
K(1)—O(4)	2.78(1)	K(2)—N(4)	2.95(1)
K(1)—O(5)	2.81(1)		
Te(1)-Pb(1)-Te(2)	94.33(4)	Te(3)-Pb(1)-Pb(2)	56.83(4)
Te(1)-Pb(1)-Te(3)	93.00(4)	Te(1)-Pb(2)-Pb(1)	57.06(4)
Te(2)-Pb(1)-Te(3)	93.24(5)	Te(2)-Pb(2)-Pb(1)	56.31(3)
Te(1)-Pb(2)-Te(2)	93.22(4)	Te(3)-Pb(2)-Pb(1)	57.14(4)
Te(1)-Pb(2)-Te(3)	93.37(5)	Pb(1)-Te(1)-Pb(2)	66.10(4)
Te(2)-Pb(2)-Te(3)	92.21(4)	Pb(1)-Te(2)-Pb(2)	65.55(3)
Te(1)-Pb(1)-Pb(2)	56.83(4)	Pb(1)-Te(3)-Pb(2)	66.03(4)
Te(2)-Pb(1)-Pb(2)	58.14(3)		

Fig. 2. The $[Pb_2Te_3]^{2-}$ anion of **2**.

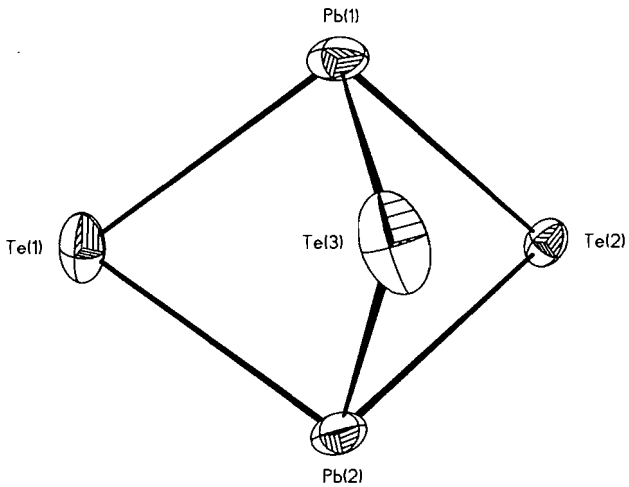

Acknowledgment

This research was supported by the U. S. National Science Foundation, Grant CHE92-24469.

References

1. R.C. Haushalter, M.M.J. Treacy, and S.B. Rice. Angew. Chem. Int. Ed. Engl. **26**, 1155 (1987).
2. Jin-S. Jung, M.J. Jun, Jung-H. Jun, and C.J. O'Connor. Inorg. Chim. Acta, **211**, 167 (1993).
3. J.H. Zhang, B. Wu, and C.J. O'Connor. Chem. Mater. **5**, 17 (1993).
4. A. Müller, E. Diemann, R. Jostes, and H. Bögge. Angew. Chem. Int. Ed. Engl. **20**, 934 (1981).
5. A. Müller, W. Jaegerman, and J.H. Enemark. Coord. Chem. Rev. **46**, 245 (1982).
6. S. Sarkar and S.B.S. Mishra. Coord. Chem. Rev. **59**, 239 (1984).
7. A. Müller and E. Diemann. Adv. Inorg. Chem. **31**, 89 (1987).
8. B. Krebs and G. Henkel. Angew. Chem. Int. Ed. Engl. **30**, 769 (1991).
9. Y. Jeannin, F. Sécheresse, S. Bernès, and F. Robert. Inorg. Chim. Acta, **198–200**, 493 (1992).
10. M.A. Ansari and J.A. Ibers. Coord. Chem. Rev. **100**, 223 (1990).
11. J.W. Kolis. Coord. Chem. Rev. **105**, 195 (1990).
12. M.G. Kanatzidis. Comments Inorg. Chem. **10**, 161 (1990).
13. M.A. Ansari, J.M. McConnachie, and J.A. Ibers. Acc. Chem. Res. **26**, 574 (1993).
14. M.G. Kanatzidis and S.-P. Huang. Coord. Chem. Rev. **130**, 509 (1994).
15. C.J. Warren, D.M. Ho, R.C. Haushalter, and A.B. Bocarsly. Angew. Chem. Int. Ed. Engl. **32**, 1646 (1993).
16. B. Eisenmann. Angew. Chem. Int. Ed. Engl. **32**, 1693 (1993).
17. C.J. Warren, D.M. Ho, and A.B. Bocarsly. J. Am. Chem. Soc. **115**, 6416 (1993).
18. C.J. Warren, S.S. Dhingra, D.M. Ho, R.C. Haushalter, and A.B. Bocarsly. Inorg. Chem. **33**, 2709 (1994).
19. C.J. Warren, R.C. Haushalter, and A.B. Bocarsly. Chem. Mater. **6**, 780 (1994).
20. H.M. Haendler, D. Mootz, A. Rabenau, and G. Rosenstein. J. Solid State Chem. **10**, 175 (1974).
21. C. Stergiou and P.J. Rentzeperis. Z. Kristallogr. **172**, 111 (1985).
22. W.S. Sheldrick and J. Kaub. Z. Anorg. Allg. Chem. **535**, 179 (1986).
23. W.S. Sheldrick and H.-J. Häusler. Z. Anorg. Allg. Chem. **557**, 105 (1988).
24. W.S. Sheldrick and H.-J. Häusler. Z. Anorg. Allg. Chem. **557**, 98 (1988).
25. W.S. Sheldrick. Z. Anorg. Allg. Chem. **562**, 23 (1988).
26. W. Milius and A. Rabenau. Z. Naturforsch. B: Chem. Sci. **43**, 243 (1988).
27. W. Milius. Z. Naturforsch. B: Chem. Sci. **44**, 990 (1989).
28. J.-H. Liao and M.G. Kanatzidis. Inorg. Chem. **31**, 431 (1992).
29. J.-H. Chou and M.G. Kanatzidis. Inorg. Chem. **33**, 1001 (1994).
30. D. Kummer and L. Diehl. Angew. Chem. Int. Ed. Engl. **9**, 895 (1970).

31. J.D. Corbett. Chem. Rev. **85**, 383 (1985).
32. R.C. Burns and J.D. Corbett. Inorg. Chem. **20**, 4433 (1981).
33. R.C. Haushalter. Angew. Chem. Int. Ed. Engl. **24**, 432 (1985).
34. R.C. Haushalter. Angew. Chem. Int. Ed. Engl. **24**, 433 (1985).
35. R.C. Haushalter. Inorg. Chim. Acta, **102**, L37 (1985).
36. S.S. Dhingra and R.C. Haushalter. Inorg. Chem. **33**, 2735 (1994).
37. S.S. Dhingra and R.C. Haushalter. J. Am. Chem. Soc. **116**, 3651 (1994).
38. R.H. Blessing. Crystallogr. Rev. **1**, 3 (1987).
39. J. de Meulenaer and H. Tompa. Acta Crystallogr. **19**, 1014 (1965).
40. G.M. Sheldrick. SHELXTL PC Version 4.1 An integrated system for solving, refining, and displaying crystal structures from diffraction data. Siemens Analytical X-Ray Instruments, Inc. Madison, Wis. 1990.
41. G.M. Sheldrick. J. Appl. Crystallogr. (1995). In preparation.
42. B. Schreiner, K. Dehnicke, and D. Fenske. Z. Anorg. Allg. Chem. **619**, 1127 (1993).
43. K.-W. Kim and M.G. Kanatzidis. Inorg. Chim. Acta, **224**, 163 (1994).
44. M. Björgvinsson, J.F. Sawyer, and G.J. Schrobilgen. Inorg. Chem. **30**, 2231 (1991).
45. M. Björgvinsson, J. Sawyer, and G.J. Schrobilgen. Inorg. Chem. **26**, 741 (1987).
46. C-W. Park, R.J. Salm, and J.A. Ibers. Angew. Chem. In press.

Can. J. Chem. Downloaded from www.nrcresearchpress.com by 80.90.12.36 on 09/08/12
For personal use only.

ansa-Metallocene imide niobium compounds

Alexander N. Chernega, Malcolm L.H. Green, and Alehandra G. Suárez

Abstract: The *ansa*-metallocene imide compounds of niobium {Nb[$Me_2C(\eta^5\text{-}C_5H_4)(\sigma\text{-}C_5H_4)$]($\eta^5\text{-}C_5H_5$)(NBu^t)} and {Nb[$Me_2C(\sigma\text{-}C_5H_4)(\eta^3\text{-}C_9H_6)$]($\eta^5\text{-}C_5H_5$)(NBu^t)} have been prepared and their crystal structures have been determined.

Key words: *ansa*, metallocene, niobium, cyclopentadienyl.

Résumé : On a préparé les composés *ansa*-métallocène imides du niobium {Nb[$Me_2C(\eta^5\text{-}C_5H_4)(\sigma\text{-}C_5H_4)$]($\eta^5\text{-}C_5H_5$)(NBu^t)} et {Nb[$Me_2C(\sigma\text{-}C_5H_4)(\eta^3\text{-}C_9H_6)$]($\eta^5\text{-}C_5H_5$)(NBu^t)} et on a déterminé leurs structures cristallines.

Mots clés : *ansa*, métallocène, niobium, cyclopentadiényle.

[Traduit par la rédaction]

There has been a current interest in *ansa*-metallocene complexes due to their application as homogeneous Ziegler-Natta catalysts for the production of isospecific polymers (1). Most *ansa*-metallocene derivatives are known for the Group 4 transition metals (2), for chromium (3), molybdenum and tungsten (4), calcium and barium (5), and samarium and ytterbium (6). Here we describe the synthesis and properties of the first examples of *ansa*-metallocenes of niobium.

Experimental

All manipulations and reactions were carried out under an atmosphere of dinitrogen (<10 ppm oxygen or water) using standard Schlenk-vessel and vacuum-line techniques or in a dry-box. Solvents were predried over activated 5 Å molecular sieves and then distilled under an atmosphere of dinitrogen from potassium (tetrahydrofuran), sodium (toluene), or sodium–potassium alloy (light petroleum (bp 40–60°C) and diethyl ether). Deuterated solvents for NMR samples were stored in ampoules with sodium ([$^2H_8$]-toluene) or dried using calcium hydride ([$^2H_2$]-dichloromethane) and transfered by vacuum distillation.

NMR spectra were recorded on Brüker AM-300 (^{1}H: 300 MHz, ^{13}C: 75.43 MHz) or AC-200 (^{1}H: 200 MHz) NMR spectrometers and referenced internally using residual protio solvent resonances (^{1}H) and solvent resonances (^{13}C) relative to tetramethylsilane (δ = 0 ppm). Low-resolution mass spectra were obtained on an AEI MS 302 mass spectrometer, updated by a data-handling system supplied by Mass Spectroscopy Services Ltd. Elemental analyses were performed by the analytical laboratory in this department.

Received November 25, 1994.

This paper is dedicated to Professor William A.G. Graham on the occasion of his 65th birthday.

A.N. Chernega, M.L.H. Green,[1] and A.G. Suárez. Inorganic Chemistry Laboratory, South Parks Road, Oxford OX1 3QR, U.K.

[1] Author to whom correspondence may be addressed. Telephone: 0865-272649. Fax: 0865-272690. E-mail: malcolm.green@icl.ox.ac.uk

Synthesis of {Nb[$Me_2C(\eta^5\text{-}C_5H_4)(\sigma\text{-}C_5H_4)$]($\eta^5\text{-}C_5H_5$)(NBu^t)} 1

A suspension of the *n*-butyllithium-generated anions of [$Me_2C(C_5H_4)_2$](7) (0.32 g, 1.73 mmol) in THF (30 mL) was treated with a solution of [Nb($\eta^5\text{-}C_5H_5$)(NBu^t)Cl_2] (8) (0.40 g, 1.33 mmol) in THF (70 mL) dropwise at room temperature and the mixture was stirred for 12 h, giving an orange-yellow solution. The volatiles were removed under reduced pressure and the residue was extracted with toluene (2 × 50 mL). After filtration, the filtrate was concentrated under reduced pressure and cooled to −80°C. After 24 h yellow crystals separated and these were collected and dried in vacuo. They were recrystallized from toluene as air-sensitive yellow crystals. Yield, 200 mg, 38%. ^{1}H NMR of the 1:1 mixture of diastereomers (the prime indicates the other isomer) (300 MHz, CD_2Cl_2, 180 K): 6.80 (1H, C_5H_4), 6.60 (1H, C_5H_4), 6.47 (1H, C_5H_4), 6.36 (1H, C_5H_4), 6.20 (1H, C_5H_4), 5.94 (5H, C_5H_5), 5.73 (1H, C_5H_4), 5.69 (1H, C_5H_4), 5.59 (1H, C_5H_4), 5.51 (1H, C_5H_4), 5.49 (1H, C_5H_4), 5.24 (5H, C_5H_5), 5.01 (1H, C_5H_4), 4.59 (1H, H10′ or H10), 4.50 (1H, H10 or H10′), 1.55 (3H, Me), 1.50 (3H, Me), 1.45 (3H, Me), 1.39 (3H, Me), 0.99 (9H, Bu^t), 0.61 (9H, Bu^t). ^{13}C–{^{1}H}NMR of the 1:1 mixture of isomers (75.43 MHz, CD_2Cl_2, 180 K): 144.7 (q, C16 or C17), 141.6 (CH, C_5H_4), 140.4 (CH, C_5H_4), 139.6 (q, C17 or C16), 126.7 (CH, C_5H_4), 126.5 (CH, C_5H_4), 121.4 (CH, C_5H_4), 114.4 (C_5H_5), 114.1 (CH, C_5H_4), 113.8 (CH, C_5H_4), 112.9 (C_5H_5), 111.0 (CH, C_5H_4), 109.0 (CH, C_5H_4), 108.4 (CH, C_5H_4), 106.7 (CH, C_5H_4), 105.1 (CH, C_5H_4), 95.6 (CH, C_5H_4), 73.6 (q, C1 or C1′), 73.0 (q, C1′ or C1), 66.1 (C10 or C10′), 62.6 (C10′ or C10), 40.1 (q, C15 or C37), 40.0 (q, C15 or C15′), 37.1 (CH_3), 35.8 (CH_3), 35.0 (Bu^t), 34.3 (Bu^t), 30.2 (CH_3), 29.6 (CH_3). There were no bands assignable to C18 and C18′ and it is assumed they are hidden under the bands assignable to the cyclopentadienyl ligands at 114.3 and 112.9 ppm. Also, the

Can. J. Chem. Downloaded from www.nrcresearchpress.com by 80.90.12.36 on 09/08/12
For personal use only.

Can. J. Chem. Downloaded from www.nrcresearchpress.com by 80.90.12.36 on 09/08/12
For personal use only.

^{13}C spectrum has one fewer band than expected for the C_5H_4 ligands and we assume that there are two bands which coincide. Mass spectrum: *m/z* 399 $[M]^+$. Anal. calcd.: C 66.2, H 7.0, N 3.5; found: C 64.4, H 7.1, N 3.25%.

Synthesis of {Nb[$Me_2C(\sigma$-$C_5H_4)(\eta^3$-$C_9H_6)$](η^5-C_5H_5)(NBu^t)} 2

A solution of [Nb(η^5-C_5H_5)Cl_2NBu^t] (9) (2.0 g, 6.06 mmol) in THF (200 mL) was treated with the dilithium salt of the 2-cyclopentadienyl,2-indenylpropane (9) (2.0 g, 7.9 mmol) in THF (minimum volume) dropwise (45 min) at room temperature and the mixture was stirred for 12 h. The volatiles were removed under reduced pressure and the residue was extracted with toluene (3 × 50 mL). After filtration the filtrate was concentrated under reduced pressure and cooled to −80°C for 24 h, giving yellow crystals. These were collected, dried in vacuo. and recrystallized from light petroleum (bp 40–60°C) to afford bright yellow crystals. Yield, 0.983 g, 36%. ^1H NMR (200 MHz, CD_2Cl_2, 230 K): 7.80 (1H, d, *J* = 8, H23 or H26), 7.34 (1H, d, *J* = 8, H23 or H26), 7.07 (1H, pseudo t, *J* = 8, H24 or H25), 6.99 (1H, pseudo t, *J* = 8, H24 or H25), 6.70 (1H, d, *J* = 3.2, H19 or H20), 6.62 (1H, br d, *J*(H11H12) 4.7), 6.15 (1H, dd, *J*(H11H12) 4.7, *J*(H12H13) 2.3, H12), 6.08 (1H, d, *J* = 3.2, H19 or H20), 5.54 (1H, pseudo t, *J*(H11H13) 2.3, *J*(H12H13) 1.7, H13), 5.40 (5H, s, H5–9), 4.32 (1H, s, H10), 2.05 (3H, s, Me), 1.80 (3H, s, Me), 0.75 (9H, s, Bu^t). ^{13}C–{^1H}NMR (75.43 MHz, CD_2Cl_2, 250 K): 160.1 (q, C14), 136.0 (q, C18 or 21 or 22), 133.6 (CH, C_5H_4 or C_9H_6), 125.7 (q, C18 or 21 or 22), 124.7 (CH, C_5H_4 or C_9H_6), 123.1 (CH, C_5H_4 or C_9H_6), 122.7 (CH, C_5H_5 or C_9H_6), 122.4 (CH, C_5H_4 or C_9H_6), 121.6 (q, C18 or 21 or 22), 119.8 (CH, C_5H_4 or C_9H_6), 119.5 (CH, C_5H_4 or C_9H_6), 107.1 (C_5H_5), 106.6 (CH, C_5H_4 or C_9H_6), 75.7 (CH, C_5H_4 or C_9H_6), 69.1 (q, C1), 63.9 (C10), 37.6 (q, C15), 32.1 (CH_3), 29.6 (CH_3), 28.4 (Bu^t). Mass spectrum: *m/z* 451 $[M]^+$, 378 $[M - NBu^t]^+$. Anal. calcd.: C 69.5, H 6.7, N 3.1; found: C 70.0, H 6.8, N 3.2%.

Crystal structure determination for compounds 1 and 2

Crystal data, data collection, and processing parameters are given in Table 1. The general procedure was as follows. A crystal was mounted in a Lindemann tube (0.7 mm) under dinitrogen and sealed with a small flame. This was transferred to the goniometer head of an Enraf–Nonius CAD4 diffractometer. Unit-cell parameters were calculated from the setting angles of 24 strong, high-angle, carefully centered reflections. Three reflections were chosen as intensity standards and were measured every 3600 s of X-ray exposure time, and three orientation control reflections were measured every 200 reflections. The data were collected at room temperature using graphite-monochromated Mo-K_α radiation (λ = 0.71069 Å) and an ω–2θ scan mode (the ratio of the scanning rates ω/θ = 1.2). Neither significant crystal decay nor movement was noted.

All data were corrected for Lorentz and polarization effects and an empirical absorption correction (10) based on azimuthal scan data was applied. Both structures were solved by direct methods. Non-hydrogen atoms were refined with anistropic thermal parameters by full-matrix least-squares procedures. An empirical absorption correction using the DIFABS (11) program was applied after isotropic convergence. For both structures all hydrogen atoms were located in the difference Fourier maps and included in the final refinement with the fixed positional and thermal parameters. A Chebyshev weighting scheme (12) was applied and the data were corrected for the effects of anomalous dispersion. All crystallographic calculations were performed using the CRYSTALS program package (13*a*) on a MicroVAX 3800 computer and neutral atom scattering factors were taken from the usual sources (13*b*). Additional material deposited as supplementary data comprises tables of H-atom coordinates, thermal parameters, and the remaining bond lengths and angles.[2]

Table 1. Crystal and data reduction parameters for **1** and **2**.

	1	**2**
Formula	$C_{22}H_{28}NNb$	$C_{26}H_{30}NNb$
M	798.8	449.4
Crystal system	Triclinic	Monoclinic
Space group	$P\bar{1}$	*C*2/*c*
a(Å)	8.5072(6)	30.082(2)
b(Å)	15.6718(9)	8.4949(6)
c(Å)	16.801(1)	16.7878(8)
α(deg)	116.15(1)	90.0
β(deg)	97.71(1)	90.33(1)
γ(deg)	97.74(1)	90.0
U(Å^3)	1944.7(3)	4290.0(5)
Z	4	8
D_c(g cm^{-3})	1.36	1.39
μ(cm^{-1})	5.9	5.5
F(000)	832	1872
ω scan width (deg)	0.81 + 0.34 tan θ	0.68 + 0.34 tan θ
ω scan speed (deg min^{-1})	1.5–10.1	1.3–10.1
Lattice segment	−*h*,*h*,−*k*,*k*,−1,*l*	−*h*,*h*,−1,*k*,−1,*l*
Crystal size (mm)	0.22 × 0.34 × 0.50	0.22 × 0.31 × 0.65
θ_{max} (deg) for data	26	31
No. of reflections:		
total	8784	6705
unique	7637	6032
in refinement	5332 (>46)	4565 (>36)
R_{merge}	0.018	0.012
No. of variables	433	253
Obs./variabl.	12.3	18.0
Weighting coeff.	12.4,−6.9,10.4	10.6,−5.2,8.6
Max, min peaks in the final difference maps (e Å^{-3})	0.88,−0.75	0.34,−0.46
R	0.039	0.026
R_w	0.043	0.031

$R = \Sigma(|F_o - F_c|\Sigma|F_o|$; $R_w = \{\Sigma w(|F_o - F_c|^2/\Sigma w|F_o|^2\}^{1/2}$.

Results and discussion

Treatment of the previously described (8) [Nb(η^5-C_5H_5)-

[2] This material can be purchased from: The Depository of Unpublished Data, Document Delivery, CISTI, National Research Council Canada, Ottawa, Canada K1A 0S2.

With the exception of the thermal parameters, these tables have also been deposited with the Cambridge Crystallographic Data Centre, and can be obtained on request from The Director, Cambridge Crystallographic Data Centre, University Chemical Laboratory, 12 Union Road, Cambridge, CB2 1EZ, U.K.

Can. J. Chem. Downloaded from www.nrcresearchpress.com by 80.90.12.36 on 09/08/12
For personal use only.

Fig. 1. (*a*) Molecular structure of {Nb[$Me_2C(\eta^5\text{-}C_5H_4)(\sigma\text{-}C_5H_4)$]($\eta^5\text{-}C_5H_5$)($NBu^t$)} **1A**. (*b*) Showing a view along the ring-centroid niobium vector. The centroid of the C_5-ring is indicated by a +. Hydrogen atoms are omitted for clarity.

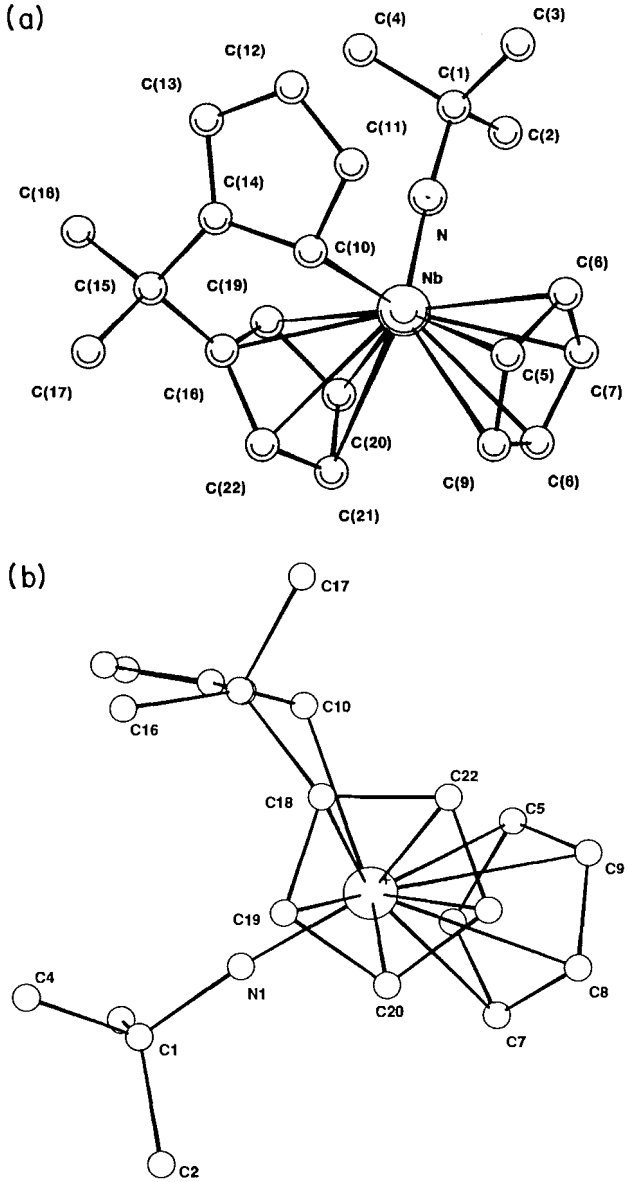

Table 2. Selected interatomic distances (Å) and angles (deg) for the two independent molecules **A** and **B** of **1**.

	Molecule **A**	Molecule **B**
Distances		
Nb—N	1.755(3)	1.758(3)
Nb—C(5)	2.530(4)	2.493(5)
Nb—C(6)	2.463(4)	2.585(4)
Nb—C(7)	2.431(4)	2.546(4)
Nb—C(8)	2.524(4)	2.467(4)
Nb—C(9)	2.586(4)	2.443(5)
Nb—C(10)	2.312(3)	2.307(4)
Nb—C(18)	2.522(3)	2.500(4)
Nb—C(19)	2.448(3)	2.431(4)
Nb—C(20)	2.431(4)	2.424(4)
Nb—C(21)	2.594(4)	2.599(4)
Nb—C(22)	2.619(4)	2.597(4)
Nb—CEN(1)	2.212	2.210
Nb—CEN(2)	2.223	2.209
N—C(1)	1.446(5)	1.446(4)
C(10)—C(11)	1.459(5)	1.471(5)
C(10)—C(14)	1.468(5)	1.470(5)
C(11)—C(12)	1.337(6)	1.352(7)
C(12)—C(13)	1.440(6)	1.425(7)
C(13)—C(14)	1.357(6)	1.365(6)
C(14)—C(15)	1.506(5)	1.512(5)
C(15)—C(18)	1.520(5)	1.508(5)
Angles		
N-Nb-C(10)	97.0(1)	97.2(1)
N-Nb-CEN(1)[a]	113.6	112.4
N-Nb-CEN(2)	113.6	113.8
C(10)-Nb-CEN(1)	104.2	105.0
C(10)-Nb-CEN(2)	98.4	97.5
CEN(1)-Nb-CEN(2)	124.0	124.8
Nb-N-C(1)	175.2(3)	174.8(3)
C(10)-C(14)-C(13)	108.6(3)	108.3(3)
C(10)-C(14)-C(15)	120.4(3)	121.6(3)
C(13)-C(14)-C(15)	130.9(4)	129.8(4)
C(14)-C(15)-C(18)	105.7(3)	104.5(3)

[a]CEN(1) and CEN(2) denote the centroids of the rings C(5)–C(9) and C(18)–C(22), respectively.

(NBu^t)Cl_2] with the dilithium salt of the dianion $[Me_2C(C_5H_4)_2]^{2-}$ in THF gave yellow crystals of {*ansa*-Nb[$Me_2C(\eta^5\text{-}C_5H_4)(\sigma\text{-}C_5H_4)$]($\eta^5\text{-}C_5H_5$) ($NBu^t$)} **1** as a 1:1 mixture of diastereomers in *ca.* 38% yield. Similarly, treatment of [Nb($\eta^5\text{-}C_5H_5$)(NBu^t)Cl_2] with the dilithium salt of the dianion $[Me_2C(C_5H_4)(C_9H_6)]^{2-}$ in THF at room temperature gave yellow crystals of {Nb[$Me_2C(\sigma\text{-}C_5H_4)(\eta^3\text{-}C_9H_6)$]($\eta^5\text{-}C_5H_5$)($NBu^t$)} **2** in ca. 36% yield. The characterizing data show that only a single diastereomer of **2** is formed. Presumably steric forces restrict formation of the other stereoisomer.

The crystal structures of **1** and **2** were determined by X-ray diffraction. The compound **1** has two chiral centres, namely, at the niobium centre, which posseses four different groups arranged in a pseudotetrahedral manner around the metal, and at the the chiral carbon of the σ-cyclopentadienyl group. The compound **1** is monomeric; the asymmetric unit contains both enantiomers **1A** and **1B** as crystallographically independent units. The enantiomers differ only very slightly in their structural parameters. Figure 1*a* shows the molecular structure of one of the two enantiomers (**1A**). Selected bond distances and angles of both molecules are given in Table 2 and the fractional atomic coordinates for all non-hydrogen atoms appear in Table 3. The metal–nitrogen bond lengths are 1.755(3) and 1.758(3) Å and the Nb-N-C(1) bond angles are almost linear: 175.2(3)° and 174.8(3)°. These values are very similar to those of the bis(η-cyclopentadienyl)imide niobium complexes [Nb(σ-C_5H_5)($\eta^5\text{-}C_5H_5$)$_2$(NBu^t)] **3** and [Nb($\eta^5\text{-}C_5H_5$)$_2$-(NBu^t)Cl] **4** in which the Nb—N bond distances and Nb-N-C(1) bond angles are 1.756(3) Å and 176.8(3)° for **3** and 1.789(4); 1.737(6) Å and 173.6(4), 179.4(5)° for **4** (14, 15). These structural data are comparable to the values found for other Nb=NR groups where the neutral NR group acts as a

Can. J. Chem. Downloaded from www.nrcresearchpress.com by 80.90.12.36 on 09/08/12
For personal use only.

Table 3. Fractional atomic coordinates and equivalent isotropic temperature factors ($Å^2$) for **1**.

Atom	*x/a*	*y/b*	*z/c*	*U*(eq)
Molecule A				
Nb	0.98957(3)	0.24431(2)	0.93437(2)	0.0327
N	0.8776(3)	0.1944(2)	0.9901(2)	0.0392
C(1)	0.7810(5)	0.1458(3)	1.0289(3)	0.0490
C(2)	0.761(1)	0.0382(5)	0.9731(6)	0.1032
C(3)	0.6222(8)	0.1760(7)	1.0336(7)	0.0899
C(4)	0.8700(8)	0.1731(7)	1.1235(5)	0.0978
C(5)	0.8401(6)	0.3191(3)	0.8497(3)	0.0524
C(6)	0.7287(5)	0.2422(5)	0.8491(3)	0.0616
C(7)	0.7820(7)	0.1558(3)	0.7947(3)	0.0598
C(8)	0.9121(7)	0.1818(4)	0.7648(3)	0.0623
C(9)	0.9470(6)	0.2791(4)	0.7970(3)	0.0564
C(10)	1.0296(4)	0.4057(2)	1.0414(2)	0.0381
C(11)	0.8860(5)	0.4332(3)	1.0761(3)	0.0475
C(12)	0.9091(5)	0.4524(3)	1.1631(3)	0.0563
C(13)	1.0692(6)	0.4415(3)	1.1916(3)	0.0545
C(14)	1.1441(4)	0.4165(3)	1.1206(2)	0.0439
C(15)	1.3089(5)	0.3931(3)	1.1117(3)	0.0490
C(16)	1.3801(7)	0.3733(4)	1.1900(3)	0.0747
C(17)	1.4256(5)	0.4782(4)	1.1140(5)	0.0721
C(18)	1.2812(4)	0.3020(3)	1.0211(3)	0.0420
C(19)	1.2220(4)	0.2061(3)	1.0050(3)	0.0433
C(20)	1.1914(5)	0.1445(3)	0.9104(3)	0.0539
C(21)	1.2451(6)	0.2019(4)	0.8698(3)	0.0588
C(22)	1.2963(5)	0.2972(3)	0.9365(3)	0.0548
Molecule B				
Nb	0.61874(3)	−0.23011(2)	0.46581(2)	0.0361
N	0.7229(3)	−0.3108(2)	0.4858(2)	0.0390
C(1)	0.8064(5)	−0.3822(3)	0.4934(3)	0.0482
C(2)	0.7259(9)	−0.4813(4)	0.4124(5)	0.0939
C(3)	0.784(1)	−0.3893(6)	0.5780(5)	0.0968
C(4)	0.9789(7)	−0.3549(6)	0.4958(9)	0.1035
C(5)	0.5996(9)	−0.2360(5)	0.3140(4)	0.0786
C(6)	0.6184(8)	−0.1380(5)	0.3705(4)	0.0736
C(7)	0.7705(7)	−0.1038(4)	0.4307(4)	0.0684
C(8)	0.8470(7)	−0.1831(5)	0.4065(4)	0.0661
C(9)	0.7399(8)	−0.2645(4)	0.3340(4)	0.0724
C(10)	0.7157(4)	−0.0975(3)	0.6076(3)	0.0435
C(11)	0.8925(5)	−0.0773(3)	0.6406(3)	0.0535
C(12)	0.9216(5)	−0.0996(4)	0.7095(3)	0.0600
C(13)	0.7711(5)	−0.1310(3)	0.7272(3)	0.0565
C(14)	0.6464(4)	−0.1281(3)	0.6688(2)	0.0414
C(15)	0.4648(4)	−0.1590(3)	0.6565(3)	0.0452
C(16)	0.4259(7)	−0.2263(4)	0.6981(4)	0.0701
C(17)	0.3896(6)	−0.0702(4)	0.7002(3)	0.0634
C(18)	0.4015(4)	−0.2126(3)	0.5550(3)	0.0427
C(19)	0.3901(4)	−0.3117(3)	0.4974(3)	0.0472
C(20)	0.3450(5)	−0.3296(4)	0.4066(3)	0.0612
C(21)	0.3129(5)	−0.2426(5)	0.4089(3)	0.0646
C(22)	0.3517(5)	−0.1714(3)	0.4974(3)	0.0568

four-electron donor ligand (16). The (ring centroid)-metal-(ring centroid) angles, 124.0 and 124.8°, are very similar to those of complexes **3** and **4**, as well as the metal–(ring centroid) distances (Nb—$Cp_{cent(1)}$ 2.212, 2.210 Å and Nb—$Cp_{cent(2)}$ 2.223, 2.209 Å). The Nb—C_{ipso} of the σ-cyclopentadienyl ligand are 2.312(3), 2.307(4) Å, which are comparable to the one in compound **3**, 2.330(3)Å (2). The bond angles C(18)-C(15)-C(14) are 105.7(3)° and 104.5(3)°.

The Nb—C bond distances of both substituted η-cyclopentadienyl ligands show that they are not coordinated in an ideal

Can. J. Chem. Downloaded from www.nrcresearchpress.com by 80.90.12.36 on 09/08/12
For personal use only.

Fig. 2. (*a*) Molecular structure of {Nb[$Me_2C(\sigma$-$C_5H_4)(\eta^3$-$C_9H_6)](\eta^5$-$C_5H_5)(NBu^t)$} **2**. (*b*) Showing a view along the ring-centroid niobium vector. The centroid of the C_5-ring is indicated by a +. Hydrogen atoms are omitted for clarity.

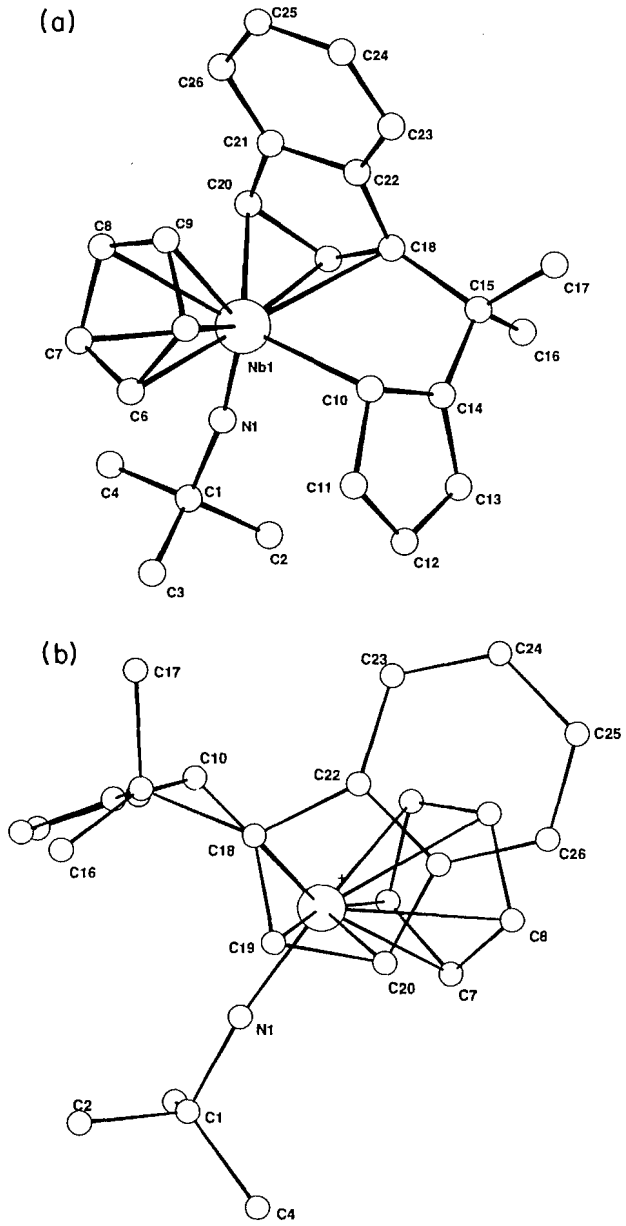

Table 4. Selected interatomic distances (Å) and angles (deg) for **2**.

Distances	
Nb—N	1.760(1)
Nb—C(5)	2.512(2)
Nb—C(6)	2.466(2)
Nb—C(7)	2.443(2)
Nb—C(8)	2.467(2)
Nb—C(9)	2.538(2)
Nb—C(10)	2.326(2)
Nb—C(18)	2.539(2)
Nb—C(19)	2.421(2)
Nb—C(20)	2.424(2)
Nb—CEN(1)	2.179
N—C(1)	1.450(2)
C(10)—C(11)	1.464(3)
C(10)—C(14)	1.474(2)
C(11)—C(12)	1.344(4)
C(12)—C(13)	1.433(4)
C(13)—C(14)	1.362(3)
C(14)—C(15)	1.507(3)
C(15)—C(18)	1.534(2)
C(18)—C(19)	1.400(2)
C(18)—C(22)	1.462(2)
C(19)—C(20)	1.414(3)
C(20)—C(21)	1.438(3)
C(21)—C(22)	1.427(2)
Angles	
N-Nb-C(10)	97.38(7)
N-Nb-C(18)	106.88(6)
N-Nb-C(19)	85.66(7)
N-Nb-C(20)	99.14(7)
C(10)-Nb-C(18)	70.73(6)
C(10)-Nb-C(19)	97.67(6)
C(10)-Nb-C(20)	126.02(6)
N-Nb-C(20)	113.2
C(10)-Nb-CEN(1)[a]	105.8
C(18)-Nb-CEN(1)	139.8
C(19)-Nb-CEN(1)	147.1
C(20)-Nb-CEN(1)	113.7
Nb-N-C(1)	169.3(1)
C(10)-C(14)-C(13)	108.3(2)
C(10)-C(14)-C(15)	120.6(2)
C(13)-C(14)-C(15)	131.0(2)
C(14)-C(15)-C(18)	104.8(1)

[a]CEN(1) denotes the centroid of the ring C(5)–C(9).

η^5-fashion to the metal, and a significant ring-slip distortion is apparent.The view of **1** through the Nb-C_5H_5 ring normal-metal vector, shown in Fig. 1*b*, reveals that the metal is displaced in the direction of the ring carbons C(30) and C(31), which are staggered with respect to the Nb—N bond. However, the deviations in the inter-ring carbon distances of the η-cyclopentadienyl ligands are not sufficiently pronounced to support an allyl-ene description of the ring distortion. The C—C distances in the unsubstituted η-C_5H_5 ring are normal. It appears that the formally 20-electron compound **1** shows structural features that are consistent with ring-slip distortions towards an 18-electron bonding mode. The crystals of **2** are composed of discrete mononuclear molecules of {Nb[$Me_2C(\eta^5$-$C_5H_4)(\eta^3$-$C_9H_6)](\eta^5$-$C_5H_5)(NBu^t)$}. The molecular structure is shown in Fig. 2*a* and 2*b*, selected distances and bond angles are given in Table 4, and the fractional atomic coordinates for all non-hydrogen atoms appear in Table 5. The most noticeable differences between **1** and **2** are a consequence of increasing steric repulsion between the bulky substituents in **2** that leads to the decrease of the dihedral angle between the C(5)–C(9) and C(18)–C(22) planes from 131.0° in **1A** and **1B** to 122.8° in **2**. There is also a decrease in the Nb—CEN(1) distance from 2.212 and 2.210 Å in **1A** and **1B** to 2.179 Å in **2**. The ring system C(18)–C(26) of **2** is planar within 0.088 Å; the dihedral angle between planes of the C(18)–C(22) and C(21)–C(26) rings is only 3.5°. The geomet-

Can. J. Chem. Downloaded from www.nrcresearchpress.com by 80.90.12.36 on 09/08/12
For personal use only.

Table 5. Fractional atomic coordinates and equivalent isotropic temperature factors ($Å^2$) for **2**.

Atom	*x/a*	*y/b*	*z/c*	*U*(eq)
Nb	0.640 053(4)	0.09909(2)	−0.013 598(8)	0.0280
N	0.590 28(5)	0.1240(2)	−0.067 75(9)	0.0359
C(1)	0.553 67(7)	0.1299(3)	−0.124 2(1)	0.0435
C(2)	0.516 30(9)	0.2258(4)	−0.088 1(2)	0.0687
C(3)	0.569 6(1)	0.2027(5)	−0.201 5(2)	0.0716
C(4)	0.537 6(1)	−0.0367(4)	−0.139 5(2)	0.0651
C(5)	0.714 59(6)	0.1366(3)	−0.077 6(1)	0.0430
C(6)	0.682 97(7)	0.1037(3)	−0.138 3(1)	0.0479
C(7)	0.668 24(8)	−0.0500(3)	−0.127 0(1)	0.0490
C(8)	0.689 81(8)	−0.1129(2)	−0.059 3(1)	0.0468
C(9)	0.719 24(6)	0.0018(3)	−0.030 2(1)	0.0431
C(10)	0.654 27(6)	0.3641(2)	0.010 4(1)	0.0354
C(11)	0.648 61(8)	0.4602(3)	−0.061 3(1)	0.0461
C(12)	0.610 8(1)	0.5433(3)	−0.055 0(2)	0.0538
C(13)	0.590 53(8)	0.5119(2)	0.020 4(1)	0.0462
C(14)	0.616 76(6)	0.4094(2)	0.061 7(1)	0.0349
C(15)	0.611 11(7)	0.3359(2)	0.142 7(1)	0.0386
C(16)	0.563 1(1)	0.3527(3)	0.172 0(2)	0.0601
C(17)	0.641 7(1)	0.4184(3)	0.203 6(1)	0.0550
C(18)	0.622 82(6)	0.1617(2)	0.130 8(1)	0.0318
C(19)	0.592 71(6)	0.0515(2)	0.100 0(1)	0.0357
C(20)	0.614 80(7)	−0.0916(2)	0.083 6(1)	0.0384
C(21)	0.658 10(7)	−0.0808(2)	0.119 8(1)	0.0376
C(22)	0.664 35(6)	0.0774(2)	0.146 16(9)	0.0330
C(23)	0.705 96(7)	0.1203(3)	0.179 5(1)	0.0432
C(24)	0.738 16(7)	0.0076(4)	0.188 3(1)	0.0520
C(25)	0.731 46(9)	−0.1478(4)	0.163 9(1)	0.0540
C(26)	0.691 92(9)	−0.1935(3)	0.129 5(1)	0.0500

rical features of the Nb═N—CBu^t group (Nb═N 1.755(3), 1.758(3) Å in **1** and 1.760(1) Å in **2**, N—C(1) 1.446(5), 1.446(4) Å in **1** and 1.450(2) Å in **2**, Nb-N-C(1) 175.2(3)°, 174.8(3)° in **1** and 169.3(1)° in **2**) are similar to those found for other Nb═NR groups (12, 13) where the neutral NR group acts as a four-electron donor ligand. The Nb—N bond distance is 1.760(1) Å in **2** and is comparable to the values found for the analogous complexes mentioned above, where the neutral NR group also acts as a four-electron donor ligand (16, 17).

The C—C distances in the five-membered ring of the indenyl ligand are as follows: C(18)—C(19) 1.400(2), C(19)—C(20) 1.414(3), C(20)—C(21) 1.438(3), C(21)—C(22) 1.427(2), and C(18)—C(22) 1.462(2) Å. These values show that the deviations in the inter-ring carbon distances are not very pronounced but are comparable with other allyl-ene descriptions of the ring distortion (18). The metal–carbon bond distances of the η^3-C_5 ring of the indenyl ligand are Nb—C(18) 2.539(2), Nb—C(19) 2.421(2), and Nb—C(20) 2.424(2) Å. The bond distance between the metal and the central carbon of the allyl portion is the shortest (see Fig. 2*b*). We note that the metal atoms in η^5-indenyl complexes also have a small slip distortion, usually in the direction of the central carbon of the allyl portion (19). We conclude that the above structural data indicate that complex {Nb(η^5-C_5H_5)[Me_2C(σ-C_5H_4)(η^3-C_9H_6)](NBu^t)} **2** has a formal 18-electron configuration.

The NMR spectra of **1** and **2** are consistent with the solution structures being the same as found in the crystalline state. Thus the ^1H and ^{13}C NMR spectra of {Nb(η^5-C_5H_5)[Me_2C(η^5-C_5H_4)(σ-C_5H_4)] (NBu^t)} **1** show the presence of two compounds in solution 1:1 ratio. The $^{13}C\{^1H\}$ NMR spectrum of **1** shows a large chemical shift difference ($\Delta\delta$ = 39 ppm) between the quaternary and the methyl carbons of the *tert*-butylimide ligand. This large value lies at the high end of the range previously recorded for *tert*-butylimide-metal derivatives (16), indicating a low electron density on the imide nitrogen due to the high degree of N→M π donation (16, 19).

The ^1H and ^{13}C NMR spectra of **1** show broad signals at room temperature, which may be due to the exchange between the η- and σ-cyclopentadienyl ligands of the C_5H_4-CMe_2-C_5H_4 ligand system. A variable temperature NMR study gave only a poorly resolved spectrum at 180 K, the lowest accessible temperature. The presence of two diastereomers increases the complexity of the spectra and for both the ^1H and ^{13}C NMR spectra it was not possible to detect all the proton and carbon signals expected for the diastereomeric mixture.

The ^1H NMR spectra of **2** at room temperature shows some broad signals and poor resolution. This suggests a degree of fluxionality or the presence of the quadrupolar moment of the ^{93}Nb nucleus (spin I = 9/2, natural abundance 100%). At 230 K the spectrum is well resolved and is given with assignment in the experimental section.

The large chemical shift difference ($\Delta\delta$ = 40 ppm) between the quaternary and the methyl carbons of the NBu^t group in the $^{13}C\{^1H\}$ NMR spectrum of **2** indicates a low electron density

on the nitrogen atom (16, 19). This is consistent with the imide ligand acting as four electron donor.

In conclusion, the formally 20-electron compound **1** shows structural features that are consistent with ring-slip distortions towards an 18-electron bonding mode and the compound **2** achieves an 18-electron configuration by virtue of the η^3-bonding of the indenyl group.

Acknowledgements

We thank the CONICET (Consejo Nacional de Investigaciones Cientificas y Técnicas, Argentina) for a fellowship to (A.G.S.).

References

1. W. Kaminsky, R. Engehausen, K. Zoumis, W. Spalek, and J. Rohrmann. Makromol. Chem., **193**, 1643 (1992); J.A. Ewen, M.J. Elder, R.L. Jones, I. Haspeslagh, J.L. Atwood, S.G. Bott, and K. Robinson. Makromol. Chem. **48/49**, 253 (1989), and references therein.
2. R.L. Halterman. Chem. Rev. **92**, 965 (1992); J.A. Smith, J. von Seyerl, G. Huttner, and H.H. Brintzinger. J. Organomet. Chem. **173**, 175 (1979); P. Burger and H.H. Brintzinger. J. Organomet. Chem. **407**, 208 (1991); J.A. Smith and H.H. Brintzinger. J. Organomet. Chem. **218**, 159 (1981).
3. H. Schwemlein, L. Zsolnai, G. Huttner, and H.H. Brintzinger. J. Organomet. Chem. **256**, 285 (1983); G. Paolucci, F. Ossola, M. Bettinelli, R. Sessoli, F. Benetollo, and G. Bombieri. Organometallics, **13**, 1746 (1994).
4. T. Mise, M. Maeda, T. Nakajima, K. Kobashi, I. Shimizu, Y. Yamamoto, and Y. Wakatsuki. J. Organomet. Chem. **473**, 155 (1994); L. Labella, A.N. Chernega, and M.L.H. Green. J. Chem. Soc. Dalton Trans. 395 (1995).
5. M. Rieckhoff, U. Pieper, D. Stalke, and F.T. Edelmann. Angew. Chem. Int. Ed. Engl. **32**, 1079 (1993).
6. F.T. Edelmann, M. Rieckhoff, I. Haiduc, and I. Silaghidumitrescu. J. Organomet. Chem. **447**, 203 (1993).
7. I.E. Nifant'ev, P.V. Ivchenko, and M. V. Borzov. J. Chem. Res. (S), 162 (1992).
8. D.N. Williams, J.P. Mitchell, A.D. Poole, U. Siemeling, W. Clegg, D.C.R. Hockless, and V.C. Gibson. J. Chem. Soc. Dalton Trans. 739 (1992).
9. M.L.H. Green and N. Ishihara. J. Chem. Soc. Dalton Trans. 657 (1994).
10. A.C.T. North, D.C. Philips, and F.S. Mathews. Acta Crystallogr. Sect. A: Cryst. Phys. Diffr. Theor. Gen. Crystallogr. **A24**, 351 (1968).
11. N. Walker and D. Stuart. Acta Crystallogr. Sect. A: Found. Crystallogr. **A39**, 158 (1983).
12. D.J. Watkin and J.R. Carruthers. Acta Crystallogr. Sect. A: Cryst. Phys. Diffr. Theor. Gen. Crystallogr. **A35**, 698 (1979).
13. (*a*) D.J. Watkin, J.R. Carruthers, and P.W. Betteridge. CRYSTALS user guide, Chemical Crystallography Laboratory, University of Oxford. 1985; (*b*) International Tables for Crystallography. Vol. 4. Kynoch Press, Birmingham. 1974.
14. M.L.H. Green, D.M. Michaelidou, P. Mountford, A.G. Suárez, and L-L Wong. J. Chem. Soc. Dalton Trans., 1593 (1994).
15. A.N Chernega, M.L.H. Green, and A.G. Suárez, J. Chem. Soc. Dalton Trans. 3031 (1993).
16. W.A. Nugent and J.M. Mayer. Metal–ligand multiple bonds. Interscience, New York. 1988; V.C. Gibson. J. Chem. Soc. Chem. Commun. 237 (1992); 1668 (1992); J. Chem. Soc. Dalton Trans. 739 (1992); G.Parkin, A.Vanasselt, D.J. Leahy, I. Whinnery, N.G. Hua, R.W. Quan, L.M. Henling, W.P. Schaefer, B.D. Santarsiero, and J.E. Bercaw. Inorg. Chem. **31**, 82 (1992).
17. (*a*) F.A. Cotton, S.A. Duraj, and W.J. Roth. J. Am. Chem. Soc. **106**, 4749 (1984); (*b*) P.A. Finn, M.S. King, P.A. Kitty, and R.E. McCarley. J. Am. Chem. Soc. **97**, 220 (1975); (*c*) L.S. Tan, G.V. Goeden, and B.L. Haymore. Inorg. Chem. **22**, 1744 (1983).
18. R.M. Kawakeski, A.L. Rheingold, W.C. Trogler, and F. Basolo. J. Am. Chem. Soc. **108**, 2460 (1986).
19. J. W. Faller, R. H. Crabtree, and A. Habib. Organometallics, **4**, 929 (1985); G.Parkin, A.Vanasselt, D.J. Leahy, I. Whinnery, N.G. Hua, R.W. Quan, L.M. Henling, W.P. Schaefer, B.D. Santarsiero, and J.E. Bercaw. Inorg. Chem. **31**, 82 (1992).

Can. J. Chem. Downloaded from www.nrcresearchpress.com by 80.90.12.36 on 09/08/12
For personal use only.

Metal complexes of biologically important ligands, LXXVIII.[1] Synthesis of palladium complexes of ferrocenyl-substituted amino acid derivatives

Doris Freiesleben, Kurt Polborn, Christian Robl, Karlheinz Sünkel, and Wolfgang Beck

Abstract: Schiff bases from ferrocene aldehyde and α-amino acidates react with $PdCl_2$ or Na_2PdCl_4 to give N,O-chelate complexes (**2***a–e*, **3**). The related *N*-ferrocenylmethylen-α-amino acid esters give, with $Pd(OAc)_2$, cyclopalladated acetate-bridged complexes (**4***a*,*b*). N,O-chelate complexes (**5–7**) are obtained from Na_2PdCl_4 with *N*-ferrocenylmethyl prolinate and-alaninate as well as with *N*,*N*-dibenzyl glycinate. The ethyl ester of *N*,*N*-dibenzylglycine and $Pd(OAc)_2$ form the cyclopalladated acetate-bridged complex **8**, while the ester of *N*-monobenzylglycine and Na_2PdCl_4 affords *trans*-$PdCl_2(L)_2$ with a monodentate N-coordinated ligand. The structures of **2***a*, **4***a*, **5**, **7**, and **9** were determined by X-ray diffraction.

Key words: ferrocene, amino acids, palladium(II) complexes, crystal structures.

Résumé : Les bases de Schiff obtenues à partir de l'aldéhyde du ferrocène et d'α-amino-acides réagissent avec le $PdCl_2$ et la Na_2PdCl_4 pour donner des complexes N,O-chélatés (**2***a–e*, **3**). Les esters apparentés des acides *N*-ferrocénylméthylène-α-aminés, par réaction avec le $Pd(OAc)_2$, conduisent aux complexes acétates pontés cyclopalladiés, **4***a*,*b*. On obtient les complexes N,O-chélatés **5–7** par réaction du Na_2PdCl_4 avec les prolinate (et alaninate) de *N*-ferrocénylméthyle et avec le glycinate de *N*,*N*-dibenzyle. L'ester éthylique de la *N*,*N*-dibenzylglycine et le $Pd(OAc)_2$ forme le complexe acétate ponté cyclopalladié **8** alors que l'ester de la *N*-monobenzylglycine et le Na_2PdCl_4 fournissent le *trans*-$PdCl_2(L)_2$ avec un coordinat monodentate N-coordiné. On a déterminé les structures des composés **2***a*, **4***a*, **5**, **7** et **9** par diffraction des rayons X.

Mots clés : ferrocène, amino-acides, complexes de palladium(II), structures cristaux.

[Traduit par la rédaction]

Introduction

Palladium compounds have found widespread application in organic synthesis (2). Coordination compounds of the type PdL_4 or PdL_2Cl_2 are used in many catalytic processes, particularly in the field of asymmetric catalysis. Besides "normal" coordination to the donor atoms of the ligands L, very frequently "cyclopalladation," especially orthopalladation, e.g., formation of a Pd—C bond in *ortho* position to the aromatic substituent bearing the coordinating functionality, has been used in stoichiometric organic transformations (3). In an effort to combine "classical" coordination chemistry with organometallic chemistry, bimetallic complexes containing a ferrocene moiety in the ligand backbone have attracted special interest, due to their potential as "redox-switchable" ligands. Many donor atom combinations have been examined, but most of them contain a nitrogen atom. For instance, many palladium complexes of P,N-donor ferrocenes such as $Fe(C_5H_4PR_2)[C_5H_3(CHRNMe_2)(PR_2)]$ have been used as catalysts in stereospecific reactions (4). Ferrocenes with N,O-donor systems have also been examined as ligands for alkali ions or Ag^+, though so far not with palladium (5), but N,S-donor derivatives coordinate to Pd^{2+} and have proven to be quite active catalysts (6). Ferrocenylalkylamines can undergo asymmetric cyclopalladation affording cyclopalladium complexes of high optical purity, which might then be used in further transformations to yield enantiomerically pure new ferrocenyl ligands (7). The formation of cyclopalladated derivatives of ferrocenylimines has also been investigated recently (8).

In the course of our studies on coordination compounds of biologically important ligands we became interested in the possibility of combining the aforementioned aspects of palladium-ferrocene chemistry with the coordination chemistry of amino acids. Ferrocenyl-substituted amino acids have been known for quite awhile (9). Also, Schiff bases from amino acids and their esters and formyl ferrocene have been reported (10) and, after reduction, have been used for the masking of peptide bridges (11). Since these complexes appeared to us as

Received November 30, 1994.

This paper is dedicated to Professor William A.G. Graham on the occasion of his 65th birthday.

D. Freiesleben, K. Polborn,[2] C. Robl,[2] K. Sünkel, and W. Beck.[3] Institut für Anorganische Chemie der Ludwig-Maximilians-Universität, Meiserstr. 1, D-80333 Munich, Germany.

[1] For Part 77 see ref. 1.
[2] X-ray structure determination.
[3] Author to whom correspondence may be addressed. Telephone: 089-5902219. Fax: 089-5902451.

Can. J. Chem. Downloaded from www.nrcresearchpress.com by 80.90.12.36 on 09/08/12
For personal use only.

Can. J. Chem. Downloaded from www.nrcresearchpress.com by 80.90.12.36 on 09/08/12
For personal use only.

Scheme 1.

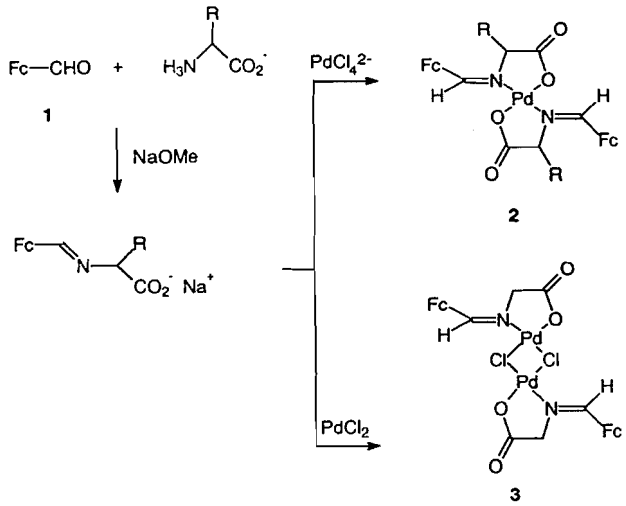

Verb.	R
2*a*	CH_3
2*b*	$CH(CH_3)_2$
2*c*	$CH_2CH(CH_3)_2$
2*d*	H

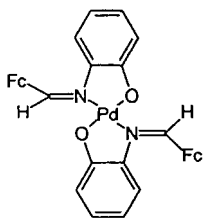

2*e*

potential N,O-donor ligands, we decided to examine their coordination behaviour towards Pd^{2+}.

Results

When ferrocenylmethylidene-substituted imino acid derivatives are generated in situ from glycine, L-alanine, L-valine, L-leucine, or anthranilic acid and formylferrocene (**1**), and are then treated with Na_2PdCl_4, the bis-N,O chelates **2***a–e* containing two ferrocene moieties per palladium ion are obtained (Scheme 1).

When the glycine derivative is treated with $PdCl_2$, the tetrametallic chloro-bridged complex **3** is formed, where only one Schiff base ligand is coordinated as an N,O donor to one Pd(II) moiety.

All complexes show characteristic IR absorptions at ca. 1650 (ν_{as} CO_2), 1620 (C=N), 490 (Pd-N), and 475 (Pd-O) cm^{-1} (in KBr). For further characterization, the crystal structure of **2***a* was determined by X-ray diffraction (vide infra).

However, when the Schiff bases obtained in situ from amino acid *esters* derived from glycine, L-alanine, and **1** were treated with $Pd(OAc)_2$ in the presence of MeOH and KOAc, orthopalladation at the ferrocene ring took place and the tetrametallic acetate-bridged complexes **4***a,b* could be isolated (Scheme 2). The IR spectra (in KBr) of **4***a,b* show the presence of the uncoordinated ester moiety by the CO absorptions at 1730–1740 cm^{-1} and the coordination of the imine nitrogen by the C=N absorptions at 1620–1640 cm^{-1} and Pd-N bands at ca. 500 cm^{-1}. For further characterization, the crystal structure of **4***a* was determined by X-ray diffraction (vide infra).

Scheme 2.

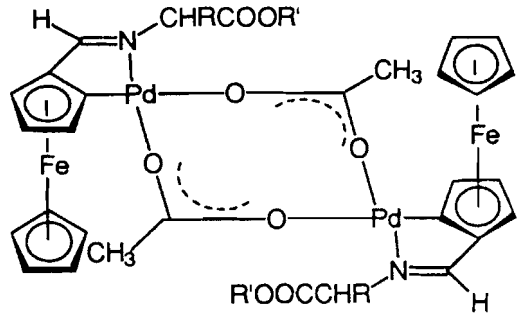

	R	R'
4*a*	H	C_2H_5
4*b*	CH_3	CH_3

Treatment of **1** with alanine in the presence of $MgCl_2$–NaOAc–MeOH or with proline in MeOH and consecutive reduction of the intermediate Schiff bases with $NaBH_4$ (11) gives *N*-ferrocenylmethylamino acidates that afford, with Na_2PdCl_4 **5**, a trimetallic structural analogue of **2** and a tetrametallic complex **6**, a structural analogue of **3** (Scheme 3).

The coordination of the carboxylate can be seen from the IR spectra (in KBr), where $\nu_{as}(CO_2)$ absorbs at 1641 (**5**) and 1655 (**6**) cm^{-1}. This was also confirmed by a X-ray structure determination of **5** (vide infra).

To summarize the results reported so far, basically two types of coordination can be observed with *N*-ferrocenylmethylidene-substituted amino acid derivatives: (*a*) N,O chelation (compounds **2**, **3**, **5**, **6**); (*b*) orthopalladation with C,N coordination (compounds **4**.)

Additionally, there is a slight variation insofar as the Pd^{2+} ions might or might not be bridged by acetate or chloride ions.

Quite interestingly, a similar coordination behaviour could be observed with *N*-benzyl derivatives of glycine or its ethyl ester. Orthopalladation of benzylamine and its *N*-monosubstituted derivatives has been reported only recently (12), while the orthopalladated α-methylated benzylamines have already found application in the resolution of chiral amines and phosphines (13). With α-phenylethylamine, formation of a $PdCl_2$ complex with two monodentate amines was also observed (13*b*). *N*-benzylglycine derivatives have been used for the extraction of metals (14).

N,*N*-Dibenzylglycine and Na_2PdCl_4, in the presence of NaOAc, yield the bis-N,O chelate **7**. Its ethyl ester reacts with palladium acetate under orthopalladation, forming a bimetallic acetate-bridged complex **8**. Finally, when *O*-ethyl-*N*-benzylglycinate is treated with Na_2PdCl_4 in the presence of NaOAc, a *trans*-$PdCl_2$ complex **9** with two monodentate *N*-coordinating amino acidates can be isolated (Scheme 4). The IR spectrum of **7** shows the coordinated CO_2 group at 1640 cm^{-1}, while the coordinated ester groups in **8** are observed at 1730 cm^{-1} and the uncoordinated ester functions in **9** at 1735 cm^{-1} (in KBr). To get more information about structural details, X-ray structure determinations of **7** and **9** were performed (vide infra).

Can. J. Chem. Downloaded from www.nrcresearchpress.com by 80.90.12.36 on 09/08/12
For personal use only.

Scheme 3.

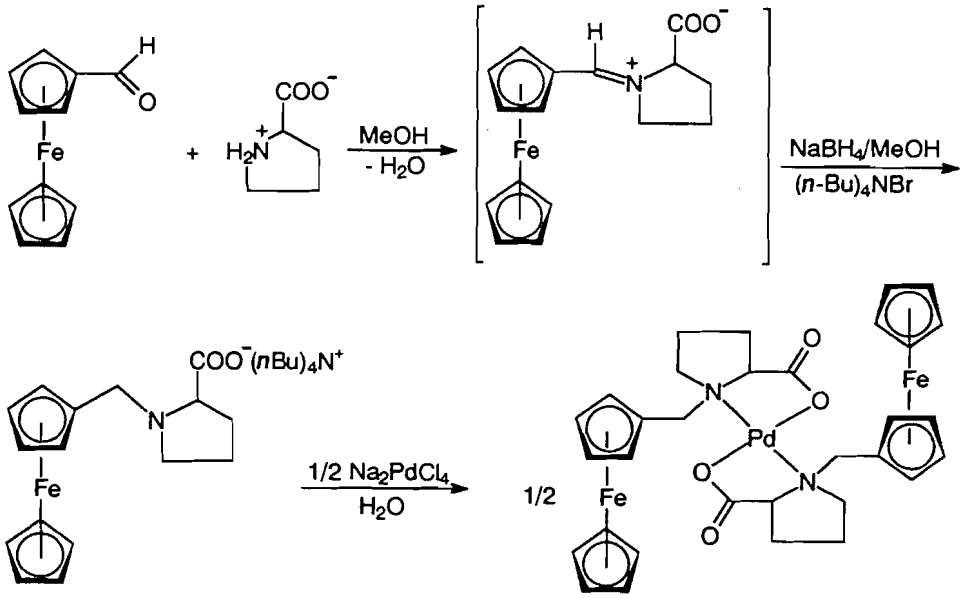

5

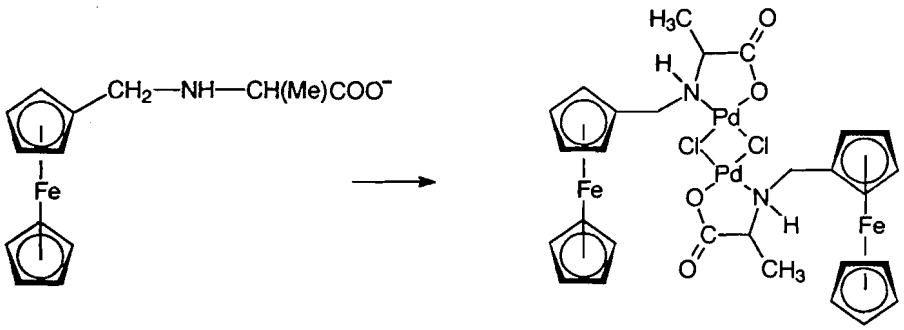

6

Crystal structure determinations

The molecular structures of the complexes **2***a*, **4***a*, **5**, **7**, and **9** were examined by X-ray diffraction. Representative views of the compounds can be seen in Figs. 1–5, experimental details of the structure determinations in Table 1, and atomic coordinates together with isotropic temperature parameters in Tables 2–6.[4] Since we are, in this context, only interested in the coordination sphere of the palladium ions, geometrical parameters of the ligand backbones will not be discussed here.

First of all, we want to look at the N,O-chelate complexes **2***a*, **5**, and **7**. All of them are bis-chelates, and all of them have *trans-N,N*/*trans-O,O* geometries. In **2***a* and **7**, this molecular symmetry is combined with a crystallographic symmetry, imposed by the Pd ions residing on an inversion centre. Consequently, complex **2***a*, derived from the chiral

Fig. 1. Molecular structure of **2***a*. Thermal ellipsoids drawn at the 20% probability level. Distances (Å): Pd...N1 2.002(3), Pd...O1 1.974(3), C12...N1 1.485(9), C11...N1 1.248(9). Angles (°): N1-Pd-O1 83.3(3), Pd-N1-C12 84.6(7), Pd-N1-C11 141.6(8), Pd-O1-C13 127.7(4).

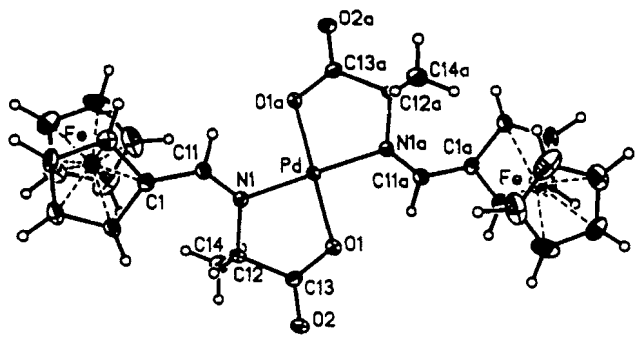

[4] Complete tables of atomic coordinates, bond lengths and angles, and anisotropic displacement coefficients can be purchased from: The Depository of Unpublished Data, Document Delivery, CISTI, National Research Council Canada, Ottawa, Canada K1A 0S2.

With the exception of the anisotropic displacement coefficients, these tables have also been deposited with the Cambridge Crystallographic Data Centre, and can be obtained on request from The Director, Cambridge Crystallographic Data Centre, University Chemical Laboratory, 12 Union Road, Cambridge, CB2 1EZ, U.K.

Can. J. Chem. Downloaded from www.nrcresearchpress.com by 80.90.12.36 on 09/08/12
For personal use only.

Scheme 4.

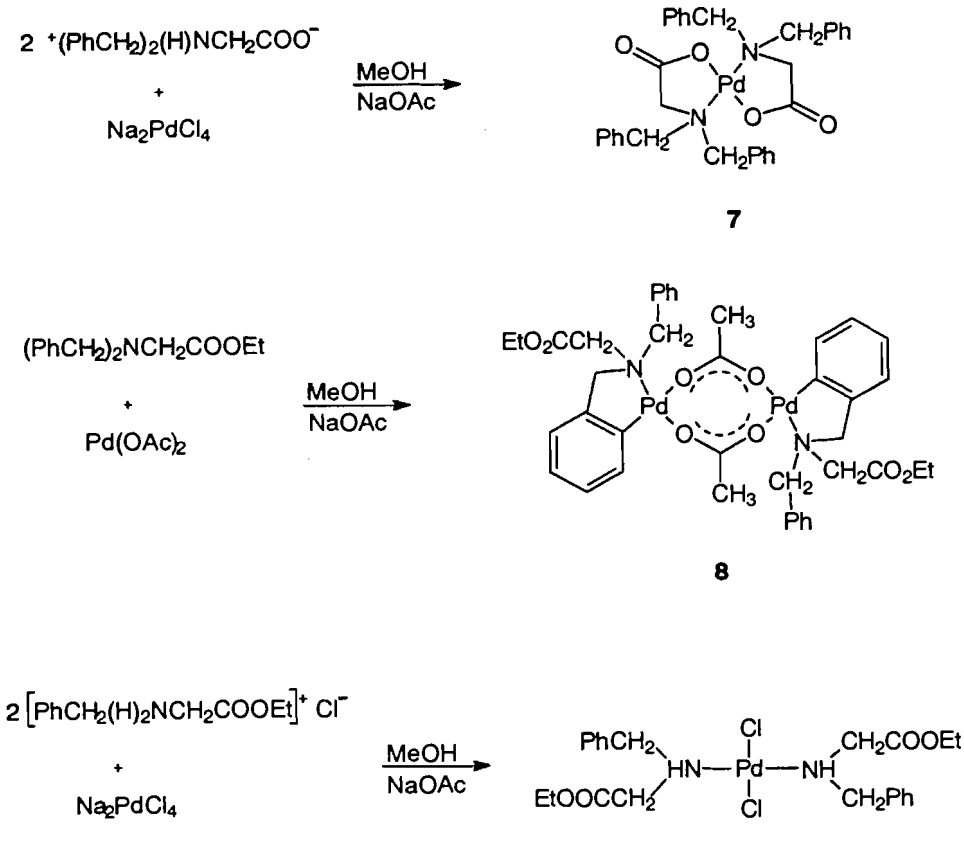

Fig. 2. Molecular structure of **4***a*. Thermal ellipsoids drawn at the 20% probability level. Distances (Å): Pd1...Pd2 2.910(2), Pd1...O1 2.136(3), Pd1...O4 2.036(3), Pd1...N1 2.024(4), Pd1...C9 1.937(6), C19...N1 1.276(7), Pd2...O3 2.135(4), Pd2...O2 2.042(3), Pd2...N2 2.023(4), Pd2...C24 1.935(5), C34...N2 1.280(7). Angles (°): C9-Pd1-N1 80.9(2), C24-Pd2-N2 81.2(2), Pd1-N1-C19 115.4(4), Pd2-N2-C34 115.7(4), Pd1-C9-C10 113.8(4), Pd2-C24-C25 113.5(4), O1-Pd1-O4 92.9(1), O2-Pd2-O3 93.7(1).

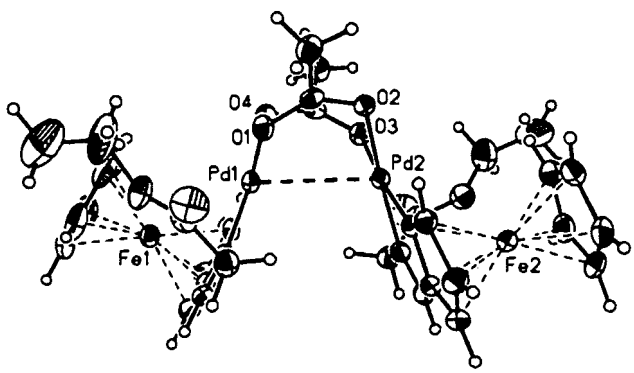

amino acid alanine, contains *both* enantiomers in the *same* molecule, and thus the crystalline material consists only of the *R,S* diastereomer. Compound **7**, being derived from the achiral glycine, cannot provide any isomers of this type. In contrast, compound **5** contains only the *S* isomer of proline. Although the nitrogen atoms become stereogenic centers by

Fig. 3. Molecular structure of **5**. Thermal ellipsoids drawn at the 20% probability level. Distances (Å): Pd...O1 1.993(5), Pd...O3 2.000(6), Pd...N1 2.041(6), Pd...N2 2.046(6), N1...C106 1.484(10), N2...C206 1.508(9). Angles (°): O1-Pd-N1 84.7(2), O1-Pd-N2 96.4(2), N2-Pd-O3 83.9(2), O3-Pd-N1 95.1(2), Pd-O1-C101 114.9(5), Pd-O3-C201 113.1(6), Pd-N1-C102 105.6(4), Pd-N2-C202 102.9(5).

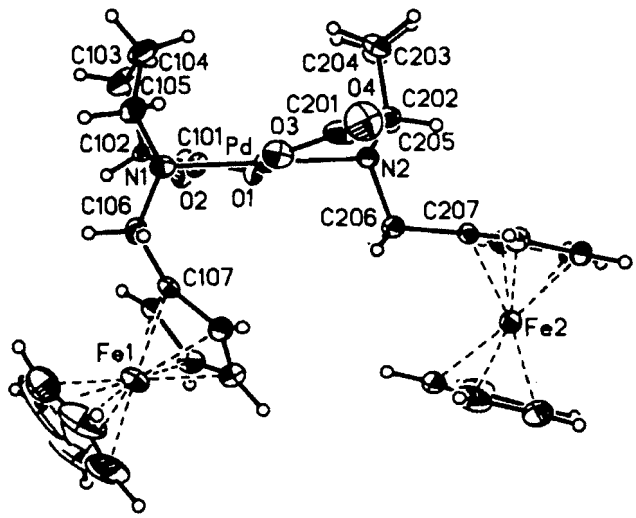

their coordination to palladium, with the *S* configuration at the α-C atom of proline, *R* configuration at the coordinating N atoms is induced for geometric reasons, and thus the only diastereomer found in the crystal is the $S_C R_N S_{C'} R_{N'}$ form,

Fig. 4. Molecular structure of **7**. Thermal ellipsoids drawn at the 20% probability level. Distances (Å): Pd...O1 1.994(3), Pd...N 2.063(4), C2...N 1.505(7). Angles (°): *N*-Pd-O1 85.2(1), Pd-N-C2 105.6(3), Pd-O1-C1 115.1(3).

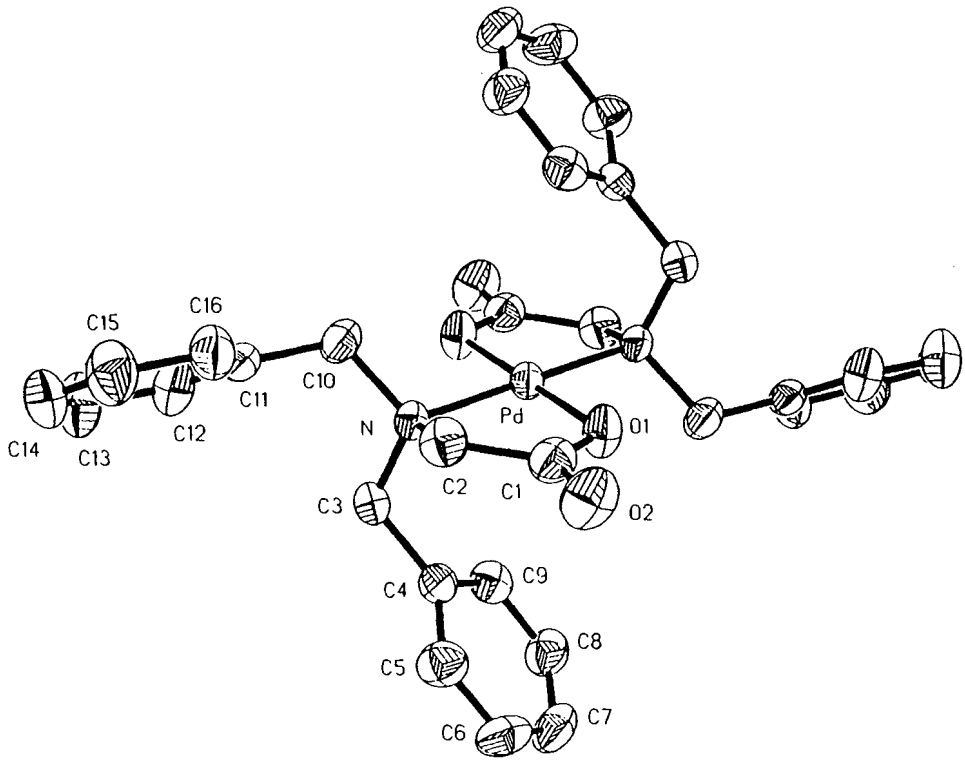

Fig. 5. Molecular structure of **9**. Thermal ellipsoids drawn at the 20% probability level. Distances (Å): Pd...Cl 2.307(1), Pd...N 2.063(3), N...C1 1.499(4), N...C8 1.476(5). Angles (°): N-Pd-Cl 88.5(1), Pd-N-C1 112.5(2), Pd-N-C8 112.4(2).

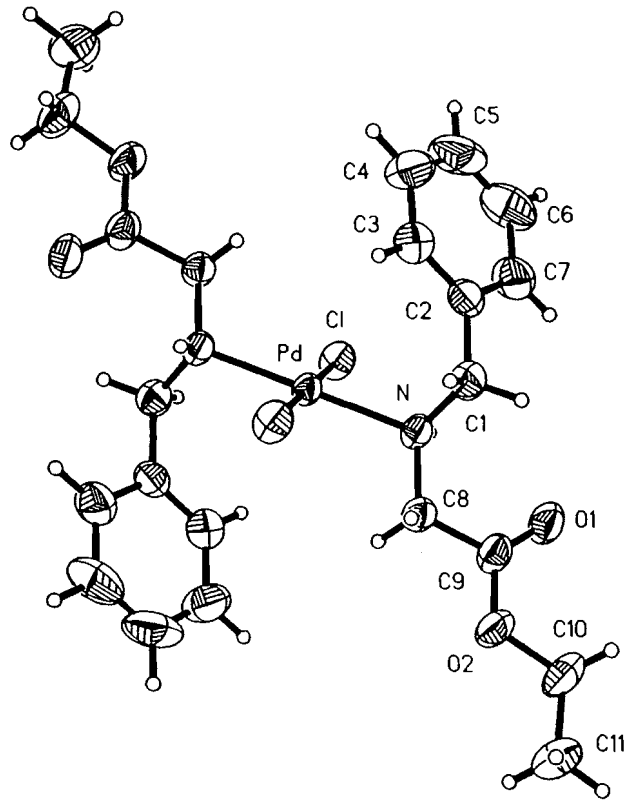

which has also been observed with other prolinate complexes.[5]

The coordination geometries around the Pd atom are essentially planar for **2***a* and **7** for crystallographic reasons, but also in **5** the sum of angles around Pd is 360.1° and Pd is thus in a planar environment as well. The best plane through the five atoms of the chelate rings in **2***a* (mean deviation 0.09 Å) includes an angle of 7° with the coordination plane; in **5**, the five atoms deviate 0.10 Å (Pd, O1, N1, etc.) and 0.15 Å (Pd, O3, N2, etc.) from their best planes, which include an angle of 21° between each other and angles of 8° and 13°, respectively, with the coordination plane.

The Pd—O distances and Pd—N distances show a slightly stronger coordination of the *imino* ligand compared with the two *amino* ligands. The chelate angles at Pd are very similar. At nitrogen and oxygen, however, the difference between the imino and amino systems becomes more obvious.

The ferrocenyl moieties are on opposite sides of the coordination plane in **2***a* (of course, due to the inversion centre at Pd), while they are on the same side in **5** with, however, two different conformations relative to the C—N bonds. Quite interestingly, one of the ferrocene units (C207–C211) is nearly coplanar with the coordination plane (angle 7°). In **7**, one of the phenyl rings "caps" each side of the coordination plane. However, no indication of any agostic interactions between Pd and the phenyl hydrogens (closest contact 2.87 Å with H9) could be obtained.

[5] With N-unsubstituted prolinates, the equivalent configuration is, of course, $S_C S_N$: see, for example, ref. 15.

Can. J. Chem. Downloaded from www.nrcresearchpress.com by 80.90.12.36 on 09/08/12
For personal use only.

Can. J. Chem. Downloaded from www.nrcresearchpress.com by 80.90.12.36 on 09/08/12
For personal use only.

Table 1. Experimental details for the crystal structure determinations.

	2a	**4a**	**5**	**7**	**9**
Formula	$C_{28}H_{28}Fe_2N_2O_4Pd*2CHCl_3$	$C_{34}H_{38}Fe_2N_2O_8Pd_2$	$C_{32}H_{36}Fe_2N_2O_4Pd$	$C_{32}H_{32}N_2O_4Pd$	$C_{22}H_{30}N_2O_4Cl_2Pd$
Formula weight	913.4	927.2	730.7	615.0	563.8
Space group	*P*-1	$P2_1/n$	$P2_12_12_1$	*C*2/*c*	*P*-1
a(Å)	7.481(2)	15.289(4)	11.180(4)	18.140(3)	5.8142(7)
b	9.449(2)	12.595(4)	11.445(3)	12.873(2)	9.733(1)
c	12.754(3)	19.557(5)	23.399(7)	13.032(2)	11.872(1)
α(°)	92.59(2)	90	90	90	103.93(1)
β(°)	93.20(2)	110.56(2)	90	91.59(1)	98.70(1)
γ(°)	96.57(2)	90	90	90	94.01(1)
V(nm^3)	0.89298	3.5261	2.9940(16)	3.0421(9)	0.6406(1)
Z	1	4	4	4	1
D_{calc}(g cm^{-3})	1.698	1.913	1.621	1.343	1.461
μ(MoK$_\alpha$) (mm^{-1})	1.783	1.747	1.581	0.636	0.952
Radiation/scan type	MoK$_\alpha$/ω	MoK$_\alpha$/ω	MoK$_\alpha$/ω	MoK$_\alpha$/2Θ	MoK$_\alpha$/ω
2Θ range (°)/ index range	4–50/±*h* ±*k* ±*l*	4–46/±*h* +*k* +*l*	2–40/±*h* ±*k* +*l*	5–50/+*h* +*k* ±*l*	5–50/+*h* ±*k* ±*l*
No. refl. coll.	3273	5330	5820	2978	2480
No. unique data (R_{int})	2804	4580 (1.08%)	2819 (2.53%)	2693 (1.45%)	2241 (1.87%)
No. observed refl. ($\|F\| \geq n\sigma(\|F\|)$)	2372 *n* = 4	3963 *n* = 4	2468 *n* = 4	2051 *n* = 3	2131 *n* = 3
Absorption correction	N/A	ψ-scan	ψ-Scan	Numerical	Numerical
min./max. Transmission		0.927/0.999	0.22/0.25	0.93/0.96	0.93/0.95
Parameters refined	205	433	370	185	151
R/R_w (g)[a]	5.13%/4.45% (0)	2.92%/2.19% (0)	2.92%/2.97% (0.0003)	4.08%/2.75% (0)	3.60%/3.20% (0)
Largest difference peak (e Å^{-3})	0.88	0.40	0.41	0.52	0.64

[a] $R = \Sigma||F_o| - |F_c||/\Sigma|F_o|$; $R_w = \{\Sigma[w(|F_o| - |F_c|)^2]/\Sigma[w|F_o|^2]\}^{1/2}$, $w^{-1} = \sigma^2_{|F|} + g|F|^2$.

The molecular structure of an orthopalladated compound was determined as well. Compound **4***a* crystallizes in the centrosymmetric space group $P2_1/n$, but both "halves" of the molecule are crystallographically independent. Since **4***a* is a glycine derivative, there is no element of central chirality, but orthopalladation leads to planar chirality in the ferrocene moiety (7). Thus, with two ferrocene moieties in the molecule of **4***a*, formation of diastereomers should be possible. However, in the crystal both ferrocene subunits show the same configuration and, because of the centrosymmetric space group, their enantiomeric counterparts are also present. The unit cell contains therefore only the $R_{Fc}R_{Fc'}/S_{Fc}S_{Fc'}$ diastereoisomeric pair. Actually, the same selectivity has been observed with an analogous orthopalladated ferrocenylmethylidene complex derived from 2,4,6-trimethylaniline as the amine compound (8*a*). The palladacycles deviate only slightly from planarity (0.03 Å at Pd1 and 0.005 Å at Pd2) and are also nearly coplanar with the cyclopentadienyl rings to which they are attached (3° in both halves). The coordination planes around the Pd^{2+} ions show only 0.03 Å (at Pd1) and 0.04 Å (at Pd2) deviation from planarity, and include angles of 6° and 3° with the corresponding chelate rings and of 35° between each other. This "folding" of the molecule has been observed with several other acetate-bridged dipalladium complexes (and adds another element of chirality to the system), while it is absent in the corresponding chloro-bridged dimers (8, 16). The acetate bridges are not planar. The close contact between the two Pd^{2+} ions is a consequence of the folding, and has been reported for other complexes of this type as well (16). The Pd—N distances lie intermediate between the values found for imino- and aminoacidate systems, presumably due to the different *trans* influence of the acetate ligand compared to a nitrogen ligand. The Pd—C distances (avg. 1.936 Å) are quite short, and consequently, the *trans* Pd—O distances (avg. 2.136 Å) are approximately 0.10 Å longer than the Pd—O bonds *trans* to the imino nitrogen. All these bond parameters are quite similar to the values reported for $Pd_2[4\text{-}OCH_3C_6H_4N{=}C(COPh)Ph]_2(OAc)_2$ (16) and $[Pd\{cpFeC_5H_3C(H){=}N\text{-}2,4,6\text{-}Me_3C_6H_2\}OAc]_2$ (8*a*). The C=N bond of the imino group (avg. 1.278 Å) is slightly elongated when compared with the situation in **2***a*, but still shorter than the literature values for the two above-mentioned complexes.

Finally, the structure of a compound with a unidentate amino acid derivative, **9**, was also determined. Here again, the Pd^{2+} ion resides on a crystallographic inversion centre. Consequently, the chiral nitrogen atom has the *R* configuration in one half of the molecule and the *S* configuration in the other. The $R_NR_{N'}$ or $S_NS_{N'}$ diastereomers are absent in the crystal.

Can. J. Chem. Downloaded from www.nrcresearchpress.com by 80.90.12.36 on 09/08/12
For personal use only.

Table 2. Fractional atomic coordinates ($\times 10^4$) and equivalent isotropic displacement coefficients ($Å^2 \times 10^3$) for **2***a*.

Atom	*x*	*y*	*z*	U_{eq}
Pd	0	0	0	34(1)
Fe	5743(1)	2930(1)	2498(1)	43(1)
O(1)	−946(6)	1406(5)	−918(4)	45(2)
O(2)	−725(7)	3715(5)	−1197(4)	57(2)
N(1)	1365(7)	1738(6)	741(5)	35(2)
C(1)	3032(9)	2911(7)	2329(6)	38(3)
C(2)	3910(9)	4288(7)	2094(6)	43(3)
C(3)	4944(10)	4832(8)	3018(7)	53(3)
C(4)	4787(10)	3862(8)	3809(7)	55(3)
C(5)	3607(9)	2675(8)	3393(6)	49(3)
C(6)	8199(12)	2343(13)	2942(8)	75(4)
C(7)	7047(15)	1162(11)	2551(13)	96(6)
C(8)	6511(13)	1407(13)	1530(12)	97(6)
C(9)	7287(15)	2671(16)	1253(9)	94(6)
C(10)	8351(11)	3257(10)	2117(10)	76(4)
C(11)	2040(9)	1764(7)	1661(6)	37(3)
C(12)	1389(9)	2980(7)	66(6)	37(3)
C(13)	−226(10)	2720(8)	−732(6)	40(3)
C(14)	3101(10)	3111(8)	−540(6)	57(3)
Cl(1)	926(4)	6104(3)	4125(3)	109(1)
Cl(2)	3486(5)	8481(3)	3969(3)	149(2)
Cl(3)	−151(6)	8787(5)	3584(4)	189(3)
C(15)	1387(13)	7651(9)	3453(8)	83(4)

The Pd—N bond length compares well with the values found in the two other compounds with a sp^3 nitrogen.

NMR Spectra

The ligands described in this paper usually display quite complicated patterns in their ^{1}H NMR spectra, due to overlapping resonances of the ferrocene part with the amino acid part. Generally, protons of substituted ferrocenes appear at $4 < \delta < 5$ ppm with multiplicities strongly dependent on the kind of substituent present. With a chiral substituent, the α as well as the β protons become diastereotopic, thus generating ABCD spin systems. Also, the resonance of the α-proton of the amino acid residue is expected in the same region of the NMR spectrum. The other protons of the amino acid usually absorb between 0.8 and 2.2 ppm, with only alanine having a really characteristic doublet absorption due to the methyl group. Finally, the proton of an imino function is expected around 8 ppm as a singlet (8) that is well separated from the other proton resonances except for the aromatic amino acidates.

It is quite clear, therefore, that unambiguous *complete* assignments of NMR spectra are either very difficult or even impossible, particularly when the formation of isomeric species has to be considered as well (vide infra). Any discussion of the species present in solution depends on the observation of well-separated signals for the imino protons in the ^{1}H NMR spectra.

Discussion

As was already mentioned, the interaction of Pd^{2+} with N-functionalized amino acid derivatives leads to formation of three different types of products. With amino acid anions, the exclusive formation of N,O chelates is observed. With amino acid esters and Na_2PdCl_4 only monodentate coordination via the nitrogen occurs, while the use of $Pd(OAc)_2$ leads to ortho-palladation. This ease of formation of cyclometallated products with $Pd(OAc)_2$ has been reported before (12*a*).

In many of the complexes presented in this paper the forma-

Table 3. Fractional atomic coordinates ($\times 10^4$) and equivalent isotropic displacement coefficients ($Å^2 \times 10^3$) for **4***a*.

Atom	*x*	*y*	*z*	U_{eq}
Pd(1)	4558(1)	817(1)	2463(1)	49(1)
Pd(2)	6498(1)	301(1)	2702(1)	46(1)
Fe(1)	3207(1)	2256(1)	3240(1)	62(1)
Fe(2)	8267(1)	911(1)	2004(1)	55(1)
O(1)	4490(2)	−185(3)	1564(2)	59(1)
O(2)	5919(2)	−910(3)	1994(2)	53(1)
O(3)	6230(2)	−439(3)	3591(2)	60(2)
O(4)	4662(2)	−436(3)	3145(2)	61(2)
O(5)	3558(3)	1262(4)	7(2)	110(3)
O(6)	2873(3)	1293(3)	832(2)	88(2)
O(7)	8189(3)	353(3)	4398(2)	82(2)
O(8)	7472(3)	871(4)	5153(2)	130(3)
N(1)	4322(2)	2161(3)	1858(2)	53(2)
N(2)	7143(3)	1570(3)	3302(2)	52(2)
C(1)	5094(3)	−840(4)	1543(3)	50(2)
C(2)	4831(3)	−1613(4)	925(3)	73(3)
C(3)	5448(4)	−742(4)	3582(3)	56(2)
C(4)	5426(4)	−1547(5)	4143(3)	94(3)
C(5)	4302(3)	2196(4)	1112(3)	68(3)
C(6)	3553(4)	1530(5)	591(3)	75(3)
C(7)	2196(4)	515(7)	406(4)	170(6)
C(8)	1370(5)	791(8)	309(5)	218(7)
C(9)	4475(3)	1817(4)	3190(3)	54(2)
C(10)	4223(3)	2861(4)	2915(3)	56(2)
C(11)	4095(3)	3513(5)	3473(3)	71(3)
C(12)	4277(4)	2872(5)	4086(3)	74(3)
C(13)	4502(3)	1848(5)	3926(3)	65(3)
C(14)	1865(4)	2744(6)	2947(6)	105(4)
C(15)	2080(4)	2088(8)	3543(5)	108(5)
C(16)	2336(5)	1116(7)	3358(6)	121(5)
C(17)	2279(5)	1180(8)	2636(6)	121(5)
C(18)	1990(4)	2194(9)	2382(4)	117(5)
C(19)	4145(3)	2986(4)	2165(3)	61(2)
C(20)	7152(4)	1776(4)	4035(3)	69(3)
C(21)	7604(5)	951(6)	4595(4)	83(3)
C(22)	8537(5)	−529(6)	4877(4)	122(4)
C(23)	9168(5)	−1117(6)	4603(4)	153(5)
C(24)	6914(3)	992(4)	1986(3)	49(2)
C(25)	7416(3)	1959(4)	2245(3)	52(2)
C(26)	7733(4)	2371(4)	1692(3)	66(3)
C(27)	7426(3)	1678(4)	1101(3)	66(2)
C(28)	6926(3)	827(4)	1271(3)	56(2)
C(29)	8873(3)	−381(5)	2609(3)	78(3)
C(30)	9322(4)	529(5)	2944(3)	83(3)
C(31)	9676(3)	1032(5)	2466(4)	93(3)
C(32)	9439(4)	437(6)	1825(4)	88(3)
C(33)	8932(4)	−446(5)	1912(4)	83(3)
C(34)	7525(3)	2217(4)	2986(3)	58(2)

Can. J. Chem. Downloaded from www.nrcresearchpress.com by 80.90.12.36 on 09/08/12
For personal use only.

Table 4. Fractional atomic coordinates ($\times 10^4$) and equivalent isotropic displacement coefficients ($Å^2 \times 10^3$) for **5**.

Atom	*x*	*y*	*z*	U_{eq}
Pd	1247(1)	4853(1)	5421(1)	41(1)
O(1)	1959(5)	3539(5)	4977(2)	56(2)
C(101)	1197(8)	2835(8)	4752(3)	54(3)
O(2)	1467(6)	1989(5)	4469(3)	95(3)
C(102)	−114(7)	3124(7)	4847(3)	51(3)
C(103)	−661(9)	3703(8)	4318(4)	93(4)
C(104)	−998(7)	4926(7)	4502(4)	80(4)
C(105)	−1285(7)	4771(7)	5128(3)	65(3)
N(1)	−318(5)	3954(5)	5331(3)	46(2)
C(106)	−690(7)	3373(7)	5869(3)	56(3)
C(107)	270(7)	2648(6)	6141(3)	41(3)
C(108)	990(8)	2964(7)	6614(3)	56(3)
C(109)	1726(8)	2030(9)	6769(4)	69(4)
C(110)	1497(7)	1121(8)	6388(4)	61(4)
C(111)	618(8)	1476(7)	5993(3)	52(3)
Fe(1)	−18(1)	1531(1)	6797(1)	60(1)
C(113)	−1763(13)	1385(28)	6926(9)	165(13)
C(114)	−1341(21)	1832(11)	7371(10)	123(8)
C(115)	−555(20)	1095(25)	7598(6)	151(10)
C(116)	−502(25)	111(25)	7249(13)	243(18)
C(112)	−1284(29)	356(20)	6845(11)	242(19)
O(3)	531(5)	6158(5)	5875(2)	60(2)
C(201)	1204(11)	7080(8)	5893(4)	71(4)
O(4)	925(7)	7981(5)	6138(3)	100(3)
C(202)	2360(8)	7009(7)	5562(3)	54(3)
C(203)	2176(10)	7386(9)	4946(4)	78(4)
C(204)	2936(9)	6588(9)	4585(4)	95(5)
C(205)	3559(8)	5775(7)	4991(3)	64(3)
N(2)	2796(5)	5788(5)	5512(3)	44(2)
C(206)	3385(6)	5336(7)	6048(3)	51(3)
C(207)	4549(7)	5935(6)	6199(3)	42(3)
C(208)	4692(8)	6906(6)	6562(3)	55(3)
C(209)	5923(9)	7093(7)	6646(3)	60(4)
C(210)	6552(7)	6266(8)	6333(3)	62(4)
C(211)	5716(8)	5537(6)	6051(3)	53(3)
Fe(2)	5457(1)	5450(1)	6904(1)	47(1)
C(212)	4580(19)	4058(14)	7204(7)	137(8)
C(213)	5769(19)	3804(10)	7140(6)	114(7)
C(214)	6473(11)	4517(12)	7469(5)	93(5)
C(215)	5711(13)	5231(11)	7752(4)	89(5)
C(216)	4559(11)	4951(14)	7611(6)	102(6)

Table 5. Fractional atomic coordinates ($\times 10^4$) and equivalent isotropic displacement coefficients ($Å^2 \times 10^3$) for **7**.

Atom	*x*	*y*	*z*	U_{eq}[a]
Pd	0	0	5000	32(1)
N	−280(2)	1552(3)	4946(3)	34(1)
O(1)	761(2)	378(2)	3990(3)	44(1)
O(2)	1152(2)	1695(3)	3047(3)	59(1)
C(1)	730(3)	1324(4)	3664(4)	43(2)
C(2)	94(3)	1984(4)	4023(4)	44(2)
C(3)	−29(3)	2072(4)	5917(4)	35(2)
C(4)	776(3)	1927(4)	6202(3)	37(2)
C(5)	1299(3)	2676(4)	5935(4)	49(2)
C(6)	2034(3)	2524(5)	6227(4)	56(2)
C(7)	2251(3)	1654(5)	6789(4)	55(2)
C(8)	1735(3)	919(4)	7061(4)	48(2)
C(9)	1008(3)	1059(4)	6768(4)	41(2)
C(10)	−1114(3)	1629(4)	4835(4)	45(2)
C(11)	−1422(3)	2725(4)	4895(4)	40(2)
C(12)	−1694(3)	3063(4)	5811(4)	52(2)
C(13)	−2003(3)	4043(5)	5893(5)	66(2)
C(14)	−2034(3)	4690(4)	5062(5)	62(2)
C(15)	−1761(3)	4359(4)	4144(5)	64(2)
C(16)	−1467(3)	3369(4)	4052(4)	52(2)

[a]The equivalent isotropic U_{eq} is calculated as one third of the trace of the orthogonal U_{ij} tensors.

Table 6. Fractional atomic coordinates ($\times 10^4$) and equivalent isotropic displacement coefficients ($Å^2 \times 10^3$) for **9**.

Atom	*x*	*y*	*z*	U_{eq}[a]
Pd	0	10000	0	33(1)
C1	3029(2)	8756(1)	547(1)	47(1)
N	901(6)	9630(3)	−1654(3)	36(1)
O(1)	3563(5)	9693(3)	−3420(2)	59(1)
O(2)	3080(5)	11997(3)	−3299(2)	59(1)
C(1)	−847(7)	8575(4)	−2567(3)	46(2)
C(2)	−1247(7)	7207(4)	−2197(3)	44(1)
C(3)	−3021(8)	7013(4)	−1589(3)	54(2)
C(4)	−3312(9)	5793(5)	−1195(4)	73(2)
C(5)	−1820(11)	4775(5)	−1422(5)	86(3)
C(6)	−93(10)	4938(5)	−2043(5)	82(2)
C(7)	227(8)	6158(4)	−2434(4)	62(2)
C(8)	1364(7)	10958(4)	−2014(3)	40(1)
C(9)	2786(7)	10770(4)	−2987(3)	46(2)
C(10)	4498(10)	12003(5)	−4209(4)	78(2)
C(11)	4391(11)	13415(5)	−4511(4)	94(3)

[a]The equivalent isotropic U_{eq} is calculated as one third of the trace of the orthogonal U_{ij} tensors.

tion of isomers is possible. These isomers might arise either from the generation of new stereogenic centers on complexation, e.g., planar chirality induced by orthopalladation, *cis/trans* isomers at the palladium ion, or *cis/trans-* isomerism around the imino functionalities.

Thus, with restricted rotation around the C=N bond, and with two such imino functions in the molecule in compounds **2** and **3**, three isomers *Z/Z*, *Z/E*, and *E/E* might be expected. For steric reasons, however, the *E/E* isomer should be strongly favoured, since it shows the least interaction between the ferrocenyl moiety and the chelate ring. This is also observed in the solid state structure of **2***a*. The ^{1}H NMR spectra of **2***a,b,d* show only one singlet for the imino protons, at δ 7.9, indicating also only one species present in solution. (It should be noted that the crystal structure determination of **2***a* indicated at least partial racemization of the amino acid. This in turn opens up the possibility of diastereoisomer formation (*R/R*, *R/S*), which should give rise to two independent NMR signal sets, which are not, however, observed.)

For the cyclopalladated compounds **4**, without any asymmetric induction by the attached amino acidate, both α positions in the substituted ferrocene ring could have been

Table 7. Elemental analyses, yields, and IR data for compounds **2–9**.

Compound	Molecular formula	%C	%H (Calcd./Found)	%N	Yield (%)	IR (Nujol/KBr) $\nu(CO_2)$	IR (Nujol/KBr) $\nu(C{=}N)$
2*a*	$C_{28}H_{28}Fe_2N_2O_4Pd$	41.50	3.48	3.28	78	1655	1620
	$\times$ 1,5 $CHCl_3$	41.91	3.81	3.37			
2*b*	$C_{32}H_{36}Fe_2N_2O_4Pd$	51.33	5.12	3.74	62	1655	1615
	$\times$ H_2O	51.20	5.01	3.72			
2*c*	$C_{34}H_{40}Fe_2N_2O_4Pd$	47.87	4.71	3.19	37	1657	1628
	$\times$ $CHCl_3$	47.41	4.77	2.97			
2*d*	$C_{26}H_{24}Fe_2N_2O_4Pd$	47.63	3.84	4.27	73	1650	1625
	$\times$ 0.5 H_2O	47.32	3.87	4.28			
2*e*	$C_{36}H_{28}Fe_2N_2O_4Pd$	53.00	4.07	3.43	27	1625	1606
	$\times$ 2.5 H_2O	52.77	4.14	3.46			
3	$C_{26}H_{24}Cl_2Fe_2N_2O_4Pd_2$	37.90	2.94	3.40	54	1650	1625
		37.40	3.02	3.38			
4*a*	$C_{34}H_{38}Fe_2N_2O_8Pd_2$	44.05	4.13	3.02	64	1737	1628
		43.23	4.15	3.03		1579	
4*b*	$C_{34}H_{38}Fe_2N_2O_8Pd_2$	44.05	4.13	3.02	58	1737	1625
		44.24	4.29	3.27		1578	
5	$C_{32}H_{36}Fe_2N_2O_4Pd$	50.12	5.26	3.65	40	1641	
	$\times$ 2 H_2O	50.14	5.58	3.55			
6	$C_{28}H_{32}Cl_2Fe_2N_2O_4Pd_2$	36.24	4.34	3.02	12	1655	
	$\times$ 4 H_2O	36.02	4.19	3.03			
7	$C_{32}H_{32}N_2O_4Pd$	57.26	5.24	3.98	82	1640	
	$\times$ 0.75 CH_2Cl_2	57.69	5.16	4.02			
	$\times$ 0.75 CH_3OH						
8	$C_{40}H_{46}N_2O_8Pd_2$	52.07	5.35	3.03	35	1730	
	$\times$ 1,5 H_2O	52.21	5.39	2.86		1585	
9	$C_{22}H_{30}Cl_2N_2O_4Pd$	46.87	5.36	4.97	70	1735	
		46.64	5.47	4.73			

attacked by Pd; thus an enantiomeric pair of the palladacycle should be generated. With two such palladacycles in a molecule, diastereomers $R_{Fc}R_{Fc'}$ and $R_{Fc}S_{Fc'}$ together with their enantiomers should be formed. With an additional centre of chirality as in **4***b*, three diastereomers: $R_{Fc}R_{Fc'}S_CS_{C'}$, $R_{Fc}S_{Fc'}S_CS_{C'}$, and $S_{Fc}S_{Fc'}S_CS_{C'}$ become possible, which should give rise to three independent (plus one equally intensive) sets of signals. The formation of at least two of these isomers (one symmetrical and one unsymmetrical) can be deduced from the ^1H NMR spectrum of **4***b*, the third isomer either being formed to a lesser extent, or its signals accidentally hidden by the other isomers.

In the corresponding *N*-dibenzylglycine derivative **8** the element of planar chirality is missing. However, the nitrogen atoms become stereogenic centres by coordination, and thus the formation of two diastereomers $R_NR_{N'}$ and $R_NS_{N'}$ together with their enantiomers should be possible. A similar argument holds for the *trans* $PdCl_2$ complex **9**. In both cases, however, the overlap of the methylene protons on one side and the phenyl protons on the other, which are all diastereotopic due to the inherent chirality, does not allow an unambiguous statement about the number of isomers formed. Due to solubility problems, the ^{13}C NMR spectra are of too poor quality to make any decisions. However, since there seems to be no source of asymmetric induction, we assume that both diastereomers are formed.

Experimental

All reactions were performed using standard Schlenk technique, under nitrogen, with N_2-saturated dry solvents. All reagents were commercially available and were used without further purification. For the NMR spectra a Jeol-GSX 270 instrument was used, for IR spectra Perkin–Elmer 841 and Nicolet 520 spectrometers. The X-ray analyses were performed on a Enraf–Nonius CAD 4 (**2***a*–**4**), Syntex R3 (**5**), and Siemens R3m/V (**7**, **9**). The programs used to solve and refine the structures were included in the Siemens–Nicolet SHELXTL-plus program package on a Microvax II computer.

Elemental analyses together with selected IR data and yields are presented in Table 7.

Bis-(*N*-ferrocenylidene-aminoacidate)-palladium(II) 2*a*–*e*

General procedure

The amino acid (1.0 mmol), dissolved in 2 mL MeOH, is

Can. J. Chem. Downloaded from www.nrcresearchpress.com by 80.90.12.36 on 09/08/12
For personal use only.

Can. J. Chem. Downloaded from www.nrcresearchpress.com by 80.90.12.36 on 09/08/12
For personal use only.

treated with a 0.5 M solution of NaOMe in MeOH until no solids or cloudiness remain. This solution is treated with 1.0 mmol formyl ferrocene (214 mg) and a small quantity of Al_2O_3. After stirring for 1 h at room temperature, the suspension is filtered and the residue washed with MeOH. The combined liquids are concentrated in vacuo to about 2 mL and then treated with 0.5 mmol Na_2PdCl_4 (147 mg). After 15 h of stirring at room temperature, the red precipitate (for **2***e* the addition of water is necessary to obtain a precipitate) is isolated and washed three times with 2 mL MeOH. Recrystallization from $CHCl_3$–hexane yields red crystals.

For the synthesis of **3**, instead of 0.5 mmol Na_2PdCl_4, 1.0 mmol $PdCl_2$ (177 mg) is added to the solution of the Schiff base.

Selected ^{1}H NMR data (270 MHz): **2***a*: 7.9s (CH=N), 4.4–4.7m, 1.8d; **2***b*: 7.9s (CH=N), 4.3m, 4.7m, 2.3m, 1.34d, 1.26d; **2***d*: 7.9s (CH=N), 4.7m, 4.4s, 4.2m; **3**: 7.9s (CH=N), 4.7m, 4.4m, 4.2m. ^{13}C NMR data (69 MHz; in $CDCl_3$): δ (*C*HN): 168.1 (for **2***a*,*c*), 169.3 (for **2***e*, **3**); δ (*C*O): 182.8 (**2***a*), 180.1 (**2***c*), 179.7 (**2***e*, **3**).

Bis(μ-acetato)-bis(*N*-ferrocenylidene-*O*-alkylamino-acidate)-dipalladium (II) 4*a*,*b*

General procedure

A solution of 1.0 mmol formylferrocene, 3 mmol Na_2CO_3 (300 mg), and 1.0 mmol *O*-ethyl- or methylamino acid hydrochloride in EtOH is refluxed for 2 h. After centrifugation the precipitate is discarded, and the solution is evaporated in vacuo to yield a dark red oil. This is dissolved in 4 mL MeOH, treated with 1.0 mmol KOAc (100 mg) and 1.0 mmol $Pd(OAc)_2$ (226 mg), and stirred for 15 h. After filtration through a Hyflo Super Cel filter aid (to remove the Pd powder also generated in the reaction) the solution is concentrated in vacuo to leave again a red oil. Several recrystallizations from CH_2Cl_2–hexane yield **4** in pure form as red crystals. ^{1}H NMR ($CDCl_3$): **4***a*: 7.4s (CH=N), 4.2–4.5m, 3.9d, 3.3q, 2.1s, 1.3t; 4b: 7.8–8.2″m″ (CH=N), 3.4–4.8m, 0.9–2.2m.

Bis(*N*-ferrocenylmethylprolinate)-palladium(II) 5

Formylferrocene 1.0 mmol, (214 mg) and 1.0 mmol L-proline (115 mg) are dissolved in 3 mL MeOH and stirred for 30 min at room temperature. The now violet solution is chilled to −78°C and treated with 5 mmol $NaBH_4$ (189 mg). While continuously stirring, the mixture is brought back to room temperature, when the solvent is stripped off in vacuo. Twenty minutes after addition of a small amount of water, 1.0 mmol NBu_4Br (322 mg) is added, and the suspension extracted with CH_2Cl_2. The organic phase is separated, dried with Na_2SO_4, filtered, and freed from solvent in vacuo. A brownish yellow powder is left. A mixture of 55 mg of this powder and 0.05 mmol Na_2PdCl_4 (15 mg) is stirred for 30 min in 1 mL of a 1:1 water–methanol mixture. Evaporation of the MeOH precipitates the product, which can be isolated by filtration and recrystallized from CH_2Cl_2 to yield yellow crystals of **5**. ^{1}H NMR ($CDCl_3$): 4.2–4.4m, 4.1s, 3.7m, 3.3m, 2.9m.

Di-μ-dichloro-*N*-ferrocenylmethylalaninate)-dipalladium(II) 6

Formylferrocene (0.3 mmol, 64 mg), dissolved in 1 mL MeOH, is treated with 0.95 mmol $MgCl_2$ (90 mg), 0.3 mmol L-alanine (27 mg), and 0.3 mmol NaOAc (25 mg). After stirring for 6 h at room temperature, the reaction mixture is chilled to −78°C and 1.5 mmol $NaBH_4$ (57 mg) is added. Over 15 h the suspension is brought back to ambient temperature. Then 1 mL 2 M HCl is added, with stirring for 20 min, to hydrolyze unreacted $NaBH_4$, after which the pH of the solution is brought to 8 by addition of 2 M NaOH. After the addition of 0.15 mmol Na_2PdCl_4 (44 mg) and stirring for 30 min, **6** can be isolated as a yellow powder.

Bis(*N*,*N*-dibenzylglycinate)-palladium(II) 7

Na_2PdCl_4 (1.0 mmol), dissolved in 8 mL MeOH, is treated with 2.0 mmol *N*,*N*-dibenzylglycine (510 mg) with stirring for 2 h. Filtration and washing with EtOH and Et_2O leaves **7** as a red powder that can be recrystallized from CH_2Cl_2–hexane. ^{1}H NMR ($CDCl_3$): 7.4–7.6m, 3.8–4.2m, 3.44s.

Bis(*N*-benzyl-*O*-ethylglycinate)-dichloro-palladium (II) 9

9 can be obtained similarly from 1.0 mmol Na_2PdCl_4, 2.0 mmol *N*-benzyl-*O*-ethylglycinate, and 2.0 mmol NaOAc. ^{1}H NMR ($CDCl_3$): 7.4–7.6m, 3.8–4.2m, 3.4m, 1.2m.

Compound 8

$Pd(OAc)_2$ (1.0 mmol, 224 mg), *N*,*N*-dibenzyl-*O*-ethylglycinate (2.0 mmol; 570 mg), and NaOAc (2.0 mmol; 164 mg) in 8 mL MeOH are stirred for 20 h at room temperature. Filtration through the filter aid removes the precipitated palladium. The solution is evaporated in vacuo, the residue taken up in CH_2Cl_2, and the solution added to Et_2O. The precipitate is discarded, and the solution chromatographed on silica gel-60 (Merck). The first yellow band, containing the product, is collected. Concentration of the solution in vacuo, followed by careful addition of hexane, yields **8** in the form of light yellow crystals. ^{1}H NMR ($CDCl_3$): 6.7–8.3m, 3.2–4.4m, 2.1s, 1.2m.

Acknowledgement

Generous support by the Deutsche Forschungsgemeinschaft, Fonds der Chemischen Industrie, and Degussa AG, Hanau, is gratefully acknowledged.

References

1. K. Severin and W. Beck. Z. Naturforsch. B: Chem. Sci. **50**, 275 (1995).
2. (*a*) S.L. Blystone. Chem. Rev. **89**, 1663 (1989), and literature cited therein; (*b*) M. Sawamura and Y. Ito. Chem. Rev. **92**, 857 (1992); (*c*) J.K. Stille. Angew. Chem. Int. Ed. Engl. **25**, 508 (1986); Angew. Chem. **98**, 504 (1986).
3. (*a*) A.D. Ryabov. Chem. Rev. **90**, 403 (1990); (*b*) Synthesis, **1985**, 233 (1985); (*c*) I. Omae. Coord. Chem. Rev. **83**, 137 (1988); (*d*) V.V. Dunina, O.A. Zalevskaya, and V.M. Potapov. Russ. Chem. Rev. **57**, 250 (1988).
4. (*a*) T. Hayashi and M. Kumada. Acc. Chem. Res. **15**, 395 (1982); (*b*) T. Hayashi. Pure Appl. Chem. **60**, 7 (1988); (*c*) A. Togni and T. Hayashi (*Editors*). Ferrocenes. VCH, Weinheim. 1995.
5. H. Plenio. Chem. Ber. **126**, 2585 (1993); P.D. Beer, J.P. Danks, M.G.B. Drew, and J.F. McAteer. J. Organomet. Chem. **476**, 63 (1994); J.C. Medina, T.T. Goodnow, M.T. Rojas, J.L. Atwood, B.C. Lynn, and G.W. Gokel. J. Am. Chem. Soc. **114**, 10583 (1992).

6. H.M. Ali, A.A. Naiini, and C.H. Brubaker, Jr. J. Mol. Catal. **77**, 125 (1992), and references cited therein.
7. (*a*) L.L. Troitskaya, L.A. Bulygina, P.V. Petrovskii, and V.I. Sokolov. Organomet. Chem. USSR, **4**, 322 (1991); (*b*) V.I. Sokolov, L.L. Troitskaya, and L.A. Bulyina. Organomet. Chem. USSR, **3**, 746 (1990); (*c*) V.I. Sokolov, L.L. Troitskaya, and O.A. Reutov. J. Organomet. Chem. **182**, 537 (1979); (*d*) M. Gruselle, B. Malezieux, V.I. Sokolov, and L.L. Troitskaya. Inorg. Chim. Acta, **222**, 51 (1994); (*e*) M. Pfeffer, J.-P. Sutter, A. DeCian, and J. Fischer. Inorg. Chim. Acta, **220**, 115 (1994).
8. (*a*) J. Blanco, E. Gayoso, J.M. Vila, M. Gayoso, C. Maichle-Mössmer, and J. Strähle. Z. Naturforsch. B: Chem. Sci. **48**, 906 (1993); (*b*) C. López, T. Sales, X. Solans, and R. Zquiak. J. Chem. Soc. Dalton Trans. 2321 (1992); (*c*) R. Bosque, C. López, J. Sales, X. Solans, and M. Font-Bardia. J. Chem. Soc. Dalton Trans. 735 (1994); (*d*) R. Bosque, M. Font-Bardia, C. López, J. Sales, J. Silver, and X. Solans. J. Chem. Soc. Dalton Trans. 747 (1994); (*e*) C. López, R. Bosque, X. Solans, M. Font-Bardia, D. Tramuns, G. Fern, and J. Silver. J. Chem. Soc. Dalton Trans. 3039 (1994); (*f*) B. Bosque, C. López, J. Sales, and X. Solans. J. Organomet. Chem. **483**, 61 (1994); (*g*) S.Q. Huo, Y.J. Wu, C.X. Du, Y. Zhu, H.Z. Yuan, and X.A. Mao. J. Organomet. Chem. **483**, 139 (1994); (*h*) Y.J. Wu, S.Q. Huo, and Y. Zhu. J. Organomet. Chem. **485**, 161 (1995).
9. (*a*) K. Schlögl. Monatsh. Chem. **88**, 601 (1957); (*b*) P.L. Pauson and J.M. Osgerby. J. Chem. Soc. 646 (1958); (*c*) A.-S. Carlström and T. Frejd. J. Org. Chem. **55**, 4175 (1990); (*d*) E. Cuingnet, S. Sergheraert, A. Tartar, and M. Dautrevaux. J. Organomet. Chem. **195**, 325 (1980); (*e*) H. Brunner, W. König, and B. Nuber. Tetrahedron: Asymmetry, **4**, 694 (1993).
10. A.M. Osman, M.A. El-Maghraby, and K.M. Hassan. Bull. Chem. Soc. Jpn. **48**, 2226 (1975).
11. H. Eckert and C. Seidel. Angew. Chem. **98**, 168 (1986); Angew. Chem. Int. Ed. Engl. **25**, 159 (1986).
12. (*a*) Y. Fuchita and H. Tsuchiya. Inorg. Chim. Acta, **209** (1993); Polyhedron, **12**, 2079 (1993); (*b*) A. Crispini, G. De Munno, M. Ghedini, and F. Neve. J. Organomet. Chem. **427**, 409 (1992).
13. (*a*) N. Gabbitas, G. Salem, M. Sterns, and A.C. Willis, J. Chem. Soc. Dalton Trans. 3271 (1993); (*b*) J. Vicente, I. Saura-Llamas, and P.G. Jones. J. Chem. Soc. Dalton Trans. 3621 (1994); (*c*) A. Togni, C. Breutel, M.C. Soares, N. Zanetti, T. Gerfin, V. Gramlich, F. Spindler, and G. Rihs, Inorg. Chim. Acta, **222**, 213 (1994); (*d*) A. Miyashita, H. Takaya, T. Souchi, and R. Noyori. Tetrahedron, **40**, 1245 (1984).
14. E. Uhlig, and K. Fischer. Z. Anorg. Allg. Chem. **539**, 195 (1986).
15. A. McL. Mathieson and H.K. Welsh. Acta Crystallogr. **5**, 599 (1952); H.C. Freeman and I.E. Maxwell. Inorg. Chem. **9**, 649 (1970); T. Ito, F. Marumo, and Y. Saito. Acta Crystallogr. Sect. B: Struct. Crystallogr. Cryst. Chem. **27B**, 1062 (1971); R. Krämer, K. Polborn, H. Wanjek, I. Zahn, and W. Beck. Chem. Ber. **123**, 767 (1990).
16. J.L. Garcia-Ruano, I. Lopez-Solera, J.R. Masaguer, C. Navarro-Ranninger, J.H. Rodriguez, and S. Martinez-Carrera. Organometallics, **11**, 3013 (1992); C. Navarro-Ranninger, I. Lopez-Solera, A. Alvarez-Valdez, J.J. Rodriguez, J.R. Masaguer, and J.L. Garcia-Ruano. J. Organomet. Chem. **476**, 19 (1994), and references cited therein.

Can. J. Chem. Downloaded from www.nrcresearchpress.com by 80.90.12.36 on 09/08/12
For personal use only.

Coordination chemistry of a mixed donor bidentate ligand with nickel. A tetrameric enolate of sodium that binds a phosphine donor

Michael D. Fryzuk, Xiaoliang Gao, and Steven J. Rettig

Can. J. Chem. Downloaded from www.nrcresearchpress.com by 80.90.12.36 on 09/08/12
For personal use only.

Abstract: The preparation of a mixed donor ligand consisting of an enolate and neutral phosphine is described and its coordination chemistry with nickel reported. The phosphino ketones R_2PCH_2COPh (R = Cy or Pr^i) are prepared by the reaction of the corresponding secondary phosphines with bromoacetophenone to form the corresponding phosphonium salts $[R_2P(H)CH_2COPh]^+Br^-$ (R = Cy or Pr^i); subsequent deprotonation leads to the neutral ketones. The enolates are formed by addition of $NaN(SiMe_3)_2$ to the neutral ketone. The crystal structure of the sodium enolate having isopropyl substituents at phosphorus displays a tetrameric structure in the solid state and there is an interaction of the phosphorus donor with the sodium anion: Na—P, 2.852(2) Å. The preparation of a series of nickel complexes was achieved by addition of the sodium enolate to the appropriate Ni(II) starting material. The structures of the nickel derivatives are reported. The catalytic behaviour of one of these complexes in the polymerization and oligomerization of ethylene is briefly described. Crystals of $\{Na[Pr^i_2PC(H)=C(O)Ph]\}_4$, **2***b*, are tetragonal, $a = b = 20.790(2)$ Å, $c = 13.539(7)$ Å, $Z = 4$, space group $I4_1/a_1$; those of $[Cy_2PC(H)=C(O)Ph](PPh_3)NiPh$, **3***a*, are triclinic, $a = 10.742(2)$ Å, $b = 19.811(3)$ Å, $c = 10.621(2)$ Å, $\alpha = 101.88(1)°$, $\beta = 119.24(1)°$, $\gamma = 91.08(1)°$, $Z = 2$, space group $P\bar{1}$; and those of $[Pr^i2PC(H)=C(O)Ph](PPh_3)NiPh$, **3***b*, are triclinic, $a = 10.219(1)$ Å, $b = 17.432(3)$ Å, $c = 9.788(1)$ Å, $\alpha = 101.18(1)°$, $\beta = 100.19(1)°$, $\gamma = 85.32(1)°$, $Z = 2$, space group $P\bar{1}$. The structures were solved by direct (**2***b*) and Patterson (**3***a* and **3***b*) methods and were refined by full-matrix least-squares procedures to $R = 0.045$, 0.044, and 0.032 ($R_w = 0.038$, 0.041, and 0.030) for 965, 4483, and 5085 reflections with $I \geq 3\sigma(I)$ respectively.

Key words: nickel, sodium enolate, homogeneous catalyst, oligomerization.

Résumé : On décrit la préparation d'un coordinat donneur mixte, formé d'un énolate et d'une phosphine neutre, et on rapporte sa chimie de coordination avec le nickel. On a prépare les phosphinocétones, R_2PCH_2COPh (R = Cy or Pr^i) par réaction des phosphines secondaires correspondantes avec la bromoacétophénone conduisant aux sels de phosphonium correspondants $[R_2P(H)CH_2COPh]^+Br^-$ (R = Cy or Pr^i) dont la dépronation conduit aux cétones neutres. On forme les énolates par addition de $NaN(SiMe_3)_2$ à la cétone neutre. La structure cristalline de l'énolate de sodium portant des substituants isopropyles sur le phosphore présente une structure trimère à l'état solide et il existe une interaction entre le phosphore donneur et l'anion sodium: Na—P, 2,852(2)Å. On a réalisé la préparation d'une série de complexes de nickel en procédant à l'addition de l'énolate de sodium sur le produit de départ approprié de Ni(II). On a déterminé les structures cristallines des dérivés du nickel. On décrit brièvement le comportement catalytique de l'un de ces complexes dans la polymérisation et l'oligomérisation de l'éthylène. Les cristaux du $\{Na[Pr^i_2PC(H)=C(O)Ph]\}_4$, **2***b*, sont tétragonaux, groupe d'espace $I4_1/a$, avec $a = b = 20,790(2)$ Å, et $c = 13,539(7)$ Å, $Z = 4$; ceux du $[Cy_2PC(H)=C(O)Ph](PPh_3)NiPh$, **3***a*, sont tricliniques, groupe d'espace $P\bar{1}$, avec $a = 10,742(2)$, $b = 19,811(3)$ et $c = 10,621(2)$ Å, $\alpha = 101,88(1)°$, $\beta = 119,24(1)°$, et $\gamma = 91,08(1)°$ et $Z = 2$ et ceux du $[Pr^i2PC(H)=C(O)Ph](PPh_3)NiPh$, **3***b*, sont tricliniques, groupe d'espace $P\bar{1}$, avec $a = 10,219(1)$, $b = 17,432(3)$ et $c = 9,788(1)$ Å, $\alpha = 101,18(1)°$, $\beta = 100,19(1)°$, $\gamma = 85,32(1)°$ et $Z = 2$. On a résolu les structures par des méthodes directes (**2***b*) et de Patterson (**3***a* et **3***b*) et on les a affinées par les

Received November 25, 1994.

This paper is dedicated to Professor William A.G. Graham, on the occasion of his 65th birthday.

M.D. Fryzuk,[1] **X. Gao, and S.J. Rettig.**[2] Department of Chemistry, University of British Columbia, 2036 Main Mall, Vancouver, BC V6T 1Z1, Canada.

[1] Author to whom correspondence may be addressed. Telephone: (604) 822-2897. Fax: (604) 822-2847. E-mail: fryzuk@chem.ubc.ca
[2] Experimental Officer: UBC Crystallographic Service.

méthodes des moindres carrés jusqu'à des valeurs de R de 0,045, 0,044, et 0,032 (R_w = 0,038, 0,041, et 0,030) pour respectivement 965, 4483, et 5085 réflexions avec $I \geq 3\sigma(I)$.

Mots clés : nickel, énolate de sodium, catalyseur homogène, oligomérisation.

[Traduit par la rédaction]

Introduction

The discovery that certain nickel(II) complexes incorporating mixed P,O donor ligands were effective catalyst precursors for ethylene oligomerization reactions in the so-called Shell-Higher-Olefin-Process (SHOP) (1–7) has sparked a number of groups to devise new ancillary ligands that can be utilized (8–14). The original preparation (1) involved reaction of a keto-phosphorus ylid of the type $Ph_3P{=}CHCOPh$ with $Ni(COD)_2$ and PPh_3 to produce, after phenyl transfer, the complex $Ni(Ph)PPh_3[Ph_2PCH{=}C(O)Ph]$. The reaction is not general since phosphorus ylids that contain two electron-rich alkyl substituents, such as $Pr^i_2PhP{=}CHCOPh$, do not transfer a phenyl to $Ni(COD)_2$ even at elevated temperatures.[3] In an effort to extend the preparation of potential SHOP catalyst precursors, the use of β-phosphinoenolates (9, 15–17) in concert with a nickel(II) starting material seemed promising since, in principle, this should allow incorporation of a variety of substituents at the phosphorus end of the mixed-donor chelate.

In this report we outline the synthesis of a mixed P,O donor ligand that has bulky electron-rich substituents attached at phosphorus. The structure of the sodium enolate of this ligand is also described along with its coordination chemistry with nickel. We also include some preliminary experiments on the catalytic behavior of these nickel derivatives.

Results and discussion

The ligand was prepared (eq. [1]) by addition of a secondary phosphine, R_2PH (R = Cy or Pr^i), to bromoacetophenone to generate the corresponding phosphonium salt, which was subsequently neutralized with methanolic NaOH to generate the keto-phosphines **1***a*, *b* as either an air- and moisture-sensitive solid (R = Cy) or a liquid (R = Pr^i). The keto-phosphines **1***a*, *b* can also be prepared via reaction of the enolate of acetophenone with the corresponding chlorophosphine, $ClPR_2$ (17). The formation of the sodium enolate derivatives **2***a*, *b* was accomplished by addition of $NaN(SiMe_3)_2$ to an ether solution of the respective keto-phosphine.

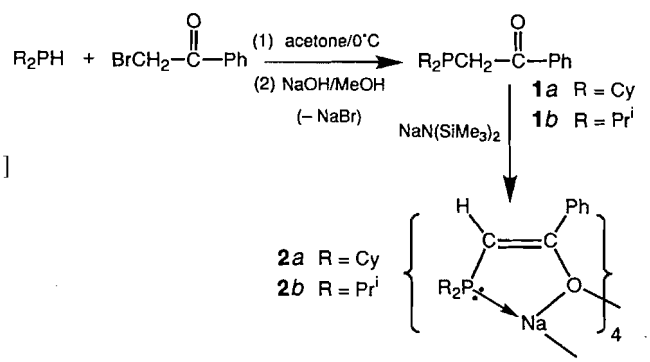

[1]

The NMR spectroscopic parameters for the sodium enolates **2***a*, *b* clearly indicate that only one diastereomer is observed in solution; the crystal structure of **2***b*, shown in Fig. 1, indicates that the *Z* enolate is present. Not only is this the expected kinetic enolate isomer (18), but the additional binding by the phosphine to the sodium cation at the enolate oxygen presumably makes this the thermodynamically most-favored isomer as well.

Fig. 1. Above: a schematic picture of the sodium β-phosphino-enolate **2***b* showing one unit of the tetramer and (below) the structure and numbering scheme from the X-ray crystal structure of the tetramer with some of the atoms removed for clarity (only the ipso carbon, C3 of the phenyl group, and the α-carbons, C9 and C12, of the isopropyls are shown). Some selected bond lengths (Å) and bond angles (°): P1—Na1 2.852(2); Na1—O1 2.431(4); Na1—O1′ 2.282(4); Na1—O1″ 2.312(4); O1—C2 1.321(5); C1—C2 1.357(6); C1—P1 1.778(5); C2—C3 1.503(7); Na1-O1-C2 119.1(3); O1-C2-C1 126.1(5); P1-C1-C2 123.6(4); Na1-P1-C1 94.8(2); P1-Na1-O1 72.67(9); Na1-O1-Na1* 84.3(1); Na1-O1-Na″ 90.7(1); Na*-O1-Na″ 87.1(1).

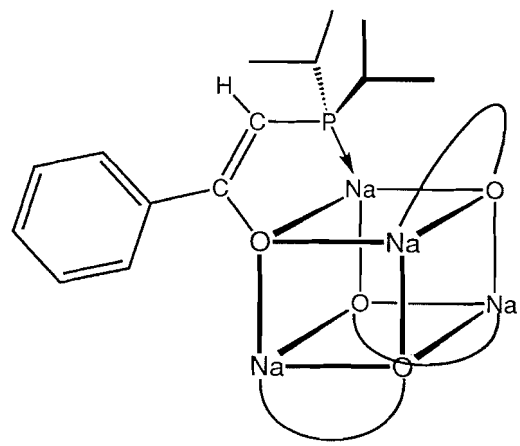

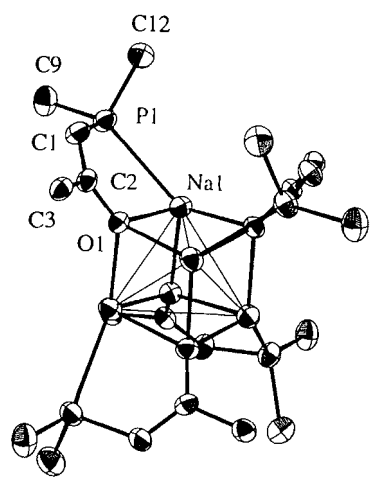

[3] X. Gao and M.D. Fryzuk, unpublished results (1993).

Can. J. Chem. Downloaded from www.nrcresearchpress.com by 80.90.12.36 on 09/08/12
For personal use only.

Can. J. Chem. Downloaded from www.nrcresearchpress.com by 80.90.12.36 on 09/08/12
For personal use only.

The X-ray crystal structure of **2*b*** (Fig. 1) displays a number of notable features. The tetrameric cubane structure is evident; in addition, the sodium atom is also coordinated by the phosphine moiety. The Na—O bond lengths are unsymmetrical and have the values of 2.282(4), 2.312(4), and 2.431(4) Å. The distance from the sodium to the phosphorus donor is 2.852(2) Å, shorter than that of 2.948(6) Å found (19) in the sodium salt of the bis(diphenylphosphino)benzyl ylid, $Na^+[Ph_2PCHPPh_2\text{-}CHPh]^-$. Other sodium–phosphorus bond lengths known are generally longer than that found in **2*b***, even when the interaction involves anionic phosphide type salts: in $[NaPHCy\cdot pmdeta]_2$, the Na—P bond distances are 2.883(8) and 2.936(7) Å (20), while in $NaPMes(SiFBu^t_2)\cdot 2THF$ the bond length is 2.890(1) Å (21).

Other than the layered aggregates of simple alkoxide salts, the structural motifs encountered in the solid-state structural analyses of sodium alkoxides and enolates, $\{NaOR\}_n$, range from tetramer ($n = 4$) to hexamer units ($n = 6$) with even non-americ structures ($n = 9$) having been found (22). In these structures, each sodium cation is generally found to be three-coordinate and sitting at the corner of the appropriate geometrical shape. In the presence of Lewis bases, adduct formation results in higher coordination numbers for the sodium and generally the formation of smaller repeating units, typically dimers or trimers although monomers are also known (23, 24). It is clear that the present cubane structure is stable enough, at least in the solid state, to tolerate the weak phosphine binding.

These sodium enolates can be used in metathetical-type reactions to prepare new coordination complexes. For example, addition of the sodium derivatives **2*a*, *b*** to suitable Ni(II) derivatives results in incorporation of the bidentate ligand (eq. [2]).

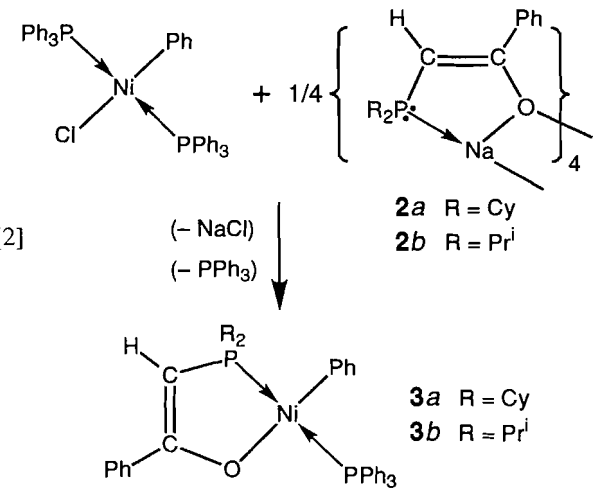

In solution, complexes **3*a*** and **3*b*** show a *trans* disposition of inequivalent phosphine donors as evidenced by the AX pattern in the $^{31}P\{^1H\}$ NPR spectrum where large $^2J_{PP}$ couplings of 272 and 275 Hz, respectively, are observed. The X-ray crystal structures of both **3*a*** and **3*b*** have been determined and both give virtually identical dimensions; only the diisopropyl derivative **3*b*** is shown in Fig. 2 along with some selected bond lengths and bond angles. The solid-state structure confirms the solution structure in that the phosphorus ligands are indeed *trans* disposed; the geometry around nickel is nearly square planar as expected. In fact, the bond angles and bond distances in both of these complexes are extremely similar to those found in the diphenylphosphino derivative $Ni(Ph)PPh_3[Ph_2PCH{=}C(O)Ph]$ mentioned earlier (1).

The preparation of these complexes can also be achieved by, first, reaction with $NiCl_2(PPh_3)_2$ to generate complex **4*a*** with the P,O ligand attached, then addition of PhMgBr to produce **3*a*** having the necessary nickel carbon bond; this is summarized in eq. [3].

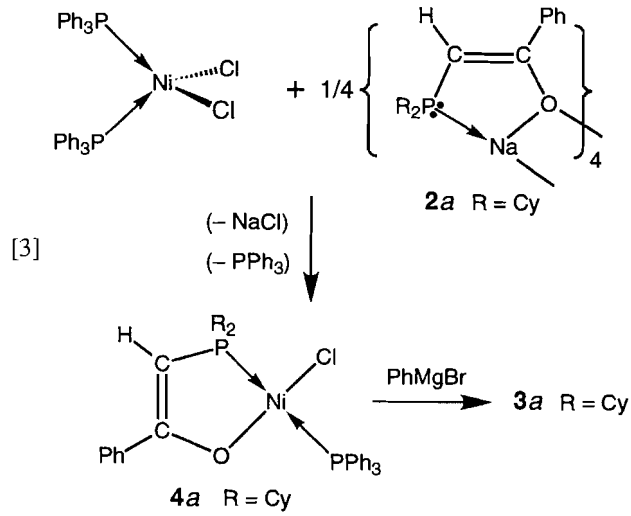

We have also examined the preparation of the corresponding allyl complex $Ni(\eta^3\text{-}C_3H_5)[Cy_2PCH{=}C(O)Ph]$ **5*a***; addition of the sodium enolate **2*a*** to allynickel dimer $[(\eta^3\text{-}C_3H_5)Ni]_2(\mu\text{-}Br)_2$ does produce the corresponding allyl complex **5*a***. However, this is accompanied by considerable amounts of decomposition products, one of which was identified as the bis(P,O)-ligand complex $Ni[Cy_2PCH{=}C(O)Ph]_2$. Subsequent investigations have shown that this reaction is very sensitive to the purity of the starting allylnickel dimer; the use of freshly recrystallized $[(\eta^3\text{-}C_3H_5)Ni]_2(\mu\text{-}Br)_2$ generates the corresponding allyl derivative **5*a*** in virtually quantitative yield.

These new nickel complexes are active in the oligomerization and polymerization of ethylene; for example, a solution of **3*b*** in toluene at 40–70°C under ethylene (2 atm; 1 atm = 101.3 kPa) produced a range of olefins (up to C_{22} as detected by GC–MS) and polyethylene (mp = 103–108°C). It would appear that the presence of an electron-rich phosphine in the bidentate, mixed-donor ligand does not seriously diminish the catalytic activity of these nickel complexes although accurate comparisons have yet to be made.

Experimental procedure

All reactions were preformed under purified nitrogen in dry, degassed solvents. NMR spectra are referenced externally to standard values as described previously (25).

$Cy_2PCH_2C(O)Ph$ (1*a*)

A solution of Cy_2PH (4.33 g, 0.0218 mol) in acetone (5 mL) was added dropwise to an acetone (20 mL) solution of $BrCH_2C(O)Ph$ (4.35 g, 0.0219 mol); the reaction is mildly exothermic. After the addition, the volatiles were removed under vacuum to yield an oil that was then dissolved in cold (0°C) MeOH (15 mL), and to it was added slowly one equiv-

Fig. 2. The structure and numbering scheme of the nickel phenyl complex **3***b*. Some selected bond lengths (Å) and bond angles (°): Ni1—P1 2.1756(7); Ni1—C1 1.893(2); Ni1—P2 2.2324(6); Ni1—O1 1.918(1); O1—C8 1.321(2); C7—C8 1.346(3); P1—C7 1.764(2); C8—C9 1.495(3); P1-Ni1-P2 174.62(3); O1-Nil-C1 178.03(9); P1-Ni1-C1 92.25(7); P2-Ni1-C1 93.12(7); P1-Ni1-O1 86.48(5); P2-Ni1-O1 88.16(5); Ni1-O1-C8 118.3(1); O1-C8-C7 122.5(2); P1-C7-C8 113.8(2); Ni1-P1-C7 98.91(7).

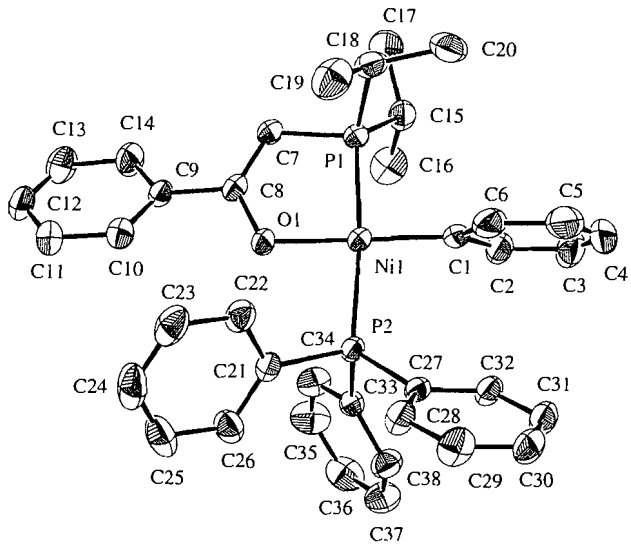

alent of NaOH (0.874) in MeOH. The resultant solution was stirred for 10 min and was then pumped to dryness. The residue was extracted with ether (2 × 25 mL), filtered to remove NaBr, dried over Na_2SO_4, then over activated molecular sieves, filtered again, and pumped to dryness. The crude product was recrystallized from pentane at –30°C to give colorless crystals in 66% (4.56 g) yield. ^{1}H NMR (C_6D_6, δ): 7.0–7.2 (m, Ph), 8.1–8.2 (m, Ph), 2.95 (d, $^2J_{PH}$ = 0.65 Hz, CH_2), 1.0–2.0 (m, Cy). ^{31}P{^{1}H} NMR (C_6D_6, δ): 0.65 (s). Anal. calcd. for $C_{20}H_{29}OP$: C 75.92, H 9.24; found: C 76.06, H 9.30.

$Pr^i_2PCH_2C(O)Ph$ (1*b*)

The same procedure as for **1***a* was followed using Pr^i_2PH and $BrCH_2C(O)Ph$ except that, after filtration, the solvent was removed under vacuum and the yellow liquid distilled at 0.001 Torr (1 Torr = 133.3 Pa) (bp 125–130°C) to give the product as a colourless liquid in 51% yield (12.05 g). ^{1}H NMR (C_6D_6, δ): 8.05–8.15 (m, Ph), 7.0–7.2 (m, Ph), 2.89 (d, $^2J_{PH}$ = 0.60 Hz, CH_2), 1.61 (d of hept, $^3J_{HH}$ = 7.05 Hz, $^2J_{PH}$ = 0.59 Hz, PCH^iPr), 1.00 (dd, $^3J_{HH}$ = 7.06 Hz, $^3J_{PH}$ = 3.09 Hz, CH_3), 0.94 (dd, $^3J_{HH}$ = 7.04 Hz, $^3J_{PH}$ = 5.58 Hz, CH_3). ^{31}P{^{1}H} NMR (C_6D_6, δ): 7.21 (s).

{Na[Cy_2PCH=C(O)Ph]}$_4$ (2*a*)

To a cold (–30°C) solution (10 mL) of the dicyclohexylphosphino ketone **1***a* (1.01 g, 3.21 mmol) diethyl ether (10 mL) was added an ethereal solution (10 mL) of $NaN(SiMe_3)_2$ (0.589 g, 3.21 mmol). The solution was allowed to warm to room temperature, stirred for 3 h, and was pumped to dryness to remove the ether and $HN(SiMe_3)_2$. The residue was recrystallized from ether–pentane to give the sodium salt **2***a* as colorless crystals. Yield: 0.90 g (83%). ^{1}H NMR (C_6D_6, δ): 7.6–7.8 (m, Ph), 6.8–7.3 (m, Ph), 4.54 (d, $^2J_{PH}$ = 5.6 Hz, C(O)=C*H*-P), 1.0–2.0 (m, Cy). ^{31}P{^{1}H} NMR (C_6D_6, δ): –26.97 (s). Anal. calcd. for $C_{20}H_{28}OPNa$: C 70.99, H 8.34; found: C 71.14, H 8.29.

{Na[Pr^i_2PCH=C(O)Ph]}$_4$ (2*b*)

Using the same procedure as above on the diisopropylphosphino ketone **1***b*, colourless crystals were obtained after recrystallization from ether–pentane. Yield: 94%. ^{1}H NMR (C_6D_6, δ): 7.65–7.8 (m, Ph), 7.1–7.3 (m, Ph), 4.49 (d, $^2J_{PH}$ = 5.85 Hz, C(O)=C*H*-P), 1.58–1.63 (m, PCH), 0.9–1.25 (m, CH_3). ^{31}P{^{1}H} NMR (C_6D_6, δ): –17.98 (s). Anal. calcd. for $C_{14}H_{20}ONaP$: C 65.11, H 7.80; found: C 64.89, H 7.96.

Ni(Ph)PPh_3[Cy_2PCH=C(O)Ph] (3*a*)

To a toluene solution (50 mL) of *trans*-Ni(PPh_3)$_2$(Ph)Cl (0.966 g, 1.39 mmol) maintained at 0°C was added dropwise a toluene solution (15 mL) of **2***a* (0.47 g, 1.39 mmol). The color of the solution went from yellow-orange to dark orange after several drops of the enolate was added. After the addition, the solution was stirred overnight, filtered, and pumped to dryness; the product was recrystallized from ether–hexanes as dark orange crystalline blocks. Yield: 0.59 g (60%). ^{1}H NMR (C_6D_6, δ): 6.7–7.7 (m, Ph), 4.5 (dd, $^2J_{PH}$ = 1.96 Hz, $^4J_{PH}$ = 0.95 Hz, C(O)=CH-P)), 2.5–1.0 (m, Cy), ^{31}P{^{1}H} NMR (C_6D_6, δ): 35.0 (d, $^2J_{PP}$ = 272.2 Hz), 20.0 (d). Anal. calcd. for $C_{44}H_{48}NiOP_2$: C 74.07, H 6.78; found: C 74.16, H 6.90.

Ni(Ph)PPh_3[Pr^i_2PCH=C(O)Ph] (3*b*)

To a slurry of *trans*-Ni(PPh_3)$_2$(Ph)Cl (0.361 g, 0.5188 mmol) in ether (40 mL) at –78°C was added an ethereal solution of 2*b* (0.134 g, 0.5188 mmol). The mixture was vigorously stirred was warmed up to room temperature after 0.5 h. The orange solution thus formed was stirred for an additional hour and was filtered. The filtrate was pumped to ≈5 mL and hexanes (20 mL) added. Removal of the solvents under vacuum gave orange crystals of 3*b*. Yield: 0.312 g (95%). ^{1}H NMR (C_6D_6, δ): 6.7–7.7 (m, 25 H, Ph), 4.47 (dd, $^2J_{PH}$ = 2.06 Hz, $^4J_{PH}$ = 0.96 Hz, PC*H*=C(O)), 1.84 (dhept, $2J_{PH}$ = 20.62 Hz, $^3J_{HH}$ = 3.48 Hz, PC*H*Me_2), 1.07 (dd, $^3J_{PH}$ = 14.29 Hz, $^3J_{HH}$ = 6.88 Hz, PCHCH_3), 1.01 (dd, $^3J_{PH}$ = 16.10 Hz, $^3J_{HH}$ = 7.08 Hz, PCHCH_3). ^{31}P{H} NMR (THF, D_2O insert, δ): 43.76 (d, $^2J_{PP}$ = 274.66 Hz), 20.76 (d). Anal. calcd. for $C_{38}H_{40}NiOP_2$: C 72.06, H 6.37; found: C 71.80, H 6.27.

Ni(Cl)PPh_3[Cy_2PCH=C(O)Ph] (4*a*)

A solution of 2*a* (0.563 g, 1.664 mmol) in toluene (5 mL) was added dropwise to a slurry of $NiCl_2(PPh_3)_2$ (1.089 g, 1.664 mmol) in toluene (15 mL). The resultant orange solution was stirred for 3 h and was filtered. The filtrate was pumped to dryness and the residue was crystallized from ether–hexanes to give compound 4*a* in 72% yield (0.8 g). ^{31}P{^{1}H} NMR (C_6D_6, δ): 41.09 (d, $^2J_{PP}$ = 325.6 Hz), 9.62 (d). Anal. calcd. for $C_{38}H_{43}ClNiOP_2$: C 67.93, H 6.45; found: C 67.79, H 6.35. Reaction of this compound with PhMgBr in ether gave Ni(Ph)PPh_3[Cy_2PCH=C(O)Ph] (3*a*), identical to that described above.

Ni(η^3-C_3H_5)[Cy_2PCH=C(O)Ph] (5*a*)

The sodium phosphino-enolate 2*a* (0.272 g, 0.8037 mmol) in toluene (10 mL) was added dropwise to a toluene solution (10

Can. J. Chem. Downloaded from www.nrcresearchpress.com by 80.90.12.36 on 09/08/12
For personal use only.

Can. J. Chem. Downloaded from www.nrcresearchpress.com by 80.90.12.36 on 09/08/12
For personal use only.

Table 1. Crystallographic data.[a]

Compound	**2**	**3*a***	**3*b***
Formula	$C_{56}H_{80}Na_4O_4P_4$	$C_{44}H_{48}NiOP_2$	$C_{38}H_{40}NiOP_2$
fw	1033.10	713.51	633.38
Color, habit	Colorless, prism	Yellow, prism	Yellow-orange, prism
Crystal size, mm	0.15 × 0.35 × 0.40	0.15 × 0.35 × 0.40	0.20 × 0.30 × 0.35
Crystal system	Tetragonal	Triclinic	Triclinic
Space group	$I4_1/a$	$P\bar{1}$	$P\bar{1}$
a, Å	20.790(2)	10.742(2)	10.219(1)
b, Å	20.790(2)	19.811(3)	17.432(3)
c, Å	13.539(7)	10.621(2)	9.788(1)
α°	90	101.88(1)	101.18(1)
β°	90	119.24(1)	100.19(1)
γ°	90	91.08(1)	85.32(1)
V, Å^3	5852(3)	1911.1(7)	1681.7(4)
Z	4	2	2
T, °C	21	21	21
D_c, g/cm^3	1.172	1.240	1.251
F(000)	2208	756	688
μ(Mo K_α), cm^{-1}	2.00	6.22	7.00
Transmission factors	0.92–1.00	0.92–1.00	0.95–1.00
Scan type	ω–2θ	ω–2θ	ω–2θ
Scan range, deg in ω	1.15 + 0.35 tan θ	1.21 + 0.35 tan θ	1.21 + 0.35 tan θ
Scan speed, deg/min	16 (up to 8 rescans)	16 (up to 8 rescans)	32 (up to 8 rescans)
Data collected	$+h, +k, +l$	$+h, \pm k, \pm l$	$+h, \pm k, \pm l$
$2\theta_{max}$, deg	45	55	60
Crystal decay, %	Negligible	Negligible	Negligible
Total no. of reflections	2148	9229	10322
Unique reflections	2013	8733	9805
R_{merge}	0.049	0.026	0.027
No. with $I \geq 3\sigma(I)$	965	4483	5085
No. of variables	154	433	380
R	0.045	0.044	0.032
R_w	0.038	0.041	0.030
gof	2.23	2.46	1.91
Max Δ/σ (final cycle)	0.005	0.05	0.001
Residual density e/Å^3	−0.16, 0.18	−0.23, 0.34	−0.20, 0.24

[a]Rigaku AFC6S diffractometer, takeoff angle 6.0°, aperture 6.0 × 6.0 mm at a distance of 285 mm from the crystal, stationary background counts at each end of the scan (scan/background time ratio 2:1), Mo K_α radiation (λ = 0.71069 Å), graphite monochromator, $\sigma^2(F^2) = [S^2(C + 4B)]/Lp^2$ (*S* = scan speed, *C* = scan count, *B* = normalized background count), function minimized $\Sigma w(|F_o| - |F_c|)^2$ where $w = 4F_o^2/\sigma^2(F_o^2)$, $R = \Sigma||F_o| - |F_c||/\Sigma|F_o|$, $R_w = (\Sigma w(|F_o| - |F_c|)^2/\Sigma w|F_o|^2)^{1/2}$, and gof = $[\Sigma w(|F_o| - |F_c|)^2/(m - n)]^{1/2}$. Values given for *R*, R_w, and gof are based on those reflections with $I \geq 3\sigma(I)$.

mL) of $[(\eta^3\text{-}C_3H_5)Ni]_2(\mu\text{-}Br)_2$ (0.144 g, 0.4018 mmol). The resultant solution was stirred overnight and was filtered to remove some black solid. The filtrate was pumped to dryness and the residue was redissolved in a minimum amount of ether, then diluted with one-third the volume of hexanes. Orange crystals deposited overnight that were identified as the bis(ligand) complex $Ni[Cy_2PCH{=}C(O)Ph]_2$. To the mother liquor was added more hexanes. Brownish-orange crystals deposited at −30°C with a yield of 0.1 g, 30%. ^1H NMR (C_6D_6, δ): 8.2–8.27 (m, *para* Ph), 7.1–7.3 (m, *ortho/meta* Ph); allyl protons: 4.97 (dddd), 4.55 (d, $^2J_{PH}$ = 1.22 Hz), 4.23 (m), 3.12 (dd, J_{HH} = 4.64 Hz, J_{HH} = 14.4 Hz), 2.32 (m); remaining proton is buried in the Cy multiplets; 1.0–2.1 (m, Cy + one allyl H). $^{31}P\{^1H\}$ NMR (C_6D_6, δ): 42.53 (s). Anal. calcd. for $C_{23}H_{333}OPNi$: C 66.54, H 8.01; found: C 66.88, H 8.07. This reaction proceeds in nearly quantitative yield if pure, recrystallized $[\eta^3\text{–}C_3H_5)Ni]_2(\mu\text{–}Br)_2$ is used.

Reaction of $Ni(Ph)PPh_3[Pr^i_2PCH{=}C(O)Ph]$ (*3b*) with ethylene

Run 1

3*b* (35 mg) was dissolved in toluene (40 mL) in a thick-walled glass bomb (80 mL) that was connected to a three-way valve; the valve was also connected to a vacuum line and an ethylene cylinder. The system outside the glass bomb was pumped, first, to remove air and, then, head space of the bomb was evacuated. After the connection to the vacuum line was closed, the bomb was opened to the ethylene cylinder. The pressure of ethylene was maintained at 2 atm during the reaction. The bomb was placed in an oil bath and the bath temperature was maintained at 40°C. After being stirred for 12 h, the slurry was filtered and the white precipitate was washed with methanol (3 × 20 mL) and dried under vacuum. Yield of polyethylene: 1.24 g. GS–MS analysis of the filtrate found

oligomers: C_{14}–C_{22}. The total amount of the oligomers was 87 mg.

Run 2

3*b* (70 mg) was used. The reaction conditions were similar to those described in Run 1, but the reaction temperature was increased to 70°C. Ten minutes after ethylene (2 atm) was introduced into the bomb, the solution became turbid. After 6 h the reaction mixture was so thick that it was difficult to stir. The reaction was stopped and the mixture was cooled to room temperature. The solid was filtered and was washed with methanol (3 × 50 mL). Yield of polyethylene: 7.05 g.

X-ray crystallographic analyses of $Na[Pr^i_2PC(H)=C(O)Ph]_4$ (2*b*), $Ni(Ph)PPh_3[Cy_2PCH=C(O)Ph]$ (3*a*), and $Ni(Ph)PPh_3[Pr^i_2PCH=C(O)Ph]$ (3*b*)

Crystallographic data appear in Table 1. The final unit-cell parameters were obtained by least squares on the setting angles for 25 reflections with 2θ = 15.6°–28.0° for **2***b*, 24.7°–30.4° for **3***a*, and 38.2°–43.1° for **3***b*. The intensities of three standard reflections, measured every 200 reflections, showed only small random fluctuations for the three data collections. The data were processed (26), corrected for Lorentz and polarization effects, and for absorption (empirical: based on azimuthal scans for three reflections).

The structure of **2***b* was solved by direct methods and those of **3***a* and **3***b* were solved by conventional heavy atom methods. The structure analyses of **3***a* and **3***b* were both initiated in the centrosymmetric space group $P\bar{1}$ on the basis of the *E*-statistics and the appearance of the Patterson functions. These choices were confirmed by the subsequent successful solutions and refinements of the structures. The tetrameric complex **2** has crystallographically imposed S_4 symmetry. The non-hydrogen atoms of all three structures were refined with anisotropic thermal parameters. Hydrogen atoms were fixed in idealized positions (C—H = 0.99 Å for **2** and 0.98 Å for **3***a* and **3***b*, $B_H = 1.2\ B_{\text{bonded atom}}$). A secondary extinction correction (Zachariasen type) was applied for **3***a*, the final value of the extinction coefficient was 5.7 (2) × 10^{-7}. Neutral atom scattering factors and anomalous dispersion corrections for all atoms were taken from the *International tables for X-ray crystallography* (27). Final atomic coordinates and equivalent isotropic thermal parameters, bond lengths and angles, hydrogen atom parameters, anisotropic thermal parameters, torsion angles, intermolecular contacts, and least-squares planes are available as supplementary material.[3]

[3] The supplementary material may be purchased from: The Depository of Unpublished Data, Document Delivery, CISTI, National Research Council Canada, Ottawa, Canada K1A 0S2.

With the exception of the tables of anisotropic thermal parameters, torsion angles, and least-squares planes, the supplementary material has also been deposited with the Cambridge Crystallographic Data Centre, and can be obtained on request from The Director, Cambridge Crystallographic Data Centre, University Chemical Laboratory, 12 Union Road, Cambridge, CB2 1EZ, U.K.

Structure factor tables are no longer being deposited and may be obtained on request from the author.

Can. J. Chem. Downloaded from www.nrcresearchpress.com by 80.90.12.36 on 09/08/12
For personal use only.

Acknowledgment

Funding for this research was provided by the Natural Sciences and Engineering Research Council of Canada.

References

1. W. Keim, F.H. Kowaldt, R. Goddard, and C. Krüger. Angew. Chem. Int. Ed. Engl. **17**, 466 (1978).
2. W. Keim. New J. Chem. **18**, 93 (1994).
3. W. Keim. J. Mol. Catal. **52**, 19 (1989).
4. W. Keim. Angew. Chem. Int. Ed. Engl. **29**, 235 (1990).
5. A. Behr, U. Freundenberg, and W. Keim. J. Mol. Catal. **35**, 9 (1986).
6. U. Müller, W. Keim, C. Krüger, and P. Betz. Angew. Chem. Int. Ed. Engl. **28**, 1011 (1989).
7. M. Peuckert and W. Keim. Organometallics, **2**, 594 (1983).
8. U. Klabunde, T.H. Tulip, D.C. Roe, and S.D. Ittel. J. Organomet. Chem. **334**, 141 (1987).
9. U. Klabunde and S.D. Ittel. J. Mol. Catal. **41**, 123 (1987).
10. U. Klabunde, R. Mulhaupt, T. Herskovitz, A.H. Janowicz, J. Calabrese, and S.D. Ittel. J. Polym. Sci. Part A: Polym. Chem. **25**, 1989 (1987).
11. P. Braunstein, D. Matt, Y. Dusausoy. J. Fischer, A. Mitschler, and L. Ricard. J. Am. Chem. Soc. **103**, 5115 (1981).
12. P. Braunstein, D.G. Kelly, A. Tiripicchio, and F. Ugozzoli. Inorg. Chem. **32**, 4845 (1993).
13. P. Braunstein, Y. Chauvin, S. Mercier, L. Saussine, A. De Cian, and J. Fisher. J. Chem. Soc. Chem. Commun. 2203 (1994).
14. H. Qichen, X. Minzhi, Q. Yanlong, X. Weihua, S. Meicheng, and T. Youqi. J. Organomet. Chem. **287**, 419 (1985).
15. S.-E. Bouaoud, P. Braunstein, D. Grandjean, D. Matt, and D. Nobel. Inorg. Chem. **25**, 3765 (1986).
16. D. Matt, M. Huhn, J. Fischer, A. De Cian, W. Klaui, I. Tkatchenko, and M.C. Bonnet. J. Chem. Soc. Dalton Trans. 1173 (1993).
17. P. Veya, C. Floriani, A. Chiesi-Villa, C. Guastini, A. Dedieu, F. Ingolf, and P. Braunstein. Organometallics, **12**, 4359 (1993).
18. H.O. House. Modern synthetic reactions. W.A. Benjamin, Don Mills, Ont. 1972.
19. H. Schmidbaur, U. Deschler, B. Zimmer-Gasser, D. Neigebauer, and U. Schubert. Chem. Ber. **113**, 902 (1980).
20. G.A. Koutsantonis, P.C. Andrews, and C.L. Raston. J. Chem. Soc. Chem. Commun. 47 (1995).
21. M. Andianarison, D. Stalke, and U. Klingebiel. Chem. Ber. **123**, 71 (1990).
22. E. Weiss. Angew. Chem. Int. Ed. Engl. **32**, 1501 (1993).
23. C. Schade and P. von Ragué Schleyer. Adv. Organomet. Chem. **27**, 169 (1988).
24. D. Seebach. Angew. Chem. Int. Ed. Engl. **27**, 1624 (1988).
25. M.D. Fryzuk. Can. J. Chem. **61**, 1347 (1983).
26. teXsan: Crystal structure analysis package. Molecular Structure Corporation, The Woodlands, Tex. 1985 and 1992.
27. International Tables for Crystallography. Vol. C. Kluwer Academic Publishers, Boston, Mass. 1992. pp. 200–206 and 219–222.

Reductions by ferrocytochrome c peroxidase: 5. Kinetics of ferricyanide reduction

Eddy Cheung and Ann M. English

Abstract: The kinetics of reduction of ferricyanide by yeast ferrocytochrome c peroxidase (CPP^{II}) were investigated as a function of ionic strength in phosphate buffers at pH 7.0 and 25 ± 1°C. The observed bimolecular rate constant (k_{12}) is 8.4×10^4 M^{-1} s^{-1} in 0.1 M phosphate. The dependence of the reaction rate on ionic strength indicates a change of −9 on the protein at pH 7.0, which is in good agreement with the total charge of −11 estimated for CCP^{II} from its amino acid content. Substituting k_{12} at infinite ionic strength (k_{12}^{∞}) into the Marcus cross relation yields an electron self-exchange rate constant (k_{11}^{∞}) for the Fe^{III}/Fe^{II} couple of CCP of 7.2×10^{-5} M^{-1} s^{-1}. This value is over four orders of magnitude higher than that calculated for the Fe^{IV}/Fe^{III} couple of CCP from literature data for cross-reactions with ferrocyanide at pH 7.0. Possible reasons for the large difference in the two CCP k_{11}^{∞} values are discussed. Literature data also allowed k_{11}^{∞} values for various other heme proteins to be determined from their cross-reactions with ferricyanide. The calculated rate constants vary by eight orders of magnitude, and the variation of k_{11}^{∞} with protein structure suggests that the redox reactivity of ferrous heme proteins towards ferricyanide is dependent on the spin state and coordination of iron, as well as on the accessibility of the heme.

Key words: cytochrome c peroxidase, ferricyanide, Marcus cross relation, electron self-exchange.

Résumé : On a étudié la cinétique de la réduction du ferricyanure par la peroxydase du ferrocytochrome c (CCP^{II}) de la levure en fonction de la force ionique de tampons de phosphate, à un pH de 7,0 et 25 ± 1°C. À 0,1 M de phosphate, la constante de vitesse bimoléculaire observée (k_{12}) est égale à $8,4 \times 10^4$ M^{-1} s^{-1}. La variation de la vitesse de réaction avec la force ionique indique que la protéine porte une charge de −9 à un pH de 7; cette valeur est en bon accord avec la charge totale de −11 évaluée pour la CCP^{II} à partir de son contenu en acide aminé. Lorsqu'on substitue la valeur de k_{12} à force ionique infinie (k_{12}^{∞}) dans l'équation de Marcus, on détermine que la constante de vitesse d'autoéchange d'un électron (k_{11}^{∞}) pour le couple Fe^{III}/Fe^{II} du CCP est égale à $7,2 \times 10^{-5}$ M^{-1} s^{-1}. Cette valeur est quatre ordres de grandeur plus grande que celle calculée pour le couple Fe^{IV}/Fe^{III} du CCP à partir des données rapportées dans la littérature pour les réactions croisées du ferrocyanure, à un pH de 7,0. On discute des raisons qui pourraient expliquer les grandes différences entre les deux valeurs k_{11}^{∞} du CCP. Les valeurs consignées dans la littérature ont permis de déterminer les valeurs de k_{11}^{∞} de diverses réactions croisées du ferricyanure avec d'autres protéines de l'hème. Les constantes de vitesses calculées varient par huit ordres de grandeur et la variation de k_{11}^{∞} avec la structure de la protéine suggère que la réactivité rédox des ions ferreux des protéines de l'hème par rapport à l'ion ferricyanure dépend de l'état de spin et de la coordination du fer ainsi que de l'accessibilité de l'hème.

Mots clés : peroxydase du cytochrome c, ferricyanure, relation croisée de Marcus, autoéchange d'électron.

[Traduit par la rédaction]

Introduction

Heme proteins carry out a diversity of functions in nature. In all instances the heme group is known to undergo redox changes. For the simple heme electron transferases, such as cytochromes c and b_5, this involves the $Fe^{II/III}$ couple (1). Heme enzymes, such as cytochrome c oxidase and heme-containing peroxidases, have more complex enzymic cycles that involve Fe^{IV}=O species (2). Hemoglobin and myoglobin (Mb) reversibly bind O_2 in nature when the iron is present in the ferrous state. However, these proteins also undergo biological and nonbiological redox reactions involving the $Fe^{II/III}$ couple (3).

Since the heme group of most heme proteins is protoporphyrin or a derivative of protoporphyrin, the redox reactivity of the heme is largely determined by the nature of the protein matrix. Despite the sensitivity of its electron-transfer reactions to medium effects, the ferri/ferrocyanide redox couple has been used extensively to probe metalloprotein electron-

Received October 4, 1994.

This paper is dedicated to Professor William A.G. Graham on the occasion of his 65th birthday.

E. Cheung[1] **and A. English.**[2] Department of Chemistry and Biochemistry, Concordia University, 1455 de Maisonneuve Blvd. West, Montreal, QC H3G 1M8, Canada.

[1] Present address: Biomira Inc., Edmonton Research Park, 2011 - 94 Street, Edmonton, AB T6N 1H1, Canada.

[2] Author to whom all correspondence may be addressed. Fax: (514) 848-2868. E-mail: english@vax2.concordia.ca

Can. J. Chem. Downloaded from www.nrcresearchpress.com by 80.90.12.36 on 09/08/12
For personal use only.

Can. J. Chem. Downloaded from www.nrcresearchpress.com by 80.90.12.36 on 09/08/12
For personal use only.

transfer mechanisms, particularly those of cytochromes and heme peroxidases (4–11). For this reason ferricyanide was chosen as an oxidant in the present study, and the reaction under investigation is the following:

$$[1] \qquad CCP^{II} + Fe(CN)_6^{3-} \underset{}{\overset{k_{12}}{\rightleftharpoons}} CCP^{III} + Fe(CN)_6^{4-}, \qquad \Delta E^o = 0.603\ V$$

where ΔE^o was calculated from the data given in footnote *d*, Table 2. The dependence of the reaction rate on salt concentration was examined in P_i buffers at pH 7.0 and room temperature.

Erman and co-workers (7, 8) have measured ferrocyanide oxidation rates by the Fe^{IV}=O (oxyferryl) heme of compound II (CpdII)[3] of CCP:

$$[2] \qquad CpdII + Fe(CN)_6^{4-} \underset{}{\overset{k_{12}}{\rightleftharpoons}} CCP^{III} + Fe(CN)_6^{3-}, \qquad \Delta E^o = 0.678$$

where the value of ΔE^o in this case was calculated from E^o = 1.087 and 0.409 V for CpdII (8) and ferricyanide (footnote *d*, Table 2), respectively. Thus, analysis in terms of the Marcus cross relation of the rate data obtained here for reaction [1] and of the literature data for reaction [2] will permit a comparison of the redox reactivity of the $Fe^{II/III}$ and $Fe^{IV/III}$ couples of CCP with the same redox reagent. This is the first application of the Marcus cross relation to reactions of two redox couples of the *same* metalloprotein with the *same* redox reagent. In addition, rate data from the literature for the reduction of ferricyanide by a number of other ferrous heme proteins are analyzed by Marcus theory with compensation for nonspecific electrostatic effects. The results, including those for CCP^{II}, are interpreted in terms of the different biological functions of the heme proteins.

Experimental

CCP was isolated from bakers' yeast according to the published procedures (12, 13) and its purity index (A_{408}/A_{280}) was 1.3. CCP^{III} concentrations were determined spectrophotometrically using an extinction coefficient of 98 mM^{-1} cm^{-1} at 408 nm (14), and ~ 3 μM CCP^{III} solutions were prepared in 5.0–200 mM sodium phosphate buffers (pH 7.0). Samples were deaerated in 1-cm cuvettes under argon for 30 min and, following the addition of 0.008% acetophenone and 2% isopropyl alcohol (which do not alter the spectral properties or activity of CCP^{III}), UV photoreduction of CCP^{III} to CCP^{II} was performed according to the procedure of Ward and Chang (15). Potassium ferricyanide solutions were prepared by weight using reagent grade material, and aliquots containing *stoichiometric* amounts of oxidant were transferred to the cuvettes by a gas-tight syringe and the solutions were rapidly mixed manually. The disappearance of CCP^{II} was monitored by following the absorbance at 440 nm on a HP 8451A rapid-scan diode-array spectrophotometer at room temperature (25 ± 1°C). A 400-nm UV cutoff filter was used to eliminate UV photoreduction by the polychromatic monitoring beam of the HP 8451A. The bimolecular rate constants were calculated from second-order (equal concentration of reagents) analysis of the rate data.

[3] **Abbreviations:** CCP, cytochrome c peroxidase; CCP^{II}, ferroCCP; CCP^{III}, ferriCCP; CpdI, compound I of CCP, which contains a ferryl (Fe^{IV}=O) heme, and an amino acid radical; CpdII, compound II of CCP, which is formed on the one-electron reduction of CpdI and contains a Fe^{IV}=O heme at pH 7 (17); Mb, myoglobin; P_i, sodium phosphate; *I*, ionic strength.

Fig. 1. Reduction of ~3 μM ferricyanide by equimolar CCP^{II} in 200 mM P_i, pH 7.0, 25 ± 1°C. Fit (solid line) to second-order kinetics (equal concentrations of reactants) over ~15 half-lives or 94% completion of the absorbance changes at 440 nm (circles); A_t and A_∞ are the absorbances at time *t* and after the reaction was completed, respectively.

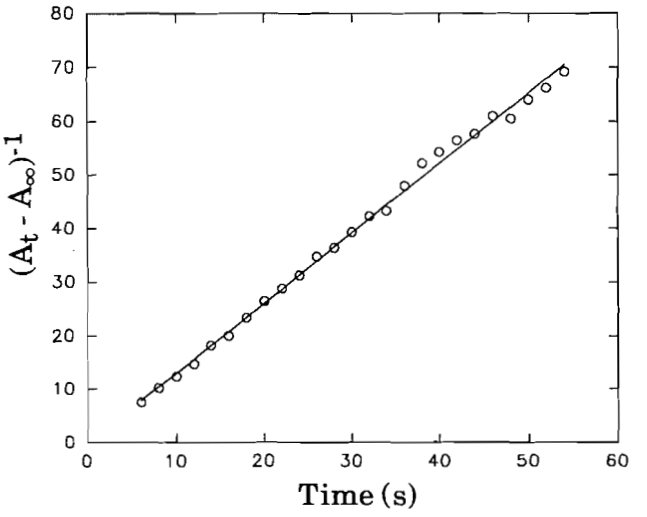

Results

The absorption maximum of CCP shifts from 408 to 440 nm upon photoreduction, with an isosbestic point at 421 nm. At 440 nm, the molar absorptivities of CCP^{II} and CCP^{III} were found to be 87 and 19 mM^{-1} cm^{-1}, respectively; hence, $\Delta\varepsilon_{440}$ = 68 nM^{-1} cm^{-1}. Figure 1 shows the fit to second-order kinetics over ~15 half-lives of the absorbance decrease at 440 nm when equal concentrations (3 μM) of CCP^{II} and $Fe(CN)_6^{3-}$ were mixed in 200 mM P_i. Excellent fits to second-order kinetics were also obtained for the 1:1 reaction in buffers containing 5.0–100 mM P_i and Table 1 lists the observed rate constants (k_{12}) as a function of P_i concentration. Because of the extreme O_2 sensitivity of CCP^{II}, it was not possible to examine reaction [1] by stopped-flow at Concordia. However, using a stopped-flow apparatus with ~1 ms time resolution in a glove box at the University of Sussex, the oxidation of ~3 μM CCP^{II} was also shown to follow second-order kinetics and to obey the simple rate law $-d[CCP^{II}]/dt = k[CCP^{II}][Fe(CN)_6^{3-}]$ under pseudo-first-order conditions with $Fe(CN)_6^{3-}$ concentrations up to 0.2 mM. Thus, unlike the reduction of ferricytochrome c by CCP^{II} (16), the reduction of $Fe(CN)_6^{3-}$ by the peroxidase is bimolecular under the conditions investigated here.

From the data presented in Table 1 it can be seen that k_{12} increases from 2.1 × 10^4 M^{-1} s^{-1} in 5.0 mM P_i to

Can. J. Chem. Downloaded from www.nrcresearchpress.com by 80.90.12.36 on 09/08/12
For personal use only.

Table 1. Observed rate constants (k_{12}) for the reduction of $Fe(CN)_6^{3-}$ by CCP^{II} in phosphate buffers, pH 7.0 at 25 ± 1°C.[a]

$[P_i]$ (mM)	Ionic strength (mM)	k_{12} (M^{-1} s^{-1})
5.0	9.3	2.1×10^4
10.0	19	4.2×10^4
15.0	28	5.1×10^4
25.0	46	6.6×10^4
50.0	93	7.6×10^4
100	186	8.4×10^4
200	372	8.7×10^4

[a]The CCP^{II} and ferricyanide concentrations were ~3 μM in each case.

8.7×10^4 M^{-1} s^{-1} in 200 mM P_i; this is consistent with both reagents being negatively charged at pH 7.0 (pI = 5.26 for CCP (17)). Although the conditions of the experiments do not allow the strict application of Debye–Hückel theory, estimates of the *effective* electrostatic charge on CCP^{II} and the rate at infinite dilution (k_{12}^0) were obtained from the ionic strength dependence of the rate constants (4, 6):

$$[3] \qquad \ln k_{12} = \ln k_{12}^0 + \frac{(2Z_1Z_2 + Z_2^2)\alpha I^{1/2}}{1 + \kappa R_1} - \frac{Z_2^2 \alpha I^{1/2}}{1 + \kappa R_2}$$

where $\alpha = 1.17$ and $\kappa = 0.329I^{1/2}$ $Å^{-1}$ for water at 25°C; Z_1, Z_2 and R_1, R_2 are the charges and radii of CCP^{II} and ferricyanide, respectively; and I = ionic strength. In eq. [3] it was assumed that the radius of the activated complex was equal to R_1 since $R_1 \gg R_2$. Equation [3] is plotted in Fig. 2(*a*) for I = 9.3–372 mM using values[4] of 23.5 and 4.5 Å (19) for R_1 and R_2, respectively. The data are a good fit to eq. [3] over the range of ionic strengths investigated, and extrapolation to $I = 0$ gives $k_{12}^0 = 1.0 \times 10^3$ M^{-1} s^{-1}. Assuming $Z_2 = -3$, the slope of the plot yields $Z_1 = -9$ for CCP^{II}.

The observed rate constant can also be related to the rate constant at infinite ionic strength (k_{12}^∞) by correcting for electrostatic interactions using Marcus-type work terms (6, 20, 21):

$$[4] \qquad \ln k_{12} = \ln k_{12}^\infty - 3.576\left[\frac{\exp(-\kappa R_2)}{1 + \kappa R_1} + \frac{\exp(-\kappa R_1)}{1 + \kappa R_2}\right] \times \frac{Z_1 Z_2}{R_1 + R_2}$$

where κ, R, and Z are as defined above. Figure 2(*b*) shows a plot of eq. [4], which is a reasonable fit to the experimental data over the ionic strength range investigated when the point at I = 9.3 mM is omitted; extrapolation to infinite ionic strength gives $k_{12}^\infty = 1.0 \times 10^5$ M^{-1} s^{-1} and the slope yields $Z_1 = -3$ for CCP^{II}. Use of eq. [4] to analyze the data reported by Jordi and Erman (7) for the oxidation of ferrocyanide by CpdII also gives a low charge (−4) for the protein. Thus, the Marcus theory treatment of electrostatic interactions appears to lead to a uniformly lower charge on CCP than that predicted from sequence data.

[4] Calculated from the molecular weight (M) of 35 350 (17) for CCP using the following equation: $R_1 = 0.717 \times M^{1/3}$ (18).

Fig. 2. Ionic strength (I) dependence of the reduction of ferricyanide by CCP^{II} in P_i buffer, pH 7.0, 25 ± 1°C. (*a*) Plot of $f(k)$ vs. $f(I)$ using eq. [3] in the text, and (*b*) plot of $f'(k)$ vs. $f'(I)$ using eq. [4] in the text, where $f(k), f(I), f'(k), f'(I)$ are defined as follows:

$$f(k) = \ln k_{obs} + \frac{Z^2 \alpha I^{1/2}}{1 + \kappa R^2}$$

$$f(I) = \frac{\alpha I^{1/2}}{1 + \kappa R_1}$$

$$f'(k) = \ln k_{obs}$$

$$f'(I) = \frac{\exp(-\kappa R_2)}{1 + \kappa R_1} + \frac{\exp(-\kappa R_1)}{1 + \kappa R_2}$$

The circles indicate the experimental points and the lines show the fits. In (*b*) the point at $f'(I) > 0.9$ was not included in the analysis.

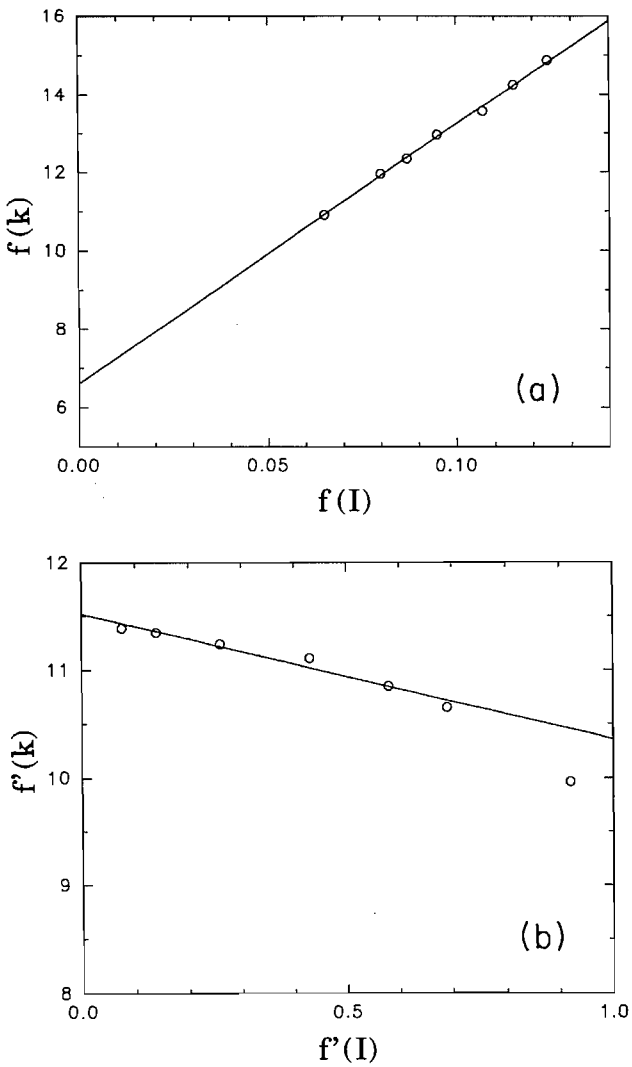

Discussion

The reduction of ferricyanide by CCP^{II} (eq. [1]) exhibited bimolecular kinetics under the experimental conditions used here (Fig. 1). This is in sharp contrast to the reduction of

Table 2. Fe^{II}/Fe^{III} homonuclear electron self-exchange rate constants at infinite ionic strength (k_{11}^{∞}) for heme proteins from their cross-reactions with $Fe(CN)_6^{3-}$.

Protein	R_1(Å)[a]	Z_1[b]	Fe^{II}/Fe^{III} [c]	ΔE_o(mV)[d]	k_{12}[e]	k_{12}^{∞}[f]	k_{11}^{∞}[g]
CCP	23.5	−11/−10	5H/5H	603	7.6×10^4	2.1×10^5	7.2×10^{-5}
Mb	18.4	3.5/4.5	5H/6H	350	1.8×10^6	1.1×10^6	4.4
Cyt c_{552}	15.8	−9/−8	6L/6L	39	4.0×10^4	1.4×10^5	5.9×10^3
Cyt c	16.6	6.5/7.5	6L/6L	147	9.2×10^6	2.9×10^6	2.4×10^4

[a]Protein radii from $R_1 = 0.717 \times M^{1/3}$ (18) and the following molecular weights: CCP 35 350; Mb 16 950; cyt c 12 360; cyt c_{552} 10 740; $R_2 = 4.5$ Å (19).

[b]Protein charges (Fe^{II}/Fe^{III} forms) estimated from sequence data as outlined in ref. 21.

[c]Coordination number and spin state of the heme Fe^{II} and Fe^{III} atoms; H, high spin; L, low spin.

[d]Redox potentials for the cross reactions assuming E^o for ferricyanide at 0.1 M ionic strength is 409 mV (Table I in ref. 21), and the following E^o (mV) values for the proteins: CCP^{III}, −194 (32); Mb^{III}, 58.8 (23); cyt c_{552}^{III}, 370 (33); and cyt c^{III}, 262 (34).

[e]Experimental second-order rate constants for the reduction of $Fe(CN)_6^{3-}$ from the following sources: CCP^{II}, Table 1, this work; Mb^{II}, in 0.1 M phosphate, pH 6.0, 19°C (5); cyt c_{552}^{II}, in phosphate buffer, pH 7.0, 23°C (Table II in ref. 33); cyt c^{II} in phosphate buffer, pH 7, $I = 0.10$ M, 25°C (9).

[f,g]k_{12}^{∞} and k_{11}^{∞} are the values corrected to infinite ionic strength for the protein cross-reaction and self-exchange rate constants, respectively. k_{11}^{∞} values were calculated using eq. [5] with $k_{22}^{\infty} = 8.76 \times 10^5$ M^{-1} s^{-1} for $Fe(CN)_6^{3-/4-}$, which was calculated from the reported value of 1.5×10^4 (Table 1 in ref. 21).

horse and yeast ferricytochromes c by CCP^{II}, which followed first-order kinetics in low and high P_i buffers (16, 22). At low P_i, cytochrome c and CCP form a stable complex so intracomplex electron transfer was expected (16). However, the electrostatically stabilized cytochrome c – CCP complex dissociates at high salt, so a conformational change in CCP^{II} was proposed to explain the first-order kinetics observed for the reduction of ferricytochrome c at high salt (16, 22). Since only bimolecular kinetics were observed for the reduction of ferricyanide, the mechanism of CCP^{II} reduction of the large (ferricytochrome c) and small (ferricyanide) oxidants is clearly different.

Analysis using eq. [3] of the ionic strength dependence of reaction [1] yields an effective charge of −9 for CCP^{II}, which is in good agreement with the value of −9.5 for CCP^{III} obtained by pH titration (7), and close to the value of −11 calculated for CCP^{II} from sequence data (17) following the procedure in ref. 21. Thus, the net charge on CCP^{II} appears to determine its reactivity with ferricyanide. This was previously shown to be the case for the reduction of ferricyanide at low ionic strength by cytochrome c_{552}, which carries a charge of −9 at pH 7.0 (4).

The Marcus cross relation has been used extensively to rationalize the reactivity of small inorganic reagents with redox proteins (6, 8, 20, 21). Assuming that the reactions possess similar adiabaticity factors, and that the precursor and successor complexes have similar stabilities, the observed bimolecular electron-transfer rate constant for the cross-reaction (k_{12}) is given by the following equation (6):

$$[5] \qquad k_{12} = (k_{11}k_{22}k_{12}f)^{1/2}$$

where k_{11} and k_{22} are the self-exchange rate constants for each of the reagents, K_{12} the equilibrium constant for the cross-reaction, and f is given by:

$$[6] \qquad \ln f = (\ln K_{12})^2/4 \ln(k_{11}k_{22}/Z^2)]$$

where Z is the collision frequency ($\sim 10^{11}$ M^{-1} s^{-1}). According to eq. [5], the bimolecular rate constant for the cross-reaction can be related to the driving force (K_{12}) for the cross-reaction and the homonuclear electron self-exchange rate constants for each of the reactants. To correct for non-specific electrostatic interactions between the proteins and the inorganic reagent, the electrostatics-corrected rate and equilibrium constants ($k_{12}^{\infty}, k_{22}^{\infty}, K_{12}^{\infty}$) were calculated as described previously (6, 20, 21), and these values were used in eq. [5]. Thus, If k_{22}^{∞} is known for the small reagent, then k_{11}^{∞} for the protein can be obtained from k_{12}^{∞}. Assuming a charge of −11 on CCP^{II}, a value of 2.1×10^5 M^{-1} s^{-1} was calculated for k_{12}^{∞} for the reduction of ferricyanide by CCP^{II}, which is similar to the value of 1.0×10^5 M^{-1} s^{-1} obtained on extrapolation of the experimental k_{12} to $I = \infty$ (eq. [4]). For $Fe(CN)_6^{3-/4-}$, k_{22}^{∞} was calculated to be 8.76×10^5 M^{-1} s^{-1} based on the reported self-exchange rate constant of 1.5×10^4 M^{-1} s^{-1} at $I = 0.1$ M (Table 1 in ref. 6). From these data a value of 7.2×10^{-5} M^{-1} s^{-1} was estimated for the self-exchange rate of CCP^{II} at infinite ionic strength (Table 2).

The value of k_{11}^{∞} gives a quantitative estimate of the electron-transfer reactivity of a protein towards the inorganic reagent used in the cross-reaction. Thus, it would be informative to compare the k_{11}^{∞} values for the Fe^{IV}/Fe^{III} and Fe^{III}/Fe^{II} couples of CCP obtained from their cross-reactions with the ferri/ferrocyanide redox couple. Ferrocyanide will rapidly reduce CpdII to CCP^{III}, and reaction [2] has been studied as a function of both ionic strength and pH (7, 8). Again, the ionic strength dependence of the rate constant is consistent with ferrocyanide seeing the net charge on the protein at pH 7.0 ($Z_1 = -9.5$ (7)). Extrapolation of k_{12} for reaction [2] (1.5×10^3 M^{-1} s^{-1} at pH 7.0 (7)) to infinite ionic strength, assuming charges of −9/−10 on $CpdII/CCP^{III}$, yields $k_{12}^{\infty} = 4.5 \times 10^3$ M^{-1} s^{-1}, and $k_{11}^{\infty} = 1.9 \times 10^{-9}$ M^{-1} s^{-1}. Hence, k_{11}^{∞} for the Fe^{IV}/Fe^{III} couple of CCP is over four orders of magnitude smaller than that for the Fe^{III}/Fe^{II} couple.

A comparison of the crystal structures of CCP^{III} and CpdI[3] revealed only small differences at the heme (24). This suggests that no major conformational changes take place on CpdI formation, and presumably also on CpdII formation.

Can. J. Chem. Downloaded from www.nrcresearchpress.com by 80.90.12.36 on 09/08/12
For personal use only.

Can. J. Chem. Downloaded from www.nrcresearchpress.com by 80.90.12.36 on 09/08/12
For personal use only.

Hence, the $>10^4$-fold variation in the reactivity of CCP^{II} and CpdII towards the $Fe(CN)_6^{3-/4-}$ couple, as reflected in the k_{11}^{∞} values, may be due to differences in the heme reorganizational energies coupled to electron transfer in CCP^{II} and CpdII. Resonance Raman data indicate that the Fe atom is high spin and 5-coordinate in both CCP^{II} and CCP^{III} (25), whereas the Fe^{IV}=O heme is 6-coordinate, low spin (26). Since cleavage of the Fe^{IV}=O bond occurs on reduction of CpdII, the inner-sphere reorganizational energy for the CpdII/CCP^{III} couple is expected to be greater than that for CCP^{II}/CCP^{III}.

The rate of reduction of CpdII by ferrocyanide increased ~100-fold on lowering the pH from 7.0 to 5.0 (7). Because of a strong pH dependence, Yandell and Yonetani (27) have suggested that proton addition to the oxene ligand in CpdII *precedes* electron transfer from ferrocyanide or other small reducing reagents. Thus, k_{11}^{∞} for CpdII/CCP^{III} derived from its cross-reactions with ferrocyanide may apply to a combined proton and electron transfer. Only a 5-fold increase was observed in the rate of ferricyanide reduction by CCP^{II} over the same pH range (A. English, unpublished results). Such a rate increase could be attributed to more favourable electrostatic interactions at pH 5.0 since CCP has a pI = 5.26 (17), suggesting that proton transfer is not rate determining in the electron-transfer reactions of CCP^{II} at neutral pH. This is consistent with the proposed site of protonation in CpdII being the oxygen atom of the Fe^{IV}=O moiety (26, 27). Therefore, the smaller k_{11}^{∞} for CpdII/CCP^{III} compared to that for CCP^{II}/CCP^{III} may be due to the existence of (partially) rate-limiting proton transfer and Fe^{IV}=O bond cleavage on reduction of CpdII.

To compare the relative reactivities of other ferrous heme proteins and CCP^{II} with the same inorganic reagent, k_{11}^{∞} values calculated from literature rate data on ferricyanide cross-reactions are listed in Table 2 for the Fe^{III}/Fe^{II} couples of CCP, Mb, and cytochromes c and c_{552}. Because of the reported sensitivity of the electron-transfer properties of ferricyanide to the medium (21), second-order rate constants, which were obtained under similar reaction conditions to those in Table 1, were chosen from the literature (footnote *e*, Table 2) to calculate the k_{11}^{∞} values listed in Table 2. The Fe^{II} forms of both deoxy Mb and CCP are 5-coordinate, high spin (28, 25), but Mb binds a water molecule on oxidation to Fe^{III}, giving rise to a 6-coordinate, high spin heme (23) whereas CCP remains 5-coordinate, high spin (25). However, despite the absence of any Fe ligation change, k_{11}^{∞} for CCP is $<10^{-5}$ that of k_{11}^{∞} for Mb. The heme group in Mb is embedded in a cleft near the surface of the molecule and ~18% of the heme is solvent-exposed (29). The heme in CCP is bound between two protein domains ~10 Å from the protein surface and only the propionate side groups of the porphyrin ring are accessible to the external environment (30, 31). Thus, a smaller k_{11}^{∞} is consistent with the reduced accessibility of the heme of CCP. The $>10^3$-fold higher electron-transfer reactivity of the cytochromes c and c_{552} compared to Mb can be largely attributed to the heme remaining 6-coordinate low spin in the Fe^{III}/Fe^{II} states of the cytochromes.

The k_{11}^{∞} values given in Table 2 can also be rationalized in terms of the biological function of the various heme proteins. Cytochromes c and c_{552} are designed to be simple electron transferases; hence, the polypeptide around the heme should promote rapid oxidation and reduction of the heme Fe. The biological function of Mb is to reversibly bind oxygen, which it does only in the ferrous state, so Mb is not expected to be as efficient as the cytochromes at transferring electrons. In fact, the protein matrix serves to reduce the autooxidation rate of oxyMb by several orders of magnitude compared to that in free hemes (35). Finally, as mentioned above, the enzymic cycle of CCP generates the highly oxidizing intermediates, CpdI and CpdII. Clearly, if the oxidizing equivalents of this protein are not to be randomly discharged, the highly reactive Fe^{IV}=O heme has to be well insulated. Nature achieves this by burying the heme ~10 Å below the protein surface and designing the surface of the protein such that its reducing substrate, ferrocytochrome c, recognizes and binds to the surface of CCP prior to electron transfer (17, 31), as confirmed in the recent X-ray structure of the CCP–cytochrome c complex (36). Access of small redox reagents to the heme appears to require diffusion ~10 Å up a channel that leads from the surface of the protein to the δ-*meso* heme edge (37). This should result in a large steric effect consistent with the small k_{11}^{∞} for CCP^{II} in Table 2.

In summary, the relative magnitudes of the protein self-exchange rate constants in Table 2 from the ferricyanide cross-reactions reflect structure–function relationships in this series of heme proteins. Of particular significance is the $>10^4$ difference in the k_{11}^{∞} values for the two redox couples of CCP estimated from the cross-reactions with ferri/ferrocyanide. This, as well as the data in Table 2, underscores the relevance of applying the Marcus cross relation to protein–small molecule data (20, 21).

Acknowledgement

This research was funded by the Natural Sciences and Engineering Research Council of Canada (NSERC).

References

1. D.W. Dixon. *In* Molecular structure and energetics: principles of enzyme activity. *Edited by* J.F. Liebman and A. Greenberg. Elsevier, New York. 1988. pp. 169–225; R.E. Dickerson and R. Timkovich. *In* The enzymes. Vol. 11. 3rd ed. *Edited by* P.D. Boyer. Academic Press, New York. 1976. Chap. 7.
2. W.A. Oertling, R.T. Kean, R. Wever, and G.T. Babcock. Inorg. Chem. **29**, 2633 (1990).
3. E. Antonini and M. Brunori. *In* Hemoglobin and myoglobin in their reactions with ligands. *Edited by* A. Neuberger and E.L. Tatum. North-Holland, Amsterdam. 1971.
4. T. Goldkorn and A. Schejter, J. Biol. Chem. **254**, 12562 (1979).
5. E. Antonini, M. Brunori, and J. Wyman. Biochemistry, **4**, 545 (1965).
6. S. Wherland and H.B. Gray. Proc. Natl. Acad. Sci. U.S.A. **73**, 2950 (1976).
7. H. Jordi and J.E. Erman. Biochemistry, **13**, 3734 (1974).
8. W.L. Purcell and J.E. Erman. J. Am. Chem. Soc. **98**, 7033 (1976).
9. P.L. Drake, R.T. Hartshorn, J. McGinnis, and A.G. Sykes. Inorg. Chem. **28**, 1361 (1989).
10. R.M. Zabinski, K. Tatti, and G.H. Czerlinski. J. Biol. Chem. **249**, 6125 (1974).
11. N. Sutin and D.R. Christman. J. Am. Chem. Soc. **83**, 1773 (1961).
12. A.M. English, M. Laberge, and M. Walsh. Inorg. Chim. Acta, **123**, 113 (1986).

13. G. Smulevich, A.R. Mantini, A.M. English, and J.M. Mauro. Biochemistry, **28**, 5058 (1989).
14. T. Yonetani and H. Anni. J. Biol. Chem. **262**, 9547 (1987).
15. B. Ward and C.K. Chang. Photochem. Photobiol. **35**, 757 (1982).
16. E. Cheung and A.M. English. Inorg. Chem. **27**, 1078 (1988).
17. H.R. Bosshard, H. Anni, and T. Yonetani. *In* Peroxidases in chemistry and biology. Vol. II. *Edited by* J. Everse, K.E. Everse, and M.B. Grisham. CRC Press, Boca Raton, Fla. 1991. Chap. 3.
18. C.R. Cantor and P.R. Schimmel. Biophysical chemistry Part II: Techniques for the study of biological structure and function. Freeman, San Francisco. 1980. p. 554.
19. B.I. Swanson and R.R. Ryan. Inorg. Chem. **12**, 283 (1973).
20. R.A. Marcus and N. Sutin. Biochim. Biophys. Acta, **811**, 265 (1985).
21. S. Wherland and H.B. Gray. *In* Biological aspects of inorganic chemistry. *Edited by* A.W. Addison, W.R. Cullen, D. Dolphin, and B.R. James. Wiley, New York. 1977. pp. 289–368.
22. A.M. English and E. Cheung. Inorg. Chim. Acta, **201**, 243 (1992).
23. R.J. Crutchley, W.R. Ellis, Jr., and H.B. Gray. J. Am. Chem. Soc. **107**, 5002 (1985).
24. S.L. Edwards, N.H. Xuong, R.C. Hamlin, and J. Krout. Biochemistry, **26**, 1503 (1987).
25. G. Smulevich, J.M. Mauro, L.A. Fishel, A.M. English, J. Kraut, and T.G. Spiro. Biochemistry, **27**, 5477 (1988).
26. C.M. Reczek, A.J. Sitter, and J. Terner. J. Mol. Struct. **214**, 27 (1989); S. Hashimoto, J. Teraoka, T. Inubushi, T. Yonetani, and T. Kitagawa. J. Biol. Chem. **261**, 11110 (1986).
27. J.K. Yandell and T. Yonetani. Biochim. Biophys. Acta, **748**, 263 (1983).
28. T. Takano. J. Mol. Biol. **110**, 537 (1977); **110**, 569 (1977).
29. E. Stellwagen. Nature, **275**, 73 (1978).
30. B.C. Finzel, T.L. Poulos, and J. Kraut. J. Biol. Chem. **259**, 13027 (1984).
31. T.L. Poulos and B.C. Finzel. Peptide Protein Rev. **4**, 115 (1984).
32. C.W. Conroy, P. Tuma, P.H. Daum, and J.E. Erman. Biochim. Biophys. Acta, **537**, 62 (1978).
33. F.E. Wood and M.A. Cusanovich. Arch. Biochem. Biophys. **168**, 333 (1975).
34. V.T. Taniguchi, W.R. Ellis Jr., V. Cammarata, J. Webb, F.C. Anson, and H.B. Gray. Adv. Chem. Ser. **201**, 51 (1982).
35. B.A. Springer, S.G. Sligar, J.S. Olson, and G.N. Philips, Jr. Chem. Rev. **94**, 669 (1994).
36. H. Pelletier and J. Kraut. Science, **258**, 1748 (1992).
37. G.D. DePillis, B.P. Sishta, A.G. Mauk, and P.R. Ortiz de Montellano. J. Biol. Chem. **266**, 19334 (1991).

Can. J. Chem. Downloaded from www.nrcresearchpress.com by 80.90.12.36 on 09/08/12
For personal use only.

Systematic substitution kinetics of the clusters $Ru_3(CO)_{11}L$ and $Ru_3(CO)_{10}L_2$ (L = P-donor ligands): The unimolecular path

Nancy M.J. Brodie and Anthony J. Poë

Can. J. Chem. Downloaded from www.nrcresearchpress.com by 80.90.12.36 on 09/08/12
For personal use only.

Abstract: The kinetics have been studied of the substitution reactions of $Ru_3(CO)_{11}L$ and $Ru_3(CO)_{10}L_2$ (L = PCy_3 (Cy = C_6H_{11}), P-*n*-Bu_3, P(*p*-$MeOC_6H_4)_3$, P(*p*-$ClC_6H_4)_3$, $P(OPh)_3$, and etpb ($P(OCH_2)_3CEt$) with $AsPh_3$ or various P-donor nucleophiles, L′, in hexane. The reactions proceed through both [L′]- independent (CO dissociative) and [L′]-dependent (associative) paths. The values of the rate constants, k_1, for the dissociative path for $Ru_3(CO)_{11}L$ can be combined with other published data and are found to fit well to the equation: $\log k_1 = \alpha + \beta_L\delta_L + \gamma_L\theta_L$. ($\beta_L$ and γ_L are constants that define how sensitive the values of $\log k_1$ are to Bodner's electronic parameter, δ_L, and to Tolman's steric parameter, θ_L, respectively.) Values of β_L and γ_L are both positive, increasing electron donicity and increasing size of L both leading to increased rates. The steric effect is more important and accounts for ca. 60% of the decrease in the free energies of activation. The effects, on the fit and on the values of β_L and γ_L, of using different electronic (Bartik's χ values) and steric (Brown's E_R values) parameters are examined and found to be small, and the question of which goodness-of-fit parameters should be used is considered. The kinetic effects of the substituents are only a small (ca. 20%) perturbation on the average free energies of activation, and the steric effect shows that use is made of only a few percent of the available ligand–ligand repulsion energy in accelerating the reactions. The second-order reactions of $M_3(CO)_{11}L$ with Me_3NO (M = Ru or Os) also fit an equation analogous to that given above and the values of β_L and γ_L obtained for these assisted CO displacement reactions are compared with those for the unimolecular, unassisted, CO dissociation. Unassisted reactions of the $Ru_3(CO)_{10}L_2$ clusters show values of β_L and γ_L that are closely similar to those for $Ru_3(CO)_{11}L$, but published data for CO dissociative reactions of some $Ru_3(CO)_9L_3$ clusters lead to much larger positive values of β_L and a large *inverse* steric effect, i.e., rates actually decrease substantially with increasing substituent size after electronic effects are allowed for. This effect is accounted for in terms of the different natures of the $Ru_3(CO)_8L_3$ intermediates.

Key words: metal carbonyls, ruthenium, clusters, kinetics, substituent effects.

Résumé : On a étudié la cinétique des réactions de substitution du $Ru_3(CO)_{11}L$ et $Ru_3(CO)_{10}L_2$ (L = PCy_3 (Cy = C_6H_{11}), P-*n*-Bu_3, P(*p*-$MeOC_6H_4)_3$, P(*p*-$ClC_6H_4)_3$, $P(OPh)_3$, et etpb ($P(OCH_2)_3CEt$) avec le $AsPh_3$ ou divers autres nucléophiles donneurs, L′, dans l'hexane. Les réactions se produisent par des voies qui dépendent (associatives) ou qui ne dépendent pas (dissociative de CO) de la [L′]. On peut combiner les valeurs des constantes de vitesse, k_1, de la voie dissociative du $Ru_3(CO)_{11}L$ avec d'autres données publiées dans la littérature et on a trouvé qu'elles peuvent facilement s'ajuster à l'équation : $\log k_1 = \alpha + \beta_L\delta_L + \gamma_L\theta_L$ (dans laquelle β_L et γ_L sont des constantes qui définissent la sensibilité des valeurs de $\log k_1$ respectivement au paramètre électronique de Bodner, δ_L, et au paramètre stérique de Tolman, θ_L. Les valeurs de β_L and γ_L sont toutes les deux positives; les vitesses de réactions augmentent avec une augmentation du caractère électrodonneur et de la grosseur de L. L'effet stérique est plus important et il est la cause de 60% de la diminution des énergies libres d'activation. On a examiné les effets, tant sur l'ajustement que sur les valeurs de β_L and γ_L, de l'utilisation de paramètres électroniques (valeurs χ de Bartik) et stériques (valeurs E_R de Brown) et on a trouvé qu'ils sont faibles et on a considéré la question de quels paramètres devraient être utilisés pour obtenir un bon ajustement. Les effets cinétiques des substituants ne correspondent qu'à de faibles (environ 20%) perturbations sur les énergies libres moyennes d'activation et l'effet stérique montre que, de l'énergie de répulsion coordinat–coordinat disponible, il n'y a qu'un faible pourcentage qui est utilisé pour accélérer les

Received November 2, 1995.

This paper is dedicated to Professor William A.G. Graham on the occasion of his 65th birthday.

N.M.J. Brodie and A.J. Poë.[1] Lash Miller Chemical Laboratories, University of Toronto, 80 St. George St., Toronto, ON M5S 1A1, Canada.

[1] Author to whom correspondence may be addressed. Telephone: (416) 978-3924. Fax: (416) 978-8775. E-mail: apoe@alchemy.chem.utoronto.ca

réactions. Les réactions du deuxième ordre du $M_3(CO)_{11}L$ avec le Me_3NO (M = Ru ou Os) peuvent aussi être ajustées à l'aide d'une équation analogue à celle donnée plus haut et on a comparé les valeurs de β_L et γ_L obtenues pour ces réactions assistées de déplacement de CO avec celle de la réaction de dissociation unimoléculaire du CO, non assistée. Les valeurs de β_L et γ_L des réactions non assistées des agrégats de $Ru_3(CO)_{10}L_2$ sont très semblables à celles du $Ru_3(CO)_{11}L$; toutefois, les données publiées dans la littérature pour les réactions dissociatives de quelques agrégats de $Ru_3(CO)_9L_3$ conduisent à des valeurs de β_L qui sont beaucoup positives et à un effet stérique *inverse*, c'est-à-dire que, après avoir tenu des effets électroniques, les vitesses diminuent considérablement avec une augmentation de la taille du substituant. On explique cet effet par les natures différentes des intermédiaires $Ru_3(CO)_8L_3$.

Mots clés : carbonyles de métaux, ruthénium, agrégats, cinétique, effets de substituants.

[Traduit par la rédaction]

Introduction

Studies of the effects of P-donor or other substituents on the rates of unimolecular substitution reactions of binary metal carbonyl clusters have appeared in the literature sparingly and sporadically throughout the last 20 years (1–7). A study of the PPh_3-substituted tetrairidium carbonyl clusters represented the first quantitative evidence that such effects did exist (1). Upon increasing n in $Ir_4(CO)_{12-n}(PPh_3)_n$ from 0 to 2 the rate constants for unimolecular substitution increased markedly. More extensive studies by Sonnenberger and Atwood (2) and Darensbourg et al. (3*a*) have been carried out on a relatively wide variety of $Ir_4(CO)_{12-n}L_n$ clusters (n = 1–3, L = As- or P-donor ligands) and the unimolecular rate constants vary substantially with the value of n and the nature of L. The results have been summarized and discussed qualitatively in terms of varying electronic and steric contributions (4). Studies of substituent effects in reactions of Co_4 (3*e*), Rh_4 (5), Ru_3 (6), and Os_3 (7) clusters have been reported but the nature and number of the substituents were not varied sufficiently for clear-cut trends to be apparent.

We have therefore undertaken a systematic study of some $Ru_3(CO)_{11}L$ and $Ru_3(CO)_{10}L_2$ clusters containing quite a wide variety of substituents, and find it possible to quantify the separate electronic and steric effects of the substituents on the rates of unimolecular substitution. The method of data analysis is also found to be useful when applied to published results for the clusters $Ru_3(CO)_9L_3$.

Experimental

The complexes $Ru_3(CO)_{11}L$ (L = $P(C_6H_{11})_3$ (PCy_3), P-*n*-Bu_3, $P(p\text{-}MeOC_6H_4)_3$, $P(OPh)_3$, $P(p\text{-}ClC_6H_4)_3$, and $P(OCH_2)_3CEt$ (etpb)) and $Ru_3(CO)_{10}L_2$ (L = PCy_3, P-*n*-Bu_3, $P(p\text{-}MeOC_6H_4)_3$, $P(OPh)_3$, and etpb) were prepared (8) from $Ru_3(CO)_{12}$ (Strem Chemicals) by published methods (9). These clusters were characterized by comparison of their IR spectra in hexane with those for identical or very similar complexes published elsewhere (9*c*). Their purity was demonstrated by their ^{31}P NMR spectra measured in hexane ($Ru_3(CO)_{11}L$) or dichloromethane ($Ru_3(CO)_{10}L_2$). The IR and ^{31}P NMR spectral data are shown in Table 1 together with the main bands shown in the UV–vis spectra. Etpb, $P(OPh)_3$, $P(OEt)_3$, P-*n*-Bu_3, PPh_3, and $AsPh_3$ were obtained and purified exactly as described previously (10). $P(p\text{-}MeOC_6H_4)_3$ and $P(p\text{-}ClC_6H_4)_3$ (Strem Chemicals) were used as received. THF (tetrahydrofuran) was distilled over sodium benzephenone under nitrogen before use. Other solvents (Aldrich reagent grade) were dried over molecular sieves. Spectra were measured with a Nicolet 10DX FTIR spectrophotometer, a Varian XL-200 NMR spectrometer, and a Cary 2300 UV–vis spectrophotometer.

Kinetic studies

Hexane solutions of $Ru_3(CO)_{11}L$ or $Ru_3(CO)_{10}L_2$ (ca. 1×10^{-4} M) containing the various nucleophiles (0.002–0.500 M) were prepared as previously described (6*d*,11). Particular care was taken to ensure that air was excluded when preparing ligand solutions of air-sensitive nucleophiles. Kinetic studies were carried out by monitoring the UV–vis spectra of pre-thermostated solutions in 10-mm cuvettes placed in the thermostated cell holder of a Cary 2300 spectrophotometer. Slower reactions were followed by repetitive scanning of groups of up to four reacting solutions. Faster reactions were monitored by following absorbance changes using the time-drive mode. Cell temperatures were measured with an iron–constantan thermocouple connected to a digital multimeter. In some cases reactions were followed using IR monitoring techniques (6*d*, 11) and employing standard Schlenk-tube methods. Samples were withdrawn from thermostated solutions of complex (ca. 5×10^{-4} M) and nucleophile (0.01–0.20 M) at timed intervals. The samples were immediately cooled and their spectra measured. Spectroscopic data for the products are shown in Table 2.

Results

Reactions of $Ru_3(CO)_{11}L$ with L′

These reactions were studied kinetically at 40°C, the highest temperature possible without some of the reactions being too fast to measure conveniently. Most reactions proceed via a mixture of unimolecular and bimolecular paths, i.e., with the rate equation $k_{obs} = k_1 + k_2[L']$. A high temperature minimizes the relative contribution of the k_2 paths to the rates.[2] Different entering ligands, L′, were also chosen to minimize the contribution of the k_2 paths and to provide sufficiently pronounced spectroscopic changes. Thus $Ru_3(CO)_{11}(PCy_3)$ and $Ru_3(CO)_{11}(P\text{-}n\text{-}Bu_3)$ are both very susceptible to nucleophilic attack and sensitive to the nature of the incoming nucleophile. $AsPh_3$ was used as the entering ligand in both cases. No [$AsPh_3$] dependence of the rates was observed and convenient increases in absorbance occurred so that good values of k_1 were easily obtained.[3] No complications from further substi-

[2] This is because unimolecular paths almost invariably have higher activation enthalpies than bimolecular ones occurring with the same compounds.

[3] The reaction of $Ru_3(CO)_{11}(PCy_3)$ with $AsPh_3$ leads to little change in the position of the UV–vis band but there is a sufficient increase in intensity for good rate data to be obtained.

Can. J. Chem. Downloaded from www.nrcresearchpress.com by 80.90.12.36 on 09/08/12
For personal use only.

Can. J. Chem. Downloaded from www.nrcresearchpress.com by 80.90.12.36 on 09/08/12
For personal use only.

Table 1. Spectroscopic data on the $Ru_3(CO)_{11}L$ and $Ru_3(CO)_{10}L_2$ clusters.

L	ν(CO), (cm^{-1})[a]	λ_{max} (nm)[b]	^{31}P NMR(ppm)[c]
$Ru_3(CO)_{11}L$			
P-*n*-Bu_3	2097(15), 2044(66), 2026(49), 2014(100), 1999(sh)(14), 1993(sh)(12), 1983(21), 1970(10)	415	16.4
P(*p*-$MeOC_6H_4)_3$	2096(18), 2044(70), 2030(sh)(36), 2024(sh)(43), 2015(100), 1986(18)	420	30.4
$P(OPh)_3$	2104(12), 2051(92), 2037(63), 2020(100), 2002(35), 1989(13)	408	128
etpb	2105(10), 2061(43), 2049(94), 2041(71), 2032(sh)(44), 2022(100), 2000(41), 1987(17)	400	125
P(*p*-$ClC_6H_4)_3$	2100(30), 2050(72), 2036(sh)(42), 2029(sh)(46), 2020(100), 1990(28), 1963(20)	416	33.4
PCy_3	2097(21), 2045(64), 2028(44), 2015(100), 1996(sh)(13), 1983(63), 1960(13)	424	49.6
$Ru_3(CO)_{10}L_2$			
P-*n*-Bu_3	2072(14), 2013(sh)(93), 1991(100), 1968(sh)(42), 1946(sh)(18)	455	15.4 (br)
P(*p*-$MeOC_6H_4)_3$	2073(25), 2018(68), 1996(100), 1974(sh)(45), 1940(sh)(23)	400, 492	30.4 (br)
$P(OPh)_3$	2088(13), 2036(78), 2009(100), 1991(sh)(35)	420	128, 129
etpb	2091(52), 2035(74), 2025(sh)(53), 2013(100), 1989(40), 1981(sh)(33)	404	125, 126, 127
P(*p*-$ClC_6H_4)_3$		400, 482	
PCy_3	2073(11), 2017(69), 1991(100), 1966(35), 1935(15)	408, 466	46 (br)

[a]Values in parentheses are intensities relative to the strongest band, taken as 100, in hexane.
[b]In hexane.
[c]$^{31}P(^1H)$ NMR spectra were measured at 20.0°C and values are relative to external H_3PO_4 (85%). Variable temperature $^{31}P(^1H)$ NMR studies were conducted on a number of the bis-substituted ruthenium clusters but this work will be discussed elsewhere.

Table 2. Spectra of products of reactions of $Ru_3(CO)_{11}L$ and $Ru_3(CO)_{10}L_2$ with L′ in hexane.

L	λ_{max}(L′)[a]	λ_{max}(L′)[b]
eptb	414 ($P(OEt)_3$)	412[c] (P(p-$MeOC_6H_4)_3$)
$P(OPh)_3$	428 ($P(OEt)_3$)	460 (PPh_3)
P-*n*-Bu_3	418 ($AsPh_3$)[d]	463 ($P(OEt)_3$)[e]
P(*p*-$ClC_6H_4)_3$	452 ($P(OPh)_3$)	388, 500 (P(p-$ClC_6H_4)_3$)
P(*p*-$MeOC_6H_4)_3$	455 ($P(OPh)_3$)[f]	490 ($P(OPh)_3$)
PCy_3	420 ($AsPh_3$)	484 ($P(OPh)_3$)

[a]For reactions of $Ru_3(CO)_{11}L$ with L′.
[b]For reactions of $Ru_3(CO)_{10}L_2$ with L′.
[c]Very broad band.
[d]IR spectrum: 2070(14), 2025(88), 2014(sh)(74), 1994(100), 1970(43), 1962(41) cm^{-1}.
[e]IR spectrum: 2044(6), 1970(100), 1941(39) cm^{-1}.
[f]IR spectrum: 2082(19), 2024(77), 2000(100), 1982(sh)(68) cm^{-1}.

tution into the products were observed (see below). The choice of reacting ligand for the substitution reactions of $Ru_3(CO)_{11}L$ (L = etpb, $P(OPh)_3$, and P(*p*-$ClC_6H_4)_3$) was made so as to generate convenient reaction times and suitably large spectroscopic changes. These three clusters were not particularly susceptible to nucleophilic attack and the subsequent reactions undergone by the product clusters, $Ru_3(CO)_{10}LL'$, were much slower than the initial reactions under the conditions used.

The reactions of $Ru_3(CO)_{11}L$ (L = P-*n*-Bu_3 and P(*p*-$MeOC_6H_4)_3$) with $AsPh_3$ and $P(OPh)_3$, respectively, were also monitored by IR techniques. This was done in order to confirm the nature of the products and to see whether any subsequent reaction of the product clusters was likely to affect the A_∞ values obtained for the initial reactions by UV–vis monitoring. The decrease of absorbance of a prominent reactant band (2044 cm^{-1}, for reactions of both clusters) was followed in a region where the products of either the initial or subsequent reactions did not absorb. The reaction of $Ru_3(CO)_{10}$(P(*p*-$MeOC_6H_4)_3$)($P(OPh)_3$) with $P(OPh)_3$ following the initial reaction of $Ru_3(CO)_{11}$(P(*p*-$MeOC_6H_4)_3$) with $P(OPh)_3$ proved to be too rapid to allow accurate values of A_∞ to be obtained when employing UV–vis monitoring but no evidence for significant further reaction of $Ru_3(CO)_{10}$(P-*n*-Bu_3)($AsPh_3$) with $AsPh_3$ was observed. UV–vis monitoring of the reactions of $Ru_3(CO)_{11}$(P-*n*-Bu_3) with $AsPh_3$ was thereby confirmed to be satisfactory in providing good values of A_∞ but all rate measurements for the reactions of $Ru_3(CO)_{11}$(P(*p*-$MeOC_6H_4)_3$) with $P(OPh)_3$ had to be obtained through IR monitoring.

The main UV–vis bands in the spectra of the reaction products are shown in Table 2 together with selected examples of their IR spectra. The intensities of the UV–vis bands were comparable with those of the reactants and there was no spectroscopic evidence for formation of appreciable amounts of mononuclear products. This is as expected since fragmentation of Ru_3 clusters seems to occur only via associative reactions (11, 12) and the small contribution of the k_2[L′] terms to k_{obs} ensures that these are quite unimportant.

The pseudo-first-order rate plots of the reactions of $Ru_3(CO)_{11}L$ with L′ to form $Ru_3(CO)_{10}LL'$ were linear for ca. 80–90% reaction. Values of k_{obs} were found to depend slightly on [L′] except when L′ was $AsPh_3$. An appropriately weighted linear least-squares analysis (7) was applied to the rate constants in order to obtain values for k_1 in the cases where an [L′]-dependent path was observed. When L′ = $AsPh_3$ the values of k_{obs} were simply averaged to give k_1, and the values of k_1 for all these reactions are also given in Table 3. The uncertainties are estimates of standard deviations that are based on a standard error, $\sigma(k_{obs})$, in each individual measurement of k_{obs} that is assumed to be the same for all the reactions. The value of $\sigma(k_{obs})$ was estimated (7) by the method of pooled variances (e.g., ref. 13).

Reactions of $Ru_3(CO)_{10}L_2$ with L′

The reactions of $Ru_3(CO)_{10}L_2$ (L = etpb, $P(OPh)_3$, PCy_3, P-*n*-Bu_3, P(*p*-$MeOC_6H_4)_3$, and P(*p*-$ClC_6H_4)_3$) with L′ were fol-

Can. J. Chem. Downloaded from www.nrcresearchpress.com by 80.90.12.36 on 09/08/12
For personal use only.

Table 3. Rate constants for the [L′]-independent path for reactions of $Ru_3(CO)_{11}L$ (at 40°C)[a] and $Ru_3(CO)_{10}L_2$ (at 25°C)[b] with L′.

L	$10^4\ k_1\ (s^{-1})^a$ (L′)	$10^4 k_1(s^{-1})^b$ (L′)
etpb	0.65 ± 0.04 ($P(OEt)_3$)	0.059 ± 0.004 ($P(p\text{-}ClC_6H_4)_3$)
$P(OPh)_3$	2.61 ± 0.17 ($P(OEt)_3$)	0.235 ± 0.010 (PPh_3)
P-*n*-Bu_3	14.5 ± 1.3 ($AsPh_3$)	0.81 ± 0.11[c]
$P(p\text{-}ClC_6H_4)_3$	9.74 ± 0.71 ($P(OPh)_3$)	0.78 ± 0.05 ($P(p\text{-}ClC_6H_4)_3$)
$P(p\text{-}MeOC_6H_4)_3$	27.5 ± 0.2 ($P(OPh)_3$)	1.37 ± 0.07 ($P(OPh)_3$)
PCy_3	134 ± 10 ($AsPh_3$)	8.60 ± 1.30[c]

[a]For reactions of $Ru_3(CO)_{11}L$ with L′. Values of k_1 were obtained by weighted least-squares analysis of $k_{obs} = k_1 + k_2[L']$ with four different values of [L′] or, when there was clearly no dependence on [L′], by averaging the four values of k_{obs}. The uncertainties are based on a standard error of ±7.2% for each measurement of k_{obs} found from the method of pooled variances applied to all 24 measurements.

[b]For reactions of $Ru_3(CO)_{10}L_2$ with L′. Unless otherwise indicated, values of k_1 were obtained as in footnote *a* and the standard error in k_{obs} was ± 6.0%.

[c]Values of k_1 were obtained from weighted least-squares analyses of $k_{obs} = k_1 + k_2[L']$ for L′ = etpb, $P(OEt)_3$, $P(OPh)_3$, P-*n*-Bu_3, PPh_3, $P(p\text{-}MeOC_6H_4)_3$, and PCy_3 (L = PCy_3 or P-*n*-Bu_3), and L′ = $P(p\text{-}MeC_6H_4)_3$ (L = P-*n*-Bu_3). Standard errors for each measurement of k_{obs} were ± 3.5% (L = P-*n*-Bu_3) and ± 4.8% (L = PCy_3).

lowed by UV–vis monitoring. However, for these reactions, the growth of the band due to the product, $Ru_3(CO)_9L_2$ L′, was monitored with time. This method of measurement was chosen because of the larger spectral changes associated with the growth of the product and the well-defined values of A_∞ that could be obtained. The $Ru_3(CO)_{10}(P(p\text{-}ClC_6H_4)_3)_2$ cluster was not isolated but was synthesized in situ from the reaction of $Ru_3(CO)_{11}(P(p\text{-}ClC_6H_4)_3)$ with excess $P(p\text{-}ClC_6H_4)_3$. Once spectroscopic examination showed that the mono-substituted cluster had disappeared, and only the bis-substituted cluster remained, the subsequent reaction of the bis-substituted cluster with additional $P(p\text{-}ClC_6H_4)_3$ was monitored.

The susceptibility to nucleophilic attack is very low for these clusters and unimolecular substitution is the only significant reaction path at low values of [L′]. The substitution reactions were conveniently studied at 25°C. Furthermore, the choice of entering group, L′, depended mainly on obtaining a suitable change in spectrum, the nucleophilicity of L′ not being as important. Since the bimolecular path was negligible or small in these reactions, there was essentially no loss of cluster due to fragmentation (12) and the products of these reactions were virtually 100% $Ru_3(CO)_{10}L_2L'$. Spectroscopic data for these products are given in Table 2.

The pseudo-first-order rate plots for these reactions were linear for ca. 90% reaction. The values of k_1 and $\sigma(k_{obs})$ were obtained as before except for the clusters $Ru_3(CO)_{10}(P\text{-}n\text{-}Bu_3)_2$ and $Ru_3(CO)_{10}(PCy_3)_2$. Reactions of these clusters were studied with a range of ligands of widely different nucleophilicity and at higher [L′] values, to be able to obtain values for k_2 as well as k_1. The values of k_2 will be discussed elsewhere. Weighted averages of the various values of k_1 obtained from the weighted linear least-squares analysis of the dependence of k_{obs} on [L′] are given in Table 3 together with values of k_1 for the other $Ru_3(CO)_{10}L_2$ clusters.

Derivation of electronic and steric profiles

The quantitative empirical characterization of separate electronic and steric effects in associative reactions of metal carbonyls with P-donor and other nucleophiles has been known to be possible for many years (10*a*, 12, 14). Similar characterization of the effects of substituents on the rates of CO dissociative reactions is much less common (15) but is equally possible. Since the rates of reaction are being examined as a function of the natures of various P donors present as substituents, rather than as nucleophiles, the parameters chosen to represent the electronic natures of the ligands should reflect their π-acidity as well as their σ-donor capacity. In principle, the balance between σ-basicity and π-acidity effects for a given ligand should depend on the nature of the metal to which it is attached, the oxidation state of the metal, the nature of other ligands, and whether the metal is bonded to other metal atoms (16), but no generally available parameters that represent such details exist. One is forced, faut de mieux, to accept the χ values of Bartik et al. (17) or the $\delta(^{13}CO)$ parameters of Bodner et al. (18), which are available for a very wide range of P donors and which reflect the σ/π balance of the ligands when present in the standard complex $Ni(CO)_3L$. These parameters are linearly related to each other (19) but the latter, although somewhat less precise,[4] have the advantage that a value is known for L = CO. They have been used successfully in analyzing a substantial number of other kinetic data (15*a*, 21).

A plot of log k_1 vs. δ_L for reactions of $Ru_3(CO)_{11}L$ is shown in Fig. 1 where it is immediately obvious that there is no general linear relationship. Steric effects are clearly important since the reactions are fastest when L = PCy_3 (Tolman cone angle (20),θ_L, = 170°) and slowest when L = CO, etpb, or $P(OEt)_3$ (θ_L = 95°, 101°, and 109°, respectively). However, the ligands $P(OPh)_3$ (θ_L = 128°) and P-*n*-Bu_3 (θ_L = 132°) are almost isosteric, and an initial quantitative measure of the electronic effect can be obtained from the gradient (β_L = 0.19 ppm^{-1}) of the line joining the values of log k_1 for these two ligands. This enables values of log k_1^0 = log k_1 − $\beta_L\delta_L$ to be calculated and a linear steric profile (i.e., a plot of log k_1° vs.

[4] The values of $\delta(^{13}CO)$ are more precise (18) than Tolman's χ values (20) but less precise than Bartik's (17).

Can. J. Chem. Downloaded from www.nrcresearchpress.com by 80.90.12.36 on 09/08/12
For personal use only.

Table 4. Dependence of log k_1 for $Ru_3(CO)_{11}L$ and $Ru_3(CO)_{10}L_2$ on electronic and steric parameters of L.

Ligand no.[a]	L	δ_L(ppm)[b]	χ_L(cm^{-1})[b]	θ(deg)[b]	E_R(kcal mol^{-1})[b]	log k_1[c]	log k_1[d]
1	CO	0	—	95	7	−4.966[e]	−6.10[e]
2	etpb	2.60	31.20	101	25	−4.184	−5.229
3	$P(OEt)_3$	3.61	21.60	109	59	−4.168[f]	—
4	$P(OPh)_3$	1.69	30.20	128	65	−3.583	−4.629
5	P-*n*-Bu_3	5.69	5.25	132	64	−2.839	−4.094
6	$P(p\text{-}ClC_6H_4)_3$	3.54	16.80	145	74	−3.011	−4.110
7	PPh_3	4.30	13.25	145	75	−3.066[g]	−4.213[g]
8	$P(p\text{-}MeOC_6H_4)_3$	4.43	10.50	145	76	−2.561	−3.863
9	PCy_3	6.32	1.40	170	116	−1.873	−3.066
10	dppm	3.52	—	121	—	—	−4.759

[a]Numbering of ligands as used in figures.
[b]See text for definitions and sources of data.
[c]For $Ru_3(CO)_{11}L$, at 40°C.
[d]For $Ru_3(CO)_{10}L_2$, at 25°C.
[e]Data from ref. 10*a*.
[f]Data from ref. 6*d*.
[g]Data from ref. 6*a*.

Fig. 1. Dependence of log k_1 on δ_L for the CO dissociative reactions of $Ru_3(CO)_{11}L$ at 40°C. Ligand numbering is taken from Table 4.

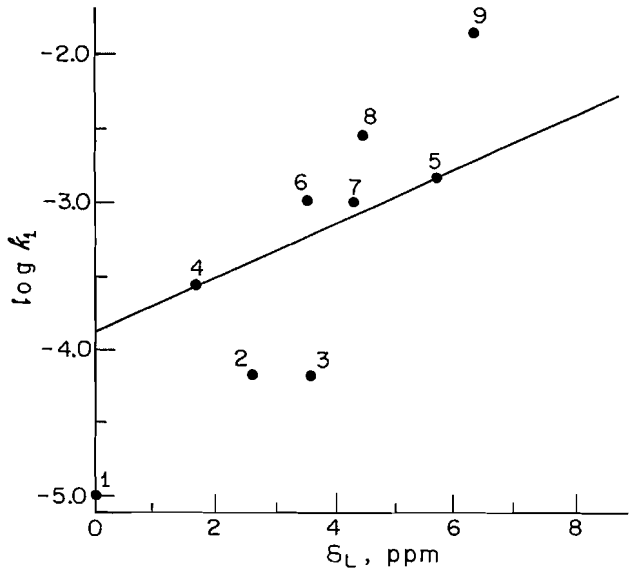

Fig. 2. Dependence of log k_1^0 (= log k_1 − $\beta_L\delta_L$) on the Tolman cone angles, θ_L, of L for the CO dissociative reactions of $Ru_3(CO)_{11}L$ (●, at 40°C) and $Ru_3(CO)_{10}L_2$ (▲, at 25°C). Ligand numbering from Table 4.

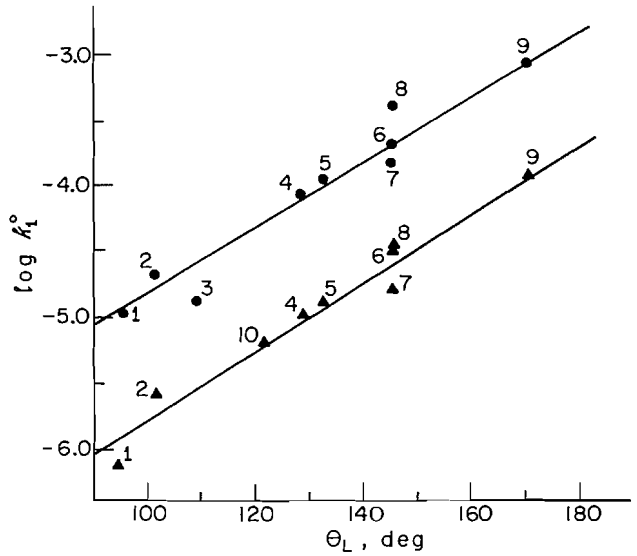

θ_L) is then obtained. This linearity shows that the data should fit eq. [1], and multiple linear regression (22) leads to the values of α, β_L, and γ_L given in Table 5.

$$[1]\quad \log k_1 = \alpha + \beta_L\delta_L + \gamma_L\theta_L$$

When data for only P-donor ligands are included, the value of β_L is not precise but is fully consistent with the initial approximate value obtained above. These parameters allow us to calculate the rate constant for L = CO, i.e., k_1 for loss of CO from $Ru_3(CO)_{12}$, and a value that is 40% higher than the experimentally observed value is obtained, showing that the procedure has quite good predictive value. If the data for L = CO are included in the analysis according to eq. [1] the fit is improved (Table 5). The RMSD is slightly reduced and $100(1 - R^2)$ decreases, the latter being a measure (23) of the extent to which the model, represented by eq. [1] and its parameters, fails to account for the data. The steric profile, obtained by using the best value of β_L, is shown in Fig. 2. An identical procedure was followed in analyzing the data for $Ru_3(CO)_{10}L_2$ and the resulting parameters are also shown in Table 5, the steric profile being shown in Fig. 2.

The use of the electronic parameter χ_L in place of δ_L inevitably leads to different values of α and β_L because of the different units, and the data for L = CO cannot be included because of the unavailability of a χ_L value (17). The value obtained for γ_L, however, is essentially identical with that obtained when δ_L was used, and the fit of the data generally is equally good (Table 5). The use of the steric parameter, E_R (24), instead of θ_L might be thought to be preferable because it is a measure of the repulsion energies between L and the other

Table 5. Kinetic parameters for the CO dissociative reactions of $Ru_3(CO)_{12-n}L_n$.

n	Electronic and steric parameters	α^a	β_L	γ_L	RMSD[b]	$100(1-R^2)$
1[c,d]	δ_L,θ_L	−7.46 ± 0.51	0.14 ± 0.07[e]	0.028 ± 0.005[f]	0.168	5.1
1[c,g]	δ_L,θ_L	−7.54 ± 0.45	0.16 ± 0.06[e]	0.028 ± 0.004[f]	0.162	3.2
1[c,d]	χ_L,θ_L	−6.07 ± 0.92	−0.025 ± 0.012[h]	0.025 ± 0.006[f]	0.165	4.9
1[c,g]	δ_L,E_R	−5.19 ± 0.28	0.17 ± 0.11[e]	0.020 ± 0.007[i]	0.291	10.5
2[j,d]	δ_L,θ_L	−8.05 ± 0.36	0.12 ± 0.05[e]	0.024 ± 0.003[f]	0.105	3.0
2[j,g]	δ_L,θ_L	−8.29 ± 0.41	0.16 ± 0.05[e]	0.025 ± 0.001[f]	0.130	2.6
3[k,g]	δ_L,θ_L	9.71 ± 0.96	0.61 ± 0.07[e]	−0.13 ± 0.01[f]	0.100	0.4
1[l,m]	δ_L,θ_L	−1.17 ± 0.33	−0.32 ± 0.06[e]	+0.015 ± 0.003[f]	0.058	5.5
1[n,m]	δ_L,θ_L	−0.88 ± 0.35	−0.20 ± 0.06[e]	+0.013 ± 0.003[f]	0.063	10.7

[a]Values of α are dependent on which electronic and steric parameters are being used.
[b]Root-mean-square deviations of log k_1(calcd.) from log k_1(expt).
[c]At 40°C.
[d]Without data for L = CO.
[e]In units of ppm^{-1}.
[f]In units of deg^{-1}.
[g]Including data for L = CO.
[h]In units of cm.
[i]In units of mol $kcal^{-1}$.
[j]At 25°C.
[k]At 80°C.
[l]For reactions of $Ru_3(CO)_{11}L$ with Me_3NO in $CHCl_3$ at 17.2°C (29).
[m]Without data for $SbPh_3$ or CO.
[n]For reactions of $Os_3(CO)_{11}L$ with Me_3NO in $CHCl_3$ at 25.2°C (29).

ligands in the reference compound $Cr(CO)_5L$. However, the fit to eq. [1] (with θ_L replaced by E_R) is considerably less good, although the value of β_L is unchanged (Table 5).

Discussion

The spectroscopic data in Tables 1 and 2 show that the reactions studied here involve the displacement of CO from $Ru_3(CO)_{11}L$ by L′ to form $Ru_3(CO)_{10}LL'$. No evidence for fragmentation of the clusters (11, 12) was obtained. Displacement of L by L′ in a rate-determining step would have led in two stages to $Ru_3(CO)_{10}L_2'$ as the product, and no evidence for this was observed either.

The reactions governed by the rate constants k_1 can therefore all be assigned to a CO dissociative process (*6d*) because the values of k_1 depend only on the nature of L and are independent of the concentrations and natures of the entering ligands. They proceed cleanly and give rise to precise rate constants. The fits of the data to eq. [1], or analogues that use different electronic or steric parameters, are generally good, the values of $100(1 - R^2)$ being small enough to show that the model represented by that equation and its parameters accounts for almost all the variation in the rates.[5] In particular, there seems to be no need for the "aryl parameter" that has recently (25) been found to contribute significantly to the values of some physicochemical parameters, including rate constants for reactions involving P-donor ligands. The fit is good even though a wide range of ligands is involved, including π-acid phosphites (16) and even CO. Inclusion of data for CO in similar analyses has been successful elsewhere (21).

A closer examination of the goodness-of-fit raises some interesting features. Specifically it is found that the data for L = $P(OEt)_3$ give the least good fit to eq. [1], especially when E_R is used as the steric parameter in which case the value of log $k_1°$ is 0.74 low. This implies that the value of E_R considerably overestimates the steric effect of this ligand in $Ru_3(CO)_{11}L$. The deviations are not due to experimental error because the kinetic data for $Ru_3(CO)_{11}(P(OEt)_3)$ are very extensive and precise (*6d*), and it is not clear why the parameters assigned to $P(OEt)_3$ lead to such a poor fit in this system.

More generally, in analyses such as these it is not sufficient to use values of R or $100(1 - R^2)$ alone as indicators of the goodness-of-fit of the model to the data (23). They need to be supplemented by the standard errors of measurement of log k_1, or the RMSD values (Table 5), which are important as indicators of the predictive merits of the analyses. Moreover, any inadequacy in the parameters describing the ligands should be investigated by measuring, as is possible with the data presented here for instance, the mean deviations, $\Delta\theta$(mean) or ΔE_R(mean), of values of θ_L or E_R from those that would lead to a perfect fit. Although this is to ascribe all the failure of the model to the steric parameters of the ligands, and nothing to the electronic parameters, the results can be informative and some values are included in Table 5. The best analyses lead to $\Delta\theta$(mean) = ± ca. 4° or ΔE_R(mean) = ± ca. 5 kcal mol^{-1}, which are quite comparable in the light of the ranges of θ_L (75°) and E_R (109 kcal mol^{-1}) for the ligands used. Although no uncertainties for E_R have been explicitly given (24), values of θ_L are believed to be good to ± ca. 2° (20) so that a signif-

[5] It must be remembered that it is generally not the *data* that are being tested (since log k values are very precise) but the *model*.

Can. J. Chem. Downloaded from www.nrcresearchpress.com by 80.90.12.36 on 09/08/12
For personal use only.

Can. J. Chem. Downloaded from www.nrcresearchpress.com by 80.90.12.36 on 09/08/12
For personal use only.

icant proportion of the deviations, and of the uncertainties of the parameters β_L and γ_L, can be ascribed to perfectly acceptable variations in the cone angles appropriate to the ligands in these clusters.

The fact that the data for L = CO fit so well to the trends determined by the P-donor substituents is interesting. The smaller number of CO ligands in the substituted clusters would be expected to require a reduction in the value of log k_1 for $Ru_3(CO)_{12}$ for statistical reasons before it could be fitted to the trends. Any such correction would lead to an increase in the deviation of the data for L = CO from the profiles but the magnitude of the correction is quite uncertain. It could be as much as log 3 if loss of CO in a substituted cluster could occur only from one particular Ru atom. At the other extreme, no correction at all would be required if it is an axial CO that dissociates and if the substituent effect is distributed equally all round the cluster so that six CO ligands are available to dissociate in each of the clusters. This is not unreasonable since axial CO ligands are more weakly bound than equatorial ones (26) and, although the products are equatorially substituted and the entering ligand becomes attached to a previously unsubstituted Ru atom, dissociation of any axial CO ligand could be rate determining. If it occurs from an already substituted Ru atom, the vacant coordination site could be transferred from that Ru atom to another after the rate-determining step (2*b*). The Ru—CO_{ax} bond lengths do not seem to depend appreciably on whether the Ru atom is substituted or not (26). Apart from any possible statistical effects, the fit of the data for L = CO to those for L = P donors must arise in part from the facts that the electronic parameters, δ_L, are actually defined relative to L = CO, and that the cone angles or E_R values are either independent of the chemical natures of the donor atoms or they are taken into account. Nevertheless the data for L = CO in $Ru(CO)_4L$ and $Mn(CO)_4LBr$ do not fit with those for the complexes where L = P donors, the rates being much faster than projected (15*a*). This may be an indication that CO dissociation from a Ru atom to which a P donor is bonded is retarded, compared with dissociation from a non-substituted Ru atom, and that the CO that dissociates from the cluster does come from an unsubstituted Ru atom. In this case some statistical correction would be required as discussed above, and the substituent effects defined by the parameters β_L and γ_L would be due to effects transmitted across the cluster.

The value of β_L for the $Ru_3(CO)_{11}L$ clusters shows that increased electron donicity of the substituents stabilizes the transition states relative to the ground states, presumably by compensating for any electron density lost by the cluster during CO dissociation. The effect is quite small and not very precise. Nevertheless, the fact that the value of β_L is ca. 2 standard deviations above zero suggests that the probability that β_L is zero or negative is only ca. 1 in 20, allowing for the six degrees of freedom involved. Analogous values of β_L for the few mononuclear carbonyls for which data are available vary from $+0.13 \pm 0.06$ ppm^{-1} to -0.11 ± 0.06 ppm^{-1} (15*a*). The value of γ_L is more precise and is positive, as are those for all the mononuclear complexes studied in this way. This would be expected from a release of steric strain as the CO leaves. The magnitude of the steric effect in the $Ru_3(CO)_{11}L$ clusters is similar to that in the mononuclear carbonyl $Ru(CO)_4L$, but smaller than those in octahedral mononuclear complexes.

The values of β_L and γ_L for the $Ru_3(CO)_{10}L_2$ clusters are surprisingly similar to those for $Ru_3(CO)_{11}L$, the small difference in the temperatures at which the reactions were studied being unlikely to affect the comparison significantly (14*d*). The second substituent evidently affects the transition states to the same extent as the ground states. The data for the $Ru_3(CO)_{10}$(dppm) cluster fit very well to the trend established by the $Ru_3(CO)_{10}L_2$ clusters. Detailed accounting for these effects is complicated by the structural changes due to the different substituents. A series of 15 Ru—P bond lengths (*d*) in mono- and bis-substituted Ru_3 clusters (26) show that they depend linearly on θ_L according to eq. [2] with a RMSD of ± 1.7 pm and with $100(1 - R^2) = 8.4\%$.

$$[2] \quad d(\text{Ru—P})/\text{pm} = (198.6 \pm 2.9) + (0.264 \pm 0.022)\theta_L$$

In addition to this, the Ru—Ru bonds *cis* to the substituents in the $Ru_3(CO)_{11}L$ clusters show a substantial increase from 282.7 pm (L = etpb) to a more or less constant value of 291 pm when $\theta_L \geq 140°$. Thus the kinetics may well reflect an increase in effective basicity of the P-donor ligands, and an increase in the Ru—P bond strengths, as the CO leaves and the Ru—P bonds can contract. A similar but less regular effect may occur because of Ru—Ru bond shortening. A number of other structural effects accompany substitution into the Ru_3 cluster (26) but these are too subtle to be incorporated into any discussion of the kinetics. Indeed, the relative simplicity of the trends in the kinetic parameters is quite surprising in view of the multiplicity of structural and energetic changes that must be taking place during formation of the transition states, but the fact remains that eq. [1] does give an excellent empirical representation of the data. These show that increasing electron donicity accounts for a decrease in activation free energies of 1.9 ± 0.9 kcal mol^{-1} while steric effects account for a decrease of 2.6 ± 0.4 kcal mol^{-1} in $\Delta G^{\ddagger}$ for the particular selection of substituents involved. The kinetic effects, though clearly noticeable, are relatively small perturbations on the overall values of $\Delta G^{\ddagger}$, which are ca. 24 ± 2 kcal mol^{-1}, and it is interesting to compare the steric effect of ca. 3 kcal mol^{-1} with the 109 kcal mol^{-1} range of E_R values. Evidently, only a very small proportion of the available repulsion energy is actually applied to increasing the rates of reaction. This implies that the steric repulsions in the transition states are only marginally less than those in the ground states, i.e., that the process of Ru—CO bond breaking, on going to the transition states, does not result in much decrease in steric repulsions. This is consistent with the proposal discussed above, that as the CO ligand moves out a P-donor ligand moves in.

A few data are available for CO dissociation from the trisubstituted clusters $Ru_3(CO)_9L_3$ (27) and these also fit well to eq. [1] with parameters as shown in Table 5. The data for L = CO (10*a*) have to be used in the analysis but the qualitative features of the results are not affected by this. The most striking features of the results are the large positive electronic effect ($\beta_L = +0.61$ ppm^{-1}) and the *inverse* steric effect, i.e., the rates of CO dissociation decrease with increasing ligand size as shown in Fig. 3. The magnitude of γ_L is such that there is almost a 10^7 change in rate attributable to a cone angle change of 50°. The activation parameters for these reactions change significantly with L and lie on an isokinetic plot with an isokinetic temperature of ca. 260°C (27). The trends were inter-

Fig. 3. Dependence of log k_1^0 on θ_L for the CO dissociative reactions of $Ru_3(CO)_9L_3$. Numbering from Table 4.

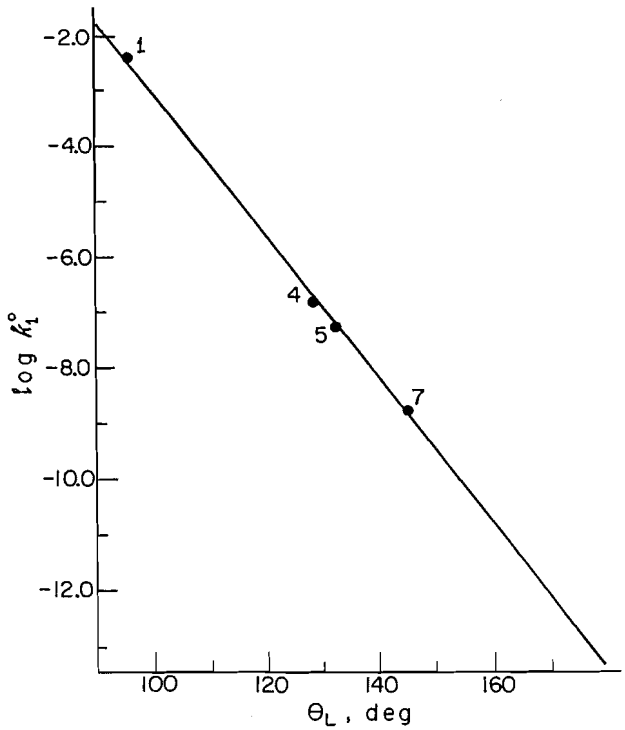

preted in terms of widely differing structures for the $Ru_3(CO)_8L_3$ intermediates, a high $\Delta H^{\neq}$ and positive $\Delta S^{\neq}$ for L = PPh_3 corresponding to a more open, loose form, and the low $\Delta H^{\neq}$ and negative $\Delta S^{\neq}$ for L = P-*n*-Bu_3 to a contracted, tightly bonded cluster. The reasons for this trend were not apparent at the time but it can now be concluded that the rates are strongly accelerated by highly donating ligands, which favour tightly bound $Ru_3(CO)_8L_3$, but are retarded by larger substituents that require more open intermediates.

Finally, it is interesting to compare the parameters in Table 5 for the unassisted dissociation of CO ligands with analogous parameters obtained (28) from published data (29) for CO displacement assisted by Me_3NO. This attacks the CO ligands at the coordinated C atom and removes them as CO_2. These reactions were studied with L = $P(OMe)_3$, $P(OEt)_3$, P-*n*-Bu_3, PPh_3, $AsPh_3$, and $SbPh_3$. Values of the highest frequency C—O stretching bands in $Ru_3(CO)_{11}L$ were available as electronic parameters and a good fit to eq. [1] can be obtained with δ_L replaced by ν_{co} (28). These same parameters can be used in an analysis (28) of corresponding data for $Os_3(CO)_{11}L$ (29). Use of δ_L in place of ν_{co} does not give a good fit unless data for $SbPh_3$ are omitted, and an inspection of the correlation between δ_L and ν_{co} suggests that this is due to an incorrectly high value of δ_L. Parameters obtained are included in Table 5 where it can be seen that the sign of β_L is negative, i.e., opposite to that for spontaneous CO dissociation. This is what would be expected since better electron donors would increase the electron density on the coordinated C atom that is undergoing nucleophilic attack. The Ru_3 cluster appears to allow a more effective transmission of the electronic effect of L than does the Os_3 cluster. Larger ligands still accelerate the reactions (i.e., the value of γ_L is positive) but to a lesser extent than for unassisted dissociation. This suggests that M—CO bond breaking is pronounced enough in the transition state for release of steric strain still to occur, but it is partially offset by the steric repulsion involved in nucleophilic attack by the Me_3NO at the C atom of a CO ligand.

Acknowledgments

We are grateful to the Natural Sciences and Engineering Research Council of Canada for support of this work.

References

1. K.J. Karel and J.R. Norton. J. Am. Chem. Soc. **96**, 6812 (1974).
2. (*a*) D.C. Sonnenberger and J.D. Atwood. J. Am. Chem. Soc. **104**, 2113 (1982); (*b*) Organometallics, **1**, 694 (1982).
3. (*a*) D.J. Darensbourg and B.J. Baldwin-Zuschke. J. Am. Chem. Soc. **104**, 3906 (1982); (*b*) D.J. Darensbourg and M.J. Incorvia. J. Organomet. Chem. **171**, 89 (1979); (*c*) Inorg. Chem. **19**, 2585 (1980); (*d*) D.J. Darensbourg, B.S. Peterson, and R.E. Schmidt, Jr. Organometallics, **1**, 306 (1982); (*e*) D.J. Darensbourg, D.J. Zalewski, and T. Delord. Organometallics, **3**, 1210 (1984).
4. A.J. Poë. *In* Metal clusters. *Edited by* M. Moskovits. Wiley, New York. 1986. Chap. 4.
5. J.R. Kennedy, F. Basolo, and W.C. Trogler. Inorg. Chim. Acta, **146**, 75 (1988).
6. (*a*) S.K. Malik and A.J. Poë. Inorg. Chem. **17**, 1484 (1978); (*b*) N.M.J. Brodie, A.J. Poë, and V.C. Sekhar. J. Chem. Soc. Chem. Commun. 1090 (1985); (*c*) B. Ambwani, S.K. Chawla, and A.J. Poë. Inorg. Chim. Acta, **133**, 93 (1987); (*d*) L. Chen and A.J. Poë. Can. J. Chem. **67**, 1924 (1989).
7. A.J. Poë and V.C. Sekhar. Inorg. Chem. **24**, 4376 (1985).
8. N.M.J. Brodie. Ph.D. Thesis, University of Toronto, 1989.
9. (*a*) M.I. Bruce, D.C. Kehoe, J.G. Matisons, B.K. Nicholson, P. Rieger, and M. Williams. J. Chem. Soc. Chem. Commun. 442 (1982); (*b*) M.I. Bruce, T. Hambley, B.K. Nicholson, and M. Snow. J. Organomet. Chem. **235**, 83 (1982); (c) M.I. Bruce, J.G. Matisons, and B.K. Nicholson. J. Organomet. Chem. **247**, 321 (1983).
10. (*a*) A.J. Poë and M.V. Twigg. J. Chem. Soc. Dalton Trans. 1860 (1974); (*b*) Inorg. Chem. **13**, 2982 (1974).
11. N.M.J. Brodie and A.J. Poë. Inorg. Chem. **27**, 3156 (1988).
12. N.M.J. Brodie, A.J. Poë, and L. Chen. Int. J. Chem. Kinet. **20**, 467 (1988).
13. J. Mandel. The statistical analysis of experimental data. Wiley–Interscience, New York. 1964.
14. (*a*) H.G. Schuster-Woldan and F. Basolo. J. Am. Chem. Soc. **88**, 1657 (1966); (*b*) E.M. Thorsteinson and F. Basolo. J. Am. Chem. Soc. **88**, 3929 (1966); (*c*) R.A. Jackson and A.J. Poë. Inorg. Chem. **18**, 3331 (1979); (*d*) K. Dahlinger, F. Falcone, and A.J. Poë. Inorg. Chem. **25**, 2654 (1986); (*e*) M. Golovin, M. Rahman, J.E. Belmonte, and W.P. Giering. Organometallics, **4**, 1981 (1985); (*f*) H.-Y Liu, K. Eriks, A. Prock, and W.P. Giering. Organometallics, **9**, 1758 (1990); (*g*) D.H. Farrar, A.J. Poë, and Y. Zheng. J. Am. Chem. Soc. **116**, 6252 (1994), and references therein.
15. (*a*) L. Chen and A.J. Poë. Inorg. Chem. **28**, 3641 (1989), and references therein; (*b*) K. Eriks, W.P. Giering, H.-Y. Liu, and A. Prock. Inorg. Chem. **28**, 1759 (1989).
16. M.M. Rahman, H.-Y. Lui, A. Prock, and W.P. Giering. Organometallics, **6**, 650, (1987).
17. T. Bartik, T. Himmler, H.-G. Schulte, and K. Seevogel. J. Organomet. Chem. **272**, 29 (1984).
18. G. Bodner, M. May, and L. McKinney. Inorg. Chem. **19**, 1951 (1980).
19. L. Chen. Ph.D. Thesis, University of Toronto, 1991.
20. C.A. Tolman. Chem. Rev. **77**, 313 (1977).

Can. J. Chem. Downloaded from www.nrcresearchpress.com by 80.90.12.36 on 09/08/12
For personal use only.

21. P. Rushman and T.L. Brown. J. Am. Chem. Soc. **109**, 3632 (1987), and references therein.
22. P.R. Bevington. Data reduction and error analysis for the physical sciences. McGraw–Hill, Toronto. 1969. p. 172.
23. C.H. Achen. Interpreting and using regression. Sage University Paper Series on Quantitative applications in the social sciences, Series No. 29. Sage Publications, Beverley Hills and London. 1982. p. 58.
24. (*a*) T.L. Brown. Inorg. Chem. **92**, 1286 (1992); (*b*) T.L. Brown and K.J. Lee. Coord. Chem. Rev. **128**, 89 (1993); (*c*) D. White and N.J. Coville. Adv. Organomet. Chem. **36**, 95 (1994).
25. M.R. Wilson, D.C. Woska, A. Prock, and W.P. Giering. Organometallics, **12**, 1742 (1993).
26. (*a*) M.R. Churchill, F.J. Hollander, and J.P. Hutchingson. Inorg. Chem. **16**, 2655 (1977); (*b*) M.I. Bruce, M.J. Liddell, C.A. Hughes, B.W. Skelton, and A.H. White. J. Organomet. Chem. **347**, 157 (1988); (*c*) N.M.J. Brodie, L. Chen, A.J. Poë, and J.F. Sawyer. Acta Crystallogr. Sect. C: Cryst. Struct. Commun. **C45**, 1314 (1989); (*d*) M.I. Bruce, M.J. Liddell, C.A. Hughes, J.M. Patrick, B.W. Skelton, and A.H. White. J. Organomet. Chem. **347**, 181 (1988).
27. (*a*) S.K. Malik and A.J. Poë. Inorg. Chem. **18**, 1241 (1979); (*b*) D.P. Keeton, S.K. Malik, and A.J. Poë. J. Chem. Soc. Dalton Trans. 1392 (1977).
28. A.J. Poë. *In* Mechanisms of inorganic and organometallic reactions. Vol. 7. *Edited by* M.V. Twigg. Plenum Press, New York. 1991. Chap. 10, p. 248.
29. J.-K. Shen, Y.-C. Gao, Q.-Z. Shi, and F. Basolo. Inorg. Chem. **27**, 4236 (1988).

Can. J. Chem. Downloaded from www.nrcresearchpress.com by 80.90.12.36 on 09/08/12
For personal use only.

Organic and inorganic templates bearing $CCo_3(CO)_9$ cluster fragments: X-ray crystal structures of $C(CH_2OCOCCl_3)_4$ and of $CH_3C(O)CHC(OH)ML_n$ where $ML_n = CCo_3(CO)_9$ or $(C_6H_5)Cr(CO)_3$

Lisa C.F. Chao, Andreas Decken, James F. Britten, and Michael J. McGlinchey

Abstract: Pentaerythritol and trichloroacetyl chloride react to yield the tetrakis-trichloroacetate ester $C(CH_2\text{-}O_2C\text{-}CCl_3)_4$, **5**, which crystallizes in the triclinic space group $P\bar{1}$ with $a = 9.874(2)$ Å, $b = 11.811(2)$ Å, $c = 12.858(3)$ Å, $\alpha = 114.35(3)°$, $\beta = 95.63(3)°$, $\gamma = 99.11(3)°$, and $V = 1326.5(5)$ Å^3 for $Z = 2$. The molecule adopts a geometry in which the trichloroacetate chains fold to produce a flattened tetrahedron, giving a molecule of approximate D_{2d} symmetry. Treatment of **5** with $Co_2(CO)_8$ gave, as the highest molecular weight product, the tris-cluster complex $C[CH_2\text{-}O_2C\text{-}CCo_3(CO)_9]_3(CH_2\text{-}O_2C\text{-}CCl_3)$, **6**, rather than the tetra-cluster $C[CH_2\text{-}O_2C\text{-}CCo_3(CO)_9]_4$, **7**. A space-filling model of **7**, derived by replacing the CCl_3 groups in **5** by $CCo_3(CO)_9$ moieties, exhibited considerable molecular crowding. Reaction of several 1,1,1-trichloroacetylacetonate salts with $Co_2(CO)_8$ gave the corresponding cluster complexes of Co(II), Co(III), or Al(III). The uncomplexed cluster ligand $CH_3C(O)CHC(OH)CCo_3(CO)_9$, **9**, crystallizes in the orthorhombic space group $Pna2_1$ with $a = 16.226(2)$ Å, $b = 11.6300(10)$ Å, $c = 9.919(2)$ Å, $V = 1871.7(4)$ Å^3 for $Z = 4$. The direction of enolization of **9** has been studied by EHMO calculations. The tendency to enolize is also found in (benzoylacetone)$Cr(CO)_3$, **17**, which crystallizes in the tetragonal space group $P4_32_12$ with $a = 10.0840(10)$ Å, $b = 10.0840(10)$ Å, $c = 25.387(5)$ Å, $V = 2581.5(6)$ Å^3 for $Z = 8$.

Key words: inorganometallic clusters.

Résumé : Le pentaérythritol et le chlorure d'acétyle réagissent pour donner l'ester tétrakis-trichloroacétate correspondant, $C(CH_2\text{-}O(O)CCCl_3)_4$, **5**, qui cristallise dans le groupe d'espace triclinique $P\bar{1}$, avec $a = 9,874(2)$, $b = 11,811(2)$ et $c = 12,858(3)$ Å, $\alpha = 114,35(3)°$, $\beta = 95,63(3)°$ et $\gamma = 99,11(3)°$, $V = 1326,5(5)$ Å^3 et $Z = 2$. La molécule adopte une géométrie dans laquelle les chaînes trichloroacétates se replie de façon à donner un tétraèdre aplati conduisant à une symétrie moléculaire qui approximativement D_{2d}. La réaction du composé **5** avec du $Co_2(CO)_8$ conduit, comme produit de poids moléculaire le plus élevé, à un complexe à trois clusters, $C[CH_2\text{-}O(O)C\text{-}CCo_3(CO)_9]_3(CH_2\text{-}O(O)C\text{-}CCl_3)$, **6**, plutôt qu'au complexe à quatre clusters, $C[CH_2\text{-}O(O)CCCo_3(CO)_9]_4$, **7**. Un modèle spatial du composé **7** obtenu en remplaçant les groupes CCl_3 du produit par des entités $CCo_3(CO)_9$ montre la présence d'un encombrement moléculaire important. La réaction de plusieurs sels 1,1,1-trichloroacétylacétonates avec du $Co_2(CO)_8$ conduit aux complexes avec clusters correspondants du Co(II), Co(III) et Al(III). Le ligand non complexé, $CH_3C(O)CHC(OH)CCo_3(CO)_9$, **9**, cristallise dans le groupe d'espace orthorhombique $Pna2_1$, avec $a = 16,226(2)$, $b = 11,6300(10)$ et $c = 9,919(2)$ Å, $V = 1871,7(4)$ Å^3 et $Z = 4$. On a étudié le sens de l'énolisation du composé **9** à l'aide de calculs d'EHMO. On a aussi déterminé la tendance à l'énolisation de la (benzoylacétone)$Cr(CO)_3$, **17**, qui cristallise dans le groupe d'espace tétragonal $P4_32_12$, avec $a = 10,0840(10)$, $b = 10,0840(10)$ et $c = 25,387(5)$ Å, $V = 2581,5(6)$ Å^3 et $Z = 8$.

Mots clés : clusters inorganométalliques.

[Traduit par la rédaction]

Received November 4, 1994.

This paper is dedicated to Professor William A.G. Graham on the occasion of his 65th birthday.

L.C.F. Chao, A. Decken, J.F. Britten, and M.J. McGlinchey.[1] Department of Chemistry, McMaster University, Hamilton, ON L8S 4M1, Canada.

[1] Author to whom correspondence may be addressed. Telephone: (905) 525-9140, ext. 23303. Fax: (905) 522-2509. E-mail: mcglinc@mcmaster.ca

Can. J. Chem. Downloaded from www.nrcresearchpress.com by 80.90.12.36 on 09/08/12
For personal use only.

Can. J. Chem. Downloaded from www.nrcresearchpress.com by 80.90.12.36 on 09/08/12
For personal use only.

Introduction

While the synthesis of large clusters is not quite the haphazard process it once was (1), there is still a rôle for serendipity. In an attempt to prepare $(OC)_9Co_3CC(O)SiR_3$, Schore and co-workers (2) obtained the 22-cobalt cluster $Co_4O[O_2C\text{-}CCo_3(CO)_9]_6$, **1**, from an unexpected self-assembly process when a mixture of $Co_3(CO)_9CCl$ and $AlCl_3$ in CH_2Cl_2 was poured over cracked ice. This molecule is important, not merely for its picturesque symmetry, but also because it bridges organometallic and coordination chemistry in a potentially controllable fashion. This concept was independently recognized by Fehlner and co-workers, who devised logical synthetic routes to such molecules as **2** through **4** (3–5). The crucial point is the existence of the $[(OC)_9Co_3C\text{-}CO_2]^-$ anion and its use in the preparation of complexes analogous to those containing bridging acetate ligands (6). These reports prompt us to communicate our own results whereby we discuss the use of poly(trichloroacetate) esters as precursors of poly-$(CO)_9Co_3C$ clusters; moreover, routes to nonacarbonyl-tricobalt-carbynyl derivatives of the ubiquitous acetylacetonate ligand are described.

Results and discussion

Clusters derived from organic templates

In recent years, the attachment of metal carbonyl fragments to surfaces has been the subject of considerable activity (7). Analogously, one can readily envisage coating a molecule of a selected shape and size with a layer of cluster fragments. Thus, one might choose to build prolate, oblate, spherical, or disk-like molecules. To investigate the viability of such a project, it was decided to attempt the synthesis of an oligo-cluster based upon a tetrahedral precursor. To this end, pentaerythritol, i.e., tetra(hydroxymethyl)methane, was treated with CCl_3-CO-Cl to yield the tetrakis-trichloroacetate ester $C(CH_2\text{-}O_2C\text{-}CCl_3)_4$, **5**. Reaction of **5** with excess $Co_2(CO)_8$ led to a complex mixture of products, several of which were separable on a column by flash chromatographic techniques. The highest molecular weight product corresponded to the tris-cluster complex $C[CH_2\text{-}O_2C\text{-}CCo_3(CO)_9]_3(CH_2\text{-}O_2C\text{-}CCl_3)$, **6**. One is tempted to ascribe the failure to isolate the tetra-cluster $C[CH_2\text{-}O_2C\text{-}CCo_3(CO)_9]_4$, **7**, to problems of steric crowding. To model this 12-cobalt molecule, it was decided first of all to obtain the X-ray crystal structure of the 12-chloro complex **5** and then to use

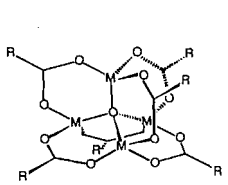

1: M=Co
2: M=Zn
R=$CCo_3(CO)_9$

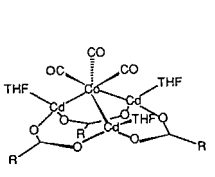

3

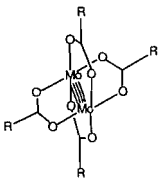

4

a molecular modelling program to replace the CCl_3 units by $CCo_3(CO)_9$ moieties.

Molecules in which a tetrahedral atom bears four identical bulky groups have been extensively studied by Iroff and Mislow (8*a*). For example, in tetrakis(trimethylsilyl)silane $Si(SiMe_3)_4$, the steric crowding causes each methyl group to mesh tightly with those in the remaining trimethylsilyl groups. $Si(SiMe_3)_4$ does not adopt T_d symmetry; instead, the twisting of the four groups lowers the symmetry to that of the rotational sub-group T, in which the C_3 axes are retained but the mirror planes are lost.

The tetra-ester **5** crystallizes in the triclinic space group $P\bar{1}$ with two molecules per unit cell. As shown in Fig. 1, the molecular structure reveals that the tetrahedral symmetry of **5** is indeed broken, but in a different fashion to that found for $Si(SiMe_3)_4$. The trichloroacetate chains fold to produce a flattened tetrahedron; they are oriented in pairwise fashion to give a molecule of approximate D_{2d} symmetry in which the C_3 axes are lost but two mirror planes and the S_4 axis are retained. The crystallographic collection parameters, atom coordinates, and selected bond length and angle data for **5** are listed in Tables 1 through 3.

Subsequently, using the modelling program ALCHEMY,[2] the four trichloromethyl units in **5** were replaced by $CCo_3(CO)_9$ fragments. These latter groups were constructed by using parameters taken from the X-ray crystal structure of $CH_3CCo_3(CO)_9$ (9). The computer-derived model of the molecule $C[CH_2\text{-}O_2C\text{-}CCo_3(CO)_9]_4$, **7**, constructed as described above and energy minimized so as to avoid unfavorable steric interactions between carbonyl ligands, appears as Fig. 2*a*; a space-filling representation of **7** is shown in Fig. 2*b*. It is apparent that the desired molecule can indeed adopt a viable conformation but it is less certain that the intermediates involved in the conversion of the CCl_3 groups into tricobalt clusters can be accommodated.

We note that other potential routes to **7** have been investi-

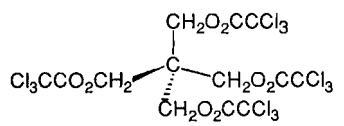

5

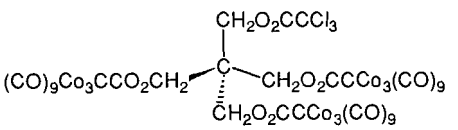

6

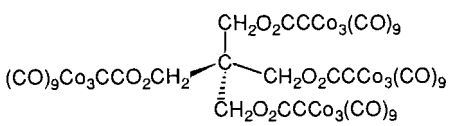

7

gated. Thus, although the acylium cation $[(OC)_9Co_3C\text{-}C{=}O]^+$ reacts readily with alcohols, phenols, or diols to give mono- or bis-clusters (10), the corresponding reaction with pentaerythritol is thwarted by the very low solubility of the tetra-alcohol in solvents that are themselves unreactive towards the organometallic acylium salt.

[2] ALCHEMY is available from Tripos Associates. St. Louis, Mo.

Can. J. Chem. Downloaded from www.nrcresearchpress.com by 80.90.12.36 on 09/08/12
For personal use only.

Fig. 1. X-ray crystal structure of $C(CH_2\text{-}O_2C\text{-}CCl_3)_4$, **5**.

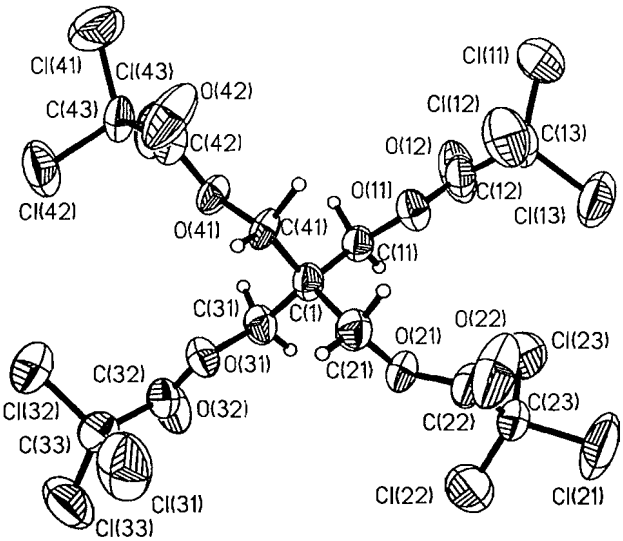

Cluster analogues of acetylacetonates

The exquisite molecules synthesized by Schore (2) and by Fehlner (3–6) depend for their existence on the stability and ready availability of the tricobalt cluster carboxylic acid $(OC)_9Co_3C\text{-}CO_2H$, which was first reported by Seyferth 20 years ago (11). However, we are unaware of any published route to the corresponding analogues of acetylacetone, i.e., $R^1\text{-}CO\text{-}CH_2\text{-}CO\text{-}R^2$, where one or both R groups are $CCo_3(CO)_9$ moieties rather than methyls. Since $RCCo_3(CO)_9$ clusters are frequently obtainable by treatment of the corresponding $RCCl_3$ precursors with dicobalt octacarbonyl, the obvious first step was to try to use 1,1,1-trichloropentan-2,4-dione (tcacH), **8**, as the cluster precursor. The ligand tcacH is readily preparable by the reaction of trichloroacetonitrile and pentan-2,4-dione with sodium acetate to give $Cl_3CC(NH_2)=CHC(O)CH_3$; subsequent treatment with concentrated HCl yields tcacH, **8**, as a colorless liquid (12, 13). However, the reaction of **8** with $Co_2(CO)_8$ does not yield useful quantities of the desired complex $CH_3\text{-}CO\text{-}CH\text{-}C(OH)\text{-}CCo_3(CO)_9$, **9**. This behavior is reminiscent of Seyferth's report that the presence of hydroxyl functionalities in the trichloromethyl precursor often limits the utility of this approach. For example, $Co_3(CO)_9C\text{-}CH_2OH$ can not be obtained directly from $Co_2(CO)_8$ and CCl_3CH_2OH (14).

From the ^1H and ^{13}C NMR spectra of tcacH, it is evident that the ligand exists in solution primarily as an enol tautomer; indeed, other electron-withdrawing groups are well known to

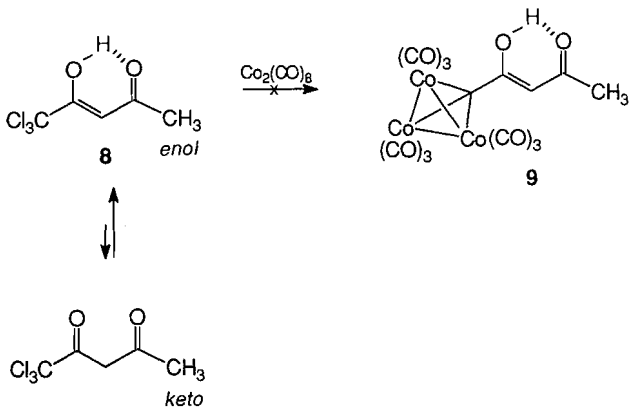

Fig. 2. (*a*) Computer-derived model of $C[CH_2\text{-}O_2C\text{-}CCo_3(CO)_9]_4$, **7**. (*b*) Computer-derived space-filling representation of $C[CH_2\text{-}O_2C\text{-}CCo_3(CO)_9]_4$, **7**.

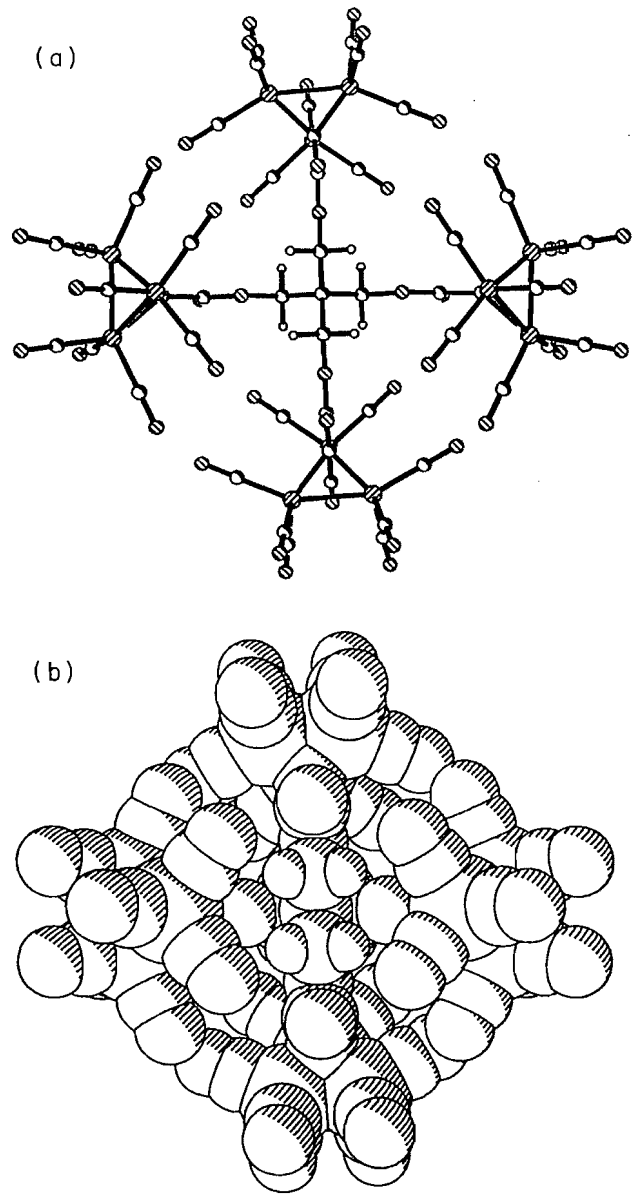

have a marked influence on the keto–enol equilibrium (15). 1,1,1-Trichloroacetylacetone, **8**, has been reported to yield complexes with a variety of di- and trivalent metals such as Cr(III), Mn(II), Fe(III), Co(II), Cu(II), and Al(III) (16). By using this approach to avoid the presence of a hydroxyl group in the ligand, we have shown that prior coordination of $[CCl_3\text{-}CO\text{-}CH\text{-}CO\text{-}CH_3]^-$ to a metal center before treatment with $Co_2(CO)_8$ does indeed lead to cluster formation, albeit in low yield. Typically, $Al(tcac)_3$, **10**, reacts with excess dicobalt octacarbonyl to yield the corresponding cluster-substituted complex **11**. The cluster **11** is conveniently identified by its FAB mass spectrum, which exhibits a [P − 1CO] peak and sequential loss of 23 carbon monoxide fragments. Moreover, one sees loss of a $Co_3(CO)_9C\text{-}C(O)CHC(O)CH_3$ fragment from the molecular ion followed by loss of 10 additional carbonyls.

Interestingly, analogous treatment of $Cu(tcac)_2$, **12**, yields,

Can. J. Chem. Downloaded from www.nrcresearchpress.com by 80.90.12.36 on 09/08/12
For personal use only.

Table 1. Structure determination summary

	5	9	17
Empirical formula	$C_{13}H_8Cl_{12}O_8$	$C_{14}H_5Co_3O_{11}$	$C_{13}H_{10}CrO_5$
Formula weight	717.6	526.0	298.21
Crystal size mm	0.20 × 0.08 × 0.25	0.30 × 0.30 × 0.33	0.25 × 0.25 × 0.25
Colour, habit	Colourless, plate	Black, parallelepiped	Red, parallelepiped
Temperature (K)	296(2)	300(2)	293(2)
Wavelength	1.54178	0.71073	0.71073
Crystal system	Triclinic	Orthorhombic	Tetragonal
Space group	$P\bar{1}$	$Pna2_1$	$P4_32_12$
Unit dimensions			
a (Å)	9.874(2)	16.226(2)	10.0840(10)
b (Å)	11.811(2)	11.6300(10)	10.0840(10)
c (Å)	12.858(3)	9.919(2)	25.387(5)
α (°)	114.35(3)	90.0	90.0
β (°)	95.63(3)	90.0	90.0
γ (°)	99.11(3)	90.0	90.0
Volume (Å^3)	1326.5(5)	1871.7(4)	2581.5(6)
Z	2	4	8
Density (calcd.) (Mg/m^3)	1.797	1.866	1.535
Absorption coeff. (mm^{-1})	11.834	2.682	0.898
F(000)	708	1032	1216
θ range (°)	2.50–55.00	3.5–23.0	2.17–27.50
Index ranges	$-10 \le h \le 10$, $0 \le k \le 12$, $-13 \le l \le 12$	$-1 \le h \le 13$, $-1 \le k \le 15$, $-1 \le l \le 21$	$-13 \le h \le 13$, $-13 \le k \le 13$, $-32 \le l \le 32$
No. reflections collected	3559	3279	6699
No. independent reflections	3349	2452	2972
No. of parameters	303	255	155
Goodness of fit on F^2	2.50	0.890	1.039
Final R indices ($I>2\sigma(I)$)	$R1$=0.0774, $wR2$=0.1106	$R1$=0.0303, $wR2$=0.0379	$R1$=0.0405, $wR2$=0.0954
R indices (all data)	$R1$=0.1039, $wR2$=0.1135	$R1$=0.0403, $wR2$=0.0410	$R1$=0.0542, $wR2$=0.1036
Extinction coefficient	0.0006(8)	N/A	N/A
Largest diff. peak (Å^{-3})	1.06	0.36	0.349
Largest diff. hole (Å^{-3})	−0.59	−0.31	−0.232

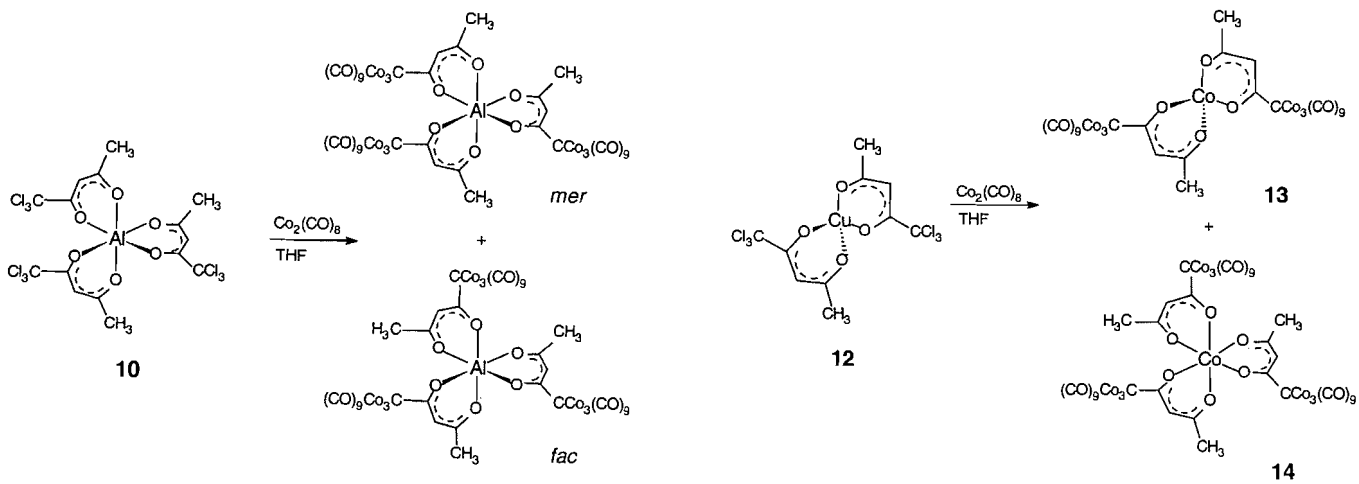

after chromatographic separation of the products, the Co(II) and Co(III) complexes **13** and **14**, respectively. Evidently, the central cobalt atoms must derive from $Co_2(CO)_8$; this observation is reminiscent of Schore's synthesis of $Co_4O[O_2C\text{-}CCo_3(CO)_9]_6$, **1**, whereby the Co(II) centers arise from decomposition of the original cobalt cluster. The octahedral systems **11** and **14** derived from trivalent metals yield *mer* and *fac* isomers and, thus far, have not allowed the isolation of single crystals suitable for a diffraction study. However, in an attempt to obtain an X-ray quality crystal of **13**, repeated chromatographic purification yielded black crystals that were subsequently shown to be the parent ligand **9**.

Recrystallization of $CH_3\text{-}CO\text{-}CH\text{-}C(OH)\text{-}CCo_3(CO)_9$, **9**,

Can. J. Chem. Downloaded from www.nrcresearchpress.com by 80.90.12.36 on 09/08/12
For personal use only.

Fig. 3. X-ray crystal structure of $CH_3C(O)CHC(OH)CCo_3(CO)_9$, **9**.

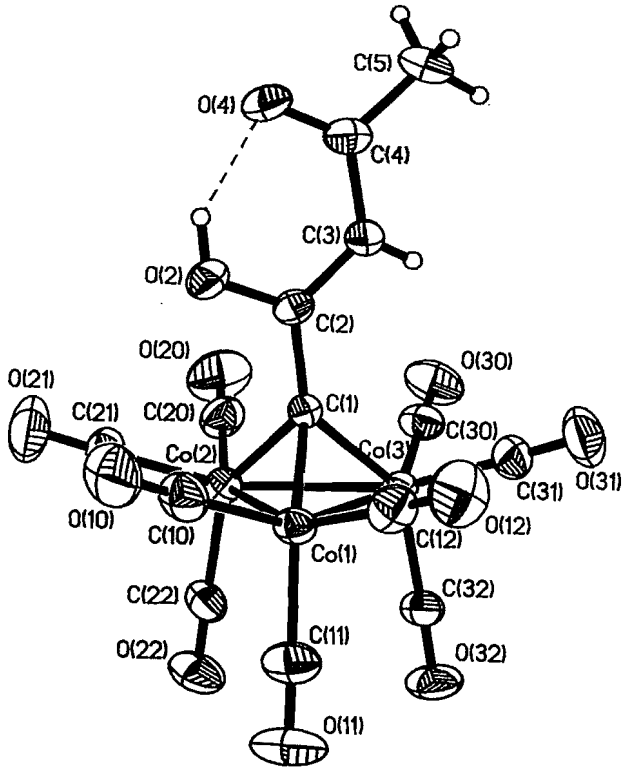

Fig. 4. The HOMO of $CH_3C(O)CHC(OH)CCo_3(CO)_9$, **9**, as the enol H migrates from (*a*) O2 to (*b*) O4.

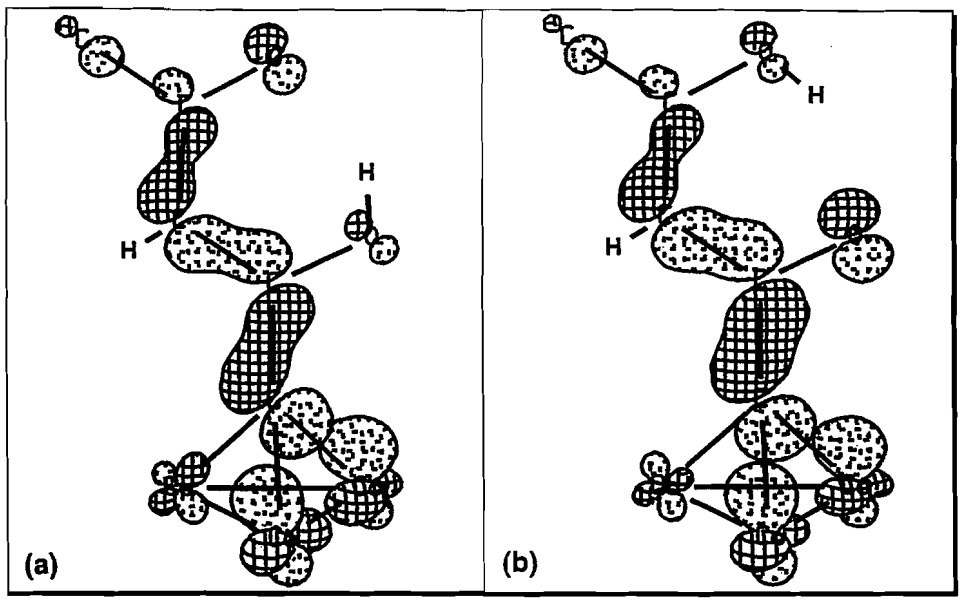

from 50/50 CH_2Cl_2/hexane gave parallelepipeds suitable for an X-ray structure determination. The cluster crystallizes in the orthorhombic space group $Pna2_1$ with four molecules in the unit cell. The crystallographic collection parameters are listed in Table 1, and atomic coordinates and selected bond length and angle data for **9** appear in Tables 4 and 5; a view of the molecule appears as Fig. 3.

Each molecule has approximate C_s symmetry with the two oxygens of the acac-type unit oriented to lie over the midpoint of a cobalt–cobalt vector. The tetrahedral Co_3C core exhibits typical bond lengths: Co—Co (2.47 Å), Co—CO (1.81 Å), and Co—C_{cap} (1.90 Å). In the solid state, the molecule exists in the enol form $CH_3C(O)$-CH=C(OH)-$CCo_3(CO)_9$, rather than as the keto tautomer. The hydroxyl moiety is at the cluster end of the five-carbon chain and the OH proton is hydrogen-bonded to the ketonic oxygen neighboring the methyl carbon. This tautomeric structure is evident from the C(2)—C(3), C(2)—O(2), C(3)—C(4), and C(4)—O(4) distances of 1.389(8), 1.320(7),

Can. J. Chem. Downloaded from www.nrcresearchpress.com by 80.90.12.36 on 09/08/12
For personal use only.

Table 2. Atomic coordinates (10^4) and equivalent isotropic displacement coefficients ($Å^2 \times 10^3$) for $C(CH_2\text{-}O_2C\text{-}CCl_3)_4$, **5**. Equivalent isotropic U defined as one third of the trace of the orthogonalized U_{ij} tensor.

Atom	x	y	z	U(eq)
Cl(11)	−2843(3)	9596(3)	7272(3)	96(2)
Cl(12)	−1030(3)	8241(3)	7943(3)	87(2)
Cl(13)	433(4)	10965(3)	9049(2)	96(2)
Cl(21)	4204(5)	12299(3)	10826(3)	131(2)
Cl(22)	5846(3)	12140(3)	9072(3)	128(2)
Cl(23)	3020(3)	12318(3)	8721(3)	109(2)
Cl(31)	8023(3)	7170(3)	3906(4)	120(2)
Cl(32)	5467(4)	5327(3)	2887(3)	131(2)
Cl(33)	6599(4)	6200(3)	5285(3)	123(2)
Cl(41)	−1240(3)	4035(3)	1274(3)	112(2)
Cl(42)	1695(3)	4438(3)	1393(3)	95(2)
Cl(43)	341(4)	6524(3)	1816(2)	90(2)
C(1)	2553(8)	8183(7)	5777(7)	44(4)
C(11)	1594(8)	9096(7)	5860(7)	45(4)
C(12)	242(9)	9731(9)	6838(7)	55(4)
C(13)	−1110(10)	9600(9)	7726(8)	64(5)
C(21)	3180(9)	8380(8)	6995(8)	56(4)
C(22)	3692(11)	10219(10)	8752(8)	65(5)
C(23)	4217(11)	11711(10)	9340(9)	78(5)
C(31)	3669(9)	8471(8)	5131(8)	52(4)
C(32)	5571(10)	7705(9)	4392(8)	57(4)
C(33)	6382(10)	6624(9)	4117(10	75(5)
C(41)	1739(9)	6809(7)	5169(6)	43(3)
C(42)	576(10)	5353(9)	3270(8)	54(4)
C(43)	351(10)	5133(9)	1987(8)	60(4)
O(11)	669(6)	8991(5)	6632(5)	52(3)
O(12)	−370(9)	10451(7)	6420(7)	93(5)
O(21)	3791(6)	9722(6)	7667(5)	59(3)
O(22)	3210(13)	9648(9)	9268(8)	131(6)
O(31)	4496(6)	7506(5)	4886(5)	52(3)
O(32)	5862(8)	8551(7)	4141(7)	86(4)
O(41)	1347(6)	6508(5)	3945(4)	49(3)
O(42)	119(10)	4582(7)	3553(6)	103(4)

Table 3. Selected bond lengths (Å) and bond angles (deg) for $C(CH_2\text{-}O_2C\text{-}CCl_3)_4$, **5**.

C(1)—C(21)	1.534(13)	C(31)-C(1)-C(21)	111.9(7)
C(21)—O(21)	1.445(9)	C(41)-C(1)-C(21)	105.4(8)
O(21)—C(22)	1.293(11)	C(41)-C(1)-C(11)	110.9(6)
C(22)—C(23)	1.575(14)	C(1)-C(21)-O(21)	107.5(8)
O(22)—C(22)	1.205(17)	C(21)-O(21)-C(22)	117.0(8)
C(23)—Cl(21)	1.746(11)	O(21)-C(22)-O(22)	125.7(9)
C(23)—Cl(22)	1.720(11)	O(22)-C(22)-C(23)	122.4(9)
C(23)—Cl(23)	1.760(13)	Cl(23)-C(23)-Cl(21)	108.9(6)

1.408(8), and 1.262(8) Å, respectively. In this structure, the C—O distances are significantly different; moreover, the enolic hydrogen can be seen in the final difference map.

We are aware of only one other structurally characterized organometallic acac-type derivative: the X-ray crystal structure of the ferrocenyl complex **15** has recently been reported, and the molecule was shown to adopt the tautomeric form in which the site of enolization is remote from the electron-donating ferrocenyl moiety (17). Analogously, in the thiophene derivative **16**, the enol-H is bonded to the oxygen adjacent to the strongly electron-withdrawing CF_3 group (18). Furthermore, it has been reported that the infrared spectrum of (benzoylacetone)$Cr(CO)_3$, **17**, indicates that in solution the enol tautomer predominates (19). From our ^{13}C NMR data, the observed keto–enol ratio in **17** is ≈1:5, but the preferred site of enolization is unknown.

Table 4. Atomic coordinates ($\times 10^4$) and equivalent isotropic displacement coefficients ($Å^2 \times 10^3$) for $CH_3C(O)CHC(OH)CCo_3(CO)_9$, **9**.

Atom	x	y	z	U(eq)
Co(1)	1862(1)	7954(1)	3043	47(1)
Co(2)	1446(1)	8633(1)	5302(1)	48(1)
Co(3)	2691(1)	7436(1)	5035(1)	43(1)
C(1)	2430(3)	8887(4)	4308(5)	40(1)
C(2)	2858(3)	9978(4)	4135(5)	43(1)
C(3)	3669(3)	10160(4)	4514(6)	50(2)
C(4)	4040(4)	11247(5)	4358(6)	57(2)
C(5)	4927(4)	11430(6)	4756(9)	83(3)
C(10)	1327(4)	9003(6)	2057(7)	67(2)
C(11)	1191(4)	6698(5)	2954(7)	68(2)
C(12)	2633(4)	7634(5)	1799(7)	65(2)
C(20)	1691(4)	9241(5)	6912(8)	72(2)
C(21)	815(4)	9809(6)	4725(8)	74(2)
C(22)	692(3)	7541(5)	5790(8)	61(2)
C(30)	3152(4)	7798(5)	6624(7)	58(2)
C(31)	3629(4)	7081(5)	4175(8)	64(2)
C(32)	2230(3)	6028(4)	5382(7)	60(2)
O(2)	2421(2)	10809(3)	3602(5)	64(1)
O(4)	3641(3)	12088(3)	3874(6)	75(2)
O(10)	1017(4)	9674(5)	1412(7)	106(2)
O(11)	784(4)	5920(5)	2925(6)	106(2)
O(12)	3131(4)	7455(5)	1011(6)	98(2)
O(20)	1845(4)	9658(5)	7906(7)	116(3)
O(21)	426(3)	10543(5)	4362(8)	117(3)
O(22)	229(3)	6843(5)	6076(6)	91(2)
O(30)	3444(3)	8045(5)	7610(6)	92(2)
O(31)	4216(3)	6869(5)	3635(7)	98(2)
O(32)	1935(3)	5167(3)	5570(6)	88(2)

In an attempt to rationalize the favored site of enolization found in the cobalt cluster **9**, molecular orbital calculations at the extended Hückel level were carried out. The crystallographically observed tautomer, in which the enol is adjacent to the cluster, is favored by ≈3.4 kcal/mol relative to the case when the OH is sited at C(4), as in $CH_3\text{-}C(OH)=CH\text{-}C(O)\text{-}CCo_3(CO)_9$. Figure 4 depicts the changes in the HOMO of **9** as the enol-H migrates from O(2) to O(4) and the C(2)—C(3) and C(3)—C(4) distances are modified accordingly. Initially (Fig. 4*a*), there is an in-plane π^* interaction between C(2) and O(2) that is augmented as the migration proceeds (Fig. 4b); that is, the system is somewhat destabilized. However, this rather simplistic approach does not account for the observed tautomer of the ferrocenyl-acac complex **15**, and it may be that a higher level of theory is needed to rationalize the behavior of such systems.

The X-ray crystal structure of (benzoylacetone)$Cr(CO)_3$, 17

It was noted previously (19) that replacement of a methyl group in acacH by an (η^6-phenyl)$Cr(CO)_3$ substituent, as in **17**, leads

Can. J. Chem. Downloaded from www.nrcresearchpress.com by 80.90.12.36 on 09/08/12
For personal use only.

Fig. 5. X-ray crystal structure of (benzoylacetone)$Cr(CO)_3$, **17**.

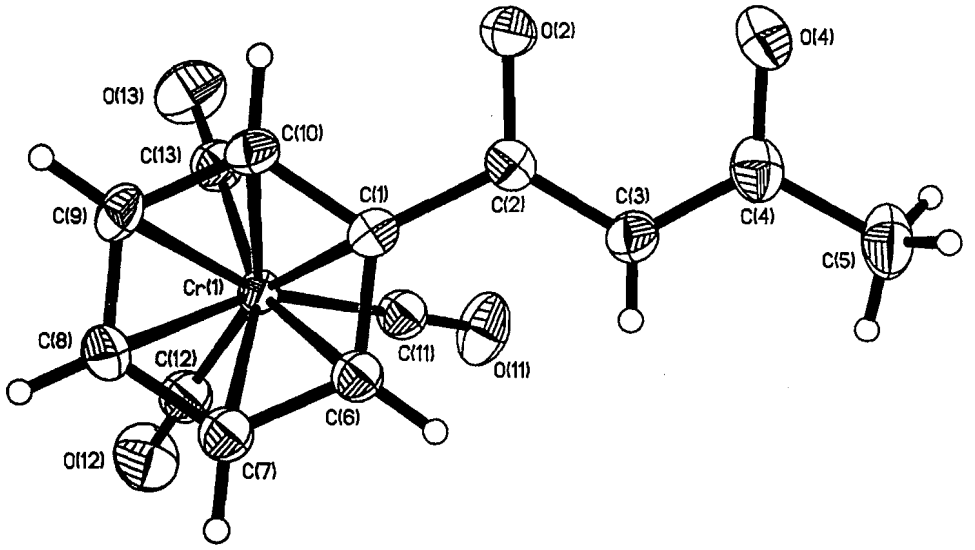

Table 5. Selected bond lengths (Å) and angles (deg) for $CH_3C(O)CHC(OH)CCo_3(CO)_9$, **9**.

C(1)—C(2)	1.456(6)	C(1)-C(2)-C(3)	123.7(4)
C(2)—C(3)	1.385(7)	C(3)-C(2)-O(2)	120.7(4)
C(3)—C(4)	1.409(7)	C(2)-C(3)-C(4)	121.0(5)
C(4)—C(5)	1.507(9)	C(3)-C(4)-C(5)	120.5(5)
O(2)—C(2)	1.309(6)	C(5)-C(4)-O(4)	118.5(5)
O(4)—C(4)	1.268(7)	C(2)-O(2)-H(2)	119.8(3)
O(2)—H(2)	0.789	C(2)-C(1)-Co(2)	126.7(3)
Co(1)—C(1)	1.899(5)	C(2)-C(1)-Co(3)	136.0(4)
Co(2)—C(1)	1.900(5)	C(2)-C(1)-Co(1)	130.7(4)
Co(3)—C(1)	1.884(4)	Co(1)-Co(2)-Co(3)	59.9(1)
Co(1)—Co(2)	2.469(1)	Co(1)-Co(3)-Co(2)	60.1(1)
Co(2)—Co(3)	2.466(1)	Co(2)-Co(1)-Co(3)	60.0(1)
Co(1)—Co(3)	2.465(1)	Co(2)-C(1)-Co(3)	81.4(2)
Co(1)—C(11)	1.824(7)	Co(1)-C(1)-Co(3)	81.3(2)
Co(2)—C(22)	1.829(6)	Co(1)-C(1)-Co(2)	81.1(2)
Co(3)—C(32)	1.832(5)	C(10)-Co(1)-C(12)	96.0(3)
C(11)—O(11)	1.120(9)	C(20)-Co(2)-C(21)	96.2(3)
C(22)—O(22)	1.142(8)	C(30)-Co(3)-C(31)	96.8(3)
C(32)—O(32)	1.126(7)	C(11)-Co(1)-C(12)	102.5(3)
		C(20)-Co(2)-C(22)	100.8(3)
		C(30)-Co(3)-C(32)	102.4(3)
		Co(1)-C(11)-O(11)	178.6(7)
		Co(2)-C(22)-O(22)	178.5(6)
		Co(3)-C(32)-O(32)	178.3(6)

Table 6. Atomic coordinates ($\times 10^4$) and equivalent isotropic displacement parameters ($Å^2 \times 10^3$) for (benzoylacetone)$Cr(CO)_3$, **17**. U(eq) is defined as one third of the trace of the orthogonalized U_{ij} tensor.

Atom	x	y	z	U(eq)
Cr(1)	9503(1)	4156(1)	249(1)	37(1)
O(4)	8513(3)	7762(3)	−1533(1)	65(1)
O(2)	7533(3)	6141(3)	−897(1)	52(1)
O(13)	9132(4)	1637(3)	−362(1)	89(1)
O(12)	11462(3)	2736(4)	931(1)	91(1)
O(11)	11848(3)	4845(3)	−423(1)	88(1)
C(5)	10275(4)	9194(4)	−1312(2)	77(1)
C(4)	9331(3)	8117(4)	−1172(1)	54(1)
C(3)	9310(3)	7524(3)	−677(1)	49(1)
C(2)	8400(3)	6532(3)	−559(1)	40(1)
C(1)	8329(3)	5870(3)	−35(1)	38(1)
C(10)	7476(3)	4773(3)	31(1)	41(1)
C(9)	7402(3)	4096(4)	515(1)	50(1)
C(8)	8185(4)	4495(4)	938(1)	52(1)
C(7)	9025(3)	5604(3)	882(1)	49(1)
C(6)	9113(3)	6274(3)	404(1)	44(1)
C(13)	9280(4)	2609(4)	−132(1)	55(1)
C(12)	10699(4)	3276(4)	675(1)	57(1)
C(11)	10941(4)	4591(3)	−168(1)	52(1)

predominantly to an enol tautomer of unknown structure. To resolve this dichotomy, an X-ray quality crystalline sample of **17** was prepared and its structure determined. (Benzoylacetone)$Cr(CO)_3$, **17**, crystallizes in the tetragonal space group $P4_32_12$ with eight molecules in the unit cell. The crystallographic collection parameters are listed in Table 1, and atomic coordinates and selected bond length and angle data for **17** appear in Tables 6 and 7; a view of the molecule appears as Fig. 5.

The acac and phenyl rings are essentially coplanar and the $Cr(CO)_3$ tripod adopts an almost staggered orientation with respect to the phenyl carbons. Although the acac portion of the molecule is clearly an enol, and the C(3) carbon is sp^2-hybridized, the C(2)—O(2) and C(4)—O(4) distances, 1.288(4) Å and 1.285(5) Å, are not significantly different. Likewise, the C(2)—C(3) and C(3)—C(4) distances, 1.390(5) Å and 1.392(5) Å, are essentially the same, perhaps indicating that the enolic H is symmetrically bonded to both oxygens. In accord with the X-ray data, the ^{13}C CPMAS spectrum of **17** exhibits peaks only for the enol tautomer.

Conclusions

Preliminary attempts to use organic templates as surfaces on which to deposit $Co_3(CO)_9C$ cluster fragments reveal that,

Can. J. Chem. Downloaded from www.nrcresearchpress.com by 80.90.12.36 on 09/08/12
For personal use only.

Table 7. Selected bond lengths (Å) and angles (degs) for (benzoylacetone)$Cr(CO)_3$, **17**.

C(1)—C(2)	1.488(4)	O(4)–C(4)–C(3)	121.0(3)
C(2)—C(3)	1.390(5)	C(3)–C(4)–C(5)	122.7(4)
C(3)—C(4)	1.392(5)	C(2)–C(3)–C(4)	120.9(3)
C(4)—C(5)	1.488(6)	O(2)–C(2)–C(3)	121.7(3)
O(2)—C(2)	1.288(4)	C(1)–C(2)–C(3)	123.2(3)
O(4)—C(4)	1.285(5)	C(10)–C(1)–C(2)	119.2(3)
Cr(1)–centroid	1.714	C(1)–C(10)–C(9)	121.1(3)
Cr(1)—C(6)	2.207(3)	C(1)–C(6)–C(7)	120.5(3)
Cr(1)—C(10)	2.207(3)	C(10)–C(9)–C(8)	120.2(3)
Cr(1)—C(1)	2.216(3)	C(6)–C(7)–C(8)	120.7(3)
Cr(1)—C(8)	2.223(3)	C(7)–C(8)–C(9)	119.5(3)
Cr(1)—C(9)	2.225(3)	C(1)–Cr(1)–C(11)	92.74(13)
Cr(1)—C(7)	2.225(3)	C(1)–Cr(1)–C(13)	115.00(14)
Cr(1)—C(11)	1.847(4)	C(1)–Cr(1)–C(12)	156.07(14)
Cr(1)—C(12)	1.848(4)	C(8)–Cr(1)–C(12)	90.2(2)
Cr(1)—C(13)	1.850(4)	C(8)–Cr(1)–C(13)	117.9(2)
C(1)—C(10)	1.412(4)	C(8)–Cr(1)–C(11)	152.0(2)
C(1)—C(6)	1.426(4)	C(11)–Cr(1)–C(12)	86.4(2)
C(10)—C(9)	1.407(4)	C(11)–Cr(1)–C(13)	89.8(2)
C(9)—C(8)	1.392(5)	C(12)–Cr(1)–C(13)	88.9(2)
C(8)—C(7)	1.410(5)	Cr(1)–C(11)–O(11)	178.8(3)
C(7)—C(6)	1.393(4)	Cr(1)–C(12)–O(12)	178.4(3)
		Cr(1)–C(13)–O(13)	178.8(3)

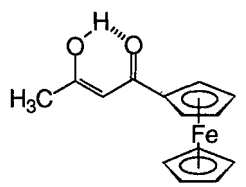

15

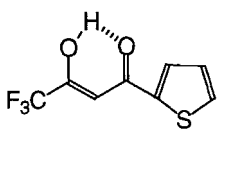

16

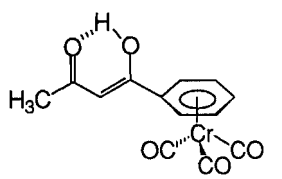

17

although the general approach of coating the central core with trichloroacetate esters is viable, care must be taken not to place too many bulky clusters in close proximity. It has also been demonstrated that coordination of the 1,1,1-trichloroacetylacetonate ligand to a variety of metal centers facilitates the construction of a range of inorganometallic clusters. The X-ray crystal structure of the parent ligand, CH_3-C(O)-CH=C(OH)-$CCo_3(CO)_9$, **9**, reveals that it exists as the enol tautomer in which the OH substituent is adjacent to the cluster moiety. Likewise, in (benzoylacetone)$Cr(CO)_3$, **17**, the 1,3-dione exists primarily in the enol form.

Experimental section

All reactions were carried out under an atmosphere of dry nitrogen employing conventional benchtop and glovebag techniques. All solvents were dried according to standard procedures before use (20). Silica gel (particle size: 20–45 μm) was employed for flash column chromatography. ^1H and ^{13}C solution NMR spectra were recorded on a Bruker AC-200 spectrometer. ^{13}C CPMAS spectra were recorded on a Bruker MSL 100 instrument. Infrared spectra were recorded on a Perkin–Elmer 283, or a Bio-Rad FTS-40 instrument using NaCl plates. Fast Atom Bombardment (FAB) was performed on a VG analytical ZAB-ZE spectrometer. 3-Nitrobenzyl alcohol was used as the sample matrix and xenon was the bombarding gas (8 keV). Melting points were determined on a Thomas Hoover capillary melting point apparatus and are uncorrected.

Preparation of $C[CH_2O_2CCCl_3]_4$, 5

$ClCOCCl_3$ (16.4 mL, 146.8 mmol) was added dropwise over a period of 1.5 h to a solution of $C(CH_2OH)_4$ (5.00 g, 36.7 mmol) and pyridine (17.0 mL, 210.2 mmol) in ether (80 mL) and was then allowed to stir for 6 h. Excess pyridine was added until the mixture was no longer acidic. The mixture was then extracted with 4 × 100 mL of 1.2 N HCl. The ether layer was dried with Na_2SO_4 and removed, leaving a white solid, **5**, which was further washed with petroleum ether (7.03 g, 9.79 mmol, 27%), mp 150–152°C. Recrystallization of **5** from diethyl ether – petroleum ether (50:50) gave X-ray quality crystals. IR (CH_2Cl_2): $\nu_{C=O}$ 1770 (s) cm^{-1}. ^1H NMR ($CDCl_3$) δ: 4.53 (s). ^{13}C NMR ($CDCl_3$) δ: 161.0 (ester carbonyl), 88.9 (CCl_3), 65.3 (CH_2), and 43.6 (tertiary *C*). Mass spectrum (DCI) *m/z* (%): 730 (100) $[M + NH_3]^+$, 677 (7) $[M - Cl]^+$, 551 (51) $[M - O_2CCCl_3]^+$, 390 (12) $[M - 2(O_2CCCl_3)]^+$, 244 (25) $[M - 4(CCl_3)]^+$, and 227 (8) $[M - 3(O_2CCCl_3)]^+$. Peaks quoted are in each case the lowest mass in each envelope and correspond to ^{35}Cl.

Reaction of 5 with $Co_2(CO)_8$

$Co_2(CO)_8$ (1.77 g, 5.12 mmol) and $C[CH_2O_2CCCl_3]_4$ (0.52 g, 0.72 mmol) in 20 mL of THF were heated at 40°C for 3.5 h. After cooling, the mixture was filtered to remove cobalt salts, and the solvent was removed in vacuo. Flash chromatography using 100% CH_2Cl_2 as eluant showed the presence of at least six different products. The first band to elute was $Co_4(CO)_{12}$, a purple-black solid (0.251 g, 0.439 mmol). The second band obtained was $C[CH_2O_2CCCo_3(CO)_9]_3(CH_2O_2CCCl_3)$, **6**, a purple oil (0.099 g, 0.059 mmol, 7%). IR (CH_2Cl_2): ν_{CO} at 2111 (w), 2067 (vs), 2048 (s); $\nu_{C=O}$ at 1607 (m, br) cm^{-1}. Mass spectrum: (*a*) (FAB^+, MCA) *m/z* (%) 1208 (18) $[M - 17CO]^+$, 1180 (18) $[M - 18CO]^+$, 1095 (38) $[M - 21CO]^+$, 1068 (20) $[M - 22CO]^+$, 1039 (42) $[M - 23CO]^+$, 984 (15) $[M - 25CO]^+$, 956 (37) $[M - 26CO]^+$, and 927 (100) $[M - 27CO]^+$. (*b*) (FAB^+) *m/z* (%) 1068 (24) $[M - CCo_3(CO)_9 - CH_2O_2CCCl_3]^+$, 1040 (68) $[M - CCo_3(CO)_9 - CH_2O_2CCCl_3 - CO]^+$, 958 (46) $[M - CCo_3(CO)_9 - CH_2O_2CCCl_3 - 4CO]^+$, 928 (100) $[M - CCo_3(CO)_9 - CH_2O_2CCCl_3 - 5CO]^+$, 844 (38) $[M - CCo_3(CO)_9 - CH_2O_2CCCl_3 - 8CO]^+$, and 760 (79) $[M - CCo_3(CO)_9 - CH_2O_2CCCl_3 - 11CO]^+$. The fourth band, a purple oil (0.033 g, 4.4%), was tentatively assigned as $C[CH_2O_2CCCo_3(CO)_9](CH_2O_2CCCl_3)_3$. IR ($CH_2Cl_2$): ν_{CO} at 2103 (w), 2050 (vs), 2042 (s); $\nu_{C=O}$ at 1606 (w) cm^{-1}. Mass spectrum: (FAB^+, MCA) *m/z* (%): 1036 (7) $[M^+]$; 1007 (27) $[M - CO]^+$; 924 (20) $[M - 4CO]^+$. Peaks quoted are in each case the lowest mass in each envelope and correspond to ^{35}Cl.

Can. J. Chem. Downloaded from www.nrcresearchpress.com by 80.90.12.36 on 09/08/12
For personal use only.

Preparation of $Cl_3CC(O)CH_2C(O)CH_3$, 8

According to the procedures of Coenen et al. (12) and of Ringel and Mayer (13), Cl_3CCN (35.0 g, 0.24 mol) and acetylacetone (25.0 g, 0.24 mol) were dissolved in 100 mL MeOH. While stirring, 50 mL of a saturated aqueous solution of sodium acetate was slowly added. The reaction mixture was stirred for 2 h and was then slowly poured into 700 mL of cold H_2O, in which a white precipitate formed immediately. It was subsequently filtered and recrystallized from hexane to give $Cl_3CC(NH_2)$=$CHC(O)CH_3$ (44.25 g, 0.22 mol, 90%). This product was then treated with 78.8 mL of concentrated HCl. Heat was evolved and NH_4Cl and an oil separated out. After cooling the solution 63.0 mL of H_2O was added. The oily layer was then treated with 118 mL of ether, dried with Na_2SO_4, and filtered. Removal of the solvent gave a liquid, which was distilled at reduced pressure (bp_{18} 100–101°C) to yield **8** as a colorless liquid (31.68 g, 0.16 mol, 71%). IR (CH_2Cl_2): $\nu_{C=O}$ at 1595 (vs) cm^{-1}. ^1H NMR ($CDCl_3$) δ: 6.10 (s, 1H, C*H* of enol), 4.05 (s, 2H, CH_2 of keto), 2.29 (s, 3H, CH_3 of keto), and 2.15 (s, 3H, CH_3 of enol). ^{13}C NMR ($CDCl_3$) δ: 186.8, 185.3 (carbonyls), 94.7 (CCl_3), 92.9 (*C*H of enol), 48.9 (CH_2 of keto), 30.1 (CH_3 of keto), and 22.9 (CH_3 of enol). Mass spectrum (EI) *m/z* (%): 202 (18) $Cl_3CC(O)CH_2C(O)CH_3$ $[M]^+$, 187 (5) $[M - CH_3]^+$; 167 (36) $[M - Cl]^+$; 152 (25) $[M - Cl - CH_3]^+$, 139 (100) $[M - Cl - CO]^+$, and 117 (27) $[M - C(O)CH_2C(O)CH_3]^+$. Peaks quoted are in each case the lowest mass in each envelope and correspond to ^{35}Cl.

Preparation of $Al[Cl_3CC(O)CHC(O)CH_3]_3$, 10

Although **10** has been reported previously and characterized by mass spectrometry (16), no synthetic procedure or NMR data are available. **8** (2.00 g, 9.83 mmol) was added to a solution of aluminum isopropoxide (0.669 g, 3.28 mmol) in 6.4 mL of benzene. After the solution was allowed to stand for 2 h, benzene and the 2-propanol produced were removed by using a rotovap to yield a white solid, **10** (1.614 g, 2.54 mmol, 78%). IR (CH_2Cl_2): $\nu_{C=O}$ 1614 (s), $\nu_{C=C}$ 1513 (s) cm^{-1}. ^1H NMR ($CDCl_3$) δ: 6.41 (s, 1H), 6.40 (s, 1H), 6.38 (s, 3H), 6.32 (s, 1H), 2.32 (s, 3H), 2.28 (s, 12H), and 2.23 (s, 3H). ^{13}C NMR ($CDCl_3$) δ: at 201.0, 200.4, 199.9 ($C(O)CCl_3$); 179.3, 178.7, 178.1 ($C(O)CH_3$); 95.1, 94.7, 94.4 (*C*H); and 28.34 (CH_3). Mass spectrum (FAB^+) *m/z* (%): 429 (79) $[M - tcac]^+$, 394 (49) $[M - tcac - Cl]^+$, 359 (24) $[M - tcac - 2Cl]^+$, 347 (28) $[M - tcac - CCl_2]^+$, 312 (25) $[M - tcac - CCl_3]^+$, and 228 (55) $[M - 2(tcac)]^+$. Peaks quoted are in each case the lowest mass in each envelope and correspond to ^{35}Cl and ^{27}Al.

Preparation of $Cu[Cl_3CC(O)CHC(O)CH_3]_2$, 12

Although **12** has been reported previously and characterized by mass spectrometry (16), no synthetic procedure is available. Copper nitrate trihydrate (2.969 g, 12.29 mmol) was dissolved in 27.5 mL of water and to this was added, with mixing, **8** (5.00 g, 24.58 mmol) and sodium acetate (2.015 g, 24.57 mmmol) in 2.75 mL water. A solid precipitated out of solution and was filtered and dried. Recrystallization from methanol yielded a grey-green solid, **12** (3.965 g, 8.46 mmol, 69%), with a melting point of 197–198°C. IR (CH_2Cl_2): $\nu_{C=O}$ 1601 (s), $\nu_{C=C}$ 1507 (s) cm^{-1}. Mass spectrum (FAB^+) shows evidence for dimerization; *m/z* (%): 729 (9) [M - tcac]$^+$, 571 (20) $[M - tcac - CHC(O)CCl_3]^+$, 528 (12) $[M - 2(tcac)]^+$, 465 (51) $[M - 2(tcac) - Cu]^+$, 458 (28) $[M - 2(tcac) - 2Cl]^+$, 416 (100) $[M - 2(tcac)\ Cu - CH_2 - Cl]^+$, 369 (66) $[M - 2(tcac) - CHC(O)CCl_3]^+$, and 348 (31) $[M - 2(tcac) - CCl_3 - Cu]^+$. Peaks quoted are in each case the lowest mass in each envelope and correspond to ^{35}Cl and ^{63}Cu.

Preparation of $Al[Co_3(CO)_9CC(O)CHC(O)CH_3]_3$, 11

10 (1.755 g, 2.77 mmol) and $Co_2(CO)_8$ (5.109 g, 14.94 mmol) in 50 mL of THF were stirred at room temperature for 1.5 h and at 40°C for 1.5 h. The resulting solution was filtered and the solvent removed *in vacuo*. Column chromatography, using as eluant ether/hexanes (1:4), yielded $Co_4(CO)_{12}$ (1.51 g, 2.64 mmol) as the first band and **11**, a brown-black oil, as the second band (0.310 g, 0.19 mmol, 7%). IR (CH_2Cl_2): ν_{CO} at 2108 (w), 2063 (vs), 2045 (s); $\nu_{C=O}$ at 1723 (m), 1601 (w), and 1525 (w) cm^{-1}. ^{13}C NMR ($CDCl_3$) δ: 220.8 ($C(O)CCo_3(CO)_9$), 196.2 (Co-*C*O's), 187.6 ($C(O)CH_3$), 117.4 (*C*H), and 29.7 (CH_3). Mass spectrum (FAB^+) *m/z* (%): 1574 (7) $[M - CO]^+$, 1518 (14) $[M - 3CO]^+$, 1378 (11) $[M - 8CO]^+$, 1294 (11) $[M - 11CO]^+$, 1238 (20) $[M - 13CO]^+$, 1210 (23) $[M - 14CO]^+$, 1182 (30) $[M - 15CO^+]$, 1154 (24) $[M - 16CO]^+$, 1126 (35) $[M - 17CO]^+$, 1077 (30) $[M - Co_3(CO)_9CC(O)CHC(O)CH_3]^+$, 1049 (25) $[M - Co_3(CO)_9CC(O)CHC(O)CH_3 - CO]$, 1014 (25) $[M - 21CO]^+$, 986 (23) $[M - 22CO]^+$, 958 (42) $[M - 23CO]^+$, 937 (50) $[M - Co_3(CO)_9CC(O)CHC(O)CH_3 - 5CO]$, 909 (68) $[M - Co_3(CO)_9CC(O)CHC(O)CH_3 - 6CO]^+$, 881 (100) $[M - Co_3(CO)_9CC(O)CHC(O)CH_3 - 7CO]^+$, 853 (70) $[M - Co_3(CO)_9CC(O)CHC(O)CH_3 - 8CO]^+$, 825 (60) $[M - Co_3(CO)_9CC(O)CHC(O)CH_3 - 9CO]^+$, and 797 (36) $[M - Co_3(CO)_9CC(O)CHC(O)CH_3 - 10CO]^+$.

Preparation of $Co[Co_3(CO)_9CC(O)CHC(O)CH_3]_2$, 13, and $Co[Co_3(CO)_9CC(O)CHC(O)CH_3]_3$, 14

12 (0.76 g, 1.62 mmol) and $Co_2(CO)_8$ (2.00 g, 5.84 mmol) were dissolved in 30 mL of THF and stirred at room temperature for 1 h and at 40°C for 1 h. This mixture was allowed to cool, and filtration and solvent removal in vacuo yielded a crude solid that was purified by flash chromatography (CH_2Cl_2/hexanes, 1:1). The first band was a brown-black oil, **13** (0.180 g, 0.162 mmol, 10%). IR of **13**, (CH_2Cl_2): ν_{CO} at 2108 (m), 2063 (vs), 2045 (s); $\nu_{C=O}$ at 1722 (vw), and 1599 (w) cm^{-1}. Mass spectrum (FAB^+) of **13**; *m/z* (%): 1109 (20) $Co[Co_3(CO)_9CC(O)CHC(O)CH_3]_2$, $[M]^+$, 1082 (12) $[M - 1CO]^+$, 1024 (73) $[M - 3CO]^+$, 998 (32) $[M - 4CO]^+$, 941 (33) $[M - 6CO]^+$, 913 (100) $[M - 7CO]^+$, 885 (77) $[M - 8CO]^+$, 857 (58) $[M - 9CO]^+$, 829 (85) $[M - 10CO]^+$, and 800 (69) $[M - 11CO]^+$. The second band was a brown-black oil, **14** (0.126 g, 0.077 mmol, 7%). IR of **14**, (CH_2Cl_2): ν_{CO} at 2107 (m), 2063 (vs), 2044 (s); $\nu_{C=O}$ at 1723 (w), 1595 (m), and 1515 (m) cm^{-1}. Mass spectrum (FAB^+) of **14**; *m/z* (%): 1521 (10) $[M - 4CO]^+$, 1353 (33) $[M - 10CO]^+$, 1297 (42) $[M - 12CO]^+$, 1157 (37) $[M - 17CO]^+$, 1129 (43) $[M - 18CO]^+$, 1024 (51) $[M - Co_3(CO)_9CC(O)CHC(O)CH_3 - 3CO]^+$, 997 (72) $[M - Co_3(CO)_9CC(O)CHC(O)CH_3 - 4CO]$, 913 (100) $[M - Co_3(CO)_9CC(O)CHC(O)CH_3 - 7CO]^+$, 885 (76) $[M - Co_3(CO)_9CC(O)CHC(O)CH_3 - 8CO$, 857 (77) $[M - Co_3(CO)_9CC(O)CHC(O)CH_3 - 9CO]$, 829 (96) $[M - Co_3(CO)_9CC(O)CHC(O)CH_3\ 10CO]^+$, and 801 (94) $[M - Co_3(CO)_9CC(O)CHC(O)CH_3 - 11CO]$. Repeated chromatography on **13** led to decomposition and yielded black crystals of **9**. Recrystallization from methylene chloride/ hexane (50:50) gave an X-ray quality sample of **9**.

Can. J. Chem. Downloaded from www.nrcresearchpress.com by 80.90.12.36 on 09/08/12
For personal use only.

Preparation of (benzoylacetone)$Cr(CO)_3$, 17

According to the literature procedure (19), (methylbenzoate)chromiumtricarbonyl (1.117 g, 4.104 mmol) and acetone (0.285 g, 4.907 mmol) in ether (20 mL) were treated with NaOEt (0.293 g, 4.309 mmol) over 1 h under N_2 atmosphere. A bright yellow precipitate formed that was filtered and then dissolved in water. Bubbling CO_2(g) resulted in the formation of an orange-red precipitate, which was extracted with ether. The ether layer was dried over Na_2SO_4, filtered, and then removed, yielding a brick-red solid, **17** (0.653 g, 2.190 mmol, 54%), mp 119–121°C [Lit. (19) mp 115–117°C]. IR (CH_2Cl_2): $\nu_{C=O}$ at 1980 (s), and 1909 (s) cm^{-1}. ^1H NMR ($CDCl_3$) δ: 5.99 (d, 2H, *ortho-H*), 5.84 (s, 1H, C*H* of enol), 5.56 (t, 1H, *para-H*), 5.28 (t, 2H, *meta-H*), 3.86 (s, 2H, CH_2 of keto), 2.31 (s, 3H, CH_3 of keto), and 2.15 (s, 3H, CH_3 of enol). ^{13}C NMR (acetone-d_6) δ: 232.6 (Cr-*C*O of enol), 232.1 (Cr-*C*O of keto), 202.3, 192.9 (*C*O of keto), 191.3, 185.3 (*C*O of enol), 97.78 (*ipso-C* of enol), 97.2, 96.1 (*para-C*, *C*H of enol), 94.7, 92.1 (*meta-C*, *ortho-C*), 53.2 (CH_2 of keto), 24.4 (CH_3 of enol). ^{13}C CPMAS; δ: 233.0 (Cr-*C*O of enol), 195.1, 183.0 (*C*O of enol), 97.3, 94.4 (*ipso-C*, *para-C*, *meta-C*, *ortho-C*, and *C*H of enol), and 26.6 (CH_3 of enol). Mass spectrum (DEI) *m/z* (%): 298 (5) $[M]^+$, 242 (8) $[M - 2CO]^+$, 214 (30) $[M - 3CO]^+$, 171 (10) $[M - 3CO - COCH_3]^+$, and 52 (100) $[Cr]^+$.

X-ray crystallography

X-ray crystallographic data for **5** were collected on a Rigaku AFC6R diffractometer with a rotating anode and graphite-monochromated Cu Kα radiation (λ = 1.54178 Å). The X-ray crystallographic data for **9** and **17** were collected on a Siemens P4 diffractometer with a rotating anode and graphite-monochromated Mo Kα radiation (λ = 0.71073 Å). The background measurements were obtained by using a stationary crystal and stationary counter at the beginning and end of the scan, each for 25% of the total scan time. The scan type used was θ–2θ. The scan rate was 32.0°/min in ω for **5**, while the scan speed was variable for **9** (1.50–60.00°/min) and for **17** (5.00–60.00°/min) in ω. In **5**, three standard reflections were measured after every 150 reflections. In **9** and **17**, three standard reflections that were measured after every 97 reflections showed no instrument instability and only minor crystal decay. The molecule **5** was solved by using Direct Methods, while for **9** and **17**, the Patterson Method was used. Both of these procedures are contained in the SHELXTL-PLUS program library (22).[3] The method of refinement was full-matrix least squares in each case. Crystal data collection parameters are listed in Table 1. Atom coordinates and selected bond lengths and angles for **5**, **9**, and **17** are collected in Tables 2 through 7.[4]

[3] SHELXTL-PLUS was written by G.M. Sheldrick. Nicolet XRD. Madison, Wis.

[4] Tables of thermal parameters, bond lengths and angles, and positional parameters for hydrogen atoms for molecules **5**, **9**, and **17** are available as supplementary material and can be purchased from: The Depository of Unpublished Data, Document Delivery, CISTI, National Research Council Canada, Ottawa, Canada K1A OS2.

Tables of bond lengths and angles and positional parameters have also been deposited with the Cambridge Crystallographic Data Centre, and can be obtained on request from The Director, Cambridge Crystallographic Data Centre, University Chemical Laboratory, 12 Union Road, Cambridge, CB2 1EZ, U.K.

Structure factor amplitudes are no longer being deposited and may be obtained directly from the author.

Molecular orbital calculations were performed via the extended Hückel method using weighted H_{ij}'s (21); orbital drawings were obtained by use of the program CACAO (22). Orbital parameters were taken from ref. 23.

Acknowledgements

Financial support from the Natural Sciences and Engineering Research Council of Canada is gratefully acknowledged. Mass spectra were obtained courtesy of Dr. Richard Smith of the McMaster Regional Centre for Mass Spectrometry, and solid state NMR data were kindly provided by Brian G. Sayer. We thank Dr. Carlo Mealli, Consiglio Nazionale delle Richerche, Florence, Italy, for the program CACAO.

References

1. R.D. Adams. *In* The chemistry of metal cluster complexes. *Edited by* D.F. Shriver, H.D. Kaesz, and R.D. Adams. VCH Publishers, Inc., New York. 1990. pp. 121–170.
2. R.L. Sturgeon, M.M. Olmstead, and N.E. Schore. Organometallics, **10**, 1649 (1991).
3. W. Cen, K.J. Haller, and T. P. Fehlner. Inorg. Chem. **30**, 3120 (1991).
4. W. Cen, K.J. Haller, and T.P. Fehlner. Organometallics, **11**, 3499 (1992).
5. (*a*) W. Cen and T.P. Fehlner. J. Am. Chem. Soc. **114**, 5451 (1992); (*b*) T.P. Fehlner (*Editor*). Inorganometallic chemistry. Plenum, New York. 1992.
6. R.C. Mehrotra and R. Bohra. Metal carboxylates. Academic Press, New York. 1983.
7. F. Quignard, A. Choplin, and J.M. Basset. J. Chem. Soc. Dalton Trans. **16**, 2411 (1994).
8. (*a*) L.D. Iroff and K. Mislow. J. Am. Chem. Soc. **100**, 2121 (1978); (*b*) L.S. Bartell, F.B. Clippard, Jr., and T.L. Boates. Inorg. Chem. **9**, 2436 (1970).
9. P.W. Sutton and L.F. Dahl. J. Am. Chem. Soc. **89**, 261 (1967).
10. D. Seyferth. Adv. Organomet. Chem. **14**, 97 (1976).
11. J.E. Hallgren, C.S. Eschbach, and D. Seyferth. J. Am. Chem. Soc. **94**, 2547 (1972).
12. M. Coenen, J. Faust, C. Ringel, and R. Mayer. J. Prakt. Chem. **27**, 239 (1965).
13. C. Ringel and R. Mayer. J. Prakt. Chem. **26**, 333 (1964).
14. D. Seyferth, J.E. Hallgren, and P.L.K. Hung. J. Organomet. Chem. **50**, 265 (1973).
15. R.L. Belford, A.E. Martell, M. Calvin. J. Inorg. Nucl. Chem. **2**, 11 (1965).
16. M.L. Morris and R.D. Koob. Org. Mass. Spectrom. **17**, 503 (1982).
17. W. Bell, J.A. Crayston, and C. Glidewell. J. Organomet. Chem. **434**, 115 (1992).
18. R.D.G. Jones. Acta Crystallogr. Sect. B: Struct. Crystallogr. Cryst. Chem. **B32**, 1224 (1976).
19. F. Calderazzo, G. Casagrande Tettamanti, and R. Ercoli. Chim. Ind. **44**, 24 (1962).
20. D.D. Perrin, W.L.F. Armarego, and D.R. Perrin. Purification of laboratory chemicals. Pergamon Press, New York. 1980.
21. (*a*) R. Hoffmann. J. Chem. Phys. **39**, 1397 (1963); (*b*) R. Hoffmann and W.N. Lipscomb. J. Chem. Phys. **36**, 2179 (1962); **36**, 3489 (1962); (*c*) J.H. Ammeter, H.-B. Bürgi, J.C. Thibeault, and R. Hoffmann. J. Am. Chem. Soc. **100**, 3686 (1978).
22. C. Mealli and D.M. Proserpio. J. Chem. Educ. **67**, 3399 (1990).
23. R.H. Summerville and R. Hoffmann. J. Am. Chem. Soc. **98**, 7240 (1976).

The syntheses and structures of the phenyl-di-μ-methylene-dirhodium complexes, $[\{(\eta^5\text{-}C_5Me_5)Rh(\mu\text{-}CH_2)\}_2(Ph)(Br)]$ and $[\{(\eta^5\text{-}C_5Me_5)Rh(\mu\text{-}CH_2)\}_2(Ph)_2]$

Zhi-Qiang Wang, Harry Adams, Neil A. Bailey, Michael L. Turner, and Peter M. Maitlis

Abstract: Reaction of PhMgBr with $[\{(\eta^5\text{-}C_5Me_5)Rh(\mu\text{-}CH_2)_2(Br)_2]$ in a halide-specific reaction gave, first, the monophenyl complex **2***a* $[\{(\eta^5\text{-}C_5Me_5)Rh(\mu\text{-}CH_2)\}_2(Ph)(Br)]$ and then the diphenyl complex **3** $[\{(\eta^5\text{-}C_5Me_5)Rh(\mu\text{-}CH_2)\}_2(Ph)_2]$. X-ray crystal structure determinations showed both molecules to have *trans* structures, $[\{(\eta^5\text{-}C_5Me_5)Rh(\mu\text{-}CH_2)\}_2(Ph)(Br)]$ ($a = 10.066(3)$, $b = 11.065(3)$, $c = 14.002(3)$ Å; $\alpha = 85.23(2)°$, $\beta = 70.10(2)°$, $\gamma = 65.22(2)°$; $U = 1328.2(6)$ Å^3; $Z = 2$; space group $P\bar{1}$, final R, 0.0586) and $[\{(C_5Me_5)Rh(\mu\text{-}CH_2)\}_2(Ph)_2]$ ($a = 17.102(8)$, $b = 10.396(4)$, $c = 16.134(7)$ Å; $U = 2869(2)$ Å^3; $Z = 4$; space group $Pccn$ (D_{2h}^{10}, No. 56), final $R = 0.0426$).

Key words : X-ray structure determination, pentamethylcyclopentadienyl, di-μ-methylene, rhodium

Résumé : La réaction du PhMgBr avec le $[\{(\eta^5\text{-}C_5Me_5)Rh(\mu\text{-}CH_2)\}_2(Br)_2]$, dans une réaction à halogénure spécifique, conduit premièrement au complexe monophénylé **2***a* $[\{(\eta^5\text{-}C_5Me_5)Rh(\mu\text{-}CH_2)\}(Ph)(Br)]$ et ensuite au complexe diphénylé **3** $[\{(\eta^5\text{-}C_5Me_5)Rh(\mu\text{-}CH_2)\}(Ph)_2]$. Des études par diffraction des rayons X ont permis de montrer que les deux molécules possèdent des structures *trans*. Pour le $[\{(\eta^5\text{-}C_5Me_5)Rh(\mu\text{-}CH_2)\}(Ph)(Br)]$, $a = 10{,}066(3)$, $b = 11{,}065(3)$ et $c = 14{,}002(3)$ Å, $\alpha = 85{,}23(2)°$ $\beta = 70{,}10(2)°$ et $\gamma = 65{,}22(2)°$, $U = 1328{,}2(6)$ Å^3, $Z = 2$, groupe d'espace $P\bar{1}$ et valeur finale de $R = 0{,}0586$ alors que pour le $[\{(\eta^5\text{-}C_5Me_5)Rh(\mu\text{-}CH_2)\}(Ph)_2]$, $a = 17{,}102(8)$, $b = 10{,}396(4)$ et $c = 16{,}134(7)$ Å, $U = 2689(2)$ Å^3, $Z = 4$, groupe d'espace $Pccn$ (D_{2h}^{10}, No. 56) et valeur finale de $R = 0{,}0426$.

Mots clés : détermination de structure, diffraction des rayons X, pentaméthylcyclopentadiényle, di-μ-méthylène, rhodium.

[Traduit par la rédaction]

Introduction

We have previously reported extensive explorations of the chemistry of the di-μ-methylene-bis(pentamethylcyclopentadienylrhodium) complexes and have shown that the $\{(\eta^5\text{-}C_5Me_5Rh)(\mu\text{-}CH_2)\}_2$ unit is unexpectedly stable, despite formally containing Rh(IV) metal centres. This has allowed the synthesis of a large number of substituted species such as $[\{(\eta^5\text{-}C_5Me_5Rh)(\mu\text{-}CH_2)\}_2(X)(Y)]$ where X, Y are anionic (e.g., halide or pseudo-halide (1–3), alkyl (4), allyl (5), benzyl (6), vinyl (7), carbonate (8), etc.) or neutral ligands (e.g., MeCN, py, CO (9), etc.). For the neutral ligands, the complexes are of course ionic and bear positive charges.

The introduction of phenyl has, however, proved quite elusive until now, and neither the mono- nor the diphenyl complex had been efficiently obtained by standard routes. For example, reactions of $[\{(\eta^5\text{-}C_5Me_5Rh)(\mu\text{-}CH_2)\}_2Cl_2]$ with phenyllithium in solvents such as toluene, tetrahydrofuran, ether, or hexane were largely unsuccessful, and only a very small amount (<10%) of the diphenyl-dirhodium complex (**3**) was isolated when phenylmagnesium bromide was reacted with $[\{(\eta^5\text{-}C_5Me_5)Rh(\mu\text{-}CH_2)\}_2Cl_2]$ in toluene. Since the chemistry of such aryl dirhodium systems is potentially of great interest, we persevered and now report the successful preparation of both the monophenyl monobromo complex, **2***a*, and the diphenyl complex, **3**, by an unexpectedly simple variation of the standard method. The key proved to be the use of the dibromo complex $[\{(\eta^5\text{-}C_5Me_5)Rh(\mu\text{-}CH_2)\}_2Br_2]$, **1**, in place of the dichloro complex $[\{(\eta^5\text{-}C_5Me_5)Rh(\mu\text{-}CH_2)\}_2Cl_2]$ to react with PhMgBr. Since there is no special reason to expect Br^- to be a better leaving group from $\eta^5\text{-}C_5Me_5Rh$ than

Received November 11, 1994.

This paper is dedicated to Professor William A.G. Graham on the occasion of his 65th birthday, and in recognition of his fine and innovative organometallic chemistry.

Z.-Q. Wang, H. Adams, N.A. Bailey, M.L. Turner, and P.M. Maitlis.[1] Department of Chemistry, The University of Sheffield, Sheffield S3 7HF, England.

[1] Author to whom correspondence may be addressed. Telephone: -44-114-2824480. Fax: -44-114-2738673. E-mail: P.Maitlis@Sheffield.ac.uk

Can. J. Chem. Downloaded from www.nrcresearchpress.com by 80.90.12.36 on 09/08/12
For personal use only.

Can. J. Chem. Downloaded from www.nrcresearchpress.com by 80.90.12.36 on 09/08/12
For personal use only.

Fig. 1. The X-ray structure of complex **2***a*, $[\{(C_5Me_5)Rh(\mu\text{-}CH_2)\}_2(Ph)(Br)]$.

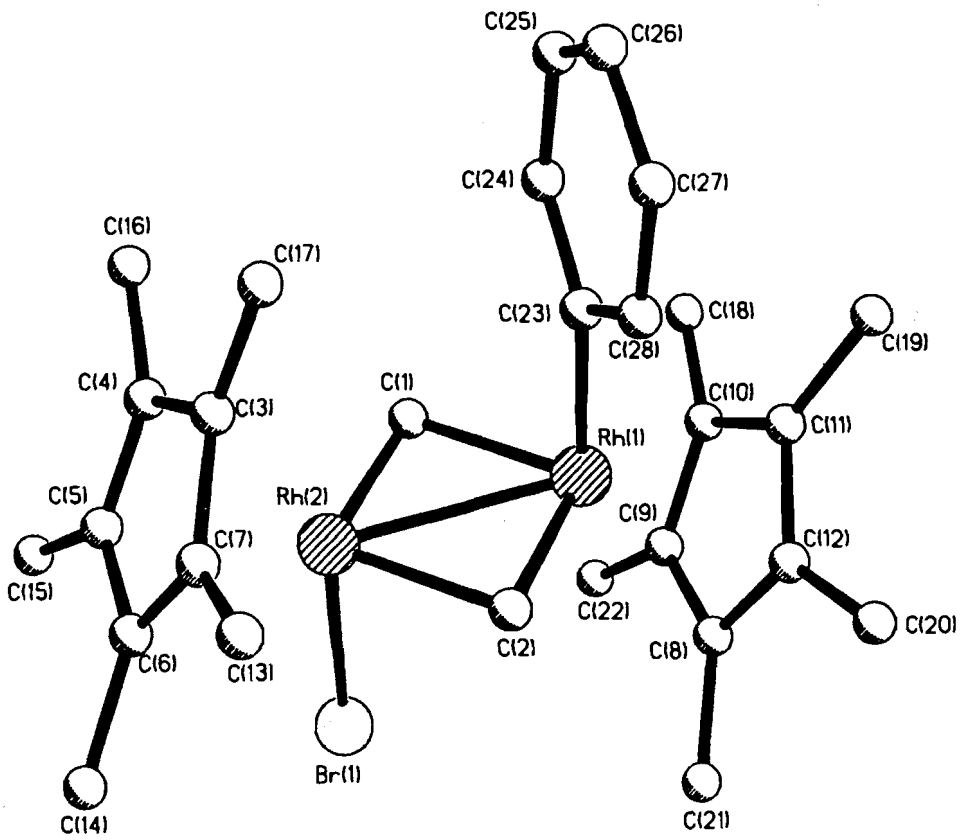

Table 1. Selected bond lengths (Å) and angles (°) for complex **2***a*, $[\{C_5Me_5)Rh(\mu\text{-}CH_2)\}_2(Ph)(Br)]$.

Rh(1)—C(1)	2.012(6)	Rh(1)—C(2)	2.024(6)
Rh(1)—C(23)	2.031(6)	Rh(1)—C(11)	2.231(6)
Rh(1)—C(10)	2.250(6)	Rh(1)—C(12)	2.264(6)
Rh(1)—C(9)	2.369(6)	Rh(1)—C(8)	2.372(6)
Rh(1)—Rh(2)	2.6410(10)	Rh(2)—C(1)	2.036(6)
Rh(2)—C(2)	2.046(6)	Rh(2)—C(6)	2.226(6)
Rh(2)—C(5)	2.224(6)	Rh(2)—C(3)	2.244(7)
Rh(2)—C(4)	2.271(7)	Rh(2)—C(7)	2.271(6)
Rh(2)—Br(1)	2.5216(11)		
C(1)-Rh(1)-C(2)	99.6(2)	C(1)-Rh(1)-C(23)	91.5(3)
C(2)-Rh(1)-C(23)	92.1(3)	C(1)-Rh(2)-Br(1)	90.0(2)
C(2)-Rh(2)-Br(1)	91.9(2)	Rh(1)-C(2)-Rh(2)	80.9(2)
Rh(1)-C(1)-Rh(2)	81.4(2)		

Cl^-, this suggests that the key step in the reaction may well be an electron transfer from the rhodium halide complex to the Grignard, which occurs more easily for bromide than for chloride.

Results and discussion

Reaction of $[\{(C_5Me_5)Rh(\mu\text{-}CH_2)\}_2Br_2]$ in toluene with 3–4 equivalents of phenylmagnesium bromide (in ether) at low temperatures gave first the bromophenyl complex **2***a*, isolated in 86% yield. If the temperature was allowed to rise to ambient during the latter part of the reaction (the other conditions remaining the same), the diphenyl complex **3** was formed, and was isolated in 45–52% yield. The yield could not be further improved due to the formation of $[\{(C_5Me_5)RhBr_2\}_2]$ (^1H NMR, δ 1.65 C_5Me_5) as by-product.

Since the phenyl dirhodium complexes have been so elusive, we have also determined the X-ray structures of **2***a* and **3** in order to see if they hold a clue to the difficulty of preparing them.

The X-ray determination showed that complex **2***a* had the expected structure (Fig. 1 and Table 1) with methylenes bridging the two rhodiums (Rh(1)—C(1) 2.012(6); Rh(1)—C(2) 2.024(6); Rh(2)—C(1) 2.036(6); Rh(2)—C(2) 2.046(6); Rh(1)—Rh(2) 2.641(1) Å). Both rhodiums are η^5-bonded to C_5Me_5 rings; in addition Rh(1) is bonded to the phenyl (Rh(1)—C(23) 2.031(6) Å) and Rh(2) to bromide (Rh(2)—Br 2.522(1) Å). The two substituents and the two rings are *trans* to each other. Both the geometry and the bond lengths are similar to those found previously in compounds of this type; however, this complex has different substituents on the two rhodiums, and hence a somewhat asymmetric $Rh(\mu\text{-}CH_2)_2Rh$ bridge is present, with the $\mu\text{-}CH_2$ slightly further from the rhodium bearing the bromine (2.036, 2.046(6) Å) than from the rhodium bearing the Ph (2.012, 2.024(6) Å). A related asymmetry is seen in the tetranuclear complex $[\{\{(C_5Me_5)Rh(\mu\text{-}CH_2)\}_2\}_2(CN)_2]^{2+}$ (3). The structures of the bromo phenyl complexes, $[(C_5Me_5)Rh(PR_3)(Ph)(Br)]$ (PR_3 = PPh_2Me, PMe_3, PPh_3, and PMe_2Ph) show Rh—Br lengths, 2.543(1), 2.533(2), 2.525(3), and 2.524(2) Å, respectively (10); thus the value of 2.522 for Rh—Br for **2***a* comes at the bottom of the

Can. J. Chem, Downloaded from www.nrcresearchpress.com by 80.90.12.36 on 09/08/12
For personal use only.

Fig. 2. The X-ray structure of complex **3**, $[\{(C_5Me_5)Rh(\mu\text{-}CH_2)\}_2(Ph)_2]$.

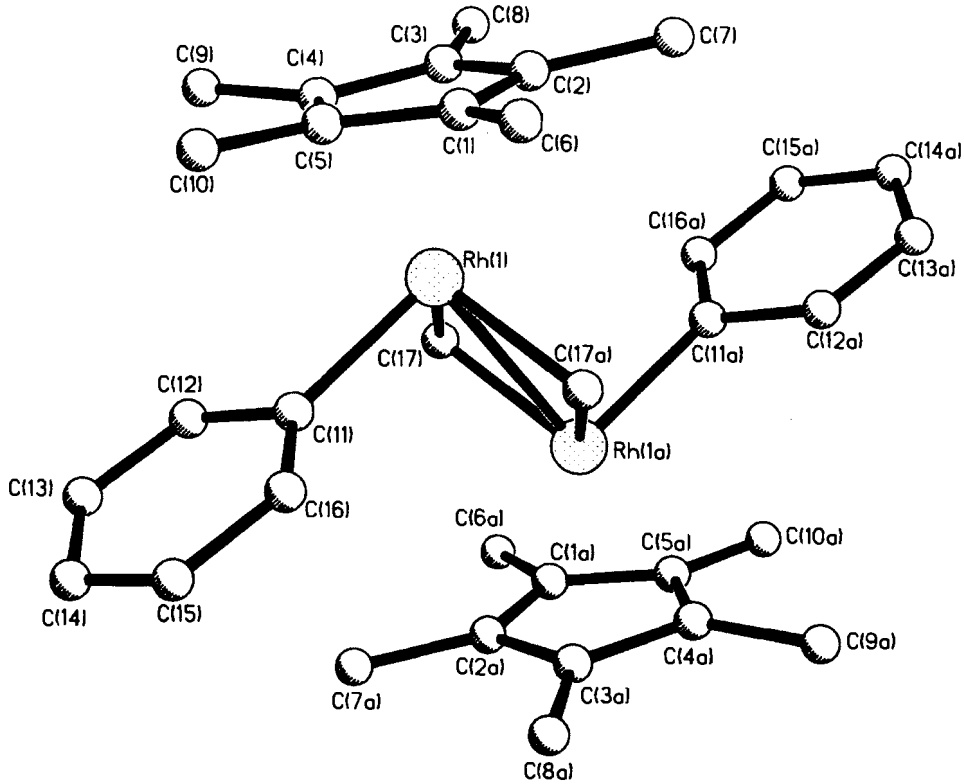

Table 2. Selected bond lengths (Å) and angles (°) for complex **3**, $[\{(C_5Me_5)Rh(\mu\text{-}CH_2)\}_2(Ph)_2]$.

Rh(1)—C(17)	2.009(6)	Rh(1)—C(11)	2.038(6)
Rh(1)—C(17)[a]	2.038(6)	Rh(1)—C(5)	2.220(6)
Rh(1)—C(4)	2.232(6)	Rh(1)—C(1)	2.278(6)
Rh(1)—C(3)	2.348(7)	Rh(1)—C(2)	2.360(6)
Rh(1)—Rh(1)[a]	2.6218(11)		
C(11)-Rh(1)-C(17)[a]	92.8(3)	C(17)-Rh(1)-C(17)[a]	99.2(2)
Rh(1)-C(17)-Rh(1)[a]	80.8(2)	C(11)-Rh(1)-C(17)	90.2(3)

[a]Symmetry transformations used to generate equivalent atoms: $-x + 1, -y, -z + 1$.

range. Similarly, the length of the Rh—C(phenyl) bond in **2***a*, 2.031 Å, is substantially shorter than those in $[(C_5Me_5)Rh(PR_3)(Ph)(Br)]$ with values of 2.065(5), 2.054(9), 2.08(1), and 2.082(6) Å, respectively, for the above series. Part of the reason for the smaller bond lengths must be the smaller size expected for Rh(IV) in **2***a* compared to that for Rh(III) in the mononuclear complexes.

The diphenyl complex **3** was characterized by elemental analysis, ^1H NMR, ^{13}C NMR, and mass spectra, and by an X-ray determination, which showed that the molecule had a *trans*-centrosymmetric structure (Fig. 2 and Table 2) with methylenes bridging the two rhodiums (Rh—CH_2, 2.009(6), 2.038(6) Å). Each rhodium is η^5-bonded to a C_5Me_5 ring and σ-bonded to a phenyl (Rh—C_6H_5 2.038(6) Å).

The Rh—Rh distances are 2.622(1) Å in **3** and 2.641(1) Å in **2***a*. While the differences are small and there are only 10 determined structures so far, these values are towards the shorter end of the range which spans 2.588(2) Å (for $[\{(C_5Me_5)Rh(\mu\text{-}CH_2)\}_2(CH{=}CH_2)_2]$ (7)) and 2.620(1) Å (for $[\{(C_5Me_5)Rh(\mu\text{-}CH_2)\}_2Me_2]$ (4)) to 2.678 Å (for $[\{(C_5Me_5)Rh)_2(\mu\text{-}CH_2)(\mu\text{-}CHMe)\}Cl_2]$ (2)) and 2.676(3) Å (for $[\{\{(C_5Me_5)Rh(\mu\text{-}CH_2)\}_2\}_2(CN)_2]^{2+}$ (3)). This suggests that substituents of low electronegativity (e.g., C) lead to shorter and stronger Rh—Rh bonds, while more electronegative substituents such as Cl lead to rather longer and presumably weaker Rh—Rh bonds. Presumably the Cl pulls some electron density out of the Rh—Rh bond. This suggestion finds support from other structural data for **2***a*; thus the Rh—Rh bond length is longer for the bromophenyl than for the diphenyl complex. Further, the angles at the rhodium bearing the phenyl are also slightly larger than those at the rhodium bearing the bromine, e.g., for CH_2-Rh-CH_2 99.6(2) against 98.1(2)°.

For the whole series of 10 structurally characterized dinuclear complexes, the Rh—CH_2 distances are all rather similar (typically 2.01–2.06 Å), within the experimental limits, as are the angles Rh-CH_2-Rh (typically 80°–83°) and CH_2-Rh-CH_2 (typically 96°–99°). The angles X-Rh-CH_2 do vary somewhat,

Can. J. Chem. Downloaded from www.nrcresearchpress.com by 80.90.12.36 on 09/08/12
For personal use only.

Table 3. Crystal data and structure refinement for complex complex **2***a*, $[\{(C_5Me_5)Rh(\mu\text{-}CH_2)\}_2(Ph)(Br)]$.

Empirical formula	$C_{28}H_{39}BrRh_2$
Formula weight	661.32
Temperature	293(2) K
Wavelength	0.71073 Å
Crystal system	Triclinic
Space group	$P\bar{1}$
Unit cell dimensions	a = 10.066(3) Å α = 85.23(2)°
	b = 11.065(3) Å β = 70.10(2)°
	c = 14.002(3) Å γ = 65.22(2)°
Volume	1328.2(6) Å^3
Z	2
Density (calculated)	1.654 Mg m^{-3}
Absorption coefficient	2.760 mm^{-1}
F(000)	664
Crystal size	0.8 × 0.4 × 0.3 mm
2θ range for data collection	3.50 to 45.00°
Index ranges	$-1 \le h \le 10$, $-11 \le k \le 11$, $-14 \le l \le 15$
Reflections collected	4302
Independent reflections	3455 (R_{int} = 0.0183)
Refinement method	Full-matrix least squares on F^2
Data/restraints/parameters	3455/0/280
Goodness-of-fit on F^2	1.044
Final R indices ($I > 2\sigma(I)$)	$R1$ = 0.0586, $wR2$ = 0.1556
R indices (all data)	$R1$ = 0.0599, $wR2$ = 0.1572
Largest diff. peak and hole	1.989 and −2.616 e Å^{-3}

but are quite close to perpendicular (85°–95°); thus the coordination about the metal atoms with respect to the two CH_2's and the R or X ligand is reasonably thought of as *fac*-octahedral. The Rh—R bond lengths in the three complexes $[\{(C_5Me_5)Rh(\mu\text{-}CH_2)\}_2R_2]$, R = Me, 2.118 av.(16) Å (4); R = Ph, 2.039(6), and R = CH=CH_2, 2.001(6) Å (7) probably reflect the different hybridizations at the carbon (and hence their different sizes), and differential π-bonding to the metal.

The two phenyl groups and the two η^5-C_5Me_5 rings in complex **3** are *trans* to each other; this arrangement is also retained in solution, as shown by the ^{1}H NMR spectra of the methylenic hydrogens. In addition to synthesizing the phenyl complexes **2***a* and **3**, we have also made the mono-*p*-tolyl and the mono-*p*-fluorophenyl complexes **2***b* and **2***c*, by the same route and in similar yield to that for **2***a*. The ^{1}H NMR spectra in the μ-CH_2 region again indicate that all the complexes have the same, *trans*, structure in solution. It is interesting that there is no indication of any dynamic behaviour (or isomerization to a *cis* isomer) in the NMR spectra of any of the complexes **2***a–c* even in acetone-d_6 down to −40°C. This contrasts with the situation in the related methylchloro complex, $[\{(\eta^5\text{-}C_5Me_5)Rh(\mu\text{-}CH_2)\}_2(Me)(Cl)]$, which is static in C_6D_6 but shows isomerization and dynamic behaviour in even slightly more polar solvents (11).

Conclusion

The di-μ-methylene-dirhodium complex $[\{(\eta^5\text{-}C_5Me_5)Rh(\mu\text{-}CH_2)\}(Br)_2]$ undergoes a halide-specific reaction with PhMgBr that gives, first, the monophenyl complex **2***a* $[\{(\eta^5\text{-}C_5Me_5)Rh(\mu\text{-}CH_2)\}_2(Ph)(Br)]$ and then the diphenyl complex **3** $[\{(\eta^5\text{-}C_5Me_5)Rh(\mu\text{-}CH_2)\}_2(Ph)_2]$. X-ray crystal structure determinations showed both molecules to have *trans* structures. There are no obvious structural features that suggest why previous attempts to make phenyl complexes of this series failed, but the success of the Grignard reaction here does appear to depend on the exclusive use of bromides.

Experimental

^{1}H NMR and ^{13}C NMR spectra were measured on a Bruker AM-250 spectrometer using the solvent as internal standard, and IR spectra on a Perkin–Elmer 1710 FT spectrometer. Elemental analyses were performed by the Sheffield University Microanalysis Service. FAB-MS spectra were recorded on a Fisons-VG ProSpec 3000 spectrometer.

All reactions were carried out under nitrogen in Schlenk tubes. Solvents were dried and distilled immediately prior to use. Phenylmagnesium bromide, *p*-fluorophenylmagnesium bromide, and *p*-tolylmagnesium bromide were purchased from Aldrich; $[\{(C_5Me_5)Rh(\mu\text{-}CH_2)\}_2Me_2]$, $[\{(C_5Me_2)Rh(\mu\text{-}CH_2)\}_2Br_2]$, and $[\{(C_5Me_5)Rh(\mu\text{-}CH_2)\}_2Cl_2]$ were prepared according to published procedures (1–9).

$[\{(\eta^5\text{-}C_5Me_5)Rh(\mu\text{-}CH_2)\}_2(C_6H_5)Br]$ (2*a*)

Phenylmagnesium bromide in ether (3.0 M; 0.1 mL, 0.3 mmol) was added dropwise over 10 min by syringe to a deep red solution of $[\{(C_5Me_5)Rh(\mu\text{-}CH_2)\}_2Br_2]$ (66.4 mg, 0.1 mmol) in freshly distilled toluene, and was cooled to −40°C. The solution was allowed to warm slowly from −40°C to −10°C over 4 h; it was then quenched with saturated aqueous NH_4Br (100 μL), and filtered. The filtrate was evaporated to dryness, and the resulting brown-red solid was extracted with pentane (3 × 50 mL) and the extract filtered and

Can. J. Chem. Downloaded from www.nrcresearchpress.com by 80.90.12.36 on 09/08/12
For personal use only.

evaporated to afford 53 mg (86%) of analytically pure **2*a*** after recrystallization from hexane. ^{1}H NMR ($CDCl_3$) δ: 1.27 and 1.56 (2 × C_5Me_5), 7.05 (dt, 2H, *o*-Ph), 6.86 (tt, 2H, *m*-Ph), 6.72 (tt, 1H, *p*-Ph); 9.28 (ddd, 2H, *J*(Rh–H) 4.5; *J*(H–H) 2 Hz, μ-CH_2), 10.26 (ddd, 2H, *J*(Rh–H) 5; *J*(H–H) 2Hz, μ-CH_2). ^{13}C NMR δ: 9.3 and 10.2 (2 × C_5Me_5), 103.6 (s) and 101.4 (d, *J* 5 Hz, C_5Me_5), 156.4 (d, *J*(Rh–C) 41 Hz, i-Ph), 138.2 (s, *o*-Ph), 121.9 (s, *m*-Ph), 127.3 (s, *p*-Ph), 178.6 (dd, *J*(Rh–C) 30 Hz, CH_2). Anal. calcd. for $C_{28}H_{39}BrRh_2$: C 50.85, H 5.9, Br 12.1%, MW 661; found: C 50.8, H 5.8, Br 12.05%, MS, FAB$^+$: *m/e* 661 (M^+, 10%).

Crystals of **2*a*** were grown from diethyl ether as red blocks; crystal dimensions 0.80 × 0.40 × 0.30 mm; the crystallographic data are summarized in Table 3. Crystal data for $C_{28}H_{39}BrRh_2$: M = 661.32. Triclinic, a = 10.066(3), b = 11.065(3), c = 14.002(3) Å, α = 85.23(2)°, β = 70.10(2)°, γ = 65.22(2)°, U = 1328.2(6) Å^3, Z = 2, D_c = 1.654 g cm^{-3}, space group $P\bar{1}$ (C_i^1, No. 2), Mo-K_α radiation ($\bar{\lambda}$ = 0.71073 Å), μ(Mo-K_α) = 27.60 cm^{-1}, F(000) = 664. Three-dimensional, room temperature X-ray data were collected in the range 3.5 < 2θ < 45° on a Siemens P4 diffractometer by the ω scan method. The 3239 independent reflections (of 4302 measured) for which $|F|/\sigma(|F|) > 4.0$ were corrected for Lorentz and polarization effects, but not for absorption. The structure was solved by direct methods and refined by full-matrix least squares on F^2. Hydrogen atoms were included in calculated positions and refined in riding mode. Refinement converged at a final R = 0.0586 (wR_2 = 0.1572 for all 4302 unique data, 280 parameters, mean and maximum δ/σ 0.000, 0.000), with allowance for the thermal anisotropy of all non-hydrogen atoms. Minimum and maximum final electron density −2.62 and 1.99 e Å^{-3}. A weighting scheme $w = 1/[\sigma^2(F_o^2) + (0.1313*P)^2 + 1.29*P]$ where $P = (F_o^2 + 2*F_c^2)/3$ was used in the latter stages of refinement. Complex scattering factors were taken from the program package SHELXL 93 (12) as implemented on the Viglen 486dx computer.

Selected bond lengths and angles, crystallographic parameters, and fractional atomic coordinates are in Tables 1, 3, and 4 respectively; further details, tables of bond lengths and angles, thermal parameters, and atomic coordinates have been deposited as supplementary material.[2]

Table 4. Atom coordinates (× 10^4) and equivalent isotropic displacement parameters (Å^2 × 10^3) for complex **2*a***, [{(C_5Me_5)Rh(μ-CH_2)}$_2$(Ph)(Br)]. U(eq) is defined as one third of the trace of the orthogonalized U_{ij} tensor.

Atom	x	y	z	U(eq)
Rh(1)	2226(1)	1924(1)	2680(1)	28(1)
Rh(2)	−406(1)	3317(1)	2329(1)	31(1)
Br(1)	−121(1)	5462(1)	2404(1)	57(1)
C(1)	40(7)	2835(7)	3657(5)	38(2)
C(2)	1822(7)	2386(7)	1346(4)	37(2)
C(3)	−1597(8)	2109(8)	2086(6)	52(2)
C(4)	−2650(8)	3040(8)	2986(5)	48(2)
C(5)	−2966(7)	4321(7)	2675(6)	45(2)
C(6)	−2200(8)	4265(7)	1585(6)	47(2)
C(7)	−1391(8)	2888(8)	1225(5)	49(2)
C(8)	4051(7)	2871(7)	2327(5)	41(2)
C(9)	3261(7)	3031(7)	3405(5)	41(2)
C(10)	3497(8)	1742(7)	3768(5)	41(2)
C(11)	4483(8)	754(7)	2936(6)	42(2)
C(12)	4789(7)	1467(7)	2032(5)	42(2)
C(13)	−576(10)	2359(11)	160(6)	80(3)
C(14)	−2391(11)	5422(9)	948(7)	76(3)
C(15)	−4019(10)	5586(9)	3333(8)	80(3)
C(16)	−3259(10)	2588(11)	4011(7)	76(3)
C(17)	−1160(11)	649(8)	2066(9)	78(3)
C(18)	3002(10)	1455(9)	4857(6)	65(2)
C(19)	5241(9)	−716(7)	2955(7)	63(2)
C(20)	5805(8)	844(10)	987(6)	69(2)
C(21)	4209(9)	3928(8)	1624(7)	62(2)
C(22)	2412(9)	4305(8)	4034(6)	58(2)
C(23)	2008(7)	182(6)	2670(5)	34(1)
C(24)	1308(8)	−298(7)	3540(5)	45(2)
C(25)	1289(10)	−1545(8)	3528(6)	60(2)
C(26)	1930(11)	−2335(8)	2639(7)	66(2)
C(27)	2675(9)	−1889(7)	1776(7)	58(2)
C(28)	2725(8)	−659(7)	1779(5)	45(2)

[{(η^5-C_5Me_5)Rh(μ-CH_2)}$_2$(4-$CH_3C_6H_4$)Br] (2*b*)

This was obtained in 82% yield from [{(C_5Me_5)Rh(μ-CH_2)}$_2$$Br_2$] and 4-tolylmagnesium bromide in ether (1 M, 0.15 mL, 0.15 mmol) by the method used for **2*a***. ^{1}H NMR ($CDCl_3$) δ: 1.26 (s, 15H, C_5Me_5), 1.53 (s, 15H, C_5Me_5); 6.64 (d, 2H; *J* 8 Hz, 2*H*-To), 6.84 (d, 2H, *J* 8 Hz, 3*H*-To), 2.11 (s, 3H, Me), 9.20 (bs, 2H, CH_2), 10.18 (dd, 2H, CH_2, *J*(Rh–H) 5 Hz, *J*(H–H) 2.0 Hz). ^{13}C NMR δ: 9.3 (s, C_5Me_5), 10.2 (s, C_5Me_5), 20.45 (s, Me), 103.5 (s, C_5Me_5), 101.4 (d, C_5Me_5, *J* 5 Hz), 137.8 (s, 2-To), 128.3 (s, 4-To), 126.8 (s, 3-To), 178.6 (dd, CH_2, *J*(Rh–C) 30 Hz). Anal. calcd. for $C_{29}H_{41}BrRh_2$: C 51.6, H 6.1, Br 11.8%, M 675; found: C 51.4, H 5.8, Br 11.75%, MS, FAB$^+$: *m/e* 675 (M^+, 20%).

[{(η^5-C_5Me_5)Rh(μ-CH_2)}$_2$(4-FC_6H_4)Br] (2*c*)

This was obtained in 82% yield from [{(C_5Me_5)Rh(μ-CH_2)}$_2$$Br_2$] and 4-fluorophenylmagnesium bromide in ether (1 M, 0.15 mL, 0.15 mmol) by the method used for **2*a***. ^{1}H NMR ($CDCl_3$) δ: 1.32 (s, 15H, C_5Me_5), 1.57 (s, 15H, C_5Me_5), 6.64 (dtd, 2H, 2*H*-C_6H_4F, *J* 8 and 2 Hz), 6.96 (dtd, 2H, 3*H*-C_6H_4F, *J* 8 and 2 Hz), 9.24 (bs, 2H, μ-CH_2), 10.18 (dd, μ-CH_2, *J*(Rh–H) 4 Hz; *J*(H–H) 1 Hz). ^{13}C NMR δ: 9.37 (s, Me), 10.18 (s, Me), 103.7 (s, C_5Me_5), 101.4 (d, C_5Me_5, *J*(Rh–C) 5 Hz), 115.7 (d, *J*(C–F) 22 Hz), 138.2(s), 128.6(s). Anal. calcd. for $C_{28}H_{38}BrFRh_2$: C 49.5, H 5.6%, M 678; found: C 49.4, H 5.7%, MS, FAB$^+$: *m/e* 678 (M^+, 25%).

[{(η^5-C_5Me_5)Rh(μ-CH_2)}$_2$$Ph_2$] (3)

Phenylmagnesium bromide in ether (3.0 M; 0.12 mL, 0.36 mmol) was added dropwise by syringe over 10 min to a deep red solution of [{(C_5Me_5)Rh(μ-CH_2)}$_2$$Br_2$] (66.4 mg,

[2] These data can be purchased from: The Depository of Unpublished Data, Document Delivery, CISTI, National Research Council Canada, Ottawa, Canada K1A 0S2.

Bond lengths and angles and hydrogen atom coordinates have also been deposited at the Cambridge Crystallographic Data Centre and can be obtained on request from The Director, Cambridge Crystallographic Data Centre, University Chemical Laboratory, 12 Union Road, Cambridge CB2 1EZ, UK.

Structure factors are no longer being deposited and can be obtained on request from the author.

Can. J. Chem. Downloaded from www.nrcresearchpress.com by 80.90.12.36 on 09/08/12
For personal use only.

Table 5. Crystal data and structure refinement for complex **3**, [{(C_5Me_5)Rh(μ-CH_2)}$_2$($Ph)_2$].

Empirical formula	$C_{34}H_{44}Rh_2$
Formula weight	658.51
Temperature	293(2) K
Wavelength	0.71073 Å
Crystal system	Orthorhombic
Space group	*Pccn*
Unit cell dimensions	a = 17.102(8) Å α = 90°
	b = 10.396(4) Å β = 90°
	c = 16.134(7) Å γ = 90°
Volume	2869(2) Å^3
Z	4
Density (calculated)	1.525 Mg m^{-3}
Absorption coefficient	1.171 mm^{-1}
F(000)	1352
Crystal size	0.7 × 0.45 × 0.3 mm
θ range for data collection	2.29 to 22.48°
Index ranges	$-1 \le h \le 18$, $-1 \le k \le 11$, $-1 \le l \le 17$
Reflections collected	2567
Independent reflections	1877 (R_{int} = 0.0244)
Absorption correction	Semi-empirical
Max. and min. transmission	0.355 and 0.294
Refinement method	Full-matrix least squares on F^2
Data/restraints/parameters	1877/0/163
Goodness-of-fit on F^2	1.078
Final R indices [$I > 2\sigma$(I)]	$R1$ = 0.0426, $wR2$ = 0.1178
R indices (all data)	$R1$ = 0.0521, $wR2$ = 0.1235
Largest diff. peak and hole	0.674 and −0.555 e Å^{-3}

0.1 mmol) in freshly distilled toluene (10 mL) cooled to −40°C. The reaction mixture was stirred at this temperature, and was allowed to warm slowly to −10°C over 2 h; it was finally allowed to warm to room temperature, where it was stirred for 6 h. The mixture was then quenched with saturated aqueous NH_4Br (100 μL), filtered, and the filtered solution quickly passed through a short Florisil column, eluting with toluene. Removal of the toluene in vacuo left a red solid, which was extracted with pentane (15 mL); removal of the pentane left 34 mg (52%) of analytically pure [{(C_5Me_5)Rh(μ-CH_2)}$_2$$Ph_2$]. ^{1}H NMR ($CD_2Cl_2$) δ: 1.12 (s, 30H, C_5Me_5), 8.90 (t, μ-CH_2, 4H, J(Rh–H) 1.5 Hz), 7.0 (dt, 4H, J 7 Hz, 1.5 Hz), 6.76 (dt, 4H, J 7 Hz, 1.5 Hz), 6.68 (dt, 2H, J 7 Hz, 1.5 Hz). ^{13}C NMR (CD_2Cl_2) δ: 9.37 (s, C_5Me_5), 102.4 (s, C_5Me_5), 121.7(s), 126.9(s), 139.4 (s), 156.6 (dd, J 43 and 10 Hz), 174.2 (t, CH_2, J(Rh–C) 29 Hz). Anal. calcd. for $C_{34}H_{44}Rh_2$: C 62.0, H 6.7, M 658; found: 61.9, 6.8%, FAB–MS: 658 (M$^+$, 100%).

Deep red oblong crystals of **3** were grown from pentane–methanol, the crystallographic data are summarized in Table 5. Crystal data for $C_{34}H_{44}Rh_2$: M = 658.51; crystal dimensions 0.70 × 0.45 × 0.3 mm. Orthorhombic, a = 17.102(8), b = 10.396(4), c = 16.134(7) Å, U = 2869(2) Å^3, Z = 4, D_c = 1.525 g cm^{-3}, space group *Pccn* (D^{10}_{2h}, No. 56), Mo-K_α radiation ($\bar{\lambda}$ = 0.71073 Å), μ(Mo-Kα) = 1.171 mm^{-1}, F(000) = 1352. Three-dimensional, room temperature X-ray data were collected in the range $3.5 < 2\theta < 45°$ on a Siemens P4 diffractometer by the ω scan method. The 1518 independent reflections (of 2567 measured) for which $|F|/\sigma(|F|) > 4.0$ were corrected for Lorentz and polarization effects, and for absorption by analysis of 10 azimuthal scans (minimum and maximum transmission coefficients 0.294 and 0.355). The structure was solved by direct methods and refined by full-matrix least squares on F^2. Hydrogen atoms were included in

Table 6. Atom coordinates (× 10^4) and equivalent isotropic displacement parameters (Å^2 × 10^3) for complex **3**, [{(C_5Me_5)Rh(μ-CH_2)}$_2$($Ph)_2$]. U(eq) is defined as one third of the trace of the orthogonalized U_{ij} tensor

	x	y	z	U(eq)
Rh(1)	4520(1)	848(1)	5322(1)	31(1)
C(1)	3750(4)	2454(7)	4817(4)	40(2)
C(2)	3382(4)	1321(7)	4554(4)	40(2)
C(3)	3158(4)	583(7)	5258(4)	44(2)
C(4)	3406(3)	1315(6)	5975(4)	40(2)
C(5)	3756(3)	2475(6)	5693(4)	39(1)
C(6)	4018(5)	3525(7)	4259(5)	66(2)
C(7)	3207(4)	950(7)	3664(4)	58(2)
C(8)	2717(4)	−629(8)	5275(5)	65(2)
C(9)	3216(4)	986(7)	6856(4)	56(2)
C(10)	4005(4)	3559(7)	6230(5)	62(2)
C(11)	5331(3)	1435(6)	6167(4)	35(1)
C(12)	5285(4)	986(6)	6993(4)	43(2)
C(13)	5759(4)	1496(7)	7602(4)	52(2)
C(14)	6304(4)	2434(7)	7421(4)	59(2)
C(15)	6356(4)	2882(7)	6622(5)	61(2)
C(16)	5868(4)	2398(7)	6014(4)	46(2)
C(17)	4712(4)	−994(6)	5640(4)	36(1)

calculated positions and refined in riding mode. Refinement converged at a final $R = 0.0426$ ($wR_2 = 0.1235$, for all 1877 data, 163 parameters, mean and maximum δ/σ 0.000, 0.001), with allowance for the thermal anisotropy of all non-hydrogen atoms. Minimum and maximum final electron density −0.555 and 0.674 e A^{-3}. A weighting scheme $w = 1/[\sigma^2(F_o^2) + (0.0708*P)^2 + 4.53*P]$ where $P = (F_o^2 + 2*F_c^2)/3$ was used in the latter stages of refinement. Complex scattering factors were taken from the program package SHELXL 93 (12) as implemented on the Viglen 486dx computer. Selected bond lengths and angles, crystallographic parameters, and fractional atomic coordinates are in Tables 2, 5, and 6, respectively; further details, tables of bond lengths and angles, thermal parameters, and atomic coordinates have been deposited.[2]

Acknowledgements

We thank the Royal Society, the Science and Engineering Research Council, and the EU Human Capital and Mobility scheme (contract no: ERBCHRXCT930147) for support.

References

1. K. Isobe, P.M. Bailey, P. Schofield, J.T. Gauntlett, A. Nutton, and P.M. Maitlis. J. Chem. Soc. Chem. Commun. 425 (1982).
2. J. Martinez, J.B. Gill, H. Adams, N.A. Bailey, I.M. Saez, and P.M. Maitlis. Can. J. Chem. **67**, 1698 (1989).
3. J. Martinez, H. Adams, N.A. Bailey, and P.M. Maitlis. J. Organomet. Chem. **405**, 393 (1991).
4. K. Isobe, A. Vázquez de Miguel, P.M. Bailey, S. Okeya, and P.M. Maitlis. J. Chem. Soc. Dalton Trans. 1441 (1983).
5. B.E. Mann, N.J. Meanwell, C.M. Spencer, B.F. Taylor, and P.M. Maitlis. J. Chem. Soc. Dalton Trans. 1555 (1985).
6. N.J. Meanwell, A.J. Smith, and P.M. Maitlis. J. Chem. Soc. Dalton Trans. 1419 (1986).
7. J. Martinez, J.B. Gill, H. Adams, N.A. Bailey, I.M. Saez, G.J. Sunley, and P.M. Maitlis. J. Organomet. Chem. **394**, 583 (1990).
8. N.J. Meanwell, A.J. Smith, H. Adams, S. Okeya, and P.M. Maitlis. Organometallics, **2**, 1705 (1983).
9. K. Isobe, S. Okeya, N.J. Meanwell, A.J. Smith, H. Adams, and P.M. Maitlis. J. Chem. Soc. Dalton Trans. 1215 (1984).
10. W.D. Jones and V.L. Kuykendall. Inorg. Chem. **30**, 2615 (1991).
11. S. Okeya, N.J. Meanwell, B.F. Taylor, K. Isobe, A. Vázquez de Miguel, and P.M. Maitlis. J. Chem. Soc. Dalton Trans. 1453 (1984).
12. G.M. Sheldrick. SHELXL 93, an integrated system for solving and refining crystal structures from diffraction data (Revision 5.1). University of Gottingen, Germany. 1993.

Can. J. Chem. Downloaded from www.nrcresearchpress.com by 80.90.12.36 on 09/08/12
For personal use only.

Tin and lead derivatives of a Schiff base – bis(orthoquinone) ligand

Bruce R. McGarvey, Andrzej Ozarowski, Zhigang Tian, and Dennis G. Tuck

Abstract: The condensation of two molecules of 3,5-di-*tert*-butylcatechol (dbc) with ammonia under oxidizing conditions is believed to proceed via a keto-imine radical. Further condensation, and subsequent reaction with tin(II) or lead(II) halides, yields complexes of identical composition, M[dbqdi]$_2$, where dbqdi is 3,5-di-*tert*-butyl-1,2-quinone-1-(2-hydroxy-3,5-di-*tert*-butylphenyl)imine anion; this name is used without prejudice as to the actual structure of the ligand. The two compounds differ in crystallographic and magnetic properties, and ESR measurements show that the tin compound has a triplet ground state. Both involve six-coordination of the metal in a distorted environment; tin is in the +IV state, but lead is +II, and there are corresponding differences in the form of the ligand. For Sn^{IV}(dbqdi)$_2$, the crystal parameters are orthorhombic, space group $C222_1$, a = 19.597(4), b = 24.375(4), c = 23.755(6) Å, Z = 8, and R = 0.073 for 1405 unique reflections. For Pb^{II}(dbqdi)$_2$, monoclinic, space group $P2_1/n$, a = 14.56(1), b = 25.967(9), c = 15.13(1) Å, β = 99.81(7)°, Z = 4, R = 0.065 for 4911 unique reflections. The different complexation behaviour is shown to be a consequence of the redox properties of the two metallic elements.

Key words: tin, lead, ESR, coordination chemistry, electron transfer.

Résumé : On croit généralement que la condensation de deux molécules de 3,5-di-*tert*-butylcatéchol (dbc) avec de l'ammoniac, dans des conditions oxydantes, se produit par le biais d'un radical céto-imine. Une condensation subséquente, avec réaction ultérieure avec des halogénures d'étain(II) ou de plomb(II), fournit des complexes de composition identique, M(dbqdi)$_2$, dans lesquels dbqdi est l'anion 3,5-di-*tert*-butyl-1,2-quinone-1-(2-hydroxy-3,5-di-*tert*-butylphényl)imine; on utilise ce nom sans égard à la structure réelle du coordinat. Les propriétés cristallographiques et magnétiques des deux composés sont différentes et les mesures de RPE indiquent que le dérivé de l'étain possède une état fondamental triplet. Les deux impliquent un niveau de coordination de six pour le métal, avec un environnement déformé; l'étain est dans un état +IV alors que pour le plomb il est de +II et on peut observer des différences correspondantes dans le forme du coordinat. Pour le Sn^{IV}(dbqdi)$_2$, les cristaux sont orthorhombiques, groupe d'espace $C222_1$, avec a = 19,597(4), b = 24,375(4) et c = 23,755(5) Å, Z = 8 et R = 0,073 pour 1405 réflexions uniques. Pour le Pb^{II}(dbqdi)$_2$, les cristaux sont monocliniques, groupe d'espace $P2_1/n$, avec a = 14,56(1), b = 25,967(9) et c = 15,13(1) Å, β = 99,81(7)°, Z = 4 et R = 0,065 pour 4911 réflexions uniques. On montre que le comportement différent de complexation est un conséquence des propriétés redox de deux éléments métalliques.

Mots clés : plomb, étain, RPE, chimie de coordination, transfert d'électron.

[Traduit par la rédaction]

Introduction

The reactions of substituted orthobenzoquinones with main group elements, or the low oxidation state derivatives of such elements, have been the subject of a number of recent papers from this laboratory. In general, the products of these processes are the appropriate catecholate or semiquinone derivatives, which have been characterized by spectroscopic and crystallographic methods. An important feature of these results is that the redox reactions in question have been shown to be one-electron transfer processes (1).

We have now extended this research to an investigation of the structure of the compounds formed when tin or lead in the +II state react with a heavily substituted catechol. Girgis and Balch (2) found that by treating an aqueous ethanol solution of 3,5-di-*tert*-butylcatechol and various divalent metal ions (Mg, Zn, Fe, Ni, Cu, Cd) with concentrated ammonium hydroxide in the presence of air, complexes of the 3,5-di-*tert*-butyl-1,2-quinone-1-(2-hydroxy-3,5-di-*tert*-butylphenyl)imine (dbqdi) anion could be formed. This name is used without prejudice since, in principle and in practice, this ligand may exist in forms varying in charge from +1 to −3, as shown in Scheme 1, and we refer to these as dbqdi-I, etc. in the discussion of our results.

All of these species may contribute in principle in the ligation of this interesting system. Many such complexes of transition metal complexes, with the metal in different oxidation

Received November 25, 1994.

This paper is dedicated to Professor William A.G. Graham on the occasion of his 65th birthday.

B.R. McGarvey, A. Ozarowski, Z. Tian, and D.G. Tuck.[1]
Department of Chemistry and Biochemistry, University of Windsor, Windsor, ON N9B 3P4, Canada.

[1] Author to whom correspondence may be addressed. Telephone: (519) 253-4232, ext. 3541. Fax: (519) 973-7098.

Can. J. Chem. Downloaded from www.nrcresearchpress.com by 80.90.12.36 on 09/08/12
For personal use only.

Can. J. Chem. Downloaded from www.nrcresearchpress.com by 80.90.12.36 on 09/08/12
For personal use only.

Scheme 1.

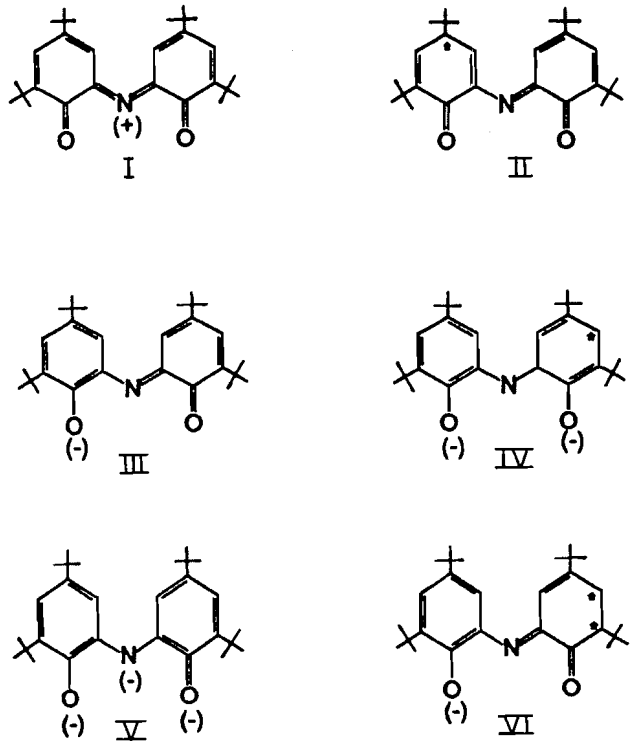

states (e.g., M^{2+}, M = Ni, Cu, Zn, Cd; M^{3+}, M = Fe, Co; M^{4+}, M = Ti, Mn) have been prepared and studied by spectroscopic, electrochemical, and X-ray crystallographic methods (2–6), but there has been relatively little work on main group analogues. In addition to the preparative work by Girgis and Balch, Stegmann, Ulmschneider, and Scheffler (7, 8) reported that a series of tin(IV) complexes could be produced from the reaction of 2-amino-4,6-di-*tert*-butylphenoxyl with aryltin(IV) halides, although the structure which they proposed has been questioned (2). One of the interesting outcomes of the present work is that reactions involving tin(II) and lead(II) halides as starting materials give rise to products with differing magnetic and structural characteristics.

Experimental section

General techniques

All the chemicals in this work were reagent grade or better, and were used as supplied. Microanalysis was carried out by Canadian Microanalytical Services Ltd. Infrared spectra in the 400–4000 cm^{-1} region were run as KBr discs on a Nicolet 5DX spectrometer, ^1H and ^{13}C NMR spectra on a Bruker AC-300L spectrometer, the UV–visible spectrum on a Shimadzu spectrometer, and ESR spectra on a Bruker ESP-300 instrument, using methods described previously (9).

Preparative

Reaction with $SnCl_2$

Tin(II) chloride (0.113 g, 0.6 mmol) was suspended in a solution of 3,5-di-*tert*-butylcatechol (0.530 g, 2.41 mmol) in 95% ethanol (50 cm^3). After addition of concentrated aqueous ammonia (5 cm^3), a stream of air was gently bubbled through the mixture, whereupon the solution turned dark blue. After overnight stirring, this solution was filtered and the dark blue solid was collected and washed with 95% ethanol (2 × 5 cm^3). The vacuum-dried product weighed 0.480 g; yield 75%, based on the proposed molecular formula. Anal. calcd. for $C_{56}H_{80}N_2O_4Sn$: C 69.8, H 8.37, N 2.91%; found: C 69.5, H 8.29, N 2.92. Crystals suitable for X-ray crystallographic analysis were obtained by recrystallization of the reaction product from methylene dichloride.

Reaction with PbF_2

(*i*) A suspension of lead difluoride (0.294 g, 1.20 mmol) in a solution of 3,5-di-*tert*-butylcatechol (1.060 g, 4.82 mmol) in 95% ethanol (50 cm^3), was treated with concentrated ammonia solution (5 cm^3), and a stream of air gently bubbled through the mixture. The solution turned dark olive-green at this point and, after about 30 min stirring, a dark black-green solid was detected. After being stirred overnight, the mixture was filtered, and the dark green solid product washed with 95% ethanol (2 × 5 cm^3). The vacuum-dried product weighed 1.010 g; yield 80%, based on the proposed molecular formula. Anal. calcd. for $C_{56}H_{80}N_2O_4Pb$: C 63.9, H 7.66, N 2.66%; found: C 63.9, H 7.57, N 2.70. Recrystallization from chloroform gave crystals suitable for X-ray crystallography.

(*ii*) In a related experiment, 3,5-di-*tert*-butyl-*o*-benzoquinone (0.265 g, 1.21 mmol) and 3,5-di-*tert*-butylcatechol (0.265 g, 1.21 mmol) reacted with lead(II) fluoride (0.147 g, 0.6 mmol). The same procedure as in (*i*) was used, except that the treatment with air was omitted. The vacuum-dried dark green product weighed 0.485 g; yield 72%. The product of this reaction had the same IR and ^1H NMR spectra as in (*i*).

Both compounds are moderately soluble in chloroform, acetone, and dichloromethane, giving dark blue (Sn) or green (Pb) solutions. The lead complex has broad strong absorption at 778, 467, 352, 293 sh, and 232 nm (cf. 793, 736, 430, 365, 300 sh, and 241 nm for the zinc complex (2).

Crystallographic analysis

(*i*) In the study of $SnO_4N_2C_{56}H_{80}$, **1**, a dark blue block crystal on a glass fibre was mounted in a Rigaku AFC6S diffractometer, equipped with graphite monochromated Mo- Kα radiation (λ = 0.71069 Å) and a rotating anode generator. Cell constants, and orientation matrices for data collection, were obtained from least-squares refinements, using 20 carefully centred reflections in the range $12.61 < 2\theta < 19.62°$. Based on the systematic absences *hkl*: $h + k \neq 2n$; 001: $l \neq 2n$, the space group was uniquely identified as $C222_1$ (no. 20), and this was confirmed by subsequent solution and refinement of the structure. Details of the intensity collection are given in Table 1.

The intensities of three representative reflections were measured after every 150 reflections. Over the course of data collection, the standards decreased by −2.1%, and a linear correction factor was applied to the results. Absorption corrections were unnecessary (cf. Table 1), but the values were corrected for Lorentz and polarization effects. The structure was solved by direct methods, and expanded using Fourier techniques. The non-hydrogen atoms were refined isotropically; hydrogen atoms on carbon were included in ideal positions but were not refined. The final cycle of full-matrix least-squares refinement was based on 1405 observed reflections ($I > 3\sigma(I)$) and 253 variable parameters, and the solution converged at

Can. J. Chem. Downloaded from www.nrcresearchpress.com by 80.90.12.36 on 09/08/12
For personal use only.

Table 1. Summary of crystal intensity data, collection, and structural refinement for tin and lead complexes of dbqdi.

	1	2
Chemical formula	$C_{56}H_{80}N_2O_4Sn$	$C_{56}H_{80}N_2O_4Pb$
M	963.95	1052.46
Crystal system	Orthorhombic	Monoclinic
Space group	$C222_1$ (No. 20)	$P2_1/n$ (No. 14)
a (Å)	19.597(4)	14.56(1)
b (Å)	24.375(4)	25.967(9)
c (Å)	23.755(6)	15.13(1)
β (deg)	—	99.81(7)
V (Å^3)	11347(3)	5634(6)
Z	8	4
F(000)	4096	2176
D_c (g cm^{-3})	1.13	1.24
Crystal dimensions/mm	0.3 × 0.3 × 0.2	0.4 × 0.4 × 0.3
μ (cm^{-1})	4.91	30.4
2θ (deg (max))	50	50
Total reflections measured	4516	10594
Unique data used ($I \geq 3\sigma$ (I))	1405	4911
T (°C)	23	23
No. of parameters	253	563
R	0.073	0.065
R'	0.065	0.072
Maximum shift/error in final cycle	0.01	0.08
Maximum, minimum peaks in final difference map (e Å^{-3})	0.70, −0.68	0.96, −1.55

Fig. 1. Structure of Sn(dbqdi)$_2$, showing the numbering system; ORTEP diagram, with atoms shown as 30% probability ellipsoids. Hydrogen atoms have been omitted for clarity.

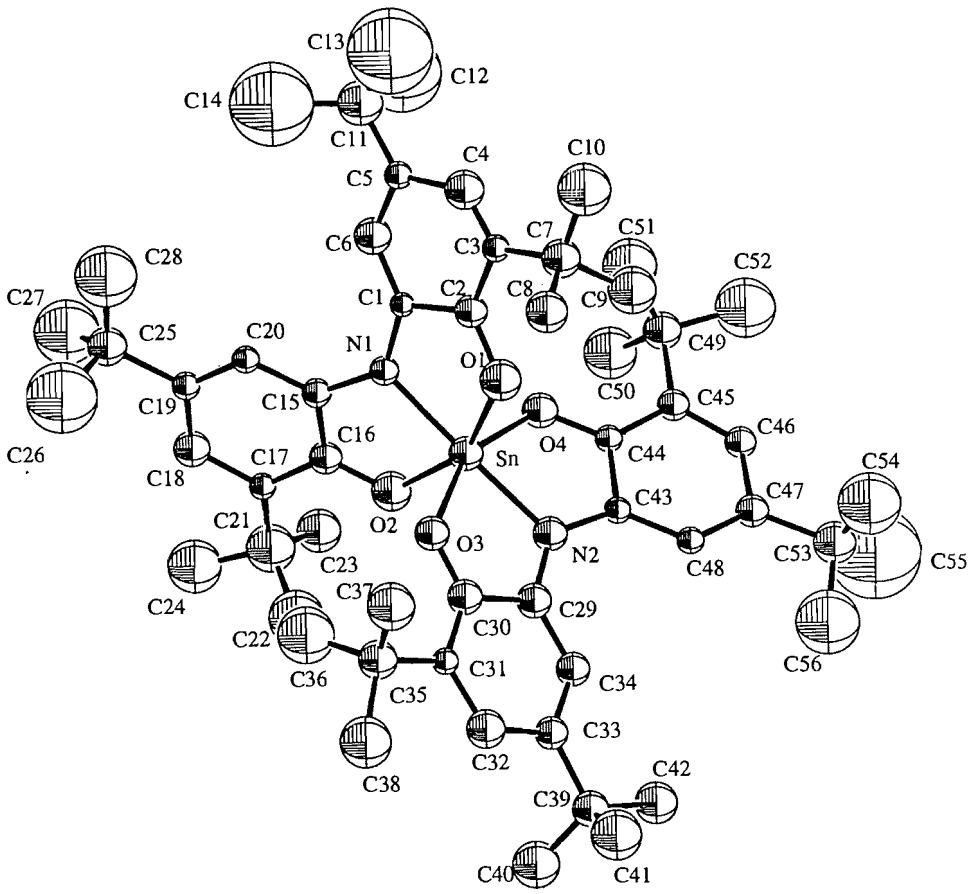

Fig. 2. Structure of $Pb(dbqdi)_2$, showing the numbering system; ORTEP diagram, with atoms shown as 30% probability ellipsoids. Hydrogen atoms have been omitted for clarity.

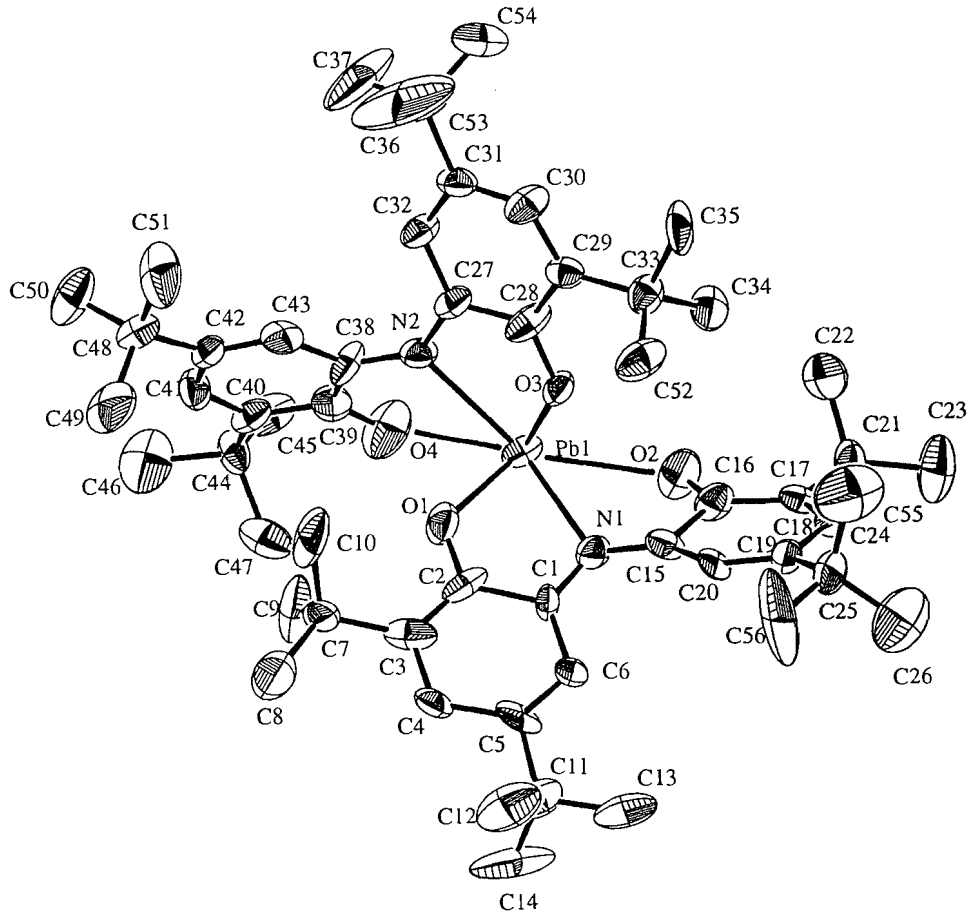

$R = 0.073$ and $R' = 0.065$. A final Fourier difference map calculation showed no peaks of chemical significance; the maximum and minimum peaks corresponded to 0.70 and -0.68 e $Å^{-3}$, respectively.

(*ii*) A dark green block crystal of $PbO_4N_2C_{56}H_{80}$, **2**, was used, with the techniques just described. Cell constants, and an orientation matrix for data collection, were obtained from a least-squares refinement using 25 carefully centred reflections in the range $25.12 < 2\theta < 29.06°$. From the systematic absences $h0l$: $h + l \neq 2n$; $0k0$: $k \neq 2n$, the space group was identified as $P2_1/n$ (no. 14), and this was confirmed by subsequent solution and refinement of the structure. Details of the intensity collection are given in Table 1.

No decay correction was applied, since the intensities of three representative reflections, measured after every 150 reflections, remained constant throughout the data collection, indicating crystal and electronic stability. An empirical absorption correction, using the program DEFABS (10), was applied with transmission factors ranging from 0.92 to 1.01; the data were also corrected for Lorentz and polarization effects. The structure was solved by direct methods. The non-hydrogen atoms were refined anisotropically, except that carbon atoms C(7)–C(13), C(17), C(38), C(41), and C(44)) were refined isotropically; hydrogen atoms on carbon were initially included in ideal positions, and subsequently refined isotropically. After several cycles of refinement, the structure converged to $R = 0.068$ and $R' = 0.083$. A final Fourier difference map calculation showed no peaks of chemical significance; the maximum and minimum peaks corresponded to 1.20 and 1.90 e $Å^3$, respectively.

In both sets of calculations, neutral-atom scattering factors were taken from Cromer and Waber (11). Anomalous dispersion effects were included in the calculations (12); the values for $\Delta f'$ and $\Delta f''$ were those published by Cromer (13). All calculations were performed using the TEXSAN (14) crystallographic software package. The structure of the molecules are shown in Figs. 1 and 2, the positional parameters are in Table 2 and 4, and the important bond distances and angles in Tables 3 and 5.

Tables of hydrogen-atom coordinates and thermal parameters, anisotropic thermal parameters for other atoms, least-squares planes, and structural data for aromatic rings and *tert*-butyl groups for each structure are available as supplementary data.[2]

[2] This supplementary data can be purchased from: The Depository of Unpublished Data, Document Delivery, CISTI, National Research Council Canada, Ottawa, Canada K1A 0S2.

Tables of hydrogen atom coordinates and structural data have also been deposited with the Cambridge Crystallographic Data Centre, and can be obtained on request from The Director, Cambridge Crystallographic Data Centre, University Chemical Laboratory, 12 Union Road, Cambridge, CB2 1EZ, U.K.

Can. J. Chem. Downloaded from www.nrcresearchpress.com by 80.90.12.36 on 09/08/12
For personal use only.

Can. J. Chem. Downloaded from www.nrcresearchpress.com by 80.90.12.36 on 09/08/12
For personal use only.

Table 2. Final fractional coordinates and thermal parameters for non-hydrogen atoms of $Sn(dbqdi)_2$ with standard deviations in parentheses.

Atom	x	y	z	B_{eq}
Sn(1)	0.0466(1)	0.2013(1)	0.0607(1)	3.17(5)
O(1)	0.014(1)	0.2814(8)	0.0470(9)	4.6(6)
O(2)	0.115(1)	0.143(1)	0.0902(10)	4.2(7)
O(3)	0.0803(9)	0.1908(9)	−0.0202(8)	3.3(5)
O(4)	−0.022(1)	0.1896(9)	0.1257(8)	3.5(5)
N(1)	0.119(1)	0.252(1)	0.098(1)	2.2(6)
N(2)	−0.028(1)	0.152(1)	0.024(1)	3.2(7)
C(1)	0.101(1)	0.305(1)	0.110(1)	1.6(6)
C(2)	0.039(2)	0.319(1)	0.083(1)	2.9(7)
C(3)	0.015(2)	0.374(1)	0.089(1)	2.0(7)
C(4)	0.042(2)	0.403(1)	0.124(1)	4.2(8)
C(5)	0.102(2)	0.392(1)	0.156(1)	2.0(7)
C(6)	0.127(2)	0.342(1)	0.146(1)	3.7(8)
C(7)	−0.043(2)	0.391(1)	0.055(2)	4.0(7)
C(8)	−0.029(2)	0.389(1)	−0.006(2)	4.9(9)
C(9)	−0.108(2)	0.353(2)	0.061(2)	6.2(10)
C(10)	−0.066(2)	0.444(2)	0.069(2)	7(1)
C(11)	0.135(2)	0.428(2)	0.198(2)	5(1)
C(12)	0.095(4)	0.410(3)	0.254(3)	17(2)
C(13)	0.106(4)	0.481(3)	0.192(3)	19(2)
C(14)	0.215(4)	0.428(3)	0.199(3)	19(2)
C(15)	0.182(2)	0.222(1)	0.111(1)	2.2(8)
C(16)	0.174(2)	0.165(2)	0.105(1)	3.0(9)
C(17)	0.233(2)	0.132(1)	0.114(1)	1.9(7)
C(18)	0.296(2)	0.159(2)	0.127(2)	3.5(9)
C(19)	0.300(2)	0.217(1)	0.130(1)	2.1(7)
C(20)	0.245(2)	0.248(1)	0.120(1)	2.2(7)
C(21)	0.226(2)	0.071(2)	0.116(2)	6(1)
C(22)	0.205(2)	0.051(2)	0.058(2)	8(1)
C(23)	0.182(2)	0.053(2)	0.157(2)	5.3(10)
C(24)	0.296(3)	0.048(2)	0.124(2)	7(1)
C(25)	0.370(2)	0.247(1)	0.141(2)	4.1(9)
C(26)	0.413(3)	0.241(3)	0.090(2)	13(1)
C(27)	0.407(3)	0.223(2)	0.191(2)	11(1)
C(28)	0.370(3)	0.306(2)	0.150(2)	10(1)
C(29)	−0.012(2)	0.130(1)	−0.028(1)	3.3(8)
C(30)	0.052(2)	0.153(1)	−0.051(1)	3.3(7)
C(31)	0.072(1)	0.133(1)	−0.101(1)	1.9(7)
C(32)	0.036(2)	0.089(1)	−0.128(1)	4.0(8)
C(33)	−0.024(2)	0.064(1)	−0.103(1)	2.9(8)
C(34)	−0.045(2)	0.085(1)	−0.053(1)	3.1(6)
C(35)	0.134(2)	0.159(2)	−0.130(2)	4.1(9)
C(36)	0.198(3)	0.152(2)	−0.090(2)	8(1)
C(37)	0.120(2)	0.217(2)	−0.140(2)	6(1)
C(38)	0.146(2)	0.128(2)	−0.188(2)	7(1)
C(39)	−0.057(2)	0.015(1)	−0.132(1)	3.6(8)
C(40)	−0.007(2)	−0.027(2)	−0.145(2)	6(1)
C(41)	−0.080(2)	0.035(2)	−0.189(2)	6(1)
C(42)	−0.118(2)	−0.006(2)	−0.101(2)	4.9(9)
C(43)	−0.090(1)	0.151(1)	0.052(1)	2.0(7)
C(44)	−0.084(2)	0.176(1)	0.108(1)	2.0(8)
C(45)	−0.143(2)	0.179(1)	0.142(1)	2.6(8)
C(46)	−0.203(2)	0.161(1)	0.119(1)	2.7(8)
C(47)	−0.212(2)	0.140(1)	0.063(2)	2.9(7)
C(48)	−0.155(2)	0.137(1)	0.032(1)	2.0(7)
C(49)	−0.136(2)	0.200(2)	0.205(1)	3.8(7)
C(50)	−0.089(2)	0.154(2)	0.238(2)	7(1)
C(51)	−0.107(2)	0.260(2)	0.208(2)	7(1)
C(52)	−0.211(2)	0.201(2)	0.231(2)	9(1)
C(53)	−0.285(2)	0.124(2)	0.042(2)	4.9(10)
C(54)	−0.317(3)	0.173(2)	0.027(2)	10(1)
C(55)	−0.323(5)	0.084(4)	0.084(4)	23(2)
C(56)	−0.277(3)	0.093(2)	−0.014(2)	11(1)
H(1)	0.021	0.438	0.130	4.982
H(2)	0.166	0.332	0.167	4.356
H(3)	−0.014	0.353	−0.016	5.554
H(4)	−0.069	0.397	−0.027	5.554
H(5)	0.006	0.415	−0.015	5.554
H(6)	−0.123	0.355	0.099	7.183
H(7)	−0.143	0.367	0.037	7.183
H(8)	−0.096	0.317	0.051	7.183
H(9)	−0.029	0.469	0.066	8.910

Fig. 3. EPR spectrum of a dilute solution of $Sn(dbqdi)_2$ in toluene at 23°C.

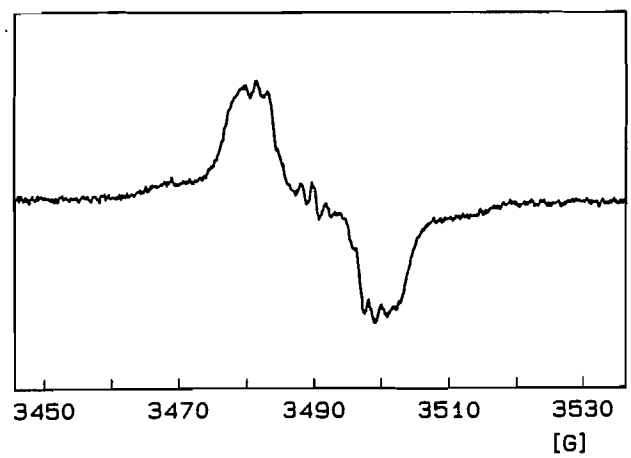

Fig. 4. ESR spectrum of a frozen toluene solution of $Sn(dbqdi)_2$ at 77 K.

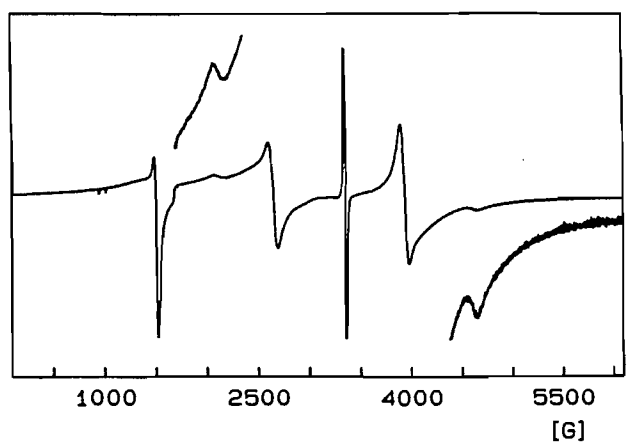

Can. J. Chem. Downloaded from www.nrcresearchpress.com by 80.90.12.36 on 09/08/12
For personal use only.

Table 3. (*a*) Bond lengths (Å) and (*b*) angles (deg) for $Sn(dbqdi)_2$, with standard deviations in parentheses.

(*a*)

Atom	Atom	Distance	Atom	Atom	Distance
Sn1	O1	2.08(2)	Sn1	O2	2.07(3)
Sn1	O3	2.05(2)	Sn1	O4	2.07(2)
Sn1	N1	2.08(3)	Sn1	N2	2.08(3)
O1	C2	1.35(3)	O2	C16	1.32(4)
O3	C30	1.29(3)	O4	C44	1.32(3)
N1	C1	1.37(4)	N1	C15	1.45(4)
N2	C29	1.38(3)	N2	C43	1.39(4)

(*b*)

Atom	Atom	Atom	Angle	Atom	Atom	Atom	Angle
O1	Sn1	O2	153.3(9)	O1	Sn1	O3	94.1(8)
O1	Sn1	O4	92.6(8)	O1	Sn1	N1	73.8(10)
O1	Sn1	N2	104.8(10)	O2	Sn1	O3	91.3(8)
O2	Sn1	O4	94.4(9)	O2	Sn1	N1	79.6(9)
O2	Sn1	N2	101.9(10)	O3	Sn1	O4	153.2(8)
O3	Sn1	N1	104.6(9)	O3	Sn1	N2	76.0(9)
O4	Sn1	N1	102.3(9)	O4	Sn1	N2	77.2(9)
N1	Sn1	N2	178(1)	Sn1	O1	C2	115(1)
Sn1	O2	C16	112(2)	Sn1	O3	C30	118(1)
Sn1	O4	C44	113(2)	Sn1	N1	C1	118(2)
Sn1	N1	C15	111(1)	C1	N1	C15	129(2)
Sn1	N2	C29	116(2)	Sn1	N2	C43	114(2)
C29	N2	C43	128(2)	N1	C1	C2	110(2)
N1	C1	C6	132(3)				
O1	C2	C1	115(2)	O1	C2	C3	125(2)
N2	C29	C34	125(3)	N1	C15	C20	123(2)
O3	C30	C29	115(2)	O2	C16	C15	120(3)
N1	C15	C16	112(3)	N2	C43	C48	129(2)
O2	C16	C17	122(3)	O4	C44	C43	117(2)
N2	C29	C30	111(2)	N2	C43	C44	111(2)
O3	C30	C31	129(3)	O4	C44	C45	123(2)

Results and discussion

Spectroscopic

The structural differences between the tin and lead derivatives of dbqdi are immediately illustrated by their ESR and NMR spectra. A solution of the tin compound in toluene at room temperature gave a complicated partially resolved ESR spectrum, centred at $g = 2.0016$, and with $A_{Sn} \sim 12$ G (Fig. 3). The spectrum of the frozen solution (Fig. 4) is clearly that of a molecule with a triplet spin state. The zero-field splitting parameters D and E which can be derived from this spectrum are $D = 0.121 \pm 0.005$ cm^{-1} and $E \sim$ O. These is also a sharp line in the centre of the spectrum, of negligible intensity, and we believe that this is due to contamination by some unidentified mono-radical species.

The magnitude of D, which measures the extent of the dipole–dipole interaction between the two spins in the $Sn(dbqdi)_2$ molecule, calls for some discussion. The value is 5–10 times higher than in a series of *cis*-$M(dbbsq)_2$ complexes (15) (M = Mg, Zn, Cd; dbbsq = 3,5-di-*tert*-butyl-1,2-benzosemiquinonate anion), for which D is typically 0.02 cm^{-1}, and $E \sim 0.0005$ cm^{-1}. In the *cis* and *trans* Sn—Sn bonded dimers $(Cl_2(dbbsq)SnSn(dbbsq)Cl_2$, in which the semiquinone ligands are of the order of 5 Å apart, the D values are 0.023 and 0.0065 cm^{-1}, respectively (9). In our previous work (15), the dipole–dipole interactions were calculated using the assumption that each of the two unpaired electrons was delocalized over one aromatic ring of dbbsq, but this approach is not applicable in the present case; even with the unrealistic assumption that the electrons are localized on each of the two nitrogen atoms bonded to tin, we calculate $D = 0.093$ cm^{-1}, which is significantly below the experimental value. This implies that we are dealing with a triplet state in which both unpaired spins are delocalized over both ligands. The EPR spectrum of a dilute liquid solution (Fig. 3) is qualitatively in agreement with this conclusion, although we have not been able to simulate this spectrum. The intensity of the EPR frozen solution spectrum increases with decreasing temperature at rate higher than changes in $1/T$, confirming that the ground state of the molecule is a triplet. We return to this point below. The zero value of E appears to be in agreement with the approximately D_{2d} symmetry of the coordination kernel of the complex, and indi-

Can. J. Chem. Downloaded from www.nrcresearchpress.com by 80.90.12.36 on 09/08/12
For personal use only.

Table 4. Final fractional coordinates and thermal parameters for non-hydrogen atoms of $Pb(dbqdi)_2$ with standard deviations in parentheses.

Atom	*x*	*y*	*z*	B_{eq}
Pb(1)	0.04438(6)	0.12328(3)	0.33811(6)	4.13(1)
O(1)	0.0318(10)	0.0457(4)	0.2631(10)	5.1(4)
O(2)	−0.084(1)	0.2022(5)	0.310(1)	7.2(5)
O(3)	0.0951(9)	0.1574(4)	0.2174(9)	4.1(3)
O(4)	0.147(1)	0.0644(7)	0.471(1)	8.2(6)
N(1)	−0.0964(10)	0.1171(5)	0.2109(10)	4.2(4)
N(2)	0.217(1)	0.0993(5)	0.330(1)	4.2(4)
C(1)	−0.113(1)	0.0701(5)	0.176(1)	3.3(4)
C(2)	−0.041(1)	0.0317(8)	0.206(1)	4.8(5)
C(3)	−0.051(2)	−0.0195(7)	0.172(2)	5.6(6)
C(4)	−0.132(1)	−0.0353(6)	0.117(1)	4.2(5)
C(5)	−0.203(2)	0.0059(6)	0.091(1)	5.0(6)
C(6)	−0.195(1)	0.0541(6)	0.116(1)	4.5(5)
C(7)	0.025(2)	−0.0610(6)	0.206(2)	6.2(7)
C(8)	0.001(2)	−0.1126(8)	0.166(2)	8.5(8)
C(9)	0.041(2)	−0.0653(8)	0.311(2)	9.1(9)
C(10)	0.116(2)	−0.0414(9)	0.173(2)	8.6(9)
C(11)	−0.294(2)	−0.0160(9)	0.031(2)	5.6(6)
C(12)	−0.274(2)	−0.043(1)	−0.054(2)	10(1)
C(13)	−0.362(2)	0.026(1)	−0.007(2)	11(1)
C(14)	−0.346(2)	−0.050(1)	0.087(2)	12(1)
C(15)	−0.134(1)	0.1579(6)	0.175(1)	4.1(5)
C(16)	−0.129(1)	0.2053(7)	0.229(1)	4.6(5)
C(17)	−0.180(1)	0.2516(6)	0.197(1)	3.7(5)
C(18)	−0.217(1)	0.2548(5)	0.112(1)	3.2(3)
C(19)	−0.217(1)	0.2125(6)	0.051(1)	4.6(5)
C(20)	−0.179(1)	0.1711(5)	0.081(1)	4.1(5)
C(21)	−0.181(2)	0.2992(6)	0.261(1)	4.9(6)
C(22)	−0.080(2)	0.3182(7)	0.290(2)	6.9(7)
C(23)	−0.244(2)	0.3417(9)	0.213(2)	9.6(9)
C(24)	−0.221(2)	0.2830(6)	0.345(2)	6.8(7)
C(25)	−0.254(2)	0.2233(7)	−0.050(2)	5.5(6)
C(26)	−0.349(2)	0.245(1)	−0.062(2)	10(1)
C(27)	0.251(1)	0.1323(7)	0.269(1)	4.3(5)
C(28)	0.184(1)	0.1636(8)	0.214(1)	5.0(6)
C(29)	0.215(1)	0.1977(6)	0.154(1)	3.7(5)
C(30)	0.311(2)	0.2004(8)	0.155(1)	5.0(6)
C(31)	0.377(1)	0.1728(6)	0.207(1)	4.3(5)
C(32)	0.347(1)	0.1386(7)	0.264(1)	4.5(5)
C(33)	0.143(1)	0.2309(7)	0.092(1)	4.5(5)
C(34)	0.081(2)	0.2661(7)	0.147(2)	6.0(7)
C(35)	0.193(2)	0.2699(7)	0.040(2)	7.2(7)
C(36)	0.481(2)	0.182(1)	0.206(2)	6.8(8)
C(37)	0.543(2)	0.159(2)	0.277(4)	22(2)
C(38)	0.252(1)	0.0577(8)	0.368(1)	4.7(5)
C(39)	0.214(2)	0.0409(7)	0.450(1)	4.8(6)
C(40)	0.253(1)	−0.0062(7)	0.492(1)	4.4(5)
C(41)	0.322(2)	−0.0309(6)	0.459(1)	4.7(5)
C(42)	0.358(1)	−0.0162(6)	0.379(1)	4.1(5)
C(43)	0.326(1)	0.0276(7)	0.339(1)	4.3(5)
C(44)	0.219(2)	−0.0225(6)	0.577(1)	4.8(6)
C(45)	0.228(2)	0.0161(10)	0.649(2)	7.1(8)
C(46)	0.267(2)	−0.072(1)	0.616(2)	9(1)
C(47)	0.111(2)	−0.0373(7)	0.552(2)	7.0(7)
C(48)	0.430(1)	−0.0512(7)	0.345(1)	4.7(5)
C(49)	0.375(2)	−0.0972(9)	0.301(2)	9.7(9)
C(50)	0.504(2)	−0.0697(9)	0.421(2)	7.9(8)
C(51)	0.479(2)	−0.0236(9)	0.277(2)	9.6(10)
C(52)	0.086(2)	0.1989(9)	0.022(2)	6.9(7)
C(53)	0.503(3)	0.164(2)	0.124(4)	21(2)
C(54)	0.507(2)	0.237(1)	0.208(4)	17(1)
C(55)	−0.183(2)	0.260(1)	−0.084(2)	11(1)
C(56)	−0.259(3)	0.1738(8)	−0.107(2)	14(1)

Table 4 (*concluded*).

cates that the structure identified in the solid state is retained in the solution phase.

The lead complex is diamagnetic, and ^1H and ^{13}C NMR spectra have been recorded (See Table 6). The ^1H spectrum is in keeping with those of corresponding zinc and cadmium species, of the parent 3,5-di-*tert*-butylcatechol, and of the related *o*-quinone. No spectrum of the free dbqdi ligand is available; paramagnetic species were present in the parent solution from which $Pb(dbqdi)_2$ was isolated (see below) and an NMR spectrum could therefore not be obtained from this source. The most obvious feature of the ^{13}C spectrum of $Pb(dbqdi)_2$ is the presence of four resonances for each type of *tert*-butyl carbon atom, and two for each of the aromatic carbon atoms. The assignments in Table 6 follow from previous work (16), and from the crystallographic results; C^1 is the highest frequency, being attached to an imido nitrogen, and C^6 is bonded to a phenolic oxygen. The asymmetry of the dbqdi ligand in this compound is consequent upon the differing Pb—O bond lengths (see below), and accounts for the four different sets of *tert*-butyl resonances, and the two different aromatic rings. The largest difference in these ^{13}C resonances is at C^1 (9.1 ppm), with smaller values of ca. 5 ppm for C^2, C^4, and C^6, and of ca. 1.5 ppm for C^3 and C^5, which carry the *tert*-butyl groups. This again is in keeping with the differences in the C—N and C—O bonds in the structure.

The infrared spectra are less informative; the most noteworthy features are the absence of both N-H and O-H modes, and of vibrations in ν(C=O) region, for each complex.

Structural

The complex $Sn(dbqdi)_2$, **1**, consists of a six-coordinate tin atom bonded to two identical ligands, with a SnO_4N_2 core which is far from octahedral in symmetry because of the constraints imposed by the ligand geometry. In contrast to the lead derivative, the tin–ligand interaction is essentially symmetrical, with two Sn—O bonds whose lengths (Sn—O(1) = 2.08(2) Å, Sn—O(2) = 2.07(3) Å; Sn—O(3) = 2.05(2) Å, Sn—O(4) = 2.07(2) Å) are identical for both ligands within experimental error. These values are close to those reported for other tin(IV) compounds, as in $Sn(trop)_2Cl_2$ (trop = tropolonate anion) (Sn—O = 2.07(s) (avg.)) (17); $Sn(malt)_2Cl_2$ (malt = 3-hydroxy-2-methyl-4-pyronate anion) (Sn—O = 2.09(1) (avg.)) (17); $[Sn(O_2C_6Cl_4)_3]^{2-}$ (Sn—O = 2.06(1) (avg.) (18); and a series of substituted phenol derivatives (Sn—O = 2.07(1) (avg.)) (19). Similar agreement can be found between *r*(Sn—N) in **1** (2.08(3) Å) and the values

Can. J. Chem. Downloaded from www.nrcresearchpress.com by 80.90.12.36 on 09/08/12
For personal use only.

Table 5. (*a*) Bond lengths (Å) and (*b*) angles (°) for b(dbqdi)$_2$, with standard deviations in parentheses.

(*a*)

Atom	Atom	Distance	Atom	Atom	Distance
Pb(1)	O(1)	2.30(1)	Pb(1)	O(3)	2.26(1)
Pb(1)	O(2)	2.80(1)	Pb(1)	O(4)	2.76(1)
Pb(1)	N(1)	2.57(1)	Pb(1)	N(2)	2.61(2)
O(1)	C(2)	1.30(2)	O(2)	C(16)	1.29(2)
O(3)	C(28)	1.31(2)	O(4)	C(39)	1.24(2)
N(1)	C(1)	1.34(2)	N(1)	C(15)	1.27(2)
N(2)	C(27)	1.41(2)	N(2)	C(38)	1.29(2)

(*b*)

Atom	Atom	Atom	Angle	Atom	Atom	Atom	Angle
O(1)	Pb(1)	O(3)	87.3(5)	O(1)	Pb(1)	N(1)	65.9(5)
O(1)	Pb(1)	N(2)	76.4(5)	O(3)	Pb(1)	N(1)	75.4(5)
O(3)	Pb(1)	N(2)	66.9(4)	N(1)	Pb(1)	N(2)	127.0(5)
Pb(1)	O(1)	C(2)	123(1)	Pb(1)	O(3)	C(28)	122(1)
Pb(1)	N(1)	C(1)	114(1)	Pb(1)	N(1)	C(15)	120(1)
C(1)	N(1)	C(15)	123(1)	Pb(1)	N(2)	C(27)	109(1)
Pb(1)	N(2)	C(38)	119(1)	C(27)	N(2)	C(38)	130(1)
N(1)	C(1)	C(2)	115(1)	N(1)	C(1)	C(6)	126(1)
N(2)	C(27)	C(28)	116(1)	N(2)	C(27)	C(32)	124(1)
N(2)	C(38)	C(39)	115(1)	O(3)	C(28)	C(27)	119(1)
O(3)	C(28)	C(29)	122(1)	N(2)	C(38)	C(43)	125(1)
O(4)	C(39)	C(40)	123(2)	O(4)	C(39)	C(38)	119(1)

Table 6. ^{1}H and ^{13}C NMR spectra of Pb(dbqdi)$_2$ and related compounds (ppm, Me_4Si = 0).

(*a*) ^{1}H NMR

Compound	Solvent	Aromatic	*t*-Bu
Pb(dbqdi)$_2$	$CDCl_3$	7.10, 6.90	1.40, 1.20
Zn(dbqdi)$_2$[a]	$CDCl_3$	7.28, 7.12	1.23, 1.13
Cd(dbqdi)$_2$[a]	$CDCl_3$	7.14	1.22, 1.19
Mg(dbqdi)$_2$[a]	$CDCl_3$	7.40, 7.20	1.26, 1.16
dbbq[b,c]	$(CD_3)_2SO$	6.97, 6.13	1.18
H_2dbc[c,d]	$(CD_3)_2SO$	6.74	1.32, 1.21

(*b*) ^{13}C NMR (in $CDCl_3$)

31.3, 30.5, 29.9, 29.2	Primary C of *t*-Bu
35.2, 35.0, 34.7, 34.1	Quaternary C of *t*-Bu
170.8, 179.9	C^1
147.0, 142.4	C^6
140.5, 139.4	C^2
137.5, 136.1	C^4
133.8, 129.1	C^5
127.9, 121.2	C^3

[a]Results from ref. 2.
[b]dbbq = 3,5-di-*tert*-butyl-1,2-benzoquinone.
[c]Results from ref. 9.
[d]dbc = 3,5-di-*tert*-butylcatechol.

in diperchlorato-tetraphenolporphinatotin(IV), for which *r*(Sn—N) = 2.073 Å (20). Longer bonds have been observed in molecules in which $NHMe_2$ is coordinated to tin phenolates (Sn—N = 2.30 Å (avg.)) (19), or in which the donor is 2-(2-pyridyl)benzimidazole (L); Sn—N for Me_2SnCl_2L = 2.422(2) and 2.447(2) Å, and for $SnBr_4L$ = 2.212(4) and 2.271(4) Å) (21). The average C—O bond length in **1** is 1.32(3) Å, between the characteristic values for C=O in *o*-semiquinones and C—O in catecholates (1). The C—N bond lengths (1.40(4) Å, avg.) and angles (C-N-C = 129(3)°) suggest that there is some double bond character.

The most immediate contrast between the tin and lead compounds lies in the M—O bonds, which are highly unsymmetrical in the latter case, with Pb—O = 2.28(2) and 2.78(2) Å. The shorter of these is similar to that in a macrocyclic Schiff base derivative of lead(II), for which Pb—O = 2.337 Å (avg.) (22); in contrast, Pb—O in the organolead(IV) compound (23) $Ph_3PbOSiPh_3$ is 2.01 Å. The larger Pb—O distance, and the Pb—N value of 2.59(2) Å, are similar to those in a lead(II) tetraimine Schiff base (2.54 and 2.67 Å (avg.), respectively) (24); in crown ether derivatives of $Pb(NO_3)_2$, Pb—O distances range between 2.645 and 3.060 Å (25, 26). In general, these results point to the presence of lead in the +II state, with one weak and one strong Pb—O bond. In keeping with the Pb—O bond distances, we find two different C—O bonds, one averaging 1.31(2) Å and the other 1.27(2), and two C—N bonds at 1.28(2) and 1.38(3) Å.

Can. J. Chem. Downloaded from www.nrcresearchpress.com by 80.90.12.36 on 09/08/12
For personal use only.

Scheme 2.

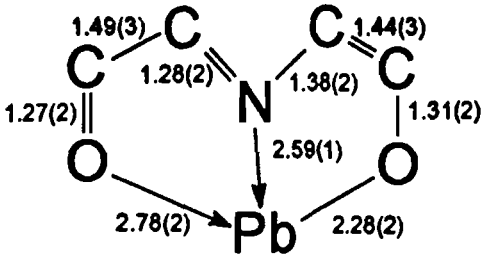

Scheme 3.

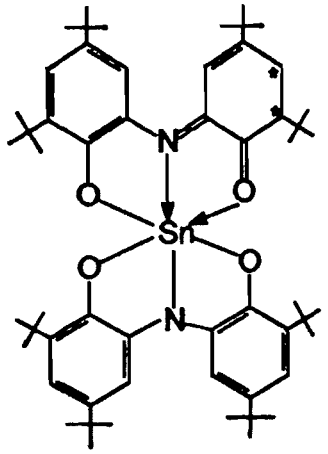

These results, and the spectroscopic data, allow some conclusions about the structure of the ligand in the two complexes. The lead complex is the easier to assign, since the diamagnetism allows only dbqdi-III and V to be considered, and since V would require lead to be in the +VI oxidation state, $Pb^{II}(dbqdi\text{-}III)_2$ is the only reasonable structure. The two Pb—O bond lengths reflect the different oxygen atoms in this form of the ligand, and point to the absence of delocalization, at least within the coordination kernel. Within the limits of the experimental errors, this is borne out by the C—N bond distances as shown in Scheme 2. The C—C bond lengths clearly do not support this idealized structure, but these bonds are part of aromatic rings so that there must be a considerable influence here from delocalization within these rings. This limitation apart, the formulation as a lead(II) complex of dbqdi-III is well founded.

The structure of the tin compound, with its triplet ground state and symmetrical Sn—O bonding, can be understood in terms of a delocalized structure, one localized form of which is shown in Scheme 3. In this formula, the ligands are portrayed as the diradical monoanion V and the anion VI, of charge −3, so that the oxidation state of tin is +IV. The C—N and C—O bonds are both of order 1¼, which is in keeping with the experimental results. A description of the actual molecular orbital scheme that leads to delocalization over the whole molecule has yet to be established.

General and preparative

The ligand dbqdi is formed by the condensation of two molecules of dbc with ammonia, followed by deprotonation, oxidation, and electron redistribution. The ESR spectrum of a

Fig. 5. (*a*) ESR spectrum of solution formed during the preparation of $Pb(dbqdi)_2$. (*b*) Simulated spectrum.

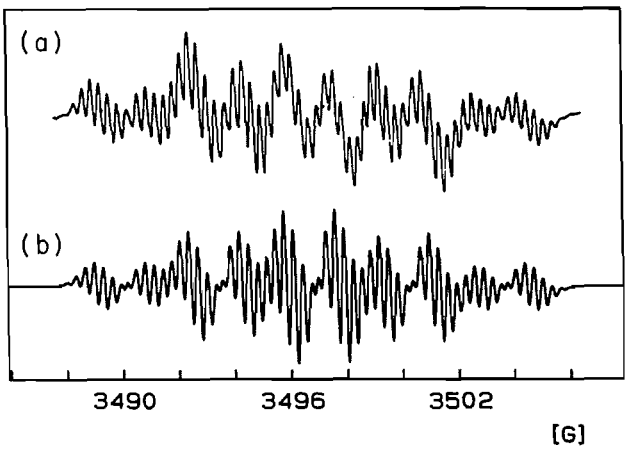

Scheme 4.

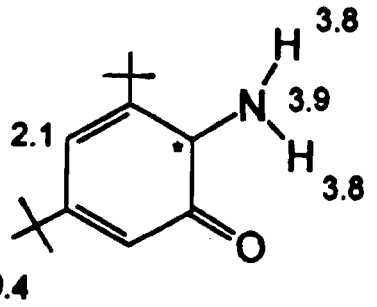

sample of the solution remaining after the synthesis and collection of the lead complex is shown in Fig. 5(*a*). There is no evidence of splitting due to coupling to a lead atom, and the spectrum can be simulated by assuming that one *tert*-butyl group ($A_H = 0.40$ G), two equivalent hydrogens with $A_H = 3.81$ G, a second hydrogen with $A_H = 2.08$ G, and a nitrogen atom with $A_N = 3.93$ G each contribute to the splitting pattern. This interpretation appears to rule out a molecule with an unpaired electron delocalized over two aromatic rings, or with an unpaired electron on one ring of a structure such as II or IV in Scheme 1, and the spectrum is tentatively assigned as being that of the species shown in Scheme 4, with the identification of the *A* values as shown. The spectrum can be reasonably simulated using these hyperfine coupling constants (Fig. 5(*b*). Further condensation of dbc at the amino site, and deprotonation, could give rise to dbqdi-III, which would be ESR-silent.

The reactions of this species with a metal ion will then depend on the redox properties of this ion. In the case of lead (II), straightforward ligation

$$[1] \quad Pb^{2+} + 2[dbqdi\text{-}III]^- \rightarrow Pb^{II}[dbqdi\text{-}III]_2$$

would give the observed diamagnetic complex in which one Pb—O bond is covalent, and the other weaker interaction is essentially weak donation from the carbonyl oxygen of the ligand. In the case of tin(II), which is a stronger reducing state than lead(II), the initial complex formation would be followed, or accompanied, by reduction of each of the ligands from

dbqdi-III to dbqdi-IV, which contains one more electron, and the subsequent delocalization to give the structure discussed above

[2] $Sn^{2+} + 2[dbqdi\text{-}III]^{-} \rightarrow Sn^{II}[dbqdi\text{-}III]_2$

[3] $\rightarrow Sn^{IV}[dbqdi\text{-}IV]_2$

[4] $\rightarrow Sn^{IV}[dbqdi\text{-}V][dbqdi\text{-}VI]$

The identification of the tin and lead derivatives of dbqdi as involving both metal and ligand in differing oxidation states is confirmed by both ESR and crystallographic evidence.

These results are compatible with earlier work on the complexes of transition metals with the dbqdi ligand, but show some of the characteristic features of main group chemistry in that the differing redox properties of tin and lead are key to understanding both the preparative route and the structural characteristics of these complexes.

Acknowledgment

This work was supported by Operating Grants (to B.R.M. and D.G.T.) from the Natural Sciences and Engineering Research Council of Canada.

References

1. D.G. Tuck. Coord. Chem. Rev. **112**, 215 (1992).
2. A.Y. Girgis and A.L. Balch. Inorg. Chem. **14**, 2724 (1975).
3. S.K. Larsen and C.G. Pierpont. J. Am. Chem. Soc. **110**, 1827 (1988).
4. B.G. Maiya, Y. Dang, and K.M. Kadish. J. Chem. Soc. Dalton Trans. 3671 (1990).
5. C.L. Simpson, S.R. Boone, and C.G. Pierpont. Inorg. Chem. **28**, 4379 (1989).
6. A. Caneschi, A. Dei, and D. Gatteschi. J. Chem. Soc. Chem. Commun. 630 (1992).
7. H.B. Stegmann and K. Scheffer. Chem. Ber. **103**, 1279 (1970).
8. H.B. Stegmann, K.B. Ulmschneider, and K. Scheffler. J. Organomet. Chem. **72**, 41 (1974).
9. T.A. Annan, B.R. McGarvey, A. Ozarowski, D.G. Tuck, and R.K. Chadha. J. Chem. Soc. Dalton Trans. 439 (1989).
10. N. Walker and D. Stuart. Acta Crystallogr. Sect. A: Found. Crystallogr. **A39**, 158 (1983).
11. D.T. Cromer and J.T. Waber. International tables for X-ray crystallography. Vol. 4. Kynoch Press, Birmingham. 1974. Table 2.2A.
12. I.A. Ibers and W.C. Hamilton. Acta Crystallogr. **17**, 781 (1964).
13. D.T. Cromer. International tables for X-ray crystallography. Vol. 4. Kynoch Press, Birmingham. 1974. Table 2.3.1.
14. TEXSAN-TEXRAY Structure analysis package. Molecular Structure Corporation, Houston, Tex. 1985.
15. A. Ozarowski, B.R. McGarvey, C. Peppe, and D.G. Tuck. J. Am. Chem. Soc. **113**, 3288 (1991).
16. T.A. Annan, Z. Tian, and D.G. Tuck. J. Chem. Soc. Dalton Trans. 19 (1991).
17. C.I.F. Denekamp, D.F. Evans, A.M.Z. Slawin, D.J. Williams, C.Y. Wong, and J.D. Woollins. J. Chem. Soc. Dalton Trans. 2375 (1992).
18. T.A. Annan, R.K. Chadha, D.G. Tuck, and K.D. Watson. Can. J. Chem. **65**, 2670 (1987).
19. G.D. Smith, V.M. Visciglio, P.E. Fenwick, and K.R. Rothwell. Organometallics, **11**, 1065 (1992).
20. W.B. Lee, S.C. Suen, F.E. Hong, J.H. Chen, T.T. Jong, and L.P. Hevang. J. Chin. Chem. Soc. (Taipei), **39**, 143 (1992).
21. T.A. Kabanes, A.D. Keramidas, D. Mantzafos, U. Russo, A. Terzis, and J.M. Tsangaris. J. Chem. Soc. Dalton Trans. 2729 (1992).
22. S.S. Tandon and V. McKee. J. Chem. Soc. Dalton Trans. 19 (1989).
23. P.G. Harrison, T.J. King, J.A. Richard, and R.C. Phillips. J. Organomet. Chem. **116**, 301 (1976).
24. H. Adams, N.A. Bailey, D.E. Fenton, R.J. Good, R. Moody, and C.O.R. De Barbarin. J. Chem. Soc. Dalton Trans. 213 (1987).
25. R.D. Rogers and A.H. Bond. Inorg. Chim. Acta, **192**, 163 (1992).
26. M.G.B. Drew, D.G. Nicholson, I. Sylte, and A.K. Vasudevan. Acta Chem. Scand. **46**, 396 (1992).

Can. J. Chem. Downloaded from www.nrcresearchpress.com by 80.90.12.36 on 09/08/12
For personal use only.

Synthesis, structure, and nonrigidity of $Os_4(CO)_{15}$, $Os_4(CO)_{13}(PMe_3)[P(OMe)_3]$, and $Os_4(CO)_{14}(CNBu^t)$

Frederick W.B. Einstein, Victor J. Johnston, Andrew K. Ma, and Roland K. Pomeroy

Can. J. Chem. Downloaded from www.nrcresearchpress.com by 80.90.12.36 on 09/08/12
For personal use only.

Abstract: The binary carbonyl $Os_4(CO)_{15}$, **1**, has been prepared by the addition of $Os(CO)_5$ to $Os_3(CO)_{10}$-(cyclooctene)$_2$ at −15°C. The related clusters $Os_4(CO)_{13}(PMe_3)[P(OMe)_3]$, **2**, and $Os_4(CO)_{14}(CNBu^t)$, **3**, have been synthesized from $Os_4(CO)_{13}(PMe_3)$ and $Os_4(CO)_{15}(CNBu^t)$, respectively. The crystal structures of **1**, **2**, and **3** reveal similar planar metal skeletons with short (2.774 (1) – 2.793 (2) Å) and long (2.978 (2) – 3.019 (2) Å) peripheral Os—Os bonds; the hinge Os—Os bond in **1–3** ranges in length from 2.936 (2) to 2.948 (1) Å. The variable temperature ^{13}C nuclear magnetic resonance spectra of **1** and **3** show that both are highly nonrigid in solution even at −120°C. The mechanism of nonrigidity is believed to be an all-equatorial, merry-go-round carbonyl exchange. The variable temperature ^{13}C nmr spectra of **2** indicate it is rigid on the nmr time scale in solution at −45°C. Carbonyl exchange is, however, observed in the spectrum at −6°C. From the mode of collapse of the signals it is believed that the lowest energy exchange processes in **3** involve axial-equatorial, merry-go-round CO exchanges in the two planes that each contain a short Os—Os bond. Crystallographic data for compound **1**: space group $C2/c$; a = 12.802 (3) Å, b = 10.217 (3) Å, c = 16.380 (5) Å, β = 91.39 (2)°; R = 0.044, 1204 observed reflections. For compound **2**: space group $P2_1/c$; a = 11.106 (7) Å, b = 16.931 (5) Å, c = 16.481 (5) Å, β = 97.71 (5)°; R = 0.051, 2117 observed reflections. For compound **3**: space group $P2_1/n$; a = 11.747 (3) Å, b = 18.009 (5) Å, c = 12.448 (2) Å, β = 92.65 (2)°; R = 0.054, 2131 observed reflections.

Key words: osmium, carbonyl, cluster, nonrigidity.

Résumé : On a préparé le complexe carbonyle binaire $Os_4(CO)_{15}$, **1**, par addition du $Os(CO)_5$ à du $Os_3(CO)_{10}$(cyclooctène)$_2$ à −15°C. On a synthétisé les agrégats apparentes $Os_4(CO)_{13}(PMe_3)[P(OMe)_3]$, **2**, et $Os_4(CO)_{14}(CNBu^t)$, **3**, à partir du $Os_4(CO)_{13}(PMe_3)$ et $Os_4(CO)_{15}(CNBu^t)$ respectivement. Les structures cristallines des composés **1, 2** et **3** révèlent que les squelettes métalliques sont plans et similaires avec des longueurs de liaisons périphériques Os—Os courtes (2,774 (1)–2,793 (2) Å) et longues (2,978 (2)–3,019 (2) Å); la longueur de la liaison charnière Os—Os des composés **1–3** varie de 2,936 (2) à 2,948 (1) Å. Les spectres de résonance magnétique nucléaire du ^{13}C à température variable des composés **1** et **3** montrent que les deux manquent grandement de rigidité, même à −120°C. On croit que ce manque de rigidité provient d'un mécanisme d'échange de carbonyle de type carrousel entièrement èquatorial. Les spectres de rmn du ^{13}C à température variable du composé **2** indiquent qu'il est rigide à l'échelle de temps de la rmn, en solution, à −45°C. On observe toutefois un échange de carbonyle à −6°C. Sur la base du mode de disparition des signaux, on croit que les processus d'échange de basse énergie dans le composé **3** impliquent des échanges de CO de type carrousel axial-équatorial dans les deux plans qui contiennent chacun une liaison Os—Os courte. Les données cristallographiques du composé **1** sont : groupe d'espace $C2/c$, avec a = 12,802 (3), b = 10,217 (3) et c = 16,380 (5) Å, β = 91,39 (2)°, et R = 0,044 pour 1204 réflexions observées. Pour le composé **2** : groupe d'espace $P2_1/c$, avec a = 11,106 (7), b = 16,931 (5) et c = 16,481 (5), β = 97,71 (5)°, et R = 0,051 pour 2117 réflexions observées. Pour le composé **3** : groupe d'espace $P2_1/n$, avec a = 11,747 (3), b = 18,009 (5) et c = 12,448 (2) Å, β = 92.65 (2)°, et R = 0,054 pour 2131 réflexions observées.

Mots clés : osmium, carbonyle, agrégat, manque de rigidité.

[Traduit par la rédaction]

Received October 25, 1994.

This paper is dedicated to Professor William A.G. Graham on the occasion of his 65th birthday.

F.W.B. Einstein, V.J. Johnston, A.K. Ma, and R.K. Pomeroy.[1] Department of Chemistry, Simon Fraser University, Burnaby, BC V5A 1S6, Canada.

[1] Author to whom correspondence may be addressed. Telephone: (604) 291-3347. Fax: (604) 291-3765. E-mail: pomeroy@sfu.ca

Can. J. Chem. Downloaded from www.nrcresearchpress.com by 80.90.12.36 on 09/08/12
For personal use only.

Introduction

Osmium forms more neutral binary carbonyl compounds than any other transition metal, with compounds with one to eight metal atoms known. The common carbonyls of osmium, namely, $Os(CO)_5$ and $Os_3(CO)_{12}$, were first prepared by Hieber and Stallmann in 1943 (1). Moss and Graham (2) described the synthesis of $Os_2(CO)_9$ in 1970; binary carbonyls with five, six, seven, and eight osmium atoms were first reported in 1972 by the Johnson and Lewis group (3).

It was not, however, until 1987 that work from this laboratory described the preparation of $Os_4(CO)_{15}$, **1**, the first tetranuclear binary carbonyl of osmium (4). Subsequently, $Os_4(CO)_{16}$ and $Os_4(CO)_{14}$ were prepared from **1** (5). The structure of **1** consists of an unusual planar "kite" Os_4 arrangement with adjacent short and long peripheral metal–metal bonds that we had observed previously in $Os_4(CO)_{14}(PMe_3)$ and rationalized in terms of three-center, two-electron metal–metal bonds (6).

Herein, we describe the details of the synthesis and structure of **1**, along with those of two related clusters, $Os_4(CO)_{13}(PMe_3)[P(OMe)_3]$, **2**, and $Os_4(CO)_{14}(CNBu^t)$, **3**. The remarkable nonrigid properties of clusters **1** – **3** as ascertained by ^{13}C nmr spectroscopy are also described. Some of the results presented here, besides appearing in a preliminary communication (4), have also been quoted as unpublished results in a review (7).

Experimental

Reactions and isolation of products were carried out under a nitrogen atmosphere with the use of standard Schlenk techniques; solvents were thoroughly dried before use. The following compounds were prepared by literature methods: $Os(CO)_5$ (8), $Os_3(CO)_{10}$(cyclooctene)$_2$ (9), $Os_4(CO)_{14}(PMe_3)$ (6), and $Os_4(CO)_{15}(CNBu^t)$ (10). An improved preparation of $Os_4(CO)_{13}(PMe_3)$ (6) is described below. The ^{13}CO-enriched clusters were prepared from ^{13}CO-enriched (~40%) $Os_3(CO)_{12}$ (11).

Infrared spectra were recorded on a Perkin–Elmer 983 spectrometer; the internal calibration of the instrument was periodically checked against the known absorption frequencies of gaseous CO. Nuclear magnetic resonance spectra were recorded on a Bruker WM400 or Bruker SY-100 spectrometer. The ^{13}C nmr spectra were obtained on ^{13}CO-enriched samples in a solvent of $CHFCl_2$–CD_2Cl_2 (~5/1) unless otherwise stated. The nmr line-shape simulation shown in Fig. 5 was carried out with a computer program written by Professor R.E.D. McClung of the University of Alberta. The microanalyses were obtained by M. K. Yang of the Microanalytical Laboratory of Simon Fraser University.

Preparation of $Os_4(CO)_{15}$ (1)

A Schlenk tube was cooled to 0°C and $Os_3(CO)_{10}$(cyclooctene)$_2$ (60 mg, 0.057 mmol) in CH_2Cl_2 (2 mL) was added along with $Os(CO)_5$ (~20 mg, ~0.06 mmol) in hexane (30 mL). The vessel was sealed and stored at −15°C for 4 d during which time dark red crystals of product formed. The mother liquor was removed and the crystals were washed with hexane and dried on the vacuum line. This yielded analytically pure $Os_4(CO)_{15}$ (48 mg, 73%) as dark red, air-stable crystals: mp 185°C (dec.). Infrared (CH_2Cl_2) ν_{CO}: 2086 (s), 2073.5 (m), 2045 (vs), 2023 (m), 2002 (sh), 1939 (m, br) cm^{-1}; ^{13}C nmr (−56°C) δ: 190.6 (4C), 188.9 (4C), 171.7 (7C). Anal. calcd. for $C_{15}O_{15}Os_4$: C 15.26, H 0.0; found: C 15.51, H, 0.0.

Improved preparation of $Os_4(CO)_{13}(PMe_3)$

A Pyrex tube was charged with $Os_4(CO)_{14}(PMe_3)$ (98 mg, 0.080 mmol) and hexane (50 mL). The stirred solution was purged with nitrogen and subjected to ultraviolet irradiation for 2.5 h (there were approximately 3 cm between the edge of the reaction vessel and the water jacket of the 200-W ultraviolet light source). The solution was purged for a further 5 min and then concentrated on the vacuum line and stored at −15°C overnight. The mother liquor was decanted from the crystals of $Os_4(CO)_{13}(PMe_3)$ (82 mg, 86%), which were dried on the vacuum line. The product was pure as determined by infrared spectroscopy (6).

Preparation of $Os_4(CO)_{13}(PMe_3)[P(OMe)_3]$ (2)

To a solution of $Os_4(CO)_{13}(PMe_3)$ (48 mg, 0.040 mmol) in hexane (60 mL) at room temperature, $P(OMe)_3$ was slowly added dropwise until the color of the solution changed from red to dark green. An infrared spectrum of the solution at this stage showed no absorptions due to $Os_4(CO)_{13}(PMe_3)$. The solvent and excess $P(OMe)_3$ were removed on the vacuum line, and the brown residue dissolved in a minimum volume of CH_2Cl_2 and chromatographed on a silica gel column (15 × 2.5 cm). A small amount of an unidentified yellow compound was eluted with hexane and discarded. The desired product was eluted as a red-green band with hexane–dichloromethane (1/1). The product-containing fractions were combined, concentrated on the vacuum line, and stored at −15°C for 4 d. The mother liquor was decanted from the red crystals of $Os_4(CO)_{13}(PMe_3)[P(OMe)_3]$ (49 mg, 92%), which were dried under vacuum: mp 127°C. Infrared (CH_2Cl_2) ν_{CO}: 2102 (m), 2075 (w), 2044 (m), 2036.5 (s), 2024 (vs), 2016 (sh), 1997.5 (m), 1977 (sh), 1970 (m), 1961 (m), 1904.5 (m) cm^{-1}; ^1H nmr ($CDCl_3$) δ: 3.65 (d, J_{PH} = 12 Hz), 1.83 (d, J_{PH} = 11 Hz); ^{13}C nmr (CH_2Cl_2–CD_2Cl_2, −44°C) δ: 214.8 (2C), 203.7 (2C, d, J_{PC} = 9.0 Hz), 201.6 (2C, d, J_{PC} = 12.3 Hz), 195.4 (1C), 178.0 (1C), 176.4 (1C), 173.3 (1C), 173.1 (1C), 173.0 (2C). Anal. calcd. for $C_{19}H_{18}O_{16}Os_4P_2$: C 17.22, H 1.37; found: C 17.66, H 1.45.

Preparation of $Os_4(CO)_{14}(CNBu^t)$

To a stirred solution of $Os_4(CO)_{15}(CNBu^t)$ (76 mg, 0.050 mmol) in CH_2Cl_2 (30 mL) was added Me_3NO (5 mg, 0.07 mmol) slurried in CH_2Cl_2; the solution changed from amber to dark green during the addition. The course of the reaction was also monitored by the disappearance of the ν_{CN} absorption at 2222 cm^{-1} in the infrared spectrum of the solution. Upon completion of the reaction, the solvent was removed on the vacuum line. The green-brown residue was dissolved in a minimum amount of CH_2Cl_2 and the resulting solution filtered through Celite. Hexane was added to the filtered solution, which was then stored at −15°C for 2 d. The mother liquor was decanted from the product, which was washed with hexane and dried on the vacuum line to afford $Os_4(CO)_{14}(CNBu^t)$ (46 mg, 62%): mp 124°C. Infrared (hexane) ν_{CN}: 2185 (m) cm^{-1}; ν_{CO}: 2110 (m), 2074.5 (s), 2066 (s), 2054.5 (s), 2045 (vs), 2030 (vs), 2015 (vs), 2005 (s), 1944.5 (m), 1933.5 (m) cm^{-1}; ^1H nmr (C_7D_8) δ: 0.96, 0.95 (ratio approximately 1:1). Anal. calcd. for $C_{19}H_9NO_{14}Os_4$: C 18.46, H 0.73, N 1.13; found: C 18.42, H 0.97, N 1.28.

Can. J. Chem. Downloaded from www.nrcresearchpress.com by 80.90.12.36 on 09/08/12
For personal use only.

Table 1. Crystal data and experimental details for complexes **1**, **2**, and **3**.

	1	**2**	**3**
Compound	$C_{15}O_{15}Os_4$	$C_{19}H_{18}O_{16}Os_4P_2$	$C_{19}H_9NO_{14}Os_4$
Formula weight	1180.8	1324.8	1235.8
Crystal system	Monoclinic	Monoclinic	Monoclinic
Space group	*C2/c*	$P2_1/c$	$P2_1/n^a$
Temperature (°C)	−73±3	23	21
a, Å	12.802 (3)	11.106 (7)	11.747 (3)
b, Å	10.217 (3)	16.931 (5)	18.009 (5)
c, Å	16.380 (5)	16.481 (5)	12.448 (2)
β, deg	91.39 (2)	97.71 (5)	92.65 (2)
Cell volume (Å^3)	2141.7	3071.0	2630.8
z	4	4	4
Density, g cm^{-3} calcd.	3.66	2.87	3.12
Abs. coeff. (cm^{-1})	237.56	166.85	193.48
Unique data	1887	4003	4607
Observ. data ($I \geq 2.5\sigma$)	1204	2117	2131
Parameters	108	275	171
R^b	0.044	0.051	0.054
$R_w{}^b$	0.060	0.053	0.050

[a]Nonstandard setting of $P2_1/c$.
[b]$R = \Sigma(||F_o| - |F_c||)/\Sigma|F_o|$; $R_w = [\Sigma w(|F_o| - |F_c|)^2/\Sigma w|F_o|^2]^{1/2}$.

X-ray structure determinations of 1, 2, and 3

The following procedure was employed for each of the three structure determinations. Additional details relating to an individual determination are given after the general procedure. A crystal of suitable size (Table 1) was mounted, in air, on an Enraf–Nonius CAD4F diffractometer. Diffraction data unless otherwise stated were collected at 21 ± 1°C with the use of graphite-monochromated Mo Kα, radiation (λ = 0.710 69 Å). Background measurements were made by extending the scan range by 25% on each side of the scan. Two standard reflections were monitored every hour during data collection, and intensity data were scaled appropriately (in each case the standard reflections varied by less than ±3% during data collection). Lorentz, polarization, and absorption corrections were applied. Accurate cell dimensions were assigned on the basis of 25 carefully centered high-angle (2θ > 25°) reflections that were widely scattered in reciprocal space.

The structures were solved either by direct methods or by inspection of a Patterson map that gave the positions of the osmium atoms. All other non-hydrogen atoms were located from Fourier difference maps alternated with least-squares refinement. Unit weights were employed initially, but weighting schemes based on counting statistics (for **2**) or on an empirical form (for **1** and **3**) were employed in the final refinements. Neutral-atom scattering factors with anomalous dispersion corrections were used (12). The computer programs used were from the NRC Vax 750/780 crystal structure system (13) or the CRYSTALS program suite (14) except that the thermal ellipsoid diagrams were made with the SNOOPI program (15). All programs were run on a MicroVAX II computer. Crystallographic data and details of each data collection are given in Table 1. Tables of thermal parameters for **1**, **2**, and **3**, and hydrogen atom coordinates for **3** have been deposited as supplementary material.[2]

$Os_4(CO)_{15}$

Crystals of **1** could not be obtained by crystallization; suitable crystals were, however, obtained directly from the synthesis when carried out as described above (i.e., at −15°C, solution unstirred). An initial data set was collected at room temperature and the structure solved by direct methods. After all the atoms were placed in the model, evidence was found that indicated the molecule was disordered in the unit cell. To better model the disorder, the data were recollected on the same crystal at −73°C and the latter data set used in subsequent refinement of the structure. The space group was determined to be either *C2/c* or *Cc* by the systematic absences. The final choice of *C2/c* (disordered) over *Cc* (ordered) was based on the refinement: the best ordered model in *Cc* had substantially worse agreement ($R = 0.052$, 120 variables) than the final disordered model in *C2/c* ($R = 0.044$, 108 variables). The asymmetric unit consists of two overlapping half molecules of $Os_4(CO)_{15}$, each of half occupancy. The two fold axis of space group *C2/c* relates the two half molecules such that one of the half molecules is equivalent to the "missing" half of the other molecule. The number of variables was limited by assigning one common isotropic temperature factor to the carbon atoms, another to the oxygen atoms, and one to each type of osmium atoms. Bond length restraints were employed during the initial stages of refinement on all Os—C and Os—O distances.

[2] These tables can be purchased from: The Depository of Unpublished Data, Document Delivery, CISTI, National Research Council Canada, Ottawa, Canada K1A OS2.

The hydrogen atom coordinates for **3** have also been deposited with the Cambridge Crystallographic Data Centre, and can be obtained on request from The Director, Cambridge Crystallographic Data Centre, University Chemical Laboratory, 12 Union Road, Cambridge, CB2 1EZ, U.K.

Can. J. Chem. Downloaded from www.nrcresearchpress.com by 80.90.12.36 on 09/08/12
For personal use only.

Table 2. Fractional coordinates for **1**.

Atom	*x/a*	*y/b*	*z/c*
Os(1)	0.4999 (3)	0.3683 (1)	0.7411 (1)
Os(2)	0.5752 (2)	0.2372 (2)	0.6063 (1)
Os(3)	0.4969 (5)	0.0799 (1)	0.7467 (2)
Os(4)	0.4248 (2)	0.2538 (2)	0.8816 (1)
O(11)	0.717 (5)	0.402 (5)	0.825 (4)
O(12)	0.282 (4)	0.423 (5)	0.665 (4)
O(13)	0.515 (3)	0.661 (3)	0.732 (2)
O(21)	0.798 (3)	0.248 (3)	0.677 (2)
O(22)	0.347 (4)	0.236 (5)	0.542 (2)
O(23)	0.622 (3)	0.488 (3)	0.515 (2)
O(24)	0.640 (3)	0.035 (4)	0.477 (2)
O(31)	0.721 (4)	0.086 (6)	0.824 (4)
O(32)	0.268 (4)	0.093 (6)	0.687 (4)
O(33)	0.560 (4)	−0.140 (4)	0.632 (3)
O(34)	0.455 (4)	−0.119 (4)	0.881 (3)
O(41)	0.641 (4)	0.227 (5)	0.971 (3)
O(42)	0.201 (3)	0.283 (4)	0.807 (2)
O(43)	0.397 (3)	0.524 (4)	0.956 (2)
O(44)	0.335 (3)	0.078 (4)	1.016 (3)
C(11)	0.637 (4)	0.374 (5)	0.796 (4)
C(12)	0.358 (4)	0.399 (5)	0.690 (4)
C(13)	0.508 (4)	0.553 (3)	0.731 (2)
C(21)	0.710 (4)	0.245 (5)	0.655 (3)
C(22)	0.421 (3)	0.237 (5)	0.564 (3)
C(23)	0.603 (4)	0.391 (4)	0.545 (3)
C(24)	0.606 (4)	0.121 (4)	0.519 (3)
C(31)	0.638 (5)	0.086 (5)	0.798 (3)
C(32)	0.358 (5)	0.092 (4)	0.709 (4)
C(33)	0.528 (4)	−0.050 (6)	0.669 (4)
C(34)	0.453 (4)	−0.043 (6)	0.830 (4)
C(41)	0.551 (3)	0.237 (5)	0.933 (2)
C(42)	0.285 (4)	0.268 (5)	0.833 (3)
C(43)	0.404 (4)	0.421 (4)	0.927 (3)
C(44)	0.364 (4)	0.134 (4)	0.959 (3)

Table 3. Bond lengths and selected angles for **1**.

Bond lengths (Å)

Os(1)—Os(2)	2.774 (1)[a]	Os(1)—Os(3)	2.948 (1)
Os(1)—Os(4)	2.775 (1)[a]	Os(2)—Os(3)	2.998 (1)[a]
Os(3)—Os(4)	2.998 (1)[a]	Os(1)—C(11)	1.96 (5)
Os(1)—C(12)	2.00 (5)	Os(1)—C(13)	1.90 (4)
Os(2)—C(21)	1.88 (5)	Os(2)—C(22)	2.08 (4)
Os(2)—C(23)	1.91 (5)	Os(2)—C(24)	1.91 (5)
Os(3)—C(31)	1.97 (6)	Os(3)—C(32)	1.88 (6)
Os(3)—C(33)	1.89 (6)	Os(3)—C(34)	1.95 (6)
Os(4)—C(41)	1.82 (4)	Os(4)—C(42)	1.94 (5)
Os(4)—C(43)	1.88 (4)	Os(4)—C(44)	1.94 (4)
C(11)—O(11)	1.15 (7)	C(12)—O(12)	1.07 (7)
C(13)—O(13)	1.11 (5)	C(21)—O(21)	1.18 (6)
C(22)—O(22)	1.00 (6)	C(23)—O(23)	1.13 (6)
C(24)—O(24)	1.20 (6)	C(31)—O(31)	1.13 (8)
C(32)—O(32)	1.19 (8)	C(33)—O(33)	1.18 (7)
C(34)—O(34)	1.14 (7)	C(41)—O(41)	1.30 (7)
C(42)—O(42)	1.16 (6)	C(43)—O(43)	1.16 (6)
C(44)—O(44)	1.16 (6)		

Selected bond angles (deg)

Os(2)-Os(1)-Os(3)	63.11 (3)	Os(3)-Os(1)-Os(4)	63.11 (3)
Os(1)-Os(2)-Os(3)	61.27 (4)	Os(1)-Os(3)-Os(2)	55.62 (3)
Os(1)-Os(3)-Os(4)	55.63 (3)	Os(1)-Os(4)-Os(3)	61.26 (4)
Os(2)-Os(1)-C(11)	93 (2)	Os(2)-Os(1)-C(13)	113 (1)
C(11)-Os(1)-C(12)	169 (2)	C(11)-Os(1)-C(13)	88 (2)
Os(3)-Os(2)-C(24)	109 (2)	C(21)-Os(2)-C(22)	174 (2)
C(21)-Os(2)-C(24)	94 (2)	Os(4)-Os(3)-C(31)	88 (2)
Os(4)-Os(3)-C(34)	77 (2)	C(31)-Os(3)-C(32)	172 (2)
C(31)-Os(3)-C(34)	90 (2)	C(33)-Os(3)-C(34)	95 (2)
Os(1)-Os(4)-C(41)	96 (2)	Os(1)-Os(4)-C(43)	90 (2)
C(41)-Os(4)-C(42)	176 (2)	C(41)-Os(4)-C(43)	92 (2)
C(43)-Os(4)-C(44)	104 (2)		

[a]Restraint was applied to this bond length.

These restraints were lifted in the final stages of the refinement. Restraints were also applied to Os—Os distances such that the chemically equivalent bond lengths were refined to their mean values. After convergence of the refinement, an empirical weighting scheme was adopted; the weight for a given reflection was given by $w = [4.35147t_0(X) + 5.6181t_1(X) + 1.65544t_2(X)]^{-1}$, where $X = |F_o|F_{max}^{-1}$ and t_n are polynomial functions of the Chebyshev series (16). Additional details of data collection and refinement are given in Table 1. Atomic positional parameters for one molecule of the disordered pair of **1** are listed in Table 2; bond lengths and selected bond angles are given in Table 3.

$Os_4(CO)_{13}(PMe_3)[P(OMe)_3]$

There was evidence for disorder of the methoxy groups of the trimethyl phosphite ligand, but this was not modelled. (Disorder is a common problem in structures with a trimethyl phosphite ligand (17).) Six weak reflections that had asymmetric backgrounds and also the largest $\langle w(|F_o| - |F_c|)^2 \rangle$ values were excluded from the final cycles of refinement. These reflections were, (−8, 4, 6), (−9, 2, 6), (11, 4, −4), (8, 7, -5), (8, 12, −6), and (8, 3, −6). There were significant peaks (2.0 (3) e Å^{-3}) near the osmium atoms (within 1 Å) in the final electron density difference map; these were likely the result of improperly modelled absorption. No peaks were observed that could be reasonably attributed to the methyl hydrogen atoms and no attempt was made to include them in calculated positions. A weighting scheme based on counting statistics was adopted during the final cycles of refinement ($K = 4 \times 10^{-4}$). Further details of the data collection and structure refinement are given in Table 1. Atomic positional parameters for **2** are presented in Table 4; important bond lengths and angles are contained in Table 5.

$Os_4(CO)_{14}(CNBu^t)$

After anisotropic refinement of the osmium atoms, an electron density difference map revealed a pair of large peaks (~4 e Å^{-3}) around each osmium atom. The peak–osmium–peak angles were approximately 180°, and the peak–peak vectors nearly parallel. Such a pattern is consistent with poorly modelled absorption or crystal twinning. The latter possibility was ruled out because the peak positions were inconsistent with chemically reasonable split osmium atom positions. An empirical absorption correction based on Ψ-scans (18) gave essentially the same agreement as the analytical correction for equivalent isotropic models with a similar pattern of peaks

Can. J. Chem. Downloaded from www.nrcresearchpress.com by 80.90.12.36 on 09/08/12
For personal use only.

Table 4. Fractional coordinates for **2**.

Atom	*x/a*	*y/b*	*z/c*
Os(1)	0.78038 (13)	0.17035 (8)	0.23725 (8)
Os(2)	0.57949 (13)	0.18132 (8)	0.11720 (8)
Os(3)	0.77657 (13)	0.06787 (8)	0.09311 (8)
Os(4)	0.98272 (14)	0.07342 (9)	0.23248 (9)
P(1)	0.4831 (9)	0.2823 (6)	0.1779 (6)
P(2)	1.0944 (14)	0.1014 (7)	0.3507 (8)
O(11)	0.899 (3)	0.3158 (14)	0.1657 (16)
O(12)	0.667 (3)	0.0564 (16)	0.3492 (16)
O(13)	0.749 (3)	0.2822 (18)	0.3747 (17)
O(21)	0.699 (3)	0.3111 (15)	0.0243 (19)
O(22)	0.449 (3)	0.0677 (14)	0.2188 (16)
O(23)	0.380 (3)	0.1556 (18)	−0.0234 (18)
O(31)	0.9184 (21)	0.1978 (13)	0.0186 (14)
O(32)	0.6444 (23)	−0.0519 (14)	0.1893 (15)
O(33)	0.5995 (25)	0.0486 (16)	−0.0617 (18)
O(34)	0.934 (3)	−0.0666 (14)	0.0424 (19)
O(41)	1.112 (3)	0.2045 (18)	0.1554 (18)
O(42)	0.870 (3)	−0.0612 (21)	0.3156 (20)
O(43)	1.159 (4)	−0.0420 (22)	0.1771 (22)
O(45)	1.030 (4)	0.0867 (20)	0.4323 (23)
O(46)	1.162 (3)	0.181 (3)	0.3665 (19)
O(47)	1.212 (4)	0.039 (3)	0.370 (3)
C(11)	0.853 (3)	0.2551 (20)	0.1876 (20)
C(12)	0.712 (3)	0.0922 (19)	0.3004 (21)
C(13)	0.765 (3)	0.2413 (20)	0.3188 (22)
C(21)	0.655 (4)	0.2585 (23)	0.0569 (24)
C(22)	0.503 (3)	0.1061 (20)	0.1824 (21)
C(23)	0.459 (4)	0.166 (3)	0.029 (3)
C(31)	0.863 (3)	0.1501 (22)	0.0468 (22)
C(32)	0.696 (3)	−0.0040 (22)	0.1537 (22)
C(33)	0.672 (3)	0.0590 (20)	0.0005 (22)
C(34)	0.880 (3)	−0.0087 (21)	0.0626 (21)
C(41)	1.059 (4)	0.155 (3)	0.192 (3)
C(42)	0.909 (5)	−0.006 (3)	0.287 (3)
C(43)	1.102 (5)	0.008 (3)	0.197 (3)
C(25)	0.574 (3)	0.3725 (19)	0.2014 (20)
C(26)	0.428 (4)	0.2566 (23)	0.2736 (24)
C(27)	0.349 (4)	0.323 (3)	0.112 (3)
C(45)	0.993 (6)	0.113 (4)	0.491 (4)
C(46)	1.107 (5)	0.258 (3)	0.377 (3)
C(47)	1.316 (8)	0.042 (4)	0.415 (5)

near the osmium atoms in the Fourier difference map. Because of these difficulties, the data reduction was carried out followed by isotropic refinement and a "pseudo" absorption correction applied by using the method of Walker and Stuart (R = 13% with no correction; R = 7% after application of DIFABS) (19)). After refinement of the model (anisotropic osmium atoms) with this "absorption" correction, the largest peaks in the electron density difference map were still near the osmium atoms, but were less than 2.5 (3) e Å^{-3} and showed a more random pattern. At this point, the methyl hydrogen atoms were included at calculated positions (d(C—H) = 0.96 Å); the positions of these atoms were not refined. The number of variables was limited by refining one common isotropic thermal motion parameter for all carbonyl oxygen atoms, one for all carbonyl carbon atoms, one for the methyl carbon atoms, and one for the hydrogen atoms. An empirical weighting scheme was employed during the final cycles of refinement with the weight, w, given by the expression $w = [26.5710t_0(X) + 40.5720t_1(X) + 24.4554t_2(X) + 8.03540t_3(X)]^{-1}$, where $X = |F_o|F_{max}^{-1}$ and t_n are polynomial functions of the Chebyshev series (16). Additional details of the data collection and structure refinement are given in Table 1; Table 6 lists the atomic positional parameters for the non-hydrogen atoms of **3**, and Table 7 contains the bond lengths and selected angles for **3**.

Table 5. Bond lengths and selected angles for **2**.

Bond lengths (Å)			
Os(1)—Os(2)	2.783 (3)	Os(1)—Os(3)	2.937 (2)
Os(1)—Os(4)	2.792 (2)	Os(2)—Os(3)	2.978 (2)
Os(3)—Os(4)	3.019 (2)	Os(1)—C(11)	1.89 (4)
Os(1)—C(12)	1.90 (4)	Os(1)—C(13)	1.83 (4)
Os(2)—P(1)	2.31 (1)	Os(2)—C(21)	1.90 (4)
Os(2)—C(22)	1.93 (4)	Os(2)—C(23)	1.86 (4)
Os(3)—C(31)	1.91 (4)	Os(3)—C(32)	1.88 (4)
Os(3)—C(33)	1.80 (5)	Os(3)—C(34)	1.85 (4)
Os(4)—P(2)	2.22 (1)	Os(4)—C(41)	1.79 (5)
Os(4)—C(42)	1.87 (5)	Os(4)—C(43)	1.88 (6)
C(11)—O(11)	1.22 (5)	C(12)—O(12)	1.17 (5)
C(13)—O(13)	1.19 (5)	C(21)—O(21)	1.18 (5)
C(22)—O(22)	1.12 (5)	C(23)—O(23)	1.16 (5)
C(31)—O(31)	1.15 (5)	C(32)—O(32)	1.19 (5)
C(33)—O(33)	1.23 (5)	C(34)—O(34)	1.22 (5)
C(41)—O(41)	1.23 (5)	C(42)—O(42)	1.15 (6)
C(43)—O(43)	1.13 (6)	P(1)—C(25)	1.84 (4)
P(1)—C(26)	1.82 (4)	P(1)—C(27)	1.86 (4)
P(2)—O(45)	1.62 (4)	P(2)—O(46)	1.54 (4)
P(2)—O(47)	1.67 (4)	O(45)—C(45)	1.19 (8)
O(46)—C(46)	1.46 (8)	O(47)—C(47)	1.29 (9)
Selected bond angles (deg)			
Os(2)-Os(1)-Os(3)	62.69 (6)	Os(3)-Os(1)-Os(4)	63.54 (6)
Os(1)-Os(2)-Os(3)	61.20 (6)	Os(1)-Os(3)-Os(2)	56.11 (6)
Os(1)-Os(3)-Os(4)	55.89 (6)	Os(1)-Os(4)-Os(3)	60.57 (6)
Os(2)-Os(1)-C(11)	89 (1)	Os(2)-Os(1)-C(13)	110 (1)
C(11)-Os(1)-C(12)	172 (2)	C(11)-Os(1)-C(13)	88 (2)
Os(3)-Os(2)-C(23)	106 (1)	C(21)-Os(2)-C(22)	178 (2)
C(21)-Os(2)-C(23)	90 (2)	C(23)-Os(2)-P(1)	97 (1)
Os(4)-Os(3)-C(31)	85 (1)	Os(4)-Os(3)-C(34)	78 (1)
C(31)-Os(3)-C(32)	171 (2)	C(31)-Os(3)-C(34)	92 (2)
C(33)-Os(3)-C(34)	94 (2)	Os(1)-Os(4)-C(41)	89 (1)
Os(1)-Os(4)-P(2)	102.0 (4)	C(41)-Os(4)-C(42)	174 (2)
C(41)-Os(4)-P(2)	86 (1)	C(43)-Os(4)-P(2)	94 (1)

Results and discussion

$Os_4(CO)_{15}$

Addition of $Os(CO)_5$ to $Os_3(CO)_{10}(COE)_2$ in hexane at −15°C afforded $Os_4(CO)_{15}$ (**1**) in approximately 70% yield (eq. 1.). Attempts to displace acetonitrile from $Os_3(CO)_{11}(CH_3CN)$ with $Os(CO)_5$ were unsuccessful. In contrast,

$$[1]\quad Os_3(CO)_{10}(COE)_2 + Os(CO)_5 \xrightarrow{-15°C} \underset{\mathbf{1}}{Os_4(CO)_{15}}$$

Can. J. Chem. Downloaded from www.nrcresearchpress.com by 80.90.12.36 on 09/08/12
For personal use only.

Table 6. Fractional coordinates for **3**.

Atom	*x/a*	*y/b*	*z/c*
Os(1)	0.1640 (1)	0.23568 (8)	0.2631 (1)
Os(2)	0.1607 (1)	0.1936 (1)	0.0471 (1)
Os(3)	0.1501 (1)	0.07616 (8)	0.2157 (1)
Os(4)	0.1492 (1)	0.14007 (9)	0.4367 (1)
O(11)	0.428 (3)	0.243 (2)	0.272 (2)
O(12)	−0.092 (3)	0.275 (2)	0.246 (2)
O(13)	0.190 (3)	0.388 (2)	0.352 (3)
O(21)	0.419 (3)	0.175 (2)	0.037 (2)
O(22)	−0.100 (3)	0.198 (2)	0.014 (3)
O(23)	0.166 (3)	0.364 (2)	0.032 (2)
O(24)	0.159 (3)	0.141 (2)	−0.178 (3)
N(31)	0.419 (2)	0.052 (2)	0.228 (2)
O(32)	−0.112 (2)	0.089 (1)	0.204 (2)
O(33)	0.137 (3)	−0.007 (2)	0.000 (3)
O(34)	0.127 (2)	−0.068 (2)	0.341 (2)
O(41)	0.412 (2)	0.130 (2)	0.454 (2)
O(42)	−0.113 (3)	−0.165 (2)	0.422 (2)
O(43)	0.174 (3)	0.258 (2)	0.610 (3)
O(44)	0.128 (3)	0.004 (2)	0.586 (3)
C(11)	0.329 (4)	0.235 (2)	0.273 (3)
C(12)	0.008 (3)	0.259 (2)	0.255 (3)
C(13)	0.174 (4)	0.327 (2)	0.308 (3)
C(21)	0.325 (4)	0.183 (3)	0.050 (4)
C(22)	0.000 (4)	0.193 (2)	0.034 (3)
C(23)	0.160 (4)	0.295 (3)	0.043 (4)
C(24)	0.145 (5)	0.162 (3)	−0.088 (5)
C(31)	0.320 (4)	0.064 (2)	0.225 (3)
C(32)	−0.011 (4)	0.088 (2)	0.210 (3)
C(33)	0.144 (3)	0.030 (2)	0.078 (3)
C(34)	0.143 (3)	−0.012 (2)	0.297 (2)
C(41)	0.309 (3)	0.132 (2)	0.435 (3)
C(42)	−0.015 (4)	0.150 (2)	0.424 (3)
C(43)	0.165 (4)	0.211 (3)	0.547 (4)
C(44)	0.130 (4)	0.056 (3)	0.528 (4)
C(1)	0.539 (3)	0.028 (2)	0.244 (3)
C(2)	0.605 (5)	0.095 (3)	0.270 (4)
C(3)	0.569 (4)	−0.003 (3)	0.135 (4)
C(4)	0.556 (5)	−0.025 (3)	0.333 (4)

$Os(CO)_4(PMe_3)$ does displace CH_3CN from $Os_3(CO)_{10}(CH_3CN)_2$ to yield $Os_4(CO)_{14}(PMe_3)$ (6). Compound **1** was isolated as dark red, air-stable crystals. Concentrated solutions of **1** in CH_2Cl_2 are red whereas dilute solutions are green. Similar dichroism (20) was observed for $Os_4(CO)_{13}(PMe_3)[P(OMe)_3]$ and $Os_4(CO)_{14}(CNBu^t)$, described below, and for $Os_4(CO)_{14}(PMe_3)$ (6).

The structure of **1** at room temperature was determined by X-ray crystallography. The structure was, however, disordered and the data were recollected at −73°C in order to better model the disorder (Experimental). The latter structure determination is discussed here; it reveals (Fig. 1) an essentially planar metal skeleton: the dihedral angle between the Os(1)Os(2)Os(3) and Os(1)Os(3)Os(4) planes is 179.0°. The Os_4 unit has adjacent short (Os(1)—Os(2) = 2.774 (1), Os(1)—Os(4) = 2.775 (1) Å) and long (Os(2)—Os(3) = Os(3)—Os(4) = 2.998 (1) Å) bonds. Although somewhat long, the diagonal Os(1)—Os(3) bond length at 2.948 (1) Å is more

Table 7. Bond lengths and selected angles for **3**.

Bond lengths (Å)

Os(1)—Os(2)	2.793 (2)	Os(1)—Os(3)	2.936 (2)
Os(1)—Os(4)	2.775 (2)	Os(2)—Os(3)	2.985 (2)
Os(3)—Os(4)	2.983 (2)	Os(1)—C(11)	1.94 (4)
Os(1)—C(12)	1.88 (4)	Os(1)—C(13)	1.74 (4)
Os(2)—C(21)	1.94 (5)	Os(2)—C(22)	1.89 (5)
Os(2)—C(23)	1.83 (5)	Os(2)—C(24)	1.78 (6)
Os(3)—C(31)	2.01 (4)	Os(3)—C(32)	1.90 (4)
Os(3)—C(33)	1.90 (4)	Os(3)—C(34)	1.89 (3)
Os(4)—C(41)	1.88 (3)	Os(4)—C(42)	1.94 (4)
Os(4)—C(43)	1.88 (4)	Os(4)—C(44)	1.92 (4)
C(11)—O(11)	1.17 (4)	C(12)—O(12)	1.21 (4)
C(13)—O(13)	1.23 (4)	C(21)—O(21)	1.14 (4)
C(22)—O(22)	1.19 (5)	C(23)—O(23)	1.25 (5)
C(31)—N(31)	1.18 (4)	C(32)—O(32)	1.18 (4)
C(33)—O(33)	1.18 (4)	C(34)—O(34)	1.17 (4)
C(41)—O(41)	1.22 (4)	C(42)—O(42)	1.17 (4)
C(43)—O(43)	1.16 (5)	C(44)—O(44)	1.18 (5)
N(31)—C(1)	1.48 (4)	C(1)—C(2)	1.47 (5)
C(1)—C(3)	1.52 (5)	C(1)—C(4)	1.47 (5)

Selected bond angles (deg)

Os(2)-Os(1)-Os(3)	62.76 (5)	Os(3)-Os(1)-Os(4)	62.91 (5)
Os(1)-Os(2)-Os(3)	60.97 (5)	Os(1)-Os(3)-Os(2)	56.27 (5)
Os(1)-Os(3)-Os(4)	55.90 (5)	Os(1)-Os(4)-Os(3)	61.19 (6)
Os(2)-Os(1)-C(11)	92 (1)	Os(2)-Os(1)-C(13)	125 (1)
C(11)-Os(1)-C(12)	167 (2)	C(11)-Os(1)-C(13)	86 (2)
Os(3)-Os(2)-C(24)	115 (2)	C(21)-Os(2)-C(22)	173 (2)
C(21)-Os(2)-C(24)	92 (2)	C(23)-Os(2)-C(24)	107 (2)
Os(4)-Os(3)-C(31)	92 (1)	Os(4)-Os(3)-C(34)	80 (1)
C(31)-Os(3)-C(32)	179 (2)	C(31)-Os(3)-C(34)	87 (2)
C(33)-Os(3)-C(34)	97 (2)	Os(1)-Os(4)-C(41)	87 (1)
Os(1)-Os(4)-C(43)	98 (1)	C(41)-Os(4)-C(42)	175 (2)
C(41)-Os(4)-C(43)	90 (2)	C(43)-Os(4)-C(44)	97 (2)

typical of an Os—Os single bond. The average Os—Os bond length in $Os_3(CO)_{12}$ of 2.877 (3) Å is usually taken as representative of the length of an Os—Os single bond in low-nuclearity osmium clusters (21).

As discussed for $Os_4(CO)_{14}(PMe_3)$ (6) these unusual bond lengths may be rationalized in terms of three-center, two-electron metal–metal bonds as shown in Chart 1. In this way, the

Chart 1.

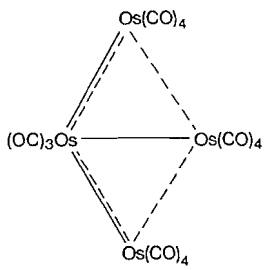

short peripheral metal–metal bonds are assigned a bond order of 1.5 and the long bonds an order of 0.5, and each osmium atom achieves an 18-electron configuration.

Many years ago Pauling proposed a simple equation for cal-

Can. J. Chem. Downloaded from www.nrcresearchpress.com by 80.90.12.36 on 09/08/12
For personal use only.

Fig. 1. Molecular structure of $Os_4(CO)_{15}$ (**1**).

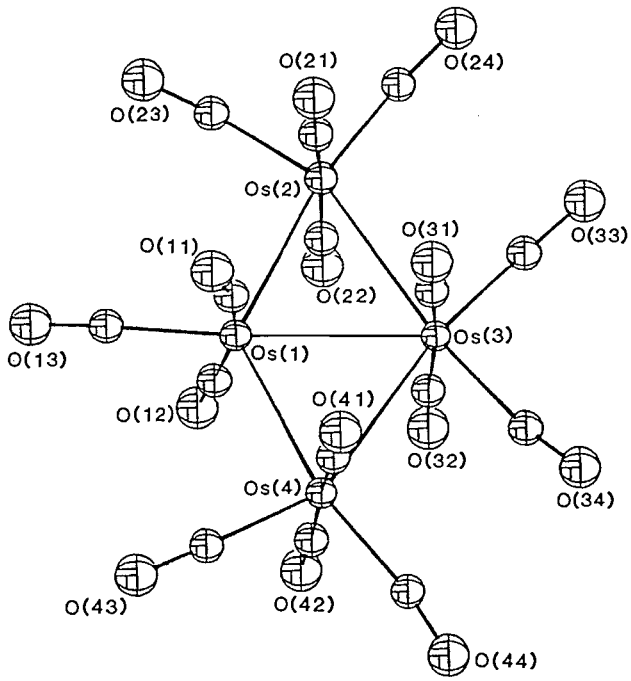

culating the bond order of a bond given its length; this is given in eq. [2] where $d(n)$ is the distance of the bond in question, d_1 is the length of a single bond of the same type, and n is the bond order (22).

$$[2] \quad d(n) = d_1 - 0.60 \log(n)$$

If a value of 2.88 Å is assumed for the length of an Os—Os single bond (the value found in $Os_3(CO)_{12}$), then application of Pauling's relationship to the Os—Os bond lengths of **1** yields a bond order of 1.5 for the short Os—Os bonds and an order of 0.6 for the long Os—Os bonds. These bond orders are therefore consistent with the interpretation shown in Chart 1. The cationic cluster $[Pt_2Au_2(PPh_3)_4(CNC_6H_3Me_2)_4]^{2+}$ has adjacent, long Pt—Au bonds that have been rationalized in terms of partial three-center, two-electron bonds (23).

An alternative electron-counting scheme for **1** is shown in Chart 2. In this scheme each Os—Os bond is considered as a

Chart 2.

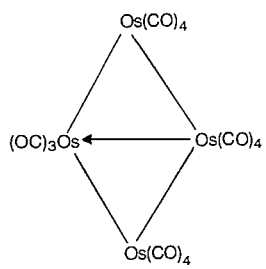

single bond but with the added feature than the diagonal (hinge) metal–metal bond is a donor–acceptor (dative) bond. Molecular orbital calculations by Mealli and Proserpio favor this interpretation (24). We have described a number of binuclear, trinuclear, and cluster compounds with unsupported Os—Os dative bonds (5, 6, 10, 25). We (26–28) and others have also proposed that in some osmium clusters donor–acceptor metal–metal bonds are present as part of the cluster framework (29). If the diagonal bond in **1**, and related clusters, is a dative metal–metal bond it is difficult to rationalize the difference in the lengths of the peripheral metal-metal bonds even allowing for the lower coordination about Os(1). Furthermore, in $Os_4(CO)_{13}(PMe_3)[P(OMe)_3]$ (described below), $Os_4(CO)_{14}(PMe_3)$ (6), and $(\eta^5\text{-}C_5Me_5)IrOs_3(CO)_{12}$ (4), the noncarbonyl ligands are not coordinated to the osmium atom that acts as the donor atom in the proposed dative metal–metal bond. In our studies of complexes with dative metal–metal bonds we have observed, not unexpectedly, that where possible the better σ-donor ligand (i.e., the noncarbonyl ligand) is bound to the donor metal–metal atom (5, 25), and in some cases this electronic preference apparently overrides considerable steric repulsions (26, 27).

It is pointed out here that there are some planar tetranuclear clusters of Ru and Os in which there are long metal–metal bonds that are not adjacent (i.e., in $Os_4(\mu\text{-}O_2CCF_3)_2(CO)_{12}$ (30), $Ru_4(\mu\text{-}PPh_2)_2(CO)_{13}$, and $Ru_4(\mu\text{-}PPh_2)_4(CO)_{10}$ (31)).

Osmium–osmium bonds are expected to have low stretching force constants and therefore the bond should be readily deformed. There are, however, innumerable trinuclear osmium clusters with a variety of ligands of varying steric bulk and yet the unbridged Os—Os bonds in these clusters are usually within ±0.05 Å of 2.877 Å, the average Os—Os length in $Os_3(CO)_{12}$. For example, in the extremely crowded molecule $Os_3(CO)_6[P(OMe)_3]_6$ (with threefold symmetry) prepared in this laboratory the Os—Os bond length is 2.927 (1) Å, and it is known that a P-donor ligand causes a lengthening of the Os—Os bond in the *trans* position (32). It is therefore probable that bond lengthening or shortening of more than ~0.05 Å from 2.877 Å can be attributed to electronic rather than steric effects. The exact nature of those electronic effects remains an intriguing problem in metal cluster chemistry.

Planar tetranuclear clusters were, until recently, rare. The butterfly and tetrahedral arrangement are the common geometries observed for tetranuclear clusters (33). The butterfly configuration is the common structure found for 62-electron clusters (**1** is a 62-electron cluster). The butterfly unit (an arachno octahedron) is also the structure most consistent with the polyhedral skeletal electron pair theory (PSEPT) for these clusters. Prior to the initial report of **1**, the only planar tetranuclear clusters without bridging ligands reported were $[Re_4(CO)_{16}]^{2-}$ (34) and $HOs_3Re(CO)_{15}$ (35). The metal–metal bond lengths in these clusters do not show the same variation as those in **1**. The structure of $HOs_3Re(CO)_{15}$ was, however, badly disordered and more recent work on $(Ph_3P)(OC)_3Re(\mu\text{-}H)Os_3(CO)_{11}$ suggests it may contain a long, unbridged Re—Os bond (28).

Planar tetranuclear osmium clusters with bridging ligands include $Os_4(\mu_3\text{-}S)(CO)_{13}$ (36) and $Cl_2SnOs_3(\mu\text{-}CH_2)(CO)_{11}$ (37). It has also been pointed out by Hoffmann[3] (see also ref. 38) that **1** is an isolobal analogue $[C_4H_7]^+$, the structure of which still remains uncertain after many years of study (39).

One of the fascinating properties of metal carbonyl clusters is their stereochemical nonrigidity (40), and the clusters

[3] R. Hoffmann, personal communication.

Can. J. Chem. Downloaded from www.nrcresearchpress.com by 80.90.12.36 on 09/08/12
For personal use only.

Fig. 2. Variable temperature ^{13}C nmr spectra of **1** (in $CHFCl_2$–CD_2Cl_2 except spectrum at −6°C: CH_2Cl_2–CD_2Cl_2).

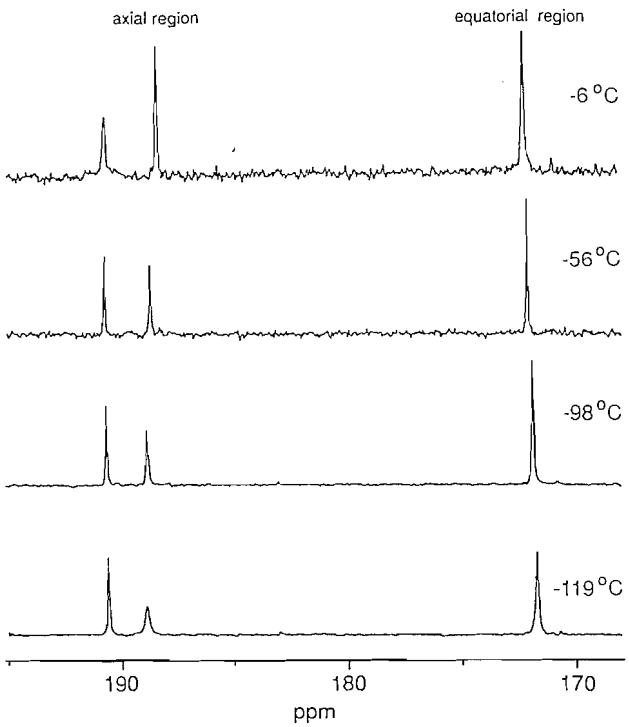

described here are no exception. Variable temperature ^{13}C nmr spectra of **1** (^{13}CO-enriched) in CD_2Cl_2–$CHFCl_2$ below 0°C are shown in Fig. 2. Because of the unusual bonding in the cluster, care must be taken when assigning resonances in a specific region of the spectrum as due to carbonyls of a certain type (i.e., axial or equatorial). For example, some of the carbonyl signals in the ^{13}C nmr spectrum of the related $Os_4(CO)_{14}(PMe_3)$, at −115°C where it is rigid, have unusual chemical shifts (6). However, by analogy to the spectra of most Os_3 clusters (41, 42) and the spectrum of $Os_4(CO)_{14}(PMe_3)$ (6), the two signals (each of intensity 4) downfield of δ 180 are confidently assigned to axial carbonyls whereas the singlet (of intensity 7) to high field of δ 175 is assigned to the equatorial carbonyl ligands.

The spectrum at −56°C is interpreted in terms of **1** with the same structure in solution as found in the solid state, but with rapid all-equatorial, merry-go-round CO-exchange taking place in the molecule; this is shown in Chart 3. This type of CO exchange has rarely been proposed for trinuclear group-8 carbonyl clusters (43). Axial-equatorial, merry-go-round CO exchange appears more common (41, 44, 45). The suggested mechanism for the low-energy carbonyl exchange in **1** is, however, consistent to that proposed for $Os_4(CO)_{14}(PMe_3)$ (6) and for $(OC)_5Cr[Os(CO)_3(PMe_3)]_2$.[4]

The spectrum of **1** at −119°C (Fig. 2) indicates CO exchange is beginning to slow on the nmr time scale: the signals δ 188.9 and 171.7 are significantly broadened relative to that at δ 190.6. This allows the assignment of the signal at δ 188.9 to the axial carbonyls on the hinge atoms that would be inequivalent in **1** if it were rigid, and therefore the signal at δ

[4] H.B. Davis and R.K. Pomeroy. Unpublished results.

Chart 3.

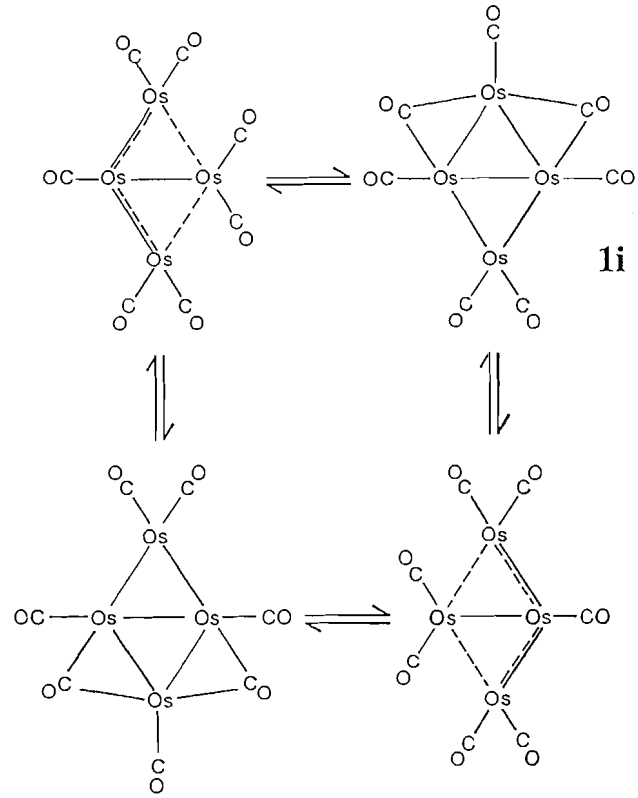

190.6 is attributed to the axial carbonyls on the wingtip metal atoms.

The low activation barrier for the CO exchange in **1** probably indicates that the intermediate with bridging carbonyls (**1i** in Chart 3) is not much higher in energy than the ground state structure of **1**. Note that in **1i** all the Os—Os bonds are considered as two-center, two-electron metal-metal bonds.

In the spectrum at −6°C there is evidence for a further fluxional process since the signal assigned to the axial carbonyls on the wingtip osmium atoms is broadened along with the signal attributed to the equatorial carbonyls. A mechanism that accounts for this observation is a threefold twist mechanism at the wingtip osmium atoms that exchanges an axial and the equatorial carbonyl ligands attached to these osmium atoms. We have proposed this type of rearrangement to account for some of the higher energy, nonrigid processes that occur in the $Os_3(CO)_{12-x}[P(OMe)_3]_x$ (x = 1–5) clusters (41, 46). (An axial-equatorial, merry-go-round CO exchange similar to that proposed for **2**, below, would cause all the signals to broaden simultaneously.)

$Os_4(CO)_{13}(PMe_3)[P(OMe)_3]$

This cluster was prepared in high yield by the addition of $P(OMe)_3$ to $Os_4(CO)_{13}(PMe_3)$ in hexane at room temperature (eq. [3]). Like **1** and $Os_4(CO)_{13}(PMe_3)$, **2** is an air-stable, red

[3] $Os_4(CO)_{14}(PMe_3) + P(OMe)_3 \longrightarrow \underset{\mathbf{2}}{Os_4(CO)_{13}(PMe_3)[P(OMe)_3]}$

solid that is dichroic in solution.

The X-ray crystal structure of **2** shows the geometry given in Fig. 3. As can be seen, the metal skeleton in **2** is essentially

Can. J. Chem. Downloaded from www.nrcresearchpress.com by 80.90.12.36 on 09/08/12
For personal use only.

Fig. 3. Molecular structure of $Os_4(CO)_{13}(PMe_3)[P(OMe)_3]$ (**2**).

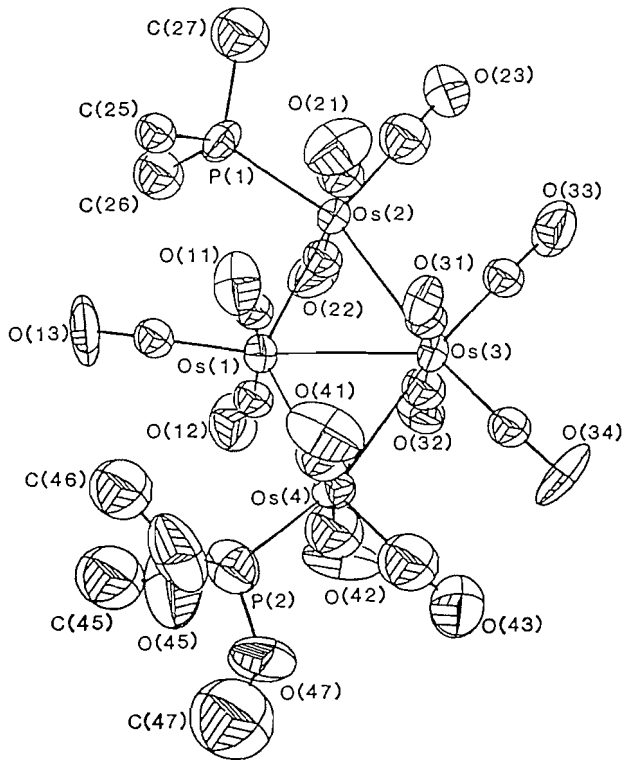

the same as that in **1**. Furthermore, the Os—Os bond lengths in **2** (and in $Os_4(CO)_{14}(PMe_3)$ and $Os_4(CO)_{14}(CNBu^t)$) are all within 0.021 Å of their counterparts in **1** (Table 8). This suggests that the difference in the length of the long and the short Os—Os bonds in these molecules cannot be attributed to packing forces or the *trans* influences of the peripheral ligands.

As expected, the phosphorus ligands occupy the sterically least encumbered sites in **2**, namely the equatorial sites that are *cis* to the $Os(CO)_3$ unit. Bulky phosphorus ligands invariably occupy equatorial sites in trinuclear metal carbonyl clusters (32, 47, 48). The Os—P distance to the phosphite at 2.22 (1) Å is shorter than that to the phosphine (2.31 (1) Å) and can be attributed to the better π-acceptor properties of the phosphite ligand (49, 50).

Variable temperature ^{13}C nmr spectra of **2** (^{13}CO-enriched) in CH_2Cl_2–CD_2Cl_2 are presented in Fig. 4. It is immediately apparent from the figure that, unlike **1** and $Os_4(CO)_{14}(PMe_3)$, **2** is rigid on the nmr time scale in solution at −45°C. The number of signals in the carbonyl region is that expected from the solid state structure of **2**.

The assignment of the carbonyl resonances shown in Fig. 4 (see also Fig. 3) is as follows. The doublets at δ 203.7 (2C) and 201.6 (2C) are assigned to the axial carbonyls on Os(2) and Os(4), respectively, by virtue of their intensity, chemical shift, and phosphorus coupling compared to those of related trinuclear osmium derivatives (41, 42). The resonances at δ 214.8 (2C) and 195.4 (1C) are assigned to the axial and equatorial carbonyls bound to Os(1), respectively, on the basis of their unusual chemical environment (a similar situation was observed in the spectrum of $Os_4(CO)_{14}(PMe_3)$ (6)). The remaining signal of intensity 2 at δ 173.0 is therefore assigned to the axial carbonyls on Os(3) (also an unusual region for such a resonance). The assignment of the remaining resonances is less straightforward; it is based on the relative chemical shifts expected (from studies on trinuclear Os compound) for signals of the equatorial carbonyls of $Os(CO)_3(L)$ (L = CO, PMe_3, $P(OMe)_3$) units, and the mode of collapse of the signals and the proposed mechanism for the exchange described below.

Table 8. Metal–metal bond lengths in **1**, $Os_4(CO)_{14}(PMe_3)$, **2** and **3**.

	1	$Os_4(CO)_{14}(PMe_3)$[a]	**2**	**3**
Os(1)—Os(2)	2.774 (1)	2.779 (2)	2.783 (3)	2.793 (2)
Os(1)—Os(4)	2.775 (1)	2.784 (2)	2.792 (2)	2.775 (2)
Os(2)—Os(3)	2.998 (1)	3.013 (2)	2.937 (2)	2.985 (2)
Os(3)—Os(4)	2.998 (1)	2.982 (2)	3.019 (2)	2.983 (2)
Os(1)—Os(3)	2.948 (1)	2.935 (2)	2.978 (2)	2.936 (2)

[a]From ref. 6.

The rearrangement to account for the low-temperature carbonyl exchange in **1** and $Os_4(CO)_{14}(PMe_3)$ involves movement of carbonyl ligands from one equatorial site to another; it is therefore not surprising that the carbonyls in **2** are far more rigid. Such a mechanism in **2** would require the migration of one of the phosphorus ligands from a wingtip Os atom to Os(1), and migration of a phosphorus ligand from one metal atom to another is known to be a high-energy process in osmium cluster chemistry (41, 51).

In the ^{13}C nmr spectrum of **2** at −6°C all the carbonyl resonances have broadened and collapsed to the base line except for those resonances assigned to the carbonyl ligands of the (hinge) $Os(CO)_4$ grouping (Fig. 4). This behavior is interpreted in terms of axial-equatorial, merry-go-round carbonyl exchanges about the short peripheral Os—Os bonds. This is shown in Chart 4. The lowest energy carbonyl exchange in $Os_3(CO)_{11}(PEt_3)$ (45) and $Os_3(CO)_{11}[P(OMe)_3]$ (41) has been interpreted as proceeding by a similar mechanism (i.e., in that plane that contains both axial and equatorial carbonyls and is also approximately orthogonal to the Os—P bond). In **2** it is proposed there are two such merry-go-round exchanges, both of which involve the axial and equatorial carbonyls on Os(1).

Careful simulation of the ^{13}C nmr spectrum at −6°C (Fig. 5) shows that the first order rate constants of the two exchange processes are slightly different: 30 ± 3 s^{-1} for the exchange that occurs in the plane that is orthogonal to the PMe_3 ligand, and 25 ± 3 s^{-1} for the exchange in the plane orthogonal to the $P(OMe)_3$ substituent. These rates translate into activation energies of ($\Delta G^{\ddagger}_{267}$) of 13.8 and 13.9 kcal mol^{-1}, respectively. In unpublished results, we have observed that the barrier to the lowest energy CO exchange in $Os_3(CO)_{11}(PMe_3)$ is lower than that in $Os_3(CO)_{11}[P(OMe)_3]$.[5]

Above room temperature the signals assigned to the CO ligands on Os(3) begin to broaden such that at 70°C (toluene–toluene-d_8 solvent) these signals have also disappeared into the base line (Fig. 4). The mechanism of how this takes place is uncertain although a localized carbonyl exchange at Os(3) as the sole mechanism can be ruled out. Given the closeness of the chemical shifts of the carbonyl resonances of the $Os(CO)_4$ grouping, such a mechanism would only cause minor broadening and rapid coalescence to a sharp signal. In other words,

[5] E. Wong, B. Gilmour, A.K. Ma, and P. K. Pomeroy. Unpublished results.

Chart 4.

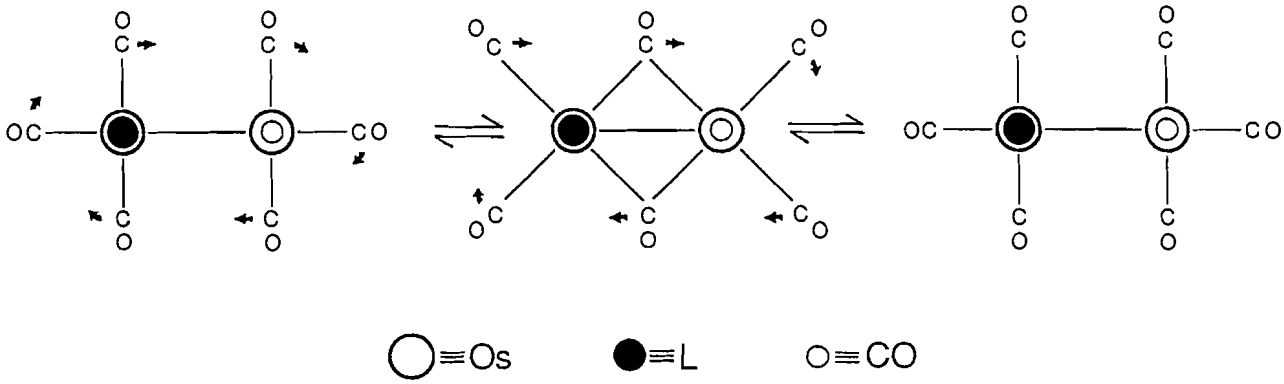

Fig. 4. Variable temperature ^{13}C nmr spectra of **2** (in CH_2Cl_2–CD_2Cl_2 except spectrum at 71°C: toluene–toluene-d_8)

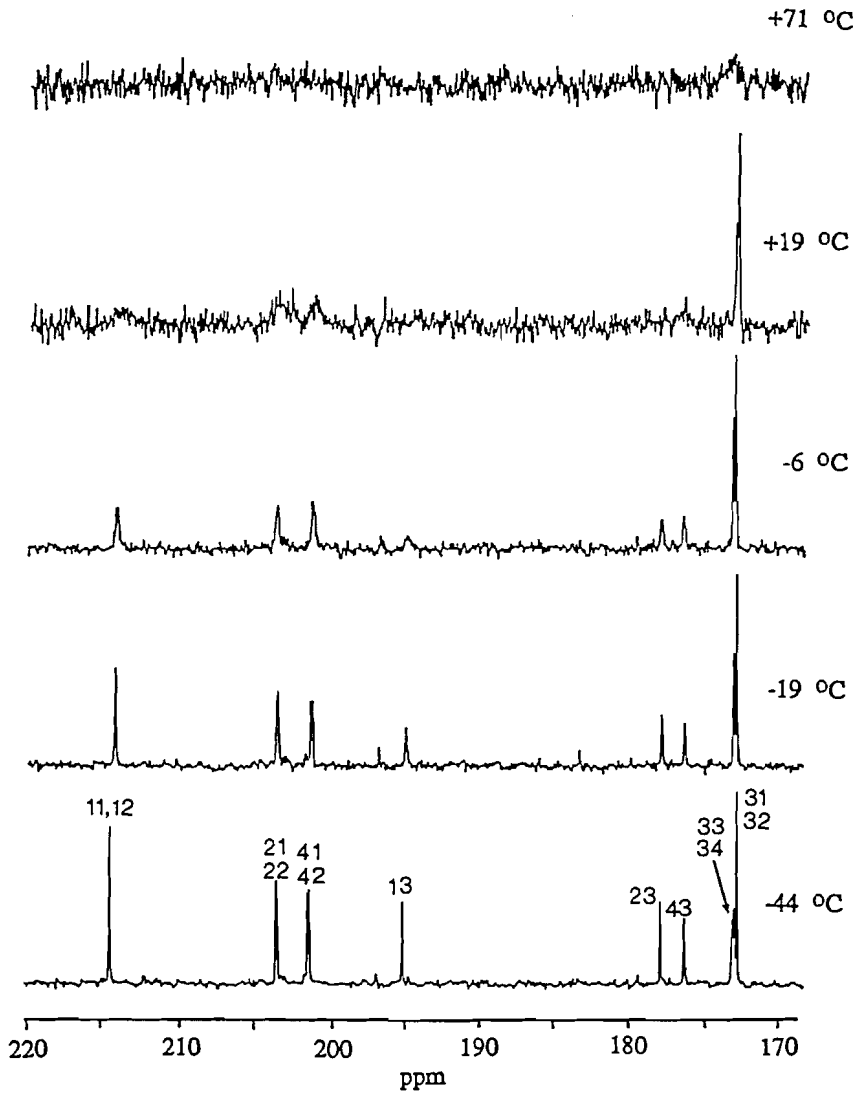

carbonyl exchange is taking place over all four osmium atoms in **2** in solution at 71°C.

$Os_4(CO)_{14}(CNBu^t)$

Dropwise addition of Me_3NO (in CH_2Cl_2) to $Os_4(CO)_{15}(CNBu^t)$ also in CH_2Cl_2 at room temperature caused a color change from amber to dark green. The progress of the reaction (eq. [4]) was monitored by infrared spectroscopy. The product, $Os_4(CO)_{14}(CNBu^t)$ (**3**), was isolated in 62% yield as dark red, air-stable crystals. The X-ray crystal

Can. J. Chem. Downloaded from www.nrcresearchpress.com by 80.90.12.36 on 09/08/12
For personal use only.

Can. J. Chem. Downloaded from www.nrcresearchpress.com by 80.90.12.36 on 09/08/12
For personal use only.

Fig. 5. Calculated (*a*) and observed (*b*) ^{13}C nmr spectra of **2** at −6°C in CH_2Cl_2–CD_2Cl_2.

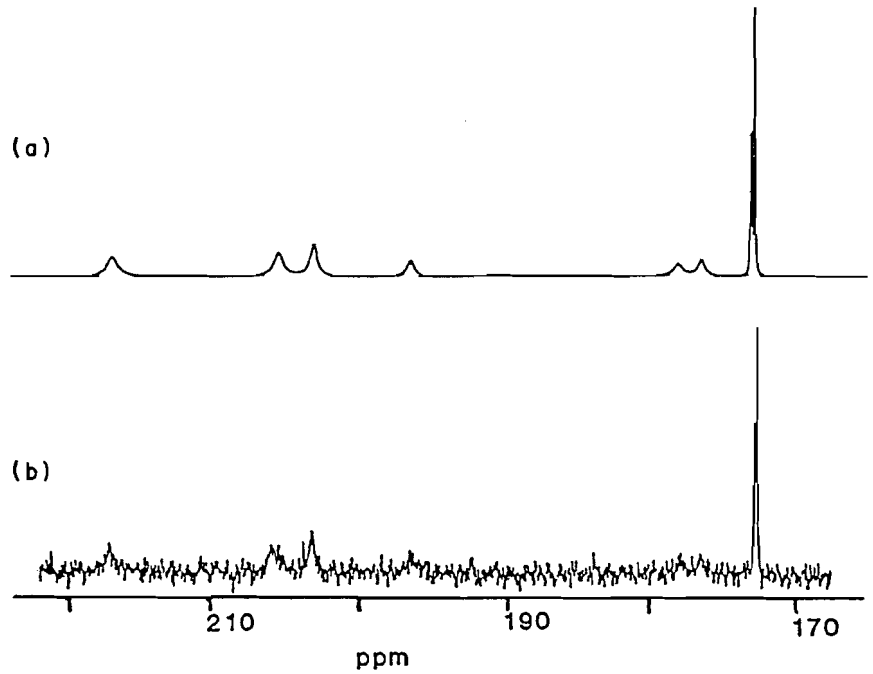

Fig. 6. Molecular structure of $Os_4(CO)_{14}(CNBu^t)$ (**3**).

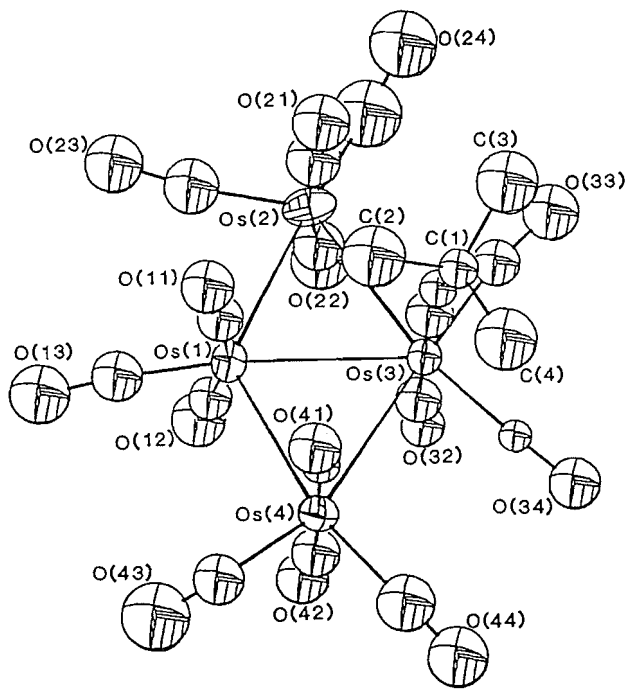

[4] $Os_4(CO)_{15}(CNBu^t) + Me_3NO \xrightarrow[62\%]{25°C} \underset{\mathbf{3}}{Os_4(CO)_{14}(CNBu^t)}$

structure of **3** again reveals (Fig. 6) a planar Os_4 skeleton with long and short peripheral Os—Os bonds (Table 8). Unlike the phosphorus-ligand derivatives of $Os_4(CO)_{15}$ (i.e., $Os_4(CO)_{14}(PMe_3)$ and **2**), the noncarbonyl ligand in **3** occupies an axial site. This was anticipated since in triosmium carbonyl clusters isocyanide ligands occupy axial rather than equatorial sites (48, 52, 53). The axial site that the isocyanide ligand occupies in **3** is, however, at the hinge osmium atom that has four terminal ligands. It might be thought that an axial site on a hinge metal atom may be sterically more hindered than an axial site on a wingtip metal atom since at the former site there are three rather than two repulsive axial-axial interactions between ligands. The Os—Os bonds that involve the Os atom (Os(3)) of the $Os(CO)_3(CNBu^t)$ grouping are, however, all longer than 2.93 Å so that the axial-axial interactions of this grouping may be less than those at the axial sites on the wingtip Os atoms since the latter metal atoms are involved in a short Os—Os bond to the other hinge Os atom (Os(1)).

The site the isocyanide ligand occupies in **3** is the site that would be expected if the Os atom of the $Os(CO)_3(CNBu^t)$ unit is acting as a net electron-donor metal atom, that is, if the electronic structure shown in Chart 2 applies to **3**. We have observed that the noncarbonyl ligand, L, in most clusters of the type $Os_5(CO)_{15}(L)$ occupies a sterically crowded site at the one osmium atom in the cluster that has four ligands coordinated to it. It is believed that this metal atom is a net electron-donor metal atom in these molecules and the better donor ligand, L, coordinated to this metal atom stablilizes the donation (26, 27).

The ^1H nmr spectrum (at an operating frequency of 100 MHz) of **3** in toluene-d_8 at ambient temperature exhibits two signals, at δ 0.95 and 0.96, of almost equal intensity. The signal at δ 0.95 was slightly broader than the other signal. The spectrum was essentially unchanged at an operating frequency of 400 MHz and with the sample at −50°C. This behaviour is interpreted in terms of two isomers present in solution that are tentatively assigned as having the solid-state structure and the isomer with the isocyanide ligand coordinated to the axial site of a wingtip osmium atom. The latter isomer is thought reasonable given that rapid carbonyl exchange in the equatorial plane in **3**, as observed in **1**, would render the remaining axial isomer equivalent to the first on the nmr time scale at room

Fig. 7. Variable temperature ^{13}C nmr spectra of **3** (in $CHFCl_2$–CD_2Cl_2).

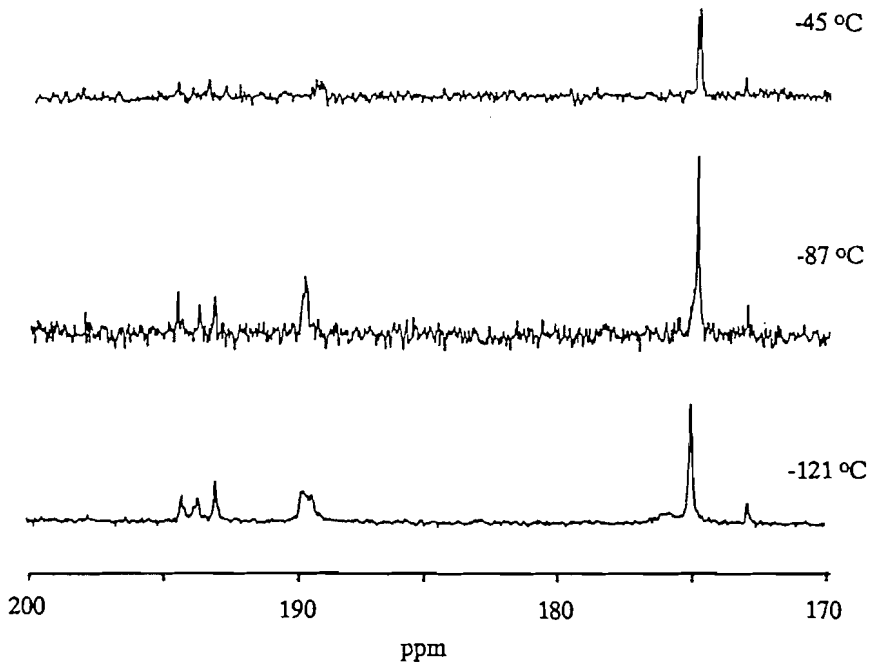

Can. J. Chem. Downloaded from www.nrcresearchpress.com by 80.90.12.36 on 09/08/12
For personal use only.

temperature. Furthermore, migration of a *tert*-butyl isocyanide ligand from one metal atom to another in a triosmium cluster has been observed previously (53). The extra broadness of the resonance at δ 0.95 may be due to quadrupolar broadening by the nitrogen atom.

Variable temperature ^{13}C nmr spectra of **3** (^{13}CO-enriched) are shown in Fig. 7. A completely satisfactory explanation of the spectra is not possible at this time. It is believed that there is rapid exchange of the equatorial carbonyl groups in the two isomers of **3** present in solution at low temperatures so as to give an averaged signal for the equatorial carbonyls of each isomer, in a similar manner to that observed for the parent **1**. The two strong signals observed in the spectrum of **3** at −45°C at δ 174.7 and 174.8 are therefore assigned to the averaged signal due to the equatorial carbonyls of the two isomers (in **1** the corresponding signal occurs at δ 171.1). These two signals of **3** become accidentally degenerate in the spectra at −87°C and −121°C. As in **1**, the axial carbonyls in the isomers of **3** are thought not to undergo rapid exchange. Because of this and the presence of the (axial) isocyanide ligand, each isomer is expected to give rise to a 2:2:1:1:1 pattern for the axial carbonyls (i.e., a total of 10 signals). The weak signals observed in the region δ 189 – 195 are assigned as due to axial carbonyls; they appear in the region expected for such resonances. The weak signal to high field of δ 175 is assigned to an axial carbonyl attached to the osmium atom of one of the isomers that has four terminal ligands; this by analogy to **2** (see above) and $Os_4(CO)_{14}(PMe_3)$ (6). Not all of the signals due to the axial carbonyls were observed, presumably due to their low intensity or to accidental degeneracy with other signals.

Although the evidence is not as strong as for **1** and $Os_4(CO)_{14}(PMe_3)$, we do believe there is rapid all-equatorial, merry-go-round carbonyl exchange in **3**. That the signal attributed to the equatorial carbonyls is slightly broadened in the spectrum at −121°C may indicate the onset of decoalescence which in turn indicates that the barrier to this process is similar to that in **1**.

Acknowledgement

We thank the Natural Sciences and Engineering Research Council of Canada for financial support. F.W.B.E. and R.K.P. acknowledge the many fruitful interactions between the members of the Chemistry Department, Simon Fraser University, and Professor Graham. R.K.P. also thanks Professor Bill Graham for his friendship and support the past 28 years.

References

1. W. Hieber and H. Stallmann. Z. Elektrochem. **49**, 288 (1943).
2. J.R. Moss and W.A.G. Graham. J. Chem. Soc. Chem. Commun. 835 (1970); J. Chem. Soc. Dalton Trans. 95 (1977).
3. C.R. Eady, B.F.G. Johnson, and J. Lewis. J. Organomet. Chem. **37**, C39 (1972); J. Chem. Soc. Dalton Trans. 2606 (1975); M. D. Vargas and J. N. Nicholls. Adv. Inorg. Chem. Radiochem. **30**, 123 (1986).
4. V.J. Johnston, F.W.B. Einstein, and R.K. Pomeroy. J. Am. Chem. Soc. **109**, 7220 (1987).
5. V.J. Johnston, F.W.B. Einstein, and R.K. Pomeroy. J. Am. Chem. Soc. **109**, 8111 (1987); Organometallics, **7**, 1867 (1988); Organometallics **9**, 2754 (1990).
6. L.R. Martin, F.W.B. Einstein, and R.K. Pomeroy. J. Am. Chem. Soc. **108**, 338 (1986); Organometallics, **7**, 294 (1988).
7. R. K. Pomeroy. J. Organomet. Chem. **383**, 387 (1990).
8. P. Rushman, G.N. van Buuren, M. Shiralian, and R.K. Pomeroy. Organometallics, **2**, 693 (1983).
9. M. Tachikawa and J.R. Shapley. J. Organomet. Chem. **124**, C19 (1977).
10. F.W.B. Einstein, V.J. Johnston, A.K. Ma, and R.K. Pomeroy. Organometallics, **9**, 52 (1990).

Can. J. Chem. Downloaded from www.nrcresearchpress.com by 80.90.12.36 on 09/08/12
For personal use only.

11. A. Becalska, R.K. Pomeroy, and W.A.G. Graham. Can. J. Chem. **67**, 1236 (1989).
12. International tables for X-ray crystallography. Vol. IV. Kynoch Press, Birmingham, England. 1974 (present distributor: Kluwer Academic, Dordrecht, Netherlands). p. 99.
13. E.J. Gabe, Y. Lepage, J.-P. Chariand, and F.L. Lee. J. Appl. Crystallogr. **22**, 384 (1989).
14. D.J. Watkin, J.R. Carruthers, and P.W. Betteridge. CRYSTALS. Chemical Crystallography Laboratory, University of Oxford, Oxford, England. 1985.
15. E.K. Davies. SNOOPI Plot Program. Chemical Crystallographic Laboratory, University of Oxford, Oxford, England. 1985.
16. J.R. Carruthers and D.J. Watkin. Acta Crystallogr. Sect. A: Cryst. Phys. Diffr. Theor. Gen. Crystallogr. **A35**, 698 (1979).
17. R.E. Cobbledick, F.W.B. Einstein, R.K. Pomeroy, and E.R. Spetch. J. Organomet. Chem. **195**, 77 (1980).
18. A.C.T. North, D.C. Phillips, and F. Mathews. Acta Crystallogr. Sect. A: Cryst. Phys. Diffr. Theor. Gen. Crystallogr. **A24**, 351 (1968).
19. N. Walker and D. Stuart. Acta Crystallogr. Sect. A: Found. Crystallogr. **A39**, 158 (1983).
20. H. Cartright. J. Chem. Educ. **63**, 984 (1986).
21. M.R. Churchill and B.G. Deboer. Inorg. Chem. **16**, 878 (1977).
22. L.C. Pauling. The nature of the chemical bond. 3rd ed. Cornell University Press, Ithaca, New York. 1960. p. 400.
23. C.E. Briant, D.I. Gilmour, and D.M.P. Mingos. J. Chem. Soc. Dalton Trans. 835 (1986).
24. C. Mealli and D.M. Proserpio. J. Am. Chem. Soc. **112**, 5484 (1990).
25. H.B. Davis, F.W.B. Einstein, P.G. Glavina, T. Jones, R.K. Pomeroy, and P. Rushman. Organometallics, **8**, 1030 (1989); J.A. Shipley, R.J. Batchelor, F.W.B. Einstein, and R.K. Pomeroy. Organometallics, **10**, 3620 (1991); R.J. Batchelor, H.B. Davis, F.W.B. Einstein, and R.K. Pomeroy. J. Am. Chem. Soc. **112**, 2036 (1990).
26. W. Wang, F.W.B. Einstein, and R.K. Pomeroy. Organometallics, **13**, 1114 (1994).
27. W. Wang, R.J. Batchelor, F.W.B. Einstein, C.-Y. Lu, and R.K. Pomeroy. Organometallics, **12**, 3598 (1993).
28. W. Wang, F. W. B. Einstein, and R. K. Pomeroy. Organometallics, **12**, 3079 (1993).
29. G.R. John, B.F.G. Johnson, and J. Lewis. J. Organomet. Chem. **181**, 143 (1979); M.I. Bruce and M.L. Williams. J. Organomet. Chem. **282**, C11 (1985); R.D. Adams and S. Wang. Organometallics, **6**, 739 (1987).
30. M.P. Diebold, S.R. Drake, B.F.G. Johnson, J. Lewis, M. McPartlin, and H.R. Powell. J. Chem. Soc. Chem. Commun. 1358 (1988); M.P. Diebold, B.F.G. Johnson, J. Lewis, V.P. Saharan, M. McPartlin, and H.R. Powell. J.Organomet. Chem. **405**, C25 (1991).
31. G. Hogarth, J.A. Phillips, F. van Gastel, N.J. Taylor, T.B. Marder, and A.J. Carty. J. Chem. Soc. Chem. Commun. 1570 (1988); J.F. Corrigan, S. Doherty, N.J. Taylor, and A.J. Carty. Organometallics, **12**, 993 (1993).
32. R.F. Alex, F.W.B. Einstein, R.H. Jones, and R.K. Pomeroy. Inorg. Chem. **26**, 3175 (1987).
33. E. Sappa, A. Tiripicchio, A.J. Carty, and G.E. Toogood. Prog. Inorg. Chem. **35**, 437 (1987).
34. M.R. Churchill and R. Bau. Inorg. Chem. **7**, 2606 (1968).
35. M.R. Churchill and F.J. Hollander. Inorg. Chem. **16**, 2493 (1977).
36. R.D. Adams, I.T. Horvàth, B.E. Segmüller, and L.-W. Yang. Organometallics, **2**, 1301 (1983).
37. N. Viswanathan, E. D. Morrison, G. L. Geoffroy, S. J. Geib, and A. L. Rheingold. Inorg. Chem. **25**, 3100 (1986).
38. C.N. Wilker and R. Hoffmann. J. Am. Chem. Soc. **105**, 5285 (1983).
39. P.C. Myhre, G.G. Webb, and C.S. Yannoni. J. Am. Chem. Soc. **112**, 8992 (1990).
40. E. Band and E.L. Muetterties. Chem. Rev. **78**, 639 (1978); G.L. Geoffroy. Acc. Chem. Res. **13**, 469 (1980); B.E. Mann. *In* Comprehensive organometallic chemistry. Vol. 3. *Edited by* G. Wilkinson, F.G.A. Stone, and E.W. Abel. Pergamon Press, Oxford. 1982. p. 89; B.F.G. Johnson and A. Rodgers. *In* The chemistry of metal cluster complexes. *Edited by* D.F. Shriver, H.D. Kaesz, and R.D. Adams. VCH Press, New York. 1990. p. 303.
41. R.F. Alex and R.K. Pomeroy. Organometallics, **6**, 2437 (1987).
42. B.E. Mann and B.F. Taylor. ^{13}C NMR data for organometallic compounds, Academic Press, New York. 1981.
43. F.A. Cotton, B.E. Hanson, and J.D. Jamerson. J. Am. Chem. Soc. **99**, 6588 (1977).
44. A.J. Deeming. Adv. Organomet. Chem. **26**, 1 (1986).
45. B.F.G. Johnson, J. Lewis, B.E. Reichert, and K.T. Schorpp. J. Chem. Soc. Dalton Trans. 1403 (1976).
46. R.F. Alex and R.K. Pomeroy. J. Organomet. Chem. **284**, 379 (1985).
47. D.J. Dahm and R.A. Jacobson. J. Am. Chem. Soc. **90**, 5106 (1968); R.E. Benfield, B.F.G. Johnson, P.R. Raithby, and G.M. Sheldrick. Acta Crystallogr. Sect. B: Struct. Crystallogr. Cryst. Chem. **B34**, 666 (1978); M.I. Bruce, J.G. Matisons, B.W. Skelton, and A.H. White. J. Chem. Soc. Dalton Trans. 2375 (1983); T. Venäläinen and T.A. Pakkanen. J. Organomet. Chem. **266**, 269 (1984); M.I. Bruce, M.J. Liddell, C.A. Hughes, J.M. Patrick, B.W. Skelton, and A.H. White. J. Organomet. Chem. **347**, 181 (1988).
48. K.-L. Lu, C.-J. Su, Y.-W. Lin, H.-M. Gau, and Y.-S. Wen. Organometallics, **11**, 3832 (1992).
49. C.A. Tolman. Chem. Rev. **77**, 313 (1977).
50. A.N. Caldwell, L. Manojlovic-Muir, and K.W. Muir. J. Chem. Soc. Dalton Trans. 2265 (1977).
51. A.J. Deeming, S. Donovan-Mtunzi, S.E. Kabir, and P.J. Manning. J. Chem. Soc. Dalton Trans. 1037 (1985).
52. M.J. Mays and P.D. Gavens. J. Chem. Soc. Dalton Trans. 911 (1980); M.I. Bruce, J.G. Matisons, R.C. Wallis, J.M. Patrick, B.W. Skelton, and A.H. White. J. Chem. Soc. Dalton Trans. 2365 (1983).
53. A.K. Ma, F.W.B. Einstein, V.J. Johnston, and R.K. Pomeroy. Organometallics, **9**, 45 (1990).

COMMUNICATION

The controlled synthesis of triosmium chain clusters

Jack Lewis and John R. Moss

Abstract: The reaction of $H_2Os_3(CO)_{12}$ with $ClSnPh_3$ in the presence of diethylamine gives exclusively the pentametallic chain compound 1,3-*ax,ax*-$Ph_3SnOs(CO)_4Os(CO)_4Os(CO)_4SnPh_3$. A similar reaction with $ClAuPPh_3$ gives 1,3-*ax,eq*-$Ph_3PAuOs(CO)_4Os(CO)_4Os(CO)_4AuPPh_3$. The di-tin compound reacts with HCl to give 1,3-*ax,ax*-$Cl_3SnOs(CO)_4Os(CO)_4Os(CO)_4SnCl_3$. These products are obtained in high yield and the reactions are selective.

Keywords: osmium carbonyl chain cluster complex.

Résumé : La réaction du $H_2Os_3(CO)_{12}$ avec le $ClSnPh_3$, en présence de diéthylamine, fournit exclusivement le composé pentamétallique linéaire 1,3-*ax,ax*-$Ph_3SnOs(CO)_4Os(CO)_4Os(CO)_4SnPh_3$. Une réaction du $ClAuPh_3$ fournit le 1,3-*ax,eq*-$Ph_3PAuOs(CO)_4Os(CO)_4Os(CO)_4AuPh_3$. Le composé contenant deux atomes d'étain réagit avec le HCl pour donner le 1,3-*ax,ax*-$Cl_3SnOs(CO)_4Os(CO)_4Os(CO)_4SnCl_3$. Ces produits sont obtenus avec des rendements élevés et les réactions sont sélectives.

Mots clés : agrégats complexes de chaînes d'osmium carbonyle.

[Traduit par la rédaction]

Introduction

Transition metal compounds containing three metals in a chain, with no bridging ligands, are relatively rare. An early example of this type of compound is the dihydride $H_2Os_3(CO)_{12}$ (1, 2). Although this compound has been known for over 25 years, its structure has never been determined due to the lack of suitable single crystals. The structure is, however, believed to be 1,3-*eq,eq*-$H_2Os_3(CO)_{12}$ by comparison with known structures of related compounds $Os_3(CO)_{12}I_2$ (3), $Os_3(CO)_{12}Cl_2$ (4), $Os_3(CO)_{12}Me_2$ (5) and on the basis of spectroscopic results (6). Since $H_2Os_3(CO)_{12}$ can be obtained in good yield from $Os_3(CO)_{12}$, it may be a useful starting material for other chain clusters. Indeed it has recently been used in the controlled assembly of new Os_6 and Os_9 clusters (7).

Received September 29, 1994.

This paper is dedicated to Professor William A.G. Graham on the occasion of his 65th birthday.

J. Lewis. University Chemical Laboratory, Lensfield Road, Cambridge CB2 1EW, England.
J.R. Moss.[1] Department Chemistry, University of Cape Town, Rondebosch 7700, South Africa.

[1] Author to whom correspondence may be addressed. Telephone: (021) 650 2535. Fax: (021) 650-3788.

Previously, it has been shown that the reaction of $SnCl_4$ with $Os_3(CO)_{12}$ leads to the formation, in high yield, of the tetrametallic chain cluster compound $ClOs_3(CO)_{12}SnCl_3$ (8) which is believed to have the 1,3-*ax,eq*-structure. This compound has more recently been shown to react with metal nucleophiles (9, 10) and the structure of $ClOs_3(CO)_{12}SnCl_2[CpW(CO)_3]$ has confirmed that it is a penta-metallic chain with 1,3-*ax,eq*-substitution (viz. *eq*-Cl and *ax*-$SnCl_2R$) at the linear triosmium centre (10). Other important triosmium dodecacarbonyl chain derivatives prepared include 1,3-*ax,ax*-$Cl_3SiOs_3(CO)_{12}SiCl_3$ (11) from $Os_3(CO)_{12}$ and $HSiCl_3$ and 1,3-*eq,eq*-$(CO)_5ReCH_2CH_2Os_3(CO)_{12}CH_2CH_2Re(CO)_5$ from $H_2Os_3(CO)_{12}$ via deprotonation with KH (12). The reaction of $Os_3(CO)_{12}$ with $ClAuPPh_3$ was originally reported to yield $ClOs_3(CO)_{12}AuPPh_3$ (13) but this compound was later found to be $Os_3(CO)_{10}(\mu\text{-}AuPPh_3)(\mu\text{-}Cl)$ with a triangulo structure (14). The reaction of $Os_3(CO)_{12}$ with halogens (15) has been found to be more complex than originally thought and shown to involve initial formation of 1,3-*ax,eq*-$Os_3(CO)_{12}X_2$ which readily isomerizes to 1,3-*eq,eq*-$Os_3(CO)_{12}X_2$ (16).

We sought to find a general route to triosmium chain cluster compounds that would go in high yields under mild conditions and which could contain functional groups that could be elaborated on. Such compounds could be precursors to inorganic polymers where the polymer is held together only by metal–metal bonds.

Can. J. Chem. Downloaded from www.nrcresearchpress.com by 80.90.12.36 on 09/08/12
For personal use only.

Can. J. Chem. Downloaded from www.nrcresearchpress.com by 80.90.12.36 on 09/08/12
For personal use only.

Results and discussion

Some years ago, Collman et al. showed that the dihydride $H_2Os(CO)_4$ could be used to build up metallic chain oligomers such as *trans*-$[Os(CO)_4(SnPh_3)_2]$ (17). Since $H_2Os_2(CO)_8$ and $H_2Os_3(CO)_{12}$ are other members of the same homologous series as $H_2Os(CO)_4$ (2), we believed that they may undergo similar reactions. Thus, starting with $H_2Os_3(CO)_{12}$, we may be able to build up chain clusters with a linear triosmium backbone.

The reaction of $H_2Os_3(CO)_{12}$ with $ClSnPh_3$ in the presence of Et_2NH readily occurred at room temperature to give quantitative conversion to a new compound (as judged by IR). The product was isolated, after recrystallization, as very pale yellow platelets, mp 214–216°C (57% yield). Elemental analysis was consistent with the molecular formula $Os_3(CO)_{12}(SnPh_3)_2$ and this was confirmed by mass spectrometry where a parent ion was seen at *m/e* 1607. Both the IR spectrum: ν(CO) (CH_2Cl_2) 2091 w 2022 vs 1945 wbr cm^{-1} and the ^{13}C NMR spectrum, in the carbonyl region: (CD_2Cl_2) δ 188.2 and δ 184.2 (approximate intensity ratio 1:2) are consistent with this compound being a pentametallic chain with the 1,3-*ax,ax*-structure. Thus, each step of the reaction sequence starting with $Os_3(CO)_{12}$ and ending in $Os_3(CO)_{12}(SnPh_3)_2$ is both highly chemo- and regioselective, in respect to the isolated products (see Scheme 1). The reasons for the compound $Os_3(CO)_{12}(SnPh_3)_2$ adopting the diaxial configuration could be both steric and electronic. We have also investigated similar reactions with other halo-tin derivatives and will report on these later.

This methodology can also be extended to other metal chlorides. Thus reaction of $H_2Os_3(CO)_{12}$ with $ClAuPPh_3$ in the presence of Et_2NH gives, after work-up and recrystallization, beige platelets of a new compound (70% yield), mp 195–198°C. Elemental analysis is consistent with the compound being the pentametallic chain $Ph_3PAuOs(CO)_4Os(CO)_4$-$Os(CO)_4AuPPh_3$. The mass spectrum (negative FAB) shows the highest *m/e* peak at ca. 1339, which may correspond to $[P - AuPPh_3 - CO]^+$. IR shows ν(CO) (CH_2Cl_2): 2117 w, 2096 m, 2044 vs, 1995 w cm^{-1}. The ^{13}C NMR spectrum in the carbonyl region (CD_2Cl_2) shows peaks at δ 190.0, 183.8, 180.4, 180.2, 176.9 (approximate intensity ratios 4:4:1:2:1). This would suggest that the *ax, eq*-isomer has been isolated.

In order to elaborate further on these pentametallic chain complexes, it is necessary to activate the complexes. The mononuclear complex $Os(CO)_4(SnPh_3)_2$ has previously been shown to give $Os(CO)_4(SnBr_3)_2$ on reaction with HBr (17). We investigated the reaction of $Ph_3SnOs_3(CO)_{12}SnPh_3$ with an excess of HCl. The reaction goes quantitatively (by IR) to give colourless needles mp 190–195°C (dec.) (81% yield after recrystallization). The mass spectrum shows the highest *m/e* peak envelope at ca. 1358, which corresponds to the parent ion for $Cl_3SnOs_3(CO)_{12}SnCl_3$. The IR shows ν(CO) (CH_2Cl_2): 2125 w, 2060 vs, 2009 w cm^{-1}, which suggests that the diaxial configuration of the $SnCl_3$ groups has been maintained in this reaction and this is further supported by the ^{13}C NMR spectrum, which shows peaks at δ 192.3 and 185.2 (intensity ratio 1:2) in CD_2Cl_2.

This work shows that it is possible to carry out reactions at a linear triosmium chain that are both highly chemoselective and regioselective. Experiments are underway to build up other chain clusters and to further elaborate the pentametallic chains described herein.

Scheme 1.

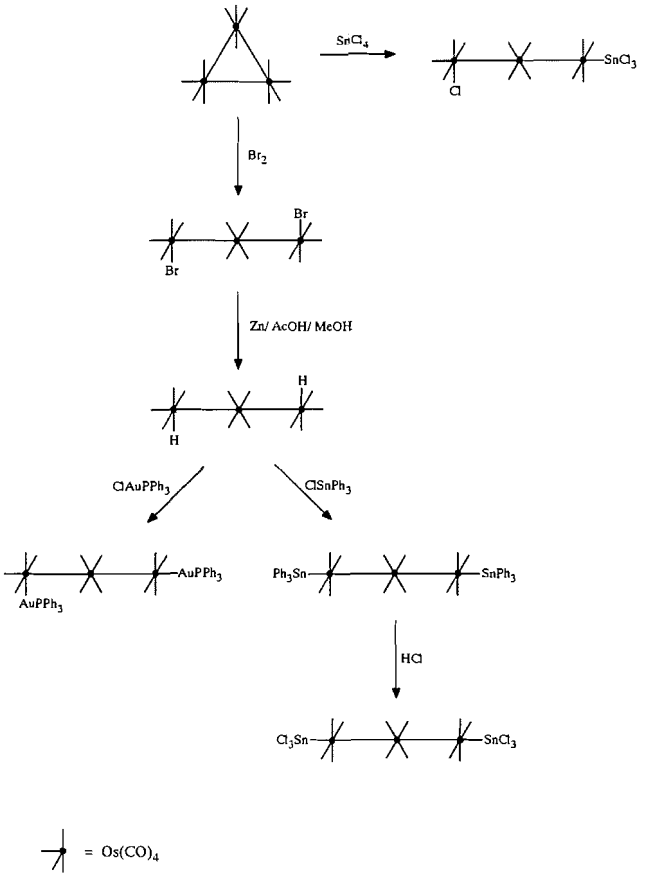

Experimental

A solution of $H_2Os_3(CO)_{12}$ (59 mg, 0.065 mmol) in dry nitrogen saturated CH_2Cl_2 (5 mL) was treated with $ClSnPh_3$ (50 mg, 0.13 mmol). An excess of NEt_2H (0.8 mL) was added and the solution stirred for 45 min. The solvent was removed under reduced pressure to give a pale yellow solid. This was recrystallised from CH_2Cl_2/CH_3OH to give very pale yellow plates of $Ph_3SnOs_3(CO)_{12}SnPh_3$ (0.057 g, 57%).

Acknowledgements

We thank the Foundation for Research and Development (South Africa) and the Bremner Travel Grant Committee for support and the University of Cape Town for sabbatical leave (for J.R.M.). J.R.M. also thanks Professor Bill Graham for introducing him to the fascinating field of osmium carbonyl chemistry.

References

1. J.R. Moss and W.A.G. Graham. J. Organomet. Chem. **23**, C47 (1970).
2. J.R. Moss and W.A.G. Graham. Inorg. Chem. **16**, 75 (1977).
3. N. Cook, L. Smart, and P. Woodward. J. Chem. Soc. Dalton Trans. 1744 (1988).
4. J.R. Moss, M.L. Niven, and E.E. Sutton. Transition Met. Chem. **13**, 429 (1988).
5. M.R. Churchill. Personal communication in J.W. Kelland and J.R. Norton. J. Organomet. Chem. **149**, 185 (1978).

6. M. Gochin and J.R. Moss. J. Organomet. Chem. **192**, 409 (1980).
7. J. Lewis and J.R. Moss. J. Organometal. Chem. **444**, C51 (1993).
8. J.R. Moss and W.A.G. Graham. J. Organomet. Chem. **18**, P24 (1969); J. Chem. Soc. Dalton Trans. 89 (1977); A. Becalska, R.K. Pomeroy, and W.A.G. Graham. Can. J. Chem. **67**, 1236 (1989).
9. S.P. Gubin, O.M. Chentsova, G.V. Burmakina, and A.A. Iogansson. Izv. Akad. Nauk SSSR, Ser. Khim. **12**, 2790 (1981).
10. D.B. Firfiray, A. Irving, and J.R. Moss. J. Chem. Soc. Chem. Commun. 377 (1990).
11. A.C. Willis, G.N. van Buuren, R.K. Pomeroy, and F.W.B. Einstein. Inorg. Chem. **22**, 1162 (1983).
12. J. Beimair, B. Niemer, K. Raab, and W. Beck. Chem. Ber. **124**, 1059 (1991).
13. C.W. Bradford and R.S. Nyholm. J. Chem. Soc. Chem. Commun. 867 (1968).
14. C.W. Bradford, W. van Bronswijk, R.J.H. Clark, and R.S. Nyholm. J. Chem. Soc. (A), 2889 (1970).
15. B.F.G. Johnson, J. Lewis, and P.A. Kilty. J. Chem. Soc. (A), 2859 (1968).
16. H.K. Sanati, A. Becalska, A.K. Ma, and R.K. Pomeroy. J. Chem. Soc. Chem. Commun. 197 (1990).
17. J.P. Collman, D.W. Murphy, E.B. Fleischer, and D. Swift. Inorg. Chem. **13**, 1 (1974).

Can. J. Chem. Downloaded from www.nrcresearchpress.com by 80.90.12.36 on 09/08/12
For personal use only.

1994 McBryde Medal Award Lecture Investigations of organized monolayer films for biosensor development[1]

Ulrich J. Krull, Michael S. Heimlich, Krishna M.R. Kallury, P.A.E. Piunno, John D. Brennan, R. Stephen Brown, and Dimitrios P. Nikolelis

Abstract: Our interests have focused on the investigation and development of biosensors that use chemically selective membranes to measure the concentration of specific species in complex media. One fundamental idea is that protein, which can bind selectively to a specific organic or biochemical species, can be incorporated into an ordered lipid or surfactant membrane assembly such that selective binding events lead to changes in the structure of the membrane (transduction) that can be measured quantitatively. The primary advantage of this method of detection is that it is applicable to interactions of enzymes, antibodies, receptors, and lectins, and it may be extended to investigations of DNA/RNA hybridization. This detection method therefore provides a sensitive generic strategy for sensor applications. The central problem to be solved is how the alteration of the structure of a membrane that is caused by binding events of protein or genetic material can give rise to an analytical signal. We have been focusing our efforts in the areas of fluorescence spectroscopy and electrochemical methods. The electrochemical methods rely on detection in changes of the permeability of membranes to ions and provide systems with very low background signal, leading to the possibility of detection of single molecular-binding events. Fluorescent systems operate on the basis that a chemically selective membrane containing a fluorescent indicator can provide an analytical signal caused by the change of the structure of the membrane due to the binding events.

Key words: fluorescence, lipid membrane, electrochemistry, receptor, biosensor.

Résumé : Nos travaux sont orientés vers l'étude et le développement de biosenseurs qui utilisent des membranes chimiquement sélectives pour mesurer la concentration d'espèces spécifiques dans des millieux complexes. Une des hypothèses fondamentales suggère que, si une protéine peut se lier sélectivement à une espèce organique ou biochimique spécifique, on peut l'incorporer dans un assemblage ordonné de lipide ou de membrane d'agent de surface; dans de telles conditions, les événements reliés à une liaison spécifique conduisent à des changements dans la structure de la membrane (transduction) que l'on peut mesurer quantitativement. L'avantage primaire de cette méthode de détection est que l'on peut l'appliquer à des interactions d'enzymes, d'anticorps, de récepteurs et de lectines et que l'on peut l'étendre à des études sur l'hybridation de ADN/ARN. Cette méthode de détection fournit alors une stratégie générique sensible pour les applications aux senseurs. Le problème central à être résolu est le suivant : comment l'altération de la structure de la membrane causée par les événements reliés à une liaison de protéine ou de matériel génétique peut-elle donner lieu à un signal analytique? On a orienté nos efforts vers la spectroscopie de fluorescence et les méthodes électrochimiques. Ces dernières sont fondées sur une détection de changements de perméabilité de membranes aux ions et elles conduisent à la possibilité de détection d'événements de liaisons moléculaires uniques. Les systèmes de fluorescence sont basés sur le fait qu'une membrane chimiquement sélective contenant un indicateur fluorescent peut fournir un signal analytique causé par un changement de structure de la membrane dû à des événements de liaison.

Mots clés : fluorescence, membrane lipidique, électrochimie, récepteur, biosenseur.

[Traduit par la rédaction]

Received June 1, 1994. Revision received January 12, 1995.

U.J. Krull,[2] S. Heimlich, K.M.R. Kallury, and P.A.E. Piunno. Chemical Sensors Group, Department of Chemistry, Erindale Campus, University of Toronto, 3359 Mississauga Road North, Mississauga, ON L5L 1C6, Canada.
J.D. Brennan. Department of Chemistry, University of Windsor, Windsor, ON N9B 3P4, Canada.
R.S. Brown. Biotechnology Research Institute, National Research Council of Canada, 6100 Royalmount Drive, Montreal, QC, H4P 2R2, Canada.
D.P. Nikolelis. Laboratory for Analytical Chemistry, Department of Chemistry, University of Athens, Panepistimiopolis, Kouponia, Athens, GR 15771, Greece.

[1] This is an invited review article based on the 1994 McBryde Medal Award Lecture presented by Professor Krull at the Annual Conference of the Canadian Society for Chemistry in Winnipeg, Manitoba, May 1994.

[2] Author to whom correspondence may be addressed. Telephone: (905) 828-5343 or 828-5413. Fax: (905) 569-4388. E-mail: ukrul@credit.erin.utoronto.ca

Can. J. Chem. Downloaded from www.nrcresearchpress.com by 80.90.12.36 on 09/08/12
For personal use only.

Can. J. Chem. Downloaded from www.nrcresearchpress.com by 80.90.12.36 on 09/08/12
For personal use only.

Fluorescence methods

The use of fluorophores that are embedded within an organized membrane has the advantages that there is no need for labelling of any portion of the selective binding protein, and that direct transduction of the extent of the selective binding interactions is achieved. Analytical assays involving tagged ligands, or complicated separation steps, are unnecessary. The membrane provides an environment in which many proteins can be embedded with retention of a high degree of biological activity. Furthermore, the membrane provides a unique intrinsic amplification since a limited number of selective molecular interactions can lead to a macroscopic spatial alteration of structure (e.g., phase transition) that concurrently influences many fluorophores that are in the membrane. We have an additional advantage to studying membrane systems because we measure fluorescence. Fluorescent probe techniques are very powerful for obtaining structural information about membranes, and we are able to study some of the fundamental physical chemistry of protein–membrane interactions.

Investigation by fluorescence spectroscopy of physically stabilized monolayer membranes requires specialized methods to improve collection of emitted radiation. We have incorporated total internal reflection fluorescence (TIRF) methods using optical fibers, and surface plasmon resonance microscopy and photopyroelectric spectroscopy methods, for investigations of immobilized membrane systems.

1. A fluorescent label for study of membrane perturbation

The quantum yield of a fluorescent molecule can be very dependent on its mobility in any specific chemical environment. It is possible, by incorporation of a fluorescent probe into a membrane, to detect selective binding events that perturb the structure of the membrane and hence alter the fluorescence intensity of the probe molecule. All our experiments have used nitrobenzoxadiazole dipalmitoylphosphatidylethanolamine (NBD-PE) as the fluorescent probe because of the similarity of its chemical structure to that of natural lipid molecules, its facile incorporation into membranes, and its potential for excitation by conventional nitrogen and argon ion lasers (1). At low concentrations (<2 mol%), the probe has little impact on the usual structure of lipid membranes. The probe partitions preferentially into areas of low order and the emission of the probe is sensitive to molecular mobility and self-quenching. While NBD-PE has been used over the last decade as a label of choice for fluorescence microscopy studies of phase structure in monolayer lipid membranes (2), it had been poorly characterized with respect to a quantitative model of emission. Such a model is of significance to interpretation of the mechanism of transduction of binding events by a membrane, and to the establishment of conditions for optimization of the S/N ratio for development of analytical systems and methods.

To investigate self-quenching (3), NBD-PE was incorporated into monolayers and vesicles composed of Egg phosphatidylcholine at concentrations of 0.1–50 mol%. Monolayer samples were dipcast onto glass slides at a pressure of 35 mN m^{-1}. Both the integrated intensity per fluorophore (quantum yield) from the vesicles and monolayers, and the mean fluorescence lifetime from the vesicles, decreased as the concentration of fluorophore in the membranes was increased. At all concentrations studied the decay of NBD-PE fluorescence was fitted to two discrete exponentials, and both lifetime components were observed to change with concentration. The complexity of the fluorescence decay did not permit the use of standard theoretical models such as the Klafter–Blumen or Stern–Volmer equations, which are normally employed to describe changes in fluorescence lifetime with changes in quencher concentration. Instead, a phenomenological approach was used to develop an empirical model of fluorescence self-quenching that could describe the observe alterations in he fluorescence lifetime and intensity. The model was based on a combination of Perrin quenching and Foerster energy transfer, and takes the following steady-state form:

$$\frac{F}{F_0} = \frac{\exp(-\pi R_c^2 C)}{1 + \pi^3 C^3 R_0^6} + \frac{\pi^3 C^3 R_0^6 \exp(-2\pi R_c^2 C)}{1 + \pi^3 C^3 R_0^6}$$

where F_0 and F are the fluorescence intensity in the absence and presence of quencher, respectively, C is the bulk concentration of fluorophore, R_c is the critical distance for trap formation, and R_0 is the Foerster energy transfer distance. The fluorescence data were fit by a model wherein NBD-PE formed non-emissive trap sites with a critical radius of R_c = 1.0 nm (Perrin quenching), with Foerster energy transfer occurring to the trap sites with an R_0 value of 2.55 nm as determined from spectral overlap integrals.

2. Transduction of selective binding events

Selective interactions of proteins located in a membrane can alter the distribution of phase structure, and such alterations can be directly visualized by fluorescence microscopy, and can be further characterized by fluorescence spectroscopy. The protein systems that we chose to study were (*a*) the selective interaction of the acetylcholine receptor with agonist/antagonist, (*b*) acetylcholinesterase with substrate, and (*c*) urease with substrate.

(i) Molecular receptor

Acetylcholine receptor (AChR) was studied because it is one of the best characterized molecular receptors with respect to structure and function in bilayer lipid membranes (BLMs). The physiological activity (electrochemical) of AchR is very sensitive to the composition of the surrounding lipid membrane, and the protein has "binding sites" for various lipids. This indicates that the effects of selective binding processes may be transmitted to the lipid matrix. Vesicles containing unlabelled AchR, NBD-PE, and soybean lecithin were prepared, and were then allowed to interact with the agonist carbamylcholine and the antagonist bungarotoxin. Fluorescence intensity enhancements were observed for both of the selective interactions, and the data were quantitatively analysed to determine the dissociation constant and the sensitivity of the fluorescence detection system (4). The experiments using carbamylcholine indicated a sensitivity of 30% relative fluorescence enhancement per μmole and a detection limit of 300 nM (linearity over only one order of magnitude). The toxin provided greater sensitivity with a detection limit of approximately 10 nM concentration. Wavelength shifts from the fluorophore were not apparent for interactions of either the carbamylcholine or the bungarotoxin, and no identification of

Can. J. Chem. Downloaded from www.nrcresearchpress.com by 80.90.12.36 on 09/08/12
For personal use only.

these species was possible based on fluorescence intensity measurements. This emphasizes a common limitation of many chemical sensors, in that unambiguous identification of binding species may not be possible if only one dimension of analytical information is available (i.e., average intensity). Time-resolved spectrofluorimetry in combination with excitation or emission energy variation provides a much greater quantity of analytical information and can be considered multidimensional in nature. Fluorescence lifetime analyses of NBD-PE in lipid vesicles containing AChR gave biexponential fits. The results of the lifetime analyses before and after enhancement of fluorescence intensity suggest that the pre-exponential factors show promise for discriminating between the agonist and toxin complexes (5). The data could not be used to provide a molecular interpretation of the origin of the two lifetime components. The results of the work with AChR demonstrated that the NBD-PE labelled lipid membranes could serve as a generic host matrix that was capable of transduction of events such as the conformational change of a molecular receptor that occurred on selective complexation with ligands. The mechanism for fluorescence transduction was consistent with a description that considers AChR perturbation of the physical and electrostatic properties of lipid membranes. The increase in fluorescence intensity of over 200%, as was seen in some of the experiments, was likely the result of changes in the self-quenching of the NBO-PE.

(ii) Enzymes

The enzyme acetylcholinesterase (AChE) was used to investigate the response of a monolayer lipid membrane to selective reactions of a hydrolytic enzyme that was known to be active in both vesicle and monolayer membranes. In this case, the mechanism for inducing reversible structural transitions within lipid membranes was based on a change of surface pH. The enzymatic catalysis of acetylcholine to acetic acid (and choline) provided a high localized hydronium ion activity at the surface of the membranes in which the enzyme was bound. Electrostatic repulsions between acidic functional groups in the headgroup region of the membrane were partly controlled by the dynamic reaction process when acetylcholine was available for the enzymatic reaction to proceed. A ratio of 7:3 DPPC/DPPA (alternatively PC/PA; dipalmitoylphosphatidylcholine and dipalmitoylphosphatidic acid) was chosen as a useful lipid mixture for examining the fluorescence response of monolayers because a significant amount of zwitterionic headgroups such as PC are necessary to promote incorporation of AChE into monolayers and because major structural changes such as phase separations are induced if a significant proportion of negatively charged headgroups such as PA are present in the membrane. AChE was deposited onto lipid monolayers that contained 1 mol% NBD-PE and were prepared at a surface pressure of 25 mN m^{-1} on a Langmuir trough, and a fluorescence microscope was used to investigate phase structure and average intensity (2, 4). The surface pressure was observed to increase to a final value of 32 mN m^{-1}. The small increase in surface pressure of the monolayer on addition of the AChE suggested that the enzyme was not interspersed deeply within the monolayer, but was likely associated with the headgroups at the membrane–water interface. Addition of 1 μmol of acetylcholine (ACh) to the subphase in the imaged region of the monolayer resulted in an increase of fluorescence intensity of about 50% with maximum signal achieved in 20 s. The signal rapidly decayed to the initial value, and the transduction by the lipid monolayers was reversible and reproducible (precision about 6%). As the quantity of ACh added to the subphase was increased the enhancement of fluorescence intensity increased, although saturation was eventually achieved. Control experiments provided no indication of intensity variation and involved the addition of electrolytes, the use of ACh without enzyme, and the use of denatured enzyme. Addition of HCl or NaOH to 7:3 DPPC:DPPA monolayers resulted in transient increases in fluorescence intensity that were similar to those observed for the reaction of AChE with ACh. Hydrochloric acid was added in 5 μmol aliquots to monolayers consisting of either pure DPPC (no enhancement observed), pure DPPA, or various mixtures of the two phospholipids to determine whether the sensitivity of transduction could be enhanced. Monolayers that contained 30 mol% or more of DPPA produced similar enhancements of fluorescence intensity (approx. 50%). Increases of fluorescence intensity did not vary systematically with the proportion of DPPA present in the monolayers, suggesting that the fluorescence signal was dependent on the degree of protonation of the PA headgroups as well as the lateral phase separation and size of domains in the imaged field. Fluorescence spectra were collected from stationary monolayers at pressures ranging from 1 to 45 mN m^{-1}. The wavelength of maximum emission due to the NBD-PE did not shift as the lateral pressure was increased, but the fluorescence intensity decreased during compression of the monolayers. This indicated that changes of fluorescence intensity were likely due to self-quenching of the fluorophore. The relative intensity at a subphase pH of 4 was always greater than at 7.4 (at constant surface area), indicating that the degree of self-quenching was decreased at the lower pH. An increase of surface pressure resulted in changes in the microscopic phase domain structure that were consistent with the growth of more condensed phases and lateral phase separation of DPPC and DPPA. DPPA has a net charge of about 1.3 at pH 7.4, and thus there is a high degree of electrostatic repulsion between headgroups. Reduction of the pH to a value of 4 reduces the anionic surface charge to a value of about 0.5 negative charges per headgroups. This decrease in headgroup–headgroup repulsion would be expected to result in a net decrease of the lateral pressure of the monolayer (at constant molecular area), which is consistent with the decrease in pressure observed in these experiments. A reduction in surface pressure would produce a change in the structure of the monolayer involving an increase in the net proportion of fluid phase, and may also promote phase separation. The higher proportion of fluid phase increases the area into which the NBD-PE may partition, and thus increases the average distance between fluorophore molecules. This leads to a decrease in self-quenching and the observed increase of fluorescence intensity (transient due to dissipation of pH gradient into large volume of subphase).

3. Towards a practical sensing configuration

The development of a portable and rugged sensing device requires that the selective recognition element be directly interfaced to the physical transducer. In the case of transducers based on fluorescent membranes, this entails stabilization of the assembly onto an optically transparent solid support such

Fig. 1. Representation of the relationship between rotational mobility (in terms of angular displacement relative to the normal to the plane of a membrane) of NBD-PE within CIMs and the probability of formation of transient trap sites. (*A*) Ionized membrane with low mobility; (*B*) neutral membrane with higher mobility.

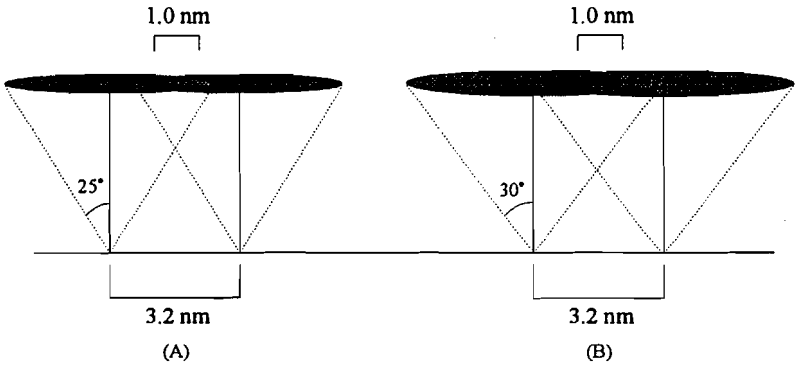

as an optical fiber. Surface stabilization of membranes must provide sufficient ruggedness to permit use over an extended period of time without severe alteration of the response characteristics of the membrane. However, the stabilization method must allow the membrane to retain characteristics of molecular mobility and fluidity that are essential for transduction of selective reactions. Our work has investigated the analytical sensitivity that can be obtained from fluorescent membranes that were stabilized onto quartz surfaces by either the Langmuir–Blodgett (L–B) dipcasting method (6, 7), or by covalent linkage of individual amphiphiles onto a surface (8, 9). Covalent immobilization of a membrane to a solid surface is a desirable alternative to L–B techniques as this methodology has the ability to produce far more stable membranes. Covalently immobilized membranes (CIMs) were prepared from species having chain lengths between 11 and 16 carbons and having a reactive silane group at one terminus and a carboxylic acid or amine functionality at the other terminus. A small amount of (1–3 mol%) of NBD-PE was partitioned into CIMs from an aqueous suspension. The enzymes AChE or urease, which both produce shifts in pH upon reaction with the substrates acetylcholine and urea, respectively, were introduced into the membranes either by adsorption or by covalent linkage directly onto the functional groups of the membranes that coated the quartz surfaces. Addition of substrate to coated wafers and optical fibers placed in aqueous solution resulted in substantial changes of fluorescence intensity from both carboxylic acid and amine functionalized membranes. For examples with adsorbed AChE, the fluorescence intensity from the monolayer could be used to distinguish changes in bulk solution concentration of ACh with a limit of detection of 2 μm ACh. For samples with colvalently immobilized urease a limit of detection of 40 μm of urea was observed. The response times were about 10–20 s for both the AChE and urease systems. An assay of enzyme activity based on fluorescence was developed, and was based on the emission of the pH probe seminaphtharhodafluor-X (10). This probe has two emission maxima, which alter in intensity relative to each other with changes of pH, providing for sensitive detection of pH changes and the use of the concept of rationing to minimize errors due to instrumental drift and photobleaching. The assay was able to measure activity from covalently immobilized enzyme on monolayer membranes (approx. 50% surface coverage by enzyme), with an accuracy of about 10% for surface areas on the order of 1 cm^2. The assay indicated that the sensitivity of the membrane-based transducers degraded tenfold over a period of 7 days when the samples were stored in phosphate buffer at 4°C.

Table 1. Slope of response of fluorescence intensity to change of pH. The pH is shifting from 4.0 to 9.0

Membrane	Slope of response to pH
Carboxylic acid	Positive
Carboxylic acid + urease	Negative
Alkylamine	Negative
Alkylamine + urease	Positive

Model for intensity changes of CIMs

An investigation of the processes responsible for changes in the intensity of NBD-PE emission in CIMs has shown that the signal is not based on direct effects of pH, polarity, surface potential, or surface charge, and that the emission intensity is strongly influenced by changes in local concentration of the fluorophore (3). Alterations in the surface charge of CIMs will change the electrostatic interactions between adjacent amphiphiles, which in turn can result in changes in the degree of rotational mobility of the covalently bound amphiphile molecules and NBD-PE. Increased rotational mobility in terms of angular distortion away from the normal to the plane of a membrane would be expected to result in an increase in the number of statistical trap sites, and therefore increases in self-quenching (Fig. 1). It is thus necessary to consider how the electrostatic interactions between an enzyme (e.g., urease) and membranes may change with pH to affect molecular mobility within a membrane. A summary of such changes and the interpretation of mechanism are presented in Table 1 and Fig. 2, respectively. The carboxylic acid membrane containing urease produced decreases in fluorescence intensity as the pH was increased, indicating that there was an increase in the self-quenching of the NBD-PE. It is likely that an increase in the area swept out by the cone associated with rotational mobility is a result of the protein occupying less surface area due to a reduction in the attractive charge interactions between the protein and the membrane. This situation would occur as a result

Can. J. Chem. Downloaded from www.nrcresearchpress.com by 80.90.12.36 on 09/08/12
For personal use only.

Can. J. Chem. Downloaded from www.nrcresearchpress.com by 80.90.12.36 on 09/08/12
For personal use only.

Fig. 2. Changes in electrostatic interactions between urease and headgroups of membranes as a function of pH, and relationship to membrane mobility. (*A*) carboxylic acid membrane with urease (shaded oval); (*B*) alkylamine membrane with urease.

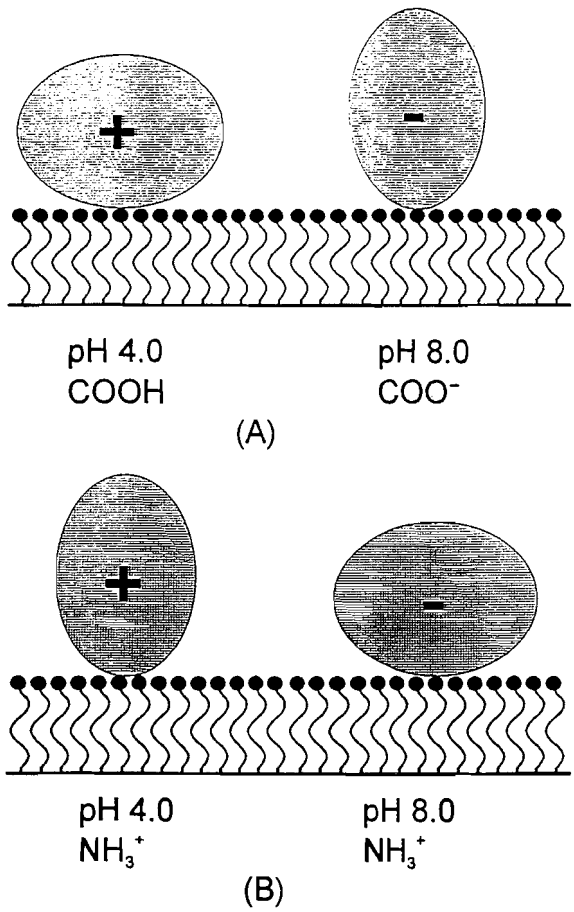

of the net charge of the protein becoming increasingly negative as the pH is raised, owing to urease having a pI of 5.1. At the same time, the carboxylic acid headgroups become negatively charged, thus repelling the protein from the surface of the membrane. The repercussions of this situation are an increase in the mobility of the fluorophores and an increase in fluorophore–fluorophore interactions (more trap sites), providing an increase in self-quenching as the pH is increased. For the alkylamine membrane, the protein again becomes more negatively charged as the pH increases from 5.1 to 9.0, but the membrane amphiphiles are positively charged and become neutral as the pH is raised. It is expected that at low pH (around 4.0) the membrane is highly positively charged while the protein is also positively charged, and thus an electrostatic repulsion should exist between the headgroups and the protein. Under these conditions, the membrane should have some degree of mobility. As the pH is raised to a value of 8.0, the protein becomes neutral and then negatively charged, while the membrane remains essentially completely ionized and positively charged. As the negative charge density of the protein increases, attractive electrostatic interactions between the protein and the membrane increase and the protein therefore interacts with a greater number of headgroups. This would reduce the mobility of the membrane and would cause decrease in the self-quenching and increases in the intensity, as observed during pH titrations.

Electrochemical methods

Natural chemoreception offers a glimpse of a biosensing system that might be replicated in a rudimentary fashion for development of practical devices. Chemoreceptive membranes consist of a bimolecular layer of lipids, which are physically associated with proteins that have molecular recognition properties, i.e., receptors. The ion channel system that is found in biological organisms is associated with rapid, reversible, sensitive, and selective chemical signalling, with unique features such as the amplification and transduction of chemical information into an electrical pulse by switching of channel conductivity.

Theoretical and experimental reports have indicated that disordered states of lipid structure, as encountered during phase transitions, are highly permeable to ions. This is relevant to the process of ion permeation through lipid membranes, as bilayer and monolayer lipid membranes can be composed of mixed phased in coexistence. The interfacial boundary between different phases in a zone of low structural order could provide a highly conductive pathway for ion permeation, ion current being modulated by aspects of molecular density, mobility, and electrostatic charge (i.e., artificial pore).

1. Control of conductivity pathways in membranes

It has been suggested that high intramembrane concentrations of 10-hydroxystearic acid (10-HSA) are responsible for changes in the permeability of gases and ions through membranes of alveolar cells of cystic fibrosis patients. Characterization of the mechanism and control of the magnitude of ion current through membranes by 10-HSA could provide an insight into the preparation of chemically selective membranes (11).

Solvent-free planar BLMs and monolayer films were prepared from a lipid mixture (by mass) containing 34% phosphatidylcholine, 19% dipalmitoylphosphatidylserine (PS), 47% cholesterol (C), and variable amounts of 10- and 12-hydroxystearic acid (0–50%). The structures of monolayer films at the air–water interface of a Langmuir–Blodgett trough were studied by pressure–area (π–A) correlations and by further correlations with microscopic phases separation as revealed by fluorescence microscopy. The ion currents through BLMs were found to increase approximately exponentially with the mole ratio of HSA (corrected for surface charge).

In a simplified view, two models for the transport process in BLMs composed of lipid, cholesterol, and 10- or 12-HSA are possible. The first model considers the hydroxyl moiety at the 10- or 12-position of the acyl chain as a "polar defect" distributed homogeneously throughout the hydrophobic interior or the membrane. The interaction of hydrated K^+ with polar hydroxyl groups would be energetically favourable in the nonpolar interior of the BLM. Therefore, the ions could be transported across the membrane via polar defects in the "hopping" mechanism. The second model considers that the same energetics associated with the first model are applicable, but that the 10- or 12-HSA is heterogeneously distributed in zones of high relative HSA concentration.

Fig. 3. Fluorescence microscopy images (full scale of image 250 μm) showing domain structure of monolayers at different pressures and with different compositions of 10-HSA. Images a, b are of monolayers that contain 12 mol% 10-HSA at average molecular areas of 0.85 and 0.50 nm^2, respectively. Images c, d are of monolayers that contain 35 mol% 10-HSA at average molecular areas of 0.85 and 0.52 nm^2, respectively.

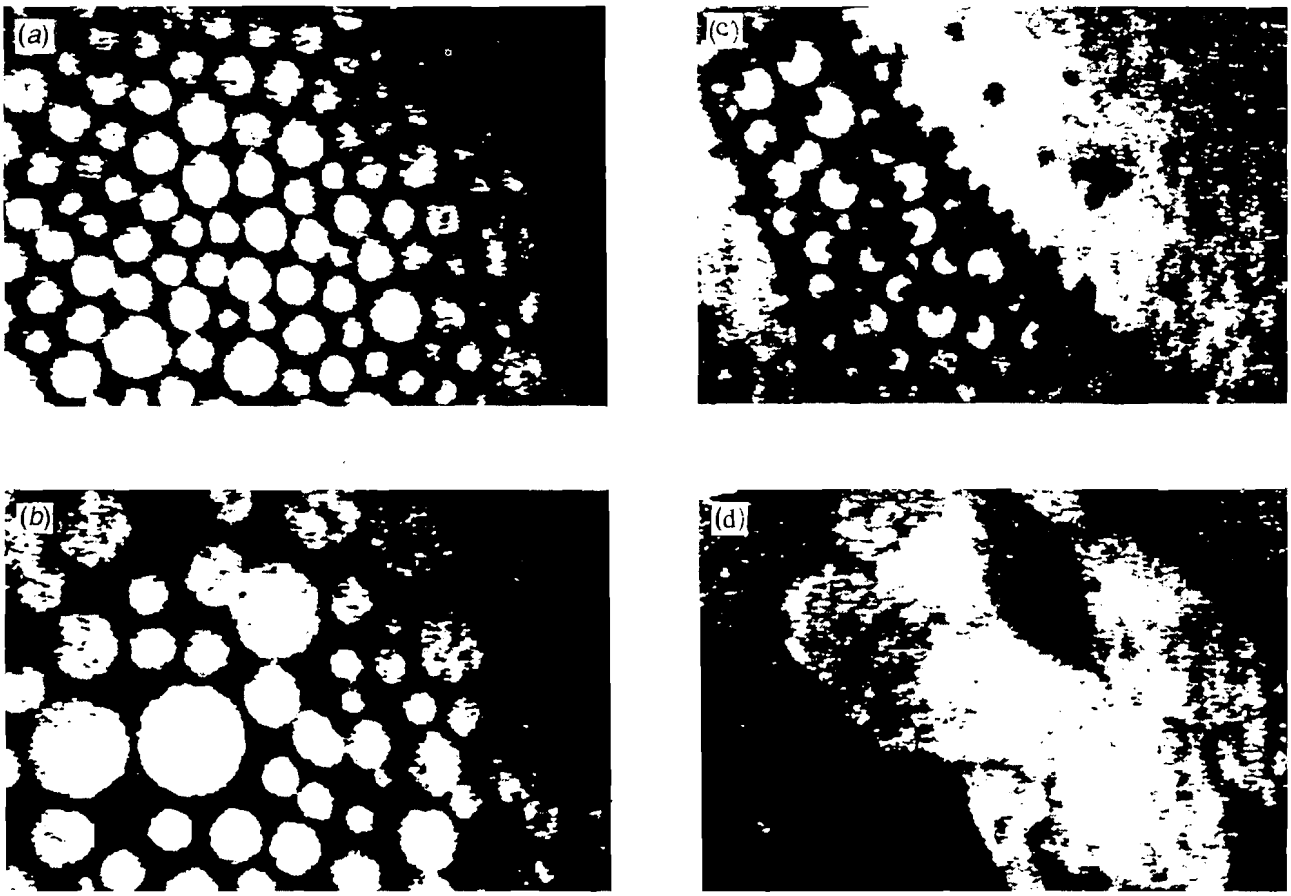

Can. J. Chem. Downloaded from www.nrcresearchpress.com by 80.90.12.36 on 09/08/12
For personal use only.

The 10- and 12-HSA have only one acyl chain, whereas the lipids (PC and DPPS) each have two acyl chains per molecule. The lipids also have a glycerol backbone that is not present in the 10- or 12-HSA. Therefore, the average molecular area decreased as the molar proportion of 10- or 12-HSA was increased. The 10- or 12-HSA has a carboxylic acid headgroup that is deprotonated at pH 7.4, indicating that the anionic form was present in the membranes used for these investigations. The negative charge present on the 10- or 12-HSA implies that electrostatic repulsion exist between 10- or 12-HSA and DPPS molecules. Hence, on structural and electrostatic principles, the 10- or 12-HSA represents an impurity in domains otherwise rich in either lipid or cholesterol components. The lowest energy state of the system could be expected to arise if the 10- or 12-HSA initially partitioned into interfacial regions between the lipid and cholesterol phases. Interfacial energetics are known to dominate cholesterol–lipid interactions at the molecular level and it is, therefore, expected that the introduction of 10- or 12-HSA would alter the phase structures in the mixed cholesterol–lipid systems.

Fluorescence microscopy indicated that 10-HSA could significantly alter the shape and distribution of domains, resulting in a substantial increase in the total interfacial area of the domains (Fig. 3). The formation of domains with "crescent" shapes has been previously linked to interfacial processes. The four-component mixture used in these experiments complicates predictions of phase structure and the extent of domain coexistence. The evolution of an inflection point in the π–A curves for a low concentration of 10-HSA could be due to the formation of a miscible eutectic mixture. The large condensation effect caused by relatively small concentrations of 10-HSA further suggests that the material is not homogeneously distributed as a bulk constituent of the monolayer, but that it is located in interfacial regions that then control phase distribution. The inflection point in the π–A isotherms occurs at a constant pressure once the concentration of 10-HSA is above 35 mol%, which suggests that an immiscible mixture is formed, resulting in a distinct phase that is rich in 10-HSA.

The appearance of a distinct phase in a BLM should alter transmembrane ion current in comparison with results obtained for lipid compositions containing less than 35 mol.% 10- or 12-HSA. There is an inflection in the trend of ion current change with HSA content of BLMs near the 35 mol.% HSA composition. The slope of ion current versus 10- or 12-HSA content is much greater for HSA compositions above 35 mol.%, indicating that a new pathway with a lower energy barrier is available for ion permeation. This pathway is likely to be associated with a phase that is rich in 10- or 12-HSA, and could involve dipolar interactions of hydroxyl residues. This cooperativity is consistent with the logarithmic relationship of

Can. J. Chem. Downloaded from www.nrcresearchpress.com by 80.90.12.36 on 09/08/12
For personal use only.

HSA composition and ion current. A further significant feature is that extrapolation of a plot to an HSA composition of zero yields an ion current substantially greater than that actually observed for BLMs that did not contain HSA. This again suggests that the HSA is heterogeneously distributed in the BLMs, in a location that affects ion current in a nonlinear fashion.

2. Critical phenomena at the BLM surface

Molecular switching systems may provide the basis for a new class of chemical sensing devices, which can be envisaged most simply as any chemically selective molecular arrangement that can exist in two or more discrete physical states. Switching between states could be represented as a change in molecular receptor conformation on binding a stimulant. However, the absolute analytical signal (e.g., ion current) associated with single ion channel events encountered in nature is usually very small, limiting the practical utility of such an analytical strategy.

A primary binding event, which locally alters the structure or electrostatic field of a lipid membrane, provides a physical change that can readily be detected by electrochemical or optical methods. Amplification of the analytical signal can be achieved by inducing a greater spatially distributed structural change caused by the selective binding event. Ideally, this concept would converge in a phase transition of the lipid membrane caused by a very limited number of receptor binding events. Such macroscopic state-switching provides opportunities for the sensing of very low concentrations of target species by monitoring the discontinuities in a relatively invariant analytical signal.

Our approach begins with the immobilization of active proteins directly onto a carefully defined lipid mixture at an air–electrolyte interface, followed by a film-casting technique for BLM formation (12). Subsequent experiments have shown that selective chemical reactions can be transduced as time-dependent singular transient ion current signals. The electrochemical event is due to the rapid reorganization of the double layer and physical structure of a BLM, and provides the basis for the construction of switchable biosensors with rapid response times and reversibility.

BLMs prepared from mixtures of a neutral lipid such as Egg phosphatidylcholine (PC) and an ionizable lipid develop an electrical double layer at the membrane–electrolyte interface. Dipalmitoylphosphatidic acid (DPPA) has two accessible ionizations with titration endpoints of about pH 4 and 7–8.5, and mixtures of PC and DPPA are very sensitive to alterations of membrane surface charge. Substantial reorganization of the phase distribution of a membrane based on the extent of DPPA ionization has considerable impact on the magnitude of the ion current and the S/N ratio. We have found electrochemical evidence that there are phase rearrangements in BLMs under certain conditions (13). As the concentration of DPPA in BLMs is increased from 0 to 20% w/w, the residual ion current through BLMs increases linearly (for pH in the range of 7–9). Between 20 and 30% w/w DPPA there is a substantial decrease in ion current that probably occurs because of an alteration of the structure of the membrane. As the content of DPPA in the membrane is increased above 30% w/w, residual ion current is again linearly related to percent composition DPPA but with a smaller slope than for the 0–20% DPPA region. It appears that 25% w/w DPPA represents a critical concentration, below which DPPA self-associates to form DPPA-rich domains, and above which DPPA and PC are distributed relatively homogeneously. Charged lipids such as DPPA can also play an important structural role for the immobilization of biochemical species at BLMs by formation by hydrogen bonds with relevant amino acid side chains of proteins. The formation of hydrogen-bonding networks enhances the immobilization, and connects regions with differing proton or electron density to provide rapid conduction between such regions.

The difficulty of selecting an initial pH to optimize the sensitivity of the response to pH of negatively charged BLMs, and to concurrently optimize the activity of chemically selective proteins, can be overcome by introducing Ca^{2+} to the bulk electrolyte solution (14). Adjustment of the intrinsic sensitivity of BLMs is achieved by selecting the lipid composition to contain concentrations of DPPA greater than 25% w/w and by related adjustments of the pH and calcium ion activity. The interaction of calcium ions with divalent negatively charged lipid (pH about 8) results in a phase separation of PC and DPPA and the formation of conductive zones in BLMs. These zones can be switched on or off by selecting a pH value of the electrolyte solution below or above 7, respectively, in the presence of a limiting Ca^{2+} concentration that depends on the DPPA composition of BLMs.

Generally the ion current magnitude is maximized for more fluid BLMs and minimized surface potential, when the ion current is the result of surface charge alterations.

3. Transduction of enzyme–substrate reactions

Electrochemical transduction of the pH changes associated with the reaction of acetylcholinesterase with acetylcholine by BLMs consisting of DPPA and PC has recently been reported (15). Acetylcholinesterase was incorporated into the BLMs so that there was a lipid-to-protein ratio of 150:1 (about 2×10^{-4} U). A transient change in current (analytical signal) appeared after a delay time of seconds to minutes (dependent on substrate concentration, Fig. 4) as a singular event after acetylcholine was added to solution. The transient signals for different concentrations of acetylcholine were approximately 10 pA in magnitude (background current 1 pA) and lasted for a period of about 1 s. These signals were due to the acetylcholine–acetylcholinesterase reaction as demonstrated by: control experiments in which acetylcholine or choline was added to the solution compartment in the absence of enzyme, by the use of denatured acetylcholinesterase, and by addition of the acetylcholinesterase inhibitor Neostigmine, which confirmed the reduction of enzyme activity as controlled by the concentration of inhibitor.

Similar experiments were done using the urea–urease system, where this second hydrolytic enzyme produced pH changes associated with the evolution of basic reaction products (16). Transient signals observed for the urea–urease system were similar in magnitude and profile, but opposite in direction, to those observed for the acetylcholinesterase-catalyzed hydrolysis of acetylcholine.

Mechanism for transduction based on electrochemical switching

Substantial conductivity differences between BLMs prepared from DPPA/PC have been observed when the membranes

Fig. 4. Calibration of the analytical signal, using in part the data of the insert. Triangles represent data from experiments at pH 5.5 and squares represent pH 8.0. The insert shows results obtained at pH 8.0 (0.1 M KCl, HEPES 10 mM, calcium ion 1 mM) with BLMs consisting of 35% DPPA when 3 μL of AChE (1.0 mg/mL) was codeposited at the air–water interface (before BLM formation). ACh concentrations (μM): (*A*) 2.20, (*B*) 5.50; (*C*) 11.0; (*D*) 22.0; (*E*) 38.5.

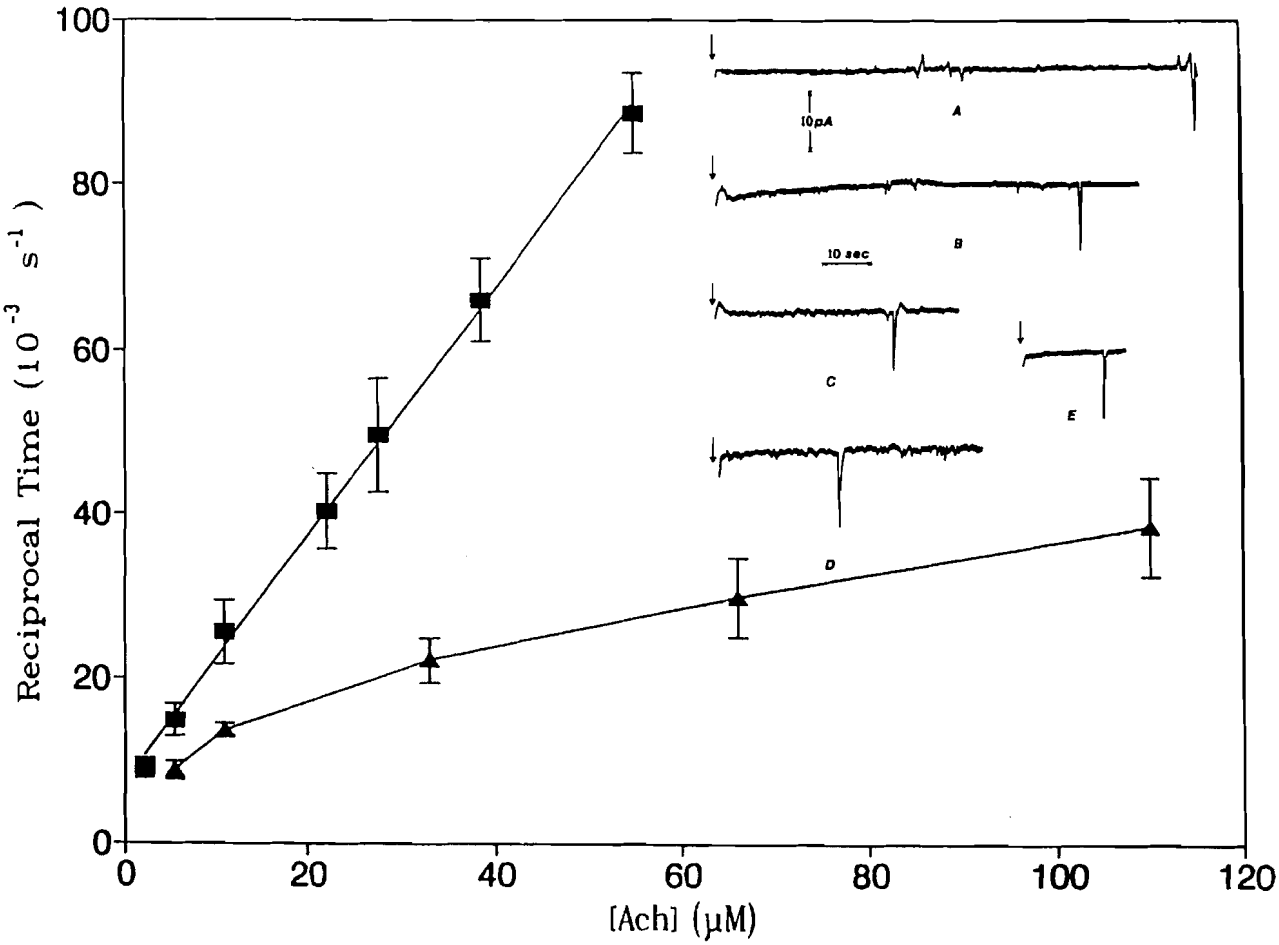

were formed at different values of pH, indicating that differences in surface charge density could alter ion permeability. If the transient currents observed for enzyme–substrate reactions were related to a well-defined steady-state BLM structure, then the current, g, would be approximated as:

$$g = A^*(1 + 0.381\sigma)$$

where A^* depends on electrolyte composition and σ is surface charge density. The surface charge density increases rapidly with pH and increases at the pK_a of the titration of DPPA, and conductivity might also be expected to change rapidly here. However, it is unlikely that this is responsible for the transient signals observed in the enzyme experiments. The surface charge density will continue to change past the pK_a as the pH continues to change, and a continuation of the trend of a change of conductivity would be expected (not a transient current response).

The appearance of a transient response has also been observed in some of our fluorescence microscopy studies of DPPA/PC monolayers at an air–water interface, during which a monolayer composed of lipids and acetylcholinesterase was rapidly exposed to a high concentration of acetylcholine. The fluorescence microscopy images indicated the presence of membranes of mixed phase structure. After a brief period of time following addition of acetylcholine (0.5–1 min) the image brightened substantially for a period of up to a few seconds, and then darkened again to a new equilibrium value of intensity. During the fluorescence "flash" there was no distinguishable change of phase structure in the fluorescence images.

The observed transient signals resulted from a change in pH at the membrane surface. However, just how the transient signal arises from a change in pH has yet to be determined. There are two possibilities, and the signal may result from a combination of these: (*i*) the signal results from rearrangements of the ions in the electrical double layer adjacent to the membrane during a rapid change of the extent of ionization of the lipids in the membrane; (*ii*) the transient results from the rearrangements of the structure of the BLM leading to a transient change in permeability of the membrane.

The mechanism of transient signal generation from BLMs prepared from DPPA/PC has been further investigated by continuous variation (titration) of pH in bulk solution to alter the surface charge density due to DPPA at the membrane surface (17).

Can. J. Chem. Downloaded from www.nrcresearchpress.com by 80.90.12.36 on 09/08/12
For personal use only.

Can. J. Chem. Downloaded from www.nrcresearchpress.com by 80.90.12.36 on 09/08/12
For personal use only.

PC is a zwitterion and thus has no net charge over the pH range of interest herein (pH 5–9). DPPA can be partially or fully ionized based on negative charges that are associated with apparent pK_a values. An electrical double layer would form at the surface of a BLM if it contained negatively charged phospholipid head groups. In a solution of 0.1 M KCl as used in these experiments, the primary layer would consist largely of potassium ions. This is significant since it is cations that are responsible for most of the ion current through these BLMs.

The surface potential of the membrane should change rapidly near the pK_a during a pH titration of the DPPA component of the membrane, and this should result in a rapid rearrangement of the double layer and therefore ion current as more cations move to compensate for the altered negative charge at the membrane. If the observed transient signal is due only to rearrangements of the electrical double layer, then the voltage change at the membrane surface when the signal is observed should correspond to that calculated by use of the Gouy–Chapman–Stern (GSC) model. If the voltage change associated with the total charge movement of an ion current transient is substantially larger than that predicted by GCS theory, then this would suggest that there s a pH-related phenomenon other than rearrangement of the electrical double layer that occurs.

During continuous pH titrations of BLMs prepared from PC/DPPA, large sharp transient signals (>10 mV) occurred at pH values between 8.1 and 7.0 (pH determined from calibration curves). For these experiments the actual pH at the surface of a BLM is lower than that in bulk solution, and can be approximated using a model of smeared uniform surface charge based on the Boltzmann relation. The increase in surface potential for an increase of DPPA content from 15 to 50% w/w would be associated with roughly an order of magnitude increase of H_3O^+ concentration at the membrane surface (for bulk solution pH in the range of 7–8), yet no clear distinction can be seen between the pH ranges at which sharp current transients were observed. The change in pH over the time course of transient signals is less than 0.1 unit, corresponding to a maximum change in potential of 2 mV as predicted by GCS theory. The area of the transient signals generally indicates that a capacitive charging potential would be of substantially larger magnitude than 2 mV. If the surface potential change of a BLM is calculated based on the pH change from the beginning of an experiment, then the magnitude of the capacitive charging phenomenon could be considered equivalent to the change of surface potential for many experiments. However, this is not the case for the largest transients, where the mismatch between theoretical surface potential and charging potential is beyond an order of magnitude. This suggests that rearrangement of the electrical double layer is not the only phenomenon responsible for the large transient signals that were observed. It would appear that during the course of the structural change the membrane becomes more permeable to ions, since the structure is less organized during the structural transition.

4. Transduction of antibody–antigen interactions

Transient ion currents similar in appearance to those associated with hydrolytic enzyme–substrate reactions were observed for an antibody–antigen interaction involving modulation of surface charge by virtue of formation of the complex (18). The thyroxin (T4) – anti-rabbit T4 interaction was chose as the immunological reaction owing to the clinical significance of T4. Recordings of signals obtained at pH 6.0 (without Ca^{2+} in bulk solution) for different concentrations of T4 with BLMs composed of 15% DPPA indicate the appearance of singular transient current signals. An important distinction in comparison to the enzyme–substrate results is that the magnitude of these transient responses is in direct proportion to the logarithm of the antigen concentration in bulk solution. Control experiments demonstrated that these signals were due to selective interactions, and involved application of antigen to BLMs in the absence of antibody, and the use of nonselective protein in the presence of antibody.

Rabbit anti-thyroxin antiserum contains antibodies with pI's between 6.3 and 9.0, whereas the pI of T4 is 5.0. Electrostatic forces are important in the mechanism of the formation of the antibody–antigen complex. The kinetics of the immunological reaction and the electrostatics of this interaction on one side of a BLM would be expected to cause a slow nonlinear double layer reorganization to occur.

The relatively constant delay times for transient current evolution for widely varying concentrations of antigen indicate that the mechanism responsible for the transient is not directly related to the charge associated with varying quantities of antigen at the BLM surface.

Similar singular current transients are not evident for BLMs composed only of PC, which may indicate that the phase structure of membranes is a predominant factor in the immobilization of immunoglobulins in BLMs, as these proteins prefer fluid areas enriched in DPPA. An increase of the pH of bulk solution (e.g., 8.0), which increases the degree of DPPA ionization (but decreases the number of hydrogen bonds between DPPA molecules) and reduces the positive charge of the antibody, results in a decrease of the signal magnitude. The presence of calcium ions in bulk solution reduces signal magnitude and dramatically delays the time for the appearance of the transient signals. BLMs can therefore be designed to provide fast and sensitive transduction of immunological interactions; e.g., detection limit of 1.0 nM of thyroxin (based on the experimental noise level of 0.7 pA) in a period of about 100 s.

5. Direct transduction of insecticides

To eliminate loss of calibration of a sensor due to denaturation of proteins, it is desirable to transduce insecticide composition into a measurable physical signal by means of selective interactions of the "stimulant" (analyze) directly with a membrane, i.e., no use of membrane-embedded receptor (19). The transduction can be designed to result from alterations of the electrostatic fields and (or) phase structure of the lipid membrane. Investigations of the direct interaction of pesticides with membranes are generally limited to absorption and permeability studies using natural cell membranes. Recently such studies have been extended beyond insecticide–acetylcholinesterase interactions to include receptors, and modulation of ion channel activity by insecticides.

Some typical pesticides were chosen for our studies and included Monocrotofos, Carbofuran, Aldicarb, and Methyl-parathion. Monocrotofos and Methyl-parathion are organophosphorus insecticides, Carbofuran is a carbamate derivative, whereas Aldicarb is an aliphatic carbamoyl-oxime. These toxicants are expected to adsorb and partition into the lipid membrane as determined by solubility parameters; the degree

Can. J. Chem. Downloaded from www.nrcresearchpress.com by 80.90.12.36 on 09/08/12
For personal use only.

of such an interaction depends largely on the chemical structure of the insecticide.

Transient current responses were observed for these experiments only for Monocrotofos and Carbofuran. A transient appeared at a relatively constant time after exposure of the membrane to monocrotofos (3.3 ± 0.3 min, $N = 5$). Similar transient current signals were obtained when using Carbofuran, and the transient signals appeared with a relatively constant delay time that was longer than that for Monocrotofos (4.8 ± 0.5 min, $N = 5$). A constant delay time of current transients was obtained when using a constant concentration (4.48×10^{-6} M) of Carbofuran (4.9 ± 0.4 min, $N = 5$), indicating that the reproducibility of the time of appearance of the signal is on the order of ca. ±9%. The magnitudes of the transient of current increased with an increase in the concentration of insecticide. Further transients of similar size were not observed over periods of 30 min after the large transient signal. The magnitude of the transient signals can be used to quantify the concentrations of Carbofuran and Monocrotofos, as the heights of the transients are linearly related to the concentration of insecticide. Reproducibility of the determination of concentration of both insecticides by use of the height of transients is about ±10%.

The transient signals have a duration of seconds or less and are indicative of alterations of the electrostatic fields of BLMs. These alterations include membrane double layer and hydrogen-bonding-network reorganizations owing to the adsorption of Monocrotofos and Carbofuran onto the membranes. These insectides are hydrophilic, which contributes to adsorption onto membranes. Monocrotofos has a structure similar to that of phosphatidic acid but the methoxy moieties impart some lipophilicity to the molecule. Both phosphatidic acid and Monocrotofos can form a hydrogen-bonding network at the membrane surface by interactions with the oxygen atoms, and alterations of such hydrogen-bonding networks are associated with reorganization of the double layer at one side of the BLM. A rapid reorganization would be observed as a phenomenon such as a transient signal.

The magnitude and sensitivity of the signal for insecticide determination depends on the quantity of DPPA in the BLM structure and the concentration of calcium ions in bulk solution. The signal magnitude is increased when the quantity of the charged lipid in the BLM is increased and (or) in the presence of calcium ions in bulk electrolyte solution. These results suggest that the presence of a phase distribution of the BLM is important for maximizing signal magnitudes.

The detection limit for Monocrotofos and Carbofuran determination measured in these experiments can be set to be three times the standard deviation of the background signal of 0.4 pA. Such a detection limit in our experiments will be 4.5×10^{-8} M and 4.8×10^{-7} M for Monocrotofos and Carbofuran, respectively. These detection limits are similar in magnitude to those obtained by electrochemical methods based on the inhibition of cholinesterases, but Monocrotofos and Carbofuran can be determined much more quickly when using detection based on BLMs.

6. Physical stabilization by surface immobilization of membranes

Development of practical devices must include mechanical stabilization of a lipid membrane onto a solid electrode, where covalent linkages between the support and the lipid/receptor molecules are desirable. To avoid the effects caused by accumulation of ions on one side of a stabilized membrane, the measurements must be made by driving the system with an a.c. voltage and by monitoring admittance with a phase-sensitive amplifier. We have described progress towards a surface-stabilized a.c. admittance modulation lipid-membrane-based biosensor that operates on the basis of control of ion permeation by artificial ion channels (20).

A portable admittance modulation measurement device was constructed, and was designed to measure both the in-phase and out-of-phase signal components for determination of "effective" ion current and membrane capacitance. The sensitivity and detection limit for the a.c. system were tested by studying the interaction of the ionophore valinomycin with planar BLMs. The electrochemical effects were observed as conductance changes of the membrane, with the limit of detection for valinomycin being at the 1 nmol dm^{-3} concentration level.

Metal electrodes were used as supports for covalent attachment of amphiphiles. Platinum electrodes with a surface area of 1 cm^2 were oxidized to provide a high density of surface hydroxyl sites. Immobilization of amphiphiles was carried out by reaction of the hydroxyl sites with silane. Gold electrodes were prepared by vacuum deposition of a 250 nm layer of the metal onto a 30 nm layer of chromium that covered borosilicate glass slides. Surface attachment of amphiphiles to this metal was achieved by sulphur–gold interactions.

A wide variety of amphiphiles differing in hydrocarbon chain length, number of chains (one or two), chain polarity, head group charge, and head group size (e.g., acidic phosphate, carboxylic acid and ester, phosphatidylcholine) were attached to both the platinum and gold surfaces. Two-step attachment procedures, as exemplified by the initial deposition of aminopropyltriethoxysilane (APTES) onto platinum followed by linkage of a 10-carbon phosphatidylcholine through an amide bond to the amino group; of APTES, often provided greater surface coverage than it an equivalent 16-carbon phosphatidylcholine had been deposited directly by the reaction of hydroxyl moieties with silane at the metal surface. Surface coverage for most experiments was in the range 40–85% as determined by X-ray photoelectron spectroscopy, and was dependent on the deposition procedure, the chain length, and the number of chains. The electrochemical results indicated that the best blockage of ion conductivity occurred when the amphiphiles contained long hydrocarbon chains. Species such as trichloro-octadecylsilane and octadecylthiol provided the best blockage, reducing the in-phase signal component by 95% for both types of metal electrode. Analogues of natural lipids such as dimyristoylphosphatidylcholine reduced the in-phase component by values of about 50%. Subsequent incubation of lipid-coated electrodes in solutions containing membrane-soluble species such as cholesterol greatly reduced the magnitude of the in-phase component of the signal to values approaching those found for BLMs. These latter electrodes were tested for response to the presence of valinomycin, and achieved detection limits in the range 10–100 nmol dm^{-3}.

A further series of analytical experiments were carried out to develop electrodes that were sensitive to pH variations, to extend the concept of control of phase domain structure to immobilized membranes. Linear 10-carbon silane and thiol

Fig. 5. Proposed scheme for development of fiber optic sensor to detect DNA hybridization.

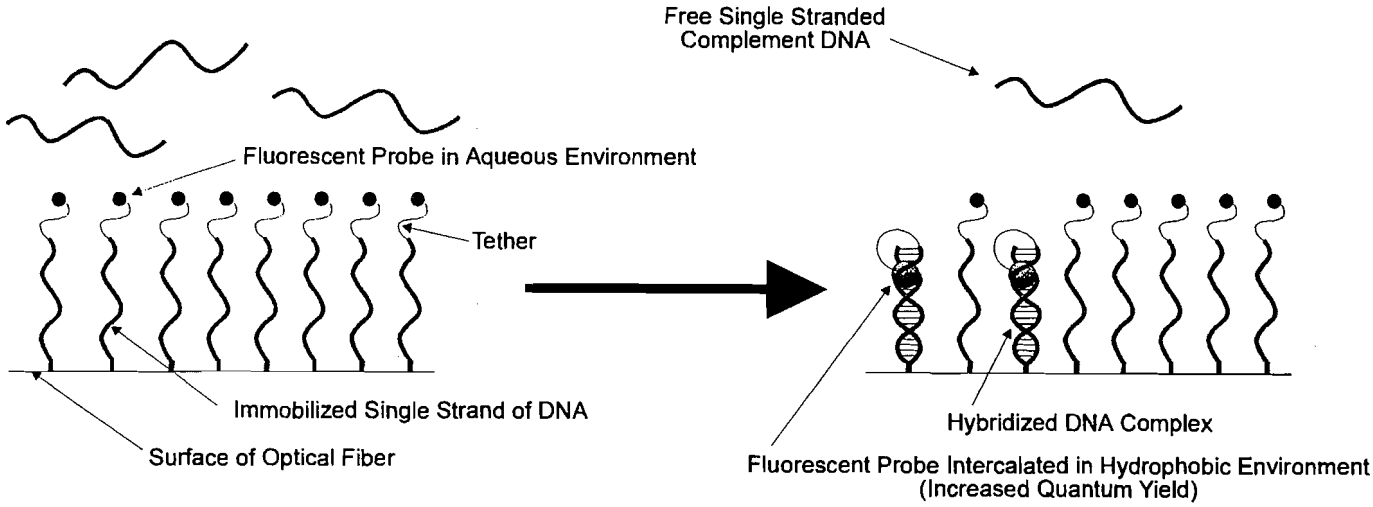

carboxylic acids were immobilized onto platinum and gold surfaces, and both systems showed good sensitivity to pH (e.g., a pH change from 7 to 8 caused a conductivity change of 25%). Modification of this system to evaluate a biosensing strategy was then done. In separate experiments, active urease and acetylcholinesterase were adsorbed onto these acidic surfaces, and urease was also covalently immobilized through the acidic functional group. The electrochemical transduction of substrates for both of these enzymes indicated the presence of time-dependent singular transients of current, thereby confirming that stabilizing sensors similar in function to BLMs could be produced. Further work involving improvement of longevity of protein function, and optimization of signal magnitude, is now underway.

New directions

We are continuing to investigate the use of organized membranes for selective chemical transduction and have recently focused attention on the use of immobilized single-stranded DNA on optical fibers for development of an analytical sensor. Fluorescent dyes are incorporated into the DNA fragments as a means of signalling the binding of DNA complement. By this approach, we can use the TIRF method for detecting binding events to "receptor" attached to an optical fiber. The use of DNA and RNA as analytical markers for applications in biotechnology and for detecting pathogenic organisms has become widespread. An important advantage provided by DNA when used as a biorecognition element is that it provides excellent chemical selectivity and outstanding chemical stability with respect to denaturation. The general focus of the research work is to use fluorescence methods to investigate hybridization of DNA (from target organism nucleus) or RNA (from cytoplasm) from sample solutions with organized monolayer membranes of complementary DNA. The specific goals of the work are to determine how the molecular organization of oriented single-stranded DNA at an interface can be controlled to permit rapid hybridization and rapid, complete dissociation of hybridized sequences using thermal and chaotropic methods. As a first step in developing this idea, we have used an automated DNA synthesizer to grow thymidylic acid icosanucleotides (dT_{20}) onto quartz optical fibers. These were then used in a TIRF configuration in a flow-through solution compartment. The covalently immobilized oligomers were able to hybridize with only complementary DNA, as indicated by the use of the fluorescent DNA stain ethidium bromide. Even without optimization, this procedure provided a detection limit of 86 ng mL^{-1} of complementary DNA, and the system could be used reversibly with a response time in the range of 20–30 min (21). We are now developing single-step immobilization schemes for attachment of complete oligomers in high density, and the use of tethered dyes (Fig. 5) so that the sensing systems are effectively internally calibrated and require no external additions of reagents for detection of hybridization.

Further work is focusing on the development of new spectroscopic techniques for investigation of monolayers at solid surfaces. Perhaps the most promising of these is the combination of photopyroelectric spectroscopy with the surface plasmon resonance achieved by the design and use of small metal particles. This approach will provide electric field enhancements at a surface for spectroscopy, and can be used to provide thermal decay pathways so as to maximize heating and therefore the sensitivity of pyroelectric detection (22). We have already demonstrated that such a sensor configuration can readily detect sub-monolayer surface coverage using low-power optical sources, and that chemically selective organized monolayer assemblies can provide substantial advantages in terms of improvements of S/N in comparison to the use of random chemically selective films (23).

Acknowledgments

We are grateful to the Natural Sciences and Engineering Research Council of Canada and to the Defense Research Establishment–Suffield for financial support of the recent work reported in this paper.

References

1. U.J. Krull, R.S. Brown, E.T. Vandenberg, and W.M. Heckl. J. Electron Microscopy Tech. **18**, 212 (1991).

Can. J. Chem. Downloaded from www.nrcresearchpress.com by 80.90.12.36 on 09/08/12
For personal use only.

2. J.D. Brennan, R.S. Brown, C.P. McClintock, and U.J. Krull. Anal. Chim. Acta, **237**, 253 (1990).
3. R.S. Brown, J.D. Brennan, and U.J. Krull. J. Chem. Phys. **100**, 6019 (1994).
4. U.J. Krull, J.D. Brennan, R.S. Brown, S. Hosein, B.D. Hougham, and E.T. Vandenberg. Analyst, **115**, 147 (1990).
5. U.J. Krull, R.S. Brown, B.D. Hougham, G. McGibbon, and E.T. Vandenberg. Talanta, **37**, 561 (1990).
6. U.J. Krull, J.D. Brennan, R.S. Brown, G. McGibbon, and K. Stewart. Int. J. Optoelectronics, **4**, 133 (1989).
7. J.D. Brennan, R.S. Brown, S.C. Ferraro, and U.J. Krull. Thin Solid Films, **203**, 173 (1991).
8. J.D. Brennan, R.S. Brown, A. DellaManna, K.M.R. Kallury, P.A.E. Piunno, and U.J. Krull. Sens. Actuators, **11**, 109 (1993).
9. J.D. Brennan, K.M.R. Kallury, and U.J. Krull. Thin Solid Films, **244**, 898 (1994).
10. J.D. Brennan, V. Kukavica, K.M.R. Kallury, and U.J. Krull. Can. J. Chem. **72**, 721 (1994).
11. D.P. Nikolelis, J.D. Brennan, R.S. Brown, G. McGibbon, and U.J. Krull. Analyst, **116**, 1221 (1991).
12. D.P. Nikolelis and U.J. Krull. Talanta, **39**, 1045 (1992).
13. D.P. Nikolelis, J.D. Brennan, R.S. Brown, and U.J. Krull. Anal. Chim. Acta, **257**, 49 (1992).
14. D.P. Nikolelis and U.J. Krull. Anal. Chim. Acta, **257**, 239 (1992).
15. D.P. Nikolelis, M.G. Tzanelis, and U.J. Krull. Anal. Chim. Acta, **281**, 569 (1993).
16. D.P. Nikolelis, M.G. Tzanelis, and U.J. Krull. Biosens. Bioelectron. **9**, 179 (1994).
17. U.J. Krull, S.L. Seethaler, J.D. Brennan, and D.P. Nikolelis. Thin Solid Films, **244**, 917 (1994).
18. D.P. Nikolelis, M.G. Tzanelis, and U.J. Krull. Anal. Chim. Acta, **282**, 527 (1993).
19. D.P. Nikolelis and U.J. Krull. Anal. Chim. Acta, **288**, 187 (1994).
20. J.D. Brennan, R.S. Brown, V. Ghaemmaghami, K.M. Kallury, M. Thompson, and U.J. Krull. *In* Chemically modified surfaces. *Edited by* H. Mottola and G. Steinmetz. Elsevier, Amsterdam. 1992. p. 275.
21. U.J. Krull, P.A.E. Piunno, R.H.E. Hudson, M.J. Damha, and H. Cohen. Anal. Chim. Acta, **288**, 205 (1994).
22. M.S. Heimlich and U.J. Krull. *In* Chemical sensor technology. Vol. 5. *Edited by* M. Aizawa. Kodansha, Tokyo. 1994. p. 117.
23. R.F. DeBono, A. Helluy, M. Heimlich, and U.J. Krull. Sensors and Actuators, **11**, 487 (1993).

Can. J. Chem. Downloaded from www.nrcresearchpress.com by 80.90.12.36 on 09/08/12
For personal use only.

1994 Merck Frosst Award Lecture New strategies for the stereoselective synthesis of natural and unnatural products via organometallic reagents and catalysts[1]

Mark Lautens, Yi Ren, Patrick Delanghe, Pauline Chiu, Shihong Ma, and John Colucci

Abstract: Samarium in the presence of diiodomethane selectively cyclopropanates an allenic alcohol to yield a methylenecyclopropane with modest to excellent diastereoselectivity. The effect of substituents at the carbinol carbon and the allenic carbon on the diastereoselectivity was investigated. A palladium catalyst was shown to promote the intramolecular cycloaddition of the methylenecyclopropane with an electron-deficient alkyne to yield a methylenecyclopentane. The reaction was stereospecific with retention of stereochemistry as proven by X-ray diffraction. Nickel catalysts accelerate the hydroalumination of oxabicyclo[3.2.1]alkenes, leading to bicyclic trialkylalanes. Upon treatment with a Lewis acid (diisobutylaluminum chloride), the trialkylalanes fragment to provide cycloheptenols. This reaction, followed by an enantioselective enzyme-catalyzed esterification, was used as a key step in a synthesis of the mevinic acid lactone.

Key words: methylenecyclopropane, palladium, stereocontrol, oxabicyclic, nickel.

Résumé : Le samarium, en présence de diiodométhane, transforme sélectivement un alcool allénique en méthylènecyclopropane avec une diastéréosélectivité allant de modeste à excellent. On a étudié l'effet d'un substituant porté par le carbone carbinolique, et par le carbone allénique, sur la diastéréosélectivité. On montre qu'une catalyse par le palladium favorise la cycloaddition intramoléculaire du méthylènecylopropane, avec un alkyne déficient en électron, pour donner un méthylènecyclopentane. La réaction est stéréospécifique avec rétention de la stéréochimie tel que l'indique la diffraction de rayons X. La catalyse par le nickel accélère l'hydroalumination des oxabicyclo[3.2.1]alcènes conduisant aux trialkylalanes bicycliques. Ces trialkylalanes traités par un acide de Lewis (chlorure de diisobutylaluminium) se fragmentent pour donner des cyclohepténols. On utilise cette réaction suivie d'une estérification catalysée par une enzyme énantiosélective comme étape clé dans une synthèse de la lactone de l'acide mévinique.

Mots clés : méthylènecyclopropane, palladium, stéréocontrôle, oxabicyclique, nickel.

[Traduit par la rédaction]

1. Introduction

New reactions and strategies are important for the stereoselective synthesis of natural and unnatural products having interesting architectures and (or) biological activity. Results are described from two of our programmes, which have as a common theme the use of cyclic molecules as templates for the control of stereochemistry in the efficient construction of natural product skeletons. An efficient method for the synthesis of stereochemically defined methylenecyclopropanes is presented and preliminary data on the stereoselectivity of transition-metal-catalyzed intramolecular cycloaddition reactions are discussed. In the second section, the use of metal catalysts in hydrometalation–fragmentation reactions leading to substituted cycloheptenols is described.

Received January 4, 1995.

This paper is dedicated, with respect, to Professor Michael J. Dignam (1931–1994).

M. Lautens,[2] Y. Ren, P. Delanghe, P. Chiu, S. Ma, and J. Colucci. Department of Chemistry, University of Toronto, Toronto, ON M5S 1A1, Canada.

[1] This paper is based on the Merck Frosst Centre for Therapeutic Research Award Lecture presented May 31, 1994, by Professor Lautens at the 77th Annual Conference of the Canadian Society for Chemistry, Winnipeg, Manitoba.

[2] Author to whom correspondence may be addressed. Telephone and Fax: (416) 978-6083. E-mail: mlautens@alchemy.chem.utoronto.ca

2. Stereochemical relay in cyclopentane formation

The use of methylenecyclopropanes as precursors to methylenecyclopentanes through a nickel- or palladium-catalyzed process has been known since the pioneering studies of Noyori, Odagi, and Takaya, and Binger and Schuchart more than 20 years ago, eq. [1] (1). The field has been reviewed

Can. J. Chem. Downloaded from www.nrcresearchpress.com by 80.90.12.36 on 09/08/12
For personal use only.

Can. J. Chem. Downloaded from www.nrcresearchpress.com by 80.90.12.36 on 09/08/12
For personal use only.

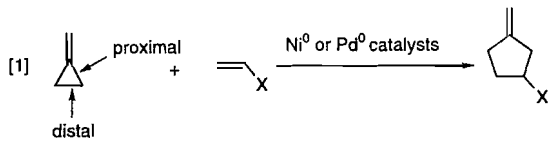

several times and only the most relevant background information is provided (2). This reaction is more complex than it appears since substrate, catalyst, and acceptor each play a role in influencing whether the distal or proximal carbon–carbon bond undergoes initial reaction with the metal. It is informative to compare the results described herein with those obtained from palladium-catalyzed trimethylenemethane (TMM) cycloadditions when attempting to resolve mechanistic issues surrounding these reactions (3).

While the intermolecular methylenecyclopropane reaction has been the most extensively studied, intramolecular versions of the cycloaddition are known. Yamago and Nakamura and Motherwell independently made the first contributions to this area (4). The example reported by Motherwell is particularly interesting since a *trans*-fused [3.3.0] system is formed, eq. [2].

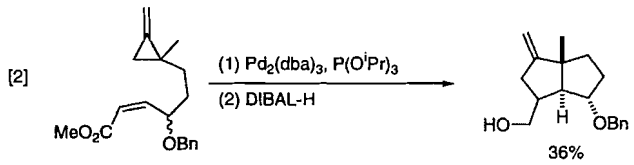

At the outset of these studies it was not known whether transition-metal-promoted cycloaddition reactions of methylenecyclopropanes catalyzed by nickel or palladium were stereospecific and (or) stereoselective and if stereochemical information could be transferred from the pre-existing stereocentres to new stereocentre(s) created in the cyclopentane, eq. [3].

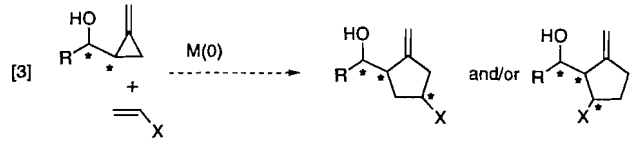

To investigate these questions, an efficient route to diastereomerically and enantiomerically enriched starting materials was essential. Furthermore, a determination of substituent effects within the methylenecyclopropane and the acceptor would define the utility of this reaction and also provide mechanistic information. While data answering all these questions is not yet in hand, progress on several fronts has been achieved.

3. Preparation of starting materials

There are many reported routes to methylenecyclopropanes in the literature (5). Unfortunately, many of these approaches are not easily adapted to preparing diastereomerically and enantiomerically pure products that have a hydroxyalkyl group (R = CH(OH)R). Two that appeared to be promising for our needs are illustrated in Scheme 1. The initial plan was to examine route "a" since we had developed access to 1,1-bimetallic compounds by a hydroxyl-directed cyclopropanation of vinyl bimetallic compounds (6).

We found that the Molander cyclopropanation (Sm, CH_2I_2, THF) (7) gave the bimetallic cyclopropanes in 75–92% yield and the diastereoselectivity was in excess of 200:1 as a result of the tributyltin moiety acting as a controlling group, eq. [4].

Scheme 1.

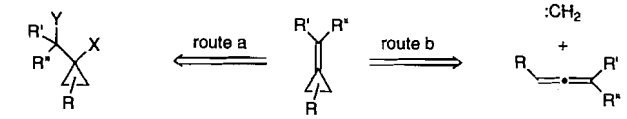

X=SiMe₃, Y=OH

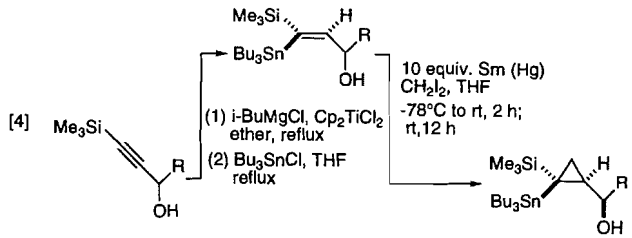

The starting 1,1-bimetallic alkenes were readily prepared in 68–85% yield by a modification of the Sato hydrometallation procedure (Cp_2TiCl_2, i-BuMgCl, Et_2O) (8). Following protection of the alcohol as the methyl ether, treatment of the cyclopropyl stannane with MeLi at 0°C gave the lithiocyclopropane, which was trapped with formaldehyde. This product does not readily undergo Peterson elimination except when the alcohol is converted to the chloride, which then reacts with Bu_4NF in THF/DMSO, eq. [5]. The overall yield for this four-step, three-pot procedure typically exceeds 50%.

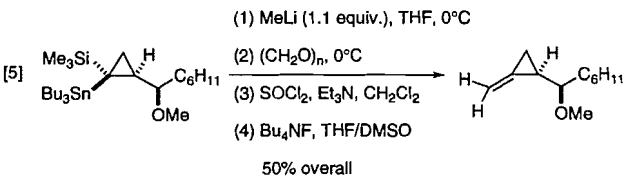

While this reaction sequence was successful, a more direct and efficient route was required. The selective cyclopropanation of an allenic alcohol would represent an ideal approach to the preparation of methylenecyclopropanes. The potential of this approach was first recognized more than 25 years ago by Bertrand and Maurin (9). However, they reported that under Simmons–Smith conditions, mono- and biscyclopropanation occurred and, furthermore, the reaction was not diastereoselective. We reexamined their results using various modifications of the Simmons–Smith reaction (10) and confirmed the lack of selectivity they reported. The best results were obtained when the sodium alkoxide of the allenic alcohol was treated with Et_2Zn–CH_2I_2. Up to 13:1 selectivity toward the olefin proximal to the hydroxy group was observed, but it was necessary to stop the reaction prior to complete consumption of starting material or an erosion in selectivity was noted.

In considering alternatives to Zn-based cyclopropanation, two observations from earlier studies using the Sm-promoted reaction of allylic alcohols suggested it might be more selective. Firstly, the oxygen of an allylic ether was a poor substrate for cyclopropanation, indicating that direction by the free hydroxyl was occurring. Secondly, homoallylic alcohols, react much more slowly than allylic alcohols, implying that the carbenoid cannot reach the more remote olefin. When an allenic alcohol was subjected to the Molander conditions we

Can. J. Chem. Downloaded from www.nrcresearchpress.com by 80.90.12.36 on 09/08/12
For personal use only.

obtained the desired product in 64% yield and the selectivity was >70:1 in favour of monocyclopropanation, eq. [6]. Using

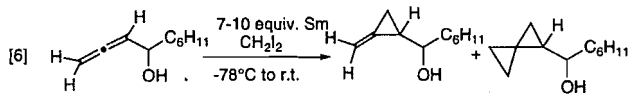

$ClCH_2I$ led to a further improvement in the yield, to 82%, with no loss of selectivity. Furthermore, under these conditions it was not necessary to add $HgCl_2$ to initiate the cyclopropanation.

With this encouraging result in hand, we prepared several more allenic alcohols using routes developed by Landor, Yamamoto, and Brandsma and co-workers, respectively, to study the effect of substitution on the diastereoselectivity (R, R′ = alkyl, H) (11).

A route to enantiomerically enriched allenic alcohols was also developed by combining an enantioselective carbonyl reduction with the Landor allenic alcohol synthesis, eq. [7].

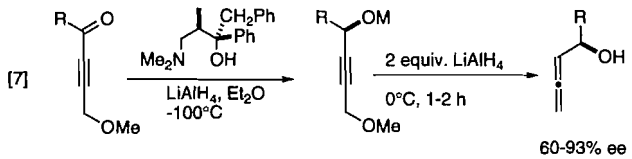

The use of a Chirald®-$LiAlH_4$ complex (12) gave the best overall results since reduction of the ynone to the propargyl alcohol could be followed by the S_N2' delivery of hydride to form the allene moiety without isolation of the intermediate. In practice this approach worked smoothly but additional $LiAlH_4$ was required following the carbonyl reduction step. This was surprising since species containing active hydride remained. We conclude that the Chirald®-$LiAlH_4$ complex is unable to effect the S_N2' reaction.

With the starting materials in hand, a determination of the substituent effects on the diastereoselectivity was undertaken. In the initial experiments with R = Cy, ratios approaching 10:1 were obtained for either CH_2I_2 or $ClCH_2I$. A correlation was observed between the steric size of the R group and the diastereoselectivity, Scheme 2. As we and others had observed previously, *n*-alkyl groups give poor and opposite selectivity (7). Smaller R groups may be capable of adopting the "inside" position, leading to the diastereomeric product. A transition state structure is shown that predicts the stereochemistry of the major diastereomer. Proof of the relative stereochemistry relied on comparison with an authentic sample prepared by an alternative route, vide infra.

The effect of substituents at other positions was also determined, Table 1. The most surprising result was that, whereas changing from R′ = H to R′ = Me had little or no effect on the diastereoselectivity, when R′ = OMe significant improvement in selectivity was observed. Clearly, electronic factors also influence the level of selectivity.

4. Proof of stereochemistry

Three different methods were used to assign the relative stereochemistry of the methylenecyclopropanes. Conversion of a 1,1-bimetallic compound of known stereochemistry to the methylenecyclopropane was used whenever possible, eq. [5].

Scheme 2.

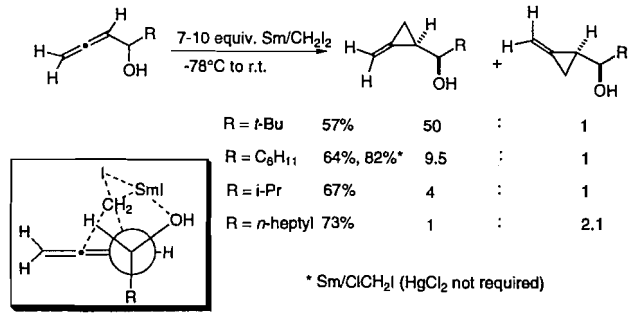

Table 1.

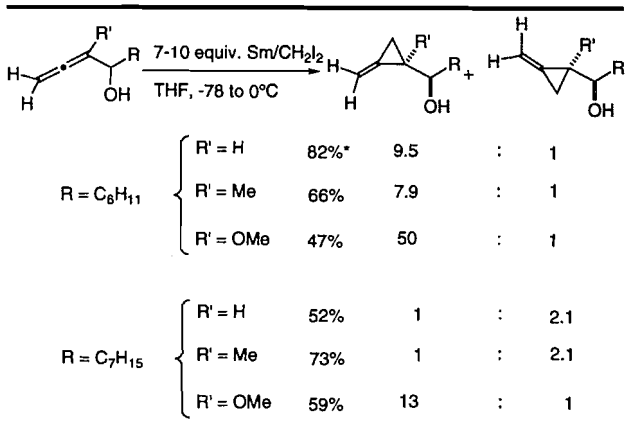

Fig. 1.

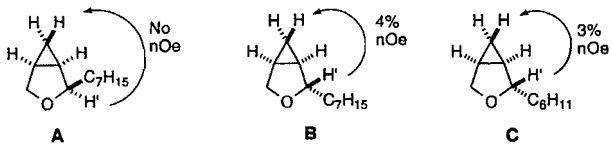

For R = cyclohexyl, R′ = OMe and Me, X-ray diffraction was used.

Nuclear Overhauser enhancements (nOe's) were also used to determine the stereochemistry. Rigid cyclic bicyclo[3.1.0] ethers were prepared by hydroboration, selective tosylation, and in situ cyclization, eq. [8]. Whereas the ether from the

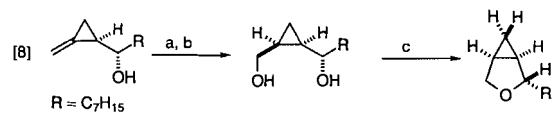

(a) BH_3 (3 equiv.), THF, 0°C. (b) H_2O_2, NaOH, EtOH, 66%. (c) *p*-TsCl (1 equiv.),Pyridine, 0°C, 83%

minor diastereomers showed a 3–4% nOe between the *endo* cyclopropyl hydrogen and H′ (**B** and **C**), no nOe was observed for the ether prepared from the major diastereomer **A**, Fig. 1. All these studies confirm that the facial selectivity of the cyclopropanation is identical irrespective of the substituent R′.

5. Intramolecular cycloadditions of methylenecyclopropanes

It was possible to address the question of stereoselectivity/

specificity in the metal-catalyzed cycloaddition by subjecting each of the diastereomeric methylenecyclopropanes to the reaction conditions and analyzing the stereochemistry of the products. Intramolecular reactions were examined first because they are known to be more efficient with substituted methylenecyclopropanes. Palladium catalysts were used because they consistently give exclusive insertion into the distal bond (1*b*,*c* and 2).

The side chain was introduced by deprotonation of the alcohol with KH–THF in the presence of 18-crown-6, addition of propargyl bromide, deprotonation of the terminal acetylene (*n*-BuLi, THF, 0°C), and addition of $ClCO_2Me$. Treatment of the substrates with $Pd_2(dba)_3$, 2 equivalents of $P(O^iPr)_3$ to Pd in toluene at reflux for 2 h, gave the cycloadducts in 70 and 72% yield, respectively, eqs. [9] and [10]. Examination of the ^1H

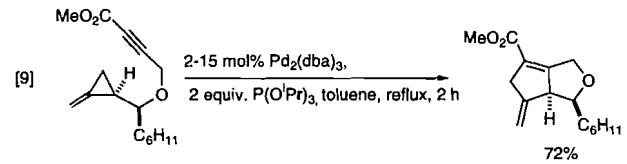

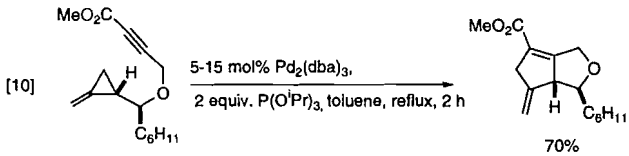

and ^{13}C NMR spectra clearly indicated that the products were not identical and that a stereospecific process had occurred (13). An X-ray structure revealed that cycloaddition with retention of configuration at the cyclopropyl stereocentre had taken place (14).

6. Conclusions

We have shown that Sm-promoted cyclopropanation of allenic alcohols is the most efficient route to the synthesis of diastereomerically enriched methylenecyclopropanes. Substitution is tolerated at every position in the allene and significant variation in the diastereoselectivity is observed as a function of steric and electronic factors. Intramolecular palladium-catalyzed cycloaddition onto an electron-deficient alkyne is stereospecific and occurs with retention of configuration. This information can be utilized in the design of natural product syntheses.

7. Stereocontrol via oxabicyclic templates

This program of research seeks to develop chemical reactions that convert a bicyclic molecule to an acyclic molecule with a resulting increase in the stereochemical content of the product. Our objective was to develop a strategy toward aldol-type products via non-carbonyl-based reactions (15). Ideally, the new strategy would avoid the iterative nature of many aldol reaction sequences. The challenges to be met include: access to all possible *syn* and *anti* products, high diastereo- and enantioselectivity, and chemical efficiency as measured by number of synthetic operations and chemical yields. Some of these objectives have been met and studies are ongoing.

Scheme 3.

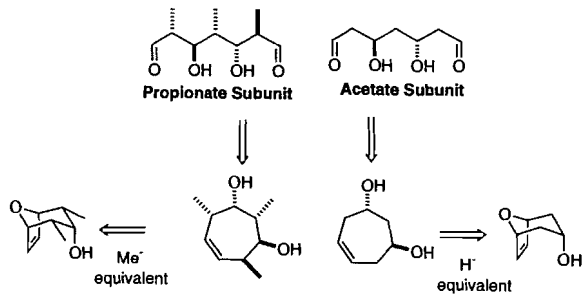

Specifically we were interested in utilizing the stereochemical information contained within oxabicyclic compounds as a route to acyclic molecules bearing acetate and propionate aldol sub-units, Scheme 3. The correct choice of starting material and nucleophile would provide access to a diverse collection of stereochemically useful products.

In a projected synthesis of ionomycin, we anticipated that the C_1–C_{23} section could be assembled from three subunits that would arise from a common starting material. The synthesis of ionomycin has been the subject of considerable interest and two total syntheses have been reported (16). Molecules of this complexity provide an opportunity to develop new strategies and test the state of the art in organic synthesis. Considerable progress toward this objective has been achieved and the methodology that is being utilized in this synthetic effort is presented.

The concept of using nucleophiles to open oxabicyclic starting materials was first reported more than 20 years ago by Caple et al. (17). Reaction of highly strained benzooxabicyclic derivatives with an organolithium and dehydration of the products gave a route to 2-substituted naphthalenes. Concurrent with our studies using cuprates and organolithium reagents with oxabicyclo[3.2.1] substrates was elegant work by Arjona, Fernandez de la Pradilla, Plumet and co-workers on the [2.2.1] series, eqs. [11], [12] (18).

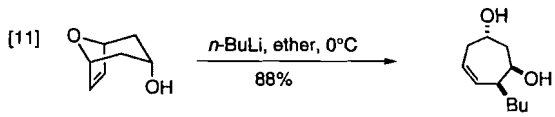

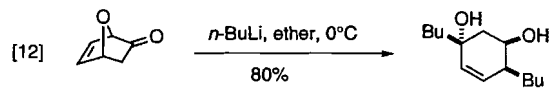

We extended the range of nucleophiles to include ring opening by a hydride source (reductive ring opening). Two sources of hydride were identified: organomagnesium reagents bearing a β-hydride react with oxabicyclic compounds in the presence of excess $MgBr_2$ but the reaction is slow and limited in scope (19*a*); a more general method uses excess DIBAL-H in refluxing hexanes (19*b*). The solvent and temperature were important variables in the latter case since the reducing agent seems to also function as a Lewis acid in assisting the opening. Other nucleophilic reducing agents such as $LiAlH_4$ are much less efficient. The optimized conditions utilized 3–5 equivalents of DIBAL-H in hexanes at reflux for 1–16 h, eq. [13]. While many substrates give good yields of the desired product, a side-product was isolated in which

Can. J. Chem. Downloaded from www.nrcresearchpress.com by 80.90.12.36 on 09/08/12
For personal use only.

reduction of the alkene occurred. Hydroalumination of the ring-opened product seems to be competitive with the initial ring-opening reaction in some cases. A technical problem is that these two products are often difficult to separate by chromatography or distillation.

[13] 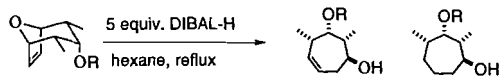

R=H, 8-12 h	83%	13%
R=Bn, 24 h	<10%	75%

A search for a more selective reducing system was initiated and the mildness of transition metal-catalyzed hydrometalations was noted (20). Nickel, palladium, zirconium, and titanium all accelerate the hydroalumination of alkenes and alkynes (20, 21). It was not clear at the outset if the hydroaluminated oxabicyclic compound could be observed or if it would undergo immediate ring opening. In the latter scenario, the product could also undergo hydroalumination, defeating the purpose of using the catalyst. Experiments to answer some of these questions were initiated.

After a survey of catalysts, Ni(0) complexes were found to be the most suitable since the reaction occurred rapidly at −78 to 0°C with 5–14 mol% of catalyst and with only 1.2 equivalents of hydrometalating agent (DIBAL-H), whereas reaction in the absence of catalyst required 5 equivalents of DIBAL-H at elevated temperatures. The trialkylalane was observed rather than the ring-opened product, as proven by deuterium trapping and oxidation studies (22).

Upon warming the trialkylalane to 70°C for 16 h, elimination occurs to provide the desired product in 65% yield accompanied by the oxabicyclic alkane in 34% yield, Scheme 4. The alkane may result from protonation of unreacted alane since elimination is quite difficult under these conditions. It is not possible to determine if epimerization precedes the *anti* elimination or if a *syn* elimination is occurring. We reasoned that addition of a Lewis acid would provide assistance to either of these processes by complexing to the bridging oxygen, thereby improving its leaving-group ability (23). Under optimized conditions, heating a mixture of the hydroaluminated product and DIBAL-Cl to 65°C gave the cycloheptenol in 88% yield.

An example of the dramatic improvement in the efficiency of this process is illustrated in the reaction of an unsubstituted oxabicyclic compound, Table 2. Using 5 equivalents of DIBAL-H in the absence of catalyst, a 1:1 mixture of the cycloheptene and cycloheptane diols was obtained. Addition of nickel avoided the formation of the alkane but the ring opening was inefficient and an equimolar amount of the oxabicyclic alkane was isolated. However, the combination of a nickel catalyst, DIBAL-H, and then a Lewis acid catalyst gave the *meso* cycloheptene diol in 85% yield with only a trace of the oxabicyclic alkane, which was easily separated. This diol was used in a synthesis of the lactone portion of mevinolin as described below (24). A second key step in the synthesis is the differentiation of the enantiotopic hydroxyl groups that was achieved by taking advantage of the high specificity of enzymes in ester formation and hydrolysis (25).

8. Synthesis of the mevinolin lactone

Mevinolin is a potent inhibitor of HMG-CoA reductase and as

Scheme 4.

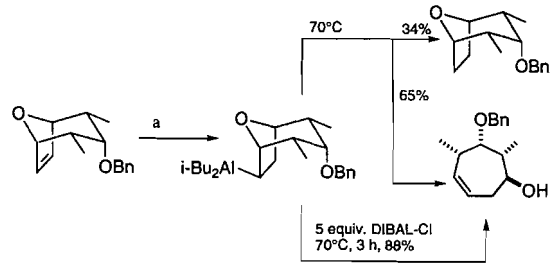

(a) 10 mol% $Ni(COD)_2$,1.2 equiv. DIBAL-H, toluene, r.t., 30 min.

Table 2.

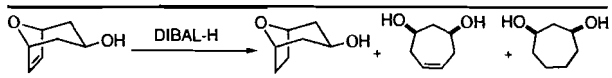

no Ni, hexanes, reflux	0	:	1	:	1
10 mol% $Ni(COD)_2$, toluene, r.t.	1	:	1	:	0
10 mol%$Ni(COD)_2$ then DIBAL-Cl, 60°C, 3-6 h	1	:	20	:	0

Scheme 5.

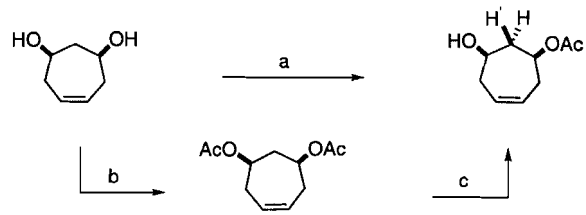

(a) Lipase AY-30, isopropenyl acetate, r.t., 4 h, 78%, 95% ee; (b) Ac_2O, Pyr, 89%; (c) Lipase PS30, pH=7.5 buffer, 54%.

a result has attracted significant attention from the synthetic and biological communities (26). The lactone moiety is essential for biological activity, whereas structural variation in the hexahydronaphthalene moiety is possible.

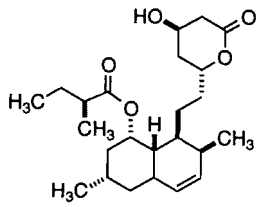

Mevinolin

As mentioned above, conversion of the *meso* diol to an enantiomerically enriched hydroxyester was achieved using an enzyme, Scheme 5. Transesterification using isopropenyl acetate and Lipase AY-30 gave the hydroxyester in 78% yield and in 95% ee as measured by Chiral GC (27). Alternatively, double acetylation of the *meso* diol furnished a *meso* diacetate, which was selectively hydrolyzed using Lipase PS30 (28). Only one enantiomer was detected under these conditions but the reaction suffered from modest yields (54%). The absolute configuration using either route to the hydroxyester was identical and was predicted based on analysis of the Mosher ester ^1H NMR spectrum at 500 MHz. The signals for H′ appear at 1.91 ppm in the major diastereomer and at 2.01 ppm in the minor diastereomer.

With ready access to the enantiomerically pure hydroxyester,

Can. J. Chem. Downloaded from www.nrcresearchpress.com by 80.90.12.36 on 09/08/12
For personal use only.

Scheme 6.

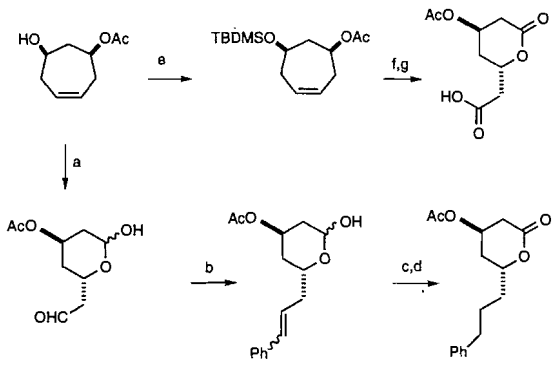

(a) O_3, PPh_3, -78°C; (b) Ph_3PCH_2BrPh, *n*BuLi, -20°C–0°C, 49% over two steps; (c) TPAP, NMO, 87%; (d) H_2, Pd-C, EtOAc, 96%; (e) TBDMSCl, DMF, imidazole, 96%; (f) $RuCl_3 \cdot xH_2O$, $NaIO_4$; (g) HF, CH_3CN, 57% over two steps.

two routes to the mevinic lactone were examined, Scheme 6. Direct ozonolytic cleavage of the olefin gave a dialdehyde, which reacted with the unprotected hydroxy group to form a lactol aldehyde that served to differentiate the two aldehyde groups. Selective reaction of the free aldehyde with a phosphorus ylide gave the olefin as a mixture of isomers (*trans*:*cis* = 2:1). Oxidation of the lactol to the lactone using TPAP/NMO (29) and hydrogenation of the olefin gave an aryl mevinic acid derivative.

Alternatively, protection of the free hydroxyl as a TBDMS ether occurred in 96% yield, Scheme 6, steps e–g. Oxidative cleavage of the double bond to the diacid followed by selective deprotection of the silyl group under acidic conditions resulted in concomitant lactonization to the lactone-acid in 57% yield. It is interesting to note that the enantiomeric product is also potentially available by cleavage of the acetate rather than the silyl moiety following the oxidation step.

9. Conclusions

Oxabicyclic compounds are readily available starting materials and they have been found to undergo novel reductive ring-opening reactions. Transition-metal-promoted hydrometalation–fragmentation using nickel catalysts and an aluminum hydride is superior to our previously reported reductive procedures, providing improved yields and milder reaction conditions. Application of this reaction represented a key step in a synthesis of the mevinic acid lactone.

Summary

Palladium catalysts promote stereospecific reactions of methylenecyclopropanes with alkynes, providing the first information on the fate of a preexisting stereocentre during the insertion and cycloaddition process. The use of a nickel catalyst in the reaction of oxabicyclic compounds opens up the potential of regio- and enantioselective reactions by the addition of phosphine ligands (30). The information obtained in these studies is currently being used in the synthesis of complex natural products.

Acknowledgements

The past and present members of my research group are thanked for their effort, experimental skill, and intellectual contributions. My colleagues in the Chemistry Department at the University of Toronto provide a stimulating environment and valuable advice. Professors Bryan Jones, Bob McClelland, Martin Moskovits, Ron Kluger, Mitch Winnik, and Adrian Brook deserve special thanks for their support. Dr. Yvan Guindon (formerly of BioMega/Boehringer Ingelheim) and Dr. Robert Young (Merck Frosst) are thanked for supporting NSERC IOR applications which funded key parts of this work. The A.P. Sloan Foundation, the Natural Sciences and Engineering Research Council (NSERC) of Canada, BioMega/Boehringer Ingelheim Research Inc., the Merck Frosst Centre for Therapeutic Research, the Petroleum Research Foundation administered by the American Chemical Society, Eli Lilly Inc., and the University of Toronto are thanked for financial support.

References

1. (*a*) R. Noyori, T. Odagi, and H. Takaya. J. Am. Chem. Soc. **92**, 5780 (1970); (*b*) P. Binger and U. Schuchardt. Angew. Chem. Int. Ed. Engl. **16**, 249 (1977); (*c*) Chem. Ber. **113**, 3334 (1980).
2. (*a*) P. Binger and H.M. Büch. Top. Curr. Chem. **135**, 77 (1987); (*b*) T. Ohta and H. Takaya. Comprehensive organic synthesis. Vol. 5. *Edited by* B.M. Trost. Pergamon Press, Oxford. 1991. p. 1185.
3. (*a*) B.M. Trost. Angew. Chem. Int. Ed. Engl. **25**, 1 (1986); (*b*) B.M. Trost, T.A. Grese, and D.M.T. Chan. J. Am. Chem. Soc. **113**, 7350 (1991), and references therein.
4. (*a*) R.T. Lewis, W.B. Motherwell, and M. Shipman. J. Chem. Soc. Chem. Commun. 948 (1988); (*b*) S. Yamago and E. Nakamura. J. Chem. Soc. Chem. Commun. 1112 (1988); (*c*) S.A. Bapuji, W.B. Motherwell, and M. Shipman. Tetrahedron Lett. **30**, 7107 (1989); (*d*) W.B. Motherwell and M. Shipman. Tetrahedron Lett. **32**, 1103 (1991); (e) H. Corlay, R.T. Lewis, W.B. Motherwell, and M. Shipman. Tetrahedron, **51**, 3303 (1995).
5. M. Lautens and P.H.M. Delanghe. J. Am. Chem. Soc. **116**, 8526 (1994), and references therein.
6. M. Lautens and P.H.M. Delanghe. J. Org. Chem. **57**, 798 (1992).
7. (*a*) G.A. Molander and J.B. Etter. J. Org. Chem. **52**, 3942 (1987); (*b*) G.A. Molander and L.S. Harring. J. Org. Chem. **54**, 3525 (1989).
8. M. Lautens and A.H. Huboux. Tetrahedron Lett. **31**, 3105 (1990), and references therein.
9. M. Bertrand and R. Maurin. Bull. Soc. Chim. Fr. 2779 (1967).
10. S.E. Denmark and J.P. Edwards. J. Org. Chem. **56**, 6974 (1991), and references therein.
11. (*a*) J.S. Cowie, P.D. Landor, and S.R. Landor. J. Chem. Soc. Perkin Trans. 1, 720 (1973); (*b*) L. Brandsma and H.D. Verkruijsse. Synthesis of acetylenes, allenes and cumulenes. Elsevier, Amsterdam. 1981. p. 43; (*c*) M. Ishiguro, N. Ikeda, and H. Yamamoto. J. Org. Chem. **47**, 2225 (1982).
12. (*a*) S. Yamaguchi, H.S. Mosher, and A. Pohland. J. Am. Chem. Soc. **94**, 9254 (1972); (*b*) S. Yamaguchi and H.S. Mosher. J. Org. Chem. **38**, 1870 (1973).
13. M. Lautens, Y. Ren, and P.H.M. Delanghe. J. Am. Chem. Soc. **116**, 8821 (1994).
14. M. Lautens, A.J. Lough, and Y. Ren. Acta Crystallogr. Submitted.
15. (*a*) M. Lautens. Pure Appl. Chem. **64**, 1873 (1992); (*b*) Synlett, 177 (1993).
16. (*a*) S. Hanessian, N.G. Cooke, B. DeHoff, and Y. Sakito. J. Am. Chem. Soc. **112**, 5276 (1990); (*b*) D.A. Evans, R.L. Dow, T.L.

Can. J. Chem. Downloaded from www.nrcresearchpress.com by 80.90.12.36 on 09/08/12
For personal use only.

Shih, J.M. Takacs, and R. Zahler. J. Am. Chem. Soc. **112**, 5290 (1990), and references therein.
17. R. Caple, G.M.S. Chen, and J.D. Nelson. J. Org. Chem. **36**, 2874 (1971).
18. O. Arjona, R. Fernandez de la Pradilla, E. Garcia, A. Martin-Domenech, and J. Plumet. Tetrahedron Lett. **30**, 6437 (1989).
19. (*a*) M. Lautens and P. Chiu. Tetrahedron Lett. **32**, 4827 (1991); (*b*) M. Lautens, P. Chiu, and J.T. Colucci. Angew. Chem. Int. Ed. Engl. **32**, 281 (1993).
20. (*a*) J.J. Eisch. Comprehensive organic synthesis. Vol. 8. *Edited by* B.M. Trost. Pergamon Press, Oxford. 1991. p. 733; (*b*) G. Wilke. Angew. Chem. Int. Ed. Engl. **27**, 185 (1988).
21. (*a*) K. Ziegler, E. Holzkamp, H. Breil, and H. Martin. Angew. Chem. **67**, 543 (1955); (*b*) J.J. Eisch and M.W. Foxton. J. Organomet. Chem. **12**, P33 (1968); (*c*) K. Fischer, K. Jonas, P. Misbach, R. Stabba, and G. Wilke. Angew. Chem. Int. Ed. Engl. **12**, 943 (1973); (*d*) J.J. Eisch and S.-G. Rhee. J. Am. Chem. Soc. **96**, 7276 (1974); (*e*) J.J. Eisch and K. C. Fichter. J. Organomet. Chem. **250**, 63 (1983).
22. P. Chiu. Ph.D. Thesis, University of Toronto (1993).
23. (*a*) G. Zweifel and J. Plamondon. J. Org. Chem. **35**, 898 (1970); (*b*) H.C. Brown and J.V.N. Vara Prasad. J. Org. Chem. **50**, 3002 (1985).
24. M. Lautens, S. Ma, and A. Yee. Tetrahedron Lett. **36**, 4185 (1995).
25. (*a*) J.B. Jones. Tetrahedron, **42**, 3351 (1986); (*b*) Y.F. Wang, J.J. Lalonde, M. Momongan, D.E. Bergbreiter, and C.H. Wong. J. Am. Chem. Soc. **110**, 7200 (1988); (*c*) R.J. Kazlauskas, A.N.E. Weissfloch, A.T. Rappaport, and L.A. Cuccia. J. Org. Chem. **56**, 2656 (1991).
26. (*a*) T. Rosen and C.H. Heathcock. Tetrahedron, **42**, 4909 (1986); (*b*) S. Valverde, J.C. Lopez, A.M. Gomez, and S. Garcia-Ochoa. J. Org. Chem. **57**, 1613 (1992), and references therein; (*c*) F.G. Kathawala. Med. Res. Rev. **11**, 121 (1991).
27. J.A. Dale and H.S. Mosher. J. Am. Chem. Soc. **95**, 512 (1973).
28. C.R. Johnson and C.H. Senanayake. J. Org. Chem. **54**, 735 (1989).
29. (*a*) W.P. Griffith, S.V. Ley, G.P. Whitcombe, and A.D. White. J. Chem. Soc. Chem. Commun. 1625 (1987); (*b*) R. Bloch and C. Brillet. Synlett, 829 (1991).
30. (*a*) M. Lautens, P. Chiu, S. Ma, and T. Rovis. J. Am. Chem. Soc. **117**, 532 (1995); (*b*) G. Giacomelli, L. Bertero, and L. Lardicci. Tetrahedron Lett. **22**, 883 (1981).

Can. J. Chem. Downloaded from www.nrcresearchpress.com by 80.90.12.36 on 09/08/12
For personal use only.

Tautomérie du 2,5-dimercapto-1,3,4-thiadiazole et synthèse de thiadiazoloacridiniques

Pascale Amiel, Abdallah Mahamoud, Pierre Brouant, Jean Pierre Galy, Jacques Barbe, Janina Karolak-Wojciechowska et Maciej Posel

Résumé : On a préparé des 2(3*H*)-thione-5-alkylthio-1,3,4-thiadiazoles dont l'arylation par différentes 9-chloroacridines a conduit, dans la pyridine servant de solvant et de base, à des 2-thione-(*N*)3-acridinyl-5-alkylthio-1,3,4-thiadiazoles. La structure moléculaire de ces composés a été précisée par spectroscopie de RMN. En outre, on a procédé à l'étude radiocristallographique d'un intermédiaire de synthèse, la 2(3*H*)-thione-5-[2′-(diéthylamino)éthylthio]-1,3,4-thiadiazole. On a ainsi mis en évidence l'existence d'une fonction thione à l'état solide, la RMN l'ayant déjà démontrée à l'état dissous. Par ailleurs, on a préparé les 2-thioacridinyl-5-alkylthio-1,3,4-thiadiazoles à partir du sel de sodium des 2-mercapto-5-alkylthio-1,3,4-thiadiazoles. On a ainsi montré que la tautomérie jouait un rôle déterminant dans la réactivité du substrat de départ.

Mots clés : acridines, thiadiazoles, tautomérie.

Abstract: Some 2(3*H*)-thione-5-alkylthio-1,3,4-thiadiazoles were prepared with a view to arylating these compounds with 9-chloroacridines. Using pyridine as solvent and base, this arylation led to the 2-thione-(*N*)3-acridinyl-5-alkylthio-1,3,4-thiadiazoles. Molecular structures of the latter were determined either by NMR spectroscopy or by referring to X-ray crystallography of the 5-(diethylaminoethylthio)-1,3,4-thiadiazole-2-thione. Thus, with respect to the tautomeric equilibrium of the compound investigated, the thione group was detected either in the solid state or in solution. In contrast, 2-acridinylthio-5-alkylthio-1,3,4-thiadiazoles were prepared by using the sodium salt of 2-mercapto-5-alkylthio-1,3,4-thiadiazoles as starting material.

Key words: acridines, thiadiazoles, tautomerism.

Introduction

On a voulu préparer des produits originaux où se retrouveraient les propriétés trypanocides des acridiniques (1, 2) et des thiadiazoles (3). Ainsi a-t-on cherché à remplacer dans les 9-thioalkylacridines, les groupements alkylés par un reste thiadiazole. On a choisi à cette fin le 2,5-dimercapto-1,3,4-thiadiazole **1**, comme produit de départ, en raison de sa réactivité particulière. En effet, cette molécule peut exister théoriquement sous les trois formes tautomères **1***a*, **1***b* et **1***c* (4–6) données dans la figure 1.

Résultats et discussion

Le but était de préparer des dérivés thioalkylés du thiadiazole **1** afin de les condenser ultérieurement avec des 9-chloroacridines **2** diversement substituées (figure 2).

On a donc d'abord synthétisé les composés monothiosubstitués **3** selon la méthode d'Inoue et al. (7) qui utilise le butanol normal à reflux en milieu alcalin avec un équivalent de réactif par rapport à **1** et, comme base, un équivalent de pyridine. Ce protocole a permis d'obtenir les dérivés **3** avec de bons rendements (environ 90%), car il évite la formation parasite de produits de dithiosubstitution comme il s'en produit par exemple en suivant d'autre conditions expérimentales décrites dans la littérature (8). On a par ailleurs voulu vérifier si la dithioalkylation du produit de départ **1** était possible par la même méthode; on a donc doublé les quantités de réactif et de base. On n'a toujours obtenu que le produit de monothiosubstitution **3**, d'ailleurs avec un rendement moins élevé que dans les conditions précédentes (environ 70%). De même, il n'a été possible de préparer par cette méthode les dérivés dithiosubstitués **4** à partir des dérivés monothiosubstitués **3** (sous forme de base

Fig. 1. Formes tautomères théoriques du 2,5-dimercapto-1,3,4-thiadiazole.

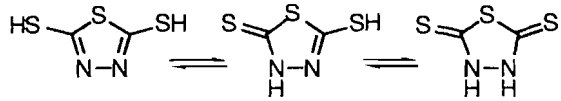

1*a* **1***b* **1***c*

Reçu le 4 juillet 1994.[1]

P. Amiel, A. Mahamoud, P. Brouant, J.P. Galy et J. Barbe.[2] Groupe d'études et de recherches en chimie thérapeutique organique et physique, Unité de recherche associée au Centre de la recherche scientifique, n° 1411, Faculté de pharmacie, 27, boulevard Jean-Moulin, 13385 Marseille Cedex 5, France.
J. Karolak-Wojciechowska et M. Posel. Technical University of Lodz, Institute of General and Ecological Chemistry, 90924 Lodz, Poland.

1 Révision reçue le 3 avril 1995.
2 Auteur à qui la correspondance doit être adressée. Téléphone : 33-91-79-38-32. Fax : 33-91-83-56-30.

Can. J. Chem. Downloaded from www.nrcresearchpress.com by 80.90.12.36 on 09/08/12
For personal use only.

Fig. 2. 9-Chloroacridines substituées utilisées dans les synthèses.

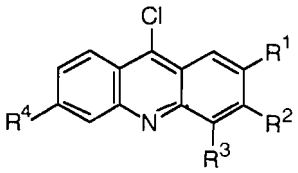

	R^1	R^2	R^3	R^4	Réf.
2a	H	H	H	H	15
2b	NO_2	H	H	H	15, 16
2c	H	NO_2	H	H	15
2d	H	NH_2	H	H	Cet article
2e	H	H	NO_2	H	17
2f	OCH_3	H	H	Cl	Aldrich

Fig. 3. Monothioalkylation et dithioalkylation du 2,5-dimercapto-1,3,4-thiadiazole.

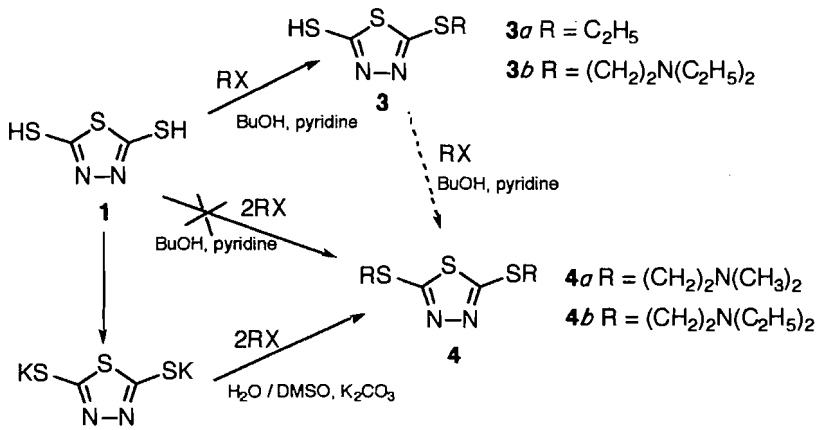

libre), qu'avec des rendements faibles (<25%). Pour obtenir les composés **4** avec de meilleurs rendements, on a donc dû alkyler le sel dipotassique du 2,5-dimercapto-1,3,4-thiadiazole (Sigma–Aldrich), dans un mélange DMSO–H_2O en présence de K_2CO_3 (9) (figure 3). Les rendements en base libre sont alors ≥ 65%.

Cependant, pour obtenir les dérivés **6** qui sont substitués sur chaque atome de soufre exocyclique par des groupements différents, le protocole décrit est inapplicable parce que les 9-chloroacridines **2** choises comme second agent d'alkylation sont, dans les conditions de l'expérience, hydrolysées en 9-acridinones. Aussi, pour obtenir ainsi les dérivés **5**, a-t-on salifié la fonction thiol libre des composés **3** (tautomérie) au moyen de méthylate de sodium. Les composés **5**, en présence de 9-chloroacridiniques, dans la pyridine et sous atmosphère inerte, ont conduit alors aux dérivés **6** recherchés.

On a pensé pouvoir échapper à la préparation des composés intermédiaires **5**, en alkylant directement les dérivés monothiosubstitués **3** dans des conditions évitant l'hydrolyse des 9-chloroacridines **2**. On a ainsi effectué les synthèses selon le mode opératoire décrit pour préparer les dérivés **6**. Les composés obtenus ont été identifiés par RMN du ^1H et RMN du ^{13}C. Ils se sont avérés être des 2-thione-*N*(3)-acridinyl-5-alkylthio-1,3,4-thiadiazoles **7** (figure 4).

Cette structure est explicable compte-tenu, chez les composés intermédiaires **3**, des résultats de la RMN du carbone 13, de ceux de l'infrarouge et de la radiocristallographie. Des exemples en sont donnés à propos du composé *3b*.

Les spectres réalisés et enregistrés, après pastillage dans le bromure de potassium ou mise en solution dans la pyridine du composé *3b*, montrent une bande vers 1480 cm^{-1} qui doit être attribuée à νC=S (6). L'intensité de cette bande est forte en raison de la probable participation de contributions ioniques du type N^+=C-S^- (10) ou N-C^+-S^- (11). À noter que cette bande n'existe pas dans le spectre de *5b*. En revanche, les bandes situées à 1435–1415 cm^{-1} sont attribuables à νC-S-R (6). Elles sont observées aussi bien chez *3b* que chez *5b*. La bande caractéristique de νSH (2245–2300 cm^{-1}) (12) ne se manifeste pas dans les spectres IR de ces composés.

Toujours pour *3b*, le spectre de RMN du ^{13}C dans le diméthylsulfoxyde hexadeutérié présente un déplacement chimique à 187,96 ppm et un autre à 156,10 ppm. Dans la pyridine-d_5, ces déplacements sont à 189,62 ppm et 157,47 ppm. On peut les attribuer aux carbones C=S et C-SR car les valeurs sont proches de celles antérieurement relevées chez les acridinethiones et les alkylthioacridines (13) : 192,9 ppm (C=S) et 146,15 ppm (C-SR). Ceci démontre donc l'existence en solution d'une forme 2-thione-5-alkylthio au lieu d'une forme 2-mercapto-5-alkylthio. La fonction thione exocyclique existant dans les composés **3** est toujours présente dans les composés **7**. En effet, la RMN du carbone 13, effectuée sur les composés de la série **7**, montre le signal

Can. J. Chem. Downloaded from www.nrcresearchpress.com by 80.90.12.36 on 09/08/12
For personal use only.

Fig. 4. Voies de synthèse des *N*- et des *S*-thiadiazoloacridiniques.

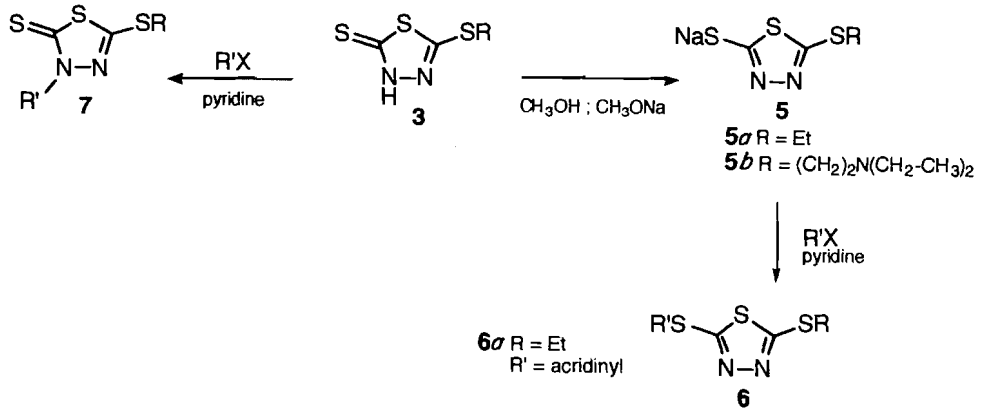

	R	R'		R	R'
7*a*	C_2H_5	2*a*	7*g*	$(CH_2)_2N(C_2H_5)_2$	2*a*
7*b*	C_2H_5	2*b*	7*h*	$(CH_2)_2N(C_2H_5)_2$	2*b*
7*c*	C_2H_5	2*c*	7*j*	$(CH_2)_2N(C_2H_5)_2$	2*c*
7*d*	C_2H_5	2*d*	7*k*	$(CH_2)_2N(C_2H_5)_2$	2*d*
7*e*	C_2H_5	2*e*	7*m*	$(CH_2)_2N(C_2H_5)_2$	2*e*
7*f*	C_2H_5	2*f*	7*n*	$(CH_2)_2N(C_2H_5)_2$	2*f*

Fig. 5. Valeurs des charges calculées pour les atomes engagés dans les réactions de substitution nucléophile.

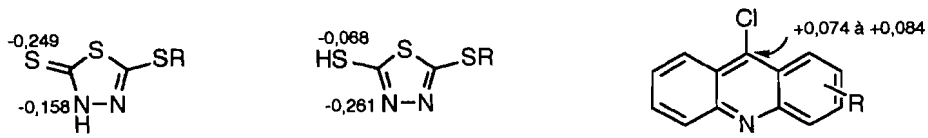

caractéristique d'un carbone engagé dans une fonction thione. Celui-ci est situé entre 187 et 190 ppm, selon le solvant utilisé.

Par ailleurs, le calcul des densités de charges faite par la méthode de Gasteiger–Hückel (Logiciel SYBYL, Tripos Assoc.), a conduit aux résultats schématisés sur la figure 5.

La charge présente sur l'azote porteur d'un hydrogène est ici significativement plus favourable à une action avec le carbone (C-9) électrophile des chloroacridiniques que celle portée par le soufre du groupement thiol. Lors de l'attaque de la base (pyridine), il devrait s'ensuivre une délocalisation de la charge négative générée par l'arrachement du proton. Cette charge sera préférentiellement portée par l'azote N(3) puisqu'on a observé que la réaction avait lieu entre cet atome et le C(9) de l'acridinique pour conduire aux molécules **7**. Il devrait s'ensuivre le mécanisme de substitution donné sur la figure 6.

Enfin, la configuration cristalline de **3***b* est rapportée sur la figure 7 : c'est celle d'une 2(3*H*)-thione-5-alkylthio-1,3,4-thiadiazole. La distance C=S correspond à une double liaison. Aucun hydrogène n'a pu être détecté autour de l'atome S(2) mais en revanche, l'hydrogène de l'atome N(3) a été mis en évidence sans ambiguïté.

Les coordonnées atomiques sont données dans le tableau 1 et les paramètres moléculaires les plus significatifs sont donnés dans les Tableau 2 et 3. Il apparaît (figure 8) que l'unité structurale consiste en deux molécules unies par des liaisons hydrogène dont les paramètres sont donnés dans le Tableau 4. L'ion chlore participe à deux liaisons hydrogène quasiment identiques N(3)-H(3)·····Cl^-·····H(6)-N(6)$^+$.

La géométrie du cycle thiadiazole est en accord avec les résultats de la littérature (14). L'atome d'azote protoné (N-6) possède une coordination tétraédrique, la somme des angles entre les substituants autres que H valant 348,5° et l'élévation de l'atome hors du plan valant 0,409(3) Å.

La radiocristallographie confirme donc ici l'existence d'une fonction thione à l'état solide, son existence à l'état dissous ayant déjà été démontrée par la RMN du carbone 13.

Conclusion

D'une part, l'alkylation du 2,5-dimercapto-1,3,4-thiadiazole **1** par un halogénure d'alkyle donne une S-alkylation pour conduire aux composés **3**. Une deuxième alkylation, suivant la première et faite dans les mêmes conditions opératoires ne donne des 2,5-dialkylthio-1,3,4-thiadiazoles qu'avec de faibles rendements. En revanche, une dialkylation en une seule étape sur le sel dipotassique de **1** permet d'augmenter les rendements. Ainsi, on met en évidence le rôle des conditions opératoires dans la réactivité de ce type de molécules qui, de plus, présentent une tautomérie prototropique. Il semble, en particulier, que le butanol favorise la monothiosubstitution.

Can. J. Chem. Downloaded from www.nrcresearchpress.com by 80.90.12.36 on 09/08/12
For personal use only.

Fig. 6. Synthèse des *N*-thiadiazoloacridiniques **7** : mécanisme réactionnel.

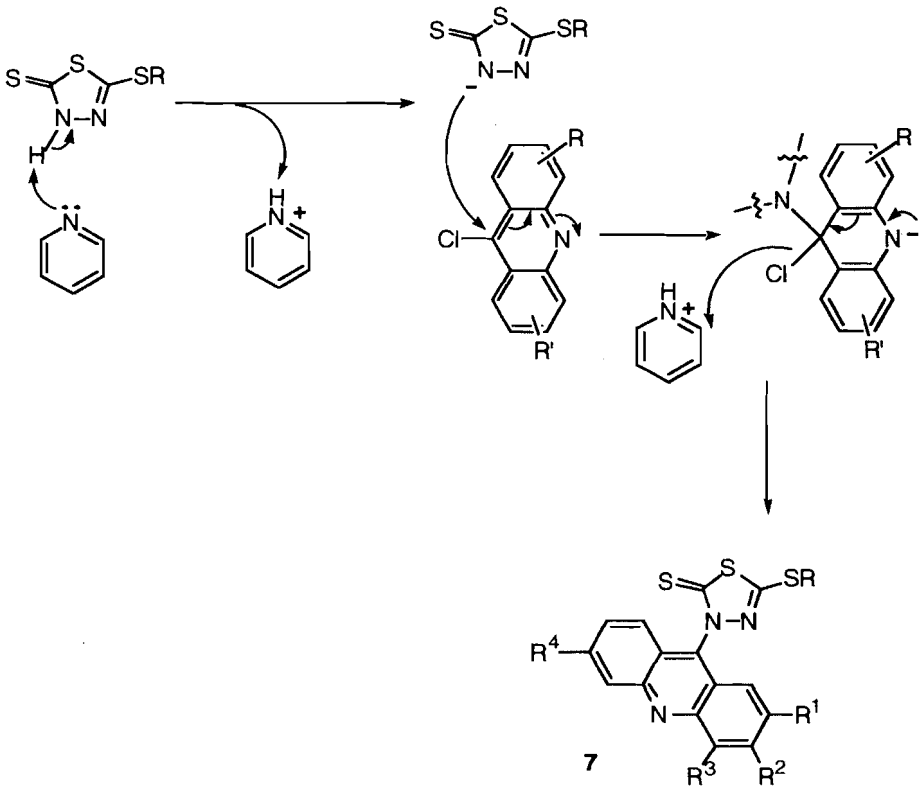

Fig. 7. Géométrie moléculaire et numérotation de **3***b*.

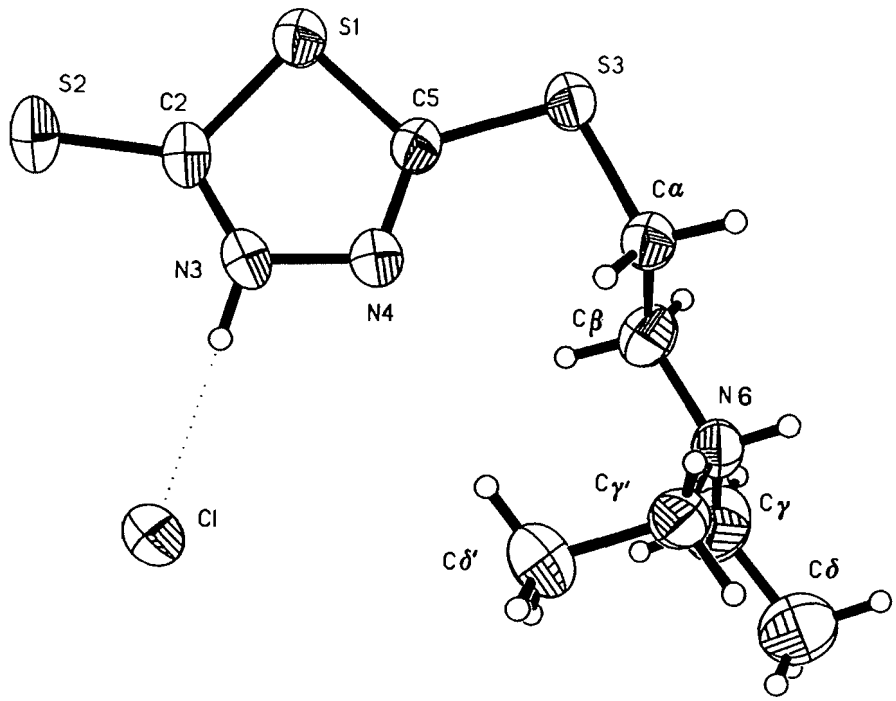

D'autre part, les sels de sodium des 2-mercapto-5-alkylthio-1,3,4-thiadiazole **4** réagissent avec les 9-chloroacridiniques pour donner les 2-acridinylthio-5-alkylthio-1,3,4-thiadiazoles **6** alors que les 2(3*H*)-thione-5-alkylthio-1,3,4-thiadiazoles **3** correspondants donnent avec les mêmes réactifs, des 2-thione-(*N*)3-acridinyl-5-alkylthio-1,3,4-thiadiazoles **7**, par condensation au niveau d'un azote intracyclique. Cette orientation particulière tient à la structure thioalkyl-thione (thioamide) et non mercapto-thioalkyl (imidothiol) des composés intermédiaires dans le milieu réactionnel.

Can. J. Chem. Downloaded from www.nrcresearchpress.com by 80.90.12.36 on 09/08/12
For personal use only.

Can. J. Chem. Downloaded from www.nrcresearchpress.com by 80.90.12.36 on 09/08/12
For personal use only.

Fig. 8. Maille élémentaire et empilement cristallin de *3b*.

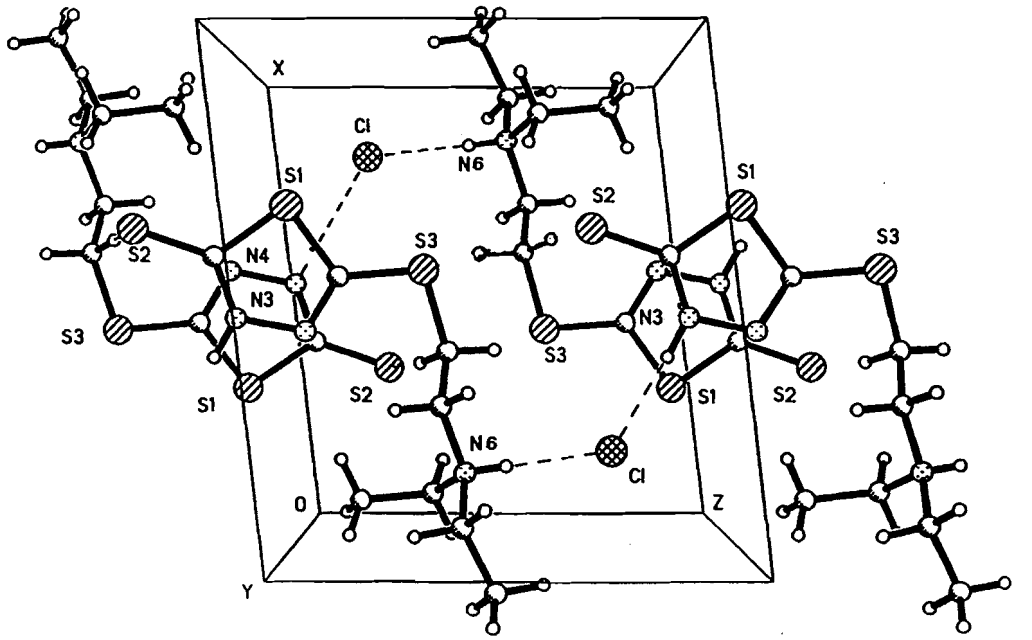

Fig. 9. Numérotation des atomes pour leur attribution en RMN du ^1H et du ^{13}C (les substituants R^1, R^2, R^3, R^4 ne sont pas mentionnés).

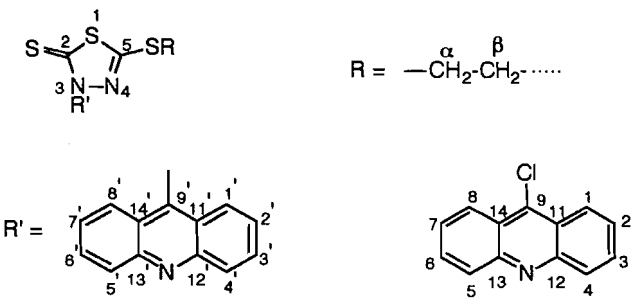

Tableau 1. Coordonnées atomiques fractionnaires ($\times 10^4$) et déviations standard.

Atome	*x/a*	*y/b*	*z/c*	U_{eq} (Å^2 × 10^2)
Cl	8028(1)	4113(1)	2608(1)	58(0.4)
S(2)	3563(1)	3633(1)	2503(1)	51(0.4)
S(1)	3124(1)	3613(1)	−862(1)	50(0.4)
S(3)	4391(1)	3691(1)	−3718(1)	47(0.4)
N(4)	5624(4)	3881(3)	−905(4)	46(1)
N(3)	5350(4)	3879(3)	557(4)	44(1)
N(6)	8423(4)	3673(3)	−4097(4)	42(1)
C(2)	4118(5)	3727(3)	843(5)	39(1)
C(5)	4529(4)	3751(3)	−1785(5)	40(1)
C(α)	6026(4)	4077(3)	−4025(5)	40(1)
C(β)	7083(5)	3359(3)	−3758(6)	46(1)
C(γ')	8910(5)	4512(4)	−3303(5)	50(1)
C(γ)	9415(6)	2917(4)	−3911(7)	71(2)
C(δ)	10730(5)	3126(5)	−4445(7)	80(2)
C(δ')	9063(6)	4452(5)	−1639(6)	82(2)

[a] $U_{eq} = (1/3)\Sigma_i\Sigma_j U_{ij} a_i^* a_j^* a_i a_j$.

Tableau 2. Longueurs de liaisons en Å et déviations standard.

S(2)—C(2)	1,667(5)	N(3)—C(2)	1,316(7)
S(1)—C(2)	1,737(4)	N(6)—C(β)	1,495(7)
S(1)—C(5)	1,738(5)	N(6)—C(γ')	1,501(7)
S(3)—C(5)	1,735(5)	N(6)—C(γ)	1,506(7)
S(3)—C(5)	1,735(5)	N(6)—C(γ)	1,512(6)
N(4)—N(3)	1,380(5)	C(γ)—C(δ')	1,493(7)
N(4)—C(5)	1,291(5)	C(γ)—C(δ)	1,495(8)

Partie expérimentale

Résonance magnétique nucléaire

La numérotation des atomes est donnée dans la figure 9. Les spectres ont été enregistrés à 20 ± 0,01°C sur un spectromètre Bruker AM 200. Les déplacements chimiques (δ ppm) ont été mesurés par rapport au tétraméthylsilane pris comme référence interne. Les constantes de couplage *J* sont exprimées en hertz.

Spectrophotométrie infrarouge

Les spectres, après pastillage à 1% dans KBr ou dissolution des produits dans la pyridine, ont été enregistrés à température ambiante sur un spectrophotomètre IRFT 57 Biorad.

Synthèses

Les analyses centésimales ont été réalisées dans le Service Commun de Microanalyse (Faculté des Sciences, Campus de St-Jérôme, Marseille) sur un autoanalyseur Technicon CHN.

3-Amino-9-chloroacridine 2d

On chauffe à reflux pendant 1 h 30, 2 g (9,5 mmol) de 3-amino-9-acridinone (15) dans 20 mL d'oxychlorure de phosphore. La solution est ensuite versée lentement dans un mélange ammoniaque – glace pilée. Le pH doit rester con-

Can. J. Chem. Downloaded from www.nrcresearchpress.com by 80.90.12.36 on 09/08/12
For personal use only.

Tableau 3. Angles de liaisons et angles de torsion en degrés et leurs déviations standard.

Angles de liaisons		Angles de torsion	
C(2)-S(1)-C(5)	89,9(2)	S(3)-C(α)-C(β)-N(6)	176,9(3)
C(5)-S(3)-C(α)	100,1(2)	N(4)-C(5)-S(3)-C(α)	−11,1(5)
N(3)-N(4)-C(5)	109,4(4)	C(5)-S(3)-C(α)-C(β)	79,9(4)
N(4)-N(3)-C(2)	119,4(4)	C(α)-C(β)-N(6)-C(γ′)	53,9(5)
C(β)-N(6)-C(γ′)	114,6(4)	C(α)-C(β)-N(6)-C(γ)	176,3(4)
C(β)-N(6)-C(γ)	110,0(4)	C(β)-N(6)-C(γ′)-C(δ′)	59,9(6)
C(γ′)-N(6)-C(γ)	113,9(4)	C(β)-N(6)-C(γ)-C(δ)	171,3(5)
S(2)-C(2)-S(1)	124,6(3)		
S(2)-C(2)-N(3)	128,1(4)		
S(1)-C(2)-N(3)	107,3(3)		
S(1)-C(5)-S(3)	120,4(3)		
S(1)-C(5)-N(4)	114,0(3)		
S(3)-C(5)-N(4)	125,7(4)		
S(3)-C(α)-C(β)	112,6(3)		
N(6)-C(β)-C(α)	112,2(4)		
N(6)-C(γ′)-C(δ′)	114,6(4)		
N(6)-C(γ)-C(δ)	114,0(5)		

Tableau 4. Caractéristiques géométriques des liaisons hydrogène et déviations standard.

Longueurs (Å)				Angles (deg)	
N(3)—H(3)	0,90(5)	H(3)—Cl	2,20(5)	N(3)-H(3)-Cl	177,2(5)
N(6)—H(6)	0,81(5)	H(6)—Cl	2,21(5)	N(6)-H(6)-Cl	175,6(5)

stamment basique. Le précipité formé est filtré, séché et rapidement repris par trois fois 750 mL d'éther éthylique chauffé à reflux. Les impuretés insolubles sont séparées par filtration et le filtrat éthéré est évaporé à sec. Rdt = 50%; F = 210–212°C (aiguilles oranges); RMN ^{1}H (DMSO-d_6) δ ppm : 6,38 (s, 2H), 6,98 (s, 1H), 7,28 (d, 1H, J = 9,3 Hz), 7,50 (m, 1H), 7,80 (m, 1H), 7,96 (d, 1H, J = 8,6 Hz), 8,41 (d, 1H, J = 9,3 Hz), 8,23 (d, 1H, J = 8,5 Hz); RMN ^{13}C (DMSO-d_6) δ ppm : 102,84 (C4), 117,83 (C11), 121,01 (C14), 122,76 (C2), 124,03 (C8), 124,46 et 124,87 (C1 et C7), 128,10 (C5), 130,19 (C6), 138,91 (C9), 148,68 (C13), 150,10 (C3 et C12). Anal. calc. pour $C_{13}H_9ClN_2$: C 68,27, H 3,93, N 12,25; trouvé : C 68,31; H 3,95; N 12,29%.

Préparation des composés ***3***

On chauffe à reflux sous agitation pendant 30 min, un mélange équimoléculaire de pyridine et de 2,5-dimercapto-1,3,4-thiadiazole dans du butanol normal. On rajoute un léger excès d'agent alkylant (1,2 pour 1). On laisse sous agitation et reflux pendant 1 nuit puis le mélange est placé au réfrigérateur. Le précipité formé est filtré, séché et recristallisé dans l'alcool éthylique absolu.

2-Mercapto-5-éthylthio-1,3,4-thiadiazole ***3***a : Rdt = 81%; F = 124°C (litt. (16, 17) : 125°C) (paillettes beiges brillantes); RMN ^{1}H (DMSO-d_6), δ ppm : 1,30 (t, 3H, J = 7,3 Hz), 3,12 (q, 2H, J = 7,3 Hz). Anal. calc. pour $C_4H_6N_2S_3$: C26,96; H 3,37; N 15,73; trouvé : C 26,98; H 3,35; N 15,68%.

Chlorhydrate du 2-mercapto-5-(2-diéthylaminoéthylthio)-1,3,4-thiadiazole ***3***b : Rdt = 88%; F = 186°C (litt. (7) : non exprimé) (paillettes blanches brillantes); IR (KBr) : 2998–2812, 1465 cm^{-1}; RMN ^{1}H (DMSO-d_6) δ ppm : 1,22 (t, 6H, J = 7,2 Hz), 3,20 (q, 4H, J = 7,2 Hz), 3,40 (m, 2H), 3,60 (m, 2H); RMN ^{13}C (DMSO-d_6) δ ppm : 8,32 (Cδ), 26,56 (Cα), 46,45 (Cγ), 49,53 (Cβ), 156,10 (C5), 187,93 (C2). RMN ^{13}C (pyridine-d_5) δ ppm : 9,19 (Cδ), 27,87 (Cα), 47,08 (Cγ), 50,49 (Cβ), 157,47 (C5), 189,62 (C2). Anal. calc. pour $C_8H_{16}ClN_3S_3$: C 33,62; H 5,60; N 14,71; trouvé : C 33,59; H 5,61; N 14,73%.

Préparation des composés ***4***a *et* ***4***b

On chauffe à 65°C sous agitation pendant 30 min une solution de sel dipotassique de 2,5-dimercapto-1,3,4-thiadazole (5 mmol) et d'agent alkylant (10 mmol) dans un mélange diméthylsulfoxyde–eau (50/50; V/V) en présence de carbonate de potassium (2 équivalents). Après refroidissement, on extrait par le chloroforme. La solution chloroformique est séchée sur sulfate de sodium anhydre, filtrée puis évaporée à sec. L'huile recueillie (base libre) est dissoute dans l'éther. Sous agitation, on rajoute de l'éther acide qui fait précipiter le dichlorhydrate. On le sépare par filtration. On le lave plusieurs fois à l'éther et on le garde 48 h au dessiccateur. La recristallisation des produits ainsi préparés n'est pas nécessaire.

2,5-Bis(diéthylaminoéthylthio)-1,3,4-thiadiazole ***4***a : Base libre : Rdt = 70%; huile jaune pâle. RMN ^{13}C ($CDCl_3$) δ ppm : 10,60 (Cδ et Cδ′), 30,45 (Cα et Cα′), 46,95 (Cγ et Cγ′), 51,25 (Cβ et Cβ′), 165,13 (C2 et C5). Dichlorhydrate : Rdt = 33%; F = 162–164°C (poudre blanche); RMN ^{1}H (D_2O) δ ppm : 1,20 (t, 12H, J = 7,3 Hz), 3,20 (q, 8H, J = 7,3 Hz), 3,50 (m, 8H). Anal. calc. pour $C_{14}H_{30}Cl_2N_4S_3$: C 39,90; H 7,12; N 13,30; trouvé : C 39,94; H 7,07; N 13,32%.

Can. J. Chem. Downloaded from www.nrcresearchpress.com by 80.90.12.36 on 09/08/12
For personal use only.

2,5-Bis(diméthylaminoéthylthio)-1,3,4-thiadiazole **4**b : Base libre : Rdt = 65%; huile jaune pâle. Dichlorhydrate : Rdt = 35%; *F* = 218–220°C (poudre blanche); RMN ^{1}H (DMSO-d_6) δ ppm : 2,73 (s, 12H), 3,36 (m, 4H), 3,65 (m, 4H). Anal. calc. pour $C_{10}H_{22}Cl_2N_4S_3$: C 32,87; H 6,02; N 15,34; trouvé : C 32,90; H 6,07; N 15,37%.

Préparation des composés **5**

On dissout 5 mmol de composé **3** sous forme de base dans 20 mL de méthanol anhydre. On rajoute goutte à goutte une quantité stoechiométrique de méthylate de sodium. Après 15 min d'agitation au bain-marie (90°C), on évapore à sec. Le résidu obtenu est trituré dans l'éther de pétrole. On recueille par filtration un précipité qui est séché. La recristallisation des produits ainsi préparés n'est pas nécessaire.

5-Éthylthio-1,3,4-thiadiazole-2-sulfure de sodium **5**a : Rdt = 89%; *F* = 188–190°C (poudre crayeuse blanche); RMN ^{1}H (D_2O) δ ppm : 1,20 (t, 3H, *J* = 7,3 Hz), 2,94 (q, 2H, *J* = 7,3 Hz); RMN ^{13}C (D_2O) δ ppm : 14,51 (Cβ), 29,68 (Cα), 163,79 (C5), 182,22 (C2). Anal. calc. pour $C_4H_5NaN_2S_3$: C 24,00; H 2,50; N 14,00; trouvé : C 24,05; H 2,53; N 14,04%.

5-Diéthylaminoéthylthio-1,3,4-thiadiazole-2-sulfure de sodium **5**b : Rdt = 90%; *F* = 64–66°C (poudre crayeuse blanche); RMN ^{1}H (D_2O) δ ppm : 0,92 (t, 6H, *J* = 7,2 Hz), 2,48 (q, 4H, *J* = 7,2 Hz), 2,72 (t, 2H, *J* = 6,4 Hz), 3,08 (t, 2H, *J* = 6,4 Hz); RMN ^{13}C (D_2O) δ ppm : 10,73 (Cδ), 31,18 (Cα), 46,92 (Cγ), 51,17 (Cβ), 162,62 (C5), 182,73 (C2). Anal. calc. pour $C_8H_{14}NaN_3S_3$: C 35,42; H 5,16; N 15,49; trouvé : C 35,45; H 5,19; N 15,54%.

2-(9′-Acridinylthio)-5-éthylthio-1,3,4-thiadiazole **6**

On chauffe à reflux sous agitation et sous courant d'azote pendant 30 min 200 mg (0,995 mmol) du sel de sodium du 2-mercapto-5-éthylthio-1,3,4-thiadiazole **5***a* dans 20 mL de pyridine anhydre. On ajoute par petites portions 210 mg (0,995 mmol) de 9-chloroacridine **2***a* et on maintient le reflux pendant 3 h. Le précipité obtenu est filtré et lavé à l'eau. Rdt = 71%; *F* = 138–140°C; RMN ^{1}H ($CDCl_3$) δ ppm : 1,33 (t, 3H, *J* = 7,3 Hz), 3,14 (q, 2H, *J* = 7,3 Hz), 7,67 (m, 2H), 7,84 (m, 2H), 8,31 (dd, 2H, *J* = 8,7 Hz), 8,70 (dd, 2H, *J* = 8,7 Hz); RMN ^{13}C ($CDCl_3$) δ ppm : 14,42 (Cβ), 28,53 (Cα), 125,80 (C3′ et C6′), 128, 26 (C2′ et C7′), 130,51 (C1′ et C8′), 130,61 (C4′ et C5′), 135,54 (C9′), 149,21 (C12′ et C13′), 164,08 (C5), 166,96 (C2); C (11′) et C (14′) ne sont pas observables. Anal. calc. pour $C_{17}H_{13}N_3S_3$: C 57,46; H 3,66; N 11,83; trouvé : C 57,49; H 3,68; N 11,87%.

Préparation des composés **7**b, **7**c, **7**e, **7**h, **7**j, **7**m

On porte à reflux sous agitation et sous courant d'azote une solution de composé **3** dans la pyridine anhydre. On ajoute 1/4 d'équivalent d'hydrure de sodium. Au bout de 30 min, on rajoute par petites portions une quantité équimoléculaire d'agent d'alkylant. On maintient le reflux pendant 5 h. Le mélange refroidi est versé dans l'eau. Le précipité formé résultant est filtré, lavé à l'eau et séché avant d'être recristallisé dans un solvant approprié précisé ci-dessous pour chaque composé après le rendement.

*2-Thione-3(*N*)-(2′-nitro)-9′-acridinyl]-5-éthylthio-1,3,4-thiadiazole* **7**b : Rdt = 65% (éther éthylique – chloroforme); *F* = 204–206°C (poudre jaune clair); RMN ^{1}H ($CDCl_3$) δ ppm : 1,45 (t, 3H, *J* = 7,4 Hz), 3,21 (q, 2H, *J* = 7,4 Hz), 7,80 (m, 2H), 8,00 (m, 1H), 8,57 (m, 3H), 8,76 (d, 1H, *J* = 2,2 Hz); RMN ^{13}C ($CDCl_3$) δ ppm : 14,56 (Cβ), 28,34 (Cα), 120,84 (C3′), 121,14 (C14′), 123,25 (C8′), 123,35 (C11′), 123,46 (C5′), 129,25 (C7′), 130,68 (C4′), 132,59 (C1′), 132,75 (C6′), 142,89 (C9′), 146,16 (C13′), 149,70 (C12′), 152,18 (C2′), 159,35 (C5), 188,11 (C2). Anal. calc. pour $C_{17}H_{12}N_4O_2S_3$: C 51,00; H 3,00; N 14,00; trouvé : C 51,05; H 2,98; N 14,08%.

*2-Thione-3(*N*)-[(3′-nitro)-9′-acridinyl]-5-éthylthio-1,3,4-thiadiazole* **7**c : Rdt = 38% (éther éthylique – chloroforme); *F* = 188–190°C (poudre rose orange); RMN ^{1}H ($CDCl_3$) δ ppm : 1,40 (t, 3H, *J* = 7,3 Hz), 3,17 (q, 2H, *J* = 7,3 Hz), 7,76 (m, 2H), 7,92 (m, 2H), 8,32–8,42 (m, 2H), 9,28 (d, 1H, *J* = 2 Hz); RMN ^{13}C ($CDCl_3$) δ ppm : 14,24 (Cβ), 27,98 (Cα), 120,64 (C2′), 123,05 (C8′), 124,02 (C14′), 124,53 (C11′), 125,28 (C1′), 127,18 (C4′), 129,93 (C7′), 130,89 (C5′), 131,91 (C6′), 140,42 (C9′), 148,08 (C13′), 148,80 (C3′), 151,66 (C12′), 158,98 (C5), 187,90 (C2). Anal. calc. pour $C_{17}H_{12}N_4O_2S_3$: C 51,00; H 3,00; N 14,00; trouvé : C 51,04; H 3,03; N 14,05%.

*2-Thione-3(*N*)-[(4′-nitro)-9′-acridinyl]-5-éthylthio-1,3,4-thiadiazole* **7**e : Rdt = 54% (éther éthylique – chloroforme); *F* = 232–234°C (poudre beige); RMN ^{1}H ($CDCl_3$) δ ppm : 1,39 (t, 3H, *J* = 7,3 Hz), 3,15 (q, 2H, *J* = 7,3 Hz), 7,71 (m, 3H), 7,96 (m, 2H) 8,16 (dd, 1H, *J* = 7,1 Hz), 8,38 (dd, 1H, *J* = 8,8 Hz); RMN ^{13}C ($CDCl_3$) δ ppm : 14,21 (Cβ), 27,95 (Cα), 119,82 (C12′), 122,87 (C8′), 123,38 (C14′), 124,32 (C2′), 125,65 (C1′), 127,07 (C7′), 129,42 (C3′), 131,11 (C5′), 131,59 (C11′), 132,00 (C6′), 140,61 (C9′), 148,97 (C4′), 150,97 (C13′), 158,79 (C5), 187,90 (C2). Anal. calc. pour $C_{17}H_{12}N_4O_2S_3$: C 51,00; H 3,00; N 14,00; trouvé : C 50,94; H 3,04; N 14,06%.

*2-Thione-3(*N*)-[(2′-nitro)-9′-acridinyl]-5-diéthylaminoéthylthio-1,3,4-thiadiazole* **7**h : Rdt = 43% (éther éthylique); *F* = 98–100°C (poudre jaune); RMN ^{1}H ($CDCl_3$) δ ppm : 0,97 (t, 6H, *J* = 7,2 Hz), 2,54 (q, 4H, *J* = 7,2 Hz), 2,83 (t, 2H, *J* = 6,9 Hz), 3,32 (t, 2H, *J* = 6,9 Hz), 7,80 (m, 2H), 8,02 (m, 2H), 8,58 (m, 2H), 8,77 (d, 1H, *J* = 2,2 Hz). Anal. calc. pour $C_{21}H_{21}N_5O_2S_3$: C 53,50; H 4,54; N 14,86; trouvé : C 53,53; H 4,55; N 14,90%.

*2-Thione-3(*N*)-[(3′-nitro)-9′-acridinyl]-5-diéthylaminoéthylthio-1,3,4-thiadiazole* **7**j : Rdt = 74% (éther éthylique); *F* = 106–108°C (poudre jaune); RMN ^{1}H ($CDCl_3$) δ ppm : 0,92 (t, 6H, *J* = 7,1 Hz), 2,48 (q, 4H, *J* = 7,1 Hz), 2,77 (t, 2H, *J* = 6,8 Hz), 3,26 (t, 2H, *J* = 6,8 Hz), 7,92–7,75 (m, 2H), 7,96 (m, 2H), 8,33–8,43 (m, 2H), 9,29 (d, 1H, *J* = 2,1 Hz); RMN ^{13}C ($CDCl_3$) δ ppm : 11,83 (Cδ), 32,65 (Cα), 47,04 (Cγ), 51,08 (Cβ), 120,65 (C2′), 123,14 (C8′), 123,50 (C14′), 124,54 (C11′), 125,36 (C1′), 127,21 (C4′), 129,86 (C7′), 130,94 (C5′), 131,88 (C6′), 140,52 (C9′), 148,14 (C12′), 148,88 (C3′), 151,71 (C13′), 159,90 (C5), 188,03 (C2). Anal. calc. pour $C_{21}H_{21}N_5O_2S_3$: C53,50; H 4,54; N 14,86; trouvé : C 53,54; H 4,56; N 14,89%.

*2-Thione-3(*N*)-[(4′-nitro)-9′-acridinyl]-5-diéthylaminoéthylthio-1,3,4-thiadiazole* **7**m : Rdt = 22% (éther éthylique); *F* =

Can. J. Chem. Downloaded from www.nrcresearchpress.com by 80.90.12.36 on 09/08/12
For personal use only.

140–142°C (poudre orange); RMN ^{1}H ($CDCl_3$) δ ppm : 0,91 (t, 6H, J = 7,1 Hz), 2,48 (q, 4H, J = 7,1 Hz), 2,76 (t, 2H, J = 6,8 Hz), 3,25 (t, 2H, J = 6,8 Hz), 7,70 (m, 3H), 7,92 (m, 2H), 8,12 (dd, 1H, J = 7,2 Hz), 8,37 (dd, 1H, J = 8,8 Hz); RMN ^{13}C ($CDCl_3$) δ ppm : 11,82 (Cδ), 32,65 (Cα), 47,03 (Cγ), 51,08 (Cβ), 119,85 (C12′), 122,95 (C8′), 123,36 (C14′), 124,35 (C2′), 125,61 (C1′), 127,16 (C7′), 129,38 (C3′), 131,12 (C5′), 131,59 (C11′), 132,00 (C6′), 140,63 (C9′), 148,95 (C4′), 150,97 (C13′), 159,80 (C5), 187,89 (C2). Anal. calc. pour $C_{21}H_{21}N_5O_2S_3$: C 53,50; H 4,54; N 14,86; trouvé : C 53,57; H 4,59; N 14,89%.

Préparation des composés 7a, 7f, 7g, 7n
On procède comme avec les composés de type **7** précédents mais sans addition d'hydrure de sodium.

*2-Thione-3(*N*)-9′-(acridinyl)-5-éthylthio-1,3,4-thiadiazole* 7a : Rdt = 79% (alcool éthylique); F = 222–224°C (poudre jaune pâle); RMN ^{1}H ($CDCl_3$) δ ppm : 1,38 (q, 3H, J = 7,3 Hz), 3,14 (t, 2H, J = 7,3 Hz), 7,59–7,89 (m, 6H), 8,35 (d, 2H, J = 8,8 Hz); RMN ^{13}C ($CDCl_3$) δ ppm : 14,24 (Cβ), 27,93 (Cα), 122,50 (C11′ et C14′), 122,80 (C3′ et C6′), 127,94 (C2′ et C7′), 130,45 (C1′ et C8′), 130,58 (C5′ et C4′), 139,75 (C9′), 149,91 (C12′ et C13′), 158,07 (C5), 187,76 (C2). Anal. calc. pour $C_{17}H_{13}N_3S_3$: C 57,46; H 3,66; N 11,83; trouvé : C 57,44; H 3,65; N 11,81%.

*2-Thione-3(*N*)-[(2′-méthoxy-6′-chloro)-9′-acridinyl)-5-éthylthio-1,3,4-thiadiazole* 7f : Rdt = 51% (alcool éthylique); F = 232–234°C (poudre jaune); RMN ^{1}H (acide trifluoroacétique, deutérié) δ ppm : 1,48 (t, 3H), 3,39 (q, 2H), 4,10 (s, 3H), 7,22 (s, 1H), 8,05 (m, 3H), 8,45 (m, 2H); RMN ^{13}C (ATFA-*d*) δ ppm : 14,63 (Cβ), 29,65 (Cα), 102,02 (C1′), 120,83 (C4′), 123,53 (C5′), 124,71 (C14′), 127,49 (C3′), 127,88 (C11′), 134,12 (C8′ ou C12′), 137,08 (C12′ ou C8′), 137,10 (C7′), 140,90 (C13′), 140,95 (C6′), 147,55 (C9′), 149,57 (C5), 166,11 (C2′), 191,62 (C2). Anal. calc. pour $C_{18}H_{14}Cl\,N_3OS_3$: C 51,48; H 3,33; N 10,01; trouvé : C 51,51; H 3,32; N 10,05%.

*2-Thione-3(*N*)-(9′-acridinyl)-5-diéthylaminoéthylthio-1,3,4-thiadiazole* 7g : Rdt = 75% (alcool éthylique); F = 178–180°C (poudre jaune vert); RMN ^{1}H ($CDCl_3$) δ ppm : 0,86 (t, 6H, J = 7,1 Hz), 2,45 (q, 4H, J = 7,1 Hz), 2,76 (t, 2H, J = 6,9 Hz), 3,24 (t, 2H, J = 6,9 Hz), 7,85–7,57 (m, 6H), 8,32 (d, 2H, J = 8,7 Hz); RMN ^{13}C ($CDCl_3$) δ ppm : 11,38 (Cδ), 31,78 (Cα), 46,81 (Cγ), 50,81 (Cβ), 122,47 (C11′ et C14′), 122,74 (C3′ et C6′), 127,84 (C2′ et C7′), 130,26 (C1′ et C8′), 130,52 (C4′ et C5′), 139,68 (C9′), 149,75 (C12′ et C13′), 158,72 (C5), 187,65 (C2). Anal. calc. pour $C_{21}H_{22}N_4S_3$: C 59,15; H 5,16; N 13,14; trouvé : C 59,14; H 5,18; N 13,17%.

*2-Thione-3(*N*)-[(2′-méthoxy-6′-chloro)-9′-acridinyl]-5-diéthylaminoéthylthio-1,3,4-thiadiazole* 7n : Rdt = 40% (éther éthylique – éther de pétrole); F = 112–114°C (poudre jaune orange); RMN ^{1}H (ATFA-*d*) δ ppm : 1,56 (signal mal résolu, 6H), 3,58 (smr, 4H), 3,94 (m, 4H), 4,37 (s, 3H), 7,50 (d, 1H, J = 1,9 Hz), 8,25–8,39 (m, 3H), 8,76 (m, 2H). Anal. calc. pour $C_{22}H_{23}Cl\,N_4OS_3$: C 53,82; H 4,68; N 11,41; trouvé : C 53,86; H 4,71; N 11,46%.

Préparation des composés 7d *et* 7k
On chauffe 30 min à reflux sous agitation et sous courant d'azote une solution de composé **3** dans la pyridine anhydre. On ajoute alors par petites portions un équivalent d'agent alkylant. On maintient le reflux pendant encore 5 h. Le mélange est ensuite refroidi et versé dans de l'éther éthylique. Il se forme un fin précipité qui est filtré et séché. On le reprend par un minimum d'eau et on alcalinise le milieu. On filtre, on lave à l'eau et on sèche le produit qui est recristallisé dans un solvant approprié précisé ci-dessous pour chaque composé après le rendement.

*2-Thione-3(*N*)-[(3′-amino)-9′-acridinyl]-5-éthylthio-1,3,4-thiadiazole* 7d : Rdt = 18% (éthanol absolu); F = 152–154°C (déc.) (poudre rouge); RMN ^{1}H ($CDCl_3$) δ ppm : 1,38 (t, 3H, J = 7,3 Hz), 3,15 (q, 2H, J = 7,3 Hz), 5,18 (s, 2H), 7,15 (d, 1H, J = 8,8 Hz), 7,35 (s, 1H), 7,40–7,60 (m, 3H), 7,77 (m, 1H), 8,29 (d, 1H, J = 8,8 Hz). Anal. calc. pour $C_{17}H_{14}N_4S_3$: C 55,13; H 3,78; N 15,13; trouvé : C 55,18; H 3,82; N 15,19%.

*2-Thione-3(*N*)-[(3′-amino)-9′-acridinyl]-5-diéthylaminoéthylthio-1,3,4-thiadiazole* 7k : Rdt = 14% (éthanol absolu); F = 138–140°C (déc.) (poudre ocre); RMN ^{1}H ($CDCl_3$) δ ppm : 0,90 (t, 6H, J = 7,1 Hz), 2,46 (q, 4H, J = 7,1 Hz), 2,75 (t, 2H, J = 6,8 Hz), 3,23 (t, 2H, J = 6,8 Hz), 4,38 (s, 2H), 7,10 (dd, 1H, J = 8,7 et 2,1 Hz), 7,35 (d, 1H, J = 2,1 Hz), 7,42–7,58 (m, 3H), 7,72 (m, 1H), 8,16 (d, 1H, J = 8,7 Hz); RMN ^{13}C ($CDCl_3$) δ ppm : 11,76 (Cδ), 32,22 (Cα), 46,83 (Cγ), 50,74 (Cβ), 106,37 (C4′), 117,69 (C11′), 120,48 (C14′), 122,57 (C8′), 122,82 (C2′), 124,11 (C1′), 125,83 (C7′), 129,17 (C5′), 130,51 (C6′), 139,59 (C9′), 148,66 (C13′), 150,26 (C3′), 151,72 (C12′), 158,89 (C5), 187,63 (C2). Anal. calc. pour $C_{21}H_{23}N_5S_3$: C 57,14; H 5,21; N 15,87; trouvé : C 57,09; H 5,23; N 15,93%.

Radiocristallographie
Le composé **3***b* a été recristallisé dans l'éthanol absolu. La détermination de la maille et l'enregistrement des intensités diffractées ont été effectués sur un diffractomètre 4 cercles KM4 (Kuma Diffraction, Wroclaw, Poland) à monochromateur au graphite pour λ (Cu) = 1,541 78 Å. Le groupe spatial et les dimensions de la maille ont été obtenues au moyen d'un ajustement par la méthode des moindres carrés à partir des positions angulaires de 25 réflexions.

On a utilisé la technique de balayage θ–2θ. On a réalisé des contrôles d'intensité toutes les 100 mesures. Les variations d'intensité se sont avérées être non significatives. Les intensités mesurées n'ont pas été corrigées pour l'absorption. On a mesuré 3040 réflexions (2787 réflexions uniques) dont 1950 respectant le critère $F > 4\sigma(F)$. Pour calculer $\sigma(F)$, on a utilisé la formule : $\sigma(F) = \sigma(F^2)/(2F^2)$ pour $F^2 > \sigma(F^2)$ et $\sigma(F) = 0{,}5\sqrt{\sigma(F^2)}$ pour $F^2 < \sigma(F^2)$.

La structure a été déterminée par méthode directe[3] avec $R(E)$ = 0,21. Les atomes d'hydrogène ont tous été localisés sur les cartes de Fourier-différences. Seuls les hydrogènes des atomes d'azote ont été inclus dans les derniers cycles d'affinement qui ont eu lieu en matrice entière tandis que les autres ont été aussi inclus dans les premiers cycles. On a affecté à tous les atomes des coefficients d'agitation thermique anisotrope à l'exception des atomes d'hydrogène pour lesquels on a utilisé un facteur d'agitation thermique isotrope correspondant à 1,5

3 G.M. Sheldrick. SHELXTL PC, Siemens Anal. X-Ray Inst. Inc. (1990).

Tableau 5. Données cristallographiques.

Formule	$C_8H_{16}N_3S_3Cl$
Dimensions du cristal, mm	0,2 × 0,2 × 0,4
Densité calculée, D_c, g cm^{-3}	1,405
Masse moléculaire relative, M_r	285, 87
Système cristallin	Monoclinique
Groupe d'espace	$P2_1/C$
Dimensions de la maille, a, Å	10,060(1)
b, Å	15,003(4)
c, Å	9,021(4)
β, deg	97,03(3)
Volume de la maille, Å^3	1351,39(5)
Nombre de molécules par maille, Z	4
μ (Cu Kα), mm^{-1}	6,63
F(000)	600
Coefficient de correction d'extinction empirique, g	0,017
Limites angulaires en θ	10 et 60
Limites d'enregistrements	h, −12 à +12; k, 0 à 19; l, 0 à 11
Nombre total de mesures	3040
Nombre total de mesures uniques	2787
Nombre de mesures avec $F > 4\sigma(F)$ utilisées pour la résolution et les affinements	1950
Facteur d'accord sur toutes les intensités mesurées, R(int)	0,035
Limite de rejet des pics de densité électronique en Fourier-différence,	
$(\Delta\rho)_{max}$ en e Å^{-3}	0,75
$(\Delta\rho)_{min}$ en e Å^{-3}	−0,43
Facteur d'accord, R	0,057
Facteur d'accord pondéré, R_w	0,058
Variation sur erreur maximum, $(\lvert\Delta/\sigma\rvert)_{max}$	<0,01
Erreur sur une observation de poids unitaire, S	4,45

fois le facteur thermique des atomes porteurs. La fonction à minimiser est $\Sigma w(|F_o| - |F_c|)^2$. Le facteur d'accord R et le facteur d'accord pondéré Rw sont donnés par : $R = \Sigma||F_o| - |F_c||/\Sigma F_o$ et $R_w = \Sigma\sqrt{w}||F_o| - |F_c||/\Sigma\sqrt{w}F_o$. Dans ces expressions $w = 1{,}0/\sigma^2$ (F_o). L'erreur sur une observation de poids unitaire est donnée par : $S = [\Sigma w(|F_o| - |F_c|)^2/(m - n)]^{1/2}$ avec m = nombre de réflexions utilisées et n = nombre de paramètres affinés.

L'enregistrement des intensités diffractées et les calculs ont été réalisés dans le Département de Cristallographie de l'Université Technologique de Lodz. Les données cristallographiques sont précisées dans le tableau 5.[4]

Remerciement

Ce travail a été réalisé dans le cadre du Programme Européen COST 815.

Bibliographie

1. A. Osuna, L.M. Ruiz-Perez, F. Gamarro, J.I. Rodriguez-Santiago, S. Castanys, D. Sharples, A.M. Galy, G. Giovannangeli, J.P. Galy, J.C. Soyfer et J. Barbe. Chemotherapy, **34**, 127 (1988).
2. H. Berny, N. Bsiri, J.J. Charbit, A.M. Galy, J.C. Soyfer, J.P. Galy, J. Barbe, D. Sharples, C.M. Mesa-Valle, C. Mascaro et A. Osuna. Arzneimit.-Forsch. **42**, 674 (1992).
3. B.P. Das, R.A. Wallace et D.W. Boykin. J. Med. Chem. **23**, 578 (1983).
4. J. Sandstrom. J. Heterocycl. Chem. **9**, 165 (1968).
5. S. Pappalardo, F. Bottino et C. Tringali. J. Org. Chem. **52**, 405 (1987).
6. G.D. Thorn. Can. J. Chem. **38**, 1439 (1960).
7. N. Inoue, T. Kojima, T. Heki et S. Hirano. Eur. Pat. Appl. 0249,239 (1987).
8. F. Bottino et S. Pappalardo. Org. Magn. Reson. **16**, 1 (1981).
9. L.E. Begin et J.E. Dunbar. U.S. Patent 4,074,049 (1978).
10. J. Chatt, L.A. Duncanson et L.M. Venanzi. Suom. Kemistil. B, **29**, 75 (1956).
11. H.M. Randall, R.G. Fowler, N. Fuson et J.R. Dangl. Infrared determination of organic structure. D. Van Nostrand, New-York. 1949.
12. B. Stanovnik et M. Tisler. Croat. Chem. Acta, **37**, 17 (1965).
13. R. Faure, J.P. Galy, E.J. Vincent, A.M. Galy, J. Barbe et J. Elguero. Spectrosc. Lett. **16**, 431 (1983).
14. J.W. Bats. Acta Crystallogr. Sect. B: Struct. Crystallogr. Cryst. Chem. **B32**, 2866 (1976).
15. A. Albert. The acridines. 2^e ed. Edward Arnold Publ., London. 1966.
16. J. Sandstrom. Ark. Kemi, **4**, 297 (1951).
17. M. Sidky, M. Mahran, M. Zayed, W. Abou et T. Hafez. Org. Prep. Proc. Int. **14**, 225 (1982).

4 Série complète de coordonnées atomiques fractionnaires et facteurs de température anisotropes peut être achetée au : Dépôt des données non publiées, Service de fourniture de documents, ICIST, Conseil national de recherches Canada, Ottawa, Canada K1A 0S2. Les facteurs de structure observés et calculés sont disponibles auprès de l'auteur correspondant.

Le tableau de coordonnées atomiques fractionnaires a aussi été déposé au Cambridge Crystallographic Data Centre, University Chemical Laboratory, 12 Union Road, Cambridge, CB2 1EZ, U.K.

Can. J. Chem. Downloaded from www.nrcresearchpress.com by 80.90.12.36 on 09/08/12
For personal use only.

Évaluation des ruptures de liaison α(C—H) centrale et terminale dans la photolyse du propène gazeux à 184,9 nm

George R. De Maré, Guy J. Collin et Hélène Deslauriers

Résumé : Nous avons repris l'étude de la photochimie du propène gazeux dans la région de l'ultraviolet lointain (λ = 184,9 nm) dans le but explicite d'apprécier les rendements quantiques des réactions de scission des liaisons α(C—H) situées de part et d'autre de la liaison double. Alors que les réactions de rupture des liaisons β(C—H) et α(C—C) sont de loin les réactions les plus importantes et constituent probablement plus de 95% des fragmentations de la molécule photoexcitée, la somme des rendements quantiques des réactions de scission α(C—H) est de l'ordre de 0,03 avec un avantage marqué (4 pour 1, comparé à 1 pour 2 statistiquement) pour la rupture de la liaison C—H centrale : ϕ(H secondaire) = 0,02 ± 0,01 et ϕ(H primaire) = 0,005 ± 0,003. L'énergie de la liaison qui se rompt est donc un facteur déterminant bien que l'énergie photonique soit nettement supérieure à celle nécessaire pour rompre ces liaisons. Les paramètres géométriques, l'énergie totale et les fréquences des modes normaux des radicaux *cis*- et *trans*-propèn-1-yle et propèn-2-yle ont été déterminés en utilisant des méthodes *ab initio* à plusieurs niveaux de théorie (bases STO-3G, 3-21G, 6-31G, 6-31G* et 6-31G**; méthodes UHF, ROHF et GVB). On trouve que le *cis*-propèn-1-yle est plus bas en énergie (0,6–1,0 kJ mol^{-1}) que le *trans*-propèn-1-yle, sauf avec la base minimale STO-3G. Les calculs prédisent que le propèn-2-yle est 14 ± 3 kJ mol^{-1} plus stable que les radicaux *cis*- et *trans*-propèn-1-yle.

Mots clés : propène, réactions unimoléculaires, photochimie, scission α(C—H), radicaux propènyles.

Abstract: The minor, α(C—H) photofragmentation processes in the far-UV photolysis of gaseous propene at λ = 184.9 nm are investigated. At this wavelength the β(C—H) and α(C—C) photofragmentation processes are of major importance, accounting for more than 95% of the primary reaction process. The total quantum yield of the three α(C—H) bond cleavage processes is close to 0.03. However ϕ(H secondary) = 0.02 ± 0.01 and the sum of the two ϕ(H primary) cleavages is 0.005 ± 0.003. Thus ϕ(H secondary)/ϕ(H primary) ≅ 4:1 whereas statistically one expects 1:2. Thus the energy of the bond that is breaking is important, even though the photon energy is much higher than that required to break it. The geometrical parameters, total energies, and fundamental frequencies of the *cis*- and *trans*-propen-1-yl and propen-2-yl radicals have been determined by *ab initio* methods at various levels of theory (STO-3G, 3-21G, 6-31G, 6-31G*, and 6-31G** basis sets; UHF, ROHF, and GVB methods). *cis*-Propen-1-yl is predicted to be 0.6–1.0 kJ mol^{-1} lower in energy than *trans*-propen-1-yl, except with the minimal STO-3G basis set. The optimizations predict that propen-2-yl is more stable than the *cis*- and *trans*-propen-1-yl radicals by 14 ± 3 kJ mol^{-1}.

Key words: propene, unimolecular reactions, photochemistry, α(C—H) cleavage, propenyl radicals.

1. Introduction

Il est bien connu que lors de la photolyse directe du propène (**M**) en phase gazeuse les réactions primaires principalement observées sont les scissions des liaisons β(C—H) et α(C—C) de la molécule photoexcitée (**M****) (1–3). Ces deux réactions produisent respectivement le radical allyle et un atome d'hydrogène d'une part et les radicaux méthyle et vinyle d'autre part :

[1] $\mathbf{M} + h\nu \rightarrow \mathbf{M}^{**}$

[2] $\mathbf{M}^{**} \rightarrow (\overline{CH_2—CH—CH_2})^* + \dot{H}$

[3] $\mathbf{M}^{**} \rightarrow (CH_2{=}\dot{C}H)^* + \dot{C}H_3$

Les espèces radicalaires R* correspondent à des entités ayant une énergie interne suffisante et sont susceptibles de se fragmenter :

[4] $(\overline{CH_2—CH—CH_2})^* \rightarrow CH_2{=}C{=}CH_2 + \dot{H}$

[5] $(CH_2{=}\dot{C}H)^* \rightarrow C_2H_2 + \dot{H}$

Ces deux dernières réactions sont en compétition avec les

Reçu le 5 janvier 1995.

G.R. De Maré.[1] Laboratoire de chimie physique moléculaire, Faculté des sciences, CP. 160/09, Université Libre de Bruxelles, av. F.D. Roosevelt 50, B-1050 Bruxelles, Belgique.
G.J. Collin et H. Deslauriers. Département des sciences fondamentales, Université du Québec à Chicoutimi, Chicoutimi, QC G7H 2B1, Canada.

1. Auteur correspondant. Téléphone : 32-2-650-4088. Fax : 32-2-650-4232. Courrier électronique (e-mail) : gdemare@ulb.ac.be

Can. J. Chem. Downloaded from www.nrcresearchpress.com by 80.90.12.36 on 09/08/12
For personal use only.

Schéma 1.

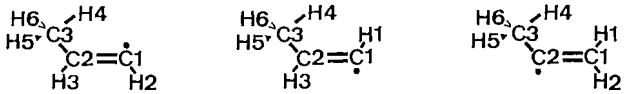

1 : *cis*-propèn-1-yle **2** : *trans*-propèn-1-yle **3** : propèn-2-yle

réactions de stabilisation par collision et sont donc observées à basse pression. Les rendements quantiques des processus primaires [2] et [3] à 184,9 nm ont été évalués respectivement à 0,63 et 0,36 ce qui, ajouté à d'autres processus primaires de plus faible importance, conduisait à un rendement quantique total de fragmentation de la molécule photoexcitée égal à 1,07 ± 0,10 (1), laissant ainsi peu de place à d'autres processus de fragmentation ou de désactivation.

Nous avons repris cette étude afin d'évaluer spécifiquement les rendements quantiques des réactions de fragmentation de type α(C—H) :

[6] $\mathbf{M}^{**} \rightarrow (CH_3—CH{=}\dot{C}H)^* + \dot{H}$

où les radicaux $(CH_3—CH{=}\dot{C}H)^*$ peuvent avoir la geométrie *cis* (**1**) ou *trans* (**2**)) (voir le Schéma 1 ci-dessus) et

[7] $\mathbf{M}^{**} \rightarrow (CH_3—\dot{C}{=}CH_2)^*(\mathbf{3}) + \dot{H}$

Les réactions déjà identifiés dans la photolyse de **M** indiquent la présence de radicaux libres thermalisés (incapables de se fragmenter dans toutes les conditions utilisées) et excités (capables de se fragmenter éventuellement à basse pression) (1). On a déjà établi que l'on pouvait considérer les rendements des radicaux allyles (ϕ = 0,62 ± 0,05) et méthyles (ϕ = 0,36 ± 0,03) ainsi que celui des atomes d'hydrogène (ϕ = 0,63 ± 0,05) indépendants de la pression totale entre 0 et 120 Torr (0 et 16 000 N m^{-2}). Les atomes d'hydrogène s'additionnent rapidement sur la double liaison de **M** en formant des radicaux isopropyles (4, 5) :

[8] $\dot{H} + \mathbf{M} \rightarrow CH_3—\dot{C}H—CH_3$

Il s'ensuit que les principales réactions secondaires sont les combinaisons (réactions [9]–[14]) et dismutations des radicaux.

[9] $2CH_3—\dot{C}H—CH_3 \rightarrow$ 2,3-diméthylbutane

[10] $2\overline{CH_2—CH—CH_2} \rightarrow$ hexa-1,5-diène

[11] $2\dot{C}H_3 \rightarrow$ éthane

[12] $CH_3—\dot{C}H—CH_3 + \overline{CH_2—CH—CH_2} \rightarrow$ 4-méthylpent-1-ène

[13] $CH_3—\dot{C}H—CH_3 + \dot{C}H_3 \rightarrow$ isobutane

[14] $\overline{CH_2—CH—CH_2} + \dot{C}H_3 \rightarrow$ but-1-ène

Nous négligerons les réactions de dismutation car les réactions mettant en jeu au moins un radical insaturé comptent en général moins de 10% de dismutation par rapport à la combinaison (5, 6). Pour la même raison on a également négligé les réactions d'addition de l'atome d'hydrogène sur le carbone centrale de **M** produisant ainsi quelques radicaux propyles primaires (4). Il faut enfin ajouter à ce tableau les réactions des radicaux vinyles thermalisés également répertoriés et mesurés dans ce système : $\phi(CH_2{=}\dot{C}H) = 0,10$ (1).

Dans la photolyse directe des but-2-ènes à λ = 184,9 nm, il a été démontré que des radicaux C_3H_5 (structure **1** et (ou) **2**) sont formés par scission d'une liaison α(C—C), réaction en compétition avec la rupture d'une liaison β(C—H) (7).[2] On aurait pu s'attendre à ce que les rapports des rendements des ruptures α(C—C)/β(C—H) soient, sinon identiques, au moins très voisins l'un de l'autre, pour les photolyses directes des isomères géométriques du but-2-ène. En fait ces rapports sont assez différents : α(C—C)/β(C—H) = 0,95 et 1,34 pour le *cis*- et le *trans*-but-2-ène, respectivement (7). Nous avons donc entrepris, en parallèle à l'étude expérimentale de la photolyse de **M**, une étude théorique des chemins réactionnels conduisant aux radicaux **1**, **2** et **3** (8).

2. Méthode

2.1 Expérimentale

Le produit **M** (Matheson, Canada) utilisé est de très haute pureté : l'analyse par chromatographie en phase gazeuse montre seulement la présence de traces de propane (160 ppm), de but-1-ène + isobutène + buta-1,3-diène (25 ± 3 ppm) et de butane normal (12 ± 3 ppm). L'hexafluorure de soufre (Merck, Sharp et Dohme, Canada) à un pureté nominale de 99,99%. Il a été utilisé tel que reçu.

Les photolyses ont été réalisées dans un appareil sans trace de mercure avec une lampe au mercure «basse pression», de telle sorte que seule la raie de résonance située à 184,9 nm est active. Les analyses chromatographiques ont été réalisées sur trois colonnes remplies (Ucon, Durapak et squalane) qui ont été décrites précédemment (1). L'actinométrie a été réalisée par comparaison en photolysant de l'éthylène dans les mêmes conditions (9). Les temps d'irradiation utilisés, combinés avec l'intensité de la lampe, ont produit un taux de transformation de **M** situé entre 0,1 et 4% dépendant de la pression. On n'a pas observé de variations significatives des rendements quantiques avec la variation du taux de conversion.

2.2 Théorique

Les optimisations de géométrie *ab initio* ont été effectués avec le programme MONSTERGAUSS (10) sur le Cray Y-MP2E/116 au Centre de Calcul «Université Libre de Bruxelles/Vrije Universiteit Brussel» en utilisant les bases classiques STO-3G (11), 3-21G (12), 6-31G (13), 6-31G* (14) et 6-31G** (14). Les minima d'énergie ont été localisés avec la technique OC (optimally conditioned variable-metric gradient minimization technique (15)).

Les méthodes UHF (Unrestricted Hartree–Fock (16)), ROHF (Restricted Open-Shell Hartree–Fock (17)) et GVB (Generalized Valence Bond (18)) ont été utilisées. Dans les calculs GVB(X) la valeur de X donne le nombre d'orbitales de valence, doublement occupées, qui sont couplées chacune à l'orbitale virtuelle correspondante dans le concept de «perfect pairing» (18).

Les fréquences des modes normaux de vibration ont été calculées avec le programme GAUSSIAN 90 (19) aux niveaux

2. Pour une discussion plus détaillée du rapport des scissions des liaisons α(C—C) et β(C—H) voir réf. 7*b*.

Can. J. Chem. Downloaded from www.nrcresearchpress.com by 80.90.12.36 on 09/08/12
For personal use only.

Tableau 1. Rendements quantiques de produits oléfiniques issus des radicaux propènyles C_3H_5[a] dans la photolyse du propène gazeux à 184,9 nm.

Propène (Torr)[b]	1,5	1,7	10,2	10,2
Hexafluorure de soufre (Torr)	—	51	—	100
Produits issus des radicaux 1 et 2				
cis-4-Méthylpent-2-ène[c]	0,0010	[d]	0,0014	[d]
Hexa-1,4-diène	<0,0015	[d]	0,0013	[d]
cis-But-2-ène	0,001	0,0035	0,0010	0,0010
trans-But-2-ène	0,0011	0,001	0,0015	0,0009
cis-Penta-1,3-diène	0,0018	[d]	0,0026	[d]
trans-Penta-1,3-diène	0,004	[d]	0,0085	[d]
Produits issus des radicaux 3				
2,3-Diméthylbut-1-ène	[d]	0,008	0,008	0,009
2-Méthylpenta-1,4-diène	0,006	0,012	0,010	0,014
Isobutène	<0,013	[d]	0,003	[d]
Isoprène	<0,0007	[d]	0,0008	[d]
Taux de transformation	3–4%		2%	

[a]L'addition de 10% d'oxygène annule les rendements quantiques de tous ces produits.
[b]1 Torr = 133 N m^{-2}.
[c]On n'a pu mesurer le rendement de l'isomère *trans*.
[d]Non-mesuré.

théoriques UHF/6-31G*//UHF/6-31G* et ROHF/6-31G*// ROHF/6-31G*.

3. Résultats et discussion

3.1 Partie expérimentale

Les résultats de quelques photolyses de **M** gazeux à 184,9 nm sont présentés dans le tableau 1. Pour les exigences de cette étude, les produits sont limités à ceux formés par la combinaison des radicaux **1**, **2** et **3** avec d'autres radicaux. (Aux taux de transformation utilisés dans cette étude les quantités des produits issues des réactions de combinaison des radicaux **1**, **2** et **3** entre eux sont trop faibles pour être mesurées.)

Les radicaux issus des fragmentations α(C—H) vont réagir avec l'ensemble des radicaux libres présents. Comme les constantes de vitesses des réactions de type radical hydrocarboné + radical hydrocarboné sont toutes similaires quel que soit le couple de radicaux hydrocarbonés mis en cause (mariage par spin antiparallèle), on admet seulement que l'importance de ces réactions est statistiquement lié aux concentrations radicalaires, négligeant l'effet de masse (20) ou tout autre facteur stérique (5, 20). Ainsi les réactions [15]–[22],

[15] **1** ou **2** + $CH_3—\dot{C}H—CH_3 \rightarrow$ *cis*- et *trans*-4-méthylpent-2-ène

[16] **1** ou **2** + $\overline{CH_2—CH—CH_2} \rightarrow$ hexa-1,4-diène

[17] **1** ou **2** + $\dot{C}H_3 \rightarrow$ *cis*- et *trans*-but-2-ène

[18] **1** ou **2** + $CH_2{=}\dot{C}H \rightarrow$ *cis*- et *trans*-penta-1,3-diène

et

[19] **3** + $CH_3—\dot{C}H—CH_3 \rightarrow$ 2,3-diméthylbut-1-ène

[20] **3** + $\overline{CH_2—CH—CH_2} \rightarrow$ 2-méthylpenta-1,4-diène

[21] **3** + $\dot{C}H_3 \rightarrow$ isobutène

[22] **3** + $CH_2{=}\dot{C}H \rightarrow$ isoprène

dovient être prises en considération. La recherche des produits de combinaison formés dans ces réactions et la mesure quantitative de leur rendement devraient permettre d'évaluer les rendements quantiques des réactions primaires [6] et [7] dans la mesure où il n'y a pas d'isomérisation des radicaux par transfert d'atome d'hydrogène.

En première approximation, les rendements quantiques des six premiers produits apparaissant au tableau 1 sont dans l'ordre d'importance des rendements quantiques des radicaux isopropyles, allyles, méthyles et vinyles observés précédemment dans la photolyse de **M** à 184,9 nm (1). Il en est de même pour les rendements quantiques des quatre derniers produits. Cependant il y a quelques différences qu'il faut discuter : étant donné que les quantités des radicaux méthyles et vinyles formées devraient être les mêmes (réaction [3]), les rendements des but-2-ènes (réaction [17]) devraient être voisins de ceux des penta-1,3-diènes (réaction [18]) et les rendements de l'isobutène (réaction [12]) proches de ceux de l'isoprène (réaction [22]). (Les rendements quantiques du *cis*-but-2-ène avec l'addition de SF_6 nous semblent erratiques : l'augmentation observée pour l'ajout de 51 Torr de SF_6 à 1,7 Torr de **M** n'est pas confirmée à plus hautre pression (tableau 1).) Mais il apparaît que les rendements en but-2-ènes sont moins élevés que ceux des penta-1,3-diènes (déficit de radicaux méthyles par rapport aux radicaux vinyles) et les rendements de l'isobutène plus élevés que ceux de l'isoprène (excès de radicaux méthyles par rapport aux radicaux vinyles). Cette dernière observation est en accord avec le fait que l'on sait qu'une

Can. J. Chem. Downloaded from www.nrcresearchpress.com by 80.90.12.36 on 09/08/12
For personal use only.

portion des radicaux vinyles excités se fragmente, donnant de l'acétylène (réaction [5], ϕ = 0,08 (1)). Les rendements des penta-1,3-diènes semblent donc trop élevés.

En tenant compte de toutes les produits mesurés et provenant de réactions impliquant les radicaux vinyles et méthyles, on trouve que le rendement en radicaux vinyles thermalisés est voisin de 0,10 et celui en radicaux méthyles de 0,36 (ce travail et réf. 1). Il y a donc un déficit en rendement des radicaux vinyles de 0,18. Notons que la réaction de fragmentation moléculaire suivante

[23] $\mathbf{M}^{**} \rightarrow CH_4 + HC{\equiv}HC$

bien que favorisée énergétiquement (6), ne peut expliquer le déficit car elle donnerait du méthane et de l'acetylène en quantités égales.

Il se peut qu'une partie des radicaux vinyles vibrationellement et (ou) électroniquement excités réagit directement avec **M** dans une réaction exceptionelle de condensation :

[24] $(CH_2{=}\dot{C}H)^* + \mathbf{M} \rightarrow (CH_3{-}\dot{C}H{-}CH_2{-}CH{=}CH_2)^*$

Suivie de l'élimination d'un atom d'hydrogène, cette condensation expliquerait l'apparent excès des penta-1,3-diènes.

Un des rapporteurs nous a demandé pourquoi on ne tenait pas compte des éventuelles réactions de condensation des autres radicaux avec **M**. Il est généralement admis que l'addition d'un radical thermalisé sur une liaison multiple à la température ambiante est très lente (énergie d'activation non-nulle et faible facteur pré-exponentiel (21)). De plus, à basse pression, l'exothermicité de cette addition est suffisante pour provoquer la décomposition du complexe (radical + oléfine) avant qu'une collision avec un troisième corps ne le stabilise.

Tenant compte de tous les produits issus des radicaux vinyles avec les radicaux **1**, **2** et **3**, sauf pour les penta-1,3-diènes et l'isoprène, l'estimation des rendements des produits issus des radicaux C_3H_5 vinyliques conduit aux valeurs suivantes : $\phi(\mathbf{3}) = 0{,}02 \pm 0{,}01$ et $\phi(\mathbf{1} + \mathbf{2}) = 0{,}005 \pm 0{,}003$. Il apparaît ainsi que la rupture de la liaison centrale ϕ(C—H) est favorisée d'un facteur 4 par rapport à la somme des ruptures des liaisons α(C—H) terminales alors que statistiquement on s'attendrait à un facteur un demi. L'énergie de dissociation de la liaison α(C—H) secondaire est légèrement inférieure à celle d'une liaison α(C—H) primaire (voir par exemple réf. 22). Il semble que l'énergie de dissociation de la liaison C—H qui se rompt (vide infra) joue un rôle déterminant bien que l'énergie fournie par le photon soit nettement supérieure à l'énergie necessaire pour rompre ces liaisons.

3.2 Calculs *ab initio*

Les géométries optimisées, les moments dipolaires et les énergies des radicaux **1**, **2** et **3**, obtenus avec les différentes méthodes de calcul *ab initio*, sont rassemblés dans les tableau 2–4, respectivement. Comme dans le cas de **M** (23), la structure la plus basse en énergie de chaque radical est de symétrie C_S avec un atome d'hydrogène du groupe méthyle situé dans le plan et au dessus de la double liaison (angles dièdres H4C3C2C1 optimisés $\equiv$ 0,00°) (8). Les résultats des calculs ne sont pas donnés ici mais notons que les structures C_S avec l'atome d'hydrogène du groupe méthyle dans le plan et dirigé vers l'extérieur sont des états de transition (maxima d'énergie) pour la rotation du groupe méthyle.

Les longueurs de liaisons obtenues avec la méthode GVB sont généralement plus grandes que celles obtenues avec la même base et les méthodes UHF et ROHF. Une exception remarquable est la liaison C1=C2 pour laquelle les valeurs optimisées UHF/STO-3G sont les plus grandes pour chaque radical. Ceci est une conséquence de la contamination de spin (influence des états électroniques supérieurs) qui est importante dans ces calculs.

Les moments dipolaires sont donnés dans les tableaux à titre indicatif. Pour les molécules les moments dipolaires obtenus avec la base STO-3G sont généralement trop petits (~50%). Enfin, les moments dipolaires obtenus avec les bases étendues se rapprochent des valeurs expérimentales mais peuvent être soit trop petits, soit trop grands (24).

3.2.1 Radicaux 1 et 2

Sauf pour les calculs avec la base minimale STO-3G, l'énergie relative du radical **1** est plus basse d'environ 1 kJ mol^{-1} que celle du radical **2**. Cette différence est vraiment minime et les enthalpies de formation des deux radicaux doivent être très proches l'une de l'autre. (Il faut encore tenir compte d'une éventuelle différence dans les «Zero Point Energies» (ZPE) (sommes des énergies vibrationnelles à 0 K; ZPE = 0,5 $\Sigma(\omega_e)$, vide infra).) Nos résultats indiquent que la difference des rapports des rendements des ruptures α(C—C) et β(C—H) obtenus dans les photolyses directes du *cis*- et du *trans*-but-2-ène à λ = 184,9 nm (α(C—C)/β(C—H) = 0,95 et 1,34, respectivement (7)) ne peut pas être expliquée par une différence dans les énergies ou enthalpies de formation des radicaux.

Que le groupe méthyle soit du même côté ou du côté opposé à l'atome d'hydrogène sur le centre radicalaire C1 ne semble pas avoir une influence majeure sur les paramêtres géometriques pour lesquelles C1 est impliqués : ainsi les valeurs de C1=C2 dans les deux radicaux, les longueurs des liaisons H2Ċ1 et H1Ċ1 et les valeurs des angles H2Ċ1C2 et H1Ċ1C2 sont similaires à chaque niveaux théorique (voir tableaux 2 et 3). Tous les calculs prédisent un élargissement de chacun des deux angles (de 10° $\pm$ 2°) par comparaison avec les angles correspondants de **M**. Ceci semble être un phénomène général : un élargissement d'environ 8° des angles HĊC concernant les centres radicalaires des radicaux *trans*-(s-*trans*)-, *trans*-(s-*cis*)-, *cis*-(s-*trans*)- et *cis*-(s-*cis*)-2-vinylcycloprop-1-yle, par comparaison avec les angles correspondant du vinylcyclopropane, est aussi prédit par les calculs *ab initio* (25). Néanmoins, notons ici que l'augmentation des angles CĊC étaient seulement d'environ 1,5° par comparaison avec les angles correspondants des rotamères du vinylcyclopropane (25). Dans ce cas les petites différences sont sans doute dues à la rigidité du cycle à trois.

Quant à la barrière à la rotation autour de la liaison double (processus **1** $\leftrightarrow$ **2**), elle serait d'environ 60 kJ mol^{-1} d'après des calculs UHF/STO-3G. Dans la photolyse de **M** à 184,9 nm, l'énergie résiduelle dans les radicaux après rupture de la liaison C—H est donc suffisante pour permettre l'isomérisation.

3.2.2 Radical 3

Pour ce radical, vu la similarité des résultats aux différents niveaux de théorie pour **1** et **2**, nous avons limités les optimisations à celles avec les bases STO-3G et 6-31G* (voir tableaux 4 et 5). L'élargissement de l'angle C1Ċ2C3 par rapport aux structures de **1**, **2** et **M** est remarquable et ressemble fort à

Can. J. Chem. Downloaded from www.nrcresearchpress.com by 80.90.12.36 on 09/08/12
For personal use only.

Tableau 2. Les paramètres géométriques, le moment dipolaire (μ) et l'énergie totale du radical **1** obtenus par optimisation complète de la géométrie à divers niveaux de théorie. Voir le schéma pour la numérotation des atomes.

	Longueur des liaisons (Å)						Angles (°)					
Méthode/base	C1C2	C2C3	H2C1	H3C2	H4C3	H(5,6)C3	C1C2C3	H2C1C2	H3C2C1	H4C3C2	μ (Debye)	Énergie (hartree)
UHF/STO-3G	1,360	1,524	1,083	1,088	1,086	1,088	123,7	130,6	120,2	111,1	0,22	−115,020 693
ROHF/STO-3G	1,299	1,524	1,084	1,087	1,085	1,088	124,4	132,1	120,3	111,0	0,25	−115,001 886
ROHF-GVB(8)/ STO-3G	1,339	1,544	1,099	1,103	1,106	1,096	123,9	131,1	120,2	110,8	0,24	−115,119 237
UHF/3-21G	1,329	1,515	1,069	1,080	1,082	1,086	123,9	134,4	119,8	110,9	0,60	−115,784 881
ROHF/3-21G	1,303	1,513	1,069	1,080	1,082	1,085	124,5	134,8	119,4	110,9	0,65	−115,775 793
ROHF-GVB(8)/ 3-21G	1,331	1,535	1,082	1,094	1,101	1,093	124,0	134,3	119,6	110,7	0,61	−115,885 007
UHF/6-31G	1,340	1,506	1,070	1,082	1,082	1,086	124,6	135,0	119,1	111,3	0,62	−116,388 630
ROHF/6-31G	1,311	1,504	1,069	1,081	1,082	1,086	125,2	135,5	118,8	111,3	0,68	−116,378 638
GVB(6)/6-31G	1,339	1,526	1,084	1,096	1,082	1,089	124,6	135,1	118,9	111,1	0,64	−116,466 613
UHF/6-31G*	1,329	1,506	1,071	1,083	1,083	1,087	124,8	134,0	118,7	111,3	0,60	−116.429 146
ROHF/6-31G*	1,305	1,506	1,072	1,082	1,083	1,087	125,2	134,2	118,3	111,1	0,64	−116.420 556
UHF/6-31G**	1,328	1,505	1,072	1,084	1,083	1,087	124,8	134,1	118,6	111,3	0,60	−116,437 747
ROHF/6-31G**	1,305	1,505	1,072	1,083	1,083	1,087	125,3	134,3	118,3	111,2	0,63	−116,429 143
GVB(1)/6-31G**	1,324	1,506	1,072	1,082	1,083	1,086	124,9	134,3	118,4	111,2	0,62	−116,456 541

Tableau 3. Les paramètres géométriques, le moment dipolaire (μ) et l'énergie relative (ΔE)[a] du radical **2** obtenus par optimisation complète de la géométrie à divers niveaux de théorie. Voir le schéma pour la numérotation des atomes.

	Longueur des liaisons (Å)						Angles (°)					
Méthode/base	C1C2	C2C3	H1C1	H3C2	H4C3	H(5,6)C3	C1C2C3	H1C1C2	H3C2C1	H4C3C2	μ (Debye)	ΔE (kJ mol^{-1})
UHF/STO-3G	1,359	1,526	1,083	1,086	1,086	1,088	124,5	130,6	119,4	111,1	0,35	−0,95
ROHF/STO-3G	1,299	1,525	1,084	1,086	1,086	1,088	125,0	132,3	119,7	111,1	0,41	−1,02
ROHF-GVB(8)/ STO-3G	1,339	1,545	1,099	1,103	1,107	1,096	124,4	131,1	119,8	110,9	0,37	−1,09
UHF/3-21G	1,329	1,520	1,070	1,077	1,083	1,085	124,5	134,4	119,3	111,2	0,84	+0,75
ROHF/3-21G	1,303	1,518	1,069	1,076	1,083	1,085	124,7	134,9	119,3	111,3	0,89	+0,87
ROHF-GVB(8)/ 3-21G	1,331	1,538	1,083	1,092	1,102	1,093	124,1	134,3	119,5	111,0	0,82	+0,64
UHF/6-31G	1,340	1,510	1,071	1,078	1,083	1,086	125,1	135,1	118,6	111,6	0,85	+0,84
ROHF/6-31G	1,311	1,509	1,070	1,078	1,083	1,085	125,4	135,8	118,6	111,7	0,91	+1,02
GVB(6)/6-31G	1,340	1,529	1,085	1,094	1,083	1,089	124,8	135,2	118,9	111,5	0,85	+0,72
UHF/6-31G*	1,329	1,510	1,072	1,079	1,084	1,087	125,0	134,2	118,6	111,5	0,80	+0,71
ROHF/6-31G*	1,305	1,509	1,073	1,079	1,084	1,086	125,1	134,5	118,6	111,5	0,84	+0,94
UHF/6-31G**	1,329	1,510	1,073	1,080	1,084	1,087	124,9	134,3	118,6	111,5	0,81	+0,83
ROHF/6-31G**	1,305	1,509	1,073	1,080	1,084	1,087	125,2	134,7	118,5	111,5	0,85	+1,06
GVB(1)/6-31G**	1,325	1,510	1,073	1,079	1,084	1,086	124,8	134,4	118,6	111,5	0,81	+0,99

[a]Relative au radical **1** (voir tableau 2).

ceux observés pour les angles H2Ċ1C2 et H1Ċ1C2 dans **1** et **2**, respectivement. Ceci confirme que les petits changements dans les valeurs des angles CĊC (~1,5°) dans les radicaux 2-vinylcycloprop-1-yles (25) sont un reflet de la contrainte de géometrie du cycle.

La liaison vinylique secondaire H3Ċ2 est moins forte que les liaisons vinyliques primaires. L'énergie de **3** relative à celle de **1** est donc située dans une fourchette de 12 à 17 kJ mol^{-1} plus basse (voir tableau 4).

Les résultats des photolyses de **M** indiquent un excès de

Can. J. Chem. Downloaded from www.nrcresearchpress.com by 80.90.12.36 on 09/08/12
For personal use only.

Tableau 4. Les paramètres géométriques, le moment dipolaire (μ) et l'énergie relative (ΔE)[a] du radical **3** obtenus par optimisation complète de la géométrie à divers niveaux de théorie. Voir le schéma pour la numérotation des atomes.

	Longueur des liaisons (Å)						Angles (°)				μ	ΔE
Méthode/base	C1C2	C2C3	H1C1	H2C1	H4C3	H(5,6)C3	C1C2C3	H1C1C2	H2C1C2	H4C3C2	(Debye)	(kJ mol^{-1})
UHF/STO-3G	1,355	1,510	1,085	1,082	1,088	1,088	133,5	122,3	121,4	110,8	0,40	−13,1
ROHF/STO-3G	1,299	1,508	1,083	1,081	1,088	1,088	135,2	122,5	121,8	110,7	0,64	−17,5
ROHF-GVB(8)/ STO-3G	1,338	1,530	1,100	1,100	1,107	1,096	133,4	122,3	121,6	110,5	0,44	−12,2
UHF/6-31G*	1,325	1,484	1,082	1,076	1,089	1,086	136,5	121,6	121,7	110,8	0,70	−13,3
ROHF/6-31G*	1,305	1,484	1,081	1,076	1,088	1,085	136,7	121,4	121,9	110,7	0,78	−14,5

[a]Relative au radical **1** (voir tableau 2).

Tableau 5. Les fréquences des modes normaux (cm^{-1}), les sommes des énergies vibrationnelles à 0 K («Zero Point Energies», ZPE = 0,5 $\Sigma(\omega_e)$ kJ mol^{-1}) et les constantes rotationelles (RC, GHz) des radicaux **1**, **2** et **3**.

		Radical					
		1		**2**		**3**	
No.	Symmétrie	A[a]	B[b]	A[a]	B[b]	A[a]	B[b]
1.	A′	3429	3429	3417	3418	3371	3382
2.		3287	3294	3315	3323	3266	3291
3.		3258	3279	3277	3280	3245	3254
4.		3196	3199	3196	3199	3180	3190
5.		1659	1851	1655	1847	1694	1891
6.		1604	1632	1598	1633	1627	1627
7.		1561	1563	1557	1559	1562	1573
8.		1356	1431	1356	1405	1524	1543
9.		1225	1239	1215	1231	1226	1242
10.		999	1011	980	1003	1024	1032
11.		912	938	962	983	940	964
12.		444	451	426	432	354	367
13.	A″	3244	3248	3247	3251	3261	3265
14.		1628	1628	1626	1626	1613	1612
15.		1153	1179	1143	1177	1145	1161
16.		896	971	928	992	938	1027
17.		642	686	673	732	529	561
18.		186	210	180	206	167	196
ZPE		183,5	186,8	183,9	187,2	183,4	186,5
RC	*A*	56,82	57,82	47,97	48,45	71,84	72,44
	B	9,53	9,63	10,06	10,21	8,70	8,80
	C	8,59	8,69	8,76	8,89	8,14	8,25

[a]UHF/6-31G*//UHF/6-31G*.
[b]ROHF/6-31G*//ROHF/6-31G*.

radicaux **3** par rapport aux facteur statistique. Cela pourrait être expliqué par un effet énergétique : dans la mercurisensibilisation du propane à 253,7 nm, le rapport de formation des radicaux isopropyles/*n*-propyle ≃ 9 tandis que le rapport statistique des liaisons (C—H secondaires)/(C—H primaires) = 1/3 (26–28). D'autres possibilités d'explication existent, par exemple une isomérisation de **1** ou **2** vers **3** par un transfert de l'atome d'hydrogène de C2 à C1 (il y a une barrière non-négligeable à ce genre de transfert en général).[3] Notons aussi que des expériences de mercurisensibilisation à 253,7 nm d'isotopomères du propane, deutériés spécifiquement, ont démontré qu'aucune isomérisation des radicaux *n*-propyles ↔

3. G.R. De Maré et E.M. Evleth. Résultats non-publiés (1995).

Can. J. Chem. Downloaded from www.nrcresearchpress.com by 80.90.12.36 on 09/08/12
For personal use only.

isopropyles ne pouvait être détectée (26). Bien que les réactions d'échanges,

[24] **1** ou **2** + **M** → **M** + **III**

puissent aussi être source d'un excédent de **3**, la réaction

[25] *n*-propyle + propane → propane + isopropyle

a été exclue dans les mercurisensibilisations du propane à 253,7 nm (26, 27). L'extension de ces résultats aux photolyses du propane ou de **M** à 184,9 nm doit être cautionée (*i*) par la plus grande énergie disponible à courte longueur d'onde et (*ii*) par la différence des états électroniques impliqués dans les processus primaires.

3.2.3 Fréquences des modes normaux

Les fréquences des modes normaux, les ZPE et les constantes de rotation des trois radicaux ont été déterminés aux niveaux UHF/6-31G*//UHF/6-31G* et ROHF/6-31G*//ROHF/6-31G* (tableau 5). Ces résultats doivent être considérées avec les géométries UHF/6-31G* et ROHF/6-31G* correspondantes (tableaux 2–4).

En général, les fréquences fondamentales déterminées par les méthodes *ab initio* utilisées dans ce travail sont surestimées de 10 à 20%. Néanmoins nous pensons qu'elles peuvent être utilisées directement pour des calculs RRKM pourvu que les fréquences pour la molécule parente soient obtenues avec la même méthode.

Les différences d'enthalpie de formation des radicaux à 0 K ($\Delta(\Delta H_f^0)$) sont obtenues en ajoutant les différences des ZPE aux énergies relatives rapportées aux tableaux 3 et 4. Les ZPE calculées pour **2** sont 0,4 kJ mol^{-1} plus élevées que celles pour **1** et donc la valeur $\Delta(\Delta H_f^0(\mathbf{2}) - \Delta H_f^0(\mathbf{1})) \simeq 1{,}1$ kJ mol^{-1}. Cette différence est trop petite pour changer les conclusions décrites ci-dessus. Notons aussi que les ZPE de **3** sont presque identiques à celles de **1**.

4. Conclusions

Dans la photochimie du propène gazeux à λ 184,9 nm, la somme des rendements quantiques des réactions de scission des liaisons α(C—H) situées de part et d'autre de la liaison double est de l'ordre de 0,03. Il y a un avantage marqué (4 pour 1, comparé à 1 pour 2 statistiquement) pour la rupture de la liaison C—H centrale: $\phi(\mathbf{3}) = 0{,}02 \pm 0{,}01$ et $\phi(\mathbf{1} + \mathbf{2}) = 0{,}005 \pm 0{,}003$. L'énergie de la liaison qui se rompte est donc importante, comme cela à déjà été observé pour la photosensibilisation du propane par le mercure triplet à 253,7 nm (26–28).

On trouve que le radical **1** est plus bas en énergie (0,6–1,1 kJ mol^{-1}) que le radical **2**, sauf avec la base minimale STO-3G. Les calculs UHF/6-31G*//UHF/6-31G* et ROHF/6-31G*//ROHF/6-31G* conduisent aux différences $\Delta(\Delta H_f^0(\mathbf{2}) - \Delta H_f^0(\mathbf{1})) = 1{,}1$ et 1,2 kJ mol^{-1} et aussi à $\Delta H_f^0(\mathbf{3}) - \Delta H_f^0(\mathbf{1}) = -13{,}4$ (UHF) et $-14{,}2$ (ROHF) kJ mol^{-1}, respectivement. Les enthalpies de formation de **1** et **2** à 0 K sont donc très voisines et on n'y trouve pas une explication pour la différence dans le rapport des scissions α(C—C)/β(C—H) dans la photolyse directe des *cis*- et *trans*-but-2-ènes à 184,9 nm (7).

5. Remerciements

Nous remercions la Division des Affaires Scientifiques et de l'Environnement de l'O.T.A.N. pour son soutien financier (CRG.920599). G.J.C. tiens à exprimer sa reconnaissance au Conseil de Recherche en Sciences Naturelles et en Génie (Canada) qui a financé une partie de cette étude. Nous remercions également MM. Earl Evleth (U. Pierre et Marie Curie, Paris) et Jean Olbregts (U. Libre de Bruxelles) pour les nombreuses discussions fructueuses au sujet de ce travail.

6. Bibliographie

1. H. Deslauriers et G.J. Collin. J. Chim. Phys. **82**, 1033 (1985).
2. G.J. Collin, H. Deslauriers et J. Deschênes. Can. J. Chem. **57**, 870 (1979).
3. P. Borrell, A. Cervenka et F.C. James. J. Chem. Soc. B, 2293 (1971).
4. J.A. Kerr et M. Parsonage. Evaluated kinetic data on gas phase addition reactions: reactions of atoms, radicals with alkenes, alkynes and aromatic compounds. CRC Press, Cleveland, Ohio. 1972. pp. 24–26.
5. E. Ratajczak et A.F. Trotman-Dickenson. OSTI, UWIST, Supplementary tables of bimolecular gas reactions 1970. pp. 87–92, et les références qui y sont citées.
6. Wing Tsang. J. Phys. Chem. Ref. Data, **20**, 221 (1991).
7. (*a*) H. Deslauriers, W. Makulski et G.J. Collin. Can. J. Chem. **65**, 1631 (1987); (*b*) G.J. Collin. Adv. Photochem. **14**, 135 (1988).
8. G.R. De Maré, E.M. Evleth, R.A. Poirier et G.J. Collin. Can. J. Chem. **72,** 1230 (1994); (*b*) En préparation.
9. G.J. Collin, H. Deslauriers et A. Wieckowski. J. Phys. Chem. **85**, 944 (1981).
10. M.R. Peterson et R.A. Poirier. University of Toronto and Memorial University, Newfoundland. 1986 MONSTERGAUSS.
11. W.J. Hehre, R.F. Stewart et J.A. Pople. J. Chem. Phys. **51**, 2657 (1969).
12. J.S. Binkley, J.A. Pople et W.J. Hehre. J. Am. Chem. Soc. **102**, 939 (1980).
13. W.J. Henre, R. Ditchfield et J.A. Pople. J. Chem. Phys. **56**, 2257 (1972).
14. P.C. Hariharan et J.A. Pople. Theor. Chim. Acta, **28**, 213 (1973); Chem. Phys. Lett. **16**, 217 (1972).
15. W.C. Davidon. Mathematical Programming, **9**, 69 (1975).
16. J.A. Pople et R.K. Nesbet. J. Chem. Phys. **22**, 571 (1959).
17. R. McWeeny et G. Dierksen. J. Chem. Phys. **49**, 4852 (1968).
18. F.W. Bobrowicz et W.A. Goddard III. *Dans* Methods of electronic structure theory. Vol. 3. *Édité par* H.F. Schaefer III. Plenum Press, New York. 1977. p. 79.
19. M.J. Frisch, M. Head-Gordon, G.W. Trucks, J.B. Foresman, H.B. Schlegel, K. Raghavachari, M. Robb, J.S. Binkley, C. Gonzalez, D.J. Defrees, D.J. Fox, R.A. Whiteside, R. Seeger, C.F. Melius, J. Baker, R.L. Martin, L.R. Kahn, J.J.P. Stewart, S. Topiol and J.A. Pople, GAUSSIAN 90 (Revision F). Gaussian Inc., Pittsburgh, Pa. 1990.
20. L. Bertrand, G.R. De Maré, G. Huybrechts, J. Olbregts et M. Toth. Chem. Phys. Lett. **5**, 183 (1970).
21. V.N. Kondrat'ev. Chemical kinetics of gas reactions. Pergamon Press Ltd., Oxford. 1964. pp. 242–246.
22. H.J. Bernstein. Trans. Faraday Soc. **58**, 2285 (1962).
23. (*a*) D.C. McKean. Int. J. Chem. Kinet. **21**, 445 (1989); (*b*) Croat. Chem. Acta, **61**, 447 (1988).
24. G.R. De Maré. J. Mol. Struct. Theochem, **253**, 199 (1992).
25. G.R. De Maré et G.J. Collin. J. Mol. Struct. Theochem, **233**, 231 (1991).
26. E. Jakubowski, P. Kebarle, O.P. Strausz et H.E. Gunning. Can. J. Chem. **45**, 2287 (1967).
27. R.A. Holroyd et G.W. Klein. J. Phys. Chem. **67**, 2273 (1963).
28. J.P. Chesick. J. Am. Chem. Soc. **86**, 3597 (1964).

Can. J. Chem. Downloaded from www.nrcresearchpress.com by 80.90.12.36 on 09/08/12
For personal use only.

Excess properties for cyclohexanone + butanols at 298.15 K

Roque Riggio, Hector E. Martinez, Norma Z. de Salas, Miriam D. de Toigo, and Juan F. Ramos

Abstract: Densities, viscosities, and refractive indexes of the binary systems cyclohexanone + *n*-butanol, + *sec*-butanol, and + 2-methyl-1-propanol have been measured at 298.15 K and atmospheric pressure, over the whole composition range. The excess values of molar volume, viscosity, Gibbs free energy of activation of viscous flow, and internal pressure were calculated from experimental measurements. Based on the variations of the excess functions with composition, conclusions about the molecular interactions in these kinds of mixtures were obtained.

Key words: excess properties, binary mixtures, butanols, cyclohexanone.

Résumé : Opérant à 298,15 K et à la pression ambiante, on a mesuré les viscosités et les indices de réfraction des systèmes binaires cyclohexanone + *n*-butanol, + *sec*-butanol et + 2-méthylpropan-1-ol, sur l'ensemble des compositions. Utilisant les données expérimentales, on a calculé les valeurs en excès du volume molaire, de la viscosité, de l'énergie libre d'activation de Gibbs de l'écoulement visqueux et de la pression interne. Sur la base des variations des fonctions d'excès avec la composition, on a tiré des conclusions concernant les interactions moléculaires de ces divers mélanges.

Mots clés : propriétés en excès, mélanges binaires, butanols, cyclohexanone.

[Traduit par la rédaction]

Can. J. Chem. Downloaded from www.nrcresearchpress.com by 80.90.12.36 on 09/08/12
For personal use only.

Introduction

In previous works we studied several binary liquid solutions of alcohols with different kinds of ketones (1–4). In this contribution we report the following excess properties: molar volumes (V^E), viscosity (η^E), molar free energy of activation of viscous flow (G^{*E}), and internal pressures (Pi^E), for the mixtures: cyclohexanone (CH) + *n*-butanol (B_1), + *sec*-butanol (B_2), and + 2-methyl-1-propanol (B_3), which were calculated from the density, viscosity, and refractive index measured.

Experimental

Materials

Components were supplied by Merk-Darmstadt (A.R. grade). All species were dried with anhydrous K_2CO_3 and fractionally distilled under a flow of nitrogen. The middle fractions were stored over 3 A molecular sieve and cyclohexanone over 4 A molecular sieve.

All solutions were prepared by weight using an H11 Mettler balance and were stored in air-tight stoppered bottles.

Density

Densities (ρ) were determined with an Anton Paar DMA46 density meter with a built-in thermostat. The accuracy was estimated to be ± 0.1 kg m^{-3}.

Viscosity

Viscosities (η) were measured with a Cannon–Fenske viscosimeter, which was calibrated with doubly distilled water and benzene. The accuracy was estimated to be $\pm 0.5\%$.

Refractive index

Refractive indexes (n_D) of pure components as well as mixtures (sodium D line) were measured with a Jena dipping refractometer with an accuracy of ± 0.00002. For the viscosity and refractive index a thermostatic water bath, whose temperature was controlled to ± 0.01°C, was used.

Results

We report in Table 1 the experimental physical properties of the pure liquids along with some literature values for comparison purposes. Densities, viscosities, and refractive indexes of the binary mixtures are reported in Table 2.

The excess functions of the binary systems can be represented by a Redlich–Kister-type equation:

$$[1] \qquad X^E = x_i x_j \sum_{k=0}^{n} a_k (2x_i - 1)^k$$

Received December 20, 1994.

R. Riggio,[1] H.E. Martinez, N.Z. de Salas, and M.D. de Toigo. Facultad de Ciencias Naturales, Universidad Nacional de Salta, Buenos Aires 177, 4400 Salta, Republica Argentina.

J.F. Ramos. Facultad de Ciencias Exactas, Universidad Nacional de Salta, Buenos Aires 177, 4400 Salta, Republica Argentina.

[1] Author to whom correspondence may be addressed. Telephone: 087-255360. Fax: 087-255513.

Table 1. Experimental physical properties of the pure liquids at 298.15 K[a]

	ρ		η		n_D	
Components	Expt.	Lit.(ref.)	Expt.	Lit.(ref.)	Expt.	Lit.(ref.)
CH	941.9	942.2[b]	1.93	2.03[b]	1.44842	—
B_1	806.0	806.0(21)	2.58	2.58(21)	1.39741	1.3973(21)
B_2	802.6	802.6(21)	3.03	3.03(21)	1.39530	1.3950(21)
B_3	797.9	797.8(21)	3.40	3.40(21)	1.39389	1.3939(21)

[a]Units: ρ, kg m^{-3}; η, mPa s.
[b]CHEMPAK. Physical Properties Database. Madison Tech. Soft. Inc., U.S.A. 1992.

Table 2. Experimental densities, viscosities, and refractive indexes at 298.15 K[a]

CH + B_1				CH + B_2				CH + B_3			
X_{CH}	ρ	η	n_D	X_{CH}	ρ	η	n_D	X_{CH}	ρ	η	n_D
0.0000	806.0	2.58	1.39741	0.0000	802.6	3.03	1.39530	0.0000	797.9	3.40	1.39389
0.0997	822.5	2.13	1.40332	0.1006	817.3	2.33	1.40093	0.1012	814.8	2.58	1.40009
0.2002	838.4	1.87	1.40907	0.2090	833.0	1.90	1.40696	0.2016	831.0	2.15	1.40605
0.3022	853.8	1.73	1.41471	0.3005	846.2	1.66	1.41199	0.2990	846.1	1.90	1.41168
0.3878	866.3	1.66	1.41929	0.4030	860.8	1.55	1.41757	0.3994	861.3	1.77	1.41734
0.5036	882.3	1.63	1.42529	0.4997	874.3	1.51	1.42274	0.5008	876.0	1.72	1.42292
0.6016	895.1	1.64	1.43019	0.6002	888.3	1.50	1.42804	0.5978	889.6	1.70	1.42815
0.6966	907.2	1.67	1.43478	0.6988	901.8	1.57	1.43316	0.6982	903.3	1.69	1.43343
0.7992	919.6	1.74	1.43955	0.8007	915.6	1.66	1.43838	0.7981	916.5	1.71	1.43855
0.8984	931.0	1.82	1.44401	0.8986	928.6	1.79	1.44333	0.8985	929.4	1.77	1.44354
1.0000	941.9	1.93	1.44842	1.0000	941.9	1.93	1.44842	1.0000	641.9	1.93	1.44842

[a] Units: ρ, kg m^{-3}; η, mPa s.

where X^E represents any of the following properties: V^E, η^E, G^{*E}, Pi^E; x_i and x_j are the mole fractions of components i and j, respectively, and a_k denotes the polynomial coefficients. In each case, the optimum number of coefficients was ascertained from an examination of the variation of the standard error of the estimate with n:

$$[2] \qquad \sigma = \left[\sum (X^E_{obs} - X^E_{cal})^2 / n_{obs} - n)\right]^{1/2}$$

where n_{obs} is the number of measurements.

The excess functions were calculated with the following equations, previously used by several authors (5–8):

$$[3] \qquad V^E = V - (x_1 V_1 + x_2 V_2)$$

$$[4] \qquad \eta^E = \eta - (x_1 \eta_1 + x_2 \eta_2)$$

$$[5] \qquad G^{*E} = RT[\ln \eta V - (x_1 \ln \eta_1 V_1 + x_2 \ln \eta_2 V_2)]$$

$$[6] \qquad Pi^E = \frac{2^{1/6}RT}{2^{1/6}V - dN^{1/3}V^{2/3}} - \left[x_1 \frac{2^{1/6}RT}{2^{1/6}V_1 - d_1 N^{1/3} V_1^{2/3}} + x_2 \frac{2^{1/6}RT}{2^{1/6}V_2 - d_2 N^{1/3} V_2^{2/3}}\right]$$

where V and η are the molar volumes and the viscosities of the mixtures; V_1, V_2, η_1 and η_2 are the molar volumes and viscosities of the pure components, respectively.

The excess internal pressures (Pi^E) of the liquid mixture were obtained (9) by the equation:

$$[7] \qquad Pi^E = Pi - (x_1 Pi_1 + x_2 Pi_2)$$

where Pi, Pi_1, and Pi_2 are the internal pressures of the mixtures and the pure components, respectively, which can be obtained from the Buchler–Hirschfelder–Curtis equation of state (10):

$$[8] \qquad Pi = \frac{2^{1/6}RT}{2^{1/6}V - dN^{1/3}V^{1/3}}$$

N is Avogadro's number and d the molecular diameter of the mixture or the pure components, calculated by the following relation (11):

$$[9] \qquad d = 2\left[\frac{n_D^2 - 1}{n_D^2 + 2} V \frac{3}{4\pi N}\right]^{1/3}$$

n_D are the refractive indexes of the mixtures or the pure components.

Table 3 shows the values of the coefficients a_k for the excess functions of the binary systems and their standard deviation, which were calculated by the method of least squares.

Discussion

When mixing an alcohol, highly associated in the pure state (12–14), with a different polar solvent, certain phenomena

Can. J. Chem. Downloaded from www.nrcresearchpress.com by 80.90.12.36 on 09/08/12
For personal use only.

Table 3. Coefficients a_k from eq. [1] and standard deviations for the binary systems at 298.15 K[a]

Systems	Coefficients	$V^E \times 10^6$	η^E	G^{*E}	P_i^E
CH + B_1	a_0	−1.5893	−2.487	−746.9	0.0193
	a_1	0.0134	1.391	309.35	−0.0019
	a_2	−0.1930	−0.953	−121.96	0.0017
	σ_y	9×10^{-3}	1×10^{-2}	1.44	7×10^{-5}
CH + B_2	a_0	0.9231	−3.914	−1121.34	−0.0087
	a_1	−0.2392	2.200	391.15	0.0029
	a_2	0.0559	−1.121	45.01	−0.0016
	σ_y	4×10^{-2}	2×10^{-2}	4.10	4×10^{-5}
CH + B_3	a_0	−0.8228	−3.752	−944.21	0.0115
	a_1	0.1139	2.396	330.84	−0.0018
	a_2	−0.0913	−2.501	−360.63	0.0018
	σ_y	5×10^{-3}	1×10^{-2}	5.06	4×10^{-5}

[a] Units: V^E, $m^3\ mol^{-1}$; η^E, mPa s; G^{*E}, cal mol^{-1}; P_i^E, kbar.

Fig. 1. Molar excess volumes of the systems at 298.15 K.

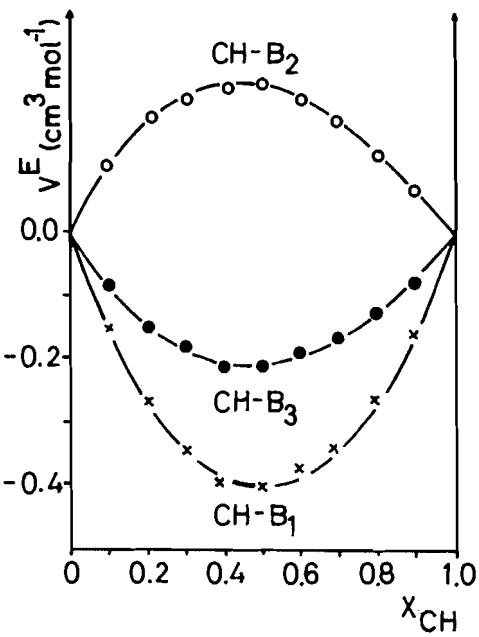

Fig. 2. Excess viscosities of the systems at 298.15 K.

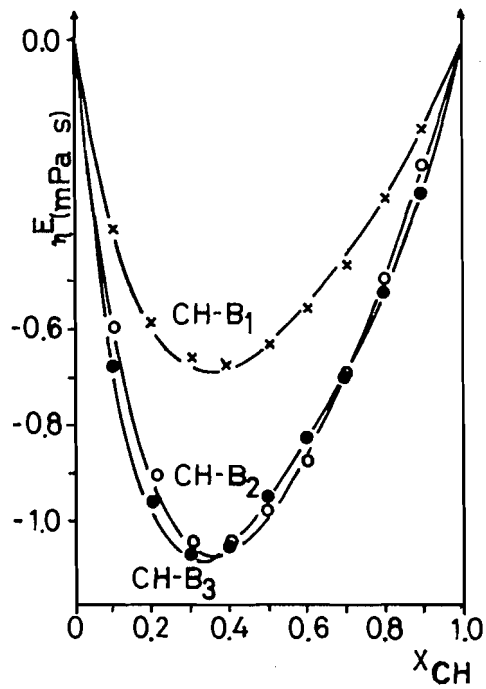

occur. Firstly, a breaking of the alcohol's associations due to hydrogen bonding takes place. Secondly, specific interactions appear in the mixtures (15). For the systems studied in this work, we justify these effects through analyses of the following excess properties: molar volume, viscosity, free energy of viscous flow, and internal pressure.

From the isothermal curves at 298.15 K in Fig. 1, excess molar volumes are plotted against composition. It can be seen that the isothermal curve at 298.15 K is positive for the CH + B_2 system, while for the CH + B_1 and CH + B_3 systems these are negative over the whole composition range. From these observations we can conclude that in all cases the alcohol's structure is broken when the mixture is formed. In the mixture containing secondary butanol (B_2) there exists a slight possibility of geometric ordering due to the OH position. Meanwhile, for the CH + B_1 system and to a lesser extent for the CH + B_3 system, both containing primary alcohols, we believe that a compensating effect produces a negative contribution to the V^E values (16, 17). The observed behaviour differences between the B_1 and B_3 mixtures and the B_2 mixture can be attributed to the higher steric freedom of the primary alcohols to form intermolecular association complexes through hydrogen bonds between the alcohol's OH and the enol form to the ketone (18). For the B_3 mixture the lower V^E negative values are probably due to the steric effect of the α-methyl group and the small keto–enol–OH associates formed.

In Fig. 2, it is observed that all mixtures present negative excess viscosity values, whose decreasing order is the following:

$$CH + B_1 \approx CH + B_3 < CH + B_2$$

Can. J. Chem. Downloaded from www.nrcresearchpress.com by 80.90.12.36 on 09/08/12
For personal use only.

Can. J. Chem. Downloaded from www.nrcresearchpress.com by 80.90.12.36 on 09/08/12
For personal use only.

Fig. 3. Molar excess free energies of viscous flow activation of the systems at 298.15 K.

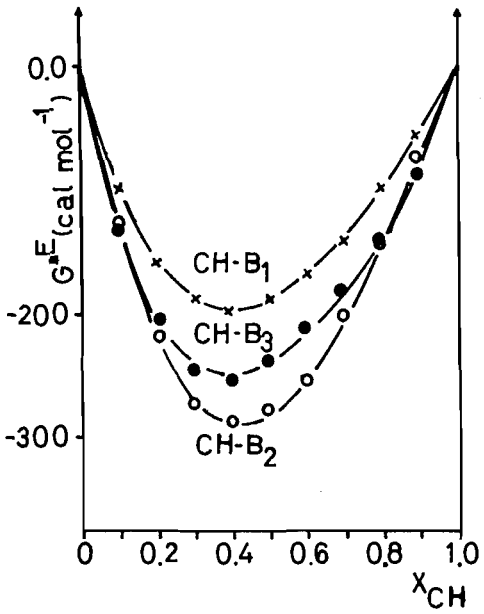

Fig. 4. Excess internal pressures of the systems at 298.15 K.

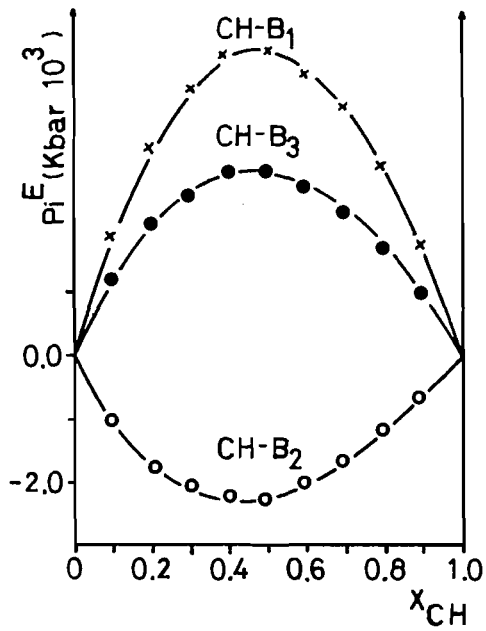

According to the above order, which is in complete agreement with the conclusions reached for the V^E behaviour, negative deviations occur when dispersion forces are preponderant (19).

Figure 3 shows the dependence of the calculated G^{*E} values upon composition. Increasing negative deviations with composition can be observed according to the following order:

$$CH + B_2 < CH + B_3 < CH + B_1$$

It is known that the strength of molecular interactions increases as G^{*E} decreases. In particular, for the above systems the interactions decrease according to the given order, which is in full accord with our previous conclusions.

On the other hand, Fig. 4 shows excess internal pressure versus composition. We can observe negative Pi^E deviations for the CH + B_2 system; meanwhile, for the CH + B_1 and CH + B_3 mixtures the opposite behaviour is present. The tendency towards negative values indicates qualitatively that the repulsion forces have a predominant effect. For those mixtures showing positive deviations the attraction forces are greater than those of repulsion. We know that cyclohexanone is present in high concentration as the enol form (20), and so it could be expected that the addition of B_1 and B_2 to cyclohexanone would cause, in these systems, keto–enol interactions. Thus our results may be in good agreement with those expected through predictions reported in the literature.

Acknowledgments

This work was supported by INENCO-CONICET-UNSa, República Argentina.

References

1. R. Riggio, J.F. Ramos, M. Hernandez Ubeda, and J.A. Espindola. Can. J. Chem. **59**, 3305 (1981).
2. H.N. Solimo, R. Riggio, and H.E. Martinez. J. Solution Chem. **15**, 283 (1986).
3. R. Riggio, M. Hernandez Ubeda, J.F. Ramos, and H.E. Martinez. J. Chem. Eng. Data, **25**, 318 (1980).
4. R. Riggio, H.E. Martinez, J.A. Espindola, and J.F. Ramos. J. Chem. Eng. Data, **29**, 11 (1984).
5. R.P. Singh and C.P. Sinha. J. Chem. Eng. Data, **30**, 470 (1985).
6. P. Cea, C. Lafuente, H. Artigas, F.M. Royo, and J. Urieta. Can. J. Chem. **72**, 1921 (1993).
7. A.M. Blanco, J. Ortega, B. Garcia, and J.M. Leal. Thermochim. Acta, **222**, 127 (1993).
8. B.P. Shukla, S.N. Dubey, and H.K. Rai. Z. Phys. Chem. Leipzig, **268**, 142 (1987).
9. J.D. Pandey, N. Pant, and B.R. Chaturvedi. Chem. Scr. **18**, 224 (1981).
10. J.O. Hirschfelder, C.F. Curtis, and R. Byron Bird. Molecular theory of gases and liquids. John Wiley & Sons, New York. 1954.
11. S. Glasstone. Tratado de Química Física. Ediciones Aguilar, Madrid. 1970.
12. H.C. Van Ness, J. Van Winkle, H.H. Richtol, and H.E. Hollinger. J. Phys. Chem. **71**, 1483 (1967).
13. G.C. Pimentel and A.L. McClellan. The hydrogen bond. W.H. Freeman and Co., San Francisco. 1960.
14. P. Huyskens. J. Mol. Struct. **100**, 403 (1983).
15. J.E. House. Trans. J. Ill. Acad. Sci. 123 (1966).
16. D.E.G. Jones, I.A. Weeks, S.C. Anand, R.W. Wetmore, and G.C. Benson. J. Chem. Eng. Data, **17**, 501 (1972).
17. G.C. Benson and O. Kiyohara. J. Chem. Eng. Data, **21**, 362 (1976).
18. F. Ratkovics and M. Lazio-Parragi. Fluid Phase Equilib. **17**, 97 (1984).
19. R.J. Fort and W.R. Moore. Trans. Faraday Soc. **62**, 1112 (1966).
20. R.D. Dunlap and R.L. Scott. J. Phys. Chem. **66**, 631 (1962).
21. J.A. Riddick and W.B. Bunger. Organic solvents. Vol. II. 3rd ed. Wiley–Interscience, New York. 1970.

Methine bases in the benzothiazole, benzoselenazole, and quinoline series, and geometry and conformational preferences of their acyl derivatives

Ajay K. Gupta, Ali Ben-Mahmud, Lisa J. Kamphuis, Jennifer L. Mueller, Suzie S. Rigby, Martin S. Gibson, Mary Frances Richardson, Linda Humeniuk, and Stanley Walker

Abstract: Dimeric structures **2***a–c* are confirmed for the "methine bases" obtained from 2-methylbenzothiazolium and -selenazolium salts and aqueous sodium hydroxide, whereas monomeric structures **3** are confirmed for methine bases similarly derived from 2-methylquinolinium salts. The latter monomers dimerize slowly on standing. Monomeric methine bases **6–9**, too hindered to dimerize, are described. 2-Acetonylidene-2,3-dihydro-3-methylbenzothiazole **10***a* and related compounds are assigned (*Z*) configurations on the basis of NOE difference spectra. Molecular mechanics calculations predict a slightly higher steric energy for the observed *s-cis* conformer of **10***a* than for the *s-trans*, indicating a stabilizing S···O interaction in the *s* conformer that need only be a few kJ mol^{-1} in magnitude. For the quinolines **13***a* and *b*, the (*E*) configuration/*s-cis* conformation is favoured. The dielectric absorption method provides a rotational energy barrier of approximately 60 kJ mol^{-1} for acetyl group relaxation in **10***a*. Oxygen–sulfur exchange is observed in the conversion of **10***a* to **12***a* by thioacetic acid.

Key words: conformation, configuration, heterocyclic compounds, S···O interaction.

Résumé : On confirme les structures dimères **2***a–2c* pour les «bases méthines» obtenues par réaction des sels de 2-méthylbenzo-thiazolium et sélénazolium avec l'hydroxyde de sodium aqueux; par ailleurs, on confirme la structure monomère **3** pour les bases méthines obtenues de la même manière à partir des sels de 2-méthylquinolinium. Laissés au repos, ces derniers monomères se dimérisent lentement. On décrit aussi les bases méthines **6–9** qui sont trop encombrées pour se dimériser. En se basant sur les différences dans les spectres d'eOn, on a attribué les configurations (*Z*) au 2-acétonylidène-2,3-dihydro-3-méthylbenzothiazole (**10***a*) et aux composés apparentés. Des calculs de mécanique moléculaire permettent de prédire que l'énergie stérique du conformère *s-cis* observé du composé **10***a* est légèrement supérieure à celle du composé *s-trans*; ces résultats indiquent que, dans le conformère *s-cis*, il existe une interaction S···O stabilisante dont l'amplitude ne doit pas dépasser quelques kJ mol^{-1}. Pour les quinoléines **13***a* et **13***b*, la configuration (*E*) avec conformation *s-cis* est favorisée. La méthode d'absorption diélectrique permet de déterminer que la barrière à l'énergie rotationnelle pour la relaxation du groupe acétyle du composé **10***a* est d'environ 60 kJ mol^{-1}. On a observé de l'échange oxygène–soufre lors de la conversion du composé **10***a* en **12***a* par de l'acide thioacétique.

Mots clés : conformation, configuration, composés hétérocycliques, interaction S···O.

[Traduit par la rédaction]

Introduction

Traditionally, treatment of quaternary salts derived from heteroaromatic bases such as 2-methylbenzothiazole or 2-methylquinoline with aqueous sodium or potassium hydroxide has been thought to give methine bases, e.g., **1**. However, the product from 2,3-dimethylbenzothiazolium perchlorate (1) was shown to be dimeric (2) and, subsequently, to possess the structure **2***a* (3); our experience in the 1,3,4-thiadiazole series has been similar (4). Formation of **2***a* under these conditions is thought to occur by addition of **1** to C2 of the antecedent quaternary cation (3). To avoid coexistence of these two species, Owen (5) used a modified base treatment of the quaternary *p*-toluenesulfonate to prepare the monomeric methine base **1** and its selenium analogue. Similar ambiguities have arisen in the quinoline series with, e.g., the product described as **3***a* being reported both as a buff and as a red solid (6, 7). We have reexamined a number of the earlier reports and confirmed the product formulations as monomeric (**1** or **3**) or as dimeric (**2**, **4**, or **5**). We have also prepared the monomeric methine bases (**6–9**); steric constraints make approach to dimeric structures improbable in these cases.

Received December 21, 1994.

A.K. Gupta, A. Ben-Mahmud, L.J. Kamphuis, J.L. Mueller, S.S. Rigby, M.S. Gibson,[1] and M.F. Richardson.[1] Department of Chemistry, Brock University, St. Catharines, ON, L2S 3A1, Canada.

L. Humeniuk and S. Walker. Department of Chemistry, Lakehead University, Thunder Bay, ON P7B 5E1, Canada.

[1] Authors to whom correspondence may be addressed.

Can. J. Chem. Downloaded from www.nrcresearchpress.com by 80.90.12.36 on 09/08/12
For personal use only.

Acyl derivatives of these methine bases, e.g. **10** and **11**, and the related thioacyl compounds **12** have attracted some attention over the years. Thus **10***a* and *b* have been prepared from 2-methylthiobenzothiazolium salts (8) and from other sources (9, 10), and in each case the same geometrical isomer has been isolated. We have encountered a similar situation in the 1,3,4-thiadiazole series, and established the (*Z*) configuration for the products with a weak hypervalent or "non-bonded" S···O interaction stabilizing the *s-cis* (*cisoid*) confirmation (4, 11). We now present evidence that again it is the (*Z*) isomers that are produced, stabilized by a S or Se···O interaction in the *s-cis* conformation (cf. ref. 12), and we provide an estimate of the internal barrier to rotation of the acetyl group in **10***a* around the acetyl – methine carbon bond. We append some observations on the related compounds **13***a* and *b* for which the (*E*) configuration/*s-cis* conformation has been proposed (13); this conformation may be stabilized by weak O···H—C3 bonding (14).

Experimental section

The following instruments were used: a Bruker AC200 spectrometer for ^{1}H NMR spectra (200 MHz; $SiMe_4$ as internal standard) and ^{13}C NMR spectra (50 MHz; solvent as internal standard); Varian Gemini 200 and Varian XL 200 spectrometers for NOE and NOE difference spectra, and a JEOL 270 spectrometer for ^{1}H–^{1}H COSY spectra; an AEI MS30 double beam mass spectrometer interfaced to a Kratos DS 55 data system and Kratos Concept 1S double focussing mass spectrometer for mass spectra (*m/z* values are quoted for the most abundant isotopic species; *m*-nitrobenzyl alcohol was used as matrix for FAB spectra). Melting points are uncorrected.

2-Methylbenzothiazole, 2-methylbenzoselenazole, and 2- and 4-methylquinolines were commercial materials, while 1-methyl-3,4-dihydroisoquinoline, 2,3-cyclopentanoquinoline, and 1,2,3,4-tetrahydroacridine were prepared by literature methods (15, 16). Quaternary salts were prepared by refluxing the base with iodomethane, iodoethane, or 3-bromopropene

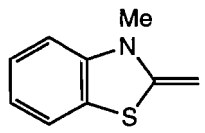

1

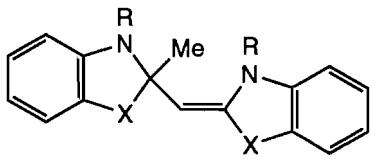

2 *a*; R = Me, X = S
b; R = Et, X = S
c; R = Me, X = Se

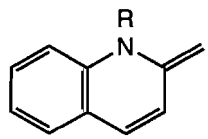

3 *a*; R = Me
b; R = Et
c; R = $CH_2CH{=}CH_2$

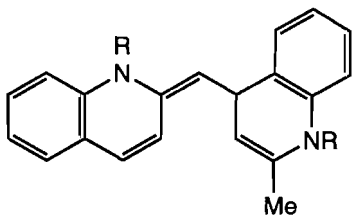

4 *a*; R = Me
b; R = Et

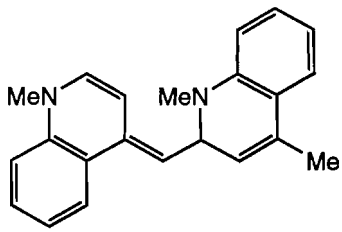

5

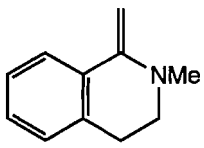

6

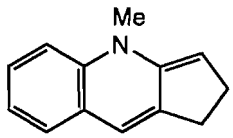

7

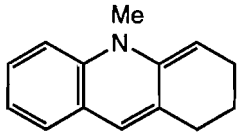

8

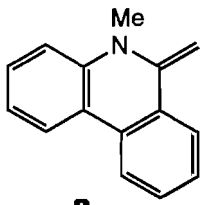

9

Can. J. Chem. Downloaded from www.nrcresearchpress.com by 80.90.12.36 on 09/08/12
For personal use only.

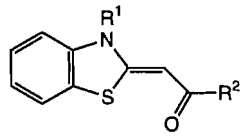

10 *a*; R^1 = Me, R^2 = Me
b; R^1 = Me, R^2 = Ph
c; R^1 = Et, R^2 = Me

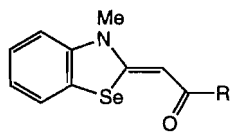

11 *a*; R = Me
b; R = Ph

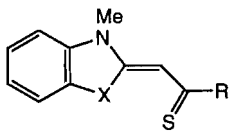

12 *a*; R = Me, X = S
b; R = Ph, X = S
c; R = NHPh, X = Se

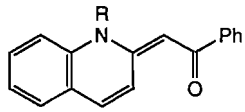

13 *a*; R = Me
b; R = Et

(allyl bromide) as appropriate. Parenthetically, 9-methylphenanthridine (17) and allyl bromide reacted slowly to give 9-methylphenanthridinium bromide.

Molecular mechanics calculations were performed as described previously (11) with Chem3D Plus, which implements Allinger's MM2 force field (18).

Dimeric methine bases: benzothiazole and benzoselenazole series

Compounds were prepared from the respective quaternary salts by reported method (1, 7, 19); spectroscopic data were as follows.

2*a*, mp 176–177°C (lit. (3) mp 178°C): the ^{1}H NMR spectrum corresponded with that reported (3); ^{1}H NMR ($CDCl_3$) δ: 1.67 (s, 3H, CH_3), 2.61 (s, 3H, CH_3), 3.24 (s, 3H, CH_3), 4.45 (s, 1H, methine CH), and 6.33–7.15 (m, 8H, arom H).

2*b*, mp 125–127°C (lit. (7) mp 126–128°C): ^{1}H NMR ($CDCl_3$) δ: 1.18 (t, 3H, CH_3), 1.27 (t, 3H, CH_3), 1.78 (s, 3H, CH_3), 3.18 (q, 2H, CH_2), 3.76 (q, 2H, CH_2), 4.55 (s, 1H, methine CH), and 6.34–7.24 (m, 8H, arom H); EI mass spectrum *m/z*: 177 (M^+, monomer, 62) and 149 (100%); FAB mass spectrum *m/z*: 354 (M^+, 5), 353 (7), and 178 (monomer + H^+, 100%).

2*c*, mp 147–149°C (lit. (19) mp 157–158°C): ^{1}H NMR ($CDCl_3$) δ: 1.88 (s, 3H, CH_3), 2.62 (s, 3H, CH_3), 3.27 (s, 3H, CH_3), 4.81 (s, 1H, methine CH), and 6.38–7.28 (m, 8H, arom H); ^{13}C NMR ($CDCl_3$) δ: 29.2, 29.7, and 32.3 (methyl carbons), 92.1 (methine carbon), 109.0, 110.2, 119.6, 120.0, 124.4, 125.5, 125.9, and 126.1 (arom. HC carbons), 121.0, 123.0, 143.8, 147.6, and 148.1 (quaternary carbons); EI mass spectrum *m/z*: 211 (M^+, monomer, 100%); FAB mass spectrum *m/z*: 422 (M^+, 35), 421 (63), and 212 (monomer + H^+, 100%).

3-Allyl-2,3-dihydro-2-methylenebenzothiazole together with its dimer (isolated by immediate extraction (cf. ref. 6) with deuteriochloroform), light brown oil that reddened on standing; ^{13}C NMR ($CDCl_3$) δ: 32.1 (CH_3, dimer), 81.0 (methine carbon, monomer), and 87.9 (methine carbon, dimer). The alternative procedure (cf. ref. 7) gave a glassy buff solid that turned red and gummy on drying in a vacuum desiccator; ^{13}C NMR ($CDCl_3$) δ: 22.2 (CH_3) and 170.0 (CO) ppm; EI mass spectrum *m/z*: 207 (M^+, $C_{11}H_{13}NOS$, 100), 165 (51), and 136 (86%).

Methine bases; quinoline, isoquinoline, and condensed quinoline series

Compounds were prepared from the respective quaternary salts and isolated by each of two general literature procedures (6; 7 and 16). For **3***a*, the earlier isolation procedure (6) gave the monomeric species, whereas the later procedure (7) gave **3***a* contaminated with **4***a*. Spectroscopic data were as follows.

3*a*, mp 70–71°C (lit. (6) mp 71–72°C); ^{1}H NMR ($CDCl_3$) δ: 3.09 (s, 3H, CH_3), 3.59 (s, 1H of methine CH_2), 3.71 (s, 1H of methine CH_2), 6.30 (d, 1H, olefinic H), 6.41 (d, 1H, olefinic H), and 6.68–7.43 (m, 4H, arom H); ^{13}C NMR ($CDCl_3$) δ: 32.8 (CH_3), 80.2 (methine carbon), 110.9 (C3), 119.0 (C4), 126.1, 126.6, 127.2, and 129.2 (arom. carbons), 122.4, 143.4, and 148.4 (quaternary carbons); EI mass spectrum *m/z*: 157 (M^+, 100%). The brick-red solid obtained on standing showed the following additional signals in the ^{13}C NMR spectrum ($CDCl_3$) δ: 30.9, 33.4, and 34.8 (CH_3), 52.4 (HC), 100.2, 104.5, 111.2, 111.4, 118.4, 120.4, 121.1, 122.0, 125.8, 126.9, 128.8, and 129.3 (arom. and vinyl HC carbons), 135.7, 136.2, 137.6, 137.7, 142.2, and 142.4 (quaternary carbons); EI mass spectrum *m/z*: 314 (M^+ of dimer, ca. 1.5%) and 157 (M^+, 100%).

3*b*, mp 76–78°C (dec.) (lit. (7) mp 79°C (dec.)); ^{1}H NMR ($CDCl_3$) δ: 1.18 (t, 3H, CH_3), 3.66 (q with two s superimposed, 4H, NCH_2 and methine CH_2), 6.30 (d, 1H, olefinic H), 6.41 (d, 1H, olefinic H), and 6.60–7.33 (m, 4H, arom. H); ^{13}C NMR ($CDCl_3$) δ: 10.0 (CH_3), 40.2 (NCH_2), 79.2 (methine carbon), 110.6 (C3), 118.9 (C4), 126.1, 127.0, 127.3, and 129.4 (arom. carbons), 122.6, 141.4, and 144.8 (quaternary carbons); FAB mass spectrum *m/z*: 172 (M + H^+, 100%). For the brick-red solid obtained on standing: FAB mass spectrum *m/z*: 343 (dimer + H^+, 4), 342 (dimer M^+, 7), 341 (dimer − H^+, 21), and 172 (monomer + H^+, 100%).

3*c* (cf. ref. 7), yellow solid, mp 80–81°C (dec., after blackening from 65°C), which darkened and finally became purple on standing; ^{13}C NMR ($CDCl_3$) δ: 40.1 (CH_2), 80.8 (methine carbon), 111.5, 119.3, 126.0, 126.9, 127.0, 129.2, and 130.6 (arom. and vinyl HC carbons), 116.7 (CH_2), 122.5, 142.0, and 145.5 (quaternary carbons).

5, mp 64°C (dec.); ^{13}C NMR ($CDCl_3$) δ: 35.7, 37.7, and 38.8 (methyl carbons), 57.8 (HC), 100.4 (methine carbon), 105.9, 110.3, 110.8, 113.3, 116.1, 116.8, 121.9, 122.4, 123.0, 123.3, 123.5, 128.5, and 133.8 (arom. and vinyl HC carbons), 129.1, 139.9, and 144.1 (quaternary carbons); EI mass spectrum *m/z*: 313 (M − H^+, ca. 1%), 312 (3), 158 (monomer M + H^+, 95), 157 (monomer M^+, 82), and 144 (100%).

6, oil: ^{1}H NMR ($CDCl_3$) δ: 2.86 (s, 3H, NCH_3), 2.91 (t, 2H, CH_2), 3.15 (t, 2H, CH_2), 3.86 (s, 1H, methine CH), 4.61 (s, 1H, methine CH), and 7.08–7.72 (m, 4H, arom. H); ^{13}C NMR ($CDCl_3$) δ: 40.6 (CH_3), 30.2 and 50.0 (2 × CH_2), 79.0 (methine carbon), 124.5, 126.1, 127.4 and 128.3 (arom. HC carbons), 131.8, 134.4, and 148.5 (quaternary carbons).

7, mp 179°C (dec.) (lit. (16) mp 170°C (dec.)); ^{1}H NMR ($CDCl_3$) δ: 2.35–2.64 (m, 4H, 2 × CH_2), 2.99 (s, 3H, CH_3), 4.30 (s, 1H, methine CH), 6.05 (s, 1H, CH), and 6.53–7.23 (m, 4H, arom. H); ^{13}C NMR ($CDCl_3$) δ: 27.8 and 28.0 (2 × CH_2), 32.8 (CH_3), 94.5 (methine carbon), 109.4, 115.3, 119.0, 125.9, and 127.3 (arom. and vinyl HC carbons), 124.6, 141.3, 144.4,

Can. J. Chem. Downloaded from www.nrcresearchpress.com by 80.90.12.36 on 09/08/12
For personal use only.

Can. J. Chem. Downloaded from www.nrcresearchpress.com by 80.90.12.36 on 09/08/12
For personal use only.

and 146.2 (quaternary carbons); EI mass spectrum *m/z*: 183 (M^+, 71) and 182 (100%).

8 (16), mp 184–185°C (dec.); ^{1}H NMR ($CDCl_3$) δ: 1.65–1.74 (m, 2H, CH_2), 2.30–2.48 (m, 4H, 2 × CH_2), 3.02 (s, 3H, CH_3), 4.44 (s, 1H, methine CH), 6.18 (s, 1H, CH), and 6.68–7.72 (m, 4H, arom. H); ^{13}C NMR ($CDCl_3$) δ: 21.6, 25.4, and 31.3 (3 × CH_2), 32.6 (CH_3), 93.5 (methine carbon), 110.3, 118.2, 121.0, 126.1, and 128.0 (arom. and vinyl HC carbons), 122.8, 132.9, 139.6, and 142.2 (quaternary carbons); EI mass spectrum *m/z*: 197 (M^+, 97) and 196 (100%).

For **9**, the quaternary salt (1.08 g, 3.2 mmol) was dissolved in DMSO (6.2 mL) prior to treatment with 1 M NaOH solution. The orange methine base **9** (0.42 g, 63%), mp 78°C (dec.), was isolated by extraction with $CDCl_3$; ^{1}H NMR ($CDCl_3$) δ: 3.25 (s, 3H, CH_3), 4.17 (s, 1H, methine CH), 4.72 (s, 1H, methine CH), and 6.83–7.91 (m, 8H, arom. H); ^{13}C NMR ($CDCl_3$) δ: 34.9 (CH_3), 82.7 (methine carbon), 112.6, 119.1, 122.0, 122.9, 124.5, 127.6, 128.6, and 129.2 (arom. HC carbons), 120.4, 129.7, 130.3, 141.5, and 145.9 (quaternary carbons); EI mass spectrum *m/z*: 207 (M^+, 100%). Exact Mass calcd. for $C_{15}H_{13}N$ 207.1049; found: 207.1064.

2-Acetonylidene-2,3-dihydro-3-methylbenzothiazole 10*a*

A mixture of 2,3-dimethylbenzothiazolium iodide (4.0 g, 14 mmol), Ac_2O (2.9 g, 28 mmol), NEt_3 (2.9 g, 29 mmol), and MeCN (15 mL) was heated under reflux for 2 h. The mixture was concentrated in vacuo and then poured into water. The crude product was collected and chromatographed on silica ($CHCl_3$–EtOAc as eluant). **10*a*** (1.5 g, 53%) crystallized from aqueous EtOH as needles, mp 158–159°C (lit. (9) mp 160–161°C); ^{1}H NMR ($CDCl_3$) δ: 2.23 (s, 3H, CH_3), 3.52 (s, 3H, CH_3), 5.84 (s, 1H, methine CH), and 7.09–7.57 (m, 4H, arom. H); ^{13}C NMR ($CDCl_3$) δ: 29.0 (CH_3), 32.3 (CH_3), 90.1 (methine carbon), 109.6, 122.1, 122.5, and 126.0 (aromatic HC carbons), 126.9, 139.7, 160.5, and 191.1 (quaternary carbons): EI mass spectrum *m/z*: 205 (M^+, 56) and 190 (100%).

2-Acetophenonylidene-2,3-dihydro-3-methylbenzothiazole 10*b*

A mixture of 2,3-dimethylbenzothiazolium iodide (1.0 g, 3.4 mmol), benzoic anhydride (0.8 g, 3.5 mmol), NEt_3 (1.0 g, 10 mmol), and MeCN (10 mL) was heated under reflux for 4 h. The oily crude product was extracted with EtOAc. Chromatography (silica; EtOAc) and crystallization from EtOH gave **10*b*** (0.7 g, 76%) as needles, mp 175–177°C (lit. (10) mp 179.5–180°C); ^{1}H NMR ($CDCl_3$) δ: 3.63 (s, 3H, CH_3), 6.52 (s, 1H, methine H), 7.12–7.65 (m, 7H, arom. H), and 8.00 (dd, 2H, arom. H); ^{13}C NMR ($CDCl_3$) δ: 32.3 (CH_3), 86.9 (methine carbon), 109.7, 122.1, 122.6, 126.3, 127.0, 128.1, and 130.6 (arom. HC carbons), 126.8, 139.4, 139.8, 162.0, and 184.2 (quaternary carbons); EI mass spectrum *m/z*: 267 (M^+, 14), 190 (10), 164 (39), and 105 (100%).

2-Acetonylidene-2,3-dihydro-3-ethylbenzothiazole 10*c*

Prepared similarly to **10*b*** (16 mmol scale; 1 h reflux), **10*c*** (0.3 g, 84%) had mp 106–108°C (lit. (9) mp 111–113°C); ^{1}H NMR ($CDCl_3$) δ: 1.40 (t, 3H, CH_3), 2.27 (s, 3H, CH_3), 4.13 (q, 2H, CH_2), 5.95 (s, 1H, methine H), and 7.00–7.80 (m, 4H, arom. H); EI mass spectrum *m/z*: 219 (M^+, 100), 204 (95), and 176 (58%).

2-Acetonylidene-2,3-dihydro-3-methylbenzoselenazole 11*a*

A mixture of 2,3-dimethylbenzoselenazolium iodide (1.0 g, 3.0 mmol), Ac_2O (0.32 g, 3.1 mmol), NEt_3 (0.29 g, 2.9 mmol), and MeCN (10 mL) was heated under reflux for 1.5 h. Isolation as for **10*a*** gave **11*a*** (0.3 g, 40%) as yellow needles, mp 163–165°C (lit. (20) mp 165°C); ^{1}H NMR ($CDCl_3$) δ: 2.24 (s, 3H, CH_3), 3.56 (s, 3H, CH_3), 6.15 (s, 1H, methine H), and 7.10–7.66 (m, 4H, arom. H); EI mass spectrum *m/z*: 253 (M^+, 69) and 238 (100%).

2-Acetophenonylidene-2,3-dihydro-3-methylbenzoselenazole 11*b*

(*a*) A mixture of 2,3-dimethylbenzoselenazolium iodide (1.0 g, 3.0 mmol), benzoic anhydride (0.6 g, 2.7 mmol), NEt_3 (0.29 g, 2.9 mmol), and MeCN (20 mL) was heated under reflux for 2 h. Chromatography (silica; EtOAc–CH_2Cl_2) and crystallization from EtOH gave **11*b*** (0.6 g, 65%) as shiny yellow plates, mp 137–139°C (lit. (21) mp 140–140.5°C); ^{1}H NMR ($CDCl_3$) δ: 3.68 (s, 3H, CH_3), 6.84 (s, 1H, methine H), 7.13–7.75 (m, 7H, arom. H), and 8.10 (dd, 2H, arom. H); EI mass spectrum *m/z*: 315 (M^+, 5), 238 (4), 212 (7), 122 (12), and 105 (100%).

(*b*) A mixture of **2*c*** (100 mg, 0.24 mmol), benzoic anhydride (110 mg, 0.49 mmol), NEt_3 (50 mg, 0.50 mmol), and $CHCl_3$ (10 mL) was heated under reflux for 1 h. Isolation as above gave **11*b*** (60 mg, 40%), mp 137–139°C, identical with the foregoing sample.

2,3-Dihydro-3-methyl-2-thioacetonylidenebenzothiazole 12*a*

A mixture of **10*a*** (500 mg, 2.44 mmol) and thioacetic acid (5 mL) was heated under reflux for 4 h. Evaporation in vacuo and trituration with EtOAc gave **12*a*** as an orange solid (350 mg, 61%) that crystallized from EtOH as orange needles, mp 187–189°C; ^{1}H NMR ($CDCl_3$) δ: 2.74 (s, 3H, CH_3), 3.68 (s, 3H, CH_3), 6.96 (s, 1H, methine H), and 7.12–7.75 (m, 4H, arom. H); EI mass spectrum *m/z*: 221 (M^+, 84), 206 (22), and 188 (100%). Exact Mass calcd. for $C_{11}H_{11}NS_2$: 221.0333; found: 221.0344.

2,3-Dihydro-3-methyl-2-thioacetophenylidenebenzothiazole 12*b*

(*a*) A mixture of 2,3-dimethylbenzothiazolium iodide (1.0 g, 3.4 mmol), carboxymethyl dithiobenzoate (0.72 g, 3.4 mmol), NEt_3 (0.36 g, 3.6 mmol), and MeCN (20 mL) was heated under reflux for 2 h. Evaporation in vacuo, chromatography (silica; $CHCl_3$), and crystallization from EtOH gave **12*b*** (0.3 g, 29%) as orange-red needles, mp 168–170°C; ^{1}H NMR ($CDCl_3$) δ: 3.84 (s, 3H, CH_3) and 7.12–7.83 (m, 10H, methine H and arom. H); EI mass spectrum *m/z*: 283 (M^+, 97), 250 (100), 221 (53), and 188 (59%). Exact Mass calcd. for $C_{16}H_{13}NS_2$: 283.0489; found: 283.0486.

(*b*) A mixture of **10*b*** (100 mg, 0.37 mmol) and thioacetic acid (3 mL) was heated under reflux for 8 h and the mixture was then concentrated in vacuo. Chromatography (silica; benzene–EtOAc) and crystallization from EtOH gave **12*b*** (60 mg, 57%), mp 166–168°C, identical with the foregoing sample.

Reaction of 2*c* with phenyl isothiocyanate

A mixture of **2*c*** (50 mg, 0.12 mmol), phenyl isothiocyanate

Can. J. Chem. Downloaded from www.nrcresearchpress.com by 80.90.12.36 on 09/08/12
For personal use only.

(20 mg, 0.15 mmol), and $CHCl_3$ (5 mL) was heated under reflux for 2 h, and the red solution was then concentrated in vacuo. Preparative TLC (silica; $CHCl_3$) and crystallization from EtOH gave the adduct **12***c* (40 mg, 78% based on phenyl isothiocyanate) as tiny yellow crystals, mp 158–160°C; ^1H NMR ($CDCl_3$) δ: 3.48 (s, 3H, CH_3), 6.58 (s, 1H, methine H), 7.12–7.68 (m, 9H, arom. H), and 8.05 (s, 1H, NH, exchangeable with D_2O); EI mass spectrum *m/z*: 346 (M^+, 100), 313 (43), and 254 (58%). Exact Mass calcd. for $C_{16}H_{14}N_2SSe$: 346.0043 (for ^{80}Se); found: 346.0027.

Results and discussion

Syntheses and characterization

Treatment of 2,3-dimethylbenzothiazolium, 3-ethyl-2-methylbenzothiazolium, and 2,3-dimethylbenzoselenazolium iodides with aqueous sodium hydroxide as originally described gave **2***a*, **2***b*, and **2***c*, respectively; these structures follow from consideration of NMR and mass spectra. 3-Allyl-2-methylbenzothiazolium bromide gave predominantly a mixture of monomeric and dimeric species (if isolated by solvent extraction) or the ring-opened amide (if isolated by filtration and desiccation) depending on the length of time in contact with water (cf. ref. 22). Similar treatment of 1,2-dimethylquinolinium iodide gave the monomeric methine base **3***a* as primary product (isolated by extraction as a buff solid (6); extraction with deuteriochloroform is useful as an aid for obtaining NMR spectra). This compound shows the methine carbon signal upfield at ca. 80 ppm and the signal due to the methine protons at ca. 3.6 ppm in its ^{13}C and ^1H NMR spectra, respectively. If, however, the product is isolated from this preparation by filtration and drying in a desiccator (7), a brick-red solid is obtained that is a mixture of monomeric and dimeric species. The ^{13}C NMR spectrum of the red solid contains 22 signals in addition to those due to **3***a* and points to the presence of **4***a*, a conclusion supported by the mass spectrum. The monomer **3***a* described above also reddens on keeping, with concomitant formation of **4***a*. The case of 1-ethyl-2-methylquinolinium salts (7) was reexamined by Metzger et al. (23) who reported obtaining mixtures of **3***b* and **4***b*. We were able to isolate **3***b* as a buff solid that reddened on keeping (7), due to the formation of **4***b*. We noted similar behaviour with 1-allyl-2-methylquinolinium bromide.

Treatment of 1,4-dimethylquinolinium iodide with aqueous sodium hydroxide solution gave a red solid that was identified as the dimeric species **5**; this turned into a purple-blue dye on exposure to air. Monomeric methine bases **6–9** were obtained from the corresponding quaternary iodides by treatment with aqueous sodium hydroxide. For these compounds, there is considerable hindrance to dimer formation and indeed no signs of dimers were detected. We conclude that a kinetically controllable procedure (cf. ref. 5) should be used to prepare monomeric methine bases from quaternary salts if a tendency to dimer formation is expected; otherwise, the aqueous base or tertiary base/acetonitrile procedures should suffice.

We turn now to the acyl and thiocyl derivatives of the methine bases in the benzothiazole and benzoselenazole series. We have used acylation of the appropriate methine base, generated in situ from the quaternary salt and triethylamine in acetonitrile, by a carboxylic chloride or anhydride to prepare **10***a–c*, and **11***a* and *b*. We also prepared **11***b* by benzolation of **2***c* (24). The Vongerichten–Rotta procedure was used to prepare **13***a* and **13***b* (13). Thioacyl derivatives have previously been made by reacting the foregoing acyl derivatives with phosphorus pentasulfide, but we have found that thioacetic acid is more convenient for the preparation of **12***a*. We had already used this reagent in the 1,3,4-thiadiazole series, where thioacetic acid had appeared to behave (unusually) as a thioacetylating agent (25). Success in the present work suggests that it plays the role of an oxygen–sulfur exchange reagent. **12***b* was prepared by thiobenzoylation of **1**, generated in situ, and **12***c* by reaction of **2***c* with phenyl isothiocyanate.

Molecular configuration

In the 1,3,4-thiadiazole series, we used N-aryl substitution (4) and X-ray crystallography (11) to determine the geometries of the acyl and thioacyl derivatives of the methine bases. In the present work, we use nuclear Overhauser effect (NOE) studies for this purpose, but first we note that the ^1H NMR spectra of representative compounds (**10***a*, **11***b*, **12***a* and *b*) in $CDCl_3$ are unchanged by running at 183 K.

First examined was **10***b* for which we deduce (*Z*) geometry. Thus, irradiation of the olefinic proton of a 0.2 M solution of **10***b* in $CDCl_3$ at δ 6.53 led to a +16.2% enhancement of the NCH_3 signal at δ 3.63. However, irradiation of the NCH_3 signal resulted in a −62.6% enhancement of the olefinic proton. This large negative enhancement was unexpected for a small molecule like **10***b*. Negative NOE's are frequently observed for macromolecules (26) that exhibit prolonged molecular motional correlation times τ_c (27). Williamson and Williams (28) have shown that negative NOE's can be observed when, by use of a viscous solvent such as Voltalef 10S (a polmer of chlorotrifluoroethylene), tumbling of the solute can be slowed down, i.e., τ_c can be prolonged. They used the observed negative NOE's to deduce the solution conformation of the antibiotic echinomycin.

A NOE difference spectrum of **10***b* (ca. 0.1 M) in $CDCl_3$ was then run. Irradiation of the NCH_3 signal at δ 3.63 led to a −24.4% enhancement of the olefinic proton at δ 6.53, a +12.5% enhancement of the aromatic proton *ortho* to the NCH_3 at δ 7.15, and a +5.3% enhancement of the aromatic protons *ortho* to the carbonyl group at δ 8.00. These enhancements were measured by normalization of the intensity of the saturated NCH_3 signal in the difference spectrum as a reference, and integrating the enhanced peaks relative to this scale. The assignment of the doublet of doublets at δ 8.00 to the aromatic protons *ortho* to the carbonyl group was further confirmed by reference to the ^1H–^1H COSY spectrum of **10***b*. The involvement of aromatic protons *ortho* to the carbonyl group in the dipolar relaxation clearly indicates molecular aggregations at high solute concentrations (29) and also helps to explain the observed large negative NOE's. In further support of molecular aggregation, irradiation of the NCH_3 protons of a 0.02 M solution of **10***b* in $CDCl_3$ led to a +7.2% enhancement of the olefinic proton.

NOE studies were used to establish the configurations of two further compounds. In the case of **10***a*, irradiation of the NCH_3 signal at δ 3.52 of a 0.2 M solution in $CDCl_3$ gave a +11% enhancement of the olefinic proton at δ 5.84, providing evidence for (*Z*) geometry. Similarly, (*Z*) geometry was established for **11***b*; irradiation of the NCH_3 signal at δ 3.68 of a 0.2

Fig. 1. The structure of **10***a* (compiled from data in ref. 30).

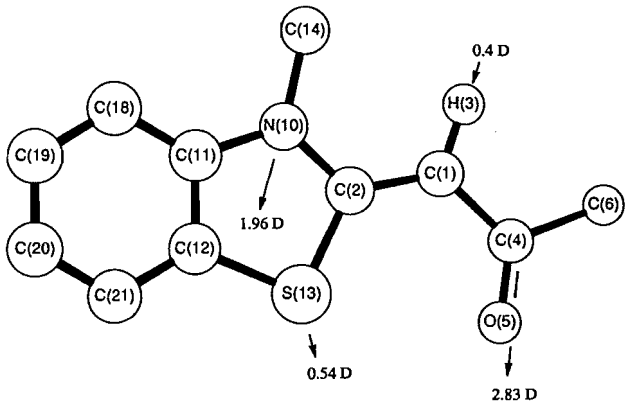

M solution in $CDCl_3$ gave a +24.1% enhancement of the olefinic proton at δ 6.84, while irradiation of the olefinic proton gave a +9.5% enhancement of the NCH_3 signal.

Molecular structure and molecular mechanics; structures 10*a* and 13*a*

The compounds **10** show a number of similarities with analogous 1,3,4-thiadiazoles reported previously. The IR carbonyl absorptions for **10***a* and *c* appear at 1604 and 1614 cm^{-1} respectively, and corresponding absorptions for a series of 2-acylidene-3-(1-cycloalkenyl)-2,3-dihydrobenzothiazoles all lie in the range 1600–1620 cm^{-1} (30). Trapani et al. (30) have reported an X-ray structure determination on one of their compounds, establishing (*Z*) geometry; we compute the S···O interatomic distance in that compound as 2.615 Å, well within the range found for corresponding 1,3,4-thiadiazoles, and indicative of a similar S···O interaction. From the coordinates given in that paper (30), we construct the model shown in Fig. 1 for compound **10***a*. The important points to note at this stage are the S···O interatomic distance (2.616 Å), the pseudo-torsion angle S(13)-N(10)-C(4)-O(5) of 1.4°, and the C(2)—C(1) and C(1)—C(4) bond orders of 1.761 and 1.374 respectively.

Using molecular mechanics, we compute the following steric energies for the (*Z*) isomer of **10***a*: *s-cis* conformer, 43.6 kJ mol^{-1}; *s-trans* (*transoid*) conformer, 38.5 kJ mol^{-1}. Corresponding energies for the (*E*) isomer are *s-cis* conformer, 52.7 kJ mol^{-1}; *s-trans* conformer, 66.4 kJ mol^{-1}. As in the thiadiazole series, the two (*Z*) conformers have lower energies than the two (*E*) conformers, and the overwhelming predominance of the (*Z*) isomer in the *s-cis* conformation in spite of a lower steric energy for the *s-trans* is an additional argument for a stabilizing S···O interaction.

For **13***a*, the argument for the (*E*) isomer existing as the *s-cis* conformer is based on the observed chemical shift for H3 in the ^1H NMR spectrum at δ 9.15, downfield due to deshielding by the proximate C=O group (13); for **13***b*, we note the corresponding signal at δ 8.89. The ^1H NMR spectrum of **13***a* in $CDCl_3$ is unchanged by running at 183 K; further, irradiation of the methine proton at δ ɔ.ϑ2 leads to a +27% enhancement of the NCH_3 signal at δ 3.62. This provides additional support for the (*E*)-*s-cis* assignment. As above, we compute the following steric energies for the (*E*) isomer: *s-cis* conformer, 49.6 kJ mol^{-1}; *s-trans* conformer, 51.0 kJ mol^{-1}. Corresponding energies for the (*Z*) isomer are *s-cis* conformer, 59.7 kJ mol^{-1}; *s-trans* conformer, 69.6 kJ mol^{-1}. The two (*E*) isomers have lower energies than the two (*Z*) isomers, and the dominant (*E*) isomer in the *s-cis* conformation may be further stabilized by weak hydrogen bonding (O···H—C3), which is not explicitly considered in the molecular mechanics calculation (14).

Fig. 2. Plot of the loss factor vs. temperature (K) at 5.02 kHz for **10***a* at a concentration of 5 wt.% solution in a polypropylene matrix (curve I). Curve II is a similar plot for pure polypropylene while curve III emerges from the subtraction of curve II from curve I at each of the experimental temperatures.

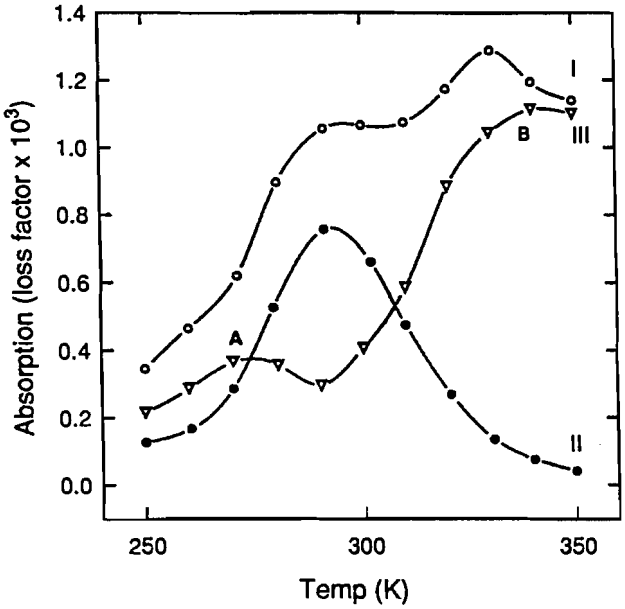

Intramolecular reorientation in 10*a*

The dielectric absorption of **10***a* has been studied with a view to determining whether the acetyl group reorients and, if so, to determine its energy barrier. The dielectric absorption method employing inert matrices (31) has, in the past 20 years, proved a most effective technique of detecting intramolecular motion and evaluating the corresponding energy barrier, and several studies have been made on acetyl group relaxation in a variety of aromatic molecules.

10*a* was dispersed in a polypropylene matrix and the dielectric absorption of its compressed disc measured at 11 temperatures at each of the following frequencies: 1010, 2020, 5020, and 10 200 Hz. This was repeated for a pure polypropylene disc, and its absorption at each temperature for a given frequency was subtracted from that of the solute-containing matrix. The results at 5020 Hz are presented in Fig. 2 where curve I gives the absorption of the solute-containing matrix, curve II that of the polypropylene, and III that for the solute itself. In case III, two absorption peaks emerge; the lower temperature peak at 276 K is designated A and the higher temperature peak, B.

The dielectric absorption technique and methods of evaluation of the results have been described previously (31–36).

It is now required to identify which of the two peaks is the intramolecular process. Molecular reorientation would account for one peak while, in view of previous studies on a wide variety of aromatic ketones, the relaxation of the acetyl

Can. J. Chem. Downloaded from www.nrcresearchpress.com by 80.90.12.36 on 09/08/12
For personal use only.

Can. J. Chem. Downloaded from www.nrcresearchpress.com by 80.90.12.36 on 09/08/12
For personal use only.

group is the most likely candidate for the other. Identification as to which peak corresponds with each of these processes is facilitated by making (rough) estimates of the dipole moment components responsible for each of the two processes. If μ_1 and μ_2 are the dipole moment components for the molecular and intramolecular processes, then the square of their values govern the intensities of each of these processes. For the present, we shall assume that the intramolecular process is acetyl group relaxation about the C(1)—C(4) bond (Fig. 1).

Published bond moment data (37, 38), shown in Fig. 1, were used in rough estimations of μ_1 and μ_2, and the inclination of the acetyl group moment to the C(2)-S(13)-C(12) group moment for the (*Z*) isomer was estimated as 25°. These estimations yielded $\mu_1 \sim 5.7$ D and $\mu_2 \sim 2.28$ D. Thus it is apparent that the intensity of the molecular relaxation process would be appreciably greater than that for the acetyl; hence the latter process is allocated to peak A and the higher temperature one to the molecular process (peak B). A temperature maximum (T_m) of about 340 K appears reasonable for the molecular process when compared with molecules such as biphenyl-4-carboxaldehyde and 9*H*-fluorene-2-carboxaldehyde, which have their molecular relaxation processes around this temperature (39) and are of a similar size.

We shall concern ourselves solely with the intramolecular process peak A. From the T_m values of 270 K, 275 K, 276 K, and 280 K at the corresponding frequencies (really frequency maximum (f_m) values) of 1010, 2020, 5020, and 10 200 Hz and the Arrhenius equation (40):

$$\log_{10} f_m = -E_A/2.303RT + A$$

where E_A is the Arrhenius energy of activation of the intramolecular process and, in our case, $T = T_m$ and A is a constant. A plot of $\log f_m$ vs. $1/T_m$ is made in Fig. 3. The f_m values may be regarded as accurate, but an error line corresponding to ±2 K was placed on the values of $1/T_m$ since partial overlap of the molecular and the intramolecular processes places some uncertainty on the determined T_m values. From the slope of the line, E_A was found to be 63 kJ mol^{-1} and its error could be greater than the normal ±10% for our dielectric procedure (32).

From the equation (39, 40):

$$E_A = \Delta H_E + RT$$

ΔH_E, the Eyring enthalpy of activation for the intramolecular process, is found to be 61 kJ mol^{-1}, that is, of the order of 60 kJ mol^{-1}.

The temperature region of absorption of this intramolecular process is fairly similar to that for acetyl group relaxation in *N*-acetylimidazole (41), which absorbs around 270 K for the frequencies employed. It is interesting to note, though, that the molecular relaxation process for this much smaller molecule occurs in the 120–160 K range, about 200 K lower than that of **10***a*.

For **10***a*, the reorientation of the acetyl group between its equilibrium positions corresponds with an asymmetrical free energy diagram in which ΔG_{E_1} and ΔG_{E_2} are the free energies of activation corresponding to the switch from the conformer of lower energy (*s-cis*) to that of the higher (*s-trans*) and to the switch from that from the higher (*s-trans*) to that of the lower

Fig. 3. Plot of $\log f_{max}$ vs. $10^3/T$ (K^{-1}) for **10***a* in a polypropylene matrix. The data correspond with process A in curve III, Fig. 2.

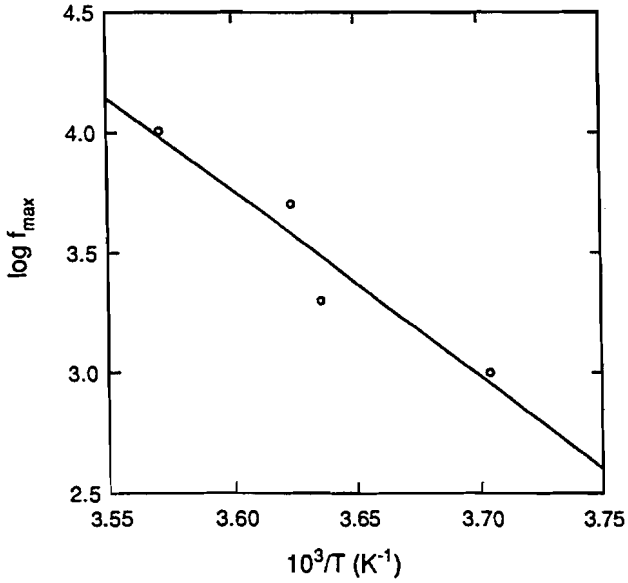

(*s-cis*), respectively, and $\Delta G°$ is the difference in free energy between the *s-cis* and *s-trans* conformers ($\Delta G_{E_1} - \Delta G_{E_2}$). The dielectric absorption method yields a free energy of activation value corresponding to the switch from the conformer with the higher energy (*s-trans*) to that of the lower (*s-cis*) (ΔG_{E_2}), and our determined ΔH_E value is for this reorientation (34*a*). The ΔH_E value for the alternative reorientation is expected to be larger since ΔS_E values are normally small for acetyl group relaxation.

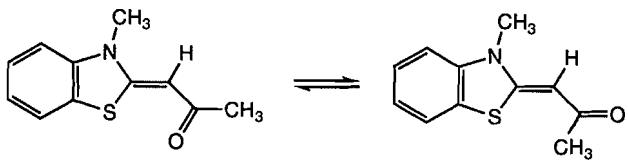

(*Z*)-s-*cis* (*Z*)-s-*trans*

The ΔH_E value of about 60 kJ mol^{-1} is to be compared with (*a*) those of 30 kJ mol^{-1} for acetyl group relaxation in acetophenone (32) and 4-acetylbiphenyl (32), which could be regarded as a typical value for simple aromatic ketones with no special conjugation effects, and (*b*) the acetyl group in *N*-acetylimidazole (41) with a value of 50 kJ mol^{-1} as a result of enhanced conjugation. Table 1 bears this out where the energy barriers for group reorientation are very similar for benzaldehyde, acetophenone, biphenyl-4-carboxaldehyde, and 4-acetylbiphenyl while appreciable increases are observed in the molecules that exhibit enhanced conjugation.

Thus, the ΔH_E value of about 60 kJ mol^{-1} for our intramolecular process is consistent with group reorientation in the more highly conjugated aldehyde and acetyl aromatic compounds, and, consequently, we assign the process to acetyl group reorientation.

We conclude that the magnitude of this ΔH_E value for acetyl group reorientation in **10***a* indicates enhanced conjugation of the keto group with the conjugated system over that in, say, acetophenone and 4-acetylbiphenyl. The value of ΔH_E for the

Table 1. ΔH_E values for group relaxation in selected carbonyl compounds.

Compound	Reference	ΔH_E (kJ mol^{-1})
Benzaldehyde	34*b*	27
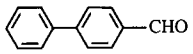	39	27
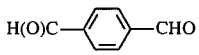	39	29
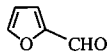	34*a*	46
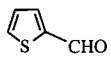	41	44
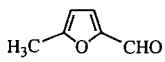	41	50
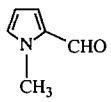	41	53
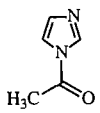	41	50

alternative reorientation, *s-cis* to *s-trans* conformer, will be larger than 60 kJ mol^{-1} because of the combination of (*a*) enhanced conjugation and (*b*) the stabilizing interaction between the S and O atoms. The latter interaction is perhaps comparable in its effect to that of a weak hydrogen bond (cf. ref. 11).

This behaviour is also predicted from the theoretical analysis (42) of **10***a* and the related molecule 2-acetonylidene-1,2-dihydro-1-methylquinoline. In the planar configurations (*Z* and *E*, respectively), the nominally double bonds of the acetonylidene side chain and adjacent ring are longer while the single bonds are shorter and exhibit some π character. The distinction between bond types returns when the acetyl group is rotated perpendicular to the ring plane. The calculations, performed at the HF/3-21G* level, predict a stabilization due to this extended conjugation. The barrier to internal rotation is found to be asymmetric, since the *s-cis* conformation allows for a further stabilizing interaction between S and O in **10***a*, and between (C3)H and O in the quinoline. This nonbonded or "closed shell" interaction is found to be a significant factor in the barrier to internal rotation, providing an additional lowering of energy for the *s-cis* conformation in each case. While the level of calculation is fairly good, given the size of these molecules, it cannot be expected to give a truly accurate prediction of barrier heights. Nevertheless, the qualitative picture is considered to be a reliable representation of the factors contributing to the stability of the preferred conformations.

Acknowledgments

We thank Dr. F. Souriel (Department of Chemistry, McGill University, Montreal, Québec) for providing NOE difference spectra, and Professor K.M. Gough (Brock University) for her interest in conducting the theoretical study (42) relevant to this work. We are grateful to the Natural Sciences and Engineering Council of Canada for financial support.

References

1. W. König and W. Meier. J. Prakt. Chem. **109**, 324 (1925).
2. O. Mumm, H. Hinz, and J. Diederichsen. Ber. Dtsch. Chem. Ges. **72**, 2107 (1939).
3. H. Larivé and R. Dennilauler. Chimia, **15**, 115 (1961); J. Metzger, H. Larivé, E. Vincent, and R. Dennilauler. J. Chim. Phys. **60**, 944 (1963).
4. T. Mohammad and M.S. Gibson. Sulfur, Phosphorus, Silicon, **70**, 243 (1992).
5. J.R. Owen. Tetrahedron Lett. **32**, 2709 (1969).
6. E. Rosenhauer, H. Hoffmann, and H. Unger. Ber. Dtsch. Chem. Ges. **59B**, 946 (1926).
7. F.M. Hamer, R.J. Rathbone, and B.S. Winton. J. Chem. Soc. 945 (1947).
8. A. van Dormael and Th. Ghys. Bull. Soc. Chim. Belg. **57**, 24 (1948).
9. L.G.S. Brooker, G.H. Keyes, R.H. Sprague, R.H. Van Dyke, E. Van Lare, G. Van Zandt, and F.L. White. J. Am. Chem. Soc. **73**, 5326 (1951).
10. V.I. Dénes, G.H. Ciurdaru, and M. Farcasan. Chem. Ber. **96**, 2691 (1963).
11. (*a*) N. Pandya, A.J. Basile, A.K. Gupta, P. Hand, C.L. MacLaurin, T. Mohammad, E.S. Ratemi, M.S. Gibson, and M.F. Richardson. Can. J. Chem. **71**, 561 (1993); (*b*) A. Kucsman and I. Kapovits. Studies in organic chemistry. Vol. 19. Organic sulfur chemistry. *Edited by* F. Bernardi, I.G. Csizmadia, and A. Mangini. Elsevier, Amsterdam. 1985. Chapt. 4.
12. V. Chandrasekhar, T. Chivers, J.F. Fait, and S.S. Kumaravel. J. Am. Chem. Soc. **112**, 5373 (1990); F.T. Burling and B.M.

Can. J. Chem. Downloaded from www.nrcresearchpress.com by 80.90.12.36 on 09/08/12
For personal use only.

Goldstein. J. Am. Chem. Soc. **114**, 2313 (1992); D.H.R. Barton, M.B. Hall, Z. Lin, S.I. Parekh, and J. Reibenspies. J. Am. Chem. Soc. **115**, 5056 (1993).
13. G. Fukata, C. O'Brien, and R.A.M. O'Ferrall. J. Chem. Soc. Perkin Trans. 2, 792 (1979); G.H. Alt. J. Org. Chem. **31**, 2384 (1966).
14. J.A.R.P. Sarma and G.R. Desiraju. Acc. Chem. Res. **19**, 222 (1986); G.R. Desiraju. Acc. Chem. Res. **24**, 290 (1991); T. Steiner and W. Saenger. J. Am. Chem. Soc. **115**, 4540 (1993).
15. W.M. Whaley and T.R. Govindachari. Organic reactions. Vol. VI. J. Wiley and Sons, Inc., New York. 1951. p. 100.
16. C.F. Koelsch. J. Org. Chem. **16**, 1362 (1951).
17. G.T. Morgan and L.P. Walls. J. Chem. Soc. 2447 (1931).
18. U. Burkert and N.L. Allinger. Molecular mechanics. ACS Monograph 177, American Chemical Society, Washington D.C. 1982.
19. L.M. Clark. J. Chem. Soc. 2313 (1929).
20. J. Bourson. Bull. Soc. Chim. Fr. 4028 (1966).
21. V.I. Dénes, Gh. Ciurdaru, and M. Farcasan. Rev. Roum. Chim. **10**, 1045 (1965); Chem. Abstr. **64**, 11403 (1966).
22. J. Metzger, H. Larivé, R. Dennilauler, and C. Gaurat. Bull. Soc. Chim. Fr. 2868 (1964).
23. J. Metzger, H. Larivé, E. Vincent, and R. Dennilauler. Bull. Soc. Chim. Fr. 46 (1967).
24. H. Wohl and J.J. Vorsanger. Bull. Soc. Chim. Fr. 3359 (1965).
25. H. Mastalerz and M.S. Gibson. J. Chem. Soc. Perkin Trans. 1, 2952 (1981).
26. P. Balaram, A.A. Bothner-By, and J. Dadok. J. Am. Chem. Soc. **94**, 4015 (1972).
27. A.E. Derome. Modern NMR techniques for chemistry research. Pergamon, Oxford. 1988. p. 103.
28. M.P. Williamson and D.H. Williams. J. Chem. Soc. Chem. Commun. 165 (1981).
29. L.F. Newcombe and S.H. Gellman. J. Am. Chem. Soc. **116**, 4993 (1994).
30. G. Trapani, A. Latrofa, A. Reho, M. Franco, G. Liso, and F. Stasi. J. Chem. Soc. Perkin Trans. 1, 1505 (1991).
31. M. Davies and J. Swain. Trans. Faraday Soc. **67**, 1637 (1971).
32. C.K. McLellan and S. Walker. Can. J. Chem. **55**, 583 (1977).
33. J. Crossley, M.A. Mazid, C.K. McLellan, P.F. Mountain, and S. Walker. (*a*) Adv. Mol. Relax. Interaction Processes, **13**, 239 (1978); (*b*) Can. J. Chem. **56**, 567 (1978).
34. (*a*) S.P. Tay, S. Walker, and E. Wyn-Jones. Adv. Mol. Relax. and Interaction Processes, **13**, 47 (1978); (*b*) A. Lakshmi, S. Walker, N.A. Weir, and J.H. Calderwood. Adv. Mol. Relax. Interact. Processes, **13**, 287 (1978).
35. M.S. Ahmed, M.A. Kashem, and S. Walker. J. Phys. Chem. **89**, 1670 (1985).
36. J. Crossley, D. Gourlay, M. Rujimethabhas, S.P. Tay, and S. Walker. J. Chem. Phys. **71**, 4095 (1979).
37. A.L. McClellan. Tables of experimental dipole moments. Vol. 2. Rahara Enterprises, El Cerrito, Calif. 1974.
38. D.B. Farmer, P.F. Mountain, and S. Walker. J. Phys. Chem. **77**, 714 (1973).
39. A. Lakshmi, S. Walker, N.A. Weir, and J.H. Calderwood. J. Chem. Soc. Faraday Trans. 2, **74**, 727 (1978).
40. N.H. Hill, W.E. Vaughan, A.H. Price, and M. Davies. Dielectric properties and molecular behaviour. van Nostrand–Reinhold, New York. 1969.
41. H.A. Khwaja, M.A. Mazid, and S. Walker. Z. Phys. Chem. (Wiesbaden), **128**, 147 (1981).
42. K.M. Gough and J. Millington. Can. J. Chem. **73**,1285 (1995).

Can. J. Chem. Downloaded from www.nrcresearchpress.com by 80.90.12.36 on 09/08/12
For personal use only.

Ab initio interpretation of conformer stabilization through S···O and C—H···O bonding in the acetyl derivatives of two representative heterocyclic methine bases

Kathleen M. Gough and Janice Millington

Abstract: *Ab initio* calculations (STO-3G and 3-21G* basis sets) have been performed on **2** and **3** to determine the most favorable structure and to provide an estimate of the barrier to internal rotation of the acyl group. The *Z* configuration is preferred in **2**, the *E* configuration in **3**, with calculated barriers to internal rotation of 79.9 and 68.7 kJ/mol, respectively, at the 3-21G* level. The wave functions from the 3-21G* calculations are analyzed with the theory of atoms in molecules. The identification of bond critical points characteristic of a closed shell interaction establishes the existence of a weak bond between S···O in **2** and between H···O in **3**, for the preferred configurations. The energy required to break this bond as well as the loss of extended conjugation throughout the hetero ring and its side chain are responsible for the asymmetry in the barrier. These findings provide a theoretical explanation for experimental observations on this class of molecules in which one conformer is preferred to any other and only one crystal structure is identified.

Key words: nonbonded sulfur–oxygen interaction, closed shell interaction, hydrogen bonding, 3-21G* basis set, theory of atoms in molecules.

Résumé : On a effectué des calculs *ab initio* (ensembles de base STO-3G et 3-21G*) sur les composés **2** et **3** dans le but de déterminer leur structure la plus favorable et d'obtenir une évaluation de la barrière à la rotation interne du groupe acyle. Les conformations préférées sont la *Z* pour le composé **2** et la conformation *E* pour le composé **3**; au niveau 3-21G*, les barrières calculées à la rotation interne sont respectivement de 79,9 et de 68,7 kJ mol^{-1}. On a analysé les fonctions d'onde obtenues par les calculs au niveau 3-21G* à l'aide de la théorie des atomes dans les molécules. L'identification de points critiques dans les liaisons, caractéristiques d'une interaction à couche fermée, permet d'établir que, dans les configurations préférées, il existe une liaison faible entre S···O dans le composé **2** et H···O dans le composé **3**. Ces résultats fournissent une explication théorique des observations expérimentales sur cette classe de molécules dans lesquelles un conformère est préféré à tous les autres et avec lesquelles on n'identifie qu'une seule structure cristalline.

Mots clés : interaction non liée soufre–oxygène, interaction à couche fermée, liaison hydrogène, ensemble de base 3-21G*, théorie des atomes dans les molécules.

[Traduit par la rédaction]

Introduction

The concept of the chemical bond is subject to a wide range of interpretations, as required by the interactions to which this term can be applied. The criteria that are accepted as defining the existence of a bond between two atoms are similarly varied. Problems arise when the nature of the interaction is far from the typical covalent behavior, as is the case for hydrogen bonding and for the so-called "hypervalent" interactions between formally nonbonded heavy atoms (1–6). While it may be more difficult to establish the existence of such weak bonds in some systems, it is nonetheless clear that such interactions do exist, and can be of vital importance in determining the stability of particular conformers and of particular crystal structures, as well as determining preferred reaction pathways.

In a recent study (1) of acyl derivatives of methine bases such as 2-acetonylidene-3,5-diaryl-2,3-dihydro-1,3,4-thiadiazole, **1**, it was proposed that some bicyclic character existed in the form of a partial hypervalent bond between S and O.

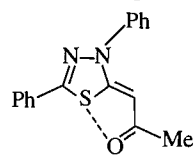

1

Received December 21, 1994.

Kathleen M. Gough[1] **and Janice Millington.** Department of Chemistry, Brock University, St. Catharines, ON L2S 3A1, Canada.

[1] Author to whom correspondence may be addressed at the Department of Chemistry, University of Manitoba, Winnipeg, MB R3T 2N2, Canada. Telephone: (204) 474-6262. Fax: (204) 275-0905. E-mail: kmgough@pauli.chem.umanitoba.ca

Can. J. Chem. Downloaded from www.nrcresearchpress.com by 80.90.12.36 on 09/08/12
For personal use only.

Can. J. Chem. Downloaded from www.nrcresearchpress.com by 80.90.12.36 on 09/08/12
For personal use only.

This conclusion was based on the observation that only one of the two possible geometrical isomers could be isolated. In addition, crystal structures showed that the S···O distance was on the order of that expected for "hypervalent" interaction. Theoretical investigations (2, 3) into the possible existence of some type of nonbonded interaction between S and O in smaller molecules with the same structural fragment have drawn the same conclusion. The evidence presented consists of calculated interatomic distances from optimized geometries, energy changes, and Mulliken population analysis. In one paper (3), a bond order was estimated from the exchange part of the second-order density matrix, according to the definition of Mayer. While this evidence is compelling, it seemed reasonable to presume that an analysis of the topological distribution of the charge density could provide further insight into the nature of the interaction. Such an analysis would also be useful for the examination of the changes in energy, molecular structure, and bonding during internal rotation and in a comparison of the *E* and *Z* configurations.

Accordingly, we present here the results of an *ab initio* study of two representative molecules: 2-acetonylidene-2,3-dihydro-3-methylbenzothiazole (**2**) and 2-acetonylidene-1,2-dihydro-1-methylquinoline (**3**).

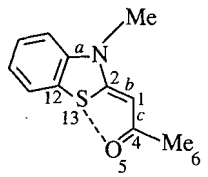

2 (*Z* configuration)

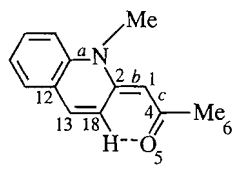

3 (*E* configuration)

In **2**, the *Z* configuration allows the S···O interaction to occur in the *s-cis* conformation, as shown; in **3**, this interaction is replaced by a possible H···O bond in the *E* configuration. In the calculations and discussion which follow, both the geometries pictured above are referred to as 0° torsion, where rotation occurs about the bond labelled *c* in the figures above. Some of the atoms are numbered for later reference and in accordance with the preceding paper. Optimized geometries were obtained with both the STO-3G and 3-21G* bases for both the 0° and 180° rotamers, and for several points along the path of internal rotation of the acetyl group, between these two extremes. The wavefunctions from the 3-21G* calculations were obtained for each geometry and analyzed with the theory of atoms in molecules (7). This topological analysis of the charge density enables one to examine the charge density between atoms, to determine whether a bond truly exists, and to examine the nature of such bonds. We have also investigated the degree of single/double bond character in the ring bonds during internal rotation and the existence of a ring-like structure. Crystal studies (1, 11) indicate that the molecules are planar; thus for the majority of the analyses, a planar constraint was imposed. Fully unconstrained calculations were performed for the 0°, 90° and 180° conformers and are compared to the constrained planar calculations.

Computational method

The starting geometries for the calculations on **2** were taken from the crystal data for a related molecule (8), in which the N-methyl group is replaced by a cyclohexenyl ring and the acyl methyl by a propyl group. Replacement by methyl groups accelerated the computations and made the topological analysis more tractable, without loss of those aspects which most strongly influenced the geometry about the nonbonded region of interest. No crystal data were available for the quinoline molecule, therefore the starting geometry was adapted from that of the thiazole.

For each molecule, the Gaussian90 molecular orbital program (9) was used to obtain the optimized geometry for the given basis set, with the following constraints. The majority of the calculations were performed with all heavy atoms coplanar, with the exception of the portion undergoing internal rotation. This choice was made because the crystal data on related compounds indicate a stable planar geometry. The internal rotation was modeled by fixing the torsional angle made between the acyl group and the defined heavy atom plane, and allowing all other parameters to relax. In the 1,3,4-thiadiazole cases, crystal data (1, 11) indicated that there might be a slight residual twist of about 1.7° of the acyl group relative to the plane; therefore several points were taken in this region. The twist angle in the benzothiazole case is 1.4° and again several points were taken in this region. The *ab initio* calculations model the gas phase behavior, where the nonplanarity may be more pronounced. Unconstrained geometry optimizations were performed for the 0°, 90°, 120°, and 180° rotamers to compare the barrier estimates and provide an upper limit to the degree of nonplanarity that might be expected.

The wave function from the optimized geometry for each rotamer was obtained with PSIG90 (10) and the topology of the charge density at selected critical points was calculated with SADDLE (10). Both programs are part of the AIMPAC suite (10), used for the analysis of atoms in molecules according to the theory developed by Bader. Bond orders can be estimated from a correlation between parameters at the bond critical points and those for bonds with well-defined bond orders. We therefore obtained these parameters for methane, ethane, ethylene, acetylene, and benzene with the 3-21G* basis for comparison with **2** and **3**.

Results and discussion

Magnitude and shape of the barriers

(a) constrained planar

The change in energy during internal rotation of the acetyl group is illustrated in Figs. 1 and 2 for the thiazole, **2**, and the quinoline, **3**, respectively. When the rest of the molecule is contrained to be planar, the 3-21G* calculated barrier to internal rotation is 75.9 kJ/mol in **2**, and only slightly lower, at 68.7 kJ/mol, in **3**. The barriers to internal rotation calculated with the STO-3G basis were 33.4 and 34.7 kJ/mol, respectively. Underestimation of the barrier is typical of these minimal basis set calculations and the 3-21G* results are to be preferred. The values are in quite good agreement with those estimated from the dielectric absorption method (11).

(b) unconstrained

The barriers drop to 74.5 and 61.8 kJ/mol, respectively, when the planarity constraint is removed. The greatest change in dihedral angle occurs in the vicinity of the N atom, at which a pyrimidal geometry would be anticipated. The dihedral angles between bonds labelled *a* and *b* (above) are:

Fig. 1. Plot of total molecular energy of thiazole **2**, during internal rotation, calculated with 3-21G* basis set.

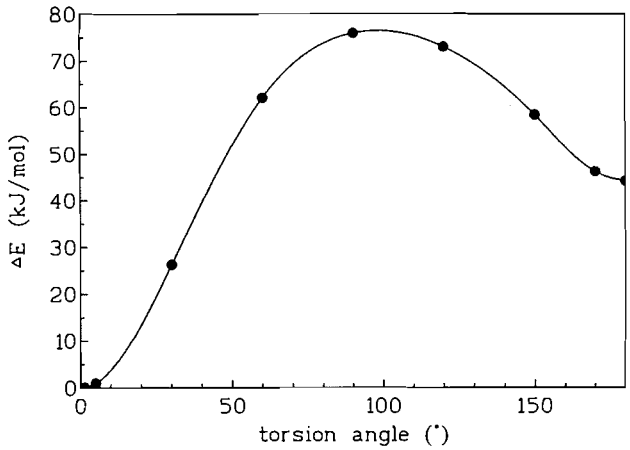

Fig. 2. Plot of total molecular energy of quinoline **3**, during internal rotation, calculated with 3-21G* basis set.

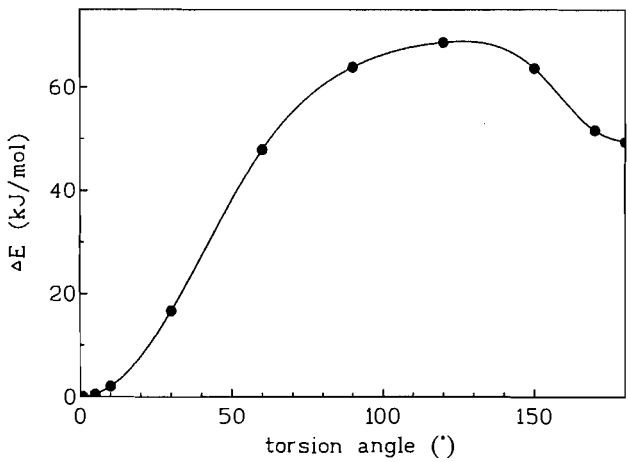

	0°	90°	180°
Thiazole(**2**)	183.9	188.8	186.0
Quinoline(**3**)	191.8	195.6	196.0

The most significant change is that the maximum in the barrier for the quinoline now occurs at 90° instead of at 120° as it appears in Fig. 2. The entire side chain remains more nearly coplanar with the S in the Z configuration (**2**) or the CH in the *E* configuration (**3**). The aromatic ring remains essentially planar throughout. This lack of tendency towards nonplanarity, combined with the crystal data, justifies our decision to examine the planar structures in more detail.

These calculated barriers are both fairly large; however, they are not inconsistent with the data estimated from the dielectric absorption method for similar compounds (11, 12). The latter estimates refer to an enthalpy difference between the 180° and 90° rotamers; however, they should provide a lower limit to the total barrier. For molecule **2**, it is suggested that the considerable height of the barrier is due to the extended conjugation between the acetonyl moiety and the ring. In both molecules, the preferred geometry is the 0° torsion. The barrier to internal rotation is significant, and its origin is of interest.

Table 1. Bond critical point parameters from standard molecules for comparison with **2** and **3**, calculated with 3-21G* basis (bond length in Å, ε and ρ (r_c) in atomic units).

					Bond order	
Molecule	Bond	Bond length	ε	ρ(r_c)	True	Est.
Ethane	C—C	1.5425	0.0	0.2178	1.0	.99
Benzene	C═C	1.3846	0.1435	0.3007	1.6	1.60
Ethene	C═C	1.3149	0.2316	0.3392	2.0	2.01
Ethyne	C≡C	1.1875	0.0	0.4077	3.0	2.88
Methane	C—H					
Ethane	C—H	1.0842	0.0110	0.2607		
Benzene	C—H	1.0721	0.0028	0.2715		
Ethene	C—H	1.0736	0.0076	0.2681		
Ethyne	C—H	1.0506	0.0	0.2777		

Clearly the hypervalent interaction should be of importance, along with loss of extended conjugation. We next use the theory of atoms in molecules to analyze the wavefunctions from the 3-21G* calculations in order to examine these factors in a more quantitative manner.

AIM properties

The theory of atoms in molecules has been presented in detail in the literature (7) and only points essential to the discussion are reviewed here. The principal properties of interest are the charge density, $\rho(\boldsymbol{r})$, the gradient ($\nabla\rho(r)$), the curvature ($\nabla^2\rho(\boldsymbol{r})$), and the ellipticity of the charge distribution (ε) at bond critical points. Within a molecule, maxima in the charge density appear at each nucleus. This density decreases as one moves away from a nucleus, then increases again as another nucleus is approached. The surface of an atom in a molecule is defined by the union of the points about the nucleus at which the charge density reaches a local minimum, that is, by the surface for which there is zero flux in the charge density. For exterior atoms, the outer surface falls away to zero at infinity, but, for practical purposes, it has been defined as the surface for which the charge density falls to 0.001 au.

A bond may be described as a *shared interaction*, where the degree of interaction may range from pure covalent to pure ionic and may include the weakly bonded interactions of interest in this study (7, 13–15). When a covalent bond forms, there is a lowering of the potential energy due to the increase in charge density between the two nuclei. If two atoms are bonded, there will be a line joining the atoms along which the charge density is maximum in the plane orthogonal to the bond path. The charge density along this line will fall to a minimum where the interatomic surface crosses the bond path, at the *bond critical point.* The three values associated with the curvature of the charge density at the bond critical point, $\nabla^2\rho(\boldsymbol{r}_c)$, are referred to as the eigenvalues of the Hessian of ρ at $\boldsymbol{r}_c$, or as λ_1, λ_2, and λ_3. The lone positive value, associated with the curvature along the bond path, is assigned to λ_3. The distribution of the charge density about a bond is frequently found to be non-uniform, as measured by the *ellipticity*, $\varepsilon = [(\lambda_1/\lambda_2) - 1]$. For the 3-21G* basis, the ellipticity varies from 0 in the C—C bond of ethane to 0.23 in ethyne (Table 1). The charge density at the bond critical point has been used to

Can. J. Chem. Downloaded from www.nrcresearchpress.com by 80.90.12.36 on 09/08/12
For personal use only.

Table 2. Properties at the bond critical point between S and O in **2**.

Torsion angle (°)	0	0.7	1.4	5	30
$\rho(r_c)$	0.0247	0.0247	0.0246	0.0242	0.0156
$\nabla^2\rho(r_c)$	0.0949	0.0949	0.0948	0.0936	0.0682
λ_1	−0.0202	−0.0202	−0.0202	−0.0191	−0.0114
λ_2	−0.0191	−0.0191	−0.0191	−0.0187	−0.0102
λ_3	0.1341	0.1341	0.1341	0.1319	0.0897
ε	0.0575	0.0574	0.0572	0.0527	0.1185
r(S···O) Å	2.6345	2.6345	2.6348	2.6440	2.8502

Table 3. Properties at the bond critical point between H and O in **3**.

Torsion angle (°)	0	1	5	10	30
$\rho(r_c)$	0.0281	0.0281	0.0279	0.0272	0.0214
$\nabla^2\rho(r_c)$	0.1139	0.1139	0.1133	0.1119	0.0961
λ_1	−0.0396	−0.0396	−0.0392	−0.0379	−0.0268
λ_2	−0.0373	−0.0373	−0.0367	−0.0357	−0.0250
λ_3	0.1908	0.1907	0.1895	0.1855	0.0480
ε	0.0618	0.0618	0.0623	0.0635	0.0726
r(H···O) Å	2.0198	2.0200	2.0233	2.0336	2.1393

Can. J. Chem. Downloaded from www.nrcresearchpress.com by 80.90.12.36 on 09/08/12
For personal use only.

obtain an estimate of the bond order in a molecule. Both parameters offer a measure of the amount of π character in a bond. A correlation between bond lengths and $\rho(r_c)$ parameters for C—C and S—S bonds has been observed in a number of studies (16). Such points exist even for very weakly interacting atoms, such as those joined by a hydrogen bond. Finally, when a molecule contains a ring, a *ring critical point* is found to exist in the charge density. At such a point, two of the three eigenvalues of the Hessian are positive and the plane of the ring represents a maximum in the charge density for any line or plane cutting through it.

Origin of the barrier

(a) Hypervalent/H-bond interactions

The structural and topological changes in the charge density accompanying rotation are listed in Tables 2–5. The parameters of interest are the bond lengths, the charge density and ellipticity at the bond critical points or ring critical points, and the estimated bond order. Tables 2 and 3 provide details of the changing interaction between the nonbonded atoms (S···O in **2** and H···O in **3**) during internal rotation. Tables 4 and 5 highlight the extended conjugation between the side chain and the ring atoms.

According to studies on weak atomic interactions (14, 15), the type of bonding found here between the S···O and H···O would be classified as a closed-shell interaction (Tables 2 and 3). The value of ρ_c is typically an order of magnitude smaller than that for a covalent bond. The curvature of the charge is still positive along the bond path, and negative in directions orthogonal to the path; however, $|\lambda_3| > |\lambda_2| \approx |\lambda_1|$. In both molecules, the bond is fairly strong, comparable to that of the hydrogen bond in the water dimer, as opposed to that found in weak van der Waals complexes between Ne or Ar and HF (7). In previous studies of closed shell interactions, the relative depletion of charge between the two atoms resulted in only a slight lowering of the potential energy and a correspondingly weak bond. The atoms were typically found to have opposite net charges and the stability of the arrangement was based mainly on the ionic-like attraction. In the present system, it appears that the interaction may also be mainly ionic, as in that of a typical hydrogen bond. The structures **2** and **3** are both too large to be analyzed fully with the AIMPAC suite. A much more detailed study of the Laplacian of the charge density, possibly on a smaller model compound, would be required if one wished to investigate the location of valence shell charge concentrations, which are the quantum mechanical counterpart of the lone pairs in VSEPR theory, and thereby ascertain the role of the sulfur *d* orbitals. The admittedly crude estimates provided by a Mulliken population analysis give charges of −0.63 (oxygen), +0.57 (sulfur) in **2** and −0.63 (oxygen), +0.34 (hydrogen) in **3**.

In both **2** and **3**, the formation of the closed-shell interaction is accompanied by the apearance of ring critical points that exhibit characteristics analogous to those of the weak bond critical points. During internal rotation, the closed-shell interaction breaks somewhere between the 30° and 60° postions. Interestingly, the weak ring critical point reforms when the methyl group is rotated to within 30° of the S or H, i.e., the 150° position, and continues on to the 180° position. The energy lowering associated with such a point is small but, since the geometry stabilization investigated here is a combination of weak factors, it is worth noting.

(b) Extended conjugation

The charge density (ρ_c) at the bond critical points of standard molecules has been obtained for this basis set (Table 1) in order to allow a bond order to be calculated from the expression (13):

$$[1] \quad n = \exp\{A(\rho - B)\}$$

Table 4. Bond critical point parameters and some estimated bond orders for S and acyl group in **2**, at 0°, 90°, and 180° rotation.

Bond	Torsion angle (°)	Bond length (Å)	ε	ρ (r_c)	Bond order (est.)
C12—S13	0.0	1.7569	0.163	0.2029	
	90.0	1.7593	0.146	0.1987	
	180.0	1.7541	0.146	0.2014	
S13–C2	0.0	1.7647	0.205	0.1997	
	90.0	1.7788	0.172	0.1939	
	180.0	1.7745	0.172	0.1953	
C2—C1	0.0	1.3500	0.272	0.3122	1.72
	90.0	1.3246	0.317	0.3275	1.88
	180.0	1.3387	0.268	0.3180	1.78
C1—C4	0.0	1.4391	0.138	0.2732	1.37
	90.0	1.4982	0.041	0.2441	1.15
	180.0	1.4625	0.096	0.2593	1.26
C4—O5	0.0	1.2291	0.058	0.3667	
	90.0	1.2116	0.018	0.3782	
	180.0	1.2206	0.033	0.3749	
C4—C6	0.0	1.5145	0.023	0.2371	1.11
	90.0	1.5144	0.034	0.2369	1.10
	180.0	1.5153	0.021	0.2364	1.11

Table 5. Bond critical point parameters and some estimated bond orders for acyl group and adjacent ring carbons in **3**, at 0°, 90°, and 180° rotation.

Bond	Torsion angle (°)	Bond length (Å)	ε	ρ (r_c)	Bond order (est.)
C12—C13	0.0	1.4426	0.063	0.2706	1.32
	90.0	1.4494	0.064	0.2667	1.35
	180.0	1.4412	0.065	0.2714	1.32
C13—C18	0.0	1.3262	0.205	0.3366	1.98
	90.0	1.3226	0.230	0.3387	2.00
	180.0	1.3255	0.221	0.3371	1.98
C18—C2	0.0	1.4591	0.049	0.2691	1.33
	90.0	1.4663	0.071	0.2590	1.26
	180.0	1.4593	0.068	0.2621	1.28
C2—C1	0.0	1.3615	0.265	0.3092	1.69
	90.0	1.3372	0.306	0.3232	1.83
	180.0	1.3523	0.261	0.3141	1.74
C1—C4	0.0	1.4511	0.128	0.2653	1.31
	90.0	1.4969	0.041	0.2450	1.16
	180.0	1.4648	0.101	0.2570	1.24
C4—C6	0.0	1.5242	0.027	0.2340	1.09
	90.0	1.5164	0.033	0.2364	1.10
	180.0	1.5189	0.017	0.2346	1.09

Can. J. Chem. Downloaded from www.nrcresearchpress.com by 80.90.12.36 on 09/08/12
For personal use only.

Can. J. Chem. Downloaded from www.nrcresearchpress.com by 80.90.12.36 on 09/08/12
For personal use only.

Fig. 3. Changes in charge density (ρ: –●–), bond length ($R_{C=C}$: --▲--), and bond ellipticity (ε: ···○···) for bonds labelled *b* and *c* in the structure of thiazole **2**. Values for ρ appear on the left axis; for $R_{C=C}$ on the right axis. Values for ellipticity range from a maximum of 0.317 au to a minimum of 0.268 au for bond *b* and 0.138 au to 0.041 au for bond *c*.

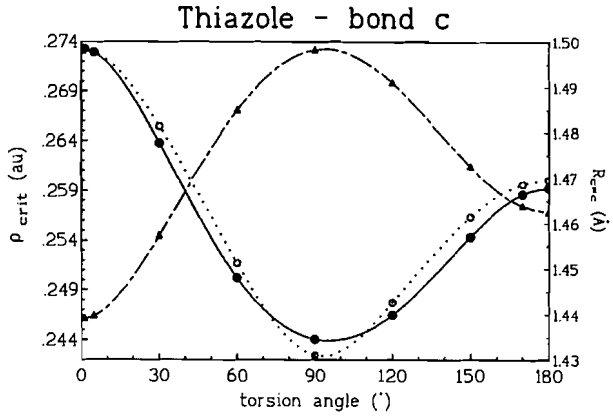

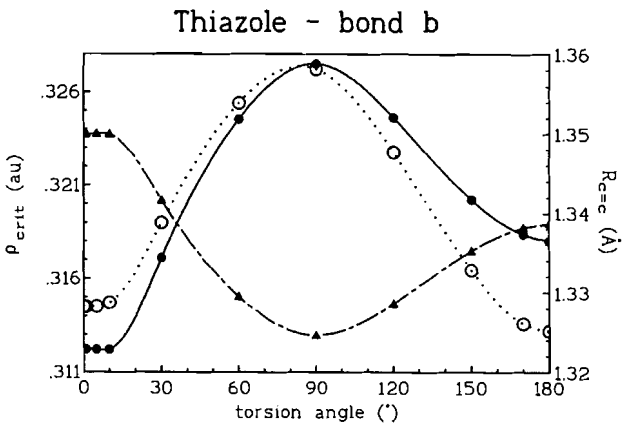

Fig. 4. Changes in charge density (ρ: –●–), bond length ($R_{C=O}$: --▲--) and bond ellipticity (ε: ···○···) for the carbonyl bonds in thiazole **2** and quinoline **3**. Values for ρ appear on the left axis; for $R_{C=O}$ on the right axis. Values for ellipticity range from a maximum of 0.053 au to a minimum of 0.021 au in the thiazole and 0.052 au to 0.024 au in the quinoline.

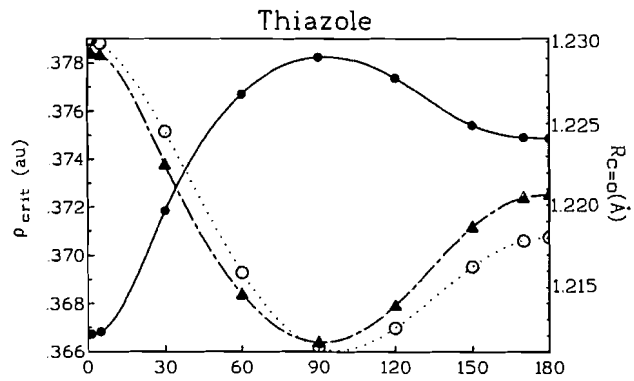

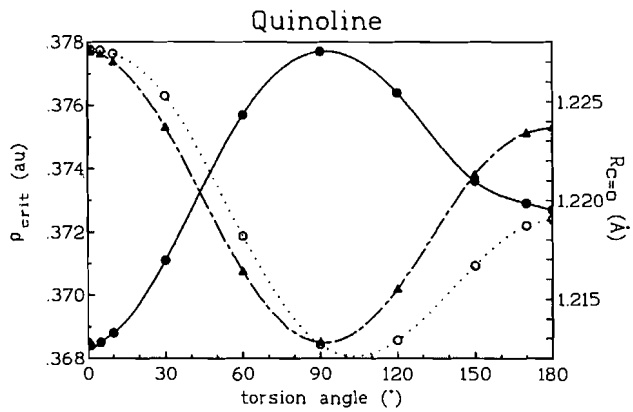

For the present study, the values of the fitted parameters are $A = 5.83$ and $B = 0.220$. The estimated bond orders for **2** and **3** are included in Tables 4 and 5. The 0° and 180° planar structures of both molecules exhibit a strong conjugative interaction. The bonds depicted as double decrease in length while the charge density about the bond becomes more elliptical, as the acyl group is rotated up out of the plane. At the same time, those designated as single become longer, and the charge density less elliptical. Typical behavior is illustrated in Fig. 3 for the bonds labelled *b* and *c* in the thiazole. As the rotation proceeds, the bond *b*, which is depicted as double, becomes shorter. The ellipticity increases, indicating an increase in the π character of the bond. The charge density at the bond critical point also increases, corresponding to the increased strength of the bond. The behavior of these properties is exactly the opposite for the bond labelled *c*, which becomes longer and weaker, while the ellipticity decreases. This nicely illustrates the loss of conjugation that occurs during the rotation. The instability of the system rises steadily as the rotation proceeds and continues to increase even after the closed-shell interaction disappears (>30°). The only obvious cause of instability is the continuing decrease in extended conjugation. The ellipticity at the bond critical point is another measure of the degree of π character in a bond. Comparison of the ellipticities of the standard bonds in Table 1 with those in Tables 4 and 5 show that the extended π bonding and the changes that occur during internal rotation are also manifested in this parameter. These data serve to further illustrate the changes in conjugation that occur during the internal rotation. A similar situation is observed for the internal rotation in the quinoline. If one assumes that the asymmetry in the barrier to internal rotation arises solely from the closed-shell interaction in the *s-cis* conformations, and that extended conjugation contributes the same amount of stability to the molecules in either the *E* or *Z* configuration, then the energy plots in Figs. 1 and 2 indicate that the closed-shell interaction is the more important, providing 45–50 kJ/mol stabilization, while the extended conjugation provides an additional 20–30 kJ/mol.

The behavior of the carbonyl bond during internal rotation is illustrated in Fig. 4, for both molecules. We note that the bond is shortest when the rotation angle is 90° and the conjugation is minimized. The bond is also less elliptical, in contrast to the C=C bond, *b*. We interpret this as indicative of the true

nature of a nonconjugated carbonyl double bond, in which the "lone pair" electrons on the oxygen actually are sharing in the bonding and the bond is more cylindrical. When the conjugation is at a maximum (0°or 180°), the increased ellipticity reflects the preference for the formation of a distinct π bond that can interact with the π bonds elsewhere along the chain. For both the C=O and C=C bonds, the conjugation results in a longer, weaker bond.

The terminal aromatic ring is altered only marginally during internal rotation, even in the 90° rotamer, and does not appear to contribute to the preference of one isomer over another. Even in the structures for which the aromatic ring is constrained to be coplanar with the hetero ring and side chain, there is almost no interaction between the two portions. However, since its presence presumably adds to the rigidity of the hetero ring, it is considered to be an essential part of the system. The bond lengths (**2**: 1.3836±0.004 and **3**: 1.388±0.009 Å) are quite similar to those in benzene. Bond orders estimated frm ρ_c and eq. [1] also indicate that the ring is essentially aromatic. This does not change during internal rotation of the acyl group.

It is interesting to compare our results with recent studies on the nature of the hydrogen bond (17, 18), which have produced the concept of the resonance-assisted hydrogen bond (rahb) in cases of homonuclear hydrogen bond formation. The latter applies to bonds of the type (O···H—O), where the oxygen atoms are part of a π conjugated fragment, such as in the enol form of a β-diketone. The authors note that extensive correlation of crystallographic data supports the notion that homonuclear hydrogen bonds are inherently different from hetero hydrogen bonds. The two cases studied in the present work fall into the latter class yet, because of their molecular structure, extended conjugation and hydrogen bonding are found to be working together to produce the most stable conformer.

From the present study, the observed stability of the 0° rotamer in **2** and **3** appears to arise from a combination of factors:

(*a*) there is a strong nonbonded interaction between the S···O and the H···O, as evidenced by the existence of a bond critical point between these atom pairs, which provides 45–50 kJ/mol stabilization energy;

(*b*) the nonbonded interaction creates a weak ring-like structure, with a ring critical point shared by the ring atoms, disappearing for a torsion >30°;

(*c*) extended conjugation contributes a further 20–30 kJ/mol to the stability of the planar configurations;

(*d*) the tendency for the molecule to pucker in the vicinity of the N atom is counterbalanced by the extended conjugation for the 0° rotamer;

(*e*) while the adjacent aromatic ring may be imparting an increased rigidity to the system, it does not participate in the electronic changes that occur during rotation.

In related experiments on a similar molecule (11), the barrier height between the 90° and 180° regions (Figs. 1 and 2) has been estimated by measuring relaxation times after promotion to the less stable configuration. This lower barrier provides an estimate of the hyperconjugation energy, and is similar to that calculated here. Finally, we note the usefulness of *ab initio* calculations in the elucidation of this problem. In particular, the charge density at the bond critical point and the bond ellipticity, obtained in the analysis of the wavefunction, should be considered in similar situations.

Acknowledgements

The authors wish to thank Prof. Martin S. Gibson for bringing this problem to our attention. This work was supported in part by a grant from the Natural Sciences and Engineering Research Council of Canada. J.M. is grateful to the Natural Sciences and Engineering Research Council of Canada for the award of an summer student research award (1993).

References

1. N. Pandya, A.J. Basile, A.K. Gupta, P. Hand, C. MacLaurin, T. Mohammed, E.S. Ratemi, M.S. Gibson, and M.F. Richardson. Can. J. Chem. **71**, 561 (1993).
2. F.T. Burling and B.M. Goldstein. J. Am. Chem. Soc. **114**, 2313 (1992).
3. (*a*) J.G. Ángyán, R.A. Poirier, Á. Kucsman, and I.G. Csizmadia. J. Am. Chem. Soc. **109**, 2237 (1987); (*b*) Á. Kucsman and I. Kapovits. *In* Studies in organic chemistry 19, Organic sulfur chemistry — theoretical and experimental advances. *Edited by* F. Bernardi, I.G. Csizmadia, and A. Mangini. Elsevier Science Publishers, Amsterdam. 1985. Chap. 4.
4. D.H.R. Barton, M.B. Hall, Z. Lin, S. I. Parekh, and J. Reibenspies. J. Am. Chem. Soc. **115**, 5056 (1993).
5. J.A.R.P. Sarma and G.R. Desiraju. Acc. Chem. Res. **19**, 222 (1986); G.R. Desiraju. Acc. Chem. Res. **24**, 290 (1991).
6. T. Steiner and W. Saenger. J. Am. Chem. Soc. **115**, 4540 (1993).
7. R.F.W. Bader. Atoms in molecules — a quantum theory. Oxford University Press, Oxford. 1990.
8. G. Trapani, A. Latrofa, A. Reho, M. Franco, G. Liso, and F. Stasi. J. Chem. Soc. Perkin Trans. 1, 1505 (1991).
9. M.J. Frisch, M. Head-Gordon, G.W. Trucks, J.B. Foresman, H.B. Schlegel, K. Raghavachari, M. Robb, J.S. Binkley, C. Gonzalez, C.F. Melius, J. Baker, R.L. Martin, L.R. Kahn, J.J.P. Stewart, S. Topiol, and J.A. Pople. Gaussian 90, Revision I. Gaussian Inc., Pittsburgh, Pa. 1990.
10. AIMPAC, McMaster University (1990); F. W. Biegler-König, R.W.F. Bader, and T.-H Tang. J. Comput. Chem. **13**, 317 (1982).
11. A.K. Gupta, A. Ben Mahmud, L.J. Kamphuis, J.L. Mueller, S.S. Rigby, M.S. Gibson, M.F. Richardson, L. Humeniuk, and S. Walker. Can. J. Chem. **73**, 1276 (1995).
12. H.A. Khawaja, M.A. Mazid, and S. Walker. Z. Phys. Chem. **128**, 147 (1981).
13. R.F.W. Bader, T.S. Slee, D. Cremer, and E. Kraka. J. Am. Chem. Soc. **105**, 5061 (1983).
14. M.T. Carroll, C. Chang, and R.F.W. Bader. Mol. Phys. **63**, 387 (1988).
15. M.T. Carroll and R.F.W. Bader. Mol. Phys **65**, 695 (1988).
16. O. Knop, R.J. Boyd, and S.C. Choi. J. Am. Chem. Soc. **110**, 7299 (1988).
17. G. Gilli, F. Belluci, V. Ferretti, and V. Bertolasi. J. Am. Chem. Soc. **111**, 1023 (1988).
18. P. Gilli, V. Bertolasi, V. Ferretti, and G. Gilli. J. Am. Chem. Soc. **116**, 909 (1994).

Can. J. Chem. Downloaded from www.nrcresearchpress.com by 80.90.12.36 on 09/08/12
For personal use only.

Ionic conductivity in the water-rich region of aqueous 2-butoxyethanol

Yoshikata Koga, Virginia J. Loo, and Kataryna T. Puhacz

Abstract: Ionic conductivities of HCl, KOH, and KCl were measured in aqueous solutions of 2-butoxyethanol (BE) at 25°C. The quantity, $\Lambda_j' = \sigma/x_j$, which is almost proportional to the molar conductivity, was extrapolated to the infinite dilution $x_j \rightarrow 0$. σ is the conductivity and x_j is the mole fraction of j(= HCl, KOH, or KCl). The plots of ${}^0\Lambda_j'$, the value of Λ_j' extrapolated to infinite dilution, against x_{BE} showed a change in slope at x_{BE} = 0.0175. The previous work from this laboratory indicated that the mixing scheme changes qualitatively at the same locus, x_{BE} = 0.0175. By mixing scheme we simply mean the way in which BE and H_2O molecules mix with each other. Assuming additivity in ${}^0\Lambda_j'$ in terms of constituent ions, those values for H^+OH^- were calculated. Plots of ${}^0\Lambda_{H^+OH^-}'$ thus calculated as a function of x_{BE} in the water-rich region, $0 < x_{BE} < 0.0175$, suggest that the hydrogen bond probability decreases in the bulk of solution, as x_{BE} increases.

Key words: aqueous 2-butoxyethanol, ionic conductivities, mixing schemes, hydrogen bond network.

Résumé : On a mesuré les conductivités ioniques du HCl, du KOH et du KCl dans des solutions aqueuses de 2-butoxyéthanol (BE) à 25°C. On a extrapolé, à dilution infinie $x_j \rightarrow 0$, la quantité $\Lambda_j' = \sigma/x_j$, qui est presque proportionnelle à la conductivité molaire. σ représente la conductivité et x_j représente la fraction molaire de j(= HCl, KOH ou KCl). Les courbes de ${}^0\Lambda_j'$, la valeur extrapolée de Λ_j' à dilution infinie, en fonction de x_{BE} montrent un changement de pente à x_{BE} = 0,0175. Les travaux antérieurs réalisés dans ce laboratoire indiquent que les schémas de mélange changent qualitativement au même point, x_{BE} = 0.0175. Par schéma de mélange nous entendons simplement la manière dont les molécules de BE et d'eau se mélangent les unes aux autres. En admettant l'additivité dans ${}^0\Lambda_j'$, en termes d'ions constitutifs, on a calculé l'additivité des ions H^+OH^-. Les courbes de ${}^0\Lambda_{H^+OH^-}'$ ainsi calculées en fonction de x_{BE} dans la région riche en eau $0 < x_{BE} < 0{,}0175$, suggèrent que la liaison hydrogène décroit probablement dans la masse de la solution lorsque x_{BE} augmente.

Mots clés : 2-butoxyéthanol aqueux, conductivités ioniques, schémas de mélange, réseau de la liaison hydrogène.

[Traduit par la rédaction]

Introduction

The mobilities of H^+ and OH^- in ice are higher by an order of magnitude than those in liquid H_2O, which are in turn considerably higher than those of other univalent ions in aqueous solutions. This is explained by the mechanism whereby H^+ and its hole (OH^-) hop cooperatively along two potential minima between two oxygen atoms in the hydrogen bond network of H_2O (1, 2). The hopping may be understood to occur as quantum mechanical tunneling (2), or via the "coherent dissipative structure." A quantum mechanical correlation exists between H^+ and H's of the surrounding H_2O molecules (3, 4). This causes H^+ or its hole (OH^-) to delocalize along the hydrogen bond network of H_2O.

The hydrogen bond network is complete in ice, while a portion of the hydrogen bonds are broken in liquid H_2O. It has been pointed out (5), however, that at moderate temperatures the hydrogen bond network of liquid H_2O is "percolated." If the diamond structure is topologically correct in liquid H_2O in terms of hydrogen bond connectivity, the bond percolation threshold will be 0.39 of the probability of intact hydrogen bonds (6). An estimate (5) indicates that hydrogen bond probability decreases as temperature increases and reaches 0.39 at about 80°C. Below this temperature, the hydrogen bond network is connected throughout the entire bulk, i.e., percolated. The high H^+ conduction in liquid water must be realized through the percolated hydrogen bond network. Thus the conductivities of H^+ or OH^- may serve as an indicator of whether or not the hydrogen bond network exists, or whether the hydrogen bond probability increases or decreases in aqueous solutions of non-electrolytes.

We have made extensive thermodynamic studies on aqueous 2-butoxyethanol (BE) (7–18). It became evident that the mixing scheme changes qualitatively at x_{BE} = 0.0175 at 25°C, as the mole fraction of BE, x_{BE}, increases. In region I, $0 < x_{BE} < 0.0175$, the partial molar enthalpy (15, 17, 18), entropy (16), and volume (12, 13) data indicate that the hydrogen bond network of H_2O is progressively enhanced as x_{BE} increases. At x_{BE} = 0.0175, however, the solution can no longer accommo-

Received October 31, 1994.[1]

Y. Koga,[2] V.J. Loo, and K.T. Puhacz. Department of Chemistry, The University of British Columbia, 2036 Main Mall, Vancouver, BC V6T 1Z1, Canada.

[1] Revision received May 10, 1995.

[2] Author to whom correspondence may be addressed. Telephone: (604) 822-3491. Fax: (604) 822-2847. E-mail: koga@chem.ubc.ca

Can. J. Chem. Downloaded from www.nrcresearchpress.com by 80.90.12.36 on 09/08/12
For personal use only.

Can. J. Chem. Downloaded from www.nrcresearchpress.com by 80.90.12.36 on 09/08/12
For personal use only.

date an additional BE in the same manner, and a different mixing scheme sets in. In region II, $0.0175 < x_{BE} < 0.5$, the solution consists of two kinds of clusters, rich in BE and in H_2O, respectively. These clusters are precursory to the phase separation with LCST at $x_{BE} = 0.06$ and 49.4°C (19), or to the nucleation of a solid solution below −3.7°C (8). That is, under appropriate conditions, they grow to macroscopic droplets or solid nuclei. At $x_{BE} \approx 0.06$, for example, when the temperature increases from below towards 49.4°C, the intensity of light scattering increases sharply (19, 20). When the temperature is lowered towards −3.7°C, the forward X-ray scattering intensity increases dramatically (7).

The purpose of the present work is to determine ionic conductivities of HCl, KOH, and KCl at infinite dilution in aqueous solutions of BE. Firstly, we wish to examine whether ionic conductivity behaves differently in regions I and II. Secondly, the conductivities of H^+ and OH^- calculated from those of the above three electrolytes may provide information about the effect of BE on the hydrogen bond network of H_2O. We note that the presence of an electrolyte dopant may affect the nature of BE–H_2O mixtures even at infinite dilution. It turns out, however, that the conductivities at infinite dilution show different behaviour in regions I and II, as shown below. A dopant apparently did not alter the existence of the two mixing schemes in BE–H_2O, at least at infinite dilution. Therefore, we tentatively assume that the mixing schemes in the binary BE–H_2O system remain the same in the ternary system (HCl, KOH, or KCl)–BE–H_2O, at infinite dilution.

Experimental

2-Butoxyethanol from Aldrich (99+%, spectroscopic grade) was used without further purification. H_2O was freshly distilled before use. A 0.1 M standard NaOH from Fisher Scientific was used to determine the concentration of a 1 M stock solution of HCl, and in turn that of KOH. KCl from Fisher Scientific (Certified ACS) was dried at 150°C overnight.

Ionic conductivities, σ, were determined by an AC bridge (YSI-35) at 60 Hz. A cell (YSI-3403) with blackened platinum electrodes was used. The nominal cell constant, k, was 1 cm^{-1}. The conductivity of the sample, σ, is calculated as

$$[1] \quad \sigma = k/R$$

where R is the resistance measured by the bridge. The cell constant, k, was calibrated using the literature value of the molar conductivity of aqueous KCl at infinite dilution (21).

Aqueous solutions containing BE in the range $0 < x_{BE} < 0.04$ and the ionic dopants (HCl, KOH, or KCl) in the range $0.0005 < x_j < 0.09$, or $0.01 < C_j < 0.5$ M (j = HCl, KOH, or KCl), were prepared by weighing. Since the three-component system (HCl, KOH, KCl)–BE–H_2O, is expected to show complicated volumetric behaviour and such data are not available, we mostly use mole fractions as concentration variables. Thus, instead of molar conductivity, $\Lambda_j = 1000\,\sigma/C_j$, we use the quotient, $\Lambda_j' = \sigma/x_j$, as the quantity almost proportional to Λ_j, particularly so at the infinite dilution.

The temperature of the bath in which conductivity measurements were made was controlled within ±0.05°C. The temperature for the KCl–BE–H_2O series was 25.0°C, while that for HCl–BE–H_2O was 24.5°C and for KOH–BE–H_2O 24.6°C.

Fig. 1. Plots of measured values of σ and x_{KOH} in KOH–BE–H_2O against x_{BE}: ●, σ; △, x_{KOH}.

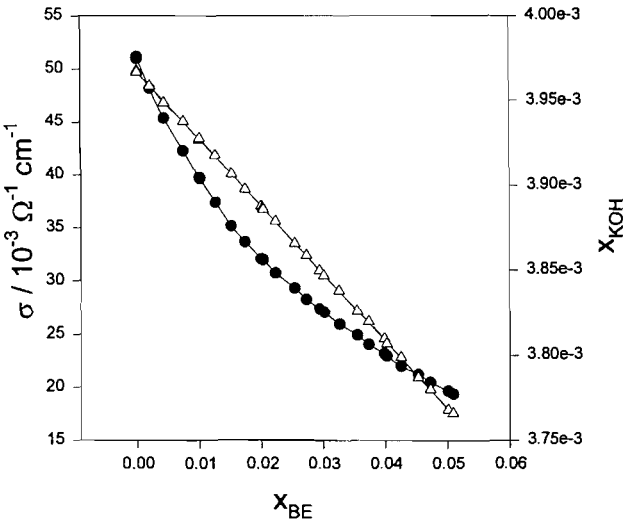

Small temperature corrections were made to the data at infinite dilution for the latter two series, using the temperature dependence for aqueous HCl and KOH (21).

Results and discussion

For pure H_2O ($x_{BE} = 0$), the molar conductivity, Λ_j, changed linearly with $\sqrt{C_j}$, as expected (21). Extrapolation to $C_j = 0$ was made to obtain Λ°_{KCl}, the value used to calibrate the cell constant (k = 1.023 cm^{-1}). The values of Λ°_{HCl} and Λ°_{KOH} were corrected for the respective temperature variation, using literature values of the temperature coefficients (21). The resulting values of Λ°_{HCl} and Λ°_{KOH} agree within 0.1% with those in ref. 21, as shown in the last two columns of Table 1. Figure 1 shows the plots of σ and x_{KOH} against x_{BE} for a series of KOH–BE–H_2O solutions starting with 0.220 M KOH solution. Small amounts of BE were added successively by weighing. Similar graphs for each starting value of C_{KOH} were obtained. From each graph, the values of σ and x_{KOH} were read off a smooth curve at fixed values of x_{BE}. For a given fixed value of x_{BE}, values of $\Lambda'_{KOH} = \sigma/x_{KOH}$ were plotted against $\sqrt{x_{KOH}}$. Extrapolation was then made to infinite dilution, $x_{KOH} \rightarrow 0$ to obtain ${}^0\Lambda'_{KOH}$ as a function of x_{BE}. The results of ${}^0\Lambda'_j$ (j = HCl, KOH, or KCl) thus obtained are listed in Table 2, after temperature corrections, assuming that the temperature coefficients are the same as that at $x_{BE} = 0$. They are plotted in Fig. 2. The uncertainty in ${}^0\Lambda'_j$ is estimated to be ±0.2 Ω^{-1} cm^{-1}, about the size of symbols in the figure. Assuming additivity in ${}^0\Lambda'_j$, the values of ${}^0\Lambda'_{H^+OH^-}$ were calculated as

$$[2] \quad {}^0\Lambda'_{H^+OH^-} = {}^0\Lambda'_{HCl} + {}^0\Lambda'_{KOH} - {}^0\Lambda'_{KCl}$$

and are listed in Table 2 and plotted in Fig. 2.

As is evident from the figure, the dependence of ${}^0\Lambda'_j$ on x_{BE} shows different behaviour in regions I and II. This suggests that the mechanisms of ionic conduction are different in each region due, no doubt, to differences in the mixing scheme. Thus, the presence of dopant ions at infinite dilution evidently

Table 1. Molar conductivities of KCl, HCl, and KOH at infinite dilution.

	${}^0\Lambda_j/\Omega^{-1}$ cm^2 mol^{-1} k = 1.023 cm^{-1}	${}^0\Lambda_j/\Omega^{-1}$ cm^2 mol^{-1} k = 1.023 cm^{-1}, 25°C This work	${}^0\Lambda_j/\Omega^{-1}$ cm^2 mol^{-1} Ref. 21, 25°C
KCl	149.8 at 25.0°C	149.8	149.8
HCl	423.3 at 24.5°C	426.5	426.2
KOH	270.0 at 24.6°C	272.0	271.8

Table 2. ${}^0\Lambda_j'$ values for j = HCl, KCl, KOH, and H^+OH^- at 25°C.

x_{BE}	${}^0\Lambda'_{KCl}/\Omega^{-1}$ cm^{-1}	${}^0\Lambda'_{KOH}/\Omega^{-1}$ cm^{-1}	${}^0\Lambda'_{HCl}/\Omega^{-1}$ cm^{-1}	${}^0\Lambda'_{HOH}/\Omega^{-1}$ cm^{-1}
0	8.2_7	15.1_0	23.7_2	30.5_5
0.00125	8.0_5	14.5_6		
0.0025	7.8_8	14.0_1		
0.0035	7.7_0	13.6_2		
0.0050	7.4_7	13.0_9	21.9_5	27.5_7
0.0060	7.3_5	12.8_0		
0.0075	7.0_7	12.3_4	21.0_0	26.2_7
0.0080	7.0_0	12.2_3		
0.0090	6.8_8			
0.0100	6.7_1	11.5_5	19.8_8	24.7_2
0.0110	6.5_7			
0.0120	6.4_3	11.0_3		
0.0125	6.3_7	10.8_4	18.8_2	23.2_9
0.0130	6.2_9			
0.0140	6.1_8	10.4_9	18.2_0	22.5_1
0.0150	6.0_4	10.2_5	17.7_6	21.9_7
0.0160	5.9_2	10.0_3	17.5_0	21.6_1
0.0165	5.8_7			
0.0170	5.8_1	9.8_6	17.1_9	21.2_4
0.0175	5.7_6	9.7_5		
0.0180	5.7_2	9.6_5	16.9_3	20.8_6
0.0185	5.6_9	9.5_4		
0.0190	5.6_6	9.4_1	16.6_2	20.3_7
0.0200	5.5_8	9.2_8	16.3_3	20.0_3
0.0220	5.3_8	8.8_6	15.6_7	19.1_5
0.0225	5.3_3			
0.0240	5.1_9	8.5_1		
0.0250	5.1_5	8.3_7	14.9_7	18.1_9
0.0260	5.0_7	8.2_4		
0.0270	5.0_1	8.0_4		
0.0280	4.9_5	8.0_0	14.3_1	17.3_6
0.0300	4.8_3	7.7_5	13.8_1	16.7_3
0.0325	4.6_9	7.4_7		
0.0350	4.5_2	7.2_3	13.0_1	15.7_2
0.0375	4.3_9	6.9_4		
0.0400	4.2_7	6.6_4	11.9_9	14.3_6

did not alter the existence of different mixing schemes I and II. This may in turn provide some assurance that the behaviour of the ionic conductivity at infinite dilution may properly reflect the hydrogen bonding nature of each mixing scheme.

Another feature to be noted in Fig. 2 is that ${}^0\Lambda'_{H^+OH^-}$ decreases sharply as x_{BE} increases. This suggests that the hydrogen bond probability actually *decreases*, as x_{BE} increases, if the ionic conduction of H^+ and OH^- occurs via the hydrogen bond network. In our earlier work, the dependence of the excess partial molar enthalpy (15, 17, 18), entropy (16), and volume (12, 13) on x_{BE} suggested the enhancement of the hydrogen bond network of H_2O in the vicinity of solute BE. It was therefore hinted that, as x_{BE} increases, the hydrogen bond probability increases progressively to the boundary at x_{BE} = 0.0175 at 25°C, at which the hydrogen bond network was thought to be complete. According to Fig. 2, therefore, this view is not correct. Rather, the hydrogen bond probability actually decreases, at least locally, as x_{BE} increases.

Can. J. Chem. Downloaded from www.nrcresearchpress.com by 80.90.12.36 on 09/08/12
For personal use only.

Can. J. Chem. Downloaded from www.nrcresearchpress.com by 80.90.12.36 on 09/08/12
For personal use only.

Fig. 2. Plots of ${}^0\Lambda_j$ against x_{BE}, for j = HCl, KOH, KCl, and H^+OH^-.

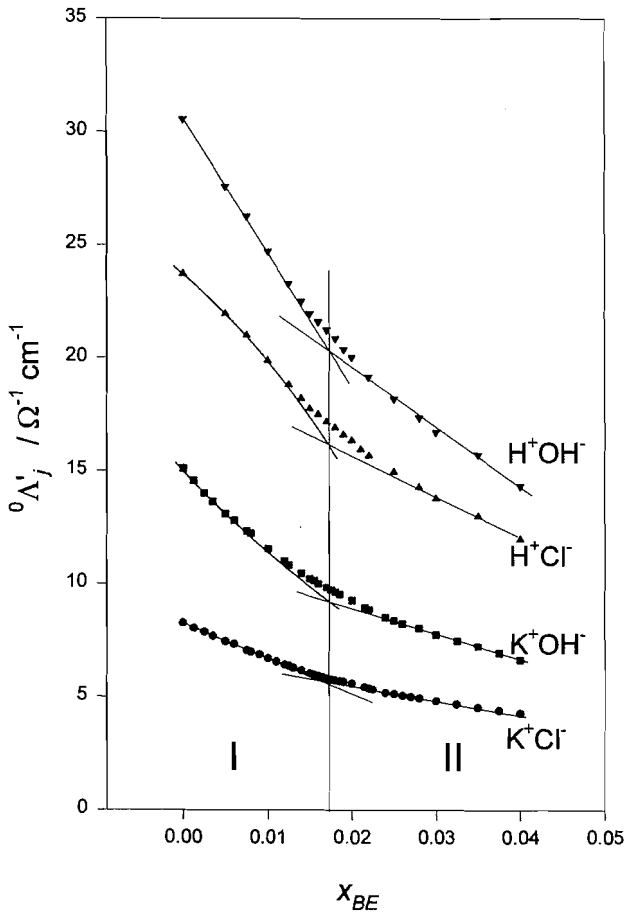

We tentatively suggest that the hydrogen bonds become stronger in the vicinity of solute BE, while the hydrogen bond probability of bulk H_2O away from BE is reduced. Noteworthy in this connection is the recent suggestion based on the results of high-resolution inelastic neutron scattering that there are two kinds of hydrogen bond with the strength ratio of 2:1 in ice Ih (22). If such possibility also exists in liquid water, the hydrogen bonds are strengthened in the vicinity of BE, which in turn weakens those of bulk water away from BE. In this view, as x_{BE} increases, the hydrogen bond probability away from BE gradually decreases to the percolation threshold, 0.39, whereupon the percolation is broken and the system consists of two kinds of regions, rich in either BE or H_2O, precursory to phase separation at higher temperatures.

A close inspection of the boundary separating mixing schemes I and II also gives some support to the latter revised view. The boundary starts at about 85°C at $x_{BE} = 0$ and ends at the incongruent melting point of an addition compound (x_{BE} = 0.0260) (8). That is, the boundary slants towards lower values of x_{BE} as the temperature increases. If the hydrogen bond were to be brought to completion at the boundary, then the boundary should slant to higher values of x_{BE} as the temperature increases, since at higher temperatures the hydrogen bond probability is lower in pure H_2O, and hence more BE molecules are needed to bring the hydrogen bond probability to unity. If, on the other hand, the hydrogen bond probability is reduced to the percolation threshold, 0.39, at the boundary, fewer BE molecules would be sufficient to bring it down to 0.39 at higher temperatures, consistent with the observed manner in which the boundary slants. Furthermore, the boundary connects smoothly to the percolation threshold of pure H_2O about 85°C.

Clearly, more spectroscopic work, inelastic neutron scattering, in particular, is needed to further elucidate the nature of this transition in the mixing scheme.

Acknowledgment

This research was supported by the Natural Sciences and Engineering Research Council of Canada in the form of an operating grant to Y.K. and first-year women summer research awards to V.J.L. (1994) and K.T.P. (1993). We thank Catherine C.M. Hui, another awardee 1992, for her preliminary work on this project. We also thank Dr. Hiroshi Ohshima, Osaka City University, for valuable discussion and suggestions.

References

1. D. Eisenberg and W. Kauzmann. *In* The structure and properties of water. Clarendon, Oxford. 1969. p. 224.
2. M. Eiger and L. DeMaeyer. *In* The structure of elctrolyte solutions. *Edited by* W.J. Harmer. John Wiley, New York. 1959. p.64.
3. C.A. Chatzidimitriou-Dreismann. Ber. Bunsen-ges. Phys. Chem. **94**, 234 (1990).
4. H. Weingartner and C.A. Chatzidimitriou-Dreismann. Nature, **346**, 548 (1990).
5. H.E. Stanley and J. Teixeira. J. Chem. Phys. **73**, 3404 (1980).
6. N.G. Parsonage and L.A.K. Staveley. *In* Disorder in crystals. Oxford University Press, Oxford. 1978. p. 84.
7. Y. Koga, K. Nishikawa, K. Yoshino, I. Tanaka, and Y. Amemiya. Chem. Phys. Lett. **228**, 53 (1994).
8. Y. Koga, T, Tanaka, T. Atake, P. Westh, and Aa. Hvidt. Bull. Chem. Soc. Jpn. **67**, 2393 (1994).
9. T. Atake and Y. Koga. Netsusokutei (Cal. Thermal. Anal. Jpn.), **21**, 130 (1994).
10. P. Westh, Aa. Hvidt, and Y. Koga. Chem. Phys. Lett. **217**, 245 (1994).
11. Aa. Hvidt and Y. Koga. Thermochim. Acta, **228**, 39 (1993).
12. Y. Koga, J. Kristiansen, and Aa. Hvidt. J. Chem. Thermodyn. **25**, 51 (1993).
13. Y. Koga. J. Phys. Chem. **96**, 10466 (1992).
14. J.V. Davies, F.W. Lau, L.T.N. Le, J.T.W. Lai, and Y. Koga. Can. J. Chem. **70**, 2659 (1992).
15. W.W.Y. Siu, T.Y.H. Wong, J.T.W. Lai, A. Chong, and Y. Koga. J. Chem. Thermodyn. **24**, 159 (1992).
16. Y. Koga. J. Phys. Chem. **95**, 4119 (1991).
17. Y. Koga, W.W.Y. Siu, and T.Y.H. Wong. J Phys. Chem. **94**, 3879 (1990).
18. W. Siu and Y. Koga. Can. J. Chem. **67**, 671 (1989).
19. N.Ito, T. Fujiyama, and Y. Udagawa. Bull. Chem. Soc. Jpn. **56**, 379 (1983).
20. T. Kato. J. Phys. Chem. **89**, 5750 (1985).
21. R.A. Robinson and R.H. Stokes. *In* Electrolyte solutions. Butterworth, London. 1965. p. 436.
22. J.-C. Li, D.K. Ross, and M.I.B. Hayes. J. Mol. Struct. **322**, 131 (1994).

A photo-oxidation of croconic acid into oxalic acid

Paul-Louis Fabre, Paule Castan, Diane Deguenon, and Nicole Paillous

Abstract: Croconic acid, $H_2C_5O_5$, is readily oxidized. This may be attested by decolorization of the solutions and by observation of oxalic acid complexes. The oxidation products are identified by ^{13}C NMR spectroscopy as oxalic and mesoxalic acids, and experimental conditions are specified. The oxidation process requires dioxygen and photons. In parallel, the electrochemical oxidation of croconic acid is studied in aqueous media and in acetonitrile. A potential–pH diagram is drawn.

Key words: croconic acid, oxalic acid, oxidation, electrochemistry, photochemistry.

Résumé : L'acide croconique $H_2C_5O_5$ est facilement oxydé, ceci est attesté par la décoloration de ses solutions et l'obtention de complexes de l'acide oxalique. Les produits d'oxydation ont été identifiés par spectroscopie RMN du ^{13}C, ce sont les acides oxalique et mesoxalique. Les conditions expérimentales requises par cette oxydation sont spécifiées, ce sont la présence de dioxygène et de lumière. Parallèlement, l'oxydation électrochimique de l'acide croconique a été étudiée dans l'eau et l'acétonitrile. Le diagramme potentiel–pH est décrit.

Mots clés : acide croconique, acide oxalique, oxydation, électrochimie, photochimie.

[Traduit par la rédaction]

Can. J. Chem. Downloaded from www.nrcresearchpress.com by 80.90.12.36 on 09/08/12
For personal use only.

Introduction

4,5-Dihydroxycyclopentenetrione **1,** commonly known as "croconic" acid, $H_2C_5O_5$, and the croconate anion $[C_5O_5]^{2-}$ have received considerable attention from both a theoretical and an experimental point of view (1–6). Croconate, like squarate or rhodizonate ions, is a member of the oxocarbon ring system, $[C_nO_n]^{2-}$, a new class of aromatic substances with planar structure containing only carbon and oxygen atoms. Both croconic and squaric acids are strong acids in aqueous solution, having pK_{A1} values of 0.80 (7) and 0.54 (8), respectively.

During the course of our investigations concerning transition metal complexes of croconic acid we attempted to prepare a manganese croconate complex. In the presence of croconic acid, 2,2′-bipyridine, and Mn(II) salt, the complex $[Mn(C_{10}H_8N_2)(C_2O_4)]_n$ was unexpectedly obtained, and was structurally identified (9). This synthesis requires the oxidation of croconic acid into oxalic acid.

Oxidation of croconic acid and of other polyketo compounds by molybdenum(VI) in acidic media has already been described by Verchere and Fleury (10–12); a transient 1/1 complex between Mo(VI) and the ionized acid was shown. Oxalic and mesoxalic acids were identified among the oxidation products. In the same way, Zubieta and co-workers described a Mo(V)–oxalate cluster obtained from polyoxomolybdate(VI) and rhodizonic acid (13). The mechanism proposed in these studies always requires electron transfer steps implying reduction of the metal. Rhodizonic acid ($H_2C_6O_6$) is known to be unstable when exposed to visible light but no study has been reported.

More recently, Zhao and Back have studied the photochemical reactions of the dianions of rhodizonic and croconic acids (14–16). In basic media, the photochemical oxidation of the croconate dianion leads to formation of the squarate dianion. Taking into account these last results and those we obtained, it seems evident that the photochemical dissociation process of croconic acid itself (acidic media) is quite different from that of its dianion (neutral or basic media). The oxalate complex we obtained during the course of our complexation process has prompted us to examine the oxidation process of croconic acid, leading to oxalic acid, in the presence or absence of manganese salts.

Received February 15, 1995.

P.-L. Fabre,[1] **P. Castan, and D. Deguenon.** Laboratoire de chimie inorganique, Université Paul Sabatier, 118 route de Narbonne, 31062 Toulouse Cedex, France.
N. Paillous. Laboratoire des IRMCP, Université Paul Sabatier, 118 route de Narbonne, 31062 Toulouse Cedex, France.

[1] Author to whom correspondence may be addressed. Telephone: 61-55-84-83. Fax: (33) 61-55-61-18.

Experimental

Materials

Croconic acid and its potassium salt were prepared according to the procedure described by Fatiadi et al. (17).

Synthesis of tetraphenylphosphonium croconate

To an aqueous solution of $P(C_6H_5)_4Cl$ (2 mmol in 10 mL), an aqueous solution of potassium croconate (1 mmol in 10 mL) is added under stirring. The solution is kept overnight on cooling and yields yellow crystals that are isolated by filtration, washed with ether, and dried under vacuo (yield 95%).

Can. J. Chem. Downloaded from www.nrcresearchpress.com by 80.90.12.36 on 09/08/12
For personal use only.

Scheme 1.

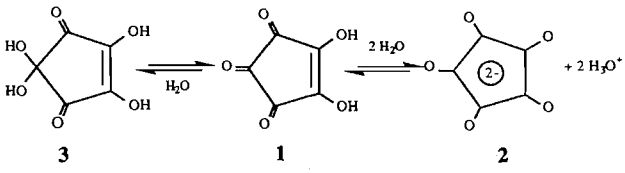

Physical measurements

IR spectra were recorded on a Perkin–Elmer 983 spectrophotometer coupled with a Perkin–Elmer infrared data station; samples were run as Nujol mulls. NMR spectra were recorded on a Brucker WM 250 Fourier transform spectrometer. UV–visible spectra were measured on a Cary 2390 spectrophotometer. Electrochemical measurements were carried out with a homemade potentiostat controlled by an Apple IIe microcomputer (18). The electrochemical cell was a conventional one with three electrodes: a working disk electrode, Cv (vitreous graphite, diameter 3 mm) or Pt (diameter 2 mm); an auxiliary electrode, Pt wire; and a reference electrode, Ag/AgCl, KCl 0.1 mol L^{-1}. EPR spectra of frozen solutions were obtained on a Bruker 200 TT spectrometer with a Bruker cryostat.

Irradiations were performed with a Muller reactor device equipped with a 200 W high-pressure mercury lamp (Osram) and an interference water cooling filter (Oriel 365FS 10–50, 25% transmission at 365 nm). The solutions of croconic acid (varying from 10^{-3} to 10^{-4} mol L^{-1}) were irradiated from 10 to 60 s in a UV quartz cell. The thickness of the cell was adjusted to obtain similar absorptions whatever the concentration. The effect of scavengers was tested under irradiation at 365 nm. NaN_3 (12 mmol L^{-1} final concentration) or DABCO (1,4-diazabicyclo[2,2,2] octane) (10 mmol L^{-1} final concentration) were added to a croconic acid solution (9×10^{-4} mol L^{-1}). We verified that the changes observed by using NaN_3 are essentially due to a pH variation.

Results and discussion

In the presence of croconic acid, 2,2′-bipyridyl, and Mn(II) salt, the complex $[Mn(C_{10}H_8N_2)(C_2O_4)]_n$ was unexpectedly obtained, and was structurally identified (9). This system requires oxidation of croconic acid into oxalic acid. At first we presumed a catalytic oxidation of croconic acid by Mn(III) traces, of which are always present in Mn(II) salts. However, it can be established that oxidation occurs even without manganese salts. Indeed, a yellow solution of croconic acid rapidly decolorized under exposure to light. The croconic acid degradation is an oxidation process. So, as a first step, the electrochemical behaviour of croconic acid was studied.

Electrochemical oxidation

According to the acidity constants of croconic acid (pK_{A1} = 0.80 and pK_{A2} = 2.24) and to hydration, the predominant forms are **1**, **2**, and **3** and depend on pH. The monoanion is not predominant.

In acid media, the oxidation process has already been reviewed (19), but the products were not isolated. Then, the electrochemical oxidation was studied in aqueous media as a function of pH. At a glassy carbon electrode, the voltammograms show, by cyclic voltammetry, the oxidation peak of croconic acid (Fig. 1). The oxidation process appears irreversible;

Fig. 1. Cyclic voltammograms at a Cv electrode in aqueous media of croconic acid 1 mol L^{-1}, potential scan speed 0.1 V s^{-1}: A: pH = 1.53; B: pH = 7.0.

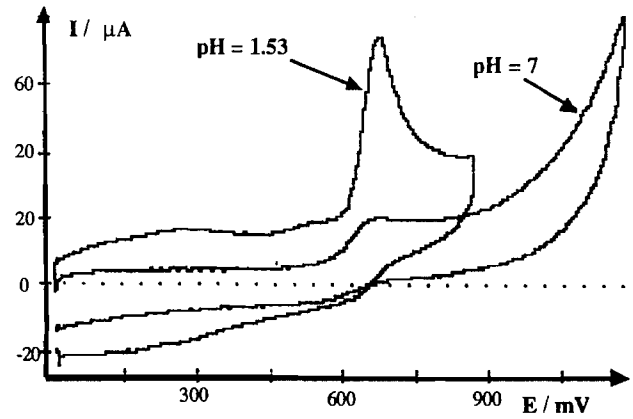

Fig. 2. Voltammograms at a rotating Cv electrode in aqueous media of croconic acid, rotation speed 1000 rpm: A: pH = 0.6, $[C_5O_5H_2]$ = 1 mmol L^{-1}; B: pH = 7.0, $[C_5O_5H_2]$ = 0.7 mmol L^{-1}.

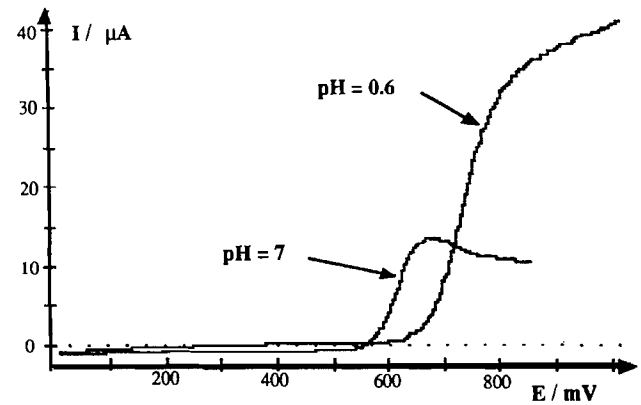

no reduction peak is observed on the backward scan. The peak current is linearly related to the square root of the potential scan speed and to the croconic acid concentration. At pH higher than 4, passivation of the electrode which disturbs the voltammetric recordings, is observed (Fig. 2); the diffusion decreases on the plateau.

Also in acid media, the diffusion wave is observed under stationary conditions at a rotating electrode, while at higher pH the wave does not present the plateau due to passivation of the electrode. Moreover, the current is lower than the current observed in acid media. This can be attributed to electrode passivation but also to a kinetic effect on the oxidation process. Effectively, by exhaustive electrolysis, coulometric integration is in agreement with a two-electron transfer whatever the pH. But in acid media electrolysis is carried out within 10 min while the basic media it requires more than an hour to be complete. The global oxidation process is expressed by the following equation:

$$H_2C_5O_5 \rightarrow C_5O_5 + 2\,H^+ + 2\,e^-$$

which gives the pentaketone **4** that exists under various hydrated forms (**4***b*, **4***c*).

Can. J. Chem. Downloaded from www.nrcresearchpress.com by 80.90.12.36 on 09/08/12
For personal use only.

Scheme 2.

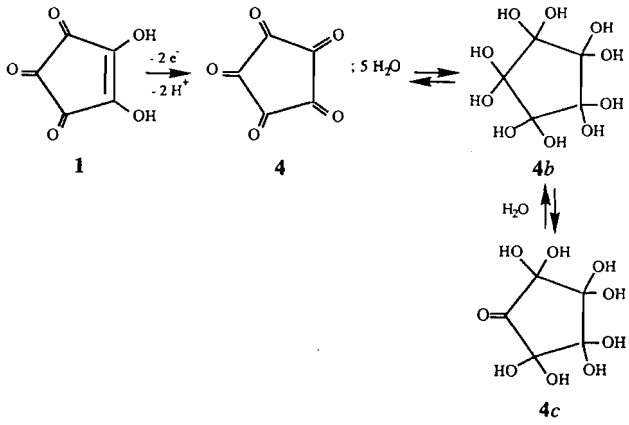

The ^{13}C NMR spectra of the resulting solution obtained by electrolysis in buffered D_2O–H_2O mixtures confirm this equation. The spectra show the hydrated form (**4***c*), which is characterized by signals at 94.8, 97.7, and 98.7 ppm ($CH(OH)_2$) and at 209.6 ppm (C=O). These are in agreement with the previously reported values: 93.0, 95.9, 96.9, and 208.0 ppm (2, 20).

According to Levich's equation for the diffusion current under stationary conditions, the diffusion coefficient of croconic acid is calculated in acid media to be $D = 5.6 \times 10^{-6}$ cm^2 s^{-1}. It is the same order of magnitude as the value reported by Sazou and Kokkinidis (19), $D = 5.5 \times 10^{-6}$ cm^2 s^{-1}.

Taking into account the half-wave potential $E_{1/2}$ measured under stationary conditions at a Cv electrode, the *E*–pH diagram is obtained (Fig. 3). This diagram is consistent with the oxidation equation where the apparent potential ($E^{\circ\prime}$) is related to the standard potential E° and to the acidity constants of croconic acid by

$$E^{\circ\prime} = E^\circ - 0.059\ \text{pH} + 0.029 \log (1 + K_{A1}/[H_3O^+] + K_{A1}K_{A2}/[H_3O^+]^2)$$

According to this equation, the potential is linearly related to −0.059 pH in acid media as observed and it should be independent of pH in basic media. In fact, at pH > 12 the potential appears to decrease with pH, which means that H^+ is involved in the oxidation process of croconate anions. It may be attributed to the formation of leuconate anions from the hydration of the pentaketone **4**:

$$C_5O_5^{2-} + 4\ H_2O \rightarrow C_5H_6O_9^{2-} + 2\ H^+ + 2\ e^-$$

or to the formation of squarate dianion according to Zhao and Back (15):

$$C_5O_5^{2-} + H_2O \rightarrow C_4O_4^{2-} + CO_2 + 2\ H^+ + e^-$$

In organic solvents (acetonitrile CH_3CN), the electrochemical behaviour of croconate dianion $[P(C_6H_5)_4]_2C_5O_5$ was studied at a platinum electrode. Under nonstationary conditions, the voltammograms show two oxidation processes (Fig. 4) that appear monoelectronic and reversible. When the potential sweep scans the two redox couples the peak ratio RI_p (reduction peak current/oxidation peak current) of the first step is slightly lower than 1 whereas it equals 1 when the potential sweep scans only the first redox couple. The peak currents are linearly related to the square root of the potential scan speed and to the croconate concentration. The oxidation process of croconate is expressed by the two successive electron transfers:

$$C_5O_5^{2-} \rightleftharpoons C_5O_5^- + e^-$$
$$C_5O_5^- \rightleftharpoons C_5O_5 + e^-$$

Under stationary conditions at a rotating Pt electrode, the voltammograms present two monoelectronic waves whose half-wave potentials are 0.28 and 0.81 V. The limiting currents are linearly related to the square root of the electrodes rotation speed and to the corconate concentration. The oxidation process is diffusion controlled as evidenced by cyclic voltammetry. According to the Levich's equation on the diffusion current under stationary conditions, the diffusion coefficient of croconate dianion is calculated to be $D = 8.0 \times 10^{-6}$ cm^2 s^{-1}. By electrolysis at a potential on the first plateau, the yellow solutions turn orange after a one-electron exchange per dianion and yield a stable radical whose EPR spectra give a *g* value of 2.0065 (6). Electrolysis of croconate dianion on the second plateau gives a two-electron exchange per dianion and yields the pentaketone **4**.

Fig. 3. Potential–pH diagram of croconic acid.

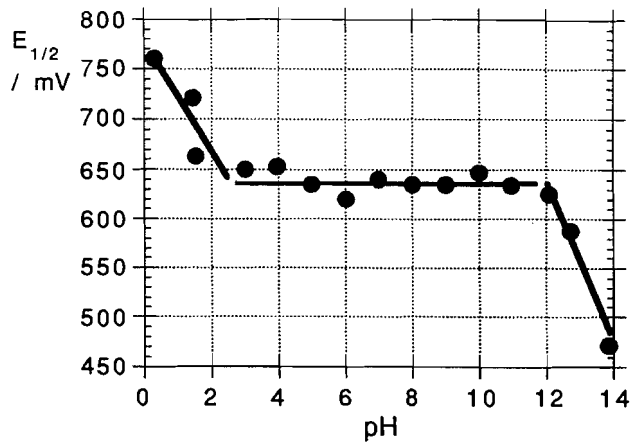

Fig. 4. Cyclic voltamograms at a Pt electrode in CH_3CN–Bu_4NClO_4 0.1 mol L^{-1} of $[P(C_6H_5)_4]_2C_5O_5$ 1 mmol L^{-1}, potential scan speed 0.1 V s^{-1}.

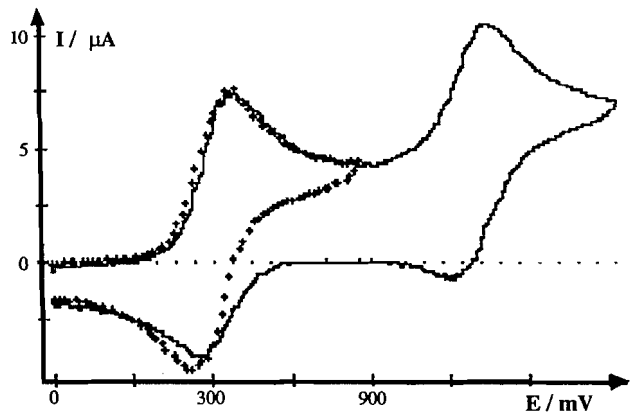

Can. J. Chem. Downloaded from www.nrcresearchpress.com by 80.90.12.36 on 09/08/12
For personal use only.

The electrochemical behaviour of croconic acid depends on the nature of the solvent. In an organic solvent, the oxidation proceeds through two monoelectronic exchanges and a long-lived radical $C_5O_5^-$ can be formed, since the EPR signal is still observed after several hours at ambient temperature. In aqueous media, the electrochemical oxidation becomes bielectronic (the radical is unstable) and yields the pentaketone more or less hydrated. So, a photoexcitation of croconic acid into radical species may activate the degradation of croconic acid. Moreover, the oxidation process depends on the acidity level.

Photochemical oxidation

Identification of products

Analysis of the resulting products in solution is achieved by ^{13}C NMR spectroscopy. ^{13}C NMR spectra of croconic acid have long been studied (2). In aqueous solution some of the carbonyl groups become hydrated and an equilibrium can be observed between the various hydrated forms.

Before light exposure, in D_2O (1.5 mL) with 0.1 mL of concentrated sulfuric acid (the oxidation process is faster in acidic medium, vide infra), we observed by NMR spectroscopy an equilibrium between the triketone form (**1**) and its monohydrate (**3**) that leads to a four-signal spectrum. The signal at 183.2 ppm is attributed to the triketone **1**, which exhibits fast exchange of the carbon sites. The croconic monohydrate **3** shows a low-frequency signal at 89.2 ppm corresponding to $C(OH)_2$ and signals at 151.6 ppm (COH) and 194.3 (C=O) ppm.

After 2 days under daylight, the yellow solution of croconic acid becomes colorless. The ^{13}C NMR spectra reveal the disappearance of croconic acid. Weak signals within the 80–100 ppm range are attributed to $C(OH)_2$ of the hydrated forms. These signals decrease with time. Moreover, two peaks at 162.9 and 173.2 are observed and related to carbonyl carbons. The ^{13}C NMR spectra of oxalic and mesoxalic acids have been recorded under the same experimental conditions. The ^{13}C NMR spectra of oxalic acid (**5**) present a single peak at 162.9 ppm while those of mesoxalic acid (**6**) present two types of signals: at 94.0 ppm the peak of the $C(OH)_2$ carbons and at 173.5 ppm the peak of the COOH carbons. Our results indicate that croconic acid oxidation leads to oxalic and mesoxalic acids through hydroxylated oxocarbons that are detected by ^{13}C NMR spectroscopy in the 80–100 ppm range. Oxalic acid is also characterized by precipitation with $CaCl_2$ (the precipitate is identified by elemental analysis and IR spectrum). By contrast, under the same conditions mesoxalic and oxalic acid solutions are stable even under irradiation. Moreover, it may be emphasized that the oxidation process of croconic acid, which is small in neutral solutions, is enhanced in acidic media and is not observed in pure D_2O.

Similarly Zhao and Back (15) observed that in neutral solutions the quantum yield for disappearance of croconate dianion was small but was substantially increased in basic solution. At pH = 12, these authors observed conversion of the croconate dianion to the squarate dianion, analogous to the conversion of rhodizonate to croconate that occurs in strong basic media and is so efficient that no other method has been developed for the preparation of croconic acid. Moreover, Stadeli et al. (2) observed in the spectra of leuconic acid (**4***b*), which is the fully hydrated form of oxidized croconic acid, a signal at ca. 195 ppm, which increases with time and was attributed to squaric acid.

Scheme 3.

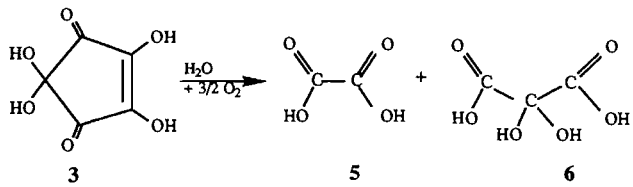

By comparison with our results, the oxidation of croconic acid in basic media is different from that in acid media. This is confirmed by the E–pH diagram of croconic acid.

Redox process

Assuming the formation of oxalic and mesoxalic acids from the oxidation of croconic acid, the redox system may be expressed as follows:

$$\underset{\mathbf{3}}{C_5H_4O_6} + 4\,H_2O \rightarrow \underset{\mathbf{5}}{C_2H_2O_4} + \underset{\mathbf{6}}{C_3H_4O_6} + 6\,H^+ + 6\,e$$

with the dioxygen system:

$$O_2 + 4\,H^+ + 4\,e^- \rightarrow 2\,H_2O$$

The overall system may be written as

$$2\,H_2C_5O_5 + 3\,O_2 + 4\,H_2O \rightarrow 2\,C_2H_2O_4 + 2\,C_3H_4O_6$$

To check this chemical balance, redox titrations by permanganate solutions were undertaken. Solutions of croconic acid exposed to dioxygen and light were titrated by $KMnO_4$ solutions. According to the oxidation of oxalic and mesoxalic acids:

$$C_2H_2O_4 \rightarrow 2\,CO_2 + 2\,H^+ + 2\,e^-$$
$$C_3H_4O_6 \rightarrow 3\,CO_2 + 4\,H^+ + 4\,e^-$$

The redox titration requires 6 electron-equivalents per croconic acid. Experimentally we found always around 6.5 (higher than 6) electrons, owing to the incomplete decomposition of the initial solution of croconic acid.

Preliminary kinetic analysis

To get more information about the oxidation pathway, we undertook preliminary kinetic studies. The croconic acid concentration can be easily monitored by electroanalytical methods or UV–visible spectroscopy. In this case, we used cyclic voltammetry at a Pt electrode.

In acid aqueous media (HCl or H_2SO_4), croconic acid solutions are electroactive at a Pt electrode. As oxalic and mesoxalic acid solutions are not electroactive at a Pt electrode in this solvent, the diffusion current is related to the croconic acid concentration and provides a monitor for kinetic studies. Moreover, the voltammograms do not show the appearance of squaric acid, which presents an oxidation peak around 0.85 V. Then, by recording the voltammograms as a function of time (Fig. 5), we observed that the peak current of croconic acid

Fig. 5. Cyclic voltammograms at a Pt electrode in H_2SO_4 0.1 mol L^{-1} of croconic acid as a function of time, potential scan speed 0.1 V s^{-1}: t = 0 h (—); t = 10 h (+++); t = 20 h 30 (×××), and t = 39 h 30 (···).

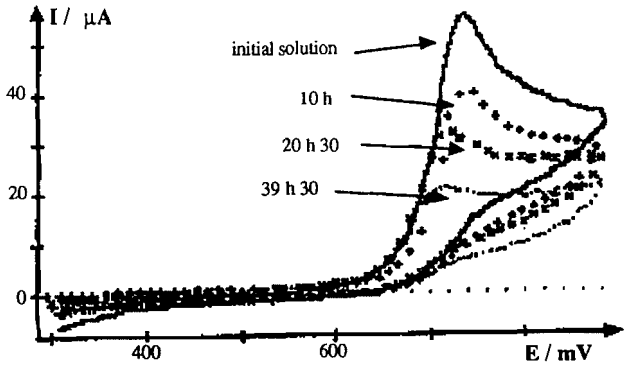

decreases with time. Kinetic determinations were then carried out under various conditions. Assuming a first-order rate, the rate constants were calculated by linear regression of $\log(I_{t=0}/I_t) = kt$.

From Fig. 6 we can point out that Mn(II) salt does not affect the oxidation speed of croconic acid; there is no catalytic effect. Croconic acid appears to be oxidized by dioxygen in acid medium and the process is photochemically activated. Under an Ar atmosphere, we did not observe any significant oxidation of the acid. Moreover, the oxidation rate increases when the acidity level increases.

From these preliminary results there are two requirements for the oxidation of croconic acid in acid media: dioxygen and photons (light). To obtain more information, the kinetics of the photo-oxidation process was followed by UV spectroscopy.

Photochemistry

Croconic acid H_2Cr presents two bands at λ = 230 nm and λ = 295 nm. These bands are displaced according to acid–base equilibria (21). The croconate dianion is characterized by a typical band at λ 363 nm (Fig. 7). This band enables us to follow the croconate concentration and the ratio $(A_0 - A_t)/A_0$ represents the degree of oxidation as a function of time. When irradiation is performed, at first the absorption at 363 nm of the solution increases. Formation of transient radical species is suggested to explain this increase. Then the whole absorption spectrum decreases as a function of time. The value of A_0 is recorded when the irradiation is stopped. In the following section we use v_0 as the initial speed of oxidation

$$v_0 = -d[H_2Cr]/dt(t = 0) = k[H_2Cr]_0^p \text{ with } \rho_0 = v_0/[H_2Cr]_0(ms^{-1})$$

The superscript p is the order rate related to croconic acid (equal to one for a first-order rate) and ρ_0 should be constant for a first-order rate.

The variation of ρ_0 as a function of croconic acid concentration shows that ρ_0 is not a constant as for a first-order rate but that it is linearly related to the concentration. Moreover, Fig. 8 shows the variation of ρ_0 with pH. It appears that ρ_0 decreases rapidly when acidity decreases.

In this way EPR spectroscopy was carried out under irradiation in order to observe the occurrence of radicals. When the solution of croconic acid was irradiated, we observed radical

Fig. 6. Pseudo-first-order rate constant of croconic oxidation measured by cyclic voltammetry at a Pt electrode: $[C_5O_5H_2]_{(t=0)}$ = 1 mmol L^{-1}; pH = 0: A, croconic acid alone; B, with 2,2 bipyridyl 0,1 mmol L^{-1}; C, with 2,2 bipyridyl, $MnCl_2$ 0,1 mmol L^{-1}; pH = 1: crononic acid alone; D, air and light; E, air and dark; F, under Ar.

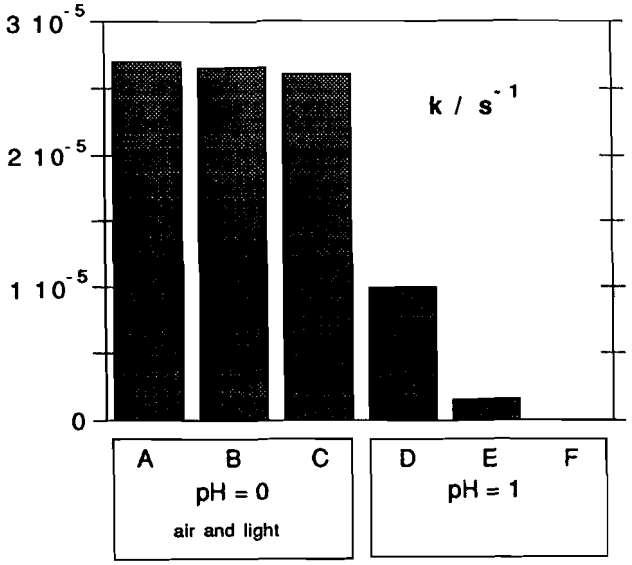

signals on the EPR spectra at g_1 = 2.0055, g_2 = 2.0045, and g_3 = 2.0038 with intensities of 1.75, 1, and 8.5, respectively. These signals are related to the presence of three different organic radicals according to the different shape of the signals. In organic aprotic solvents the electrochemical oxidation of croconate dianion leads to a stable radical whose EPR spectra gives a g value of 2.0065.

According to all these results, three major parameters appear in the oxidation process of croconic acid:

1. pH. Oxidation occurs in acidic media. From Fig. 8, ρ_0 appears linearly related to pH and reaches 0 in neutral medium. The slope of the ρ_0 variations in acid media gives a crossing point at pH 4.7. This value has the same order of magnitude as the pK_A of the HO_2, radical (22), which can yield singlet dioxygen by deprotonation (23). However, in this case the kinetic parameter should be higher at high pH values and this pathway cannot be retained. Alternatively, the variation of ρ_0 may be related to the acidity constants of croconic acid, that is, to the relative domains of the species. At low pH, the protonated form (**1**) or its hydrated form (**3**) are predominant and easily oxidized. At pH > 4, the croconate dianion (**2**) is predominant and, due to is high delocalization, is too stable to undergo an oxidation process (solutions of $K_2C_5O_5$ do not turn colorless).

2. Dioxygen is necessary according to the overall process. The involvement of singlet dioxygen is not indicated since the reaction rate is not significantly modified by classical scavengers of singlet dioxygen such as sodium azide or DABCO. The reaction is inhibited in D_2O while it would be accelerated as in the case of a singlet dioxygen oxidation.

3. Light enhances the croconic acid oxidation. The EPR signals observed under irradiation suggest that reaction is due to a radical pathway. As shown by isobestic points in the UV spectra, the decomposition of form **3** is achieved via an intermediate product. Moreover, the increase of absorbance under

Can. J. Chem. Downloaded from www.nrcresearchpress.com by 80.90.12.36 on 09/08/12
For personal use only.

Can. J. Chem. Downloaded from www.nrcresearchpress.com by 80.90.12.36 on 09/08/12
For personal use only.

Fig. 7. UV–vis spectra of croconic acid solution after irradiation sequences (5 s).

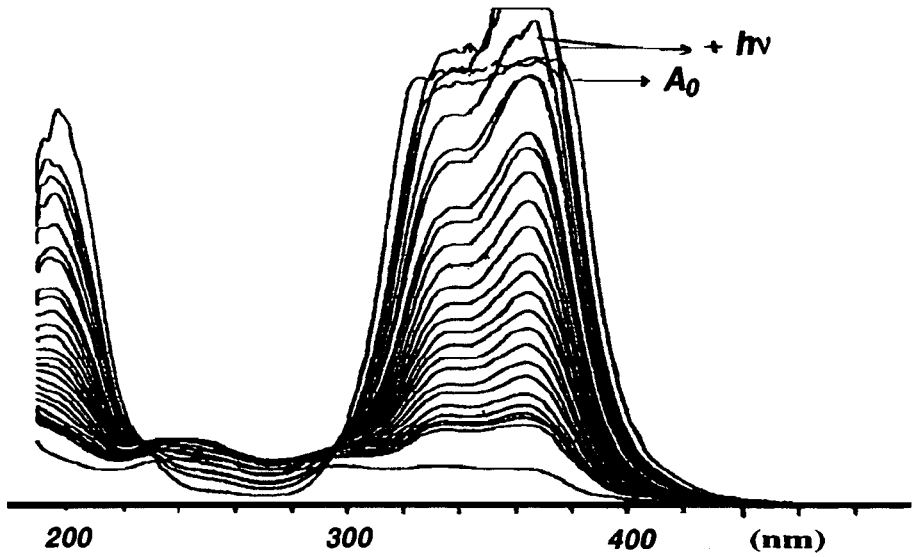

Fig. 8. Variation of the kinetics parameter ρ_0 versus pH.

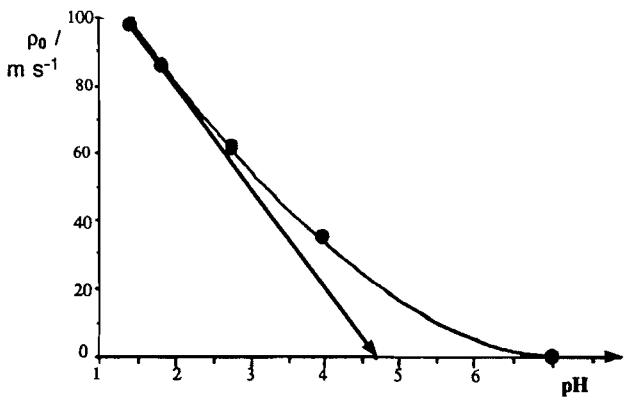

irradiation may be attributed to the transient formation of a radical. In basic media where the dianion $C_5O_5^{2-}$ is the predominant form, excited $C_5O_5^{2-*}$ (**3***) can yield the radical anion $C_5O_5^{-}$ (15, 16) or be deactivated by dioxygen (16).

Transposition of croconate dianion oxidation (15, 16) in acid medium would lead to the following sequence:

$$C_5O_6H_4 + h\nu \rightarrow C_5O_6H_4^*$$

$$\underset{\mathbf{3}^*}{C_5O_6H_4^*} + \underset{\mathbf{3}}{C_5O_6H_4} + 3\,H_2O \rightarrow \underset{\mathbf{4}c}{C_5O_9H_8} + \underset{\mathbf{7}}{C_5O_6H_6}$$

The formation of compound **7** requires the preliminary reduction of croconic acid. On the basis of the EPR signals observed, it is suggested that this reduced product may occur from an electron transfer between a molecule of croconic acid in the excited state and another molecule in the ground state, leading to the subsequent formation of the croconic radical anion (this assumption is in agreement with the bimolecular character of the reaction). The oxidation of the diene **7** may be

Scheme 4.

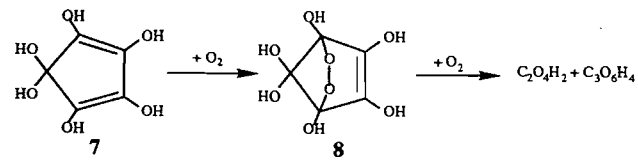

expressed either by a 1,4 addition as proposed in Scheme 4 or by two 1,2 additions of oxygen (24).

Conclusion

Oxocarbon compounds are reported to present interesting properties as ligands. They also undergo redox processes that enable $[C_nO_n]^{2-}$ conversions. Moreover, in this work croconic acid has been shown to be oxidized into oxalic and mesoxalic acids in acid media. These results are in agreement with those of Verchere and Fleury (10–12) on the oxidation of croconic acid and other polyketo compounds with metal salts in acidic media. The main difference in the oxidation products in acidic and basic media arises from the acido-basic properties of croconic acid; this is supported by the potential–pH data for croconic acid. Similarly, the electrochemical oxidation and the photooxidation are different in acidic and basic media.

References

1. N.C. Baenziger and J.J. Hegenbarth. J. Am. Chem. Soc. **86**, 3250 (1964).
2. W. Stadeli, R. Hollenstein, and W. von Philipsborn. Helv. Chim. Acta, **60**, 948 (1977).
3. R.I. Gelb, L.M. Schwartz, D.A. Laufer, and J.O. Yardley. J. Phys. Chem. **81**, 1268 (1977).
4. W.H. Flygare and R.C. Benzon. J. Mol. Phys. **20**, 225 (1970).
5. D. Eggerding and R. West. J. Am. Chem. Soc. **98**, 3641 (1976).
6. R. West. *In* Oxocarbons. Academic Press, New York. 1980.
7. L.M. Schwartz, R.I. Gelb, and O. Yardley. J. Phys. Chem. **79**, 2246 (1975).
8. L.M. Schwartz and O. Howard. J. Phys. Chem. **75**, 1978 (1971).

9. D. Deguenon, G. Bernardinelli, J.P. Tuchagues, and P. Castan. Inorg. Chem. **29**, 3031 (1990).
10. J.F. Verchere and M.B. Fleury. Bull. Soc. Chim. Fr. 2611 (1972).
11. J.F. Verchere and M.B. Fleury. J. Less-Common Met. **36**, 133 (1974).
12. J.F. Verchere and M.B. Fleury. J. Less-Common Met. **54**, 135 (1977).
13. Q. Chen, S. Liu, and J. Zubieta. Angew. Chem. Int. Ed. Engl. **27**, 1724 (1988).
14. G. Iraci and M.H. Back. Can. J. Chem. **66**, 1293 (1988); B. Zhao and M.H. Back. Can. J. Chem. **69**, 528 (1991).
15. B. Zhao and M.H. Back. Can. J. Chem. **70**, 135 (1992).
16. B. Zhao and M.H. Back. Int. J. Chem. Kinet. **26**, 25 (1994).
17. A.J. Fatiadi, H.S. Isbell, and W.F. Sager. J. Res. Natl. Bur. Stand. Sect. A: **67**: 1225 (1963).
18. P. Cassoux, R. Dartiguepeyron, P.L. Fabre, and D. de Montauzon. Actual Chim. **1–2**, 79 (1985), Electrochim. Acta, **30**, 1485 (1985).
19. D. Sazou and G. Kokkinidis. Can. J. Chem. **65**, 397 (1987).
20. W. Stadeli, R. Hollenstein, and W. von Philipsborn. Helv. Chim. Acta, **60**, 955 (1977).
21. K. Yamada, N. Mizumo, and Y. Hirata. Bull. Chem. Soc. Jpn. **31**, 543 (1958).
22. B.H. Bielski. J. Photochem. Photobiol. **28**, 645 (1978).
23. S.S. Miller, K. Zahir, and A. Haim. Inorg. Chem. **24**, 3978 (1985).
24. A.A. Frimer. Chem. Rev. **79**, 359 (1979); J. Erikensen, C.S. Foste, and T.L. Parker. J. Am. Chem. Soc. **99**, 6455 (1977).

Can. J. Chem. Downloaded from www.nrcresearchpress.com by 80.90.12.36 on 09/08/12
For personal use only.

The acidity and tautomerism of β-diketones in aqueous solution

John W. Bunting, James P. Kanter, Raymond Nelander, and Zhennan Wu

Abstract: The acidity and keto–enol tautomerism of a series of symmetrical β-diketones ($RCOCH_2COR$ (**1**): R = methyl (*a*), phenyl (*b*), 3-pyridinyl (*c*), 4-pyridinyl (*d*), 3-(*N*-methyl)pyridinio (*e*), and 4-(*N*-methyl)pyridinio (*f*)) and two series of unsymmetrical β-diketones ($RCOCH_2COCH_3$ (**7***a*–**7***f*) and $RCOCH_2COC_6H_5$ (**8***a*–**8***f*)) have been investigated in aqueous solution at 25°C and ionic strength 0.1. Values of pK_a^{eq} were measured spectrophotometrically, and the acidities of the enols (pK_a^E) were obtained from the analysis of the pH dependence of the buffer catalysis for the general acid-catalyzed protonation of the enolate conjugate bases. These data in turn allowed the calculation of the acidities of the keto tautomers (pK_a^K) and the equilibrium constants for enolization (K_E = [Enol]/[Keto]). In general, K_E is greater for the symmetrical ketones (**1**) than for the corresponding R-substituted unsymmetrical ketones (**7** and **8**). K_E is much more sensitive to the nature of the R substituent in these three series of β-diketones than in the corresponding series of β-keto esters and amides. Correlations between pK_a^K for **8** and **7** combined with the known acidities of the corresponding β-keto esters and amides provide the first accurate estimates of the acidities of dimethyl malonate (pK_a = 13.0) and malonamide (pK_a = 12.5) in aqueous solution.

Key words: acidity, tautomerism, β-diketones.

Résumé : Opérant en solutions aqueuses, à 25°C et à une force ionique de 0,1, on a étudié l'acidité et l'isomérie céto–énolique d'une série de β-dicétones symétriques ($RCOCH_2COR$ (**1**) : R = méthyl (*a*), phényl (*b*), 3-pyridyle (*c*), 4-pyridyle (*d*), 3-(*N*-méthyl)pyridinio (*e*) et 4-(*N*-méthyl)pyridinio (*f*)) et de deux séries de β-dicétones non symétriques ($RCOCH_2CORCH_3$ (**7***a*–**7***f*) et $RCOCH_2COC_6H_5$ (**8***a*–**8***f*)). On a mesuré les pK_a^{eq} spectrophotométriquement et on a déterminé les acidités des énols (pK_a^E) par une analyse de la relation entre la dépendance sur le pH de la catalyse du tampon sur la protonation par catalyse acide générale des bases conjuguées énolates. Ces données permettent ensuite de calculer les acidités des céto-tautomères (pK_a^K) et les constantes d'équilibre de l'énolisation (K_E = [Énol]/[Cétone]). En général, la valeur de K_E est plus grande pour les cétones symétriques (**1**) que pour les cétones non symétriques correspondantes substituées par des groupes R (**7** et **8**). La valeur de K_E est beaucoup plus sensible à la nature du substituant R dans ces trois séries de β-dicétones que dans les séries correspondantes de β-cétoamides. Des corrélations entre les valeurs des pK_a^K des composés **7** et **8** combinées avec les acidités connues des β-cétoesters et β-cétoamides correspondants fournissent les premières évaluations précises des acidités du malonate de diméthyle (pK_a = 13,0) et du malonamide (pK_a = 12,5) en solution aqueuse.

Mots clés : acidité, tautomérie, β-dicétones.

[Traduit par la rédaction]

Introduction

In aqueous solution, β-diketones (**1** = KH) exist in equilibrium with their keto–enol isomers (**2** = EH) and the corresponding enolate anion (**3** = E^-) as described in Scheme 1. Titration of the equilibrium mixture of KH and EH gives an apparent acid ionization constant, K_a^{eq} (eq. [1]), which may be described by the ionization constant of either tautomer and the equilibrium ratio of the enol and keto tautomers, K_E = [EH]/[KH], as shown in eqs. [2] and [3].

$$[1] \quad K_a^{eq} = [H^+][E^-]/([KH] + [EH])$$

$$[2] \quad pK_a^{eq} = pK_a^K + \log (1 + K_E)$$

$$[3] \quad pK_a^{eq} = pK_a^E + \log (1 + 1/K_E)$$

pK_a^{eq} is usually readily determined by spectrophotomeric titration in aqueous solutions buffered at various pH values. In principle, the measurement of any one of pK_a^K, pK_a^E, or K_E then allows the evaluation of all equilibrium constants in Scheme 1 using eqs. [2] and [3]. Aqueous solutions of acetylacetone (**1**: R = CH_3) have been examined a number of times (1–10), and there is general agreement that at equilibrium approximately 20% of this diketone exists in the form of the enol (**2**: R = CH_3) near room temperature. However, there have been relatively few studies of other β-diketones in aqueous solution (4, 7, 11–13), and thus there is little information

Received August 16, 1994.

J.W. Bunting,[1] J.P. Kanter, R. Nelander, and Z. Wu.
Department of Chemistry, University of Toronto, Toronto, ON M5S 1A1, Canada

[1] Deceased February 20, 1995.

Can. J. Chem. Downloaded from www.nrcresearchpress.com by 80.90.12.36 on 09/08/12
For personal use only.

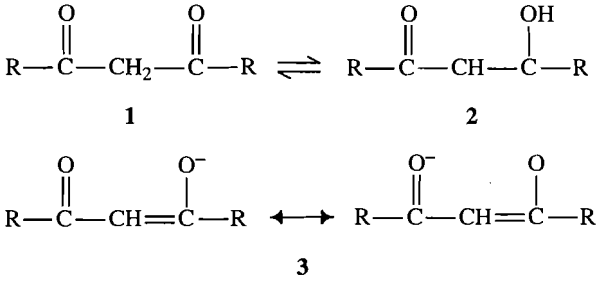

1 2

3

Scheme 1.

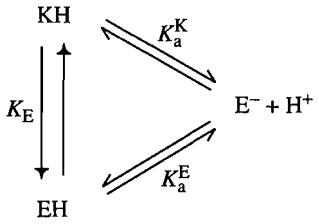

available on the dependence of each of the three equilibrium constants of Scheme 1 upon the nature of the R substituents in **1**, which represents symmetrical β-diketones, or upon R^1 and R^2 in **4**, which represents unsymmetrical species ($R^1 \neq R^2$).

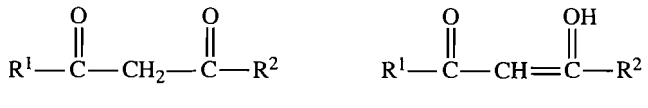

4 5

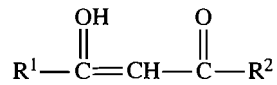

6

The study of unsymmetrical β-diketones introduces an additional complication, which is not relevant for symmetrical β-diketones, and is of no significance for β-keto esters or amides that we have recently examined (14). Unsymmetrical β-diketones (**4**) can enolize to give a pair of enol structural isomers (**5** and **6**). Thus the generation of enols by O-protonation of the enolate ion derived from **4** will in general give a mixture of these two enol species, and so the pK_a^E and K_E defined in terms of Scheme 1 will contain a contribution from the equilibrium ratio of **5**: **6**. This limitation will complicate the interpretation of the structural dependences of pK_a^E and K_E and also relationships between pK_a^K and pK_a^E such as those which were developed (14) for β-keto esters and amides.

The current work reports an investigation of the equilibria for the deprotonation and tautomerism of 15 β-diketones in aqueous solution. These species include six symmetrical ketones (**1***a*–**1***f*; see Table 1), six β-keto methyl ketones (**7***a*–**7***f*; see Tables 1 and 2; note that **1***a* = **7***a*), and six β-keto phenyl ketones (**8***a*–**8***f*; note that **8***a* = **7***b* and **8***b* = **1***b*). Useful linear free energy relationships are established between pK_a^K values for the various classes of β-diketones and the corresponding β-keto esters and amides (14). We have also found that the enol contents of β-keto esters and amides are not, in general, a reasonable basis for the confident prediction of the enol contents of similarly substituted β-diketones.

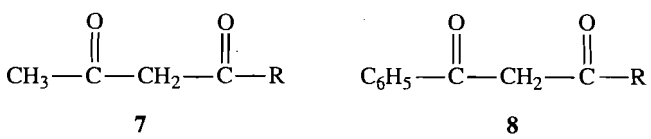

7 8

Experimental

2,4-Pentanedione (acetylacetone **1***a*), 1-phenyl-1,3-butanedione (benzoylacetone **7***b*), and 1,3-diphenyl-1,3-propanedione (dibenzoylmethane **1***b*) are commercially available. All other neutral β-diketones were prepared by the condensation of the enolate anion of 3- or 4-acetylpyridine with the appropriate methyl ester. A detailed synthesis of **1***c* is described below. Each pyridyl β-diketone was methylated by treatment with methyl bromide in acetone solution in a pressure bottle at room temperature for 24 h. All products were characterized by ^1H NMR spectroscopy in CD_3SOCD_3; in general these spectra indicated the presence of a mixture of the keto and enol tautomers in this solvent (13).

1,3-Di-3-pyridinyl-1,3-propanedione (1*c*)

Methyl nicotinate (2.5 g) was dissolved in 3-acetylpyridine (10 mL). An 80% dispersion of sodium hydride in mineral oil (0.6 g) was added to this solution, with constant stirring, over a period of 30 min. The mixture was stirred and refluxed for a further 2.5 h during which time the solution became bright yellow. The product solution was cooled to room temperature, diluted with diethyl ether (40 mL), and neutralized with a few drops of concentrated HCl. A saturated aqueous solution of sodium chloride (20 mL) was added, and the product was collected by exhaustive extraction with methylene chloride. These extracts were dried over magnesium sulfate, and the solvent was removed on the rotary evaporatory. The resulting oil was treated with a 1:1 mixture of diethyl ether and hexane (10 mL). After refrigeration overnight, large pale-yellow crystals of **1***c* were obtained, and recrystallized from 2-propanol in 78% overall yield; mp 198–200°C (lit. (15) mp 199–201°C; (16) mp 198°C).

The following β-diketones were similarly prepared: **1***d*, mp 152–154°C; **7***c*, mp 81–83°C (lit. (17) 81–82°C); **7***d*, mp 66–67°C (lit. (18) mp 66–67°C); **8***c*, mp 119–121°C; **8***d*, mp 83–84°C (lit. (18) mp 83–84°C).

The following bromide salts were also obtained: **1***e*·$(Br^-)_2$, mp 243°C (dec.); **1***f*·$(Br^-)_2$, mp 248°C (dec.); **7***e*·Br^-, mp 142°C (dec.); **7***f*·Br^-, mp 152°C (dec.); **8***e*·Br^-, mp 210–212°C; **8***f*·Br^-, mp 255–257°C.

pK_a measurements

The spectrophotometric measurements of pK_a^{eq} and the evaluation of pK_a^K in pH-jump experiments by stopped-flow spectrophotometry closely followed the methods described in detail in our recent work (14). All experimental data are for aqueous solutions of ionic strength of 0.1 (KCl + buffer) at 25°C, with the exception of data for dibenzoylmethane (**1***b*) for which limited aqueous solubility required the addition of 10% acetonitrile to all aqueous solutions.

Can. J. Chem. Downloaded from www.nrcresearchpress.com by 80.90.12.36 on 09/08/12
For personal use only.

Can. J. Chem. Downloaded from www.nrcresearchpress.com by 80.90.12.36 on 09/08/12
For personal use only.

Fig. 1. The pH dependence of the absorption spectrum of **7***e* (0.101 mM) in aqueous solution. Spectra are at pH 4.00 (spectrum 1), 6.03, 6.23, 7.02, and 8.50 (spectrum 5).

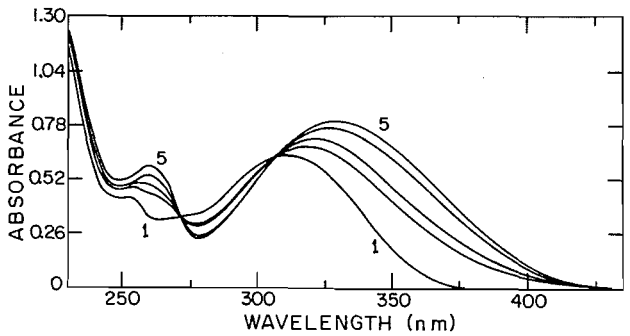

Fig. 2. The pH dependence of the absorption spectrum of **1***e* (0.0454 mM) in aqueous solution. Spectra are at pH 2.08 (spectrum 1), 3.47, 4.00, 4.51, 5.04, 5.52, and 7.04 (spectrum 7).

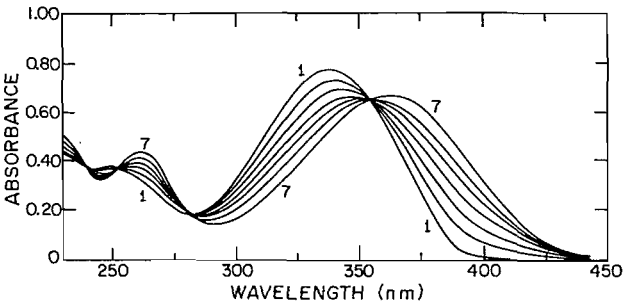

Results

Figures 1 and 2 display the pH-dependence of the electronic absorption spectra of two of the ketones examined in this study. These two examples, which are typical of the spectral observations for all diketones in the current study, are chosen to demonstrate pH-dependent spectra for a β-diketone (**7***e*) that predominates over its enol tautomer, and a diketone (**1***e*) that exists mainly as the enol isomer. In basic solution, each enolate conjugate base displays an intense long-wavelength absorption maximum. These λ_{max} are listed in Tables 1 and 2, and vary systematically in the order: methyl < phenyl < 3-pyridyl < 4-pyridyl < 3-(*N*-methyl pyridinio) < 4-(*N*-methyl pyridinio) for the enolates; i.e., systematically from *a*–*f* for the conjugate bases from each of **1**, **7**, and **8**. The same ordering of λ_{max} values was also observed (14) for the enolate conjugate bases of the corresponding β-keto esters and amides. All symmetrical enolate ions (**3**) have longer wavelength absorption maxima (Table 1) than do the corresponding unsymmetrical enolate ions from each of **7** and **8** (Table 2). The corresponding enol (**2***f*) has λ_{max} = 353 nm.

The pH dependence of the absorbance at constant wavelength in the vicinity of λ_{max} of the enolate was used to evaluate pK_a^{eq} for the equilibrated tautomeric mixtures from each of **1**, **7**, and **8**. Values of pK_a^{eq} are listed in Tables 1 and 2.

The acidities of the enols (pK_a^E) were calculated form the pH dependence of buffer catalysis of the ketonization reactions in pH-jump experiments in which a solution of the enolate conjugate base was rapidly acidified in the stopped-flow spectrophotometer. This technique, and the algebraic treatment of the kinetic data that allows the calculation of pK_a^E, have recently been described (14) in some detail. Values of pK_a^E are included in Tables 1 and 2. These tables also include K_E calculated from eq. [3], and pK_a^K, which was subsequently calculated from eq. [2].

For **1***e* and **1***f* there was no observable time-dependent absorbance change upon acidification of the enolate species. This implies that the conjugate acid species is predominantly the enol tautomer in these two cases and that $pK_a^{eq} = pK_a^E$. For **8***d* and **8***f*, the time-dependent absorbance changes upon acidification of the enolate were quite small. In these two cases, values of pK_a^E were still measurable; however, these enol acidities are within experimental error of pK_a^{eq}, and so accurate values of K_E and pK_a^K are not directly accessible by the current experimental method. The estimates of pK_a^K in Tables 1 and 2 for these two species are based upon the linear free energy relationships that are developed below.

Discussion

The data in Tables 1 and 2 represent the most extensive set of data that are currently available for the structural dependence of the equilibrium constants defined in Scheme 1 for β-diketones in aqueous solution. Before discussing the trends in these data it is important to appreciate a limitation that is inherent in the current experimental method for the evaluation of K_E and pK_a^K. The calculation of these two parameters requires a significant difference between pK_a^{eq} and pK_a^K. If K_E (= [Enol]/[Keto]) < 1, this difference is large and accurate values of K_E and pK_a^K are obtained. However, $pK_a^E \approx pK_a^{eq}$ for those species for which the tautomeric ratio lies heavily in favour of the enol tautomer, and accurate numerical values of K_E are not accessible. Our experience from both the current study and our earlier work (14) is that K_E should be less than 5 for the quantitative analysis of structural effects upon K_E and pK_a^K. This limit will be adopted in the correlation analyses of equilibrium constants that are presented below, although we will also show that the linear free energy relationships that we have developed do allow an alternative route to the estimation of pK_a^K (and consequently K_E) when this equilibrium constant is not directly accessible experimentally.

Acidities of keto and enol tautomers

A well-defined relationship between the acidities of the β-keto methyl ketones (**7**) and the structurally related β-keto phenyl ketones (**8**) is shown in Fig. 3. This figure includes data points for the methyl esters and amides of acetoacetic and benzoylacetic acids in addition to the β-diketones of the current study. The correlation line in Fig. 3 is defined by eq. [4], which in turn allows the estimation of pK_a^K for **8***d* and **8***f* (Table 2).

$$[4]\quad pK_a^K(\mathbf{8}) = 0.98(\pm 0.05)pK_a^K(\mathbf{7}) - 0.2(\pm 0.2) \qquad (r = 0.995;\ n = 6)$$

Similar linear correlations can be demonstrated between pK_a^K values for β-keto methyl ketones (**7**) and β-keto methyl esters (**9**) (eq. [5]), β-keto phenyl ketones (**8**) and β-keto methyl esters (**9**) (eq. [6]), β-keto methyl ketones (**7**) and β-keto amides (**10**) (eq. [7]), and β-keto phenyl ketones (**8**) and β-keto amides (**10**) (eq. [7]). The slope parameters in eqs. [5]–

Table 1. Equilibrium constants for deprotonation and tautomerization of symmetrical β-diketones (**1**) and their enols (**2**).[a]

No.	R	λ_{max} (log ε)[b]	pK_a^{eq}	pK_a^E	pK_a^K	K_E
1*a* = **7***a*	CH_3	292 (4.41)	8.79	8.03	8.71	0.21
1*b* = **8***b*[c]	C_6H_5	347 (4.17)	8.71	8.64	≈7.9	≈6
1*c*	3-C_5H_4N	350 (4.04)	7.23	7.04	6.78	1.8
1*d*	4-C_5H_4N	356 (4.05)	5.51	5.45	≈4.65	≈6
1*e*	3-($C_5H_4NCH_3^+$)	362 (4.17)	4.82	4.82	(3.2)[d]	40
1*f*	4-($C_5H_4NCH_3^+$)	403 (3.99)	3.07	3.07	(0.7)[d]	200

[a]In aqueous solution, ionic strength 0.1, at 25°C. K_E is calculated from eq. [3] for **1***a*–**1***d*, and from eq. [2] for **1***e* and **1***f*.
[b]Longest wavelength absorption maximum in the spectrum of the enolate conjugate base.
[c]All data are for aqueous solutions containing 10% acetonitrile.
[d]Average of the values calculated from eqs. [9] and [10].

Table 2. Equilibrium constants for deprotonation and tautomerization of unsymmetrical β-diketones (**7** and **8**) and their enols.[a]

No.	R	λ_{max} (log ε)[b]	pK_a^{eq}	pK_a^E	pK_a^K	K_E
7*b* = **8***a*	C_6H_5	320 (4.09)	8.77	8.39	8.53	0.72
7*c*	3-C_5H_4N	322 (3.75)	7.64	7.15	7.47	0.48
7*d*	4-C_5H_4N	327 (4.13)	7.39	7.16	7.00	1.4
7*e*	3-($C_5H_4NCH_3^+$)	329 (3.93)	6.24	5.53	6.15	0.24
7*f*	4-($C_5H_4NCH_3^+$)	377 (3.79)	5.97	5.92	≈5.0	≈8
8*c*	3-C_5H_4N	347 (4.14)	7.62	7.37	7.26	1.3
8*d*	4-C_5H_4N	350 (4.22)	7.30	7.27(7.18)[c]	(6.7)[d]	3
8*e*	3-($C_5H_4NCH_3^+$)	354 (4.12)	6.15	5.84	5.86	0.97
8*f*	4-($C_5H_4NCH_3^+$)	388 (3.96)	5.92	5.89	(4.7)[d]	16

[a]In aqueous solution, ionic strength 0.1, at 25°C. K_E was calculated from eq. [3] in all cases excepting **8***d* and **8***f* for which eq. [2] was used (see text).
[b]Longest wavelength absorption maximum in the spectrum of the enolate base.
[c]Calculated from eq. [3] for $K_E = 3$.
[d]Calculated from eq. [4].

Can. J. Chem. Downloaded from www.nrcresearchpress.com by 80.90.12.36 on 09/08/12
For personal use only.

[8] demonstrate that β-diketones are somewhat less sensitive to variation in the R substituent of the acyl functional group than are the less acidic β-keto esters and amides

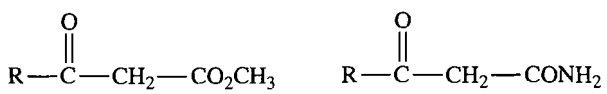

9 **10**

[5] $pK_a^K(\mathbf{7}) = 0.80(\pm0.08)pK_a^K(\mathbf{9}) + 0.4(\pm0.3)$ $(r = 0.982; n = 6)$

[6] $pK_a^K(\mathbf{8}) = 0.77(\pm0.09)pK_a^K(\mathbf{9}) + 0.2(\pm0.3)$ $(r = 0.975; n = 6)$

[7] $pK_a^K(\mathbf{7}) = 0.78(\pm0.07)pK_a^K(\mathbf{10}) + 0.7(\pm0.3)$ $(r = 0.984; n = 6)$

[8] $pK_a^K(\mathbf{8}) = 0.75(\pm0.08)pK_a^K(\mathbf{10}) + 0.6(\pm0.3)$ $(r = 0.977; n = 6)$

Interpolation in these correlation equations can be used to predict pK_a^K for some related species. Equation [5] and pK_a^K= 10.60 for methyl acetoacetate (**7**: R = OCH_3) (14) predicts pK_a^K = 12.9 for dimethyl malonate (**9**: R = OCH_3). Equation [6] and pK_a^K = 10.28 for methyl benzoylacetate (**8**: R = OCH_3) (14) lead to pK_a^K = 13.0 for this same malonate diester. These predictions are similar to the pK_a = 13.3 for diethyl malonate (19) that is the only experimental value we have been able to locate for the acidity of a malonate diester in aqueous solution, although the experimental basis of this value is unclear.

A similar analysis using pK_a^K = 10.41 for acetoacetamide and pK_a^K = 10.04 for benzoylacetamide (14) leads to pK_a^K = 12.5 for malonamide (**10**: R = NH_2) from both eqs. [7] and [8]. We have been unable to find a literature value for the acidity of this diamide in aqueous solution. Williams and Xia (20) have recently estimated $K_E = 4 \times 10^{-10}$ for the enolization of malonamide. These values of pK_a^K and K_E then allow the cal-

Can. J. Chem. Downloaded from www.nrcresearchpress.com by 80.90.12.36 on 09/08/12
For personal use only.

Fig. 3. Correlation between pK_a^K for **8** and pK_a^K for **7** (*a–e* as defined in Table 2), including data for methyl esters (**9** = E) and amides (**10** = A) of acetoacetic and benzoylacetic acids. The correlation line is defined by eq. [4].

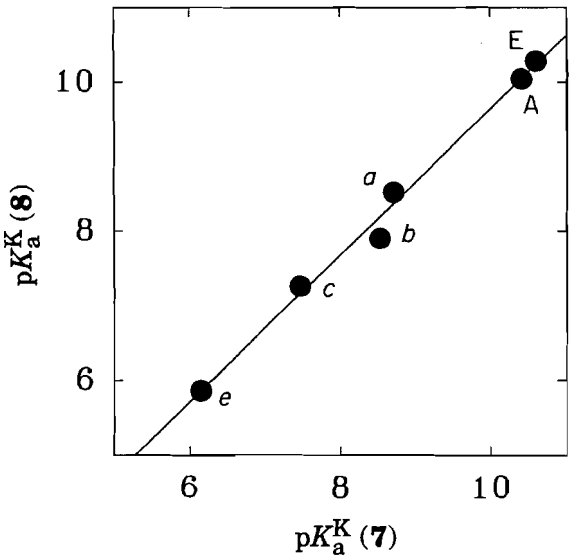

culation of pK_a^E = 3.1 for the enol of malonamide using Scheme 1.

Figure 4 shows a linear relationship (eq. [9]) between pK_a^K for symmetrical β-diketones (**1**) and pK_a^K for the corresponding unsymmetrical β-keto methyl ketones (**7**). A similar linear relationship (eq. [10]) also exists between pK_a^K for **1** and pK_a^K for the unsymmetrical β-keto phenyl ketones (**8**). The pK_a^K data estimated above for the diester and diamide of malonic acid appear to be consistent with these relationships. Equations [9] and [10] can be used to estimate for **1***e* and **1***f* (see Table 1) for which we have been unable to demonstrate any β-diketone tautomer upon acidification of solutions of the enolate conjugate bases in pH-jump experiments. The calculated K_E ratios then confirm the predominance of the enol tautomers in these two cases.

[9] $pK_a^K(\mathbf{1}) = 2.22(\pm0.15)pK_a^K(\mathbf{7}) - 10.6(\pm0.5)$ $(r = 0.990; n = 6)$

[10] $pK_a^K(\mathbf{1}) = 2.16(\pm0.12)pK_a^K(\mathbf{8}) + 9.4(\pm0.4)$ $(r = 0.993; n = 6)$

[11] $pK_a^K(\mathbf{8}) = 1.05(\pm0.06)pK_a^E(\mathbf{7}) - 0.1(\pm0.1)$ $(r = 0.993; n = 6)$

Since the experimentally measured pK_a^E values contain contributions from more than one enol tautomer of **7** and **8**, we did not expect to find simple relationships for pK_a^E that are analogous to those reported above for pK_a^E. However, Figs. 5 and 6 show that some approximate relationships involving pK_a^E do exist. Thus, there appears to be a linear relationship between the pK_a^E values for the enols of **7** and **8** (Fig. 5 and eq. [11]) although β-keto esters and amides, which give a single enol, deviate somewhat from the relationship for the β-diketones. Figure 6

Fig. 4. Correlations between pK_a^K for **1** and **7** (*a–e* as defined in Tables 1 and 2), including data for dimethyl malonate (A) and malonamide (E) evaluated from eq. [4] as examples of **1**. The correlation line is defined by eq. [9].

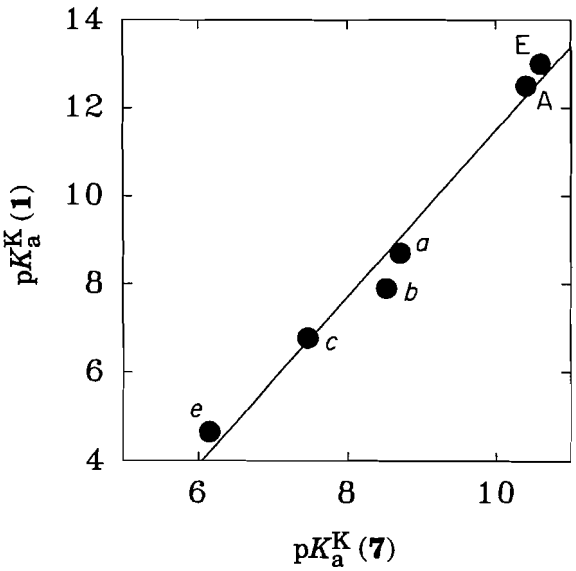

demonstrates the dependence of pK_a^E upon pK_a^K for **1**, **7**, and **8**. The correlation line in Fig. 6 corresponds to eq. [12], which is defined for the symmetrical β-diketones (**1**). The data for the unsymmetrical ketones, apart from the 3-(*N*-methyl pyridinio) derivatives (**7***e* and **8***e*), are also consistent with eq. [12].

[12] $pK_a^E(\mathbf{2}) = 0.68(\pm0.07)pK_a^K(\mathbf{1}) + 2.6(\pm0.5)$ $(r = 0.981; n = 6)$

Structural effects upon K_E

It is apparent from Table 2 that K_E is smaller for β-keto methyl ketones (**7**) than for the corresponding β-keto phenyl ketones (**8**) bearing the same R substituent. This enhanced enol content for phenyl ketones over methyl ketones is dramatized by the 30-fold greater K_E for dibenzoylmethane (**1***b*) than for acetylacetone (**1***a*); this is presumably attributable to the styrene-like conjugation that is present in the enols of phenyl ketones. For the symmetrical β-diketones (**1**) enol content increases in the order: methyl < 3-pyridyl < phenyl ≈ 4-pyridyl << 3- and 4-(*N*-methyl puridinio). With the exception of R = 3-(*N*-methyl pyridinio), this same order is essentially preserved for **7** and **8**, although the enol content is clearly smaller for R = phenyl than for R = 4-pyridyl in these two series of unsymmetrical ketones. For **7***e* and **8***e*, the enol content is unusually small in comparison with the high enol content of the symmetrical 3-(*N*-methyl pyridinio) diketone (**1***e*). For both **7***e* and **8***e*, K_E is of similar magnitude to that found for **7***a* and **8***a* and more than 10-fold smaller than for the isomeric 4-(*N*-methyl pyridinio) species (**7***f* and **8***f*). We have no simple explanation for the unique effects from the 3-(*N*-methyl pyridinio) substituents in symmetrical and unsymmetrical β-diketones, other than to suggest that the predominant enol, for reasons unknown, may be that which enolizes on the side of the acetyl and benzoyl groups, respectively (i.e., **5**: $R^2 = CH_3$ or C_6H_5), rather than

Fig. 5. Correlation between pK_a^K for the enols of **8** and **7** (*a–e* as defined in Table 2). The correlation line is defined by eq. [11]. The data for methyl esters (**9** = E) and amides (**10** = A) of acetoacetic and benzoylacetic acids are not included in this relationship.

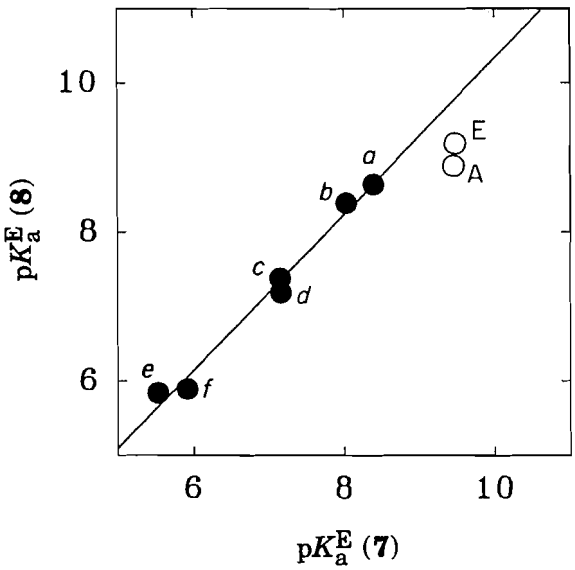

Fig. 6. The relationship between pK_a^E and pK_a^K for **1** (filled circles), **7** (empty circles), and **8** (filled triangles). The correlation line is eq. [12] defined for symmetrical ketones (**1**) only.

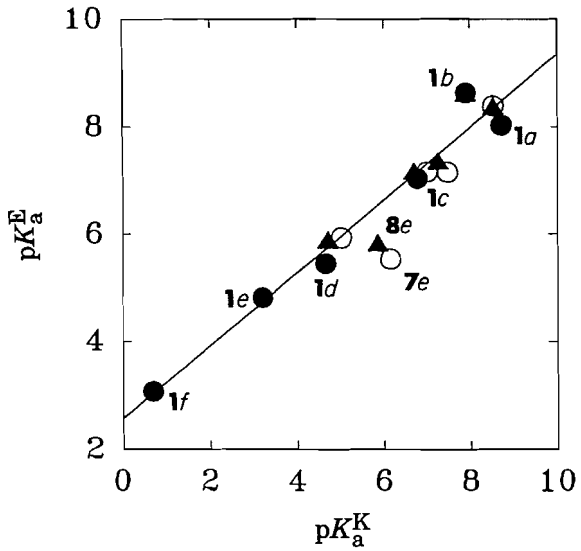

rather than towards the 3-pyridinio carbonyl group (i.e., **6**: R^1 = 3-($C_5H_4NCH_3^+$)).

The strong dependence of K_E upon R for β-diketones in Tables 1 and 2 is in marked contrast with the relative insensitivity of K_E to the same six R substituents in β-keto esters and amides (**9** and **10** with R substituents *a–f* as defined in Tables 1 and 2) (14). All of these β-keto esters and amides predominate over their enol tautomers (enol contents in the range 6–22%) in aqueous solution, with K_E for each of **9** and **10** being smaller than for the corresponding R-substituted diketone in Table 2. For each of **9** and **10**, K_E varies less than 4-fold, with little difference between the enol contents for R = methyl and R = phenyl. For both **9** and **10**, K_E is largest for R = 4-pyridyl, with approximately a 2-fold decrease in enol content upon N-methylation of either the 3- or 4-pyridyl derivatives. This latter observation is in marked contrast to the dramatic increase in K_E that is indicated in Tables 1 and 2 upon methylation of **1***c*, **1***d*, **7***d*, and **8***d*.

The foregoing comparisons make it clear that, in general, substituent effects upon K_E from the acyl groups in β-keto esters and amides cannot be used as a general guide to the effects of these same acyl groups upon the enol contents of β-diketones. While this result may initially appear somewhat surprising, in fact there should be significant differences between the roles of substituent effects upon enol stability for β-keto esters (and amides), symmetrical β-diketones, and unsymmetrical β-diketones. For **9** and **10**, enolization is only expected towards the ketone, and not towards the formal carbonyl group of the ester or amide unit. In these cases, the dependence of K_E upon R gives a direct indication of the influence of R upon the relative stabilities of ketones and their isomeric enols. For symmetrical diketones, two R groups are changed simultaneously and, while there is only one enol species, the effects of the two R groups upon the stability of **2** will probably be quite different. For unsymmetrical β-diketones, there is the additional problem that the experimentally determined K_E contains contributions from two structurally isomeric enols (**5** and **6**) and the likelihood that the equilibrium ratio of [**5**]/[**6**] will also be dependent upon R^1 and R^2.

Acknowledgement

We appreciate the support of this work by the Natural Sciences and Engineering Research Council of Canada.

References

1. G. Schwarzenbach and E. Felder. Helv. Chim. Acta, **27**, 1044 (1944); **27**, 1701 (1944).
2. M.L. Eidenhoff. J. Am. Chem. Soc. **67**, 2073 (1945).
3. B. Eistert, E. Merkel, and W. Reiss. Chem. Ber. **87**, 1513 (1954).
4. P. Rumpf and R. La Rivière. C. R. Hebd. Seances Acad. Sci. **244**, 1501 (1957).
5. A.S.N. Murthy, A. Balasubramanian, C.N.R. Rao, and T.R. Kasturi. Can. J. Chem. **40**, 2267 (1962).
6. M.L. Ahrens, M. Eigen, W. Kruse, and G. Maass. Ber. Bunsenges. Phys. Chem. **74**, 380 (1970).
7. P. Alcais and R. Brouillard. J. Chem. Soc. Perkin Trans. 2, 1214 (1972).
8. C.F. Bernasconi and R.D. Bunnell. Isr. J. Chem. **26**, 420 (1985).
9. M. Moriyasu, A. Kato, and Y. Hashimoto. J. Chem. Soc. Perkin Trans. 2, 515 (1986).
10. J. Emsley and N.J. Freeman. J. Mol. Struct. **161**, 193 (1987).
11. J.-P. Calmon and P. Maroni. Bull. Soc. Chim. Fr. 2532 (1965).
12. S. Forsén and M. Nilsson. *In* The chemistry of the carbonyl group. Vol. 2. *Edited by* J. Zabicky. Interscience, London. 1970. Chap. 3.

Can. J. Chem. Downloaded from www.nrcresearchpress.com by 80.90.12.36 on 09/08/12
For personal use only.

14. J.W. Bunting and J.P. Kanter. J. Am. Chem. Soc. **115**, 11 705 (1993).
15. M. Ferles, S. Kafka, A.S. Ankava, and M. Sputova. Collect. Czech. Chem. Commun. **46**, 1169 (1981).
16. A. Babska, L. Bielski, L. Kuczynski, S. Respond, and H. Witek. Pol. J. Pharmacol. Pharm. **25**, 175 (1973).
17. L.F. Kuick and H.J. Adkins. J. Am. Chem. Soc. **57**, 143 (1935).
18. E. Belgodere, R. Bossio, F. De Sio, S. Maraccini, and R. Repino. Heterocycles, **20**, 504 (1983).
19. R.G. Pearson and J.M. Mills. J. Am. Chem. Soc. **72**, 1692 (1950).
20. D.L.H. Williams and L. Xia. J. Chem. Soc. Chem. Commun. 985 (1992); J. Chem. Soc. Perkin Trans. 2, 1429 (1993).

Can. J. Chem. Downloaded from www.nrcresearchpress.com by 80.90.12.36 on 09/08/12
For personal use only.

A multinuclear NMR study of the cycloaddition reaction of $SNSAsF_6$ with *tert*-butylphosphaacetyline $(CH_3)_3CCP$ leading to the 5-*tert*-butyl-1,3,2,4-dithiazaphospholium $(CH_3)_3C\overline{CPSNS}^+$ cation; a preliminary account of the novel exchange of a cyclic phosphorus by nitrogen in the reaction of $(CH_3)_3C\overline{CPSNS}^+$ with azide N_3^- leading to 5-*tert*-butyl-1,3,2,4-dithiadiazolyl $(CH_3)_3C\overline{CNSNS}^{\cdot}$

Simon Parsons, Jack Passmore, Xiaoping Sun, and Manfred Regitz

Abstract: The cycloaddition reaction of SNS^+ (as the AsF_6^- salt) with 5-*tert*-butylphosphaacetyline $(CH_3)_3CCP$ in sulfur dioxide solution at −60°C gave $(CH_3)_3C\overline{CPSNS}^+$, the first identified example of a 1,3,2,4-dithiazaphospholium heterocycle $R\overline{CPSNS}^+$. The cycloadduct was characterized by multinuclear NMR (^1H, ^{13}C, ^{14}N, ^{15}N, ^{31}P) spectroscopy at low temperature. Reduction of 6π $(CH_3)_3C\overline{CPSNS}^+$ in situ with $SbPh_3$ in the presence of Me_4NCl led to a radical, which may be the 7π *tert*-butyl-1,3,2,4-dithiazaphospholyl $(CH_3)_3C\overline{CPSNS}^{\cdot}$. The reaction of 5-*tert*-butyl-1,3,2,4-dithiazaphospholium $(CH_3)_3C\overline{CPSNS}^+$ with azide N_3^- surprisingly gave the previously known 5-*tert*-butyl-1,3,2,4-dithiadiazolyl $(CH_3)_3C\overline{CNSNS}^{\cdot}$. The conversion of $(CH_3)_3C\overline{CPSNS}^+$ to $(CH_3)_3C\overline{CNSNS}^{\cdot}$ by the net replacement of a cyclic phosphorus with nitrogen is unprecedented.

Key words: dithiazaphospholium, dithiazaphospholyl, cycloaddition, multinuclear NMR, ESR.

Résumé : La réaction de cycloaddition du SNS^+ (sous forme de sel de AsF_6^-) avec le *tert*-butylphosphaacétyline $(CH_3)_3CCP$ en solution dans le bioxyde de soufre à −60°C donne le $(CH_3)_3C\overline{CPSNS}^+$, qui est le premier exemple identifié d'un 1,3,2,4-dithiazaphospholium hétérocyclique $R\overline{CPSNS}^+$. On a caractérisé l'adduit

Received February 7, 1995.

S. Parsons,[1] J. Passmore,[2] and X. Sun. Department of Chemistry, The University of New Brunswick, Fredericton, NB E3B 6E2, Canada.
M. Regitz. Department of Chemistry, The University of Kaiserslautern, Erwin-Schrodinger-Strasse, D-6750 Kaiserslautern, Germany.

[1] Present address: Department of Chemistry, The University of Edinburgh, King's Buildings, West Mains Road, Edinburgh EH9 3JJ, Scotland.
[2] Author to whom correspondence may be addressed. Telephone: (506)453-4821. Fax: (506)453-4981. E-mail: PASSMORE@UNB.CA.

Can. J. Chem. Downloaded from www.nrcresearchpress.com by 80.90.12.36 on 09/08/12
For personal use only.

cyclique par spectroscopie de RMN de noyaux multiples (^1H, ^{13}C, ^{14}N, ^{15}N, ^{31}P) à basse température. La réduction in situ du $(CH_3)_3CCPSNS^+$ 6π avec le $SbPh_3$ en présence de Me_4NCl conduit à un radical, qui peut être le *tert*-butyl-1,3,2,4-dithiazaphospholyl 7π $(CH_3)_3CCPSNS^{\cdot}$. La réaction du 5-*tert*-butyl-1,3,2,4-dithiazaphospholium $(CH_3)_3CCPSNS^+$ avec l'azoture N_3^- conduit de façon surprenante au 5-*tert*-butyl-1,3,2,4-dithiadiazolyl $(CH_3)_3CCNSNS^{\cdot}$ connu antérieurement. La transformation du $(CH_3)_3CCPSNS^+$ en $(CH_3)_3CCNSNS^{\cdot}$ où un phosphore cyclique est remplacé par l'azote est sans précédent.

Mots clés: dithiazaphospholinium, dithiazaphospholyl, cycloaddition, RMN de noyaux multiples, RPE.

[Traduit par la rédaction]

Can. J. Chem. Downloaded from www.nrcresearchpress.com by 80.90.12.36 on 09/08/12
For personal use only.

Introduction

Previous investigations showed that SNS^+ (as the AsF_6^- salt) undergoes quantitative symmetry-allowed cycloaddition reactions with a variety of nitriles, alkynes, and SN^+ (1) to give five-membered rings. The kinetics of the cycloadditions with C≡N, C≡C, and C=C bonds show (1*e*) that the rate of reaction is inversely proportional to the ionization energy of the latter, implying that the cycloaddition proceeds via the interaction of the LUMO of SNS^+ (acceptor) with the HOMO of the multiple bond (donor). Thus, the cycloadditions of SNS^+ are the simplest of any of the 1,3-dipole-type species. We predicted that a number of other unsaturated molecules, including the phosphaalkynes RC≡P, should undergo thermodynamically favourable cycloadditions based on a bonds formed/bonds broken model (2). On the basis that the rate of these cycloadditions should be inversely proportional to ionization energy (IP = 9.70 eV for $(CH_3)_3CCP$, a low IP relative to other molecules that cycloadd to SNS^+ (1*e*)), we expected that $(CH_3)_3CCP$ would undergo a fast thermodynamically allowed concerted cycloaddition reaction with SNS^+. These predictions (2) are confirmed by this work. Reference has been made (3) to the cycloadditions of SNS^+ with the doubly bonded C=N, P=N, P=P, and N=N bonds[3] as we had previously predicted (2), but no experimental evidence was provided. However, reactions of SNS^+ with double bonds may be expected to be more complex than those with triple bonds, as the reactions of SNS^+ with olefins form a mixture of 1:1 and 2:1 olefin–SNS^+ cycloadducts in liquid SO_2 at room temperature or lower (1*c*, 2). In addition, the claim has been made (4) for the preparation of $(CH_3)_3CCPSNSAsF_6$ on the basis that a radical was produced on the reduction of the isolated salt, which was attributed to $(CH_3)_3CCPSNS^{\cdot}$. However, no direct evidence was given for the $(CH_3)_3CCPSNS^+$ cation, and the radical is very unlikely $(CH_3)_3CCPSNS^{\cdot}$ (see below). In this paper, a multinuclear NMR study of the cycloaddition reaction of $SNSAsF_6$ with *tert*-butylphosphaacetyline $(CH_3)_3CCP$ in sulfur dioxide solution at −60°C is described. This gives 5-*tert*-butyl-1,3,2,4-dithiazaphospholium $(CH_3)_3CCPSNS^+$, the first identified example of any 1,3,2,4-dithiazaphospholium heterocycle $RCPSNS^+$. We show in this work that $(CH_3)_3CCPSNSAsF_6$ readily decomposed on attempted isolation at room temperature. The ESR spectral parameters (1:1:1 triplet with g = 2.0045, a^N = 1.467 mT, a^P not observed) for the radical, said to be $(CH_3)_3CCPSNS^{\cdot}$ (4) given on reduction of the isolated product $(CH_3)_3CCPSNSAsF_6$, do not fit a SNS·-containing radical in which the SNS moiety is connected to a conjugated system as would be expected for $(CH_3)_3CCPSNS^{\cdot}$. The ESR data are, however, consistent with a radical in which the $SNS^{\cdot}$ moiety is connected to a nonconjugated fragment. Previous investigations have shown (1*f*, 2, 5) that a variety of such conjugated $SNS^{\cdot}$-containing radicals have very similar g (2.005–2.008) and a^N (1.10 ± 0.03 mT) values that are substantially different from the a^N values (1.28 ± 0.03 mT) of the nonconjugated radicals in which the two sulfurs are bonded to a saturated moiety (Table 1). Therefore, the identity of this radical is very likely not $(CH_3)_3CCPSNS^{\cdot}$ as proposed (4). In this work, an attempted generation of the 5-*tert*-butyl-1,3,2,4-dithiazaphospholyl $(CH_3)_3CCPSNS^{\cdot}$ radical was carried out by in situ reduction of $(CH_3)_3CCPSNS^+$ (as the AsF_6^- salt) at low temperature with $SbPh_3$ in the presence of Me_4NCl. In addition, reaction of $(CH_3)_3CCPSNS^+$ with cesium azide CsN_3 in liquid SO_2 was performed, which surprisingly gave the previously known 7π 5-*tert*-butyl-1,3,2,4-dithiadiazolyl $(CH_3)_3CCNSNS^{\cdot}$ radical. The conversion of $(CH_3)_3CCPSNS^+$ to $(CH_3)_3CCNSNS^{\cdot}$ by the net replacement of a cyclic phosphorus with nitrogen is unprecedented, although baffling rearrangements are not unusual in sulfur nitrogen chemistry (6, 7*a*, 19). A preliminary account of this work has been briefly described in a conference presentation (7*b*).

[3] Manuscripts in preparation quoted in ref. 3.

Experimental section

Instrumentation and reagents

Multinuclear NMR spectra were recorded with Varian Associates XL-200 MHz (as described (8) for ^1H and ^{13}C spectra) and UNITY 400 MHz spectrometers. For the UNITY 400 MHz spectrometer, the spectra were accumulated in 72K (^{13}C), 12K (^{14}N), 128K (^{15}N), or 115K (^{31}P) data points, and obtained unlocked. ^{13}C spectra were run at 100.58 MHz with a spectral width of 30.0 kHz (0.46 Hz/data point, acquisition time 1.200 s, pulse width 12.0 μs) with ^1H decoupling. ^{14}N spectra were run at 28.90 MHz with a spectral width of 12.0 kHz (1.47 Hz/data point, acquisition time 0.501 s, pulse width 40 μs, 1000 scans). ^{15}N spectra were run at 40.54 MHz with a spectral width of

Table 1. ESR parameters[a] of various SNS•-containing radicals.

Radical	g^b		a^N (mT)[b]	
	By Sutcliffe	By Schriver	By Sutcliffe	By Schriver
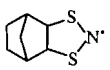	2.0064		1.31	
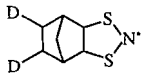	2.0064		1.31	
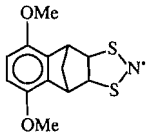	2.0065		1.28	
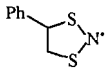	2.0061		1.23	
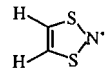	2.0065	2.007	1.07	1.07
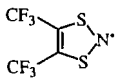	2.0062	2.005	1.15	1.13
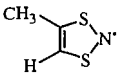		2.006		1.07
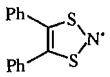	2.0063		1.08	
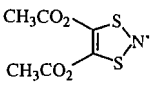	2.0065	2.006	1.10	1.08
	2.0077		1.10	
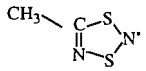	2.0052	2.0068	1.13	1.08
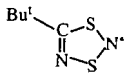	2.0048	2.006	1.10	1.10
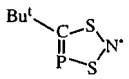		2.0059[c] (this work)		1.14[c] (this work)
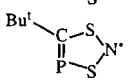	2.0045		1.467	

[a]All the SNS•-containing radicals have very similar g values (2.005–2.008), characteristic of the unpaired electron delocalized along the SNS moiety. All the SNS•-containing radicals for which the SNS moiety is bonded to a conjugated system have very close a^N values (1.10 ± 0.03 mT); however, the radicals for which the SNS moiety is bonded to a saturated system have greater a^N values (ca. 1.3 mT).

[b]The g and a^N values are taken from ref. 5 (for Bu^{t}CPSNS• by Sutcliffe, the values are taken from ref. 4); the g and a^N values by Schriver are taken from ref. 2.

[c]For Bu^{t}CPSNS• (g = 2.0059, a^N = 1.14 mT) (this work), the g value fits the SNS•-containing radicals, and the a^N value fits the radicals for which the SNS• moiety is connected to a conjugated system.

20.0 kHz (0.31 Hz/data point, acquisition time 3.198 s, pulse width 20 μs, 2000 scans). ^{31}P spectra were run at 161.93 MHz with a spectral width of 90.0 kHz (0.69 Hz/data point, acquisition time 0.640 s, pulse width 10 μs). The pulse widths quoted correspond to tip angles of 58° (^{13}C), 60° (^{14}N), and 55° (^{15}N, ^{31}P). Spectra were referenced externally to a solution of TMS in SO_2 (^{1}H and ^{13}C), neat CH_3NO_2 (^{14}N and ^{15}N), and 3 M H_3PO_4 in D_2O (^{31}P). ESR spectra were recorded as the first derivative

Can. J. Chem. Downloaded from www.nrcresearchpress.com by 80.90.12.36 on 09/08/12
For personal use only.

Table 2. Multinuclear NMR data[a] for 1,3,2,4-dithiazaphospholium and related analogues.

$(CH_3)_3CCP$	$(CH_3)_3\overline{CCPSNS}^{+}$[b]	$(CH_3)_3\overline{CCN''SN'S}^{+}$	$H_3\overline{CC'SNSC''H}^{+}$
$\delta(^1H) = 1.21$(d) $^4J_{HP} = 0.88$	$\delta(^1H) = 1.6$(s)		
$\delta(^{13}C) = 184.8$(d) $^1J_{CP} = 38.5$	$\delta(^{13}C) = 237.5$(d) $^1J_{CP} = 104.4$		
CP	$\overline{CPSNS}^{+}$		
$\delta(^{13}C) = 36.4$(d) $^2J_{CP} = 18.2$ *tert*-C	$\delta(^{13}C) = 43.2$(d) $^2J_{CP} = 12.8$ *tert*-C		
$\delta(^{13}C) = 31.3$(d) $^3J_{CP} = 6.0$ CH_3	$\delta(^{13}C) = 35.7$(d) $^3J_{CP} = 7.0$ CH_3		
$\delta(^{31}P) = -69.2$(s)	$\delta(^{31}P) = 389.2$(s) $\delta(^{31}P) = 316$[c] $\delta(^{31}P) = 393$[d]	$\delta(^{14}N) = +28$, N″ $\Delta\nu_{1/2} = 870$	$\delta(^{13}C) = 167$, C″
	$\delta(^{14}N) = 37.5$ $\Delta\nu_{1/2} = 790$ $\delta(^{15}N) = 30.8$ $\Delta\nu_{1/2} = 4.8$	$\delta(^{14}N) = -28$, N′ $\Delta\nu_{1/2} = 580$	

[a]Singlet and doublet are represented by s and d, respectively. The ^1H and ^{31}P spectral data of $(CH_3)_3CCP$ in SO_2 solution were obtained using a Varian XL-200 MHz NMR spectrometer at room temperature. The ^{13}C spectral data of $(CH_3)_3CCP$ (TMS in C_6D_6 as reference) are taken from ref. 7. The spectral data of $(CH_3)_3\overline{CCPSNS}^{+}$ (1.4 M) were obtained using a Varian UNITY-400 MHz NMR spectrometer at −60°C (AsF_6^- anion, SO_2 solvent). The spectral data for $(CH_3)_3\overline{CCNSNS}^{+}$ and $H_3\overline{CCSNSCH}^{+}$ were previously obtained (1*e*) using a Varian XL-200 MHz NMR spectrometer at room temperature.

[b]The integration in the ^{14}N spectrum implied that ca. 20% SNS^+ ($\delta(^{14}N) = -90.8$ ppm, $\Delta\nu_{1/2} = 6$ Hz) remained unreacted at the time the spectrum was obtained, indicating that the reaction was likely incomplete at this point. No SNS^+ was detected in the weaker ^{15}N spectrum, possibly because of the much lower signal-to-noise ratio and (or) differences in the ^{15}N relaxation times.

[c]^{31}P chemical shift calculated by eq. [2].

[d]^{31}P chemical shift calculated by eq. [3].

of the absorption curve in the X-band with a locally modified Varian E-4 spectrometer using DPPH as a field marker.

$SNSAsF_6$ was prepared as described (9). *tert*-Butylphosphaacetyline $(CH_3)_3CCP$ was used as received (10) from Professor M. Regitz. The NMR (^1H, ^{31}P) spectra of $(CH_3)_3CCP$ in liquid SO_2 were recorded at room temperature using a Varian XL-200 MHz spectrometer. See Table 2 for data obtained in this work and from the literature (11). The NMR studies established that $(CH_3)_3CCP$ did not react with SO_2 under ambient conditions, therefore SO_2 is a suitable solvent for $(CH_3)_3CCP$.

Multinuclear NMR (^{14}N, ^{15}N, ^{31}P, ^{13}C, ^1H) spectroscopic studies on the cycloaddition reaction of $SNSAsF_6$ with *tert*-butylphosphaacetyline $(CH_3)_3CCP$

The reaction was performed in a 10 mm NMR tube (fitted with a J. Young "O-Ringette" type valve) in situ. SO_2 (2.82 g) and $(CH_3)_3CCP$ (0.281 g, 2.81 mmol) were successively condensed onto $SNSAsF_6$ (0.764 g, 2.86 mmol) at −196°C. The contents were warmed to −60°C, immediately giving a bright yellow solution. The solution was kept at this temperature for 4 h. The multinuclear NMR (in the time sequence of ^{15}N, ^{14}N, ^{13}C, ^{31}P, and ^1H) spectra[4] were recorded using a Varian UNITY 400 MHz spectrometer at −60°C. The ^1H spectrum was taken on the decoupling coil. The cycloadduct $(CH_3)_3\overline{CCPSNS}AsF_6$ was shown to decompose in liquid SO_2 at room temperature after 4 h, giving a complex mixture in solution and a black precipitate (^1H NMR: a group of peaks at 1.0–1.5 ppm) with almost all the detectable phosphorus in solution converted to PF_6^- anion (^{31}P NMR: $\delta = -143.6$ ppm (int 100%), septet, $^1J_{PF} = 712.5$ Hz and four unassigned peaks between −20 and −110 ppm (int less than 8%)). NMR data of the reaction product $(CH_3)_3\overline{CCPSNS}^{+}$ are shown in Table 2. The data for the starting material $(CH_3)_3CCP$ and for the related heterocycles $(CH_3)_3\overline{CCNSNS}^{+}$ and $H\overline{CSNSCCH_3}^{+}$ are also included for comparison.

[4] Actual spectra deposited. Copies of material on deposit may be purchased from: The Depository of Unpublished Data, Document Delivery, CISTI, National Research Council Canada, Ottawa, Canada K1A 0S2.

Can. J. Chem. Downloaded from www.nrcresearchpress.com by 80.90.12.36 on 09/08/12
For personal use only.

Can. J. Chem. Downloaded from www.nrcresearchpress.com by 80.90.12.36 on 09/08/12
For personal use only.

Reduction of the 5-*tert*-butyl-1,3,2,4-dithiazaphospholium $(CH_3)_3CCPSNS^+$ cation with $SbPh_3$ in the presence of Me_4NCl

The reactions were performed in situ in a two-bulbed (ca. 15 cm^3) vessel incorporating a 4 mm quartz ESR tube and a medium frit.[5] SO_2 (1.55 g) and $(CH_3)_3CCP$ (0.0299 g, 0.299 mmol) were successively condensed onto $SNSAsF_6$ (0.0148 g, 0.0554 mmol) at −196°C. The contents were warmed to −60°C, immediately giving a bright yellow $(CH_3)_3CCPSNSAsF_6$ solution. The solution was kept at this temperature for 2 h and then quickly poured through a precooled (ca. −40°C) glass frit (to avoid possible decomposition of the cycloadduct) onto the solid mixture of $SbPh_3$ (0.020 g, 0.0566 mmol) and Me_4NCl (0.014 g, 0.128 mmol) in the second bulb at −40°C, immediately giving an orange solution. This solution was then diluted with preweighed $CFCl_3$ (7.38 g) and part of it transferred into the attached ESR tube, which was subsequently flame sealed at −196°C. The ESR spectrum was recorded at room temperature, showing a 1:1:1 triplet with g = 2.0059(3) and a^N = 1.14(2) mT.[4] The ESR signal completely disappeared on exposure of this sample to room light for one day at room temperature. A low-temperature (−60°C) ESR spectrum was recorded on another similarly prepared sample, showing an essentially identical 1:1:1 triplet (g = 2.0057, a^N = 1.13 mT, and a^P not observed),[4] which disappeared on exposure to light at room temperature.

Reaction of the 5-*tert*-butyl-1,3,2,4-dithiazaphospholium $(CH_3)_3CCPSNS^+$ cation with azide N_3^- leading to 5-*tert*-butyl-1,3,2,4-dithiadiazolyl $(CH_3)_3CCNSNS^{\cdot}$

The reactions were performed similarly to the reduction of $(CH_3)_3CCPSNS^+$ as described above. The mixture of $SNSAsF_6$ (0.0160 g, 0.0599 mmol) and $(CH_3)_3CCP$ (0.0584 g, 0.583 mmol) in liquid SO_2 (1.48 g) gave a bright yellow $(CH_3)_3CCPSNSAsF_6$ solution, which was then quickly poured onto an excess CsN_3 (0.039 g, 0.224 mmol) at −40°C, immediately giving an orange solution. This orange solution was diluted with $CFCl_3$ (7.30 g), and part of it was transferred into the attached ESR tube, which was subsequently flame sealed at −196°C. The ESR spectrum[4] was recorded on this sample at −60°C, showing hyperfine 1:1:1 triplets of a 1:1:1 triplet due to two nonequivalent ^{14}N (I = 1); g = 2.0060, $a^{N'}$ = 1.08 mT, $a^{N''}$ = 0.06 mT. The pattern and g and a^N values of the spectrum are characteristic of those of 1,3,2,4-dithiadiazolyl $RCN''SN'S^{\cdot}$ radicals (g = 2.005–2.007, $a^{N'}$ = 1.08–1.11 mT) (1*f*, 2, 5, 7*a*) and almost identical to an authentic sample of $(CH_3)_3CCN''SN'S^{\cdot}$ (g = 2.0071, $a^{N'}$ = 1.09 mT, $a^{N''}$ = 0.06 mT) (13). On exposure to room light for 2 weeks at room temperature, the ESR spectrum[4] exhibited a weaker signal of a 1:2:3:2:1 quintet (g = 2.011, a^N = 0.53 mT) (cf. $(CH_3)_3CCNSSN^{\cdot}$: g = 2.012, a^N = 0.52 mT) (13) coincident with disappearance of the three-line pattern, indicating that the $(CH_3)_3CCN''SN'S^{\cdot}$ had photochemically rearranged to $(CH_3)_3CCNSSN^{\cdot}$ as we have previously demonstrated (7*a*, 13). The ESR studies of another similarly prepared sample also showed the formation of $(CH_3)_3CCNSNS^{\cdot}$ and its subsequent partial rearrangement to $(CH_3)_3CCNSSN^{\cdot}$.

[5] The experimental techniques have been described in ref. 12.

Fig. 1. The optimized (RHF, STO-3G) geometries of the 6π 1,3,2,4-dithiazaphospholium $HCPSNS^+$ cation.

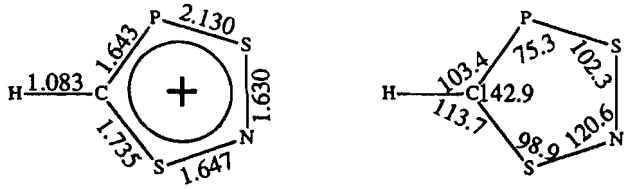

Molecular orbital calculations

The geometries of the hydrogen derivative of 6π 1,3,2,4-dithiazaphospholium $HCPSNS^+$ were optimized, and its electronic structure was then examined by molecular orbital calculations on the basis of the optimized geometries. The geometry optimization (Fig.1) and the subsequent MO calculations were performed with the Gaussian 92 program at the STO-3G (RHF) level.

Results and discussion

Multinuclear NMR spectroscopic studies of the cycloaddition reaction of $SNSAsF_6$ with *tert*-butylphosphaacetyline $(CH_3)_3CCP$

When $SNSAsF_6$ was mixed with an excess of $(CH_3)_3CCP$ in liquid SO_2 at −60°C, the colour of the solution immediately turned to bright yellow (different from the yellow colour of $SNSAsF_6$). The rapid colour change and subsequent NMR studies indicated that the cycloaddition of SNS^+ with $(CH_3)_3CP$ (eq. [1]) was likely relatively fast[6]

[1] $(CH_3)CCP + SNSAsF_6 \rightarrow (CH_3)_3CCPSNSAsF_6$

The initial reaction product underwent decomposition at room temperature to give a complex mixture (^1H and ^{31}P NMR), which hindered its isolation. The attempted isolation of $(CH_3)_3CCPSNS^+$ as the $AlCl_4^-$ salt was unsuccessful, probably as a consequence of the decomposition of the cation during the anion exchange[7] and (or) subsequent work-up. Therefore,

[6] On the basis of the correlation of the rate of SNS^+ cycloaddition to the ionization potential of the multiple bonds C≡N (IP 12–14 eV), C≡C (IP 11–13 eV), and C=C (IP = 10.5 for C_2H_4) bonds (1*e*, *g*)), the cycloaddition reaction of $(CH_3)_3CCP$ (IP=9.70 eV) would be expected to be fast.

[7] The attempted isolation of $(CH_3)_3CCPSNSAlCl_4$ was performed by reacting CsCl with $(CH_3)_3CCPSNSAsF_6$ in situ in liquid SO_2 followed by the evacuation of SO_2 and in situ reaction of the product (expected to be the covalent $(CH_3)_3CCPSNSCl$) with $AlCl_3$ in CH_2Cl_2 (expected to give $(CH_3)_3CCPSNSAlCl_4$). The recovered solid product was characterized by ^1H NMR, showing, however, a group of unassignable resonances (spectrum deposited), indicating that a complex mixture was formed.

Can. J. Chem. Downloaded from www.nrcresearchpress.com by 80.90.12.36 on 09/08/12
For personal use only.

the cycloadduct was characterized in situ at −60°C by multinuclear NMR (^{1}H, ^{13}C, ^{14}N, ^{15}N, ^{31}P) spectroscopy.

The NMR (^{1}H, ^{13}C, ^{31}P) resonances of the cycloadduct $(CH_3)_3C\overline{CPSNS}^+$ appeared at lower field relative to those of $(CH_3)_3CCP$ (see Table 2), characteristic of the formation of the deshielded cation (cf. the cycloadditions of nitriles (1*e*, *f*)). The ^{14}N spectrum of $(CH_3)_3C\overline{CPSNS}^+$ exhibited a broader signal (δ = 37.5 ppm, $\Delta\nu_{1/2}$ = 790 Hz) than that (δ = −28 ppm, $\Delta\nu_{1/2}$ = 580 Hz) of the corresponding N′ in the nitrogen analogue $(CH_3)_3C\overline{CN''SN'S}^+$ (1*e*)), consistent with the replacement of N″ by the larger P. The magnitude of $^1J(^{31}P, ^{13}C)$ of $(CH_3)_3C\overline{CPSNS}^+$ (104 Hz) is surprisingly greater than that of $(CH_3)_3CCP$ (38.5 Hz). However, this is characteristic of a decrease in the CP bond order,[8] and indicates the presence of a C=P double bond. Neilson and co-workers showed (15) that for various acyclic phosphaalkenes (C=P), the ^{31}P chemical shifts are directly proportional to the $^1J_{PC}$ coupling constants. Using Neilson's plot of $\delta(^{31}P)$ versus $^1J_{PC}$ for various C=P containing molecules (Fig. 1 in ref. 15), $\delta(^{31}P)$ = 389 ppm (observed for $(CH_3)_3C\overline{CPSNS}^+$) corresponds to $^1J_{PC}$ = 99 Hz (observed 104 Hz for $(CH_3)_3C\overline{CPSNS}^+$). Alternatively, $^1J_{PC}$ = 104 Hz (observed for $(CH_3)_3C\overline{CPSNS}^+$) corresponds to $\delta(^{31}P)$ = 402 ppm (observed 389 ppm for $(CH_3)_3C\overline{CPSNS}^+$). This further supports the presence of a C=P double bond in the heterocyclic $(CH_3)_3C\overline{CPSNS}^+$. The ^{15}N spectrum of $(CH_3)_3C\overline{CPSNS}^+$ exhibited a singlet (δ = 30.8 ppm, $\Delta\nu_{1/2}$ = 4.8 Hz), and the $^2J(^{31}P, ^{15}N)$ coupling was not observable (estimated from the ^{15}N linewidth to be smaller than 4 Hz). This is in the range found for $^2J(^{31}P, ^{15}N)$ for heterophospholes $-\overline{NCPCC}$ (typically 0–9 Hz), while $^1J(^{31}P, ^{15}N)$ for heterophospholes $-\overline{NPCCC}$ are typically 80–90 Hz (16), which further supports the identity of the $\overline{CPSNS}^+$ ring. Our NMR results (refer to Table 1) also quantitatively fit eqs. [2] and [3], which were previously established for the correlations of the ^{31}P chemical shift ($\delta(^{31}P)$) of various =P- moiety containing acyclic and heterocyclic compounds to the ^{14}N (14,16) and ^{13}C (14,17) chemical shifts ($\delta(^{14}N)$ and $\delta(^{13}C)$, respectively) of the corresponding =N- (replacement of P by N) and =CH- (replacement of P by CH) moieties in analogous acyclic and heterocyclic compounds.

[2] $\delta(^{31}P) = 1.33\delta(^{14}N) + 279$

[3] $\delta(^{31}P) = 4.88\delta(^{13}C) - 422$

In addition, the difference (59 ppm) between the $\delta(^{15}N)$ of $(CH_3)_3C\overline{CPSNS}^+$ (30.8 ppm) and $\delta(^{14}N)$ of N′ in $(CH_3)_3C\overline{CN''SN'S}^+$ (−28 ppm) (1*e*, 2) is comparable to those for $CH_3\overline{NCPCN}'$ and the nitrogen analogue $CH_3\overline{NCNCN}'$ (the difference in $\delta(^{14}N)$ for N′ is ca. 50 ppm) (16) and for $CH_3-\overline{CCPN(CH_3)N}'$ and the nitrogen analogue $H\overline{CCNN(CH_3)N}'$ (the difference in $\delta(^{14}N)$ for N′ is ca. 40 ppm) (16). Thus, the formation of the new type of 6π heterocyclic 1,3,2,4-dithiazaphospholium $-\overline{CPSNS}^+$ is further evidenced by a careful examination of its ^{31}P and ^{14}N (^{15}N) chemical shifts. The multinuclear NMR spectroscopic studies establish the presence of 5-*tert*-butyl-1,3,2,4-dithiazaphospholium $(CH_3)_3-\overline{CCPSNS}^+$, reasonably formed by the symmetry-allowed cycloaddition reaction of SNS^+ with *tert*-butylphosphaacetyline $(CH_3)_3CCP$. This is the first example of any 1,3,2,4-dithiazaphospholium heterocycle.

The ab initio calculations showed that the frontier molecular orbitals of 6π $H\overline{CPSNS}^+$ (HOMO and LUMO) consist of conjugated p_π orbitals (p_π coefficients on $H\overline{CPS'NS}^+$ (HOMO, LUMO): C (0.50, 0.08), P (0.63, 0.28), S′(0.18, −0.57), N (−0.35, 0.80), and S (−0.39, −0.47)) similar to the previous known nitrogen analogue $H\overline{CNSNS}^+$ (p_π coefficients on $H\overline{CN'S'NS}^+$ (HOMO, LUMO): C (−0.26, 0.12), N′(0.04, 0.17), S′(0.73, −0.54), N (0.09, 0.83), and S (−0.65, −0.51)). The CP bond order[9] obtained from the calculated CP bond distance of 1.643 Å (Fig. 1) is ca. two, supporting the proposed C=P double bond in the cycloadduct by NMR studies. In addition, the sum of the bond orders in the SNS moiety is ca. three (each SN bond possesses bond order 1.4), and the sum of bond orders for all the bonds in the cationic heterocycle is estimated to be ca. seven and can represented by valence bond structures **1** and **2**.

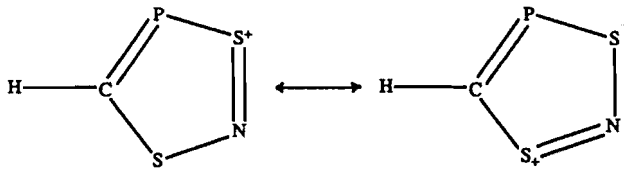

1 **2**

All these results support the proposed identity of the heterocyclic $\overline{CPSNS}^+$ cation.

Reduction of the 6π 5-*tert*-butyl-1,3,2,4-dithiazaphospholium $(CH_3)_3C\overline{CPSNS}^+$ cation to a radical that may be the 7π 5-*tert*-butyl-1,3,2,4-dithiazaphospholyl $(CH_3)_3C\overline{CPSNS}^{\cdot}$

$SNSAsF_6$ cycloadds to $(CH_3)_3CCP$ in liquid SO_2 to give the 6π $(CH_3)_3C\overline{CPSNS}AsF_6$. Since $(CH_3)_3C\overline{CPSNS}AsF_6$ under-

[8] The $^1J(^{31}P, ^{13}C)$ of phosphaalkenes (C=P) (30–112 Hz) are generally larger than those of phosphaalkynes (C≡P) (14–56 Hz) (14).

[9] The bond orders are calculated by Pauling's equation (18):

bond order = 10 exp [−(D_b − D_1)/0.711]

where D_b is the bond length (optimized or observed), and D_1 is the sum of the radii of the two atoms the bond order between which is one. The covalent radii used are as follows (12): r_C = 0.772 Å, r_P = 1.10 Å, r_S = 1.04 Å, and r_N = 0.70 Å.

goes decomposition to a complex mixture at room temperature, instead of reducing a recovered $SNSAsF_6/(CH_3)_3CCP$ reaction product as was performed in previous work (4), in this work the $(CH_3)_3CCPSNS^+$ cation was prepared and reduced in situ at −40°C using excess $SbPh_3$ in the presence of Me_4NCl (eq. [4]),

[4] $(CH_3)_3CCPSNSAsF_6 + 1/2\ SbPh_3 + Me_4NCl \rightarrow (CH_3)_3CCPSNS^{\cdot} + 1/2\ SbPh_3Cl_2 + Me_4NAsF_6$

immediately giving a radical species the ESR spectrum of which exhibited a 1:1:1 triplet (due to the coupling to ^{14}N (I = 1)) with g = 2.0059 and a^N = 1.14 mT. This is reasonably attributed to a new type of heterocyclic 7π 5-*tert*-butyl-1,3,2,4-dithiazaphospholyl $(CH_3)_3CCPSNS^{\cdot}$ (cf. the previously known $(CH_3)_3CCNSNS^{\cdot}$ (13)) by comparison with various conjugated SNS· moiety containing heterocyclic radicals (g = 2.005 − 2.007, a^N = 1.10 ± 0.03) (Table 1). The a^P coupling was not observable even at −60°C.[10] The a^N values for the proposed $(CH_3)_3CCPSNS^{\cdot}$ radical obtained in this work (a^N = 1.10 mT) and the radical previously obtained (a^N = 1.467 mT) (4) are substantially different. The reason for this difference (ca. 0.33 mT) is not clear but, most likely, the previous attempted generation of $(CH_3)_3CCPSNS^{\cdot}$ (4) was not successful because of decomposition of the original $(CH_3)_3CCPSNSAsF_6$ at room temperature (as demonstrated earlier in this paper) prior to the reduction.

The novel exchange of a cyclic phosphorus by nitrogen in the reaction of $(CH_3)_3CCPSNS^+$ with azide N_3^- leading to 5-*tert*-butyl-1,3,2,4-dithiadiazolyl $(CH_3)_3CCNSNS^{\cdot}$

In contrast to the possible formation of 5-*tert*-butyl-1,3,2,4-dithiazaphospholyl $(CH_3)_3CCPSNS^{\cdot}$ by reduction of the 5-*tert*-butyl-1,3,2,4-dithiazaphospholium $(CH_3)_3CCPSNS^+$ cation according to eq. [2], reaction of $(CH_3)_3CCPSNS^+$ with cesium azide CsN_3 in liquid SO_2 gave another radical species the ESR spectrum of which at −60°C surprisingly exhibited hyperfine 1:1:1 triplets of a 1:1:1 triplet (g = 2.0060, $a^{N'}$ = 1.08 mT, $a^{N''}$ = 0.06 mT), characteristic of the previously known 7π 5-*tert*-butyl-1,3,2,4-dithiadiazolyl $(CH_3)_3CCNSNS^{\cdot}$. Consistently, as expected, this radical on photolysis rearranged to 5-*tert*-butyl-1,2,3,5-dithiadiazolyl $(CH_3)_3CCNSSN^{\cdot}$ identified by ESR (1:2:3:2:1 quintet) (7*a*, 13). It is noteworthy that the reduction of $(CH_3)_3CCPSNS^+$ by $SbPh_3$ in the presence of Me_4NCl gave a radical the low-temperature ESR spectrum of which only gave a 1:1:1 triplet reasonably attributable to $(CH_3)_3CCPSNS^{\cdot}$, but did not give a hyperfine structure. In addition, this sample did not undergo a photochemical rearrangement as in the case for $(CH_3)_3CCNSNS^{\cdot}$ under similar conditions, but instead decomposed to diamagnetic species in room light. All the results unambiguously show that the reaction of 5-*tert*-butyl-1,3,2,4-dithiazaphospholium $(CH_3)_3CCPSNS^+$ with azide N_3^- gave the previously known 5-*tert*-butyl-1,3,2,4-dithiadiazolyl $(CH_3)_3CCNSNS^{\cdot}$ radical. The conversion of $(CH_3)_3CCPSNS^+$ to $(CH_3)_3CCNSNS^{\cdot}$ by the net replacement of a cyclic phosphorus with nitrogen is unprecedented.

The following two possible mechanisms (Schemes 1 and 2) are proposed[11] to account for the reaction of $(CH_3)_3CCPSNS^+$ with N_3^- leading to $(CH_3)_3CCPSNS^{\cdot}$. The initial step of this reaction may involve a cycloaddition of N_3^- ($^-N{=}N^+{=}N^-$) to the C=P bond leading to **2** (Scheme 1). Alternatively, it may also involve an attack of terminal nitrogen on N_3^- on the carbon of **1** leading to **6** (Scheme 2). On elimination of N_2 **2** and **6** give fused bicyclic molecules **3** and **7**, respectively. The potential molecular strain in the three-membered CNP ring in **3** may induce a ring opening, giving **4**. The phosphorus on both **4** and **7** may possibly be abstracted on reaction with the solvent SO_2 ($P_xS_yO_z$) and, as a result, the final product **5** (identified by ESR) is formed.

The previous investigations showed (6, 7*a*) that sulfur-nitrogen-containing compounds often undergo complex structural rearrangements, e.g., the isomerization of 1,3,2,4-dithiadiazolyl radicals (7*a*) and scrambling reactions of sulfur diimides (6). This preliminary work shows another example of the baffling features involved in the chemistry of sulfur nitrogen compounds.

Conclusions

The previous investigations showed that the SNS^+ cation (as the AsF_6^- salt) undergoes general extensive cycloaddition reactions with various nitriles, alkynes, alkenes, and SN^+ (1). In this work, the generality of this type of pseudo 1,3-dipolar cycloaddition has been extended to the phosphaalkyne $(CH_3)_3CCP$ to lead to the first example of a new class of heterocyclic compound 1,3,2,4-dithiazophospholium $(CH_3)_3CCPSNS^+$ (eq. [1]). This cationic cycloadduct was character-

[10] An explanation for the coupling constant $a^P \simeq 0$ was sought by a comparison of the coefficients of p_π SOMO of $HCPSNS^{\cdot}$ (ROHF, STO-3G) on N (0.97) and P (0.08), and total spin densities of $HCPSNS^{\cdot}$ (UHF, STO-3G)) in the *s*-orbitals for N (0.042) and P (0.001) (cf. optimized $HCN'SNS^{\cdot}$: p_π coefficients N (0.95) and N′ (0.08); *s*-orbital spin density N (0.048) and N′ (0.001)). The optimized geometries (bond lengths (Å) and angles (°)) for $HCPSNS^{\cdot}$ (ROHF, STO-3G) are given below: H—C (1.080), C—P (1.621), P—S′(2.115), S′—N (1.742), N—S (1.749), C—S (1.751); ∠SCP (146.4), ∠CPS′(75.2), ∠PS′N (103.2), ∠S′NS (115.0), ∠NSC (100.1), ∠S′CH (113.7), ∠HCP (100.5). These low-level calculations imply that the value of a^P may indeed be very small. Much higher level calculations are needed before the point can be viewed as settled. However, the calculation of the molecular isotropic and anisotropic hyperfine tensors (coupling constants) has been said to be one of the most challenging tasks in computational chemistry (19).

[11] The reaction mechanisms were proposed by Professor Z. Valenta of this Department.

Can. J. Chem. Downloaded from www.nrcresearchpress.com by 80.90.12.36 on 09/08/12
For personal use only.

Can. J. Chem. Downloaded from www.nrcresearchpress.com by 80.90.12.36 on 09/08/12
For personal use only.

Scheme 1.

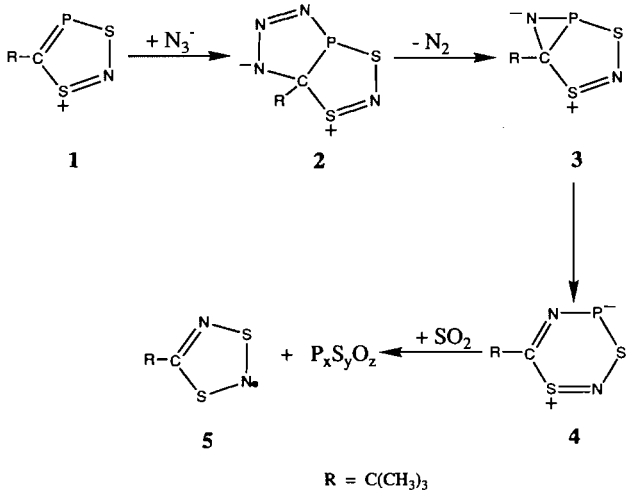

Scheme 2.

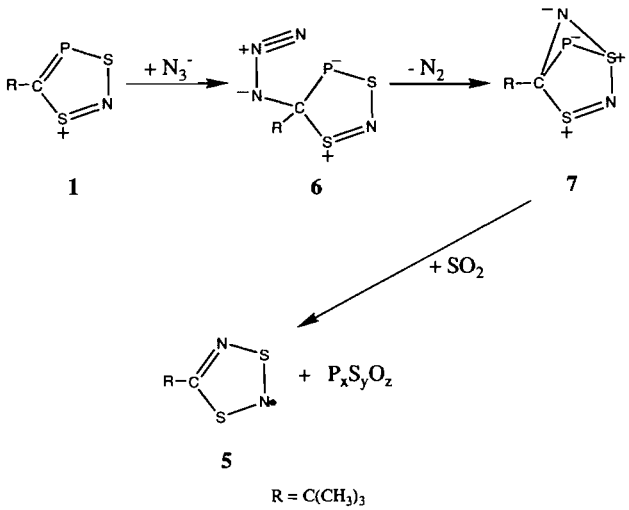

ized by multinuclear NMR (^{1}H, ^{13}C, ^{14}N, ^{15}N, ^{31}P) spectroscopy. The ^{31}P chemical shift of $(CH_3)_3C\overline{CPSNS}^+$ fits well with eqs. [2] and [3] for correlations of a variety of =P- containing compounds to the corresponding nitrogen =N- and hydrocarbon =CH- containing analogues, supporting the identity of this new class of five-membered ring $\overline{CPSNS}^+$, and it is further supported by *ab initio* calculations. This work suggests that other triply bonded species X≡Y containing one or more heavier atoms of groups 14 and 15[12] may also cycloadd to SNS^+ in the readily prepared $SNSAsF_6$ (9) in the convenient solvent SO_2 at low temperatures, leading to the formation of new classes of five-membered rings readily characterizable by multinuclear NMR spectroscopy. In addition, our results imply that isolation of the salts of these cations in the solid state will necessitate exchange of AsF_6^- by other anions, e.g., $AlCl_4^-$.

[12] SNS^+ also cycloadds to the XS≡N (X = F, Cl, Br) (1*e*, 2) triple bond containing a heavier atom (of group 16) to give $X\overline{SNSNS}^+$, although the reaction is not likely a symmetry-allowed concerted cycloaddition.

Reduction of the 6π $(CH_3)_3C\overline{CPSNS}^+$ cation with $SbPh_3$ in the presence of Me_4NCl may have given $(CH_3)_3C\overline{CPSNS}^{\cdot}$, the first member of a new class of 7π 1,3,2,4-dithiazophospholyl radicals, supported by ESR spectroscopy, showing a 1:1:1 triplet with $g = 2.0059$ and $a^N = 1.14$ mT. However, splitting from ^{31}P was not observed, possibly because the a^P value is very small.

Reaction of 5-*tert*-butyl-1,3,2,4-dithiazaphospholyl $(CH_3)_3C\overline{CPSNS}^+$ (as the AsF_6^- salt) with azide N_3^- in liquid SO_2 surprisingly gave the previously known 7π 5-*tert*-butyl-1,3,2,4-dithiadiazolyl $(CH_3)_3C\overline{CNSNS}^{\cdot}$ radical. The conversion of $(CH_3)_3C\overline{CPSNS}^+$ to $(CH_3)_3C\overline{CNSNS}^{\cdot}$ by the net replacement of a cyclic phosphorus with nitrogen is unprecedented.

The synthesis of a new radical, possibly $(CH_3)_3C\overline{CPSNS}^{\cdot}$, and $(CH_3)_3C\overline{CNSNS}^{\cdot}$ from $(CH_3)_3C\overline{CPSNS}^+$ suggests that this cation, and those like it, are likely to open up even more unusual chemistry.

Acknowledgements

We thank Dr. P. Penner for obtaining NMR spectra using a Varian UNITY 400 MHz spectrometer, Dr. S. Mattar and Mr. R. McGregor for recording low-temperature ESR spectra of $(CH_3)_3C\overline{CNSNS}^{\cdot}$ (S.M.) and $(CH_3)_3C\overline{CPSNS}^{\cdot}$ (R.M.), respectively, and Professor Z. Valenta for suggesting the reaction mechanisms. We also thank the Natural Sciences and Engineering Research Council of Canada (NSERC) and the University of New Brunswick (X.S.) for financial support, and the Canadian Commonwealth Scholarship and Fellowship Committee for a graduate scholarship (S.P.).

References

1. (*a*) G.K. MacLean, J. Passmore, M.N.S. Rao, M. J. Schriver, P.S. White, D. Bethell, R.S. Pilkington, and L.H. Sutcliffe. J. Chem. Soc. Dalton Trans. 1405 (1985); (*b*) G.K.MacLean, J. Passmore, M.J. Schriver, P.S. White, D. Bethell, R.S. Pilkington, and L.H. Sutcliffe. J. Chem. Soc. Chem. Commun. 807 (1983); (*c*) N. Burford, J.P. Johnson, J. Passmore, M.J. Schriver, and P. S. White. J. Chem. Soc. Chem. Commun. 966 (1986); W.V.F. Brooks, S. Brownridge, J. Passmore, M.J. Schriver, and X. Sun. J. Chem. Soc. Dalton Trans. Submitted; (*d*) J. Passmore and M.J. Schriver. Inorg. Chem. **27**, 2749 (1988); (*e*) S. Parsons, J. Passmore, M.J. Schriver, and X. Sun. Inorg. Chem. **30**, 3342 (1991); (*f*) J. Passmore, X. Sun, and S. Parsons. Can. J. Chem. **70**, 2972 (1992); (*g*) S. Parsons and J. Passmore. Acc. Chem. Res. **27**, 101 (1994); (*h*) W.V.F. Brooks, T.S. Cameron, S. Parsons, J. Passmore, and M.J. Schriver. Inorg. Chem. **33**, 6230 (1994).
2. M.J. Schriver. Ph.D Thesis, University of New Brunswick. 1988.
3. A.J. Banister, I. Lavender, S.E. Lawrence, J.M. Rawson, and W.J. Clegg. J. Chem. Soc. Chem. Commun. 29 (1994).
4. Y.-L. Chung, S.A. Fairhurst, D.G. Gillies, K.F. Preston, and L.H. Sutcliffe. Magn. Reson. Chem. **30**, 666 (1992).
5. S. Rolfe, D. Griller, K.U. Ingold, and L.H. Sutcliffe. J. Org. Chem. **44**, 3515 (1979); K.F. Preston and L.H. Sutcliffe. Magn. Reson. Chem. **28**, 189 (1990).

6. R.T. Oakley. Prog. Inorg. Chem. **36**, 299 (1988); A.W. Cordes, R.C. Haddon, and R.T. Oakley. The chemistry of inorganic ring systems. *Edited by* R. Steudel. Elsevier, Amsterdam 1992. Chap. 16, p. 295.
7. (*a*) N. Burford, J. Passmore, and M.J. Schriver. J. Chem. Soc. Chem. Commun. 140 (1986); N. Burford, J. Passmore, and X. Sun. Phosphorus, Sulfur Silicon Relat. Elem., **93/94**, 487 (1994); X. Sun. Ph.D Thesis, University of New Brunswick, 1995; J. Passmore and X. Sun. Inorg. Chem. Submitted; (*b*) S. Parsons, J. Passmore, and X. Sun. Phosphorus, Sulfur Silicon Relat. Elem., **93/94**, 435 (1994).
8. S. Parsons, J. Passmore, M.J. Schriver, and P.S. White. Can. J. Chem. **68**, 852 (1990).
9. E.G. Awere and J. Passmore. J. Chem. Soc. Dalton Trans. 1343 (1992).
10. G. Becker, H. Schmidt, G. Uhl, and W. Uhl. Inorg. Synth. **27**, 249 (1990).
11. G. Becker, G. Gresser, and W. Uhl. Z. Naturforsch. **36b**, 16 (1981).
12. M.P. Murchie, R. Kapoor, J. Passmore, and G. Schatte. Inorg. Synth. In press.
13. W.V.F. Brooks, N. Burford, J. Passmore, M.J. Schriver, and L.H. Sutcliffe. J. Chem. Soc. Chem. Commun. 69 (1987).
14. K. Karaghiosoff. Multiple bonds and low coordination in phosphorus chemistry. *Edited by* M. Regitz and O.J. Scherer. Thieme Medical Publishers Inc., New York. 1990. pp. 463–471.
15. R.J. Thoma, C.A. Prieto, and R.H. Neilson. Inorg. Chem. **27**, 784 (1988).
16. A. Schmidpeter and B. Wrackmeyer. Z. Naturforsch. **41b**, 553 (1986).
17. K. Karaghiosoff and A. Schmidpeter. Phosphorus Sulfur, **29**, 73 (1988).
18. L. Pauling The nature of the chemical bond. 3rd ed. Cornell University Press, Ithaca, N.Y. 1960.
19. S.M. Mattar, C. Kennedy, and C. Bourque. Chem. Phys. Lett. **227**, 539 (1994); D. Feller, D. Glendening, E.A. McCullough, and R.J. Miller. J. Chem. Phys. **99**, 2829 (1993); B. Engles and S.D. Peyerimhoff. Mol. Phys. **67**, 583 (1989); D. Feller and E.R. Davidson. J. Chem. Phys. **80**, 1006 (1984).

Can. J. Chem. Downloaded from www.nrcresearchpress.com by 80.90.12.36 on 09/08/12
For personal use only.

A study of the negative ion FABMS of tris(perfluorophenyl)phosphine and related compounds: matrix effects

Mandapati Saraswathi, Jack M. Miller, and Tim R.B. Jones

Abstract: The mass spectra of tris(perfluorophenyl)phosphine obtained under negative ion Fast Atom Bombardment conditions showed formation of an unusual ion at *m/z* 397 attributed to $((C_6F_5)_2PO_2)^-$. The matrix effects involved in this reaction are discussed. Negative ion FAB spectra of tris(perfluorophenyl)arsine and tris(perfluorophenyl)stibine are also reported.

Key words: pentafluorophenylphosphine, -arsine, -stibine; negative ion FABMS; matrix effects.

Résumé : Les spectres de masse d'ions négatifs du tris(perfluorophényl)phosphine obtenus par bombardement à l'aide d'atomes rapides montrent la formation d'un ion inhabituel à *m/z* 397 que l'on attribue à l'espèce $((C_6F_5)_2PO_2)^-$. On discute de l'effet de matrice impliqué dans cette réaction. On rapporte également les spectres d'ions négatifs FAB du tris(perflurophényl)arsine et du tris(perfluorophényl)stibine.

Mots clés : pentafluorophénylphosphine, pentafluorophénylarsine, pentafluorophénylstibine, ions négatifs FABMS, effet de matrice.

[Traduit par la rédaction]

Can. J. Chem. Downloaded from www.nrcresearchpress.com by 80.90.12.36 on 09/08/12
For personal use only.

Introduction

Liquid matrices used in FABMS can produce adverse effects in analysis of organic and organometallic compounds. For example, low surface activity of analytes may result in poor response in the spectra. Since extensive chemical noise or background may be produced by the matrices, this can interfere in characterization of analytes (1). Therefore, the selection of matrix plays a vital role in FABMS.

In addition, many groups have reported (2–11) both expected and unexpected reactions of FAB matrices with analytes. Protonation in the FAB matrix of organic analytes such as nucleosides (2), chlorin (3), organic dyes (4), and peptides (5) is common. Reductive dehalogenation reactions have also been observed during FABMS analysis of halogenated compounds including nucleotides (6), nucleosides (7), phenylalanine (8), and phenothiazine drugs (9). In other work, an impurity of ammonium chloride in a thioglycerol FAB matrix yielded $(M + NH_4)^+$ ions from valinomycin with almost complete exclusion of the $(M + H)^+$ ion (10), and the formation of adduct ions with analytes in radical reactions induced by glycerol as a FAB matrix has been reported (11).

Chemical reactions, more complicated than simple protonation and adduct formation, can also occur in the FAB source. For example, Schiff-base product formation with formaldehyde generated from glycerol matrix was observed during the analysis of angiotensin (12). In addition to the FAB matrix giving unexpected and (or) unwanted reactions in FAB mass spectra, other side reactions with the metal probe tips have also been reported (13, 14). Copper cluster formation with fomblin oil (13) and exchange reactions of copper metal with metal in organometallic samples (14) occurred when copper probe tips were used. Stainless steel tips eliminated most but not all of these effects (15).[2]

The undesirable reactions of liquid matrices may provide valuable information or insights into the chemical reactivity of analytes (16). As one part of a study of these reactions, we wish to report the formation of an unusual ion at *m/z* 397 from tris(perfluorophenyl)phosphine with a 3-nitrobenzyl alcohol (NBA) matrix under negative ion FAB.

Results and discussion

The negative ion FAB mass spectrum of tris(perflurophenyl)phosphine (**1**) obtained using NBA as matrix is given in Fig. 1, with the corresponding positive ion spectrum for comparison. The most abundant ions observed in the negative ion spectrum are at *m/z* 167(100%) and 397(81%). Other important ions are at *m/z* 148, 249, 315, 365, 381, 513, 529, and 532 (molecular ion), though the latter is very weak compared to that of the positive ion spectrum. The electron capture ability of this compound is surprisingly poor. The perfluorophenyl anion (*m/z* 167) is the base peak in the spectrum. The same ion is more abundant in the spectra of tris(perfluorophenyl)arsine (**2**) and tris(perfluorophenyl)stibine (**3**) (Table 1). The negative ion FAB spectrum of **1** has entirely different ion intensities than its positive ion electron impact spectrum (17). This is in sharp contrast to related Group V perfluoro-triptycene ana-

Received December 14, 1994.

M. Saraswathi, J.M. Miller,[1] and T.R.B. Jones. Department of Chemistry, Brock University, St. Catharines, ON L2S 3A1, Canada.

[1] Author to whom correspondence may be addressed. Telephone: (905) 688-5550, ext. 3402. Fax: (905) 682-9020. E-mail: jmiller@sandcastle.cosc.brocku.ca

[2] Also, J.M. Miller and A. Fulcher. Unpublished observations.

Fig. 1. FAB spectra of $(C_6F_5)_3P$–NBA: (i) negative ion; (ii) positive ion.

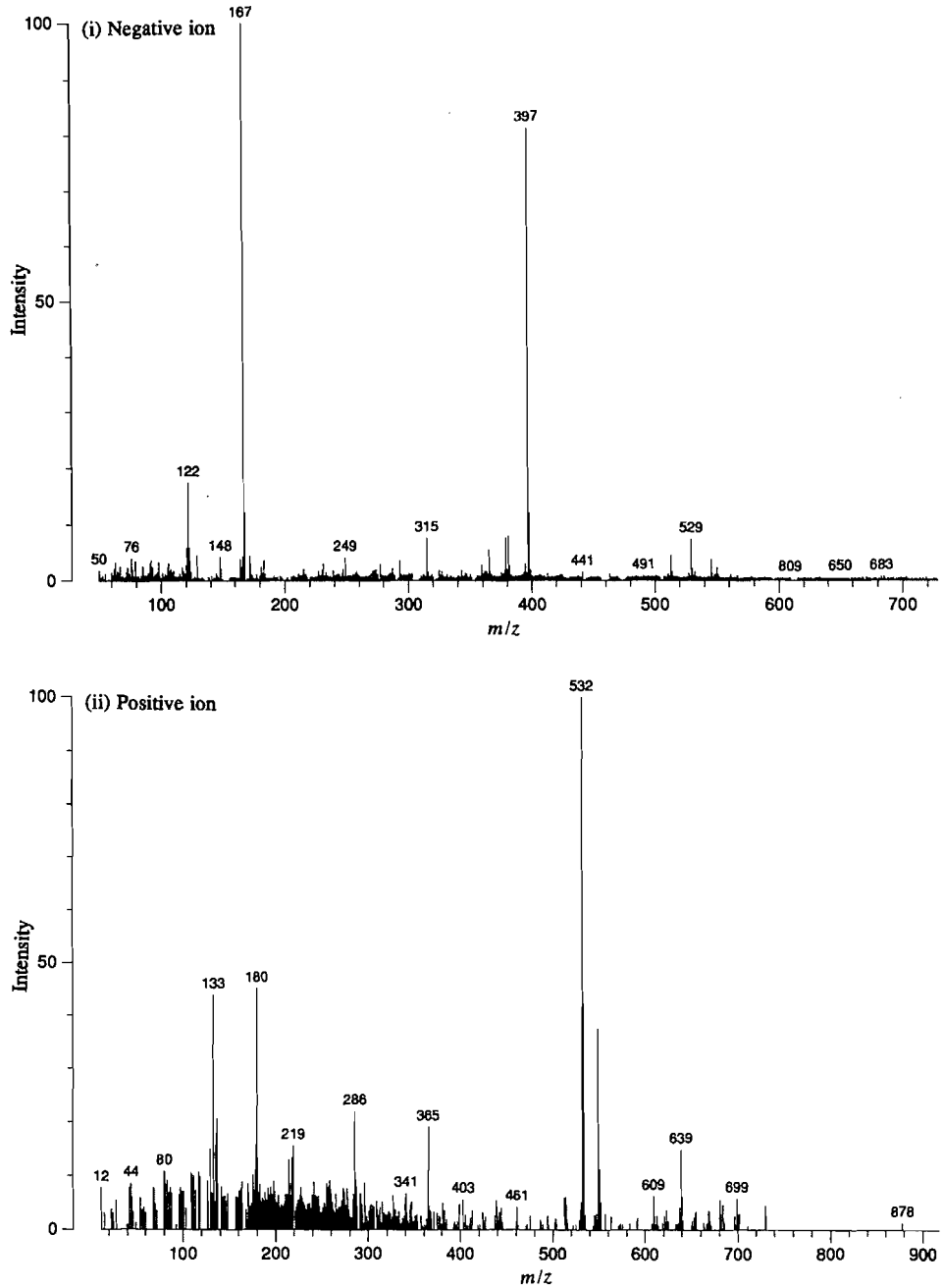

logs described previously (18) where the negative ion FAB spectra closely resembled the positive ion EI spectra. The high oxidation potentials of the Group V elements may cause the parent negative ions to be very weak, though the fluoroaromatic rings might be considered as good electron acceptors. Thus, tris(perfluorophenyl)amine (**4**) did not give good spectra under negative ion FAB conditions. The clearly delineated fragmentation of **1** obtained under negative ion FAB conditions using NBA as a matrix is given in Scheme 1. Collision-induced dissociation techniques were used to probe the ion structures, especially that of the ion at *m/z* 397.

We also see, in the spectrum of **1**, other ions at *m/z* 549, 578, and 685 that do not arise directly by simple ionization of the analyte. These additional ions are $(M + 17)^-$, $(M + 46)^-$, and $(M + 153 \text{ or NBA})^-$, respectively. The metastable and collision-induced dissociation spectra of the molecular ion of **1** (*m/z* 532) show that loss of perfluorophenyl from the molecular ion is a facile process. Loss of PF_2 from the $(C_{12}F_{10}P)^-$ ion (*m/z* 365) produces another abundant ion at *m/z* 296 and $(M - F)^-$, $(C_{12}F_{10}P - F_2)^-$, $(C_{12}F_{10}P - C_6F_4)^-$, and $(C_{12}F_{10}P - PF_3)^-$ are the other minor ions. However, the ion at *m/z* 397 is not produced in the unimolecular decomposition of the molecular ion of **1**. This suggests the involvement of the FAB matrix in the formation of the *m/z* 397 ion. Precursors are not detected

Can. J. Chem. Downloaded from www.nrcresearchpress.com by 80.90.12.36 on 09/08/12
For personal use only.

Can. J. Chem. Downloaded from www.nrcresearchpress.com by 80.90.12.36 on 09/08/12
For personal use only.

Table 1. Negative ion FABMS of $(C_6F_5)_3X$ with NBA matrix[a]

Ions	X		
	P	As	Sb
$(M)^{-\bullet}$	2	1	5
$(M + OH - HF)^-$	7	3	1
$(M - F)^-$	4	2	1
$(M - C_6F_5)^-$	5	7	3
$(C_{12}F_9)^-$ {*m/z*: 315}	8	10	6
$(C_{12}F_7)^-$ {*m/z*: 277}	3	4	4
$(C_6F_5)^-$	100	100	100
$(C_6F_4)^-$	4	3	2
Other ions	3(249)	8(425)	2(775)
	81(397)	1(729)	
	7(381)		

[a]Relative abundances of fragment ions above 1% are presented.

Scheme 1. Fragmentation of molecular ion (*m/z* 532) of **1** under negative ion FAB.

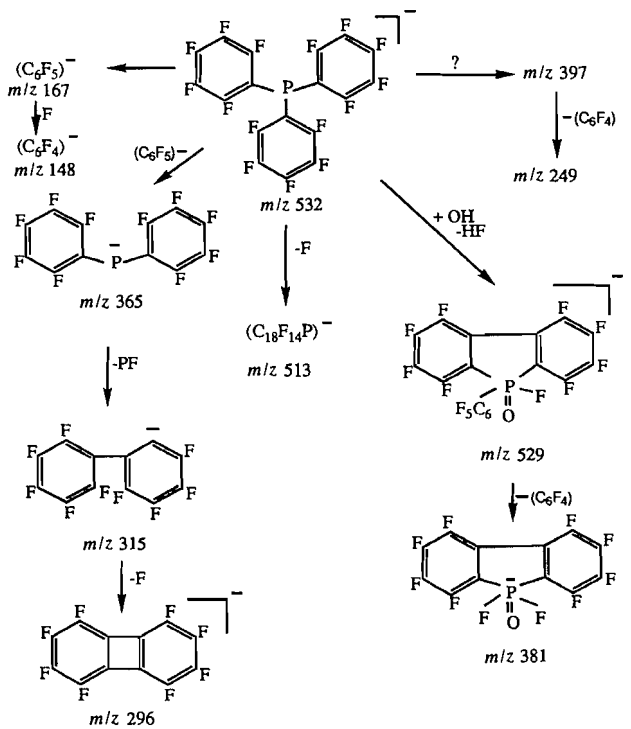

in B^2/E linked scan studies of the 397 ion. However, the metastable spectrum of the adduct ion of **1** with NBA (i.e., *m/z* 685) produced three abundant ions at *m/z* 397, 532 [$M^{-\bullet}$ of $P(C_6F_5)_3$], and 684 (Fig. 2).

The fragmentation in the first field-free region of the other ions with masses above that of the molecular ion, i.e., at *m/z* 549 and 578 (Fig. 2), also produced an ion at *m/z* 397 as a major fragment. The ion at *m/z* 529, obtained in the negative ion FAB spectrum of **1**, may be generated by the addition of an OH group and subsequent loss of HF from the molecular ion in an NBA matrix, which is a source of hydroxy radicals (19). The metastable ion spectrum of *m/z* 529 showed loss of oxygen as a major process, to produce an ion at *m/z* 513 (Fig. 2). The *B/E* spectrum of the 578 ion also showed the formation of

Scheme 2. Metastable ion fragmentation of *m/z* 397.

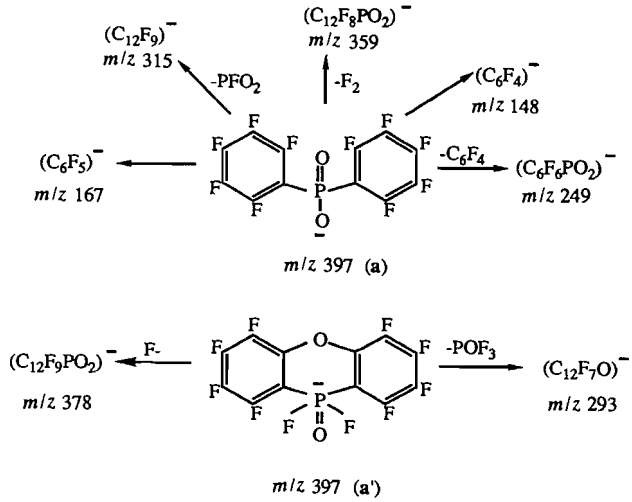

a 529 ion. The ion at *m/z* 578 could be made up of a mass 532 species bound to NO_2. This would account for the formation of *m/z* 397, but not of 529. Surprisingly, the *B/E* linked scan study of the 549 ion did not produce the 529 ion, suggesting that it may not be the hydroxyl adduct. The formulation of *m/z* 549 thus remains elusive, though it may be related to an NBA adduct of the 397 species.

The positive ion FAB of **1** in an NBA matrix did give the molecular ion as the base peak and other ions at *m/z* 365, 549, and 639 (Fig. 1). Formation of the unexpected 397 ion was not observed. The negative ion FAB spectra of **1** and tris(perfluorophenyl)phosphine oxide recorded with matrices containing hydroxy groups such as NBA, glycerol, 3-mercapto-1,2-propanediol, and 2,2′-thiodiethanol also showed the formation of an *m/z* 397 ion. However, this ion is not produced from a 2-nitrophenyloctylether matrix. The mestastable ion spectra of the 397 ion obtained from **1** and tris(perfluorophenyl)phosphine oxide using NBA and glycerol are found to be similar (Fig. 3). The position of the 397 ion was not shifted when the spectra were recorded with the addition of deuterium oxide to NBA or glycerol matrices. These experiments further establish that hydrogen radicals produced from selvedge are not directly involved in the formation of the 397 ion, though hydroxilic matrices are necessary. The origin of the 397 ion could not be established from B^2/E linked scan studies. This can be attributed to either the rapid decomposition of precursor ions and (or) to the formation of this species in the selvedge itself through the oxidation of the phosphine. The ion at *m/z* 549 might have also formed in the matrix. On unimolecular decomposition this yields primarily the 397 ion by the loss of 152 mass units. This suggests that the ion at *m/z* 549 could be the (NBA − H) adduct of the 397 species.

Multiple high-resolution mass measurements of the 397 ion obtained from **1** with an NBA matrix fit the elemental composition of $C_{12}F_{10}PO_2$ (calcd: 396.94859; theoretical: 396.94763; Δ = 2.4 ppm). Chemical ionization experiments carried out with tris(perfluorophenyl)phosphine and tris(perfluorophenyl)phosphine oxide failed to form a 397 ion. These experiments, together with the requirement for a hydroxilic matrix, clearly suggest that formation of the 397 ion must involve the matrix in a vital role. Based on these results, two structures for the *m/z* 397 ion are proposed, **a** and **a′** (Scheme 2). Formation

Fig. 2. Metastable negative ion FAB spectra of $(C_6F_5)_3P$–NBA: (i) *m/z* 685; (ii) *m/z* 578; (iii) *m/z* 549; and (iv) *m/z* 529.

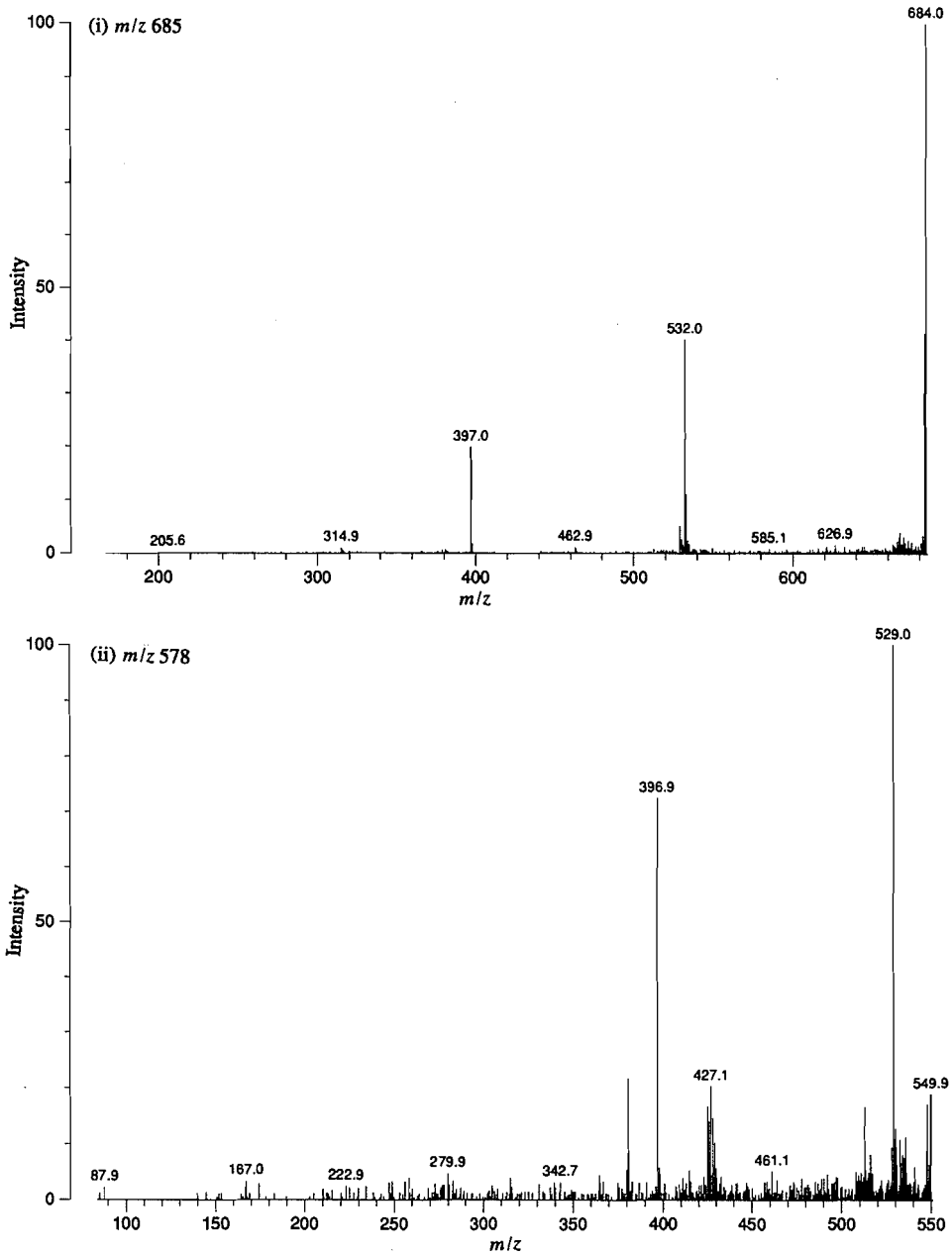

of mestastable ions at *m/z* 148, 167, 249, 315, and 359 from the 397 ion can be explained using structure **a**, and the remaining ions at *m/z* 293 and 378 can arise more readily from structure **a′**. Both structural types are consistent with species previously identified in the EI and positive ion FAB spectra of various Group V derivatives. The ion at *m/z* 397 thus is likely to be a mixture of **a** and **a′**, with the same empirical formulae. This ion formation is analogous to the solution chemistry oxidation of phosphine.

Conclusions

The matrices possessing hydroxy groups used for recording FABMS tris(perfluorophenyl)phosphine resulted in the formation of an unusual ion at *m/z* 397 by the oxidation of phosphorus(III) to phosphorus(V). The radical differences between the positive and negative ion FAB spectra and the EI spectrum serve as a warning that interpretation of mass spectra based solely on a single ionization technique can lead to

Can. J. Chem. Downloaded from www.nrcresearchpress.com by 80.90.12.36 on 09/08/12
For personal use only.

Fig. 2 (*concluded*).

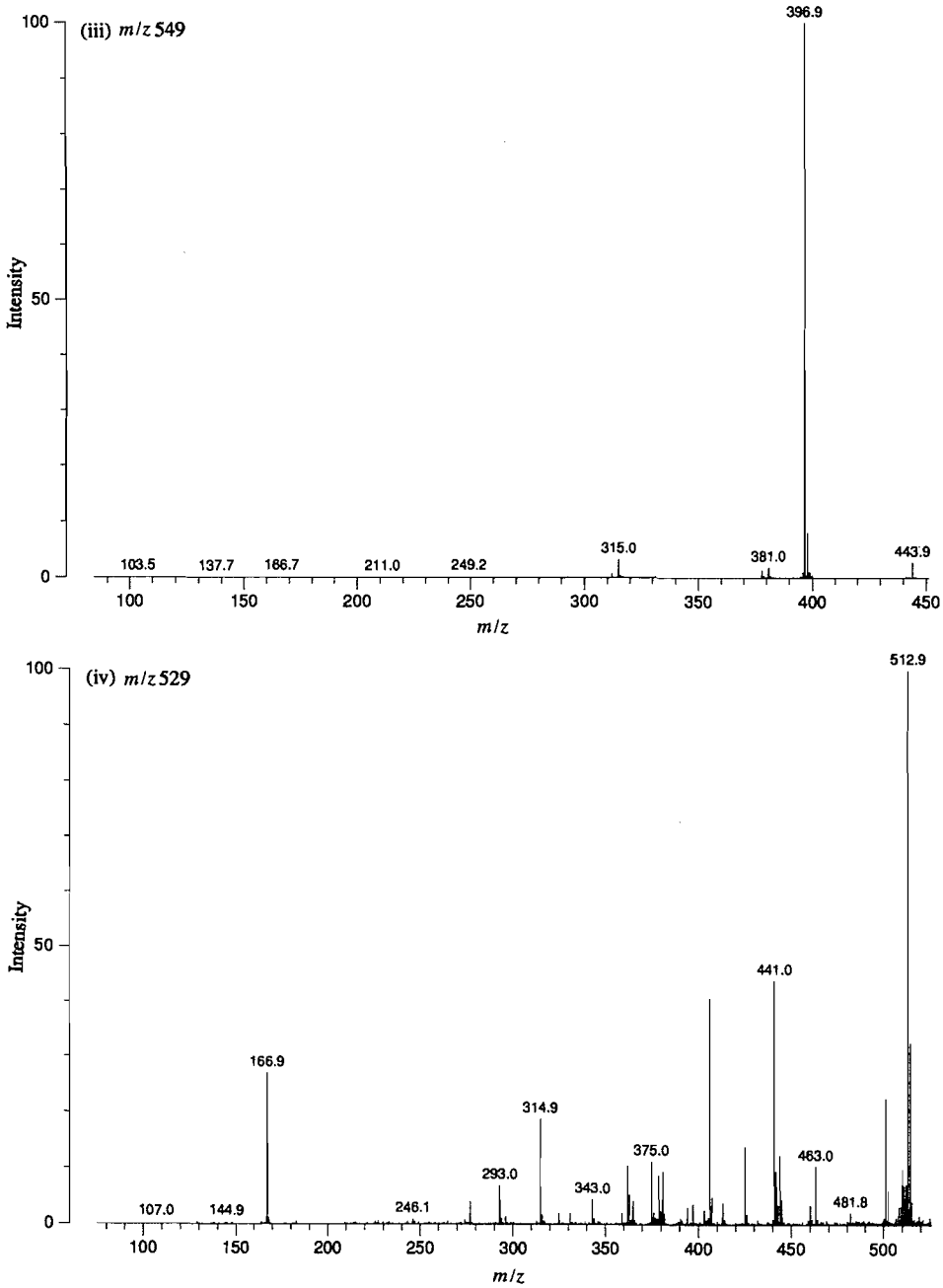

Can. J. Chem. Downloaded from www.nrcresearchpress.com by 80.90.12.36 on 09/08/12
For personal use only.

errors unless that technique is well understood for a particular compound class. For these compounds, the EI spectra are probably the best. In the negative ion FAB spectrum the *m/z* 397 species appears to be a reaction product involving the matrix rather than something involving preferential ionization of impurities.

Experimental

Compounds **1–3** utilized in this study were prepared according to procedures described in the literature: **1** (20), **2** and **3** (21); compound **4** was obtained from Fluorochem Limited. Compounds 2-nitrophenyl octyl ether (Fluka), 3-nitrobenzyl alcohol, 3-mercapto-1,2-propanediol, 2,2′-thiodiethanol, glycerol, and deuterium oxide (Aldrich) were used without further purification.

FAB mass spectra were recorded on a Kratos concept 1S mass spectrometer, interfaced to a Kratos DART/MACH3 data system. The standard concept FAB source was used with an Ion Tech Fast Atom Gun. Ionization was achieved using

Fig. 3. Metastable negative ion FAB spectra of *m/z* 397: (i) $(C_6F_5)_3P$–NBA; (ii) $(C_6F_5)_3P$–glycerol; (iii) $(C_6F_5)_3PO$–NBA; and (iv) $(C_6F_5)_3PO$–glycerol.

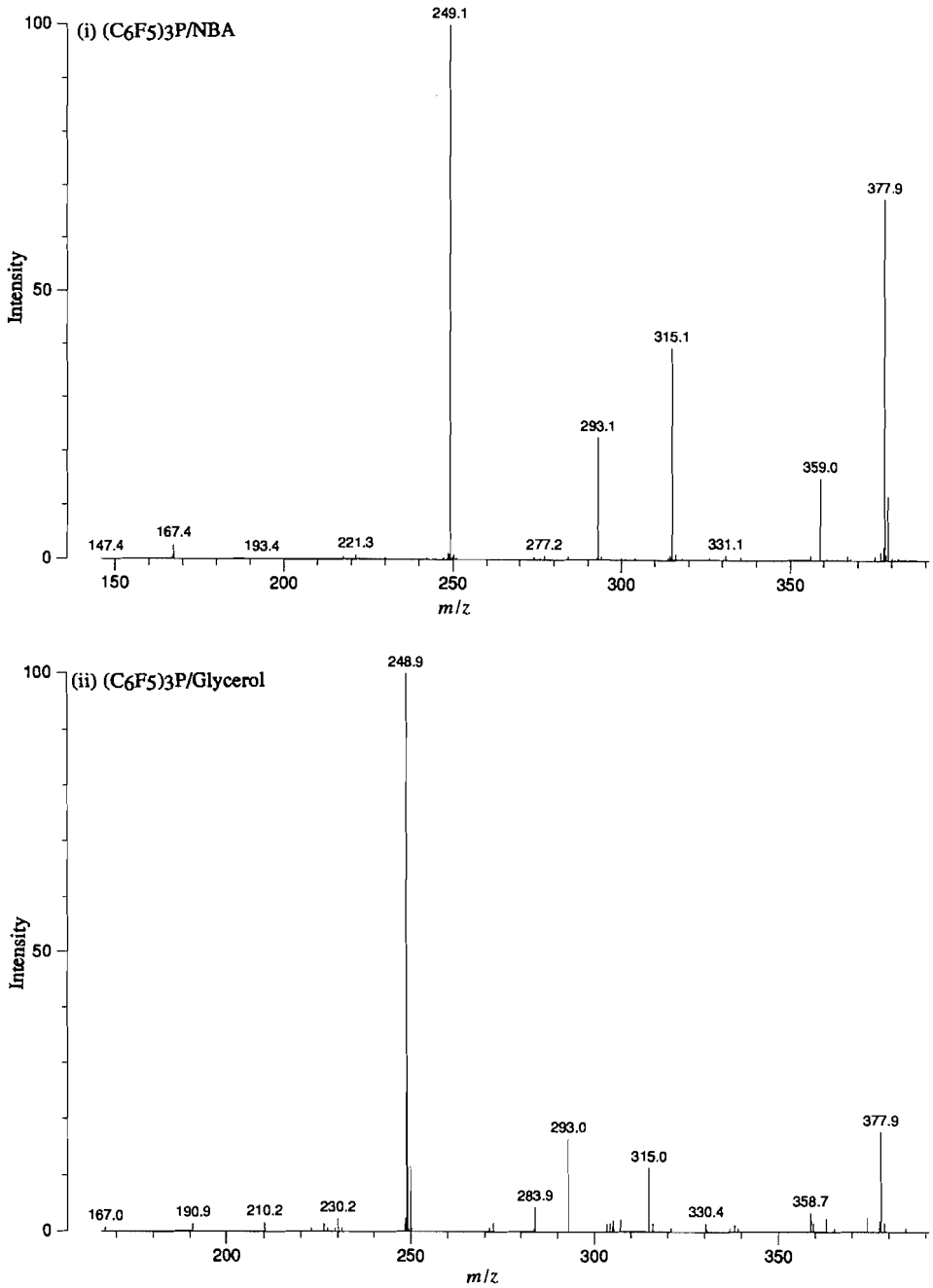

Can. J. Chem. Downloaded from www.nrcresearchpress.com by 80.90.12.36 on 09/08/12
For personal use only.

xenon fast atoms generated with 6–8 kV and 1 mA emission current. The pressure in the source was (1–2) × 10^{-5} Torr (1 Torr = 133.3 Pa). The source was operated at room temperature. Samples dissolved in the matrix were placed on 1 mm diameter stainless steel probe tips. A 8 kV accelerating potential was used at a resolving power of 1000 for recording low-resolution spectra and 10 000 for Exact Mass measurement. The data system was calibrated with a mixture of sodium iodide, rubidium iodide, and cesium iodide (1:1:1 molar ratio); spectra were acquired, averaged, and the matrix background was subtracted using the data system. Helium was used as the collision gas for recording Collisionally Activated Dissociation (CAD) spectra and the pressure of helium was adjusted to reduce the main beam intensity by 30–35% of its original value. Daughter ion and precursor ion scans were recorded by keeping B/E and B^2/E, respectively, constant.

Fig. 3 (*concluded*).

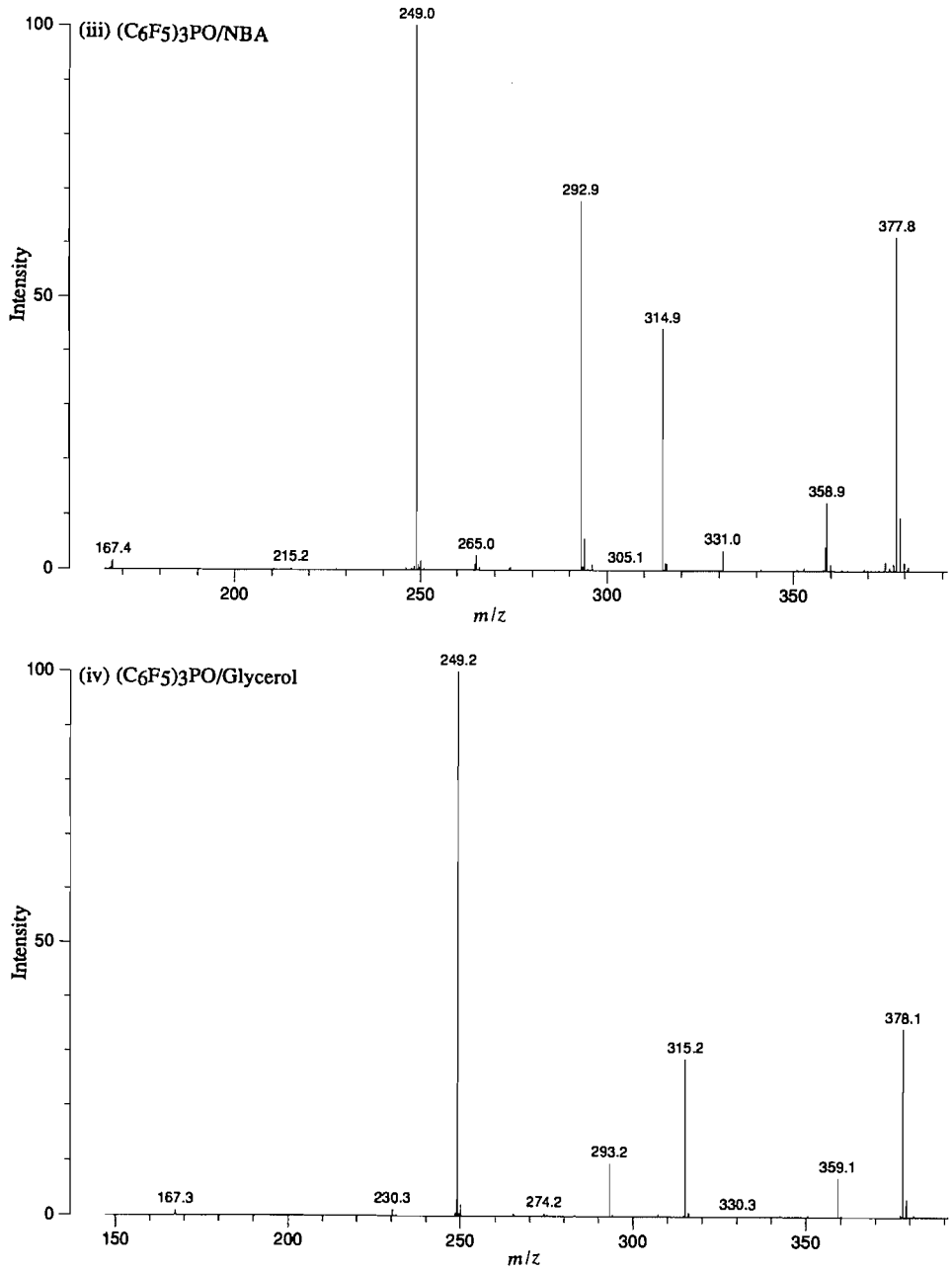

Can. J. Chem. Downloaded from www.nrcresearchpress.com by 80.90.12.36 on 09/08/12
For personal use only.

Acknowledgment

The authors thank the Natural Sciences and Engineering Research Council of Canada (NSERC) for operating and equipment grants to J.M. Miller.

References

1. (*a*) W.V. Ligon, Jr. and S.B. Dorn. Int. J. Mass Spectrom. Ion Processes, **57**, 75 (1984); (*b*) **61**, 113 (1984).
2. R.L. Cerny and M.L. Gross. Anal. Chem. **57**, 1160 (1985).
3. P. Schulze, D. Kush, A. Meier, and F.P. Montforts. Org. Mass. Spectrom. **29**, 496 (1994).
4. (*a*) P.J. Gale, B.L. Bentz, B.T. Chait, F.H. Field, and R.J. Cotter. Anal. Chem. **58**, 1070 (1986); (*b*) G. Pelzer, E. DePauw, D. Viet Dung, and J. Marien. J. Phys. Chem. **88**, 5065 (1984); (*c*) M.H. Florencio and W. Heerma. Org. Mass Spectrom. **28**, 657 (1993).
5. (*a*) B.D. Mussellmann and J.T. Watson. Biomed. Mass Spectrom. **14**, 247 (1989); (*b*) B.L. Schwartz, B.W. Erickson, M.M. Bursey, and G.D. Marbury. Org. Mass Spectrom. **28**, 113 (1993).

6. (*a*) H.M. Schiebel, P. Schulze, W.D. Stohrer, D. Leibfritz, B. Jastorff, and K.M. Mauer. Biomed. Mass Spectrom. **12**, 170 (1985).
7. (*a*) S.K. Seithi, C.C. Nelson, and J.A. McClosky. Anal. Chem. **56**, 1975 (1984); (*b*) S.M. Musser and J.A. Kelley. Org. Mass Spectrom. **28**, 672 (1993).
8. T. Nakamura, H. Nagaki, and T. Kinoshita. Bull. Chem. Soc. Jpn. **58**, 2798 (1985).
9. R.W. Edom, G. McKay, J.W. Hubbard, and K.K. Midha. Biol. Mass Spectrom. **20**, 585 (1991).
10. M.A. Baldwin and K.J. Welham. Org. Mass Spectrom. **21**, 235 (1986).
11. (*a*) T. Keough, F.S. Ezra, A.F. Russell, and J.D. Pryne. Org. Mass Spectrom, **21**, 241 (1987); (*b*) T. Keough. Int. J. Mass Spectrom. Ion Processes, **86**, 155 (1988).
12. W.D. Lehman, M. Kessler, and W.A. Konig. Biomed. Mass Spectrom. **11**, 217 (1984).
13. S.A. Martin, C.E. Costello, and K. Biemann. Anal. Chem. **54**, 2362 (1982).
14. P.R. Ashton and M.E. Rose. Org. Mass Spectrom. **21**, 388 (1986).
15. A. Fulcher. Brock University, M.Sc. Thesis. 1988.
16. (*a*) M.E. Rose, C. Longstaff, and P.D.G. Dean. Biomed. Mass Spectrom. **10**, 512 (1983); (*b*) A. Liguori, G. Sindona, and N. Uccella. J. Am. Chem. Soc. **108**, 7488 (1986).
17. A.T. Rake and J.M. Miller. J. Chem. Soc. A, 1881 (1970).
18. N.A.A. Ai-Jabar, J.B. Jones, D.S. Brown, A.H. Colligan, A.G. Massey, J.M. Miller, and J.W. Nye. Appl. Organomet. Chem. **3**, 459 (1989).
19. R.D. Bowen, T.N. Danks, D. Mitchell, and S.E. Thomas. Org. Mass Spectrom. **23**, 674 (1988).
20. L.A. Wall, R.E. Donadio, and W.J. Pummer. J. Am. Chem. Soc. **82**, 4846 (1960).
21. M. Fild, O. Glemser, and G. Christoph. Angew. Chem. Int. Ed. Engl. **3**, 801 (1964).

Can. J. Chem. Downloaded from www.nrcresearchpress.com by 80.90.12.36 on 09/08/12
For personal use only.

1-Deoxy-D-xylulose

Isaac A. Kennedy, Thomas Hemscheidt, James F. Britten, and Ian D. Spenser

Abstract: 1-Deoxy-D-xylulose (= 1-deoxy-D-*threo*pentulose) is a precursor of thiamin (Vitamin B_1) and of pyridoxine (Vitamin B_6) in bacteria. The synthesis of a [2,3-$^{13}C_2$] bond-labeled sample of the compound, to be used for investigations of the biosynthesis of the two vitamins, is described. In aqueous solution 1-deoxy-D-xylulose exists mainly as the open chain ketone. In methanol solution the compound exists as a mixture of the open chain ketone and the two corresponding epimeric furanoses. In acid solution the compound yields a dimeric anhydride, di-β-1-deoxy-D-xylulofuranose 2,3′:3,2′-dianhydride, whose structure was established by X-ray crystallography.

Key words: [2,3-$^{13}C_2$]-1-deoxy-D-xylulose, di-β-1-deoxy-D-xylulofuranose 2,3′:3,2′-dianhydride, 5-*O*-benzyl-3,4-*O*-isopropylidene-1-deoxy-D-xylulose, 4-*O*-benzyl-2,3-*O*-isoproylidene-D-threose.

Résumé : Dans les bactéries, le 1-désoxy-D-xylulose (= 1-désoxy-D-*thréo*pentulose) est un précurseur de la thiamine (vitamine B_1) et de la pyridoxine (vitamine B_6). On décrit la synthèse d'un échantillon de ce composé marqué sur les liaisons [2,3-$^{13}C_2$] qui sera utilisé dans des études de la biosynthèse des deux vitamines. En solution aqueuse, le 1-désoxy-D-xylulose existe principalement sous la forme d'une chaîne cétonique ouverte. En solution dans le méthanol, le composé existe sous la forme d'un mélange de la chaîne cétonique ouverte et des deux furanoses épimères correspondants. En solution acide, le composé fournit un anhydride dimère, le 2,3′:3,2′-dianhydride du di-β-1-désoxy-D-xylulofuranose, dont on a déterminé la structure par diffraction des rayons X.

Mots clés : [2,3-$^{13}C_2$]-1-désoxy-D-xylulose, 2,3′:3,2′-dianhydride du di-β-1-désoxy-D-xylulofuranose, 5-*O*-benzyle-3,4-*O*-isopropylidène-1-désoxy-D-xylulose, 4-*O*-benzyle-2,3-*O*-isoproylidène-D-thrèose.

[Traduit par la rédaction]

Introduction

The natural occurrence of 1-deoxy-D-xylulose (= 1-deoxy-D-*threo*pentulose) was first reported in 1976 (1). The compound was obtained from an isolate of *Streptomyces hygroscopicus*, and its structure and stereochemistry were deduced from its mass spectrum and on the basis of the identification of its reduction product as a mixture of 1-deoxy-D-xylitol and 1-deoxy-D-lyxitol, by comparison of their ^{1}H NMR spectra, GLC retention times, and optical rotation values with those of authentic specimens prepared from D-xylose and D-lyxose, respectively (2).

It was subsequently found that a wide range of microorganisms show enzymic activity leading to the formation of 1-deoxy-D-xylulose as well as of 1-deoxy-L-xylulose, by acyloin type condensation of pyruvic acid with D-glyceraldehyde or L-glyceraldehyde, respectively (3), a reaction that is catalysed by pyruvate dehydrogenase (E.C. 1.2.4.1) (4) and is accompanied by decarboxylation. Another enzyme, acetoin dehydrogenase (E.C. 1.1.1.5), found in the same microorganisms, generates 1-deoxy-D-xylulose or its enantiomer by reaction of D- or L-glyceraldehyde, respectively, with acetoin or methylacetoin instead of with pyruvic acid, yielding acetaldehyde or acetone, respectively, as the second product (4).

Received February 15, 1995.

I.A. Kennedy, T. Hemscheidt, J.F. Britten, and I.D. Spenser.[1] Department of Chemistry, McMaster University, Hamilton, ON L8S 4M1, Canada.

[1] Author to whom correspondence may be addressed. Telephone: (905) 525-9140, ext. 23245. Fax: (905) 522-2509. E-mail: spenser@mcmail.cis.mcmaster.ca

1-Deoxy-D-xylulose is described as a crystalline compound, $C_5H_{10}O_4$, mp 61–63°C (1), 62–63°C (3), $[\alpha]_D$ +46 (*c* 1, H_2O)(1), +33.6 (*c* 1, H_2O)(3). Since the crystalline compound shows strong carbonyl absorption at 1710 cm^{-1} (2, 4), it follows that it exists as the open chain ketone (2). 1-Deoxy-L-xylulose, mp 63–65°C, $[\alpha]_D$ −33 (*c* 1, H_2O) (3) showed similar characteristics.

The appearance of three methyl singlets in the ^{1}H NMR spectrum ((D_2O or [D_6]DMSO) δ: 2.15 (80%), 1.31, 1.23 ppm (together 20%, signal at 1.31 more intense than signal at 1.23)) (2), ((D_2O) δ: 2.50 (72%), 1.69 (20%), 1.64 (6%); 3.75–4.70 (4H, m) ppm) (3) leads to the conclusion that in solution the compound exists as a mixture in which the open chain ketone predominates over the two anomeric furanoses, one of which is more abundant than the other.

Several chemical syntheses of 1-deoxyxylulose have been reported. Derivatives of the L-enantiomer, prepared from threonamide (5, 6), had been reported long before the compound had been isolated from natural sources. Two syntheses of 1-deoxy-D-xylulose ($[\alpha]_D^{21}$ +34 (*c* 1, H_2O)) were devised in connection with investigations of thiamin biosynthesis, one starting with derivatives of D-glyceraldehyde and acetaldehyde, the other from D-arabinose (7). The former method was employed to prepare a sample of 1-deoxy-D-[1,1,1-$^2H_3$]xylulose, the latter to generate a sample of the [1,1,1,(*RS*)-5-$^2H_4$]derivative. Both of these labeled compounds were shown to be incorporated into the thiazole nucleus of thiamin in *Escherichia coli* (7). The latter compound served as a precursor also of pyridoxine in *E. coli* (8). Another synthesis (9), leading to racemic 1-deoxyxylulose, starts from xylitol, a *meso* compound.

Can. J. Chem. Downloaded from www.nrcresearchpress.com by 80.90.12.36 on 09/08/12
For personal use only.

None of these syntheses were suitable for the preparation of the ^{13}C-labeled sample we required for our investigation of pyridoxine biosynthesis. What was needed was a sample of 1-deoxy-D-xylulose bond-labeled with ^{13}C at C-2,3, in order to test the direct incorporation of the substrate into pyridoxol without cleavage of the C-2,C-3 bond. This bond is one of only two bonds that are formed *de novo* when pyridoxine is derived from [1,2,3,4,5,6-$^{13}C_6$]glucose (10). To prove that 1-deoxy-D-xylulose is a late intermediate on the route from glucose into pyridoxine, it must be shown that the intact C-2,3 bond of the deoxypentulose is incorporated into pyridoxine.

Results and discussion

The major determinant in the design of the synthesis of ^{13}C-labeled compounds is the availability of ^{13}C-labeled starting materials that are not exorbitantly expensive. This factor becomes overriding when two contiguous carbon atoms in the target compound are to be enriched with ^{13}C.

This paper describes a synthesis of [2,3-$^{13}C_2$]-1-deoxy-D-xylulose (**14**) that starts with triethyl phosphono[1,2-$^{13}C_2$]acetate (**2**), or from ethyl bromo[1,2-$^{13}C_2$]acetate. Ethyl bromoacetate is a convenient starting material for preparation of triethyl phosphonoacetate (11). Both doubly labeled compounds are commercially available. The key intermediate of the route is [1,2-$^{13}C_2$]-4-*O*-benzyl-2,3-*O*-isopropylidene-D-threose (**10**), from which the target compound, [2,3-$^{13}C_2$]-1-deoxy-D-xylulose (**14**), is obtainable in four steps. The route to **10** proceeds by a sequence that has been well explored in the preparation of the corresponding unlabeled compounds, employing the Sharpless titanium-catalyzed asymmetric epoxidation procedure, followed by Payne and Pummerer rearrangement (12, 13). Unlabeled 4-*O*-benzyl-2,3-*O*-isopropylidene-D-threose (**18**) is accessible (14–16) in two steps from (−)-2,3-*O*-isopropylidene-D-threitol ([4*R*,5*R*]-4,5-di(hydroxymethyl)-2,2-dimethyl-1,3-dioxolane) (**15**), a compound that is commercially available.

Condensation of *O*-benzylglycolaldehyde (**1**) with triethyl phosphono[1,2-$^{13}C_2$]acetate (**2**) (cf. refs. 17–19) under conditions known to yield the *E* isomer exclusively (ref. 20, and footnote 9 of ref. 12) gave ethyl [1,2-$^{13}C_2$]-4-benzyloxy-*E*-but-2-enoate (**3**) in 79% yield. Reduction with diisobutyl aluminium hydride (cf. refs. 19, 21) gave [1,2-$^{13}C_2$]-4-benzyloxy-*E*-but-2-en-1-ol (**4**) in quantitative yield. This compound was subjected to the Sharpless asymmetric epoxidation procedure (cf. refs. 12, 13, 19, and 22), using D-(−)-diisopropyl tartrate in the presence of titanium tetraisopropropoxide, giving [1,2-$^{13}C_2$]-(2*R*,3*R*)-4-benzyloxy-2,3-epoxybutan-1-ol (**5**) in 86% yield. Payne and Pummerer rearrangements (12, 13) then yielded, in sequence, [1,2-$^{13}C_2$]-(2*R*,3*R*)-4-benzyloxy-1-phenylthiobutane-2,3-diol (**6**), then the corresponding 2,3-isopropylidene derivative, [1,2-$^{13}C_2$]-(2*R*,3*R*)-4-benzyloxy-2,3-*O*-isopropylidene-1-phenylthiobutane-2,3-diol (**7**), followed by the corresponding sulfoxide (**8**) and the *gem*-acetoxy sulfide (**9**). In basic solution the latter undergoes hydrolysis accompanied by inversion (13, 23), to yield the labeled key intermediate, [1,2-$^{13}C_2$]-4-*O*-benzyl-2,3-*O*-isopropylidene-D-threose ([4,4′-$^{13}C_2$]-(4*S*,5*R*)-5-benzyloxymethyl-4-formyl-2,2-dimethyl-1,3-dioxolane)(**10**). The overall yield of **10** from **6** was 71%.

Grignard reaction of **10** with methyl magnesium chloride gave a 2.5:1 diastereomeric mixture of the corresponding methyl carbinols, [2,3-$^{13}C_2$]-5-*O*-benzyl-3,4-*O*-isopropylidene-1-deoxy-D-xylitol and -lyxitol (**11**) in 90% yield. The mixture was oxidized with pyridinium dichromate (24) to yield [2,3-$^{13}C_2$]-5-*O*-benzyl-3,4-*O*-isopropylidene-1-deoxy-D-xylulose (**12**) in 88% yield. Acid hydrolysis removed the isopropylidene protecting group to give [2,3-$^{13}C_2$]-5-*O*-benzyl-1-deoxy-D-xylulose (**13**) (yield 88%), which, on hydrogenolysis in the presence of 10% palladium/carbon gave the desired product, [2,3-$^{13}C_2$]-1-deoxy-D-xylulose (**14**) in quantitative yield. Overall, 10 g bond labeled starting material (**2**) furnished 0.95 g bond labeled 1-deoxy-D-xylulose (**14**) (16% yield).

In preparation for the labeled synthesis, the new steps of the above reaction sequence, from the key intermediate (**10**) to the final product (**14**), were explored with unlabeled material. Unlabeled 4-*O*-benzyl-2,3-*O*-isopropylidene-D-threose (**18**) was obtained in two steps from (−)-2,3-*O*-isopropylidene-D-threitol [(4*R*,5*R*)-4,5-di(hydroxymethyl)-2,2-dimethyl-1,3-dioxolane] (**15**) (Aldrich), by oxidation (15, 16) of the monobenzyl derivative, (4*R*,5*R*)-5-benzyloxymethyl-4-hydroxymethyl-2,2-dimethyl-1,3-dioxolane (**16**) (14). The utility of the *tert*-butyldimethylsilyl protecting group was also investigated. 4-*O*-(*tert*-butyldimethylsilyl)-2,3-*O*-isopropylidene-D-threose (**19**) was obtained from **15** via **17** in two analogous steps (25).

Nonstereospecific Grignard methylation of the aldehyde group of **18** or of **19** with methyl magnesium chloride yielded a diastereomeric mixture (5:2 and 3:2, respectively, for **20** and **21**) of 5-protected-3,4-*O*-isopropylidene-1-deoxy-D-xylitol and -lyxitol. Oxidation of each of the two diastereomeric mixtures, **20** or **21**, either with pyridinium dichromate (24) or with oxalyl chloride – DMSO (26) gave the corresponding 5-protected-3,4-*O*-isopropylidene-1-deoxy-D-xylulose (**22**, **23**) in 90% and 78% yield, respectively.

Conversion of the 5-*tert*-butyldimethylsilyl derivative (**23**) into free 1-deoxy-D-xylulose (**27**), either stepwise, using tetrabutylammonium fluoride to yield 3,4-*O*-isopropylidene-1-deoxy-D-xylulose (**26**), followed by hydrolysis with dilute acid, or directly, with sodium fluoride in HCl solution, gave the final product in very poor (ca. 25%) yield. Silyl protection was therefore abandoned in favour of benzyl protection.

Simultaneous removal of both the benzyl (27) and the isopropylidene (27, 28) protecting groups from 5-*O*-benzyl-3,4-*O*-isopropylidene-1-deoxy-D-xylulose (**22**) using boron trichloride gave the deoxypentulose (**27**) in poorer yield (26%) than stepwise removal of the two groups. Presumably side reactions occur and the reagent and the product form a complex that resists separation even after repeated addition of methanol, followed by flash chromatography. Hydrogenolytic debenzylation of 5-*O*-benzyl-3,4-*O*-isopropylidene-1-deoxy-D-xylulose (**22**) gave 3,4-*O*-isopropylidene-1-deoxy-D-xylulose (**26**) in 95% yield, from which 1-deoxy-D-xylulose (**27**) was obtained in 75% yield by acid hydrolysis. Conversely, acid hydrolysis of 5-*O*-benzyl-3,4-*O*-isopropylidene-1-deoxy-D-xylulose (**22**) gave 5-*O*-benzyl-1-deoxy-D-xylulose (**24**) in 88% yield. Hydrogenolysis in the presence of Pd/C then gave the free 1-deoxy-D-xylulose (**27**) in 95% yield. The latter deprotection sequence was chosen for the labeled synthesis.

When 1-deoxy-D-xylulose (**27**) was prepared from 3,4-*O*-isopropylidene-1-deoxy-D-xylulose (**26**) by acid hydrolysis, and the solution was concentrated without complete removal of acid, a crystalline compound was obtained whose physical

Can. J. Chem. Downloaded from www.nrcresearchpress.com by 80.90.12.36 on 09/08/12
For personal use only.

Scheme 1. Synthesis of [2,3-$^{13}C_2$]-1-deoxy-D-xylulose (**14**) from *O*-benzylglycolaldehyde (**1**) and triethyl [1,2-$^{13}C_2$]phosphonoacetate (**2**). ▬ = ^{13}C–^{13}C.

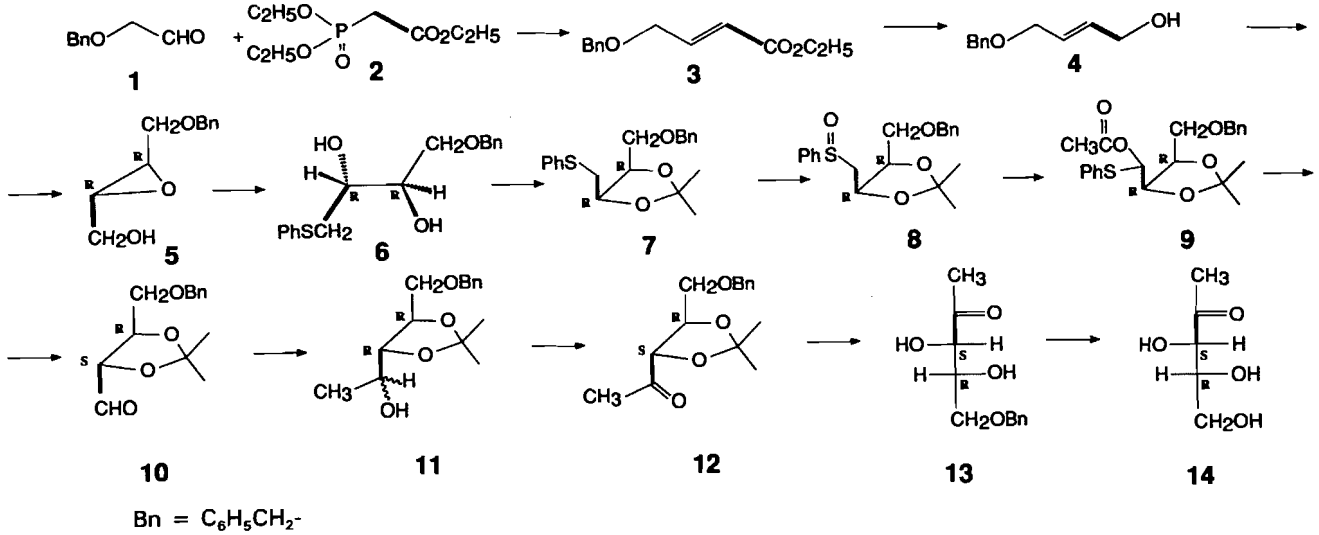

Bn = $C_6H_5CH_2$-

Scheme 2. Synthesis of 1-deoxy-D-xylulose (**27**) from (−)-2,3-*O*-isopropylidene-D-threitol (**15**).

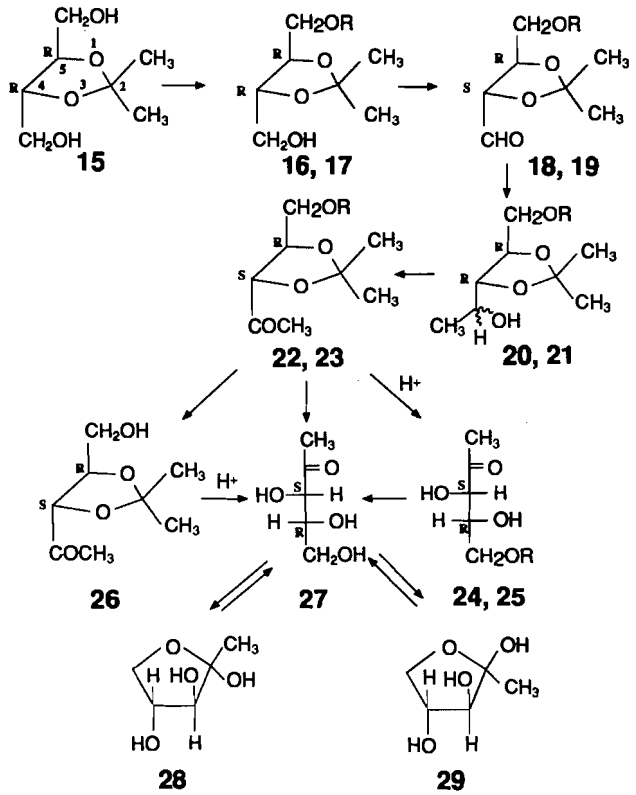

16, 18, 20, 22, 24 R = $C_6H_5CH_2$-
17, 19, 21, 23, 25 R = *tert*-butyldimethylsilyl-

constants (mp 145–146°C, $[\alpha]_D^{20}$ −55.2 (*c* 1, CH_3OH)) were different from those reported (1,3) for 1-deoxy-D-xylulose (**27**).

The structure of this compound was determined by X-ray crystallography. The compound was found to be di-β-1-deoxy-D-xylulofuranose 2,3′:3,2′-dianhydride (**30**), a dimer of β-1-deoxy-D-xylulofuranose (**29**). X-ray structure analysis of **30** (Fig. 1) showed it to contain a non-crystallographic twofold axis relating the two furanose rings, which adopt puckered conformations, with the two methylene groups, C(5) and C(5′), out of plane towards the same side of the molecule. Intramolecular bonding is normal. The OH groups at C(4) and C(4′) are strongly hydrogen bonded: The oxygen atom O(4) forms a hydrogen bond to HO(4′) of one of the neighbouring dimers (at $x+1, y-1, z$: 2.888(1) Å) and the H of O(4) interacts with the furanose ring oxygen, O(5′), of another (at $x, y-1, z$: 2.957(1) Å). This results in a two-dimensional sheet perpendicular to the crystallographic *c*-axis, with the methyl groups (C(1) and C(1′)) on one face and the methylene groups (C(5) and C(5′)) on the other. The crystallographic screw axes (2_1) stack these sheets in the *c*-direction, with methylenes facing methylenes, and methyls intertwined with methyls. The atomic coordinates and equivalent isotropic temperature factors are listed in Table 1.

Experimental

The starting material for the synthesis of 1-deoxy-D-xylulose (**27**) was a commercial product, (−)-2,3-*O*-isopropylidene-D-threitol ((4*R*,5*R*)-4,5-di(hydroxymethyl)-2,2-dimethyl-1,3-dioxolane) (**15**) (Aldrich). This was converted into 4-*O*-benzyl-2,3-*O*-isopropylidene-D-threose (**18**) as well as into 4-*O*-(*tert*-butyldimethylsilyl)-2,3-*O*-isopropylidene-D-threose (**19**) in analogy with published procedures that were employed to synthesize the L-enantiomers. Monobenzylation of (**15**) (14) gave 4-*O*-benzyl-2,3-*O*-isopropylidene-D-threitol (**16**) from which **18** was obtained (15, 16) by Swern oxidation (26). Monosilylation of **15** (25) gave 4-*O*-(*tert*-butyldimethylsilyl)-2,3-*O*-isopropylidene-D-threitol (**17**), Swern oxidation of which gave **19** (25).

(4*R*,5*R*)-5-Benzyloxymethyl-4-(2′-(*RS*)-hydroxyethyl)-2,2-dimethyl-1,3-dioxolane (5-*O*-benzyl-3,4-*O*-isopropylidene-1-deoxy-D-xylitol plus 5-*O*-benzyl-3,4-*O*-isopropylidene-1-deoxy-D-lyxitol) (20)

Methyl magnesium chloride (3 M in THF, Aldrich, 2 equivalents) was added dropwise to a stirred solution of **18** ($[\alpha]_D^{20}$ −19.4 (*c* 1.30, $CHCl_3$); lit. (16) $[\alpha]_D^{21}$ of enantiomer +16.8 (*c*

Can. J. Chem. Downloaded from www.nrcresearchpress.com by 80.90.12.36 on 09/08/12
For personal use only.

Scheme 3. Formation of di-β-1-deoxy-D-xylulofuranose 2,3′:3,2′-dianhydride (**30**) by dimerization of β-1-deoxy-D-xylulofuranose (**29**).

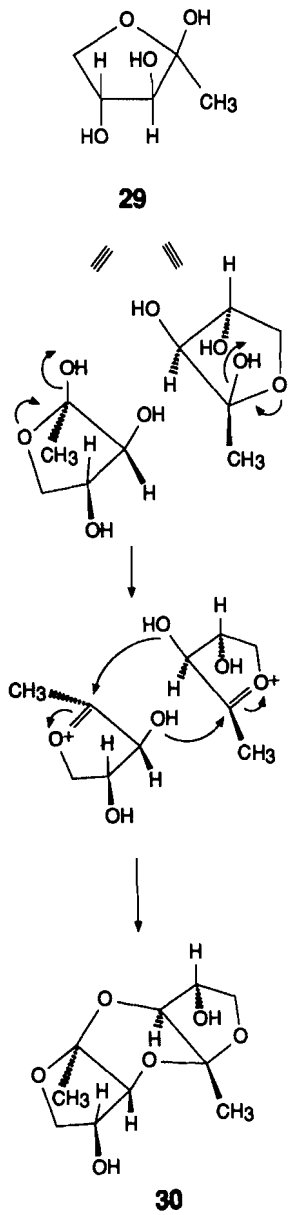

1.10, $CHCl_3$)) (3.3 g, 13.2 mmol) in dry tetrahydrofuran (25 mL) at 0°C and stirring was continued overnight. After dilution with ether (40 mL), the mixture was poured carefully into an ice-cold saturated aqueous solution of ammonium chloride. The phases were separated and the aqueous layer was extracted with ether (2 × 20 mL). The organic extracts were combined, dried over anhydrous $MgSO_4$, filtered, and evaporated. The residual oil was purified by flash chromatography (10% ethyl acetate – petroleum ether) to yield 3.2 g (91%) of a 2.5:1 mixture of the two diastereomers **20**. ^{1}H NMR (200 MHz, $CDCl_3$) δ: 1.13 (d, 3H, J = 6.3 Hz, CH_3CHOH), 1.33 (s, 6H, $(CH_3)_2$), 2.75 (br s, 1H, OH), 3.33–3.81 (m, 4H, 2(OCH), (CH_2O)), 3.95–4.05 (m, 1H, CHOH), 4.53 (s, 2H, OCH_2Ph), 7.26 (m, 5H, C_6H_5). ^{13}C NMR (50.3 MHz, $CDCl_3$) δ: 137.2,

Fig. 1. Thermal ellipsoid diagram of **30**. (50% probability for C and O; hydrogen atoms are represented by circles of arbitrary size).

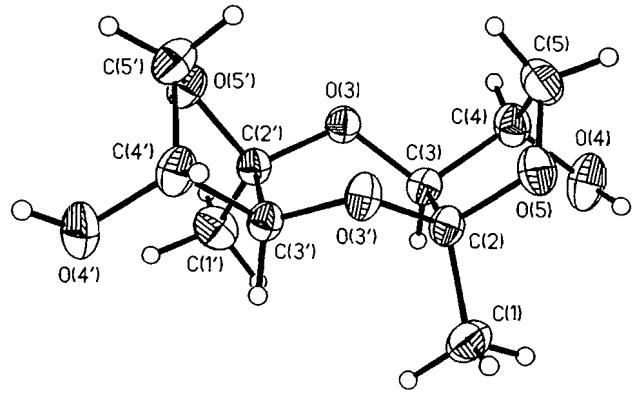

Table 1. Atomic coordinates (×10^4) and equivalent isotropic displacement parameters (Å^2 × 10^3) for **30**.

Atom	x	y	z	U(eq)[a]
C(1)	837(2)	−106(2)	1358(1)	36(1)
C(2)	1800(2)	716(1)	2517(1)	24(1)
C(3)	4169(2)	1272(1)	2367(1)	25(1)
O(3)	4482(1)	2922(1)	2843(1)	26(1)
C(4)	5371(2)	91(2)	3267(1)	33(1)
O(4)	5860(2)	−1449(1)	2648(1)	44(1)
C(5)	3707(2)	−156(2)	4278(1)	36(1)
O(5)	1780(1)	−423(1)	3546(1)	32(1)
C(1′)	4071(2)	4692(2)	976(1)	36(1)
C(2′)	3168(2)	4159(1)	2239(1)	24(1)
C(3′)	809(2)	3548(1)	2180(1)	24(1)
O(3′)	529(1)	2093(1)	2927(1)	27(1)
C(4′)	−424(2)	4935(2)	2842(1)	30(1)
O(4′)	−928(2)	6159(1)	1908(1)	40(1)
C(5′)	1236(2)	5539(2)	3790(1)	34(1)
O(5′)	3192(1)	5554(1)	3072(1)	31(1)

[a] U(eq) is defined as one third of the trace of the orthogonalized U_{ij} tensor.

128.4 (2×), 127.8 (2×), 108.9, 82.8, 82.3, 77.4, 73.7, 70.9, 70.5, 67.8, 67.3, 27.1, 26.8, 19.6, 19.1. Anal. calcd. for $C_{15}H_{22}O_4$: C 67.64, H 8.33; found: C 67.39, H 8.13.

(4*S*,5*R*)-4-Acetyl-5-benzyloxymethyl-2,2-dimethyl-1,3-dioxolane (5-*O*-benzyl-3,4-*O*-isopropylidene-1-deoxy-D-xylulose) (22)

Pyridinium dichromate (24) (8.60 g, 22.8 mmol) was added to a solution of **20** (3.0 g, 11.3 mmol) in DMF (15 mL) and the mixture was stirred for 24 h. Water (30 mL) was then added and the mixture extracted with ether (3 × 40 mL). The combined ether extract was washed with brine, dried over anhydrous $MgSO_4$ and concentrated to give an oily residue. Flash chromatography (10% ether – petroleum ether) of the residual oil gave the product (**22**) as a colourless oil (2.7 g, 90%). $[\alpha]_D^{20}$ −16.4 (*c* 1.54, CH_2Cl_2). ^{1}H NMR (200 MHz, $CDCl_3$) δ: 1.42 (s, 3H, CH_3), 1.54 (s, 3H, CH_3), 2.34 (s, 3H, CH_3CO), 3.62–3.71 (m, 1H, OCH), 3.73–3.79 (m, 1H, OCHCO), 4.21

Can. J. Chem. Downloaded from www.nrcresearchpress.com by 80.90.12.36 on 09/08/12
For personal use only.

Can. J. Chem. Downloaded from www.nrcresearchpress.com by 80.90.12.36 on 09/08/12
For personal use only.

(s, 2H, OCH_2), 4.63 (s, 2H, $CH_2C_6H_5$), 7.22–7.38 (m, 5 H, C_6H_5). ^{13}C NMR (50.3 MHz, $CDCl_3$) δ: 208, 137.6, 128.1 (2×), 127.3 (3×), 110.7, 81.6, 77.0, 73.2, 69.9, 26.6, 26.1, 26.0. Anal. calcd. for $C_{15}H_{20}O_4$: C 68.16, H 7.63; found: C 68.06, H 7.71.

5-*O*-Benzyl-1-deoxy-D-xylulose (24)

5-*O*-Benzyl-3,4-*O*-isopropylidene-1-deoxy-D-xylulose (**22**) (1.0 g, 3.8 mmol) was dissolved in 50 mL of a solution prepared by mixing CH_3CN, H_2O, and 2 M HCl in the ratio 90:6:3 (29). The mixture was stirred for 24 h and was then concentrated, and CH_2Cl_2 (30 mL) was added.

The solution was washed with saturated Na_2CO_3 (2 × 5 mL) and brine. The organic layer was concentrated after drying over Na_2SO_4 and chromatographed on silica gel (230–400 mesh) using the following solvents: 50% ether – petroleum ether until a yellowish fraction came off, then CH_2Cl_2, and finally 5% methanol – CH_2Cl_2 to afford 0.75 g (87%) **24** as a colourless oil. $[\alpha]_D^{20}$ +51.6 (*c* 1.32, CH_2Cl_2). ^1H NMR (200 MHz, $CDCl_3$) δ: 2.22 (s, CH_3), 2.34 (d, 1H, *J* = 7.7 Hz, OH), 3.55 (m, 1H, CH), 3.58 (s, 1H, OH), 3.65 (d, 1H, *J* = 4.5 Hz, COCH), 4.13–4.19 (m, 2H, CH_2O), 4.51 (s, 2H, $OCH_2C_6H_5$), 7.28 (m, 5H, C_6H_5). ^{13}C NMR (50.3 MHz, $CDCl_3$) δ: 208.1, 137.6, 128.4 (2×), 127.9, 127.8 (2×), 76.3, 73.6, 71.0, 70.4, 25.5. HRMS calcd. for $C_{12}H_{17}O_4$ (M^+ + 1): 225.1127; found: 225.1123. Anal. calcd. for $C_{12}H_{16}O_4 \cdot 0.25\ H_2O$: C 63.00, H 7.27; found: C 62.65, 62.95; H 7.18, 7.08.

(4*R*,5*R*)-5-*O*-(*tert*-Butyldimethylsilyl)oxymethyl-4-(2′-(*RS*)-hydroxyethyl)-2,2-dimethyl-1,3-dioxolane (5-*O*-(*tert*-butyldimethylsilyl)-3,4-*O*-isopropylidene-1-deoxy-D-xylitol plus 5-*O*-(*tert*-butyldimethylsilyl)-3,4-*O*-isopropylidene-1-deoxy-D-lyxitol) (21)

Methyl magnesium chloride (1 M in THF, Aldrich, 3 equivalents) was added dropwise to a stirred solution of **19** (1.4 g) in dry THF (25 mL) at 0°C and the mixture was stirred overnight and allowed to reach room temperature. It was then refluxed for 1 h, cooled, diluted with cold ether (40 mL), and was then added dropwise to an ice-cold saturated aqueous solution of ammonium chloride (75 mL). The phases were separated and the aqueous phase was extracted with ether (3 × 50 mL). The organic extracts were combined, washed with water (2 × 40 mL) and saline (2 × 40 mL), dried over anhydrous $MgSO_4$, filtered, and evaporated. The residual oil was purified by flash chromatography (10% ethyl acetate – hexane 1:3), followed by bulb-to-bulb distillation (oven temp. 140°C, 0.2 Torr; 1 Torr = 133.3 Pa). Yield 1.0 g, (70%) with respect to **19**, mixture of two diastereomers ca. 3:2.

Major, less polar diastereomer: $[\alpha]_D^{20}$ −23.0 (*c* 2.89, $CHCl_3$). ^1H NMR: (500 MHz, $CDCl_3$) δ: 0.1 (s, 6H, $SiMe_2$), 0.9 (s, 9H, Si-*t*Bu), 1.25 (d, 3H, *J* = 6.2 Hz, CH_3CHOH), 1.38, 1.39 (2 × s, 6H, $C(CH_3)_2$), 3.65 (m, 2H, $SiOCH_2$), 3.8 (m, 1H, OCH), 3.89 (m, 2H, OCH, *C*HOH). ^{13}C NMR (75 MHz, $CDCl_3$) δ: 108.9, 84.3, 79.6, 68.3, 64.4, 27.1, 27.0, 26.0, 19.5, 18.2, −5.4. MS(EI) *m/z*: 275 ($M^+ - CH_3$, 10%), 175 (25), 157 (14), 133 (14), 131 (93), 117 (57), 89 (11), 83 (21), 75 (100). HRMS calcd. for $C_{13}H_{27}O_4Si$ ($M^+ - CH_3$): 275.1679; found: 275.1672.

Minor, more polar diastereomer: $[\alpha]_D^{20}$ −7.9 (*c* 1.58, $CHCl_3$). ^1H NMR: (500 MHz, $CDCl_3$) δ: 0.065 (s, 6H, $SiMe_2$), 0.89 (s, 9H, Si-*t*Bu), 1.21 (d, 3H, *J* = 6.2 Hz, CH_3CHOH), 1.39, 1.40 (2 × s, 6H, $C(CH_3)_2$), 3.73 (m, 2H, $SiOCH_2$), 3.8 (m, 2H, 2 OCH), 3.94 (m, 1H, *C*HOH). ^{13}C NMR (75 MHz, $CDCl_3$) δ: 109.2, 82.7, 77.6, 67.5, 63.8, 27.3, 27.2, 25.9, 19.7, 18.3, −5.5. MS(EI) *m/z*: 275 ($M^+ - CH_3$, 12%), 245 (5), 187 (8), 175 (35), 157 (14), 131 (92), 117 (58), 99 (27), 83 (21), 75 (100). HRMS calcd. for $C_{13}H_{27}O_4Si$ ($M^+ - CH_3$): 275.1679; found: 275.1692.

(4*S*,5*R*)-4-Acetyl-5-(*tert*-butyldimethylsilyl)oxymethyl-2,2-dimethyl-1,3-dioxolane (5-*O*-(*tert*-butyldimethylsilyl)-3,4-*O*-isopropylidene-1-deoxy-D-xylulose) (23)

To a stirred solution of oxalyl chloride (0.31 mL, 3.6 mmol, 1.2 equiv.) in dry CH_2Cl_2 (6 mL) at −78°C was added dropwise a solution of DMSO (0.5 mL, 7.2 mmol, 2.4 equiv.) in CH_2Cl_2 (3 mL) over 5 min. After stirring for 15 min, a solution of **21** (0.9 g, 3.1 mmol) in dry CH_2Cl_2 (6 mL) was added over 5 min. and stirring was continued for 2 h at −78°C. Triethylamine (1.7 mL, 12 mmol, 4 equiv.) in CH_2Cl_2 (5 mL) was then added to the reaction mixture and the temperature was allowed to rise to room temperature over 1.5 h. The mixture was diluted with 5 volumes anhydrous ether, the solution was filtered through a Celite pad, and the filtrate was concentrated in vacuo. The residual oil was diluted with ether and washed with water (2 × 5 mL) and salt solution (5 mL). The ether layer was dried over $MgSO_4$, filtered, and evaporated. The 5-*O*-(*tert*-butyldimethylsilyl)-3,4-*O*-isopropylidene-1-deoxy-D-xylulose (**23**) so obtained was purified by flash chromatography with 10% ethyl acetate in hexane (Yield 0.7 g). $[\alpha]_D^{20}$ −20.0 (c 2.23, $CHCl_3$). ^1H NMR (500 MHz, $CDCl_3$) δ: 0.09 (s, 6H, $SiMe_2$), 0.9 (s, 9H, Si-*t*Bu), 1.43, 1.46 (2 × s, 6H, $C(CH_3)_2$), 2.29 (s, 3H, $COCH_3$), 3.76 (dd, 1H, *J* = 3.9, 11.3 Hz, CH_2O), 3.88 (dd, 1H, *J* = 3.5, 11.3 Hz, CH_2O), 4.06 (m, 1H, $CHCH_2$), 4.32 (d, 1H, *J* = 7.5 Hz, *C*HCO). ^{13}C NMR (75 MHz, $CDCl_3$) δ: 109.2, 82.7, 77.6, 67.5, 63.8, 27.3, 27.2, 25.9, 19.7, 18.3, −5.5. MS(EI) *m/z*: 288 (M^+, 0.3%), 273 ($M^+ - CH_3$, 3.2) 245 (14),231 (26), 187 (22), 173 (31), 145 (35), 143 (23), 131 (31), 117 (100), 101 (33), 89 (14), 86 (40), 84 (63), 75 (66), 73 (80). HRMS calcd. for $C_{14}H_{28}O_4Si$: 288.1757; found: 288.1784.

(4*S*,5*R*)-4-Acetyl-5-hydroxymethyl-2,2-dimethyl-1,3-dioxolane (3,4-*O*-isopropylidene-1-deoxy-D-xylulose) (26)

*A. By debenzylation of 5-*O*-benzyl-3,4-*O*-isopropylidene-1-deoxy-D-xylulose (22)*

A mixture of the benzyl ether **22** (0.16 g, 0.61 mmol) and pre-equilibrated 10% palladium/carbon (Aldrich, wet Degussa type) (0.1 g) in 95% ethanol (6 mL) was hydrogenated (30, 31) for 3 h at room temperature and atmospheric pressure. The mixture was filtered through Celite, and the filtrate evaporated at reduced pressure to afford a white solid. The solid residue was redissolved in a small amount of MeOH and applied to a column of alumina (neutral, Brockmann, Activity 1), equilibrated with CH_2Cl_2. The column was washed with 5% MeOH in CH_2Cl_2. The product (0.10 g, 95%) slowly formed a semisolid mass upon evaporation of the solvent. $[\alpha]_D^{20}$ −19.2 (*c* 1.83, CH_3OH). ^1H NMR (200 MHz, $CDCl_3$) δ: 1.37 (s, 3H, CH_3), 1.41 (s, 3H, CH_3), 2.25 (s, 3H, CH_3CO), 2.22 – 2.36 (br s, 1H, OH), 3.66 (dd, 1H, *J* = 12.0, 4.1 Hz, O-C*H*H), 3.84 (dd, 1H, *J* = 12.0, 3.4 Hz, O-C*H*H), 4.04 (ddd, 1H, *J* = 7.9, 4.1, 3.4 Hz, O-C*H*-CH_2), 4.20 (d, 1H, *J* = 7.9 Hz, O-C*H*-CO). ^{13}C NMR (50.3 MHz, $CDCl_3$) δ: 209.1, 110.7, 81.6, 78.0, 62.2, 26.7, 26.5, 26.0.

Can. J. Chem, Downloaded from www.nrcresearchpress.com by 80.90.12.36 on 09/08/12
For personal use only.

B. By desilylation of 5-O-(tert-*butyldimethylsilyl*)-*3,4*-O-*isopropylidene-1-deoxy-*D*-xylulose (**23**)*

A 0.4 M solution of **23** (0.1 g) in THF was reacted with a 1 M solution of tetrabutylammonium fluoride (2 equiv.) in THF at 0°C with stirring under nitrogen. The progress of the reaction was monitored by TLC (silica gel, pet. ether – ethyl acetate 7:3). When reaction appeared complete (ca. 1 h) the mixture was concentrated in vacuo and the residue applied to a column of alumina (neutral, Brockmann, Activity III), equilibrated with CH_2Cl_2. The column was washed with two bed volumes of CH_2Cl_2 and was then eluted with two bed volumes each of 1% MeOH in CH_2Cl_2, 2% MeOH in CH_2Cl_2 and 3% MeOH in CH_2Cl_2. The product, obtained in poor yield (20–25%) upon evaporation of the solvent, elutes in the 2% and 3% fractions.

A similarly poor yield of 1-deoxy-D-xylulose (**27**) wa obtained when **23** was simultaneously desilylated and hydrolyzed with aqueous HF.

1-Deoxy-D-xylulose (27)

Method A

Acid hydrolysis of 3,4-*O*-isopropylidene-1-deoxy-D-xylulose (**26**) (100 mg, 0.57 mmol) with 2 M HCl in acetonitrile, following the procedure for the conversion of **22** into **24**, gave 1-deoxy-D-xylulose (**27**) (58 mg, 75%), together with a number of unidentified byproducts that gave discrete spots on TLC. One of these by-products, which was obtained in 10% yield (13 mg), was isolated as a crystalline compound and identified as **30** (see below).

Method B

Hydrogenolysis of 5-*O*-benzyl-1-deoxy-D-xylulose (**24**) (0.50 g, 2.2 mmol) in the presence of Pd/C (see conversion of **22** into **26**) gave 1-deoxy-D-xylulose (**27**) (0.29 g, 97%).

Method C

Boron trichloride (1 M in CH_2Cl_2, Aldrich, 2.4 mL, 2.4 mmol) (27, 28) was added dropwise to a solution of 5-*O*-benzyl-3,4-*O*-isopropylidene-1-deoxy-D-xylulose (**22**) (0.13 g, 0.49 mmol) in CH_2Cl_2 (2 mL) at −78°C. The reaction mixture was warmed to 0°C for 30 min. and then to room temperature for an additional 30 min. Excess BCl_3 was removed under vacuum and 95% aqueous methanol (10 mL) was added and the mixture concentrated. This process was repeated and the crude concentrate chromatographed on neutral alumina (1% MeOH – CH_2Cl_2) to afford a mixture of the cyclized products (**28** and **29**) as an oil (17 mg, 26%).

In aqueous solution, the product exists mainly as the open chain deoxypentulose **27** (66%), together with a 1:1 mixture of the anomeric α and β furanoses **28** and **29** (33%). $[\alpha]_D^{20}$ +22.4 (*c* 1.10, H_2O);[2] (lit. (7) $[\alpha]_D^{21}$ +34 (*c* 1, H_2O)). ^{1}H NMR (200 MHz, D_2O) δ: 1.35, 1.39 (anomers), 2.21 (open chain)(total 3H, 3 s, in the ratio 16:15:67, CH_3), 3.52–3.78 (m, 2H, OCH_2), 4.07–4.33 (m, 2H, CHCH). ^{13}C NMR (50.3 MHz, H_2O) δ: 216.7,79.7, 74.0, 64.7, 28.2.

In methanol solution the product exists mainly as a 1:1 mixture of the two oily cyclized products **28** and **29** (17 mg, 26%). ^{1}H NMR (200 MHz, CD_3OD) δ: 1.27 (s, CH_3), 1.32 (s, CH_3)(anomeric ratio ca. 1:1), 3.19–3.23 (m, 2H, 2(OH)), 3.29–3.33 (m, 4H, 2 × 2(OH)), 3.45–3.74 (m, 4H, 2 × CH_2O), 3.90–4.20 (m, 4H, 2 × (CH, CH)). ^{13}C NMR (50.3 MHz, CD_3OD) δ: 110.4, 105.9; 85.1, 83.8; 79.2. 77.8; 72.8, 71.6; 19.1, 16.9 (ratio of anomers 1:1).

Di-β-1-Deoxy-D-xylulofuranose 2,3′:3,2′-dianhydride (30)

The dimeric compound (**30**) was obtained as colourless crystals in 10% yield as a by-product in the preparation of **27** from **26** by acid hydrolysis (method A). It was recrystallized from methanol/CH_2Cl_2. Melting point: 145–146°C. $[\alpha]_D^{25}$ −55.2 (*c* 1, CH_3OH). ^{1}H NMR (200 MHz, CD_3OD) δ: 1.41 (s, 6H 2×CH_3), 3.60 – 3.70 (m, 4H, 2 × CH_2O), 4.02 (m, 2H, 2 × C*H*OH), 4.12 (d, 2H, *J* = 2.7 Hz, 2 × CH), 4.78 (s, 2H, 2 × OH). ^{13}C NMR (50.3 MHz, CD_3OD) δ: 105.0, 83.0, 77.9, 74.3, 21.6. Anal. calcd. for $C_{10}H_{16}O_6$: C 51.72, H 6.95; found: C 51.09, H 6.84.

Crystal data:

$C_{10}H_{16}O_6$ fw = 232.23

Monoclinic, $a = 6.2580(10)$, $b = 7.999(2)$, $c = 10.547(2)$ Å, β = 90.52(3)°, $V = 527.9(2)$ Å^3, $Z = 2$, $\rho_c = 1.461$ g cm^{-3}, $\mu = 0.121$ mm^{-1} (296(2)° K, MoKα$_1$, λ = 0.71073 Å).

A single crystal of **30** (0.40 × 0.25 × 0.08 mm^3) was glued to a glass fibre. X-ray diffraction data were collected on a Siemens P4 diffractometer with a Mo rotating anode. Variable speed scans (4° – 60°/min in ω, 0.37° in ω on either side of the Kα split) were used for θ–2θ scans of the full sphere of reflections in the range $3.5° < 2\theta < 60.0°$. Three standard reflections were measured after every 97 measurements. No decay was observed. 3386 reflections were collected, and 186 low-angle reflections were recollected at lower power to determine the intensities of several reflections that had overflowed the counter (scale factor = 6.5). Merging of the data resulted in 2953 independent reflections ($R_{int} = 0.019$). Absorption and extinction corrections were not required.

The SHELXTL programs (32) were used for structure solution, refinement, and preparation of diagrams and tables. Direct methods provided a model of all non-hydrogen atoms in the polar space group $P2_1$. Anisotropic refinement and a difference Fourier synthesis revealed all hydrogen atoms, which were subsequently refined isotropically. Full-matrix weighted least-squares refinement on F^2 of 209 parameters using 2953 reflections with $F^2 > -3\sigma$ gave a goodness of fit $S = 1.043$ and a $wR2 = 0.088$, where $S = [\Sigma[w(F_o^2 - F_c^2)^2]/(m-n)]^{1/2}$ for *m* reflections and *n* parameters; $wR2 = [\Sigma[w(F_o^2 - F_c^2)^2]/\Sigma[w(F_o^2)^2]]^{1/2}$; and $w = 1/[\Sigma^2(F_o^2) + (0.0597P)^2]$, $P = [\max(0,F_o^2)/3] + [2F_c^2/3]$.

The traditional *R* equals 0.035, for all values of *F*. The largest difference peak and hole were 0.226 and −0.192 e/Å^3. The absolute configuration of **30** follows from that of its precursor (**27**) whose synthesis from starting materials of known absolute configuration is here described. Scattering factors (33) and anomalous scattering corrections (34) were taken from International Tables for Crystallography, Vol. C.[3]

[2] The value of $[\alpha]_D$ was found to vary from preparation to preparation, due to variation in the proportions of the open chain (**27**) and furanose (**28, 29**) forms that were present.

[3] Tables of bond lengths and angles, of anisotropic temperature factors, of hydrogen atom parameters, of torsion angles, and of least-squares planes may be purchased from: The Depository of Unpublished Data, Document Delivery, CISTI, National Research Council Canada, Ottawa, Canada K1A 0S2.

Tables of bond lengths, bond angles, and hydrogen atom parameters have also been deposited with the Cambridge Crystallographic Data Centre, and can be obtained on request from The Director, Cambridge Crystallographic Data Centre, University Chemical Laboratory, 12 Union Road, Cambridge, CB2 1EZ, U.K.

Can. J. Chem. Downloaded from www.nrcresearchpress.com by 80.90.12.36 on 09/08/12
For personal use only.

Synthesis of [2,3-$^{13}C_2$]-1-deoxy-D-xylulose (14)

The starting materials, ethyl [1,2-$^{13}C_2$]bromoacetate (Cambridge Isotopes), triethyl [1,2-$^{13}C_2$]phosphonoacetate (**2**) (Aldrich), and *O*-benzylglycolaldehyde (benzyloxyacetaldehyde (Aldrich)) (**1**), were commercial products. Ethyl [1,2-$^{13}C_2$]bromoacetate was converted into triethyl [1,2-$^{13}C_2$]phosphonoacetate (**2**) in 95% yield by a published method (11).[4] Each step in the synthetic sequence leading to the labeled end product was performed repeatedly on a small scale. The products of individual preparations of a given intermediate were combined for the next step, when necessary. A total of 10 g **2** was converted into 0.95 g **14**, a net yield of 16%.

Triethyl [1,2-$^{13}C_2$]phosphonoacetate (2): bp 100–102°C at 0.6 torr (lit. (11) bp 109–109.5°C at 0.8 torr). ^{1}H NMR (200 MHz, $CDCl_3$) δ: 1.25 (t, 3H, J = 7.1 Hz, ester CH_2CH_3), 1.31 (t, 6H, J = 7.1 Hz, 2(PO-CH_2CH_3)), 2.92 (ddd, 2H, $^1J_{^{13}C,H}$ = 128.9 Hz, $J_{P,H}$ = 21.6 Hz, $^2J_{^{13}C,H}$ = 7.4 Hz, $^{13}CH_2{}^{13}CO$), 4.06 – 4.23 (m, 6H, 3(OCH_2CH_3)). ^{13}C NMR (50.3 MHz, $CDCl_3$) δ: 165.8 (dd, $J_{^{13}C,^{13}C}$ = 58.4 Hz, $J_{^{13}C,P}$ = 7.0 Hz), 62.7, 62.6, 61.5, 34.3 (dd, $J_{^{13}C,P}$ = 134.5 Hz, $J_{^{13}C,^{13}C}$ = 58.4 Hz), 16.3, 16.2, 14.0.

*Ethyl [1,2-$^{13}C_2$]-4-benzyloxy-*E*-but-2-enoate (3) (17–19)*

Triethyl [1,2-$^{13}C_2$]phosphonoacetate (**2**) (2.0 g, 8.9 mmol, Aldrich) in benzene (6 mL) was added dropwise over 20 min to a suspension of NaH (220 mg, 9 mmol) in benzene (30 mL) at 22°C. The mixture was stirred for 1.5 h at 22°C and *O*-benzylglycolaldehyde (**1**) (1.35 g, 9.0 mmol, Aldrich) in benzene (5 mL) was added dropwise over 10 min. A gelatinous precipitate began to form as the aldehyde was added. The mixture was stirred for 3 h, water was added, and the layers separated. The aqueous layer was washed with ether (3×) and the combined organic extracts were dried over $MgSO_4$. Concentration followed by chromatography (5% ether – hexanes) on silica gel (230–400 mesh) gave **3** (1.5 g, 78%) as a colourless oil. ^{1}H NMR (200 MHz, $CDCl_3$) δ: 1.25 (t, 3H, J = 7.1 Hz, O-CH_2CH_3), 4.10–4.23 (m, 4H, CH_2-CH=, O-CH_2CH_3), 4.52 (s, 2H, CH_2-C_6H_5), 6.11 (tddd, 1H, $J_{^{13}C,H}$ = 164.0 Hz, $^3J_{H,H}$ = 15.8 Hz, $^2J_{^{13}C,H}$ = 3.3, $^2J_{H,H}$ = 2.0 Hz, ^{13}C-H), 6.88–7.05 (m, 1H, C-H), 7.27–7.34 (m, 5 H, C_6H_5). ^{13}C NMR (50.3 Hz, $CDCl_3$) δ: 166.2 (d, J = 75.49 Hz), 144.1 (d, J = 70.5 Hz), 137.6, 128.4 (2×), 127.7, 127.5 (2×), 121.3 (d, J = 75.5 Hz), 72.6, 68.5 (d, J = 6.0 Hz), 60.3, 14.2. MS (EI) *m/z*: 222 (M^+, 1%), 193 (2), 110 (10), 91 (100); (CI) *m/z*: 240 ($M^+ + NH_3$, 100%), 223 ($M^+ + 1$, 16). HRMS calcd. for $^{13}C_2C_{11}H_{16}O_3$: 222.1166; found: 222.1166.

*[1,2-$^{13}C_2$]-4-Benzyloxy-*E*-but-2-en-1-ol (4) (19)*

Diisobutyl aluminium hydride (21) (1.5 M solution in toluene, Aldrich, 9.4 mL, 14.1 mmol) was added dropwise over 10 min to a solution of **3** (1.25 g, 5.6 mmol) in methylene chloride (30 mL) at 0°C (cf. ref. 21). After stirring for 6 h, excess methanol was added while the temperature was maintained between 0 and 5°C. The resulting white gelatinous precipitate was filtered through celite, washed with hot methanol, and the filtrate was concentrated. Chromatography (20% ethyl acetate – petroleum ether) on silica gel (230–400 mesh) gave **4** (1.0 g, 99%) as a colourless oil. ^{1}H NMR (200 MHz, $CDCl_3$) δ: 1.38 (br s, 1H, OH), 4.12 (dm, 2H, J = 148.4 Hz, $^{13}CH_2$-O), 5.89 (dm, 1H, J = 148.9 Hz, =^{13}CH), 5.74–5.90 (m, 1H, =CH), 7.26–7.39 (m, 5 H, C_6H_5). ^{13}C NMR (50.3 MHz, $CDCl_3$) δ: 138.1, 132.2 (d, J = 45.9 Hz), 128.4 (2×), 127.7 (2×), 127.6, 72.3, 70.1, 62.9 (d, J = 46.0 Hz). MS (CI) *m/z*: 198 ($M^+ + NH_3$, 100%), 163 ($M^+ + H - H_2O$, 11).

[1,2-$^{13}C_2$]-(2R,3R)-4-Benzyloxy-2,3-epoxybutan-1-ol ([1,2-$^{13}C_2$]-(2R,3R)-4-benzyloxymethyl-2-hydroxymethyl-2,3-oxirane) (5) (12, 19, 22)

To a solution of methylene chloride (80 mL) at −20°C was added sequentially titanium tetraisopropropoxide (2.8 mL, 9.35 mmol) and D-(−)-diisopropyl tartrate (2.5 mL, 11.7 mmol) in methylene chloride (5 mL) and the mixture stirred for 10 min. [1,2-$^{13}C_2$]-4-Benzyloxy-*E*-but-2-en-1-ol (**4**) (1.5 g, 8.3 mmol) in methylene chloride (5 mL) was added and the mixture stirred for 2 h at −20°C and then stored overnight at −18°C. After 18 h, aqueous saturated Na_2SO_4 solution (8 mL) and ether (8 mL) were added to the reaction mixture, which was stirred for 1 h at 22°C. After filtration through Celite, the filtrate was concentrated and diluted with ether (63 mL). 1 N NaOH solution (14 mL) was added to the ethereal solution and the resulting mixture stirred 30 min at 0°C. The ether layer was separated and the aqueous layer washed with ether (2×). The combined ether extracts were washed with brine, dried, and concentrated. Chromatography (20% ethyl acetate – petroleum ether) on silica gel (230–400 mesh) gave **5** as a colourless oil (1.4 g, 86%). $[\alpha]_D^{20}$ +28.8 (*c* 1.68, CH_2Cl_2) (lit. (14) $[\alpha]_D^{22}$ of enantiomer: −21 (*c* 0.97, $CHCl_3$)). ^{1}H NMR (200 MHz, $CDCl_3$) δ: 2.13 (br s, 1H, OH), 2.60–3.37 (m, 2H, O-CH, O-CH*H*), 3.43–3.79 (m, 3H, $^{13}CH_2$-OH, O-C*H*H), 3.90–4.41 (m, 1H, O-^{13}CH), 4.57 (AB q, 2H, J = 12.1 Hz, O-CH_2), 7.32–7.38 (m, 5H, C_6H_5). ^{13}C NMR (50.3 MHz, $CDCl_3$) δ: 137.7, 128.4 (2×), 127.7 (2×), 73.3, 69.6, 61.1 (d, J = 46.2 Hz), 55.7 (d, J = 46.2 Hz), 54.4. MS (EI) *m/z*: 195 (M^+ − H, 5%), 177 (3), 107 (92), 91 (100); (CI) *m/z*: 214 ($M^+ + NH_3$, 100%). HRMS calcd. for $^{13}C_2C_9H_{13}O_3$ (M^+ − H): 195.0932; found: 195.0962.

[1,2-$^{13}C_2$]-(2R,3R)-4-Benzyloxy-1-phenylthiobutane-2,3-diol (6) (12)

A solution of the epoxide **5** (580 mg, 3.0 mmol) in *tert*-butanol (15 mL) was mixed with a 0.5 M NaOH solution (15 mL, 7.5 mmol) and nitrogen gas was passed vigorously through the mixture for 40 min. The mixture was then heated to reflux in a nitrogen atmosphere and thiophenol (400 μL, 40 mmol) in *tert*-butanol (3 mL) was added over 3 h by syringe pump. The reaction mixture was cooled to room temperature, the layers were separated, and the aqueous layer was washed with methylene chloride (3 × 5 mL). The combined organic extracts were washed successively with 1 N NaOH solution, water, and brine, dried over $MgSO_4$, and concentrated to afford the crude diol as a solid. Recrystallization from methylene chloride and hexanes affords **6** as white needles, mp 102–103°C (470 mg, 52%). $[\alpha]_D^{20}$ −22.2 (*c* 1.11, CH_2Cl_2) (lit. (12) $[\alpha]_D^{25}$ of enantiomer: +40.3 (*c* 0.77, EtOH)). ^{1}H NMR (200 MHz, $CDCl_3$) δ: 2.55–3.00 (m, 3H, $^{13}CHHSC_6H_5$, 2(OH)), 3.29–3.36 (m, 1H, CH*H*SC_6H_5), 3.55–4.10 (m, 4H, O-CH_2, 2(O-CH)), 4.53 (s, 2H, O-CH_2-C_6H_5), 7.14–7.39 (m, 10H, 2(C_6H_5)). ^{13}C NMR (50.3 MHz, $CDCl_3$) δ: 135.0, 129.8 (2×), 129.0 (2×), 128.5 (2×), 127.9 (2×), 127.8 (2×), 126.6, 73.6,

[4] Literature references in this section refer to non-enriched (and in one case (19) singly enriched) compounds.

Can. J. Chem. Downloaded from www.nrcresearchpress.com by 80.90.12.36 on 09/08/12
For personal use only.

71.9, 70.3 (d, J = 38.22 Hz), 38.0 (d, J = 38.22 Hz). MS (EI) *m/z*: 306 (M^+, 15%), 167 (20), 124 (43), 91 (100). HRMS calcd. for $^{13}C_2C_{15}H_{20}O_3S$: 306.1200; found: 306.1208.

[4,4′-$^{13}C_2$]-(4R,5R)-5-Benzyloxymethyl-4-phenylthiomethyl-2,2-dimethyl-1,3-dioxolane ([3,4-$^{13}C_2$]-(2R,3R)-2,3-O-isopropylidene-1-benzyloxy-4-phenylthiobutane-2,3-diol, ([3,4-$^{13}C_2$]-(2R,3R)-2,3-O-isopropylidene-1-benzyl-4-phenylthiobutan-1,2,3-triol) (7) (12)

Diol **6** (320 mg, 1.0 mmol) in methylene chloride (10 mL) was treated with 2,2-dimethoxypropane (250 μL, 2.2 mmol) and phosphorus oxychloride (1 drop) was added. The solution was stirred overnight at 22°C. 15% Aqueous NaOH solution (5 drops) was added and the mixture stirred for 30 min. After adding water, the layers were separated and the organic fraction dried and concentrated to afford **7** as a colourless oil (360 mg, 99%). A small amount of the product was chromatographed (5% ether – petroleum ether) on silica gel (230 – 400 mesh) for analysis. Compound **7** slowly reverts to **6** when kept in the refrigerator for several days. $[\alpha]_D^{20}$ −2.27 (c 1.01, CH_2Cl_2). ^{1}H NMR (200 MHz, $CDCl_3$) δ: 1.34 (s, 3H, CH_3), 1.46 (s, 3H, CH_3), 3.31 (dm, 2H, J = 77.5 Hz, $^{13}CH_2$-S-C_6H_5), 3.53 – 3.64 (m, 2H, O-CH_2), 4.31 (dm, 1H, J = 150.4 Hz, O-^{13}CH), 4.31 – 4.37 (m, 1H, O-CH), 4.56 (AB q, 2H, J = 12.0 Hz, O-$CH_2C_6H_5$), 7.17 – 7.37 (m, 10 H, 2(C_6H_5)). ^{13}C NMR (50.3 MHz, $CDCl_3$) δ: 137.6, 135.9, 129.4 (2×), 128.9 (2×), 128.4 (2×), 127.8 (2×), 126.2 (2×), 108.8, 76.1, 75.7 (d, J = 40.39), 73.6, 68.4, 39.9 (d, J = 40.39), 28.0, 25.4. MS (EI) *m/z*: 346 (M^+, 7%), 199 (5), 167 (25), 109 (12), 91 (100). HRMS calcd. for $^{13}C_2C_{18}H_{24}O_3S$: 346.1513; found: 346.1523.

[4,4′-$^{13}C_2$]-(4R,5R)-5-Benzyloxymethyl-4-phenylthiomethyl-2,2-dimethyl-1,3-dioxolane sulfoxide ([3,4-$^{13}C_2$]-(2R,3R)-2,3-O-isopropylidene-1-benzyloxy-4-phenylthiobutane-2,3-diol sulfoxide) (8) (12)

m-Chloroperoxybenzoic acid (50–55%, 200 mg, ca. 0.58 mmol) dissolved in methylene chloride (6 mL) was added from a dropping funnel to **7** (200 mg, 0.58 mmol) in methylene chloride (6 mL) at −20°C. After stirring for 1 h, the mixture was washed with 1 N NaOH solution (2×), water (2×), and brine, dried ($MgSO_4$), and concentrated to afford the oily product (206 mg, 99%) as a mixture of diastereomers. This product was used without further purification for the next step. When the preparation of the sulfoxide is carried out on a large scale (>1 g starting material) further oxidation takes place and a significant amount of the sulfone (>5%) is formed as a by-product. ^{1}H NMR (200 MHz, $CDCl_3$) δ: 1.29, 1.42, 1.43, 1.49 (s, 6H, 2(CH_3)), 2.31 – 3.20 (m, 2H, $^{13}CH_2$-S), 3.24 – 3.75 (m, 2H, O-CH_2), 4.18 – 4.61 (m, 3H, O-^{13}CH, O-$CH_2C_6H_5$), 4.93 – 5.12 (m, 1H, O-CH), 7.14 – 7.71 (m, 10 H, 2(C_6H_5)). ^{13}C NMR (50.3 MHz, $CDCl_3$) δ: 137.7, 131.2, 131.1, 129.2 (2×), 129.0 (2×), 128.3 (2×), 128.2 (2×), 127.7 (2×), 124.6 (2×), 123.6, 108.7, 108.6, 76.0, 75.4, 75.2, 73.4, 73.2, 71.5 (d, J = 39.9 Hz), 70.5 (d, J = 40.0 Hz), 68.2, 66.7, 66.1, 59.6 (d, J = 40.1 Hz), 57.6 (d, J = 40.0 Hz), 27.7, 25.2. MS (EI) *m/z*: 363 (M^+ + 1, 1%), 237 (16), 125 (52), 91 (100). HRMS calcd. for $^{13}C_2C_{18}H_{25}O_4S$ (M^+ + 1): 363.1550; found: 363.1533.

[4,4′-$^{13}C_2$]-(4R,5R)-5-Benzyloxymethyl-4-(α-RS-α-acetoxy-α-phenylthio)methyl-2,2-dimethyl-1,3-dioxolane ([3,4-$^{13}C_2$]-(2R,3R)-2,3-O-isopropylidene-1-benzyloxy-4-phenylthio-4-acetoxybutane-2,3-diol) (9) (12)

Sodium acetate (2.70 g, 33 mmol) was added to **8** (2.10 g, 5.8 mmol) dissolved in acetic anhydride (50 mL) and the mixture refluxed under nitrogen for 8 h. After cooling to room temperature, the reaction mixture was washed successively with saturated $NaHCO_3$ solution, water, and brine, dried ($MgSO_4$), and concentrated. Chromatography (10% ether – hexanes) afforded the oily product **9** (1.65 g, 73%) as a 5:1 mixture of diastereo-mers. ^{1}H NMR (200 MHz, $CDCl_3$) δ: 1.32, 1.46, 1.48 (s, 6H, 2(CH_3)), 1.90, 2.06 (1:4.7) (s, 3H, $COCH_3$), 3.52–3.80 (m, 2H, O-CH_2), 4.28 (dm, 1H, J = 143.5 Hz, O-^{13}CH), 4.37 (m, 1H, O-CH), 5.59 (m, 2H, O-$CH_2C_6H_5$), 6.12 (dm, 1H, J = 143.5 Hz, ^{13}CH-S), 7.26–7.50 (m, 10 H, 2(C_6H_5)). ^{13}C NMR (50.3 MHz, $CDCl_3$) δ: 169.0, 137.5, 134.5, 133.5 (2×), 130.7, 128.2 (3×), 128.6, 128.5 (2×), 128.3 (2×), 128.1, 127.7, 127.5, 109.2, 81.9, 80.6, 79.6, 79.1, 78.2, 77.3, 76.8, 76.6, 75.6, 73.3, 66.1, 27.0, 25.3, 24.8, 20.9. MS (EI) *m/z*: 404 (M^+, 1%), 344 (4), 295 (3), 145 (53), 91 (100); (CI) *m/z*: 422 (M^+ + NH_3, 18%), 354 (100).

[4,4′-$^{13}C_2$]-(4R,5R)-5-Benzyloxymethyl-4-formyl-2,2-dimethyl-1,3-dioxolane ([1,2-$^{13}C_2$]-4-O-benzyl-2,3-O-isopropylidene-D-threose, [1,2-$^{13}C_2$]-(2S,3R)-4-O-benzyl-2,3-O-isopropylidene-2,3,4-trihydroxybutanal, [4,4′-$^{13}C_2$]-(2S,3R)-5-(phenylmethoxy)methyl]-2,2-dimethyl-1,3-dioxolane-4-carboxaldehyde) (10) (23)

Potassium carbonate (1.30 g, 9.0 mmol) was added to a solution of **9** (1.50 g, 3.8 mmol) in methanol (50 mL) and the mixture stirred overnight at 22°C. Under these conditions hydrolysis of the acetoxy phenylthio function is accompanied by inversion (13, 23). The solvent was removed in vacuo, methylene chloride (15 mL) was added, and the mixture was washed with 0.5 N NaOH solution (2×) and brine. Drying ($MgSO_4$) followed by concentration gave the crude aldehyde **10** (940 mg, 99%), which was used without further purification since it is reported (16) that the intensity of the CHO proton signal drops to one half after 12 h. ^{1}H NMR (200 MHz, $CDCl_3$) δ: 1.41 (s, 3H, CH_3), 1.48 (s, 3H, CH_3), 3.30–3.90 (m, 3H, O-^{13}CH, O-CH_2), 4.15–4.32 (m, 1H, O-CH), 4.59 (s, 2H, $CH_2C_6H_5$), 7.28–7.34 (m, 5 H, C_6H_5), 9.73 (ddd, 1H, J = 178.0 Hz, 26.0 Hz, 1.40 Hz, ^{13}CHO).

[4,4′-$^{13}C_2$]-(4R,5R)-5-Benzyloxymethyl-4-(2′-(RS)-4-hydroxyethyl-2,2-dimethyl-1,3-dioxolane ([2,3-$^{13}C_2$]-5-O-benzyl-3,4-O-isopropylidene-1-deoxy-D-xylitol plus [2,3-$^{13}C_2$]-5-O-benzyl-3,4-O-isopropylidene-1-deoxy-D-lyxitol) (11)

Grignard methylation of [1,2-$^{13}C_2$]-4-*O*-benzyl-2,3-*O*-isopropylidene-D-threose (**10**) and work-up was carried out, starting with 900 mg (3.6 mmol) **10** as described for the unlabeled compound (**18** → **20**). Yield 870 mg (91%). Ratio of diastereomers 2.5:1. ^{1}H NMR (200 MHz, $CDCl_3$) δ: 1.20 (m, 6H, 2(CH_3)), 1.33, 1.34 (s, 3H, $^{13}CHCH_3$, 2.5:1), 2.80 (br s, 1H, OH), 3.21–3.72 (m, 3H, O-CH_2, O-CH), 3.91–4.22 (m, 2H, O-^{13}CH, ^{13}CH-OH), 4.53 (s, 2H, $CH_2C_6H_5$), 7.26–7.29 (m, C_6H_5). ^{13}C NMR (50.3 MHz, $CDCl_3$) δ: 137.7, 137.5, 128.4 (2×), 127.8 (2×), 127.6, 109.1, 109.0, 82.9 (d, J = 42.8), 82.3 (d, J = 40.8), 81.9, 81.2, 73.6, 67.8 (d, J = 42.3), 67.5 (d, J = 40.8), 27.1, 26.9, 19.9, 19.7. MS (EI) *m/z*: 268 (M^+, 0.5%), 269 (M^+ + H, 6), 253 (54), 210 (20), 91 (100); (CI) *m/z*: 286 (M^+ + NH_3, 30%), 268 (9). HRMS calcd. for $^{13}C_2C_{13}H_{23}O_4$ (M^+ + H): 269.1663; found: 269.1664.

[2,3-$^{13}C_2$]-5-O-Benzyl-3,4-O-isopropylidene-1-deoxy-D-xylulose ([4,4'-$^{13}C_2$]-(4S,5R)-4-acetyl-5-benzyloxymethyl-2,2-dimethyl-1,3-dioxolane) (12)

Oxidation of **11** and work-up was carried out, starting with 1.40 g (5.3 mmol) **11**, as described for the unlabeled compound (**20** → **22**). Yield 1.30 g (93%). $[\alpha]_D^{20}$ −17.4 (*c* 1.50, CH_2Cl_2). ^{1}H NMR (200 MHz, $CDCl_3$) δ: 1.41 (s, 3H, CH_3), 1.45 (s, 3H, CH_3), 2.24 (d, 3H, *J* = 4.0 Hz, $CH_3{}^{13}CO$), 3.59–3.82 (m, 3H, O-CH_2, O-^{13}CH), 4.14–4.21 (m, 1H, O-CH), 4.58 (s, 2H, $CH_2C_6H_5$), 7.29–7.32 (m, 5H, C_6H_5). ^{13}C NMR (50.3 MHz, $CDCl_3$) δ: 208.2 (d, *J* = 45.9 Hz), 137.7, 128.2 (2×), 127.5 (2×), 110.9, 81.7 (d, *J* = 45.9 Hz), 77.0, 73.4, 70.1, 26.8, 26.1 (2×). MS (EI) *m/z*: 266 (M^+, 3%), 222 (11), 91 (100); (CI) *m/z*: 284 ($M^+ + NH_3$, 94%), 267 (M^+ + H, 70), 209 (100). HRMS calcd. for $^{13}C_2C_{13}H_{20}O_4$: 266.1428; found: 266.1425.

[2,3-$^{13}C_2$]-5-O-Benzyl-1-deoxy-D-xylulose (13)

Hydrolysis of 5-*O*-benzyl-3,4-*O*-isopropylidene-1-deoxy-D-xylulose (**12**) (600 mg, 2.3 mmol) and work-up was carried out as described for the unlabeled compound (**22** → **24**). Yield 460 mg (90%). $[\alpha]_D^{20}$ 50.43 (*c* 1.25, CH_2Cl_2). ^{1}H NMR (200 MHz, $CDCl_3$) δ: 2.23 (dd, 3H, *J* = 6.04 Hz, 1.27 Hz, $CH_3{}^{13}CO$), 2.8 (br s, 1H, OH), 3.39 (s, 1H, OH), 3.57–3.60 (m, 2H, O-CH_2), 3.78–4.22 (m, 2H, O-^{13}CH, O-CH), 4.53 (s, 2H, $CH_2C_6H_5$), 7.24–7.37 (m, 5 H, C_6H_5). ^{13}C NMR (50.3 MHz, $CDCl_3$) δ: 208.1 (d, *J* = 39.1 Hz), 137.4, 128.2 (2×), 127.6 (3×), 77 (d, *J* = 39.4 Hz), 73.3, 70.7, 70.5, 25.5. MS (EI) *m/z*: 227 (M^+ + H, 2%), 226 (M^+, 0.5), 136 (5), 91 (100); (CI) *m/z*: 244 ($M^+ + NH_3$, 100). HRMS calcd. for $^{13}C_2C_{10}H_{17}O_4$ (M^+ + H): 227.1194; found: 227.1192.

[2,3-$^{13}C_2$]-1-Deoxy-D-xylulose (14)

Hydrogenolysis of the benzyl ether **13** (300 mg, 1.3 mmol) in the presence of 10% palladium/carbon, as described for the unlabeled compound (**24** → **27**), gave [2,3-$^{13}C_2$]-1-deoxy-D-xylulose (**14**) in quantitative yield (180 mg) as a colourless oil. ^{1}H NMR (200 MHz, CD_3OD) δ: 1.23–1.37 (m, 3H, $CH_3{}^{13}$C-OH), 2.16 (dd, 3H, *J* = 6.1 Hz, 4.9 Hz, $CH_3{}^{13}CO$) ($CH_3{}^{13}$C-OH:$^{13}COCH_3$ = 2.1:1), 3.15–3.23 (m, 2H, 2(OH)), 3.24–4.6 (m, 5 H, CH-^{13}CH, O-CH_2, OH). ^{1}H NMR (200 MHz, D_2O) δ: 1.30–1.34 m, 3H, $CH_3{}^{13}$C-OH), 2.17 (d, *J* = 4.66 Hz, $CH_3{}^{13}CO$) ($CH_3{}^{13}$C-OH:$CH_3{}^{13}CO$ = 1:1.5), 3.40–4.41 (m, 4H, O-CH_2, ^{13}CH-CH). ^{13}C NMR (50.3 MHz, CD_3OD) δ: 212.2 (d, *J* = 41.4 Hz), 110.6 (d, *J* = 49.5 Hz), 105.8 (d, *J* = 46.4 Hz), 85.1 (d, *J* = 47.0 Hz), 83.6 (d, *J* = 48.9 Hz), 78.4 (d, *J* = 41.4 Hz), 77.6, 72.6, 71.2, 19.1, 16.8, 16.6. ^{13}C NMR (50.3 MHz, D_2O) δ: 213.1 (d, *J* = 40.6 Hz), 109.4 (d, *J* = 48.5 Hz) 105.5 (d, *J* = 47.1 Hz), 82.7 (d, *J* = 46.9 Hz), 81.3 (d, *J* = 46.5 Hz), 77.2 (d, *J* = 41.2 Hz), 78.3, 72.8, 71.8, 16.9, 14.8. MS (CI) *m/z*: 154 ($M^+ + NH_3$, 90%), 136 (M^+, 100), 119 (70), 101 (36).

Acknowledgment

This investigation was supported by a research grant (GM50778) (to I.D.S) from the National Institute of General Medical Sciences, U.S. Public Health Service, which is gratefully acknowledged.

References

1. L. Slechta and L.E. Johnson. J. Antibiot. **29**, 685 (1976).
2. H Hoeksema and L. Baczynskij. J. Antibiot. **29**, 688 (1976).
3. A. Yokota and K. Sasajima. Agric. Biol. Chem. **48**, 149 (1984).
4. A. Yokota and K. Sasajima. Agric. Biol. Chem. **50**, 2517 (1986).
5. M.L. Wolfrom and R.B. Bennett. J. Org. Chem. **30**, 458 (1965).
6. A. Ishizu, K. Yoshida, and N. Yamazaki. Carbohydr. Res. **23**, 23 (1972).
7. S. David, B. Estramareix, J.-C. Fischer, and M. Therisod. J. Chem. Soc. Perkin Trans. 1, 2131 (1982).
8. R.E. Hill, B.G. Sayer, and I.D. Spenser. J. Am. Chem. Soc. **111**, 1916 (1989).
9. T. Shono, Y. Matsumura, H. Hamaguchi, and S. Naitoh. J. Org. Chem. **48**, 5126 (1983).
10. R.E. Hill, B.G. Sayer, and I.D. Spenser. J. Chem. Soc. Chem. Commun. 612 (1986).
11. J. Wolinsky and K.L. Erickson. J. Org. Chem. **30**, 2208 (1965).
12. T. Katsuki, A.W.M. Lee, P. Ma, V.S. Martin, S. Masamune, K.B. Sharpless, D. Tuddenham, and F.J. Walker. J. Org. Chem. **47**, 1373 (1982).
13. S.Y. Ko, A.W.M. Lee, S. Masamune, L.A. Reed III, K.B. Sharpless, and F.J. Walker. Tetrahedron, **46**, 245 (1990).
14. E. Hungerbühler and D. Seebach. Helv. Chim. Acta, **64**, 687 (1981).
15. T. Mukaiyama, K. Suzuki, and T. Yamada. Chem. Lett. 929 (1982).
16. T. Mukaiyama, K. Suzuki, T. Yamada, and F. Tabusa. Tetrahedron, **46**, 265 (1990)
17. G. Solladie, C. Frechou, J. Hutt, and G. Demailly. Bull. Soc. Chim. Fr. 827 (1987).
18. G. Solladie, J. Hutt, and C. Frechou. Tetrahedron Lett. **28**, 61 (1987).
19. Y. Yabe, D. Guillaume, and D.H. Rich. J. Am. Chem. Soc. **110**, 4043 (1988).
20. J. Villieras, M. Rambaud, and M. Graff. Tetrahedron Lett. **26**, 53 (1985).
21. E. Winterfeldt. Synthesis, 617 (1975).
22. K.C. Nicolaou, R.A. Daines, J. Uenishi, W.S. Li, D.P. Papahatjis, and T.K. Chakraborty. J. Am. Chem. Soc. **110**, 4672 (1988).
23. A.W.M. Lee, V.S. Martin, S. Masamune, K.B. Sharpless, and F.J. Walker. J. Am. Chem. Soc. **104**, 3515 (1982).
24. E.J. Corey and G. Schmidt. Tetrahedron Lett. 399 (1979).
25. H. Iida, N. Yamazaki, and Ch. Kibayashi. J. Org. Chem. **52**, 3337 (1987).
26. A.J. Mancuso, S.-L. Huang, and D. Swern. J. Org. Chem. **43**, 2480 (1978).
27. D.R. Williams, D.L. Brown, and J.W. Benbow. J. Am. Chem. Soc. **111**, 1923 (1989).
28. T.J. Tewson and M.J. Welch. J. Org. Chem. **43**, 1090 (1978).
29. C.C. Wei, S. De Bernardo, J.P. Tengi, J. Borgese, and M. Weigele. J. Org. Chem. **50**, 3462 (1985).
30. C.H. Heathcock and R. Ratcliffe. J. Am. Chem. Soc. **93**, 1746 (1971).
31. J.S. Bindra and A. Grodski. J. Org. Chem. **43**, 3240 (1978).
32. G. Sheldrick. SHELXTL, v5. Crystallographic software package. Siemens Industrial Automation, Inc., Madison, Wis. 1994.
33. A.J.C. Wilson (*Editor*). International tables for crystallography. Vol. C. Kluwer Academic Publishers, Dordrecht. 1992. Table 6.1.1.4.
34. A.J.C. Wilson (*Editor*). International tables for crystallography. Vol. C. Kluwer Academic Publishers, Dordrecht. 1992. Table 4.2.6.8.

Can. J. Chem. Downloaded from www.nrcresearchpress.com by 80.90.12.36 on 09/08/12
For personal use only.

Comparison of calcium complexation of some carboxylic acids derived from D-glucose and D-fructose

Hélène Bazin, Alain Bouchu, Gérard Descotes, and Michelle Petit-Ramel

Abstract: The aim of this work was to compare calcium sequestering behaviour of 11 carboxylic acids derived from carbohydrates, and to study the influence of molecular structure on the calcium complexation. For this purpose, various carboxylic acids derived from methyl D-glucopyranoside, methyl D-fructopyranoside, and methyl D-fructofuranoside were synthesized and studied using an ion selective electrode to determine calcium complex formation constants. Complexation sites of carbohydrate skeletons were determined using ^{13}C NMR.

Key words: Ca(II) complexation, carboxylic acids, fructofuranosides, fructopyranosides, glucopyranosides.

Résumé : Le but de ce travail est de comparer la complexation des ions calcium de 11 dérivés carboxyliques de sucres, et d'étudier l'influence de leur structure moléculaire sur cette complexation. Pour cela, divers acides carboxyliques dérivés des D-glucopyranoside, D-fructopyranoside et D-fructofuranoside de méthyle ont été synthétisés. Les constantes des équilibres de complexation ont été determinées à l'aide d'une électrode sélective réversible aux ions calcium. Les sites de complexation des squelettes sucres ont été déterminés par rmn ^{13}C.

Mots clés : complexation du Ca(II), acides carboxyliques, fructofuranosides, fructopyranosides, glucopyranosides.

Introduction

It is well known that the use of sodium tripolyphosphate (STP) in detergent formulations as a calcium and magnesium sequestering agent is subject to regulation because it leads to eutrophication of surface waters including lakes and seas (1–5). For this reason, extensive studies have been carried out with the aim of finding an alternative for STP that meets all requirements. The main demands of such substitutes are good sequestration (Ca and Mg), good biodegradability/biocompatibility, low price, good solubility in water, and nontoxicity.

Up to now the intensive search for substitutes for STP has resulted in only a few systems meeting the technical, commercial, and environmental requirements. These substitutes include complexing agents (nitrilotriacetate (NTA) and citrate), a precipitating agent (sodium carbonate), and an inorganic ion exchanger (zeolite NaA).

The now commonly used alternative for STP is zeolite NaA (6–9), an inorganic ion exchanger that has several attractive properties: it is cheap, the calcium binding is satisfactory, and the substance is nontoxic. However, there are also some drawbacks involved in its use, namely, low solubility in water and slow binding of magnesium, especially at lower washing temperatures (6, 9, 10). Moreover, deposits (incrustations) formed on the fabrics during the washing process do not dissolve. In view of these negative aspects, a so-called cobuilder is added, which prevents the formation of incrustation and acts as a carrier, transporting the calcium and the magnesium ions to the zeolite NaA (9).

Polyacrylate and copolymers of acrylate and maleate are widely used for this purpose and they generally show optimal performance for incrustation inhibition. These copolymers are reported to be physiologically safe (11) but they are not biodegradable, which makes their long-term application unattractive.

For this reason, the development of (bio-)degradable detergent additives is of considerable importance. Carbohydrates may serve as an alternative starting material for the preparation of polycarboxylic acids since (*i*) carbohydrates are inexpensive renewable materials and (*ii*) carbohydrate-derived products are expected to be readily (bio-)degradable via hydrolysis of the acid-labile acetal bonds.

In the last decade ether carboxylic acids derived from carbohydrates have been of importance because of their multiple properties. They can be obtained by several reactions (Fig. 1*a*): oxidation of carbohydrate with or without ring opening, carboxymethylation, ethoxylation of carbohydrate with subsequent hydrolysis of hydroxyl to carboxyl groups, graft copolymerization of carbohydrates with acrylic acid (or derivatives), and cyanoethylation followed by subsequent hydrolysis of nitriles to carboxyl groups.

Actually, the most useful and most studied products are oxidized (12–19) and carboxymethylated (13, 20, 21) polysaccha-

Received February 15, 1995.

H. Bazin and G. Descotes. Laboratoire de chimie organique II, Unité de recherche associée nº 463 du Centre national de la recherche scientifique, Université Lyon I, F-69622 Villeurbanne, France.
A. Bouchu. 2-Eridania Béghin-Say, Centre d'entreprises et d'innovation (CEI), B.P. 2132, F-69603 Villeurbanne, France.
M. Petit-Ramel.[1] Laboratoire d'instrumentation et de chimie analytique en solution (LICAS), Université Lyon I, F-69622 Villeurbanne, France.

[1] Author to whom correspondence may be addressed. Telephone: 72-44-84-95. Fax: 72-43-13-30.

Can. J. Chem. Downloaded from www.nrcresearchpress.com by 80.90.12.36 on 09/08/12
For personal use only.

Fig. 1. (*a*) Synthesis of ether carboxylic acids from carbohydrates. (*b*) Studied carboxylic acids derived from carbohydrates.

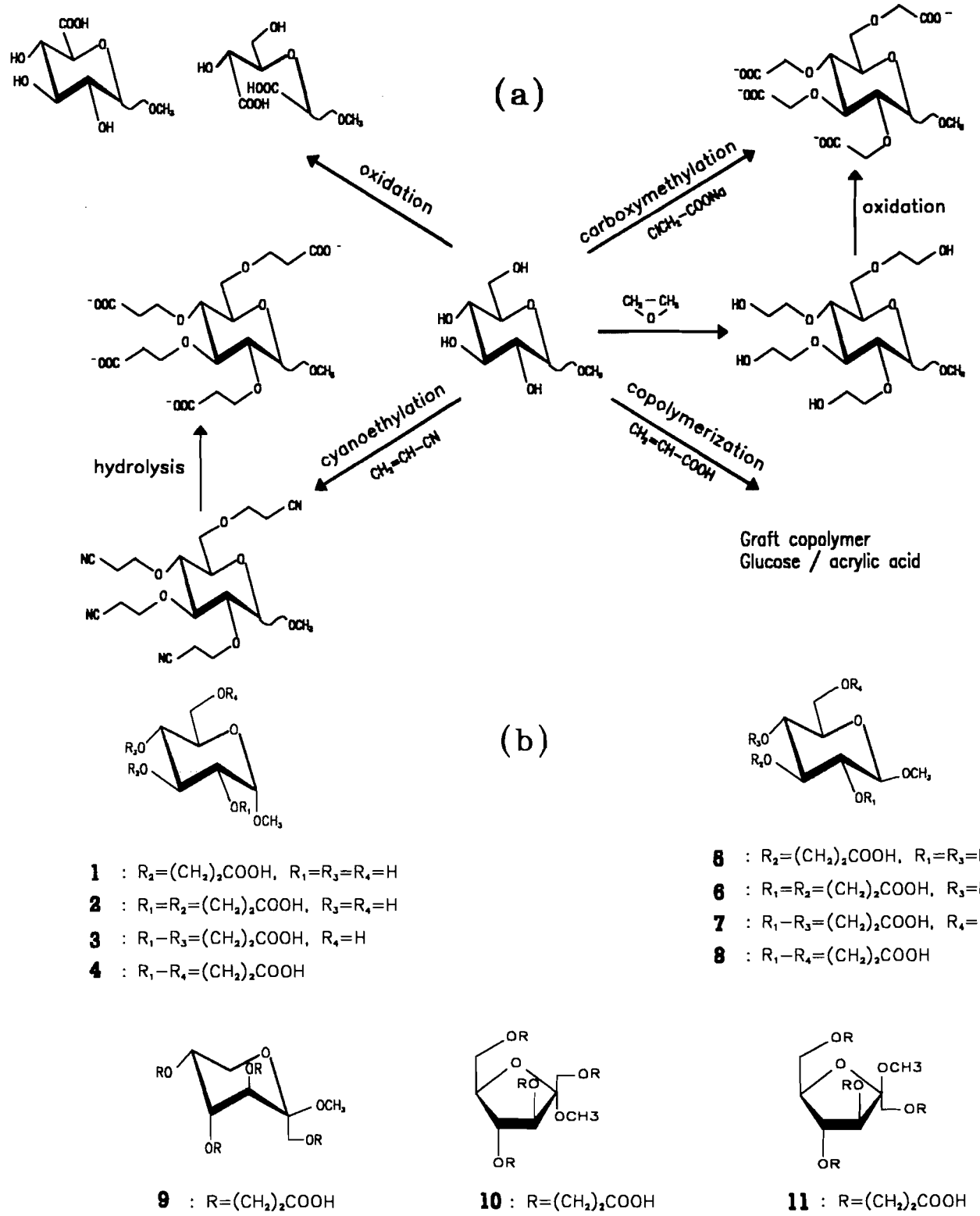

rides. The first are obtained by periodic oxidation of polysaccharides with cleavage of vicinal diol, the second by carboxymethylation of polysaccharides. These latter show better calcium sequestering capacity than STP.

Oxidation products of adduct carbohydrate – ethylene oxide present good performance, but the cost of this oxidation method limits its industrial application (22, 23).

Copolymerization of carbohydrate with acrylic acid leads to a graft copolymer, which possesses good anti-incrustation properties (24–27).

Can. J. Chem. Downloaded from www.nrcresearchpress.com by 80.90.12.36 on 09/08/12
For personal use only.

Can. J. Chem. Downloaded from www.nrcresearchpress.com by 80.90.12.36 on 09/08/12
For personal use only.

Currently, the number of ether carboxylic acids obtained by hydrolysis of cyanoethylated carbohydrates is limited. However, nitriles, which are carboxylic acid precursors, make the cyanoethylation a very attractive way to obtain such compounds.

Consequently we first synthesized carboxylic acids from carbohydrates by cyanoethylation and subsequent hydrolysis of the nitriles to carboxylic acids (Fig. 1*b*). We then determined the calcium complex formation constants of these acids, using a calcium selective electrode.

Study of carboxylic derivatives of methyl D-glucopyranoside **1–8** permits us to particularize the influence of both carboxylic groups and anomeric configuration on calcium sequestering properties. Comparison of percarboxylic derivatives of methyl D-glucopyranoside, **4** and **8**, methyl D-fructopyranoside, **9**, and methyl D-fructofuranoside, **10** and **11**, allows us to compare, on the one hand, the influence of the carbohydrate and, on the other hand, the influence of the pyranic or furanic ring on the calcium complexation.

Experimental

Syntheses of carboxylic acids **1–11** derived from carbohydrates have been described in a previous work (28). These new carboxylic acids were obtained by cyanoethylation of protected or unprotected D-glucose and D-fructose. The acidic alcoholysis of these cyanoethylated carbohydrates leads to the corresponding methyl esters, which were saponified to the carboxylic acids. All new cyanoethylated compounds, methyl esters, and carboxylic acids were fully characterized by ^1H and ^{13}C NMR and microanalysis.

The stability constants of the calcium complexes were determined using a calcium selective electrode. A Corning digital 250 expanded-scale pH-meter, a calcium electrode Tacussel F 2112 Ca, and a single-junction Tacussel XR 100 reference electrode were used to follow the variation in Ca^{2+} activity of an aqueous $CaCl_2$ solution by titration with a sequestering compound. All titrations were carried out under an atmosphere of nitrogen at 25 + 0.5°C.

The calibration curve of the calcium ion selective electrode was obtained by measuring the activity of Tacussel aqueous standard $CaCl_2$ solutions (10^{-2}, 5×10^{-3}, 10^{-3}, 5×10^{-4}, 10^{-4}, and 5×10^{-5} M).

The pH-meter was calibrated and the electrode assembly standardized at pH 3.00, pH 7.00, and pH 10,00 with buffer solutions obtained from Aldrich.

Determination at fixed sequestering compound concentration

Aqueous sodium hydroxide (maintained under nitrogen atmosphere) was added to 100 mL of an aqueous $CaCl_2$ solution (μ = 0.1 M, KCl) and 2 mL of an aqueous sequestering compound solution (0.1 M) to obtain pH variations of 0.1.

Determination at fixed pH

The polycarboxylate compound (2.0 mL of 0.1 M aqueous solution) was added in 20 portions to 100 mL of an aqueous $CaCl_2$ solution (μ = 0.1 M, KCl). The pH was fixed at 10 by adding aqueous NH_3.

The protonation constants of each carboxylic acid were determined by protometric measurements.

^{13}C (50.32 MHz) NMR spectra were recorded on a Bruker AC 200 spectrometer.

Results and discussion

After validation of our measurements and our data processing with α-hydroxyacids, complexation by the carboxylic acids **1–11** was examined.

α-Hydroxyacids

For this group the reference compounds were racemic lactic acid, HOOC-CHOH-CH_3; malic acid, HOOC-CHOH-CH_2COOH; and citric acid, HOOC-COH-$(CH_2COOH)_2$.

Calcium complexation depends on the pH of the solution and, although detergency studies are made at basic pH, we first considered the pH influence on the calcium complexation at a constant [ligand]/[calcium] ratio (Fig. 2*a*) and, second, the calcium ion concentration versus the ligand concentration at a constant alkaline pH (Fig. 2*b*).

Metal and ligand concentrations were fixed, respectively, at 10^{-3} M and 2×10^{-3} M and measurements were carried out between pH 3 and 12 (Fig. 2*a*). In the case of citric acid, the concentration of the uncomplexed calcium remains weak and constant at pH higher than 6.5, when the total deprotonation of the three carboxylic groups is effective. In the case of malic and lactic acids and at pH higher than the latter deprotonation constant, the free calcium concentration is more important and fluctuating. For pH higher than 10.5–11, the observed fast decrease in the free calcium concentration can be explained by calcium carbonate precipitation.

At pH 10, metal concentration was fixed at 10^{-3} M and ligand concentration varied from 0 to 2×10^{-3} M. It can be seen from Fig. 2*b* that citrate is a better complexant than malate and lactate. This major difference in the complexation behaviour of these acids can be explained by the lower acidity constant of the hydroxyl group (K_{OH}) for citric acid. This hydroxyl is easily ionized at basic pH and can take part in the calcium complex in alcoholate form. For concentrations of malic and lactic acids ranging from 0.7 to 1.2×10^{-3} M and 0 to 10^{-3} M, respectively, an irregular decrease in the free calcium concentration is observed. This anomaly can be explained by the coexistence of polynuclear complexes or complexes of variable stoechiometry and their corresponding equilibra.

Complex constants

The stability constants of calcium complexes (Table 1) were calculated using two complementary methods. Under the defined experimental conditions (6.5–11 pH range and a [ligand]/[Ca(II)] ratio of 1:1) and according to Craggs et al. (34), protonated species can be neglected and we can assume that the stoechiometry of the complexes is 1:1, expressed by the complexation equilibrium :

$$[1] \quad Ca^{2+} + L^{n-} \rightleftharpoons CaL^{2-n}$$

$$K = \frac{[CaL^{2-n}]}{[Ca^{2+}][L^{n-}]}$$

The stability constant K of the complex is easily calculated (eqs. [2] and [3]) from the initial and experimental concentra-

Can. J. Chem. Downloaded from www.nrcresearchpress.com by 80.90.12.36 on 09/08/12
For personal use only.

Fig. 2. Citric, malic, and lactic acids: (*a*) pH influence on the calcium complexation. (*b*) Calcium complexation according to ligand concentration. (*c*) Stability constants for citric, malic, and lactic acids.

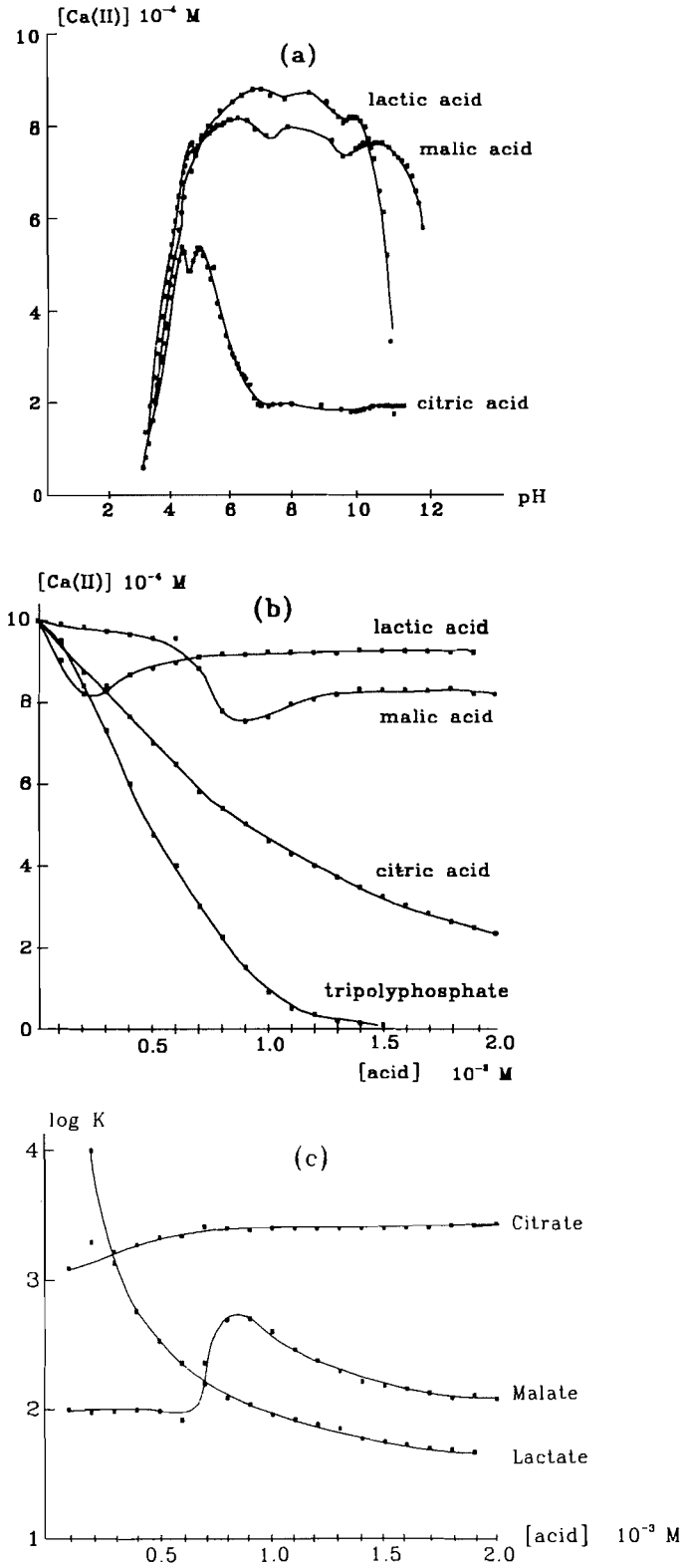

Fig. 3. Carboxylic acids derived from methyl D-glucopyranoside: (*a*) Calcium complexation according to the ligand concentration. (*b*) Calcium complexation by anomeric mono- and dicarboxylic acids. (*c*) Stability constants according to the ligand concentration.

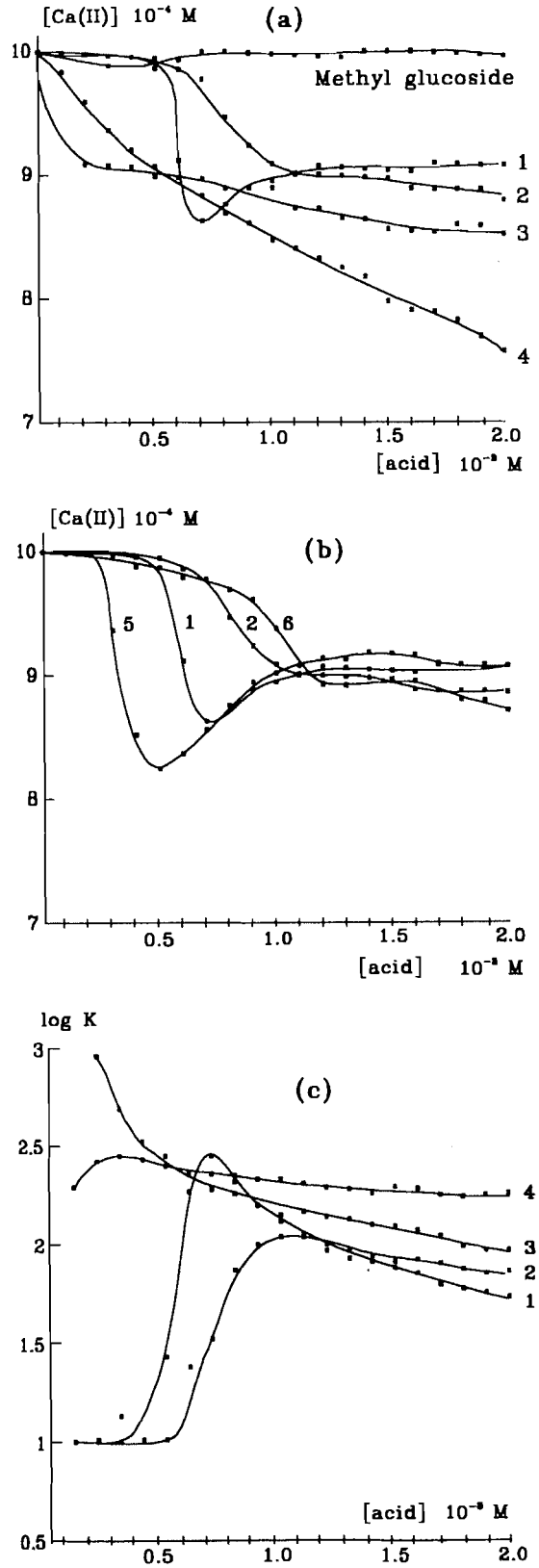

Table 1. Protonation constants and stability constants of the ligands and Ca(II) complexes.

	Protonation constants[a]					Complexation constants		
Acid	log K_1	log K_2	log K_3	log K_{OH}	Ref.	log K	L:Ca	Ref.
Citric	5.10(02)	3.93(02)	2.58(02)	12.42	29	3.24[a]	2:1	30
Malic	4.49(01)	3.14(02)		15.46	29	2.24[b]	2:1	31
Lactic	3.60(01)			15.10	33	1.55[c]	3:1	32

[a]μ = 0.5 ($NaNO_3$), 25°C.
[b]$\mu \rightarrow 0$, 25°C.
[c]μ = 0.1 (KCl), 25°C.
Values in parentheses are the standard deviation corresponding to the last significant digits (2σ).

Table 2. Calcium complexation stability constants for citric, malic, and lactic acids

Acid	log K calculated from [Ca(II)] = f([acid])	log K calculated from [Ca(II)] = f(pH)	log K	Ref.
Citric	3.41[a] (03)	3.55[a] (06)	3.24[a]	30
Malic	2.25[a] (31)	2.21[a] (24)	2.24[b]	31
Lactic	1.63[a] (25)	1.99[a] (27)	1.55[c]	32

[a]μ = 0.1 (KCl), 25°C.
[b]$\mu \rightarrow 0$, 25°C.
[c]μ = 0.1 (KCl), 25°C.
Values in parentheses are the standard deviation corresponding to the last significant digits (2σ).

Table 3. Protonation constants for carboxylic derivatives from methyl D-glucopyranoside at 25°C, μ = 0.1 (KCl)

Compound		log K_n	log K_{n-1}	log K_{n-2}	log K_{n-3}
n = 1	**1**	4.26(01)			
	5	4.11(01)			
n = 2	**2**	4.15(01)	4.90(01)		
	6	4.11(02)	5.21(05)		
n = 3	**3**	3.81(01)	4.65(01)	5.41(02)	
	7	3.97(09)	4.62(05)	5.44(06)	
n = 4	**4**	3.75(01)	4.43(01)	5.05(01)	5.77(01)

Values in parentheses are the standard deviation corresponding to the last significant digits (2σ).

tions in calcium and ligand as, $[Ca^{2+}]_0$, $[L^{n-}]_0$, $[Ca^{2+}]$

$$[2] \quad [L^{n-}] : [CaL^{2-n}] = [Ca^{2+}]_0 - [Ca^{2+}]$$
$$[3] \quad [L^{n-}] = [L^{n-}]_0 - [CaL^{2-n}]$$

For a constant [ligand]/[Ca(II)] ratio of 2:1, and in the pH range corresponding to the complex formation, the calculation of the stability constant depends on the average of the concentrations in free calcium (Fig. 2*a*).

At pH 10, the complexation constant can be calculated from each set of experimental points. The stability constant of citric acid is quite invariant (Fig. 2*c*) because of the strong complexation with the three carboxylic groups. As expected, the calculation range can be considered above the 1:1 [ligand]/[Ca(II)] ratio, in good agreement with the assumption of major formation of the 1:1 complex.

Table 2 shows that both experimental approaches are entirely satisfactory and lead to comparable average values. As these calculated constants are in excellent agreement with those reported in the literature, this study shows that the experimental procedures are reliable and perfectly reproducible.

Carboxylic derivatives from methyl D-glucopyranosides

Quantitative information about interactions between protons and functional groups of the ligand may conventionally be given by the general formation equilibria constants Kq of the species HqL. Standard derivations are calculated from the residual variance and the matrix of variances by a pit-mapping method (29).

Protonation constants for **1**–**7** are given in Table 3. This table shows that the first acidity increases with an increasing number of carboxylic groups. For each anomer α and β, these constants are comparable.

Metal and ligand concentrations were fixed, respectively, at 10^{-3} and 2×10^{-3} M and the measurements were carried out between pH 3 and 12. For each compound, the free calcium concentration fluctuates more than those observed for citric, malic, and lactic acids. There is a free calcium concentration level for each compound. This level is smallest with the tetracarboxylic acid.

At pH 10, metal concentration was fixed at 10^{-3} M and

Can. J. Chem. Downloaded from www.nrcresearchpress.com by 80.90.12.36 on 09/08/12
For personal use only.

Table 4. Stability constants for calcium complexes with carboxylic acids derivatived from D-glucose and D-fructose at $\mu = 0.1$ (KCl), 25°C.

Compound	log K calculated from [Ca(II)] = f([acid])	log K calculated from [Ca(II)] = f(pH)
1	**1.89**(20)	**1.95**(28)
5	**1.85**(18)	**1.93**(20)
2	**1.94**(12)	**2.01**(24)
6	**1.93**(10)	**1.95**(34)
3	**2.07**(12)	**2.12**(30)
7	—	**2.05**(20)
4	**2.28**(04)	**2.24**(32)
8	—	**2.18**(22)
9	**2.25**(12)	
10–11	**2.13**(16)	

Values in parentheses are the standard deviation corresponding to the last significant digits (2σ).

Fig. 4. Carboxylic acids derived from methyl D-fructoside.
(*a*) Calcium complexation according to the ligand concentration.
(*b*) Stability constants according to the ligand concentration.

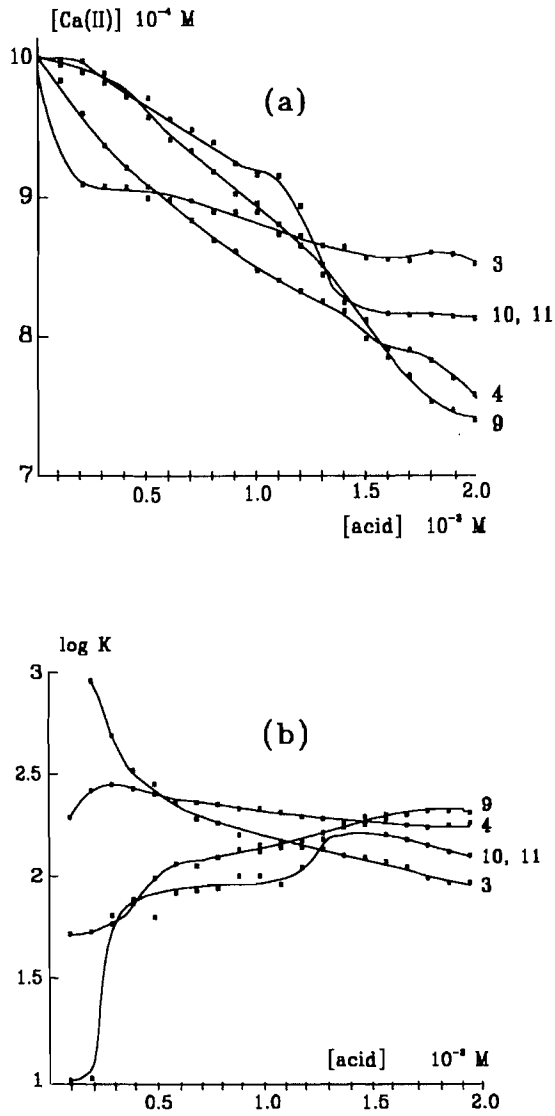

ligand concentration varied from 0 to 2×10^{-3} M. To demonstrate the influence of the number of carboxylic groups, we have included the methyl α-D-glucopyranoside, which has no carboxylic group. Figure 3*a* shows that an increasing number of carboxylic groups has a favourable effect on the calcium sequestering strength.

To determine whether the behaviour of α anomers differs from that of β anomers, the calcium complexation of mono- and dicarboxylic acids, **1**, **5** and **2**, **6**, have been compared (Fig. 3*b*). In the ligand concentration range from 0 to 0.7×10^{-3} M, Fig. 3*b* shows that β anomer **5** is a better complexant than α anomer **1**, and in the ligand concentration range from 0 to 1.1×10^{-3} M, the α anomer **2** is a better complexant than β anomer **6**. So for low ligand concentrations, the anomeric configuration has a significant influence on the calcium complexation. This effect is more pronounced for ligands having fewer carboxylic groups.

Complex constants

Stability constants for α anomers, calculated from the relation [Ca(II)] = f(ligand), are represented according to the ligand concentration (Fig. 3*c*). **4** shows similar behaviour to citric acid. Its stability constants are almost the same for the region of ligand concentration from 0 to 2×10^{-3} M. For **1**, **2**, and **3**, stability constants are stable over the ligand concentration range 10^{-3} to 2×10^{-3} M. The average values calculated in the previous interval are given in Table 4, with the complex constants calculated from the relation [Ca(II)] = f(pH).

This table shows that the two experimental methods lead to comparable values and, for a [ligand]/[calcium] ratio of 2:1, the α and β anomers have the same complexation strength.

Carboxylic derivatives from methyl D-fructosides

Measurements at pH 10 were the only ones performed. Since the anomeric configuration has no effect on the calcium complexation for tetracarboxylic compounds (see results obtained with methyl D-glucopyranoside derivatives), the tetracarboxylic derivatives from methyl α- and β-D-fructofuranoside **10** and **11** have not been separated.

Results of the calcium complexation at pH 10 obtained for tetracarboxylic derivatives from methyl β-D-fructopyranoside

Can. J. Chem. Downloaded from www.nrcresearchpress.com by 80.90.12.36 on 09/08/12
For personal use only.

Fig. 5. Chemical shift variations induced by the calcium complexation for acids derived from methyl D-glucopyranoside. (*a*) Dicarboxylic acid **2**. (*b*) Tricarboxylic acid **3**. (*c*) Tetracarboxylic acid **4**.

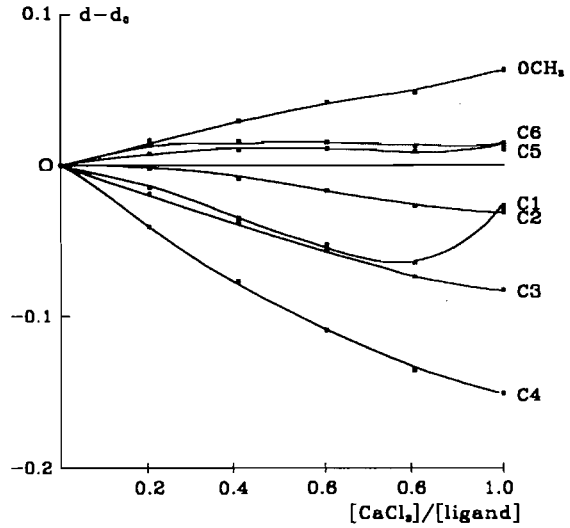

(a)

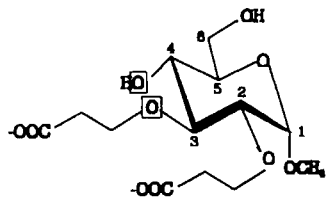

2

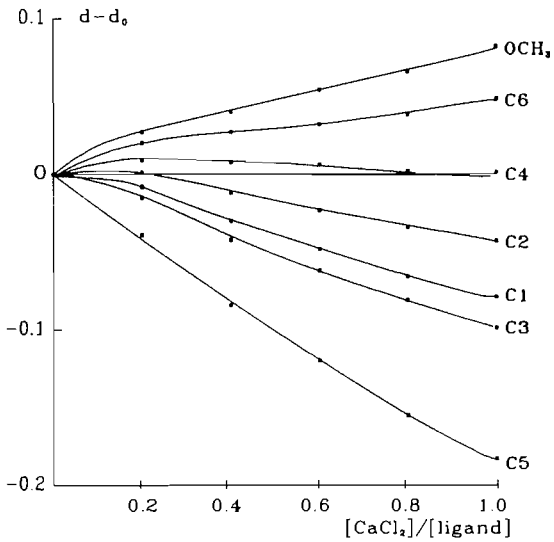

(b)

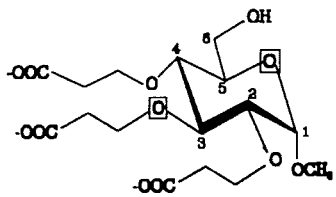

3

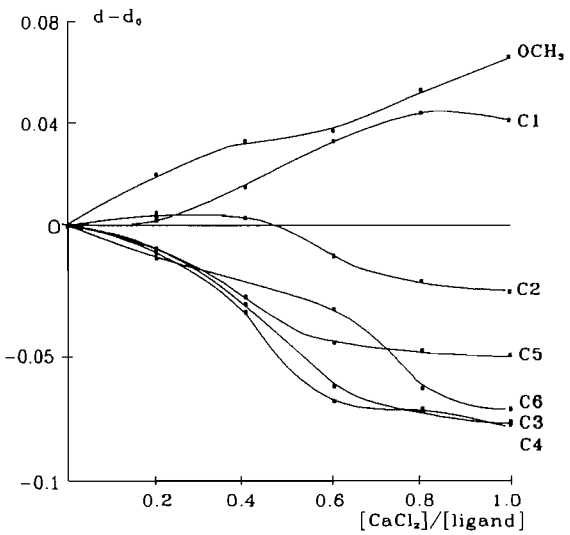

(c)

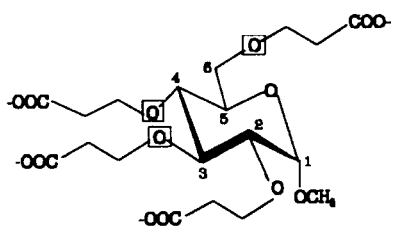

4

Can. J. Chem. Downloaded from www.nrcresearchpress.com by 80.90.12.36 on 09/08/12
For personal use only.

Fig. 6. Chemical shift variations induced by the calcium complexation for the carboxylic acid derived from methyl D-fructofuraanoside. (*a*) α Anomer **10**. (*b*) β Anomer **11**.

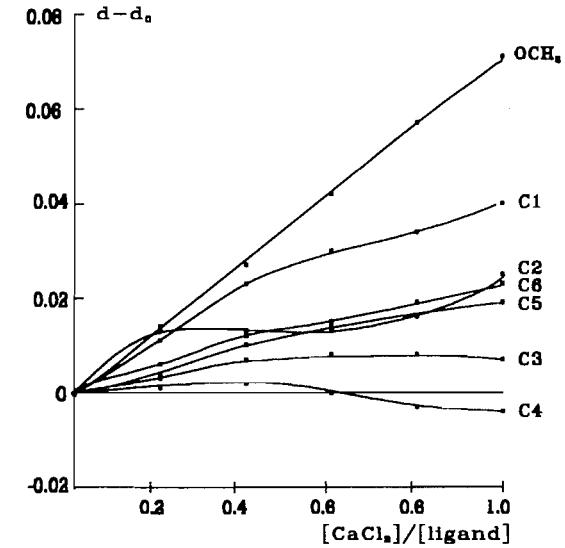

(a)

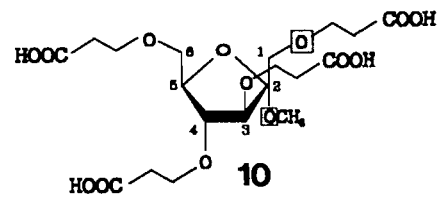

10

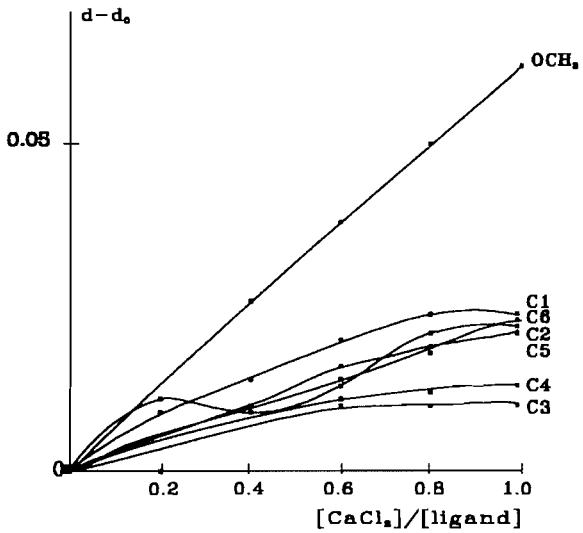

(b)

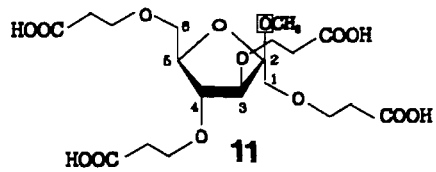

11

9 and methyl α- and β-D-fructofuranoside **10** and **11** are reported in Fig. 4*a* with the curves previously obtained for tri- and tetracarboxylic derivatives from methyl α-D-glucopyranosides **3** and **4**.

As we have seen, the tetrasubstituted derivatives **4**, **9**, **10**, and **11** are better complexants than the tricarboxylic derivative **3**. For a [ligand]/[calcium] ratio of 2:1 and for the tetracarboxylic compounds **4**, **9**, **10**, and **11**, the derivatives from methyl D-fructofuranoside **10** and **11** are the least active and the derivative from methyl β-D-fructopyranoside **9** is the most active.

Complex constants

Figure 4*b* illustrates the variation of stability constants for **3**, **4**, **9**, **10**, and **11** with ligand concentration. Although at a [ligand]/[Ca(II)] ratio of 2:1 **9** is more active than **4**, its stability constants are less stable than those of **4**.

The stability constants calculated in the ligand concentration range 0 to 2×10^{-3} M illustrate this observation (Table 4).

Determination of the calcium complexation sites for the carbohydrate skeletons

Upon complexation of calcium ions by a ligand, the relaxation times and the chemical shifts of the carbons are perturbed. These perturbations are more important if the carbon in question is near a complexation site (35, 36). The complexation sites for the carbohydrate skeletons of **2**, **3**, **4**, **10**, and **11** have been so determined using ^{13}C NMR, by measurements of chemical shift variation of the carbons of the ligand with increasing calcium concentration, after verification that addition of a salt that is inert towards complexation (sodium chloride, and addition of calcium chloride) to an aqueous solution of methyl α-D-glucopyranoside (which presents no calcium complexation under our experimental conditions) does not lead to great variations of chemical shift for the ring carbons. ^{13}C NMR spectra of the ligands with increasing calcium chloride concentrations, [ligand]/[Ca(II)] ratio from 0 to 1, have been obtained and the variations of chemical shift induced by

Can. J. Chem. Downloaded from www.nrcresearchpress.com by 80.90.12.36 on 09/08/12
For personal use only.

the calcium complexation are represented according to the ratio [ligand]/[Ca(II)].

Methyl α-D-glucopyranoside derivatives 2, 3, and 4

For the dicarboxylic derivative **2**, the highest chemical shift variations are obtained for the C3 and C4. So the oxygens on C3 and C4 are the privileged complexation sites (Fig. 5*a*).

For tricarboxylic derivative **3**, the more perturbated chemical shifts are obtained for the C5 and C3, showing privileged complexation sites by the ring oxygen and the oxygen on C3 (Fig. 5*b*).

For tetracarboxylic derivative **4**, the highest chemical shift variations are obtained for the C4, C3, and C6. So the oxygens on C4, C3, and C6 are the privileged complexation sites (Fig. 5*c*).

Methyl α- and β-D-fructofuranoside derivatives 10 and 11

Figures 6*a* and 6*b* show that the carbons having the highest chemical shift variations are the carbons C2 and C1 for the α anomer **10** and the carbon C1 for the β anomer **11**.

Conclusion

Calcium sequestering properties of 11 carboxylic derivatives from methyld D-glucopyranoside, methyl D-fructopyranoside, and methyl D-fructofuranoside have been studied using a calcium selective electrode and introducing a precise and reproductible procedure.

Study of the citric, malic, and lactic acids allowed us to set up two experimental approaches for the calcium complexation measurement. The first follows the variations in free calcium concentration with the pH, the second, with the ligand concentration. These two processes lead to the corresponding complex formation constants, which are in excellent agreement with those reported in the literature. If the pH is fixed, as in the case of the detergency studies, the second process, which is moreover more precise, must be used.

Although these carboxylic acids are biodegradable, their calcium sequestering properties are less effective than those of citric acid. In addition, at pH 10 and for a temperature higher than 50°C, a de-etherification of carboxyethyl groups occurs, leading to the free carbohydrate. So the use of such compounds is not appropriate in the case of the usual laundry products.

Moreover, from a fundamental point of view, at the time of the study of calcium complexation for the carboxylic derivatives of methyl D-glucopyranoside, we emphasize that the calcium complexation strength *increases* with increasing number of carboxylic groups. Although the tetracarboxylic derivative **4** is less effective than citric acid, its calcium complexation behaviour being similar, for a [ligand]/[Ca(II)] ratio higher than 1, the anomeric configuration has no effect on the calcium complexation, and for a [ligand]/[Ca(II)] ratio smaller than 1, the anomeric configuration has a significant effect on the calcium complexation, when the compound contains fewer carboxylic groups.

Comparison of the complexing properties of the tetracarboxylic derivatives from methyl D-glucopyranoside, methyl D-fructopyranoside, and methyl D-fructofuranoside shows that (*i*) pyranic derivatives seem more effective than furanic derivatives, and (*ii*) for pyranic rings, the complex stability for derivatives of methyl D-glucopyranoside and methyl D-fructopyranoside is almost identical, but for a [ligand]/[Ca(II)] ratio of 2:1, the first is the more effective.

The ^{13}C NMR study of the calcium complexes, which allows us to easily determine the calcium complexation sites, shows that (*i*) for the derivatives of methyl D-glucopyranoside, in addition to the carboxylic groups, the oxygen on C3 is the only common complexation site, (*ii*) for the derivatives of methyl D-fructofuranoside, complexation sites differ for each anomer.

References

1. G.L. Phillips. Water Pollut. Control (Maidstone, Engl.), **83**, 400 (1984).
2. A.V. Gray. J. Inst. Water Eng. Sci. **39**, 173 (1985).
3. J.V. DePinto, T.C. Young, and L.M. McIlroy. Environ. Sci. Technol. **20**, 752 (1986).
4. H.N.S. Weichers and J.J.C. Heynike. Water SA, **12**, 99 (1986).
5. M. Dwyer, S. Yeoman, J.F. Lester, and R. Perry. Environ. Technol. **11**, 263 (1990).
6. P. Berth. J. Am. Oil Chem. Soc. **55**, 52 (1978).
7. P. Berth. Tenside Deterg. **15**, 176 (1978).
8. H. Krueszmann, P. Vogel, H. Hloch, and H. Carlhoff. Seifen, Öle, Fette, Wachse, **105**, 3 (1979).
9. P. Berth, M. Berg, and K. Hachmann. Tenside Deterg. **20**, 276 (1980).
10. M.S. Nieuwenhuizen, A.H. Ebaid, M. van Duin, A.P.G. Kieboom, and H. van Bekkum. Tenside Deterg., **21**, 221 (1984).
11. W.J. Wirth. Proc. World Conf. Detergents, 2nd, Montreux. *Edited by* A.R. Baldwin. The American Oil Chemist's Society, 1987. p. 138.
12. C.A. Wilham, J.A. McGuire, A.M. Mark, and C.L. Mehltretter. J. Am. Oil. Chem. Soc. **47**, 522 (1970).
13. M. Diamantaglou, H. Magerlein, and R. Zielke. Tenside Deterg. **14**, 250 (1977).
14. A.C. Besemer and H. van Bekkum. Starch/Stärke, **46**, 95 (1994).
15. C.L. Mehltretter. Starch/Stärke, **37**, 294 (1985).
16. M. Floor, L.P.M. Hafsteed, W.P.T. Groenland, L.A.Th. Verhaar, A.P.G. Kieboom, and H. van Bekkum. Recl. Trav. Chim. Pays-Bas, **108**, 384 (1989).
17. M.S. Nieuwenhuizen, A.P.G. Kieboom, and H. van Bekkum. J. Am. Oil. Chem. Soc. **60**, 120 (1983).
18. M.S. Nieuwenhuizen, A.P.G. Kieboom, and H. van Bekkum. Starch/Stärke, **37**, 192 (1985).
19. M. Floor, J.A. Peters, H. van Bekkum, and A.P.G. Kieboom. Carbohydr. Res. **203**, 19 (1990).
20. J.W. Green. Methods Carbohydr. Chem. **3**, 322 (1963).
21. F.L. Diehl (Procter and Gamble Co.). US Patent No. 3,723,332 (1973); Chem. Abstr. **79**, 20664d (1973).
22. K.H. Schoenwaelder, E.I. Leupold, W. Gohla, F.J. Dany, and M. Schlingmann (Hoechst AG). Ger. Offen. DE 3,928,310 (1991); Chem. Abstr. **114**, 231068s (1991).
23. H. Fiege and K. Wedemeyer. Z. Angew. Chem. **93**, 812 (1981).
24. K. Engelskirchen and J. Galinke (Henkel and Cie G.m.b.H.). Ger. Offen. 2,334,162 (1974); Chem. Abstr. **81**, 27565x (1974).
25. K. Driemel, K. Bunthoff, and H. Nies (Grillo Werke). Ger. Offen. DE 3,714,732 (1988); Chem. Abstr. **110**, 156587 (1988).
26. K. Driemel, K. Bunthoff, H. Nies, and D. Rohe (Grillo Werke). DE 3;834,237 (1990); Chem. Abstr. **114**, 145873u (1990).
27. W. Denziger, H. Hartmann, A. Kud, R. Baur, J. Feldmann, and H.J. Raubenheimer (BASF AG). DE 4.003,172 (1991); Chem. Abstr. **115**, 256935f (1991).
28. H. Bazin, A. Bouchu, and G. Descotes. J. Carbohydr. Chem. In press.
29. I. Khalil, M. Petit-Ramel, and C. Barbier-Chapelet. Can. J. Chem. **56**, 1919 (1978).

Can. J. Chem. Downloaded from www.nrcresearchpress.com by 80.90.12.36 on 09/08/12
For personal use only.

30. F. Bosch Reig and F. Burriel Marti. Inf. Quim. Anal. **23**, 5 (1969).
31. R.P. Bell and G.M. Waind. J. Chem. Soc. 2357 (1951).
32. R. Gosh and V.S.K. Nair. J. Inorg. Nucl. Chem. **32**, 3025 (1970).
33. D. Jalon, M. Petit-Ramel, and G. Thomas David. Bull. Soc. Chim. Fr. **12**, 21 (1983).
34. A. Craggs, G.J. Moody and J.D.R. Thomas. Analyst (London), **104**, 961 (1979).
35. M.S. Nieuwenhuizen, A.P.G. Kieboom, and H. van Bekkum. Recl. J. R. Neth. Chem. Soc. **101**, 339 (1982).
36. M. Floor, J.A. Peters, H. van Bekkum, and A.P.G. Kieboom. Carbohydr. Res. **19**, 203 (1990).

Can. J. Chem. Downloaded from www.nrcresearchpress.com by 80.90.12.36 on 09/08/12
For personal use only.

Synthesis of 3-substituted tetrahydroisoquinolines by acid-catalyzed cyclization of *p*-toluenesulfonamides of *N*-benzyl aminoacetaldehyde derivatives

Viviana L. Ponzo and Teodoro S. Kaufman

Abstract: The acid-catalyzed cyclization of *p*-toluenesulfonamides of *N*-benzyl aminoacetaldehyde, or their acetalic counterparts, usually yields 1,2-dihydroisoquinolines. However, cyclization of intermediates bearing a substituent α to the carbonyl group affords 3-substituted 2-*p*-toluenesulfonyl tetrahydroisoquinolin-4-ol derivatives, capable of further transformation into the related 1,2,3,4-tetrahydroisoquinolines.

Key words: 3-substituted tetrahydroisoquinolines, MY336-a analog, acid-catalyzed cyclization, tetrahydroisoquinolin-4-ol derivatives.

Résumé : La cyclisation, catalysée par un acide, des *p*-toluènesulfonamides du *N*-benzylaminoacétaldéhyde ou de leurs acétals équivalents conduit habituellement aux 1,2-dihydroisoquinoléines. Cependant, la cyclisation des intermédiaires portant un substituant en position α du carbonyle conduit aux dérivés 2-*p*-toluènesulfonyl tétraisoquinolin-4-ol substitués en position 3, pouvant subir des transformation plus poussées en donnant les 1,2,3,4-tétrahydroisoquinoléines apparentées.

Mots clés : tétrahydroisoquinoléines substituées en position 3, analogue du MY336-a, cyclisation catalysée par un acide, dérivés du tétrahydroisoquinolin-4-ol.

[Traduit par la rédaction]

Can. J. Chem. Downloaded from www.nrcresearchpress.com by 80.90.12.36 on 09/08/12
For personal use only.

The synthesis of isoquinolines and 2-*p*-toluenesulfonyl-1,2-dihydroisoquinolines by acid-catalyzed cyclization of *p*-toluenesulfonamides of *N*-benzylaminoacetaldehyde acetals was first reported by Jackson and co-workers (1); it is a modification of the Pomeranz–Fritsch process, which has been used as a synthetic tool of importance in the preparation of a variety of isoquinoline systems (2). A salient feature of this sequence is the possibility of synthesizing the relatively uncommon and difficult to obtain heterocycles carrying a 7,8-substitution pattern on the isocyclic ring.

The original strategy was modified by Boger et al. (3) and more recently by Castedo and co-workers (4), enhancing its synthetic power. Additionally, as part of a study on the total synthesis of the novel β-adrenergic receptor antagonist MY336-a (**1**) bearing a 1,3-disubstituted heterocyclic ring, we recently reported the successful obtention of a 1-substituted 1,2,3,4-tetrahydroisoquinoline from the related *p*-toluenesulfonyl 1,2-dihydroisoquinoline precursor (5).

In a further extension of this series of work, we wish to report the applicability of the Jackson sequence to the elaboration of 3-substituted tetrahydroisoquinolines through the syntheses of prototypes **2** and **3**, and the obtention of **4**, which embodies the 3,7,8-oxygenated substituent array present in **1**.

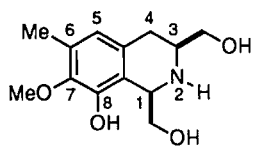

MY336-a, **1**

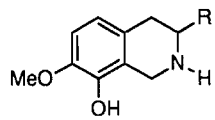

2 R= Me
3 R= CH_2CH_2OH
4 R= CH_2OH

Although many 3-substituted isoquinolines have been synthesized by alternative routes, it has been reported that the formation of 3-alkylisoquinolines is difficult or fails in the Pomeranz–Fritsch synthesis (6), and it is known that isoquinolines and dihydroisoquinolines having alkyl, aryl, or aralkyl groups in the 3 position have generally been obtained in lower yield than derivatives unsubstituted in that position, by the Bischler–Napieralski procedure (7).

As shown in Scheme 1, for the preparation of the simplest prototype (**2**), the known aldehyde **5** (8) was reductively aminated with alanine ethyl ester to afford the secondary amine **6**, which readily provided intermediate **7** in 76% overall yield upon reaction with *p*-toluenesulfonyl chloride. Functional group interconversion furnished the required substrates for cyclization; thus, **7** in THF–ethanol was reduced with lithium

Received December 21, 1994.

V.L. Ponzo and T.S. Kaufman.[1] Instituto de Química Orgánica de Síntesis (CONICET-UNR) and Facultad de Ciencias Bioquímicas y Farmacéuticas, Universidad Nacional de Rosario, Suipacha 531, (2000) Rosario, Argentina.

[1] Author to whom correspondence may be addressed. Telephone: 54-41-370477. Fax: 54-41-370346.

Can. J. Chem. Downloaded from www.nrcresearchpress.com by 80.90.12.36 on 09/08/12
For personal use only.

Scheme 1.

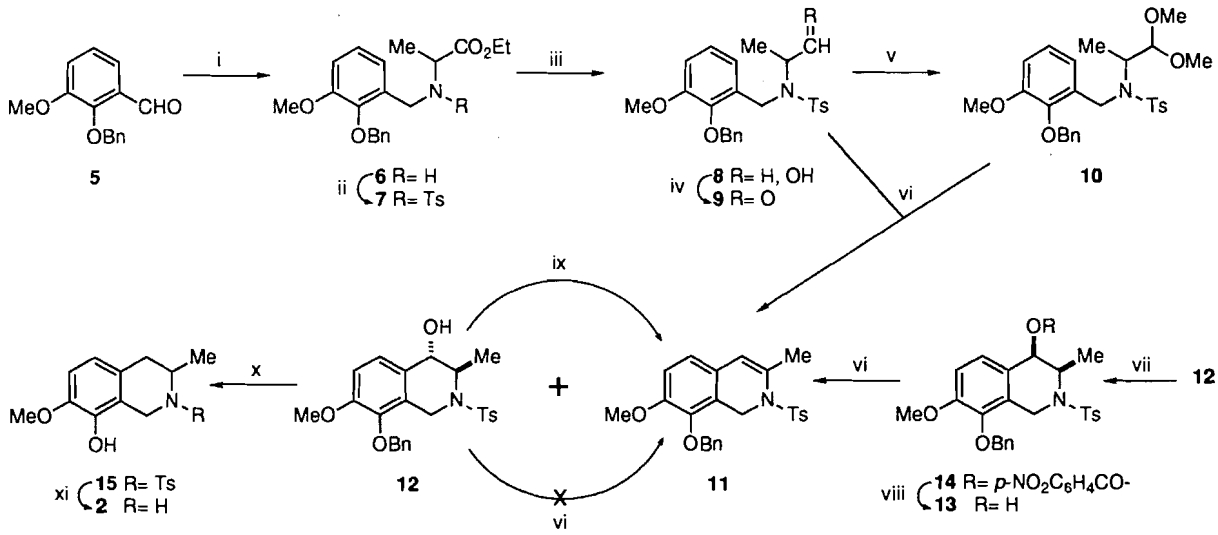

(i) AlaOEt.HCl, TEA, H_2/PtO_2, EtOH; (ii) TsCl, pyridine, CH_2Cl_2; (iii) LiBr, $NaBH_4$, THF-EtOH, 40°C; (iv) 1. $(COCl)_2$, DMSO, CH_2Cl_2, TEA, -60°C; (v) 2,2-DMP, TsOH, MeOH, room temp.; (vi) 6N HCl, dioxane, reflux; (vii) Ph_3P, DEAD, p-$NO_2C_6H_4CO_2H$, benzene; (viii) NaOH, MeOH; (ix) $CuSO_4/SiO_2$, $Cl_2CHCHCl_2$, 100°C; (x) H_2, 10% Pd/C, HCl, MeOH; (xi) 1. Na, NH_3, -33°C, 2. NH_4Cl, -33°C to room temp.

Fig. 1.

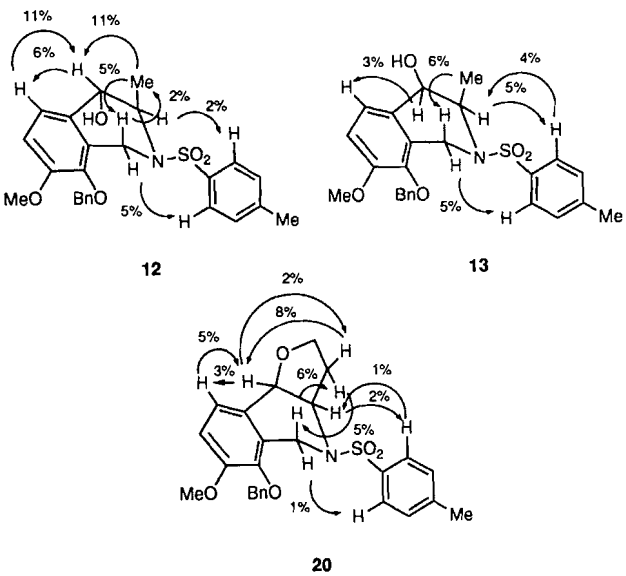

borohydride, generated in situ (9), to alcohol **8**, which was immediately reoxidized to the related aldehyde **9** following the procedure of Swern, and, finally, acetalization of **9** with 2,2-dimethoxypropane in methanol under *p*-toluenesulfonic acid catalysis furnished **10** in 80% yield from **7**.

Heating under reflux a dioxane solution of acetal **10** containing 4 equivalents of 6 N hydrochloric acid smoothly led to a 1:5.8 mixture of cyclized products in combined 82% yield. These were identified as the expected, light-sensitive, 1,2-dihydroisoquinoline derivative **11** and a 3-methyl-1,2,3,4-tetrahydroisoquinolin-4-ol to which structure **12** was assigned based on the small $J_{H\text{-}3,H\text{-}4}$ value observed and the nOe data shown in Fig. 1. The same product distribution was observed upon cyclization of aldehyde **9**.

Scheme 2.

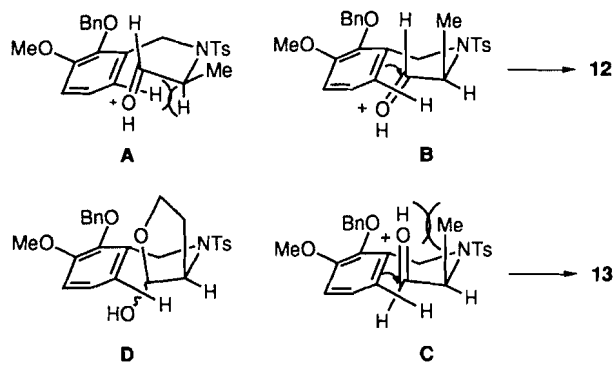

The isolation of **12** as the main cyclization product was puzzling, since this transformation usually provides 1,2-dihydroisoquinolines. The causes of this reaction outcome were studied. Careful inspection of Dreiding models suggested that, due to the steric interaction between the hydrogen atom α to the carbonyl group and the aromatic proton located in the ring closure position (**A**, Scheme 2), cyclization could only be accomplished by an aromatic ring attack on the intermediate carbonium ion, formed by protonation either of the acetalic or (most probably) of the aldehydic moieties, from the same face of the 3-substituent.

In this analysis, the aromatic ring would be capable of attacking either one of two different conformations of the protonated carbonyl, the most favored one being that in which it is antiperiplanar (**B**) with the 3-substituent and gives rise to **12** through a chair-like transition state. On the other hand, attack to the synperiplanar conformation (**C**), producing the diastereoisomeric compound **13**, should be disfavored due to the interaction between the protonated oxygen and the 3-methyl group, resulting in a diminished yield of the latter. Since alcohol **13** could not be isolated, it was supposed that it would

Can. J. Chem. Downloaded from www.nrcresearchpress.com by 80.90.12.36 on 09/08/12
For personal use only.

easily dehydrate to afford the observed 1,2-dihydroisoquinoline derivative **11**, while the lack of a *trans* β-hydrogen atom would preclude the dehydration of **12** under the acidic reaction conditions.

To test this hypothesis, chromatographically purified **12** was exposed to the same cyclization conditions. However, this attempt to obtain **11** met with failure, since only some decomposition of the alcohol was detected and no evidence of formation of the dehydrated product was found.

Interestingly, it was reported (10) that structurally related 3,4-dihydroisoquinolines, obtained through a Bischler–Napieralski type cyclization and carrying a 3*R**,4*S** substitution pattern, were resistant to dehydration when PCl_5 was employed as cyclodehydration agent, while its substitution by P_2O_5 afforded isoquinolines by a process similar to that of the Pictet–Gams reaction. Resistance to dehydration with PCl_5 was explained as being a result of the disfavored formation of the required intermediate carbocation.

Dehydration of **12** was acceptably accomplished either by treating the alcohol with hexamethylphosphoric triamide (HMPA) as reported by Monson (11), a procedure that does not require a *trans* orientation of the hydroxyl and the β-hydrogen for elimination to occur, or by heating the alcohol in 1,1,2,2-tetrachloroethane with anhydrous copper(II) sulfate adsorbed on silica gel (12). Although the mechanisms of these dehydrations are not clear, the formation of intermediates with carbonium cationic character is invoked in both cases.

The behaviour of epimeric alcohol **13** was also verified. To this end, **12** was submitted to a Mitsunobu reaction as modified by Martin, employing *p*-nitrobenzoic acid as the acidic component to overcome the usually low yields associated with the serious steric hindrance around the reacting group (13). As expected, the reaction was not very clean, but afforded the required *p*-nitrobenzoate **14**, which provided **13** in 50% overall yield from **12** after brief exposure to a methanolic solution of sodium hydroxide. Comparison of $J_{H\text{-}3,H\text{-}4}$ and nOe data of **12** and **13** (Fig. 1) confirmed the proposed configurational assignments for both alcohols.

To our satisfaction, **11** was obtained in 80% yield as the sole isolable product when the epimerized alcohol **13** was subjected to the standard cyclization conditions.

To finish the proposed synthesis, **12** was submitted to a palladium-catalyzed hydrogenolysis in hydrochloric acid – methanol to cleanly afford **15**, which was reductively detosylated to furnish model compound **2** in 37% overall yield from **5**.

Curiously, in spite of precedents on related systems (14), 1,2-dihydroisoquinoline **11** proved to be resistant to catalytic double bond hydrogenation, while its treatment with sodium in liquid ammonia gave a complex mixture of products; thus, the unexpected obtention of **12** provided a short and easy entry into the target 3-substituted tetrahydroisoquinoline.

Tempted with the possibility of obtaining optically active cyclized compounds, the synthetic scheme was repeated employing L-alanine ethyl ester as starting material. Unfortunately, racemization of the chiral center during the cyclization step gave **12** in its racemic form, as evidenced by duplication of the H-5, H-6, and 7-methoxyl signals in its ^1H NMR spectrum when recorded in benzene-d_6 employing (+)-Eu(hfc)$_3$ as chiral shift reagent.

Next, the cyclization of a less flexible model was studied in order to better understand the factors affecting this process and

Scheme 3.

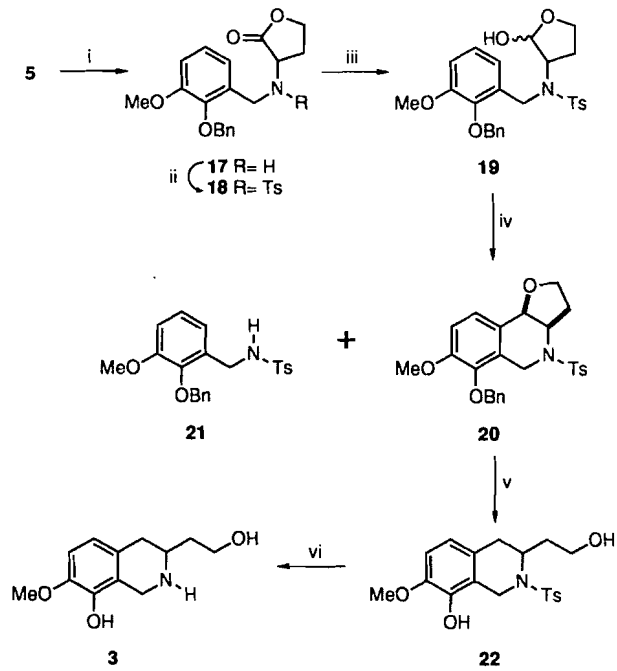

(i) 2-amino-γ-butyrolactone. HBr, (**16**. HBr), TEA, H_2/PtO_2, EtOH; (ii) TsCl, pyridine, CH_2Cl_2; (iii) DIBAH, toluene, -45°C; (iv) 6N HCl, dioxane, 140°C; (v) H_2, 10% Pd/C, H_2SO_4, MeOH; (vi) 1. Na,NH_3, -33°C, 2. NH_4Cl, -33°C to room temp.

to evaluate the possibility of synthesizing 1,2,3,4-tetrahydroisoquinolines carrying functional groups on the C-3 side chain amenable to further elaboration.

Compound **3** was selected as the synthetic target based on the ready availability of the starting 2-amino-γ-butyrolactone (**16**), capable of being reduced to a masked aldehyde suitable for cyclization in a few steps, and embodying a ring that should restrict the direction of the attack by the aromatic moiety, since the protonated intermediate (**D**, Scheme 2) can only adopt a synperiplanar orientation with regard to the C-3 substituent.

Platinum-catalyzed reductive amination of **5** with amine **16** furnished compound **17**, which was transformed into the related *p*-toluenesulfonamide **18** by reaction with *p*-toluenesulfonyl chloride (Scheme 3). Partial reduction of the latter with diisobutyl aluminium hydride (DIBAH) in toluene at −45°C afforded an unseparable mixture of epimeric lactols **19** ready for cyclization, in an acceptable 50% overall yield from **5**.

When heated in dioxane containing 4 equivalents of 6 N hydrochloric acid, the lactols sluggishly cyclized to give significant decomposition after 75 min and a modest 52% yield of product, to which the expected structure **20** was assigned based on its ^1H NMR signals and nOe data analysis as depicted in Fig. 1. An increase in acid concentration to 6.5 equivalents was detrimental, causing a further decrease in yield to 41%, whereas keeping the heating bath at 140°C shortened the reaction time to 45 min and resulted in 69% recovery of **20**. In addition, 7% of *p*-toluenesulfonamide **21** was isolated; this is known to be produced when cyclization is difficult or impeded (1).

To complete the synthesis, **20** was submitted to a palladium-on-charcoal-catalyzed hydrogenation to give **22** and,

Scheme 4.

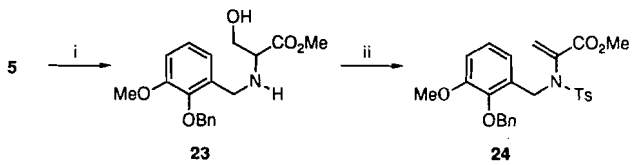

(i) SerOMe.HCl, TEA, H_2/PtO_2, EtOH; (ii) TsCl, pyridine, CH_2Cl_2

Scheme 5.

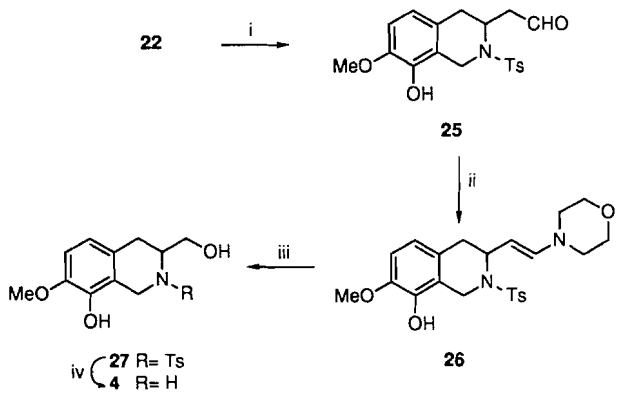

(i) $(F_3CCO)_2O$, DMSO, CH_2Cl_2, -60°C, TEA; (ii) morpholine, 4 Å molecular sieves, benzene; (iii) 1. O_3, Et_2O, -78°C, 2. $NaBH_4$, MeOH; (iv) 1. Na, NH_3, -33°C, 2. NH_4Cl, -33°C to room temp.

finally, this sulfonamide was reductively detosylated, furnishing the 1,2,3,4-tetrahydroisoquinoline **3** in 86% overall yield for both steps.

Having obtained models **2** and **3**, attention was turned to the synthesis of **4**. Unfortunately, the first approach and most direct route to the target proved unsuccessful, as depicted in Scheme 4.

While reductive amination of **5** with serine methyl ester efficiently provided **23**, reaction of this amine with *p*-toluenesulfonyl chloride in pyridine – methylene chloride gave only α,β-unsaturated ester **24** under an ample variety of conditions. This was not surprising, since many serine ester derivatives have shown a tendency towards β-elimination in the presence of base (15, 16).

We then envisaged a second plan, involving a one-carbon degradation of intermediate **22**. As shown in Scheme 5, this was achieved by Swern oxidation of the starting alcohol to **25** in 69% yield, followed by convenient transformation of this aldehyde into its related enamine **26** by reaction with morpholine in benzene under 4Å molecular sieves catalysis (17). Without purification, **26** was ozonized at −78°C (18) employing a sodium borohydride based reductive work-up of the intermediate ozonides, which afforded alcohol **27**. This, in turn, was detosylated with sodium in refluxing liquid ammonia to give **4**, an analog of **1**, in 60% overall yield from **25**.

In conclusion, an effective strategy for the synthesis of 3-substituted tetrahydroisoquinolines by proper modifications of Jackson's sulfonamido acetal cyclization strategy is reported through the elaboration of prototypes **2** and **3**. The first Jackson-type cyclization of a lactol was carried out, leading to a furo[3,4-*b*]isoquinoline derivative, the first such tricyclic structure to be prepared using this route. In addition, as demonstrated by the elaboration of a lower partial analog of MY336-a, the ready availability of the present synthetic scheme seems suitable as a strategy for the first total synthesis of the natural product. This work is underway.

Experimental section

Melting points were measured on an Ernst Leitz hot-stage microscope apparatus and are uncorrected. IR spectra were taken on a Bruker IFS 25 spectrometer with solid samples as KBr pellets and liquid samples as films. ^1H and ^{13}C NMR spectra were recorded in deuteriochloroform unless otherwise stated, on a Bruker AC-200E instrument at 200.13 and 50.32 MHz, respectively, with tetramethylsilane as the internal standard. ^{13}C NMR resonances corresponding to two carbon atoms are designated with an asterisk, while those assigned to three carbons are marked with #. High-resolution mass spectral data were obtained from UMYMFOR (Buenos Aires). All reactions were carried out in a dry nitrogen atmosphere.

General procedure for the reductive amination of 5 and synthesis of *p*-toluenesulfonamides

The amine salt, triethylamine, and pre-reduced platinum oxide in absolute ethanol were successively added to a solution of **5** in absolute ethanol. The reaction was stirred at room temperature under hydrogen at atmospheric pressure until no starting material remained. The catalyst was separated by centrifugation, the volatiles were evaporated under reduced pressure, and the oily residue was dissolved in a 10:1 mixture of methylene chloride – pyridine.

A 0.58 M solution of *p*-toluenesulfonyl chloride in the same solvent was added dropwise to the above solution cooled in an ice-water bath. After stirring overnight, brine (50 mL) was added and the products were extracted with diethyl ether (3 × 50 mL). The combined ethereal extracts were successively washed with 1 N hydrochloric acid (2 × 10 mL), saturated sodium hydrogen carbonate (10 mL), and brine (2 × 10 mL), then dried over sodium sulfate and concentrated under reduced pressure. The residue was flash-chromatographed.

Ethyl-2-[*N*-(2-benzyloxy-3-methoxyphenyl)methyl-*N*-(*p*-toluenesulfonyl)]aminopropanoate (7)

By the general method, reaction of alanine ethyl ester hydrochloride (790 mg, 5.13 mmol), triethylamine (0.714 mL, 5.13 mmol), platinum oxide (70 mg), and **5** (1241 mg, 5.13 mmol) in absolute ethanol (25 mL) provided amine **6** (1619 mg, 92%) as an oil; IR (film): 3750–3100, 2978, 2954, 1730, 1586, 1478, 1274, 1184, 1082, 986, 752, and 698 cm^{-1}; ^1H NMR δ: 1.22 (3H, t, J = 11 Hz, OCH_2CH_3), 1.25 (3H, d, J = 7 Hz, $CHCH_3$), 1.90 (1H, br s, $w_{1/2}$ = 15 Hz, NH), 3.30 (1H, q, J = 7 Hz, $CHCH_3$), 3.70 (2H, q, J = 11 Hz, OCH_2CH_3), 3.88 (3H, s, OCH_3), 4.10 (2H, ABq, J = 7.1 Hz, Δδ = 0.07, $ArCH_2N$), 5.04 (2H, s, OCH_2Ph), 6.86 (1H, dd, J = 1.8, 7.7 Hz, ArH), 6.90 (1H, dd, J = 1.8, 7.7 Hz, ArH), 7.07 (1H, t, J = 7.7 Hz, ArH), and 7.31–7.49 (5H, m, ArH of benzyl); ^{13}C NMR δ : 14.10, 16.82, 46.67, 55.73, 55.93, 60.42, 74.77, 111.51, 121.62, 123.88, 127.78, 128.14*, 128.23*, 133.82, 137.79, 146.09, 152.62, and 175.33.

Following the general method, the reaction of the *p*-toluenesulfonyl chloride solution (7.2 mL, 4.19 mmol) with **6** (1250 mg, 3.64 mmol) in methylene chloride – pyridine (22

Can. J. Chem. Downloaded from www.nrcresearchpress.com by 80.90.12.36 on 09/08/12
For personal use only.

Can. J. Chem. Downloaded from www.nrcresearchpress.com by 80.90.12.36 on 09/08/12
For personal use only.

mL) gave sulfonamide **7** (1502 mg, 83%) as an oil; IR (film): 2988, 2940, 1736, 1596, 1584, 1478, 1334, 1220, 1160, 1070, 982, 862, 760, 702, and 662 cm^{-1}; ^1H NMR δ: 1.02 (3H, t, J = 7 Hz, CH_2CH_3), 1.18 (3H, d, J = 7.3 Hz, $CHCH_3$), 2.41 (3H, s, $ArCH_3$), 3.80 (3H, s, OCH_3), 3.82 (2H, q, J = 7 Hz, CH_2CH_3), 4.40 (2H, s, $ArCH_2N$), 4.50 (1H, q, J = 7.3 Hz, $CHCH_3$), 5.01 (2H, ABq, J = 18 Hz, Δδ = 0.09, OCH_2Ph), 6.85 (1H, dd, J = 1.8, 7.9 Hz, ArH), 7.04 (1H, t, J = 7.9 Hz, ArH), 7.13 (1H, dd, J = 1.8, 7.9 Hz, ArH), 7.29–7.39 (5H, m, ArH of benzyl), and 7.43 (4H, ABq, J = 8.5 Hz, Δδ = 0.37, ArH of *p*-toluenesulfonamide); ^{13}C NMR δ: 13.58, 16.30, 21.31, 43.68, 55.42, 55.62, 60.81, 74.46, 111.16, 120.81, 123.79, 127.35*, 127.83, 128.19*, 128.35*, 129.19*, 132.09, 136.92, 137.37, 143.04, 144.51, 152.06, and 170.86; HRMS calcd. for $C_{27}H_{31}NO_6S$: 497.1872; found: 497.1891.

2-[*N*-(2-Benzyloxy-3-methoxyphenyl)methyl-*N*-(*p*-toluenesulfonyl)]amino-γ-butyrolactone (18)

Following the general procedure, reaction of the hydrobromide of **16** (750 mg, 4.13 mmol), triethylamine (0.575 mL, 4.13 mmol), platinum oxide (70 mg), and aldehyde **5** (1000 mg, 4.13 mmol) in absolute ethanol (25 mL) afforded **17** (1230 mg, 91%) as an oil; IR (film): 3600–3100, 2938, 1778, 1584, 1478, 1378, 1274, 1170, 1018, 982, 754, and 700 cm^{-1}; ^1H NMR δ: 1.80–1.90 (1H, br s, $w_{1/2}$ = 10 Hz, NH), 1.91–2.09 (1H, m, $CHCH_2$), 2.22–2.43 (1H, m, $CHCH_2$), 3.32–3.46 (1H, m, $CHC{=}O$), 3.78 (2H, s, $ArCH_2N$), 3.90 (3H, s, OCH_3), 4.07 (1H, dt, J = 6.4, 9.3 Hz, CH_2O), 4.30 (1H, dt, J = 2.4, 9.3 Hz, CH_2O), 5.05 (2H, ABq, J = 11 Hz, Δδ = 0.10, OCH_2Ph), 6.88 (1H, d, J = 7.9 Hz, ArH), 6.95 (1H, dd, J = 2.1, 7.9 Hz, ArH), 6.98 (1H, dd, J = 2.1, 7.9 Hz, ArH), and 7.30–7.48 (5H, m, ArH of benzyl); ^{13}C NMR δ: 29.75, 46.30, 54.62, 55.27, 65.19, 74.46, 111.33, 121.23, 123.64, 127.53, 127.87*, 127.91*, 132.68, 137.22, 145.65, 152.18, and 176.76.

By the general procedure, addition of the *p*-toluenesulfonyl chloride solution (1.4 mL, 0.81 mmol) to **17** (225 mg, 0.69 mmol) dissolved in methylene chloride – pyridine (4 mL) provided **18** (422 mg, 88%) as an oil; IR (film): 2938, 1784, 1598, 1478, 1336, 1274, 1160, 1088, 1020, and 754 cm^{-1}; ^1H NMR δ: 2.12–2.29 (2H, m, $CHCH_2$), 2.43 (3H, s, $ArCH_3$), 3.89 (3H, s, OCH_3), 3.98–4.32 (3H, m, $CHCH_2$), 4.29 (2H, q, J = 10.1 Hz, $ArCH_2N$), 4.99 (2H, ABq, J = 11 Hz, Δδ = 0.08, OCH_2Ph), 6.86 (1H, dd, J = 3, 8 Hz, ArH), 7.00 (1H, d, J = 8 Hz, ArH), 7.02 (1H, dd, J = 3, 8 Hz, ArH), 7.32 (5H, s, ArH of benzyl), and 7.55 (4H, ABq, J = 8.3 Hz, Δδ = 0.53, ArH of *p*-toluenesulfonamide); ^{13}C NMR δ: 21.13, 27.17, 44.68, 55.38, 56.37, 64.89, 74.29, 111.61, 120.68, 123.93, 127.50*, 127.79, 128.02*, 128.44*, 129.12*, 130.05, 136.24, 136.71, 143.35, 144.56, 152.03, and 172.87; HRMS calcd. for $C_{26}H_{27}NO_6S$: 481.1559; found: 481.1572.

Methyl-2-[*N*-(2-benzyloxy-3-methoxyphenyl)methyl-*N*-(*p*-toluenesulfonyl)]aminopropenoate (24)

Employing the general procedure, serine methyl ester hydrochloride (1098 mg, 7.06 mmol), triethylamine (0.982 mL, 7.06 mmol), platinum oxide (80 mg), and aldehyde **5** (1708 mg, 7.06 mmol) in absolute ethanol (28 mL) afforded **23** (2263 mg, 92%) as an oil; IR (film): 3600–3080, 2950, 1734, 1654, 1586, 1478, 1376, 1274, 1206, 1182, 1080, and 754 cm^{-1}; ^1H NMR δ: 2.10 (2H, br s, $w_{1/2}$ = 17 Hz, NH and OH), 3.35 (1H, dd, J = 4.5, 5.9 Hz, $CHCO_2CH_3$), 3.55 (1H, dd, J = 5.9, 10.8 Hz, CH_2OH), 3.64 (3H, s, CO_2CH_3), 3.70 (2H, d, J = 4.3 Hz, $ArCH_2N$), 3.71 (1H, dd, J = 4.5, 10.8 Hz, CH_2OH), 3.89 (3H, s, OCH_3), 5.04 (2H, s, OCH_2Ph), 6.87 (1H, d, J = 8.4 Hz, ArH), 6.88 (1H, d, J = 7.4 Hz, ArH), 7.04 (1H, dd, J = 7.4, 8.4 Hz, ArH), and 7.31–7.45 (5H, m, ArH of benzyl); ^{13}C NMR δ: 46.28, 51.50, 55.36, 61.52, 61.91, 74.46, 111.36, 121.32, 123.71, 127.56, 127.87*, 127.97*, 132.91, 137.33, 145.70, 152.25, and 172.93.

By the general procedure, reaction of the *p*-toluenesulfonyl chloride solution (0.65 mL, 0.38 mmol) with **23** (50 mg, 0.15 mmol) in methylene chloride – pyridine (1 mL) provided **24** (61 mg, 85%) as a solid, mp 113.5-115°C (hexane – diethyl ether); IR(KBr): 2946, 1728, 1632, 1586, 1480, 1342, 1272, 1162, 1074, 982, 798, and 712 cm^{-1}; ^1H NMR δ: 2.44 (3H, s, $ArCH_3$), 3.52 (3H, s, CO_2CH_3), 3.86 (3H, s, OCH_3), 4.47 (2H, s, $ArCH_2N$), 4.91 (2H, s, OCH_2Ph), 5.41 (1H, s, $C{=}CH_2$), 6.12 (1H, s, $C{=}CH_2$), 6.83 (1H, d, J = 7.5 Hz, ArH), 6.86 (1H, d, J = 7.5 Hz, ArH), 7.04 (1H, t, J = 7.5 Hz, ArH), 7.32 (5H, s, ArH of benzyl), and 7.47 (4H, ABq, J = 8.2 Hz, Δδ = 0.40, ArH of *p*-toluenesulfonamide); ^{13}C NMR δ: 21.39, 46.47, 51.96, 55.56, 74.74, 111.67, 121.57, 124.01, 127.03, 127.71*, 127.84*, 128.16*, 128.27*, 129.17*, 129.47, 135.51, 135.56, 137.23, 143.36, 152.23, and 164.05; HRMS calcd. for $C_{26}H_{27}NO_6S$: 481.1559; found: 481.1553.

2-[*N*-(2-Benzyloxy-3-methoxyphenyl)methyl-*N*-(*p*-toluenesulfonyl)]aminopropan-1-ol (8)

To a solution of sulfonamide **7** (1120 mg, 2.25 mmol) in a 1:1 THF–EtOH mixture (30 mL) were successively added lithium bromide (392 mg, 4.51 mmol) and sodium borohydride (172 mg, 4.51 mmol). The reaction was stirred overnight at 40°C, then 10% w/v citric acid solution (10 mL) was added, the organic solvents were evaporated under reduced pressure, and the reaction products were extracted with ethyl acetate (3 × 30 mL). The extract was dried, concentrated, and chromatographed, affording **8** as an oil (870 mg, 85%); IR (film): 3490, 3030, 2970, 2942, 1600, 1586, 1478, 1328, 1270, 1154, 1090, 1030, 970, 854, 816, 756, 658, and 622 cm^{-1}; ^1H NMR δ: 0.74 (3H, d, J = 6.9 Hz, $CHCH_3$), 1.78 (1H, dd, J = 6.9, 7.2 Hz, $CHCH_3$), 2.43 (3H, s, $ArCH_3$), 3.16 (2H, t, J = 7.2 Hz, CH_2OH), 3.89 (3H, s, OCH_3), 4.19 (2H, ABq, J = 16 Hz, Δδ = 0.12, $ArCH_2N$), 5.01 (2H, ABq, J = 11.3 Hz, Δδ = 0.15, OCH_2Ph), 6.86 (1H, dd, J = 1.6, 8.1 Hz, ArH), 7.10 (1H, t, J = 8.1 Hz, ArH), 7.23 (1H, dd, J = 1.6, 8.1 Hz, ArH), 7.34 (5H, s, ArH of benzyl), and 7.45 (4H, ABq, J = 8 Hz, Δδ = 0.36, ArH *p*-toluenesulfonamide); ^{13}C NMR δ: 13.45, 21.29, 40.84, 55.56, 55.73, 64.18, 74.95, 111.35, 120.86, 124.33, 126.82, 127.97*, 128.24*, 128.44*, 129.45*, 132.20, 137.09, 137.54, 143.00, 144.43, and 152.17; HRMS calcd. for $C_{25}H_{29}NO_5S$: 455.1766; found: 455.1783.

2-[*N*-(2-Benzyloxy-3-methoxyphenyl)methyl-*N*-(*p*-toluenesulfonyl)]aminopropanal dimethyl acetal (10)

A methylene chloride solution of dimethyl sulfoxide (4.26 mL, 9.32 mmol) was dropwise added in 2 min to a stirred solution of oxalyl chloride (4.66 mmol) in the same solvent (3 mL) cooled to −60°C. After 5 min, a solution of alcohol **8** (707 mg, 1.55 mmol) in methylene chloride (3 mL) was incorporated dropwise. The mixture was stirred for 15 min at −60°C, followed by addition of triethylamine (1.73 mL, 12.43 mmol). Then it was left to react for 15 min at −60°C and 15 min at

Can. J. Chem. Downloaded from www.nrcresearchpress.com by 80.90.12.36 on 09/08/12
For personal use only.

room temperature; the reaction was quenched with brine (10 mL) and the product was extracted with diethyl ether (3 × 30 mL). The extracts were combined, dried over sodium sulfate, concentrated under reduced pressure, and chromatographed to furnish aldehyde **9** (672 mg, 95%); IR (film): 3030, 2962, 2898, 1736, 1598, 1482, 1352, 1336, 1274, 1158, 1078, 1012, 976, 814, 750, and 664 cm^{-1}; ^1H NMR δ: 1.03 (3H, d, J = 7 Hz, $CHCH_3$), 2.44 (3H, s, $ArCH_3$), 3.87 (3H, s, OCH_3), 3.94 (1H, q, J = 7 Hz, $CHCH_3$), 4.18 (2H, ABq, J = 15 Hz, Δδ = 0.07, $ArCH_2N$), 4.98 (2H, s, OCH_2Ph), 6.87 (1H, t, J = 5.2 Hz, ArH), 7.05 (2H, d, J = 5.2 Hz, ArH), 7.32 (5H, s, ArH of benzyl), 7.46 (4H, ABq, J = 8.3 Hz, Δδ = 0.40, ArH of *p*-toluenesulfonamide), and 9.32 (1H, s, CHO); ^{13}C NMR δ: 11.06, 21.41, 43.43, 55.68, 61.78, 74.96, 112.07, 121.51, 124.31, 127.22*, 128.07, 128.31*, 128.46*, 129.68#, 128.88, 137.06, 143.59, 145.48, 152.39, and 198.90.

Tosic acid (16 mg, 0.085 mmol) and 2,2-dimethoxypropane (0.30 mL) were successively added to a solution of aldehyde **9** (193 mg, 0.426 mmol) in absolute methanol (8 mL). After stirring overnight at room temperature, saturated sodium hydrogen carbonate (1 mL) and brine (10 mL) were added and the alcohol was removed under reduced pressure. The reaction products were extracted with diethyl ether (3 × 40 mL), dried over sodium sulfate, concentrated, and chromatographed to give acetal **10** (210 mg, 99%) as a solid, mp 107–108.5°C (hexane – diethyl ether); IR (KBr): 3030, 2936, 2836, 1598, 1586, 1478, 1452, 1340, 1272, 1158, 1088, 972, 816, 756, and 658 cm^{-1}; ^1H NMR δ: 0.84 (3H, d, J = 6.9 Hz, $CHCH_3$), 2.41 (3H, s, $ArCH_3$), 3.01 (3H, s, $CHOCH_3$), 3.18 (3H, s, $CHOCH_3$), 3.87 (3H, s, OCH_3), 3.98 (1H, dq, J = 6.9 , 5.2 Hz, $CHCH_3$), 4.07 (1H, d, J = 5.2 Hz, $CH(OCH_3)_2$), 4.30 (2H, s, $ArCH_2N$), 5.01 (2H, ABq, J = 11 Hz, Δδ = 0.05, OCH_2Ph), 6.83 (1H, dd, J = 1.4, 8 Hz, ArH), 7.05 (1H, t, J = 8 Hz, ArH), 7.19 (1H, dd, J = 1.4, 8 Hz, ArH), 7.30–7.43 (5H, m, ArH of benzyl), and 7.45 (4H, ABq, J = 8.4 Hz, Δδ = 0.40, ArH of *p*-toluenesulfonamide); ^{13}C NMR δ: 12.06, 21.33, 42.22, 54.28, 54.64, 55.05, 55.71, 74.56, 105.96, 110.92, 121.05, 123.74, 127.16*, 127.83, 128.23#, 129.29#, 132.79, 137.62, 137.92, 142.81, 144.68, and 152.10; HRMS calcd. for $C_{27}H_{33}NO_6S$: 499.2028; found: 499.2035.

Cyclization of aldehyde 9 to (3*R**,4*S**)-8-benzyloxy-4-hydroxy-7-methoxy-3-methyl-2-(*p*-toluenesulfonyl)-1,2,3,4-tetrahydrosoquinoline (12) and 8-benzyloxy-1,2-dihydro-7-methoxy-3-methyl-2-(*p*-toluenesulfonyl)isoquinoline (11)

Aldehyde **9** (65 mg, 0.144 mmol) in dioxane (0.7 mL) containing 6 N hydrochloric acid (0.01 mL, 4 equiv.) was heated under reflux for 20 min; the solution was cooled to room temperature, made basic with saturated sodium hydrogen carbonate (0.5 mL), diluted with brine (5 mL), and extracted with ethyl acetate (3 × 30 mL). The combined extracts were washed with brine (5 mL), dried, and concentrated under reduced pressure to give a crude that was chromatographed, yielding 1,2-dihydroisoquinoline **11** as an oil (9 mg, 12%); IR (film): 3032, 2924, 2840, 1598, 1492, 1348, 1272, 1162, 1088, 1038, 812, 708, and 630 cm^{-1}; ^1H NMR δ: 2.21 (3H, s, CH_3-3), 2.25 (3H, s, $ArCH_3$), 3.81 (3H, s, OCH_3), 4.55 (2H, s, H-1), 4.98 (2H, s, OCH_2Ph), 6.02 (1H, s, H-4), 6.47 (2H, ABq, J = 8.2 Hz, Δδ = 0.17, H-5 and H-6), 7.18 (4H, ABq, J = 8.4 Hz, Δδ = 0.46, ArH of *p*-toluenesulfonamide), and 7.30–7.45 (5H, m, ArH of benzyl); ^{13}C NMR δ: 21.14, 22.01, 44.66, 55.78, 74.80, 110.60, 118.96, 119.46, 123.59, 125.04, 126.81*, 128.05, 128.32#, 128.39*, 128.52*, 135.17, 135.26, 137.03, 142.77, and 152.00; HRMS calcd. for $C_{25}H_{25}NO_4S$: 435.1504; found: 435.1511.

Increasing the polarity of the eluent furnished alcohol **12** (52 mg, 70%) as a solid, mp 111–113°C (hexane – diethyl ether); IR (KBr): 3346, 2968, 2886, 1606, 1598, 1492, 1346, 1278, 1166, 1068, 958, 820, 750, and 674 cm^{-1}; ^1H NMR δ: 0.59 (3H, d, J = 6.9 Hz, CH_3-3), 2.30 (1H, br s, $w_{1/2}$ = 15 Hz, OH), 2.43 (3H, s, $ArCH_3$), 3.56 (1H, d, J = 16.8 Hz, H-1_{ax}), 3.90 (3H, s, OCH_3), 4.28 (1H, br s, H-4), 4.33 (1H, dq, J = 6.9, 2.0 Hz, H-3), 4.71 (1H, d, J = 16.8 Hz, H-1_{eq}), 5.13 (2H, ABq, J = 12 Hz, Δδ = 0.11, OCH_2Ph), 6.84 (2H, ABq, J = 8 Hz, Δδ = 0.13, H-5 and H-6), 7.30–7.38 (5H, m, ArH of benzyl), and 7.50 (4H, ABq, J = 8.2 Hz, Δδ = 0.42, ArH of *p*-toluenesulfonamide); ^{13}C NMR δ: 12.60, 21.42, 38.95, 54.14, 55.74, 70.65, 74.23, 111.75, 125.90, 126.53, 126.71, 127.23*, 128.09, 128.34*, 128.42*, 129.63*, 136.34, 137.23, 143.08, 143.37, and 151.90; HRMS calcd. for $C_{25}H_{27}NO_5S$: 453.1609; found: 453.1590.

(3*aR**,3*bR**)-6-Benzyloxy-7-methoxy-4-(*p*-toluenesulfonyl)-2,3,3*a*,3*b*,4,5-hexahydrofuro[3,4-*b*]isoquinoline (20)

A solution of DIBAH in toluene (1.5 M, 0.63 mL, 0.94 mmol) was added dropwise to a stirred solution of lactone **18** (430 mg, 0.894 mmol) in toluene (10 mL) at −45°C. When no starting material remained (TLC) saturated ammonium chloride was added (5 mL), the reaction was warmed to room temperature, and the products were extracted with diethyl ether (4 × 20 mL). The organic extracts were dried over sodium sulfate, concentrated under reduced pressure, and chromatographed to afford lactols **19** as an inseparable mixture (353 mg, 82%); IR (film): 3534, 2924, 1598, 1478, 1160, and 660 cm^{-1}.

The above mixture of lactols (200 mg, 0.43 mmol) was dissolved in dioxane (10 mL) and 6 N hydrochloric acid (0.25 mL, 1.52 mmol) was added dropwise. After heating the vigorously stirred biphasic system at 140°C for 45 min, it was cooled to room temperature, the acid was carefully neutralized with saturated sodium hydrogen carbonate, brine (7 mL) was added, and the reaction products were extracted with diethyl ether (4 × 25 mL). Drying, concentration, and chromatographic purification of the combined ethereal extracts provided **20** (140 mg, 69%) as a solid, mp 107–108°C (hexane – diethyl ether); IR (KBr): 2928, 1598, 1496, 1330, 1278, 1160, 1088, 920, 814, and 700 cm^{-1}; ^1H NMR δ: 1.70–1.90 (1H, m, $CHCH_2$), 2.09–2.25 (1H, m, $CHCH_2$), 2.42 (3H, s, $ArCH_3$), 3.60–3.75 (2H, m, CH_2O), 3.69 (1H, d, J = 16.2 Hz, H-1_{ax}), 3.86 (3H, s, OCH_3), 4.67 (2H, br s, H-3 and H-4), 4.87 (1H, d, J = 16.2 Hz, H-1_{eq}), 4.98 (2H, s, OCH_2Ph), 6.6 (2H, ABq, J = 8.4 Hz, Δδ = 0.14, H-5 and H-6), 7.28–7.48 (5H, m, ArH of benzyl), and 7.31 (4H, ABq, J = 8 Hz, Δδ = 0.41, ArH of *p*-toluenesulfonamide); ^{13}C NMR δ: 21.25, 29.53, 38.18, 55.57, 55.71, 65.43, 74.00, 74.73, 111.27, 124.90, 125.97, 126.97*, 127.98, 128.29*, 128.37*, 129.22#, 136.12, 137.19, 142.96, 143.00, and 151.95; HRMS calcd. for $C_{26}H_{27}NO_5S$: 465.1610; found: 465.1602.

An increase in solvent polarity produced the elution of **21** (12 mg, 7%), as a solid, mp 105–106°C (hexane – diethyl ether); IR (KBr): 3260, 2948, 1588, 1482, 1322, 1274, 1160,

Can. J. Chem. Downloaded from www.nrcresearchpress.com by 80.90.12.36 on 09/08/12
For personal use only.

1052, 986, and 750 cm^{-1}; ^1H NMR δ: 2.38 (3H, s, $ArCH_3$), 3.85 (3H, s, OCH_3), 3.91 (2H, d, J = 6.5 Hz, $ArCH_2N$), 4.75 (1H, t, J = 6.5 Hz, NH), 4.95 (2H, s, OCH_2Ph), 6.72 (1H, dd, J = 2, 8 Hz, ArH), 6.83 (1H, dd, J = 2, 7.7 Hz, ArH), 6.90 (1H, dd, J = 7.7, 8 Hz, ArH), 7.22–7.33 (5H, m, ArH of benzyl), and 7.38 (4H, ABq, J = 8.3 Hz, Δδ = 0.41, ArH of *p*-toluenesulfonamide); ^{13}C NMR δ: 21.27, 42.95, 55.57, 74.54, 112.03, 121.29, 123.98, 126.80*, 128.05, 128.28#, 128.31*, 129.24, 130.15, 136.63, 136.86, 142.82, 145.11, and 152.13; HRMS calcd. for $C_{22}H_{23}NO_4S$: 397.1348; found: 397.1350.

Dehydration of alcohol 12 to 1,2-dihydroisoquinoline 11

Anhydrous copper(II) sulfate supported on silica gel (17.7 mg, 1:3 w/w, 1.1 equiv.) was added to a solution of the alcohol (8 mg, 0.018 mmol) in 1,1,2,2-tetrachloroethane (1 mL). The mixture was heated and stirred for 1 h at 100°C. After separation of the catalyst by centrifugation, the supernatant was chromatographed, affording **11** (6 mg, 80%).

(3*S,4*S**)-8-Benzyloxy-4-hydroxy-7-methoxy-3-methyl-2-(*p*-toluenesulfonyl)-1,2,3,4-tetrahydroisoquinoline (13) by Mitsunobu inversion of alcohol 12**

Diethylazodicarboxylate (0.33 mL, 2.1 mmol) was added dropwise to a stirred solution of alcohol **12** (200 mg, 0.43 mmol), triphenylphosphine (550 mg, 2.1 mmol), and *p*-nitrobenzoic acid (320 mg, 1.9 mmol) in dry benzene (20 mL) at room temperature. The solution was stirred for 4 h, whereupon the volatile components were removed under reduced pressure and the residue was chromatographed, yielding the *p*-nitrobenzoate **14** (130 mg, 50%) as a solid, mp 64–65°C (hexane – diethyl ether); IR (KBr): 2942, 1726, 1608, 1526, 1496, 1350, 1266, 1162, 1090, 980, 812, 736, 718, and 670 cm^{-1}; ^1H NMR δ: 0.83 (3H, d, J = 6.8 Hz, CH_3-3), 2.41 (3H, s, $ArCH_3$), 3.87 (1H, d, J = 16.8 Hz, H-1_{ax}), 3.90 (3H, s, OCH_3), 4.68 (1H, dq, J = 5.3, 6.8 Hz, H-3), 4.71 (1H, d, J = 16.8 Hz, H-1_{eq}), 5.10 (2H, ABq, J = 11.2 Hz, Δδ = 0.08, OCH_2Ph), 6.05 (1H, d, J = 5.3 Hz, H-4), 6.90 (2H, ABq, J = 8.6 Hz, Δδ = 0.09, H-5 and H-6), 7.30–7.40 (5H, m, ArH of benzyl), 7.46 (4H, ABq, J = 8.3 Hz, Δδ = 0.42, ArH of *p*-toluenesulfonamide), and 8.27 (4H, ABq, J = 9.1 Hz, Δδ = 0.10, ArH of *p*-nitrobenzoate); ^{13}C NMR δ: 10.92, 21.41, 39.44, 48.38, 55.79, 71.08, 74.33, 111.44, 121.70, 123.62, 123.82*, 126.76, 127.07*, 128.22*, 128.42*, 128.54*, 129.65, 130.75*, 134.96, 136.68, 137.14, 143.04, 143.37, 150.74, 151.63, and 163.84.

Sodium hydroxide (50 mg) was added to a solution of ester **14** (100 mg, 0.16 mmol) in methanol (4 mL). After stirring for 1 h at room temperature, the solution was neutralized with 1 N hydrochloric acid, brine (5 mL) was added, the organic solvent was removed under reduced pressure, and the reaction products were extracted with diethyl ether (3 × 15 mL). Chromatographic purification of the dried and concentrated extract afforded alcohol **13** as an oil (74 mg, 100%); IR (film): 3504, 2920, 2850, 1654, 1598, 1492, 1438, 1324, 1280, 1162, 1074, 1026, 814, 736, and 670 cm^{-1}; ^1H NMR δ: 0.64 (3H, d, J = 6.8 Hz, CH_3-3), 1.65 (1H, br s, $w_{1/2}$ = 13 Hz, OH), 2.41 (3H, s, $ArCH_3$), 3.75 (1H, d, J = 16.9 Hz, H-1_{ax}), 3.89 (3H, s, OCH_3), 4.33 (1H, dq, J = 6.8, 5.6 Hz, H-3), 4.64 (1H, d, J = 16.9 Hz, H-1_{eq}), 4.81 (1H, bd, J = 5.6 Hz, H-4), 5.06 (2H, ABq, J = 11.3 Hz, Δδ = 0.09, OCH_2Ph), 7.07 (2H, ABq, J = 8.6 Hz, Δδ = 0.34, H-5 and H-6), 7.22–7.39 (7H, m, ArH of benzyl and ArH of *p*-toluenesulfonamide), and 7.64 (2H, d, J = 8.3 Hz, ArH of *p*-toluenesulfonamide); ^{13}C NMR δ: 21.37*, 39.59, 50.99, 55.74, 68.31, 74.16, 111.42, 121.46, 125.97, 127.02*, 128.05, 128.31#, 128.43*, 129.58*, 136.71, 137.27, 142.71, 143.17, and 151.01; HRMS calcd. for $C_{25}H_{27}NO_5S$: 453.1609; found: 453.1595.

Dehydration of alcohol 13 to 1,2-dihydroisoquinoline 11

A solution of alcohol **13** (80 mg, 0.18 mmol) in dioxane (0.7 mL) and 6 N hydrochloric acid (0.12 mL, 4 mol. equiv.) was heated under reflux for 20 min and cooled to room temperature, then saturated sodium hydrogen carbonate (0.5 mL) and brine (5 mL) were added and the products were extracted with ethyl acetate (3 × 30 mL). The extracts were washed with brine (5 mL), dried, and the solvent was removed under reduced pressure to give a crude, chromatography of which furnished 1,2-dihydroisoquinoline **11** as an oil (63 mg, 80%).

General method for the reductive detosylation of 2-(*p*-toluenesulfonyl)-1,2,3,4-tetrahydroisoquinolines

A solution of the sulfonamide in dry THF was added to anhydrous liquid ammonia contained in a three-necked flask, fitted with a Dry Ice – acetone condenser protected with a sodium hydroxide tube and an ammonia inlet. With rapid stirring, sodium metal contained in a graduated glass tube was slowly added to the solution until the characteristic blue color persisted for about 10 min. The reaction was quenched with ammonium chloride (4 mol. equiv.), the solvent was evaporated at room temperature, and the residue was mixed with methanol (2 mL). The methanolic solution was mixed with silica gel, the solvent was removed under reduced pressure, and the adsorbed reaction product was chromatographed.

8-Hydroxy-7-methoxy-3-methyl-1,2,3,4-tetrahydroisoquinoline (2)

To a solution of alcohol **12** (20 mg, 0.044 mmol) in methanol (2 mL) were added 10% Pd/C (3 mg) and 6 N hydrochloric acid (0.5 mL). The reaction was stirred overnight under hydrogen at 3 atm (1 atm = 101.3 kPa), then the catalyst was separated by centrifugation and washed twice with methanol (0.5 mL). Solvent evaporation under reduced pressure and chromatography provided **15** (15 mg, 98%) as an oil; IR (film): 3440, 2922, 2848, 1596, 1498, 1332, 1282, 1158, 1068, 960, 816, 724, and 670 cm^{-1}; ^1H NMR δ: 0.95 (3H, d, J = 6.8 Hz, CH_3-3), 2.38 (3H, s, $ArCH_3$), 2.43 (1H, dd, J = 1.8, 10.8 Hz, H-4_{ax}), 2.97 (1H, dd, J = 5.4, 10.8 Hz, H-4_{eq}), 3.85 (3H, s, OCH_3), 4.06 (1H, d, J = 16.5 Hz, H-1_{ax}), 4.45 (1H, ddd, J = 1.8, 5.4, 6.8 Hz, H-3), 4.80 (1H, d, J = 16.5 Hz, H-1_{eq}), 5.70 (1H, br s, OH), 6.61 (2H, ABq, J = 7.9 Hz, Δδ = 0.16, H-5 and H-6), and 7.48 (4H, ABq, J = 8.3 Hz, δ = 0.49, ArH of *p*-toluenesulfonamide); ^{13}C NMR δ: 16.43, 21.34, 34.43, 38.38, 47.25, 56.01, 109.21, 117.94, 119.91, 125.20, 127.09*, 129.45*, 137.01, 141.46, 142.91, and 144.14.

Following the general detosylation procedure, a solution of sulfonamide **15** (20 mg, 0.058 mmol) in THF (0.8 mL) was added to anhydrous liquid ammonia (4 mL). After reaction with sodium, ammonium chloride quench, and the usual work-up, tetrahydroisoquinoline **2** (10 mg, 90%) was recovered as a solid, mp 226–230°C (methanol – diethyl ether); IR (KBr): 3700–2500, 2940, 2926, 1588, 1500, 1384, 1288, 1242, and 880 cm^{-1}; ^1H NMR δ (D_2O, HOD at δ_H 4.60): 1.27 (3H, d, J = 6.5 Hz, CH_3-3), 2.63 (1H, dd, J = 10.3, 17.3 Hz, H-4), 2.89

Can. J. Chem. Downloaded from www.nrcresearchpress.com by 80.90.12.36 on 09/08/12
For personal use only.

(1H, dd, J = 4.5, 17.3 Hz, H-4), 3.39 (1H, ddt, J = 4.5, 6.5, 10.3 Hz, H-3), 3.67 (3H, s, OCH_3), 4.12 (2H, ABq, J = 16.2 Hz, $\Delta\delta$ = 0.22, H-1), and 6.70 (2H, ABq, J = 8.4 Hz, $\Delta\delta$ = 0.23, H-5 and H-6); ^{13}C NMR δ (D_2O, dioxane at δ_C 66.64): 18.82, 33.06, 41.62, 50.89, 57.67, 113.52, 116.52, 121.20, 125.88, 143.36, and 146.93; HRMS calcd. for $C_{11}H_{15}NO_2$: 193.1103; found: 193.1097.

8-Hydroxy-3-(2-hydroxyethyl)-7-methoxy-1,2,3,4-tetrahydroisoquinoline (3)

To a solution of compound **20** (150 mg, 0.322 mmol) in a 2:1 methanol – diethyl ether mixture (3 mL) were added 10% Pd/C (15 mg) followed by 7.2 N sulfuric acid (0.30 mL), and the reaction was stirred overnight under hydrogen at 4 atm. The catalyst was separated by centrifugation, the solvent was removed under reduced pressure, and the crude product was chromatographed, yielding **22** (119 mg, 98%) as needles, mp 160–160.5°C (hexane – ethyl acetate); IR (KBr): 3750–3300, 2930, 1498, 1328, 1282, 1158, 1062, 954, 874, 722, and 676 cm^{-1}; ^1H NMR δ: 1.53–1.64 (2H, m, $CHCH_2$), 2.36 (3H, s, $ArCH_3$), 2.38 (1H, dd, J = 1.9, 12.9 Hz, H-4_{ax}), 2.63 (1H, dd, J = 5.9, 12.9 Hz, H-4_{eq}), 3.63 (1H, dt, J = 4.3 Hz, 11.9, CH_2OH), 3.78 (1H, dt, J = 6.5, 11.9 Hz, CH_2OH), 3.84 (3H, s, OCH_3), 4.25 (1H, d, J = 17.7 Hz, H-1_{ax}), 4.44 (1H, m, H-3), 4.79 (1H, d, J = 17.7 Hz, H-1_{eq}), 5.80 (2H, br s, $w_{1/2}$ = 13 Hz, ArOH and CH_2OH), 6.57 (2H, ABq, J = 8.3 Hz, $\Delta\delta$ = 0.19, H-5 and H-6), and 7.44 (4H, d, J = 8.2 Hz, $\Delta\delta$ = 0.47, ArH of *p*-toluenesulfonamide); ^{13}C NMR δ: 21.29, 31.77, 34.28, 38.78, 48.01, 55.93, 58.51, 109.13, 117.35, 119.63, 124.84, 126.65*, 129.51*, 137.11, 141.50, 143.08, and 144.22.

By the general procedure, a solution of sulfonamide **22** (30 mg, 0.080 mmol) in THF (0.9 mL) was added to anhydrous liquid ammonia (7 mL). Reaction with a slight excess of sodium was followed by ammonium chloride quench and the usual work-up to provide tetrahydroisoquinoline **3** (16 mg, 88%) as a yellowish solid, mp 254–257.5°C (methanol – diethyl ether); IR (KBr): 3700–2200, 3400, 2942, 1502, 1438, 1292, 1090, 878, and 618 cm^{-1}; ^1H NMR δ (D_2O, HOD at δ_H 4.60): 1.60–1.90 (2H, m, CH_2CH_2OH), 2.63 (1H, dd, J = 10.5, 17 Hz, H-4_{ax}), 2.84 (1H, dd, J = 4.6, 17 Hz, H-4_{eq}), 3.25–3.40 (1H, m, H-3), 3.54–3.67 (2H, m, CH_2OH), 3.61 (3H, s, OCH_3), 4.04 (2H, ABq, J = 16.3 Hz, $\Delta\delta$ = 0.24, H-1), and 6.63 (2H, ABq, J = 8.4 Hz, $\Delta\delta$ = 0.22, H-5 and H-6); ^{13}C NMR δ (D_2O, dioxane at δ_C 66.64): 32.47, 36.49, 43.19, 54.42, 58.70, 60.37, 114.50, 117.94, 122.25, 126.71, 144.56, and 148.07; HRMS calcd. for $C_{12}H_{17}NO_3$: 223.1208; found: 223.1209.

3-Formylmethyl-8-hydroxy-7-methoxy-2-(*p*-toluenesulfonyl)-1,2,3,4-tetrahydroisoquinoline (25)

A methylene chloride solution of dimethyl sulfoxide (0.695 mL, 1.33 mmol) was added dropwise in 2 min to a stirred solution of trifluoroacetic anhydride (0.67 mmol) in the same solvent (1.5 mL) cooled to −60°C. After stirring for 15 min, a solution of alcohol **22** (125 mg, 0.33 mmol) in methylene chloride (1 mL) was incorporated dropwise. After a 15 min reaction period, triethylamine (0.23 mL, 1.66 mmol) was added and left to react for 15 min at −60°C and 15 min at room temperature; then brine (10 mL) was added and the reaction product was extracted with diethyl ether (3 × 25 mL). The extracts were combined, dried over sodium sulfate, concentrated under reduced pressure, and chromatographed to furnish aldehyde **25** (86 mg, 69%); IR (film): 3444, 2922, 2842, 1720, 1498, 1332, 1284, 1160, 1090, 964, 816, 728, and 676 cm^{-1}; ^1H NMR δ: 2.39 (3H, s, $ArCH_3$), 2.50 (2H, dd, J = 1.5, 6.9 Hz, CH_2CHO), 2.52 (1H, dd, J = 2.5, 15.9 Hz, H-4_{ax}), 2.88 (1H, dd, J = 5.5, 15.9 Hz, H-4_{eq}), 3.85 (3H, s, OCH_3), 4.16 (1H, d, J = 17.1 Hz, H-1_{ax}), 4.77 (1H, d, J = 17.1 Hz, H-1_{eq}), 4.80 (1H, ddd, J = 2.5, 5.5, 6.9 Hz, H-3), 5.74 (1H, s, OH), 6.60 (2H, ABq, J = 8.3 Hz, $\Delta\delta$ = 0.18, ArH), 7.47 (4H, ABq, J = 7.4 Hz, $\Delta\delta$ = 0.43, ArH of *p*-toluenesulfonamide), and 9.67 (1H, t, J = 1.5 Hz, CHO); ^{13}C NMR δ: 21.37, 32.18, 39.09, 45.55, 46.63, 56.00, 109.39, 117.61, 119.89, 124.32, 127.05*, 129.60*, 136.43, 141.56, 143.38, 144.45, and 199.57; HRMS calcd. for $C_{19}H_{21}NO_5S$: 375.1140; found: 375.1149.

8-Hydroxy-3-hydroxymethyl-7-methoxy-2-(*p*-toluenesulfonyl)-1,2,3,4-tetrahydroisoquinoline (27)

To a solution of aldehyde **25** (50 mg, 0.132 mmol) in dry benzene (2 mL) were successively added powdered activated 4Å molecular sieves (150 mg) and morpholine (0.017 mL, 0.198 mmol). After stirring overnight at room temperature, the solids were decanted by centrifugation and washed twice with anhydrous benzene (1 mL). The organic solution was evaporated under reduced pressure to give enamine **26** (56 mg, 95%) as a yellowish oil; IR (film): 2958, 2852, 1650, 1498, 1330, 1284, 1160, 1062, 946, 728, and 664 cm^{-1}; ^1H NMR δ: 2.39 (3H, s, $ArCH_3$), 2.56 (1H, dd, J = 10.5, 15.6 Hz, H-4_{ax}), 2.88 (4H, t, J = 4.7 Hz, CH_2NCH_2), 3.14 (1H, dd, J = 8.3, 15.6 Hz, H-4_{eq}), 3.58 (4H, t, J = 4.7 Hz, CH_2OCH_2), 3.70 (1H, d, J = 16.5 Hz, H-1_{ax}), 3.84 (3H, s, OCH_3), 4.01 (1H, d, J = 13.8 Hz, NCH=C*H*), 4.05 (1H, dd, J = 8.3, 10.5 Hz, H-3), 4.78 (1H, d, J = 16.5 Hz, H-1_{eq}), 4.82 (1H, br s, $w_{1/2}$ = 8 Hz, OH), 5.93 (1H, d, J = 13.8 Hz, N-C*H*=CH), 6.62 (2H, ABq, J = 8.3 Hz, $\Delta\delta$ = 0.15), and 7.48 (4H, ABq, J = 8.2 Hz, $\Delta\delta$ = 0.48, ArH of *p*-toluenesulfonamide); ^{13}C NMR δ: 21.35, 35.11, 39.03, 46.28*, 52.80, 55.92, 67.91*, 95.55, 109.07, 118.24, 119.63, 125.42, 127.57*, 128.19, 129.15*, 136.74, 141.46, 142.47, and 144.13.

A solution of enamine **26** (50 mg, 0.112 mmol) in dry diethyl ether (2 mL) was cooled to −78°C and treated with ozonized oxygen until no starting material was left as determined by TLC. The intermediate ozonides were reacted with excess sodium borohydride in methanol for 1.5 h at −78°C and 30 min at room temperature. Then, 10% citric acid (5 mL) was added, the organic solvents were removed under reduced pressure, and the reaction products were extracted with diethyl ether (3 × 20 mL). The combined extracts were dried and chromatographed to furnish alcohol **27** (30 mg, 73%) as an oil; IR (film): 3500, 2926, 1498, 1336, 1284, 1162, 1090, 968, 814, and 666 cm^{-1}; ^1H NMR δ: 2.39 (1H, br s, $w_{1/2}$ = 16 Hz, CH_2OH), 2.42 (3H, s, $ArCH_3$), 2.70 (1H, dd, J = 3.2, 12.1 Hz, H-4_{ax}), 2.96 (1H, dd, J = 6, 12.1 Hz, H-4_{eq}), 3.71 (1H, dd, J = 5.1, 11.1 Hz, CH_2OH), 3.74 (1H, d, J = 15.7 Hz, H-1_{ax}), 3.83 (1H, dd, J = 3.4, 5.1 Hz, CH_2OH), 3.84 (3H, s, OCH_3), 4.02–4.12 (1H, m, H-3), 4.74 (1H, d, J = 15.7, H-1_{eq}), 5.86 (1H, br s, ArOH), 6.70 (2H, ABq, J = 8.4 Hz, $\Delta\delta$ = 0.08, ArH), and 7.54 (4H, ABq, J = 8.0 Hz, $\Delta\delta$ = 0.43, ArH of toleuensulfonamide); ^{13}C NMR δ: 21.35, 40.49, 43.39, 44.01, 55.98, 64.55, 109.21, 118.73, 119.62, 126.79, 127.40*, 129.63*, 133.49, 141.69, 143.50, and 144.56; HRMS calcd. for $C_{18}H_{21}NO_5S$: 363.1140; found: 363.1133.

8-Hydroxy-3-hydroxymethyl-7-methoxy-1,2,3,4-tetrahydroisoquinoline (3)

Following the general reductive detosylation procedure, a solution of sulfonamide **27** (30 mg, 0.083 mmol) in THF (0.9 mL) was added to anhydrous liquid ammonia (7 mL) and left to react with a slight excess of sodium. Ammonium chloride quench and the usual work-up provided tetrahydroisoquinoline **4** (15 mg, 87%) as a solid, mp 238–241°C (methanol–diethyl ether); IR (KBr): 3418, 3370, 3298, 2934, 1624, 1502, 1438, 1334, 1286, 1116, 1040, 922, and 810 cm^{-1}; ^1H NMR δ (D_2O, HOD at δ_H 4.60): 3.23–3.29 (1H, m, H-3), 3.54 (2H, dd, J = 3.3, 5.4, CH_2OH), 3.85 (3H, s, OCH_3), 3.88 (1H, dd, J = 5.3, 11.3, H-4_{ax}), 4.00 (1H, dd, J = 3.7, H-4_{eq}), 4.05 (2H, ABq, J = 16.1, Δδ = 0.10, H-1), and 6.76 (2H, ABq, J = 8.6, Δδ = 0.13, ArH); ^{13}C NMR δ (D_2O, dioxane at δ_C 66.64): 35.39, 40.74, 44.25, 56.45, 64.89, 112.34, 116.50, 119.85, 125.08, 141.64, and 145.96; HRMS calcd. for $C_{11}H_{15}NO_3$: 209.1052; found: 209.1051.

Acknowledgements

We thank the International Foundation for Science (IFS), Fundación Antorchas, CONICET, and Universidad Nacional de Rosario for support of this work. Fruitful discussions with Dr. E.A. Rúveda are also gratefully acknowledged.

References

1. A.J. Birch, A.H. Jackson, and P.V.R. Shannon. J. Chem. Soc. Perkin Trans. 1, 2185 (1974).
2. A.J. Birch, A.H. Jackson, and P.V.R. Shannon. J. Chem. Soc. Perkin Trans. 1, 2190 (1974); A.H. Jackson and G.W. Stewart. J. Chem. Soc. Chem. Commun. 149 (1971); A.H. Jackson, G.W. Stewart, G.A. Charnock, and J.A. Martin. J. Chem. Soc. Perkin Trans. 1, 1911 (1974).
3. D.L. Boger, C.H. Brotherton, and M.D. Kelley. Tetrahedron, **37**, 3977 (1981).
4. A. García, L. Castedo, and D. Domínguez. Synlett, 271 (1993).
5. T.S. Kaufman. J. Chem. Soc. Perkin Trans. 1, 403 (1993).
6. W.J. Gensler. Org. React. **6**, 194 (1951).
7. W.M. Whaley and T.R. Govindachari. Org. React. **6**, 94 (1951).
8. T.S. Kaufman. Synth. Commun. **23**, 473 (1993).
9. Y. Hamada, M. Shibata, T. Sugiura, S. Kato, and T. Shioiri. J. Org. Chem. **52**, 1252 (1987).
10. D. Badía, E. Domínguez, and I. Tellitu. Tetrahedron, **48**, 4419 (1992).
11. R.S. Monson. Tetrahedron Lett. 567 (1971); R.S. Monson and D.N. Priest. J. Org. Chem. **36**, 3826 (1971).
12. T. Nishiguchi, N. Machida, and E. Yamamoto. Tetrahedron Lett. **28**, 4565 (1987).
13. S.F. Martin and J.A. Dodge. Tetrahedron Lett. **32**, 3017 (1991).
14. R.D. Clark, Jahangir, and J.A.Langston. Can. J. Chem. **72**, 23 (1994).
15. S.J. Blarer. Tetrahedron Lett. **26**, 4055 (1985).
16. J.A. Bajgrowicz, A. El Hallaoui, R. Jacquier, Ch. Pigiere, and Ph. Viallefont. Tetrahedron Lett. **25**, 2759 (1984).
17. K. Taguchi and F.H. Westheimer. J. Org. Chem. **36**, 1570 (1971).
18. B. Witkop. J. Am. Chem. Soc. **78**, 2873 (1956).

Can. J. Chem. Downloaded from www.nrcresearchpress.com by 80.90.12.36 on 09/08/12
For personal use only.

Kinetic resolution of sulfoxides with pendant acetoxy groups using cholesterol esterase: substrate mapping and an empirical rule for chiral phenols

Alessio N. Serreqi and Romas J. Kazlauskas

Can. J. Chem. Downloaded from www.nrcresearchpress.com by 80.90.12.36 on 09/08/12
For personal use only.

Abstract: Sulfoxides are valuable chiral auxiliaries because they direct the formation of carbon–carbon bonds. As a route to enantiomerically pure sulfoxides, we examined hydrolase-catalyzed kinetic resolution by hydrolysis of a pendant acetoxy group. Screening hydrolases for the enantioselective hydrolysis of the acetate in 2-(methylsulfinyl)phenyl acetate, **1***b*, identified cholesterol esterase (CE) as the most enantioselective enzyme. The enantiomeric ratio, *E*, ranged from 10 to 25, favoring the (*R*) configuration at sulfur. Competing chemical hydrolysis of **1***b* caused the large range in the measured values of *E*. A small-scale (250 mg) resolution of (±)-**1***b* yielded (*S*)-**1***b* with >99% ee (11% yield) after recrystallization. Changing the methyl substituent to phenyl or *n*-butyl did not significantly change the enantioselectivity (*E* = 10 and 15, respectively), but changing it to a chloromethyl substituent lowered the enantioselectivity slightly (*E* = 5). Changing the phenyl acetate to a naphthyl acetate (2-(phenylsulfinyl)phenyl acetate vs. 1-(phenylsulfinyl)-2-naphthyl acetate) increased the enantioselectivity from 10 to 19. In all cases CE favored the (*R*)-sulfoxide. To aid the design of new resolutions with CE, we propose an empirical rule that accounts for the observed enantiopreference of CE toward these 5 sulfoxides and 15 other chiral aryl acetates. This empirical rule uses both the size of the substituents and their conformational preferences to predict which enantiomer reacts faster.

Key words: kinetic resolution, lipase, cholesterol esterase, sulfoxides, empirical rule.

Résumé : Les sulfoxydes sont des auxiliaires chiraux utiles parce qu'ils orientent la formation de liaisons carbone–carbone. Dans le but d'obtenir des sulfoxydes énantiomériquement purs, on a examiné la possibilité d'utiliser une résolution cinétique catalysée par une hydrolase impliquant l'hydrolyse d'un groupe acétoxy. Une évaluation des hydrolases pour leur capacité à effectuer l'hydrolyse énantiosélective de l'acétate de 2-(méthylsulfinyl)phényle, **1***b*, a permis d'identifier l'estérase de cholestérol (CE) comme l'enzyme le plus énantiosélectif. Le rapport énantiomérique, *E*, varie de 10 à 25 et il favorise la configuration (*R*) au niveau du soufre. L'hydrolyse chimique compétitive du composé **1***b* provoque les grandes variations observées dans les valeurs mesurées de *E*. Une résolution préparative à faible échelle (250 mg) du composé (±)-**1***b* conduit, après recristallisation, au (*S*)-**1***b* avec un ee >99% (rendement de 11%). Lorsqu'on change le substituant de méthyle à phényle ou *n*-butylé, il n'y a pas de changement significatif d'énantiosélectivité (*E* = 10 et 15, respectivement); toutefois, si on le remplace par un chlorométhyle, l'énantiosélectivité est légèrement diminuée (*E* = 5). Si l'on remplace l'acétate de phényle par l'acétate de naphtyle (acétate de 2-(phénylsulfinyl)phényle vs. acétate de 1-(phénylsulfinyl)-2-naphtyle) l'énantiosélectivité passe de 10 à 19. Dans tous les cas, la CE favorise le (*R*)-sulfoxyde. Dans le but d'aider au développement de nouvelles résolutions à l'aide de la CE, on propose une règle empirique qui permet de tenir compte des énantiopréférences observées pour la CE vis-à-vis de ces 5 sulfoxydes et de 15 autres acétates arylés chiraux. Ces règles empiriques font appel à la fois à la grosseur des substituants et à leurs préférences conformationnelles pour prédire quel énantiomère réagira le plus rapidement.

Mots clés : résolution cinétique, lipase, estérase de cholestérol, sulfoxydes, règle empirique.

[Traduit par la rédaction]

Received January 17, 1995.

A.N. Serreqi and R.J. Kazlauskas.[1] Department of Chemistry, McGill University, 801 Sherbrooke St. W., Montréal, QC H3A 2K6, Canada.

[1] Author to whom correspondence may be addressed. Telephone: (514) 398-7228. Fax: (514) 398-3797. E-mail: romas_kazlauskas@maclan.mcgill.ca

Can. J. Chem. Downloaded from www.nrcresearchpress.com by 80.90.12.36 on 09/08/12
For personal use only.

Introduction

Chiral sulfoxides (1) are useful chiral auxiliaries to direct the formation of carbon–carbon bonds (2). Examples include: electrophilic additions to anions at the α- or β-carbon, nucleophilic addition to the C=C bond of vinyl sulfoxides or a carbonyl β to the sulfoxide, radical reactions at the α-carbon, and Diels–Alder reactions of vinyl sulfoxides.

Two classes of enantioselective syntheses are the best current routes to enantiomerically pure sulfoxides (3): (*1*) stereospecific displacements at sulfites, sulfinates, and related compounds with established chirality at sulfur and (*2*) enantioselective oxidation of sulfides. Stereospecific displacements of menthol from *O*-menthyl *p*-tolylsulfinate remain the most common synthetic methods because the starting sulfite is easily prepared (4). Recent research identified several alternate starting compounds that yield sulfoxides after one (5) or two (6) displacements at the sulfur stereocenter. Examples of enantioselective oxidations of sulfides that yield sulfoxides with >90% ee include oxidations with a modified Sharpless reagent (7), chiral oxaziridines (8), titanium complexes of binaphthol (9), chloroperoxidase (10), and microorganisms (11). Recent comparisons of several of these reagents found that they complement one another (12). A related approach is to introduce carbon stereocenters in the sulfides and then use an achiral reagent for oxidation (for recent examples, see ref. 13).

Another route to enantiomerically pure sulfoxides is resolution. Although some resolutions relied on complexation (14), enantioselective oxidation (15), or reduction (16), the most successful resolutions used hydrolase-catalyzed reactions, Fig. 1. Almost 30 years ago Reid et al. (17) used pepsin to catalyze the enantioselective hydrolysis of sulfites with the structure PhOS(O)OR. Although hydrolysis yielded achiral product, the unreacted sulfite was enriched in one enantiomer. More recently, researchers resolved sulfoxides by hydrolyzing pendant ester groups in sulfoxides. Ohta et al. (18) resolved sulfinylacetates and sulfinylpropanoates by a microbe-catalyzed hydrolysis. Burgess et al. (19) resolved these compounds using the more readily accessible *Pseudomonas* K-10 lipase from Amano. Cardellicchio et al. resolved the related methyl (*Z*)-3-arylsulfinylpropenoates with lipase from *Candida rugosa* (CRL) or α-chymotrypsin (20), while Allenmark and Andersson (21) resolved a series of 2-(alkylsulfinyl)benzoates with CRL. Similarly, Mikolajczyk et al. used hydrolases for the enantioselective synthesis of sulfoxides by hydrolysis of the meso diesters (22). In all but one of these hydrolase-catalyzed reactions, the sulfur stereocenter lay in the acid portion of the ester.

In this paper, we examine the ability of lipases to resolve sulfur stereocenters that lie in the alcohol portion of the ester. We

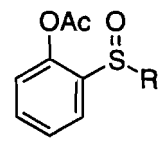

1*b*, R = CH_3
2*b*, R = CH_2Cl
3*b*, R = *n*-C_4H_9
4*b*, R = Ph

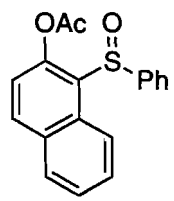

5*b*

Fig. 1. Enantiomerically enriched sulfoxides and sulfinates prepared by enantioselective hydrolysis. (*a*) Racemic sulfoxides and sulfinates that were resolved by enantioselective hydrolysis. The absolute configuration of the favored enantiomer is shown where known. (*b*) Meso sulfoxides that were desymmetrized by enantioselective hydrolysis. In all but one example, the sulfoxide lies in the acid portion of the ester. Abbreviations: PLE = pig liver esterase; α-CT = α-chymoptrypsin; lipase K 10 = lipase from *Pseudomonas* sp. type K 10 from Amano; CRL = lipase from *Candida rugosa*.

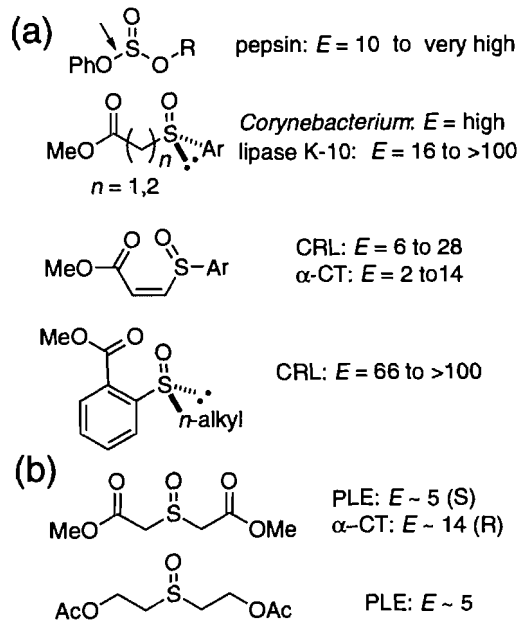

used lipases to resolve 2-(alkylsulfinyl)phenyl acetates, **1*b***–**3*b***, 2-(phenylsulfinyl)phenyl acetate, **4*b***, and 1-(phenylsulfinyl)-2-naphthyl acetate, **5*b***. The enzyme cholesterol esterase showed the highest enantioselectivity for these substrates, but these enantioselectivities were only moderate; enantiomeric ratios ranged from 5 to 25. In addition, we use this data and previous data from similar chiral aryl acetates to propose an empirical rule. The empirical rule accounts for the observed enantiopreference of CE toward these compounds and may be useful for the design of new CE-catalyzed resolutions, especially the resolution of remote stereocenters and non-carbon stereocenters.

Results

Synthesis and resolution of sulfoxides

Sulfoxides **1*b***–**5*b*** were prepared by standard chemical procedures, Scheme 1. Oxidation of 2-(methylthio)phenol followed by acetylation gave 2-(methylsulfinyl)phenyl acetate, **1*b***. Chlorination of **1*b*** using *N*-chlorosuccinimide gave the chloromethylsulfoxide, **2*b***. To prepare **3*b*** and **4*b***, we deprotonated anisole with butyllithium and quenched this anion with the appropriate disulfide. Removal of the methyl group, oxidation at sulfur, and acetylation gave **3*b*** and **4*b***. Preparation of the naphthyl derivative **5*b*** started from 1-bromo-2-naphthol protected as the ethoxymethyl ether. The Grignard reagent prepared from this bromide was quenched with phenylsulfinyl

Scheme 1.

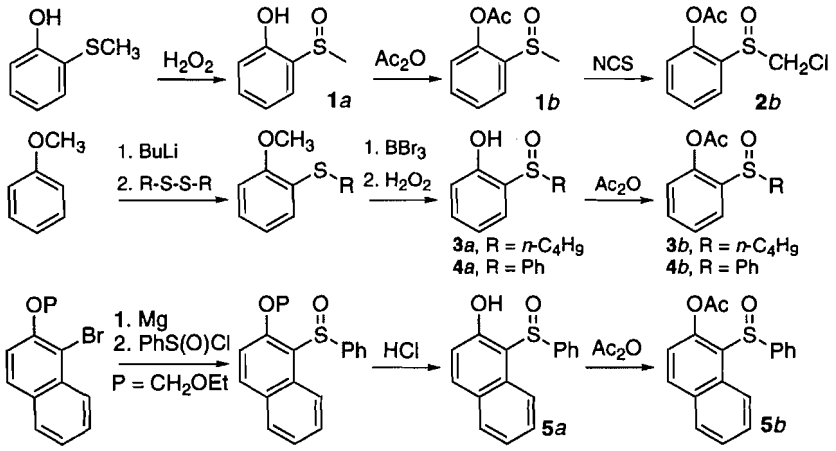

chloride, then deprotected and acetylated to give **5***b*. When we used the benzyl protecting group, the Grignard reagent formed in very low yield; when we used the methyl protecting group, its removal required BBr_3, which also reacted with other parts of the molecule. Previous researchers made **1***a* and **3***a* by reaction of 2-mercaptophenol with an alkyl halide followed by oxidation with hydrogen peroxide (23). Both methods appear comparable.

Using substrate **1***b*, we screened commercial lipases and esterases for their ability to catalyze the enantioselective hydrolysis of the acetoxy group, Table 1, eq [1]. Pancreatic

[1] 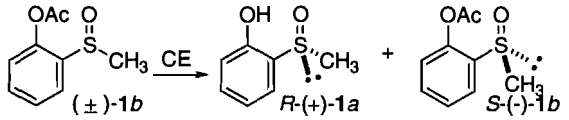

cholesterol esterase (CE) showed the highest enantioselectivity. The enantiomeric ratio, *E* (24), for this reaction ranged from 10 to 25, indicating modest to good enantioselectivity. Two other lipases, lipase from *Candida rugosa* (CRL) and lipase from *Aspergillus niger* (ANL), also showed modest enantioselectivity, $E = 7 \pm 2$ and 9 ± 2, respectively. The enantiomeric ratio for the other enzymes was less than 4.

Competing chemical hydrolysis of **1***b* caused the large range in the measured enantiomeric ratio for the CE-catalyzed reaction. The half-life for nonenzymatic hydrolysis of **1***b* was approximately 40 h under the conditions used for enzymatic reactions: phosphate buffer (10 mM, pH 7.0) stirred with an equal volume of ethyl ether.[2] We measured lower enantiomeric ratios when the reaction times were long, consistent with more chemical hydrolysis. We made no correction for this chemical hydrolysis. For the less enantioselective enzymes, this chemical hydrolysis did not significantly affect the measured enantiomeric ratio.

The facile chemical hydrolysis of **1***b* is consistent with the electron-withdrawing effect of the methylsulfinyl substituent. Indeed, the pK_a of the leaving phenol, **1***a*, is 7.06 (25), similar to that for *p*-nitrophenol, whose pK_a is 7.14 (26). Esters of *p*-nitrophenol also hydrolyze slowly in neutral aqueous solutions. Although competing chemical hydrolysis is a disadvantage of using a reactive ester, the more rapid enzymatic reaction is an advantage. CE catalyzed the hydrolysis of **1***b* 200 times faster than a natural substrate, cholesterol acetate, under the same conditions: 33 vs. 0.17 U/mg, respectively.

A crude preparation of CE, pancreas acetone powder, also showed a similar enantioselectivity toward **1***b*, Table 1. In previous resolutions of binaphthols, we also found that this crude preparation showed the same enantioselectivity as purified CE (27). We used this pancreas acetone powder to resolve 250 mg of **1***b*. At 56% conversion, the remaining substrate, (*S*)-**1***b*, had 77% ee corresponding to an *E* of 9.2. We removed phenol **1***a* as the phenolate by washing with sodium carbonate solution.[3] After recrystallization of (*S*)-**1***b* from toluene–hexane, we isolated 28 mg with >99% ee, 11% yield. The maximum yield is 50% in a resolution.

Cholesterol esterase catalyzed the hydrolysis of similar acetoxysulfoxides **2***b*–**5***b* with similar enantioselectivities: 5–19. Changing the methyl substituent in **1***b* to chloromethyl in **2***b* lowered the enantioselectivity from 10–25 to 5. Changing the methyl substituent in **1***b* to butyl or phenyl in **3***b* or **4***b* had little effect on enantioselectivity: *E* was 14 and 10, respectively. Changing from phenyl acetate **4***b* to naphthyl acetate **5***b* increased the enantioselectivity from 10 to 19. For CRL- and ANL-catalyzed hydrolyses of **5***b*, the enantiomeric ratios were 6 and 3, respectively.

Cholesterol esterase favored the (*R*) enantiomer for all five substrates. We established the absolute configuration of **1***b* and **4***b* by comparing their optical rotations to known rotations in the literature, see Experimental section. We also tentatively assigned (*R*) absolute configurations to the favored enantio-

[2] The rate of nonenzymic hydrolysis of **1***b* decreased at 0°C ($t_{1/2}$ = 600 h). Replacing the ethyl ether phase with chloroform or hexane also decreased the rate of hydrolysis ($t_{1/2}$ > 100 d, 180 h, respectively, at room temperature). We also checked for racemization of **1***a* and **1***b*. When stirred in aqueous solution overnight, we observed partial hydrolysis of **1***b* and partial racemization of both **1***a* and **1***b* at pH 4, partial hydrolysis of **1***b* and complete racemization of both **1***a* and **1***b* at pH 8, and complete hydrolysis of **1***b* and complete racemization of the resulting **1***a* at pH 10. However, when an organic phase was present as in the enzyme reaction, this racemization was completely suppressed. Over 4 d at pH 8.6 or 6.9 we detected no racemization of **1***a* or **1***b* when we added hexane–isopropanol (9:1) as a second phase. We did observe a small amount of hydrolysis of **1***b* under these conditions.

[3] This extraction procedure racemized **1***a*. See footnote 1

Can. J. Chem. Downloaded from www.nrcresearchpress.com by 80.90.12.36 on 09/08/12
For personal use only.

Table 1. Enantioselectivity of hydrolases towards sulfoxides **1***b*–**5***b*.

Substrate	Enzyme[a]	Activity,[b] U/mg	Conv.,[c] %	ee_p, %[d] (config)	ee_s, %[d] (config)	E[e]
1*b*	CE	33	50	62(*R*)	66	10–25
1*b*	CE[f]	0.019	52	72	42	9–22
1*b*	CRL	0.018	36	67(*R*)	37	7 ± 2
1*b*	ANL	0.059	45	57(*R*)	47	9 ± 2
1*b*	PPL	0.041	28	48(*R*)	20	3.4
1*b*	RML	0.056	49	3(*S*)	8	1.1
1*b*	PCL	0.11	67	33(*R*)	68	3.8
1*b*	K10	0.037	40	45(*R*)	29	3.5
2*b*	CE[f]	0.027	26	55	30(*S*)[g]	4.6
3*b*	CE	5.8	38	80	48(*S*)[g]	14
4*b*	CE	0.94	41	73(*R*)	50	10
4*b*	CRL	0.036	37	nd	34(*S*)	5.2
4*b*	ANL	0.023	39	nd	12(*R*)	1.6
4*b*	PPL	0.005	38	nd	18(*S*)	2.2
5*b*	CE	6.90	43	82(*R*)[g]	62	19
5*b*	CRL	0.0092	46	56(*R*)[g]	48	5.6
5*b*	ANL	0.17	44	33(*R*)[g]	26	2.5
5*b*	ACE	$<7 \times 10^{-3}$	—	—	—	—

[a]CE = cholesterol esterase; PPL = lipase from porcine pancreas; CRL = lipase from *Candida rugosa* (synonym *C. cylindracea*); ANL = lipase from *Aspergillus niger* (Amano AP-6); RML = lipase from *Rhizomucor miehei* (Amano MAP-10); K-10 = lipase from *Pseudomonas* sp. (Amano K-10); PCL = lipase from *Pseudomonas cepacia* (Amano P30); ACE = electric eel acetylcholine esterase.

[b]U/mg = μmol ester hydrolyzed per minute per mg of solid.

[c]The % conversion was determined either from the amount of base consumed during hydrolysis or calculated from the enantiomeric excess of the starting material (ee_s) and product (ee_p) using conv. = $ee_s/(ee_s+ee_p)$.

[d]The enantiomeric purity of **1***a*, **1***b*, **2***a*, and **2***b* were determined by HPLC using a Chiralcel OB column. The enantiomeric purities of **3***b*-**5***b* were determined by ^{1}H NMR in the presence of (+)-Eu(hfc)$_3$. Compounds **3***a*-**5***a* were acetylated and the enantiomeric purities of the acetates were measured by ^{1}H NMR in the presence of (+)-Eu(hfc)$_3$.

[e]E = enantiomeric ratio, which measures the preference of the enzyme for one enantiomer over the other (See ref. 24). The *E* listed is an average of at least two reactions. The values of ee and %conv. are for one of these reactions and may not give exactly the *E* shown. Reference 34 includes experimental details of the enzyme hydrolysis and work-up for similar compounds.

[f]Pancreas acetone powder, a crude preparation of cholesterol esterase, was used as the catalyst.

[g]Tentative assignment of absolute configuration based on the relative chemical shift of the favored enantiomer in the ^{1}H NMR in the presence of Eu(hfc)$_3$.

mers of **2***b*, **3***b*, and **5***b* based on relative positions of the acetyl methyl ^{1}H NMR resonance in the presence of Eu(hfc)$_3$. The resonance for the fast-reacting enantiomer appeared downfield of the resonance for the slow-reacting enantiomer for all five acetoxysulfoxides. The other hydrolases also favored (*R*)-**1***b* except lipase from *Rhizomucor miehei* (RML), which favored (*S*)-**1***b*, but with low enantioselectivity. CRL favored the (*R*) enantiomers of **4***b* and **5***b* with moderate enantioselectivity, but ANL showed low enantioselectivity and favored (*S*)-**4***b* and (*R*)-**5***b*.

Empirical rule to predict the enantiopreference of CE toward chiral aryl esters

An empirical rule that predicts the enantiopreference of CE toward secondary alcohols, Fig. 2*a* (28), does not apply to the sulfoxides resolved in this paper. To include these substrates, we propose an extension of this secondary alcohol rule to chiral aryl esters, Fig. 2*b*. Like the earlier rule, the extension uses the size of the substituents to predict which enantiomer will react faster.

Figure 3 summarizes all reported resolutions of chiral aryl esters with CE. The first group of substrates, Fig. 3*a*, are rigid. They include binaphthols (27) and thiobinaphthol (29), spiro compounds (27), helicene derivatives (30),[4] and α-tocopherols (32, 33). To apply the rule, we simply chose the enantiomer whose shape best matched the schematic in Fig. 2*b*. Of the 11 examples, 10 fit the empirical rule. The exception (spirobiindanol where R = H) showed only a slight enantiopreference for the other enantiomer.

[4] The authors reported a (+) rotation for a quinone derived from oxidation of the favored enantiomer. We tentatively assign this as the (*P*) configuration shown because (+)-[5]-helicene has the (*P*) configuration (31).

Can. J. Chem. Downloaded from www.nrcresearchpress.com by 80.90.12.36 on 09/08/12
For personal use only.

Can. J. Chem. Downloaded from www.nrcresearchpress.com by 80.90.12.36 on 09/08/12
For personal use only.

Fig. 2. Empirical rules for the observed enantiopreference of cholesterol esterase. (*a*) Cholesterol esterase favors the enantiomers of secondary alcohols with the shape shown, where M represents a medium substituent such as methyl and L represents a large substituent such as phenyl. For details see ref. 28. (*b*) A proposed extension of this empirical rule to chiral aryl esters. With the aryl ester oriented in the plane of the paper, cholesterol esterase favors the enantiomer with the larger substituent, L, to the lower right and behind the plane of the paper.

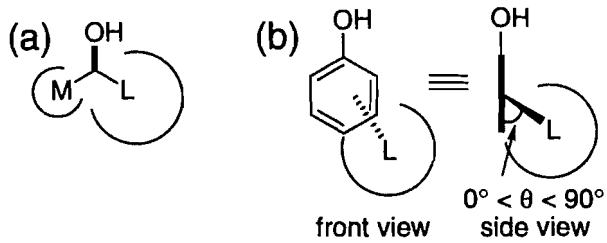

The second group of substrates comprises the sulfoxides resolved in this paper and the related phosphines and phosphine oxides resolved previously (34), Fig. 3*b*. These substrates are flexible because a single bond links the stereocenter to the aryl ring. Rotation about this bond allows both enantiomers to adopt conformations that resemble the aryl ester rule. However, these conformations are diastereomeric so one enantiomer adopts this conformation more easily.[5] We suggest that this enantiomer will react faster. Thus, applying the aryl ester rule to flexible substrates requires the researcher to compare the stabilities of the conformations whose shape matches the rule. The fast-reacting enantiomer is the one whose conformation lies lower in energy.

We compared the stabilities of enantiomers of sulfoxides **1***b*–**5***b* in conformations that resemble the rule using molecular mechanics and indeed found that the conformation for the fast-reacting (*R*) enantiomer lay 0.60–1.7 kcal/mol lower in energy, Table 2. Figure 4 compares the conformations for (*R*)- and (*S*)-**5***b*. When (*R*)-**5***b* orients the phenyl substituent as suggested by the rule, it lies 1.7 kcal/mol lower in energy that the corresponding conformation of (*S*)-**5***b*. This difference is probably due to the favorable eclipsed orientation of the sulfoxide oxygen and naphthyl ring for (*R*)-**5***b* and the less favorable *gauche* orientation of these groups in (*S*)-**5***b* (35).

A similar comparison of conformations that resemble the rule, for phosphine oxides **6** and **7**, also found that the fast-reacting (*R*)-enantiomers lay lower in energy, Table 2. For **6**, the energy difference between the local minima was 0.40 kcal/mol. For **7**, only the fast-reacting enantiomer had a local minimum that resembled the rule, so we compared the energies at $\theta = 45°$,[6] the middle of the range suggested in the rule, $0° > \theta > 90°$. The fast-reacting enantiomer lay 0.78 kcal/mol lower at

[5] Enantiomers have identical energies for their global minima and for the ensemble of all conformations, but two particular conformations may be diastereomeric and therefore differ in energy.

[6] θ is the dihedral angle between the aryl ring and the largest substituent as defined in Fig. **2***b*.

Fig. 3. Structures of the fast-reacting enantiomers in CE-catalyzed resolutions of chiral aryl esters. (*a*) Rigid substrates. Ten of the eleven substrates follow the rule; one spirobiindanol (R = H) does not. (*b*) Flexible substrates: sulfoxides, phosphine oxides, and phosphines (ref. 34). Table 2 summarizes the enantioselectivity of CE toward these substrates.

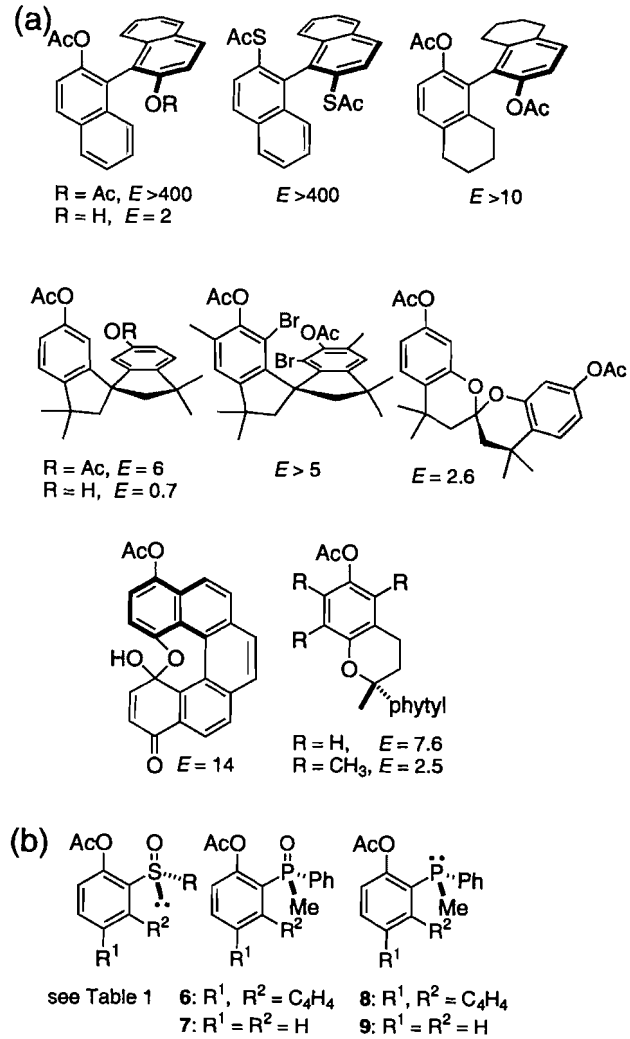

45° and by a similar amount throughout the range, Fig. 5. The conformation for the fast-reacting enantiomer lies lower in energy because the oxygen on phosphorus eclipses the aromatic ring. In the slow-reacting enantiomer the methyl group on phosphorus eclipses the aromatic ring. Both X-ray crystal structures and semi-empirical calculations showed that an oxygen on phosphorus favors a nearly eclipsed orientation to an aromatic ring (36).

The fast-reacting enantiomers of phosphines **8** and **9** also lay at lower energy when we compared conformations that resembled the rule. We found no local minima that resemble the rule, so we again compared the energies at $\theta = 45°$ where the difference was 1.6 kcal/mol for **8**, Fig. 6, and 0.80 kcal/mol for **9**. The conformation for the fast-reacting enantiomer is more stable because the lone pair, not the methyl, eclipses the aromatic ring. Such conformations have been previously identified as low-energy conformations (37).

Fig. 4. Conformations of sulfoxide **5***b* that resemble the aryl ester rule. Both enantiomers have local minima that place the largest group (phenyl) into the orientation required by the rule. However, the conformation for the (*R*)-**5***b* (fast reacting) lies 1.7 kcal/mol lower in energy than the conformation for the (*S*)-**5***b* (slow reacting). In (*R*)-**5***b*, the sulfoxide oxygen eclipses the aryl ring, while in (*S*)-**5***b* the sulfoxide oxygen lies *gauche* to the aryl ring. This difference allows (*R*)-**5***b* to more easily adopt a conformation that resembles the aryl ester rule. Structures and relative energies were calculated using molecular mechanics. Gray indicates carbon atoms, stippling indicate oxygen atoms, diagonal stripes indicate the sulfur atom, and the small light gray ball represents the sulfur lone pair.

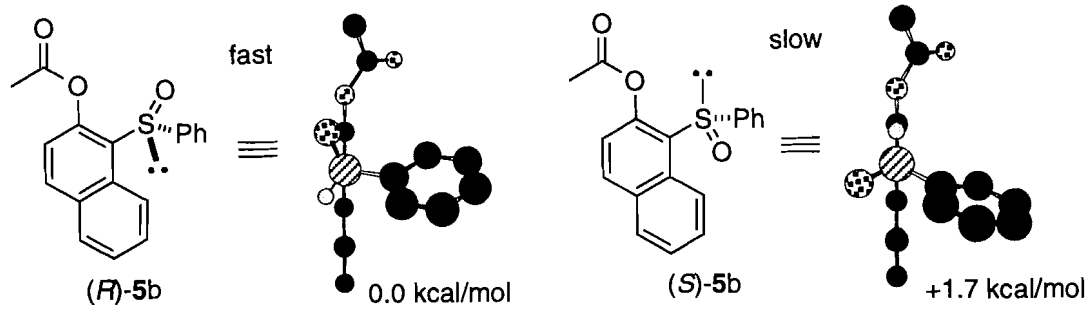

Fig. 5. Conformational energies of the two enantiomers of phosphine oxide **7** in conformations that resemble the chiral aryl ester rule. The fast-reacting enantiomer lies at lower energy throughout the range $0° > \theta > 90°$. The energy difference at $\theta = 45°$ is 0.78 kcal/mol. The fast-reacting enantiomer lies at lower energy because the oxygen, not the methyl, eclipses the aryl ring. Gray indicates carbon atoms, stippling indicates oxygen atoms, and vertical stripes indicate the phosphorus atom.

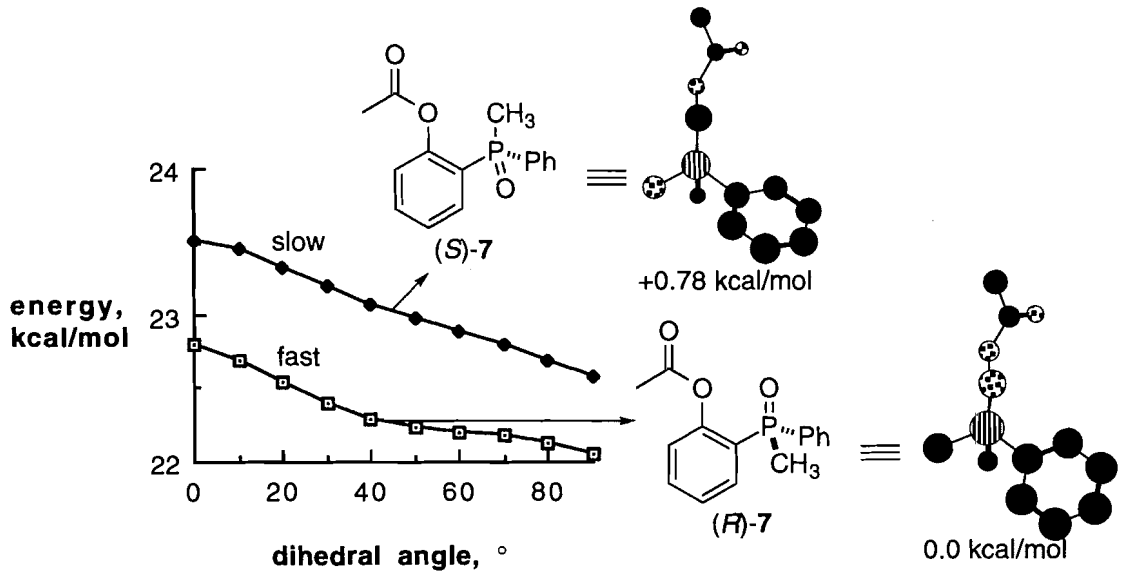

In summary, the aryl ester rule in Fig. 2*b* reliably predicts which enantiomer reacts faster with CE for 16 of the 17 examples. For rigid substrates, one simply choses the enantiomer whose shape best matches the rule. For flexible substrates, one compares the stabilities of the two enantiomers in conformations that resemble the rule and chooses the more stable one.

Discussion

Cholesterol esterase resolved sulfoxide **1***b* with moderate enantioselectivity ranging from 10 to 25. Using this resolution, we prepared (*S*)-**1***b* with >99% ee, but in modest yield. Cholesterol esterase also resolved four other sulfoxides, **2***b*–**5***b*, with similar enantioselectivity, suggesting that this resolution may be useful for a wide range of substrates. Indeed, we recently reported the resolution of several phosphines and phosphine oxides using a similar approach (34).

The degree of enantioselectivity was lower than previous resolutions (20, 21) where the sulfoxide was in the acid portion of the ester. Thus, putting the sulfoxide in the alcohol portion does not seem to be a good general strategy for resolution of sulfoxides. Nevertheless, several synthetic applications of arylsulfoxides require a methoxy or other alkoxy group oriented *ortho* to the sulfinyl group for high enantioselectivity (38). For these applications, our kinetic resolution may be a good route to the enantiomerically pure sulfoxides.

We also proposed an extension of the empirical rule for sec-

Can. J. Chem. Downloaded from www.nrcresearchpress.com by 80.90.12.36 on 09/08/12
For personal use only.

Fig. 6. Conformational energies of the two enantiomers of phosphine **8** in conformations that resemble the chiral aryl ester rule. The fast-reacting enantiomer lies at lower energy throughout the range $0° > \theta > 90°$, but both enantiomers have similar energies at $\theta = 90°$. The energy difference at $\theta = 45°$ is 1.6 kcal/mol. The fast-reacting enantiomer lies at lower energy because the lone pair, not the methyl, eclipses the aryl ring. Gray indicates carbon atoms, stippling indicates oxygen atoms, vertical stripes indicate the phosphorus atom, and the small light gray ball represents the phosphine lone pair.

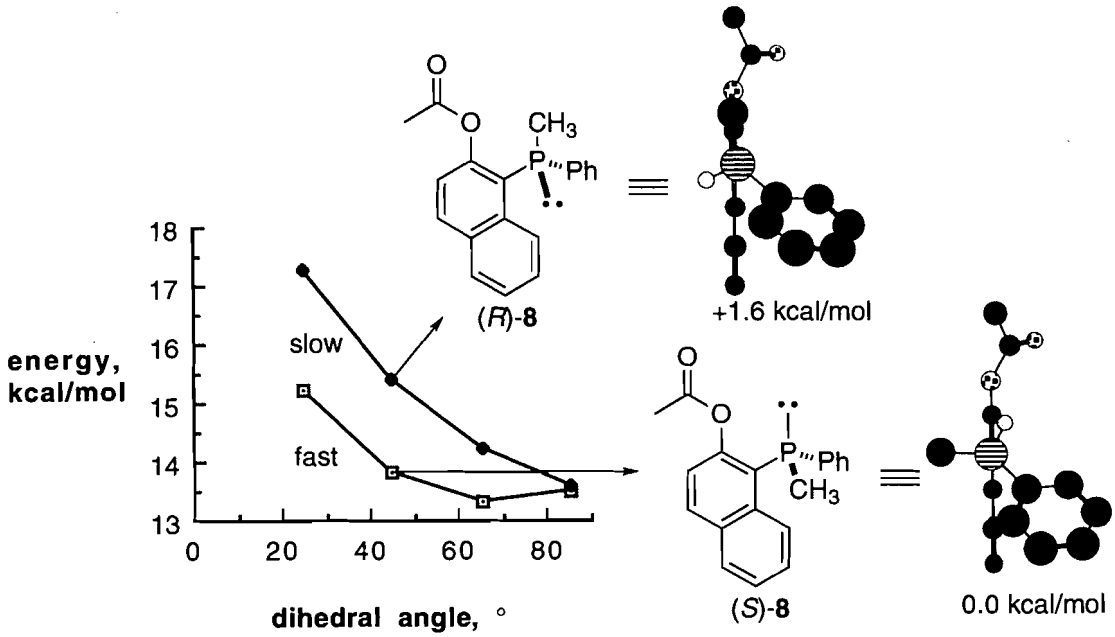

Table 2. Angles and relative energies of conformations that resemble the aryl ester rule.

Substrate	θ(fast)[a]	θ(slow)[b]	ΔEnergy[c]	E[d]
1*b*	88°	53°	1.1	10–25
2*b*[e]	87°	77°	0.60	5
3*b*	83°	81°	1.6	14
4*b*	83°	66°	1.7	10
5*b*	80°	62°	1.7	19
6	52°	63°	0.40	32
7	17°	(45°)[f]	0.78[g]	4
8	(45°)[f]	(45°)[f]	1.6	5
9	(45°)[f]	(45°)[f]	0.80	4

[a]The dihedral angle between the aryl ring and the large group as defined in Fig. 2*b* for the local minimum, which resembles the rule for the fast-reacting enantiomer. Some local minima may also be global minima.

[b]Same as in note *a*, but for the slow-reacting enantiomer.

[c]$\text{Energy}_{\text{slow}} - \text{Energy}_{\text{fast}}$ in kcal/mol. The positive values indicate that the conformation for the fast-reacting enantiomer lies lower in energy.

[d]Enantioselectivity of CE toward these substrates. Data for **6–9** are from ref. 34.

[e]The chlorine atom oriented *anti* to the sulfoxide oxygen.

[f]This enantiomer had no local mimimum where $0° < \theta < 90°$. The energy difference is for the middle of this range, $\theta = 45°$. Unless otherwise noted, the energy differences were similar throughout the entire range.

[g]Difference at 45° for both enantiomers.

ondary alcohols to include chiral aryl esters. For rigid substrates, the enantiomer that resembles the schematic in Fig. 2*b* indeed reacted faster for 10 of the 11 examples. For the flexible substrates, this empirical rule required a comparison of conformational energies. We compared these energies using molecular mechanics and found that in all nine cases the fast-reacting enantiomer was the one that more easily adopted a conformation that resembled the rule. Although the calculated energy differences were small, <2 kcal/mol, we believe most errors cancelled because we compared the conformations of enantiomers. Indeed, the calculated conformational preferences were consistent with the experimentally determined conformational preferences of sulfoxides, phosphine oxides, and phosphines.

Without this empirical rule, CE appeared to have an opposite enantiopreference toward sulfoxides and phosphines. When we compared the 3-D structures of the fast-reacting enantiomers, we found that the lone pair of the phospine overlapped, not the lone pair of the sulfoxide, but the oxygen. (Compare the structures of the fast-reacting sulfoxide in Fig. 4 with the fast-reacting phospine in Fig. 6). However, our empirical rule explains this difference. For the sulfoxide, the oxygen, not the sulfoxide lone pair, favors the eclipsed orientation to the aromatic ring, while for the phosphine the lone pair favors this orientation. In the most stable conformation both the sulfoxide and phosphine have a similar orientation of the large substituent.

The empirical rule currently predicts only which enantiomer reacts faster and not the degree of enantioselectivity. For both the rigid and flexible substrates, most of the enantioselectivities range from moderate to good, with a few excellent enantioselectivities. There is no obvious structural feature that distinguishes the substrates resolved with excellent enantioselectivity from the others. For the flexible substrates, we looked for a correlation between the degree of enantioselectivity and the difference in conformational energies in Table 2,

Can. J. Chem. Downloaded from www.nrcresearchpress.com by 80.90.12.36 on 09/08/12
For personal use only.

Can. J. Chem. Downloaded from www.nrcresearchpress.com by 80.90.12.36 on 09/08/12
For personal use only.

but found only a moderate correlation. This is consistent with the notion that both differences in conformational energies and interactions in the active site will contribute to enantioselectivity.

Crystallographers have not yet solved the three-dimensional structure of mammalian cholesterol esterase, but they have solved the structure of CRL, a related enzyme. This structure showed that the active site indeed contains large and medium-sized pockets as suggested by the secondary alcohol rule (39). Our extension to chiral aryl esters suggests that within the large pocket, one side is more open than the other and that this difference determines the enantiopreference of CE toward chiral phenols. The structure of CRL indeed shows more space on the side of this large pocket suggested by the empirical rule. Although there are fewer examples, this chiral aryl rule may also apply to CRL. For the sulfoxides **1***b*, **4***b*, and **5***b*, CRL was less enantioselective than CE; however, for the phosphines and phosphine oxides, CRL was more enantioselective (34).

This empirical rule may be useful in the design of new CE-catalyzed resolutions. Up until now most lipase-catalyzed resolutions involve stereocenters close to the ester group. One current goal is to extend the usefulness of lipases by resolving stereocenters distant from the ester and to resolve non-carbon stereocenters. This empirical rule may help identify good examples.

Experimental section

General

Cholesterol esterase (CE) from porcine pancreas was purchased from Genzyme, Boston, Mass. Lipase from *Candida rugosa* (also known as *C. cylindracea* (40)), acetylcholine esterase, porcine pancreas lipase, and bovine pancreas acetone powder were purchased from Sigma Chemical Co., St. Louis, Mo. Lipase from *Pseudomonas cepacia* (lipase P-30), lipase from *Rhizomucor miehei* (MAP-10, synonym *Mucor miehei* (40)), lipase from *Aspergillus niger* (AP-6), and lipase from *Pseudomonas* K10 (lipase-K10) were purchased from Amano International Enzyme Co., Troy, Va. One unit of hydrolase activity, U, corresponds to one μmol of ester group hydrolyzed per minute. Silica gel 70–230 mesh, 60Å (Aldrich, Milwaukee, Wis.) was used for flash chromatography. All other reagents were purchased from Aldrich Chemical Company. Melting points are uncorrected. Tetrahydrofuran and benzene were dried by distillation from sodium under nitrogen with benzophenone as an indicator. Methylene chloride was distilled from sodium hydride and stored over 4Å molecular sieves. Silica gel plates (0.25 mm, Whatman) with G-UV-254 indicator were used for TLC. Mass spectra were acquired using electron ionization conditions (70 eV). ^{1}H NMR spectra were recorded in $CDCl_3$ at 200 MHz using tetramethylsilane as the internal reference. Unless otherwise noted, ^{13}C NMR spectra were recorded in $CDCl_3$ at 75 MHz and were proton decoupled. Either $CDCl_3$ (77.0 ppm) or tetramethylsilane was used as the internal reference. Enzyme assays and reactions were run as described previously for phosphine oxides (34).

(±)-2-(Methylsulfinyl)phenol, ***1****a*

Hydrogen peroxide (24 mL of a 30% soln., 0.21 mol) was added dropwise to a stirred solution of 2-(methylthio)phenol (25 g, 0.18 mol) in acetic acid (100 mL) that was kept at room temperature with a water bath. After addition was complete the reaction mixture was stirred for 45 min. The acetic acid was removed as an azeotrope with toluene by rotary evaporation. The residue dissolved in ethyl acetate (200 mL) and was washed with saturated $NaHCO_3$ solution (2 × 200 mL) and water (200 mL). The organic phase was dried over $MgSO_4$, filtered, and concentrated by rotary evaporation to a solid. Recrystallization from toluene yielded pale yellow crystals, 25.5 g (92%): mp 126–127°C (lit. (23) mp 127–128°C); ^{1}H NMR δ: 7.92–6.89 (m, 4H), 2.95 (s, 3H); ^{13}C NMR δ: 159.1, 133.0, 124.8, 123.4, 119.9, 119.4, 41.7; MS *m/z*: 156 ($M^{+\bullet}$, 93), 141 (100), 113 (49), 109 (11), 65 (22), 63 (11); The mass spectrum and ^{1}H NMR spectrum agree with those reported previously (23).

(±)-2-(Methylsulfinyl)phenyl acetate, ***1****b*

Acetic anhydride (8.5 mL, 90 mmol) was added to a stirred solution of **1***a* (7.2 g, 46 mmol) and pyridine (5.7 mL, 70 mmol) in CH_2Cl_2 (300 mL). The mixture was refluxed for 8 h, when a TLC showed that the reaction was complete. The mixture was cooled, washed with saturated $NaHCO_3$ solution (2 × 500 mL) and with H_2O (500 mL). The organic phase was dried over $MgSO_4$, filtered, and concentrated by rotary evaporation to an oil that solidified on standing. Recrystallization from toluene–hexane yielded white crystals, 7.6 g (82%): mp 85–86°C; R_f = 0.16 (ethyl acetate – hexane, 1:1); ^{1}H NMR δ: 7.98–7.16 (m, 4H), 2.78 (s, 3H), 2.34 (s, 3H); ^{13}C NMR δ: 168.3, 146.0, 137.6, 132.0, 127.2, 124.7, 122.6, 42.2, 20.6; MS *m/z*: 198 ($M^{+\bullet}$, 11), 156 (87), 141 (100), 113 (18), 109 (10), 43 (13); HRMS calcd. for $C_9H_{10}O_3S$: 198.0351; found: 198.0347.

(±)-2-(Chloromethylsulfinyl)phenyl acetate, ***2****b*,

was prepared by chlorination of **1b** as described by Satoh et al. (41) for a similar (methylsulfinyl)benzene. Purification by column chromatography on silica gel eluted with hexane – ethyl acetate (3:1) gave a yellow oil, (22%): R_f = 0.22 (hexane – ethyl acetate, 3:1); ^{1}H NMR δ: 7.98–6.91 (m, 4H), 4.64 (d, 1H, J = 16 Hz), 4.41 (d, 1H, J = 16 Hz), 2.35 (s, 3H); MS *m/z*: 234 ($(M + 2)^{+\bullet}$, 2), 232 ($M^{+\bullet}$,4), 190 (27), 141 (100), 113 (27), HRMS calcd. for $C_9H_9O_3ClS$: 231.9961; found: 231.9960.

1-Methoxy-2-(butylthio)benzene was prepared as described below for 1-methoxy-2-(phenylthio)benzene: yellow oil (82%); R_f = 0.40 (hexane – ethyl acetate, 19:1); ^{1}H NMR δ: 7.45–6.77 (m, 4H), 3.90 (s, 3H, OCH_3), 2.90 (t, 2H, J = 7 Hz), 2.0–1.3 (m, 4H), 0.93 (t, 3H, CH_3, J = 7 Hz). ^{13}C NMR (50 MHz) δ: 156.0, 128.0, 125.9, 124.6, 120.4, 109.9, 55.9, 32.0, 31.5, 22.7, 14.4; MS *m/z*: 196 ($M^{+\bullet}$, 70), 153 (18), 140 (100), 138 (17), 125 (24). Previous researchers reported a similar ^{1}H NMR spectrum, except for the δ3.90 resonance, which they observed at δ3.50 (42).

(±)-2-(Butylsulfinyl)phenol, ***3****a*, was prepared as described below for **4***a*. The methyl group in 1-methoxy-2-(butylthio)benzene was removed with BBr_3 and the resulting 2-(butylthio)phenol was purified by column chromatography on silica gel eluted with hexane to give a yellow oil (40%): R_f = 0.59 (hexane – ethyl acetate, 9:1); ^{1}H NMR δ: 7.8–6.6 (m, 4H), 2.68 (t, 2H, J = 7 Hz), 1.8–1.2 (m, 4H), 0.88 (t, 3H, CH_3, J = 7 Hz). Oxidation with hydrogen peroxide yielded **3***a* as an

Can. J. Chem. Downloaded from www.nrcresearchpress.com by 80.90.12.36 on 09/08/12
For personal use only.

oil (71%): R_f = 0.23 (hexane – ethyl acetate, 3:1); ^{1}H NMR δ: 7.37–6.86 (m, 4H), 3.05 (m, 2H), 1.70 (m, 2H), 1.44 (m, 2H), 0.92 (t, 3H, CH_3, J = 7 Hz); ^{13}C NMR δ: 159.9, 132.8, 125.4, 121.3, 119.6, 119.4, 55.0, 24.4, 21.7, 13.6; MS *m/z*: 198 ($M^{+\bullet}$, 46), 142 (87), 124 (87), 96 (100), 65 (20), 57 (25), 41 (18). Previous researchers reported a similar mass spectrum and ^{1}H NMR spectrum (23).

(±)-2-(Butylsulfinyl)phenyl acetate, ***3***b, was prepared by acetylation of ***3****a* as described below for ***5****a*; yellow oil (62%): R_f = 0.36 (hexane – ethyl acetate, 3:1); ^{1}H NMR δ: 8.0–7.1 (m, 4H), 3.1–2.7 (m, 2H), 2.33 (s, 3H, $COCH_3$), 1.95–1.30 (m, 4H) 0.95 (t, 3H, CH_3, J = 7 Hz); ^{13}C NMR δ: 168.2, 146.2, 135.8, 127.0, 125.5, 122.6, 55.2, 24.1, 21.7, 13.6; MS *m/z*: 240 ($M^{+\bullet}$, 4), 198 (31), 142 (18), 124 (38), 96 (32), 43 (30); HRMS calcd. for $C_{12}H_{16}O_3S$: 240.0820; found: 240.0822.

1-Methoxy-2-(phenylthio)benzene

To a solution of anisole (1.0 mL, 9.2 mmol) in dry THF (7 mL) cooled to −78°C under nitrogen was added butyllithium (3.4 mL of a 2.5 N soln. in hexanes, 1.1 equiv.) and the resulting solution was stirred at 0°C for 1.5 h. Diphenyldisulfide (2.21 g, 10.1 mmol) dissolved in THF (7 mL) was added to the reaction mixture and stirred at room temperature for 2 h. The reaction was quenched by the addition of water (10 mL) and the products were extracted with diethyl ether (3 × 20 mL). The organic phase was washed with 10% NaOH solution (20 mL), H_2O (20 mL), and saturated NaCl solution (20 mL) and dried over $MgSO_4$, filtered, and concentrated by rotary evaporation. Column chromatography on silica gel eluted with hexane – ethyl acetate (99:1) afforded a yellow oil, 1.49 g (75%): R_f = 0.21 (hexane – ethyl acetate, 99:1); ^{1}H NMR δ: 7.38–6.89 (m, 9H), 3.88 (s, 3H); ^{13}C NMR δ: 157.2, 134.4, 131.5, 131.3, 129.0, 128.3, 127.0, 123.9, 121.1, 110.8, 55.8; MS *m/z*: 216 ($M^{+\bullet}$, 100), 210 (17), 183 (10), 168 (11). Previous researchers reported a similar ^{1}H NMR (43).

(±)-2-(Phenylsulfinyl)phenol, ***4***a

Boron tribromide (10 mL of a 1 N solution in CH_2Cl_2, 2.5 equiv.) was added to a solution of 1-methoxy-2-(phenylthio)benzene (0.84 g, 3.9 mmol) in dry CH_2Cl_2 (25 mL) cooled to −23°C under nitrogen. The resulting solution was stirred for 1 h at −23°C, then stirred for 24 h at room temperature. The organic phase was washed with H_2O (30 mL), saturated $NaHCO_3$ solution (30 mL), and H_2O (30 mL), then dried over $MgSO_4$, filtered, and concentrated by rotary evaporation. Column chromatography on silica gel eluted with hexane – ethyl acetate (9:1) afforded 2-(phenylthio)phenol as an oil, 0.63 g (80%): R_f = 0.28 (hexane); IR (neat): 3357 (OH), 3058, 1576, 1471, 1191, 738, 688 cm^{-1}; ^{1}H NMR δ: 7.55–6.91 (m, 9H), 6.52 (s, 1H, OH, exchanges with D_2O); ^{13}C NMR (50 MHz) δ: 156.3, 136.2, 135.1, 131.6, 128.6, 126.2, 125.5, 120.7, 115.7, 115.1; MS *m/z*: 202 ($M^{+\bullet}$, 100), 96 (23). Previous researchers prepared this sulfide in low yield by another route (44). To prepare ***4****a*, hydrogen peroxide (0.25 mL of a 33% solution, 1.1 equiv.) was added to a solution of 2-(phenylthio)phenol (0.48 g, 2.4 mmol) in acetic acid (5 mL) at room temperature and stirred for 1 h. The acetic acid was removed by rotary evaporation to give a yellow solid. Recrystallization from toluene gave white crystals, 0.38 g (74%): mp 163–164°C (lit. (45) mp 164–165 °C); R_f = 0.37 (hexane – ethyl acetate, 3:1); ^{1}H NMR δ: 7.72–6.87 (m); ^{13}C NMR δ: 159.4, 143.6, 133.1, 131.4, 129.5, 126.0, 124.8, 123.1, 119.9, 119.6; MS *m/z*: 218 ($M^{+\bullet}$, 100), 170 (59), 141 (19), 125 (22), 110 (36), 94 (41), 77 (26, C_6H_5+).

(±)-2-(phenylsulfinyl)phenyl acetate, ***4***b, was prepared by acetylation of ***4***a using the procedure described below for ***5***b: yellow oil, 0.18 g (50%); R_f = 0.18 (hexane – ethyl acetate, 3:1); ^{1}H NMR δ: 7.97–7.12 (m, 9H), 2.24 (s, 3H); ^{13}C NMR (50 MHz) δ: 166.9, 146.2, 143.5, 136.3, 131.4, 130.7, 128.6, 126.3, 125.2, 124.8, 122.5, 21.3; MS *m/z*: 260 ($M^{+\bullet}$, 12), 219 (14), 218 (100), 170 (40), 125 (11), 110 (18), 109 (11), 94 (18); HRMS calcd. for $C_{14}H_{12}O_3S$: 260.0507; found: 260.0503.

(±)-2-(Ethoxymethoxy)-1-(phenylsulfinyl)naphthalene

Magnesium turnings (0.24 g, 10 mmol) and 1-bromo-2-(ethoxymethoxy)naphthalene (2.56 g, 9.1 mmol) were added to dry THF (20 mL.). Once the Grignard reaction was initiated, the solution was refluxed for 45 min. Upon cooling to room temperature, benzenesulfinyl chloride (46) (1.46 mL, 9.1 mmol) dissolved in THF (10 mL) was added dropwise. The reaction mixture was refluxed for 15 min, then cooled and poured into 1% HCl (20 mL). The products were extracted with ethyl acetate (3 × 25 mL) and the combined extracts were dried over $MgSO_4$, filtered, and concentrated by rotary evaporation. Column chromatography on silica gel eluted with hexane – ethyl acetate (4:1) afforded an oil, 0.51 g (17%): R_f = 0.12 (hexanes – ethyl acetate, 4:1); ^{1}H NMR δ: 8.67 (d, 1H, J = 10 Hz), 7.95–7.15 (m, 10H), 5.37 (d, 1H, J = 12 Hz), 5.24 (d, 1H, J = 12 Hz), 4.05 (q, 2H, J = 8 Hz), 3.6 (t, 3H, J = 10 Hz).

(±)-2-(Hydroxy)-1-naphthylphenylsulfoxide, ***5***a

Concentrated HCl (3 drops) was added to a solution of (±)-2-(ethoxymethoxy)-1-(phenylsulfinyl)naphthalene (0.50 g, 1.5 mmol) in methanol (10 mL). The solution was refluxed for 45 min, then the solvent was removed by rotary evaporation and the residue dissolved in ethyl acetate (20 mL). The organic phase was washed with saturated $NaHCO_3$ (10 mL), then with saturated NaCl (10 mL), and dried over $MgSO_4$, filtered, and concentrated by rotary evaporation to a yellow oil, 0.35 g (75%): R_f = 0.41 (hexanes – ethyl acetate, 3:1); ^{1}H NMR δ: 8.25–6.82 (m); MS *m/z*: 284 ($M^{+\bullet}$, 6), 268 (31), 252 (100), 220 (34), 191 (23), 146 (36). This material was used in the next step without further purification.

(±)-2-Acetoxy-1-naphthylphenylsulfoxide, ***5***b

Sodium carbonate (0.16 g, 1.5 mmol), *N,N*-dimethyl-4-aminopyridine (14 mg, 0.11 mmol), and acetic anhydride (0.17 g, 1.7 mmol) were added to a solution of ***5****a* (0.35 g, 1.1 mmol) in ethyl acetate (10 mL) and the mixture was stirred for 12 h. The reaction mixture was washed with 1% HCl (10 mL), saturated NaCl (10 mL), and dried over $MgSO_4$, filtered, and concentrated by rotary evaporation. Column chromatography on silica gel eluted with hexane – ethyl acetate (4:1) afforded an oil, 0.29 g (86%): R_f = 0.19 (hexanes – ethyl acetate, 4:1); ^{1}H NMR δ: 8.72–7.15 (m, 11H), 2.35 (s, 3H); MS *m/z*: 310 ($M^{+\bullet}$, 18), 268 (100), 252 (35), 220 (85), 159 (51).

Can. J. Chem, Downloaded from www.nrcresearchpress.com by 80.90.12.36 on 09/08/12
For personal use only.

Enantiomeric purity

Enantiomers of **1***a*, **1***b*, **2***a*, and **2***b* were separated by HPLC on a chiral stationary phase (Chiralpak OB – tribenzoylated cellulose on silica gel, Daicel Chemical Industries, Ltd. Fort Lee, N.J.) eluted with hexane–isopropanol (4:1) at 0.5 mL/min. Samples were dissolved in eluting solvent at a concentration of 1 mg/mL. **1***a*: $k'_S = 1.26$, $k'_R = 2.08$, $\alpha = 1.65$; **1***b*: $k'_S = 8.07$, $k'_R = 8.34$, $\alpha = 1.37$; **2***a*: $k'_S = 1.28$, $k'_R = 1.74$, $\alpha = 1.36$; **2***b*: $k'_S = 6.80$, $k'_R = 9.28$, $\alpha = 1.36$. For **3–5**, the acetates and phenols were separated by chromatography on silica gel eluted with toluene – ethyl ether (9:1) for **3** and **4** or hexane – ethyl acetate (4:1) for **5**. Kagan and co-workers recently reported an enantiomeric enrichment of sulfoxides during silica gel chromatography due to dimerization of the sulfoxides (47). We combined all the fractions containing the acetates or the phenols to avoid any such enrichment. The enantiomeric purity of the isolated **3***b*–**5***b* was determined by ^{1}H NMR in the presence of Eu(hfc)$_3$ (approximately 1.5 equiv.). The acetyl methyl resonances were separated by 8 Hz under these conditions. The enantiomeric purity of **3***a*–**5***a* was determined in the same manner after acetylation with acetic anhydride as described above.

Absolute configuration

Phenol **1***a*, isolated from a CE-catalyzed resolution of **1***b* was converted to (*R*)-(+)-1-methoxy-2-(methylsufinyl)benzene and its optical rotation was compared to that reported in the literature. Potassium carbonate (1.5 equiv.) and CH_3I (1.5 equiv.) were added to **1***a* dissolved in acetone (5 mL) and the suspension was stirred for 12 h at room temperature. The acetone was removed by rotary evaporation. The residue was suspended in ethyl acetate (5 mL) and washed with 1% HCl (5 mL), then saturated NaCl (5 mL), dried over $MgSO_4$, filtered, and concentrated under vacuum to an oil: $[\alpha]_D$ (obsd) +65 (*c* 3.2, acetone) (lit. (48) $[\alpha]_D$ −25.8 (*c* 3.2, acetone) for the (*S*) enantiomer with 8% ee). Similarly (*R*)-(+)-1-methoxy-2-(phenylsulfinyl)benzene was prepared from **4***a* isolated from a CE-catalyzed resolution: $[\alpha]_D$ (obsd) +44 (*c* 0.03, MeOH) (lit. (49) (*R*)-(+): $[\alpha]_D$ +275 (*c* 1.03, acetone)). The absolute configurations of the enantiomers of **2***b*, **3***b*, and **5***b*, which reacted faster with CE, were also assigned the (*R*) configuration based on the relative positions of the acetyl methyl ^{1}H NMR resonance in the presence of Eu(hfc)$_3$. The resonance for the fast-reacting enantiomer appeared downfield of the resonance for the slow-reacting enantiomer for all five acetoxysulfoxides.

Resolution of (±)-1*b* with pancreas acetone powder

Bovine pancreas acetone powder (an inexpensive source of CE, 210 mg, Sigma) and crude sodium taurocholate (329 mg, Sigma) were added to a mixture of phosphate buffer (25 mL, 10 mM, pH 7.0 and diethyl ether (25 mL). The pH was readjusted to 7.0 and a solution of (±)-**1***b* (251 mg, 1.27 mmol) in diethyl ether (25 mL) was added. The pH was maintained at 7.0 with a pH stat, which controlled the addition of NaOH (0.505 N). At the 56% conversion, LiCl (1 g) was added to break up the emulsion and the reaction mixture was extracted with ethyl acetate – ethanol (9:1, 3 × 55 mL). The combined extracts were dried over $MgSO_4$, filtered, concentrated by rotary evaporation, and redissolved in toluene (25 mL). This toluene solution was washed with saturated Na_2CO_3 solution (1 × 20 mL) to remove **1***a*.[2] The toluene solution was then washed with H_2O (20 mL), saturated NaCl solution (20 mL), dried over $MgSO_4$, filtered, and concentrated to give (*S*)-**1***b* as an oil, 77% ee. Recrystallization from toluene–hexane yielded white crystals, 28 mg, 0.14 mmol, 11% yield from a maximum 50% in a resolution, >99% ee by HPLC. The TLC and ^{1}H NMR of (*S*)-**1***b* were identical to that for the racemate.

Conformational analysis of 1–9

Local minima and their relative energies were calculated using molecular mechanics using HyperChem revision 3 (Hypercube, Waterloo, Ont.) with default MM+ parameters. Structures were minimized first using a steepest decent algorithm and then with a conjugate gradient to an rms error of <0.005. When we found no local minimum in the range $0° > \theta > 90°$, we compared several fully minimized structures with a fixed θ as shown in Figs. 5 and 6.

Acknowledgments

We thank the Natural Sciences and Engineering Research Council of Canada, le Fonds pour la formation de chercheurs et l'aide à la recherche (Québec), and the McGill Faculty of Graduate Research for financial support.

References

1. K.K. Andersen. *In* The chemistry of sulphones and sulphoxides. *Edited by* S. Patai, Z. Rappaport, and C.J.M. Stirling. Wiley, New York. 1988. pp. 55–94,
2. T. Satoh and K. Yamakawa. Synlett, 455 (1992); A.J. Walker. Tetrahedron: Asymmetry, **3**, 961 (1992); G. Solladié. Synthesis, 185 (1981); G.H. Posner. Acc. Chem. Res. **20**, 72 (1987).
3. H.B. Kagan and F. Rebiere, Synlett, 643 (1990).
4. K.K. Andersen. Tetrahedron Lett. 93 (1962); J. Drabowicz, B. Bujinicki, and M. Mikolajczyk. J. Org. Chem. **47**, 3325 (1982); G. Solladié. Synthesis, 185 (1981).
5. J.P. Marino, S. Bogdan, and K. Kimura. J. Am. Chem. Soc. **114**, 5566 (1992); D.A. Evans, M.M. Faul, L. Colombo, J.J. Bisaha, J. Clardy, and D. Cherry. J. Am. Chem. Soc. **114**, 5977 (1992); I. Fernández, N. Khiar, J.M. Llera, and F. Alcudia. J. Org. Chem. **57**, 6789 (1992); M. Wills, R.J. Butlin, and I.D. Linney. Tetrahedron Lett. **33**, 5427 (1992); J.K. Whitesell and M.-S. Wong. J. Org. Chem. **59**, 597 (1994).
6. F. Rebiere and H.B. Kagan. Tetrahedron Lett. **30**, 3659 (1989); F. Rebiere, O. Samuel, L. Ricard, and H.B. Kagan. J. Org. Chem. **56**, 5991 (1991); S.C. Benson and J.K. Snyder. Tetrahedron Lett. **32**, 5885 (1991).
7. F. Di Furia, G. Modena, and R. Seraglia. Synthesis, 325 (1984); P. Pitchen, M. Deshmukh, E. Dunach, and H.B. Kagan. J. Am. Chem. Soc. **106**, 8188 (1984); S.H. Shao, O. Samuel, and H.B. Kagan. Org. Synth. **68**, 49 (1989).
8. F.A. Davis, R.T. Reddy, W. Han, and P.J. Carroll. J. Am. Chem. Soc. **114**, 1428 (1992).
9. N. Komatsu, M. Hashizume, T. Sugita, and S. Uemura. J. Org. Chem. **58**, 4529 (1993).
10. S. Colonna, N. Gaggero, L. Casella, G. Carrea, and P. Pasta. Tetrahedron: Asymmetry, **3**, 95 (1992); H. Fu, H. Kondo, Y. Ichikawa, G.C. Look, and C.-H. Wong. J. Org. Chem. **57**, 7265 (1992). Related oxidation catalyzed by cyclohexanone monooxygenase: G. Carrea, B. Redigolo, S. Riva, S. Colonna, N. Gaggero, E. Battistel, and D. Bianchi. Tetrahedron: Asymmetry, **3**, 1063 (1992).
11. Review: H.L. Holland. Chem. Rev. **88**, 473 (1988). Recent reports: M. Madesclaire, A. Fauve, J. Metin, and A. Carpy. Tetrahedron: Asymmetry, **1**, 311 (1990); P.H. Buist and D.M.

Can. J. Chem. Downloaded from www.nrcresearchpress.com by 80.90.12.36 on 09/08/12
For personal use only.

Marecak. J. Am. Chem. Soc. **113**, 5877 (1991); H.L. Holland, C.G. Rand, P. Viski, and F.M. Brown. Can. J. Chem. **69**, 1989 (1991); C.C.R. Allen, D.R. Boyd, H. Dalton, N.D. Sharma, S.A. Haughey, R.A.S. McMordie, B.T. McMurray, G.N. Sheldrake, and K. Sproule. J. Chem. Soc. Chem. Commun. 119 (1995).
12. C. Rossi, A. Fauve, M. Madesclaire, D. Roche, F.A. Davis, and R.T. Reddy. Tetrahedron: Asymmetry, **3**, 629 (1992); C.M. Rayner, M.S. Sin, and A.D. Westwell. Tetrahedron Lett. **33**, 7237 (1992).
13. R. Breitschuh and D. Seebach. Synthesis, 1170 (1992); A.M. Bernard and P.P. Piras. Synth. Commun. **22**, 2789 (1992); G.O. Danelon, E.G. Mata and O.A. Mascaretti. Tetrahedron Lett. **34**, 7877 (1993).
14. F. Toda, K. Tanaka, and S. Nagamatsu. Tetrahedron Lett. **25**, 4929 (1984); F. Toda, K. Mori, Y. Matsuura, and H. Akai, J. Chem. Soc. Chem. Commun. 1591 (1990).
15. N. Komatsu, M. Hashizume, T. Sugita, and S. Uemura. J. Org. Chem. **58**, 7624 (1993); T. Kawasaki, N. Watanabe, T. Sugai, and H. Ohta. Chem. Lett. 1611 (1992).
16. R.L. Crumble, B.S. Deol, J.E. Nemorin, and D.D. Ridley. Aust. J. Chem. **31**, 1965 (1978); S. Iriuchijima and N. Kojima. Agric. Biol. Chem. **42**, 451 (1978).
17. T.W. Reid, T.P. Stein, and D. Fahrney. J. Am. Chem. Soc. **89**, 7125 (1967).
18. H. Ohta, Y. Kato, and G. Tsuchihasi. Chem. Lett. 217 (1986).
19. K. Burgess, I. Henderson, and K.-K. Ho. J. Org. Chem. **57**, 1290 (1992); K. Burgess and I. Henderson. Tetrahedron Lett. **30**, 3633 (1989).
20. C. Cardellicchio, F. Naso, and A. Scilimati. Tetrahedron Lett. **35**, 4635 (1994).
21. S.G. Allenmark and A.C. Andersson. Tetrahedron: Asymmetry, **4**, 2371 (1993).
22. M. Mikolajczyk, P. Kielbasinski, R. Zurawinski, M. Wieczorek, and J. Blaszczyk. Synlett, 127 (1994).
23. A.O. Pedersen, G. Schroll, and S.-O. Lawesson. Tetrahedron, **26**, 4449 (1970).
24. C.S. Chen, Y. Fujimoto, G. Girdaukas, and C.J. Sih. J. Am. Chem. Soc. **104**, 7294 (1982).
25. U. Folli, D. Iarossi, and F. Taddei. J. Chem. Soc. Perkin Trans. 2, 848 (1973).
26. W.P. Jencks and J. Regenstein. *In* Handbook of biochemistry. 2nd ed. *Edited by* H.A. Sober. CRC Press, Cleveland, Ohio. 1970. p J-195.
27. R.J. Kazlauskas. J. Am. Chem. Soc. **111**, 4953 (1989); Org. Synth. **70**, 60 (1991).
28. R.J. Kazlauskas, A.N.E. Weissfloch, A.T. Rappaport, and L.A. Cuccia. J. Org. Chem. **56**, 2656 (1991).
29. M. Kiefer, R. Vogel, G. Helmchen, and B. Nuber. Tetrahedron, **50**, 7109 (1994).
30. L. Liu and T.J. Katz. Tetrahedron Lett. **31**, 3983 (1990).
31. H.J. Bestman and W. Both. Angew. Chem. Intl. Ed. Engl. **11**, 296 (1972); J.-P. Mazleyrat and Z. Welvart. Nouv. J. Chim. **7**, 491 (1983).
32. E. Mizuguchi, M. Takemoto, and K. Achiwa. Tetrahedron: Asymmetry, **4**, 1961 (1993).
33. A. Moore, G.W. Burton, and K.U. Ingold. J. Am. Chem. Soc. **116**, 6945 (1994); competitive experiment in the presence of taurocholate.
34. A.N. Serreqi and R.J. Kazlauskas. J. Org. Chem. **59**, 7609 (1994).
35. S. Ianelli, A. Musatti, M. Nardelli, R. Benassi, U. Folli, and F. Taddei. J. Chem. Soc. Perkin Trans. 2, 49 (1992), and references therein.
36. P. Ugliengo, J. Ahmed, D. Viterbo, M. Calleri, and M. Ceruti. Gazz. Chim. Ital. **119**, 487 (1989); P. Ugliengo, J. Ahmed, D. Viterbo, and M. Ceruti. Gazz. Chim. Ital. **119**, 493 (1989).
37. M. Chin, G.L. Durst, S.R. Head, P.L. Bock, and J.A. Mosbo. J. Organomet. Chem. **470**, 73 (1994).
38. S.G. Pyne, A.R. Hajipour, and K. Prabakaran. Tetrahedron Lett. **35**, 645 (1994); P. Renaud and T. Bourquard. Tetrahedron Lett. **35**, 1707 (1994); C. Bolm and P. Müller. Tetrahedron Lett. **36**, 1625 (1995).
39. P. Grochulski, Y. Li, J.D. Schrag, and M. Cygler. Protein Sci. **3**, 82 (1994).
40. Catalogue of Fungi/Yeasts. 17th ed. American Type Culture Collection, Rockville, Md. 1987.
41. T. Satoh, T. Oohara, Y. Ueda, and K. Yamakawa. J. Org. Chem. **54**, 3130 (1989).
42. F.A. Davis, L.A. Jenkins, and R.L. Billmers. J. Org. Chem. **51**, 1033 (1986).
43. M. Hori, T. Kataoka, H. Shimizu, M. Miyagaki, and T. Takagi. Chem. Pharm. Bull. **22**, 2030 (1974).
44. T. Schaeffer, S.R. Salaman, T.A. Wildman, and P.D. Clark. Can. J. Chem. **60**, 342 (1982).
45. E.D. Amstutz, I.M. Husberger, and J.J. Chessick. J. Am. Chem. Soc. **73**, 1220 (1951).
46. F. Kurzer. *In* Organic syntheses. Coll. Vol. 4. *Edited by* N. Rabjohn. John Wiley, New York. 1963. pp. 937–939.
47. P. Diter, S. Taudien, O. Samuel, and H.B. Kagan. J. Org. Chem. **59**, 370 (1994).
48. B. Dudzinski, P. Lyzwa, M. Mikolajczyk, and J. Drabowicz. *In* Proceedings of the Fourth International Symposium on Cyclodextrins. *Edited by* O. Huber and J. Szejtli. Kluwer Academic, Amsterdam. 1988. pp. 503–507.
49. M. Moriyama, T. Yoshimura, N. Furukawa, T. Numata, and S. Oae. Tetrahedron, **32**, 3003 (1976).

Regiocontrolled functionalization of seven-membered ring via nucleophilic cycloheptenyl-η^3-allyltitanium complexes

Jan Szymoniak, Didier Felix, Jack Besançon, and Claude Moïse

Can. J. Chem. Downloaded from www.nrcresearchpress.com by 80.90.12.36 on 09/08/12
For personal use only.

Abstract: A new "electron-reversed" method for the functionalization of a seven-membered ring is developed. Cycloheptenyl-η^3-allyltitanocene complexes derived from cycloheptatriene react with aldehydes or carbon dioxide to afford, respectively, the mixture of isomeric 1,4- and 1,3-cycloheptadienyl carbinols **3***a–e* and **2***a–e* or methyl esters **7** and **6**. The **3/2** and **7/6** ratios increase with increasing steric hindrance in the electrophile. Moreover, these may be significantly increased by introducing *tert*-butyl substituents on the Cp rings of the starting titanocene dichloride. The regiochemistry of the reaction was rationalized in terms of the equilibrium between the two envisageable allylic complexes. The reaction constitutes the first direct entry to functionalized 1,4-cycloheptadienes, some of which are related to biologically active compounds.

Key words: η^3-allyltitanium complexes, cycloheptadiene derivatives, regiocontrol, electron reversal.

Résumé : Une nouvelle méthode de type inversion de polarité de fonctionnalisation du cycle à sept atomes de carbone est présentée. Les cycloheptenyl-η^3-allyltitanocenes, obtenus à partir du cycloheptatrième, sont opposés à divers aldéhydes ou au dioxyde de carbone. Il en résulte des mélanges de cyclohepta-1,4 et -1,3-diényl carbinols (respectivement **3** et **2**) ou d'esters méthyliques (**7** et **6**). Les rapports **3/2** et **7/6** augmentent avec la taille de l'éléctrophile utilisé. Par ailleurs, on observe une nette augmentation de ce rapport par l'introduction du groupe *tert*-butyle sur chacun de cycles cyclopentadiényles du dichlorure de titanocène de départ. La régioseléctivité de la réaction est interprétée en terme d'équilibre entre les deux complexes allyliques possibles. La réaction offre une approche directe des dérivés de cyclohepta-1,4-diène d'intérêt biologique.

Mots clés : complexes η^3-allyltitane, dérivés cycloheptadiènes, régiosélectivité, inversion de polarité.

The significant synthetic interest in allyl organometallics lies especially in that they can be used for the stereocontrolled construction of open-chain systems (1). Allylation reactions that involve nucleophilic attack of various allylic metals on electrophiles such as aldehydes, ketones, imines, and Michael acceptors have been extensively studied (2). The allylic organometallic method has been successfully applied for the stereoselective synthesis of a number of segments that are commonly found in biologically active compounds (3).

Besides the ability to control the stereochemical course of the reaction, the transition-metal-based allyl organometallics can lead to reversed polarity equivalents (Umpolung). In this matter, in our recent communication we reported a procedure for the transformation of cycloheptatriene into the cycloheptenyl-η^3-allyltitanocene complexes (4). The latter can be related to simpler η^3-allyltitanocenes, which are efficient allylation agents known to add to aldehydes in a regio- and stereocontrolled fashion (5). To the best of our knowledge, there are no precedents, however, for the use of alkenyl-η^3-allyltitanocenes (6) as nucleophilic allyl reagents. We therefore focused our attention on the synthetic use of the cycloheptenyl-η^3-allyltitanocenes formed. The complex mixtures were reacted in situ with aldehydes **1***a–e* to produce, in good yield, isomeric homoallylic alcohols **2***a–e* and **3***a–e* (Scheme 1).[2] The **3/2** ratio was noted to increase with increasing size of aldehyde.

In seeking to expand the scope of this new methodology concerning the functionalization of seven-membered rings,[3] we decided to explore the reactivity of the complexes **A** and **B** towards other electrophiles. Moreover, we undertook studies of allylation reaction regioselectivity, in particular aimed at improving the **3/2** product ratio. Indeed, the reaction could provide a first straight entry to 1,4-cycloheptadienes substituted at the 6 position (analogous to **3**), closely related to biologically active molecules (8).

Received January 31, 1995.

J. Szymoniak,[1] D. Felix, J. Besançon, and C. Moïse.[1] Laboratoire de synthèse et d'électrosynthèse organométalliques associé au Centre national de la recherche scientifique (Unité de recherche associée n° 1685), Faculté des sciences, 6 bd Gabriel, 21 000 Dijon, France.

[1] Authors to whom correspondence may be addressed.

[2] The products were obtained after basic work-up (Na_2Co_3) followed by usual chromatography purification. Alternatively, trimethylsilyl ethers of the corresponding alcohols can be prepared directly by a simple treatment of the reaction mixture with Me_3SiCl.

[3] Up to now, methodologies using organometallic chemistry have usually involved a nucleophile addition to the cationic cycloheptadiene-iron, -molybdenum, or -palladium complexes; see ref. 7.

Scheme 1.

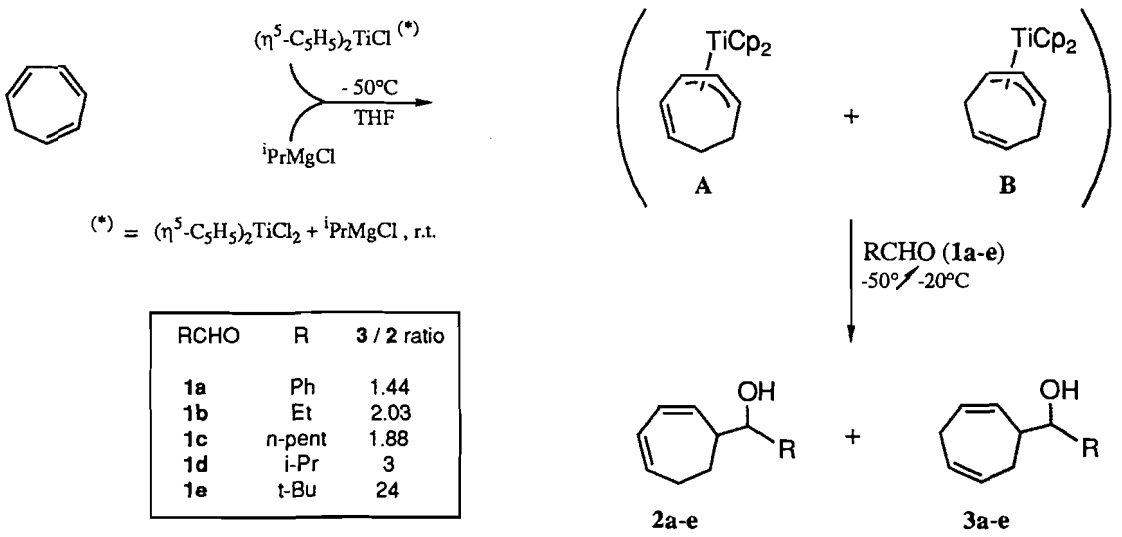

RCHO	R	3 / 2 ratio
1a	Ph	1.44
1b	Et	2.03
1c	*n*-pent	1.88
1d	i-Pr	3
1e	t-Bu	24

Scheme 2.

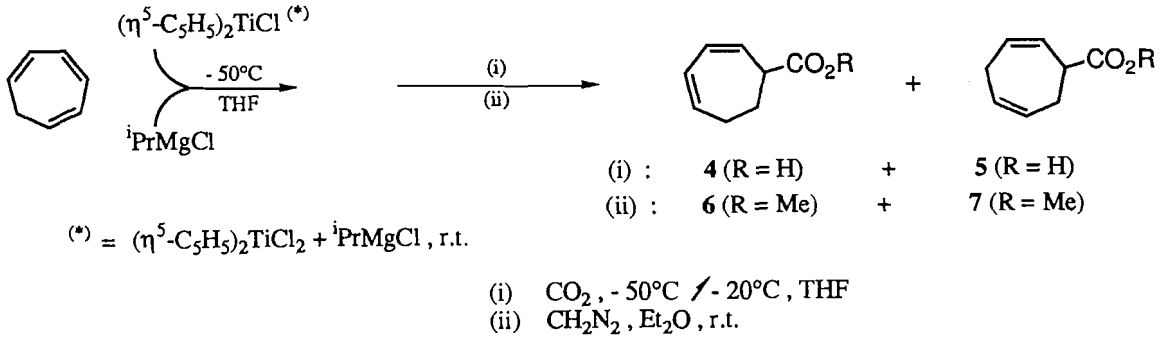

Results and discussion

Carbon dioxide has been shown to insert into η^3-allyltitanium(III) reagents to afford, after hydrolysis, the corresponding β,γ-unsaturated carboxylic acids (9). We have reacted this small, symmetrical electrophile with the cycloheptenyl-η^3-allyltitanium complexes **A**/**B**, prepared in situ by the reaction of preformed Cp_2TiCl and isopropylmagnesium chloride in the presence of cycloheptatriene. The resulting crude mixture of carboxylic acids **4** and **5** was treated with diazomethane and chromatographed to give corresponding isomeric esters **6** and **7** (Scheme 2). It must be mentioned that the major product **7** is a direct starting material for the preparation of biologically active molecules of marine origin (10). The five-step synthesis of **7**, involving a rearrangement of functionalized vinylcyclopropanes, has been reported in the literature (11).

The ratio of **7**/**6** = 1.22 is not surprising in light of the evolution of the regioselectivity observed for aldehydes (Scheme 1). The overall data indicate that steric effects play a leading part in the control of regioselectivity. The increase of the **3**/**2** product ratio as the size of electrophile increases, may be related to the greater steric hindrance for complex **A** (related to **2**) compared with complex **B** (related to **3**). In fact, two opposing factors can operate here. The electronic factor should favour complex **A**, owing to the conjugation of the vinyl group with the allyl system. However, to gain the maximum resonance energy, the conjugation in **A** involves a planar arrangement of five of the seven carbon atoms of the ring. As a result, increased steric hindrance should exist in **A**, probably due to interaction with the titanocene part.

To obtain additional insight into the regiochemical outcome of the reaction we decided to enhance steric bulk in the complexes by introducing *tert*-butyl substituents into both cyclopentadienyl rings. We assumed that such a supplementary hindrance should alter the regioselectivity of the addition step. Therefore, substituted titanocene dichloride $(^t BuCp)_2TiCl_2$ was prepared and used as a precursor for the formation of cycloheptenyl-η^3-allyltitanium complexes ^{t}**A** and ^{t}**B**. The complexes added in situ with aldehydes **1***a–e* or carbon dioxide to produce, respectively, homoallyl alcohols **2***a–e* and **3***a–e* or acids **4** and **5** (esters **6** and **7** after diazomethane methylation). The reactions were carried out as previously, and overall yields of the products (**2**+**3**) appeared closely similar to those obtained for the reactions using Cp_2TiCl_2. Likewise for the latter, the major regioisomers **3***a–e* were obtained as stereochemically pure products by ^{1}H and ^{13}C NMR as well as by GC-coupled mass spectroscopy. Similarly, minor compounds **2***a*, **2***d*, and **2***e* possess spectral characteristics that are consistent with their single stereoisomer structure. On the other hand, compounds **2***b* and **2***c*, derived from less sterically hindered aldehydes, show evidence (^{13}C NMR and GC–MS) of the presence of two stereoisomers.

The molar ratios relative to the pairs of regioisomers **3**/**2** and **7**/**6** (**5**/**4**) together with the corresponding ratios obtained

Can. J. Chem. Downloaded from www.nrcresearchpress.com by 80.90.12.36 on 09/08/12
For personal use only.

Table 1. Molar ratios of regioisomers **3/2** and **7/6**.

Electrophile		Products	**3/2** or **7/6** ratio	
RCHO (**1**)	R		(Cp_2TiCl_2) using reactions	$(Cp^tBu)_2TiCl_2$ using reactions
1*a*	C_6H_5	**3***a*+**2***a*	1.44	3.16
1*b*	C_2H_5	**3***b*+**2***b*	2.03	2.44
1*c*	*n*-C_5H_{11}	**3***c*+**2***c*	1.88	2.84
1*d*	$(CH_3)_2CH$	**3***a*+**2***a*	3	15.66
1*e*	$(CH_3)_3C$	**3***a*+**2***a*	24	
	CO_2	**7**+**6**	1.22	4

Fig. 1.

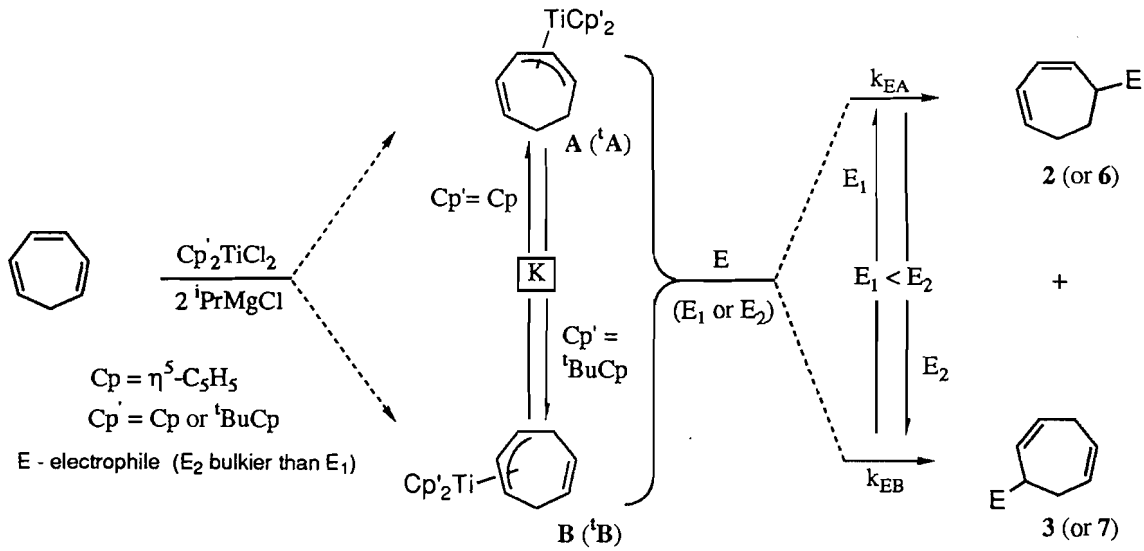

previously from the nonsubstituted cyclopentadienyl-ring-bearing complexes **A** and **B** are summarized in Table 1.[4] Comparison of these two series of values shows that the supplementary hindrance introduced into the cycloheptenyl-η^3-allyltitanocenes does affect the regioselectivity of the reaction. Indeed, the **3/2** (**7/6**) ratio increases significantly for all electrophiles used. This phenomenon agrees with the postulate of the steric demands being greater for complex **A** than for complex **B**.

Quenching experiments contributed further to the clarification of the regiochemistry. The complex mixtures **B/A** and **^{t}B/^{t}A** were trapped with gaseous HCl. The ratios of the resulting 1,4- vs. 1,3-cycloheptadiene, determined by ^{1}H NMR and gas chromatography, were 0.82 and 1.15, respectively. We assumed them to approach the **B/A** and **^{t}B/^{t}A** equilibrium levels. Indeed, the ratio was lower for nonsubstituted complexes (**B/A**) (than for the substituted ones (**^{t}B/^{t}A**). On the other hand, both values were significantly lower than any of the corresponding **3/2** ratios from Table 1.

More detailed studies, particularly in kinetics, are needed to elucidate the regiochemistry of the reaction. However, a plausible hypothesis implies an equilibrium between **A** and **B** (Fig. 1), possibly ensured by dehydrometallation followed by a rehydrometallation process. Such an equilibrium, disturbed by the reacting electrophile, can be assumed on account of the variable **3/2** product ratio,which was systematically higher than the corresponding **B/A** (**^{t}B/^{t}A**) values. The regiochemistry of the reaction is thus determined in the kinetically controlled addition of the electrophile to the equilibrated mixture of **A** and **B** (Fig. 1). In this context, the increase of the **3/2** product ratio with size of attacking electrophile suggests that the steric demands are more strict on the path to the transition state starting from **A** than on that starting from **B**. Because of the presumed reactant-like transition state for the allyltitanation reactions (12), the above statement agrees favorably with the thermodynamic postulate of the sterically disfavoured complex **A**. An introduction of the supplementary bulky group into the titanocene unit destabilizes complex **^{t}A** much more than complex **^{t}B**, leading to the higher **B/A** equilibrium level (1.15 = **^{t}B/^{t}A** > **B/A** = 0.82). Indeed, the **3/2** ratio increases for all the electrophiles used. This effect appears to be particularly pronounced when a bulky aldehyde, e.g., isobutyraldehyde (**1***d*), is used (**3/2** ratio change from 3 to 15.7).

The above hypothesis is true only if the complexes **A** and **B** are interconverted at a rate slower than that at which the rapid electrophilic addition occurs. Nevertheless, an opposite trend cannot be completely ruled out at present. If Curtin–Hammett conditions apply, only differences in the kinetics of electrophilic addition will affect the regiochemical outcome of the

[4] The molar ratios of the regioisomers **3/2** and **7/6** (**5/4**) were established by ^{1}H NMR, using crude reaction mixtures.

Can. J. Chem. Downloaded from www.nrcresearchpress.com by 80.90.12.36 on 09/08/12
For personal use only.

Scheme 3.

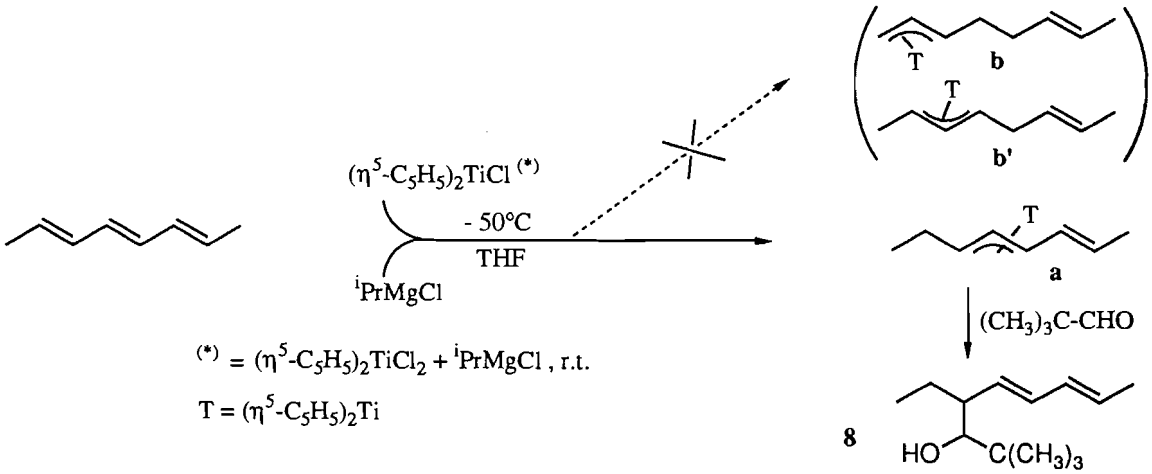

reaction. In any case, although steric factors play a major role in determining regioselectivity, the reactivity of the electrophile must still be taken into account. For example, benzaldehyde reacts least selectively with **B/A** but is more sterically hindered than either propionaldehyde or hexanal (Table 1). Furthermore, the less hindered CO_2 reacts more selectively with ^{t}**B**/^{t}**A** than most of the aldehydes examined.

Additional insight into the specific role of the steric factor in the *cyclic* alkenyl-η^3-allyltitanocenes is provided by an experiment in which a *linear* triene, namely 2,4,6-octatriene, was used as substrate (Scheme 3). The preparation of the corresponding allyltitanocene(s) and its(their) reaction with pivalic aldehyde (**1***e*) were carried out according to the usual protocol. The only product obtained in good yield was the conjugated homoallylic alcohol **8**. Such a result indicates a strong preference for the formation of the conjugated complex **a**, to the detriment of the totally absent isolated complexes **b** and **b′**. The absence of the steric factor for acyclic complexes is an especially striking fact, since the most bulky aldehyde was employed here as an electrophile.

Conclusion

The "reversed polarity" approach to the functionalization of a seven-membered ring is of synthetic interest since (*i*) it offers a simple opportunity to introduce electrophile reagents directly into the cycloheptatriene, and (*ii*) it provides a first straight entry to the 6-substituted 1,4-cycloheptadienes. Indeed, the regiochemical trends that are analyzed make possible further improvement of the 1,4 vs. 1,3 product ratio. Due to the high stereoselectivity exhibited for the former, the reaction employing chiral allyltitanium reagent (13) could open a direct way to optically active 1,4 derivatives of biological interest.

Experimental section

General

Organometallic reactions were run under argon atmosphere using vacuum line techniques. The solvents used were distilled under argon from sodium benzophenone ketyl. Aldehydes **1***a–e*, cycloheptatriene, titanocene dichloride, and isopropylmagnesium chloride (2 M solution in THF) were purchased from Aldrich Chemical Co. Aldehydes and cycloheptatriene were distilled under argon prior to use. 2,4,6-Octatriene was prepared by a reported procedure (14). ^{1}H and ^{13}C NMR spectra were recorded at 400 and 100.53 MHz, respectively. Mass spectra were obtained by the EI (70 eV) technique. Gas chromatography (GC) was carried out on 30 m × 0.25 mm copper column packed with methyl silicone with a flow rate of 1.6 mL/min. Column flash chromatography was performed on silica gel 60 (Merck) by using hexane:diethyl ether (8:2 to 95:5 v/v) as eluents.

Representative procedure for the preparation of cycloheptadienyl carbinols 2 and 3

Isopropylmagnesium chloride (1.5 mL, 2 M solution in THF) was added by syringe at room temperature under argon to a stirred suspension of titanocene dichloride[5] (0.75 g, 3.02 mmol) in 20 mL of THF. After stirring for 30 min the resulting green solution of Cp_2TiCl was cooled to −50°C. Freshly distilled cycloheptatriene (0.41 g, 4.5 mmol) and a second portion of isopropylmagnesium chloride (1.5 mL) were simultaneously added, dropwise via syringes. After stirring for 10 min at −50°C, pivalic aldehyde (0.26 g, 3.02 mmol) was added neat by syringe and the mixture was allowed to warm gradually to −20°C over a period of 30 min. The reaction mixture was poured into a separatory funnel containing ether (100 mL), and treated with saturated aqueous $NaHCO_3$ (25 mL). The ether layer was separated and the aqueous layer was extracted with ether. The combined ether layers were dried over $MgSO_4$ and concentrated in vacuo. The residue was diluted with ether/hexane = 2/1 (20 mL) and the titanium derivatives separated by filtration (the major portion of titanocene dichloride can be recovered by acidifying the aqueous layer). The solvent was removed in vacuo. Purification by flash chromatograpy on silica gel column eluting with hexane/ether (5/1) afforded the isomeric homoallylic alcohols **2***e* (0.016 g, 3%) and **3***e* (0.39 g, 73%).

2*e* : IR (neat): 3475, 1650, 1610 cm^{-1}; ^{1}H NMR (C_6D_6) δ: 5.92–5.86 (m, 1H), 5.84–5.74 (m, 3H), 2.86 (d, J = 6.7 Hz, 1H), 2.66 (m, 1H), 2.50–2.39 (m, 1H), 2.22–2.12 (m, 1H), 1.74–1.66 (m, 1H), 1.63–1.53 (m, 1H, H-5 decoupling: ddd,

[5] Alternatively (^{t}BuCp)$_2$TiCl$_2$ was used, resulting in the closely similar overall (**3+2**) yields, and the increased **3/2** product ratio (Table 1).

Can. J. Chem. Downloaded from www.nrcresearchpress.com by 80.90.12.36 on 09/08/12
For personal use only.

Can. J. Chem. Downloaded from www.nrcresearchpress.com by 80.90.12.36 on 09/08/12
For personal use only.

J = 13.1, 9.6, 4.2 Hz), 1.39 (d, J = 6.7 Hz, 1H, D_2O exchangeable), 0.89 (s, 9H); ^{13}C NMR {^1H} ($CDCl_3$) δ: 135.6, 132.5, 127.8, 124.5, 84.7, 41.9, 36.2, 32.6, 29.4, 26.7; DEPT ^{13}C NMR: disappearance of 36.2; MS *m/z*: 180 (M^+, 20), 123 (100), 105, 95, 79.

3*e* : IR (neat): 3417, 2957, 1648; ^1H NMR (C_6D_6)δ: 5.91 (dd, J = 11.5, 6.0 Hz, 1H), 5.73 (dddd, J = 11.5, 6.2, 6.0, 2.3 Hz, 1H), 5.63 (dddd, J = 11.5, 6.0, 6.0, 2.3 Hz, 1H), 5.50 (ddd, J = 11.5, 6.9, 6.0 Hz, 1H, coupled with H-7), 3.42 (m, 1H), 3.25 (br s, 1H), 2.24–2.16 (m, 1H, coupled with H=1), 2.11–1.96 (m, 3H), 1.58 (br s, 1H, D_2O exchangeable), 0.92 (s, 9H); ^{13}C{^1H} NMR ($CDCl_3$) δ: 134.2, 131.8, 130.9, 130,4. 83.4, 41.3, 36.2, 27.3, 26.6, 26.5; DEPT ^{13}C NMR: disappearance of 36.2; MS *m/z*: 123 ($M^+ - CMe_3$), 105, 94, 79 (100).

The spectral data of homoallylic alcohols **2***a–d* and **3***a–d* obtained similarly are as follows.

2*a* (29%): ^1H NMR (C_6D_6) δ: 7.23–7.03 (m, 5H), 6.06 (dd, J = 4.0, 11.1 Hz, 1H), 5.87–5.60 (m, 3H), 4.34 (dd, J = 5.1, 8.0 Hz, 1H), 2.70 (m, 1H), 2.10–2.02 (m, 2H), 1.70–1.60 (m, 3H); ^{13}C{^1H} NMR ($CDCl_3$) δ: 144.0, 134.9, 133.6, 127.2, 126.4, 125.5, 78.2, 47.5, 30.4, 30.0.

3*a* (42%): ^1H NMR (C_6D_6) δ: 7.26–7.04 (m, 5H), 5.89–5.64 (m, 3H), 5.47 (dd, J = 4.5, 11.5 Hz, 1H), 4.51 (dd, J = 4.0, 7.5 Hz, 1H), 3.54 (m, 1H), 2.12–2.03 (m, 2H), 1.96–1.86 (m, 2H), 1.60 (d, J = 4.0 Hz, 1H, D_2O exchangeable); ^{13}C {^1H} NMR ($CDCl_3$) δ: 143.3, 132.7, 132.4, 130.8, 129.7, 128.8, 127.0, 126.8, 77.8, 49.2, 27.2.

2*b* (25%): ^1H NMR (C_6D_6) δ: 5.95–5.50 (m, 4H), 3.88 (pseudoquad., J = 6.7 Hz), 2.28–2.00 (m, 3H), 1.85–1.60 (m, 3H), 1.38 (pseudoquintet, J = 6.9 Hz, 2H), 0.90 (t, J = 7.0 Hz, 3H);^{13}C {^1H} NMR ($CDCl_3$) δ: 136.5, 136.1, 134.6, 134.5, 126.3, 125.9, 124.8, 124.6, 77.2, 75.7, 46.9, 46.7, 29.7, 29.0, 28.9, 26.9, 26.3, 10.4, 10.3; MS[6] *m/z*: 152 (M^+, 23), 123 (41), 95 (100), 91 (90), 79 (95), 67 (79).

3*b* (50%): ^1H NMR (C_6D_6) δ: 5.87–5.56 (m, 4H), 3.43 (pseudoquad., J = 6.0 Hz, 1H), 3.23–3.14 (m, 1H), 2.30–2.02 (m, 4H), 1.65 (br s, 1H, D_2O exchangeable), 1.43 (pseudoquintet, J = 7.0 Hz, 2H), 0.94 (t, J = 7.0 Hz, 3H); ^{13}C NMR{^1H} ($CDCl_3$) δ: 132.0, 131.7, 130.5, 129.2, 76.7, 45.0, 27.0, 26.8, 10.6; MS *m/z*: 152 (M^+, 7), 91 (100), 77 (70), 65 (40).

2*c* (25%): ^1H NMR (C_6D_6) δ: 5.90–5.73 (m, 1H), 3.51–3.40 (m, 1H), 2.41–2.32 (m, 1H, coupled with δ 3.45), 2.20–2.12 (m, 1H), 2.10–1.98 (m, 1H), 1.90–1.79 (m, 1H), 1.77–1.67 (m, 1H), 1.51–1.38 (m, 3H), 1.38–1.15 (m, 6H), 0.82 (t, J = 6.8 Hz, 3H); ^{13}C NMR{^1H} ($CDCl_3$) δ: 134.6, 134.4, 133.3, 126.0, 125.8, 124.8, 124.6, 76.7, 74.2, 47.4, 47.2, 34.2, 32.0, 31.9, 29.9, 25.9, 22.7, 18.9, 17.2; MS[6] *m/z* 194 (M^+, 16), 123 (90), 95 (100), 79 (95).

3*c* (48%): ^1H NMR (C_6D_6) δ: 5.86–5.75 (m, 1H), 5.68–5.61 (m, 3H), 3.56 (pseudoquintet, J = 4.2 Hz, 1H), 3.23 (m, 1H, coupled with δ 3.56), 2.25–2.18 (m, 2H), 2.12–2.01 (m, 2H), 1.54–1.38 (m, 3H), 1.35–1.18 (m, 6H), 0.88 (t, J = 6.8 Hz, 3H); ^{13}C NMR{^1H} ($CDCl_3$) δ: 132.3, 132.0, 130.6, 129.1, 76.8, 45.4, 34.2, 32.0, 26.7, 25.8, 22.7, 14.1; MS *m/z*: 194 (M^+, 4), 94 (100), 79 (95).

2*d* (18%):^1H NMR (C_6D_6) δ: 5.85–5.70 (m, 3H), 5.65–5.57 (m, 1H), 3.04 (pseudotriplet, J = 7.0 Hz, 1H), 2.50–2.39 (m, 1H, coupled with δ: 3.04), 2.05–1.70 (m, 5H), 0.90 (d, J = 7.0 Hz, 3H), 0.72 (d, J = 7.0 Hz, 3H); ^{13}C NMR{^1H} ($CDCl_3$) δ: 134.6, 132.9, 126.7, 124.9, 81.3, 44.04, 31.4, 30.4, 29.7, 22.8, 18.0; MS *m/z*: 165 ($M^+ - 1$, 4), 94 (50), 79 (100).

3*d* (55%): ^1H NMR (C_6D_6) δ: 5.90–5.72 (m, 3H), 5.47 (dd, J = 6.0, 11.2 Hz, 1H, coupled with δ 3.26), 3.26 (m, 1H), 3.17 (pseudotriplet, J = 7.0 Hz, 1H), 2.23–2.00 (m, 5H), 1.73 (m, 1H), 0.98 (d, J = 7.0 Hz, 3H), 0.78 (d, J = 7.0 Hz, 3H); ^{13}C NMR{^1H} ($CDCl_3$) δ: 132.4, 131.9, 131.3, 128.9, 80.6, 42.6, 30.9, 26.6, 19.6, 18.3; DEPT ^{13}C NMR: reversed δ 26.66 and 26.62; MS *m/z*: 166 (M^+, 25), 123 (100), 95 (84), 91 (47), 79 (75), 67 (50).

Reaction of cycloheptenyl-η³-allyltitanocene complexes with carbon dioxide: esters 6 and 7

The cycloheptenyl-η³-allyltitanium complex mixture was obtained as described above, in two separated reduction steps: Cp_2TiCl (3 mmol in about 25 mL of THF), formed at first at room temperature, was then allowed to react within 10 min with the second equivalent of iso-C_3H_7MgCl in the presence of cycloheptatriene (0.41 g, 4.5 mmol, 1.5 equiv.) at −50°C. Carbon dioxide was then passed through the reaction mixture at −50°C, with stirring for 10 min, and the temperature was allowed to rise to −20°C over a 0.5 h period. The mixture was treated with 2 M HCl and air was passed, with stirring, through the solution for 5 min. The solution was diluted with 140 mL of ether/hexane = 9/1 and the precipitate of titanocene chloride was recovered by filtration. The organic layer was extracted with two portions of 0.5 M NaOH (2 × 15 mL). The aqueous layer was acidified with 2 M HCl and extracted with ether (3 × 40 mL). The ethereal layer was washed with brine to pH 4−5, and concentrated in vacuo to provide the crude mixture of acids **4** and **5**.[4] The corresponding methyl esters **6** and **7**[4] were prepared by using excess diazomethane in ether and were purified by chromatography on silica gel, eluting with hexane/ether = 95/5.

6 (0.15 g, 33%): ^1H NMR (C_6D_6) δ: 7.12 (br s, 1H), 5.85–5.72 (m, 3H), 3.33 (s, 3H), 2.20 (m, 1H), 2.05–1.96 (m, 2H), 1.52 (pseudoquintet, 2H); ^{13}C NMR{^1H} (CD_3COCD_3) δ: 168.2, 144.5, 132.5, 129.7, 123.8, 52.1, 32.1, 31.4, 29.1; MS *m/z*: 152 (M^+, 22), 137 (8), 121 (10), 93 (44), 91 (100), 77 (58).

7 (0.18 g, 39%): ^1H NMR (C_6D_6) δ: 6.73 (ddd, J = 1.8, 3.6, 11.4 Hz, 1H), 6.02 (dd, J = 4.7, 11.4 Hz, 1H), 5.74–5.65 (m, 2H), 3.42 (s, 3H), 3.20 (m, 1H), 2.1–1.98 (m, 2H); ^{13}C NMR{^1H} (CD_3COCD_3) δ: 174.6, 135.5, 131.2, 126.7, 125.4, 47.9, 31.1, 26.6, 26.5; MS *m/z*: 152 (M^+, 26), 137 (10), 121 (8), 93 (52), 91 (100), 77 (59).

Addition of octenyl η³-allyltitanocene to pivalic aldehyde: dienol 8

Cp_2TiCl was obtained as described above, starting from 4 mmol (1.00 g) of titanocene dichloride. The stirred solution of Cp_2TiCl in 30 mL of THF was cooled to −50°C and the freshly distilled 2,4,6-octatriene (0.43 g, 4 mmol) was added via syringe, simultaneously with a second portion of isopropylmagnesium chloride (2 mL, 2 M solution in THF). After 10 min stirring at −50°C, pivalic aldehyde (0.34 g, 4 mmol) was added slowly via syringe and the temperature was allowed to rise to −20°C over a 0.5 h period. The basic ($NaHCO_3$) work-up was performed as outlined above. The crude homoallylic alcohol **8** was obtained as a sole product

[6] MS identical for both diastereomers.

that was further purified by flash chromatography (hexane/ether = 12/1) (0.54 g, 69%, EE probably; traces of an another stereoisomer (<5%) were observed by ^{1}H and ^{13}C NMR). ^{1}H NMR (C_6D_6) δ: 5.64–5.61 (m, 1H), 5.49–5.33 (m, 3H), 3.32–3.27 (m, 1H), 3.21–3.15 (m, 1H), 1.91 (pseudoquad., J = 6.3 Hz, 1H), 1.60 (br s, 1H, D_2O exchangeable), 1.51 (dd, J = 1.7, 6.7 Hz, 3H), 1.01 (s, 9H), 0.89 (t, J = 5.5 Hz, 3H); ^{13}C NMR{^{1}H} (C_6D_6) δ: 132.8, 132.2, 130.8, 124.9, 81.9, 44.5, 36.5, 27.9, 26.7, 14.7, 13.9; MS *m/z*: 195 (M^+ – H, 31), 179 (27), 151 (50), 110 (65), 95 (42).

Quenching of cycloheptenyl-η^3-allyltitanocene complexes with gazeous HCl

The complex mixture was obtained by the procedure outlined above, in two separate reduction steps at room temperature and then at −50°C. The protonation was performed at −50°C by passing gazeous HCl over a 10 min period. After the conventional basic ($NaHCO_3$) treatment, the ratios of 1,4- to 1,3-cycloheptadiene were established by GC chromatography as well as by ^{1}H NMR. They were equal to 0.82 and 1.15 for the reactions using Cp_2TiCl_2 and Cp'_2TiCl_2, respectively.

References

1. (*a*) Y. Yamamoto. Acc. Chem. Res. **20**, 243 (1987); (*b*) R.W. Hoffman. Angew. Chem. Int. Ed. Engl. **26**, 489 (1987).
2. (*a*) W. Roush. *In* Comprehensive organic synthesis. Vol. 2. *Edited by* B. Trost, I. Fleming, and C.H. Heathcock. Pergamon Press, New York. 1991. p. 1; (*b*) Y. Yamamoto and N. Asao. Chem. Rev. **93**, 2207 (1993).
3. (*a*) C.H. Heathcock. *In* Asymmetric synthesis. Vol. 3. *Edited by* J.D. Morrison. Academic Press, New York. 1984. p. 111; (*b*) S. Masamune, W. Choy, J.S. Peterson, and L.R. Sita. Angew. Chem. Int. Ed. Engl. **26**, 489 (1987).
4. J. Szymoniak, D. Felix, and C. Moïse. Tetrahedron Lett. 8613 (1994).
5. F. Sato, S. Iijima, and M. Sato. Tetrahedron Lett. 243 (1981).
6. H. Lehmkuhl and S. Fustero. Liebigs Ann. Chem. **9**, 1353 (1980).
7. (*a*) A.J. Pearson and K. Chang. J. Org. Chem. **58**, 1228 (1993); (*b*) A.J. Pearson, S. Mallik, R. Mortezaei, M.W.D. Perry, R.J. Shively, Jr., and W.J. Youngs. J. Am. Chem. Soc. **112**, 8034 (1990); (*c*) H.E. Schink, H. Pettersson, and J.-E. Bäckvall. J. Org. Chem. **56**, 2769 (1991).
8. D.G. Mueller, H. Kawai, B. Stache, E. Foelster, and W. Boland. Experientia, **46**, 534 (1990).
9. F. Sato, S. Iijima, and M. Sato. J. Chem. Soc. Chem. Commun. 180 (1981).
10. M.J. Garson. Chem. Rev. **93**, 1699 (1993), and references therein.
11. T. Kajiwara, Y. Sasaki, F. Kimura, and A. Hatanaka. Agric. Biol. Chem. **45**, 1461 (1981).
12. S. Collins, W.P. Dean, and D.G. Ward. Organometallics, **7**, 2289 (1988).
13. R.O. Duthaler and A. Hafner. Chem. Rev. **92**, 807 (1992).
14. B.M. Jacobson, G.M. Arvanitis, C.A. Eliasen, and R. Mitelman. J. Org. Chem. **50**, 194 (1985).

Can. J. Chem. Downloaded from www.nrcresearchpress.com by 80.90.12.36 on 09/08/12
For personal use only.

A novel PC-based gravimetric autotitrator with a multi-solution delivery system

Mark A. Hetherington, Min Chen, and R. Stephen Reid

Abstract: The development of a novel PC-based gravimetric autotitrator is described. A single electronic balance serves as the weight buret for the delivery of three different solutions. It is therefore possible to add titrand and titrant under automated control. Investigation of the standard nickel(II)–glycinate–proton equilibrium system was used to evaluate performance.

Key words: titrator, titration, potentiometry, automated control.

Résumé : On décrit le développement d'un appareil d'autotitrage gravimétrique basé sur un ordinateur personnel. Une seule balance électronique sert de burette à mesurer pour la distribution de trois solutions différentes. Il est donc possible d'ajouter les substances titrantes et à titrer sous contrôle automatisé. Dans le but d'évaluer la performance de la méthode, on a étudié le système standard en équilibre : nickel(II)–glycinate–proton.

Mots clés : appareil de titrage, titration, potentiométrie, contrôle automatisé.

Can. J. Chem. Downloaded from www.nrcresearchpress.com by 80.90.12.36 on 09/08/12
For personal use only.

Introduction

Equilibrium potentiometric studies can yield acid dissociation and complexation constant data of high precision. However, the collection of the necessary data (possibly hundreds of data points per titration) is time-consuming, tedious, and repetitive; automation of this process is thus highly desirable.

A number of PC-based autotitrators with various software design and hardware configurations (1–7) have been reported previously. Delivery control has been accomplished in one of two ways. In volumetric designs (1–3), a digitally controlled buret is employed; electronic pulses from the computer advance a piston of a motor-driven syringe. The volume added at any stage is proportional to the number of pulses sent. While a wide variety of autotitration systems is commercially available, these are both expensive and insufficiently flexible for equilibrium titration work (8).

In gravimetric designs (4–7), a titrant reservoir is placed on an analytical balance. The computer controls an on–off valve set in the delivery tube from the reservoir to a titration vessel. The current reservoir weight is sensed by the computer and hence the weight of any titrant added can be inferred.

Gravimetric delivery systems display several advantages over their volumetric counterparts. The precision and accuracy of weighing is intrinsically higher than that involved in measuring volumes (9). Even a modestly priced electronic analytical balance can yield a resolution of 0.1 mg (i.e., 0.1 μL). Such balances are also readily interfaceable. Further, delivery of titrant by weight eliminates problems due to solution density fluctuations caused by temperature variations.

An ideal autotitration system for speciation studies would require the operator merely to input the titration parameters and supply the titrant, titrand, and, where applicable, solutions for dilution or ionic strength control. The system would then handle sample preparation, introduction, titration, and disposal. The autotitrator described in this paper was developed as another step towards this ideal system. It uses a single electronic balance to serve as the "weight buret" and can currently accommodate up to three separate solution delivery vessels.

Received February 13, 1995.

M.A. Hetherington, M. Chen, and R.S. Reid.[1] Department of Chemistry, University of Saskatchewan, Saskatoon, SK S7N 5C9, Canada.

[1] Author to whom correspondence may be addressed. Telephone: (306) 966-4673. Fax: (306) 966-4730. E-mail: reid@sask.usack.ca

Experimental

pH measurement

All pH measurements were made with a Fisher Accu-pHast standard combination glass body pH electrode (Cat. No. 13-620-296) and a Fisher Accumet pH meter (model 825MP). The electrode was calibrated following the suggested NIST (National Institute of Standards and Technology) method. First, a set of primary standard solutions are prepared, the pH of which have been accurately determined (NIST, ref. 10). The electrode is then calibrated using these primary solutions. Since these NIST solutions are only stable for a few hours, a set of stable commercial buffer solutions are then standardized using the NIST solutions, yielding secondary standards that can then be used for routine recalibration.

A 0.05 molal solution of potassium hydrogen phthalate (KHP), which has been ground and dried, in H_2O at 25°C is assigned a NIST pH of 4.008. A solution that is 0.025 molal in both KH_2PO_4 and Na_2HPO_4 has an NIST pH of 6.865 at the same temperature (10). The electrode was calibrated using these solutions and subsequently the stable commercial buffers (BDH) with nominal pH values of 4.00 and 7.00 were analyzed as unknown solutions and their exact pH values recorded.

Fig. 1. Hardware architecture of the computer-controlled gravimetric autotitrator.

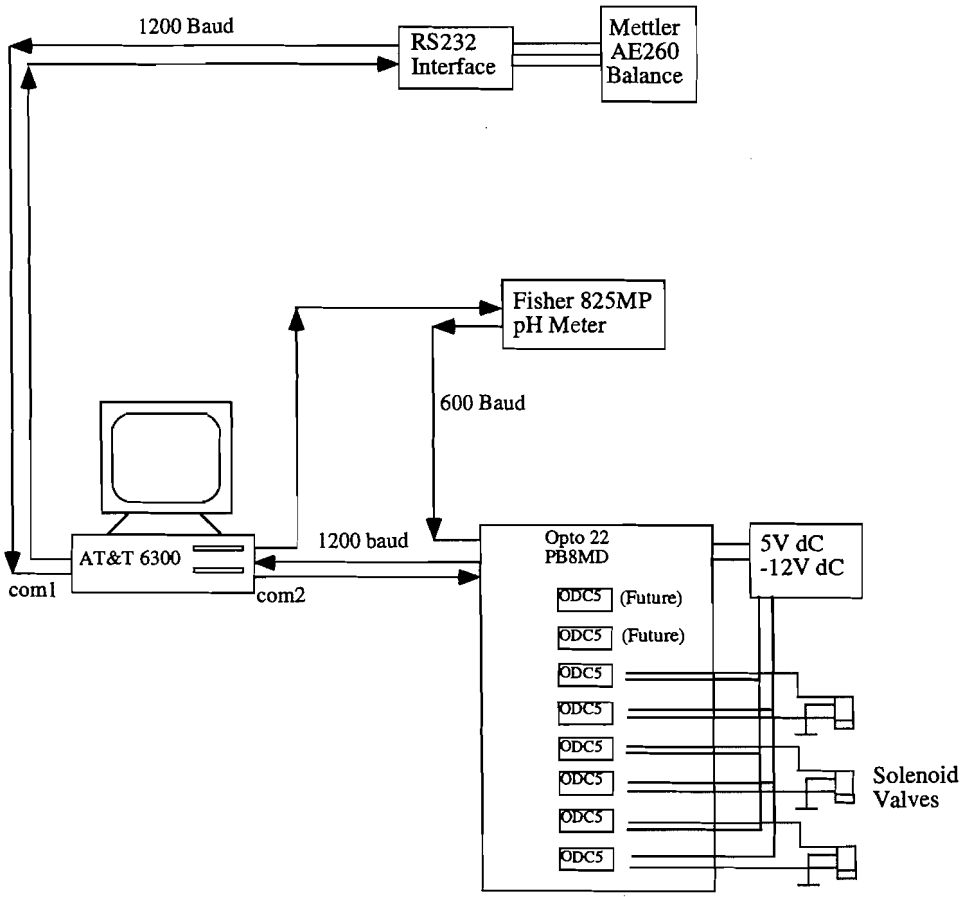

A temperature of 25°C was maintained using a water bath equipped with a Haake D1 circulator and cold water cooling coil.

Preparation of solutions for system validation

Unless otherwise specified, all chemicals were purchased from BDH (British Drug Houses, Toronto, Ont.) and were used as received. Corning Mega-Pure™ water (doubly-distilled, deionized) was used throughout for all solutions. All solutions for this study, with the exception of titrant and KHP solution, were prepared in a solvent containing 0.29 M NaCl and 0.01 M HCl for a total ionic strength of 0.3 M. The acid concentration of this solvent was determined to be 0.01115 ± 0.0010 M′ by titration of samples dispensed from one of the reservoirs on the balance with NaOH titrant from another of the reservoirs. M′ is used to denote "weight molarity," i.e., moles of solute per kilogram of solution. This is a convenient unit to use when titrating gravimetrically.

The NaOH titrant was made, using proper procedures to ensure absence of carbonate (11), by dilution of a saturated solution to volume with water. The NaOH concentration was determined as 0.08651 ± 0.0001 M′ by titration of samples of standard solution of the primary standard KHP prepared as described below.

The standard KHP solution, 0.05305 M′ in 0.14 M KNO_3, was prepared using ground and dried KHP and KNO_3 as supplied. The weight molarity of the solution was calculated by determining the weight of solution as the difference between the weight of a 250 mL volumetric flask before and after being filled and made up to the mark.

A standard solution of 0.2036 ± 0.00026 M′ nickel chloride was made by dissolving $NiCl_2 \cdot 6H_2O$ in solvent and bringing it to volume in a 250 mL volumetric flask. This stock $NiCl_2$ solution was standardized by titration with a standard EDTA solution in ammonia buffer using a Murexide indicator. This EDTA solution was in turn standardized by titration of a 0.03048 M standard nickel solution prepared by dissolving nickel metal in a 1:1 mixture of concentrated HNO_3 and water and quantitatively transferring and bringing to volume in a precalibrated 250 mL volumetric flask. The EDTA solution, prepared by dissolving the disodium salt in water, was found to have a concentration of 0.02096 ± 0.00008 M.

A stock solution of glycine hydrochloride was prepared by dissolving enough glycine hydrochloride in 1 L of solvent to make a ~0.03 M solution. The concentration was found to be 0.0306 ± 0.0002 M′.

Hardware

A Mettler AE160 electronic balance (Mettler Instrument Corp., Princeton, N.J.) equipped with an RS232C interface (commercially available from Mettler) was used as the weight buret for the titrator system. The computer-controlled valves were made by the General Valve Corporation, Fairfield, N.J. (part no. 2-26-900). The titration vessel is stirred magnetically.

An AT&T 6300WGS microcomputer was used to control

Can. J. Chem. Downloaded from www.nrcresearchpress.com by 80.90.12.36 on 09/08/12
For personal use only.

Fig. 2. General layout of the titration system: M: microenclosure; R: titrant reservoirs; V: valves; D: delivery tubing; T: titration vessel; P: tubing positioner.

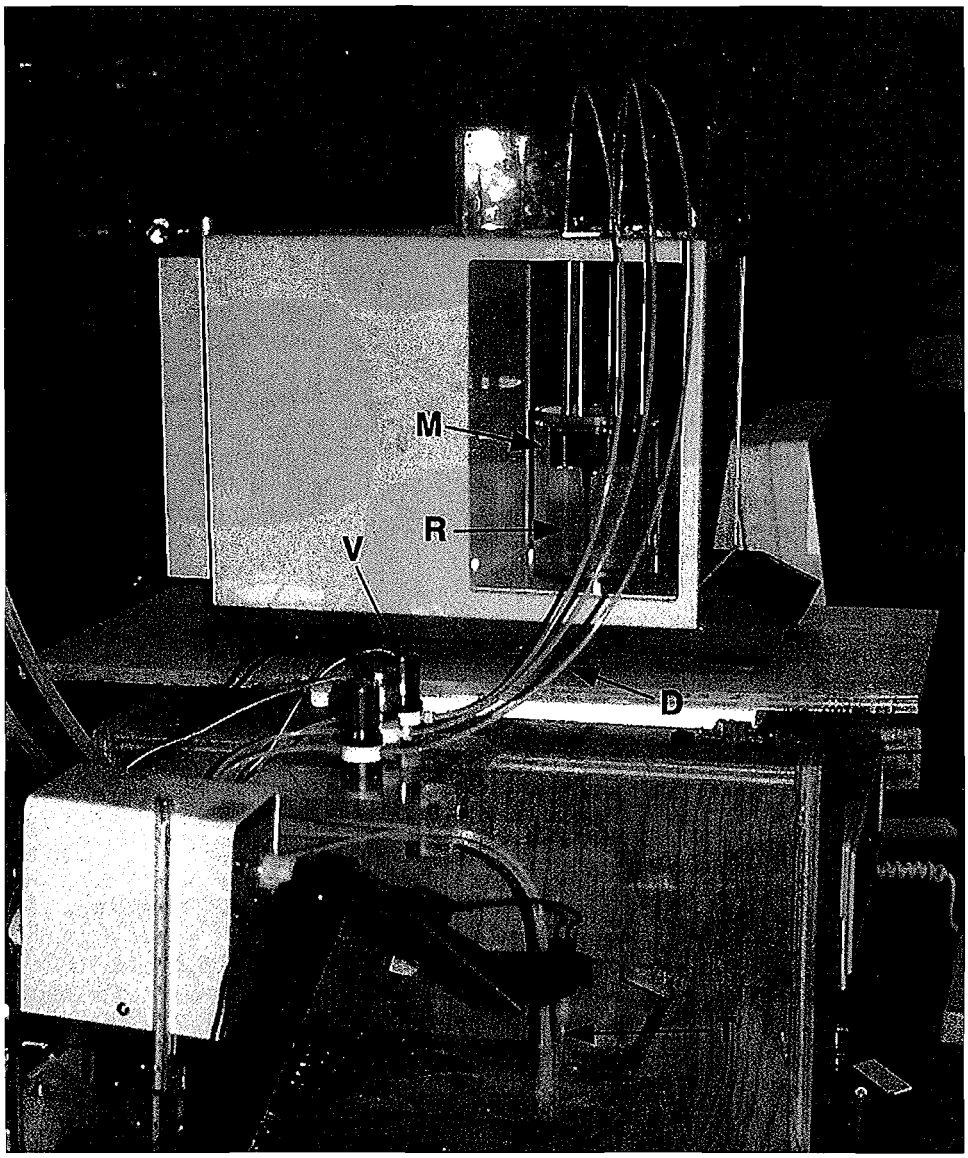

Can. J. Chem. Downloaded from www.nrcresearchpress.com by 80.90.12.36 on 09/08/12
For personal use only.

the system. The pH meter and analytical balance are interfaced to the computer via proprietary RS232 interfaces.

The computer is equipped with only two serial ports and there are three components to interface. To allow interfacing of several devices to the computer, and also allow for future expansion, an Opto 22 8-point intelligent digital and analog Input/Output (I/O) controller (PB8MD, Opto 22 Inc., Hunting Beach, CA 92649, U.S.A.) was employed. This setup routes the input data from the pH meter, and the control pulses to the valves, through a single computer serial port. Figure 1 shows the hardware architecture. Figure 2 shows the general layout of the whole system.

To enable fine flow rate control a micrometer-controlled needle restriction valve (Fig. 3) was constructed and set in line with the solution delivery tubing. The flow rate can thus be correlated with a setting on the micrometer head, and set reproducibly.

Solution delivery system

The titrant is delivered by gravity (the reservoir is elevated above the titration vessel by a distance of about 30 cm). The flow is controlled by latching on/off solenoid valve(s) that are opened and closed by separate 12 V, 700 mA pulses under computer control via the Opto controller. A siphon tube enters each solution reservoir through a small hole in the cap. The tube is held so that a very small annulus is maintained between the inside edge of the hole and the tube. Thus, the only point of physical contact between the reservoir and the rest of the delivery system is where the tube touches the liquid. Previous studies (5) have shown this to be preferable to systems involving tubulated reservoir bottles, where tension in the delivery tubing inevitably contributes to instability in balance readings. Teflon tubing, 1.48 mm i.d. and 3.00 mm o.d., was chosen for all delivery tubing because it is stiff enough to allow reproducible tubing alignment, flexible enough to work with effec-

Can. J. Chem. Downloaded from www.nrcresearchpress.com by 80.90.12.36 on 09/08/12
For personal use only.

Fig. 3. Micrometer-controlled needle restriction valve. Arrows indicate direction of liquid flow. F: end-fittings; M: micrometer head; N: "needle;" P: Plexi-glas block.

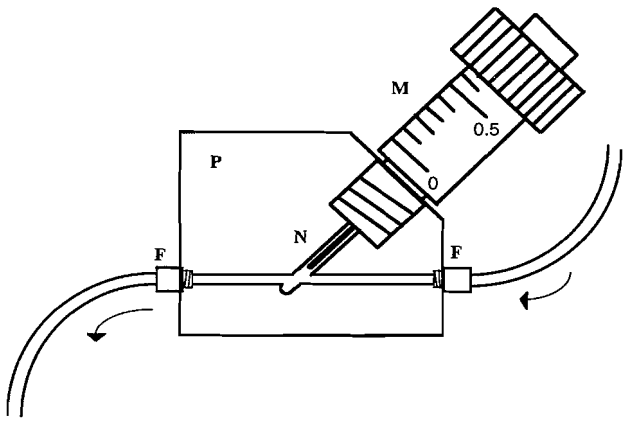

tively, and easy to rinse. The titration vessel is a 10 mL glass vessel placed in the constant temperature bath. A Plexiglas cap is used to locate the pH sensor and solution delivery tubes in position. It also holds a gas delivery tube; titrations are performed under a "blanket" of argon to minimize any effects related to atmospheric carbon dioxide.

Figure 4 shows the electronic balance and "microchamber" constructed to address the issues of evaporation and contamination common to a dip-tube type system. The microchamber was developed to reduce the exchangeable air space above the solution reservoirs. The chamber consists of a clear circular Plexiglas enclosure that can slide up and down on steel supports so solutions may be changed or replenished. An O-ring in the base of the microchamber seals it against the floor of the balance when in the lowered (operating) position. The use of this chamber has reduced the evaporation to around 0.01 mg/min or ~5 mg per 8 h working day and could be reduced further if all fittings and casings of the balance itself were sealed from the room environment. The concentration changes during the course of a series of titrations can be shown to be negligible under these operating conditions. SUPERQUAD (see below) is capable of refining the titrant concentration so corrections can also be made at the point of data analysis if required.

SASKWATCH — software control program

SASKWATCH, from **SASK**atoon **W**eight **A**utotitrator **C**ontrol **H**andler, is the control program for the autotitrator, written in Turbo Pascal version 5.0 (Borland International Inc., Scotts Valley, Calif.).

The operator inputs control parameters and performs various tasks through a series of control menus. Firstly, the parameters for the titration are input. The operator will choose between pH or mV mode for the signal from the pH meter and select initial and final pH or mV values for the titration.

Extensive studies of the relationship between valve open time and the resultant weight of solution delivered showed this to display essentially straight-line behaviour. The slope and intercept of this line for each delivery channel can be entered directly, or determined experimentally by a subroutine. The computer then "knows" how long a given valve must be left open in order for a specified weight of solution to be delivered.

Fig. 4. Electronic balance with microchamber (M) and solution reservoir (R).

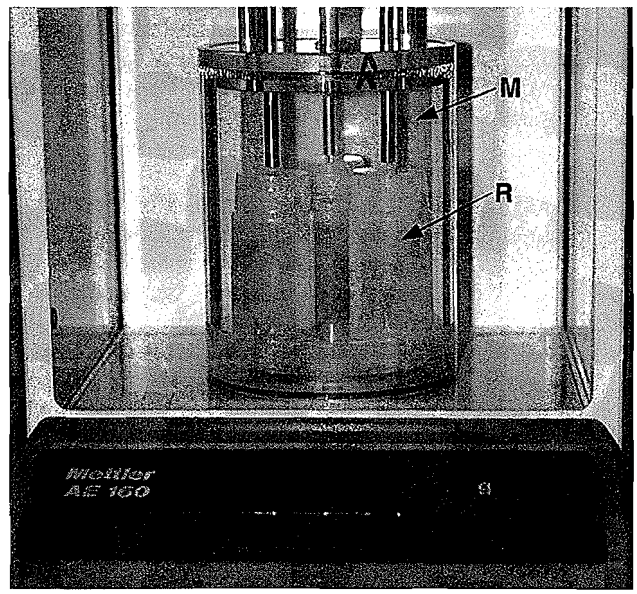

Three types of titration can be selected. The simplest involves the delivery of a constant weight of titrant between successive points in the titration. This is suitable for rapid, "survey" titrations, but not for accurate speciation work. (A weight increment small enough to locate points precisely will result in far too many data points in buffer regions.)

More complex to implement, but more useful, is a constant pH (or mV) increment between points. This requires prediction of the future shape of the titration curve. Analytically, this is impossible in the absence of the very information the titration is being performed to elicit; however, a reasonable approximation can be found using the hyperbolic extrapolation routine of Smit and Smit (12). The three most recent data points (pH as a function of weight of titrant added) are mathematically fitted to a hyperbolic model. It is then assumed that the new point also lies on this path; hence, the weight increment required can be calculated by entering the desired "target pH" into the model. In practice, this works well; for instance, if a typical pH increment of 0.20 is selected, actual increment observed are typically within 0.02 of this. (Note that since the actual weight delivered and the actual resultant pH are recorded for every point, the slight inadequacy in prediction capability does *not* represent an error in the actual data recorded.)

The constant pH increment titration has the disadvantage that too many data will be collected in the endpoint regions, and much time will be taken waiting for pH stabilization according to stringent criteria (see below). A *combination type* titration is also implemented, where constant pH increment mode is enabled until the required weight additions become small, when they default to a minimum value (i.e., constant weight increment mode). This mode gives a better distribution of data points, and is the one we normally use.

Since both pH electrode response and complexation reactions can take a finite time, the routine also checks that equilibrium has been reached before "accepting" a pH reading into the stored data-set. A user-selectable number of individual

readings (typically 10) is input, and the slope in the pH versus time response is calculated. If this is significantly different from zero (the stringency test is also user-selectable) then the measurements are rejected, and the cycle repeated after a short wait. This continues until equilibrium is judged to have been reached or a "time out" period is exceeded. The mean of the most recent set of measurements is then stored.

Titrator operation

Firstly, the sample addition routine is used. The operator is asked to select a valve number (2 or 3) corresponding to the desired solution and position on the balance pan. Each vessel has its own delivery tubing and computer-interfaced control valve. By keeping a record of which valve was opened last, the titrator "knows" which solution has been delivered. Next, a prompt for weight of sample to be added appears and the valve is opened for the required time calculated on the basis of a prior flow rate calibration for that valve.

After the desired samples from all reservoirs have been added, titration parameters are input, as above, and titration is performed. Various prompts ensure the readiness of the various hardware components. The first titrant addition is made. On the basis of the recent shape of the titration curve and a flow calibration made prior to the start of titration, the computer predicts the valve open time required to reach the next desired weight or pH value. This cycle continues unattended and finishes when the preset maximum weight or pH range is met or exceeded. At this time an output file, consisting essentially of pH (or mV) and titrant weight data pairs, is created. All data analysis and subsequent presentation were performed on an IBM compatible PC, after data transfer from the titrator computer via floppy diskette.

Experimental approach for the nickel(II)–glycinate–proton study

The study involves the determination of the two acid dissociation constants for glycine, the formation constants for the three Ni–Gly complexes, and various important solution parameters. Since there are at least five equilibria involved in this system, a systematic approach is necessary; the important solution parameters are standardized first and the equilibrium constants are then determined one at a time in "building block" fashion as suggested in a previous study (13). Figure 5 shows the equilibrium scheme for the nickel(II)–glycine system.

The NaOH titrant was standardized by filling one of the solution reservoirs with the KHP standard solution and a second with the titrant. The sample addition routine was used to dispense samples of the KHP, which were then titrated as usual. To determine the apparent molar ionic product of water (pK^c_W) and the acid concentration, samples of solvent, contained in one of the reservoirs, were titrated with the NaOH titrant, contained in a second reservoir. Next the solvent was replaced by the glycine standard solution and the dissociation constants for glycine were obtained by titrating samples of glycine with NaOH. Finally, the third reservoir was filled with the nickel standard solution and the formation constants for Ni(II)–Gly were found by titrating samples of Ni(II)–Gly prepared with Ni:Gly ratios ranging from 1:1 to 1:4. The resulting formation and acid dissociation constants were then compared with those of the interlaboratory study to determine if errors were present in the experimental system.

Fig. 5. Equilibrium scheme and definition of formation constants for the nickel(II)–glycine system.

$$H_2Gly^+ \underset{}{\overset{K_{a1}}{\rightleftharpoons}} HGly \overset{K_{a2}}{\rightleftharpoons} Gly^+ \underset{K_{f1}}{\rightleftharpoons} NiGly^+ \underset{K_{f2}}{\rightleftharpoons} Ni(Gly)_2 \underset{K_{f3}}{\rightleftharpoons} Ni(Gly)_3^-$$

$$K_{f1} = \frac{[NiGly^+]}{[Ni^{2+}]\,[Gly^-]} \qquad K_{f2} = \frac{[Ni(Gly)_2]}{[Gly^-]\,[NiGly^+]}$$

$$K_{f3} = \frac{[Ni(Gly)_3^-]}{[Gly^-]\,[Ni(Gly)_2]}$$

Results and discussion

All titration data was processed using SUPERQUAD (14). Processing times were typically 0.5–5 min, depending on the speed of the PC employed. The NaOH concentration was determined by keeping the number of millimoles of KHP and the value of pK^c_W (set at the value of 13.76 determined previously (7, 13)) constant and refining the NaOH concentration, "electrode parameter" $E^{0\prime}$, and the pK_a values for KHP. The acid concentration and pK^c_W were determined by keeping the NaOH concentration constant and refining $E^{0\prime}$, pK^c_W, and HCl concentration.

Once the solution parameters were determined, the dissociation constants were found by refining the total millimoles of glycine and proton, both pK_a values for glycine, and $E^{0\prime}$ while keeping the NaOH concentration and pK^c_W constant. The acid dissociation constant pK_{a1} was found to be 2.43 ± 0.02 and pK_{a2} was 9.63 ± 0.03. Following published recommendations, only data in the range $2.0 < pH < 9.5$ were used for the determination of these equilibrium constants (7).

The formation constants for the various Ni(II)–Gly complexes were determined by refining the total millimoles of proton and glycine, the logarithm of the formation constants log K_{f1}, log K_{f2}, and log K_{f3}, and $E^{0\prime}$ while keeping pK^c_W, total millimoles of nickel, both dissociation constants, and the NaOH concentration constant.

As previously suggested, data in the range $2.5 < pH < 9$ were input for fitting these constants except for Ni(II):Gly ratios less than 1:2, in which case usable data are only available in the pH range $2.5 < pH < 8$. Above this range, pH readings were erratic, signalling that precipitation of nickel hydroxide had commenced. Below this range, acid error in the electrode led to large residual values that compromised the goodness of fit.

The weighted mean values and associated standard deviations for the formation constants were determined using the values from all titration data. These values are log K_{f1} = 5.65 ± 0.02, log K_{f2} = 4.71 ± 0.03, and log K_{f3} = 3.50 ± 0.02. As

Can. J. Chem. Downloaded from www.nrcresearchpress.com by 80.90.12.36 on 09/08/12
For personal use only.

Table 1. SUPERQUAD results for the nickel(II)–glycine–proton system.

Value	(25°C, 1.0 M)[a]	(25°C, 1.0 M)[b]	(25°C, 0.3 M)[c]	(25°C, 0.3 M)[d]
pK_{a1}	2.44(3)[e]	2.42(2)	2.43(1)	2.43(3)
pK_{a2}	9.62(4)	9.65(1)	9.63(1)	9.62(2)
$\log K_{f1}$	5.55(7)	5.62(4)	5.64(1)	5.65(1)
$\log K_{f2}$	4.70(1)	4.75(5)	4.73(1)	4.71(3)
$\log K_{f3}$	3.50(3)	3.57(3)	3.50(1)	3.50(2)
pK_w^c	13.69(3)	—	13.76(1)	13.76(2)

[a]Reference 7.
[b]Reference 15.
[c]Reference 13.
[d]This work.
[e]Numbers in parentheses are standard deviations.

shown in Table 1, these values compare well with those reported in the literature, including previous studies from this laboratory.

The titration system is being used in a variety of metal–ligand speciation studies involving Gd, Hg, Cu, and other metal ions.

Conclusion

A novel PC-based single-buret multi-solution autotitrator has been developed for use in speciation studies. Validation was performed by investigating the well-characterized nickel(II)–glycine complex system. The formation and dissociation constants thus obtained were in good agreement with the accepted literature values. The system as described is capable of collecting the quality, high-precision data required for such speciation studies.

Acknowledgements

We wish to thank Mr. A. Leyland for his assistance in the construction of some of the hardware. Financial support from the Natural Sciences and Engineering Research Council of Canada and the University of Saskatchewan is also gratefully acknowledged.

References

1. H. Gampp, M. Maceder, A.D. Zuberbuhler, and T.A. Kaden. Talanta, **27**, 513 (1980).
2. G. Velinov, N. Todoror, and S. Karamphilov. Talanta, **30**, 687 (1983).
3. A. Braithwaite, C.C. Hills, and F.J. Smith. Comput. Appl. Lab. **2**, 115 (1984).
4. R. Guevremont and B. Kratochvil. Anal. Chem. **50**, 1945 (1978).
5. B. Kratochvil and J.E. Nolan. Anal. Chem. **56**, 586 (1984).
6. J.R. Chipperfield and D.E. Webster. Anal. Chim. Acta, **197**, 373 (1987).
7. A.P. Arnold, S.A. Diagnault, and D.L. Rabenstein. Anal. Chem. **57**, 1112 (1985).
8. A. Avdeef and J. Comer. Am. Lab. **110**, Feb. (1987).
9. B. Kratochvil and C. Maitra. Int. Lab. **13**, 24 (1983).
10. R.G. Bates. Determination of pH: theory and practice. 2nd ed. John Wiley & Sons. New York. 1973.
11. W.E. Harris and B. Kratochvil. An introduction to chemical analysis. Saunders Golden Sunburst Series, Saunders College Publishing, Philadelphia, Pa. 1981.
12. J.C. Smit and H.C. Smit. Anal. Chim. Acta, **143**, 45 (1982).
13. M. Chen. Ph.D. Dissertation, University of Saskatchewan, Saskatoon. 1991.
14. P. Gans, A. Sabatini, and A. Vacca. J. Chem. Soc. Dalton Trans. 1195 (1985).
15. A. Braibanti, F. Dallavalle, G. Mori, and M. Pasquali. Gazz. Chim. Ital. **113**, 407 (1983).

Can. J. Chem. Downloaded from www.nrcresearchpress.com by 80.90.12.36 on 09/08/12
For personal use only.

Molecular and electronic structures of the purple chromophore $RC(NH_2)(NSePh)$ (R = H, 4-$CH_3C_6H_4$)

Tristram Chivers, Katherine McGregor, Masood Parvez, Ignacio Vargas-Baca, and Tom Ziegler

Can. J. Chem. Downloaded from www.nrcresearchpress.com by 80.90.12.36 on 09/08/12
For personal use only.

Abstract: The reaction of Li[4-$CH_3C_6H_4C(NSiMe_3)_2$] with PhECl (E = S, Se) in a 1:1 molar ratio produces the monosubstituted derivatives 4-$CH_3C_6H_4C(NEPh)[N(SiMe_3)_2]$ (**3***b*, E = Se; **3***d*, E = S). The thermolysis of **3***b* at 130°C produces $PhSeN(SiMe_3)_2$ and 4-$CH_3C_6H_4CN$. Crystals of **3***b* slowly acquire a purple stain upon prolonged standing at 23°C owing to the formation of 4-$CH_3C_6H_4C(NH_2)(NSePh)$ (**4***c*, λ_{max} = 551 nm). The formamidine derivative $HC(NH_2)(NSePh)$ (**4***a*, λ_{max} = 472 nm) was isolated from the reaction of $HCN_2(SiMe_3)_3$ with PhSeCl (1:3 molar ratio) in dichloromethane. The structure of **4***a* was shown by X-ray crystallography to involve a *syn* configuration at the >C=N- bond and hydrogen bonding between amino nitrogen atoms. The crystals of **4***a* are monoclinic, space group $P2_1$ (No. 4), with *a* = 7.514(1), *b* = 5.575(1), *c* = 8.925(1) Å, β = 100.71(1)°, *V* = 367.40(6) Å^3, and *Z* = 2. The final *R* and R_w values were 0.055 and 0.060, respectively. The ^1H and ^{77}Se NMR spectra indicate that both **4***a* and **4***c* exist as a mixture of tautomers in THF solution. DFT calculations for the model tautomers $HC(NH_2)(NER)$ and HC(NH)(NHER) (E = S, Se; R = H, Ph) show that the former is more stable in all cases, but the difference in total bonding energy is smaller for selenium than for sulfur (17.5 vs. 29 kJ mol^{-1}). The visible absorption band for **4***a* is assigned to the HOMO–LUMO transition (ΔE = 2.90 eV, λ_{max} = 427 nm) of the minor tautomer.

Key words: formamidine, tautomer, selenium, purple chromophore.

Résumé : La réaction du Li[4-$CH_3C_6H_4C(NSiMe_3)_2$] avec le PhECl (E = S, Se), dans un rapport molaire de 1 : 1, conduit à la formation des dérivés monosubstitués 4-$CH_3C_6H_4C(NEPh)[N(SiMe_3)_2]$ (**3***b*, E = Se; **3***d*, E = S). La thermolyse du composé **3***b* à 130°C fournit du $PhSeN(SiMe_3)_2$ et 4-$CH_3C_6H_4CN$. Les cristaux du produit **3***b* acquièrent lentement une couleur violette lorsqu'on les laisse à 23°C pour une période prolongée; cette couleur est due à la formation du 4-$CH_3C_6H_4C(NH_2)(NSePh)$ (**4***c*, λ_{max} = 551 nm). On a isolé le dérivé formamidine $HC(NH_2)(NSePh)$ (**4***a*, λ_{max} = 472 nm) du milieu réactionnel de la $HCN_2(SiMe_3)_3$ avec le PhSeCl (rapport molaire 1 : 3) dans le dichlorométhane. Faisant appel à la diffraction des rayons X, on a montré que la structure du composé **4***a* implique une configuration *syn* au niveau de la liaison >C=N- et des liaisons hydrogènes entres les atomes des azotes aminés. Les cristaux du composé **4***a* sont monocliniques, groupe d'espace $P2_1$ (No. 4), avec *a* = 7,514(1), *b* = 5,575(1), *c* = 8,925(1) Å, β = 100,71(1)°, *V* = 367,40(6) Å^3, and *Z* = 2. Les valeurs finales de *R* et R_w sont respectivement de 0,055 et 0,060. Les spectres RMN du ^1H et du ^{77}Se indiquent que, en solution dans le THF, les deux composés **4***a* et **4***c* existent chacun sous la forme d'un mélange de tautomères. Des calculs DFT sur les tautomères modèles $HC(NH_2)(NER)$ et HC(NH)(NHER) (E = S, Se; R = H, Ph) montrent que, dans tous les cas, le premier est le plus stable; toutefois, la différence en énergie totale de liaison est plus faible pour le sélénium que pour le soufre (17,5 vs. 29 kJ mol^{-1}). La bande d'absorption dans le visible du composé **4***a* est attribuée à la transition des OM HO et BV (ΔE = 2,90 eV, λ_{max} = 427 nm) du tautomère mineur.

Mots clés : formamidine, tautomère, sélénium, chromophore violet.

Introduction

Organoselenium-nitrogen compounds, e.g., *N*-(phenylselenenyl)-*o*-quinone imine (1), have attracted attention recently, partly on account of their applications in organic synthesis (2). Cyclic oligomers of the type $(RSeN)_4$ (R = Me, ^{i}Pr, Ph) have been spectroscopically identified (3) and the structure of $(HSeN_4)$ has been determined by ab initio calculations (4). In an attempt to make related eight-membered rings of the type $(RC)_2N_4(SeR)_2$ we found that the reaction of $PhCN_2(SiMe_3)_2$ with $RSeCl_3$ (R = Me, Ph) unexpectedly produces the intensely coloured diazenes **1***a* (λ_{max} = 502 nm) and **1***b* (λ_{max} = 553 nm) (5). The diazene **1***b* is formed in better yields, via the resonance-stabilized radical $PhC(NSePh)_2^{\bullet}$ (**2**), from the reaction of $PhCN_2(SiMe_3)_2$ with three molar equivalents of PhSeCl (6). The monosubstituted derivative **3***a* was obtained as an oil contaminated with a purple impurity, tentatively assumed to be the diazene **1***b*, when this reaction was con-

Received March 28, 1995.

T. Chivers,[1] K. McGregor, M. Parvez, I. Vargas-Baca, and T. Ziegler. Department of Chemistry, The University of Calgary, Calgary, AB T2N 1N4, Canada.

[1] Author to whom correspondence may be addressed. Telephone: (403) 220-5741. Fax: (403) 289-9488. E-mail: chivers@acs.ucalgary.ca

Can. J. Chem. Downloaded from www.nrcresearchpress.com by 80.90.12.36 on 09/08/12
For personal use only.

ducted with a 1:1 molar ratio (6). We have now prepared pure samples of **3*b*** as white crystals and observed that in the solid state these crystals develop a purple taint after several weeks at room temperature. We report here investigations of the thermolysis and hydrolysis of **3*b*** that have led to the identification of the purple chromophore and theoretical calculations that elucidate the origin of the low-energy electronic transition. The X-ray crystal of structure of $HC(NH_2)(NSePh)$ is also described.

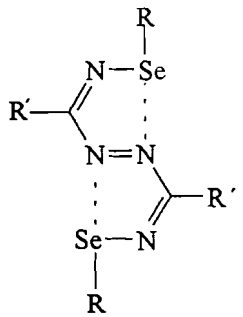

1*a*, R = Me, R′ = Ph
1*b*, R = R′ = Ph
1*c*, R = Ph, R′ = 4-$CH_3C_6H_4$

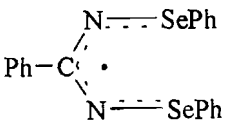

2

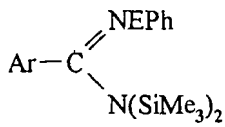

3*a*, Ar = Ph, E = Se
3*b*, Ar = 4-$CH_3C_6H_4$, E = Se
3*c*, Ar = Ph, E = S
3*d*, Ar = 4-$CH_3C_6H_4$, E = S

Experimental

Reagents and general procedures

Solvents were dried by treatment with the appropriate drying agent and freshly distilled before use. All reactions and the manipulation of moisture-sensitive products were carried out under an atmosphere of nitrogen by using Schlenk techniques or a Vacuum Atmospheres drybox. Li[4-$CH_3C_6H_4C(NSiMe_3)_2$] (7), $HCN_2(SiMe_3)_3$ (8), and $PhSeN(SiMe_3)_2$ (9) were prepared by literature methods. $LiN(SiMe_3)_2$ was obtained from Aldrich and recrystallized from hexanes – diethyl ether before use. PhSeCl (Aldrich) was used as received. PhSCl was prepared from Ph_2S_2 (Aldrich) and SO_2Cl_2 in CCl_4.

Instrumentation

^1H and ^{77}Se NMR spectra were run on Bruker ACE-200 and Bruker AM-400 spectrometers, respectively, operating at 200.132 and 76.132 MHz. ^{77}Se NMR chemical shifts are reported relative to Me_2Se. UV–visible spectra were determined by using a Cary 5E spectrophotometer. Infrared spectra were recorded as Nujol mulls (KBr plates) on a Mattson 4030 FTIR spectrometer. Elemental analyses were performed within the Chemistry Department at the University of Calgary.

Preparation of 4-$CH_3C_6H_4C(NSePh)[N(SiMe_3)_2]$, 3*b*

A solution of PhSeCl (1.91 g, 10 mmol) in CH_2Cl_2 (20 mL) was added dropwise (20 min) to a solution of Li[4-$CH_3C_6H_4C(NSiMe_3)_2$] (10 mmol) in diethyl ether (60 mL) at −78°C. The yellow reaction mixture was allowed to warm slowly to 23°C to produce a white precipitate of LiCl. Solvent was removed under vacuum to give a yellow oil, which was extracted with hexanes (2 × 50 mL). The hexanes were removed under vacuum to give a yellow solid, which was recrystallized from a *minimum* volume of pentane at −18°C, yielding **3*b*** as an off-white solid (1.1 g, 2.5 mmol, 25%). ^1H NMR ($CDCl_3$) δ: 7.22–7.76 (m, 9H, $CH_3C_6H_4$ and SeC_6H_5), 2.40 (s, 3H, $CH_3C_6H_4$), 0.31 (s, 18H, $Si(CH_3)_3$). ^{77}Se NMR (THF) δ: 779 (s).

Preparation of 4-$CH_3C_6H_4C(NSPh)[N(SiMe_3)_2]$, 3*d*

The compound **3*d*** was obtained in 50% yield from PhSCl and Li[4-$CH_3C_6H_4C(NSiMe_3)_2$] by a procedure similar to that described for the preparation of **3*b***. ^1H NMR ($CDCl_3$) δ: 7.21–7.79 (m, 9H, $CH_3C_6H_4$ and SC_6H_5), 2.41 (s, 3H, $CH_3C_6H_4$), 0.27 (s, 18H, $Si(CH_3)_3$). Anal. calcd. for $C_{19}H_{30}N_2SSi_2$: C 62.12, H 7.82, N 7.24; found: C 62.15, H 7.90, N, 7.88.

Preparation of 4-$CH_3C_6H_4C(NH_2)(NSPh)$, 4*b*

A stoichiometric amount of methanol was added to a solution of **3*d*** (0.36 g, 1.0 mmol) in THF (10 mL). The reaction mixture was heated gently during 10 min and then the volatile materials were removed under vacuum to give 4-$CH_3C_6H_4C(NH_2)(NSPh)$ as a colourless solid (0.22 g, 0.90 mmol, 90%). IR (cm^{-1}): 2723 m, 2674 m, 1627 m, 1304 m, 1153 m, 1086 m, 1022 m, 829 m, 769 m, 735 s, 688 m. ^1H NMR (CD_2Cl_2) δ: 7.75–7.50 (m, 4H, $CH_3C_6H_4$), 7.40–7.10 (m, 5H, SC_6H_5), 5.11 (s, 2H, NH_2), and 2.37 (s, 3H, $CH_3C_6H_4$). Anal. calcd. for $C_{14}H_{14}N_2S$: C 69.39, H 5.82, N 11.56; found: C 70.26, H 6.23, N 11.62.

Preparation of 4-$CH_3C_6H_4C(NH_2)(NSePh)$, 4*c*

4-$CH_3C_6H_4C(NH_2)(NSePh)$ was obtained in 40% yield as dark purple crystals by the treatment of **3*b*** with methanol in a manner similar to that described above for the preparation of **4*b***. IR (cm^{-1}): 2721 m, 2671 m, 1306 m, 1261 m, 1018 m, 966 m, 822 m, 768 m, 733 s, 688 m, 669 m. UV–vis: λ_{max} 551 nm, ε(apparent) 8000 M^{-1} cm^{-1}.[2] ^1H NMR (CD_2Cl_2) δ: 8.35–8.20 (m, 2H, $CH_3C_6H_4$), 7.90–7.75 (m, 2H, $CH_3C_6H_4$), 7.70–7.10 (m, 14H, $CH_3C_6H_4$ and C_6H_5), 5.12 (s, 4H, NH_2), 2.45 (s, 3H, $CH_3C_6H_4$), and 2.38 (s, 3H, $CH_3C_6H_4$). Anal. calcd. for $C_{14}H_{14}N_2Se$: C 58.14, H 4.88, N 9.69; found: C 58.75, H 4.56, N 9.73.

Reaction of $HCN_2(SiMe_3)_3$ with PhSeCl

A solution of PhSeCl (3.16 g, 17 mmol) in CH_2Cl_2 (20 mL) was added dropwise to a solution of $HCN_2(SiMe_3)_3$ (1.49 g, 5.7 mmol) in (20 mL) at −78°C. The reaction mixture was allowed to warm slowly to 23°C with stirring and the colour of the solution changed from yellow to orange-red and, finally, to dark purple. After 16 h solvent was removed under vacuum to give a black solid, which was extracted with hexanes (3 × 15 mL). Removal of hexanes under vacuum yielded PhSeSePh

[2] The apparent molar extinction coefficients of **4*a*** and **4*c*** were calculated as the absorbance at the maximum divided by the total concentration and the optical path length.

Can. J. Chem. Downloaded from www.nrcresearchpress.com by 80.90.12.36 on 09/08/12
For personal use only.

Table 1. Crystal data for $HC(NH_2)(NSePh)$.

Parameter	Value	Parameter	Value
Formula	$C_7H_8N_2Se$	Z	2
Mol. wt.	199.11	D_{calc}, g cm^{-3}	1.800
	Monoclinic	$F(000)$	196
Space group	$P2_1$	μ(MoKα), cm^{-1}	50.28
a, Å	7.514(1)	T, °C	23.0
b, Å	5.575(1)	R	0.055
c, Å	8.925(1)	R_w	0.060
β, deg	100.71(1)		
V, Å^3	367.40(6)		

(2.28 g, 7.3 mmol) tainted with the purple product. The solid residue was recrystallized from CH_2Cl_2 to give dark-brown crystals of $HC(NSePh)(NH_2)$ **4***a* (0.55 g, 2.8 mmol, 48%). IR (cm^{-1}): 2721 m, 2672 m, 1306 m, 1284 m, 1167 m, 1153 m, 1063 m, 1020 m, 893 m, 771 m, 685 m. UV–vis (CH_2Cl_2): λ_{max} 472 nm, ε(apparent) 3200 M^{-1} cm^{-1}.[2] ^{1}H NMR (CD_2Cl_2) δ: 9.79 (s, 1H, C*H*), 7.90–7.80 and 7.60–7.30 (m, C_6H_5 and CH, ~10H). ^{77}Se NMR (CD_2Cl_2) δ: 988 (s), and 912 (s). Anal. calcd. for $C_7H_8N_2Se$: C 42.00, H 4.03, N 14.00; found: C 42.16, H 3.17, N 13.95.

Crystal structure determination of $HC(NSePh)(NH_2)$

A dark brown plate-like crystal of **4***a* (0.09 × 0.30 × 0.45 mm) with a metallic lustre was obtained from CH_2Cl_2–heptane (2:10) at 14°C, mounted on a glass fibre, and coated with epoxy. Pertinent crystallographic data are listed in Table 1. The unit cell constants were determined from the setting angles of 22 reflections with $28.57 < 2\theta < 35.56°$. All measurements were made on a Rigaku AFC6S diffractometer with the ω–2θ scan technique. An empirical absorption correction using the program DIFABS (10) was applied. The data were corrected for Lorentz and polarization effects.

The structure was solved by heavy-atom methods and expanded using Fourier techniques (11). The non-hydrogen atoms were refined anisotropically. The C atoms of the benzene ring were constrained to be a regular hexagon; H atoms were located from a difference map and were included in the final rounds of calculations at geometrically idealized positions. Atomic scattering factors (12, 13), corrected for anomalous dispersion (14), were used. Data processing was carried out using TEXSAN (15) and the structure was solved and refined using SHELX76 (16). Positional parameters are given in Table 2 and selected bond distances and bond angles are summarized in Table 3.

Hydrogen atom parameters, anisotropic thermal parameters, torsion angles, and complete tables of bond lengths and bond angles have been deposited.[3]

[3] Supplementary material mentioned in the text may be purchased from: The Depository of Unpublished Data, Document Delivery, CISTI, National Research Council of Canada, Ottawa, Canada, K1A OS2.

Tables of hydrogen atom parameters and bond lengths and angles have also been deposited with the Cambridge Crystallographic Data Centre and can be obtained on request from The Director, Cambridge Crystallographic Data Centre, University Chemical Laboratory, 12 Union Road, Cambridge, CB2 IEZ, U.K.

Table 2. Atomic coordinates (× 10^4) and U_{eq} (Å^2 × 10^3) of non-hydrogen atoms for $HC(NH_2)(NSePh)$.

Atom	*x/a*	*y/b*	*z/c*	U_{eq}
Se	1405(2)	143	1544(2)	47(1)
N(1)	2063(19)	3259(27)	1625(16)	54(4)
N(2)	4394(16)	2205(28)	274(15)	49(4)
C(1)	3343(21)	3911(35)	939(18)	54(5)
C(2)	−610(15)	−77(19)	2552(13)	49(4)
C(3)	−1881(15)	1771(19)	2417(13)	55(5)
C(4)	−3334(15)	1625(19)	3185(13)	64(7)
C(5)	−3315(15)	−370(19)	4088(13)	54(7)
C(6)	−2244(15)	−2218(19)	4223(13)	55(5)
C(7)	−791(15)	−2072(19)	3455(13)	53(5)

Table 3. Experimental and calculated values of selected bond distances (Å) and bond angles (deg) for $HC(NH_2)(NSePh)$.

	Experimental	Calculated
C(1)—N(2)	1.43(0.02)	1.38
C(1)—N(1)	1.28(0.02)	1.29
N(1)—Se(1)	1.80(0.01)	1.88
C(2)—Se(1)	1.90(0.01)	1.91
N(2)-C(1)-N(1)	121.9(1.6)	129.3
C(1)-N(1)-Se(1)	118.5(1.2)	116.0
C(2)-Se(1)-N(1)	106.2(0.5)	98.27

Calculations

All calculations were based on approximate density functional theory within the local density approximation (17), using the ADF program system developed by Baerends et al. (18, 19), and vectorized by Raveneck (20). The numerical integration was based on a scheme developed by Becke (21). All molecular dimensions were fully optimized, by a procedure based on the method developed by Versluis and Ziegler (22). All bonding energies were evaluated by the generalized transition state method due to Ziegler and Rauk (23). This treatment also allows for a detailed energy decomposition of the total bonding energy into steric and single orbital contributions (24). A double-ζ STO basis (18) was employed for the *ns* and *np* shells of the main group elements. This basis set was augmented by a 3*d* STO function for sulfur, 4*d* STO for selenium, and for hydrogen a 2*p* STO was used as polarization. Electrons in lower shells were treated by the frozen core approximation (18). A set of auxiliary (26) *s*, *p*, *d*, *f*, and *g* STO functions, centered on the different nuclei, was used in order to fit the molecular density and present Coulomb and exchange potentials accurately in each SCF cycle.

Energy differences were calculated by augmenting the local density approximation (LDA) energy expression by Vosko et al. (27) with Becke's exchange corrections (28) and Perdew's nonlocal correlation correction (29).

Results and discussion

Synthesis of 4-$CH_3C_6H_4C(NEPh)[N(SiMe_3)_2]$ (*3b*, E = Se; *3d* E = S)

The monosubstituted compounds **3***b* and **3***d* were obtained as

Can. J. Chem. Downloaded from www.nrcresearchpress.com by 80.90.12.36 on 09/08/12
For personal use only.

Fig. 1. ORTEP diagram for $HC(NH_2)(NSePh)$ showing atom labelling; 50% probability ellipsoids are shown for non-hydrogen atoms.

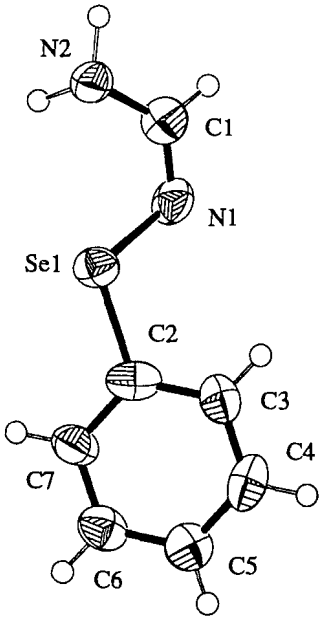

moisture-sensitive white crystals by the reaction of $Li[4\text{-}CH_3C_6H_4C(NSiMe_3)_2]$ with PhSeCl or PhSCl, respectively. The use of the lithium derivative rather than $4\text{-}CH_3C_6H_4C(NSiMe_3)_3$ (6) yields a cleaner, more easily purified product, particularly in the case of the selenium derivative **3***b*. The ^1H NMR spectrum of **3***b* is almost identical to that of analytically pure **3***d* and the ^{77}Se NMR spectrum exhibits a singlet at δ 779 ppm (cf. δ (^{77}Se) 995 ppm for **1***c* (30)). Nevertheless, satisfactory analytical data could not be obtained for **3***b* even on samples that appeared to be pure on the basis of ^1H and ^{77}Se NMR spectra.

Crystalline samples of **3***b* develop a dark purple taint over a period of several weeks at 23°C even when stored under an argon atmosphere. The thermal decomposition of solid **3***b* at 130°C for 12 h produces $PhSeN(SiMe_3)_2$ (δ (^{77}Se) 682 ppm, cf. lit. δ 684 ppm (9)) and $4\text{-}CH_3C_6H_4CN$, which was identified by IR and ^1H NMR spectroscopy. No evidence for the formation of **1***c* in the solid state decomposition of **3***b* was obtained. Thus it seems unlikely that the purple chromophore that is produced slowly in crystalline samples is **1***c*. The decomposition of **3***b* in THF solution does, however, produce the diazene **1***c*, together with Ph_2Se_2 and $PhSeN(SiMe_3)_2$, all of which were identified by the ^{77}Se NMR spectrum of the purple solution.

Spectroscopic characterization and X-ray structure of $HC(NH_2)(NSePh)$

Although trithiolated benzamidines of the type $ArCN_2(SPh)_3$ are thermally unstable at room temperature (6), the corresponding formamidine derivative $HCN_2(SPh)_3$ can be isolated as colourless crystals.[4] By contrast, the reaction of $HCN_2(SiMe_3)_3$ with three molar equivalents of PhSeCl produced $HC(NH_2)(NSePh)$, **4***a*, presumably as a result of hydrolysis during the work-up procedure. Both the ^1H NMR spectrum and the ^{77}Se NMR spectrum of **4***a*, which shows two resonances at δ 988 and δ 912 ppm, suggest the existence of two tautomeric forms in solution. Compound **4***a* exhibits an intense visible absorption band at 472 nm in CH_2Cl_2 solution.

[4] T. Chivers and I. Vargas-Baca. Unpublished results.

Fig. 2. Packing diagram for $HC(NH_2)(NSePh)$.

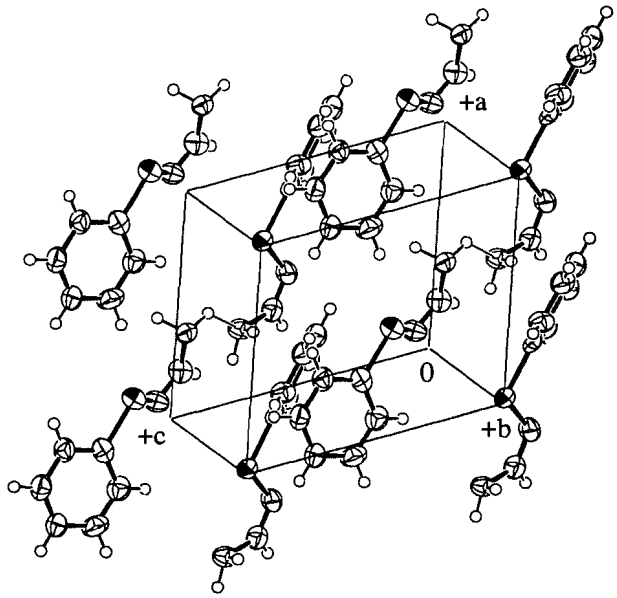

The structure of **4***a* was determined by X-ray crystallography. An ORTEP drawing with the atomic numbering scheme is displayed in Fig. 1. Selected bond lengths and bond angles are summarized in Table 3. The molecule **4***a* adopts a *syn* configuration with respect to the C(1)═N(1) double bond, as has been observed for **1***a* (5). The N-C-N-Se unit is nearly planar, with a dihedral angle of −7.5°, and the phenyl ring is twisted by 37.5° with respect to the N-C-N plane. As indicated in Fig. 2, the molecules in the crystal lattice are connected by hydrogen bonds between nitrogen atoms of amino groups (N---N′ separation of 3.00 Å with N2---H′-N2′ angle of 124°; primed atoms at symmetry position: $1\text{-}x, y\text{-}½, \text{-}z$). The C—N bond distances of 1.43(2) and 1.28(2) Å are typical for single and double bonds, respectively (31). The Se—N bond distance of 1.80(1) Å is comparable to the value 1.817(3) Å observed for the selenium-substituted diazene **1***a* (5) and somewhat shorter than the single bond value of 1.87 Å (32).

Hydrolysis of $4\text{-}CH_3C_6H_4C(NEPh)[N(SiMe_3)_2]$ (E = S, Se)

The purple colour of $HC(NH_2)(NSePh)$ suggested that hydrolysis might be an explanation for the purple taint apparent in aged crystals of the monosubstituted compound **3***b*. Consequently **3***b* and, for comparison, **3***d* were deliberately converted to the expected hydrolysis products $4\text{-}CH_3C_6H_4C(NH_2)(NEPh)$ (**4***b*, E = S; **4***c* E = Se) by the addition of methanol. The ^1H NMR spectrum of the pale yellow sulfur derivative, which remains unchanged down to −90°C, is consistent with the sole existence of the tautomer **4***b*′ in solution. By contrast, the ^1H NMR and ^{77}Se NMR spectra of $4\text{-}CH_3C_6H_4C(NH_2)(NSePh)$ (**4***c*) suggest the existence of both tautomers **4***c*′ and **4***c*″ in approximately the same amounts in CD_2Cl_2 solutions at room temperature. Furthermore, the selenium derivative **4***c* is dark purple and exhibits an intense visible absorption band at 551 nm. For comparison the diazene **1***b* exhibits a visible absorption band at 553 nm with a shoulder at 580 nm (6).

Table 4. Total bonding energies (B.E.) and electronic transition energies (ΔE) for $HC(NH_2)(NER)$ and HC(NH)[NH(ER)] (E = S, Se; R = H, Ph).

	B.E.[a]	ΔE[b]	λ_{max}[c]
$HC(NH_2)(NSH)$	−4 062.99	4.34	286
HC(NH)[NH(SH)]	−4 033.77	3.74	332
$HC(NH_2)(NSPh)$	−10 553.07	3.44	360
HC(NH)[NH(SPh)]	−10 512.21	3.11	398
$HC(NH_2)(NSeH)$	−3 959.71	3.89	319
HC(NH)[NH(SeH)]	−3 942.22	3.34	371
$HC(NH_2)(NSePh)$	−10 484.45	3.30	376
HC(NH)[NH(SePh)]	−10 459.57	2.90	427

[a]In kJ mol^{-1}.
[b]In eV.
[c]In nm.

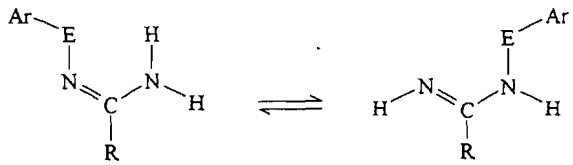

4a′, E = Se, Ar = Ph, R = H
4b′, E = S, Ar = Ph, R = 4-$CH_3C_6H_4$
4c′, E = Se, Ar = Ph, R = 4-$CH_3C_6H_4$

4a″
4b″
4c″

DFT calculations for $HC(NH_2)(NSeR)$ and HC(NH)[NH(SeR)]

To compare the relative stabilities of the amino and imino tautomers **4a′–c′** and **4a″–c″**, respectively, and to provide an explanation of the purple colour of the selenium derivatives, approximate density functional theory (DFT) calculations (33) were carried out on the model compounds $HC(NH_2)(NER)$ and HC(NH)[NH(ER)] (E = S, Se; R = H, Ph) (33). The results are summarized in Table 4. The calculated structural parameters for the amino derivative $HC(NH_2)(NSePh)$ are compared with the corresponding experimental values for **4c** in Table 3. Bond distances are reproduced within 0.05 Å for the organic moiety and 0.10 Å for the bonds to the heavy element. Larger differences are observed between calculated and experimental values of the bond angles, probably as a result of the intermolecular hydrogen bonding interactions in the solid state.

The calculations show that the amino tautomers **4a′** are always more stable than the imino tautomers **4a″**, due to the larger π delocalization. Selenium forms a weaker π-bond than sulfur with nitrogen. Consequently, the energy barrier between the tautomers is smaller for the selenium derivatives. This is consistent with the NMR spectroscopic data, which showed the existence of two tautomers in solution for the selenium derivatives **4a** and **4c**, whereas only the amino tautomer is evident in the ^1H NMR spectrum of **4b**. The lowest energy electronic transition for all the model compounds is the HOMO $[n_E] \rightarrow$ LUMO[π*(C═N)] transition. In the amino tautomers mixing of the chalcogen lone pair and π*(C═N) MOs increases the HOMO–LUMO gap so that the electronic transitions are of higher energy than the corresponding transition for the imino tautomer. The replacement of the H substituent on the chalcogen in the model compounds by an aryl group raises the energy of the lone pair so that the predicted value of the electronic transition for the imino tautomer HC(NH)[NH(SePh)] is 427 nm, in reasonable agreement with the experimental value of 472 nm for **4a**. On the other hand, on the basis of NMR spectroscopic evidence, the sulfur derivative **4b** exists only as the amino tautomer and exhibits no absorption in the visible region consistent with the predicted trend of higher transition energies for the sulfur compounds compared to their selenium analogues (see Table 4).

Conclusions

The purple chromophore formed from RC(NSePh)$[N(SiMe_3)_2]$ (R = H, aryl) in solution or, more slowly, in the solid state has been identified as the hydrolysis product RCN_2H_2SePh, which, for R = H, adopts a *syn* conformation in the solid state. In contrast to the corresponding sulfur derivatives, which form only the amino tautomer $RC(NH_2)(NSPh)$ in solution, the selenium compounds exist as a mixture of amino and imino tautomers, $RC(NH_2)(NSePh)$ and RC(NH)(NHSePh), respectively. DFT calculations suggest relatively close values of the total bonding energies for the two tautomers in the case of the selenium derivatives. The calculations also indicate that the purple colour of the Se compounds can be attributed to the HOMO $[n_E] \rightarrow$ LUMO[π*(C═N)] transition of the imino tautomer.

Acknowledgements

We thank the Natural Sciences and Engineering Research Council of Canada for financial support and Dirección General de Asuntos del Personal Académico – Universidad Nacional Autónoma de México (DGAPA-UNAM) for a graduate scholarship (I. V.-B.).

References

1. D.H.R. Barton, A.G. Brewster, S.V. Ley, and M.N. Rosenfeld. J. Chem. Soc. Chem. Commun. 147 (1977).
2. (*a*) E.J. Corey and P. Caprino. J. Am. Chem. Soc. **111**, 5472 (1989); (*b*) N.R. Kotecha, S.V. Ley, and S. Mantegani. Synlett, 396 (1992).
3. D.H.R. Barton and S.I. Pareck. J. Am. Chem. Soc. **115**, 948 (1993).
4. D.H.R. Barton, M.B. Hall, Z. Lin, and S.I. Pareck. J. Am. Chem. Soc. **115**, 955 (1993).
5. V. Chandrasekhar, T. Chivers, J.F. Fait, and S.S. Kumaravel. J. Am. Chem. Soc. **112**, 5373 (1990).
6. V. Chandrasekhar, T. Chivers, S.S. Kumaravel, M. Parvez, and M.N.S. Rao. Inorg. Chem. **30**, 4125 (1991).
7. R.T. Boeré, R.T. Oakley, and R.W. Reed. J. Organomet. Chem. **331**, 161 (1987).
8. A.W. Cordes, C.D. Bryan, W.M. Davis, R.H. de Laat, S.H. Glarum, J.D. Goddard, R.C. Haddon, R.G. Hicks, D.K. Kennepohl, R.T. Oakley, S.R. Scott, and N.P.C. Westwood. J. Am. Chem. Soc. **115**, 7332 (1993).
9. A.V. Zibarev, M.A. Fedorov, and G.G. Furin. Izv. Akad. Nauk S.S.S.R. Ser. Khim. **4**, 829 (1989).
10. DIFABS: N. Walker and D. Stuart. Acta Crystallogr. Sect. A: Found. Crystallogr. **A39**, 158 (1983).
11. DIRDIF 92: P.T. Beurskens, G. Admiraal, G. Beurskens, W.P. Bosman, S. Garcia-Granda, R.O. Gould, J.M.M. Smits, and C.

Can. J. Chem. Downloaded from www.nrcresearchpress.com by 80.90.12.36 on 09/08/12
For personal use only.

Smykalla. The DIRDIF program system, Technical Report of the Crystallography Laboratory, University of Nijmegen, The Netherlands. 1992.
12. D.T. Cromer and J.T. Walker. International tables for X-ray crystallography. Vol. IV. Kynoch Press, Birmingham, England. 1974.
13. R.F. Stewart, E.R. Davidson, and W.T. Simpson. J. Chem. Phys. **42**, 3175 (1965).
14. D.T. Cromer and D. Liberman. J. Chem. Phys. **53**, 1891 (1970).
15. TEXSAN: Crystal structure analysis packages. Molecular Structure Corporation, The Woodlands, Tex. 1985 and 1992.
16. G.M. Sheldrick. SHELX76. A program for crystal structure analyses. University Chemical Laboratory, Cambridge, England. 1976.
17. (*a*) O. Gunnarsson and I. Lundquist. Phys. Rev. B: Solid State, **10**, 1319 (1974); (*b*) Phys. Rev. B: Solid State, **13**, 4274 (1976); (*c*) O. Gunnarsson, M. Johnson, and I. Lundquist. Phys. Rev. B: Condens. Matter, **20**, 3136 (1979).
18. E.J. Baerends, D.E. Ellis, and P. Ros. Chem. Phys. **2**, 41 (1973).
19. E.J. Baerends. Ph.D. Thesis, Frije Universiteit, Amsterdam. 1975.
20. W. Ravenek. *In* Algorithms and applications on vector and parallel computers. *Edited by* H.J.J. Riele, Th.J. Dekker, and H.A. van de Horst. Elsevier, Amsterdam. 1987.
21. A.D. Becke. J. Chem. Phys. **88**, 2547 (1988).
22. L. Versluis and T. Ziegler. J. Chem. Phys. **88**, 322 (1988).
23. T. Ziegler and A. Rauk. Theor. Chim. Acta, **46**, 1 (1977).
24. T. Ziegler. *In* Metal–ligand interactions: from atoms, to clusters, to surfaces. *Edited by* D.R. Salahub and N. Russo. Kluwer Academic Publishers, Amsterdam. 1992.
25. (*a*) J.G. Snijders, E.J. Baerends, and P. Vernoijs. At. Data Nucl. Data Tables, **26**, 483 (1982); (*b*) P. Vernoijs, J.G. Snijders, and E.J. Baerends. Slater type basis functions for the whole periodic system. Internal Report, Frije Universiteit, Amsterdam. 1981.
26. J. Krijn and E.J. Baerends. Fitfunctions in the HFS method. Internal Report, Frije Universiteit, Amsterdam. 1984.
27. S.H. Vosko, L. Wilk, and M. Nusair. Can. J. Phys. **58**, 1200 (1990).
28. A.D. Becke. Phys. Rev. A: At. Mol. Opt. Phys. **38**, 2938 (1988).
29. (*a*) J.P. Perdew. Phys. Rev. B: Condens. Matter, **33**, 8822 (1986); (*b*) Phys. Rev. B: Condens. Matter, **34**, 7406 (1986).
30. T. Chivers, K. McGregor, and M. Parvez. Inorg. Chem. **33**, 2364 (1994).
31. A.F. Wells. Structural inorganic chemistry. 5th ed. Clarendon Press, Oxford, England. 1984.
32. F. Wasaki, H. Murakami, N. Yamazaki, M. Yasui, M. Tomura, and N. Matsumura. Acta Crystallogr. Sect. C: Cryst. Struct. Commun. **C47**, 998 (1991).
33. T. Ziegler. Chem Rev. **91**, 651 (1991).

Can. J. Chem. Downloaded from www.nrcresearchpress.com by 80.90.12.36 on 09/08/12
For personal use only.

ADDITIONS AND CORRECTIONS/AJOUTS ET CORRECTIONS

Naresh Pandya, Anthony J. Basile, Ajay K. Gupta, Patrick Hand, Cindy L. MacLaurin, Taj Mohammad, Elaref S. Ratemi, Martin S. Gibson, and Mary Frances Richardson. 2-Acylidene-3,5-diaryl-2,3-dihydro-1,3,4-thiadiazoles and related compounds: a question of hypervalent S...O interactions. Can. J. Chem. **71**, 561 (1993).

On p. 569, the structural formula for **15***a* and *b* should have a positive charge on N3:

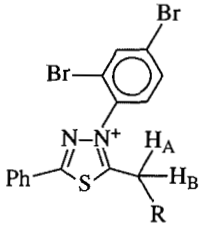

15*a*: R = Me
15*b*: R = Ph

George R. De Maré, Yurii N. Panchenko, Alexander V. Abramenkov, and Charles W. Bock. An empirically corrected quantum mechanical potential energy curve of internal rotation of acryloyl fluoride, CH_2═CH-CF═O. Can. J. Chem. **71**, 656 (1993).

The value of F_4 in the last column of Table 2 should be 0.0231 instead of 0.2306. All calculations involving the Fourier coefficients were carried out with the correct values of these coefficients.

Can. J. Chem. Downloaded from www.nrcresearchpress.com by 80.90.12.36 on 09/08/12
For personal use only.

^{1}H, ^{19}F, and ^{13}C nuclear magnetic resonance approaches to the barrier to rotation about the Csp^2—Csp^3 bond in 1,1,1-trifluoro-2-phenylethane. Proximate coupling constants and molecular orbital computations

Ted Schaefer, Paul Hazendonk, and David M. McKinnon

Abstract: The ^{1}H, ^{19}F and $^{13}C\{^{1}H\}$ nuclear magnetic resonance spectra of 1,1,1-trifluoro-2-phenylethane, **1**, in CS_2–C_6D_{12}, acetone-d_6, and benzene-d_6 solutions, on analysis, yield long-range coupling constants from which are derived the apparent twofold barriers to rotation about the Csp^2—Csp^3 bonds. The twofold barrier is 9.0(2) kJ/mol, independent of solvent, 4.0 kJ/mol larger than that of ethylbenzene, also independent of solvent. The theoretical barrier heights for the free molecules at the post-Hartree–Fock level of molecular orbital theory (frozen-core MP2/6-31G*) also differ by 4 kJ/mol, but are about 1 kJ/mol higher than the experimental estimates. The perpendicular conformer is the most stable for both molecules. Comparisons are made with the benzyl halides, in which the internal barriers are remarkably sensitive to solvent. A spin–spin coupling constant over five formal bonds, ^{5}J(H, F), involving the *ortho* protons in **1**, is +0.74(2) Hz and is discussed in some detail in terms of its dependence on internuclear distances (possible through-space interactions). The solvent perturbations of ^{3}J(H, F) and of ^{2}J(C, F) are of opposite sign. Other long-range coupling constants or their absence are also pointed out. For example, those between ^{19}F and ^{13}C nuclei or protons at the *meta* position are effectively zero; at the *para* position they are significant.

Key words: 1,1,1-trifluoro-2-phenylethane; ^{1}H, ^{19}F, and ^{13}C NMR; long-range spin–spin coupling constants; through-space ^{1}H, ^{19}F spin–spin coupling constants; internal rotational potential; molecular orbital computations of internal potential.

Résumé : L'analyse des spectres de résonance magnétique nucléaire du ^{1}H, du ^{19}F et du $^{13}C\{H\}$ du 1,1,1-trifluoro-2-phényléthane, **1**, en solution dans du CS_2–C_6D_{12}, dans de l'acétone-d_6 ou du benzène-d_6, permet d'obtenir les constantes de couplage à longue distance à partir desquelles on peut dériver les barrières binaires apparentes à la rotation autour des liaisons Csp^2—Csp^3. La barrière binaire est de 9,0(2) kJ/mol, elle est indépendante du solvant et elle est 4,0 kJ/mol plus élevée que celle de l'éthylbenzène qui est aussi indépendante du solvant. Les hauteurs des barrières théoriques des molécules libres, évaluées par la théorie des orbitales moléculaires à un niveau post-Hartree–Fock (MP2/6-31G* à référence fixée), diffèrent aussi par 4,0 kJ/mol; elles sont toutefois environ 1 kJ/mol plus élevées que les évaluations expérimentales. Dans les deux molécules, le conformère perpendiculaire est le plus stable. On a fait des comparaisons avec les halogènures de benzyle dans lesquels les barrières internes sont particulièrement sensibles au solvant. La constante de couplage spin–spin à travers cinq liaisons formelles, ^{5}J(H, F), impliquant les protons *ortho* du composé **1** est égale à +0,74(2) Hz; on en discute en détail en fonction de sa dépendance sur les distances internucléaires (interactions possibles à travers l'espace). Les perturbations des solvants sur les ^{3}J(H, F) et ^{2}J(C, F) sont de signes opposés. On spécifie aussi d'autres constantes de couplage à longue distance et, dans les cas appropriés, leur absence. Par exemple, ces constantes entre les noyaux ^{13}C et ^{19}F ou les protons en position *méta* sont effectivement égales à zéro; en position *para*, elles sont significatives.

Mots clés : 1,1,3-trifluoro-2-phényléthane; RMN du ^{1}H, du ^{13}C et du ^{19}F; constantes de couplage spin–spin à longue distance; constantes de couplage spin–spin ^{1}H, ^{19}F à travers l'espace; potentiel de rotation interne; calculs d'orbitales moléculaires du potentiel interne.

Received April 3, 1995.

T. Schaefer,[1] P. Hazendonk, and D.M. McKinnon. Department of Chemistry, University of Manitoba, Winnipeg, MB R3T 2N2, Canada.

[1] Author to whom correspondence may be addressed. Telephone: (204) 474-9335. Fax: (204) 275-0905.

Can. J. Chem. Downloaded from www.nrcresearchpress.com by 80.90.12.36 on 09/08/12
For personal use only.

Can. J. Chem. Downloaded from www.nrcresearchpress.com by 80.90.12.36 on 09/08/12
For personal use only.

Introduction

This report presents theoretical and experimental assessments of the potential hindering rotation about the Csp^2—Csp^3 bond in 1,1,1-trifluro-2-phenylethane, **1**. Comparisons are made with similar and extensive data for ethylbenzene (1–4) and other benzyl derivatives. A secondary aim of this study concerns the through-space or proximate component of the spin–spin coupling constant over five formal bonds, $^5J(^{19}F, H\text{-}2)$, between the fluorine-19 nuclei and the *ortho* protons in **1**.

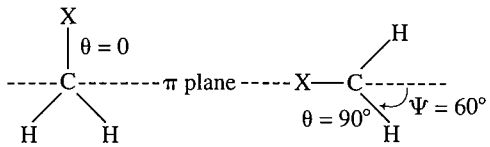

A **B**

All theoretical and experimental studies agree that **A** is the conformer of lowest, **B** that of highest, energy for the ethylbenzene (X = CH_3). Disagreement exists as to the difference in energies between **A** and **B**, the twofold component of the internal rotational potential; the numbers lie between 4.2 and 9.2 kJ/mol (3, 4). Molecular orbital calculations imply the presence of a fourfold component, V_4, in the rotational potential, of the same sign as V_2 and probably no larger than one-fifth of the magnitude of the latter (1, 2). If this statement holds, then V_2 is probably less than 6 kJ/mol in solution and also, as indicated by the invariance of the barrier-dependent $^6J(H, CH_2)$ to solvent (1), quite insensitive to the local environment of the molecule. The assumption of a pure twofold potential in solution yield V_2 as 5.0 kJ/mol (1). The rotational spectrum for the vapor (2) is consistent with a V_2 of 4.9(7) and a V_4 of 0.9 kJ/mol, as well as with a vanishing V_4 and a V_2 of 7.8(7) kJ/mol. The presence of a significant magnitude for V_4 has not been shown experimentally.

The origin of the barrier to internal rotation in ethylbenzene has been discussed in terms of steric repulsion (1), which destabilizes **B**, a molecular orbital model invoking four-electron (overlap) repulsion (5), minimized in **A**, as well as in terms of hyperconjugative stabilization of **A** (6, 7). An indirect approach (7) suggests that the hyperconjugative component is 1.2 ± 0.3 kJ/mol, the hyperconjugative ability of the C—C bond being larger than that of the C—H bond in the side chain. While this number must be regarded with circumspection (7), because no other measurements of hyperconjugative contributions to conformational energies appear to exist for neutral molecules, intuition suggests that the electronegative fluorine substituents in **1** may act to reduce the hyperconjugative interaction with the aromatic π system, that is, to destabilize **A**. Turning to **B**, considerations of size suggest that this conformer is more energetic for **1** than for ethylbenzene. Alternatively, attractive forces between the ^+C–F^- and *ortho* ^-C–H^+ dipoles will counteract the steric repulsion and, depending on their relative magnitude, **B** may actually be more stable relative to **A** in **1** than in ethylbenzene.

With these possibilities in hand, it appears sensible to compute the internal rotational potential for free **1**, to predict its geometry at a reliable level of molecular orbital theory (for use by molecular spectroscopists), and to compare these data with measurements of the internal barrier for **1** in solvents of varying polarity. The long-range spin–spin coupling constant between the methylene and *para* ring protons is sensitive, in principle, to the potential opposing the motion about the Csp^2—Csp^3 bond (1).

Experimental

The 1,1,1-trifluoro-2-phenylethane, **1**, was prepared as described (8). Dilute solutions of **1** in CS_2–C_6D_{12}–TMS–C_6F_6, acetone-d_6–TMS–C_6F_6, and benzene-d_6–TMS–C_6F_6 solvent mixtures (see Table 1 for details) were filtered into 5 mm o.d. nmr sample tubes, were degassed by at least four freeze–pump–thaw cycles, and the tubes were then flame-sealed to produce reasonably symmetric tops. The nmr measurements utilized an AM 300 Bruker spectrometer.

As many as 64 free induction decays (200 for ^{13}C), using acquisition times of 40 s (34 s for ^{13}C), were added, and were preceded by extensive shimming, monitored by the decays from internal reference compounds. After zero-filling to four times the size of the data table and the application of small amounts of resolution enhancement, Fourier transformation yielded spectra with a resolution of 0.003, 0.006, and 0.030 Hz/point for ^1H, ^{19}F, and ^{13}C nuclei, respectively.

Molecular orbital computations[2] on **1** and **2** used the computer program GAUSSIAN 92 (10). Bond angles and lengths were optimized but the atoms of the phenyl group were constrained to a plane during the optimizations. INDO MO FPT computations of spin–spin coupling constants (11, 12) utilized various computed geometries. Energies and coupling constants were fit to Fourier series in the conformational angles, θ and ψ (see **A** and **B**).

Results and discussion

Spectral analyses

The spectra were analyzed with the computer program NUMARIT (13), as extensively reworked by R. Sebastian and K. Marat in this laboratory. Tables 1 and 2 present the extracted spectral parameters. Figure 1 displays part of the ^{19}F nmr spectrum of the CF_3 group in **1**, demonstrating that $^5J(H, F)$ is positive. In Fig. 2 one multiplet of the ^1H nmr spectrum of the CH_2 group in **1** shows the agreement attained between theory and experiment of protons coupled to eight other nuclei. The $^{13}C\{^1H\}$ spectra were also subjected to analysis so as to find the precision available from these first-order spectra.

Theoretical internal barriers

Table 3 presents the components of theoretical barriers to internal rotation about the Csp^2—Csp^3 bond in **1**. As expected, **A** lies at the bottom of the potential (θ = 0), which is dominated by the twofold component. For the split-valence basis sets, V_2 is 11.3, 10.8, and 10.5 kJ/mol for the RHF 6-31G, 6-31G*, and 6-31G** bases, respectively. The correlation-gradient, MP2/6-31G*, energies at θ = 0 and θ = 90° differ by 10.04 kJ/mol. In comparison, for ethylbenzene the V_2 values are 6.0 kJ/mol for both RHF 6-31G* bases (1, 2) and a single-point MP2/6-31G*//6-31G* barrier height is 5.8 kJ/mol (2). Theoretically, therefore, the hindering potential in **1** is 4–5 kJ/mol larger than in ethylbenzene.

Figures 3 and 4 present the planar and perpendicular MP2/

[2] For details of the notation for the various basis sets and the MP2 approximation to electron correlation, see ref. 9.

Table 1. The ^{1}H and ^{19}F nmr spectral parameters for 1,1,1-trifluro-2-phenylethane, **1**, at 300.135 MHz, 282.362 MHz, and 300 K in three environments.

Parameter	Solvent			Parameter	Solvent		
	CS_2/C_6D_{12}[a]	Acetone-d_6[b]	Benzene-d_6[c]		CS_2/C_6D_{12}[a]	Acetone-d_6[b]	Benzene-d_6[c]
ν(F)	26,897.416[d]	27 660.288	27 396.884	^4J(H, CH_2)	−0.527	−0.520[g]	−0.528
$\nu(CH_2)$	968.854[e,f]	1062.027	837.761	^5J(H, CH_2)	0.267	0.264(1)[g]	0.261
$\nu_2 = \nu_6$	2151.556	2211.607	2080.961	^6J(H, CH_2)	−0.344	−0.350(1)[g]	−0.345
$\nu_3 = \nu_5$	2172.815	2212.761	2107.007	^5J(H, CF_3)	+0.735	+0.759	+0.741
ν_4	2168.254	2203.323	2103.795	^6J(H, CF_3)	0.006	0.010	0.002
$^3J(CH_2, F)$	10.721	11.269	10.954	^7J(H, CF_3)	±0.071	±0.070	±0.061
$^3J_{23} = {}^3J_{56}$	7.714	7.722	7.724	Root-mean-square deviation	0.007	0.010	0.006
$^3J_{34} = {}^3J_{45}$	7.504	7.523(1)	7.516				
$^4J_{26}$	1.958	1.965(2)	1.964	Largest absolute difference	0.016	0.021	0.014
$^4J_{24} = {}^4J_{46}$	1.239	1.238(1)	1.264	Transitions calculated	2579	2662	2170
$^4J_{35}$	1.438	1.443(1)	1.445	Assigned transitions	1976	1850	1992
$^5J_{25} = {}^5J_{36}$	0.602	0.596(1)	0.602	Assigned peaks	799	523	856

[a]As a 4.7 mol% solution in CS_2, containing also 10 mol% of C_6D_{12}, 0.5 mol% of TMS, and 0.25 mol% of C_6F_6.
[b]As a 5.3 mol% solution in acetone-d_6 with 0.5 mol% of TMS and 0.25 mol% of C_6F_6.
[c]As a 6.3 mol% solution in benzene-d_6 with 0.5 mol% of TMS and 0.25 mol% of C_6F_6.
[d]In Hz at 282.3624 MHz to high frequency of internal C_6F_6.
[e]In Hz at 300.1349 MHz to high frequency of internal TMS.
[f]Unless otherwise noted the standard deviations are less than 0.001 Hz.
[g]The small range of the aromatic proton chemical shifts entailed correlations of as large as 0.5 between a number of the spectral parameters.

Table 2. The $^{13}C\{^1H\}$ nmr spectral parameters for 1,1,1-trifluoro-2-phenylethane, **1**, at 75.4689 MHz and 300 K.

Parameter	Solvent[a]		
	CS_2–C_6D_{12}	Acetone-d_6	Benzene-d_6
ν-β	125.532	127.246	126.454
ν-α	40.292	40.097	40.014
ν_1	130.067[b]	131.460	130.455
$\nu_2 = \nu_6$	130.050[b]	131.121	130.358
$\nu_3 = \nu_5$	128.022	128.797	128.173
ν_4	128.628	129.401	128.796
^1J(C, F)	−276.88[c]	−275.81	−276.52
^2J(C, F)	(+)29.79	(+)29.23	(+)29.46
^3J(C, F)	(+)2.90	(+)3.07	(+)2.96
^4J(C, F)	0.70[e]	0.68	0.71
^5J(C, F)	0.02[d,e]	0.03	0.02
^6J(C, F)	0.29[e]	0.30	0.29

[a]For the samples described in Table 1.
[b]Assigned on the assumption that $|^3J(C, F)| > |^4J(C, F)|$, shifts in ppm relative to internal TMS.
[c] ^nJ(C, F) are precise to at least 0.01 Hz, as given by spectral analytical procedures.
[d]Estimated from comparisons of line widths.
[e]Signs are unknown, but see text.

Fig. 1. The ^{19}F nmr spectrum of a 6.3 mol% solution of 1,1,1-trifluoro-2-phenylethane, in benzene-d_6 at 282.36 MHz and at 300 K, is shown at the bottom. The scale is in Hz to high frequency of internal C_6F_6. The computed spectrum at the top uses the spectral parameters in Table 1, with a linewidth of 0.045 Hz and ^5J(H, F) = +0.7 Hz. In the middle, the simulated spectrum has ^5J(H, F) = −0.7 Hz. A ^7J(H, F) of 0.07 Hz is present in all spectra.

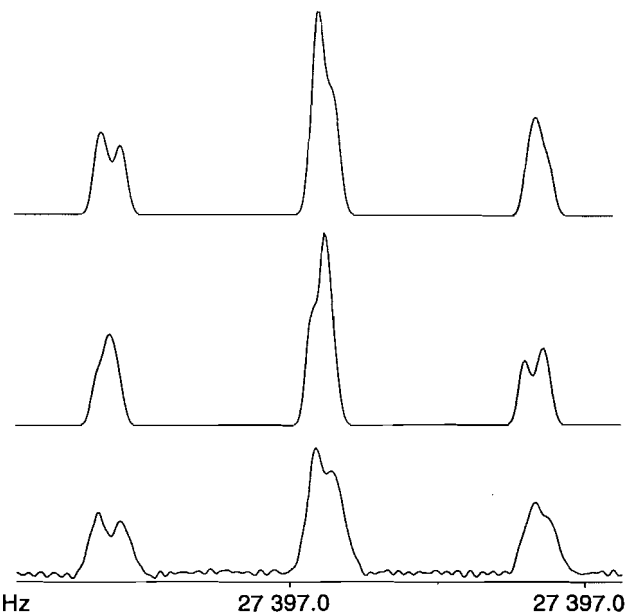

6-31G* geometries of **1**, of possible use to molecular spectroscopists. Note the opening of the exocyclic CCC bond angles in the planar form, implying repulsive destabilization of **A**.

Experimental barriers in solution

The long-range coupling constants between the methylene and ring protons are all functions of the angle ψ (see **B**). In particular, ^6J(H, CH_2) = ^6J is proportional to $\sin^2\psi$ (1) which, in turn, has an expectation value dependent on the torsional potential about the Csp^2—Csp^3 bond (14). One may write $^6J = {}^6J_{90}\langle\sin^2\psi\rangle$, where $^6J_{90}$ is the value at $\psi = 90°$. $^6J_{90}$ decreases in magnitude as the electronegativity of the substituent on the

Can. J. Chem. Downloaded from www.nrcresearchpress.com by 80.90.12.36 on 09/08/12
For personal use only.

Fig. 2. The ^{1}H nmr spectrum of one of the methylene multiplets of a 4.7 mol% solution of 1,1,1-trifluoro-2-phenylethane in CS_2–C_6D_{12} is compared with the computed spectrum. The scale is in Hz at 300.135 MHz to high frequency of internal TMS, at 300 K.

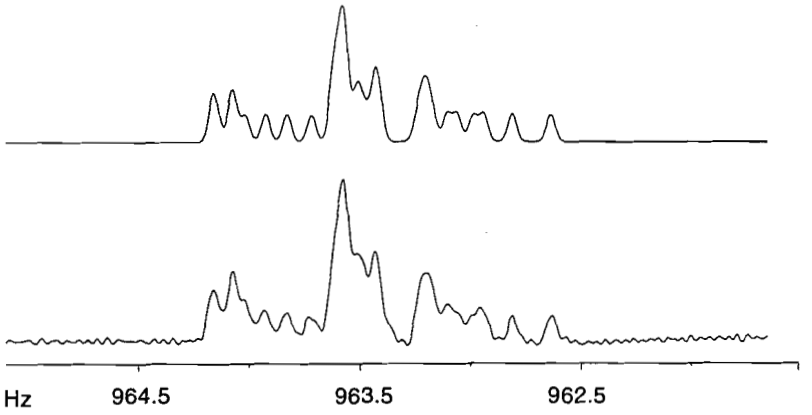

Fig. 3. The MP2/6-31G* geometry of the perpendicular, most stable, structure of 1,1,1-trifluoro-2-phenylethane is shown. The projection of the a C—H bonds onto a plane perpendicular to the phenyl plane illustrates that their torsion angle is 29.8° in the *J* method discussed in the text. The Csp^2-Csp^3-Csp^3 angle is 111.8°.

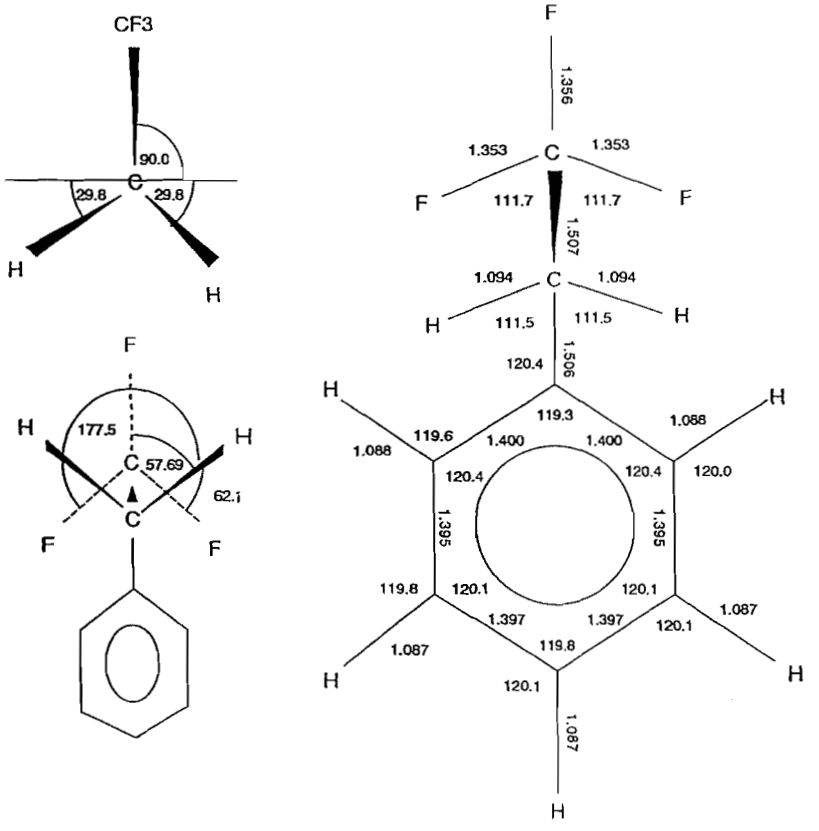

methylene group increases (smaller σ–π hyperconjugative overlap). For example, it is −1.20 Hz for X = H (15) and −0.95 Hz for X = F, as determined (16) experimentally. Other $^6J_{90}$ values are −1.02 Hz for X = OH or OCH_3 (17) and −1.16 Hz for X = CH_3 (1). The electronegativity on the Pauling scale is 3.46 for X = CF_3, leading[3] to $^6J_{90}$ = −1.03 Hz for **1**. It fol-

[3] Our INDO MO FPT computations for X = H, F, and CF_3 yield $^6J_{90}$ as −1.22, −1.07, and −1.14 Hz, respectively, qualitatively in agreement with a reduction in the magnitude of $^6J_{90}$ caused by an electronegative substituent. The experimental value (16) for X = F is 0.12 Hz lower in magnitude than the theoretical; the empirical value of $^6J_{90}$ for X = CF_3, used in the text, is 0.11 Hz lower in magnitude than that given by the INDO parameterization.

Can. J. Chem. Downloaded from www.nrcresearchpress.com by 80.90.12.36 on 09/08/12
For personal use only.

Can. J. Chem. Downloaded from www.nrcresearchpress.com by 80.90.12.36 on 09/08/12
For personal use only.

Fig. 4. The MP2/6-31G* geometry of the high-energy conformer of 1,1,1-trifluoro-2-phenylethane illustrates the opening of the bond angles in the side chain, possibly indicative of steric strain.

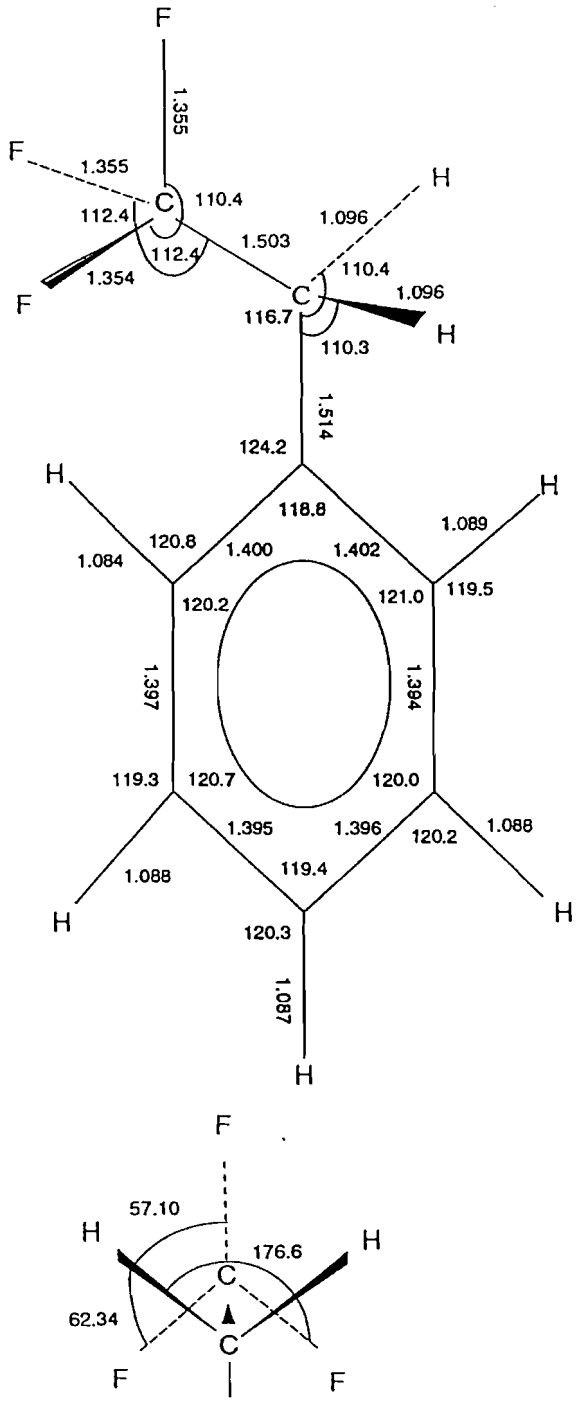

lows that $\langle \sin^2\psi \rangle = 0.336$, where the average of ^6J for the three solutions (Table 1) is used. From a hindered rotor model (14), the apparent V_2 follows as 9.0 kJ/mol, 4.0 kJ/mol higher than given by the same approach for ethylbenzene in a range of solvents (1, 3). The MP2/6-31G*, correlation-gradient computation for the free molecule has the barrier height as 10.04 kJ/mol, which is 4.2 kJ/mol higher than that from a similar calculation for ethylbenzene (see above). Considering possible errors in theory and experiment, it seems possible to conclude that, for both molecules, the two methods essentially agree about the barrier heights. By implication, the internal rotational potentials in both molecules, one polar, the other not, are insensitive to environment (note the essentially equal $^6J(H, CH_2)$ numbers for **1** in the three solvents in Table 1) or, pushing the evidence, the barrier heights in both molecules are about 1 kJ/mol lower in solution than in the vapor. While the dipole moment of ethylbenzene is only 0.6 D (2), that of **1** is computed as 2.53 D for **A** and 2.42 D for **B** (MP2/6-31G*), which are similar to the 2.32 D measured for CH_3CF_3 (18). To first order in reaction field theory (19), a large solvent perturbation of the internal potential is therefore not anticipated.

Table 3. The theoretical components of the potential function hindering rotation about the Csp^2—Csp^3 bond in 1,1,1-trifluoro-2-phenylethane, **1**.

Basis	V_2[a,b]	V_4	V_6	V_8	$\langle \sin^2\theta \rangle$[c]
AM1	3.93(1)	−0.08(1)	−0.59(1)	−0.27(1)	0.319
STO-3G	7.63(2)	−0.37(2)	0.23(2)	−0.05(2)	0.204
6-31G	11.29(1)	0.58(1)	−0.19(1)	−0.15(1)	0.125
6-31G*	10.77(2)	1.14(2)	−0.21(2)	−0.19(2)	0.123
6-31G**	10.48(1)	1.09(1)	−0.17(1)	−0.17(1)	0.127_5

[a]In kJ/mol, numbers in parentheses being standard errors.

[b]In the perpendicular form, **A**, defined by $\theta = 0$, the minimum computed energies in a.u. are −597.441 228 (STO-3G), −605.161 984 (6-31G), −605.365 304 (6-31G*), −605.377 477 (6-31G**), and −606.887 011 (MP2/6-31G*). The barrier height for the post-Hartree–Fock calculation is 10.04 kJ/mol.

[c]The expectation value of $\sin^2\theta$ at 300 K, being related to that of $\sin^2\psi$ (see **B**) by $\langle \sin^2\theta \rangle = 1.5 - 2 \langle \sin^2\psi \rangle$ for tetrahedral angles at the methylene carbon atom.

The presence of a hyperconjugative component of the barrier in **1** cannot be established at present. At first sight, the absence of any hyperconjugative interaction between the CH_2CF_3 group and the aromatic π system is indicated by the essential equality of the chemical shifts of H-4 and C-4 in **1** and benzene (20, 21); hence the barrier should have no such component. However, as a referee points out, the equality of shifts could also reflects a combination of C–H hyperconjugation and π-electron polarization by the remote CF_3 group or, indeed, opposing C–H and C–C hyperconjugation.

An intriguing contrast exists between these data and the solvent effects on the internal rotational potentials of the benzyl halides. According to the ^6J method above, for benzyl fluoride **A** is stabilized by 1.7 ± 0.4 kJ/mol when the solvent is changed from CS_2 to acetone-d_6 (16); in the former solvent the twofold potential, with **A** also at the minimum, is only 0.7(2) kJ/mol. Similarly, for benzyl chloride, the apparent twofold barriers are 8.8 ± 0.4 and 11.2 ± 0.4 kJ/mol in the two solvents (22). A different method, based on residual intramolecular dipolar coupling constants, measured for the compounds dispersed in nematic solvents, also yields barriers for X = F, Cl, Br, I that increase in magnitude as the polarity of the medium rises (23, 24). For example, in the least polar solvent the (assumed) V_2 is 8.96 ± 0.06 kJ/mol, when X = Cl, rising to 11.05 ± 0.14 kJ/mol in the most polar nematic medium (24); the dielectric constants of these media are not given.

Can. J. Chem. Downloaded from www.nrcresearchpress.com by 80.90.12.36 on 09/08/12
For personal use only.

The reasons for the contrast between the benzyl halides, X = F to I, and X = CF_3 or CH_3, escape us; **1** is certainly at least as polar as any of the benzyl halides. One possibility (5) for the halides might be that **A** is favored by electrostatic forces between the $^+C–X^-$ and *ortho* $^-C–H^+$ dipoles; these are proportional to the reciprocal of the effective dielectric constant and thus the old question again arises. What is the effective dielectric constant at the site of the interaction of the intramolecular charges on the molecular periphery when the molecule is immersed in a solvent of bulk dielectric constant? The similar magnitudes of the changes in potential, caused by the same solvents, for X = F or Cl, even though the barriers are substantially different, are consistent with this electrostatic origin: the dipole moments of benzyl fluoride and chloride and essentially equal, that is, the $^+C–X^-$ dipoles are very similar. While this rationalization is consistent with the insensitivity to solvent of the barrier in ethylbenzene (1), it appears as inconsistent with the behaviour of **1**. The Mulliken charges (MP2/6-31G*) are $-0.38e$ on fluorine and $+0.21e$ on *ortho* hydrogen atoms. The qualitative difference is that the C—F bonds are staggered about the *ortho* C—H bonds in **B** for **1**, whereas the C—F bond lies in the molecular plane when X = F. Perhaps further discussion should await confirmation by another method of the solvent independence of the internal rotational potential of **1**.

^4J(H, CH_2) and ^5J(H, CH_2) in 1

^4J(H, CH_3) in toluene has been written as $-1.08\sin^2\psi - 0.32\cos^2\psi$, the first term referring to a π-electron contribution, the second to a σ-electron component (25). If the coefficient of the term in $\sin^2\psi$ is multiplied by 1.03/1.20, as indicated from the treatment above the ^6J(H, CH_2) in **1**, then ^4J(H, CH_2) becomes −0.524 Hz because $\langle\sin^2\psi\rangle$ is 0.336. This number happens to agree exactly with the average of the measured numbers in Table 1.

In toluene, ^5J(H, CH_2) apparently (15) obeys the relationships, $0.336\sin^2\psi + 0.322\sin^2(\psi/2)$. Again, reduction of the σ, π maximum by 1.03/1.20 and noting that $\langle\sin^2(\psi/2)\rangle$ is 0.5 for any combination of evenfold terms in the internal rotational potential yields ^5J(H, CH_2) as 0.258 Hz, in reasonable agreement with the average, 0.264(3) Hz, of the values in Table 1. These two calculations assume that the σ-electron terms are independent of X, which may be unwarranted, so that the present agreements between experimental and theoretical numbers for ^4J(H, CH_2) and ^5J(H, CH_2) could be accidental.

^5J(H, CF_3) and proximate coupling mechanisms

The long-range coupling constants between ^{19}F nuclei and ring protons in **1** (Table 1) demonstrate a relatively large ^5J(H, CF_3) of + 0.74(2) Hz. The ^7J(H, CF_3) of magnitude 0.07(1) Hz is most likely a σ,π transmitted coupling constant, whose magnitude is consistent with the undetectable ^6J(H, CF_3). The latter is also expected to have a component transmitted by the π electrons, but smaller than ^7J(H, CF_3), perhaps only about 25% as large, as found for σ,π interactions in toluene. On that basis, ^5J(H, CF_3) may contain a σ,π component of comparable magnitude to ^7J(H, CF_3). The implication, that ^5J(H, CF_3) is dominated by other coupling mechanisms,[4] is assessed as follows.

[4] For a recent, extensive review of the theoretical and physical aspects of spin–spin coupling constants and, in particular, of through-space or proximate modes of the transmission of nuclear spin-state information, see ref. 26.

Fig. 5. ^5J(H-2, CF) is plotted as a function of the dihedral angle of the C(*ortho*)C (*ipso*)CF fragment in **1**. The INDO MO FPT values show that a close approach of H-2 and the fluorine atom leads to a large, negative ^5J. The circles refer to the C—F bond, which remains distant from the *ortho* C—H bond for all conformations. As the C—C(F_3) bond moves out of the phenyl plane, some rotation about this bond occurs, leading to a minimum in one H, F distance at a dihedral angle near 40° (6-31G* geometry). The predicted ^5J, to be compared with measurement, is obtained by averaging two values, equally displaced from 90° (H-2 and H-6 are isochronous).

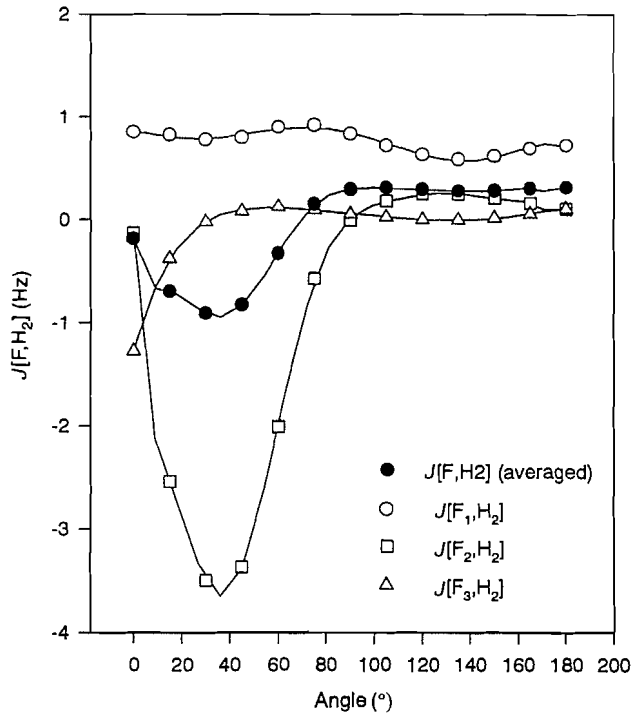

Figure 5 displays the INDO MO FPT values of ^5J(H, CF_3) as a function of the torsion angle between the Csp^3—Csp^3 bond and the aromatic plane (6-31G* geometries). As expected from various computational schemes (26), a close approach of the atoms containing the coupled nuclei leads to a negative, through-space coupling constant (the in-plane conformer has F-1 far from H-2, the CF_3 group being in a nearly staggered conformation about the *ortho* C—H bond). The prediction of a change in sign of ^5J(H, CF_3), from negative to positive, for an out-of-plane angle between 60° and 70° is qualitatively consistent with the 90 ± arc $(\langle\sin^2\theta\rangle)^{1/2}$ of 65.5° or 114.5° derived from the coupling constants in the previous section. A positive shift of about 0.5 Hz in the computed coupling constants would produce semiquantitative agreement with measurement. Another representation of the sensitivity of ^5J(H, CF_3) to nonbonded interatomic distances is developed in Figs. 6 and 7. Figure 6 displays the RHF 6-31G* distances between the ^{19}F nuclei and the *ortho* proton as a function of the torsion angle in Fig. 5 (as the angle increases the CF_3 group also rotates somewhat about the Csp^2—Csp^3 bond in order to relieve steric strain). Figure 7 demonstrates the high sensitivity of ^5J(H, CF_3) to the internuclear distance in regions where it is smaller than the sum of the van der Waals radii of hydrogen and fluorine. The change in sign from positive to negative

Can. J. Chem. Downloaded from www.nrcresearchpress.com by 80.90.12.36 on 09/08/12
For personal use only.

Fig. 6. The distances between the ^{19}F nuclei and the *ortho* proton in **1** are plotted as a function of the angle by which the C—C(F_3) bond twists out of the ring plane. One ^{19}F nucleus remains far from the proton, another approaches it most closely at about 40° because rotation about the C—C(F_3) bond also occurs during the out-of-plane twist, no doubt in order to relieve steric repulsion (6-31G* geometries).

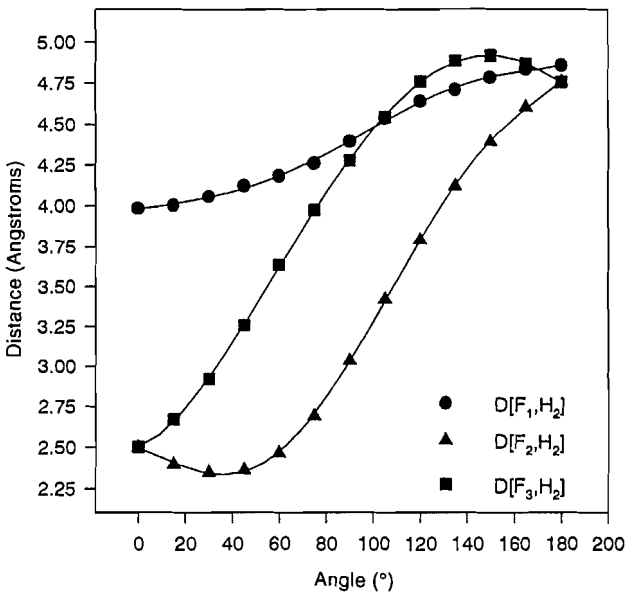

for a given ^{19}F nucleus occurs very near 3.0 Å; the average coupling constant is −0.33 Hz at a 60° torsion from the aromatic plane, +0.15 Hz at 75°.

Although the present computations and measurements of ^5J(H, CF_3) in **1** are not entirely compatible, theory yielding numbers somewhat too small, measurements on a derivative of **1** in which the CF_3 group lies much nearer the aromatic plane, on average, would test the prediction of a negative ^5J(H, CF_3).

In $C_6H_5OCF_3$, ^5J(H, CF_3) is +1.03(1) Hz (27). The magnitude of the barrier to rotation is uncertain, although it appears that the perpendicular conformer is most stable, as indicated by 6-31G computations (27) and by alternative internal rotational potentials derived from residual dipolar coupling constants measured for solutions in nematic solvents (28). In the 4-fluoro derivative, ^5J(H, CF_3) is +0.95Hz (27). Of course, if through-space interactions are important, it is then expected that their magnitudes depend crucially on the details of geometry, small differences in bond angles and lengths leading to significant changes in ^5J(H, CF_3).

The challenge to the theory of proximate coupling constants is emphasized by the following examples. In 2-trifluoromethylbenzaldehyde, in which the C—H bond of the formyl group spends most of its time wedged between two C—F bonds, ^5J(H, CF_3) is +2.2 Hz (29), yet INDO MO FPT calculations find a negative value. In 2-hydroxybenzotrifluoride, a negative ^5J(OH, CF_3) is in qualitative agreement with theory (30). In other words, the sign and magnitude of ^5J(H, CF_3) depend on the site of the CF_3 group as well as that of the proton.

$^3J(CH_2, F)$

In Table 1 it is shown that $^3J(CH_2, F)$ in **1** increases from 10.72 Hz in CS_2–C_6D_{12} to 11.27 Hz in acetone-d_6 solution. For CH_3CF_3, a reaction field model (31) of the solvent dependence of $^3J(CH_2, F)$ predicts an increase of 0.62 Hz, in close agreement with the 0.55 Hz measured for **1**. $^3J(CH_3, F)$ is reported as 12.8 Hz for CH_3CF_3, state not given (32). The value of 10.95 Hz for **1** in benzene-d_6 solution is consistent with an effective dielectric constant rather larger than anticipated in reaction field models (19). Some ^nJ(C, F) values for **1** also display an intrinsic solvent dependence (Table 2), discussed below.

$^nJ(^{13}C, ^{19}F)$ in 1

^1J increases algebraically in going from CS_2 to acetone-d_6 solution, as expected from an electrostatic model (31). In contrast, the positive ^2J(C, F) decreases as polarity of the solvent increases. This striking behaviour is opposite to that of ^2J(H, F) in CHF_3, where decreases[5] are dominated by van der Waals interactions with the solvent (33) molecules and attributed to perturbations of the orbital contributions to the coupling constant. Were ^2J(C, F) negative in **1**, the solvent perturbations could be attributed to an increase in a positive Fermi contact contribution, caused by bond polarizations (31). As it is, the experimental observations remain unexplained; all ^2J(C, F) are thought to be positive (34), and its INDO MO FPT value for **1** is 4 Hz.

^3J(C, F) is computed to be positive and rather insensitive to θ, while ^4J(C, F) can be written as $-0.06 + 0.51\sin^2(\phi/2) - 0.64\sin^2\phi + 0.28\sin^2 2\phi$, where φ is the angle by which the C—C(F_3) bond twists *out* of the phenyl plane. Experimentally, $\langle\sin^2\phi\rangle$ is 0.87, $\langle\sin^2(\phi/2)\rangle$ is 0.5 for an evenfold potential, and $\langle\sin^2 2\phi\rangle$ is estimated as 0.46 so that the theoretical value of ^4J(C, F) follows as −0.22 Hz. It is of interest that the signs of ^4J(C, F) and ^5J(H, F) are predicted to be opposite (in Fig. 5 one must take a rough mean for arc $\sin^2\phi \sim 65°$ or 115° to obtain an estimate of the theoretical ^5J(H, F), and find about 0.2 Hz). Because the experimental value of ^5J(H, F) is +0.74(2) Hz and that of ^4J(C, F) is ± 0.70(2) Hz, the sign of the latter should be determined (not an easy experiment for **1**).[6]

^5J(C, F) in **1** is ≤0.03 Hz in magnitude and, it may be noted, ^6J(H, CF_3) is undetectable (Table 1); both involve the *meta* site in **1**. The *para* position, however, yields a ^6J(C, F) of 0.30(2) Hz in magnitude and a ^7J(H, CF_3) of 0.07 Hz. If these two coupling constants are transmitted through the π-electron system, they should be proportional to Q^CCH and Q^HCH, respectively. The hyperfine parameters are a measure of spin polarization by spin density in the 2*pz* orbital of the *para* C—H bond, causing parallel and antiparallel spin orientations of the proton and ^{13}C nucleus, respectively. Q^CCH/Q^HCH is −1.6 (3) for neutral (diamagnetic) molecules, whereas $|^6J$(C, F)/^7J(H, CF_3)| is 4 in **1**. Therefore another coupling mechanism may be present for ^6J(C, F), its nature unknown.

[5] ^2J(H, F) is 79.14(2), 79.29(2), and 79.47(2) Hz in CS_2, C_6H_6, and $(CH_3)_2C{=}O$ solutions, respectively (33), and is 79.69(2) Hz for the vapor at about 72 atm (1 atm = 101.3 kPa), whereas ^2J(C, F) in **1** is 29.79(1), 29.46(1), and 29.23 Hz for these solvents.

[6] Such an experiment would provide comparisons with theory and experiment (35) for ^5J(H,F) and ^4J(C,F) measured on aromatic compounds in which a ring C—F bond lies near a ^{13}C—H bond of a methyl group on a side chain. In these compounds the ratio, $^4J/^5J$, can change sign as the C—F and C—H bonds move away from a common plane.

Fig. 7. ^5J(H, F) is plotted as a function of the distance between the ^{19}F nuclei and the *ortho* proton in **1**. These distances occur as the C—C(F_3) bond twists away from the plane of the phenyl group (6-31G* geometries). The one outlier (a solid circle) may well be a misleading datum.

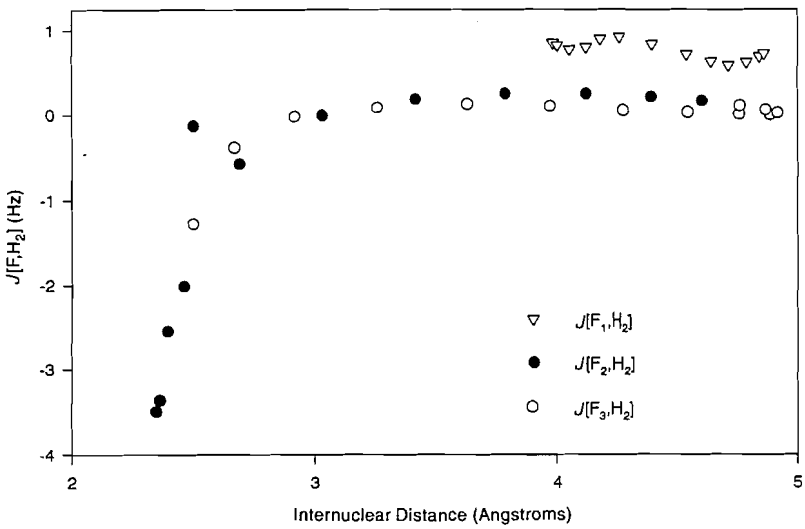

Can. J. Chem. Downloaded from www.nrcresearchpress.com by 80.90.12.36 on 09/08/12
For personal use only.

Acknowledgments

We thank the Natural Sciences and Engineering Research Council of Canada for financial assistance. The referees are thanked for cogent criticism.

References

1. T. Schaefer, G.H. Penner, and R. Sebastian. Can. J. Chem. **65**, 873 (1987).
2. W. Caminati, D. Damiani, G. Corbelli, B. Velino, and C.W. Bock. Mol. Phys. **74**, 885 (1991).
3. T. Schaefer, W.K. Chan, R. Sebastian, R. Schurko, and F.E. Hruska. Can. J. Chem. **72**, 1972 (1994).
4. J. Kao. J. Am. Chem. Soc. **109**, 3817 (1987), and references therein.
5. G.H. Penner, T. Schaefer, R. Sebastian, and S. Wolfe. Can. J. Chem. **65**, 1845 (1987).
6. W.J. Hehre, L. Radom, and J.A. Pople. J. Am. Chem. Soc. **94**, 1496 (1972).
7. T. Schaefer, R.W. Schurko, and G.M. Bernard. Can. J. Chem. **72**, 1780 (1994).
8. C.H. DePuy and A.L. Schultz. J. Org. Chem. **39**, 878 (1974).
9. W.J. Hehre, L. Radom, P.v.R. Schleyer, and J.A. Pople. Ab initio molecular orbital theory. Wiley, New York. 1986.
10. M.J. Frisch, G.W. Trucks, M. Head-Gordon, P.M.W. Gill, M.W. Wong, J.B. Foresman, B.G. Johnson, H.B. Schlegel, M.A. Robb, E.S. Replogle, R. Gomperts, J.L. Andres, K. Raghavachari, J.S. Binkley, C. Gonzalez, R.L. Martin, D.J. Fox, D.J. Defrees, J. Baker, J.J.P. Stewart, and J.A. Pople. GAUSSIAN 92, Revision C. Gaussian, Inc., Pittsburgh, Pa. 1992.
11. J.A. Pople, J.W. McIver, Jr., and N.S. Ostlund. J. Chem. Phys. **49**, 2960 (1968); **49**, 2965 (1968).
12. J.A. Pople and D.L. Beveridge. Approximate molecular orbital theory. McGraw Hill, New York. 1970.
13. A.R. Quirt and J.S. Martin. J. Magn. Reson. **5**, 318 (1971); J.S. Martin, A.R. Quirt, and K.E. Worvill. The NMR program library. Daresbury Laboratory, Daresbury, U.K.
14. W.J.E. Parr and T. Schaefer. Acc. Chem. Res. **13**, 400 (1980).
15. T. Schaefer, R. Sebastian, and G.H. Penner. Can. J. Chem. **63**, 2597 (1985).
16. T. Schaefer, C. Beaulieu, R. Sebastian, and G.H. Penner. Can. J. Chem. **68**, 581 (1990).
17. R. Laatikainen and K. Tuppurainen. J. Chem. Soc. Perkin Trans. **2**, 121 (1987).
18. R.G. Schulman, B.P. Dailey, and C.H. Townes. Phys. Rev. **78**, 145 (1950).
19. R.J. Abraham and E. Bretschneider. *In* Internal rotation in molecules. *Edited by* W.J. Orville-Thomas. J. Wiley and Sons, New York. 1974. Chap. 13.
20. W.J. Hehre, R.W. Taft, and R.D. Topsom. Prog. Phys. Org. Chem. **12**, 159 (1976).
21. D.E. Ewing. Org. Magn. Reson. **12**, 499 (1979).
22. T. Schaefer, R. Sebastian, and G.H. Penner. Can. J. Chem. **64**, 1372 (1986).
23. G. Celebre, G. DeLuca, M. Longeri, and J.W. Emsley. Mol. Phys. **67**, 239 (1989).
24. G. Celebre, G. DeLuca, M. Longeri, and A. Ferrarini. Mol. Phys. **83**, 309 (1994).
25. M. Barfield, C.J. Fallick, K. Hata, S. Sternhell, and P.W. Westerman. J. Am. Chem. Soc. **105**, 217 (1983).
26. R.H. Contreras and J.C. Facelli. Annu. Rep. NMR Spectrosc. **27**, 255 (1993).
27. T. Schaefer, G.H. Penner, R. Sebastian, J. Peeling, and C. Beaulieu. Can. J. Chem. **69**, 1047 (1991).
28. M. Barnes, J.W. Emsley, T.J. Horne, G.M. Warms, G. Celebre, and M. Longeri. J. Chem. Soc. Perkin Trans. 2, 1807 (1989).
29. T. Schaefer, S.R. Salman, and T.A. Wildman. Can. J. Chem. **58**, 2364 (1980).
30. J.B. Rowbotham, M. Smith, and T. Schaefer. Can. J. Chem. **53**, 986 (1975).
31. M. Barfield and M.D. Johnston, Jr. Chem. Rev. **73**, 53 (1973).
32. N. Muller and D.T. Carr. J. Phys. Chem. **67**, 112 (1963).
33. T. Schaefer, H.M. Hutton, and S.R. Salman. Can. J. Chem. **57**, 1877 (1979).
34. F.J. Weigert and J.D. Roberts. J. Am. Chem. Soc. **93**, 2361 (1971).
35. I.D. Rae, J.A. Weigold, R.H. Contreras, and G. Yamamoto. Magn. Reson. Chem. **30**, 1047 (1992).

The enols of acetic acid and methyl acetate

J. Peter Guthrie and Zhi Liu

Abstract: We have determined the heat of formation of 1,1-dimethoxyethene, $\Delta H_f(l) = -75.56 \pm 0.87$ kcal mol^{-1}, by measuring the heat of hydrolysis. The heat of vaporization, 8.47 ± 0.10 kcal mol^{-1}, was estimated from the boiling points at various pressures. The standard entropy of gaseous 1,1-dimethoxyethene, $82.02 \pm 2.$ cal deg^{-1} mol^{-1}, was calculated using frequencies obtained by MO calculations at the 6-31G** level. The free energy of transfer, 1.02 ± 1, was estimated by additivity with allowance for a distant polar interaction. Thus the free energy of formation in aqueous solution, $\Delta G_f(aq) = -37.07 \pm 1.48$ kcal mol^{-1}, could be calculated. The free energies of hydrolysis for enol ethers appear to be insensitive to structure; we used an average value and so calculated the values of the free energies of formation of the enols of acetic acid and methyl acetate, -67.90 ± 1.67 and -52.48 ± 1.53 kcal mol^{-1}, respectively. These values are in good agreement with other recent evaluations. This method should be applicable to related enols.

Key words: enols, thermodynamics, heat of formation, entropy, ketene acetal.

Résumé : On a déterminé la chaleur de formation du 1,1-diméthoxyéthène, $\Delta H_f(l) = -75,56 \pm 0,87$ kcal mol^{-1}, à partir de la mesure de sa chaleur d'hydrolyse. On a évalué sa chaleur de vaporisation, $8,47 \pm 0,10$ kcal mol^{-1}, à partir de ses points d'ébullition à diverses pressions. Utilisant les fréquences obtenues à partir de calculs d'OM au niveau 6-31G**, on a calculé que l'entropie standard du 1,1-diméthoxyéthène à l'état gazeux est de $82,02 \pm 2.$ cal deg^{-1} mol^{-1}. Utilisant une additivité qui tient compte d'une interaction polaire à distance, on a évalué l'énergie libre de transfert à $1,02 \pm 1$. On a donc pu calculer que l'énergie libre de formation en solution aqueuse est de $\Delta G_f(aq) = -37,07 \pm 1,48$ kcal mol^{-1}. Les énergies libres d'hydrolyse des énols semblent insensibles à la structure; on a utilisé une valeur moyenne et on a pu ainsi calculer les valeurs des énergies libres de formations des énols de l'acide acétique et de l'acétate de méthyle qui seraient respectivement de $-67,90 \pm 1,67$ et $-52,48 \pm 1,53$ kcal mol^{-1}. Ces valeurs sont en bon accord avec d'autres évaluations récentes. Cette méthode devrait être applicable à des énols apparentés.

Mots clés : énols, thermodynamique, chaleur de formation, entropie, acétal du cétène.

Introduction

Kresge, Wirz, and co-workers (1–6) have determined the enol contents of simple aldehydes and ketones and, more recently, of mandelic acid (7). As yet the only routes to the enol content of acetic acid are an indirect thermodynamic argument that we have presented (8), and an indirect kinetic analysis of deuterium exchange kinetics (8). The carbon pK_a values of acetic acid (8) and ethyl acetate (9) have been calculated from kinetics of exchange.

We have now determined the heat of formation of 1,1-dimethoxyethene, and have calculated a value of the free energy of formation in aqueous solution based on this heat of formation. We have examined a possible way to estimate the free energy change for the hypothetical hydrolysis reactions leading to the enol of methyl acetate and the enol of acetic acid. These calculations lead to values in good agreement with those reported earlier, suggesting that the new estimation procedure is valid.

Received September 13, 1994.[1]

J.P. Guthrie[2] and Z. Liu. Department of Chemistry, University of Western Ontario, London, ON N6A 5B7, Canada.

[1] Revision received June 9, 1995.

[2] Author to whom correspondence may be addressed. Telephone: (519) 661-2166. Fax: (519) 661-3022.

Results

1,1-Dimethoxyethene was prepared by the literature procedure (10) and purified by distillation in vacuum. Despite careful pre-treatment of the glassware with base, to avoid any acid-catalyzed polymerization, we found that the distilled sample invariably contained a few percent of impurity. The impurity increased in amount over time, and precipitated as a white, noncrystalline solid. This material was separated, and its ^{1}H nmr spectrum in $CDCl_3$ was recorded; this spectrum showed the peaks expected for poly (-C(OCH$_3$)$_2$-CH$_2$-). Since a simple ketal will not react in aqueous sodium hydroxide solution, the effect of this impurity on the heat of reaction was assumed to be simply that of dilution of the sample.

The observed heat of reaction for process [1], see Table 1, was -33.30 ± 0.85 kcal mol^{-1} for a sample shown by nmr analysis to be 94% pure. The true heat of reaction was therefore calculated to be -35.43 ± 0.85 kcal mol^{-1}.

[1] $CH_2{=}C(OCH_3)_2(l) + 2\ H_2O\ (soln) \rightleftharpoons CH_3COOH\ (soln) + 2\ CH_3OH\ (soln)$

Correcting to the standard state for all species, using data from Table 1, leads to a heat of reaction for process [2], as -17.79 ± 0.86 kcal mol^{-1}.

Can. J. Chem. Downloaded from www.nrcresearchpress.com by 80.90.12.36 on 09/08/12
For personal use only.

Can. J. Chem. Downloaded from www.nrcresearchpress.com by 80.90.12.36 on 09/08/12
For personal use only.

Table 1. Heats of reaction and solution.[a]

Compound	ΔH	Compound	ΔH
$CH_2{=}C(OCH_3)_2$	−32.62	H_2O	0[b]
	−34.25	CH_3OH	−1.72
	−33.03		−1.70
Avg.	−33.30 ± 0.85		−1.84
CH_3COOH	−14.11	Avg.	−1.75 ± 0.08
	−14.15		
Avg.	−14.13 ± 0.02		

[a]All at 25°C in 0.1 N aqueous sodium hydroxide solution; enthalpies are in kcal mol^{-1}.

[b]No detectable heat change on injection of distilled water.

Table 2. Thermodynamic data.[a]

Compound	$\Delta H_f(l)$[b]	$\Delta G_f(aq)$[c]
H_2O	−68.32 ± 0.01	−56.69 ± 0.01
CH_3OH	−57.15 ± 0.07	−42.14 ± 0.15
CH_3CH_2OH		−43.44 ± 0.16
CH_3COOH	−115.70 ± 0.08	−94.35 ± 0.38
CH_3COOCH_3		−78.92 ± 0.60
$CH_2{=}C(OCH_3)_2$	−75.56 ± 0.87[d]	−37.07 ± 1.48[e]
$CH_2{=}C(OCH_3)(OH)$		−52.48 ± 1.53[e]
$CH_2{=}C(OH)_2$		−67.90 ± 1.67[e]
$CH_2{=}CH(OH)$		−24.84 ± 0.21
$CH_2{=}C(CH_3)(OH)$		−27.02 ± 0.60
$CH_2{=}CH(OCH_3)$		−9.99 ± 0.51
$CH_2{=}C(CH_3)(OCH_3)$		−12.55 ± 1.11
$CH_2{=}C(Ph)(OH)$		8.68 ± 0.43
$CH_2{=}C(Ph)(OCH_3)$		23.49 ± 0.46

[a]Standard states are the pure liquid and 1 M aqueous solution with an infinitely dilute reference state. The standard state for aqueous water is the pure liquid. Enthalpies and Gibbs free energies are in kcal mol^{-1}.

[b]From ref. 25 unless otherwise noted.

[c]From ref. 14 unless otherwise noted.

[d]Calculated from the observed enthalpy of reaction and the known enthalpies of formation of the other reactants and products.

[e]Calculated as described in the text.

[2] $CH_2{=}C(OCH_3)_2(l) + 2\ H_2O\ (l)$

$$\rightleftharpoons CH_3COOH(l) + 2\ CH_3OH\ (l)$$

Now it is possible to calculate the heat of formation of liquid 1,1-dimethoxyethene, using heats of formation from the literature: Table 2. The value so calculated is −75.56 ± 0.87 kcal mol^{-1}. To determine the heat of vaporization, we measured the boiling point at reduced pressures, using a small-scale apparatus (11). The boiling point data, Table 3, can be fitted to the equation: $\log p = 8.587 - 2068/T$. At each pressure, the heat of vaporization was calculated from the boiling point, using the empirical relationship that we have reported (12). The average heat of vaporization so determined was 8.47 ± 0.28 kcal mol^{-1}; the error is taken as the weighted average error in the original correlation (12). This allows calculation of the heat of

Table 3. Vapor pressures and heat of vaporization for $CH_2{=}C(OCH_3)_2$.[a]

p (Torr)	t (°C)	ΔH_{vap} (kcal mol^{-1})
760	89	8.30
133	47	8.47
121	45	8.49
78	36	8.56
69	30	8.56
	Avg.	8.47 ± 0.10

[a]Calculated as described in the text.

formation of 1,1-dimethoxyethene in the gas phase as −67.09 ± 0.90 kcal mol^{-1}.

The entropy was estimated in several independent ways. First we applied Benson's group additivity method (13). Since no value for the group contribution for an sp^2 carbon bonded to two oxygens, $[C_d(O)_2]$ has been reported, we used $[C_d(C)_2]$ as an approximation; such approximations are generally reasonably close (13, 14). This estimation procedure led to a value of $S°(g) = 87.43$ cal deg^{-1} mol^{-1}. Next we used MM3 to estimate the entropy by way of vibrational frequencies and statistical mechanics; this required using estimated values of two parameters for which no values were available. Although the force constant for O-C_d-O bending is likely to be close to 0.6 md Å rad^{-2}, and the preferred angle to 120° (the values we chose), the torsional parameters are harder to guess. The value of the entropy turned out to be moderately sensitive to the exact values used, varying from 82.9 to 86.3 cal deg^{-1} mol^{-1} depending on the values used for the unknown torsional parameters for the C(sp^2)—O bond of a ketene acetal. Finally we employed molecular orbital methods to estimate the vibrational frequencies that were then used to calculate the entropy by statistical mechanics. AM1 led to a value of 86.05 cal deg^{-1} mol^{-1}; GAUSSIAN 92[3] at the 6-31G* level led to a value of 81.94 cal deg^{-1} mol^{-1}, and at the 6-31G** level to a value of 82.02. These calculations used the default scale factor of 1/1.12 to correct the calculated frequencies. We used the entropy from GAUSSIAN 92 at the 6-31G** level for further calculations, and assign an uncertainty of ± 2 cal deg^{-1} mol^{-1}.

From the enthalpy and entropy we can calculate the free energy of formation in the gas phase as −38.09 ± 1.09 kcal mol^{-1}. Finally, we need to estimate the free energy of transfer from the gas phase to aqueous solution, in order to calculate the free energy of formation in water. The free energy of transfer cannot be measured directly because of the rapid hydrolysis of the ketene acetal, even in aqueous hydroxide solution (15). We estimate the free energy of transfer by making use of the sequence: isobutene: 2-methoxypropene: 1,1-dimethoxyethene, assuming that the effects of replacing CH_3 by OCH_3 are constant except that there will be a distant polar interaction (16, 17) for the two methoxy groups in 1,1-dimethoxyethene.

[3] GAUSSIAN 92, Revision D.2. M.J. Frisch, G.W. Trucks, M. Head-Gordon, P.M.W. Gill, M.W. Wong, J.B. Foresman, B.G. Johnson, H.B. Schlegel, M.A. Robb, E.S. Replogle, R. Gomperts, J.L. Andres, K. Raghavachari, J.S. Binkley, C. Gonzalez, R.L. Martin, D.J. Fox, D.J. Defrees, J. Baker, J.J.P. Stewart, and J.A. Pople, Gaussian, Inc., Pittsburgh, Pa. 1992.

Can. J. Chem. Downloaded from www.nrcresearchpress.com by 80.90.12.36 on 09/08/12
For personal use only.

For lack of information allowing a better correction we will assume that this is the same as the interaction in $CH_2(OCH_3)_2$ (17), namely 1.56 kcal mol^{-1}. Thus we end up with an estimated free energy of transfer of 1.02 kcal mol^{-1} for 1,1-dimethoxyethene, to which we assign an uncertainty of ±1 kcal mol^{-1}. This allows us to calculate the free energy of formation in aqueous solution as −37.07 ± 1.48 kcal mol^{-1}.

As a check we calculated the free energy of transfer using AMSOL 1.0[4] (18); this led to a value of 0.12 kcal mol^{-1} for the standard states that we use. AMSOL seems to give values within 1.5 kcal mol^{-1} of the true value for various compounds that have been tested (18). We will use the value estimated above, but consider AMSOL a confirmation of the approximate correctness of the estimate.

Now we would like to calculate the free energies of formation of the enols of methyl acetate and acetic acid. The problem here is to estimate the effect of substituents on the free energy of hydrolysis of an enol ether. For sp^3 hybridized carbon, the free energy change for process [3] is moderately sensitive to electron withdrawal from the central carbon by R^1, R^2 and R^3 (19).

[3] 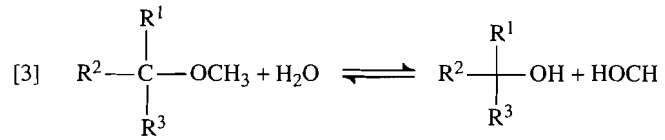

The slope of a plot of ΔG vs. $\Sigma\sigma^*$ for R^1, R^2 and R^3 is 0.63. On the other hand, for esters where OR is attached to an sp^2 hybridized carbon the free energy change is almost totally insensitive to electron withdrawal. For R = CF_3, CH_3, pCH_3O-C_6H_4, C_6H_5, pNO_2-C_6H_4, ΔG = +1.65 (20), +1.70 (21), +1.17 (22), +1.26 (22), +1.21 (22) (all for reaction in water, where the standard state of water is the pure liquid at unit activity). There does appear to be an effect on changing from an aliphatic to an aromatic acyl substituent, but within each series the effect of drastic change in substituents is very small.

[4]

[5] 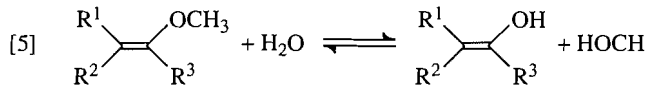

We therefore propose, as a speculation to be tested, that for enol ethers as well, the free energy change for the hypothetical hydrolysis [5] will be very insensitive to the nature of R^1, R^2, and R^3. First we will calculate a weighted average value from the data available in the literature. From the data in Table 2 we can calculate free energy changes for these hydrolysis reactions, as shown in Table 4. The weighted average value is −0.86 ± 0.39. Now using this weighted average value for the free energy changes in reactions [6] and [7] we can calculate

[6] $CH_2{=}C(OCH_3)_2$ (aq) + H_2O (l)

$\rightleftharpoons CH_2{=}C(OCH_3)(OH)$ (aq) + CH_3OH (aq)

[4] QCPE606, Quantum Chemical Program Exchange, Indiana University.

Table 4. Free energy of hydrolysis of enol ethers.[a]

Enol ether	ΔG_{hydrol}
$CH_2{=}CH(OCH_2CH_3)$	−1.6 ± 0.57
$CH_2{=}C(CH_3)(OCH_3)$	0.08 ± 1.27
Cyclohexenyl-OCH_3	−0.48 ± 1.38
$CH_2{=}C(Ph)(OCH_3)$	−0.26 ± 0.65
Average	−0.56 ± 0.63
Weighted average	−0.86 ± 0.39

[a]In aqueous solution at 25°C, calculated using the free energies of formation in Table 3. Gibbs free energies are in kcal mol^{-1}.

[7] $CH_2{=}C(OCH_3)(OH)$ (aq) + H_2O (l)

$\rightleftharpoons CH_2{=}C(OH)_2$ (aq) + CH_3OH (aq)

the free energies of formation for the enols of methyl acetate, −52.48 ± 1.53 kcal mol^{-1}, and of acetic acid, −67.90 ± 1.67

[8] CH_3-CO-OCH_3 (aq) $\rightleftharpoons CH_2{=}C(OCH_3)(OH)$ (aq)

[9] CH_3-CO-OH_3 (aq) $\rightleftharpoons CH_2{=}C(OH_3)$ (aq)

kcal mol^{-1}. With these energies in hand we can calculate free energy changes for the enolization processes; ΔG_8 = 26.44 ± 1.64 kcal mol^{-1}, pK_E = 19.4 ± 1.2, ΔG_9 = 26.45 ± 1.71 kcal mol^{-1}, pK_E = 19.4 ± 1.3.

Discussion

These results for acetic acid, pK_E = 19.4 ± 1.3, may be compared with expectations based on disproportionation calculations, where the enol content of acetic acid was predicted to be pK_E = 21 ± 2 (8), or the prediction based on deuterium exchange into acetic acid, pK_E = 19.3 ± 2.2 (8).

For methyl acetate, we predict a pK_E of 19.4 ± 1.2, in agreement with a value based on kinetics of exchange in aqueous solution (9).

The thermochemical approach reported in this paper should have some generality, and could make more pK_E values accessible to indirect determination. The major limitation that we see is the assumption that the free energy change for the hypothetical hydrolysis process leading from an enol ether to an enol will be the same as for simple models. This seems reasonable in the absence of large substituent effects, but cannot be assumed to apply if there are large resonance or field effects from substituents.

Given the markedly different pK_a values of the enols of mandelic acid (7) and simple aldehydes and ketones (23), it is surprising that the assumption of similar free energies of hydrolysis for the enol ethers holds as well as it does. Since the various procedures leading to enol contents for acetic acid or methyl acetate, including the present work, lead to consistent results, it suggests that the assumption is valid. We still feel that extrapolation to compounds with strong electron-withdrawing substituents would require new model compounds.

Experimental

Materials

Bromoacetaldehyde dimethyl acetal, potassium metal, and

terpineol were purchased from Aldrich, and used without further purification. 1,1-Dimethoxyethene was prepared by reaction of bromoacetaldehyde dimethyl acetal with the potassium salt of terpineol, following the literature procedure (10). The nmr spectrum ($CDCl_3$) showed two sharp peaks at d 3.08 and 3.64 in a ratio of 1:3. There were additional peaks at 1.41 and 3.26 that were attributed to polymer. On standing, a sample of 1,1-dimethoxyethene deposited a white solid, the nmr spectrum of which consisted mainly of these two peaks. The sample of 1,1-dimethoxyethene used for calorimetry was 94% monomer and 6% polymer.

Methods

The nmr spectra were recorded on a Varian Gemini 300 instrument. Vapor pressures were determined using a small-scale boiling point apparatus (11). Heats of reaction and solution were determined using a homemade calorimeter, as previously described (24). The reaction solvent was 0.1 N NaOH.

Acknowledgments

We thank the Natural Sciences and Engineering Research Council of Canada for financial support of this work. We thank Dr. T.L. Amyes for communicating results of her studies of exchange in methyl acetate prior to publication.

References

1. Y. Chiang, A.J. Kresge, and J. Wirz. J. Am. Chem. Soc. **106**, 6392 (1984).
2. Y. Chiang, A.J. Kresge, Y.S. Tang, and J. Wirz. J. Am. Chem. Soc. **106**, 460. (1984).
3. Y. Chiang, A.J. Kresge, M. Capponi, and J. Wirz. Helv. Chim. Acta, **69**, 1331. (1986).
4. Y. Chiang, A.J. Kresge, J.A. Santaballa, J. Wirz. J. Am. Chem. Soc. **110**, 5506 (1988).
5. Y. Chiang, M. Hojatti, J.R. Keefe, A.J. Kresge, N.P. Schepp, and J. Wirz. J. Am. Chem. Soc. **109**, 4000 (1987).
6. Y. Chiang, A.J. Kresge, and P.A. Walsh. J. Am. Chem. Soc. **108**, 6314 (1986).
7. Y. Chiang, A.J. Kresge, P. Pruszynski, N.P. Schepp, and J. Wirz. Angew. Chem. Int. Ed. Engl. **29**, 792 (1990).
8. J.P. Guthrie. Can. J. Chem. **71**, 2123 (1993).
9. T.L. Amyes and J.P. Richard. To be published.
10. E.J. Corey, J.D. Bass, R. LeMahieu, and R.B. Mitra. J. Am. Chem. Soc. **86**, 5570 (1964).
11. S.R. Hoover, H. John, and E.F. Mellon. Anal. Chem. **25**, 1940 (1953).
12. J.P. Guthrie. Can. J. Chem. **64**, 635 (1986).
13. S.W. Benson. Thermochemical kinetics. Wiley, New York. 1976.
14. J.P. Guthrie. Can. J. Chem. **70**, 1042 (1992).
15. A. Kankaanpera and H. Tuominen. Suom. Kemistil. **40**, 270 (1967).
16. J. Hine and P.K. Mookerjee. J. Org. Chem. **40**, 292 (1975).
17. J.P. Guthrie. Can. J. Chem. **69**, 1893 (1991).
18. C.J. Cramer and D.G. Truhlar. J. Am. Chem. Soc. **113**, 8305 (1991).
19. J.P. Guthrie. Can. J. Chem. **53**, 898 (1975).
20. J.P. Guthrie. Can. J. Chem. **54**, 202 (1976).
21. A.R. Fersht and W.P. Jencks. J. Am. Chem. Soc. **92**, 5442 (1970).
22. J. Guthrie, D. Pike, and Y. Lee. Can. J. Chem. **70**, 1671 (1992).
23. J.R. Keefe and A.J. Kresge. *In* The chemistry of enols. *Edited by* Z. Rappoport. Wiley, Chichester. 1990. p. 399.
24. J.P. Guthrie. J. Am. Chem. Soc. **96**, 3608 (1974).
25. D.D. Wagman, W.H. Evans, V.B. Parker, R.H. Schumm, I. Halow, S.M. Bailey, K.L. Churney, and R.L. Nuttall. J. Phys. Chem. Ref. Data, Suppl. 2, **11**, (1982).

Can. J. Chem. Downloaded from www.nrcresearchpress.com by 80.90.12.36 on 09/08/12
For personal use only.

Synthesis of (*S*)-4-hydroxy-α-lapachone and biotransformation of some 4-chromanones by *Mortierella isabellina* ATCC 42613

Herbert L. Holland, Jia Qi, and T. Samuel Manoharan

Abstract: 1-Methoxy-2-naphthol was converted by MOM ether formation, lithiation at C-3, reaction with 3,3-dimethylacryloyl chloride, cyclization, and oxidation using cerium ammonium nitrate to 4-keto-α-lapachone (2,2-dimethyl-4-keto-1-oxa-1,2,3,4-tetrahydroanthra-5,10-quinone). Reduction by biotransformation using *Mortierella isabellina* ATCC 42613 gave (*S*)-4-hydroxy-α-lapachone in high (>95%) optical purity. Reduction of several 2,2-dimethyl-4-chromanones to the corresponding (*S*)-alcohols by *M. isabellina* is also reported.

Key words: biotransformation, chemoenzymatic, 4-hydroxy-α-lapachone, *Mortierella isabellina*.

Résumé : Faisant appel à la série de réactions suivantes, formation d'éther MOM, lithiation en C-3, réaction avec du chlorure de 3,3-diméthylacryloyle, cyclisation et oxydation à l'aide du nitrate d'ammonium cérique, on a transformé le 1-méthoxynapht-2-ol en 4-céto-α-lapachone (2,2-diméthyl-4-céto-1-oxa-1,2,3,4-tétrahydroanthra-5,10-quinone). Sa réduction par biotransformation utilisant de la *Mortierella isabellina* ATCC 42613 conduit à la (*S*)-4-hydroxy-α-lapachone avec une pureté optique élevée (>95%). On rapporte aussi la réduction de plusieurs 2,2-diméthyl-4-chromanones en alcools-(*S*) correspondants par la *M. isabellina*.

Mots clés : biotransformation, chemoenzymatique, 4-hydroxy-α-lapachone, *Mortierella isabellina*.

Introduction

The biotransformation of 4-chromanone (**1**) by *Mortierella isabellina* ATCC 42613 can be used to prepare (*S*)-4-chromanol (**2**) in high yield and enantiomeric purity (Scheme 1) (1). (*S*)-4-Hydroxy-α-lapachone (**3**), which possesses the (*S*)-4-chromanol functional unit, has been isolated from the Japanese Kisasage tree *Catalpa ocata* (2, 3) and from the heartwood of the Brazilian *Zeyhera tuberculosa* (4), and has been shown to possess antineoplastic properties (4). The racemate of **3** was prepared by Gupta and Khanna in a non-regioselective synthesis (5, 6), and by Tapia's group in a route involving construction of the aromatic ring via Diels–Alder addition to a suitably substituted quinone (7), but preparation of the natural chiral material has not hitherto been reported. To develop a route to (*S*)-**3** based on chiral reduction of an appropriately substituted keto precursor we have examined the biotransformation by *M. isabellina* of a number of substituted 4-chromanones (**4**, **8**, and **13**). The syntheses of these compounds and their biotransformations by *M. isabellina* are presented, together the preparation of (*S*)-4-hydroxy-α-lapachone (**3**) by *M. isabellina*-catalyzed reduction of 2,2-dimethyl-4-keto-1-oxa-1,2,3,4-tetrahydroanthra-5,10-quinone.

Received May 18, 1995.

H.L. Holland,[1] **J. Qi, and T.S. Manoharan.** Department of Chemistry, Brock University, St. Catharines, ON L2S 2A1, Canada.

[1] Author to whom correspondence may be addressed. Telephone: (905) 688-5550, ext. 3406. Fax: (905) 688-2789.

Scheme 1. Preparation of (*S*)-4-chromanol.

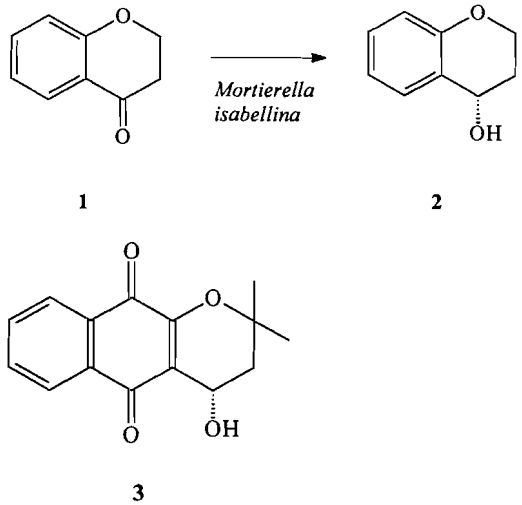

Results and discussion

To investigate the effect of methyl substitution at C-2 on the stereochemistry of biotransformation of a chromanone, the 2,2-dimethyl-substituted substrate **4** was prepared by a modification of ApSimon's method (8) and subjected to biotransformation using *M. isabellina* (Scheme 2). The desired (*S*)-alcohol **5** was produced in good yield, but its enantiomeric excess (40%) was low. The absolute stereochemistry of this and other reduction products described below was assigned in two ways: firstly, in accord with the observation that *M. isa-*

Can. J. Chem. Downloaded from www.nrcresearchpress.com by 80.90.12.36 on 09/08/12
For personal use only.

Scheme 2. Biotransformation of 2,2-dimethyl-4-chromanone.

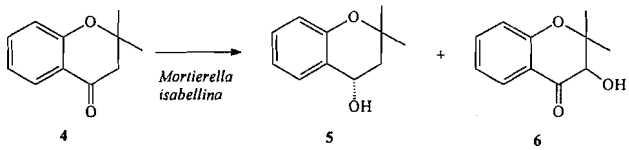

bellina reduces benzylic ketones according to Prelog's rule to give (*S*) benzylic carbinols (1, 9), and secondly by the observation that addition of the chiral ^{1}H nmr shift reagent tris[3-(heptafluoropropylhydroxymethylene)-*d*-camphorato] europium(III) to a non-racemic benzylic alcohol results in a ^{1}H nmr spectrum in which the carbinol hydrogen of the -C*H*(OH)- unit can be resolved into two baseline-separated signals in the 10–20 ppm region. In all cases examined using alcohols of known configuration, the signal attributable to the (*S*) enantiomer is upfield and that of the (*R*) enantiomer downfield (1, 10, 11). In addition to the production of **5**, biotransformation of **4** by *M. isabellina* also resulted in formation of a minor product, hydroxyketone **6**, whose stereochemistry was not examined.

A route to 4-hydroxy-α-lapachone via a precursor such as **7** was first considered. Prior to undertaking synthesis of the latter, we examined reduction of 2,2-dimethyl-5,8-dimethoxychroman-4-one (**8**). Chroman-4-ones with this substitution

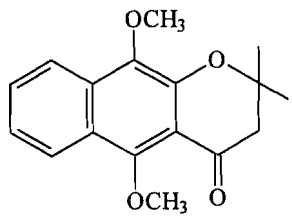

7

pattern have not been reported, and we developed the synthesis of **8** from 2,5-dimethoxyphenol as outlined in Scheme 3. Biotransformation of **8** by *M. Isabellina* (Scheme 3) gave the alcohol (*S*)-**9** in high yield (99%) and in an enantiomeric purity exceeding 95%. A ^{1}H nmr analysis in the presence of tris[3-(heptafluoropropylhydroxymethylene)-*d*-camphorato] europium(III) failed to reveal any (*R*) enantiomer; addition of controlled amounts of synthetic (±)-**9** to the biotransformation product followed by nmr analysis confirmed the (*S*) configuration of the latter by the gradual appearance of a C*H*OH signal downfield from that of the original sample.

Biotransformation of the chroman **10** (Scheme 4) also gave **9**, but in racemic form. Additional products were obtained and assigned structures **11** and **12** on the basis of homonuclear nOe experiments. It was clear from mass spectral and ^{1}H nmr analysis that **11** was a mono-O-demethyl derivative of the substrate, and the site of demethylation was shown to be O(5) by the absence of nOe enhancement of the benzylic methylene protons upon irradiation of the remaining O-methyl signal at δ 3.77 ppm. Similarly, **12** was clearly a phenolic derivative of substrate; nOe experiments involving irradiation of the C-5 methoxy signal at δ 3.74 ppm showed an enhancement of only the benzylic methylene protons at δ 2.74, while irradiation of the C-8 methoxy resonance resulted only in enhancement of

Scheme 3. Synthesis and biotransformation of 5,8-dimethoxy-2,2-dimethyl-4-chromanone (**8**).

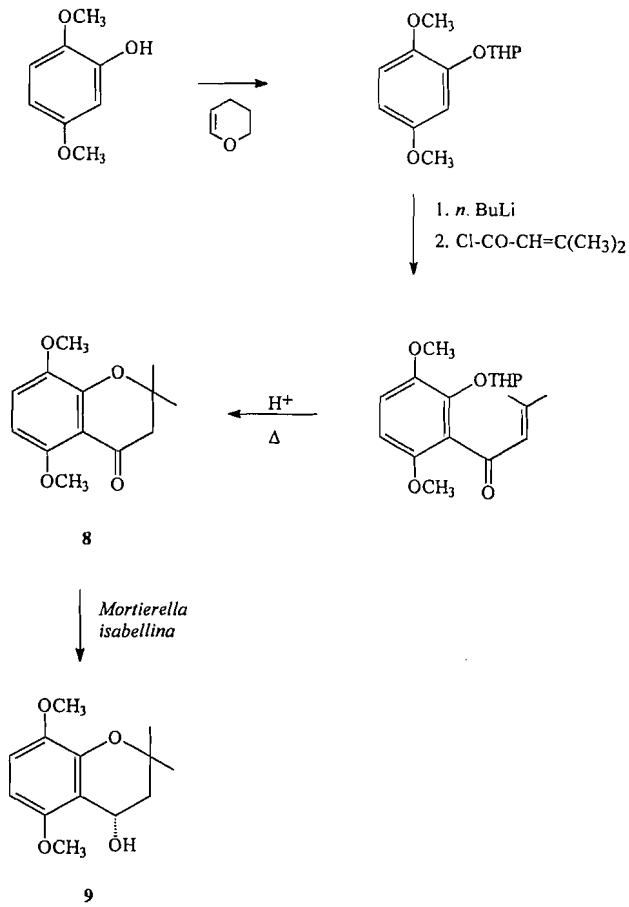

Scheme 4. Biotransformation of 5,8-dimethoxy-2,2-dimethylchroman (**10**).

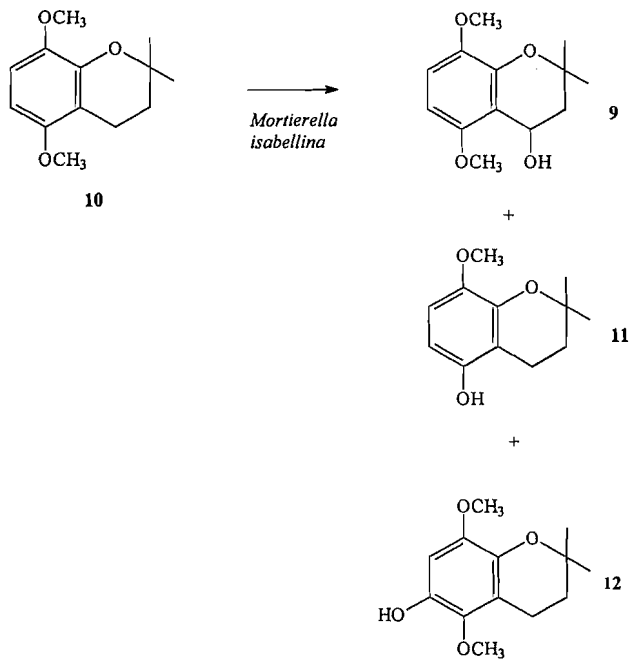

Can. J. Chem. Downloaded from www.nrcresearchpress.com by 80.90.12.36 on 09/08/12
For personal use only.

Can. J. Chem. Downloaded from www.nrcresearchpress.com by 80.90.12.36 on 09/08/12
For personal use only.

the C-7 aromatic hydrogen signal. During investigation of the synthesis and biotransformation of 6,7-benzo-5,8-dimethoxy-2,2-dimethyl-4-chromanone **7** as a route to **3**, we were unsuccessful in attempts to prepare **7** by a route analogous to that of Scheme 3. Although lithiation of a protected phenol intermediate analogous to that shown in Scheme 3 was achieved (evidenced by incorporation of deuterium label when quenched with D_2O), reaction of this species with dimethylacryolyl chloride did not afford the desired ketone, resulting only in formation of intractable product mixtures. We therefore turned our attention to the monomethoxy analogue **13**, whose synthesis from 1-methoxy-2-naphthol is shown in Scheme 5. In contrast to the THP protection of Scheme 3, we found here that protection of the phenolic group as a MOM ether facilitated purification of intermediates. It was also necessary, again in contrast to the route of Scheme 3, to use *tert*-butyllithium for lithiation of the intermediate protected phenol.

Biotransformation of **13** by *M. isabellina* gave the (*S*) alcohol **14** (Scheme 5), but the enantiomeric purity was low (32%) and phenolic side-products were obtained. However, given that the presence of a substituent *ortho* to the carbonyl group undergoing biocatalytic reduction apparently results in enhancement of the optical purity of the resulting (*S*) alcohol (cf. results from **4** vs. **8**), we examined the quinone **15** (4-ketolapachone), obtained by ceric ion oxidation of **13** (Scheme 6). Biotransformation of **15** by *M. isabellina* resulted in the formation of (+)-4-hydroxy-α-lapachone (**3**) in acceptable yield and high (>95%) enantiomeric purity. The absolute configuration of the (+) (natural) enantiomer of **3** has been assigned as (*S*) by application of the extended dibenzoate chirality rule to the CD spectrum of its benzoate ester (2). The configuration of our product is thus established. Furthermore, under conditions described above where racemic alcohols give cleanly resolved signals in chiral nmr analysis, we were unable to detect any (*R*)-**3** in our product. The reactions of Schemes 5 and 6 therefore represent the first asymmetric synthesis of the natural enantiomer of (*S*)-(+)-4-hydroxy-α-lapachone.

Although spectral data of our synthetic sample matched those reported in the literature for both natural (2–4) and synthetic (5–7) 4-hydroxy-α-lapachone, we observed discrepancies in physical data. This material has been variously reported as a yellow oil (natural (2, 4) and synthetic racemate (7)) and a yellow solid with mp 117–119°C (synthetic racemate (6)), whereas our material melted at 67°C. Furthermore, natural 4-hydroxy-α-lapachone has a reported rotation, $[\alpha]_D$ +27.4, whereas our sample showed $[\alpha]_D$ +39.7 under the same conditions. From this it may be inferred that the natural material is not optically pure, possessing an enantiomeric purity of 69%. To confirm this our sample of **3** was converted to the acetate **16** in order to compare the data obtained therefrom with those reported for synthetic racemic **16** and for **16** obtained by acetylation of natural 4-hydroxy-α-lapachone. Again, although our spectral data for **16** matched those reported (2), the mp and rotation data were disparate, the latter confirming the conclusion that natural 4-hydroxy-α-lapachone is not optically pure as isolated. Our sample of **16** has $[\alpha]_D$ −22.7 whereas the acetate of natural 4-hydroxy-α-lapachone has $[\alpha]_D$ −14.2, corresponding to ee = 63% (2).

We therefore suggest that our synthesis of (*S*)-(+)-4-hydroxy-α-lapachone gives enantiomerically pure material, whereas the natural product is not enantiomerically homogeneous. Whether this results from an aspect of its biosynthesis or the occurrence of partial racemization during the extraction procedure is unknown.

Scheme 5. Synthesis and biotransformation of 6,7-benzo-2,2-dimethyl-8-methoxy-4-chromanone (**13**).

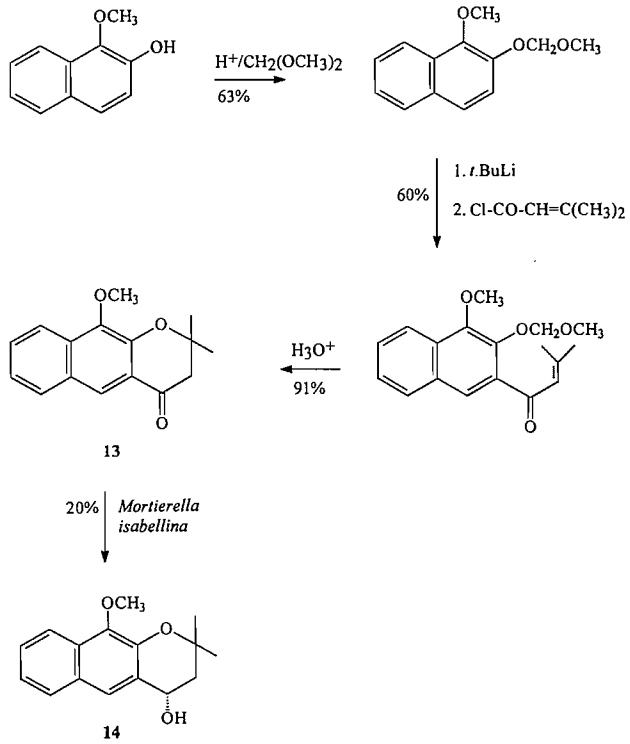

Scheme 6. Preparation of (*S*)-4-hydroxy-α-lapachone (**3**) and the acetate (**16**).

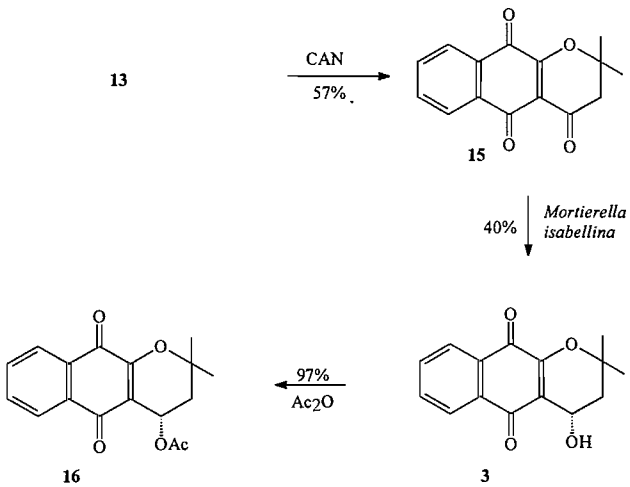

Experimental

Apparatus, materials, and methods

Melting points were determined on a Kofler heating stage. Infrared spectra were recorded with an Analect 6260FX spec-

Can. J. Chem. Downloaded from www.nrcresearchpress.com by 80.90.12.36 on 09/08/12
For personal use only.

trometer. The nmr spectra were recorded at 200 MHz (routine ^1H) or 50 MHz (routine ^{13}C) with a Bruker AC200 spectrometer using $CDCl_3$ as solvent and $CHCl_3$ as internal standard. ^{13}C signals are assigned as primary (p), secondary (s), tertiary (t), or quaternary (q) from analysis of JMOD spectra. Enantiomeric ratios were examined by ^1H nmr analysis in the presence of sufficient tris[3-(heptafluoropropylhydroxymethylene)-*d*-camphorato] europium(III) to cause shifting of the C*H*OH signals under investigation to δ 10–20 ppm. Homonuclear nOe difference spectra were obtained at McMaster University using a Bruker AM500 spectrometer. Optical rotations were obtained in the stated solvent at ambient temperature with a Rudolph Autopol III polarimeter. Mass spectra were obtained with a Kratos 1S instrument operating in EI mode. Thin-layer chromatography (tlc) was performed on Merck silica gel 60F-254 and flash column chromatography used silica gel, 230–400 mesh. Microanalyses were performed by Guelph Chemical Laboratories, Guelph, Ontario.

Maintenance of microorganisms

Mortierella isabellina ATCC 42613 was obtained from the American Type Culture Collection, Rockville, Md., and was maintained on 4% malt agar slopes, grown at 27°C, and stored at 4°C.

Preparation of bicyclic substrates

*2,2-Dimethyl-4-chromanone (**4**)*

Based on a procedure of ApSimon et al. (8), a mixture of *o*-hydroxyacetophenone (13.5 g), pyrrolidine (12.2 g), dry acetone (6 g), and toluene (100 mL) was stirred under argon for 4 days. The mixture was then acidified with 5% HCl, and the organic layer was separated and washed with saturated aqueous NaCl (3 × 50 mL), dried, and evaporated. The residue was dissolved in dichloromethane and passed through a short column of Florisil using dichloromethane as eluent. The effluent was washed with 5% KOH (4 × 50 mL), dried, and evaporated. Crystallization of the residue from ethanol gave the title compound in 65% yield; mp 90°C; ^1H nmr δ: 1.46 (6H, s), 2.72 (2H, s), 6.90–7.01 (2H, m), 7.46 (1H, d of t), and 7.85 (1H, d of d) ppm; ^{13}C nmr δ: 26.6 (2C, p), 48.8 (s), 77.6 (q), 118.3 (t), 120.3 (q), 120.6 (t), 126.5 (t), 136.1 (t), 160.0 (q), and 192.4 (q) ppm.

*5,8-Dimethoxy-2,2-dimethyl-4-chromanone (**8**)*

A mixture of 2,5-dimethoxyphenol (7 g), dihydropyran (16.5 mL), and concentrated HCl (2 drops) was stirred overnight under an argon atmosphere. Dichloromethane (100 mL) was then added, and the resulting solution washed with 10% NaOH (2 × 20 mL). The organic layer was dried and evaporated, and the residue purified by Kugelrohr distillation (120–130°C/0.7 Torr; 1 Torr = 133.3 Pa) to yield 8.7 g (82%) of 2,5-dimethoxyphenol tetrahydropyranyl ether as a colourless oil; ^1H nmr δ: 1.55–1.75 (4H, m), 1.85–2.0 (6H, m), 3.55–4.05 (8H, m and two s), 5.59 (1H, t), 6.45–6.51 (1H, m), and 6.78–6.85 (2H, m) ppm; ms *m/z*(%): 238(1.4), 180(1), 166(1), 154(100), 139(63), 125(9), 111(22), 85(24). This material was dissolved in dry THF (400 mL), and the solution was placed under an argon atmosphere and cooled to 0°C. A solution of *n*-BuLi (14 mL, 2.8 M in hexane) was then added slowly and with stirring at such a rate as to maintain the reaction temperature below 5°C. On completion of addition, the cooling bath was removed and the mixture stirred at room temperature for 2 h. The system was then cooled to −65°C and 3,3-dimethylacryloyl chloride (4.2 mL) was added slowly. The system was left to warm to ambient temperature overnight, then water (100 mL) was added. The resulting mixture was stirred for 15 min and then extracted with chloroform. The organic phase was dried and evaporated to yield a viscous oil (14 g) that was directly dissolved in chloroform (30 mL). To this solution was added dilute HCl (60 mL, 6 M), and the resulting mixture was stirred at room temperature for 2 h. The solution was then extracted with chloroform (3 × 200 mL) and the extract dried and evaporated. The residue was subjected to Kugelrohr distillation at 125–135°C/0.5 Torr to give 5,8-dimethoxy-2,2-dimethyl-4-chromanone (1.27 g). Further product was obtained by chromatography of the residue from the Kugelrohr distillation using 50–60% ethyl acetate – hexane as eluent; mp 143–145°C (from ethyl acetate); ir (KBr) ν_{max}: 1694 cm^{-1}; ^1H nmr δ: 1.50 (6H, s), 2.72 (2H, s), 3.84 and 3.87 (each 3H, s), 6.39 and 7.0 (2H, ABq) ppm; ^{13}C nmr δ: 26.3 (2C, p), 50.2 (s), 56.1 (p), 56.9 (p), 79.2 (q), 101.6 (t), 111.3 (q), 118.4 (t), 143.0 (q), 151.3 (q), 153.8 (q), 191.3 (q) ppm; ms *m/z*(%): 236(64), 221(31), 206(6), 181(58), 180(100), 165(21), 151(31), 137(54), 123(45). Anal. calcd. for $C_{13}H_{16}O_4$: C 66.09, H 6.83%; found: C 65.79, H 6.65%.

*5,8-Dimethoxy-2,2-Dimethylchroman (**10**)*

Lithium aluminum hydride (1.0 g) was added to a stirred solution of 5,8-dimethoxy-2,2-dimethyl-4-chromanone (2.7 g) in dry THF (200 mL), and resulting mixture stirred and heated under reflux for 1 h. The mixture was then cooled, ethyl acetate (5 mL) added, and the reaction mixture stirred for a further 30 min at room temperature. A saturated aqueous solution of sodium sulfate (200 mL) was then added, and the mixture extracted with chloroform (3 × 150 mL). The extract was dried and evaporated and the residue chromatographed on silica gel. Elution with 30–40% ethyl acetate – hexane gave (±)-5,8-dimethoxy-2,2-dimethyl-4-chromanol (**9**, 2.3 g, 85%), obtained as a colourless solid following crystallization from ethyl acetate – hexane; mp 99–101°C; ir (KBr) ν_{max}: 3520 cm^{-1}; ^1H nmr δ: 1.41 and 1.48 (each 3H, s), 1.95–2.15 (2H, m), 3.50 (1H, s, exchanges with D_2O), 3.81 and 3.85 (each 3H, s), 5.0 (1H, t), 6.35 and 6.74 (2H, ABq) ppm; ^{13}C nmr δ: 26.8 (p), 27.2 (p), 40.2 (s), 55.5 (p), 56.7 (p), 60.8 (t), 75.1 (q), 100.1 (t), 111.2 (t), 114.0 (q), 132.1 (q), 143.7 (q), 152.3 (q) ppm; ms m/z(%): 238(66), 205(36), 183(33), 182(100), 167(18), 153(5), 139(19), 107(11). Anal. calcd. for $C_{13}H_{18}O_4$: C 65.53, H 7.61%; found: C 65.56, H 7.80%.

Concentrated HCl (12 mL) was added to a solution of the alcohol **9** (0.44 g) in chloroform (6 mL) and the resulting mixture stirred overnight at room temperature. Water (10 mL) was then added and the mixture was extracted with chloroform (3 × 25 mL). The extract was dried and evaporated, and the residue subjected to chromatography. Elution with 30–40% ethyl acetate – hexane gave 2,2-dimethyl-5,8-dimethoxychromene (0.34 g, 84%); mp 62–64°C; ^1H nmr δ: 1.45 (6H, s), 3.76 and 3.79 (each 3H, s), 5.56 and 6.63 (2H, ABq), and 6.29 and 6.68 (2H, ABq) ppm; ms *m/z*(%): 220(25), 205(100), 190(12), 175(24), 157(6), 91(5), 77(5).

To a solution of the above olefin (0.34 g) in ethyl acetate (6 mL) was added 10% palladium/carbon catalyst (50 mg). Overnight hydrogenation using a Parr apparatus at 19 psig (1

Can. J. Chem. Downloaded from www.nrcresearchpress.com by 80.90.12.36 on 09/08/12
For personal use only.

psi = 6.9 kPa) followed by filtration and evaporation of the filtrate gave 5,8-dimethoxy-2,2-dimethylchroman (**10**, 0.31 g, 91%); mp 56–58°C; ^{1}H nmr δ: 1.38 (6H, s), 1.78 (2H, t), 2.66 (2H, t), 3.78 and 3.81 (each 3H, s), 6.29 and 6.66 (2H, ABq) ppm; ^{13}C nmr δ: 17.4 (s), 26.6 (2C, p), 32.2 (s), 55.5 (p), 56.6 (p), 74.1 (q), 99.5 (t), 109.2 (t), 111.4 (q), 120.5 (q), 143.3 (q), 151.8 (q); ms *m/z*(%): 222(100), 167(84), 166(69), 151(6), 137(21), 123(15). Anal. calcd. for $C_{13}H_{18}O_3$: C 70.24, H 8.16%; found: C 70.62%, H 7.82%.

Biotransformations of bicyclic substrates

General procedures

Two slopes of *Mortierella isabellina* ATCC 42613 were used to inoculate 15 1 L Erlenmeyer flasks each containing 200 mL of an autoclaved medium composed of glucose (40 g), soybean flour (5 g), yeast extract (5 g), sodium chloride (5 g), and dibasic potassium phosphate (5 g) per L of distilled water. The flasks were allowed to stand overnight at 27°C, then were placed on a rotary shaker at 180 rpm, and growth continued for a further 72 h at 27°C. The fungus was then harvested by centrifugation (IEC chemical centrifuge) and resuspended in 15 1 L Erlenmeyer flasks each containing 200 mL of distilled water. Substrate (1 g in 30 mL of 95% ethanol) was then distributed among the flasks, which were replaced on the rotary shaker at 180 rpm, at 27°C, for a further 72 h. The fungus and aqueous medium were then separated by filtration as before, the aqueous medium extracted with dichloromethane (continuous extraction, 72 h), and the fungus discarded. Concentration of the medium extract gave the crude product, which was examined by tlc, using ether or 10% methanol – ether as solvent, and then subjected to flash chromatography. The yields and ee values quoted below refer to purified, homogeneous material, and arise from the combination of (only) homogeneous column fractions without further purification (e.g., crystallization) that could lead to changes in stereochemical enrichment values.

*2,2-Dimethyl-4-chromanone (**4**)*

Biotransformation of **4** (1 g) by the above procedure gave the following products in order of elution. (*S*)-2,2-Dimethylchroman-4-ol (**5**, 0.78 g); ir (KBr) ν_{max}: 3353 cm^{-1}; ^{1}H nmr δ: 1.26 and 1.39 (each 3H, s), 1.71–2.11 (2H, m), 2.90 (1H, br. s, exchanges D_2O), 4.75 (1H, d of t), and 6.73–7.42 (4H, m) ppm; ^{13}C nmr δ: 25.8 (p), 26.4 (p), 42.5 (s), 63.5 (t), 75.1 (q), 117.1 (t), 120.2 (t), 124.3 (q), 127.6 (t), 128.1 (t), and 153.2 (q) ppm; ms *m/z*(%): 178(60), 145(70), 123(57), 122(100), 121(71); $[\alpha]_D$ +8.4 (*c* 2.0, chloroform); ee 40% based on integration of C*H*OH and C-5H nmr signals in the presence of Eu(tfc)$_3$. 2,2-Dimethylchroman-3-ol-4-one (**6**, 42 mg); ir (KBr) ν_{max}: 1694, 3467 cm^{-1}; ^{1}H nmr δ: 1.22 (3H, s), 1.65 (3H, s), 3.78 (1H, br s, exchanges D_2O), 4.43 (1H, s), and 6.92–7.84 (4H, m) ppm; ^{13}C nmr: 17.2 (p), 26.9 (p), 77.0 (s), 83.5 (q), 118.4 (t), 188.9 (q), 121.1 (t), 126.7 (t), 136.6 (t), 159.5 (q), 194.4 (q); ms *m/z*(%): 192(68), 178(12), 163(53), 148(17), 121(100). M$^+$ calcd. for $C_{11}H_{12}O_3$: 192.0786; found: 192.0790.

*5,8-Dimethoxy-2,2-dimethyl-4-chromanone (**8**)*

Biotransformation of **8** (0.25 g) using four 1 L Erlemeyer flasks as described above gave, following extraction and chromatography with 30–50% ethyl acetate – hexane, (*S*)-5,8-dimethoxy-2,2-dimethylchroman-4-ol (**9**, 0.25 g, 99%); mp 67–69°C; nmr and mass spectral data identical with those described above for (±)-**9**; $[\alpha]_D$ +7.5 (*c* 1.5, ethanol); ee >95% based on ^{1}H nmr analysis of the C*H*OH signal in the presence of Eu(tfc)$_3$.

*5,8-Dimethoxy-2,2-dimethylchroman (**10**)*

Exposure of **10** (0.35 g) to *M. isabellina* (2 L of culture in 10 Erlenmeyer flasks) for 72 h followed by extraction as described above gave a crude extract (0.15 g) that was subjected to chromatography using 20–60% ethyl acetate – hexane as eluent and gave, in order of elution, 5,8-dimethoxy-2,2-dimethylchroman (**10**, 50 mg); 2,2-dimethyl-5-hydroxy-8-methoxychroman (**11**, 6 mg), as an oil; ^{1}H nmr δ: 1.37 (6H, s), 1.80 (2H, t, *J* = 7 Hz), 2.65 (2H, t, *J* = 7 Hz), 3.77 (3H, s), and 6.24/6.58 (2H, ABq) ppm; ^{13}C nmr δ: 17.4 (s), 26.6 (2C, p), 32.1 (s), 56.7 (p), 74.1 (q), 104.1 (t), 110.0 (q), 110.1 (t), 143.1 (q), 144.5 (q), 147.8 (q) ppm; ms *m/z*: M$^+$ 208; an oil (33 mg), which was further purified by preparative tlc (alumina) using chloroform as eluent to give 5,8-dimethoxy-2,2-dimethylchroman-4-ol (**9**, 5 mg), identified by spectral comparisons with authentic material; $[\alpha]_D$ 0; and 5,8-dimethoxy-2,2-dimethyl-6-hydroxychroman (**12**, 10 mg), as an oil; ^{1}H nmr δ: 1.35 (6H, s), 1.76 (2H, t, *J* = 7 Hz), 2.74 (2H, t *J* = 7 Hz), 3.74 and 3.77 (each 3H, s), and 6.43 (1H, s) ppm; ^{13}C nmr δ: 17.8 (s), 26.6 (2C, p), 32.2 (s), 56.2 (p), 60.8 (p), 73.6 (q), 98.2 (t), 115.5 (q), 137.0 (q), 137.4 (q), 140.8 (q), and 145.6 (q) ppm; ms *m/z*: M$^+$ 238.

Synthesis of 6,7-benzo-2,2-dimethyl-8-methoxy-4-chromanone (**13**)

A solution of 1-methoxy-2-naphthol (12) (6.26 g) and *p*-toluenesulfonic acid (0.1 g) in dichloromethane (80 mL) containing dimethoxymethane (25 mL) was heated under reflux (argon atmosphere) overnight in an apparatus fitted with a Soxhlet apparatus containing 40 g of activated 3 Å molecular sieves. The mixture was then cooled, triethylamine (1 mL) added, and the resulting solution washed (2 × 10% aqueous sodium hydroxide followed by saturated NaCl), dried, and evaporated. The residue was passed through a column of silica gel using 2% ethyl acetate – hexane as eluent to give 4.85 g (63%) of 1-methoxy-2-(methoxymethoxy)-naphthalene as a pale yellow oil; ^{1}H nmr δ: 3.53 (3H, s), 3.99 (3H, s), 5.27 (2H, s), 7.4–8.1 (6H, m) ppm; ^{13}C nmr δ: 58.2 (p), 61.1 (p), 96.0 (s), 116.7 (t), 121.4 (t), 124.1 (t), 124.5 (t), 126.0 (t), 127.6 (t), 129.0 (q), 130.6 (q), 144.0 (q), 145.0 (q) ppm; ms *m/z*(%): 218(100), 188(24), 173(71), 145(37), 127(33). M$^+$ calcd. for $C_{13}H_{14}O_3$: 218.0943; found: 218.0941.

A solution of *tert*-butyllithium (8.2 mL, 1.4 M in pentane) was added slowly to a stirred solution of 1-methoxy-2-(methoxymethoxy)-naphthalene (2.0 g) in dry THF (30 mL) under an argon atmosphere at −80°C. The resulting green solution was allowed to reach room temperature, stirred at that temperature for 1 h, and then recooled to −80°C. Upon slow addition of 3,3-dimethylacryolyl chloride (1.4 mL), the reaction mixture became pale yellow. The reaction was stirred overnight at room temperature, and then worked up by addition of aqueous THF and extraction with chloroform. The organic extract was washed with 10% aqueous sodium hydroxide, saturated sodium bicarbonate solution, and saturated sodium chloride, and then dried and evaporated. Chromatography (silica gel, 30% ethyl acetate – hexane) afforded 1.7 g (60%) of 3-(3′,3′-

Can. J. Chem. Downloaded from www.nrcresearchpress.com by 80.90.12.36 on 09/08/12
For personal use only.

dimethylacryloyl)-1-methoxy-2-(methoxymethoxy)-naphthalene as a pale yellow oil; ^{1}H nmr δ: 2.01 (3H, s), 2.26 (3H, s), 3.52 (3H, s), 4.04 (3H, s), 5.18 (2H, s), 6.68 (1H, t), and 7.5–8.1 (5H, m) ppm; ms *m/z*(%): 300(21), 285(9), 256(26), 200(34) relative to 83(100). M^+ calcd. for $C_{18}H_{20}O_3$: 300.1362; found: 300.1386.

The above compound (4.32 g) was dissolved in a mixture of THF (90 mL) and 6 M sulfuric acid (10 mL) and the resulting solution refluxed overnight. The solution was then cooled, neutralized by addition of 5% aqueous sodium hydroxide solution, and the resulting mixture extracted with chloroform. The extract was washed with saturated sodium bicarbonate solution, dried, and evaporated to give a residue that, following chromatography, afforded 6,7-benzo-2,2-dimethyl-8-methoxy-4-chromanone (**13**, 3.35 g, 91%); mp 94–95.5°C from ethyl acetate – hexane; ^{1}H nmr δ: 1.55 (6H, s), 2.85 (2H, s), 4.03 (3H, s), 7.36 (1H, t), 7.54 (1H, t), 7.67 (1H, d), 8.08 (1H, d), and 8.28 (1H, s) ppm; ^{13}C nmr δ: 27.0 (2C, p), 49.7 (s), 61.0 (p), 70.0 (q), 121.3 (t), 122.0 (t), 123.0 (t), 124.7 (t), 126.1 (q), 126.6 (t), 130.0 (t), 132.6 (q), 142.5 (q), 146.2 (q), and 193.0 (q) ppm; ms *m/z*(%): 256(100), 241(16), 201(49), 200(64), 185(25), 157(44). M^+ calcd. for $C_{16}H_{16}O_3$: 256.1099; found: 256.1119. Anal. calcd. for $C_{16}H_{16}O_3$: C 74.98, H 6.29%; found: C 74.61, H 6.60%.

Biotransformation of 6,7-benzo-2,2-dimethyl-8-methoxy-4-chromanone (13)

Using a 72 h growth of *M. isabellina* (600 mL of culture in three 1 L Erlenmeyer flasks), the title ketone (0.18 g) was converted to (*S*)-6,7-benzo-2,2-dimethyl-8-methoxychroman-4-ol (**14**, 35 mg), isolated as an oil by chromatography on silica gel using a 2% ether – benzene stepwise gradient elution; ^{1}H nmr δ: 1.36 (3H, s), 1.53 (3H, s), 1.92 and 2.24 (each 1H, dd), 2.4 (1H, br. s, exchanges D_2O), 3.95 (3H, s), 5.02 (1H, t), 7.36 (2H, m), 7.69 (1H, d), 7.73 (1H, s), and 8.04 (1H, d) ppm; ^{13}C nmr δ: 25.9 (p), 29.4 (p), 42.8 (s), 60.7 (p), 64.1 (t), 75.8 (q), 120.9 (t), 121.5 (t), 123.7 (t), 125.9 (t), 127.6 (t), 128.0 (q), 128.4 (q), 128.6 (q), 141.4 (q), and 142.8 (q) ppm; ms *m/z*(%): 258(46), 240(60), 225(100), 210(30), 202(81), 187(55). M^+ calcd. for $C_{16}H_{18}O_3$: 258.1256; found: 258.1270; $[\alpha]_D$ +24.8 (*c* 0.5, ethanol), ee 32% based on ^{1}H nmr analysis of the C*H*OH signal in the presence of Eu(tfc)$_3$. Also obtained from chromatography was a pale green oily material (11 mg) tentatively identified as a phenolic derivative of **14** by the following spectral data: ^{1}H nmr δ: 1.33 (3H, s), 1.51 (3H, s), 1.9 and 2.2 (each 1H, dd), 3.92 (3H, s), 4.95 (1H, t), 6.31 (1H, br. s, exchanges D_2O), 6.94 (1H, s), 7.03 and 7.88 (2H, ABq), and 7.41 (1H, s) ppm; ms *m/z*(%): 274(2), 256(10), 241(9), 226(4) relative to 83(100). Lack of material and instability of the product precluded further analysis.

Synthesis of 4-hydroxy-α-lapachone

4-Keto-α-lapachone (15)

A solution of 6,7-benzo-2,2-dimethyl-8-methoxy-4-chromanone (**13**, 0.2 g) in acetonitrile (2 mL) was cooled to 0°C and then a solution of ceric ammonium nitrate (2.18 g) in water (10 mL) was added at 0°C over a period of 5 min. The mixture was stirred for a further 30 min at 0°C, water (20 mL) was added, and the resulting solution was extracted with chloroform. The extract was dried and concentrated to a volume of 30 mL. The resulting solution was then aerated and refluxed for 24 h. After this period the cooled solution was washed (saturated aqueous sodium bicarbonate), dried, and evaporated. Chromatography of the residue gave 4-keto-α-lapachone (**15**, 0.11 g, 57%) as a yellow solid, mp 161–164°C (from benzene–hexane) (lit. (2) mp 163–165°C); ir ν_{max}: 1689, 1714 cm^{-1}; ^{1}H nmr δ: 1.62 (6H, s), 2.77 (2H, s), 7.76 (2H, m), and 8.10 (2H, m) ppm; ^{13}C nmr δ: 26.1 (2C, p), 48.7 (s), 84.4 (q), 112.9 (q), 126.3 (t), 127.0 (t), 130.8 (q), 132.0 (q), 133.3 (t), 135.4 (t), 162.4 (q), 180.0 (q), 180.6 (q), and 189.7 (q) ppm; ms *m/z*(%): 256 (73), 201 (98), 173(47), 104(100).

(S)-4-Hydroxy-α-lapachone (3)

Biotransformation of the ketone **15** (0.41 g) with a culture of *M. isabellina* in eight 1 L Erlenmeyer flasks as outlined above, followed by chromatography of the extract, gave (*S*)-4-hydroxy-α-lapachone (**3**, 0.2 g, 49%) as a yellow solid, mp 67°C (lit. (2) yellow syrup (*S*); (6) mp 117–119°C (racemate); (7) yellow oil (racemate); (4) yellow oil (*S*);); ir ν_{max}: 1645, 1683, 3505 cm^{-1}; ^{1}H nmr δ: 1.44 (3H, s), 1.55 (3H, s), 2.08 (2H, dd), 3.80 (1H, br s, exchanges D_2O), 4.97 (1H, t), 7.70 (2H, m), and 8.08 (2H, m) ppm; ^{13}C nmr δ: 26.7 (p), 27.1 (p), 39.6 (s), 60.0 (t), 79.8 (q), 120.4 (q), 126.0 (t), 126.6 (t), 131.2 (q), 131.9 (q), 133.4 (t), 134.3 (t), 154.1 (q), 180.1 (q), and 186.1 (q) ppm; ms *m/z*(%): 258(24), 243(10), 203(93), 176(69), 146(87), 105(50), 83(100). M^+ calcd. for $C_{15}H_{14}O_4$: 258.0892; found: 258.0888. $[\alpha]_D$ +39.7 (*c* 1.3, methanol) (lit. (2) $[\alpha]_D$ +27.4 (methanol)), ee >95% by ^{1}H nmr analysis of the C*H*OH signal in the presence of Eu(tfc)$_3$.

(S)-4-Acetoxy-α-lapachone (16)

Acetic anhydride (1 mL) was added to a solution of (*S*)-4-hydroxy-α-lapachone (**3**, 0.071 g) in dry pyridine (2 mL) and the mixture allowed to stand overnight at room temperature. The usual work-up afforded a yellow residue that, on chromatography, afforded (*S*)-4-acetoxy-α-lapachone (**16**, 0.08 g, 97%). Crystallization from ethanol gave a pale yellow solid, mp 145–148.5°C (lit. (6) mp 136–138°C (racemate); (7) mp 138.5–139.5°C (racemate); (4) mp 118–120°C (*S*); (2) mp 139.5–140.5°C (*S*)); ir ν_{max}: 1616, 1651, 1683, 1739, 2931, 2979 cm^{-1}; ^{1}H nmr δ: 1.51 (3H, s), 1.56 (3H, s), 2.15 (5H, s + m), 6.10 (1H, dd), 7.72 (2H, m), and 8.10 (2H, m) ppm; ^{13}C nmr δ: 21.0 (p), 25.4 (p), 28.8 (p), 38.1 (s), 60.6 (t), 78.7 (q), 116.7 (q), 126.3 (t), 131.1 (q), 132.0 (q), 133.2 (t), 134.4 (t), 155.8 (q), 170.0 (q), 179.9 (q), and 182.7 (q) ppm; ms *m/z*(%): 300(0.6), 258(100), 243(12), 225(9), 201(71). M^+ calcd. for $C_{16}H_{16}O_5$: 300.0998; found: 300.1004. $[\alpha]_D$ −22.7 (*c* 1.3, methanol) (lit. (2) $[\alpha]_D$ −14.2 (*c* = 1.03, methanol)).

Acknowledgements

We are grateful to Mr. T. Jones (Brock University) for the mass spectral data, and to Dr. D.W. Hughes (McMaster University, Hamilton, Ontario, Canada), for the 500 MHz ^{1}H NMR spectra. Financial support was provided by the Natural Sciences and Engineering Research Council of Canada.

References

1. H.L. Holland, T.S. Manoharan, and F. Schweizer. Tetrahedron: Asymmetry, **2**, 335 (1991); Preparative biotransformations, module 2:4.1. *Edited by* S.M. Roberts. J. Wiley, Chichester. 1992.

2. H. Inouye, T. Okuda, and T. Hayashi. Chem. Pharm. Bull. **23**, 384 (1975).
3. S. Ueda, K. Inoue, Y. Shiobara, I. Kimura, and H. Inouye. Planta Med. **40**, 168 (1980).
4. M.L. Duarte Weinberg, O.R. Gottlieb, and G.G. De Oliveira. Phytochemistry, **15**, 570 (1976).
5. R.B. Gupta and R.N. Khanna. Curr. Sci. **46**, 337 (1977).
6. R.B. Gupta and R.N. Khanna. Ind. J. Chem. (B), **16**, 35 (1978).
7. C. Saitz B., J.A. Valderrama, R. Tapia, F. Farina, and M.C. Paredes. Synth. Commun. **22**, 955 (1992).
8. J.W. ApSimon, L.W. Herman, and C. Huber. Can. J. Chem. **63**, 2589 (1985).
9. V. Prelog. Pure Appl. Chem. **9**, 119 (1964).
10. H.L. Holland, E.J. Bergen, P.C. Chenchaiah, S.H. Khan, B. Munoz, R.W. Ninniss, and D. Richards. Can. J. Chem. **65**, 502 (1987).
11. H.L. Holland, F.M. Brown, B. Munoz, and R.W. Ninniss. J. Chem. Soc. Perkin Trans. 2, 1557 (1988).
12. F.R. Hewgill and B.S. Middleton. J. Chem. Soc. (C), 2316 (1967).

Can. J. Chem. Downloaded from www.nrcresearchpress.com by 80.90.12.36 on 09/08/12
For personal use only.

Association between halothane and oxygenated solvents by ^{1}H NMR spectroscopy

Marcela Tkadlecová, Jaroslav Havlíček, and Vladimír Dohnal

Abstract: Using ^{1}H NMR spectroscopy the complex-formation equilibria between halothane (2-bromo-2-chloro-1,1,1-trifluoroethane) and methyl *tert*-butyl ether or tetrahydrofuran in various inert solvents (hexane, heptane, decane, cyclohexane) were measured as a function of temperature. For two different association models (ideal solution and athermal solution), assuming only the formation of a 1:1 H-bonded complex, the equilibrium constants and the standard enthalpies of the complex-formation reaction were calculated. The ideal solution model provides values of the equilibrium constant that differ for different inert solvents. The athermal solution model makes this false solvent effect much smaller. For the low halothane concentration used, its dimerization was neglected. This assumption was verified experimentally.

Key words: ^{1}H NMR, association, complex formation, halothane.

Résumé : Utilisant la spectroscopie RMN du ^{1}H, on a mesuré l'influence de la température sur l'équilibre de formation de complexes entre l'halothane (2-bromo-2-chloro-1,1,1-trifluoroéthane) et l'oxyde de méthyle et de *tert*-butyle ou le tétrahydrofurane, dans divers solvents inertes (hexane, heptane, décane, cyclohexane). On a calculé les enthalpies standard de la réaction de formation des complexes pour deux modèles différents d'associations (solutions idéales et athermales) ne supposant que la formation de complexes 1 : 1 par liaisons hydrogènes. Les valeurs de la constante d'équilibre obtenues à l'aide du modèle de la solution idéale diffèrent pour chacun des solvants inertes. Le modèle de la solution athermale conduit à un faux effet de solvant qui est beaucoup plus faible. Pour les faibles concentrations d'halothane utilisées, on a négligé sa dimérisation. On a vérifié cette hypothèse expérimentalement.

Mots clés : RMN du ^{1}H, association, formation de complexes, halothane.

[Traduit par la rédaction]

1. Introduction

Due to the highly acidic hydrogen atom in the molecule of 2-bromo-2-chloro-1,1,1-trifluoroethane (halothane) a strong complexation via hydrogen bonding occurs when this bromofreon is mixed with efficient proton acceptors, such as oxygenated solvents. We have studied this interesting class of systems within a broader long-term project on haloalkane-containingmixtures. Recently, we reported extensive thermodynamic data (vapor–liquid equilibria (1), excess enthalpies (2), excess heat capacities (3), excess volumes (3)) for mixtures of halothane with oxygenated solvents, documenting the governing effect of complex formation on thermodynamic solution properties. Using several association models, a detailed analysis of the data has been carried out (4) for halothane + methyl-*tert*-butyl ether, + tetrahydrofuran, + 2-propanone, and + methyl acetate and quantitative information concerning the degree of complexation and stability of the complexes has been obtained. For these systems, a very good simultaneous description of vapor–liquid equilibria and thermal properties has been achieved by simple association models, the resulting solvation enthalpies agreeing well with the results obtained by quantum mechanical calculations.

^{1}H NMR spectroscopy provides an alternative technique for studing complex formation. Since the work on association in the systems of chloroform with acetone or triethylamine (5) appeared, ^{1}H NMR has often been applied to the study of association phenomena. Self-association has been studied in alcohols (6, 7) and simple organic acids (8–11) as well as in complex organic molecules (12, 13). Hetero-association has been investigated in systems of phenol with oxygenated solvents (14, 15), amides (14), fluoroalkanes (16), and in systems of acetonitrile with amides (17, 18). Solvent effects in these measurements have been observed and discussed (10, 14).

In this work, ^{1}H NMR spectroscopy was employed to measure complex formation between halothane and methyl *tert*-butyl ether (MTBE) or tetrahydrofuran (THF) in several inert solvents. The values of the equilibrium constants and the standard enthalpies of complex formation obtained were compared with those derived from thermodynamic measurements.

Received December 14, 1994.

M. Tkadlecová[1] and J. Havlíček. Department of Analytical Chemistry, Institute of Chemical Technology, 166 28 Prague 6, Czech Republic.
V. Dohnal. Department of Physical Chemistry, Institute of Chemical Technology, 166 28 Prague 6, Czech Republic.

[1] Author to whom correspondence may be addressed. Telephone: (+42 2) 3115772. Fax: (+42 2) 24310273. E-mail: Marcela. Tkadlecova@vscht.cz

Can. J. Chem. Downloaded from www.nrcresearchpress.com by 80.90.12.36 on 09/08/12
For personal use only.

Can. J. Chem. Downloaded from www.nrcresearchpress.com by 80.90.12.36 on 09/08/12
For personal use only.

Experimental

Materials

Halothane (Spofa Praha, >99.9% stabilized with 0.01 mass % of thymol), hexane, heptane, and cyclohexane (all Lachema Brno, p.a.) were used after distillation and drying with molecular sieves. MTBE (Fluka, 99.5%) and THF (Aldrich, HPLC grade, 99.9%) were used without purification. Decane (Aldrich, 99%) was dried with molecular sieves.

Instrumentation

A Varian NMR spectrometer, model Gemini 300 HC, with a variable-temperature accessory was used, the working frequency being 300.075 MHz. The homogeneity of the magnetic field was adjusted on a sample tube with deuterated acetone and then the measurements were performed without lock. Like the acetone sample, all measured samples had similar volumes of about 1 mL to maintain the field homogeneity. Each sample was measured three times with four scans and pulse width 6° after the initial 10 min temperature equilibration.

The ^{1}H NMR signal of halothane is a quartet due to ^{1}H–^{19}F coupling (coupling constant 5.2 Hz). Its chemical shift was referenced to the signal of an inert solvent. To justify such referencing, tetramethylsilane was added to some samples after the difference between the chemical shift of halothane and that of inert solvent was measured. It was observed that the chemical shifts of inert solvent and oxygenated solvent are independent of sample composition; only the chemical shift of halothane changes due to the association. The reproducibility of the measured chemical shift differences was ±0.5 Hz. The temperature of the sample, stable within ±0.1 K, was calibrated by means of methanol or ethylene glycol temperature calibration set.

Sample preparation

For each system (halothane + MTBE or + THF in various inert solvents) 10 samples were prepared directly in the sample tubes by means of weighing, from the following stock solutions: (*a*) mixture of halothane in inert solvent, (*b*) mixture of oxygenated solvent in inert solvent (samples 2–6) or pure oxygenated solvent (samples 7–10), and (*c*) inert solvent (not used for samples 6 and 10). Relatively large sample volumes (1 mL) were used in order to minimize the volume of the vapor phase and to decrease the influence of inaccuracy in weighing.

Let x_A^0 and x_B^0 stand for the analytical mole fractions of halothane and oxygenated solvent, respectively. In all samples prepared, x_A^0 were similar and less than 0.05 to suppress the effect of possible halothane dimerization. For such low concentrations of halothane in our samples the self-association of halothane was neglected (see also discussion). The chemical shift measured for sample 1 (halothane in inert solvent without MTBE or THF) was considered to be the chemical shift of the monomeric halothane. The mole fraction x_B^0 of MTBE or THF in the prepared samples increased approximately in the following sequence: 0, 0.007, 0.015, 0.03, 0.05, 0.07, 0.15, 0.30, 0.50, 0.75, to obtain roughly constant increments in the chemical shift difference measured.

Procedure

Assuming only 1:1 complex formation between halothane and oxygenated solvent (4), the observed chemical shift of halothane δ_{obs} is given as the weighted arithmetic mean of the shift corresponding to the proton in the uncomplexed form δ_A and that corresponding to the proton in the complexed form δ_{AB}

$$\delta_{obs} = \frac{n_A^0 - n_{AB}}{n_A^0}\,\delta_A + \frac{n_{AB}}{n_A^0}\,\delta_{AB}$$

where n_A^0 is the analytical molar amount of halothane and n_{AB} is the molar amount of the complex in equilibrium. The value of δ_A is obtained for sample 1 (mixture of halothane and inert solvent without oxygenated solvent). Then,

$$\Delta\delta_{obs} = \delta_{obs} - \delta_A = \frac{n_{AB}}{n_A^0}\,(\delta_{AB} - \delta_A) = \frac{n_{AB}}{n_A^0}\,D$$

where D is the difference between the chemical shifts δ_{AB} and δ_A. Thus, nine $\Delta\delta_{obs}$ values corresponding to the compositions of samples 2–10 were obtained for each system at a given constant temperature. To analyze these experimental data, i.e., to calculate the equilibrium constant of complex formation, two simple association models were used.

Ideal association model

The simplest model assumes that the mixture of true species (A, B, AB) forms an ideal solution. The equilibrium constant for the complex-formation reaction (A + B → AB) in terms of mole fractions can be expressed as follows

$$K = \frac{x_{AB}}{x_A x_B} = \frac{n_{AB}(n_A^0 + n_B^0 + n_I - n_{AB})}{(n_A^0 - n_{AB})(n_B^0 - n_{AB})}$$

where n_B^0 and n_I are the added molar amounts of the oxygenated and the inert solvent, respectively.

Athermal association model

In this model, the mixture of true species is considered to be nonideal, its nonideality originating solely from differences in species sizes. The Flory–Huggins expression employed to describe the activity coefficients of the species involved (i = A, B, AB) is

$$\gamma_i = \frac{\Phi_i}{x_i}\,\exp\left(1 - \frac{\Phi_i}{x_i}\right)$$

where Φ_i are the volume fractions of true species

$$\Phi_i = \frac{r_i n_i}{\sum_j r_j n_j}$$

r_j being the size parameter of the j-species. The van der Waals volumes normalized by Abrams and Prausnitz (19) were used as the size parameters in this work (halothane 3.5682, MTBE 4.0678, THF 2.9415, hexane 4.4998, heptane 5.1742, decane 7.1974, cyclohexane 4.0464). Under the assumption $r_{AB} = r_A + r_B$, the equilibrium constant can be expressed as follows:

$$K = \frac{x_{AB}}{x_A x_B} \times \frac{\gamma_{AB}}{\gamma_A \gamma_B} = \frac{r_A + r_B}{r_A r_B} \times \frac{n_{AB}(r_A n_A^0 + r_B n_B^0 + r_I n_I)}{(n_A^0 - n_{AB})(n_B^0 - n_{AB})} e^{-1}$$

To estimate the values of parameters K and D for a given model, an objective function must be minimized. The objective function considered here assumes equal standard deviations at all points and is given by the sum of the squares of differences between calculated and experimental values of quantity $\Delta\delta_{obs}$. The best parameters were calculated by means of an optimization procedure based on the method of conjugate gradients (20).

For the ideal association model approximate values of parameters K and D can also be calculated according to Nakano et al. (14). Their linearized formula, derived for the equilibrium constant expressed in terms of molarities, was modified for the equilibrium constant expressed in terms of mole fractions as follows

$$\frac{n_B^0}{n_I \Delta\delta_{obs}} = \frac{K+1}{KD} \times \frac{n_A^0 + n_B^0 - n_{AB}}{n_I} + \frac{1}{KD}$$

The iteration starts with $n_{AB} = 0$ in all points. Using linear regression the values of parameters K and D and then new values of n_{AB} at each point are calculated, until the values of K and D are constant.

Nakano's iterative method converges very quickly, but its estimates are not well justified statistically. They provided, however, a good initial approximation for calculating the best values of parameters by minimizing the objective function mentioned above. For the athermal association model the optimization started with parameters found for the ideal association model.

Results

For all systems, the measurements were carried out at three temperatures: approximately 297, 303, and 310 K. The association in the system of halothane with MTBE was measured in four inert solvents: hexane, decane, heptane (two measurements), and cyclohexane (two measurements). For duplicate measurements newly prepared samples were used. The reproducibility, as judged by the differences in calculated values of K and D for the replicates, is for heptane fully comparable with the uncertainties of the determination, $\sigma(K)$ and $\sigma(D)$, but for cyclohexane is somewhat worse. Therefore, cyclohexane was not used in the measurements on halothane with THF.

The optimized values of K and D with their standard deviations and the standard deviation of fit are given for each system and temperature in Table 1 (ideal association model) and Table 2 (athermal association model). Using the values of K at three different temperatures of each system the value of ΔH with its standard deviation for each system was calculated from the van't Hoff equation.

The van't Hoff plots are shown for the ideal association model and the athermal association model in Figs. 1 and 2, respectively. In both figures, the results inferred previously from thermodynamic measurements (4) are plotted for comparison (solid lines). Dotted lines in Fig. 2 represent the van't Hoff plots, obtained for the system of halothane with MTBE or THF by averaging the $K_{298.15}$, ΔH values from measurements in different inert solvents. The parameters $K_{298.15}$, ΔH of these straight lines are given in Table 3.

Discussion

Comparison of models used

From a comparison of Figs. 1 and 2 it is clear that the ideal association model produces a false solvent effect. The optimized values of K decrease and the values of D increase in the following order of inert solvents: cyclohexane, hexane, heptane, and decane, the pattern being the same for systems with MTBE and THF (cyclohexane was not used for systems with THF). The athermal association model makes the differences between individual inert solvents used significantly smaller and more random, which can easily be seen qualitatively from the comparison of Figs. 1 and 2 and quantitatively from comparison of Tables 1 and 2.

Using the athermal association model, the range of K values obtained for different solvents at a given temperature decreased 5 times for systems with MTBE and 8 times for systems with THF as compared with the ideal association model. The parameter D should be temperature independent; its variation decreased 4 times for MTBE and 5 times for THF. There was also some improvement in the variation of ΔH values: 1.5 times for MTBE and 2 times for THF. The standard deviation of fit did not change significantly with the use of the athermal association model. Also, the differences in values of correlation coefficients for the van't Hoff plots between the two models used were insignificant. These values were mostly greater than 0.999 and never less than 0.993.

Let us stress that the better performance of the athermal association model has not been achieved by increasing the number of fitted parameters. The adjustable parameters are the same as in the ideal association model, i.e., K and D. However, it turns out that the parameters evaluated for the model of athermal association have a better physical significance than those obtained for ideal association model.

Comparison with results from thermodynamics

The aim of this work was to compare the results from ^{1}H NMR measurements with those calculated from thermodynamic measurements. For this purpose, the values of $K_{298.15}$ and ΔH obtained from the NMR measurements in different inert solvents were averaged, and calculated average values are listed in Table 3 together with the results from ref. 4. The comparison is given for the athermal association model, which performed better both on the spectroscopic (better physical significance of the evaluated parameters) and the thermodynamic data (significantly smaller standard deviation of fit).

As can be seen from Table 3 the agreement between the association parameters derived from spectroscopy and from thermodynamics is qualitative rather than quantitative. The qualitative agreement consists in the fact that, for the system halothane + THF, both the spectroscopic and the thermodynamic measurements imply a higher degree of complexation (higher $K_{298.15}$) and a lower stability of the respective com-

Can. J. Chem. Downloaded from www.nrcresearchpress.com by 80.90.12.36 on 09/08/12
For personal use only.

Can. J. Chem. Downloaded from www.nrcresearchpress.com by 80.90.12.36 on 09/08/12
For personal use only.

Table 1. Ideal association model: optimized parameters K, D, standard deviation of fit σ, and calculated ΔH values.

Halothane +	T (K)	$K \pm \sigma(K)$	$D \pm \sigma(D)$ (Hz)	σ (Hz)	$\Delta H \pm \sigma(\Delta H)$ (kJ/mol)
MTBE	296.95	4.58 ± 0.17	371.8 ± 5.1	2.5	
In heptane	302.65	4.00 ± 0.09	377.0 ± 3.4	1.5	−14.6 ± 1.5
I	309.35	3.61 ± 0.07	369.9 ± 2.9	1.2	
MTBE	296.85	4.53 ± 0.05	376.9 ± 1.5	0.8	
In heptane	302.75	4.03 ± 0.05	377.3 ± 1.6	0.8	−16.3 ± 0.7
II	309.85	3.44 ± 0.06	383.1 ± 2.7	1.1	
MTBE	297.15	6.45 ± 0.12	355.5 ± 2.2	1.3	
In cyclohexane	303.15	5.55 ± 0.07	353.8 ± 1.6	0.8	−15.6 ± 1.7
I	310.15	4.95 ± 0.07	350.5 ± 1.8	0.9	
MTBE	297.45	6.64 ± 0.22	356.1 ± 3.5	2.3	
In cyclohexane	303.75	5.91 ± 0.18	354.2 ± 3.3	2.0	−15.2 ± 0.2
II	310.05	5.18 ± 0.09	351.1 ± 2.1	1.2	
MTBE	297.45	5.15 ± 0.12	368.2 ± 3.0	1.7	
In hexane	303.95	4.54 ± 0.12	369.2 ± 3.3	1.7	−13.6 ± 0.6
	311.55	4.02 ± 0.07	366.7 ± 2.5	1.1	
MTBE	298.15	3.34 ± 0.12	401.7 ± 5.1	2.2	
In decane	303.55	2.94 ± 0.10	405.2 ± 5.1	2.0	−16.8 ± 0.6
	309.65	2.56 ± 0.10	409.2 ± 6.1	2.0	
THF	296.95	5.11 ± 0.09	376.2 ± 2.1	1.4	
In heptane	302.65	4.63 ± 0.07	375.2 ± 1.9	1.2	−14.3 ± 0.7
	309.35	4.05 ± 0.06	379.4 ± 1.9	1.1	
THF	297.95	6.12 ± 0.16	363.3 ± 2.9	2.1	
In hexane	303.35	5.53 ± 0.14	365.0 ± 3.0	2.1	−14.2 ± 0.1
	309.65	4.94 ± 0.13	364.4 ± 3.2	2.0	
THF	297.95	3.63 ± 0.08	400.2 ± 3.2	1.7	
In decane	303.25	3.22 ± 0.08	404.7 ± 3.7	1.8	−16.8 ± 0.03
	309.75	2.80 ± 0.07	409.9 ± 3.9	1.7	

plex (less negative ΔH) than for halothane + MTBE. The quantitative agreement is, however, less specific.

For an exact quantitative comparison, it should be considered that the athermal association model in ref. 4 was applied with equal van der Waals volumes of the nominal components ($r_A = r_B$). If the same simplification, such as in ref. 4, is used, the values of $K_{298.15}$ from spectroscopy are about 10% greater for MTBE and 10% smaller for THF as compared to the values in Table 3. Then, the quantitative comparison of $K_{298.15}$ is as follows: the values from spectroscopy are roughly 1.5 times higher than those from thermodynamics both for MTBE and for THF, the relative difference between MTBE and THF being kept the same (15%). The spectroscopic and thermodynamic values of ΔH agree within about 1.5 kJ/mol, the former being more negative.

The lack of quantitative agreement might be caused by different experimental conditions in the two types of measurements; when compared to the thermodynamic measurements, the NMR data were obtained in the presence of an inert solvent and at much lower halothane concentrations.

The observed systematic differences between individual inert solvents and the effort to eliminate this false solvent effect enabled us to choose the better model from the two association models used. Although the chosen athermal association model diminished the solvent effect significantly, it can hardly be considered fully realistic, since it accounts only for molecular size differences while all non-chemical interactions are neglected.

To judge the influence of the different concentration ranges for which the experimental data were obtained (i.e., $x_A^0 < 0.05$ for the NMR measurements and the whole composition range for the thermodynamic measurements), the extent of halothane dimerization was explored.

Dimerization of halothane

In all calculations above, the dimerization of halothane was neglected. This essential assumption was verified as follows:

(*a*) For five dilute solutions of halothane in hexane with x_A^0 uniformly covering a range from 0.01 to 0.05, the chemical shift of halothane was measured and extrapolated to $x_A^0 = 0$. The value of the chemical shift of the monomeric halothane, $\delta_A = 1688.0 \pm 0.3$ Hz (5.6253 ± 0.0010 ppm) obtained in this way at 297.85 K is 1.5 Hz smaller than the chemical shift of halothane measured for sample 1 with hexane as inert solvent. This difference is small and should be suppressed by referencing the measured chemical shift of halothane for the

Can. J. Chem. Downloaded from www.nrcresearchpress.com by 80.90.12.36 on 09/08/12
For personal use only.

Table 2. Athermal association model: optimized parameters K, D, standard deviation of fit σ, and calculated ΔH values.

Halothane +	T (K)	$K \pm \sigma(K)$	$D \pm \sigma(D)$ (Hz)	σ (Hz)	$\Delta H \pm \sigma(\Delta H)$ (kJ/mol)
MTBE	296.95	4.78 ± 0.16	357.1 ± 4.1	2.4	
In heptane	302.65	4.21 ± 0.08	359.7 ± 2.6	1.4	−13.9 ± 1.4
I	309.35	3.81 ± 0.07	351.1 ± 2.3	1.1	
MTBE	296.85	4.73 ± 0.04	361.7 ± 1.1	0.7	
In heptane	302.75	4.23 ± 0.04	360.1 ± 1.2	0.7	−15.5 ± 0.6
II	309.85	3.64 ± 0.06	362.8 ± 2.0	1.0	
MTBE	297.15	5.01 ± 0.08	359.8 ± 1.9	1.1	
In cyclohexane	303.15	4.30 ± 0.05	358.7 ± 1.5	0.8	−15.8 ± 1.8
I	310.15	3.83 ± 0.06	355.8 ± 2.0	0.9	
MTBE	297.45	5.20 ± 0.15	358.5 ± 3.2	2.0	
In cyclohexane	303.75	4.62 ± 0.12	356.8 ± 3.0	1.8	−15.3 ± 0.2
II	310.05	4.04 ± 0.06	354.0 ± 1.7	0.9	
MTBE	297.45	4.57 ± 0.09	363.4 ± 3.0	1.5	
In hexane	303.95	4.03 ± 0.09	363.6 ± 2.8	1.5	−13.4 ± 0.6
	311.55	3.57 ± 0.06	360.4 ± 2.2	1.1	
MTBE	298.15	5.24 ± 0.17	355.6 ± 3.2	2.2	
In decane	303.55	4.68 ± 0.14	353.1 ± 3.0	2.0	−14.6 ± 0.6
	309.65	4.16 ± 0.14	350.0 ± 3.4	2.0	
THF	296.95	6.60 ± 0.10	347.1 ± 1.5	1.3	
In heptane	302.65	6.02 ± 0.08	343.3 ± 1.3	1.2	−13.1 ± 0.6
	309.35	5.33 ± 0.07	343.1 ± 1.3	1.1	
THF	297.95	6.72 ± 0.16	345.2 ± 2.2	2.0	
In hexane	303.35	6.10 ± 0.14	343.8 ± 2.2	1.9	−13.4 ± 0.1
	309.65	5.48 ± 0.13	340.9 ± 2.3	1.9	
THF	297.95	6.95 ± 0.13	343.7 ± 1.9	1.8	
In decane	303.25	6.28 ± 0.13	341.4 ± 2.0	1.8	−14.2 ± 0.1
	309.75	5.59 ± 0.11	337.9 ± 2.0	1.7	

Table 3. Comparison of $K_{298.15}$, ΔH values obtained for the system halothane + MTBE or THF in this work (NMR) and from thermodynamic measurements (TD).

	NMR		TD	
Halothane +	$K_{298.15} \pm \sigma(K)$	$\Delta H \pm \sigma(\Delta H)$ (kJ/mol)	$K_{298.15} \pm \sigma(K)$	$\Delta H \pm \sigma(\Delta H)$ (kJ/mol)
MTBE	4.83 ± 0.12	−14.8 ± 0.4	3.26 ± 0.01	−13.6 ± 0.3
THF	6.70 ± 0.13	−13.5 ± 0.3	3.67 ± 0.02	−11.8 ± 0.2

individual sample to the sample 1. The temperature dependence of the chemical shift of halothane in sample 1 was found to be insignificant. The differences in the measured chemical shifts of halothane in individual inert solvents for sample 1 are also small (within ±1.5 Hz from the signal of halothane in hexane) and comparable to the standard deviations of fit of the complex formation experiments given in Tables 1 and 2.

(*b*) An additional six samples of halothane+hexane with x_A^0 covering the whole composition range were prepared and the chemical shifts of halothane were measured. The changes in chemical shift of halothane due to dimerization are small (about 40 Hz for pure halothane), while the maximal measured values of $\Delta\delta_{obs}$ for the case of association with MTBE or THF were greater than 300 Hz.

Supposing the formation of linear dimer and the athermal solution ($r_{AA} = 2r_A$), the optimal values of the dimerization constant and the difference between chemical shift of dimer and monomer were found by minimizing the sum of squares of differences between experimental and calculated values of chemical shifts of halothane. The calculation was very unstable; the model of ideal solution did not converge.

Can. J. Chem. Downloaded from www.nrcresearchpress.com by 80.90.12.36 on 09/08/12
For personal use only.

Fig. 1. Ideal association model: experimental van't Hoff plot for systems of halothane with MTBE (hollow symbols) or THF (full figures) as measured in several inert solvents; △ ▽ ▲ heptane, ○ ● hexane, □ ■ decane, ◁ ▷ cyclohexane. Solid lines are van't Hoff plots calculated from thermodynamic data.

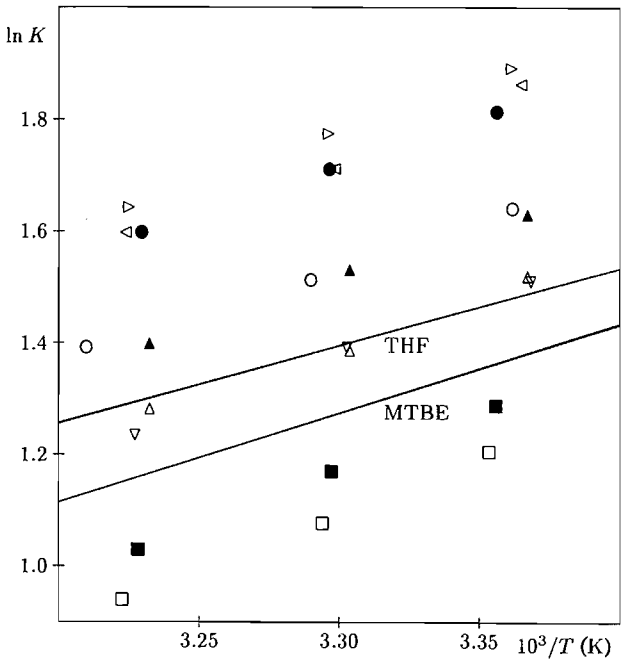

Fig. 2. Athermal association model: experimental van't Hoff plot for systems of halothane with MTBE (hollow symbols) or THF (full figures) as measured in several inert solvents, △ ▽ ▲ heptane, ○ ● hexane, □ ■ decane, ◁ ▷ cyclohexane. Dotted lines average measurements for all the inert solvents used (for parameters of these lines see Table 3), solid lines are calculated from thermodynamic data.

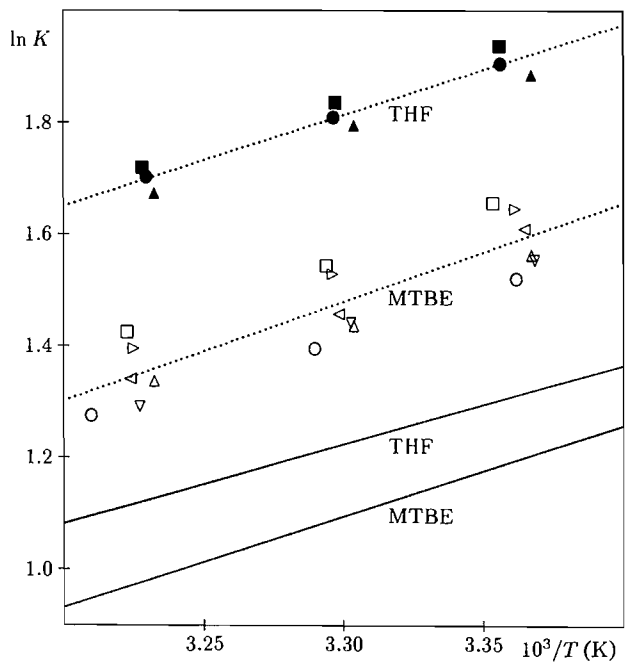

Therefore only the model of athermal association was used. For 297.85 K the following values were estimated: dimerization constant 0.091 ± 0.010 and chemical shift of dimer 2154 ± 41 Hz (7.18 ± 0.14 ppm), standard deviation of fit being 0.4 Hz.

Having determined the value of the self-association constant of halothane, it can be readily found that, for $x_A^0 < 0.05$, less than 1% of halothane is dimerized. Thus, our spectroscopic measurements should be virtually unaffected by the self-association of halothane.

In concentrated halothane solutions, however, the extent of halothane dimerization increases, reaching nearly 15% for pure halothane. Through comparison of the excess Gibbs energy values calculated for the system halothane + MTBE or THF it was found that the values of $K_{298.15}$ from thermodynamics would be about 20% higher if self-association of halothane were accounted for. Thus, the influence of halothane self-association on the results derived from thermodynamics turns out to be significant and its complete neglect can at least partially explain the lack of quantitative agreement between the results from spectroscopy and those from thermodynamics.

References

1. D. Fenclová and V. Dohnal. J. Chem. Thermodyn. **25**, 689 (1993).
2. M. Costas, S. Perez-Casas, V. Dohnal, and D. Fenclová. Thermochim. Acta, **213**, 23 (1993).
3. V. Dohnal, M. Costas, and D. Fenclová. Thermochim. Acta, **214**, 183 (1993).
4. V. Dohnal, D. Fenclová, M. Bureš, and M. Costas. J. Chem. Soc. Faraday Trans. **89**, 1025 (1993).
5. C.M. Huggins, G.C. Pimentel, and J.N. Shoolery. J. Chem. Phys. **23**, 1244 (1955).
6. W.B. Dixon. J. Phys. Chem. **74**, 1396 (1970).
7. M. Rappon and R.M. Johns. J. Mol. Liq. **40**, 155 (1989).
8. M.A. Goldman and M.T. Emerson. J. Phys. Chem. **77**, 2295 (1973).
9. A.M. Rajab and E.A. Noe. J. Am. Chem. Soc. **112**, 4697 (1990).
10. N. Muller and P.I. Rose. J. Phys. Chem. **69**, 2564 (1965).
11. N. Muller and O.R. Hughes. J. Phys. Chem. **70**, 3975 (1966).
12. D.F. Nogales, J.-S. Ma, and D.A. Lightner. Tetrahedron, **49**, 2361 (1993).
13. F. Aradi. Magn. Reson. Chem. **28**, 246 (1990).
14. M. Nakano, M.I. Nakano, and T. Higuchi. J. Phys. Chem. **71**, 3954 (1967).
15. Y.S. Bogachev, S.S. Berestova, and N.M. Kotova. Zh. Obshch. Khim. **61**, 1394 (1991).
16. M. Shibakami and A. Sekiya. Bull. Chem. Soc. Jpn. **66**, 315 (1993).
17. A.G. Krestov, M.Y. Nikiforov, and G.A. Kerakosyan. Zh. Fiz. Khim. **64**, 1769 (1990).
18. A.G. Krestov, M.Y. Nikiforov, and G.A. Kerakosyan. Zh. Fiz. Khim. **65**, 187 (1991).
19. D.S. Abrams and J.M. Prausnitz. AICHE J. **21**, 116 (1975).
20. R. Fletcher and C.M. Reeves. Comput. J. **7**, 149 (1964).

Application pratique des réseaux neuro mimétiques aux données spectroscopiques (infrarouge et masse) en vue de l'élucidation structurale

D. Cabrol-Bass, C. Cachet, C. Cleva, A. Eghbaldar et T.P. Forrest

Résumé : Au cours de ces trois dernières années, des recherches intensives menées indépendamment par plusieurs équipes ont montré que les réseaux neuro mimétiques à couches peuvent être utilisés pour analyser les données spectroscopiques en vue de la détermination de structures moléculaires et que leurs performances s'approchent de celles de spécialistes chevronnés. La construction de tels réseaux, leur apprentissage et l'évaluation de leurs performances requièrent des bases de données spectrales et structurales de taille importante, des logiciels spécialisés, des machines performantes et des temps de calculs non négligeables. Cependant, une fois ces réseaux mis au point, leur utilisation pratique peut se faire directement au laboratoire d'analyse, c'est à dire sur des machines de faible coût (type PC), avec un minimum de manipulations et dans un temps très bref. Dans cet article on rappelle la méthodologie de mise au point des réseaux neuro mimétiques pour l'interprétation des données spectroscopiques et on présente un logiciel permettant d'appliquer ces réseaux sur un ordinateur de type PC couplé ou non avec les spectromètres infrarouge et de masse. Ce logiciel accepte comme données d'entrée, d'une part la description des réseaux à appliquer, et d'autre part les spectres à interpréter numérisés, l'un et l'autre sous forme de fichiers ASCII. Cette approche permet d'appliquer les réseaux neuro mimétiques directement au laboratoire d'analyse avec des ressources informatiques limitées.

Mots clés : réseaux neuromimétiques, spectres infrarouge, spectres de masse, détermination de structure.

Abstract: In the last few years, intensive research by several groups has shown that neural networks can be used to analyse spectral data for structural elucidation, and that their performance approaches that of an expert in the field. The construction of such networks, their training and evaluation, requires large structural and spectral databases and significant computational resources and time. However, once the network has been completed it can be used very effectively for practical applications on an ordinary desktop computer. In this article we describe the methodology for creating such a network for infrared and mass spectra, and present a program for use on a personal computer, either connected to a spectrometer or independently. The program accepts data in ASCII format, both for the network description and for the spectral information. This approach permits the use of neural networks in an analytical laboratory with limited computational resources.

Key words: neural networks, infrared spectroscopy, mass spectroscopy, structure determination.

Introduction

Après les premiers travaux de McCulloch et Pitts (1), puis ceux de Rosenblatt sur le perceptron (2), il aura fallu attendre ces dernières années pour voir se développer des applications des réseaux neuro mimétiques en Chimie. Depuis le début des années 90, leur nombre n'a cessé de croître rapidement, en particulier dans les domaines de la classification automatique et de la prévision de propriété. D'excellents articles de synthèse (3–5) et un ouvrage (6) présentant les applications des réseaux neuro mimétiques en Chimie ont été publiés récemment. L'intérêt des réseaux neuro mimétiques pour l'interprétation et la classification des données spectroscopiques résulte de leurs qualités intrinsèques, en particulier, (*i*) la tolérance au bruit de fond : l'information étant délocalisée sur l'ensemble des connexions entre neurones, une perturbation éventuelle de quelques données n'entraîne pas une dégradation irrémédiable des performances des réseaux; (*ii*) l'aptitude à la généralisation : il n'est pas nécessaire d'apprendre exhaustivement tous les cas de figure possibles d'un problème pour pouvoir classer un nouveau jeu de données.

Un réseau neuro mimétique, dans sa forme la plus simple (réseau à couches non-récurrent), est constitué de plusieurs unités élémentaires de traitement appelées cellules (ou neurones) organisées en couches. Chaque cellule i d'une couche est reliée à toutes les cellules j de la couche précédente au travers des connexions affectées d'un poids W_{ij}. La première couche, qui reçoit l'information à traiter, est appelée couche d'entrée (ou rétine), la dernière, qui produit les réponses du réseau, est appelée couche de sortie (ou couche de décision).

Reçu le 17 janvier 1995.

D. Cabrol-Bass, C. Cachet, C. Cleva et A. Eghbaldar. LARTIC Université de Nice Sophia-Antipolis, Nice, France.
T.P. Forrest.[1] Department of Chemistry, Dalhousie University, Halifax, NS B3H 4J3, Canada.

[1] Auteur à qui adresser toute correspondance. E-mail : forrest@ac.dal.ca

Can. J. Chem. Downloaded from www.nrcresearchpress.com by 80.90.12.36 on 09/08/12
For personal use only.

Can. J. Chem. Downloaded from www.nrcresearchpress.com by 80.90.12.36 on 09/08/12
For personal use only.

Chaque cellule constitue une unité élémentaire de traitement qui effectue la sommation pondérée des valeurs qui lui sont transmises (éq. [1]), puis applique au résultat obtenu net_i, une fonction de transfert, généralement de type sigmoïde (éq. [2]) :

$$[1] \quad net_i = \Sigma_j W_{ij} \cdot out_j + \theta_i$$

$$[2] \quad out_i = \frac{1}{1 + \exp(-k \cdot net_i)}$$

equations dans lesquelles θ_i est une valeur ajustable appelée bias, W_{ij} est le poids de la connexion entre les cellules i et j, net_i est le résultat de la sommation effectuée par éq. [1], out_i est le résultat de l'application de la fonction de transfert [2], il constitue une des entrées des cellules de la couche suivante, et k est un paramètre ajustable de la fonction de transfert.

Le comportement collectif des neurones permet de simuler, de manière rudimentaire, quelques facultés du système nerveux (simulation neuro mimétique), notamment l'apprentissage et la mémorisaiton, et leur confère ainsi une certaine aptitude à la reconnaissance et la généralisation.

La mise en oeuvre d'une application avec un réseau à couches non récurrent s'effectue généralement en trois phases : apprentissage, évaluation, application.

L'apprentissage se fait à partir d'un ensemble d'exemples (ensemble d'apprentissage) qui sont présentés au réseau plusieurs fois. Quand on dit présentés, on entend que les exemples sont appliqués en entrée pour que le réseau modifie au fur et à mesure les poids associés à ses connexions afin d'adapter sa réponse en sortie en fonction des exemples présentés (apprentissage non supervisé) et éventuellement des réponses attendues (apprentissage supervisé). Une présentation complète de l'ensemble d'apprentissage est appelé cycle d'apprentissage ou epoch. Il existe différents algorithmes d'apprentissages (rétropropagation du gradient, gradient conjugué, «line search», etc.); leur description dépasse le cadre de cet article, voir par exemple la référence 4.

L'évaluation consiste à présenter au réseau un ensemble d'exemples (ensemble de test) et à mesurer la qualité de ses réponses. Suivant les objectifs que l'on se fixe on peut chercher à évaluer la capacité du réseau à reconnaître les exemples qu'on lui a soumis lors de l'apprentissage (mémorisation). Dans ce cas, l'ensemble de test sera extrait de l'ensemble d'apprentissage. Mais dans la plupart des applications on s'intéresse à la capacité du réseau à généraliser son aptitude de reconnaissance à des exemples nouveaux (prévision). Dans ce cas, l'ensemble de test doit être constitué d'examples qui ne font pas partie de l'ensemble d'apprentissage. Dans le cas où le nombre d'exemples est limité, on peut employer une procédure dite de «cross-validation» dans laquelle les exemples utilisés en phase d'évaluation sont extraits tour à tour de l'ensemble d'exemples disponibles. Evidemment, il y a une dégradation des performances quand on passe de la mémorisation à la prévision. En particulier, si on pousse l'apprentissage trop loin, le réseau risque de mémoriser des détails non significatifs des exemples de l'ensemble d'apprentisage et ceci au détriment de sa capacité de généralisation. On parle alors de sur-apprentissage. Evidemment si la qualité des réponses n'est pas jugée satisfaisante, il faut modifier l'architecture du réseau et (ou) le codage de l'information présentée en entrée et (ou) la méthode d'apprentissage. Les phases d'apprentissage et d'évaluation sont donc étroitement liées et, pour l'heure, il n'existe pas de méthode qui permette d'aboutir à de bons résultats sans coup férir.

L'application consiste à exploiter un réseau, dont les performances après apprentissage et évaluation sont jugées acceptables, pour classer des exemples dont on ne sait pas s'ils figurent ou non dans les ensembles d'apprentissage ou de test et par conséquent dont les réponses ne sont pas connues a priori. L'hypothèse sous-jacente est que ces nouveaux exemples sont tirés d'une population ayant les mêmes caractéristiques que la population parente dont ont été extraits les ensembles d'apprentissage et de test et que, par conséquent, les performances attendues seront au moins aussi bonnes que celles observées en prévision.

Comme l'ont montré van Est et al. (7), le développement d'applications concrètes des réseaux neuro mimétiques pour l'analyse des données spectroscopiques fait intervenir plusieurs niveaux. En amont se trouve la recherche informatique portant sur les réseaux eux-mêmes (nouvelles architectures, nouveaux modes d'apprentissage, optimisation des paramètres, etc.). Puis, exploitant les résultants précédents, peuvent se développer des travaux de recherche appliquée dont l'objectif est d'aboutir à des réseaux efficaces pour un type de problème donné. Enfin, ces réseaux pourront être incorporés dans des logiciels destinés aux analyses de laboratoire; ces derniers ne doivent avoir à se préoccuper ni de l'architecture des réseaux ni de leurs modes internes de fonctionnement, mais les utiliseront simplement comme des outils destinés à faciliter leur travail d'interprétation. Dans le présent travail, on s'intéresse à ce dernier niveau en proposant un logiciel pouvant être utilisé sur une machine de type PC, couplé ou non avec les spectromètres. Ce logiciel est capable d'appliquer des réseaux, préalablement mis au point, par nous mêmes ou par d'autres, à des spectres de masse et infrarouge pour en tirer des informations structurales.

Réseaux neuro mimétiques et interprétation des données spectroscopiques

Dans l'application qui nous préoccupe, les réseaux neuro mimétiques sont utilisés pour déduire des informations structurales relatives à une molécule inconnue à partir de données spectrales. Le vecteur d'entrée est donc constitué d'une série de valeurs réelles qui décrivent le spectre considéré, tandis que le vecteur de sortie est constitué d'une série d'indicateurs qui caractérisent certains éléments structuraux de la molécule.

Vecteur d'entrée

En ce qui concerne le vecteur d'entrée, il faut distinguer le cas où le spectre à traiter est continu (spectre de bandes) de celui où il est discontinu (spectre de raies). Les spectres infrarouge seront pris comme exemples des spectres continus et les spectres de masse comme exemples des spectres de raies.

Pour les premiers (infrarouge) on peut décomposer la plage de fréquences du spectre en un certain nombre d'intervalles, chacun de ces intervalles constituant un élément du vecteur d'entrée. La plage de fréquences toutes entière peut être divisée en intervalles d'égale largeur (8–12) ou, au contraire, certaines parties plus riches en informations peuvent être découpées plus finement que d'autres (13, 14) ou même on

Can. J. Chem. Downloaded from www.nrcresearchpress.com by 80.90.12.36 on 09/08/12
For personal use only.

peut ne retenir que certaines parties spécifiques du spectre (15). Récemment, Meyer et al. (16) ont appliqué au spectre infrarouge une analyse en composantes principales pour construire des vecteurs d'entrée de faible dimensionalité (de 4 à 10) représentatifs de l'ensemble du spectre.

Pour chaque intervalle, deux types de codage ont été utilisés jusqu'à présent. Dans le premier (8, 9, 15) chaque élément du vecteur d'entrée reçoit une valeur égale à zéro lorsqu'il n'y a pas de bande dans l'intervalle qui lui est associé et une valeur proportionnelle à l'intensité de la bande, comprise entre zéro et un, dans le cas contraire. Cette manière de coder le spectre revient à le transformer en un spectre de raies et fait perdre l'information relative à la largeur et à la forme des bandes. Dans le second type de codage, on associe à chaque intervalle, la valeur de l'absorption en son milieu (10, 17), ou la valeur moyenne sur l'intervalle (11, 13). Ces valeurs sont généralement normalisées entre zéro et un. Ceci s'apparente à une numérisation du spectre et le vecteur ainsi obtenu conserve plus d'informations. La transformation par analyse en composantes principales (16) réduit considérablement la dimensionalité du vecteur d'entrée tout en conservant la plus grande quantité d'information.

Pour les spectres du second type (spectres de masse) s'il paraît simple d'associer l'intensité de chacune des valeurs du rapport *m/z* à un élément du vecteur d'entrée, cette solution est à écarter pour deux raisons.

1. Les spectres de masse ne sont pas très reproductibles, en particulier au niveau de l'intensité des pics. Pour résoudre ce problème, on utilise des modes de codage de l'intensité des pics qui permettent d'atténuer les variations trop importantes. Deux types de codages se sont révélés les plus efficaces : le codage logarithmique (18) qui permet d'atténuer les variations d'intensité et le codage par seuillage (19, 20) qui consiste à fixer en seuils ordonnés et à affecter à chaque pic le seuil atteint par son intensité. Dans le cas où il n'y a qu'un seul seuil, on parle de codage binaire (21, 22).

2. Les informations structurales contenues dans un spectre de masse sont de nature très variée. La plage utile de valeurs du rapport *m/z* étant comprise entre 40 et 440 environ, on obtiendrait, si on retenait toutes ces valeurs, un vecteur d'entrée dont la dimension serait de l'ordre de 400. En fait, un grand nombre de ces pics ne sont pas pertinents et en pratique on n'en retient qu'un certain nombre considérés comme caractéristiques de certains motifs structuraux. Mais il n'y a pas que les pics eux-mêmes qui puissent être associés à des informations structurales. Il y a également des séries de pics, des pics isotopiques ou des différences clefs (M − 18, M − 28, ...) qui sont caractéristiques d'une ou plusieurs famille(s) de composés. En plus des rapports *m/z* retenus, on ajoute donc au vecteur d'entrée d'autres descripteurs construits par autocorrélation, sommation, moyennisation, etc. (23–25).

Il apparaît donc que, dans un cas comme dans l'autre, le spectre numérisé ne peut pas être utilisé tel quel, mais qu'il faut lui faire subir certaines transformations pour constituer le vecteur d'entrée.

Vecteurs de sortie

En ce qui concerne les vecteurs de sortie, on utilise généralement des indicateurs de la présence (valeur 1) ou de l'absence (valeur 0) de motifs structuraux (sous structures) (8–11, 14, 16), mais d'autres sortes d'informations structurales comme par exemple le type de substitution aromatique (15), le type d'alcool (7) ou la classe de composé (12, 17, 24–26) peuvent également figurer comme éléments additionnels du vecteur de sortie. Dans ce dernier cas, un autre réseau spécifique à chaque classe peut être utilisé pour raffiner la classification, voire identifier spécifiquement chaque composé; on parle alors de réseaux hiérarchiques (13, 24). Une application particulière de ce type a été développée par Tanabe et al. (27) en infrarouge. Un premier réseau effectue une classification en 40 catégories (les éléments du vecteur de sortie sont alors des indicateurs d'appartenance à ces classes). Pour chacune d'entre elles, un deuxième réseau effectue alors la reconnaissance des composés (les éléments du vecteur de sortie étant ici associés individuellement à un composé spécifique). Le vecteur de sortie peut aussi être utilisé pour contruire une clef permettant de retrouver rapidement un spectre particulier dans une collection de spectres (28).

Architecture

La définition des vecteurs d'entrée et de sortie détermine corrélativement le nombre de neurones (cellules) des couches d'entrée (*NE*) et de sortie (*NS*). Il a été montré que les réseaux ayant une couche intermédiaire (couche cachée) ont des performances légèrement supérieures aux réseaux qui n'en possèdent pas (9, 11). Il reste donc à fixer le nombre de (*NC*) cellules dans cette couche et éventuellement le nombre de couches cachées. Ce nombre dépend aussi du nombre d'exemples disponibles pour effectuer l'apprentissage. En effet, il est souhaitable de limiter la taille des réseaux pour éviter le phénomène de sur-apprentissage. Une règle empirique, pas toujours respectée, donne comme valeur indicative $NC = 2NE + NS$, mais la plupart des auteurs fixent ce nombre arbitrairement ou sur la base d'essais plus ou moins systématiques.

Le tableau 1 donne l'architecture des réseaux employés par différents auteurs ainsi que le type de codage du vecteur d'entrée.

Ensembles d'apprentissage et de test

La conduite des phases d'apprentissage et de test requiert la constitution d'ensembles d'exemples formés des spectres et des structures correspondantes, ces spectres et structures étant transformés respectivement en vecteurs d'entrée et de sortie avant leur utilisation. La taille et la composition de ces ensembles sont très importantes. En effet, il faut qu'ils soient représentatifs de la population de molécules dont on cherchera à établir la structure une fois le réseau mis au point. Par ailleurs, le nombre de connexions pouvant être assez élevé, il faut disposer d'un nombre d'exemples suffisamment grand pour réduire l'indétermination portant sur les poids de ces connexions. Les ensembles sont le plus souvent constitués par tirage aléatoire parmi les collections d'exemples disponibles. Il est néanmoins nécessaire de vérifier que les distributions dans ces ensembles des motifs structuraux retenus pour constituer le vecteur de sortie sont bien représentatives de leurs distributions dans la population parente. Cette précaution n'est pas toujours respectée par tous les auteurs. Pour compenser la faible représentation de certains motifs structuraux dans la population parente, Smits et al. (13) introduisent dans l'ensemble d'apprentissage le même exemple plusieurs fois, ou construisent des exemples «synthétiques» par simulation

Tableau 1. Types et architecture des réseaux.

Référence	Spectra	Codage[a]	*NE*	*NC*	*NS*	Type de réseau
8	IR	P	256	0	128	Simple
9	IR	P	256	34	36	Simple
10	IR	I	128	40	32	Simple
11	IR	I	284	0; 33	1 ou 12	Simple
12	IR	I	422	4	1–3	Simple
14	IR	I	752	18–80	35	Simple
13	IR	I	268	0; 33	2–12	Hiérarchique
15	IR	I	48–96	0; 27; [31, 11][b]	3	Spécialisé
16	IR	ACP/I	4–10	30	13	Simple
17	IR	P	13–462	18	6–9	Simple
24	SM	D + P	494	12–64	36	Hiérarchique
25	SM	D + P	8–10	16–20	1	Simple
27	IR	I	250	40	40	Hiérarchique
29	IR	I	284	30	12	Simple
[c]	SM	D + P	234	40	17	Simple

[a]Codage : D par descripteurs, P par pics, I par l'intensité, ACP/I analyse en composante principale sur intensité. *NE*, *NC*, *NS* : nombre de cellules dans les couches d'entrée, cachée, de sortie.
[b]Réseau avec deux couches cachées.
[c]Voir note 3.

Tableau 2. Taille des ensembles d'apprentissage et de test, et programmes utilisés.

Référence	NApl	NTest	NTest/NApl	Programme
8	6695	541	0,08	PASCAL
9	2499	416	0,17	PASCAL + C
10	100	50	0,50	PASCAL
11	212	236	1,11	NEUROSHELL
12	10	25	2,50	PASCAL
13	266–726	252–650	0,95–0,90	ANNET
14	609	1328		PASCAL
15	100	78	0,78	ANSIM
16	700	384	1,83	PASCAL
17	48	9	0,19	BRAINMAKER
24	31 926	12 671[a]	0,17[b]	BP (C)
25	226–288	569–2608	2,52–10,09	PASCAL
27	1129	[c]	[c]	NEUROSIM/L
29	300	884	2,95	ASPIRIN
[d]	495	493	1,00	ASPIRIN

[a]Parmi les 12671 exemples de test, 7261 figurent dans l'ensemble d'apprentissage.
[b]Valeur calculée en ne tenant compte que des exemples qui ne figurent pas dans l'ensemble d'apprentissage.
[c]Réseau utilisé uniquement en reconnaissance.
[d]Voir note 3.

ou modification d'exemples existants. Dans le même but, et pour sortir des minima locaux dans lesquels le réseau peut se trouver, Klawun et Wilkins (14) proposent de poursuivre l'apprentissage avec une sur-représentation des cas «difficiles». Malgré les réserves de principe que peut susciter cette manière de procéder, il semble que les performances du réseau en soient sensiblement améliorées. La taille des spectrothèques disponibles étant forcément limitée et les temps d'apprentissage augmentant rapidement avec le nombre des exemples retenus, on est toujours contraint de faire un compromis. Le tableau 2 donne les tailles des ensembles d'apprentissage et de test utilisés dans les travaux cités en références. Il est à noter que pour la plupart d'entre eux, les ensembles de test sont de taille inférieure aux ensembles d'apprentissage. Dans ces conditions, il est difficile d'apprécier la capacité des réseaux à généraliser.

Programmes employés

ANSIM Scientific Application International Cooperation (n'est plus distribué commercialement).

ANNET Laboratory for Analytical Chemistry, University of Nijmegen, Toernooiveld 1, 6525 ED Nijmegen, Netherlands.

ASPIRIN Release V5.0 MITRE Signal Processing Labo-

Can. J. Chem. Downloaded from www.nrcresearchpress.com by 80.90.12.36 on 09/08/12
For personal use only.

ratory Technical Report MP-91W00050. The Mitre Corporation. 7525 Colshire Drive, McLean, VA 22102, U.S.A.

BP Programme en C extrait de réf. 30.

BRAINMAKER California Scientific Software, 160 E. Montecito #E, Sierra Madre, CA 91024, U.S.A.

NEUROSHELL Ward Systems Group Inc., 245 W. Patrick St., Frederick, MD 21701, U.S.A.

NEUROSIM/L Fujitsu Ltd, 1-17-25 Shinkamata, Ota-Ku, Tokyo 144, Japan. (NEUROSIM/L est une carte accélératrice dédiée à la simulation de réseaux neuro mimétique à couches qui dispose d'un logiciel spécifique).

PASCAL Programme développé par les auteurs en PASCAL.

Conduite de l'apprentissage

L'algorithme classique de la rétropropagation du gradient est le plus utilisé pour l'apprentissage des réseaux multicouches. Les paramètres de l'apprentissage (vitesse d'apprentissage et inertie) sont souvent ajustés empiriquement de sorte que la convergence du réseau soit rapidement obtenue.

En ce qui concerne le nombre d'épochs, il importe que l'apprentissage soit interrompu avant que le réseau n'entre dans la phase de sur-apprentissage au cours de laquelle il commence à mémoriser des détails non significatifs des spectres, ce qui détériorerait son aptitude à la généralisation. Deux types de critères sont utilisés comme condition d'arrêt. Des critères a priori qui interrompent l'apprentissage dès que l'erreur globale du réseau (somme des carrés des écarts) ou l'erreur globale cumulée sur une sous-population tirée au hasard devient inférieure à un seuil fixé arbitrairement à l'avance. Ces critères conduisent à de bons résultats pour des réseaux mono-sortie mais, pour les réseaux multi-sorties, ils ignorent les disparités qui peuvent exister dans la rapidit de convergence pour chaque motif structural à reconnaître. On peut également utiliser une condition d'arrêt optimisée. Il s'agit en fait de suivre, au fur et à mesure de l'apprentissage, les performances du réseau sur un ensemble de test et ce pour chaque sortie. On peut dès lors mettre fin à l'apprentissage lorsque le niveau de performances ne s'améliore plus et avant que le sur-apprentissage ne commence à le dégrader. Ce critère serait sans doute parfait si les performances optimales étaient toutes obtenues simultanément pour toutes les sorties, ce qui est rarement le cas. Il faut alors trouver un compromis entre les différents optima afin de fixer un nombre de cycles d'apprentissage en tenant compte de la plus ou moins grande rapidité de convergence des sorties. Si les disparités sont trop importantes, il peut être préférable de séparer en deux réseaux distincts les sorties qui convergent rapidement de celles qui demandent un plus grand nombre de cycles d'apprentissage.

Evaluation des performances

Pour évaluer les performances des réseaux, aussi bien en reconnaissance qu'en prévision, on utilise deux catégories d'indicateurs : ceux construits à partir des écarts entre les valeurs de sortie calculées par le réseau et les valeurs attendues, et ceux qui se fondent sur les réposes obtenues après classification. Pour effectuer cette classification, chaque valeur de sortie *So* (valeur réelle généralement comprise entre 0 et 1) doit être convertie en une réponse booléenne $R \in$ [**Vrai**, **Faux**] relative à la présence de l'élément structural qui lui est associé. On adopte souvent une logique trimodale en ajoutant la valeur **Indéfini**. Pour cela il est nécessaire de fixer des seuils : *SA* seuil d'acceptation et *SR* seuil de rejet, tels que $R =$ **Faux** pour *So* inférieur à *SR*; $R =$ **Indéfini** pour *So* compris entre *SR* et *SA* inclusivement et $R =$ **Vrai** pour *So* supérieur à *SA*. Les valeurs des seuils *SA* et *SR* sont le plus souvent fixées arbitrairement mais peuvent aussi être optimisées en fonction du critère de performance retenu (11).

Il est très difficile de comparer rigoureusement les performances des réseaux décrits par les différents auteurs car ils n'utilisent pas tous les même indicateurs. De plus, des indices portant le même nom ne sont pas toujours définis de la même façon. Par exemple, un des indices les plus fréquemment mis en avant : le taux de réponses exactes, est parfois calculé en ajoutant au score la valeur 1 pour les réponses correctes (sans faire la distinction entre réponses positives et négatives) et 0,5 pour les cas douteux, tandis que d'autres auteurs ne comptent que les réponses correctes. De plus, l'ensemble des données nécessaires à la comparaison des résultats obtenus n'est pas toujours publié. Certains indices, en particulier le taux global de réponses exactes, dépendent de la probabilité a priori de trouver le ou les motifs structuraux considérés, donc de leurs proportions dans les populations étudiées, et donnent souvent une image exagérément flatteuse des performances réelles du réseau. La question de la validation et de l'évaluation des réseaux est discutée dans la référence 31; pour une revue critique des indices utilisés voir Sbirrazzuoli et al. (29).

Malgré ces difficultés de comparaison, il ressort clairement des travaux publiés que les réseaux neuro mimétiques à couches atteignent, dans le domaine qui nous intéresse, des niveaux de performances égaux ou supérieurs aux méthodes utilisées classiquement pour la classification des spectres (26, 32). Certains essais, qui demandent à être confirmés, montrent même que leurs performances supportent la comparaison avec celles d'étudiants avancés (15) voire de praticiens expérimentés (13), cependant cette conclusion reste controversée (12).

Application pratique au laboratoire d'analyse

Les logiciels répertoriés dans le tableau 2, col. 5 sont spécifiquement conçus pour faciliter la construction de nouveaux réseaux, la conduite de leur apprentisage et l'évaluation de leurs performances, mais ne sont pas bien adaptés à une utilisation pratique au laboratoire d'analyse. En effet, pour ce type d'utilisation, il est nécessaire de disposer d'un logiciel qui : (*i*) construise automatiquement le vecteur d'entrée à partir du spectre du composé inconnu en fonction des caractéristiques retenues pour le réseau spécifique à appliquer; (*ii*) soumette ce vecteur d'entrée au réseau dont l'architecture et les poids des connexions auront été préalablement déterminés au cours de la phase d'apprentissage; (*iii*) calcule le vecteur de sortie; (*iv*) applique éventuellement la méthode de seuillage retenue pour produire les réponses concernant les différents motifs structuraux à reconnaître; (*v*) permette éventuellement d'appliquer plusieurs réseaux pour une même molécule inconnue et donne une présentation synthétique des résultats obtenus.

Une telle application en spectroscopie infrarouge a été

Can. J. Chem. Downloaded from www.nrcresearchpress.com by 80.90.12.36 on 09/08/12
For personal use only.

Fig. 1. Schéma fonctionnel du programme ANNE pour le traitement d'un spectre.

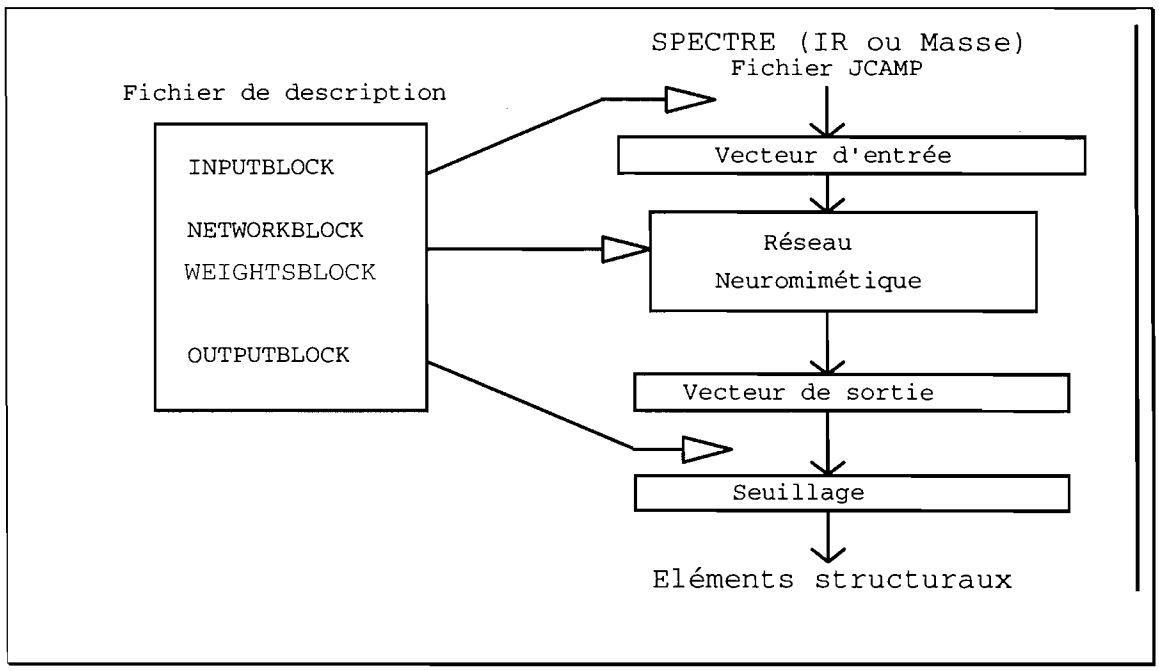

développée récemment par van Est et al. (7) sur mini-ordinateur VAX sous VMS. Les fichiers décrivant les réseaux (architecture et poids) qui résultent de la phase d'apprentissage conduite sur une station Sun SPARC sont préalablement chargés sur le VAX. Le spectre infrarouge du composé inconnu au format standard JCAMP-DX (33) est ensuite transmis du spectromètre à un PC par la voie série RS232 suivant le protocole KERMIT, puis du PC au mini-ordinateur VAX par le réseau Ethernet suivant le protocole NFS. Cette solution n'est pas généralisable aux laboratoires d'analyse qui n'ont pas tous accès à un réseau Ethernet ni à un mini-ordinateur VAX, aussi avons-nous préféré développer un programme unique, dénommé ANNE (Artificial Neural Network Executable), qui puisse être exploité entièrement sur un PC standard fonctionnant sous MS-DOS, tel que ceux généralement couplés aux spectromètres et s'appliquant aussi bien à la spectroscopie infrarouge qu'à la spectrométrie de masse. Contrairement aux apprentissages qui peuvent être assez longs, la conversion des spectres et l'application d'un réseau est extrêmement rapide et il n'y a pas d'immobilisation du PC.

Après apprentissage effectué sur station UNIX à l'aide du logiciel ASPIRIN et détermination par optimisation des valeurs des seuils, toutes les informations relatives à un réseau particulier et au mode de codage des spectres sont rassemblées dans un fichier de description ASCII dont le format est inspiré du standard JCAMP.

Ce fichier se compose des sections ou blocs suivants : (*i*) un en-tête qui permet d'identifier le réseau et spécifie le type de spectroscopie utilisée; (*ii*) le bloc de description du réseau (NETWORKBLOCK) qui contient la topologie du réseau (nombre de noeuds dans chaque couche), et qui spécifie la fonction de transfert utilisée (*iii*) le bloc de description du vecteur d'entrée (INPUTBLOCK) qui contient les informations nécessaires au prétraitement du spectre brut pour construire le vecteur d'entrée; (*iv*) le bloc de description des sorties (OUTPUTBLOCK) qui contient pour chaque sortie le nom de l'élément structural correspondant, les valeurs des seuils et éventuellement les degrés de confiances attribués à chaque réponse; (*v*) le bloc des poids (WEIGHTSBLOCK) qui contient les valeurs des bias et des poids des connections entre cellules.

Le début de chaque bloc et chaque champ d'information à l'intérieur d'un bloc est précédé d'un label qui permet de l'identifier. Les dits labels sont placés en début de ligne et commencent par ##. Seul le block de description du vecteur d'entrée a un contenu qui dépend du type de spectroscopie. Les spécifications complètes du fichier de description des réseaux sont données en annexe. Des exemples de fichiers de description sont contenus avec des fichiers spectres et le programme exécutable ANNE dans la disquette de démonstration qui peut être obtenue auprès des auteurs.[2]

Ces fichiers (un par réseau) peuvent être distribués aux utilisateurs du laboratoire d'analyse par tout système de transfert de fichiers, voire sur disquette. En fait, rien n'impose que ces fichiers résultent du logiciel ASPIRIN que nous utilisons. Si on respecte son format (voir annexe) il peut contenir les résultats obtenus avec n'importe quel autre logiciel de simulation de réseaux neuro mimétiques. L'application des réseaux ainsi décrits est prise en charge par le programme ANNE, lequel est écrit en Pascal orienté objet (Turbo Pascal 6.0). L'architecture des réseaux ainsi que les dimensions des vecteurs d'entrée et de sortie étant variables d'une application à l'autre, il a fallu prévoir une allocation dynamique de la mémoire pour les grandes matrices et vecteurs manipulés par le programme. Pour cela, nous avons fait appel aux unités contenues dans «Object Professional» de Turbo Power Software.

Les spectres à interpréter doivent être disponibles au format

[2] Pour obtenir une copie du programme exécutable ainsi que des exemples de fichiers de description des réseaux envoyer une disquette 3,5 HD formatéee à D.C-B.

Can. J. Chem. Downloaded from www.nrcresearchpress.com by 80.90.12.36 on 09/08/12
For personal use only.

Fig. 2. Système de menu du programme ANNE.

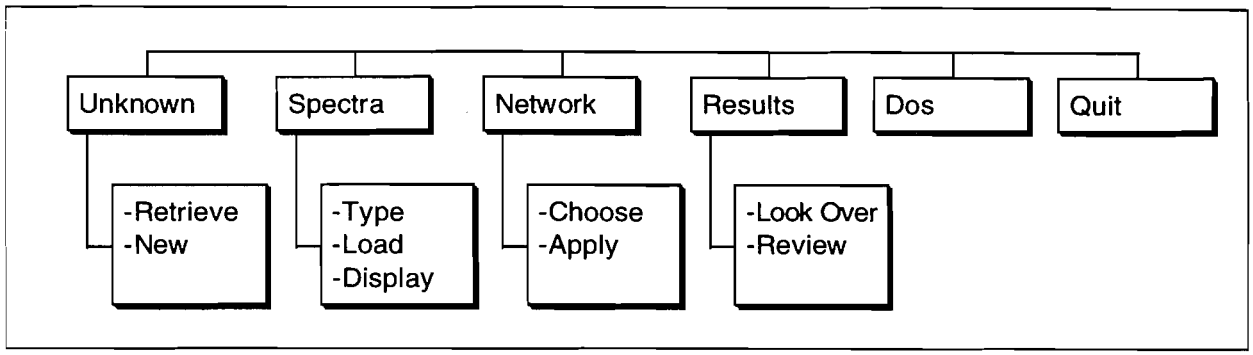

Unknown

Retrieve : Reprise de l'étude d'une structure déjà partiellement élucidée.

New : Initialisation de l'étude d'une nouvelle substance de structure inconnue.

Spectra

Type : Choix du type de spectroscopie.

Load : Chargement du spectre correspondant à la substance en cours d'étude.

Display : Visualisation du spectre à l'écran.

Network

Choose : Choix du réseau neuro mimétique et chargement des poids.

Apply : Application du réseau au spectre sélectionné puis examen des résultats obtenus pour décider de leur rejet ou de leur archivage.

Results

Review : Examen de la synthèse des conclusions relatives à la substance étudiée tirées par tous les réseaux employés précédemment et archivés.

Look over : Examen des résultats du dernier réseau appliqué.

DOS : Accès au système d'exploitation.

standard JCAMP-DX (33). Pour les spectres infrarouge cela ne pose pas de problème; en effet, la plupart des spectromètres disposent de cette facilité. Les données seront enregistrées suivant la spécification ##XYDATA=(X++(Y..Y)). Cela n'est pas aussi simple pour les spectres de masse pour lesquels le standard JCAMP-DX n'est pas aussi répandu. Aussi peut-il être nécessaire d'écrire un programme de conversion pour disposer du spectre de masses au format JCAMP-DX; dans ce cas, les données seront enregistrées suivant la spécification ##XYDATA=(XY..XY).

Le programme ANNE est doté d'une interface utilisateur organisée autour d'un menu hiérarchique dont les options principales sont représentées dans la figure 2. Le système dispose d'un système d'aide contextuelle qui rend inutile la consultation d'un manuel d'utilisation. Les opérations sont logiquement effectuées dans l'ordre des options et sous options proposées par le menu, mais il est possible de revenir en arrière ou de procéder dans un ordre différent.

Le premier traitement effectué lors de l'application d'un réseau par le programme consiste à convertir le spectre expérimental en vecteur d'entrée, conformément aux spécifications contenues dans la partie INPUTBLOCK du fichier de description du dit réseau. Les spécifications pour cette conversion sont différentes suivant le type de spectre, mais le résultat est le même, à savoir : le vecteur d'entrée constitué d'une série de nombres réels. Dans le cas d'un spectre infrarouge, les spécifications de conversion sont simples puisqu'elles consistent seulement à préciser quelles sont les plages de fréquences à prendre en compte et la résolution à retenir pour chacune d'entre elles. Pour les spectres de masse il est bien connu que l'utilisation exclusive des intensités des pics est insuffisante et qu'il faut leur adjoindre des descripteurs supplémentaires construits à partir de ces pics. La syntaxe adoptée pour la partie INPUTBLOCK permet de spécifier la plupart des descripteurs utilisés classiquement (23–25). Si nécessaire, il est facile d'implémenter de nouveaux descripteurs dans l'unité Pascal contenant les routines de conversion des spectres de masse. Le temps total de chargement et de conversion d'un spectre d'une part et de chargement et d'application d'un réseau d'autre part ne dépasse pas 1 s sur un PC 486DX à 33 MHz.

Pour une même spectroscopie, plusieurs réseaux peuvent avoir été mis au point et pourront être appliqués l'un après l'autre aux mêmes données spectrales. Evidemment, les conversions à effectuer peuvent être différentes pour chacun d'eux. Les résultats obtenus par le réseau employé et pour chacune de ses sorties sont présentés immédiatement accompagnés, s'il y a lieu, de l'indication du degré de confiance qui s'y rattache. L'ensemble des résultats obtenus, pour une même substance de structure inconnue, par tous les réseaux qui auront été employés est présenté d'une manière synthétique grâce à l'option Review (voir figure 3). Cette présentation permet de mettre en évidence les convergences, complémentarités et éventuelles divergences dans les conclusions obtenues par les différents réseaux appliqués.

Exemple d'application

À titre d'exemple, nous utiliserons les résultats obtenus avec deux réseaux : l'un traitant les spectres infrarouge (29), l'autre les spectres de masse[3] qui permettent de reconnaître des motifs structuraux assez généraux figurant dans le tableau 3.

[3] A. Eghbaldar. À paraître.

Can. J. Chem. Downloaded from www.nrcresearchpress.com by 80.90.12.36 on 09/08/12
For personal use only.

Tableau 3. Motifs structuraux reconnus par deux réseaux en IR[a] et SM[b] et performances atteintes en généralisation.

Type de motif	Motifs structuraux reconnus en IR	SR	SA	GQ	EQ	Motifs structuraux reconnus en SM	SR	SA	GQ	EQ
Oxygéné	IR1 : hydroxyle	0,456	0,680	84,7	64,8	SM1 : hydroxyle (à	0,495	0,518	81,6	51,2
	IR2 : alcool primaire	0,448	0,648	94,9	61,5	l'exclusion des acides				
	IR3 : acide carboxylique	0,448	0,648	93,5	64,7	et imides)				
	IR4 : ester	0,448	0,648	94,8	71,5	SM2 : acide carboxylique	0,300	0,301	89,1	32,5
	IR5 : aldehyde	0,448	0,648	95,9	44,9	SM3 : ester	0,500	0,501	70,7	41,0
	IR6 : cetone	0,456	0,680	87,3	28,6	SM4 : carbonyle (à l'exclusion des acides, amides et cétones conjuguées)	0,386	0,409	66,8	31,8
Azoté	IR7 : amine ou amide primaire ou secondaire	0,444	0,726	86,5	40,5	SM5 : amine	0,485	0,555	85,9	51,2
						SM6 : amide	0,253	0,256	92,4	20,7
	IR8 : amine ou amide					SM7 : imine ($R_2C{=}NR$)	0,198	0,199	95,2	47,5
	primaire	0,448	0,648	93,1	50,1	SM8 : imine ($R_2C{=}NH$)	0,400	0,600	96,5	45,0
Halogéné						SM9 : R-Cl	0,373	0,585	90,4	56,6
						SM10 : R-F	0,220	0,902	99,3	49,7
Sans hétéroatome	IR9 : alcène	0,439	0,615	82,1	17,3	SM11 : alcène ($R_2C{=}CH_2$)	0,301	0,302	93,1	40,8
						SM12 : alcène ($R_2C{=}CR_2$)	0,489	0,497	76,5	46,4
	IR10 : aromatique					SM13 : aromatique				
	(hydrocarboné)	0,439	0,615	83,5	66,3	(hydrocarboné)	0,305	0,327	90,4	80,9
	IR11 : *gem* diméthyle	0,448	0,648	93,1	47,9	SM14 : R-CH_3	0,280	0,351	84,0	44,2
	IR12 : méthylène	0,448	0,648	70,6	40,7	SM15 : R-$(CH_2)_n$-R	0,517	0,564	77,3	45,9
						SM16 : R-$(CH)_nR_2$	0,649	0,718	71,9	34,7
						SM17 : R-$(C)_n$-R_3	0,550	0,572	77,9	48,5

[a]Architecture : NE = 284, NC = 30, NS = 12. Nombre d'exemples : NApl = 300, NTest = 884, Nombre d'epochs = 198.
[b]Architecture : NE = 234, NC = 40, NS = 17. Nombre d'exemples : Napl = 495, Ntest = 493; Nombre d'époch s = 1500.

Can. J. Chem. Downloaded from www.nrcresearchpress.com by 80.90.12.36 on 09/08/12
For personal use only.

Fig. 3. Extrait d'écarn montrant une partie des résultats obtenus avec deux réseaux différents.

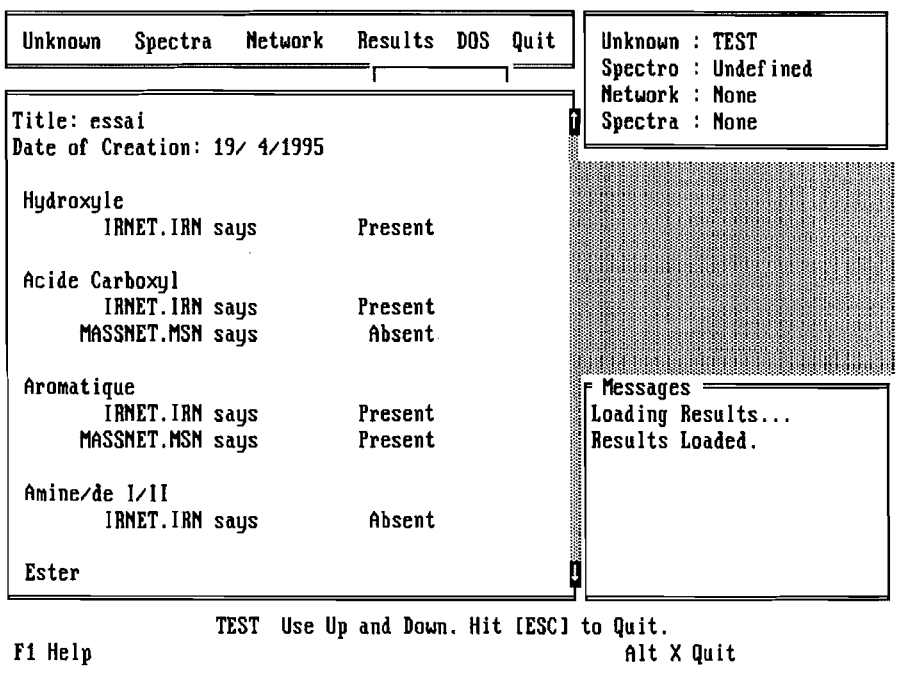

Can. J. Chem. Downloaded from www.nrcresearchpress.com by 80.90.12.36 on 09/08/12
For personal use only.

Dans ce tableau, nous avons porté les valeurs des seuils de SR et SA utilisées pour décider respectivement de l'absence ou de la présence du motif structural. Figurent également les valeurs de deux indicateurs de performance des réseaux : la qualité globale (GQ) et la qualité extra-statistique (EQ). La qualité globale est définie par le rapport du nombre de réponses exactes au nombre d'exemples traités $GQ = (IPc + IAc)/N_t$, avec IPc = nombre de réposes positives correctes, IAc = nombre de réposes négatives, N_t = nombre total de cas traités. Cette grandeur est souvent la seule donnée par les auteurs; bien qu'ayant une significant simple, elle peut donner une idée exagérément optimiste des performances d'un réseau car elle inclut la probabilité a priori de trouver une réponse exacte. Aussi avons-nous introduit (29) la qualité extra-statistique (EQ) qui ne présente pas cet inconvénient et qui permet une comparaison plus fine des performances de différents réseaux. $EQ = (GQ - S_t)/(1 - S_t)$; avec $S_t = 1 + 2P_i + 2P_i^2$ probabilité a priori de répondre juste lorsque la proportion du motif i dans la population est P_i. La qualité extra statistique représente donc l'amélioration relative apportée par le réseau par rapport à la probabilité a priori de répondre juste.

Les performances atteintes sont très satisfaisantes pour tous les motifs structuraux étudiés. On observe cependant des différences entre les deux types de spectroscopie. En particulier on note que, comme on pouvait s'y attendre, la spectroscopie infrarouge est plus efficace pour reconnaître les groupements fonctionnels, notamment oxygénés. La spectrométrie de masse, de son côté, donne des indications plus variées et plus fiables sur le squelette hydrocarboné.

Pour la très grande majorité des molécules mono ou polyfonctionnelles examinées, tous les motifs structuraux présents sont bien reconnus. Les réponses faussement négatives sont rares et correspondent dans la plupart des cas à des situations particulières (équilibre céto-énoliques, molécules particulièrement encombrées, interactions entre groupes fonctionnels voisins, conjugaison, etc...).

Par exemple, pour l'acide benzoïque tous les motifs structuraux présents ou absents sont correctement identifiés par les deux réseaux à l'exception du groupe acide carboxylique. Celui-ci est détecté sans ambiguïté comme étant présent par le réseau (IRNET.IRN) opérant sur le spectre infrarouge (motif IR3, $So = 0.990$) mais n'est pas reconnu par le réseau (MASSNET.MSN) en spectrométrie de masse (motif SM2, $So = 0.024$) ainsi que cela apparaît dans l'extrait d'écran de la figure 3. Cette apparente contradiction entre les réponses fournies par les deux réseaux s'explique et peut être tournée en avantage. En effet, nous avons observé que les réponses fournies par le réseau en spectrométrie de masse sont fortement influencées par le fait que le motif structural recherché est porté ou non par un système aromatique. En particulier, pour le groupe «Acide carboxylique» le réseau en spectrométrie de masse ne donne de réponses positives que pour les acides aliphatiques alors que le réseau en infrarouge donne des réponses positives pour tous les types d'acides. Dans le cas présent, l'existence du noyau aromatique étant détectée sans ambiguïté par les deux techniques (Motif IR10, $So = 0.997$. Motif SM13, $So = 0.732$), on peut facilement conclure que le groupe acide carboxylique détecté en infrarouge est porté par le noyau aromatique et que c'est pour cette raison qu'il n'est pas détecté en spectrométrie de masse. Dans ce cas particulièrement simple il est donc facile de construire la structure correcte. Evidemment, pour des structures plus complexes on ne peut pas espérer obtenir aussi facilement une solution complète. Cependant l'utilisation combinée des deux spectroscopies, qui se trouve facilitée par le programme ANNE, permet de tels recoupements qui facilitent l'élaboration d'une structure.

Conclusion

Les réseaux neuro mimétiques constituent une technique de classification des données spectrales dont les performances égalent ou dépassent celles des techniques employées plus classiquement.

Si leur mise au point peut être longue et demander des équipement informatiques spécifiques, leur application au laboratoire d'analyse peut se faire avec des matériels largement disponibles. Le logiciel présenté permet d'exploiter très simplement cette technique. Pour chaque substance de structure inconnue dont on dispose des spectres, le programme présente sous la forme d'un tableau synthétique l'ensemble des réponses fournies par les différents réseaux neuro mimétiques mis en oeuvre. Les convergences, complémentarités et divergences éventuelles dans les conclusions sont ainsi clairement mises en évidence. Evidemment, l'utilité de ce programme se trouvera renforcée par la disponibilité de réseaux neuro mimétiques performants permettant de déduire la présence ou l'absence de motifs structuraux plus nombreux et variés que ceux disponibles pour l'instant. La construction et l'apprentissage de tels réseaux est en cours dans notre laboratoire. Le format de description des réseaux que nous proposons permet l'échange des réseaux entre équipes utilisant des matériels et des logiciels différents.

Références

1. W.S. McCulloch et W. Pitts. Bull. Math. Biophys. **5**, 115 (1943).
2. F. Rosenblatt. Psychol. Rev. **65**, 386 (1986).
3. J.A. Burns et G.M. Whitesides. Chem. Rev. **93**, 2583 (1993).
4. B.J. Wythoff. Chemom. Intell. Lab. Syst. **18**, 115 (1993).
5. J. Gasteiger et J. Zupan. Angew. Chem. Int. Ed. Engl. **32**, 503 (1993).
6. J. Zupan et J. Gasteiger. Neural networks for chemists. VCH Publishers, New York. 1993.
7. Q.C. van Est, P.J. Schoenmakers, J.R.M. Smits et W.P.M. Nijssen. Vib. Spectrosc. **4**, 263 (1993).
8. E.W. Robb et M.E. Munk. Mikrochim. Acta (Wien), **1**, 131 (1990).
9. M.E. Munk, M.S. Madison et E.W. Robb. Mikrochim. Acta (Wien), **2**, 505 (1991).
10. M. Meyer et T. Weigelt. Anal. Chim. Acta, **265**, 183 (1992).
11. D. Ricard, C. Cachet, D. Cabrol-Bass et T.P. Forrest. J. Chem. Inf. Comput. Sci. **33**, 202 (1993).
12. T. Visser, H.J. Luinge et J. van der Maas. Anal. Chim. Acta, **296**, 141 (1994).
13. J.R.M. Smits, P. Schoenmakers, A. Stehmann, F. Sijstermans et G. Kateman. Chemom. Intell. Lab. Syst. **18**, 27 (1993).
14. C. Klawun et C.L. Wilkins. Chem. Inf. Comput. Sci. **34**, 984 (1994).
15. U.M. Weigel et R.J. Herges. Chem. Inf. Comput. Sci. **32**, 723 (1992).
16. M. Meyer, K. Meyer et H. Hobert. Anal. Chim. Acta, **282**, 407 (1993).
17. R. Fesseden et L. Györgyi. J. Chem. Soc. Perkin Trans. 2, 1755 (1991).

18. K.S. Haraki. The self-training interpretive and retrieval system: improved substructure perception. Cornell University, Ithaca, N.Y. 1980.
19. D.R. Scott. Anal. Chim. Acta, **211**, 11 (1988).
20. D.R. Scott. Chemom. Intell. Lab. Syst. **4**, 47 (1988).
21. S.L. Grotch. Anal. Chem. **42**, 1214 (1970).
22. G. Van Marlen et J.H. Van den Hende. Anal. Chim. Acta, **112**, 143 (1979).
23. H. Lohninger et K. Varmuza. Anal. Chem. **59**, 236 (1987).
24. B. Curry et D.E. Rumelhart. Tetrahedron Comput. Methodol. **3**, 213 (1990).
25. H. Lohninger. *Dans* software development in chemistry. Vol. 5. *Édité par* J. Gmehling. Springer Verlag, Berlin, Heidelberg. 1991. pp. 159–168.
26. H. Lohninger et F. Stancl. Fresenius J. Anal. Chem. **344**, 186 (1992).
27. K. Tanabe, T. Tamura et H. Uesaka. Appl. Spectrosc. **46**, 807 (1992).
28. C. Klawun et C.L. Wilkins. Anal. Chem. **67**, 374 (1995).
29. N. Sbirrazzuoli, C. Cachet, D. Cabrol-Bass et T.P. Forrest. Neural Comput. Appl. **1**, 229 (1993).
30. J.L. McClelland et D.E. Rumelhart. Exploration in parallel distributed processing: a handbook of models, programs, and exercises. MIT Press, Cambridge, Mass. 1988.
31. G. Kateman et J.R.M. Smits. Anal. Chim. Acta, **277**, 179 (1993).
32. W. Werther, H. Lohninger, F. Stancl et K. Varmuza. Chemom. Intell. Lab. Syst. **22**, 63 (1994).
33. R.S. McDonald et P.A. Wilks, Jr. Appl. Spectrosc. **42**, 151 (1988).

Annexe : Specifications du fichier de description des reseaux

Nom : XXXXX.MSN ou IRN

Les informations figurant en police `Courier Bold` telles que : ##INPUTBLOCK sont des mots réservés (labels) qui doivent apparaître tels quels. Les informations données en police *Times Roman Italique* doivent être remplacées par une donnée.

Le fichier est constitué d'un en-tête et de quatre blocs : le bloc de description de l'architecture du réseau, le bloc de description du vecteur d'entrée, le bloc de descriptions vecteur de sortie et le bloc des poids des connexions.
Chaque bloc et chaque type d'information à l'intérieur d'un bloc est précédé d'un label qui permet de l'identifier.
Les labels sont placés en début de ligne et commencent par ##
Le fichier se termine par une ligne contenant le label ##END

Structure générale

En-tête
##NETWORKBLOCK
Bloc de description de l'architecture du réseau
##INPUTBLOCK
Bloc de description du vecteur d'entrée (dépend du type de spectroscopie)
##OUTPUTBLOCK
Bloc de description du vecteur de sortie
##WEIGHTSBLOCK
Bloc contenant les poids des connexions
##END

Can. J. Chem. Downloaded from www.nrcresearchpress.com by 80.90.12.36 on 09/08/12
For personal use only.

En-tête

Contenu du Fichier	Commentaire
##TITLE = *Texte libre*	
##ORIGIN = *Texte libre*	
##DATATYPE = *Spectro*	*Spectro* = Type de spectroscopie. *Spectro* = **MASS.SPECTRA** ou Spectro = **INFRARED SPECTRA**

Bloc de description de l'architecture du réseau

Contenu du Fichier	Commentaire
##NETWORKBLOCK	Label de début du bloc
##NBINPUT = *Nbinput*	*Nbinput* = Nombre de cellules dans la couche d'entrée
##NBHIDDEN = *NbHidden*	*NbHidden* = Nombre de cellules dans la couche cachée
##NBOUTPUT = *NbOutput*	*NbOutput* = Nombre de cellules dans la couche de sortie
##ACTFUNCT = *FunctType*	*FunctType* = Type de fonction d'activation *FunctType* = **1** Fonction linéaire entre [−1, +1] de pente k *FunctType* = **2** Fonction linéaire entre [0, +1] de pente k *FunctType* = **3** Fonction sigmoïde entre [−1, +1] *FunctType* = **4** Fonction sigmoïde entre [0, +1]
##KPARAM = k	k = Paramètre de la fonction d'activation. Pour la fonction pente k = pente Pour la fonction sigmoïde $1/(1 + \exp(-kx))$

Bloc de description du vecteur d'entrée
Pour les spectres infrarouge :

Contenu du Fichier	Commentaire
##INPUTBLOCK	Label de début du bloc
##CONVTYPE = *ConvType* [1]	*ConvType* = Type de conversion à effectuer sur les données *ConvType* ∈ [0, 1, 2, 3] *ConvType* = 0 : Les données ne sont pas modifiées. 1 : Les données sont ramenées en absorbance. 2 : Les données sont normalisées à 1 par rapport à la plus grande valeur. 3 : Les données sont transformées en pourcentage de transmitance.
##NBRANGES = *NbRanges* Li Ls R	*NbRanges* = Nombre de plages à prendre en compte *NbRanges* lignes suivantes : *Li* = limite inférieure de la plage *Ls* = Limite supérieure de la plage *R* = résolution dans la plage.

Can. J. Chem. Downloaded from www.nrcresearchpress.com by 80.90.12.36 on 09/08/12
For personal use only.

Pour les spectres de masse :
Nota : les nombres entre crochets renvoient aux remarques figurant à la suite du tableau.

Contenu du Fichier	Commentaire
##INPUTBLOCK	Label de début du bloc
##CONVTYPE = *ConvType* [1]	*ConvType* = Type de conversion à effectuer sur les données [2] *ConvType* ∈ {0, 1, 2} *ConvType* = 0 : Les données ne sont pas modifiées. 1 : Les données sont codées par seuillage 2 : Les données sont transformées par l'équation [3] Si *ConvType* = 1, les lignes suivantes préciseront le nombre de niveaux et les seuils:
##NBLEVELS = *NbLevels* *Seuil Valeur*	*NbLevels* = Nombre de niveaux de seuillage [4] *NbLevels* Lignes suivantes : *Seuil* = Seuil supérieur de chaque niveau *Valeur* = Valeur attribuée aux signaux entrant dans ce niveau
##DETECTLEVEL = *DetectLevel*	*DetectLevel* = Valeur du seuil de détection d'un pic. [5].
##NBRANGES = *NbRanges* *Li Ls*	*NbRanges* = Nombre de plages à prendre en compte [6] *NbRanges* lignes suivantes : *Li* = Limite inférieure de la plage *Ls* = Limite supérieure de la plage
##NBPEAKS = *NbPeaks* *MZ*	*NbPeaks* = Nombre de pics individuels à prendre en compte [7]. *NbPeaks* Lignes suivantes : *MZ* = Valeur du rapport M/Z de chaque pic à prendre en compte.
##NBDIFFERENCES = *NbDiff* *DX*	*NbDiff* = Nombre de différences clefs à prendre en compte [8] *NbDiff* Lignes suivantes : *DX* = Valeur telle que M/Z = M-DX est à prendre en compte
##NBSETS = *NbSets* *NbPs* $M_1\ M_2\ \ldots\ M_{NbPs}$	*NbSets* = Nombre d'ensembles de pics à prendre en compte [8]. 2x*NbSets* lignes suivantes : *NbPS* = Nombre de pics dans un ensemble $M_1\ M_2\ \ldots\ M_{NbPs}$: Valeurs des rapports M/Z des pics de l'ensemble considéré.
##NBSERIES = *NbSeries* *Raison Début*	*NbSeries* = Nombre de séries de pics à prendre en compte [9]. *NbSeries* lignes suivantes : *Raison* = Raison de la série *Débutt* = Rapport M/Z du premier pic de la série.
##NBPATTERNS = *NbPatterns* *NbPT* $M_i\ I_i$	*NBPatterns* = Nombre de "Patterns" à prendre en compte [10] *NbPattern* Groupes de lignes suivantes *NbPt* = Nombre d'éléments dans le pattern *NbPT* Lignes suivantes : $M_i\ I_i$: valeurs du rapport M/Z et de l'intensité du *i* ième pic du "Pattern".
##NBATCSUMS = *NbAtcSums* *Patc*	*NbAtcSums* = Nombre de sommes d'autocorrélations à prendre en compte [11] *NbAtcSums* lignes suivantes : *Patc* = paramètre d'autocorrélation
##NBCONSTSUMS = *NbCstSums* *PSum*	*NbCstSums* = Nombre de sommes constantes à prendre en compte [12] *NbCstSums* lignes suivantes : *PSum* = Paramètre de somme constante
##NBISOTOPIC = *NbIsotop* *DecIsoptop*	*NbIsotop* = Nombre de pics isotopiques à prendre en compte [13] *NbIsotop* lignes suivantes : *DecIsotop* décalage isotopique

[1] Seul le paramètre ##CONVTYPE = *ConvType* est obligatoire et doit figurer en premier, les autres sont facultatifs et peuvent être donnés dans n'importe quel ordre. Cet ordre détermine l'ordre des éléments dans le vecteur d'entrée.

[2] Les spectres sont normalisés entre 0 et 1 par rapport au pic de base préalablement à tout traitement.

[3] $I_M = (\log_2(1 + L_M/1000))^{1/2}$

[4] Le codage par seuillage permet d'effectuer une transformation non-linéaire sur les signaux.
Exemple :
##NBLEVELS = 4
0.2 0.0
0.6 0.4
0.8 0.8
1.0 1.0

Can. J. Chem. Downloaded from www.nrcresearchpress.com by 80.90.12.36 on 09/08/12
For personal use only.

Les signaux dont l'intensité I est $0.0 < I <= 0.2$ recevront la valeur 0.0
$0.2 < I <= 0.6$ recevront la valeur 0.4
$0.6 < I <= 0.8$ recevront la valeur 0.8
$0.8 < I <= 1.0$ recevront la valeur 1.0

[5] Les signaux dont la valeur d'intensité après codage est inférieure au seuil indiqué par *DetectLevel* sont affectés de la valeur 0. Cette opération ne s'applique pas aux pics isotopiques.

[6] Toutes les valeurs de *M/Z* dans les plages ($Li <= M/Z <= Ls$) ainsi définies constituent autant d'éléments du vecteur d'entrée.
Exemple :
##NBRANGES = 1
40 220
Retient toutes les valeurs comprises entre 40 et 220 bornes incluses comme autant d'éléments du vecteur d'entrée.

[7] Ajoute les pics énumérés comme éléments du vecteur d'entrée.
Exemple :
##NBPEAKS = 5
112
124
141
156
167
Retient toutes les valeurs correspondantes à *M/Z* = 112, 124, 141, 156, 167 comme éléments du vecteur d'entrée.

[8] Ajoute les pics M – DX comme éléments du vecteur d'entrée
Exemple :
##NBDIFFERENCES = 4
18
28
46
54
Retient toutes les valeurs à M – 18, M – 28, M – 46 et M – 54 comme éléments du vecteur d'entrée.

[9] Ajoute la moyenne des valeurs de chaque ensemble défini comme élément du vecteur d'entrée.
Exemple :
##NBSETS = 2
4
79 81 93 95
6
55 67 81 91 95 107
Ajoute les éléments $\frac{1}{4}(I_{79} + I_{81} + I_{93} + I_{95})$ et $\frac{1}{6}(I_{55} + I_{67} + I_{81} + I_{91} + I_{95} + I_{107})$ au vecteur d'entrée.

[10] Ajoute un indice de similarité avec un schéma prototypique (pattern) défini. Pour chaque schéma défini par un vecteur prototype formé des intensités correspondantes à une série de valeurs de *M/Z*, cet indice est calculé en faisant le produit scalaire de ce vecteur prototype par le vecteur extrait du spectre pour les mêmes valeurs du rapport *M/Z* (25).
Exemple :
##NBPATTERNS = 1
4
41 0.60
55 0.34
67 0.31
79 0.41
Ajoute la valeur du produit scalaire entre le vecteur prototype Vp = [0.60, 0.34, 0.31, 0.41] et le vecteur extrait du spectre pour les mêmes valeurs de *M/Z* Vs = $[I_{41}, I_{55}, I_{67}, I_{79}]$ au vecteur d'entrée.

[11] Ajoute les sommes d'autocorrélations normalisées au vecteur d'entrée (23).
Exemple :
##NBNBATCSUMS = 1
14
Ajoute la valeur de AC(14)/AC(0) au vecteur d'entrée.
$AC(\Delta m) = \sum_{m=1}^{m=L-\Delta m} I_m \cdot I_{m+\Delta m}$ avec Δm paramètre d'autocorrélation et L plus forte masse.

[12] Ajoute des termes *Cps* dits «constant summ» définis par réf. 24 au vecteur d'entrée.
Exemple :
##NBNCONSTSUMS = 1
28
Ajoute la valeur de $Cps = (\sum_m I_m \cdot I_{M+ps-m})/I_B$ pour ps = 28; I_B : intensité du pic de base. *ps* : masse de la partie commune.
Nota : Les pics intervenant dans le produit sont tels que la somme de leur valeur de *M/Z* est égale à la masse moléculaire M + le paramètre choisi ps.

Can. J. Chem. Downloaded from www.nrcresearchpress.com by 80.90.12.36 on 09/08/12
For personal use only.

[13] Ajoute les intensités des pics isotopiques spécifiés au vecteur d'entrée. Noter que cette intensité échappe à l'application du paramètre *DetectLevel.*

Bloc de description du vecteur de sortie

Contenu du Fichier	Commentaire
##OUTPUTBLOCK	Label de début du bloc
##NBINTERVALS = *NbIntervals*	*NbIntervals* = Nombre d'intervalles à prendre en compte
##INTVLBLS	*NbIntvbls* lignes suivantes
Labeli	*Labeli* = Etiquette associée au *i* ième intervalle
##OUTPUTLBL	Nboutput lignes suivantes
I OutputLbl CutPt1 ... Cuptj	*I* = Output number *OutputLbl* = Output label *CutPt1* = Premier point de coupure *CutPtj* = jième point de coupure *Nota* : pour chaque sortie, il y a *Intervals-1* points de coupure.
##CONFLEVELS	Degrés de Confiances *Nboutput* lignes suivantes
I Cf1 ... Cfj	*I* = Output number *Cf1* = Degré de confiance du premier intervalle *Cfj* = Degré de confiance du jème intervalle *Nota :* pour chaque sortie, il y a NbIntervals degrés de confiance. Une valeur 0 pour un degré de confiance signifie qu'il n'est pas attribué.

Exemple :

```
##OUTPUTBLOCK
##NBINTERVALS = 3
##INTVLBLS
Absent
Indéterminé
Présent
##OUTPUTLBL
1    Hydroxyl     0.200    0.600
2    Carbonyle    0.220    0.580
3    Ethylénic    0.120    0.760
4    N-H          0.300    0.630
##CONFLEVELS
1    0.85         0        0.92
2    0.95         0        0.96
3    0.78         0        0.82
4    0.92         0        0.86
```

Remarque : les valeurs ci-dessus sont arbitraires.

Can. J. Chem. Downloaded from www.nrcresearchpress.com by 80.90.12.36 on 09/08/12
For personal use only.

Description du contenu du WEIGHTSBLOCK
Ce bloc est constitué d'un extrait du fichier des poids tel qui est produit par ASPIRIN.
Les premières lignes sont éliminées.

Contenu du Fichier	Commentaire
##WEIGHTSBLOCK	Label de début du bloc
Layer: *NetName*:**Output_Layer**	Début de description de la couche de sortie. *NetName*: = Nom du réseau 2 × *NbOutput* Lignes suivantes
Nodes [*i*, **0**]:	*i* = Numéro du noeud (**0** est une constante)
Bias = **BiasValue**	BiasValue = Valeur du Bias pour ce noeud
Connection from *Netname*:**Hidden_Layer**:	2 × NbOutput Lignes suivantes
Node [*i*, **0**]:	*i* = Numéro du noeud (**0** est une constante)
Wi0 Wi1 Wi2 Wij	*Wij* : Poids des connexions entre la couche cachée et le noeud *i* de la couche de sortie. Il y a donc *NbHidden* valeurs.
Layer: *NetName*:**Hidden_Layer**	Début de description de la couche cachée *NetName*: = Nom du réseau 2 × *NbHidden* Lignes suivantes
Node [*i*, **0**]:	*i* = Numéro du noeud (**0** est une constante)
Bias = *BiasValue*	*BiasValue* = Valeur du Bias pour ce noeud
Connection from $INPUTS:	
Node [*1*, **0**]:	*i* = Numéro du noeud (**0** est une constante)
Wi0 Wi1 Wi2 Wij	*Wij* : Poids des connexions entre la couche d'entrée et le noeud *i* de la couche de sortie. Il y a donc *NbInput* valeurs.

Can. J. Chem. Downloaded from www.nrcresearchpress.com by 80.90.12.36 on 09/08/12
For personal use only.

Poly *N*-(2-cyanoethyl)pyrrole as a selective film for the thickness-shear-mode acoustic wave sensor

Zhiping Deng, David C. Stone, and Michael Thompson

Abstract: Poly *N*-(2-cyanoethyl)pyrrole films have been synthesized by electrochemical polymerization and characterized by cyclic voltammetry, scanning electron microscopy, and X-ray photoelectron spectroscopy. Polymeric coatings prepared on the surface of a thickness-shear-mode acoustic wave sensor have been used to examine response selectivity to a number of gas-phase probe molecules. The responses of the poly *N*-(2-cyanoethyl)pyrrole based sensor are compared with the parent polypyrrole device and rationalized in terms of the molecular interactions between probes and polymer films. The polar cyano functionality enhances interactions with analytes such as acetonitrile.

Key words: gas sensor, thickness-shear-mode acoustic wave sensor, poly *N*-(2-cyanoethyl)pyrrole film, polypyrrole film, conducting polymer.

Résumé : On a synthétisé des films de poly *N*-(2-cyanoéthyl)pyrrole par polymérisation électrochimique et on les a caractérisés par voltampérométrie cyclique, microscopie électronique à balayage et par spectroscopie photoélectronique des rayons X. On a utilisé les revêtements polymériques préparés sur la surface d'un senseur d'onde acoustique dans le mode de cisaillement de l'épaisseur pour examiner la sélectivité de la réponse à un certain nombre de molécules sondes en phase gazeuse. On a comparé les réponses du senseur basé sur le poly-*N*-(2-cyanoéthyl)pyrrole avec celles de l'équivalent ne portant que le polypyrrole parent et on a rationalisé les différences en fonction d'interactions moléculaires entre les sondes et les films de polymère. Une fonction polaire cyano augmente les interactions avec les produits à analyser, comme acétonitrile.

Mots clés : senseur de gaz, senseur d'onde acoustique dans le mode cisaillement de l'épaisseur, film de poly-*N*-(2-cyanoéthyl)pyrrole, film de polypyrrole, polymère conducteur.

Can. J. Chem. Downloaded from www.nrcresearchpress.com by 80.90.12.36 on 09/08/12
For personal use only.

Introduction

Films or coatings of polypyrrole (PPY) and its derivatives have proven to be extremely useful in the fabrication of gas-phase chemical sensors (1). These materials possess unique electronic, magnetic, and optical properties that allow their molecular recognitive capabilities to be coupled directly with electronic circuits in a sensor configuration (2). The ease of preparation by electrochemical polymerization together with their chemical stability under normal conditions have contributed to the application of polypyrroles in various sensing systems for more than a decade (3, 4).

Polypyrrole films display fast reversible changes in conductivity when exposed to gases or vapours (5). This phenomenon makes them attractive for application as chemical sensors based on conductivity changes. Bartlett and Ling-Chung (6) investigated the behaviour of a sensor with respect to reversible changes in the presence of various saturated organic vapours. They found that the response of a polypyrrole film to a gas depended on both the nature of the analyte and the semiconducting properties of the polymer.

Polypyrrole has also been used as a chemically selective layer on thickness-shear-mode (TSM) acoustic wave devices for gas sensing. Adsorption of gas-phase species into the polypyrrole layer causes a shift in the series resonant frequency of the piezoelectric crystal. The Sauerbrey equation (7) can then be used to describe the resulting relationship between mass change and frequency shift. This sensing process involves sorption of the molecules both on and into the polymer film, and so is dependent on film structure and functionality. For example, using a combination of polypyrrole-coated TSMs with optical spectroscopy and work function measurements, Topart and Josowicz (8) were able to study the interaction between methanol and polypyrrole. The combination of conductivity together with piezoelectric measurements has also been employed to examine the interaction between polypyrrole and different vapours (9). Slater et al. (10), for example, showed that simultaneous recording of mass and conductivity changes could be employed to overcome the problem of moisture interference in piezoelectric response.

The properties of polypyrrole (and its derivatives) can be modified both chemically and electrochemically (11), allowing fine tuning of its capabilities for selective adsorption. In this context, Wallace and co-workers (12, 13) reported the use of polypyrrole film as a stationary phase in liquid chromatography and concluded that subjecting the films to different

Received March 28, 1995.

Z. Deng, D.C. Stone, and M. Thompson.[1] Department of Chemistry, University of Toronto, 80 St. George Street, Toronto, ON M5S 1A1, Canada.

[1] Author to whom correspondence may be addressed. Telephone: (416) 978-3575. Fax: (416) 978-8775.

Can. J. Chem. Downloaded from www.nrcresearchpress.com by 80.90.12.36 on 09/08/12
For personal use only.

potentials affected their selectivity, thus altering the partition coefficients.

Thompson and co-workers (14) have studied the effect of different oxidation states of the polymer film with respect to TSM sensor response to several organic gas-phase probes. Their results demonstrated that changing the oxidation state could lead to an enhancement of selectivity and sensitivity. For instance, the greatest sensitivity for toluene was achieved with the neutral polymer, the oxidized form gave the best results for ammonia, while for methanol either extreme oxidation or reduction was preferable. Elliott and co-workers (15, 16) also investigated the absorption of neutral organic species in aqueous solution to the poly(*N*-methyl)pyrrole film in detail. They observed that the partition of dichloromethane into the reduced form is approximately twice that into the oxidized form of poly(*N*-methyl)pyrrole.

The general selectivity of polypyrrole-based sensors is considered poor, however, somewhat limiting their application for detecting gases and vapours. Strategies used to improve their molecular recognitive capability have included the incorporation of different counterions into the polypyrrole film, since this was found to change the morphology of thin films and the concentration of chemical defects (17, 18). Alternative approaches include chemical derivatization (19) and the use of sensor arrays with pattern recognition techniques (10).

In the present work, we describe the fabrication and study of conducting poly *N*-(2-cyanoethyl)pyrrole (PCPY) films, which are expected to provide improved selectivity for certain gases due to the presence of the cyano group.

Experimental

Materials

Methanol, toluene, acetonitrile, triethylamine (Aldrich), and tetrabutylammonium perchlorate (Fluka) were all of analytical reagent grade and used as received. Pyrrole and 1-(2-cyanoethyl)pyrrole were purchased from Aldrich and vacuum-distilled before use.

Equipment

Electrochemical polymerization was carried out in the TSM cell as described previously (14). 9 MHz Gold-coated piezoelectric crystals (International Crystal Manufacturing Co., Oklahoma) were used as the working electrodes (0.25 cm^2 gold on each side) in the polymerization. A combined platinum–Ag/AgCl electrode (Metrohm) functioned as the counter and reference electrode, respectively. All polymer films were deposited onto the electrode from freshly prepared solutions. Either cyclic potential or step potential deposition was performed using a potentiostat (model RDE4, Pine Instrument Company). Before the electropolymerization, electrolyte solutions containing the monomer were degassed by purging with nitrogen for 20 min.

Scanning electron microscopy (SEM) was performed using a Hitachi S-570 SEM with an accelerating voltage of 18 kV. The samples were coated with a very thin gold film by sputter-coating for 60 s at a current of 20 mA. To measure the thickness of the polymers, the polymer-coated crystals were broken across the centre of the electrode.

X-ray photoelectron spectra (XPS) were obtained with a Leybold Max 200 XPS system using an unmonochromatized Mg Kα X-ray source with an analysis area of 2 mm × 4 mm. The source was run at 15 kV and 20 mA. The survey spectra and quantitative atomic measurements were acquired with a pass energy of 192 eV, while high-resolution spectra were obtained with a pass energy of 48 eV. Features in the resultant spectra due to excitation from weaker X-ray satellite lines were subtracted out using an algorithm supplied by the manufacturer. Relative atomic percentages were derived from spectra run in low-resolution mode, normalized to unit transmission of the spectrometer. The sensitivity factors used for the normalized spectra were empirically derived by Leybold. Deconvolution of the high-resolution spectra was again performed using software provided with the spectrometer.

TSM experiments were performed using the oscillator method described previously (14). The conducting polymers used in the current paper are all in the oxidized state as prepared. The oscillation frequency was measured by a universal frequency counter (Hewlett–Packard model 5334B) interfaced to a Macintosh II computer. Data were collected every 6 s.

Gas generation

A gas sample system was designed and constructed to control the flow rate and concentration of the test vapours (Fig. 1). This system employs three bubblers in series to generate the vapour from the corresponding liquid. This is connected as the "sample loop" of a six-port chromatographic injection valve, which allows the bubbler to be isolated from the rest of the flow system at both ends. Separate lines are incorporated to allow dilution of the sample vapour stream and purging of the cell containing the TSM. Mass flow meters (Cole–Parmer) are used in conjunction with needle valves to set and control the flow rates through the bubbler, bypass, dilution, and purge lines. Check valves are also included in each line to allow further isolation of those parts of the system not in use at any one time. Stainless steel components and PTFE tubing were used in all parts of the system where organic vapours could be present.

In normal operation, helium was passed through the bubbler and purge lines continuously at a flow rate of 30 mL/min, a switching valve being used to switch them to the detector cell as appropriate. The concentration of each sample vapour was determined by passing the sample stream through a cold trap for a specific period of time and then weighing the condensed liquid. The values obtained were 45 ± 5 (methanol), 10 ± 3 (toluene), 34 ± 4 (acetonitrile), 29 ± 3 (triethylamine), and 15 ± 5 (water) mg/L. Relative standard deviation for repeated exposure of a given film to a single analyte was typically 1–4%. For different films, the response to the same analyte showed a relative standard deviation of 2–8%. It was also found that the same film could be successfully reused following exposure to different analyte vapours.

Results and discussion

Electrochemical polymerization

Cyclic voltammetry is widely employed to investigate kinetics of electrode processes for electrochemical polymerization and to characterize the resulting polymer film (20). Figure 2 shows typical cyclic voltammograms of the electrochemical polymerization of 0.1 M 1-(2-cyanoethyl)pyrrole in acetonitrile containing 0.1 M tetrabutylammonium perchlorate as the sup-

Fig. 1. Schematic diagram of the gas generation device.

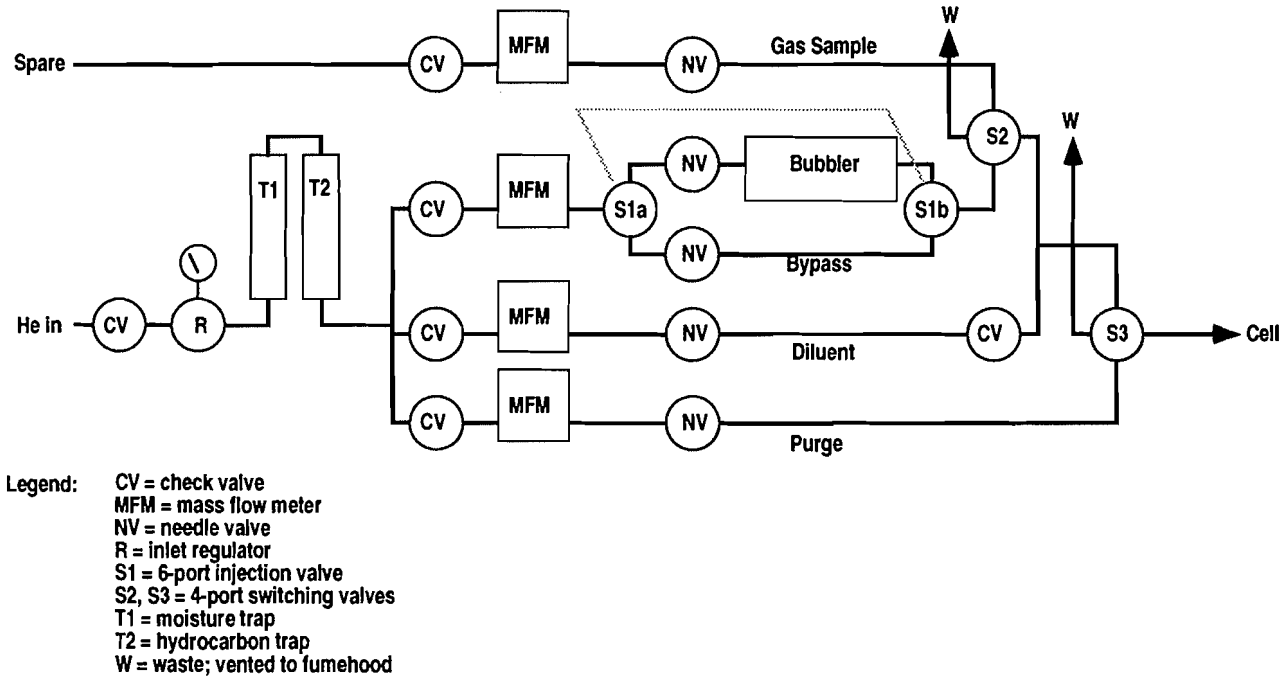

Fig. 2. Cyclic voltammogram of polymerization of 1-(2-cyanoethyl)pyrrole (0.1 M) and 0.1 M tetrabutylammonium perchlorate – acetonitrile at scan rate of 100 mV/s. Scan potential range is from 0.0 to 1.2 V vs. Ag/AgCl (3 M).

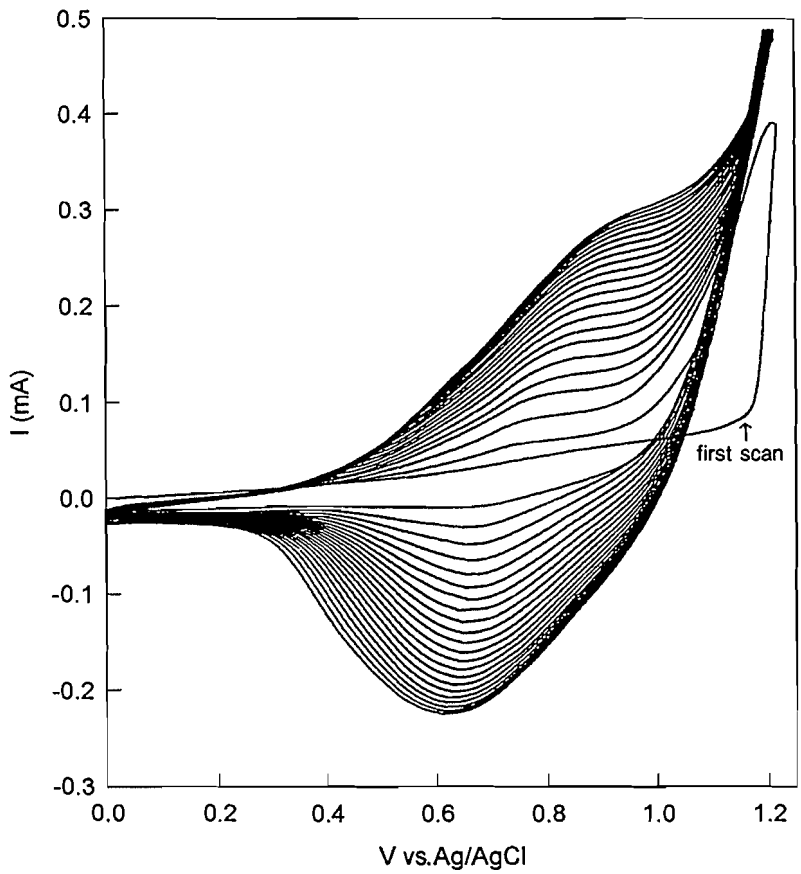

Can. J. Chem. Downloaded from www.nrcresearchpress.com by 80.90.12.36 on 09/08/12
For personal use only.

Can. J. Chem. Downloaded from www.nrcresearchpress.com by 80.90.12.36 on 09/08/12
For personal use only.

Fig. 3. Cyclic voltammogram of PCPY in 0.1 M tetrabutylammonium perchlorate – acetonitrile without monomer. Scan potential is from 0.0 to 1.2 V. (1) 20; (2) 40; (3) 60; (4) 80; (5) 100 mV/s.

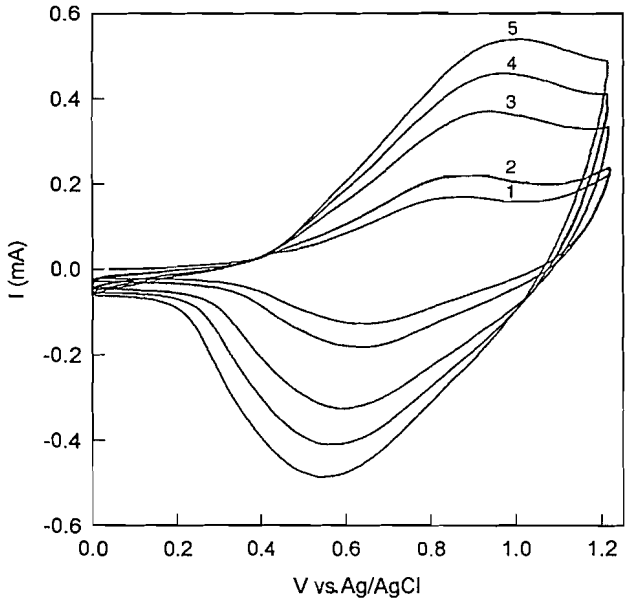

porting electrolyte. The voltammograms were obtained using a cyclic potential from 0.0 to 1.2 V vs. Ag/AgCl (3 M) at a scan rate of 100 mV/s. On the first scan, the current increases sharply upon reaching +1.1 V, indicating the beginning of monomer oxidation. The oxidation potential for 1-(2-cyanoethyl)pyrrole is higher than that for pyrrole because of the steric and electronic effects of the side chain in the 1-(2-cyanoethyl)pyrrole. The inductive effect of this side chain makes oxidation of the monomer more difficult (3). The anodic peak on the second scan is at about +0.7 V, which corresponds to the oxidation of PCPY. As polymerization proceeds, the peak potential moves towards higher potentials, while the corresponding peak current continues to increase until it stops after 22 scans. The rate of current increase is fastest over the initial cycles, then becomes increasingly slower. The anodic peak shift is variously attributed to electrochemical polarization due to a heterogeneous electron transfer, ohmic polarization of film or solution, the mobility of the counterion due to the porosity of the thin film, and a decrease in the film conductivity (21). The cathodic peak for the second cycle is at ca. +0.64 V, which corresponds to the reduction of PCPY. During reduction of the polymer, counteranions (ClO_4^- in this system) diffuse out of the polymer film. It is not surprising that the cathodic peak is much broader than the anodic peak since the counterions diffuse out slowly. The cathodic peak potential also moved to lower potential values with successive scans.

Figure 3 shows the scan rate dependence of the cyclic voltammogram of PCPY in the same electrolyte solution but without the monomer. Well-defined anodic and cathodic peaks were observed. The anodic peak shifts to more positive potential whereas the cathodic peak moves toward lower potential as the scan rate increases, thus increasing the difference between both peaks. The other feature of the cyclic voltammogram is that both anodic and cathodic peaks are very broad, which is characteristic of slow diffusion of the dopant anions in and out of the polymer film (20, 22).

Fig. 4. The dependence of anodic current on the scan rate.

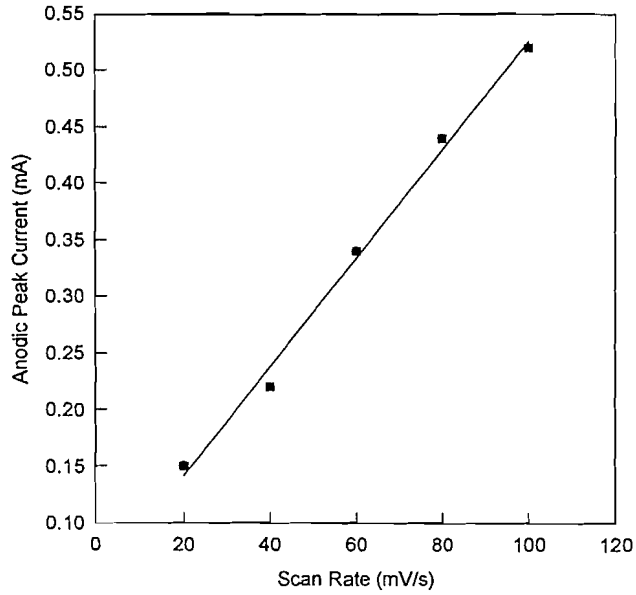

The anodic peak current values in Fig. 3 can be plotted as a function of the scan rate, which helps to determine the mechanism of the electrode process. The graph is shown in Fig. 4. A very linear dependence is obtained, indicating that the electrode process is not controlled by diffusion of electroactive species to the electrode surface. Furthermore, it can be concluded that the electroactive species is effectively localized on the electrode surface (23–25).

Scanning electron microscopy

The morphology of the polymer as electrochemically formed on the electrode of the TSM was examined by SEM. Both normal (microscopically rough) and smooth (optically flat) TSMs were used in order to study the effect of the roughness of the underlying surface. It was found that for very thin films of PCPY deposited using either a step potential (+1.2 V, 40 s) or cyclic voltammetry (10 scans), the polymer film follows the morphology of the electrode very closely. As the film thickness increases, the morphology becomes increasingly different from that of the underlying electrode. Figure 5*a* shows the photomicrograph for a thick film (+1.2 V, 3 min) deposited onto a rough TSM. As the polymer grows on the surface, it assumes a globular form that increasingly fills in the cavities comprising the underlying surface. This results in a "lumpy," non-uniform surface. Figure 5*b* shows the film formed under identical conditions on a smooth TSM. This film was considerably less "lumpy," showing a more consistent film thickness in keeping with the flatness of the underlying electrode. Based on the frequency shifts in air for the deposition process, the same amount of polymer was deposited in each case (~140 μg per side), giving globular films, although the resulting film surface area was greater for the rough than for the smooth TSM. Similar results were obtained for PPY films, and are consistent with results obtained for other polypyrrole derivatives by this group (14). The side view of the same film (Fig. 5*c*) can be used to estimate the film thickness, which was about 2 μm. It is interesting to compare the polymer films pre-

Fig. 5. Scanning electron micrographs of PCPY; (*a*) rough Au surface; (*b*) smooth Au surface, (*c*) as (*b*), side view.

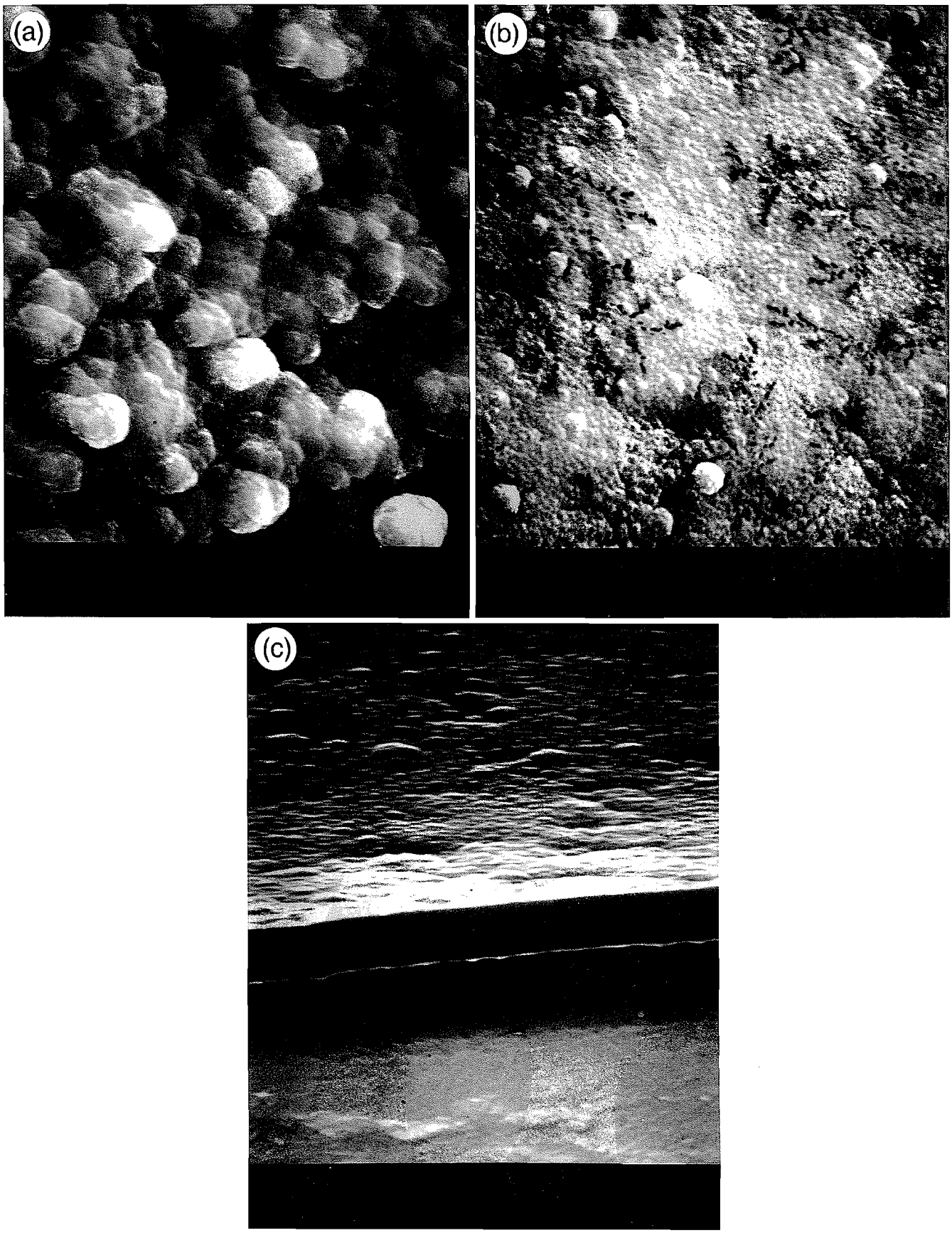

Can. J. Chem. Downloaded from www.nrcresearchpress.com by 80.90.12.36 on 09/08/12
For personal use only.

Fig. 6. C(1*s*) X-ray photoelectron spectrum of PCPY.

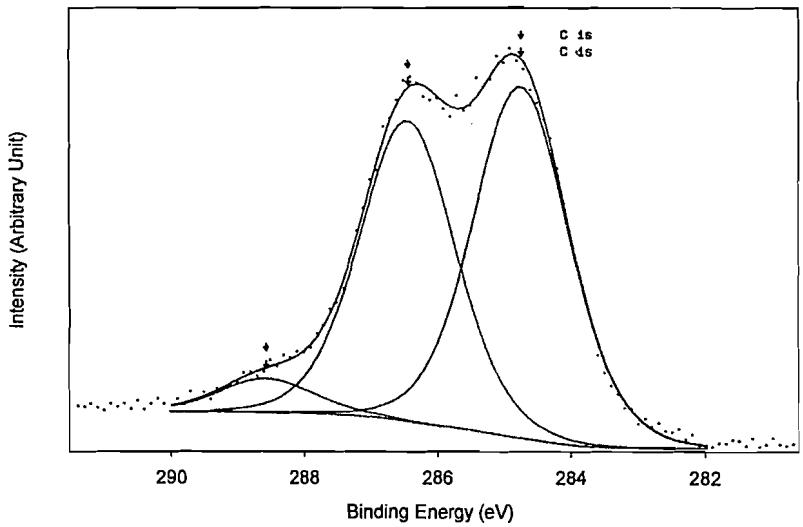

pared by cyclic voltammetry with those prepared using the step potential method. Although very similar in appearance, the former were found to be more compact, uniform, and less cracked than the latter.

X-ray photoelectron spectra

The C(1*s*) core level spectrum is shown in Fig. 6. The C 1s peak can be deconvoluted into three peaks, corresponding to 284.6, 286.3, and 288.4 eV. The carbon peaks are asymmetric and skewed toward the high-binding-energy side. The peak at 284.6 eV is complex and cannot be assigned to one specific species. It has previously been assigned to the α and β carbons of the pyrrole ring (26). The difference in binding energy between the α and β carbon atoms has been reported as 0.9 eV (27, 28), but the individual lines are difficult to resolve. The peak at 286.3 eV (with intensity almost equal that of the peak at 284.6 eV) is attributed to the carbon atom in the cyano group. This is in disagreement with the assignment previously made with reference to PPY (29), where the peak at 286.2 eV was attributed to carbon bound to the ClO_4^- counterion and the peak at 288.5 eV to the cyano group of trapped acetonitrile solvent. Standard spectra of poly(acrylonitrile) (PAN) and poly(methacrylonitrile) (PMAN), however, have both been used to assign the cyano carbon to 286.7 eV (30). To confirm the assignment, a polypyrrole film was prepared at +1.0 V under identical solution conditions to the PCPY film and XPS analysis performed in the same way. The C 1*s* peak assignments and relative intensities are summarized in Table 1. Comparing the intensities for peaks 1 and 2 shows that the ratio increases from 1:0.30 for PPY to 1:0.90 for PCPY, suggesting that the peak at 286.3 eV arises from both trapped solvent and the inherent cyano group of the PCPY film. As further support for this assignment, it is noted that Barber et al. (31) gave the cyano carbon in pure acetonitrile as 287.3 eV The third peak (288.4 eV) is therefore assigned to a carbonyl group, which could arise from either atmospheric oxidation or interaction with the perchlorate counterion.

The N (1*s*) spectrum contains only one major peak at 400.0 eV and does not yield significant additional information. The Cl (2*p*) spectrum consists of two pairs of overlapped peaks that can be deconvoluted into four peaks at 200.8, 202.3, 207.5, and 209.4 eV representing the $2p_{1/2}$ and $2p_{3/2}$ peaks for two different Cl species. The peak at the lower binding energy can be assigned to Cl^-, which might have leaked from the reference electrode. The peak on the high-binding side is generally attributed to perchlorate ions from the supporting electrolyte.

Table 1. (*a*) Relative peak intensities in the C(1*s*) region for PPY and PCPY.

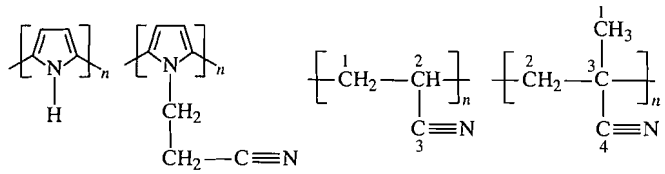

	Peak no.		
	1	2	3
Binding energy (eV)	284.6	286.3	288.4
PPY			
peak intensity	72.3 ± 5	21.4 ± 5	6.3 ± 3
PCPY			
Peak intensity	50.2 ± 3	45.3 ± 4	4.5 ± 2

(*b*) Relative peak intensities in the C(1*s*) region for PAN.[a]

	Peak no.		
	1	2	3
Binding energy (eV)	285.48	286.35	286.73
Peak intensity	34	33	33

(*c*) Relative peak intensities in the C(1*s*) for PMAN.[a]

	Peak no.			
	1	2	3	4
Binding energy (eV)	285.00	285.41	286.46	286.74
Peak intensity	25	25	25	25

[a]Reference 30.

Can. J. Chem. Downloaded from www.nrcresearchpress.com by 80.90.12.36 on 09/08/12
For personal use only.

Table 2. Boiling points and solvation parameters for gas probes.[a]

Solute	bp(°C)	R_2	π_2^*	α_2^H	β_2^H	log L^{16}
Acetonitrile	82	0.237	0.75	0.09	0.44	1.560
Toluene	110	0.601	0.55	0.00	0.14	3.344
Methanol	65	0.278	0.40	0.37	0.41	0.922
Water	100	0.000	0.43	0.33	0.65	0.260
Triethylamine	89	0.101	0.15	0.00	0.67	3.077

[a]References 32, 33.

Can. J. Chem. Downloaded from www.nrcresearchpress.com by 80.90.12.36 on 09/08/12
For personal use only.

Interaction with volatile vapours

To elucidate the dominant mechanisms of interaction for different gases with the PCPY film, five probe molecules were employed, each of which is capable of interacting with the surface in different ways. Possible interactions include π–π overlap, dipole–dipole, hydrogen bond formation, and Lewis acid–base combinations. The responses of PCPY to these probes are compared with those of PPY. Table 2 summarizes the solvation parameters for the probe molecules used in the context of a linear solvation energy relationship for solute – stationary phase interactions in GLC (32, 33). Here, the polarizability parameter R_2 is a measure of the ability of a solute to interact through n and π electrons while the polarity parameter π_2^* is a measure of the ability to support dipole–dipole and dipole – induced dipole interactions. Similarly, the parameters α_2^H and β_2^H indicate the relative gas-phase hydrogen bond acidities and basicities, while log L^{16} accounts for dispersion interactions. All these parameters provide a relative scale for comparing different analytes (34) and, since no quantitative data are available to characterize the solubility properties of both PPY and PCPY films, it is difficult to interpret the results only by these parameters.

Assuming that the Sauerbrey equation is valid for the experimental conditions used, the appropriate frequency shifts yield a direct comparison of the mass of each analyte sorbed on or into the film once the dynamic steady-state response has been reached. Consideration of the number of analyte molecules corresponding to this added mass, however, reveals that this will be influenced by film thickness and porosity, and by the relative rates of adsorption and desorption. The latter will in turn depend on the number and strength of analyte–film interactions, the analyte volatility, the temperature, and the gas-phase molar concentration. In addition, different concentrations were obtained for each analyte, and, since each analyte has a different volatility, it is therefore difficult to normalize the results in order to make a valid comparison between analytes without making some further assumptions. The steady-state frequency shifts obtained for each film–analyte combination were therefore recalculated for a constant film thickness. The validity of this approach is ensured by our results, which demonstrate that there is a linearity between the frequency responses and film thickness. The normalized frequency shifts, which were typically calculated from the average of five consecutive measurements, are listed in Table 3.

The mass uptake under static conditions, which corresponds to the plateau on the curve of frequency against time, represents the equilibrium of sorption between gas and solid phases, which is determined by the thermodynamic factor associated with the interactions between vapor and polymer. The equilibrium involved can be described quantitatively by the partition coefficient, which is related to the frequency shifts by the following equation (35, 36):

$$K = \frac{\Delta f_v \rho}{\Delta f_s C_v}$$

where Δf_v is the sensor frequency shift caused by the vapor sorption C_v is the vapor concentration (gm cm^{-3}), and Δf_s the initial frequency shift due to the deposition of coating. ρ is the density of coating material, 1.48 and 1.40 g cm^{-3} for PPY and PCPY, respectively, obtained from the TSM device measurement in this work. The K and log K values calculated are shown in Table 4. More quantitative information about the solubility interaction can be obtained from the log K value, which is a function of the solvation parameters of the solute (33). It is found that the partition coefficient of acetonitrile for PCPY is twice as large as that for PPY, while K of methanol for PCPY is 1.7 times that for PPY. The K values of toluene for PCPY decrease to one tenth, and the magnitude of K of triethylamine for PCPY also drops to half, compared with those for PPY. The partition coefficients of water for both PPY and PCPY films are almost identical. The K value of methanol for PPY in our work is consistent with that reported in literature (36) if the differences in concentration are taken into account.

An alternative approach is to normalize the frequency shifts by the molar concentration in the gas phase to preclude the factor of molecular weight. The frequency responses thus calculated are shown in Fig. 7. Comparing first the responses of each film to the same analyte, it can be seen that there is a marked decrease in response on going from PPY to PCPY for toluene and triethylamine, whereas an increase is observed for acetonitrile, water, and methanol. The results can be explained by considering the nature of the interaction with the polymer film. The main interaction for toluene will presumably be through π–π stacking of the benzene and pyrrole sub-units, as indicated by its large values for R_2 and log L^{16}. The net favorable interactions are the result of π–σ attractions that overcome π–π electron repulsion. These electrostatic forces determine the geometry of the interaction while van der Waals forces contribute to the magnitude of the interaction (37). Toluene can also interact with PPY through either an orthogonal π–HN bonded model or a non-orthogonal orientation π–dipole interaction (38). Geometric orientation is therefore an important factor for the interaction of toluene with PPY. It was reported that PPY has a helical structure (39–42); however, the presence of the cyanoethyl side chain would be expected to block the helical channel, thus preventing toluene from effectively interacting with the pyrrole ring. Hence, the lowest frequency response of PCPY to toluene could be attributed to the steric effect of the pendant side chain. Although triethylamine has one of the lowest polarizability parameters (R_2), it also has a dispersion parameter (log L^{16}) similar to that of toluene. Furthermore, it is capable of forming a hydrogen bond with the pyrrole N-H (in PPY), which is obviously missing in the case of PCPY. Thus a similar effect would be predicted, i.e., a decrease in response on going from a PPY to a PCPY film, as in fact is observed. Although hydrogen-bonding interactions can be expected to be stronger than π-electron or dispersion interactions, the fact that triethylamine has a higher volatility than toluene explains why the relative responses (corrected for

Table 3. Frequency decreases for TSM-sensor-coated PPY or PCPY films (Hz).

Vapours	Acetonitrile	Toluene	Water	Methanol	Triethylamine
PPY	1875 ± 62	845 ± 19	2581 ± 53	2183 ± 42	1065 ± 45
PCPY	4560 ± 79	83 ± 7	2863 ± 49	3870 ± 76	573 ± 12
Ratio[a]	2.4	0.1	1.1	1.8	0.5

[a]Ratio of the response of PCPY to that of PPY.

Table 4. (*a*) Partition coefficient K and log K values from TSM-sensor-coated PPY.

Vapor	Acetonitrile	Toluene	Water	Methanol	Triethylamine
K	3264	5002	10186	2872	2174
log K	3.51	3.70	4.01	3.45	3.34

(*b*) Partition coefficient K and log K values from TSM-sensor-coated PCPY.

Vapor	Acetonitrile	Toluene	Water	Methanol	Triethylamine
K	7511	465	10689	4816	1106
log K	3.88	2.67	4.03	3.68	3.04

Fig. 7. The responses of TSM-coated PPY or PCPY films to different vapours. The data from Table 3 were normalized with respect to the molar concentration of the vapour.

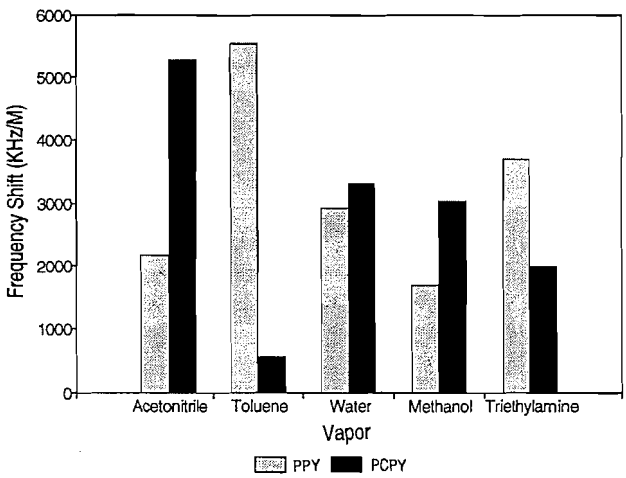

gas-phase molar concentration) should be different in the case of PPY film. The larger response for triethylamine than for toluene for PCPY film is somewhat harder to rationalize, but could well be a function of the shape of the adsorption isotherms for these two analytes, which in turn depends on the volatility of the respective vapours and the strength of the interaction between them and the polymers (43), as well as the assumptions made in the normalization procedure adopted.

Considering the remaining three analytes, acetonitrile is expected to interact with PPY via π–HN (44, 45), but with PCPY principally through dipole–dipole interaction (46) as shown in Figs. 8*a*, *b*, and *c*. Since the cyano group is one of the most polar functionalities, the dipole–dipole interaction between acetonitrile and PCPY is possibly stronger than the π–HN interaction in the case of PPY. Water and methanol are expected to interact through hydrogen bonding, which is through NH—O with PPY (44, 45) and CN—HO with PCPY

Fig. 8. Schematic of the interaction between various analytes and polymer films. (*a*) Acetonitrile interacts with PPY through NH-π; (*b*) and (*c*) acetonitrile interacts with PCPY through dipole–dipole; (*d*) methanol interacts with PPY through hydrogen bonding; (*e*) methanol interacts with PCPY by hydrogen bonding; (*f*) methanol interacts with PCPY through dipole–dipole.

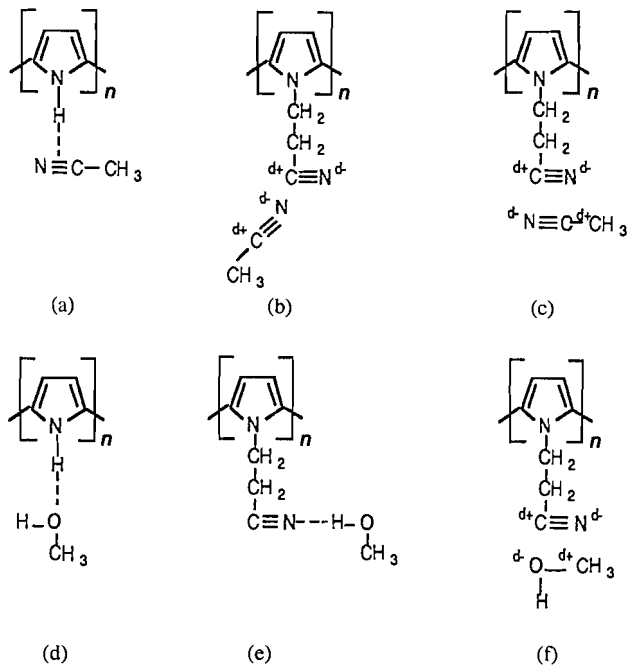

(46) or through π–HO with both polymers (Figs. 8*d* and *e*) (38). Thus the increased response to each analyte on going from PPY to PCPY can be explained by the introduction of the highly polar cyano group, providing an additional dipole–dipole interaction (Fig. 8*f*). Interestingly, the order of responses for the PPY film follows the boiling point order for these three compounds, indicating that at room temperature there is insufficient difference in the relative strengths of specific interactions to overcome simple condensation effects

Can. J. Chem. Downloaded from www.nrcresearchpress.com by 80.90.12.36 on 09/08/12
For personal use only.

(this relationship is not observed if the different gas-phase concentrations are not taken into account). If the ratio of the PCPY to PPY responses from Table 3 is calculated for each analyte, values of 2.4, 1.1, and 1.8 are obtained for acetonitrile, water, and methanol, respectively. Comparing the polarizability (R_2), polarity (π_2^*), and dispersion parameters (log L^{16}) for these three analytes suggests that the principal reasons for these differences are the polarizability and polarity (i.e., dipole–dipole interactions) rather than the ability to form hydrogen bonds with the PCPY cyano group through H-bond donation.

Conclusions

PCPY films provide an additional material for forming chemically selective surfaces on TSM acoustic wave sensors. The highly polar nature of the cyano group allows interaction through alternate mechanisms to hydrogen bonding (for example), so PCPY-coated sensors could usefully be incorporated into sensor arrays where it is the pattern of responses, rather than an absolute value from a single device, that provides the sensor signal and allows a degree of selectivity to be obtained. These films may be deposited electrochemically, and have been characterized in terms of their morphology, surface functional groups, and response to different gas-phase probe molecules. The results of these studies can be correlated with solubility parameters and rationalized on the basis of an understanding of the morphology and structure of the PCPY film. Future work will attempt to correlate these findings with conductivity measurements.

Acknowledgement

Support for this work from the Natural Sciences and Engineering Research Council of Canada is gratefully acknowledged. We also thank K.M.R. Kallury, University of Toronto, for assistance with the XPS measurements.

References

1. J.M. Charlesworth, A.C. Partridge, and N. Garrard. J. Phys. Chem. **97**, 5418 (1993).
2. P.R. Teasdale and G.G. Wallace. Analyst, **118**, 329 (1993).
3. A.F. Diaz and J. Bargon. *In* Handbook of conducting polymers. Vol. 1. *Edited by* T.A. Skotheim. Marcel Dekker, New York. 1986. pp. 81–115.
4. A.F. Diaz, K.K. Kanazawa, and G.P. Gardini. J. Chem. Soc. Chem. Commun. **14**, 635 (1979).
5. J.J. Miasik, A. Hopper, and B.C. Tofield. J. Chem. Soc. Faraday Trans. 1, **82**, 1117 (1982).
6. P.N. Barlett and S.K. Ling-Chung. Sens. Actuators, **20**, 287 (1989).
7. G.Z. Sauerbrey. J. Phys. **155**, 206 (1959).
8. P. Topart and M. Josowicz. J. Phys. Chem. **96**, 8662 (1992).
9. Y. Kunugi, K. Nigorikawa, Y. Harima, and K. Yamashita. J. Chem. Soc. Chem. Commun. **7**, 873 (1994).
10. J.M. Slater, J. Paynter, and E.J. Watt. Analyst, **118**, 379 (1993).
11. M.D. Imisides, R. John, P.J. Riley, and G.G. Wallace. Electroanalysis, **3**, 879 (1991).
12. D.M.T. O'Riordan and G.G. Wallace. Anal. Chem. **58**, 128 (1986).
13. M.J. Spemer, P.R. Teasdale, and G.G. Wallace. Anal. Chim. Acta, **263**, 71 (1992).
14. S.J. Vigmond, K.M.R. Kallury, V. Gheammaghami, and M. Thompson. Talanta, **39**, 449 (1992).
15. D.L. Feldheim, M.Krejcik, S.M. Hendrickson, and C.M. Elliott. J. Phys. Chem. **98**, 5714 (1994).
16. D.L. Feldheim, S.M. Hendrickson, M. Krejcik, and C.M. Elliott. J. Phys. Chem. **99**, 3288 (1995).
17. H. Ge and G.G. Wallace. J. Chromatogr. **588**, 25 (1991).
18. M.E.G. Lyons, C.H. Lyons, C. Fitzgerald, and T. Bannor. Analyst, **118**, 361 (1993).
19. M.E.H. Amrani, M.S. Ibrahim, and K.C. Persaud. Mater. Sci. Eng. **C: 1**, 17 (1993).
20. Y. Wei, C.C. Chan, J. Tian, G.W. Jang, and K.F. Hsuch. Chem. Mater. **3**, 888 (1991).
21. A. Yassar, J. Roneali, and F. Garnier. Macromolecules, **22**, 804 (1989).
22. J.R. Reynolds, S.G. Hsu, and H.J. Arnott. J. Polym. Sci. B: Polym. Phys. **27**, 2081 (1989).
23. T.R. Jow, K.Y. Jen, R.L. Elsenbaumer, and L.M. Shacklette. Synth. Met. **14**, 53 (1986).
24. G. Tourillon. *In* Handbook of conducting polymers. Vol. 1. *Edited by* T.A. Skotheim. Marcel Dekker. New York. 1986. pp. 293–350.
25. E.W. Tsai, S. Basak, J.P. Ruiz, J.R. Reynolds, and K. Rajeshwar. J. Electrochem. Soc. **136**, 3683 (1989).
26. P. Pfluger and G.B. Street. J. Chem. Phys. **80**, 544 (1984).
27. U. Gelius, C.J. Allan, G. Johansson, H. Siegbahn, D.A. Allison, and K. Siegbahn. Phys. Scr. **3**, 237 (1971).
28. D.T. Clark and D.M. Lilley. J. Chem. Phys. Lett. **9**, 234 (1971).
29. G. Morea, L. Sabbatini, P.G. Zambonin, A.J. Swift, R.H. West, and J.C. Vickerman. Macromolecules, **24**, 3630 (1991).
30. G. Beamson and D. Briggs. High resolution XPS of organic polymers: The Scienta ESCA300, database. Wiley, New York. 1992. pp. 184–186.
31. M. Barber, J.A. Connor, M.F. Guest, I.H. Hillier, M. Schwarz, and M. Stacey. J. Chem. Soc. Faraday Trans. 2, **69**, 551 (1973).
32. M.H. Abraham, G.S. Whiting, R.M. Doherty, and W.J. Shuely. J. Chem. Soc. Perkin Trans. **2**, 1451 (1990).
33. M.H. Abraham, G.S. Whiting, R.M. Doherty, and W.J. Shuely. J. Chem. Soc. Perkin Trans. **2**, 1851 (1990).
34. D.S. Ballantine, Jr. S.L. Rose, J.W. Grate, and H. Wohltjen. Anal. Chem. **58**, 3058 (1986).
35. J.W. Grate, S. Arthur, D.S. Ballantine, Jr., H. Wohltjen, M.H. Abraham, R.A McGill, and P. Sasson. Anal. Chem. **60**, 869 (1988).
36. P. Topart and M. Josowicz. J. Phys. Chem. **96**, 7824 (1992).
37. A.C. Hunter and J.K.M. Sanders. J. Am. Chem. Soc. **112**, 5525 (1990).
38. R.A. Jones and G.P. Bean. The chemistry of pyrrole. Academic Press, New York. 1977. pp. 439–445.
39. R. Yang, D.F. Evans, L. Christensen, and W.A. Hendrickson. J. Phys. Chem. **94**, 6117 (1990).
40. G.R. Mitchell and A.J. Geri. J. Phys. D: Appl. Phys. **20**, 1346 (1987).
41. F. Garnier, G. Tourillon, J.Y. Barraud, and H.J. Dexpert. Mater. Sci. **20**, 2687 (1985).
42. R. Yang, K.M. Dalsin, D.F. Evans, L. Christensen, and W.A. Hendrickson. J. Phys. Chem. **93**, 511 (1989).
43. E.T. Zellers, S.A. Batterman, M. Han, and S.J. Patrash. Anal. Chem. **67**, 1092 (1995).
44. D.J. Chadwick. *In* Pyrroles. *Edited by* R.A. Jones. Wiley, New York. 1990. pp. 1–103.
45. M. Josowicz, J. Janata, K.Ashley, and S. Pons. Anal. Chem. **59**, 253 (1987).
46. J. Grundnes. *In* The chemistry of the cyano group. *Edited by* Z. Rappoport. Wiley, New York. 1970. pp. 123–166.

Can. J. Chem. Downloaded from www.nrcresearchpress.com by 80.90.12.36 on 09/08/12
For personal use only.

The crystal and molecular structure of chlorotriphenyl(isoquinolinium-1-carboxylato)tin(IV)

Frank E. Smith, Lian Ee Khoo, Lian Sai Chia, and Rosemary C. Hynes

Abstract: The synthesis and crystal structure of the 1:1 complex formed between triphenyltin chloride and isoquinoline-1-carboxylic acid ($[Ph_3SnCl:C_{10}H_7NO_2]$) is described. The tin(IV) atom is found to be five coordinate, being bound to three phenyl groups, the chlorine atom, and an oxygen from isoquinoline-1-carboxylic acid. The geometry around the tin atom is that of a trigonal bipyramid, with the three phenyl groups occupying the equatorial positions, and the apical sites taken by the chlorine atom and a carboxyl oxygen from the isoquinoline-1-carboxylic acid. The crystals are triclinic, space group $P\bar{1}$, with $a = 17.932(12)$ Å, $b = 17.935(15)$ Å, $c = 18.686(12)$ Å, $\alpha = 63.16(5)°$, $\beta = 81.70(6)°$, $\gamma = 68.45(6)°$, $V = 4986(6)(10)$ Å^3, $Z = 8$, and $D_{calc} = 1.486$ Mg m^{-3}. The final residual is $R_F = 0.050$, on 8375 reflections with $I_{net} > 2.5\sigma(I_{net})$. Two of the cell dimensions are equivalent and there are four molecular units in the unit cell, so precautions are described for ensuring that correct space-group determination had been made and that some concealed symmetry in the final structure had not been overlooked.

Key words: triorganotin, complex, isoquinoline-1-carboxylic acid, fungicidal activity.

Résumé : On décrit la synthèse et la structure cristalline du complexe 1 : 1 formé entre le chlorure de triphénylétain et l'acide isoquinoléine-1-carboxylique ($[Ph_3SnCl : C_{10}H_7NO_2]$). On a trouvé que l'atome d'étain(IV) est pentacoordiné; il est lié à trois groupes phényles, à un atome de chlore et à un oxygène de l'acide isoquinoléine-1-carboxylique. La géométrie autour de l'atome d'étain est une bipyramide trigonale dans laquelle les trois groupes phényles occupent les positions équatoriales alors que les positions apicales sont occupées par l'atome de chlore et un oxygène carboxylique de l'acide isoquinoléine-1-carboxylique. Les cristaux sont tricliniques, groupe d'espace $P\bar{1}$, avec $a = 17,932(12)$, $b = 17,935(15)$ et $c = 18,686(12)$ Å, $\alpha = 63,16(5)°$, $\beta = 81,70(6)°$ et $\gamma = 68,45(6)°$, $V = 4986(6)(10)$ Å^3, $Z = 8$ et $D_{calc} = 1,486$ Mg m^{-3}. La valeur résiduelle finale, $R_F = 0,050$, pour 8375 réflexions avec $I_{net} > 2,5\sigma(I_{net})$. Deux des dimensions de la cellule sont équivalentes et il y a quatre unités moléculaires par motif cellulaire; on décrit donc les précautions qu'il faut prendre pour s'assurer que le groupe d'espace a bien été déterminé et que certaines symétries cachées de la structure finale n'ont pas été omises.

Mots clés : triorganoétain, complexe, acide isoquinoléine-1-carboxylique, activité fongicide.

[Traduit par la rédaction]

Introduction

In almost all instances, carboxylic acids form tin complexes in their deprotonated (carboxylate) forms, but there are a few cases of coordination to tin by the electrically neutral acids (1). For example, picolinic acid and quinaldic acid have been reported to form complexes with triphenyltin chloride (2, 3) and isothiocyanate (4). In each of these complexes, the structures are similar, with the acid in the form of its zwitterion behaving as a monodentate ligand and bonding to the triphenyltin moiety via a carboxylate oxygen. The resulting five-coordinate organotin species have a trigonal bipyramidal geometry, but are held together in pairs through hydrogen bonding. The hydrogen bonding may be between the heterocyclic N-atoms and uncoordinated carboxylate oxygens of different molecules in the pair (2), or through uncoordinated water molecules positioned between the two units (3, 4).

These compounds, as well as displaying most unusual structures, have also shown promising fungicidal activity (5). The use of triphenyltin compounds as fungicides is well documented (6–11). However, when fungicides are to be used on living vegetation, the phytocidal properties of the compounds are also of great significance. Triphenyltin chloride adducts have been shown to possess a high fungicidal to phytocidal ratio (12) and we have therefore been prompted to commence the synthesis of a series of analogous complexes between

Received May 27, 1994.[1]

F.E. Smith.[2] Chemistry Department, Laurentian University, Sudbury, ON P3E 2C6, Canada.
L.E. Khoo and L.S. Chia. School of Science, Nanyang Technological University, 469, Bukit Timah Road, Singapore 1025. Singapore.
R.C. Hynes. Biochemistry Department, University of Toronto, Toronto, ON M5S 1A1, Canada.

[1] Revision received May 12, 1995.
[2] Author to whom correspondence may be addressed. Telephone: (705) 675-1151, ext. 2101. Fax: (705) 675-4844. E-mail: fsmith@nickel.laurentian.ca

Can. J. Chem. Downloaded from www.nrcresearchpress.com by 80.90.12.36 on 09/08/12
For personal use only.

Can. J. Chem. Downloaded from www.nrcresearchpress.com by 80.90.12.36 on 09/08/12
For personal use only.

triphenyltin chloride and other protonated carboxylic acids containing heterocyclic nitrogen atoms. We describe here the synthesis and crystal structure of one such complex, that formed between triphenyltin chloride and isoquinoline-1-carboxylic acid.

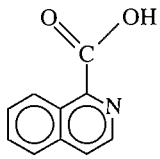

Isoquinoline-1-carboxylic acid

Experimental

Preparation of chlorotriphenyl(isoquinolinium-1-carboxylato)tin(IV)

The 1:1 adduct, Ph_3SnCl:isoquinoline-1-carboxylic acid, was obtained as a white crystalline solid in good yield (90%) by mixing hot ethanol solutions containing stoichiometric quantities of triphenyltin chloride and isoquinoline-1-carboxylic acid. The complex crystallized in the refrigerator, was filtered off, washed with cold ethanol, and then recrystallized from ethanol (mp 125–127°C (dec.)). Microanalyses were performed at Universiti Sains Malaysia. Analytical data for $Ph_3SnCl:C_{10}H_7NO_2$: Anal. calcd. for $C_{28}H_{22}NO_2ClSn$(%): C 60.19, H 3.92, N 2.51; found(%): C 59.92, H 4.07, N 2.42.

X-ray analysis

Space group and cell dimensions

The crystals are triclinic, space group $P\bar{1}$ with a = 17.932(12) Å, b = 17.935(15) Å, c = 18.686(12) Å, α = 63.16(5)°, β = 81.70(6)°, γ = 68.45(6)°, V = 4986(6)(10) Å^3, Z = 8, and D_{calc} = 1.486 Mg m^{-3}. Crystal dimensions: 0.33 × 0.30 × 0.30 mm. Empirical formula: $C_{28}H_{22}NO_2ClSn$ or $[Ph_3SnCl:C_{10}H_7NO_2]$. FW = 558.62, F(000) = 2226.85, μ = 1.16 mm^{-1}, λ = 0.70930 Å.

Data collection, structure solution and refinement

Cell dimensions were obtained from 25 reflections with 2θ in the range 30°–40°. The intensity data were collected at 293 K on a Rigaku model AFC6S diffractometer run by the TEXRAY[3] diffractometer control program, using the $\theta/2\theta$ scan mode and $Mo_{K\alpha}$ radiation (λ = 0.70930 Å). A total of 13 408 reflections were measured, of which 12 904 were unique. Of these, 8375 had $I_{net} > 2.5\sigma(I_{net})$ and merging R was 4.6% for 504 pairs of symmetry-related reflections. The h, k, and l ranges were −17 to 19, 0 to 19, and −17 to 20, respectively, and $2\theta_{max}$ was 45°. Absorption corrections were made from four ψ-scan curves (13). The minimum and maximum transmission factors are 0.665 and 0.770. The structure was solved by direct methods (SOLVER (14)), followed by a difference Fourier. Refinement was by block-diagonal least-squares cycles. Phenyl rings were refined as rigid groups with carbons anisotropic. All hydrogens were given calculated positions and assigned fixed isotropic thermal parameters equal to 0.01 + U_{eq} of the bonded atom. All other atoms were refined anisotropically. The final least-squares cycle was calculated with 216 atoms and 1045 parameters and 8375 out of 12 904 reflections. Weights based on counting statistics were used. Final residuals are R_F = 0.050, R_W = 0.045 for data with $I_{net} > 2.5\sigma(I_{net})$, R_F = 0.099, R_W = 0.047 for all data. The goodness of fit was 1.67. Maximum shift/error was 0.094. In the last difference Fourier map, the top peak was 0.670 e/Å^3, and the deepest hole was −0.560 e/Å^3. Scattering factors were taken from the literature (15). Structure solution and refinement was performed using the NRCVAX system of crystal structure solving programs (14).

[3] The Molecular Structure Corporation, Woodlands, Tex., U.S.A.

Fig. 1. Molecular structure and atom numbering scheme.

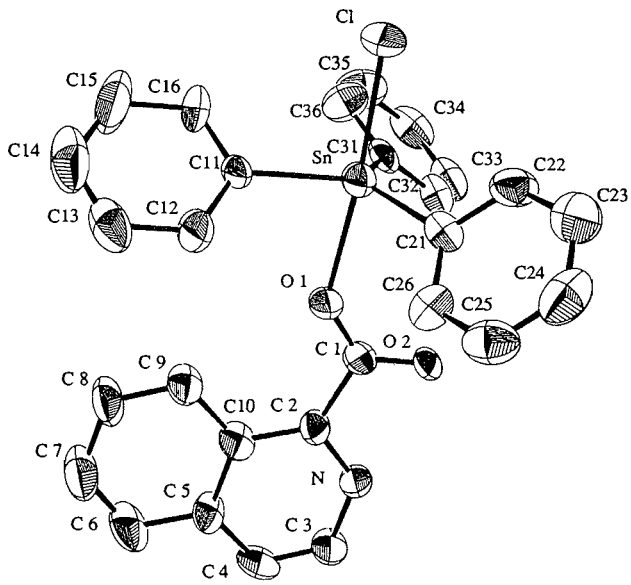

Fig. 2. Packing in the unit cell.

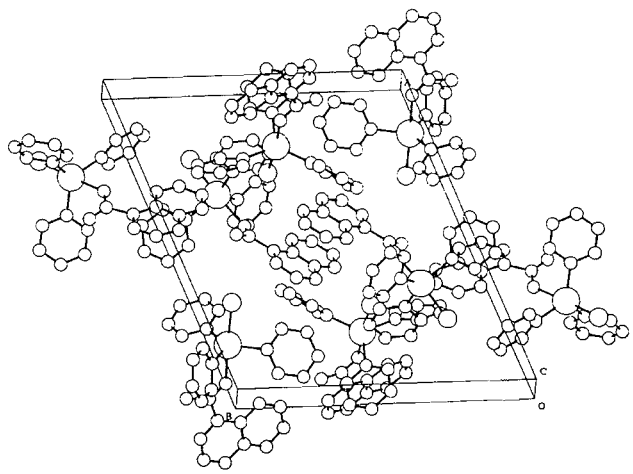

Results and discussion

The tin(IV) atom is found to be five coordinate, being bound to three phenyl groups, the chlorine atom, and an oxygen from isoquinoline-1-carboxylic acid. The geometry around the tin atom is that of a trigonal bipyramid, with the three phenyl groups occupying the equatorial positions, and the apical sites taken by the chlorine atom and a carboxyl oxygen from the isoquinoline-1-carboxylic acid. The molecular structure and crystallographic numbering scheme are shown as an ORTEP

Table 1. Atomic parameters x, y, z and B_{eq}. ESDs refer to the last digit printed.

	x	y	z	B_{eq}[a]
SnA	0.21910(4)	0.47993(4)	0.19415(4)	3.37(4)
C1A	0.29562(17)	0.41830(18)	0.32120(15)	4.62(17)
O 1A	0.1450 (4)	0.5269 (4)	0.0777 (4)	4.1 (4)
O 2A	0.0844 (4)	0.6748 (4)	0.0231 (4)	4.0 (4)
NA	0.0222 (5)	0.6789 (5)	−0.0954 (4)	3.7 (5)
C 1A	0.1021 (6)	0.5997 (6)	0.0262 (5)	3.4 (6)
C 2A	0.0665 (5)	0.5988 (6)	−0.0430 (5)	3.1 (5)
C 3A	−0.0125 (7)	0.6948 (6)	−0.1630 (6)	4.9 (7)
C 4A	−0.0012 (7)	0.6277 (7)	−0.1811 (6)	5.2 (7)
C 5A	0.0454 (6)	0.5407 (6)	−0.1312 (6)	3.6 (6)
C 6A	0.0594 (7)	0.4664 (7)	−0.1474 (7)	5.2 (8)
C 7A	0.1026 (7)	0.3828 (7)	−0.0956 (7)	5.9 (8)
C 8A	0.1348 (7)	0.3675 (7)	−0.0250 (7)	5.2 (7)
C 9A	0.1239 (6)	0.4348 (6)	−0.0053 (6)	4.0 (6)
C10A	0.0796 (6)	0.5247 (6)	−0.0588 (5)	3.5 (6)
C11A	0.2559 (4)	0.3525 (3)	0.1934 (4)	3.6 (6)
C12A	0.2826 (4)	0.3401 (4)	0.1244 (3)	4.7 (7)
C13A	0.3012 (4)	0.2567 (5)	0.1259 (4)	6.6 (9)
C14A	0.2932 (5)	0.1857 (4)	0.1965 (5)	7.6 (10)
C15A	0.2665 (5)	0.1981 (4)	0.2656 (4)	8.3 (10)
C16A	0.2479 (4)	0.2815 (4)	0.2640 (3)	5.8 (8)
C21A	0.2804 (3)	0.5708 (4)	0.1233 (4)	3.2 (6)
C22A	0.3093 (4)	0.6068 (4)	0.1612 (3)	4.9 (8)
C23A	0.3540 (4)	0.6620 (4)	0.1185 (4)	6.5 (9)
C24A	0.3699 (4)	0.6813 (4)	0.0379 (4)	6.0 (8)
C25A	0.3411 (4)	0.6454 (4)	0.0000 (3)	5.0 (7)
C26A	0.2963 (4)	0.5901 (4)	0.0427 (4)	4.1 (6)
C31A	0.1084 (3)	0.5167 (4)	0.2510 (4)	3.4 (6)
C32A	0.0559 (4)	0.6045 (4)	0.2201 (3)	3.9 (7)
C33A	−0.0160 (3)	0.6276 (4)	0.2580 (4)	5.3 (8)
C34A	−0.0355 (3)	0.5628 (5)	0.3268 (4)	5.3 (8)
C35A	0.0169 (4)	0.4749 (4)	0.3577 (3)	6.3 (9)
C36A	0.0888 (4)	0.4519 (3)	0.3198 (4)	4.9 (7)
SnB	0.66803(4)	0.76446(5)	0.24160(4)	3.85(4)
C1B	0.78798(16)	0.79980(18)	0.17401(16)	5.11(17)
O 1B	0.5613 (4)	0.7217 (4)	0.3048 (4)	4.4 (4)
O 2B	0.5291 (4)	0.7634 (4)	0.4050 (4)	4.3 (4)
NB	0.4304 (4)	0.6747 (5)	0.4662 (4)	3.4 (4)
C 1B	0.5255 (5)	0.7230 (6)	0.3675 (5)	3.4 (6)
C 2B	0.4684 (5)	0.6016 (6)	0.3801 (5)	3.3 (6)
C 3B	0.3794 (6)	0.6299 (6)	0.5068 (6)	4.1 (6)
C 4B	0.3737 (6)	0.5671 (6)	0.4877 (6)	4.2 (6)
C 5B	0.4183 (6)	0.5505 (6)	0.4253 (6)	4.1 (6)
C 6B	0.4144 (6)	0.4855 (6)	0.4063 (6)	4.6 (7)
C 7B	0.4588 (7)	0.4703 (7)	0.3435 (7)	5.7 (8)
C 8B	0.5063 (7)	0.5200 (8)	0.3006 (7)	6.4 (9)
C 9B	0.5124 (7)	0.5847 (7)	0.3158 (6)	4.6 (7)
C10B	0.4733 (5)	0.6638 (6)	0.4048 (5)	3.3 (5)
C11B	0.6554 (5)	0.7022 (5)	0.1722 (4)	4.4 (7)
C12B	0.7094 (4)	0.6185 (5)	0.1829 (4)	6.9 (9)
C13B	0.6976 (5)	0.5761 (4)	0.1408 (5)	8.7 (12)
C14B	0.6319 (6)	0.6174 (6)	0.0880 (5)	8.9 (12)
C15B	0.5779 (5)	0.7011 (6)	0.0773 (4)	9.2 (13)
C16B	0.5896 (4)	0.7435 (4)	0.1194 (5)	7.0 (9)
C21B	0.7341 (4)	0.6833 (4)	0.3530 (3)	4.0 (6)
C22B	0.7358 (4)	0.5960 (4)	0.3984 (4)	5.7 (8)

Can. J. Chem. Downloaded from www.nrcresearchpress.com by 80.90.12.36 on 09/08/12
For personal use only.

Table 1 (*continued*).

	x	*y*	*z*	B_{eq}[a]
C23B	0.7799 (5)	0.5432 (3)	0.4706 (4)	6.0 (8)
C24B	0.8222 (4)	0.5778 (5)	0.4974 (3)	5.8 (8)
C25B	0.8204 (4)	0.6651 (5)	0.4519 (4)	6.6 (9)
C26B	0.7764 (5)	0.7179 (3)	0.3797 (4)	6.0 (9)
C31B	0.5947 (4)	0.9003 (3)	0.2081 (4)	4.3 (7)
C32B	0.6296 (3)	0.9621 (5)	0.1985 (4)	5.5 (8)
C33B	0.5830 (5)	1.0520 (4)	0.1707 (4)	7.1 (9)
C34B	0.5016 (5)	1.0800 (3)	0.1526 (4)	6.9 (9)
C35B	0.4668 (3)	1.0182 (5)	0.1623 (4)	7.5 (10)
C36B	0.5134 (4)	0.9284 (4)	0.1900 (4)	5.1 (7)
SnC	0.18736(4)	0.94435(5)	0.26286(4)	3.71(4)
C1C	0.31707(18)	0.87313(20)	0.34032(18)	6.06(21)
O 1C	0.0701 (4)	1.0032 (4)	0.1839 (4)	4.0 (4)
O 2C	0.0311 (4)	1.1511 (4)	0.1172 (4)	4.5 (4)
NC	−0.0948 (4)	1.1603 (5)	0.0544 (5)	4.0 (5)
C 1C	0.0265 (6)	1.0772 (6)	0.1354 (5)	3.4 (6)
C 2C	−0.0406 (5)	1.0800 (6)	0.0909 (5)	3.1 (6)
C 3C	−0.1590 (6)	1.1762 (7)	0.0115 (7)	5.4 (7)
C 4C	−0.1702 (7)	1.1101 (7)	0.0040 (7)	5.4 (8)
C 5C	−0.1145 (6)	1.0226 (6)	0.0413 (5)	3.6 (6)
C 6C	−0.1253 (7)	0.9528 (7)	0.0314 (6)	4.9 (8)
C 7C	−0.0684 (7)	0.8700 (7)	0.0672 (6)	5.3 (8)
C 8C	−0.0046 (7)	0.8532 (6)	0.1122 (6)	5.0 (8)
C 9C	0.0078 (6)	0.9185 (6)	0.1223 (6)	4.2 (7)
C10C	−0.0483 (5)	1.0058 (6)	0.0869 (5)	3.2 (6)
C11C	0.1665 (4)	0.8221 (3)	0.3009 (3)	3.8 (6)
C12C	0.2298 (3)	0.7449 (5)	0.3079 (4)	5.2 (8)
C13C	0.2151 (4)	0.6664 (4)	0.3296 (4)	6.3 (8)
C14C	0.1370 (5)	0.6650 (4)	0.3442 (4)	7.0 (9)
C15C	0.0737 (4)	0.7421 (5)	0.3372 (4)	6.0 (8)
C16C	0.0884 (4)	0.8206 (4)	0.3156 (4)	4.7 (7)
C21C	0.2478 (4)	0.9863 (4)	0.1536 (3)	3.3 (6)
C22C	0.3062 (4)	0.9214 (3)	0.1347 (4)	5.8 (8)
C23C	0.3490 (4)	0.9463 (5)	0.0644 (4)	6.5 (9)
C24C	0.3334 (4)	1.0361 (6)	0.0130 (3)	6.3 (9)
C25C	0.2751 (4)	1.1011 (4)	0.0319 (3)	5.4 (8)
C26C	0.2323 (3)	1.0762 (4)	0.1022 (4)	4.4 (7)
C31C	0.1265 (4)	1.0241 (4)	0.3263 (4)	4.0 (7)
C32C	0.0432 (4)	1.0637 (5)	0.3224 (4)	6.3 (9)
C33C	0.0058 (4)	1.1136 (5)	0.3654 (5)	7.9 (10)
C34C	0.0517 (5)	1.1238 (5)	0.4123 (5)	8.3 (11)
C35C	0.1350 (5)	1.0842 (6)	0.4163 (4)	9.3 (13)
C36C	0.1724 (3)	1.0343 (5)	0.3733 (4)	6.8 (10)
SnD	0.73735(5)	1.22057(5)	0.28939(4)	4.18(5)
C1D	0.80086(19)	1.29826(19)	0.16270(17)	6.21(23)
O 1D	0.6821 (4)	1.1359 (4)	0.4038 (4)	4.4 (4)
O 2D	0.5925 (4)	1.2245 (4)	0.4530 (4)	4.6 (5)
ND	0.5506 (5)	1.0949 (5)	0.5651 (4)	4.0 (5)
C 1D	0.6278 (6)	1.1533 (6)	0.4499 (5)	3.5 (6)
C 2D	0.5990 (6)	1.0759 (6)	0.5105 (5)	3.3 (6)
C 3D	0.5194 (7)	1.0357 (7)	0.6247 (6)	4.9 (7)
C 4D	0.5359 (7)	0.9529 (7)	0.6301 (6)	5.7 (8)
C 5D	0.5862 (7)	0.9289 (7)	0.5729 (6)	4.7 (7)
C 6D	0.6042 (7)	0.8445 (6)	0.5746 (6)	5.5 (8)
C 7D	0.6515 (8)	0.8234 (7)	0.5182 (7)	6.8 (9)

Can. J. Chem. Downloaded from www.nrcresearchpress.com by 80.90.12.36 on 09/08/12
For personal use only.

Table 1 (*concluded*).

	x	*y*	*z*	B_{eq}[a]
C 8D	0.6862 (8)	0.8834 (8)	0.4589 (7)	6.7 (9)
C 9D	0.6710 (7)	0.9655 (7)	0.4548 (6)	5.2 (7)
C10D	0.6206 (6)	0.9899 (6)	0.5109 (6)	3.9 (6)
C11D	0.7972 (4)	1.0917 (4)	0.2907 (4)	4.9 (7)
C12D	0.7802 (4)	1.0766 (5)	0.2289 (4)	5.5 (8)
C13D	0.8130 (5)	0.9916 (6)	0.2318 (4)	6.8 (10)
C14D	0.8627 (5)	0.9219 (4)	0.2964 (5)	7.7 (10)
C15D	0.8797 (4)	0.9371 (4)	0.3582 (4)	8.0 (10)
C16D	0.8470 (4)	1.0220 (5)	0.3553 (4)	6.2 (8)
C21D	0.7837 (4)	1.2612 (5)	0.3589 (4)	4.2 (6)
C22D	0.7976 (4)	1.2089 (4)	0.4413 (4)	4.8 (7)
C23D	0.8306 (5)	1.2342 (5)	0.4862 (3)	7.0 (10)
C24D	0.8497 (5)	1.3118 (6)	0.4488 (5)	7.8 (11)
C25D	0.8357 (5)	1.3642 (4)	0.3665 (5)	9.9 (13)
C26D	0.8027 (5)	1.3389 (4)	0.3215 (3)	6.6 (9)
C31D	0.6201 (3)	1.2879 (5)	0.2350 (4)	4.1 (7)
C32D	0.5933 (4)	1.3798 (5)	0.1887 (4)	5.5 (8)
C33D	0.5178 (5)	1.4231 (3)	0.1509 (4)	6.5 (8)
C34D	0.4690 (3)	1.3745 (5)	0.1593 (4)	6.6 (9)
C35D	0.4957 (4)	1.2826 (5)	0.2056 (5)	6.9 (9)
C36D	0.5712 (4)	1.2393 (3)	0.2435 (4)	5.6 (8)

The following atoms are the symmetry equivalents:

Name	*x*	*y*	*z*			
NCa	0.09478	0.83971	−0.05443	$-x$	2.000 $-y$	$-z$
NDb	0.44935	0.90507	0.43494	1.000 $-x$	2.000 $-y$	1.000 $-z$
NAa	−0.02222	1.32112	0.09538	$-x$	2.000 $-y$	$-z$
NBb	0.56958	1.32532	0.53385	1.000 $-x$	1.000 $-y$	1.000 $-z$

[a] B_{eq} is the mean of the principal axes of the thermal ellipsoid.

Can. J. Chem. Downloaded from www.nrcresearchpress.com by 80.90.12.36 on 09/08/12
For personal use only.

[16] plot in Fig. 1 while Fig. 2 is a drawing illustrating the packing in the very large unit cell, which contains four molecular units designated A, B, C, and D. The final fractional coordinates of non-hydrogen atoms with equivalent isotropic thermal parameters are listed in Table 1, while the bond lengths and bond angles for the complex are in Tables 2 and 3, respectively. Calculated hydrogen atom parameters and anisotropic thermal parameters have been deposited as Tables S-1, S-2, and S-3, respectively.[4]

Once the space group had been determined as $P\bar{1}$ with two of the cell dimensions equivalent and four molecular units in the unit cell, it became essential to ensure that the space-group had been correctly determined and that some concealed symmetry in the final structure had not been overlooked. The crystallographic software used, NRCVAX [14], provides routines for cell reduction (CREDUC) and the identification of missed symmetry (MISSYM), both of which were run to double check this most unusual cell. The cell reduction program did identify a pseudo-monoclinic cell. The transformation:

$$\begin{bmatrix} -1 & 0 & 0 \\ 0 & -1 & 2 \\ 0 & 1 & 0 \end{bmatrix}$$

gives an A-centred monoclinic cell with dimensions a = 17.932, b = 33.360, c = 17.935 Å, β = 111.55°, but the δ (deviation of α and γ from 90 degrees) is unacceptably high at 2.343°. Further analysis confirmed the original space-group determination to have been correct.

There are two close contacts with an adjacent trigonal bipyramidal molecule and we propose that these dissymmetric trigonal bipyramidal units are linked together by hydrogen bonding into centrosymmetrically related pairs (A–C and B–D). While it proved impossible to locate the acidic protons on the electron density map, it appears that they are situated between the molecules in each dimer in such a position as to facilitate the formation of hydrogen bonds between each of the

[4] These data can be purchased from: The Depository of Unpublished Data, Document Delivery, CISTI, National Research Council Canada, Ottawa, Canada K1A 0S2. Calculated and observed structure factors may be obtained from the author. The tables of hydrogen atom parameters have also been deposited with the Cambridge Crystallographic Data Centre, and can be obtained on request from The Director, Cambridge Crystallographic Data Centre, University Chemical Laboratory, 12 Union Road, Cambridge, CB2 1EZ, U.K.

Can. J. Chem. Downloaded from www.nrcresearchpress.com by 80.90.12.36 on 09/08/12
For personal use only.

Table 2. Bond distances in angstroms.

Sn(A)—Cl(A)	2.489(3)	Sn(C)—O(1C)	2.361(6)
Sn(A)—O(1A)	2.359(6)	Sn(C)—Cl(C)	2.501(4)
O(1A)—C(1A)	1.250(11)	O(1C)—C(1C)	1.245(11)
O(2A)—C(1A)	1.240(10)	O(2C)—C(1C)	1.242(11)
NA—C(2A)	1.330(11)	NC—C(2C)	1.326(11)
NA—C(3A)	1.354(11)	NC—C(3C)	1.368(13)
C(1A)—C(2A)	1.531(12)	C(1C)—C(2C)	1.533(12)
C(2A)—C(10A)	1.420(12)	C(2C)—C(10C)	1.423(12)
C(3A)—C(4A)	1.331(14)	C(3C)—C(4C)	1.340(15)
C(4A)—C(5A)	1.398(14)	C(4C)—C(5C)	1.417(14)
C(5A)—C(6A)	1.423(13)	C(5C)—C(6C)	1.427(13)
C(5A)—C(10A)	1.431(13)	C(5C)—C(10C)	1.423(13)
C(6A)—C(7A)	1.356(15)	C(6C)—C(7C)	1.371(16)
C(7A)—C(8A)	1.387(15)	C(7C)—C(8C)	1.379(16)
C(8A)—C(9A)	1.358(13)	C(8C)—C(9C)	1.365(13)
C(9A)—C(10A)	1.436(13)	C(9C)—C(10C)	1.415(13)
Sn(B)—Cl(B)	2.473(3)	Sn(D)—Cl(D)	2.500(4)
Sn(B)—O(1B)	2.292(6)	Sn(D)—O(1D)	2.328(6)
O(1B)—C(1B)	1.258(11)	O(1D)—C(1D)	1.251(11)
O(2B)—C(1B)	1.236(11)	O(2D)—C(1D)	1.224(11)
NB—C(3B)	1.359(12)	ND—C(2D)	1.322(12)
NB—C(10B)	1.335(11)	ND—C(3D)	1.368(12)
C(1B)—C(10B)	1.537(13)	C(1D)—C(2D)	1.556(13)
C(2B)—C(5B)	1.431(13)	C(2D)—C(10D)	1.441(13)
C(2B)—C(9B)	1.427(13)	C(3D)—C(4)	1.362(15)
C(2B)—C(10B)	1.419(13)	C(4D)—C(5D)	1.412(15)
C(3B)—C(4B)	1.365(14)	C(5D)—C(6D)	1.412(14)
C(4B)—C(5B)	1.399(14)	C(5D)—C(10D)	1.438(14)
C(5B)—C(6B)	1.390(14)	C(6D)—C(7D)	1.357(16)
C(6B)—C(7B)	1.395(16)	C(7D)—C(8D)	1.410(17)
C(7B)—C(8B)	1.370(17)	C(8D)—C(9D)	1.364(15)
C(8B)—C(9B)	1.358(14)	C(9D)—C(10D)	1.399(14)

uncoordinated carboxylic acid oxygen atoms and heterocyclic nitrogen atoms of the two molecules in the dimer. A very similar hydrogen bonding scheme was found for the analogous complex of picolinic acid with triphenyltin chloride (2), for which the position of the acidic proton was located precisely. In the picolinic acid complex, the acidic proton is bonded to the nitrogen of the pyridine ring. The acid is thus coordinated in the form of a zwitterion. Each acidic proton is involved in a bifurcated hydrogen bond to the corresponding uncoordinated carboxylate oxygen atoms in each member of the pair of centrosymmetrically related molecules, thus holding the two molecules in close proximity.

We believe the hydrogen bonding scheme present in the title complex to be very similar to that found for the analogous picolinic acid complex, with the acidic protons H-bonding to the symmetry-related O(2) of another molecule. Figure 3 is a schematic drawing the intra- and inter-molecular close N–O contacts in both sets of hydrogen-bonded dimeric pairs. The distances given show that the two pairs have almost identical configurations. Table 4 gives a selection of bond distances and interatomic separations for the title complex (molecule A and dimer A–C) and the picolinic acid complex.

The similarity in the atomic separations listed in Table 4 is consistent with the two related compounds having a similar hydrogen bonding scheme. If the acidic protons are included

Fig. 3. Inter- and intramolecular N—O distances in the dimeric units of the title complex.

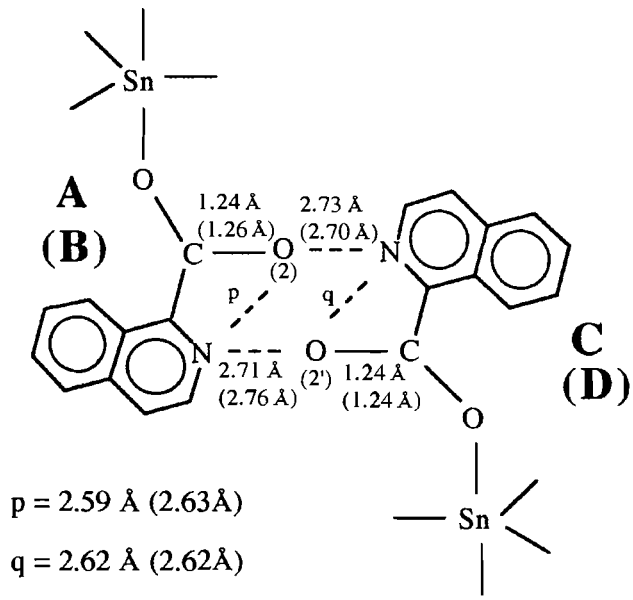

in calculated positions for a zwitterionononic structure, with the N—H bond distances set at 0.977 Å, the O–H separations may be calculated. When this is done, the O–H distances, averaged over the four molecular units, are 2.19 Å (same molecule) and 1.88 Å (between molecules). The corresponding distances for the picolinic acid complex are 2.17 and 1.73 Å, respectively.

In a recent review (1) it has been pointed out that the hydrogen bonding schemes of Ph_3SnX complexes with protonated carboxylic acids fall into one of two categories, distinguished by the Sn–O(2) separation. Where the hydrogen bonding between the monomers involves the participation of an uncoordinated water molecule (3, 4), the Sn–O(2) distance is found to be about 3.3 Å, whereas for direct hydrogen bonding as reported for the picolinic acid complex (2) this distance is about 3.8 Å. It is significant to note that the Sn–O(2) distance for the title compound is 3.77 Å, giving further support for the hydrogen bonding model proposed.

The Sn–O(1) distance of 2.359 Å for the title complex is comparable to those found for the quinaldic acid (2.350 Å (3)) and picolinic acid (2.347 Å (2)) complexes. These values are somewhat larger than the Sn—O bond lengths of 2.25 Å in dichlorodimethylbis(pyridine-*N*-oxide)tin(IV) (17), 2.317 Å in aquachlorotriphenyl(2,2′:6′,2″-terpyridyl)tin(IV) (18), or 2.25 Å in aquaisothiocyanatotriphenyl(2,2′:6′,2″-terpyridyl)tin(IV) (19). The elongation of Sn–O distance in the protonated carboxylic acid complexes is probably partially due to the double-bond character of the C—O bonds. The Sn–Cl distance of 2.489 Å is also very similar to that found in the picolinic (2.515 Å (2)), and quinaldic acid (2.526 Å (3)) complexes and within the range of Sn–Cl distances (2.32–2.58 Å) in other chloro complexes (20).

We have found that only those carboxylic acids with a carboxyl group that is α to the heterocyclic nitrogen atom are able to form complexes in the protonated form with triphenyltin chloride. Thus, we were unable to prepare such complexes between nicotinic or isonicotinic acids and Ph_3SnCl.

Can. J. Chem. Downloaded from www.nrcresearchpress.com by 80.90.12.36 on 09/08/12
For personal use only.

Table 3. Bond angles in degrees.

Cl(A)-Sn(A)-O(1A)	175.25(16)	Cl(C)-Sn(C)-O(1C)	174.85(17)
Sn(A)-O(1A)-C(1A)	135.9(5)	Sn(C)-O(1C)-C(1C)	137.7(6)
C(2A)-NA-C(3A)	124.4(8)	C(2C)-NC-C(3C)	122.8(8)
O(1A)-C(1A)-O(2A)	128.1(8)	O(1C)-C(1C)-O(2C)	127.8(8)
O(1A)-C(1A)-C(2A)	117.7(7)	O(1C)-C(1C)-C(2C)	117.8(8)
O(2A)-C(1A)-C(2A)	114.2(7)	O(2C)-C(1C)-C(2C)	114.5(8)
NA-C(2A)-C(1A)	113.9(7)	NC-C(2C)-C(1C)	114.2(7)
NA-C(2A)-C(10A)	118.4(8)	NC-C(2C)-C(10C)	119.9(8)
C(1A)-C(2A)-C(10A)	127.6(8)	C(1C)-C(2C)-C(10C)	125.8(8)
NA-C(3A)-C(4A)	119.5(8)	NC-C(3C)-C(4C)	120.9(9)
C(3A)-C(4A)-C(5A)	121.3(8)	C(3C)-C(4C)-C(5C)	119.4(9)
C(4A)-C(5A)-C(6A)	123.7(9)	C(4C)-C(5C)-C(6C)	119.2(9)
C(4A)-C(5A)-C(10A)	118.4(8)	C(4C)-C(5C)-C(10C)	119.7(8)
C(6A)-C(5A)-C(10A)	117.9(8)	C(6C)-C(5C)-C(10C)	121.1(9)
C(5A)-C(6A)-C(7A)	121.4(9)	C(5C)-C(6C)-C(7C)	116.5(9)
C(6A)-C(7A)-C(8A)	120.6(9)	C(6C)-C(7C)-C(8C)	122.7(9)
C(7A)-C(8A)-C(9A)	121.5(9)	C(7C)-C(8C)-C(9C)	122.3(9)
C(8A)-C(9A)-C(10A)	120.0(9)	C(8C)-C(9C)-C(10C)	118.3(9)
C(2A)-C(10A)-C(5A)	118.0(8)	C(2C)-C(10C)-C(5C)	117.2(8)
C(2A)-C(10A)-C(9A)	123.3(8)	C(2C)-C(10C)-C(9C)	123.5(8)
C(5A)-C(10A)-C(9A)	118.7(8)	C(5C)-C(10C)-C(9C)	119.2(8)
Cl(B)-Sn(B)-O(1B)	175.91(17)	Cl(D)-Sn(D)-O(1D)	174.02(17)
Sn(B)-O(1B)-C(1B)	132.1(6)	Sn(D)-O(1D)-C(1D)	134.7(6)
C(3B)-NB-C(10B)	123.2(8)	C(2D)-ND-C(3D)	123.1(8)
O(1B)-C(1B)-O(2B)	128.3(8)	O(1D)-C(1S)-O(2D)	128.6(9)
O(1B)-C(1B)-C(10B)	116.3(8)	O(1D)-C(1D)-C(2D)	116.8(8)
O(2B)-C(1B)-C(10B)	115.3(8)	O(2D)-C(1D)-C(2D)	114.5(8)
C(5B)-C(2B)-C(9B)	118.7(8)	ND-C(2D)-C(1D)	113.6(8)
C(5B)-C(2B)-C(10B)	117.0(8)	ND-C(2D)-C(10D)	120.6(8)
C(9B)-C(2B)-C(10B)	124.3(8)	C(1D)-C(2D)-C(10D)	125.9(8)
NB-C(3B)-C(4B)	119.5(8)	ND-C(3D)-C(4D)	120.9(9)
C(3B)-C(4B)-C(5B)	120.4(9)	C(3D)-C(4D)-C(5D)	118.8(9)
C(2B)-C(5B)-C(4B)	119.5(8)	C(4D)-C(5D)-C(6D)	121.3(10)
C(2B)-C(5B)-C(6B)	119.5(9)	C(4D)-C(5D)-C(10D)	120.8(9)
C(4B)-C(5B)-C(6B)	121.0(9)	C(6D)-C(5D)-C(10D)	117.9(9)
C(5B)-C(6B)-C(7B)	120.3(9)	C(5D)-C(6D)-C(7D)	120.3(10)
C(6B)-C(7B)-C(8B)	119.5(9)	C(6D)-C(7D)-C(8D)	121.0(9)
C(7B)-C(8B)-C(9B)	123.2(10)	C(7D)-C(8D)-C(9D)	121.0(10)
C(2B)-C(9B)-C(8B)	118.9(10)	C(8D)-C(9D)-C(10D)	119.1(10)
NB-C(10B)-C(1B)	113.7(8)	C(2D)-C(10D)-C(5D)	115.8(9)
NB-C(10B)-C(2B)	120.2(8)	C(2D)-C(10D)-C(9D)	123.5(9)
C(1B)-C(10B)-C(2B)	126.1(8)	C(5D)-C(10D)-C(9D)	120.6(9)

Table 4. Selected bond distances and interatomic separations for $Ph_3SnCl{\cdot}L$ (molecular unit A/dimer A–C).

	Bond/interatomic distances (Å)	
Atom pair	Title complex	Picolinic acid complex (2)
Sn—O(1)	2.359(6)	2.347(3)
Sn—Cl	2.489(3)	2.515(1
C(1)—O(1)	1.250(11)	1.256(3)
C(1)—O(2)	1.240(10)	1.232(3)
N---O(2)	2.593(11)	2.661(5)
N---O(2′)	2.726(12)	2.651(5)

As was previously pointed out (3, 4), it would therefore appear that the presence of the α nitrogen is essential for the formation of this type of complex, probably to facilitate the proton transfer process, which is essentially the conversion of the hydrogen bond between the acidic proton and the heterocyclic nitrogen in the free acid into a covalency in the complex (there now being a hydrogen bond in place of the former covalency between the acidic proton and the carboxylate oxygen).

Acknowledgements

We thank Nanyang Technological University and the Laurentian University Research Fund (LURF) for financial assistance and Ms. Anna Yee for technical assistance.

References

1. E.R.T. Tiekink. Appl. Organomet. Chem. **5**, 1 (1991).
2. L. Prasad, E.J. Gabe, and F.E. Smith. Acta Crystallogr. Sect. B: Struct. Crystallogr. Cryst. Chem. **B38**, 1325 (1982).
3. E.J. Gabe, F.L. Lee, L.E. Khoo, and F.E. Smith. Inorg. Chim. Acta, **105**, 103 (1985).
4. E.J. Gabe, F.L. Lee, L.E. Khoo, and F.E. Smith. Inorg. Chim. Acta, **112**, 41 (1986).
5. F.E. Smith, D. Okioga, and L.E. Khoo. Int. Pest Control, **22**, 61 (1980).
6. A.G. Davies and P.J. Smith. *In* Comprehensive organometallic chemistry. Vol. 2. *Edited by* G. Wilkinson, F.G.A. Stone, and E.W. Abel. Pergamon Press, New York. 1982.
7. A.G. Davies and P.J. Smith. *In* Advances in inorganic chemistry and radiochemistry. Vol. 23. *Edited by* H.J. Emeleus and A.G. Sharpe. Academic Press, New York. 1980. p. 1.
8. S.J. Blunden and A. Chapman. *In* Organometallic compounds in the environment. *Edited by* P.J. Craig. John Wiley and Sons, New York. 1986. p. 111.
9. S. Nicklin and M.W. Robson. Appl. Organomet. Chem. **2**, 487 (1988).
10. M.H. Gitlitz. Adv. Chem. Ser. **157**, 167 (1976).
11. A.J. Crowe. Appl. Organomet. Chem. **1**, 143 (1987).
12. R.C. Poller. The chemistry of organotin compounds. Academic Press, New York. 1970. p. 271.
13. D.C. Phillips, A.C.T. North, and F.S. Mathews. Acta Crystallogr. **24**, 351 (1968).
14. E.J. Gabe, Y. Le Page, J-P. Charland, F.L. Lee, and P.S. White. J. Appl. Crystallogr. **22**, 384 (1989).
15. International tables for X-ray crystallography. Vol. IV. 2nd ed. Kynoch Press, Birmingham, England. 1974. p. 99.
16. C.K. Johnson. ORTEP. Report ORNL-5138, Oak Ridge National Laboratory, Oak Ridge, Tenn. 1976.
17. E.A. Blom, B.R. Penfold, and W.T. Robinson. J. Chem. Soc. A, 913 (1969).
18. L. Prasad, F.L. Lee, Y. Le Page, and F.E. Smith. Acta Crystallogr. Sect. B: Struct. Crystallogr. Cryst. Chem. **B38**, 259 (1982).
19. L. Prasad and F.E. Smith. Acta Crystallogr. Sect. B: Struct. Crystallogr. Cryst. Chem. **B38**, 1815 (1982).
20. P.G. Harrison, T.J. King, and J.A. Richards. J. Chem. Soc. Dalton Trans. 1723 (1974).

Can. J. Chem. Downloaded from www.nrcresearchpress.com by 80.90.12.36 on 09/08/12
For personal use only.

Electrochemistry of methylidyne and 1,2,3,5-dithiadiazole complexes of iron and nickel and a reinterpretation of the composition of "$PhCN_2S_2Fe_2(CO)_6$"[1]

René T. Boeré, Klaus H. Moock, Vicki Klassen, Joel Weaver, Dieter Lentz, and Heike Michael-Schulz

Can. J. Chem. Downloaded from www.nrcresearchpress.com by 80.90.12.36 on 09/08/12
For personal use only.

Abstract: The title compounds have been studied in CH_2Cl_2 by cyclic voltammetry. Nonacarbonyldi(μ_3-methylidyne)triiron, $[Fe_3(CO)_9(\mu_3\text{-}CX)_2]$ (X = F, Cl, Br, H), undergo chemically reversible $1e^-$ reduction (−0.72 to −0.88 V vs. SCE) and irreversible oxidation (+1.59 to +1.72 V); the compound for which X = F displays a second, irreversible reduction (−1.96 V). Using reduction potentials of comparable μ_3-E (E = S, Se, NPh, PPh) clusters, μ_3-methylidyne ligands are shown to be strongly basic, comparable to PPh and NPh and more basic than S or Se. The methylidyne clusters are both more difficult to oxidize and reduce than isomeric alkyne clusters $[Fe_3(CO)_9(C_2R_2)]$, indicative of greater thermodynamic stability. The complexes previously formulated as $[Fe_2(CO)_6(S_2N_2CC_6H_4X)]$ (X = H, CF_3, OCH_3) are reversibly reduced (−1.59 to −1.70 V) and irreversibly oxidized (+1.0 to 1.3 V), unlike free dithiadiazole radicals, which are reversibly oxidized around +0.8 V. This behaviour is not consistent with the ring-centered free radical claimed for the case where X = H; instead we find conclusive evidence that these are diamagnetic complexes of the 3-*H*-1,2,3,5-dithiadiazolines, $[Fe_2(CO)_6(S_2N\{NH\}CC_6H_4X)]$ (ν_{NH} = 3376–3381 cm^{-1}; δ_{NH} = 6.55–7.1 ppm). Dicyclopentadienyldithiadiazoledinickel, $[Ni_2Cp_2(S_2N_2CC_6H_5)]$, is both reversibly reduced (–0.79 V) and oxidized (+0.45 V); and irreversibly oxidized at +1.9 V. This is consistent with an unpaired electron, and only the nickel cluster has an ESR signal (g = 2.0410, no resolved hyperfine splitting). Extended Hückel theory locates the free electron in a SOMO restricted to Ni, C, and S atoms.

Key words: electrochemistry, organometallic, methylidyne, dithiadiazole, dithiadiazoline.

Résumé : On a étudié les composés mentionnés dans le titre par voltampérométrie cyclique dans du CH_2Cl_2. Le nonacarbonyldi(μ_3-méthylidyne)fer, $[Fe_3(CO)_9(\mu_3CX)_2]$ (X = Cl, Br, H), subit une réduction à $1é^-$ chimiquement réversible (−0,72 à −0,88 V vs. SCE) et une oxydation irréversible (+1,59 à +1,72 V); le composé dans lequel X = F présente une deuxième réduction irréversible (−1,96 V). Utilisant les potentiels de réduction d'agrégats μ_3E (E = S, Se, NPh, PPh), on montre que les coordinats μ_3-méthylidyne sont fortement basiques, comparables à PPh et NPh et plus basiques que S ou Se. Les agrégats méthylidynes sont à la fois plus difficiles à oxyder et plus difficiles à réduire que les agrégats alcyniques isomères $[Fe_3(CO)_9(C_2R_2)]$; ceci indique une plus grande stabilité thermodynamique. Contrairement aux radicaux dithiadiazoles libres qui sont oxydés d'une façon réversible à environ +0,8 V, les complexes pour lesquels on avait proposé antérieurement la structure $[Fe_2(CO)_6(S_2N_2CC_6H_4X)]$ (X = H, CF_3, OCH_3) sont réduits d'une manière réversible (−1,59 à −1.70 V) et ils sont oxydés d'une manière irréversible (+1,0 à +1,3 V). Ce comportement n'est pas en accord avec l'existence d'un radical libre centré sur un cycle, tel qu'il avait été préconisé pour le cas où X = H; on trouve plutôt des données concluantes indiquant que ceux-ci sont des complexes diamagnétiques des 3-*H*-1,2,3,5-dithiadiazolines, $[Fe_2(CO)_6(S_2N\{NH\}CC_6H_4X)]$ (ν_{NH} = 3376–3381 cm^{-1}; δ_{NH} = 6,55–7,1 ppm). Le dicyclopentadiényldithiadiazoledinickel, $[Ni_2Cp_2(S_2N_2CC_6H_5)]$, est aussi bien réduit (–0.79 V) qu'oxydé (+0,45 V) d'une façon réversible et il est oxydé irréversiblement à +1,9 V. Ce comportement est en accord avec la présence d'un électron non apparié et seul l'agrégat du nickel possède un signal en rpe (g = 2,0410, sans

Received April 6, 1995.

R.T. Boeré,[2] K.H. Moock,[3] V. Klassen, and J. Weaver. Department of Chemistry, University of Lethbridge, Lethbridge, AB T1K 3M4, Canada.

D. Lentz and H. Michael-Schulz. Institut für Anorganische und Analytische Chemie, Freie Universität Berlin, Fabeckstraße 34-36, 14195 Berlin, Germany.

[1] Part of this work was presented at the 7th International Symposium on Ring Systems (IRIS), Banff, Canada, August, 1994.

[2] Author to whom correspondence may be addressed. Telephone: (403) 329-2045; Fax: (403) 329-2057. Internet: boere@hg.uleth.ca

[3] Current address: Research School of Chemistry, Australian National University, ACT0200, Australia.

couplage hyperfin résolu). Des calculs d'orbitales moléculaire d'après la théorie de Hückel étendue permettant de localiser l'électron libre dans une SOMO restreinte aux atomes de Ni, C et S.

Mots clés : électrochimie, organométallique, méthylidyne, dithiadiazole, dithiadiazoline.

[Traduit par la rédaction]

Introduction

Electrochemical studies of organometallic compounds can give useful insights into their behavior and electronic structure. The enhanced chemical reactivity of many low-valent organometallic compounds, compared to classical coordination compounds, requires the use of special handling techniques, including specialized electrochemical cells and the use of nonaqueous solvents. In this work we use cyclic voltammetry to study several organometallic cluster compounds using an original cell design that is equally capable of operating under a vacuum or a carbon monoxide atmosphere (1). The methylidyne complexes $[Fe_3(CO)_9(\mu\text{-}CX)_2]$, **1**, (X = F, Cl, Br, H) (2) and the so-called dithiadiazole complexes $[Fe_2(CO)_6(S_2N_2CPh)]$, **2***a*, and $[Ni_2Cp_2(S_2N_2CPh)]$ **3** (3) were investigated. (Cp stands for η^5-C_5H_5.) The latter two were claimed to be paramagnetic organometallic clusters. In fact we discovered that all the iron carbonyl clusters including **2***a* have a similar electrochemical behavior. However, the nickel cyclopentadienyl complex behaved differently. It was reminiscent of the paramagnetic parent 1,2,3,5-dithiadiazole ring system, **4** (4). This led us to question the validity of the claim that **2***a* contains a ligand-centered unpaired electron.

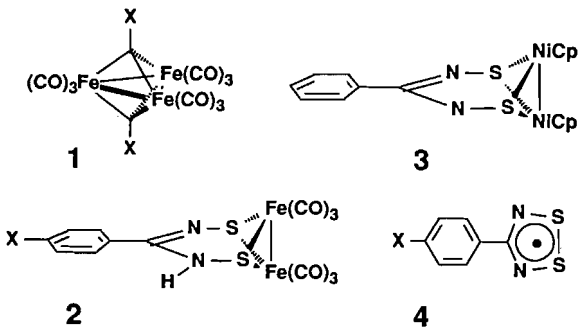

To further assess this problem we prepared two 4-substituted aryl analogues to **2***a* with better solubility and convenient NMR spectral patterns, $[Fe_2(CO)_6(S_2N_2CC_6H_4X)]$, X = OCH_3, **2***b*, and X = CF_3, **2***c*. A detailed spectroscopic investigation of these complexes using mass spectrometry, ^1H and ^{13}C NMR, ESR, and electronic absorption spectroscopy conclusively demonstrates that **2** should be reformulated as complexes of the 3-*H*-1,2,3,5-dithiadiazolines $[Fe_2(CO)_6(S_2N\{NH\}CC_6H_4X)]$ (X = H, OCH_3, CF_3), and that they are in fact diamagnetic. However, we have also established that **3** is definitely a paramagnetic species with the unpaired electron located mostly on C, S, and Ni atoms. A preliminary account of this work has appeared (5).

Results

Electrochemistry

$Fe_3(CO)_9(\mu_3\text{-}CX)_2$ ***1***a *X = F,* ***1***b *X = Cl,* ***1***c *X = Br,* ***1***d *X = H*

Figure 1 shows the cyclic voltammogram (cv) of **1***a* in CH_2Cl_2.

Fig. 1. Cyclic voltammogram of $[Fe_3(CO)_9(CF)_2]$, **1***a*, in CH_2Cl_2 containing 0.5 M $^nBu_4NPF_6$ electrolyte.

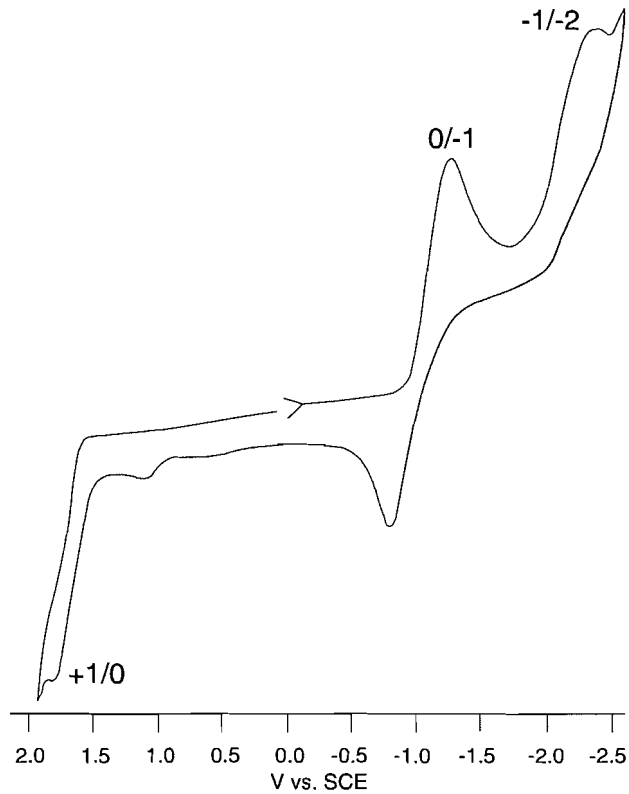

In the cv, one reversible first reduction wave with $\mathscr{E}_{1/2}$ = −0.88 V vs. SCE and an irreversible second reduction wave at −1.96 V are observed. Under the conditions stated in Table 1, an irreversible oxidation occurs within the range of solvent stability at $\mathscr{E}_a$ = +1.58 V. Experiments with a CO atmosphere in the electrochemical cell show a slight improvement of the reversibility of the oxidation and reduction steps in the cv. This effect has been noted before for structurally similar bicapped clusters $[Fe_3(CO)_8(\mu_3\text{-}E)_2]$ (6).

Reversible reductions were found for the corresponding chloro, bromo, and hydrido clusters with half-wave potentials at −0.72, −0.74, and −0.86 V vs. SCE, respectively. None of these clusters had a second reduction step within the solvent stability field. Irreversible oxidation steps are observed at +1.68, +1.72, and +1.59 V.

$[Fe_2(CO)_6(S_2N\{NH\}C\text{-}C_6H_4\text{-}X)]$, **2**a *X = H,* **2**b *X = OCH_3,* **2**c *X = CF_3*

Figure 2 shows the cv of **2***a* in CH_2Cl_2 at +25°C and a scan rate of 100 mV s^{-1}. Under these conditions a reversible one-electron reduction at $\mathscr{E}_{1/2}$ = −1.70 V and an irreversible oxidation at +1.2 V are observed. The oxidation step remained strictly irreversible even at scan rates of 10 V s^{-1} and temperatures

Can. J. Chem. Downloaded from www.nrcresearchpress.com by 80.90.12.36 on 09/08/12
For personal use only.

Can. J. Chem. Downloaded from www.nrcresearchpress.com by 80.90.12.36 on 09/08/12
For personal use only.

Table 1. Electrochemical data.[a]

Compound	Process:	$\mathscr{E}_1$	$\mathscr{E}_2$	$\mathscr{E}_3$
$Fe_3(CO)_9(\mu_3\text{-}CF)_2$		+1.58[b,c]	−0.88	−2.0[b,d]
$Fe_3(CO)_9(\mu_3\text{-}CCl)_2$		+1.68[b,c]	−0.72	
$Fe_3(CO)_9(\mu_3\text{-}CBr)_2$		+1.72[b,c]	−0.74	
$Fe_3(CO)_9(\mu_3\text{-}CH)_2$		+1.59[b,c]	−0.86	
$Fe_2(CO)_6(S_2N_2HCC_6H_4CF_3)$[e]		+1.3[b,c]	−1.57[f]	
$Fe_2(CO)_6(S_2N_2HCC_6H_5)$[e]		+1.2[b,c]	−1.70	
$Fe_2(CO)_6(S_2N_2HCC_6H_4OCH_3)$[e]		+1.0[b,c]	−1.69[f]	
$Ni_2(Cp)_2(S_2N_2CC_6H_5)$		+1.9[b,c]	+0.45	−0.79
$S_2N_2CC_6H_4CF_3$[g]		+0.86	−0.73	
$S_2N_2CC_6H_5$[g]		+0.78	−0.82	
$S_2N_2CC_6H_4OCH_3$[g]		+0.73	−0.85	

[a]From cyclic voltammetry at a Pt electrode in CH_2Cl_2 containing 0.5 M NBu_4PF_6 electrolyte, referenced to SCE such that $\mathscr{E}_{1/2}$ = +0.48 V for $[Cp_2Fe]^{+/0}$; potentials are $\mathscr{E}_{1/2}$ measured under reversible conditions at a scan rate ν = 100 mV s^{-1} at 25°C, unless otherwise noted.

[b]Irreversible behaviour at scan rates ν = 50–1000 mV s^{-1} at 25°C.

[c]Anodic peak potential.

[d]Cathodic peak potential.

[e]Additional peaks occur in voltammogram at +0.5 and −1.1 V after scanning through oxidation process at $\mathscr{E}_1$.

[f]Reversible conditions at ν = 200 mV s^{-1} at −20°C

[g]Reference 4*b*.

Fig. 2. Cyclic voltammogram of $[Fe_2(CO)_6(S_2N\{NH\}CC_6H_5)]$, **2***a*, in CH_2Cl_2 containing 0.5 M $^nBu_4NPF_6$ electrolyte. The peaks marked with an asterisk only occur after scanning through the oxidation process.

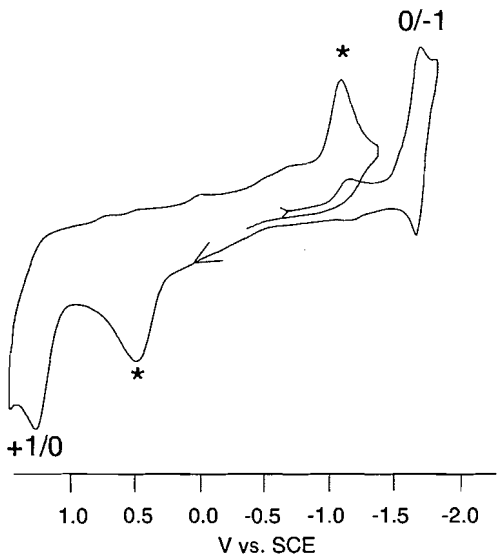

below −50°C. On scanning through the oxidation process new signals at −1.1 V and +0.5 V, marked by asterisks in the figure, initially appear before, on repeated scanning, all signals vanish. Scans omitting the oxidation process show the reversible reduction process undiminished over a period of several hours, and with no evidence of the decomposition signals. The electrochemical behavior of **2***b* and **2***c* is very similar to that of **2***a*, with the reversible reduction at $\mathscr{E}_{1/2}$ = −1.69 V and −1.59 V, the irreversible oxidation at +1.0 V and +1.3 V, respectively (Table 1), and secondary signals at −1.1 V and +0.5 V.

Fig. 3. Cyclic voltammogram of $[Ni_2(Cp)_2(S_2N_2CC_6H_5)]$, **3**, in CH_2Cl_2 containing 0.5 M $^nBu_4NPF_6$ electrolyte.

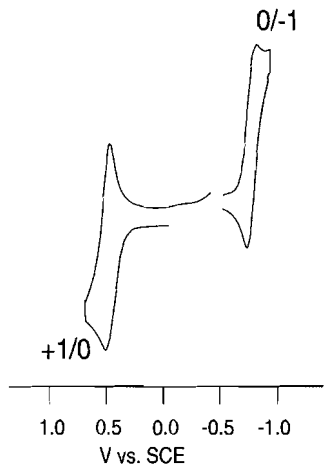

*$Ni(Cp)_2(S_2N_2CC_6H_5)$, **3**.*

Figure 3 shows the cv of the nickel complex in CH_2Cl_2. Fully reversible reduction and oxidation processes are observed at $\mathscr{E}_{1/2}$ = −0.79 V and $\mathscr{E}_{1/2}$ = +0.45 V, respectively. A second, irreversible oxidation process could also be observed at +1.9 V. Repeated scanning through this second oxidation causes the disappearance of all signals in the voltammogram. However, in contrast to the iron complexes, the complete cv can be recovered by reconditioning the electrode through holding the potential at −2.0 V for about a minute.

We noticed considerable similarity in the redox properties of the iron carbonyl clusters **1** and **2**. First, they all have a reversible first reduction $\mathscr{E}_2$; secondly, they all have an irreversible oxidation process $\mathscr{E}_1$; thirdly, the separation between

Table 2. Selected solution IR data for $[Fe_2(CO)_6(S_2N_2HCC_6H_4X]$, **2**.[a]

Assignment	**2***a*	**2***b*	**2***c*	Conditions
ν(N-H)	3376	3381	3377	$CHCl_3$, conc.
ν(C≡O)	2073 (1)[b]	2071 (2)	2074 (2)	CS_2, dilute
ν(C≡O)	2035 (3)	2034 (3)	2037 (3)	CS_2, dilute
ν(C≡O)	2001 (2)	2000 (3)	2004 (3)	CS_2, dilute
ν(C≡O)	1995 (2)	1994 (3)	1997 (3)	CS_2, dilute

[a]Recorded in 0.2 mm NaCl cavity cell.
[b]Relative intensity of ν(C≡O) bands given in parentheses.

Table 3. NMR parameters for $[Fe_2(CO)_6(S_2N_2HCC_6H_4X]$, **2**.[a]

Assignment[b]	**2***a*	**2***b*	**2***c*
H_2	[c]	7.47(8.5)[d]	7.67(8.5)[d]
H_3	[c]	6.91(8.5)[d]	7.60(8.5)[d]
H-N	6.55	6.65[d]	7.1[d] br
X	—	3.82[d]	—
$C_{1'}$	158.53	158.76	158.11[d]
C_1	136.68	129.13	140.21[d]
C_2	129.05	127.37	127.36[d]
C_3	126.14	114.23	126.44[d] *q*(3.7)
C_4	131.32	162.05	130.74[d] *q*(32.8)
X	—	55.42	126.39[d] *q*(272.3)
C≡O	206.9 br	207.0 br	209.2[d] br

[a]In ppm, relative to internal TMS, coupling constants in Hz given in parentheses where appropriate; recorded in $CDCl_3$, unless otherwise noted.
[b]Atom numbering scheme:

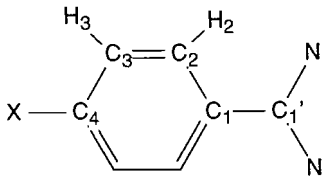

[c]Multiplet, 7.51–7.37 ppm, integrating to 5H.
[d]In CD_2Cl_2.

$\mathscr{E}_1$ and $\mathscr{E}_2$ is of similar magnitude: 2.40–2.46 V for **1** and 2.69–2.87 V for **2**. In view of the claim that **2***a* contains an unpaired electron centered on the heterocyclic ring (3*a*), we were surprised by the absence of a facile, reversible oxidation process, as invariably observed for 1,2,3,5-dithiadiazole radicals, whose electrochemistry has been exhaustively studied (4). On the other hand, the nickel cluster **3** displays such a process, identified as $\mathscr{E}_2$ in Table 1, where for comparative purposes the potentials of the parent heterocycles are also listed. Complex **3** is reversibly oxidized at a considerably less positive potential compared to S_2N_2CPh (+0.45 vs. +0.78 V). The very different electrochemical behaviour of **2** and **3**, which are otherwise quite similar clusters derived from the same heterocycles, led us to carefully compare their spectroscopic properties.

Solution studies

That the structures of **2***b,c* are similar to the butterfly structure of **2***a*, for which a crystal structure is known (3*a*), is readily proven by IR spectroscopy. In the CO stretching region, in CS_2 solution, all three have virtually identical absorptions both in frequency and relative intensity (Table 2). There is a very small but consistent trend in ν(C≡O) values: each band moves slightly to higher wave number with increasing electron-withdrawing character of the remote substituent. The bands are also strikingly similar to those of related thiolate clusters (for example, $[Fe(CO)_3SC_2H_5]_2$: 2070, 2034, 2000, 1987 cm^{-1}) (7), which also possess the butterfly structure. In contrast to the solution spectra, solid-state spectra recorded either as Nujol mulls or as KBr pellets show each CO band split into two, indicative of substantial symmetry lowering in the crystal.

Clusters **2** provide well-resolved NMR spectra typical for diamagnetic species, i.e., without paramagnetic line broadening or unusual chemical shifts (5), whereas the parent dithiadiazole radicals **4** show broad featureless NMR spectra consistent with their paramagnetism. The ^1H and ^{13}C chemical shifts (Table 3) are within the range observed for a wide variety of aryl-C(NS~)$_2$ compounds that we have previously studied (8). The samples of **4** were sealed under vacuum to prevent the facile reaction with oxygen (8*a*). The ^1H spectra show, in addition to the typical A_2B_2 aromatic peaks, one relatively broad peak with variable chemical shift (range: 6–7 ppm) integrating to 1H. This latter peak disappeared on shaking the solution with a little D_2O (5). Supposing this to be a hydrogen atom attached to one of the nitrogen atoms of the dithiadiazole ligand, we returned to solution IR spectroscopy using much more concentrated solutions in $CHCl_3$, which has an open window above 3000 cm^{-1}. All three complexes showed a weak but relatively sharp peak around 3380 cm^{-1}, assigned to ν(N-H) (9).

ESR spectra

We were unable to obtain an ESR signal even from concentrated solutions of pure samples of **2**, which is consistent with diamagnetism, in agreement with the NMR and electrochemical evidence. Figure 4 shows the isotropic ESR spectrum of **3** in solution. It displays a strong signal without any hyperfine structure. The *g*-value is 2.0410 and the peak-to-trough separation is 0.69 mT. This is very similar to the ESR signal reported for the paramagnetic cobalt cluster $[Co_3Cp_3(\mu_3\text{-}S)_2]I$, which has a broad single line and a *g*-value of 2.05 (10). In extremely dilute solutions in CH_2Cl_2, an additional, weak, five-line pattern is observed, which can be identified as the parent radical **4** by its *g*-value of 2.011 and a_N of 0.49 mT (4*b*, 11). This very small amount of **4** probably results from thermal or photochemical dissociation of the cluster. The absence of the familiar five-line pattern in the ESR spectrum of **3** indicates that the distribution of the unpaired electron in the clus-

Can. J. Chem. Downloaded from www.nrcresearchpress.com by 80.90.12.36 on 09/08/12
For personal use only.

Can. J. Chem. Downloaded from www.nrcresearchpress.com by 80.90.12.36 on 09/08/12
For personal use only.

Table 4. Electronic absorption spectra of **2** and **3**[a]

Compound	λ_1 ε_1	λ_2 ε_2	λ_3 ε_3	λ_4 ε_4	λ_5 ε_5	λ_6 nm ε_6 M^{-1} cm^{-1}
2*a*	473	394(sh)	322	256(sh)	232	
	1110	*1280*	*22 500*	*28 800*	*38 900*	
2*b*	471	396(sh)	325	276(sh)	234	
	1094	*2670*	*25 900*	*22 600*	*37 200*	
2*c*[b]	474	380(sh)	332(sh)	268(sh)	233	
	934	*4490*	*8630*	*24 600*	*36 000*	
3	876[c]	500(sh)	399	346	326	243
	900	*2100*	*22 800*	*24 900*	*24 700*	*23 200*

[a]All spectra were recorded using 1 cm quartz cuvettes in dry CH_3CN.
[b]The appearance of this spectrum differs due to the marked lower intensity of λ_3.
[c]This band measured at extreme wavelength limit of spectrophotometer, and values are only approximate.

Fig. 4. Solution ESR spectrum of **3** in degassed CH_2Cl_2 (*a*) at 10^{-6} M, showing the additional presence of a small five-line pattern with $g = 2.010$ with $a_N = 0.5$ mT, and (*b*) at 10^{-4} M where this minor component is not visible. The main signal has $g = 2.0410$.

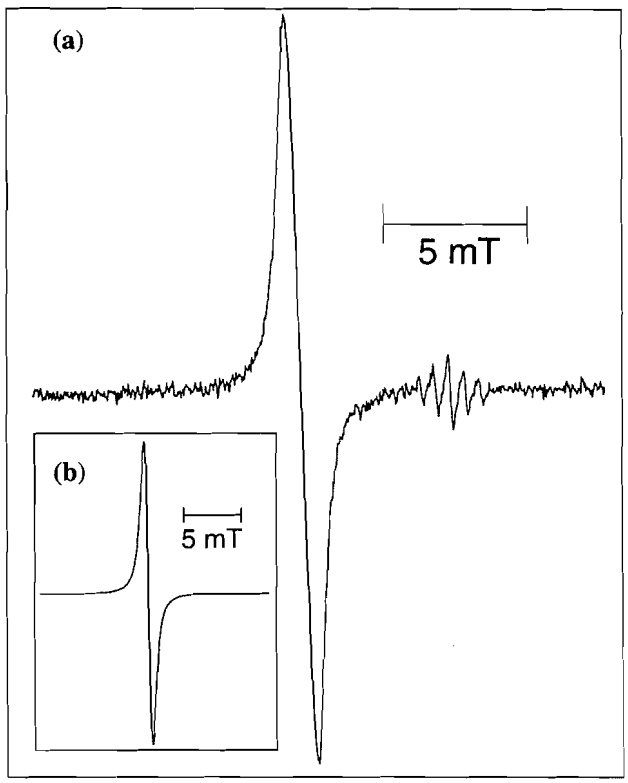

ter is quite different than in the parent heterocycle. This conclusion is supported by the EHMO calculations reported below.

Electronic spectra

We have measured the electronic absorption spectra of **2** and **3** in CH_3CN solution (Table 4). The contrast in their properties seen electrochemically is repeated here. Complexes **2** absorb in the blue (~470 nm) and in the UV (322 and 232 nm). For comparison, the electronic spectrum of diamagnetic $Fe_2S_2(CO)_6$ consists of three bands at 476, 333, and 278 nm. The intensity of the 333 nm band is 11 900 (12). The low-energy band in this cluster is considered to be due to transitions within the metal–metal bonding orbitals, i.e., it is cluster centered. Complex **3** has a visible band considerably higher in energy (399 nm) and three UV bands (346, 326, and 243 nm); in addition there is a weak band at very low energy (876 nm). Apart from the low-energy band, this spectrum is quite similar to that reported (up to 820 nm) for the paramagnetic cluster $[Ni_3Cp_3(\mu_3S)_2]$, which has a visible band at 396 nm and two UV bands (13). These results are in qualitative agreement with the EHMO calculations reported below.

Discussion

Electron counting

Iron–carbon clusters with the analytical formula $Fe_3(CO)_9C_2R_2$ can exist according to Wade's rules (14) in at least two possible stereo isomers. Compounds of type I are well known as trinuclear alkyne clusters, **5** (15). Only recently with the synthesis of the series of methylidyne clusters $Fe_3(CO)_9(\mu_3\text{-}CX)_2$, **1**, (X = F, Cl, Br, H) have examples of type II been found (2). Both are *closo* polyhedra with $n = 5$, where n represents the number of skeletal polyhedron vertices, and with 12 (i.e., $2n+2$) skeletal electrons (14). Each CX ligand acts as a three-electron donor. By this treatment, the C—C bonds in the type I complexes are considered as part of the skeletal framework. Both types are 54e$^-$ clusters and fit the 18-electron rule.

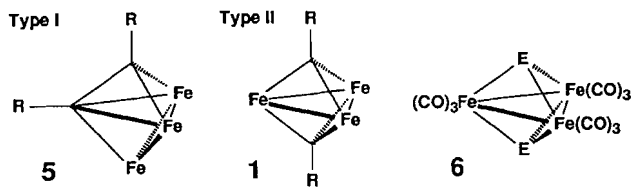

Iron–sulfur clusters of the general formula $Fe_2(CO)_6(SLig)_2$, where Lig refers to any one of a direct S—S bond, terminal σ-bonded groups (Me, Et), or some sort of indirect bridge, i.e., including the ring-opened dithiadiazole ligands in **2**, are all tetrahedral clusters with $(2n+4)$ skeletal bonding electrons.

Can. J. Chem. Downloaded from www.nrcresearchpress.com by 80.90.12.36 on 09/08/12
For personal use only.

They do not fit Wade's rules in any simple way. However, they do fit the $18e^-$ rule precisely, with each S atom acting as a three-electron ligand. According to the evidence presented in this work, we conclude that **2** are electron-precise $36e^-$ clusters formed from a dithiadiazoline ligand, while **3** is a $39e^-$ species formed from the parent dithiadiazole. The precise electron count in the latter is complicated by the question of whether or not it has a Ni—Ni bond.

This leaves only consideration of the formal oxidation states of the metals in these clusters. In both **2***a* and **3** the S—S bonds have opened up considerably on cluster formation (from 2.09 in the dimer to 2.93 and 2.905 Å in the two clusters (3)). If this is considered to be due to oxidative addition to the metals, then formally we are dealing with complexes of the $[S_2N_2CR]^{2\bullet-}$ and $[S_2N_2HCR]^{2-}$ ligands and hence with metals in Fe^+ and Ni^{2+} oxidation states. In much the same way, S_2N_2 forms complexes through oxidative addition that are formally derivatives of $S_2N_2^{2-}$ (16).

Comparison of redox potentials for 1

The electrochemical behaviour of the parent triiron cluster $[Fe_3(CO)_{12}]$ (17), alkyne clusters $[Fe_3(CO)_9(RCCR)]$, **5**, (15*f*), and bicapped trigonal planar clusters $[Fe_3(CO)_8(\mu_3\text{-}E)_2]$, E = S, Se, NPh, PPh, **6** (6), has been studied in detail. In general, the triiron clusters all undergo a reversible one-electron reduction step. In addition, further electrode processes, such as a second reduction or an oxidation step, are also observed but are usually less well defined.

The type I alkyne complexes **5***a* (R = Me), **5***b* (R = Et), and **5***c* (R = Ph) undergo a first reduction at −0.47, −0.49, and −0.36 V, respectively, and a second reversible reduction at −0.65, −0.60, −0.67 V, as well as irreversible oxidation at +1.29, +1.42, +1.35 (anodic peak potentials), all measured in CH_2Cl_2 (15*f*). There is a small difference in potential between the first and second reductions of these type I complexes. This has been attributed to thermodynamic effects accompanying a structural reorganization from a *closo* to a *nido* geometry, based on solution IR and NMR evidence (15*f*). The much greater separation between the sequential reductions in **1** suggests that such a rearrangement does not readily occur for the type II clusters. Comparison of the redox potentials of type I and II clusters is complicated by differences in substituents at C. However, the closest similarity in properties might be expected between **1***d* (R = H) and **5***a* (R = Me). We see that the μ_3-methylidyne is almost 0.4 V harder to reduce, as well as 0.3 V harder to oxidize, than the dimethylacetylene cluster. Thus the electrochemical stability range, defined as the difference between the potentials at which oxidation and reduction occur, is significantly greater for **1** than for **5**.

The capped trigonal planar type II clusters **6** are of directly comparable structure to **1**. In all cases the initial reduction is reversible with the comparable potentials at −0.61 V (S), −0.56 V (Se), −0.86V (NPh) (6*a*), and −0.79V (PPh) (6*b*) measured in THF solution. The first reductions of **1**, irrespective of the nature of R, are more comparable to these heteroatom capped clusters than to the isomeric type I alkyne clusters. Bond et al. have suggested that, so long as the free energy of solvation for a series of compounds is similar and there are no major structural changes during the reduction process, then the reduction potentials should reflect the energy of the LUMO (17*a*). Since these conditions are likely to apply to the tri-capped clusters, the reduction potentials serve as a measure of their LUMO energies. These therefore provide an insight into the relative basicity of the capping groups, since substitution with a more basic ligand should raise the energy of the LUMO, making reduction more difficult. On this basis μ_3-methylidyne ligands are strongly basic, comparable to PPh and NPh, and more basic than S.

All of these results corroborate earlier conclusions emphasizing the stability of the alkylidyne clusters and in particular the high degree of covalency of the Fe—Fe and Fe—C bonding (18). The electronic structure of **1***a* has been studied by Extended Hückel as well as SCF methods in C_{3h} symmetry (i.e., with one C≡O group on each iron lying in the plane of the iron triangle) (18*a*). In the oxidation process, electrons are removed from the *e″* HOMO **7** and **8**, which are Fe—C_{apical} as well as Fe—Fe bonding. The experimental evidence suggests that removal of electrons from these orbitals leads to cluster fragmentation. Reduction involves occupation of the *a′* LUMO **9**, which is Fe—Fe anti-bonding but does not involve the capping ligands.

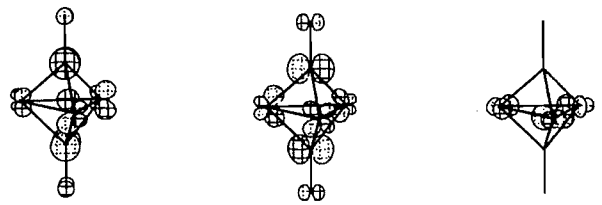

7 8 9

Comparison of redox potentials for 2

The reduction potentials may be compared to those of $[Fe_2(CO)_6S_2]$ (19) and $[Fe_2(CO)_6(SR)_2]$ (R = Me, Et, $S(CH_2)_nS$, n = 2,3) (20), which have been studied by cyclic voltammetry. The "naked" disulfide cluster has been shown to undergo a complex redox process in THF solution, in which the radical anion forms in an electrochemically irreversible (but chemically well-defined) process at −1.53 V and dimerizes to give $[Fe_4S_4(CO)_{12}]^{2-}$. The dimer is subsequently reduced to the dianion $[Fe_2S_2(CO)_6]^{2-}$ at −2.46 V. This process can be reversed, with the first reoxidation at −2.2 V and the second at −0.63 V (19). This interesting process is rather difficult to compare with the reversible reduction of **2**.

Under a CO atmosphere, $[Fe_2(CO)_6(SR)_2]$ are reduced quasi-reversibly or reversibly. Bridged systems, i.e. those with $S(CH_2)_nS$ dithiolate ligands, were found to be electrochemically the best behaved. The potentials range from −1.1 to −1.2 V using DMF as the solvent (20). The ~0.5 V difference between these values and the −1.6 to −1.7 V recorded for the reduction of **2** may in part be solvent related, since the strongly coordinating solvent DMF is expected to move reduction potentials to a less negative value compared to the weakly interacting dichloromethane used in our study. Thus, the electrochemical reductions of $[Fe_2(CO)_6(SR)_2]$ and **2** are roughly comparable and the ring-opened dithiadiazoline ligand in **2** may be considered an exotic form of a bridging dithiolate.

Comparison of redox potentials for 3

There is no directly comparable disulfide with the same cluster structure as **3**. Instead $[CpNi(CO)]_2$ reacts with elemental sulfur to yield the paramagnetic cluster $[Ni_3Cp_3(\mu_3\text{-}S)_2]$ (13*a*).

Can. J. Chem. Downloaded from www.nrcresearchpress.com by 80.90.12.36 on 09/08/12
For personal use only.

The electrochemistry of this cluster has been studied in benzonitrile (13*c*), acetonitrile, acetone, and methylene chloride (13*b*). The central redox processes are qualitatively similar to those observed for **3**. Reversible oxidation (+0.09 V in CH_2Cl_2) and reversible reduction (−0.81 V) as well as irreversible oxidation (+0.97 V in CH_2Cl_2) are observed. The electrochemical reversibility of this first oxidation of $[Ni_3Cp_3(\mu_3\text{-}S)_2]$ has been substantiated by chemical synthesis of the cation. In CH_3CN and PhCN the second oxidation is reversible and further irreversible oxidation is observed. Thus, $[Ni_3Cp_3(\mu_3\text{-}S)_2]$ is considerably easier to oxidize than **3** (in accord with its greater electron richness), but its reduction is very comparable to that of **3**.

Solid-state structures of 2

The evidence originally presented for the claim that **2***a* contains a ring-centered unpaired electron consisted of (*i*) magnetic susceptibility measurements, which were not fully discussed, and (*ii*) the presence of short N...N contacts in the single-crystal X-ray crystal structure (3*a*). However, these short contacts fit both in *length* and *direction* for hydrogen bonding between an N—H unit and a nitrogen atom on the adjacent molecule. The short intermolecular distance between N(1) and N(2) is 2.84 Å. If a hydrogen atom is attached to N(2) at the calculated position for an sp^2 hybridized nitrogen atom and with d(N—H) = 0.95 Å, the distance from H to N(1) in the adjacent molecule is 2.03 Å. Similarly, attachment to N(1) with the same bond length gives a distance H to N(2) of 2.12 Å. These values are very similar to the average of 2.20 Å tabulated in ref. 21 for a wide range of N—H...N bonds. If the material prepared by these authors was indeed a dithiadiazoline complex as suggested here, the magnetic results and the five-line ESR signals they obtained may have been due to co-crystallization of uncoordinated **4***a*, which is apparently a common occurence in this chemistry.[4] The splitting of the carbonyl bands in the IR spectra of solid samples of **2** is consistent with the unsymmetrical dithiadiazoline structure we have proposed, as is the inequivalence in the C—N bond lenghts of 1.295(8) and 1.348(7) found in the crystal structure of **2***a*.

MO description of 2 and 3

EHMO descriptions of **2** and **3**, as *radicals*, using S_2N_2CH as a model ligand have been published (3). We have been able to repeat the essential features of these calculations, although in our hands the parameters published in ref. 3 lead to very different results; the parameters we have used are listed in Table 5. The makeup of the highest filled orbitals of **2** turns out to be very sensitive to parameter choice.[5] Using the best choice of parameters, in our judgment, we find for the purported radical that the singly occupied molecular orbital (SOMO) of **2** is indeed **11**, a sulfur and nitrogen lone-pair-type orbital almost entirely localized on the ligand, as previously claimed (3*a*). At slightly lower energy is the first doubly occupied orbital, **10**, derived from the S—S σ bond in the free heterocycle. The LUMO **12** is derived from the ligand π_4 orbital, and has a large contribution from the carbon monoxide carbon atoms. However, as we have demonstrated, **2** is not a free radical, but rather a diamagnetic cluster containing $S_2N\{NH\}CR$. What is the consequence of attaching a hydrogen atom to a ring nitrogen atom? The answer to this question is addressed in Fig. 5. Attachment of a hydrogen atom to one of the ring nitrogen atoms in a reasonable geometry stabilizes **11′** sufficiently so that it falls below **10′**, which then becomes the HOMO of the new cluster.

Fig. 5. Schematic representation of the effect of H coordination to a nitrogen lone pair in a model version of **2** using HCN_2S_2 as the ligand. Stabilization of **11′** (viewed here in the plane of the dithiadiazole ligand) occurs, leaving **10′** as the HOMO of the dithiadiazoline-containing cluster.

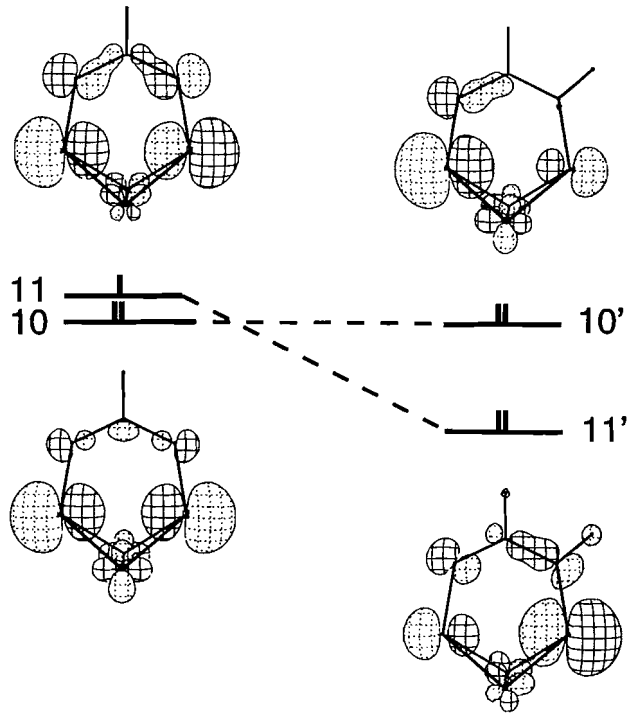

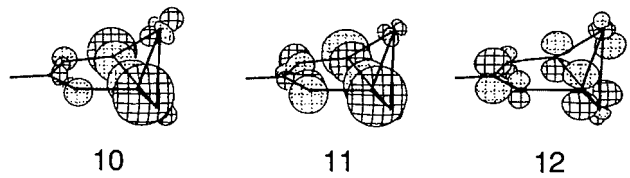

In contrast to **2**, the makeup of the frontier orbitals of model **3** is quite insensitive to parameter choice for sulfur and nitrogen. Essentially the same picture develops using the two H_{ii}

[4] A.J. Banister. Private communication.

[5] Such sensitivity to Hückel parameters also applies to $[Fe_2S_2(CO)_6]$ (22) and $[Fe_2S_2(CO)_6]^{2-}$ (23), which have been intensively studied by a wide variety of computational methods. DeKock et al. have reported HFS calculations on both compounds. We found that the best approximation to the HFS calculation on the neutral cluster (22*d*) using EHMO could be achieved using"standard" H_{ii} for N and S. Yet for the dianion (23*a*) much better agreement was obtained if the H_{ii} of DeKock and Gray were employed (24). Andersen et al. also used these latter parameters in their EHMO calculations (22*c*). Since **2** is geometrically and electronically more closely related to the dianion, we decided to employ the DeKock and Gray H_{ii}. The choice has a profound influence on the frontier orbitals of **2**: with standard H_{ii}, the HOMO is Fe–Fe σ bonding, similar to the a_1 orbital calculated by all methods to be HOMO of $[Fe_2S_2(CO)_6]$. This orbital is HOMO-3 in **2** when using the DeKock and Gray H_{ii}.

choices. The LUMO **15** is a combination of the ligand π_4 orbital and Cp contributions. The SOMO **14** is made up from ligand π_3 (35%), Ni 3*d* (40%), and the Cp (25%). It has a node at the ring nitrogen atoms. This description is similar to that published previously (3*b*), and explains the absence of coupling noted above for the ESR spectrum of **3** since the major isotopes of C, S, and Ni have $I = 0$. The highest doubly occupied orbital, **13**, is a S,N lone-pair orbital very similar to **11**.

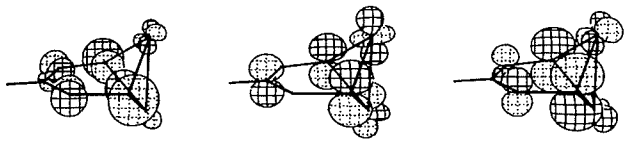

13 14 15

Although the discussion here must be regarded as tentative until high-level calculations are performed, we find a satisfying explanation of the fact that **3** is stable as a radical while **2** is not. Due to the two extra valence electrons in the nickel cluster, the unpaired electron donated by **4** is accommodated in an anti-bonding orbital with significant participation by the back-bonding Cp ligands. This orbital has very similar topology to the LUMO of **2**, which is also capable of accepting an additional electron, as demonstrated by the reversible one-electron reduction reported above. On the other hand, the hypothetical radical form of **2** would need to accommodate the unpaired electron in the ring σ orbital **11** (or alternatively in a metal–metal bonding MO, using "standard" parameters.) This configuration is too reactive, resulting in hydrogen abstraction, and the loss of the 37th valence electron to a localized N—H bond. Fundamentally these are not unexpected results. For example, while ferrocene is electron-precise, nickelocene is a $20e^-$ metallocene. The higher effective nuclear charge of nickel over iron accounts for the lowering of the energy of the anti-bonding orbitals. Nickel clusters are simply more likely to be stable when electron-rich than are iron clusters.

Formation of the dithiadiazole and dithiadiazoline complexes

The reaction sequences leading to **2** and **3** are complex. First of all, the dithiadiazole radicals themselves are not capable of reducing $Fe_3(CO)_{12}$ to the radical anion (17). The same is true for $[CpNi(CO)]_2$, which undergoes an irreversible $2e^-$ reduction only at -2.4 V (25). This would seem to rule out the involvement of an ETC mechanism for CO displacement from the parent clusters. Substitution is accompanied, at least formally, by oxidative addition. It may be that the final electron count is controlled more by the cluster electronic structure than by the nature of the dithiadiazole ligand. In the case of **3**, the cluster tolerates electron-richness, but **2** resists deviation from the $18e^-$ count. The "excess" electron may then be dumped out onto the ligand, where H-atom abstraction may then be invoked to explain the formation of the dithiadiazoline. (In this regard, the use of toluene as the solvent may be significant, since this is a well-known source for H abstraction.) Whatever mechanism is proposed to deal with these observations must also account for the low yields of these reactions, which never seem to exceed 50% of theory.

There are clear similarities here with the reaction of S_4N_4 and $Ni(CO)_4$, which results after work-up in the formation of $Ni(S_2N_2H)_2$, i.e., a complex of the protonated form of $S_2N_2^{2-}$, or $S_2N_2H^-$ (26). On the other hand, with $CpCo(CO)_2$ the complex $CpCoS_2N_2$ is obtained, formally derived from $S_2N_2^{2-}$ (16). The reactions of binary thiazenes with organometallic complexes are also not well understood, involve complex redox changes, and may very well involve the intermediacy of free radicals. We believe that the reactions of **4** with transition metals are useful models for the even more complex reactions of the binary compounds, and are therefore worthy of further investigation. Work on the elucidation of the mechanism whereby stable free-radical heterocycles interact with metal clusters is in progress, as are attempts to produce the redox changes identified for **3** by chemical means.

Experimental section

General

$Fe_3(CO)_9(\mu_3\text{-}CX)_2$ (X = F, Cl, Br, H) (2), $[RC_6H_4CN_2S_2]_2$ (R = H, CH_3O, CF_3) (8*a*), $[Fe_2(CO)_6(S_2N\{NH\}CPh)]$ (3*a*), and $[Cp_2Ni_2(S_2N_2CPh)]$ (3*b*) were prepared by published procedures. Solvents were reagent grade, and distilled from sodium wire (toluene) or from P_2O_5 (CH_2Cl_2). Unless otherwise indicated, all procedures were performed under an atmosphere of purified N_2 using a dry-box, Schlenk ware, and vacuum-line techniques. Infrared spectra were recorded on a BOMEM MB102 Fourier transform spectrometer. Electronic absorption spectra were obtained in 1.00 cm quartz cuvettes on a Varian DMS 100S spectrophotometer. ESR spectra were collected using a spectrometer constructed from a Bruker ESP300E console, microwave bridge, signal bridge, field controller, and Hall controller connected to an older electromagnet. NMR spectra were acquired at 250.13 (^1H) and 62.90 (^{13}C) MHz on a Bruker AC250-F spectrometer. Mass spectra were recorded by the Mass Spectrometry Center, University of Alberta, Canada. Elemental analyses were performed by MHW Laboratories, Phoenix, Ariz., U.S.A.

Preparation of $[Fe_2(CO)_6(S_2N\{NH\}CC_6H_4OCH_3)]$, 2*b*

$CH_3OC_6H_4CN_2S_2$ (0.50 g, 2.37 mmol) and $[Fe_3(CO)_{12}]$ (1.23 g, 2.44 mmol) were stirred in 100 mL toluene under N_2. The mixture was slowly heated to 95°C over a period of 3 h until tlc analysis (silica with 1:1 CH_2Cl_2–hexanes eluant) indicated disappearance of $Fe_3(CO)_{12}$. After cooling to room temperature unreacted solid material was removed by filtration and the solvent removed under vacuum. The crude product was recrystallized from hot toluene to give orange crystals, 0.48 g (0.98 mmol, 41% yield), mp 165–169°C (dec). Anal. calcd. for $C_{14}H_8Fe_2N_2O_7S_2$: C 34.17, H 1.64, N 5.69, S 13.03%, found: C 34.12, H 1.59, N 5.47, S 12.94%.

Preparation of $[Fe_2(CO)_6(S_2N\{NH\}CC_6H_4CF_3)]$, 2*c*

$CF_3C_6H_4CN_2S_2$ (0.25 g; 1.0 mmol) and $Fe_3(CO)_{12}$ (0.34 g; 0.67 mmol) in 75 mL toluene were heated for 8 h while the temperature was slowly increased to 70°C, and were stirred until all the $Fe_3(CO)_{12}$ was consumed (tlc). The solution was then filtered hot, and the filtrate reduced to dryness. Recrystallization of the residue from toluene–hexanes gave 0.27 g (0.51 mmol, 51% yield) of fine orange needles (dec. 165°C). In some reactions extraction of the solids from the first filtration with CH_2Cl_2 yielded some additional product. Anal. calcd. for $C_{14}H_5F_3Fe_2N_2O_6S_2$: C 31.73, H 0.95, N 5.29, S 12.10%; found: C 31.90, H 1.16, N 5.53, S 12.00%.

Can. J. Chem. Downloaded from www.nrcresearchpress.com by 80.90.12.36 on 09/08/12
For personal use only.

Can. J. Chem. Downloaded from www.nrcresearchpress.com by 80.90.12.36 on 09/08/12
For personal use only.

Table 5. Parameters used in Extended Hückel calculations

Orbital		H_{ii} (eV)	ζ_1	ζ_2	C_1^a	C_2^a
H	1*s*	−13.6	1.3			
C	2*s*	−21.4	1.625			
	2*p*	−11.4	1.625			
N	2*s*	−25.6	1.95			
	2*p*	−13.2	1.95			
O	2*s*	−32.3	2.275			
	2*p*	−14.8	2.275			
S	3*s*	−20.7	1.817			
	3*p*	−11.6	1.817			
Fe	4*s*	−9.17	1.900			
	4*p*	−5.37	1.900			
	3*d*	−12.7	5.350	1.80	0.5366	0.6678
Ni	4*s*	−9.11	1.825			
	4*p*	−5.15	1.125			
	3*d*	−13.4	5.750	2.00	0.5683	0.6292

[a]Coefficients used in the double-ζ expansion of the *d* orbitals.

Electrochemistry

Cyclic voltammetric (cv) studies (scan rates v = 20–5000 mV s^{-1}) were made with a PAR 173 potentiostat in combination with a PAR 175 programmer and recorded on a Houston Graphics 2000 XY plotter or a Hewlett Packard 181 storage oscilloscope. Electrochemical experiments were performed on a platinum three-electrode system with the platinum working electrode either a 0.5 mm Pt wire or a 0.5 mm diameter Pt micro-tip. A positive feedback circuitry was employed to minimize *iR* drop losses. The vacuum-tight all-glass electrochemical cell has been described in detail elsewhere (1). The cell was charged with the supporting electrolyte (NBu_4PF_6) at a concentration of 0.05 mol L^{-1}. After heating of the electrolyte at +90°C for 12 h on the vacuum line to remove traces of water, the solvent (dry degassed CH_2Cl_2) was transferred under vacuum. Compounds under investigation and ferrocene acting as an internal reference compound were added to the cell using break-seal techniques. The ferricenium/ferrocene couple was determined in this system at +0.48 V vs. SCE at 25°C. For experiments under a CO atmosphere a slight positive pressure (1.1–1.2 atm; 1 atm = 101.3 kPa) was used to fill the electrochemical cell with the gas on a vacuum line.

Extended Hückel MO calculations

EHMO calculations were performed using CACAO 4.0 running on a 25 MHz 486 Intel-based personal computer (27). Parameters employed are listed in Table 5. Geometries used are based on idealizations of the structures as determined by X-ray crystallography (3).

Supplementary data

Infrared spectroscopic and mass spectral data for **2***b* and **2***c* have been deposited.[6]

[6] The supplementary material can be purchased from: The Depository of Unpublished Data, Document Delivery, CISTI, National Research Council Canada, Ottawa, Canada K1A 0S2.

Acknowledgments

This work was supported by the Natural Sciences and Engineering Research Council of Canada, the University of Lethbridge research fund (R.T.B.), the Deutsche Forschungsgesellschaft and Fonds der Chemischen Industrie, Germany (D.L. and H.M.S.). K.H.M. acknowledges the award of a Feodor-Lynen Fellowship by the Alexander von Humboldt Foundation. V.K. was supported by an NSERC undergraduate research award. We thank the University of Lethbridge for the purchase of the NMR spectrometer, and Prof. John Weil, University of Saskatchewan, Saskatoon, Canada, for the use of the ESR spectrometer. The assistance of Dr. Michael Mombourquette and Suzanne Manley with the acquisition of the ESR spectra is gratefully acknowledged.

References

1. K.H. Moock and M.H. Rock. J. Chem. Soc. Dalton Trans. 2459 (1993).
2. (*a*) D. Lentz, I. Brüdgam, and H. Hartl. Angew. Chem. **97**, 115 (1985); Angew. Chem. Int. Ed. Engl. **24**, 119 (1985); (*b*) D. Lentz and H. Michael. Inorg. Chem. **28**, 3396 (1989); (*c*) Chem. Ber. **123**, 1481 (1990).
3. (*a*) A.J. Banister, I.B. Gorrell, W. Clegg, and K.A. Jørgensen. J. Chem. Soc. Dalton Trans. 2229 (1989); (*b*) J. Chem. Soc. Dalton Trans. 1105 (1991).
4. (*a*) R.T. Boeré and K.H. Moock. J. Am. Chem. Soc. **117**, 4755 (1995); (*b*) R.T. Boeré, K.H. Moock, and M.Z. Parvez. Z. Anorg. Allgem. Chem. **620**, 1589 (1994); (*c*) C.M. Aherne, A.J. Banister, I.B. Gorrell, M.I. Hansford, Z.V. Hauptman, A.W. Luke, and J.M. Rawson. J. Chem. Soc. Dalton Trans. 967 (1993).
5. V. Klassen, K. Preuss, K.H. Moock, and R.T. Boeré. Phosphorus Sulfur Silicon Relat. Elem. **93–94**, 449 (1994).
6. (*a*) T.M. Bockman and J.K. Kochi. J. Am. Chem. Soc. **109**, 7725 (1987); (*b*) H.H. Ohst and J.K. Kochi. J. Am. Chem. Soc. **108**, 2897 (1986).
7. J.A. De Beer and R.J. Haines. J. Organomet. Chem. **24**, 757 (1970).
8. (*a*) R.T. Boeré, K.H. Moock, S. Derrick, W. Hoogerdijk, K. Preuss, J. Yip, and M. Parvez. Can. J. Chem. **71**, 473 (1993); (*b*) R.T. Boeré, J. Fait, K. Larsen, and J. Yip. Inorg. Chem. **31**, 1417 (1992); (*c*) R.T. Boeré, J. Eng, K. Preuss, M. Parvez, C.D. Bryan, and A.W. Cordes. Can. J. Chem. **72**, 1171 (1994).
9. R.M. Silverstein, G.C. Bassler, and T.C. Morril. Spectrometric identification of organic compounds. 5th ed. Wiley, New York. 1991.
10. P.D. Frisch and L.F. Dahl. J. Am. Chem. Soc. **94**, 5082 (1972).
11. R.T. Boeré, R.T. Oakley, R.W. Reed, and N.P.C. Westwood. J. Am. Chem. Soc. **111**, 1180 (1989).
12. E. Bayer, H. Eckstein, H. Hagenmaier, D. Josef, J. Koch, P. Krauss, A. Röder, and P. Schretzmann. Eur. J. Biochem. **8**, 33 (1969).
13. (*a*) H. Vahrenkamp, V.A. Uchtman, and L.F. Dahl. J. Am. Chem. Soc. **90**, 3272 (1968); (*b*) T.E. North, J.B. Thoden, B. Spencer, and L.F. Dahl. Organometallics, **12**, 1299 (1993); (*c*) T. Madach and H. Vahrenkamp. Chem. Ber. **114**, 505 (1981).
14. K. Wade. Adv. Inorg. Chem. Radiochem. **18**, 1 (1976).
15. (*a*) W. Hübel, E.H. Braye, A. Clauss, E. Weiss, U. Küerke, D.A. Brown, G.S.D. King, and C.J. Hoogzand. Inorg. Nucl. Chem. **9**, 204 (1959); (*b*) J.F. Blount, L.F. Dahl, C. Hoogzand, and W.J. Hübel. J. Am. Chem. Soc. **88**, 292 (1966); (*c*) E. Sappa, A. Tiripicchio, and P. Braunstein. Chem. Rev. **83**, 203 (1983); (d) G. Granozzi, E. Tondello, M. Casarin, S. Aime, and D. Osella. Organometallics, **2**, 430 (1983); (*e*) V. Busetti, G. Granozzi, S. Aime, R. Gobetto, and D. Osella. Organometallics, **3**, 1510

(1984); (*f*) D. Osella, R. Gobetto, and P. Montanegro. Organometallics, **5**, 1247 (1986).
16. (*a*) R.T. Boeré, B. Klassen, and K.H. Moock. J. Organomet. Chem. **467**, 127 (1994); (*b*) T. Chivers and F. Edelmann. Polyhedron, **5**, 1661 (1986).
17. (*a*) A.M. Bond, P.A. Dawson, B.M. Peak, B.H. Robinson, and J. Simpson. Inorg. Chem. **16**, 2199 (1977); (*b*) D. Miholová, J. Klíma, and A. A. Vlcek. Inorg. Chim. Acta, **27**, L67 (1978).
18. (*a*) M. Casarin, D. Ajo, D. Lentz, R. Bertoncello, and G. Granozzi. Inorg. Chem. **26**, 465 (1987); (*b*) M. Casarin, A. Gulino, D. Lentz, H. Michael-Schulz, and A. Vittadini. Inorg. Chem. **32**, 1383 (1993).
19. F.T. Al-Ani and J.P. Pickett. J. Chem. Soc. Dalton Trans. 2329 (1988).
20. A. Darchen, H. Mousser, and H. Patin. J. Chem. Soc. Chem. Commun. 968 (1988).
21. W.C. Hamilton and J.A. Ibers. Hydrogen bonding in solids. W.A. Benjamin, New York. 1968. p. 16.
22. (*a*) B.K. Teo, M.B. Hall, R.F. Fenske, and L.F. Dahl. J. Organomet. Chem. **70**, 413 (1974); (*b*) Inorg. Chem. **14**, 3103 (1975); (*c*) E.L. Anderson, T.P. Fehlner, A.E. Foti, and D.R. Salahub. J. Am. Chem. Soc. **102**, 7422 (1980); (*d*) R.L. DeKock, E.J. Baerends, and A. Oskam. Inorg. Chem. **22**, 4158 (1983).
23. (*a*) R.L. DeKock, E.J. Baerends, and R. Hengelmolen. Organometallics, **3**, 289 (1984); (*b*) T.D. Weatherhill, T.B. Rauchfuss, and R.A. Scott. Inorg. Chem. **25**, 1466 (1986).
24. R.L DeKock and H. B. Gray. Chemical structure and bonding. Benjamin/Cummings Publishing Co., Menlo Park, Calif. 1980.
25. R.E. Dessy, P.M. Weissman, and R.L. Pohl. J. Am. Chem. Soc. **88**, 5117 (1966).
26. M. Göhring and A. Debo. Z. Anorg. Allgem. Chem. **273**, 319 (1953).
27. C. Mealli and D. M. Proserpio. J. Chem. Educ. **67**, 399 (1990)

Can. J. Chem. Downloaded from www.nrcresearchpress.com by 80.90.12.36 on 09/08/12
For personal use only.

Synthesis of acetylenedicarboxylic acid esters and asymmetric Diels–Alder reactions of the bis(methyl (*S*)-lactyl) ester

James L. Charlton, Gaiklean Chee, and Heather McColeman

Abstract: A general method has been developed for the preparation of acetylenedicarboxylic acid esters and applied to the synthesis of both achiral and chiral esters. Diels–Alder reactions of one of the chiral esters, the bis(methyl (*S*)-lactyl) ester, with various types of dienes, such as phenylbutadiene, orthoquinodimethanes, and isobenzofuran, have been investigated. Moderate asymmetric induction was observed in reactions with dienes bearing an α-hydroxyl group. In one case, an unusual solvent-induced reversal of asymmetric induction was observed.

Key words: acetylenedicarboxylic acid esters, phenylbutadiene, orthoquinodimethanes, isobenzofurans, Diels–Alder, asymmetric.

Résumé : On a développé une méthode générale de préparation des esters de l'acide acétylènedicarboxylique et on l'a appliquée à la synthèse d'esters tant achiraux que chiraux. On a étudié les réactions de Diels–Alder de l'un des esters chiraux, l'ester bis((*S*)-lactyle de méthyle), avec divers types de dienes, tels que le phénylbutadiène, les orthoquinodiméthanes et l'isobenzofurane. Avec les dienes portant un groupe α-hydroxyle, on a observé une induction asymétrique modérée. Dans un cas, on a observé une inversion inhabituelle de l'induction asymétrique induite par un solvant.

Mots clés : esters de l'acide acétylènedicarboxylique, phénylbutadiène, orthoquinodiméthanes, isobenzofuranes, Diels–Alder, asymétrique.

[Traduit par la rédaction]

Can. J. Chem. Downloaded from www.nrcresearchpress.com by 80.90.12.36 on 09/08/12
For personal use only.

Introduction

The simple dialkyl esters of acetylenedicarboxylic acid (ADA) such as the dimethyl, diethyl, and dimenthyl can be prepared in good yield by direct esterification of the acid, and these esters have been widely used in studies of intermolecular Diels–Alder reactions with numerous types of dienes (see ref. 1 for a few examples). In some cases, direct esterification of ADA is complicated by the addition of the alcohol to the reactive triple bond polarized by the carboxylate groups (2). This side reaction has hindered the preparation of more complicated ADA esters such as the diaryl esters, which can only be prepared in moderate yield (~14%) by direct esterification of either ADA or acetylenedicarbonyl chloride (3). The preparation of complex ADA esters is, in fact, a very difficult task and it is noteworthy that literature reports of ADA ester derivatives, other than the simple dialkyl esters, are infrequent (3). Chiral esters of ADA, except for the menthyl ester, have been neglected as dienophiles in studies of asymmetric Diels–Alder reactions and the disregard of these compounds is attributed to difficulties encountered in their preparation. In addition, esters of alcohols that contain ester groups themselves, such as methyl lactate, cannot be prepared by direct esterification of ADA because the ester groups of the alcohols are susceptible to side reactions such as transesterification and hydrolysis. We would now like to report the full details of a general method for the preparation of ADA esters that is applicable to the synthesis of all types of ADA esters (Scheme 1).

Scheme 1.

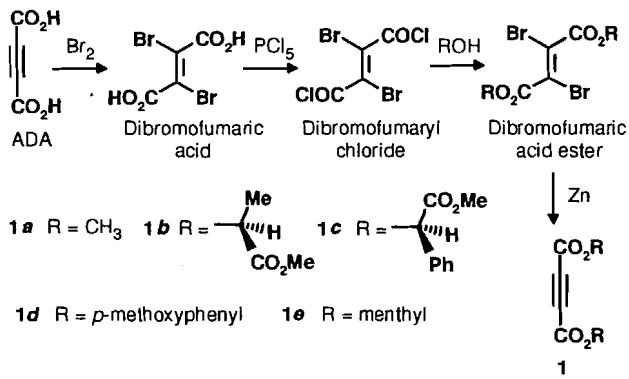

Asymmetric induction in Diels–Alder reactions of the fumarate or acrylate of methyl lactate has been the subject of numerous studies (4), and we considered that studies of the analogous ester of ADA might be equally worthwhile. The

Received January 27, 1995.

J.L. Charlton,[1] G. Chee, and H. McColeman. Department of Chemistry, University of Manitoba, Winnipeg, MB R3T 2N2, Canada.

[1] Author to whom correspondence may be addressed. Telephone: (204) 474-9267. Fax: (204) 275-0905.

Can. J. Chem. Downloaded from www.nrcresearchpress.com by 80.90.12.36 on 09/08/12
For personal use only.

Scheme 2.

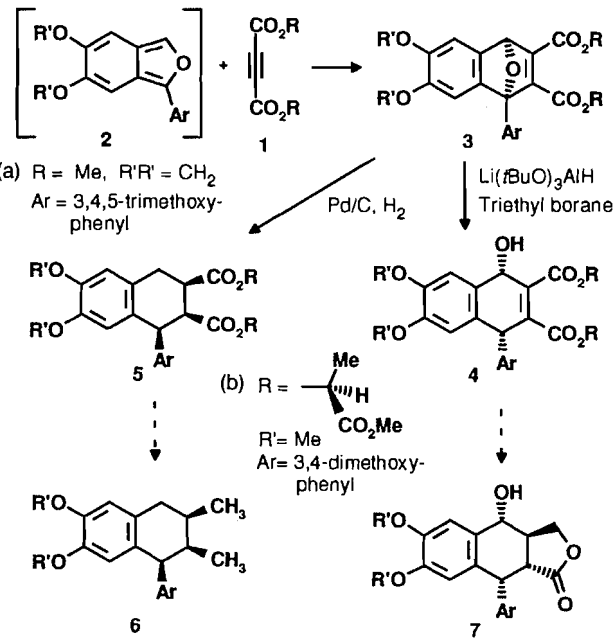

approach in Scheme 1 makes possible the preparation of the lactyl ADA ester **1***b*, and a study has been undertaken of its Diels–Alder reactions with various dienes such as phenylbutadiene (5), orthoquinodimethanes (*o*-QDMs) (6), and isobenzofurans (7). These dienes have been used extensively in organic synthesis for the construction of biaryl, aryltetralin, and naphthalene compounds. For instance, Rodrigo and co-workers have previously shown that an isobenzofuran can be trapped by dienophiles such as dimethyl ADA ester **1***a* to give a racemic cycloadduct that can then be hydrogenated with Pd/C to afford the corresponding tetralin **5***a* (see Scheme 2, series (a)) (8). In addition, the oxygen bridge can also be reductively cleaved by lithium tri-*tert*-butoxyaluminumhydride and triethyl borane to afford the corresponding 1,4-*cis*-dihydro naphthol **4***a* (9). The method should be applicable to the asymmetric synthesis of aryltetralin lignans, as proposed in Scheme 2. If cycloadduct **3***b* could be formed from isobenzofuran **2** and lactyl ADA ester **1***b* with the absolute stereochemistry shown, it could then be reduced stereoselectively to an aryltetralin with podophyllotoxin (**7**) or norisoguaiacin (**6**) relative and absolute stereochemistry, compounds that show antitumor and antibacterial activity, respectively (10).

Results and discussion

A. Synthesis of acetylenedicarboxylic acid esters

The ADA esters were prepared according to the procedures shown in Scheme 1 and briefly described in a preliminary communication (11). The general approach involves esterification of dibromofumaryl chloride followed by 2,3-dibromo elimination to afford the acetylenic diester in excellent yield. Dibromofumaryl chloride can be prepared by bromination of ADA followed by treatment with phosphorus pentachloride. Other than the bromination of ADA (80%), every step afforded a yield of >90% with no addition to the triple bond, transesterification, or hydrolysis. Bromination of a neutral aqueous solution of the potassium salt of ADA in the presence of sodium bromide proceeded smoothly. Phosphorus pentachloride rather than thionyl chloride was used for the preparation of dibromofumaryl chloride since the latter caused the liberation of bromine, which led to formation of unidentified by-products. The esterification of the acid chloride was carried out in carbon tetrachloride using pyridine as a catalyst at ice temperature. Of all the steps leading to the acetylenic esters, zinc-promoted debromination of dibromofumarate was the most troublesome due to the necessity to change the reaction conditions as the type of the diester changed. This was especially obvious in the case of bis(methyl (*S*)-lactyl) and bis(methyl (*R*)-mandelyl) esters of dibromofumaric acid. The former could be reduced with granular zinc in refluxing THF in 4 h, while the latter required the much more activated amalgamated zinc. In addition, the preparation of the mandelyl ADA ester **1***c* from the dibromofumarate using amalgamated zinc dust in refluxing THF for 1 h gave rise to the fumarate and maleate of the corresponding ester as by-products (3–4% each). Under the same condition, these products, which result from the reduction of the triple bond, were not observed in the preparation of lactyl ADA ester **1***b*. The reason for this is not known. It was found that the mandelyl ADA ester **1***c* and its fumarate were inseparable by chromatography. However, we discovered that α-hydroxy-*o*-QDM, which is a short-lived intermediate that can be prepared thermally from benzocyclobutenol (12), reacted with the fumarate at a faster rate than with the acetylenic ester. Therefore, treating a mixture of mandelyl ADA ester **1***c* and its fumarate with a trace amount of benzocyclobutenol in refluxing toluene allowed almost complete removal of the 4% fumarate as a cycloadduct after chromatography. The removal of the fumarate can be monitored by the disappearance of the olefinic protons at 7.06 ppm.

Although the approach in Scheme 1 does not offer any superiority over direct esterification methods for simple dialkyl esters of ADA (**1***a* and **1***e*), it does provide a method for the synthesis of complex ADA esters. The previously reported bis(*p*-methoxyphenyl) ester of ADA (**1***d*), which could be prepared only in 14–15% yield by direct esterification of ADA or acetylenedicarbonyl chloride (3), could now be prepared using the approach in Scheme 1 in an overall yield of >70%. Similarly, two new chiral esters of ADA, the lactyl ester **1***b* and mandelyl ester **1***c*, which could not be obtained by any direct esterification method, were also synthesized in excellent yield.

B. Asymmetric Diels–Alder reactions of bis(methyl (*S*)-lactyl) acetylenedicarboxylate (1*b*)

The Diels–Alder reactions of lactyl ADA ester **1***b* with various types of dienes were investigated. The dienes chosen for study were phenylbutadiene, various *o*-QDMs (α-hydroxy, α-phenyl-α′-hydroxy, α-hydroxy-α-phenyl, and α-phenyl), and an aryl isobenzofuran.

(*E*)-1-Phenyl-1,3-butadiene (13) was reacted with lactyl ADA ester **1***b* in refluxing xylenes to give a mixture of two diastereomers (**8**/**9**) in a 1:1.3 ratio,[2] as determined by integration of the four methoxy singlets between 3.5 and 3.8 ppm in

[2] Absolute stereochemistry of the major cycloadduct was not determined.

Can. J. Chem. Downloaded from www.nrcresearchpress.com by 80.90.12.36 on 09/08/12
For personal use only.

Scheme 3.

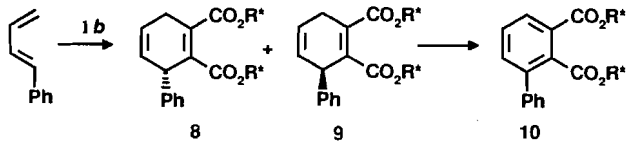

Scheme 4.

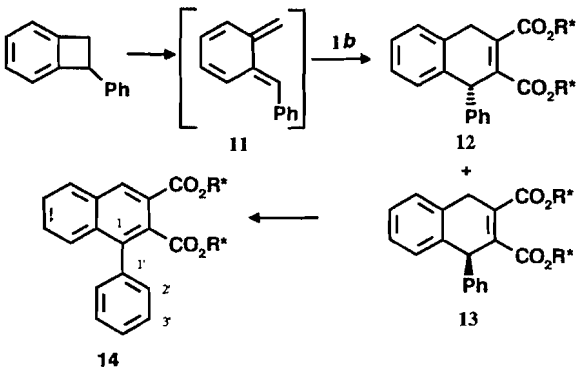

Scheme 5.

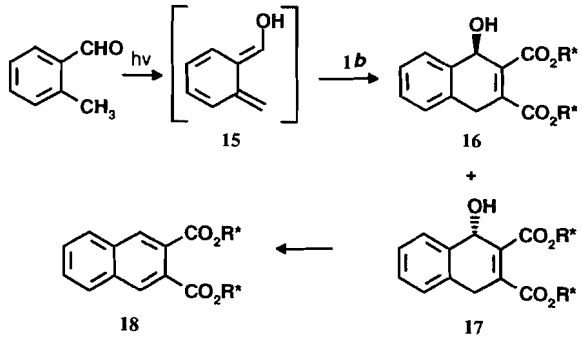

Scheme 6.

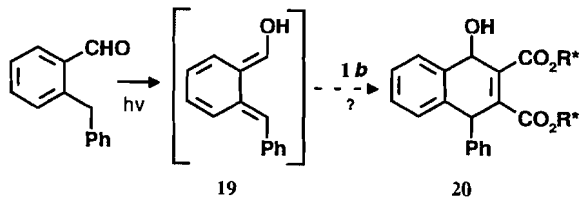

Scheme 7.

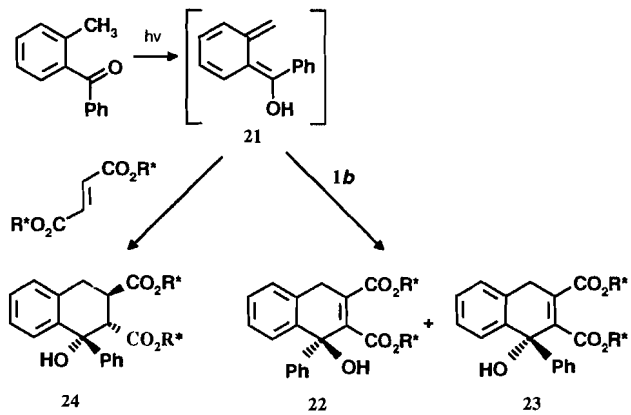

the NMR spectrum. Carrying out the reaction in methylene chloride at room temperature using $MeAlCl_2$ as catalyst gave only a slightly improved 1:2 mixture of the two diastereomers. The diastereomers were not separated but were further dehydrogenated to the biaryl **10** using Pd/C in refluxing xylenes, in order to confirm their structures (Scheme 3).

α-Phenyl-*o*-QDM (**11**), prepared thermally from α-phenylbenzocyclobutene (14) in refluxing toluene, reacted nonselectively with ADA ester **1*b*** to give a mixture of two diastereomers (**12/13**) in a 1:1.4 ratio[2] (see Scheme 4). In view of the poor diastereoselectivity, no attempt was made to separate the two diastereomers. The structures were confirmed by aromatization using Pd/C in refluxing xylenes to afford the phenylnaphthalene **14**. This aromatized product showed an interesting ^{13}C NMR feature in that 10 instead of 8 aromatic CH peaks were observed. This indicates that the C-2′ and C-3′ were not identical to C-6′ and C-5′, respectively, on the NMR time scale at room temperature, and the reason for this is attributed to the restricted rotation about the C1—C1′ bond of the molecule. Restricted rotation in arylnaphthalene derivatives giving rise to atropisomers has been studied elsewhere (15) but, to the best of our knowledge, the observed ^{13}C NMR properties of these compounds have not been reported.

α-Hydroxy-*o*-QDM (**15**), formed by the irradiation of 2-methylbenzaldehyde in benzene at room temperature, was reacted with lactyl ADA ester **1*b***. The addition was highly diastereoselective, generating a mixture of two fairly unstable diastereomers **16** and **17** (1:5 ratio),[2] which dehydrated slowly to give naphthol **18** upon standing at room temperature (Scheme 5). When α-hydroxy-*o*-QDM was generated thermally from benzocyclobutenol (12) in refluxing benzene, only the naphthol **18** was isolated.

o-QDM **19** was generated photochemically from *o*-benzylbenzaldehyde since its thermal precursor, *trans*-2-phenylbenzocyclobuten-1-ol, tends to be very difficult to prepare (16). Disappointingly, the aldehyde did not form a trappable *o*-QDM **19** on irradiation in the presence of ADA ester **1*b***, probably due to quenching of the triplet aldehyde by the dienophile (**4*b***)(Scheme 6).

α-Hydroxy-α-phenyl-*o*-QDM (**21**), generated by irradiation of 2-methylbenzophenone, was reacted with lactyl ADA ester **1*b*** to give a mixture of two diastereomers **22** and **23** (1:2.1 ratio),[2] which were characterized by NMR spectroscopy. The structures of the diastereomers were confirmed by dehydration using pTsOH in refluxing benzene to afford the phenylnaphthalene **14**. The reaction is depicted in Scheme 7.

Although the diastereoselectivity of the reaction was synthetically unsatisfactory, an interesting phenomenon was observed during the search for other solvents that might improve diastereoselectivity. When polar solvents such ethyl acetate, acetone, acetonitrile, or methanol were used, the ratio of the two diastereomers was reversed, as shown in Table 1.

To examine if a similar effect would occur with another dienophile carrying the same chiral auxiliary, an experiment was carried out using methyl (*S*)-lactyl fumarate as dienophile. In solvents such as benzene, acetone, and ethyl acetate, the reaction afforded predominantly diastereomer **24** (>90%

Can. J. Chem. Downloaded from www.nrcresearchpress.com by 80.90.12.36 on 09/08/12
For personal use only.

Table 1. Solvent effects on the diastereofacial selectivity in the Diels–Alder reaction of α-hydroxy-α-phenyl-*o*-QDM (**21**) with bis(methyl (*S*)-lactyl) acetylenedicarboxylate (**1***b*).

Solvent	Ratio of isomer[a] A : B
Hexane–benzene	1 : 2
Benzene	1 : 2.1
Ethyl acetate	2.2 : 1
Acetone	2.4 : 1
Acetonitrile	2 : 1
Methanol	2 : 1

[a]Measured using the integration ratios of two methyl doublets between 1.2 and 1.4 ppm of their ^{1}H NMR ($CDCl_3$) spectra.

de) as given in Scheme 7.[3] In methanol, the diastereoselectivity of the reaction was reduced, affording two diastereomers in a 1:1.4 ratio, with **24** remaining as the major isomer. Solvent effects on Diels–Alder reactions are well known and can result in notable improvement in reaction rates, *endo*/*exo* diastereoselectivity, and diastereofacial selectivity (18). The phenomena have been explained by solvophobicity and electrostatic interactions of the solute and solvent (19). In all cases studied, the enhancement of the *endo*/*exo* or diastereofacial selectivities was observed, but no one has reported the unusual solvent-induced reversal of asymmetric induction in Diels–Alder reactions. A solvent-induced reversal of asymmetric induction has been observed in the photodeconjugation of an α,β-unsaturated lactyl ester (20). As well, the $TiCl_4$-catalysed Diels–Alder reaction of lactyl fumarate with cyclopentadiene yields a preferred product of opposite configuration to that of the uncatalysed reaction (21). A complete understanding of the effect of solvents on the asymmetric control of the Diels–Alder reaction of ADA ester **1***b* and *o*-QDM **21** will require further study.

The last diene used for the study of a Diels–Alder reaction of ADA ester **1***b* was isobenzofuran **2***b*, generated using a modified literature procedure, via phthalan **26** by the acid-catalysed elimination reaction of hydroxyacetal **25** (Scheme 8)(22). Precursor **25** was reacted with ADA ester **1***b* in the presence of a catalytic amount of glacial acetic acid at 95°C for 20 min, giving the aromatized cycloadduct naphthol **29** as a major product (80 ± 5%), and two bridged cycloadducts (**27** and **28**) as minor products (20 ± 5%) in a 1:1.2 ratio,[2] as determined by the integration of two pairs of lactyl doublets between 1.0 and 1.6 ppm. Using $MeAlCl_2$ or Et_2AlCl in place of glacial acetic acid as a catalyst for the formation of isobenzofuran **2***b* and for the Diels–Alder reaction, at either room temperature or at 70°C, failed to afford any cycloadduct from hydroxyacetal **25** and ester **1***b*.

[3] The assignment of the absolute and relative stereochemistry of diastereomer **24** was made on the basis of previous work on a similar compound. Because the chiral auxiliary of the dienophile employed in this study had the opposite stereochemistry to that used previously, a reverse facial selectivity in the Diels–Alder reaction was assumed. (ref. 17).

Scheme 8.

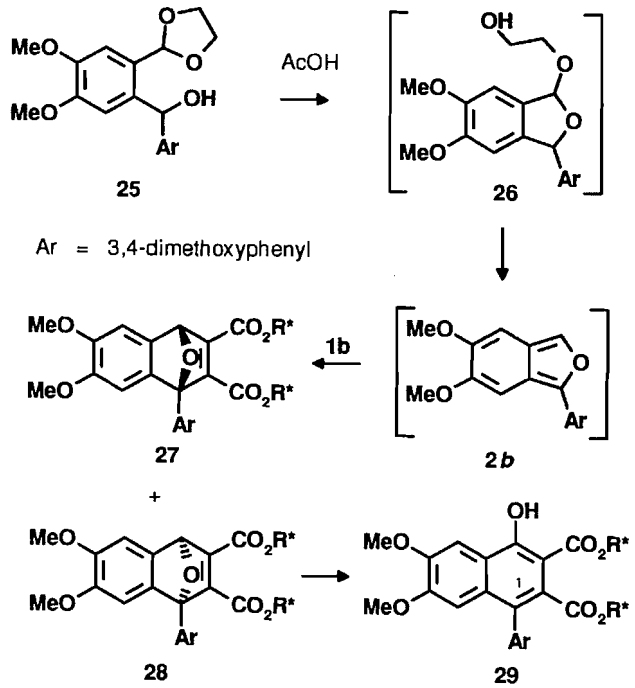

Since the formation of **27** and **28** showed no diastereoselectivity, no attempt was made to isolate the bridged cycloadducts, and the crude product was reacted further in the presence of acid to convert both minor products to the naphthol, which was isolated in 80% yield after chromatography. Its ^{1}H NMR spectrum showed an interesting feature in that most of the characteristic peaks of naphthol **29** were split into doublets. Similar to phenylnaphthalene **14**, the phenomenon is attributed to the restricted rotation about the C1—C1′ bond, which causes naphthol **29** to exist in two diastereomeric forms as observable in the NMR spectrum. Further investigations on the hindered rotation of arylnaphthalene lignans are under progress and will be reported in the near future.

The results for the Diels–Alder reactions of ADA ester **1***b* with various types of diene are summarized in Table 2. The dienes without an α-hydroxy group afforded stable cycloadducts but, disappointingly, gave poor diastereoselectivity. This was only marginally increased in the presence of the Lewis acid $MeAlCl_2$. In reactions with *o*-QDMs, diastereofacial selectivity was poorer than when using the fumarate of methyl lactate, which is known to give de's of >95% (4). Even though reasonable diastereoselectivity was observed in reactions with α-hydroxy-*o*-QDMs, the cycloadducts tended to be fairly unstable due to their ease of dehydration. The reaction of isobenzofuran **2***b* with ADA ester **1***b* appeared nonselective, and was not suitable for use in the preparation of diastereomerically pure aryltetralins. The use of the Lewis acids Et_2AlCl or $MeAlCl_2$ in this reaction entirely stopped cycloadduct formation.

Experimental

A description of general instrumentation, procedures for the irradiation experiments, and identification and characterization of compounds has been provided previously (4).

Table 2. Yields and diastereomer ratios of the Diels–Alder reactions of bis(methyl (*S*)-lactyl) acetylenedicarboxylate (**1***b*) with various dienes.

Type of diene	Cycloadducts (% yield)[a]	Ratio of two diastereomers[b]	Aromatization product (% yield)[c]
Phenylbutadiene	82	1:1.3	92
	75[d]	1:2[d]	
11	62	1:1.3	90
15	46	1:5	39
21	82	1:2	80
2*b*	20	1:1.2	80

[a]After chromatography.
[b]Measured using the integration ratios of their ^{1}H NMR ($CDCl_3$) spectra.
[c]Either isolated from the cycloaddition reactions, or after specific treatments of the cycloadducts for structural confirmation (see Experimental).
[d]$MeAlCl_2$ catalysed (see Experimental).

Can. J. Chem. Downloaded from www.nrcresearchpress.com by 80.90.12.36 on 09/08/12
For personal use only.

A. Synthesis of acetylenedicarboxylic acid esters

Dibromofumaric acid

A modification of a literature procedure was used (23). An aqueous solution of KOH (2 M, ca. 20 mL) was added to the monopotassium salt of acetylenedicarboxylic acid (5.51 g, 36.3 mmol) with stirring until the resulting solution became neutral. Bromine (6.33 g, 39.6 mmol) was added to sodium bromide (18.7 g, 0.18 mol) in water (80 mL), and this solution was then added to the neutral solution of ADA. Water was added to the mixture to give a total volume of 150 mL. The brown color of the solution discharged after 2 h in the dark at room temperature. It was left standing for a further day. The colorless solution was acidified with concentrated HCl to pH 1–2, and extracted with ethyl acetate (4 × 20 mL). The organic layer was washed with saturated sodium bisulfite (3 × 20 mL), dried ($MgSO_4$), and concentrated in vacuo to give a colorless solid (9.44 g). The product was recrystallized from THF–hexanes to give colorless needles (8.0 g, 80%); mp 237–238°C, identical to that reported previously (24); IR (CH_2Cl_2): 1697 cm^{-1}; ^{13}C NMR (H_2O/D_2O) δ: 113.10 (2 × C), 168.61 (2 × CO); mass spectrum *m/e* (rel %): 276 (1.3), 274 (2.4), 272 (1.2), 186 (4), 184 (6), 182 (3), 151 (16), 149 (17), 106 (95), 104 (100).

Dibromofumaryl chloride

The compound was prepared according to Ott's procedure (24). Dibromofumaric acid (4.69 g, 17.1 mmol), petroleum ether (30 mL), and phosphorus pentachloride (7.17 g, 34.4 mmol) were stirred together at room temperature until the precipitate dissolved (ca. 5 h). The solution was poured onto crushed ice and stirred for 15 min. The organic layer was separated, dried ($MgSO_4$), and concentrated in vacuo to give a pale yellow liquid (4.87 g, 92%). IR (CH_2Cl_2): 1779 cm^{-1}. ^{13}C NMR ($CDCl_3$) δ: 114.64 (2 × C), 162.00 (2 × CO); mass spectrum *m/e* (rel %): 312 (4.5), 310 (5.5), 277 (24), 275 (36), 257 (10), 256 (14), 249 (25), 247 (35), 213 (18), 211 (11), 184 (17), 133 (98), 131 (100). Exact Mass calcd. for $C_4{}^{79}Br^{81}Br^{35}Cl_2O_2$: 309.7621; found: 309.7578.

General procedure for the preparation of dibromofumarates (except for the dimethyl ester)

To the alcohol (3.18 mmol) and pyridine (0.255 g, 3.22 mmol) in CCl_4 (20 mL) at 0°C under nitrogen, was added dibromofumaryl chloride (0.497 g, 1.60 mmol) in CCl_4 (10 mL), dropwise, over a period of 10 min. The mixture was stirred for 20 min and then at room temperature for another 40 min. It was washed with water (2 × 20 mL), 5% sodium bicarbonate (4 × 20 mL), and water (2 × 20 mL). The organic layer was dried ($MgSO_4$) and concentrated in vacuo.

Bis(methyl (R)*-lactyl) dibromofumarate*: A yellow liquid (93%); $[\alpha]_D^{20}$ −22.4 (*c* 0.923, $CHCl_3$); IR (CH_2Cl_2): 1748 cm^{-1}; ^{1}H NMR ($CDCl_3$) δ: 1.61 (d, 6H, *J* = 7.05), 3.79 (s, 6H), 5.27 (q, 2H, *J* = 7.06); ^{13}C NMR ($CDCl_3$) δ: 16.71 (2 × CH_3), 52.57 (2 × CH_3), 70.84 (2 × CH), 112.66 (2 × C), 161.24 (2 × CO), 169.65 (2 × CO); mass spectrum *m/e* (rel %): 367 (15.0), 365 (15.1), 345 (7), 343 (15), 341 (8), 293 (15), 291 (15), 183 (37), 155 (14), 86 (100). Anal. calcd. for $C_{12}H_{14}Br_2O_8$: C 32.31, H 3.16; found: C 32.43, H 3.21.

Bis(p-*methoxyphenyl) dibromofumarate*: A pale yellow solid (96%); mp 146–148°C; IR (CH_2Cl_2): 1700 cm^{-1}; ^{1}H NMR ($CDCl_3$) δ: 3.81 (s, 6H), 6.93 (d, 4H, *J* = 9.08), 7.15 (d, 4H, *J* = 9.10); ^{13}C NMR ($CDCl_3$) δ: 55.63 (2 × CH_3), 113.26 (2 × C), 114.64 (4 × CH), 121.75 (4 × CH), 143.42 (2 × C), 157.89 (2 × C), 160.85 (2 × CO); mass spectrum *m/e* (rel %): 486 (M^+, 2.0), 365 (3), 363 (6), 361 (4), 326 (8), 284 (4), 282 (5), 124 (100), 123 (48), 109 (95). Anal. calcd. for $C_{18}H_{14}Br_2O_6$: C 44.47, H 2.90; found: C 44.47, H 2.86.

Bis(methyl (S)*-mandelyl) dibromofumarate*: A colorless liquid that crystallized upon standing (93%); mp 61–63°C; $[\alpha]_D^{20}$ −103.3 (*c* 1.462, $CHCl_3$); IR (CH_2Cl_2): 1749, 1751 cm^{-1}; ^{1}H NMR ($CDCl_3$) δ: 3.77 (s, 6H), 6.07 (s, 2H), 7.39–7.41 (m, 6H), 7.48–7.51 (m, 4H); ^{13}C NMR ($CDCl_3$) δ: 52.88 (2 × CH_3), 76.36 (2 × CH), 113.09 (2 × C), 127.65 (4 × CH), 128.86 (4 × CH), 129.62 (2 × CH), 132.46 (2 × C), 161.22 (2 × CO), 167.87 (2 × CO); mass spectrum *m/e* (rel %): 407 (2.0), 405 (4.4), 403 (2.3), 189 (14), 150 (31), 149 (100.0) 121 (36), 118 (22), 105 (45). Anal. calcd. for $C_{22}H_{18}Br_2O_8$: C 46.34, H 3.18; found: C 46.58, H 3.18.

Dimenthyl dibromofumarate: A colorless oil that crystallized upon standing (100%); mp 82–85°C; $[\alpha]_D^{20}$ −55 (*c* 0.418,

Can. J. Chem. Downloaded from www.nrcresearchpress.com by 80.90.12.36 on 09/08/12
For personal use only.

$CHCl_3$); IR (CH_2Cl_2): 1732 cm^{-1}; ^1H NMR ($CDCl_3$) δ: 0.79 (d, 6H, J = 6.92), 0.84–0.93 (m, 2H), 0.92 (d, 6H, J = 7.11), 0.94 (d, 6H, J = 6.67), 1.11 (m, 4H), 1.50 (m, 4H), 1.71 (br d, 4H), 2.02 (dp, 2H, J = 2.73, 6.96), 2.06 (m, 2H), 4.84 (dt, 2H, J = 4.39, 10.91); ^{13}C NMR ($CDCl_3$) δ: 16.02 (2 × CH_3), 20.72 (2 × CH_3), 21.95 (2 × CH_3), 23.20 (2 × CH_2), 25.95 (2 × CH), 31.45 (2 × CH), 34.06 (2 × CH_2), 40.19 (2 × CH_2), 46.90 (2 × CH), 77.78 (2 × CH), 112.01 (2 × C), 161.84 (2 × CO); mass spectrum *m/e* (rel %): 395 (0.5), 273 (1.7), 271 (3.6), 269 (1.8), 149 (17), 139 (22), 138 (50), 123 (31), 95 (94), 81 (85). Anal. calcd. for $C_{24}H_{38}Br_2O_4$: C 52.38, H 6.96; found: C 52.54, H 7.04.

Dimethyl dibromofumarate

A mixture of dibromofumaryl chloride (0.425 g, 1.38 mmol) and methanol (4 mL) was refluxed under nitrogen for 2 h. The solvent was evaporated and the precipitate was dissolved in dichloromethane (5 mL), then washed with 5% sodium bicarbonate (3 × 10 mL) and water (2 × 10 mL). The dichloromethane layer was dried ($MgSO_4$) and concentrated in vacuo to give a colorless solid (0.393 g, 94%); mp 36–37°C; IR (CH_2Cl_2): 1744 cm^{-1}; ^1H NMR ($CDCl_3$) δ: 3.91 (s, 6H); ^{13}C NMR ($CDCl_3$) δ: 53.68 (2 × OCH_3), 112.70 (2 × C), 162.59 (2 × CO); mass spectrum *m/e* (rel %): 304 (14), 302 (28), 300 (15), 273 (48), 271 (97), 269 (51), 223 (30), 221 (30), 195 (15), 193 (17), 149 (20), 147 (20), 133 (35), 131 (35). Exact Mass calcd. for $C_6H_6Br_2O_4$: 301.8612; found: 301.8606.

General procedure for the preparation of acetylenedicarboxylates (not including the bis(methyl (R)-mandelyl) and dimenthyl esters)

Dibromofumarate (1 mmol), dry THF (10 mL), and granular zinc (0.4 g, 6 mmol) were refluxed under nitrogen for 2–5 h depending on the type of ester (Note: the bis(*p*-methoxyphenyl) ester required a catalytic amount of I_2). The granular zinc was filtered off and THF evaporated. The brown residue was dissolved in dichloromethane (5 mL) and washed with water (4 × 10 mL). The organic phase was dried ($MgSO_4$) and concentrated in vacuo.

*Dimethyl acetylenedicarboxylate (**1**a)*: The reaction was complete after 2 h reflux with granular zinc. A colorless liquid was obtained (93%), ^1H NMR ($CDCl_3$) δ: 3.85 (s, 6H); ^{13}C NMR ($CDCl_3$) δ: 53.42 (2 × CH_3), 74.63 (C≡C), 152.12 (2 × CO), identical to that reported previously.[4]

*Bis(methyl (S)-lactyl) acetylenedicarboxylate (**1**b)*: The reaction was complete after 4 h reflux with granular zinc. A yellow oil that crystallized upon standing was obtained (95%). The solid was recrystallized from ethyl acetate–hexane; mp 78–81°C; $[\alpha]_D^{20}$ +8.0 (*c* 0.365, CHCl3); IR (CH_2Cl_2): 1732, 1760 cm^{-1}; ^1H NMR ($CDCl_3$) δ: 1.57 (d, 6H, J = 7.05), 3.78 (s, 6H), 5.23 (q, 2H, J = 7.06); ^{13}C NMR ($CDCl_3$) δ: 16.74 (2 × CH_3), 52.70 (2 × CH_3), 70.72 (2 × CH), 74.98 (C≡C), 150.76 (2 × CO), 169.47 (2 × CO); mass spectrum *m/e* (rel %): 255 (2.0), 227 (13), 183 (100), 155 (49), 111 (45.9), 87 (31), 83 (51), 80 (39). Anal. calcd. for $C_{12}H_{14}O_8$: C 50.35, H 4.93; found: C 50.10, H 4.95.

*Bis(p-methoxyphenyl) acetylenedicarboxylate (**1**d)*: This reaction required a 5 h reflux with granular zinc and I_2 (20 mg). A colourless oil that crystallized upon standing was obtained (93%); mp 146–147°C; ^1H NMR ($CDCl_3$) δ: 3.81 (s, 6H), 6.91 (br d, 4H, J = 9.14), 7.09 (br d, 4H, J = 9.15), identical to that previously reported (3); ^{13}C NMR ($CDCl_3$) δ: 55.61 (2 × CH_3), 75.96 (C≡C), 114.66 (4 × CH), 121.82 (4 × CH), 143.00 (2 × C), 150.32 (2 × C), 157.97 (2 × CO).

*Bis(methyl (R)-mandelyl) acetylenedicarboxylate (**1**c)*: Bis-(methyl (*R*)-mandelyl) dibromofumarate (71 mg, 0.12 mmol), dry THF (3 mL), and amalgamated zinc dust (47 mg, 0.72 mmol) were refluxed under nitrogen for 1 h. The solution was worked up as in the general procedure above to give a pale yellow liquid (47 mg, 95%). The ^1H NMR spectrum of the crude product showed the presence of two by-products (3–4% each). One was identified as the fumarate of methyl (*R*)-mandelate by comparison to an authentic sample (25), while the other appeared to be the maleate ester (see below). The fumarate was inseparable from mandelyl ester **1***c* by chromatography. This by-product could be removed by reacting the crude product (40 mg) with a small amount of benzocyclobutenol (12) (6 mg) in refluxing toluene (2 mL) for 30 min, followed by chromatography with 10% ethyl acetate – hexanes, which afforded the pure mandelyl ester **2** (38 mg, 85%); $[\alpha]_D^{20}$ −45.6 (*c* 0.485, $CHCl_3$); IR (CH_2Cl_2): 1761, 1735 cm^{-1}; ^1H NMR ($CDCl_3$) δ: 3.75 (s, 6H), 6.03 (s, 2H), 7.39–7.48 (m, 10H); ^{13}C NMR ($CDCl_3$) δ: 52.96 (2 × CH_3), 75.11 (C≡C), 76.18 (2 × CH), 127.70 (4 × CH), 128.92 (4 × CH), 129.76 (2 × CH), 132.22 (2 × C), 150.64 (2 × CO), 167.64 (2 × CO); mass spectrum *m/e* (rel %): 351 (M−CO_2CH_3, 1.0), 189 (6), 159 (10), 150 (31), 149 (24), 118 (66), 105 (80), 91 (100), 77 (71). Anal. calcd. for $C_{22}H_{18}O_8$: C 64.39, H 4.42; found: C 65.38, H 4.42.[5]

Bis(methyl (R)-mandelyl) maleate: mp 73–74°C; $[\alpha]_D^{20}$ −173 (*c* 0.15, $CHCl_3$); IR (CH_2Cl_2): 1755, 1763 cm^{-1}; ^1H NMR ($CDCl_3$) δ: 3.68 (s, 6H), 5.90 (s, 2H), 6.43 (s, 2H), 7.35 (br s, 10H); ^{13}C NMR ($CDCl_3$) δ: 52.61 (2 × CH_3), 75.07 (2 × CH), 127.62 (4 × CH), 128.71 (4 × CH), 129.23 (2 × CH), 129.78 (2 × CH), 133.18 (2 × C), 163.77 (2 × CO), 168.59 (2 × CO); mass spectrum *m/e* (rel %): 255 (6), 248 (2), 165 (3), 150 (50), 149 (100), 121 (42), 105 (31), 91 (22), 77 (30). Anal. calcd. for $C_{22}H_{20}O_8 \cdot EtOAc$: C 62.39, H 5.64; found: C 62.71, H 5.16.

*Dimenthyl acetylenedicarboxylate (**1**e)*: Dimenthyl dibromofumarate (75 mg, 0.13 mmol), dry THF (3 mL), and amalgamated zinc dust (84 mg, 1.28 mmol) were stirred under nitrogen at room temperature for 16 h. The solution was worked up as in the general procedure described above to give a colorless solid (46 mg, 92%); mp 131–133°C; $[\alpha]_D^{20}$ −79.1 (*c* 0.139, $CHCl_3$); IR (CH_2Cl_2): 1726 cm^{-1}; ^1H NMR ($CDCl_3$) δ: 0.77 (d, 6H, J = 6.93), 0.91 (d, 6H, J = 6.99), 0.92 (d, 6H, J = 6.50), 0.85–0.93 (m, 2H), 1.06 (m, 4H), 1.44 (m, 4H), 1.70 (m, 4H), 1.89 (dp, 2H, J = 2.64, 6.94), 2.03 (m, 2H), 4.84 (dt, 2H, J = 4.44, 10.92); ^{13}C NMR ($CDCl_3$) δ: 16.10 (2 × CH_3), 20.70 (2 ×

[4] Dimethyl acetylenedicarboxylate is commercially available. Its chemical information can be obtained from The Aldrich Catalog Handbook of Fine Chemicals 1994–1995, Aldrich Chemical Company, Inc., Milwaukee, Wis., pp. 548 (1994), and references cited therein.

[5] The unsatisfactory data of the elemental analysis of ADA ester **2** can probably be attributed to the difficulty in complete removal of the trace amount of the corresponding fumarate.

Can. J. Chem. Downloaded from www.nrcresearchpress.com by 80.90.12.36 on 09/08/12
For personal use only.

CH_3), 21.91 (2 × CH_3), 23.27 (2 × CH_2), 26.08 (2 × CH), 31.47 (2 × CH), 33.99 (2 × CH_2), 40.45 (2 × CH_2), 46.80 (2 × CH), 74.87 (C≡C), 77.66 (2 × CH), 151.61 (2 × CO); mass spectrum *m/e* (rel %): 139 (24), 138 (49), 129 (16), 123 (30), 95 (100), 83 (90), 81 (82). Anal. calcd. for $C_{24}H_{38}O_4 \cdot 1.5$ EtOAc: C 68.93, H 9.64; found: C 68.95, H 9.62.

B. Diels–Alder reactions of bis(methyl (*S*)-lactyl) acetylenedicarboxylate

(E)-1-Phenyl-1,3-butadiene

A modified literature procedure was used (13). *n*-Butyllithium (2.0 M, 5.6 mL, 11.2 mmol) was added dropwise to a suspension of methyltriphenylphosphonium bromide (3.95 g, 11.0 mmol) in ether (30 mL) under N_2 in an ice bath. The precipitate dissolved and the solution was stirred for 30 min and then cooled to −78°C, followed by dropwise addition of *trans*-cinnamaldehyde (1.39 g, 10.5 mmol) in ether (10 mL). The mixture was gradually warmed to room temperature and stirred for another 2 h. The colorless precipitate was filtered off with the aid of Celite, and the filtrate was concentrated in vacuo. The residue was redissolved in petroleum ether (10 mL) and eluted through a short silica gel column, washed with petroleum ether (ca. 20 mL), and the collected solution concentrated in vacuo to leave a pale yellow liquid (0.75 g, 55 %), which was used in the next reaction without purification.

*Cycloadducts **8** and **9***

A mixture of (*E*)-1-phenyl-1,3-butadiene (0.177 g, 1.36 mmol), **1***b* (0.118 g, 0.41 mmol), and hydroquinone (2 mg) in xylenes (4 mL) was refluxed under N_2 for 6 h. The resulting solution was run through a short silica gel column and rinsed with hexanes to remove xylenes. The product was then eluted with ethyl acetate and concentrated in vacuo to give a pale yellow liquid (0.17 g), containing mainly two diastereomers in a 1:1.3 ratio, as determined by ^{1}H NMR spectroscopy.[2] The product was chromatographed using 25% ethyl acetate – hexanes to give an oil (0.14 g, 82%); IR (CH_2Cl_2): 1745 cm^{-1}; ^{1}H NMR ($CDCl_3$, a mixture of two diastereomers) δ: 1.23 (d, 3H, *J* = 7.01), 1.25 (d, 4H, *J* = 6.95), 1.50 (d, 3H, *J* = 7.06), 1.53 (d, 4H, *J* = 7.05), 3.12 (m, 2.3H), 3.30 (m, 2.3H), 3.59 (s, 3H), 3.60 (s, 4H), 3.74 (s, 3H), 3.76 (s, 4H), 4.44 (m, 2.3H), 4.95 (q, 1H, *J* = 6.99), 5.09 (q, 1.3H, *J* = 6.99), 5.20 (q, 1H, *J* = 7.09), 5.23 (q, 1.3H, *J* = 7.06), 5.80 (m, 4.6H), 7.15–7.30 (m, 11.7H); mass spectrum *m/e* (rel %): 414 (M−H_2, 2.0), 312 (34), 225 (78), 181 (100), 153 (33), 149 (31). Exact Mass (CIMS, NH_4^+) calcd. for $C_{22}H_{24}O_8 \cdot NH_4$: 434.1815; found: 434.1780.

*Lewis acid-catalyzed Diels–Alder reaction of **1**b and phenylbutadiene*

A mixture of phenylbutadiene (55 mg, 0.43 mmol), **1***b* (15.5 mg, 0.054 mmol), and $MeAlCl_2$ (1.0 M in hexanes, 0.22 mL, 0.21 mmol) in CH_2Cl_2 (2 mL) was stirred under nitrogen at room temperature for 20 h. The mixture was diluted with CH_2Cl_2 (10 mL), washed with water (3 × 10 mL), dried ($MgSO_4$), and concentrated to afford a brown residue (60 mg). The ^{1}H NMR spectrum of the crude product showed the presence of two diastereomers in a 1:2 ratio, with the chemical shifts identical to those of cycloadducts **8** and **9**. The product was chromatographed using 25% ethyl acetate – hexanes to give an oil (17 mg, 75%).

*Biaryl **10***

A mixture of diastereomers **8** and **9** (70 mg, 0.17 mmol) was refluxed with Pd/C (0.3 g) in xylenes (4 mL) for 10 h. The mixture was filtered through a short column of silica gel, and rinsed with hexanes to remove xylenes. The product was eluted with ethyl acetate and concentrated to leave a pale yellow oil (65 mg, 92%); $[\alpha]_D^{20}$ −21.8 (*c* 0.625, $CHCl_3$); IR (CH_2Cl_2): 1743 cm^{-1}; ^{1}H NMR ($CDCl_3$) δ: 1.26 (d, 3H, *J* = 6.99), 1.61 (d, 3H, *J* = 7.04), 3.62 (s, 3H), 3.8 (s, 3H), 5.25 (q, 1H, *J* = 6.96), 5.33 (q, 1H, *J* = 7.04), 7.37–7.41 (m, 5H), 7.55 (m, 2H), 8.06 (dd, 1H, *J* = 4.80, 7.90); ^{13}C NMR ($CDCl_3$) δ: 16.68 (CH_3), 16.94 (CH_3), 52.12 (CH_3), 52.33 (CH_3), 69.52 (2 × CH), 127.81 (CH), 127.97 (CH), 128.15 (2 × CH), 128.94 (2 × CH), 129.02 (CH), 129.34 (CH), 133.80 (C), 134.55 (CH), 138.90 (C), 141.06 (C), 164.81 (C), 167.19 (C), 170.59 (C), 170.74 (C); mass spectrum *m/e* (rel %): 414 (M^+, 10), 311 (47), 225 (85), 152 (19), 84 (100). Exact Mass calcd. for $C_{22}H_{22}O_8$: 414.1314; found: 414.1293.

*Cycloadducts **12** and **13***

A mixture of **1***b* (0.10 g, 0.35 mmol) and α-phenylbenzocyclobutene (**14**) (95 mg, 0.52 mmol) in toluene (5 mL) was refluxed for 5 h. The solution was concentrated in vacuo to give an oily residue that was chromatographed using 25% ethyl acetate – hexanes to afford a mixture of two diastereomers (**12** and **13**, 0.10 g, 62%) in a 1:1.3 ratio, as determined by ^{1}H NMR spectroscopy;[2] IR (CH_2Cl_2): 1750 cm^{-1}; ^{1}H NMR ($CDCl_3$, a mixture of two diastereomers) δ: 1.35 (d, 4H, *J* = 7.02), 1.36 (d, 3H, *J* = 7.02), 1.52 (d, 4H, *J* = 7.02), 1.57 (d, 3H, *J* = 7.29), 3.64 (s, 4H), 3.67 (s, 3H), 3.77 (s, 3H), 3.78 (s, 4H), 3.84 (dd, 1.3H, *J* = 3.4, 22.2), 3.85 (dd, 1H, *J* = 3.4, 22.2), 4.02 (dd, 1H, *J* = 4.39, 21.9), 4.06 (dd, 1.3H, *J* = 4.4, 22.36), 5.06 (q, 1.3H, *J* = 7.02), 5.18 (m, 2.3H), 5.26 (m due to overlap of two quartets, 2.3H), 7.13–7.25 (m, 21H); mass spectrum *m/e* (rel %): 464 (M−H_2, 6), 362 (19), 275 (30), 231 (54), 202 (32), 119 (66) 116 (63). Exact Mass (CIMS, NH_4^+) calcd. for $C_{26}H_{26}O_8 \cdot NH_4$: 484.1971; found: 484.1937.

*Phenylnaphthalene **14***

A mixture of diastereomers **12** and **13** (50 mg, 0.11 mmol) and Pd/C (0.30 g) in xylenes (5 mL) was refluxed for 20 h. The work-up procedure for biaryl **10** was used to give a yellow oil (45 mg, 90%); $[\alpha]_D^{20}$ +13.7 (*c* 0.54, $CHCl_3$); IR (CH_2Cl_2): 1744 cm^{-1}; ^{1}H NMR ($CDCl_3$) δ: 1.21 (d, 3H, *J* = 6.97), 1.66 (d, 3H, *J* = 7.04), 3.63 (s, 3H), 3.77 (s, 3H), 5.18 (q, 1H, *J* = 6.97), 5.39 (q, 1H, *J* = 7.04), 7.13–7.53 (m, 8H), 8.01 (br d, 1H, *J* = 8.02), 8.67 (s, 1H); ^{13}C NMR ($CDCl_3$) δ: 16.71 (CH_3), 17.06 (CH_3), 52.09 (CH_3), 52.36 (CH_3), 69.41 (CH), 69.49 (CH), 124.13 (C), 127.03 (CH), 127.63 (CH), 127.83 (CH), 127.96 (CH), 128.04 (CH), 129.11 (CH), 129.32 (CH), 129.94 (C), 130.41 (CH), 130.53 (CH), 131.72 (CH), 132.39 (C), 134.27 (C), 136.29 (C), 139.16 (C), 164.91 (C), 167.25 (C), 170.66 (C), 170.91 (C); mass spectrum *m/e* (rel %): 464 (M^+, 37), 361 (41), 275 (100), 231 (20), 202 (62). Exact Mass calcd. for $C_{26}H_{24}O_8$: 464.1471; found: 464.1499.

*Cycloadducts **16** and **17**, and naphthol **18***

1*b* (0.145 g, 0.51 mmol) and 2-methylbenzaldehyde (4*a*) (0.303 g, 2.5 mmol) were irradiated in benzene (10 mL) for 2.5

Can. J. Chem. Downloaded from www.nrcresearchpress.com by 80.90.12.36 on 09/08/12
For personal use only.

h and then concentrated in vacuo. Chromatography of the crude product using 25% ethyl acetate – hexanes afforded two fairly unstable diastereomers (**16** and **17**, 96 mg, 46%) in a 1:5 ratio, as determined by ^{1}H NMR spectroscopy.[2] IR (CH_2Cl_2): 3489 (OH), 1742 cm^{-1}; ^{1}H NMR ($CDCl_3$, major diastereomer) δ: 1.57 (d, 3H, J = 7.08), 1.60 (d, 3H, J = 7.10), 3.69 (dd, 1H, J = 4.64, 23.0), 3.99 (dd, 1H, J = 3.77, 23.05), 3.78 (s, 3H), 3.81 (s, 3H), 5.29 (q, 1H, J = 7.06), 5.45 (q, 1H, J = 7.12), 5.72 (t, 1H, J = 4.16), 7.20–7.38 (m, 3H), 7.79 (dd, 1H, J = 1.89, 6.93). A by-product (81 mg, 39%) was also isolated from the chromatography of the crude diastereomers. It was identified as the naphthol **18**; $[\alpha]_D^{20}$ +24.6 (*c* 0.46, $CHCl_3$); IR (CH_2Cl_2): 1746 cm^{-1}; ^{1}H NMR ($CDCl_3$) δ: 1.56 (d, 6H, J = 7.07), 3.73 (s, 6H), 5.33 (q, 2H, J = 7.05), 7.57 (dd, 2H, J = 3.19, 3.24), 7.88 (dd, 2H, J = 3.24, 3.3), 8.30 (s, 2H); ^{13}C NMR ($CDCl_3$) δ: 17.02 (2 × CH_3), 52.39 (2 × CH_3), 69.55 (2 × CH), 127.72 (2 × C), 128.77 (4 × CH), 130.72 (2 × CH), 133.47 (2 × C), 166.54 (2 × C), 171.10 (2 × C); mass spectrum *m/e* (rel %): 388 (M^+, 16), 285 (54), 199 (100), 171 (14), 149 (15). Exact Mass calcd. for $C_{20}H_{20}O_8$: 388.1158; found: 388.1150.

*Cycloadducts **22** and **23***

1*b* (69 mg, 0.24 mmol) and 2-methylbenzophenone (78 mg, 0.40 mmol) were irradiated in benzene for 2 h. The reaction mixture was concentrated in vacuo and chromatographed (ethyl acetate – hexanes) to give a mixture of two diastereomers (**22** and **23**, 95 mg, 82%) in a 1:2.1 ratio, as shown in the ^{1}H NMR spectrum.[2] IR (CH_2Cl_2): 3458 (OH), 1741 cm^{-1}; ^{1}H NMR ($CDCl_3$, mixture of two diastereomers) δ: 1.24 (d, 3H, J = 7.02), 1.34 (d, 6.3H, J = 7.05), 1.56 (d, 3H, J = 7.04), 1.57 (d, 6.3H, J = 7.05), 3.68 (s, 3H), 3.74 (s, 6.3H), 3.76 (s, 6.3H), 3.79 (s, 3H), 3.85 (d, 3.1H, J = 22.58), 4.02 (d, 2.1H, J = 22.57), 4.03 (d, 1H, J = 22.74), 4.43 (s, 2.1H), 4.69 (s, 1H), 5.15 (m due to overlap of four quartets, 6.2H), 7.16–7.59 (m, 27.9H); mass spectrum *m/e* (rel %): 464 ($M-H_2O$, 32), 361 (34), 301 (26), 275 (100), 202 (53). Exact Mass calcd. for $C_{26}H_{24}O_8$: 464.1470; found: 464.1442. A mixture of diastereomers **22** and **23** (20 mg, 0.04 mmol) was refluxed with *p*-TsOH (6 mg) in benzene for 1 h. The solution was filtered through a short silica gel column, and concentrated in vacuo to give an oily residue (16 mg, 80%), that had an NMR spectrum identical to that of phenylnaphthalene **14** (see above).

*Cycloadduct **24***

Methyl (*S*)-lactyl fumarate (4*a*) (140 mg, 0.48 mmol) and 2-methylbenzophenone (93 mg, 0.47 mmol) were irradiated in benzene for 20 h and then concentrated in vacuo. The ^{1}H NMR spectrum of the crude product showed the presence of predominantly one diastereomer (>90% de), and a by-product (ca. 20%) that was identified as the maleate of methyl (*S*)-lactate by comparison to an authentic sample (4*a*). The cycloadduct and the maleate were inseparable by chromatography. The latter could be removed by reacting the crude product (0.233 g) with an excess of benzocyclobutenol (12) (0.15 g) in refluxing toluene for 5 h, followed by chromatography with 15–25% ethyl acetate – hexanes, which afforded the pure cycloadduct **24** (0.10 g, 44%) (17); $[\alpha]_D^{20}$ +48.6 (*c* 0.500, $CHCl_3$); IR (CH_2Cl_2): 3436, 1744 cm^{-1}; ^{1}H NMR ($CDCl_3$) δ: 1.13 (d, 3H, J = 7.05), 1.54 (d, 3H, J = 7.02), 3.15 (dd, 1H, J = 11.96, 16.32), 3.43 (dd, 1H, J = 4.32, 16.33), 3.57–3.82 (m, 2H), 3.68 (s, 3H), 3.77 (s, 3H), 4.20 (s, 1H, OH), 4.90 (q, 1H, J = 7.04), 5.12 (q, 1H, J = 7.09), 6.91 (d, 1H, J = 7.13), 7.02–7.42 (m, 8H); ^{13}C NMR ($CDCl_3$) δ: 16.29 (CH_3), 16.84 (CH_3), 32.76 (CH_2), 39.34 (CH), 52.29 (CH_3), 52.55 (CH_3), 55.01 (CH), 68.78 (CH), 68.90 (CH), 76.29 (C), 126.22 (2 × CH), 126.61 (CH), 126.97 (CH), 127.60 (2 × CH), 127.68 (CH), 128.10 (CH), 130.21 (CH), 133.30 (C), 140.36 (C), 146.60 (C), 171.16 (CO), 171.50 (CO), 171.63 (CO), 174.17 (CO); mass spectrum *m/e* (rel %): 466 (0.3, $M-H_2O$), 334 (10), 274 (16), 231 (45.3), 205 (100), 202 (57). Exact Mass calcd. for $C_{26}H_{26}O_8$: 466.1628; found: 466.1657.

*Arylnaphthol **29***

1*b* (0.10 g, 0.35 mmol) and hydroxyacetal **25** (22) (0.16 g, 0.41 mmol) were dissolved in a minimum amount of dichloromethane (ca. 0.5 mL), and then maintained at 95°C in the presence of glacial acetic acid (0.18 mL) for 20 min. The NMR spectrum of the crude product (1 mg in $CDCl_3$) showed the presence of naphthol **29** (80 ± 5%), and two diastereomers (**26** and **27**, 20 ± 5%). The remainder of the crude mixture was reacted for another 20 min, and then chromatographed using 25–35% ethyl acetate – hexanes to give a colorless solid (0.17 g, 80%); mp 69–72°C; $[\alpha]_D^{20}$ +27 (*c* 1.05, $CHCl_3$); IR (CH_2Cl_2): 3350, 1739 cm^{-1}; ^{1}H NMR ($CDCl_3$) δ: 1.01 (d, 3H, J = 6.85), 1.07 (d, 3H, J = 6.85), 1.57 (d, 3H, J = 7.02), 1.58 (d, 3H, J = 7.01), 3.65 (d, 6H, J = 4.12), 3.73 (d, 6H, J = 1.99), 3.78 (s, 6H), 3.86 (d, 6H, J = 4.08), 3.94 (d, 6H, J = 0.88), 4.05 (s, 6H), 5.16 (dq, 2H, J = 4.79, 6.84), 5.40 (dq, 2H, J = 2.46, 7.02), 6.73 (d, 2H, J = 5.81), 6.88–6.97 (m, 6H), 7.74 (s, 2H), 12.00 (d, 2H, J = 3.52); ^{13}C NMR ($CDCl_3$) δ: 16.25 (CH_3), 16.30 (CH_3), 16.67 (CH_3), 16.73 (CH_3), 51.93 (2 × OCH_3), 52.30 (2 × OCH_3), 55.57 (2 × OCH_3), 55.75 (2 × OCH_3), 55.78 (2 × OCH_3), 55.89 (2 × OCH_3), 69.18 (OCH), 69.23 (OCH), 69.97 (2 × OCH), 100.47 (2 × C), 102.67 (2 × CH), 105.73 (2 × CH), 110.49 (CH), 110.62 (CH), 114.16 (CH), 114.25 (CH), 119.77 (2 × C), 123.28 (CH), 123.36 (CH), 127.43 (2 × C), 128.30 (C), 128.37 (C), 128.98 (C), 129.00 (C), 132.31 (2 × C), 148.17 (C), 148.24 (C), 148.39 (C), 148.47 (C), 149.69 (2 × C), 152.38 (2 × C), 159.43 (C), 159.50 (C), 167.18 (CO), 167.30 (CO), 168.82 (CO), 168.89 (CO), 170.03 (2 × CO), 170.28 (2 × CO); mass spectrum *m/e* (rel %): 600 (M^+, 11), 496 (17), 410 (100), 84 (14). Exact Mass calcd. for $C_{30}H_{32}O_{13}$: 600.1842; found: 600.1847.

Acknowledgments

We are grateful to the Natural Sciences and Engineering Research Council of Canada for financial support of this project. The financial assistance of the University of Manitoba in the form of a Postgraduate Fellowship is also acknowledged. We acknowledge the assistance of W. Buchannon and T. Foniok in providing mass spectral and NMR spectroscopic services.

References

1. (*a*) R.O. Angus, Jr. and R.P. Johnson. J. Org. Chem. **48**, 273 (1983); (*b*) W. H. Hersh and R.G. Bergman. J. Am. Chem. Soc. **105**, 5846 (1983); (*c*) B.J. Arnold, S.M. Mellows, P.G. Sammes, and T.W. Wallace. J. Chem. Soc. Perkin Trans. 1, 401 (1974); (*d*) E. Block and R. Stevenson. J. Chem. Soc. Perkin Trans. 1, 308 (1973); (*e*) J. Mann, S.E. Piper, and L.K.P. Yeung. J. Chem. Soc. Perkin Trans. 1, 2081 (1984).
2. E. Winterfeldt. Angew. Chem. Int. Ed. Engl. **6**, 423 (1967).

3. M. Alvaro, H. Garcia, M.A. Miranda, and J. Primo. Tetrahedron, **48**, 3437 (1992).
4. (*a*) J.L. Charlton, G. Plourde, K. Koh, and A.S. Secco. Can. J. Chem. **67**, 574 (1989); (*b*) Can. J. Chem. **68**, 2022 (1990); (*c*) J.L. Charlton, K. Koh, and G.L. Plourde. Can. J. Chem. **68**, 2028 (1990); (*d*) J.L. Charlton, K. Koh, and G.L. Plourde. Tetrahedron Lett. **30**, 3279 (1989).
5. (*a*) C. Rucker, D. Lang, J. Sauer, H. Friege, and R. Sustmann. Chem. Ber. **113**, 1663 (1980); (*b*) R.G. Hall and S. Trippett. Tetrahedron Lett. **23**, 2603 (1982); (*c*) J. Drexler, R. Lindermayer, M.A. Hassan, and J. Sauer. Tetrahedron Lett. **26**, 2555 (1985).
6. J.L. Charlton and M.M. Alauddin. Tetrahedron, **43**, 2873 (1987), and references cited therein.
7. R. Rodrigo. Tetrahedron, **44**, 2093 (1988), and references cited therein.
8. G. Weeratunga, D. Rajapaksa, and R. Rodrigo. J. Org. Chem. **50**, 5902 (1985).
9. R.J. Moss and B. Rickborn. J. Org. Chem. **50**, 1381 (1985).
10. W. Donald MacRae and G.H.N. Towers. Phytochemistry, **23**, 1207 (1984).
11. J.L. Charlton and G.L. Chee. Tetrahedron Lett. **35**, 6243 (1994).
12. P.G. Sammes. Tetrahedron, **32**, 405 (1976).
13. G. Wittig and U. Schollkopf. Chem. Ber. **87**, 1318 (1954).
14. L. Horner, P.V. Subramaniam, and K. Eiben. Liebigs Ann. **714**, 91 (1986).
15. (*a*) R.A. Friedel, M. Orchin, and L. Reggel. J. Am. Chem. Soc. **70**, 199 (1948); (*b*) D.M. Hall, S. Ridgwell, and E.E. Turner. J. Chem. Soc. 2498 (1954); (*c*) T. Gilchrist, R. Hodges and A.L. Porte. J. Chem. Soc. 1780 (1962); (*d*) N.S. Bhacca and R. Stevenson. J. Org. Chem. **28**, 1638 (1963).
16. D.I. MacDonald and T. Durst. J. Org. Chem. **53**, 3663 (1988).
17. J.L. Charlton, S. Maddaford, K. Koh, S. Boulet, and M.H. Saunders. Tetrahedron: Asymmetry, **4**, 645 (1993).
18. C. Reichardt. *In* Solvents and solvent effects in organic chemistry; VCH, Weinheim. 1988.
19. M.F. Ruiz-Lopez, X. Assfeld, J.I. Garcia, A. Mayoral, and L. Salvatella. J. Am. Chem. Soc. **115**, 8780 (1993), and references cited therein.
20. J.L. Charlton and V.C. Pham. Tetrahedron Lett. **33**, 6073 (1992).
21. H. Hartmann, A.F.A. Hady, J. Weetman, and G. Helmchen. Angew. Chem. Int. Ed. Engl. **26**, 1143 (1987).
22. B.A. Keay, H.P. Plaumann, D. Rajapaksa, and R. Rodrigo. Can. J. Chem. **61**, 1987 (1983).
23. L. Eichelberger. J. Am. Chem. Soc. **48**, 1320 (1926).
24. E. Ott. Ann. Chem. **392**, 265 (1912).
25. J.L. Charlton and K. Koh. Synlett, 133 (1990).

Can. J. Chem. Downloaded from www.nrcresearchpress.com by 80.90.12.36 on 09/08/12
For personal use only.

Unsymmetrical dienophiles and their reactions with *ortho*-quinodimethanes

James L. Charlton, David Bogucki, and Peng Guo

Abstract: Three unsymmetrical chiral dienophiles have been synthesized and their reactivities with α-hydroxy-*ortho*-quinodimethanes have been assessed. Thus, the methyl (*S*)-lactyl esters of *trans*-4-bromocrotonate and *trans*-4-acetoxycrotonate (**1** and **2**) and mono (methyl (*S*)-lactyl) fumarate **3** were synthesized. Each was reacted with α-hydroxy-*o*-quinodimethane and α-hydroxy-α-phenyl-*o*-quinodimethane. While reaction with α-hydroxy-*o*-quinodimethane gave synthetically useful yields of cycloadducts with high regioselectivity and diastereoselectivity, the corresponding reactions with α-hydroxy-α-phenyl-*o*-quinodimethane were less successful. The reaction of **3** with α-hydroxy-α′-phenyl-*o*-quinodimethane also gave a mixture of cycloadducts.

Key words: *ortho*-quinodimethanes, lignans, Diels–Alder, asymmetric, lactate.

Résumé : On a synthétisé trois diénophiles chiraux non symétriques et on a évalué leurs réactivités avec les α-hydroxy-*ortho*-quinodiméthanes. On a ainsi synthétisé les *trans*-4-bromocrotonoate et *trans*-4-acétoxycrotonoate (**1** et **2**) et le monofumarate (**3**) de ((*S*)-lactyle de méthyle). On a les a tous fait réagir avec l'α-hydroxy-*ortho*-quinodiméthane et l'α-hydroxy-α-phényl-*ortho*-quinodiméthane. Alors que la réaction de l'α-hydroxy-*ortho*-quinodiméthane fournit des rendements synthétiquement utiles de cycloadduits avec de fortes régiosélectivités et diastéréosélectivités, les réactions correspondantes avec l'α-hydroxy-α-phényl-*ortho*-quinodiméthane ne conduisent pas au même succès. La réaction du composé **3** avec l'α-hydroxy-α′-phényl-*ortho*-quinodiméthane conduit aussi à un mélange de cycloadduits.

Mots clés : *ortho*-quinodiméthanes, lignanes, Diels–Alder, asymétrique, lactate.

[Traduit par la rédaction]

Introduction

In several publications we have demonstrated the use of both methyl lactyl fumarate and methyl mandelyl fumarate in asymmetric Diels–Alder reactions with *ortho*-quinodimethanes (*o*-QDMs) and the elaboration of the corresponding cycloadducts into naturally occurring lignans (1). An example of the synthesis of (−)-deoxypodophyllotoxin is shown in Scheme 1 (1*a*).

One of the pitfalls in using a symmetrical dienophile such as bis(methyl lactyl) or (methyl mandelyl) fumarate in such reactions is that it is often difficult to later chemically differentiate between the two ester groups in the cycloadduct. A potential solution to this problem is to use an unsymmetrical dienophile. While a number of unsymmetrical chiral dienophiles have been used in Diels–Alder reactions (see the extensive list of references in ref. 2), we were particularly interested in 4-halo or 4-oxy derivatives of crotonic acid esters as these dienophiles would provide a route to the butyrolactone functionality often found in aryl tetralin lignans such as deoxypodophyllotoxin (see Scheme 1). Although these dienophiles should be more useful in later functional group transformations, it remained to be determined if they would show sufficiently high yield, regioselectivity, diastereoselectivity (*endo* vs. *exo*), and asymmetric induction to make them synthetically useful. To this end we have synthesized the methyl (*S*)-lactyl esters of *trans*-4-bromocrotonate and *trans*-4-acetoxycrotonate, **1** and **2**. The mono (methyl (*S*)-lactyl) ester of fumaric acid, **3**, was also prepared. Methyl lactyl esters were chosen as the reactions of methyl lactyl esters of acrylates and fumarates have been very stereoselective in reactions with α-hydroxy-*o*-quinodimethanes. Each ester was reacted with α-hydroxy-*o*-quinodimethane and α-hydroxy-α-phenyl-*o*-quinodimethane. **3** was also reacted with α-hydroxy-α′-phenyl-*o*-quinodimethane.

Scheme 1.

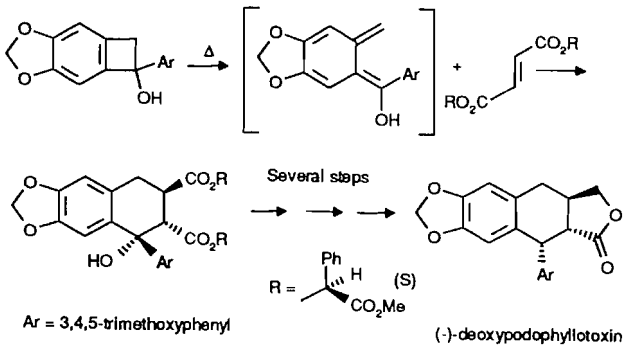

Results and discussion

The crotonate esters **1** and **2** were synthesized[2] from 4-bromo-

Received May 2, 1995.

J.L. Charlton,[1] D. Bogucki, and P. Guo. Department of Chemistry, University of Manitoba, Winnipeg, MB R3T 2N2, Canada.

[1] Author to whom correspondence may be addressed. Telephone: (204) 474-9267. Fax: (204) 275-0905.

[2] Based on our previous experience (1) we assume that no epimerization of the lactyl group occurs during formation of the esters.

Can. J. Chem. Downloaded from www.nrcresearchpress.com by 80.90.12.36 on 09/08/12
For personal use only.

Can. J. Chem. Downloaded from www.nrcresearchpress.com by 80.90.12.36 on 09/08/12
For personal use only.

Scheme 2.

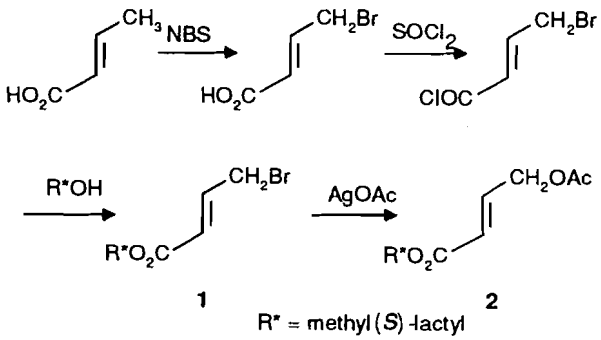

Scheme 3.

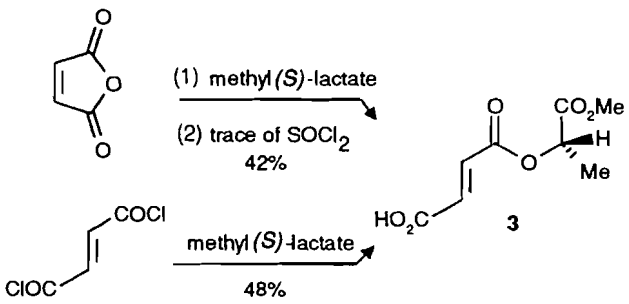

Scheme 4.

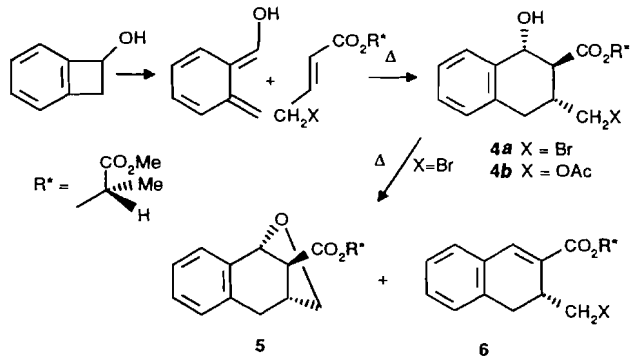

Scheme 5.

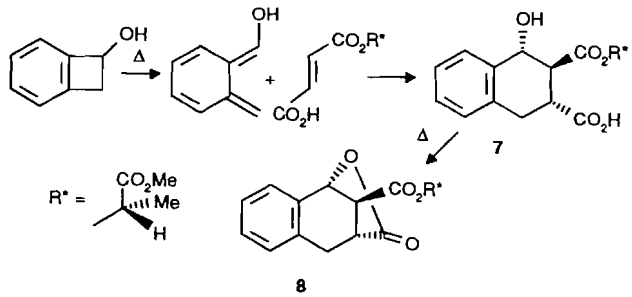

crotonic acid, which in turn was prepared using the method of Pinza and Pifferi (3*a*) as shown in Scheme 2. Mono (methyl (*S*)-lactyl) fumarate, **3**, was prepared by two methods as shown in Scheme 3. Using a modified literature procedure (4), methyl (*S*)-lactate was mixed with maleic anhydride (1:1) to give the mono (methyl (*S*)-lactyl) maleate intermediate. Without purification, this intermediate was isomerized to the fumarate in the presence of a catalytic amount of thionyl chloride to give **3** in 42% yield. In the second method, **3** was prepared in 48% yield by heating a 1:1 mixture of methyl (*S*)-lactate and fumaryl chloride.

Thermolysis of benzocyclobutenol (5)[3] was used as the method for generating α-hydroxy-*o*-QDM and assessing its reactivity with **1**, **2**, and **3**. To prepare the cycloadduct with 4-bromocrotonate **1**, 1.8 equivalents of benzocyclobutenol were refluxed with **1** in benzene for 70 h at which time a further 1.6 equivalents of benzocyclobutenol were added and the solution refluxed for a further 95 h. The solution was evaporated and chromatographed (EtOAc–hexanes) to give cycloadduct **4***a* (89%). The structure of the cycloadduct **4***a* was established from its ^{1}H NMR spectrum and by its conversion to the ether **5** on refluxing in toluene (see Scheme 4). Carrying out the cycloaddition reaction itself in refluxing toluene also gave primarily the ether **5** along with the elimination product **6.**

The cycloadduct of 4–acetoxycrotonate **2** with α-hydroxy-*o*-QDM was likewise prepared by refluxing **2** with 2 equivalents of benzocyclobutenol in toluene for 67 h. Evaporation of the toluene and chromatography (EtOAc–hexanes) gave cycloadduct **4***b* in 76% yield. The cycloadduct was assigned the structure **4***b* (see Scheme 4) on the basis of its spectral properties. The absolute stereochemistries of cycloadducts **4***a* and **4***b* were assigned on the basis of our previous experience with methyl lactyl unsaturated esters reacting with hydroxy-*o*-QDMs (1*c*, *d*, *f*, *g*, *h*, and *j*), but the assignment should be regarded as tentative. Although the precise diastereoselectivity and regioselectivity for the formation of **4***a* and **4***b* is unknown, it should be noted that there were only very minor peaks in the ^{1}H NMR spectra of the crude products that could be attributed to isomeric cycloadducts.

Dienophile **3** was reacted with α-hydroxy-*o*-QDM by adding benzocyclobutenol (2.7 equivalents) to a refluxing solution of **3** in toluene and refluxing for a further 2 h. Passage through a short silica gel column (EtOAc), evaporation, and crystallization from EtOAc–hexane gave cycloadduct **7** in 42% yield (see Scheme 5). Further concentration of the mother liquors gave crystals of the lactone **8** in 5% yield, identified by comparison with an authentic sample whose absolute and relative stereochemistry had been previously assigned (1*j*). The cycloadduct **7** closed readily to the lactone **8** on standing for a few days in methylene chloride solution, thereby providing confirmation of both the absolute and relative stereochemistry assigned to **7**.

From the above encouraging results it appears that the three unsymmetrical dienophiles **1**, **2**, and **3** all react with α-hydroxy-*o*-QDMs giving synthetically useful levels of regioselectivity, diastereoselectivity, and asymmetric induction. In a previous paper we proposed that hydrogen bonding between the lactyl chiral auxiliary and the hydroxyl of the *o*-QDM is very important in the reactions of lactyl substituted dienophiles and α-hydroxy-*o*-QDMs (1*d*). It appears that it is equally important in these reactions, leading to products with the lactyl ester group adjacent to and *trans* (*exo* addition), to the neighboring hydroxyl group.

To investigate the scope of these reactions we have also studied the addition of **1**, **2**, and **3** with α-hydroxy-α-phenyl-*o*-quinodimethane **9** (see Scheme 6). This *o*-QDM is a model for other similar oxygenated *o*-QDMs that we have found useful

[3] For preparation of benzocyclobutenol see ref. 5(*b*).

Scheme 6.

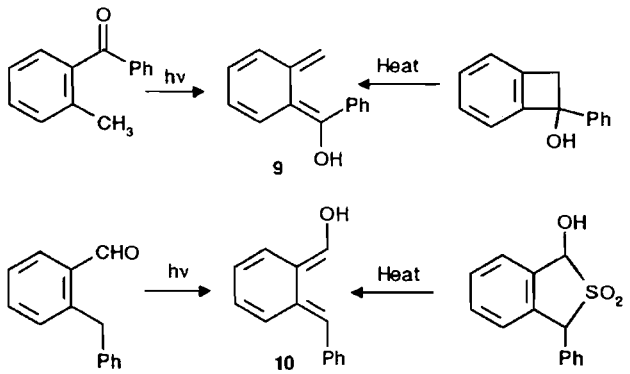

in asymmetric lignan synthesis. Unfortunately none of the three unsymmetrical dienophiles reacted with α-hydroxy-α-phenyl-*o*-quinodimethane **9** to give a cycloadduct with reasonable stereo- or regioselectivity. **1** and **2** did not react at all with the *o*-QDM generated either photochemically from 2–methylbenzophenone, or thermally from -phenylbenzocyclobutenol (1*c*). Dienophile **3** did react with the *o*-QDM **9** generated from benzocyclobutenol, but the ^{1}H NMR spectrum of the crude product indicated that it was a mixture of at least four isomeric cycloadducts. Dienophile **3** was also reacted with *o*-QDM **10**, generated either photochemically or thermally from its corresponding sulfone as shown in Scheme 6. Thermal generations of *o*-QDM **10** from the sulfone in the presence of dienophile **3** gave a mixture of four cycloadducts while the photochemical reaction gave back only starting materials.

Experimental

A description of general instrumentation, procedures for the irradiation experiments, and identification and characterization of compounds have been provided previously (1).

4-Bromo-(methyl (*S*)-lactyl) crotonate, 1

Crotonic acid (5.01 g, 58.2 mmol) was refluxed in a solution of CCl_4 (50 mL) containing NBS (10.53 g, 59.16 mmol) and benzoyl peroxide (210 mg, 0.867 mmol) under a N_2 atmosphere for 4.5 h. The solution was cooled, kept at 5°C for 16 h, and the resulting colorless precipitate (succinimide) filtered off. Thionyl chloride (6.40 ml, 87.7 mmol) was added to the solution, which was then stirred at 60°C in a 100 mL round-bottom flask fitted with a condenser and drying tube ($CaCl_2$) for 4 h. The solution was cooled to room temperature, the solvent evaporated and several small portions of CCl_4 evaporated, from the remaining liquid. The crude acid chloride was refluxed in CCl_4 (20 ml) in the presence of methyl (*S*-lactate (8.30 ml, 86.9 mmol) under a drying tube ($CaCl_2$) for 66.5 h. After cooling the solution to room temperature and evaporating the solvent, the crude product was chromatographed on silica gel (8% EtOAc – hexanes) to give a light yellow liquid (5.83 g, 40%): $[\alpha]_D^{25}$ −12.6 (*c* 0.95, $CHCl_3$); IR ($CHCl_3$): 1719 (CO) cm^{-1}; ^{1}H NMR ($CDCl_3$) δ: 1.53 (d, 3H, *J* = 7.1), 3.76 (s, 3H), 4.02 (dd, 2H, *J* = 1.2, 7.2), 5.17 (q, 1H, *J* = 7.1), 6.10 (dd, 1H, *J* = 1.2, 15.4), 7.08 (dt, 1H, *J* = 7.3, 15.4); ^{13}C NMR ($CDCl_3$) δ: 17.0 (CH_3), 28.9 (CH_2), 52.4 (CH_3), 68.8 (CH), 123.7 (CH), 143.0 (CH), 164.6 (C), 171.0 (C); mass spectrum (NH_4^+ CI) *m/z* (relative intensity): 253/251 ([M + H]$^+$, 3), 221/219 (3), 193/191 (12), 171 (15), 166/164 (9), 149/147 (100), 121/119 (8), 113 (13), 68 (70). Anal. calcd. for $C_8H_{11}O_4Br$: C 38.27, H 4.42; found: C 38.49, H 4.34.

4-Acetoxy-(methyl (*S*)-lactyl) crotonate, 2

4-Bromo-(methyl (*S*)-lactyl) crotonate (1.00 g, 3.98 mmol) and silver acetate (731 mg, 4.38 mmol) in acetic acid (26 mL) were stirred at 100°C under a drying tube ($CaCl_2$) for 22 h. The solution was filtered to remove precipitate, which was washed with EtOAc. Water was added to the filtrate and the whole extracted with EtOAc. The EtOAc layers were combined, washed with saturated $NaHCO_{3\ (aq)}$, water, dried ($MgSO_4$), and evaporated. The crude product was chromatographed on silica gel (10% EtOAc – hexanes) giving a colorless liquid (685 mg, 75%): $[\alpha]_D^{25}$ −11.4 (*c* 2.30, $CHCl_3$); IR ($CHCl_3$): 1742 (CO) cm^{-1}; ^{1}H NMR ($CDCl_3$) δ: 1.53 (d, 3H, *J* = 7.1), 2.13 (s, 3H), 3.76 (s, 3H), 4.76 (dd, 2H, *J* = 2.0, 4.5), 5.18 (q, 1H, *J* = 7.1), 6.11 (dt, 1H, *J* = 2.0, 15.8), 7.02 (dt, 1H, *J* = 4.5, 15.8); ^{13}C NMR ($CDCl_3$) δ: 17.0 (CH_3), 20.7 (CH_3), 52.4 (CH_3), 62.4 (CH_2), 68.7 (CH), 121.1 (CH), 142.6 (CH), 164.9 (C), 170.2 (C), 171.1 (C); mass spectrum (NH_4^+ CI) *m/z* (relative intensity): 231 ([M + H]$^+$, 1), 171 (22), 127 (21), 85 (100), 55 (24); HRMS calcd. for $C_8H_{11}O_4$ ($M^+ - CH_3CO_2$) 171.0657; found: 171.0657.

Mono (methyl (*S*)-lactyl) fumarate, 3

Method 1

A procedure similar to that used to prepare monomethyl fumarate was used (4). Maleic anhydride (1.02 g, 10.4 mmol) and methyl (*S*)-lactate (1.4 mL, 15 mmol) were mixed until a homogeneous solution was obtained. Thionyl chloride (0.05 mL) was added and the mixture heated on a steam bath for 10 min. After cooling, the solution was made basic with aqueous 5% $NaHCO_3$, washed with CH_2Cl_2, acidified with 10% aqueous HCl, and extracted with CH_2Cl_2. The combined organic extracts were dried ($MgSO_4$) and evaporated to leave a colorless oil (0.85 g, 42%): $[\alpha]_D^{20}$ −8.6 (*c* 0.91, $CHCl_3$); IR (CH_2Cl_2): 1736, 1711 cm^{-1}; ^{1}H NMR ($CDCl_3$) δ: 1.55 (d, 3H, *J* = 7.1), 3.76 (s, 3H), 5.21 (q, 1H, *J* = 7.1), 6.90 (d, 1H, *J* = 15.7), 7.08 (d, 1H, *J* = 15.6), 10.6 (br s, 1H); ^{13}C NMR ($CDCl_3$) δ: 16.9 (CH_3), 52.7 (CH_3), 69.6 (CH), 133.9 (CH), 134.4 (CH), 164.0, 169.2, 170.9 (CO); mass spectrum *m/z* (relative intensity): 157 (2), 143 (23), 113 (25), 99 (100), 85 (6). Anal. calcd. for $C_8H_{10}O_6$: C 47.65, H 4.99; found: C 47.30, H 4.99. The proton NMR also exhibited peaks consistent with the presence of a small amount (ca. 6%) of the isomeric maleate ester; ^{1}H NMR ($CDCl_3$) δ: 1.57 (d, 3H, *J* = 7.1), 3.78 (s, 3H), 5.25 (q, 1H, *J* = 7.1), 6.41 (d, 1H, *J* = 12.5), 6.47 (d, 1H, *J* = 12.6).

Method 2

Fumaryl chloride (5 mL, 47.4 mmol) and methyl (*S*)-lactate (5 mL, 52.4 mmol) were heated at 100–110°C under nitrogen for 30 h. Water (30 mL) was added and the aqueous phase was made basic with solid sodium carbonate. The aqueous phase was extracted with CH_2Cl_2, acidified with 10% aqueous HCl, and extracted again with CH_2Cl_2. The latter extract was dried and evaporated to leave a dark oil (5.5 g, 58%). The oil was purified by chromatography on silica gel using 30% EtOAc –

Can. J. Chem. Downloaded from www.nrcresearchpress.com by 80.90.12.36 on 09/08/12
For personal use only.

Can. J. Chem. Downloaded from www.nrcresearchpress.com by 80.90.12.36 on 09/08/12
For personal use only.

hexanes as eluant to give a colorless oil (4.56 g, 48%). All physical data were identical to those given above.

Cycloadduct 4*a*

Benzocyclobutenol (37.5 mg, 0.312 mmol) and 4–bromo-(methyl-(*S*)-lactyl)-crotonate (42.8 mg, 0.170 mmol) were refluxed in benzene (3.0 mL) under a drying tube ($CaCl_2$) for 70 h. More benzocyclobutenol (33.0 mg, 0.275 mmol) was added and refluxing of the solution continued for 95 h. The solvent was evaporated and the crude product chromatographed on silica gel (8% EtOAc – hexanes) to give a light yellow liquid (56.3 mg, 89%): $[\alpha]_D^{25}$ −65.8 (*c* 0.28, $CHCl_3$); IR ($CHCl_3$): 3504 (OH), 1747 (CO) cm^{-1}; ^1H NMR ($CDCl_3$) δ: 1.58 (d, 3H, *J* = 7.2), 2.55 (m, 1H, H-3), 2.80 (dd, 1H, *J* = 9.6, 10.6, H-2), 2.95 (d, 2H, *J* = 8.0), 3.52 (dd, 1H, *J* = 3.4, 10.3, H-4), 3.57 (dd, 1H, *J* = 5.7, 10.3, H-4), 3.83 (s, 3H), 4.04 (br s, 1H), 4.99 (d, 1H, *J* = 9.5, H-1), 5.31 (q, 1H, *J* = 7.2), 7.12 (d, 1H, *J* = 6.8), 7.24 (m, 2H), 7.67 (d, 1H, *J* = 7.1); ^{13}C NMR ($CDCl_3$) δ: 16.7 (CH_3), 32.9 (CH_2), 35.8 (CH), 37.3 (CH_2), 53.0 (CH_3), 53.5 (CH), 69.0 (CH), 71.7 (CH), 126.3 (CH), 126.6 (CH), 127.5 (CH), 128.1 (CH), 133.9 (C), 136.8 (C), 172.5 (C), 173.5 (C); mass spectrum (NH_4^+ CI) *m/z* (relative intensity), 390–388 ([M + NH_4]$^+$, 32), 372–370 (M^+, 90), 355–353 (38), 308 (28), 273 (30), 251–249 (100), 240–238 (31), 187 (88), 158 (36), 141 (61), 128 (52), 115 (27), 91 (28); HRMS calcd. for $C_{16}H_{19}O_5{}^{81}Br$: 372.0395; found: 372.0394; HRMS calcd. for $C_{16}H_{19}O_5{}^{79}Br$: 370.0415; found: 370.0418.

Ether 5 and elimination product 6

Benzocyclobutenol (98.8 mg, 0.822 mmol) and 4–bromo-(methyl-(*S*)-lactyl)-crotonate (99.5 mg, 0.396 mmol) were refluxed in toluene (3.5 mL) with a drying tube ($CaCl_2$) for 71 h and the solvent was evaporated. A ^1H NMR spectrum of the crude product mixture indicated that cycloadduct **4**a, plus elimination and ether products **5** and **6**, were present in a ratio of 4.5:1.0:1.7, respectively. Chromatography on silica gel (5% EtOAc – hexanes) gave samples of compounds **6** and **5** as pale yellow liquids. Elimination product **6**: $[\alpha]_D^{25}$ +35.3 (*c* 0.59, $CHCl_3$); IR ($CHCl_3$): 1713 (CO) cm^{-1}; ^1H NMR ($CDCl_3$) δ: 1.60 (d, 3H, *J* = 7.1), 3.04 (m, 2H), 3.29 (m, 2H), 3.55 (m, 1H, H-4), 3.78 (s, 3H), 5.26 (q, 1H, *J* = 7.0), 7.28 (m, 4H), 7.68 (s, 1H, H-1); ^{13}C NMR ($CDCl_3$) δ: 17.0 (CH_3), 30.5 (CH_2), 33.2 (CH_2), 34.8 (CH), 52.4 (CH_3), 68.9 (CH), 127.1 (CH), 128.5 (C), 128.8 (CH), 129.0 (CH), 130.6 (CH), 131.2 (C), 134.4 (C), 139.2 (CH), 165.6 (C), 171.2 (C); mass spectrum *m/z* (relative intensity), 354–352 (M^+, 5), 251–249 (8), 169 (18), 155 (100), 141 (33), 128 (13), 115 (13), 59 (11); HRMS calcd. for $C_{16}H_{17}O_4{}^{81}Br$: 354.0289; found: 354.0300; HRMS calcd. for $C_{16}H_{17}O_4{}^{79}Br$: 352.0310; found: 352.0324. Ether **5**: $[\alpha]_D^{25}$ −32.7 (*c* 0.28, $CHCl_3$); IR ($CHCl_3$): 1744 (CO) cm^{-1}; ^1H NMR ($CDCl_3$) δ: 1.36 (d, 3H, *J* = 7.0), 2.81 (d, 1H, *J* = 17.5, H-4), 3.04 (m, 1H, H-3), 3.42 (m, 2H, H-2, H-4), 3.50 (s, 3H), 3.83 (d, 1H, J = 8.3, H-10), 4.16 (m, 1H, H-10), 4.95 (q, 1H, *J* = 7.0), 5.01 (d, 1H, *J* = 5.1, H-1), 7.16 (m, 4H); ^{13}C NMR ($CDCl_3$) δ: 16.7 (CH_3), 33.8 (CH_2), 35.6 (CH), 48.6 (CH), 52.2 (CH_3), 68.7 (CH), 74.3 (CH_2), 76.8 (CH), 126.1 (CH), 127.9 (CH), 128.3 (CH), 129.0 (CH), 133.7 (C), 137.6 (C), 168.9 (C), 170.6 (C); mass spectrum *m/z* (relative intensity), 290 (M^+, 7), 186 (19), 158 (19), 142 (71), 129 (100), 115 (13), 91 (19), 71 (60); HRMS calcd. for $C_{16}H_{18}O_5$: 290.1155; found: 290.1152.

Cycloadduct 4*b*

Benzocyclobutenol (220 mg, 1.83 mmol) and 4–acetoxy-(methyl-(*S*)-lactyl)-crotonate (206 mg, 0.895 mmol) were refluxed in toluene (2.0 mL) with a drying tube ($CaCl_2$) for 67 h and the solvent was evaporated. The crude product was chromatographed on silica gel (5% and 10% EtOAc – hexanes consecutively) to give a light yellow liquid (240 mg, 76%): $[\alpha]_D^{25}$ −45.9 (*c* 0.70, $CHCl_3$); IR (CH_2Cl_2): 3484 (OH), 1736 (CO) cm^{-1}; ^1H NMR ($CDCl_3$) δ: 1.56 (d, 3H, *J* = 7.1), 2.05 (s, 3H), 2.57 (m, 1H, H-3), 2.70 (dd, 1H, *J* = 9.6, 10.9, H-2), 2.80 (m, 1H, H-4), 2.93 (dd, 1H, *J* = 5.7, 16.6, H-4), 3.82 (s, 3H), 3.97 (d, 1H, *J* = 4.1), 4.06 (dd, 1H, *J* = 4.3, 11.1, H-10), 4.16 (dd, 1H, *J* = 5.8, 11.1, H-10), 5.00 (dd, 1H, *J* = 3.3, 9.4, H-1), 5.27 (q, 1H, *J* = 7.2), 7.10 (d, 1H, *J* = 7.1), 7.23 (m, 2H), 7.65 (m, 1H); ^{13}C NMR ($CDCl_3$) δ: 16.6 (CH_3), 20.8 (CH_3), 31.3 (CH_2), 34.3 (CH), 51.8 (CH), 52.9 (CH_3), 66.1 (CH_2), 69.0 (CH), 71.6 (CH), 126.2 (CH), 126.6 (CH), 127.4 (CH), 128.0 (CH), 133.9 (C), 137.0 (C), 170.8 (C), 172.3 (C), 173.9 (C); mass spectrum *m/z* (relative intensity): 350 (M^+, 2), 272 (54), 203 (40), 187 (62), 168 (87), 158 (100), 141 (61), 129 (57), 115 (20), 91 (24), 85 (32), 59 (18); HRMS calcd. for $C_{18}H_{22}O_7$: 350.1365; found: 350.1365.

Cycloadduct 7 and lactone 8

Mono (methyl (*S*)-lactyl) fumarate **3** (0.247 g, 1.2 mmol) and 4 Å molecular sieves (0.2 g) in toluene (6 mL) were heated to reflux. Benzocyclobutenol (0.38 g, 3.2 mmol) in methylene chloride (5 mL) was added portionwise over 20 min, and the solution stirred for another 2 h. After passing through a short silica gel column (EtOAc) the solution was evaporated to leave an oil that crystallized from EtOAc–hexanes (4:1) giving colorless crystals (01.64 g, 42%), mp 152–153°C: $[\alpha]_D^{25}$ −78.4 (*c* 0.90, $CHCl_3$); IR (CH_2Cl_2): 3503, 1738 cm^{-1}; ^1H nmr ($CDCl_3$) δ: 1.60 (t, 3H, *J* = 7.15), 3.05 (m, 2H), 3.25 (m, 2H), 3.82 (s, 3H), 4.96 (d, 1H, *J* = 9.5, H-1), 5.34 (q, 1H, *J* = 7.16), 7.13–7.26 (m, 4H), 7.71 (d, 1H, *J* = 7.4); ^{13}C nmr ($CDCl_3$) δ: 16.6 (CH_3), 31.4 (CH_2), 40.4 (CH), 50.4 (CH), 53.1 (CH_3), 69.1 (CH), 70.9 (CH), 126.8 (CH), 126.9 (CH), 127.6 (CH), 132.8 (C), 136.5 (C), 172.9 (C), 173.9 (C), 179.1 (C); mass spectrum *m/z* (relative intensity): 304 (3), 200 (17), 156 (27), 128 (100), 45 (53). Anal. calcd. for $C_{16}H_{18}O_7$: C 59.62, H 5.63; found: C 59.30, H 5.64. Further concentration of the mother liquors from above gave another colorless crystalline compound (0.019 g, 5%) that proved to be the lactone **8;** properties are identical to those previously reported in the literature (1j).

Acknowledgements

We are grateful to the Natural Sciences and Engineering Research Council of Canada for financial support of this project.

References

1. (*a*) J.L. Charlton and D.E. Bogucki. J. Org. Chem. **60**, 588 (1995); (*b*) S.P. Maddaford and J.L. Charlton. J. Org. Chem. **58**, 4132 (1993); (*c*) J.L. Charlton, S.P. Maddaford, K. Koh, S. Boulet, and M.H. Saunders. Tetrahedron: Asymmetry, **4**, 645 (1993); (*d*) J.L. Charlton and S. Maddaford. Can. J. Chem. **71**, 827 (1992); (*e*) J. L. Charlton and K. Koh. J. Org. Chem. **57**, 1514 (1991); (*f*) J.L. Charlton, K. Koh, and G.L. Plourde. Can.

J. Chem. **68**, 2028 (1990); (*g*) J.L. Charlton and K. Koh. Synlett, 333 (1990); (*h*) J.L. Charlton, G.L. Plourde, K. Koh, and A.S. Secco. Can. J. Chem. **68**, 2022 (1990); (*i*) J.L. Charlton, K. Koh, and G.L. Plourde. Tetrahedron Lett. **30**, 3279 (1989); (*j*) J.L. Charlton, G.L. Plourde, K. Koh, and A.S. Secco. Can. J. Chem. **67**, 574 (1989).

2. P. Mathivanan and U. Maitra. J. Org. Chem. **60**, 364 (1995).
3. M. Pinza and G. Pifferi. J. Pharm. Sci. **67**, 120 (1978).
4. P.G. Campbell, G. Sumrell, and C.H. Schramm. J. Org. Chem. **26**, 697 (1961).
5. (*a*) P.G. Sammes. Tetrahedron, **32**, 405 (1976); (*b*) W.A. Bubb and S. Sternhell. Aust. J. Chem. **28**, 1685 (1976).

Can. J. Chem. Downloaded from www.nrcresearchpress.com by 80.90.12.36 on 09/08/12
For personal use only.

The thioformamidyl group as an α-substituent in carbocations

M. Bertone, D.L.J. Vuković, A. Cunje, C.F. Rodriquez, E. Lee-Ruff, and A.C. Hopkinson

Abstract: *Ab initio* molecular orbital calculations at MP2(FULL)/6-311G(d,p) or MP2(FULL)/6-31G(d,p) are reported for carbocations $RR'CCHO^+$, $RR'CCHS^+$, $RR'CCONH_2^+$, and $RR'CCSNH_2^+$ where R and R′ are H, CH_3, c-C_3H_5, and C_6H_5. Primary (R = R′ = H), secondary (R = H, R′ = alkyl or phenyl), and tertiary (R = R′ = CH_3) ions prefer the cyclic oxiranyl or thiiranyl structure **9**, with the open structure **8** being a transition structure for ring opening. Tertiary carbocations with R = R′ = phenyl or cyclopropyl and the 9-thioformamidyl-9-fluorenyl cation have the open structure. Isodesmic reactions show $CONH_2$ to be weakly stabilizing in the methyl cation, and $CSNH_2$ has a larger stabilizing effect, roughly equivalent to that of a methyl group. An α-thioamide substituent is less stabilizing in the ethyl cation and even less stabilizing in the isopropyl cation. In $C_6H_5CHCSNH_2^+$ the $CSNH_2$ group is slightly destabilizing and, by extrapolation, is more destabilizing in $Ar_2CCSNH_2^+$. The rearrangement of the α-thioformamidyl-benzyl cation to benzothiophene is calculated to have a low barrier, 15.4 kcal/mol at HF/6-31G(d,p).

Key words: molecular orbitals, destabilized carbocations, rearrangement.

Résumé : On a effectué des calculs d'orbitales moléculaires *ab initio* aux niveaux MP2(FULL)/6-311G(d,p) ou MP2(FULL)/6-31G(d,p) pour les carbocations $RR'CCHO^+$, $RR'CCHS^+$, $RR'CCONH_2^+$ et $RR'CCSNH_2^+$ dans lesquels R et R′ sont égaux à H, CH_3, cyclo-C_3H_5 et C_6H_5. Pour les ions primaires (R = R′ = H), secondaires (R = H et R′ = alkyle ou phényle) et tertiaires (R = R′ = CH_3) les structures préférées sont les oxiranyles et thiiranyles cycliques (**9**) alors que la structure ouverte (**8**) intervient comme structure de transition pour l'ouverture du cycle. Les carbocations tertiaires avec R = R′ = phényle ou cyclopropyle ainsi que le carbocation 9-thioformamidyl-9-fluorényle existent dans la structure ouverte. Les réactions isodesmiques montrent que le $CONH_2$ est faiblement stabilisant dans le cation méthyle alors que le $CSNH_2$ possède un effet stabilisant plus important, approximativement équivalent de celui du groupe méthyle. Un substituant α-thioamide est moins stabilisant dans le cation éthyle et encore moins stabilisant dans le cation isopropyle. Dans le $C_6H_5CHCSNH_2^+$ le groupe $CSNH_2$ est légèrement moins déstabilisant et, par extrapolation, il est plus déstabilisant dans le $Ar_2CCSNH_2^+$. On a calculé que la barrière au réarrangement du cation α-thioformamidyl-benzyle en benzothiophène est relativement faible, 15,4 kcal/mol au niveau HF/6-31G(d,p).

Mots clés : orbitales moléculaires, carbocations déstabilisés, réarrangement.

[Traduit par la rédaction]

Electron-deficient molecules are extremely sensitive to substituent effects and the highest sensitivity ever observed is for the generation of methyl cations CH_2X^+ from methanes CH_3X in the gas phase (1). Carbocations, in general, are electron-deficient species that can be stabilized by π-donating substituents such as NH_2, OCH_3, and F, and that usually are destabilized by electron-withdrawing groups (2–9). However, when electron-withdrawing substituents like CN, COOR, $CONR_2$, COR, $PO(OR)_2$, CF_3, NO_2, SOR, and SO_2R are attached directly to the cationic carbon, the adjacent empty *p*-orbital on carbon induces these substituents to become π donors and, consequently, ions containing these substituents are less destabilized than expected (for reviews, see ref. 10). The chemistries of a wide variety of "destabilized" carbocations have been studied extensively, and some ions are sufficiently stable to be observed directly by UV and NMR spectroscopy (11–14).

Carbocations containing the thioamide group are particularly interesting since this substituent appears to be stabilizing in carbocations containing another destabilizing group, but to be destabilizing in less electron-deficient carbocations (14, 15). Such substituents, which change their electronic character depending upon their molecular environment, are said to be amphielectronic.

Stabilization by $CSNH_2$ may occur through two types of interaction. In the first, π donation leads to delocalization of the positive charge onto the sulfur, i.e., there is a large contribution from resonance structure **1***b* and this implies a shortening of the C—C bond and a lengthening of C—S. This interaction is maximized by the thioamide group being coplanar with $R'RC^+$. Hartree–Fock level *ab initio* molecular orbital calculations have shown structure **1***b* to be an important con-

Received March 28, 1995.

M. Bertone, D.L.J. Vuković, A. Cunje, C.F. Rodriquez, E. Lee-Ruff, and A.C. Hopkinson.[1] Department of Chemistry, York University, North York, ON M3J 1P3, Canada.

[1] Author to whom correspondence may be addressed. Telephone: (416) 736-5246. Fax: (416) 736-5936.

Can. J. Chem. Downloaded from www.nrcresearchpress.com by 80.90.12.36 on 09/08/12
For personal use only.

Can. J. Chem. Downloaded from www.nrcresearchpress.com by 80.90.12.36 on 09/08/12
For personal use only.

tributor to the parent ion (R = R′ = H) but to be of little importance for the oxygen analogue (16).

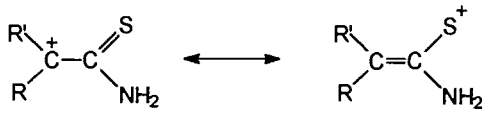

1*a* 1*b*

The second possible stabilizing interaction, neighbouring group participation, involves rotation about the C^+–$CSNH_2$ bond to form the sulfur-bridged ion, **2**, in which the charge is delocalized over both heteroatoms and the cationic carbon. Earlier *ab initio* studies have shown the amino group to be strongly stabilizing in both thiiranyl and oxiranyl cations and structure **2***c* is the best representation of this ion (16).

Previously only the parent amino-substituted thiiranyl cation (R = R′ = H) was studied at the MP2(FC)/6-31G(d,p)//HF/6-31G(d) level of theory (16). By extrapolation from the more extensive study on the oxiranyl cations it seemed probable that increased substitution would favour the ring-opened structure, **1**, but sulfur is a better bridging atom than oxygen making it difficult to predict which of the $RR'CCSNH_2^+$ ions would be cyclic. We now present a theoretical study of the relationship between structures **1** and **2** as a function of the stabilizing ability of substituents R and R′, using several combinations of H, CH_3, c-C_3H_5, and C_6H_5. The inclusion of electron correlation systematically favours the cyclic ion **2** over the open ion, **1**, and for this reason, molecular size permitting, electron correlation is included in the optimisation of most structures.

Spectral data on α-(*N*,*N*-dimethylthioformamidyl)-diphenylmethyl cations have been interpreted in terms of the open ion, **3**, a structure similar to that observed for the oxygen analogues (11, 17). Ion **3** rapidly rearranges to benzothiophene **5** at room temperature, with **4** being suggested as an intermediate (14, 17). In intermediate **4**, the aromaticity of one phenyl group has been destroyed and the other phenyl group cannot formally carry the positive charge, but it is possible to draw resonance structures in which the charge is located on the heteroatoms. Intuitively this structure seemed likely to be high on the potential energy surface and we therefore extended our study to include the energy profile for the rearrangement of **3** into **4**.

Computational details

Ab initio molecular orbital calculations were performed using GAUSSIAN 92 (18). For structures **1** and **2** of cations $RR'CSNH_2^+$, for methanes RR′CHCSNH$_2$, and for a limited number of the oxygen analogues of these compounds, structure optimizations using gradient techniques (19) were carried out at the HF/6-31G(d,p) level (20). For some open ions it was necessary to initially fix the two substituents R and R′ to be coplanar with the thioamide group in order to prevent the structures from collapsing into the cyclic ions **2**. Subsequent

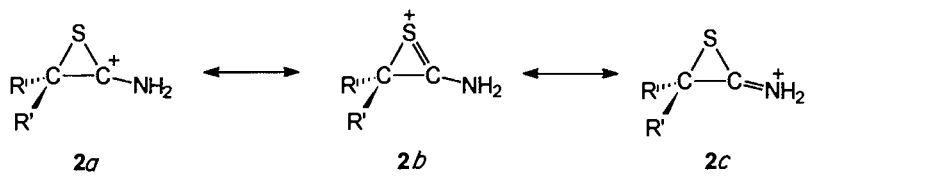

2*a* 2*b* 2*c*

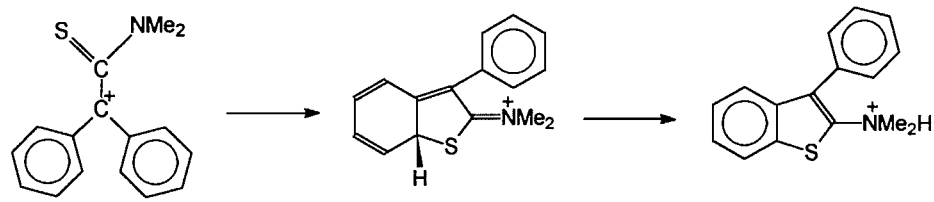

3 4 5

optimization, releasing all constraints, followed by harmonic vibrational frequency calculations, determined whether the structures were at minima or were transition structures. All structures were subsequently optimized using correlated wavefunctions, with MP2(FULL)/6-31G(d,p) (21) calculations used for the smaller molecules, and MP2(FC)/3-21G(d) calculations for ions containing two cyclopropyl substituents or one or more phenyl groups. The 9-thioformamidyl substituted fluorenyl cation was optimized at HF/6-31G(d,p) and at MP2(FC)/3-21G(d) (22). Structures **6** and **7**, in which the amino group of the thioamides has been replaced by H (thereby reducing the relative stability of the cyclic ion), have been optimized at HF/6-31G(d,p) and at MP2(FULL)/6-311G(d,p) for R = R′ = H and R = R′ = CH_3. Structures for ion **7** in which R = R′ = c-C_3H_5 and R = R′ = C_6H_5 have been optimized at MP2(FC)/3-21G(d).

Total energies, relative energies, and zero-point energies are given in Table 1, and some key structural details are in Table 2. Data for the thioacetamides are given in Table 3.

6 7

Table 1. Total energies (hartrees) of thiiranyl and oxiranyl cations and their ring-opened isomers.

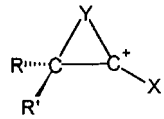

9

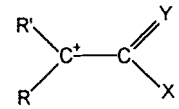

8

R, R′	HF/6-31G(d,p)[a]	ZPE[b,c]	MP2(FULL)/6-311G(d,p)[a,d]	HF/6-31G(d,p)[a]	ZPE[b,c]	MP2(FULL)/6-311G(d,p)[a,d]
(*a*) **Thioaldehydes** (X = H, Y = S)						
H,H	−474.64666(0)	26.3(0)	−475.24905(0)	−474.62647(11.3)	24.9(1)	−475.20165(28.3)
CH_3, CH_3	−552.74827(4.8)	58.1(0)	−553.70736(0)	−552.75543(0)	57.8(0)	−553.68777(12.0)
c-C_3H_5, c-C_3H_5[g]				(−702.93547)[e]		
C_6H_5, C_6H_5[g]				(−928.46518)[e]		
(*b*) **Aldehydes** (X = H, Y = O)						
H, H	−151.97131(0)	27.1(0)	−152.52219(0)	−151.94891(12.3)	25.3(1)	−152.47458(28.1)
CH_3, CH_3	−230.08382(13.2)	59.9(0)	−230.99031(0.3)	−230.10267(0)	58.5(0)	−230.98862(0)
c-C_3H_5, c-C_3H_5[g]				(−381.71520)[e]		
C_6H_5, C_6H_5[g]				(−607.74145)[e]		
(*c*) **Thioamides** (X = NH_2, Y = S)						
H, H	−529.75126(0)	37.0(0)	−530.33212(0)	−529.68015(42.7)	35.1(1)	−530.25847(44.3)
CH_3, H	−568.79977(0)	53.7(0)	−569.53229(0)	−568.74878(29.8)	51.5(1)	−569.47437(34.1)
CH_3, CH_3	−607.84627(0)	70.1(0)	−608.73254(0)	−607.80665(23.2)	68.4(1)	−608.68242(29.8)
c-C_3H_5, H			−[643.12470(0)][f]			−[643.10817(9.2)][f]
	−645.67552	74.4(0)	−646.68915(0)	−645.65705(10.4)	73.2(1)	−646.66506(13.9)
c-C_3H_5, c-C_3H_5				−761.59864(0)	111.2(0)	[−758.65967(0)][f]
C_6H_5, H	−759.31931(0)	85.4(0)	[−756.36898(0)][f]	−759.30526(8.4)	85.0(1)	[−756.34314(15.8)][f]
C_6H_5, C_6H_5			(−983.72091)[e]			[−985.17305][f]
Fluorenyl			[−984.00801][f]	−987.73151(0)	119.9(0)	
(*d*) **Amides** (X = NH_2, Y = O)						
H, H	−207.08124(0)	38.6(0)	−207.70124(0)	−207.02312(33.8)	35.9(1)	−207.62627(44.3)
CH_3, CH_3	−285.18754(0)	71.4(0)	−286.10972(0)	−285.17276(7.2)	69.3(1)	−286.07959(21.7)
C_6H_5, H[g]				−436.68287		
C_6H_5, C_6H_5[g]				(−662.50586)[e]		

[a]Relative energies in kcal/mol, after inclusion of zero-point energies, are given in parentheses.
[b]Zero-point energies (kcal/mol), calculated at HF/6-31G(d,p), were scaled by a factor of 0.89.
[c]Number of imaginary frequencies is in parentheses.
[d]For X = H, MP2(FULL) calculation at 6-311G(d,p) (23,24); for X = NH_2, MP2(FULL) calculations at 6-31G(d,p).
[e]Calculated at HF/3-21G(d).
[f]Calculated at MP2(FC)/3-21G(d).
[g]For these ions attempts at optimizing the cyclic structure resulted in ring-opening.

Results and discussion

1. Structural details; factors that determine whether the ion is cyclic or open

a) Open ions 8

Structures **1** and **6** may be generalized as **8**. For aldehydes (**8**, X = H, Y = O or S) when R and R′ are both H, the open ion is higher in energy than the cyclic ion **9** at HF/6-31G(d,p) and inclusion of electron correlation further increases the relative stabilization of the cyclic structure. When both R and R′ are CH_3, the open ions have lower energies than the cyclic isomers, but inclusion of electron correlation results in $(CH_3)_2CCHS^+$ becoming cyclic, while the oxygen analogue remains open but with a very low potential for bending into the cyclic structure.

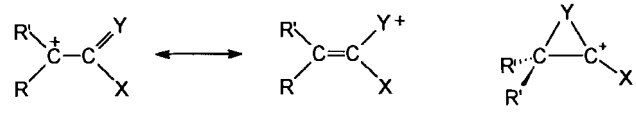

8*a* **8*b*** **9**

Aldehydes substituted with R = R′ = C_6H_5 and c-C_3H_5 have open structures at HF/3-21G(d). The $(c\text{-}C_3H_5)_2CCHY^+$ ions have the two cyclopropyl groups perpendicular to the plane defined by CCHY and coincident with the formally vacant *p*-orbital on C^+, thereby having the configuration in which the cyclopropyl groups can most effectively donate electron density to the cationic carbon. The $(C_6H_5)_2CCHY^+$ ions have the plane of CHY rotated out of the plane defined by $C_{ipso}C^+C_{ipso}$ (by 17° for Y = O and 45° for Y = S) but large C^+CY angles indicate that there is no tendency for neighbouring group participation. The phenyl groups are prevented from being copla-

Can. J. Chem. Downloaded from www.nrcresearchpress.com by 80.90.12.36 on 09/08/12
For personal use only.

Can. J. Chem. Downloaded from www.nrcresearchpress.com by 80.90.12.36 on 09/08/12
For personal use only.

Table 2. Structural parameters[a] for cyclic and open cations.

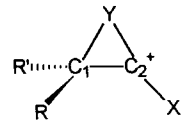

9

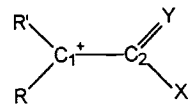

8

R, R′	C1—C2	C2—Y	C1—Y	C2—X	∠C1C2Y	C1—C2	C2—Y	C2—X	∠C1C2Y
(*a*) **Thioaldehydes** (X = H, Y = S)[b]									
R = R′ = H	1.451	1.605	1.911	1.085	77.2	1.405	1.661	1.088	118.0
R = R′ = CH_3	1.445	1.613	1.994	1.087	81.2	1.455	1.635	1.091	122.0
R = R′ = c-C_3H_5[c]						1.491	1.594	1.071	125.7
R = R′ = C_6H_5[c]						1.486	1.596	1.075	123.9
(*b*) **Aldehydes** (X = H, Y = O)[b]									
R = R′ = H	1.433	1.241	1.618	1.088	74.1	1.483	1.226	1.095	115.0
R = R′ = CH_3	1.439	1.238	1.762	1.091	81.9	1.535	1.208	1.101	119.2
R = R′ = c-C_3H_5[c]						1.527	1.203	1.079	122.8
R = R′ = C_6H_5[c]						1.524	1.204	1.077	122.6
(*c*) **Thioamides** (X = NH_2, Y = S)[d]									
R = R′ = H	1.448	1.652	1.884	1.295	74.6	1.408	1.721	1.330	113.5
R = CH_3, R′ = H	1.488	1.652	1.913	1.298	75.9	1.425	1.697	1.337	113.7
R = R′ = CH_3	1.446	1.653	1.942	1.300	77.3	1.456	1.675	1.348	119.4
R = H, R′ = c-C_3H_5	1.445	1.650	1.968	1.301	78.7	1.463	1.656	1.350	120.7
R = R′ = c-C_3H_5[e]						1.498	1.636	1.319	115.3
R = H, R′ = C_6H_5[e]	1.468	1.665	2.115	1.309	84.7	1.502	1.640	1.331	126.6
R = R′ = C_6H_5[c]						1.504	1.635	1.325	116.1
Fluorenyl[e]						1.481	1.637	1.317	113.2
(*d*) **Amides** (X = NH_2, Y = O)[d]									
R = R′ = H	1.428	1.285	1.571	1.289	70.6	1.453	1.257	1.342	113.9
R = R′ = CH_3	1.433	1.280	1.648	1.296	74.6	1.528	1.230	1.346	117.1
R = H, R′ = C_6H_5[e]						1.519	1.194	1.336	120.7
R = R′ = C_6H_5[c]						1.525	1.212	1.340	119.3

[a]Bond lengths are in angstroms, angles in degrees.
[b]Optimized at MP2(FULL)/6-311G(d,p).
[c]Optimized at HF/3-21G(d).
[d]Optimized at MP2(FULL)/6-31G(d,p).
[e]Optimized at HF/6-31G(d,p).

Table 3. Total energies (hartrees) of amidylmethanes.

				Key structural parameters[b]		
Methane	HF/6-31G(d,p)	ZPE[a]	MP2(FULL)/6-31G(d,p)	C—C	C—Y	C—N
CH_3CONH_2	−207.98897	43.7	−208.62845	1.513	1.227	1.367
CH_3CSNH_2	−530.62207	43.0	−531.21751	1.507	1.643	1.351
$CH_3CH_2CSNH_2$	−569.65975	60.3	−570.40565	1.510	1.644	1.350
c-$C_3H_5CH_2CSNH_2$	−646.53020	81.1	−647.55622	1.510	1.644	1.350
$C_6H_5CH_2CSNH_2$	−760.17611	92.1	−757.22642[c]	1.525	1.663	1.320
$(CH_3)_2CHCSNH_2$	−608.69643	77.0	−609.59563	1.516	1.644	1.350

[a]Zero-point energies (kcal/mol) have been scaled by a factor of 0.89.
[b]Bond lengths in angstoms.
[c]Optimized at MP2(FULL)3-21G(d).

nar by interaction between *ortho* hydrogens, and the angle of twist is ≈22° for Y = O and ≈29° for Y = S.

For ions **8** in which R and R′ do not stabilize an adjacent cationic carbon, then valence bond structure **8***b* permits delocalization of charge onto the heteroatom, Y. This structure is of greatest significance when R = R′ = H and, from the structural data on H_2CCHS^+ in Table 2, it is clear from the short C—C distance (1.405 Å) and the long C—S distance (1.661 Å) that structure **8***b* is a major contributor. A Mayer bond order analysis (25) on this structure (at HF/6-31G(d,p)) shown in **8***c* gave bond orders of 1.266 for C—C and 1.639 for C-S, indicating that **8***a* is more important than **8***b*, but that the contribution from the latter is quite large. The structural data on the oxygen analogues H_2CCHO^+, C—C 1.483 Å and C-O 1.226 Å, are much closer to standard single and double bonds, respectively, indicating the valence bond structure **8***b* is less important in the oxygen-containing ions.

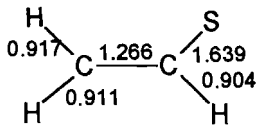

8*c*

In carbocations containing an α-amide group (**8**, X = NH_2, Y = S or O) the amino group heavily stabilizes the cyclic structure through contributions from structures **2***c*. For example, for H_2CCHS^+ the cyclic ion **9** is lower in energy than the open ion **8** by 28.3 kcal/mol, while for the thioamide ion $H_2CCSNH_2^+$ the difference is 44.3 kcal/mol. A consequence of this stabilization is that α-amide substituted ions containing R groups that stabilize the open structure do not always prefer the open structure. Thioamide substituted ions with either R = R′ = CH_3 or with one R group C_6H_5 or c-C_3H_5 are then cyclic. Similarly, $(CH_3)_2CCONH_2^+$ is calculated to be cyclic, a result that is contrary to experimental evidence that ion $(CH_3)_2CCON(CH_3)_2^+$, generated under solvolytic conditions, is an open ion (26). Ion $C_6H_5CHCONH_2^+$ has the open structure **8** at HF/6-31G(d,p) with all the atoms almost coplanar (oxygen and phenyl eclipse) but, since inclusion of electron correlation consistently favours the cyclic structure, it is possible that higher level calculations would show the cyclic structure to be preferred. Similar comments apply to tertiary carbocations (R = R′ = C_6H_5 or c-C_3H_5). At HF/3-21G(d) ions $(C_6H_5)_2CCYNH_2^+$ (Y = O or S) have the amide group twisted approximately 90° out of the plane defined by $C_{ipso}C^+C_{ipso}$, in the appropriate conformation for bridging but, as shown by C⁺CY angles of 119.3° (Y = O) and 116.1° (Y = S), there is no evidence of bridging. For ion $(C_6H_5)_2CCSNH_2^+$, however, inclusion of electron correlation at MP2(FC)/3-21G(d) resulted in a decrease in angle C⁺CS to 91.5°.

The 9-thioformamidyl-9-fluorenyl cation has the planar thioamidyl group perpendicular to the fluorenyl ring structure, with angle C⁺CS varying from 114.5° at HF/3-21G(d) to 84.0° at MP2(FC)/3-21G(d) and 113.2° at HF/6-31G(d,p). Clearly, the amount of neighbouring group participation is dependent on the level of calculation, probably indicating a low potential for the ring-opening vibrational mode, and at the levels of theory used here it is not possible to give a definitive answer as to whether these more heavily substituted ions are cyclic or open. Experimentally, solutions of diphenylmethyl and fluorenyl cations containing an α-$CSNMe_2$ group are intensely coloured, with spectra similar to those of unsubstituted ions, providing strong evidence that the ions have the open structure (17).

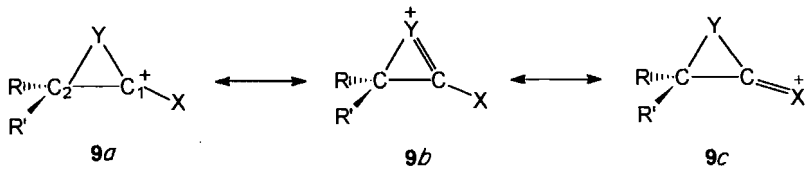

9*a* **9***b* **9***c*

(b) Cyclic ions

It is only possible to optimize cyclic structures **9** for oxiranyl and thiiranyl cations when they are at minima on the potential energy surface. Other ions ring open to form a rotamer of **8** in which the CXY plane is coplanar with the empty *p*-orbital on C⁺. The Y—C2 distance and C2C1Y angle both increase as the electron-donating abilities of R and R′ increase. For all the cyclic aldehydes the C2—Y distances are considerably longer than standard single C—Y bonds (~1.80 Å for C—S and ~1.43 Å for C-O) (2), the C1—Y distances are close to C=Y double bond distance (~1.61 Å for C=S and ~1.22 Å for C=O), and the C1—C2 distances are intermediate between single and double bonds (~1.54 Å for C—C, ~1.34 Å for C=C) (2). For ions that we have classified as cyclic, angle C2C1Y varies between 74° and 82°.

The results of a Mayer bond order analysis (25) on CH_2CHS^+, the ion with the smallest C2C1Y angle, are shown on structure **10**. The C1—S bond order of 1.680 indicates considerable double bonding between these atoms, but both C1—C2 and C2—S have bond orders close to one and must be considered to be single bonds. Clearly then resonance structure **9***b* (X = H, Y = S) is the best way of representing this ion.

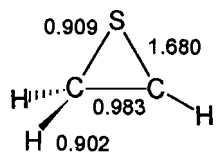

10

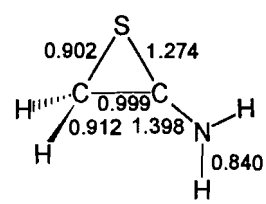

11

For cyclic ions where X = NH_2, much of the positive charge in **9** is transferred onto the nitrogen and structure **9***c* becomes a major contributor. This requires a double bond between C and N and the average C—N distance for these ions (~1.30 Å) is close to that for a standard C=N distance (C=N is 1.27 Å, C—N is 1.47 Å). The cyclic amide ions have less charge delo-

Can. J. Chem. Downloaded from www.nrcresearchpress.com by 80.90.12.36 on 09/08/12
For personal use only.

Can. J. Chem. Downloaded from www.nrcresearchpress.com by 80.90.12.36 on 09/08/12
For personal use only.

calization onto Y than the equivalent aldehyde-containing ions and this is reflected in longer C1—Y distances (by 0.04–0.06 Å). Comparison of the bond orders calculated for the cyclic thioamide **11** (X = NH_2, Y = S, R = R′ = H) with those for the cyclic thioaldehyde **10** show the C1—S bond order to be much smaller (1.274 compared with 1.680), but there is still some double bond character in the ring. In **11** the C—N bond has the highest bond order (1.398). This indicates some double bond character, but less than implied by the short bond length.

The barrier to ring opening of the cyclic ion, the energy difference between structures **9** and **8**, decreases as angle C2C1Y increases. This crude relationship is best illustrated by the thioamide series where, when R = R′ = H the angle is 74.6° and the barrier is 44.3 kcal/mol, when R = R′ = CH_3 the angle is 77.3° and the barrier 29.8 kcal/mol, when R = H, R′ = c-C_3H_5 the angle is 78.7° and the barrier 13.9 kcal/mol, and when R = H, R′ = C_6H_5 the angle is 84.7 and the barrier 8.4 kcal/mol.

2. Stabilization energies of α-substituents in carbocations

(a) Substituents in methyl cations CH_2X^+

The methyl cations are extremely electron deficient and any substituent X in CH_2X^+ ions is a potential source of electron density. The ability of a substituent to stabilize the methyl cation can be assessed from the isodesmic reaction in eq. [1] where a positive energy indicates that R is stabilizing in the cation. This approach has been used extensively to assess the stabilities of cations. In our earlier study of ions

[1] $CH_2R^+ + CH_4 \rightarrow CH_3^+ + CH_3R$

CH_2COX^+ (X = CH_3, NH_2, OH and F), we found that, using the open ions, **8**, in eq. [1], groups CHO, $COCH_3$, and $CONH_2$ were stabilizing, and COOH and COF were destabilizing (16). By contrast, ions CH_2CHS^+ and $CH_2CSNH_2^+$ were found to be strongly stabilized (ΔE for eq. [1] was 30.6 kcal/mol for CH_2CHS^+ and 35.7 kcal/mol for $CH_2CSNH_2^+$). We have now reevaluated ΔE for eq. [1] for $CH_2CONH_2^+$ and $CH_2CSNH_2^+$ using structures optimized at MP2(FULL)/6-31G(d,p), and the resulting ΔE values of 10.3 kcal/mol and 37.4 kcal/mol, respectively (Table 5), are in good agreement with the earlier values obtained with lower level theory (16).

To put the stabilization energies provided by amidyl substituents onto a comparative scale, we have used eq. [1] to calculate ΔE for methyl cations substituted by methyl, vinyl, cyclopropyl, and phenyl substituents. The total energies for these methanes and methyl cations are given in Table 4 and the stabilization energies are in Table 5. For these hydrocarbon substituents, the MP2(FULL)/6-31G(d,p) calculations consistently give higher ΔE values than the HF level calculations, with the difference being in the range 6–12 kcal/mol. For several of these ions accurate experimental enthalpies of formation are available (25) and stabilization energies calculated from these data, shown in the last column of Table 5, are within ±2 kcal/mol of the values calculated at MP2(FULL)/6-31G(d,p). Only for the cyclopropylcarbinyl cation, where the experimental enthalpy is not well established, is there a large difference between experiment and theory. From the stabilization energies in Table 5, then, we conclude that the relative stabilizing abilities of substituents in the methyl cation are $CONH_2$(open) < $CSNH_2$(open) ≈ CH_3 < $CONH_2$(cyclic)≈ $CH{=}CH_2$ < c-C_3H_5≈C_6H_5 < $CSNH_2$(cyclic). In making these comparisons it should be noted that the stabilization energies calculated for the cyclic amide substituted ion, **2**, are not for isodesmic reactions and, for these reactions, inclusion of electron correlation increases the stabilization by larger amounts (>20 kcal/mol).

(b) Thioamide as an α-substituent in cations $RCHX^+$ and $RR'CX^+$

The question as to whether an α-thioamidyl group is destabilizing in a secondary carbocation $RCHCSNH_2^+$, where the other substituent R is stabilizing, can be addressed by using the reaction in eq. [2] (Table 6). Considering the open structure, **1**, the thioamidyl group stabilizes the ethyl cation by 16.5 kcal/mol, compared with 37.4 kcal/mol for the stabilization of

[2] $RCHCSNH_2^+ + RCH_3 \rightarrow RCH_2^+ + RCH_2CSNH_2$

the methyl cation. In the cyclopropylcarbinyl cation, c-$C_3H_5CHCSNH_2^+$, the thioamidyl group is stabilizing by 7.9 kcal/mol, while in the benzyl cation $C_6H_5CHCSNH_2^+$ it is destabilizing by 1.9 kcal/mol. However, neighbouring group participation results in each of these open structures being transition structures that collapse into cyclic structure **2**. Using structure **2** in eq. [2] produces a reaction that is not isodesmic but for which the stabilization energies for all ions are positive.

Replacement of the remaining hydrogen atom attached to the cationic carbon by an electron-donating group creates a tertiary carbocation and it is ions of this type that have been observed and characterized under stable ion conditions (14, 17). The size of these ions, $Ar_2CCSNMe_2^+$, precludes the use of high level *ab initio* calculations at this time, but we have calculated the stabilization energy provided by the thioamidyl group in the isopropyl cation by using eq. [3].

[3]

Based on the open structure, **1**, the thioamidyl group is stabilizing but by only 8.0 kcal/mol. Thus the stabilization energies resulting from an α-$CSNH_2$ group in methyl, ethyl, and isopropyl cations are 37.4, 16.5, and 8.0 kcal/mol, respectively. By comparison, using experimental enthalpies of formation, an α-methyl substituent stabilizes the methyl, ethyl, and isopropyl cations by 43.4, 19.8, and 19.9 kcal/mol (27).

An α-thioamidyl substituent is slightly destabilizing in the open benzyl cation $C_6H_5CHCSNH_2^+$ and, since a second phenyl group contributes additional stabilization, the α-thioamidyl group is expected to be more destabilizing in the diphenylmethyl cation, $(C_6H_5)_2CCSNH_2^+$. Furthermore, our geometry optimizations on $(C_6H_5)_2CCSNH_2^+$ have shown this ion to prefer the open structure, in keeping with the experi-

Can. J. Chem. Downloaded from www.nrcresearchpress.com by 80.90.12.36 on 09/08/12
For personal use only.

Table 4. Total energies (hartrees) and zero-point energies (kcal/mol) for hydrocarbons RCH_3 and methyl cations RCH_2^+.

R	HF/6-31G(d,p)	ZPE[a]	MP2(FULL)/6-31G(d,p)	
(*a*) **Methanes RCH_3**				
H	−40.20170	26.4	−40.36986	
CH_3	−79.23824	44.2	−79.55371	
CH_2CH_3	−118.27616	61.3	−118.74088	
$CH = CH_2$	−117.08161	47.5	−117.51908	
c-C_3H_5	−156.10916	65.2	−156.70304	
C_6H_5	−269.75388	76.1	−270.72798	(−268.85227)[c]
(*b*) **Methyl cations RCH_2^+**				
H	−39.23630	18.6	−39.35120	
CH_3[b]	−78.32095	36.0	−78.60118	
$CH = CH_2$	−116.20208	40.8	−116.59575	
c-C_3H_5	−155.24008	57.9	−155.79926	
C_6H_5	−268.89920	69.9	−269.83096	(−267.97199)[c]
$(CH_3)_2CH^+$	−117.39376	52.7	−117.81491	

[a]HF level harmonic frequencies scales by a factor of 0.89.
[b]Non-classical (bridged) ion.
[c]At MP2(FC)/3-21G(d).

Table 5. Substituent effects in monosubstituted-methyl cations using eq. [1].

	ΔE_{el}[a] from eq. [1]		
R	HF/6-31G(d,p)	MP2(FULL)/6-31G(d,p)	$\Delta H_{rxn,\,298}$[a,b]
CH_3	30.2	41.5	43.5
$CH = CH_2$	53.9	59.8	58.0
c-C_3H_5	60.4	72.1	(59.7)
C_6H_5	69.5	76.4	76.2
$CONH_2$	−0.3 (36.2)[c]	10.3 (57.4)[c]	
$CSNH_2$	14.7 (59.4)[c]	37.4 (83.6)[c]	

[a]Energies are in kcal/mol.
[b]Experimental enthalpies of formation used to calculate these numbers were taken from ref. 25.
[c]Ions containing $CONH_2$ and $CSNH_2$ were assumed to have the open structure, **1**. The numbers in parentheses are calculated using the more stable cyclic ions, **2**.

Table 6. Effect of $CSNH_2$ as an α-substituent in ions $RR'CCSNH_2^+$ as calculated from $RR'CCSNH_2^+ + RR'CH_2 \rightarrow RR'CH^+ + RR'CHCSNH_2$.

R, R′	HF/6-31G(d,p)	MP2(FULL)/6-31G(d,p)[a]
(*a*) **Assuming $RR'CCSNH_2^+$ has the open structure, 1**		
H, H	14.7	37.4
H, CH_3	4.0	16.5
H, c-C_3H_5	−2.6	7.9
H, C_6H_5	−10.1	−1.9[b]
CH_3, CH_3	−4.6	8.0
(*b*) **Assuming $RR'CCSNH_2^+$ has the cyclic structure, 2**		
H,H	59.4	83.6
H, CH_3	36.0	49.7
H, c-C_3H_5	9.0	23.0
H, C_6H_5	−1.3	14.3[b]
CH_3, CH_3	20.2	39.5

[a]Energies are in kcal/mol.
[b]Calculated at MP2(FC)/3-21G(d).

Can. J. Chem. Downloaded from www.nrcresearchpress.com by 80.90.12.36 on 09/08/12
For personal use only.

mental observation that ions $Ar_2CCSNMe_2^+$ have the open structure (17). We therefore conclude that an α-thioamidyl group is destabilizing in diarylmethyl cations.

3. Rearrangement of the α-thioformamidyl-benzyl cation

Our interest in the thioformamidyl group as an α-substituent in carbocations was initiated by our discovery that α-(*N*,*N*-dimethylthioformamidyl)-diarylmethyl cations, $Ar_2CCSNMe_2^+$, undergo cyclization to form benzothiophenes, with substitution occurring in the phenyl group containing the more electron-donating substituent (14,17). A plausible mechanism for this reaction involves nucleophilic attack by sulfur on the aryl group that carries the larger fraction of the positive charge. Structure optimization on $Ph_2CCSNH_2^+$ established that both phenyl groups are rotated ~26° relative to the plane defined by the two ipso carbons and the two exocyclic carbons. The thioformamidyl group is rotated ~90° relative to this plane, placing the sulfur atom in a position to attack a phenyl group from above. In an unsymmetrically substituted ion, the aryl group containing the more electron-donating substituents lies more closely in the plane and the other aryl group rotates further out of plane, thereby making the electron-rich aryl group the more accessible for nucleophilic attack. Semi-empirical calculations at the AM1 level showed that for *p*-$CH_3OC_6H_4,C_6H_5CCSNH_2^+$ the transition state for attack on the substituted ring is lower in energy than that for attack on the phenyl.

The α-(*N*,*N*-dimethylthioformamidyl)benzyl cation also rearranges to a benzothiophene and we have modelled this reaction theoretically at HF/6-31G(d,p) by examining the rearrangement of the sulfur-bridged ion **12** (structure **9** with R = C_6H_5, R′ = H, X = NH_2, Y = S) to the initial product of cyclization, the benzothiophene protonated at the bridging carbon, ion **13**. The transition structure for this reaction was located by first mapping the surface, using the *ortho* carbon-sulfur distance as a reaction coordinate, and then optimizing, using the eigenvector-following method (28), the transition structure associated with the highest point on the profile (transition structure **14**). Ion **13** is 14 kcal/mol below **12** and the barrier to its formation, via **14**, is 15.4 kcal/mol above **12**. Ion **15**, the structure through which **12** racemizes, is only 8.4 kcal/mol above **12**. Some of the key geometric parameters for structures **12–15** are given in Fig. 1.

Ion **13**, the intermediate in the ring-closing reaction, is the only protonated 2-aminobenzothiophene that we have examined at HF/6-31G(d,p), but at HF/3-21G(d) the N-protonated isomer **16** is 8.3 kcal/mol lower than **13** while the S-protonated isomer, **17**, is 18.4 kcal/mol higher than **13**.

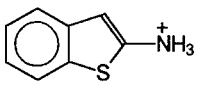

16

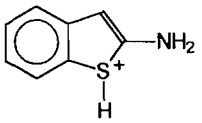

17

In isomer **13**, the phenyl group has been disrupted and the geometric parameters for structure **13** reveal an alternation of bond lengths around the carbon framework. The C—N distance of 1.305 Å, while slightly longer than that in **12** (1.279 Å), clearly indicates a large amount of π-delocalization from nitrogen.

Conclusions

Ab initio molecular orbital calculations show that primary (CH_2X^+) and secondary ($RCHX^+$) carbocations in which X = CHO, CHS, $CONH_2$, and $CSNH_2$ have a cyclic structure **9** involving an oxiranyl or thiiranyl ring. The amino group of the amide substituent stabilizes the cyclic structure by delocalizing the positive charge on to the nitrogen and the amide-substituted ions consequently have a higher barrier to ring opening than the aldehyde-substituted ions. Tertiary ions $RR'CX^+$, where R = R′ = CH_3, are also cyclic, but for ions in which R = R′ = cyclopropyl or phenyl, the cations have the open structure.

In methyl cations all substituents are stabilizing and, by use of isodesmic reactions, we have shown that the amide group, $CONH_2$, has a very small effect while the thioamide $CSNH_2$, is almost as stabilizing as the methyl group. In secondary carbocations, $RCHCSNH_2^+$, the stabilization resulting from $CSNH_2$ is considerably smaller when R = CH_3, and is negative (i.e., destabilizing) when R is C_6H_5. In the only tertiary ion we were able to calculate at MP2(FULL)/6-31G(d,p), ion $(CH_3)_2CCSNH_2^+$, the thioamide group is stabilizing but by only 8.0 kcal/mol. From all these data, it is clear that the $CSNH_2$ group attached to a cationic carbon stabilizes very electron-deficient carbocations even without any involvement from neighbouring group participation. However, in tertiary ions $RR'CCSNH_2^+$, where both R and R′ are powerful electron

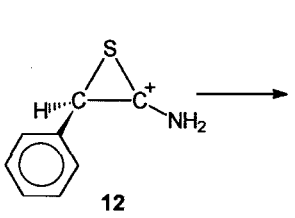

12

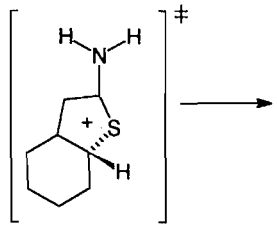

14

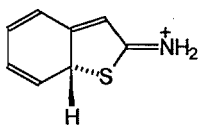

13

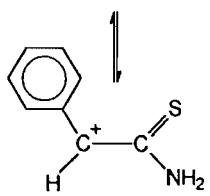

15

Fig. 1. Geometric parameters and total energies (hartrees) for isomers of $C_8H_8SN^+$. Bond lengths in angstroms, bond angles in degrees.

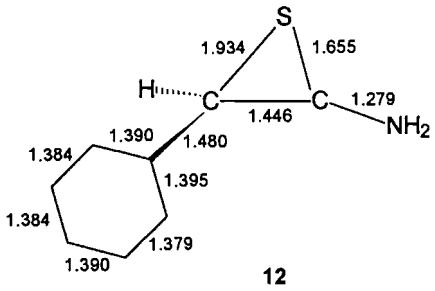

12

E= -759.31931 (min)

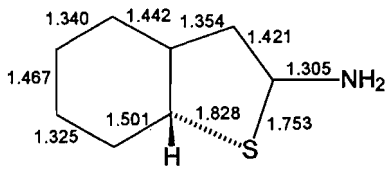

13

E= -759.34236 (min)

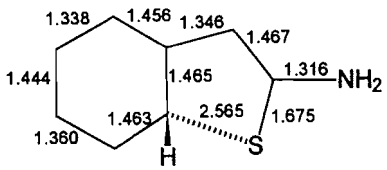

14

E= -759.29428 (t. s.)

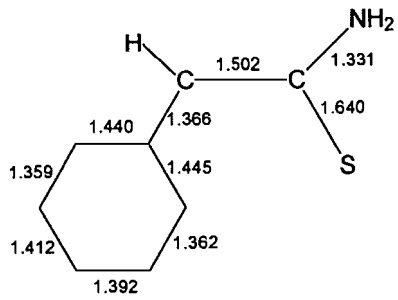

15

E= -759.30526 (t. s.)

donors, the open structure is preferred and, from the result on $C_6H_5CHCSNH_2^+$ and noting the trend in stabilization resulting from substitution by one and two methyl groups, we conclude that $CSNH_2$ will be destabilizing in $(C_6H_5)_2CCSNH_2^+$.

In solution, 2,2-diaryl-2-chloro-*N*,*N*-dimethylthioacetamide and α-*N*,*N*-dimethylthioformamidyl-diarylmethyl cations undergo facile ring closure to form benzothiophenes and the monoaryl derivatives also undergo this reaction, but more slowly. The ease of this reaction implies a low barrier to rearrangement and the calculated barrier of 15.4 kcal/mol for the rearrangement of $C_6H_5CHCSNH_2^+$ to the protonated benzothiophene is consistent with these experimental observations.

Acknowledgements

We thank A.E. Ketvirtis and S. Quan for technical assistance and the Natural Sciences and Engineering Research Council of Canada for financial support.

References

1. R.W. Taft, R.H. Martin, and F.W. Lampe. J. Am. Chem. Soc. **87**, 2490 (1965).
2. W.J. Hehre, L. Radom, P.v.R. Schleyer, and J.A. Pople. *Ab initio* molecular orbital theory. John Wiley and Sons, New York. 1986
3. Y. Apeloig, P.v.R. Schleyer, and J. A. Pople. J. Am. Chem. Soc. **99**, 1291 (1977).
4. R.T. Brownlee and D.J. Craik. J. Am. Chem. Soc. **105**, 872 (1983).
5. J.A. Pople, Y. Apeloig, and P.v.R. Schleyer. Chem. Phys. Lett. **85**, 489 (1982).
6. M.H. Lien and A.C. Hopkinson. J. Mol. Struct. (Theochem), **121**, 1 (1985).
7. J.C. White, R.J. Cave, and E.R. Davidson. J. Am. Chem. Soc. **110**, 6308 (1988).
8. A.C. Hopkinson and M.H. Lien. Can. J. Chem. **63**, 3582 (1985).
9. A.C. Hopkinson and M.H. Lien. J. Am. Chem. Soc. **108**, 2843 (1986).
10. (*a*) J.P. Bégué and M. Charpentier-Morize. Acc. Chem. Res. **13**, 207 (1980); (*b*) P.G. Gassman and T.T. Tidwell. Acc. Chem. Res. **16**, 279 (1983); (*c*) X. Creary. Acc Chem. Res. **18**, 3 (1985); (*d*) X. Creary (*Editor*). Advances in carbocation chemistry. JAI Press Inc., Greenwich, Conn. 1989; (*e*) X. Creary. Chem. Rev. **91**, 1625 (1991).
11. (*a*) A.C. Hopkinson, L.H. Dao, P. Dupperouzel, M. Maleki, and E. Lee-Ruff. J. Chem. Soc. Chem. Commun. 727 (1983); (*b*) L.H. Dao, M. Maleki, A.C. Hopkinson, and E. Lee-Ruff. J. Am. Chem. Soc. **108**, 5237 (1986); (*c*) D. Fletcher, F.J. Ablenas, A.C. Hopkinson, and E. Lee-Ruff. Tetrahedron Lett. **27**, 4853 (1986); (*d*) L.J. Johnston, P. Kwong, A. Shelemay, and E. Lee-Ruff. J. Am. Chem. Soc. **115**, 1664 (1993).
12 (*a*) G.A. Olah, G.K.S. Prakash, M. Arvangaghi, V.V. Krishnamurthy, and S.C. Naran. J. Am. Chem. Soc. **102**, 6640 (1980); (*b*) **106**, 2378 (1984).
13. (*a*) G.A. Olah, M. Arvanaghi, and G.K.S. Prakash. J. Am. Chem. Soc. **104**, 1628 (1982); (*b*) G.A. Olah, G.K. Prakash, and M. Arvanaghi. J. Am. Chem. Soc. **102**, 6640 (1980).
14. F.J. Ablenas, B.E. George, M. Maleki, R. Jain, A.C. Hopkinson, and E. Lee-Ruff. Can. J. Chem. **65**, 1800 (1987).
15. X. Creary and T. Aldridge. J. Org. Chem. **56**, 4280 (1991).
16. M.H. Lien and A.C. Hopkinson. J. Am. Chem. Soc. **110**, 3788 (1988).

Can. J. Chem. Downloaded from www.nrcresearchpress.com by 80.90.12.36 on 09/08/12
For personal use only.

17. K. Kalamatianos. M.Sc. Thesis, York University. 1989.
18. M.J. Frisch, G.W. Trucks, M. Head-Gordon, P.M.W. Gill, J.B. Forseman, B.G. Johnson, H.B. Schlegel, M.A. Robb, E.S. Replogle, R. Gomperts, J.L. Andres, K. Raghavachari, J.S. Binkley, C. Gonzalez, R.L. Martin, D.J. Fox, D.J. Defrees, J. Baker, J.J.P. Stewart, and J.A. Pople. GAUSSIAN 92, Revision C.4. Gaussian, Inc., Pittsburgh, Pa. 1992.
19. H.B. Schlegel. J. Comput. Chem. **3**, 214 (1982).
20. W.J. Hehre, R. Ditchfield, and J.A. Pople. J. Chem. Phys. **56**, 2257 (1972); (*b*) P.C. Hariharan and J.A. Pople. Theor. Chim. Acta, **28**, 213 (1973).
21. C. Moller and M.S. Plesset. Phys. Rev. **46**, 618 (1934); (*b*) J.S. Binkley and J.A. Pople. Int J. Quantum Chem. **9**, 229 (1975).
22. M.M. Francl, W.J. Pietro, W.J. Hehre, J.S. Binkley, M.S. Gordon, D.J. DeFrees, and J.A. Pople. J. Chem. Phys. **77**, 3654 (1982).
23. M.J. Frisch, J.A. Pople, and J.S. Binkley. J. Chem. Phys. **80**, 3265 (1984).
24. (*a*) R. Krishnan, J.S. Binkley, R. Seeger, and J.A. Pople. J. Chem. Phys. **72**, 650 (1980); (*b*) A.D. McLean and G.S. Chandler. J. Chem. Phys. **72**, 5639 (1980).
25. I. Mayer. Int. J. Quantum Chem. **29**, 73 (1986); **29**, 477 (1986).
26. X. Creary, S. McDonald, and M.D. Eggers. Tetrahedron Lett. **26**, 811 (1985).
27. S.G. Lias, J.E. Bartmess, J.F. Liebman, R.D. Levin, and W.G. Mallard. J. Phys. Chem. Ref. Data, Supplement. 1988.
28. (*a*) J. Baker. J. Comput. Chem. **7**, 385 (1986); (*b*) J. Comput. Chem. **8**, 563 (1987); (*c*) J. Simons, P. Jorgensen, H. Taylor, and J. Ozment. J. Phys. Chem. **87**, 2745 (1983); (*d*) C.J. Cerjan and W.H. Miller. J. Chem. Phys. **75**, 2800 (1981); (*e*) A. Bannerjee, N. Adams, J. Simons, and R. Shepard. J. Phys. Chem. **89**, 52 (1985).

Can. J. Chem. Downloaded from www.nrcresearchpress.com by 80.90.12.36 on 09/08/12
For personal use only.

^{1}H and ^{13}C nuclear magnetic resonance and molecular orbital studies of the internal rotational potential and of spin–spin coupling transmission in phenylallene

Ted Schaefer, Scott Kroeker, and David M. McKinnon

Abstract: The ^{1}H nuclear magnetic resonance spectra of phenylallene, diluted in acetone-d_6 and benzene-d_6, yield long-range coupling constants over as many as eight formal bonds between the ring and side-chain protons. These are discussed in terms of σ- and π-electron spin–spin coupling mechanisms, which are sensitive to the torsion angle between the allenyl and phenyl fragments. The torsion angle is assessed by means of molecular orbital computations of the internal rotational potential, whose height is calculated as 16.0 kJ/mol at the MP2/6-31G* level of correlation-gradient theory. Comparison with experimental and theoretical internal rotational potentials for styrene suggests that steric repulsions in the planar form of styrene amount to about 4 kJ/mol. In a field of 7.0 T, phenylallene is partially aligned, entailing a positive dipolar coupling constant between the methylene protons, from which absolute signs of the spin–spin coupling constants involving these protons can be inferred. Such coupling constants over seven and eight bonds, to the *meta* and *para* protons, are taken as being mediated by the extended π-electron system, providing a measure of π-electron contributions to coupling constants between *meta* protons and those in side chains (spin correlation). Some coupling constants between protons and ^{13}C nuclei in the side chain, as well as between ring protons and these ^{13}C nuclei, are also discussed in terms of spin coupling mechanisms. Solvent perturbations of one-bond proton–carbon coupling constants in the allenyl group do not follow the usual pattern in which an increase in polarity of the solvent is associated with an increase in the magnitude of the coupling constant.

Key words: ^{1}H NMR, phenylallene; ^{1}H NMR, long-range spin–spin coupling constants in phenylallene; phenylallene, internal rotational potential, molecular orbital computations; molecular orbital calculations, an internal rotational potential in phenylallene.

Résumé : Les spectres RMN du ^{1}H du phénylallène, en solution dans l'acétone-d_6 et le benzène-d_6, permettent de tirer les constantes de couplage sur des distances allant jusqu'à huit liaisons formelles, entre les protons du cycle et ceux de la chaîne latérale. On les discute en fonction des mécanismes de couplage spin–spin des électrons σ et π qui sont sensibles à l'angle de torsion entre les fragments allényle et phényle. On évalue l'angle de torsion par des calculs d'orbitales moléculaires du potentiel de rotation interne dont la hauteur a été évaluée à 16,0 kJ/mol au niveau MP2/6-31G* de la théorie de corrélation du gradient. Une comparaison des potentiels expérimental et théorique de rotation interne du styrène suggère que les répulsions stériques dans la forme planaire du styrène sont de l'ordre de 4 kJ/mol. Dans un champ de 7,0 T, le phénylallène est partiellement aligné impliquant une constante de couplage dipolaire positive entre les protons du méthylène et à partir de laquelle on peut déduire les constantes de couplage spin–spin de ces protons. On considère que ces constantes de couplages s'étendant sur sept et huit liaisons, vers les protons *méta* et *para*, sont rendues possibles par le système étendu d'électrons π et qu'elles fournissent une mesure des contributions des électrons π aux constantes de couplage entre les protons *méta* et ceux de la chaîne latérale (corrélation de spin). On fait appel aux mécanismes de couplage de spin pour discuter aussi de quelques constantes de couplage entre des protons et des noyaux ^{13}C de la chaîne latérale, comme celles entre les protons du cycle et des noyaux ^{13}C. Les perturbations par les solvants des constantes de couplage proton–carbone à travers une liaison dans le groupe allényle ne suivent pas le patron

Received May 8, 1995.

T. Schaefer,[1] S. Kroeker, and D.M. McKinnon. Department of Chemistry, University of Manitoba, Winnipeg, MB R3T 2N2, Canada.

[1] Author to whom correspondence may be addressed. Telephone: (204) 474-9335. Fax: (204) 275-0905.

Can. J. Chem. Downloaded from www.nrcresearchpress.com by 80.90.12.36 on 09/08/12
For personal use only.

habituel selon lequel une augmentation de la polarité du solvant est associée à une augmentation de l'amplitude de la constante de couplage.

Mots clés : RMN du ^{1}H; phénylallène; constantes de couplage spin–spin à longue distance; potentiel de rotation interne; calculs d'orbitales moléculaires.

[Traduit par la rédaction]

Introduction

One aim of this report is to compare the computed barriers to internal rotation in phenylallene, **1**, and styrene, **2**. In the planar conformer of **2** the indicated repulsions oppose the π-electron conjugation favouring planarity. Whether, in fact, there exists a (small) barrier to planarity in **2** is a matter of disagreement (1–8) between experimental and theoretical data. The β-CH bond is absent in **1**, while ^{13}C nmr chemical shifts indicate (9) rather similar π conjugational energies in the two molecules. Hence the barriers to rotation about the bond between the fragments in **1** and **2** may, by subtraction, represent a first approximation to the steric destabilization of planar **2**. Accordingly, molecular orbital computations of the internal rotational potential in **1** are reported here and are compared with similar computations (5, 6, 10) on styrene.

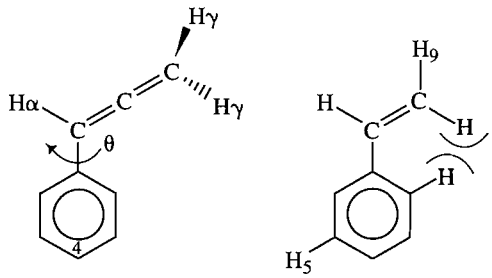

1 **2**

A second aim of this work is the analysis of the ^{1}H nmr spectra of **1**. In particular, the long-range spin–spin coupling constants over four to eight formal intervening bonds, between the protons on the side chain and those in the phenyl group, are obtained. The dependence of such coupling constants on the conformational angle, θ (see **1**), and hence on the internal rotational potential, has been discussed in detail for styrene and a number of its derivatives (3, 11, 12). A similar discussion for phenylallene does not appear to be available and is given below. It also happens that the spectral pattern for the phenyl group in acetone-d_6 solution is unique and is illustrated.

In addition, some coupling constants between protons and ^{13}C nuclei within the side chain are presented and compared with earlier measurements. Long-range coupling constants of the ring protons with the ^{13}C nuclei in the allenyl fragment are also given and are discussed in terms of coupling mechanisms.

Experimental

Phenylallene, **1**, was prepared from 1,1-dibromo-2-phenylcyclopropane, itself constructed using styrene, bromoform, and potassium hydroxide, exactly as described in the recent literature (13). Dilute solutions of **1** (see Table 1 for details) in benzene-d_6 and acetone-d_6 were filtered into 5 mm o.d. nmr tubes and were then degassed by at least five cycles of the freeze–pump–thaw procedure. The tubes were flame-sealed under vacuum such that reasonably symmetric tops were produced.

The ^{1}H nmr spectra were obtained from an AM 300 Bruker spectrometer at a probe temperature of 300 K. Typically, 32 free induction decays were coadded, using acquisition times of 30 s and a digital resolution of 0.017 Hz/point after zero-filling to twice the original data table. A small amount of resolution enhancement and Fourier transformation produced spectra whose line widths at half-height were about 0.03 Hz. Final shimming procedures used the free induction decays from internal tetramethylsilane (TMS). Similar procedures were used for the ^{13}C nmr spectra, except that acquisition times were 20 s, digital resolution was 0.027 Hz/point, and the number of coadded free induction decays was as large as 1800.

The signs of the coupling constants between the ring and γ protons (see **1**) were determined by partial decoupling (14) experiments in which the transitions of the α protons were irradiated for given spin states of the γ protons, while detecting those of the ring protons. The signs of the coupling constants in Table 1 follow on the basis that $^4J_{\alpha\gamma}$ is negative, as it is if ^3J(H, CH_3) in 1-chloro-1,2-butadiene is positive (15–17). The sign of the dipolar coupling between the γ protons in **1** is consistent with the absolute signs in Table 1 (see below).

Molecular orbital computations on phenylallene employed various basis sets[2] in the program GAUSSIAN 92 (18), as well as the AM1 algorithm (19). The conformational angle, θ, was fixed at 15° intervals between 0° (planar) and 90° (perpendicular) while all other angles and bond lengths were optimized during the SCF cycles, with the constraint, however, that the phenyl moiety remain planar. Some post-Hartree–Fock correlation-gradient calculations, MP2/6-31G* (frozen-core), were done for the planar and perpendicular conformations. The relative energies at various θ values were fit to

$$V(\theta) = \Sigma_n V_n \sin^2 (n\theta/2)$$

where n is the foldedness of the term contributing to the internal rotational potential. Expectation values at 300 K of $\sin^2\theta$ were calculated from these potentials.

Results and discussion

Spectral analyses

Analyses of the ^{1}H nmr spectra employed the program NUMARIT (21), rather extensively reworked by R. Sebastian and renamed NUMMRIT. The spectra were treated as arising from ABB'CC'XY_2 spin systems. A satisfactory fit to the methylene proton (Y_2) region could not be had in the absence of a *positive* dipolar coupling between them. Table 1 presents the spectral parameters. The finite dipolar coupling means that the phenylallene molecules are partially aligned in the field, B_0. In the planar conformation the interproton vector of the methylene group lies perpendicular to the molecular plane. Because of the sign of the diamagnetic anisotropy of the mol-

[2] An explanation of the notation and the meaning of the basis sets, and a description of the MP2 approximation to electron correlation, can be found in ref. 20.

Can. J. Chem. Downloaded from www.nrcresearchpress.com by 80.90.12.36 on 09/08/12
For personal use only.

Table 1. The ^{1}H nmr spectral parameters for phenylallene at 300 MHz and 300 K in acetone-d_6 and benzene-d_6 solutions.

	Solvent			Solvent	
Parameter	Acetone-d_6[a]	Benzene-d_6[b]	Parameter	Acetone-d_6[a]	Benzene-d_6[b]
$\nu_2 = \nu_6$	2193.069[c,d]	2164.446	$^4J_{2\alpha} = {}^4J_{6\alpha}$	−0.376[e]	−0.380
$\nu_3 = \nu_5$	2192.251	2133.865	$^5J_{3\alpha} = {}^5J_{5\alpha}$	0.282[e]	0.286
ν_4	2158.755	2101.517	$^6J_{4\alpha}$	−0.213	−0.211
ν_α	1875.078	1813.465	$^6J_{2\gamma} = {}^6J_{6\gamma}$	−0.583[e]	−0.579
ν_γ	1550.259	1458.000	$^7J_{3\gamma} = {}^7J_{5\gamma}$	0.207[e]	0.205
$^3J_{23} = {}^3J_{56}$	7.779	7.777	$^8J_{4\gamma}$	−0.610	−0.604
$^3J_{34} = {}^3J_{45}$	7.470[f]	7.442	$^2D_{\gamma\gamma}$	+0.012[g]	+0.015
$^4J_{24} = {}^4J_{46}$	1.214(2)[f]	1.243	Calculated transitions	826	826
$^4J_{26}$	1.914(2)	1.903	Assigned transitions	622	617
$^4J_{35}$	1.427(2)	1.433	Peaks observed	320	405
$^5J_{25} = {}^5J_{36}$	0.609	0.605	Largest difference	0.017	0.011
$^4J_{\alpha\gamma}$	−6.856	−6.811	Root-mean-square deviation	0.008	0.005

[a]As a 5.1 mol% solution in acetone-d_6, containing also 0.5 mol% TMS.
[b]As a 5.1 mol% solution in benzene-d_6, containing also 0.5 mol% TMS.
[c]In Hz at 300.137, MHz to high frequency of internal TMS.
[d]Unless otherwise noted, the standard deviations are ≤0.001 Hz.
[e]These parameters are correlated by 0.55.
[f]These parameters are correlated by 0.88.
[g]The dipolar coupling is positive.

Fig. 1. The ^{1}H nmr spectrum of the methylene protons at 300 MHz and 300 K for a 5.1 mol% solution of phenylallene benzene-d_6 is shown at the bottom of the figure. At the top the best theoretical spectrum is shown in the absence of a dipolar coupling constant between these protons; the rest of the ^{1}H nmr spectrum, containing transitions from the α and the phenyl protons, agrees well with experiment. The middle spectrum has the dipolar coupling constant for the methylene protons as +0.0150(4) Hz. A negative sign, relative to those of the spin–spin coupling constants involving these protons, did not allow a fit of theory to experiment.

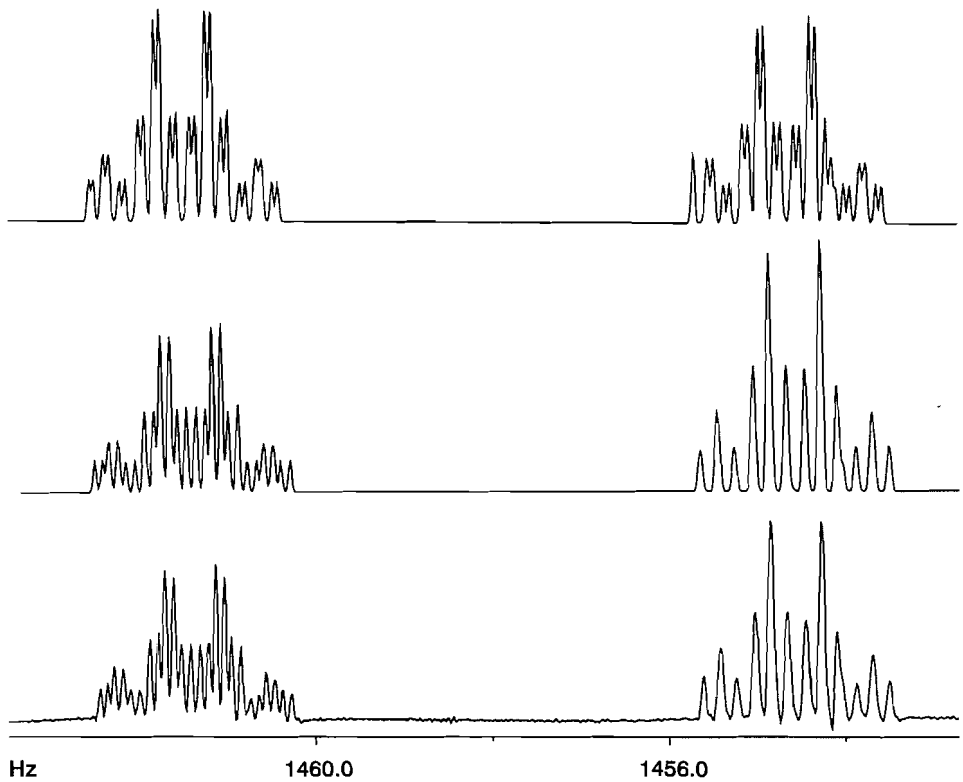

Can. J. Chem. Downloaded from www.nrcresearchpress.com by 80.90.12.36 on 09/08/12
For personal use only.

Fig. 2. The ^{1}H nmr spectra, experimental and theoretical, are shown for the phenyl protons of phenylallene as a 5.1 mol% solution in acetone-d_6 (300 MHz and 300 K). The *para* protons resonate at 2158.75 Hz to high frequency of internal TMS. The *ortho* and *meta* protons differ in their chemical shifts by 0.82 Hz (0.0027 ppm). In consequence, their spectrum is dominated by two bands of peaks separated by roughly 4.3 Hz, the average of the coupling constants between the *para* proton and the *ortho* and *meta* protons (in Table 1, $^3J_{34} + {}^4J_{24}$ is 8.68 Hz). Some of the weak peaks in the *para* region are obscured by noise in this spectrum; they do exist.

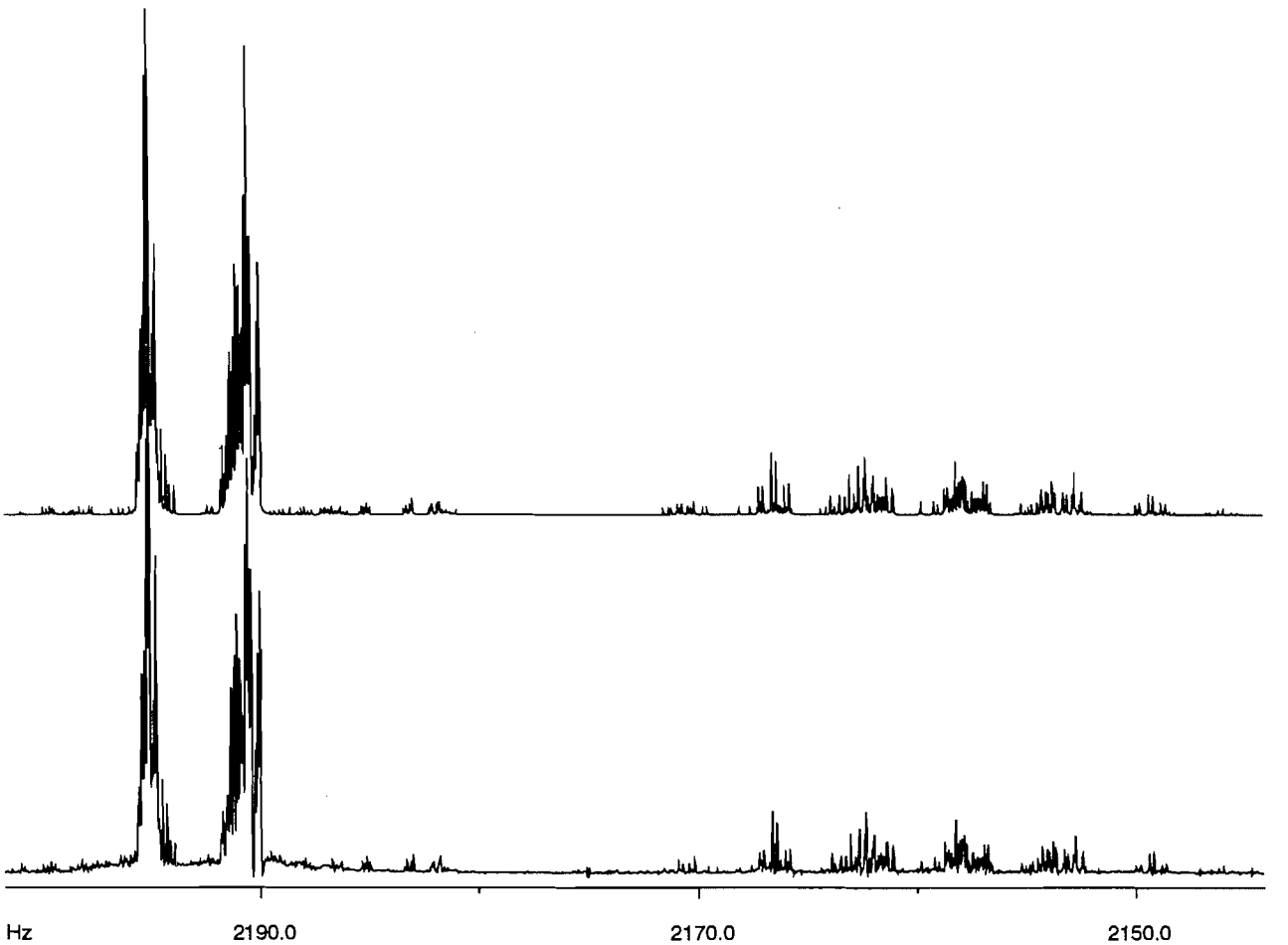

ecule and because $\langle \sin^2\theta \rangle$ is about 0.1 (see below), a positive dipolar coupling constant is indeed anticipated (22, 23). Figure 1 illustrates the spectral consequences.

The dipolar coupling constant is +0.0124(5) in acetone-d_6 and +0.0150(4) Hz in benzene-d_6 solution. It cannot be concluded that either the alignments or the internal barriers differ in the two solutions.[3] Because the magnitudes of the dipolar coupling constants drop off as the cube of the internuclear distance, one may conclude that the three-bond, or *ortho*, coupling constants in Table 1 are uncertain to within about 0.003 Hz. Similarly, introduction of a dipolar coupling between the α and *ortho* protons did not improve the spectral fits. Because, in addition, proton–proton coupling constants within a phenyl group are solvent dependent,[4] this dependence being rather

[3] At 500 MHz one should have 0.033 and 0.042 Hz for the dipolar coupling constants at 300 K, still rather small. A procedure designed to obtain the alignment factors and the diamagnetic anisotropy, independently of the complications due to internal rotation, would involve deuteration at, say, the *para* position of the phenyl ring (22, 23).

[4] This fact has been documented for a wide variety of benzene derivatives in this laboratory. The pattern of the solvent dependencies in Table 1 is the same as in the other molecules; $^4J_{24}$ *decreases* in the more polar solvent, for example.

Table 2. Some ^nJ(H, ^{13}C) values for phenylallene, **1**

	^{13}C nucleus		
Proton	C-α[a]	C-β[b]	C-γ[c]
H-4[d,e]	0.91[5]	(−)0.42[6,f]	0.28[7]
H-3, H-5	0.80[4]	(+)0.22[5,f]	(−)0.04 ± 0.02[6]
H-2, H-6	5.36[3]	(−)0.62[4,f]	0.43[5]
H_α	162.53(158.65)[1,g]	−3.45(−3.27)[2]	7.18(6.99)[3]
H_γ	8.16(8.08)[3]	−4.46(−4.46)[2]	168.23(167.25)[1]

[a] At 94.391 (94.273) ppm with respect to internal TMS in benzene-d_6 (acetone-d_6).

[b] At 209.868 (210.404) ppm.

[c] At 78.605 (78.887) ppm.

[d] Superscripts indicate the number of intervening bonds between the nuclei; numbers in parentheses refer to acetone-d_6 solutions.

[e] Unless otherwise noted, standard deviations, as given by spectral analyses, were less than 0.01 Hz.

[f] In acetone-d_6 solution, in which the *ortho* and *meta* protons have almost identical chemical shifts (Table 1), the spectral consequences of virtual coupling show that ^4J(C-β, H-2) and ^5J(C-β, H-3) have opposite signs.

[g] The signs of $^{1,2,3}J$(H,C) within the allenyl moiety are known (52).

Can. J. Chem. Downloaded from www.nrcresearchpress.com by 80.90.12.36 on 09/08/12
For personal use only.

Table 3. The theoretical conformational energies of phenylallene in kJ/mol.

θ(deg)	0	STO-3G[a]	6-31G	6-31G*	6-31G**	MP2/6-31G*
0	0.00	0.00	0.00	0.00	0.00	0.00[b]
15	0.38	1.13	0.87	0.79	0.78	—
30	1.52	4.38	3.44	3.15	3.13	—
45	3.31	9.25	7.43	6.86	6.84	—
60	5.28	14.54	11.98	11.15	11.12	—
75	6.81	18.67	15.70	14.69	14.66	—
90	7.42	20.29	17.21	16.16	16.12	16.04[b]

[a]The total computed energies for the planar (θ = 0) conformer with the STO-3G to MP2/6-31G* bases were −341.182 752, −345.295 485, −345.414 641, −345.429 114, and −346.543 821 au, in that order.

[b]These represent correlation-gradient (optimization of geometry in the post-Hartree–Fock procedure) calculations.

Table 4. Comparisons of the theoretical components of the internal rotational potentials for styrene, **2**, and phenylallene, **1**.

Component (kJ/mol)	AM1	STO-3G		6-31G		6-31G*		6-31G**
	1[a]	**1**	**2**[b]	**1**	**2**[c]	**1**	**2**[d]	**1**
V_2	7.42(1)	20.26(2)	16.28(8)	17.16(3)	13.19(15)	16.07(5)	12.02(1)	16.06(5)
V_4	−0.41(1)	−0.88(2)	−3.00(7)	−1.15(3)	−3.18(15)	−1.22(5)	−3.13(1)	−1.20(5)

[a]An AM1 value for the height of the potential for styrene (24) is 6.07 kJ/mol.

[b]Reference 5.

[c]Reference 10.

[d]Reference 6. A slightly better fit is obtained if a V_6 of −0.1 kJ/mol is included in the fit.

larger (Table 1) than the expected dipolar coupling constants, and because they are not germane to the aims of this paper, this matter was not investigated further.

The chemical shifts of the *ortho* and *meta* protons of phenylallene differ by only 0.82 Hz in the acetone-d_6 solution. In consequence, the spectral pattern of the ring protons is at first confusing and, to our knowledge, of a kind not available in the literature. Figure 2 therefore displays the computed and measured ring proton spectra for the acetone-d_6 solution.

Some ^{13}C nmr data for the allenic group are shown in Table 2. The signs of the coupling constants within the side chain involving the ring protons are based on theory or analogous compounds.

The theoretical internal rotational potential of 1

The theoretical energies, employing various basis sets, are reproduced in Table 3 for various values of the torsion angle, θ. The twofold and fourfold components of the internal rotational potential, derived from these energies, are given in Table 4, in which comparisons are made with similar values for styrene. It has been recommended (24) that AM1 potential heights for styrene and similar molecules be scaled by a factor of 1.9 ± 0.25; the value for phenylallene is then 14.1 ± 1.9 kJ/mol. This value will not be discussed further, except to note that it comes close to 16.0 kJ/mol, as obtained from the MP2/6-31G* (frozen core) approach, a correlation-gradient calculation.

For styrene, **2**, the experimental barrier height is either 12.8(1) kJ/mol, based on supersonic jet fluorescence spectroscopy (1), or 13.8(2) kJ/mol, as obtained from microwave spectroscopy (2). In Table 4 it can be seen that the 6-31G value, at 13.2 kJ/mol, agrees best with these values whereas a larger basis set, 6-31G*, gives a lower barrier.[5] From the viewpoint of the unknown barrier in phenylallene, it is interesting, first, that each basis set yields a barrier higher by very close to 4.0 kJ/mol than for styrene and, second, that the first approximation to electron correlation energies, MP2/6-31G*, does not alter the computed barrier.[6] This difference of 4.0 kJ/mol is here taken as a first estimate of the destabilization of the planar form of styrene due to the steric repulsion between the *ortho* and β-*cis* C—H bonds (see **2**). A trial potential energy curve which included a term in $E_s \cos^{12}\theta$, and used to fit the deuterium quadrupolar splitting of styrene-α-*d*, itself partially oriented in a magnetic field, suggested that E_s, the steric repulsion energy, was probably less than 4.2 kJ/mol (4).

Figures 3 and 4 give the MP2/6-31G* structure of the planar and perpendicular forms of phenylallene, probably of use to molecular spectroscopists. According to the potentials in Table 4, the expectation values of $\langle\cos^2\theta\rangle$ at 300 K are 0.90 and

[5] A post-Hartree–Fock computation (6) for styrene, MP4(SDQ)/6-31G//HG/6-31G, has the barrier height as only 10.4 kJ/mol. For differing views about the basis set dependence of computed barriers in benzene derivatives, and the reliability of various approaches to accounting for electron correlation, see refs. 25 and 26.

[6] For styrene the MP2/6-31G* barrier is 1.1 kJ/mol lower than the 6-31G* barrier (6).

Can. J. Chem. Downloaded from www.nrcresearchpress.com by 80.90.12.36 on 09/08/12
For personal use only.

Table 5. INDO MO FPT computations of ^nJ(H,H) and ^nJ(H,C) in Hz in phenylallene. $\theta = 0$ corresponds to a planar molecule.

Coupling constant[a]	A	$B(\sin^2\theta)$	$C(\cos^2\theta)$	$D(\sin^2(\theta/2))$	Factors[b]
^6J(H-4, H-α)≡$^6J_{4\alpha}$	—	−1.01	−0.23	—	0.69
^5J(H-4, C-α)	1.23	−0.33	—	—	0.76
^5J(H-3, H-α)≡$^5J_{3\alpha}$	—	0.36	0.25	0.81	0.42
^4J(H-3, C-α)	0.71	—	−0.13	−0.17	—
^4J(H-2, H-α)≡$^4J_{2\alpha}$	—	−1.22	−0.50	−0.19	—
^3J(H-2, C-α)	4.55	—	0.77	1.05	—
^6J(H-4, C-β)	—	−0.47	−0.66	—	0.66
^5J(H-3, C-β)	—	0.34	0.42	0.45	—
^4J(H-2, C-β)	—	−0.62	−0.77	−0.26	0.68
^8J(H-4, H-γ)≡$^8J_{4\gamma}$	—	−0.06	−0.79	—	0.85
^7J(H-4, C-γ)	—	0.05	0.52	—	0.59
^7J(H-3, H-γ)≡$^7J_{3\gamma}$	—	0.36	0.52	—	0.41
^6J(H-3, C-γ)	—	−0.18	−0.31	0.10	—
^6J(H-2, H-γ)≡$^6J_{2\gamma}$	—	−0.39	−0.96	—	0.64
^5J(H-2, C-γ)	—	0.36	0.66	0.06	0.65

[a]The 6-31G** geometries were used for ^nJ(H,H) and 6-31G geometries for ^nJ(H,C); this will not alter the qualitative functional relationships presented here, while only semiquantitative agreement of the coefficients, *A–D*, with experiment would be anticipated at best.

[b]The factor by which the ^nJ from theory has to be multiplied in order to reproduce experiment; it is assumed that $\langle\sin^2\theta\rangle$ is 0.103 and that the internal rotational potential is evenfold, so that $(\sin^2(\theta/2))$ is 0.5. It is notorious that INDO MO FPT computations overestimate σ-electron contributions, particularly for possible all-*trans* pathways; in such situations the factor will be smaller than in others (compare $^5J_{3\alpha}$ and $^8J_{4\gamma}$, for example).

Can. J. Chem. Downloaded from www.nrcresearchpress.com by 80.90.12.36 on 09/08/12
For personal use only.

0.83 for **1** and **2**, respectively, at the 6-31G level of theory, implying somewhat lower conjugation in the latter. The chemical shifts of the C-4 nuclei,[7] often taken (9) as indicative of the extent of π-electron transfer, are, respectively, 128.5, 126.6, and 127.6 ppm for benzene, **1**, and **2** (9). As expected from the $\langle\cos^2\theta\rangle$ values, unity corresponding to most effective π overlap, the allenyl group transfers slightly more electron density to the phenyl moiety than does the vinyl fragment. The argument is, not that allenyl is a better intrinsic π donor than vinyl, but that the steric forces, which act conformationally to somewhat inhibit π conjugation in styrene, are absent in phenylallene. The *para* protons in **1** are also somewhat more shielded, by 0.03 ppm, than those in **2**, in acetone-d_6 solution. However, the shift for **2** was measured at a concentration of 16 mol% (28), that for **1** at 5.1 mol%.

Long-range coupling constants, ^nJ(H,H)

INDO MO FPT computations (29–31) yielded ^nJ(H,H) as a function of the torsion angle and were fit to plausible functions of this angle, as summarized in Table 5. In all the functional relationships discussed below, the units of ^nJ are Hz.

(a) The γ protons

Theoretically, $^8J_{4\gamma} = -0.79(1) + 0.73(3)\sin^2\theta$, or, equivalently, $-0.06\sin^2\theta - 0.79\cos^2\theta$ and strongly implies the π-electron-mediated coupling mechanism indicated in **A**. In **A**, the benzene plane lies perpendicular to the page, so that its $2p\pi$ orbitals are oriented in the plane of the page. Therefore, in the planar conformer of **1**, the methylene plane is also parallel to the page. A crossed arrow indicates the spin state of the proton. The usual σ–π spin polarization mechanism, defined by a negative hyperfine interactive parameter, Q^{H}CH, leads to the parallel orientation of the π electron at C-4. The electron spin correlation along the extended π-electron system yields the indicated spin state at C-β. Another σ–π, or hyperconjugative, interaction involving the γ-proton and defined by the positive hyperfine interaction parameter, Q^{H}CCH, then leads to the spin state of the γ proton. Hence the two protons possess parallel spin states, defining a negative $^8J_{4\gamma}$.

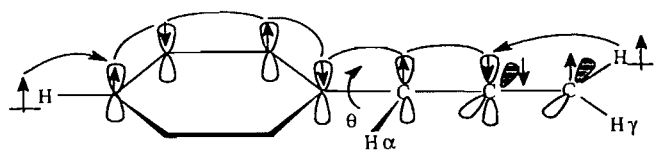

A

As θ increases from zero, as in **A**, the π-electron spin correlation decreases and disappears at $\theta = 90°$. The computed θ dependence of ^8J agrees with this model. The semiempirical, INDO MO FPT, computational scheme predicts the qualitative conformational dependence of long-range coupling constants rather well (32), particularly for pure π-electron mechanisms, but is not expected, in general, to provide quantitative results. One approach to a calibration of the computations, for the present molecule, is to compare the measured $^4J_{\alpha\gamma}$, also a π-electron coupling constant (17), with the computed number. These are -6.8_3 and -8.0 Hz, respectively, the ratio being 0.85. Reduction of the computed ^8J values by this factor[8] leads to $^8J_{4\gamma} = -0.67(1) + 0.62(2)\sin^2\theta$. This equation

[7] Reference 9 does not appear to give the ^{13}C nmr chemical shifts for **1**, although they are quoted in ref. 27 as coming from the former.

Can. J. Chem. Downloaded from www.nrcresearchpress.com by 80.90.12.36 on 09/08/12
For personal use only.

predicts $\langle \sin^2\theta \rangle$ as 0.102(4) at 300 K, based on an $^8J_{4\gamma}$ of −0.607 Hz (Table 1).

It so happens that this expectation value agrees exactly with those computed from the 6-31G* or 6-31G** potentials (Table 4). It is also true that $^8J_{4\gamma}$ is essentially the same in the two solvents. Naturally, it does not follow that the internal rotational potential of phenylallene is independent of solvent. Yet, this certainly appears to be true for ethylbenzene[9] in a variety of solvents (34). The spin–spin coupling constants of styrene and a number of its derivatives have been interpreted (3, 11) on the basis of such an independence, although a contrary conclusion was reached (4) from partially averaged quadrupolar coupling constants in deutero derivatives of styrene. The simplest assumption at present, consistent with the available evidence, is that the internal potential in phenylallene is not affected by the present solvents. The ensuing discussion of other coupling constants makes this assumption.

$^7J_{3\gamma} = {}^7J_{5\gamma} \equiv {}^7J$ is 0.206 Hz. It is unlikely (33) that this coupling constant is transmitted by other than the π-electron mechanism discussed for $^8J_{4\gamma}$. The sign can be understood from the spin orientations in structure **A**, the smaller magnitude than that of $^8J_{4\gamma}$ from the notion that spin correlation for atoms belonging to different classes (starred, unstarred) is larger in magnitude than between atoms of the same class (37, 38). A suggestive set of numbers is the Hückel bond orders, being 0.667 for *ortho*, −0.333 for *para*, and zero for *meta*, carbon atoms in benzene. The INDO MO FPT results for $^7J_{3\gamma}$ do not seem sensible, given by $0.52\cos^2\theta + 0.36\sin^2\theta$ and leading to a value of 0.36 Hz in the perpendicular conformer. One expects $^7J_{3\gamma}$ to become very small, that is, to vanish essentially at $\theta = 90°$. A derivative of **1** with a very large average θ is needed to confirm this expectation.

In terms of the present model, $^7J_{3\gamma}/^8J_{4\gamma} = -0.34$ is a measure of the ratio of the π-electron contributions, at *meta* and *para* sites, to coupling constants involving nuclei in the side chain of benzene derivatives. There has been uncertainty about this ratio, for example, in toluene (39) and other alkyl benzene derivatives (40). Because, say, ^5J(H, CH) in such compounds has a stereospecific σ-electron component (39, 41), subtraction of a known π-electron component from the measured value would increase the precision with which conformational populations could be deduced.

As to $^6J_{2\gamma}$, its striking aspect is the near equality with $^8J_{4\gamma}$; the former is −0.581(3) Hz, the latter, −0.607(4) Hz (the numbers are averages for the two solutions). The implication, that the π-electron contributions to these coupling constants are effectively equal, is unexpected from the viewpoint of bond orders available from molecular orbital theory (42–45), where J is proportional to the square of a mobile bond order.

[8] Of course, this approach does not take into account any computational errors at the C-4 site nor the computation of the π-electron spin correlation at the C-1, C-α sites. However, judging by similar computations for $^7J_{4\beta}$ in styrene, also a pure π-electron coupling constant (33), and the rather good agreement with the available experimental data (3, 28, 33), this calibration is reasonable.

[9] The internal rotational potential in the relatively polar molecule, benzyl fluoride, changes by 2 kJ/mol in passing from CS_2 to acetone-d_6 solution (35); its dipole moment is 1.77 D in benzene solution (36). The computed dipole moments for phenylallene are 0.078 D for the planar and 0.076 D for the perpendicular conformers (6-31G**).

Fig. 3. The MP2/6-31G* (frozen-core) structure of the planar conformer of phenylallene may well be of interest to molecular spectroscopists. The computed rotational constants are 4.579 23, 0.993 14, and 0.820 72 GHz at the equilibrium geometry. The height of the internal rotational barrier is calculated as 16.0 kJ/mol, so that this structure is presumably somewhat more to the point than that of the perpendicular structure in Fig. 4. A high-level computed structure for allene is available (63), as is an MP2/6-31G* structure (64). The latter has a C=C length of 1.313 Å (experiment, 1.308 Å). Comparison with the MP2/6-31G* structure above for phenylallene suggests a slight lengthening of the Cα—Cβ bond, implying some delocalization into the C1—Cα bond.

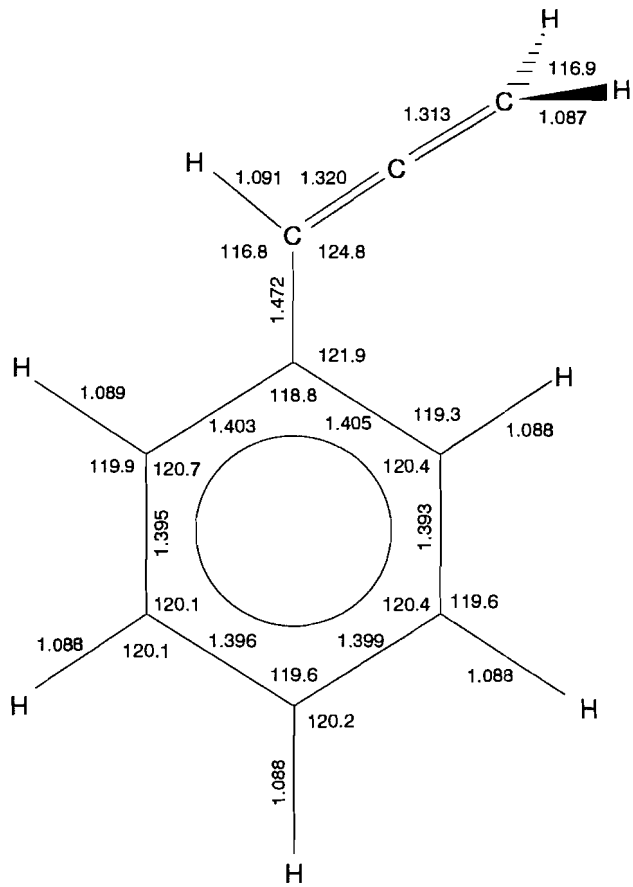

However, in various formulations based on valence bond theory (37, 43), J is proportional to a bond order, variously defined (43, 45). Some formulations (46) yield nearly equal contributions of the π-electrons to the coupling constants between *ortho* and between *para* protons in benzene. While it is perhaps unexpected that spin correlation between *para* sites is comparable to that between *ortho* sites, it may be noted that $^8J_{4\gamma}$ has two coupling pathways via the aromatic π-electron systems, $^6J_{2\gamma}$ only one.[10]

The INDO MO FPT computation yields $^6J_{2\gamma} = -0.96\cos^2\theta - 0.39\sin^2\theta$. After reduction by a factor of 0.85, as for $^8J_{4\gamma}$, this result implies a $^6J_{2\gamma}$ of −0.33 Hz in the perpendicular conformer, inexplicable in the present model in the absence of an

[10] It is amusing that the ratio of the magnitudes of the Coulson (Hückel) bond orders for *para* and *ortho* sites is one-half; there exists no theoretical justification, however, for a proportionality of J^π to the magnitude of the Hückel bond order.

Fig. 4. The MP2/6-31G* structure of the *perpendicular* conformer of phenylallene. There are some significant predicted changes in bond angles at the first exocyclic carbon atom (see Fig. 3). The exocyclic Csp^2–Csp^2 bond length has lengthened by nearly 0.02 Å. The computed rotational constants are 4.182 14, 0.967 747, and 0.867 967 GHz. Note that the side chain is not drawn in projection, it being more convenient to indicate bond parameters in the structure as drawn.

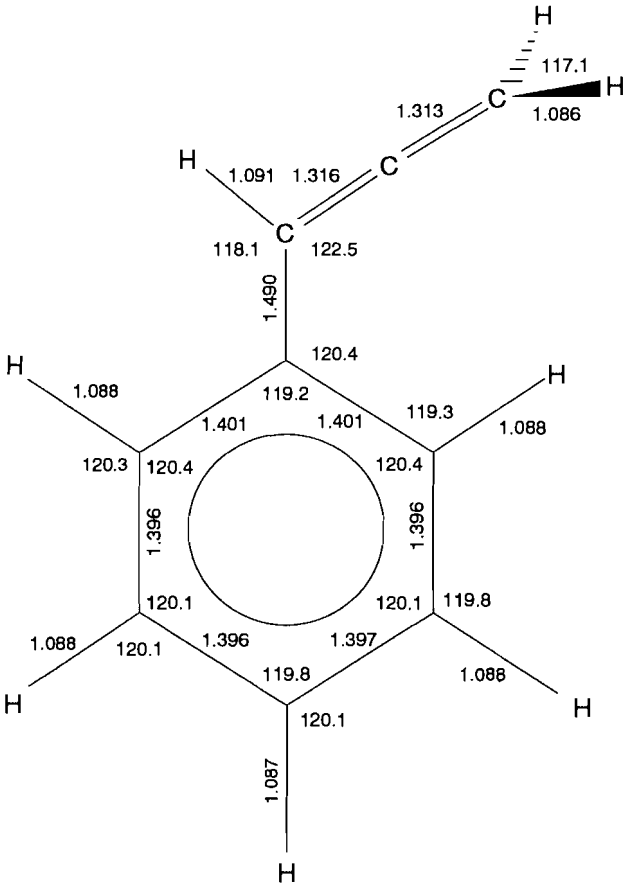

additional mechanism operative at $\theta = 90°$. A similar situation holds for ^5J(H-2, C-γ) below.

(b) The α proton

The coupling constant, $^6J_{4\alpha}$, in styrene consists of two components, one due to a π-electron mechanism analogous to the one in **A** and the other arising from a σ,π mechanism. The former depends on $\cos^2\theta$, the latter on $\sin^2\theta$ (33). One formulation (3) has $^6J_{4\alpha} = -0.149\cos^2\theta - 0.597\sin^2\theta$, another (47) yields $-0.130\cos^2\theta - 0.800\sin^2\theta$. On the assumption that $\langle\sin^2\theta\rangle$ is 0.103 for phenylallene, the first equation would yield $^6J_{4\alpha}$ in this molecule as −0.195 Hz, the second as −0.199 Hz. The experimental value is −0.212(2) Hz (Table 1). The INDO MO FPT//6-31G** computations for phenylallene give $^6J_{4\alpha} = -0.228(1)\cos^2\theta - 1.009(1)\sin^2\theta$, an overestimate of the magnitudes, as also found for styrene (3). Reduction of both terms by a factor of 0.69 would produce agreement with a $\langle\sin^2\theta\rangle$ of 0.103, that is $^6J_{4\alpha} = -0.157(1)\cos^2\theta - 0.696(1)\sin^2\theta$.

Turning to $^5J_{3\alpha}$, one may note that INDO MO FPT methods are notorious for an overestimation of the σ-electron component of such coupling constants, toluene (39, 41) and benzaldehyde (48) being only two examples. Indeed, for phenylallene, the INDO MO FPT//6-31G** expression is $^5J_{3\alpha} = 0.25\cos^2\theta + 0.36\sin^2\theta + 0.81\sin^2(\theta/2)$. For an evenfold potential, $\langle\sin^2(\theta/2)\rangle$ is 0.5, so that $^5J_{3\alpha}$ is computed as 0.67 Hz, in contrast to the measured value of 0.284(2) Hz. For benzaldehyde and toluene derivatives there is evidence (49, 50) that ^5J effectively vanishes at $\theta = 0°$ (not an all-*trans* pathway). An empirical expression for $^5J_{3\alpha}$ can be developed as follows. The π- and σ,π-electron contributions at $\theta = 0°$ are taken as 34% (see the discussion of plain58$J_{4\gamma}$ and $^7J_{3\gamma}$) of those assessed above for $^6J_{4\alpha}$, that is, 0.053 and 0.237 Hz, respectively. Together with the experimental value of $^5J_{3\alpha}$, one then has $^5J_{3\alpha} = 0.05\cos^2\theta + 0.24\sin^2\theta + 0.42\sin^2\theta/2$, an expression more likely to correspond to reality than that found theoretically. One might argue that, because ^5J in benzaldehyde vanishes at $\theta = 0°$, also for an sp^2 carbon atom in the side chain, so should ^5J in phenylallene. However, ^6J in benzaldehyde is undetectable (51), corresponding to the large internal barrier, and implying a negligible π component also of ^5J, that is, at $\theta = 0°$.

Finally $^4J_{2\alpha} = -0.50(8)\cos^2\theta - 1.22(1)\sin^2\theta - 0.19(1)\sin^2(\theta/2)$, theoretically. The experimental value is −0.378(3) Hz. An empirical procedure, based on the behaviour of $^{6,8}J_\gamma$ and $^6J_{4\alpha}$, yields $^4J_{2\alpha} = -0.16\cos^2\theta - 0.70\sin^2\theta - 0.32\sin^2(\theta/2)$.

A test of all these empirical relationships would require a derivative characterized by a large effective torsion angle.

The dipolar coupling constant, $D_{\gamma\gamma}$

At a torsion angle, θ, of zero, $D_{\gamma\gamma}$ must be positive, as follows (22, 23) from the known partial alignment of aromatic molecules in the magnetic field of the spectrometer. If the anisotropy of the diamagnetic susceptibility were known, as well as the proton, proton distance in the methylene group in phenylallene, $D_{\gamma\gamma}$ could be related to the torsional potential: $D_{\gamma\gamma}$ must be negative for the perpendicular conformer ($\theta = 90°$). If the calculated torsional potential is correct and if the molecule orients in the same way as benzene, then the signs of $^{6,7,8}J_\gamma$ given in Table 1 are absolute and independent of the sign determinations described above.

Some $^nJ(^1H, ^{13}C)$ for phenylallene

Table 2 contains the $^nJ(^1H, ^{13}C)$ values accessible by analysis of the ^{13}C nmr spectral of **1**, mainly in benzene-d_6 solution.

(a) $^nJ(H,C)$ within the side chain

One striking fact is the *decrease* in ^1J(H,C) in passing from benzene-d_6 to acetone-d_6 solution.[11] The decrease is 3.9 Hz for ^1J(H,C-α) and 1.0 Hz for ^1J(H,C-γ). In most cases[12] an increase is observed (53, 54) in passing to the more polar environment, as predicted by models in which the electric field from the solvent causes a redistribution of charge in the whole molecule carrying the C—H bond (53). If the charge redistri-

[11] For the neat compound, containing also 10% v/v benzene-d_6 and 5% v/v TMS, ^1J(H,C-α) is 161.5(3) Hz (52). Reference 52 collects all available ^nJ(H,C) values within the allenyl group for numerous allenes and also points out discrepancies of sign and magnitude for earlier data.

[12] For example, for the olefinic protons in 1,3-dioxole, ^1J(H,C) increases when moving from benzene-d_6 to acetone-d_6 solution (55).

Can. J. Chem. Downloaded from www.nrcresearchpress.com by 80.90.12.36 on 09/08/12
For personal use only.

Can. J. Chem. Downloaded from www.nrcresearchpress.com by 80.90.12.36 on 09/08/12
For personal use only.

bution is confined to the C—H bond, then a decrease is indeed calculated (53). Why this should be true for the allenyl moiety is unknown and needs further study for a number of its derivatives. ^1J(H,C) in such compounds has been correlated with dual substituent parameters (56).

Solvent perturbations of ^2J(H,C) and ^3J(H,C) have not been reported previously; they amount to a few percent in Table 2.

(b) $^nJ(^1H, ^{13}C)$*, ring protons to side chain* ^{13}C *nuclei*

(i) The para *proton coupling constants*: Consider first the coupling constants involving the *para* proton, $^{5,6,7}J$(H-4,C). ^5J(H,C-α) is 0.91 Hz; its computed dependence on θ can be written as $1.23 - 0.33 \sin^2\theta$, and is larger than the +0.65 Hz measured (57) for the corresponding coupling constant in toluene and the 0.5 Hz reported for benzoic acid (58). The coupling constant in toluene has been interpreted as a σ–π interaction, proportional to $Q^{H}CHQ^{C}CC$. Both hyperfine interactions are negative and refer to π-electron spin densities on the contiguous aromatic carbon atoms (57). In **1**, C-α is sp^2 hybridized, so that an additional hyperfine interaction comes from π spin density on C-α (see structure **A**). This contribution can be thought of as involving parameters describing the polarization of orbitals, containing *s* character and centered on C-α, by the π density on C-α (59). The net result is a negative contribution to ^5J(H-4, C-α). As θ increases from 0° to 90°, the INDO computations indicate a decrease of 0.33 Hz, corresponding to cessation of spin correlation between the π-electrons on C-1 and C-α. The INDO MO FPT numbers are again too large, apparently. Taking $\langle\sin^2\theta\rangle$ as 0.103, as in the discussion of the proton–proton coupling constants, together with the requirement that theory fit experiment, leads to $0.94 - 0.25 \sin^2\theta$ for the coupling constant. Of course, this relationship assumes that theory overestimates both contributions by the same factor; this is not known.

As to ^6J(H-4, C-β), the computed numbers are reproduced by $-0.47 \sin^2\theta - 0.66 \cos^2\theta$, written in this way to emphasize the possible π-electron and σ,π-electron (hyperconjugative) components. The demand, as above, that the coefficients lead to agreement with the measurement of (−)0.42 Hz, leads to the expression, $^6J = -0.31 \sin^2\theta - 0.43 \cos^2\theta$. If true, then the σ,π hyperfine parameter, $Q^{C}CCCsp > 0$, and proportional to $\sin^2\theta$, is 0.44 of the magnitude of the σ,π hyperfine parameter, $Q^{H}CCH$, characterizing $^6J_{4\alpha}$ in a previous section. The π-electron contribution, the term in $\cos^2\theta$, should decrease more than the σ,π term as θ takes on large values.

^7J(H-4, C-γ) is 0.28 Hz, which theoretically follows $0.52 \cos^2\theta + 0.05 \sin^2\theta$, indicating a coupling constant transmitted via spin correlation in the extended system and, if the usual reduction in the theoretical parameters is applied, one has $0.31 \cos^2\theta + 0.03 \sin^2\theta$. The π-electron correlation at C-β favours their parallel orientation, as in structure **A** (Hund's rule). Hence the positive coupling constant can be thought of as being a result of the positive product, $Q^{H}CHQ^{C}CC\gamma$, which outweighs the negative contribution proportional to $Q^{H}CHQ^{C\gamma}C\gamma$. Just like ^8J(H-4, H-γ), ^7JH,C) should become very small or vanish when the π-electron conjugation between the aromatic and allenic moieties is removed at θ = 90°.

(ii) The ortho *proton coupling constants*: Turning to $^{3,4,5}J$(H,C) for the *ortho* protons, the theoretical vicinal coupling constant ^3J(H-2, C-α) is given by $4.55 + 0.77 \cos^2\theta + 1.05 \sin^2(\theta/2)$. The theoretical expression suggests a π-electron contribution of about 0.77 Hz and a θ-dependent substituent effect from C-β. For an evenfold potential, $\langle\sin^2(\theta/2)\rangle = 0.5$, and with a $\langle\sin^2\theta\rangle$ of 0.103 one has ^3J(H,C) as 5.76 Hz, whereas the measured value is 5.36 Hz. In toluene, ^3J(H,C) is 4.62 Hz (57). At least part of the higher magnitude in **1** may be attributed to a π-electron contribution via the partial double bond between C-1 and C-α, the term in $\cos^2\theta$, as well as the larger length of the exocyclic Csp^2—Csp^3 bond in toluene.

The INDO numbers for ^4J(H-2, C-β) are represented by $-0.63 \sin^2\theta - 0.76 \cos^2\theta - 0.26 \sin^2(\theta/2)$. Multiplication by a factor of 0.68 produces agreement with the measured −0.63(3) Hz.

For ^5J(H-2, C-γ), the INDO numbers are reproduced by $0.36 \sin^2\theta + 0.66 \cos^2\theta + 0.06 \sin^2(\theta/2)$. The term in $\cos^2\theta$ represents the transmission of spin-state information by the extended π-electron system, most effective in the planar conformation. The term in $\sin^2\theta$ is puzzling because it has a maximum in the perpendicular conformation of **1** but cannot be a β σ,π contribution of the sort involved in ^6J(H-4, C-β). Were this true, ^7J(H-4, C-γ) should also have a substantial value at φ = 90°, yet does not. The measured ^5J(H-2, C-γ) is 0.43 Hz; the theoretical expression, if multiplied by 0.65, would yield that number.

(iii) The meta *proton coupling constants*: ^4J(H-3, C-α) has a theoretical formulation, $0.71 - 0.13 \cos^2\theta - 0.17 \sin^2(\theta/2)$, implying a π-electron contribution of −0.13 Hz in the planar molecule and a negative substituent perturbation with a maximum magnitude when the C-α, C-β bond extends the all-*trans* bond arrangement. The π-electron contribution to ^4J(H,H) in benzene is −0.23(2) Hz (60). The experimental value of 0.80 Hz is larger than the 0.51 Hz predicted by theory, the only example in which this inversion occurs, and suggests that INDO underestimates the σ-electron component of ^4J(H,C) for the famous W configuration of the intervening bonds in an aromatic system.

^5J(H-3, C-β) can be written, theoretically, as $0.42 \cos^2\theta + 0.34 \sin^2\theta + 0.45 \sin^2(\theta/2)$. The first term represents the π-electron component in the extended π system in the planar form, the second term a putative σ,π component, and the last term would then account for a σ-electron contribution. This relationship predicts 0.63 Hz for ^5J(H-3, C-β), while the measured value is less than half as large. The overestimate is similar to that for ^5J(H-3, H-α).

Finally, ^6J(H-3, C-γ) computes as $-0.31 \cos^2\theta - 0.18 \sin^2\theta + 0.10 \sin^2(\theta/2)$. The positive σ-electron term, in $\sin^2(\theta/2)$, has a precedent in one of a similar magnitude predicted (33) for the all-*trans* ^6J(H-5, H-9) in styrene (see **2**) and confirmed in 3-fluorostyrene (61). However, the predicted value of ^6J(H-3, C-γ) in **1** is −0.25 Hz and is measured as ±0.04 ± 0.02 Hz. To assess which term, or perhaps all, are faulty in the theory also requires a phenylallene derivative characterized by a large θ.

^{13}C nuclear magnetic resonance chemical shifts

The ^{13}C nmr chemical shifts of the allenyl moiety in Table 2 display solvent perturbations as large as 0.54 ppm and of varying sign and are also different from those reported for a solution of **1** in $CDCl_3$ (62). Satisfactory computations of these shifts for the free molecule are now possible, judging from the results for allene (63).

Can. J. Chem. Downloaded from www.nrcresearchpress.com by 80.90.12.36 on 09/08/12
For personal use only.

Acknowledgments

This work was aided by the Natural Sciences and Engineering Research Council of Canada. The referees are thanked for helpful criticism.

References

1. J.M. Hollas, H. Musa, T. Ridley, P.H. Turner, K.H. Weisenberger, and V. Fawcett. J. Mol. Spectrosc. **94**, 437 (1982).
2. W. Caminati, B. Vogelsanger, and A. Bauder. J. Mol. Spectrosc. **128**, 384 (1988).
3. T. Schaefer, R. Sebastian, and G.H. Penner. Can. J. Chem. **66**, 584 (1988).
4. K.L. Facchine, S.W. Staley, P.C.M. van Zijl, P.K. Mishra, and A.A. Bothner-By. J. Am. Chem. Soc. **110**, 4900 (1988).
5. T. Schaefer and G.H. Penner. Chem. Phys. Lett. **114**, 526 (1985).
6. S. Tsuzuki, K. Tanabe, and E. Osawa. J. Phys. Chem. **94**, 6175 (1990), and references therein.
7. M. Head-Gordon and J.A. Pople. J. Phys. Chem. **97**, 1147 (1993).
8. R. Hargitai, P.G. Szalay, G. Pongor, and G. Fogarasi. J. Mol. Struct. (Theochem), **306**, 293 (1994).
9. D.E. Ewing. Org. Magn. Reson. **12**, 499 (1979).
10. C.W. Bock, M. Trachtman, and P. George. Chem. Phys. **93**, 431 (1985).
11. T. Schaefer and R. Sebastian. Can. J. Chem. **68**, 1383 (1990).
12. T. Schaefer, J. Peeling, G.H. Penner, A. Lemire, and R. Sebastian. Can. J. Chem. **63**, 24 (1985).
13. T.-y.R. Chen, M.R. Anderson, S. Crossman, and D.G. Peters. J. Org. Chem. **52**, 1231 (1987).
14. D.F. Evans and J.P. Maher. Proc. Chem. Soc. (London), 208 (1961).
15. E.I. Snyder and J.D. Roberts. J. Am. Chem. Soc. **84**, 1582 (1962).
16. S.L. Manatt and D.D. Elleman. J. Am. Chem. Soc. **84**, 1579 (1962).
17. M. Karplus. J. Chem. Phys. **33**, 1842 (1960).
18. M.J. Frisch, G.W. Trucks, M. Head-Gordon, P.M.W. Gill, M.W. Wong, J.B. Foresman, B.G. Johnson, H.B. Schlegel, M.A. Robb, E.S. Replogle, R. Gomperts, J.L. Andres, K. Raghavachari, J.S. Binkley, C. Gonzalez, R.L. Martin, D.J. Fox, D.J. Defrees, J. Baker, J.J.P. Stewart, and J.A. Pople. GAUSSIAN 92, Revision C. Gaussian, Inc., Pittsburg, Pa. 1992.
19. M.J. Dewar, E.G. Zoebisch, E.F. Healy, and J.J.P. Stewart. J. Am. Chem. Soc. **107**, 3902 (1985).
20. W.J. Hehre, L. Radom, P.v.R. Schleyer, and J.A. Pople. *Ab initio* molecular orbital theory. Wiley and Sons, New York. 1986.
21. J.S. Martin, A.R. Quirt, and K.E. Worvill. The NMR program library. Daresbury Laboratory, Daresbury, U.K.
22. E.W. Bastiaan, J. Bulthuis, and C. MacLean. Magn. Reson. Chem. **24**, 723 (1986).
23. E.W. Bastiaan, C. MacLean, P.C.M. van Zijl, and A.A. Bothner-By. Annu. Rep. NMR Spectrosc. **19**, 35 (1987).
24. B. Coussens, K. Pierloot, and R.J. Meier. J. Mol. Struct. (Theochem), **259**, 331 (1992).
25. R.J. Meier. J. Phys. Chem. **97**, 10248 (1993).
26. M. Head-Gordon and J.A. Pople. J. Phys. Chem. **97**, 10250 (1993).
27. E. Breitmaier and W. Voelter. Carbon-13 nmr spectroscopy. 3rd ed. VCH Publishers, New York. 1987.
28. H. Nies, H. Bauer, K. Roth, and D. Rewicki. J. Magn. Reson. **39**, 521 (1980).
29. J.A. Pople, J.W. McIver, Jr., and N.S. Ostlund. J. Chem. Phys. **49**, 2960 (1968); **49**, 2965 (1968).
30. J.A. Pople and D.L. Beveridge. Approximate molecular orbital theory. McGraw Hill Book Co., New York. 1970.
31. P.A. Dobosh and N.S. Ostlund. Quantum Chemistry Program Exchange, **11**, 281 (1975).
32. R.H. Contreras and J.C. Facelli. Annu. Rep. NMR Spectrosc. **27**, 255 (1993).
33. M. Barfield, C.J. Macdonald, I.R. Peat, and W.F. Reynolds. J. Am. Chem. Soc. **93**, 4195 (1971).
34. T. Schaefer, G.H. Penner, and R. Sebastian. Can. J. Chem. **65**, 873 (1987).
35. T. Schaefer, C. Beaulieu, R. Sebastian, and G.H. Penner. Can. J. Chem. **68**, 581 (1990).
36. M.T. Rogers. J. Am. Chem. Soc. **69**, 457 (1947).
37. H.M. McConnell. J. Chem. Phys. **30**, 126 (1959).
38. M. Barfield and B. Chakrabarti. J. Am. Chem. Soc. **91**, 4346 (1969).
39. T. Schaefer, R. Sebastian, and G.H. Penner. Can. J. Chem. **63**, 2597 (1985).
40. T. Schaefer, R. Sebastian, and G.H. Penner. Can. J. Chem. **66**, 1495 (1988).
41. R. Wasylishen and T. Schaefer. Can. J. Chem. **50**, 1852 (1972).
42. M. Barfield, C.J. Fallick, K. Hata, S. Sternhell, and P.W. Westerman. J. Am. Chem. Soc. **105**, 2178 (1983).
43. M. Barfield, M.J. Collins, J.E. Gready, S. Sternhell, and C.W. Tansey. J. Am. Chem. Soc. **111**, 4285 (1989).
44. J.E. Gready, K. Hata, S. Sternhell, and C.W. Tansey. Aust. J. Chem. **43**, 593 (1990).
45. H.M. McConnell. J. Mol. Spectrosc. **1**, 11 (1957).
46. M. Randic and X. Guo. Int. J. Quantum Chem. **49**, 215 (1994).
47. R. Laatikainen, E. Kolehmainen, T. Kuokkanen, and K. Tuppurainen. J. Magn. Reson. **78**, 9 (1988).
48. I.R. Peat and W.F. Reynolds. Can. J. Chem. **48**, 2403 (1974).
49. T. Schaefer and C.S. Takeuchi. Can. J. Chem. **67**, 1022 (1989).
50. T. Schaefer, R. Sebastian, D.M. McKinnon, P.W. Spevack, K.J. Cox, and C.S. Takeuchi. Can. J. Chem. **71**, 960 (1993).
51. T. Schaefer and C.S. Takeuchi. Can. J. Chem. **67**, 827 (1989).
52. N.J. Koole, M.J.A. de Bie, and P.E. Hansen. Org. Magn. Reson. **22**, 146 (1984).
53. M. Barfield and M.D. Johnston, Jr. Chem. Rev. **73**, 53 (1973), and references therein.
54. I. Ando and G.A. Webb. Org. Magn. Reson. **15**, 111 (1981).
55. T. Schaefer, K. Chum, D. McKinnon, and M.S. Chauhan. Can. J. Chem. **53**, 2734 (1975).
56. W. Runge. Prog. Phys. Org. Chem. **13**, 315 (1981).
57. M. Hansen and H.J. Jakobsen. J. Magn. Reson. **20**, 520 (1975).
58. J.L. Marshall and R. Seiwell. Org. Magn. Reson. **8**, 419 (1976).
59. M. Karplus and G.K. Fraenkel. J. Chem. Phys. **35**, 1312 (1961).
60. J.B. Rowbotham and T. Schaefer. Can. J. Chem. **52**, 496 (1974).
61. T. Schaefer and R. Sebastian. Can. J. Chem. **68**, 1383 (1990).
62. W. Runge and J. Firl. Ber. Bunsen-ges. Phys. Chem. **79**, 913 (1975).
63. J. Gauss. J. Chem. Phys. **99**, 3629 (1993).
64. D.W. Rogers and F. McLafferty. J. Phys. Chem. **99**, 1375 (1995).

Electrochemical and spectroscopic behavior of trifluoromethylacetophenone in aqueous and micellar medium

Elodie Liotier, Guy Mousset, and Christine Mousty

Can. J. Chem. Downloaded from www.nrcresearchpress.com by 80.90.12.36 on 09/08/12
For personal use only.

Abstract: The electrochemical behavior of 4-trifluoromethylacetophenone (TFMA) has been studied in aqueous ($2 \leq pH \leq 10$), micellar, and ethanolic solutions using polarographic techniques. A slow hydration process of the carbonyl group has been observed by means of polarography and UV–visible spectrophotometry. Besides the well-known pH dependence of the electroreduction of aromatic ketones, C—F bond cleavages concomitant to the ketone reduction occur under electrolysis conditions in alkaline medium (pH = 10) at a very negative potential (−1.7 V), leading to the formation of 4-methylacetophenone, which is reduced at this potential with formation of the carbinol and of symmetrical and dissymmetrical pinacols. Finally, the reduction of TFMA has been performed in the presence of chiral surfactants in order to test their ability to induce an asymmetric induction.

Key words: 4-trifluoromethylacetophenone, 4-methylacetophenone, electroreduction, micellar medium, chiral surfactants, hydration, C—F bond fission.

Résumé : Une étude polarographique de la 4-trifluorométhylacétophénone (TFMA) a été réalisée en milieux aqueux ($2 \leq pH \leq 10$), micellaire et éthanolique. Un phénomène d'hydratation lente de la fonction carbonyle a été mis en évidence en polarographie et en spectroscopie UV–visible. Des électrolyses préparatives ont été menées aux différents pH étudiés. Outre la formation des carbinols et pinacols diastéréoisomères attendus, une coupure des liaisons C—F concomitante à la réduction de la fonction carbonyle se produit lors de l'électrolyse en milieu basique (pH = 10) à un potentiel assez négatif (−1,7 V). La 4-méthylacétophénone est alors formée et est elle-même réductible à ce potentiel pour conduire au carbinol et à des pinacols symétriques et dissymétriques. Nous avons également réalisé la réduction de la TFMA en présence de tensioactifs chiraux afin de tester leur potentialité au niveau de l'induction asymétrique sur les produits de réduction.

Mots clés : 4-trifluorométhylacétophénone, 4-méthylacétophénone, électroréduction, milieu micellaire, agents tensioactifs chiraux, hydratation, coupure d'une liaison C—F.

Introduction

Previous papers from this laboratory have reported on the mechanism of electrochemical reduction of aromatic ketones derived from acetophenone in aqueous or in micellar medium (1, 2) and in the presence of cyclodextrins (3). In particular, the dimerization reaction leading to diastereomeric pinacols has been investigated in these media. The present work extends these studies to trifluoromethylacetophenone (TFMA).

Indeed, the presence of a CF_3 group on the aromatic ring of aromatic ketones causes a significant shift of the corresponding half-wave reduction potentiel ($E_{1/2}$) to less negative values (4), making the electrochemical study in aqueous medium easier. However, in aqueous solutions, numerous carbonyl compounds are known to be subject to complex equilibria involving hydration–dehydration of the carbonyl group and keto–enol and acid–base equilibria; these result in the formation of both geminal-diols and enols or carbanion enolates according to the pH (5–7). Moreover, the reduction of trifluoromethyl compounds in aqueous and nonaqueous solutions may also involve C—F bond fission (8–13).

In this work, both the electrochemical and spectroscopic behavior of TFMA have been investigated in various protic solvents such as aqueous, micellar, and ethanolic solutions.

Received April 3, 1995.

E. Liotier, G. Mousset, and C. Mousty.[1] Laboratoire d'électrochimie organique, thermodynamique et électrochimie en solution, Unité de recherche associée au Centre national de la recherche scientifique n° 434, Université Blaise Pascal, 24 avenue des Landais, 63177 Aubière Cédex, France.

[1] Author to whom correspondence may be addressed. Telephone: 33-73-40-71-57. Fax: 33-73-27-44-43.

Results

1. Polarographic study

pH effects

The shape of the polarograms of TFMA changes significantly over the pH range 2–10 (Fig. 1). In acidic medium (pH < 5), two successive polarographic waves (A_1 and A_2) are observed. In the pH range 2–5, the half-wave potential of the first one

Table 1. Critical micellar concentration of surfactants used.

Compound	Formula	Symbol	CMC (M)	Reference
β-*N*-Glucosyl-*N*-heptylurea	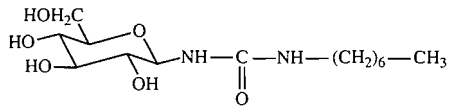	GHU	8×10^{-2}	14
2-*O*-Lauroyl saccharose	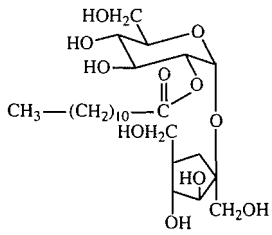	LS	7.5×10^{-4}	15
1-*S*-Octyl β-D-thioglucopyranoside	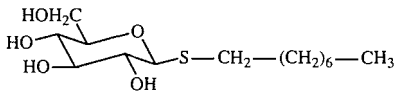	OTG	9×10^{-3}	16
Polyoxyethylene dodecyl ether	$C_{12}H_{25}$—(O—CH_2—CH_2)$_{23}$—OH	BRIJ35	6×10^{-5}	17

Can. J. Chem. Downloaded from www.nrcresearchpress.com by 80.90.12.36 on 09/08/12
For personal use only.

Fig. 1. Polarographic curves of 1×10^{-3} M TFMA recorded in different aqueous buffer solutions ($v = 4$ mV s^{-1}).

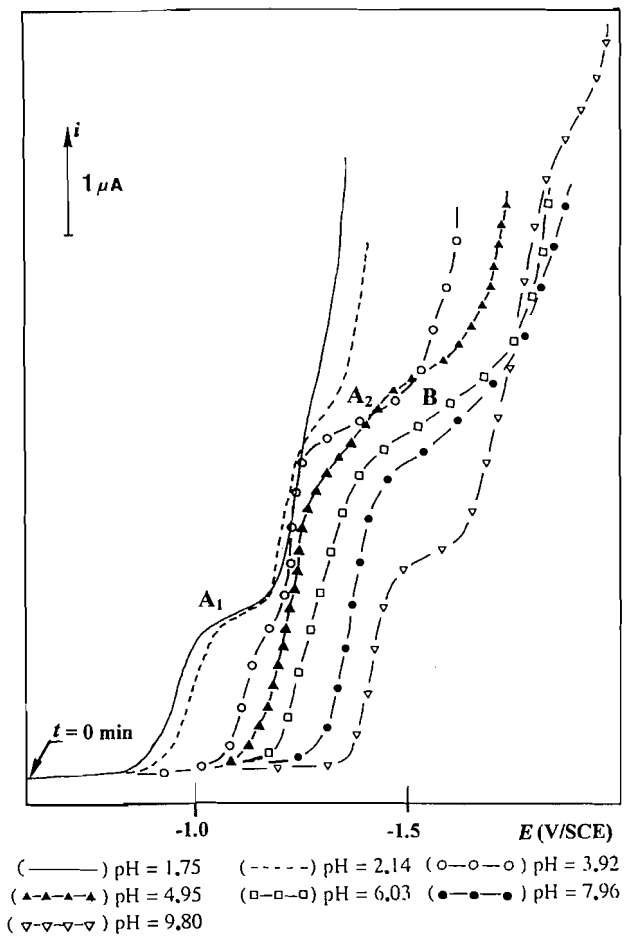

(A_1) shows a linear shift to more negative values by about 70 mV per pH unit (Fig. 2*a*). The height of the second wave A_2 is approximately equal to that of the first one and its half-wave potential ($E_{1/2} = -1.2$ V) is independent of pH from the value at which it first becomes discernible (pH 2) to the value at which it merges with the first wave (pH 5) to give a new wave B (Figs. 1, 2*a*). The half-wave potential of this wave B becomes slightly more negative as the pH is increased ($\Delta E_{1/2}$ / ΔpH $\cong$ 40 mV). Finally, in basic medium (pH 10) its limiting current decreases and a fourth wave (C) appears at more negative potential ($E_{1/2} = -1.72$ V), very close to the electrolyte reduction limit.

We have noticed that the wave heights of TFMA (i_{dA} and i_{dB}) decrease slowly with time (Fig. 2*b*) and that, in 50/50 ethanol/water solutions, the wave heights are constant but systematically smaller, even for the first scan, than in aqueous solutions ($0.6 \times i_{dH_2O}$) (Figs. 3, 4). These current variations with time prevent any accurate coulometric determination of the electron number involved in the electroreduction of TFMA at the different pH values.

Micellar medium effects

In the presence of surfactants, polarographic curves of TFMA are modified according to the nature of surfactants added (Figs. 3–5). In the presence of GHU, a surfactant that forms micelles but at a very high critical micellar concentration (CMC) (Table 1), the shape of the polarographic wave is not modified (Fig. 3). However, in weakly acidic solutions, addition of nonionic surfactants such as BRIJ35, OTG, and LS at a concentration superior to their respective CMC (Table 1) causes a shift of the reduction waves toward more negative potentials (Figs. 3, 5). In basic medium (Fig. 4), the addition of BRIJ35 has two major effects: first, wave B is shifted toward more positive potentials (curve 2) and its intensity is higher ($i_{dB} = 3.34$ μA) than in aqueous solution at the same pH ($E_{1/2} =$

Fig. 2. (*a*) Variation of half-wave potentials of waves A_1, A_2 and B as a function of pH. (*b*) Variation of $i_{d\,(A_1 + A_2)}$ as a function of time.

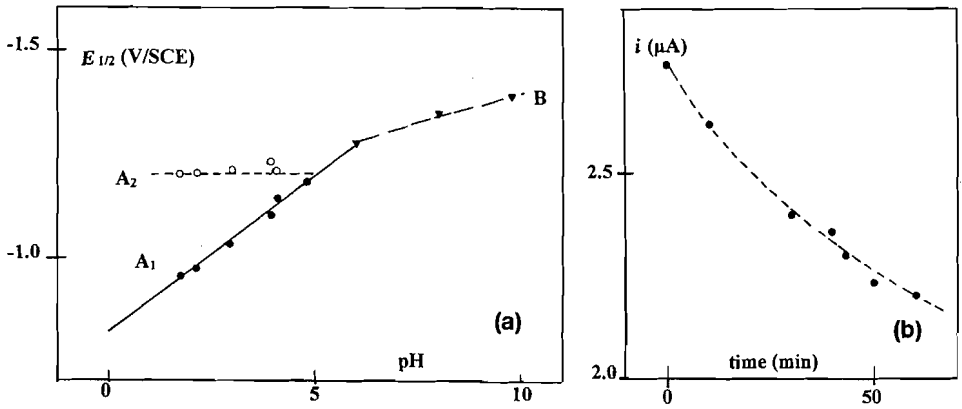

Fig. 3. Polarographic curves of 1×10^{-3} M TFMA at pH = 4: (1) with 1×10^{-3} M GHU; (2) with 1×10^{-3} M BRIJ35; (3) in 50/50 water/ethanol solution.

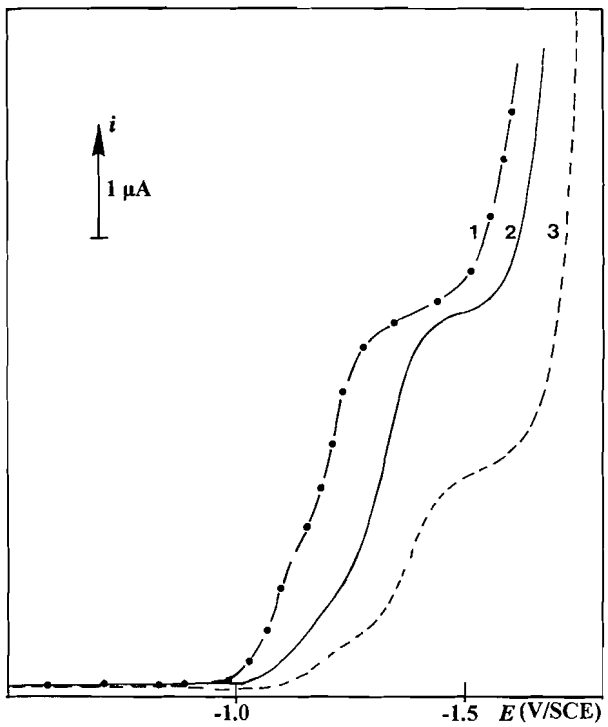

Fig. 4. Polarographic curves of 1×10^{-3} M TFMA at pH = 10: (1) without surfactant; (2) with 1×10^{-3} M BRIJ35; (3) in 50/50 water/ethanol solution.

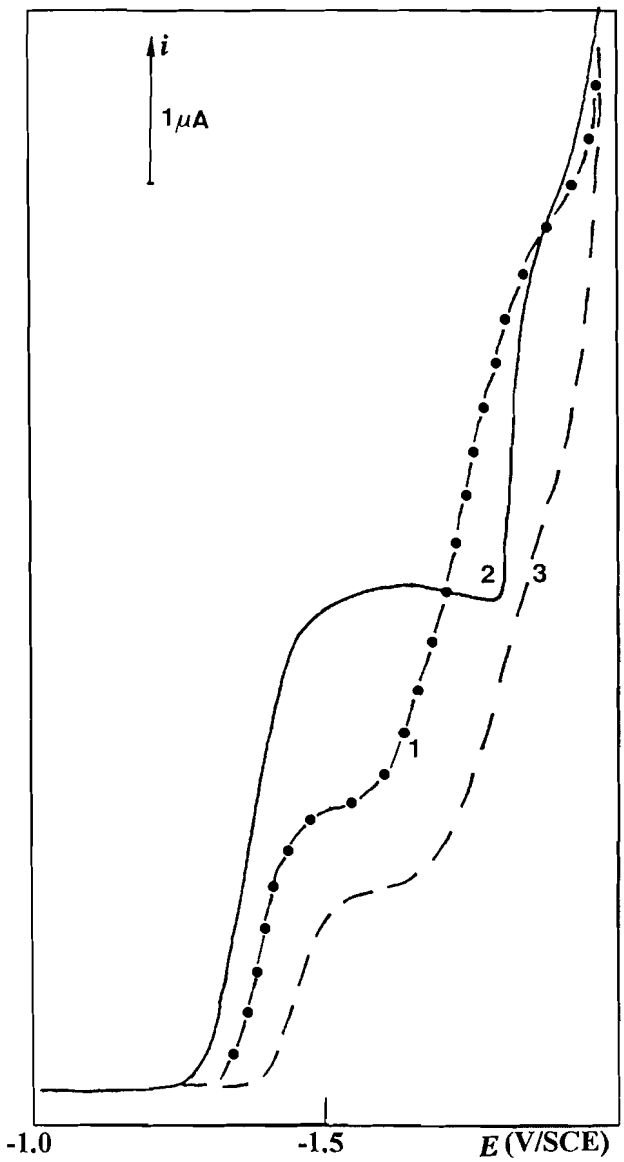

-1.40 V and $i_{dB} = 2.0$ μA, curve 1), and second, wave C is shifted toward negative potentials. Therefore it appears that in the presence of BRIJ35, the reduction of TFMA becomes roughly independent of the pH of the solution from pH 4 to pH 10 and occurs at $E_{1/2} \cong -1.35$ V (Figs. 3 and 4).

2. Preparative controlled-potential electrolyses

In aqueous solutions

Electrolyses of TFMA were performed in the different buffer solutions used, allowing an assignment of the reaction products obtained at a fixed potential corresponding to each of the four waves A_1, A_2, B, and C. The relative quantities of ketone (TFMA), carbinol (C1), and pinacols (P1) were determined

Can. J. Chem. Downloaded from www.nrcresearchpress.com by 80.90.12.36 on 09/08/12
For personal use only.

Table 2. ^{1}H NMR signals (DMSO-d_6) of ketones and reduction products

Compound	AA'BB' pattern	O*H*	C*H*$_3$	HO-C-*H*
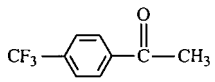 (TFMA)	8.19, 7.94	—	2.69(s)	—
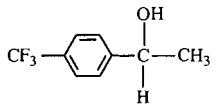 (C_1)	7.71, 7.60	5.44(d)	1.34(d)	4.80(qd)
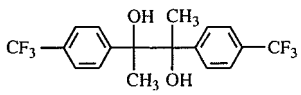 (P_1) Pinacol *meso*	7.80, 7.66	5.35(s)	1.28(s)	—
(P_1) Pinacol *dl*	7.45, 7.32	5.51(s)	1.70(s)	—
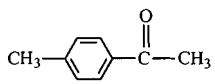 (MA)	7.89, 7.36	—	2.70(s) 2.48(s)	—
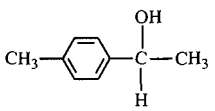 (C_2)	7.25, 7.14	5.11(d)	2.30(s) 1.32(d)	4.72(qd)
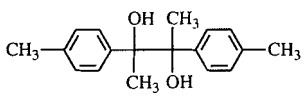 (P_2) Pinacol *meso*	7.34, 7.05	4.77(s)	2.55(s) 1.25(s)	—
(P_2) Pinacol *dl*	7.99, 6.94	4.90(s)	2.25(s) 1.45(s)	—

from ^{1}H NMR spectral analysis (Table 2). The values are summarized in Table 3.

In acidic medium (pH 3), a coulometric *n* value of 1 was obtained upon electrolysis at a potential on the diffusion plateau of the first wave (A_1). It corresponds to the formation of pinacols (P_1) as major products. Electrolysis at the potential of the second wave (A_2) gave a coulometric *n* value of 1.3 for which both pinacols (P_1) and carbinol (C_1) were obtained. Reduction of TFMA at a potential situated on the diffusion plateau of the second wave B in the pH 5 solution produced mainly carbinol (C_1). A higher than expected *n* value is obtained (Table 3). It could result from a beginning of C—F bond cleavages even at this pH value (vide infra).

Finally, controlled-potential electrolysis at −1.72 V in a pH 10 buffer solution yielded mainly pinacols (P_1) but also numerous other compounds. At least the different products were separated by GC (DB1 column) and identified by mass spectrometry coupled with gas chromatography (Table 4) and by assignment of their ^{1}H NMR signals, especially in the aromatic region, by comparison with NMR spectra of authentic samples (Table 2). Except for TFMA and its reduction products (the carbinol (C_1) and the pinacols (P_1)), there were methylacetophenone (MA) and its corresponding carbinol (C_2) and pinacols (P_2) (Tables 2 and 4). The chemical and electrochemical reduction of MA gave the authentic samples used for identification. The GC peaks arising at 47.6 and 48.2 min might correspond to two mixed diastereomeric pinacols (P3).

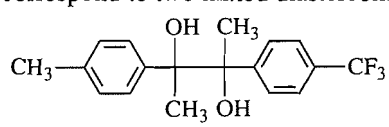

(P_3)

This hypothesis has been confirmed by analysis of the frag-

Can. J. Chem. Downloaded from www.nrcresearchpress.com by 80.90.12.36 on 09/08/12
For personal use only.

Table 3. Electrolysis of TFMA in aqueous solutions.

pH	Potential of electrolysis (V/SCE)	Electricity consumed ($F\ mol^{-1}$)	% TFMA	% C_1	% P_1	Pinacols/ carbinol	dl/*meso*
3	−1.05	1.0	8	<5	88	—	0.9
3	−1.20	1.3	19	41	39	0.95	0.9
5	−1.45	3.0	—	>95	—	—	—
10	−1.70	3.1	6[a]	14[a]	38*	2.71	2

[a]The percentages of other reduction products are given in the results section.

Table 4. EIGC data of TFMA electrolysis at pH 10 (E_{appl} = −1.70 V).

Peak	*t* (min)	Mass	Compound
P1	11.2	188	TFMA
P2	14.1	190	C_1
P3	16.1	136	C_2
P4	16.6	134	MA
P5	44.7	378	P_1 *dl*
P6	45.8	378	P_1 *meso*
P7	47.6	324	P_3
P8	48.2	324	P_3
P9	51.3	270	P_2 *dl*
P10	51.5	270	P_2 *meso*

Fig. 5. Polarographic curves of 1×10^{-3} M TFMA at pH = 5: (1) without surfactant; (2) with 1×10^{-2} M OTG; (3) with 1×10^{-2} M LS.

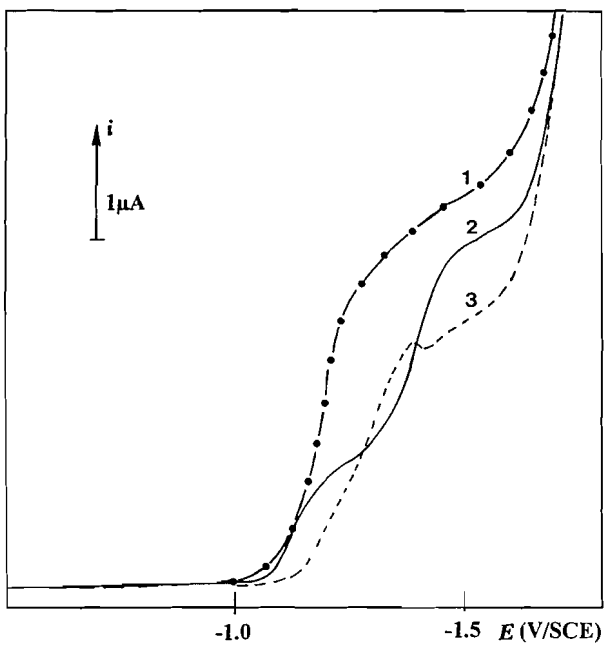

ments observed in EIGC mass spectra. The ^1H NMR spectra registered for the unseparable mixture of carbinols and pinacols show, in the aromatic area, a set of AA′BB′ signals characteristic of *p*-disubstituted benzene rings located for the dissymmetrical pinacols at 7.73 (2H, Ar), 7.63 (2H, Ar), 7.41 (2H, Ar), 7.09 (2H, Ar) and 7.46 (2H, Ar), 7.34 (2H, Ar), 7.41 (2H, Ar), 7.09 (2H, Ar). The relative quantities of ketones and

Fig. 6. UV absorption spectra of TFMA: (*a*) in acetonitrile (1) $C = 3.33 \times 10^{-5}$ M, (2) $C = 1 \times 10^{-3}$ M, 3) $C = 1 \times 10^{-2}$ M; (*b*) in aqueous solution (pH = 4) (1) $C = 3.33\ 10^{-5}$ M, (2) $C\ 1 \times 10^{-3}$ M.

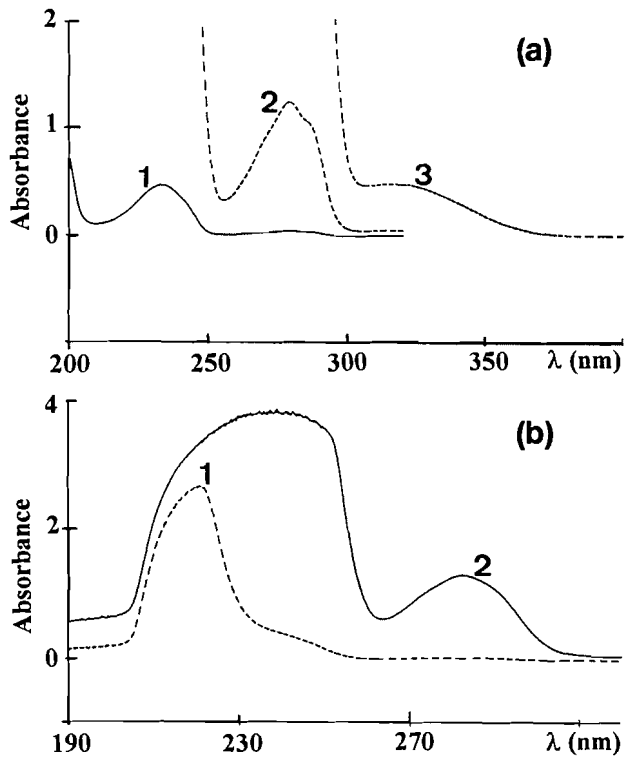

reduction products estimated, from the GC and NMR data, are the following: TFMA 6%, C_1 14 %, P_1 38 %, MA <2%, C_2 28%, P_2 3%, P3 11%.

In micellar medium

Electrolyses of TFMA were also performed in the presence of chiral surfactants (2.5×10^{-2} M LS and 5×10^{-2} M OTG) at pH 5 ($E_{appl} = -1.43$ V). Carbinol (C_1) obtained as reduction product, after its identification by ^1H NMR, was analyzed by GC on a LIPODEX-E column that allows good separation of the two enantiomers (*R* and *S*). There was no asymmetric induction (enantiomeric excess ≤ 0.05).

3. UV spectroscopic studies

In acetonitrile, TFMA shows a strong π–π* absorption band (K) at 239 nm, a medium-intensity benzenoid band (B) at about 277 nm (ε = 1000), and a weak band corresponding to the *n*–π* transition (λ_{max} = 316 nm, ε = 50) (Fig. 6*a*). The lat-

Can. J. Chem. Downloaded from www.nrcresearchpress.com by 80.90.12.36 on 09/08/12
For personal use only.

Can. J. Chem. Downloaded from www.nrcresearchpress.com by 80.90.12.36 on 09/08/12
For personal use only.

Fig. 7. Variation of absorbance at 284 nm as a function of time in various media: (*a*) aqueous buffer solution (pH = 4); (*b*) aqueous buffer solution (pH = 4) + 1×10^{-3} M BRIJ; (*c*) 50/50 water/ethanol solution.

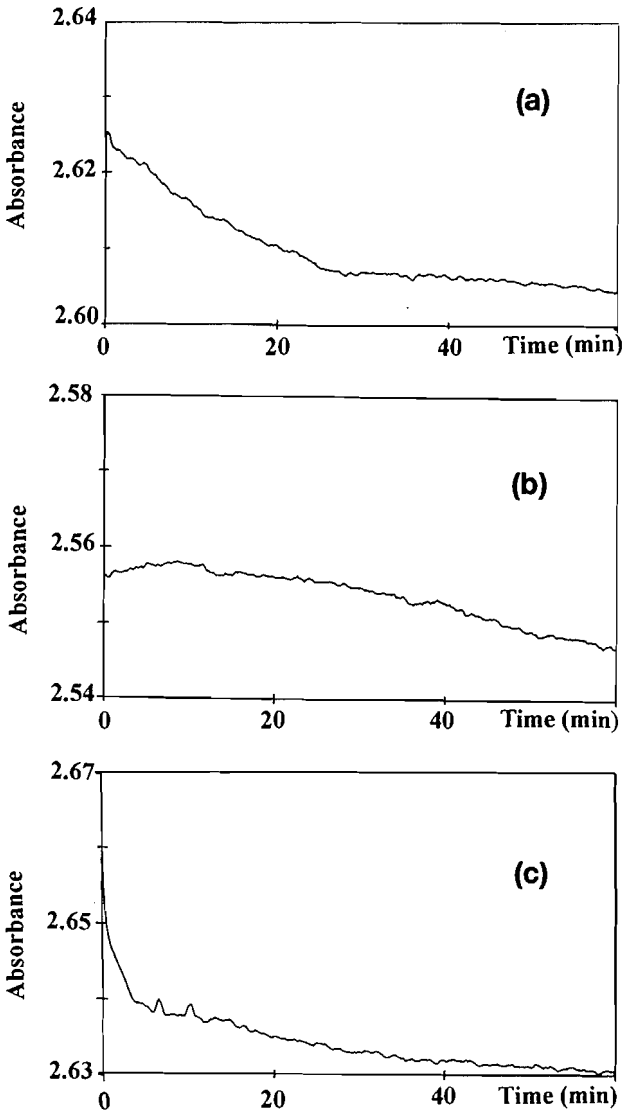

ter disappears in aqueous solution because of the low solubility of TFMA in water. Under these conditions, we observe only two strong bands (λ_{max} (K) = 221 nm, ε = 80 000 and, λ_{max} (B) = 284 nm, ε = 1300) (Fig. 6*b*).

Information on hydration of TFMA can be obtained both from the decrease of the carbonyl absorption band and from the shift of the strong aromatic absorption at 284 nm. Indeed, absorbance of the n–π^* transition is directly proportional to the concentration of free carbonyl compound present in the solution; however, we cannot use it because of the low intensity of the band. On the other hand, hydration of the carbonyl group suppresses delocalization, and the aromatic π–π^* absorption band at 284 nm is progressively replaced by another corresponding to the aromatic hydrocarbon absorption situated at lower wavelength. The kinetics of hydration of TFMA was therefore followed by the decrease of the absorbance at 284 nm as a function of time (Fig. 7).

In aqueous solution (pH 4), we observe that the absorbance at 284 nm decreases regularly with time (Fig. 7*a*). The presence of BRIJ 35 in the solution causes first the stabilization of absorbance with, further, a slower decrease than in water solution (Fig. 7*b*). On the contrary, in hydroalcoholic solution, we observe a rapid decrease of the absorbance (Fig. 7*c*).

Discussion

The substitution of acetophenone with the CF_3 electron- withdrawing group enhances the hydration property of the carbonyl function (5). For example, α,α,α-trifluoroacetophenone has frequently been chosen as a model compound to study hydration–dehydration and acid–base equilibria involving the geminal diol group -$C(OH)_2CF_3$ (6, 7). In the case of TFMA, the evolution of the polarographic curves (Fig. 2*b*) and of the spectrophotometric spectra (Fig. 7*a*) as a function of time in aqueous solution strongly suggests that the carbonyl group is involved in a slow hydration–dehydration equilibrium ($k_h \cong 10^{-4}$ s^{-1}, a value estimated from polarographic and UV spectroscopy data) leading to the non-reducible geminal diol form. The rate of carbonyl hydration is expected to be sensitive to electronic effects occurring in the 4-substituted phenacyl derivatives; for example, a value of $k_h \cong 10^{-6}$ s^{-1} had been calculated for the 4-methylacetophenone (18). In the presence of the neutral surfactant (BRIJ35), the ketone is solubilized in the polyoxyethylene (O-CH_2-CH_2-)$_n$ region of the micelles (19) where the hydration reaction is slightly inhibited. In ethanolic solutions, the hemiacetal is more rapidly formed than the *gem*-diol, leading to an immediate decrease of the absorption wave.

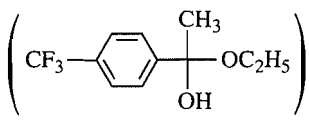

It is generally accepted that aromatic ketones are reduced according to the pH of the solution, with the formation of carbinol or pinacols in various amounts (1, 20, 21). The presence of a CF_3 group in the TFMA causes a shift of half-wave reduction potentials to less negative values ($\Delta E_{1/2} \cong 25$ mV) (4), making the study in aqueous solution easier.

In acidic medium, as previously reported by Stocker et al. (22), electrolysis at the first reduction step A_1 (E_{appl} (A_1) = −1.05 V) yields pinacols (Table 3). The ketyl radical results from the reduction of the protonated ketone (wave A_1 in Fig. 1 and in Scheme 1). It can further be involved either in a dimerization reaction leading to the pinacols (P_1) (see Scheme 1), with little preference in the steric approach (*dl*/*meso* = 0.9) (22), or in a second reduction step (A_2) at more negative potential (E_{appl} (A_2) = −1.20 V) (Fig. 1) leading to the carbinol (C_1) (see wave A_2 in Fig. 1 and in Scheme 1). In the case of acetophenone, this second wave lies in the potential range where the discharging of protons occurs in acidic medium (1). With TFMA, at a potential corresponding to wave A_2, the reduction and the dimerization reactions are in competition and the same percentage of pinacols and carbinol is obtained (Table 3). The half-wave potential of wave A_1 shifts to more negative values as the pH of the solution is increased, and merges with A_2 into a single two-electron wave at pH 5, a value of pH slightly lower than that obtained with benzaldehyde and acetophenone (21) probably due to the presence of the CF_3 group. When the electrolysis potential becomes more negative (on the plateau of wave B), the reduction process prevails as regards the

Can. J. Chem. Downloaded from www.nrcresearchpress.com by 80.90.12.36 on 09/08/12
For personal use only.

Scheme 1.

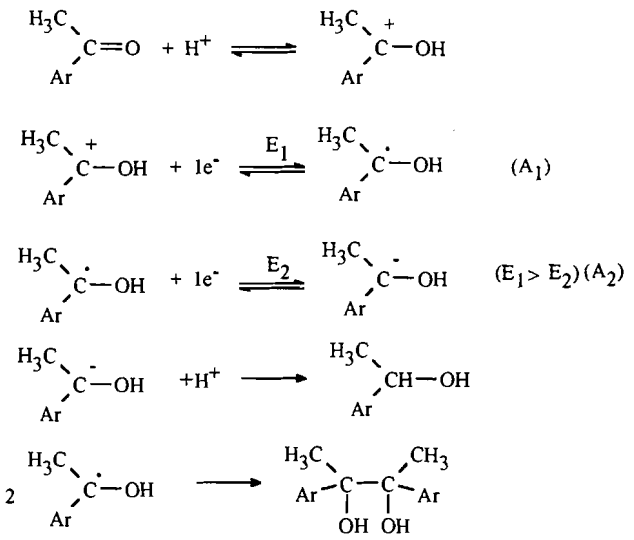

Scheme 2.

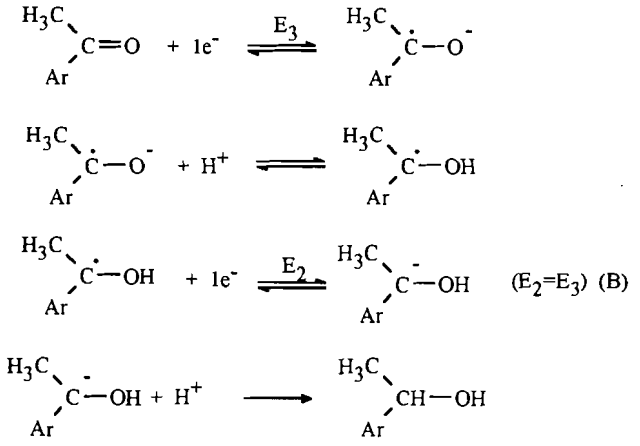

dimerization, and all the molecules are reduced to form the carbinol (Table 3).

In alkaline medium, the ketone can also be reduced directly to form the anion-radical, which after protonation is reduced to form the carbinol (Scheme 2).

However, when the proton concentration decreases, the electropinacolization involving radical–radical, radical–substrate, or ion–substrate coupling (22, 23) becomes prevalent with, as a consequence, a decrease of the wave height (i_{dB}) (Fig. 1).

Contrary to the results previously published by Stocker et al. (22), we obtained a relatively high yield of pinacols after electrolysis in basic medium at a potential ($E_{appl} = -1.7$ V) corresponding to the fourth reduction step (see wave C of Fig. 1) (Table 2). The ratio *dl/meso* for diastereomeric pinacols is 2, in agreement with the value generally reported for these alkaline media (24). Moreover, under our electrolysis conditions at very negative potential, one may consider a possible C—F. bond cleavage concomitant to the ketone reduction (22). In aqueous solution, it has been reported that the successive reductive removal of the three fluorine atoms of trifluoromethyl compounds can be carried out at a single potential (−1.7 V in the case of TFMA) (8, 9, 13). For such a cleavage the presence of an activating group in the molecule is clearly necessary as demonstrated by the fact that trifluoromethylbenzene itself is non-reducible even at more cathodic potentials than −2.0 V vs. SCE (13), while for aromatic compounds bearing a sulfamyl function, a trifluoromethyl substituent is reduced to the methyl group at −1.76 V in aqueous solution (8).

The protonation of the intermediates is slower in alkaline medium, and a competition between the protonation of the radical-anion (Scheme 2) and the loss of a fluoride anion, as proposed by Coleman et al. (12) in the case of trifluoro-benzylesters, can occur (Scheme 3).

Scheme 3.

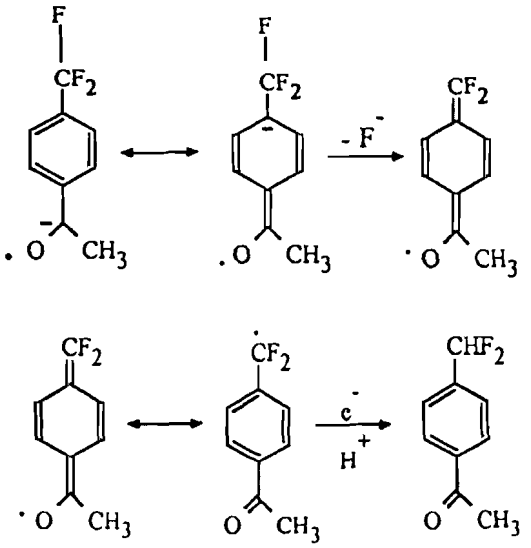

Three consecutive cleavages of fluorine bonds from the trifluoromethyl group lead to the formation of methylacetophenone (MA), which bas been found in the reduction products of TFMA at pH 10 (Table 4). This ketone is further reduced under these conditions with the formation of its carbinol (C_2) and pinacols (P_2) as reduction products, characterized in EIGC mass spectrometry and ^{1}H NMR by comparison with authentic samples.

The shape of polarograms depends on the nature of the surfactants present in the solution (Figs. 3–5), more precisely, on their micellar properties (CMC) but also on their adsorption mode at the mercury electrode (2). In the presence of nonionic surfactants such as BRIJ35, LS, and OTG at a concentration higher than their CMC, the electroreduction of TFMA occurs at roughly the same potential ($E_{1/2} \cong -1.35$ V) whatever the buffer solution. In the presence of GHU, a surfactant that does not form micelles at the concentration used (14), the polarograms have the same evolution with pH as in aqueous solutions. Moreover, tensammetric curves have shown that at the same concentration, LS appears to be more strongly adsorbed than OTG and GHU.[2] This fact can explain the small hump observed on the polarogram recorded in the presence of LS. These results strongly suggest that TFMA is solubilized in the hydrophobic core of the micelles of BRIJ35, LS, and OTG, inside which chemical reactions, such as hydration and protonation are inhibited.

[2] C. Mousty, unpublished results.

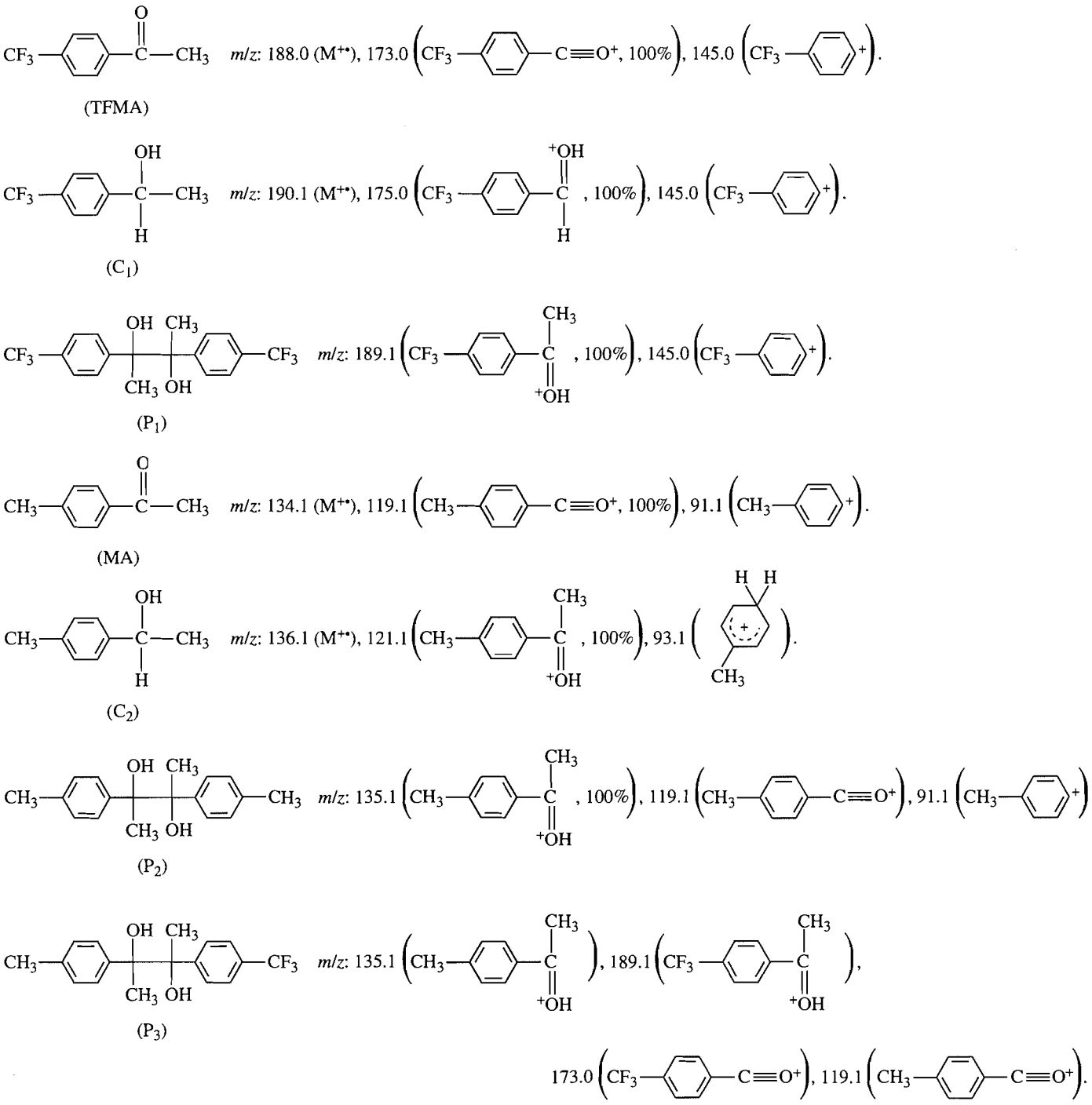

Chiral micelle systems can be used as a simple analogue to mimic the stereochemistry of enzyme reactions. However, few examples of asymmetric induction for the reduction of prochiral substrates in chiral micelles have been described. In particular, two papers report the reduction, by sodium borohydride, of phenylalkylketones in aqueous micelles of chiral surfactants such as trialkylmethylammonium bromides (25), dodecyl glucopyranoside, and dodecyl glucopyranouranate (26), giving optically active carbinols with enantioselectivities of up to 17.7% (25) and 98% (26), respectively. As a means of comparison, we have performed the electroreduction of TFMA in chiral micelles of OTG and LS. Contrary to the latter results, we do not observe any significant chiral induction. Indeed, hydrophobic interactions play an important role in the enantioselectivity. The bonding of prochiral ketone with chiral micelles is a dynamic process that would certainly be improved by the presence of a long alkyl chain in the ketone molecules. Such investigations are in progress in our group.

Experimental

Aqueous solutions ($2 \leq pH \leq 10$) were prepared with McIlvaine (acidic medium) and Britton Robinson (basic medium) buffer solutions. The ionic strength was adjusted to 0.5 M by

Can. J. Chem. Downloaded from www.nrcresearchpress.com by 80.90.12.36 on 09/08/12
For personal use only.

adding KCl. 4-Trifluoromethylacetophenone (TFMA) (Aldrich), 4-methylacetophenone (MA) (Janssen), polyoxyethylene dodecyl ether (BRIJ35) (Fluka), and 1-*S*-octyl β-D-thioglucopyranoside (OTG) (Aldrich) were used as received. The β-*N*-glucosyl-*N*-heptylurea (GHU) and the 2-*O*-lauroyl saccharose (LS) were provided by Professor Plusquellec (14, 15). The critical micellar concentrations (CMC) of these nonionic surfactants are given in Table 1.

Polarographic current voltage curves were recorded by means of a Tacussel PRG5 polarograph. The drop time was kept constant at 1 s with an electromagnetic hammer. The outflow of mercury was 0.64 mg s^{-1} for a mercury height of 50 cm. During all electrochemical measurements, we used a saturated calomel electrode (SCE) as reference; the cell was thermostated at 30°C and maintained under an inert atmosphere by argon previously saturated by flowing through the TFMA solution. The TFMA solutions were obtained by diluting a concentrated DMF stock solution (0.1 M) into the aqueous electrolytic medium.

Preparative controlled-potential electrolyses were carried out in a three-compartment glass cell joined by two sintered glasses. The cathodic compartment contained 100 mL of buffer solution, 400 mg of TFMA, a reference electrode, an Ar tube, and a mercury pool of 13 cm^2 as the working electrode. The anode was a glassy carbon electrode. When the electrolyses were stopped, the solutions were neutralized and extracted twice with 50 mL ethyl ether.

The reduction products were column chromatographed on silica gel (eluent cyclohexane/ethyl acetate 7/3) and finally analyzed by gas chromatography (GC) on a DB1 or a LIPODEX-E column and by NMR spectroscopy (^{1}H, 400 MHz, DMSO-d_6) (Table 2). Authentic samples of the carbinols were obtained by chemical reduction of TFMA with sodium borohydride.

Methylacetophenone (MA) was used as a reference product, its corresponding carbinol was obtained by chemical reduction with $NaBH_4$, and the pinacols were synthesized by a controlled-potential electrolysis at pH 10, $E_{appl} = -1.70$ V. NMR data for these compounds are given in Table 2.

Mass spectra (EIGC) were obtained from the "Service Central d'analyse" of CNRS (see preceding page).

UV absorption spectra were recorded with a Uvikon 941 spectrophotometer using a matched pair of 1 cm fused quartz cells.

Acknowledgment

We acknowledge the contribution of Professor Plusquellec, Laboratoire de Chimie organique et des substances naturelles (URA 1467) from the École Nationale Supérieure de Chimie of Rennes, for supplying the LS and GHU.

References

1. A. Honorat and P. Martinet. Electrochim. Acta, **28**, 1703 (1983).
2. (*a*) C. Mousty and G. Mousset. New J. Chem. **16,** 1063 (1992); (*b*) *In* Electrochemistry in colloids and dispersion. *Edited by* R.A. MacKay and J. Texter. VCH Publishers, New York. 1992. pp. 291–301.
3. R. Prime, A.M. Martre, G. Mousset, and P. Pouillen. Bull. Soc. Chim. Fr. **127**, 18 (1991).
4. R.O. Loutfy and R.O. Loutfy. Tetrahedron, **29**, 2251 (1973).
5. W.A. Sheppard and C.M. Sharts. *In* Organic fluorine chemistry. Benjamin, New York. 1969. p. 437.
6. W.J. Scott and P. Zuman. J. Chem. Soc. Faraday Trans. **72**, 1192 (1976).
7. W.J. Scott and P. Zuman. Anal. Chim. Acta, **126**, 71 (1981).
8. A.I. Cohen, B.T. Keeler, N.H. Coy, and H.L. Yale. Anal. Chem. **34**, 216 (1962).
9. J.H. Stocker and R.M. Jenevein. Chem. Commun. 934 (1968).
10. J.P. Coleman, H.G. Gilde, J.H.P. Utley, and B.C.L. Weedon. Chem. Commun. 738 (1970).
11. C.P. Andrieux and J.M. Saveant. Bull. Soc. Chim. Fr. 2090 (1973).
12. J.P. Coleman, Naser-Ud-Din, H.G. Gilde, J.H.P. Utley, and B.C.L. Weedon. J. Chem. Soc. Perkin Trans. 2, 1903 (1973).
13. H. Lund and N.J. Jensen. Acta Chem. Scand. **328**, 263 (1974).
14. D. Plusquellec, C. Brenner-Henaff, P. Leon-Ruaud, S. Duquenoy, M. Lefeuvre, and H. Wroblewski. J. Carbohydr. Chem. **13**, 737 (1994).
15. C. Chauvin, K. Baizko, and D. Plusquellec. J. Org. Chem. **58**, 2291(1993).
16. S. Saito and T. Tsuchiya. Biochemistry, **222**, 829 (1984).
17. P. Becher and A. Harrikiko. J. Colloid Interface Sci. **27**, 634 (1968)
18. I. M. Kovach, Q. Zhao, M. Keane, and R. Reyes. J. Am. Chem. Soc. **115**, 10471 (1993).
19. J.H. Fendler, E.J. Fendler, G.A. Infante, P.S. Shih, and L.K. Patterson. J. Am. Chem. Soc. **97**, 89 (1975).
20. E. Laviron. Collect. Czech. Chem. Commun. **30**, 4219 (1965).
21. E. Laviron and J.C. Lucy. Bull. Soc. Chim. Fr. **7**, 2202 (1966).
22. J.H. Stocker, R.M. Jenevein, and D.H. Kern. J. Org. Chem. **34**, 2810 (1969).
23. L. Nadjo and J.M. Saveant. J. Electroanal. Chem. **44**, 327 (1973).
24. J.H. Stocker and R.M. Jenevein. J. Org. Chem. **33**, 294 (1968).
25. Y. Zhang, W. Fan, P. Lu, and W. Wang. Synth. Commun. **18**, 1495 (1988).
26. H. Yong-Zheng and Y. Ohi-Ming. Acta Chim. Sin. **46**, 239 (1988).

Can. J. Chem. Downloaded from www.nrcresearchpress.com by 80.90.12.36 on 09/08/12
For personal use only.

On the relationship between the order parameter $\langle P_2(\cos\theta)\rangle$ and the shape of orientation distributions

Claude-Paul Lafrance, Anne Nabet, Robert E. Prud'homme, and Michel Pézolet

Abstract: The molecular orientation is generally expressed by an "order parameter," $\langle P_2\rangle$, which depends on both the angular position and the shape of the orientation distribution. This parameter is an average made over all orientations of the structural units studied in a sample and, consequently, a given $\langle P_2\rangle$ value can correspond to different orientation distributions. In this article, model distributions are used to show the relationship between the shape, width, and angular position of the center of the orientation distribution on the $\langle P_2\rangle$ coefficient, for the case where the distribution of the molecular chains exhibits cylindrical symmetry with respect to the reference direction. A significant difference is observed between the order parameters calculated for distributions of Gaussian and Lorentzian shapes with similar width at half-height. The variation of the $\langle P_2\rangle$ coefficient as a function of the width at half-height, $W_{1/2}$, and of the position of the center of the distribution, θ_C, is analyzed. Figures showing the range of $W_{1/2}$–θ_C coordinates that can correspond to a given $\langle P_2\rangle$ value are presented. As an example, the influence on the order parameter of the disorder between the different domains of phospholipid samples (mosaic spread) and of the conformational disorder in the acyl chains of these molecules is also studied. This example permits the evaluation of the magnitude of the errors that can be introduced in calculations of the tilt angle of the molecular chains in the case of distributions of finite widths or of bimodal character.

Key words: orientation, orientation function, phospholipid bilayers, conformational disorder, mosaic spread.

Résumé : L'orientation moléculaire est généralement exprimée par un paramètre d'ordre, $\langle P_2\rangle$, dont la valeur dépend à la fois de la position angulaire et de la forme de la distribution d'orientation. Ce paramètre d'ordre constitue une moyenne faite sur toutes les orientations des unités structurales étudiées dans un échantillon et, en conséquence, une valeur de $\langle P_2\rangle$ donnée peut correspondre à différentes distributions d'orientation. Des distributions modèles sont utilisées afin de montrer l'influence de la forme, de la largeur et de la position angulaire du centre de la distribution d'orientation sur le coefficient $\langle P_2\rangle$, pour le cas où les chaînes moléculaires possèdent une symétrie cylindrique par rapport à la direction de référence. Une différence significative est observée entre les paramètres d'ordre calculés pour des distributions de formes Gaussienne et Lorentzienne de même largeur à mi-hauteur. La variation du coefficient $\langle P_2\rangle$ en fonction de la largeur à mi-hauteur, $W_{1/2}$, et de la position du centre de la distribution, θ_C, est analysée. Des figures montrant la plage de coordonnées $W_{1/2}$–θ_C pouvant correspondre à une valeur de paramètre d'ordre donnée sont présentées. À titre d'exemple, la variation du coefficient $\langle P_2\rangle$ en fonction du désordre entre les différents domaines d'échantillons de phospholipides et en fonction du désordre conformationnel dans les chaînes acyles de ces molécules est également étudiée. Cet exemple permet d'évaluer l'importance des erreurs pouvant être introduites dans le calcul de l'angle d'inclinaison des chaînes moléculaires dans le cas de distributions de largeur finie ou de caractère bimodal.

Mots clés : orientation, fonction d'orientation, bicouches de phospholipides, désordre conformationnel, désordre entre les différents domaines.

Can. J. Chem. Downloaded from www.nrcresearchpress.com by 80.90.12.36 on 09/08/12
For personal use only.

Introduction

The occurrence of orientation at the molecular level has a considerable importance in macromolecular science, since it gives directional properties to materials. In the last two decades, numerous publications have dealt with the characterization of orientation in oriented polymer films and fibers (1–5), in biological membranes (6, 7), and in liquid crystals (3). Measurements of molecular orientation are now commonly conducted in various fields of research, yet the literature gives many examples where conclusions drawn from such measurements seem to overlook limitations related either to the characterization method itself or to the mathematical significance of the order parameter calculated from the experiment.

Recently, Myers and Cooper (8) analyzed some of the errors that can arise in the determination of orientation of polymers by infrared spectroscopy. More specifically, the

Received February 17, 1995.

C.-P. Lafrance, A. Nabet, R.E. Prud'homme,[1] and M. Pézolet.[1] Département de chimie and Centre de recherches en sciences et ingéniérie des macromolécules, Université Laval, QC G1K 7P4, Canada.

[1] Authors to whom correspondence may be addressed. Telephone: (418) 656-2481. Fax: (418) 626-7916. E-mail: michel.pezolet@chm.ulaval.ca

Can. J. Chem. Downloaded from www.nrcresearchpress.com by 80.90.12.36 on 09/08/12
For personal use only.

problems caused by the imperfect polarizer behavior, by the improper determination of the chain conformation, and by the assumption of an inaccurate value of the angle between the chain axis and the transition dipole moment were discussed. Furthermore, Ahn and Franses (9) mentioned the possible influence of the width of the orientation distribution on the tilt angle calculated from infrared spectroscopy measurements of Langmuir–Blodgett films. Following this line, the present article focusses on the interpretation of the order parameter, taking into account the fact that orientation distributions at the molecular level are neither necessarily very narrow nor can always be considered as of unimodal character.

Generally, the molecular orientation is expressed by an "order parameter" or "orientation function," $\langle P_2(\cos\theta)\rangle$, or $\langle P_2\rangle$, which is the second-order coefficient of a series expansion of the orientation distribution (1–5). Although all the techniques generally used to study the molecular orientation allow the calculation of the $\langle P_2\rangle$ coefficient, wide-angle X-ray diffraction (WAXD) and infrared spectroscopy (IR) are often preferred over other characterization methods. The main advantage of X-ray diffraction is that the orientation distribution of different crystal planes can be measured directly, giving the width, the shape, and the position of the maximum of the distribution. The orientation of the crystal phase is then completely defined, and all the $\langle P_n\rangle$ coefficients of the series expansion can be determined (1, 10–12). On the other hand, infrared spectroscopy is a simple, fast, and reliable method that can be used to calculate the $\langle P_2\rangle$ coefficient for amorphous or crystalline samples, in either solid, gel, or liquid crystalline phases (4, 6).

The $\langle P_2\rangle$ coefficient depends not only on the angular position of the orientation distribution but also on its shape and width, since it is an average made over all orientations in the sample. Thus, the $\langle P_2\rangle$ value can be used, for example, to discuss the evolution of orientation in a series of polymer samples deformed to different draw ratios. However, the knowledge of this sole coefficient does not allow the unambiguous determination of the inclination of structural units in a sample. The objective of this paper is, first, to emphasize the fact that the $\langle P_2\rangle$ coefficient is an average and to give guidelines on the interpretation of this order parameter. The relationship between the $\langle P_2\rangle$ coefficient and the shape, width, and angular position of the orientation distribution will be discussed. A comparison with the calculation of $\langle P_n\rangle$ coefficients from X-ray diffraction will be made, using model distributions, since WAXD allows the direct measurement of the orientation distribution, and thus offers a practical method to visualize the effect of the shape and position of the distribution on the $\langle P_2\rangle$ value. These simulations will demonstrate that the discrimination between different types of orientation distribution, all having the same $\langle P_2\rangle$ value, can be made when $\langle P_n\rangle$ coefficients of higher orders are known. Yet it will be shown that, even in this case, the possibility of differentiating between certain orientation distributions depends on the precision of the $\langle P_n\rangle$ values obtained from the experiment, and it can still be difficult if only a few coefficients are known ($n \leq 8$).

The final section of this paper presents an evaluation of the errors that can be introduced in angular calculations by assuming a single and narrow orientation distribution model when the actual distribution can exhibit a finite width or possess a bimodal character. For this purpose, the influence on the $\langle P_2\rangle$ coefficient of the disorder that can be present in phospholipid samples will be analyzed. Phospholipids are the main constituents of biological membranes and, since the properties of membranes depend on the molecular orientation of their constituents, several studies have appeared in the literature dealing with the orientation of the acyl chains of these molecular assemblies. This system has been chosen to illustrate the influence of the shape of orientation distribution on the order parameter because different types of disorder occur in phospholipid samples. The "mosaic spread," i.e., the disorientation between different domains of phospholipid samples deposited on a support, gives an example of the broadening of an orientation distribution by the superimposition of a second distribution. Besides, the occurrence of conformational disorder, which can be introduced either thermally or by the interaction of phospholipids with peptides and proteins, can be used as a model to illustrate the discrepancy between interpretations of orientation measurements arising when the distribution is of bimodal character rather than unimodal. Figures will be shown to evaluate the influence of both types of disorder in molecular orientation studies.

Fig. 1. The Euler angles θ, ϕ, and ψ defining the orientation of a set of molecular coordinates **a**, **b**, **c** with respect to a macroscopic reference system x, y, z. θ and ϕ describe the orientation in space of the molecular chain axis **c**, while ψ refers to the rotation of the **a** and **b** molecular axes around **c**.

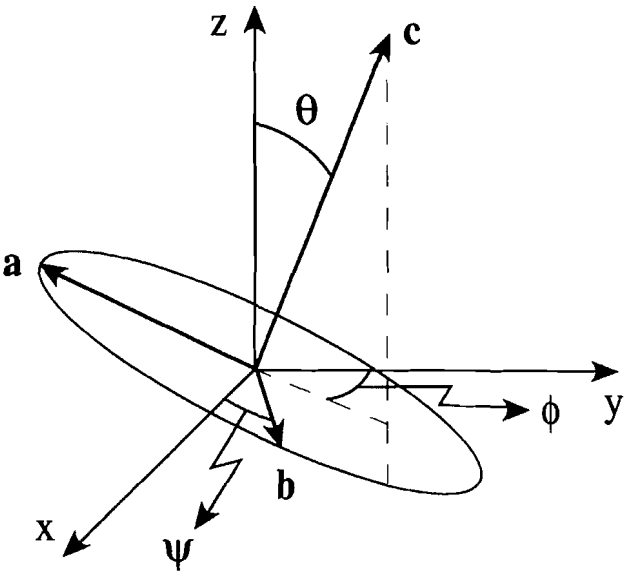

Theory

Characterization of the molecular orientation by a series of Legendre polynomials

The orientation in space of a set of orthogonal axes (**abc**), for example, the crystal axes of an orthorhombic unit cell, can be completely described with respect to a macroscopic reference frame (xyz) by using the Euler angles θ, ϕ, and ψ (1), as shown in Fig. 1. Defining **c** as the molecular chain axis, the angle θ describes the inclination of the chain with respect to z, ϕ describes the position of its projection in the xy plane, while the angle ψ describes the rotation of the unit cell around its **c** axis. The orientation distribution of structural units in polymer

Can. J. Chem. Downloaded from www.nrcresearchpress.com by 80.90.12.36 on 09/08/12
For personal use only.

or biological samples can be characterized by using a variety of mathematical functions, the aim of the procedure being to associate one or several index values to the sample investigated. By reference to the boundaries of the function, these index values are then indicative of the degree and of the type of orientation distribution that is present. With respect to the coordinate system defined in Fig. 1, the orientation distribution of the structural units, $N(\theta, \phi, \psi)$, can be mathematically expressed as a series expansion in spherical harmonics (13–16). However, this mathematical treatment can often be simplified by the presence of transverse isotropy of the distribution of the molecular chain axis in the samples, i.e., isotropy in the *xy* plane. The problem then reduces to the description of the orientation of a unique axis, **c**, with respect to a reference direction, *z*. For distributions of such cylindrical symmetry, the distribution $N(\theta)$ can be characterized by using a series of Legendre polynomials, $P_n(\cos\theta)$ (1, 2, 10, 17):

$$[1] \quad N(\theta) = \sum_{n=0}^{\infty} (n + 1/2)\langle P_n\rangle P_n(\cos\theta)$$

where the normalization term $(n + \frac{1}{2})$ ensures the convergence of the series, while the coefficients $\langle P_n\rangle$ are the values that are determined experimentally. All the odd-order terms in eq. [1] are equal to zero because of the symmetry with respect to the mirror plane perpendicular to the *z* axis. The first even-order Legendre polynomials are given by:

$$P_0(\cos\theta) = 1$$

$$[2] \quad P_2(\cos\theta) = \tfrac{1}{2}(3\cos^2\theta - 1)$$

$$P_4(\cos\theta) = \tfrac{1}{8}(35\cos^4\theta - 30\cos^2\theta + 3)$$

The $\langle P_n\rangle$ coefficients of eq. [1] for a given structural unit are obtained by averaging the orientation of all units in the sample. For an isotropic sample, all coefficients are equal to zero, except $\langle P_0\rangle$, which is always equal to unity. For an oriented sample exhibiting an infinitely narrow distribution centered at an angle θ_C, the $\langle P_n\rangle$ coefficients take the value of the corresponding polynomial at this angle. Since all polynomials have their maximum value of unity at $\theta = 0°$, $\langle P_2\rangle = 1$ for structural units oriented perfectly parallel to the reference direction, while $\langle P_2\rangle = 0$ and -0.5 for a perfect orientation at $\theta = 54.7°$ and 90°, respectively.

All characterization methods used for molecular orientation studies allow the calculation of the $\langle P_2\rangle$ coefficient (1, 2). Raman spectroscopy and polarized fluorescence measurements also give the $\langle P_4\rangle$ value, and coefficients up to $\langle P_8\rangle$ can be obtained by NMR spectroscopy. Only wide-angle X-ray diffraction allows the calculation of all $\langle P_n\rangle$ coefficients, because the shape of the orientation distribution of crystal planes is measured directly by this technique.

For a system composed of several nested orientation distributions, each of these showing cylindrical symmetry, for example, *i* about the symmetry axis *z*, *j* about *i*, and *k* about *j*, the Legendre addition theorem can be used to calculate the relation between the global $\langle P_n\rangle$ coefficients obtained from the measurement and the coefficients characterizing each distribution. If, in the above example, γ is defined as the angle between *k* and the reference direction *z*, this theorem states that

Fig. 2. Geometric representation for the study of the orientation of a molecular axis **c** inclined at θ from the reference direction *z*, using measurements made for a structural unit **S** located at β from **c** and at γ from *z*. The distributions of **c** about *z* and of **S** about **c** both exhibit cylindrical symmetry.

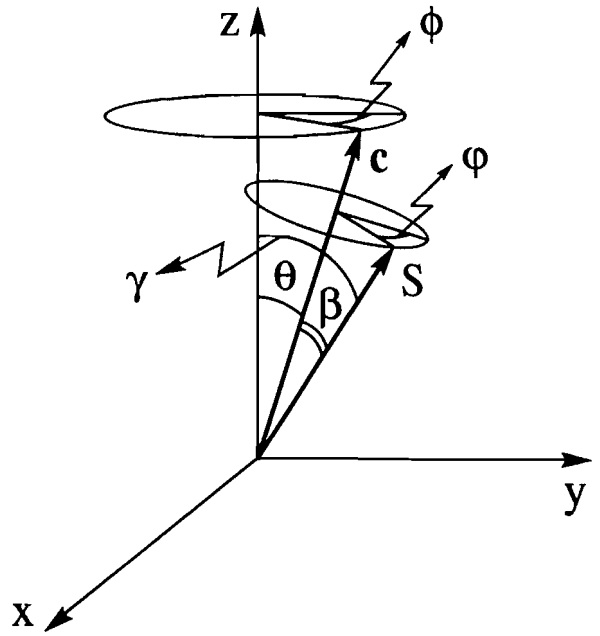

the global $\langle P_n\rangle_\gamma$ measured for this system is equal to the product of the $\langle P_n\rangle$ values characterizing each of the distributions:

$$[3] \quad \langle P_n\rangle_\gamma \equiv \langle P_n\rangle_{kz} = \langle P_n\rangle_{kj}\langle P_n\rangle_{ji}\langle P_n\rangle_{iz}$$

This property of the Legendre polynomials can be used to isolate the contributions from nested orientation distributions to the global $\langle P_2\rangle_\gamma$ coefficient calculated from the experiment. Let us consider the determination of the $\langle P_2\rangle_{cz}$ coefficient, which characterizes the orientation of the molecular chain **c** with respect to the reference direction *z*, by taking measurements relative to a structural unit **S**, which is inclined at an angle β from **c**, as is depicted in Fig. 2. The structural units studied could be, for example, the normal to a set of crystal planes studied by WAXD, or the dipole transition moment of a vibration studied by infrared spectroscopy. Since both the distributions of **S** with respect to **c** and of **c** with respect to *z* exhibit cylindrical symmetry, then that of **S** with respect to *z* also possesses this symmetry. Using eq. [3], the measured $\langle P_2\rangle_\gamma$ or $\langle P_2\rangle_{Sz}$ coefficient characterizing the orientation of the units **S** inclined at the angle γ with respect to *z* is related to the $\langle P_2\rangle_{cz}$ coefficient by:

$$[4] \quad \langle P_2\rangle_\gamma \equiv \langle P_2\rangle_{Sz} = \langle P_2\rangle_{Sc}\langle P_2\rangle_{cz}$$

Since the angle β is generally considered as fixed, i.e., the orientation distribution of **S** about **c** is infinitely narrow, then $\langle P_2\rangle_{Sc} = P_2(\cos\beta)$, and the $\langle P_2\rangle_{cz}$ is calculated by the equation:

$$[5] \quad \langle P_2\rangle_{cz} = \frac{\langle P_2\rangle_{Sz}}{P_2(\cos\beta)}$$

Can. J. Chem. Downloaded from www.nrcresearchpress.com by 80.90.12.36 on 09/08/12
For personal use only.

Discussion

Relationship between the $\langle P_2 \rangle$ coefficient and the orientation distribution

The relationship between the $\langle P_2 \rangle$ coefficient and the shape and angular position of the orientation distribution can be illustrated through the calculation of the $\langle P_n \rangle$ coefficients from the intensity distribution measured by wide-angle X-ray diffraction, $I(\theta)$. Considering Fig. 2, it can be seen that the fraction of chains **c** oriented at any angle θ is proportional to the circumference of the base of the cone described by the rotation of **c** about *z*, i.e., it is proportional to $N(\theta) \sin \theta$. For a given set of crystal planes, the diffracted intensity measured at an angle θ, $I(\theta)$, is proportional to the number of planes inclined at this angle, and the $\langle P_n \rangle$ coefficients are thus given by (1, 10, 17):

$$[6] \quad \langle P_n \rangle = \frac{\int_0^{\pi/2} I(\theta) \sin \theta \, P_n(\cos \theta) \, d\theta}{\int_0^{\pi/2} I(\theta) \sin \theta \, d\theta}$$

The model orientation distributions $I(\theta)$ used here are obtained by a 50% Gaussian – 50% Lorentzian sum, the functions being defined by:

$$[7] \quad \text{Gaussian: } I_G(\theta) = I_C \exp[-\ln 2((\theta - \theta_C)/\omega_{1/2})^2]$$

$$\text{Lorentzian: } I_L(\theta) = I_C[1 + (\sqrt{2} - 1)((\theta - \theta_C)/\omega_{1/2})^2]^{-2}$$

where I_C, θ_C, and $\omega_{1/2}$ represent, respectively, the maximum intensity, the center, and the half-width at half-height of the distribution. For the Lorentz-type function, the expression in the square brackets is raised to a –2 power instead of –1 for a classical Lorentzian, which causes a faster decrease of the tail of the distribution. The function then becomes equivalent to a Pearson VII function with an adjustable parameter $m = 2$ (11, 12). This shape of Lorentzian function is used here because, for highly oriented polymers, the orientation distribution of the crystal planes measured by wide-angle X-ray diffraction exhibits a mixed Gaussian–Lorentzian character, which is well approximated by a 50%G–50%L sum of the functions given in eq. [7] (10–12). Moreover, as will be discussed further, the analysis of data from the literature indicates that the 50%G–50%L sum also gives a good fit of the shape of the mosaic spread in supported phospholipid samples.

Table 1 gives $\langle P_2 \rangle$ values calculated using a Gaussian, a Lorentzian, and a sum of 50% Gaussian – 50% Lorentzian functions, for distributions centered at $\theta_C = 0°$ with full-widths at half-height ($W_{1/2} = 2\omega_{1/2}$) between 5° and 20°. It is observed that the shape of the orientation distribution has a considerable influence on the order parameter. For example, the $\langle P_2 \rangle$ coefficient calculated for the Lorentzian and the Gaussian–Lorentzian sum shows a significant deviation from unity when $W_{1/2} = 10°$, whereas that obtained for the Gaussian function is still close to the value for perfect parallel orientation. It has been assumed in different studies that the shape of orientation distributions can be well approximated by a Gaussian function (9, 18, 19). However, the exponential form of this type of function produces a rapid decrease of the tail of the curves, and mathematical simulations made using a Gaussian or another function of exponential form generally fall below the experimental distributions in the low-density region of the curves (10, 18, 20, 21). Comparisons made between orientation distributions measured by X-ray diffraction and mathematical simulations have shown that, for oriented polymers, a function of mixed Gaussian and Lorentzian character (Pearson VII function) gives a much better fit than the Gaussian shape (10–12, 21).

Table 1. $\langle P_2 \rangle$ coefficient calculated for orientation distributions generated using the Gaussian and Lorentzian functions defined in eq. [7] and a 50%–50% sum of these functions for different values of the full-width at half-height of the distribution, $W_{1/2}$ (in degrees).

$W_{1/2}$	Gauss	50% G + 50% L	Lorentz
5	1.00	0.98	0.97
10	0.98	0.94	0.91
15	0.96	0.89	0.85
20	0.94	0.85	0.79

Figure 3 illustrates the calculation of the $\langle P_2 \rangle$ coefficient for three different orientation distributions defined by a 50% Gaussian – 50% Lorentzian sum. The distribution curves, $I(\theta)$, are shown on the left-hand side of the figure, together with the curves showing the variation as a function of θ of the second-order Legendre polynomial $P_2(\cos \theta)$ and of the sine function. Distributions I and II are centered at $\theta_C = 25°$, with a full-width at half-height of 5° and 40°, respectively, while distribution III has its maximum at 54.7°, with $W_{1/2} = 10°$. The expressions evaluated in the numerator and denominator integrals of eq. [6] are plotted in the three graphs on the right-hand side of Fig. 3 for the different orientation distributions. The $\langle P_2 \rangle$ value is calculated from the ratio of the area under the full curve divided by that under the dotted curve. For the narrow distribution I, the shape of these two curves is identical, and the value of the $\langle P_2 \rangle$ coefficient, 0.72, is close to the value of the $P_2(\cos \theta)$ function at $\theta = 25°$, which is equal to 0.732. Distribution II multiplies the Legendre polynomial curve over a broader range, showing significant intensity up to angles where $P_2(\cos \theta) < 0$. The full curve corresponding to the numerator of eq. [6] thus takes negative values at $\theta > 54.7°$. Moreover, the dotted curve relative to the normalization term $I(\theta) \sin \theta$ defines a considerable area in comparison with the full curve, and is shifted towards the high angles because the sine function increases with θ. These two factors give a much lower $\langle P_2 \rangle$ value of 0.45 for distribution II as compared to that obtained for the intensity distribution I, even if both exhibit their maximum at $\theta_C = 25°$.

Distribution III is centered at the angle where the $P_2(\cos \theta)$ polynomial is equal to zero. Therefore, the numerator of eq. [6] gives both positive and negative areas in the corresponding graph of the right-hand side of Fig. 3 and the $\langle P_2 \rangle$ coefficient is negligible, even if the $I(\theta)$ curve exhibits a considerable orientation. Thus, an orientation measurement giving $\langle P_2 \rangle = 0$ can be interpreted either as an indication of an ordered system centered around $\theta = 54.7°$, or as a completely isotropic system.

A given $\langle P_2 \rangle$ value can correspond either to a narrow distribution centered at the angle θ_{narrow} where the Legendre polynomial is equal to the calculated coefficient, or to a broad distribution centered at an angle between θ_{narrow} and 0° (positive $\langle P_2 \rangle$ values) or between θ_{narrow} and 90° (negative $\langle P_2 \rangle$

Fig. 3. Calculation of the $\langle P_2 \rangle$ coefficient from eq. [6] for three different model intensity distributions $I(\theta)$. The $\langle P_2 \rangle$ values for distributions I, II, and III are given in the corresponding graphs of the right-hand side of the figure, showing the curves for $[I(\theta)\ P_2(\cos\theta)\ \sin\theta]$ (solid line) and $[I(\theta)\ \sin\theta]$ (dotted line).

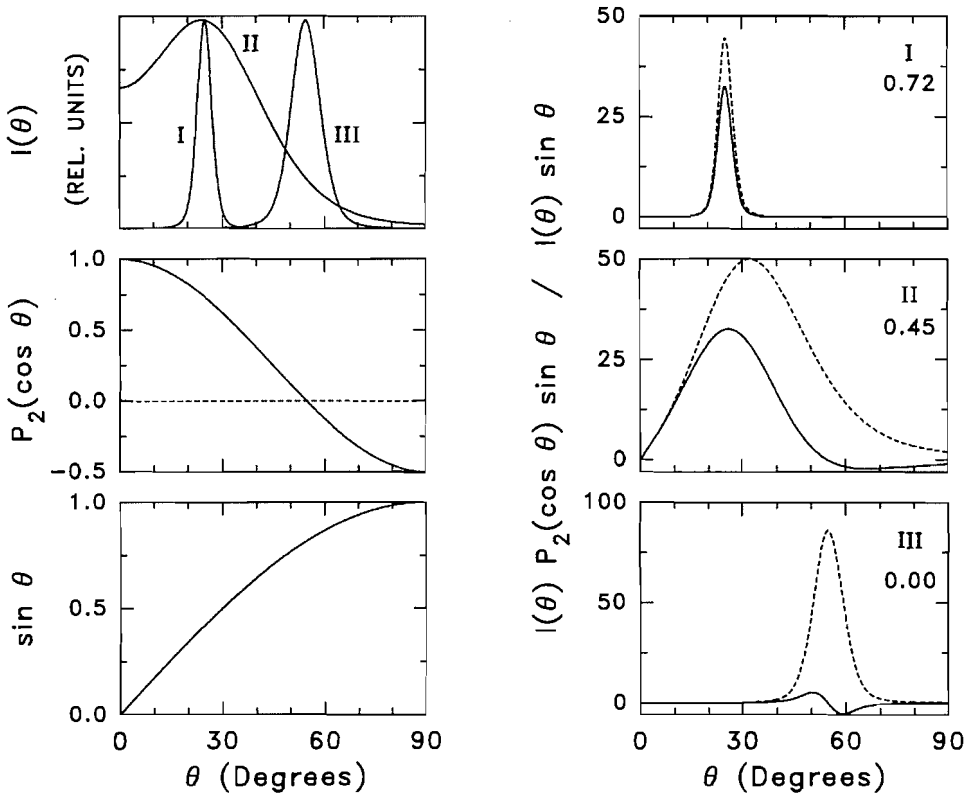

values). This is illustrated in Fig. 4, which presents different orientation distributions that were constructed using a 50% Gaussian – 50% Lorentzian sum, or the addition of two such functions. Despite the obvious differences in the position and in the width of the peaks, all distributions give the same $\langle P_2 \rangle$ coefficient. The first distribution is centered at $\theta_C = 24°$ and its $\langle P_2 \rangle$ coefficient takes the value of the polynomial at this angle, 0.750, since it is sufficiently narrow ($W_{1/2} = 2.5°$). The second and third distributions are broader than the first one and are centered at angles $\theta_{narrow} < 24°$. The two distributions at the bottom of the figure show that it is not possible to determine whether this order parameter corresponds to a unimodal or a bimodal distribution. To obtain this information, it is necessary to calculate higher order $\langle P_n \rangle$ coefficients, using X-ray diffraction, NMR, Raman, or polarized fluorescence spectroscopy. The knowledge of the $\langle P_2 \rangle$ and $\langle P_4 \rangle$ coefficients, with sufficient accuracy, can rule out some types of orientation distribution, as it is seen by comparing the $\langle P_4 \rangle$ values in Fig. 4, but the unambiguous discrimination between some distributions requires still higher order coefficients. Since the precision on $\langle P_n \rangle$ coefficients obtained in orientation studies is at best 0.01 (for example, by comparing results from different crystal planes in WAXD (10–12, 22) or from different IR bands), the distinction between the second, fourth, and fifth distributions displayed in Fig. 4 is not possible from their $\langle P_4 \rangle$ values, but could be made on the basis of the $\langle P_8 \rangle$ coefficients.

The interpretation of the type and degree of orientation cannot be made on the sole basis of the $\langle P_2 \rangle$ value unless the coefficient is close to the boundaries of the $P_2(\cos\theta)$ polynomial. $\langle P_2 \rangle$ coefficients close to 1.0 or to −0.5 clearly indicate that the sample studied is highly oriented, with its chains oriented nearly parallel or perpendicular to the reference direction, respectively. However, a $\langle P_2 \rangle$ value close to zero can be obtained for an isotropic sample, or for a highly oriented sample where the molecular chains are oriented around $\theta = 54.7°$, or for a sample possessing a broad orientation distribution at an intermediate angle.

Figure 5*a* shows a three-dimensional representation of the variation of the $\langle P_2 \rangle$ coefficient as a function of the width at half-height $W_{1/2}$ and of the position θ_C of a mixed Gaussian – Lorentzian orientation distribution. As stated above, for a very narrow distribution, the $\langle P_2 \rangle$ coefficient is equal to the value of the second-order Legendre polynomial (eq. [2]) at the angle corresponding to the center of the distribution. Thus, for $W_{1/2} = 0°$, the $P_2(\cos\theta)$ curve is obtained, with a maximum of unity at $\theta = 0°$ and a minimum of −0.50 at $\theta = 90°$. The broadening of the orientation distribution causes a decrease of the absolute value of the $\langle P_2 \rangle$ coefficient, except for distributions centered around $\theta = 54.7°$, which are always characterized by a $\langle P_2 \rangle$ value near zero. Figure 5b gives iso-$\langle P_2 \rangle$ curves obtained by joining the θ_C and $W_{1/2}$ coordinates corresponding to identical $\langle P_2 \rangle$ values, i.e., these curves represent the intersection between horizontal planes and the three-dimensional surface of Fig. 5*a*. It can be observed that the $\langle P_2 \rangle$ values near

Can. J. Chem. Downloaded from www.nrcresearchpress.com by 80.90.12.36 on 09/08/12
For personal use only.

Can. J. Chem. Downloaded from www.nrcresearchpress.com by 80.90.12.36 on 09/08/12
For personal use only.

Fig. 4. Values of the $\langle P_4 \rangle$ and $\langle P_8 \rangle$ coefficients, for different orientation distributions, all having the same order parameter $\langle P_2 \rangle = 0.750$.

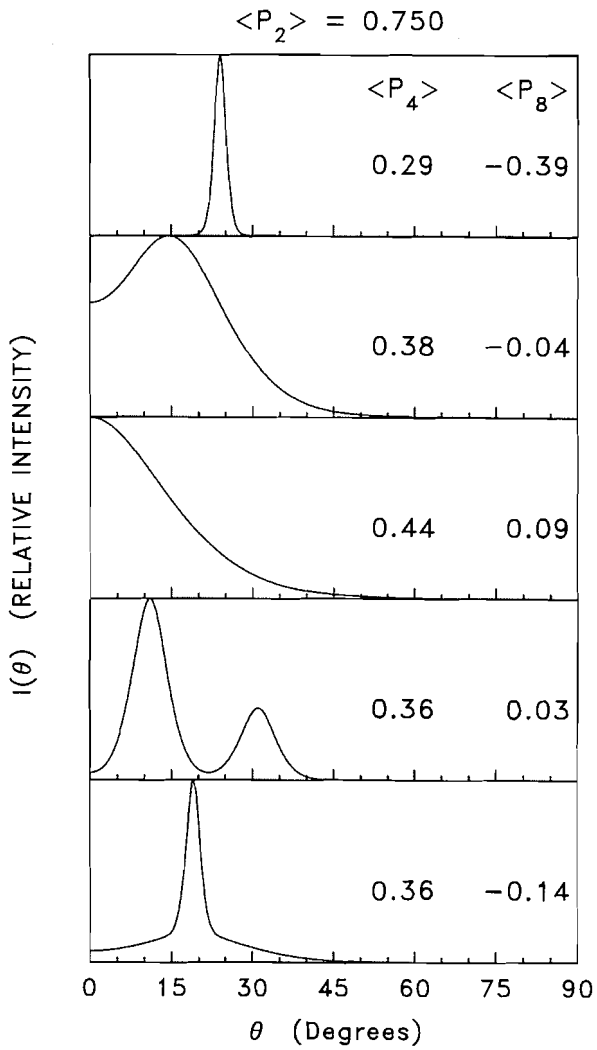

Fig. 5. (*a*) Three-dimensional representation of the variation of the $\langle P_2 \rangle$ coefficient as a function of the full-width at half-height ($W_{1/2}$) and of the position of the maximum (θ_C) of the orientation distribution. (*b*) Iso-$\langle P_2 \rangle$ curves for different values of the coefficient as a function of $W_{1/2}$ and θ_C.

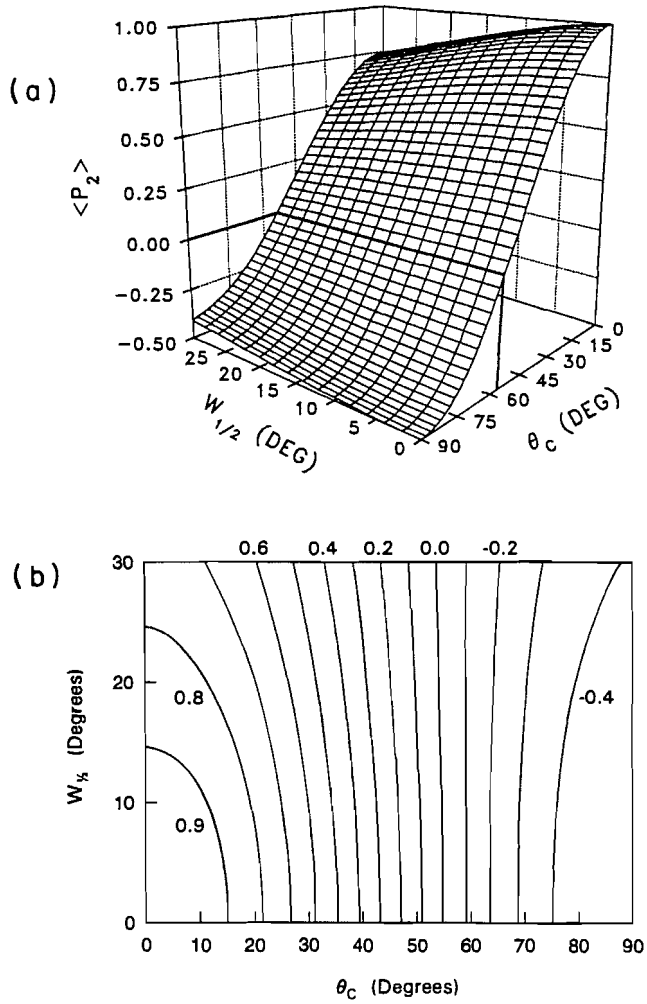

the extremum of the function vary significantly with the width and position of the center of the distribution. For example, a $\langle P_2 \rangle$ coefficient equal to 0.90 can be obtained for a narrow distribution located at $\theta_C = 15°$ as well as for a distribution with $W_{½} = 14.5°$ and centered at $\theta_C = 0°$. In comparison, for the $\langle P_2 \rangle = 0.50$ curve, the θ_C value varies only by 8°, from approximately 35° to 27°, when the width of the distribution increases from nearly zero to $W_{½} = 30°$. For unimodal distributions, Fig. 5*b* can be used to determine the range of $\theta_C - W_{1/2}$ coordinates corresponding to a given value of the $\langle P_2 \rangle$ coefficient.

Calculation of angles from the $\langle P_2 \rangle$ coefficient

In many instances, the $\langle P_2 \rangle$ coefficient is used as an orientation index, which indicates the evolution of the molecular orientation in a series of samples. For example, the $\langle P_2 \rangle_c$ value is frequently plotted as a function of the draw ratio, λ, in order to study the variation of the molecular chain orientation occurring during the deformation of polymers. However, the $\langle P_2 \rangle$ coefficient is also sometimes used to calculate the angle between a given structural unit in the sample and the reference direction. For example, infrared measurements of the $\langle P_2 \rangle_\gamma$ coefficient for two different bands can be used to determine the angle β between the dipole transition moment and the molecular chain for the second vibration, provided that this angle is known for the first one and that the orientation distribution of the chains and of both vibrations exhibit cylindrical symmetry. In other cases, the $\langle P_2 \rangle_\gamma$ coefficient is also used to calculate the apparent tilt angle, θ_{app}, of the molecular chains with respect to the reference direction, *z*:

$$[8] \quad \theta_{app} = \arccos\left[\frac{2\langle P_2 \rangle_\gamma}{3P_2(\cos\beta)} + \frac{1}{3}\right]^{1/2}$$

However, such angular calculations are justified only in the case of very narrow orientation distributions, since the $\langle P_2 \rangle_\gamma$ coefficient depends on both the shape and the angular position of the center of the distribution, as was discussed in the preceding section. Therefore, it is important to evaluate the magnitude of the errors that can be introduced when calculations are made using eq. [8], assuming a narrow and unimodal ori-

Fig. 6. Curves describing the apparent angle θ_{app} (eq. [8]) between the phospholipid acyl chain axis and the normal to the surface of the sample as a function of the molecular chain orientation θ_C: (*a*) for different values of the mosaic spread order parameter $\langle P_2 \rangle_{mz}$; (*b*) for different fractions of methylene groups in and between *gauche* conformers x_g (in %).

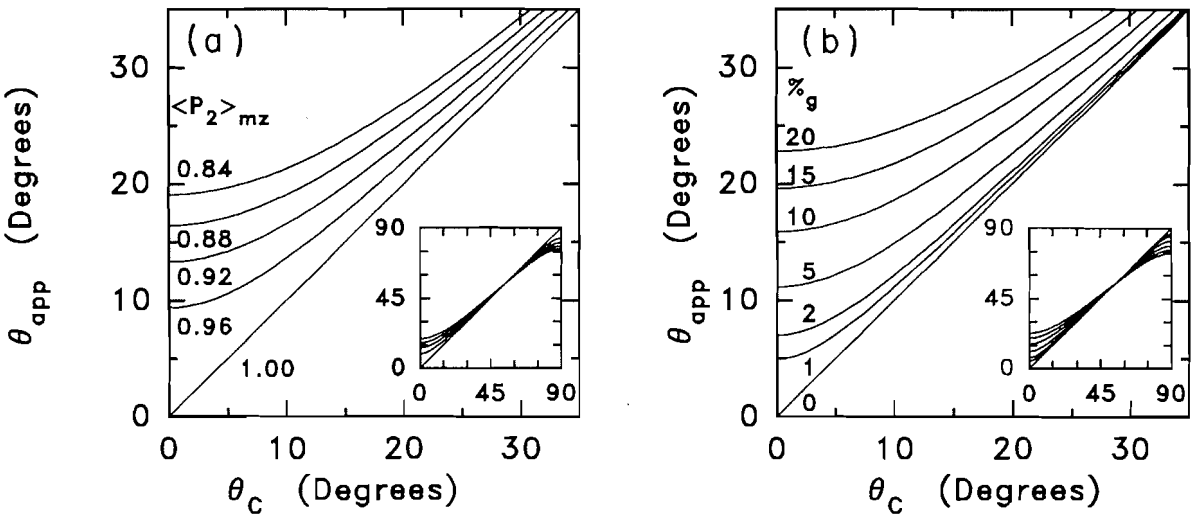

entation distribution whereas the real shape of this distribution is unknown. To achieve this, it is convenient to analyze results of studies where calculations of this sort are made. Orientation studies of phospholipid bilayers by infrared spectroscopy have been chosen for this purpose, since this characterization method gives the $\langle P_2 \rangle$ coefficient only, whereas the orientation of the lipid acyl chains can be affected by different types of disorder.

Orientation measurements of phospholipid bilayers

Phospholipid molecules, which are the main constituents of biological membranes, are built of two acyl chains linked to a polar head group (6). These molecules form bilayer structures, where the carbon chains form the inner hydrophobic part of the membrane, while the polar heads are exposed to the aqueous media on both sides of the membrane. The properties of these molecular assemblies are temperature dependent, with a phase transition occurring at the so-called "melting temperature," T_m. In the gel phase ($T < T_m$), the conformation of the carbon chains is generally considered as all-*trans*, whereas in the liquid crystalline phase ($T > T_m$), *gauche* bonds are present in the acyl chains. Attenuated total reflectance (ATR) and tilted angle transmission infrared spectroscopy are frequently used to investigate the molecular orientation in phospholipid bilayers (6, 7).

The $\langle P_2 \rangle_\gamma$ coefficient measured for samples deposited on a solid substrate, as it is done in orientation studies of biological membranes by infrared spectroscopy, can be considered as resulting from three different orientation contributions. First, the angle β between the transition dipole moment and the molecular chain introduces a factor equal to $P_2(\cos \theta)$ in the calculation, assuming that the orientation of the dipole with respect to the chain can be represented by a delta function, as is done in eq. [5]. It is noteworthy that Zbinden (23) and, more recently, Myers and Cooper (8) pointed out that there can be inaccurate assumptions regarding the β values for vibrations that are frequently used in orientation studies. In cases where discrepancies are obtained when the molecular chain axis orientation is calculated from different vibrations, this factor should thus be considered. The $\langle P_2 \rangle_\gamma$ coefficient also takes into account two orientation distributions, one resulting from the inclination of the chains with respect to the normal to the surface of the membrane, and the other from the disorder of the different membrane domains on the surface of the support. This latter type of disorder is generally referred to as the mosaic spread. Using the Legendre addition theorem (eq. [3]), the $\langle P_2 \rangle_\gamma$ value measured for such samples can be written as:

$$[9] \quad \langle P_2 \rangle_\gamma = \langle P_2 \rangle_{mz} \langle P_2 \rangle_{cm} P_2(\cos \beta)$$

where the subscripts mz and cm refer to the orientation distributions of the membrane domains with respect to the support and to that of the molecular chains in the membrane, respectively.

Values of $W_{1/2}$ ranging from 5° to 15° are common for the mosaic spread of supported samples measured in studies of biological membranes (18, 24–30). However, knowing the width at half-height of the distribution is not sufficient to assess the effect of this disorder on the measurements, since the shape of the distribution is also important, as is demonstrated in Table 1. $\langle P_2 \rangle_{mz}$ values of 0.92 ± 0.02 were calculated for freeze-fractured multilayered purple membrane samples studied by electron microscopy measurements (18, 31), which showed an orientation distribution curve with $W_{1/2} \approx 12.5°$ (18). A comparison with the results presented in Table 1 indicates that the shape of such a distribution is definitely not Gaussian, and would better be described by a 50% Gaussian – 50% Lorentzian distribution. A curve-fitting analysis of the results of Stamatoff et al. (28), who studied multilayered DPPC samples by X-ray diffraction, also indicates that the mosaic spread distribution in biological membranes is not purely Gaussian. The exponential form of the Gaussian function produces a rapid decrease of the tail of this distribution, which falls below the experimental points. Comparing

Can. J. Chem. Downloaded from www.nrcresearchpress.com by 80.90.12.36 on 09/08/12
For personal use only.

Can. J. Chem. Downloaded from www.nrcresearchpress.com by 80.90.12.36 on 09/08/12
For personal use only.

the Gaussian, Lorentzian, and the 50%G–50%L curves, the latter showed the best correlation with the experimental data.

It can thus be concluded that the mosaic spread in phospholipid bilayer samples exhibits a shape that can be approximated by a Gaussian – Lorentzian sum. Considering the values given in Table 1 for this type of distribution, it appears that the influence of the $\langle P_2 \rangle_{mz}$ coefficient in orientation studies cannot be neglected. Figure 6*a* shows curves that demonstrate the deviation between the apparent angle θ_{app} calculated by eq. [8] and the actual center θ_C of narrow orientation distributions (delta functions) for different $\langle P_2 \rangle_{mz}$ values. It is observed that the superimposition of the mosaic spread over the molecular chain distribution can cause a significant discrepancy between these two angles, particularly near $\theta_C = 0$ and 90°.

Another factor that could affect the interpretation of orientation measurements of phospholipids is the presence of *gauche* conformers in the acyl chains of the lipids. In the liquid crystalline phase, the presence of *gauche* conformers precludes the definition of a chain axis, and orientation measurements by IR spectroscopy can thus only be considered as indicative of the average orientation of the studied vibrations. For the gel phase, the tilt angle between the acyl chains and the normal to the bilayer could be calculated using eq. [8] in cases where the preparation conditions provide a narrow ($W_{1/2} < 5°$) mosaic spread, or if a good estimate of the $\langle P_2 \rangle_{mz}$ coefficient can be obtained for samples prepared by a given procedure. Nevertheless, provided that this condition is fulfilled, it is still necessary to determine the shape of the orientation distribution.

For phospholipids in the gel phase, it is frequently assumed that the acyl chains of the lipid are in the all-*trans* conformation (32). However, several studies by infrared (6, 33–35), NMR (36, 37), and Raman (38, 39) spectroscopy have shown that approximately a 2–7% fraction of *gauche* conformers is probably already present at temperatures below the transition, accounting for an average of 0.5–1.0 *gauche* bond per chain. The *gauche* rotamers are probably located mostly in kinks (*gtg'*) or jogs (*gttg'*) (34, 40, 41), which are not too disruptive of side-to-side order in the bilayer, or form end-*gauche* methyl groups (38). Moreover, the insertion of peptides or proteins in membranes can also introduce conformational disorder in the phospholipid acyl chains. A simple calculation (40) can be made to evaluate the influence of the nonplanar conformers on the orientation measurements of lipid acyl chains. Let us consider a bimodal distribution of the orientation of the methylene groups, with a first population of *trans* conformers oriented along the molecular chain axis, and a second oriented at 60° from this axis, with respective fractions x_t and x_g. Neglecting the presence of double *gauche* conformers, the x_g population is composed of the CH_2 groups located at the *gauche* bonds and of those between the *g* and *g'* conformers. The global $\langle P_2 \rangle_{CH_2}$ coefficient for this bimodal distribution is given by:

$$[10] \quad \langle P_2 \rangle_{CH_2} = x_t \langle P_2 \rangle_t + x_g \langle P_2 \rangle_g$$

It is assumed again that the orientation distributions of the x_t and x_g populations both exhibit cylindrical symmetry with respect to the reference direction and that the orientation of the CH_2 groups in the x_g fraction can be represented by a delta function inclined at 60° from the acyl chain axis. Then, $\langle P_2 \rangle_t = \langle P_2 \rangle_{cz}$ and the Legendre addition theorem leads to:

$$[11] \quad \langle P_2 \rangle_g = \langle P_2 \rangle_{cz} P_2(\cos 60°)$$

where the subscripts *z* and *c* represent the reference direction and the molecular chain axis, respectively. Using $x_g = (1 - x_t)$ and introducing eq. [11] in eq. [10] gives the equation:

$$[12] \quad \langle P_2 \rangle_{CH_2} = (1.125x_t - 0.125) \langle P_2 \rangle_{cz}$$

Assuming that $\langle P_2 \rangle_{cz} = P_2(\cos \theta_C)$, i.e., the orientation distribution of the acyl chains centered at θ_C is very narrow, the $\langle P_2 \rangle_{CH_2}$ coefficient calculated by eq. [12] can be used to evaluate, through eq. [8], the apparent angle between the chains and the membrane normal, θ_{app}. Figure 6*b* presents curves describing the variation of θ_{app} as a function of the orientation of the molecular chain axis θ_C for different percentages of methylene groups in the x_g population. These curves show that, even for a fraction $x_g \leq 5\%$, the presence of the *gauche* conformers in the phospholipid hydrocarbon chains can result in a significant error in the calculation of the chain tilt in the membrane. As it was observed in Figs. 5 and 6*a*, distributions oriented around $\theta_C = 0°$ are influenced more strongly than those centered at higher angles. However, even for phospholipids with chains oriented at 20°–35° from the reference direction, a range that encompasses the tilt angle values measured for several phospholipids (29, 42–44), *trans–gauche* isomerization could introduce some errors in the determination of the chain tilt angle by IR spectroscopy measurements at temperatures below the transition temperature. For example, for molecular axis orientations θ_C of 20° and 35°, θ_{app} values of 21.1° and 35.5° are calculated, respectively, if $x_g = 2\%$, while values of 22.6° and 36.2° are obtained for $x_g = 5\%$.

Conclusions

This article presents an analysis of the relationship between the order parameter $\langle P_2 \rangle$ and the width, the shape, and the position of the maximum θ_C of the orientation distribution. It is shown that distributions of different widths, shapes, and θ_C can give the same order parameter. Therefore, to determine unambiguously the characteristics of the actual orientation distribution, the $\langle P_2 \rangle$ coefficient is generally not sufficient and higher order coefficients are necessary. In cases where only the $\langle P_2 \rangle$ is known, the tilt angle θ_C between the molecular chain axis and the reference direction can be calculated from the order parameter only if the distribution is unimodal and very narrow because, in this particular case, the $\langle P_2 \rangle$ coefficient is close to the value of the $P_2(\cos \theta_C)$ polynomial. For broad distributions, or for distributions featuring more than one maximum, the $\langle P_2 \rangle$ value has to be considered as an average, which cannot be used to calculate the tilt angle.

The above conclusions have also been applied to the determination of the acyl chain orientation in phospholipid samples, frequently studied by infrared spectroscopy, a method that allows only the calculation of the $\langle P_2 \rangle$ coefficient. The order parameter obtained for supported phospholipid samples contains three different contributions, arising from the mosaic spread, from the orientation of the lipid molecules in the bilayers, and from the orientation of the transition dipole moment of the vibration used for the calculation. Our simulations show that the presence of mosaic spread and that of conformational disorder cannot be neglected in orientation studies. The anal-

ysis of the probable influence of these two parameters indicates that errors of a few degrees can be made in the determination of the tilt angle of the acyl chains of the lipids. The deviations between the apparent tilt angle and the true center of the orientation distribution are larger for distributions centered close to 0 or 90°.

Acknowledgements

This work was made possible through financial support from the Natural Sciences and Engineering Research Council of Canada and from the Department of Education of Québec (FCAR program).

References

1. I.M. Ward (*Editor*). Structure and properties of oriented polymers. J. Wiley and Sons, New York. 1975.
2. I.M. Ward (*Editor*). Developments in oriented polymers. Vol. 1. Applied Science, London. 1982.
3. I.M. Ward (*Editor*). Developments in oriented polymers. Vol. 2. Elsevier Applied Science, London. 1987.
4. B. Jasse and J.L. Koenig. J. Macromol. Sci.-Rev. Macromol. Chem. **C17**, 61 (1979).
5. J.L. White and M. Cakmak. *In* Encyclopedia of polymer engineering and science. Vol. 10. 2nd ed. *Edited by* H. Mark, N. Bikales, C. Overberger, and G. Menges. J. Wiley and Sons, New York. 1987. pp. 595–636.
6. U.P. Fringeli and H.H. Günthard. *In* Molecular biology, biochemistry and biophysics. Vol. 31. *Edited by* E. Grell. Springer-Verlag, Berlin. 1981. pp. 270–332.
7. E. Goormaghthigh and J.M. Ruysschaert. *In* Molecular description of biological membranes by computer aided conformational analysis. Vol. I. *Edited by* R. Brasseur. CRC Press, Boca Raton, Fla. 1990. pp. 285–329.
8. C.W. Myers and S.L. Cooper. Appl. Spectrosc. **48**, 72 (1994).
9. D.J. Ahn and E.J. Franses. Thin Solid Films, **224**, 971 (1994).
10. C.-P. Lafrance, M. Pézolet, and R.E. Prud'homme. Macromolecules, **24**, 4948 (1991).
11. C.-P. Lafrance, J. Debigaré, and R.E. Prud'homme. J. Polym. Sci. Polym. Phys. Ed. **31**, 255 (1993).
12. C.P. Lafrance and R.E. Prud'homme. Polymer, **35**, 3927 (1994).
13. H.D. Deas. Acta Crystallogr. **5**, 542 (1952).
14. R.-J. Roe and W.R. Krigbaum. J. Chem. Phys. **40**, 2608 (1964).
15. R.-J. Roe. J. Appl. Phys. **36**, 2024 (1965).
16. S. Nomura, H. Kawai, I. Kimura, and M. Kagiyama. J. Polym. Sci. Part A-2: **8**, 383 (1970).
17. W.R. Krigbaum and R.-J. Roe. J. Chem. Phys. **40**, 737 (1964).
18. N.A. Clark, K.J. Rothschild, D.A. Luippold, and B.A. Simon. Biophys. J. **31**, 65 (1980).
19. R. Hentschel, H. Sillescu, and H.W. Spiess. Polymer, **22**, 1516 (1981).
20. D.I. Bower. J. Polym. Phys. Polym. Phys. Ed. **19**, 93 (1981).
21. P. Sajkiewicz, and A. Wasiak. J. Appl. Crystallogr. **23**, 88 (1990).
22. A.P. Unwin, D.I. Bower, and I.M. Ward. Polymer, **26**, 1605 (1985).
23. R. Zbinden. Infrared spectroscopy of high polymers. Academic Press, New York. 1964. Chap. 5, pp. 166–233.
24. A.E. Blaurock. J. Mol. Biol. **93**, 139 (1975).
25. R. Henderson. J. Mol. Biol. **93**, 123 (1975).
26. M.P. Heyn, R.J. Cherry, and U. Müller. J. Mol. Biol. **117**, 607 (1977).
27. G. Büldt, H.U. Gally, J. Seelig, and G. Zaccai. J. Mol. Biol. **134**, 673 (1979).
28. J.B. Stamatoff, W.F. Graddick, L. Powers, and D.E. Moncton. Biophys. J. **25**, 253 (1979).
29. S. Tristam-Nagle, R. Zhang, R.M. Suter, C.R. Worthington, W.-J. Sun, and J.F. Nagle. Biophys. J. **64**, 1097 (1993).
30. J.F. Nagle. Biophys. J. **64**, 1110 (1993).
31. K.J. Rothschild and N.A. Clark. Biophys. J. **25**, 473 (1979).
32. G. Zaccai, G. Büldt, A. Seelig, and J. Seelig. J. Mol. Biol. **134**, 693 (1979).
33. U.P. Fringeli. Biophys. J. **34**, 173 (1981).
34. R. Mendelsohn, M.A. Davies, J.W. Brauner, H.F. Schuster, and R.A. Dluhy. Biochemistry, **28**, 8934 (1989).
35. L. Senak, D. Moore, and R. Mendelsohn. J. Phys. Chem. **96**, 2749 (1992).
36. J.H. Davis. Biophys. J. **27**, 339 (1979).
37. J.H. Davis. Biochim. Biophys. Acta, **737**, 117 (1983).
38. N. Yellin and I.W. Levin. Biochemistry, **16**, 642 (1977).
39. B.P. Gaber and W.L. Peticolas. Biochim. Biophys. Acta, **465**, 260 (1977).
40. A. Seelig and J. Seelig. Biochemistry, **13**, 4839 (1974).
41. L. Senak, M.A. Davies, and R. Mendelsohn. J. Phys. Chem. **95**, 2565 (1991).
42. M.J. Janiak, D.M. Small, and G.G. Shipley. Biochemistry, **15**, 4575 (1976).
43. F. Jähnig, K. Harlos, H. Vogel, and H. Eibl. Biochemistry, **18**, 1459 (1979).
44. P. Yeagle (*Editor*). The structure of biological membranes. CRC Press, Boca Raton, Fla. 1992.

Can. J. Chem. Downloaded from www.nrcresearchpress.com by 80.90.12.36 on 09/08/12
For personal use only.

Preparation of *ortho*-hydroxyalkylanilines as *ortho*-quinone methide imine precursors via an aminoborane complex

David Migneault, Michael A. Bernstein, and Cheuk K. Lau

Abstract: A general process for *ortho*-specific hydroxyalkylation of secondary anilines has been developed. *N*-Methylanilinochlorophenylboranes react readily with aryl aldehydes, and with α,β-unsaturated or saturated aliphatic aldehydes to give the corresponding *ortho*-hydroxyalkylanilines in good yield. Thermolysis of the latter generated the corresponding *ortho*-quinone methide imine, which can participate in an electrocyclic or intramolecular [4+2] cycloaddition reaction to give various dihydro- and tetrahydroquinoline derivatives. Application of the method to the syntheses of 5-aza analogs of hexahydrocannabinol is demonstrated.

Key words: quinone methide imine, *ortho*-hydroxyalkylaniline, azacannabinoids.

Résumé : On a mis au point un processus général pour effectuer l'hydroxyalkylation *ortho*-spécifique d'anilines secondaires. Les *N*-méthylanilinochlorophénylboranes réagissent facilement avec les aldéhydes aryliques et aliphatiques saturés ou α,β-insaturés pour fournir les *ortho*-hydroxyalkylanilines correspondantes avec de bons rendements. La thermolyse de ces dernières permet de générer les imines correspondantes de *ortho*-quinométhide qui peuvent participer dans des réactions électrocycliques ou de cycloaddition intramoléculaires [4+2] pour donner divers dérivés de la dihydro- et de la tétrahydroquinoléine. On a démontré l'application de cette méthode à la synthèse d'analogues 5-aza de l'hexahydrocannabinol.

Mots clés : imine de quinométhide, *ortho*-hydroxyalkylaniline, azacannabinoïdes.

[Traduit par la rédaction]

Introduction

ortho-Quinone methide imines **1** are highly reactive and useful synthetic intermediates. A variety of nitrogen-containing heterocycles have been prepared by the reaction of *ortho*-quinone methide imines with an olefin via cycloaddition or electrocyclic reactions (1–10). These highly reactive and unstable intermediates can be generated by flash vacuum pyrolysis of *ortho*-aminobenzyl alcohols or their *tert*-butoxycarbonylamino derivatives (2, 3), pyrolytic decarboxylation of dihydro-1,3-benzoxazin-2-ones (4), photolytic or thermal extrusion of SO_2 from 2,1-benzisothiazoline 2,2-dioxides (5, 6) fluoride-induced 1,4-elimination of [*ortho*-[(trimethylsilyl)alkylamino]-benzyl]trimethyl ammonium iodide (7), photodecarbonylation of oxindol (8), thermal ring cleavage of 2-azidoindole (9), and thermal tautomerization of *N*-phenylbenzoazetine (10).

Recently we reported the preparation of various substituted 2-phenyl-4*H*-1,3,2-benzodioxaborines, stable *ortho*-quinone methide precursors, by treating a phenol with an aldehyde in the presence of dichlorophenylborane (11). Herein we report the extension of this methodology to prepare a variety of *N*-methyl-2-hydroxyalkylanilines and their thermolysis to generate the corresponding *ortho*-quinone methide imines **1** under fairly mild conditions. Trapping of the latter with an olefin via an eletrocyclic or an intramolecular [4+2] cycloaddition reaction led to the syntheses of *N*-methyl-2-alkyl-1,2-dihydroquinolines as well as 5-aza analogs of hexahydrocannabinol (Scheme 1).

Received April 5, 1995.

D. Migneault, M.A. Bernstein, and C.K. Lau.[1] Medicinal Chemistry Department, Merck Frosst Centre For Therapeutic Research, P.O. Box 1005, Pointe Claire – Dorval, QC H9R 4P8, Canada

[1] Author to whom correspondence may be addressed. Telephone: (514) 428-8622. Fax: (514) 695-0693.

Results and discussion

ortho-Hydroxyalkylation of *N*-methylaniline

ortho-Specific hydroxyalkylation of aniline can be achieved quite readily by *ortho*-lithiation of *tert*-butoxycarbonylaniline followed by trapping of the resulting anion with the appropriate aldehyde (3, 12). Reaction of an aldehyde with *N*-methylanilinodichloroborane, prepared from *N*-methylaniline and boron trichloride *in situ*, provided a non-basic alternative. However, the latter reaction works well with benzaldehyde but poorly with aliphatic aldehydes (13). With our recent success in *ortho*-hydroxyalkylation of phenol using dichlorophenylborane as the complexing agent (11), we decided to investigate the use of this reagent to prepare *ortho*-hydroxyalkylanilines.

Using the procedure we reported for *ortho*-hydroxyalkylation of phenol (11), reaction of *N*-methylaniline with dichlorophenylborane and benzaldehyde in the presence of triethylamine in dichloromethane at 0°C gave a very poor yield of the corresponding benzyl alcohol. However, reaction of the preformed *N*-methylanilinochlorophenylborane **7***a* with benzaldehyde, in the presence of diisopropylethylamine at

Can. J. Chem. Downloaded from www.nrcresearchpress.com by 80.90.12.36 on 09/08/12
For personal use only.

Scheme 1.

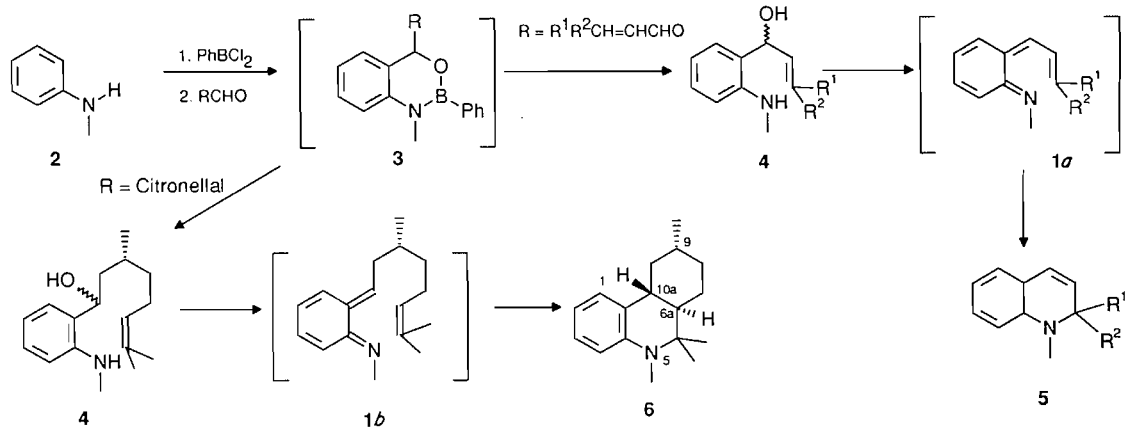

Table 1. Preparation of *o*-hydroxyalkyl aniline.

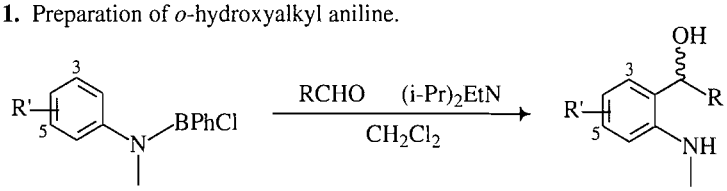

7 4

	R	R'	Temp. (°C)	Time (h)	Product	(yield %)[a]
7*a*	Ph	H	0	1.5	4*a*	(90)
		H	−20	1.5	4*b*	(71)
		H	−20	0.5	4*c*	(55)
		H	−20	0.8	4*d*	(75)
		H	0–20	1.5	4*e*	(65)
	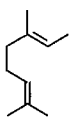	H	−20	3	4*f*	(59)
	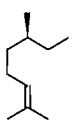	H	0–20	3	4*g*	(81)
7*b*	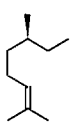	3-OMe 5-OMe	−20	2	4*h* 4*i*	(32) (34)

[a]Isolated yield.

0°C, gave 90% yield of the desired benzyl alcohol **4***a* (3) (Table 1). The presumed intermediate, 2,4-diphenyl-3,1,2-benzoxazaborine **3***a*, was not isolated. The yield of **4***a* was comparable to that reported by Sugasawa et al. using boron trichloride (13). It was thus of interest to study the scope and limitations of this reaction to determine whether **7** would react readily with aliphatic aldehydes in good yield. Thus, reaction of **7** with a series of α,β-unsaturated aldehydes was first investigated. A stock solution of **7** was prepared in advance according to the procedure of Sugasawa et al. (13). This solution could be stored at 0°C for more than 2 weeks without deterioration. In a typical procedure, a solution of **7** (11 mmol) in dichloroethane was added dropwise to a mixture of the aldehyde (10 mmol) and diisopropylethylamine (20 mmol) in dichloromethane at −20°C. The mixture was stirred at −20°C to 0°C for the appropriate time. The results are summarized in

Can. J. Chem. Downloaded from www.nrcresearchpress.com by 80.90.12.36 on 09/08/12
For personal use only.

Table 2. Synthesis of dihydroquinolines.

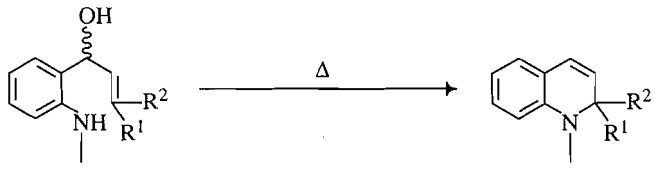

4 **5**

Substrate	Method[a]	Temp. (°C)	Time (h)	Product (yield %)[b]			
4*b*	A	180	0.75	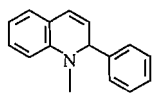 (43)		**4***b*	(27)
	B	80	20	(57)			
				5*a*			
4*c*	A	130	5	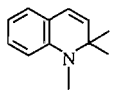 (53)		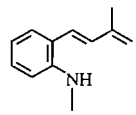	(16)
				5*b*		**9**	
4*d*	A	130	22.5	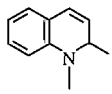 (51)		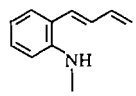	(10)
				5*c*		**10**	
	B	80	20	Decomposition			
4*e*	A	180	20	Decomposition			
	B	80	20	Decomposition			
4*f*	A	139	1.5	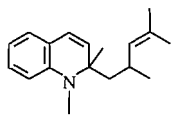 (21)		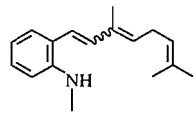	(48)
				5*d*		**11**	

[a]Method A: The substrate was refluxed in the corresponding solvent only. Method B: The substrate was refluxed in the corresponding solvent in the presence of 3 molar equivalents of phenylboronic acid and 0.3 molar equivalents of propionic acid.

[b]Isolated yield.

Scheme 2.

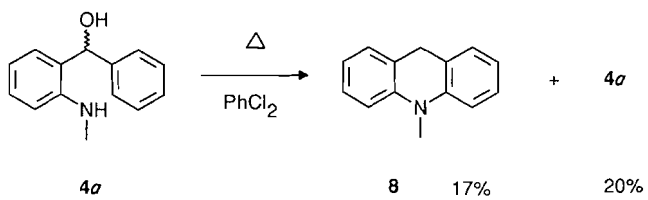

4*a* **8** 17% 20%

Table 1. Reaction of **7***a* with cinnamaldehyde gave a 71% yield of the corresponding allylic alcohol **4***b*. Similarly, **7***a* reacts readily with 3-methyl-2-butenal, crotonaldehyde, and acrolein to give **4***c* (55%), **4***d* (75%), and **4***e* (65%), respectively. With citral, the *ortho*-hydroxyalkylated product **4***f* was isolated in 59% yield. (*R*)-(+)-Citronellal, a saturated aliphatic aldehyde, was found to react quite readily with **7***a* to give the corresponding alcohols **4***g* as a 1:1 mixture of diastereomers in 81% yield. Reaction of 3-methoxy-*N*-methylanilinochlorophenylborane **7***b* with (*R*)-(+)-Citronellal gave 66% yield of the corresponding alcohols as a 1:1 mixture of regioisomers **4***h* and **4***i*. Both **4***h* and **4***i* are themselves composed of 1:1 mixtures of diastereomers. The two diastereomers of **4***i* were separable by chromatography while those of **4***h* were not.

Electrocyclic reactions of *ortho*-quinone methide imines

The benzylic and allylic alcohol substituted anilines **4** thus prepared are all well disposed for electrocyclic reactions. Thermolysis of the benzyl alcohol **4***a* in refluxing 1,2-dichlorobenzene (180°C) for 0.75 h gave only a 17% yield of the corresponding 10-methyl-9,10-dihydroacridine **8** (4) (Scheme 2), presumably via the *ortho*-quinone methide imine intermediate **1**. No trace of the corresponding acridine was detected. The yield was not improved by extending the reaction time or by raising the reaction temperature to 250°C. In contrast, flash vacuum thermolysis of **4***a* at 600°C gave a much better yield of the corresponding dihydroacridine derivative (4).

Dehydration and electrocyclization of the allylic alcohol derivatives **4***b*–**4***d* was more successful and the results are summarized in Table 2. Thermolysis of the cinnamyl alcohol derivative **4***b* in refluxing dichlorobenzene (180°C) for 0.75 h gave a 43% yield of the desired 1-methyl-2-phenyl-1,2-dihydroquinoline **5***a* (14). A significant amount of starting material (27%) was also recovered. Extending the reaction time

Can. J. Chem. Downloaded from www.nrcresearchpress.com by 80.90.12.36 on 09/08/12
For personal use only.

Table 3. Synthesis of 5-azacanabinoids.

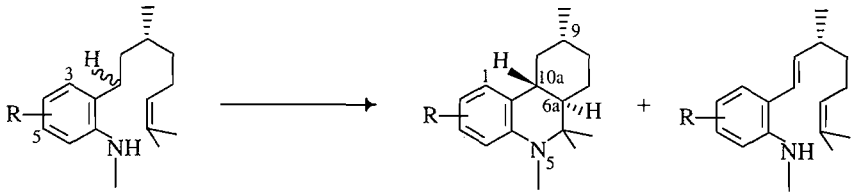

4 **6** **12**

Substrate	R	Method[a]	Temp. (°C)	Time (h)	Product	ratio	(yield %)[b]
4*g*	H	A	180	0.75	**6***a* **12***a*	1.4:1	(69)
		B	110	32		6.6:1	(71)
4*h*	3-MeO	A	130	2	**6***b* **12***b*	0:1	(73)
		B	180	1.5		1:1	(70)
4*i*	5-MeO	A	80	20	**6***c* **12***c*	10:1	(51)
		B	180	0.25		1:0	(61)

[a]Method A: The substrate was refluxed in the corresponding solvent only. Method B: The substrate was refluxed in the corresponding solvent in the presence of 3 molar equivalents of phenylboronic acid and 0.3 molar equivalents of propionic acid.

[b]Isolated yield.

resulted in lower yields due to decomposition. At a lower temperature (refluxing benzene), the reaction took 5 h to complete. More by-products were formed and the yield of **5***a* was significantly lower. In our previous work, it was found that the *ortho*-quinone methides could be generated more readily from 2-phenyl-4*H*-1,3,2-benzodioxaborin than the corresponding *ortho*-hydroxyalkyl phenol (11). It was hoped that the analogous 2-phenyl-4*H*-3,1,2-benzoxazaborin would behave similarly to afford the *ortho*-quinone methide imine more readily. Thus, a mixture of alcohol **4***b*, phenylboronic acid (3 equivalents), and a catalytic amount of propionic acid was refluxed in benzene for 20 h with concomitant removal of water. No trace of the corresponding 2-phenyl-4*H*-1,3,2-benzoxaborin was observed during this reaction, but a slightly better yield of **5***a* (57%) was isolated after chromatography. Electrocyclization of **4***c* was achieved in refluxing xylene (130°C), giving the corresponding *N*-methyl-2,2-dimethyl-1,2-dihydroquinoline **5***b* in 53% yield. Another product, **9**, formed by dehydration of the side chain, was also obtained in 16% yield. Similarly, thermolysis of the crotyl alcohol derivative **4***d* at 130°C gave 51% yield of the cyclized product **5***c* (12) and a 15% yield of the dehydrated product **10**. Attempts to limit the formation of the dehydrated products by using the phenylboronic acid procedures described above for **4***b* resulted in extensive decomposition. Apparently **4***c* and **4***d* are much more acid sensitive than **4***b*. Thermolysis of the unsubstituted allyl alcohol **4***e* at various temperatures and conditions failed to give any electrocyclized product. Either starting material was recovered or decomposition resulted when the reaction was performed at higher temperature. Thermolysis of the allylic alcohol derived from citral **4***f* in refluxing xylene gave mainly the dehydrated product **11** (48%) and only a 21% yield of the cyclized product **5***d*, an aza analog of cannabichromene. None of the product derived from the [2+4] cycloaddition with the terminal olefin, which would have led to the synthesis of a 5-aza analog of tetrahydrocannabinol, was detected. Reducing the temperature by refluxing **4***f* in benzene gave only **11** and none of the desired product **5***d*.

Syntheses of 5-aza tetrahydrocannabinoid analogs

Intramolecular trapping of *ortho*-quinone methide imines by an olefin via flash vacuum pyrolysis of *ortho*-hydroxyalkylaniline at 600°C has been reported (3). Our newly developed methodology of *ortho*-hydroxalkylation of aniline can provide such substrates quite readily. We investigated the application of this methodology for the preparation of 5-*aza* analogs of hexahydrocannabinol. Alcohols **4***g*, **4***h*, and **4***i* described in Table 1 were prepared for this purpose from Citronellal (Scheme 1 and Table 3). Thus, thermolysis of **4***g* in refluxing dichlorobenzene for 0.75 h gave a 69% yield of a 1.4 to 1 mixture of the expected cycloaddition product **6***a* and the dehydrated product **12***a*. However, thermolysis of **4***g* in the presence of phenylboronic acid and a catalytic amount of propionic acid in refluxing toluene for 32 h gave 71% of **6***a* and **12***a* in a ratio of 6.6:1. The two compounds were separated after repeated chromatography. Only a single optically active diastereomer of **6***a* ($[\alpha]_D^{25}$ +43 (*c* 1.2, $CHCl_3$)) was obtained. The stereochemistry of **6***a* is identical to that of the natural hexahydrocannabinol as confirmed by 2D COSY and decoupling NMR experiments. The vicinal coupling constant of the aliphatic signal of H-10a at δ 2.42 (d, t) across the ring junction, *J*(6a,10a), was measured to be 11.1 Hz; this is consistent with a *trans* ring junction. The equatorial orientation of the 9-Me group and boat conformation of the saturated carbonaceous ring was deduced from the analysis of the (highest field) H-10ax (δ 0.86). This proton appeared as an apparent quartet, due to approximately equal geminal and two *trans* diaxial vicinal couplings (11.4 Hz). H-9 is therefore axial, and the methyl substituent is equatorial. The ^{13}C NMR spectrum is consistent with the structure.

Thermolysis of the 3-methoxyaniline derivative **4***h* in dichlorobenzene or xylene gave no trace of the cyclized product **6***b*. Only the dehydration product **12***b* was isolated. However, after refluxing **4***h* with phenylboronic acid and a catalytic amount of propionic acid in 1,2-dichlorobenzene for 1.5 h, a 1:1 mixture of **6***b* and **12***b* was isolated in a 70% yield.

Can. J. Chem. Downloaded from www.nrcresearchpress.com by 80.90.12.36 on 09/08/12
For personal use only.

Can. J. Chem, Downloaded from www.nrcresearchpress.com by 80.90.12.36 on 09/08/12
For personal use only.

An analytical sample of **6*b*** was obtained after repeated chromatography of the mixture. The compound was found to be optically active, ($[\alpha]_D^{25}$ −51 (*c* 4.2, $CHCl_3$)). The aliphatic region of the ^1H NMR spectrum is virtually identical to that of **6*a***, indicating it has the same stereochemistry. The ^{13}C NMR spectrum is again consistent with the indicated structure.

In contrast, thermolysis of the 5-methoxyaniline derivative **4*i*** in refluxing benzene in the presence of phenylboronic acid and a catalytic amount of propionic acid for 20 h gave 51% of the desired cyclized product **6*c*** and the dehydrated product **12*c*** in the ratio of 10:1. Using the same method but refluxing in 1,2-dichlorobenzene for only 0.25 h, the yield of **6*c*** was increased to 61%. No trace of the dehydrated product **12*c*** was observed. The ^1H NMR and ^{13}C NMR spectra of compound **6*c*** are very similar to those of compounds **6*a*** and **6*b***, and are consistent with the indicated structure.

In summary, we have shown that *ortho*-hydroxyalkylation of *N*-methylaniline via *N*-methylanilinochlorophenylborane is a general and efficient process that works well with aromatic, α,β-unsaturated, and saturated aliphatic aldehydes. The *N*-methyl-*ortho*-hydroxyalkylanilines thus obtained are useful precursors of *o*-quinone methide imines. We have also shown that the latter can be generated pyrolytically from *N*-methyl-*ortho*-hydroxyalkylanilines much more readily in the presence of phenylboronic acid. With the 2-alkyl chain properly substituted with an olefin, the resulting *o*-quinone methide imines can either undergo a facile electrocyclic reaction to give *N*-methyl-2-alkyl-1,2-dihydroquinolines or they may undergo an intramolecular cycloaddition reaction to give polycyclic tetrahydroquinoline derivatives. The method was applied to the synthesis of several analogs of 5-azahexahydrocannabinol.

Experimental

General information

Proton nuclear magnetic resonance spectra were obtained on a Varian 200, Brucker ARX 400 and Brucker ARX 500 spectrometers. Reported boiling points are those observed during distillation with a Kugelrohr apparatus and are uncorrected. Melting points were measured on a Buchi 510 melting point apparatus and are uncorrected. Low-resolution mass spectral analyses were performed by the Oneida Research Services, Inc. of Whitesboro, N.Y. Exact masses were obtained by high-resolution mass spectroscopy performed by Dr. O. Maimer of McGill University, Montreal, Québec. Elemental analyses were performed by Guelph Chemical Laboratories Ltd., Guelph, Ontario. Flash chromatography was performed using Merck silica gel 60, 230–400 mesh and tlc using Merck silica gel 60F 254 sheets.

General procedure A

Preparation of N-*methyl*-ortho-*hydroxyalkylanilines*

A stock solution of *N*-methylanilinochlorophenylborane **7*a*** was prepared by adding dichlorophenylborane (100 mmol) to a solution of *N*-methylaniline (100 mmol) in 1,2-dichloroethane (100 mL) at 0°C. The resulting mixture was refluxed for 2 h under a rapid stream of nitrogen to remove the HCl formed. The mixture was cooled to give a 0.8 M cloudy solution that could be stored at 0°C for more than 6 weeks without deterioration. In a typical procedure, a solution of **7** (11 mmol) in dichloroethane was added dropwise to a mixture of the aldehyde (10 mmol) and diisopropylethylamine (20 mmol) in dichloromethane at −20°C. The mixture was stirred at −20°C to 0°C for the appropriate time, quenched with ammonium hydroxide (not needed for benzaldehyde and saturated aliphatic aldehydes), and then filtered through a short pad of silica gel. The filtrate was concentrated and the residue was chromatographed on silica gel and eluted with EtOAc–hexane (0–20%).

*(2-Methylaminophenyl)-phenylmethanol (**4**a)*

Following the general procedure A, benzaldehyde (1.06 g, 10 mmol) was reacted with **7*a*** to give, after chromatography, 1.95 g (90%) of the title compound **4*a*** (3); mp 122–125°C; ir (film): 3420 (NH), 3250 (OH) cm^{-1}; ^1H nmr (200 MHz, $CDCl_3$), δ: 2.40 (bs, 1H), 2.77 (s, 3H, N-CH_3), 4.55 (bs, 1H), 5.84 (br s, 1H, CHO), 6.70 (m, 2H), 6.90 (m, 1H), 7.25 (m, 6H). Anal. calcd. for $C_{14}H_{14}NO$: C 78.84, H 7.09, N 6.56; found: C 78.71, H 7.10, N 6.43.

*1-(2-Methylaminophenyl)-3-phenylprop-2-en-1-ol (**4**b)*

According to general procedure A, cinnamaldehyde (1.32 g, 10 mmol) was reacted with **7*a*** at −20°C for 1.5 h to give, after chromatography, 1.70 g (71%) of the title compound as a solid; mp 76–78°C; ir (film): 3325 (NH), 3150 (OH) cm^{-1}; ^1H nmr (200 MHz, $CDCl_3$), δ: 2.87 (s, 3H, N-CH_3), 2.16 (br s , 1H), 4.9 (br s, 1H), 5.43(m, 1H), 6.60 (m, 4H), 7.30 (m, 7H). Exact Mass calcd. for $C_{16}H_{18}NO$ (M+1): 240.1388; found: 240.1388. Anal. calcd. for $C_{16}H_{17}NO$: C 80.30, H 7.16, N 5.85; found: C 80.26, H 7.33, N 5.71.

*3-Methyl-1-(2-methylaminophenyl)-but-2-en-1-ol (**4**c)*

According to general procedure A, 3-methyl-2-butenal (841 mg, 10 mmol) was reacted with **7*a*** (11 mmol) at −20°C for 0.5 h to give, after chromatography, 1.05 g (55%) of the title compound; ir (film): 3100–3600 (NH, OH) cm^{-1}; ^1H nmr (200 MHz, CD_3COCD_3), δ: 1.70 (d, 3H, J = 1.2 Hz), 1.72 (d, 3H, J = 1.2 Hz), 2.80 (d, 3H, J = 5.3 Hz, N-CH_3), 4.22 (d, 1H, J = 4.0 Hz, OH), 5.38 (d, 1H, J = 5.38 Hz), 5.40 (d, 1H, J = 5.40 Hz), 5.65 (m, 1H), 6.60 (m, 2H), 7.10 (m, 2H); ms, *m/z*: 192 (M+1), 174.

*(2-Methylaminophenyl)-but-2-1-ol (**4**d)*

According to general procedure A, crotonaldehyde (701 mg, 10 mmol) was reacted with **7*a*** (11 mmol) at −20°C for 0.75 h to afford, after chromatography, 1.33 g (75%) of the title compound as an oil; ir (film): 3100–3600 (NH, OH) cm^{-1}; ^1H nmr (200 MHz, CD_3COCD_3), δ: 1.67 (d, 3H, J = 5.0 Hz), 2.79 (d, 3H, J = 5.3 Hz, N-CH_3), 4.36 (d, 1H, J = 4.0 Hz, OH), 5.10 (m, 1H), 5.25 (bs, 1H), 5.80 (m, 2H), 6.60 (m, 2H), 7.10 (m, 2H); ms, *m/z*: 178 (M+1), 177, 160.

*(2-Methylaminophenyl)-prop-2-en-1-ol (**4**e)*

According to general procedure A, acrolein (200 mg, 3.56 mmol) was reacted with **7*a*** (11 mmol) at 0°C for 0.5 h, then at room temperature for 0.75 h, to afford, after chromatography, 375 g (65%) of the title compound as an oil; ir (film): 3100–3600 (NH, OH) cm^{-1}; ^1H nmr (200 MHz, CD_3COCD_3), δ: 2.80 (d, 3H, J = 5.2 Hz, N-CH_3), 4.52 (d, 1H, J = 4.3 Hz, OH), 5.10 (dt, 1H, J = 10.4, 1.6 Hz), 5.18 (m, 2H), 5.3 (dt, 1H, J = 17.2, 1.8 Hz), 6.18 (m, 1H), 6.56 (m, 2H), 7.10 (m, 2H). Anal. calcd.

Can. J. Chem. Downloaded from www.nrcresearchpress.com by 80.90.12.36 on 09/08/12
For personal use only.

for $C_{10}H_{13}NO$: C 73.59, H 8.03, N 8.58; found: C 73.54, H 8.19, N 8.44.

*1-(2-Methylaminophenyl)-3,7dimethylocta-2,6-dien-1-ol (**4**f)*
According to general procedure A, citral (1.522 g, 10 mmol) was reacted with **7***a* (11 mmol) at −20°C for 3 h to afford, after chromatography, 1.522 g (59%) of the title compound as a mixture of 2-(*E*) and 2-(*Z*) isomers, in a ratio of 2.4:1. An analytical pure sample of each isomer was obtained by repeated chromatography. The less polar alcohol (an oil) exhibited: ir (film): 3100–3600 (NH, OH) cm^{-1}; ^1H nmr (200 MHz, CD_3COCD_3), δ: 1.57 (s, 3H), 1.63 (s, 3H), 1.75 (d, 3H, J = 1.3 Hz), 2.15, (m, 4H), 2.82 (s, 3H, N-CH_3), 4.18 (d, 1H, J = 4.0 Hz, OH), 5.10 (m, 1H, NH), 5.42 (m, 2H), 5.68 (dd, 1H, J = 8.9, 1.1 Hz), 6.50 (m, 2H), 7.10 (m, 2H). The more polar alcohol (an oil) exhibited: ^1H nmr (200 MHz, CD_3COCD_3), δ: 1.58 (s, 3H), 1.65 (s, 3H), 1.69 (d, 3H, J = 1.4 Hz), 2.10 (m, 4H), 2.83 (s, 3H, N-CH_3), 4.22 (d, 1H, J = 4.3Hz, OH), 5.10 (m, 1H, NH), 5.35 (m, 2H), 5.63 (dd, 1H, J = 8.6, 1.1 Hz), 6.55 (m, 2H), 7.10 (m, 2H). Exact Mass calcd. for $C_{17}H_{26}NO$ (M+1): 260.2014 ; found: 260.2014.

*(3R)-1-(2-Methylaminophenyl)-3,7-dimethyloct-6-en-1-ol (**4**g)*
According to general procedure A, (*R*)-(+)-Citronellal (Sigma, 85% pure, $[\alpha]_D$ +11.8) (1.54 g, 10 mmol) was reacted with **7***a* (11 mmol) at 0°C for 0.5 h, then at 20°C for 3 h, to afford, after chromatography, 2.12 g of the title compound as a 1:1 mixture of diastereomers (81%); ^1H nmr (400 MHz, CD_3COCD_3), resolved signals of the mixture, δ: 0.93 (d, 3H, J = 6.5 Hz), 0.95 (d, 3H, J = 6.4 Hz), 1.56 (s, 3H), 1.60 (s, 3H), 1.62 (s, 3H), 1.68 (s, 3H), 2.79 (s, 3H, N-CH_3), 2.80 (s, 3H, N-CH_3), 5.05 (m, 1H, CH═C), 5.12 (m, 1H, CH═C), 5.41 (bs, 1H, NH), 5.44 (bs, 1H, NH); other resonances, δ: 1.12 (m, 1H), 1.20 (m, 1H), 1.35 (m), 1.70 (m), 1.90 (m), 4.30 (m, 2H, OH), 4.77 (m, 2H, CHO), 6.56 (m, 4H), 6.98 (m, 2H), 7.07 (m, 2H). Anal. calcd. for $C_{17}H_{27}NO$: C 78.11, H 10.41, N 5.36; found: C 78.23, H 10.48, N 4.92.

*(3R)-1-(2-Methoxy-6-methylaminophenyl)-3,7-dimethyloct-6-en-1-ol (**4**h) and (3R)-1-(4-methoxy-6-methylamino-phenyl)-3,7-dimethyloct-6-en-1-ol (**4**i)*
According to general procedure A, (*R*)-(+)-citronellal (1.54 g, 10 mmol) was reacted with **7***b* (11 mmol) at −20°C for 2 h and at 20°C for 0.5 h to afford, after chromatography, 32% of **4***h* and 34% of **4***i*. Compound **4***h* is an inseparable 1:1 mixture of diastereomers: ^1H nmr (400 MHz, CD_3COCD_3), resolved signals of **4***h*, δ: 0.91 (d, 3H, J = 6.6 Hz), 0.95 (d, 3H, J = 6.6 Hz), 1.56 (s, 3H), 1.60 (s, 3H), 1.63 (s, 3H), 1.66 (s, 3H), 2.76 (s, 3H, N-CH_3), 2.77 (s, 3H, N-CH_3), 3.72 (s, 3H, OCH_3), 3.73 (s, 3H, OCH_3), 4.32 (d, 1H, J = 3.5 Hz, OH), 4.34 (d, 1H, J = 3.6 Hz, OH), 5.05 (bt, 1H, J = 7.1 Hz, CH═C), 5.12 (bt, 1H, J = 7.1 Hz, CH═C), 5.50 (m, 2H, CHO), 6.05 (bs, 2H, NH), 6.23 (d, 2H, J = 8.3 Hz), 6.25 (d, 4H, J = 8.2 Hz), 7.00 (t, 1H, J = 8.2 Hz); other resonances, δ: 1.15 (m, 2H), 1.30 (m, 2H), 1.40 (m, 2H), 1.50 (m, 2H), 1.70 (m, 2H), 2.0 (m, 4H). Exact Mass calcd. for $C_{18}H_{30}NO_2$ (M+1): 292.2276; found: 292.2276. The two diastereomers of compound **4***i* were separated by repeated chromatography. The less polar isomer: ^1H nmr (400 MHz, CD_3COCD_3), δ: 0.91 (d, 3H, J = 6.6 Hz), 1.18 (m, 1H), 1.42 (m, 2H), 1.60 (s, 3H), 1.66 (s, 3H), 1.65 (m, 2H), 1.97 (m, 2H), 2.78 (d, 3H, J = 5.2 Hz, N-CH_3), 3.73 (s, 3H), 4.13 (d, 1H, J = 4 Hz, OH), 4.72 (m, 1H, CHO), 5.12 (bt, 1H, J = 7.2 Hz, CH═C), 5.48 (bs, 1H, NH), 6.11 (m, 2H), 6.88 (d, 1H, J = 8.8 Hz); ^{13}C nmr (100.6 MHz, CD_3COCD_3), δ: 17.7, 19.6, 25.9, 26.2, 30.4, 38.5, 43.62, 55.1, 72.1, 97.7, 100.3, 122.5, 125.8, 128.4, 131.3, 150.2, 161.1. The more polar isomer of **4***i* : ^1H nmr (400 MHz, CD_3COCD_3), δ: 0.94 (d, 3H, J = 6.8 Hz), 1.13 (m, 1H), 1.40 (m, 1H), 1.48 (m, 1H), 1.56 (s, 3H), 1.63 (s, 3H), 1.65 (m, 2H), 1.80 (m, 1H), 1.95 (m, 1H), 2.78 (d, 3H, J = 5.2 Hz, N-CH_3), 3.73 (s, 3H), 4.16 (d, 1H, J = 3.9 Hz, OH), 4.70 (m, 1H, CHO), 5.05 (bt, 1H, J = 7.2 Hz, CH═C), 5.48 (bs, 1H, NH), 6.10 (d, 1H, J = 7.4 Hz), 6.12 (s, 1H), 6.86 (d, 1H, J = 7.8 Hz); ^{13}C nmr (100.6 MHz, CD_3COCD_3), δ: 17.8, 20.6, 25.9, 26.1, 30.2, 30.4, 37.7, 43.3, 55.1, 72.9, 97.7, 100.3, 121.9, 125.8, 128.7, 131.2, 150.3, 161.2. Exact Mass calcd. for $C_{18}H_{30}NO_2$ (M+1) : 292.2276; found: 292.2276.

*Preparation of 10-methyl 9,10-dihydroacridine (**8**)*
A solution of **4***a* (203 mg, 0.95 mmol) in 1,2-dichlorobenzene (6 mL) was heated to reflux for 40 min. The reaction mixture was poured directly onto a silica gel column and eluted with EtOAc–hexane to give 32 mg (17%) of the title compound **8** (3) and 44 mg (20%) of recovered starting material. The title compound is a solid, mp 91–93°C; ^1H nmr (200 MHz, CD_3COCD_3), δ: 3.39 (s, 3H), 3.85 (s, 2H), 6.90 (m, 4H), 7.20 (m, 4H). Anal. calcd. for $C_{14}H_{13}N$: C 86.12, H 6.71, N 7.17; found: C 86.19, H 6.87, N 7.11.

General procedure B

*Thermolysis 1-(2-methylaminophenyl)-3-phenyl-prop-2-en-1-ol (**4**b)*
A solution of **4***b* (995 mg, 4.16 mmol) in 1,2-dichlorobenzene (30 mL) was heated to reflux for 40 min. The solution was cooled and then poured directly onto a silica gel column and eluted with 0–5% Et_2O–hexane to give 398 mg (43.3%) of 1-methyl-2-phenyl-1,2-dihydroquinoline **5***a* (14) and 270 mg (27%) of recovered starting material. The cyclized product **5***a* is a solid, mp 82–84°C; ir (KBr): 1580, 1490, 735 cm^{-1}; ^1H nmr (300 MHz, $CDCl_3$), δ: 2.72 (s, 3H, N-CH_3), 5.15 (dd, 1H, J = 4.8, 1.3 Hz), 5.67 (dd, 1H, J = 9.8, 4.8 Hz), 6.38 (d, 2H, J = 9.8 Hz), 6.43 (d, 2H, J = 7.9 Hz), 6.61 (dt, 1H, J = 7.4, 1.0 Hz), 6.92 (dd, 1H, J = 7.3, 1.5 Hz), 7.1 (dt, 1H, J = 8.1, 1.6 Hz), 7.40 (s, 5H). Exact Mass calcd. for $C_{16}H_{16}N$ (M+1): 222.1283; found: 222.1283.

*Thermolysis of 3-methyl-1-(2-methylaminophenyl)-but-2-en-1-ol (**4**c)*
According to general procedure B, a solution of **4***c* (768 mg, 4.02 mmol) in xylene (21 mL) was heated to reflux for 5 h to give, after chromatography, 53% of 1,2,2-trimethyl-1,2-dihydroquinoline **5***b* and 16% of the elimination product [2-(3-methylbuta-1,3-dienyl)-phenyl]-methylamine **9**. Compound **5***b* : ir (film): 2960, 1595, 1490 cm^{-1}; ^1H nmr (200 MHz, CD_3COCD_3), δ: 1.32 (s, 6H, CH_3), 2.79 (s, 3H), 5.46 (d, 1H, J = 9.8 Hz), 6.24 (d, 1H, J = 9.8 Hz), 6.5 (dt, 2H, J = 8.2, 1.0 Hz), 6.80 (dd, 1H, J = 7.1, 1.7 Hz), 7.01 (dt, 1H, J = 7.8, 1.7 Hz); ^{13}C nmr (100.6 MHz, CD_3COCD_3), δ: 27.3, 30.5, 56.6, 110.5, 116.4, 121.6, 123.8, 126.5, 128.5, 132.2, 145.0. Exact Mass calcd. for $C_{12}H_{16}N$ (M+1): 174.1283; found: 174.1283. Compound **9** : ir (film): 3430 (NH), 1600, 1500 cm^{-1}; ^1H nmr

Can. J. Chem. Downloaded from www.nrcresearchpress.com by 80.90.12.36 on 09/08/12
For personal use only.

(200 MHz, CD_3COCD_3), δ: 1.95 (s, 3H), 2.82 (d, 3H), 4.95 (bs, 1H, NH), 5.00 (m, 2H), 6.60 (m, 2H), 6.75 (s, 2H), 7.12 (dt, 1H, J = 7.9, 1.4 Hz), 7.32 (dd, 1H, J = 7.5, 1.3 Hz); ^{13}C nmr (100.6 MHz, CD_3COCD_3), δ: 18.8, 30.9, 110.3, 117.1, 117.5, 122.9, 124.1, 127.2, 128.9, 133.9, 142.3, 146.6. Exact Mass calcd. for $C_{12}H_{16}N$ (M+1): 174.1283; found: 174.1283.

*Thermolysis of (2-methylaminophenyl)-but-2-en-1-ol (**4**d)*

According to general procedure B, a solution of **4***d* (979 mg) in xylene (29 mL) was heated to reflux for 22 h to give, after multiple chromatography, 446 mg (51%) of 1,2-dimethyl-1,2-dihydroquinoline **5***c* and 86 mg (10%) of [2-(buta-1,3-dienyl)-phenyl]-methylamine **10**. Compound **5***c*: ir (film): 2960, 1595, 1495, 680 cm^{-1}; ^{1}H nmr (200 MHz, CD_3COCD_3), δ: 1.07 (d, 3H, J = 6.3 Hz), 2.84 (s, 3H), 4.11(quintet, 1H, J = 6.2 Hz), 5.68 (dd, 1H, J = 9.7, 5.3 Hz), 6.30 (d, 1H, J = 9.8 Hz), 6.45 (m, 2H), 6.84 (dd, 1H, J = 7.3, 1.6 Hz), 7.01 (dt, 1H, J = 7.8, 1.5 Hz); ^{13}C nmr (100.6 MHz, CD_3COCD_3), δ: 18.2, 35.8, 55.3, 110.5, 116.5, 122.5, 124.9, 126.7, 127.0, 129.0, 145.0. Anal. calcd. for $C_{11}H_{13}N$: C 82.97, H 8.23, N 8.80; found: C 82.94, H 8.11, N 9.15. Compound **10**: ir (film): 3300–3500 (NH) cm^{-1}; ^{1}H nmr (200 MHz, CD_3COCD_3), δ: 2.87 (s, 3H), 3.75 (bs, 1H), 5.17 (dd, 1H, J = 9.2, 1.7 Hz), 5.35 (dd, 1H, J = 16.9, 2.0 Hz), 6.30 (m, 2H), 6.70 (m, 3H), 7.11 (dd, 1H, J = 7.5, 1.5 Hz), 7.22 (dt, 1H, J = 7.8, 1.6 Hz); ^{13}C nmr (100.6 MHz, CD_3COCD_3), δ: 30.7, 109.6, 116.4, 119.0, 122.6, 126.8, 128.8, 130.0, 132.4, 133.7, 146.7. Exact Mass calcd. for $C_{11}H_{14}N$ (M+1): 160.1126; found: 160.1126.

*Thermolysis of 1-(2-methylaminophenyl)-3,7dimethylocta-2,6-dien-1-ol (**4**f)*

According to general procedure B, a solution of **4***f* (195 mg, mixture of *cis* and *trans* isomers) was heated to reflux in xylene for 1.5 h to give, after multiple chromatography, 39 mg (21%) of 1,2-dimethyl-2-(4-methylpent-3-enyl)-1,2-dihydroquinoline **5***d* and 78 mg (48%) of [2-(3,7-dimethylocta-1,3,6-trienyl)-phenyl]-methylamine **11** as a complex mixture of isomers. Compound **5***d*: ir (film): 2960, 2920, 1600, 1580 780 cm^{-1}; ^{1}H nmr (200 MHz, $CDCl_3$), δ: 1.27 (m, 1H), 1.30 (s, 3H), 1.52 (s, 3H), 1.63 (s, 3H), 2.02 (m, 3H), 2.76 (s, 3H), 5.10 (m, 1H), 5.33 (d, 1H, J = 9. 9 Hz), 6.33 (d, 1H, J = 9.9 Hz), 6.44 (d, 1H, J = 8.2 Hz), 6.54 (dt, 1H, J = 7.3 Hz, 1.0 Hz), 6.77 (dd, 1H, J = 7.7, 1.0 Hz), 6.98 (dt, 1H, J = 9.3, 1.5 Hz); ^{13}C nmr (100.6 MHz, CD_3COCD_3), δ: 17.6, 23.9, 25.7, 27.3, 30.2, 41.5, 60.1, 109.3, 115.7, 121.0, 124.3, 125.0, 126.5, 129.0, 130.0, 131.5, 145.5. Exact Mass calcd. for $C_{17}H_{24}N$ (M+1): 242.1909; found: 242.1909.

*Thermolysis of (3*R*)-1-(2-methylaminophenyl)-3,7-dimethyloct-6-en-1-ol (**4**g)*

According to general procedure B, a solution of **4***g* (1.276g, 4.889 mmol) in 1,2-dichlorobenzene (25 mL) was heated to reflux for 0.75 h to afford, after multiple chromatography, 474 mg (40%) of (6a*R*,9*R*,10a*R*)-5,6,6,9-tetramethyl-5,6,6a,7,8,9,10,10a-octahydrophenanthridine **6***a* and 342 mg (29%) of (3*R*)-(1*E*)-[2-(3,7-dimethylocta-1,6-dienyl)-phenyl]-methylamine **12***a*. Compound **6***a*: $[\alpha]_D$ +43 (*c* 1.2, $CHCl_3$); ir (film): 2960, 2930, 1600, 1580, 780 cm^{-1}; ^{1}H nmr (500 MHz, CD_3COCD_3), δ: 0.86 (q, 1H, J = 11.4 Hz, H-10ax), 0.94 (dt, 1H, J = 12.7, 3.5 Hz, H-8ax), 0.97 (d, 3H, J = 6.6 Hz), 0.99 (s, 3H), 1.23 (m, 1H, H-7ax), 1.25 (m, 1H, H-6a), 1.28 (s, 3H), 1.56 (m, 1H, H-9ax), 1.81 (m, 1H, H-8eq), 1.90 (m, 1H, H-7eq), 2.42 (dt, 1H, J = 11.1, 4.0 Hz, H-10a), 2.49 (m, 1H, H-10eq), 2.85 (s, 3H), 6.55 (m, 2H), 7.10 (m, 2H); ^{13}C nmr (100.6 MHz, CD_3COCD_3), δ: 19.1, 22.8, 26.2, 28.2, 32.2, 32.4, 35.0, 35.6, 40.1, 47.6, 57.1, 111.6, 115.5, 124.7, 126.9, 145.9. Exact Mass calcd. for $C_{17}H_{26}N$ (M+1): 244.2065; found: 244.2065. Compound **12***a*: ir (film): 3430 (NH) 2950, 2900, 1600, 1500, 740 cm^{-1}; ^{1}H nmr (500 MHz, $CDCl_3$), δ: 1.14 (d, 3H, J = 6.7 Hz), 1.45 (m, 2H), 1.65 (s, 3H), 1.74 (d, 3H, J = 1.0 Hz), 2.07 (m, 2H), 2.35 (m, 1H), 2.91 (s, 3H), 3.81 (bs, 1H), 5.16 (m, 1H), 5.96 (dd, 1H, J = 15.6, 8.0 Hz), 6.37 (d, 1H, J = 15.6 Hz), 6.67 (d, 1H, J = 8.1 Hz), 6.75 (m, 1H), 7.2 (m, 2H); ^{13}C nmr (100.6 MHz, CD_3COCD_3), δ: 15.9, 17.7, 20.1, 25.7, 25.9, 30.9, 37.1, 37.2, 109.9, 117.3, 123.7, 124.6, 127.3, 128.1, 131.4, 139.5, 145.9. Anal. calcd. for $C_{17}H_{25}N$: C 83.89, H 10.35, N 5.75; found: C 83.86, H 9.88, N 5.72. Exact Mass calcd. for $C_{17}H_{26}N$ (M+1): 244.2065; found: 244.2065.

*Thermolysis of (3*R*)-1-(2-methoxy-6-methylaminophenyl)-3,7-dimethyloct-6-en-1-ol (**4**h)*

According to general procedure B, a solution of **4***h* (161 mg, 0.4 mmol) in xylene (2.5 mL)was heated under reflux for 2 h to afford 111 mg (73%) of (3*R*)-(1*E*)-[2-(3,7-dimethylocta-1,6-dienyl)-3-methoxyphenyl]-methylamine **12***b*; ^{1}H nmr (400 MHz, $CDCl_3$), δ: 1.08 (d, 3H, J = 6.7 Hz), 1.39 (m, 2H), 1.59 (s, 3H), 1.67 (s, 3H), 2.02 (m, 2H), 2.30 (m, 1H), 2.81 (s, 3H), 3.75 (s, 3H), 4.25 (bs, 1H, NH), 5.12 (bt, 1H, J = 6.1 Hz), 5.86 (dd, 1H, J = 16.4, 7.8 Hz), 6.20 (d, 1H, J = 16.4 Hz), 6.29 (s, 1H), 6.31 (s, 1H), 7.07 (t, 1H, J = 8.2 Hz); ^{13}C nmr (100.6 MHz, CD_3COCD_3), δ: 17.8, 21.3, 25.9, 26.7, 31.2, 38.0, 38.7, 55.7, 100.7, 104.1, 121.4, 125.6, 128.8, 131.6, 141.0, 148.9, 158.5. Exact Mass calcd. for $C_{18}H_{28}NO$ (M+1): 274.2170; found: 274.2171.

General procedure C

*Thermolysis of 1-(2-methylaminophenyl)-3-phenylprop-2-en-1-ol (**4**b) in the presence of phenylboronic acid*

A mixture of **4***b* (100 mg, 0.42 mmol), phenylboronic acid (153 mg, 1.26 mmol), and propionic acid (9.3 mg, 0.126 mmol) in benzene (6 mL) was refluxed for 20 h with concomitant removal of water. The mixture was concentrated in vacuum and the residue was chromatographed on silica gel, eluting with 2.5% EtOAc–hexane to give 52.8 mg (57%) of **5***a*.

*Thermolysis of (3*R*)-1-(2-methylaminophenyl)-3,7-dimethyloct-6-en-1-ol (**4**g) in the presence of phenylboronic acid*

According to general procedure C, a mixture of **4***g* (200 mg, 0.76 mmol), phenylboronic acid (250 mg, 2.06 mmol), and propionic acid (15 mg, 0.21 mmol) in 5 mL of toluene was refluxed for 32 h to give, after chromatography, 132 mg (71%) of a mixture of **6***a* and **12***a* in the ratio of 6.6:1.

*Thermolysis of (3*R*)-1-(2-methoxy-6-methylaminophenyl)-3,7-dimethyloct-6-en-1-ol (**4**h) in the presence of phenylboronic acid*

According to general procedure C, a mixture of **4***h* (200 mg, 0.69 mmol), phenylboronic acid (250 mg, 2.06 mmol), and propionic acid (15 mg, 0.21 mmol) in 5 mL of 1,2-dichloro-

benzene was refluxed for 1.5 h to give, after chromatography, 132 mg (70%) of a mixture of (6a*R*,9*R*,10a*R*)-1-methoxy-5,6,6,9-tetramethyl-5,6,6a,7,8,9,10,10a-octahydrophenanthridine **6***b* and **12***b* in the ratio of 1:1. An analytical sample of **6***b* was obtained by multiple chromatography. Compound **6***b*: $[\alpha]_D$ −51 (*c* 4.2, $CHCl_3$); ^{1}H nmr (400 MHz, CD_3COCD_3), δ: 0.61 (q, 1H, *J* = 11.4 Hz, H-10ax), 0.77 (s, 3H), 0.91 (d, 3H, *J* = 6.5 Hz), 1.10 (m, 2H), 1.30 (s, 3H), 1.44 (dt, 1H, *J* = 11.3, 2.3 Hz), 1.61 (m, 1H), 1.87 (m, 1H), 1.94 (m, 1H), 2.48 (dt, 1H, *J* = 10.7, 2.2 Hz), 2.79 (s, 3H), 2.95 (m, 1H), 3.76 (s, 3H), 6.31 (d, 1H, *J* = 8.1 Hz), 6.34 (d, 1H, *J* = 8.4 Hz), 6.97 (t, 1H, *J* = 8.3 Hz); ^{13}C nmr (100.6 MHz, $CDCl_3$), δ: 15.9, 22.7, 26.1, 28.8, 33.0, 33.1, 36.1, 37.3, 40.6, 50.2, 55.1, 55.9, 100.4, 107.6, 115.3, 126.8, 148.5, 158.4. Exact Mass calcd. for $C_{18}H_{28}NO$ (M+1): 274.2170; found: 274.2171.

*Thermolysis of (3*R*)-1-(4-methoxy-6-methylaminophenyl)-3,7-dimethyloct-6-en-1-ol (**4***i*) in the presence of phenylboronic acid*

According to general procedure C, a mixture of **4***i* (291 mg, 1 mmol), phenylboronic acid (365 mg, 3 mmol), and propionic acid (22 mg, 0.3 mmol) in benzene (10 mL) was refluxed for 20 h to give, after chromatography, 140 mg (51%) of a mixture of (6a*R*,9*R*,10a*R*)-3-methoxy-5,6,6,9-tetramethyl-5,6,6a,7,8,9,10,10a-octahydrophenanthridine **6***c* and (3*R*)-(1*E*)-[2-(3,7-dimethylocta-1,6-dienyl)-5-methoxyphenyl]methylamine **12***c* in the ratio of 10:1. An analytical sample of **6***c* was obtained by multiple chromatography. Compound **6***c*: $[\alpha]_D$ +37 (*c* 4.5, $CHCl_3$); ^{1}H nmr (400 MHz, CD_3COCD_3), δ: 0.83 (q, 1H, *J* = 11.6 Hz, H-10ax), 0.98 (d, 3H, *J* = 6.5 Hz), 1.0 (s, 3H), 1.20 (m, 2H), 1.22 (m, 1H), 1.29 (s, 3H), 1.54 (m, 1H), 1.82 (m, 1H), 1.89 (m, 1H), 2.37 (dt, 1H, *J* = 10.3, 2.7 Hz), 2.45 (m, 1H), 2.83 (s, 3H), 3.71 (s, 3H), 6.12 (d, 1H, *J* = 2.4 Hz), 6.16 (dd, 1H, *J* = 8.3, 2.4 Hz), 7.0 (d, 1H, *J* = 8.3 Hz); ^{13}C nmr (100.6 MHz, CD_3COCD_3), δ: 19.1, 23.1, 26.5, 28.7, 32.4, 33.0, 35.8, 36.0, 41.3, 48.9, 55.1, 57.7, 99.2, 100.7, 120.2, 125.9, 147.8, 160.0. Exact Mass calcd. for $C_{18}H_{28}NO$ (M+1): 274.2170; found: 274.2172. Insufficient compound **12***c* was available for complete characterization. The reaction was repeated with 225 mg (0.77 mmol) of **4***i* in refluxing 1,2-dichlorobenzene for 0.25 h to give 129 mg (61%) of **6***c* with no trace of **12***c*.

References

1. C.W.G. Fishwick and D.W. Jones. *In* The chemistry of quinonoid compounds. Vol. 2. *Edited by* S. Patai and Z. Rappoport. John Wiley and Sons Ltd., New York. 1988. pp. 403–453.
2. Y.-L. Mau and V. Boekelheide. J. Org. Chem. **45**, 1547 (1980).
3. C.W.G. Fishwick, R.C. Storr, and P.W. Manley. J. Chem. Soc. Chem. Commun. 1304 (1984).
4. I. Hodgetts, S.J. Noyce, and R.C. Storr. Tetrahedron Lett. **25**, 5435 (1984).
5. M. Lancaster and D.J.H. Smith. J. Chem. Soc. Chem. Commun. 471 (1980).
6. K. Wojciechowski. Tetrahedron, **49**, 7277 (1993).
7. Y. Ito, S. Miyata, M. Nakatsuka, and T. Saegusa. J. Am. Chem. Soc. **103**, 5250 (1981).
8. M. Fisher and F. Wagner. Chem. Ber. **102**, 3486 (1969).
9. E. Foresti, P. Spagnolo, and P. Zanirato. J. Chem. Soc. Perkin Trans. 1, 1354 (1989).
10. E.M. Burgess and L. McCullagh. J. Am. Chem. Soc. **88**, 1580 (1966).
11. C.K. Lau, M. Mintz, M.A. Bernstein, and C. Dufresne. Tetrahedron Lett. **34**, 5527 (1993).
12. J.M. Muchowski and M.C. Venati. J. Org. Chem. **45**, 4798 (1980).
13. T. Sugasawa, T. Toyoda, M. Adachi, and K. Sasakura. J. Am. Chem. Soc. **100**, 4842 (1978).
14. R.C. Elderfield and B.H. Wark. J. Org. Chem. **27**, 543 (1962).

Can. J. Chem. Downloaded from www.nrcresearchpress.com by 80.90.12.36 on 09/08/12
For personal use only.

Volumetric properties of (water + diethanolamine) systems

Yadollah Maham, Tjoon T. Teng, Alan E. Mather, and Loren G. Hepler

Abstract: Densities of completely miscible (water + methyldiethanolamine) and (water + ethyldiethanolamine) systems have been measured over the full range of compositions at temperatures from 25 to 80°C. Results of these measurements have been used in calculating excess molar volumes and partial molar volumes of each component. We have also identified different measures of the thermal expansion of these systems and have calculated some of these derivative quantities. The partial molar volumes and their derivatives with respect to temperature provide a basis for extending our understanding of molecular interactions in these (water + organic) systems.

Key words: diethanolamines, excess molar volumes, partial molar volumes, expansivities, aqueous solutions.

Résumé : Opérant à des températures allant de 25 à 80°C, on a mesuré les densités des systèmes complètement miscibles (eau + méthyldiéthanolamine) et (eau + éthyldiéthanolamine) sur l'ensemble des plages de composition. On a utilisé ces résultats pour calculer les volumes molaires en excès et les volumes molaires partiels de chacun des composants. On a aussi identifié différentes mesures de l'expansion thermique de ces systèmes et on a calculé quelques-unes de ces quantités dérivées. Les volumes molaires partiels et leurs dérivées par rapport à la température fournissent une base pour étendre notre compréhension des interactions dans ces systèmes (eau + composé organique).

Mots clés : diéthanolamines, volumes molaires en excès, volumes molaires partiels, expansivité, solutions aqueuses.

[Traduit par la rédaction]

Introduction

Various (water + alkanolamine) systems are used for removal of acidic gases such as carbon dioxide and especially hydrogen sulfide from gas streams in the natural gas and petroleum industries and are of increasing importance in treating acidic gas streams in several chemical production industries. Knowledge of several properties, including densities at several temperatures, is required for engineering design and for subsequent operations, as summarized by Astarita et al. (1).

In addition to the well-established industrial uses of experimental data for these completely miscible (water + alkanolamine) systems, there is interest in using volumetric data in combination with molecular theories or models of solutions to extend our understanding of molecular interactions in (water + organic) systems. Because much of our focus in this paper is on the volumetric properties of an alkanolamine at infinite dilution in water, we cite two theoretical investigations (2, 3) that focussed on the temperature dependence of partial molar volumes of aqueous solutes. We also call attention to subsequent theory by Yoshimura and Nakahara (4), a useful review by Davis (5), and recent theory by Marcus (6). Some of each of these cited works is devoted to volumetric properties of (water + organic) systems, and some of the theoretical work by Marcus (6) is specifically concerned with volumetric properties of (water + alkanolamine) systems.

There have been two recent reports (7, 8) of volumetric properties of (water + alkanolamine) systems. We also call attention to several other reports (7–23) of volumetric properties of (water + organic) systems, which include experimental results or methods of analysis that are related to our work.

Received April 24, 1995.

Y. Maham, T.T. Teng,[1] A.E. Mather, and L.G. Hepler.[2]
Department of Chemistry and Department of Chemical Engineering, University of Alberta, Edmonton, AB T6G 2G2, Canada.

[1] Present address: School of Industrial Technology, Universite Sains Malaysia, Penang, Malaysia.

[2] Author to whom correspondence may be addressed. Telephone: (403) 492-2762. Fax: (403) 492-8231.

Experimental

Methyldiethanolamine [$CH_3N(C_2H_4OH)_2$, MDEA] and ethyldiethanolamine [$C_2H_5N(C_2H_4OH)_2$, EDEA] from Aldrich Chemical Company were stated to be 99% and 98+% pure. Results of titrations with standardized hydrochloric acid were consistent with purities slightly better than 99% for both MDEA and EDEA, which were then used as received. Mixtures of these ethanolamines with doubly distilled water were made by mass, with care being taken to minimize exposure to air (carbon dioxide).

Densities were measured with an Anton Paar DMA 45 density meter, which was calibrated with dry air and distilled water at each temperature, making use of densities of water from Kell (24). Accuracies of most of our densities are about $\pm(3 \times 10^{-5})$ g cm^{-3}, with accuracies of a few densities (especially at the higher temperatures) being about $\pm(8 \times 10^{-5})$ g cm^{-3}. Temper-

Can. J. Chem. Downloaded from www.nrcresearchpress.com by 80.90.12.36 on 09/08/12
For personal use only.

Can. J. Chem. Downloaded from www.nrcresearchpress.com by 80.90.12.36 on 09/08/12
For personal use only.

Table 1. Mole fractions, densities, and excess molar volumes for water (1) + methyldiethanolamine (2, MDEA) mixtures.[a]

	25°C		30°C		40°C		50°C		60°C		70°C		80°C	
x_2	d	V^E	d	V^E	d	V^E	d	V^E	d	V^E	d	V^E	d	V^E
0.0000	0.997 04	0.000	0.995 65	0.000	0.992 22	0.000	0.998 04	0.000	0.983 20	0.000	0.977 77	0.000	0.971 80	0.000
0.0079	1.001 28	−0.044	0.999 68	−0.043	0.996 12	−0.044	0.991 85	−0.046	0.986 68	−0.043	0.981 29	−0.046	0.975 36	−0.049
0.0176	1.006 18	−0.101	1.004 50	−0.101	1.000 69	−0.102	0.996 09	−0.102	0.990 92	−0.102	0.985 28	−0.104	0.979 01	−0.103
0.0364	1.014 93	−0.220	1.012 91	−0.218	1.008 60	−0.218	1.003 58	−0.216	0.997 98	−0.214	0.991 84	−0.211	0.985 31	−0.208
0.0612	1.024 61	−0.379	1.022 26	−0.375	1.017 27	−0.369	1.011 61	−0.363	1.005 47	−0.356	0.999 08	−0.353	0.992 04	−0.343
0.0923	1.034 14	−0.570	1.031 33	−0.561	1.025 54	−0.547	1.019 25	−0.534	1.012 60	−0.522	1.005 66	−0.512	0.998 12	−0.493
0.1322	1.042 43	−0.778	1.039 24	−0.765	1.032 82	−0.744	1.025 86	−0.722	1.018 64	−0.701	1.010 66	−0.667	1.003 29	−0.657
0.1859	1.048 81	−0.989	1.045 28	−0.972	1.038 26	−0.943	1.030 80	−0.915	1.023 13	−0.885	1.015 21	−0.858	1.007 12	−0.827
0.2526	1.052 09	−1.154	1.048 39	−1.136	1.041 03	−1.104	1.033 22	−1.070	1.025 35	−1.039	1.017 43	−1.015	1.008 87	−0.965
0.3021	1.052 76	−1.224	1.049 06	−1.210	1.041 54	−1.177	1.033 64	−1.143	1.025 60	−1.106	1.017 64	−1.083	1.009 12	−1.033
0.3658	1.052 18	−1.252	1.048 39	−1.238	1.040 74	−1.203	1.032 08	−1.134	1.024 76	−1.136	1.016 76	−1.113	1.008 29	−1.062
0.5026	1.048 63	−1.144	1.044 97	−1.145	1.037 20	−1.110	1.029 27	−1.085	1.021 28	−1.054	1.013 03	−1.015	1.004 53	−0.952
0.5653	1.046 88	−1.056	1.043 10	−1.052	1.035 50	−1.032	1.027 61	−1.011	1.019 62	−0.980	1.011 75	−0.968	1.003 45	−0.915
0.6960	1.043 14	−0.798	1.039 52	−0.814	1.031 80	−0.788	1.024 00	−0.779	1.016 06	−0.751	1.008 02	−0.725	1.000 03	−0.690
0.7997	1.040 50	−0.558	1.036 84	−0.575	1.029 12	−0.553	1.021 41	−0.555	1.013 38	−0.518	1.005 60	−0.515	0.997 70	−0.484
0.8989	1.038 32	−0.314	1.034 58	−0.328	1.026 87	−0.308	1.019 20	−0.319	1.011 38	−0.301	1.003 56	−0.295	0.995 70	−0.265
0.9475	1.037 31	−0.185	1.033 57	−0.201	1.025 86	−0.183	1.018 16	−0.192	1.010 38	−0.179	1.002 60	−0.177	0.994 78	−0.149
1.0000	1.035 90	0.000	1.032 00	0.000	1.024 45	0.000	1.016 66	0.000	1.009 00	0.000	1.001 24	0.000	0.993 67	0.000

[a]Units are g cm^{-3} for densities (d) and are cm^3 mol^{-1} for excess molar volumes (V^E).

Table 2. Mole fractions, densities, and excess molar volumes for water (1) and ethyldiethanolamine (2, EDEA) + mixtures.[a]

	25°C		30°C		40°C		60°C		80°C	
x_2	d	V^E	d	V^E	d	V^E	d	V^E	d	V^E
0.0000	0.997 04	0.000	0.995 65	0.000	0.992 22	0.000	0.983 20	0.000	0.971 80	0.000
0.0026	0.998 37	−0.020	0.996 89	−0.019	0.993 38	−0.019	0.984 03	−0.016	0.972 75	−0.020
0.0056	0.999 45	−0.036	0.998 14	−0.039	0.994 70	−0.042	0.985 35	−0.042	0.973 60	−0.040
0.0112	1.002 52	−0.087	1.000 88	−0.086	0.997 28	−0.090	0.987 43	−0.086	0.975 50	−0.084
0.0244	1.008 51	−0.196	1.006 61	−0.194	1.002 43	−0.194	0.991 74	−0.186	0.979 39	−0.185
0.0392	1.014 33	−0.318	1.012 69	−0.326	1.008 00	−0.324	0.996 31	−0.307	0.982 87	−0.291
0.0582	1.021 25	−0.488	1.018 93	−0.486	1.013 49	−0.475	1.001 13	−0.458	0.986 19	−0.416
0.0810	1.027 51	−0.674	1.024 61	−0.664	1.018 41	−0.643	1.004 20	−0.593	0.988 85	−0.547
0.1062	1.031 93	−0.844	1.028 87	−0.833	1.022 00	−0.802	1.005 87	−0.708	0.990 59	−0.672
0.1468	1.036 37	−1.078	1.032 67	−1.053	1.025 17	−1.012	1.007 95	−0.892	0.991 75	−0.836
0.1896	1.037 96	−1.251	1.034 13	−1.226	1.026 18	−1.175	1.008 87	−1.057	0.991 59	−0.964
0.2351	1.037 96	−1.380	1.033 72	−1.341	1.025 09	−1.266	1.008 12	−1.166	0.990 51	−1.057
0.2949	1.036 45	−1.477	1.032 38	−1.447	1.024 00	−1.386	1.005 29	−1.202	0.988 62	−1.137
0.4071	1.031 52	−1.478	1.027 61	−1.461	1.019 25	−1.404	1.001 87	−1.286	0.984 22	−1.156
0.4904	1.027 76	−1.393	1.023 69	−1.367	1.015 41	−1.316	0.998 13	−1.200	0.981 07	−1.101
0.6031	1.022 83	−1.178	1.018 52	−1.134	1.010 58	−1.111	0.993 32	−0.989	0.976 27	−0.876
0.6772	1.019 91	−0.999	1.015 77	−0.968	1.007 83	−0.948	0.991 16	−0.877	0.974 03	−0.747
0.7598	1.016 70	−0.744	1.012 93	−0.751	1.004 26	−0.657	0.988 59	−0.689	0.971 96	−0.602
0.8692	1.013 08	−0.386	1.009 44	−0.412	1.001 68	−0.417	0.985 52	−0.402	0.969 40	−0.367
0.9330	1.011 75	−0.230	1.007 86	−0.229	0.999 85	−0.206	0.983 94	−0.223	0.967 91	−0.198
1.0000	1.010 00	0.000	1.006 11	0.000	0.998 27	0.000	0.982 21	0.000	0.966 38	0.000

[a]Units are g cm^{-3} for densities (d) and are cm^3 mol^{-1} for excess molar volumes (V^E).

atures of the water bath were stable to ±0.001° during the time required to measure a density and were known to ±0.01°C, as measured with a Guildline platinum resistance thermometer.

Results

Experimental results (mole fractions and densities) and one kind of derived result (excess molar volume, V^E) are reported in Table 1 for (water + MDEA) systems and in Table 2 for (water + EDEA systems). The excess molar volume is defined by

$$[1] \quad V^E = V_m - x_1V_1^* - x_2V_2^*$$

in which V_m represents the volume of a mixture containing a total of one mole of (water + alkanolamine), x_1 and x_2 are mole

Can. J. Chem. Downloaded from www.nrcresearchpress.com by 80.90.12.36 on 09/08/12
For personal use only.

Fig. 1. Densities of (water + alkanolamine) systems at 25°C. DEA (densities from ref. 8) represents diethanolamine. MDEA and EDEA (densities from Tables 1 and 2) represent methyldiethanolamine and ethyldiethanolamine. All of these densities decrease with increasing temperature.

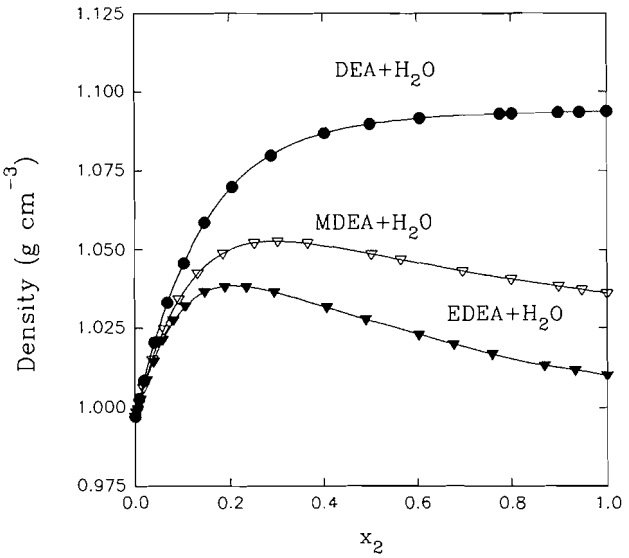

fractions of water and alkanolamine, respectively, and V_1^* and V_2^* are the molar volumes of the corresponding pure liquids. Equation [1] can also be expressed as

$$[2] \quad V^E = [x_1M_1 + x_2M_2)/d] - (x_1M_1/d_1^*) - (x_2M_2/d_2^*)$$

in which M_1 and M_2 represent molar masses of water and alkanolamine, respectively, and d, d_1^*, and d_2^* represent densities of a mixture of specified mole fraction, of pure water, and of pure alkanolamine, respectively. The values of V^E listed in Tables 1 and 2 were calculated from mole fractions, molar masses, and densities by way of eq. [2].

The general trends of density and V^E with increasing mole fraction of alkanolamine are illustrated in Figs. 1 and 2.

Calculations and discussion

The partial molar volume of a component ($\overline{V}_i$) is defined by

$$[3] \quad \overline{V}_i = (\partial V/\partial n_i)_{T,p,n,j}$$

Differentiation of eq. [1] and combination with eq. [3] leads (25, 26) to the following equations for the partial molar volumes of water ($\overline{V}_1$) and of alkanolamine ($\overline{V}_2$):

$$[4] \quad \overline{V}_1 = V^E + V_1^* - x_2(\partial V^E/\partial x_2)_{p,T}$$

$$[5] \quad \overline{V}_2 = V^E + V_2^* + (1 - x_2)(\partial V^E/\partial x_2)_{p,T}$$

Equations equivalent to [4] and [5] are presented in the useful review by Davis (5).

A convenient way to carry out the differentiations specified in eq. [4] and eq. [5] can begin with equations that will fit the V^E results that are reported in Tables 1 and 2. For this purpose we use equations of the Redlich–Kister form:

Fig. 2. Excess molar volumes of (water + alkanolamine) systems at 25°C. See legend for Fig. 1.

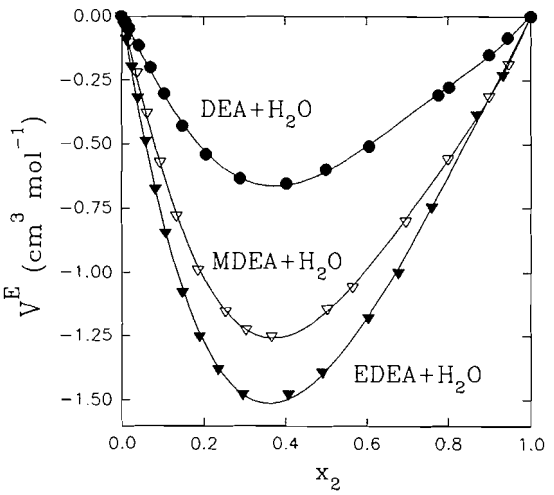

$$[6] \quad V^E = x_2(1 - x_2)\sum A_n(1 - 2x_2)^{n-1}$$

Redlich–Kister coefficients (A_n) are listed in Table 3 for the (water + MDEA) and (water + EDEA) systems.

Differentiation of eq. [6] with respect to x_2 and combination of the result of differentiation with eqs. [4] and [5] leads to the following equations for the partial molar volumes of water ($\overline{V}_1$) and of alkanolamine ($\overline{V}_2$):

$$[7] \quad \overline{V}_1 = V_1^* + x_2\sum A_n(1 - 2x_2)^{n-1} - 2x_2(1 - x_2)\sum A_n(n - 1)(1 - 2x_2)^{n-2}$$

$$[8] \quad \overline{V}_2 = V_2^* + (1 - x_2)^2\sum A_n(1 - 2x_2)^{n-1} + 2x_2(1 - x_2)^2\sum A_n(n - 1)(1 - 2x_2)^{n-2}$$

Much of our present interest is in the partial molar volume of water at infinite dilution ($\overline{V}_1^\circ$) in an alkanolamine and in the partial molar volume of an alkanolamine at infinite dilution ($\overline{V}_2^\circ$) in water. We therefore set $x_2 = 1$ in eq. [7] and $x_2 = 0$ in eq. [8] to obtain

$$[9] \quad \overline{V}_1^\circ = V_1^* + \sum A_n(-1)^{n-1}$$

and

$$[10] \quad \overline{V}_2^\circ = V_2^* + \sum A_n$$

Equations [7] and [8] permit calculation of the partial molar volumes of each component (not at infinite dilution) conveniently and with the accuracy that is justified by the accuracy of the experimental data; we have used these equations for this purpose as reported later in this paper. But it should be recognized that the Redlich–Kister equation [6] and its derivative equations [7] and [8] are intended to provide the best overall fit of the data in convenient form with a minimum number of adjustable parameters. It is known, however, that the Redlich–Kister equation and especially its derivatives do not always provide the best representation of properties of either component at infinite dilution in the other component. Therefore, we

Can. J. Chem. Downloaded from www.nrcresearchpress.com by 80.90.12.36 on 09/08/12
For personal use only.

consider two alternatives to eqs. [9] and [10] for evaluation of $\overline{V}_1^\circ$ and $\overline{V}_2^\circ$.

As shown previously (8), the apparent molar volume of water in alkanolamine ($V_{\phi,1}$) and the apparent molar volume of alkanolamine in water ($V_{\phi,2}$) can be calculated as

$$[11] \quad V_{\phi,1} = V_1^* + (V^E/x_1) = V_1^* + [V^E/(1 - x_2)]$$

and

$$[12] \quad V_{\phi,2} = V_2^* + (V^E/x_2)$$

Simple graphical or analytical extrapolation of $V_{\phi,1}$ to $x_1 = 0$ ($x_2 = 1$) leads to the desired value of $\overline{V}_1^\circ$ and similar extrapolation of $V_{\phi,2}$ to $x_2 = 0$ leads to the desired value of $\overline{V}_2^\circ$. Perron et al. (17) have used an equivalent method based on extrapolation of the "reduced volume" represented by V^E/x_1x_2 to $x_2 = 1$ or 0 to obtain equally accurate values of partial molar volumes at infinite dilution.

The methods of obtaining $\overline{V}_2^\circ$ by way of eq. [10], extrapolation of $V_{\phi,2}$, or extrapolation of V^E/x_1x_2 are all satisfactory and lead to similar results having good accuracy. On the other hand, because we have few V^E values for x_2 near unity (small x_1), accuracies of $\overline{V}_1^\circ$ values are less good, especially for those derived from Redlich–Kister coefficients and eq. [9]. The values of $\overline{V}_1^\circ$ that we cite later have all been obtained by extrapolation of $V_{\phi,1}$ values to $x_1 = 0$.

Before using the equations above with our experimental results for calculation of partial molar volumes, we turn to consideration of thermal expansion. The thermal expansion of a pure substance is often expressed in terms of the coefficient of thermal expansion, defined as $\alpha^* = (1/V^*)(\partial V^*/\partial T)_p$. It is more convenient for us to omit the $(1/V^*)$ and to consider the molar expansivity (E_i^*) of a pure substance (i) defined as

$$[13] \quad E_i^* = (\partial V_i^*/\partial T)_p$$

For a mixture the corresponding definition of the molar expansivity in terms of the molar volume represented by V is

$$[14] \quad E = (\partial V/\partial T)_{p,\text{composition}}$$

Similarly, we define a partial molar expansivity ($\overline{E}_i$) as

$$[15] \quad \overline{E}_i = (\partial \overline{V}_i/\partial T)_{p,\text{composition}}$$

Differentiation of a well-known equation for the molar volume of a mixture ($V = x_1\overline{V}_1 + x_2\overline{V}_2$) with respect to temperature and combination with the definitions expressed by eqs. [13]–[15] gives us

$$[16] \quad E = x_1\overline{E}_1 + x_2\overline{E}_2$$

as a relationship between the molar expansivity of the mixture and the partial molar expansivities of the components.

Following earlier investigations (2, 3) of the dependence of $\overline{V}_2^\circ$ on temperature in relation to "structure-making" and "structure-breaking" solutes in water, we will be concerned with

$$[17] \quad (\partial \overline{E}_2^\circ/\partial T) = (\partial^2 \overline{V}_2^\circ/\partial T^2)_p$$

Table 3. Redlich–Kister equation fitting coefficents for aqueous mixtures of MDEA and EDEA at different temperatures.

t(°C)	A_1	A_2	A_3	A_4	A_5
	A_6				
MDEA+H_2O					
25	−4.5812	−2.2030	−1.4972	−2.5745	1.0238
	4.3152				
30	−4.5786	−1.9919	−1.3480	−2.8341	0.6551
	4.6423				
40	−4.4631	−2.0014	−1.2001	−2.3123	0.6219
	3.7439				
50	−4.3402	−1.8654	−1.1196	−1.9030	0.2339
	3.2168				
60	−4.2408	−1.8335	−0.8315	−2.2435	0.0216
	3.5168				
70	−4.1587	−2.0470	−0.5444	−0.6750	−0.3915
	1.8772				
80	−3.9280	−2.1569	−0.7843	0.4236	0.0705
	0.2199				
EDEA+H_2O					
25	−5.5059	−2.3111	−1.3882	−6.6162	0.5630
	7.6422				
30	−5.3179	−1.9982	−2.1017	−7.3522	1.2242
	8.2524				
40	−5.1370	−2.0636	−1.6073	−6.1220	0.6667
	6.6420				
60	−4.6746	−1.8071	−1.4997	−3.9663	0.1072
	4.1077				
80	−4.2014	−2.1729	−1.4730	−2.0330	0.0118
	2.3025				

Because we and others have expressed our experimental results in terms of excess molar volumes, it is useful to consider the effect of temperature on the excess volume by differentiating eq. [1] with respect to temperature, defining the excess molar expansivity as

$$[18] \quad E^E = (\partial V^E/\partial T)_{p,\text{composition}}$$

and thence obtaining

$$[19] \quad E^E = E - x_1E_1^* - x_2E_2^*$$

All of our V^E values are negative (Tables 1 and 2 and Fig. 2), as is common for other completely miscible (water + polar organic) systems. These V^E values become less negative with increasing temperature, as is also common.

Partial molar volumes of water ($\overline{V}_1$) and of alkanolamines ($\overline{V}_2$) can be calculated for all compositions by using the Redlich–Kister coefficients (Table 3) in eqs. [7] and [8]. An illustration of the results of such calculations for the partial molar volumes of MDEA over the complete range of compositions and several temperatures is provided in Fig. 3. Several previous investigators (for examples see refs. 7, 8, 12, 14, 21, and 23) have observed similar minima in graphs of $\overline{V}_2$ against mole fraction (as in Fig. 3) for various alcohols and other polar organics in water.

Koga and colleagues (19, 23) have used partial molar vol-

Can. J. Chem. Downloaded from www.nrcresearchpress.com by 80.90.12.36 on 09/08/12
For personal use only.

Table 4. Partial molar volumes[a] of MDEA and EDEA at infinite dilution in water ($\overline{V}_2°$) and of water at infinite dilution in MDEA and in EDEA ($\overline{V}_1°$).

t (°C)	$\overline{V}_2°$(MDEA)	$\overline{V}_1°$(in MDEA)	$\overline{V}_2°$(EDEA)	$\overline{V}_1°$(in EDEA)
25	109.5	14.2	124.6	14.4
30	110.0	14.0	125.1	14.4
40	110.7	14.4	126.1	14.7
50	111.4	14.3		
60	112.5	14.6	128.0	14.7
70	113.1	14.8		
80	113.8	15.5	130.3	15.3

[a]Units of $\overline{V}_1°$ and $\overline{V}_2°$ are $cm^3\ mol^{-1}$.

Fig. 3. Partial molar volumes of MDEA in water at several temperatures. ●, 25°C; ▽, 40°C; ▼, 60°C; □, 80°C.

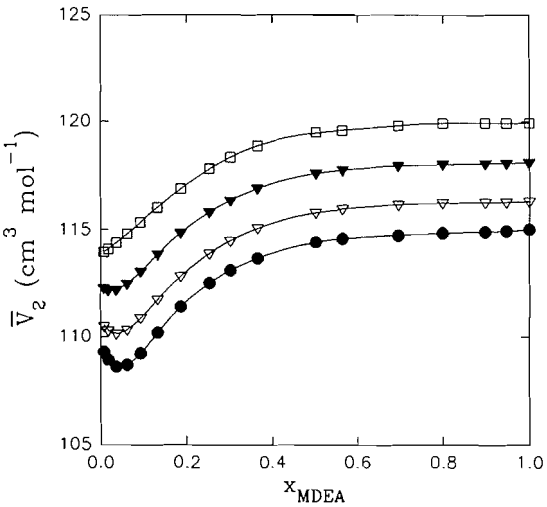

umes and several other thermodynamic properties as a basis for deducing detailed "pictures" of solute–solute, solute–water, and water–water interactions over ranges of composition for (water + 2-butoxyethanol) and (water + dimethyl sulfoxide) systems. Pagé, Huot, and Jolicoeur (7) have used their collection of thermodynamic properties (volumes, compressibilities, and heat capacities) of the (water + ethanolamine) system as a basis for their picture of molecular interactions. One of the reasons for undertaking the present investigation and also our earlier investigation (8) of the volumetric properties of other (water + alkanolamine) systems was to obtain some of the data needed for forming similar pictures of molecular interactions in these systems; calorimetric measurements are in progress. Because development of credible pictures along the lines described by Koga (19, 23) and Jolicoeur (7) requires an extensive array of thermodynamic data, we turn now to sim pler analyses that can be carried out with only our presently reported results.

Previous investigators of dilute aqueous solutions have used several criteria as a basis for describing some solutes as "structure makers" and other solutes as "structure breakers". One such classification (2, 3) is based on the sign of $d^2\overline{V}_2°/dT^2$; a positive sign corresponds to a structure-making solute while a negative sign corresponds to a structure-breaking solute. In Table 4 we list the values of partial molar volumes of MDEA and of EDEA at several temperatures at infinite dilution in water ($\overline{V}_2°$). Graphs of $\overline{V}_2°$ of MDEA and of EDEA against temperature give straight lines with positive slopes. Values of the slopes $d\overline{V}_2°/dT$ are 0.08 $cm^3\ mol^{-1}\ K^{-1}$ for MDEA and 0.10 $cm^3\ mol^{-1}\ K^{-1}$ for EDEA. Because of the linearity of $\overline{V}_2°$ against temperature, $d^2\overline{V}_2°/dT^2 = 0$ within the accuracies of our results over the temperature range 25–80°C, which means (according to the criterion of temperature dependence of partial molar volumes) that these solutes cause no net or overall structure-making or structure-breaking effects in water. It was observed earlier (8) that values of $d\overline{V}_2°/dT$ are positive and values of $d^2\overline{V}_2°/dT_2 = 0$ for other alkanolamines in water, which led to the same conclusion about these solutes being neither net structure makers nor net structure breakers.

Partial molar volumes of water at infinite dilution in MDEA and in EDEA are listed in Table 4. Accuracies of these values do not justify making any statement about $d^2\overline{V}_1°/dT^2$, but it is clear that the first derivatives $d\overline{V}_1°/dT$ are positive. All of the $\overline{V}_1°$ values are smaller than the corresponding molar volumes of pure water (V_1*) at the same temperature. This observation is consistent with the idea that the molar volume of pure water is a sum of the "actual" molecular volumes plus the "empty" volume that arises from the hydrogen-bonded "open" structure of liquid water. Partial molar volumes (8) of water at infinite dilution in other alkanolamines at several temperatures are also smaller than corresponding values of V_1* and have been interpreted similarly.

Sakurai and Nakagawa (18) have measured densities of dilute solutions of water in benzene and in several *n*-alkanols at several temperatures. They have used these densities and corresponding compositions in evaluating the partial molar volumes of water at infinite dilution (represented here by $\overline{V}_1°$) in each solvent at several temperatures. Their values of $\overline{V}_1°$ for water at infinite dilution in methanol, ethanol, *n*-propanol, and *n*-butanol at each temperature from 5 to 45°C are substantially smaller than corresponding values of V_1* and are consistent with the interpretation above.

We also note that the partial molar volumes of water in alkanols increase with number of atoms of carbon per molecule of alkanol in the sequence ethanol through *n*-octanol and that the difference between V_1* and $\overline{V}_1°$ values decreases with increasing number of atoms of carbon per molecule of alkanol. This effect is sufficiently large that the values of $\overline{V}_1°$ for water in *n*-octanol are *larger* than the corresponding values of V_1* at the higher temperatures (35 and 45°C). This observation leads us to suggest that our earlier (see above) explanation for values of $\overline{V}_1°$ being smaller than corresponding values of V_1* is probably incomplete and might even be largely mistaken.

The values of $\overline{V}_1°$ reported by Sakurai and Nakagawa (18)

for water in alkanols in the sequence ethanol through *n*-octanol and also for water in benzene lead to positive values of $d\overline{V}_1°/dT$, as also reported here and previously (8) for water in alkanolamines. All of these positive values of $d\overline{V}_1°/dT$ are consistent with the general observation that dV/dT is positive for most pure substances and most solutions. But they have also reported that $d\overline{V}_1°/dT$ is negative for water in methanol, for which neither they nor we have any satisfactory explanation.

Sakurai and Nakagawa (18) have also reported values of $V_1°$ for water in benzene that are substantially larger (3–4 cm^3 mol^{-1}) than corresponding values of V_1*. It seems reasonable to suggest that this unusual difference can be explained on the basis of disruption of the "stacked layers structure" of liquid benzene, with a consequent increase in volume. It may also be that a similar explanation involving disruption of reasonably closely packed alkane chains is appropriate for the relatively large values of $\overline{V}_1°$ for water in the larger alkanols.

We (11, 15) and others (9, 10, 13, 16, 17) have used partial molar volumes ($\overline{V}_2°$) of many organics in water to develop additivity schemes that might contribute to our understanding of organic–water interactions and that are certainly useful for predicting partial molar volumes for organic solutes in water. A few of these investigations (especially ref. 16) have led to additivity schemes for partial molar expansivities. Our further developments along these lines, based on our own and other recently reported volumes and expansivities, will be reported later.

Acknowledgement

We thank the Natural Sciences and Engineering Research Council of Canada for grants in support of this and other research on the properties of (water + organic) systems.

References

1. G. Astarita, D.W. Savage, and A. Bisio. Gas treating with chemical solvents. John Wiley & Sons, New York. 1983.
2. L.G. Hepler. Can. J. Chem. **47**, 4613 (1969). Note that the vertical axis in Fig. 2 of ref. 2 should be labelled V_2^0.
3. J.L. Neal and D.A.I. Goring. J. Phys. Chem. **74**, 658 (1970).
4. Y. Yoshimura and M. Nakahara. Bull. Chem. Soc. Jpn. **61**, 1887 (1988)
5. M.I. Davis. Chem. Soc. Rev. 127 (1993).
6. Y. Marcus. J. Chem. Soc. Faraday Trans. **91**, 427 (1995).
7. M. Pagé, J.-Y. Huot, and C. Jolicoeur. Can. J. Chem. **71**, 1064 (1993).
8. Y. Maham, T.T. Teng, L.G. Hepler, and A.E. Mather. J. Solution Chem. **23**, 195 (1994).
9. S. Cabani, G. Conti, and L. Lepori. J. Phys. Chem. **76**, 1338 (1972); **78**, 1030 (1974).
10. S. Cabani, G. Conti, and E. Matteoli. J. Solution Chem. **5**, 751 (1976).
11. O. Enea, P.P. Singh, and L.G Hepler. J. Solution Chem. **11**, 719 (1977).
12. G. Roux, G. Perron, and J.E. Desnoyers. J. Solution Chem. **7**, 639 (1978).
13. H. Høiland. J. Solution Chem. **9**, 857 (1980).
14. G.C. Benson and O. Kiyohara. J. Solution Chem. **9**, 791 (1980).
15. O. Enea, C. Jolicoeur, and L.G. Hepler. Can. J. Chem. **58**, 704 (1980).
16. S. Cabani, P. Gianni, V. Mollica, and L. Lepori. J. Solution Chem. **10**, 563 (1981).
17. S. Cabani, G. Conti, E. Matteoli, and M.R. Tine. J. Chem. Soc. Faraday Trans. **77**, 2385 (1981).
18. M. Sakurai and T. Nakagawa. J. Chem. Thermodyn. **14**, 269 (1982); **16**, 171 (1984).
19. J.V. Davies, F.W. Lau, L.T.N. Le, J.T.W. Lai, and Y. Koga. Can. J. Chem. **70**, 2659 (1992).
20. G. Perron, L. Couture, and J.E. Desnoyers. J. Solution Chem. **21**, 433 (1992).
21. G. Perron, F. Quirion, D. Lambert, J. Ledoux, L. Ghaicha, R. Bennes, M. Privat, and J.E. Desnoyers. J. Solution Chem. **22**, 107 (1993).
22. L.E. Strong, M. Bowe, J. White, and K. Abi-Selah. J. Solution Chem. **23**, 541 (1994).
23. J.T.W. Lai, F.W. Lau, D. Robb, P. Westh, G. Nielsen, C. Trandum, A. Hvidt, and Y. Koga. J. Solution Chem. **24**, 89 (1995).
24. G.S. Kell. J. Chem. Eng. Data, **20**, 97 (1975).
25. S.E. Wood and R. Battino. Thermodynamics of chemical systems. Cambridge University Press, Cambridge, U.K. 1990.
26. W.E. Acree, Jr. Thermodynamic properties of nonelectrolyte solutions. Academic Press, New York. 1984.

Can. J. Chem. Downloaded from www.nrcresearchpress.com by 80.90.12.36 on 09/08/12
For personal use only.

Crystal and molecular structure of *Z*- and *E*-1,2-dichloro-1,2-bis(2-chlorophenyl)-ethylene. An X-ray and NMR study

Luciano Antolini, Ugo Folli, Dario Iarossi, Adele Mucci, Silvia Sbardellati, and Ferdinando Taddei

Abstract: The crystal structures of the title compounds were determined by single crystal X-ray diffraction techniques. The molecule of the *Z* isomer, which crystallizes in the monoclinic space group *C2/c* with $Z = 4$ in a cell of dimensions $a = 14.891(2)$, $b = 10.780(2)$, $c = 8.769(1)$ Å, $\beta = 97.47(2)°$, $V = 1395.7(7)$ Å^3, has crystallographic twofold symmetry. The *E* form crystallizes in the orthorhombic space group *Pbca* with $a = 11.730(1)$, $b = 6.932(1)$, $c = 16.841(1)$Å, $V = 1369.4(2)$ Å^3, and $Z = 4$. Its molecules have crystallographically dictated $\bar{1}$ symmetry. In both isomers the phenyl rings are roughly perpendicular to the average ethylene plane. The atoms characterizing this plane show significant deviations from planarity in the *Z* isomer. Marked bond-angle distortions at the ethene carbons of both structures are observed. The ^{1}H and ^{13}C NMR spectra of the compounds were measured and, particularly in the case of the ^{1}H chemical shifts, fall into two quite separate spectral regions. At low temperature, two conformational isomers, those with different relative orientation of the C—Cl bonds of the phenyl rings, are observed in the spectrum of each compound.

Key words: chlorostilbenes, overcrowded molecules, X-ray structure, conformations, NMR spectroscopy.

Résumé : On a déterminé les structures cristallines des composés mentionnés dans le titre à l'aide de techniques de diffraction des rayons X sur des cristaux uniques. La molécule de l'isomère *Z*, qui cristallise dans le groupe d'espace *C2/c*, avec $a = 14,891(2)$, $b = = 10,780(2)$, $c = 8,769(1)$ Å, $\beta = 97,47(2)°$, $V = 1395,7(7)$ Å^3, et $Z = 4$, possède une symétrie cristallographique binaire. La forme *E* cristallise dans le groupe d'espace orthorhombique *Pbca* avec $a = 11,730(1)$, $b = 6,932(1)$ et $c = 16,841(1)$ Å, $V = 1369,4(2)$ Å^3, et $Z = 4$. Ses molécules existent dans une symétrie $\bar{1}$ dictée par sa cristallographie. Dans les deux isomères, les noyaux phényles sont approximativement perpendiculaires au plan moyen de l'éthyléne. Dans l'isomère *Z*, les atomes caractérisant ce plan présentent des déviations significatives par rapport à la planéité. Dans les deux structures, on a observé des distorsions marquées dans les angles de liaison des carbones de l'éthène. On a déterminé les spectres RMN du ^{1}H et du ^{13}C et les déplacements chimiques, particulièrement du ^{1}H, sont divisés en deux régions spectrales bien distinctes. À basse température, dans chacun des composés, on a observé deux isomères conformationnels qui différent par l'orientation relative des liaisons C—Cl par rapport aux noyaux phényles.

Mots clés : chlorostilbènes, molécules encombrées, structure par rayons X, conformations, spectroscopie RMN.

[Traduit par la rédaction]

Introduction

The reductive coupling of benzotrichloride in anaerobic conditions in the presence of metal ions in low states of oxidation yields (1 – 4) tolane tetrachloride, which is partly dehalogenated to a mixture of *Z*- and *E*-1,2-dichloro-1,2-bis(phenyl)ethylene. When iron(II) chloride is employed, dehalogenation does not take place even in boiling acetonitrile solution (5). We have found that, when (2-chloro)benzotrichloride is reacted with iron(II) chloride, extensive dehalogenation occurs at room temperature to yield *Z*- (**1**) and *E*-1,2-dichloro-bis(2-chlorophenyl)ethylene (**2**), the *E*/*Z* isomer ratio being close to unity. The overcrowded character of the coupling product formed from (2-chloro)benzotrichloride probably accounts for the relative ease with which dehalogenation occurs.

Received February 6, 1995.

L. Antolini, U. Folli, D. Iarossi, A. Mucci, S. Sbardellati, and F. Taddei.[1] Dipartimento di Chimica, Università, Via Campi 183, 4110 Modena, Italy.

[1] Author to whom correspondence may be addressed. Telephone: 0039-59-378432. Fax: 0039-59-373543

Scheme 1

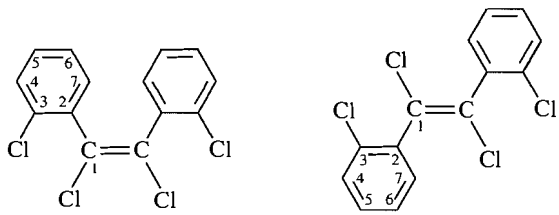

1 **2**

In view of the presence of *ortho* substituents and of the chlorine atoms in the ethene fragment, compounds **1** and **2** should be conformationally hindered, and the *ortho* chlorine atoms should give rise to additional conformational preferences owing to the relative orientation of the corresponding C—Cl bonds.

Accordingly, these molecules were studied both in the solid state (X-ray spectroscopy) and in solution (NMR spectroscopy), in order to discover the extent of the constraints hindering internal rotation of the rings and the structure of the conformational minima. The results of the NMR analysis

Can. J. Chem. Downloaded from www.nrcresearchpress.com by 80.90.12.36 on 09/08/12
For personal use only.

Can. J. Chem. Downloaded from www.nrcresearchpress.com by 80.90.12.36 on 09/08/12
For personal use only.

should afford useful insight into the presence and quantity of their *E* and *Z* isomers in reaction mixtures.

Experimental

Compounds

2-Chlorobenzotrichloride (Aldrich) (5.50 g, 19.6 mmol) was dissolved in CH_3CN (80 mL) (previously distilled from P_2O_5 in Ar atmosphere). Ar was bubbled into the solution in order to obtain an inert atmosphere in the reaction apparatus. $FeCl_2 \cdot 4H_2O$ (11.91 g, 59.9 mmol) was then introduced and the mixture stirred for 7 h at 45–50°C. The reaction was quenched by dilution with water (500 mL). The precipitated organic material was filtered, thoroughly washed, first with water and then with cyclohexane (to remove colour), and dried in a vacuum desiccator over P_2O_5. The crude product (2.15 g, 69%) had mp 115–160°C and consisted of only two compounds (*E* and *Z* isomers) as revealed by TLC (SiO_2, petroleum ether bp 30–40°C/ethyl ether 3:1)and GLC (HPS cross-linked 5% PH ME silicon; *E*/*Z* ratio 45:55). Anal. calcd. for $C_{14}H_8Cl_4$: C 52.9, H, 2.5; found: C 53.5, H 2.5%.

Dissolution of the crude in hot acetone, followed by slow cooling at room temperature, yielded a fraction of almost pure *E* isomer, which was further purified by crystallization from isopropyl alcohol; mp 170–172°C (100% purity by TLC and GLC analysis); a crystal was selected for X-ray diffraction. From the acetone mother liquor, by concentration and refrigeration at 0°C, a fraction rich in the *Z* isomer was isolated, and was further purified by crystallization from *n*-hexane and finally from isopropyl alcohol; mp 125–127°C (100% purity by TLC and GLC analysis); a crystal was selected for X-ray analysis. For the high- and low-melting isomer, melting points of 170°C and 139°C, respectively, have been reported (6).

X-ray structure determination

The selected crystals were sealed in a glass capillary and transferred directly to an Enraf-Nonius CAD4 diffractometer. All measurements were carried out at room temperature under the conditions summarized in Table 1, which also contains information relating to data reductions and structure determinations.

Major calculations were carried out on a VAX 6310 computer with the use of the SHELX-86 program (8) for structure solution, SHELX-76 (9) for least-squares refinements and source of scattering factors, and ORTEP (10) for molecular drawings. Final fractional atomic coordinates and equivalent isotropic thermal parameters are given in Tables 2 and 3 for the *Z* and *E* forms, respectively.[2]

[2] Tables of anisotropic thermal parameters for non-hydrogen atoms, complete bond distances and bond angles, torsion angles, selected least-squares planes, and stereoviews of unit cell contents may be purchased from: The Depository of Unpublished Data, Document Delivery, CISTI, National Research Council Canada, Ottawa, ON K1A 0S2, Canada.

Structure factor amplitudes are no longer being deposited and may be obtained directly from the authors.

Tables of bond lengths and angles and stereoviews of unit cells have also been deposited with the Cambridge Crystallographic Data Centre, and can be obtained on request from the Director, Cambridge Crystallographic Data Centre, University Chemical Laboratory, 12 Union Road, Cambridge, CB2 1EZ, U.K.

NMR measurements

The spectra were measured with a Bruker AMX-400 spectrometer operating at 400.13 and 100.61 MHz for ^1H and ^{13}C nuclei, in $CDCl_3$ solution (0.1 M). Chemical shifts are given as δ values referring to TMS. The acquisition time was 5–6 s for ^1H and 1–2 s for ^{13}C spectra. ^{13}C NMR data were obtained from ^1H-detected chemical shift correlation via heteronuclear multiple-quantum coherence (HMQC) (11) and ^1H-detected heteronuclear multiple-bond correlation (HMBC) (12) experiments with standard pulse sequences. The delay Δ_1 = 3.07 ms was employed for the evolution of ^1J(CH) in HMQC and for the low-pass *J*-filter in HMBC, and the delay Δ_2 = 50 ms for the long-range coupling constant evolution in HMBC; AQ = 0.6 s and the resolution in *f*1 before zero-filling was 0.1–0.2 ppm.

Results and discussion

Table 4 lists selected interatomic distances and bond and torsion angles for both structures. The molecule of the *Z* isomer (Fig. 1) lies on a crystallographic twofold axis, whereas that of the *E* form (Fig. 2) has an inversion center at the midpoint of the ethene bond. Hence, in both cases, the asymmetric unit contains one half molecule.

The conformation of the molecules can be described in terms of torsion angles around the C(1)—C(2) bond or by means of the dihedral angle between mean planes through the ethene and phenyl moieties. These torsional (see Table 4) and dihedral angles (80.1° and 82.2° for the *Z* and *E* forms, respectively) show that the phenyl groups have quite similar and roughly normal orientations with respect to the ethene plane. This conformation differs significantly from those observed for the *Z* and *E* isomers of tetrachlorostilbene (1,2-dichloro-1,2-bis(4-chlorophenyl)ethylene) (13, 14), characterized by torsion angles of about 54 and 75°, respectively. It appears that the larger dihedral angles between the phenyl rings and the ethene plane in these compounds can be attributed mainly to the repulsive interaction between the Cl(1) and Cl(2) atoms (Table 4). The dihedral angles become smaller in the 4-chlorophenyl analogues since in their case the repulsive interaction involves the Cl(1) and H atoms. The phenyl rings make a dihedral angle of 69.7° between themselves in the *Z* form, whereas they are exactly parallel, for reasons of symmetry, in the *E* isomer. It should also be pointed out that the six atoms belonging to the ethene fragment of the *Z* isomer display relevant distortions from coplanarity, with atomic deviations ranging from +0.056 to −0.056 Å. Similar, but slightly larger, distortions from planarity were also observed in the ethene moiety of *Z*-dichlorostilbene (13) and, in both cases, could be determined by short, nonbonded intramolecular interactions. A Cl(1)···Cl(1′) separation of 3.07 Å was observed in the above-cited compound, which compares with a value of 3.139(1) Å in our *Z* isomer.

There are no significant differences between corresponding bond distances in compounds **1** and **2** and they compare well with those reported for *E*- and *Z*-dichlorostilbene (13). In both structures, the ethene fragment suffers from considerable strain in the bond angles, which deviate significantly from 120°. An increase in the C(1′)-C(1)-C(2) bond angles (see Table 4) and a parallel decrease in the Cl(1)-C(1)-C(2) angles is observed as well. These angular deformations are more

Table 1. Crystal data and summary of intensity data collection and structure refinement of 1,2-dichloro-1,2-bis-(2-chlorophenyl)ethylene.

Compound	**1** (*Z* isomer)	**2** (*E* isomer)
Formula	$C_{14}H_8Cl_4$	$C_{14}H_8Cl_4$
Molecular weight	318.030	318.030
Crystal system	Monoclinic	Orthorhombic
Space group	*C2/c* (No. 15)	*Pbca* (No. 61)
Temperature, °C	20	20
Cell constants	25 reflections with $\theta > 8°$	25 reflections with $\theta > 13°$
a, Å	14.891(2)	11.730(1)
b, Å	10.780(2)	6.932(1)
c, Å	8.769(1)	16.841(1)
β, deg	97.47(2)	90
Cell volume, Å^3	1395.7(7)	1369.4(2)
Z	4	4
D_{calcd}, g cm^{-3}	1.513	1.542
F(000)	640	640
Diffractometer/scan	CAD4, ω–2θ	CAD4, ω–2θ
Radiation (λ, Å)	Graphite monochromated MoKα (0.71069)	
Reflections measured	$-19 \le h \le 19$, $0 \le k \le 14$, $0 \le l \le 11$	$-1 \le h \le 15$, $-1 \le k \le 9$, $-1 \le l \le 22$
2θ limits, deg	4.0–56.0	4.0–56.0
Scan width, deg	1.10 + 0.35 tan θ	0.80 + 0.35 tanθ
Scan speed limits, deg min^{-1}	1.3–5.5	1.1–5.5
Standard reflections	2 every 1 h	2 every 1 h
Decay of standards	14.5%	0.7%
No. of collected reflections	1781	2214
No. of observed reflections	1224 with $I \ge 3\sigma(I)$	1095 with $I \ge 3\sigma(I)$
No. of unique reflections	1140 (R_{int} = 0.014)	801(R_{int} = 0.017)
Max. crystal dimensions, mm	0.35 × 0.33 × 0.30	0.35 × 0.30 × 0.12
μ, cm^{-1}	7.5	7.7
Range of relative transmission factors[a]	0.971–0.999	0.840–0.999
Corrections applied	LP, decay, and absorption	LP and absorption
Structure solution	Direct methods	Direct methods
Treatment of H atoms	Refined isotropically	Ref. isotropically with common *B*
No. of varied parameters	99	95
Weights	$1.0/[\sigma^2(F_o) + 0.00062F_o^2]$	$1.18/[\sigma^2(F_o) + 0.00029F_o^2]$
GOF	1.39	1.72
Max. Δ/σ	0.001	0.006
$R = \Sigma\|\|F_o\| - \|F_c\|\|/\Sigma\|F_o\|$	0.032	0.030
R_w	0.035	0.033
Δρ: max. – min., e Å^{-3}	+0.43 −0.21	+0.29 −0.22
Secondary extinction	No evidence	0 weight to 1 strong low-order reflection

[a]Based on empirical ψ scan (7).

likely to be due to short, nonbonded intramolecular interactions between atoms of *o*-chlorophenyl substituents and the chlorines attached to the ethene fragment than to electronic effects.

The molecular packing of compounds **1** and **2** is characterized by a lack of short van der Waals contacts. In both cases, only three interatomic distances less than 3.60 Å were observed; the shortest ones are a Cl(2)···Cl(2) contact of 3.421(1) Å in the *Z* isomer, and a Cl(1)···C(4) separation of 3.464(3) Å in the *E* form. Nevertheless, the crystal packing of the *Z* isomer shows evidence of weak π–π interactions between the molecules stacked in the 1 0 −1 direction. The stacking distance between mean planes through phenyl rings is 3.621 Å, and the shortest C···C contact 3.640(4) Å. The molecules of the *E* isomer are stacked along the *b* direction, but at a distance of one axis length (6.932 Å). The closest, albeit weak, ring–ring interactions occur between phenyl groups whose mean planes make a dihedral angle of 61.3°. In both isomers, the ring chlorine atoms are oriented in such a way as to allow the rings to come close together. The ^1H and ^{13}C chemical shifts measured at 300 and 240 K for compounds **1** and **2** are reported in Table 5. The δ values were obtained fom 1D spectra, whereas the assignment was performed through 2D inverse detection: HMQC (11) and HMBC (12) experiments were performed and ^1H chemical shifts were simulated with the DNMR5 program (15). The signal assignment is mostly

Can. J. Chem. Downloaded from www.nrcresearchpress.com by 80.90.12.36 on 09/08/12
For personal use only.

Can. J. Chem. Downloaded from www.nrcresearchpress.com by 80.90.12.36 on 09/08/12
For personal use only.

Table 2. Final fractional coordinates and equivalent isotropic temperature factors[a] for *Z*-1,2-dichloro-bis(2-chlorophenyl)-ethylene (**1**).

Atom	*x*	*y*	*z*	B_{eq}, Å^2
Cl(1)	0.40915(3)	−0.02030(5)	0.13697(8)	4.99(2)
Cl(2)	0.29588(4)	0.21328(5)	0.33677(7)	4.78(2)
C(1)	0.4622(1)	0.1168(2)	0.2021(2)	3.21(7)
C(2)	0.4177(1)	0.2310(2)	0.1340(2)	3.18(7)
C(3)	0.3412(1)	0.2815(2)	0.1847(2)	3.27(7)
C(4)	0.2992(2)	0.3863(2)	0.1181(3)	4.07(8)
C(5)	0.3353(2)	0.4423(2)	−0.0013(3)	4.8(1)
C(6)	0.4113(2)	0.3950(2)	−0.0542(3)	5.1(1)
C(7)	0.4521(2)	0.2895(2)	0.0124(3)	4.44(9)
H(4)	0.244(2)	0.414(2)	0.154(3)	4.9(5)[b]
H(5)	0.314(2)	0.512(2)	−0.047(4)	6.2(7)[b]
H(6)	0.438(2)	0.431(3)	−0.139(3)	6.6(7)[b]
H(7)	0.502(2)	0.255(2)	−0.031(3)	5.1(5)[b]

[a]B_{eq} is defined as one-third of the trace of the orthogonalized B_{ij} tensor.
[b]Isotropic *B*.

Table 3. Final fractional coordinates and equivalent isotropic temperature factors[a] for *E*-(1,2)-dichloro-bis(2-chlorophenyl)-ethylene (**2**).

Atom	*x*	*y*	*z*	B_{eq}, Å^2
Cl(1)	0.50325(7)	0.75216(9)	0.57282(4)	4.84(3)
Cl(2)	0.67864(6)	0.7681(1)	0.39312(5)	5.45(4)
C(1)	0.4914(2)	0.5923(3)	0.4935(2)	3.5(1)
C(2)	0.4571(2)	0.6815(4)	0.4170(1)	3.3(1)
C(3)	0.5357(2)	0.7705(3)	0.3675(2)	3.4(1)
C(4)	0.5019(3)	0.8592(4)	0.2978(2)	4.1(1)
C(5)	0.3894(3)	0.8579(5)	0.2773(2)	4.6(1)
C(6)	0.3104(3)	0.7703(5)	0.3239(2)	4.8(1)
C(7)	0.3429(3)	0.6831(5)	0.3946(2)	4.3(1)
H(4)	0.555(2)	0.917(4)	0.270(2)	4.2(3)[b]
H(5)	0.368(2)	0.917(4)	0.234(2)	4.2(3)[b]
H(6)	0.231(3)	0.769(4)	0.314(2)	4.2(3)[b]
H(7)	0.284(2)	0.623(4)	0.431(2)	4.2(3)[b]

[a]B_{eq} is defined as one-third of the trace of the orthogonalized B_{ij} tensor.
[b]Common isotropic *B*.

based on the fact that only H(7) affords a correlation with C(1) in the HMBC spectrum. The spectral lines of the protons show different widths at half-height, indicating that slow internal rotation(s) occur. The ^{1}H spectrum of compound **1** is closer to first order and the signals of the single protons are at higher field than in compound **2**. The sharpest signals are those at 7.13 ppm and the broadest those at 7.25 ppm. The ^{1}H spectrum of compound **2** is strongly coupled and contains two groups of signals with the same integrated area, one within 7.45–7.52 ppm and the other within 7.32–7.38 ppm. On lowering the sample temperature to 240 K, the spectrum of each compound shows the presence of two chemical species, in the ratio 85/15 for compound **1** and 45/55 for compound **2**. In the ^{13}C spectrum of **2**, the splitting of a number of signals is observed already at 300 K and all the signals are split at 240 K, yet for compound **1** this occurs only at 240 K.

The internal rotation process in these molecules can occur

Table 4. Main molecular dimensions in 1,2-dichloro-bis(2-chlorophenyl)ethylenes.

	Z form (**1**)	*E* form (**2**)
Interatomic distances (Å)		
Cl(1)—C(1)	1.737(2)	1.741(2)
C(1)—C(1′)[a]	1.315(3)	1.313(5)
C(1)—C(2)	1.486(2)	1.484(3)
C(3)—Cl(2)	1.734(2)	1.730(3)
Cl(1)···Cl(1′)	3.139(1)	4.270(1)
Cl(1)···Cl(2)	3.609(1)	3.660(1)
Bond angles (°)		
C(1′)-C(1)-Cl(1)	121.69(6)	118.7(3)
C(1′)-C(1)-C(2)	123.86(9)	126.3(3)
Cl(1)-C(1)-C(2)	114.4(1)	115.0(2)
C(3)-C(2)-C(7)	117.8(2)	118.3(2)
C(3)-C(2)-C(1)	122.6(2)	121.7(2)
C(7)-C(2)-C(1)	119.6(2)	120.0(2)
C(4)-C(3)-C(2)	122.0(2)	121.1(3)
C(4)-C(3)-Cl(2)	118.1(2)	119.6(2)
C(2)-C(3)-Cl(2)	119.9(1)	119.3(2)
Torsional angles (°)		
Cl(1)-C(1)-C(1′)-Cl(1′)	1.3(4)	180
C(2)-C(1)-C(1′)-C(2′)	8.0(5)	180
C(3)-C(2)-C(1)-C(1′)	−103.7(3)	−100.1(4)
C(7)-C(2)-C(1)-C(1′)	82.2(4)	77.6(3)

[a]Primed atoms are related to unprimed ones by the symmetry transformation $1 - x$, y, $1/2 - z$ of the reference coordinates for the *Z* form, and by the symmetry transformation $1 - x$, $1 - y$, $1 - z$ for the *E* form.

Fig. 1. ORTEP drawing of *Z*-1,2-dichloro-1,2-bis(2-chlorophenyl)ethylene with atom labelling scheme. Thermal ellipsoids for non-H atoms enclose 50% probability. Primed atoms are related to unprimed ones by the symmetry transformation $1 - x$, y, $1/2 - z$ of the reference coordinates.

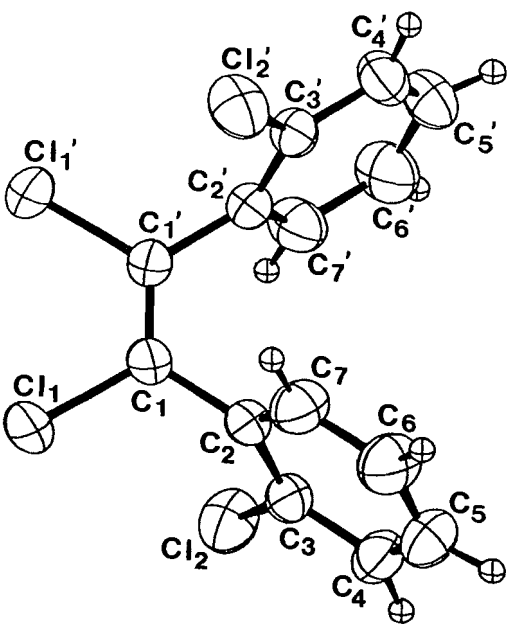

Can. J. Chem. Downloaded from www.nrcresearchpress.com by 80.90.12.36 on 09/08/12
For personal use only.

Table 5. ^1H and ^{13}C chemical shifts (δ values) measured at 300 and 240 K in $CDCl_3$ solution.

	1			2			
	300 K	240 K		300 K		240 K	
Isomer amount (%):		85	15			55	45
H(4)	7.27	7.28	7.25	7.48		7.49	7.49
H(5)	7.13	7.16	7.16	7.36		7.38	7.38
H(6)	7.05	7.05	7.09	7.36		7.38	7.38
H(7)	7.25	7.22	7.21	7.48	7.45	7.49	7.46
C(1)	130.22	130.27	130.47	128.08	128.08	127.98	128.24
C(2)	135.70	135.40	134.55	135.73	135.40	135.40	135.35
C(3)	133.22	133.08	133.70	133.03	133.48	132.85	133.27
C(4)	129.62	129.74	130.23	129.85	130.08	129.96	130.17
C(5)	130.50	130.87	130.54	130.60	130.60	130.96	130.91
C(6)	126.82	127.16	126.48	127.20	126.97	127.47	127.27
C(7)	130.08	130.08	131.95	130.68	130.60	130.77	130.62

Fig. 2. The structure of *E*-1,2-dichloro-1,2-bis(2-chlorophenyl)-ethylene with atom labelling scheme. Thermal motion ellipsoids enclose 50% probability. Primed atoms are related to unprimed ones by the symmetry transformation $1 - x$, $1 - y$, $1 - z$ of the reference coordinates.

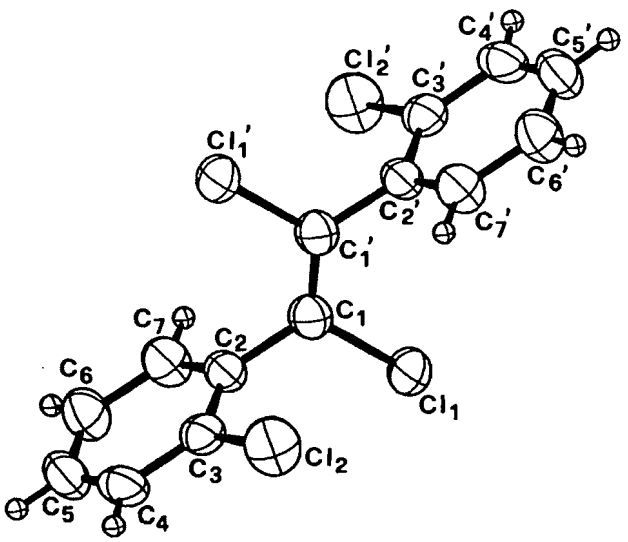

around the hexocyclic C(sp^2)—C(sp^2) bond and the conformational minimum is expected for the phenyl ring almost perpendicular to the plane of the double bond, owing to the presence of the chlorine atom on C(1). Two orientations are nevertheless expected, which we will label *syn* and *anti*, in view of the fact that the C—Cl bonds on the phenyl rings can be located on the same or opposite side with respect to the ethylenic plane. The rotational minima for the phenyl rings almost perpendicular to the double-bond plane are found from semi-empirical AM1/MNDO (16) calculations, and the *anti* are more stable than the *syn* conformations in compounds **1** and **2**. The *anti* form is that found in the solid state structure of these compounds.

The higher field ^1H resonance in compound **1** with respect to compound **2**, for the *syn* and *anti* forms, can probably be attributed to reciprocal screening due to the ring current effect, which should be less efficient in the *E* isomer, **2**. It is trickier to justify the small relative ^1H chemical shifts of the *anti* and *syn* forms in each compound, which would appear to depend mainly on the orientation of the protons with respect to the C—Cl bonds of the phenyl rings and from other effects that are difficult to quantify.

Acknowledgements

The authors have warmly appreciated financial support from the Italian Ministero dell'Università e della Ricerca Scientifica (MURST) and leave to use the X-ray and NMR spectrometers and VAX 6310 computer of the Interdipartimental Centers (CIGS and CICAIA) of Modena University.

References

1. T.A. Cooper and T. Takeshita. J. Org. Chem. **36**, 3517 (1971).
2. T. Shirafuji, Y. Yamamoto, and H. Nozaki. Bull. Chem. Soc. Jpn. **44**, 1994 (1971).
3. K. Onuma, J. Yamashita, and H. Hashimoto. Bull Chem. Soc. Jpn. **46**, 333 (1972).
4. T.A. Cooper. J. Am. Chem. Soc. **95**, 4158 (1973).
5. A. Cornia, U. Folli, S. Sbardellati, and F. Taddei. J. Chem. Soc. Perkin Trans. 2, 1847 (1993).
6. J.B. Firth and T.H. Smith. J. Chem. Soc. 337 (1936).
7. A.C.T. North, D.C. Phillips, and F.S. Mathews. Acta Crystallogr. Sect. A: Cryst. Phys. Diffr. Theor. Gen. Crystallogr. **A24**, 351 (1968).
8. G.M. Sheldrick. SHELX-86. Program for crystal structure solution. University of Göttingen, Göttingen, Germany. 1986.
9. G.M. Sheldrick. SHELX-76. Program for crystal structure determination. University Chemical Laboratory, Cambridge, England. 1976.
10. C.K. Johnson. ORTEP. Report ORNL-3794. Oak Ridge National Laboratory, Oak Ridge, Tenn. 1965.
11. A. Bax, R.H. Griffey, and B.L. Hawkins. J. Magn. Reson. **55**, 301 (1983).
12. A. Bax and M.F. Summers. J. Am. Chem. Soc. **108**, 2093 (1986).
13. R. Norrestam, S. Hovmöller, P. Tor-Björn, R. Göthe, and C.A. Wachtmeister. Acta Crystallogr. Sect. B: Struct. Crystallogr. Cryst. Chem. **B33**, 370 (1977).
14. A.J. de Kok and C. Romers. Acta Crystallogr. Sect. B: Struct. Crystallogr. Cryst. Chem. **B34**, 2477 (1978).

15. D.S. Stefenson and G. Binsch. DNMR5: Iterative nuclear magnetic resonance program for unsaturated exchange-broadening bandshapes. QCPE Program 365, Quantum Chemistry Program Exchange, Indiana University, Bloomington, Ind. 1979.

16. M.J.S. Dewar, E.G. Zoebisch, E.F. Healy, and J.J.P. Stewart. J. Am. Chem. Soc. **107**, 3902 (1985).

Can. J. Chem. Downloaded from www.nrcresearchpress.com by 80.90.12.36 on 09/08/12
For personal use only.

Action of tetrabutylammonium tribromide with *para*-substituted chalcones in protic and aprotic media

Jacques Berthelot, Yamina Benammar, and Bernard Desmazières

Abstract: Bromination of the double bond of *para*-substituted chalcones under mild conditions in aprotic solvents is accomplished with high yields using tetrabutylammonium tribromide ($TBABr_3$). In methanol, the main reaction is (α-β) bromomethoxylation. Stereoselectivity, regioselectivity, and chemioselectivity of this bromomethoxylation reaction are described.

Key words: bromination, bromomethoxylation, tetrabutylammonium tribromide, (α-β) dibromodihydrochalcones, α-bromo,β-methoxydihydrochalcones.

Résumé : La bromation de la double liaison ethylènique de chalcones *para*-substituées a été effectuée en utilisant le tribromure de tétrabutylammonium ($TBABr_3$). Cette réaction, dans les solvants aprotiques, se produit dans des conditions douces et les rendements obtenus sont élevés. Dans le méthanol, le produit majoritaire correspond à une (α-β) bromométhoxylation. Les aspects stéréo, régio et chémiosélectifs de cette réaction de bromométhoxylation sont envisagés.

Mots clés : bromination, bromométhoxylation, tribromure de tétrabutylammonium, (α-β) dibromodihydrochalcones, α-bromo-β-méthoxydihydrochalcones.

Can. J. Chem. Downloaded from www.nrcresearchpress.com by 80.90.12.36 on 09/08/12
For personal use only.

(α-β) Dibromodihydrochalcones **I** and α-bromo,β-methoxydihydro chalcones **II** are interesting intermediates in the synthesis of biologically active cyclic compounds such as pyrazolines (1), pyrimidines (2), imidazoles (1), aziridines (2), and quinoxalines (3). Some chalcones are also used as precursors in the synthesis of natural compounds such as flavones (4). Compounds **I** are usually prepared using bromine (alone or with an excess of bromide) or *N*-bromosuccinimide (NBS) in weakly polar, aprotic solvents (CCl_4, $CHCl_3$, CH_2Cl_2). Yields are limited by secondary reactions, e.g., bromination of aromatics (4). The members of group **II** are normally prepared in methanol (after several days of heating) using either bromine, NBS in excess, or methylhypobromite. Yields are limited, and compounds **I** are produced as by-products. Yields for the group **II** compounds improve when an excess of NBS in hot methanol is used in the presence of acids, bromine, or silver salts (5, 6). Group **II** compounds can also be synthesized by high-temperature methanolysis of the dibromo products **I**; however, this reaction is not general, as it depends strongly on the nature of the aromatic substituents (4).

We have used tetrabutylammonium tribromide ($TBABr_3$) to perform regioselective bromination of activated aromatics (phenols and amines) (7) in high yields and without polymerization. $TBABr_3$ (a stable, non-hygroscopic solid) is easy to use under mild conditions and, unlike bromine, it is neither corrosive nor toxic. We hoped that use of this reagent to perform room temperature bromination of chalcones might lead to improved yields in the synthesis of **I** or **II**.

Received February 14, 1995.

J. Berthelot,[1] Y. Benammar, and B. Desmazières. Laboratoire de chimie organique structurale, Unité de recherche associée n° 506, boîte 45, Université P. et M. Curie, 4, Place Jussieu, 75252 Paris, Cédex 05, France.

[1] Author to whom correspondence may be addressed; Fax: 33 1 44272568.

Results

We used *para*-substituted chalcones in the (*E*) configuration as reactants. The products (**I** and **II**) were characterized by physical and spectroscopic methods and were positively identified by comparison with authentic samples.

(a) In aprotic solvents

In $CHCl_3$ one equivalent of $TBABr_3$ was found to nearly quantitatively brominate one equivalent of chalcone (Table 1) at room temperature.

[1] X-PhCOCH=CHPh-Y + $TBABr_3$
1 **2**

→ X-PhCOCHBr-CHBrPh-Y + TBABr
I **3**

Sonication (50 kHz) of the reactant mixture at 20°C greatly reduced reaction times and increased yields of the (α-β) dibromo compounds to more than 95% in all cases (Table1). In order to optimize the experimental conditions, chalcone **1***a* was used as a model reactant with different solvents, $CHCl_3$, CCl_4, CH_2Cl_2, or CH_3CN (Table 2). At 60°C the bromination reaction was faster (3 h), but the yield was lower (50%) due to polymerization of the enone system. As seen in Table 2, the best yields were obtained by sonicating stoichiometric proportions of the reactants, in chloroform at room temperature.

Can. J. Chem. Downloaded from www.nrcresearchpress.com by 80.90.12.36 on 09/08/12
For personal use only.

Table 1. Bromination of chalcones by $TBABr_3$, at 20°C, in $CHCl_3$.

	Compounds						
	1*a*	**1***b*	**1***c*	**1***d*	**1***e*	**1***f*	**1***g*
X:	H	MeO	MeO	Br	NO_2	H	H
Y:	H	MeO	H	H	H	MeO	Cl
Magnetic stirring							
Time (h)	20	20	25	55	62	25	50
Yield (%)[a] of **I**	97	95	93	92	91	95	92
Ultrasound							
Time (h)	3.5	4	4	9	10	4	8
Yield (%)[a] of **I**	98	98	97	95	95	97	97

[a]Yield of pure isolated products.

Table 2. Stoichiometric action of $TBABr_3$ on **1***a* (magnetic stirring).

Experiment	Solvent	*T* (°C)	Time (h)	Yield (%)**I**	Yield (%) **1***a*
1	$CHCl_3$	20	20	95	—
2[a]	$CHCl_3$	20	4	98	—
3	CCl_4	20	20	70	28
4	CH_3CN	20	20	81	18
5	CH_2Cl_2	20	20	90	Traces
6	$CHCl_3$	60	3	50	Resins
7	CCl_4	76	2	40	Resins
8[b]	$CHCl_3$	20	16	93	—
9[b]	$CHCl_3$	60	2.5	52	Resins

[a]Sonication.
[b]Two equivalents of $TBABr_3$.

With each chalcone, only the (α-β) dibromo compound **I** was obtained as a racemic mixture of *erythro* isomers. Bromination of double bonds by bromine has been studied in a large number of solvents, and its mechanism is well known (5, 8, 9). However, few studies of bromination by Br_3^- have been reported. Generally, this anion is generated in situ by reaction of bromine with excess Br^- (7). Bellucci et al. have proposed the following mechanism for tribromide in $CHCl_3$ (10) (Scheme 1).

This *trans* addition was confirmed by the reconversion of the dibromides back to the initial chalcones using an excess of iodide (11).

(b) In methanol

Enone bromination with bromine, NBS, or methyl hypobromite in methanol gives three main products, namely, the dibrominated (D.B.) and the (α-β) bromomethoxylated regioisomers whose proportions depend on the experimental conditions (12) (Scheme 2).

Substitution reactions (when alkyl groups are present), electrophilic addition to aryl moieties, enone polymerization, and formation of secondary derivatives (β brominated or β methoxybrominated ketones) can also occur concurrently (13).

The reaction in methanol was performed in the same way as in aprotic solvents. Compound **1***a* was used as a model to study this reaction. The results are summarized in Table 3.

The best yield of the C_α compound was obtained at 20°C with sonication (experiment 3); there was no evidence for the formation of the C_β regioisomer and no secondary products or polymerization (except at 60°C). Yields of the dibrominated compound were small (about 5%) except in the $CHCl_3$–MeOH mixture. After 3 days of stirring in methanol, in the absence or presence of $TBABr_3$, the dibromide can be recov-

Scheme 1

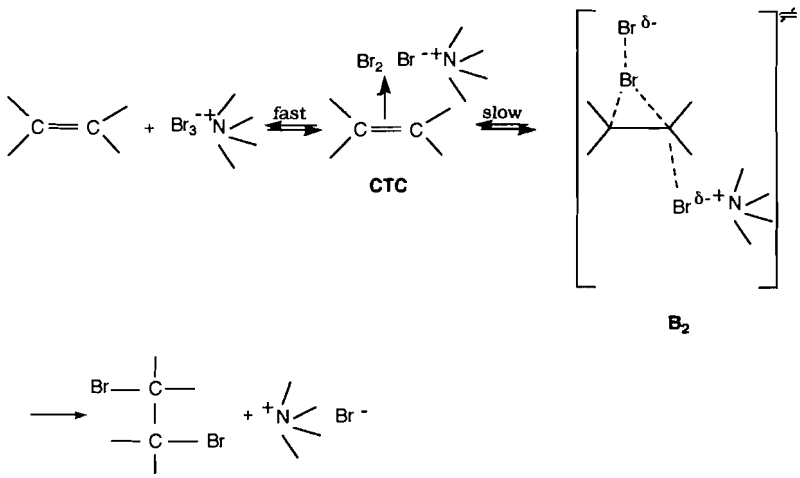

Scheme 2

$$ArCOCH{=}CHAr' \xrightarrow[MeOH]{TBABr_3} \underset{(D.B.)}{ArCOCHBr{-}CHBrAr'} + \underset{(C_\alpha)}{ArCOCHBr{-}CH(OMe)Ar'} + \underset{(C_\beta)}{ArCOCH(OMe){-}CHBrAr'}$$

Table 3. Stoichiometric action of $TBABr_3$[a] with **1***a* in methanol, at 20°C,[b] with stirring.[c]

Experiment	Time (h)	D.B. (%)	C_α (%)	C_β (%)	Yield (%) **I**[d]
1	48	5	90	—	95
2	40	5	91	—	96
3	6	3	93	—	96
4	18	Trace	50	—	50 + resins
5[e]	48	7	87	—	94
6[f]	48	5	89	—	94
7[g]	35	45	51	—	96

[a]Experiment 2: 1.8 $TBABr_3$.
[b]Experiment 4: 60°C.
[c]Experiment 3: Sonication.
[d]Pure and isolated.
[e]With NaBr.
[f]With $NaHCO_3$.
[g]In 50 mL MeOH – 50 mL $CHCl_3$.

ered intact, and there was no noticeable formation of methoxylated derivatives. This result eliminates the possibility that the formation of the dibrominated compound is a first step, followed by partial methanolysis.When an excess of NaBr (or $NaHCO_3$) was added, there was no noticeable modification of the chemioselectivity.

Results obtained with *para*-substituted chalcones

Based on the results obtained with **1***a*, reactions with the *para*-substituted chalcones were carried out using stoichiometric proportions at room temperature in methanol.

Regardless of the mixing conditions (stirring or sonication), the same results were obtained with each chalcone. The only noticeable difference was the accelerated rate of reaction when ultrasound was used. In all cases, global yields were almost quantitative. Polymerization and formation of by-products were inhibited, and bromination was slower than in $CHCl_3$. Only chalcones bearing an electron-withdrawing group (Br or NO_2) on the aromatic ring vicinal to the carbonyl group are transformed into a mixture of the two (α-β) bromomethoxylated regioisomers. Chalcones containing an electron-donating group (**1***b*, **1***c*, **1***f*) give quantitatively the C_α brominated derivative. With regard to chemioselectivity, it appears that the yield of the dibrominated compound increases when the reaction time increases. It is worth noting the essential role that the solvent plays in this reaction (8, 9). The equilibrium constant for the reaction $Br_3^- \leftrightarrows Br_2 + Br^-$ is strongly dependent on the nature of the solvent ($K_D = (7–9) \times 10^{-6}$ in aprotic solvents such as $CHCl_3$ or CH_3CN, but $K_D = 5 \times 10^{-3}$ in methanol) (8) Since the reaction is slow in methanol (from 25 to 72 h depending on the enone), the two brominating reagents (Br_2 and Br_3^-) must be present simultaneously, and bromination by $TBABr_3$ in methanol seems to be a complex process. Presumably the chalcones with electron donors give Markovnikov additions where product arises from normal nucleophilic capture β to the carbon bearing the C(O)Ar unit. Electron withdrawers change the electronic distribution and the relative α/β attack in MeOH. This interpretation is supported by the results obtained by Heasley et al., who studied the reaction of Br-Cl with (α-β) unsaturated esters (14).

Table 4. Action of $TBABr_3$ with chalcones in methanol at 20°C.

Chalcone	Time (h) Stirring	Sonication	D.B. (%)	C_α (%)	C_β (%)	Global yield (%)
1*a*	48	8	5[a]	90[a]	—	95[a]
1*b*	25	4	—	97[a]	—	97[a]
1*c*	28	4.5	—	98[a]	—	98[a]
1*d*	72	11	18[a]	18	56	92
1*e*	72	11	22[a]	20	50	92
1*f*	30	4.5	—	97[a]	—	97[a]
1*g*	70	10.5	15[a]	77[a]	—	92[a]

[a]Yields for pure, isolated compound.

While the bromination of alkenes by Br_2 is a basic reaction in organic chemistry, the electrophilic addition of Br_3^- to ethylenic compounds is uncommon, except when it occurs indirectly. The use of $TBABr_3$ in synthesis of brominated chalcones is interesting and useful as it allows excellent yields, without polymerization as a side reaction, under mild reaction conditions. The essential role of the solvent is confirmed in these reactions.

Experimental

General remarks

All chalcones, with the exception of **1***a*, which was purchased from Aldrich Chemical Co, were prepared according to the usual method, the Claisen–Schmidt reaction. The appropriate aldehydes and acetophenones were used in equimolecular proportions in ethanol and were treated with an aqueous NaOH solution (20–40%) (15). $TBABr_3$ was obtained from Janssen Chemica. Melting points were measured using a Köfler hot bench. ^1H NMR spectra were recorded using an AC 200 Bruker spectrometer (200 MHz, solution in $CDCl_3$, internal reference TMS, chemical shifts in ppm). Mass spectra (MS) were obtained using a Ribermag R10–10 C quadrupolar mass spectrometer.

The purity of the products was checked by thin-layer chromatography (stationary phase: fluorescent silica gel, mobile phase: diethyl ether – hexane in variable proportions, generally about 20%:80%, respectively). Purification was performed by preparative chromatography on fluorescent silica gel (Merck PF-254, 20 cm × 20 cm plates, thickness 0.1 cm), using diethyl ether and hexane as eluent.

As the dibrominated and bromomethoxylated compounds are thermally unstable, it was not possible to use gas chromatography.

A standard ultrasonic cleaning bath (50 kHz) was used (at room temperature) for reactions requiring sonication.

Reaction conditions

Reactions were generally performed at room temperature, 2×10^{-3} mol of chalcone and 2×10^{-3} mol of $TBABr_3$ were dissolved in 100 cm^3 of solvent. The reactions were carried out using either mechanical stirring or ultrasound. The initially red-colored solution changed gradually to yellowish and finally became colourless, at which point the reaction was

Can. J. Chem. Downloaded from www.nrcresearchpress.com by 80.90.12.36 on 09/08/12
For personal use only.

Can. J. Chem. Downloaded from www.nrcresearchpress.com by 80.90.12.36 on 09/08/12
For personal use only.

complete, as confirmed by TLC. The solvent was evaporated and the residue, dissolved in diethyl ether, was washed first with aqueous 5% sodium thiosulfate solution and finally with water. After evaporation of the solvent, a colorless oil was obtained.

In the case of bromination reactions performed in aprotic medium, the pure dibrominated compound was readily precipitated by addition of a small amount of ethanol.

For reactions performed in methanol, the putative dibrominated compound was crystallized by adding a few drops of ethanol. After separation of the dibrominated compound, the remaining solution, which contained the bromomethoxylated compound (or the two regioisomers in the case of **1***d* and of **1***e*), was purified using preparative chromatography.

(α-β) Dibromo dihydrochalcones I: APhCOCH$_\alpha$Br-CH$_\beta$BrPhB

All of these compounds were characterized by ^{1}H NMR, the -CHBr-CHBr- system of vicinal *erythro* dibrominated compounds giving two doublets between 5 and 5.9 ppm, with a coupling constant $J_{\alpha\beta} = J_{\beta\alpha}$ of 10–12 Hz (17). These latter values are characteristic of two protons in the *anti* position. The compounds were identified by comparison with samples prepared according to literature data (identical physical constants and spectroscopic properties).

I*a*: mp 160°C (lit. (16*a*) mp 160°C); NMR δ_H 7.3–8.2 (10H, m), 5.65 (1H(β), d, $J_{\beta\alpha}$ 12.5 Hz), 5.85 (1H(α), d, $J_{\alpha\beta}$ 12.5 Hz), MS (EI) *m/z*: 287–289 ((M − Br)$^{+\cdot}$, 10%), 208 ((M−2Br)$^+$, 30%), 105 ((PhCO)$^+$, 100%).

I*b*: mp 149°C (lit. (16*b*) mp 148°C); NMR δ_H: 6.9 (2H, dd), 7.3 (2H, d), 8.15 (2H, d), 5.1 (1H(β), d, $J_{\beta\alpha}$ 10 Hz), 5.25 (1H(α), d, $J_{\alpha\beta}$ 10 Hz), 3.75 (3H, s); MS (EI) *m/z*: 426–428–430 (M$^{+\cdot}$, 20%), 268 ((M − 2Br)$^+$, 45%), 135 ((MeOPhCO)$^+$, 100%).

I*c*: mp 160°C (lit. (16*c*) mp 159°C); NMR δ_H: 6.9–8.1 (9H, m), 5.2 (1H(β), d, $J_{\beta\alpha}$ 10 Hz), 5.8 (1H(α), d, $J_{\alpha\beta}$ 10 Hz), 3.85 (3H, s); MS (EI) *m/z*: 396–398–400 (M$^{+\cdot}$, 5%), 317–319 ((M−Br)$^+$, 5%), 238 ((M − 2Br)$^+$, 55%), 135 ((MeOPhCO)$^+$, 100%).

I*d*: mp 183°C (lit. (16*d*) mp 184°C); NMR δ_H: 7.3–7.9 (9H, m), 5.45 (1H(β), d, $J_{\beta\alpha}$ 11 Hz), 5.55 (1H(α), d, $J_{\alpha\beta}$ 11 Hz), MS (EI) *m/z*: 365–367–369 ((M − Br)$^+$, 15%), 286–288 ((M−2Br)$^+$, 25%), 207 ((M − 3Br)$^+$, 60%), 183–185 ((BrPhCO)$^+$, 50%), 131 ((PhCH=CHCO)$^+$, 70%), 105 ((PhCO)$^+$, 75%), 77 (Ph$^+$, 100%).

I*e*: mp 194°C (lit. (16*e*) mp 194°C); NMR δ_H: 7.3–7.5 (5H, m), 8–8.4 (4H, m), 5.7 (1H(β), d, $J_{\beta\alpha}$ 12 Hz), 5.9 (1H(α), d, $J_{\alpha\beta}$ 12 Hz), MS (EI) *m/z*: 332–334 ((M − Br)$^+$, 10%), 253 ((M − 2Br)$^+$, 25%), 150 ((NO$_2$PhCO)$^+$, 100%), 103 ((PhCH=CH)$^+$, 90%).

I*f*: mp 140°C (lit. (16*f*) mp 140°C); NMR δ_H: 6.85 (2H, d), 7–7.45 (5H, m), 7.7–8 (2H, m), 5.5 (1H(β) ; d, $J_{\beta\alpha}$ 12 Hz), 5.75 (1H(α), d, $J_{\alpha\beta}$ 12 Hz), 3.75 (3H, s), MS (EI) *m/z*: 396–398–400 (M$^{+\cdot}$, 1%), 317–319 ((M − Br)$^+$, 10%), 238((M − 2Br)$^+$, 28%), 105 ((PhCO)$^+$, 100%).

I*g*: mp 176°C (lit. (16*g*) mp 178°C); ^{1}H NMR δ_H: 7.4–8.1 (9H, m), 5.6 (1H(β), d, $J_{\beta\alpha}$ 12 Hz), 5.75 (1H(α), d, $J_{\alpha\beta}$ 12 Hz), MS (EI) *m/z*: 400–402–404–406 (M$^{+\cdot}$, 2%), 365–367–369 ((M − Cl)$^+$, 5%), 321–323–325 ((M − Br)$^+$, 5%), 105 ((PhCO)$^+$, 100%).

α-Bromo β-methoxy dihydrochalcones II: APhCOCH$_\alpha$Br-CH$_\beta$(OMe)PhB

As previously mentioned, the chalcones **1***a, b, c, f,* and *g* give only one bromomethoxylated regioisomer **II**. The compounds **II***a, b, c, f,* and *g* were purified using preparative chromatography as mentioned above and were identical to compounds prepared according to the literature. ^{1}H NMR spectra display characteristic doublets (between 5 and 5.9 ppm) corresponding to the -CH(Br)-CH(OMe)- system and a singlet between 3.1 and 3.8 ppm (3H) corresponding to the β methoxy.

In the case of **II***d* and **II***e*, a mixture of two bromomethoxylated regioisomers C$_\alpha$ and C$_\beta$ was obtained after purification by preparative chromatography. These two isomers were not separated using GC (because of their thermal instability) or liquid chromatography (TLC or HPLC). They were characterized by ^{1}H NMR and mass spectroscopy. The relative abundances of the two isomers were determined by ^{1}H NMR. The regioisomers **II***e* have not been described previously. Only the **II***d* C$_\alpha$ compound was known previously (16*e*), but a similar preparation resulted in an unstable oil containing the two regioisomers.

II*a*: mp 78°C (lit. (16*h*) mp 77°C); NMR δ_H: 7.25–8.2 (10H, m), 5.15 (1H(α), d, $J_{\alpha\beta}$ 11.7 Hz), 4.75 (1H(β), d, $J_{\beta\alpha}$ 11.7 Hz), 3.1 (3H, s), MS (EI) *m/z*: 287–289 ((M − OCH$_3$)$^+$, 90%), 121 ((PhCHOCH$_3$)$^+$, 100%), 105 ((PhCO)$^+$, 75%).

II*b*: mp 110°C (lit. (16*i*) mp 109°C); NMR δ_H: 7.9 (2H, d), 7.3 (2H, d), 7.0 (4H, d), 5.2 (1H(α), d, $J_{\alpha\beta}$ 10 Hz), 4.8 (1H(β)), d, $J_{\beta\alpha}$ 10 Hz), 3.85 (3H, s), 3.2 (s, 3H); MS (EI) *m/z*: 299 ((M − Br)$^+$, 40%), 151 ((MeOPhCHOCH$_3$)$^+$, 100%), 135 ((CH$_3$OPhCO)$^+$, 95%), ((PhCHOMe)$^+$, 30%).

II*c*: mp 125°C (lit. (16*j*) mp 126°C); NMR δ_H: 7.8–8.0 (2H, m), 7.4–7.2 (5H, m), 7.0 (2H, d), 5.1 (1H(α), d, $J_{\alpha\beta}$ 10 Hz), 4.8 (1H(β), d, $J_{\beta\alpha}$ 10 Hz), 3.8 (3H, s), 3.2 (3H, s); MS (EI) *m/z* : 348–350 (M$^{+\cdot}$, 3%), 238 ((M−(Br + OCH$_3$)$^+$, 28%), 207 ((M − (Br + 2OCH$_3$))$^+$, 20%), 135 ((CH$_3$OPhCO)$^+$, 100%), 121 ((PhCHOCH$_3$)$^+$, 55%), 105 ((PhCO)$^+$, 35%).

II*f*: mp 102°C (lit. (16*k*) mp 102°C); NMR δ_H: 7.7–8.0 (2H, m), 7.4–7.0 (5H, m), 6.9–6.8 (2H, m), 5.1 (1H(α), d, $J_{\alpha\beta}$ 9.8 Hz), 4.7 (1H(β), d, $J_{\beta\alpha}$ 9.8 Hz), 3.75 (3H, s), 3.1 (3H, s), MS (EI) *m/z*: 348–350 (M$^{+\cdot}$, 5%), 238 (M − (Br + OCH$_3$))$^+$, 35%), 207 ((M − (Br + 2OCH$_3$))$^+$, 10%), 151 ((MeOPhCHOCH$_3$)$^+$, 100%), 105 ((PhCO)$^+$, 80%).

II*g*: mp 118°C (lit. (16l) mp 115°C); NMR δ_H: 7.3–8. (9H, m), 5.1 (1H(α), d, $J_{\alpha\beta}$ 12 Hz), 4.7 (1H(β), d, $J_{\beta\alpha}$ 12 Hz), 3.15 (3H, s); MS(EI) *m/z*: 321–323–325 ((M − OCH$_3$)$^+$, 1%), 273–275 ((M − Br)$^+$, 20%), 155–157 ((ClPhCHOCH$_3$))$^+$, 80%), 105 ((PhCO)$^+$, 100%).

The mixture of the two regioisomers of **II***d* was an oil. MS (EI) *m/z*: 365–367–369 ((M − OMe)$^+$, 1%), 317–319 ((M − Br)$^+$, 5%), 227–229 ((BrPhCOCH(OCH$_3$)$^+$, 35%), 183–185 ((BrPhCO)$^+$, 30%), 121 ((PhCHOCH$_3$)$^+$, 100%). The peak at *m/z* 227–229 is characteristic of the presence of C$_\beta$, the peak at 121 indicates the presence of C$_\alpha$.

(α) BrPhCOCH$_\alpha$Br-CH$_\beta$(OMe)Ph: NMR δ_H: 7.1–7.8 (aromatic H, m), 4.9 (1H(α), d, $J_{\alpha\beta}$ 12.5 Hz), 4.6 (1H(β), d, $J_{\beta\alpha}$ 12.5 Hz), 3.1 (3H, s). This is consistent with the *erythro* structure (17).

(β) BrPhCOCH$_\alpha$(OMe)-CH$_\beta$BrPh: NMR δ_H: 7.1–7.8 (aromatic H, m), 5.05 (1H(α), d, $J_{\alpha\beta}$ 12,5 Hz), 4.7 (1H(β), d, $J_{\beta\alpha}$ 12.5 Hz), 3.3 (3H, s). This is consistent with the *erythro* structure (17).

Comparison of the singlet integrations corresponding to the three protons of the methoxy groups of each regioisomer gives the ratio (α)/(β) = 1/3.

Similarly, for the mixture of the regioisomers of **II***e*: MS (EI) *m/z*: 332–334 ($(M-OCH_3)^+$, 5%), 253 ($(M - (Br + OCH_3)^+$, 25%), 194 ($(NO_2PhCOCH(OCH_3)^+$, 35%), 150 ($(NO_2PhCO)^+$, 95%), 121 ($(PhCH(OCH_3)^+$, 100%). The peak at *m/z* 194 indicates the presence of C_β and the peak at 121 the presence of C_α.

(α) $NO_2PhCOCH_\alpha Br\text{-}CH_\beta(OCH_3)Ph$: NMR δ_H: 8.3–7.3 (aromatic H, m), 4.6 (1H(α), d, $J_{\alpha\beta}$ 12.6 Hz), 4.4 (1H(β), d, $J_{\beta\alpha}$ 12.6 Hz), 3.4 (3H, s). This is consistent with the *erythro* structure (17).

(β) $NO_2PhCOCH_\alpha(OMe)\text{-}CH_\beta BrPh$: NMR δ_H: 8.3–7.3 (aromatic H, m), 4.7 (1H(α), d, $J_{\alpha\beta}$ 12.6 Hz), 4.5 (1H(β), d, $J_{\beta\alpha}$ 12.6 Hz), 3.6 (3H, s). This is consistent with the *erythro* structure (17). As described above, we obtained (α)/(β) = 2/3.

References

1. M.G. Joshi and K.N. Wadodkar. Indian J. Chem. **20B**, 1090 (1981).
2. F.G. Weber and H. Liepert. Z. Chem. **25**, 175 (1985).
3. V.D. Orlov, N.P. Vorobeva, N.N. Demenkova, V.S. Chesnovki, and F.G. Yaramanko. Khim. Geterotsikl. Soedin. **3**, 328 (1988).
4. J.A. Donnely and C.L. Higginbotham. Tetrahedron, **46**, 7219 (1990).
5. P.B.D. De La Mare and R. Bolton. Electrophilic additions to unsaturated systems. 2nd ed. Elsevier, Oxford, London. 1982. Chap. 7, p. 113.
6. L.C. Vishwakarma and J.S. Walia. J. Indian Chem. Soc. **53**, 156 (1976).
7. J. Berthelot, C. Guette, P.L. Desbene, J.J. Basselier, P. Chaquin, and D. Masure. Can. J. Chem., **67**, 2061 (1989).
8. M.F. Ruasse, J. Aubard, and P. Monjoint. J. Chim. Phys. **82**, 539 (1985); M.F. Ruasse. Adv. Phys. Org. Chem. **28**, 207 (1993).
9. M.F. Ruasse. Acc. Chem. Res. **23**, 87 (1990).
10. G. Belluci, R. Blanchini, R. Ambrosetti, and G. Ingrosso. J. Org. Chem. **50**, 3313 (1985).
11. R.S. Raghavan, K. Velayutham, and V. Rajendran. Indian J. Chem. **23 A**, 466 (1984).
12. V.L. Heasley, T.J. Louie, D.K. Luttul, M.D. Millar, M.B. Moore, D.F. Nogales, A.M. Sauerbrey, A.B. Shevel, T.Y. Shibuya, M.S. Stanley, D.F. Schellhamer, and G.E. Heasley. J. Org. Chem. **53**, 2199 (1988).
13. V.L. Heasley, D.F. Schellhamer, T.L. Carter, D.E. Gipe, R.K. Gipe, R.C. Green, J. Nordeen, T.D. Rempel, and D.W. Spaite. Tetrahedron Lett. **22**, 2467 (1981).
14. V.L. Heasley, D.W. Spaite, and D.F. Schellhamer. J. Org. Chem. **44**, 2608 (1979).
15. A.I. Vogel. Practical organic chemistry. 3rd ed. Longmans, Green and Co., London 1957. p. s718.
16. Beilsteins Handbuch der Organischen Chemie. 5th ed. Julius Springer, Berlin. (*a*) **7–III**, 2154; (*b*) **8–III**, 2703; (*c*) **8–III**, 1340; (*d*) **7–III**, 2157; (*e*) **7–II**, 382; (*f*) **8–III**, 1346; (*g*) **7–I**, 238; (*h*) **8–II**, 204; (*i*) **8–I**, 704; (*j*) **8–III**, 2705; (*k*) **8–III**, 2706; (*l*) **8–III**, 1349 (1981).
17. K. Yates and R.S. McDonald. J. Org. Chem. **38**, 2465 (1973).

Can. J. Chem. Downloaded from www.nrcresearchpress.com by 80.90.12.36 on 09/08/12
For personal use only.

Kinetics and mechanism of the oxidation of the sulphite ion by the Mn(III)–cydta complex ion

Uttra Chandrawat, Aditya Prakash, and Raj N. Mehrotra

Abstract : The reinvestigated oxidation of S(IV), HSO_3^-/SO_3^{2-} ions, by $[Mn(cydta)(OH_2)]^-$ confirmed that S(IV) is oxidized in two parallel paths; the order with respect to [S(IV)] is one in one of the paths and two in the other. The nature of the dependence of the rate on $[H^+]$ is also confirmed. However, the rapid scan of the reaction mixture and measurement of the initial absorbance of the reaction mixture at different wavelengths at the beginning of the reaction suggest an outer-sphere mechanism. The rate parameters are of the same order as obtained in known reactions of an outer-sphere mechanism and this mechanism is further supported by the Marcus cross relation.

Key words: kinetics, outer-sphere mechanism, $[Mn(cydta)]^-$, SO_3^{2-}.

Résumé : Un réexamen de la réaction d'oxydation du S(IV), des ions HSO_3^-/SO_3^{2-}, par le $[Mn(cydta)(OH_2)]^-$ a permis de confirmer que le S(IV) est oxydé par deux voies parallèles; l'ordre de la réaction par rapport au [S(IV)] est de un dans l'une des voies et de deux dans l'autre. On a aussi confirmé la nature de la dépendance de la vitesse de réaction sur la $[H^+]$. Toutefois, un balayage rapide du mélange réactionnel et une mesure de l'absorbance initiale du mélange réactionnel à diverses longueurs d'onde au début de la réaction suggèrent l'existence d'un méchanisme de couche externe. Les paramètres de vitesse sont du même ordre que ceux obtenus dans des réactions connues de mécanisme de couche externe et ce dernier est aussi supporté par la relation croisée de Marcus.

Mots clés : cinétique, mécanisme de couche externe, $[Mn(cydta)]^-$, SO_3^{2-}.

[Traduit par la rédaction]

Introduction

The oxidation of S(IV) (HSO_3^-/SO_2^{2-}) by metal ions has the following unusual feature: both one- and two-electron net oxidations occur, and the product may be sulphate, the dithionate ion, or, more often, a mixture (1). The oxidation of the S(IV) ion, a subject of much attention in the past, is of current interest (2). Parallel first- and second-order dependence on [S(IV)] were suggested in an inner-sphere mechanism with the assumption that $cydta^{4-}$ acted as a pentadentate ligand allowing S(IV) to occupy the sixth coordination site of manganese(III) (3). There are, however, both early (4) and recent (5) literature references suggesting that $[Mn(cydta)(OH_2)]^-$ is a seven-coordinated complex in which $cydta^{4-}$ is a hexadentate ligand in aqueous $[Mn(cydta)(OH_2)]^-$ solution and the seventh coordination site is occupied by water. The same is true for the complex solution in methanol (6). Therefore this reinvestigation was considered desirable. The previous results (3), the parallel first- and second-order paths in [S(IV)] and an increase in the rate with pH, are confirmed although the inverse rate dependence on $[H^+]$ is linked to a first-order path in [S(IV)] rather than a path second-order in [S(IV)] (3). Similarly, the reaction path with $S_2O_5^{2-}$ accounts for the second-order path in [S(IV)]. In addition to the spectral evidence, which did not support the formation of an inner-sphere complex (though the formation of a precursor complex is not excluded), other evidence, such as comparison of the estimated rates of electron transfer with other outer-sphere reactions (5) including the oxidation of dithionite ion (7) and the application of the Marcus cross-relation (8), are indicative of an outer-sphere mechanism.

Received April 6, 1995.

U. Chandrawat, A. Prakash, and R.N. Mehrotra.[1] Department of Chemistry, Jai Narain Vas University, Jodhpur 342 005, India.

[1] Author to whom correspondence may be addressed. Telephone: 0091-0291-40840. Note: reprints not available.

Experimental

Materials

Acetic (Sarabhai-M, GR) and perchloric (E. Merck, GR) acids were standardized against a standard alkali. Sodium acetate (Sarabhai, GR) solution was prepared by weight. An approximate $Mn(ClO_4)_2$ (G.F. Smith) solution, prepared in dilute perchloric acid, was standardized against a standard EDTA solution using PAR (4-(2-pyridylazo)-resorcinol) indicator (9). *trans*-Cyclohexane-1,2-diamine-*N*,*N*,*N*′,*N*′-tetraacetic acid (cydta) was obtained from Baker and Sigma. All chemicals, certified or reagent grade, were used as received.

The Mn(III) complex was prepared by the oxidation of $[Mn(cydta)]^{2-}$ by PbO_2 in dilute sulphuric acid (10). The use of excess PbO_2 was avoided because it causes the oxidation of H_4cydta to formaldehyde. The $PbSO_4$ and PbO_2 were filtered

Can. J. Chem. Downloaded from www.nrcresearchpress.com by 80.90.12.36 on 09/08/12
For personal use only.

Can. J. Chem. Downloaded from www.nrcresearchpress.com by 80.90.12.36 on 09/08/12
For personal use only.

through a sintered crucible and the pH of the filtrate was adjusted to 4. The stock solution, stored in a refrigerator, was suitably diluted in the desired buffer and standardized spectrophotometrically at 510 nm ($\epsilon = 345$ dm^3 mol^{-1} cm^{-1} at pH <6) (4). The pH was checked with an Agrionic pH meter. Twice-distilled water, purged with nitrogen for at least 1 h, was used for the preparation of solutions.

The freshly prepared sodium sulphite (Baker, Analyzed grade) solution was standardized iodometrically (11). An acetate concentration of 0.06 mol dm^{-3} was present in the buffered solution prepared by mixing sodium acetate and acetic acid solutions in the required ratio (12).

Rate measurements

The rate of the reaction was measured, under pseudo-first-order conditions ($[SO_3^{2-}] \gg [Mn(cydta)(OH_2)^-]$), in terms of the disappearance of $[Mn(cytda)(OH_2)]^-$ at 510 nm using a Union Giken RA-401 stopped-flow spectrophotometer. The temperature of the reactant solutions (±0.1°C) in storage cylinders was maintained at the desired temperature by circulating water from a Haake D8G circulatory water bath. Several measurements were made on a particular run, storing good stopped-flow traces for averaging and calculation of k_{obs}, the pseudo-first-order rate constant. The standard deviation for the k_{obs} values was <5% at low $[SO_3^{2-}]$ and between 5 and 10% at high $[SO_3^{-2}]$.

Test for free radical

The addition of 1 mL of acrylonitrile to solutions of $[Mn(cytda)(OH_2)]^-$ and SO_3^{2-}, purged with nitrogen, did not show cloudiness even on long standing. However, a curdy precipitate of polyacrylonitrile obtained on mixing these solutions indicated the formation of free radicals during the reaction.

Rapid scanning

A rapid scan of the reaction mixture covering 48 nm on either side of 510 nm, Fig. 1, was recorded on a Union Giken RA-415 stopped-flow spectrophotometer using a 3.5 nm slit and the spent reaction mixture as the reference. This short range, sufficient for the detection of the newly formed species, is recorded over a period of a few milliseconds after mixing. The spectra, top to bottom, were recorded at 3, 5, 9, 13, 15, and 17 ms after mixing. The decreasing absorbance, over a period much less than the period over which the reaction was studied, did not represent the formation of an intermediate because the concentration of such an intermediate, if formed, is likely to increase with time unless its rate of decomposition is faster than its rate of formation. In that case the reaction is unlikely to proceed through an intermediate complex. Hence, the decrease in the absorbance is probably due to the reduction of $[Mn(cydta)(OH_2)]^-$ ion.

In another experiment the initial absorbance of the stopped-flow traces at the time of initiation of the reaction were measured over 470–610 nm at 10 nm intervals. These were compared with the absorbance obtained when S(IV) solution was replaced with water but using the same $[Mn(cydta)(OH_2)]^-$ solution. No significant changes in the absorbance were noted at any of the wavelengths used. Hence it is concluded that no new species was formed on mixing solutions of $[Mn(cydta)(OH_2)]^-$ and S(IV).

Fig. 1. The successive rapid scan spectra of the reaction mixture ($10^4[Mn(cydta)^-] = 4.0$, $10^2[\text{sulphite}]_0 = 1.08$ mol dm^{-3}, pH 4.27 at 25.3°C) recorded at 510 nm with an interval of 0 ms and a gate time 1 ms. The spectrum starting from top to bottom corresponds to the times 3 (●), 5 (○), 9 (△), 13 (△), 15 (□), and 17 (■) ms after mixing.

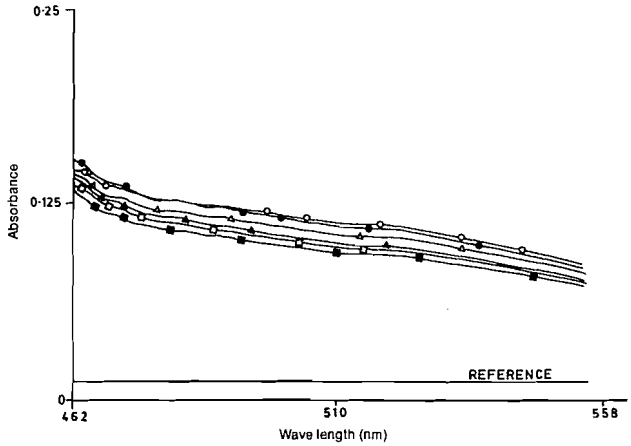

Results

Stoichiometry

The stoichiometry of the reaction was determined using excess $[Mn(cydta)(OH_2)]^-$ over [S(IV)] at different pH values and ionic strengths. The low pH's, 3.32 and 3.72, were selected particularly because $S_2O_6^{2-}$ is a significant product of sulphite radical recombination at low pH (13). The two solutions were introduced into the stopped-flow apparatus and the final absorbance at 510 nm was read from the stopped-flow trace, and $\Delta[Mn(cydta)(OH_2)^-]$ was calculated for a given [S(IV)]. In the control experiment the initial absorbance of the $[Mn(cydta)(OH_2)]^-$ solution was measured by replacing the sulphite solution with degassed distilled water. A value of $\Delta[Mn(cydta)(OH_2)^-]/\Delta[SO_3^{2-}] = 1.97 \pm 0.03$ indicated a 2:1 stoichiometry consistent with eq. [1].

$$[1]\quad 2[Mn(cydta)(OH_2)]^- + SO_3^{2-} + H_2O \rightarrow 2[Mn(cydta)(OH_2)]^{2-} + SO_4^{2-} + 2H^+$$

The stoichiometry, estimating excess unreacted sulphite by back titrating with iodine, remained inconclusive because of the scattered ratio values and irreproducible results (14). This is attributed to air oxidation of sulphite (15). In a qualitative test, sulphite ion was removed by the addition of formaldehyde, which forms an adduct (2*e*). Product analysis indicated that sulphate ion was the principal product. The dithionate ion was, however, not detected.

Dependence on [S(IV)]

The plot between k_{obs} and [S(IV)], Fig. 2, indicates that k_{obs} increased more rapidly than the increase in [S(IV)]. However, the plots of $k_{obs}/[S(IV)]$ against [S(IV)], Fig. 3, are linear with intercepts at all temperatures.

Dependence on pH

The effects of $[H^+]$ on the observed rate, Table 1, indicates that

Can. J. Chem. Downloaded from www.nrcresearchpress.com by 80.90.12.36 on 09/08/12
For personal use only.

Fig. 2. The concave-up plot of k_{obs} against $[sulphite]_0$ ($10^4[Mn(cydta)^-] = 4.0$, $[CH_3COO^-] = 0.06$, $\mu = 0.16$ mol dm^{-3} at pH 4.27 at 25°C).

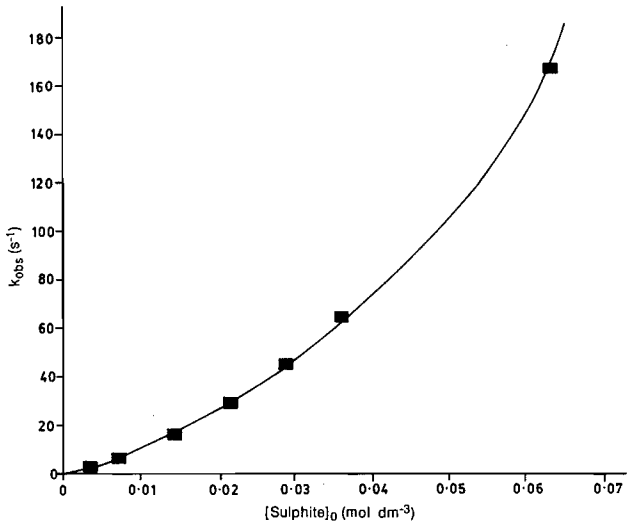

Table 1. The dependence of k_{obs} on pH at 25°C. $10^4[Mn(cydta)^-] = 4.0$, $10^3[SO_3^{2-}] = 7.2$, $\mu = 0.4$ mol dm^{-3}.

pH	3.8	4.08	4.4	4.66	5.05
k_{obs} (s^{-1})	3.12	4.54	7.80	13.0	28.7

the rate increases with pH. A linear plot with an intercept, Fig. 4, is obtained when $k_{obs}/[SO_3^{2-}]$ is plotted against $[H^+]^{-1}$.

Effect of ionic strength

The effect of ionic strength, not studied by previous workers (3), was investigated with $LiClO_4$ (Table 2) because sodium ions, at times, produce medium effects (16). At relatively high ionic strengths (μ), the Davies equation [2] (17) is applicable. The required plot between $\log k_{obs}$ and $\sqrt{\mu}/(1 + \sqrt{\mu})$ was linear with the slope value 1.7, indicating that the reactants are similarly charged and have one and two charges, respectively.

$$[2] \quad \log k_{obs} = \log k_0 + m(\sqrt{\mu}/(1 + \sqrt{\mu}))$$

Effect of $[SO_4^{2-}]$

The addition of Na_2SO_4, at constant ionic strength ($NaClO_4$), had no effect on the rate. The k_{obs} value, measured over $[SO_4^{2-}] = (0.4 - 4.0) \times 10^{-4}$ mol dm^{-3} ($10^4[Mn(cydta)(OH_2)^-] = 4.0$, $10^3[SO_3^{2-}] = 7.2$, $[CH_3CO_2^-] = 0.06$, $\mu = 0.4$ mol dm^{-3}, pH 4.27 at 25°C) was 6.87 ± 0.33 s^{-1}. It indicated the absence of any reversible step involving SO_4^{2-} in the mechanism.

Effect of $[Mn(cydta)^{2-}]$

The effect of the addition of $[Mn(cydta)^{2-}]$ ($0.2–2.0 \times 10^{-4}$ mol dm^{-3}) on the rate ($10^4[Mn(cydta)(OH_2)^-] = 4.0$, $10^3[SO_3^{2-}] = 7.2$, $[CH_3CO_2^-] = 0.06$, $\mu = 0.3$ mol dm^{-3}, pH 4.27 at 25°C) indicated that the k_{obs} value, 4.66 ± 0.06 s^{-1}, was independent of $[Mn(cydta)^{2-}]$. This excluded the possibility of a reversible step during the electron transfer.

Effect of acrylamide

The rates, measured at different concentrations of acrylamide, decreased with increasing acrylamide concentration. This indicates that an equilibrium reaction in which free radicals and the reduced oxidant are generated is not rate determining. If it were so, the removal of the free radicals by a scavenger would have resulted in an increase in the forward rate.

Fig. 3. The plot of $k_{obs}/[sulphite]_0$ against $[sulphite]_0$ at $\mu = 0.16$ mol dm^{-3} and temperature 8.5 (■), 16.5 (+), 25 (□), and 31.6°C (▲).

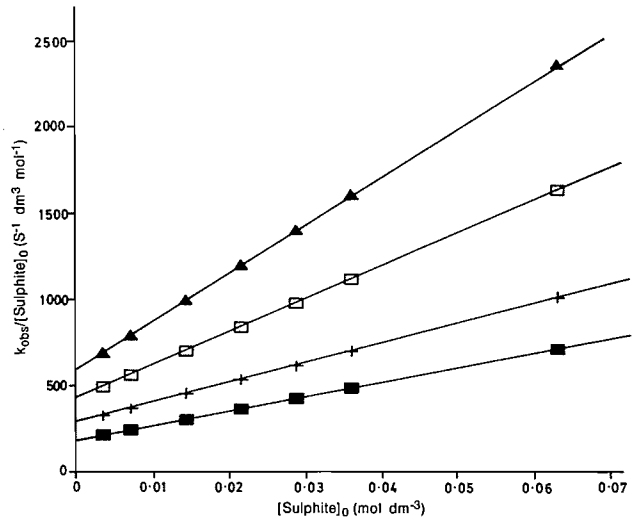

Fig. 4. The plot of $k_{obs}/[sulphite]_0$ against $[H^+]^{-1}$ ($10^4[Mn(cydta)^-] = 4.0$, $10^3[sulphite] = 7.2$ and $\mu = 0.4$ mol dm^{-3} at 25°C).

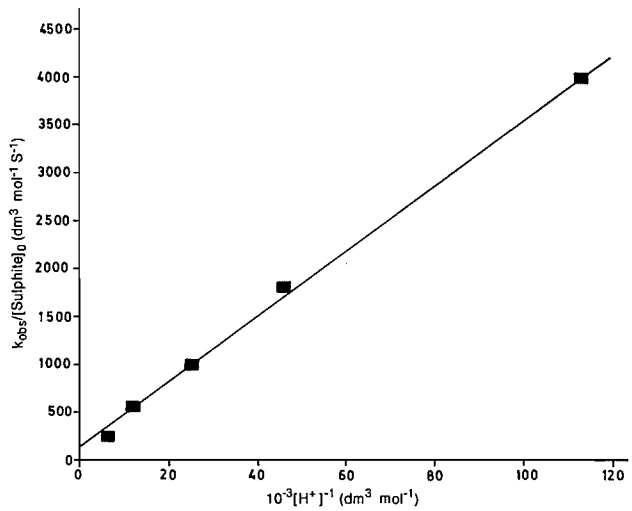

Table 2. Dependence of k_{obs} on the initial ionic strength at 25°C. $10^4[Mn(cydta)^-] = 4.0$. $10^3[SO_3^{2-}] = 10.8$, $[CH_3COO^-] = 0.06$ mol dm^{-3} at pH 4.27.

μ(mol dm^{-3})	0.16	0.40	0.516	1.0
k_{obs} (s^{-1})	5.57	7.97	9.22	12.6

Mechanism and discussion

Mechanism

The retarding effect of H^+ could arise either from the equilib-

rium [3] with $pK_a = 6.79$ (18), or the equilibrium [3*a*] with $pK_h = 8.1$ (4).

$$[3]\quad HSO_3^- \overset{K_a}{\rightleftharpoons} H^+ + SO_3^{2-}$$

$$[3a]\quad [Mn(cydta)(OH_2)]^- \overset{K_h}{\rightleftharpoons} [Mn(cydta)(OH)]^{2-} + H^+$$

Since the difference between the pK_a and pK_h values is more than one unit, the equilibrium [3*a*] is less likely to affect the kinetics rates. Moreover, the deprotonated $[Mn(cydta)(OH)]^{2-}$ ion associated with a reduced potential (19) may prove to be a poor oxidant in comparison to the $[Mn(cydta)(OH_2)]^-$ ion. Thus the retarding effect of H^+ is ascribed to the greater reactivity of SO_3^{2-} ion.

The formation of an intermediate in the proposed mechanism is not emphasized because in a reaction where the observed rate constant is a product of a rate and a preequilibrium constant, such speculation is probably unwarranted (20). This does not mean that the formation of a precursor complex is excluded although the spectrophotometric measurements did not hint at the formation of any newer species.

In view of the stoichiometry and kinetic results and the consideration that SO_4^{2-} ion is the only oxidation product, the following mechanism based on simple reactions is proposed.

$$[3]\quad HSO_3^- \overset{K_a}{\rightleftharpoons} H^+ + SO_3^{2-}$$

$$[4]\quad 2HSO_3^- \overset{Q_d}{\rightleftharpoons} S_2O_5^{2-} + H_2O$$

$$[5]\quad [Mn(cydta)(OH_2)]^- + SO_3^{2-} \overset{k}{\longrightarrow} [Mn(cydta)(OH_2)]^{2-} + SO_3^-$$

$$[6]\quad [Mn(cydta)(OH_2)]^- + S_2O_5^{2-} \overset{k_1}{\longrightarrow} [Mn(cydta)(OH_2)]^{2-} + SO_3^- + SO_2$$

$$[7]\quad [Mn(cydta)(OH_2)]^- + SO_3^- \overset{k_7}{\longrightarrow} [Mn(cydta)(OH_2)]^{2-} + SO_3$$

$$[8]\quad SO_3 + H_2O \overset{\text{fast}}{\longrightarrow} SO_4^{2-} + 2H^+$$

where the product of the ionic charges in the rate-determining steps [5] and [6] is 2, a value in fair agreement with the slope value 1.7 obtained in the Davies plots.

The protonation (21) of HSO_3^- to yield SO_2 is not considered because the pK_a of H_2SO_3 is 1.6 and, therefore, is unlikely to be a significant species under the conditions of the study. The formation of $S_2O_5^{2-}$ in reaction [4], $Q_d = 0.088$ dm^3 mol^{-1} (22), and reducing the complex in the rate-limiting reaction [6] explains the parallel second-order term in [S(IV)] in the rate law.

The existence of SO_3^- radical in aqueous solution is supported by esr (23). The SO_3^- radicals can also decay through reactions [9] and [10] as well as reaction [7]. The recently estimated values of k_9 and k_{10} are 1.8×10^8 and 2.3×10^8 dm^3 mol^{-1} s^{-1}, respectively (24).

$$[9]\quad SO_3^- + SO_3^- \overset{k_9}{\longrightarrow} S_2O_6^{2-}$$

$$[10]\quad SO_3^- + SO_3^- \overset{k_{10}}{\longrightarrow} SO_3 + SO_3^{2-}(SO_4^{2-} + SO_2)$$

Reaction [7] is required both by the stoichiometry and the effect of acrylamide on the rate. Further, its precedence over reactions [9] and [10] is evident from its value, 1×10^9 dm^3 mol^{-1} s^{-1}, estimated in $[Ru(NH_3)_4(phen)]^{2+}$ oxidation of sulphite ion (2*e*). Though the exact value for the present case can not be estimated (beyond our facilities), yet there is no reason to believe that it might be much different. The irreversible hydrolysis of SO_3 in reaction [8] is known to be rapid.

The above sequence of reactions leads to the rate law in eq. [11], which could be expressed as eq. [12] with the proviso that $1 \gg K_a[H^+]^{-1} + Q_d[HSO_3^-]^2$ because of the small values of K_a and Q_d and $[H^+]$ and $[HSO_3^-]$ used.

$$[11]\quad \frac{-d[Mn(cydta)(OH_2)^-]}{dt} = \frac{2(kK_a[H^+]^{-1} + k_1Q_d[HSO_3^-])[Mn(cydta)(OH_2)^-][HSO_3^-]}{1 + K_a[H^+]^{-1} + Q_d[HSO_3^-]}$$

$$[12]\quad \frac{k_{obs}}{[HSO_3^-]} = 2(kK_a[H^+]^{-1} + k_1Q_d[HSO_3^-])$$

Equation [12] is consistent with the linearity of the plots in Figs. 3 and 4. The close agreement in the values of kK_a, 0.0179 (intercept, Fig. 3) and 0.0173 s^{-1} (slope, Fig. 4), and that of $k_1Q_d = 1.57 \times 10^4$ (slope, Fig. 3) and 1.55×10^4 dm^6 mol^{-2} s^{-1} (intercept, Fig. 4) from two different plots supports the rate law and the mechanism.

The values of k and k_1, Table 3, were deduced from the least-squares values of the intercepts ($= kK_a[H^+]^{-1}$) and slopes ($= k_1Q_d$) of the plots in Fig. 3 at various temperatures. The respective activation parameters deduced from these values are also reported there.

Discussion

The results of the stoichiometry and the retarding effect of H^+ of the previous study (3) are confirmed. The inverse H^+ ion dependence is, however, linked with a path first-order in [S(IV)] rather than to a path second-order in [S(IV)] (3). This inversion is due to the proposed reactions of SO_3^{2-} and $S_2O_5^{2-}$; the former is responsible for the inverse H^+ ion dependence whereas the latter is independent of $[H^+]$.

Further, no difficulty is seen in the reaction between $S_2O_5^{2-}$ and $[Mn(cydta)(OH_2)]^-$ because $k_1 \approx 10^5$ dm^3 mol^{-1} s^{-1} is much less than its estimated (3) rate (two orders higher than the rate of diffusion-controlled reactions) for its reaction with $[Mn(cydta)(OH)]^{2-}$ ion. The other area of disagreement is the inner-sphere mechanism (3).

The focal point for the inner-sphere mechanism was that hexadentate $cydta^{4-}$ acted as a pentadentate ligand (3). It is not clear why one carboxylato arm behaved differently from the others in the otherwise seven-coordinated complex (4, 5). The first step in the accommodation of S(IV) in the seven-coordinated manganese ion would involve bond rupture between the carboxylato arm and the metal centre. The rate of such a process is considered to be less rapid than the rate of electron transfer as in the outer-sphere oxidation of dithionite by $[Mn(cydta)(OH_2)]^-$ (7). The present reaction more closely resembles the dithionite reaction. The reactive species SO_3^{2-} and $S_2O_5^{2-}$ are identical with SO_2^- and $S_2O_4^{2-}$ and so is the

Can. J. Chem. Downloaded from www.nrcresearchpress.com by 80.90.12.36 on 09/08/12
For personal use only.

Table 3. The values of k ($dm^3\ mol^{-1}\ s^{-1}$) and k_1 ($dm^3\ mol^{-1}\ s^{-1}$) at different temperatures and μ = 0.16 mol dm^{-3} and related activation parameters.

Temperature (°C)	8.5	16.5	25.0	31.6
$10^{-4}\ k$	7.18	13.0	22.2	34.6
	$\Delta H^{\ddagger} = 48 \pm 1$ kJ mol^{-1}		$\Delta S^{\ddagger} = 12 \pm 4$ J $K^{-1}\ mol^{-1}$	
$10^{-4}\ k_1$	4.73	6.48	10.9	16.0
	$\Delta H^{\ddagger} = 38 \pm 3$ kJ mol^{-1}		$\Delta S^{\ddagger} = -28 \pm 4$ J $K^{-1}\ mol^{-1}$	

Table 4. Data for Marcus cross relation.

No.	Complex	μ	r_2 (Å)	ln k_{12} (ref.)	ln k_{22} (ref.)	ln K_{12}	E^0 (ref.)	ln k_{11}	ln f_{12}	L.H. side of eq. [17]
1.	$[Ru(NH_3)_4phen]^{3+}$	0.1	4.4	10.5(2*e*)	16.3(30)	−7.8	0.52(2*e*)	4.89	−0.77	2.91
2.	MnO_4^-	0.1	3.5	11.8(31)	6.58(32)	−6.21	0.56(33)	23.5	−0.39	17.3
3.	$[Os(bpy)_3]^{3+}$	0.1	6.8	16.6(2*f*)	21.4(34)	4.67	0.84(2*f*)	1.48	−0.08	6.15
4.	$*[Ru(bpy)_3]^{2+}$	0.1	6.8	12.6(35)	18.4(36)	4.67	0.84(2*f*)	−1.51	−0.08	3.16
5.	$[IrBr_6]^{2-}$	0.1	4.5	12.7(37)	19.1(38)	4.67	0.84(35)	−0.75	−0.15	3.92
6.	$[IrCl_6]^{2-}$	0.1	4.4	10.9(34)	12.2(39)	6.62	0.89(40)	3.18	−0.34	9.80
7.	$[Fe(bpy)_3]^{3+}$	0.1	6.8	19.2(34)	20.0(41)	13.2	1.06(42)	0.37	−1.01	13.6
8.	$[Fe(phen)_3]^{3+}$	1.0	6.8	15.3(43)	20.0(44)	14.4	1.09(45)	−5.39	−1.13	9.01
9.	$[Ru(bpy)_3]^{3+}$	0.1	6.8	21.5(35)	19.8(40)	21.1	1.26(34)	−0.85	−2.68	20.2
10.	$[Mn(cydta)(OH_2)]^-$	0.4	6	11.6[a]	1(7)	4.67	0.84(4)	18.3	−0.144	23.0

[a]This work.

Can. J. Chem. Downloaded from www.nrcresearchpress.com by 80.90.12.36 on 09/08/12
For personal use only.

equilibrium governing the formation of the dimeric species. The rate-determining constants are also similar. Further, if the predicted (3) association constant ($\approx 10^{-2}$) between the metal and S(IV) is taken into consideration then k and k_1 values are further increased, lending more support to the outer-sphere mechanism. The rate of exchange of water (25), $4.4 \times 10^8\ s^{-1}$, coordinated to the seventh site, prevented its substitution by S(IV).

The other factors negating an inner-sphere mechanism include the recent suggestion (2*f*) that access by S(IV) to the metal centre is needed for the formation of dithionate, which presently is not an oxidation product. The approach of a negatively charged species to the carboxylate side is considered electrostatically unfavourable, and the presence of the cyclohexane substituent on the diamine side prevents adequate donor–acceptor orbital overlap (5).

The outer-sphere nature of the reaction is finally examined in the light of Marcus theory (8) given by the following equations (26).

$$[13]\quad k_{12} = (k_{11}k_{22}K_{12}f_{12})^{1/2}W_{12}$$

$$[14]\quad \ln f_{12} = \frac{(\ln K_{12} + (w_{12} - w_{21})/RT)^2}{4(\ln (k_{11}k_{22}/Z^2) + (w_{11} + w_{22})/RT)}$$

$$[15]\quad W_{12} = \exp((w_{11} + w_{22} - w_{12} - w_{21})/2RT)$$

$$[16]\quad w_{ij} = \frac{z_i z_j e^2}{D\sigma_{ij}(1 + \beta\sigma_{ij}\sqrt{\mu})}$$

where k_{12} is the rate constant for electron transfer from SO_3^{2-} to the oxidant, k_{11} is the self-exchange rate constant for the SO_3^-/SO_3^{2-} couple, k_{22} is the self-exchange rate constant for the various complexes (used as oxidants), K_{12} is the equilibrium constant for the various electron-transfer reactions, W_{12} is the electrostatic work term, w_{ij} is the work required to bring ions i and j (charges z_i and z_j) to the separation distance σ_{ij} (equal to the sum of the radii of the ions), D is the static dielectric constant of the medium, $\beta = (8\pi Ne^2/1000D\mathbf{K}T)^{1/2}$, Z is the collision rate, a value 1×10^{25} is used for Z^2 (27), R is the gas constant (kcal $mol^{-1}\ K^{-1}$), and $\mathbf{K}$ is the Boltzmann constant. The radius of SO_3^- and SO_3^{2-} is taken as 3 Å.

Assuming the adiabatic nature of the self-exchange reactions, eq. [13] could be rearranged to eq. [17].

$$[17]\quad 2\ln k_{12} - \ln f_{12} - 2\ln W_{12} - \ln k_{22} = \ln k_{11} + \ln K_{12}$$

The plot of eq. [17] for the data in Table 4 is linear, Fig. 5, though the points corresponding to MnO_4^- and $[Mn(cydta)(OH_2)]^-$ show considerable deviation. The least-squares value of the slope, excluding the MnO_4^- and $[Mn(cydta)(OH_2)]^-$ points, is 0.83 ± 0.09 ($r^2 = 0.942$), in fair agreement with the expected value of unity. The intercept results in a value of k_{11} equal to 8 $dm^3\ mol^{-1}\ s^{-1}$, which is in fair agreement with the recently estimated value 4 $dm^3\ mol^{-1}\ s^{-1}$ (2*f*).

The deviation corresponding to MnO_4^- is attributed to the formation of an inner-sphere complex (2*f*). The same is not true for $[Mn(cydta)(OH_2)]^-$ for it is felt that this complex is not similar to the complexes listed in Table 4. This observation is based on the fact that inclusion of the rate of oxidation of vanadium(IV) by $[Mn(cydta)(OH_2)]^-$ with those by polyaza macrocycle– (28) and tris(polypyridine)–metal complexes (29) for treatment by the Marcus theory resulted in two separate straight lines, as shown earlier (29), one each for the

Fig. 5. The plot of $2 \ln k_{12} - \ln f_{12} - 2 \ln W_{12} - \ln k_{22}$ against $\ln K_{12}$.

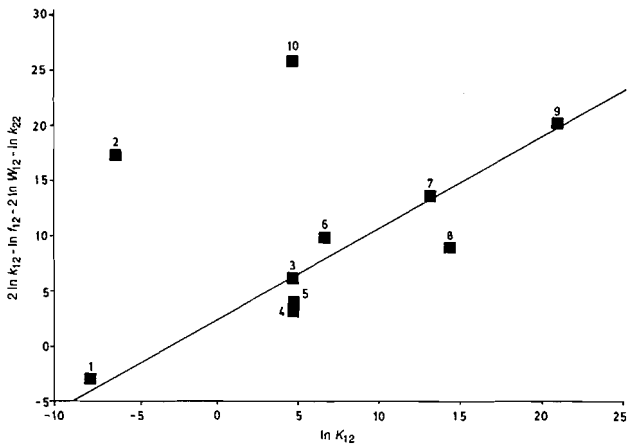

polyaza macrocycle and tris(polypyridine) complexes, with the point corresponding to the Mn complex falling on the straight line of the polyaza macrocycle complexes. Both polyaza macrocycle and tris(polypyridine) complexes oxidize vanadium(IV) by an outer-sphere mechanism (28, 29). Hence, $[Mn(cydta)]^-$ shows greater resemblance to the polyaza macrocycle complexes than to the polypyridine complexes.

In conclusion, the reaction, which not only shows similarities with the rate and mechanism of a similar known outer-sphere reaction (7) but also has rates similar to those of several other outer-sphere reactions (5), cannot be considered as an inner-sphere reaction on the simple assumption that $cydta^{4-}$ is acting as a pentadentate ligand. However, a further study of this interesting reducing agent by polyaza macrocycle complexes, known to be outer-sphere oxidants (28), is needed to test the strict compliance with the Marcus theory (8) because $[Mn(cydta)]^-$ has shown greater resemblance to polyaza macrocycle complexes than polypyridine complexes in V(IV) oxidation. We plan to undertake this study in the near future.

Acknowledgements

We thank the Department of Science and Technology for providing financial assistance for the stopped-flow instrument, and the Council of Scientific and Industrial Research for financing the project and awarding a Junior Research Fellowship to U.C. We sincerely thank Professor D.H. Macartney, Queen's University, for a critical preview of the manuscript and for allowing his program for the calculations presented in Table 4.

References

1. (*a*) D.M. Yost and H. Russell, Jr. Systematic inorganic chemistry. Prentice-Hall, New York. 1944. p. 358; (*b*) W.C.E. Higginson and J.W. Marshall. J. Chem. Soc. 447 (1957).
2. (*a*) P. Bhargava and K.S. Gupta. Ind. J. Chem. **32A**, 201 (1993); (*b*) T. Ernst, M. Cifert, and M. Wilgosky. Int. J. Chem. Kinet. **24**, 887 (1992); (*c*) M. Ali, S.K. Saha and P. Banerjee. Bull. Chem. Soc. Jpn. **64**, 2497 (1991); (*d*) J. Chem. Soc. Dalton Trans. 187 (1990); (*e*) R. Sarala, M.S. Islam, S.B. Rabin, and D.M. Stanbury. Inorg. Chem. **29**, 1133 (1990); (*f*) R. Sarala and D.M. Stanbury. Inorg. Chem. **29**, 3456 (1990); (*g*) D.W. Carlyle. J. Am. Chem. Soc. **94**, 4525 (1972).
3. V.M. Bobba, G. Giraudi, and E. Mentasti. Transition Met. Chem. **13**, 256 (1988).
4. R.E. Hamm and M.A. Suwyn. Inorg. Chem. **6**, 139 (1967).
5. D.H. Macartney and D.W. Thompson. Inorg. Chem. **28**, 2195 (1989).
6. B.L. Pohand and R. Stewart. Can. J. Chem. **50**, 3432 (1972).
7. Raj N. Mehrotra and Ralph G. Wilkins. Inorg. Chem. **19**, 2177 (1980).
8. R.A. Marcus. J. Phys. Chem. **72**, 891 (1968), and references therein.
9. L. Meites (*Editor*). Handbook of analytical chemistry. McGraw–Hill, New York. 1963. p. 3-182.
10. G. Giraudi and E. Mentasti. Transition Met. Chem. **6**, 230 (1981).
11. I.M. Kolthoff, E.B. Sandell, E.J. Meehan, and S. Bruckenstein (*Editors*). Qualitative chemical analysis. 4th ed. Macmillan, New York. 1969. p. 857.
12. A.I. Vogel. Textbook of qualitative inorganic analysis. 4th ed. Longman, London. 1986. p. 45.
13. T.E. Ericksen. J. Chem. Soc. Faraday Trans. 1, **70**, 208 (1974); Radiochem. Radioanal. Lett. **16**, 147 (1974).
14. L.J. Kirschenbaum, I. Kouadio, and E. Mentasti. Polyhedron, **8**, 1299 (1989).
15. S.E. Schwartz (*Editor*). Trace atmospheric constituents. Wiley, New York. 1983. pp. 117 and 147.
16. (*a*) D.L. Toppen and R.G. Linck. Inorg. Chem. **10**, 2635 (1971); (*b*) C. Lavalee and T.W. Newton. Inorg. Chem. **11**, 2616 (1972).
17. C.W. Davies. Ion-association. Butterworth, Washington, D.C. 1962.
18. L.G. Sillén and A.E. Martell. Stability constants of metal ion complexes. Special Publication 25, Chemical Society, London. 1971. p. 133.
19. A. Chakraborty. Comments Inorg. Chem. **4**, 1 (1985).
20. S.J. Patton and C.H. Brubaker. Inorg. Chem. **12**, 1402 (1973).
21. R.M. Smith and A.E. Martell. Critical stability constants. Vol. 6. Plenum, New York. 1989. pp. xvi and 450.
22. R.E. Connick, T.M. Tam, and E. Von Deuster. Inorg. Chem. **21**, 103 (1982).
23. (*a*) R.O.C. Norman and P.M. Storey. J. Chem. Soc. B, 1009 (1971); (*b*) B.D. Flockhart, K.J. Irvin, R.C. Pink, and B.D. Sharma. J. Chem. Soc. Chem. Commun. 339 (1971).
24. S.J. Waygood and W.J. McElroy. J. Chem. Soc. Faraday Trans. **88**, 1525 (1992).
25. M.S. Zetter. Inorg. Chem. **14**, 1027 (1975).
26. R.G. Wilkins. Kinetics and mechanism of reactions of transition metal complexes. 2nd ed. VCH, Weinheim. 1991. p. 267.
27. D.H. Macartney and N. Sutin. Inorg. Chem. **24**, 3403 (1985).
28. D.H. Macartney, A. McAuley, and O.A. Olubuyide. Inorg. Chem. **24**, 307 (1985).
29. D.H. Macartney. Inorg. Chem. **25**, 2222 (1986).
30. G.M. Brown and N. Sutin. J. Am. Chem. Soc. **101**, 883 (1979).
31. L.I. Simandi, M. Jaky, C.R. Savage, and Z.A. Schelly. J. Am. Chem. Soc. **107**, 4220 (1985).
32. O.L. Spiccia and T.W. Swaddle. Inorg. Chem. **26**, 2265 (1987).
33. A.J. Bard, R. Parsons, and J. Jordon (*Editors*). Standard potentials in aqueous solution. Marcel Dekker, New York. 1985. p. 437.
34. G. Nord, B. Pedersen, and O. Farver. Inorg. Chem. **17**, 2233 (1978).
35. C. Cruetz, N. Sutin, and B.S. Brunschwig. J. Am. Chem. Soc. **101**, 1297 (1979).
36. N. Sutin and C. Cruetz. *In* Inorganic and organometallic photochemistry. *Edited by* M.S. Wrighton. American Chemical Society, Washington, D.C. 1978. pp. 1–27.
37. W.K. Wilmarth, D.M. Stanbury, J.E. Byrd, H.N. Po, and C.-P. Chua. Coord. Chem. Rev. **51**, 155 (1983).
38. D.M. Stanbury, W.K. Wilmarth, S. Khalaf, H.N. Po, and J.E. Byrd. Inorg. Chem. **19**, 2715 (1980).
39. P. Hurwitz and K. Kustin. Trans. Faraday Soc. **62**, 427 (1966).

Can. J. Chem. Downloaded from www.nrcresearchpress.com by 80.90.12.36 on 09/08/12
For personal use only.

40. D.W. Margerum, K.L. Chellappa, F.P. Bossu, and G.L. Bruce. J. Am. Chem. Soc. **97**, 6894 (1975).
41. I. Ruff and M. Zimonyi. Electrochim. Acta, **18**, 515 (1973).
42. A.A. Schilt. Analytical applications of 1,10-phenanthroline and related compounds. Pergamon, New York. 1969. p. 118.
43. D.W. Carlyle. J. Am. Chem. Soc. **94**, 4525 (1972).
44. B.S. Brunschwig, C. Creutz, D.H. Macartney, T.-K. Sham, and N. Sutin. Faraday Discuss. Chem. Soc. **74**, 113 (1982).
45. A.A. Schilt. Analytical applications of 1,10-phenanthroline and related compounds. Pergamon, New York. 1969. pp. 36, 107, and 122.

Can. J. Chem. Downloaded from www.nrcresearchpress.com by 80.90.12.36 on 09/08/12
For personal use only.

Étude thermodynamique des trois isomères de l'acide chlorobenzoïque. Partie II[1]

Raphaël Sabbah et Aaron Rojas Aguilar

Résumé : Notre calorimètre isopéribolique à bombe rotative, précédemment décrit, a été modifié : (*i*) en diminuant et en stabilisant les échanges thermiques entre le système calorimétrique et le milieu extérieur; (*ii*) en modifiant son thermomètre de mesure; (*iii*) en lui associant un système informatisé de robotique, d'acquisition et de traitement des signaux thermiques. Après avoir vérifié la bonne marche de l'appareil ainsi modifié et réalisé l'étalonnage du système calorimétrique, nous avons déterminé à 298,15 K et par calorimétrie de combustion les enthalpies de formation à l'état condensé des trois isomères de l'acide chlorobenzoïque. En associant ces valeurs à celles de leurs enthalpies de sublimation à 298,15 K, nous avons pu déterminer leurs enthalpies de formation à l'état gazeux. Les valeurs expérimentales des fonctions thermodynamiques $-\Delta_c H_m^0$ (s, 298,15 K), $-\Delta_f H_m^0$ (s, 298,15 K), $\Delta_{sub} H_m^0$ (298,15 K) et $-\Delta_f H_m^0$ (g, 298,15 K) sont données pour les acides 2-chloro-benzoïque, 3-chlorobenzoïque et 4-chlorobenzoïque. À partir de l'enthalpie d'atomisation expérimentale de ces trois acides, une valeur enthalpique a été proposée pour la liaison C_b—Cl dans ce type de composés. Les valeurs expérimentale et théorique de l'énergie de conjugaison sont compatibles. Une discussion sur la stabilité relative de quelques dérivés monosubstitués de l'acide benzoïque étudiés au laboratoire est aussi développée.

Mots clés : thermodynamique, calorimétrie de combustion, analyse thermique différentielle; acide 2-chlorobenzoïque, acide 3-chlorobenzoïque, acide 4-chlorobenzoïque, enthalpies de combustion, de formation, énergie de conjugaison, enthalpies d'atomisation, de liaisons intramoléculaires, substance d'intercomparaison.

Abstract: Our isoperibol rocking-bomb calorimeter, previously described, has been modified to: (*i*) reduce and stabilize the heat exchange between the calorimetric system and its surroundings; (*ii*) change its thermometer; (*iii*) associate with it a computer program for the robotics of different steps of an experiment, data acquisition, and determination of the thermodynamic quantities. After testing these modifications and calibrating the calorimetric system, the enthalpies of formation in the condensed state and at 298.15 K of the three isomers of chlorobenzoic acid have been determined by combustion calorimetry. Associating these values with those of their enthalpies of sublimation previously measured, we determined their enthalpies of formation in the gaseous state. The experimental values of the thermodynamic functions $-\Delta_c H_m^0$ (s, 298.15 K), $-\Delta_f H_m^0$ (s, 298.15 K), $\Delta_{sub} H_m^0$ (298.15 K), and $-\Delta_f H_m^0$ (g, 298.15 K) are given for 2-chlorobenzoic acid, 3-chlorobenzoic acid, and 4-chlorobenzoic acid. From the experimental value of the enthalpy of atomization, it has been possible to determine an enthalpy value for the C_b—Cl bond. The experimental and theoretical values of the resonance energy of the three isomers are compatible. The relative stability of some monosubstituted derivatives of benzoic acid studied in our laboratory is also discussed.

Key words: thermodynamics, combustion calorimetry, differential thermal analysis; 2-chlorobenzoic acid, 3-chlorobenzoic acid, 4-chlorobenzoic acid, enthalpies of combustion, of formation, resonance energy, enthalpies of atomization, of intramolecular bonds, reference material.

1. Introduction

Plusieurs travaux ayant pour but la mise en évidence du lien existant entre grandeurs énergétiques et structure dans les composés organiques ont été réalisés au laboratoire depuis quelques années. L'étude thermodynamique des dérivés monosubstitués de l'acide benzoïque en fait partie. Après avoir étudié les acides aminobenzoïques (1, 2) et les acides hydroxybenzoïques (3), nous avons entrepris au début de cette décennie, l'étude partielle des dérivés halogénés (Cl, Br, I) par calorimétrie de sublimation et par analyse thermique différentielle (4–6). Le présent travail se propose de compléter cette étude dans le cas des dérivés chlorés par calorimétrie de combustion. Il permettra d'apporter une contribution au niveau des liaisons intramoléculaires et de la stabilité relative des molécules d'acide benzoïque monosubstituées.

Signalons au passage que les travaux réalisés jusqu'ici sur l'étude des propriétés thermodynamiques des trois isomères

Reçu le 25 mai 1995.

R. Sabbah[2] et A. Rojas Aguilar. Centre de thermodynamique et de microcalorimétrie du Centre national de la recherche scientifique, 26, rue du 141e R.I.A., 13331 Marseille Cedex 03, France.

1. La première partie correspond à la référence 4.
2. À qui les demandes de tirés-à-part devront être adressées.

Can. J. Chem. Downloaded from www.nrcresearchpress.com by 80.90.12.36 on 09/08/12
For personal use only.

Fig. 1. Exemple de thermogramme $T = f(t)$ relatif à une expérience de combustion. T_j = température de la jaquette; T_i = température initiale de l'eau du seau; T'_i = température de cette eau au moment de la mise de feu; T_f = température maximale atteinte par cette eau; T'_f = température de cette eau en fin d'expérience; les temps t_i, t'_i, t_f, t'_f correspondent à T_i, T'_i, T_f, T'_f.

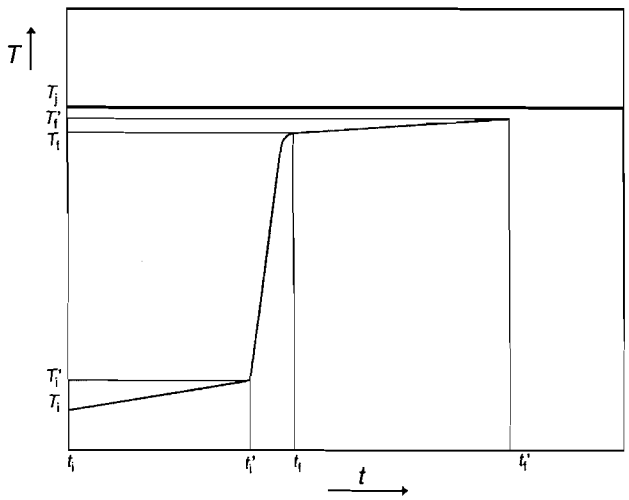

de l'acide chlorobenzoïque sont très peu nombreux. La majeure partie d'entre eux traite de la combustion du dérivé *para* en vue de pouvoir le proposer comme substance d'intercomparaison en calorimétrie de combustion de substances chlorées (7, 8).

2. Partie expérimentale

2.1. Produits

Les acides chlorobenzoïques utilisés dans ce mémoire sont des produits Fluka (pour l'acide 2-chlorobenzoïque, pureté : 98%) et Aldrich (pour les acides 3-chlorobenzoïque, pureté : >99% et 4-chlorobenzoïque, pureté : 99%). Ces trois substances ont été repurifiées par sublimations successives, trois fois dans le cas des acides 2-chloro- et 4-chlorobenzoïques et deux fois dans le cas de l'acide 3-chlorobenzoïque, sous une pression résiduelle de 1,3 Pa à 373 K.

La pureté des échantillons ainsi traités a été déterminée par analyse thermique différentielle; elle est de (99,95 ± 0,01), (99,94 ± 0,01) et (99,92 ± 0,01) mol% respectivement pour les isomères *ortho*, *méta* et *para*.

Les autres substances citées dans ce travail ont été utilisées telles que : anhydrique arsénieux (Merck; 99,5%), permanganate de potassium (Prolabo; 99,5%), nitrate d'argent (Prolabo; 99,8%), iodate de potassium (Prolabo; 99,9%), acide chlorhydrique (Prolabo; R.P. p.a.), brome (Fluka; 99,5%), hexachloroplatinate de sodium (Fluka; >99%).

Toutes les solutions décrites dans ce travail ont été préparées à partir d'une eau distillée et déminéralisée.

L'oxygène utilisé dans nos expériences de combustion est un produit Air Liquide N45; son degré de pureté est égal à 99,995% (fraction molaire d'azote : $<10^{-5}$).

2.2. Appareillage, technique et mode opératoire

Pour réaliser l'étude objet de ce mémoire, nous avons utilisé la calorimétrie de combustion et l'analyse thermique différentielle.

2.2.1. Calorimétrie de combustion

Elle a été réalisée à l'aide d'un calorimètre isopéribolique semblable au modèle mis au point et utilisé à l'Argonne National Laboratory (9), précédemment décrit dans la référence 2 et auquel ont été apportées certaines modifications visant : (*i*) la diminution et la stabilisation des échanges thermiques entre le système calorimétrique et le milieu extérieur; (*ii*) la modification de son thermomètre de mesure; (*iii*) l'association d'un système informatisé de robotique, d'acquisition et de traitement des signaux thermiques.

Ce calorimètre est constitué de deux parties : une enceinte extérieure et un seau intérieur. L'enceinte extérieure est un récipient à double paroi renfermant de l'eau maintenue à (298,15 ± 0,002) K à l'aide d'une régulation électronique conçue, réalisée et mise au point par les services techniques du Centre et dont l'élément sensible est une thermistance (Fenwall GB32) de 2 kΩ à 298,15 K. Afin de lui éviter des fluctuations de température trop brutales, l'enceinte extérieure a été recouverte sur sa périphérie d'un revêtement en mousse de polyuréthane de 50 mm d'épaisseur. Par ailleurs et pour la même raison, ce calorimètre est placé dans une salle thermorégulée dont la variation de température n'excède pas ±0,1 K dans la journée.

L'enceinte extérieure abrite le seau calorimétrique. Il existe entre ces deux parties une couche d'air d'environ 10 mm. Ce seau peut recevoir, outre la bombe rotative et le système d'engrenages qui lui est solidaire, une résistance chauffante de 86 Ω alimentée par trains d'ondes à partir d'une tension alternative de 220 V, un agitateur rotatif ayant la forme d'une hélice et 2880 g d'eau distillée pesée au 1/10 de gramme à l'aide d'une balance (Mettler, modèle P5-11).

La bombe utilisée est de forme cylindrique ($\phi_{ext} = 8$ cm, $h =$ 16,5 cm). Elle est réalisée à partir d'un alliage à haute teneur en nickel (Parr, modèle 1004) et est revêtue d'une épaisseur de 0,5 mm de platine pur. Son volume utile est de 0,347 dm^3. Elle est équipée d'un jeu d'engrenages qui lui permet de se mouvoir selon deux axes perpendiculaires. Elle comporte deux électrodes de mise de feu et deux robinets à pointeaux permettant l'entrée et la sortie des gaz.

La température de l'eau du seau calorimétrique est déterminée à l'aide d'une thermistance linéarisée de 5,6 kΩ à 298,15 K (Betatherm 36K53A3) que nous avons étalonnée entre 293 et 303 K. La valeur de sa résistance en fonction du temps est mesurée à l'aide d'un multimètre numérique Keithley modèle 2001, sensible au millième d'ohm.

Le signal électrique issu de ce multimètre est traité à l'aide d'un ordinateur et d'un programme informatique mis au point au laboratoire. Celui-ci gère l'évolution de la température du seau calorimétrique avant et pendant la période initiale, pendant les périodes principale et finale, et commande (*a*) la mise de feu à la substance étudiée par l'intermédiaire d'un courant redressé fourni par une source de 6 V traversant un fil de platine de 0,05 mm d'épaisseur, de 45 mm de longueur, tendu entre les deux électrodes; (*b*) la rotation de la bombe réalisée 180 s après la mise de feu. Trente rotations s'effectuant en 216 s se sont avérées nécessaires pour assurer l'homogénéité du système réactionnel après combustion.

Avec ce système de détection, nous pouvons déterminer avec fiabilité T'_i et T_f à $\pm 3 \times 10^{-5}$ K ainsi que les pentes des parties rectilignes de la courbe $T = f(t)$ (fig. 1) correspondant aux périodes initiale et finale.

Can. J. Chem. Downloaded from www.nrcresearchpress.com by 80.90.12.36 on 09/08/12
For personal use only.

Can. J. Chem. Downloaded from www.nrcresearchpress.com by 80.90.12.36 on 09/08/12
For personal use only.

Lorsqu'on travaille avec une substance solide, comme c'est le cas ici, celle-ci est mise sous forme de pastilles à l'aide d'une presse (Parr, modèle 2811). Les expériences préliminaires réalisées avec les trois isomères ayant conduit à des combustions incomplètes lorsque $m \geq 0{,}8$ g, nous avons été contraints, afin de les éviter, d'utiliser une substance auxiliaire favorisant la combustion en plaçant nos pastilles à l'intérieur d'un sachet confectionné par nos soins à partir de film de polythène de 50 μm d'épaisseur. Par ailleurs et afin de travailler dans les meilleures conditions de substitution, on s'arrange pour que la masse de substance brûlée (pastille + sachet de polythène), déterminée au μg près à l'aide d'une balance Mettler, modèle M5, fournisse en brûlant une variation de température ΔT aussi voisine que possible de celle qui est obtenue lors de l'étalonnage du système calorimétrique à partir de la combustion d'acide benzoïque. On place l'ensemble pastille + sachet dans un creuset en platine ayant une capacité de 3 cm^3. Le fil de platine, ci-dessus mentionné, est relié à cet ensemble à l'aide d'un fil de coton d'environ 50 mm de longueur. Les masses de ces deux fils sont, elles aussi, pesées au μg près. À chaque pesée, on associe la valeur de la pression atmosphérique du moment, du degré hygrométique et de la température de l'air ambiant pour pouvoir calculer la masse réelle de la pastille, du sachet de polythène, des fils de coton et de platine et du creuset.

Avant chaque expérience, on introduit 20 cm^3 de solution 0,0589 M d'anhydride arsénieux (As_2O_3) dans la bombe. Ce volume est nécessaire pour réduire le chlore contenu dans la substance à l'état d'ions chlorures (Cl^-). La pression d'oxygène à l'intérieur de la bombe est de 3,04 MPa. Une fois garnie, la bombe est placée dans le seau calorimétrique contenant l'eau distillée. Elle est maintenue verticale à l'aide d'un ressort métallique dont l'autre extrémité est fixée à une borne électrique solidaire et isolée du seau. Ce ressort sert de conducteur du courant électrique nécessaire pour porter au rouge le fil de platine permettant à la combustion de démarrer. Le seau, fermé par un couvercle, est placé à l'intérieur de la jaquette isotherme.

2.2.2. Analyse thermique différentielle

Cette technique nous a permis de déterminer le degré de pureté de nos substances. L'appareillage et le mode opératoire sont consignés dans les références 10 et 11.

2.3. Préparation des solutions titrées

2.3.1. Permanganate de potassium ($KMnO_4$) : 6,5 g de cette substance ont été dissous à chaud dans 2 dm^3 d'eau. Après décantation et filtration, la solution obtenue a été stockée dans un flacon de couleur brune. Sa concentration ($c = 0{,}0202$ M) a été déterminée à partir d'une solution titrée d'acide oxalique 0,05 M.

2.3.2. Anhydride arsénieux (As_2O_3) : 12 g de ce composé ont été dissous à chaud dans 1 dm^3 d'eau. Après décantation et filtration, la concentration de la solution obtenue ($c = 0{,}0589$ M) a été déterminée à partir de la liqueur précédente de permanganate de potassium.

2.3.3. Nitrate d'argent ($AgNO_3$) : 17 g de cette substance ont été dissous dans 1 dm^3 d'eau. La concentration de cette solution ($c = 0{,}1007$ M) a été déterminée par dosage à partir d'une solution titrée de chlorure de sodium 0,1 M.

2.4. Analyse de la phase liquide

La solution issue de la bombe après combustion est étendue à 200 cm^3.

À part le dosage des ions hexachloroplatinates $(PtCl_6)^{2-}$ réalisé par spectrophotométrie dans le visible, tous les autres dosages ont été effectués par potentiométrie en utilisant une électrode de référence au calomel et une électrode de mesure en platine (dans le cas du dosage de la solution de $KMnO_4$ et de As_2O_3) et d'argent (dans le cas du dosage de Cl^-). Généralement deux à trois essais ont été réalisés pour chaque dosage. L'exactitude et la reproductibilité des mesures sont supérieures à 99,5%.

Signalons au passage que nous n'avons pas trouvé dans nos solutions une concentration significative en acides nitrique et nitreux.

Tous les dosages potentiométriques ont été réalisés en utilisant des microburettes de 2 ou (et) 5 cm^3 (protégées de la lumière dans le cas de la solution de permanganate de potassium).

2.4.1. Dosage de As_2O_3

Les analyses sont réalisées à partir de la liqueur titrée de $KMnO_4$ décrite ci-dessus sur 20 cm^3 de solution initiale de As_2O_3 ou issue de la bombe après combustion, additionnées de 10 cm^3 d'acide chlorhydrique 6 M et d'une goutte de solution 0,0025 M d'iodate de potassium. Nous avons pris le soin de vérifier à plusieurs reprises et un mois après l'essai que la concentration des solutions analysées n'avait pas changé.

2.4.2. Dosage de $(PtCl_6)^{2-}$

Une quantité (2 cm^3) de solution issue de la bombe après combustion est additionnée de 2 cm^3 d'eau déminéralisée, d'une goutte de brome liquide et d'une solution saturée de bromure de sodium. Le brome en excès est éliminé en faisant passer un courant d'air comprimé dans la solution ainsi obtenue. On ajoute alors 1 cm^3 d'une solution d'iodure de potassium à 1% et on complète le volume de la solution ainsi préparée à 7 cm^3 par addition d'eau déminéralisée. La détermination spectrophotométrique de la concentration en ions $(PtCl_6)^{2-}$ se fait dans le visible (à 490 μm). L'étalonnage préalable de l'appareil a été réalisé à partir de solutions titrées d'hexachloroplatinate de sodium (Na_2PtCl_6).

2.4.3 Dosage de Cl^-

Afin de vérifier que tout le chlore contenu dans la substance brûlée est bien passé sous la forme de Cl^- et de $(PtCl_6)^{2-}$, des analyses d'ions chlorures ont été réalisées sur 10 cm^3 de solution issue de la bombe après combustion en utilisant la solution titrée de $AgNO_3$ décrite dans le paragraphe 2.3.3. La valeur moyenne du chlore total trouvée est de $(99{,}7 \pm 0{,}3)$%.

Nous avons aussi pris la précaution de vérifier que la solution issue de la bombe après combustion ne contenait pas d'ions Au^{3+} pouvant provenir de l'attaque par l'acide chlorhydrique de l'or éventuellement présent au niveau des soudures des deux électrodes sur le couvercle de la bombe. Cette vérification a été réalisée en utilisant la réaction de Au^{3+} avec I^- (provenant d'une solution de KI) et en dosant, par iodométrie à partir d'une solution titrée de thiosulfate de sodium, l'iode ainsi formé (12).

2.5. Oxydation catalytique de As_2O_3 en As_2O_5 par l'oxygène en présence de platine

Dans le cas de la combustion de dérivés chlorés, la présence de la solution d'anhydride arsénieux dans la bombe est indispensable si l'on veut que tout le chlore contenu dans la substance

Can. J. Chem. Downloaded from www.nrcresearchpress.com by 80.90.12.36 on 09/08/12
For personal use only.

étudiée passe après combustion à l'état d'ions chlorures (une légère partie du chlore est cependant complexée sous la forme d'ions hexachloroplatinates et dosée par spectrophotométrie).

Il a été montré qu'en présence d'oxygène (sous une pression de 3,04 MPa) le revêtement platiné de la bombe catalysait l'oxydation de As_2O_3 en As_2O_5 (13). Il était donc indispensable de connaître exactement la fraction de As_2O_3 ainsi oxydée entre le moment du garnissage de la bombe et celui de sa rotation.

Deux méthodes peuvent être utilisées pour déterminer la quantité de As_2O_3 ainsi oxydée. L'une d'elles, décrite par Stridh (13), consiste à mesurer le pH d'une solution de As_2O_3 additionnée d'une autre de As_2O_5, la concentration de ces deux solutions étant connue. On établit la courbe pH = [$c(As_2O_5)$] et on l'utilise ensuite pour déterminer, à partir du pH des solutions recueillies après combustion, la concentration en As_2O_5 formé. Une seconde méthode consiste à réaliser l'étalonnage du système calorimétrique en plaçant dans la bombe 20 cm^3 de la solution de As_2O_3 et à déterminer par titrage potentiométrique les quantités de As_2O_3 avant et après expérience. À partir de la courbe pH = [$c(As_2O_5)$] ci-dessus mentionnée, on peut se rendre compte que si la concentration en As_2O_5 dépasse 10^{-3} mol dm^{-3}, la variation du pH en fonction de la concentration de As_2O_5 devient faible, ce qui rend imprécise la détermination de cette concentration dans les solutions issues de la combustion. En conséquence, la seconde méthode donnant, dans ce cas, des résultats plus exacts et plus reproductibles est préférée à la première. Nos expériences ont permis de constater que (2,7 ± 0,3)% de As_2O_3 se trouvant dans la solution initiale s'oxydaient catalytiquement. Nous en avons tenu compte dans le calcul de la concentration initiale de la solution de As_2O_3 utilisée.

À noter que l'oxydation catalytique de As_2O_3 en As_2O_5 est surtout prépondérante entre le moment du garnissage de la bombe et celui de sa rotation. En effet, la formation de HCl entraîne une diminution du pH de la solution initiale, ce qui a pour effet de réduire l'oxydation catalytique de As_2O_3 (12).

2.6. Analyse de la phase gazeuse

Après chaque combustion et détente de la phase gazeuse à 101,3 kPa, nous avons vérifié, à l'aide des tubes de Dräger, l'absence dans celle-ci de chlore et de monoxyde de carbone.

3. Résultats

Nous avons consigné dans le tableau 1 les grandeurs physiques à 298,15 K des substances utilisées qui interviennent dans les calculs menant aux résultats expérimentaux.

L'étalonnage du système calorimétrique, consistant à déterminer son équivalent énergétique (U_{calor}), a été effectué à l'aide de l'acide benzoïque (échantillon 39i du NIST) dans les mêmes conditions que la mesure de l'énergie de combustion des acides chlorobenzoïques. C'est ainsi qu'un gramme d'acide benzoïque, comprimé sous la forme de deux pastilles, a été brûlé en présence de 20 cm^3 de solution 0,0589 M de As_2O_3. Nous trouvons U_{calor} = (14 995,7 ± 1,4) J K^{-1}.

Les résultats expérimentaux obtenus par calorimétrie de combustion et correspondant à la réaction :

$$ClC_6H_4CO_2H(s) + 7\ O_2(g) + 598\ H_2O(l) \rightarrow 7\ CO_2(g) + [HCl{\cdot}600\ H_2O](l)$$

sont consignés dans les tableaux 2–4. Les grandeurs thermodynamiques à l'état standard qui les accompagnent ont été calculées à partir des valeurs expérimentales en utilisant un programme informatique écrit par nos soins, tenant compte des corrections dites de Washburn et des données de la littérature. Dans le calcul de l'enthalpie de formation de nos substances à l'état condensé, nous avons adopté pour $\Delta_f H_m^0$ (g, 298,15 K, CO_2), $\Delta_f H_m^0$ (l, 298,15 K, H_2O) et $\Delta_f H_m^0$ (l, 298,15 K, ($HCl{\cdot}600\ H_2O$)) respectivement les valeurs (−393,51 ± 0,13) kJ mol^{-1} (14), (−285,830 ± 0,042) kJ mol^{-1} (14) et (−166,62 ± 0,08) kJ mol^{-1} (15).

À part l'acide 4-chlorobenzoïque qui a fait l'objet de plusieurs travaux par calorimétrie de combustion dans le but de l'ériger comme substance d'intercomparaison dans l'étude des substances chlorées (7, 8) par cette technique, les deux autres isomères ont été très peu étudiés (16, 17).

Les valeurs de l'enthalpie de combustion de l'isomère *para*, obtenues avec un appareillage comparable au nôtre et consignées dans la littérature, sont comprises entre −3062,8 et −3065,4 kJ mol^{-1} (7, 16–21). En conséquence, notre résultat (−3065,6 ± 0,5) kJ mol^{-1} est tout à fait compatible avec ces valeurs.

En ce qui concerne les deux autres isomères, seules deux valeurs de l'enthalpie de combustion pour chacun d'eux existent dans la littérature (16, 17). L'une d'elles, obtenue avec un appareillage doté de bombe rotative (17), est égale à (−3088,3 ± 0,7) kJ mol^{-1} pour l'isomère *ortho* et à (−3068,5 ± 1,5) kJ mol^{-1} pour l'isomère *méta*. Comme nous pouvons le constater, ces deux valeurs sont en parfait accord avec nos résultats (cf. tableaux 2 et 3).

4. Discussion

L'ensemble des résultats expérimentaux consignés dans le tableau 5 permet la détermination de certaines grandeurs énergétiques liées à la structure des molécules étudiées.

4.1. Energie de conjugaison

Les trois molécules d'acides chlorobenzoïques étudiées dans ce mémoire sont conjuguées. En conséquence, nous avons essayé de déterminer, d'abord, leur énergie de conjugaison expérimentale, puis avons comparé celle-ci à la valeur théorique obtenue en utilisant la méthode de calcul décrite dans la référence 22.

L'énergie de conjugaison est, par définition, égale à la différence entre l'énergie réelle de la molécule et l'énergie qu'elle aurait si les divers systèmes insaturés qu'elle comporte étaient indépendants. Sur le plan pratique, pour la déterminer, nous utilisons les enthalpies standard de combustion à l'état gazeux de la molécule réelle et de la molécule fictive non conjuguée. La première de ces grandeurs s'obtient expérimentalement tandis que la seconde nécessite le recours aux systématiques. En ce qui nous concerne, nous avons utilisé celle de Klages qui est consignée dans la référence 23. Quant au calcul de l'énergie de conjugaison théorique, nous avons utilisé la méthode décrite dans la référence 22 en utilisant le jeu de paramètres suivant :

Pour la liaison C—Cl, $\alpha Cl = \alpha + 2{,}125\ \beta_0$ et $\beta C—Cl = 0{,}750\ \beta_0$ (24), k(C—Cl) = 4 × 10^2 N m^{-1}, d_0(C—Cl) = 1,7.

Pour la fonction acide (2, 22) :

Tableau 1. Grandeurs physiques des substances utilisées à 298,15 K.

Substance	Formule brute	M^a (g mol^{-1})	ρ (g cm^{-3})	$-(\partial U/\partial P)_T$ (J g^{-1} MPa^{-1})	C_p (J K^{-1} g^{-1})	$-\Delta_c u^0$ (s, 298,15 K) (J g^{-1})
Acide benzoïque	$C_7H_6O_2$	122,1234	1,32(28)	0,12(28)	1,21(28)	26413,9(29)
Polythène	$(CH_2)_n$	14,0269	0,92(30)	0,055(30)	2,22(30)	46371(31)
Coton	$CH_{1,791}O_{0,850}$	27,4157	1,50(28)	0,29(28)	1,7(28)	16399(32)
Acide 2-chlorobenzoïque	$C_7H_5O_2Cl$	156,5682	1,544(33)	0,068(18)	0,93(17)	
Acide 3-chlorobenzoïque	$C_7H_5O_2Cl$	156,5682	1,544(33)	0,068(18)	0,93(17)	
Acide 4-chlorobenzoïque	$C_7H_5O_2Cl$	156,5682	1,540(34)	0,068(18)	0,93(17)	

[a]Valeurs calculées à partir du tableau des masses atomiques de 1991 (27).

Tableau 2. Combustion de l'acide 2-chlorobenzoïque à 298,15 K.

m(subst.) (g)	m(poly.) (g)	m(coton) (g)	m(Pt) (g)	$n_f(As_2O_3)$ (10^{-4} mol)	$n_f(H_2PtCl_6)$ (10^{-5} mol)	ΔT (K)	$-\Delta U_{IBP}$ (J)	$-W_1$ (J)	W_2 (J)	$-\Delta_c U^0_m$ (s, 298,15 K) (kJ mol^{-1})
0,935 971	0,082 720	0,002 232	4,341 849	7,60	1,4	1,492 06	22 515	3872	179	3088,73
0,938 067	0,081 959	0,001 966	4,338 291	7,19	1,2	1,492 50	22 522	3833	191	3087,50
0,949 199	0,083 176	0,001 816	4,332 196	7,07	1,2	1,510 85	22 799	3887	195	3087,31
0,933 391	0,088 817	0,001 856	4,329 984	6,69	$0,8_5$	1,508 42	22 762	4149	206	3087,61
0,953 630	0,085 678	0,002 066	4,328 635	6,74	$0,9_3$	1,525 41	23 019	4007	206	3087,63

$-\Delta_c U^0_m$ (s, 298,15 K) = (3087,76 ± 0,25) kJ mol^{-1}
$-\Delta_c H^0_m$ (s, 298,15 K) = (3087,76 ± 0,25) kJ mol^{-1}

ΔT : variation exacte de la température du système calorimétrique.
ΔU_{IBP} : variation de l'énergie interne de la bombe et de son contenu.
W_1 : énergie de combustion de la substance auxiliaire et du coton.
W_2 : corrections pour passer à l'état standard.
$n_f(As_2O_3)$: nombre de moles de As_2O_3 à l'état final.

Tableau 3. Combustion de l'acide 3-chlorobenzoïque à 298,15 K.

m(subst.) (g)	m(poly.) (g)	m(coton) (g)	m(Pt) (g)	$n_f(As_2O_3)$ (10^{-4} mol)	$n_f(H_2PtCl_6)$ (10^{-5} mol)	ΔT (K)	$-\Delta U_{IBP}$ (J)	$-W_1$ (J)	W_2 (J)	$-\Delta_c U^0_m$ (s, 298,15 K) (kJ mol^{-1})
0,919 798	0,082 891	0,001 961	4,354 988	6,97	$0,6_3$	1,465 48	22 114	3876	203	3069,97
0,924 138	0,083 282	0,001 961	4,351 536	6,89	1,0	1,473 14	22 230	3894	207	3071,50
0,926 975	0,086 541	0,002 071	4,350 401	7,52	1,6	1,485 11	22 411	4047	188	3069,86
0,923 028	0,086 125	0,001 901	4,348 866	7,95	1,1	1,477 07	22 289	4025	173	3068,70
0,931 239	0,093 181	0,002 181	4,347 214	8,08	1,3	1,478 56	22 312	3893	170	3068,21

$-\Delta_c U^0_m$ (s, 298,15 K) = (3069,65 ± 0,57) kJ mol^{-1}
$-\Delta_c H^0_m$ (s, 298,15 K) = (3069,65 ± 0,57) kJ mol^{-1}

ΔT : variation exacte de la température du système calorimétrique.
ΔU_{IBP} : variation de l'énergie interne de la bombe et de son contenu.
W_1 : énergie de combustion de la substance auxiliaire et du coton.
W_2 : corrections pour passer à l'état standard.
$n_f(As_2O_3)$: nombre de moles de As_2O_3 à l'état final.

Can. J. Chem. Downloaded from www.nrcresearchpress.com by 80.90.12.36 on 09/08/12
For personal use only.

Tableau 4. Combustion de l'acide 4-chlorobenzoïque à 298,15 K.

m(subst.) (g)	m(poly.) (g)	m(coton) (g)	m(Pt) (g)	$n_f(As_2O_3)$ (10^{-4} mol)	$n_f(H_2PtCl_6)$ (10^{-5} mol)	ΔT (K)	$-\Delta U_{IBP}$ (J)	$-W_1$ (J)	W_2 (J)	$-\Delta_c U^0_m$(s, 298,15 K) (kJ mol^{-1})
0,899 897	0,082 910	0,001 956	4,374 964	8,79	1,1	1,433 98	21 639	3877	145	3065,07
0,923 676	0,076 779	0,002 206	4,374 131	8,96	1,3	1,445 37	21 811	3596	141	3063,57
0,932 645	0,083 877	0,001 091	4,368 073	8,78	1,1	1,479 25	22 322	3907	147	3066,79
0,935 879	0,080 108	0,001 906	4,366 811	8,46	1,0	1,472 30	22 217	3746	157	3063,91
0,922 835	0,081 740	0,001 881	4,364 892	8,38	1,2	1,461 90	22 060	3821	159	3067,38
0,933 140	0,081 159	0,001 856	4,362 364	7,19	$0,8_5$	1,476 18	22 276	3794	197	3067,99
0,928 742	0,082 216	0,002 251	4,360 990	8,43	1,2	1,470 78	22 194	3849	158	3066,01
0,931 944	0,082 691	0,001 931	4,359 200	8,05	1,4	1,476 38	22 279	3866	171	3064,66
0,939 468	0,087 507	0,002 117	4,353 541	6,72	$0,6_4$	1,503 91	22 694	4093	212	3064,58

$-\Delta_c U^0_m$ (s, 298,15 K) = (3065,55 ± 0,52) kJ mol^{-1}
$-\Delta_c H^0_m$ (s, 298,15 K) = (3065,55 ± 0,52) kJ mol^{-1}

ΔT : variation exacte de la température du système calorimétrique.
ΔT_{IBP} : variation de l'énergie interne de la bombe et de son contenu.
W_1 : énergie de combustion de la substance auxiliaire et du coton.
W_2 : corrections pour passer à l'état standard.
$n_f(As_2O_3)$: nombre de moles de As_2O_3 à l'état final.

Tableau 5. Grandeurs thermodynamiques des acides chlorobenzoïques à 298,15 K.

Substance	$-\Delta_c H^0_m$ (s, 298,15 K) (kJ mol^{-1})	$-\Delta_f H^0_m$ (s, 298,15 K) (kJ mol^{-1})	$\Delta_{sub} H^0_m$ (298,15 K)[a] (kJ mol^{-1})	$-\Delta_f H^0_m$ (g, 298,15 K) (kJ mol^{-1})
Acide 2-chlorobenzoïque	3087,8 ± 0,2	405,1 ± 0,5	100,9 ± 0,5	304,2 ± 0,7
Acide 3-chlorobenzoïque	3069,7 ± 0,6	423,2 ± 0,8	101,4 ± 0,4	321,8 ± 0,9
Acide 4-chlorobenzoïque	3065,6 ± 0,5	427,3 ± 0,7	102,5 ± 0,4	324,8 ± 0,8

[a]Valeurs empruntées à la référence 4.

αO-(H) = α + 2,500 β_0 $\quad$ βC-O-(H) = 1,080 β_0
αO = α + 0,875 β_0 $\quad$ βC-O = 1,375 β_0
αC = α + 0,250 β_0

(β_0 est l'intégrale de recouvrement dans la molécule de benzène et a, pour valeur absolue, 131,7 kJ mol^{-1}). Les calculs effectués nous ont permis d'obtenir les résultats consignés dans le tableau 6.

Comme nous pouvons le constater, il existe un accord satisfaisant entre les différentes valeurs expérimentales et théoriques de l'énergie de conjugaison.

Tableau 6. Energie de conjugaison des trois acides chlorobenzoïques.

Substance	$E_{conj,exp}$(kJ mol^{-1})	$E_{conj,théor}$(kJ mol^{-1})
Acide 2-chlorobenzoïque	209	217
Acide 3-chlorobenzoïque	223	216
Acide 4-chlorobenzoïque	226	217

4.2. Enthalpie d'atomisation

Pour déterminer la somme des enthalpies des liaisons intramoléculaires d'une molécule, il est indispensable de connaître son enthalpie d'atomisation. Celle-ci, à l'état standard et à la température T, est liée à la transformation suivante : molécule (considérée comme gaz idéal, état fondamental, T) $\rightarrow$ atomes (chacun d'eux, considéré comme gaz idéal, état fondamental, T).

Sur le plan expérimental, à une température donnée, si l'on considère une molécule de formule générale : $C_aH_bO_cCl_d$, la réaction d'atomisation s'écrit :

$$C_aH_bO_cCl_d(g) \rightarrow aC(g) + bH(g) + cO(g) + dCl(g)$$

L'enthalpie liée à cette réaction s'appelle «enthalpie d'atomisation expérimentale» et est égale à :

$$\Delta_{a,exp}H^0_m = a\Delta_fH^0_mC(g) + b\Delta_fH^0_mH(g) + c\Delta_fH^0_mO(g) + d\Delta_fH^0_mCl(g) - \Delta_fH^0_mC_aH_bO_cCl_d(g).$$

Aussi, à partir de l'enthalpie de formation d'une molécule à l'état gazeux et de celle des différents constituants C, H, O et Cl, que l'on emprunte aux tables (14) et qui, à 298,15 K, valent respectivement : (716,67 ± 0,44), (217,997 ± 0,006), (249,17 ± 0,10) et (121,302 ± 0,008) kJ mol^{-1}, est-il possible de calculer son enthalpie d'atomisation expérimentale. Nous trouvons pour les trois molécules d'acides chlorobenzoïques les valeurs consignées dans le tableau 7.

Pour déterminer l'enthalpie de liaison $H(C_b—Cl)$ dans les molécules d'acides chlorobenzoïques, nous sommes partis de $\Delta_{a,exp}H^0_m$ (298,15 K). En effet, on sait que l'enthalpie d'atomisation est égale à la somme des enthalpies des liaisons intramoléculaires compte tenu des facteurs de stabilisation et de déstabilisation.

Can. J. Chem. Downloaded from www.nrcresearchpress.com by 80.90.12.36 on 09/08/12
For personal use only.

Can. J. Chem. Downloaded from www.nrcresearchpress.com by 80.90.12.36 on 09/08/12
For personal use only.

Tableau 7. Enthalpie d'atomisation expérimentale des trois acides chlorobenzoïques et de la liaison (C_b—Cl).

Substance	$\Delta_{a,exp}H_m^0$ (298,15 K) (kJ mol^{-1})	H(Cb—Cl) (kJ mol^{-1})
Acide 2-chlorobenzoïque	7031 ± 2	338,7
Acide 3-chlorobenzoïque	7048 ± 2	354,6
Acide 4-chlorobenzoïque	7051 ± 2	358,6

Pour ce qui est des liaisons C_b—C_b du cycle benzénique, nous avons utilisé le procédé de calcul consigné dans la référence 25. Celui-ci fait intervenir un paramètre lié à la géométrie de la molécule (l'indice de liaison l_{rs} entre deux atomes directement liés r et s) obtenu à partir du calcul théorique de l'énergie de conjugaison (fig. 2). La relation reliant H_{rs} à l_{rs} s'écrit : (H_{rs}/kJ mol^{-1}) = 246,0 l_{rs} + 342,6.

Quant à H(C_b—H), H(C_b—C) et H(C_b—COOH), nous avons utilisé les valeurs 415,88; 351,56 et 1657,35 kJ mol^{-1} (26). Ainsi, dans le cas présent, pour calculer H(C_b—Cl), cela revient à retrancher de $\Delta_{a,exp}H_m^0$ (298,15 K) la part énergétique des différentes liaisons ci-dessus mentionnées. Le calcul effectué nous a permis d'obtenir les valeurs consignées dans le tableau 7. Nous avons adopté la valeur moyenne de 356,6 kJ mol^{-1} pour H(C_b—Cl) dans les acides chlorobenzoïques. Le même calcul, réalisé avec la molécule de chlorobenzène, nous a donné H(C_b—Cl) = 348,7 kJ mol^{-1}.

4.3. Stabilité relative de quelques dérivés monosubstitués de l'acide benzoïque

Ayant précédemment étudié au laboratoire les acides aminobenzoïques (2), hydroxybenzoïques (3) et, dans le présent travail, les acides chlorobenzoïques, il nous a paru intéressant de comparer la stabilité relative de ces dérivés monosubstitués de l'acide benzoïque à partir des valeurs de leur enthalpie de formation à l'état gazeux et à 298,15 K consignées dans le tableau 8.

Au sujet des dérivés *ortho* et *para*, cette comparaison fait ressortir que les isomères *ortho* seraient plus stables lorsque X (substituant) = OH ou NH_2. L'inverse est observé lorsque X = Cl. Dans le premier cas, cette stabilité serait vraisemblablement due à la formation d'une liaison hydrogène intramoléculaire entre l'atome d'oxygène du carbonyle et celui d'hydrogène de la fonction hydroxyle ou aminée. À l'effet stérique, qui en est partiellement la cause dans le second cas, vient s'ajouter, à notre avis, un effet de répulsion électrostatique entre l'atome de chlore et celui d'oxygène du carbonyle.

La comparaison des isomères *ortho* dans le cas où X = OH ou NH_2 permet de se rendre compte que la stabilité du dérivé hydroxylé est supérieure à celle du dérivé aminé. La chélation semble s'affaiblir en passant de l'acide hydroxybenzoïque à l'acide aminobenzoïque. Cette observation rejoint celle que nous avions faite à la suite de l'étude de ces mêmes composés par calorimétrie de sublimation et consignée dans un précédent travail (3). Elle trouve une confirmation dans l'ouvrage de Julg (35) à propos de l'énergie mise en jeu par la liaison hydrogène intramoléculaire dans les acides hydroxybenzoïque et aminobenzoïque : O—H···O (25 kJ mol^{-1}), N—H···O (11 kJ mol^{-1}).

Enfin, on note que, quel que soit l'isomère considéré, la stabilité semble croître dans l'ordre X = NH_2, Cl, OH et serait due à une conjugaison qui s'intensifierait en passant des acides amino, aux chloro et aux hydroxybenzoïques (cf. tableau 8).

Signalons, pour terminer, que les conclusions consignées dans ce paragraphe auraient pu être déduites en prenant comme élément de comparaison les valeurs de l'énergie de conjugaison des molécules consignées dans le tableau 8.

Fig. 2. Indices de liaison dans les molécules des trois acides chlorobenzoïques.

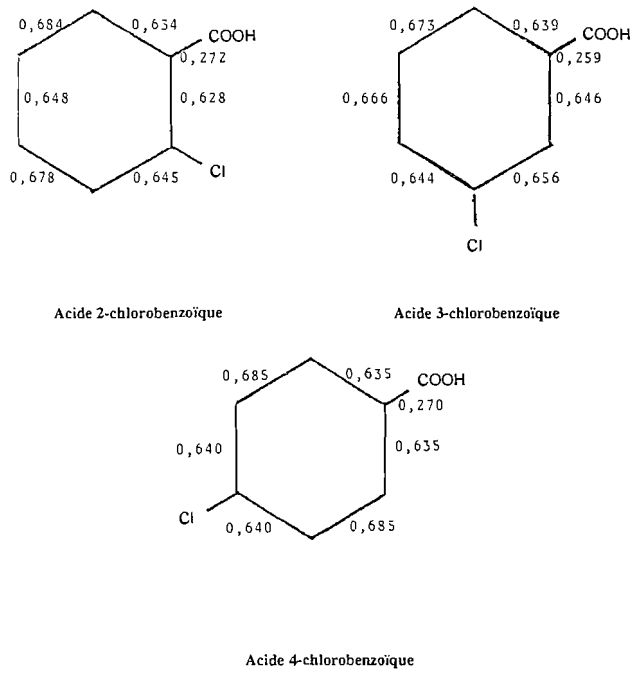

Tableau 8. Enthalpie de formation à l'état gazeux et à 298,15 K de quelques dérivés monosubstitués de l'acide benzoïque et leur énergie de conjugaison.

Substituant X =	$-\Delta_fH_m^0$ (g, 298,15 K) (kJ mol^{-1})			Référence bibliographique
	ortho	*méta*	*para*	
NH_2	296,2	289,3	293,9	2
OH	495,8	469,1	492,7	3
Cl	304,2	321,8	324,8	Ce travail
	$E_{conj,exp}$(kJ mol^{-1})			
	ortho	*méta*	*para*	
NH_2	208	199	203	2
OH	268	238	262	3
Cl	209	223	226	Ce travail

4.4. Peut-on ériger l'acide chloro-4 benzoïque au rang de substance d'intercomparaison en calorimétrie de combustion des substances chlorées?

À cette question, des chercheurs (17, 18) avant nous ont répondu par l'affirmative considérant que ce composé possède les propriétés requises dans un tel cas : stable, possédant une faible pression de vapeur saturante, non-hygroscopique, facile

à manipuler et à stocker, ignition aisée. Vis-à-vis de ces propriétés, nous n'avons aucun commentaire à faire. Par contre, comme nous l'avons indiqué dans le paragraphe 2.2.1. et quel que soit l'isomère, à partir d'une certaine masse ($m \geq 0{,}8$ g) de substance et dans nos conditions expérimentales, il nous a été très difficile d'obtenir une combustion complète sans la présence de substance auxiliaire (dans notre cas le polythène dont la part énergétique représente 4,2 % de l'énergie totale dissipée). Signalons au passage que Hu et al. (18) utilisent, dans certaines de leurs expériences avec l'acide 4-chlorobenzoïque, l'huile de paraffine comme substance auxiliaire.

L'incertitude qui accompagne nos valeurs expérimentales représente l'écart moyen, $\sigma_m = \pm\{(x - x_0)^2/n(n-1)\}^{1/2}$, x étant chacune des n valeurs entrant dans le calcul de la moyenne x_0. Lorsque la valeur expérimentale est fonction de plusieurs variables, l'incertitude calculée tient compte de l'erreur sur chacune de ces variables.

Remerciements

Les auteurs tiennent à remercier les services techniques du Centre pour l'aide qu'ils leur ont apportée dans les travaux de modification du calorimètre isopéribolique à bombe rotative ainsi que M. Juan Antonio Guardado Perez pour sa contribution dans la remise en route de cet appareil. L'un de nous (A.R.A.) remercie le Consejo Nacional de Ciencia y Technologia (CONACYT) pour l'octroi d'une bourse lui ayant permis de préparer, au laboratoire, une thèse dont ce travail constitue la première partie.

Bibliographie

1. R. Sabbah, R. Chastel et M. Laffitte. Can. J. Chem. **52**, 2201 (1974).
2. M. Nabavian, R. Sabbah, R. Chastel et M. Laffitte. J. Chim. Phys. **74**, 115 (1977).
3. R. Sabbah et T.H.D. Le. Can. J. Chem. **71**, 1378 (1993).
4. R. Sabbah et H. Hirtz. Bull. Chem. Soc. Fr. **128**, 26 (1991).
5. Z.C. Tan et R. Sabbah. Sci. China, Ser. B: **37**, 641 (1994).
6. Z.C. Tan et R. Sabbah. Thermochim. Acta, **231**, 109 (1994).
7. J.B. Pedley, R.D. Naylor et S.P. Kirby. Thermochemical data of organic compounds. 2nd ed. Chapman and Hall, London. 1986.
8. S. Sunner et M. Månsson. (*Editors*). IUPAC – Experimental chemical thermodynamics. Vol. 1. Combustion calorimetry. Pergamon, Oxford. 1979.
9. W.N. Hubbard, C. Katz et G. Waddington. J. Phys. Chem. **58**, 142 (1954).
10. R. Sabbah et I. Antipine. J. Therm. Anal. **32**, 1929 (1987).
11. R. Sabbah et L. El Watik. J. Therm. Anal. **36**, 2299 (1990).
12. G. Charlot. Les méthodes de la chimie analytique. Analyse quantitative minérale. 4è ed. Månsson, Paris. 1961.
13. G. Stridh. J. Chem. Thermodyn. **7**, 703 (1975).
14. Report of the Codata Task Group on Key Values for Thermodynamics. J. Chem. Thermodyn. **10**, 903 (1978).
15. D.D. Wagman, W.H. Evans, V.B. Parker, I. Holow, S.M. Bailey et R.H. Schumm. NBS Technical Note 270-3, Washington, 1968.
16. L. Smith, L. Bjellerup, S. Krook et H. Westermark. Acta Chem. Scand. **7**, 65 (1953).
17. W.H. Johnson et E.J. Prosen. J. Res. Natl. Bur. Stand. Sect. A: **78**, 683 (1974).
18. A.T. Hu, G.S. Sinke, M. Månsson et B. Ringner. J. Chem. Thermodyn. **4**, 203 (1972).
19. V.P. Kolesov, G.M. Slavutskaya et T.S. Papina. Russ. J. Phys. Chem. **46**, 474 (1972).
20. V.A. Platanov, Yu. N. Simulin et R.V. Dzhagatspanyan. Russ. J. Phys. Chem. **55**, 1209 (1981).
21. S.N. Hajiev, M.J. Agarunov et H.G. Nurullaev. J. Chem. Thermodyn. **6**, 713 (1974).
22. R. Sabbah, M. Gilbert et A. Julg. Thermochim. Acta, **10**, 345 (1974).
23. G.W. Wheland. Resonance in organic chemistry. Wiley, New York. 1955.
24. A. Julg et O. Julg. Exercices de chimie quantique. Dunod, Paris. 1967.
25. R. Sabbah et I. Antipine. Bull. Soc. Chim . Fr. 392 (1987).
26. R. Sabbah et M. Laffitte. Thermochim. Acta, **25**, 376 (1978).
27. Atomic weights of the elements 1991. Pure Appl. Chem. **64**, 1519 (1992).
28. W.D. Good et N.K. Smith. J. Chem. Eng. Data, **14**, 102 (1969).
29. J.D. Cox, H.A. Gundry et A.J. Head. Trans. Faraday Soc. **60**, 653 (1964).
30. J.D. Cox et G. Pilcher. Thermochemistry of organic and organometallic compounds. Academic Press, London. 1970.
31. S. Skoulika et R. Sabbah. C.R. Acad. Sci. Paris, **295**, 657 (1982).
32. M. Coten et R. Sabbah. Thermochim. Acta, **49**, 307 (1981).
33. G. Ferguson et G.A. Sim. Acta Crystallogr. **14**, 1262 (1961).
34. R.S. Miller, I.C. Paul et D.Y. Curtin. J. Am. Chem. Soc. **96**, 6334 (1974).
35. A. Julg. Chimie théorique. Dunod, Paris. 1964.

Can. J. Chem. Downloaded from www.nrcresearchpress.com by 80.90.12.36 on 09/08/12
For personal use only.

1-Aminocyclohexene-2,4-dicarbonitrile derivatives. Syntheses and structural study

Antonio Lorente, Carmen Galan, Isabel Fonseca, and Juliana Sanz-Aparicio

Abstract: Substituted 1-aminocyclohexene-2,4-dicarbonitriles were obtained by reaction of α,β-unsaturated nitriles (two equivalents) with benzyl cyanide. By recrystallization from ethanol one diastereomeric racemate was isolated in each case. The cyclohexene structures were established from spectroscopic data (IR, MS, and one- and two-dimensional NMR). Relative stereochemical configurations and conformational preferences in the solid state of cyclohexenes **2** and **3** and propanedicarbonitrile **1** were established from X-ray crystallography. Crystals of **1** ($C_{17}H_{14}N_2$) belong to the orthorhombic space group *Pbca*. Cell dimensions are $a = 17.168(7)$, $b = 21.612(5)$, $c = 7.508(2)$ Å, $V = 2785(7)$ Å^3. Final $R = 0.078$ and $R_w = 0.091$; 1363 reflections were observed. The compound **2** ($C_{26}H_{21}N_3$) crystallizes in the monoclinic space group $P2_1/n$ with $Z = 4$. The crystal data for **2** are $a = 7.743(1)$, $b = 24.420(1)$, $c = 11.164(1)$ Å, $\beta = 102.65(1)°$, $V = 2059.7(3)$ Å^3. Final $R = 0.046$ and $R_w = 0.059$; 2701 reflections were observed. Crystals of **3** ($C_{16}H_{17}N_3$) belong to the triclinic space group $P\bar{1}$. Cell dimensions are $a = 14.582(1)$, $b = 7.283(1)$, $c = 7.116(1)$ Å, $\alpha = 110.84(0)°$, $\beta = 85.92(0)°$, $\gamma = 97.81(1)°$, $V = 696.9(2)$ Å^3. Final $R = 0.047$ and $R_w = 0.052$; 2227 reflections were observed. The cyclohexene ring in **2** and **3** exists as a sofa rather then as a half-chair conformation.

Key words: 1-aminocyclohexenes, α,β-unsaturated nitriles, benzyl cyanide.

Résumé : On a obtenu les 1-aminocyclohex-1-ène-2,4-dicarbonitriles substitués par réaction de nitriles α,β-insaturés (deux équivalents) avec du cyanure de benzyle. Par recristallisation, on a obtenu dans chaque cas un racémique diastéréoisomère. On a déterminé les structures des cyclohexènes par des données spectroscopiques (IR, SM et RMN en une ou deux dimensions). Pour établir les configurations stéréochimiques relatives et les préférences conformationnelles des cyclohexènes **2** et **3** et du propanedicarbonitrile **1** à l'état solide, on a fait appel à la diffraction des rayons X. Les cristaux du composé **1** ($C_{17}H_{14}N_2$) sont orthorhombiques, groupe d'espace *Pbca*, avec $a = 17,168(7)$, $b = 21,612(5)$ et $c = 7,508(2)$ Å, $V = 2785(7)$ Å^3. $R = 0,078$ et $R_w = 0,091$ pour 1363 réflexions observées. Les cristaux du composé **2** ($C_{26}H_{21}N_3$) sont monocliniques, groupe d'espace $P2_1/n$, avec $a = 7,743(1)$, $b = 24,420(1)$ et $c = 11,164(2)$ Å, $\beta = 102,65(1)°$, $V = 2059,3(3)$ Å^3. $R = 0,046$ et $R_w = 0,059$ pour 2701 réflexions observées. Les cristaux du composé **3** ($C_{16}H_{17}N_3$) sont tricliniques, groupe d'espace $P\bar{1}$, avec $a = 14,582(1)$, $b = 7.283(1)$ et $c = 7,116(1)$ Å, $\alpha = 110,84(0),°$ $\beta = 85,92(0)°$ et $\gamma = 97,81(1)°$, $V = 696,9(2)$ Å^3. $R = 0,047$ et $R_w = 0,052$ pour 2227 réflexions observées. Les cycles des cyclohexènes des composés **2** et **3** existent dans la conformation sofa plutôt que dans la conformation demi-chaise.

Mots clés : 1-aminocyclohexènes, nitriles α,β-insaturés, cyanure de benzyle.

Introduction

The base-catalyzed dimerizations of α,β-unsaturated dinitriles allow the synthesis of aminocyclohexenes (1, 2) and amino-1,3-cyclohexadienes (3–8), which can be hydrolyzed to the corresponding cyclohexanones or cyclohexenones, respectively. Conformational analysis of cyclohexenes and their derivatives have been performed by different experimental (9) and theoretical methods (10). In most cases the lowest-energy conformation is the half-chair; however, the presence of substituent or fused rings can lead to conformations that are close to the ideal sofa arrangement. In this paper we describe the synthesis and structural study of 1-aminocyclohexene-2,4-dicarbonitriles **2** and **3**.

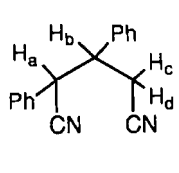

1

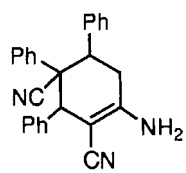

2

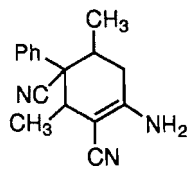

3

When benzyl cyanide was reacted with cinnamonitrile in sodium methoxide – methanol solution we obtained 1-amino-

Received October 31, 1994[1]

A. Lorente[2] and C. Galan. Departamento de Química Orgánica, Universidad de Alcalá, 28871 Alcalá de Henares, Madrid, Spain.
I. Fonseca and J. Sanz-aparicio. Unidad Estructural de Investigacion de Cristalografía, Instituto Rocasolano, Consejo Superior de Investigaciones Cientificas, Serrano 119, 28006 Madrid, Spain.

[1] Revision received May 26, 1995.
[2] Author to whom correspondence may be addressed. Telephone: 341-8854691. Fax: 341-8854660.

Can. J. Chem. Downloaded from www.nrcresearchpress.com by 80.90.12.36 on 09/08/12
For personal use only.

Can. J. Chem. Downloaded from www.nrcresearchpress.com by 80.90.12.36 on 09/08/12
For personal use only.

3,4,5-triphenylcyclohexene-2,4-dicarbonitrile (**2**) whereas, when the reaction was performed with sodium 2-propoxide in 2-propanol, 1,2-diphenyl-1,3-propanedicarbonitrile (**1**) was obtained. By reaction of **1** with another equivalent of cinnamonitrile in a sodium methoxide – methanol solution the cyclohexene **2** was obtained. Similarly the reaction of crotononitrile with benzyl cyanide, in similar conditions to those employed in the preceding case, afforded 2,4-dimethyl-3-phenyl-1,3,5-pentanetricarbonitrile (**4**) and its cyclization product: 1-amino-3,5-dimethyl-4-phenylcyclohexene-2,4-dicarbonitrile (**3**). The same reaction with NaH as the base in dimethylformamide (DMF) affords **3** as the sole product of the reaction.

Experimental

General

All melting points were taken in open capillary tubes on a Büchi SMP-20 and are uncorrected. IR spectra were measured as KBr pellets on a Perkin–Elmer 883 spectrophotometer. Mass spectra were recorded on a Hewlett–Packard 5988 spectrometer at 70 eV. ^{1}H and ^{13}C NMR spectra were recorded on a Varian UNITY-300 spectrometer at 303 K. The recording conditions were: ^{1}H NMR (299.949 MHz), 2% w/v solutions, acquisition time 3 s, spectral width 4000 Hz, and pulse width 11 μs. Conventional irradiation was used for the double resonance experiments. ^{13}C NMR (75.429 MHz) spectra were recorded using 5% w/v solutions, acquisition time 1 s, delay time 2 s, spectral width 16 500 Hz, and pulse width 3.6 μs. The homonuclear (COSY 45°) and heteronuclear (XHCORD) shift correlation experiments were performed by using standard Varian pulse sequences. Microanalyses were carried out in a Perkin–Elmer Elemental Analyzer model 240B.

X-ray diffraction

The crystals were mounted on an automatic four-circle diffractometer (Enraf–Nonius CAD-4 or Philips PW 1100). Cell parameters were obtained by least-squares refinement and intensity data were collected using graphite monochromatized radiation (MoKα on CAD-4 and CuKα on Philips) and the ω–2θ scan technique; two standard reflections measured every 100 reflections showed no intensity variation. Lorentz and polarization corrections were applied. The structures were determined by direct methods using the programs MITHRIL (11) and MULTAN 80 (12). The H atoms for compounds **1** and **3** were located on a difference map and, for compound **2**, on a difference map and by geometrical calculations. All H atoms were introduced in the refinement. In compound **1** all the parameters of the H atoms were maintained fixed but in compounds **2** and **3** the coordinates were refined, while the thermal parameters were fixed. An empirical weighting scheme (13) was applied in order to give no trends in $\langle w\Delta^2F\rangle$ vs. $\langle|F_o|\rangle$ and $\langle\sin\theta/\lambda\rangle$. The atomic scattering factors and anomalous dispersion were taken from International Tables for X-ray crystallography (14). The computation was made on a VAX 11/750 with XRAY70 (15), PARST (16), and Xtal 3.0 (17) programs. Experimental and X-ray structural data for compounds **1–3** are collected in Table 1.

Synthesis of 1,2-diphenyl-1,3-propanedicarbonitrile (1)

To a solution of sodium (230 mg, 10 mmol) in dry propan-2-ol (30 mL), benzyl cyanide (1.17 g, 10 mmol) and cinnamonitrile (1.29 g, 10 mmol) were added. The reaction mixture was stirred at room temperature for 3 h and then poured into ice-water (200 mL). The solid material thus obtained was filtered and recrystallized from propan-2-ol, 75% yield. Anal. calcd. for $C_{17}H_{14}N_2$: C 82.90, H 5.73, N 11.37; found: C 82.70, H 5.60, N 11.51.

By fractional recrystallization from propan-2-ol diastereomeric racemates α(1*R*,2*S*; 1*S*,2*R*) and β(1*R*,2*R*; 1*S*,2*S*) were individually isolated.

(1R,2S; 1S,2R) isomer: mp 124–125°C (lit. (18) mp 123°C). IR ν: 2242, 1494, 1453, and 1429 cm^{-1}; MS *m/e*: 246 (M^+, 28%), 178 (14), 131 (67), 130 (100), 128 (18), 118 (48), 117 (86), 116 (58), 104 (47), 103 (74), 102 (40), 101 (14), 90 (38), 89 (58), 88 (14), 78 (26), and 77 (64).

(1R,2R; 1S,2S) isomer: mp 132–133°C. IR ν: 2243, 1492, 1454, and 1434 cm^{-1}; MS *m/e*: 247 (M^+ + 1, 11%), 246 (M^+, 35), 178 (20), 131 (66), 130 (100), 118 (40), 117 (84), 116 (58), 90 (28), 89 (56), 88 (11), 78 (19), and 77 (63).

Synthesis of 1-amino-3,4,5-triphenylcyclohexene-2,4-dicarbonitrile (2)

Procedure A

To a solution of sodium (690 mg, 30 mmol) in dry methanol (75 mL), benzyl cyanide (1.76 g, 15 mmol) and cinnamonitrile (3.87 g, 30 mmol) were added. The reaction mixture was stirred at 50°C for 8 h and at room temperature for 12 h and was then concentrated to dryness. The oily residue was dissolved in ethanol (50 mL) and precipitated by addition of diethyl ether. The solid thus obtained was purified by recrystallization from ethanol; 66% yield, mp 271–272°C. IR ν: 3464, 3365, 3230, 2236, 2182, 1636, and 1604 cm^{-1}; ^{13}C NMR (acetone-d_6) δ: 35.78 (C-6), 47.47 (C-5), 54.15 (C-3), 56.60 (C-4), 76.18 (C-2), 119.32 and 119.99 (CN), 128.05, 128.21, 128.42, 128.77, 128.93, 129.25 and 130.66 (Co, m, p, aromatics), 136.73, 138.35 and 140.18 (C_{ipso}), and 158.64 (C-1); MS *m/e*: 375 (M^+, 13%), 227 (30), 226 (42), 205 (13), 204 (14), 171 (33), 170 (100), 169 (93), 155 (13), 150 (21), 143 (19), 142 (17), 130 (22), 115 (21), and 77 (16). Anal. calcd. for $C_{26}H_{21}N_3$: C 83.17, H 5.64, N 11.19; found: C 83.10, H 5.79, N 11.02.

Procedure B

To a solution of sodium (69 mg, 3 mmol) in dry methanol (20 mL), 1,2-diphenyl-1,3-propanedicarbonitrile (**1**) (738 mg, 3 mmol) and cinnamonitrile (387 mg, 3 mmol) were added. The reaction mixture was heated at 50°C for 8 h and then poured into ice-water (200 mL). The precipitate thus obtained was filtered and recrystallized from ethanol; 69% yield.

Synthesis of 2,4-dimethyl-1-phenyl-1,3,5-pentanetricarbonitrile (4) and 1-amino-3,5-dimethyl-4-phenylcyclohexene-2,4-dicarbonitrile (3)

Procedure A

To a solution of sodium (920 mg, 40 mmol) in dry methanol (100 mL), benzyl cyanide (2.34 g, 20 mmol) and crotononitrile (2.68 g, 40 mmol) were added. The reaction mixture was stirred at 50°C for 8 h and then concentrated in vacuo. The oily residue thus obtained was dissolved in diethyl ether (100 mL) and washed with water (3 × 50 mL). The organic phase was

Can. J. Chem. Downloaded from www.nrcresearchpress.com by 80.90.12.36 on 09/08/12
For personal use only.

Table 1. Crystal data, data collection, and structure refinement for compounds **1–3**.

	1	2	3
Formula	$C_{17}H_{14}N_2$	$C_{26}H_{21}N_3$	$C_{16}H_{17}N_3$
Crystal size (mm)	0.24 × 0.37 × 0.35	0.32 × 0.31 × 0.23	0.27 × 0.31 × 0.37
Molecular weight	246.116	375.472	251.330
Crystal system	Orthorombic	Monoclinic	Triclinic
Space group	*Pbca*	$P2_1/n$	$P\bar{1}$
Unit cell determination	25 reflections	50 reflections	67 reflections
	(10 < 2θ < 26)	(10 < 2θ < 37)	(13 < 2θ < 90)
a (Å)	17.168(7)	7.743(1)	14.582(1)
b (Å)	21.612(5)	24.420(1)	7.283(1)
c (Å)	7.508(2)	11.164(1)	7.116(1)
α (°)			110.842(3)
β (°)		102.65(1)	85.923(5)
γ (°)			97.81(1)
V (Å^3)	2785.7(7)	2059.7(3)	696.9(2)
D_c (g cm^{-3})	1.1746	1.2108	1.1977
Z	8	4	2
μ (cm^{-1})	0.652	0.671	5.325
F (000)	1040	792	268
λ	0.7107(MoKα)	0.7107(MoKα)	1.5418(CuKα)
Scanning range for θ	2 < θ < 28	2 < θ < 28	2 < θ < 65
Reflections measured	4061	4996	2361
Reflections observed	1363	2701	2227
($I > 2\sigma(I)$ criterion)			
hkl range	0/24, 0/30, 0/10	−10/10, 0/32, 0/14	−17/17, −8/8, 0/8
Final max shift/error	0.1	0.1	0.02
Final *R*	0.078	0.046	0.047
Final R_w	0.091	0.059	0.052

dried ($MgSO_4$) and concentrated under vacuum. The crude product was purified by flash chromatography on a silica gel column (diameter 6 cm) (hexane – ethyl acetate, 3:1) affording first **4**; 6% yield, bp (3 Torr; 1 Torr = 133.3 Pa) 167°C. IR ($CHCl_3$) ν: 2245, 2185, 1494, 1455, and 1422 cm^{-1}; ^{1}H NMR (CD_3CN) δ: 1.11 (d, 3H, CH_3, J = 6.60 Hz), 1.17 (d, 3H, CH_3, J = 6.60 Hz), 2.26–2.56 (m, 5H, aliphatics), 4.04 (d, 1H, H-1, J = 6.60 Hz), and 7.36–7.47 (m, 5H, aromatics); MS *m/e*: 251 (M^+, 15%), 211 (11), 184 (30), 183 (46), 156 (15), 144 (79), 143 (69), 142 (19), 128 (17), 117 (89), 116 (69), 115 (55), 108 (100), 91 (19), 90 (14), 89 (25), and 77 (23). Anal. calcd. for $C_{16}H_{17}N_3$: C 76.46, H 6.82, N 16.72; found: C 76.81, H 6.70, N 17.01.

On continuing elution with the same mixture of solvents a second product **3** was obtained, and was recrystallized from ethanol; 8% yield, mp 203–204°C. IR ν: 3432, 3347, 3243, 2237, 2187, and 1654 cm^{-1}; ^{1}H NMR (acetone-d_6) δ: 0.71 (d, 3H, CH_3-C5, $J_{Me,b}$ = 6.36 Hz), 0.98 (d, 3H, CH_3-C3, $J_{Me,a}$ = 6.79 Hz), 2.39 (ddd, 1H, **Hd**, $J_{c,d}$ = −17.68 Hz, $J_{b,d}$ = 4.95 Hz, $J_{a,d}$ = 0.98 Hz), 2.61 (m, 1H, **Hb**), 2.64 (m, 1H, **Hc**, $J_{b,c}$ = 12.06 Hz, $J_{a,c}$ = 2.20 Hz), 2.96 (m, 1H, **Ha**), 5.62 (br s, 2H, NH_2), and 7.35–7.55 (m, 5H aromatics); ^{13}C NMR (acetone-d_6) δ: 16.85 (CH_3-C3), 17.44 (CH_3-C5), 35.35 (C-6), 36.25 (C-5), 39.85 (C-3), 56.02 (C-4), 76.84 (C-2), 118.76 and 119.45 (CN), 128.29, 128.89 and 129.85 (Co, m, p aromatics), 138.16 (C_{ipso}), and 156.95 (C-1).

Procedure B

To a suspension of 80% sodium hydride (1.2 g, 40 mmol) in anhydrous DMF (50 mL), benzyl cyanide (2.34 g, 20 mmol) and crotononitrile (2.68 g, 40 mmol) were added. The mixture was stirred at room temperature for 48 h and then the solvent was removed in vacuo. The residue thus obtained was treated with diethyl ether to give a solid that was filtered and recrystallized from ethanol; 41% yield.

Results and discussion

Description of the structure of 1,2-diphenyl-1,3-propanedicarbonitrile (1)

The crude product of the reaction is a diastereomeric racemic mixture arbitrarily designated α and β (diastereomeric ratio (^{1}H NMR) α:β ca. 65:35). The assignment of relative configurations to the diastereomeric racemates α (1*R*,2*S*; 1*S*,2*R*) and β (1*R*,2*R*; 1*S*,2*S*) was performed by X-ray diffraction of a monocrystal of the α diastereomer obtained by recrystallization of the crude diastereomeric mixture from propan-2-ol.

X-ray analysis

Figure 1 displays a view of the molecule with atomic numbering. Selected bond lengths, bond angles, and torsion angles are shown in Table 2. See Table 8 for coordinates and thermal parameters. Successive isotropic and anisotropic refinement cycles showed large temperature factor values for atoms C3, N3, N5, C23, and C24, which suggests a certain disorder; this may explain the high values of the *R* factors. All lengths and angles have normal values, except for the distance C24—C25,

Fig. 1. Molecular plot of **1** showing the atom numbering with displacement ellipsoids drawn (17) at the 50% probability level.

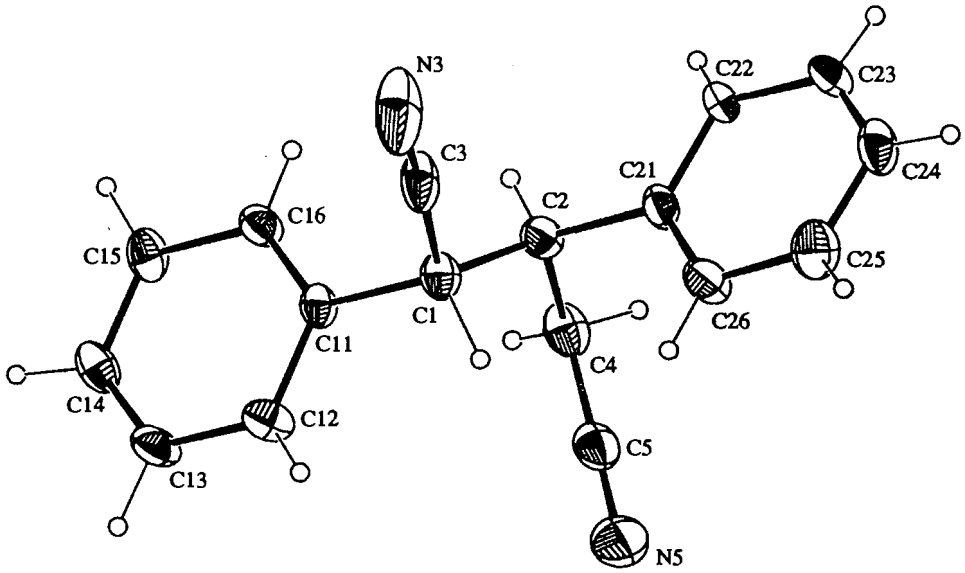

Table 2. Selected bond lengths (Å), bond angles (deg), and torsion angles (deg) for **1**.

(*a*) Bond lengths

C1—C2	1.532(9)	C2—C21	1.547(8)
C1—C3	1.458(10)	C3—C21	1.547(8)
C1—C11	1.545(8)	C3—N3	1.132(13)
C2—C4	1.528(10)	C5—N5	1.156(13)

(*b*) Bond angles

C3-C1-C21	110.0(5)	C2-C4-C5	112.9(6)
C2-C1-C11	113.6(5)	C4-C5-N5	178.1(8)
C1-C2-C21	111.4(5)	C1-C11-C16	117.5(5)
C1-C2-C4	111.6(5)	C1-C11-C12	122.5(5)
C4-C2-C21	111.5(5)	C2-C21-C26	118.5(5)
C1-C3-N3	176.9(8)	C2-C21-C22	122.4(5)

(*c*) Torsion angles

C3-C1-C11-C12	66.8(8)	C11-C1-C2-C4	−56.0(7)
C2-C1-C11-C12	−56.1(8)	C1-C2-C21-C22	45.6(8)
C3-C1-C11-C16	−112.4(6)	C1-C2-C21-C26	−135.5(6)
C2-C1-C11-C16	124.7(6)	C1-C2-C4-C5	−57.1(8)
C3-C1-C2-C21	55.4(7)	C4-C2-C21-C22	−79.8(8)
C3-C1-C2-C4	−179.2(6)	C4-C2-C21-C26	99.1(7)
C11-C1-C2-C21	178.6(5)	C21-C2-C4-C5	68.2(8)

which is shorter than the expected value. The molecule consists of a central chain with two cyano groups and two phenyl rings attached to it. The torsion angles around C1—C2 are C3-C1-C2-C4 −179.2 (6)° and C11-C1-C2-C21 178.6 (5)°. The phenyl rings, which form an angle of 11.4(2)° between them, are above and below the central chain, C11 being −1.175(6) Å and C21 at 1.183(6) Å out of the plane formed by C3-C1-C2-C4. There are no other intermolecular forces than van der Waals.

Spectral properties

The IR spectrum shows the C≡N stretching frequency at 2242 (α) and 2243 (β) cm^{-1}. The ^1H NMR chemical shifts and splitting patterns are also consistent with the suggested structure. The aliphatic protons appear as a four-spin ABCM system, which was analysed by means of the LAOCOON III program (19). The magnetic parameters deduced from this analysis are shown in Table 3.

Can. J. Chem. Downloaded from www.nrcresearchpress.com by 80.90.12.36 on 09/08/12
For personal use only.

Table 3. ^{1}H NMR parameters for the diastereomeric racemates of (±)-1,2-diphenyl-1,3-propanedicarbonitrile (**1**).

	Chemical shifts, δ (ppm)			Coupling constants, *J* (Hz)	
	α isomer	β isomer		α isomer	β isomer
H-**a**	4.29 ± 0.02	4.19 ± 0.01	**Ha-Hb**	7.91 ± 0.02	6.50 ± 0.02
H-**b**	3.39 ± 0.02	3.47 ± 0.01	**Ha-Hc**	0.72 ± 0.02	0.34 ± 0.02
H-**c**	2.79 ± 0.02	2.97 ± 0.01	**Ha-Hd**	0.65 ± 0.02	0.62 ± 0.03
H-**d**	2.65 ± 0.02	2.85 ± 0.01	**Hb-Hc**	6.47 ± 0.02	9.51 ± 0.03
Ph[a]	7.09–7.23 (m, 4H)	7.15–7.26 (m, 4H)	**Hb-Hd**	7.02 ± 0.02	5.49 ± 0.03
	7.26–7.46 (m, 6H)	7.32–7.36 (m, 6H)	**Hc-Hd**	−17.01 ± 0.02	−16.97 ± 0.02

[a]Directly measured from the spectra.

Table 4. Selected bond lengths (Å), bond angles (deg), and torsion angles (deg) for **2**.

(*a*) Bond lengths

C1—C2	1.581(3)	C3—C21	1.530(3)
C1—C6	1.523(3)	C4—C5	1.508(3)
C1—C7	1.526(3)	C5—C6	1.364(3)
C2—C3	1.565(3)	C5—N27	1.348(3)
C2—C13	1.542(3)	C6—C28	1.428(3)
C2—C19	1.485(4)	C19—N20	1.132(4)
C3—C4	1.527(4)	C28—N29	1.155(3)

(*b*) Bond angles

C6-C1-C7	111.7(2)	C2-C3-C4	110.4(2)
C2-C1-C7	112.0(2)	C4-C3-C21	110.6(2)
C2-C1-C6	112.2(2)	C3-C4-C5	112.1(2)
C1-C2-C19	108.4(2)	C4-C5-N27	114.4(2)
C1-C2-C13	110.2(2)	C4-C5-C6	120.3(2)
C1-C2-C3	107.3(2)	C6-C5-N27	125.2(2)
C13-C2-C19	110.1(2)	C1-C6-C5	125.5(2)
C3-C2-C19	109.2(2)	C5-C6-C28	119.0(2)
C3-C2-C13	111.5(2)	C1-C6-C28	115.4(2)
C2-C3-C21	115.9(2)	C2-C19-N20	179.5(3)
		C6-C28-N29	176.5(3)

(*c*) Torsion angles

C6-C1-C2-C3	40.3(2)	C2-C1-C7-C12	89.8(3)
C1-C2-C3-C4	−64.7(2)	C1-C2-C13-C14	117.4(2)
C2-C3-C4-C5	53.5(3)	C1-C2-C13-C18	−63.5(3)
C3-C4-C5-C6	−17.6(3)	C3-C2-C13-C14	−123.5(2)
C4-C5-C6-C1	−6.1(4)	C3-C2-C13-C18	55.6(3)
C2-C1-C6-C5	−6.7(3)	C2-C3-C21-C22	−114.0(3)
C6-C1-C7-C8	36.6(3)	C2-C3-C21-C26	70.2(3)
C2-C1-C7-C8	−90.3(3)	C4-C3-C21-C22	119.4(3)
C6-C1-C7-C12	−143.3(2)	C4-C3-C21-C26	−56.4(3)

Description of the structure of 1-amino-3,4,5-triphenylcyclohexene-2,4-dicarbonitrile (2)

Recrystallizations from ethanol of the crude reaction afforded a single diastereomer whose relative configuration (3*S*,4*S*,5*R*; 3*R*,4*R*,5*S*) was determined by X-ray diffraction.

X-ray analysis

Selected bond lengths, bond angles, and torsion angles are collected in Table 4. See Table 9 for coordinates and thermal parameters. Figure 2 displays a view of the molecule with atomic numbering. The delocalization between the donor N27 and the acceptor cyano group is reflected in the molecular dimensions: the C5—C6 distance of 1.364(3) Å is significantly longer than the C=C bond in ethylene (1.336(2) Å) (20) and in unsubstituted cyclohexene (1.335(3) Å) (21); there is a corresponding shortening of the C5—N27 (1.348(4) Å) bond rela-

Can. J. Chem. Downloaded from www.nrcresearchpress.com by 80.90.12.36 on 09/08/12
For personal use only.

Fig. 2. Molecular plot of **2** showing the atom numbering with displacement ellipsoids drawn (17) at the 50% probability level.

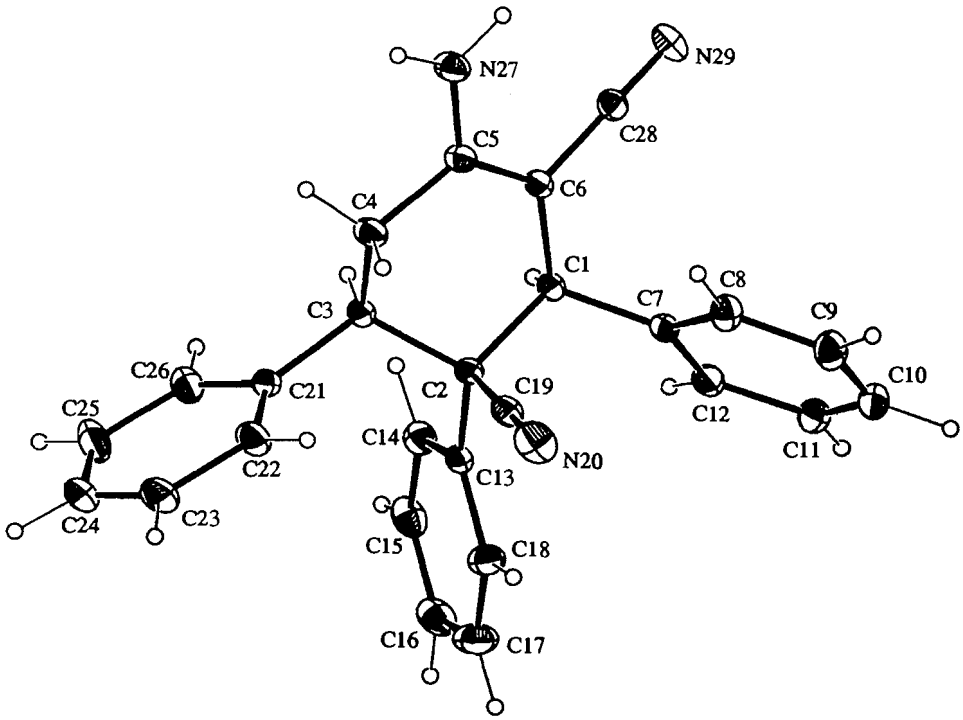

Table 5. Geometry of intra- and intermolecular hydrogen bonds for **2**.

A—B.....C	AB	BC	AC	ABC
C14—H14.....N20(0)	0.99(4)	2.75(4)	3.433(4)	126(3)
C4—H42.....N29(1)	1.00(4)	2.60(3)	3.253(4)	123(3)
C9—H9.....N27(2)	1.03(4)	2.59(4)	3.458(4)	143(3)
N27—H271.....N29(1)	0.90(4)	2.41(3)	3.257(3)	156(3)
N27—H272.....N20(3)	0.93(4)	2.43(4)	3.171(4)	136(3)

Symmetry code:
(0) *X*, *Y*, *Z*
(1) $+X - 1/2, -Y + 1/2, +Z - 1/2$
(2) $+X + 1, +Y, +Z$
(3) $+X - 1/2, -Y + 1/2, +Z + 1/2$

tive to the normal C(sp^2)—N (1.426 Å) bond (22). The lengthening of the C1—C2 and C2—C3 bonds is a consequence of intramolecular interactions (23) between the neighbouring groups attached to the carbon atoms in positions 1, 2, and 3. The steric hindrance is alleviated by the molecule taking up a sofa conformation (see ring torsional angles in Table 4); the phenyl groups at C2 and C3 are in an equatorial position and the one at C1 in a quasi-equatorial orientation while the cyano group at C2 is in an axial orientation. H1 and H41 are in quasi-axial, H3 in axial, and H42 in quasi-equatorial positions. There are two weak N...N hydrogen bonds (Table 5) (24, 25). There are one intramolecular (C14—H14...N20) and two intermolecular (C4—H42...N29, C9—H9...N27) short contacts that can reasonably be described as hydrogen bonds according to Taylor and Kennard (26). The molecules are held together by this network of hydrogen bonds and by van der Waals forces.

Spectroscopic data

The IR spectrum shows the N-H stretching frequency at 3464, 3365, and 3230 cm^{-1}, and the C≡N stretching frequency at 2236 (unconjugated) and 2182 (conjugated) cm^{-1}. The 300 MHz spectrum of compound **2** was analyzed iteratively (19) and the best computed data of chemical shifts and coupling constants are given in Table 6. The values of $^3J_{bc}$ and $^3J_{bd}$ are in agreement with those calculated by application of the empirical equation of Haasnoot et al. (27) for the vicinal torsion angles expected for an axial–quasi-axial and axial–quasi-equatorial relationship between Hb–Hc and Hb–Hd, respectively. The magnitude of the homoallylic coupling constants ($^5J_{ad} < 1$Hz, $^5J_{ac} > 1$Hz) indicate that protons **a** and **c** are in a quasi-axial and **d** in a quasi-equatorial orientation. The assignment of carbon resonances has been made on the basis of the proton–carbon shift correlation spectrum.

Can. J. Chem. Downloaded from www.nrcresearchpress.com by 80.90.12.36 on 09/08/12
For personal use only.

Table 6. ^{1}H NMR parameters for the 1-amino-3,4,5-triphenyl-cyclohexene-2,4-dicarbonitrile (**2**).

	Chemical shifts δ (ppm)		Coupling constants *J* (Hz)
H-**a**	4.44 ± 0.01	**Ha**-**Hc**	1.88 ± 0.01
H-**b**	4.09 ± 0.01	**Ha**-**Hd**	0.73 ± 0.01
H-**c**	3.30 ± 0.01	**Hb**-**Hc**	12.48 ± 0.01
H-**d**	2.86 ± 0.01	**Hb**-**Hd**	4.74 ± 0.01
NH_2[a]	5.90 (br s)	**Hc**-**Hd**	−17.62 ± 0.01
Ph[a]	6.90–7.40 (m)		

[a]Directly measured from the spectrum.

Fig. 3. Molecular plot of **3** showing the atom numbering with displacement ellipsoids drawn (17) at the 50% probability level.

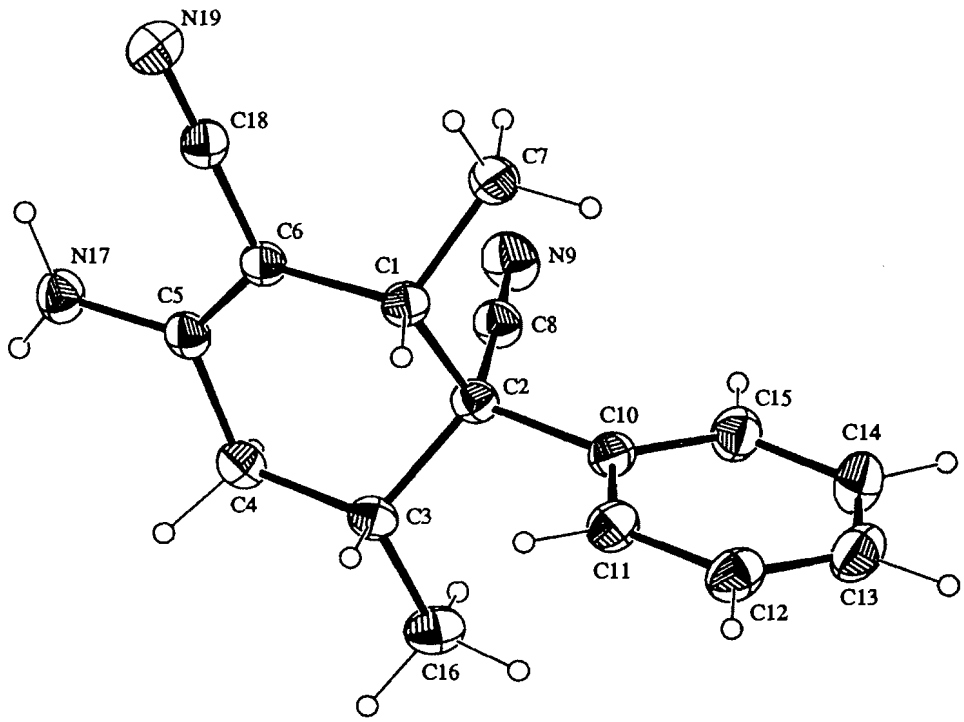

Can. J. Chem. Downloaded from www.nrcresearchpress.com by 80.90.12.36 on 09/08/12
For personal use only.

Description of the structure of 1-amino-3,5-dimethyl-4-phenylcyclohexene-2,4-dicarbonitrile (3)

The crude product of the reaction is a diastereomeric racemic mixture that affords a single diastereomer on recrystallizing from ethanol. The assignment of the relative configuration (3*R*,4*R*,5*R*; 3*S*,4*S*,5*S*) to this diastereomer was performed by X-ray diffraction.

X-ray analysis

Selected bond lengths, bond angles, and some torsion angles are collected in Table 7. Coordinates and thermal parameters are shown in Table 10. Figure 3 displays a view of the molecule with atomic numbering. As in the cyclohexene **2** there is a delocalization between the amino and the cyano groups: the double bond C5═C6 in the cyclohexene is longer than in ethylene and unsubstituted cyclohexene while C5—N17 and C6—C18 are shorter than standard values but, in both cases, very similar to the values found in **2**. However the distances C1—C2 and C2—C3 have normal values because of the less bulky substituents. The steric hindrance due to the substituents at C2 causes lengthening of the C2—C8 bond. Here also, as a consequence of the steric hindrance, the cyclohexene **3** adopts a sofa conformation (see ring torsional angles in Table 7). The methyl and phenyl groups at C2 and C3 are positioned equatorially and the methyl group at C1 is in a quasi-equatorial orientation. There are two hydrogen bonds between the amino and the cyano groups. The two hydrogen atoms of the amine group are involved in intermolecular hydrogen bonding with the N atoms of the cyano groups. The geometry of these hydrogen bonds is as follows: (*i*) N17...N(19(1) 3.053 (2) Å, H171...N19(1) 2.16(3) Å, N17—H171...N19(1) 161(2)° and (*ii*) N17...N9(2) 3.225(2) Å, H172...N9(2) 2.56(3) Å, N17—

Can. J. Chem. Downloaded from www.nrcresearchpress.com by 80.90.12.36 on 09/08/12
For personal use only.

Table 7. Selected bond lengths (Å), bond angles (deg), and torsion angles (deg) for **3**.

(*a*) Bond lengths

C1—C2	1.541(2)	C3—C16	1.506(2)
C1—C6	1.519(2)	C4—C5	1.486(2)
C1—C7	1.529(2)	C5—C6	1.359(2)
C2—C3	1.556(2)	C5—N17	1.351(2)
C2—C8	1.487(2)	C6—C18	1.406(2)
C2—C10	1.532(2)	C8—N9	1.142(3)
C3—C4	1.528(2)	C18—N19	1.145(2)

(*b*) Bond angles

C6-C1-C7	111.5(1)	C4-C3-C16	110.4(1)
C2-C1-C7	112.2(1)	C3-C4-C5	115.7(1)
C2-C1-C6	110.3(1)	C4-C5-N17	115.6(1)
C1-C2-C10	110.6(1)	C4-C5-C6	120.6(1)
C1-C2-C8	107.1(1)	C6-C5-N17	123.8(2)
C1-C2-C3	108.3(1)	C1-C6-C5	124.6(1)
C8-C2-C10	110.6(1)	C5-C6-C18	117.6(1)
C3-C2-C10	111.3(1)	C1-C6-C18	117.7(2)
C3-C2-C8	108.7(1)	C2-C8-N9	177.4(2)
C2-C3-C16	113.7(1)	C2-C10-C15	119.5(1)
C2-C3-C4	110.7(1)	C2-C10-C11	122.4(1)
		C6-C18-N19	179.0(2)

(*c*) Torsion angles

C2-C1-C6-C18	−159.3(1)	C3-C2-C10-C15	−61.2(2)
C7-C1-C6-C5	147.9(1)	C1-C2-C3-C4	61.8(1)
C2-C1-C6-C5	22.5(2)	C1-C2-C3-C16	−173.3(1)
C7-C1-C6-C18	−33.9(2)	C8-C2-C3-C16	70.6(2)
C6-C1-C2-C10	−173.9(1)	C8-C2-C3-C4	−54.3(1)
C6-C1-C2-C8	65.4(1)	C10-C2-C3-C16	−51.5(2)
C6-C1-C2-C3	−51.7(1)	C10-C2-C3-C4	−176.4(1)
C7-C1-C2-C10	61.1(2)	C2-C3-C4-C5	−40.1(2)
C7-C1-C2-C8	−59.6(2)	C16-C3-C4-C5	−166.8(1)
C7-C1-C2-C3	−176.7(1)	C3-C4-C5-C6	8.9(2)
C1-C2-C10-C11	−120.5(2)	C3-C4-C5-N17	−172.3(1)
C1-C2-C10-C15	59.3(2)	C4-C5-C6-C1	0.2(2)
C8-C2-C10-C11	−2.0(2)	C4-C5-C6-C18	−178.0(1)
C3-C2-C10-C11	119.0(2)	N17-C5-C6-C1	−178.5(1)
C8-C2-C10-C15	177.8(1)	N17-C5-C6-C18	3.3(2)

H172...N9(2) 131(2)°. Symmetry code: (1) $-x+1, -y+1, -z+1$; (2) $-x+1, -y, -z$. The molecules are held together by these hydrogen bonds and by van der Waals forces.

Supplementary data for compounds **1–3** are available.[3]

Spectroscopic data

The IR spectrum shows the N-H stretching frequency at 3432, 3347, and 3243 cm^{-1}. The unconjugated and conjugated C≡N stretching appear at 2237(w) and 2187(s) cm^{-1}, respectively.

^1H and ^{13}C NMR

The aliphatic protons appear as a ten-spin complex $ABCDX_3Y_3$ system. The assignment of proton resonances has been made on the basis of the proton–proton shift correlation spectrum and double resonance experiments. In acetone at 300 MHz the signals due to **Ha**, **Hd**, CH_3-C3, and CH_3-C5 appear well differentiated. Overlapping resonances between **Hb** and **Hc** signals were observed. The assignment of all signals was made feasible by a homonuclear 2D COSY 45° experiment ($CDCl_3$). The multiplet at 2.96 ppm (**Ha**) displays a strong correlation with the doublet at 0.98 ppm (CH_3-C3) and a weak correlation (homoallylic coupling) with the signals centered at 2.39 (**Hd**) and 2.64 (**Hc**) ppm. The multiplet at 2.61 ppm (**Hb**)

[3] X-ray data for compounds **1–3** have been deposited as supplementary material and can be purchased from: The Depository of Unpublished Data, Document Delivery, CISTI, National Research Council Canada, Ottawa, Canada K1A 0S2. Tables of atomic coordinates and of bond lengths and angles have also been deposited with the Cambridge Crystallographic Data Centre, and can be obtained on request from The Director, Cambridge Crystallographic Data Centre, University Chemical Laboratory, 12 Union Road, Cambridge, CB2 1EZ, U.K.

Can. J. Chem. Downloaded from www.nrcresearchpress.com by 80.90.12.36 on 09/08/12
For personal use only.

Table 8. Coordinates and thermal parameters as $U_{eq} = (1/3).\text{sum}[U_{ij}.a_i^*.a_j^*.a_i.a_j.\cos(a_i,a_j)].10^3$ for compound **1**.

Atom	x	y	z	U_{eq}
C1	−0.1052(3)	0.1132(3)	0.4251(8)	56(2)
C2	0.4388(3)	0.3847(3)	0.3973(8)	56(2)
C3	−0.0586(4)	0.0797(4)	0.2943(10)	81(3)
C4	−0.1079(3)	0.1492(4)	0.7458(9)	69(3)
C5	−0.1281(4)	0.2112(4)	0.6953(9)	69(3)
C11	0.3129(3)	0.0841(3)	0.0608(8)	49(2)
C12	0.3010(3)	0.4736(3)	0.4951(8)	57(2)
C13	−0.2742(3)	0.0010(3)	0.5113(8)	60(2)
C14	0.1644(3)	0.0356(4)	0.0503(8)	61(2)
C15	−0.3233(3)	0.0934(4)	0.3840(9)	65(3)
C16	−0.2499(3)	0.1190(3)	0.3792(8)	61(2)
C21	0.0210(3)	0.3566(3)	0.0802(8)	53(2)
C22	0.0342(3)	0.1965(4)	0.4834(9)	69(3)
C23	0.1093(4)	0.2201(4)	0.4686(10)	80(3)
C24	0.1703(3)	0.1907(4)	0.5541(11)	74(3)
C25	0.1564(3)	0.1385(4)	0.6470(11)	71(3)
C26	0.0823(3)	0.1149(3)	0.6619(10)	65(2)
N3	0.4749(4)	0.0515(5)	0.3072(13)	168(4)
N5	−0.1439(4)	0.2607(4)	0.6496(11)	102(3)

Table 9. Coordinates and thermal parameters as $U_{eq} = (1/3).\ \text{sum}[U_{ij}.a_i^*.a_j^*.a_i.a_j.\cos(a_i,\ a_j)].10^3$ for compound **2**.

Atom	x	y	z	U_{eq}
C1	0.5473(3)	0.3736(1)	0.4491(2)	31(1)
C2	0.4973(3)	0.3754(1)	0.3034(2)	32(1)
C3	0.3011(3)	0.3551(1)	0.2627(2)	37(1)
C4	0.2866(4)	0.2951(1)	0.2980(2)	46(1)
C5	0.3631(4)	0.2854(1)	0.4331(2)	37(1)
C6	0.4747(3)	0.3229(1)	0.4999(2)	33(1)
C7	0.7469(3)	0.3796(1)	0.4988(2)	35(1)
C8	0.8566(4)	0.3338(1)	0.5192(3)	45(1)
C9	1.0388(4)	0.3396(2)	0.5650(3)	57(1)
C10	1.1116(4)	0.3905(2)	0.5907(3)	60(1)
C11	1.0050(5)	0.4364(2)	0.5719(3)	58(1)
C12	0.8215(4)	0.4312(1)	0.5247(3)	45(1)
C13	0.5198(3)	0.4339(1)	0.2578(2)	35(1)
C14	0.6393(4)	0.4464(1)	0.1864(3)	49(1)
C15	0.6537(5)	0.5001(2)	0.1459(3)	67(2)
C16	0.5492(5)	0.5409(1)	0.1756(3)	63(1)
C17	0.4299(5)	0.5288(1)	0.2463(3)	55(1)
C18	0.4145(4)	0.4757(1)	0.2872(3)	45(1)
C19	0.6150(4)	0.3369(1)	0.2559(2)	40(1)
N20	0.7043(4)	0.3077(1)	0.2189(2)	62(1)
C21	0.2136(4)	0.3640(1)	0.1271(2)	41(1)
C22	0.0728(4)	0.4002(2)	0.0980(3)	58(1)
C23	−0.0200(5)	0.4067(2)	−0.0236(3)	74(2)
C24	0.0281(5)	0.3766(2)	−0.1152(3)	68(2)
C25	0.1691(5)	0.3410(2)	−0.0884(3)	63(1)
C26	0.2630(4)	0.3348(1)	0.0337(3)	52(1)
N27	0.3030(3)	0.2398(1)	0.4783(2)	48(1)
C28	0.5201(4)	0.3177(1)	0.6308(3)	38(1)
N29	0.5523(4)	0.3159(1)	0.7365(2)	52(1)

Table 10. Coordinates and thermal parameters as $U_{eq} = (1/3).\ \text{sum}[U_{ij}.a_i^*.a_j^*.a_i.a_j.\cos(a_i,\ a_j)].10^4$ for compound **3**.

Atom	x	y	z	U_{eq}
C1	0.7311(1)	0.1082(3)	0.3801(3)	487(7)
C2	0.7450(1)	−0.0859(3)	0.2033(2)	470(7)
C3	0.6632(1)	−0.2440(3)	0.2106(3)	504(7)
C4	0.5704(1)	−0.1810(3)	0.1816(3)	546(7)
C5	0.5605(1)	0.0328(3)	0.2878(3)	496(7)
C6	0.6337(1)	0.1616(3)	0.3769(3)	482(7)
C7	0.8052(1)	0.2774(3)	0.3788(3)	652(9)
C8	0.7409(1)	−0.0440(3)	0.0152(3)	541(8)
N9	0.7351(1)	−0.0081(3)	−0.1278(3)	737(9)
C10	0.8388(1)	−0.1531(3)	0.2180(3)	507(7)
C11	0.9061(1)	−0.1769(3)	0.0668(3)	677(9)
C12	0.9905(2)	−0.2364(4)	0.0876(4)	847(12)
C13	1.0082(2)	−0.2743(4)	0.2558(4)	811(11)
C14	0.9417(2)	−0.2530(3)	0.4058(4)	735(10)
C15	0.8576(1)	−0.1932(3)	0.3874(3)	616(8)
C16	0.6741(2)	−0.4485(3)	0.0591(3)	674(9)
N17	0.4746(1)	0.0837(3)	0.2832(2)	619(7)
C18	0.6185(1)	0.3604(3)	0.4802(3)	534(8)
N19	0.6051(1)	0.5203(3)	0.5648(3)	708(8)

Fig. 4. Notation for aliphatic hydrogens of cyclohexenes **2** and **3**.

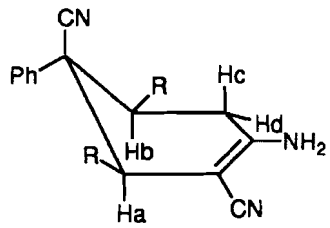

correlates strongly with the doublet at 0.71 ppm (CH_3-C5) and, finally, the multiplets at 2.61 (**Hb**) and 2.64 (**Hc**) ppm correlate with the multiplet at 2.39 ppm (**Hd**). To strengthen these assumptions double resonance (DR) experiments were performed in acetone-d_6 at 300 MHz. On saturating the CH_3-C3 signal at 0.98 ppm the multiplet at 2.96 ppm collapses to an apparent double doublet. By irradiation of the CH_3-C5 signal at 0.71 ppm the multiplet at 2.61 collapses to a double doublet. On saturating the **Ha** signal at 2.96 ppm the multiplet at 2.39 collapses to a double doublet and the doublet at 0.98 collapses to a singlet. Finally, by irradiation of the **Hd** signal at 2.39 ppm the multiplet at 2.96 collapses to an apparent quartet and the multiplets centered at 2.61 and 2.64 ppm simplify. As in the cyclohexene **2**, the magnitude of the homoallylic coupling ($^5J_{ad}$ and $^5J_{ac}$) attests that protons **a** and **c** are in a quasi-axial and **d** in a quasi-equatorial orientation.

The assignment of carbon resonances has been made on the basis of APT and proton–carbon shift correlation spectra.

Acknowledgments

This work was supported by the Comunidad Autónoma de Madrid (Spain) Grant C061/91.

References

1. M.R.S. Weir and J.B. Hyne. Can. J. Chem. **43**, 772 (1965).
2. N. Martín-León, M. Quinteiro, C. Seoane, and J.L. Soto. Liebigs Ann. Chem. 101 (1990).
3. J.K. Williams. J. Org. Chem. **28**, 1054 (1963).
4. M.R.S. Weir and J.B. Hyne. Can. J. Chem. **41**, 2905 (1963).
5. M.R.S. Weir and J.B. Hyne. Can. J. Chem. **42**, 1443 (1964).
6. K. Gewald and W. Schill. J. Prakt. Chem. **313**, 678 (1971).
7. J. Mirek, M. Adamczyk, and M. Mokrosz. Synthesis, 296 (1980).
8. K. Takabe, S. Ohkawa, and T. Katagiri. Synthesis, 358 (1981).
9. F.A.L. Anet. *In* The conformational analysis of cyclohexenes, cyclohexadienes and related hydroaromatic compounds. *Edited by* P.W. Rabideau. VCH Publishers, New York. 1989. pp. 3–45.
10. K.B. Lipkowitz. *In* The conformational analysis of cyclohexenes, cyclohexadienes and related hydroaromatic compounds. *Edited by* P.W. Rabideau. VCH Publishers, New York. 1989. pp. 213–265.
11. C.J. Gilmore. MITHRIL. A computer program for the automatic solution of crystal structures from X-ray data. Dept. of Chemistry, University of Glasgow, Glasgow, Scotland. 1983.
12. P. Main, S.J. Fiske, S.E. Hull, L. Lessinger, G. Germain, J.P. Declercq, and M.M. Woolfson. MULTAN 80. A system of computer programs for the automatic solution of crystal structures from X-ray diffraction data. Univs. of York, England, and Louvain, Belgium. 1980.
13. M. Martínez-Ripoll and F.H. Cano. PESOS program, Instituto Rocasolano, Consejo Superior de Investigaciones Cientificas, Serrano, Madrid, Spain. 1975.
14. International tables for X-ray crystallography. Vol. IV. Kynoch Press, Birmingham, England. 1974.
15. J.M. Stewart, F.A. Kundell, and J.C. Baldwin. The XRAY 70 system. Computer Science Center, University of Maryland, College Park, Md., U.S.A. 1970.
16. M.A. Nardelli. Comput. Chem. **7**, 95 (1983).
17. S.R. Hall and J.M. Stewart (*Editors*). Xtal 3.0 reference manual. Univs. of Western Australia, Australia, and Maryland, U.S.A. 1990.
18. J. Boyer, R.J.P. Corriu, R. Perz, and C. Reye. Tetrahedron, **39**, 117 (1983).
19. S. Castellano and A.A. Bothner-By. J. Chem. Phys. **41**, 3863 (1964).
20. L.S. Bartell, E.A. Roth, C.D. Hollowell, K. Kuchitsu, and J.E. Young. J. Chem. Phys. **42**, 2683 (1965).
21. J.F. Chiang and S.H. Bauer. J. Am. Chem. Soc. **91**, 1898 (1969).
22. H.L. Ammon, P.H. Mazzochi, M.C. Regan, and E. Colicelli. Acta Crystallogr. Sect. C: Cryst. Struct. Commun. **C45**, 1722 (1989).
23. A.J. Tenon, N'Dédé Erby, A. Voglozin, E. Degny, and T.Y. N'Guessan. Acta Crystallogr. Sect. C: Cryst. Struct. Commun. **C45**, 622 (1989).
24. J. Kozisek, M. Dunaj-Jurco, U. Grobe, and H. Kohler. Acta Crystallogr. Sect. C: Cryst. Struct. Commun. **C46**, 2422 (1990).
25. K. Yamaguchi, A. Ohsawa and Ch. Kawabata. Acta Crystallogr. Sect. C: Cryst. Struct. Commun. **C46**, 1749 (1990).
26. R. Taylor and O. Kennard. J. Am. Chem. Soc. **104**, 5063 (1982).
27. C.A.G. Haasnoot, F.A.A.M. de Leeuw, and C. Altona. Tetrahedron, **36**, 2783 (1980).

Can. J. Chem. Downloaded from www.nrcresearchpress.com by 80.90.12.36 on 09/08/12
For personal use only.

A study of the Reformatsky reaction on formylcoumarins

Lakshmi Narayan Dutta, Manju Bhattacharyya, and Asoke Kumar Sarkar

Abstract: The reactions of bromozinc enolate reagents on formylcoumarins (**1**, **2**) afforded spiro-γ-lactones (**15–18**), furan derivatives (**13**, **14**), and coumarinylcarbinols (**3**, **4**) as highly unusual products along with the expected β-hydroxyesters (**5–12**). Stereochemical features of some of these products turned out to be highly informative and were unambiguously corroborated.

Key words: formylcoumarins, unusual Reformatsky products, stereochemistry.

Résumé : Les énolates bromozinciques réagissent sur les formylcoumarines (**1**, **2**) pour donner les β-hydroxyesters attendus (**5–12**) ainsi que des spiro-γ-lactones (**15–18**), des dérivés furaniques (**13**, **14**) et coumarinylcarbinols (**3**, **4**) dont les caractéristiques stéréochimiques, corroborées dans certains cas sans ambiguïté, fournissent d'importantes informations.

Mots clés : formylcoumarines, produits Reformatsky inattendus, stéréochimie.

[Traduit par la rédaction]

Can. J. Chem. Downloaded from www.nrcresearchpress.com by 80.90.12.36 on 09/08/12
For personal use only.

The Reformatsky reaction is of enormous research interest (1, 2) though it has found very limited application to coumarin systems (3). We have recently studied (4) this reaction on coumarinyl methyl ketones in order to assess various selectivities of this versatile reagent for the synthesis of naturally occurring coumarins (5). The success of these investigations prompted us to undertake further study of this reaction on formylcoumarins (1, 2). This ultimately uncovered some highly interesting and uncommon findings, which we wish to report in this communication.

Results

4-Formylcoumarin (**1**) and 4-formyl-7-methoxycoumarin (**2**), prepared through SeO_2 oxidation (6) of the respective 4-methylcoumarins on treatment with the Reformatsky reagents generated as bromozinc enolates from α-bromoesters of acetic, propionic, *n*-butyric, and *iso*-butyric acids in benzene, afforded the expected β-hydroxyesters[2] (**5–12**) in 40% yield.[3] In addition to these products, each reaction afforded the corresponding alcohol (**3**, **4**) as a relatively polar component in 20% yield, presumably formed through the simple reduction of the formyl group in **1** and (or) **2**. This observation is highly unusual under Reformatsky conditions and the reaction pathway most likely proceeds via a SET mechanism (7).

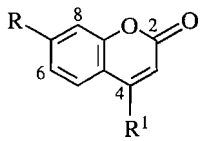

1 R = H; R^1 = CHO
2 R = OMe; R^1 = CHO
3 R = H; R^1 = CH_2OH
4 R = OMe; R^1 = CH_2OH
5 R = H; R^1 = $CH(OH)CH_2CO_2Et$
6 R = OMe; R^1 = $CH(OH)CH_2CO_2Et$
7 R = H; R^1 = $CH(OH)CHMeCO_2Et$
8 R = OMe; R^1 = $CH(OH)CHMeCO_2Et$
9 R = H; R^1 = $CH(OH)CHEtCO_2Et$
10 R = OMe; R^1 = $CH(OH)CHEtCO_2Et$
11 R = H; R^1 = $CH(OH)CMe_2CO_2Et$
12 R = OMe; R^1 = $CH(OH)CMe_2CO_2Et$
19 R = H; R^1 = CH_2OAc
20 R = OMe; R^1 = CH_2OAc

The identity of the above alcohols (**3**, **4**) could be conclusively established through the preparation of authentic samples of **3** and **4** by $NaBH_4$ reduction of **1** and **2**, respectively. These simple monomeric reduction products **3** and **4** could ultimately be converted into their corresponding acetates **19** and **20**, having mp's of 99 and 168°C. Since we failed to detect any pinacol products, viz., CouCH(OH)CH(OH)Cou, in any of the Reformatsky reactions performed, it is reasonable to assume that the initial anion radical produced from **1** and **2** must have free access to a proton source (8), most likely the α-bromoester.

Using the bromozinc enolate generated from ethyl α-bromoacetate, the formylcoumarins (**1**, **2**) afforded the corresponding β-hydroxyesters (**5**, **6**), whose preferred conformation turned out to be **5***a* and **6***a*, respectively, as the β-H of

Received March 30, 1995.

L.N. Dutta,[1] M. Bhattacharyya, and A.K. Sarkar. Department of Chemistry, Jadavpur University, Calcutta 700 032, India.

[1] Author to whom correspondence may be addressed.

[2] These products along with others described, excepting **13***a* and **17**, gave satisfactory C, H analyses and the expected spectral (UV, IR, ^1H NMR and MS) data; with **13***a* and **17**, their UV, IR, and ^1H NMR spectra are consistent with their proposed structures.

[3] All yields reported are calculated on the basis of the recovery (approximately 30%) of the starting material.

Can. J. Chem. Downloaded from www.nrcresearchpress.com by 80.90.12.36 on 09/08/12
For personal use only.

these β-hydroxyesters appeared in their ^{1}H NMR spectra at about δ 5.54 as a doublet of a doublet (J = 4, 8 Hz) in complete agreement with the Karplus equation (9). Further, these preferred conformers are in full conformity with conformational analysis if due contributions of hydrogen bonding and nonbonded steric interaction in all their plausible conformations are taken into consideration (10). Analogously, the β-hydroxyesters (**11**, **12**) obtained from the bromozinc enolate of α-bromo-iso-butyrate may have their preferred conformation as **11***a* and **12***a*.

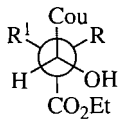

5*a*,**6***a* R = H$_a$; R^1 = H$_b$
11*a*,**12***a* R,R^1 = Me
7*a*,**8***a* R = Me; R^1 = H
7*b*,**8***b* R = H; R^1 = Me
9*a*,**10***a* R = Et; R^1 = H
9*b*,**10***b* R = H; R^1 = Et.

Cou = 4-Coumarinyl/7-methoxy-4-coumarinyl

When bromozinc enolates generated from esters of α-bromopropionic acid and α-bromo-*n*-butyric acid were allowed to react with **1** and **2**, a relatively polar semisolid material was eluted in each case from the column chromatogram. ^{1}H NMR spectra of these semisolids revealed them to be the corresponding β-hydroxyesters (**7**, **9** from **1** and **8**, **10** from **2**), but upon more careful scrutiny of each of their spectra the presence of two different signals for the alcohol methine proton was observed at δ 5.4 and δ 5.0, respectively, in a 1:1 ratio. Not surprisingly, this 1:1 mixture was the diastereomeric *erythro* and *threo* β-hydroxyesters, which have been better referred to as "pref" and "parf" (11). However, what was surprising was the fact that the reaction fails to record any diastereoselectivity, contrary to a number of reports (4, 12).

Fortunately, each of the above mixtures of diastereomeric alcohols (**7**–**10**) could be resolved into their pure components (**7***a*–**10***a* and **7***b*–**10***b*) through extensive column, chromatographic separation, where the respective *erythro* alcohols (**7***a*–**10***a*) migrated out earlier than the corresponding *threo* alcohols (**7***b*–**10***b*). The alcoholic methine proton appeared at ~δ 5.4 (1H, d, J = 4 Hz) in the *erythro* alcohols (**7***a*–**10***a*) and at ~δ 5.0 (1H, d, J = 8 Hz) in the *threo* alcohols (**7***b*–**10***b*). Conformational analysis (10) suggests the preferred conformation of the *erythro* alcohols to be **7***a*–**10***a* and the *threo* alcohols to be **7***b*–**10***b*. This prediction was corroborated by the observed coupling constant of the alcoholic methine protons, which had ^3J values of 4 Hz for **7***a*–**10***a* and 8 Hz for **7***b*–**10***b*, and are in excellent agreement with the J values predicted simply from the Karplus equation (9).

It should be mentioned at this stage that the reaction of bromozinc enolate derived from α-bromo-*n*-butyrate with **1** and **2** afforded relatively nonpolar yellow solids having mp's of 119 and 64°C, respectively, in low yield (~8%). From ^{1}H and ^{13}C NMR spectra (Table 1) as well as 2D COSY (^{1}H–^{1}H) studies (13) these compounds were characterized as furan derivatives **13** and **14**. These furans could be formed through cyclization of diaddition adducts **13***a* and **14***a*, respectively, followed by their unusual dehydrogenation. This was further substantiated by the fact that **13***a* could be detected in trace amounts (^{1}H

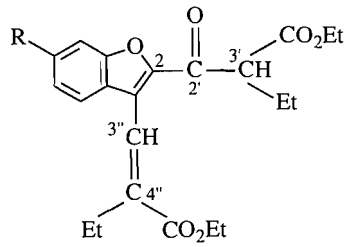

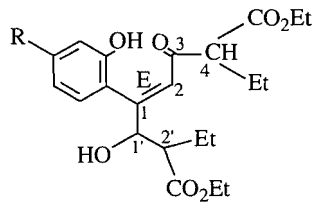

13 R = H
14 R = OMe

13*a* R = H
14*a* R = OMe

NMR spectrum fully consistent with its assigned structure). The configuration of the double bond indicated in the α,β-unsaturated ester moiety in **13** and **14** was initially assigned as *E* due to their presumed formation from the respective β-hydroxyesters (4, 14). Finally NOE (13) studies unequivocally confirmed the *E* configuration of the olefinic double bond in **13** and **14**. In **13** an enhancement in the intensity of the 3″-H at δ 8.56 was noticed on irradiation of the 4″-$CO_2CH_2CH_3$ methylene at δ 4.14. This close proximity in space of 3″-H and the methylene group of 4″-$CO_2CH_2CH_3$ further suggests the preferred conformation of this α,β-unsaturated ester moiety as *s-trans*.

To our pleasant surprise the Reformatsky reaction on **1** and **2**, employing α-bromo-iso-butyrate, afforded a few additional minor products e.g., **15** and **16** from **1** and **17** and **18** from **2**. IR spectra of all these minor products indicated the presence of a highly characteristic absorption of a γ-lactone carbonyl stretching (15) at ~1770 cm^{-1}. This tempted us to assign the presence of a spiro-γ-lactone moiety in all these compounds and, upon careful consideration of the mechanistic aspects of their possible genesis, intermediate **21** was seen as the most plausible precursor. The presence of a relatively shielded methylene group at δ 3.91 (2H, q, J = 7 Hz) of one of the two ethoxycarbonyl groupings in **15** and **18** plausibly suggests a configuration of these two as **15***a* and **18***a* wherein one for the ethoxycarbonyl groups falls directly above the σ-plane of the aromatic nucleus in their most populated preferred conformation. This sort of shielding is not expected if the configuration is represented as **15***b* and **18***b*.

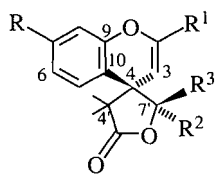

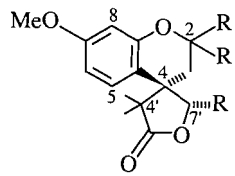

15 R,R^2 = H; R^1,R^3 = CMe$_2$CO$_2$Et
16 R,R^3 = H; R^1,R^2 = CMe$_2$CO$_2$Et
18 R = OMe; R^1,R^3 = CMe$_2$CO$_2$Et; R^2 = H

17 R = CMe$_2$CO$_2$Et

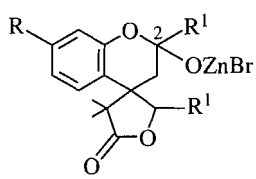

21 R = H, OMe; R^1 = CMe$_2$CO$_2$Et

Moreover, the above assignment of **15***a* and **18***a* is further

Can. J. Chem. Downloaded from www.nrcresearchpress.com by 80.90.12.36 on 09/08/12
For personal use only.

Table 1. ^{13}C NMR spectral assignments of Reformatsky products **13**, **14**, and **18**

Assignment of specific carbon	Chemical shift (δ), nature of carbon (p/s/t/q)		
	13	**14**	**18**
C – 2	x, q[a]	155.9, q	152.9, q
C – 3	x, q	110.4, q	95.9, t
C – 4	130.9, t	121.7, t	49.7, q
C – 5	123.7, t	110.5, t	129.5, t
C – 6	124.2, t	154.7, q	109.7, t
6 – OMe	—	55.5, p	—
C – 7	116.1, t	101.0, t	153.1, q
7 – OMe	—	—	55.3, p
C – 8	x, q	161.9, q	101.3, t
C – 9	x, q	113.4, q	160.0, q
C – 10	—	—	109.0, q
C – 2′	x, q	196.7, q	46.3, q
2′ Me_2	—	—	14.0 and 13.8, p
2′ – $CO_2CH_2CH_3$	—	—	174.7, q; 61.0, s; 20.0, p
C – 3′	56.8, t	56.7, t	—
3′ – CH_2CH_3	19.8, s; 11.8, p	20.2, s; 11.9, p	—
3′ – $CO_2CH_2CH_3$	x, q; 60.2, s; 13.8, p	167.8, q; 60.2, s; 13.9, p	—
C – 3″	126.4, t	127.5, t	—
C – 4′	—	—	51.2. q
4′ Me_2	—	—	21.9 and 22.2, p
C – 4″	x, q	135.0, q	—
4″ – CH_2CH_3	21.9, s; 13.0, p	22.0, s; 13.1, p	—
4″ – $CO_2CH_2CH_3$	x, q; 61.3, s; 14.2, p	169.7, q; 61.3, s; 14.2, p	—
C – 5′	—	—	179.8, q
C – 7′	—	—	84.2, t
8′ CMe_2	—	—	45.6, q; 20.1 and 19.9, p
8′ – $CO_2CH_2CH_3$	—	—	175.4, q; 61.0, s; 22.7, p

[a]x, q: Chemical shifts of such quaternary carbons could not be unambiguously detected.

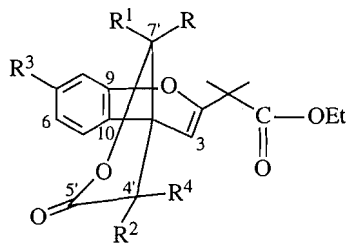

15*a* R,R^3 = H; R^1 = CMe_2CO_2Et; R^2,R^4 = Me
16*a* R^1,R^3 = H; R = CMe_2CO_2Et; R^2,R^4 = Me
18*a* R = H; R^1 = CMe_2CO_2Et; R^3 = OMe; R^2,R^4 = Me
15*b* R,R^1 = Me; R^3,R^4 = H; R^2 = CMe_2CO_2Et
16*b* R,R^1 = Me; R^2,R^3 = H; R^4 = CMe_2CO_2Et
18*b* R,R^1 = Me; R^2 = CMe_2CO_2Et; R^3 = OMe; R^4 = H

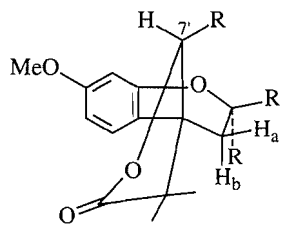

17*a* R = CMe_2CO_2Et

substantiated from the reaction of **1** through the isolation of another spiro-γ-lactone (**16**) in which the relative shielding of the protons of the methylene group in one of the ethoxycarbonyl functions is not observed. In addition, both the lactone methine proton and vinylic methine proton in **16** appeared as a doublet with a *J* value of 4 Hz. This is possible only if the two coupled protons assume a W-type orientation (16), thus demanding the configuration as represented in **16***a*. This type of coupling is not found with **15***a* and **18***a*, in agreement with our proposition. It is interesting to point out at this stage that another spiro-γ-lactone (**17**) was isolated from the reaction of **2**, having an ^1H NMR spectrum in agreement with the configuration as depicted in **17***a*, with a close resemblance to **16***a* from a configurational standpoint. It should be emphasized at this stage that the proposed structures **17***a* and **18***a* are in full agreement with their ^{13}C NMR (Table 1) and 2D COSY (^1H–^1H) spectra (13).

The formation of spiro-γ-lactones (**15***a*, **16***a*, **18***a*) delineated above necessitates the consumption of 3 moles of bromozinc enolate per mole of formylcoumarins (**1**, **2**), and involves a 1,4-addition to the conjugated coumarin carbonyl, along with 1,2-additions to the aldehyde and coumarin carbonyls, via **21** as a plausible intermediate, followed by further usual modifications. The genesis of **17***a* is most likely ratio-

Table 2. Physical data of compounds **3–20**.

Compound	Yield (%)	Melting/boiling point (°C)	Mol. formula	Calcd. C	Calcd. H	Found C	Found H
3	20	138	$C_{10}H_8O_3$	68.18	4.5	68.2	3.91
4	20	187	$C_{11}H_{10}O_4$	64.07	4.85	64.03	3.98
5*a*	33	62	$C_{14}H_{14}O_5$	64.12	5.34	63.94	5.28
6	33	80	$C_{15}H_{16}O_6$	61.64	5.47	60.98	5.49
7*a*	29	110	$C_{15}H_{16}O_5$	65.21	5.79	65.3	5.81
7*b*		115–120/0.3–0.4 Torr					
8*a*	32	114	$C_{16}H_{18}O_6$				
8*b*		139		62.74	5.88	62.75	5.78
9*a*	30	112–117/0.2–0.5 Torr		66.20	6.20	66.3	6.28
9*b*		130–135/0.3–0.6 Torr	$C_{16}H_{18}O_5$				
10*a*	36	135	$C_{17}H_{20}O_6$	63.75	6.25	63.67	6.21
10*b*		109		63.75	6.25	63.71	6.23
11	34	116	$C_{16}H_{18}O_5$	66.20	6.20	66.18	6.10
12	31	125	$C_{17}H_{20}O_6$	63.75	6.25	63.55	6.55
13	7	119	$C_{22}H_{26}O_6$	68.39	6.73	68.37	6.68
13*a*	7	111	$C_{22}H_{30}O_7$	65.02	7.38	64.98	7.29
14	16	64	$C_{23}H_{28}O_7$	66.34	6.73	66.29	6.70
15	13	90–96/0.5–0.6 Torr					
16	17	80	$C_{26}H_{34}O_7$	68.12	7.42	68.14	7.43
17	12	97–100/0.3–0.4 Torr					
18	14	94	$C_{27}H_{36}O_8$	66.39	7.37	66.37	7.33
19	89	99	$C_{12}H_{10}O_4$	66.05	4.58	65.98	5.49
20	83	168	$C_{13}H_{12}O_5$	62.90	4.83	62.91	4.81

All bp's recorded in the table are temperature/pressure; (1 Torr = 133.3 Pa) for sublimation of the compounds which happen to be semisolid in nature.

Can. J. Chem. Downloaded from www.nrcresearchpress.com by 80.90.12.36 on 09/08/12
For personal use only.

nalized by 1,2-addition of a further mole of bromozinc enolate at the C-2 centre of **21**. Moreover, the isolation of the various products suggests that 1,2-addition to the aldehyde most likely involves minimum energy of activation.

Finally, it may be concluded that the Reformatsky reaction of formyl coumarins, using α-bromoacetate and α-bromopropionate, is highly chemoselective. Relatively less chemoselectivity has been observed with the more bulky bromozinc enolates generated from α-bromo-*n*-buryrate and iso-butyrate. Thus the Reformatsky reaction should prove to be an attractive method for the elaboration of different types of side chains in coumarin. It is highly interesting to note that the formation of spiro-γ-lactone and furan derivatives is unique, and there are almost no reports in the literature in which a substrate takes up more than 1 mole of bromozinc enolate reagent to afford such products. The reduction of the aldehyde function to the corresponding alcohol, observed under Reformatsky reaction conditions, also constitutes a highly unusual finding.

Experimental procedure

Boiling points and melting points are uncorrected. UV spectra were taken in aldehyde-free ethanol on a Hitachi U-2000 spectrophotometer. IR spectra were recorded in KBr with a Hitachi 270-30 data processor. The ^{1}H NMR spectra were determined in $CDCl_3$ on JEOL FX100 FT and Hitachi R600 FT spectrometers using TMS as internal standard. Mass spectra were recorded on a Finnigan Mat 1020C spectrometer operating at 70 eV and a Shimadzu model Gems QP 1000DA spectrometer. ^{13}C NMR spectra were run on a Bruker WH 250 spectrometer that was also used for the NOE studies and 2D homounuclear (^{1}H–^{1}H) COSY experiments.

Reformatsky reaction with 1 and 2 employing various ethyl α-bromoesters of acetic, propionic, *n*-butyric, and isobutyric acids

General procedure

The respective Reformatsky reagents were prepared by heating at reflux the corresponding α-bromoesters (17.1 mmol) along with zinc wool (1.11 g, 16.97 mmol) and a pinch of iodine in dry benzene under anhydrous conditions. Formylcoumarin **1** (1 g, 5.75 mmol in 50 mL of dry benzene) or **2** (1 g, 4.90 mmol in 50 mL of dry benzene) was added dropwise after all the zinc wool had dissolved and, after complete addition, refluxing was continued for a further period of 12 h while the nitrogen atmosphere was maintained throughout. The reaction mixture was finally cooled and decomposed by the addition of 20% sulphuric acid (100 mL) in the cold. The benzene layer was removed and the aqueous layer was extracted with $CHCl_3$ (3 × 50 mL). The combined benzene and chloroform extracts were washed with saturated brine solution (3 × 50 mL), followed by washing with aqueous saturated $NaHCO_3$ solution (3 × 30 mL). The solution was finally dried over anhydrous sodium sulphate and evaporation of the solvent afforded the respective crude products from which all of the pure products (**3–18**) were isolated by extensive column chromatography over silica gel (Table 2).

Can. J. Chem. Downloaded from www.nrcresearchpress.com by 80.90.12.36 on 09/08/12
For personal use only.

*$NaBH_4$ reduction of **1** and **2**, respectively, to the corresponding alcohols **3** and **4***

Formylcoumarin **1** (500 mg, 2.88 mmol) or **2** (500 mg, 2.45 mmol) was taken up in 50 mL methanol, an solid $NaBH_4$ (4.0 g, 0.11 mol) was added slowly in portions. After stirring overnight the mixture was decomposed with dilute hydrochloric acid until the solution became acidic; it was extracted with ethyl acetate (3 × 50 mL) and finally dried over anhydrous sodium sulphate. Removal of solvent afforded the respective reduction products **3** and **4**, in 95% yield, which were ultimately crystallized from methanol (Table 2).

*Preparation of acetates (**19**, **20**) of the respective reduction products (**3**, **4**)*

The reduction products, **3** (100 mg, 0.57 mmol) and **4** (100 mg, 0.49 mmol) obtained either as Reformatsky reaction product or as $NaBH_4$ reduction product from **1** and **2**, respectively, were separately warmed with 2 mL of acetic anhydride and a catalytic amount of fused sodium acetate under anhydrous condition for 1 h, and decomposed with crushed ice. The resulting mass was neutralized with solid $NaHCO_3$ and finally extracted with $CHCl_3$ (3 × 10 mL). The combined chloroform extracts were washed with brine (3 × 15 mL) and dried over anhydrous sodium sulphate. Evaporation of the solvent afforded the respective acetates (**19**, **20**), which were finally crystallized from a $CHCl_3$ – petroleum ether mixture (Table 2).

*Separation of diastereomeric alcohols, **7–10** into pure diastereomers, **7a** and **7b**, **8a** and **8b**, **9a** and **9b**, **10a** and **10b**, respectively*

The crude mixture of diastereomeric alcohols (**7–10**) was subjected to extensive and careful column chromatography over silica gel using 10% ether – petroleum ether mixture as eluant. In all experiments the *erythro* diastereomers **7***a*, **8***a*, **9***a*, **10***a* eluted first, followed by the polar *threo* diastereomers **7***b*, **8***b*, **9***b*, and **10***b*, respectively.

In a typical experiment 200 mg of alcohol, **8**, was fed into a column of silica gel and was eluted with 10% ether – petroleum ether mixture. The *erythro* diastereomer **8***a* (40 mg) migrated out first, followed by a mixture of *erythro* and *threo* diastereomers (100 mg). After this the nonpolar *threo* diastereomer, **8***b* (50 mg), in pure form, could be eluted from the same chromatogram.

Spectral characteristics of new products

3: IR: 3080, 1723, 1605 cm^{-1}; UV: 225 nm (log ε 2.80), 381 (2.25); ^1H NMR: 2.49 (1H, t, J = 7 Hz, OH), 4.92 (2H, dd, J = 1.5, 7 Hz, CH_2OH), 6.64 (1H, t, J = 1.5 Hz, 3-H), 7.20–7.68 (4H, complex, aromatic protons).

4: IR: 3360, 1710, 1675, 1600 cm^{-1}; UV: 225 nm (log ε 2.75), 381 (2.50); ^1H NMR: 3.82 (3H, s, OCH_3), 4.72 (2H, dd, J = 1, 7 Hz, CH_2OH), 5.58 (1H, t, J = 7 Hz, OH), 6.30 (1H, t, J = 1 Hz, 3-H), 6.90 (1H, d, J = 2 Hz, 8-H), 6.94 (1H, dd, J = 2, 7 Hz, 6-H), 7.60 (1H, d, J = 7 Hz, 5-H).

5: IR: 3449, 1725, 1720, 1605 cm^{-1}; UV: 250 nm (log ε 3.85), 322 (3.97); ^1H NMR: 1.24 (3H, t, J = 8 Hz, $CO_2CH_2CH_3$), 2.62 (1H, dd, J = 4, 18 Hz, 2′-H_b), 2.83 (1H, dd, J = 8, 18 Hz, 2′-H_a) 3.68 (1H, bs, OH), 4.20 (2H, q, J = 8 Hz, $CO_2CH_2CH_3$), 5.41 (1H, dd, J = 4, 8 Hz, 1′-H), 6.66 (1H, d, J = 1 Hz, 3-H), 7.25–7.49 (4H, complex, aromatic protons); MS: 262 (100, $M^{+\cdot}$), 244 (4.3, $M^{+\cdot} - H_2O$), 234 (1.2, $M^{+\cdot} - CO$), 217 (10.8, $M^{+\cdot} - CO - OH$), 216 (18.5, $M^{+\cdot} - CO - H_2O$), 199 (8.1, $M^{+\cdot} - OEt - H_2O$), 189 (10.8, $M^{+\cdot} - OH - CO - C_2H_4$), 188 (27.5, $M^{+\cdot} - H_2O - CO - C_2H_4$), 175 (23.7, $M^{+\cdot} - CH_2CO_2Et$), 174 (43.5, $M^{+\cdot} - CH_2CO_2Et - H$), 171 (10.8, $M^{+\cdot} - H_2O - CO - OEt$), 147 (45.6, $M^{+\cdot} - CH_2CO_2Et - CO$), 146 (35.3, $M^{+\cdot} - CH_2CO_2Et - H - CO$).

6: IR: 3310, 1720, 1700, 1600 cm^{-1}; UV: 242 nm (log ε 3.80), 311 (3.92); ^1H NMR: 1.30 (3H, t, J = 8 Hz, $CO_2CH_2CH_3$), 2.68 (1H, dd, J = 8, 18 Hz, 2′-H_a), 2.85 (1H, dd, J = 4, 18 Hz, 2′-H_b), 3.95 (3H, s, OCH_3), 4.25 (2H, q, J = 8 Hz, $CO_2CH_2CH_3$), 5.49 (1H, dd, J = 4, 8 Hz, 1′-H), 6.76 (1H, d, J = 1 Hz, 3H), 6.84 (1H, d, J = 2 Hz, 8-H), 6.89 (1H, dd, J = 2, 8 Hz, 6H), 7.57 (1H, d, J = 8 Hz, 5-H); MS: 292 (100, $M^{+\cdot}$), 274 (85, $M^{+\cdot} - H_2O$), 264 (2.1, $M^{+\cdot} - CO$), 247 (7.2, $M^{+\cdot} - CO - OH$), 246 (3.1, $M^{+\cdot} - CO - H_2O$), 229 (9.3, $M^{+\cdot} - OEt - H_2O$), 205 (19.2, $M^{+\cdot} - CH_2CO_2Et$), 204 (34, $M^{+\cdot} - CH_2CO_2Et - H$), 201 (12.7, $M^{+\cdot} - H_2O - CO - OEt$), 190 (19.5, $M^{+\cdot} - HCO_2Et - CO$), 177 (70.2, $M^{+\cdot} - CH_2CO_2Et - CO$), 176 (41.4, $M^{+\cdot} - CH_2CO_2Et - H - CO$), 148 (34, $M^{+\cdot} - CO - CH_2CO_2Et - CHO$).

7*a*: IR: 3452, 1712, 1688, 1604 cm^{-1}; UV: 225 nm (log ε 4.79), 311 (3.84); ^1H NMR: 1.16 (3H, d, J = 7 Hz, 2′-CH_3), 1.26 (3H, t, J = 7 Hz, $CO_2CH_2CH_3$), 2.88 (1H, dq, J = 4, 7 Hz, 2′-H), 3.26 (1H, d, J = 4 Hz, OH), 4.26 (2H, q, J = 7 Hz, $CO_2CH_2CH_3$), 5.56 (1H, br t, J = 4 Hz, 1′-H), 6.72 (1H, d, J = 1 Hz, 3-H), 7.20–7.60 (4H, complex, aromatic protons); MS: 276 (57.8, $M^{+\cdot}$), 258 (1.7, $M^{+\cdot} - H_2O$), 230 (12.4, $M^{+\cdot} - H_2O - CO$), 215 (3.00, $M^{+\cdot} - H_2O - CO - CH_3$), 203 (18.4, $M^{+\cdot} - OH - CO - C_2H_4$), 202 (21.0, $M^{+\cdot} - CO - H_2O - C_2H_4$), 176 (15.5, $M^{+\cdot} - CO - H_2O - C_2H_4 - C_2H_2$), 175 (100, $M^{+\cdot} - CHMeCO_2Et$), 174 (78.1, $M^{+\cdot} - CHMeCO_2Et - H$), 147 (52.4, $M^{+\cdot} - CHMeCO_2Et - CO$), 145 (17.2, $M^{+\cdot} - CHOHCHMeCO_2Et$).

7*b*: IR: 3448, 1730, 1606 cm^{-1}; UV: 225 nm (log ε 4.78), 314 (3.49); ^1H NMR: 1.12 (3H, d, J = 7 Hz, 2′-CH_3), 1.20 (3H, t, J = 7 Hz, $CO_2CH_2CH_3$), 3.00 (1H, dq, J = 7, 8 Hz, 2′-H), 3.80 (1H, d, J = 8 Hz, OH), 4.15 (2H, q, J = 7 Hz, $CO_2CH_2CH_3$), 5.06 (1H, br t, J = 8 Hz, 1′-H), 6.48 (1H, d, J = 1 Hz, 3-H), 7.23–7.80 (4H, complex, aromatic protons).

8*a*: IR: 3304, 1752, 1710, 1614 cm^{-1}; UV: 218 nm (log ε 4.07) 323 (3.70); ^1H NMR: 1.06 (3H, d, J = 7 Hz, 2′-CH_3), 1.16 (3H, t, J = 7 Hz, $CO_2CH_2CH_3$), 3.02 (1H, dq, J = 4, 7 Hz, 2′-H), 3.68 (1H, d, J = 4 Hz, OH), 3.86 (3H, s, OCH_3), 4.25 (2H, q, J = 7 Hz, $CO_2CH_2CH_3$), 5.44 (1H, br t, J = 4 Hz, 1′-H), 6.44 (1H, d, J = 1 Hz, 3-H), 6.80–7.28 (3H, complex, aromatic protons).

8*b*: IR: 3307, 1732, 1702, 1614, 1554 cm^{-1}; UV: 219 nm (log ε 3.99), 324 (3.70); ^1H NMR: 1.07 (3H, d, J = 7 Hz, 2′-CH_3), 1.26 (3H, t, J = 7 Hz, $CO_2CH_2CH_3$), 2.75 (1H, dq, J = 7, 8 Hz, 2′-H), 3.68 (1H, d, J = 8 Hz, OH), 3.88 (3H, s, OCH_3), 4.18 (2H, q, J = 7 Hz, $CO_2CH_2CH_3$), 5.00 (1H, br t, J = 8 Hz, 1′-H), 6.28 (1H, d, J = 1 Hz, 3-H), 6.83–7.24 (3H, complex, aromatic protons).

9*a*: IR: 3499, 1720, 1710, 1600 cm^{-1}; UV: 225 nm (log ε 4.65), 325 (3.72); ^1H NMR: 0.81 (3H, t, J = 7 Hz, 2′-CH_2CH_3), 1.22 (3H, t, J = 7 Hz, $CO_2CH_2CH_3$), 1.72 (2H, quin, J = 7 Hz, 2′-CH_2CH_3), 2.72 (1H, dt, J = 4, 7 Hz, 2′-H), 3.52 (1H, bs, OH), 4.24 (2H, q, J = 7 Hz, $CO_2CH_2CH_3$), 5.40 (1H, br d, J = 4 Hz, 1′-H), 6.70 (1H, d, J = 1 Hz, 3-H), 7.02–7.58 (4H, complex, aromatic protons).

9*b*: IR: 3400, 1730, 1710, 1605 cm^{-1}; UV: 225 nm (log ε 4.67),

Can. J. Chem. Downloaded from www.nrcresearchpress.com by 80.90.12.36 on 09/08/12
For personal use only.

325 (3.56); ^{1}H NMR: 0.96 (3H, t, J = 7 Hz, 2′-CH_2CH_3), 1.22 (3H, t, J = 7 Hz, $CO_2CH_2CH_3$), 1.80 (2H, quin, J = 7 Hz, 2′-CH_2CH_3), 2.48 (1H, dt, J = 8, 7 Hz, 2′-H), 3.84 (1H, s, OH), 4.11 (2H, q, J = 7 Hz, $CO_2CH_2CH_3$), 5.08 (1H, br d, J = 8 Hz, 1′-H), 6.42 (1H, d, J = 1 Hz, 3-H), 7.20–7.64 (4H, complex, aromatic protons).

10*a*: IR: 3460, 1730, 1718, 1605 cm^{-1}; UV: 219 nm (log ε 3.84), 324 (3.66); ^{1}H NMR: 0.84 (3H, t, J = 7 Hz, 2′-CH_2CH_3), 1.24 (3H, t, J = 7 Hz, $CO_2CH_2CH_3$), 1.80 (2H, dq, J = 4, 7 Hz, 2′-CH_2CH_3), 2.72 (1H, dt, J = 4, 7 Hz, 2′-H), 3.65 (1H, br d, J = 4 Hz, OH), 3.84 (3H, s, OCH_3), 4.23 (2H, q, J = 7 Hz, $CO_2CH_2CH_3$), 5.35 (1H, t, J = 4 Hz, 1′-H), 6.52 (1H, d, J = 1 Hz, 3-H), 6.84–7.61 (3H, complex, aromatic protons); MS: 320 (35.6, $M^{+\cdot}$), 275 (7.3, $M^{+\cdot}$ − ȮEt), 257 (7.7, $M^{+\cdot}$ − ȮEt − H_2O), 229 (12.1, $M^{+\cdot}$ − ȮEt − H_2O − CO), 218 (7.7, $M^{+\cdot}$ − ȮEt − CO − Ėt), 206 (100, $M^{+\cdot}$ − ĊHEtCO$_2$Et + Ḣ), 205 (69.1. $M^{+\cdot}$ − ĊHEtCO$_2$Et), 204 (58.4, $M^{+\cdot}$ − ĊHEtCO$_2$Et − Ḣ), 178 (80.1, 206 − CO), 149 (50.2, 178 − ĊHO), 148 (51.9, 178 − CH_2O).

10*b*: IR: 3450, 1730, 1715, 1620 cm^{-1}; UV: 218 nm (log ε 4.20), 323 (4.04); ^{1}H NMR: 1.00 (3H, t, J = 7 Hz, 2′-CH_2CH_3), 1.21 (3H, t, J = 7 Hz, $CO_2CH_2CH_3$), 1.84 (2H, dq, J = 7, 8 Hz, 2′-CH_2CH_3), 3.82 (1H, dt, J = 7, 8 Hz, 2′-H), 3.55 (1H, d, J = 8 Hz, OH), 3.88 (3H, s, OCH_3), 4.18 (2H, q, J = 7 Hz, $CO_2CH_2CH_3$), 5.10 (1H, t, J = 8 Hz, 1′-H), 6.32 (1H, d, J = 1 Hz, 3-H), 6.84–7.64 (3H, complex, aromatic protons); MS: 320 (47.7, $M^{+\cdot}$), 275 (6.3, $M^{+\cdot}$ − ȮEt), 229 (12.6, $M^{+\cdot}$ − ȮEt − H_2O − CO), 218 (4.5, $M^{+\cdot}$ − ȮEt − CO − Ėt), 206 (100, $M^{+\cdot}$ − ĊHEtCO$_2$Et + Ḣ), 205 (65.8, $M^{+\cdot}$ − ĊHEtCO$_2$Et), 204 (64.0, $M^{+\cdot}$ − ĊHEtCO$_2$Et − Ḣ), 178 (64.0, 206 − CO), 149 (28.8, 178 − ĊHO), 148 (27.9, 178 − CH_2O).

11: IR: 3372, 1725, 1720, 1604 cm^{-1}; UV: 219 nm (log ε 4.24), 314 (4.02); ^{1}H NMR: 1.19 (3H, s, 2′-CH_3), 1.28 (3H, s, 2′-CH_3), 1.28 (3H, t, J = 7 Hz, $CO_2CH_2CH_3$), 3.28 (1H, d, J = 4 Hz, OH), 4.22 (2H, q, J = 7 Hz, $CO_2CH_2CH_3$), 5.42 (1H, d, J = 4 Hz, 1′-H), 6.60 (1H, d, J = 1 Hz, 3-H), 7.24–7.82 (4H, complex, aromatic protons); MS: 290 (4.72, $M^{+\cdot}$), 244 (1.7, $M^{+\cdot}$ − EtOH), 227 (0.1, $M^{+\cdot}$ − ȮEt − H_2O), 217 (2.81, $M^{+\cdot}$ − ĊO$_2$Et), 185 (6.0, $M^{+\cdot}$ − Ṁe − ĊO$_2$Et − ȮH), 175 (27.0, $M^{+\cdot}$ − ĊMe$_2$CO$_2$Et), 174 (11.2, $M^{+\cdot}$ − ĊMe$_2$CO$_2$Et − Ḣ), 147 (11.2, $M^{+\cdot}$ − ĊMe$_2$CO$_2$Et − CO), 116 (100, $M^{+\cdot}$ − CO − ĊHOHCMe$_2$CO$_2$Et − Ḣ).

12: IR: 3456, 1732, 1714, 1606 cm^{-1}; UV: 219 nm (log ε 4.23), 327 (4.11); ^{1}H NMR: 1.12 (3H, s, 2′-CH_3), 1.20 (3H, s, 2′-CH_3), 1.20 3H, t, J = 7 Hz, $CO_2CH_2CH_3$), 3.54 (1H, d, J = 4 Hz, OH), 3.86 (3H, s, OCH_3), 4.37 (2H, q, J = 7 Hz, $CO_2CH_2CH_3$), 5.32 (1H, d, J = 4 Hz, 1′-H), 6.40 (1H, d, J = 0.5 Hz, 3-H), 6.80–7.72 (3H, complex, aromatic protons).

13: IR: 1735, 1685, 1595 cm^{-1}; UV: 255 nm (log ε 4.15), 360 (3.83); ^{1}H NMR: 1.02 (3H, t, J = 7 Hz, 3′-CH_2CH_3), 1.18 (3H, t, J = 7 Hz, 4″-CH_2CH_3), 1.20 (3H, t, J = 7 Hz, 3′-$CO_2CH_2CH_3$), 1.34 (3H, t, J = 7 Hz, 4″-$CO_2CH_2CH_3$), 2.04 (2H, quin, J = 7 Hz, 3′-CH_2CH_3), 2.60 (2H, q, J = 7 Hz, 4″-CH_2CH_3), 4.14 (2H, q, J = 7 Hz, 4″-$CO_2CH_2CH_3$ and 1H, hidden under q, 3′-H), 4.16 (2H, q, J = 7 Hz, 3′-$CO_2CH_2CH_3$), 7.00–7.98 (4H, complex, aromatic protons), 8.56 (1H, s, 3″-H); MS: 386 (64.3, $M^{+\cdot}$), 371 (100, $M^{+\cdot}$ − CH_3), 343 (5.8, $M^{+\cdot}$ − CH_3 − C_2H_4), 341 (16.5, $M^{+\cdot}$ − ȮEt), 340 (5.4, $M^{+\cdot}$ − EtOH), 314 (13.4, $M^{+\cdot}$ − ĊO$_2$Et + Ḣ), 313 (21.4, $M^{+\cdot}$ − ĊO$_2$Et), 271 (15.2, $M^{+\cdot}$ − ĊHEtCO$_2$Et), 197 (12.5, $M^{+\cdot}$ − ĊHEtCO$_2$Et − HCO$_2$Et); 2D Cosy (^{1}H–^{1}H): strong cross peaks for 4-H with 5-H; 5-H with 6-H; 4″-$CO_2CH_2CH_3$ with 4″-$CO_2CH_2CH_3$; 3′-$CO_2CH_2CH_3$ with 3′-$CO_2CH_2CH_3$; 3′-CH_2CH_3 with 3′-CH_2CH_3 and 3′-H; 4″-CH_2CH_3 with 4″-CH_2CH_3, whereas 3″-H with 4″-$CO_2CH_2CH_3$ (weak); NOE study: increment (29%) in intensity of methylene signal at δ 4.14 for 4″-$CO_2CH_2CH_3$ on irradiation of 3″-H signal at δ 8.56, increment (26%) intensity of 3″-H on irradiation of methylene signal of 4″-$CO_2CH_2CH_3$.

13*a*: IR: 3405, 1710, 1705, 1615 cm^{-1}; ^{1}H NMR: 0.90 (3H, t, J = 7 Hz, 2′-CH_2CH_3), 1.08 (3H, t, J = 7 Hz, 4-CH_2CH_3), 1.24 (3H, t, J = 7 Hz, 2′-$CO_2CH_2CH_3$), 1.34 (3H, t, J = 7 Hz, 4-$CO_2CH_2CH_3$), 1.80 (2H, m, 2′-CH_2CH_3), 1.90 (1H, br, 1′-OH), 2.56 (2H, m, 4-CH_2CH_3), 2.72 (1H, m, 2′-H), 4.20 (2H, q, J = 7 Hz, 2′-$CO_2CH_2CH_3$), 4.21 (2H, q, J = 7 Hz, 4-$CO_2CH_2CH_3$ and 1H, hidden under methylene signals, 4-H), 5.18 (1H, d, J = 4 Hz, 1′-H), 7.02–7.52 (5H, complex, 4 aromatic protons and 1 olefinc proton), 8.04 (1H, s, phenolic OH).

14: IR: 1730, 1725, 1680, 1595 cm^{-1}; UV: 260 nm (log ε 4.30), 360 (4.24); ^{1}H NMR: 1.04 (3H, t, J = 7 Hz, 3′-CH_2CH_3), 1.10 (3H, t, J = 7 Hz, 4″-CH_2CH_3), 1.18 (3H, t, J = 7 Hz, 3′-$CO_2CH_2CH_3$), 1.34 (3H, t, J = 7 Hz, 4″-$CO_2CH_2CH_3$), 2.04 (2H, quin, J = 7 Hz, 3′-CH_2CH_3), 2.59 (2H, q, J = 7 Hz, 4″-CH_2CH_3), 3.82 (3H, s, OCH_3), 4.16 (2H, q, J = 7 Hz, 4″-$CO_2CH_2CH_3$ and 1H, hidden under q, 3′-H), 4.24 (2H, q, J = 7 Hz, 3′-$CO_2CH_2CH_3$), 6.80–7.81 (3H, complex, aromatic protons), 8.44 (1H, s, 3″-H); MS: 416 (52.6, $M^{+\cdot}$), 401 (100, $M^{+\cdot}$ − CH_3), 373 (6.3, $M^{+\cdot}$ − CH_3 − CO), 371 (8.0, $M^{+\cdot}$ − ȮEt), 370 (2.6, $M^{+\cdot}$ − EtOH), 343 (12.5, $M^{+\cdot}$ − ĊO$_2$Et), 342 (1.7, $M^{+\cdot}$ − HCO$_2$Et), 301 (8.0, $M^{+\cdot}$ − ĊHEtCO$_2$Et), 227 (4.5, $M^{+\cdot}$ − ĊHEtCO$_2$Et − HCO$_2$Et); 2D Cosy (^{1}H–^{1}H): strong cross peaks for 3′-CH_2CH_3 with 3′-CH_2CH_3; 4″-CH_2CH_3 with 4″-CH_2CH_3; 3′-$CO_2CH_2CH_3$ with 3′-$CO_2CH_2CH_3$, 4″-CH_2CH_3 with 4″-$CO_2CH_2CH_3$; 3′-H with 3′-CH_2CH_3; 4-H with 5-H.

15: IR: 1785, 1730, 1595 cm^{-1}; UV: 212 nm (log ε 5.08) 277 (4.60); ^{1}H NMR: 0.65, (3H, s, CH_3), 1.21 (3H, s, CH_3), 1.29 (6H, t, J = 7 Hz, 2-$CO_2CH_2CH_3$), 1.35 (3H, s, CH_3), 1.49 (3H, s, CH_3), 1.50 (3H, s, CH_3), 1.59 (3H, s, CH_3), 3.88 (2H, q, J = 7 Hz, $CO_2CH_2CH_3$), 4.20 (2H, q, J = 7 Hz, $CO_2CH_2CH_3$), 5.20 (1H, s, 3-H), 5.44 (1H, s, 7′-H), 6.95–7.28 (4H, complex, aromatic protons); MS: 458 (1.0, $M^{+\cdot}$), 429 (1.0, $M^{+\cdot}$ − Ėt), 387 (25.6, $M^{+\cdot}$ − C_2H_4 − CO − Ṁe), 299 (5.0, $M^{+\cdot}$ − ĊMe$_2$CO$_2$Et − Ėt − Ṁe) 286 (100, $M^{+\cdot}$ − ĊMe$_2$CO$_2$Et − CO − C_2H_5), 273 (30.6, 299 − C_2H_2), 271 (10.0, 299 − CO), 213 (23.4), 131 (24.3).

16: IR 1790, 1740, 1595 cm^{-1}; UV: 204 nm (log ε 4.74), 276.5 (3.92); ^{1}H NMR: 1.10–1.42 (24H, six CH_3 and two $CO_2CH_2CH_3$), 4.18 (2H, q, J = 7 Hz, $CO_2CH_2CH_3$), 4.22 (2H, q, J = 7 Hz, $CO_2CH_2CH_3$), 4.65 (1H, d, J = 5 Hz, 3-H), 4.83 (1H, d, J = 5 Hz, 7′-H), 6.89–7.29 (4H, complex, aromatic protons); MS: 458 (12.6, $M^{+\cdot}$), 387 (34.5, $M^{+\cdot}$ − C_2H_4 − CO − Ṁe), 359 (18.5), 299 (24.5, $M^{+\cdot}$ − ĊMe$_2$CO$_2$Et − Ėt − Ṁe), 286 (100, $M^{+\cdot}$ − ĊMe$_2$CO$_2$Et − CO − C_2H_5), 273 (10.4, 299 − C_2H_2), 271 (10.3, 299 − CO).

17: IR: 1775, 1725, 1600 cm^{-1}; UV: 217 nm (log ε 4.69), 282 (3.76); ^{1}H NMR: 0.79 (3H, s, CH_3), 1.03 (3H, s, CH_3), 1.13 (3H, s, CH_3), 1.23 (3H, s, CH_3). 1.25 (3H, t, J = 7 Hz, $CO_2CH_2CH_3$), 1.28 (3H, s, CH_3), 1.30 (3H, s, CH_3), 1.36 (3H, t, J = 7 Hz, $CO_2CH_2CH_3$), 1.39 (3H, s, CH_3), 1.40 (3H, t, J = 7 Hz, $CO_2CH_2CH_3$), 1.62 (3H, s, CH_3), 2.14 (1H, bd, J = 12 Hz, $3H_a$), 2.62 (1H, dd, J = 4, 12 Hz, 3-H_b), 3.24 (1H, br d, J = 4

Hz, 7′-H), 3.74 (3H, s, OCH_3), 4.14 (2H, q, J = 7 Hz, $CO_2CH_2CH_3$), 4.16 (2H, q, J = 7 Hz, $CO_2CH_2CH_3$), 4.22 (2H, q, J = 7 Hz, $CO_2CH_2CH_3$), 7.36 (1H, dd, J = 0.5, 7 Hz, 6-H), 7.41 (1H, d, J = 0.5 Hz, 8-H), 7.77 (1H, d, J = 7 Hz, 5H); 2D Cosy (^{1}H–^{1}H): strong cross peaks for $3H_a$ with $3H_b$; 7′-H with 3-H_b; 5-H with 6-H.

18: IR: 1775, 1723, 1595 cm^{-1}; UV: 221 nm (log ε 5.01), 283 (4.25); ^{1}H NMR: 1.08 (3H, s, CH_3), 1.18 (3H, s, CH_3), 1.38 (6H, t, J = 7 Hz, 2-$CO_2CH_2CH_3$), 1.22 (3H, s, CH_3), 1.33 (3H, s, CH_3), 1.45 (3H, s, CH_3), 1.63 (3H, s, CH_3), 3.84 (3H, s, OCH_3), 3.91 (2H, q, J = 7 Hz, $CO_2CH_2CH_3$), 4.18 (2H, q, J = 7 Hz, $CO_2CH_2CH_3$), 4.71 (1H, s, 3-H), 5.44 (1H, s, 7′-H), 6.55 (1H, d, J = 1.5 Hz, 8-H), 6.70 (1H, dd, J = 1.5, 7 Hz, 6-H), 7.31 (1H, d, J = 7 Hz, 5-H); MS: 488 (8.9, $M^{+\cdot}$), 458 (6.3, $M^{+\cdot} - CH_2O$), 417 (25.1, $M^{+\cdot} - C_2H_4 - CO - Me$), 329 (25.9, $M^{+\cdot} - CMe_2CO_2Et - E - Me$), 317 (18.8, $M^{+\cdot} - CMe_2CO_2Et - CO - C_2H_4$), 316 (100, $M^{+\cdot} - CMe_2CO_2Et - CO - C_2H_4 - H$), 303 (5.1); 2D Cosy (^{1}H–^{1}H): strong cross peaks for 7′-$CO_2CH_2CH_3$ with 7′-$CO_2CH_2CH_3$; 2-$CMe_2CO_2CH_2CH_3$ with 2-$CMe_2CO_2CH_2CH_3$; 5-H with 6-H; 6-H with 8-H.

Acknowledgements

The authors thank Prof. Dr. W. Kraus and Dr. B. Vogler (Hohenheim Universität, Stuttgart), Dr. B.G. Hazra (National Chemical Laboratory, Pune), and Dr. P.K. Bhattacharyya (Bhaba Atomic Research Centre, Bombay) for spectral measurements. Thanks are also due to the authorities of Jadavpur University for a fellowship to one of us (M.B.).

References

1. A. Fürstner. Synthesis, 571 (1989).
2. J. Boersma. *In* Comprehensive organometallic chemistry. Vol. 2. *Edited by* G. Wilkinson. Pergamon Press, Oxford. 1982. p. 823.
3. P.J. Brogden, C.D. Gabbutt, and J.D. Hepworth. *In* Comprehensive heterocyclic chemistry. Vol. 3. *Edited by* A.R. Katritzky and C.W. Rees. Pergamon Press, Oxford. 1984. p. 681.
4. L.N. Dutta, N.C. Sinha, and A.K. Sarkar. Ind. J. Chem. **27B**, 801 (1988).
5. R.D.H. Murray. Fortschr. Chem. Org. Naturst. **58**, 83 (1991).
6. K. Ito and J. Sawarobori. Chem. Pharm Bull. **31**, 3014 (1983).
7. W. Carruthers. Some modern methods in organic synthesis. 3rd ed. Cambridge University Press, Cambridge. 1986. p. 436.
8. T.H. Lowry and K.S. Richardson. Mechanism and theory in organic chemistry. 3rd ed. Harper and Row Publishers, New York. 1987. p. 683.
9. D.H. Williams and I. Fleming. Spectroscopic methods in organic chemistry. 4th ed. McGraw Hill, London. 1987. p. 92.
10. E.L. Eliel, N.L. Allinger, S.J. Angyal, and G.A. Morrison. Conformational analysis. Wiley Interscience, New York. 1965. p. 13.
11. F.A. Carey and M.E. Kuehne. J. Org. Chem. **47**, 3811 (1982).
12. C.H. Heathcock. *In* Asymmetric synthesis. Vol. 3. *Edited by* J.D. Morrison. Academic Press, Orlando, Fla. 1983. p. 144.
13. J.K.M. Sanders and B.K. Hunter. Modern NMR spectroscopy. Oxford University Press, Oxford. 1987. p. 300.
14. H.O. House. Modern synthetic reactions. 2nd ed. Benjamin Cummings, Redwood City, Calif. 1972. p. 629.
15. R.M. Silverstein, G.C. Bassler, and T.C. Morrill. Spectrometric identification of organic compounds. 4th ed. John Wiley and Sons, New York. 1981. p. 122.
16. E. Pretsch, T. Clerc, J. Seibl, and W. Simon. Strukturaufklärung Organischer Verbindungen. Springer-Verlag, Berlin. 1976. H 190.

Can. J. Chem. Downloaded from www.nrcresearchpress.com by 80.90.12.36 on 09/08/12
For personal use only.

8790

Peptide models XI. Substitution effects on peptide chains. The magnitude of side-chain–backbone interactions in oligopeptides HCO-(NHCHRCO)$_n$-NH$_2$ for R = CH$_3$. An ab initio study

M.A. McAllister, G. Endredi, W. Viviani, A. Perczel, P. Csaszar, J. Ladik, J.-L. Rivail, and I.G. Csizmadia

Abstract: The stabilization effect of the Me group with respect to H has been determined for peptides of the type HCO-(NH-CHR-CO)$_n$-NH$_2$ for $1 \leq n \leq 3$. It was found that for the Me group the stabilization energy was in the vicinity of 5.4 kcal/mol. The site of substitution had no appreciable effect on the stabilization energy. The stabilization energy for monomethyl substitution (R = CH$_3$) ranged from 5.21 to 5.60 kcal/mol. For dimethyl substitution the values were between 10.53 and 10.81 kcal/mol, and for trimethyl substitution it was 15.99 kcal/mol.

Key words: stabilization effects of substituents, oligopeptide conformations, ab initio study on HCO-(NHCHRCO)$_n$-NH$_2$.

Résumé : On a déterminé l'effet de stabilisation du groupe méthyle par rapport à l'hydrogène dans les peptides du type HCO-(NH-CHR-CO)$_n$-NH$_2$ dans lesquels $1 \leq n \leq 3$. On a trouvé que l'énergie de stabilisation du groupe méthode est d'environ 5,4 kcal/mol. Le site de substitution n'a pas d'effet appréciable sur l'énergie de stabilisation. L'énergie de stabilisation pour la monosubstitution (R = CH$_3$) varie de 5,21 à 5,60 kcal/mol. Les énergies de stabilisation provoquées par deux méthyles s'établissent entre 10,53 et 10,81 kcal/mol alors que celle associée à une substitution par trois méthyles est égale à 15,99 kcal/mol.

Mots clés : effets de stabilisation de substituents, conformations des oligopeptides, étude ab initio de HCO-(NHCHRCO)$_n$-NH$_2$.

[Traduit par la rédaction]

Received September 13, 1994.[1]

M.A. McAllister. Department of Chemistry, University of North Texas, Denton, TX 76203, U.S.A.

G. Endredi and J. Ladik. Institute of Theoretical Chemistry and Laboratory of the National Foundation for Cancer Research, Friedrich-Alexander University, Erlangen-Nürnberg, Egerlandstrasse 3, D-91056 Erlangen, Germany.

W. Viviani. Instituto de Bioquimica, Universidade de Sao Paolo, Sao Paolo, Brazil.

A. Perczel. Department of Biochemistry, University of Oxford, Oxford OX1 2QU, U.K., and Department of Organic Chemistry, Institute of Chemistry, Eötvös Lorand University, H-1117 Budapest, Hungary.

P. Csaszar. Department of Chemistry, University of Toronto, Toronto, ON M5S 1A1, Canada, and APOTEX, Inc., 150 Signet Drive, Weston, ON M9L 1T9, Canada.

J.-L. Rivail. Laboratoire de chimie theorique, Unité associée n° 510 au Centre national de la recherche scientifique, Université de Nancy I, BP 239, F-54506 Vandoeuvre-les-Nancy Cedex, France.

I.G. Csizmadia.[2] Institute for Theoretical Chemistry and Laboratory of the National Foundation for Cancer Research, Friedrich-Alexander University, Erlangen-Nürnberg, Egerlandstrasse 3, D-91056 Erlangen, Germany; Department of Organic Chemistry, Institute of Chemistry, Eötvös Lorand University, H-1117 Budapest, Hungary; Department of Chemistry, University of Toronto, Toronto, ON M5S 1A1, Canada; and Laboratoire de chimie théorique, Unité associée n° 510 au Centre national de la recherche scientifique, Université de Nancy I, BP 239, F-54506 Vandoeuvre-les-Nancy Cedex, France.

[1] Revision received June 6, 1995.

[2] Author to whom correspondence may be addressed. Telephone: (416) 978-3598. Fax: (416) 978-1631. E-mail: icsizmad@alchemy.chem.utoronto.ca

Can. J. Chem. Downloaded from www.nrcresearchpress.com by 80.90.12.36 on 09/08/12
For personal use only.

Can. J. Chem. Downloaded from www.nrcresearchpress.com by 80.90.12.36 on 09/08/12
For personal use only.

Introduction

The use of ab initio molecular orbital calculations to investigate substituent effects on chemical reactions has become commonplace (1, 2). Recently Wiberg et al. used this methodology to study the electronic effect of substitution on several classes of organic compounds including hydrocarbons (3, 4), alkenes (5), and carbonyls (6). Similarly, Tidwell et al. have used this technique to investigate substituent effects on highly reactive intermediates, ones which are not easily accessible via experiment. These included ketenes (7), allenes (8), isocyanates (9), diazomethanes (10), fulvenones (11), and diazocyclopolyenes (11). In the field of peptide chemistry, recent studies of single amino acid diamides generated from glycine, alanine, and valine have been subjected to an analogous study (12–15) in order to investigate substituent effects of the various side chains found in amino acids. However, this methodology has not, as yet, been applied to the study of oligopeptides. Recent studies on the polyalanine systems For-Ala-Ala-NH_2 (16–18) and For-Ala-Ala-Ala-NH_2 (19) have made available the necessary data for studying substituent effects on these systems.

The Ramachandran map, $E = E(\phi, \psi)$, associated with single amino acid diamides, HCO-NH-CHR-CO-NH_2, has nine discrete conformations as shown schematically in Fig. 1. These nine conformational centres, which can clearly be identified (13) on the Ramachandran potential energy surface (PES), have been labelled by subscripted Greek letters (α_D, α_L, β_D, β_L, γ_D, γ_L, δ_D, δ_L, ε_D, and ε_L).

Methodology

Ab initio calculated properties of all compounds under study were determined from full geometry optimizations at the HF/3-21G level of theory (20) using the GAUSSIAN 92 program (21). In all cases the geometry optimizations were terminated only when the root-mean-square force (gradient) along the internal coordinates was less then 6.5×10^{-5} au. Previous studies (17, 18) have revealed that a more stringent convergence criterion does not lead to significant changes in either the calculated molecular energy or structure. In particular, dihedral angles (ϕ and ψ) of selected alanine dipeptide triamides were found to change no more than ±0.4° when the gradient convergence criterion was increased 10-fold (16).

The energy values obtained from the ab initio computations are total energies for the molecule as a whole and therefore no direct comparison is possible when dealing with different compounds. This difficulty has been encountered in the studies of a series of substituted molecules and the problem was solved by considering so-called isodesmic reactions (1–11) where the number of identical bond types is conserved during the reaction. To be able to compare the conformational energy of peptides with different side chains we have proposed the use of similar reasoning (12–15). Thus, the isodesmic reaction can be represented by eq. [1].

[1] For-(NH-CH_2-CO)$_n$-NH_2 + n(R-CH_3)

→ For-(NH-CHR-CO)$_n$-NH_2 + n(CH_4)

Equation [1] is an isodesmic reaction that compares the relative effects of changing a substituent (R) on a peptide backbone (NH-CHR-CO)$_n$ to that of a simple alkane (R-CH_3). Thus, a calculated ΔE that is greater than zero (endothermic) for the above reaction would indicate that the substituent (R) prefers to be on the alkane rather than on the peptide. Similarly, if the ΔE for the reaction is less than zero (i.e., exothermic) then the substituent preferentially stabilizes the peptide relative to the alkane. From previous studies (3), we know that when R = CH_3 there is only a minimal substituent effect on R-CH_3. We can thus assume that the main substituent effect emerging from this analysis is due to stabilizing or destabilizing effects on the peptide backbone itself.

Fig. 1. Idealized PES topology for a single amino acid residue involving two complete cycles of rotation in both ϕ and ψ (the location of the minima are specified by their names in terms of subscripted Greek letters).

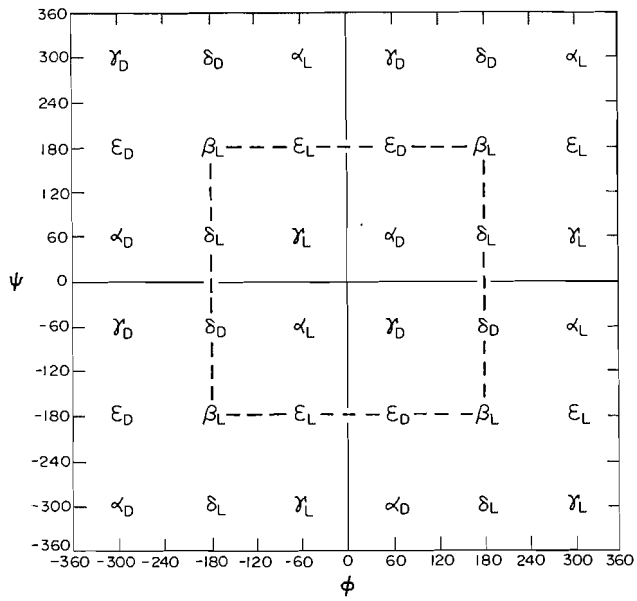

The corresponding stabilization energy is defined by eq. [2].

[2] $\Delta E^{R}_{stabil} = E_X$[For-(NH-CHR-CO)$_n$-$NH_2$] + nE(CH_4)

$- \{E_{\gamma_L}$[For-(NH-CH_2-CO)$_n$-NH_2] + nE[R-CH_3]$\}$

In eq. [1], For-(NH-CH_2-CO)$_n$-NH_2 stands for oligo- or poly-glycine, where For- is the N-terminal formyl (HCO-) protecting group and -NH_2 is the C-terminal amide protecting group. For-(NH-CHR-CO)$_n$-NH_2 is a homo-peptide with degree of polymerization n and R stands for the side chain of the amino acid residue. In eq. [2] ΔE^{R}_{stabil} is the stabilization energy, E_X[For-(NH-CHR-CO)$_n$-NH_2] is the energy of any homo oligo-peptide, with degree of polymerization n in conformation X, and E_{γ_L}[For-(NH-CH_2-CO)$_n$-NH_2] is the energy of oligo-glycine diamide in its reference conformation (γ_L)$_n$. Finally, E(CH_4) and E(R-CH_3) are energy values of the appropriate hydrocarbons.

In this calculation the glycine residues (For-(NH-CH_2-CO)$_n$-NH_2) are always in their global minimum energy conformation (poly γ_L); the hydrocarbons R-CH_3 and CH_4 are also considered in their global minimum energy conforma-

Table 1. The variation of stabilization energy (ΔE^R_{stabil}) with relative energy ($\Delta E^R_{X-\gamma_L}$) for various backbone (BB) conformations.[a]

BB conformation (x)	Gly[b] R = H		Ala R = Me		Val (χ_1 = 60°) R = iPr		Val (χ_1 = 180°) R = iPr		Val (χ_1 = 300°) R = iPr	
	$\Delta E^R_{X-\gamma_L}$	ΔE^R_{stabil}	$\Delta E^R_{X-\gamma_L}$	ΔE^R_{stabil}	$\Delta E^R_{X-\gamma_L}$	ΔE^R_{stabil}	$\Delta E^R_{X-\gamma_L}$	ΔE^R_{stabil}	$\Delta E^R_{X-\gamma_L}$	ΔE^R_{stabil}
α_D	—	—	5.95	0.36	8.73	3.33	6.75	1.35	7.89	2.49
α_L	—	—	—	—	—	—	—	—	—	—
β_L	0.65	0.65	1.25	−4.34	1.99	−3.41	3.35	−2.05	1.81	−3.59
γ_D	0.00	0.00	2.53	−3.07	5.27	−0.12	2.21	−3.19	5.65	0.25
γ_L	0.00	0.00	0.00	−5.60	0.00	−4.74	0.00	−5.40	0.00	−5.04
δ_D	3.27	3.27	7.31	1.71	7.94	2.55	9.05	3.65	10.93	5.47
δ_L	3.27	3.27	3.83	−1.77	4.23	−1.17	—	—	3.29	−2.11
ε_D	—	—	8.16	2.57	12.35	6.95	10.76	5.36	11.04	5.64
ε_L	—	—	—	—	—	—	—	—	—	—

[a]Energy values are in kcal/mol. The definition of ΔE^R_{stabil} is given in eqs. [2] and [3]. The following fully optimized hydrocarbon energy values (HF/321G) were used in eq. [2] to calculate ΔE^R_{stabil}: E(Me-H) = −39.976 877 hartree; E(Me-Me) = −78.793 948 hartree; E(Me-^{i}Pr) = −156.434 471 hartree.

[b]For Gly, b = 0. Thus $\Delta E^R_{stabil} = \Delta E^R_{X-\gamma_L}$.

tion, while the compound studied, i.e., For-(NH-CHR-CO)$_n$-NH$_2$, may be in any desired conformation. ΔE^R_{stabil}, then, is a measure of the change in energy associated with transfering the group R from the hydrocarbon R-CH$_3$ to a glycine residue, plus the change in energy associated with the peptide conformational change when it goes from its global minimum (i.e., poly γ_L) to the chosen conformation (X). For the X = poly γ_L conformations the large negative values of ΔE^R_{stabil} indicate that the R group is more stabilizing for the amino acid backbone than is the hydrocarbon.

In contrast to the above, for a given peptide, the various conformations can be compared in terms of their relative energies with respect to the global minimum, which is defined by eq. [3].

$$[3] \qquad \Delta E^R_{X-\gamma_L} = E(\text{given conformation:X}) - E(\text{global minimum})$$

Scheme 1 below shows the labeling scheme used to define the bonding in the mixed dipeptides and tripeptides. These schemes are used to define the folding parameters "d" and "τ", which have been introduced previously (16–18).

For the mixed dipeptide triamides,

$$d_{model} = {}^2H^d—{}^4H^d$$

$$\tau_{model} = {}^2H^d—C^1\alpha—C^2\alpha—{}^4H^d$$

For the mixed tripeptides,

$$d^1{}_{model} = {}^1H^d—C^1\alpha$$

$$d^2{}_{model} = {}^2H^d—C^3\alpha$$

$$\tau^1{}_{model} = {}^1H^d—C^3\alpha—C^2\alpha—C^1\alpha$$

$$\tau^2{}_{model} = {}^2H^d—C^1\alpha—C^2\alpha—C^3\alpha$$

In all cases, the corresponding d_{crit} and τ_{crit} values are obtained by replacing the necessary H—C bond distances with a value of 1.515 Å and the H—N bond distances with a value of 1.462 Å, as was done previously (16–19).

Scheme 1.

Labeling Scheme for Mixed Dipeptides

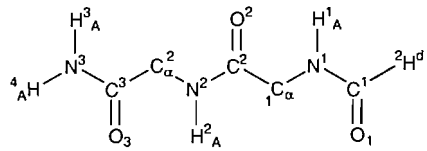

Labeling Scheme for Mixed Tripeptides

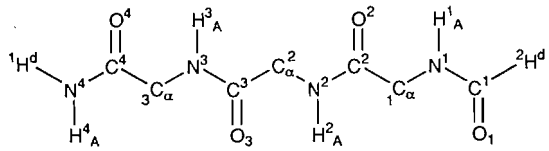

Results

Calculated values of $\Delta E^R_{X-\gamma_L}$ and ΔE^R_{stabil} for monopeptides, that is, diamides of glycine, alanine, and valine, are given in Table 1, and are shown graphically in Fig. 2. Table 2 contains the total energies of the 49 stable conformations of For-Ala-Ala-NH$_2$ dipeptides, as well as the corresponding $\Delta E^R_{X-\gamma_L}$ and ΔE^R_{stabil} values (which are plotted in Fig. 3*a*). Table 3 and Fig. 3*b* show the calculated $\Delta E^R_{X-\gamma_L}$ and ΔE^R_{stabil} values for the tripeptide For-Ala-Ala-Ala-NH$_2$.

Table 4 contains energetic and structural data for the mixed dipeptides. Table 5 contains the corresponding information for the mixed tripeptides.

Can. J. Chem. Downloaded from www.nrcresearchpress.com by 80.90.12.36 on 09/08/12
For personal use only.

Fig. 2. Variation of stabilization energy (ΔE^{R}_{stabil}) for alanine diamide, as computed for conformer X, with relative energy ($\Delta E^{R}_{X-\gamma_L} = E^{R}_{X} - E^{R}_{\gamma_L}$) with respect to its γ_L conformer (in kcal/mol units). The equivalent information for glycine diamide and valine diamide is also shown for the sake of comparison.

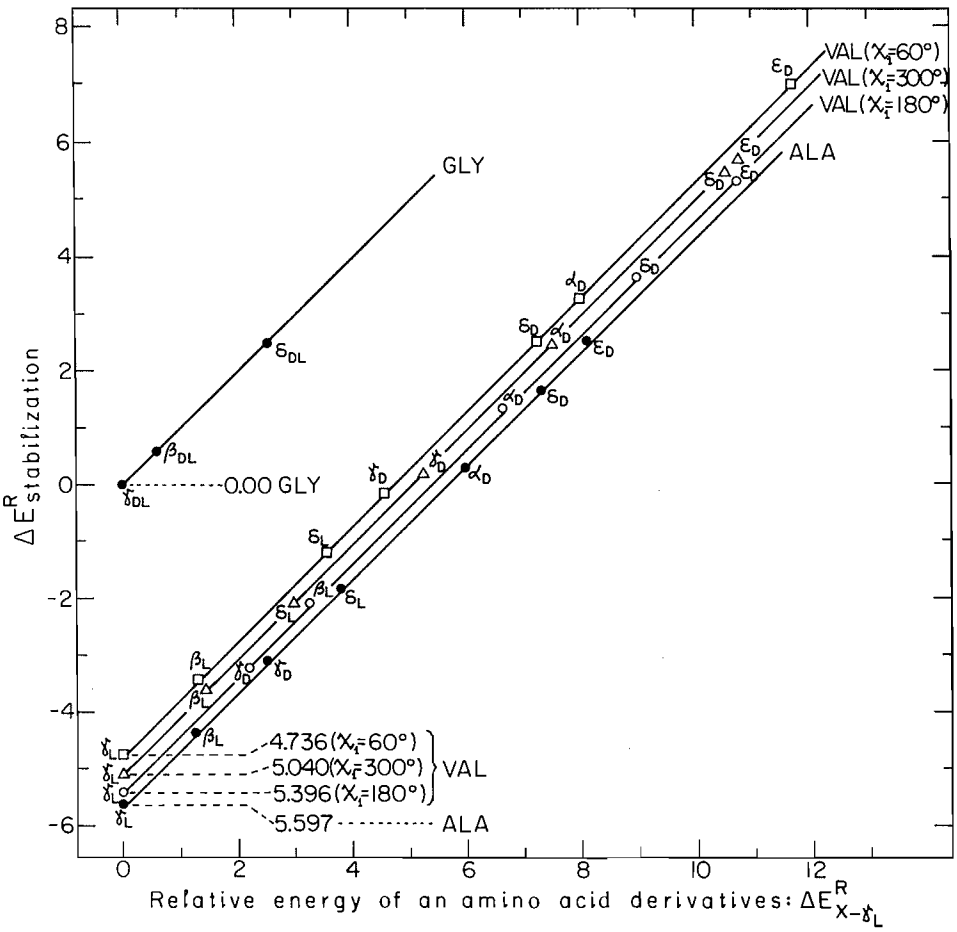

Discussion

It should perhaps be emphasized that Figs. 2 and 3 may be misleading in the sense that the same information is given on both the horizontal and the vertical axes. This is necessarily so, since all that is done is the shifting of the reference state as illustrated by Fig. 4. However, such representations as shown in Figs. 2 and 3 are useful because they show graphically the spread of energy values as well as the continually decreasing y-intercept.

(i) Monopeptides

Methyl substitution (from R = H to R = Me) at the α-carbon of a simple peptide such as HCO-NH-CHR-CO-NH_2 is stabilizing the backbone in its γ_L conformation in excess of 5 kcal/mol. The various ΔE^{Me}_{stabil} values span the following range:

$$-5.60 \text{ kcal/mol} \leq \Delta E^{Me}_{stabil} \leq +2.57 \text{ kcal/mol}$$
$$\gamma_L \qquad\qquad \epsilon_D$$

It is interesting to note that the ^{i}Pr group is a better electron donor than Me; therefore more extensive stabilization is expected from the ^{i}Pr group. However, ^{i}Pr is bulkier than Me and therefore steric hindrance would be somewhat destabilizing. Consequently, the Me and ^{i}Pr stabilization become approximately equivalent (14).

$$\Delta E^{Me}_{stabil} \approx \Delta E^{iPr}_{stabil}$$

This is clearly illustrated in Table 1 and Fig. 2.

(ii) Homodipeptides

A total of 49 conformations for HCO(-NH-CHMe-CO)$_2$-NH_2 have been obtained by geometry optimization (16, 17) and the stabilization energy ($\Delta E^{Me,Me}_{stabil}$) of each of these conformations has now been calculated. The various $\Delta E^{Me,Me}_{stabil}$ values span the following range

$$-10.81 \text{ kcal/mol} \leq \Delta E^{Me,Me}_{stabil} \leq +4.56 \text{ kcal/mol}$$

Can. J. Chem. Downloaded from www.nrcresearchpress.com by 80.90.12.36 on 09/08/12
For personal use only.

Can. J. Chem. Downloaded from www.nrcresearchpress.com by 80.90.12.36 on 09/08/12
For personal use only.

Table 2. Energetics[a] of alanine dipeptides (For-Ala-Ala-NH_2).

BB conformation (x)	Energy (hartrees)	ΔE^R_{stabil}	$\Delta E^R_{X-\gamma_L}$
$\alpha_D\alpha_D$	−656.956 139	−6.08	4.73
$\alpha_D\beta_L$	−656.954 609	−5.12	5.69
$\alpha_D\delta_D$	−656.949 915	−2.17	8.64
$\alpha_D\delta_L$	−656.950 469	−2.52	8.29
$\alpha_D\gamma_D$	−656.950 869	−2.77	8.04
$\alpha_D\gamma_L$	−656.956 058	−6.03	4.78
$\alpha_L\delta_L$	−656.958 697	−7.68	3.13
$\beta_L\alpha_D$	−656.952 663	−3.90	6.91
$\beta_L\beta_L$	−656.960 419	−8.77	2.05
$\beta_L\delta_D$	−656.949 998	−2.23	8.59
$\beta_L\delta_L$	−656.955 673	−5.79	5.03
$\beta_L\varepsilon_D$	−656.949 539	−1.94	8.87
$\beta_L\gamma_D$	−656.956 752	−6.46	4.35
$\beta_L\gamma_L$	−656.961 052	−9.16	1.65
$\delta_D\alpha_D$	−656.943 013	2.16	12.97
$\delta_D\beta_L$	−656.951 769	−3.34	7.48
$\delta_D\delta_D$	−656.940 844	3.52	14.33
$\delta_D\varepsilon_D$	−656.941 230	3.28	14.09
$\delta_D\varepsilon_L$	−656.654 315	−4.94	5.88
$\delta_D\gamma_D$	−656.948 001	−0.97	9.84
$\delta_D\gamma_L$	−656.952 531	−3.82	7.00
$\delta_L\alpha_D$	−656.948 190	−1.09	9.72
$\delta_L\beta_L$	−656.956 570	−6.35	4.46
$\delta_L\delta_D$	−656.945 712	0.46	11.28
$\delta_L\varepsilon_D$	−656.954 078	−4.79	6.03
$\delta_L\gamma_D$	−656.954 474	−5.03	5.78
$\delta_L\gamma_L$	−656.958 063	−7.29	3.53
$\varepsilon_D\beta_L$	−656.950 278	−2.40	8.41
$\varepsilon_D\delta_D$	−656.939 187	4.56	15.37
$\varepsilon_D\delta_L$	−656.955 958	−5.97	4.85
$\varepsilon_D\varepsilon_D$	−656.940 468	3.76	14.57
$\varepsilon_D\gamma_D$	−656.947 257	−0.51	10.31
$\varepsilon_D\gamma_L$	−656.952 062	−3.52	7.29
$\gamma_D\alpha_D$	−656.952 458	−3.77	7.04
$\gamma_D\beta_L$	−656.952 732	−3.94	6.87
$\gamma_D\delta_D$	−656.949 771	−2.08	8.73
$\gamma_D\delta_L$	−656.953 949	−4.71	6.11
$\gamma_D\varepsilon_D$	−656.949 096	−1.66	9.15
$\gamma_D\varepsilon_L$	−656.953 218	−4.25	6.57
$\gamma_D\gamma_D$	−656.956 213	−6.13	4.69
$\gamma_D\gamma_L$	−656.960 326	−8.71	2.11
$\gamma_L\alpha_D$	−656.955 569	−5.72	5.09
$\gamma_L\beta_L$	−656.957 037	−6.64	4.17
$\gamma_L\delta_D$	−656.956 465	−6.28	4.53
$\gamma_L\delta_L$	−656.958 574	−7.61	3.20
$\gamma_L\varepsilon_D$	−656.955 072	−5.41	5.40
$\gamma_L\varepsilon_L$	−656.954 742	−5.20	5.61
$\gamma_L\gamma_D$	−656.959 946	−8.47	2.34
$\gamma_L\gamma_L$	−656.963 681	−10.81	0.00

[a]ΔE^R values given in kcal/mol.

The least stable conformation (+4.56 kcal/mol) turned out to be the $\varepsilon_D\delta_D$ and the most stable conformation (−10.81 kcal/mol) is the $\gamma_L\gamma_L$ conformation. The six existing homo-

Fig. 3. (*a*) Variation of stabilization energy (ΔE^R_{stabil}) for dialanine diamide, as computed for conformer X, with relative energy ($\Delta E^R_{X-(\gamma_L)_2} = E^R_X - E^R_{(\gamma_L)_2}$) with respect to its $(\gamma_L)_2$ conformer. (*b*) Variation of stabilization energy (ΔE^R_{stabil}) for trialanine diamide, as computed for conformer X, with relative energy ($\Delta E^R_{X-(\gamma_L)_3} = E^R_X - E^R_{(\gamma_L)_3}$) with respect to its $(\gamma_L)_3$ conformer.

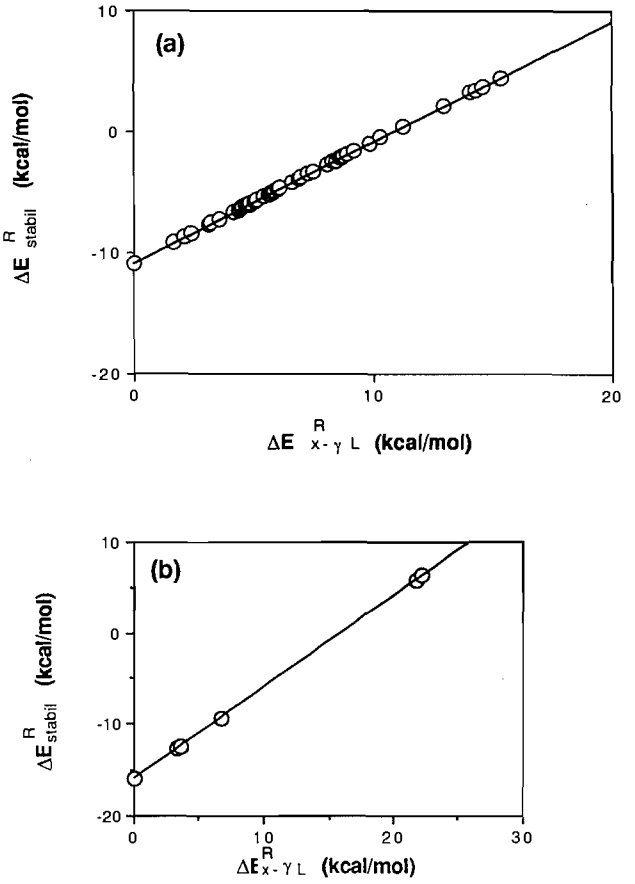

conformations (19) of For-Ala-Ala-NH_2 have the following stabilization energy values:

		$\Delta E^{Me,Me}_{stabil}$
adad	$\alpha_D\alpha_D$	−6.08
blbl	$\beta_L\beta_L$	−8.77
dddd	$\delta_D\delta_D$	+3.52
eded	$\varepsilon_D\varepsilon_D$	+3.76
gdgd	$\gamma_D\gamma_D$	−6.13
glgl	$\gamma_L\gamma_L$	−10.81

The results are summarized in Table 2 and illustrated in Fig. 3*a*.

(iii) Homotripeptides

A total of six diagonal conformations for HCO(-NH-CHMe-CO)$_3$-NH_2 have been computed (17) and the following range

Table 3. Energetics[a] of alanine tripeptides (For-Ala-Ala-Ala-NH_2).

Conformation (x)	Energy (hartrees)	ΔE^{R}_{stabil}	$\Delta E^{R}_{X-\gamma_L}$
$\alpha_D\alpha_D\alpha_D$	−901.447 981	−12.47	3.52
$\beta_L\beta_L\beta_L$	−901.448 327	−12.68	3.31
$\delta_D\delta_D\delta_D$	−901.418 164	6.25	22.24
$\varepsilon_D\varepsilon_D\varepsilon_D$	−901.418 849	5.82	21.81
$\gamma_D\gamma_D\gamma_D$	−901.442 887	−9.27	6.72
$\gamma_L\gamma_L\gamma_L$	−901.453 598	−15.99	00.00

[a]ΔE^{R} values given in kcal/mol.

of stabilization energy values has been found.

$$-15.99\text{kcal/mol} \leq \Delta E^{Me,Me,Me}_{stabil} \leq +6.25\text{kcal/mol}$$
$$(\gamma_L\gamma_L\gamma_L) \qquad (\delta_D\delta_D\delta_D)$$

This is illustrated in Fig. 3*b* and summarized in Table 3.

The results for the alanine homooligopeptide diamides shown in Figs. 2, 3*a*, and 3*b* are summarized in Fig. 5, where b_1, b_2, and b_3 are the intercepts for ΔE_{stabil} with respect to the $\Delta E^{R}_{X-\gamma_L} = E_{rel}$ corresponding to the stabilization energy at the $(\gamma_L)_n$ conformation.

(iv) Mixed dipeptides and tripeptides

The energetics of systematic replacement of α-hydrogens in For-Gly-Gly-NH_2 with Me groups to give the corresponding For-Ala-Gly-NH_2, For-Gly-Ala-NH_2, and For-Ala-Ala-NH_2 are depicted in Fig. 6. The approximately −5.4 kcal/mol stabilization energy per Me substitution is apparent and there is only a negligible difference in stability between For-Gly-Ala-NH_2 and For-Ala-Gly-NH_2.

Fig. 4. The shifting of the reference state for changing from $\Delta E^{R}_{X-(\gamma_L)n}$ to ΔE^{R}_{stabil}.

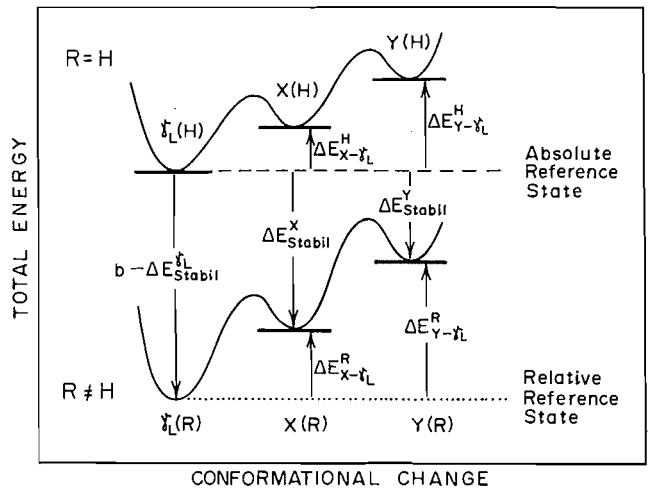

Table 4. Calculated (HF/3-21G) parameters for mixed dipeptides.[a]

Parameter	Dipeptides			
	Gly-Gly	Ala-Gly	Gly-Ala	Ala-Ala
Energy (hartree)	−579.312 309	−618.138 034	−619.137 973	−656.963 681
ϕ_1	−82.6	−84.0	−82.9	−84.2
ϕ_2	−83.5	−83.7	−84.8	−84.9
ψ_1	63.5	66.6	63.6	67.0
ψ_2	63.3	63.4	66.2	66.4
χ_1	—	63.8	—	64.0
χ_2	—	—	63.3	63.3
ω_0	−175.7	−176.2	−175.8	−174.4
ω_1	−176.6	−179.0	−176.9	−174.1
ω_2	−178.3	−178.3	179.0	−178.9
Force (RMS)	1.6×10^{-5}	1.0×10^{-5}	1.1×10^{-5}	2.1×10^{-5}
Force (Max)	4.1×10^{-5}	3.6×10^{-5}	3.5×10^{-5}	6.4×10^{-5}
d_{model}	7.95	7.95	7.92	7.92
d_{crit}	8.79	8.79	8.75	8.76
τ_{model}	164.3	168.3	163.5	167.8
τ_{crit}	165.0	169.0	164.0	166.4
$O_1—H^2_A$	2.00	2.01	2.01	2.02
$O_2—H^3_A$	2.00	2.00	2.00	2.00
ΔE_{rel}	00.00	00.00	00.00	00.00
S.E.	00.00	−5.43	−5.39	−10.81

[a]All dipeptides were in their global minimum ($\gamma_L\gamma_L$) conformation. All distances given in Å, angles given in degrees (°). Forces are in atomic units (au). Relative energy values are in kcal/mol.

Can. J. Chem. Downloaded from www.nrcresearchpress.com by 80.90.12.36 on 09/08/12
For personal use only.

Can. J. Chem. Downloaded from www.nrcresearchpress.com by 80.90.12.36 on 09/08/12
For personal use only.

Table 5. Calculated (HF/3-21G) parameters for mixed tripeptides.[a]

Parameter	Gly-Gly-Gly	Gly-Gly-Ala	Gly-Ala-Gly	Ala-Gly-Gly	Ala-Ala-Gly	Ala-Gly-Ala	Gly-Ala-Ala	Ala-Ala-Ala
Energy (hartree)	−784.976 902	−823.802 467	−823.802 280	−823.802 691	−862.628 051	−862.628 259	−862.627 822	−901.453 577
ϕ_1	−82.3	−82.2	−82.4	−83.6	−83.7	−83.4	−82.4	−83.8
ϕ_2	−82.6	−83.0	−84.2	−82.9	−84.5	−83.1	−84.5	−84.6
ϕ_3	−83.7	−85.0	−83.8	−83.6	−83.9	−85.0	−85.1	−85.2
ψ_1	63.2	63.2	63.5	66.3	66.8	66.2	63.5	66.8
ψ_2	61.8	62.0	65.4	62.0	65.5	62.0	65.6	65.7
ψ_3	63.3	66.0	63.4	63.2	63.3	65.9	66.3	66.3
χ_1	—	—	—	63.7	63.8	63.7	—	63.8
χ_2	—	—	63.0	—	63.0	—	63.0	63.1
χ_3	—	63.1	—	—	—	63.2	63.2	63.2
ω_0	−175.9	−175.9	−176.0	−176.3	−176.4	−176.3	−175.9	−176.3
ω_1	−176.9	−176.9	−177.3	−179.3	−179.9	−179.2	−177.3	−179.8
ω_2	−175.5	−175.9	−178.4	−175.6	−178.3	−175.9	−178.6	−178.6
ω_3	−178.6	178.9	−178.7	−178.6	−178.5	178.9	178.8	178.8
Force (RMS)	6.5×10^{-5}	4.5×10^{-5}	1.1×10^{-5}	1.9×10^{-5}	3.1×10^{-5}	5.2×10^{-5}	2.2×10^{-5}	1.6×10^{-5}
Force (Max)	2.6×10^{-4}	1.4×10^{-4}	4.9×10^{-5}	5.8×10^{-5}	1.4×10^{-4}	2.1×10^{-4}	8.5×10^{-5}	7.0×10^{-5}
d^1_{model}	8.36	8.33	8.36	8.37	8.37	8.33	8.33	8.34
d^1_{crit}	8.78	8.74	8.79	8.79	8.80	8.75	8.76	8.77
d^2_{model}	8.35	8.35	8.31	8.35	8.32	8.35	8.31	8.32
d^2_{crit}	8.77	8.77	8.72	8.77	8.73	8.76	8.73	8.73
τ^1_{model}	164.5	163.7	169.1	164.7	169.0	163.8	168.3	168.3
τ^1_{crit}	163.0	162.0	167.5	163.1	167.5	162.1	166.6	166.6
τ^2_{model}	162.6	162.3	161.9	166.6	166.1	166.1	161.6	165.8
τ^2_{crit}	164.8	164.5	164.1	168.8	168.4	168.3	163.8	168.0
$O_1—H^2_A$	1.98	1.98	1.99	1.98	2.00	2.00	1.99	2.00
$O_2—H^3_A$	1.97	1.98	1.98	1.97	1.98	1.98	1.99	1.99
$O_3—H^4_A$	1.99	1.99	1.99	1.99	1.99	1.99	2.00	2.00
ΔE_{rel}	00.00	00.00	00.00	00.00	00.00	00.00	00.00	00.00
S.E.	00.00	−5.33	−5.21	−5.47	−10.67	−10.80	−10.53	−15.98

[a]All dipeptides were in their global minimum ($\gamma_L\gamma_L\gamma_L$) conformation. All distances given in Å, angles given in degrees. Forces are in atomic units (au). Relative energy values are in kcal/mol.

Can. J. Chem. Downloaded from www.nrcresearchpress.com by 80.90.12.36 on 09/08/12
For personal use only.

Fig. 5. Variation of stabilization energy (ΔE^{R}_{stabil}) for HCO-(NH-CHR-CO)$_n$-NH$_2$ with $1 \leq n \leq 3$, as computed for conformer X, with relative energy ($\Delta E^{R}_{X-(\gamma_L)n} = E^{R}_{X} - E^{R}_{(\gamma_L)n}$) with respect to its $(\gamma_L)_n$ conformers.

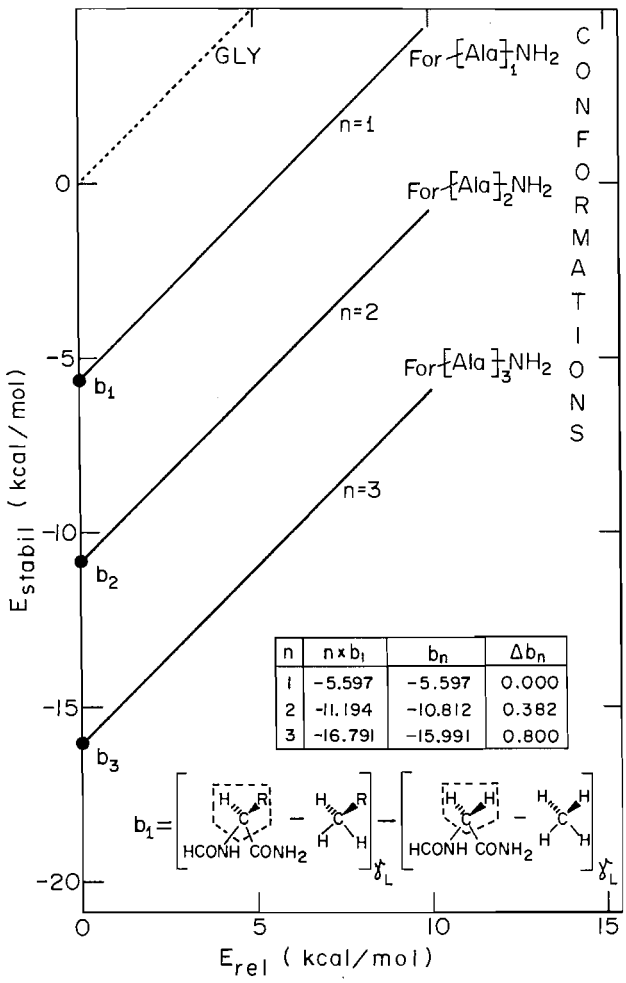

n	n x b_1	b_n	Δb_n
1	-5.597	-5.597	0.000
2	-11.194	-10.812	0.382
3	-16.791	-15.991	0.800

Similar information is presented for tripeptides in Fig. 7. Again, the Me substitution appears to be reasonably constant and the different isomers have practically the same stability.

If the Me stabilization energy were strictly constant then the stabilization could be fit to a straight line:

$$\Delta E_{stabil} = (b_1) \times n$$

where the variable n is the degree of polymerization of the peptide For-(NH-CHMe-CO)$_n$-NH$_2$ and the slope b_1 is the stabilization exerted by a single Me group for a monopeptide ($n = 1$).

Figure 8 indicates that this is only approximately true. As the diagonal broken line shows, there is an ever increasing systematic deviation from such a simple rule. Since this systematic deviation represents a reduction in stabilization energy it seems reasonable to assume that such a destabilizing phenomenon demonstrates steric hindrance due to Me crowding.

Such a phenomenon is also encountered in partially Me-substituted tripeptides. For example: For-Ala-Gly-Ala-NH$_2$ (denoted as Me, H, Me) is more stable than For-Ala-Ala-

Fig. 6. Energetics of systematic Me substitution of Gly-Gly leading to Ala-Ala.

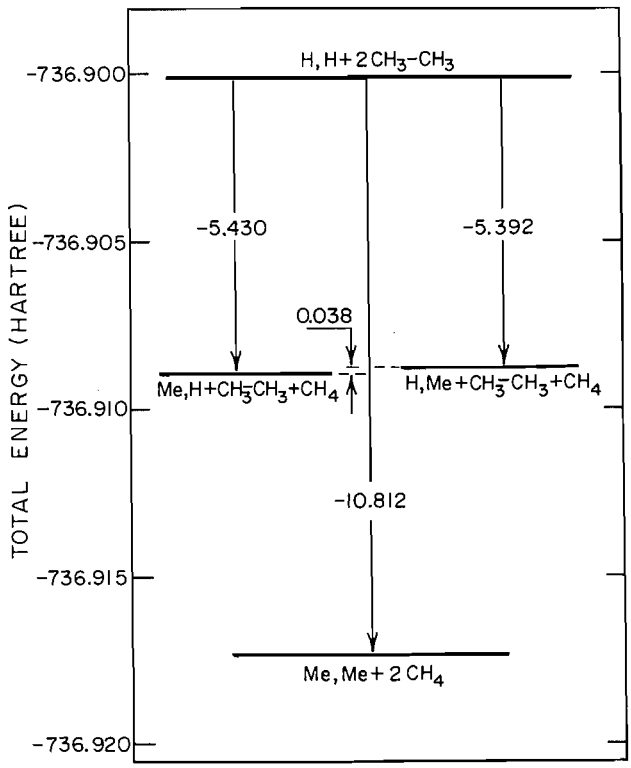

Fig. 7. Energetics of systematic Me substitution of Gly-Gly-Gly leading to Ala-Ala-Ala.

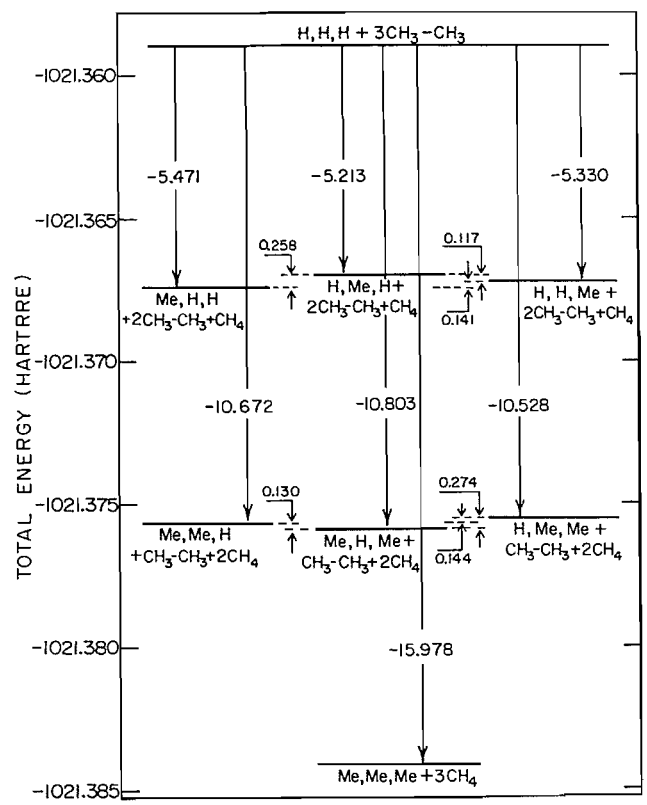

Fig. 8. Variation of stabilization energy with increasing degree of polymerization for $(Gly)_n$ and $(Ala)_n$ and mixed systems.

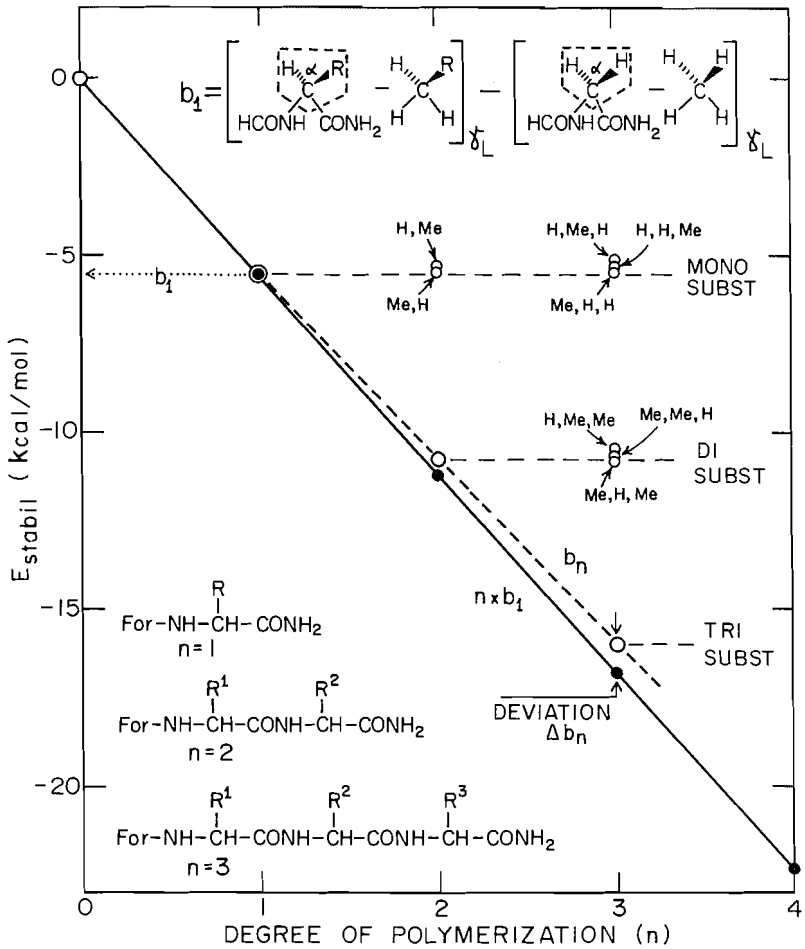

Fig. 9. Energetics of isodesmic Me–H exchange in di- and tripeptides (energy differences are given in kcal/mol).

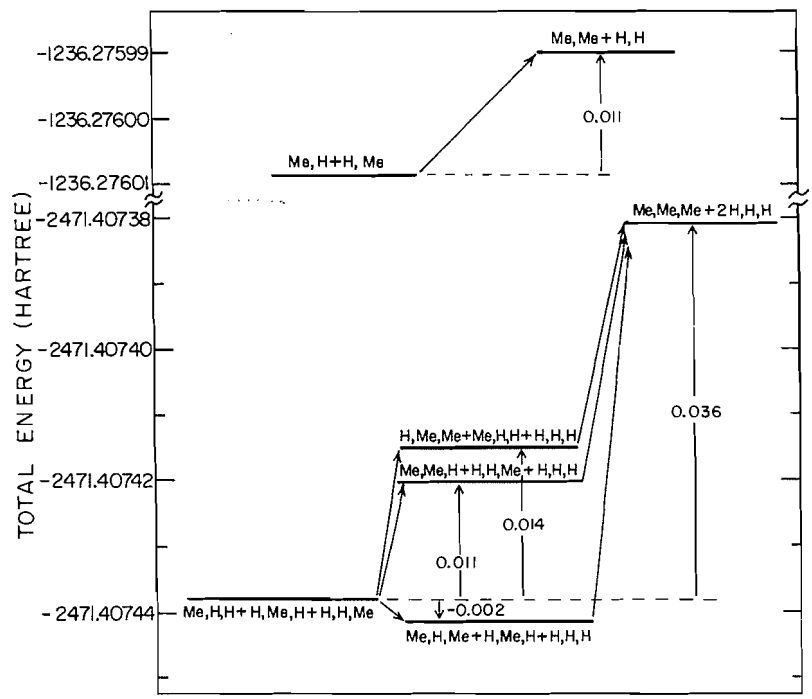

Can. J. Chem. Downloaded from www.nrcresearchpress.com by 80.90.12.36 on 09/08/12
For personal use only.

Gly-NH_2 (denoted as Me, Me, H) and For-Gly-Ala-Ala-NH_2 (denoted as H, Me, Me). Figure 9, presenting the energetics of Me transfer via isodesmic reactions, also underlines this phenomenon.

In summary, it is also clear from Fig. 8, for both $n = 2$ and $n = 3$, that Me substitution in the N-terminal amino acid residue (i.e., near the formyl protecting group) stabilizes the oligopeptide slightly more than substitution at the C-terminal amino acid residue (i.e., near the amide protecting group). Also, substitution at the central amino acid residue in the case of $n = 3$ represents somewhat less effective destabilization than either one of the terminal substitutions in tripeptides.

Concluding remarks

As a result of the present work, the stabilization of all oligopeptide and protein conformations can now be related to the standard conformation $(\gamma_L)_n$ of polyglycine.

$$\begin{array}{l} \text{-Gly-Gly-Gly-} + CH_3\text{-}CH_2\text{-OH} + CH_3\text{-}CH_3 + CH_3\text{-}CH_2\text{-Ph} \\ \quad \gamma_L \ \ \gamma_L \ \ \gamma_L \\ \qquad \Big\downarrow \ \Delta E_{\text{stabil}} = b_{\text{Ser}} + b_{\text{Ala}} + b_{\text{Phe}} < 0 \\ \text{-Ser-Ala-Phe-} \qquad + 3\ CH_4 \\ \quad \gamma_L \ \ \gamma_L \ \ \gamma_L \\ \qquad \Big\downarrow \ \Delta E^{\text{Me}}_{\gamma_L \rightarrow \alpha_D} > 0 \\ \text{-Ser-Ala-Phe-} \qquad + 3\ CH_4 \\ \quad \gamma_L \ \ \alpha_D \ \ \gamma_L \end{array}$$

The value of b_{Ala} is presented here for different degrees of polymerization ($1 \leq n \leq 3$). The value of b_{Ser} has been published recently (22) for various side-chain orientations, and the value of b_{Phe} will be published shortly (23). When stabilization energies are available for all amino acid residues, in every possible side-chain conformation, then the stabilization energy will be available for all backbone folding, and every possible short-range, backbone–side-chain interaction. The only stabilization or destabilization forces that lie outside of such an approach are the long-range side-chain–backbone and side-chain–side-chain interactions.

Acknowledgment

The authors wish to express their gratitude to the University of Toronto Center for High Performance Computing for the generous donation of Cray computer time at the Pittsburgh Supercomputer Center, and to the Leibnitz Computing Centre of the Bavarian Academy of Sciences for providing CPU time on their Cray YMP/8 Supercomputer. The continued financial support of the Natural Sciences and Engineering Research Council of Canada is gratefully acknowledged. This research was also supported in part by a grant from the Hungarian Scientific Research Foundation (OTKA Nos. T-017192 and F-013799).

References

1. W.J. Hehre, L. Radom, P.v.R. Schleyer, and J.A. Pople. Ab initio molecular orbital theory. Wiley, New York. 1986.
2. P.v.R. Schleyer. Pure Appl. Chem. **59**, 1647 (1987).
3. K.B. Wiberg and C.M. Breneman. J. Am. Chem. Soc. **112**, 8765 (1990).
4. K.B. Wiberg. J. Org. Chem. **56**, 544 (1991).
5. K.B. Wiberg and K.E. Laidig. J. Org. Chem. **57**, 5092 (1992).
6. K.B. Wiberg, C.M. Hadad, P.R. Roblen, and J. Cioslowski. J. Am. Chem. Soc. **114**, 8644 (1992).
7. L. Gong, M.A. McAllister, and T.T. Tidwell. J. Am. Chem. Soc. **113**, 6021 (1991).
8. M.A. McAllister and T.T. Tidwell. J. Org. Chem. **59**, 4506 (1994).
9. M.A. McAllister and T.T. Tidwell. J. Chem. Soc. Perkin Trans. 2, 2239 (1994).
10. M.A. McAllister and T.T. Tidwell. J. Am. Chem. Soc. **114**, 6553 (1992).
11. M.A. McAllister and T.T. Tidwell. J. Am. Chem. Soc. **114**, 5362 (1992).
12. W. Viviani, J.-L. Rivail, and I.G. Csizmadia. Theor. Chim. Acta, **85**, 189 (1993).
13. A. Perczel, J.G. Ángyán, M. Kajtár, W. Viviani, J.-L. Rivail, J.-F. Marcoccia, and I.G. Csizmadia. J. Am. Chem. Soc. **113**, 6256 (1991).
14. W. Viviani, J.-L. Rivail, A. Perczel, and I.G. Csizmadia. J. Am. Chem. Soc. **115**, 8321 (1993).
15. M.A. McAllister, A. Perczel, P. Csaszar, W. Viviani, J.-L. Rivail, and I.G. Csizmadia. J. Mol. Struct. **288**, 161 (1993).
16. M.A. McAllister, A. Perczel, P. Csaszar, and I.G. Csizmadia. J. Mol. Struct. **288**, 181 (1993).
17. A. Perczel, M.A. McAllister, P. Csaszar, and I.G. Csizmadia. J. Am. Chem. Soc. **115**, 4849 (1993).
18. A. Perczel, M.A. McAllister, P. Csaszar, and I.G. Csizmadia. Can. J. Chem. **72**, 2050 (1994).
19. M. Cheung, M.E. McGovern, T. Jin, D.-C. Zhao, M.A. McAllister, O. Farkas, A. Perczel, P. Csaszar, and I.G. Csizmadia. J. Mol. Struct. **309**, 151 (1994).
20. J.S. Binkley, J.A. Pople, and W.J. Hehre. J. Am. Chem. Soc. **102**, 939 (1980).
21. M.J. Frisch, G.W. Trucks, M. Head-Gordon, P.M.W. Gill, M.W. Wong, J.B. Forseman, B.G. Johnson, H.B. Schlegel, M.A. Robb, E.S. Replogle, R. Gomperts, J.L. Andres, K. Raghavachari, J.S. Binkley, C. Gonzalez, R.L. Martin, D.J. Fox, D.J. Defrees, J. Baker, J.J.P. Stewart, and J.A. Pople. GAUSSIAN 92. Gaussian Inc., Pittsburg, Pa. 1992.
22. O. Farkas, A. Perczel, J.-F. Marcoccia, M. Hollosi, and I.G. Csizmadia. J. Mol. Struct. (THEOCHEM), **331**, 27 (1995).
23. O. Farkas, M.A. McAllister, J. Ma, A. Perczel, M. Hollosi, and I.G. Csizmadia. J. Mol. Struct. (THEOCHEM). In press.

Can. J. Chem. Downloaded from www.nrcresearchpress.com by 80.90.12.36 on 09/08/12
For personal use only.

Application of median filtering to noisy data

David C. Stone

Abstract: The properties and application of the median filter are investigated using both simulated and real data for signals evolving with time. Comparison is made with existing numerical techniques for drift compensation and noise reduction in analytical measurements such as the moving average and Savitzky–Golay digital filters. The median filter provides a means for dealing with "spiky" noise and separating peaks from a slowly changing baseline, even when the exact nature of the drift and noise distribution is not known. Median filtering is a useful and complementary addition to existing digital filtering techniques, being mathematically robust and readily implemented on any computer platform.

Key words: median filtering, signal noise, signal processing, digital filters, chemometrics, data smoothing.

Résumé : Utilisant des données simulées ainsi que réelles de signaux évoluant avec le temps, on a étudié les propriétés et le domaine d'application du filtre médian. On a effectué une comparaison de cette méthode avec les techniques numériques existantes pour la compensation de la dérive et pour la réduction du bruit dans des mesures analytiques telles que la moyenne pondérée et les filtres digitaux de Savitzky–Golay. Le filtre médian fournit une façon de tenir compte du bruit à pointes et de séparer les pics d'une ligne de base qui se modifie lentement, même lorsque la nature exacte de la dérive et de la distribution du bruit n'est pas connue. Le filtrage médian est une addition utile et complémentaire aux techniques existantes de filtrage digital, il est mathématiquement robuste et il peut facilement être mis en place sur toutes sortes d'ordinateurs.

Mots clés : filtrage médian, bruit de signal, étude des signaux, filtres digitaux, chimiométrique, aplanissement des données.

[Traduit par la rédaction]

Introduction

Many measurements in analytical chemistry involve recording the evolution of some dependent variable (the signal) with an independent variable increasing in discrete steps. The most obvious examples are the measurement of time-dependent phenomena in kinetic studies, although with the increasing use of computers many wavelength-dependent measurements can be described in the same terms. This has led to the development of various numerical methods for dealing with noisy or drifting signals, ranging from the simple to the complex (1–3). The method of choice for a particular situation will be determined by factors such as the nature of the measurement and noise, the magnitude of the signal-to-noise ratio, the computational and programming resources available, and the time scale for the required calculations. Different methods may also be considered where calculations must be performed in real time as data are collected rather than following completion of the measurement cycle. Thus while sophisticated and powerful procedures are increasingly being applied to analytical situations, there is still a place for simple mathematical procedures that can be accomplished with a minimum of computational expenditure and programming experience. One such method is the technique of median filtering. Originally described by Tukey (4) in the 1970s, median filtering has previously been applied to image (5) and speech processing (6). For example, many image-processing programs that provide "sharpening" or "edge extraction" functions exploit median filtering to achieve this.

It is difficult to say how widely median filtering has been employed in analytical chemistry, although it is likely that averaging techniques and polynomial smoothing are both considerably more prevalent. Papers explicitly on median filters and their properties are rare within the chemical literature (7, 8), while the technique is not as well covered in chemometrics texts as other methods of noise reduction. Median filtering can, however, be usefully applied to problems in analytical chemistry as demonstrated by the recent original work of Moore and Jorgenson (7). They applied this method to the extraction of peaks from chromatograms having strongly drifting baselines, and were able to show that it provided a superior performance to the mathematically more complex Butterworth and Chebyshev digital filters. More recently Camus and Larson (8) applied median filtering to noise reduction in atom probe analysis. This paper is of particular interest because it highlights the implicit assumption often made that the noise distribution is Gaussian. In this case the distribution is binomial (an event with probability q will occur m times out of n trials where m is an integer, $0 \leq m \leq n$), so filters developed for Gaussian noise do not perform well, distorting important features of the data. A more familiar example of this situation might be photon-counting measurements, in which errors are described by the Poisson distribution.

Received February 16, 1995.

D.C. Stone.[1] Department of Chemistry, University of Toronto, Toronto, ON M5S 1A1, Canada.

[1] Telephone: (416) 978-6568. Fax: (416) 978-8775. E-mail: dstone@chem.utoronto.ca

Can. J. Chem. Downloaded from www.nrcresearchpress.com by 46.23.64.124 on 09/08/12
For personal use only.

Can. J. Chem. Downloaded from www.nrcresearchpress.com by 46.23.64.124 on 09/08/12
For personal use only.

In this paper, the properties of the median filter are explored for situations common in analytical chemistry using synthetic transient response data, and its performance is compared to other, readily implemented digital filters. The transient functions chosen represent both continuous and discontinuous, symmetrical and asymmetrical functions. The baseline correction method of Moore and Jorgenson is also further evaluated in terms of the integrity of the extracted peak profile as well as the recovered peak area. Finally, the median filter is demonstrated using "worse case scenario" data from a surface acoustic wave based chemical sensor system.

Experimental

Instrumentation

The surface acoustic wave – gas chromatographic combination used in this work is a development of a system described previously (9). Briefly, a surface acoustic wave (SAW) device is used as the frequency-controlling element in a radio frequency oscillator circuit, and is situated in a GC detector oven immediately at the outlet of a capillary column. Under these circumstances, the oscillation frequency is perturbed by mass eluting from the column and adsorbing to the SAW surface. The recorded chromatographic peaks are therefore a function of both the evolving eluate concentration and the adsorption kinetics at the sensor surface. In the current system, both channels of a quartz 52 MHz dual delay-line SAW device are electrically connected in parallel and exposed to a single gas stream. A second, external SAW device is used as a signal reference source. Measurements can be made by monitoring either the difference frequency between the two SAWs, or recording the frequency of the detector SAW directly.

The oscillation frequency of the SAW device was monitored continuously using an HP5328A counter (Hewlett Packard) connected to an Apple™ Macintosh® II computer via an IEEE 488 interface bus (National Instruments). Mixtures of up to six components were injected on to a J&W 30 m × 0.53 mm DB-Wax capillary column (Chromatographic Specialities, Inc.). Chemicals used were either analytical grade and used as received or were freshly distilled before use. Confirmation of the chromatogram was obtained using an FID detector in series with the SAW device and an HP3390A recording integrator (Hewlett Packard).

Software

Data collection and analysis were performed using custom software written and compiled using Think C™ 6.0 (Symantec Corp.). The median filtering subroutines were written using methods derived from Press et al. (10). Additional smoothing and filtering were achieved using the generalized Savitzky–Golay method (sliding or initial-point least-squares smoothing) as implemented by Gorry (11). The software also includes routines for peak height, width, and area calculation, baseline subtraction, and curve fitting. Peaks are defined by the user in a special window by drawing a straight line across the base of the peak as identified visually; all peak calculations are then performed within this region.

A second program was written to generate artificial data for more detailed analysis of the filter. This allowed data sets describing a variety of functions to be constructed with or without the addition of specific noise distributions. Comparison of the original and filtered data was achieved by exporting the data to a spreadsheet program for analysis and plotting.

Fig. 1. The effect of filtering on outliers and steps: (A) smoothing by a moving average filter ($r = 3$); (B) smoothing by a median filter ($r = 3$). (—) original data, (+) filtered data.

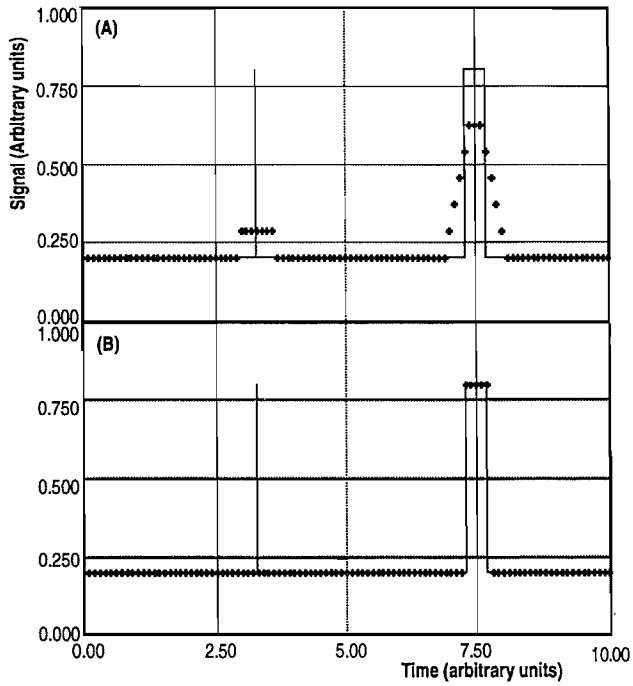

Results and discussion

General description of filter properties

A common technique for improving the signal-to-noise ratio of data evolving with time is the moving average (MA) filter (ref. 2, p. 175). In essence, the kth value is replaced with the arithmetic mean of all the values in the range $(k - r)$ to $(k + r)$ of a moving "window" of rank r and width $(2r + 1)$. It should be noted that the first and last r values are "lost" from the data in the process. An alternative scheme involves bin (or boxcar) averaging, where each kth value is replaced with the mean of j replicate determinations. This latter approach is satisfactory where the rate of data collection is much greater than the rate of any change in the measured signal and the noise is normally distributed. When the sampling rate is low relative to the rate of change of the signal, however, this can result in a significant distortion of the measured profile.

A simple calculation can readily show that a single outlier affects the mean greatly, resulting in a rectangular "step" of width $2r + 1$ in the filtered data. In the same way it can be shown that passing a MA filter over a step function will result in a ramp of width $2r + 1$ centred at the point of the step, since each successive window will contain a greater number of larger values (Fig. 1A). Recognition of this sensitivity of the mean to outliers has resulted in increasing interest in "robust" (nonparametric) statistical methods (12). Such methods are attractive since it is readily demonstrated that the median is considerably less sensitive to outliers than the mean. Furthermore, there are no assumptions concerning the nature of the noise distribution implicit in their use. From a computational

viewpoint, however, the median could be considered as less efficient since calculation requires sorting the data into either ascending or descending order. For a set of n values x_i the median is calculated as

$$[1] \quad m = x_k; \qquad k = \frac{(n+1)}{2} \qquad (n \text{ odd})$$

$$[2] \quad m = \frac{(x_k + x_l)}{2}; \qquad k = n/2;\ l = (n/2) + 1 \qquad (n \text{ even})$$

Since this is a selection process it is possible to speed up the calculation by using a variation of the Quicksort method in which only those subsets containing the required kth value are sorted (10). In this modification a further improvement in speed can be obtained for even $n > 100$ by equating the median to the $(n/2)$th value, avoiding two sorts (for the two centre values). With these considerations in mind, implementation of the median filter (ME) is essentially the same as for the moving average filter: For $r > 0$, the kth point in the filtered data corresponds to the median of the unfiltered values in the window $(k - r)$ to $(k + r)$. As with the moving average filter, the first and last r points are lost. Again, a simple calculation serves to illustrate the properties of this filter. When a median filter (moving average using the median instead of the mean) with $r = 1$ is passed over a single outlier, the outlying value will always be at the extreme end of the ranked data, and so will never become the median value. Similarly, when a median filter is passed over a step function it can readily be appreciated that the median value will become the higher value precisely when the centre of the window is at the step point *provided* that the window is narrower than the step function (Fig. 1B). This clearly demonstrates the importance of careful selection and optimization of filter parameters when applying digital filtering to experimental data.

Figure 2 shows the effects of applying both filters to an artificially generated chromatographic peak, which is essentially a continuous function (Gaussian) with a slight asymmetry introduced by virtue of monitoring the evolving profile at a fixed point over time rather than at a fixed time over distance (13). For the data used here the retention time and variance were 3.00 min and 0.004 min^2, respectively, while the actual peak consisted of ≈40 data points. Both filters caused a decrease in observed peak height with increasing r, although for small r the ME filter showed a smaller reduction. They also gave rise to increased peak widths, although the median filter did so at a slower rate. The two filters showed opposite behaviour with increasing r for other peak properties such as observed area and retention time, however. Thus the MA filter gave constant area and retention time, while the ME filter showed reduced area and a slight increase in retention time (3.00 to 3.08 min for $r = 0$ to $r = 15$). These results can be directly attributed to the difference in mathematical properties of the median and mean, which also explain the flat-topped, truncated peaks produced by the median filter. The latter are produced whenever the data points are symmetrically distributed about a single minimum or maximum, i.e., the values on one side are the mirror image of those on the other. In fact it can be shown (Fig. 3) that there is a relationship between r and the number of identical values about the centre, n_c. For n even, symmetrically distributed points,

Fig. 2. The effect of filtering on a chromatographic peak. Upper: (A) original data; (B) smoothing by a moving average filter ($r = 8$); (C) smoothing by a median filter ($r = 8$). Data are spaced every 0.01 min. Lower: plot of relative peak height versus filter rank for both filters.

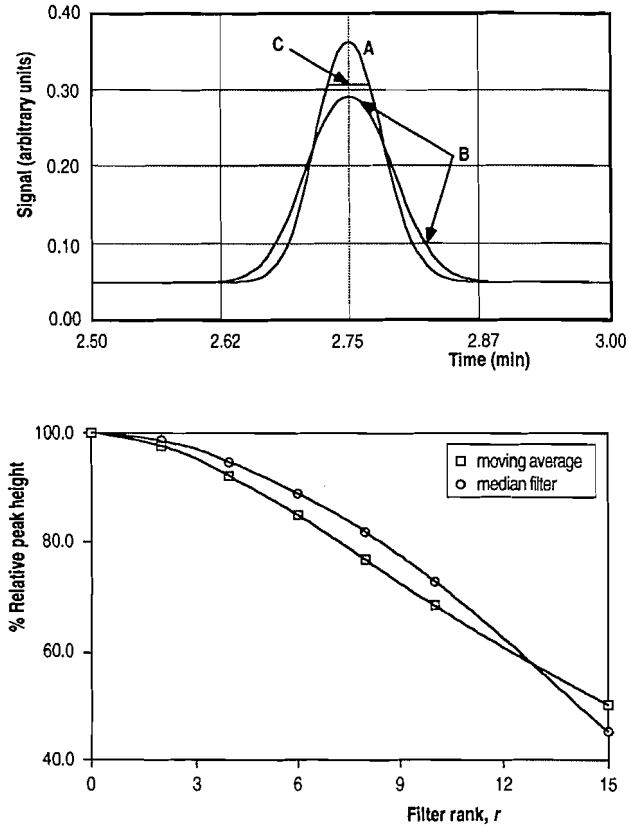

Fig. 3. Origin of peak truncation for the median filter. The median of the $(k - 1)$th window is identical to the $(k - 1)$th value. The median of the kth window is equal to the $(k - 1)$th and $(k + 1)$th values, not the kth value.

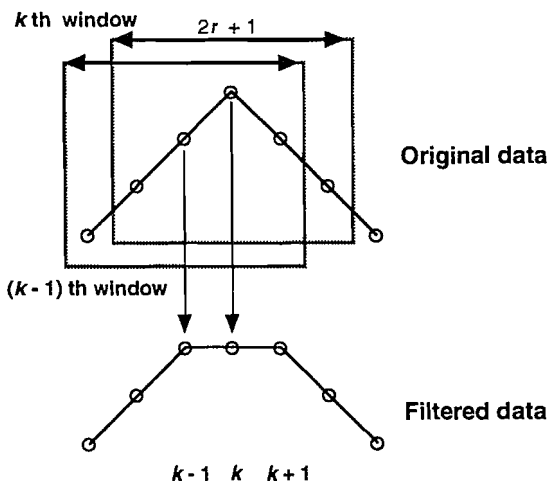

$$[3] \quad n_c = r \text{ for } r \text{ odd}, r > 1$$

$$[4] \quad n_c = r + 1 \text{ for } r \text{ even}, r > 0$$

and for n odd, symmetrically distributed points,

Can. J. Chem. Downloaded from www.nrcresearchpress.com by 46.23.64.124 on 09/08/12
For personal use only.

Table 1. Effect of filtering on peak shape for the chromatogram of Fig. 2.

	RMS deviation[a]	
Rank r	Median	Average
4	0.0024	0.0071
8	0.0118	0.0221
15	0.0470	0.0502

[a]Root-mean-sum of the square of the differences between ith points in the original and filtered chromatograms.

Table 2. Effect of filtering on peak shape for the profile of Fig. 4.

	RMS deviation[a]	
Rank r	Median	Average
4	0.000 36	0.0064
8	0.001 06	0.0157
15	0.003 29	0.0345

[a]Same as Table 1.

[5] $n_c = r + 2$ for r odd, $r > 0$

[6] $n_c = r + 1$ for r even, $r > 0$

The effect of filtering on overall peak shape can be evaluated by calculating the root mean square of the differences between filtered and unfiltered data, i.e.,

[7] $$\text{distortion} = \sqrt{\frac{1}{n}\sum_{i=1}^{n}(y_i - y_i')^2}$$

Such calculations showed that both filters caused increasing distortion of overall peak shape, the MA filter having the greater effect (Table 1).

A discontinuous, asymmetrical peak shape was generated using exponential functions. This type of transient would be encountered, for example, in flow injection analysis using a well-stirred mixing tank with a step concentration input function. The moving average and median filters were again applied to these data, and their effect evaluated as before (Fig. 4). Both filters caused approximately the same decrease in peak height with increasing rank (97.7% of maximum for r = 15) while the peak width increased slightly. Times for peak maximum were unchanged for the ME filter but decreased markedly for the MA filter (86.0% of original for r = 15). A similar truncation of the peak maximum was observed for the ME filter as before, but the moving average filter caused a much larger distortion of the overall peak shape (Table 2). In particular, the time at which the concentration first increases was masked by the moving average filter. Note also that the severity of all these effects for both filters depends on the number of points sampled during evolution of the profile: the higher the sampling rate and the broader the profile, the lower the relative distortion of the filtered to original signals.

Fig. 4. The effect of filtering on an exponential peak shape: (A) original data; (B) smoothing by a moving average filter (r = 10); (C) smoothing by a median filter (r = 10). Inset: close-up of the peak maximum showing truncation of the peak by the median filter. Data are spaced every 0.01 min.

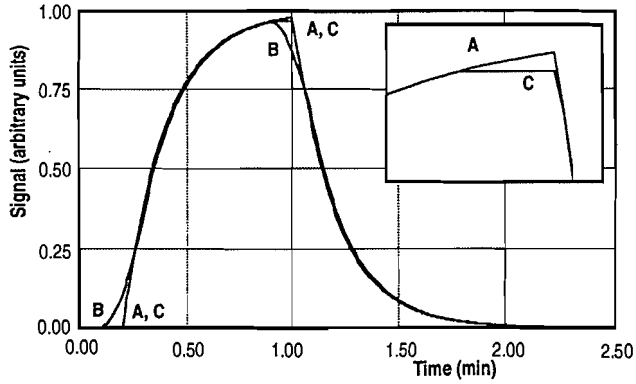

Effect of noise on filter performance

The effect of measurement noise was investigated by superposing known noise functions onto the original data shown in Fig. 1 and repeating the filtering calculations. The noise values were generated using methods outlined in Press et al. (10) to give three different distributions: (*i*) uniform random deviates with zero mean and ranges ±0.02, 0.05, and 0.10; (*ii*) normally distributed deviates with zero mean and standard deviations of 0.02, 0.05, and 0.10; and (*iii*) exponentially distributed deviates with zero mean multiplied by scaling factors of 0.02, 0.05, and 0.10. As expected, the median filter successfully removed the spike from the data while retaining the step function for all three noise types. (Note, however, that when r is greater than or equal to the width of the step function in the data (r = 5 in this case) the step function will be completely removed.) This is to be expected since, as we have seen, the mathematical properties of the median filter favour application to data where edge retention is important (5). In the same way, the moving average filter gave rise to the same features as shown in Fig. 1B. Both filters were successful in reducing baseline noise as measured by the standard deviation, there being a significant difference in s between filtered and unfiltered data as measured by the F-test (p = 0.05). Using the same measure, there was no significant difference between the standard deviations for the two different filters. Similar results were obtained by Camus and Larson for a simulated composition profile with superposed binomially distributed noise (8).

Filter performance for drift compensation

Moore and Jorgenson (7) used median filtering to extract chromatographic peaks from data with a drifting baseline by first using the filter to completely remove the peak of interest and then subtracting the baseline to obtain the peak in the absence of drift. As long as the filter rank was greater than or equal to the number of points in the peak, accurate peak areas and heights were obtained on comparing the filtered and unfiltered data. A similar procedure was carried out using the data of Fig. 2 added to known baseline drift and noise functions. Initial cal-

Can. J. Chem. Downloaded from www.nrcresearchpress.com by 46.23.64.124 on 09/08/12
For personal use only.

Table 3. Evaluation of median filtering for correction of baseline drift.

No.	Description[a]	Noise range[b]	Baseline slope[c]	r	% area	% height	% width
1	Original	None	0.000 00	50	99.82	100.00	100.00
2	1 + S 7.5/0.01	None	0.008 23	50	98.76	99.68	100.00
3	As 2	0.02	0.008 23	50	100.51	101.59	100.00
4	2 + R 0.25/0.14	0.02	0.247 59	40	67.45	82.22	86.67
5	As 4	0.02	0.247 59	90	81.45	90.16	93.33
6	1 + S 3.5/0.04	None	0.070 46	50	92.84	96.83	100.00
7	As 6	0.02	0.070 46	50	95.24	100.95	100.00
8	1 + S 3.5/0.02	None	0.035 06	40	95.31	98.10	100.00
9	As 8	None	0.035 06	90	100.19	100.32	100.00
10	1 + S 3.5/0.01	None	0.017 80	40	97.79	99.05	100.00
11	As 10	None	0.017 80	60	98.78	99.68	100.00
12	As 10	None	0.017 80	90	99.95	100.00	100.00
13	1 + R 0.07/0.10	None	0.070 00	40	90.38	95.87	100.00
14	1 + R 0.03/0.10	None	0.030 00	40	95.16	98.10	100.00
15	1 + R 0.01/0.10	None	0.010 00	40	98.22	99.37	100.00
16	1 + R 0.05/0.10	None	0.050 00	40	91.67	96.51	100.00
17	1 + R 0.10/0.10	None	0.100 00	40	87.22	94.29	93.33
18	1 + R 0.20/0.10	None	0.200 00	40	78.15	88.89	93.33

[a]S *X/Y*: sine curve with period *X* minutes and amplitude *Y*; R *X/Y*: linear ramp with slope *X* and intercept *Y*.

[b]Uniform random deviates with zero mean and indicated range.

[c]Measured adjacent to peak for ramp functions and by interpolation across peak for sine functions, arbitrary units.

culations were performed using a filter of rank 40 since there were approximately this many points in the peak. The performance of this method of baseline correction was evaluated in terms of the recovered peak area as a percentage of the starting peak area, and the results are summarized in Table 3.

In general terms, the technique worked well provided that the slope of the baseline within the peak envelope did not change rapidly, although a slight rise of the baseline, after filtering, on the trailing side of the peak was observed in some cases. This is a result of the properties of the median when applied to data having a varying slope, and results in a slight dip below zero in the baseline-subtracted peak. With the data analysed here, 95% or better of the original peak area (based on the area before addition of simulated drift) was recovered using $r = 40$ when the magnitude of the baseline slope under the peak was less than ≈ 0.04 (for comparison, the peak height/width ratio was 2.10). The recovered area could be improved for any degree of baseline drift by increasing the width of the window used in the filter, but this also resulted in a considerable increase in the time taken to perform the filtering operation.

In terms of the other peak parameters, the recovered peak heights and widths (width at half-maximum height) follow the same basic pattern as the areas, although the extent of the variation is lower. For example, when only 67% of the area was recovered, 82% of the height and 87% of the width were recovered. Peak retention times were only shifted relative to the peak of Fig. 2 when artificial noise was added to the signal, typically giving a variation of less than 0.3%.

Comparison with other digital filters

A common approach to filtering noise is the application of Savitzky–Golay (SG) smoothing (14–18). This technique also uses a moving window; however, a polynomial is fitted through the points in the window by the method of least squares. (The MA filter can therefore be considered as a zero-order SG filter.) The success of this technique lies in the fact that fitting can be achieved by simple convolution with a set of integer weights, rendering it computationally fast and simple. An added benefit is that derivatives can easily be obtained during the smoothing process by calculating the appropriate weights, explaining the widespread use and popularity of the method. Although the first and last r points are again lost on smoothing the data, Gorry (11) has developed a refinement that retains these values. In the following discussion, the exact filter will be identified using Savitzky and Golay's notation, *XaYZ*, where *X* is the width ($= 2r + 1$), *Y* the order of the polynomial, and *Z* the order of the differential.

The effect of applying SG smoothing to the data of Fig. 1, both with and without added noise, was investigated using r values of 2, 5, and 7 and both second- and third-order polynomials. The noise distributions used were as follows: normal with mean zero and standard deviation ± 0.05; uniform with mean zero and range ± 0.05; and exponential with mean zero and scale factor 0.05. Some typical results are shown in Fig. 5. Note that at sharp edges the filter produces ripples that widen as the filter rank is increased. This is a result of trying to fit a polynomial function across a discontinuity: similar results would be obtained with filters based on the fast Fourier transform (FFT) algorithm such as the Butterworth and Chebyshev filters (7, 19). Savitzky–Golay smoothing also reduces the height and increases the width of such features as spikes and steps. Note that the smoothing gives rise to a curving baseline in the same way that sharp edges give rise to ripples. A one-tailed *F*-test was used to see if there was a significant improvement between the baseline standard deviations of the filtered

Can. J. Chem. Downloaded from www.nrcresearchpress.com by 46.23.64.124 on 09/08/12
For personal use only.

Can. J. Chem. Downloaded from www.nrcresearchpress.com by 46.23.64.124 on 09/08/12
For personal use only.

Fig. 5. The effect of a 15a20 Savitzky–Golay smoothing on the data of Fig. 1 with added uniform noise. See text for further details.

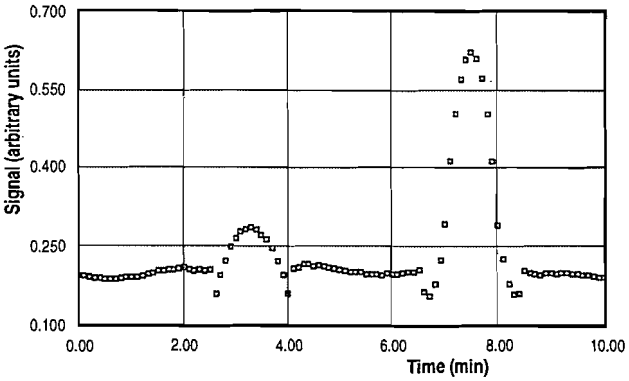

and unfiltered data for each noise function over increasing time frames. Generally, it was found that while all the filters used here reduced baseline noise significantly over long time periods, a significant reduction was only obtained over short periods with normally distributed noise. When the moving average and median filters were applied to the same data, the results were the same as in the absence of the noise functions. Camus and Larson report that a MA filter of rank 9 gave a better reduction in noise than a ME filter of equal rank for a sloping function with binomially distributed noise, whereas the median filter showed a significantly better performance for a step function, in keeping with the results obtained here.

Figure 6 shows the performance of the three different filters for three data sets, each containing 1000 points and having a different noise distribution function. A filter rank of zero indicates the unfiltered data. For comparison, Camus and Larson presented similar calculations using a binomial noise distribution and median, moving average, and parabolic filters. As expected, all filters successfully reduce noise as r is increased for flat baselines regardless of the noise distribution, although the magnitude of the reduction in variance decreases exponentially with increasing r. For exponential and normal noise functions, there is little to choose between the ME and MA filters if the sole criterion is reduction in baseline variance. For uniform and binomial noise distributions, the MA filter gives the better performance for the same rank *provided* that the data do not contain a discontinuity, such as a step function. Both the MA and ME filters perform better than the SG filter for exponential and normal noise distributions. This is because (for the same rank) the noise reduction capability of SG filters decreases with order and, as mentioned previously, the MA filter is a SG filter of rank zero. For uniform deviates the SG filter would be preferred to the ME on the basis of computational speed only.

A similar study was performed on the peak of Fig. 2 in order to compare the performance of the different filters with regard to peak shape: different noise functions were added to the original data, and the filters applied prior to peak shape analysis. All SG filters studied were third-order polynomials (i.e., *X*a30 filters). Since the original data set is a continuous function with superposed noise, the SG filter produced increasingly smooth peaks as the window width was increased. The baseline was also flattened out, exhibiting similar features as noted above. In comparison, the ME filter gave rise to increasingly

Fig. 6. Effect of the Savitzky–Golay, median and moving average filters on different baseline noise distributions as a function of filter rank r. (A) Exponential noise with zero mean and scale factor 0.05; (B) Gaussian noise with zero mean and standard deviation 0.05; (C) uniform random noise with zero mean and range ±0.05. Noise is expressed as the standard deviation relative to that of the unfiltered data.

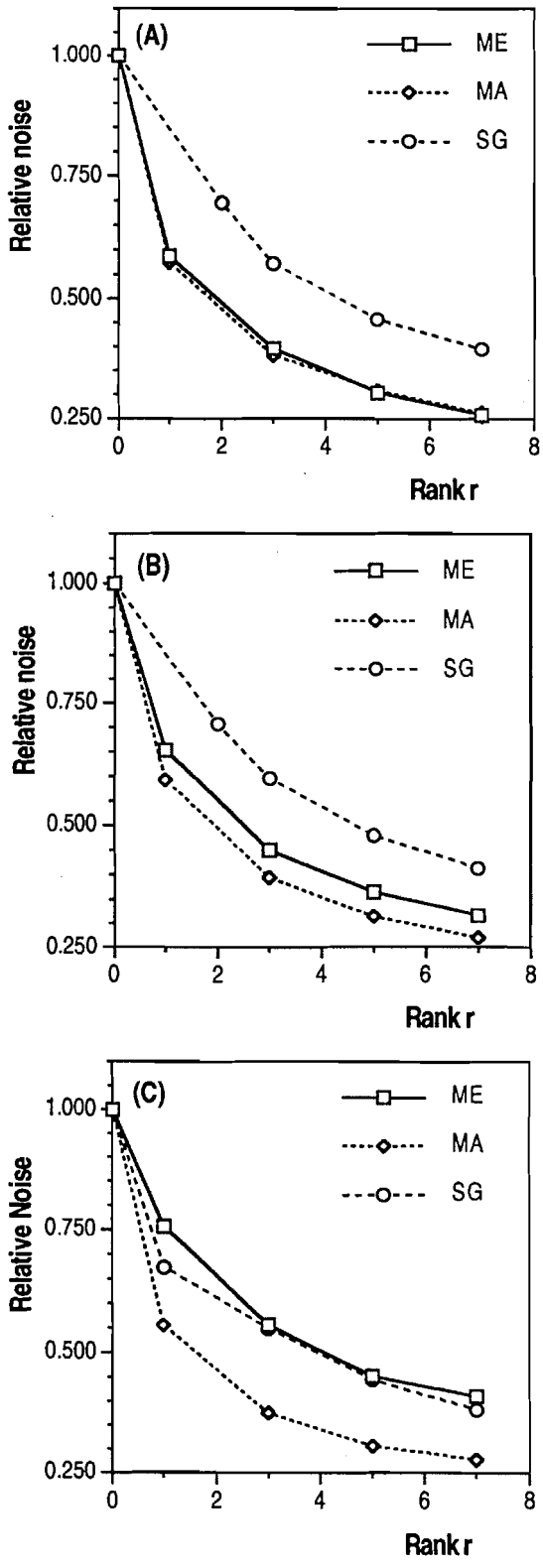

Fig. 7. Distortion produced by different filters on noisy data. Original = data of Fig. 2; exponential = exponential noise with scale factor 0.02; Gaussian = normally distributed noise with zero mean and standard deviation ±0.02; uniform = random distribution with zero mean and range ±0.02; medX = median filter of rank X; aveX = moving average filter of rank X.

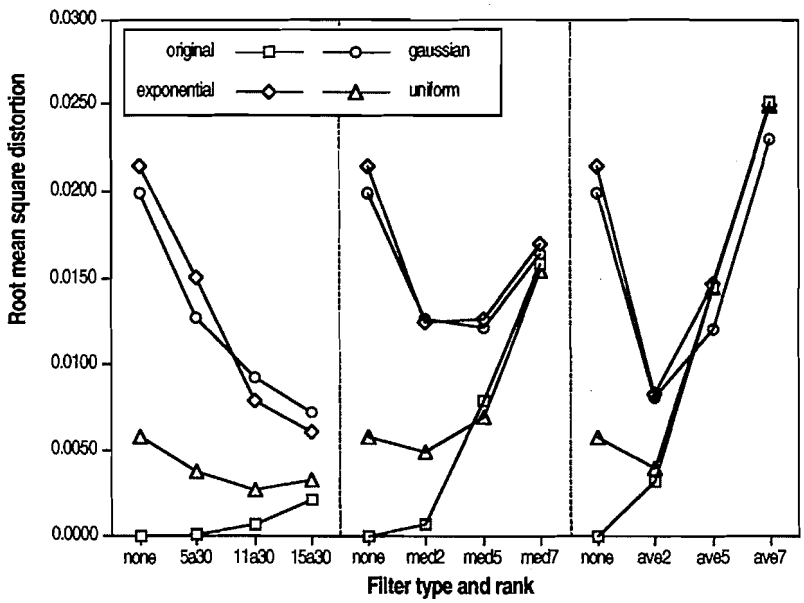

truncated, flat-topped peaks as described earlier. The MA filter again had a similar effect on the baseline, while the peaks were of the expected shape. Analysing the peak parameters showed that both the ME and MA filters gave a decrease in peak height and an increase in width at half height with increasing r as noted above, the ME filter showing the slower rate of change. Results for the SG filter were harder to interpret because of the added noise, but comparing results for the same analysis performed on the original peak showed that the SG filter increased area and decreased height while leaving the width at half height and retention time unaffected. Similar results have been obtained by Enke and Nieman for Gaussian and Lorentzian peaks (16). Results for the ME and MA filters were identical to those noted earlier.

The effect of filtering on overall peak shape was also studied by comparing the noisy peak (filtered and unfiltered) with the original noise-free data by calculating the distortion as described above. The results are summarized in Fig. 7 and show two effects: (*i*) an initial decrease due to noise reduction followed by (*ii*) increasing "true" distortion due to the filter properties. Note that in the absence of any superposed noise all the filters cause increasing distortion with increasing r, the least effect occurring with the SG filter and the greatest with the moving average. With a uniform noise distribution of zero mean and range ±0.02 there appears to be an optimum filter rank for reducing peak distortion for all three filters, corresponding to the balance of the two processes already outlined. The rapid increase in distortion measured for the ME and MA filters can be attributed to the peak truncation and increasing inclusion of the baseline, respectively. For normal (Gaussian) and exponential ("spiky") distributions, the best results were obtained for the SG filter with increasing rank: significant reductions in distortion were also achieved using the ME and MA filters, but this was reversed if the rank was increased beyond an optimal value.

Table 4. Comparison of approximate calculation times for different filters.

	Time[a] (s)		
r	ME	MA	SG
1	0.82	0.10	0.07
7	1.75	0.30	0.33
12	4.55	0.45	0.55
40	16.8	1.30	n/a[b]

[a]Calculations performed on the same 1000 point data set using a Macintosh II with 68020 processor and 68881 co-processor.

[b]The specific implementation of the routine to calculate weight tables for SG filtering was limited to a rank of 25 for practical reasons.

The final comparison between these three filters is concerned with the time taken to perform the necessary computations. Table 4 summarizes the time required to complete filtering of the same 1000 point data set for different filter parameters. These results were obtained using the implementations described in the experimental section, with the exception that median calculations were performed using a full data sort. The reason for this was that the faster median implementation described earlier was found to be faulty whenever the routine was applied to a window containing a sequence of identical values. Clearly, if this error was remedied calculation times could be improved. Although calculation times on different platforms will to some extent be implementation and compiler dependent, generally faster times will be obtained on more recent personal computers.

Other digital filtering techniques that have been applied to

Can. J. Chem. Downloaded from www.nrcresearchpress.com by 46.23.64.124 on 09/08/12
For personal use only.

Fig. 8. SAW–GC response for injection of 0.20 μL of 1:1 toluene:2-nitrotoluene (by volume) using T_{inj} = 207°C, T_{col} = 178°C, T_{det} = 72°C, and T_{saw} = 57.6°C. 2-Nitrotoluene peak (*a*) in the presence of electrical noise, and (*b*) after application of the median filter, r = 1. Note: no coating on the quartz SAW device. For other details, see text and ref. 9.

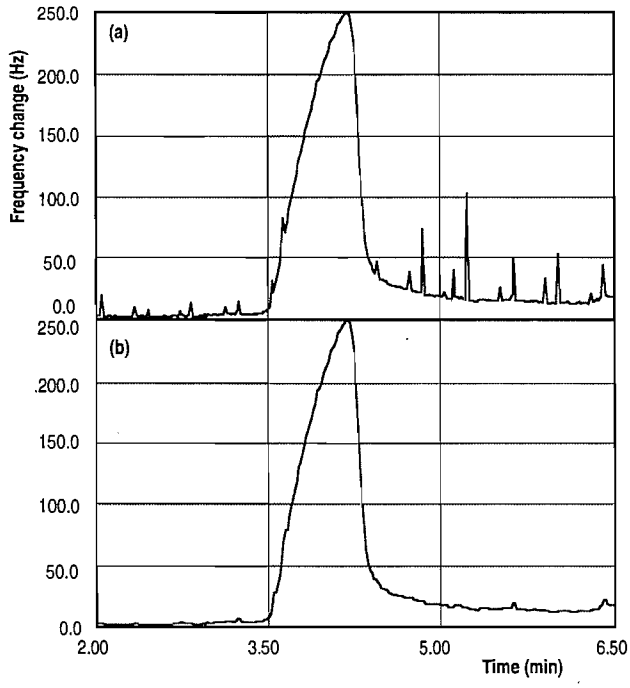

analytical signals are based on either Fourier Transform or Kalman filtering techniques (1–3). Unlike the methods described so far, these techniques require more detailed knowledge of the nature of the signal and any noise or drift associated with it. In addition, they represent a significant increase in mathematical and computational complexity. A good example of this is the recent application of a modified extended Kalman filter incorporating least median of squares (robust) regression to detect and correct drifting calibration in graphite furnace-AAS while minimizing the effect of outliers and the number of recalibration measurements (20). One potential advantage of Kalman filtering is that it is not necessary to know the exact physical relationship describing the evolving signal, as long as a suitable mathematical function can be found that accurately describes the observed behaviour. To obtain good results with this technique, however, it is essential to have good estimates of the system and measurement noise. Another potential problem with FFT-based filters (such as the previously mentioned Butterworth and Chebyshev filters) is that they can introduce features into the data that may constitute an interference from an analytical viewpoint. A more detailed comparison with these filters is beyond the scope of the present article.

Application to transient sensor signals

As described in the experimental section, median filtering has been implemented in the software used to collect and analyse data from a SAW–GC combination. The reason for this was that under certain conditions with the particular configuration used, the SAW response can be subject to noise resulting from the heating circuits of the GC turning on and off. This noise is characteristically a regularly spaced, single-point "spike" in the data and thus ME filtering represents a logical choice for its removal. An example is shown in Fig. 8 both before and after filtering. Since the noise peaks are only a single point, they can be successfully removed using r = 1, ensuring minimal distortion of the analyte peak profiles. Both SG and moving average filters would not be as successful in removing such features.

A hazard in the use of any form of data processing is overprocessing, i.e., applying a sequence of processing techniques that produce a good picture but in the process completely mask the quality of the original measurement. For completeness, an example is given in Fig. 9. This shows results deliberately obtained from the SAW–GC system under a "worst-case" scenario: a badly aged SAW device operating at elevated temperature and close to the edge of the oscillators' stable region combined with an old, contaminated capillary column and injection port septum. Application of ME filtering with subsequent SG smoothing to restore a rounded appearance to the analyte peaks gives a reasonable chromatogram, but in the process has generated one spurious peak and significantly altered peak heights and areas. Multiple filter passes and combinations of techniques can make poor data look good, but they do not make it better. As always, it is the responsibility of the operator to exercise judgement on both the quality of the data and the required level and sophistication of filtering applied to it prior to analysis.

Conclusions

Like any other digital processing technique, median filtering has its advantages and disadvantages. It has been demonstrated that, compared to moving average and Savitzky–Golay filtering, ME filtering is particularly effective at removing noise spikes from experimental data. When applied in this manner, low filter ranks should be used ($1 \leq r \leq 3$) to ensure successful filtering with minimal distortion of the original signal. Likewise, ME filtering is particularly well suited to situations in which retention of sharp edges and discontinuities in the data are important. Median filtering can also be successfully applied to peak measurement in the presence of drifting baselines as previously demonstrated by Moore and Jorgenson (7). In addition to the conditions identified by these authors, it has been demonstrated here that the relative baseline slope is important in determining the accuracy of peak areas and heights obtained by this method.

In more general terms, a moving average or Savitzky–Golay filter may be preferred in situations were large filter ranks are required for successful smoothing of noisy data, but once again careful attention must be paid to the nature of the signal being processed and the information required from it: if peak heights are important, for example, an SG filter may well be preferable to an MA filter. Finally, a simple median filter could be implemented for real-time smoothing of experimental data as an alternative to other techniques, provided that large values of r are not required. Median filtering is thus a useful complement to existing data-processing methods for instrumental measurements.

Can. J. Chem. Downloaded from www.nrcresearchpress.com by 46.23.64.124 on 09/08/12
For personal use only.

Fig. 9. SAW–GC chromatogram showing overprocessing of very noisy data: (*a*) original data for a six-component mixture of organic compounds; (*b*) the same data following median filtering ($r = 2$) and SG smoothing (15a20).

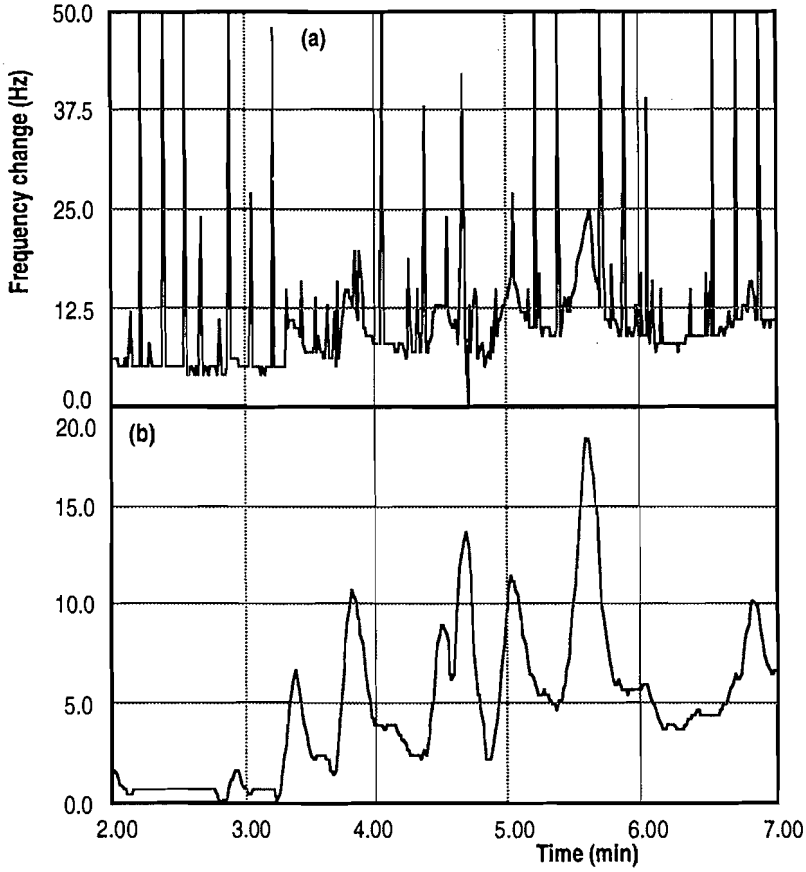

Can. J. Chem. Downloaded from www.nrcresearchpress.com by 46.23.64.124 on 09/08/12
For personal use only.

Acknowledgment

I would like to thank Michael Thompson (University of Toronto, Canada) for providing the opportunity to perform this work; M. Donata Frank (University of Toronto, Canada) for the SAW–GC measurements; and Peter A. Gorry (University of Manchester, England) for providing a FORTRAN listing of his generalized Savitzky–Golay routine. This work was supported in part by the Institute for Chemical Science and Technology, Canada.

References

1. S.D. Brown. Anal. Chim. Acta, **181**, 1 (1986).
2. R.G. Brereton. Chemometrics: applications of mathematics and statistics to laboratory systems. Ellis Horwood, New York. 1990.
3. C.L. Erickson, M.J. Lysaght, and J.B. Callis. Anal. Chem. **64**, 1155A (1992).
4. J.W. Tukey. Exploratory data analysis. Addison-Wesley, Reading, Mass. 1977.
5. T.S. Huang (*Editor*). Two-dimensional digital signal processing II: Transforms and median filters. Springer-Verlag, Berlin. 1981.
6. L.R. Rabiner, M.R. Sambur, and C.E. Schmidt. IEEE Trans. Acoust. Speech Signal Process. **23**, 552 (1975).
7. A.W. Moore and J.W. Jorgenson. Anal. Chem. **65**, 168 (1993).
8. P.P. Camus and D.J. Larson. Appl. Surf. Sci. **76/77**, 416 (1994).
9. M. Thompson and D.C. Stone. Anal. Chem. **62**, 1895 (1990).
10. W.H. Press, S.A. Teukolsky, W.T. Vettering, and B.P. Flannery. Numerical recipes in C: The art of scientific computing. 2nd ed. Cambridge University Press, Cambridge. 1992. pp274ff, 341ff.
11. P.A. Gorry. Anal. Chem. **62**, 570 (1990).
12. J.N. Miller. Analyst, **118**, 455 (1993).
13. P.J. Karol. Anal. Chem. **61**, 1937 (1989).
14. A. Savitzky and M.J.E. Golay. Anal. Chem. **36**, 1627 (1964).
15. J. Steinier, Y. Termonia, and J. Deltour. Anal. Chem. **44**, 1906 (1972).
16. C.G. Enke and T.A. Nieman. Anal. Chem. **48**, 705A (1976).
17. A. Proctor and P.M.A. Sherwood. Anal. Chem. **52**, 2315 (1980).
18. P.D. Wentzall, T.P. Doherty, and S.R. Crouch. Anal. Chem. **59**, 367 (1987).
19. R.W. Hamming. Digital filters. 3rd ed. Prentice Hall, Englewood Cliffs, N.J. 1989.
20. D. Wienke, T. Vijn, and L. Buydens. Anal. Chem. **66**, 841 (1994).

Dosage comparatif des produits issus de la dégradation alcaline des hexoses

Marie-France Dubois, Luc Rigal et Antoine Gaset

Résumé : L'analyse quantitative du glucose, du fructose, du mannose, du sorbose, du psicose, et parallèlement des acides lactique, glycérique, glycolique, formique et acétique issus du traitement alcalin des hexoses est étudiée par chromatographie liquide haute performance ionique, couplée à un détecteur à ampérométrie pulsée avec deux colonnes Carbopac Dionex en série pour les sucres et à un conductimètre avec une colonne HPICE AS1 Dionex pour les acides. Cette méthode sensible et fiable ne nécessite aucun prétraitement des échantillons. Elle est comparée à la chromatographie liquide haute performance sur colonnes Biorad HPX87C et HPX87P montées en série pour les sucres et sur colonne Interaction ORH 801 pour les acides ainsi qu'au dosage enzymatique. Elle est appliquée à la comparaison du comportement du fructose, du glucose et du mannose en milieu alcalin.

Mots clés : hexoses, acides polyhydroxylés, isomérisation, dégradation alcaline, chromatographie liquide haute performance ionique.

Abstract: The mixture of hexoses and carboxylic acids produced by alkaline degradation of fructose was analyzed quantitatively by high-performance liquid chromatography. A pulsed amperometric detector with two Carbopac Dionex columns in series was employed in the assay of sugars (glucose, fructose, mannose, sorbose, and psicose), while a conductimeter with an HPICE AS1 Dionex column was employed for carboxylic acids (lactic, glyceric, glycolic, formic, and acetic). This sensitive and reproducible method obviated sample pretreatment. The results were compared with those of enzymatic assays and HPLC determinations using Biorad HPX87C and HPX87P columns in series for the sugars, and an Interaction ORH 801 column for the carboxylic acids. The behaviour of fructose, glucose, and mannose in alkaline medium was compared.

Key words: hexoses, polyhydroxylic acids, isomerization, alkaline degradation, high-performance ionic liquid chromatography.

Can. J. Chem. Downloaded from www.nrcresearchpress.com by 80.90.12.36 on 09/08/12
For personal use only.

Introduction

La dégradation alcaline des hexoses conduit à un très grand nombre de produits (1). Il se forme essentiellement des sucres isomères de l'hexose de départ (fructose, glucose, mannose, sorbose, psicose...) (2) ainsi que des acides polyhydroxylés (acides lactique, glycolique, glycérique, formique et acétique...) (3).

L'analyse de ces composés de dégradation est très importante dans de nombreux domaines : dans l'alimentaire, car ils influencent la saveur et la couleur des produits (4–6); dans les traitements des liqueur noires issues des procédés papetiers (7–9); et dans l'industrie de transformation des sucres (10–14) et en particulier pour l'optimisation de la production de l'acide lactique (15–20).

Les principales méthodes analytiques utilisées pour le dosage de tels milieux sont : (*i*) la chromatographie liquide haute performance (CLHP) sur colonne, de type silice greffée par des groupements amino propyl ou de type échangeurs d'ions sous forme Ca^{2+} ou Pb^{2+}, pour les sucres (21–28), ou de type silice greffée par des groupements C_8 ou C_{18} ou du type échangeurs d'ions sous forme H^+, pour les acides (6, 29–31).

La détection est alors assurée par réfractométrie dans le cas des sucres et des acides ou par spectrophotométrie UV, plus sensible, dans le cas des acides. Pour les sucres, la spectrophotométrie visible après ajout-post colonne est de moins en moins utilisée (28). Ce type d'analyse impose des prétraitements de neutralisation et déminéralisation du fait de la mise en oeuvre de solvants organiques dans le cas des colonnes type silice greffée, ou de résine échangeuse d'ions dans le cas de la chromatographie d'échange.

(*ii*) les méthodes enzymatiques : ces techniques, du fait même de la spécificité de l'enzyme employée, permettent le dosage sélectif du produit. Cependant, elles nécessitent un essai par produit à doser, et dans certains cas, un prétraitement de décoloration. Enfin, ces enzymes ne sont disponibles que pour quatre de nos produits (32, 33) (glucose, fructose, mannose et acide lactique).

(*iii*) la chromatographie en phase gazeuse, par exemple sur colonne type OV 101, pour les sucres (34–36), CP Sil 5 pour les acides (15, 37–39), couplée à un détecteur à ionisation de flamme : les sucres et les acides doivent subir préalablement une dérivation après neutralisation et lyophilisation (40). Cette dernière est assez délicate dans le cas des mélanges de

Reçu le 3 mars 1994.[1]

M.-F. Dubois, L. Rigal[2] et A. Gaset. Laboratoire de chimie agro-industrielle, Institut national polytechnique de Toulouse, École nationale supérieure de chimie de Toulouse, 118, route de Narbonne, 31077 Toulouse Cédex, France.

[1] Révision reçue le 26 mai 1995.
[2] Auteur à qui adresser toute correspondance. Téléphone : 61 17 57 22. Fax : 61 17 57 30.

Fig. 1. Séparation CLHP de glucose, fructose, mannose, sorbose et psicose sur les 2 colonnes Aminex HPX 87C et Aminex HPX 87P montées en série. Température de la colonne : 85°C. Eluant : eau désionisée. Débit de l'éluant : 0,3 mL/min.

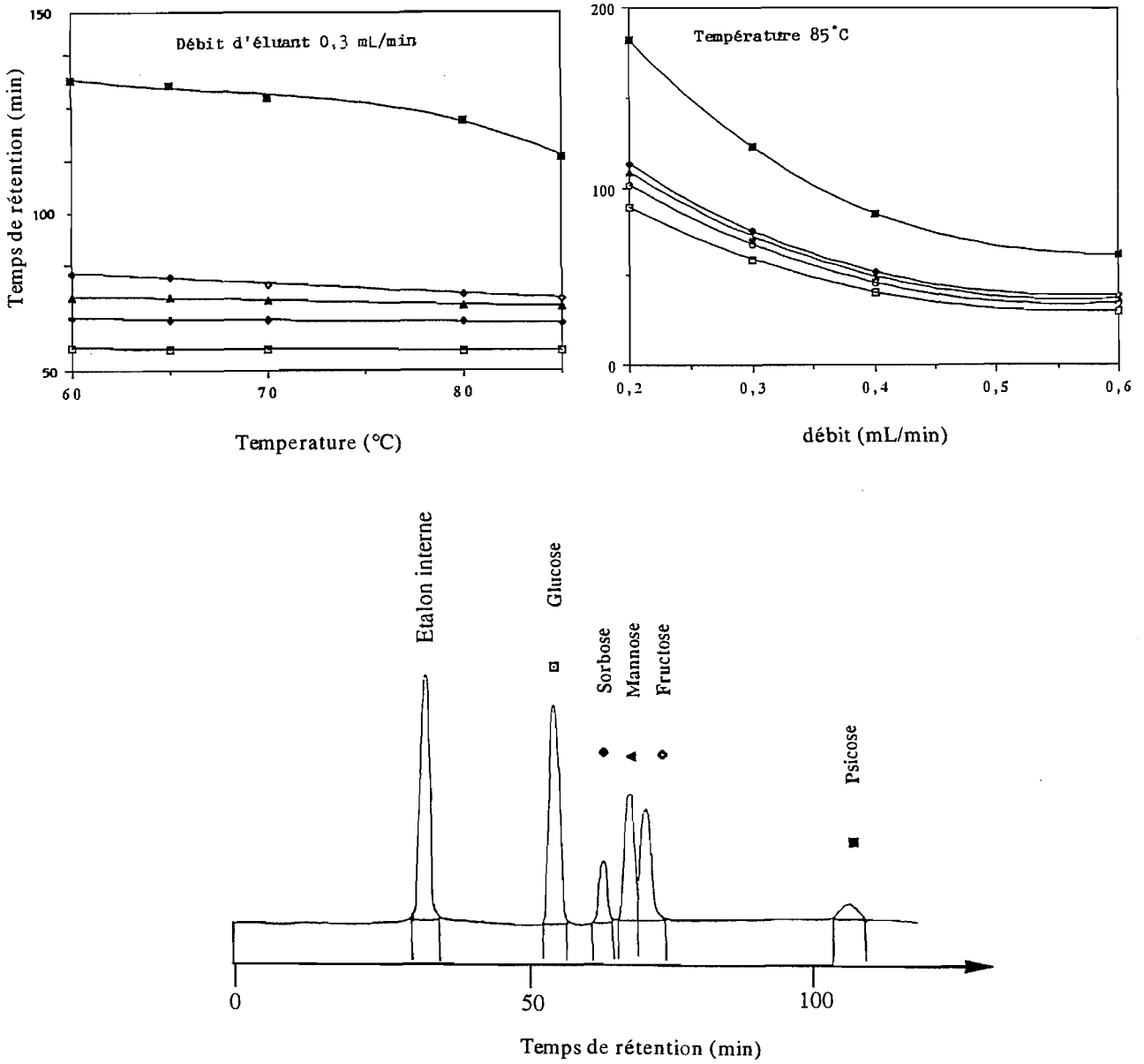

sucres et d'acides. Elle risque de provoquer une modification du milieu. De plus, l'acide formique et l'acide acétique ne pourront pas être dosés dans les mêmes conditions d'analyses.

Pour notre part, nous nous sommes intéressés à la mise au point d'une méthode d'analyse fiable et sensible des principaux hexoses et acides polyhydroxylés rencontrés dans les milieux issus du traitement basique du fructose, du glucose ou du mannose.

La chromatographie liquide haute performance ionique (CLHPI) couplée à l'ampérométrie pulsée pour les sucres (41–44) et à la conductimétrie pour les acides (45, 46) élimine les contraintes imposées par les autres méthodes analytiques (prétraitement des milieux, décoloration...). Notre objectif est d'optimiser ces deux méthodes CLHPI en vue de suivre l'évolution en fonction du temps de neuf composés issus de la dégradation alcaline des sucres.

Partie expérimentale

Réactifs et étalons

Tous les produits sont de pureté élevée, pour analyse :

Sucres étalons : D-fructose (Fluka 47 739), D-glucose (Prolabo 24 379-294), D-mannose (Aldrich 11 285-5), D-sorbose (Roquette Frères 80078), D-psicose (Sigma P-1275), D-galactose (Prolabo 24 333 183), Cellobiose (Prolabo 22 558 120), Arabitol (Sigma A 3381).

Acide étalons : acide DL-lactique (sodium salt) (Fluka 71 720), acide acétique (sodium salt) (Merck 6268), acide formique (Fluka 06 440), acide glycérique (calcium salt) (Fluka 50 036), acid glycolique (Fluka 50 590), acid pimelique (Fluka 80 500), acide propionique (Fluka 81 910).

Can. J. Chem. Downloaded from www.nrcresearchpress.com by 80.90.12.36 on 09/08/12
For personal use only.

Fig. 2. Séparation CLHPI de glucose, fructose, mannose, sorbose et psicose avec deux colonnes Carbopac montées en série. Température : 20°C. Débit d'éluant : 1 mL/min, éluant E_1 : NaOH 100 mM, E_2 : H_2O, gradient étagé : 0–4 min : 15% E_1; 4–100 min : 100% E_2; 100–125 min : 100% E_1; 125–145 min : 15% E_1. Ajout post-colonne : 300 mM de soude.

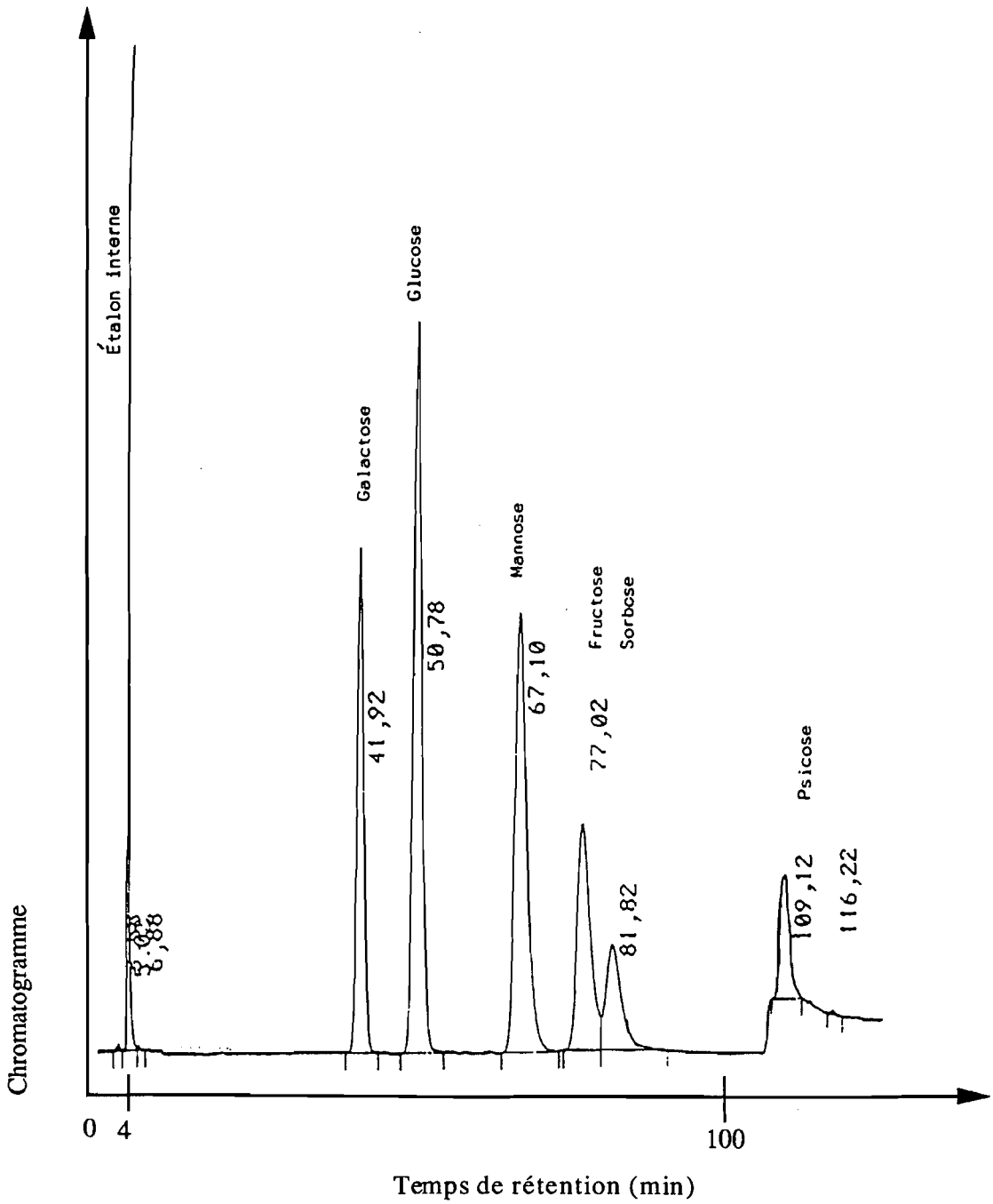

Réactifs pour les éluants : soude (Baker 7067), acide octane sulfonique (Dionex 35 362), tétrabutylammonium hydroxyde (Janssen 17 6610), acide sulfurique (Fluka 84 720), propanol-2 (Chromasol SDS).

Méthodes de dosage

Chromatographie liquide haute performance (CLHP)

Un chromatographe liquide équipé avec une pompe Perkin Elmer Isocratique 250, une vanne Rhéodyne 7 125 (boucle d'injection 20 μL), un réfractomètre Perkin Elmer LC25, un chauffe-colonne Croco Cil™ et un intégrateur LDC, Milton Roy CI 10B ont été utilisés.

Pour les sucres, les colonnes sont de type échangeur de cation forte sous forme Ca^{2+} ou Pb^{3+} (Bio-Rad Aminex HPX 87C and HPX 87P; 300 mm × 7,8 mm i.d.) monté avec une précolonne (cartouche Biorad Microguard). L'éluant est l'eau désionisée. L'étalon interne est le cellobiose.

Can. J. Chem. Downloaded from www.nrcresearchpress.com by 80.90.12.36 on 09/08/12
For personal use only.

Tableau 1. Comparaison du dosage du glucose, du fructose, du mannose et de l'acide lactique par les méthodes CLHP, enzymatique et CLHPI.

Composé	Dosage CLHP après prétraitement (g/L)	Dosage enzymatique après prétraitement (g/L)	Dosage enzymatique sans prétraitement (g/L)	Dosage CLHPI sans prétraitement (g/L)
Glucose	1,41	1,35	1,66	1,73
Fructose	0,88	0,96	1,03	1,07
Mannose	1,08	1,05	1,18	1,24
Acide lactique	7,24	7,47	7,90	8,00

Fig. 3. Chromatogramme d'un milieu réactionnel de dégradation alcaline du fructose sur la colonne Interaction ORH 801. Température de la colonne : 35°C. Eluant : H_2SO_4 0,01 N. Débit d'éluant : 0,6 mL/min.

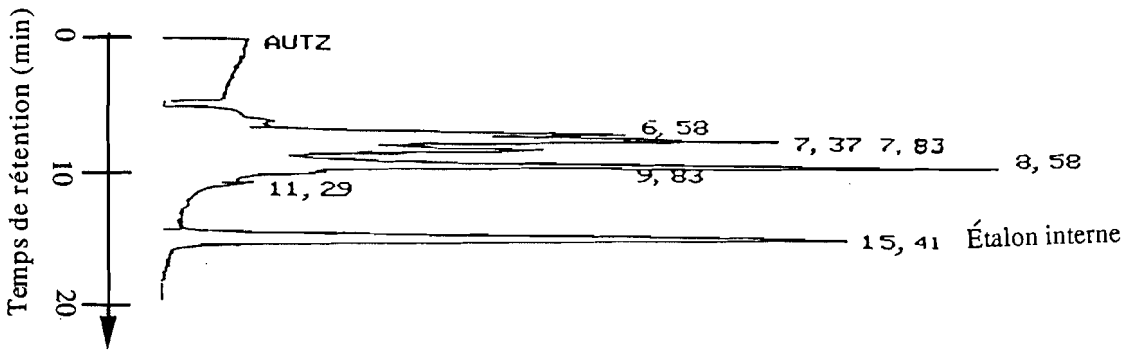

Pour les acides, la colonne est de type échangeur de cation forte sous forme H^+ (300 mm × 6,5 mm i.d.) monté avec une précolonne (cartouche Interaction Ionguard). L'éluant est l'acide sulfurique 0,01 N. L'étalon interne est l'acide pimélique.

Chromatographie liquide ionique haute performance (CLHPI)

Le système de chromatographie ionique utilisé est le BioLC Dionex avec une boucle d'injection de 50 µL et équipé de deux manières différentes pour les analyses de sucres et pour celles des acides.

Pour les sucres : Les séparations sont réalisées sur une ou deux colonnes Carbopac (250 mm × 4 mm i.d.) commercialisées par la Société Dionex, montées en série, reliées à une précolonne Carbopac PA1 Dionex. Les deux types d'éluants utilisés sont de l'eau désionisée, avec une résistivité de 18 MΩ et une solution de soude à 150 mM.

Dans le cas de la réalisation d'un gradient ou d'un gradient étagé à l'aide de ces deux éluants, un ajout post-colonne de soude 300 mM juste avant la cellule du détecteur par ampérométrie pulsée (PAD) est nécessaire afin d'éviter de trop grands changements de pH lors de la détection, et de stabiliser ainsi la ligne de base.

L'étalon interne utilisé est l'arabitol. Les caractéristiques du PAD sont : électrode en or; potentiels appliqués : $E_1 = 0{,}05$ V, $E_2 = 0{,}60$ V, $E_3 = -0{,}60$ V; durées d'application : $t_1 = 480$ ms, $t_2 = 120$ ms, $t_3 = 60$ ms.

Pour les acides : Les conditions d'analyse pour les acides sont : colonne HPICE AS1 (250 mm × 8 mm i.d.) de la Société Dionex, éluant solution d'acide octane sulfonique 1 mM et de propanol-2 à 2% dans l'eau désionisée, régénérant tétrabutylammoniumhydroxyl (TBAOM), étalon interne acide propionique, conductimètre sensibilité 30 µS.

Enzymologie

Les dosages sont réalisés suivant les tests de Boehringer et Mannheim (1 112 821, 139 106, 131 229).

Préparation des échantillons

Obtention de mélanges réactionnel type

Dans un ballon de 500 mL muni d'un agitateur mécanique, d'un réfrigérant et d'un thermomètre, le sucre en solution dans l'eau (100 mL) est thermostaté à la température choisie, sous agitation. La base (NaOH) en solution dans 100 mL d'eau est alors additionnée. En fin de réaction (9 h) le milieu réactionnel est refroidi dans un bain d'eau et de glace pilée.

Traitement des milieux réactionnels

Pour l'analyse des échantillons par CLHPI ou enzymologie, les échantillons sont simplement dilué dans l'eau désionisée (dosages enzymatiques et des sucres par CLHPI) ou dans l'éluant (dosages des acides en CLHPI). Dans ce dernier cas le pic négatif qui correspondrait à l'eau injectée, de conductivité plus faible que celle de l'éluant est supprimé.

Dans le cas de l'analyse par CLHP, pour le dosage des acides, les milieux réactionnels sont prétraités sur résines échangeuses d'ions H^+ (Lewatit S100) afin d'éliminer les cations présents dans la solution, puis dilués dans l'eau désionisée. Pour le dosage des sucres, les milieux réactionnels sont neutralisés et déminéralisés par percolation sur résine acide (Lewatit S100 forme H^+) puis basique (Lewatit MP62 forme OH^-). Ils sont ensuite dilués si nécessaire dans l'eau désionisée.

Can. J. Chem. Downloaded from www.nrcresearchpress.com by 80.90.12.36 on 09/08/12
For personal use only.

Can. J. Chem. Downloaded from www.nrcresearchpress.com by 80.90.12.36 on 09/08/12
For personal use only.

Fig. 4. Séparation CLHPI des acides lactique, glycolique, glycérique, formique et acétique sur la colonne Dionex HPICE AS1. Température : 21°C. Eluant : solution d'acide octane sulfonique 1 mM et de propanol-2 à 2% dans l'eau désionisée. Débit d'éluant : 0,3 mL/min.

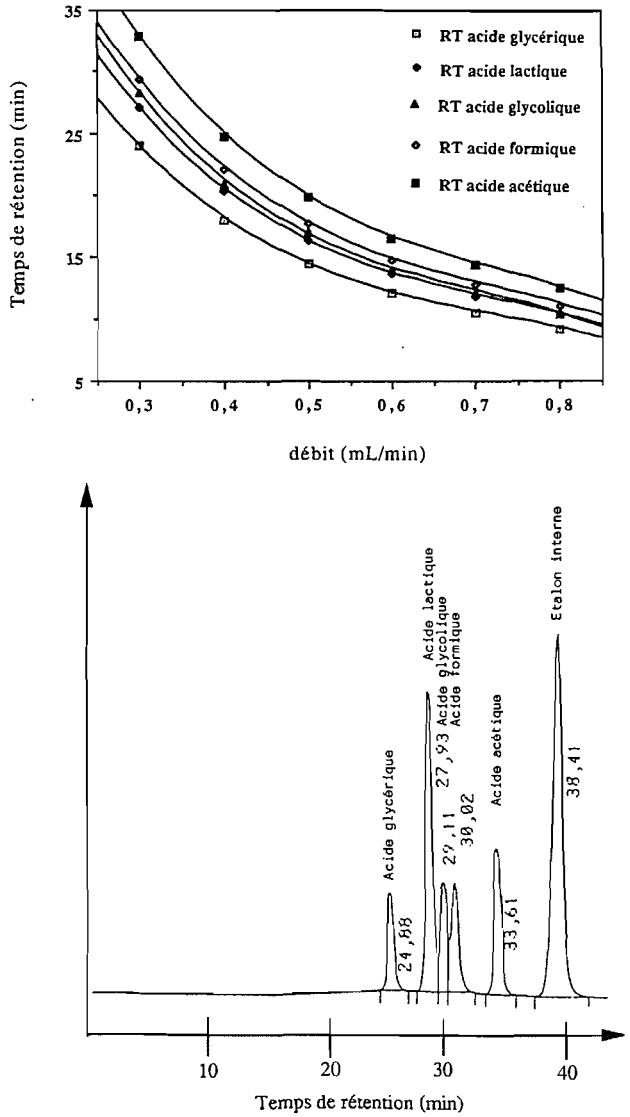

Résultats et discussion

1. Analyse des sucres

L'analyse des sucres en CLHP sur colonne calcium ou plomb ne permet pas la séparation satisfaisante du glucose, fructose, mannose, sorbose et psicose. Par contre, avec les deux colonnes Ca^{2+} et Pb^{2+} montées en série, une diminution de la température et du débit de l'éluant améliore la séparation (figure 1). Cependant cette technique nécessite le traitement préalable des milieux réactionnels (neutralisation et déminéralisation).

La chromatographie liquide haute performance ionique par échange d'ion permet de résoudre cette difficulté. Cette technique présente l'avantage de mettre en œuvre des résines stables de pH = 0–14 et de ne nécessiter que des temps d'équilibrage très court. La détection ampérométrique pulsée est spécifique, sensible et compatible avec un gradient d'élution, grâce à l'ajout post-colonne de soude concentrée (41, 42). La sensibilité autorise de grandes dilutions de l'échantillon ce qui élimine de nombreux problèmes d'interférences avec la matrice. Les milieux réactionnels, dans le cas du traitement alcalin des hexoses peuvent donc être injectés sans prétraitement, après simple dilution.

Tableau 2. Comparaison du comportement du fructose, du glucose et du mannose en milieu basique concentré.

	Sucre de départ		
Produit	Fructose[a]	Glucose[a]	Mannose[a]
Fructose	0,001	0,001	0,036
Glucose	0,007	0,013	0,033
Mannose	0,01	0,014	0,116
Galactose	0	0	0
Sorbose	0	Trace	Trace
Psicose	0	Trace	Trace
Acide lactique	1,292	0,816	0,73
Acide glycérique	0,107	0,086	0,069
Acide glycolique	0,030	0,085	0,073
Acide formique	0,179	0,176	0,23
Acide acétique	0,03	0,036	0,045

[a]Mole de produit formé/mole de sucre introduit. Conditions opératoires : concentration en sucre = 25 g/L; NaOH = 2 M; 9 h; 40°C.

Dans le cas d'une seule colonne Carbopac, la séparation des différents sucres à doser n'est pas satisfaisante en dépit des changements de force éluante, de gradient et de débit. Afin d'augmenter l'efficacité de séparation, deux colonnes Carbopac ont été montées en série. La réalisation d'un gradient étagé dans le cas de l'utilisation de ces deux colonnes a permis d'obtenir une séparation correcte de l'ensemble des sucres (figure 2). Dans ces conditions, l'analyse quantitative de ces hexoses est obtenue avec une bonne précision ($x \pm 0{,}02\,x$). La gamme de concentration utilisée pour nos essais après ajout de l'étalon interne est de 10 à 200 ppm. Cependant, la limite de détection pour les sucres avec le PAD est largement inférieure puisqu'elle se situe autour de quelques picomoles injectées (42).

La comparaison des résultats obtenus selon les méthodes, CLHP, enzymatique et CLHPI dans le cas du dosage de glucose, fructose et mannose contenus dans un milieu réactionnel (tableau 1) montre que : le prétraitement de neutralisation et de déminéralisation impératif pour l'analyse CLHP conduit à une sous-estimation des sucres; et lorsque le milieu réactionnel est peu coloré, les concentrations en sucre obtenues par la voie enzymatique sans prétraitement et par CLHPI sont voisines. Cependant, dans le cas de milieux réactionnels trop colorés, le dosage enzymatique n'est plus fiable sans prétraitement de décoloration. Celui-ci constitue une source d'erreur.

Cette méthode de dosage par CLHPI permet donc de doser de façon fiable sensible et directe, le glucose, le mannose, le fructose, le sorbose et le psicose. De plus, cette méthode à permis de mettre en évidence la présence de galactose dans les milieux réactionnels issus du traitement alcalin du fructose, du glucose ou du mannose.

Fig. 5. Cinétique d'isomérisation du fructose. Concentration initiale en fructose : 100 g/L; NaOH : 0,3 M; température : 40°C.

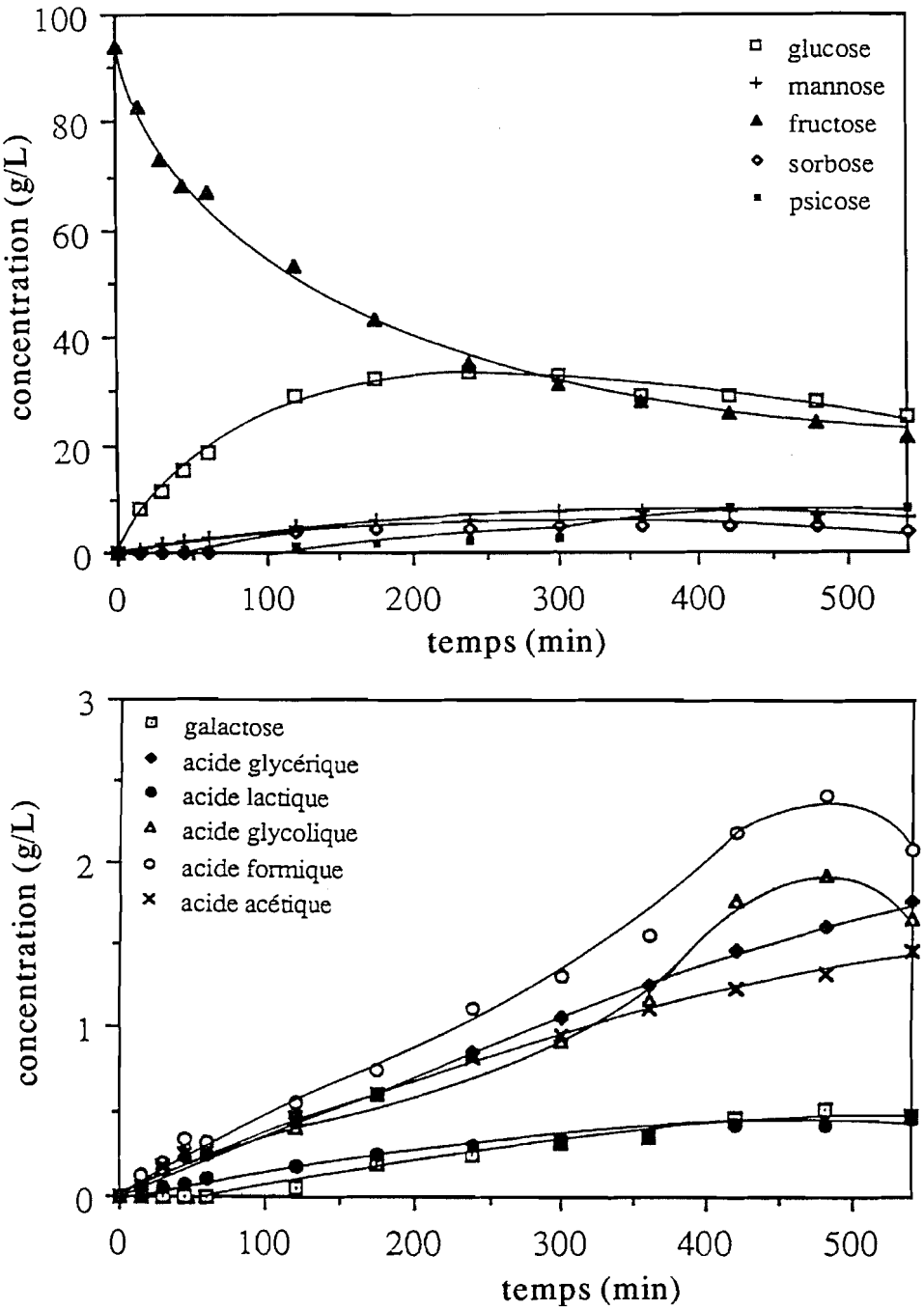

Can. J. Chem. Downloaded from www.nrcresearchpress.com by 80.90.12.36 on 09/08/12
For personal use only.

2. Analyses des acides carboxyliques polyhydroxylés

L'analyse des acides en CLHP sur colonne échangeuse sous forme H^+ nécessite le prétraitement des milieux réactionnels afin déliminer les cations présents dans la solution. Sur ce type de colonne on peut détecter les sucres et les acides. Cependant, leurs temps de rétention sont très voisins et l'analyse d'un milieu réactionnel issu de la dégradation alcaline du fructose ne permet pas de les doser de façon satisfaisante dans le mélange (figure 3).

De plus, la comparaison du dosage de l'acide lactique par cette méthode et la méthode enzymatique avant et après prétraitement de décationisation sur résines échangeuses montre que ce dernier est à l'origine d'une sous-estimation des concentrations (tableau 1).

Le dosage par chromatographie liquide ionique haute performance résoud cette difficulté. En effet, comme dans le cas des sucres, le prétraitement n'est plus nécessaire. Dans les conditions d'utilisations standards (débit d'éluant 0,8 mL/min), les acides sont mal séparés. La diminution du débit permet d'améliorer cette séparation (figure 4).

Les résultats obtenus pour les concentrations en acide lactique sont comparables à ceux obtenus par dosage enzyma-

Fig. 6. Cinétique d'isomérisation du glucose. Concentration initiale en glucose : 100 g/L; NaOH : 0,3 M; température : 40°C.

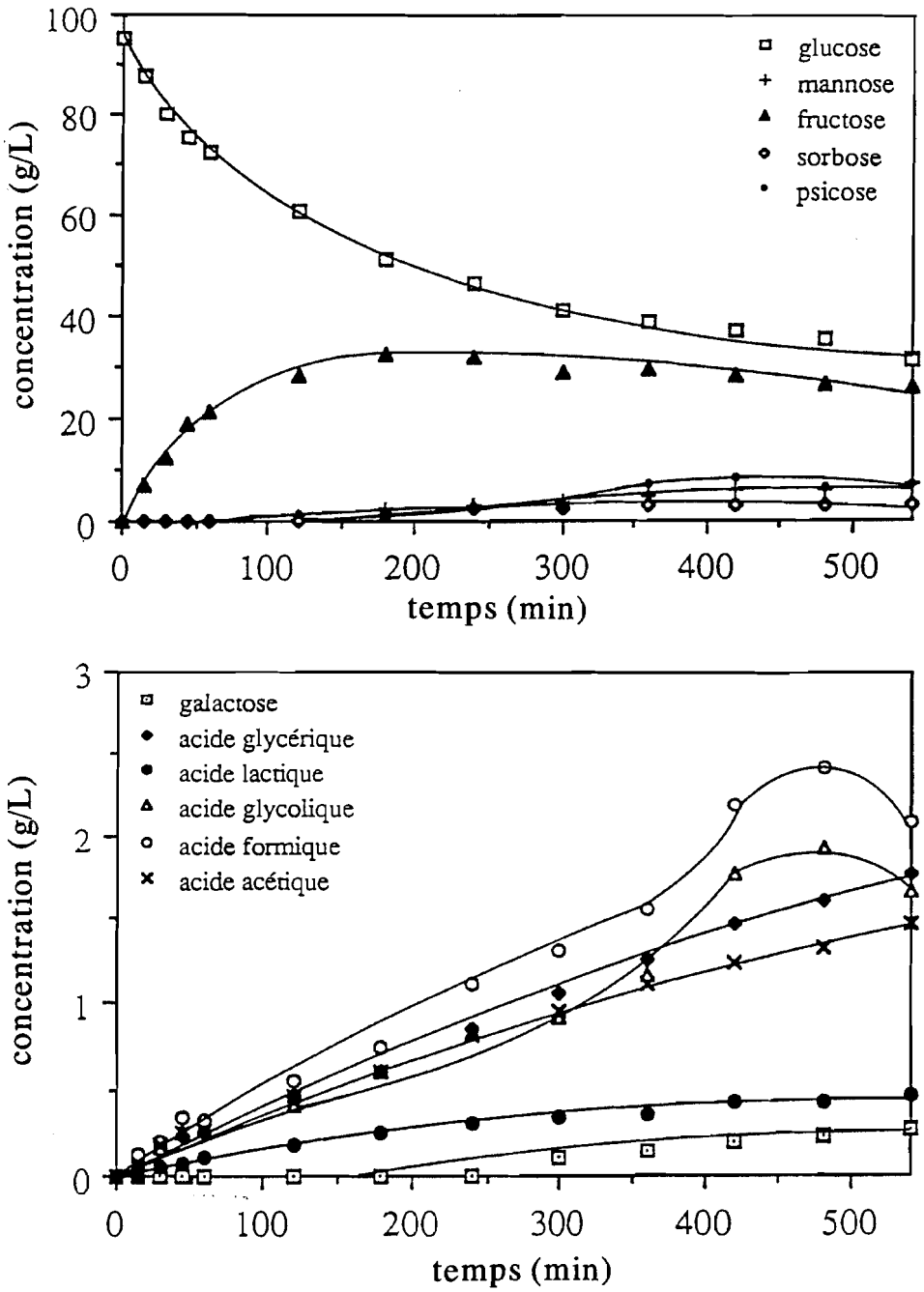

tique sans prétraitement (tableau 1). De plus, cette méthode chromatographique permet de doser les acides glycérique, glycolique, acétique et formique, ce qui n'était pas le cas des autres méthodes. L'analyse quantitative de ces cinq acides est obtenue avec une bonne précision ($x \pm 0{,}025\ x$). Grâce au système de suppression chimique, le bruit de fond est diminué et la sensibilité augmentée. Nous avons travaillé dans une gamme de concentration après dilution de 10 à 20 ppm. Celle-ci pourra être déplacée vers des concentrations plus faibles sans difficulté.

3. Application au cas de mélanges réactionnels

L'évolution des constituants de milieux réactionnels issus de traitements alcalins du fructose, du glucose et du mannose a été suivie grâce à la méthode de dosage par CLHPI. L'étude cinétique de la transformation du fructose en glucose et en mannose, et inversement, en solution alcaline a été menée par de nombreux auteurs (21, 24, 34, 35, 47–52). Cependant, si la formation du psicose a été prise en considération par quelques auteurs (21, 49, 52, 53), celles due sorbose et du galactose ne l'ont été que plus rarement (2, 21, 54–56). Les résultats obtenus par nos soins confirment la différence de comportement des trois hexoses vis-à-vis de l'action de la soude :

(*i*) Dans des conditions opératoires de faible concentration en base, l'isomérisation du fructose en glucose et mannose (figure 5) est plus rapide que celle du glucose (figure 6) et

Can. J. Chem. Downloaded from www.nrcresearchpress.com by 80.90.12.36 on 09/08/12
For personal use only.

Fig. 7. Cinétique d'isomérisation du mannose. Concentration initiale en mannose : 100 g/L; NaOH : 0,3 M; température : 40°C.

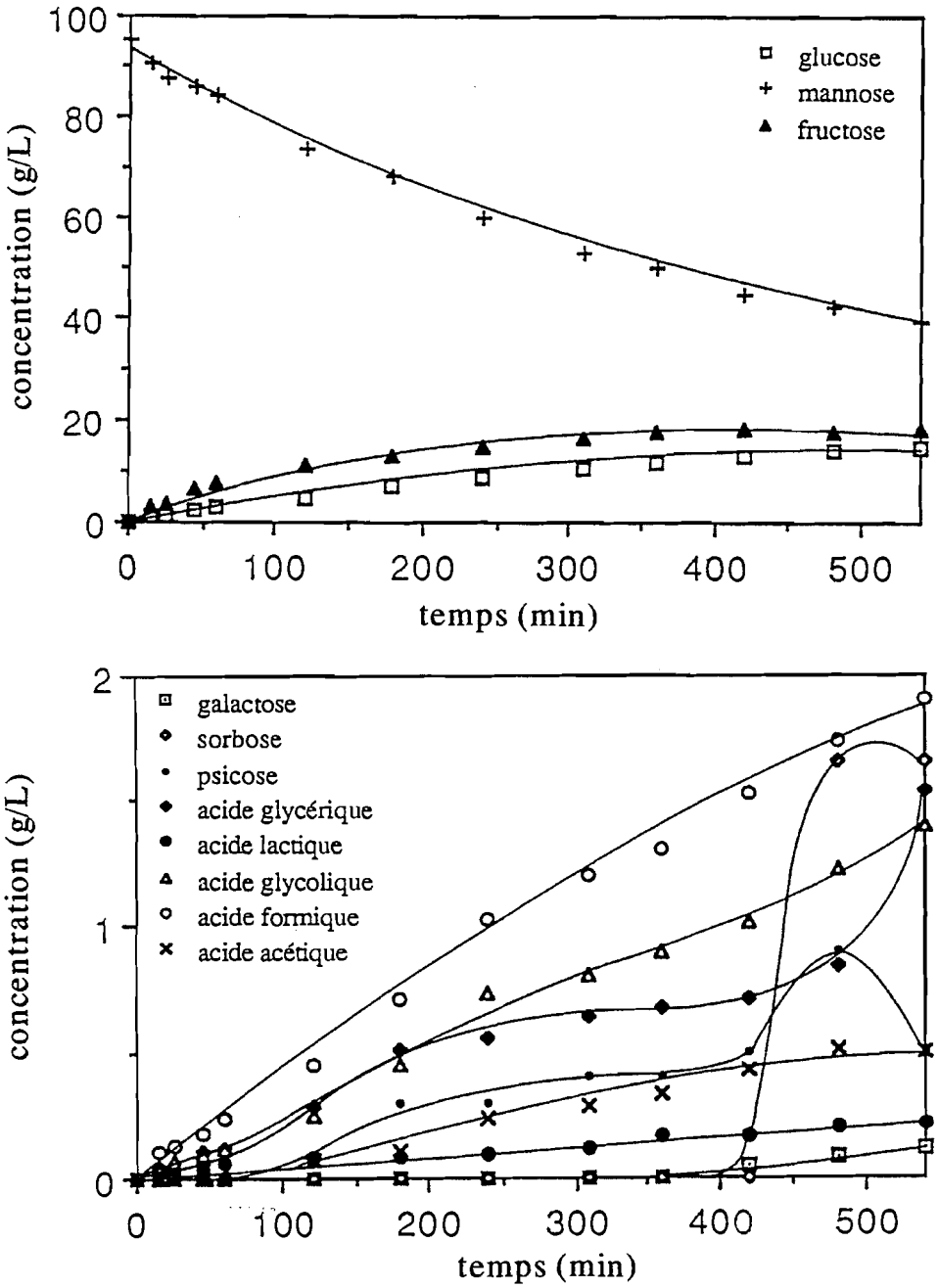

surtout du mannose (figure 7) (24). L'apparition du sorbose, du psicose et du galactose, qui mettent en jeu des mécanismes plus complexes (2, 21) est nettement plus lente. Cependant, à partir du fructose ou du glucose, le sorbose et le psicose atteignent après quelques heures de réaction, des concentrations à peine plus faibles que celle du mannose. L'apparition du galactose, dans ces deux cas, est retardée et il ne se forme qu'en proportion plus faible que les acides. À partir du mannose, le psicose n'est obtenu qu'en concentration très faible, et les formations du galactose et du sorbose sont très retardées.

(*ii*) Dans ces mêmes conditions de faible concentration en base, la formation de l'acide lactique est nettement défavorisée par rapport à celle des autres acides. Par contre, à forte concentration en soude, et pour une faible concentration initiale en monosaccharide, c'est l'acide lactique qui devient majoritaire (tableau 2). Ici aussi, l'ordre de réactivité vis-à-vis de l'action des bases est fructose > glucose > mannose.

Conclusion

L'analyse quantitative des sucres issus de la dégradation d'un hexose en milieu alcalin est obtenue avec les meilleurs résultats par la méthode chromatographique liquide ionique. Bien que cette séparation soit relativement longue, elle permet de doser exactement glucose, fructose, mannose, surbose, psi-

Can. J. Chem. Downloaded from www.nrcresearchpress.com by 80.90.12.36 on 09/08/12
For personal use only.

cose sans prétraitement. En outre, elle permet de mettre en évidence la présence de galactose. L'augmentation de la capacité des résines utilisées dans les colonnes Carbopac devrait permettre de diminuer les durées d'analyses. La chromatographie liquide haute performance sur les colonnes plomb et calcium en série a confirmé la présence de ces sucres et le dosage enzymatique des trois principaux sucres (glucose, fructose et mannose) a permis une vérification quantitative. Les acides issus de ce même traitement sont également dosés grâce à une seconde analyse par chromatographie liquide ionique et le dosage de l'acide lactique est confirmé par enzymologie. Cette méthode d'analyse permet donc d'envisager l'étude de l'optimisation de l'obtention de l'acide lactique par traitement alcalin des monosaccharides en milieu concentré.

Remerciements

Les auteurs remercient la Société Applexion rédaction complète.

References

1. J.U. Nef. Justus Liebigs Ann. Chem. **357**, 214 (1907).
2. H. El Khadem, S. Ennifar et H.S. Isbell. Carbohydr. Res. **185**, 51 (1989).
3. J.M. De Bruijn, A.P.G. Kieboom et H. Van Bekkum. Recl. Trav. Chim. Pays-Bas, **105**, 176 (1986).
4. R.D. Rocklin, A. Henshall et R.B. Rubin. Am. Lab. (Shelton, Conn.), **34**, March (1990).
5. Z. Hu, Z.G. Liu et X. Quian. Shipin Yu Fajao Gongye, **1**, 8 (1987); Chem. Abstr. **106**, 212 632q (1987).
6. R.T. Marsili, H. Ostapenko, R.E. Simmons et D.E. Green. J. Food Sci. **46**, 52 (1981).
7. I.A. Antipova, S.A. Medvedeva, L.N. Petrushenko, et V.A. Babkin. Khim. Drev. **2**, 46 (1981); Chem. Abstr. **94** (22), 1769665y (1981).
8. P.O. Bethge et K. Lindstrom. Analyst (Cambridge, U.K.), **99** (1175), 137 (1974).
9. A.N. Ivanov, L.G. Popova, V.N. Piyalkin et Y.I. Chernousov. Izv. Vyssh. Uchebn. Zaved. Lesn. Zh. **16**, 118 (1973); Chem. Abstr. **80** (12), 61258 P (1973); **17**, 108 (1974); Chem. Abstr. **81**, 123197 Z. (1974).
10. M. Kiely et M. O'Sullivan. Sucr. Belge Sugar Ind. Abstr. **95**, 83 (1976).
11. J.F.T. Oldfiedld, R. Parslow et M. Shore. Int. Sugar J. **75**, 3 (1973); **75**, 44 (1973).
12. R. Detavernier, J.P. Ducatillon et G. Deruy. Sucr. Fr. **124** (71), 133 (1983).
13. D.F. Charles. Int. Sugar J. **83** (991), 195 (1981).
14. N. Kubadinow. Zuckerindustrie (Berlin), **112**, 700 (1987).
15. J.M. De Bruijn, A.P.G. Kieboom, H. Van Bekkum et P.W. Van Der Poel. Int. Sugar J. **86** (1027), 195 (1984).
16. J.M. De Bruijn, A.P.G. Kieboom et H. Van Bekkum. Recl. Trav. Chim. Pays-Bas, **105**, 176 (1986).
17. H.S. Isbell, H.L. Frush, C.W.R. Wade et C.E. Hunter. Carbohydr. Res. **9**, 163 (1969).
18. A.P.G. Kieboom et H. Van Bekkun. Starch conversion technology. Marcel Dekker, New York. 1985.
19. G. Mantovani et G. Vaccari. Ind. Sacc. Ital. **83**, 4 (1990).
20. J. Michelet, A. Deschamps et J.M. Lebeault. Colloq. Soc. Fr. Microbiol. 39 (1982).
21. H.S. El Khadem, S. Ennifar et H.S. Isbell. Carbohydr. Res. **169**, 13 (1987).
22. M. Makkee, A.P.G. Kieboom, H. Van Bekkum et P.W. Van Der Poel. Int. Sugar J. **86**, 195 (1984).
23. A.J. Shaw et G.T. Tsao. Carbohydr. Res. **60**, 327 (1978).
24. G. De Wit, A.P.G. Kieboom et H. Van Bekkum. Carbohydr. Res. **74**, 157 (1979).
25. K. Aitzetmuller. J. Chromatogr. **156**, 354 (1978).
26. D.L. Hendrix, R.E. Lee et J.G. Baust. J. Chromatogr. **210**, 45 (1981).
27. B. Porsch. J. Chromatogr. **253**, 49 (1982).
28. A. Meunier, M. Caude et R. Rosset. Analusis, **14**, 363 (1986).
29. D.F. Charles. Int. Sugar J. **83** (991), 169 (1981).
30. N. Kubadinow. Zuckerindustrie (Berlin), **107**, 1107 (1982).
31. C. Gonnet, M. Marichy et N. Philippe. Analusis, **7**, 370 (1979).
32. F. Bandion et M. Valenta. Mitt. Klosterneuburg, **27**, 4 (1977).
33. G. Henniger et L. Mascaro. J. Assoc. Off. Anal. Chem. **68**, 1021 (1985).
34. T. Vuorinen et E. Sjostrom. Carbohydr. Res. **108**, 23 (1982).
35. C. Kooyman, K. Vellenga et H.G.J. De Wilt. Carbohydr. Res. **54**, 33 (1977).
36. J.A. Rendleman et J.E. Hodge. Carbohydr. Res. **15**, 83 (1979).
37. R. Detavernier, J.P. Ducatillon et G. Deruy. Sucr. Fr. **124** (71), 133 (1983).
38 J.M. MacLeod et R. Schroeder. J. Wood Chem. Technol. **2**, 187 (1982).
39. W.J. Hughes et T.M. Thorpe. J. Food. Sci. **52**, 1078 (1987).
40. G. Petersoon. Carbohydr. Res. **33**, 47 (1974).
41. J.L. Peschet. Le Technoscope de Biofutur, **28**, 10 (1989).
42. J.L. Peschet et A. Giacalone. Industrie Agro-Alimentaire, 18 (1991) Juillet/Août (Cahier Scientifique et Technique).
43. W.R. La Course, D.A. Mead, Jr. et D.C. Johnson. Anal. Chem. **62**, 220 (1990).
44. R.D. Rocklin et C.A. Phohl. J. Liq. Chromatogr. **6**, 1577 (1983).
45, R.D. Rocklin, R.W. Slingsby et C.A. Pohl. J. Liq. Chromatogr. **9**, 757 (1986).
46. H. Small, T.S. Stevens et W.C. Bauman. Anal. Chem. **47**, 1801 (1975).
47. M.L. Mirza, F. Ul, H. Nasim et M. Akram. J. Pure Appl. Sci. **4**, 9 (1985).
48. J.C. Sowden et R. Schaffer. J. Am. Chem. Soc. **74**, 499 (1952); **74**, 505 (1952).
49. C.H. Bamford et J.R. Collins. Proc. R. Soc. London, Ser. A: **228**, 100 (1955).
50. A.P.G. Kieboom et H. Van Bekkum. Recl. Trav. Chim. Pays-Bas, **103**, 1 (1984).
51. E.R. Garret et J.F. Young. J. Org. Chem. **35**, 3502 (1970).
52. J.M. De Bruijn. Thèse T.H. Delft, The Netherlands, (1986).
53. S. Passeron et E. Recondo. J. Chem. Soc. 813 (1965).
54. M.L. Wolfrom et J.N. Schumacher. J. Am. Chem. Soc. **77**, 3318 (1955).
55. J.C. Swoden et R.R. Thompson. J. Am. Chem. Soc. **80**, 1435 (1958).
56. M.G. Blair et J.C. Sowden. J. Am. Chem. Soc. **77**, 3323 (1955).

Can. J. Chem. Downloaded from www.nrcresearchpress.com by 80.90.12.36 on 09/08/12
For personal use only.

A two-dimensional copper(I) polymer containing both molecular rod and anionic bridges: synthesis and crystal structure of (μ-chloro)-(μ-pyrazine)copper(I)

J.M. Moreno, J. Suarez-Varela, E. Colacio, J.C. Avila-Rosón, M.A. Hidalgo, and D. Martin-Ramos

Abstract: The crystal structure of bright-red crystals of the bidimensional polynuclear diamagnetic (μ-chloro)(μ-pyrazine)copper(I) complex has been analyzed from X-ray diffraction data. The structure was solved by the heavy-atom method. Full-matrix least-squares refinement based on 673 reflections with $F > 4\sigma(F)$ converged to a final $R = 0.043$ and $R_w = 0.048$. Crystals of this complex are monoclinic, space group $P2/c$, $a = 3.814(1)$, $b = 6.356(1)$ and $c = 11.497(5)$ Å; $\beta = 96.04(2)°$, $Z = 2$. The structure consists of planes of copper(I) atoms linked by pyrazine and Cl^- bridges, each Cu(I) being in a distorted tetrahedral environment formed by two chloride ions and two nitrogen atoms belonging to two pyrazine molecules, with bond distances of Cu—Cl = 2.349(1) and Cu—N = 2.038(4) Å. Vibrational and electronic spectroscopy of the title compound is also reported.

Key words: two-dimensional copper(I)–pyrazine complexes.

Résumé : Utilisant les données de la diffraction des rayons X, on a déterminé la structure cristalline des cristaux rouge brillant du complexe diamagnétique polynucléaire bidimensionnel (μ-chloro)(μ-pyrazine)cuivre(I). On a résolu la structure par la méthode des atomes lourds et on l'a affinée par la méthode des moindres carrés (matrice complète) jusqu'à des valeurs finales de $R = 0{,}043$ et $R_w = 0{,}048$ pour 673 réflexions avec $F > 4\sigma(F)$. Les cristaux du complexe sont monocliniques, groupe d'espace $P2/c$, avec $a = 3{,}814(1)$, $b = 6{,}356(1)$ et $c = 11{,}497(5)$ Å; $\beta = 96{,}04(2)°$, $Z = 2$. La structure est formée de plans d'atomes de cuivre(I) liés par des ponts pyrazine et chlore; chaque Cu(I) comporte un environnement tétraédrique déforme formé par deux ions chlores et deux atomes d'azote appartenant à deux molécules de pyrazine et les distances des liaisons sont Cu—Cl = 2,349(1) et Cu—N = 2,038(4) Å. On rapporte aussi les spectres de vibration et électronique du composé mentionné dans le titre.

Mots clés : complexes bidimensionnels cuivre(I)–pyrazine.

[Traduit par la rédaction]

Introduction

Numerous examples of pyrazine-bridged derivatives of copper(II) complexes have been prepared and structurally characterized in order to study the ability of the pyrazine bridge to mediate the magnetic exchange interaction in new one- (1–4) and two-dimensional (5–8) materials. However, pyrazine-bridged metal complexes are not only interesting because of their magnetic properties. Thus, Hoskins and Robson proposed (9) that infinite-ordered frameworks may be formed by linking together tetrahedral or octahedral metal centres through rodlike connecting ligands, such as pyrazine. These coordination polymers (9–12) present potential utility in host–guest chemistry, ion exchange, and heterogeneous catalysis. A significant part of the research in this field has concerned systems assembled by using copper(I) salts and *N,N'*-donor bidentate linear ligands with different rod lengths. Despite this, since the copper(I)–pyrazine dimers reported in the early 1960s by Lever et al. (13, 14) nearly three decades passed until Thompson and co-workers described the first one-dimensional structurally described pyrazine-bridged copper(I) complex (15), and, to the best of our knowledge, only a few one- (15–17), two- (17–19), and three-dimensional (19) pyrazine-

Received April 20, 1995.

J.M. Moreno, J. Suarez-Varela, and E. Colacio.[1] Departamento de Química Inorgánica, Facultad de Ciencias, Universidad de Granada, 18071-Granada, Spain.
J.C. Avila-Rosón. Departamento de Química Analítica. Facultad de Ciencias. Universidad de Granada. 18071-Granada, Spain.
M.A. Hidalgo. Centro de Instrumentacion Cientifica, Universidad de Granada. 18071-Granada, Spain.
D. Martin-Ramos. Departamento de Mineralogía y Petrología, Facultad de Ciencias, Universidad de Granada, 18071-Granada, Spain.

[1] Author to whom correspondence may be addressed. Fax: +34 58 243322. E-mail: ECOLACIO@UGR.ES

Can. J. Chem. Downloaded from www.nrcresearchpress.com by 46.23.64.124 on 09/08/12
For personal use only.

bridged copper(I) complexes have been reported so far. Furthermore, it should be stressed that several of these compounds were obtained by serendipitous reduction of copper (II) to copper(I) (15, 18, 19).

In the present work we report on the crystal structure of a new two-dimensional (μ-chloro)(μ-pyrazine)copper(I) polymer obtained by accidental reduction of copper(II) in the presence of *N,N*-3,4-dimethylphenyl(carboxymethyl)glycine.

Experimental

Physical measurements

Microanalyses of C, N, and H, and measurements of electronic and infrared spectra were carried out as already reported (20).

Syntheses

N,N-*3,4-dimethylphenyl(carboxymethyl)glycine*

This compound was synthesized according to the methods described in the literature (21).

(μ-Chloro)(μ-pyrazine)copper(I)

The title compound was obtained by using standard crystal-growing techniques in gels. The procedure was as follows: a solution (5 mL) of silica gel (pH = 5, ρ = 1.059 g cm^{-3}), prepared with sodium metasilicate (Merck) solution (pH = 11.2) and HCl (1 M), containing 0.5 g (2.07 mmol) of $Cu(NO_3)_2 \cdot 3H_2O$ was added to a glass test tube. When the coagulation took place, 3 mL of silica gel without the copper salt were added and also allowed to coagulate. After gelling, 10 mL of an aqueous solution (adjusted to pH = 8 with NaOH 6 M) formed by 0.49 g (2.07 mmol) of *N,N*-3,4-dimethylphenyl(carboxymethyl)glycine and 1 g (12.49 mmol) of pyrazine were poured on the gel. After 2 weeks suitable reddish crystals for single X-ray diffraction were formed, mechanically separated from the gel, and washed with distilled water. Experiments were performed at room temperature (about 20°C). Anal. calcd. for $C_4H_4N_2ClCu$: C 26.83, H 2.25, N, 15.64, Cu 35.48; found: C 26.97, H 2.31, N 15.33, Cu 35.65. Infrared spectrum (v = very, w = weak, m = medium, s = strong), ν(pyrazine) cm^{-1}; 3075, 3020 w (b_{1u}, b_{3u}); 1474 m (b_{1u}); 1408 s (b_{3u}); 1155 s (b_{1u}); 1110 m (b_{2g}); 1046 m (b_{1u}); 800 s (b_{2u}); 594 w (b_{3g}) and 446 s (b_{2u}); 306 vw ν(Cu-Cl).

X-ray data collection and structure determination

Single-crystal data collection was performed at ambient temperature with a Siemens–Stoe AED-2 four-circle diffractometer using monochromatized Mo K_α radiation (λ = 0.710 69 Å). The unit cell parameters for the red crystals were obtained from least-squares refinement of 25 reflections ($25 > 2\theta > 35°$). Crystal data: $C_4H_4N_2ClCu$, M = 179.08, monoclinic, space group $P2/c$, a = 3.814(1), b = 6.356(1), c = 11.497(5) Å, β = 96.04(2)°, U = 277.19(15) $Å^3$, Z = 2, D_c = 2.146 g cm^{-3}, $F(000)$ = 176, μ(Mo K_α) = 4.31 mm^{-1}.

A total of 999 independent reflections (R_{int} = 2.35%) out of 5168 were collected by the ω–2θ scan mode ($3 > 2\theta > 65°$) with variable scan rate from 0.6° to 3.6° min^{-1} depending on the intensity. A total of 673 reflections with $F > 4\sigma(F)$ were considered to have observable intensity and were used in the structure analysis. Intensities of three check reflections measured after every 90 min showed only statistical variation. The data were corrected for Lorentz and polarization effects and for absorption (empirical, based on azimuthal scans for three reflections). Transmission factors ranged from 0.927 to 1.000.

Table 1. Atomic coordinates (×10^4) and equivalent isotropic displacement coefficients ($Å^2 \times 10^4$).

Atom	x	y	z	U_{eq}[a]
Cu	0	2020(1)	2500	38(1)
Cl	5000	−135(2)	2500	39(1)
N(1)	0	3794(4)	1017(3)	30(1)
C(2)	1256(8)	3079(6)	0000	33(2)
C(3)	−1264(9)	5771(5)	0960(4)	31(2)

[a] U_{eq} defined as one third of the trace of the orthogonalized U_{ij} tensor.

The structure was solved by a combination of Patterson and Fourier techniques by using the SHELXTL-PLUS program package (22) on a MicroVAX II computer. In the final refinement, all non-hydrogen atoms were refined anisotropically. Hydrogen atoms were placed at their calculated positions and only their thermal parameters were refined. The function minimized was $\Sigma w(\Delta F)^2$ ($w = 1/\sigma_F^2$), resulting in a final $R = \Sigma||F_o| - |F_c||/\Sigma|F_o|$ value of 0.0434 and $R_w = [\Sigma w(|F_o| - |F_c|)^2/\Sigma w|F_o|^2]^{1/2} = 0.0475$. Maximum and minimum peaks in the final Fourier synthesis were 0.48 and −0.50 e $Å^{-3}$. The goodness-of-fit ratio was 0.81 for 40 parameters (data-to-parameter ratio = 16.8/1). Atomic coordinates for the non-hydrogen atoms are listed in Table 1. Hydrogen atom parameters, anisotropic thermal parameters, and structure factors have been deposited.[2]

Results and discussion

The (μ-pyrazine)(μ-chloro)copper(I) complex was obtained by accidental reduction of Cu(II) to Cu(I) in the reaction medium. In this process, the glycine derivative might act as reduction agent, since, as we have previously shown, the 2,6-dimethylphenylglycinato can be easily oxidized to oxalato anion in the presence of Cu(II) (20). Nevertheless, because of reduction of Cu(II) in the presence of 2,3-dimethylpyrazine has been reported (18), a possible mechanism in which the pyrazine derivative acts as reduction agent cannot be disregarded.

The electronic spectrum of the complex shows the presence of a single band at 600 nm. Since no d–d transitions are expected for a d^{10} complex, this band has been assigned to a metal-to-ligand charge transfer transition (MLCT). These MLCT bands appear at slightly higher energies, within the visible region, in most of Cu(I)–pyrazine complexes, affording orange or yellow colours (15–19). The positions of these bands depend upon the pyrazine substituents since methyl groups make pyrazine a poorer π acceptor (16). In our com-

[2] Copies of material for deposit may be purchased from: The Depository of Unpublished Data, Document Delivery, CISTI, National Research Council of Canada, Ottawa, Canada K1A 0S2.

With the exception of the anisotropic thermal parameters, this material has also been deposited with the Cambridge Crystallographic Data Centre, and can be obtained on request from The Director, Cambridge Crystallographic Data Centre, University Chemical Laboratory, 12 Union Road, Cambridge, CB2 1EZ, U.K.

Can. J. Chem. Downloaded from www.nrcresearchpress.com by 46.23.64.124 on 09/08/12
For personal use only.

Can. J. Chem. Downloaded from www.nrcresearchpress.com by 46.23.64.124 on 09/08/12
For personal use only.

Fig. 1. A view of the coordination about the copper atom; 40% probability thermal ellipsoids are shown for the non-hydrogen atoms.

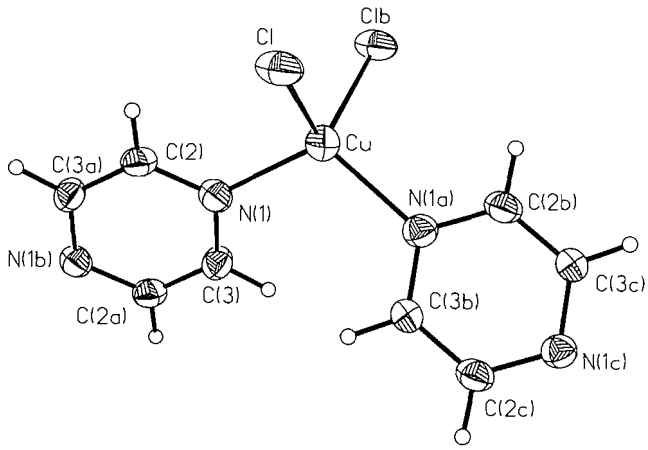

plex, the shift of the MLCT toward lower energies might be attributed to the substitution of two N-donor ligands by two bridging chloride ions, which would decrase the HOMO–LUMO gap. Nevertheless, a detailled molecular orbital calculation should be carried out in order to obtain a best understanding of this effect.

The IR spectrum of free pyrazine shows two absorption bands at 804 and 417 cm^{-1} in the 900–400 cm^{-1} region. It is this latter band that gives more information about the coordination mode of the pyrazine. Thus, this band is shifted to higher frequencies as a consequence of the pyrazine coordination to the metal ions. Nevertheless, the position of this band, when not split, gives little useful information about the pyrazine coordination mode, as has already been pointed out (6, 15). The IR spectrum of our complex shows, as the most significant feature, a single band centred at 446 cm^{-1}, which corresponds to a symmetrical bridging coordinated pyrazine with not very strong interaction, its value being in the low-frequency range for bridging pyrazines (6, 15, 16). The remaining bands observed (experimental section) correspond to those previously assigned (15, 23). An additional Cu–Cl absorption band appears at 306 cm^{-1}.

Up to now, all the copper(I)–pyrazine complexes described in the literature (15–19) show the pyrazine as the only bridging ligand. It should be noted that this complex is new in the sense that it incorporates two different kinds of bridging ligands in the structure, namely the pyrazine and the chloride ion. The only precedents for this kind of complex are limited to those of composition Cu_2LX_2 (13, 14) and CuLX (14) (where L = pyrazine, methylpyrazine, and dimethylpirazine; and X = Cl^-, Br^-, I^-, or CN), but none were examined by X-ray diffraction.

The most relevant feature of the structure is the disposition of the Cu(I) ions in two-dimensional lattices. Within each layer the metal ions are bridged by two chloride ions and two pyrazine ligands. Thus, each copper ion is tetracoordinated, giving rise to a CuN_2Cl_2 chromophore. A view of the chromophore together with the atomic labelling scheme is given in Fig. 1, while bond lengths and angles are listed in Table 2. This four-coordinate environment is compatible with two idealized geometries: tetrahedral and square-planar. The procedure proposed by Muetterties and Guggenberger (24) locates the coordination polyhedron at 1% of the $T_d \leftrightarrow D_{4h}$ deformation pathway, the geometry being almost that of an idealized tetrahedron. Within the coordination polyhedron both Cu—Cl and Cu—N bond distances of 2.349(1) and 2.038(4) Å, respectively, fall well withinin the range of those previously reported for related compounds (15–19, 25, 26) and do not deserve further comment.

Table 2. Bond lengths (Å) and angles (deg).

Cu—Cl	2.349(1)	Cu-N(1)	2.038(4)
N(1)—C(2)	1.335(6)	N(1)-C(3)	1.344(6)
C(2)—C(3)^{I}	1.373(7)		
Cl-Cu-N(1)	104.8(1)	Cl-Cu-Cl^{II}	108.5(1)
N(1)-Cu-Cl^{II}	113.0(1)	N(1)-Cu-N(1)^{III}	112.8(2)
Cu-Cl-Cu^{IV}	108.5(1)	Cu-N(1)-C(2)	121.6(3)
Cu-N(1)-C(3)	123.1(3)	C(2)-N(1)-C(3)	115.3(4)
N(1)-C(2)-C(3)^{I}	122.8(4)	N(1)-C(3)-C(2)^{I}	121.9(4)

I = $-x$, $1-y$, $-z$; II = $x-1$, y, z; III = $-x$, y, $\frac{1}{2}-z$; IV = $x+1$, y, z

Fig. 2. A perspective view of a two-dimensional layer within the packing.

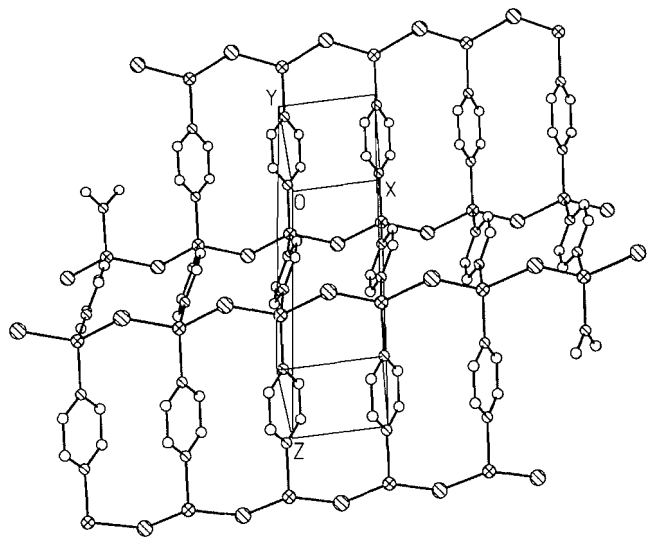

The layers, see Fig. 2, can be described as formed by two types of perpendicular monodimensional zigzag chains crossing at the copper atoms. Chains of the first type run along the *c* axis and have pyrazine as bridging ligand, while those of the second type extend parallel to the *a* axis containing bridging chloride anions. Then, the three-dimensional crystal structure is achieved by stacking of two-dimensional layers along the *b* axis. Intralayer Cu···Cu distances are 3.814 and 6.883 Å for Cu-Cl-Cu and Cu-pyz-Cu, respectively. In the tridimensional network pyrazine rings stack with a distance of 3.814 Å, which suggests some degree of extensive π–π cloud interactions.

It seems that the presence of bridging chloride anions in the structure prevents the formation of a 3–D scaffold-like material. The inclusion of chloride anions in the structure affords the following effects: Firstly, the value of the metal–chloride–metal angle is in our case (*ca.* 109°) far from the theoretical value of 180° given by Hoskins and Robson (9).

Table 3. Bond lengths and angles for pyrazine derivatives in some copper complexes.

Compound	Reference	C—N (Å)	C—C (Å)	N-C-C (°)	C-N-C (°)
Cu(Cl)(pyz)	This work	1.335, 1.344	1.373	121.9, 122.8	115.3
Pyrazine	27	1.334	1.378	122.4	115.8
$Cu(hfac)_2(pyz)$[a]	1	1.33	1.38	121, 123	115
$[Cu(hfac)_2]_2(pyz)$	1	1.33, 1.38	1.36	122	116
$Cu(NO_3)_2(pyz)$	2	1.33	1.387	120.64	118.73
$Cu(ClO_4)_2(pyz)_2$	4	1.344	1.382	122	116
$[Cu_2(tampyz)Cl_2]Cl_2 \cdot 2\frac{1}{4}H_2O$[b]	5	1.334	1.382	115.1, 118.8	122.4
$Cu(CH_3SO_3)_2(pyz)_2$	6	1.340, 1.343	1.388, 1.392	121.6–122.4	115.4–116.8
$Cu(NCO)_2(mepyz)_2$[c]	7	1.335, 1.338	1.370, 1.394	121.7	116.6
$Cu(CF_3SO_3)(pyz)_2$	15	1.330–1.335	1.361–1.381	121.5–123.3	114.8–116.1
$Cu(CF_3SO_3)(2,5\text{–mepyz})_2$[d]	16	1.322–1.347	1.381–1.494	118.3–124.5	116.5–117.0

[a]hfac = 1,1,1,5,5,5-hexafluoropentane-2,4-dionato.
[b]tampyz = 2,3,5,6-tetrakis(aminomethyl)pyrazine.
[c]mepyz = methylpyrazine.
[d]2,5-mepyz = 2,5-methylpyrazine.

Secondly, rodlike ligands yield larger metal–metal distances than do chloride ions. While the first effect could be responsible for the difficulty in arranging the atoms geometrically to built up scaffold-like structures (9), the latter might prevent the formation of cavities large enough to allow the formation of interpenetrating frameworks (12).

As for the pyrazine rings, these are located on an inversion centre, being, as usual, planar within the experimental error. Nevertheless, some values of bond lengths and angles are significantly different from those found for free pyrazine (27) and bridging copper-pyrazine complexes (1–8, 15–17). Moreover, comparison of pyrazine bond lengths and angles in our complex with those reported in the literature, Table 3, reveals that the distortions in the former are of different sign. Thus, the distortions in the reported complexes, compared with free pyrazine, show a marked trend towards increasing the C—C and C-N-C values, while the N—C and N-C-C values remain almost constant. However, in our complex the C—C and C-N-C values are significantly lower and the C—N bond distances slightly longer. The increase of the C-N-C angle when pyrazine is coordinated has been justified on the basis of electronic reasons (2), since the involvement of the lone-pair electrons on the nitrogen atom in bonding to the copper atom reduces the repulsion between lone-pair and ring electrons. Taking into account that the above-mentioned electronic reasons support similar distortion in our compound, the observed distortions may be attributed to steric effects arising from the manner in which the copper, μ-pyrazine, and μ-chloro entities are held together to form the bidimensional lattice.

Acknowledgements

The authors thank Direccion General de Investigacion Cientifica y Technica (DGICYT) (PB91/0725) and Junta de Andalucía for financial support.

References

1. R.C.E. Belford, D.E. Fenton, and M.R. Truter. J. Chem. Soc. Dalton Trans. 17 (1974).
2. A. Santoro, A.D. Mighell, and C.W. Reimann. Acta. Crystallogr. Sect B: Struct. Crystallogr. Cryst. Chem. **B26**, 979 (1970).
3. C.J. O'Connor, C.L. Klein, R.J. Majeste, and M.L. Trefonas. Inorg. Chem. **21**, 64 (1982).
4. M. Ferigo, P. Bonhôte, W. Marty, and H. Stoecli-Evans. J. Chem. Soc. Dalton Trans. 1549 (1994).
5. J. Darriet, M.S. Haddad, E.N. Duesler, and D.N. Hendrickson. Inorg. Chem. **18**, 2679 (1979).
6. J.S. Haynes, S.J. Rettig, J.R. Sams, R.C. Thompson, and J. Trotter. Can. J. Chem. **65**, 420 (1987).
7. T. Otieno, S.J. Rettig, R.C. Thompson, and J. Trotter. Inorg. Chem. **32**, 4384 (1993).
8. M. Graf, H. Stoeckli-Evans, C. Whitaker, P.A. Marioni, and W. Marty. Chemia, **47**, 202 (1993).
9. B.F. Hoskins and R. Robson. J. Am. Chem. Soc. **112**, 1546 (1990).
10. R.W. Gable, B.F. Hoskins, and R. Robson. J. Chem. Soc. Chem. Commun. 1677 (1990).
11. B.F. Abrahams, M.J. Hardie, B.F. Hoskins, R. Robson, and E.E. Sutherland. J. Chem. Soc. Chem. Commun. 1049 (1994).
12. L. Carlucci, G. Ciani, D.M. Proserpio, and S. Sironi. J. Chem. Soc. Chem. Commun. 2755 (1994).
13. A.B.P. Lever, J. Lewis, and R.S. Nyholm. Nature, **189**, 58 (1961).
14. A.B.P. Lever, J. Lewis, and R.S. Nyholm. J. Chem. Soc. 3156 (1963).
15. T. Otieno, S.J. Rettig, R.C. Thompson, and J. Trotter. Can. J. Chem. **67**, 1964 (1989).
16. T. Otieno, S.J. Rettig, R.C. Thompson, and J. Trotter. Can. J. Chem. **68**, 1901 (1990).
17. S. Kitagawa, M. Munakata, and T. Tanimura. Inorg. Chem. **31**, 1714 (1992).
18. M.M. Turnbull, G. Pon, and R.D. Willett. Polyhedron, **10**, 1835 (1991).
19. T. Otieno, S.J. Rettig, R.C. Thompson, and J. Trotter. Inorg. Chem. **32**, 1607 (1993).
20. J. Suarez-Varela, J.M. Dominguez-Vera, E. Colacio, J.C. Avila-Roson, M.A. Hidalgo, and D. Martin-Ramos. J. Chem. Soc. Dalton Trans. 2143 (1995).
21. J.M. Salas-Peregrin, J.C. Avila-Rosón, M. Román-Ceba, and J. Suárez-Varela. Thermochim. Acta, **89**, 151 (1985).
22. SHELXTL PLUS program. X-ray Instrument Group, Nicolet Instrument Corp., Madison, Wis. 1990.

Can. J. Chem. Downloaded from www.nrcresearchpress.com by 46.23.64.124 on 09/08/12
For personal use only.

23. M. Goldstein and W.D. Unsworth. Spectrochim. Acta, **27A**, 1055 (1971).
24. E.L. Muetterties and L.J. Guggenberger. J. Am. Chem. Soc. **96**, 1748 (1974).
25. S. Lindroos and P. Lumme. Acta Crystallogr. Sect. C: Cryst. Struct. Commun. **C46**, 2039 (1990).
26. E.B. Fleischer, D. Jeter, and R. Florian. Inorg. Chem. **13**, 1042 (1974).
27. P.J. Wheatley. Acta Crystallogr. **10**, 182 (1957).

Can. J. Chem. Downloaded from www.nrcresearchpress.com by 46.23.64.124 on 09/08/12
For personal use only.

Thermodynamic properties of the $NiCl_2$–$CoCl_2$–KCl system

Peter J. Tumidajski and Christopher A. Pickles

Abstract: The thermodynamic behavior of $NiCl_2$ in $NiCl_2$–$CoCl_2$–KCl ternary solutions was investigated using formation cells of the type, (−)Ni/$NiCl_2$–$CoCl_2$–KCl/C, $Cl_{2\,(gas,\,1\,atm)}$ (+). The values of the $NiCl_2$ activity coefficients indicate a non-ideal system consonant with the formation of complex species. The $NiCl_2$ activity coefficients at 1000 K were fitted to the polynomial equation,

$$\ln \gamma = (-1225 + 363t - 3186t^2 + 8385t^3 - 6369t^4)Y^2 + (6776 - 1639t + 14803t^2 - 41112t^3 + 32405t^4)Y^3 + (-8665 + 1842t - 16964t^2 + 48873t^3 - 39440t^4)Y^4$$

where

$$Y = 1 - X_{KCl} \text{ and } t = \frac{X_{CoCl_2}}{X_{CoCl_2} + X_{NiCl_2}}$$

The experimental data were limited to the ranges $0 \leq t \leq 0.80$ and $0.10 \leq Y \leq 0.5$.

Key words: molten salt, thermodynamic properties, nickel chloride, non-ideal solution, complex species.

Résumé : Utilisant des cellules de formation du type (−) Ni/$NiCl_2$–$CoCl_2$–KCl/C, $Cl_{2(gaz,\,1\,atm)}$(+), on a étudié le comportement thermodynamique du $NiCl_2$ dans des solutions ternaires de $NiCl_2$–$CoCl_2$–KCl. Les valeurs des coefficients d'activité du $NiCl_2$ indiquent que le système n'est pas idéal, ce qui est en accord avec la formation d'espèces complexes. Les coefficients d'activé du $NiCl_2$ à 1000 K peuvent être ajustés à l'équation polynomiale

$$\ln \gamma = (-1225 + 363t - 3186t^2 + 8385t^3 - 6369t^4)Y^2 + (6776 - 1639t + 14803t^2 - 41112t^3 + 32405t^4)Y^3 + (-8665 + 1842t - 16964t^2 + 48873t^3 - 39440t^4)Y^4$$

dans laquelle $Y = 1 - X_{KCl}$ et

$$t = \frac{X_{CoCl_2}}{X_{CoCl_2} + X_{NiCl_2}}$$

Les données expérimentales sont limitées par $0 \leq t \leq 0{,}80$ et $0{,}10 \leq Y \leq 0{,}5$.

Mots clés : sels fondus, propriétés thermodynamiques, chlorure de nickel, solution non idéale, espèces complexes.

[Traduit par la rédaction]

Introduction

In previous publications from the authors, the thermodynamic properties of charge asymmetric molten salt solutions of metal chlorides with alkali halide solvents have been investigated by EMF measurements (1–7). The measurements provide valuable and practical information on: the feasibility of new processes for the recovery of metals by fused salt electrolysis, and high-temperature batteries and energy storage devices.

The thermodynamic properties of the charge asymmetric molten salt solutions, such as the exothermic enthalpies and activities with pronounced negative deviations from ideality, indicate the formation of complex species. The concept of complex formation in molten salts has been described in detail elsewhere (1, 6). Briefly, a molten salt complex like $(MCl_{z+r})^{r-}$ is a local configuration where a cation M^{z+} is surrounded by $(z + r)Cl^-$ anions.

[1] $$MCl_z + r \cdot ACl \leftrightarrow (MCl_{z+r})^{r-} + r \cdot A^+$$

Within the complex itself, the M—Cl bond distances and, accordingly, the corresponding bond energies, are different from the M—Cl bond distances in the noncomplexed pure molten MCl_z state. However, because of overall electrical neu-

Received April 3, 1995.

P.J. Tumidajski.[1] Materials Laboratory, Building M-20, National Research Council of Canada, Ottawa, ON K1A 0R6, Canada.
C.A. Pickles. Department of Materials and Metallurgical Engineering, Queen's University, Kingston, ON K7L 3N6, Canada.

[1] Author to whom correspondence may be addressed. Telephone: (613) 993-4028. Fax: (613) 954-5984. E-mail tumidajski@irc.lan.nrc.ca

Can. J. Chem. Downloaded from www.nrcresearchpress.com by 46.23.64.124 on 09/08/12
For personal use only.

Can. J. Chem. Downloaded from www.nrcresearchpress.com by 46.23.64.124 on 09/08/12
For personal use only.

trality, the anions and cations occupy single anionic and cationic lattice sites within the quasi-lattice structure of the ionic solution. Thus, the $(MCl_{z+r})^{r-}$ entities are not discrete ions on single anionic sites. A perturbation in the cation to anion bond distance within the continuum of the molten ionic phase is regarded as evidence of a complex species.

Previous work has focused on the thermodynamic state of the metal ions (and the complex) by control of the solvent composition with mixed halide solvents. The situation where the thermodynamic behavior of solutions in which two metal cations compete for the available chloride anionic ligands has not heretofore been reported. Accordingly, this paper reports on the thermodynamic behavior of the $NiCl_2$–$CoCl_2$–KCl solutions.

Experimental

The $NiCl_2$, $CoCl_2$, and KCl were spectroscopic grade and anhydrous. They were received in sealed ampoules from APL Engineered Materials (Urbana, Illinois). They were packed under argon gas. The chemicals were used without further purification. Nickel electrodes were polished with fine emery paper, and then washed several times with a 10 volume percent HF solution, distilled water, and acetone. Weighing, handling, and the transfer of all chemicals was conducted inside a glove box filled with anhydrous argon gas where the oxygen and moisture were always kept below 5 ppm.

The cell design was similar to the chloride formation cells described elsewhere (3, 4, 7). The cell consisted of a nickel metal electrode immersed in the $NiCl_2$–$CoCl_2$–KCl molten solution of known composition and a graphite chlorine electrode which also dipped into a molten solution of the same composition. The two cell compartments were separated by an asbestos fiber diaphragm fused into silica glass. The cell reaction is

$$[2] \quad Ni_{(s)} + Cl_{2(g,\,1\,atm)} = \underline{NiCl_2}$$

where, $\underline{NiCl_2}$ represents the $NiCl_2$ in the $NiCl_2$–$CoCl_2$–KCl solution. The corresponding Nernst equation is

$$[3] \quad E_{cell} = E^0_{NiCl_2} - \frac{RT}{2F}\ln(\gamma_{NiCl_2}X_{NiCl_2})$$

where F is Faraday's constant of 96 487 J V^{-1} mol^{-1}, R is the universal gas constant given as 8.3144 J K^{-1} mol^{-1}, and T is the absolute temperature in Kelvin. The standard state in all cases is pure liquid $NiCl_2$ at the temperature of the experiments. $E^0_{NiCl_2}$ is the standard potential for the formation of pure liquid $NiCl_2$. Values for $E^0_{NiCl_2}$ were obtained from a previous investigation (8).

Initially, the cell was heated for 24 h in a furnace while anhydrous argon gas passed over the salts to remove any residual moisture. Then, EMFs were measured with a Hewlett Packard model 3468B multimeter. Reversibility was confirmed by temperature cycling and with polarization tests. For a complete description of the temperature cycling procedure and the polarization test refer to previous reports (1, 4). In all cases, the cell EMF returned to within ±2 mV of the original cell EMF. Cell EMFs were also corrected for the thermoelectric potential between the nickel and the graphite electrodes.

Fig. 1. Cell voltage versus temperature for the $Y = 0.10$ composition.

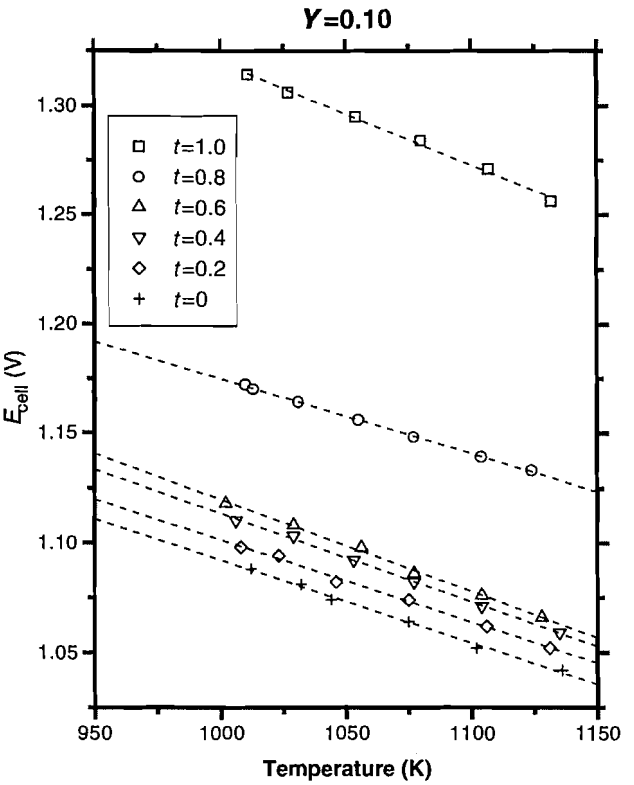

The values ranged from 1 to 5 mV over the range of experimental temperatures. The temperature upper limit was determined by subjective observation of vapor loss from the melt.

Results and discussion

Cell EMFs have been plotted against temperature in Figs. 1–3 for $Y = 0.1$, $Y = 0.25$, and $Y = 0.50$, respectively. The broken lines in Fig. 1–3 indicate the least-squares lines through the experimental data points. Table 1 summarizes the statistical treatment of the least-squares lines, which have been expressed in the form $E = A + BT$, where E is the cell EMF in volts and T is the temperature in Kelvin. Melt compositions have been expressed in terms of the following variables:

$$[4] \quad Y = 1 - X_{KCl}$$

$$[5] \quad t = \frac{X_{CoCl_2}}{X_{CoCl_2} + X_{NiCl_2}}$$

All measured cell potentials are reported with a positive sign as they represent spontaneous overall cell reactions. The correlation coefficients in Table 1 indicate that the relationship between EMF and temperature is linear. The estimate for the standard deviations of cell EMF for the regression of cell EMF on temperature is less than ±2 mV for all points. Further, the measured EMF values were stable and reproducible to within ±1 mV.

Values for $\ln \gamma_{NiCl_2}$ at 1000 K were calculated with eq. [3]. The values are summarized in Table 2. It can be seen that γ_{NiCl_2} deviates markedly from ideal behavior in consonance

Can. J. Chem. Downloaded from www.nrcresearchpress.com by 46.23.64.124 on 09/08/12
For personal use only.

Table 1. Cell EMF as a function of temperature for the $NiCl_2$–$CoCl_2$–KCl system.

		$E_{cell} = A + BT$ (V)			
Y	t	A	$B \times 10^4$	Corr. coeff.	T (K)
0.10	0.80	1.516	−3.410	−0.999	1010–1124
0.10	0.60	1.539	−4.194	−0.998	1002–1128
0.10	0.40	1.517	−4.038	−0.999	1006–1135
0.10	0.20	1.475	−3.737	−0.998	1008–1131
0.10	0	1.469	−3.768	−0.997	1012–1136
0.25	0.80	1.472	−4.275	−0.997	897–1018
0.25	0.60	1.475	−4.618	−0.991	886–941
0.25	0.40	1.471	−4.629	−0.983	868–1003
0.25	0.20	1.570	−5.852	−0.999	849–936
0.25	0	1.539	−5.646	−0.996	857–960
0.50	0.80	1.419	−5.625	−0.978	882–1015
0.50	0.60	1.361	−5.351	−0.999	907–1009
0.50	0.40	1.469	−6.601	−0.988	893–1008
0.50	0.20	1.467	−6.745	−0.990	908–1018
0.50	0	1.280	−4.952	−0.991	968–1032

Fig. 2. Cell voltage versus temperature for the $Y = 0.25$ composition.

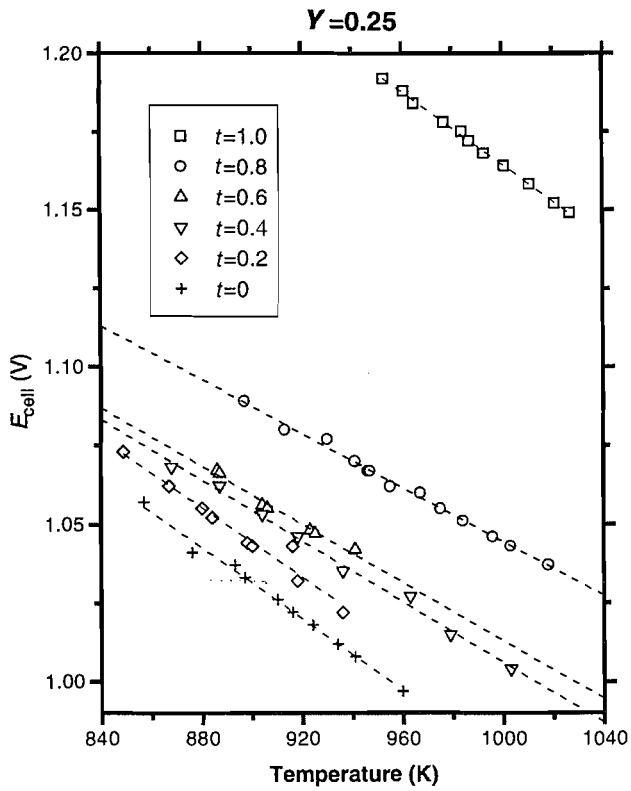

Fig. 3 Cell voltage versus temperature for the $Y = 0.50$ composition.

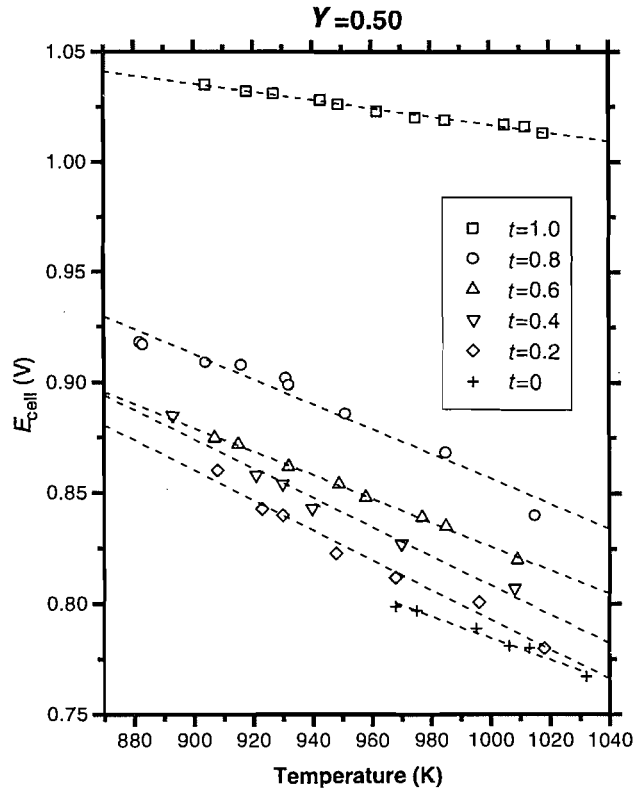

with the thermodynamic behavior commonly associated with complex formation in fused salts. When Y is constant, the values of γ_{NiCl_2} do not vary appreciably with changes in t. It appears that the thermodynamic state of $NiCl_2$ in the ternary solution is mainly defined by the behavior of $NiCl_2$ in the binary $NiCl_2$–KCl solution with only minor influence by the addition of $CoCl_2$. Conversely, when t is constant and Y varies, then there a definite dependence of γ_{NiCl_2} on Y (i.e., with the availability of the chloride anions).

The experimental values of $\ln \gamma_{NiCl_2}$ at 1000 K were fitted to a polynomial function of Y and t in the manner described previously (9). The resultant equation is

$$[6]\quad \ln \gamma = (-1225 + 363t - 3186t^2 + 8385t^3 - 6369t^4)Y^2 + (6776 - 1639t + 14803t^2 - 41112t^3 + 32405t^4)Y^3 + (-8665 + 1842t - 16964t^2 + 48873t^3 - 39440t^4)Y^4$$

Table 2. Values of ln γ_{NiCl_2} for the $NiCl_2$–$CoCl_2$–KCl ternary system at 1000 K.

t	Y	ln γ_{NiCl2}
0	0.10	−6.340
0	0.25	−4.535
0	0.50	−0.815
0.20	0.10	−6.331
0.20	0.25	−4.538
0.20	0.50	−0.785
0.40	0.10	−6.325
0.40	0.25	−4.809
0.40	0.50	−0.858
0.60	0.10	−6.066
0.60	0.25	−4.506
0.60	0.50	−0.860
0.80	0.10	−6.651
0.80	0.25	−4.545
0.80	0.50	−0.875

Therefore, eq. [6] can be used to calculate the $NiCl_2$ thermodynamic properties for any composition in the ternary $NiCl_2$–$CoCl_2$–KCl solution at 1000 K. And, in conjunction with the Gibbs–Duhem equation, the integral thermodynamic properties at 1000 K can be calculated for the ternary solution.

Conclusions

1. The thermodynamic properties of $NiCl_2$ in the $NiCl_2$–$CoCl_2$–KCl ternary solution indicate marked deviations from ideality in consonance with nickel complex formation.
2. The addition of $CoCl_2$ to the $NiCl_2$–KCl solution has a minor influence on the nickel chloride activity.
3. Values of ln γ_{NiCl_2} were fitted to a polynomial equation at 1000 K. The equation can be used to calculate the thermodynamic properties of $NiCl_2$ for any composition in the ternary melt within the composition range $0 \leq t \leq 0.80$ and $0.10 \leq Y \leq 0.5$.

References

1. P.J. Tumidajski and S.N. Flengas. J. Electrochem. Soc. **137**, 2717 (1990).
2. P.J. Tumidajski and S.N. Flengas. J. Electrochem. Soc. **138**, 1659 (1991).
3. P.J. Tumidajski and S.N. Flengas. Can. J. Chem. **69**, 462 (1991).
4. P.J. Tumidajski and S.N. Flengas. Can. J. Chem. **63**, 1080 (1985).
5. P.J. Tumidajski and S.N. Flengas. Proc. Int. Symp. Molten Salts, 7th, Montreal. 1990. *Edited by* J. Wilkes, C. Hussey, S.N. Flengas, and Y. Ito. The Electrochemical Society, N.J. p. 410.
6. P.J. Tumidajski and S.N. Flengas. Proc. Int. Symp. Molten Salts, 5th, Las Vegas, Nev. 1986. *Edited by* M.L. Saboungi, K. Johnson, D.S. Newman, and D. Inman. The Electrochemical Society, N.J. p. 551.
7. C.A. Pickles and S.N. Flengas. J. Electrochem. Soc. **131**, 2069 (1984).
8. D.C. Hamby and A.B. Scott. J. Electrochem. Soc. **115**, 704 (1968).
9. A.D. Pelton and S.N.Flengas. Can. J. Chem. **47**, 2283 (1969).

Can. J. Chem. Downloaded from www.nrcresearchpress.com by 46.23.64.124 on 09/08/12
For personal use only.

Structural characterization of the O-chain polysaccharide from *Proteus mirabilis* strain 7570

Dušan Uhrín, Vandana Chandan, and Eleonora Altman

Abstract: The O-chain polysaccharide produced by *Proteus mirabilis* strain 7570 was shown by chemical analysis and 1D and 2D NMR spectroscopy to be a high molecular weight acidic linear polymer of tetrasaccharide repeating units, composed of D-galacturonic acid, 2-acetamido-2-deoxy-D-galactose, and 2-acetamido-2-deoxy-D-glucose (2:1:1). In addition, native O-chain was randomly substituted by O-acetyl groups.

Key words: *Proteus*, lipopolysaccharide, O-chain, structure, NMR.

Résumé : L'analyse chimique et la spectroscopie RMN 1D et 2D ont montré que la chaîne O-spécifique produite par la souche 7570 de *Proteus mirabilis* est un polymère linéaire et acide, de haut poids moléculaire, constitué d'un tétrasaccharide répétitif, composé d'acide D-galacturonique, de 2-acétamido-2-désoxy-D-galactose, et de 2-acétamido-2-désoxy-D-glucose (2 : 1 : 1). De plus, la chaîne O-spécifique native est substituée de manière stochastique par des groupements O-acétyles.

Mots clés : *Proteus*, lipopolysaccharide, chaîne O-spécifique, structure, RMN.

Can. J. Chem. Downloaded from www.nrcresearchpress.com by 46.23.64.124 on 09/08/12
For personal use only.

Introduction

Proteus mirabilis, a common uropathogen, can cause urinary tract infections in hospitalized hosts and in patients with anatomic abnormalities or with local damage of urinary tract (1). Bladder and kidney stones (2) and bacteraemia (3) are other complications of *P. mirabilis* infection. Postulated virulence factors of *P. mirabilis* include fimbria-mediated adherence to uroepithelial cells via fimbriae, hydrolysis of urea by urease, haemolysin-induced cytotoxicity, swarming motility, IgA protease activity, and destruction of kidney epithelium by invasion (4). The severity of the disease caused by *P. mirabilis* has been attributed to its ability to degrade urea, which may lead to formation of struvite or carbonate-apatite struvite stones (5). In addition, exopolysaccharides of pathogenic strains of *Proteus* have been hypothesized to be potential virulence factors accelerating crystal growth (5). Here we report the structure of the O-antigen of *P. mirabilis* strain 7570 (ATCC 51286) isolated from a patient with struvite urolithiasis and serotyped as 0:23,56 by passive agglutination.

Experimental

LPS isolation and O-polysaccharide (O-PS) preparation

Cells of *P. mirabilis* strain 7570 were grown in brain heart infusion (BHI) broth (Difco) in a 75 L IF-75 fermenter (New Brunswick Scientific) at 37°C over 18 h and harvested in 1% phenol solution. *Proteus mirabilis* LPS was extracted by a modified enzyme – hot aqueous phenol method as described by Johnson and Perry (6). The well-separated aqueous and phenol layers were dialyzed against tap water until phenol free and lyophilized. The lyophilizates were dissolved in 1% saline (w/v) and, following the removal of insoluble material by low-speed centrifugation, the clear solutions were subjected to ultracentrifugation (105 000 × *g*, 4°C, 12 h) to obtain the LPS as precipitated gels. The LPS gels from the aqueous layer were dissolved in distilled water and lyophilized to give purified LPS in ca. 2% yield (based on dry cell weight). To obtain O-PS, aqueous LPS was subjected to mild acid hydrolysis in 1% (v/v) acetic acid at 100°C for 2 h and the insoluble lipid A was removed by centrifugation. The concentrated supernatant was dissolved in pyridinium acetate (0.05 M, pH 4.5) and fractionated by gel filtration on a Sephadex G-50 column (Pharmacia, 2 × 90 cm) with the same buffer as eluent. Fractions of the eluate (10 mL) were collected automatically and analyzed colorimetrically for neutral aldose (7), aminoglycose (8), hexuronic acid (9), phosphate (10), and 3-deoxy-2-octulosonate (11).

Analytical methods

GLC was done with a Hewlett–Packard 5890 series II gas chromatograph fitted with a hydrogen flame detector using a capillary column (0.32 mm × 30 m) containing fused silica DB-17 (J&W Scientific); an initial temperature of 180°C was held for 2 min, followed by an increase to 240°C at 4°C/min.

High-performance anion exchange chromatography (HPAEC) was performed using a Dionex HPLC system fitted with a CarboPac PA1 pellicular anion exchange column (4 × 250 mm) with pulsed amperometric detection (PAD). The flow rate was 1.0 mL/min. The following pulse potentials

Received April 10, 1995.

D. Uhrín,[1] V. Chandan, and E. Altman.[2] Institute for Biological Sciences, National Research Council of Canada, Ottawa, ON K1A 0R6, Canada.

[1] On leave from the Institute of Chemistry, Slovak Academy of Sciences, 842 38 Bratislava, Slovakia. This is NRCC Publication No. 39497.

[2] Author to whom correspondence may be addressed. Telephone: (613) 990-0904. Fax: (613) 941-1327.

Can. J. Chem. Downloaded from www.nrcresearchpress.com by 46.23.64.124 on 09/08/12
For personal use only.

were used: $E1$ = 0.05 V; $E2$ = 0.6 V; $E3$ = −0.8 V. The response time of the PAD was set to 360 ms for the pulse duration range of 2. Prior to injection the column was equilibrated with a 85:15 mixture of 150 mM NaOH (eluent A) and 1 M sodium acetate in 150 mM NaOH (eluent B). For the uronic acid determination the O-chain was hydrolyzed with 10 N hydrochloric acid for 15 min at 90°C. The isocratic separation of acidic monosaccharides was achieved with a 1:1 mixture of eluents A and B. The absolute configurations of glycoses were established by GLC–MS of their trimethylsilylated (*R*)-2-butyl glycoside derivatives (12). Neutral monosaccharides were determined by GLC as their alditol acetate derivatives. The O-PS was hydrolysed with 2 M trifluoroacetic acid for 17 h at 100°C. The liberated glycoses were reduced ($NaBH_4$) and acetylated as previously described (13).

O-deacetylation of O-PS

O-PS (20 mg) was treated with 5% ammonium hydroxide (2 mL) at 37°C overnight. The excess of ammonia was removed by flushing with a stream of nitrogen, and the solution was lyophilized.

Carbodiimide reduction of O-PS

O-Deacetylated (O-deAc) O-PS (10 mg) was dissolved in distilled water (3 mL) and the pH adjusted to pH 4.7 with 0.5 N HCl. After addition of 1-ethyl-3-(3-dimethylaminopropyl)carbodiimide (30 mg), the stirred mixture was maintained at pH 4.7 with 0.05 N HCl. When the consumption of hydrochloric acid ceased, sodium borodeuteride (60 mg) was added, and the reaction was allowed to proceed for 17 h at room temperature. The mixture was neutralized with dilute acetic acid, dialyzed extensively against distilled water, and lyophilized. The residue was subjected to a repeated carbodiimide reduction following the procedure described above. The final product was purified on Sephadex G-50 gel filtration column eluted with distilled water (yield, 4.6 mg).

Methylation analysis

Samples of the carbodiimide-reduced O-deAc O-PS (2 mg) were methylated according to the Hakomori procedure and the methylated products were extracted into dichloromethane (5 × 0.5 mL). Methylation product was subjected to methanolysis with 3% (w/v) methanolic hydrogen chloride at 80°C for 4 h, followed by neutralization with silver carbonate. The concentrated residue was hydrolyzed with 2 M trifluoroacetic acid (1 mL) for 7 h at 100°C and, following concentration to dryness, reduced with sodium borodeuteride in water over 17 h at room temperature. The solution was acidified with 10% acetic acid and the reaction mixture was evaporated under a stream of N_2, followed by evaporation from methanol containing 10% acetic acid (5 × 0.5 mL) to remove borate. The residual alditols were acetylated by heating with acetic anhydride:pyridine mixture (1:1, 1 mL) at 100°C for 1 h and analyzed by GLC–MS.

SDS-PAGE

LPS preparations were subjected to SDS-PAGE with the Laemmli buffer system (14). The 4% stacking gel and the 12.5% separating gel did not contain SDS (15).

NMR spectroscopy

NMR spectra were obtained on a Bruker AMX 500 spectrometer using standard Bruker software. The observed ^1H chemical shifts are reported relative to internal acetone (2.225 ppm) and the carbon chemical shifts are quoted relative to the methyl group of internal acetone (31.07 ppm). The O-deAc O-PS sample was exchanged twice with D_2O and measured at 35°C using 10 mg dissolved in 0.5 mL of D_2O. Acquisition and processing of respective 2D NMR experiments were done as described previously (16).

General methods

Concentrations were made up under reduced pressure and below 40°C. Optical rotations were determined at 20°C in 10 cm microtubes using a Perkin–Elmer model 243 polarimeter.

Results and discussion

Extraction of *P. mirabilis* strain 7570 cells by the modified lysozyme phenol–water extraction procedure, followed by purification of the LPS by repeated ultracentrifugation afforded an aqueous-phase LPS (yield, 1.13 g). The silver-stained profiles of purified aqueous-phase LPS gave a pattern typical of the smooth type although the bands representing LPS with shorter O-chains were more pronounced than the SDS-PAGE banding pattern of *Salmonella enteritidis* or *Escherichia coli* LPS (Fig. 1). The lack of staining of the upper LPS bands could be due to the inability of the material to enter the gel, possibly because of a high concentration of charged groups in the O-chain PS (see below). Partial hydrolysis of the S-type LPS with hot dilute acetic acid gave an insoluble lipid A, and gel-filtration of the water-soluble products on Sephadex G-50 afforded an O-PS fraction eluting in the void volume of the system (yield, 9.3%). It was homogeneous with respect to hexuronic acid and 2-amino-2-deoxyglycose components and had $[\alpha]_D$ +100 (*c* 1.59, water). Anal. found: C 38.00, H 5.03, N 2.67, ash 6%.

Hydrolysis of the carbodiimide-reduced O-PS ($NaBD_4$), followed by GLC–MS analysis of the $NaBH_4$-reduced and acetylated product, showed it to be composed of 2-amino-2-deoxy-D-glucose, 2-amino-2-deoxy-D-galactose, and D-galactose-6,6-d_2 (1:1:2). The presence of galacturonic acid was further confirmed by high-performance anion-exchange chromatography of the hydrolysis products of the native O-PS. The D configuration of glycoses was established by capillary GLC of the trimethylsilylated derivatives of their (*R*)-2-butyl glycosides. Methanolysis of the methylated carbodiimide-reduced O-PS, followed by hydrolysis, reduction ($NaBD_4$), and acetylation of the resulting alditol methyl ethers (Table 1) showed the O-chain to be composed of a linear repeating tetrasaccharide unit containing the following linked glycoses: [→4)-D-Gal$_p$A-(1→, →2)-D-Gal$_p$A-(1→, →3)-D-Glc$_p$NAc-(1→ and →3)-D-Gal$_p$NAc-(1→].

The ^1H NMR spectrum of the native O-PS exhibited a heterogeneity due to the presence of the *O*-acetyl groups. The complex pattern was simplified after O-deacetylation, and subsequent 2D NMR analysis confirmed that the sample consisted of a single molecular species. The ^1H NMR spectrum of the O-deAc O-PS showed, inter alia, signals for two *N*-acetyl groups at 2.01 (3H) and 2.15 (3H) ppm, together with four anomeric signals at 4.54, 4.835, 4.945, and 5.405 ppm (Table 2), consistent with the proposed tetrasaccharide repeating unit. The anomeric resonances were labelled **a**, **b**, **c**, and **d** according to the descending chemical shifts in the ^1H NMR spec-

Can. J. Chem. Downloaded from www.nrcresearchpress.com by 46.23.64.124 on 09/08/12
For personal use only.

Table 1. GLC–MS analysis of the methylated carbodiimide reduced O-chain polysaccharide of *Proteus mirabilis* strain 7570.

Alditol acetate derivative	T_{GM}[a]	Molar ratio[b]
1,5-Di-*O*-acetyl-2,3,4,6-tetra-*O*-methylgalactitol-1,6,6-d_3	1.06	0.11
1,4,5-Tri-*O*-acetyl-2,3,6-tri-O-methylgalactitol-1,6,6-d_3	1.31	0.35
1,2,5-Tri-*O*-acetyl-3,4,6-tri-*O*-methylgalactitol-1,6,6-d_3	1.35	1.00
1,3,5-Tri-*O*-acetyl-2-deoxy-4,6-di-*O*-methyl-2-(*N*-methylacetamido)-glucitol-1-*d*	2.38	0.29
1,3,5-Tri-*O*-acetyl-2-deoxy-4,6-di-*O*-methyl-2-(*N*-methylacetamido)-galactitol-1-*d*	2.41	0.21

[a]Retention time of the derived alditol acetate relative to that of 1,5-di-*O*-acetyl-2,3,4,6-tetra-*O*-methylglucitol.

[b]Relative to 1,2,5-tri-*O*-acetyl-3,4,6-tri-*O*-methylgalactitol-1,6,6-d_3.

Fig. 1. SDS-PAGE (12.5%) pattern of LPS from *Proteus mirabilis* strain 7570 (lane 1), *Escherichia coli* O111 strain 003 (lane 2), and *Salmonella enteritidis* strain 27655-36 (lane 3).

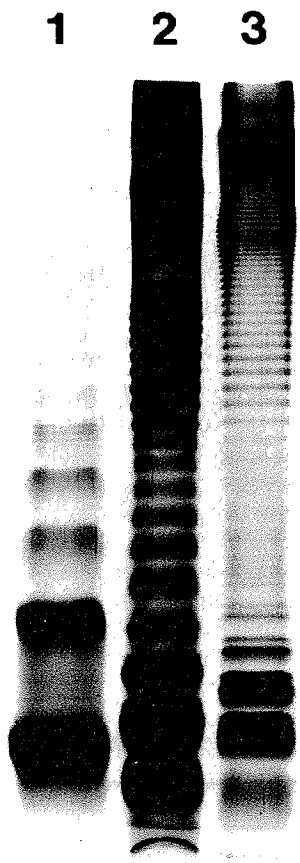

trum. The resolution-enhanced ^{1}H NMR spectrum of O-deAc O-PS (see top trace of the 2D NOESY spectrum, Fig. 2) indicated, on the basis of large $J_{1,2}$ values, that residues **c** and **d** had β-D-configuration, while residues **a** and **b** yielded broad singlets precluding an immediate determination of their anomeric configuration.

^{1}H resonances of the O-deAc O-PS were partially assigned using a 2D proton chemical shift correlated spectroscopy (COSY) and a total correlated spectroscopy (TOCSY). A series of 2D TOCSY spectra was acquired using mixing times of 25, 45, and 90 ms. The magnetization transfer from H-1 stopped at H-4 in residue **d**, while it was relayed only as far as H-3 for residues **a** and **b**, possibly due to small $J_{1,2}$ values and (or) fast spin–spin relaxation. The observed transfer from H-4 to H-3 and H-2 in **a** and **b** residues allowed, however, the identification of H-4**a** and H-4**b** signals as overlapping singlets at 4.38 ppm. No transfer to H-5 protons was observed in either **a**, **b**, or **d** residue as expected for a *galacto*-pyranosyl configuration. All the resonances for the residue **c** were identified and its β-D-Glc$_p$ configuration was established.

The sequence and the position of the glycosidic linkages in the O-deAc O-PS were determined by a 2D nuclear Overhauser effect spectroscopy (NOESY), which in addition enabled the ^{1}H assignments of H-5 resonances in residues **a**, **b**, and **d** and those of H-6,6′ in the residue **b**. Four 2D NOESY spectra were acquired using mixing times of 50, 100, 150, and 200 ms, allowing for discrimination between the direct NOE cross peaks and the peaks due to the spin diffusion (Fig. 2). The H-5 resonances of residues **a**, **b**, and **d** were located on the basis of H-4/H-5 and H-3/H-5 NOE cross peaks. However, the NOEs between H-5 and H-6,6′ were established for the residue **b** only, suggesting that residues **a** and **d** are oxidized at C-6. In addition, the NOEs between protons of one of the $NCOCH_3$ groups and H-2**c** and H-4**c** resonances were observed, indicating the presence of the *N*-acetyl group in the residue **c**. No NOEs were observed for the protons of the other *N*-acetyl group. Characteristic intraresidue NOEs were detected between H-1 and H-2 protons in the residues **a** and **b**, indicating their α-D-configuration. The sequence of the glycoses in the repeating unit of the O-PS was established from the following observed interglycosidic NOEs: 1**a** → 2**c** and 3**c**; 1**b** → 4**a**; 1**c** → 2**d**; and 1**d** → 3**b**.

To resolve the ambiguity in the **a** → **c** linkage and also to verify the structure determined via ^{1}H NMR spectroscopy, a ^{13}C NMR spectrum of O-deAc O-PS was analyzed and assigned on the basis of ^{13}C–^{1}H correlated (2D HMQC) and proton-relayed ^{13}C–^{1}H correlated (2D HMQC-TOCSY) experiments (Table 3). In the 2D HMQC spectrum only cross peaks between directly attached protons and carbons are observed, while in the 2D HMQC-TOCSY spectrum additional cross peaks are detected for any given carbon, corresponding to other protons within the same residue. The intensity of these cross peaks depends on the magnitude of coupling constants between the protons involved and on the length of the TOCSY mixing time. For short mixing times only immediate neighbours of a particular proton are

Table 2. ^{1}H NMR chemical shift data for the O-deAc O-PS of *P. mirabilis* strain 7570.

Residue	Glycosyl unit	H-1	H-2	H-3	H-4	H-5	H6	H6′	$COCH_3$
a	→4)-α-D-Gal$_p$A-(1→	5.405	3.90	3.94	4.38	4.24	—	—	—
b	→3)-α-D-Gal$_p$NAc-(1→	4.945	4.31	4.00	4.385	4.34	3.74	3.71	2.01
c	→3)-β-D-Gal$_p$NAc-(1→	4.835	3.77	3.77	3.665	3.39	3.89	3.705	2.15
d	→2)-β-D-Gal$_p$A-(1→	4.54	3.67	3.70	4.14	4.07	—	—	—

Fig. 2. A 500 MHz 2D NOESY spectrum of O-deAC O-PS acquired using a mixing time of 150 ms. The following cross peaks appeared due to the spin diffusion, as deduced from 2D NOESY spectra acquired with shorter mixing times: 1**d**/4**b**, 1**d**/5**b**, and 3**b**/3**d**.

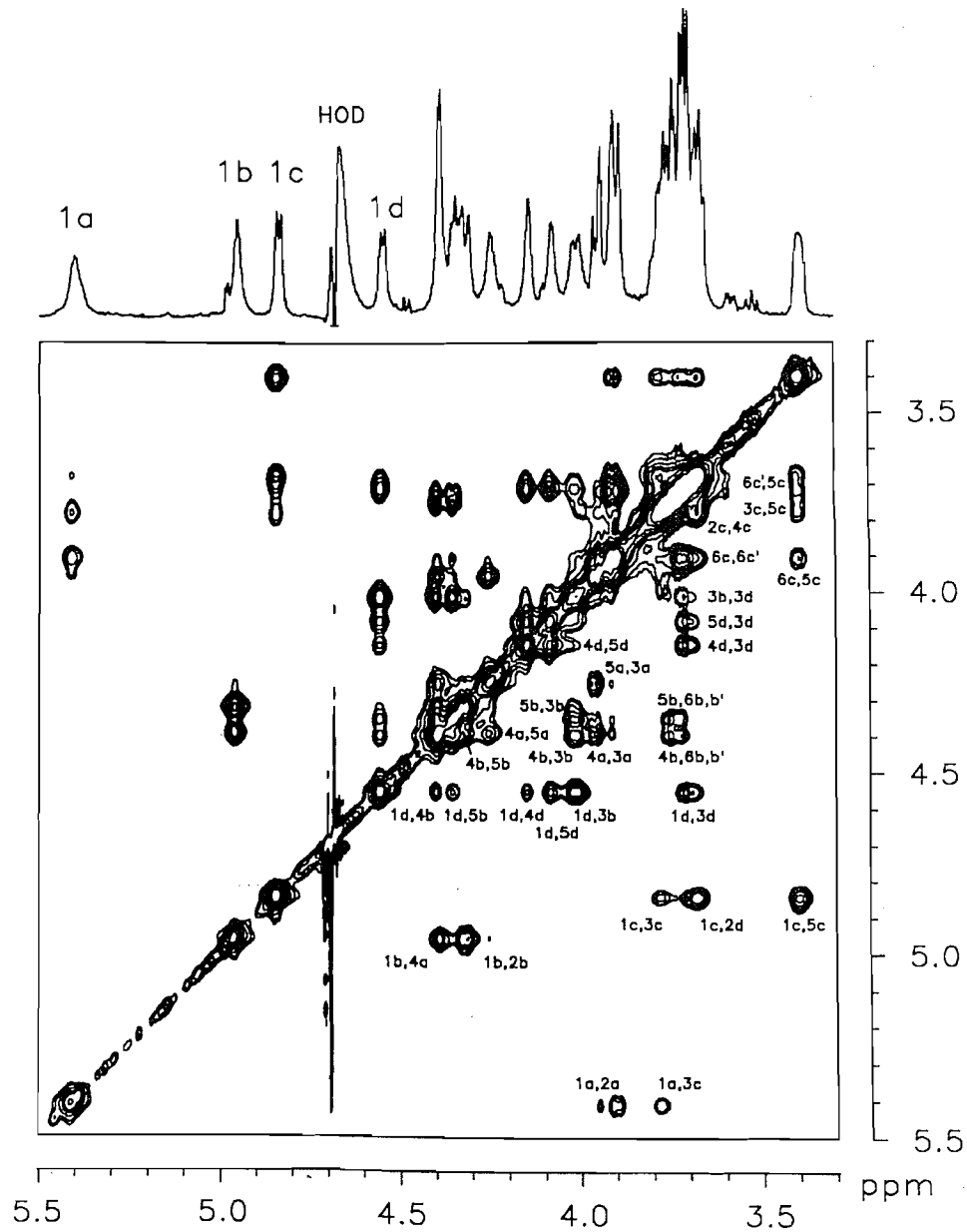

observed, while for longer mixing periods more remote protons might also appear. Therefore, when two proton resonances are overlapped, while their corresponding carbon resonances are separated, it is possible by a combination of 2D HMQC and 2D HMQC-TOCSY experiments with a short mixing time to establish the neighbouring protons for each carbon and thus deduce the carbon assignment (16).

In the case of O-deAc O-PS, two protons (H-2**c**, 3**c**) reso-

Can. J. Chem. Downloaded from www.nrcresearchpress.com by 46.23.64.124 on 09/08/12
For personal use only.

Table 3. ^{13}C NMR chemical shift data for the O-deAc O-PS of *P. mirabilis* strain 7570.

Residue	Glycosyl unit	C-1	C-2	C-3	C-4	C-5	C-6	$COCH_3$	$COCH_3$
a	→4)-α-D-Gal$_p$A-(1→	101.3	69.2	69.7	80.0	—[a]	174[b]	—	—
b	→3)-α-D-Gal$_p$NAc-(1→	99.8	49.2	78.0	70.0	71.5	61.5	23.0	175.4
c	→3)-β-D-Gal$_p$NAc-(1→	102.5	55.2	82.6	71.5	76.3	61.5	23.8	174.9
d	→2)-β-D-Gal$_p$A-(1→	103.1	78.0	75.1	71.3	—[a]	174[b]	—	—

[a]Not observed.
[b]Broad signal.

nating at 3.77 ppm were correlated on the basis of a 2D HMQC experiment with carbon signals at 82.58 and 55.17 ppm. These ^{13}C chemical shifts are characteristic for a carbon involved in glycosidic linkage and a carbon carrying an *N*-acetyl group, respectively. In the subsequent 2D HMQC-TOCSY experiment, acquired using a short mixing time (16 ms), a relay signal at 4.84 ppm (H-1**c**) was observed at 55.17 ppm but not at 82.58 ppm. This implies that the *N*-acetyl group is present at C-2**c**, while the C-3**c** is involved in a glycosidic linkage. In a similar manner, the assignments of the remaining carbons involved in glycosidic linkages were established by a combination of HMQC and HMQC-TOCSY experiments, confirming the results of the homonuclear experiments.

The position of the second *N*-acetyl group was determined from the HMQC spectrum where a cross peak between the H-2**b** proton (4.31 ppm) and a ^{13}C signal at 49.19 ppm, characteristic of the α-linked 2-amino-*galacto*-pyranosyl residue, was observed (17). In addition, the expected cross peaks between the H-5**a** and H-5**d** and their corresponding carbons were not observed in the HMQC spectrum. These ^{13}C signals were also missing in the 1D ^{13}C spectrum of O-deAc O-PS, possibly due to the fast spin–spin relaxation of C-5 signals in the residues **a** and **d**. The ^{13}C resonances of their respective carboxyl groups (C-6) appeared as one very broad signal at 174 ppm.

The combined chemical and NMR evidence permits the structure of the O-antigen to be established as a linear tetrasaccharide repeating unit **1**.

$$[\rightarrow 4)\text{-}\alpha\text{-D-Gal}_p\text{A-}(1\rightarrow 3)\text{-}\beta\text{-D-Glc}_p\text{NAc-}(1\rightarrow 2)\text{-}\beta\text{-D-Gal}_p\text{A-}(1\rightarrow 3)\text{-}\alpha\text{-D-Gal}_p\text{NAc-}(1\rightarrow]_n$$
$$\mathbf{a} \qquad \mathbf{c} \qquad \mathbf{d} \qquad \mathbf{b}$$
$$+ \text{O-Ac}$$

1

It has been suggested that the acidic nature of the O-polysaccharides of *P. mirabilis* contributes to the formation of stones in the alkaline environment created by the bacterial urease activity. Most of these polysaccharides contain acidic components, such as uronic acids, phosphate groups, and, less frequently, pyruvate ketals and lactic acid (18). Partial O-acetylation has been reported in several O-specific polysaccharides of *P. mirabilis*.

Acknowledgements

We express our appreciation to J.L. Penner, University of Toronto, for serotyping the *P. mirabilis* strain. F. Cooper provided GLC–MS analyses, and large-scale cell production was carried out by D.W. Griffith.

References

1. K.F. Fairley, A.G. Bond, and P. Habersberger. Lancet, **2**, 427 (1967).
2. D.P. Griffith, D.M. Musher, and C. Itin. Invest. Urol. **13**, 346 (1976).
3. U. Setia, I. Serventi, and P. Lorenz. Arch. Intern. Med. **144**, 1633 (1984).
4. H.L.T. Mobley and G.R. Chippendale. J. Infect. Dis. **161**, 525 (1990).
5. R.J.C. McLean, J.C. Nickel, K.-J. Cheng, and J.W. Costerton. Crit. Rev. Microbiol. **16**, 37 (1988).
6. K.G. Johnson and M.B. Perry. Can. J. Microbiol. **22**, 29 (1976).
7. M. Dubois, K.A. Gilles, J.K. Hamilton, P.A. Rebers, and F. Smith. Anal. Chem. **28**, 350 (1956).
8. R. Gatt and E.R. Berman. Anal. Biochem. **15**, 167 (1965).
9. N. Blumenkrantz and G. Asboe-Hansen. Anal. Biochem. **54**, 484 (1973).
10. P.S. Chen, T.Y. Toribara, and H. Warner. Anal. Chem. **28**, 1756 (1956).
11. D. Aminoff. Biochem. J. **81**, 384 (1965).
12. G.J. Gerwig, J.P. Kamerling, and J.F.G. Vliegenthart. Carbohydr. Res. **77**, 1 (1979).
13. S.W. Gunner, J.K.N. Jones, and M.B. Perry. Can. J. Chem. **39**, 1892 (1961).
14. U.K. Laemmli and M. Favre. J. Mol. Biol. **80**, 575 (1973).
15. P.J. Hitchcock and T.M. Brown. J. Bacteriol. **154**, 269 (1983).
16. D. Uhrín, J.-R. Brisson, L.L. MacLean, J.C. Richards, and M.B. Perry. J. Biomol. NMR, **4**, 615 (1994).
17. P. Colson and R.R. King. Carbohydr. Res. **47**, 1 (1976).
18. Y.A. Knirel, E.V. Vinogradov, A.S. Shashkov, Z. Sidorczyk, A. Rozalski, I. Radziejewska-Lebrecht, and W. Kaca. J. Carbohydr. Chem. **12**, 379 (1993).

Can. J. Chem. Downloaded from www.nrcresearchpress.com by 46.23.64.124 on 09/08/12
For personal use only.

Aggregation of squaraine dyes: Structure–property relationships and solvent effects

Andrew J. McKerrow, Erwin Buncel, and Peter M. Kazmaier

Can. J. Chem. Downloaded from www.nrcresearchpress.com by 46.23.64.124 on 09/08/12
For personal use only.

Abstract: In characterizing the UV–visible absorption properties of a series of seven anilino class squaraine dyes in dimethyl sulfoxide (DMSO) – water mixtures, spectral features characteristic of aggregation were observed. These included hypsochromic and hypochromic shifts of the absorption maximum, relative to the nonassociated state of these dyes. Previously aggregation of this class of squaraine dyes had only been reported in studies of Langmuir–Blodgett (LB) films prepared with squaraine dyes. In the present study two distinctly different and novel solution dye aggregates, designated as type A and type B, were identified on the basis of their characteristic absorption properties. The type A aggregate was characterized by an absorption maximum that was hypsochromically and hypochromically shifted, in comparison with that of the nonassociated dyes, and had a secondary absorption occurring at approximately the same wavelength at which nonassociated squaraine dyes absorb. These spectral features are believed to be the result of a "face-to-face" alignment of molecules in the aggregate. The type B aggregate featured a broad absorption typically from 525 to 700 nm. Based on similarities between the spectral features of type B aggregates and LB films of surfactant squaraines, the alignment of molecules in the solution aggregate was believed to be such that the electron-deficient squarylium moieties interacted with the electron-rich dialkylamino phenyl moieties. Certain squaraine dyes that were investigated as part of this study were found to form both type A and type B aggregates, depending upon the composition of the DMSO–water medium. Typically, the type A aggregate formed preferentially in media of intermediate DMSO content (50–70% DMSO) and the type B aggregate in more water-rich media (<20% DMSO). In the intervening region it was possible to monitor spectroscopically a dynamic conversion from the type B aggregate to the type A aggregate. An examination of structure–property relationships indicated that dyes with less hydrophobic N-alkyl substituents formed only type A aggregates. Squaraine dyes with more hydrophobic N-alkyl substituents were found to form type B aggregates in water and type A aggregates in some DMSO–water mixtures. A model of squaraine aggregation was proposed in which the type A squaraine aggregate was "thermodynamically" preferred while the type B aggregate was "kinetically" preferred. The stability of the type B aggregate was proposed to be enhanced by increasing hydrophobicity of the N-alkyl substituents and decreased by increasing amounts of DMSO in the solvent system.

Key words: squaraine dyes, aggregation, crystallochromy, solvent effects.

Résumé : Opérant dans des mélanges diméthylsulfoxyde–eau, on a déterminé les propriétés d'absorption dans l'UV–visible d'une série de sept colorants squaraïne de la classe de anilino; elles permettent d'observer des caractéristiques spectrales typiques d'agrégation. Celles-ci incluent des déplacements hypsochromes et hypochromes des maxima d'absorption par rapport à l'état non associé de ces colorants. Antérieurement, des agrégations de colorants squaraïne de cette classe n'avaient été rapportées que dans des études de films de Langmuir–Blodgett (LB) préparés avec des colorants squaraïne. Dans la présente étude, en se basant sur les propriétés caractéristiques d'absorption, on a identifié deux nouveaux colorants agrégés en solution, distinctement différents et désignés respectivement de type A et de type B. L'agrégat de type A est caractérisé par une absorption maximale qui, par comparaison avec les colorants non associés, est hypsochromatiquement et hypochromiquement déplacé et qui présente une absorption secondaire se produisant approximativement à la même longueur d'onde que celle des colorants squaraïne non associés. On croit que ces caractéristiques spectrales sont le résultat d'un alignement face à face des molécules dans l'agrégat. L'agrégat de type B est caractérisé par une absorption large qui s'étale d'une façon typique entre 525 et 700 nm. En se basant sur des similarités entre les caractéristiques spectrales des agrégats de type B et les films LB des agents de surface squaraïnes, on croit que l'alignement de molécules dans la solution agrégée est telle que les portions

Received May 4, 1995.

A.J. McKerrow and E. Buncel. Department of Chemistry, Queen's University, Kingston, ON K7L 3N6, Canada. Telephone: (613) 545-2616. Fax: (613) 545-6669
P.M. Kazmaier. Xerox Research Centre of Canada, Mississauga, ON L5K 2L1, Canada. Telephone: (905) 823-7091. Fax: (905) 822-7022.

électrodéficientes squarylium interagissent avec les portions dialkylaminophényles riches en électron. On a trouvé que certains colorants squaraïnes utilisés dans cette étude forment des agrégats aussi bien du type A que du type B dépendant de la composition du milieu DMSO–eau. D'une façon typique, les agrégats de type A se forment préférentiellement dans un milieu contenant une quantité intermédiaire (50–70%) de DMSO alors que les agrégats de type B se forment dans des milieux plus riches en eau (<20% de DMSO). Dans la région intermédiaire, il est possible de détecter d'une façon spectroscopique une conversion dynamique des agrégats de type B en agrégats de type A. Un examen des relations structure–propriété indique que les colorants portant des substituants N-alkyles moins hydrophobiques ne forment que des agrégats de type A. On a trouvé que les colorants squaraïne avec des substituants N-alkyles plus hydrophobiques forment des agrégats de type B dans l'eau et des agrégats de type A dans certains mélanges de DMSO–eau. On propose un modèle d'agrégation de la squaraïne dans lequel l'agrégat de type A de la squaraïne est préféré d'un point de vue thermodynamique alors que l'agrégat de type B est cinétiquement préféré. On suggère que la stabilité des agrégats de type B est augmentée avec une augmentation de l'hydrophobicité des substituants N-alkyles et qu'elle diminue avec une augmentation des quantités de DMSO dans le système de solvant.

Mots clés : colorants squaraïne, agrégation, cristallochromie, effets de solvant.

[Traduit par la rédaction]

Introduction

Since their initial preparation in 1965 (1), the squaraine dyes have been studied using a wide range of experimental and theoretical methods. These include studies of the solution state properties using UV–visible (2), fluorescence emission (2, 3), and nuclear magnetic resonance (NMR) spectroscopies (4), as well as electrochemical techniques (5). The properties of these dyes in the solid state have been investigated using single crystal (6) and X-ray powder diffraction techniques (5), while a number of workers have prepared Langmuir–Blodgett thin films incorporating squaraine dyes (7).

As part of our studies of the squaraine dyes we recently reported the observation of novel solution aggregates of a squaraine dye in mixtures of dimethyl sulfoxide (DMSO) and water (8).

When squaraine **4** was added to DMSO–water mixtures with greater than 70% DMSO, spectroscopic characterization of the solutions showed an absorption indicative of the nonassociated squaraine, $\lambda_{max} \simeq 664$ nm, $\varepsilon_{664} \simeq 300\,000\ M^{-1}\ cm^{-1}$, Fig. 1.

In media of between 50 and 70 v/v% DMSO–water we reported that the introduction of squaraine **4**, in a trifluoroethanol (TFE) solution, resulted in solutions with an absorption maximum at 530 nm, $\varepsilon_{530} \simeq 80\,000\ M^{-1}\ cm^{-1}$, and a secondary absorption at approximately 650 nm. The solutions had an absorption spectrum identical to Fig. 2 (spectrum 7). The reduced intensity and large hypsochromic shift of the absorption maximum, in comparison with the spectral features of the nonassociated dye observed in more DMSO-rich media, indicated that aggregation had occurred. This was the first reported example of a solution squaraine aggregate and for the purposes of this paper associated squaraines characterized by such a shift of the absorption maximum and a secondary absorption at longer wavelengths will be referred to as *type A aggregates*.

In DMSO–water mixtures with less than 20% DMSO the addition of squaraine **4**, in TFE solution, yielded solutions characterized by a broad absorption maximum from 550 nm to 700 nm, similar to Fig. 2 (spectrum 1). This absorption was also hypochromically shifted, relative to the intensity of the absorption maximum of the nonassociated dye, and squaraine aggregates that feature these absorption characteristics will henceforth be denoted as *type B aggregates*.

Fig. 1. UV–visible absorption spectrum of squaraine **4** in DMSO.

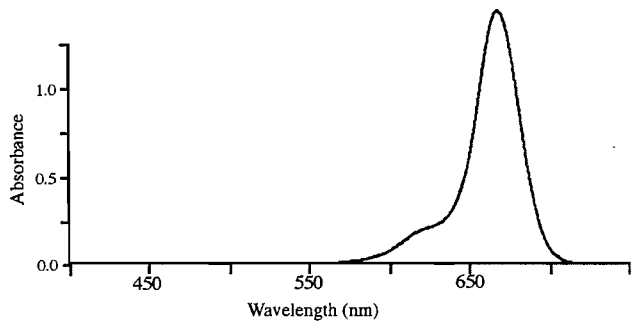

Fig. 2. UV–visible absorption spectra of squaraine **4** in 30 v/v% DMSO–water monitored at 12 min intervals after sample preparation, showing the dynamic conversion from a type B aggregate (spectrum 1) to a type A aggregate (spectrum 7).

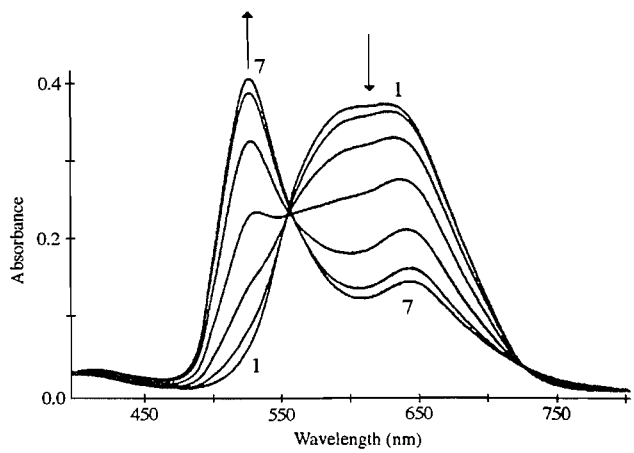

In the intervening region (20–50% DMSO) we reported that the type B aggregate formed initially on addition of the squaraine **4** – TFE solution to the binary solvent system. Over time, *a dynamic conversion from the type B aggregate to the type A aggregate was observed*, see Fig. 2. As the amount of DMSO cosolvent increased, the rate of this dynamic conversion was found to increase.

Can. J. Chem. Downloaded from www.nrcresearchpress.com by 46.23.64.124 on 09/08/12
For personal use only.

Can. J. Chem. Downloaded from www.nrcresearchpress.com by 46.23.64.124 on 09/08/12
For personal use only.

Prior to these observations, the only published reports concerning the aggregation of squaraine dyes dealt with the association of surfactant squaraine dyes in Langmuir–Blodgett thin films (7). In these studies aggregation could be detected by characterizing the thin films using UV–visible absorption spectroscopy. Subsequently other workers have reported the solution state aggregation of squaraine dyes (9).

Through the study of these novel dye aggregates there is the potential to better understand both the intrinsic molecular properties of these dyes, and their intermolecular interactions. Accordingly, a comprehensive investigation of the aggregation properties of this class of squaraine dyes was undertaken. The goals of these studies included gaining an understanding of (*i*) the effect on aggregation of various functional groups in the dye, (*ii*) the nature of the DMSO solvent effect on squaraine aggregation, and (*iii*) the spatial relationship between molecules in the two aggregate types.

Experimental investigations of these aggregation phenomena involved a spectrophotometric study of bis(4-di-*n*-butylamino-2-hydroxyphenyl)squaraine, **4**, and six other squaraine dyes in a series of DMSO–water mixtures. The other dyes included bis(4-dimethylamino-2-hydroxyphenyl)squaraine, **1**, bis(4-diethylamino-2-hydroxyphenyl)squaraine, **2**, bis(4-di-*n*-propylamino-2-hydroxyphenyl)squaraine, **3**, and bis(4-di-*n*-octylamino-2-hydroxyphenyl)squaraine, **5**. Bis(4-di-*n*-butylamino-2-hydroxy-6-methylphenyl)squaraine, **6**, and bis(8-hydroxy-9-julolidinyl)squaraine, **7**, were also included in these studies.

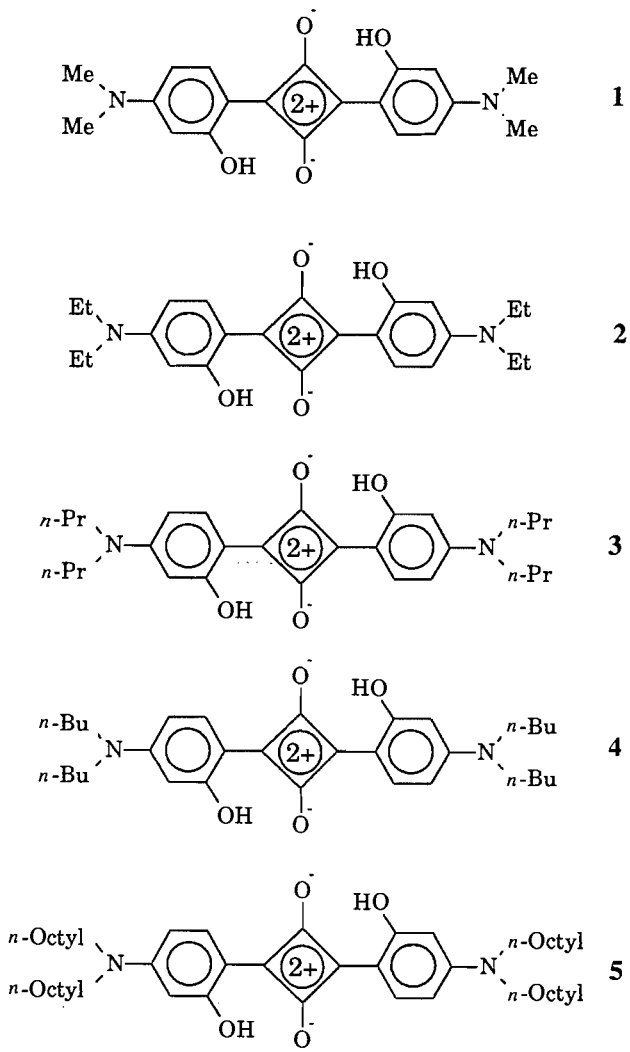

Experimental

Synthesis

Squaraine dyes were prepared using the method of Sprenger and Ziegenbein (10) in which two equivalents of aromatic dialkylamine were reacted with one equivalent of squaric acid in a toluene–1-butanol solvent system. Details concerning the preparation of these dyes will be published elsewhere.

Squaraine aggregation studies

Purification of reagents and preparation of solutions

Considerable care was taken in the purification of reagents and preparation of solutions for these experiments. All glassware was soaked overnight in a bath of Decon-75, washed with copious amounts of distilled water, and oven dried.

Dimethyl sulfoxide was freshly distilled from calcium hydride. Distilled and doubly deionized water was refluxed for 4 h in order to remove CO_2, and cooled under a stream of nitrogen. Binary DMSO–water mixtures were prepared for these studies by accurately determining the mass of each component in the mixtures. Organic solvents used in the preparation of dye stock solutions included 2,2,2-trifluoroethanol, acetone, and *N*,*N*-dimethylacetamide. These solvents were of spectroscopic grade and were purified, when necessary, according to standard procedures (11).

Stock solutions of each dye were freshly prepared in an appropriate solvent and characterized by UV–visible absorption spectroscopy prior to each experiment. The physical properties of the stock solutions of the squaraine dyes included in this study are reported in Table 1. Bis(4-dimethylamino-2-hydroxyphenyl)squaraine, **1**, was found to be highly insoluble and as a result a saturated stock solution was prepared in *N*,*N*-dimethylacetamide and the excess dye was removed by filtration. The concentration of this solution was estimated to be 6×10^{-6} M, based on an estimated extinction coefficient of $\varepsilon_{646} = 350\,000\ M^{-1}\ cm^{-1}$ for the absorption maximum at 646 nm that is typical for dyes of this class (2).

Spectrophotometric method

Reproducible results were obtained in the spectrophotometric studies by preparing samples in a consistent manner. This involved introducing 2 mL of the appropriate DMSO–water mixture into a 10-mL round-bottom flask that was fitted with a stirring bar, a rubber septum, and flushed with nitrogen. An aliquot of the dye stock solution (maximum 1 v/v%, unless otherwise noted) was then added quickly to the mixture and stirring continued for 30 s, followed by sonication for 60 s. The solution was transferred quickly by syringe into a quartz cuvette and placed in a Cary 3 UV–visible spectrophotometer fitted with a thermostated cell compartment at 25°C. The absorption spectrum of the sample was recorded immediately and at intervals of 10–15 min for at least 1 h. These experiments were performed either in duplicate or triplicate. Samples were subsequently stored for later analysis. Due to experimental limitations squaraine **1** could not be studied in

Table 1. Spectroscopic properties of squaraine dyes that were used in the aggregation study.

Squaraine	λ_{max} (nm)	ε (M^{-1} cm^{-1})	Solvent[a]
Bis (4-dimethylamino-2-hydroxyphenyl), **1**	646	350 000	*N,N*-DMA
Bis (4-diethylamino-2-hydroxyphenyl), **2**	638	318 000	TFE
Bis (4-di-*n*-propylamino-2-hydroxyphenyl), **3**	647	343 000	Acetone
Bis (4-di-*n*-butylamino-2-hydroxyphenyl), **4**	645	331 000	TFE
Bis (4-di-*n*-octylamino-2-hydroxyphenyl), **5**	645	358 000	Acetone
Bis (4-di-*n*-butylamino-2-hydroxy-6-methylphenyl, **6**	665	345 000	TFE
Bis (8-hydroxy-9-julolidinyl), **7**	676	348 000	*N,N*-DMA

[a]TFE corresponds to 2,2,2-trifluoroethanol, *N,N*-DMA to *N,N*-dimethylacetamide.

Can. J. Chem. Downloaded from www.nrcresearchpress.com by 46.23.64.124 on 09/08/12
For personal use only.

Fig. 3. (*a*) UV–visible absorption spectra of squaraine **1** in 10 v/v% *N,N*-dimethylacetamide-water monitored at 10 min intervals after sample preparation. (*b*) UV–visible absorption spectra of squaraine **2** in 30 v/v% DMSO–water monitored at 10 min intervals after sample preparation. (*c*) UV–visible absorption spectra of squaraine 6 in 40 v/v% DMSO–water monitored at 10 min intervals after sample preparation, showing the dynamic conversion from a type B aggregate (spectrum 1) to a type A aggregate (spectrum 9).

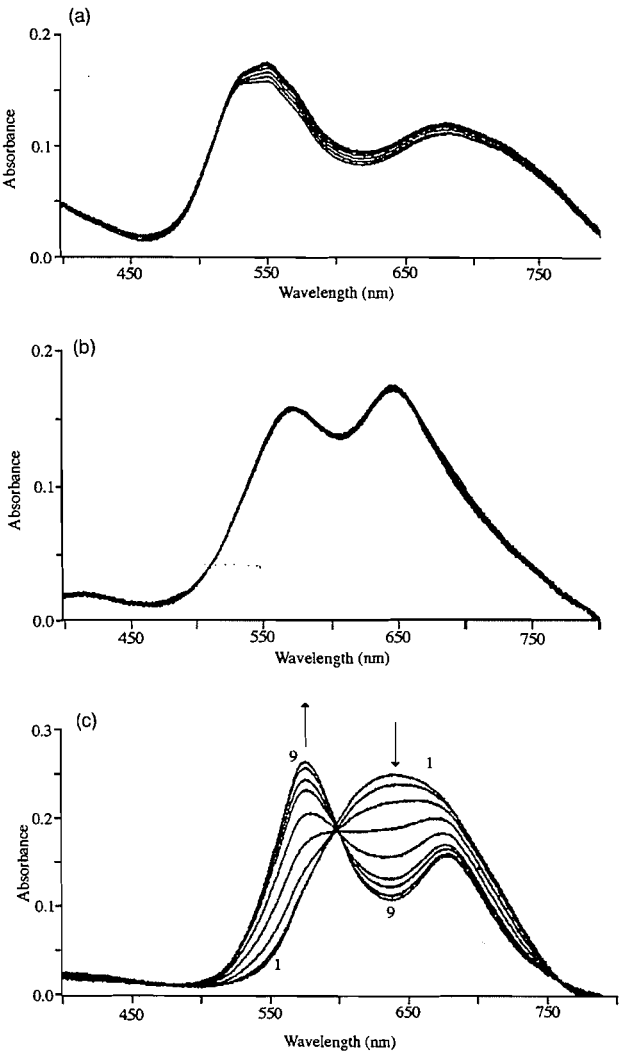

DMSO–water mixtures but rather an aliquot of the dye in a *N,N*-dimethylacetamide stock solution was diluted 10-fold with water.

Results and discussion

1. Classification of squaraine aggregates: Classes A, B, and A/B

In these studies the aggregation properties of seven squaraine dyes were investigated as a function of solvent composition using a series of DMSO–water mixtures. Characterization of these solutions for several hours after preparation and again after at least 1 day, via UV–visible absorption spectroscopy, delineated the spectroscopic properties of these aggregates over both the short and long term. As a summary, it is useful to group these compounds into three classes based on the impact of solvent composition on aggregation in the short-term experiments.

Class A squaraines formed only *type A aggregates* when self-association occurred. Bis(8-hydroxy-9-julolidinyl)squaraine, **7**, was included in this class, as addition of this dye in an *N,N*-dimethylacetamide stock solution to water and mixtures of between 10 and 50 v/v% DMSO–water resulted in solutions whose spectroscopic properties were similar to those of the previously defined type A aggregates.

When a stock solution of bis(4-dimethylamino-2-hydroxyphenyl)squaraine, **1**, in *N,N*-dimethylacetamide was diluted 10-fold with water the resulting solution was found to feature a broad absorption at 550 nm, $\varepsilon_{550} \simeq 81\ 000\ M^{-1}\ cm^{-1}$, and a secondary absorption at 684 nm, Fig. 3*a*. These spectral features are diagnostic of aggregation phenomena and are similar to that observed when squaraine **4** was introduced into mixtures of between 50 and 70% DMSO. In both cases aggregation resulted in a hypsochromic and hypochromic shift of the absorption maximum and a secondary absorption at longer wavelengths. Based on this similarity, it was concluded that squaraine **1** formed type A aggregates in 10 v/v% *N,N*-dimethylacetamide–water.

In media of less than 50% DMSO, bis(4-diethylamino-2-hydroxyphenyl)squaraine, **2**, was characterized by two absorptions at 566 and 645 nm, Fig. 3*b*. In 10 v/v% DMSO–water these two absorptions were of similar intensity, $\varepsilon_{566} \simeq \varepsilon_{645} \simeq 55\ 000\ M^{-1}\ cm^{-1}$, but as the DMSO content of the medium increased, the intensity of the longer wavelength absorption increased to eventually become the dominant absorption in the 40% DMSO mixture, $\varepsilon_{657} \simeq 71\ 000\ M^{-1}\ cm^{-1}$.

The absorption spectrum of aggregates of squaraine **2** and

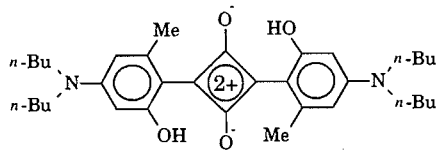

6

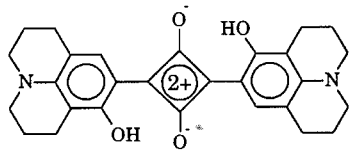

7

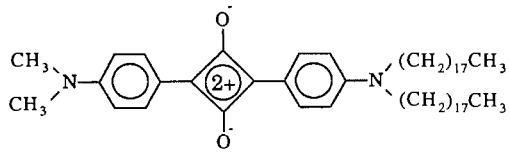

8

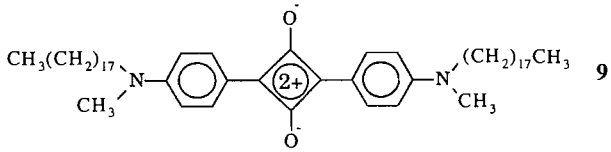

9

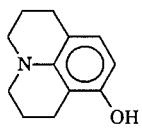

10

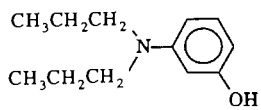

11

the typical type A aggregate are similar in that both feature two absorptions that are hypochromically shifted in comparison with nonassociated dyes. In both cases one absorption occurs at approximately the same wavelength at which the nonassociated dye absorbed while the second absorption was hypsochromically shifted by at least 100 nm. For squaraine **4**, as well as other dyes in this study, the longer wavelength absorption of the type A aggregate was the less intense of the two absorptions. For squaraine **2** this was not the case but, based on the similar splitting of the absorption spectrum, this dye is considered to form type A aggregates in media of less than 50% DMSO.

The spectral characteristics of the type A aggregates that formed with squaraine dyes **1**, **2**, and **7** are summarized in Table 2. The range of DMSO–water solvent compositions in which squaraines **2** and **7** formed aggregates or were nonassociated is reported in Table 3.

Class B squaraines were found to form only *type B aggregates* when self-association occurred. In these studies only bis(4-di-*n*-octylamino-2-hydroxyphenyl)squaraine, **5**, was included in this class. Solutions of squaraine **5** that were prepared in water and media of 10–80 v/v% DMSO–water were all characterized by spectral features characteristic of a type B aggregate, i.e., a broad absorption from 550 to 725 nm. These solutions are stable over the 1 h monitoring period. Spectroscopic characterization of these solutions after at least 3 days revealed that the aggregates prepared in 0–60% DMSO did not change, while the type B aggregate in 70% DMSO converted to a type A aggregate.

The third group of dyes are the *Class A/B squaraines* that were found to form type A aggregates in mixtures of intermediate DMSO composition, and type B aggregates in water-rich media. For dyes in this class a dynamic conversion from type B aggregates to type A aggregates was also spectroscopically observed in some solvent media. The previously reported aggregation properties of bis(4-di-*n*-butylamino-2-hydroxyphenyl)squaraine, **4**, are typical of a Class A/B dye (8). Experiments with squaraine **4** that were carried out as part of the present study also demonstrate that the type B aggregate of squaraine 4 that formed in water could be converted to a type A aggregate by altering the solvent composition to 50 v/v% DMSO, a solvent composition in which the type A aggregate was known to be stable. The type A aggregate that forms in 50% DMSO was not affected, however, by changing the solvent composition to 6.25% DMSO–water, a solvent composition in which the type B aggregate was generally observed with squaraine **4**.

The aggregation properties of bis(4-di-*n*-propylamino-2-hydroxyphenyl)squaraine, **3**, were very similar to those of squaraine **4**, although the range of solvent compositions in which the type A and B aggregates formed differed, see Table 3. Spectroscopic characterization of the aggregate solutions of squaraine **3** several days after preparation revealed that the type B aggregates that formed in water had changed to type A aggregates.

Bis(4-di-*n*-butylamino-2-hydroxy-6-methylphenyl)squaraine, **6**, was classified as a Class A/B dye as it formed type A or B aggregates depending upon solvent composition. A dynamic conversion from type B to type A aggregates was observed for squaraine **6** in 40 and 50 v/v% DMSO–water. The dye was initially found to aggregate yielding a type B aggregate, Fig. 3*c* (spectrum 1). Over the 1 h monitoring period this absorption decreased in intensity while an absorption at 575 nm developed. Upon equilibration the squaraine solutions were characterized by absorptions diagnostic of type A aggregates, Fig. 3*c* (spectrum 9). As was observed with squaraines **3** and **4**, the rate of conversion from the type B aggregate to the type A aggregate was found to increase with increasing DMSO content.

The spectroscopic properties of the type A and B aggregates that formed with these three dyes are reported in Table 2 and the solvent compositions in which aggregation occurred are reported in Table 3.

With several of the dyes in this study it was observed that when the dye existed in the nonassociated state the intensity of the characteristic squaraine absorption decreased over time. The rate of loss of the chromophore was also found to decrease as the amount of water in the solvent system decreased. This phenomenon could be the result of a slow precipitation of the dye out of solution and (or) a chemical reaction occurring in the DMSO–water solvent system that results in chromophore loss. Other workers have noted a slow fading of the colour of aqueous squaraine solutions and attributed it to attack of hydroxide on the central squaraine ring (12). Such a situation could certainly occur in these studies and similar problems may also affect the long-term stability of the aggregated squaraine dyes.

Can. J. Chem. Downloaded from www.nrcresearchpress.com by 46.23.64.124 on 09/08/12
For personal use only.

Table 2. Spectroscopic properties of typical aggregates of squaraine dyes **1–7** that were identified in the short-timeframe experiments and the DMSO–water compositions in which they formed.

Squaraine	Type A aggregates			Type B aggregates	
	λ_{max} (sh)	ε_{max}	Solvent composition	Absorption range (ε)	Solvent composition
Class A					
Bis (4-dimethylamino-2-hydroxyphenyl), **1**	550 (684)	81 000	[a]		
Bis (4-diethylamino-2-hydroxyphenyl), **2**	566 and 645	55 000	40–0		
Bis (8-hydroxy-9-julolidinyl), **7**	572 (682)	78 000	50–0		
Class B					
Bis (4-di-*n*-octylamino-2-hydroxyphenyl), **5**				550–725 (80 000)	80–0
Class A/B					
Bis (4-di-*n*-propylamino-2-hydroxyphenyl), **3**	523 (650)	78 000	40–10	530–750 (83 000)	0
Bis (4-di-*n*-butylamino-2-hydroxyphenyl), **4**	538 (650)	76 000	70–20	550–700 (80 000)	20–0
Bis (4-di-*n*-butylamino-2-hydroxy-6-methylphenyl, **6**	575 (680)	95 000	70–40	550–750 (90 000)	30–0

[a]Solvent composition: 10% *N,N*-dimethylacetamide in water.

Table 3. Range of solvent compositions over which squaraines **1–7** formed type A or type B aggregates (denoted A or B) or were nonassociated (denoted N).

Squaraine	Solvent composition (v/v% DMSO–water) 0 20 40 60 80 100
Class A	
Bis (4-dimethylamino-2-hydroxyphenyl), **1**	[a]
Bis (4-diethylamino-2-hydroxyphenyl), **2**	A | N
Bis (8-hydroxy-9-julolidinyl), **7**	A | N
Class B	
Bis (4-di-*n*-octylamino-2-hydroxyphenyl), **5**	B | N
Class A/B	
Bis (4-di-*n*-propylamino-2-hydroxyphenyl), **3**	B | B→A | A | N
Bis (4-di-*n*-butylamino-2-hydroxyphenyl), **4**	B | B→A | A | N
Bis (4-di-*n*-butylamino-2-hydroxy-6-methylphenyl, **6**	B | B→A | A | N

[a]Solvent composition: 10% *N,N*-dimethylacetamide in water.

Can. J. Chem. Downloaded from www.nrcresearchpress.com by 46.23.64.124 on 09/08/12
For personal use only.

2. UV–visible absorption properties of type A and B squaraine aggregates

The optical absorption properties of aggregates that formed with the seven squaraine dyes used in these studies result from electronic transitions to states that are dependent on the relative spatial orientation of molecules (13). Although specific features of the type A and B aggregates varied within this family of dyes, their general spectroscopic properties were similar. Therefore, it may be possible to gain an understanding of the spatial orientation of molecules in the squaraine aggregates by examining the spectral features of the type A and B aggregates.

Squaraines **2**, **3**, and **4** were characterized in DMSO-rich media in the nonassociated state with absorption maxima in the region from 650 to 665 nm. The type A aggregates of this series of dyes featured a major absorbance that was both hypsochromically and hypochromically shifted, relative to the nonassociated dye, and was observed in the region between 523 and 566 nm. Typically these aggregates also featured a secondary absorbance at ca. 650 nm. In DMSO-rich media

Can. J. Chem. Downloaded from www.nrcresearchpress.com by 46.23.64.124 on 09/08/12
For personal use only.

squaraines **6** and **7** were characterized by an absorption maximum at 682 nm. Type A aggregates that formed with these dyes featured absorption maxima that occurred between 572 and 580 nm and a less intense absorbance at the same wavelength as the nonassociated dye.

In terms of the qualitative observations regarding dye aggregation (14) and exciton theory (13), these hypsochromically shifted absorption maxima indicate that the dyes formed aggregates with many molecules whose transition dipoles were parallel. This corresponds to an aggregate with a "face-to-face" packing of dye molecules.

These results are consistent with the results of a study by Law and Chen of surfactant squaraine dyes (*7a*). In their investigation, monolayers of suitable squaraine dyes were prepared using the Langmuir–Blodgett film technique and the absorption properties of these monolayers measured. The unsymmetrical dye 1-(4-dimethylaminophenyl)-3-(4-di-*n*-octadecylaminophenyl) squaraine, **8**, formed a stable monolayer in which Law and Chen concluded that there was a slightly offset face-to-face packing of molecules. The absorption properties of this monolayer were identical to those of the type A aggregate identified in the present study, thus indicating that similar intermolecular interactions were occurring in both instances.

A possible explanation for the characteristic minor absorbance of the type A aggregate involves attributing it to an absorption by nonassociated dye. This suggestion is not supported by the studies of squaraine **4** at dilute concentrations (10^{-7} M), which indicate that in general the minor absorbance in the type A aggregate does not correspond to absorption by nonassociated dye.

Alternatively, this absorption could result from a transition within the face-to-face aggregates that is not accounted for by exciton theory.

The spectroscopic features of the type B aggregates of squaraines **3**, **4**, **5**, and **6** are essentially identical as each was characterized by a broad absorption from 500 to 750 nm. Comparisons of the absorption spectra of these dyes in the nonassociated state and as type B aggregates demonstrate that the absorption intensity of the latter is considerably less than the former, 80 000 versus 300 000 M^{-1} cm^{-1}, respectively. Such a hypochromic shift is diagnostic of aggregation phenomena. Unlike the type A aggregates, however, the type B aggregate lacked a shift in the absorption maximum that can be readily correlated with exciton theory.

On the basis of the width of the absorption of this aggregate, ca. 250 nm, it can be concluded that this peak represents the summation of several optical transitions. These multiple transitions occur at energies above and below the absorption energy of the nonassociated dye. In terms of the exciton model, dimer absorbances that are near the monomer absorbance energy correspond to aggregate geometries for which the angular relationship between chromogens approaches the nodal point at 55°. Such a situation was reported by Fuhrhop et al. in studies of protoporphyrin IX glycosamides in which dimerization resulted in a broadened Soret band that lacked an appreciable exciton shift (15). Accordingly, the spectroscopic features of the type B aggregate could be indicative of multiple absorbances from an aggregate of molecules with varying orientations that are greater and less than 55°.

An alternative explanation of the absorption features of the type B aggregate of these squaraine dyes would involve intermolecular interactions that are not considered by the exciton model. In their study of surfactant squaraine dyes Law and Chen reported that bis(4-(*N*-methyl-*N*-octadecylamino)phenyl) squaraine, **9**, formed monolayers that were stabilized by charge transfer interactions between adjacent molecules (*7a*). These interactions were the result of an alignment of molecules in the monolayer that permitted the electron-deficient squarylium moieties to interact with the electron-rich dialkylamino phenyl moieties. The spectroscopic properties of the monolayer of squaraine **9** were similar to those of the type B aggregate, suggesting that the spatial orientation of molecules in the solution aggregates was similar.

3. Structure-property relationships and the role of the DMSO–water solvent medium in squaraine aggregation

To better understand the aggregation properties of the seven squaraine dyes in this study it is instructive to examine the role that molecular functionality and the DMSO–water solvent system plays in aggregation. One group of dyes that should be compared includes the bis(4-dialkylamino-2-hydroxyphenyl)squaraines with N-alkyl substituents that include methyl, ethyl, *n*-propyl, *n*-butyl, and *n*-octyl groups. To further investigate the role of molecular structure on aggregation phenomena the behaviour of bis(4-di-*n*-butyl-2-hydroxyphenyl)-squaraine and bis(4-di-*n*-butyl-2-hydroxy-6-methylphenyl)-squaraine as well as bis(4-di-*n*-propylamino-2-hydroxyphenyl)squaraine and bis(8-hydroxy-9-julolidinyl)squaraine should be compared.

(a) Comparison of the aggregation properties of squaraine dyes with varying N-alkyl substituents

Comparison of the short-term aggregation properties of the five bis(4-di-*N*-alkylamino-2-hydroxyphenyl)squaraine dyes with varying N-alkyl substituents shows that these compounds were considerably different, Table 3. As the effect of the squaraine ring and the hydroxyl functionality should be the same for all of these dyes, it is reasonable to propose that the difference in their aggregation characteristics is related to particular properties of the N-alkyl substituents. One would expect that the electronic influence of the five different substituents would not vary appreciably with increasing chain length, and this assertion is consistent with the results of electrochemical studies of squaraine dyes (5). However, it would be expected that the influence of *hydrophobic interactions* would be greater for squaraine dyes with longer alkyl chains.

Several workers have reported that alkyl substitution in dye molecules affects their aggregation properties. Iyer and Singh studied the sodium salts of a series of 1-amino-4-alkylaminoanthraquinone-2-sulfonic acids with alkyl substituents including methyl, ethyl, *n*-propyl, and *n*-butyl (16). For this class of compounds self-association proceeded only as far as the dimer state. With alkyl chains of increasing length the critical aggregation concentration, hereafter referred to as the CAC, was found to decrease. Thermodynamic studies of the dimerization of these dyes were consistent with explanations of hydrophobic interactions based on water-structure arguments. In other studies it was noted that dyes with alkyl functionality tended to have lower CACs and form higher order aggregates with increasing alkyl chain length (17).

It is reasonable to assume that van der Waals forces would

Can. J. Chem. Downloaded from www.nrcresearchpress.com by 46.23.64.124 on 09/08/12
For personal use only.

be primarily responsible for the self-association of dye molecules with short alkyl chains. Based on the above discussion, hydrophobic forces would also be expected to contribute significantly to the free energy of association for dyes with moderate to long alkyl chains.

The aggregation properties of the bis(4-dialkylamino-2-hydroxyphenyl)squaraine dyes with methyl, ethyl, *n*-propyl, *n*-butyl, and *n*-octyl chains can be interpreted on the basis of these arguments. The dyes in this series with methyl and ethyl substituents were found to form type A aggregates. *Since shorter alkyl chains are associated with minor hydrophobic effects, it is proposed that the free energy of association for the formation of type A aggregates with these two dyes does not feature a significant additional contribution from hydrophobic interactions.*

The free energy of aggregation for bis(4-di-*n*-octylamino-2-hydroxyphenyl)squaraine, **5**, is expected to include a considerable additional contribution due to hydrophobic interactions, resulting in a decrease in the CAC and an increased degree of aggregation, in comparison with squaraine dyes with shorter alkyl chains. *That this dye with increased hydrophobicity should form an aggregate with a different spatial orientation of chromophores (the type B species) relative to the aggregate formed with the less hydrophobic dyes (the type A species) was not anticipated.*

Bis(4-di-*n*-propylamino-2-hydroxyphenyl)squaraine, **3**, and bis(4-di-*n*-butylamino-2-hydroxyphenyl)squaraine, **4**, both formed type B aggregates in water that were stable over the 1 h monitoring period. Based on a comparison with other dyes in this series, these results indicated that aggregation of these two dyes in this medium was subject to the same influences that resulted in the formation of the type B aggregate of squaraine **5**.

To further probe this phenomenon of squaraine aggregation it is worthwhile to examine the effects of adding these dyes to binary DMSO–water mixtures.

The preparation of aggregated dyes in aqueous media containing organic cosolvents is generally believed to decrease the degree of aggregation and increase the CAC (17). Both of these observations reflect a change in the free energy of aggregation that favours the nonassociated dye and (or) destabilizes the aggregate. Studying a series of dyes in DMSO–water mixtures should therefore provide an estimate of the relative stabilities of their aggregates.

Bis(4-diethylamino-2-hydroxyphenyl)squaraine, **2**, formed stable type A aggregates in DMSO–water mixtures up to and including 40 v/v% DMSO–water. In media of greater than 50% DMSO the dye existed in a nonassociated state. These results indicated that, as expected, with increasing DMSO content there is a shift in the association equilibrium towards the monomeric state. Monitoring these solutions over time revealed no changes in the spectroscopic properties of the aggregate solutions.

Both bis(4-di-*n*-propylamino-2-hydroxyphenyl)squaraine, **3**, and bis(4-di-*n*-butylamino-2-hydroxyphenyl)squaraine, **4**, formed type B aggregates in water and, relative to squaraine **2**, the alkyl substituents on these dyes were more hydrophobic. These dyes, therefore, were expected to be strongly aggregated and were found to aggregate over a similar range of solvent mixtures as squaraine **2**, Table 3.

In addition to the cosolvent "weakening" these dye aggregates, so that the nonassociated state eventually became more favoured in DMSO-rich media, it was also noted that in mixtures of DMSO–water it was possible to observe a conversion from the type B to type A aggregate. The response time of aggregate solutions to perturbations that render them in a non-equilibrium state depends on the strength of their mutual association. Weakly associated dye aggregates will rapidly shift towards the monomeric state upon dilution or elevation of temperature. This change in equilibrium can be detected by a rapid increase in the intensity of the absorption ascribed to the monomer. For strongly aggregated dyes it is found that the time required to reestablish equilibrium after changes in conditions can range from minutes to days (18). The slow change in the properties of strongly aggregated solutions is generally referred to as "aging" and can be readily monitored by absorption spectroscopy.

The type B aggregate that formed with bis(4-di-*n*-propylamino-2-hydroxyphenyl)squaraine, **3**, in water was found to have converted to a type A aggregate when analyzed by UV–visible absorption spectroscopy several days later. This result would indicate that the type A aggregate was thermodynamically preferred and that the type B aggregate should be considered as a thermodynamically less stable aggregate. The slow aging of the type B aggregate solution to a type A species would indicate that the molecules in this ensemble were strongly bound.

By introducing squaraine **3** into mixtures of DMSO–water it was possible to affect the aggregate stability, relative to that in water, and thereby alter this aging process. In the range of solvent compositions from 10 to 20 v/v% DMSO–water the thermodynamics of aggregation were sufficiently different than in water so that conversion from type B to type A aggregates could be monitored over a 1 h period. Given that a similar conversion was observed in water, the cosolvent appears to aid in this process. With increasing DMSO content, 30 and 40 % DMSO, only the type A aggregate was observed and presumably the aggregate stability continued to decrease with increasing DMSO content.

For bis(4-di-*n*-butylamino-2-hydroxyphenyl)squaraine, **4**, a similar solvent-dependent conversion from a type B to type A aggregate was observed and the enhanced stability of its type B aggregate in DMSO–water mixtures, relative to squaraine **3**, could be related to the greater hydrophobicity of this dye.

Bis(4-di-*n*-octylamino-2-hydroxyphenyl)squaraine, **5**, is believed to be the most hydrophobic dye in this study, forming type B aggregates in DMSO–water mixtures up to and including 80% DMSO, and in solvent compositions up to 60% DMSO these aggregates were stable for at least 3 days. In a DMSO-rich medium of 70% DMSO squaraine **5** initially formed a type B aggregate but after several days conversion to a type A aggregate had occurred. This was clearly a similar aging phenomenon as that observed with squaraines **3** and **4**. The fact that this only occurred in DMSO-rich media and after several days is indicative of the ability of the N-alkyl substituents of increasing hydrophobicity to stabilize the type B aggregate, although this was not ultimately the most stable aggregation state.

Unusual effects of DMSO on aggregation of hydrophobic molecules have previously been observed. Uehara et al. studied aggregation of chlorophyll *a* in binary DMSO–water mixtures as a means of modelling the states of aggregation of this compound that are observed in vivo (19). Using UV–visible absorp-

Can. J. Chem. Downloaded from www.nrcresearchpress.com by 46.23.64.124 on 09/08/12
For personal use only.

tion spectroscopy these workers were able to identify three different colloidal forms of chlorophyll *a* and to determine that the solvent composition controlled which aggregate formed.

Langhals and Balli also reported dynamic aggregation effects in DMSO–water mixtures (20). Studying a series of dimethinemerocyanine dyes containing long alkyl chains it was reported that these compounds formed J aggregates, i.e., aggregates that absorbed light at a longer wavelength than the absorption maximum of the nonassociated dye, at concentrations as low as 5×10^{-8} M. Furthermore, upon addition of the dyes to DMSO–water mixtures it was observed by absorption spectroscopy that an initial aggregate formed and converted over time to a second aggregate with a longer wavelength absorption, a J aggregate. These dynamic aggregation effects are similar to the present squaraine aggregation studies.

*(b) Comparison of the aggregation properties of bis(4-di-*n*-butylamino-2-hydroxyphenyl)squaraine, **4**, and bis(4-di-*n*-butylamino-2-hydroxy-6-methylphenyl)squaraine, **6***

The aggregation properties of squaraines **4** and **6** were found to be similar, i.e., they formed type B aggregates in water, a conversion from type B to type A aggregates was observed in some DMSO–water mixtures, while in DMSO-rich media only type A aggregates were observed. Comparison of the structures of these dyes reveals that their only difference is that squaraine **6** has a methyl group substituted *ortho* to the squaraine ring in the C(6) position.

The presence of the methyl group adjacent to the four-membered ring could result in a steric interaction between this alkyl group and the C-O group on the squaraine ring. This would result in a twisting of the phenyl rings out of the plane of the four-membered ring and a bathochromic shift of the absorption maximum (2). The degree of twisting is a function of the magnitude of the repulsive forces and may be counterbalanced by the proposed intramolecular hydrogen bonding involving the phenyl hydroxyl group and a squaraine C-O group (2, 5).

The energies associated with the van der Waals forces all feature a r^{-6} dependence on separation distance and are expected to diminish rapidly at large intermolecular separations. As a result of these distance requirements it is believed that planar molecules, which can closely pack, are the most likely to form stable aggregates. The stability of the aggregates formed with squaraine **6** and squaraine **4** did not differ appreciably. Thus, it may be concluded that distortions in molecular geometry that resulted from steric interactions involving the methyl substituents in squaraine **6** were not sufficient to destabilize aggregates that formed with this dye.

In the preceding discussion of squaraine dyes **1**–**5** it was noted that factors associated with increasing hydrophobicity of the N-alkyl groups were related to the formation of type B aggregates in water. For the squaraines **4** and **6** the hydrophobicity of their N-alkyl substituents was the same. The presence of the methyl group in squaraine **6** could have further affected the hydrophobicity of the dye.

Studies of the free energy of transfer of pure hydrocarbons into water can be shown to provide a quantitative measure of the hydrophobic effect (21). Although predictions concerning hydrophobic interactions between solutes that are based on such thermodynamic studies can be misleading (22), they still serve as a means of estimating the hydrophobicity of solutes. For example, the free energies of transfer of benzene and toluene from their liquid state into water are 4.6 and 5.4 kcal mol^{-1}, respectively (23). This comparison demonstrates that introduction of a methyl group into an aromatic ring increases its hydrophobic effect. A similar substitution in the squaraine dyes should have slightly increased the hydrophobicity of squaraine **6** relative to squaraine **4**.

The DMSO solvent effect on aggregation of these two dyes is similar to that discussed previously for the dyes with varying N-alkyl substituents.

*(c) Comparison of the aggregation properties of bis(4-di-*n*-propylamino-2-hydroxyphenyl)squaraine, **3**, and bis(8-hydroxy-9-julolidinyl)squaraine, **7***

Comparison of the aggregation properties of squaraines **3** and **7** in water can provide a subtle means of probing the role of molecular functionality in influencing self-association. The compounds 8-hydroxyjulolidine, **10**, and 3-di-*n*-propylaminophenol, **11**, are similar in that each consists of a 3-aminophenol moiety and N-alkyl functionality involving a three-carbon chain. For 8-hydroxyjulolidine these propyl chains are bonded to the aromatic ring but no such restriction is present in 3-di-*n*-propylaminophenol. The squaraine dyes that are prepared with these two compounds are anticipated to have differing electronic and hydrophobic properties. For bis(8-hydroxy-9-julolidinyl)squaraine, **7**, the fused alkyl chains should support delocalization of the lone pair of electrons on the nitrogen into the phenyl ring. Experimental evidence in support of this has been garnered from studies of the electrochemical (5) and UV–visible absorption properties of similar squaraines (2). This change in the electronic characteristics of the dye is not expected to significantly alter its aggregation properties.

In terms of hydrophobic interactions it is not necessarily apparent how squaraine **3** and **7** would compare. Once again, although not strictly comparable, it is constructive to look for insights from studies of hydrophobic effects. Thermodynamic studies of hydrophobic solutes have demonstrated that the free energy of transfer, a measure of the hydrophobic effect, increases with increasing internal degrees of freedom (24). For linear and branched alkanes this is believed to be mainly an entropic effect. The increase in hydrophobic effect due to increased internal degrees of freedom is demonstrated by the experimentally measured standard free energies of solution of tetrahydrofuran and 1-butanol that are reported to be 1.72 and 2.35 kcal mol^{-1}, respectively, at 25°C (24). Investigations of aliphatic alcohols and their corresponding ethers have demonstrated that enthalpic factors are also significant (25).

These investigations of hydrophobic effects for alkanes and cyclic hydrocarbons would indicate that bis(8-hydroxy-9-julolidinyl)squaraine, **7**, should be less hydrophobic than bis(4-di-*n*-propylamino-2-hydroxyphenyl)squaraine, **3**. This is consistent with the observation that squaraine **7** forms type A aggregates in water but squaraine **3** forms type B aggregates under the same conditions.

The DMSO solvent effect on the aggregation of squaraines **3** and **7** can be understood on the basis of the previous discussion.

4. A thermodynamic model of squaraine dye aggregation

In the discussion of structure–property relationships it was proposed that the introduction of substituents of increasing

Can. J. Chem. Downloaded from www.nrcresearchpress.com by 46.23.64.124 on 09/08/12
For personal use only.

hydrophobicity into anilino-class squaraine dyes should have increased the degree of aggregation and decreased the CAC. The DMSO–water solvent effect studies provided qualitative support for these changes in the association equilibria. In addition, the thermodynamic relationship between these type A and type B aggregates can be proposed on the basis of the results of these studies.

Both spectroscopic monitoring of aggregate solutions and minimum concentration studies demonstrated that the Class A/B dyes were found to rapidly aggregate upon addition to water, indicating that the nonassociated form of these dyes was not stable in these media. For squaraines **3**, **4**, and **6**, energetically favorable self-association yielded the type B aggregate. Monitoring squaraine **3** in water over time revealed a conversion to the type A aggregate. This dynamic aggregate conversion indicates that the type B aggregate could be considered to be "kinetically" preferred while the type A aggregate was "thermodynamically" preferred.

The results of the DMSO–water solvent effect studies are consistent with this interpretation of the events associated with squaraine aggregation. The addition of organic cosolvent to water is expected to destabilize the aggregates, relative to the nonassociated state (18). With increasing amounts of DMSO the nonassociated form of the dye eventually is stabilized. In intermediate solvent mixtures the type B aggregate was destabilized by DMSO cosolvent, resulting in a more facile conversion to the type A aggregate than was observed in water.

The assignment of the type A aggregate as the thermodynamically preferred aggregate in water and DMSO–water media was supported by the medium effect studies with squaraine **4**. These investigations showed that the type B aggregate of squaraine **4** in water would convert to a type A species by dilution to 50% DMSO. However, the type A aggregate in 50 v/v% DMSO–water did not convert to the type B species by dilution to 6.25% DMSO, a medium in which the type B aggregate formed on initial mixing.

The preceding discussion of structure–property relationships noted that factors associated with the introduction of hydrophobic functionality into these dyes resulted in the formation of type B aggregates. In the case of bis(4-di-*n*-octylamino-2-hydroxyphenyl) squaraine, **5**, the only Class B dye in these studies, its type B aggregates were sufficiently stable in the short-timeframe experiments that they formed in DMSO–water mixtures in which all other squaraines had either converted to the type A aggregate or were nonassociated. The slow conversion of type B aggregates of squaraine **5** to type A aggregates that was observed in 70% DMSO demonstrates that the first aggregate species to form is not the most thermodynamically stable state, although conversion to type A aggregates in more water-rich media did not occur over a period of several weeks.

Conclusions

In this study the aggregation properties of seven squaraine dyes were investigated in a series of DMSO–water mixtures using UV–visible absorption spectroscopy. In general it was found that when aggregation occurred these dyes formed one or both of two novel solution aggregates, designated as type A and type B, depending upon the composition of the mixed solvent system.

The spectroscopic properties of the type A aggregate can be interpreted within the framework of exciton theory as being diagnostic of a face-to-face packing of molecules in the aggregate. This is consistent with the results of a study of monolayers of surfactant squaraine dyes reported by Law and Chen (*7a*). The spectroscopic properties of the type B aggregate cannot readily be interpreted by exciton theory.

The propensity of the squaraine dyes to form one or both types of aggregates can be understood through an examination of structure–property relationships. Specifically, squaraine dyes with less hydrophobic N-alkyl substituents, i.e., methyl and ethyl, formed only the type A aggregates in these studies. Dyes with more hydrophobic substituents, i.e., *n*-butyl or *n*-octyl, formed type B aggregates in water that would convert over time to type A aggregates. The change in the spatial orientation of chromophores that was observed with more hydrophobic squaraines was not anticipated. In these studies the DMSO cosolvent served to destabilize the aggregate, thereby aiding in the conversion of type B aggregates to type A and, in sufficient quantities, leading to complete dissociation of the dyes.

Based on these observations, a thermodynamic model of squaraine dye aggregation has been proposed in which the type B aggregate is kinetically preferred while the type A aggregate is thermodynamically preferred. Increasing hydrophobicity of the dye is believed to stabilize the type B aggregate while increasing amounts of DMSO destabilize the type B aggregate, resulting in a more facile conversion to the type A species.

Acknowledgments

Financial support for this research was provided by the Natural Sciences and Engineering Research Council of Canada through a University–Industry Cooperative Research Development Grant and by the Xerox Research Centre of Canada.

References

1. J. Treibs and K. Jacob. Angew. Chem. Int. Ed. Engl. **4**, 694 (1965).
2. K.-Y. Law. J. Phys. Chem. **91**, 5184 (1987).
3. (*a*) L.F.V. Ferreira, S.M.B. Costa, and E.J. Pereira. Photochem. Photobiol. **55**, 361 (1991); (*b*) K.-Y. Law. Chem. Phys. Lett. **150**, 357 (1988); (*c*) V. Rehak and G. Israel. Chem. Phys. Lett. **132**, 236 (1986).
4. (*a*) P.M. Kazmaier, G.K. Hamer, and R.A. Burt. Can. J. Chem. **68**, 530 (1990); (*b*) K.-Y. Law. J. Phys. Chem. **93**, 5925 (1989).
5. K.-Y. Law, J.S. Facci, F.C. Bailey, and J.F. Yanus. J. Imaging Sci. **34**, 31 (1990).
6. (*a*) J. Bernstein and E. Goldstein. Mol. Cryst. Liq. Cryst. **164**, 213 (1988); (*b*) J. Bernstein, M. Tristani-Kendra, and C.J. Eckhardt. J. Phys. Chem. **90**, 1069 (1986); (*c*) Y. Kobayashi, M. Goto, and M. Kurahashi. Bull. Chem. Soc. Jpn. **59**, 311 (1986).
7. (*a*) K.-Y. Law and C.C. Chen. J. Phys. Chem. **93**, 2533 (1989); (*b*) M. Matsumoto, T. Sekiguchi, H. Tanaka, M. Tanaka, T. Nakamura, H. Tachibana, E. Manda, Y. Kawabata, and M. Sugi. J. Phys. Chem. **93**, 5877 (1989); (*c*) M. Matsumoto, T. Sekiguchi, H. Tanaka, M. Tanaka, T. Nakamura, H. Tachibana, E. Manda, and Y. Kawabata. Chem. Lett. 1085 (1988); (*d*) M. Tanaka, T. Sekiguchi, M. Matsumoto, T. Nakamura, E. Manda, and Y. Kawabata. Thin Solid Films, **160**, 299 (1988); (*e*) M. Matsumoto, T. Nakamura, M. Tanaka, T. Sekiguchi, H. Komizu, S.Y. Matsuzaki, E. Manda, Y. Kawabata, S. Saito, S. Iizima, and M. Sugi. Bull. Chem. Soc. Jpn. **60**, 2737 (1987); (*f*) Y. Kawabata, T. Sekiguchi, M. Tanaka, T. Nakamura, H. Komizu,

K. Honda, E. Manda, M. Saito, M. Sugi, and S. Iizima. J. Am. Chem. Soc. **107**, 5270 (1985).
8. E. Buncel, A.J. McKerrow, and P.M. Kazmaier. J. Chem. Soc. Chem. Commun. 1242 (1992).
9. (*a*) K. Liang, K.-Y. Law, and D.G. Whitten. J. Phys. Chem. **98**, 13379 (1994); (*b*) S. Das, T.L. Thanulingam, K.G. Thomas, P.V. Kamat, and M.V. George. J. Phys. Chem. **97**, 13620 (1993).
10. H.-E. Sprenger and W. Ziegenbein. Angew. Chem. Int. Ed. Engl. **5**, 894 (1966).
11. D.D. Perrin and W.L.F. Armarego. Purification of laboratory chemicals. 3rd ed. Permagon, Oxford. 1988.
12. M. Forster and R.E. Hester. J. Chem. Soc. Faraday Trans. 1, **78**, 1847 (1982).
13. M. Kasha. *In* Molecular processes in radiation biology. *Edited by* L. Augenstein and R. Mason. Academic, New York. 1964.
14. D.G. Duff and C.H. Giles. *In* Water: a comprehensive treatise. Vol. 4. *Edited by* F. Franks. Plenum, New York. 1975. pp. 169–207.
15. J.-H. Fuhrhop, C. Demoulin, C. Boettcher, J. Koning, and U. Siggel. J. Am. Chem. Soc. **114**, 4159 (1992).
16. S.R.S. Iyer and G.S. Singh. J. Soc. Dyers Colour. **89**, 128 (1973).
17. (*a*) A. Datyner and M.T. Pailthorpe. J. Colloid Interface. Sci. **76**, 557 (1980); (*b*) A. Datyner, A.G. Flowers, and M.T. Pailthorpe. J. Colloid Interface Sci. **74**, 71 (1980); (*c*) D.G. Duff, D.J. Kirkwood, and D.M. Stevenson. J. Soc. Dyers Colour. **93**, 303 (1977).
18. E. Coates. J. Soc. Dyers Colour. **85**, 355 (1969).
19. K. Uehara, K. Shibata, H. Nakamura, and M. Tanaka. Chem. Lett. 1445 (1982).
20. E. Langhals and H. Balli. Helv. Chem. Acta, **68**, 1782 (1985).
21. C. Tanford. The hydrophobic effect: formation of micelles and biological membranes. 2nd ed. Wiley, New York. 1980. pp. 5–28.
22. A. Ben-Naim. Hydrophobic interactions. Plenum. New York. 1980. p. 25.
23. S.J. Gill, N.F. Nichols, and I. Wadso. J. Chem. Thermodyn. **8**, 445 (1976).
24. F. Franks. *In* Water: A comprehensive treatise. Vol. 4. *Edited by* F. Franks. Plenum, New York. 1975. pp. 1–93.
25. M.H. Abraham. J. Am. Chem. Soc. **102**, 5910 (1980).

Can. J. Chem. Downloaded from www.nrcresearchpress.com by 46.23.64.124 on 09/08/12
For personal use only.

1,3-Dioxan-5-ones: synthesis, deprotonation, and reactions of their lithium enolates

Marek Majewski, D. Mark Gleave, and Pawel Nowak

Abstract: A general synthetic route to 2-alkyl- and 2,2-dialkyl-1,3-dioxan-5-ones, using tris(hydroxymethyl)-nitromethane as the starting material, is described. Deprotonation of these compounds was studied. It was established that these dioxanones could be deprotonated with LDA; however, the reduction of the carbonyl group via a hydride transfer from LDA, giving the corresponding dioxanols, often competed with deprotonation. The reduction could be minimized by using Corey's internal quench procedure to form silyl enol ethers and was less pronounced in 2,2-dialkyldioxanones (ketals) than in 2-alkyldioxanones (acetals). Self-aldol products were observed when dioxanone lithium enolates were quenched with H_2O. Addition reactions of lithium enolates of dioxanones to aldehydes were *threo*-selective as predicted by the Zimmerman–Traxler model. Dioxanones having two different alkyl groups at the 2-position were deprotonated enantioselectively by chiral lithium amide bases with enantiomeric excess (ee) of up to 70%.

Key words: 1,3-dioxan-5-ones, enantioselective deprotonation, chiral lithium amides.

Résumé : On décrit une méthode générale de synthèse des 2-alkyl- et 2,2-dialkyl-1,3-dioxan-5-ones qui fait appel au tris(hydroxyméthyl)nitrométhane comme produit de départ. On a étudié la déprotonation de ces composés. Il a été établi que ces dioxanones peuvent être déprotonées par le LDA; toutefois, ces déprotonations sont souvent accompagnées par des réductions du groupe carbonyle, via un transfert d'hydrure provenant du LDA, conduisant aux dioxanols correspondants. Il est possible de minimiser la réduction en utilisant la méthode de piégeage interne de Corey conduisant à la formation d'éthers énoliques silylés; la réduction est moins prononcée avec les 2,2-dialkyldioxanones (cétals) qu'avec les 2-alkyldioxanones (acétals). On a observé des produits d'autoaldolisation lorsqu'on piège les énolates lithiés de la dioxanone avec de l'eau. Les réactions d'addition des énolates de lithium des dioxanones sur les aldéhydes sont *threo*-sélectives comme on peut le prédire à l'aide du modèle de Zimmerman–Traxler. Sous l'influence d'amidures de lithium chiraux, les dioxanones possédant deux groupes alkyles différents en position 2 sont déprotonées d'une façon énantiosélective avec un ee allant jusqu'à 70%.

Mots clés : 1,3-dioxan-5-ones, déprotonation énantiosélective, amidures de lithium chiraux.

[Traduit par la rédaction]

Introduction

2-Alkyl- and 2,2-dialkyl-1,3-dioxan-5-ones (**2**) constitute a group of interesting heterocyclic compounds about which relatively little is known. These compounds can be considered simply as acetal and ketal protected forms of 1,3-dihydroxyacetone, a key building block in nature. A common way to synthesize both natural and unnatural carbohydrates and their analogues is to use enzyme-catalyzed aldol reactions of 1,3-dihydroxyacetone phosphate (1, 2). One drawback to this reaction is that it is only suitable for certain aldehydes: nonhindered aliphatic, α-heteroatom-substituted, and differently protected alkoxy aldehydes are common substrates; however, severely hindered aliphatic or α,β-unsaturated aldehydes do not react (2). Furthermore, aromatic aldehydes are either poor substrates or are unreactive.

We became interested in dioxanones during a study of enantioselective deprotonation of C_s symmetrical ketones (3, 4). 1,3-Dioxan-5-ones, which are nonsymmetrically substituted at the 2-position, belong to the C_s symmetry point group and are conformationaly biased and, for these reasons, can be considered promising candidates for enantioselective deprotonation with chiral lithium amide bases. Enolates of these dioxanones can be viewed as synthetic equivalents of the dihydroxyacetone enolate, and it was hoped that the enolates will react readily with both aromatic and hindered aliphatic aldehydes.

The differences in free energy between conformers of dioxanones having equatorial substituents at the 2-position and the corresponding axial conformers (*A* values) are greater than these observed for cyclohexanones (5). This was expected to cause higher selectivity in enantioselective deprotonation experiments with dioxanones than with analogous cyclohexanones, according to Koga's original observations (6). However, this expectaction did not materialize (vide infra).

M. Majewski,[1] D.M. Gleave, and P. Nowak. Department of Chemistry, University of Saskatchewan, 110 Science Pl., Saskatoon, SK S7N 5C9, Canada.

[1] Author to whom correspondence may be addressed. Telephone: (306) 966 4671. Fax: (306) 966 4730. E-mail: MAJEWSKI@sask.usask.ca

Can. J. Chem. Downloaded from www.nrcresearchpress.com by 46.23.64.124 on 09/08/12
For personal use only.

Can. J. Chem. Downloaded from www.nrcresearchpress.com by 46.23.64.124 on 09/08/12
For personal use only.

Scheme 1.

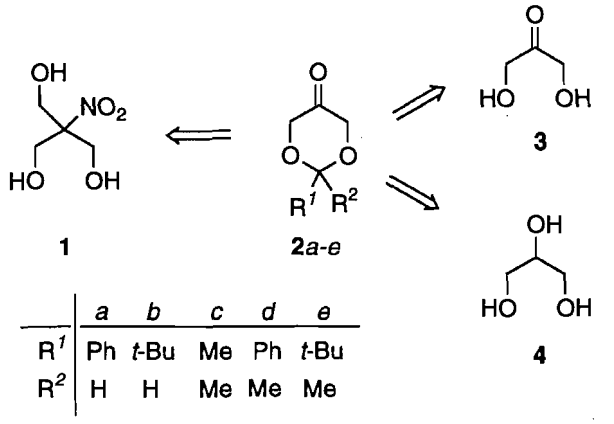

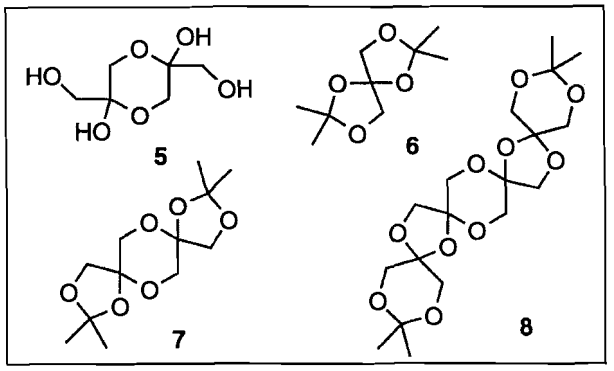

Enolate chemistry of dioxanones has not been explored before. To the best of our knowledge enolization of dioxanones has been performed in only two instances and in both cases the reaction constituted part of a multi-step synthesis: (*i*) In 1988 Hirama et al., as part of the Avermectin project, reported the aldol reaction of a derivative of 4-hydroxymethyl-2,2-dimethyldioxan-5-one (7). (*ii*) In 1990 Francl, Swindell, and co-workers described the deprotonation of 2,2-dimethyldioxan-5-one by LDA, followed by reaction of the resulting enolate with MeI (8).

Of special note is the work done by Enders et al. on the enantioselective alkylation of 2,2-dimethyldioxan-5-one using the SAMP/RAMP hydrazone methodology (9).

Results and discussion

Synthesis of dioxanones

At the onset of this work several 2-alkyl- and 2,2-dialkyl-1,3-dioxa-5-ones were known (10); however, we encountered a number of problems when trying to repeat their syntheses. In an effort to devise a reasonably efficient, reproducible route to dioxanones we first attempted two obvious approaches: starting from dihydroxyacetone (**3**) or 1,2,3-propanetriol (**4**, Scheme 1). Both strategies were unsuccessful. 1,3-Dihydroxyacetone is commercially available in the form of a stable dimer **5**, which can be degraded to dihydroxyacetone at elevated temperatures. Numerous attempts to obtain compound **2***c* via a reaction of either the dimer or the monomer with acetone under acidic conditions produced variable amounts of the compounds **6**, **7** (major product), and **8**. It seems that the dimer reacts faster with ketones than the monomer.

Scheme 2.

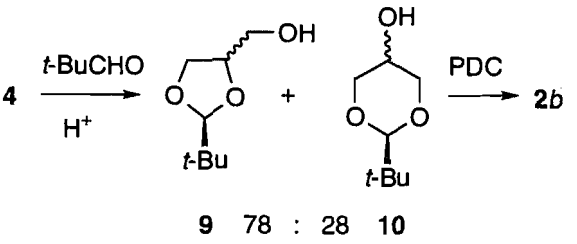

Scheme 3.

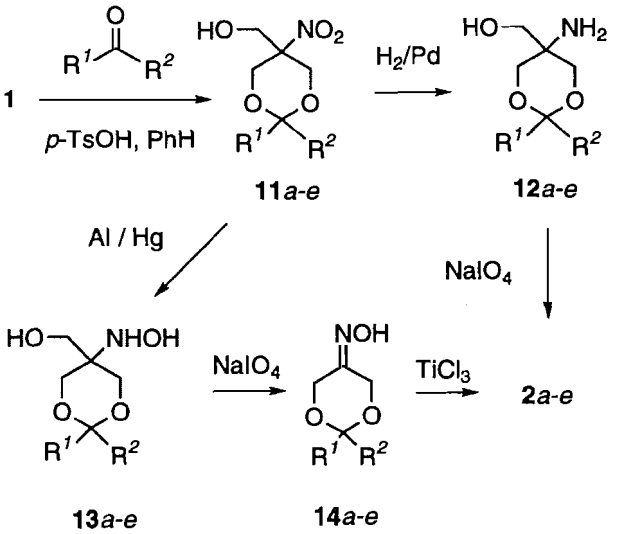

Condensation of 1,2,3-propanetriol (**4**) with pivalaldehyde yielded predominantly two diastereoisomeric dioxolanes **9** (Scheme 2) (11). All attempts (Swern, Collins, Fetizon's, PDC, and Jones conditions were tried) to oxidize the minor dioxanol (**10**) to the corresponding dioxanone **2***b* either failed or gave low yields, presumably due to instability of the dioxanone product.

2-Phenyl-1,3-dioxan-5-one (**2***a*) had been synthesized by several groups using tris(hydroxymethyl)nitromethane (**1**) as the starting material (10*a*,*c*,*d*). We were able to refine this strategy and devise two pathways for synthesis of all the dioxanones **2***a–e* used in this study (Scheme 3). Condensation of **1** with aldehydes and ketones proceeded well. The next step, aluminum amalgam reduction of a nitro compound analogous to **11***a–e* (i.e., **11***f*: R^1 = H; R^2 = CH_2CH_2Ph) was previously reported by Trost et al. to give the corresponding amine **12***f* (10*f*). In our hands the hydroxylamines **13***a–e* were always produced, often together with the corresponding amines, which complicated the purification. The last reaction in this pathway, hydrolysis with $TiCl_3$, was capricious and thus, albeit the pathway **1** → **11** → **13** → **2** proved a viable strategy, a better method was sought. In the end, the strategy via a catalytic hydrogenation under high pressure (**1** → **11** → **12** → **2**) gave higher overall yields and was more amenable to scaling up.

With the problem of synthesis of dioxanones **2***a–e* solved, the stage was now set for deprotonation experiments.

Lithium enolates of 1,3-dioxan-5-ones

Our initial attempts to deprotonate phenyldioxanone **2***a* and

Scheme 4.

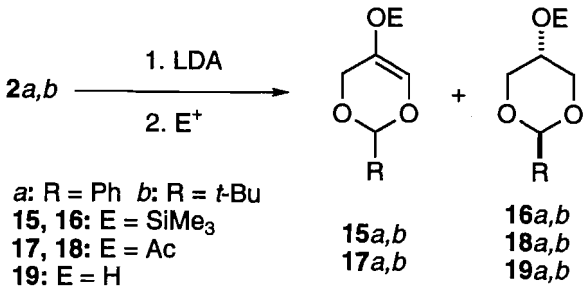

Scheme 5.

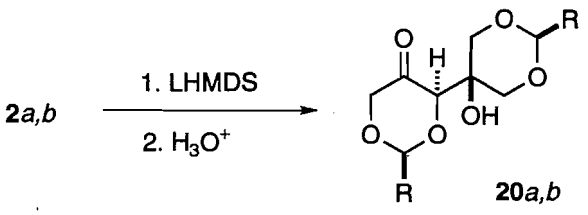

tert-butyldioxanone **2***b* with LDA were not successful. Treatment of either **2***a* or **2***b* with LDA (THF; −78°C) followed by addition of either acetic anhydride or chlorotrimethylsilane yielded two products in each case. In addition to the expected enol ethers or esters (**15**, **17**; Scheme 4), products arising from LDA behaving as a reducing agent were obtained (compounds **16** and **18**). The amounts of reduction products were substantial (40–65%), and clearly rendered the deprotonation experiments inefficient. In all cases these componds were *trans* and no sign of the *cis* product was observed. This is consistent with the axial attack of the reducing agent.

When aldol experiments were attempted on the enolates of both dioxanones (**2***a*, **2***b*) using pivalaldehyde or benzaldehyde as electrophiles, the dioxanols **19***a* and **19***b* were obtained as the major products under a variety of conditions. Isolated yields ranged from 40 to 68%.

Reduction by LDA is well precedented (for a review, see ref. 12). In our case the reduction was an undesirable side reaction, and so various reaction parameters were probed in an effort to control the reaction system. The first variable tested was the solvent: Et_2O, THF, and DME were tried in experiments with compound **2***b*. Formation of the dioxanol **19***b* as, respectively, 81, 63, and 64% of the isolated products was observed. Diethyl ether clearly favors reduction whilst the reaction in DME was much less clean than in other solvents and several unidentified side products were detected.

The observation that the amount of reduction could be increased using ether as the solvent led to a more thorough investigation, with TMS-Cl and Ac_2O used to trap the lithium alkoxide. Dioxanyl ethers **16***a,b* and esters **18***a,b* were obtained in high yields (72–89%). Thus, LDA could be used efficiently for diastereoselective reduction of dioxanones.

We found that the reduction could be minimized by using Corey's internal quench procedure for the formation of silyl enol ethers (13). With LDA as base only 5% reduction was observed with both dioxanones **2***a* and **2***b* under internal quench conditions (cf., the Experimental section, procedure B4*b*). Also, replacing LDA with lithium amides derived from amines that lack any α-hydrogens (i.e., LiTMP or LHMDS) prevented reduction (12). Reaction of dioxanones with lithium amides can thus be successfully controlled and, depending on the conditions, either enolization or reduction might be the major pathway. The procedures to avoid reduction should be applicable to other cases like ours, where reduction with LDA is undesirable.

Scheme 6.

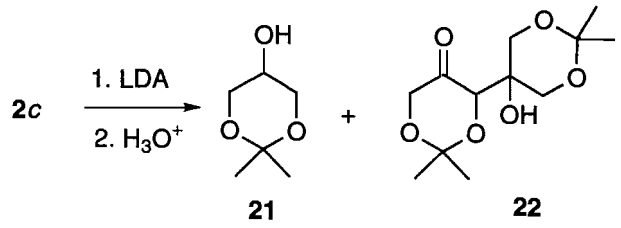

Aldol addition reactions

Attempted aldol addition of the Li enolate of *tert*-butyldioxanone **2***b* (generated with LHMDS or LiTMP to avoid reduction) to benzaldehyde yielded large quantities of recovered starting material. Modifications such as increasing the amount of the base (to two equivalents), prolonging the reaction time (to 90 min), and warming to 0°C had little effect. These results were surprising because both LHMDS and LiTMP had given high yields in the formation of silyl enol ethers using the internal quench procedure.

An experiment whereby the dioxanone was treated with LHMDS at 0°C in ether, and after 2 h quenched with water, was done with the intention of determining whether the enolization was clean. The results with both **2***a* and **2***b* were disappointing. Neither reaction was particularly "clean." A small amount of dioxanone decomposition was thought to have occurred. In the case of phenyldioxanone this was evidenced by the presence of benzaldehyde (approximately 30%). In both cases the major constituent of the crude reaction mixture was the self-aldol product (**20**) (Scheme 5).

Ketones usually do not suffer from self-aldolization unless they are exceptionally reactive (14*a*). Dioxanones belong to the class of α-alkoxyketones, which are known to be very electrophilic with the reactivity approaching that of aldehydes (14*b*). Self-aldol addition of α-alkoxyketones is precedented (15).

Further work on 1,3-dioxan-5-ones revealed that the acetals (**2**, R^1 or R^2 = H) were less stable, and more prone to reduction and to self-aldolization than the ketals (**2**, R^1 and R^2 = alkyl). Accordingly, we decided to investigate enolization reactions of 2,2-dimethyl-1,3-dioxan-5-one (**2***c*). Deprotonation of this compound with LDA followed by aqueous quench (Scheme 6) gave very little of the reduction product **21** (5% in THF and 17% when Et_2O was used as the solvent) and substantial amounts of the self-aldol product **22** (up to 64%).

Somewhat surprisingly, aldol reaction of the lithium enolate of **2***c* with benzaldehyde worked well both under rapid quench (in this method the ketone is added to LDA followed immediately by addition of the aldehyde) (3) and normal conditions and a mixture of two diasteroisomeric aldol products (**23***a* and **24***a*; Scheme 7) was formed in up to 76% yield (the ratio of *threo*:*erythro* isomers was 65:35). Other aldehydes (heptanal, cyclohexanecarbaldehyde, cinnamaldehyde) gave similar results, with cyclohexanecarbaldehyde being the most

Can. J. Chem. Downloaded from www.nrcresearchpress.com by 46.23.64.124 on 09/08/12
For personal use only.

Can. J. Chem. Downloaded from www.nrcresearchpress.com by 46.23.64.124 on 09/08/12
For personal use only.

Table 1. Enantioselective deprotonation of dioxanone **2e**.

Entry	Lithium amide	LiCl	ee (%)[a]	Yield (%)[b]
1	**25**a	—	10 (–)	43
2		0.5 equiv.	4 (–)	63
3	**25**b	—	13 (+)	32
4		0.5 equiv.	39 (+)	56
5	**25**c	—	60 (–)	32
6		0.5 equiv.	70 (–)	63
7	**26**a	—	18 (–)	58
8		0.5 equiv.	60 (–)	51
9	**26**b	—	50 (–)	41
10		0.5 equiv.	60 (–)	41
11	**27**	—	23 (+)	28
12		0.5 equiv.	20 (+)	51

[a]The symbol (+) or (–) refers to the sign of the $[\alpha]_D$ of the major enantiomer.

[b]Yields of isolated, purified product **23***c*.

diastereoselective; the ratio of *threo* and *erythro* isomers **23***b* and **24***b* in this case was greater than 90:10. It seems that the self-aldol reaction occurs primarily when the lithium enolate of a dioxanone is quenched with water, while quenching with an aldehyde leads to a reasonably clean aldol product.

The lithium enolate of dioxanone **2***e* reacted with cyclohexanecarbaldehyde and gave only one diastereoisomer of the corresponding aldol (*cis-threo* **23***c*) to the limit of NMR detection. Thus, the aldol addition of dioxanone lithium enolate was successfully realized and proved *threo*-selective in agreement with the Zimmerman–Traxler model (14*a*).

Enantioselective deprotonation

Deprotonation of the dioxanone **2***e* with chiral bases **25–27** was studied. The nonracemic enolates were trapped as the aldol product **23***c* and the enantiomeric excess (ee) was measured by NMR using the chiral shift reagent $Eu(hfc)_3$. The results are presented in Table I. Generally, the enantioselectivities were modest. Addition of LiCl (0.5 equivalents) resulted in a measurable improvement of enantioselectivity in most cases. This effect of LiCl on enantioselective deprotonation is precedented (16), and it is likely that lithium chloride changes the aggregation of chiral lithium amides (17). Aldols derived from dioxanones

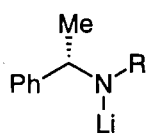

25*a*: R = Me
25*b*: R = CH_2Ph
25*c*: R = $CHPh_2$

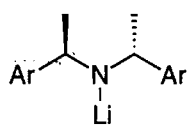

26*a*: Ar = Ph
26*b*: Ar = 2-naphtyl

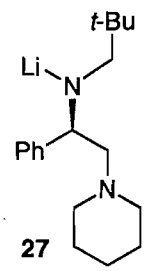

27

proved prone to decomposition during column chromatography and, although the conversion in most cases was high (the starting material was consumed) and the NMR spectra of the crude products appeared reasonably clean, the yields of pure aldols (after column chromatography) were low.

Conclusions

Synthesis and selected reactions of five 2-alkyl- and 2,2-dialkyl-1,3-dioxan-5-ones were studied. A general synthetic route, using tris(hydroxymethyl)nitromethane as the starting material, was developed for dioxanones. It has been established that dioxanones can be successfully deprotonated; however, reduction by LDA, giving the corresponding dioxanols, can compete with deprotonation. Reduction could be maximized by using ether as solvent and could be minimized by using Corey's internal quench procedure to form silyl enol ethers and by use of dioxanones derived from ketones, rather than from aldehydes. Formation of self-aldol products was observed when dioxanone Li enolates were quenched with H_2O.

Scheme 7.

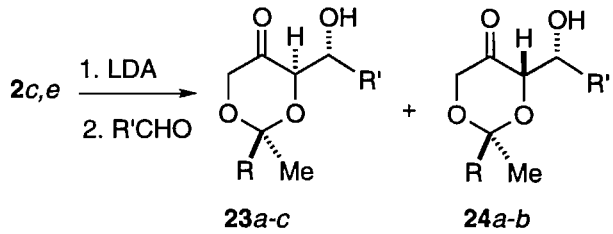

23*a-c* **24***a-b*

a R = Me; R' = Ph
b R = Me; R' = cyclohexyl
c R = *t*-Bu; R' = cyclohexyl

Aldol addition reactions of lithium enolates of 2,2-dimethyl- and 2-*tert*-butyl-2-methyl-1,3-dioxan-5-ones (**2***c* and **2***e*) to various aldehydes were *threo*-selective as predicted by the Zimmerman–Traxler model. Diastereoselectivities in excess of 95:5 were observed.

Dioxanones having two different alkyl groups at the 2-position were deprotonated enantioselectively by chiral lithium amide bases in the presence of LiCl with ee of up to 70%.

Experimental Section

General methods

All air-sensitive reactions were carried out under argon. Diethyl ether, THF, DME, benzene, and hexane were dried with sodium and distilled under nitrogen from sodium benzophenone ketyl. Diisopropylamine, triethylamine, pyridine, and TMEDA were distilled from CaH_2 under argon and stored over 4 Å molecular sieves. Aldehydes were freshly distilled and stored under argon. Chiral amines were distilled under reduced pressure and stored over 4 Å molecular sieves. TMSCl was distilled under argon from CaH_2 and stored over Reillex™ 402 (Aldrich®) (18). Ac_2O was freshly distilled and stored under argon. *n*-BuLi was periodically titrated using 2,5-dimethoxybenzyl alcohol as indicator.

Flash chromatography (19) was carried out using Merck Kieselgel 60 (230–400 mesh), and all TLC was performed on precoated plates (Merck, silica gel 60, F254). The spots were detected using UV light, iodine, or by dipping a plate in an aqueous solution containing phosphomolybdic acid, $Ce(SO_4)_2$ and H_2SO_4 followed by charring on a hot plate. Melting points are uncorrected. NMR spectra were recorded at 300 MHz (^1H) and 75 MHz (^{13}C), $CDCl_3$ was used as solvent unless otherwise stated, and TMS was used as internal standard. The multiplicity of ^{13}C NMR signals was determined by *J*-modulation (20).

Can. J. Chem. Downloaded from www.nrcresearchpress.com by 46.23.64.124 on 09/08/12
For personal use only.

Polyacetals 6, 7, and 8

A solution of dihydroxyacetone monomer (5 mmol) was prepared by refluxing the dimer (451 mg, 2.5 mmol) in acetone (15 mL) overnight. Then, *p*-TsOH·H_2O (10 mg) was added and the mixture was stirred at room temperature. Progress of the reaction was monitored by GC. After 46 h the acetone was removed in vacuo and $CHCl_3$ was added. After washing with saturated aqueous $NaHCO_3$ solution (15 mL) and water (2 × 10 mL) the solution was dried ($MgSO_4$) and chloroform was removed to yield a white solid (310 mg) that comprised **6**, **7**, and **8** (19:64:17). The products were separated by flash chromatography (SiO_2, hexane:AcOEt), which yielded pure **6** (30 mg), **7** (152 mg), and **8** (66 mg).

Compound 6

White solid. R_f 0.24 (4:1 hexane:AcOEt); mp 145–146°C. IR: 1294 cm^{-1}. ^1H NMR δ: 4.10 (2H, d, J = 9.1 Hz), 3.96 (2H, d, J = 9.1 Hz), 1.48 (6H, s), 1.39 (6H, s). ^{13}C NMR δ: 110.8, 109.1, 71.5, 26.4, 26.2. MS (CI-NH_3), *m/z* (rel. intensity): 189 ($[M + 1]^+$, 1), 173 (36), 131 (13), 115 (100), 72 (63). A correct elemental analysis could not be obtained.

Compound 7

White solid. R_f 0.39 (4:1 hexane:AcOEt), mp 160-162°C. IR: 1305, cm^{-1}. ^1H NMR δ: 4.18 (2H, d, J = 11.5 Hz), 4.04 (2H, d, J = 9.3 Hz), 3.74 (2H, d, J = 9.3 Hz), 3.63 (2H, d, J = 11.5 Hz), 1.51 (6H, s), 1.45 (6H, s). ^{13}C NMR δ: 112.0, 100.3, 71.8, 65.4, 26.6, 26.3. MS (CI-NH_3), *m/z* (rel. intensity): 278 ($[M + 18]^+$, 9), 261 ($[M + 1]^+$, 100), 245 (21), 220 (60), 203 (19), 185 (26), 172 (22), 131 (32), 127 (31), 114 (33), 72 (38). Anal. calcd. for $C_{12}H_{20}O_6$: C 55.37, H 7.74; found: C 55.24, H 7.51.

Compound 8

White solid. R_f 0.10 (4:1 hexane:AcOET); mp 199–202°C. IR: 1305 cm^{-1}. ^1H NMR δ: 4.00 (4H, dd, J = 11.4, 9.4 Hz), 3.87 (4H, d, J = 11.7 Hz), 3.74 (4H, d, J = 9.4 Hz), 3.60 (4H, dd, J = 11.7, 11.4 Hz), 1.51 (6H, s), 1.45 (6H, s). ^{13}C NMR δ: 112.1, 100.4, 89.2, 71.6, 63.7, 63.4, 26.6, 26.3. MS (CI-NH_3), *m/z* (rel. intensity): 422 ($[M + 18]^+$, 6), 350 (41), 333 (67), 292 (100), 185 (54), 129 (46), 114 (41), 72 (36). Anal. calcd. for $C_{18}H_{28}O_{10}$: C 53.46, H 6.98; found: C 53.60, H 7.15.

Synthesis of 2-alkyl-1,3-dioxan-5-ones and 2,2-dialkyl-1,3-dioxan-5-ones (refs. 10*b–d, f*)

*5-Hydroxymethyl-5-nitro-1,3-dioxanes (**11**)*

General procedure A1: An aldehyde (or ketone) (50 mmol) was added to a solution of tris(hydroxymethyl)nitromethane (7.556 g, 50 mmol) and *p*-TsOH·H_2O (95 mg, 0.5 mmol) in benzene (150 mL). The mixture was refluxed overnight under a Soxhlet filled with 4 Å molecular sieves. The benzene was removed in vacuo, saturated aqueous $NaHCO_3$ solution (50 mL) was added, and the mixture was extracted with ethyl acetate (3 × 50 mL). Drying ($MgSO_4$) and removal of solvent generally afforded the nitrodioxane in a sufficiently high state of purity for the next stage of the synthesis.

*5-Hydroxymethyl-5-hydroxylamino-1,3-dioxanes (**13**)*

General procedure A2: A 2% aqueous solution of $HgCl_2$ (200 mL) was added to the reaction vessel containing aluminum foil (5.395 g) that had been cut into approximately 1 cm^2 squares. The mixture was swirled for 20 s and then decanted. The foil was successively washed (as quickly as possible) with ethanol (200 mL) and diethyl ether (200 mL) before addition of the nitrodioxane (20 mmol) in 10% aqueous THF (250 mL). The reaction vessel was immediately cooled to 0°C and a vigorous reaction ensued with strong evolution of hydrogen gas. The mixture was stirred for 30 min (at which time TLC indicated no starting material remained), then filtered, and the filter cake was washed with acetone (100 mL). The organic solvents were removed in vacuo and the resulting aqueous solution was extracted with ethyl acetate (2 × 50 mL), dried ($MgSO_4$), and concentrated. The crude hydroxylaminodioxane was used without additional purification.

*1,3-Dioxan-5-one oximes (**14**)*

General procedure A3: To a solution of hydroxylamine (10 mmol) in methanol (75 mL) was added KH_2PO_4 (1.361 g, 10 mmol). The solution was cooled to 0°C; then a solution of $NaIO_4$ (2.353 g, 12 mmol) in water (75 mL) was added dropwise over a period of 5 min. The solution generally turned blue, then green, then yellow-orange, and a thick white suspension appeared. After 30 min the mixture was filtered and the filter cake washed with chloroform (50 mL). After removal of organic solvents in vacuo $Na_2S_2O_3$ was added in small portions, with stirring, until the brown colour of iodine disappeared. Extraction with AcOEt (3 × 75 mL) followed by drying ($MgSO_4$) and removal of solvent yielded the oxime; smaller amounts of dioxanone were also typically observed.

*1,3-Dioxan-5-ones (**2**)*

General procedure A4: An aqueous, freshly prepared solution of $TiCl_3$ (15 mmol, 1 M) was added to a solution of oxime (5 mmol) and ammonium acetate (4.625 g, 60 mmol) in dioxane (40 mL) at 0°C. The mixture was stirred vigorously and the progress of the reaction was monitored by TLC. After 45 min the mixture was extracted with diethyl ether (5 × 50 mL) and dried ($MgSO_4$). The crude material was purified by flash chromatography (SiO_2).

*5-Amino-5-hydroxymethyl-1,3-dioxanes (**12**)*

General procedure A5: A solution of **11** (150 mmol) in EtOH (300 mL) was vigorously mixed with Raney nickel (0.5 g), filtered, and fresh Ra-Ni (5 g) was added. The mixture was then hydrogenated, with stirring, in a high-pressure Parr reactor (85°C; 1400 psi of H_2) for 4 h (1 psi = 6.9 kPa). The catalyst was then filtered off and the solvent was removed (roto-vap), affording crude compound **12**, which was generally subjected to oxidative cleavage with $NaIO_4$ (procedure A6) without purification.

*1,3-Dioxan-5-ones (**2**)*

General procedure A6: A cold solution of $NaIO_4$ (120 mmol) in H_2O (300 mL) was added to a solution of **12** (100 mmol) in 1:1 MeOH:H_2O at 0°C. The resulting mixture was stirred at 0°C for 15 min – 1.5 h, filtered, and extracted with CH_2Cl_2 (10 × 50 mL). After drying ($MgSO_4$) and removal of the solvents (rotovap; bath temp. <30°C), the crude dioxanone **2** was purified by short-path distillation (Kugelrohr).

Can. J. Chem. Downloaded from www.nrcresearchpress.com by 46.23.64.124 on 09/08/12
For personal use only.

2-Phenyl-1,3-dioxan-5-one (2*a*) (ref. 10*i*)

*Compound 11*a
Procedure A1 afforded white solid in 88% yield. ^{1}H NMR showed that the product contained two isomers in a ratio of 88:12. *Major isomer*: R_f 0.22 (1:1 hexane:AcOEt); mp 120–121°C. IR: 3416 cm^{-1}. ^{1}H NMR δ: 7.53–7.40 (5H, m), 5.65 (1H, s), 4.93 (2H, d, J = 12.9 Hz), 4.71 (1H, t, J = 4.6 Hz), 4.26 (2H, d, J = 12.9 Hz), 3.91 (2H, d, J = 4.6 Hz). ^{13}C NMR (acetone-d_6) δ: 138.4, 129.3, 128.4, 126.6, 101.7, 88.2, 69.0, 63.5. MS (CI-NH_3), *m/z* (rel. intensity): 257 ([M + 18]$^+$, 68), 240 ([M + 1]$^+$, 100), 238 (23), 210 (15), 105 (38). Anal. calcd. for $C_{11}H_{13}NO_5$: C 55.22, H 5.48, N 5.86; found: C 55.15, H 5.52, N 5.92. *Minor isomer*: R_f 0.58 (1:1 hexane:AcOEt); mp 83–85°C. IR: 3481 cm^{-1}. ^{1}H NMR δ: 7.55–7.32 (5H, m), 5.52 (1H, s), 4.60 (2H, d, J = 11.6 Hz), 4.41 (2H, d, J = 6.4 Hz), 4.28 (2H, d, J = 11.6 Hz), 2.05 (1H, t, J = 6.4 Hz). ^{13}C NMR (acetone-d_6) δ: 138.1, 129.6, 128.7, 126.9, 101.9, 83.1, 67.6, 63.2. MS (CI), *m/z* (rel. intensity): 257 ([M + 18]$^+$, 100), 240 ([M + 1]$^+$, 41), 227 (23), 210 (25), 195 (21), 105 (27).

*Hydroxylamine 13*a
Procedure A2 afforded a white solid, in 89% yield, that was a mixture of two isomers (88:12). *Major isomer*: mp 134–135°C, IR: 3392, 3251, 3228 cm^{-1}. ^{1}H NMR δ: 7.50 (2H, m), 7.38 (3H, m), 5.47 (1H, s), 4.31 (2H, d), 3.79 (2H, d), 3.50 (2H, s). ^{13}C NMR (acetone-d_6) δ: 139.4, 129.2, 128.5, 126.8, 102.0, 69.0, 61.8, 58.0. MS (CI-NH_3), *m/z* (rel. intensity): 226 ([M + 1]$^+$, 76), 210 (100), 194 (33), 121 (42), 73 (42). Anal. calcd. for $C_{11}H_{15}NO_4$: C 58.66, H 6.71, N 6.22; found: C 58.44, H 6.67, N 6.13.

*Amine 12*a
Procedure A5 afforded **12***a* in quantitative yield; mp 115–117°C (lit. (10*c*) mp 117–118°C). One isomer. ^{1}H NMR δ: 7.52–7.47 (m, 2H), 7.40–7.32 (m, 3H), 5.40 (s, 1H), 3.90 (d, 2H, J = 11.0 Hz), 3.84 (d, 2H, J = 11.0 Hz) 3.40 (s, 2H), 2.70 (br s, 3H).

*Oxime 14*a
Procedure A3 afforded a yellow oil, comprising 86% oxime **14***a* and 14% ketone **2***a*. The mixture was separated by flash chromatography (SiO_2, 8:1 PhH:AcOEt); the ketone was eluted first, followed by the oxime (white solid, 64%). R_f 0.50 (1:1 hexane:AcOEt); mp 82–85°C; IR: 3367, 1452 cm^{-1}. ^{1}H NMR δ: 8.93 (1H, s), 7.57–7.45 (2H, m), 7.45–7.32 (3H, m), 5.65 (1H, s), 5.30 (1H, d, J = 15.7 Hz), 4.63 (1H, d, J = 14.3 Hz), 4.53 (1H, d, J = 14.3 Hz), 4.44 (1H, d, J = 15.7 Hz). ^{13}C NMR δ: 151.0, 137.1, 129.2, 128.3, 126.0, 100.5, 66.4, 62.1. MS (CI-NH_3), *m/z* (rel. intensity): 194 ([M + 1]$^+$, 59), 179 (100), 105 (24).

*2-Phenyl-1,3-dioxan-5-one (2*a*) (ref. 10*i*)*
Procedure A4 afforded the crude material, which was purified by flash chromatography (8:1 benzene:ethyl acetate) and yielded the ketone **2***a* as a white solid (60%). R_f 0.42 (1:1 hexane:AcOEt). ^{1}H NMR δ: 7.56–7.36 (5H, m), 5.90 (1H, s), 4.51 (2H, d, J = 15 Hz), 4.50 (2H, d, J = 15 Hz). ^{13}C NMR δ: 204.2, 136.7, 129.3, 128.4, 126.1, 98.9, 72.4. Procedure A6 afforded **2***a* in 26% yield (reaction time 20 min).

2-*tert*-Butyl-1,3-dioxan-5-one (2*b*) (ref. 10*h*)

*Compound 11*b
Procedure A1 yielded the crude product (90%), which was a mixture of two isomers (64:36). *Major isomer*: R_f 0.70 (1:1 hexane:AcOEt), mp 102–103 °C. IR: 3523 cm^{-1}. ^{1}H NMR δ: 4.42 (2H, d, J = 11.5 Hz), 4.28 (2H, d, J = 6.7 Hz), 4.11 (1H, s), 4.01 (2H, d, J = 11.5 Hz), 2.02 (1H, t, J = 6.7 Hz), 0.92 (9H, s). ^{13}C NMR δ: 108.1, 62.9, 67.5, 62.4, 34.7, 24.4. MS (CI-NH_3), *m/z* (rel. intensity): 237 ([M + 18]$^+$, 100), 220 ([M + 1]$^+$, 16), 218 (22), 175 (18), 162 (65). *Minor isomer*: R_f 0.37 (1:1 hexane:AcOEt); mp 166–167°C. IR: 3575, 3436 cm^{-1}. ^{1}H NMR δ: 4.86 (2H, dd J = 12.8, 1.4 Hz), 4.14 (1H, s), 3.88–3.77 (4H, m), 1.76 (1H, t, J = 6.1 Hz), 0.88 (9H, s). ^{13}C NMR (acetone-d_6) δ: 107.4, 88.1, 68.6, 63.4, 34.9, 24.2. MS (CI-NH_3), *m/z* (rel. intensity): 237 ([M + 18]$^+$, 100), 220 ([M + 1]$^+$, 4), 190 (14), 175 (21), 162 (20), 86 (16). Anal. calcd. for $C_9H_{17}NO_5$: C 49.31, H 7.82, N 6.39; found: C 49.23, H 7.71, N 6.17.

*Hydroxylamine 13*b
Procedure A2: White solid, 85% yield. Mixture of two isomers (56:44). *Major isomer*: R_f 0.21 (5% MeOH in $CHCl_3$); mp 164–165°C. IR: 3475, 3269, 3214 cm^{-1}. ^{1}H NMR δ: 4.14 (2H, d, J = 11.8 Hz), 4.06 (1H, s), 3.94 (1H, v br s), 3.53 (2H, d, J = 11.8 Hz), 3.46 (2H, s), 0.92 (9H, s). ^{13}C NMR (acetone-d_6) δ: 107.9, 68.8, 62.0, 58.0, 35.2, 24.7. MS (CI-NH_3), *m/z* (rel. intensity): 206 (100), 190 (87), 174 (37), 158 (17), 148 (13), 101 (21). Anal. calcd. for $C_9H_{19}NO_4$: C 52.67, H 9.33, N 6.82; found: C 52.77, H 9.57, N 6.64.

*Amine 12*b
Procedure A5 afforded **12***b* in quantitative yield as a mixture of two isomers in a ratio of 69:31 (by GC; isomers were not separated); mp 154–158°C. IR (KBr): 3343.5, 3307.6, 3187.1, 1046.6 cm^{-1}. ^{1}H NMR (*major isomer*): 4.05 (s, 1H), 3.75 (d, 2H, J = 11.0 Hz), 3.58 (d, 2H, J = 11.0 Hz), 3.30 (m, 1H) 2.60 (br s, 3H), 0.93 (s, 9H); (*minor isomer*): 4.03 (s, 1H), 3.95 (d, 2H, J = 11.0 Hz), 3.75 (d, 2H, J = 11.0 Hz), 3.30 (m,1H), 2.60 (br s, 3H), 0.90 (s, 9H). ^{13}C NMR (*major isomer*): 108.0, 73.8, 64.3, 50.6, 34.7, 24.4; (*minor isomer*): 107.6, 73.0, 64.2, 48.9, 34.5, 24.5. MS (CI-NH_3): 191 (M + 2, 11), 190 (M + 1, 100), 122 (9), 101 (14).

*Oxime 14*b
Procedure A3: Crude material was a yellow solid that comprised 86% oxime (**14***b*) and 14% ketone (**2***b*). Separated by flash chromatography (SiO_2, 3:1 hexane:AcOEt), the oxime was the second component to be eluted (white solid, 69%). R_f 0.28 (3:1 hexane:AcOEt); mp 98–100°C. IR: 3282 cm^{-1}. ^{1}H NMR δ: 7.15 (1H, s), 5.19 (1H, d, J = 15.7 Hz), 4.48 (1H, d, J = 14.2 Hz), 4.31 (1H, d, J = 14.2 Hz), 4.24 (1H, s), 4.21 (1H, d, J = 15.7 Hz), 0.93 (9H, s). ^{13}C NMR δ: 151.9, 107.0, 66.3, 62.2, 35.1, 24.5. MS (CI-NH_3), *m/z* (rel. intensity): 174 ([M + 1]$^+$, 87), 116 (100), 86 (11). Anal. calcd. for $C_8H_{15}NO_3$: C 55.47, H 8.73, N 8.09; found: C 55.40, H 8.87, N 7.99.

*2-tert-Butyl-1,3-dioxan-5-one (2*b*) (ref. 10*h*)*
Procedure A4 yielded the crude material, which was purified by flash chromatography (SiO_2, 3:1 hexane:AcOEt). White solid, 50% yield. R_f 0.39 (3:1 hexane:AcOEt). ^{1}H NMR δ:

Can. J. Chem. Downloaded from www.nrcresearchpress.com by 46.23.64.124 on 09/08/12
For personal use only.

4.43 (2H, d, J = 18.0 Hz), 4.43 (1H, s), 4.27 (2H, d, J = 18.0 Hz), 0.97 (9H, s).
Procedure A6 afforded **2***b* in 50% yield (reaction time 20 min).

2,2-Dimethyl-1,3-dioxan-5-one (2*c*) (refs. 8, 9)

Compound ***11***c *(ref. 21)*
Procedure A1: Acetone (25 mL, 340 mmol) was added to a solution of p-TsOH·H_2O (190 mg, 1 mmol) and tris(hydroxymethyl)nitromethane (15.112 g, 100 mmol) in benzene (150 mL). The mixture was refluxed overnight under a Soxhlet extractor containing 4 Å molecular sieves. Solvents were removed in vacuo and saturated aqueous $NaHCO_3$ solution (200 mL) was added. The mixture was extracted with AcOEt (4375 mL), dried ($MgSO_4$), and the solvent was removed to yield an off-white solid (14.651 g, 77%). R_f 0.31 (1:1 hexane:AcOEt); mp 123–125°C. IR: 3426 cm^{-1}. ^1H NMR δ: 4.46 (2H, d, J = 13.0 Hz), 4.14 (2H, d, J = 13.0 Hz), 3.94 (2H, s), 3.78 (1H, s), 1.43 (3H, s), 1.32 (3H, s). ^{13}C NMR (acetone-d_6) δ: 98.6, 87.1, 63.0, 61.2, 25.3, 20.1. MS (CI-NH_3), m/z (rel. intensity): 209 ([M + 18]$^+$, 100), 192 ([M + 1]$^+$, 91), 176 (82), 162 (37), 146 (45), 127 (28). Anal. calcd. for $C_7H_{13}O_5N$: C 43.98, H 6.85, N 7.33; found: C 44.10, H 7.09, N 7.19.

Amine ***12***c
Procedure A5 afforded **12***c* in 93% yield; mp 63–65°C (hexane:Et_2O 1:1) (lit. (10*i*) mp 54.5–55.5°C; (10*j*) 72–73°C). IR (KBr): 3325, 3262, cm^{-1}. ^1H NMR δ: 3.76 (d, 2H, J = 12.0 Hz), 3.52 (d, 2H, = 12.0 Hz), 3.48 (s, 2H), 2.30 (br s, 3H), 1.41 (s, 3H), 1.39 (s, 3H). ^{13}C NMR δ: 98.3, 67.2, 65.1, 50.1, 24.7, 22.2; MS (CI-NH_3), m/z: (rel. intensity): 162 (M + 1, 100%), 146 (15), 104 (52), 73 (97). Anal. calcd. for $C_7H_{15}NO_3$: C 52.17, H 9.32, N 8.69; found: C 52.18, H 9.65, N 8.65.

Oxime ***14***c *and 2,2-dimethyl-1,3-dioxan-5-one (2*c*) (refs. 8, 9)*
Procedures A2, A3: Aluminum amalgam reduction of the nitrodioxane (**11***c*) yielded a complex mixture thought to comprise hydroxylamine, primary amine, and oxime. The mixture was not amenable to separation and was immediately submitted to the oxidative cleavage conditions. The amount of dioxanone in the crude product mixture from oxidative cleavage was maximized by allowing the reaction to proceed for 38 h. The crude material typically comprised 60% dioxanone (**2***c*) and 40% oxime (**14***c*). The mixture was separated by flash chromatography (SiO_2, 4:1 hexane:AcOEt).
14*c*. R_f 0.12 (4:1 hexane:AcOEt). IR: 3360 cm^{-1}. ^1H NMR δ: 4.60 (2H, s), 4.27 (2H, s), 1.41 (6H, s). ^{13}C NMR δ: 155.7, 100.0, 59.1, 57.4, 23.5. MS (CI-NH_3), m/z (rel. intensity): 163 (4), 146 (100), 130 (15), 98 (72), 58 (11).
2*c*. R_f 0.31 (4:1 hexane:AcOEt). IR: 1738 cm^{-1}. ^1H NMR δ: 4.16 (4H, s), 1.46 (6H, s). ^{13}C NMR δ: 207.5, 99.7, 66.3, 23.0. MS (CI-NH_3), m/z (rel. intensity): 131 ([M + 1]$^+$, 100), 72 (11), 58 (10).
Procedure A6 afforded **2***c* in 49% yield (reaction time 15 min).

2-Phenyl-2-methyl-1,3-dioxan-5-one (2*d*)

Compound ***11***d
Modified procedure A1 (1.1 equivalents of tris(hydroxymethyl)nitromethane were used and the reaction mixture was refluxed for 87 h) yielded **11***d* as an off-white solid (76%) that was isomerically pure; mp 129–130°C. IR: 3510, 1548 cm^{-1}. ^1H NMR δ: 7.52–7.34 (5H, m), 4.64 (2H, d, J = 12.5 Hz), 3.85 (2H, d, J = 12.5 Hz), 3.68 (2H, d, J = 6.1 Hz), 1.74 (1H, t, J = 6.1 Hz), 1.53 (3H, s). ^{13}C NMR (acetone-d_6) δ: 139.7, 129.3, 128.6, 126.7, 101.4, 87.8, 63.4, 63.3, 31.4. MS (CI-NH_3), m/z (rel. intensity): 271 ([M + 18]$^+$, 15), 254 ([M + 1]$^+$, 100), 238 (20), 224 (35), 105 (31). Anal. calcd. for $C_{12}H_{15}NO_5$: C 56.91, H 5.97, N 5.53; found: C 56.77, H 6.12, N 5.39.

Hydroxylamine ***13***d *and amine* ***12***d
Procedure A2 yielded a white solid (87%) that comprised 50% primary amine (**12***d*) and 50% hydroxylamine (**13***d*). The mixture could be separated by flash chromatography (SiO_2, methanol:AcOEt); however, oxidative cleavage was generally performed on the mixture.
13*d*. R_f 0.71 (1:1 MeOH:AcOEt); mp 139–140°C. IR: 3397 cm^{-1}. ^1H NMR δ: 7.47–7.28 (5H, m), 3.80 (2H, d, J = 11.6 Hz), 3.66 (2H, d, J = 11.6 Hz), 3.27 (2H, s), 1.44 (3H, s). ^{13}C NMR (acetone-d_6) δ: 141.2, 129.3, 128.4, 127.1, 101.0, 63.3, 61.8, 57.9, 32.0. MS (CI-NH_3), m/z (rel. intensity): 240 ([M + 1] + , 100), 224 (45), 192 (28), 121 (88), 104 (52), 73 (20). Anal. calcd. for $C_{12}H_{17}NO_4$: C 60.24, H 7.16, N 5.85; found: C 60.21, H 6.96, N 5.88.
12*d*. R_f 0.37 (1:1 MeOH:AcOEt); mp 166–168°C. IR: 3345, 3278 cm^{-1}. ^1H NMR δ: 7.45–7.37 (5H, m), 3.67 (2H, d, J = 11.2 Hz), 3.50 (2H, d, J = 11.2 Hz), 3.22 (2H, br s), 3.17 (2H, s), 1.46 (3H, s). ^{13}C NMR (acetone-d_6) δ: 142.7, 129.2, 128.4, 127.1, 100.6, 70.1, 69.6, 64.8, 31.8. MS (CI-NH_3), m/z (rel. intensity): 225 (M + 2, 13), 224 (M + 1, 100), 192 (7), 135 (18), 105 (8), 104 (34), 73 (22). Anal. calcd. for $C_{12}H_{17}NO_3$: C 64.55, H 7.67, N 6.27; found: C 64.56, H 7.84, N 6.22.
Procedure A5 afforded **12***d* in quantitative yield.

Oxime ***14***d *and 2-phenyl-2-methyl-1,3-dioxan-5-one (2*d*)*
Modified procedure A3 (two equivalents of $NaIO_4$ and half an equivalent of KH_2PO_4 were used) yielded a mixture of dioxanone **2***d* and oxime **14***d* (44:56). The mixture was separated by flash chromatography (SiO_2, 6:1 hexane:AcOEt), ketone eluted first (41%), followed by oxime (54%).
14*d*. R_f 0.23 (4:1 hexane:AcOEt). IR: 3350, 1458 cm^{-1}. ^1H NMR δ: 7.56–7.32 (5H, m), 4.79 (1H, d J = 16.5 Hz), 4.37 (1H, d, J = 16.5 Hz), 4.37 (1H, d, J = 13.8 Hz), 4.27 (1H, d, J = 13.8 Hz), 1.61 (3H, s). ^{13}C NMR δ: 155.2, 140.8, 128.4, 128.1, 125.9, 101.3, 60.3, 58.1, 28.4. MS (CI-NH_3), m/z (rel. intensity): 208 ([M + 1]$^+$, 100), 192 (66), 130 (10), 105 (13).
2*d*. R_f 0.44 (4:1 hexane:AcOEt). IR: 1751 cm^{-1}. ^1H NMR δ: 7.59–7.34 (5H, m), 4.27 (2H, d, J = 17.1 Hz), 4.12 (2H, d, J = 17.1 Hz), 1.67 (3H, s). ^{13}C NMR δ: 206.6, 140.7, 128.2, 128.1, 125.5, 100.7, 67.1, 26.7. MS (CI-NH_3), m/z (rel. intensity): 193 ([M + 1]$^+$, 100), 177 (24), 105 (13). Anal. calcd. for $C_{11}H_{12}O_3$: C 68.73, H 6.29; found: C 68.56, H 6.02.
Procedure A6 afforded **2***d* in 92% yield (reaction time 30 min).

2-*tert*-Butyl-2-methyl-1,3-dioxan-5-one (2*e*)

Compound ***11***e
Modified procedure A1 (two equivalents of pinacolone were used and the mixture was refluxed for 48 h) yielded the crude product (83%) as an off-white solid comprising two

Can. J. Chem. Downloaded from www.nrcresearchpress.com by 46.23.64.124 on 09/08/12
For personal use only.

isomers (68:32). *Major isomer*: R_f 0.38 (1:1 hexane:AcOEt), mp 92–94°C. IR: 3429, 3337 cm^{-1}. ^1H NMR δ: 4.63 (2H, d, J = 13.2 Hz), 4.03 (2H, d, J = 13.2 Hz), 3.82 (2H, d, J = 6.1 Hz), 1.80 (1H, t, J = 6.1 Hz), 1.37 (3H, s), 0.91 (9H, s). ^{13}C NMR (acetone-d_6) δ: 102.6, 87.8, 63.3, 62.0, 39.3, 24.2, 11.4. MS (CI-NH_3), m/z (rel. intensity): 235 ([M + 2]$^+$, 13), 234 ([M + 1]$^+$, 100), 218 (9), 176 (21). Anal. calcd. for $C_{10}H_{19}NO_5$: C 51.78, H 8.63, N 5.87; found: C 51.72, H 8.31, N 5.88.

Compound ***13e***
Procedure A2: White solid, 87% yield. Mixture of isomers (64:36). *Major isomer*: mp 159–161°C. IR: 3487, 3273 cm^{-1}. ^1H NMR δ: 3.88 (2H, d, J = 12.0 Hz), 3.75 (2H, d, J = 12.0 Hz), 3.48 (2H, s), 1.35 (3H, s), 0.99 (9H, s). ^{13}C NMR (acetone-d_6) δ: 105.3, 61.9, 61.8, 57.8, 39.9, 24.7, 11.5. MS (CI-NH_3), m/z (rel. intensity): 220 ([M + 1]$^+$, 64), 204 (100), 188 (67), 172 (56), 130 (41), 104 (48), 73 (31). Anal. calcd. for $C_{10}H_{21}NO_4$: C 54.77, H 9.65, N 6.39; found: C 55.04, H 9.82; N 6.32.

Compound ***12e***
Procedure A5: White solid, 98% yield. Mixture of two isomers in a ratio of 77:23 (not separated); mp 82–87°C (hexane). IR (KBr): 3252 cm^{-1}; ^1H NMR δ *(major isomer)*: 3.85 (dtr, 2H, J_1 = 1.5, J_2 = 12.0 Hz), 3.48 (dtr, 2H, J_1 = 1.5, J_2 = 12.0 Hz), 3.28 (s, 2H), 1.70 (brs, 3H), 1.32 (s, 3H), 1.03 (s, 9H), *(minor isomer)*: 3.75 (s, 2H), 3.67 (d, 2H, J = 11.5 Hz), 3.58 (d, 2H, J = 11.5 Hz), 1.70 (br s, 3H), 1.38 (s, 3H), 0.97 (s, 9H); ^{13}C NMR δ *(major isomer)*: 102.5, 67.3, 64.9, 50.5, 39.4, 24.5, 11.2; *(minor isomer)*: 102.0, 66.2, 64.6, 49.0, 39.2, 24.6, 11.3; MS (CI-NH_3), m/z: 204 (M + 1, 100%), 188 (11), 146 (22), 115 (50), 104 (73), 86 (32), 73 (52). Anal. calcd. for $C_{10}H_{21}NO_3$: C 59.09, H 10.41, N 6.89; found: C 59.18, H 10.37, N 6.79.

Compound ***14e***
Procedure A3: The crude product was a greenish solid that contained an oxime:ketone mixture (80:20). The mixture was separated by flash chromatography (SiO_2, hexane:AcOEt). Oxime (***14e***) eluted first (white solid, 52%). R_f 0.18 (6:1 hexane: AcOEt); mp 64–65°C. IR: 3284, 3162, 1162 cm^{-1}. ^1H NMR δ: 7.50 (1H, br s), 4.77 (1H, d, J = 17 Hz), 4.62 (1H, d, J = 17 Hz), 4.40 (1H, d, J = 14.5 Hz), 4.29 (1H, d, J = 14.5 Hz), 1.34 (3H, s), 1.01 (9H, s). ^{13}C NMR δ: 155.7, 104.1, 61.2, 58.6, 40.3, 25.0, 16.1. MS (CI-NH_3), m/z (rel. intensity): 189 ([M + 2]$^+$, 12), 188 ([M + 1]$^+$, 100), 172 (10), 130 (37). Anal. calcd. for $C_9H_{17}NO_3$: C 57.73, H 9.15, N 7.48; found: C 57.77, H 9.32, N 7.29.

*2-tert-Butyl-2-methyl-1,3-dioxan-5-one (**2e**)*
Procedure A4: $TiCl_3$ hydrolysis was generally performed on the crude oxime:ketone mixture obtained in the preceding step without additional purification.
2e. R_f 0.44 (6:1 hexane:AcOEt); mp 47-49°C. IR: 1736 cm^{-1}. ^1H NMR δ: 4.33 (2H, d, J = 18.5 Hz), 4.25 (2H, d, J = 18.5 Hz), 1.37 (3H, s), 1.04 (9H, s). ^{13}C NMR δ: 207.9, 103.6, 68.8, 40.4, 25.2, 15.9. MS (CI-NH_3), m/z (rel. intensity): 173 ([M + 1]$^+$, 100), 115 (29). Anal. calcd. for $C_9H_{16}O_3$: C 62.76, H 9.36; found: C 62.91, H 9.50.
Procedure A6 (reaction time 5h) afforded ***2e*** in 63%.

Enolization and reactions of dioxanones.
General procedure B
Diisopropylamine (0.08 mL, 0.55 mmol) was dissolved in THF (3 mL) and cooled to 0°C. *n*-BuLi (0.24 mL of a 2.3 M solution in hexanes; 0.55 mmol) was added, dropwise, and the solution was stirred for 15 min before cooling to −78°C. Dioxanone **2** (0.50 mmol) in THF (1.5 mL) was then added dropwise over 5 min. The resulting mixture was stirred for 30 min at −78°C and was then treated with an appropriate electrophile, stirred for a specific length of time, and then quenched with saturated aqueous NH_4Cl solution (2 mL) at −78°C. After warming to room temperature, saturated $NaHCO_3$ solution was added (5 mL) and the mixture was extracted with Et_2O (3 × 5 mL). The combined organic extracts were washed with brine (1 × 10 mL) and dried ($MgSO_4$). Removal of solvents in vacuo yielded the crude product(s).

The above procedure was followed in experiments with chiral lithium amide bases with the following modifications: (*i*) reaction time for deprotonation of the amine with BuLi was 90 min. (*ii*) In experiments with LiCl the chloride was added as 0.56 M solution in THF to the lithium amide, the mixture was stirred for 30 min, cooled to −78°C and the dioxanone was added. The enantiomeric excess was measured by ^1H NMR using $Eu(hfc)_3$ as the chiral shift reagent.

(B1) Enol acetates
Acetic anhydride (0.24 mL, 2.5 mmol) was added, as the electrophile, to the solution of the enolate generated as above. After stirring for between 30 min and 1 h at −78°C the reaction was quenched with water. Standard work-up yielded the crude enol acetate, usually accompanied by the acetate of the product of reduction.

(B2) Aldols
The aldehyde, typically PhCHO (0.50 mmol), was added in one portion to the enolate solution and the solution was stirred at −78°C for 15 min. Standard work-up yielded the crude aldol products.

(B3) Protonation
After the dioxanone (0.50 mmol) had been stirred with LDA (0.55 mmol) for 30 min, the reaction was quenched with saturated aqueous NH_4Cl solution. Work-up in the usual manner yielded a mixture that was typically analysed by GC and (or) ^1H NMR.

(B4) Silylation
(a) External quench: TMSCl (0.32 mL, 2.5 mmol) was added, as the electrophile, immediately followed by Et_3N (1 mL) and the mixture was allowed to warm to room temperature. The excess TMSCl, Et_3N, and THF were removed in vacuo and saturated aqueous $NaHCO_3$ (10 mL) was added. Extraction with ether (3 × 5 mL), drying ($MgSO_4$), and removal of solvent yielded the crude product mixture.
(b) Internal quench: TMSCl (0.32 mL, 2.5 mmol) was added to a solution of LDA (0.55 mmol) in THF (3 mL), followed by the dropwise addition of dioxanone (0.5 mmol) in THF (1.5 mL) over 3 min. After 1 min Et_3N (1 mL) was added and the mixture was allowed to warm up to room temperature. Work-up identical to that for the external quench procedure was performed.

Can. J. Chem. Downloaded from www.nrcresearchpress.com by 46.23.64.124 on 09/08/12
For personal use only.

*5-Trimethylsilyloxy-2-phenyl-1,3-diox-4-ene (**15**a) and* trans-*2-phenyl-1,3-dioxan-5-ol trimethylsilane (**16**a)*

Procedure B4*a* yielded yellow oil (99%) consisting of **15***a* and **16***a* (60:40 by ^{1}H NMR).

15*a*. IR (Neat): 1456, 1380 cm^{-1}. ^{1}H NMR δ: 7.57–7.32 (5H, m), 6.52 (1H, s), 5.65 (1H, s), 4.42 (1H, d, J = 14.7 Hz), 4.20 (1H, d, J = 14.7 Hz), 0.24 (9H, s). ^{13}C NMR δ: 136.8, 134.3, 130.1, 129.1, 128.3, 126.2, 97.8, 66.0, 0.0. MS (EI), *m/z* (rel. intensity): 250 ([M]$^+$, 19), 217 (12), 179 (69), 129 (100), 105 (31), 73 (42). A correct analysis could not be obtained.

16*a*. R_f 0.57 (4:1 hexane:AcOEt); IR: 1253 cm^{-1}. ^{1}H NMR δ: 7.52–7.32 (5H, m), 5.40 (1H, s), 4.21 (2H, dd, J = 11.2, 5.1 Hz), 3.96 (1H, m), 3.60 (2H, dd, J = 11.2, 10.1 Hz), 0.15 (9H, s). ^{13}C NMR δ: 137.6, 128.9, 128.2, 126.0, 101.0, 72.2, 61.7, −0.1. MS (EI), *m/z* (rel. intensity): 253 ([M + 1]$^+$, 33), 252 ([M]$^+$, 19), 180 (67), 132 (34), 116 (90), 101 (100), 73 (61). Anal. calcd. for $C_{13}H_{20}SiO_3$: C 61.87, H 7.99; found: C 62.11, H 8.01. Procedure B4*b* resulted in formation of 5% of **16***b* and 95% of **15***b* as established by GLC.

*5-Trimethylsilyloxy-2-*tert*-butyl-1,3-diox-4-ene (**15**b) and* trans-*2-*tert*-butyl-1,3-dioxan-5-ol trimethylsilane (**16**b)*

Procedure B4*a*: Yellow oil. Crude yield 91%. Product distribution: 44% **15***b* and 56% **16***b*. Preliminary purification of mixture was by distillation (Kugelrohr); components could not be separated, and were characterized via independent synthesis.

15*b*. IR (neat): 1403, 1252 cm^{-1}. ^{1}H NMR δ: 63.7 (1H, s), 4.24 (1H, s), 4.20 (1H, d, J = 14.5 Hz), 4.08 (1H, d, J = 14.5 Hz), 0.95 (9H, s), 0.20 (9H, s). ^{13}C NMR δ: 133.8, 130.0, 104.1, 66.2, 34.3, 24.6, 0.0. MS (EI), *m/z* (rel. intensity): 259 ([M + 39]$^+$,79), 230 ([M]$^+$, 12), 216 (52), 147 (19), 73 (100). Anal. calcd. for $C_{11}H_{22}O_3Si$: C 57.35, H 9.63; found: C 56.87, H 10.00.

16*b* R_f 0.32 (20:1 hexane:AcOEt). IR: 1462, 1112 cm^{-1}. ^{1}H NMR δ: 4.05 (2H, dd, J = 11.2, 5.1 Hz), 3.98 (1H, s), 3.75 (1H, m), 3.32 (2H, dd, J = 11.2, 10.1 Hz), 0.90 (9H, s), 0.12 (9H, s). ^{13}C NMR δ: 107.4, 72.0, 62.0, 34.5, 24.8, 0.0. MS (EI), *m/z* (rel. intensity): 232 ([M]$^+$, 16), 176 (100), 130 (73), 117 (65), 101 (77), 73 (87). Anal. calcd. for $C_{11}H_{24}O_3Si$: C 56.85, H 10.41; found: C 57.07, H 10.24.

*5-Acetyloxy-2-phenyl-1,3-diox-4-ene (**17**a) and* trans-*2-phenyl-1,3-dioxan-5-ol acetate (**18**a) (ref. 10*a*)*

Procedure B1: Crude mixture contained a mixture of **17***a* (48%) and **18***a* (52%), which were separated by flash chromatography (SiO_2, 4:1 hexane:AcOEt). Compound **17***a* was eluted first (20%), followed by **18***a* (22%).

17*a*. R_f 0.47 (4:1 hexane:AcOEt); mp 58–60°C. IR: 1764 cm^{-1}. ^{1}H NMR δ: 7.58–7.32 (5H, m), 6.85 (1H, s), 5.83 (1H, s), 4.72 (1H, d, J = 14.4 Hz), 4.35 (1H, d, J = 14.4 Hz), 2.18 (3H, s). ^{13}C NMR δ: 169.2, 136.2, 135.9, 130.8, 129.4, 128.4, 126.3, 98.5, 64.4, 20.5. MS (CI-NH_3), *m/z* (rel. intensity): 238 ([M + 18]$^+$, 38), 179 (25), 165 (36), 132 (100), 106 (41). Anal. calcd. for $C_{12}H_{12}O_4$: C 65.45, H 5.49; found: C 65.66, H 5.55

18*a*: R_f 0.30 (4:1 hexane:AcOEt); mp 108–109°C (lit. (10*a*) mp 118°C).

*5-Acetyloxy-2-*tert*-butyl-1,3-diox-4-ene (**17**b) and* trans-*2-*tert*-butyl-1,3-dioxan-5-ol acetate (**18**b)*

Crude product (60%; yellow oil) contained a mixture of **17**b and **18**b (43:57) that was purified by flash chromatography (SiO_2, 10:1 hexane:AcOEt). The components could not be separated and were characterized via independent synthesis.

17*b*. R_f 0.19 (15:1 hexane:AcOEt). IR: 1759 cm^{-1}. ^{1}H NMR δ: 6.67 (1H, s), 4.48 (1H, d, J = 14.3 Hz), 4.45 (1H, s), 4.16 (1H, d, J = 14.3 Hz), 2.14 (3H, s), 0.96 (9H, s). ^{13}C NMR δ: 169.3, 135.8, 130.3, 104.5, 64.3, 34.3, 24.3, 20.5. MS (CI-NH_3), *m/z* (rel. intensity): 218 ([M + 18]$^+$, 100), 200 ([M]$^+$, 9), 157 (15), 132 (50), 129 (20), 115 (16). Anal. calcd. for $C_{10}H_{16}O_4$: C 59.98, H 8.05; found: C 60.22, H 7.99.

18*b*. R_f 0.47 (4:1 hexane:AcOEt). IR: 1750 cm^{-1}. ^{1}H NMR δ: 4.85 (1H, tt, J = 10.4, 5.3 Hz), 4.23 (2H, dd, J = 10.9, 5.3 Hz), 4.03 (1H, s), 3.42 (2H, dd, J = 10.9, 10.4 Hz), 2.04 (3H, s), 0.91 (9H, s). ^{13}C NMR δ: 169.8, 107.6, 68.3, 63.0, 34.7, 24.7, 20.8. MS (CI-NH_3), *m/z* (rel. intensity): 220 (M + 18]$^+$, 18), 203 ([M + 1]$^+$, 47), 145 (85), 117 (100), 86 (29). Anal. calcd. for $C_{10}H_{18}O_4$: C 59.39, H 8.97; found: C 59.47, H 9.12.

trans-*2-Phenyl-1,3-dioxan-5-ol (**19**a)*

Crude product (obtained according to procedure B3) contained 81% **19***a* and 19% starting material **2***a*. Purification by flash chromatography (SiO_2, hexane:AcOEt) gave **19***a* as clear liquid (83%). Spectral properties were in agreement with literature values (10*i*).

trans-*2-*tert*-Butyl-1,3-dioxan-5-ol (**19**b)*

Crude product (obtained according to procedure B3 in Et_2O) contained 89% **19***b* and 11% starting material **2***b*. Purification was by flash chromatography (SiO_2, hexane:AcOEt). White solid. R_f 0.22 (4:1 hexane:AcOEt). IR: 3297 cm^{-1}. ^{1}H NMR δ: 4.18 (2H, dd, J = 11.0, 5.2 Hz), 4.00 (1H, s), 3.85 (1H, m), 3.33 (2H, dd, J = 11.0, 10.0 Hz), 1.43 (1H, d, J = 5.5 Hz), 0.92 (9H, s). ^{13}C NMR δ: 107.5, 71.6, 61.4, 34.5, 24.8. MS (CI-NH_3), *m/z* (rel. intensity): 178 ([M + 18]$^+$, 62), 161 ([M + 1]$^+$, 70), 103 (100).

19*b* via inverse addition: A solution of LDA (0.50 mmol) in ether (2 mL) was added, dropwise, to a solution containing dioxanone **1***b* (72 mg, 0.45 mmol) in ether (3 mL) at −78°C. The mixture was stirred for 1 h before quenching with saturated aqueous NH_4Cl solution. Work-up in the usual manner yielded a mixture (65:35) of alcohol **19***b* and ketone **2***b*.

*4-(1-Hydroxy-4-*tert*-butyl-3,5-dioxanyl)-2-*tert*-butyl-1,3-dioxan-5-one (**20**b)*

To a solution of HMDS (0.15 mL, 0.69 mmol) in diethyl ether (3 mL) at −5°C was added, dropwise, *n*-BuLi (0.37 mL of a 1.88 M solution in hexanes). The solution was stirred for 90 min before cooling to −78°C. A solution of dioxanone **2***b* (53 mg, 0.33 mmol) in ether (1.5 mL) was added dropwise over 5 min. The solution was allowed to warm to 0°C and was stirred for 2 h, after which time the reaction was quenched with saturated aqueous NH_4Cl solution (2 mL). After warming to room temperature, saturated aqueous $NaHCO_3$ solution (10 mL) was added and the mixture was extracted with ether (2 × 8 mL). The organic extracts were combined and washed with brine (2 × 15 mL). Drying and removal of solvents yielded the crude product mixture, which was purified by flash chromatography (SiO_2, 10:1 hexane:AcOEt). Self-aldol **20***b* was isolated as an oil (18 mg, 34%). R_f 0.47 (4:1 hexane:AcOEt). IR: 3571, 1738 cm^{-1}. ^{1}H NMR δ: 5.13 (1H, s), 4.36 (2H, s), 4.14

Can. J. Chem. Downloaded from www.nrcresearchpress.com by 46.23.64.124 on 09/08/12
For personal use only.

(1H, dd, J = 11.8, 3.2 Hz), 4.06 (1H, s), 4.01 (1H, dd, J = 11.7, 3.3 Hz), 3.96 (1H, d, J = 2.0 Hz), 3.71 (1H, d, J = 11.7 Hz), 3.64 (1H, d, J = 11.7 Hz), 3.15 (1H, d, J = 2.0 Hz), 0.96 (9H, s), 0.93 (9H, s). ^{13}C NMR δ: 203.9, 107.8, 103.4, 80.5, 74.7, 72.5, 72.3, 71.4, 35.2, 34.8, 24.6, 24.5. MS (CI-NH_3), *m/z* (rel. intensity): 334 ([M + 18]$^+$, 100), 317 ([M + 1]$^+$, 74), 259 (53), 248 (57), 173 (21), 101 (33).

*2,2-Dimethyl-1,3-dioxan-5-ol (**21**) (ref. 22)*

To a solution of $NaBH_4$ (20 mg, 0.53 mmol) in i-PrOH (4 mL) at 0°C was added dioxanone **2***c* (114 mL, 0.96 mmol). The solution was stirred for 30 min before quenching with water (2 mL). The mixture was extracted with ether (2 × 5 mL) and the combined organic extracts washed with saturated aqueous NaCl solution (15 mL), dried ($MgSO_4$), and the solvents removed in vacuo. The crude material was purified by flash chromatography (SiO_2, 1:2 hexane:AcOEt) to afford a clear liquid (77 mg, 61%). R_f 0.27 (1:2 hexane:AcOEt). ^{1}H NMR δ: 4.07 (2H, dd, J = 12.1, 1.1 Hz), 3.75 (2H, dd, J = 12.1, 1.7 Hz), 3.53 (1H, m), 2.84 (1H, d, J = 10.2 Hz), 1.46 (3H, s), 1.43 (3H, s). ^{13}C NMR δ: 98.4, 65.2, 63.5, 27.7, 19.5.

*4-(1-Hydroxy-4,4-dimethyl-3,5-dioxanyl)-2,2-dimethyl-1,3-dioxan-5-one (**22**)*

Procedure B3 (THF; 0.5 equiv. of LDA) yielded a mixture comprising 38% dioxanone **2***c*, 4% alcohol **21**, and 58% **22**. Removal of the more volatile components under high vacuum (0.1 Torr, 16 h; 1 Torr = 133.3 Pa) yielded **22** in a high state of purity (oil, 44%). R_f 0.26 (1:1 hexane:AcOEt). IR: 3460, 1747 cm^{-1}. ^{1}H NMR δ: 4.48 (1H, s), 4.28 (1H, d, J = 17.2 Hz), 4.13 (1H, d, J = 12.1 Hz), 4.03 (1H, d, J = 11.7 Hz), 4.00 (1H, d, J = 17.2 Hz), 3.85 (1H, d, J = 12.1 Hz), 3.67 (1H, d, J = 11.7 Hz), 2.83 (1H, br s), 1.49 (3H, s), 1.47 (3H, s), 1.45 (3H, s), 1.42 (3H, s). ^{13}C NMR δ: 208.2, 101.0, 98.2, 73.8, 68.6, 67.2, 65.1, 64.4, 23.8, 23.5, 23.1, 23.0. MS (CI-NH_3), *m/z* (rel. intensity): 278 ([M + 18]$^+$, 24), 261 ([M + 1]$^+$, 45), 220 (100), 131 (17). Anal. calcd. for $C_{12}H_{20}O_6$: C 55.37, H 7.74; found: C 55.27, H 7.60.

General procedure for rapid quench aldol reactions of 2*c* (ref. 3)

A solution of dioxanone **2***c* (50 μL, 0.42 mmol) in 1.5 mL THF was added, dropwise, to a solution of LDA (0.46 mmol) in THF (3 mL) at −78°C. The aldehyde (0.42 mmol) was then added immediately, in one portion. Stirring was continued for 2 min prior to quenching with saturated aqueous NH_4Cl solution (2 mL). The solution was allowed to warm to room temperature, then was worked up in the usual manner.

*4-(Hydroxyphenylmethyl)-2,2-dimethyl-1,3-dioxan-5-one (**23**a, **24**a)*

Procedure B2 afforded crude product (yellow oil, 86 mg, 92%) containing the *threo* and *erythro* isomers[2] **23***a* and **24***a* (64:36). A pure sample of each compound was obtained by flash chromatography (SiO_2, 4:1 hexane:AcOEt); the *threo* isomer (23) **23***a* (30 mg, 32%) eluted first, followed by the *erythro* compound **24***a* (25 mg, 28%).

23*a*. R_f 0.18 (4:1 hexane: AcOEt). IR: 3494, 1741 cm^{-1}. ^{1}H NMR δ: 7.26–7.45 (5H, m), 4.91 (1H, dd, J = 7.7, 3.1 Hz), 4.35 (1H, dd, J = 7.7, 1.4 Hz), 4.27 (1H, dd, J = 17.5, 1.4 Hz), 4.04 (1H, d, J = 17.5 Hz), 3.62 (1H, d, J = 3.1 Hz), 1.37 (3H, s), 1.25 (3H, s). ^{13}C NMR δ: 211.0, 139.2 128.1, 127.1, 101.2, 76.1, 72.7, 66.7, 23.6, 23.2. MS (CI-NH_3), *m/z* (rel. intensity): 254 ([M + 18]$^+$, 100), 237 ([M + 1]$^+$, 15), 178 (19), 131 (54). Anal. calcd. for $C_{13}H_{16}O_4$: C 66.09, H 6.83; found: C 66.23, H 6.73.

24*a*. R_f 0.13 (4:1 hexane:AcOEt). IR: 3473, 1750 cm^{-1}. ^{1}H NMR δ: 7.45–7.30 (5H, m), 5.24 (1H, dd, J = 8.0, 2.7 Hz), 4.48 (1H, dd, J = 2.7, 1.5 Hz), 4.30 (1H, dd, J = 17.1, 1.5 Hz), 4.06 (1H, d, J = 17.1 Hz), 2.78 (1H, d, J = 8.0 Hz), 1.49 (3H, s), 1.37 (3H, s). ^{13}C NMR δ: 207.4, 140.1, 128.3, 127.9, 126.5, 101.0, 78.0, 71.3, 67.2, 24.3, 23.3. MS (CI-NH_3), *m/z* (rel. intensity): 255 (M + 19, 14), 254 (M + 18, 100), 237 (M + 1, 11), 219 (31), 196 (13), 179 (18), 178 (31), 165 (36), 161 (59), 131 (52), 130 (11), 124 (33), 113 (46), 105 (18), 94 (10), 76 (32), 72 (25). Anal. calcd. for $C_{13}H_{16}O_4$: C 66.09, H 6.83; found: C 66.11, H 6.70.

*4-(Cyclohexylhydroxymethyl)-2,2-dimethyl-1,3-dioxan-5-one (**23**b, **24**b).*

Procedure B2 afforded crude product (oil, 97 mg, 95%) containing the *threo* isomer[2] **23***b* and a small amount of the *erythro* isomer[2] **24***b* (less than 10% by NMR). Purification by flash chromatography (SiO_2; 4:1 hexane:AcOEt; R_f 0.32) afforded **23***b* (70 mg, 69%) as a yellow solid (mp 64–66°C). IR (KBr): 3531, 1737 cm^{-1}. ^{1}H NMR δ: 4.28 (dd, 1H, J_1 = 17.5, J_2 = 1.5 Hz), 4.21 (dd, 1H, J_1 = 7.5, J_2 = 1.5 Hz), 4.03 (d, 1H, J = 17.5 Hz), 3.69 (m, 1H), 3.00 (br s, 1H), 1.92–1.47 (m, 7H), 1.47 (s, 3H), 1.44 (s, 3H), 1.44–1.09 (m, 4H); ^{13}C NMR δ: 212.0, 100.9, 74.1, 73.3, 66.6, 38.3, 29.5, 26.4, 26.3, 26.2, 26.0, 23.7, 23.6; MS (CI); *m/e* (rel. intensity): 260 (M + 18, 100), 243 (M + 1, 65), 95 (11), 72 (16). Anal. calcd. for: $C_{13}H_{22}O_4$: C 64.44, H 9.15; found: C 64.68, H 9.17.

cis-*4-(Cyclohexylhydroxymethyl)-2-*tert*-butyl-2-methyl-1,3-dioxan-5-one (**23**c) (ref. 23)*

Procedure B2, followed by purification by flash chromatography (SiO_2, 8:1 hexane:AcOEt), yielded **23***c* as an oil (53 mg, 61%). R_f 0.38 (4:1 hexane:AcOEt). IR (KBr): 3530, 1731 cm^{-1}. ^{1}H NMR δ: 4.36 (dd, 1H, J = 18.0 Hz, J = 1.5 Hz), 4.30 (d, 1H, J = 5.5 Hz), 4.22 (d, 1H, J = 18.0 Hz), 3.73 (ddd, 1H, J_1 = 3.5, J_2 = 5.5 Hz, J_3 = 5.5 Hz), 2.91 (d, 1H, J = 3.5 Hz), 1.83–1.75 (m, 3H), 1.75–1.60 (m, 4H), 1.45 (s, 3H), 1.35–1.10 (m, 6H), 1.06 (s,9H). ^{13}C NMR δ: 210.2, 103.3, 76.4, 75.7, 69.5, 40.0, 38.7, 29.2, 27.1, 26.3, 26.2, 26.0, 25.0, 15.7. MS (CI-isobutane), *m/z* (rel. intensity): 286 (M + 2, 14), 285 (M + 1, 68), 227 (26), 185 (11), 173 (18), 167 (20), 113 (12), 101 (100), 95 (26). Anal. calcd. for: $C_{16}H_{28}O_4$: C 67.57, H 9.92; found: C 67.82, H 10.15. $[\alpha]_D^{24}$ −34.5 (*c* 0.8, MeOH) for the sample having 67% ee (by ^{1}H NMR).

[2] The aldol stereostructural assignments (*threo* vs. *erythro* isomers; compounds **23***a–c* and **24***a, b*) were made by NMR on the basis of the well-known "rule of thumb" based on the analysis of a large number of coupling constants in ^{1}H NMR spectra and chemical shifts in ^{13}C NMR spectra (cf. ref. 23). All assumptions inherent in this analysis apply. To determine the relative configuration (*cis* or *trans*) in compound **23***c* a crystal structure of a derivative of this compound was obtained (the full crystallographic data will be published elsewhere).

Acknowledgements

We are grateful to Natural Sciences and Engineering Research Council of Canada and to the University of Saskatchewan for financial support of this work. We thank Professor J. W. Quail for help in establishing the relative configuration of compound **23***c*.

References

1. M.D. Bednarski. *In* Comprehensive organic synthesis. Vol. 2. *Edited by* B.M. Trost. Pergamon Press, Oxford. 1991. p. 455.
2. M.D. Bednarski, E.S. Simon, N. Bischofberger, W-D. Fessner, M-J. Kim, W. Lees, T. Saito, H. Waldmann, and G.M. Whitesides. J. Am. Chem. Soc. **111**, 628 (1989).
3. M. Majewski and D.M. Gleave. J. Org. Chem. **57**, 3599 (1992).
4. M. Majewski and R. Lazny. Tetrahedron Lett. **35**, 3653 (1994).
5. (*a*) F.A. Carey and R.J. Sundberg. Advanced organic chemistry. Part A. 3rd ed. Plenum Press, New York. 1990. p. 146; (*b*) M.J.O. Anteunis, D. Tavernier, and F. Barremans. Heterocycles, **4**, 293 (1976).
6. (*a*) R. Shirai, M. Tanaka, and K. Koga. J. Am. Chem. Soc. **108**, 543 (1986); (*b*) M. Majewski and J. MacKinnon. Can. J. Chem. **72**, 1699 (1994).
7. M. Hirama, T. Noda, S. Itô, and C. Kabuto. J. Org. Chem. **53**, 706 (1988).
8. M.M. Francl, G. Hansell, B.P. Patel, and C.S. Swindell. J. Am. Chem. Soc. **112**, 3535 (1990).
9. (*a*) D. Enders and B. Bockstiegel. Synthesis, 493 (1989); (*b*) D. Enders and U. Jegelka. Tetrahedron Lett. **34**, 2453 (1993).
10. (*a*) J.C. Joachims and Y. Kobayashi. Tetrahedron Lett. 575 (1974); (*b*) Y. Kobayashi, J. Lambrecht, J.C. Joachims, and U. Burkert. Chem. Ber. **111**, 3442 (1978); (*c*) A.A. Marei and R.A. Raphael. J. Chem. Soc. 886 (1960); M.H. Chang and R.J. Crawford. Can. J. Chem. **59**, 2556 (1981); (*e*) H. Vorbröggen. Acta Chem. Scand. Ser. B, **36**, 420 (1981); (*f*) B.M. Trost, S.A. King, and T. Schmidt. J. Am. Chem. Soc. **111**, 5902 (1989); (*g*) P.M. Collins, A.S. Travis, and K.N. Tsiquaye. J. Chem. Soc. Perkin Trans. 1, 1895 (1974); (*h*) Y. Senda, T. Teresawa, J. Ishiyama, S. Kamiyama, and S. Imaizumi. Bull. Chem. Soc. Jpn. **62**, 2948 (1989); (*i*) J.C. Joachims, Y. Kobayashi, and E. Skrzelewski. Tetrahedron Lett. 571 (1974).
11. (*a*) M. Trister and H. Hibbert. Can. J. Res. Sect. B: **14**, 415 (1937); (*b*) A.J. Showler and P.A. Darley. Chem. Rev. **67**, 427 (1967); (*c*) A. Piasecki and B. Burczyk. Pol. J. Chem. **54**, 367 (1980).
12. M. Majewski and D.M. Gleave. J. Organomet. Chem. **470**, 1 (1994).
13. E.J. Corey and A.W. Gross. Tetrahedron Lett. **25**, 495 (1984).
14. (*a*) C.H. Heathcock. *In* Comprehensive organic synthesis. Vol. 2. *Edited by* B. M. Trost. Pergamon Press, Oxford. 1991. p. 140; (*b*) E.R. Thornton and G. Das. J. Am. Chem. Soc. **112**, 5360 (1990).
15. (*a*) B. Rickborn and S. Mirsadeghi. J. Org. Chem. **51**, 986 (1986); (*b*) M. Fedoronko, M. Petrusová, V. Kovácik. Collect. Czech. Chem. Commun. **50**, 2252 (1985); (*c*) B. Föshlisch, D. Krimmer, E. Gehrlach, and D. Käshammer. Chem. Ber. **121**, 1585 (1988); D. Seebach, R. Naef, and G. Calderari. Tetrahedron, **40**, 1313 (1984).
16. (*a*) M. Majewski and R. Lazny. Tetrahedron Lett. **35**, 3653 (1994); (*b*) B.J. Bunn, P.J. Cox, and N.S. Simpkins. Tetrahedron, **49**, 207 (1993); (*c*) B.J. Bunn, N.S. Simpkins, Z. Spavold, and M.J. Crimmin. J. Chem Soc. Perkin Trans. 1, 3113 (1993).
17. (*a*) D.B. Collum. Acc. Chem. Res. **26**, 227 (1993); (*b*) P.G. Williard and M.J. Hintze. J. Am. Chem. Soc. **112**, 8602 (1990).
18. D.K. Hutchinson. Aldrichimica Acta, **19**, 58 (1986).
19. W.C. Still, M. Kahn, and A. Mitra. J. Org. Chem. **43**, 2923 (1979).
20. D.W. Brown, T.T. Nakashima, and D.L. Rabenstein. J. Magn. Reson. **45**, 302 (1981).
21. G. B. Linden and M.H. Gold. J. Org. Chem. **21**, 1175 (1956).
22. G.J.F. Chittenden. Carbohydr. Res. **91**, 85 (1981).
23. C.H. Heathcock. *In* Asymmetric Synthesis. Vol. 3. *Edited by* J.D. Morrison. Academic Press, New York. 1984. pp. 112–115.

Can. J. Chem. Downloaded from www.nrcresearchpress.com by 46.23.64.124 on 09/08/12
For personal use only.

Organic nitrates, thionitrates, peroxynitrites, and nitric oxide: a molecular orbital study of the $RXNO_2 \rightleftharpoons RXONO$ (X = O, S) rearrangement, a reaction of potential biological significance

Dale R. Cameron, Alison M.P. Borrajo, Brian M. Bennett, and Gregory R.J. Thatcher

Abstract: The rearrangement of organic thionitrate to sulfenyl nitrite potentially mediates the release of nitric oxide from organic nitrates, such as nitroglycerin, in the presence of thiol. The biological activity of these nitrovasodilators is proposed to result from release of nitric oxide in vivo. The thionitrate rearrangement bears analogy to the rearrangement of peroxynitrous acid to nitric acid, which has been proposed to mediate the biological toxicity of nitric oxide and superoxide. In this paper, the two concerted rearrangement processes and competing homolytic reactions are explored using molecular orbital calculations at levels up to MP4SDQ/6-31G*//MP2/6-31G*. Examination of structure and energy for all conformers and isomers of $RSONO_2$ (R = H, Me), models for organic thionitrates and their isomers, demonstrates that structures corresponding to thionitrates and sulfenyl nitrates are of similar energy. Free energies of reaction for homolysis of these compounds are low ($\Delta G_0 < 19$ kcal/mol), whereas the barrier for concerted rearrangement is large ($\Delta G^{\neq}$(aq.) = 56 kcal/mol). The larger barrier for concerted rearrangement of peroxynitrous acid to nitric acid ($\Delta G^{\neq}$(aq.) = 60 kcal/mol) again compares unfavourably with homolysis ($\Delta G_0 < 11$ kcal/mol for homolysis to NO_2 or $^{\cdot}NO$). The transition state structures, confirmed by normal mode and intrinsic reaction coordinate analysis, indicate that considerable structural reorganization is required for concerted rearrangement of the ground state species. These results suggest that concerted rearrangement is not likely to be a viable step in either biological process. However, rearrangement via homolysis and radical recombination may provide an energetically accessible pathway for peroxynitrous acid rearrangement to nitric acid and rearrangement of thionitrate to sulfenyl nitrite. In this case, NO_2 will be a primary product of both reactions.

Key words: thionitrate, nitric oxide, peroxynitrite, nitrovasodilator, nitrate.

Résumé : Le réarrangement des thionitrates organiques en nitrites de sulfényle pourrait éventuellement permettre de dégager, en présence de thiols, de l'oxyde nitrique à partir de nitrates organiques, comme la nitroglycérine. Il est suggéré que l'activité biologique de ces nitrovasodilatateurs est le résultat d'une expulsion in vivo d'oxyde nitrique. Le réarrangement thionitrate ressemble au réarrangement de l'acide peroxynitreux en acide nitrique qui serait la cause de la toxicité biologique de l'oxyde nitrique et du superoxyde. Dans ce travail, utilisant des calculs d'orbitales moléculaires à des niveaux allant jusqu'à MP4SDQ/6-31G*//MP2/6-31G*, on a examiné les deux processus concertés du réarrangement et les réactions homolytiques qui leur font compétition. Un examen de la structure et de l'énergie de chacun des conformères et des isomères des $RSONO_2$ (R = H, Me), modèles des thionitrates organiques et de leurs isomères, permet de démontrer que les structures correspondant aux thionitrates et aux nitrites de sulfényles sont d'énergies semblables. Les énergies libres de réaction pour l'homolyse de ces composés sont basses ($\Delta G_0 < 19$ kcal/mol) alors que la barrière pour le réarrangement concerté est élevée ($\Delta G^{\neq}$(aq) = 56 kcal/mol). La barrière encore plus élevée observée pour le réarrangement concerté de l'acide peroxynitreux en acide nitrique ($\Delta G^{\neq}$(aq) = 60 kcal/mol) donne à nouveau lieu à une comparaison non favorable avec l'homolyse ($\Delta G_0 < 11$ kcal/mol pour l'homolyse en NO_2 ou en $^{\cdot}NO$). Les structures des états de transition, confirmées par une analyse du mode normal et des coordonnées de la réaction

Received May 10, 1995.

D.R. Cameron, A.M.P. Borrajo, and G.R.J. Thatcher.[1] Department of Chemistry, Queen's University, Kingston, ON K7L 3N6, Canada.
B.M. Bennett. Department of Pharmacology and Toxicology, Queen's University, Kingston, ON K7L 3N6, Canada.

[1] Author to whom correspondence may be addressed. Telephone: (613) 545-2640. Fax: (613) 545-6669.

Can. J. Chem. Downloaded from www.nrcresearchpress.com by 80.90.12.36 on 09/08/12
For personal use only.

intrinsèque, indiquent qu'une réorganisation structure importante est requise pour un réarrangement concerté des espèces dans l'état fondamental. Ces résultats suggèrent qu'il est peu probable que le réarrangement concerté soit une étape viable dans l'un ou l'autre des processus biologiques. Toutefois, un réarrangement par le biais d'une homolyse et d'une recombinaison de radicaux peut s'avérer une voie énergétiquement accessible pour le réarrangement de l'acide peroxynitreux en acide nitrique et pour le réarrangement du thionitrate en nitrite de sulfényle. Dans ce cas, le NO_2 sera le produit primaire de chacune de ces réactions.

Mots clés : thionitrate, oxyde nitrique, peroxynitrite, nitrovasodilatateur, nitrate.

[Traduit par la rédaction]

Introduction

Nitric oxide is the subject of substantial, current interest, stimulated by recent evidence suggesting many varied biological roles for NO, extending beyond vasodilation to immune function and neurotransmission (1). Furthermore, there is significant interest in the toxicology and pharmaceutical applications of ·NO and ·NO-releasing agents (2). Interestingly, glyceryl trinitrate (GTN, nitroglycerin), which has been used since 1879 in the treatment of angina pectoris (3), is now widely believed to exert its therapeutic effect through release of nitric oxide (·NO) in vivo (4). Several simple organic nitrates ($RONO_2$) in addition to GTN, including erythrityltetranitrate, isosorbide dinitrate, and isoidide dinitrate, are effective and clinically important vasodilators (5). A substantial body of evidence supports the hypothesis that the vasodilatory activity of these organic nitrates, and indeed of other potent vasodilators such as nitroprusside and molsidomine, is largely the result of activation of guanylate cyclase (GCase) leading to an elevated level of intracellular cGMP, which mediates vascular smooth muscle relaxation. Consideration of pharmacological data has led to the conclusion that activation of GCase by nitrovasodilators is effected by binding of a common proximal ligand to a heme site. There is some consensus in the literature that this ligand is ·NO and that Endothelium Derived Relaxing Factor (EDRF) is in fact ·NO or a nitrosothiol (RSNO) (6). The exact biotransformation mechanism by which GTN is converted to ·NO or nitrosothiol remains unresolved. A sulfhydryl-dependent biotransformation pathway requires mediation by either glutathione-S-transferase (GST) or non-enzymically by a free thiol, possibly cysteine (7). The early, seminal hypothesis of Ignarro et al. (4*a*) proposed that organic nitrates enter the smooth muscle cell where breakdown occurs by an enzymic or non-enzymic process to yield inorganic nitrite. The pathway rests on the intermediacy of inorganic nitrite (NO_2^-), which must be converted to ·NO (eqs. [1]–[3]). Although this pathway was accepted for many years, substantial evidence now exists against the intermediacy of NO_2^- in the biotransformation of GTN (8).

[1] $RONO_2 + R'SH \xrightarrow{R'SH} NO_2^- + R'SSR' + ROH$

[2] $NO_2^- + H^+ \longrightarrow HONO \xrightarrow{-O_2} \cdot NO$

[3] $\cdot NO + R''SH \xrightarrow{-O_2} R''SNO$

The task then is to formulate a chemically reasonable mechanism for the conversion of GTN to ·NO mediated by thiol (RSH). Such a mechanism may be simply drawn as involving the initial formation of a thionitrate ($RSNO_2$), which rearranges to a sulfenyl (RSONO) or sulfinyl nitrite (RS(O)NO) (eqs. [4], [5]). Either of these nitrites may be drawn as forming NO on homolysis. Although a similar mechanism appeared in the pharmacological literature in recent years, no experimental work or computational studies have been reported to support this mechanism (4*c*, 9). Furthermore, it is of interest that this mechanism is analogous to that recently proposed by Koppenol et al. for the rearrangement reaction between peroxynitrous and nitric acids (10). This peroxynitrite rearrangement, itself, is of substantial biological significance, as it is proposed to mediate the biological toxicity of ·NO and superoxide (eqs. [6], [7]).

[4] $RONO_2 + R'SH \rightarrow R'SNO_2 + NO_2^- + H^+$

[5] $R'SNO_2 \rightleftharpoons [R'SONO \rightleftharpoons R'S(O)NO] \rightarrow \cdot NO + R'SO\cdot$

[6] $\cdot NO + \cdot O_2^- \rightarrow OONO^-$

[7] $OONO^- + H^+ \rightarrow HOONO \rightleftharpoons HONO_2$

The molecular orbital calculations reported within examine the thermodynamics, reaction barriers, and reaction profiles for the thionitrate and peroxynitrite rearrangements and the thermodynamics of related competing homolytic processes. The results allow comparison of the two rearrangement processes, examination of the viability of these and competing processes as general reactions of biological significance, and speculation as to modes of catalysis. Activation barriers for the rearrangement processes are calculated at levels up to MP4SDQ/6-31G*//MP2/6-31G* with aqueous solvation energies applied and structures along the reaction coordinate examined by intrinsic reaction coordinate (IRC) and Natural Bond Orbital (NBO) analysis.

Methodology

Isomers of methyl thionitrate and $HSNO_2$ were employed as truncated models of organic thionitrates and their isomers. The energy and structure for each isomer of $MeSNO_2$ was calculated employing full geometry optimization at the following levels: AM1 (11), PM3 (12), HF/6-31G*//HF/6-31G* and MP2/6-31G*//HF/6-31G* using GAUSSIAN 92 (13) on an IBM RISC 6000/355, and SPARTAN 3.0[2] on an SGI Iris Indigo, employing the standard basis sets supplied (14). Energies and structures for the isomers of $HSNO_2$ were calculated employing full geometry optimization at the following levels: PM3,

[2] SPARTAN v.3.0. Wavefunction, Inc. 18401 Von Karman, no. 210, Irvine, CA 92715, U.S.A.

Can. J. Chem. Downloaded from www.nrcresearchpress.com by 80.90.12.36 on 09/08/12
For personal use only.

Can. J. Chem. Downloaded from www.nrcresearchpress.com by 80.90.12.36 on 09/08/12
For personal use only.

HF/6-31G*//HF/6-31G*, MP2/6-31G*//HF/6-31G*, MP2/6-31G*//MP2/6-31G*, and MP4SDQ/6-31G*//MP2/6-31G*. Energies and structures for the isomers of $HONO_2$ were calculated employing full geometry optimization at the following levels: PM3, HF/6-31G*//HF/6-31G*, MP2/6-311G**//HF/6-31G*, MP2/6-31G*//MP2/6-31G*, and MP4SDQ/6-31G*//MP2/6-31G*, with the exception of the rearrangement transition state, which was obtained at levels up to MP2/6-311G**//HF/6-31G*. Energies and structures for free radical species were calculated employing full geometry optimization at the levels UMP2/6-31G*//UMP2/6-31G* and UMP4SDQ/6-31G*//UMP2/6-31G*. All MP calculations use the frozen-core approximation. For selected structures, pre-orthogonal NBO overlap matrices were obtained and second-order perturbational analyses and full NBO analyses performed with GAUSSIAN 92 (15). Mulliken charges and charges derived from the electrostatic potential (CHELP) were recorded for each structure (16). The continuum dielectric solvation models employed for aqueous solvation energies were SM3-PM3 (17) as implemented in SPARTAN and the CDM model of Lim and Chan.[3] These models were applied using geometries obtained at the ab initio level. The identity of stationary points was confirmed by calculation of analytical frequencies at the appropriate level. Thermochemical data were obtained by normal mode analysis and calculation of analytical frequencies (using SPARTAN 4.0 for RMP2 structures. Free energies, enthalpies of reaction (ΔG, ΔH), and free energies of activation ($\Delta G^{\ddagger}$) were calculated from various reactants including a PdV term for dissociative processes. Transition state structures for both rearrangement reactions were located by full optimization using linear synchronous transit geometries (obtained using SPARTAN) as starting points. The character of these transition state structures was confirmed by (*i*) analysis of the normal mode associated with the single imaginary frequency, and (*ii*) IRC analysis (at the RHF/6-31G* level, using GAUSSIAN 92) along the reaction coordinate from transition state to ground states (19). The term ground state is used throughout to indicate stationary points on the calculated potential energy surfaces possessing zero imaginary frequencies. The more correct terms, reactant and product, lead to confusion, since the two rearrangement reactions discussed in this paper are considered in forward and reverse directions. Frequencies and zero point energies (E_{ZP}) are scaled by 0.9 (20). A discussion on the suitability of the 6-31G* basis set in calculations at the MP2 level for methyl nitrate and nitric acid has appeared previously (21).

Results

Thorough exploration of the conformational space for nitric acid isomers has been reported by Hehre and co-workers (21*b*), therefore only one isomer of nitric acid (**1**) and the *cis* (**2c**) and *trans* (**2t**) isomers of peroxynitrous acid were studied herein (Scheme 1, Table 1). However, in the absence of previous work, a thorough study of the isomers of the thionitrates, $HSNO_2$ and CH_3SNO_2, was required. Several rotamers were located of structures corresponding to sulfenyl nitrites (RSONO (**3H**, R = H; **3M**, R = Me)), in addition to conformers of sulfinyl nitrites (RS(O)NO (**4H**, R = H; **4M**, R = Me)) and thionitrate ($RSNO_2$ (**5H**, R = H; **5M**, R = Me)) (Scheme 1, Table 1, Table 2, Fig. 1). The identity of these structures as energy minima and first- or second-order saddle points was confirmed by calculation of analytical frequencies (Table 1, Fig. 1). A greater range of conformers was located for the Me series due to the additional S—C bond rotational barriers. Calculations at the HF/6-31G* level show sulfenyl nitrite (**3**) and thionitrate (**5**) isomers to be of similar energy (Table 1, Fig. 1, Fig. 2), in particular in comparison to their oxygen congeners, nitric and peroxynitrous acid, where the latter is considerably the less stable. Estimation of the influence of aqueous solvation through various solvation approximations demonstrates little difference in energy between the thionitrate and sulfenyl nitrite isomers and their conformers (Table 1, Fig. 1). Thus sulfenyl nitrites are predicted to be of similar stability to their thionitrate isomers in the gas phase and solution. Comparison of energies obtained from geometry optimization at the MP2 level of **3H**, **4H**, and **5H** does not significantly change this conclusion, but at this level the structure of the sulfinyl nitrites (**4H**) is lost upon geometry optimization to yield association complexes of NO with HSO (Tables 1, 2, 5). Again at the higher MP4//MP2 level sulfenyl nitrites and thionitrates are seen to be of similar energy (Tables 1, 5). The experimentally observed frequencies in *tert*-butyl thionitrate associated with NO_2 a stretch, NO_2 s stretch, and NO_2 bend are 1301, 1265, and 831 cm^{-1}, compared with 1322, 1226, and 806 cm^{-1} calculated for $HSONO_2$. The N=O stretch in HSONO is calculated at $\approx$1593 cm^{-1} (**3Hcs**, **3Hca**), suggesting the possibility for experimental detection of transient sulfenyl nitrite species.

We previously calculated structures and energies for all conformers of $HSNO_2$ and CH_3SNO_2 by full geometry optimization using the semi-empirical AM1 and PM3 Hamiltonians and ab initio calculation at the lower RHF/3-21G* level (22). At these lower levels of calculation, geometrical parameters for the isomeric thionitrates and sulfenyl nitrite structures are reproduced reasonably consistently when compared to the data at the higher levels of calculation. However, molecular energy is highly dependent on method and basis set (22). This is illustrated for the $HSNO_2$ series, in which molecular energies at the PM3 level show sulfinyl nitrites as the most stable structures, whereas at the HF/6-31G*//HF/6-31G* sulfenyl nitrites are most stable (Fig. 2). Comparison of these data and those at higher levels of calculation suggest that, for these and related molecules, the minimal level of calculation must include MP2/6-31G* energies, although a lower level of geometry optimization may be accommodated.

Scheme 1.

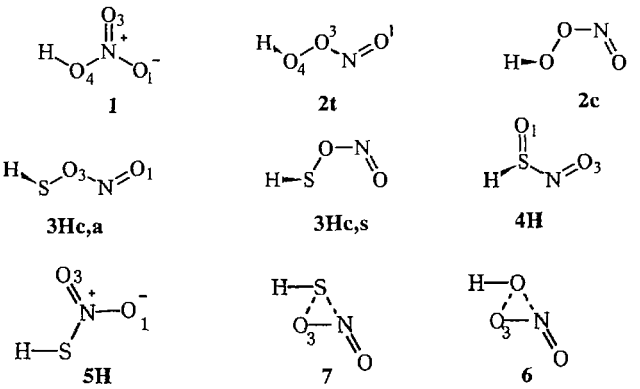

[3] C. Lim and S.K. Chan. Institute of Biomedical Sciences, Academica Sinica, Taipei, Taiwan. See ref. 18.

Table 1. Energies, atomic charges, solvation energies, and thermochemical data used for calculation of reaction free energies and activation parameters for peroxynitrous acid isomers, thionitrate isomers, and free radical species.

	Molecular energies, hartrees					CHELP charges, e^f				Energies, kcal/mol				
	E(MP2/HF)[a]	E(HF/HF)[b]	E(MP2/MP2)[c]	E(MP4/HF)[d]	E(MP4/MP2)[e]	S/O	N	O1	O3	PM3/SM3[g]	CDM aq[h]	Hv[i]	$E_{ZP}{}^i$ scaled	$S_{tot}{}^i$, cal mol^{-1} K^{-1}
1	−280.306 466	−279.444 264	−280.165 222	−280.154 395	−280.162 059	−0.48	0.98	−0.42	−0.52	−4.95	−6.58	17.76	15.73	62.9
2t	−280.241 355	−279.392 624	−280.104 788	−280.105 470	−280.114 903	−0.42	0.17	−0.17	−0.02	−9.84	−3.63	16.44	14.26	64.3
2c	−280.245 153	−279.394 064	−280.109 544	−280.097 715	−280.118 316	−0.36	0.14	−0.08	−0.13	−9.43	−3.45	16.46	14.29	64.5
3Hca	−602.755 007	−602.113 029	−602.765 339	—	−602.783 963	−0.07	0.19	−0.08	−0.19	−8.73	−1.65	13.80	11.65	67.5
3Hcs	−602.758 652	−602.113 810	−602.768 875	—	−602.784 758	−0.03	0.24	−0.09	−0.29	−8.63	−2.21	13.69	11.39	69.4
4H	−602.731 862	−602.079 326	−602.762 885	—	—	0.14	0.06	0.09	−0.04	−20.4	−10.29	13.37	11.27	68.2
5H	−602.769 034	−602.109 326	−602.776 681	—	−602.785 647	−0.06	0.58	−0.34	−0.39	−9.36	−5.40	14.72	12.75	66.2
6	−280.146 333	−279.231 336	—	−280.001 351	—	−0.25	0.19	−0.25	−0.21	−7.09	−4.47	15.12	12.79	67.2
7	−602.676 299	−602.000 729	−602.684 283	—	−602.694 485	0.04	0.33	−0.24	−0.34	−14.55	−4.70	12.90	11.10	66.3
OH	—	—	−75.521 033	—	−75.535 043	—	—	—	—	—	—	4.82	5.35	42.6
OOH	—	—	−150.479 673	—	−150.514 352	—	—	—	—	—	—	8.13	9.04	53.3
HSO	—	—	−473.170 714	—	−473.193 557	—	—	—	—	—	—	6.23	6.94	56.2
HS	—	—	−398.161 942	—	−398.181 733	—	—	—	—	—	—	3.57	3.97	44.5
NO_2	—	—	−204.560 248	—	−204.554 793	—	—	—	—	—	—	5.67	6.36	57.5
NO	—	—	−129.558 900	—	−129.568 250	—	—	—	—	—	—	5.03	5.60	47.6

Note: MP2 level calculations and data on radical species have been published previously.

[a]MP2/6-311G**//HF/6-31G* for **1–2**, **6**; MP2/6-31G*//HF/6-31G* for **3–5**, **7**.

[b]HF/6-31G*//HF/6-31G*.

[c]MP2/6-31G*//MP2/6-31G*.

[d]MP4SDQ/6-31G*//HF/6-31G*.

[e]MP4SDQ/6-31G*//MP2/6-31G*.

[f]For MP2 geometry (**3**, **4**, **5**, **7**); HF geometry (**1**, **2**, **6**).

[g]For MP2 geometry, except **1–2**, **6** HF geometry.

[h]Using HF//HF charges and geometries (**1**, **2**, **6**); MP2//MP2 charges and geometries (**3**, **4**, **5**, **7**).

[i]MP2//MP2 **1–3**, **5**, **7** and free radical species; HF//HF for **4**, **6**; HF//HF data, for other compounds, used to obtain data in Fig. 4*a* is not shown.

Can. J. Chem. Downloaded from www.nrcresearchpress.com by 80.90.12.36 on 09/08/12
For personal use only.

Can. J. Chem. Downloaded from www.nrcresearchpress.com by 80.90.12.36 on 09/08/12
For personal use only.

Table 2. Bond lengths (Å) and bond angles for selected structures optimized at MP2/6-31G* (H series) or HF/6-31G* (Me series).

	d(N—O1)	*d*(N—O3)	*d*(S—O3)	*d*(S—N)	*d*(R—S)	∠(SON)	∠(ONO)	∠(SNO)	∠(RSZ)
HSONO **3Hca**	1.177	1.537	1.691	—	1.346	108.9	108.9	—	98.0
$HSONO_2$ **5H**	1.232	1.231	—	1.804	1.341	—	127.8	118.2	93.0
HS(O)NO **4H**	—	1.182	1.558	2.529	1.370	—	50.6	85.4	105.3
HSONO **3Hcs**	1.167	1.608	1.669	—	1.348	112.6	113.2	—	99.4
MeSONO **3Mcs**	1.151	1.358	1.684	—	1.800	120.4	115.8	—	100.4
MeSONO **3Mca**	1.148	1.372	1.671	—	1.798	113.1	110.4	—	99.6
$MeSNO_2$ **5M**	1.187	1.189	—	1.763	1.802	—	126.7	119.1	100.2
MeS(O)NO **4M**	—	1.159	1.462	1.816	1.797	—	—	112.0	91.6

Fig. 1. Structures, structural labels, and relative molecular energies (kcal/mol) for methyl thionitrate isomers. First- and second-order saddle points (two imaginary frequencies) are indicated by superscripts(‡). Energies are MP2/6-31G*//HF/6-31G* + E_{ZP} with aqueous solvation energies (SM3) indicated in parentheses. The stereochemical labels employed to indicate isomer geometry are applied in an identical fashion to the H series (**3H**, **4H**, **5H**).

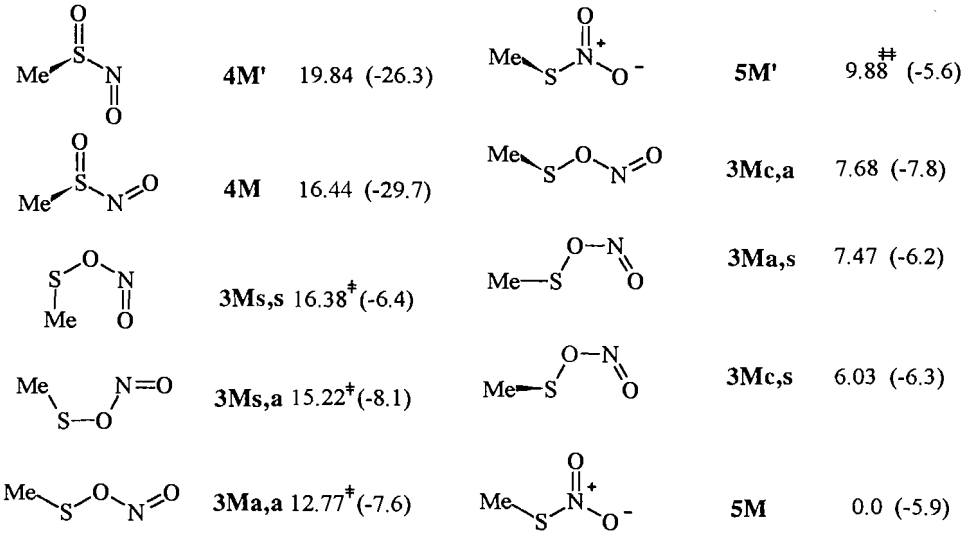

Fig. 2. Relative molecular energies for conformers of **3H**, **4H**, **5H** calculated at semi-empirical and ab initio levels: PM3 + E_{ZP}; HF/6-31G*//HF/6-31G* + E_{ZP}

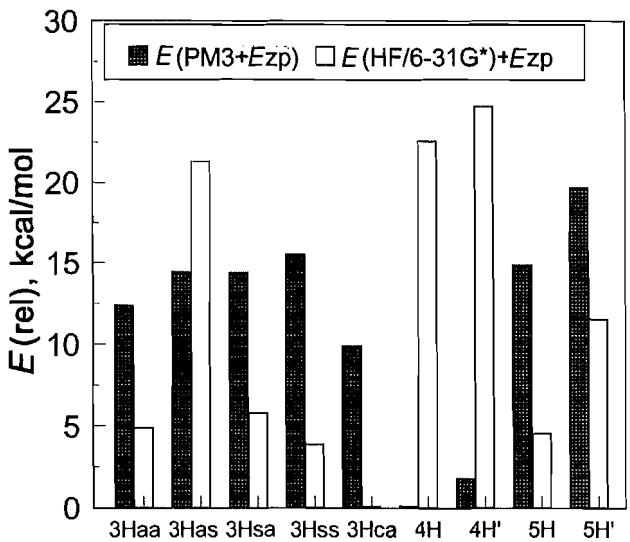

Calculations on NO_2 and other free radical species treated in this present paper have been reported previously (23). The purpose of the calculations reported within is to provide comparative thermodynamic parameters for the homolytic dissociations of the nitric acid and thionitrate isomers. Energies obtained at the UMP4SDQ/6-31G*//UMP2/6-31G* level (Table 1) are used with zero point energy (E_{ZP}) corrections and vibrational data to yield free energy, enthalpy, and entropy of reaction for homolysis (Tables 3–5; Figs. 3, 4, 6, 7). For comparison with these calculations, the experimentally estimated O—O bond energy in peroxynitrous acid is ≈20 kcal/mol (24). Calculated values of $\langle S^2 \rangle$ are in the range 0.76–0.78 (doublets) and reveal little spin contamination. Projected PMP2 energies with annihilation of contaminating spin states deviate from UMP2 energies by 0.8 kcal/mol for thiyl radical to 2.7 kcal/mol for nitric oxide. Extension of electron correlated effects from the MP2 to MP4SDQ level leads to differences in relative molecular energies for radical and other species, modifying quantitative reaction energies but not altering qualitative conclusions made from data calculated at the MP2 level (Tables 1, 4, 5).

The free energy profile for rearrangement of isomers of per-

Can. J. Chem. Downloaded from www.nrcresearchpress.com by 80.90.12.36 on 09/08/12
For personal use only.

Table 3. Relative molecular energies and free energies (at 298 K) for HXNOO species and radical products, calculated at MP4SDQ/6-31G*//MP2/6-31G* level, kcal/mol.

	HOONO **2c**	$HONO_2$ **1**	NO + HOO	NO_2 + HO
ΔE	−22.41	−49.86	0.00	−4.54
$\Delta E(+E_{ZP})$	−22.80	−48.80	0.00	−7.50
ΔG	−9.74	−35.41	0.00	−6.97
	HSONO**3Hcs**	$HSNO_2$ **5H**	HSO + NO	HS + NO_2
ΔE	−30.26	−30.82	−15.86	0.00
$\Delta E(+E_{ZP})$	−29.20	−28.40	−13.60	0.00
ΔG	−17.54	−16.15	−14.38	0.00

Fig. 3. Thermochemical data for (*a*) peroxynitrous acid, nitric acid, and related free radical species; (*b*) thionitrate, sulfenyl nitrite, and related free radical species. Free energies of reaction shown are at the MP4SDQ/6-31G*//MP2/6-31G* level, in kcal/mol (see Table 3).

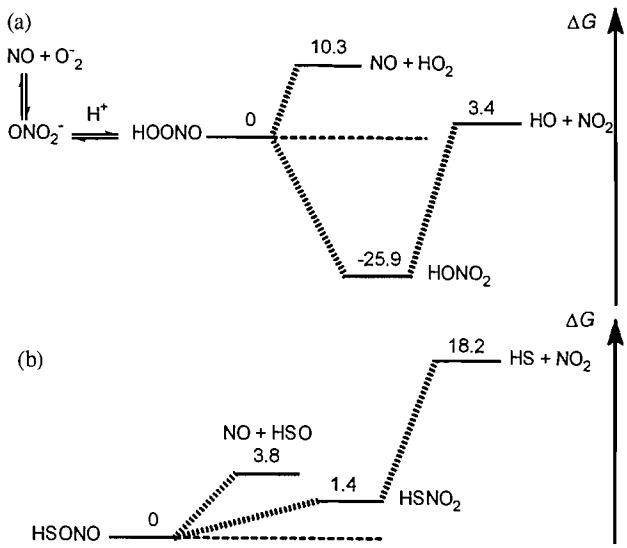

oxynitrous acid with nitric acid was explored by varying several bond angles and bond lengths separately and in combination, approximating the reaction coordinate, at various levels of calculation. However, in each case, the "reaction profile" proceeded to plateau approximately 65–100 kcal/mol above peroxynitrous acid, whereupon "dissociation" of the molecule occurred. A transition state for rearrangement was instead located by geometry optimization from the linear synchronous transit structure generated from high-energy conformers of $HONO_2$ and HOONO (Fig. 5). Clearly, destruction of the O-N-O-O plane is essential for transition state location and indeed reaction. To confirm that this structure corresponded to the transition state for rearrangement, the imaginary frequency corresponding to the reaction coordinate and structures along the intrinsic reaction coordinate were examined. One imaginary frequency was located corresponding to the reaction coordinate (-2143 cm^{-1}, RHF frequency) and the reaction profile generated from the IRC did indeed correspond to rearrangement of peroxynitrous acid to nitric acid (Fig. 6). Examination of structures along the IRC from *trans*-peroxynitrous acid (**2t**) to nitric acid demonstrates clearly the initial rotation about the O—O bond to place HO orthogonal to the plane of the nitro moiety (O-N-O) (Fig. 6). Reaction proceeds by lengthening of the O—O distance and migration of HO towards nitrogen and thence relaxation to the planar nitric acid

Fig. 4. Reaction coordinate – free energy profiles for homolysis and rearrangement. (*a*) Free energy profile for peroxynitrite rearrangement. Relative free energies below line are at MP4SDQ/6-31G*//MP2/6-31G* and those above line (and $\Delta G^{\neq}$) are MP4SDQ/6-31G*//HF/6-31G* + *E*(CDM-aq.sol), in kcal/mol (see Tables 1, 4). (*b*) Free energy profile for thionitrate rearrangement. Relative free energies below line are at MP4SDQ/6-31G*//MP2/6-31G* and those above line (and $\Delta G^{\neq}$) are MP4SDQ/6-31G*//MP2/6-31G* + *E*(CDM-aq.sol.), in kcal/mol (see Tables 1, 5). *E*(CDM-aq.sol.) is derived from CDM data.

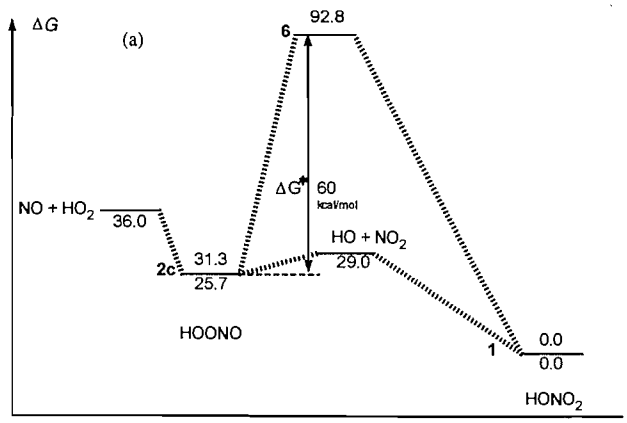

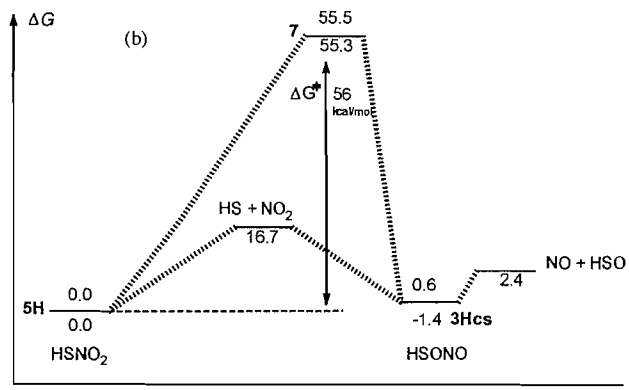

Fig. 5. Structural data for peroxynitrite (**6**) and thionitrate (**7**) rearrangement transition states obtained by optimization at HF/6-31G* and MP2/6-31G*, respectively. See Figs. 6 and 7 for stereochemical representations.

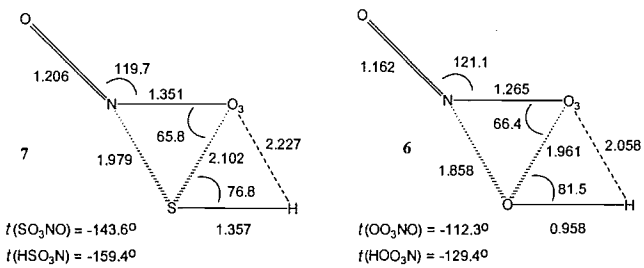

structure. In addition, the proximity of the hydrogen to the oxygen O3 along the entire reaction profile is clear. Although the O3···H distance reaches 2.0 Å and there is likely electrostatic stabilization between these two centres, NBO analysis reveals no significant charge transfer interactions indicative of stronger hydrogen bonding.

The reaction energy profile depicted uses the N— OH distance as the *x*-axis reaction coordinate (Fig. 6). The profile generated using the mass-scaled internal coordinate (not shown) is smooth and more symmetric; however, use of the N—OH distance as the reaction coordinate provides a profile that clearly demonstrates a curious and informative "discontinuity" at d(HO—N) ≈ 2.2 Å. This discontinuity lies at the crossover between the two processes, torsional and scissile. The first process is initial torsional rotation about the bond between the oxygen (O3) and nitrogen in peroxynitrous acid (**2t**), to place HO orthogonal to the O-N-O plane. This structure is close to the transition state for rotation about this O—N bond. The second process, structural deformation of this "rotamer" through O—O bond elongation, migration, and cleavage, is associated with the large energy barrier.

The reaction energy profile for thionitrate rearrangement was located in a similar manner to that for peroxynitrite. IRC energies and structures were calculated at the HF/6-31G*//HF/6-31G* level and reveal a similar reaction pathway to the peroxynitrite rearrangement. However, the dislocation of HS from the nitro plane (O-N-O) is much less marked than that of HO in the related rearrangement. Reaction again proceeds from the *trans* isomer, in this case sulfenyl (**5Hca**), to the planar thionitrate (**3H**). Again the proximity of the hydrogen with the bridging oxygen along the profile is noted and, again, NBO analysis did not provide evidence of a hydrogen bond involving significant charge transfer. Since the energies of the **5Hca** and **5Hcs** conformers are close and dependent on level of calculation, this rearrangement reasonably may proceed equally from either conformer. The structures and energies of the ground and transition state species were reoptimized at the MP4SDQ/6-31G*//MP2/6-31G* level (Fig. 7) with normal mode analysis (Table 1, Table 2, Fig. 5). The imaginary frequency corresponding to the reaction coordinate for **7** is at -886 cm^{-1} (MP2 frequency).

Combination of the thermodynamic data for homolysis with activation energies for rearrangement allows construction of free energy profiles for reactions of peroxynitrite (Fig. 4*a*) and thionitrate (Fig. 4*b*). Relative molecular energies, enthalpies, and free energies have been calculated at a number of different levels with zero point energies (E_{ZP}) and aqueous solvation approximations (Tables 3, 4, and 5). The PM3-SM3, CDM, and other solvation models applied do not yield consistent values for aqueous solvation energies, presumably owing to lack of parameterization for molecules similar to those in this study (Table 1). Cramer and Truhlar state that the PM3-SM3 model may give anomalously positive solvation energy values for nitroaliphatics partly because of unusual atomic charges at N in PM3 level calculations; SM2 performs equally poorly (17). Comparison of PM3 electrostatic charges at atoms with those from MP2 calculations (Table 1) demonstrates the anticipated large positive charges at N in **1H** and **5H** at the PM3 level: +1.81 (HF geometry) and +1.44 (MP2 geometry), respectively. The CDM aqueous solvation model utilizes charges from the ab initio calculations and does indicate PM3-SM3 to yield a relatively positive solvation energy for **1H**, but not for **5H**. In addition, the choice of charge type, electrostatic, Mulliken, or natural, has a significant effect on CDM solvation energies. Clearly, use of the calculated aqueous solvation energies is limited to indication of the magnitude of perturbation of the reaction free energies calculated in the gas phase, on transfer to aqueous solvent (Table 1). For these small neutral molecules this perturbation is small relative to the large activation free energies. At the highest level of calculation employed and with (CDM) solvation energies applied, it can be estimated that the free energy of activation in aqueous solution at 298 K for peroxynitrous acid rearrangement to nitric acid is 60 kcal/mol and that for rearrangement of thionitrate to sulfenyl nitrite is 56 kcal/mol (Fig. 4).

Discussion

GTN biotransformation

Two general pathways for organic nitrate biotransformation may be described, characterized as sulfhydryl dependent and heme dependent (4, 7, 25). There is substantial debate about whether the sulfhydryl-dependent pathway requires glutathione-S-transferase (7*c*). However, it has been conclusively demonstrated that GTN in the presence of specific, simple thiols is capable of activation of guanylate cyclase (7*d*). Therefore, it has been postulated that in the presence of these specific thiols ·NO is a minor product of the reaction of thiol with GTN. The major product of reaction of GTN with all thiols at neutral pH is inorganic nitrite (8). Early hypotheses required generation of ·NO or nitrosothiol from the initial nitrite product (4*a*). In recent years, alternative postulates have appeared widely, involving thionitrate as an intermediate, with further reaction such as (*a*) subsequent reduction to nitrosothiol (for example, ref. 26), or (*b*) concerted rearrangement to sulfinyl and sulfenyl nitrites (4*c*, 9). Indeed, a chemically reasonable mechanism may be drawn, in which thionitrate partitions between thiolysis yielding nitrite ion and concerted rearrangement to the sulfenyl or sulfinyl nitrite (Scheme 2). Support for the subsequent homolytic generation of ·NO may be drawn from (*a*) the reported facile homolytic decomposition of the related sulfenyl and sulfinyl nitrates (27), and (*b*) the relative stability and ease of generation of sulfinyl radicals (28). However, only one paper has appeared, by Oae et al., directed at the reactivity of thionitrates, and this work did not deal with aqueous solution (29). The paper of Oae et al. yields only circumstantial evidence for rearrangement, in that sulfonyl species are observed

Can. J. Chem. Downloaded from www.nrcresearchpress.com by 80.90.12.36 on 09/08/12
For personal use only.

Fig. 6. Reaction energy profile for rearrangement of peroxynitrous acid (**2t**, right-hand side) to nitric acid (**1**, left-hand side), generated from IRC analysis on the HF/6-31G*//HF/6-31G* transition state. The N—OH distance is chosen as the reaction coordinate and *x*-axis. Use of the mass-scaled internal coordinate as reaction coordinate yields a smooth profile without discontinuity. The reaction coordinate shown is chosen to better illustrate the dynamics of rearrangement. Structures along the reaction profile are shown with nitrogen and the terminal oxygen eclipsed as shown by the appended Newman projection.

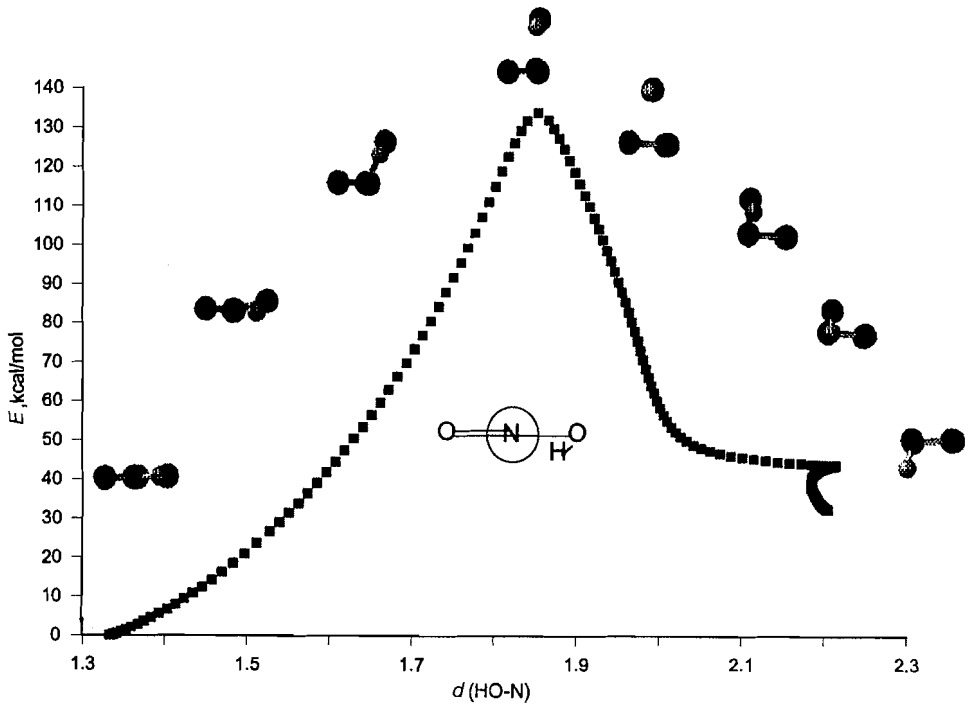

Fig. 7. Reaction energy profile for rearrangement of thionitrate $HSNO_2$ (**5H**, left-hand side) to sulfenyl nitrite HSONO (**3Hca**, right-hand side), generated from IRC analysis on the HF/6-31G*// HF/6-31G* transition state. The S—N distance is chosen as the reaction coordinate and *x*-axis. Structures along the reaction profile are shown with nitrogen and the terminal oxygen eclipsed as shown by the appended Newman projection.

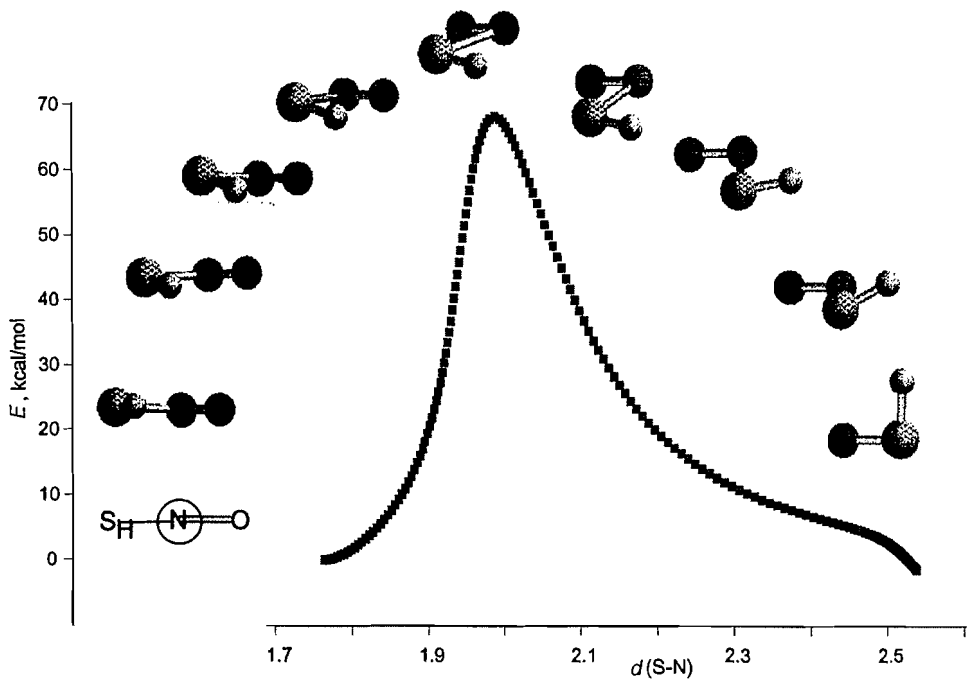

Can. J. Chem. Downloaded from www.nrcresearchpress.com by 80.90.12.36 on 09/08/12
For personal use only.

Table 4. Relative molecular energies and free energies of peroxynitric acid isomers, free radical products, and the rearrangement transition state, kcal/mol.

	G_{rel}(MP2)[a]	ΔE(MP4/MP2)[b]	ΔE(HF/HF)[c]	ΔE(MP2/HF)[d]	ΔE(MP4/HF)[b]	ΔE(MP4/MP2) + E_{ZP}[b]
NO + HOO	52.61	49.86	—	—	—	48.80
NO_2 + HO	36.50	45.32	—	—	—	41.30
$HONO_2$ **1**	0.00	0.00	0.00	0.00	0.00	0.00
HOONO**2t**	36.11	29.59	32.40	40.86	30.70	28.10
HOONO**2c**	33.15	27.445	31.50	38.47	35.60	26.10
HOONO**6**	—	—	133.61	100.48	96.00	—

[a]MP2/6-31G*//MP2/6-31G*.
[b]MP4SDQ/6-31G*//MP2/6-31G*.
[c]HF/6-31G*//HF/6-31G*.
[d]MP2/6-311G**//HF/6-31G*.

Table 5. Relative molecular energies and enthalpies (at 298 K) of thionitrate isomers, free radical products, and the rearrangement transition state, kcal/mol.

	ΔE(MP2/MP2)[a]	ΔE(HF/HF)[b]	ΔE(MP2/HF)[c]	ΔE(MP2/MP2)[a] + E_{ZP}[e]	ΔH(MP4/MP2)[d]	ΔE(MP4/MP2)[d] + E_{ZP}[f]
HSONO **7**	57.98	70.96	58.19	58.14	55.85	56.42
$HSNO_2$ **5H**	0.00	2.81	0.00	0.00	0.80	0.80
$HSNO_2$ **5H′**	6.17	10.40	6.43	7.80		
HSONO**3Haa**	12.40	4.81	13.28	12.89		
HSONO**3Has**	6.37	1.17	6.87	7.52		
HSONO**3Hsa**	12.32	5.51	13.26	12.75		
HSONO**3Hss**	7.92	3.35	8.62	8.63		
HSOBI**3Hca**	7.12	0.49	8.80	7.12	0.61	0.76
HSONO**3Hcs**	4.90	0.00	6.51	5.87	0.00	0.00
HS(O)NO**4H**	8.68	21.64	23.32	10.07		
HS(O)NO**4H′**	23.49	24.03	27.23	24.64		
NO + HSO	29.53	—	—	—	14.04	15.62
NO_2 + HS	34.19	—	—	—	27.88	29.20

[a]MP2/6-31G*//MP2/6-31G*.
[b]HF/6-31G*//HF/6-31G*.
[c]MP2/6-31G*//HF/6-31G*.
[d]MP4SDQ/6-31G*//MP2/6-31G*.
[e]HF on HF geometries.
[f]MP2 on MP2 geometries.

Scheme 2.

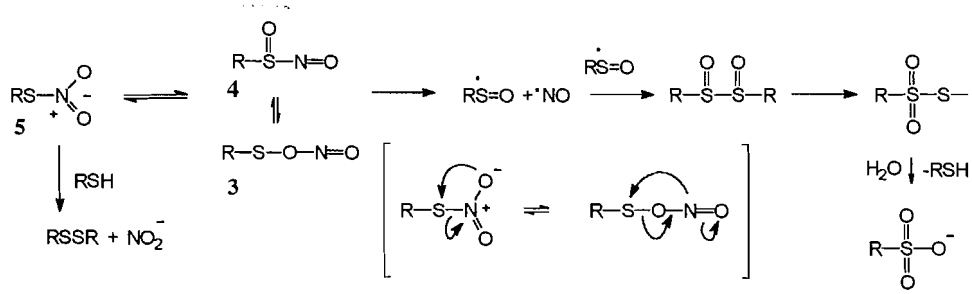

as products of thionitrate decomposition, presumably from sulfinyl radical recombination (30) (Scheme 2). However, we have recently demonstrated ·NO generation from *tert*-butyl thionitrate in aqueous solution at neutral pH and ambient temperature using an ·NO selective Clarke-type electrode (ISO-NO, World Precision Instruments) (Thatcher and Lock, unpublished results). The question to be answered is whether this ·NO may derive from sulfenyl nitrite after rearrangement of the initially formed thionitrate (Scheme 2).

Thionitrates, sulfenyl and sulfinyl nitrites

The few thionitrates studied to date are reactive species, only

Can. J. Chem. Downloaded from www.nrcresearchpress.com by 80.90.12.36 on 09/08/12
For personal use only.

Can. J. Chem. Downloaded from www.nrcresearchpress.com by 80.90.12.36 on 09/08/12
For personal use only.

tertiary alkyl thionitrates having sufficient stability for storage. Sulfinyl and sulfenyl nitrites have not been isolated and similarly can be expected to be high-energy species. Sulfenyl nitrates have been observed to undergo rapid homolysis in aqueous solution to NO_2 and sulfinyl radical, yielding a sulfonothioate product by radical recombination (27). Although the planar thionitrate is the only stable conformer, there are several low-energy sulfenyl nitrite conformers. The calculations on the isomers of $MeSNO_2$ and $HSNO_2$ demonstrate that structures corresponding to thionitrates and sulfenyl nitrites are of similar energy at the highest level of calculation with electron correlation incorporated at the MP2 or MP4SDQ//MP2 levels (Tables 3, 5; Fig. 1). Structures corresponding to sulfinyl nitrites are not stable at the highest level of geometry optimization. The lowest energy sulfenyl nitrite conformers are 1–7 kcal/mol higher in energy than the thionitrate in the H and Me series of compounds, except with inclusion of electron correlation at the MP4SDQ level when the sulfenyl nitrites become marginally more stable (Fig. 1, Table 5). Thus rearrangement of thionitrate to sulfenyl nitrite appears thermodynamically accessible.

Thionitrate rearrangement

The thermodynamic viability of rearrangement of thionitrate to sulfenyl nitrite, in light of competing homolytic fission to NO_2 and thiyl radical, can be judged from the data shown in Figs. 3 and 4 (Tables 2 and 5). Indeed comparison with data for $^{\cdot}NO$ and sulfinyl radical gives information on the homolysis of the sulfenyl nitrite itself. Clearly, rearrangement of thionitrate to sulfenyl nitrite is thermodynamically viable: $\Delta G_0(aq) = 0.6$ kcal/mol. Competitive homolysis to NO_2 and sulfinyl radical reflects a low S—N bond dissociation energy: $\Delta G_0 = 16.7$ kcal/mol (Fig. 4). However, the lower free energy of reaction of sulfenyl nitrite to yield $^{\cdot}NO$ and thiyl radical ($\Delta G_0 = 3.8$ kcal/mol, Fig. 3) suggests that, with a low barrier to rearrangement, this pathway would be viable for $^{\cdot}NO$ generation from the initially formed thionitrate (Scheme 2). It remains to examine the energy barrier of the thionitrate → sulfenyl nitrite rearrangement step.

Inspection of the HOMO and other close-lying occupied orbitals for thionitrate reveals problems in terms of orbital symmetry for a simple concerted reaction via migration of HS along the nitro (ONO) plane. Indeed, the transition state located for the rearrangement reaction has the sulfur dislocated out of the nitro plane, although S, O, N, and O are coplanar in both ground states. If the rearrangement is viewed from the sulfenyl nitrite, reaction is initiated by rotation about the SO—NO and HS—ON bonds followed by S—O bond elongation and migration of sulfur to nitrogen (Fig. 7). The free energy of activation for the rearrangement of thionitrate (**5H**) is 56 kcal/mol in the gas phase at the highest level of calculation. The PM3-SM3 model suggests a small relative stabilization of the transition state from aqueous solvation (Table 1), but the CDM model yields a negligible reduction of the barrier, which remains at 56 kcal/mol at 25°C. This activation barrier is clearly substantial, especially in light of the small bond dissociation energies associated with the S—O and S—N bonds of the ground states. The size of this barrier provoked us to examine the similar peroxynitrite rearrangement. This reaction had been proposed in the literature, supported by MO calculations.

Peroxynitrite rearrangement

The rearrangement mechanism proposed by Koppenol et al. is founded upon comparison of molecular orbital calculations with experimental data (10). A mechanism via homolytic dissociation of peroxynitrous acid and radical recombination of hydroxyl radical and nitrogen dioxide was rejected, partly on the basis of an estimated $\Delta S^{\ddagger}$ of 1–5 cal mol^{-1} K^{-1}, which was argued to be too low for a homolytic reaction. Instead, a concerted rearrangement mechanism was proposed in which peroxynitrous acid undergoes concerted migration of OH from O to N via a high-energy rotamer to yield nitric acid as product. The free energy barrier to rearrangement was presented as 17 kcal/mol (PM3 level). The authors reported location of a "potential transition state" at the PM3 level with ∠OON = 80° and d(O—O) = 1.8 Å (cf. Fig. 5), although no confirmation by normal mode analysis was provided. Subsequent calculations at the RHF/6-31G** level on peroxynitrous acid conformers did not locate any transition states, but a speculative rearrangement mechanism was expounded (31). Previous to this work, the conformational space of peroxynitrous acid had been fully explored at the RHF and MP2/6-31G* levels by Hehre and co-workers (21*b*).

The formation of peroxynitrite species and isomerization in the gas phase are also of interest in atmospheric chemistry. Atkinson et al. proposed that alkyl nitrates formed from reaction of peroxy radicals with nitric oxide might result from rearrangement of the peroxynitrite to the nitrate via a cyclic transition state akin to the transition state located in the present calculations (a flattened analogue of **6** was drawn) (32). However, these workers emphasized a rearrangement proceeding from a vibrationally and chemically excited peroxynitrite, for which a reaction energy profile was drawn. Burkholder et al. suggested a similar rearrangement of peroxynitrous to nitric acid, again via a high-energy form of peroxynitrous acid (24).

The rearrangement pathway mapped by IRC analysis from location of the transition state structure (Figs. 5, 6, and 7) shows similarity to that speculated upon by Koppenol and Klasinc (31). The initial process is rotation about the O—N bond of peroxynitrous acid towards the rotamer with the HO oxygen orthogonal to the nitro (ONO) plane, in simile with the thionitrate rearrangement mechanism. However, in this reaction further dislocation of the oxygen from the nitro plane is required to permit orbital overlap in the transition state (Fig. 6). The underestimation of the barrier for rearrangement in previous work results from the assumption that the initial, simple torsional motion surmounts the barrier to rearrangement. In fact, the very substantial barrier results from the bond lengthening and bending processes associated with migration of oxygen consequent to the initial rotational motion. The free energy of activation for rearrangement of peroxynitrous acid at 25°C with aqueous solvation corrections applied is 60 kcal/mol. The substantial hypothetical barrier for rearrangement of nitric acid to peroxynitrous acid ($\Delta G^{\ddagger}$ (aq.) = 93 kcal/mol) allows comparison with the rearrangement of thionitrate to sulfenyl nitrite ($\Delta G^{\ddagger}$ (aq.) = 56 kcal/mol). The higher barrier is compatible with the more extreme geometrical distortion required to reach the transition state in the peroxynitrite rearrangement.

Rearrangement versus homolysis

It has been clearly demonstrated experimentally that peroxynitrite in aqueous solution isomerizes to nitrate via peroxynitrous acid (33). Equally, it can be simply demonstrated that

Can. J. Chem. Downloaded from www.nrcresearchpress.com by 80.90.12.36 on 09/08/12
For personal use only.

alkyl thionitrate spontaneously yields ·NO in aqueous solution. However, the substantial barriers to reaction, calculated for the concerted rearrangement processes involved, strongly argue against such concerted rearrangements mediating the observed experimental phenomena. The free energies of reaction associated with the competitive homolytic processes are calculated to be low: ≈17 kcal/mol for dissociation of thionitrate to NO_2 and thiyl radical; and ≈3 kcal/mol for dissociation of peroxynitrous acid to NO_2 and hydroxyl radical. Rearrangement via homolysis and radical recombination appears a more likely pathway for both reactions. Of course, the concerted rearrangement processes may be susceptible to catalysis. Indeed, the limited range of thiols, which in the presence of GTN are able to activate GCase, all possess a β-carboxylate group; for example, thiosalicylic acid (*7a*, *d*). The ability of a β-carboxylate or carboxylic acid group to participate in intramolecular base, nucleophilic, and acid catalysis is well documented. We are currently exploring potential catalytic pathways experimentally and through further MO calculations. The present calculations cannot rule out a nonconcerted ionic or diradical rearrangement. However, the low free energy for homolysis of the S—O bond of thionitrate coupled with that for dissociation of sulfenyl nitrite to ·NO suggests that a homolysis–recombination pathway is more reasonable (eq. [8], Fig. 4). If separation and diffusion of the initial geminate pair competes with recombination, NO_2 may be released before ·NO in both thionitrate and peroxynitrite rearrangements. The question then to be addressed is whether NO_2 may mediate some of the biological activity of organic nitrates and toxicity of ·NO.

[8] $R'SNO_2 \rightarrow \{R'S^{\cdot}\ {}^{\cdot}NO_2\} \rightarrow R'SONO \rightarrow R'SO^{\cdot} + {}^{\cdot}NO$

Conclusions

1. Structures representing thionitrates and conformers of sulfenyl nitrites are of similar energy at the higher levels of calculation employed, including electron correlation at the MP4SDQ//MP2 and MP2 levels. Structures corresponding to sulfinyl nitrites do not represent stable equilibrium geometries at the MP2 level of calculation.
2. Free energies of reaction for homolysis of thionitrates, sulfenyl nitrites, and peroxynitrous acid, at 298 K, all lie below 17 kcal/mol. The free energy for homolysis of nitric acid is 29 kcal/mol.
3. Structural reorganization to reach the transition states for concerted rearrangement of thionitrate to sulfenyl nitrite and peroxynitrous acid to nitric acid requires destruction of the ONOX plane of the ground states (X = S, O).
4. The energy barriers for concerted rearrangement of peroxynitrous acid and thionitrate are substantial: $\Delta G^{\ddagger}$ (aq.) = 60 kcal/mol and 56 kcal/mol, respectively.
5. The small energies of homolysis and the large activation barriers to concerted rearrangement suggest that the most reasonable mechanism for rearrangement involves homolysis followed by radical recombination. In this case, NO_2 is an initial product of reaction.

Acknowledgments

This work was supported by the Heart and Stroke Foundation of Ontario (Grant no. A2259) and Queen's University. Felicity Wowk, Jen Barbour, Jodi Lock, and Christine Robb are thanked for preliminary calculations.

References

1. J.S. Stamler, D.J. Singel, and J. Loscalzo. Science, **258**, 1898 (1992); H-J Galla. Angew. Chem. Int. Ed. Engl. **23**, 378 (1993); T.G. Traylor and V.S. Sharma. Biochemistry, **31**, 2847 (1992).
2. D.A. Wink, R.W. Nims, J.F. Darbyshire, D. Christodoulou, I. Hanbauer, G.W. Cox, F. Laval, J. Laval, J.A. Cook, M.C. Krishna, W.G. DeGraff, and J.B. Mitchell. Chem. Res. Toxicol. **7**, 519 (1994); J.A. Hrabie, J.R. Klose, D.A. Wink, and L.K. Keefer. J. Org. Chem. **58**, 1472 (1993); S.A. Lipton, Y-B Choi, Z-H Pan, S.Z. Lei, H-S. V. Chen, N.J. Sucher, J. Loscalzo, D.J. Singel, and J.S. Stamler. Nature, **364**, 626 (1993); S. Tamir, R.S. Lewis, TdeR. Walker, W.M. Deen, J.S. Wishnok, and S.R. Tannenbaum. Chem. Res. Toxicol. **6**, 895 (1993).
3. J. Abrams. Am. J. Cardiol. pp. 1B–3B (1992), and following articles.
4. (*a*) L.J. Ignarro, H. Lippton, J.C. Edwards, W.H. Baricos, A.L. Hyman, P.J. Kadowitz, and C.A. Grueter. J. Pharmacol. Exp. Ther. **218**, 739 (1981); (*b*) G.S. Marks. J. Physiol. Pharmacol. **65**, 1111 (1987); (*c*) R.A. Yeates. Arzneim-Forsch. **42**, 1314 (1992).
5. B.M. Bennett. Trends Pharmacol. Sci. **15**, 245 (1994); W.R. Kukovetz and S. Holzman. Eur. J. Clin. Pharmacol. **38**, S9 (1990).
6. M. Feelisch, M. te Poel, R. Zamora, A. Deussen, and S. Moncada. Nature, **368**, 62 (1994); S. Moncada, R.M.J. Palmer, and E.A. Higgs. Pharmacol. Rev. **43**, 109 (1991).
7. (*a*) M. Feelisch and E. Noack. Eur. J. Pharmacol. **142**, 465 (1987); (*b*) R.A. Yeates, M. Schmid, and M. Leitold. Biochem. Pharmacol. **38**, 1749 (1989); (*c*) M.A. Kurz, T.D. Boyer, R. Whalen, T.E. Peterson, and D.G. Harrison. Biochem. J. **292**, 545 (1993); (*d*) S. Chong and H-L. Fung. Biochem. Pharmacol. **42**, 1433 (1991).
8. C. Romanin and W.R. Kukovetz. J. Mol. Cell Cardiol. **20**, 389 (1988).
9. M. Feelisch. J. Cardiovasc. Pharmacol. **17** (S3), 25 (1991).
10. W.H. Koppenol, J.J. Moreno, W.A. Pryor, H. Ischiropoulos, and J.S. Beckman. Chem. Res. Toxicol. **5**, 834 (1992).
11. M.J.S. Dewar, E.G. Zoebisch, E.F. Healy, and J.J.P. Stewart. J. Am. Chem. Soc. **107**, 3902 (1985).
12. J.J.P. Stewart. J. Comput. Chem. **10**, 209 (1989); **10**, 221 (1989).
13. M.J. Frisch, G.W. Trucks, M. Head-Gordon, P.M.W. Gill, M.W. Wong, J.B. Foresman, B.G. Johnson, H.B. Schlegel, M.A. Robb, E.S. Replogle, R. Gomperts, J.L. Andes, K. Raghavachari, J.S. Binkley, C. Gonzalez, R.L. Martin, and D.J. GAUSSIAN 92, Revision C, Gaussian Inc., Pittsburgh, Pa. 1992.
14. M.M. Francl, W.J. Pietro, W.J. Hehre, J.S. Binkley, M.S. Gordon, D.J. DeFrees, and J.A. Pople. J. Am. Chem. Soc. **104**, 5039 (1982); R. Krishnan, M.J. Frisch, and J.A. Pople. J. Chem. Phys. **72**, 4244 (1980); J.S. Binkley and J.A. Pople. Int. J. Quantum. Chem. **9**, 229 (1975).
15. J.P. Foster and F. Weinhold. J. Am. Chem. Soc. **102**, 7211 (1980); A.E. Reed and F. Weinhold. J. Chem. Phys. **78**, 4066 (1983); A.E. Reed, R.B. Weinstock, and F. Weinhold. J. Chem. Phys. **83**, 735 (1985); J.E. Carpenter and F. Weinhold. J. Mol. Struct. (Theochem), **169**, 41 (1988).
16. L.E. Chirlian and M.M. Francl. J. Comput. Chem. **8**, 894 (1987).
17. C.J. Cramer and D.G. Truhlar. J. Comput. Chem. **13**, 1089, (1992); J. Comput.-Aided Mol. Des. **6**, 629 (1992).
18. S.L. Chan and C. Lim. J. Phys. Chem. **98**, 692 (1994).

19. C. Gonzalez and H.B. Schlegel. J. Phys. Chem. **90**, 2154 (1989).
20. W.J. Hehre, L. Radom, P.v.R. Schleyer, and J.A. Pople. Ab initio molecular orbital theory. John Wiley & Sons, Toronto. 1986.
21. (*a*) T.J. Lee and J.E. Rice. J. Am. Chem. Soc. **114**, 8247 (1992); (*b*) M.P. McGrath, M.M. Francl, F.S. Rowland, and W.J. Hehre. J. Phys. Chem. **92**, 5353 (1988).
22. D.R. Cameron. Ph.D. Thesis, Queen's University, 1994.
23. D. Yu, A. Rauk, and D.A. Armstrong. J. Phys. Chem. **96**, 6031 (1992).
24. J.B. Burkholder, P.D. Hammer, and C.J. Howard. J. Phys. Chem. **91**, 2136 (1987); D.J. Benton and P. Moore. J. Chem. Soc. A, 3179 (1970).
25. B.M. Bennett, B.T. McDonald, and M.J. St James. J. Pharmacol. Exp. Ther. **261**, 716 (1992); H. Schroder. J. Pharmacol. Exp. Ther. **262**, 298 (1992).
26. E. Noack and M. Feelisch. Basic Res. Cardiol. **86** (S2), 37 (1991).
27. Y.J. Park, H.H. Shin, and Y.H. Kim. Chem. Lett. 1483 (1992); R.M. Toppin and N. Kharasch. J. Org. Chem. **27**, 4353 (1962); S. Oae and K. Ikura. J. Chem. Soc. Jpn. **38**, 58 (1965).
28. C. Chatgilialoglu. *In* The chemistry of sulfones and sulfoxides. *Edited by* S. Patai and C.J.M. Rapaport. Wiley, New York. 1988. Chap. 24.
29. S. Oae, K. Shinhama, K. Fujimori, and H.K. Yong. Bull. Chem. Soc. Jpn. **53**, 775 (1980).
30. P.L. Folkins and D.N. Harpp. J. Am. Chem. Soc. **113**, 8998 (1991), and references therein.
31. W.H. Koppenol and L. Klasinc. Int. J. Quantum Chem. **S20**, 1 (1993).
32. R. Atkinson, W.P.L. Carter, and A.M. Winer. J. Phys. Chem. **87**, 2012 (1983).
33. M. von Gretzel, A. Henglein, and S. Taniguchi. Ber. Bunsen-Ges. Phys. Chem. **74**, 292 (1970).

Can. J. Chem. Downloaded from www.nrcresearchpress.com by 80.90.12.36 on 09/08/12
For personal use only.

Structure–sweetness relationships for fructose analogs. Part III. 3-Deoxy-D-*erythro*-hexulose (3-deoxy-D-fructose): composition in solution and evaluation of sweetness

Walter A. Szarek, Robert J. Rafka, Te-Fang Yang, and Olivier R. Martin

Abstract: As part of continuing studies on the structural features responsible for the intense sweetness of D-fructose, 3-deoxy-D-*erythro*-hexulose (3-deoxy-D-fructose, **1**) was prepared, its solution composition was determined, and its taste was evaluated. In aqueous solution, 3-deoxy-D-fructose exists as a complex mixture of five tautomeric forms in which the β-D-pyranose form is preponderant (52.5% at 22°C) and the α-D-pyranose form is the least abundant (5%). Quite remarkable is the behavior of the open-chain *keto* form of **1**: its content increases from 7.5% at 22°C, to 36% at 82°C, and to 47% at 97°C, making this form the preponderant one at high temperatures. 3-Deoxy-D-fructose was found to be sweet, albeit probably not as sweet as D-fructose. The hydroxyl group at C-3 is thus not an essential function of the glycophore of D-fructose. The significance of this result is discussed in relation to the evidence already available and the divergent theories that have been proposed to explain the origin of the sweet taste of D-fructose.

Key words: 3-deoxy-D-*erythro*-hexulose (3-deoxy-D-fructose), sweetness, solution composition.

Résumé : La poursuite d'études sur les attributs structuraux responsables pour la douceur intense du D-fructose nous a conduit à préparer le 3-désoxy-D-*érythro*-hexulose (3-désoxy-D-fructose, **1**), à déterminer sa composition en solution et à évaluer son goût. En solution aqueuse, le 3-désoxy-D-fructose existe sous forme d'un mélange complexe de cinq formes tautomères dans lequel la forme β-D-pyranose est prépondérante (52.5% à 22°C) et la forme α-D-pyranose est la moins abondante (5%). Le comportement de la forme à chaîne ouverte *céto* est tout-à-fait remarquable : présente à 7.5% à 22°C, sa concentration augmente à 36% à 82°C et à 47% à 97°C, ce qui en fait la forme la plus abondante à haute température. Le 3-désoxy-D-fructose est doux, cependant probablement pas aussi doux que le D-fructose. Le groupement hydroxyle en C-3 apparaît ainsi ne pas être une fonction essentielle du glycophore du D-fructose. L'importance de ce résultat est discuté en relation avec les données déjà disponibles et les théories divergentes qui ont été proposées pour expliquer l'origine de la douceur du D-fructose.

Mots clés : 3-désoxy-D-*érythro*-hexulose (3-désoxy-D-fructose), caractère sucré, composition d'une solution.

Introduction

The origin of the intense sweetness of D-fructose, the sweetest of the natural sugars (1), has been the object of much debate (2). While the lipophilic component X of the presumed tripartite AH–B–X glycophore (3) can be attributed to one of the methylene groups (2), the assignment of the hydrogen bond donor (AH) and acceptor (B)-couple remains unresolved. As part of continuing studies on deoxy ketohexoses designed to probe the role of individual hydroxyl groups in the glycophore of D-fructose, we have already shown (4) that the 5-OH group is not essential for the sweet response since 5-deoxy-D-*threo*-hexulose (5-deoxy-D-fructose) is nearly as sweet as D-fructose. We have now completed studies on 3- and 4-deoxy-D-fructose (3-deoxy-D-*erythro*- and 4-deoxy-D-*threo*-hexulose). We report, in this article, the composition of 3-deoxy-D-*erythro*-hexulose (**1**) in solution and an evaluation of its sweet taste. The properties of 4-deoxy-D-*threo*-hexulose will be reported separately.

A brief summary of the attempts to rationalize the sweet taste of D-fructose will serve to place our results in proper perspective. In early studies, Shallenberger (1, 5) had proposed that the anomeric hydroxyl group (HO-2) and the oxygen atom at C-1 (O-1) of β-D-fructopyranose (**2**), the major form of D-fructose in solution (6), constituted the AH–B site of the glycophore. This assignment was supported, in particular, by

Received May 4, 1995.

W.A. Szarek[1] **and R.J. Rafka.** Department of Chemistry, Queen's University, Kingston, ON K7L 3N6, Canada.
T.-F. Yang and O.R. Martin. Department of Chemistry, State University of New York, Binghamton, NY 13902-6000, U.S.A.

[1] Author to whom correspondence may be addressed. Telephone: (613) 545-2643. Fax: (613) 545-6532.

Can. J. Chem. Downloaded from www.nrcresearchpress.com by 46.23.64.124 on 09/08/12
For personal use only.

Can. J. Chem. Downloaded from www.nrcresearchpress.com by 46.23.64.124 on 09/08/12
For personal use only.

the reduced sweetness of analogs **3** (β-D-arabinose) and **4** (1,5-anhydro-D-mannitol) lacking the CH_2OH and the 2-OH groups, respectively (7). This model does not take into consideration the other hydroxyl groups of the molecule and does not explain the considerable difference in sweetness between D-fructose and its C-5 epimer, L-sorbose: as it exists almost exclusively as α-L-sorbopyranose **5** in solution (6), this ketose

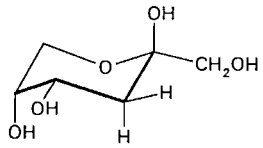

1

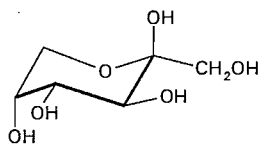

2

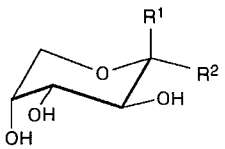

3 $R^1 = OH, R^2 = H$
4 $R^1 = H, R^2 = CH_2OH$

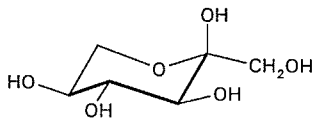

5

is, structurally, very closely related to β-D-fructopyranose; it is, however, nearly devoid of sweet taste. The molecular properties of the two ketoses have been compared using IR spectral data (8) and by means of theoretical calculations (9–11), in attempts to explain this difference of sweetness. In one of these attempts (10), the results have suggested that the assignment of the AH–B couple in β-D-fructopyranose should be reversed, making HO-1 the hydrogen bond donor and O-2 the acceptor. Interestingly, the examination of IR data led Mathlouthi and Portmann (12) to propose the same revised assignment. In 1988, on the basis of intensity–time studies of the sweetness of sugars, Birch et al. (13, 14) suggested that the anomeric center may play no direct role and that the AH–B component of the glycophore was the 3,4-α-glycol system. Very recently, Lichtenthaler and Immel (2) have defined and calculated molecular hydrophobicity potential profiles for sugars, which provide a global description of the hydrophilic and hydrophobic regions in the molecule. This approach seems to lend support to Birch's proposal since it was found that the zone of greatest hydrophilicity in β-D-fructopyranose was centered around the 4-OH group, thus possibly making this group essential for sweetness. This is also consistent with our prediction that the O-4 atom would be the most attractive site for protonation (9). Of relevance are also the observations that both the 6-thio- (15) and the 6-carba- (16) analogs of β-D-fructopyranose are intensely sweet, presumably as a result of the expansion of the hydrophobic region of the molecule (2). Our studies on 3- and 4-deoxy-D-fructose were expected to contribute further evidence towards a better understanding of the origin of the sweetness of D-fructose.

Results and discussion

Synthesis

3-Deoxy-D-fructose (**1**) is not available from natural sources, although its presence has been detected in caramel mixtures by glc analysis (17); an enzyme catalyzing the reduction of 3-deoxyglucosone to **1** has been recently isolated from porcine liver (18). The first synthesis of **1** was reported by Kuhn et al. (19) (multistep synthesis from D-glucosamine). Compound **1** has also been obtained by way of the Perkow reaction of 1,3,4,5,6-penta-*O*-acetyl-*keto*-D-fructose with trimethyl phosphite (20) and by way of isomerization reactions of 3-deoxy-D-*arabino*- or *ribo*-hexoses (21). However, radical deoxygenation procedures make this deoxy ketose readily available: treatment of the 3-*O*-(imidazolylthiocarbonyl) derivative of 1,2:4,5-di-*O*-isopropylidene-D-fructopyranose (**6**) (22) with tributyltin hydride, as described by Rasmussen et al. (23), afforded, after 20 min at reflux temperature in toluene, compound **7** in 87% yield (lit. (23): 65% after a reaction time of several hours). 3-Deoxy-D-fructose (**1**) was obtained by deacetonation of **7** in 2:1 (v/v) acetone–water in the presence of an acidic ion-exchange resin, purification by chromatography, and recrystallization from hot ethanol (overall yield from **6**: 68%). During the course of the present studies, the synthesis of **1** by essentially the same procedure was reported by Dills (24).

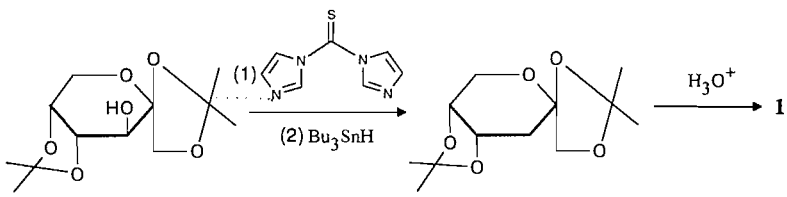

6 **7**

Composition of 1 in solution

Upon dissolution of a solid sample in D_2O at room temperature, 3-deoxy-D-fructose (**1**) rapidly equilibrates into a mixture in which five different forms are clearly discernible (^1H NMR, ^{13}C NMR). Integration of the signals of the protons at the deoxy position indicates a composition (Table 1) reminiscent of that of D-fructose: the β-pyranose form is predominant (52.5%), the α- and β-furanose forms are relatively abundant (20% and 15%), and the α-pyranose form is minor (5%). The major difference with D-fructose is a much larger proportion of *keto* form (7.5%): that the removal of a secondary substituent from D-fructose increases the content of acyclic form is consistent with the well-known influence of the number of substituents on the position of the tautomeric equilibrium (25). While the *keto* form is hardly detectable in D-fructose (0.5–0.8%) (26), its highly deoxygenated analogs exist completely (e.g., 6-hydroxy-2-hexanone (27)) or largely (e.g., 1,6-dihydroxy-2-hexanone (28)) in the open-chain form in aqueous solution. It is remarkable that we had not observed the *keto* form in the spectra of the 5-deoxy isomer of **1**, namely 5-deoxy-D-*threo*-hexulose, in our previous studies of this compound (4). This can be explained by the fact that the β-pyranose form of 5-

Table 1. Equilibrium composition of **1** at room temperature (22°C).[a,b]

Solvent	β-Pyranose (%)	α-Pyranose (%)	β-Furanose (%)	α-Furanose (%)	*keto* form (%)
D_2O	52.5	5	15	20	7.5
CD_3OD	41	10	16	24	9

[a]By integration of ^1H NMR signals.

[b]For comparison, the composition of D-fructose at 31°C in D_2O is the following (25): β*p*, 65%; α*p*, 2.5%; β*f*, 25%; α*f*, 6.5%; *k*, 0.8%.

deoxy-D-fructose is especially favorable (no axial substituents) and it is the only one to be actually detected (see also ref. 29). The stability of this tautomeric form is probably also responsible, in part, for the unusual behavior of 5-deoxy-D-fructose and its aldose isomer (5-deoxy-D-glucose) towards glucose isomerase (aldose → ketose isomerization exclusively) (29). The equilibrium composition of **1** in CD_3OD has also been determined and the results are reported in Table 1.

The NMR signals of the two H-3 protons of the different forms of **1** in solution (D_2O as well as CD_3OD) occur in a wide chemical-shift range (1.75–2.75 ppm in D_2O) with relatively little overlap and therefore provide a great deal of structural information. The protons at C-3 of the major, β-pyranose form (**1**β*p*) are nearly equivalent in D_2O and form a higher-order spin system; however, the ^1H NMR parameters of **1**β*p* can be readily obtained from the spectrum of **1** in CD_3OD, in which the equilibration of **1** is slower than in D_2O (~2 h) and the signals of H-3e and H-3a are well separated. The coupling constants for **1**β*p* (Table 2) clearly indicate that H-4 is axial and H-5 equatorial and, therefore, that the β-pyranose form of **1** adopts the same $^2C_5$ conformation as β-D-fructopyranose in solution (6). The ^1H NMR parameters detectable for the minor α-pyranose tautomer (**1**α*p*) suggest that its conformation is the alternate $^5C_2$ chair form. Thus, both anomers adopt the conformation in which the anomeric OH group is axial, a situation that prevails also for most 2-hexuloses (6): these conformations are predicted, on the basis of simple relative free energy calculations (30), to be the more stable ones (**1**β*p*: $^2C_5$, 1.7; $^5C_2$, 5.05. **1**α*p*: $^2C_5$, 3.45; $^5C_2$, 2.75 kcal/mol; note: because of the absence of an OH group at C-3, the contribution of the anomeric effect was taken as 0.85 kcal/mol).

The proportion of furanose forms in an equilibrated solution of **1** is similar to that observed in D-fructose; however, as a result of the absence of a substituent at C-3, which suppresses *gauche* interactions with the substituents at the anomeric carbon, the ratio of anomers is much closer to 1, with the α-anomer being predominant (α/β ratio: ~1.3 in **1**, ~0.25 in D-fructose). The absence of significant differences in the ^{13}C

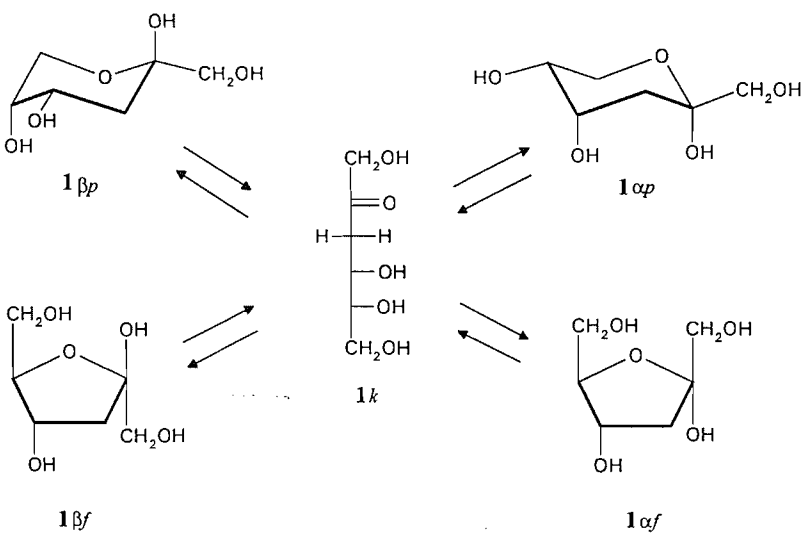

NMR parameters of **1**α*f* and **1**β*f* (e.g., δ C-2 = 106.14 and 106.47 ppm) and in the H,H-coupling constants makes the assignment of the anomeric configuration of the furanose forms difficult. However, it is noted that the difference in chemical shift between the two protons at C-3 (Δδ (H-3A,3B)) is much larger (0.5 ppm) in one anomer than in the other (0.12 ppm), the average chemical shift being about the same (Table 2). The large difference was attributed to the anomer (α) in which *one* of the two H-3's is *cis* with respect to two oxygen atoms, and the small difference to the anomer (β) in which each H-3 is *cis* with respect to one oxygen atom. This assignment is entirely corroborated by the data reported (31) for the methyl furanosides of 2-deoxy-DL-*erythro*-pentose (Δδ (H-3A,3B): α-anomer, 0.48; β-anomer, 0.12 ppm).

The study of the composition of **1** in aqueous solution at variable temperature revealed an unusual behavior (Table 3): while the proportion of α,β-furanose and α-pyranose forms remained roughly constant as the temperature of the solution was raised, the content of *keto* form increased sharply at the expense of the β-pyranose tautomer. The *keto* form actually became the major tautomeric form at temperatures above 80°C! This behavior is in contrast with that of D-fructose (6,

Can. J. Chem. Downloaded from www.nrcresearchpress.com by 46.23.64.124 on 09/08/12
For personal use only.

Table 2. ^{1}H NMR parameters for **1** at room temperature (22°C).

	CD_3OD^a	D_2O^b				
	β-Pyranose	β-Pyranose	α-Pyranose	β-Furanose	α-Furanose	*keto* form
H-1A	3.41 AB	3.49 s	3.46 AB	3.58 s	3.54 s	4.38 AB
H-1B						
H-3A	1.70[c] dd	1.80[e]	1.91 dd	2.15 dd	1.925 dd	2.65 dd
H-3B	1.89[d] t		1.98 dd	2.27 dd	2.425 dd	2.745 dd
H-4	~4.0 ddd	4.09 ddd		4.41 ~q	4.26 dt	
H-5	3.70 br s	3.85 br s		3.93 ~q	4.15 ~q	
H-6A	~3.69 dd	3.74 dd		3.65 dd	3.505 dd	
H-6B	4.0 d	4.01 dd		3.75 dd	3.71 dd	
$J_{1A,1B}$	11.2		11.8			19.3
$J_{3A,3B}$	12.6	13[e]	14.8	13.6	14.2	16.2
$J_{3A,4}$	5.0	5.3[e]	~4	7.2	4.0	9.1
$J_{3B,4}$	12	12[e]	5.1	7.2	7.4	3.8
$J_{4,5}$	3.0	3.2		5.6	4.2	
$J_{5,6A}$	2.2	2.2		6.2	5.5	
$J_{5,6B}$	0	1.2		3.8	3.6	
$J_{6A,6B}$	11.0	12.8		12.1	12.3	

[a]Spectrum in CD_3OD: immediately after dissolution of the solid sample; β-pyranose form >90%. Internal standard: δ HCD_2OD 3.31. Partial data for other forms present in an equilibrated solution of **1** in CD_3OD are given in the experimental section.

[b]Spectrum in D_2O: equilibrated solution (24 h). Internal standard: δ CH_3CN 2.05.

[c]H-3 equatorial. Also exhibits $^4J_{3e,5}$ = 0.7 Hz.

[d]H-3 axial.

[e]Strongly coupled system with Δδ = 3 Hz. The coupling constants have been determined by simulation of the H-3A,3B,4 system; all the lines of the simulated system matched the observed lines within ±0.1 Hz.

Table 3. Effect of temperature on the composition of **1** in D_2O.[a]

T (°C)	β-Pyranose (%)	α-Pyranose (%)	β-Furanose (%)	α-Furanose (%)	*keto* form (%)
4	60	5	13	19	3
22	52.5	5	15	20	7.5
52	41	6	15	21	17
62	28	5	19	23	25
82	20	4	18	22	36
97[b]	15	7	13	17	47

[a]Compositions at temperatures different from room temperature (22°C) are less accurate than the composition at 22°C.

[b]Sample was recovered unchanged after having been heated at this temperature.

26, 32) and other ketoses (6) for which the decrease of the β-pyranose form at higher temperatures is usually accompanied by an increase of the furanose forms. As expected on the basis of entropic factors, the *keto* form of D-fructose also increases with temperature (26, 33) (a 12.5-fold increase of its concentration between 30 and 80°C has been recently reported (34)), but, because of the small initial concentration, its content remains below 10%. Interestingly, a similar temperature dependence has been observed by Angyal et al. (35) for 1-deoxy-D-fructose (6% *keto* form at 37°C, 26% at 85°C), the β-pyranose form remaining, however, preponderant, even at 85°C. The presence of a large amount of *keto* form at high temperature in 1- and 3-deoxy-D-fructose is probably attributable primarily to electronic factors that affect the reactivity of that form: the removal of either vicinal hydroxy group indeed decreases the reactivity of the carbonyl function and thus

Can. J. Chem. Downloaded from www.nrcresearchpress.com by 46.23.64.124 on 09/08/12
For personal use only.

Can. J. Chem. Downloaded from www.nrcresearchpress.com by 46.23.64.124 on 09/08/12
For personal use only.

makes the *keto* form energetically comparable to the other tautomeric forms.

Evaluation of sweetness of 1

The sweetness of 5% and 10% (w/v) aqueous solutions of 3-deoxy-D-fructose was evaluated by three trained panelists[2] who compared, in two sessions, the taste of these two solutions with that of recently prepared (0.5–1 h) 2, 5, and 10% solutions of D-fructose, 5 and 10% solutions of sucrose, and aged tap water. The 5% solution of 3-deoxy-D-fructose was judged to be less sweet than the 5% sucrose solution, with two panelists noting a slightly bitter aftertaste. At higher concentration (10%), the solution was judged to be sweeter than a 5% solution of sucrose, although less sweet than a 10% solution of D-fructose or sucrose with, again, some additional taste sensations.

Thus, 3-deoxy-D-fructose is sweet, although probably not as sweet as D-fructose itself. The comparison is made difficult by the fact that the concentration of the presumed sweet form, i.e., the β-D-pyranose tautomer, is substantially lower for **1** (~45–50%) than it is for D-fructose (~60–65%) at physiological temperature. Furthermore, one cannot exclude the possibility that a minor form also contributes to the sweetness of the ketose. Nevertheless, this result clearly indicates that the 3-OH group is not an essential function of the glycophore of D-fructose, a finding that seems to support the attribution of the primary AH–B site to the hydroxyl functions at C-1 and C-2 of the parent ketose. However, we believe, in agreement with Lichtenthaler and Immel (2), that the hydrophilic component of the D-fructose glycophore is not limited to a single α-glycol group. In view of the evidence currently available and the results presented here, we propose that the hydroxyl groups at C-1 and C-2 form the dominant AH–B system and the hydroxyl groups at C-3 and C-4 form a secondary hydrophilic site, in which the 4-OH is the more important function. This interpretation is supported by our studies on 4-deoxy-D-*threo*-hexulose, which will be the subject of a forthcoming publication.

Experimental

^{1}H NMR spectra were recorded at 360.13 MHz on a Bruker AM-360 spectrometer, and ^{13}C NMR spectra at 90.56 or 100.6 MHz on Bruker AM-360 or AM-400 spectrometers, respectively. Chemical shifts (δ) are given in ppm downfield from Me_4Si. Spectra were recorded in D_2O containing 1,4-dioxane (^{13}C NMR: δ 67.26) or acetonitrile (^{13}C NMR: δ CH_3CN 119.8; ^{1}H NMR: δ 2.05 ppm downfield from $Me_3Si(CH_2)_3SO_3Na$) as the internal standard, or in CD_3OD (δ HCD_2OD 3.31). Coupling constants (Hz) were obtained from first-order analyses of the ^{1}H NMR spectra, with the exception of the signals of H-3A,3B of **1**β*p* in D_2O (see Table 2); the simulation of this spin system was performed using PCPMR (Serena Software) on an IBM-compatible personal computer. For the ^{13}C NMR spectra recorded in the APT-mode, (+) or (−) are used to indicate a positive (quaternary and methylene) or a negative (methine and methyl) amplitude of the signals.

[2] Each panelist distinguished among the basic tastes in the test described by Spencer (36) as well as correctly ranked the sweetness of sucrose solutions in the test described by Cameron (37).

3-Deoxy-D-*erythro*-hexulose (1) ("3-deoxy-D-fructose")

To a solution of 3-deoxy-1,2:4,5-di-*O*-isopropylidene-β-D-*erythro*-hexulopyranose **3** (23) (2.07 g, 8.45 mmol) in a mixture of acetone (25 mL) and water (50 mL) was added Amberlite IR-120(H^+) ion-exchange resin (6 g), and the mixture was stirred for 24 h at room temperature. The liquid was then decanted from the resin, passed through a bed of Amberlite IR-45(OH^-) ion-exchange resin (~6 g), and concentrated. The residual, crude **1**, was purified by column chromatography (2:1:0.1 (v/v/v) dichloromethane–ethanol–water, solvent system *A*) and recrystallization from ethanol; a total mass of 1.15 g (83%) of crystalline **1** was obtained in three crops; mp 111–112°C (lit. (19) mp 112–114°C; lit. (21*a*) mp 113–115°C); R_f 0.33 (solvent *A*); $[\alpha]_D$ −43.8 (2 min) → −40.0 (40 min) (*c* 1.6, H_2O) (lit. (19) $[\alpha]_D$ −69 (4 min) → −43.5 (40 min) (*c* 1.0, H_2O); lit. (21*a*) $[\alpha]_D$ −70.1 (3 min) → −42.5 (40 min) (*c* 1.0, H_2O)); ν_{max} (KBr): 3300 (br, OH), 1450, 1275, 1255, 1210, 1150, 1080, 1055, 1030, 980, 880, 860, 790, 735, and 710 cm^{-1}; ^{13}C NMR: immediately after dissolution in D_2O (100.6 MHz, CH_3CN as internal standard; β-pyranose form almost exclusive), δ: 42.11 ((−) C-3), 64.57, 68.14 ((−) C-1,6), 65.55, 67.83 ((+) C-3,4), 97.96 ((−) C-2); equilibrated solution in D_2O (90.56 MHz, 1,4-dioxane as the internal standard; signals labeled "s" (small) belong to a minor component (α-pyranose or *keto* form)), δ: 35.07 ((−), s), 42.12 (−), 42.17 (−), 42.27 (−), 60.39 ((−), s), 62.23 (−), 63.09 (−), 63.18 (−), 64.65 (−), 65.56, 65.60 (+), 65.91 (−), 66.17 (−), 66.50 ((−), s), 66.80 ((+), s), 67.48 ((+), s), 67.89 (+), 68.22 (−), 68.58 ((+), s), 68.63 ((−), s), 71.69 (+), 72.02 (+), 74.96 ((+), s), 86.40 (+), 86.96 (+), 97.10 ((−), s, C-2 (α-pyranose)), 98.03 ((−), C-2 (β-pyranose)), 106.14 and 106.47 ((−), C-2 (α,β-furanoses)), and 212.51 (s, C-2 (*keto* form)). ^{1}H NMR data: see Table 2. Partial data for an equilibrated solution of **1** in CD_3OD, α-furanose form, δ: 1.845 (dd, $J_{3A,3B}$ = 13.5 Hz, $J_{3A,4}$ = 4.5 Hz, H-3A), 2.43 (dd, $J_{3B,4}$ = 7.5 Hz, H-3B), 4.05 (~q, $J_{4,5}$ ~4.5 Hz, H-5), 4.20 (dt, H-4); β-furanose form, δ: 2.15 (d, $J_{3,4}$ = 6.9 Hz, H-3's), 3.87 (~q, $J_{4,5}$ = 5.2 Hz, H-5), 4.35 (dt, H-4); α-pyranose form, δ: ~1.85 (dd, $J_{3A,3B}$ = 14.3 Hz, H-3A), 1.99 (dd, $J_{3B,4}$ = 4.0 Hz, H-3B); *keto* form, δ: 2.57 (dd, $J_{3A,3B}$ = 15 Hz, $J_{3A,4}$ = 8.9 Hz, H-3A), 2.72 (dd, $J_{3B,4}$ = 3.6 Hz, H-3B).

Acknowledgments

The authors are grateful to the Natural Sciences and Engineering Research Council of Canada for financial support in the form of a grant to W.A.S.

References

1. R.S. Shallenberger. (*a*) Pure Appl. Chem. **50**, 1409 (1978); (*b*) Zuckerindustrie, **104**, 121 (1979).
2. F.W. Lichtenthaler and S. Immel. *In* Sweet-taste chemoreception. *Edited by* M. Mathlouthi, J.A. Kanters, and G.G. Birch. Elsevier Applied Science, London and New York. 1992. pp. 21–53.
3. (*a*) R.S. Shallenberger. Taste chemistry. Blackie Academic & Professional, London. 1993; (*b*) *In* Sweet-taste chemoreception. *Edited by* M. Mathlouthi, J.A. Kanters, and G.G. Birch. Elsevier Applied Science, London and New York. 1992. pp. 75–90.
4. O.R. Martin, S.-L. Korppi-Tommola, and W.A. Szarek. Can. J. Chem. **60**, 1857 (1982).
5. R.S. Shallenberger and T.E. Acree. Nature, **216**, 480 (1967).

6. S. Angyal and G.S. Bethell. Aust. J. Chem. **29**, 1249 (1976).
7. (*a*) M.G. Lindley and G.G. Birch. J. Sci. Food Agric. **26**, 117 (1975); (*b*) G.G. Birch. CRC Crit. Rev. Food Sci. Nutr. **8**, 54 (1976).
8. W.A. Szarek, S.-L. Korppi-Tommola, H.F. Shurvell, V.H. Smith, Jr., and O.R. Martin. Can. J. Chem. **62**, 1512 (1984).
9. W.A. Szarek, S.-L. Korppi-Tommola, O.R. Martin, and V.H. Smith, Jr. Can. J. Chem. **62**, 1506 (1984).
10. R.J. Woods, V.H. Smith, Jr., W.A. Szarek, and A. Farazdel. J. Chem. Soc. Chem. Commun. 937 (1987); R.J. Woods, W.A. Szarek, and V.H. Smith, Jr. Can. J. Chem. **69**, 1917 (1991).
11. R.J. Woods, W.A. Szarek, and V.H. Smith, Jr. J. Am. Chem. Soc. **112**, 4732 (1990).
12. M. Mathlouthi and M.O. Portmann. J. Mol. Struct. **237**, 327 (1990).
13. G.G. Birch, S. Shamil, and Z. Shepherd. Experentia, **42**, 1232 (1986).
14. G.G. Birch and S. Shamil. J. Chem. Soc. Faraday Trans. 1, **84**, 2635 (1988).
15. M.G. Lindley, R.S. Shallenberger, and R.L. Whistler. J. Food Sci. **41**, 575 (1976).
16. (*a*) T. Suami, S. Ogawa, M. Takata, K. Yasuda, A. Suga, K. Takei, and Y. Uematsu. Chem. Lett. 719 (1985); (*b*) S. Ogawa, Y. Uematsu, S. Yoshida, N. Sasaki, and T. Suami. J. Carbohydr. Chem. **6**, 471 (1987).
17. T. Severin, J. Hiebel, and H. Popp-Ginsbach. Z. Lebensm.-Unters. Forsch. **178**, 284 (1984).
18. Z.-Q. Liang, F. Hayase, and H. Kato. Eur. J. Biochem. **197**, 373 (1991).
19. R. Kuhn, H. J. Haas, and A. Seelinger. Chem. Ber. **94**, 2534 (1961).
20. J. Thiem, D. Rasch, and H. Paulsen. Chem. Ber. **109**, 3588 (1976).
21. (*a*) S. Kucar. Collect. Czech. Chem. Commun. **41**, 2592 (1976); (*b*) S. Kucar, J. Zamocky, and K. Linek. Czech. Patent 180,856 (Sept. 15, 1979); (*c*) V. Bilik, L. Petrus, and J. Zamocky. Czech. Patent 188,003 (Mar. 15, 1982).
22. R.F. Brady, Jr. Carbohydr. Res. **15**, 35 (1970).
23. J.R. Rasmussen, C.J. Slinger, R.J. Kordish, and D.D. Newman-Evans. J. Org. Chem. **46**, 4843 (1981).
24. W.L. Dills, Jr. Carbohydr. Res. **208**, 276 (1990).
25. S.J. Angyal. Adv. Carbohydr. Chem. Biochem. **42**, 15 (1984), and refs. cited.
26. (*a*) W. Funcke, C. Von Sonntag, and C. Triantaphylides. Carbohydr. Res. **75**, 305 (1979); (*b*) W.J. Goux. J. Am. Chem. Soc. **107**, 4320 (1985).
27. J.E. Whiting and J.T. Edwards. Can. J. Chem. **49**, 3799 (1971).
28. W.A. Szarek, O.R. Martin, R.J. Rafka, and T.S. Cameron. Can. J. Chem. **63**, 1222 (1985).
29. J.R. Durrwachter, D.G. Drueckhammer, K. Nozaki, H.M. Sweers, and C.-H. Wong. J. Am. Chem. Soc. **108**, 7812 (1986).
30. S.J. Angyal. Aust. J. Chem. **21**, 2737 (1968).
31. B.M. Arshava, Yu. E. Raifel'd, and S.M. Makin. Zh. Org. Khim. **26**, 778 (1990).
32. B. Schneider, F. W. Lichtenthaler, G. Steinle, and H. Schiweck. Liebigs Ann. Chem. 2443 (1985).
33. L.D. Hayward and S.J. Angyal. Carbohydr. Res. **53**, 13 (1977).
34. V.A. Yaylayan and A.A. Ismail. J. Carbohydr. Chem. **11**, 149 (1992).
35. S.J. Angyal, G.S. Bethell, D.E. Cowley, and V.A. Pickles. Aust. J. Chem. **29**, 1239 (1976).
36. H.W. Spencer. *In* sweetness and sweeteners. *Edited by* G.G. Birch, L.F. Green, and C.B. Coulson. Applied Science Publishers, London. 1971. pp. 112–129.
37. (*a*) A.T. Cameron. Trans. R. Soc. Can. Sect. 3, **37**, 11 (1943); (*b*) Can. J. Res. Sect. E: **22**, 46 (1944).

Can. J. Chem. Downloaded from www.nrcresearchpress.com by 46.23.64.124 on 09/08/12
For personal use only.

Investigations of aluminum hydroxyphosphates and activated sludge by ^{27}Al and ^{31}P MAS NMR

Stephen J. Duffy and Gary W. vanLoon

Abstract: High-resolution solid-state ^{27}Al and ^{31}P MAS NMR has been used to investigate the nature of aluminum- and phosphorus-containing solids formed during wastewater treatment. Although difficult to characterize by conventional techniques, these amorphous solids can be characterized by MAS NMR, providing information about their short-range ordering. In the present study, most of the solids were precipitated under conditions of high alkalinity, similar to those encountered during wastewater treatment. The ageing time of the aluminum hydroxide prior to the addition of phosphate (t_1), the ageing time of the aluminum hydroxyphosphates after the addition of phosphate (t_2), and the phosphorus to aluminum molar ratio were controlled while the effects of changing the parameters were examined. It was found that the aluminum MAS NMR chemical shift was related to the amount of phosphate present in the solid, which in turn was related to t_1, t_2, and the P:Al molar ratio. The results also lend support to the hypothesis that phosphate removal occurs through an adsorption process onto amorphous aluminum hydroxide, rather than through direct precipitation of aluminum phosphate. The increased understanding of aluminum and phosphate chemistry and the species formed during wastewater treatment will be useful in optimizing wastewater treatment processes.

Key words: aluminum, phosphate, NMR, activated sludge, wastewater treatment.

Résumé : On a utilisé la RMN MAS du ^{27}Al et du ^{31}P pour étudier la nature de solides, contenant du phosphore et de l'aluminium, formés au cours du traitement des eaux usées. Même s'ils sont difficiles à caractériser par les techniques conventionnelles, ces solides amorphes peuvent facilement être caractérisés par la RMN MAS et on obtient ainsi des informations sur leur arrangement à courte distance. Dans la présente étude, la plupart des solides ont été précipités dans des conditions d'alcalinité élevée semblables à celles utilisées durant le traitement des eaux usées. Le temps de vieillissement de l'hydroxyde d'aluminium avant l'addition du phosphate (t_1), le temps de vieillissement des hydroxyphosphates d'aluminium après l'addition du phosphate (t_2) et les rapports molaires du phosphore à l'aluminium ont été contrôlés alors que les effets d'un changement de ces paramètres ont été examinés. On a trouvé que le déplacement chimique de l'aluminium dans la RMN MAS est relié à la quantité de phosphate présente dans le solide qui, à son tour, est relié à t_1, à t_2 et au rapport molaire P : Al. Les résultats supportent aussi l'hypothèse selon laquelle l'enlèvement du phosphate se produit par un processus de surface sur l'hydroxyde d'aluminium plutôt que par une précipitation directe du phosphate d'aluminium. La meilleure compréhension de la chimie de l'aluminium et des phosphates ainsi que des espèces qui se forment au cours du traitement des eaux usées sera utile pour l'optimisation de ces procédés de traitement.

Mots clés : aluminium, phosphate, RMN, boues activées, traitement des eaux usées.

[Traduit par la rédaction]

Introduction

Point-source pollutant discharges from municipal wastewater treatment facilities are recognised as having a major impact on water quality and the surrounding ecosystems. Since the early 1970s, phosphates have been identified as a pollutant of specific concern with regard to eutrophication of water bodies (1). To reduce the amount of this element entering receiving waters from point sources, one cost-effective and efficient phosphorus removal method includes addition of alum to the wastewater stream as part of an integrated treatment system. One such system, the activated sludge process (ASP) is a method of treating wastewater biologically under aerobic conditions in order to reduce the biological oxygen demand (BOD). At many locations, ASP treatment plants have been modified in a simple manner to incorporate the addition of alum as a part of the overall process. Where this has been done, it has usually been possible to reduce the phosphorus content of discharges to less than 1 mg L^{-1}. However, even this level of residual phosphorus is sufficient to cause significant accumulation of phosphate nutrient in sensitive ecosystems and therefore further stringent controls on wastewater effluent quality may be required.

Alum or other aluminum additives serve two interconnected purposes in the wastewater treatment process. The first is to aid in coagulation and flocculation of organic and inor-

Received March 24, 1995.

S.J. Duffy and G.W. vanLoon.[1] Department of Chemistry, Queen's University, Kingston, ON K7L 3N6, Canada.

[1] Author to whom correspondence may be addressed. Telephone: (613) 545-2633. Fax: (613) 545-6669. E-mail: vanloong@qucdn.queensu.ca.

Can. J. Chem. Downloaded from www.nrcresearchpress.com by 46.23.64.124 on 09/08/12
For personal use only.

Can. J. Chem. Downloaded from www.nrcresearchpress.com by 46.23.64.124 on 09/08/12
For personal use only.

ganic colloidal material and the second is to precipitate soluble inorganic phosphate from the wastewater stream. Optimizing effectiveness and efficiency in carrying out these processes requires a knowledge of the behaviour of aluminum throughout its "lifetime" in the treatment system.

Soluble phosphates are effectively precipitated from wastewater by aluminum(III) under conditions of high alkalinity, leaving very low residual concentrations, often lower than 0.2 mg L^{-1}. On the other hand, a portion of the particulate phosphates that are formed does not settle in the clarifier and is subsequently discharged from the treatment system; these fine materials are consequently the principal form of phosphorus released into the receiving water (2).

Often, when the chemistry of phosphorus removal is discussed, a very simple but chemically inadequate description of the reaction of phosphate with alum-derived aluminum ion is given by eq. [1] (3–5).

[1] $Al^{3+} + PO_4^{3-} \longrightarrow AlPO_4$ (s)

In many cases, however, the aluminum (Al^{3+}) is injected at a point in the treatment system where the concentration of soluble phosphate is very low and the simple stoichiometry indicated by eq. [1] could not be correct.

Alum additions during the activated sludge process have been done at various locations; frequently the point chosen is within but near the exit of the aeration chamber. For example, Plant A at Kingston Township Pollution Control Plant (KTPCP) adds alum at this point and measurements show that the soluble phosphorus concentration just upstream from the point of addition is approximately 0.5 mg L^{-1} (2). The coagulant dose is 5 mg L^{-1} aluminum, which corresponds to a 1:11.5 molar ratio of phosphorus to aluminum. The 0.5 mg L^{-1} concentration of soluble phosphorus at this location compares with a concentration of between 2 and 4.5 mg L^{-1} soluble phosphorus in the aerator influent. This indicates that a large fraction of soluble phosphorus has been removed in the aerator itself.

If the formation of aluminum phosphate is not a direct precipitation process as shown in eq. [1], then it is important to know how the phosphorus is subsequently removed from solution. The answer to this question may provide insight into the conditions required to maximize the dephosphorization capability of alum. It is known that when alum, in the form of a hydrated aluminum(III) ion, is added to a high alkalinity wastewater with a typical pH of approximately 7, its principal reactions are a series of rapid successive hydrolysis steps, ultimately resulting in the precipitation of amorphous aluminum hydroxide.

One hypothesis for phosphorus removal involves phosphate adsorbing onto the newly formed amorphous aluminum hydroxide, producing an aluminum phosphate solid. Goldshmid and Rubin addressed a similar issue and reported that the solid phases identified in precipitates were $AlPO_4$, $Al_3(OH)_3(PO_4)_2$, and $Na_3Al_5H_6(PO_4)_8$, depending on the conditions of precipitation (6).

In this paper we examine the nature of the solid aluminum precipitates from both a well-characterized laboratory system and an activated sludge process, using magic angle spinning (MAS) nuclear magnetic resonance (NMR) spectroscopy as well as several other techniques.

High-resolution solid-state MAS NMR has recently become an important tool for providing specific chemical and structural information of a type that has been unattainable by more traditional means (7–13). X-ray diffraction (XRD) analysis is one of the traditional methods and is used to determine the crystalline nature of solid materials. However, when dealing with solids that are not highly ordered on a molecular level, an X-ray diffraction pattern cannot be obtained. It is with such XRD amorphous solids, having a lower level of molecular order, that MAS NMR is particularly useful for interpreting structures (14). Since both aluminum and phosphorus have nuclei, ^{27}Al and ^{31}P, respectively, that are favourable for NMR analysis, this technique is particularly suitable for examining aluminum- and phosphorus-containing solids. While NMR has seen little application in dephosphorization studies, it has been applied to structural analysis of aluminophosphate molecular sieves or zeolites (15–17).

Three parameters from the MAS NMR spectra may be used in interpreting the structures of amorphous aluminum hydroxides, aluminum phosphates, and aluminum hydroxyphosphates: chemical shifts, the relative size of peaks, and the degree of sharpness associated with each signal. Of these, the most important is the ^{27}Al chemical shift; its value depends primarily on the coordination number for the aluminum and on the nature of the neighbouring atoms. Shown in Table 1 are ^{27}Al and ^{31}P MAS NMR chemical shifts for aluminum oxides, aluminum hydroxides, and aluminum phosphates reported in various sources. The octahedral forms of aluminum appear separated from tetrahedral forms by about 50–80 ppm, while smaller differences, up to 25 ppm, are due to the nature of the aluminum neighbours. In the case of tetrahedral aluminum, Muller, Gessner et al. showed that in situations where the nearest neighbours were AlO_4, SiO_4, or PO_4 the chemical shifts ranged between 71 and 87 ppm, 50 and 67 ppm, and 33 and 45 ppm, respectively (11). The size of a peak in a spectrum is generally a reflection of the amount of element in a particular structural environment, while the peak widths can indicate the extent of molecular order. In a qualitative way, the narrower the peak, the more ordered the system. Table 2 summarizes XRD results and NMR peak widths measured at half peak height for a number of the solids investigated in the present study. The ^{27}Al MAS NMR spectra that had peak widths less than 10 ppm were from samples that had been identified as being crystalline, while spectra that had peaks widths greater than 10 ppm were generally associated with XRD amorphous material.

The differences in the ^{31}P MAS NMR chemical shifts are smaller than those for ^{27}Al since a single type of coordination associated with PO_4 tetrahedra is involved in all cases. However, the small change in chemical shifts that are a consequence of changing environments near the phosphate groups can also be used as evidence for particular structures.

In this paper we have synthesized aluminum hydroxide, aluminum phosphate, and aluminum hydroxyphosphate precipitates, using a variety of conditions related to wastewater treatment. We also obtained sludge samples from a local treatment plant and examined the ^{27}Al and ^{31}P MAS NMR spectra of the various solids.

Experimental methods

Chemicals

Reagent grade $NaHCO_3$ and KH_2PO_4 were used to prepare

Table 1. ^{27}Al and ^{31}P MAS NMR spectral peak positions for some aluminum compounds.

Sample	Al coordination	MAS NMR chemical shift/ppm ^{27}Al	MAS NMR chemical shift/ppm ^{31}P	Reference
$[Al(H_2O)_6]^{3+}$ (soln. species)	6	0	—	Standard This study
Gibbsite $Al(OH)_3$	6	8	—	This study
Aluminum hydroxide $Al(OH)_3$	6	8.1	—	20
Corundum α-Al_2O_3	6	5	—	18
$Al(OH)_4^-$ (soln. species)	4	80	—	11
Sodium aluminate β-$NaAlO_2$	4	77	—	18
Berlinite $AlPO_4$	4	33.2 26.3	−24.8	17
Variscite $AlPO_4 \cdot 2H_2O$	6	—	−18.6	26
Metavariscite $AlPO_4 \cdot 2H_2O$	6	−13.2	−19.3	17
$Al(H_2PO_4)_3$	6	−16.6	—	25
$Al(H_2O)_3(H_2PO_4)(HPO_4)$	6	−7.6	—	17
Anaerobically digested sludge		—	2.47	26
Soil containing 580 ppm P		—	1.75	27

aqueous solutions of 0.833 mol L^{-1} carbonate species and 0.323 mol L^{-1} phosphate species. These solutions plus commercial grade liquid alum ($Al_2(SO_4)_3 \cdot 14H_2O$ 48% w/v) obtained from KTPCP and distilled deionized water were used to prepare most of the solids precipitated in the laboratory. Other chemicals included Fisher Certified aluminum hydroxide and aluminum chloride hexahydrate, Baker Analyzed Reagent aluminum sulfate 16-hydrate, aluminium phosphate (variscite), and ICN Pharmaceuticals aluminum metaphosphate ($Al(PO_3)_3$).

Laboratory preparation of solid samples

Three types of aluminum solids were prepared in the laboratory: (*i*) aluminum hydroxides precipitated at high alkalinity, (*ii*) aluminum hydroxyphosphates precipitated at high alkalinity, and (*iii*) aluminum phosphates precipitated at low pH. The solids formed at high alkalinity were prepared by one of two methods. The first method involved adding alum alone or prior to the addition of phosphate. The second method involved adding phosphate first, and then alum. In both methods, 25.00 mL of bicarbonate solution and sufficient distilled deionized water (DDW) to bring the final volume to 100 mL were first mixed in a 150 mL beaker. Following this, 0.860 mL of alum and 1.00, 5.00, or 50.00 mL of the phosphate solution were added in the appropriate order. The molar ratios of phosphorus to aluminum in solution used were therefore 0.17, 0.87, or 8.7, respectively. Using an Eppendorf™ micropipet, the alum was added into a solution while it was being smoothly mixed using a single-blade stirrer at 350 rpm. The actual quantity of aluminum added was 50 mg, as determined by atomic absorption spectroscopy (AAS) analysis. The aluminum phosphate solid precipitated at low pH was prepared by mixing aqueous solutions containing equimolar amounts of aluminum and phosphorus without further adjustment of pH; the pH after mixing was near 3.

The time allowed for the aluminum hydroxide to age prior to the filtration or addition of phosphate is referred to as t_1. On the other hand, t_2 refers to the ageing time after the phosphate addition and prior to the solid being filtered. Actual values of t_1 and t_2 were established for each experiment and are documented in the results and discussion section.

Samples were filtered using either a 0.45 μm filter or a porcelain filter crucible and were dried for approximately 2 h at 110°C and then weighed. Further drying at the same temperature effected only small additional weight losses, never larger than 5%. Some whole or partial samples were heated at 800°C for 16 h in a muffle furnace and were reanalyzed by MAS NMR or X-ray diffraction, or digested with hydrochloric acid and analyzed for aluminum by AAS and for phosphorus using a molybdenum blue procedure.

Four aerator sludge samples were obtained from plant A of the KTPCP. The first two samples were retrieved from a loca-

Can. J. Chem. Downloaded from www.nrcresearchpress.com by 46.23.64.124 on 09/08/12
For personal use only.

Table 2. Comparison of the ^{27}Al MAS NMR signal peak width (determined at half peak height) and XRD results for some of the prepared aluminum solids, shown with the particular ageing times and P:Al molar ratios used.

Sample name	Ageing times t_1/min	Ageing times t_2/h	P:Al ratio	Peak width/ppm	XRD results
PAl-2	0	2	0.17	20.5	Amorphous
PAl-3	1	2	0.17	21.7	Amorphous
Calcined PAl-9	0	2	0.87	4.3	Crystalline, matches JCPDS 20-45, unknown structure
Calcined PAl-11	0	2	8.7	5.7	Crystalline, sharp pattern, melange of 2 or 3 structures
Calcined PAl-13	0	192	0.87	4.6	Crystalline, ill-defined pattern
Calcined PAl-14	1	2	0.87	4.0	Crystalline, ill-defined pattern
Calcined PAl-15	1	2	8.7	7.4	Crystalline, sharp pattern, melange of 2 or 3 structures
PAl-16	0	696	0.17	21.1	Amorphous
Al-2	41 760	0	0.0	26.3	Amorphous
Gibbsite $Al(OH)_3$	Reagent		0.0	6.9	Crystalline, gibbsite
Variscite $AlPO_4 \cdot 2H_2O$	Reagent		1.0	2.2	Crystalline, ill-defined pattern
Calcined variscite ($AlPO_4$)	Reagent		1.0	8.0	Crystalline, berlinite
PAl-1	Formed under acid conditions		1.0	4.0	Crystalline, unidentified phases
Calcined PAl-1	Formed under acid conditions		1.0	3.9 2.1	Crystalline, $KAlP_2O_7$ (36-1459) plus unidentified phases

Can. J. Chem. Downloaded from www.nrcresearchpress.com by 46.23.64.124 on 09/08/12
For personal use only.

tion just prior to alum addition, the third sample was obtained from a location just downstream from the alum addition point, and the fourth sample was obtained from the sludge being recycled into the aeration chamber.

Sample analyses

A duplicate series of aluminum hydroxyphosphates were analyzed for aluminum, phosphorus, and water in order to determine the molecular formulas. Samples were prepared using the second method described earlier with the P:Al molar ratios of 0.17, 0.87, and 8.7. The t_1 was 0 min and t_2 was 2 h for each sample. After determining the quantity of aluminum and phosphorus (the latter assuming a HPO_4^{2-} species), the amount of hydroxide associated with the solid material was determined by means of a charge balance calculation. The amount of water associated with the solid, previously dried to near constant weight at 110°C, was determined by the weight loss of the solid after heating at 800°C for 16 h, taking into account the water produced from the released hydroxides. A simple example of this process is given in eq. [2].

$$[2] \quad Al(HPO_4)(OH)\cdot H_2O \xrightarrow[16\ h]{800°C} AlPO_4 + 2\ H_2O$$

In the above hypothetical situation the aluminum undergoes a conversion from an octahedral to a tetrahedral arrangement. This is also consistent with the ^{27}Al MAS NMR data, which indicated an octahedral aluminum prior to heating at 800°C and a tetrahedral aluminum after heating, as shown in the results and discussion below.

Guinier–deWolff patterns were obtained by XRD analysis and were compared to patterns for known aluminum and phosphorus compounds.

Can. J. Chem. Downloaded from www.nrcresearchpress.com by 46.23.64.124 on 09/08/12
For personal use only.

Table 3. Peak maxima in ^{27}Al MAS NMR spectra for aluminum hydroxide solids prepared by precipitating 50 mg of aluminum and aged for the time (t_1) shown. Samples were dried at 110°C and calcined. Peaks are listed in order of decreasing size.

Sample	t_1/h	Chemical shift/ppm[a] 110°C	Chemical shift/ppm[a] Calcined	Al source
Al-1 amorphous $Al(OH)_3$	2	8 Br	nd	Alum
Al-2 amorphous $Al(OH)_3$	696	8 Br	8 Br 64 Br	Alum
Al-3 $Al(OH)_3$	2568	−7 Br 3 Br −20 Br	76 Sh	Alum
Al-4 amorphous $Al(OH)_3$	0.017	8 Br	nd	Alum
Al-5 amorphous $Al(OH)_3$	0.017	8 Br	9 Br 66 SmBr	$AlCl_3$
Al-6 $Al(OH)_3$	2568	−8 Br 4 Br −20 Br	76 Sh	$AlCl_3$
$Al(OH)_3$ gibbsite	reagent	8 Sh −5 Sm	9 Br 63 SmBr	—

[a]Results are referenced to a static signal from a 0.2 M solution of aluminum nitrate. Sh = sharp, Sm = small, Br = broad, nd = not determined.

NMR methods

MAS NMR analyses were conducted on laboratory chemical reagents, on solids precipitated from solutions prepared in the laboratory, and on sludge samples retrieved from plant A at KTPCP. The ^{27}Al MAS NMR spectra were obtained on a Bruker AM-400 solid-state high-resolution NMR spectrometer operating at a field of 9.4 T, using a 5 mm VT multinuclear ultra-high-speed double-tuned MAS probe. The ^{27}Al frequency of 104.2 MHz and sample spinning rates of 6–11 kHz were used. Depending on the sample, between 100 and 3200 free induction decays were performed at a repetition time of 1 s and a pulse length of 2 μs. Samples were packed into zirconia rotors, which contained 0.03% Al or less. The ^{27}Al MAS NMR chemical shifts are referenced to a static signal obtained from a 0.2 M aqueous solution of $Al(NO_3)_3$.

The ^{31}P MAS NMR spectra were obtained on a Bruker CXP-200 solid-state high-resolution NMR spectrometer using a ^{13}C cross-polarization magic angle spinning (CP-MAS) accessory probe and a field of 4.7 T. The ^{31}P frequency of 80.98 MHz and sample spinning rates of 3–5 kHz were used. Depending on the sample, between 16 and 32 000 free induction decays were performed at a repetition time of 5 s and a pulse length of 3 μs. The ^{31}P NMR chemical shifts are referenced to solid $(NH_4)H_2PO_4$.

Results and discussion

Investigations of aluminum hydroxide precipitated in the absence of phosphate

The results of the ^{27}Al MAS NMR analyses on a number of samples of amorphous aluminum hydroxide of various ages, t_1, are reported in Table 3. The dominant peak in all samples appeared near 8 ppm (Fig. 1) in agreement with results for six-coordinate aluminum hydroxide solids as reported by Hayashi (18), Bradley and Hanna (19), and Kunnar et al. (20). When the source of aluminum (aluminum sulfate or aluminum chloride), the method of precipitation (good mixing or none), or age of aluminum (t_1 equal to 2 h or 29 d) was varied, no quantifiable difference was found in the MAS NMR signal. This is unlike previous experimental results using the "Ferron method" where decreasing aluminum reactivity (reflecting increasing crystallinity) was observed as the amorphous aluminum hydroxide aged or when the hydroxide was prepared without good mixing (21). The contrasting results reflect the variation in sensitivity of the two methods with respect to assessing molecular order.

While there was no significant difference between NMR spectra of samples aged up to 29 d, the t_1 = 107 d samples (Al-3 and Al-6) had signals that were broader and with chemical

Can. J. Chem. Downloaded from www.nrcresearchpress.com by 46.23.64.124 on 09/08/12
For personal use only.

Fig. 1. ^{27}Al MAS NMR spectrum of amorphous aluminum hydroxide (sample Al-1), $t_1 = 2$ h, prepared by precipitating alum at high alkalinity. Spinning side bands appear on either side of the main signal about 85 ppm away.

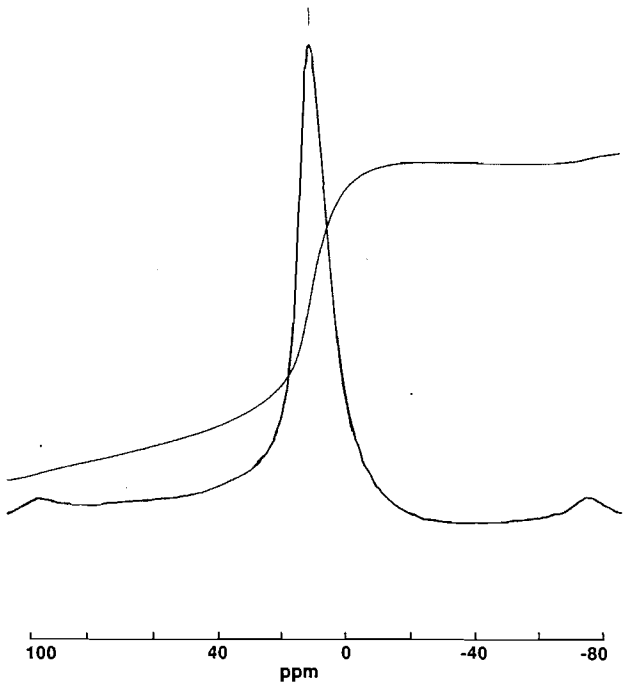

Fig. 2. ^{27}Al MAS NMR spectrum of aluminum hydroxide solid (sample Al-3), $t_1 = 2568$ h, prepared by precipitating alum at high alkalinity. Spinning sides bands are not shown.

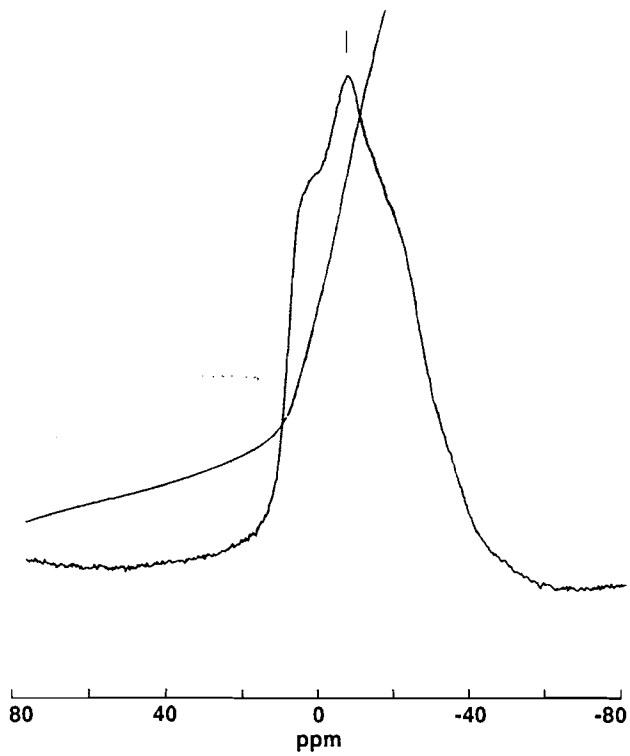

shifts centred at −7 ppm (Fig. 2). During the extended ageing, there was a rise in the solution pH to near 10, as a result of re-equilibration of atmospheric CO_2 and the carbonate species. A high pH is known to favour the formation of bayerite during crystallization and would also cause partial resolubilization of aluminum as $AlOH_4^-$. In highly alkaline solutions the aluminum hydroxide solid is known to have a negatively charged surface (22). This could affect both the structure of the solid in solution and the solid recovered after filtering and cause the observed shift in the NMR chemical signal that was obtained.

Much more significant changes in the NMR spectra were observed when the precipitates were heated. Phase transitions that solid aluminum hydroxides and oxyhydroxides undergo upon heating have been reviewed by Mackenzie and Berggren (23). A simplified sequence involving the major transitions observed for aluminum hydroxide can be represented by eq. [3]:

$$[3]\quad \text{amorphous } Al(OH)_3 \xrightarrow[\approx 300°C]{-H_2O} \gamma\text{-}Al_2O_3 \xrightarrow[>1000°C]{} \alpha\text{-}Al_2O_3$$

where α-Al_2O_3 (corundum) is heat stable up to 1950°C. Dollimore indicated that heating freshly precipitated aluminum hydroxide to a temperature of 800°C or higher eventually produces corundum (24).

Our samples were subjected to heating at 800°C for 16 h (from now on referred to as being calcined) and the MAS NMR results (Table 3) indicate partial conversion of aluminum coordination to a tetrahedral form, consistent with the formation of γ-Al_2O_3. The spectra had two broad peaks, the smaller one centred at 65 ppm characteristic of a tetrahedral signal and the original octahedral signal centred near 8 ppm (Fig. 3). However, samples Al-3 and Al-6, both of which had been aged (t_1) for 107 d, after being calcined gave a single sharp peak at 76 ppm indicating complete conversion of aluminum to a tetrahedral form (Fig. 4). The spectrum was identical to that reported for β-$NaAlO_2$ (sodium aluminate) in Table 2.

Investigation of aluminum phosphate precipitated at low pH

MAS NMR spectra were obtained on solid samples of variscite, $AlPO_4 \cdot 2H_2O$, aluminum metaphosphate, $Al(PO_3)_3$, and the solid prepared by reacting equimolar amounts of phosphorus and aluminum at pH 3 (PAl-1). The peak positions are shown in Table 4. Variscite gave a large sharp peak at −11 ppm that is similar to the octahedral aluminum signal at −13.2 ppm reported by Blackwell and Patton (17). When the sample of variscite was calcined, the ^{27}Al MAS NMR spectrum changed to having a sharp peak at 38 ppm and a second smaller peak at 31 ppm, producing berlinite (determined by XRD), similar again to the results reported by Blackwell and Patton (17).

Since sample PAl-1 had been prepared by precipitating aluminum phosphate under acid (pH 3) conditions, no hydroxide would be formed and the product would be expected to be essentially $AlPO_4$. The ^{27}Al MAS NMR results showed a sharp peak at −11 ppm and a second, smaller, overlapping peak at −9 ppm, similar to the spectrum of variscite (Fig. 5). The XRD measurements on PAl-1 indicated that it was crystalline but of unknown structure; the lines did not match the spectrum for variscite. After sample PAl-1 had been calcined, two distinct forms of aluminum phosphate were identified

Can. J. Chem. Downloaded from www.nrcresearchpress.com by 46.23.64.124 on 09/08/12
For personal use only.

Fig. 3. ^{27}Al MAS NMR spectrum of calcined amorphous aluminum hydroxide (sample Al-5), t_1 = 1 min, prepared by precipitating aluminum (chloride) at high alkalinity. Spinning side bands appear on either side of the main signal about 85 ppm away.

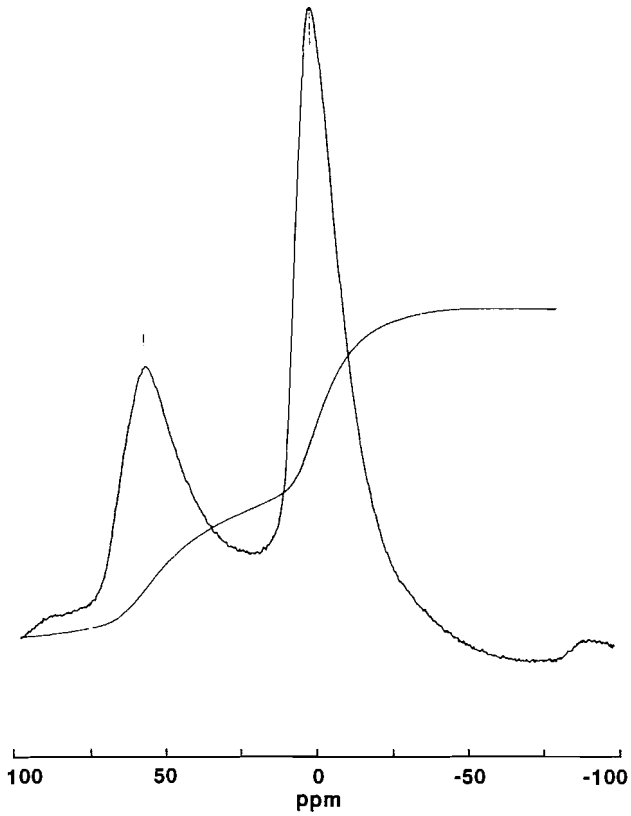

(Fig. 6). The tetrahedral aluminum signal at 38 ppm indicated anhydrous $AlPO_4$, while the octahedral resonance at −16 ppm had been previously described by Muller et al. as characteristic of solid $Al(H_2PO_4)_3$ (25).

The solids mentioned above were also characterized by ^{31}P MAS NMR analyses and the peak positions are shown in Table 4. The spectrum obtained from variscite had a peak at −19 ppm close to the −19.3 ppm reported by Blackwell and Patton (17). PAl-1 had a signal at −18 ppm, again indicating that the solid is similar to variscite. However, the NMR spectrum of the calcined PAl-1 sample indicated the presence of two environments for phosphorus as there were two peaks, one at −22 ppm and the other at −27 ppm, while calcined variscite had only one peak at −23 ppm.

Investigations of aluminum hydroxyphosphates precipitated at high alkalinity

In a wastewater treatment plant, aluminum is precipitated under conditions of high alkalinity in the presence of phosphate, and aluminum hydroxyphosphates are formed. We therefore studied the precipitates formed under similar conditions in the laboratory. Aluminum hydroxyphosphates are solids that may be thought of as intermediate between aluminum hydroxide and aluminum phosphate. We would expect this composition to be reflected in the NMR chemical shifts.

Fig. 4. ^{27}Al MAS NMR spectrum of calcined aluminum hydroxide (sample Al-3), t_1 = 2568 h, prepared by precipitating aluminum (chloride) at high alkalinity. Spinning side bands appear on either side of the main signal about 90 ppm away.

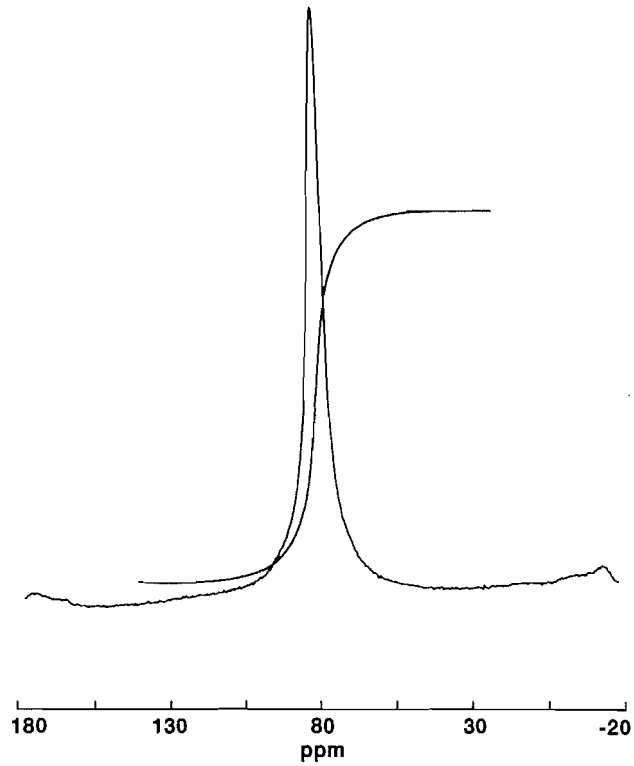

Influence of t_1 on the ^{27}Al MAS NMR spectra

Table 5 summarizes the MAS NMR peak positions for a series of six solids precipitated from solutions with high alkalinity and an equilibrium pH near 7. When investigating the effect of varying t_1, the molar ratio of added P:Al was 0.17; in some typical cases this is near the ratio at the point of alum addition in a treatment plant. Alum was added to solutions without phosphate and the precipitates were aged for times, t_1, ranging from 1 to 9000 min. Phosphate was then added and the precipitate was allowed to equilibrate with the solution for a constant time, t_2, of 2 h. One other solid was formed with phosphate present at the time of alum addition; t_1 was equal to 0 min and t_2 was equal to 2 h for this sample.

Each of the MAS NMR spectra of the precipitates showed a large broad peak (the peak width ranged from 18 to 22 ppm at half peak height) with the maximum located between 4 and 6 ppm, close to the 8 ppm signal obtained for the amorphous aluminum hydroxide samples and far from the variscite signal at −11 ppm. The consistent position of the peak in all cases indicated that, regardless of the age of the aluminum hydroxide, the solid that was formed after being in contact with phosphate still contained aluminum only in octahedral coordination. Samples with t_1 of 0 and 1 min were both clearly amorphous materials as no lines were observed in the XRD spectrum.

It was especially interesting that there was no apparent difference between the NMR results for the precipitate formed when phosphate was present in the solution prior to the addition of alum (t_1 of 0 min) and the precipitates that had been

Table 4. Peak maxima in ^{27}Al and ^{31}P MAS NMR spectra for aluminum phosphate solids that were dried at 110°C and calcined. Peaks are listed in order of decreasing size.

	Chemical shift/ppm[a]			
	^{27}Al		^{31}P	
	110°C	Calcined	110°C	Calcined
$AlPO_4 \cdot 2H_2O$ Variscite	−11 Sh 8 Sm[b]	38 Sh 31 Sh 7 Sm[b]	−20 Sh	−23 Sh
$Al(PO_3)_3$ Aluminum metaphosphate	−21 Sh 39 Sm	nd	−51 Sh	nd
PAl-1 (precipitated under acidic (pH = 3) conditions, P:Al = 1	−11 Sh −8 Sh 43 SmBr	−16 Sh 38 Sh	−18 Sh 8 SmSh	−22 Sh −27 Sh

[a]The aluminum chemical shift is referenced to a 0.2 M static aluminum nitrate solution and the phosphorus chemical shift is referenced to solid ammonium dihydrogen phosphate. Sh = sharp, Sm = small, Br = broad, nd = not determined.

[b]Aluminum hydroxide impurity.

Fig. 5. ^{27}Al MAS NMR spectrum of $AlPO_4 \cdot 2H_2O$ (variscite). Spinning side bands appear on either side of the main signal about 85 ppm away.

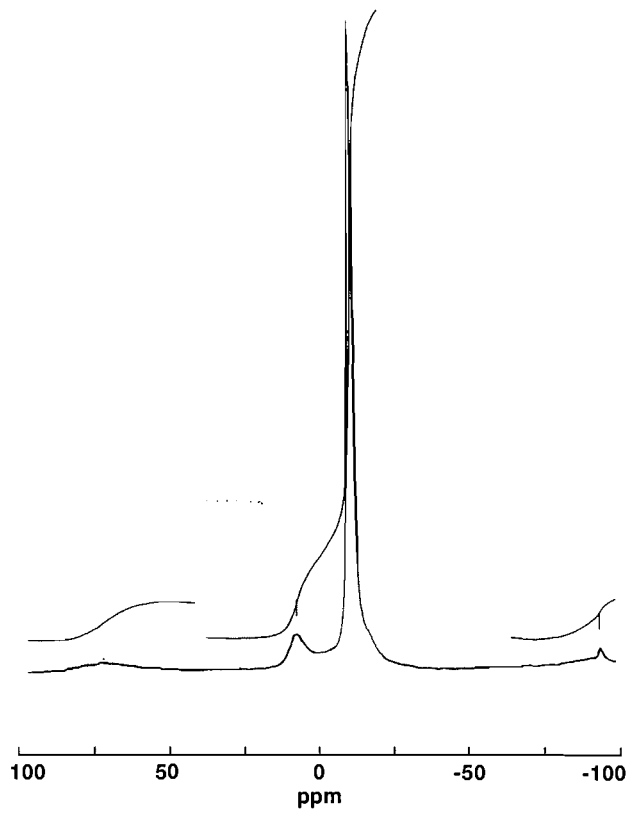

Fig. 6. ^{27}Al MAS NMR spectrum of calcined aluminum phosphate (sample PAl-1), P:Al = 1.0, prepared by precipitating aluminum (chloride) under acid (pH = 3) conditions in the presence of phosphate.

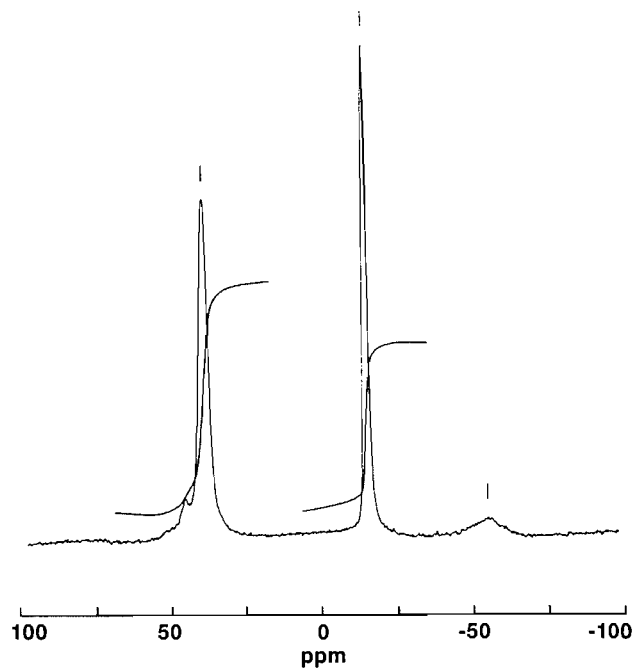

allowed to age for 1 or 10 min before adding phosphate. Where t_1 was 0 min, it was possible that aluminum could have reacted directly with phosphate, while in the latter cases aluminum hydroxide had precipitated before phosphate addition and the only method of phosphate removal was through post-precipitation adsorption processes. The similar NMR spectra for all samples suggest that, in no case, was there significant evidence for direct coordination between phosphate and aluminum ion.

There are, however, important differences between NMR spectra of aluminum hydroxide alone and aluminum hydroxide that was allowed to react with phosphate. In the latter cases only, ageing of the hydroxide (t_1) caused the ^{27}Al NMR peak maximum to shift downfield. It appeared that the shift was

Can. J. Chem. Downloaded from www.nrcresearchpress.com by 46.23.64.124 on 09/08/12
For personal use only.

Table 5. Peak maxima for ^{27}Al and ^{31}P MAS NMR spectra for aluminum hydroxyphosphates (P:Al ratio = 0.17) that were dried at 110°C and calcined. Peaks are listed in order of decreasing size. t_2 was 2 h for each sample. Also shown are the corresponding integrated values for the ^{31}P MAS NMR signals.

		Chemical shift/ppm[a]			
		^{27}Al		^{31}P	
Sample	t_1/min	110°C[b]	Calcined	110°C	^{31}P Integrated signal
PAl-2	0	4 Br	39 Br 13 Br 53 Br	−11 Br	795
PAl-3	1	4 Br	nd	−11 Br	732
PAl-4	10	4 Br	33 Br 5 Br 53 Br	−11 Br	650
PAl-5	100	5 Br	nd	−11 Br	558
PAl-6	1000	6 Br	5 Br 39 Br 56 Br	−11 Br	549
PAl-7	9000	6 Br	7 Br 65 Br 40 Br	−9 Br	187

[a]The aluminum chemical shift is referenced to a 0.2 M static aluminum nitrate solution and the

Table 6. Amount of phosphorus (from a total of 5 mg) removed by aluminum hydroxide at various ages (t_1) after reaction for 10 min (t_2) and the integrated ^{31}P MAS NMR signal for solids prepared using 50 mg phosphorus with a t_2 of 2 h.

t_1/min	Amount of P adsorbed/mg	Integrated ^{31}P MAS NMR signal
0	3.2	795
1	2.4	732
10	1.6	650
100	1.2	558
1000	0.5	549
9000	—	187

related to the presence of phosphate in the precipitate. Table 6 shows that the size of the peak, reflecting the amount of phosphate that was adsorbed, decreased with increasing t_1. Maximum uptake of phosphate occurred when t_1 = 0 but the maximum value could never exceed a ratio of 0.17 P:Al in this experiment. Therefore, the presence of phosphate in the precipitate caused the NMR peak to shift toward the position of the peak for variscite but, because the amount of phosphate was small, the final position was still far from the value associated with variscite, where the P:Al ratio is 1. A second feature of NMR spectra of samples with phosphate differing from those of samples without phosphate was the presence of two small broad peaks centred near 30 and 60 ppm, indicating other minor aluminum components of possible tetrahedral coordination (Fig. 7).

Influence of t_1 on the NMR spectra for the calcined aluminum hydroxyphosphate solids

NMR spectra of the calcined aluminum hydroxyphosphate precipitates gave evidence of the heterogeneous composition of the amorphous material. A large, broad, composite peak with maxima occurring at 39, 13, and 53 ppm (Fig. 8) was obtained for the calcined sample PAl-2 prepared with t_1 equal to 0. However, the calcined sample with t_1 equal to 9000 min (PAl-7), gave only a small peak at 40 ppm while broad signals at 7 and 65 ppm were much larger (Fig. 9). It appeared that the broad signal from calcined PAl-2 was a combination of overlapping peaks due to different aluminum components: possibly $AlPO_4$, which has a signal near 40 ppm, Al_2O_3 with a signal near 60 ppm, and $Al(OH)_3$ near 8 ppm. As the phosphate content of the series of six samples decreases, the ^{27}Al MAS NMR spectra began to more closely resemble the two peaks obtained from the calcined aluminum hydroxide samples that were discussed earlier.

Influence of t_1 on the ^{31}P MAS NMR spectra

The ^{31}P MAS NMR peak maxima for samples in the series with t_1 values ranging from 0 to 9000 min, and t_2 constant at 2 h, are also shown in Table 5. The spectra obtained for each of these samples consisted of one broad signal centred near −11

Can. J. Chem. Downloaded from www.nrcresearchpress.com by 46.23.64.124 on 09/08/12
For personal use only.

Can. J. Chem. Downloaded from www.nrcresearchpress.com by 46.23.64.124 on 09/08/12
For personal use only.

Fig. 7. ^{27}Al MAS NMR spectrum of amorphous aluminum hydroxyphosphate (sample PAl-5), t_1 = 100 min, t_2 = 2 h, P:Al = 0.17, prepared by precipitating alum at high alkalinity followed by the addition of phosphate. Spinning side bands appear on either side of the main signal about 80 ppm away.

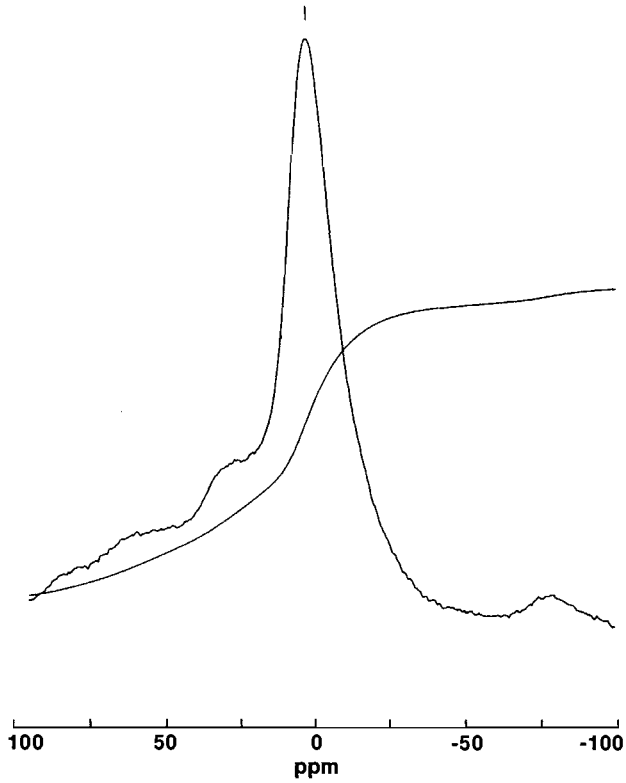

Fig. 8. ^{27}Al MAS NMR spectrum of calcined amorphous aluminum hydroxyphosphate (sample PAl-2), t_1 = 0 min, t_2 = 2 h, P:Al = 0.17, prepared by precipitating alum at high alkalinity in the presence of phosphate.

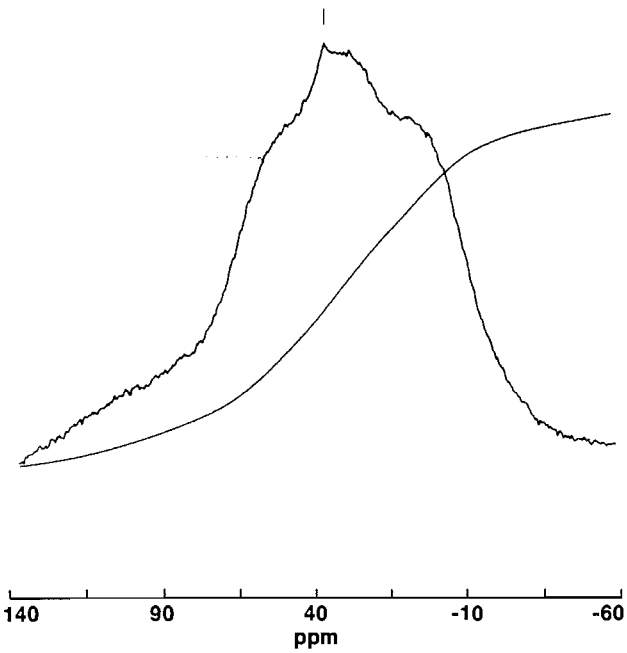

Fig. 9. ^{27}Al MAS NMR spectrum of calcined amorphous aluminum hydroxyphosphate (sample PAl-7), t_1 = 9000 min, t_2 = 2 h, P:Al = 0.17, prepared by precipitating alum at high alkalinity followed by the addition of phosphate.

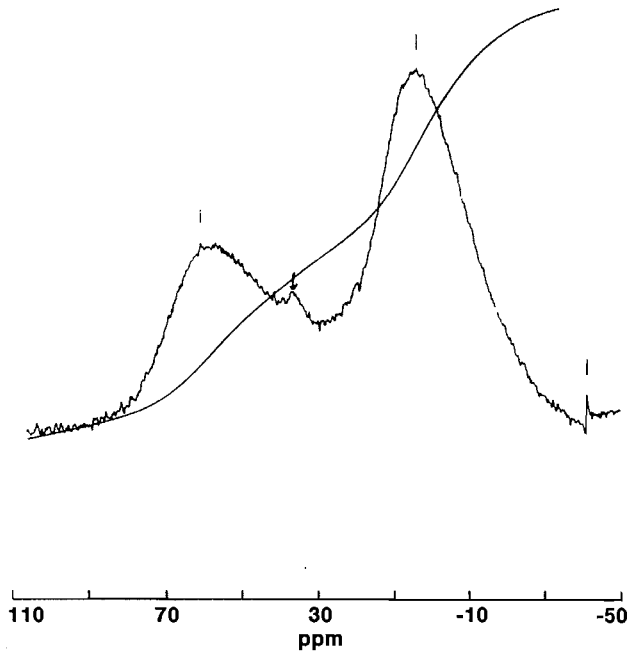

ppm, quite different from the variscite result of −19 ppm. For this set, the instrument parameters (including the number of scans) were held constant so that the integrated signal could be taken as proportional to the amount of phosphate adsorbed by the aluminum hydroxide. Although no calibration was carried out, the integrated peak areas showed that phosphorus content increased with decreasing values of t_1 (Table 6).

Influence of t_2 and the P:Al molar ratio on the nature of solid aluminum hydroxyphosphate

The influence of ageing in the presence of phosphate, t_2, and of the P:Al molar ratio on the structure of the aluminum hydroxyphosphate precipitates was also investigated. To ensure maximum phosphorus removal, a t_1 of 0 was chosen for all samples. Ageing times of 2 h and 3.5 months were chosen for t_2, and P:Al molar ratios of 0.17, 0.87, and 8.7 were used.

The MAS NMR peak maxima are shown in Table 7. As the P:Al molar ratio was increased from 0.17 to 0.87 and then to 8.7, the chemical shift of the main NMR peak moved from 4 to −4 ppm and then to −10 ppm (Figs. 10, 11, and 12). The extent of upfield shift was related to the amount of phosphate coordinated to the aluminum as noted above, except that, in this experiment, the difference was larger because the amount of phosphate was much higher than had been previously used. The larger proportion of phosphate in the precipitate was also reflected in the mass of the solids obtained. After drying at 110°C the masses of precipitates for material prepared using P:Al molar ratios of 0.17, 0.87, and 8.7 were in the ratios 1:1.6:2.3. After analysis for aluminum, phosphorus and water, the formulas of these solids were calculated to be $Al(HPO_4)_{0.16}(OH)_{2.7}\cdot 1.0H_2O$, $Al(HPO_4)_{0.8}(OH)_{1.4}\cdot 0.8H_2O$, and $Al(HPO_4)_{1.2}(OH)_{0.6}0.5H_2O$ for the three molar ratios, respectively. It is interesting that the molar ratio of phosphorus

Table 7. Peak maxima for ^{27}Al and ^{31}P MAS NMR spectra for aluminum hydroxyphosphates that were dried at 110°C and calcined. Peaks are listed in order of decreasing size. t_1 was 0 min for each sample.

			Chemical shift/ppm[a]			
			^{27}Al		^{31}P	
Sample	t_2/h	P:Al ratio	110°C	Calcined	110°C	Calcined
PAl-2	2	0.17	4 Br 30 SmBr 60 SmBr	39 Br 13 Br 53 Br	−11 Br	−15 Br
PAl-8	2880	0.17	6 Br	9 Br 65 Br	2 Br	0 Br
PAl-9	2	0.87	−4 Br 21 SmBr 45 SmBr	39 Sh 10 Sh	−8 Br	−28 Br
PAl-10	2592	0.87	−1 Br 29 SmBr 55 SmBr	45 Br 14 Br 65 Br	−4 Br	−9 Br
PAl-11	2	8.7	−10 Br 45 SmBr 14 SmBr	40 Sh 46 Sh	−8 Br	−14 Sh −9 Sh −27 Sh −1 Sh
PAl-12	2592	8.7	−7 Br 44 SmBr 19 SmBr	nd	nd	nd

[a]The aluminum chemical shift is referenced to a 0.2 M static aluminum nitrate solution and the phosphorus chemical shift is referenced to solid ammonium dihydrogen phosphate. Sh = sharp, Sm = small, Br = broad, nd = not determined.

to aluminum in the third solid is 1.2, greater than that of the 1:1 ratio in $AlPO_4$.

The NMR spectra of these samples also showed a small broad signal in the tetrahedral region and another effect of increasing the P:Al molar ratio was to augment this contribution. The presence of a strong broad signal at 45 ppm, near the location for $AlPO_4$, became more pronounced at the P:Al molar ratios of 0.87 and 8.7, such that it was clear that a tetrahedral aluminum was formed as a minor component of the precipitate (Figs. 10–12).

When the precipitate was allowed to remain in contact with the phosphate-containing solution for an extended time (t_2 = 3.5 months) the octahedral peak shifted from 4 to 6 ppm, from −4 to −1 ppm, and from −10 to −7 ppm for the 0.17, 0.87, and 8.7 molar ratio samples, respectively. This indicates that during the long ageing process there had been a loss of adsorbed phosphate that was likely related to the rise in pH noted earlier.

The ^{27}Al MAS NMR spectra of the calcined samples having a t_2 of 2 h and P:Al molar ratios of 0.87 and 8.7 (PAl-9 & PAl-11) are shown in Figs. 13 and 14. There were strong sharp signals at 39 ppm and at 40 and 46 ppm, respectively; both are characteristic of tetrahedral aluminum, which is the expected form after heating. The peak maxima for the ^{31}P MAS NMR spectra are also shown in Table 7.

Alum assisted activated sludge samples

Sludge samples retrieved from plant A of the KTPCP were analyzed by ^{27}Al and ^{31}P MAS NMR and the peak maxima from the resulting spectra are reported in Table 8. Each aluminum NMR spectrum contained a single broad peak near −1 ppm along with a broad shoulder peak centred near 55 ppm (Fig. 15). The chemical shift of the main peak indicates that there was a substantial quantity of phosphate associated with the aluminum in this material, similar to that used for the laboratory-prepared samples with the P:Al molar ratio of 0.87. The calcined sludge samples gave a single sharp NMR peak at 39 ppm (Fig. 16), which also occurred with calcined samples that had been prepared using a P:Al molar ratio of 0.87. The results indicated that the sludge contained aluminum solids that were mostly octahedral and that there was an approximately equal quantity of phosphorus and aluminum in the

Can. J. Chem. Downloaded from www.nrcresearchpress.com by 46.23.64.124 on 09/08/12
For personal use only.

Can. J. Chem. Downloaded from www.nrcresearchpress.com by 46.23.64.124 on 09/08/12
For personal use only.

Fig. 10. ^{27}Al MAS NMR spectrum of amorphous aluminum hydroxyphosphate, (sample PAl-2), $t_1 = 0$ min, $t_2 = 2$ h, P:Al = 0.17, prepared by precipitating alum at high alkalinity in the presence of phosphate.

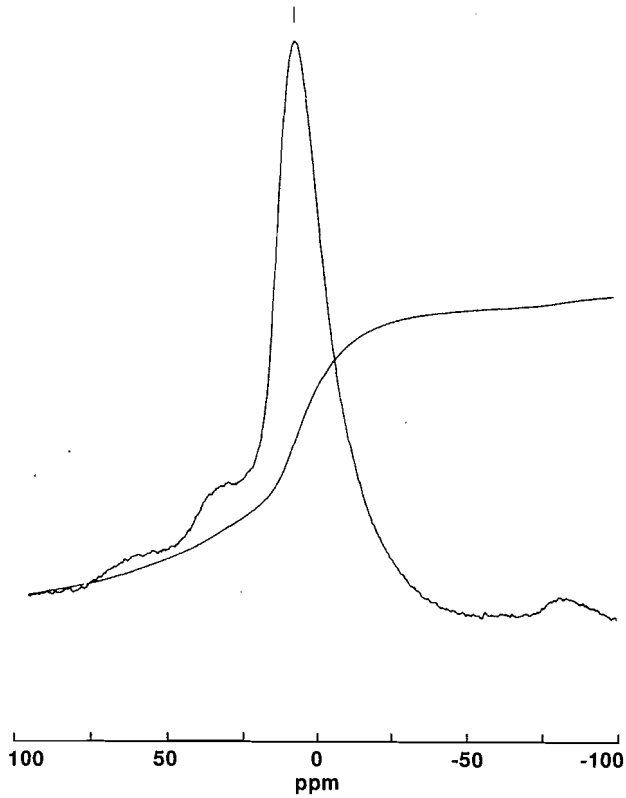

Fig. 11. ^{27}Al MAS NMR spectrum of amorphous aluminum hydroxyphosphate (sample PAl-9), $t_1 = 0$ min, $t_2 = 2$ h, P:Al = 0.87, prepared by precipitating alum at high alkalinity in the presence of phosphate.

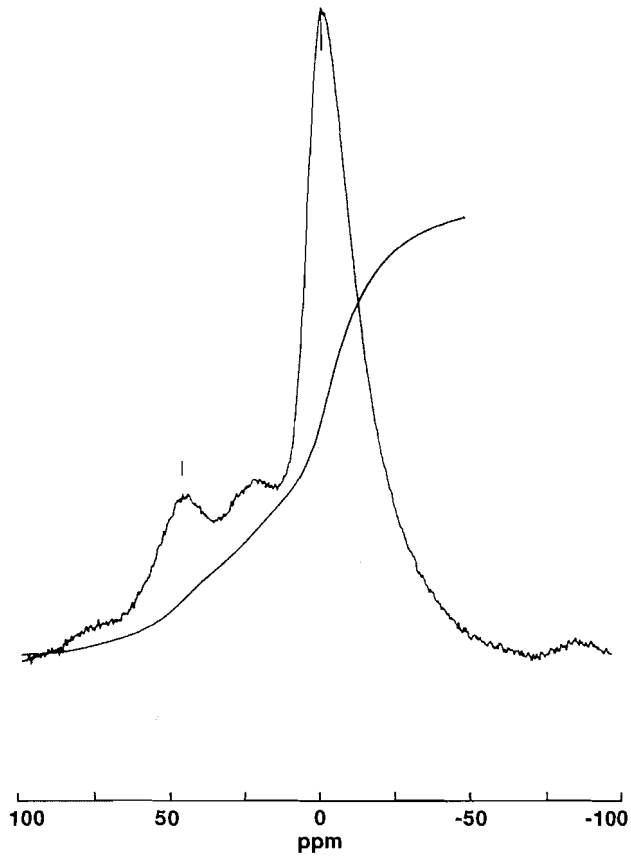

Table 8. Peak maxima for ^{27}Al and ^{31}P MAS NMR spectra for aerator sludge samples obtained from an activated sludge treatment plant, dried at 110°C and calcined, and listed in order of decreasing peak size.

		Chemical shift/ppm[a]			
		^{27}Al		^{31}P	
Sample	Aerator location	110°C	calcined	110°C	calcined
S-1	Before alum addition	−2 Br 55 SmBr	39 Sh	−8 Br	−28 Br
S-2	Before alum addition	0 Br 55 SmBr	39 Sh	−8 Br	−28 Br 2 SmBr
S-3	After alum addition	−1 Br 58 SmBr	39 Sh	−8 Br	−28 Br 2 SmBr
S-4	Secondary recycle	−0 Br 46 SmBr	39 Sh	−8 Br	−28 Br 2 SmBr

[a]The aluminum chemical shift is referenced to a 0.2 M static aluminum nitrate solution and the phosphorus chemical shift is referenced to solid ammonium dihydrogen phosphate. Sh = sharp, Sm = small, Br = broad.

sludge. Chemical analysis of the aerator sludge confirmed this by showing that the particulate aluminum and phosphorus concentrations were 107.9 and 96.5 mg L^{-1}, respectively, corresponding to a molar ratio of 0.78 (2). The small broad peak at 55 ppm is an indication that a portion of aluminum exists in the tetrahedral form and is possibly due to an aluminum oxide.

The peak maxima results of the ^{31}P MAS NMR spectra are also reported in Table 8. Each sample had a broad signal at −8

Can. J. Chem. Downloaded from www.nrcresearchpress.com by 46.23.64.124 on 09/08/12
For personal use only.

Fig. 12. ^{27}Al MAS NMR spectrum of amorphous aluminum hydroxyphosphate (sample PAl-11), $t_1 = 0$ min, $t_2 = 2$ h, P:Al = 8.7, prepared by precipitating alum at high alkalinity in the presence of phosphate.

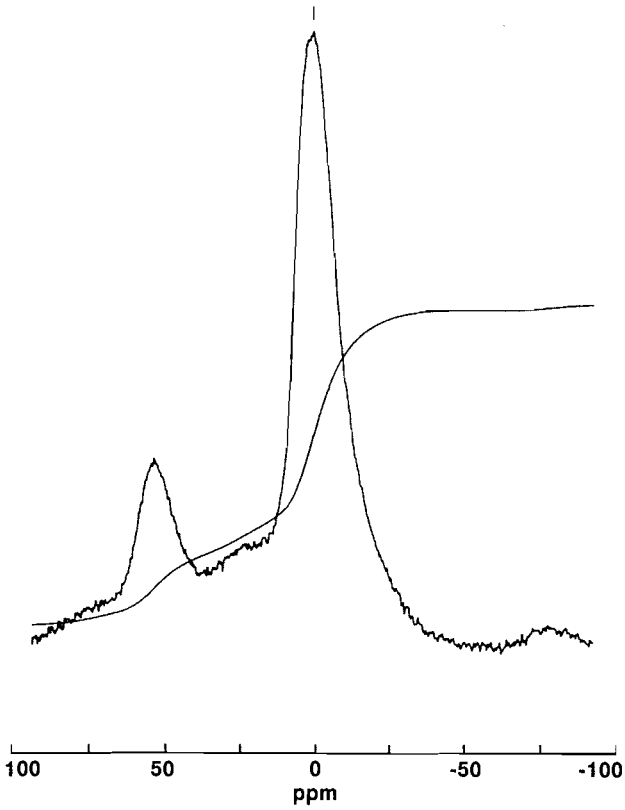

Fig. 13. ^{27}Al MAS NMR spectrum of calcined amorphous aluminum hydroxyphosphate (sample PAl-9), $t_1 = 0$ min, $t_2 = 2$ h. P:Al = 0.87, prepared by precipitating alum at high alkalinity in the presence of phosphate. Spinning side bands appear on either side of the main signal about 80 ppm away.

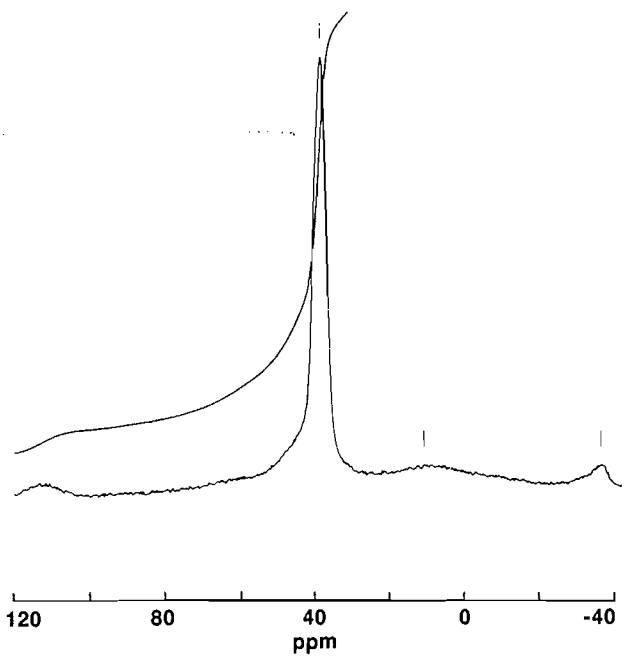

Fig. 14. ^{27}Al MAS NMR spectrum of calcined amorphous aluminum hydroxyphosphate (sample PAl-11), $t_1 = 0$ min, $t_2 = 2$ h, P:Al = 8.7, prepared by precipitating alum at high alkalinity in the presence of phosphate. One spinning side band appears at −50 ppm.

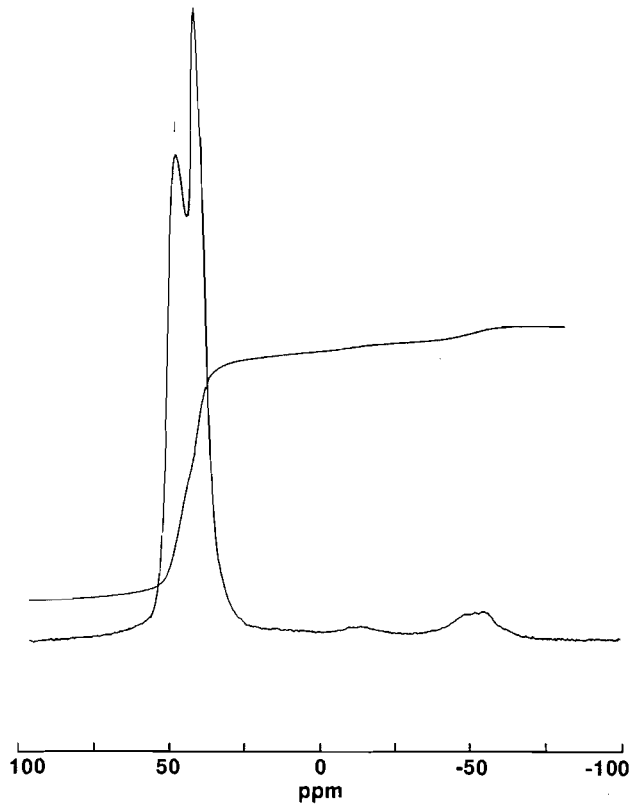

Fig. 15. ^{27}Al MAS NMR spectrum of an aerator sludge (sample S-1). The sample was obtained at a point upstream from the alum addition location in an activated sludge treatment plant in Kingston, Ontario.

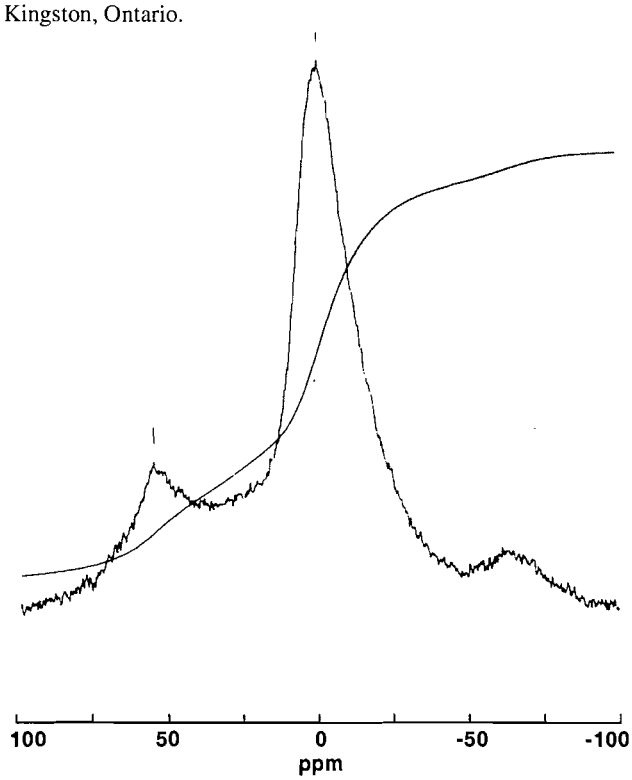

Fig. 16. ^{27}Al MAS NMR spectrum of calcined aerator sludge (sample S-1). The sample was obtained at a point upstream from the alum addition location in an activated sludge treatment plant in Kingston, Ontario. Spinning side bands appear on either side of the main peak 90 ppm away.

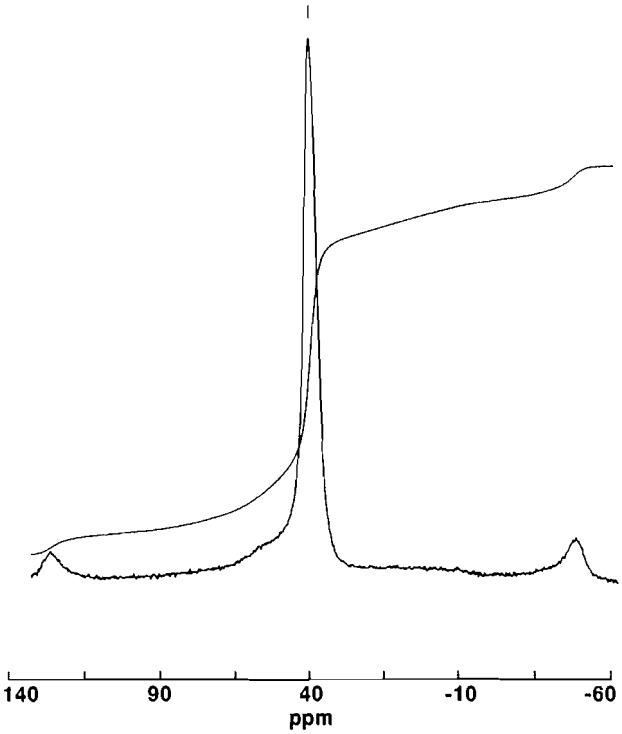

ppm that was similar to those obtained from samples precipitated at high alkalinity, but different from that of variscite at −19 ppm. The calcined samples had a signal at −28 ppm, again similar to that obtained for the samples prepared with a molar ratio of 0.87, but different from the calcined variscite sample.

Summary

The technique of high-resolution solid-state ^{27}Al MAS NMR provides useful information concerning structures of amorphous aluminum hydroxide and hydroxyphosphate solids. The ^{31}P MAS NMR, while not as informative, provided data that supported the observations from the aluminum NMR results. The ^{27}Al MAS NMR analysis showed that amorphous aluminum hydroxides and aluminum hydroxyphosphates contained mostly octahedral aluminum. In the case of the aluminum hydroxyphosphates, a formula such as $Al(HPO_4)_{0.8}(OH)_{1.4}0.8\ H_2O$, based on both the NMR information and chemical analysis, would best represent the structure of the amorphous material formed in a wastewater treatment process. The ^{27}Al MAS NMR results also showed that when these solids were calcined the aluminum was converted from an octahedral to a tetrahedral coordination.

Other results obtained using MAS NMR were consistent with a process in which aluminum hydrolyzes immediately upon entry into a highly alkaline wastewater stream followed by subsequent removal of phosphate by an adsorption process onto the surface of the hydrous aluminum oxide. The formation of tetrahedral $AlPO_4$ occurred, but only to a small extent and only under conditions of high ratios of soluble phosphate to soluble aluminum (in this case, a molar ratio of 8.7), which are unlikely to exist in the ASP. With increasing phosphorus content of the solids, the aluminum NMR results showed an upfield shift of the NMR signal (from 4 to −10 ppm). A trend related to the age of the aluminum (t_1) was also established; this indicated that with increased age prior to phosphate addition, less phosphorus was adsorbed onto the solid. The trend was again followed by observing the upfield shift of the MAS NMR signal. The degree of mixing at the time of alum addition made no difference in the form of the aluminum solid as observed by MAS NMR.

Acknowledgements

The authors wish to thank Ms. Sue Blake for assistance in performing the MAS NMR measurements, Prof. R.D. Heyding for carrying out XRD measurements on many of the solids, and Prof. B.K. Hunter for helpful discussions. Thanks are also due to David Cybulski for work performed and the Natural Sciences and Engineering Research Council of Canada and the School of Graduate Studies at Queen's University for financial support.

References

1. R.W. Slater and G.E. Bangay. *In* Phosphorus management strategies for lakes. *Edited by* C.R. Loehr, C.S. Martin, and W. Rast. Ann Arbor Science, Ann Arbor, Mich., 1980. pp. 13–25.
2. S.J. Duffy, J.E. Deutschman, and G.W. vanLoon. Water Pollut. Res. J. Can. **29**, 487 (1994).
3. R.P.G. Bowker and H.D. Stensel. *In* Phosphorus removal from wastewater. Noyes Data Corp., Park Ridge, N.J. 1990. pp. 54–81.
4. S.G. Nutt. Water Pollut. Res. J. Can. **26**, 495 (1991).
5. R.W. Ockershausen. Water Wastes Eng. **11**, 56 (1974).
6. T. Goldshmid and A.J. Rubin. Sep. Sci. Technol. **23**, 2269 (1988).
7. W.P. Rothwell, J.S. Waugh, and J.P. Yesinowski. J. Am. Chem. Soc. **102**, 2637 (1980).
8. D. Muller, W. Gessner, H. Behrens, and G. Scheler. Chem. Phys. Lett. **79**, 59 (1981).
9. D. Muller, D. Hoebbel, and W. Gessner. Chem. Phys. Lett. **84**, 25 (1981).
10. D. Muller, E. Jahn, G. Ladwig, and U. Haubenreisser. Chem. Phys. Lett. **109**, 332 (1984).
11. D. Muller, W. Gessner, A. Samoson, E. Lippmaa, and G. Scheler. J. Chem. Soc. Dalton Trans. 1277 (1986).
12. S.F. Dec, G.E. Maciel, and J.J. Fitzgerald. J. Am. Chem. Soc. **112**, 9069 (1990).
13. B.A. Huggins and P.D. Ellis. J. Am. Chem. Soc. **114**, 2098 (1992).
14. A.K. Cheetham and P. Day. *In* Solid state chemistry techniques. Clarendon Press, Oxford. 1987. p. 206.
15. J.A. Martens, B. Verlinden, M. Mertens, P.J. Grobet, and P.A. Jacobs. *In* Zeolite synthesis. American Chemical Society, Washington, D.C. 1989. pp. 305–328.
16. J. Klinowski. Anal. Chim. Acta, **283**, 929 (1993).
17. C.S. Blackwell and R.L. Patton. J. Phys. Chem. **88**, 6135 (1984).
18. S. Hayashi. Annu. Rep. NMR Spectrosc. **28**, 77 (1994).
19. S.M. Bradley and J.V. Hanna. J. Chem Soc. Chem. Commun. 1249 (1993).
20. A.C. Kunwar, A.R. Thompson, H.S. Gutowsky, and E. Oldfield. J. Magn. Reson. **60**, 467 (1984).

Can. J. Chem. Downloaded from www.nrcresearchpress.com by 46.23.64.124 on 09/08/12
For personal use only.

21. S.J. Duffy and G.W. vanLoon. Environ. Sci. Technol. **28**, 1950 (1994).
22. J.A. Davis and J.D. Hem. *In* The environmental chemistry of aluminum. *Edited by* G. Sposito. CRC Press, Boca Raton, Fla. 1989. pp. 185–220.
23. R.C. MacKenzie and G. Berggren. *In* Differential thermal analysis. *Edited by* R.C. MacKenzie. Academic Press Inc., New York. 1970. pp. 271–302.
24. D. Dollimore. *In* Thermal analysis – techniques & applications. *Edited by* E.L. Charsley and S.B. Warrington. The Royal Society of Chemistry, Cambridge. 1992. pp. 238–264.
25. D. Muller, I. Grunze, E. Hallas, and G.Z. Ludwig. Anorg. Allg. Chem. **500**, 80 (1983).
26. Z.R. Hinedi, A.C. Chang, and J.P. Yesinowski. Soil Sci.Soc. Am. J. **53**, 1053 (1989).
27. R.J.P. Williams. J. Chem Soc. Chem. Commun. 1051 (1981).

Can. J. Chem. Downloaded from www.nrcresearchpress.com by 46.23.64.124 on 09/08/12
For personal use only.

Base-catalyzed ring openings of benzocyclobutenones and -ols

J.C. Bradley and T. Durst

Abstract: The base-catalyzed ring opening of a number of isomeric *E*- and *Z*-benzylidenebenzocyclobutenones and -ols has been studied in both protic and aprotic solvents. Cleavage of the C1—C2 bond results in the formation of stilbenes with mainly, and at times exclusively, retained stereochemistry. For the alcohols, these results point to an oxyanion-induced carbon–carbon bond cleavage leading to a vinyl anion that is protonated with retention of configuration in the protic solvents rather than to an electrocyclic ring opening to an alkoxy *o*-quinodimethane. Reaction of the *Z* isomer of benzylidenebenzocyclobutenol with methyllithium in THF at 20°C causes isomerization to the *E* isomer, cleavage of the C1—C2 bond, and recyclization of the resultant isomerized vinyl anion.

Key words: benzylidenebenzocyclobutenones, base-catalyzed ring opening; benzylidenebenzocyclobutenols, base-catalyzed ring opening.

Résumé : On a étudié l'ouverture de cycle catalysée par les bases, en solvants protiques ainsi qu'aprotiques, d'un certain nombre de *E* et *Z* benzylidènebenzocyclobuténones et -ols. Le clivage de la liaison C1—C2 conduit à la formation de stilbènes qui, d'une façon générale et quelquefois exclusive, conservent la stéréochimie de départ. Pour les alcools, ces résultats suggèrent l'existence d'un clivage de liaison carbone–carbone induit par un oxyanion qui conduit à un anion vinylique qui, dans les solvants protiques, subit plutôt une protonation avec rétention de configuration qu'une ouverture électrocyclique de cycle conduisant à une alkoxy-*o*-diquinométhane. La réaction de l'isomère *Z* du benzylidènebenzocyclobuténol avec le méthyllithium dans le THF, à 20°C, provoque une isomérisation en isomère *E*, un clivage de la liaison C1—C2 et une recyclisation de l'anion vinylique isomérisé qui en résulte.

Mots clés : benzylidènebenzocyclobuténones, benzylidènebenzocyclobuténols, ouverture de cycle catalysée par les bases.

[Traduit par la rédaction]

Can. J. Chem. Downloaded from www.nrcresearchpress.com by 46.23.64.124 on 09/08/12
For personal use only.

Introduction

The base-catalyzed cleavage of benzocyclobutenones, **1**, and -butenols, **2**, has been studied by a number of authors with the view of determining the selectivity between the cleavage of the aryl CO bond (C1—C7), bond (a), leading to phenylacetic acids and the benzyl CO bond (C1—C2), bond (b), resulting in the formation of *o*-toluic acids (1–5). In the case of benzocyclobutenols, the question of whether the intermediate obtained upon cleavage of bond (b) is best described as a benzylic carbanion, **3**, or, a 1-alkoxy-*o*-quinodimethane, **4**, has also been addressed (6). Factors that alter the ratio of the bond (a) to bond (b) cleavage in benzocyclobutenones are easily rationalized. In the case of **1** (R = H), treatment with hydroxide ion gives approximately equal amounts of phenylacetic and *o*-toluic acids (1). Addition of an anion-stabilizing group either in the aromatic ring or at the 2-position results in predictable changes in the bond (a) to (b) ratio. For example, treatment of 6-methoxybenzocyclobutenone with ethanolic KOH leads almost exclusively to 3-methoxyphenylacetic acid (2, 3), while replacement in **1** of an α-hydrogen by a bromine results only in the rupture of bond (b) (4) (Scheme 1).

Treatment of benzocyclobutenols with strong bases in alcohols or water gives almost exclusive cleavage of the (b) bond, affording *o*-methylbenzaldehydes (1, 5, 6). The rate of ring opening in the oxyanion **5** is considerably accelerated relative to that in **2** and requires only minutes at temperatures as low as −78°C. In contrast, the thermal ring opening in **2** occurs at a synthetically useful rate in refluxing toluene. The rate enhancement has been touted as an example of an oxyanion-accelerated electrocyclic ring opening (6).

Choy and Yang (6*a*) have attempted to determine, by trapping experiments with dimethyl fumarate and dimethyl maleate, whether **3** or **4** is the representation of the ring better opened hybrid. The results were, however, somewhat ambiguous. Approximately 80% of the cycloaddition products obtained from **2** (R = H) upon treatment with NaH in THF at 0°C in the presence of dimethyl maleate had retained the *cis* geometry of the dienophile, but in 20% the stereochemical integrity of the alkene was lost. A similar reaction of **2** (R = Ph) at −78°C gave only the expected Diels–Alder product. These results could be explained by a combination of a concerted cycloaddition beginning with **4** and a competing tandem Michael addition–cyclization pathway commencing with **3** or, more simply, by assuming that the Michael addition

Received January 2, 1995.

J.C. Bradley and T. Durst.[1] Ottawa–Carleton Chemistry Institute, Department of Chemistry, University of Ottawa, Ottawa, ON K1N 6N5, Canada.

[1] Author to whom correspondence may be addressed. Telephone: (613) 562-5800, ext. 6072. Fax: (613) 562-5170.

Scheme 1.

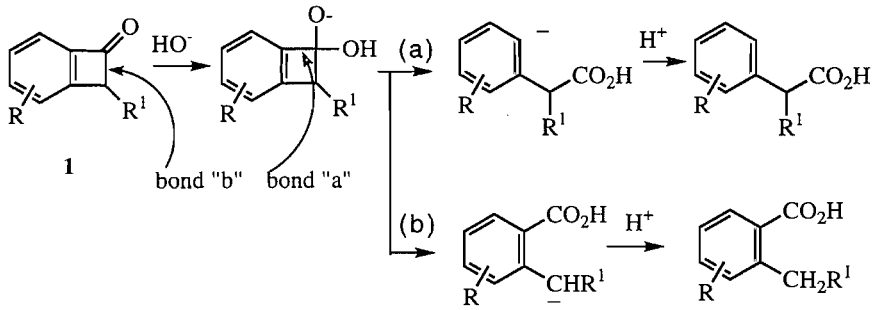

Scheme 2.

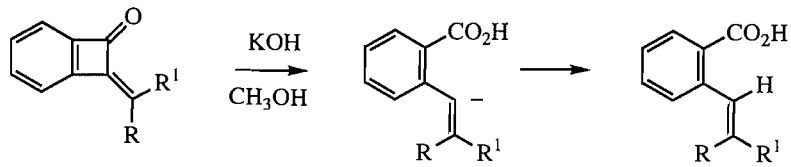

6E, R = Ph, R^1 = H
6Z, R= H, R^1 = Ph

8, R = Ph, R^1 = H
9, R = H, R^1 = Ph

7E, R = H, R^1 = Ph
7Z, R = Ph, R^1 = H

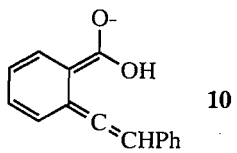

10

intermediate from **3** and dimethyl maleate is partly isomerized prior to cyclization when R = H at 0°C, but not at −78°C when R = Ph. A study by Swenton et al. (*6b*) with a different substrate also addressed the above question; it too failed to give a definitive answer. A very recent paper by Olofson and coworkers (7) reports that the ring opening of the sodium salts of **5** in the presence of aromatic aldehydes affords excellent yields of δ-lactols. Benzylic anions, e.g. 3, are assumed to be intermediates (8).

Access to both isomeric benzylidenebenzocyclobutenones **6***E* and **6***Z* (*8a*) and a variety of related benzocyclobutenols provided us with a unique opportunity to probe the nature of the intermediates obtained upon cleavage of bond (b) in these compounds under basic conditions. If the ring-opened intermediate is best described as a vinyl carbanion, such cleavage should result in the formation of the acids **7***Z* from **6***E* via **8** and **7***E* from **6***Z* via **9**. These expectations are based on the reasonable assumption that the vinyl anions **8** and **9** maintain their stereochemical integrity and protonate with retention of configuration (9). In contrast, description of the intermediate as an alkoxy-*o*-quinodimethane leads to the allenic derivative **10** from both **6***E* and **6***Z*. Subsequent protonation should lead to the same product mixture from both **6***E* and **6***Z* (Scheme 2).

Discussion and results

(a) Benzylidenebenzocyclobutenones in protic media

Reaction of **6***E* and **6Z** with methanolic KOH at 25°C afforded a 4:1 mixture of (a) to (b) cleavage products in the case of **6***E* and 1:5 for **6***Z*. Importantly, the (b) bond cleavage products were formed exclusively with retention of configuration. No crossover products were detected in the NMR of the crude products obtained from either **6***E* or **6***Z*. The higher (b) to (a) cleavage in **6***Z* vs. **6***E* is likely due to the greater strain in the alkoxide derived from the *Z* isomer compared to that from the *E* isomer, thereby weakening the C1—C2 bond. Similar results were obtained when $CH_3O^-Na^+/CH_3OH$ was used as the basic medium except that somewhat lower (a) to (b) ratios were observed: 2:1 for **6***E* and 1:7 for **6***Z*. These results are consistent with the description of the intermediates in the ring opening of **6***E* and **6***Z* as the vinyl anions **8** and **9**, respectively, rather than the allene alkoxide **10**.

Treatment of the 4,5-methylenedioxybenzylidenebenzocyclobutenones **11** with KOH in methanol gave higher values for the (a) to (b) ratios than those obtained with **6**. Only the bond (a) cleavage product **12** was observed with **11***E* while **11***Z* gave a 1:1 mixture of **13** and **14**. Again, the bond (b) cleavage product **14** was uncontaminated with its geometric isomer, constistent with a vinyl anion intermediate, Scheme 3.

(b) Benzylidenebenzocyclobutenols

Reaction of the tertiary alcohol **15***Z* with 5 N KOH afforded a 13:1 mixture of the (b) vs. (a) cleavage products **16** and **17**, respectively, while **15***E* gave a 1:1 mixture of **17** and **18**. The observed stereochemistry of the (b) cleavage products **16** and **18** is consistent only with a vinyl carbanion intermediate. The product **17** was tentatively identified by NMR and GC–MS. It appeared to be formed as a roughly equal mixture of the two possible geometric isomers from both **15***E* and **15***Z*. Isomerization of this α,β-unsaturated ketone via a hydroxide ion addition-elimination sequence should be quite facile.

Interestingly, the *Z* alcohol **19** afforded a 6:1:1 mixture of

Can. J. Chem. Downloaded from www.nrcresearchpress.com by 46.23.64.124 on 09/08/12
For personal use only.

Scheme 3.

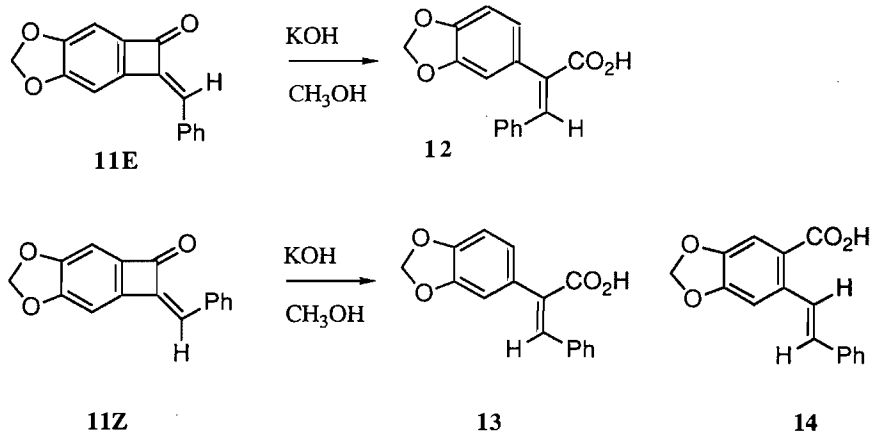

Table 1. Relative amounts of cleavage products from benzylidenebenzocyclobutanols.

15*E*, R = Ph	—	**18**, R = Ph (1)	**17**, R = Ph (1)
15*Z*, R = Ph	**16**, R = Ph (13)	—	**17**, R = Ph (1)
19*Z*, R = CH_3	**20***E*, R = CH_3 (6)	**20***Z*, R = CH_3 (1)	**21**, R = CH_3 (1)
22*E*, R = H	R = CH_3 (6)	R = H (2.5)	R = H (1)
22*Z*, R = H	R = CH_3 (6)	R = H (1)	—

the (b) cleavage products **20***E* and **20***Z* and the (a) cleavage product **21**. Analysis of the results of the reaction of **19***E* in methanolic KOH was complicated by further reaction of the products due to the refluxing methanol reaction conditions required to break the cyclobutene ring. Finally in this series, the secondary alcohols **22***E* and *Z* gave even higher loss of stereochemical integrity in the (b) bond fragmentation products. These results are summarized in Table 1.

Overall, the results obtained in the base-catalyzed fragmentaion of the above benzylidenebenzocyclobutenols are consistent with a vinyl carbanion rather than the allenic alkoxide description for the intermediate, The observed trend: complete stereochemical retention in the (b) cleavage products from **15***E* and *Z*, to some loss in the products obtained from **19***Z* and even more from those derived from **22***E* and **22***Z*, indicates a decreasing barrier to inversion in the vinyl anion **23** on going from R = Ph to CH_3 to H. This suggests an increasing contribution of the allenic alkoxide resonance hybrid **24** as the R group becomes smaller, thereby lowering the barrier to inversion.

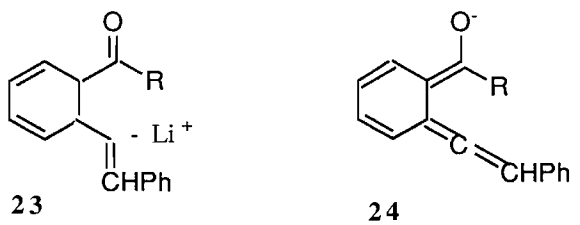

23 **24**

R = H, CH_3, Ph

(c) Reactions in aprotic media

The alkoxy anion-induced ring cleavage starting with the alcohols **22***E* and *Z* was also studied under aprotic conditions with the hope of trapping or observing spectroscopically the ring-opened anionic intermediates.

Thus addition of 1 equivalent of CH_3Li to a solution of **22***Z* in THF at −78°C gave a ^{13}C NMR spectrum that corresponded to the alkoxide **27***Z*. No significant changes were observed upon warming to near 0°C, but on further warming to about 20°C for 1 h the spectrum changed and corresponded to one containing **27***E* as the major component. No further changes were observed when the solution was left at 20°C for an additional 16 h. Quenching of the solution gave **22***E* as the major product. Similar treatment of **22***E* resulted in the recovery of the starting material.

Reaction of **22***Z* with 2 equivalents of CH_3Li in THF at room temperature afforded a mixture of products: recovered **22***Z*, isomerization product **22***E*, and the ring-opened products **25** and **26** in a ratio of 0.1:1.1:0.2 as judged by GC analysis. The structures of the alcohols **25** and **26** were assigned on the basis of their spectroscopic properties and via unambiguous synthesis from the corresponding 2-formylstilbenes.

Can. J. Chem. Downloaded from www.nrcresearchpress.com by 46.23.64.124 on 09/08/12
For personal use only.

Scheme 4.

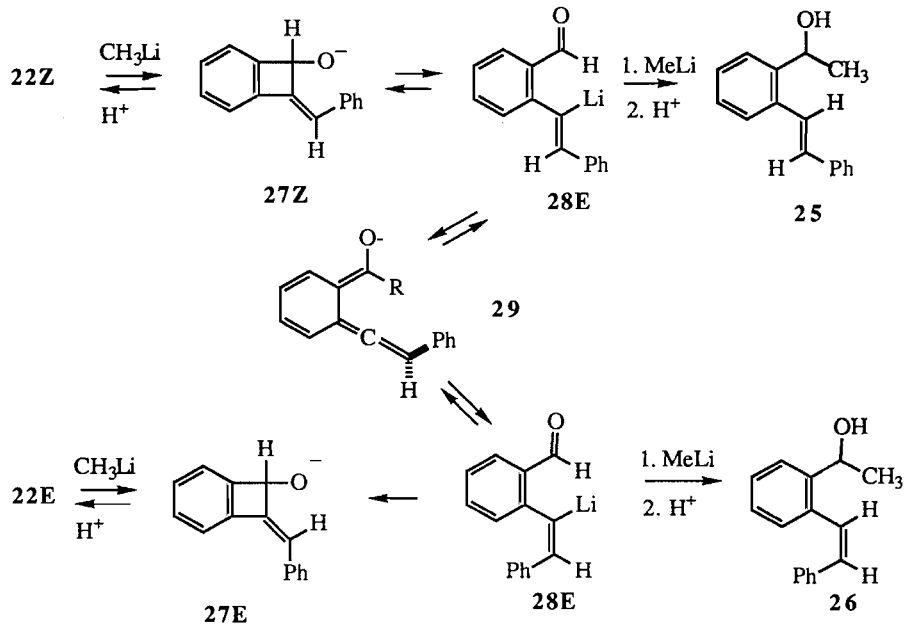

These results are interpreted as shown in Scheme 4. The lithio alkoxide **27***Z* is stable to 0°C, but opens to the vinyllithium derivative **28***E* when warmed to 20°C. In the absence of rapid quenching by a protic solvent, this species can isomerize to **28***Z* and then recyclize to **27***E*. Both **28***E* and **28***Z* are trapped by the excess CH_3Li to give the alcohols **25** and **26**, respectively.

Surprisingly, the reaction of **22***Z* with 10 equivalents of CH_3Li at room temperature did not result in a larger percentage of trapping of the aldehydes **28***E* and **28***Z* with CH_3Li. Instead, these conditions retarded considerably the isomerization of **22***Z* to **22***E*, giving ratios of **22***Z*:**22***E*:**25** + **26** of 3:1:0.2 (GC analysis). We initially postulated that "protection" of the alkoxide **27***Z* toward ring opening might be due to a second metallation either at the *ortho* aromatic or a vinyl position and that such a metallation stabilizes the alkoxide, thereby making ring opening more difficult. When this was tested by quenching the reaction mixture with D_2O, no deuterium incorporation was found in the recovered **22***Z* by MS, suggesting possible stabilization of **27***Z* by the excess CH_3Li via aggregation (10).

Conclusions

The anionic ring opening of the C1—C2 bond in benzylidenebenzocyclobutenols and -ones is most readily explained as occurring via carbon–carbon cleavage resulting in vinyl anions rather than an oxyanion-promoted electrocyclic ring opening. This decision is based on the trapping of the aldehyde-vinyllithium intermediates **27***E*/*Z* with CH_3Li, and the observation that the base-catalyzed ring openings in protic media result in the formation of stilbenes with retention of configuration. It is difficult to explain these results assuming that the intermediates have alkoxyallenic (*o*-quinodimethane) structures.

Experimental section

General

Details concerning the purification of solvents and reagents, chromatographic procedures, and the aquisition of spectroscopic data have been described in earlier publications (8).

Reaction of E*-2-benzylidenebenzocyclobutenone,* **6***E, with KOH*

A solution of **6***E* (47 mg) in methanolic KOH (5 N, 3 mL) was warmed to 40°C for 1.5 h and then kept at room temperature for a further 18 h. The solution was acidified with 5 mL of 5 N HCl and extracted thoroughly with ether. The yield of acids, a 4:1 mixture of *E*-2,3-diphenylpropenoic acid (11) (δ: 7.95, s, CHPh) and 2-(*Z*-2-phenylethenyl)-benzoic acid **7***Z* (12) (δ: 6.62, d, J = 12.4 Hz, CHPh), was 50.6 mg (96%). The mixture was esterified with ethereal diazomethane and the resultant esters were separated by radial chromatography (silica gel, 1:1 hexane–CH_2Cl_2).

For methyl *E*-2,3-diphenylpropenate (13): IR: 1709 cm^{-1}; ^1H NMR, δ: 3.77 (3H, s), 6.96–7.04 (2H, m), 7.08–7.23 (5H, m), 7.3–7.4 (3H, m), 7.85 (lH, s); ^{13}C NMR, δ: 52.4, 127.8, 128.2, 128.7, 129.1, 129.7, 130.6, 132.4, 134.6, 135.9, 140.5, 168.4; HRMS, calcd. for $C_{16}H_{14}O_2$: 238.0994; found: 238.0999.

For the methyl ester of **7***Z*: ^1H NMR, δ: 3.87 (3H,s), 6.63 (lH, d, J = 12.4 Hz), 7.0–7.3 (9H, m), 7.96 (lH, m); ^{13}C NMR, δ: 52.0, 126.9, 127.1, 128.0, 129.2, 129.3, 129.6, 130.4, 130.6, 131.1, 131.9, 136.7, 139.6, 167.5; HRMS, calcd. for $C_{16}H_{14}O_2$: 238.0994; found: 238.0998.

Reaction of 2-benzylidenebenzocyclobutenone, **6***Z, (8*a*) with KOH*

The enone **6***Z* (50 mg) was treated as above yielding 49.2 mg of a 5:1 mixture of 2-(*E*-2-phenylethenyl)-benzoic acid (14), **7***E*, (δ = 7.02, J = 16.4 Hz) and *Z*-2,3-diphenylpropenoic acid (11) (δ = 7.08, CHPh). Treatment with diazomethane afforded the corresponding esters .

For methyl *Z*-2,3-diphenylpropenoate: ^1H NMR, δ: 3.76 (3H, s), 7.02 (lH, s), 7.2–7 5 (10H, m); ^{13}C NMR, δ: 52.2, 126.5 (2), 128.2, 128.4, 128.5, 128.7, 131.6, 134..9, 135.7,

Can. J. Chem. Downloaded from www.nrcresearchpress.com by 46.23.64.124 on 09/08/12
For personal use only.

Can. J. Chem. Downloaded from www.nrcresearchpress.com by 46.23.64.124 on 09/08/12
For personal use only.

136.9, 170.1; HRMS, calcd. for $C_{16}H_{14}O_2$: 238.0994; found: 238.0974.

For the methyl ester of **7*E***: ^{1}H NMR, δ: 3.92 (3H, s), 7.00 (lH, d, J = 16.2 Hz), 7.23–7.39 (4 H, m) 7.50 (lH, t, J = 8 Hz), 7.55 (2H, d, J = 8 Hz), 7.71 (lH, d, J = 8 Hz), 7.92 (lH, dd, J = 8, 1.4 Hz), 7.98 (lH d, J = 16.2 Hz); ^{13}C NMR, δ:52.1, 126.8 (2), 126.9, 127.1 127.4, 128.5, 128.6, 130.6, 131.4, 132.1 137.4, 139.2, 167.8; HRMS, calcd. for $C_{16}H_{14}O_2$: 238.0994; found: 238.0989.

Reaction of E-*2-benzylidene-4,5-methylenedioxybenzocyclobutenone,* ***11****E, (8a) with aqueous KOH*

The enone **11*E***, (8*a*) (59.5 mg) was allowed to react in 3 mL of methanolic KOH for 22 h at room temperature. Work-up, as above, afforded 62.4 mg of **12** as a yellowish solid, insoluble in common organic solvents. IR (KBr): 3500–2700 cm^{-1}; ^{1}H NMR(D_2O/K_2CO_3), δ: 5.93 (2H, s), 6.62 (lH, dd, J = 8.0, 1.7 Hz), 6.66 (lH, dd, J = 1.7, 0.5 Hz), 6.82 (lH, dd, J = 8.0, 0.5 Hz), 7.0–7.2 (6H, m), 7.42(1H, s).

Reaction of Z-*2-benzylidene-4,5-methylenedioxybenzocyclobutenone,* ***11****Z, (7a) with aqueous KOH*

This compound (8*a*) (50.2 mg) when reacted in the same manner as **11*E*** afforded a mixture whose ^{1}H NMR (D_2O/K_2CO_3) was interpreted as a 1:1 mixture of **13** and **14** with the key peaks occurring at δ: 7.0 (d, J = 16 Hz) for **13** and 6.85 (lH, dd, J = 8.0, 1.5 Hz), 7.09 (lH, d, J = 1.5 Hz) for **14**. These compounds were not further characterized.

Cleavage reactions of E- *and* Z-*1-phenyl-2-benzylidenebenzocyclobutenone,* ***15****E and* ***15****Z*

Solutions of these compounds (8*b*) in 5 N methanolic KOH were kept at room temperature for 3 days and then worked up by acidifying the solution and extracting with ether, as above. The products were characterized by ^{1}H NMR. Ratios were determined by GC. See Table 1.

From **15*Z*** the major product was 2′-benzoyl-*trans*-stilbene, **16**. ^{1}H NMR, δ:7.04 (IH, d, J = 16.3 Hz), 7.18 (lH, d, J = 16.2 Hz), 7.1–7.9 (14H, m); MS.: 284 (100, $M^{+\cdot}$), 283 (16), 265 (9), 207 (35), 206 (23), 178 (41), 77 (24); HRMS, calcd. for $C_{21}H_{16}O$: 284.1201; found: 284.1220.

From **15*E***, the major products were separated by silica gel radial chromatography plates using 2:1 hexanes–CH_2Cl_2. 2′-Benzoyl *cis*-stilbene, **18**, had ^{1}H NMR, δ:6.48 (lH, d, J = 12.2 Hz), 6.60 (1H, d, J = 12.2 Hz), 7.06–7.18 (5H, m), 7.28–7.33 (3H, m), 7.36–7.44 (3H, m), 7.53 (lH, t, J = 7.3 Hz), 7.44, (2H, d, J = 7.0 Hz); ^{13}C NMR, δ: 126.7 127.2, 128.1, 128.3 128.5, 128.6, 129.0, 130.1, 130.2, 130.3, 131.4, 133.0, 133.6, 136.9, 137.6, 138.6, 197.8; MS: 284 (100, $M^{+\cdot}$); HRMs, calcd. for $C_{21}H_{16}O$: 284.1201; found: 284.1212.

l-Benzoyl-1,2-diphenylethylene, **17**, was obtained as a 1:1 mixture of isomers. The ^{1}H NMR, spectrum of the mixture showed absorption only in the δ = 7–8 ppm region. The carbonyl carbons of the two isomers occurred at δ = 197.3 and 199.3. The MS of the mixture had peaks at 284 (95, $M^{+\cdot}$), 207 (10, M − C_6H_5), 206 (23, M − C_6H_6), 179 (25, M − PhCO), 105 (100, $PhCO^+$).

Preparation of E-*2-benzylidene-1-methylbenzocyclobutenol,* ***19****E*

To a solution of 96 mg benzocyclobutenone **6*E*** (0.46 mmol) in THF (10 mL) at 78°C was added 0.92 mmol of CH_3Li. The reaction mixture was stirred for 30 min at 78°C, allowed to warm to room temperature, and quenched with saturated NH_4Cl solution. Further work-up followed by chromatography (1:3 hexane:CH_2Cl_2, increasing to pure CH_2Cl_2) afforded 94 mg (91%) of **19*E*** as a colorless solid mp 78–79°C; ^{1}H NMR, δ: 1.74 (3H, s), 2.56 (lH, OH), 6.48 (1H, s), 7.2–7.6 (9H); ^{13}C NMR, δ: 23.5, 82.4, plus 12 peaks from 117–155 ppm; MS: 222 ($M^{+\cdot}$, 100), 221 (M − H, 52), 207 (M − CH_3, 60), 179 (M − CH_3CO, 63), 178 (83); HRMS, calcd. for $C_{16}H_{14}O$: 222.1044; found: 222.1054. Anal. calcd.: C 86.45, H 6.35; found: C 86.32, H 6.56.

Preparation of Z-*2-benzylidene-1-methylbenzocyclobutenol,* ***19****Z*

Using the same procedure as above and on a similar scale, the *Z* isomer **19*Z***, mp 114–116°C was obtained in 43% yield from **6*Z*** (the low yield is due to the instability of **19*Z*** under basic conditions). ^{1}H NMR, δ: 1.74 (3H, s) 2.65 (1 H, OH), 6.56 (1H, s), 7.2–7.5 (7H, m), 7.70 (2H, d, J = 8.2 Hz); ^{13}C NMR, δ: 22.8, 83.7, plus 12 additional resonances between 118 and 154 ppm; MS 222 ($M^{+\cdot}$, 100), 221 (M−H, 48), 207 (M − CH_3), 52), 179 (M − CH_3CO, 53), 178 (68); HRMS, calcd. for $C_{16}H_{14}O$: 222.1044; found: 222.10057. Anal. calcd.: 86.45, H 6.35, found: C 86.28, H 6.51.

Reaction of ***19****Z with KOH*

This reaction was carried out in 5 N methanolic KOH for 45 min at room temperature. A ^{1}H NMR spectrum of the crude product showed four methyl peaks at δ = 2.59, 2.51, and 2.29 (and 2.23) in an approximate 6:1:1 ratio. These peaks were assigned to **20*E***, **20*Z***, and the isomers of **21**, respectively (see below). GC monitoring of a second run showed that these ratios did not change significantly when the reaction was continued for 3 days prior to work-up. Careful silica gel chromatography (radial) with 2:1 hexanes/CH_2Cl_2 afforded almost pure **20*E*** and **20*Z***.

For **20*E***: (11) IR ($CHCl_3$): 1683 cm^{-1}; ^{1}H NMR, δ: 2.60 (3H, s), 6.96 (1H, d, J = 16.3 Hz), 7.2–7.7 (10H, m); ^{13}C NMR, δ: 29.8, 126.8, 127.1, 127.3, 127.4, 127.8, 128.6, 129.0, 131.5, 131.6, 137.2, 137.3 (2×), 202.1; MS 222($M^{+\cdot}$, 100), 221 (17), 207 (M−CH_3, 52), 179 (M − CH_3CO, 63).

For **20*Z***: ^{1}H NMR, δ: 2.52 (3H, s), 6.61 (1H, d, J = 12.1 Hz), 6.89 (1H, d, J = 12.2 Hz), 6.95–7.4 (8H, m), 7.6–7.8 (1H, m); ^{13}C NMR, δ: 41.9, 127.0, 127.2, 128.1, 129.2(2×) 130.1, 130.4, 131.1, 131.6, 136.6, 137.7, 137.8, 201.

These isomers could not be completely separated.

Reaction of ***19****E with KOH*

When **19*E*** was dissolved in 5 N methanolic KOH, no reaction was observed (GC) after 3 days. The reaction mixture was then refluxed for 30 min. The ^{1}H NMR, spectrum of the crude product was very complicated. It revealed one significant peak at δ = 2.53, which was attributed to **20*Z***. The assignment of this peak as indicating the presence of **20*Z*** was verified by comparing GC retention times with those of an authentic sample.

Preparation of Z-*2-benzylidenebenzocyclobutanol,* ***22****Z*

To a solution of **6*Z*** (114 mg, 0.55 mmol) in methanol (5 mL) was added $NaBH_4$ (61 mg). The mixture was stirred for 30 min

at room temperature and then poured into a mixture of ether (10 mL) and 1% HCl (10 mL). Separation, reextraction of the aqueous phase with ether, and evaporation of the combined organic phase afforded a crude product, which was passed through a short silica gel plug. The yield of **22***E* was 114 mg, 99%. IR: 3577 cm^{-1}(OH); ^1H NMR, δ: 2.35 (lH, d, J = 10.9 Hz, OH), 5.78 (lH, d, J = 10.8 Hz), 6.59 (s, lH), 7.20–7.4 (7H, m), 7.62 (2H, d, J = 8 Hz); MS: 208 (100, $M^{+\cdot}$), 207 (43, M−H), 179 (64, M − CHO), 178 (74); HRMS, calcd. for $C_{15}H_{12}O$: 208.0890; found: 208.0888. Anal. calcd. for $C_{15}H_{12}O$: C 86.54, H 5.77; found: C 86.40, H 5.93.

Preparation of Z*-2-benzylidenebenzocyclobutenol,* 22E
The same procedure as for **22***Z* afforded 97% of **22***E*. IR: 3580 cm^{-1}; ^1H NMR, δ: 2.51 (lH, s, OH), 5.49 (s, lH), 6.50 (s, lH), 7.2–7.6 (m, 9H); MS: 208 (100, $M^{+\cdot}$), 207 (45, M − H), 179 (66, M − CHO), 178 (73); HRMS, calcd. for $Cl_{15}H_{12}O$: 208.0888; found: 208.0896. Anal. calcd. for $C_{15}H_{12}O$: C 86.54, H 5.77; found: C 86.35, H 5.83.

Reaction of 22Z *and* 22E *will methanolic KOH*
The alcohol **22***Z* was stirred with 5 N KOH for 3.5 h at room temperature. Work-up afforded a mixture of two aldehydes, which were partially separated by radial chromatography (3:1 hexane/CH_2Cl_2).

2′-Formyl-*trans*-stilbene: mp 79–81°C (lit. (11*b*) mp 80–82°C; ^1H NMR, δ: 7.05 (lH, d, J = 16.3 Hz), 7.26–7.46 (6H, m), 7.54–7.61 (3H, m), 7.71 (lH, d, J = 7.8 Hz), 10.31 (lH, s), ^{13}C NMR, δ: 12 aromatic and alkene signals from 126.4–140.9, 192.0 (CHO); MS: 208 (100, $M^{+\cdot}$), 207(31), 179(40, M − CHO), 178 (50), 165 (25), 105 (35), 89 (22); HRMS, calcd. for $C_{15}H_{12}O$: 208.0888; found: 208.0900.

2′-Formyl-*cis*-stilbene (15): ^1H NMR, δ: 6.82 (lH, d, J = 12.2 Hz), 6.97 (1H, d, J = 12.2 Hz), 7.00–7.04 (2H, m), 7.11–7.1 6 (3H, m), 7.27 (lH, d, J = 7.5 Hz), 7.35–7.5 (2H, m), 7.87 (lH, dd, J = 1.5, 7.7 Hz), 10.23 (lH, s). The MS was almost identical with that of the *trans* isomer. This product was not further characterized since it could not be completely separated from the *trans* isomer.

The cleavage of **22***E* under the above conditions was followed by g.c. The major products had identical retention times with those of the *trans* and *cis* stilbenes, above. The ratio of *cis* to trans isomers was approximately 2.5:1. A small amount of an aldehyde (δ = 9.74) isomeric with the above products (GC–MS) was also detected.

Reaction of 22E *and* 22Z *with methyllithium in THF*
These reactions were carried out by addition of the appropriate amount of CH_3Li to a solution of **22***E* or **22***Z* in THF at −78°C or at room temperature. The room temperature reactions were allowed to proceed for 40 min. Work-up involved quenching with aqueous NH_4Cl and extraction with ether. Product ratios were based on ^1H NMR analysis of the crude reaction mixtures. Authentic samples of the alcohols **25** (characteristic ^1H NMR peaks, δ:1.50 (3H, d, J = 6.4 Hz), 5.27 (lH, q, J = 6.4 Hz), 6.95 (lH, d, J = 16.0 Hz)), and **26** (characteristic ^1H NMR peaks at δ: 1.41 (3H, d, J = 6.4 Hz), 5.12 (lH, q, J = 6.4 Hz), 6.63 (lH, d, J = 12.2 Hz), 6.74 (lH, d, J = 12.3 Hz)). Authentic samples were prepared for comparison by reacting **20***E* and **20***Z*, respectively, with CH_3Li.

Acknowledgements

The finacial support of the Natural Sciences and Engineering Research Council of Canada in the form of an operating grant (T.D.) and a P.G.S. Fellowship to J.-C. Bradley (1989–1993) is gratefully acknowledged.

References

1. M.P. Cava and H.K. Muth. J. Am. Chem. Soc. **82**, 652 (1960).
2. R.V. Stevens and G.S. Bisacchi. J. Org. Chem. **47**, 2396 (1982).
3. J.O. Amputian and F. Stansfield. J. Chem. Soc. Perkin Trans. 1, 1949 (1974).
4. (*a*) M.P. Cava, D. Mangold, and K. Muth. J. Org. Chem. **29**, 2947 (1964); (*b*) M.P. Cava, D.R. Napier, and R.J. Pohl. J. Am. Chem. Soc. **85**, 2076 (1963).
5. (*a*) M.E. Jung, P.Y. Lam, M.M. Mansuri, and L.M. Speltz. J. Org. Chem. **50**, 1087 (1985).
6. (*a*) W. Choi and H. Yang. J. Org. Chem. **53**, 5796 (1988); (*b*) J.S. Swenton, D.K. Jackson, M.J. Manning, and P.W. Raynolds. J. Am. Chem. Soc. **100**, 6182 (1978).
7. J.J Fitzgerald, A.R. Pagano, V.M. Sakoda, and R.A. Olofson. J. Org. Chem. **59**, 4117 (1994).
8. (*a*) J.C. Bradley and T. Durst. J. Org. Chem. **56**, 5459 (1991); (*b*) J.C. Bradley, T. Durst, and A.J. Williams. J. Org. Chem. **57**, 6575 (1992).
9. (*a*) P.K. Chou and S.R. Kass. J. Am. Chem. Soc. **113**, 4357, (1991); (*b*) W.H. Walborsky and L.M. Turner. J. Am. Chem. Soc. **94**, 2273 (1972).
10. D. Seebach. Angew. Chem. Int. Ed. Engl. **27**, 1624 (1988).
11. J. Klein and E. Shekhor. Isr. J. Chem. **6**, 701 (1968); (*b*) R.E. Buckles and K. Bremer. Org. Synth. Coll. Vol. **IV**, 777 (1967).
12. D.F. DeTar and L.A. Carpino. J. Am. Chem. Soc. **78**, 475 (1956).
13. (*a*) G. Berti Tetrahedron, **4**, 393, (1958); (*b*) J. Org. Chem. **24**, 1934 (1959).
14. A.T. Reid, J.T. Sharp, H.R. Sood, and P.T. Thorogood. J. Chem. Soc. Perkin Trans. 1, 2543 (1973).
15. (*a*) A.A. Baum. J. Am. Chem. Soc. **94**, 6866 (1974); (*b*) C.C. Leznoff and S. Greenberg. Can. J. Chem. **54**, 3824 (1976).

Can. J. Chem. Downloaded from www.nrcresearchpress.com by 46.23.64.124 on 09/08/12
For personal use only.

On the Baylis–Hillman reaction of acrylate, acrylonitrile, and acrolein with some non-enolizable α-dicarbonyl compounds: synthesis of phytotoxic bipolaroxin models

George M. Strunz, Richard Bethell, Glen Sampson, and Peter White

Abstract: The Baylis–Hillman reaction of acrylonitrile, methyl acrylate, and acrolein with several cyclic α-dicarbonyl compounds was investigated. Whereas acrylonitrile reacted with most of these ketones, giving good yields of the expected 1'-cyanovinyl carbinols, the more sterically demanding methyl acrylate failed to undergo the reaction. Attempted Baylis–Hillman reaction of acrolein with the 1,2-dicarbonyl substrates usually resulted in polymers but, in two cases, the desired α-substituted acroleins were obtained. An alternative route to such compounds was developed, employing a Grignard – allylic oxidation sequence. In bioassays, some of the products, embodying the functionality believed responsible for the phytotoxicity of the sesquiterpene bipolaroxin, inhibited germination of lettuce seeds. This activity diminished with time.

Key words: Baylis–Hillman, acrylonitrile, acrylate, acrolein, α-dicarbonyl, bipolaroxin, phytotoxicity.

Résumé : Nous avons étudié la réaction de Baylis–Hillman sur l'acrylonitrile, l'acrylate de méthyle ainsi que l'acroléine avec plusieurs composés α-dicarbonyliques cycliques. Tandis que l'acrylonitrile réagit avec la plupart de ces cétones, fournissant les carbinols 1'-cyanovinyliques attendus avec de bons rendements, l'acrylate de méthyle, à cause de sa plus grande exigence stérique, ne réagit pas de tout. Quand la réaction de Baylis–Hillman fut essayée avec l'acroléine et les composés α-dicarbonyliques, seulement des polymères furent obtenus à l'exception de deux cas, où les acroléines α-substituées furent obtenues. Utilisant la réaction de Grignard, suivie d'une oxidation allylique, une autre route pour produire ces composés fut developpée. Quelques-uns de ces produits, possédant la structure partielle que l'on croit responsable de la phytotoxicité du sesquiterpène bipolaroxin, ont inhibé la germination des semences de laitue. Cet activité a diminué avec le temps.

Mots clés : Baylis–Hillman, acrylonitrile, acrylate, acroléine, composés α-dicarbonyliques, bipolaroxin, phytotoxicité.

Can. J. Chem. Downloaded from www.nrcresearchpress.com by 46.23.64.124 on 09/08/12
For personal use only.

Introduction

The sesquiterpene bipolaroxin, **1**, is a phytotoxic metabolite produced by *Bipolaris cynodontis*, a pathogen of Bermuda grass, *Cynodon dactylon* (L.), which is considered an important weed species in certain agricultural systems (1). The mechanism proposed to account for the phytotoxicity of bipolaroxin (by analogy with the suggested mode of action of 7-hydroxycostal (2)) involves conjugate addition of a nucleophile to the enal system, giving an intermediate such as **II**, followed by a fragmentation resulting in release of the phytotoxic agent acrolein (Scheme 1) (1).

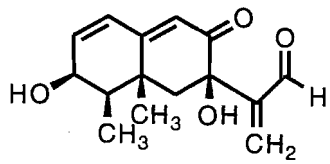

1

The hydroxy enal system, believed to confer phytotoxicity upon bipolaroxin, is reminiscent of functionality **IX** accessible via the Baylis–Hillman reaction (Scheme 2) (3); in fact, bipolaroxin is *formally* derivable by a Baylis–Hillman-type condensation involving one carbonyl group of the diketone **III** (in Scheme 1) and acrolein. As all steps in the Baylis–Hillman sequence appear to be reversible (cf. ref. 4), the release of acrolein in vivo by bipolaroxin may be analogous to a "biologically catalyzed" retro-Baylis–Hillman-type process.

We were intrigued by the possibility that simple Baylis–Hillman products derived from acrolein and suitable α-diketones (or aldehydes) might, like bipolaroxin, release acrolein on interaction with certain (intracellular?) plant con-

Received June 5, 1995.

G.M. Strunz[1] **and R. Bethell.** Canadian Forest Service — Maritimes Region, P.O. Box 4000, Fredericton, NB E3B 5P7, Canada.
G. Sampson and P. White. Nova Scotia Agricultural College, Truro, NS B2N 5E3, Canada.

[1] Author to whom correspondence may be addressed. Telephone: (506) 452-3531. Fax: (506) 452-3525.

Can. J. Chem. Downloaded from www.nrcresearchpress.com by 46.23.64.124 on 09/08/12
For personal use only.

Scheme 1.

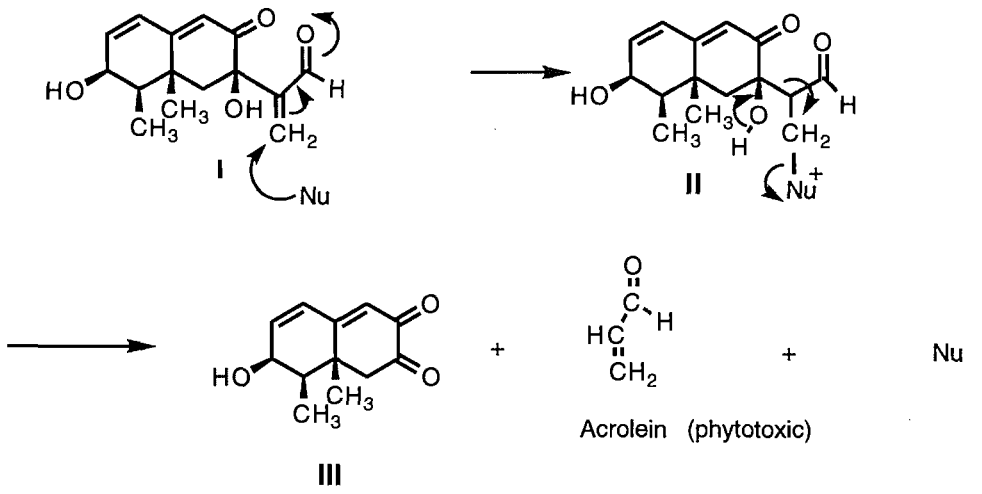

Scheme 2. W = electron-withdrawing group, e.g., -CHO, -COR, -COOR, -CN; R = alkyl or aryl; R′ = usually H.

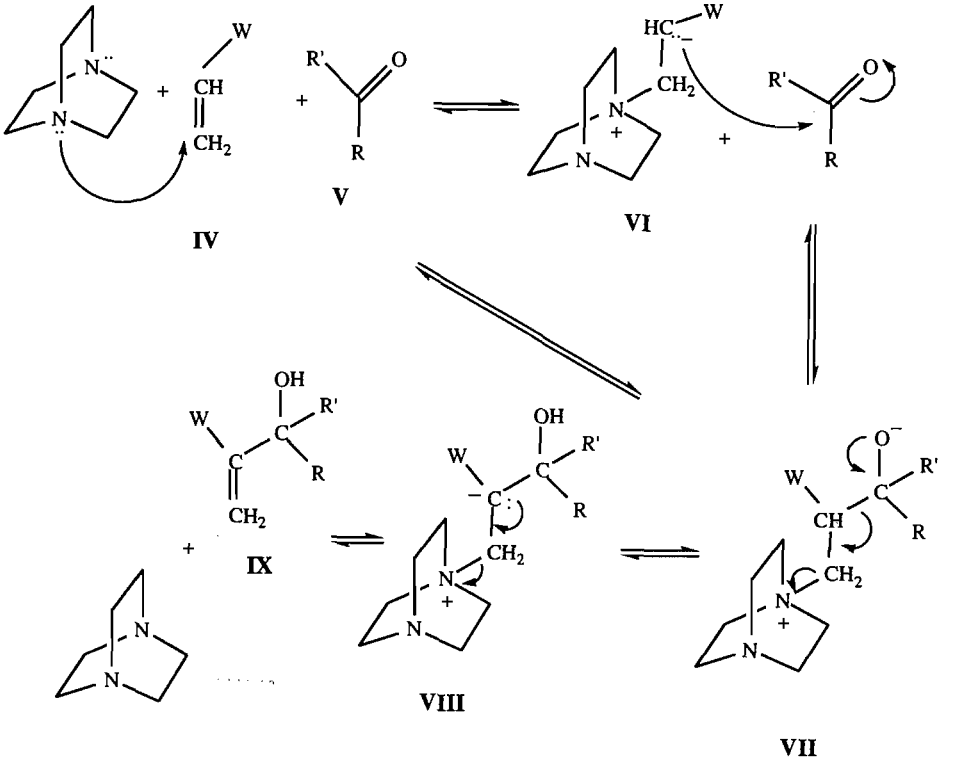

stituents, thus providing support for the proposed mechanism of action of the natural phytotoxin and perhaps even suggesting leads for development of useful, environmentally benign, herbicides.

Acrolein features rarely as the conjugated carbonyl substrate (nucleophilic partner) in Baylis–Hillman-type condensations (with aldehydes), clearly because of its propensity to form oligomers or polymers under the basic catalysis employed. We considered that this hurdle might perhaps be surmounted by selection of appropriate reaction conditions. For example, successful condensations of acrolein with aldehydes have been reported under high (kbar) pressure, which effects a dramatic acceleration in the rates of Baylis–Hillman reactions (5). Alternatively, the desired hydroxy enals might in principle be accessible by selective reduction of the corresponding Baylis–Hillman-derived hydroxy acrylates or acrylonitriles.

In contrast to aldehydes, *ketones* are not generally considered to be reactive carbonyl partners in Baylis–Hillman reactions (again, except under high pressure (5)). It appeared to us that the enhanced reactivity of certain α-diketones towards aldol-type reactions (cf. ref. 6) might perhaps make them suitable partners for reaction with Baylis–Hillman-type vinyl carbanion equivalents. Indeed, α-keto esters have been found to possess the requisite reactivity (7).

This paper reports our investigation into the preparation of

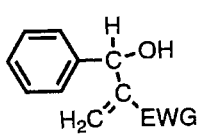

2 ***a*** **(EWG=CHO)**
b **(EWG=CO_2Me)**
c **(EWG=CN)**

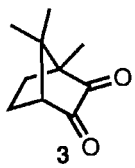

3

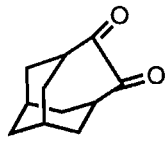

4

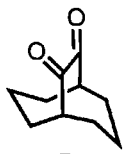

5

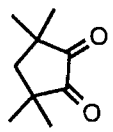

6

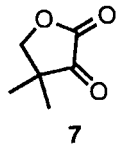

7

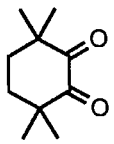

8

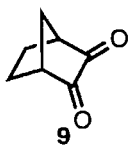

9

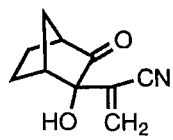

10

compounds embodying functionality **IX**, via the Baylis–Hillman reaction of non-enolizable α-dicarbonyl precursors (**V**, R′ = COR″) with the "activated olefins" acrolein, methyl acrylate, and acrylonitrile (**IV**, W = CHO, CO_2Me, CN) (Scheme 2). The hydroxy enals obtained from successful reaction with acrolein were tested for phytotoxic activity in bioassays.

Results and discussion

As a prelude to this study, the behavior of acrolein with an aldehyde electrophile under typical Baylis–Hillman conditions was first examined. Reaction of acrolein with a large excess of benzaldehyde, no solvent, and 0.1 equivalent of either 1,4-diazabicyclo[2.2.2]octane (DABCO) or 3-quinuclidinol (3-QDL) as catalyst afforded, after 4 days at ambient temperature, a 12% yield (based on acrolein) of the desired hydroxy enal, **2***a*. In contrast, methyl acrylate and acrylonitrile gave, on 3-QDL catalyzed reaction with benzaldehyde under similar conditions, the Baylis–Hillman products, **2***b* and **2***c*, in yields of 85% and 82%, respectively.

Although this result did not augur well for the proposed use of acrolein in the Baylis–Hillman reaction, we proceeded to explore its feasibility with α-diketones as the electrophilic partners. In the absence of solvent, cyclohexane-1,2-dione exists as a tautomeric mixture containing about 40% of the enol form (8), and it appeared unlikely to be a suitable substrate for Baylis–Hillman reaction, a conjecture attested by the complex mixture resulting from its reaction with acrylonitrile and DABCO.[2] It was clear that any potential α-dicarbonyl substrate must be **non-enolizable**, leading us to the selection, for study purposes, of the readily available[3] 1,2-naphthoquinone, acenaphthenequinone, camphorquinone **3**, homoadamantane-2,3-dione **4** (9), bicyclo[3.3.2]decane-9,10-dione **5**, 3,3,5,5-tetramethylcyclopentane-1,2-dione **6**, dihydro-4,4-dimethyl-2,3-furandione **7**, and 3,3,6,6-tetramethylcyclohexane-1,2-dione **8** (10).

Racemic camphorquinone **3** readily underwent the 3-QDL catalyzed Baylis–Hillman reaction with acrylonitrile, affording, after 15 days at ambient temperature, the keto-hydroxynitrile, **11***c*, in 73% yield. The product was obtained as a single isomer, whose regio- and stereochemistry were tentatively assigned on the basis of the nuclear Overhauser enhancement between the hydroxylic proton and the C-4 bridgehead proton, as well as the protons of one of the two methyl groups on C-7. (*endo* Attack is, of course, expected to be favored for steric reasons.) A minor product, **12** (ca. 12%) , arising either from reaction of acrylonitrile dimer with **3**, or by conjugate addition to **11***c* of the anion derived from a second molecule of acrylonitrile, was obtained in some runs.

In contrast, treatment of camphorquinone **3** with methyl acrylate in the presence of 3-QDL for 17 days afforded unchanged camphorquinone and no trace of Baylis–Hillman product **11***b*. This result may be attributed to the hindered nature of the camphorquinone carbonyl groups, and the difference in steric demand between nitrile and ester. Perhaps not surprisingly, therefore, all attempts to prepare the desired model, **11***a*, directly

[2] R. Bethell and G.M. Strunz. Unpublished results.

[3] 1,2-Naphthoquinone, acenaphthenequinone, and compounds **3**, **6**, and **7** are commercially available. The 1,2-diketones **4**, **8**, and **9** were prepared essentially using literature procedures (9–11) (with some minor experimental modifications). Compound **5** was prepared from bicyclo[3.3.1]nonan-9-one by reduction of the corresponding cyanohydrin silyl ether, Tiffeneau-Demyanov ring expansion (12), and selenium dioxide oxidation of the ring-expanded ketone (cf. ref. 9). Norbornane-2,3-dione **9**, an apparently logical candidate for testing, is reported to be unstable (11), undoubtedly a contributing factor in the unsatisfactory results obtained on attempting the Baylis–Hillman reaction with acrylonitrile (8% yield of product **10**) Accordingly, it was not investigated further (with acrolein) in the present study. Neither of the conjugated aryl diones 1,2-naphthoquinone nor acenaphthenequinone was sufficiently reactive to afford satisfactory yields of Baylis–Hillman products with acrylonitrile,[2] and their reaction with acrolein was not pursued.

Can. J. Chem. Downloaded from www.nrcresearchpress.com by 46.23.64.124 on 09/08/12
For personal use only.

Can. J. Chem. Downloaded from www.nrcresearchpress.com by 46.23.64.124 on 09/08/12
For personal use only.

Scheme 3.

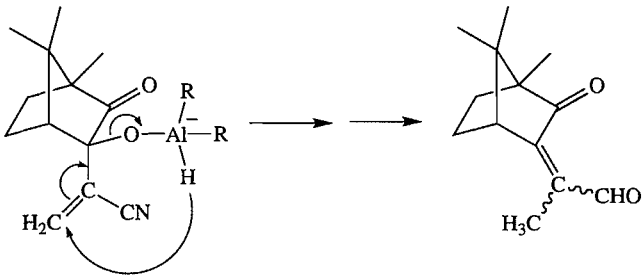

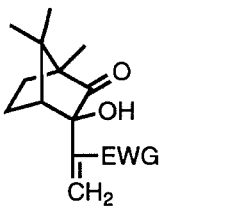

11 *a* **(EWG=CHO)**
b **(EWG=CO_2Me)**
c **(EWG=CN)**

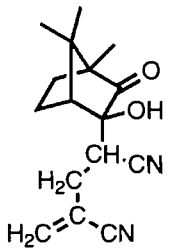

12

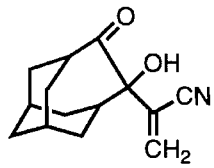

13

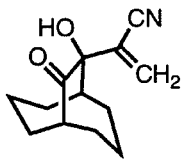

14

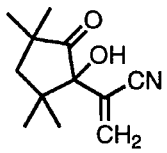

15

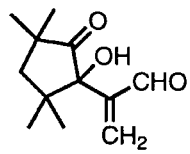

16

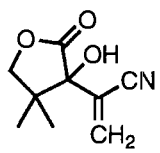

17

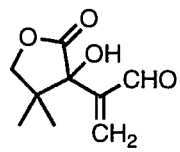

18

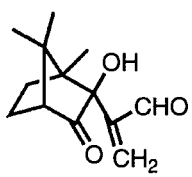

19

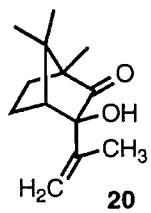

20

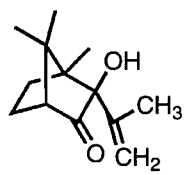

21

by Baylis–Hillman reaction of **3** with acrolein were unsuccessful. Reaction, either in the presence or absence of solvent (THF, benzene) catalyzed by DABCO, triethylamine, 3-hydroxyquinuclidine, 1,5,7-triazabicyclo[4.4.0]dec-5-ene on polystyrene, or triphenylphosphine (3), at temperatures ranging from −78°C to room temperature, or with ultrasonic radiation (13), resulted in polymerization of acrolein and, typically, recovery of unchanged camphorquinone, **3**.

Attempts to reduce **11***c* selectively to the desired aldehyde **11***a* using a wide variety of reagents and conditions (DIBAL, $LiAlH_2(OEt)_2$, $LiAlH_4$,Et_3SiH/Lewis acid, $SnCl_2$/HCl (Stephen reduction), etc.) were unsuccessful, vitiating the hope that interaction of the reducing reagent with the hydroxyl group might produce a complex capable of delivering hydrogen to the unhindered nitrile group. Only in the case of $LiAlH_2(OEt)_2$ was an aldehydic product isolated (albeit in low yield), but here accompanied by conjugate reductive displacement of the hydroxyl group. A possible mechanism for this transformation is depicted in Scheme 3. Results observed on treatment of benzaldehyde and the series of 1,2-dicarbonyl compounds **3–8** with acrylonitrile and acrolein under catalysis by 3-QDL are compiled in Table 1. As mentioned above, methyl acrylate afforded an 85% yield of the hydroxy acrylate **2***b* on reaction with benzaldehyde, but failed to give a Baylis–Hillman product with *any* of the α-dicarbonyl compounds. Of the α-dicarbonyl compounds tested, only 3,3,5,5-tetramethyl-

Can. J. Chem. Downloaded from www.nrcresearchpress.com by 46.23.64.124 on 09/08/12
For personal use only.

cyclopentane-1,2-dione **6** and the ketolactone **7** proved to be satisfactory substrates for Baylis–Hillman reaction with acrolein. In contrast to the readiness of 3,3,5,5-tetramethylcyclopentane-1,2-dione **6** to undergo the Baylis–Hillman reaction with acrolein and acrylonitrile, all attempts to effect the process with 3,3,6,6-tetramethylcyclohexane-1,2-dione **8**, under similar conditions, furnished unchanged diketone. This result may be attributed both to greater steric inhibition of nucleophilic attack at the carbonyl groups of **8**, and the lack of enhanced reactivity associated with "eclipsing" the two carbonyl groups (as in **6**).

It has previously been noted that the Baylis–Hillman reaction of acrylate esters, CH_2=CHCOOR, with aldehydes as electrophiles, is significantly influenced by steric and electronic properties of the R group (4). Furthermore, β-substituted acrylates (e.g., crotonyl systems) do not undergo the reaction even under high-pressure conditions (3). The sensitivity of the reaction to steric effects is highlighted in the present study by the dramatic contrast observed between the behavior of acrylonitrile and methyl acrylate, the former reacting readily with most of the 1,2-dicarbonyl compounds and the (more sterically demanding) ester failing to give *any* of the corresponding Baylis–Hillman products.

Notwithstanding the successful preparation of **16** and **18**, the Baylis–Hillman reaction is clearly not a generally useful synthesis of the desired keto hydroxy enal system **IX** (W = CHO, R′ = COR″). An alternative, more versatile approach was therefore briefly explored, using camphorquinone **3** as substrate, in order to augment the number of compounds available for bioassay. Reaction of **3** with the Grignard reagent prepared from 2-bromopropene and allylic oxidation of the product **20** provided a viable, if not wholly satisfactory solution, affording **11***a* in ca. 25% yield. Regioisomer **19**, resulting from *endo* attack of the Grignard reagent at the C-2 carbonyl was also obtained (25% via **21**) by this procedure. The structure and stereochemistry of these compounds were confirmed by nOe experiments.

Five hydroxy enal models, **2***a*, **11***a*, **16**, **18**, and **19** were thus readily accessible by simple methodology for phytotoxicity testing. Compound **16**, prepared in a single step by the Baylis–Hillman reaction, and **11***a* and **19**, accessible via a Grignard – allylic oxidation sequence, feature the keto hydroxy enal functional array present in bipolaroxin. As the liberation of acrolein, believed responsible for the phytotoxicity of bipolaroxin, is triggered by conjugate addition of a nucleophile to the enal system, it was clearly important to ascertain initially the in vitro stability of these compounds in aqueous medium. Accordingly, compound **16**, considered representative of the series, was dissolved in the minimum volume of methanol and stirred for 24 h at ambient temperature with aqueous buffers at pH 3.0, 7.0, and 10. Both TLC analysis and quantitative recovery of unaltered starting material attested to the relative stability of the hydroxy enal system in neutral and acidic aqueous medium (pH 7.0 and 3.0). On the other hand, the treatment at pH 10 predictably resulted in virtually quantitative conversion of **16** back to its diketone precursor **6**.

Bioassay results showing the ability of some of the hydroxyacroleins and acrylonitriles, as well as their precursor carbonyl compounds, to inhibit germination of lettuce seeds during an 8 day period (an indicator of phytotoxic activity) are compiled in Table 2. For seeds placed on agar in wells treated with 100 ppm solutions,[4] the ketolactone **7** did not show significant inhibition after 8 days, whereas the derived hydroxyacrolein **18** strongly inhibited germination (and the corresponding acrylonitrile **17** was also active). On the other hand, neither the α-diketone **6** nor its derivatives **16** or **15** were inhibitory at this concentration. Whereas camphorquinone **3** and the derived hydroxyacrolein **11***a* were essentially devoid of activity, the isomeric hydroxyacrolein **19** showed significant inhibition.

From these data, one can conclude that although the phytotoxicity of bipolaroxin may indeed result from in vivo liberation of acrolein as suggested (1, 2), structural features besides the presence of the implicated keto hydroxy enal functional array are necessary for the bioactivity. Interestingly, *both* benzaldehyde *and* its hydroxyacrolein derivative **2***a* strongly inhibited germination when applied at 100 ppm, indicating a different mode of action, at least in the former case.

When the bioassay period was extended to 16 days, inhibitory effects on germination and seedling growth were dramatically attenuated and were no longer detectable even for the 500 ppm treatments with any of the test compounds other than **17**, benzaldehyde, and **2***a*.

Experimental

General

Melting points were determined on a hot-stage apparatus and are uncorrected. Infrared spectra were recorded on a Philips Pye Unicam PU9516 infrared spectrophotometer. Accurate mass measurements were made on a Kratos MS-50 instrument. NMR spectra were recorded in $CDCl_3$ on a Varian XL-200 spectrometer operating at a frequency of 200.068 MHz for ^1H, and on a Varian Unity 400 operating at a frequency of 399.946 MHz for ^1H and100.564 MHz for ^{13}C.

2-[1′-(1′-Hydroxy-2′-oxo-3′,3′,5′,5′-tetramethylcyclopentyl)]-propenal 16

Acrolein (0.17 mL, 2.5 mmol) was added to a solution of 3,3,5,5-tetramethyl-1,2-cyclopentanedione **6** (382 mg, 2.5 mmol) in dry THF (5 mL) containing 3-quinuclidinol (3-QDL) (70 mg, 0.25 mmol). The reaction mixture was stirred at ambient temperature in a closed vessel for 3 days, when additional acrolein (0.17 mL, 2.5 mmol) was added. Stirring was continued for a further 2 days until TLC analysis indicated that reaction was complete. Water was then added and the mixture was extracted with ether (4 × 10 mL). The extracts were dried over $MgSO_4$ and removal of solvent on a rotary vacuum evaporator afforded the crude product (601 mg) as an orange-colored oil. Flash chromatography on silica gel (eluent: hexane-EtOAc, 5:1) furnished 379 mg (72%) of pure keto hydroxy enal **16** as an almost colorless oil; IR ($CHCl_3$): 3550 (sharp), 3500–3200, 3000–2800, 1740, 1690, 1455, 1370, 1300 cm^{-1}; ^1H NMR ($CDCl_3$, 200 MHz) δ: 0.82 (3H, s), 1.05 (3H, s), 1.23 (3H, s), 1.23 (3H, s), 1.84 (2H, ABq, J_{AB} = 13.0 Hz, $\Delta\nu$ = 76.1 Hz), 3.65 (1H, s), 6.35 (1H, s), 6.50 (1H, s), 9.52 (1H, s); HREIMS, *m/z* (relative intensity) (ion): 210.1251 (5) (M^+) (calcd. for $C_{12}H_{18}O_3$: 210.1256), 195 (3) ($M-CH_3$), 182 (6) (M − CO),

[4] All of the compounds tested inhibited germination of lettuce seeds when the concentration was increased to 10 000 ppm.

Table 1. Yields of Baylis–Hillman products from benezaldehyde and 1,2-dicarbonyl compounds **3–8** with acrylonitrile and acrolein.

Electrophilic carbonyl partner	Anion derived from $CH_2{=}CHCN$	Anion derived from $CH_2{=}CHCHO$
	Baylis–Hillman product (yield)	
PhCHO	**2***c* (82%)	**2***a* (12%)
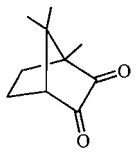 **3**	**11***c* (73%)	Polymer
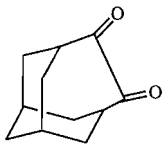 **4**	**13** (70%)	Polymer
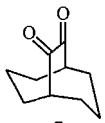 **5**	**14** (71%)	Polymer
6	**15** (100%)	**16** (72)%
7	**17** (81%)	**18** (32)%
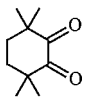 **8**	0	Polymer

Table 2. Inhibition of germination of lettuce seed by synthetic 2-substituted acroleins and acrylonitriles.

	Concentration (PPM) (Activity)						
Compound	50	100	250	500	1000	2000	10000
PhCHO	+++	+++	+++	+++	+++	+++	+++
2*a*	++	+++	+++	++	+++	+++	+++
15	+	–	++	+	+	++	+++
18	+++	+++	+++	+++	+++	+++	+++
17	++	++	–	+	+++	++	+++
19	–	++	++	++	+++	++	+++

Can. J. Chem. Downloaded from www.nrcresearchpress.com by 46.23.64.124 on 09/08/12
For personal use only.

Can. J. Chem. Downloaded from www.nrcresearchpress.com by 46.23.64.124 on 09/08/12
For personal use only.

154 (100) ($M - C_4H_8$), 139 (12) ($M - C_4H_8 - CH_3$), 126 (63) ($M - C_5H_8O$), 125 (65) ($M - C_5H_9O$), 111 (45) ($M - C_5H_8O - CH_3$), 97 (12) $(C_7H_{13})^+$.

2-[1′-(1′-Hydroxy-2′-oxo-3′,3′,5′,5′-tetramethylcyclopentyl)]-acrylonitrile 15

3,3,5,5-Tetramethyl-1,2-cyclopentanedione **6** (301 mg, 1.95 mmol) and 3-QDL (50 mg, 0.195 mmol) were dissolved in acrylonitrile (5.0 mL). The solution was stirred at ambient temperature in a closed vessel for 3 days. Ether was added and the mixture was washed with water and brine and dried over $MgSO_4$. Removal of solvent on a rotary vacuum evaporator afforded 402 mg (100%) of chromatographically pure **15** as a pale brown solid, mp 104°C; IR ($CHCl_3$): 3550 (sharp), 3400–3200, 3000–2850, 2240, 1740, 1460 cm^{-1}; ^1H NMR ($CDCl_3$, 400 MHz) δ: 1.05 (3H, s), 1.09 (3H, s), 1.22 (3H, s), 1.25 (3H, s), 1.92 (2H, ABq, J_{AB} = 13.2 Hz, $\Delta\nu$ 69.6 Hz), 2.77 (1H, br s), 6.18 (1H, s), 6.25 (1H, s); HREIMS, *m/z* (relative intensity) (ion): 207.1259 (14) M^+) (calcd. for $C_{12}H_{17}NO_2$: 207.1260), 123 (100) ($M - C_5H_8O$), 108 (7) ($M - C_5H_8O - CH_3$).

Baylis–Hillman reaction of acrylonitrile and camphorquinone

Racemic camphorquinone **3** (2.530 g, 22 mmol) and 3-QDL (280 mg, 2.2 mmol) were dissolved in acrylonitrile (15.0 mL). The solution was stirred in a closed vessel at ambient temperature for 18 days, during which time the color changed from yellow to dark red. After addition of water, the mixture was extracted thoroughly with ether and the extracts were washed with brine and dried over $MgSO_4$. The crude amorphous product obtained on removal of solvent on a rotary vacuum evaporator was purified by flash chromatography on silica gel. Elution with hexane–EtOAc (5:1) afforded pure **11***c* (3.517 g; 73%) as a white solid, mp 73°C; IR ($CHCl_3$): 3550 (sharp), 3100–2850, 2220, 1750 cm^{-1}; ^1H NMR ($CDCl_3$, 400 MHz) δ: 0.87 (3H, s), 1.00 (3H, s), 1.01 (3H, s), 1.24–1.40 (2H, m), 1.59–1.66 (1H, m), 1.86–1.96 (1H, m), 2.21 (1H, d, J = 4.8 Hz), 3.49 (1H, br s), 5.68 (1H, s), 5.87 (1H, s); ^{13}C NMR ($CDCl_3$) δ: 9.2 (q), 20.3 (q), 21.9 (q), 22.6 (t), 27.8 (t), 45.5 (s), 51.2 (d), 58.9 (s), 79.1 (s), 116.5 (s), 124.9 (s), 130.0 (t), 215.8 (s); FABMS (NOBA matrix): 220 (19) ($M^+ + H$), 219 (23) (M^+), 204 (6) ($M - CH_3$), 202 (13) ($M - OH$), 174 (100).

A minor by-product **12** (718 mg; 12%) eluted after **11***c*; IR $CHCl_3$): 3550, 3000–2850, 2275, 2240, 1740 cm^{-1}; ^1H NMR ($CDCl_3$, 400 MHz) δ: 0.92 (3H, s), 1.00 (3H, s), 1.05 (3H, s), 1.21–1.28 (1H, m), 1.38–1.45 (1H, m), 1.63–1.70 (1H, m), 1.89–1.99 (1H, m), 2.29 (1H, d, J = 4.4 Hz), 2.50–2.53 (2H, ~t), 3.62–3.66 (1H, m), 3.80–3.84 (1H, m), 5.86 (1H, s), 6.18 (1H, s); ^{13}C NMR ($CDCl_3$) δ: 9.4 (q),19.1 (d), 20.3 (q), 22.3, 22.3 (t/q), 28.7 (t), 45.7 (s), 52.4 (d), 59.9, 60.0 (t/s), 83.2 (s), 116.0 (s), 117.3 (s), 121.6 (s), 133.8 (t), 212.9 (s); HREIMS, *m/z* (relative intensity) (ion): 272.1521 (1) (M^+) (calcd. for $C_{16}H_{20}N_2O_2$: 272.1525), 244 (11) ($M - CO$), 243 (10) ($M - CHO$), 229 (5) ($M - CO - CH_3$), 189 (3) ($C_{11}H_{13}N_2O$), 188 (6) ($C_{11}H_{12}N_2O$), 83 (100) (C_6H_{11}).

3-Phenyl-3-hydroxy-2-methylenepropanonitrile 2*c*

Standard procedure as above: acrylonitrile (0.66 mL, 10 mmol), benzaldehyde (5 mL), DABCO (112 mg, 1 mmol), ambient temperature, 8 days. The crude product obtained on work-up was purified by flash chromatography on silica gel. Elution with hexane–EtOAc (2:1) furnished 1.3 g (82% from acrylonitrile) of chromatographically pure **2***c* as a clear colorless oil; IR ($CHCl_3$): 3600 (sharp), 3550–3200, 3150–2800, 2240, 1490, 1455, 1395 cm^{-1}; ^1H NMR ($CDCl_3$, 200 MHz) δ: 3.98 (2H, ABq, J_{AB} = 3.9 Hz, $\Delta\nu$ = 514 Hz), 6.01 (1H, d, J = 1.2 Hz), 6.09 (1H, d, J = 1.6 Hz), 7.38 (5H, s); HREIMS, *m/z* (relative intensity) (ion): 159.0687 (36) (M^+) (calcd. for $C_{10}H_9NO$: 159.0684), 107 (100) (C_7H_7O), 79 (52) (C_6H_7), 77 (48) (C_6H_5).

Methyl 3-phenyl-3-hydroxy-2-methylenepropanoate 2*b*

Standard procedure: methyl acrylate (1.15 mL, 12.8 mmol), benzaldehyde (10 mL), DABCO (143 mg, 1.28 mmol), ambient temperature, 8 days. The crude product obtained after work-up was purified by flash chromatography on silica gel. Elution with hexane–EtOAc (2:1) furnished 2.09 g (85% from methyl acrylate) of chromatographically pure **2***b* as a clear colorless oil; IR ($CHCl_3$): 3600 (sharp), 3550–3300, 3100–2850, 1720, 1630 cm^{-1}; ^1H NMR ($CDCl_3$, 200 MHz) δ: 3.00 (1H, br), 3.73 (3H, s), 5.57 (1H, br), 5.83 (1H, t, J = 1.2 Hz), 6.34 (1H, d, J = 0.8 Hz), 7.26–7.40 (5H, m); HREIMS, *m/z* (relative intensity) (ion): 192.0798 (41) (M^+) (calcd. for $C_{11}H_{12}O_3$: 192.0786), 105 (100) (C_7H_5O),191 (38) ($C_{11}H_{11}O_3$), 160 (49) ($C_{10}H_8O_2$), 159 (11) ($C_{10}H_7O_2$), 132 (47)(C_9H_8O).

3-Phenyl-3-hydroxy-2-methylenepropanal 2*a*

Standard procedure: acrolein (1.00 mL, 15.0 mmol), benzaldehyde (10 mL), DABCO (141 mg, 1.3 mmol), ambient temperature, 8 days. The crude product, obtained after work-up, was purified by flash chromatography on silica gel. Elution with hexane–EtOAc (3:1) furnished 292 mg (12% from acrolein) of chromatographically pure **2***a* as a clear colorless oil; IR ($CHCl_3$): 3600 (sharp), 3550–3300, 3150–2700, 1685 cm^{-1}; ^1H NMR ($CDCl_3$, 200 MHz) δ: 4.20 (2H, ABq, J_{AB} = 4.3 Hz, $\Delta\nu$ 571 Hz), 6.16 (1H, s), 6.44 (1H, s), 7.26–7.38 (5H, m), 9.58 (1H, s); HREIMS, *m/z* (relative intensity) (ion): 162.0666 (34) (M^+) (calcd. for $C_{10}H_{10}O_2$: 162.0681), 161 (100) ($C_{10}H_9O_2$),107 (14) (C_7H_7O), 105 (19) (C_7H_5O), 79 (28) (C_6H_7).

Dihydro-4,4-dimethyl-3-hydroxy-3-(1′-cyanovinyl)-2-furanone 17

Standard procedure: dihydro-4,4-dimethyl-2,3-furandione (**7**) (499 mg, 3.9 mmol), 3-QDL (100 mg, 0.78 mmol), acrylonitrile (5.0 mL), ambient temperature, 24 h. Flash chromatography (silica gel; hexane–EtOAc, 3:1) of the crude product obtained on work-up afforded **17** (508 mg, 81% from ketolactone) as a colorless crystalline solid, mp 71°C; IR ($CHCl_3$): 3550 (sharp), 3500–3100, 3000–2850, 2250, 1780, 1465, 1400, 1370 cm^{-1}; ^1H NMR ($CDCl_3$, 200 MHz) δ:1.13 (3H, s), 1.19 (3H, s), 3.55 (1H, s), 4.09 (2H, ABq, J_{AB} = 8.9 Hz, $\Delta\nu$ = 22.9 Hz), 6.15 (1H, s), 6.26 (1H, s); HREIMS, *m/z* (relative intensity) (ion): 136.0756 (7) ($M^+ - H - CO_2$) (calcd. for $C_8H_{10}NO$: 136.0763), 122 (100) (C_7H_8NO).

Dihydro-4,4-dimethyl-3-hydroxy-3-(1′-formylvinyl)-furanone 18

To a solution of dihydro-4,4-dimethyl-2,3-furandione **7** (533 mg, 4.2 mmol) in dry THF containing 3-QDL (105 mg, 0.83 mmol) was added acrolein (0.3 mL, 4.5 mmol). The mixture was stirred at ambient temperature in a closed vessel for 3

Can. J. Chem. Downloaded from www.nrcresearchpress.com by 46.23.64.124 on 09/08/12
For personal use only.

days. (Addition of more acrolein during the course of the reaction did not enhance the yield.) Flash chromatography (silica gel; hexane–EtOAc, 2:1) of the crude product obtained on work-up afforded **18** (240 mg, 31% from ketolactone) as a pale yellow crystalline solid, mp 77°C; IR ($CHCl_3$): 3600–3200, 3150–2800, 1775, 1730, 1685, 1465, 1380 cm^{-1}; ^1H NMR ($CDCl_3$, 200 MHz) δ: 0.91 (3H, s), 1.18 (3H, s), 3.95 (1H, br), 3.99 (2H, ABq, J_{AB} = 8.8 Hz, $\Delta\nu$ = 35.4 Hz), 6.39 (1H, s), 6.56 (1H, s), 9.57 (1H, s); HREIMS, *m/z* (relative intensity) (ion): 139.0757 (4) ($M^+ - H - CO_2$) (calcd. for $C_8H_{11}O_2$: 139.0759), 125 (100) ($C_7H_9O_2$), 107 (12) (C_7H_7O).

2-Oxo-3-(*endo*)-hydroxy-3-(*exo*)-(1′-cyanovinyl)-bicyclo[2.2.1]heptane 10[5]

A solution of 2-norbornanone (2.88 g, 26.1 mmol) in xylenes (ca. 10 mL) was heated at 135°C with selenium dioxide (3.861 g, 35.0 mmol) for 4 h. The (crude) yellow-orange solid obtained after filtration and removal of solvent in vacuo was dissolved in acrylonitrile (ca. 5 mL) and 3-QDL (436 mg, 3.4 mmol) was added. The red reaction mixture was stirred at ambient temperature in a closed vessel for 24 h. The crude material obtained on work-up was purified on silica gel and **10** (366 mg, 8% from 2-norbornanone) was eluted with hexane–EtOAc (2:1). The product **10** was a colorless solid, mp 83°C; IR ($CHCl_3$): 3550, 3000–2850, 2220, 1750 cm^{-1}; ^1H NMR ($CDCl_3$, 400 MHz) δ: 1.60–1.69 (3H, m), 1.75–1.79 (1H, m), 1.88–1.96 (1H, m), 2.05–2.12 (1H, m), 2.70–2.72 (1H, m), 2.83–2.84 (1H, m), 3.26 (1H, s), 5.79 (1H, s), 6.03 (1H, s); ^{13}C NMR ($CDCl_3$) δ: 19.7 (t), 27.1 (t), 32.4 (t), 44.4 (d), 48.8 (d), 80.1 (s), 116.3 (s), 123.5 (s), 133.1 (t), 215.4 (s); HREIMS, *m/z* (relative intensity) (ion): 177.0796 (7) (M^+) (calcd. for $C_{10}H_{11}NO_2$: 177.0790), 149 (13) ($M^+ - CO$), 108 (100) (C_6H_6NO).

Acrylonitrile-homoadamantane-2,3-dione reaction

Standard procedure: homoadamantane-2,3-dione **4** (prepared according to ref. 10 with some modifications) (98 mg, 0.55 mmol), 3-QDL (15 mg, 0.01 mmol), acrylonitrile (ca 5 mL), ambient temperature, 24 h. Flash chromatography (silica gel; hexane–EtOAc, 2:1) of the crude product obtained on work-up afforded **13** (88 mg,70%) as a colorless crystalline solid, mp 78°C; IR ($CHCl_3$): 3500, 2950, 2240, 1700, 1450 cm^{-1}; ^1H NMR ($CDCl_3$, 200 MHz) δ: 1.63–2.14 (11H, m), 2.32–2.34 (1H, m), 2.88–2.97 (2H, m), 3.75 (1H, br), 5.49 (1H, s), 5.99 (1H, s); HREIMS, *m/z* (relative intensity) (ion): 231.1260 (52) (M^+) (calcd. for $C_{14}H_{17}NO_2$: 231.1260), 203 (26) ($M^+ - CO$), 202 (16) ($M^+ - H - CO$), 121 (23) (C_9H_{13}), 108 (42) (C_8H_{12}), 107 (24) (C_8H_{11}), 95 (75) (C_7H_{11}), 79 (100) (C_6H_7).

Acrylonitrile–bicyclo[3.3.2]decane-9,10-dione reaction

Standard procedure: bicyclo[3.3.2]decane-9,10-dione **5** (48.5 mg, 0.29 mmol) (prepared from bicyclo[3.3.1]nonan-9-one by reduction of the corresponding cyanohydrin silyl ether, Tiffeneau–Demyanov ring expansion (13), and selenium dioxide oxidation of the ring-expanded ketone (cf. ref. 10)), 3-QDL (10 mg, 0.079 mmol), acrylonitrile (5.0 mL), ambient temperature, 24 h. Preparative TLC (silica gel; hexane–EtOAc, 5:1) of the crude product obtained on work-up afforded **14** (43 mg, 68%) as a colorless crystalline solid, mp 90°C; IR ($CHCl_3$): 3600–3400, 3000–2800, 2240, 1690, 1450 cm^{-1}; ^1H NMR ($CDCl_3$, 200 MHz) δ: 1.46–2.00 (11H, m), 2.14–2.19 (1H, m), 2.55–2.57 (1H, m), 3.08–3.13 (1H, m), 3.5 (1H, br), 5.50 (1H, s), 5.99 (1H, s); HREIMS, *m/z* (relative intensity) (ion): 219.1256 (5) (M^+) (calcd. for $C_{13}H_{17}NO_2$: 219.1260), 191 (49) ($M^+ - CO$), 176 (12) ($M^+ - CO - CH_3$), 162 (20) ($C_{10}H_{12}NO$), 148 (15) ($C_9H_{10}NO$), 134 (12) (C_8H_8NO), 121 (28) (C_7H_7NO), 120 (10) (C_7H_6NO), 96 (100) (C_7H_{12}).

Reaction of camphorquinone with Grignard reagent from 2-bromopropene

Camphorquinone (racemic) **3** (1.87 g,11.3 mmol) in anhydrous THF was added under argon during 15 min to the Grignard reagent prepared from 2-bromopropene (1.02 mL, 11.5 mmol) and magnesium turnings (280 mg, 11.5 mg atom) in THF at −78°C. The mixture was stirred at the same temperature under an argon atmosphere for 2 h and the reaction was then quenched by addition of saturated NH_4Cl solution. Flash chromatography (silica gel; hexane–EtOAc, 5:1) of the crude product obtained on conventional work-up gave a clean mixture of regioisomeric products resulting from (*endo* sterically favored) attack of the reagent at the 2- or the 3-carbonyl group of camphorquinone. NMR analysis of the mixture indicated that the ratio of products arising from attack at C-2 and C-3, respectively, was about 6:5. Repeated flash chromatography of the mixture using the same solvent system allowed the isomers to be separated and isolated as crystalline solids. Their structures could be distinguished on the basis of nOe experiments, in particular the nOe enhancement between the hydroxyl and the bridgehead protons in the 3-hydroxy-3-isopropenyl isomer **20**, and its absence in the "C-2" regioisomer, **21**. The latter was the less polar product, mp 45°C; IR ($CHCl_3$): 3600–3500 (sharp), 3300–3200 (br), 3000–2800, 1730 cm^{-1}; ^1H NMR ($CDCl_3$, 400 MHz) δ: 0.95 (3H, s), 1.07 (3H, s), 1.08 (3H, s), 1.45–1.55 (2H, m), 1.61–1.68 (1H, m), 1.82–1.86 (4 H), 2.18–2.20 (1H, d), 2.32 (1H, s), 4.69 (1H, s), 4.83 (1H, d, J = 0.8 Hz); HREIMS, *m/z* (relative intensity) (ion): 208.1455 (33) (M^+) (calcd. for $C_{13}H_{20}O_2$: 208.1464), 111 (100) ($C_7H_{11}O$) ($M^+ - C_6H_9O$), 193 (13) ($M^+ - CH_3$), 153 ($C_9H_{13}O_2$) ($M^+ - C_4H_7$), 152($C_9H_{12}O_2$) ($M^+ - C_4H_8$), 140 (21) ($C_8H_{12}O_2$), 137 (15) ($C_9H_{13}O$), 126 ($C_7H_{10}O_2$), 121 (10) (C_9H_{13}).

The 3-hydroxy-3-isopropenyl isomer **20** had mp 57°C; IR ($CHCl_3$): 3600–3500 (sharp), 3500–3200 (br), 3000–2800, 1730 cm^{-1}; ^1H NMR ($CDCl_3$, 400 MHz) δ: 0.95 (3H, s), 0.98 (3H, s), 1.05 (3H, s), 1.32–1.42 (2H, m), 1.59 (1H, m), 1.79–1.84 (4H), 2.07 (1H, d, J = 4.4 Hz), 2.28 (1H, s), 4.72 (1H, s), 4.82 (1H, s); HREIMS, *m/z* (relative intensity) (ion): 208.1462 (26) (M^+) (calcd. for $C_{13}H_{20}O_2$: 208.1464), 180 (32) ($M^+ - CO$), 137 (12) ($C_9H_{13}O$) ($M^+ - C_4H_7O$), 97 (100) (C_6H_9O), 84 (71) (C_6H_{12}), 69 (13) (C_5H_9), 69 (13) (C_4H_5O).

Keto-hydroxyenal 11*a*

To the 3-hydroxy-3-isopropenyl Grignard product **20** (472 mg, 2.27 mmol) in dry methylene chloride (ca. 10 mL) was added selenium dioxide (504 mg, 4.5 mmol) and *tert*-butyl hydroperoxide (0.9 mL of 90% solution, 9.1 mmol). The mixture was heated under gentle reflux for 6 days. When cool, the mixture was filtered, and the filtrates were washed with water and brine and dried over $MgSO_4$. The crude product, obtained after removal of solvent in vacuo, was subjected to flash chro-

[5] Stereochemistry tentatively assigned, based on presumably preferred *exo* attack of nucleophile on carbonyl.

matography on silica gel (hexane–EtOAc, 5:1), affording 328 mg (65%) of chromatographically pure **11***a* as an orange-colored oil; IR ($CHCl_3$): 3600–3500 (sharp), 3100–2800, 1745, 1690 cm^{-1}; ^1H NMR ($CDCl_3$, 200 MHz) δ: 0.95 (3H, s), 0.99 (3H, s), 1.10 (3H, s), 1.20–1.34 (2H, m), 1.54–1.68 (1H, m), 1.76–1.91 (1H, m), 2.51 (1H, d, J = 4.4 Hz), 2.86 (1H, br), 6.07 (1H, s), 6.21 (1H, s), 9.57 (1H, s); HREIMS, *m/z* (relative intensity) (ion): 222.1259 (21) (M^+) (calcd. for $C_{13}H_{18}O_3$: 222.1256), 194 (15), ($M^+ - CO$), 179 (35) ($M^+ - CO - CH_3$), 138 (100) ($C_8H_{10}O_2$) ($M^+ - C_5H_8O$), 125 (13) ($C_7H_9O_2$) ($M^+ - C_6H_9O$), 123 (11) ($C_7H_7O_2$) ($M^+ - C_6H_{11}O$), (121) (11) (C_8H_9O), 95 (18) (C_7H_{11}).

Keto-hydroxyenal 19

Procedure as for isomer **11***a* using 2-hydroxy-2-isopropenyl precursor **21** (240 mg, 1.15 mmol) in methylene chloride (5.0 mL), selenium dioxide (256 mg, 2.3 mmol), and *tert*-butyl hydroperoxide (0.46 mL of 90% solution, 4.6 mmol). The product, **19**, was obtained after chromatography as a yellow oil in a yield of 179 mg (70%); IR ($CHCl_3$): 3600–3500 (sharp), 3100–2900, 1750, 1680 cm^{-1}; ^1H NMR ($CDCl_3$, 200 MHz) δ: 0.97 (3H, s), 1.03 (3H, s), 1.12 (3H, s), 1.16–1.27 (1H, m), 1.43–1.71 (2 H, m), 1.80–1.91 (1H, m), 2.29 (1H, d, J = 4.8 Hz), 3.60 (1H, br), 6.18 (1H, s), 6.23 (1H, s), 9.54 (1H, s); HREIMS, *m/z* (relative intensity) (ion): 222.1250 (11) (M^+) (calcd. for $C_{13}H_{18}O_3$: 222.1256), 221 (34) ($M^+ - H$), 207 (28) ($M^+ - CH_3$), 205 (30) ($M^+ - OH$), 179 (17) ($M^+ - CO - CH_3$), 161 (14) ($M^+ - CO - CH_3$-H_2O), 151 (12) ($C_6H_{11}O_2$) ($M^+ - C_4H_7O$), 125 (100) ($C_7H_9O_2$) ($M^+ - C_6H_9O$), 121 (C_9H_{13}), 112 (17) ($C_6H_8O_2$) ($M^+ - C_7H_{10}O$), 111 (31) ($C_6H_7O_2$) ($M^+ - C_7H_{11}O$), 109 (26) (C_8H_{13}), 109 (21) (C_7H_9O), 97 (28) (C_6H_9O), 95 (55) (C_7H_{11}).

Bioassays

Bioassay wells consisted of 10 mL test tubes containing 7 mL of autoclaved 8% water–agar that had been allowed to harden. A 10 000 ppm stock solution in ethyl acetate and a dilution series of each test compound in the same solvent was prepared. A 500 μL volume of the appropriate test solution was deposited as a layer on the surface of the agar in each well. The solvent was allowed to evaporate in a laminar air flow, leaving a residue of the compound on the agar surface. (In cases where capillary attraction and rapid crystallization deposited the compounds on the sides of the test tubes rather than on the agar, the crystals were redissolved in 500 μL of ethyl acetate and the solvent evaporated again.) Controls were untreated and solvent treated.

Four or five sterilized leaf lettuce seeds were then placed in contact with the treated agar surface in each vial, and the vials were wrapped in foil to maintain sterile conditions and exclude light (four replicates per treatment). After 8 days, inhibition of germination was rated visually. In Table 2, the score "+++" indicates maximum inhibition (usually seed coat split with no radicle development). The designation "−" indicates normal (or near normal) germination and seedling growth (seedling length) relative to controls.

Acknowledgements

Financial support from the Canadian Forest Service Green Plan BICOVER Network and from the Ontario Ministry of Natural Resources (ARIO) is gratefully acknowledged. We are indebted to Dr. Peter Penner, University of New Brunswick, for recording some of the NMR spectra, and to Mr. Dan Drummond, UNB, for the mass spectra.

References

1. F. Sugawara, G. Strobel, L.E. Fisher, G.D. VanDuyne, and J. Clardy. Proc. Natl. Acad. Sci. U.S.A. **82**, 8291 (1985).
2. J.A. Schneider and K. Nakanishi. J. Chem. Soc. Chem. Commun. 353 (1983).
3. S.E. Drewes and G.H.P. Roos. Tetrahedron, **44**, 4653 (1988).
4. Y. Fort, M.C. Berthe, and P. Caubere. Tetrahedron, **48**, 6371 (1992).
5. J.S. Hill and N.S. Isaacs. Tetrahedron Lett. **27**, 5007 (1986).
6. G.M. Strunz and C.M. Yu. Can. J. Chem. **66**, 1081 (1988).
7. D. Basavaiah, T.K. Bharathi, and V.V.L. Gowriswari. Tetrahedron Lett. **28**, 4351 (1987); D. Basavaiah and V.V.L. Gowriswari. Synth. Commun. **19**, 2461 (1989).
8. E.S. Gould. Mechanism and structure in organic chemistry. Holt, Rinehart and Winston, New York. 1959. p. 376.
9. J.L.M.A. Schlatmann, J.G. Korsloot, and J. Schut. Tetrahedron, **26**, 949 (1970).
10. N.J. Leonard and P.M. Mader. J. Am. Chem. Soc. **72**, 5388 (1950).
11. K. Alder, H.K. Schafer, H. Esser, H. Krieger, and R. Reubke. Justus Liebigs Ann. Chem. **593**, 23 (1955).
12. P.A.S. Smith and D.R. Baer. Org. React. **11**, 157 (1960).
14. G.H.P. Roos and P. Rampersadh. Synth. Commun. **23**, 1261 (1993).

Can. J. Chem. Downloaded from www.nrcresearchpress.com by 46.23.64.124 on 09/08/12
For personal use only.

Studies on the transannular Diels–Alder reaction of 15-membered macrocyclic trienes containing a *trans-trans* diene. Part I: Synthesis and isomerization of various model cyclopentadecatrienes[1]

Dennis G. Hall, Renate Müller, and Pierre Deslongchamps

Abstract: The transannular Diels–Alder reaction of 15-membered macrocyclic trienes with a *trans-trans-cis* (TTC) olefin geometry can lead to A.B.C.[6.6.7] tricyclic products of *trans-syn-trans* (TST) and *cis-syn-cis* (CSC) stereochemistry whereas the TTT isomers can produce the *trans-anti-cis* (TAC) and *cis-anti-trans* (CAT) tricycles. In order to study the influence of the position (pro-6.6 or pro-6.7) and the nature (alkyl, alkoxymethyl, or formyl) of the dienophile substituent, a set of 10 model cyclopentadecatrienes was prepared. The synthesis of appropriately functionalized trisubstituted dienophile and diene synthons, as well as their coupling reactions affording acyclic precursors, is described in this paper (first in a series of two). A mild and efficient macrocyclization protocol yielded the required methyl- or alkoxymethyl-substituted cyclic substrates. Further transformations led to the formyl-substituted ones. In particular, the TTT macrocycles containing an enal as a dienophile could be completely isomerized to the corresponding TTC thermodynamic isomers in acidic aqueous media.

Key words: transannular, Diels–Alder, 15-membered ring, A.B.C.[6.6.7] tricycles, diterpene.

Résumé : La réaction de Diels–Alder transannulaire des triènes macrocycliques à 15 membres ayant une géométrie *trans-trans-cis* (TTC) peut mener aux produits tricycliques A.B.C.[6.6.7] de stéréochimie *trans-syn-trans* (TST) et *cis-syn-cis* (CSC) tandis que les isomères TTT peuvent produire les tricycles *trans-anti-cis* (TAC) et *cis-anti-trans* (CAT). Dans le but d'étudier l'influence de la position (pro-6.6 ou pro-6.7) et la nature (alkyle, alkoxyméthyle ou formyle) du substituant sur le diénophile, un ensemble de 10 cyclopentadécatriènes modèles fut préparé. La synthèse de synthons diénophiles trisubstitués et dienes adéquatement fonctionnalisés ainsi que leur réaction de couplage fournissant les précurseurs acycliques sera décrite dans cet article (le premier dans une série de deux). Un protocole de macrocyclisation doux et efficace a fourni les substrats cycliques désirés substitués d'un méthyle ou d'un groupement alkoxyméthyle. Des transformations subséquentes ont mené aux dérivés substitués avec un groupement formyle. En particulier, les macrocycles TTT contenant un énal comme diénophile ont pu être complètement isomérisés, en milieu aqueux acide, aux isomères thermodynamiques TTC correspondants.

Mots clés : transannulaire, Diels–Alder, cycle à 15 membres, tricycles A.B.C.[6.6.7], diterpène.

Introduction

One major goal of contemporary organic synthesis is to raise chemical efficiency by allowing a methodology, or a reaction, to accomplish the construction of complex structures in a minimal number of steps (1). Such efforts from our laboratory (2) and others (3) have led to the development of a promising synthetic stategy: the transannular Diels–Alder (TADA) reaction. In this case, the [4+2] cycloaddition of macrocyclic trienes is associated with a smaller energy of activation than that of acyclic trienes. This is a great benefit of the TADA strategy, leading to the one-step formation of tricyclic compounds possessing four new stereogenic centers. We have indeed exploited this higher state of reactivity in the past by successfully employing cycloaddition partners normally associated with poor reactivity. Such examples include enol ethers (4) and unactivated tetrasubstituted alkenes (5) as dienophiles as well as open-chain dienes with a strongly disfavored *trans-cis* geometry (6).[3]

Received March 20, 1995.

D.G. Hall, R. Müller, and P. Deslongchamps.[2] Laboratoire de synthèse organique, Département de chimie, Faculté des sciences, Université de Sherbrooke, Sherbrooke, QC J1K 2R1, Canada.

[1] Taken in part from D.G. Hall; Ph.D. Thesis, 1995.

[2] Author to whom correspondence may be addressed. Telephone: (819) 821-7002. Fax: (819) 821-7910. E-mail: dlnchamp@structure.chimie.usherb.ca

[3] The superiority of the TADA approach versus its intramolecular variant, the IMDA reaction (7), was further demonstrated by us (2) and by Schreiber and co-workers (3*d*). In each of these examples, a given triene failed to undergo the desired cycloaddition even at high temperatures whereas prior cyclization gave highly reactive cyclic trienes, which indeed gave satisfaction to their conceptors by reacting smoothly at low temperatures.

Can. J. Chem. Downloaded from www.nrcresearchpress.com by 46.23.64.124 on 09/08/12
For personal use only.

Can. J. Chem. Downloaded from www.nrcresearchpress.com by 46.23.64.124 on 09/08/12
For personal use only.

Scheme 1.

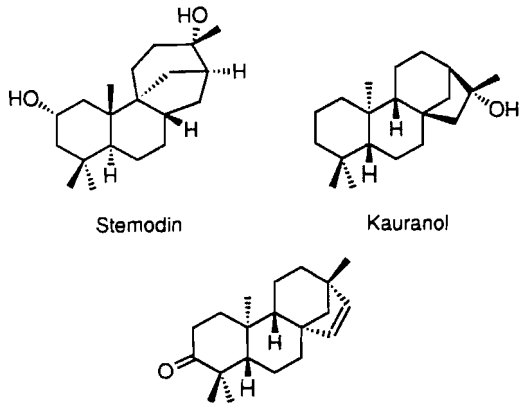

Previous fundamental studies from our group concentrated on 13- and 14-membered macrocyclic trienes, leading, respectively, to A.B.C.[6.6.5] and [6.6.6] tricycles (2). A logical step in extending the scope of the TADA strategy is to explore other systems such as 15-membered macrocyclic trienes. The resulting A.B.C[6.6.7] tricyclic compounds are part of a substructure found in a substantial number of naturally occurring compounds such as the stemodanes, kauranes, and stachanes (8). Some significant examples are illustrated in Scheme 1.

We wish to report in this article the full details of our investigation on the TADA reaction of 15-membered macrocyclic trienes bearing a *trans-trans* (TT) diene and various dienophiles with either *trans* (T) or *cis* (C) geometry.[4]

In comparison with their lower homologs, these larger substrates are likely to require higher temperatures to collapse into tricycles owing to larger activation parameters ($\Delta H^{\neq}$ and $\Delta S^{\neq}$). In other words, proximity effects are expected to show a reduced influence along the reaction pathway. Whereas the 14-membered TTC and TTT macrocyclic trienes[5] were concomitantly undergoing the TADA reaction under macrocyclization conditions (80°C) (*6b*), the 15-membered trienes should be isolable on the basis of the aforementioned arguments. Accordingly, an investigation of the reaction conditions will be a possible issue. A study of dienophile substituent effects (nature, geometry, and position) is indeed highly desirable in order to identify and understand the factors controlling stereoselection. To this end, a set of model cyclopentadecatrienes containing an *E,E*-diene moiety was devised (Scheme 2). These substrates were planned to bear a methyl, a methoxymethyl (MOM)-protected hydroxymethyl, or a formyl substituent on the dienophile, either placed at a position leading to a substitution at the angular [6.6] or [6.7] ring junction. In principle, by virtue of *endo* or *exo* approaches, TTT macrocycles (**1–5**) can lead to two tricyclic diasteromers, namely of *trans-anti-cis* (TAC) (**1a–5a**) and CAT (**1b–5b**) stereochemistry at ring junctions. In turn, the TTC geometrical isomers (**6–10**) can give tricycles of *trans-syn-trans* (TST) (**5a–10a**) and CSC (**5b–10b**) stereochemistry. The construction of conveniently functionalized dienophile and diene synthons, as well as their elaboration into macrocyclic trienes **1–10**, is described in this article (Part I).

Methods and discussion

Our general retrosynthetic approach for the synthesis of model macrocyclic substrates **1–10** is outlined in Scheme 3. This simple convergent strategy, using preformed diene and dienophile synthons with malonate connectors, is based on our earlier work on smaller ring systems (2). Thus, macrocyclic trienes are obtained through anionic cyclization of the corresponding chlorotrienes. The latter derive from a coupling reaction of a diene-substituted malonate anion with a homoallylic chloride. The appropriately functionalized dienophile synthons (methyl or MOMO-methyl) are prepared by a methodology allowing the obtention of both geometric isomers in pure form. Position isomerism, i.e., a pro-6.6 or pro-6.7 dienophile substituent,[6] depends on the selected site of substitution in the coupling reaction. Finally, formyl-substituted macrocyclic trienes are accessed via a hydrolysis–oxidation sequence on the corresponding MOMO-methyl analogs.

Preparation of *E,E* dienes 21 and 23

The basic strategy for the preparation of *trans-trans* diene synthons **21** and **23**, as illustrated in Scheme 4, employs Horner–Emmons methodolgy for stereoselective olefination (10). Mono-protection of propanediol as a tetrahydropyranyl ether, followed by Swern oxidation (11), gave aldehyde **12**. Condensation of the latter with the sodium anion of ethyl diisopropyl phosphonoacetate yielded the *E* α,β-unsaturated ester **13**. Diisobutylaluminum hydride reduction then furnished allylic alcohol **14** in high yield. A second oxidation–olefination–reduction sequence led to alcohol **17**, which was protected as its *tert*-butyldiphenylsilyl ether **18**. The homoallylic alcohol function was liberated through acidic alcoholysis of the tetrahydropyranyl ether[7] to give **19**. Mesylation of the latter followed by nucleophilic substitution with the sodium anion of dimethyl malonate resulted in the isolation of diene synthon **21**. Protecting group interchange could be realized by silyl ether cleavage with fluoride ion, yielding alcohol **22**, which was acylated with pivaloyl chloride to give **23**.

Preparation of *E* dienophile 28 and *Z*-30

An *E/Z* mixture of trisubstituted alkene **26**, prepared according to our previously reported method (*6a*), was treated with tetra-*n*-butylammonium fluoride to give alcohols **27** and **29**, which were separated by chromatography although with some difficulties (Scheme 5). Each of these could be activated prior to the subsequent coupling reaction by formation of the corresponding methanesulfonate esters **28** and **30**.

Preparation of *Z* dienophile 40 and *E* 47

The syntheses of isomeric (methoxymethoxy)methyl-substituted dienophiles **40** and **47** (Scheme 6) also relies on a Horner-Emmons reaction, using α-diethylphosphono-γ-butyrolactone (12) to generate a 47:53 **33*E*/33*Z*** mixture upon con-

[4] For preliminary communications of this work see ref. 9.

[5] The letters (C and T) refer to the olefin geometry of the macrocycles only; the first two letters refer to the diene geometry and the last one to that of the dienophile.

[6] The pro-6.7 and pro-6.6 nomenclature refers to the respective C1 (R^1) and C2 (R^2) angular positions on the resulting tricycles (see Scheme 2).

[7] L. Ruest, S. Lamothe, and P. Deslongchamps. Unpublished results.

Can. J. Chem. Downloaded from www.nrcresearchpress.com by 46.23.64.124 on 09/08/12
For personal use only.

Scheme 2.

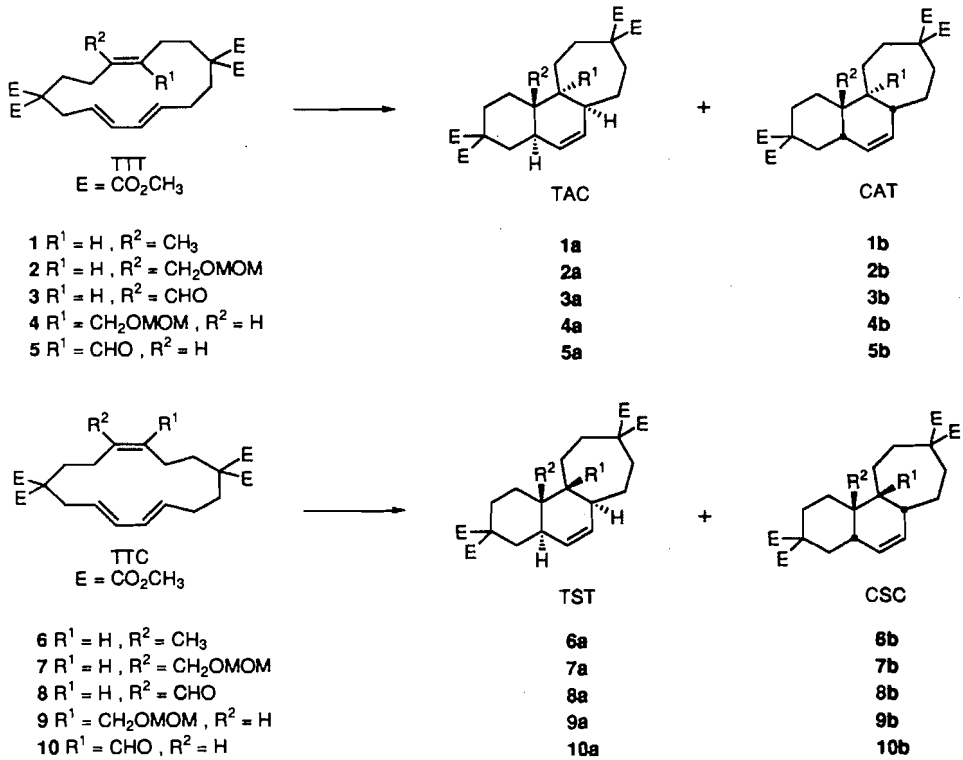

Scheme 3. Retosynthetic plan.

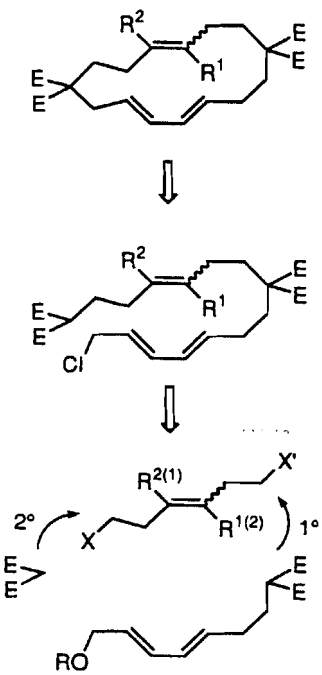

densation with aldehyde **32**. Such a lack of selectivity was desirable to fulfill our needs in both isomers as the resulting *E* and *Z* alkylidene lactones can be easily separated on silica gel chromatography. Confirmation of double bond geometries came from ^{1}H nmr nOe experiments where only one lactone, evidently **33***E*, showed some enhancement between the allylic methylenes. The *Z* synthon **40** was constructed by making use of the same straightforward sequence applied for the recently reported synthesis of the *E* isomer **47** (13). To this end, lactone **33***Z* was subjected to a four-step sequence dealing with some unstable intermediates that had to be reacted without delay. Diisobutylaluminum hydride reduction furnished a crude mixture of **34** and **35** that was then treated with manganese dioxide, yielding homogeneous aldehyde **35**. Acetylation of the remaining alcohol function gave **36** and sodium borohydride reduction furnished pure allylic alcohol **37** in 56% overall yield from **33***Z*. Protection of alcohol **37** as a MOM ether gave **38**. Then, methanolysis of the acetate group led to the isolation of alcohol **39**, the ready precursor of mesylate **40**.

Preparation of *Z* dienophile 49

Compared to **40**, the preparation of **49** was envisaged for coupling with the diene synthon at the opposite extremity of the unsymmetrical dienophile, thus eventually leading to macrocycles with alkoxymethyl substitution at the pro-6.6 position. Desilylation of **38** with fluoride ion followed by mesylation of the resulting alcohol **48** furnished the desired dienophilic coupling partner **49** (Scheme 7).

Synthesis of TTT macrocyclic substrate 1 and TTC 6

As shown in Scheme 3, the elaboration of acyclic trienes into the desired macrocycles starts with the coupling reaction of an appropriately functionalized diene synthon with the required dienophile counterpart. The syntheses of isomeric macrocyclic trienes TTT **1** and TTC **6** with a methyl substituent on the dienophile use the same reaction sequence, performed in parallel from both *E* and *Z* alkenes **28** and **30** (Scheme 8). Thus, the sodium anion derived from diene-substituted malonate **21** was alkylated with the aforementioned homoallylic

Can. J. Chem. Downloaded from www.nrcresearchpress.com by 46.23.64.124 on 09/08/12
For personal use only.

Scheme 4. Diene synthesis.

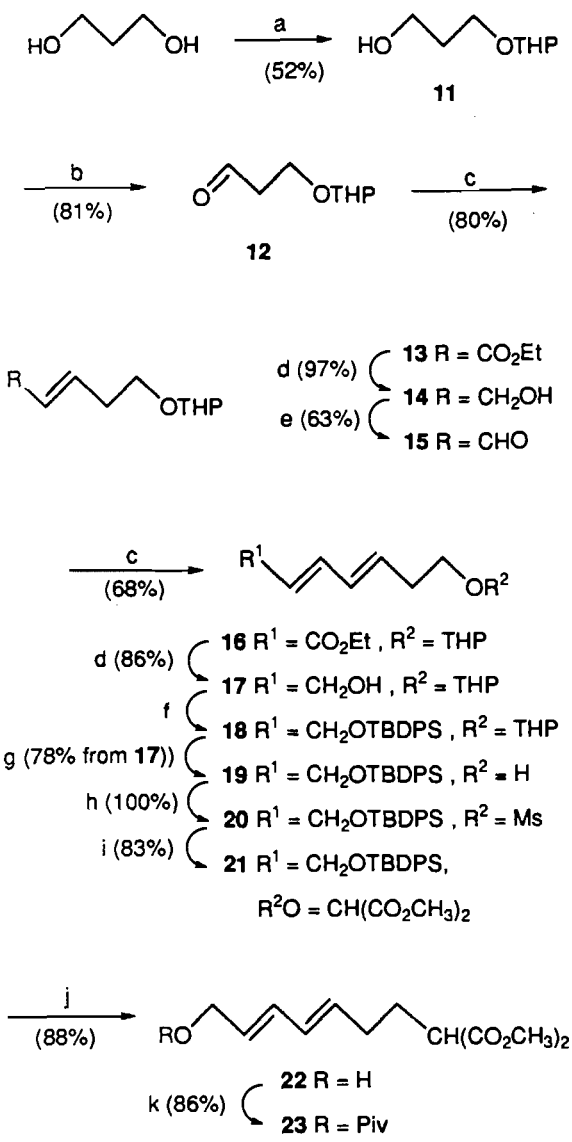

(a) 3,4-dihydro-2H-pyran, PTSA, CH_2Cl_2, 0°C, 3 h.
(b) $(COCl)_2$, DMSO, Et_3N, CH_2Cl_2, -78°C to rt, 1 h.
(c) NaH, THF, 0°C; then $(iPr)_2P(O)CH_2CO_2Et$, cool to -78°C; then **12** or **15**, -78°C to rt, 1 h.
(d) DIBALH, Et_2O, -78°C, 1 h.
(e) PCC, 3 A m.s., CH_2Cl_2, rt, 1.5 h.
(f) imidazole, TBDPSCl, THF, rt, 1 h.
(g) PPTS, iPrOH, reflux, 1 h.
(h) Et_3N, MsCl, CH_2Cl_2, 0°C, 1 h.
(i) NaH, DMF, rt; then $CH_2(CO_2CH_3)_2$; then **20** in THF, KI, 70-75°C, 15 h.
(j) TBAF, THF, rt, 3 h
(k) Et_3N, DMAP, $(CH_3)CCOCl$, 0°C, 2 h; rt, 1 h.

methanesulfonate esters **28** and **30** and added sodium iodide, to give the respective trienes **50** and **56** in good yields. The tetrahydropyranyl protecting group was removed under transacetalization conditions to afford alcohols **51** and **57**. The introduction of a second malonate connecting unit was performed through another sequence of mesylation – dimethyl malonate alkylation, as described above for diene **21**, yielding

Scheme 5. Synthesis of methyl-substituted dienophiles.

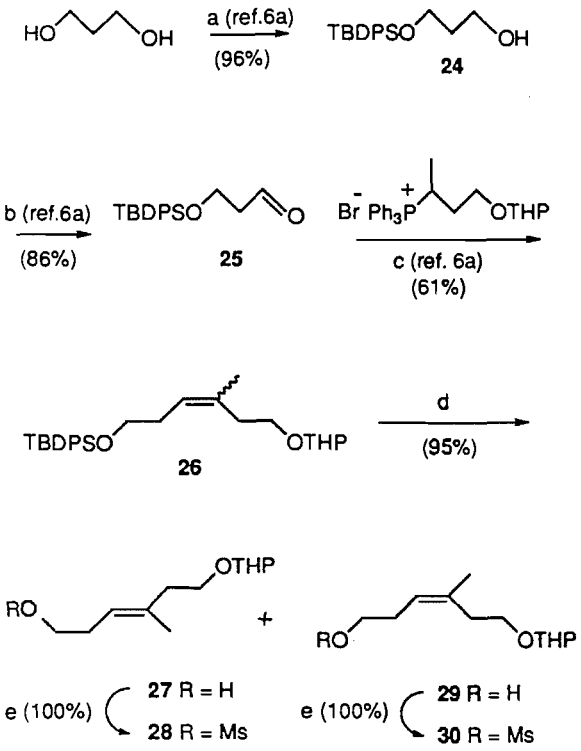

(a) imidazole, TBDPSCl, rt, 25 h.
(b) $(COCl)_2$, DMSO, Et_3N, CH_2Cl_2, -78°C to rt, 1 h.
(c) nBuLi, THF, 0°C, 3 h.
(d) TBAF, THF, 0°C, 1 h; separation.
(e) Et_3N, MsCl, rt, 2 h.

pentadecatrienes **53** and **59**. Silyl ether cleavage of the latter compounds gave the respective alcohols **54** and **60**. These intermediates were then chlorinated using the method of Collington and Meyers (14), and the corresponding sensitive chlorides **55** and **61** were immediately cyclized at 75°C under our usual pseudo-high-dilution conditions (syringe pump addition over >10 h into a stirred cesium carbonate suspension), affording high yields of TTT macrocycle **1** and TTC isomer **6**.

Following our expectation as discussed in the introduction, no Diels–Alder products were observed under these mild conditions. Also, no detectable amount of dimerization products was formed. The conservation of the double bond geometries in macrocyclic products **1** and **6** and all others in this article has been confirmed by comparing ^1H nmr data with those of their corresponding triene precursors. Finally, the structures of the macrocyclic trienes described herein were rigorously established by spectroscopic methods including ^1H and ^{13}C nmr, ir, and low- and high-resolution ms.

Synthesis of TTT macrocyclic substrate 4 and TTC 9

The synthetic pathway for isomeric macrocyclic trienes **4** and **9** is similar to that previously described for **1** and **6**. Thus, *E,E* diene **23** was coupled to the *Z* dienophile synthon **40**, affording triene **62** (Scheme 9). The alcohol function was deprotected to give **63**, which was mesylated and substituted with the sodium anion of dimethyl malonate, yielding tetraester **65**.

Can. J. Chem. Downloaded from www.nrcresearchpress.com by 46.23.64.124 on 09/08/12
For personal use only.

Scheme 6. Synthesis of alkoxymethyl-substituted dienophiles.

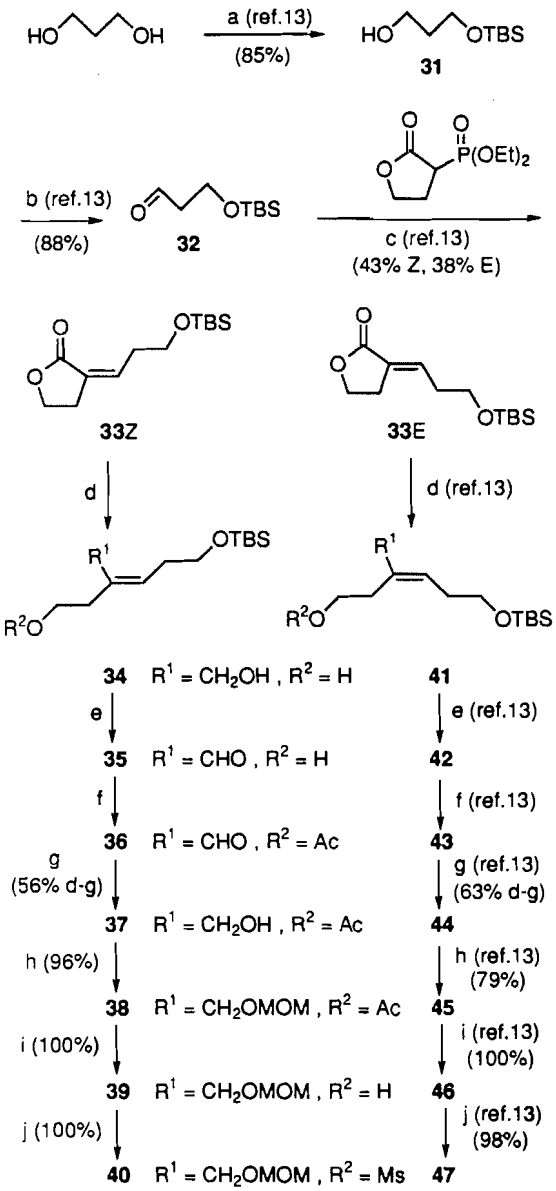

(a) imidazole, TBSCl, THF, rt, 36 h.
(b) $(COCl)_2$, DMSO, Et_3N, CH_2Cl_2, -78°C to rt, 1 h.
(c) NaH, C_6H_6; then α-diethylphosphono-γ-butyrolactone, rt to 60°C; then **32**, 60°C, 0.5 h.
(d) DIBALH, Et_2O, -78C, 1 h. (e) MnO_2, $CHCl_3$, r t, 3 h
(f) Ac_2O, Et_3N, DMAP, CH_2Cl_2, 0°C, 2 h.
(g) $NaBH_4$, CH_3OH, 0°C, 1 h.
(h) DIPEA, MOMCl, CH_2Cl_2, rt, 20 h
(i) K_2CO_3, CH_3OH, rt, 3 h. (j) Et_3N, MsCl, CH_2Cl_2, 0°C, 3 h.

The pivaloyl ester was cleaved to give alcohol **66** and chlorination of this intermediate gave chloride **67**. This chlorotriene was cyclized under the usual conditions, giving TTT macrocyclic triene **4** in high yield. This compound gave nice crystals and X-ray diffraction analysis confirmed its structure[8] and thereby that of previous intermediates, including the *Z/E* geometrical assignment on alkylidene lactones **33**. The TTC isomer **9** was synthesized through an identical sequence starting from the *E* dienophile synthon **47**.

[8] M. Drouin, D.G. Hall, and A.G. Michel. Unpublished results.

Scheme 7. Preparation of dienophile synthon **49**.

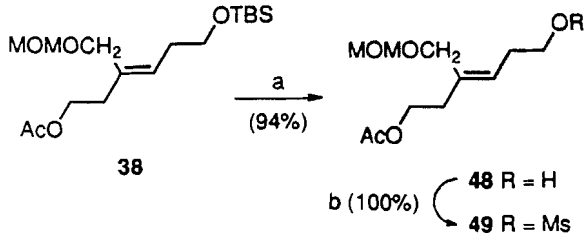

(a) TBAF, THF, rt, 1 h. (b) Et_3N, MsCl, CH_2Cl_2, 0°C, 1 h

Synthesis of TTT macrocyclic substrate 2

TTT macrocyclic triene **2** bearing an alkoxymethyl substituent at the pro-6.6 position was constructed from building blocks **21** and **49** (Scheme 10). Upon anionic coupling according to the usual conditions, triene **74** was isolated in moderate yield. The acetate protecting group was cleaved to yield **75** and the installment of a second malonate connecting unit led to the obtention of tetraester **77**. Desilylation of the latter intermediate gave alcohol **78**, which was transformed into the corresponding chloride **79**. Cyclization of this chlorotriene afforded the TTT macrocyclic triene **2** in high yield. Except for signals ascribed to the pro-6.6 substituent, ^1H nmr spectra of **2** and **1** were virtually identical.

Transformation of alkoxymethyl-substituted macrocycles into formyl-substituted macrocyclic substrates 5, 10, and 3

Upon hydrolysis of the methoxymethyl protecting group of **4**, alcohol **80** was isolated in high yield (Scheme 11). Manganese dioxide oxidation of this allylic alcohol afforded TTT formyl-substituted macrocyclic triene **5**. Macrocyclic triene **9** was also subjected to the same conditions, this time using the Dess–Martin periodinane (15) as the oxidant, yielding aldehyde **10**. In turn, aldehyde **3** was obtained via **82** in high yield from MOM ether **2**.

The *trans* to *cis* enal isomerization of 3 and 5 to 8 and 10; synthesis of 7

Upon treatment with a small amount of 1 N aqueous hydrochloric acid in tetrahydrofuran for a few hours, TTT formyl-substituted macrocyclic trienes **3** and **5** could be entirely transformed in almost quantitative yields to their parent TTC macrocycles **8** and **10** (Scheme 11). This alkene chemical inversion process[9] was unambiguously confirmed by comparing nmr data with an authentic sample of **10** originating from **9** by the direct route described above. This olefin inversion indicates that having three *E*-double bonds is a highly unfavorable situation for our 15-membered macrocycles. This trend is probably further reinforced by the preferred *transoid* conformation of the diene moiety, which can be deduced from the X-ray structure of **4** and ^1H nmr coupling constants[10] on some macrocyclic trienes described herein.

[9] Presumably occurring through an addition–elimination mechanism: protonation of the aldehyde carbonyl triggers nucleophilic attack (by chlorine ion or water) at the distal alkene carbon. Rotation of the sp^3 rehybridized bond and elimination restores the double bond with net inversion. For a review on alkene inversion, see ref. 16.

[10] The usual vicinal constants between central hydrogens of a 1,3 diene are the following (17): $J_{transoid}$: ~10 Hz; J_{cisoid}: ~5 Hz.

Scheme 8. Synthetic sequence for **1** and **6**.

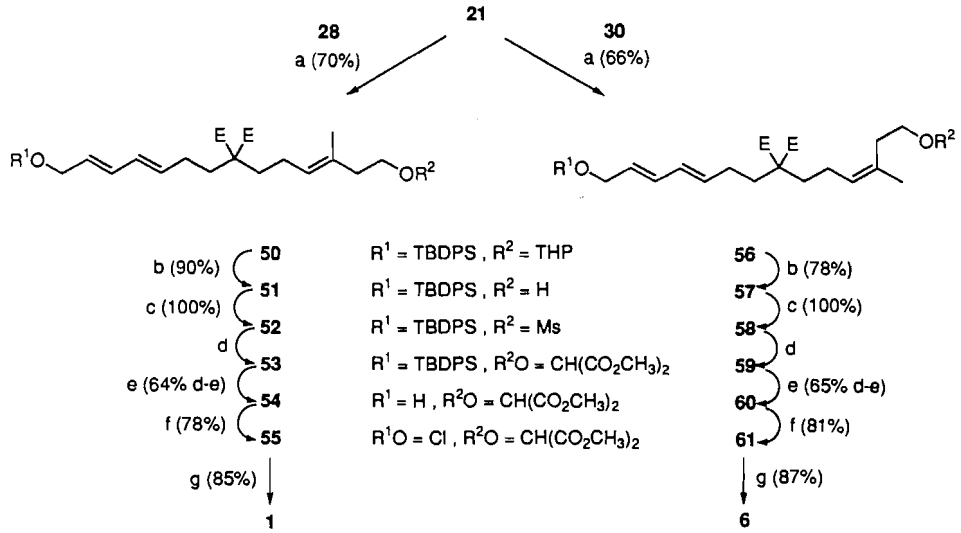

(a) NaH, DMF; then **21**, 40°C, 1 h; then **28** or **30** in THF, KI, 70°C, 12 h. (b) PPTS, iPrOH, reflux, 1 h.
(c) Et_3N, MsCl, CH_2Cl_2, rt, 1 h. (d) NaH, THF, rt; then $CH_2(CO_2CH_3)_2$, 0.5 h; then **52** or **58** in THF, KI, 75°C, 18 h.
(e) TBAF, THF, rt, 3 h. (f) LiCl, s-collidine, MsCl, DMF, rt, 1-2.5 h. (g) Cs_2CO_3, DMF/THF, 75°C; then **55** or **62** in DMF/THF by slow addn within 12-20 h, final [ ] c.a. 0.004 M.

Scheme 9. Synthetic sequence for **4** and **9**.

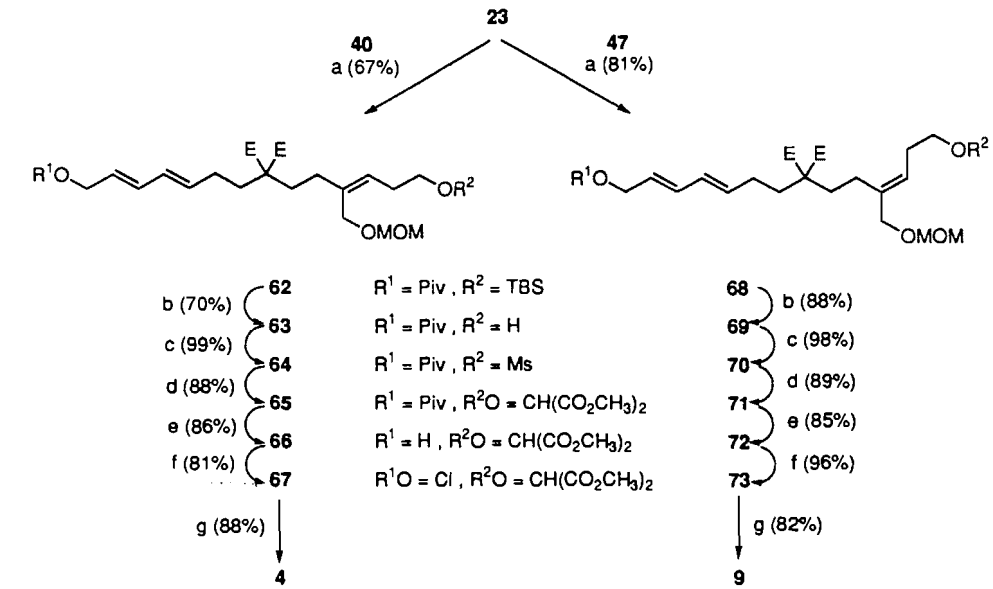

(a) NaH, DMF; then **23**, 40°C, 1 h; then **40** or **47** in THF, KI, 70°C, 18 h. (b) TBAF, THF, rt, 4.5 h.
(c) Et_3N, MsCl, CH_2Cl_2, 0°C, 1.5 h. (d) NaH, THF, 40°C; then $CH_2(CO_2CH_3)_2$, 0.5h; then **64** or **70** in THF, KI, 75°C, 12 h.
(e) NaOMe, MeOH, rt, 5 h. (f) LiCl, s-collidine, MsCl, DMF, 0°C, 4 h. (g) Cs_2CO_3, DMF/THF, 75°C; then **67** or **73** in DMF/THF by slow addn within 12 h, final [ ] c.a. 0.004 M.

Although the *transoid* conformation of 1,4-disubstituted *E,E* 1,3-dienes minimizes allylic strain compared to the compact *cisoid* conformation (18), it has the effect of orienting the two ring chains in opposite directions. As a result, there is less conformational freedom for the remaining methylenes, and a *Z* geometry at the dienophile double bond is thus preferable in alleviating this situation since it returns the two ring chains in the same direction. This thermodynamic preference was corroborated by performing molecular modeling experiments (Fig. 1). Energy minimization of ester-truncated TTT **5** and

Can. J. Chem. Downloaded from www.nrcresearchpress.com by 46.23.64.124 on 09/08/12
For personal use only.

Can. J. Chem. Downloaded from www.nrcresearchpress.com by 46.23.64.124 on 09/08/12
For personal use only.

Fig. 1. AM1 optimized structures in s-*cis* enal conformation with truncated ester functions.

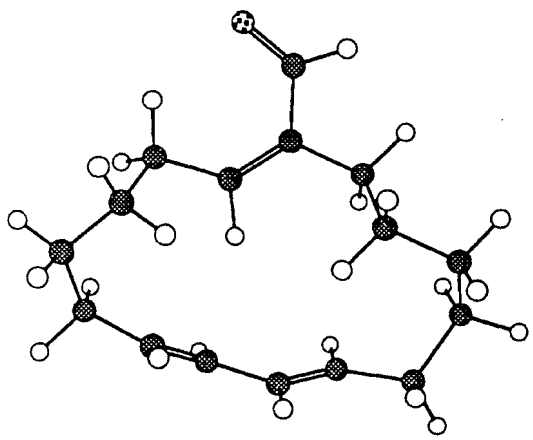

TTT **5** (E = H)
$\Delta H°_f$ = - 38.2 kcal/mol

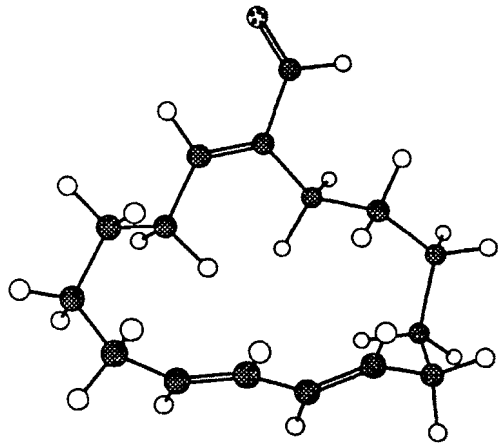

TTC **10** (E = H)
$\Delta H°_f$ = - 41.3 kcal/mol

TTC **10** using the semi-empirical Hamiltonian AM1 (19) gave a much lower $\Delta H°_f$ (3.1 kcal/mol) for the TTC isomer.[11]

Due to their propensity for enal inversion, manipulation of TTT macrocyclic substrates **3** and **5** needed special attention.[12] However, this behaviour could be exploited most advantageously to save time and effort on synthesis and gain access to more macrocyclic substrates from a single one. For instance, it was shown above that $MOMOCH_2$-substituted macrocyclic triene **2** could be transformed to TTC formyl-substituted derivative **8**. Then, sodium borohydride reduction of the aldehyde function yielded allylic alcohol **83** and protection of the latter with methoxymethyl chloride afforded model macrocyclic substrate **7** (Scheme 11). Thus, the enal inversion process carried out on **3** provided a short access to **7**, skirting a much longer route starting from a performed *cis* dienophilic building block.

Conclusion

In summary, the present paper describes the efficient and highly convergent preparation of a set of model 15-membered macrocyclic trienes **1**–**10** containing a *trans-trans* diene. Various trisubstituted dienophile building blocks with *E* or *Z* geometry, and bearing a methyl, MOMO-methyl, or formyl substituent, were prepared and coupled with a diene synthon to eventually give acyclic triene precursors. A smooth macrocyclization protocol afforded high yields (>85%) of the aforementioned cyclopentadecatrienes, which, unlike their lower homologs, were found insensible to a TADA transformation at the temperature of macrocyclization (75°C). Also, it was found that TTT macrocyclic trienes with an enal moiety as a dienophile could be isomerized quantitatively to their corresponding TTC congeners in aqueous acidic media. This observation gave many insights into the relative stability and conformational behaviour of our model macrocyclic trienes. A

Scheme 10. Synthetic sequence for **2**.

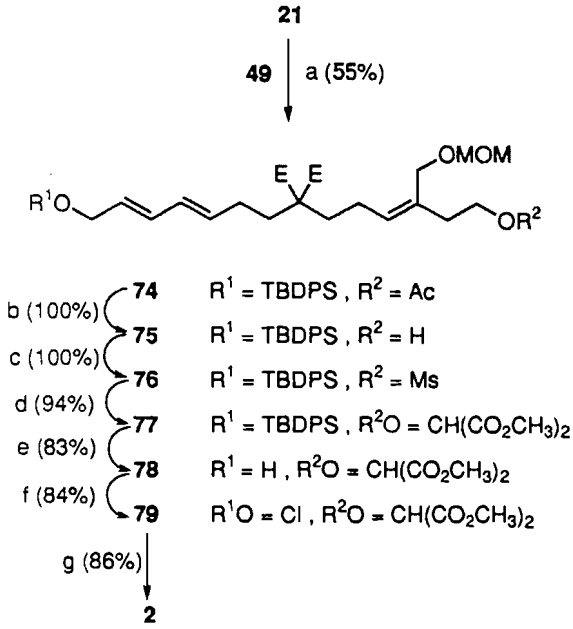

(a) NaH, DMF; then **21**, 40°C, 1 h; then **49** in THF, KI 75°C, 12 h. (b) K_2CO_3, MeOH, rt, 3 h.
(c) Et_3N, MsCl, CH_2Cl_2, 0°C, 1.5 h.
(d) NaH, THF, 40°C; then $CH_2(CO_2CH_3)_2$, 0.5 h; then **76** in THF, KI, 75°C, 15 h. (e) TBAF, THF, rt, 2.5 h.
(f) LiCl, s-collidine, MsCl, DMF, 0°C, 2.5 h.
(g) Cs_2CO_3, DMF/THF, 75°C; then **79** in DMF/THF by slow addn within 15 h, final [ ] c.a. 0.004 M.

[11] Computational procedure: all the calculations were done at the RHF level. Input files for MOPAC 6.00 were generated by importing X-ray structure **4** and an analogue of **9** ($R^1 = nBu_3Sn$, Scheme 2, M. Drouin and G. Falardeau. Unpublished results) into SYBYL 6.01 (Tripos Associates, Inc.: 16995 Hanley Rd., Suite 303, St. Louis, Missouri 63144-2913) for IBM RISC 6000 computers. Ester-truncated **5** and **10** were then minimized with either a s-*cis* or s-*trans* dienophile conformation using Maximin force field within SYBYL and were submitted to AM1 for full optimization. The s-*trans* conformers (not shown) were higher in energy although with a comparable $\Delta\Delta H°_f$ (2.4 kcal/mol).

[12] MnO_2 oxidation of **80** and **82** tends to give minor amounts of the TTC aldehydes **10** and **8** with prolonged reaction times.

Scheme 11. Final transformations and isomerization of macrocycles.

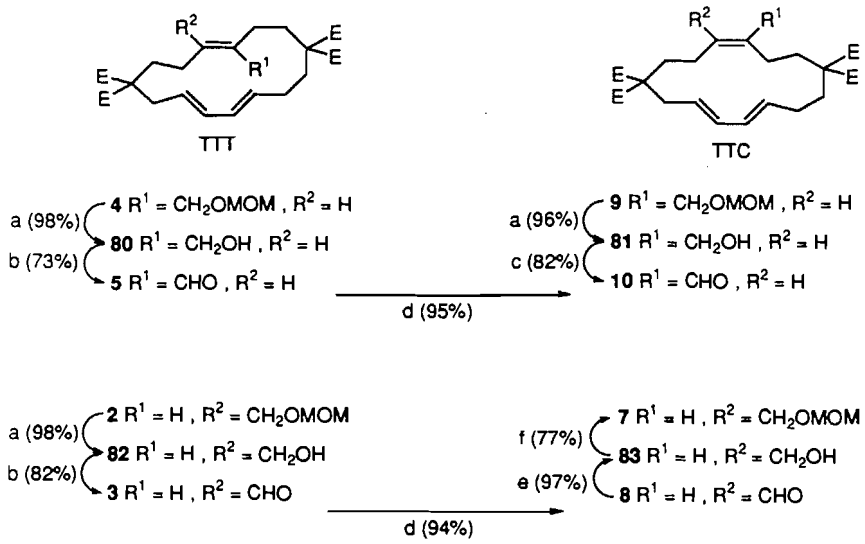

(a) conc. $HCl_{(aq)}$ / H_2O / MeOH, 60°C, 2-6 h. (b) MnO_2, CH_2Cl_2, rt. (c) Dess-Martin periodinane, CH_2Cl_2, rt, 1 h. (d) 1N $HCl_{(aq)}$, THF, rt, 3-12 h. (e) $NaBH_4$, MeOH/THF, 0°C, 1 h (f) DIPEA, MOMCl, CH_2Cl_2, rt, 5 h.

study of their reactivity toward the transannular Diels–Alder reaction leading to A.B.C.[6.6.7] tricyclic compounds is described in the following paper of this issue (Part II).

Experimental

General

For the benefit of homogeneity in the nomenclature of analogous series of compounds, substituent numbering was kept constant in spite of the existing rules. Reactions were performed under nitrogen atmosphere with oven- (150°C) or flame-dried glassware. All solvents were dried and distilled shortly before use: diethyl ether and tetrahydrofuran (sodium – benzophenone ketyl); benzene, dichloromethane, dimethylformamide, and dimethyl sulfoxide (calcium hydride); methanol (magnesium–iodine). Most amines were dried over calcium hydride and distilled, dimethyl malonate was distilled as such, and methanesulfonyl chloride was dried over phosphorus pentoxide and distilled. Cesium carbonate, lithium chloride, and potassium iodide were flame-dried under reduced pressure before use. All other starting materials and reactants were obtained commercially and used as such or purified by standard means. All solvents and reactants purified and dried were stored under nitrogen. Analytical (0.25 mm) and preparative thin-layer chromatography (desorption solvent: ethyl acetate) were carried out on prcoated glass plates with silica gel 60F-250 (Merck). Materials were detected by visualization under an ultraviolet lamp and by dipping into a solution of phosphomolybdic acid (10% in ethanol) followed by heating on a hot plate. For flash chromatography, Merck Kieselgel silica gel 60 (230–400 Mesh A.S.T.M.) was used. All solvents used in chromatography were distilled. Concentration of organic solutions implies evaporation on a rotary evaporator followed by reduced pressure (>0.5 Torr; 1 Torr = 133.3 Pa).

The infrared (ir) spectra were taken on a Perkin–Elmer 681 spectrophotometer or on a Perkin–Elmer 1600 FT-ir spectrometer. Proton nuclear magnetic resonance (nmr) spectra were recorded on a Bruker WM-250 or Bruker AC-300 instrument. The following abbreviations were used: br, broad; s, singlet; d, doublet; dd, doublet of doublet; t, triplet; q, quartet; qn, quintet; and m, multiplet. Chemical shifts are reported in δ values relative to chloroform (7.26 ppm) or benzene (7.15 ppm) as internal standard. Proton-decoupled carbon nmr spectra used chloroform (77.00 ppm) or benzene (126.00 ppm) as internal standard. Where necessary, decoupling experiments and two-dimensional techniques were performed. Mass spectral (ms) assays were obtained on a VG Micromass ZAB-2F instrument. Melting points of crystalline materials were determined on a Büchi M-50 or on a Reichert apparatus and are uncorrected. Crystallographic analyses were performed on a Enraf–Nonius CAD-4 diffractometer (Mo Kα radiation; λ = 0.70930 Å).

3-Tetrahydropyranyloxy propanol (11)

3,4-Dihydro-2*H*-pyran (81 mL, 0.89 mol) was added to a solution of 1,3-propanediol (161 mL, 2.23 mol) and *p*-toluenesulfonic acid (5.93 g, 31 mmol) in dichloromethane (250 mL) at 0°C. The mixture was stirred 3 h and a saturated sodium bicarbonate solution (200 mL) was added. The organic phase was segregated and the aqueous layer was extracted with ethyl acetate (3 × 100 mL). The combined organic layers were dried with anhydrous magnesium sulfate, filtered, and concentrated. The crude product was purified by flash chromatography (10–50% ethyl acetate in hexanes) to afford 73.7 g (52%) of alcohol **11** as an oil; ir (CH_2Cl_2): 3620, 3540, 2950, 2880 cm^{-1}; ^1H nmr (250 MHz) ($CDCl_3$) δ (ppm): 4.59 (1H, dd, J = 4.5 Hz, 2.5 Hz, -O-CH-O-), 3.99–3.72 (4H, m) and 3.65–3.45 (2H, m) (3 × $-CH_2O-$), 2.45 (1H, m, -OH), 1.95–1.40 (8H, m, 4 × $-CH_2-$); ^{13}C nmr (75 MHz, $CDCl_3$) δ (ppm): 98.92, 65.51, 62.33, 60.54, 32.01, 30.46, 25.15, 19.48;

Can. J. Chem. Downloaded from www.nrcresearchpress.com by 46.23.64.124 on 09/08/12
For personal use only.

Can. J. Chem. Downloaded from www.nrcresearchpress.com by 46.23.64.124 on 09/08/12
For personal use only.

ms *m/e*: 159 (M^+ − H). Exact Mass calcd. for $C_8H_{15}O_3$: 159.1021; found: 159.1026 ± 0.0005.

3-Tetrahydropyranyloxypropanal (12)

Dimethyl sulfoxide (23.5 mL, 0.36 mol) in dichloromethane (70 mL) was added over a 10 min period to a solution of oxalyl chloride (14.5 mL, 0.17 mol) in dichloromethane (315 mL) at −78°C. The flask was stirred 20 min and the alcohol **11** (24.1 g, 0.15 mol) in dichloromethane (140 mL) was added over a 25 min period. The solution was stirred 45 min and triethylamine (96 mL, 0.69 mol) was added. The thick white mixture was allowed to warm to room temperature for 1 h and water (200 mL) was added, followed by extractions with dichloromethane (3 × 100 mL). The combined organic phases were washed with water (2 × 70 mL), saturated aqueous sodium chloride (150 mL), dried over anhydrous magnesium sulfate, filtered, and concentrated. The crude material was then purified by flash chromatography (25% ethyl acetate in hexanes) giving aldehyde **12** (19.22 g, 81%); ir (CH_2Cl_2): 2950, 2880, 2740, 1725 cm^{-1}; ^1H nmr (250 MHz) ($CDCl_3$) δ: 9.81 (1H, t, J = 2.0 Hz, -CHO), 4.62 (1H, dd, J = 4.0 Hz, 2.5 Hz, -OCHO-), 4.09 (1H, dt, J = 10.5 Hz, 6.0 Hz, -O*H*CHCH$_2$CHO), 3.90–3.78 (1H, m, -(CH$_2$)$_3$-*H*CHO-), 3.75 (1H, dt, J = 10.5 Hz, 6.0 Hz, -OHC*H*CH$_2$CHO), 3.58-3.45 (1H, m, -(CH$_2$)$_3$-HC*H*O-), 2.69 (2H, dt, J = 6.0 Hz, 2.0 Hz, -C*H*CHO), 1.90–1.40 (6H, m, -CH(C*H*$_2$)$_3$CH$_2$O-); ^{13}C nmr (75 MHz, $CDCl_3$) δ (ppm): 201.30, 99.00, 62.25, 61.21, 43.82, 30.48, 25.73, 19.32; ms *m/e*: 159 (MH^+), 157 (M^+ − H). Exact Mass calcd. for $C_8H_{13}O_3$: 157.0864; found: 157.0868 ± 0.0005.

(*E*)-Ethyl 5-tetrahydropyranyloxy-2-pentenoate (13)

A solution of ethyl diisopropylphosphonoacetate (45.98, 0.183 mol) in tetrahydrofuran (100 mL) was added dropwise over a period of 0.5 h to a stirred suspension of sodium hydride (5.84 g, 0.147 mol, 60% in mineral oil) in tetrahydrofuran (600 mL) cooled to 0°C. After stirring for 10 min, the solution was cooled to −78°C and a solution of aldehyde **12** (19.2 g, 0.121 mol) in tetrahydrofuran (240 mL) was added within 0.5 h. Stirring was continued for 15 min and the reaction mixture was allowed to warm to room temperature (~1 h). A solution of saturated aqueous ammonium chloride was added and the mixture was extracted thrice with diethyl ether. The combined organic layers were washed with brine, dried over anhydrous magnesium sulfate, filtered, concentrated, and the residue was purified by flash chromatography (17% ethyl acetate in hexanes), yielding ester **13** (22.12 g, 80% colorless oil); ir (CH_2Cl_2): 2950, 1715, 1655 cm^{-1}; ^1H nmr (250 MHz) ($CDCl_3$) δ (ppm): 6.99 (1H, dt, J = 15.5 Hz, 7.0 Hz, -C*H*=CHCO$_2$Et), 5.90 (1H, dt, J = 15.5 Hz, 1.5 Hz, -CH=C*H*CO$_2$Et), 4.60 (1H, m, -OCHO-), 4.19 (2H, q, J = 7.0 Hz, -CO$_2$C*H*$_2$CH$_3$), 3.86 (1H, dt, J = 9.5 Hz, 6.5 Hz, -O*H*CH-CH$_2$CH=), 3.90–3.80 (1H, m, -(CH$_2$)$_3$*H*CHO-), 3.51 (1H, dt, J = 9.5 Hz, 6.5 Hz, -OHCHCH$_2$CH=), 3.55–3.47 (1H, m, -(CH$_2$)$_3$HC*H*O-), 2.51 (2H, ddt, J = 6.5 Hz, 6.5 Hz, 1.5 Hz, -CH=CH-C*H*$_2$-), 1.87–1.45 (6H, m, -CH(C*H*$_2$)$_3$CH$_2$O-), 1.29 (3H, t, J = 7.0 Hz, -CO$_2$CH$_2$C*H*$_3$); ms *m/e*: 227 (M^+ − H), 183 (M^+ − EtO).

(*E*)-5-Tetrahydropyranyloxy-2-pentenol (14)

Diisobutylaluminum hydride (381 mL, 0.381 mol, 1.0 M in dichloromethane) was added to a cooled solution (−78°C) of ester **13** (39.5 g, 0.173 mol) in diethyl ether (1.5 L). After stirring for 1 h at −78°C methanol (200 mL) was added and the mixture was allowed to warm to room temperature and washed with a 30% aqueous solution of disodium tartrate (4 × 400 mL). The combined aqueous phases were extracted with diethyl ether (3 × 200 mL) and the resulting organic layers were dried over anhydrous magnesium sulfate, filtered, and concentrated, yielding pure alcohol **14** (31.13 g, 97%, colorless oil); ir (CH_2Cl_2): 3600, 3460, 2950 cm^{-1}; ^1H nmr (250 MHz, $CDCl_3$) δ (ppm): 5.78 (2H, m, -CH=CH-), 4.09 (3H, m, -OCHO-, -C*H*$_2$OH), 3.90–3.80 (1H, m, -(CH$_2$)$_3$*H*CHO-), 3.77 (1H, dt, J = 9.5 Hz, 7.0 Hz, -O*H*CHCH$_2$CH=), 3.52–3.45 (1H, m, -CH$_2$)$_3$HC*H*O-), 3.44 (1H, dt, J = 9.5 Hz, 7.0 Hz, -OHC*H*CH$_2$CH=), 2.40–2.30 (2H, m, -CH=CHC*H*$_2$-), 1.90–1.41 (7H, m, -CH(C*H*$_2$)$_3$CH$_2$O-, OH); ms *m/e*: 185 (M^+ − H).

(*E,E*)-Ethyl 7-tetrahydropyranyloxy-2,4-heptadienoate (16)

Pyridinium chorochromate (24.0 g, 0.111 mol) was added to a stirred suspension of alcohol **14** (13.8 g, 0.074 mol) and powdered 3 Å molecular sieves (32 g) in dichloromethane (400 mL) at 0°C. The mixture was allowed to warm to room temperature and stirred for 1.5 h. Then, diethyl ether (1 L) was added and the reaction mixture was filtered over a short pad of silica gel. The solvent was evaporated and the residue was purified by flash chromatography (35% ethyl acetate in hexanes), giving aldehyde **15** (8.3 g, 63%, colorless oil). This material was immediately reacted with diisopropylphosphonoacetate, following the procedure described for the preparation of **13**, yielding ester **16** (7.62 g, 68%, colorless oil) after purification by flash chromatography (20% ethyl acetate in hexanes); ir (neat): 2940, 2870, 1715, 1645 cm^{-1}; ^1H nmr (250 MHz, $CDCl_3$) δ (ppm): 7.25 (1H, dd, J = 15.5 Hz, 10.0 Hz, -C*H*=CH-CO$_2$Et), 6.25 (1H, dd, J = 15.5 Hz, 10.0 Hz, -CH$_2$CH=C*H*-), 6.14 (1H, dt, J = 15.5 Hz, 6.5 Hz, -CH$_2$C*H*=C*H*-), 5.80 (1H, d, J = 15.5 Hz, -CH=C*H*CO$_2$Et), 4.59 (1H, m, -OCHO-), 4.19 (2H, q, J = 7.0 Hz, CO$_2$C*H*$_2$CH$_3$), 3.90–3.80 (1H, m, -(CH$_2$)$_3$*H*CHO-), 3.82 (1H, dt, J = 9.5 Hz, 6.5 Hz, THPO-*H*CH-), 3.55–3.45 (1H, m, -(CH$_2$)$_3$HC*H*O-), 3.45 (1H, dt, J = 9.5 Hz, 6.5 Hz, THPO-HC*H*CH$_2$-), 2.47 (2H, dt, J = 6.5 Hz, THPOCH$_2$C*H*$_2$CH=), 1.90–1.45 (6H, m, -CH(C*H*$_2$)$_3$CH$_2$O-), 1.29 (3H, t, J = 7.0 Hz, CO$_2$CH$_2$C*H*$_3$); ^{13}C nmr (75 MHz, $CDCl_3$) δ (ppm): 167.69, 144.64, 140.50, 129.89, 119.77, 98.78, 66.10, 62.20, 60.16, 33.32, 30.58, 25.36, 19.42, 14.22; ms *m/e*: 254 (M^+), 209 (M^+ − OEt).

(*E-E*)-1-*tert*-Butyldiphenylsiloxy-2,4-heptadien-7-ol (19)

Using the procedure employed for the preparation of **14**, ester **16** (6.95 g, 27.4 mmol) was treated with diisobutylaluminum hydride (40.1 mL, 60.2 mmol, 1.5 M in toluene) in diethyl ether (220 mL), giving the crude alcohol **17** (5.0 g, 86%). This material was dissolved in tetrahydrofuran (150 mL) and imidazole (4.02 g, 59.0 mmol), followed by addition of *tert*-butyldiphenylchlorosilane (7.4 mL, 28 mmol), The solution was stirred 1 h at room temperature and saturated aqueous ammonium chloride (100 mL) was added. The resulting mixture was extracted with hexanes – diethyl ether (1:1, 3 × 100 mL) and the combined organic phases were washed with brine, dried over anhydrous magnesium sulfate, filtered, and concentrated to give the crude silyl ether **18**. Pyridinium *p*-toluenesulfonate (0.73 g, 2.9 mmol) was added to a solution of crude **18** in isopropanol (250 mL). The solution was stirred under reflux for

Can. J. Chem. Downloaded from www.nrcresearchpress.com by 46.23.64.124 on 09/08/12
For personal use only.

1 h and allowed to cool to room temperature. Solid potassium carbonate (0.6 g) was added under stirring and the mixture was filtered and concentrated. The crude product was purified by flash chromatography (25% ethyl acetate in hexanes), affording dienic alcohol **19** (6.70 g, 78% from **16**, colorless oil); ir (CH_2Cl_2): 3600, 2940, 1690 cm^{-1}; ^1H nmr (250 MHz, $CDCl_3$) δ (ppm): 7.71–7.66 (4H, m) and 7.43–7.34 (6H, m) (2 × Ph); 6.35–6.12 (2H, m, -CH=C*H*-C*H*=CH-), 5.77–5.59 (2H, m, -C*H*=CH-CH=C*H*-), 4.23 (2H, d, J = 5.0 Hz, TBDPSOCH_2CH=), 3.69 (2H, m, -CH_2OH), 2.36 (2H, dt, J = 6.5 Hz, 6.5 Hz, =CHCH_2CH_2OH), 1.40 (1H, m, OH), 1.06 (9H, s, -Si$(CH_3)_3$); ms *m/e*: 309 (M^+ − *t*Bu).

(*E,E*)-8-*tert*-Butyldiphenylsiloxy-1,1-bis(methoxycarbonyl)-4,6-octadiene (21)

Methanesulfonyl chloride (1.49 mL, 19.2 mmol) was added to a cooled solution (0°C) of alcohol **19** (6.70 g, 18.3 mmol) and triethylamine (3.83 mL, 27.4 mmol) in dichloromethane (220 mL). After stirring at 0°C for 1 h, the reaction mixture was poured into water and extracted with dichloromethane (3 × 150 mL). The combined organic layers were washed with brine (50 mL), dried over anhydrous magnesium sulfate, filtered, and concentrated to give the crude mesylate **20** (8.15 g, 100%), which was immediately used for the next reaction.

Dimethylmalonate (10.5 mL, 91.5 mmol) was added dropwise to a suspension of sodium hydride (3.29 g, 82.3 mmol, 60% dispersion in mineral oil) in dimethylformamide (180 mL) and stirred until the bubbling had stopped. A solution of the crude mesylate **20** in tetrahydrofuran (180 mL) and potassium iodide (0.61 g, 3.60 mmol) were added to the clear solution. The reaction mixture was stirred 15 h at 70–75°C and allowed to cool to room temperature. Aqueous saturated ammonium chloride (200 mL) was added and the mixture was extracted with ether–hexanes (1:2, 1 × 400 mL, 3 × 100 mL). The combined organic layers were dried over anhydrous magnesium sulfate, filtered, and concentrated. The residue was purified by flash chromatography (20% ethyl acetate in hexanes) to give the alkylation product **21** (7.31 g, 83% from **19**, colorless oil); ir (neat): 3080–3000, 2960, 2860, 1755, 1740 cm^{-1}; ^1H nmr (250 MHz, $CDCl_3$) δ (ppm): 7.69–7.66 (4H, m) and 7.43–7.34 (6H, m) (2 × Ph), 6.24 (1H, dd, J = 15.0 Hz, 10.5 Hz, TBDPSOCH$_2$CH=C*H*-CH=CH-), 6.06 (1H, dd, J = 15.0 Hz, 10.5 Hz, TBDPSOCH$_2$CH=CH-C*H*=CH-), 5.68 (1H, dt, J = 15.0 Hz, 5.0 Hz, TBDPSOCH$_2$C*H*=CH-), 5.58 (1H, dt, J = 15.0 Hz, TBDPSOCH$_2$CH=CH-CH=C*H*-), 4.22 (2H, br d, J = 5.0 Hz, TBDPSOCH_2CH=), 3.74 (6H, s, -CH$(CO_2CH_3)_2$), 3.40 (1H, t, J = 7.5 Hz, -C$H(CO_2CH_3)_2$), 2.18–2.09 (2H, m, =HCCH_2CH_2-), 2.06–1.97 (2H, m, =HCCH$_2$CH_2-), 1.06 (9H, s, -SiC$(CH_3)_3$; ^{13}C nmr (62.5 MHz, $CDCl_3$) δ (ppm): 169.7, 135.5, 133.6, 131.6, 131.3, 130.7, 129.6, 127.6, 64.1, 52.4, 50.8, 30.1, 28.3, 26.8, 19.2; ms *m/e*: 480 (M^+), 423 (M^+ − *t*Bu). Exact Mass calcd. for $C_{28}H_{36}O_5Si$: 480.2332; found: 480.2324 ± 0.0014.

(*E,E*)-1,1-bis(Methoxycarbonyl)-4,6-octadien-1-ol (22)

To a solution of silyl ether **21** (1.40 g, 2.9 mmol) in tetrahydrofuran (24 mL) was added tetra-*n*-butyl ammonium fluoride (3.2 mL, 3.2 mmol, 1.0 M in tetrahydrofuran) and the flask was stirred 3 h at room temperature. Aqueous saturated ammonium chloride (10 mL) was added and the mixture was extracted with diethyl ether (4 × 50 mL). The combined organic layers were washed with brine (5 mL), dried over anhydrous magnesium sulfate, filtered, and concentrated. The crude product was purified by flash chromatography (50% ethyl acetate in hexanes), yielding alcohol **22** (0.62 g, 88%, colorless oil); ir (neat): 3460 (br), 3020, 2980–2840, 1745 cm^{-1}; ^1H nmr (250 MHz, $CDCl_3$) δ (ppm): 6.21 (1H, dd, J = 15.5 Hz, 10.5 Hz, HOCH$_2$CH=C*H*-CH=), 6.06 (1H, dd, J = 15.5 Hz, 10.5 Hz, HOCH$_2$CH=CH-C*H*=CH), 5.76 (1H, dt, J = 14.5 Hz, 6.5 Hz, HOCH$_2$C*H*=CH-), 5.64 (1H, dt, J = 14.5 Hz, 7.0 Hz, HOCH$_2$CH=CH-CH=C*H*-), 4.17 (2H, dd, J = 5.5 Hz, 5.5 Hz, HOCH_2CH=), 3.74 (6H, s, 2 × CH_3O-), 3.38 (1H, t, J = 7.0 Hz,- CH_2C$H(CO_2CH_3)_2$), 2.15 (2H, dt, J = 7.0 Hz, 7.0 Hz, =CHCH_2CH_2-), 2.02 (2H, dt, J = 7.0 Hz, 7.0 Hz, =CHCH$_2$CH_2-), 1.32 (1H, t, J = 5.5 Hz, *H*OCH$_2$-); ms *m/e*: 224 (M^+−H_2O). Exact Mass calcd. for $C_{12}H_{16}O_4$: 224.1049; found: 224.1037 ± 0.0006.

(*E,E*)-8-Pivaloyloxy-1,1-bis(methoxycarbonyl)-4,6-octadiene (23)

To a cooled solution (0°C) of alcohol **22** (0.494 g, 2.04 mmol) in dichloromethane (20 mL) were successively added triethylamine (0.85 mL, 6.1 mmol), a few crystals of 4-dimethylaminopyridine (cat.), and trimethylacetyl chloride (0.75 mL, 6.1 mmol). The solution was stirred 2 h at 0°C, then 1 h at room temperature, and a saturated aqueous solution of ammonium chloride (15 mL) was added. The mixture was extracted with dichloromethane (3 × 50 mL) and the combined organic layers were washed with water (5 mL) and brine (5 mL), dried with anhydrous magnesium sulfate, filtered, and concentrated. The crude product was purified by flash chromatography (5% ethyl acetate in hexanes), giving pivaloyl ester **23** (0.575 g, 86%, yellowish oil); ir (neat): 2990–2840, 1735 (br) cm^{-1}; ^1H nmr (250 MHz, $CDCl_3$) δ (ppm): 6.23 (1H, dd, J = 15.0 Hz, 10.5 Hz, PivOCH$_2$CH=C*H*-CH=), 6.05 (1H, dd, J = 15.0 Hz, 10.5 Hz, PivOCH$_2$CH=CH-C*H*=CH-), 5.66 (2H, dt, J = 15.0 Hz, 6.0 Hz, PivOCH$_2$C*H*=CH-CH=C*H*-), 4.56 (2H, d, J = 6.0 Hz, PivOCH_2CH=), 3.74 (6H, s, 2 × CH_3O-), 2.23–1.92 (4H, m, -CH_2CH_2CH$(CO_2CH_3)_2$), 1.21 (9H, s, $(CH_3)_3CCO_2$-); ^{13}C nmr (75 MHz, $CDCl_3$) δ (ppm): 177.95, 169.44, 133.41, 130.56, 125.28, 64.37, 52.27, 50.62, 38.55, 29.97, 27.95, 26.98; ms *m/e*: 241 (M^+ − $(CH_3)_3CO$). Exact Mass calcd. for $C_{12}H_7O_5$: 241.1076; found: 241.1074 ± 0.0007.

(*E*)-3-Methyl-1-tetrahydropyranyloxy-3-hexen-6-ol (27) and (*Z*)-3-methyl-1-tetrahydropyranyloxy-3-hexen-6-ol (29)

A crude mixture of inseparable *cis* and *trans* isomers **26** (7.79 g, 17.2 mmol) was dissolved in tetrahydrofuran (160 mL) and cooled to 0°C. Tetra-*n*-butylammonium fluoride (18.9 mL, 18.9 mmol, 1.0 M in tetrahydrofuran) was added and the solution was stirred 1 h at 0°C. The volatiles were then evaporated to near-dryness and the residue was purified by flash chromatography (5% acetone, 45% dichloromethane in hexanes) giving **29** (0.940 g, 26%), **27** (0.872 g, 24%), and a nonseparated fraction (1.65 g, 45%):

cis Isomer **29**: ir ($CHCl_3$): 3420, 2950 cm^{-1}; ^1H nmr (250 MHz, $CDCl_3$) δ (ppm): 5.27 (1H, t, J = 7.5 Hz, -C*H*=C(CH_3)-), 4.58 (1H, m, -OCHO-), 3.86 (1H, dt, J = 9.5 Hz, 7.0 Hz, -*H*CHOTHP), 3.90–3.80 (1H, m, -$(CH_2)_3$*H*CHO-), 3.64–3.58 (2H, m, HOCH_2-), 3.55–3.45 (1H, m, -$(CH_2)_3$HC*H*O-), 3.46 (1H, dt, J = 9.5 Hz, 6.5 Hz,

Can. J. Chem. Downloaded from www.nrcresearchpress.com by 46.23.64.124 on 09/08/12
For personal use only.

-HC*H*OTHP), 2.43–2.27 (4H, m, -C*H*$_2$CH=C(CH$_3$)C*H*$_2$-), 1.18 (1H, m, -OH), 1.90–1.50 (6H, m, -(C*H*$_2$)$_3$CH$_2$O-), 1.77 (3H, s, -CH$_3$); ^{13}C nmr (62.5 MHz, CDCl$_3$) δ (ppm): 135.1, 123.1, 98.7, 65.2, 62.0, 31.9, 31.2, 30.3, 25.2, 23.3, 19.3; ms *m/e*: 214 (M$^+$), 199 (M$^+$ − CH$_3$).

trans Isomer **27**: ir (CHCl$_3$): 3420, 2960 cm^{-1}; ^{1}H nmr (250 MHz, CDCl$_3$) δ (ppm): 5.20 (1H, tq, *J* = 7.7 hz, *J* ≈ 1Hz, -C*H*=C(CH$_3$)-), 4.57 (1H, m, -OCHO-), 3.90–3.80 (1H, m, -(CH$_2$)$_3$*H*CHO-), 3.81 (1H, dt, *J* = 9.5 Hz, 7.0 Hz, -*H*CHOTHP), 3.60 (2H, m, -C*H*$_2$OH), 3.48 (1H, dt, *J* = 9.5 Hz, 6.5 Hz, -HC*H*OTHP), 3.55–3.45 (1H, m, -(CH$_2$)$_3$HC*H*O-), 2.34–2.28 (4H, m, -C*H*$_2$CH=C(CH$_3$)C*H*$_2$-), 1.90–1.50 (7H, m, -(C*H*$_2$)$_3$CH$_2$O-, OH), 1.68 (3H, d, *J* = 1.0 Hz, -CH$_3$); ^{13}C nmr (62.5 MHz, CDCl$_3$) δ (ppm): 135.6, 121.8, 98.8, 66.0, 62.4, 62.1, 39.7, 31.4, 30.6, 25.4, 19.6, 16.4; ms *m/e*: 214 (M$^+$), 199 (M$^+$ − CH$_3$).

(*Z*)-3-Hydroxymethyl-1-acetoxy-6-*tert*-butyldimethylsiloxy-3-hexene (37)

Diisobutylaluminum hydride (17.2 mL, 26.0 mmol, 1.5 M in toluene) was added over a few minutes to a solution of lactone **33***Z* (3.00 g, 11.7 mmol) in diethyl ether (90 mL) at −78°C. The solution was stirred for 2.5 h after which methanol (15 mL) was added and the mixture allowed to warm to room temperature. It was then extracted with a 30% aqueous solution of disodium tartrate (4 × 25 mL) and the combined aqueous phases were extracted with diethyl ether (4 × 50 mL). The combined organic layers were washed with brine (25 mL), dried with anhydrous magnesium sulfate, and filtered over a short pad of silica gel. Concentration of the solvents left a mixture (2.59 g, ~85%) of diol **34** along with aldehyde **35**, originating from incomplete reduction. This sensitive material was immediately used for the next step by dilution into chloroform (70 mL). Manganese dioxide (10.0 g, 117 mmol) was added and the mixture was stirred 12 h (more manganese dioxide might be needed depending on its activity), after which it was filtered over a pad of Celite (rinsed with chloroform). The filtrate was concentrated to give 2.37 g (theoretically: 9.2 mmol, ~84%) of crude aldehyde **35** (homogeneous by TLC). Without delay, the latter intermediate was dissolved in dichloromethane (200 mL) and the solution was cooled to 0°C. Acetic anhydride (4.05 mL, 43 mmol), triethylamine (6.05 mL, 43 mmol), and 4-dimethylaminopyridine (a few crystals, cat.) were successively added. The solution was stirred 3 h at 0°C and aqueous saturated ammonium chloride (100 mL) was then added. The mixture was extracted with dichloromethane (3 × 100 mL) and the combined organic layers were washed with water (30 mL) and brine (30 mL), dried with anhydrous magnesium sulfate, filtered, and concentrated. The residue was purified by flash chromatography (40% ethyl acetate in hexanes), yielding pure unstable acetate **36** (2.40 g, 87%, colorless oil), which was immediately reacted in the following step. A 0.91 g portion of **36** (3.03 mmol) was dissolved in methanol (50 mL) and the solution was cooled to 0°C. Sodium borohydride (87 mg, 2.8 mmol) was added and the mixture was stirred 45 min at 0°C. A solution of aqueous saturated ammonium chloride (25 mL) was added and the bulk of methanol was evaporated. The resulting mixture was diluted with water (15 mL) and extracted with diethyl ether (4 × 50 mL). The combined organic layers were dried over anhydrous magnesium sulfate, filtered, and evaporated. The crude product was purified by flash chromatography (20–70% ethyl acetate in hexanes), affording allylic alcohol **37** (0.75 g, 83% (56% overall from **33***Z*), colorless oil); ir (neat): 3460 (br), 2990, 1740 cm^{-1}; ^{1}H nmr (250 MHz, CDCl$_3$) δ (ppm): 5.38 (1H, t, *J* = 8.0 Hz, =C*H*CH$_2$-), 4.18 (2H, t, *J* = 7.0 Hz, -C*H*$_2$OAc), 4.08 (2H, s, -C*H*$_2$OH), 3.62 (2H, t, *J* = 6.0 Hz, -CH$_2$OTBS), 2.44 (2H, t, *J* = 7.0 Hz, -C*H*$_2$CH$_2$OAc), 2.40 (1H, br, -OH), 2.32 *H* (2H, dt, *J* = 8.0 Hz, 6.0 Hz, -C*H*$_2$CH$_2$OTBS), 2.03 (3H, s, CH$_3$CO$_2$-), 0.88 (9H, s, -SiC(CH$_3$)$_3$), 0.06 (6H, s, -Si(CH$_3$)$_2$); ms *m/e*: 245 (M$^+$ − (CH$_3$)$_3$C). Exact Mass calcd. for C$_{11}$H$_{21}$O$_4$Si: 245.1209; found: 245.1208 ± 0.0007.

(*Z*)-3-(Methoxymethoxy)methyl-1-acetoxy-6-*tert*-butyldimethylsiloxy-3-hexene (38)

To a solution of *Z* allylic alcohol **37** (0.74 g, 2.5 mmol) in dichloromethane (50 mL) were successfully added diisopropylethylamine (1.3 mL, 7.5 mmol) and methoxymethyl chloride (0.37 mL, 4.9 mmol). The reaction mixture was stirred for 20 h at room temperature, after which a saturated solution of ammonium chloride (15 mL) was added. The mixture was extracted with dichloromethane (3 × 50 mL) and the combined organic layers were washed with water (5 mL) and brine (5 mL), dried with anhydrous magnesium sulfate, filtered, and concentrated. Purification of the residue by flash chromatography (30% ethyl acetate in hexanes) furnished compound **38** (0.82 g, 96%, colorless oil); ir (neat): 2990–2820, 1740, 1470 cm^{-1}; ^{1}H nmr (250 MHz, CDCl$_3$) δ (ppm): 5.48 (1H, t, *J* = 7.5 Hz, =C*H*CH$_2$-), 4.60 (2H, s, -OCH$_2$O-), 4.17 (2H, t, *J* = 7.0 Hz, -C*H*$_2$OAc), 4.09 (2H, s, -CH$_2$OMOM), 3.59 (2H, t, *J* = 7.0 Hz, -CH$_2$OTBS), 3.37 (3H, s, -OCH$_3$), 2.43 (2H, t, *J* = 7.0 Hz, -C*H*$_2$CH$_2$OAc), 2.32 (2H, dt, *J* = 7.0 Hz, 7.0 Hz, -C*H*$_2$CH$_2$OTBS), 2.03 (3H, s, CH$_3$CO$_2$-), 0.88 (9H, s, -SiC(CH$_3$)$_3$), 0.04 (6H, s, -Si(CH$_3$)$_2$); ms *m/e*: 289 (M$^+$ − (CH$_3$)$_3$C). Exact Mass calcd. for C$_{13}$H$_{25}$O$_5$Si: 289.1471; found: 289.1477 ± 0.0008.

(*Z*)-3-(Methoxymethoxy)methyl-6-*tert*-butyldimethylsiloxy-3-hexenol (39)

Potassium carbonate (30 mg, 0.22 mmol) was added to a solution of compound **38** (0.38 g, 1.10 mmol) in methanol (12 mL). The solution was stirred 3 h at room temperature and then diluted with diethyl ether (25 mL). The resulting mixture was filtered over a short column of silica gel (rinsed with diethyl ether) and the filtrate was concentrated to give pure alcohol **39** (0.34 g, 100%, colorless oil); ir (neat): 3425 (br), 2990–2840 cm^{-1}; ^{1}H nmr (250 MHz, CDCl$_3$) δ (ppm): 5.53 (1H, t, *J* = 8.0 Hz, =C*H*CH$_2$-), 4.63 (2H, s, -OCH$_2$O-), 4.09 (2H, s, -CH$_2$OMOM), 3.70 (2H, t, *J* = 6.0 Hz, -CH$_2$OH), 3.62 (2H, t, *J* = 6.5 Hz, -CH$_2$OTBS), 3.38 (3H, s, -OCH$_3$), 2.44–2.30 (4H, m, -C*H*$_2$C=CHC*H*$_2$-), 1.80 (1H, br, -OH), 0.88 (9H, s, -SiC(CH$_3$)$_3$), 0.04 (6H, s, -Si(CH$_3$)$_2$); ms *m/e*: 243 (M$^+$ − MOMO). Extract Mass calcd. for C$_{13}$H$_{27}$O$_2$Si: 243.1780; found: 243.1777 ± 0.0007.

(*Z*)-(Methoxymethoxy)methyl-1-acetoxy-3-hexen-6-ol (48)

To a solution of **38** (0.445 g, 1.28 mmol) in tetrahydrofuran (10 mL) was added tetra-*n*-butylammonium fluoride (1.35 mL, 1.35 mmol, 1 M in tetrahydrofuran) and one drop of triethylamine as an acid scavenger. The reaction mixture was stirred for 1 h at room temperature after which a saturated solution of aqueous ammonium chloride (10 mL) was

Can. J. Chem. Downloaded from www.nrcresearchpress.com by 46.23.64.124 on 09/08/12
For personal use only.

added. The resulting mixture was extracted with diethyl ether (4 × 30 mL) and the combined organic layers were washed with brine (5 mL), dried with anhydrous magnesium sulfate, filtered, and concentrated. The residue was purified by flash chromatography (30 → 80% ethyl acetate in hexanes), giving alcohol **48** (0.28 g, 94%, colorless oil); ir (neat): 3460 (br), 2990–2820, 1750 cm^{-1}; ^1H nmr (300 MHz, $CDCl_3$) δ (ppm): 5.48 (1H, t, J = 7.5 Hz, =C*H*CH_2-), 4.61 (2H, s, -OCH_2O-), 4.17 (2H, t, J = 7.0 Hz, -CH_2OAc), 4.10 (2H, s, -CH_2OMOM), 3.63 (2H, t, J = 7.0 Hz, -C*H*$_2$OH), 3.37 (3H, s, -OCH_3), 2.44 (2H, t, J = 7.0 Hz, -C*H*$_2CH_2OAc$), 2.35 (2H, dt, J = 7.0 Hz, 7.0 Hz, -C*H*$_2CH_2OH$), 2.03 (3H, s, CH_3CO_2-), 1.93 (1H, s, -OH); ^{13}C nmr (75 MHz, $CDCl_3$) δ (ppm): 171.11, 134.70, 128.70, 95.50, 64.05, 62.98, 61.78, 55.44, 34.82, 31.29, 20.99; ms *m/e*: 201 (M^+ − CH_3O), 187 (M^+ − CH_3OCH_2). Exact Mass calcd. for $C_9H_{15}O_4$: 187.0970; found: 187.0968 ± 0.0005.

(*E,E,E*)-3-Methyl-14-*tert*-butyldiphenylsiloxy-7,7-bis(methoxycarbonyl)-1-tetrahydropyranyloxy-tetradeca-3,10,12-triene (50)

To a solution of *E* hexenol **27** (0.556 g, 2.60 mmol) in dichloromethane (32 mL) were successively added triethylamine (0.55 mL, 3.9 mmol) and methanesulfonyl chloride (0.21 mL, 2.70 mmol). After stirring at room temperature for 2 h, the reaction mixture was poured into water (50 mL) and extracted with dichloromethane (4 × 25 mL). The combined organic layers were washed with brine, dried with anhydrous magnesium sulfate, filtered, and concentrated to give crude mesylate **28** (0.761 g, ~100%). This sensitive material was immediately used for the next step.

A solution of malonate **21** (0.921 g, 1.92 mmol) in dimethylformamide (11 mL) was added to a suspension of sodium hydride (82.0 mg, 2.05 mmol, 60% dispersion in mineral oil) in dimethylformamide (11 mL). After stirring at 35–40°C for 1 h, the reaction mixture became clear and a solution of crude mesylate **28** in tetrahydrofuran (22 mL), followed by anhydrous potassium iodide (68 mg, 0.40 mmol), was added and the reaction flask was stirred at ~70°C for 12 h. Saturated aqueous ammonium chloride (75 mL) was added and the resulting mixture was extracted with diethyl ether – hexanes (1:1, 5 × 75 mL). The combined organic phases were washed with water and brine, dried with anhydrous magnesium sulfate, filtered, and concentrated. The residue was purified by flash chromatography (10% ethyl acetate in hexanes), affording the coupling product **50** (0.902 g, 70%, colorless oil) along with recovered malonate **21** (210 mg, 23%); ir (CH_2Cl_2): 2960–2880, 1730 cm^{-1}; ^1H nmr (250 MHz, $CDCl_3$) δ (ppm): 7.69–7.66 (4H, m) and 7.43–735 (6H, m) (2 × Ph); 6.23 (1H, dd, J = 15.0 Hz, 10.0 Hz, TBDPSOCH_2CH=C*H*-), 6.07 (1H, dd, J = 15.0 Hz, 5.0 Hz, TBDPSOCH_2CH=CH-C*H*=), 5.71–5.55 (2H, m, -C*H*=CH-CH=C*H*-), 5.16 (1H, m, -*H*C=C(CH_3)-), 4.59 (1H, m, -OCHO-), 4.22 (2H, d, J = 4.5 Hz, -CH_2OTBDPS), 3.90–3.67 (2H, m, -*H*CHOTHP + -$(CH_2)_3$*H*CHO-), 3.71 (6H, s, 2 × CH_3O-), 3.52–3.41 (2H, m, -HC*H*OTHP + -$(CH_2)_3$HC*H*O-), 2.27 (2H, t, J = 7.0 Hz, -CH_2CH_2OTHP), 2.05–1.80 (8H, m, -CH_2CH_2-C(CO_2CH_3)$_2$CH_2CH_2-), 1.80–1.50 (6H, m -CH(CH_2)$_3$-CH_2O-), 1.62 (3H, s, CH_3-), 1.05 (9H, s, -SiC(CH_3)$_3$); ms *m/e*: 676 (M^+), 619 (M^+ − *t*Bu), 591 (M^+ − THP).

(*E,E,E*)-3-Methyl-14-*tert*-butyldiphenylsiloxy-7,7-bis(methoxycarbonyl)-tetradeca-3,10,12-trien-1-ol (51)

A solution of tetrahydropyranyl ether **50** (0.894 g, 1.32 mmol) and pyridinium *p*-toluenesulfonate (33.5 mg, 0.13 mmol) in isopropanol (17 mL) was stirred under reflux for 1 h. The solution was allowed to cool to room temperature and potassium carbonate (60 mg) was added. The mixture was stirred 15 min and filtered on a fritted glass funnel and concentrated. Purification of the residue by flash chromatography (30% ethyl acetate in hexanes) gave alcohol **51** (0.712 g, 90%, colorless oil); ir (neat): 3450, 2980–2880, 1735 cm^{-1}; ^1H nmr (250 MHz, $CDCl_3$) δ (ppm): 7.69–7.65 (4H, m) and 7.43–7.34 (6H, m) (2 × Ph); 6.23 (1H, dd, J = 15.0 Hz, 10.5 Hz, -C*H*=CHCH_2OTBDPS), 6.06 (1H, dd, J = 15.0 Hz, 10.5 Hz, =C*H*-CH=CH-CH_2OTBDPS), 5.67 (1H, dt, J = 15.0 Hz, 4.5 Hz, =C*H*CH_2OTBDPS), 5.65–5.55 (1H, m, =C*H*(CH_2)$_2$-), 5.20 (1H, m, -C*H*=C(CH_3)-), 4.22 (2H, dd, J = 4.5 Hz, 1 Hz, -CH_2OTBDPS), 3.72 (6H, s, 2 × CH_3O-), 3.66 (2H, m, -CH_2OH), 2.23 (2H, t, J = 6.0 Hz, -CH_2CH_2OH), 2.03–1.97 (4H, m) and 1.97–1.91 (4H, m) (-(CH_2)$_2$C(CO_2CH_3)$_2$-(CH_2)$_2$-); 1.62 (3H, d, J = 1.0 Hz, -CH=C(C*H*$_3$)-), 1.39 (1H, m, OH), 1.05 (9H, s, -Si(CH_3)$_3$); ms *m/e*: 592 (M^+), 535 (M^+ − *t*Bu).

(*E,E,E*)-4-Methyl-1,1,8,8-tetrakis(methoxycarbonyl)-pentadeca-4,11,13-trien-15-ol (54)

To a cooled solution (0°C) of alcohol **51** (0.705 g,1.19 mmol) and triethylamine (0.25 mL, 1.8 mmol) in dichloromethane (15 mL) was added methanesulfonyl chloride (0.097 mL, 1.25 mmol). After stirring at room temperature for 1.5 h the reaction mixture was poured into water (50 mL) and extracted with dichloromethane (5 × 30 mL). The combined organic layers were washed with brine, dried with anhydrous magnesium sulfate, filtered, and concentrated to give the crude mesylate **52** (0.799 g, ~100%). This sensitive material was immediately consumed in the next step.

Dimethyl malonate (0.68 mL, 6.0 mmol) was added dropwise to a stirred suspension of sodium hydride (0.21 g, 5.4 mmol, 60% dispersion in mineral oil) in dimethylformamide (14 mL). After ~30 min at room temperature the reaction mixture became clear and a solution of crude mesylate **52** in tetrahydrofuran (14 mL), followed by anhydrous potassium iodide (40 mg, 0.24 mmol), was added. The flask was stirred at 70–75°C for 18 h after which aqueous saturated ammonium chloride (50 mL) was added. The resulting mixture was extracted with petroleum ether – diethyl ether (2:1, 5 × 25 mL) and the combined organic layers were dried over anhydrous magnesium sulfate, filtered, and concentrated. The residue was purified by flash chromatography (20% ethyl acetate in hexanes), giving alkylation product **53** (0.860 g) contaminated with dimethyl malonate. This material was dissolved in tetrahydrofuran (12 mL) and tetra-*n*-butylammonium fluoride (1.20 mL, 1.20 mmol, 1 M in tetrahydrofuran) was added. The reaction mixture was stirred at room temperature for 3 h, after which the bulk of the solvent was evaporated. The residue was purified by flash chromatography (50% ethyl acetate in hexanes), yielding alcohol **54** (0.357 g, 64% overall from **51**, colorless oil); ir (neat): 3520, 2970–2880, 1735 cm^{-1}; ^1H nmr (250 MHz, $CDCl_3$) δ (ppm): 6.20 (1H, dd, J = 15.0 Hz, 10.5 Hz, $HOCH_2$CH=C*H*-), 6.06 (1H, dd, J = 15.0 Hz, 10.5 Hz, $HOCH_2$CH=CH-C*H*=), 5.74 (1H, dt, J = 15.0 Hz, 6.0 Hz,

Can. J. Chem. Downloaded from www.nrcresearchpress.com by 46.23.64.124 on 09/08/12
For personal use only.

$HOCH_2CH$=), 5.64 (1H, dt, J = 15.0 Hz, 3.0 Hz, $HOCH_2CH$=CH-CH=), 5.14–5.06 (1H, m, -CH=C(CH_3)-), 4.16 (2H, d, J = 6.0 Hz, -CH_2OH), 3.73 (6H, s, 2 × CH_3O-), 3.71 (6H, s, 2 × CH_3O-), 3.32 (1H, t, J = 7.0 Hz, -CH(CO_2CH_3)$_2$), 2.04–1.84 (13H, m, 6 × -CH_2-, OH), 1.57 (3H, d, J = 1.0 Hz, -CH=C(CH_3)-); ms *m/e*: 468 (M^+), 450 ($M^+ - H_2O$).

(*E,E,E*)-4-Methyl-1,1,8,8-tetrakis(methoxycarbonyl)-cyclopentadeca-4,11,13-triene (1)

Methanesulfonyl chloride (0.023.0 mL, 0.30 mmol) was added to a cooled solution (0°C) of alcohol **54** (46.3 mg, 0.099 mmol), anhydrous lithium chloride (25.2 mg, 0.594 mmol), and s-collidine (0.039 mL, 0.297 mmol) in dimethylformamide (1.0 mL). The reaction mixture was stirred at 0°C for 30 min (a thick white preciptate appeared after ~10 min), then warmed at room temperature for 2.5 h, after which it was poured into ice–water (~20 mL) and extracted with diethyl ether – petroleum ether (1:1, 4 × 25 mL). The combined organic layers were successively washed with saturated aqueous cupric sulfate (2 × 15 mL), water and brine, dried with anhydrous magnesium sulfate, filtered, and concentrated. The residue was quickly purified by flash chromatography on a short column (25% ethyl acetate in hexanes), affording unstable allylic chloride **55** (37.5 mg, 78%, colorless oil), which was used without delay for the following macrocyclization reaction.

To a vigorously stirred suspension of dry cesium carbonate (195 mg, 0.59 mmol) in dimethylformamide–tetrahydrofuran (5 mL:5 mL) at ~75°C was slowly added allylic chloride **55** (37.5 mg, 0.077 mmol) in dimethylformamide–tetrahydrofuran (3.5 mL:3.5 mL) via syringe pump within 11 h (final concentration: 4.5 × 10^{-3} M). After additional stirring for 13 h, the reaction mixture was allowed to cool to room temperature, filtered through a fritted glass funnel, and concentrated (the rotary evaporator was connected to an oil pump to remove dimethylformamide). The residue was purified by flash chromatography (15% ethyl acetate in hexanes) and crystallized from ethyl acetate – hexanes (mp 188–131°C), giving TTT macrocyclic triene **1** (29.6 mg, 85%, white solid); ir -CH_2Cl_2): 2980–2860, 1730 cm^{-1}; ^{1}H nmr (250 MHz, $CDCl_3$) δ (ppm): 6.04 (2H, m, -HC=CH-CH=CH-), 5.51–5.25 (2H, m, -HC=CH-CH=CH-), 5.02 (1H, m, -C(CH_3)=CH-), 3.74 (6H, s, 2 × CH_3O-), 3.72 (6H, s, 2 × CH_3O-), 2.75 (2H, d, J = 7.5 Hz, =CHCH_2C(CO_2CH_3)$_2$-), 2.16–1.95 (8H, m) and 1.85–1.65 (4H, m) (6 × -CH_2-); 1.54 (3H, s, -CH=C(CH_3)-); ^{1}H nmr (250 MHz, C_6D_6) δ (ppm): 5.89–5.73 (2H, m, -CH=CH-CH=CH-), 5.48 (1H, dt, J = 14.5 Hz, 7.5 Hz, -(CH_3O_2C)$_2$CCH_2CH=), 5.25 (1H, dt, J = 14.5 Hz, 7.5 Hz, -CH=CH(CH_2)$_2$-), 5.06 (1H, tq, J = 7.0 Hz, 1.5 Hz, -CH=C)CH_3)-), 3.32 (6H, s, 2 × CH_3O-), 3.31 (6H, s, 2 × CH_3O-), 2.97 (2H, d, J = 7.0 Hz, -(CH_3O_2C)$_2$CCH_2CH=), 2.36–2.21 (6H, m, 3 × -CH_2CH=), 2.06–1.83 (6H, m, 3 × -CH_2-), 1.41 (3H, d, J = 1.5 Hz, -CH=C)CH_3)-); ^{13}C nmr (62.5 MHz, $CDCl_3$) δ (ppm): 172.0, 136.0, 135.5, 134.5, 130.8, 124.9, 124.5, 58.3, 57.2, 52.5, 52.4, 35.6, 31.1, 30.2, 29.8, 29.1, 27.1, 20.3, 16.7; ms *m/e*: 450 (M^+), 435 ($M^+ - CH_3$). Exact Mass calcd. for $C_{24}H_{34}O_8$: 450.2253; found: 450.2246 ± 0.0013.

(3*Z*,10*E*,12*E*)-3-Methyl-14-*tert*-butyldiphenylsiloxy-7,7-bis(methoxycarbonyl)-1-tetrahydropyranyloxy-tetradeca-3,10,12-triene (56)

Using the procedure employed for the preparation of **28**, *Z* hexenol **29** (0.606 g, 2.83 mmol) was transformed into the corresponding crude mesylate **30** (0.825 g, ~100%). It was immediately reacted with malonate **21** (1.20 g, 2.50 mmol) as described for **50**, yielding the coupling product **56** (1.17 g, 66% from **29**, colorless oil) along with recovered malonate **21** (0.140 g, 12%); ir (CH_2Cl_2): 2980–2860, 1730 cm^{-1}; ^{1}H nmr (250 MHz, $CDCl_3$) δ (ppm): 7.69–7.65 (4H, m) and 7.46–7.33 (6H, m) (2 × Ph); 6.22 (1H, dd, J = 15.0 Hz, 10.0 Hz, TBDPSOCH_2CH=CH-), 6.05 (1H, dd, J = 15.0 Hz, 10.0 Hz, TBDPSOCH_2CH=CH-CH=), 5.68 (1H, dt, J = 15.0 Hz, 5.0 Hz, TBDPSOCH_2CH=), 5.67–5.54 (1H, m, TBDPSOCH_2CH=CH-CH=CH-), 5.22–5.15 (1H, m, -CH=C(CH_3)-), 4.61–4.57 (1H, m, -OCHO-), 4.23 (2H, d, J = 5.0 Hz, TBDPSOCH_2-), 3.90–3.80 (1H, m, -(CH_2)$_3$$H$CHO-), 3.76 (1H, dt, J = 9.0 Hz, 7.5 Hz, -HCHOTHP) 3.71 (6H, s, 2 × CH_3)-), 3.55–3.45 (1H, m, -(CH_2)$_3$HCHO-), 3.41 (1H, dt, J = 9.0 Hz, 7.5 Hz, -HCHOTHP), 2.30 (2H, t, J = 7.5 Hz, =CH_2CH_2OTHP), 2.02–1.96 (4H, m) and 1.96–1.90 (4H, m) (-(CH_2)$_2$-C(CO_2CH_3)-(CH_2)$_2$-); 1.71 (3H, s, -CH=C(CH_3)-), 1.90–1.45 (6H, m, -CH(CH_2)$_3$$CH_2$O-), 1.05 (9H, s, -SiC($CH_3$)$_3$); ms *m/e*: 676 ($M^+$), 619 ($M^+$ – *t*Bu), 591 (M^+ – THP).

(3*Z*,10*E*,12*E*)-3-Methyl-14-*tert*-butyldiphenylsiloxy-7,7-bis(methoxycarbonyl)-tetradeca-3,10,12-trienol (57)

Using the procedure described for the preparation of **51**, triene **56** (1.17 g, 1.73 mmol) was transformed into alcohol derivative **57** (0.80 g, 78%, colorless oil); ir $CHCl_3$): 3610, 3980–3840, 1730 cm^{-1}; ^{1}H nmr (250 MHz, $CDCl_3$) δ (ppm): 7.70–7.65 (4H, m) and 7.46–7.34 (6H, m) (2 × Ph); 6.24 (1H, dd, J = 15.0 Hz, 10.0 Hz, TBDPSOCH_2CH=CH-), 6.06 (1H, dd, J = 15.0 Hz, 10.0 Hz, TBDPSOCH_2CH=CH-CH=), 5.68 (1 H, dt, J = 15.0 Hz, 5.0 Hz, TBDPSOCH_2CH=), 5.68–5.55 (1H, m, TBDPSOCH_2CH=CH-CH=CH-), 5.33–5.23 (1H, m, -CH=C(CH_3)-), 4.22 (2H, d, J = 5.0 Hz, TBDPSOCH_2-), 3.72 (6H, s, 2 × CH_3O-), 3.72–3.62 (2H, m, -CH_2OH), 2.29 (2H, t, J = 6.5 Hz, -CH_2CH_2OH), 2.05–1.97 (4H, m) and 1.97–1.90 (4H, m) (-(CH_2)$_2$C(CO_2CH_3)$_2$-(CH_2)$_2$-); 1.72 (3H, d, J = 1.0 Hz, -CH=C(CH_3)-), 1.45 (1H, m, -OH), 1.06 (9H, s, -SiC(CH_3)$_3$); ms *m/e*: 592 (M^+), 535 (M^+ – *t*Bu).

(4*Z*,11*E*,13*E*)-4-Methyl-1,1,8,8-tetrakis(methoxycarbonyl)-pentadeca-4,11,13-trien-15-ol (60)

Using the procedure described for the preparation of **54**, alcohol **57** (0.737 g, 1.24 mmol) was successively mesylated (**58**, 0.835 g, ~100%) and alkylated with dimethyl malonate (reaction time, 15 h). Silyl ether cleavage of **59** yielded pure alcohol **60** (0.451 g, 65% overall from **57**, colorless oil); ir ($CHCl_3$): 3500, 2980–2880, 1735 cm^{-1}; ^{1}H nmr (250 MHz, $CDCl_3$) δ (ppm): 6.20 (1H, dd, J = 15.0 Hz, 10.0 Hz, $HOCH_2$- CH=CH-), 6.05 (1H, dd, J = 15.0 Hz, 10.0 Hz, $HOCH_2$-CH=CH-CH=), 5.75 (1H, dt, J = 15.0 Hz, 6.0 Hz, $HOCH_2$CH=), 5.71–5.61 (1H, m, $HOCH_2$CH=CH-CH=CH-), 5.18–5.10 (1H, m, -CH=C-(CH_3)-), 4.16 (2H, d, J = 6.0 Hz, $HOCH_2$-), 3.73 (6H, s, 2 × CH_3O-), 3.72 (6H, s, 2 × CH_3O-), 3.31 (1H, t, J = 7.0 Hz, -CH(CO_2CH_3)$_2$), 2.15–1.75 (13H, m, 6 × -CH_2-, OH), 1.67 (3H, s, -CH=C(CH_3)-); ms *m/e*: 450 (M^+ – H_2O).

Can. J. Chem. Downloaded from www.nrcresearchpress.com by 46.23.64.124 on 09/08/12
For personal use only.

(4*Z*,11*E*,13*E*)-4-Methyl-1,1,8,8-tetrakis(methoxycarbonyl)-cyclopentadeca-4,11,13-triene (6)

Using the procedure described for the preparation of **1**, alcohol **60** (0.351 g, 0.75 mmol) was transformed (reaction time, 1 h) into the corresponding allylic chloride **61** (297 mg, 81%, colorless oil). Macrocyclization of the latter (0.227 g, 0.467 mmol) proceeded within 20 h of slow addition with 5 h of further stirring (**61** dissolved in dimethylformamide–tetrahydrofuran (25 mL:25 mL) and added to cesium carbonate in the same solvent at 70°C (33 mL:33 mL; final concentration: 4.1×10^{-3} M), yielding TTC macrocyclic triene **6** (0.183 g, 87%, white solid, crystallized: mp 119–138°C); ir ($CHCl_3$): 2960–2860, 1730 cm^{-1}; ^1H nmr (250 MHz, $CDCl_3$) δ (ppm): 6.25–6.10 (2H, m, -CH=C*H*-C*H*=CH-), 5.83–5.70 (1H, m) and 5.66–5.53 (1H, m) (-C*H*=CH-CH=C*H*-); 5.00–4.92 (1H, br t, $J = 7.0$ Hz, -C*H*=C(CH_3)-, 3.74 (6H, s, 2× CH_3O-), 3.71 (6H, s, 2 × CH_3O-), 2.67 (2H, d, J = 7.5 Hz, -(CH_3O_2C)$_2$CC*H*$_2$CH=), 2.12–1.92 (4H, m), and 1.97–1.85 (2H, m) (3 × -CH_2CH=); 1.85–1.80 (4H, m) and 1.70–1.55 (2H, m) (3 × -CH_2-); 1.63 (3H, s, -CH=C(C*H*$_3$)-); ^1H nmr (250 MHz, C_6D_6) δ (ppm): 6.00–5.72 (3H, m, -(CH_3O_2C)$_2$CCH$_2$C*H*=C*H*-C*H*=CH-), 5.62 (1H, dt, $J = 14.0$ Hz, 7.0 hz, -CH=CH-CH=C*H*-), 5.12 (1H, tq, $J = 8.0$ Hz, 1.5 Hz, -C*H*=C(CH_3)-), 3.33 (12H, s, 4 × CH_3O-), 2.83 (2H, d, $J = 6.5$ Hz, -(CH_3O_2C)CC*H*$_2$CH=), 2.30–2.05 (6H, m, 3 × -C*H*$_2$CH=), 2.05–1.88 (4H, m), and 1.88–1.74 (2H, m) (3 × -CH_2-); 1.69 (3H, d, J = 1.5 Hz, -CH=C(C*H*$_3$)-); ^{13}C nmr (62.5 MHz, $CDCl_3$) δ (ppm): 172.1, 171.9, 135.1, 134.1, 133.6, 131.2, 125.5 (2), 59.1, 56.7, 52.5, 52.4, 37.0, 31.4, 31.3, 30.4, 26.6, 25.5, 23.3, 22.0; ms *m/e*: 450 (M^+), 435 ($M^+ - CH_3$). Exact Mass calcd. for $C_{24}H_{34}O_8$: 450.2253; found: 450.2263 ± 0.0013.

(3*Z*,10*E*,12*E*)-4-(Methoxymethoxy)methyl-1-*tert*-butyldimethysiloxy-7,7-bis(methoxycarbonyl)-14-pivaloyloxy-tetradeca-3,10,12-triene (62)

To a cooled (0°C) solution of *Z* hexenol **39** (0.322 g, 1.09 mmol) in dichloromethane (8 mL) were successively added triethylamine (0.21 mL, 1.52 mmol) and methanesulfonyl chloride (0.093 mL, 1.20 mmol). After stirring at 0°C for 1 h, water (10 mL) was added and the mixture was extracted with dichloromethane (4 × 15 mL). The combined organic layers were washed with brine (5 mL), dried over anhydrous magnesium sulfate, filtered, and concentrated. The crude compound was quickly purified by flash chromatography (30% ethyl acetate in hexanes) on a short column, yielding pure mesylate **40** (0.415 g, 100%, colorless oil). This sensitive material was immediately used for the following coupling reaction.

A solution of malonate **23** (0.356 g, 1.09 mmol, coevaporated several times with benzene) in dimethylformamide (1.0 mL) was added to a stirred suspension of sodium hydride (45.0 mg, 1.12 mmol, 60% dispersion in mineral oil) in dimethylformamide (2.0 mL). After stirring at 40°C for 1 h, hydrogen evolution ceased and the yellowish mixture became clear. Then, a solution of the above mesylate **40** in tetrahydrofuran (3.0 mL), followed by potassium iodide (93 mg, 0.53 mmol), was added and the reaction flask was stirred 6 h at 75°C and 12 h at ~65°C. A solution of aqueous saturated ammonium chloride (20 mL) was added and the resulting mixture was extracted with diethyl ether – petroleum ether (1:2, 4 × 30 mL). The combined organic phases were washed with brine, dried over anhydrous magnesium sulfate, filtered, and concentrated. The residue was purified by flash chromatography (1° dichloromethane for removing starting malonate **23**, 2° 30% ethyl acetate in hexanes), yielding coupling product **62** (0.445 g, 67%, colorless oil) and recovered malonate **23** (0.12 g, 10%); ir (neat): 2990–2840, 1740 (br) cm^{-1}; ^1H nmr (250 MHz, $CDCl_3$) δ (ppm): 6.22 (1H, dd, J = 15.0 Hz, 10.5 Hz, PivOCH$_2$CH=C*H*-CH=), 6.05 (1H, dd, J = 15.0 Hz, 10.5 Hz, PivOCH$_2$CH=CH-C*H*=), 5.77–5.57 (2H, m, -C*H*=CH-CH=C*H*-), 5.42 (1H, br t, $J = 7.5$ Hz, =CH-*HC*=), 4.59 (2H, s, -OCH$_2$O-), 4.56 (2H, br d, $J = 6.5$ Hz, PivOC*H*$_2$CH=), 4.05 (2H, s, -C*H*$_2$OMOM), 3.71 (6H, s, 2 × -CO_2CH_3), 3.59 (2H, t, J = 7.0 Hz, -C*H*$_2$OTBS), 2.30 (2H, dt, J = 7.0 Hz, 7.0 Hz, -C*H*$_2$CH$_2$OTBS), 2.13–1.84 (8H, m, -(C*H*$_2$)$_2$C(CO_2CH_3)$_2$ -(C*H*$_2$)$_2$-), 1.20 (9H, s, (CH_3)$_3$ CCO_2-), 0.88 (9H, s, -SiC(CH_3)$_3$), 0.04 (6H, s, -Si(CH_3)$_2$); ^{13}C nmr (62.5 MHz, $CDCl_3$) δ (ppm): 178.00, 171.69, 136.34, 134.24, 133.68, 129.80, 126.32, 125.12, 95.45, 64.42, 64.23, 62.69, 57.02, 55.07, 52.13, 38.59, 34.47, 31.76, 31.46, 31.26, 29.65, 27.06, 25.79, 18.16, −5.37; ms *m/e*: 597 ($M^+ - CH_3$), 555 (M^+ − C(CH_3)$_3$). Exact Mass calcd. for $C_{31}H_{53}O_9Si$: 597.3459; found: 597.3453 ± 0.0018.

3*Z*,10*E*,12*E*)-4-(Methoxymethoxy)methyl-7,7-bis(methoxycarbonyl)-14-pivaloyloxy-tetradeca-3,10,12-trienol (63)

To a solution of silyl ether **62** (0.440 g, 0.72 mmol) in tetrahydrofuran (6 mL) was successively added tetra-*n*-butylammonium fluoride (0.76 mL, 0.75 mmol, 1 M in tetrahydrofuran) and triethylamine (one drop, used as an acid scavenger). The solution was stirred at room temperature for 4.5 h, after which aqueous saturated ammonium chloride (10 mL) was added. The resulting mixture was extracted with diethyl ether (4 × 30 mL) and the combined organic phases were washed with brine, dried over anhydrous magnesium sulfate, filtered, and concentrated. The crude product was purified by flash chromatography (70% ethyl actetate in hexanes), giving alcohol **63** (0.345 g, 96%, colorless oil); ir (neat): 3480 (br), 2990–2820, 1730 cm^{-1}; ^1H nmr (250 MHz, $CDCl_3$) δ (ppm): 6.22 (1H, dd, J = 15.0 Hz, 10.0 Hz, PivOCH$_2$CH=C*H*-), 6.05 (1H, dd, J = 15.0 Hz, 10.0 Hz, PivOCH$_2$CH=CH-C*H*=), 5.78–5.57 (2H, m, -C*H*=CH-CH=C*H*-), 5.46 (1H, br t, J = 8.0 Hz, -CH=C-), 4.60 (2H, s, -OCH$_2$O-), 4.56 (2H, br d, $J = 7.0$ Hz, PivOC*H*$_2$CH=), 4.06 (2H, s, -C*H*$_2$OMOM), 3.71 (6H, s, 2 × -CO_2CH_3), 3.64 (2H, t, J = 6.0 Hz, -C*H*$_2$OH), 3.37 (3H, s, CH_3O-), 2.35 (2H, dt, J = 6.0 Hz, 6.0 Hz, -C*H*$_2$CH$_2$OH), 2.16–1.82 (8H, m, -(C*H*$_2$)$_2$-C(CO_2CH_3)$_2$-(C*H*$_2$)$_2$-), 1.86–1.50 (1H, br, -OH), 1.20 (9H, s, (CH_3)$_3$$CCO_2$-); ms *m/e*: 466 ($M^+ - CH_3OH$), 436 ($M^+$ − MOM). Exact Mass calcd. for $C_{25}H_{38}O_8$: 466.2566; found: 466.2557 ± 0.0014.

(4*Z*,11*E*,13*E*)-5-(Methoxymethoxy)methyl-1,1,8,8-tetrakis(methoxycarbonyl)-15-pivaloyloxy-pentadeca-4,11,13-triene (65)

To a cooled solution (0°C) of trienol **63** (0.340 g, 0.68 mmol) and triethylamine (133 μL, 0.96 mmol) in dichloromethane (8 mL) was added methanesulfonyl chloride (59 μL, 0.75 mmol). After stirring at 0°C for 1.5 h, water (10 mL) was added and the mixture was extracted with dichloromethane (4 × 25 mL). The combined organic layers were washed with brine (10 mL), dried over anhydrous magne-

Can. J. Chem. Downloaded from www.nrcresearchpress.com by 46.23.64.124 on 09/08/12
For personal use only.

sium sulfate, filtered, and concentrated. The crude compound was quickly purified by flash chromatography (40% ethyl acetate in hexanes) on a short column, yielding pure mesylate **64** (0.392 g, 99% colorless oil). This sensitive material was immediately used for the following alkylation reaction.

Dimethyl malonate (0.39 mL, 3.38 mmol) was added dropwise to a stirred suspension of sodium hydride (0.120 g, 3.05 mmol, 60% dispersion in mineral oil) in dimethylformamide (3.0 mL). After ~30 min at 40°C, hydrogen evolution ceased and the solution became clear. Then, a solution of the above mesylate in tetrahydrofuran (3.0 mL), followed by potassium iodide (56 mg, 0.34 mmol), was added and the reaction flask was stirred 5 h at 75°C and 12 h at 40°C. A solution of aqueous saturated ammonium chloride (50 mL) was added and the resulting mixture was extracted with diethyl ether – petroleum ether (1:2, 4 × 25 mL). The combined organic phases were washed with brine (5 mL), dried with anhydrous magnesium sulfate, filtered, and concentrated. The residue was purified by flash chromatography (25% ethyl acetate in hexanes), giving product **65** (0.365 g, 88%, colorless oil); ir (neat): 3000–2840, 1735 cm^{-1}; ^1H nmr (250 MHz, $CDCl_3$) δ (ppm): 6.22 (1H, dd, J = 15.0 Hz, 10.0 Hz, $PivOCH_2CH{=}CH$-), 6.05 (1H, dd, J = 15.0 Hz, 10.0 Hz, $PivOCH_2CH{=}CH\text{-}CH{=}$), 5.77–5.57 (2H, m, -$CH$=CH-CH=$CH$-), 5.36 (1H, br d, J = 7.0 Hz, -CH=C-), 4.57 (2H, s, -OCH_2O-), 4.55 (2H, d, J = 6.0 Hz, $PivOCH_2CH{=}$), 4.01 (2H, s, -CH_2OMOM), 3.74 (6H, s, 2 × -CO_2CH_3), 3.71 (6H, s, 2 × CO_2CH_3), 3.36 (1H, t, J = 7.5 Hz, -$CH(CO_2CH_3)_2$), 3.35 (3H, s, CH_3O-), 2.20–1.82 (12H, m, 6 × -CH_2-), 1.20 (9H, s, $(CH_3)_3CCO_2$-); ms *m/e*: 581 (M^+ − CH_3O), 549 (M^+ − $MOMOH_2$). Exact Mass calcd. for $C_{30}H_{44}O_{11}$: 581.2960; found: 581.2956 ± 0.0023.

(4*Z*,11*E*,13*E*)-5-(Methoxymethoxy)methyl-1,1,8,8-tetrakis(methoxycarbonyl)-pentadeca-4,11,13-trien-15-ol (66)

A solution of sodium methoxide (1.2 mL, 1.18 mmol, 1.0 M in methanol; freshly prepared from sodium and anhydrous methanol) was added to triene **65** (0.362 g, 0.59 mmol) in methanol (3.0 mL). The solution was stirred at room temperature for 5 h (3.6 mL of sodium methoxide solution were added after 2 h), after which aqueous saturated ammonium chloride (10 mL) was added. The resulting mixture was extracted with diethyl ether (6 × 30 mL) and ethyl acetate (25 mL). The combined organic layers were dried over anhydrous magnesium sulfate, filtered, and concentrated. The crude product was purified by flash chromatography (65% ethyl acetate in hexanes), affording alcohol **66** (0.268 g, 86%, colorless oil); ir (neat): 3450 (br), 2980–2820, 1730 cm^{-1}; ^1H nmr (250 MHz, $CDCl_3$) δ (ppm): 6.20 (1H, dd, J = 15.0 Hz, 10.0 Hz, $HOCH_2CH{=}CH$-), 6.06 (1H, dd, J = 15.0 Hz, 10.0 Hz, $HOCH_2CH{=}CH\text{-}CH{=}$), 5.82–5.57 (2H, m, -$CH$=CH-CH=$CH$-), 5.36 (1H, br t, J = 7.0 Hz, -CH=C-), 4.57 (2H, s, -OCH_2O-), 4.16 (2H, br d, J = 6.0 Hz, $HOCH_2$-), 4.01 (2H, s, -CH_2OMOM), 3.74 (6H, s, 2 × -CO_2CH_3), 3.71 (6H, s, 2 × -CO_2CH_3), 3.36 (1H, t, J = 6.5 Hz, -$CH(CO_2CH_3)_2$), 3.36 (3H, s, CH_3O-), 2.25–1.78 (12H, m, 6 × -CH_2-), 1.46–1.27 (1H, br, -OH); ms *m/e*: 510 (M^+ − H_2O). Exact Mass calcd. for $C_{26}H_{38}O_{10}$: 510.2465; found: 510.2471 ± 0.0015.

(4*Z*,11*E*,13*E*)-5-(Methoxymethoxy)methyl-1,1,8,8-tetrakis(methoxycarbonyl)-cyclopentadeca-4,11,13-triene (4)

Methanesulfonylchloride (0.047 mL, 0.60 mmol) was added to a cooled solution (0°C) of alcohol **66** (0.264 g, 0.50 mmol), s-collidine (0.083 mL, 0.63 mmol), and lithium chloride (25 mg, 0.58 mL) in dimethylformamide (1.0 mL). The reaction mixture was stirred at 0°C for 1.5 h (a thick white precipitate appeared after ~10 min), after which s-collidine (17 μL), lithium chloride (5 mg), and methanesulfonyl chloride (10 μL) were added in order to complete the reaction (2 h of additional stirring at 0°C). The reaction mixture was then poured into ice-water (10 mL) and extracted with diethyl ether – petroleum ether (1:1, 4 × 25 mL). The combined organic layers were successively washed with aqueous saturated cupric sulfate (5 mL) and brine (2 × 5 mL), dried with anhydrous magnesium sulfate, filtered, and concentrated. The residue was quickly purified by flash chromatography (40% ethyl acetate in hexanes) over a short column, affording unstable allylic chloride **67** (0.220 g, 81%, colorless oil). This material was used without delay for the following macrocyclization reaction.

To a vigorously stirred suspension of cesium carbonate (0.790 g, 2.42 mmol) in dimethylformamide–tetrahydrofuran (30 mL:30 mL) at 75°C was slowly added the above allylic chloride **67** (coevaporated several times with benzene) in dimethylformamide–tetrahydrofuran (20 mL:20 mL) via syringe pump within 12 h (final concentration: 4 × 10^{-3} M). After additional stirring for 5 h, the reaction mixture was allowed to cool to room temperature, filtered through a fritted glass, and concentrated (the rotary evaporator was connected to an oil pump for removing dimethylformamide). The residue was purified by flash chromatography (25% ethyl acetate in hexanes), giving pure TTT macrocyclic triene **4** (0.181 g, 88%, foamy solid). A sample of this compound could be recrystallized in dichloromethane–hexanes, giving small needles (mp 53–58°C) from which a suitable one was submitted to X-ray crystallographic analysis for structure confirmation; ir (neat): 3000–2780, 1730 cm^{-1}; ^1H nmr (300 MHz, $CDCl_3$) δ (ppm): 6.00 (1H, dd, J = 14.0 Hz, 10.0 Hz, -HC=CH-CH=CH-), 5.95 (1H, dd, J = 14.0 Hz, 10.0 Hz, -HC=CH-CH=CH-), 5.55 (1H, dt, J = 14.0 Hz, 6.5 Hz, -HC=CH-CH=CH-), 5.40–5.27 (2H, m, -HC=CH-CH=CH,-CH=C-), 4.55 (2H, s, -OCH_2O-), 3.94 (2H, s, -CH_2OMOM), 3.71 (6H, s, 2 × -CO_2CH_3), 3.69 (6H, s, 2 × -CO_2CH_3), 3.34 (3H, s, CH_3O-), 2.74 (2H, d, J = 8.0 Hz, -$(CH_3O_2C)_2CCH_2CH{=}$), 2.20–2.00 (6H, m, 3 × -$CH_2CH{=}$), 2.00–1.85 (4H, m) and 1.85–1.70 (2H, m) (3 × -CH_2-); ^{13}C nmr (75 MHz, $CDCl_3$) δ (ppm): 171.95, 171.90, 136.76, 135.20, 134.03, 131.82, 130.32, 124.86, 95.72, 64.51, 58.40, 58.21, 55.17, 52.56, 52.35, 35.79, 31.98, 29.67, 29.11, 27.96, 27.87, 19.99; ms *m/e*: 510 (M^+), 478 (M^+ − CH_3OH), 448 (M^+ − MOMOH). Exact Mass calcd. for $C_{24}H_{32}O_8$: 448.2092; found: 448.2105 ± 0.0013.

(4*Z*,11*E*,13*E*)-5-Hydroxymethyl-1,1,8,8-tetrakis(methoxycarbonyl)-cyclopentadeca-4,11,13-triene (80)

The $MOMOCH_2$-substituted TTT macrocycle **4** (20.0 mg, 0.039 mmol) was stirred 2.0 h in a concentrated hydrochloric acid – water–methanol solvent mixture (0.5:1.0:8.5,1.0 mL) at 60°C. The solution was then allowed to cool to room temper-

Can. J. Chem. Downloaded from www.nrcresearchpress.com by 46.23.64.124 on 09/08/12
For personal use only.

ature and a solution of aqueous saturated sodium bicarbonate (5 mL) was added under stirring. The resulting mixture was extracted with diethyl ether (3 × 20 mL) and ethyl acetate (2 × 10 mL). The combined organic layers were dried with anhydrous magnesium sulfate, filtered, and concentrated, yielding pure alcohol **80** (18.0 mg, 98%, white foamy solid); ir (neat): 3480 (br), 3000–2840, 1730 cm^{-1}; ^1H nmr (300 MHz, $CDCl_3$) δ (ppm): 6.08–5.91 (2H, m, -CH=C*H*-C*H*=CH-), 5.57 (1H, dt, *J* = 14.0 Hz, 7.0 Hz, -C*H*=CH-CH=CH-), 5.35 (1H, dt, *J* = 14.0 Hz, 7.5 Hz, -CH=CH-CH=C*H*-), 5.28 (1H, t, *J* = 6.5 Hz, -CH=C-), 4.07 (2H, s, $-CH_2OH$), 3.73 (6H, s, 2 × $-CO_2CH_3$), 3.72 (6H, s, 2 × $-CO_2CH_3$), 2.76 (2H, d, *J* = 7.5 Hz, $(CH_3O_2C)_2CCH_2CH$=), 2.20–2.04 (6H, m, 3 × $-CH_2CH$=), 2.04=1.90 (4H, m) and 1.90–1.78 (2H, m) (3 × $-CH_2-$); 1.60 (1H, br, -OH); ms *m/e*: 466 (M^+), 448 ($M^+ - H_2O$). Mass Exact calcd. for $C_{24}H_{34}O_9$: 466.2203; found: 466.2195 ± 0.0014.

(4*Z*,11*E*,13*E*)-5-Formyl-1,1,8,8-tetrakis(methoxycarbonyl)-cyclopentadeca-4,11,13-triene (5)

To a stirred solution of TTT macrocyclic trienol **80** (35.0 mg, 0.075 mmol) in dichloromethane (1.5 mL) at room temperature were added a few crystals of sodium acetate buffer and manganese dioxide (65 mg, 0.75 mmol, additional quantities might be added depending on the degree of activity of this reagent). The solution was stirred 16 h, after which it was filtered through a small Celite column with a thin pad of silica gel on the top (prewashed with dichloromethane). The column was rinsed with dichloromethane and the filtrate was concentrated, yielding formyl-substituted TTT macrocyclic triene **5** (25.5 mg, 73%, white solid, contaminated with <5% of the TTC isomer); ir (neat): 2970, 2930, 2855, 1730, 1670 cm^{-1}; ^1H nmr (250 MHz, C_6D_6) δ (ppm): 9.79 (1H, s, -CHO), 6.04 (1H, t, *J* = 7.5 Hz, -C*H*=CCHO), 5.79 (1H, dd, *J* = 15.0 Hz, 10.0 Hz, -CH=C*H*-CH=CH-), 5.61 (1H, dd, *J* = 15.0 Hz, 10.0 Hz, -CH=CH-C*H*=CH-), 5.45 (1H, dt, *J* = 15.0 Hz, 7.0 Hz, -C*H*=CH-CH=CH-), 5.26 (1H, dt, *J* = 15.0 Hz, 7.5 Hz, -CH=CH-CH=C*H*-), 3.35 (6H, s, 2 × $-CO_2CH_3$), 3.31 (6H, s, 2 × $-CO_2CH_3$), 2.81 (2H, d, *J* = 7.0 Hz, $-(CH_3O_2C)_2CCH_2CH$=), 2.35–1.85 (12H, m, 3 × $-CH_2CH_2-$); ^{13}C nmr (62.5 MHz, C_6D_6) δ (ppm): 189.36, 171.76, 171.50, 150.66, 138.44, 136.83, 135.92, 130.57, 125.83, 58.71, 58.53, 52.15, 51.98, 36.93, 32.06, 31.13, 29.85, 28.20, 24.14, 20.21; ms *m/e*: 464 (M^+), 446 ($M^+ - H_2O$). Exact Mass calcd. for $C_{24}H_{32}O_9$: 464.2046; found: 464.2035 ± 0.0018.

(*E,E,E*)-5-Formyl-1,1,8,8-tetrakis(methoxycarbonyl)-cyclopentadeca-4,11,13-triene (10)

To a solution of formyl-substituted TTT macrocyclic triene **5** (20.0 mg, 0.043 mmol) in tetrahydrofuran (1.0 mL) was added a solution of aqueous hydrochloric acid (1 N, 2 drops). The mixture was stirred 3 h at room temperature, after which a few crystals of sodium bicarbonate were added. The flask was stirred for 10 min and the content was evaporated to near-dryness. The residue was purified by flash chromatography (25% ethyl acetate in hexanes), yielding TTC isomer **10** (19.0 mg, 95%, clear oil); ir (neat): 2960 (br), 2860, 2720, 1730 (br), 1685 cm^{-1}; ^1H nmr (300 MHz, $CDCl_3$) δ (ppm): 9.25 (1H, s, -CHO), 6.33 (1H, t, *J* = 7.5 Hz, -C*H*=CCHO-), 6.25–6.08 (2H, m, -CH=C*H*-C*H*=CH-), 5.75 (1H, dt *J* = 14.5 Hz, 7.0 Hz, -C*H*=CH-CH=CH-), 5.62 (1H, dt, *J* = 14.5 Hz, 7.0 Hz, -CH=CH-CH=C*H*-), 3.78 (6H, s, 2 × $-CO_2CH_3$), 3.76 (6H, s, 2 × $-CO_2CH_3$), 2.72 (2H, d, *J* = 7.5 Hz, $-(CH_3O_2C)CCH_2CH$=), 2.33–2.20 (2H, m), and 2.13–1.70 (10H, m) (3 × $-CH_2CH_2-$); ^1H nmr (300 MHz, C_6D_6) δ (ppm): 9.03 (1H, s, -CHO), 5.95–5.45 (5H, m, -CH=CH-CH=CH-, -C*H*=CCHO-), 3.59 (6H, s, 2 × $-CO_2CH_3$), 3.33 (6H, s, 2 × $-CO_2CH_3$), 2.76 (2H, d, *J* = 7.0 Hz, $-(CH_3O_2C)_2CCH_2CH$=), 2.30–1.85 (12H, m, 3 × $-CH_2CH_2-$); ^{13}C nmr (75 MHz, $CDCl_3$) δ (ppm): 194.40, 171.75, 171.31, 153.03, 143.07, 135.35, 134.07, 130.50, 125.52, 58.84, 56.53, 52.63, 52.37, 37.42, 31.71, 30.21, 29.98, 29.72, 27.84, 23.62, 17.53; ^{13}C nmr (75 MHz, C_6D_6) δ (ppm): 194.06, 171.92, 171.47, 152.37, 143.57, 135.91, 134.36, 130.88, 125.84, 59.29, 56.97, 52.16 (br), 38.15, 32.22, 31.00 (br), 30.58, 38.42, 30.09, 28.07, 24.02, 18.15; ms *m/e*: 464 (M^+), 446 ($M^+ - H_2O$). Exact Mass calcd. for $C_{24}H_{32}O_9$: 464.2046; found: 464.2040 ± 0.0014.

(*E,E,E*)-4-(Methoxymethoxy)methyl-1-*tert*-butyldimethylsiloxy-7,7-bis(methoxycarbonyl)-14-pivaloyloxy-tetradeca-3,10,12-triene (68)

Using the procedure employed for the preparation of **62**, *E* hexenol **46** (1.92 g, 6.30 mmol) was transformed into the corresponding mesylate **47** (2.38 g, 99%, colorless oil). It was immediately reacted with malonate **23** (1.83 g, 5.60 mmol) in dimethylformamide–tetrahydrofuran (15 mL:15 mL) for 9 h at 75°C. The coupling product **68** (2.77 g, 81%, clear yellowish oil) was obtained through flash chromatography purification; ir (neat): 2960, 1733 cm^{-1}; ^1H nmr (300 MHz, $CDCl_3$) δ (ppm): 6.19 (1H, dd, *J* = 15.0 Hz, 10.5 Hz, PivOCH_2CH=C*H*-), 6.03 (1H, dd, *J* = 15.0 Hz, 10.5 Hz, PivOCH_2CH=CH-C*H*=), 5.70–5.50 (2H, m, -C*H*=CH-CH=C*H*-), 5.44 (1H, t, *J* = 7.0 Hz, -C=CH-), 4.57 (2H, s, $-OCH_2O-$), 4.53 (2H, d, *J* = 6.0 Hz, PivOCH_2CH=), 3.92 (2H, s, $-CH_2OMOM$), 3.69 (6H, s, 2 × $-CO_2CH_3$), 3.59 (2H, t, *J* = 7.0 Hz, $-CH_2OTBS$), 3.33 (3H, s, CH_3O-), 2.21 (2H, dt, *J* = 7.0 Hz, 7.0 Hz, $-CH_2CH_2OTBS$), 2.05–1.90 (8H, m, $-(CH_2)_2-C(CO_2CH_3)_2-(CH_2)_2-$), 1.17 (9H, s, $(CH_3)_3CCO_2-$), 0.85 (9H, s, $-SiC(CH_3)_3$), 0.03 (6H, s, $-Si(CH_3)_2$); ^{13}C nmr (75 MHz, $CDCl_3$) δ (ppm): 178.16, 171.68, 136.34, 134.23, 133.67, 129.88, 125.98, 125.18, 95.35, 71.17, 64.54, 62.57, 57.15, 55.17, 52.30, 38.67, 31.90, 31.40, 31.21, 27.29, 27.11, 25.86, 23.00, 18.24, −5.37; ms *m/e*: 597 ($M^+ - CH_3$), 555 ($M^+ - C(CH_3)_3$). Exact Mass calcd. for $C_{31}H_{53}O_9Si$: 597.3459; found: 597.3453 ± 0.0018.

(*E,E,E*)-4-(Methoxymethoxy)methyl-7,7-bis(methoxycarbonyl)-14-pivaloyloxy-tetradeca-3,10,12-trienol (69)

Using the procedure followed for the preparation of **63**, silyl ether **68** (2.70 g, 4.40 mmol) was cleaved, yielding alcohol **69** (1.93 g, 88% colorless oil) after purification by flash chromatography (25 → 70% ethyl acetate in hexanes); ir (neat): 3470, 2980–2860, 1730 cm^{-1}; ^1H nmr (300 MHz, $CDCl_3$) δ (ppm): 6.22 (1H, dd, *J* = 15.0 Hz, 10.5 Hz, PivOCH_2CH=C*H*-), 6.06 (1H, dd, *J* = 15.0 Hz, 10.5 Hz, PivOCH_2CH=CH-C*H*=), 5.74–5.56 (2H, m, -C*H*=CH-CH=C*H*-), 5.49 (1H, t, *J* = 7.0 Hz, -C=CH-), 4.61 (s, 2H, $-OCH_2O-$), 4.56 (2H, d, *J* = 6.5 Hz, PivOCH_2CH=), 3.97 (s, 2H, $-CH_2OMOM$) 3.73 (6H, s, 2 × $-CO_2CH_3$), 3.67 (2H, t, *J* = 6.5 Hz, $-CH_2OH$), 3.37 (3H, s, $-OCH_3$), 2.31 (2H, dt, *J* = 6.0 Hz, 6.0 Hz, $-CH_2CH_2OH$), 2.05–1.95 (8H, m, $-(CH_2)_2C(CO_2CH_3)_2-CCH_2)_2-$), 1.57 (1H,

Can. J. Chem. Downloaded from www.nrcresearchpress.com by 46.23.64.124 on 09/08/12
For personal use only.

br, -OH), 1.20 (9H, s, $(CH_3)_3CCO_2$-); ^{13}C nmr (75 MHz, $CDCl_3$) δ (ppm): 178.10, 171.61, 137.31, 134.05, 133.60, 129.82, 125.61, 125.09, 95.36, 71.21, 64.43, 61.83, 57.05, 55.15, 52.24, 38.55, 31.96, 31.40, 30.90, 27.17, 26.99, 22.93; ms *m/e*: 467 ($M^+ - OCH_3$), 436 ($M^+ -$ MOMOH). Exact Mass calcd. for $C_{25}H_{39}O_8$: 467.2645; found: 467.2634 ± 0.0014.

(*E,E,E*)-5-(Methoxymethoxy)methyl-1,1,8,8-tetrakis (methoxycarbonyl)-15-pivaloyloxy-pentadeca-4,11,13-triene (71)

Using the procedure described for the preparation of **65**, trienol **69** (1.386 g, 2.78 mmol) was successively mesylated (**70**, 1.57 g, 98%, colorless oil) and alkylated with dimethyl malonate (reaction time, 12 h at 75°C), yielding the alkylation product **71** (1.40 g, 89%, colorless oil); ir (neat): 2980–2800, 1730 cm^{-1}; ^{1}H nmr (300 MHz, $CDCl_3$) δ (ppm): 6.22 (1H, dd, *J* = 15.0 Hz, 10.5 Hz, $PivOCH_2CH$=C*H*-), 6.06 (1H, dd, *J* = 15.0 Hz, 10.5 Hz, $PivOCH_2CH$=CH-C*H*=), 5.72–5.60 (2H, m, -C*H*=CH-CH=C*H*-), 5.41 (1H, t, *J* = 7.0 Hz, -C=CH-), 4.60 (2H, s, $-OCH_2O$-), 4.56 (2H, d, *J* = 6.0 Hz, $PivOCH_2CH$=), 3.94 (2H, s, $-CH_2OMOM$), 3.73 (6H, s, 2 × $-CO_2CH_3$), 3.72 (6H, s, 2 × $-CO_2CH_3$), 3.36 (3H, s, $-OCH_3$), 3.36 (1H, t, *J* = 7.0 Hz, -C*H*$(CO_2CH_3)_2$), 2.12–1.86 (12H, m, 3 × $-CH_2CH_2$-), 1.20 (9H, s, $(CH_3)_3CCO_2$-); ^{13}C nmr (75 MHz, $CDCl_3$) δ (ppm): 177.84, 171.38, 169.32, 136.29, 133.99, 133.49, 126.69, 127.28, 125.03, 95.16, 70.78, 64.30, 56.90, 54.98, 52.13, 50.56, 31.70, 31.09, 28.29, 27.05, 26.92, 24.74, 22.69; ms *m/e*: 581 ($M^+ - CH_3O$), 549 ($M^+ - MOMOH_2$). Exact Mass calcd. 581.2960; found: 581.2956 ± 0.0023.

(*E,E,E*)-5-(Methoxymethoxy)methyl-1,1,8,8-tetrakis-(methoxycarbonyl)-pentadeca-4,11,13-trien-15-ol (72)

Using the procedure followed for the preparation of alcohol **66**, pivaloyl ester **71** (1.40 g, 2.30 mmol) was treated with sodium methoxide (0.014 mmol; reaction time, 5 h) to give alcohol **72** (1.03 g, 85%, colorless oil) after flash chromatography purification (30% ethyl acetate in hexanes); ir: 3500 (br), 2950, 1735 cm^{-1}; ^{1}H nmr (300 MHz, $CDCl_3$) δ (ppm): 6.20 (1H, dd, *J* = 15.0 Hz, 10.5 Hz, $HOCH_2CH$=C*H*-), 6.07 (1H, dd, *J* = 15.0 Hz, 10.5 Hz, $HOCH_2CH$=CH-C*H*=), 5.80–5.60 (2H, m, -C*H*=CH-CH=C*H*-), 5.41 (1H, t, *J* = 7.0 Hz, -C=CH-), 4.60 (2H, s, $-OCH_2O$-), 4.16 (2H, d, *J* = 6.5 Hz, $HOCH_2$-), 3.93 (2H, s, $-CH_2OMOM$), 3.73 (6H, s, 2 × $-CO_2CH_3$), 3.72 (6H, s, 2 × $-CO_2CH_3$), 3.36 (3H, s, $-OCH_3$), 3.36 (1H, t, *J* = 7.0 Hz, -CH$(CO_2CH_3)_2$), 2.12–1.85 (13H, m, 3 × $-CH_2CH_2$-, -OH); ^{13}C nmr (75 MHz, $CDCl_3$) δ (ppm): 171.58, 169.52, 136.36, 133.07, 130.96, 130.44, 130.14, 127.34, 95.30, 70.89, 63.02, 57.10, 55.13, 52.37, 52.26, 50.76, 31.84, 31.17, 28.37, 27.18, 24.84, 22.82; ms *m/e*: 510 ($M^+ - H_2O$). Exact Mass calcd. for $C_{26}H_{38}O_{10}$: 510.2465; found: 510.2471 ± 0.0015.

(*E,E,E*)-5-(Methoxymethoxy)methyl-1,1,8,8-tetrakis-(methoxycarbonyl)-cyclopentadeca-4,11,13-triene (9)

Using the procedure followed for the preparation of TTT macrocyclic triene **4**, trienol **72** (1.10 g, 2.08 mmol) was transformed (reaction time, 4 h; ~25% of the initial quantity of reagents were added after 3 h to complete the reaction) into the corresponding allylic chloride **73** (1.11 g, 96%, colorless oil, obtained through filtration of the $MgSO_4$ dried organic phase over a fritted glass funnel containing a ~2 cm silica gel pad). This material was immediately macrocyclized (final concentration: 3 × 10^{-3} M), yielding pure TTC macrocyclic triene **9** (0.85 g, 82%, foamy oil that slowly solidifies in the refrigerator); ir (neat): 2950, 1730 cm^{-1}; ^{1}H nmr (300 MHz, $CDCl_3$) δ (ppm): 6.20–6.07 (2H, m, -CH=C*H*-C*H*=CH-), 5.80–5.58 (2H, m, -C*H*=CH-CH=C*H*-), 5.34 (1H, t, *J* = 7.0 Hz, -C=CH-), 4.51 (2H, s, $-OCH_2O$-), 3.79 (2H, s, $-CH_2OMOM$), 3.72 (12H, s, 4 × $-CO_2CH_3$), 3.32 (3H, s, $-OCH_3$), 2.67 (2H, d, *J* = 7.0 Hz, $-(CH_3O_2C)_2CCH_2CH$=), 2.13–1.70 (12H, m, 3 × $-CH_2CH_2$-); ^{13}C nmr (75 MHz, $CDCl_3$) δ (ppm): 171.94, 171.83, 135.10, 134.98, 133.66, 130.85, 128.93, 126.11, 94.96, 70.58, 59.35, 56.92, 55.24, 52.61, 52.43, 37.69, 32.96, 30.31, 29.49, 27.63, 22.54, 21.34; ms *m/e*: 510 (M^+), 478 ($M^+ - CH_3OH$), 448 ($M^+ -$ MOMOH). Exact Mass calcd. for $C_{26}H_{38}O_{10}$: 510.2465; found: 510.2462 ± 0.0015.

(*E,E,E*)-5-Hydroxymethyl-1,1,8,8-tetrakis(methoxycarbonyl)-cyclopentadeca-4,11,13-triene (81)

Using the procedure followed for the preparation of TTT macrocyclic trienol **80**, MOM ether **9** (0.300 g, 0.59 mmol) was cleaved (reaction time, 6 h; temperature: 60–65°C) into the corresponding alcohol **81** (0.264 g, 96%, clear oil, obtained through filtration of the $MgSO_4$ dried organic phase over a fritted glass funnel containing a ~2 cm thick silica gel pad); ir (neat): 3540 (br), 3000–2850, 1730 cm^{-1}; ^{1}H nmr (300 MHz, $CDCl_3$) δ (ppm): 6.19–6.06 (2H, m, -CH=C*H*-C*H*=CH-), 5.76–5.68 (1H, m, -C*H*=CH-CH=CH-), 5.60 (1H, dt, *J* = 14.0 Hz, 7.0 Hz, -CH=CH-CH=C*H*-), 5.29 (1H, t, *J* = 7.0 Hz, -CH=C-), 3.86 (2H, s, $-CH_2OH$), 3.71 (12H, s, 4 × $-CO_2CH_3$), 2.65 (2H, d, *J* = 7.5 Hz, $-(CH_3O_2C)_2CCH_2CH$=), 2.12–1.70 (12H, m, 3 × $-CH_2CH_2$-), 1.57 (1H, br s, -OH); ^{13}C nmr (75 MHz, $CDCl_3$) δ (ppm): 171.97, 171.77, 135.00, 133.70, 130.81, 126.42, 125.98, 125.54, 66.57, 59.41, 56.86, 51.49 (br), 37.52, 32.95, 30.24, 29.54, 27.56, 22.33, 21.03; ms *m/e*: 466 (M^+), 448 ($M^+ - H_2O$). Exact Mass calcd. for $C_{24}H_{34}O_9$: 466.2203; found: 466.2194 ± 0.0013.

Direct route to 10

To a stirred solution of TTC macrocyclic trienol **81** (0.207 g, 0.44 mmol) in dichloromethane (4 mL) was added to Dess–Martin periodinane (0.226 g, 0.53 mmol). The mixture was stirred 1.0 h at room temperature, then diluted with diethyl ether (100 mL) and quenched with aqueous saturated sodium bicarbonate (25 mL). Pentahydrated sodium thiosulfate (~1.0 g, ~3.5 mmol) was added and the mixture was vigorously stirred for 15 min. The organic layer was separated and washed with aqueous saturated sodium bicarbonate (3 mL), water (5 mL), dried with anhydrous magnesium sulfate, filtered, and concentrated. The residue was purified by flash chromatography (20% ethyl acetate in hexanes), yielding formyl-substituted TTC macrocyclic triene **10** (0.169 g, 82%, white foam), identical to the one prepared from *trans-cis* enal inversion on **5**.

(3*Z*,10*E*,12*E*)-3-(Methoxymethoxy)methyl-1-acetoxy-7,7-bis(methoxycarbonyl)-14-*tert*-butyldiphenylsiloxy-tetradeca-3,10,12-triene (74)

Using the procedure employed for the preparation of **62**, *Z* hexenol **48** (0.275 g, 1.66 mmol) was transformed into the corresponding purified (flash chromatography: 50% ethyl acetate in hexanes) mesylate **49** (0.367 g, 100%, colorless

Can. J. Chem. Downloaded from www.nrcresearchpress.com by 46.23.64.124 on 09/08/12
For personal use only.

oil). It was immediately reacted with malonate **21** (0.535 g, 1.12 mmol) in dimethylformamide–tetrahydrofuran (2.5 mL: 2.5 mL) for 12 h at 75°C. The coupling product **74** (0.425 g, 55%, colorless oil) was obtained through flash chromatography purification (15 → 40% ethyl acetate in hexanes) along with a 0.22 g recovered mixture of both coupling substrates; ir (neat): 3080–3000, 2990–2840, 1740 (br) cm^{-1}; ^1H nmr (250 MHz, $CDCl_3$) δ (ppm): 7.72–7.63 (6H, m) and 7.45–7.33 (4H, m) (2 × Ph); 6.23 (1H, dd, J = 15.0 Hz, 11.0 Hz, TBDPSOCH$_2$CH=C*H*-), 6.07 (1H, dd, J = 15.0 Hz, 11.0 Hz, TBDPSOCH$_2$CH=CH-C*H*=), 5.75–5.50 (2H, m, -C*H*=CH-CH=C*H*-), 5.42 (1H, br t, J = 6.0 Hz, -CH=C-), 4.59 (2H, s, -OCH$_2$O-), 4.22 (2H, br d, J = 5.0 Hz, TBDPSOC*H*$_2$CH=), 4.16 (2H, t, J = 7.0 Hz, -CH$_2$OAc), 4.04 (2H, s, -C*H*$_2$OMOM), 3.72 (6H, s, 2 × -CO$_2$CH$_3$), 3.36 (3H, s, CH$_3$O-), 2.41 (2H, t, J = 7.0 Hz, -C*H*$_2$CH$_2$OAc), 2.04 (3H, s, CH$_3$CO$_2$-), 2.05–1.85 (8H, m, -(C*H*$_2$)$_2$C(CO$_2$CH$_3$)$_2$-(C*H*$_2$)$_2$-), 1.05 (9H, s, -SiC(CH$_3$)$_3$); ^{13}C nmr (62.5 MHz, $CDCl_3$) δ (ppm): 171.71, 170.94, 135.46, 133.63, 132.63, 132.24, 131.48, 130.50, 129.56, 128.47, 127.93, 127.58, 95.39, 64.06, 63.91, 63.00, 57.03, 55.19, 52.27, 34.40, 32.72, 32.14, 27.21, 26.74, 22.57, 20.86, 19.15; ms *m/e*: 694 (M^+), 662 ($M^+ - CH_3OH$), 649 (M^+ − MOM). Exact Mass calcd. for $C_{39}H_{54}O_9Si$: 694.3537; found: 694.3546 ± 0.0021.

(3*Z*,10*E*,12*E*)-3-(Methoxymethoxy)methyl-7,7-bis (methoxycabonyl)-14-*tert*-butyldiphenylsiloxy-tetradeca-3,10,12-trienol (75)

To a solution of acetate **74** (0.410 g, 0.58 mmol) in methanol (10 mL) was added anhydrous potassium carbonate (16 mg, 0.12 mmol). The reaction mixture was stirred at room temperature for 3 h, after which it was diluted with diethyl ether (25 mL) and filtered on a silica gel column (rinsed with diethyl ether). The filtrate was concentrated, yielding pure alcohol **75** (0.383 g, 100%, colorless oil); ir (neat): 3450 (br), 3080–3000, 2980–2820, 1735 cm^{-1}; ^1H nmr (250 MHz, $CDCl_3$) δ (ppm): 7.72–7.63 (6H, m) and 7.45–7.32 (4H, m), (2 × Ph), 6.23 (1H, dd, J = 15.0 Hz, 11.0 Hz, TBDPSOCH$_2$CH=C*H*-), 6.07 (1H, dd, J = 15.0 Hz, 11.0 Hz, TBDPSOCH$_2$CH=CH-C*H*=), 5.75–5.53 (2H, M, -C*H*=CH-CH=C*H*-), 5.48 (1H, br t, J = 7.0 Hz, -CH=C-), 4.62 (2H, s, -OCH$_2$O-), 4.22 (2H, br d, J = 5.0 Hz, TBDPSOC*H*$_2$CH=), 4.05 (2H, s, -CH$_2$OMOM), 3.72 (6H, s, 2 × -CO$_2$CH$_3$), 3.75–3.65 (2H, m, -CH$_2$OH), 3.37 (3H, s, CH$_3$O-), 2.35 (2H, t, J = 6.0 Hz, -C*H*$_2$CH$_2$OH), 2.27–2.11 (1H, br, -OH), 2.10–1.85 (8H, m, -(C*H*$_2$)$_2$-C(CO$_2$CH$_3$)$_2$-(C*H*$_2$)$_2$-), 1.05 (9H, s, -SiC(CH$_3$)$_3$); ms *m/e*: 620 ($M^+ - CH_3OH$), 595 ($M^+ - C(CH_3)_3$). Exact Mass calcd. for $C_{36}H_{48}O_7Si$: 620.3169; found: 620.3174 ± 0.0024.

(4*Z*,11*E*,13*E*)-4-(Methoxymethoxy)methyl-1,1,8,8-tetrakis(methoxycarbonyl)-15-*tert*-butyldiphenyl-siloxypentadeca-4,11,13-triene (77)

Using the procedure described for the preparation of **65**, trienol **75** (0.378 g, 0.58 mmol) was successively mesylated (**76**, 0.425 g, 100%, colorless oil) and alkylated with dimethyl malonate (reaction time; 15 h), yielding product **77** (0.420 g, 94%, colorless oil); ir (neat): 3100–3000, 3000–2800, 1735 (br) cm^{-1}; ^1H nmr (250 MHz, $CDCl_3$) δ (ppm): 7.72–7.65 (6H, m) and 7.48–7.32 (4H, m) (2 × Ph); 6.22 (1H, dd, J = 15.0 Hz, 10.0 Hz, TBDPSOCH$_2$CH=C*H*-), 6.06 (1H, dd, J = 15.0 Hz, 10.0 Hz, TBDPSOCH$_2$CH=CH-C*H*=), 5.75–5.51 (2H, m, -C*H*=CH-CH=C*H*-), 5.45–5.32 (1H, m, -CH=C-), 4.57 (2H, s, -OCH$_2$O-), 4.22 (2H, br d, J = 5.5 Hz, TBDPSOC*H*$_2$CH=), 4.01 (2H, s, -C*H*$_2$OMOM), 3.74 (6H, s, 2 × -CO$_2$CH$_3$), 3.72 (6H, s, 2 × -CO$_2$CH$_3$), 3.36 (1H, t, J = 7.0 Hz, -C*H*(CO$_2$CH$_3$)$_2$), 3.35 (3H, s, CH$_3$ O-), 2.18–1.84 (12H, m, 6 × -CH$_2$-), 1.05 (9H, s, -SiC(CH$_3$)$_3$); ms *m/e*: 766 (M^+), 709 (M^+ − *t*Bu). Exact Mass calcd. for $C_{42}H_{58}O_{11}Si$: 766.3748; found: 766.3766 ± 0.0022.

(4*Z*,11*E*,13*E*)-4-(Methoxymethoxy)methyl-1,1,8,8-tetrakis(methoxycarbonyl)-pentadeca-4,11,13-trien-15-ol (78)

Using the procedure followed for the preparation of **63**, silyl ether **77** (0.410 g, 0.54 mmol) was cleaved (reaction time, 20 min at 0°C, then 2.5 h at room temperature, extractions: 3 × 30 mL diethyl ether, then 2 × 20 mL ethyl acetate), yielding alcohol **78** (0.234 g, 83% (with 5% **77**), colorless oil) after purification through flash chromatography (40 → 70% ethyl acetate in hexanes); ir (neat): 3500 (br), 3000–2800, 1735 (br) cm^{-1}; ^1H nmr (250 MHz, $CDCl_3$) δ (ppm): 6.19 (1H, dd, J = 14.5 Hz, 10.5 Hz, HOCH$_2$CH=C*H*-), 6.06 (1H, dd, J = 14.5 Hz, 10.5 Hz, HOCH$_2$CH=CH-CH=), 5.82–5.57 (2H, m, -C*H*=CH-CH=C*H*-), 5.44–5.31 (1H, m, -CH=C-), 4.57 (2H, s, -OCH$_2$O-), 4.17 (2H, br d, J = 6.0 Hz, HOC*H*$_2$-), 4.00 (2H, s, -C*H*$_2$OMOM), 3.74 (6H, s, 2 × -CO$_2$CH$_3$), 3.72 (6H, s, 2 × -CO$_2$CH$_3$), 3.36 (1H, t, J = 7.0 Hz, -C*H*(CO$_2$CH$_3$)$_2$), 3.35 (3H, s, CH$_3$O-), 2.20–1.88 (13H, m, 6 × -CH$_2$-, -OH); ms *m/e*: 510 ($M^+ - H_2O$). Exact Mass calcd. for $C_{26}H_{38}O_{10}$: 510.2465; found: 510.2456 ± 0.0015.

(4*Z*,11*E*,13*E*)-4-(Methoxymethoxy)methyl-1,1,8,8-tetrakis(methoxycarbonyl)-cyclopentadeca-4,11,13-triene (2)

Using the procedure described for the preparation of **4**, alcohol **78** (0.230 g, 0.44 mmol) was transformed (reaction time, 2.5 h; no additional reagents were needed) into the corresponding allylic chloride **79** (0.197 g, 84%, colorless oil). Macrocyclization of the latter (90 mg, 0.16 mmol) proceeded within 13 h of slow addition, with 2 h of further stirring (**79** dissolved in dimethylformamide–tetrahydrofuran (5 mL:5 mL) and added to cesium carbonate in the same solvent (12 mL:12 mL); final concentration; 4 × 10^{-3} M), yielding pure TTT macrocyclic triene **2** (72 mg, 86%, foamy solid); ir (neat): 3000–2800, 1730 cm^{-1}; ^1H nmr (300 MHz, $CDCl_3$) δ (ppm): 6.02 (1H, dd, J = 14.0 Hz, 10.0 Hz, -CH=C*H*-CH=CH-), 5.99 (1H, dd, J = 14.0 Hz, 10.0 Hz, -CH=CH-C*H*=CH-), 5.48 (1H, dt, J = 6.5 Hz, 6.5 Hz, -C*H*=CH-CH=CH-), 5.31 (1H, dt, J = 7.0 Hz, 7.0 Hz, -CH=CH-CH=C*H*-), 5.26 (1H, t, J = 6.5 Hz, 6.5 Hz, -CH=C-), 4.59 (2H, s, -OCH$_2$O-), 3.96 (2H, s, -CH$_2$OMOM), 3.74 (6H, s, 2 × -CO$_2$CH$_3$), 3.72 (6H, s, 2 × -CO$_2$CH$_3$), 3.37 (3H, s, CH$_3$O-), 2.77 (2H, d, J = 7.5 Hz, -(CH$_3$O$_2$C)$_2$-CC*H*$_2$CH=), 2.20–2.07 (4H, m) and 2.07–1.93 (4H, m) and 1.93–1.85 (2H, m) and 1.85–1.72 (2H, m) (6 × -CH$_2$-); ^{13}C nmr (75 MHz, $CDCl_3$) δ (ppm): 171.89, 136.21, 135.72, 134.99, 130.80, 129.36, 124.99, 95.75, 64.67, 58.18, 57.05, 55.26, 52.61, 52.50, 35.49, 30.22, 29.97, 29.07, 27.82, 26.80, 20.03; ms *m/e*: 5.10 (M^+), 478 ($M^+ - CH_3OH$). Exact Mass calcd. for $C_{26}H_{38}O_{10}$: 510.2465; found: 510.2456 ± 0.0015.

Can. J. Chem. Downloaded from www.nrcresearchpress.com by 46.23.64.124 on 09/08/12
For personal use only.

(4*Z*,11*E*,13*E*)-4-Hydroxymethyl-1,1,8,8-tetrakis(methoxycarbonyl)-cyclopentadeca-4,11,13-triene (82)

Using the procedure followed for the preparation of TTT macrocyclic trienol **80**, the MOM ether of **2** (0.111 g, 0.218 mmol) was cleaved (reaction time, 5 h; filtration of the magnesium sulfate dried organic extracts over a fritted glass funnel filled with a 2 cm thick pad of silica gel), yielding alcohol **82** (0.109 g, 98%, white foamy solid); ir (neat): 3500 (br), 2990–2820, 1730 cm^{-1}; ^1H nmr (300 MHz, $CDCl_3$) δ (ppm): 6.14–5.91 (2H, m, -CH=C*H*-C*H*=CH-), 5.46 (1H, dt, *J* = 14.0 Hz, 7.0 Hz, -C*H*=CH-CH=CH-), 5.30 (1H, dt, *J* = 14.0 Hz, 7.0 Hz, -CH=CH-CH=C*H*-), 5.19 (1H, t, *J* = 7.0 Hz, -C=CH-), 4.04 (2H, s, -CH_2OH), 3.72 (6H, s, 2 × -CO_2CH_3), 3.69 (6H, s, 2 × -CO_2CH_3), 2.76 (2H, d, *J* = 7.5 Hz, -(CH_3O_2C)$_2$CCH_2CH=), 2.15–1.72 (12H, m, 3 × -CH_2CH_2-); ^{13}C nmr (300 MHz, $CDCl_3$) δ (ppm): 171.86 (br), 137.72, 136.04, 135.60, 130.75, 128.26, 125.03, 60.20, 58.09, 56.97, 52.55, 52.43, 35.44, 30.22, 29.03, 27.73, 26.49, 19.88; ms *m/e*: 466 (M^+ − H_2O), 435 (M^+ − OCH_3). Exact Mass calcd. for $C_{24}H_{34}O_9$: 466.2203; found: 466.2199 ± 0.0014.

(4*Z*,11*E*,13*E*)-4-Formyl-1,1,8,8-tetrakis(methoxycarbonyl)-cyclopentadeca-4,11,13-triene (3)

Using the procedure followed for the preparation of formyl-substituted TTT macrocyclic triene **5**, TTT macrocyclic trienol **82** (10.5 mg, 0.023 mmol) was oxidized (reaction time, 4 h; additional manganese dioxide was added at three occasions), yielding TTT macrocycle **3** (8.5 mg, 82%, foamy solid, contaminated with <5% of the TTC isomer; NOTE: oxidation with the Dess–Martin periodinane followed by $Na_2S_2O_3$ work-up gave 73% with no isomerization); ir (neat): 2950, 2840, 1730 cm^{-1}; ^1H nmr (300 MHz, C_6D_6) δ (ppm): 9.83 (1H, s, -CHO), 5.96 (1H, t, *J* = 7.5 Hz, -(CHO)C=C*H*-), 5.80–5.62 (2H, m, -CH=C*H*-*HC*=HC-), 5.71 (1H, dt, *J* = 14.5 Hz, 7.0 Hz, -C*H*=CH-CH=CH-), 5.12 (1H, dt, *J* = 14.5 Hz, 7.0 Hz, -CH=CH-CH=C*H*-), 3.32 (6H, s, 2 × -CO_2CH_3), 3.30 (6H, s, 2 × -CO_2CH_3), 2.95 (2H, d, *J* = 7.0 Hz, -(CH_3O_2C)$_2$CCH_2CH=), 2.30–1.90 (12H, m, 3 × -CH_2CH_2); ^1H nmr (300 MHz, $CDCl_3$) δ (ppm): 9.97 (1H, s, -CHO), 6.38 (1H, t, *J* = 8.0 Hz, -(CHO)C=C*H*-), 6.00 (1H, dd, *J* = 14.5 Hz, 10.5 Hz, -CH=C*H*-CH=CH-), 5.89 (1H, dd, *J* = 14.5 Hz, 10.5 Hz, -CH=CH-C*H*=CH-), 5.46 (1H, br dt, *J* = 14.5 Hz, 6.0 Hz, -C*H*=CH-CH=CH-), 5.32 (1H, dt, *J* = 14.5 Hz, 7.5 Hz, -CH=CH-CH=C*H*-), 3.72 (12H, br s, 4 × -CO_2CH_3), 2.73 (2H, d, *J* = 7.5 Hz, -(CH_3O_2C)$_2$CCH_2CH=), 2.33–2.22 (2H, m) and 2.18–2.05 (4H, m) and 2.05–1.85 (6H, m) (3 × -CH_2CH_2-); ^{13}C nmr (75 MHz, C_6D_6) δ (ppm): 189.11, 171.64, 171.43, 148.70, 140.10, 135.76, 135.19, 131.51, 126.62, 58.45, 57.61; 52.13, 52.07, 36.22, 31.85, 30.47, 29.93, 27.84, 23.01, 19.90; ms *m/e*: 464 (M^+), 446 (M^+ − H_2O), 433 (M^+ − OCH_3). Exact Mass calcd. for $C_{24}H_{32}O_9$: 464.2046; foound: 464.2040 ± 0.0014.

(*E*,*E*,*E*)-4-Formyl-1,1,8,8-tetrakis(methoxycarbonyl)-cyclopentadeca-4,11,13-triene (8)

Using the procedure described for the preparation of formyl-substituted TTC macrocyclic triene **10**, TTT macrocyclic trienal **3** (72 mg, 0.15 mmol) was isomerized (reaction time, 12 h) to the TTC isomer **8** (68 mg, 94%, colorless foam); ir (neat): 2960, 2860, 2720, 1730 cm^{-1}; ^1H nmr (300 MHz, $CDCl_3$) δ (ppm): 9.29 (1H, s, -CHO), 6.26 (1H, br t, *J* = 7.0 Hz, -(CHO)C=C*H*-), 6.21–6.09 (2H, m, -CH=C*H*-C*H*=CH-), 5.74 (1H, dt, *J* = 14.5 Hz, 7.0 Hz, -C*H*=CH-CH=CH-), 5.42 (1H, dt *J* = 14.5 Hz, 7.5 Hz, -CH=CH-CH=C*H*-), 3.75 (6H, s, 2 × -CO_2CH_3), 3.73 (6H, s, 2 × -CO_2CH_3), 2.72 (2H, d, *J* = 7.5 Hz, -(CH_3O_2C)$_2$CCH_2CH=), 2.20–1.95 (10H, m) and 1.80–1.65 (2H, m) (3 × -CH_2CH_2-); ^1H nmr (300 MHz, C_6D_6) δ (ppm): 9.08 (1H, s, -CHO), 5.87–5.76 (3H, m, -CH=C*H*-C*H*=CH-, -(CHO)C=C*H*-), 5.55–5.44 (2H, m, -C*H*=CH-CH=C*H*-), 3.46 (96H, s, 2 × -CO_2CH_3), 3.34 (6H, s, 2 × -CO_2CH_3), 2.96 (2H, d, *J* = 7.5 Hz, -(CH_3O_2C)$_2$CCH_2CH=); 2.15–1.97 (8H, m) and 1.97–1.75 (2H, m) and 1.75–1.62 (2H, m) (3 × -CH_2CH_2-); ^{13}C nmr (75 MHz, $CDCl_3$) δ (ppm): 194.52, 171.63, 171.50, 153.72, 142.40, 135.23, 133.86, 131.31, 125.07, 58.89, 56.23, 52.68 (br), 35.94, 31.52, 30.97, 29.72, 26.79, 23.13, 17.15; ^{13}C nmr (75 MHz, C_6D_6) δ (ppm): 193.87, 171.67, 152.89, 142.89, 135.79, 133.61, 131.83, 125.43, 59.23, 56.83, 52.31, 52.13, 36.76, 32.42, 31.75, 30.44, 26.99, 23.88, 17.85; ms *m/e*: 464 (M^+), 446 (M^+ − H_2O), 433 (M^+ − OCH_3). Exact Mass calcd. for $C_{24}H_{32}O_9$: 464.2046; found: 464.2040 ± 0.0014.

(*E*,*E*,*E*)-4-Hydroxymethyl-1,1,8,8-tetrakis(methoxycarbonyl)-cyclopentadeca-4,11,13-triene (83)

To a cooled solution (0°C) of TTC-macrocyclic trienal **8** (42 mg, 0.091 mmol) in methanol–tetrahydrofuran (1:1, 2 mL), was added sodium borohydride (3.5 mg, 0.091 mmol). The solution was stirred 1 h, after which a solution of aqueous ammonium chloride (5 mL) was added. The aqueous phase was extracted with diethyl ether (3 × 10 mL) and ethyl acetate (2 × 10 mL) and the combined organic layers were washed with brine, dried over anhydrous magnesium sulfate, and filtered over a fritted glass funnel filled with a 1.5 cm thick silica gel pad (rinsed with ethyl acetate). The filtrate was concentrated, leaving pure alcohol **83** (41 mg, 97%, colorless oil); ir (neat): 3540 (br), 2955, 2860, 1730 cm^{-1}; ^1H nmr (300 MHz, $CDCl_3$) δ (ppm): 6.23–6.10 (2H, m, -CH=C*H*-C*H*=CH-), 5.78 (1H, dt, *J* = 14.5 Hz, 7.0 Hz, -C*H*=CH-CH=CH-), 5.57 (1H, dt, *J* = 14.0 Hz, 7.0 Hz, -CH=CH-CH=C*H*-), 5.24 (1H, t, *J* = 8.0 Hz, -C=CH-), 3.98 (2H, br s, -CH_2OH), 3.72 (6H, s, 2 × -CO_2CH_3), 3.70 (6H, s, 2 × -CO_2CH_3), 2.67 (2H, d, *J* = 7.0 Hz, -(CH_3O_2C)$_2$CCH_2CH=), 2.12–1.60 (13H, m, 3 × -CH_2CH_2, -OH); ^{13}C nmr (75 MHz, $CDCl_3$): 171.99, 171.75, 138.03, 135.32, 133.56, 131.34, 126.65, 125.34, 66.85, 59.02, 56.53, 52.63, 52.49, 36.44, 31.84, 30.97 (2), 26.61, 21.69, 21.32; ms *m/e*: 466 (M^+), 448 (M^+ − H_2O). Exact Mass calcd. for $C_{24}H_{34}O_9$: 466.2203; found: 466.2198 ± 0.0013.

(*E*,*E*,*E*)-4-(Methoxymethoxy)methyl-1,1,8,8-tetrakis(methoxycarbonyl)-cyclopentadeca-4,11,13-triene (7)

To a solution of TTC-macrocyclic trienol **83** (41 mg, 0.088 mmol) in dichloromethane (1.5 mL), were successively added diisopropylethylamine (0.046 mL, 0.26 mmol) and methoxymethyl chloride (0.014 mL, 0.18 mmol). The mixture was stirred 5 h at room temperature, after which a solution of aqueous saturated ammonium chloride (5 mL) was added. The resulting mixture was extracted with dichloromethane (3 × 10 mL) and the combined organic layers were washed with brine, dried over anhydrous magnesium sulfate, filtered, and concentrated. The residue was purified by flash chromatography (30% ethyl acetate in hexanes), yielding TTC macrocycle **7**

(34 mg, 77%, foamy oil); ir (neat): 2950, 1735 cm^{-1}; ^1H nmr (300 MHz, $CDCl_3$) δ (ppm): 6.22–6.10 (2H, m, -CH=C*H*-C*H*=CH-), 5.78 (1H, dt, J = 15.0 Hz, 7.0 Hz, -C*H*=CH-CH=CH-), 5.55 (1H, dt, J = 15.0 Hz, 7.0 Hz, -CH=CH-CH=C*H*-), 5.27 (1H, t, J = 8.0 Hz, -C=CH-), 4.56 (2H, s, -OCH_2O-), 3.87 (2H, s, -CH_2OMOM), 3.72 (6H, s, 2 × CO_2CH_3), 3.70 (6H, s, 2 × CO_2CH_3), 3.34 (3H, s, -OCH_3), 2.68 (2H, d, J = 7.0 Hz, -$(CH_3O_2C)_2CCH_2CH$=); 2.12–1.97 (4H, m) and 1.97–1.78 (6H, m) and 1.78–1.63 (2H, m) (3 × -CH_2CH_2-); ^{13}C nmr (75 MHz, $CDCl_3$) δ (ppm): 172.00, 171.75, 135.23, 133.55, 131.44, 129.26, 127.70, 125.40, 95.49, 71.28, 59.08, 56.66, 55.23, 52.54, 36.69, 32.00, 31.09, 30.90, 26.55, 21.93, 21.69; ms *m/e*: 510 (M^+) 478 ($M^+ - CH_3OH$), 448 (M^+ − MOMOH). Exact Mass calcd. for $C_{26}H_{38}O_{10}$: 510.2465; found: 510.2471 ± 0.0015.

Acknowledgements

This research was financially supported by the Natural Sciences and Engineering Research Council of Canada (NSERC, Ottawa) and by the "Ministère de l'Enseignement Supérieur et de la Science (Fonds FCAR, Québec)." D.G.H. thanks NSERC for a 1967 Postgraduate Award. We wish to acknowledge the help of Dr. Solo Goldstein and Prof. Yves L. Dory for the molecular modeling calculations, and Mr. Gilles Provencher for his technical assistance in the preparation of some intermediates.

References

1. (*a*) L.F. Tietze and U. Beifuss. Angew. Chem. Int. Ed. Engl. **32**, 131 (1993); (*b*) T.-L. Ho. Tandem organic reactions. Wiley, New York. 1992; (*c*) H.M.R. Hoffmann. Angew. Chem. Int. Ed. Engl. **31**, 1332 (1992); (*d*) B.M. Trost. Science, **254**, 1471 (1991); (*e*) P. Deslongchamps. Bull. Soc. Chim. Fr. II, **9**, 349 (1984).
2. P. Deslongchamps. Pure Appl. Chem. **24**, 43 (1991).
3. (*a*) S.H. Jung, Y.S. Lee, H. Park, and D.-S. Kwon. Tetrahedron Lett. **36**, 1051 (1995); (*b*) W.R. Roush, J.S. Warmus, and A.B. Works. Tetrahedron Lett. **34**, 4427 (1993); (*c*) T. Takahashi, Y. Sakamoto, and T. Doi. Tetrahedron Lett. **33**, 3519 (1992); (*d*) J.A. Porco, Jr., F.J. Schoenen, T.J. Stout, J. Clardy, and S.L. Schreiber. J. Am. Chem. Soc. **112**, 7410 (1990).
4. M. Quimpère, L. Ruest, and P. Deslongchamps. Can. J. Chem. **70**, 2335 (1992).
5. J.Y. Roberge, P. Giguère, Y.L. Dory, P. Soucy, and P. Deslongchamps. Can. J. Chem. **72**, 1820 (1994).
6. (*a*) A. Ndibwami, S. Lamothe, D. Guay, R. Plante, P. Soucy, S. Goldstein, and P. Deslongchamps. Can. J. Chem. **71**, 695 (1993); (*b*) A. Ndibwami, S. Lamothe, P. Soucy, S. Goldstein, and P. Deslongchamps. Can. J. Chem. **71**, 714 (1993).
7. W.R. Roush. *In* Comprehensive organic synthesis. Vol. 4. *Edited by* B.M. Trost. Pergamon Press, Oxford. 1991. pp. 513–550.
8. (*a*) T.K. Devon and A.I. Scott. *In* Handbook of naturally occurring compounds, Vol. II. Terpenes. Academic Press, New York. 1972; (*b*) T. Kametani (*Editor*). Heterocycles: Supplement no. 2. Sendai, Japan. June, 1983.
9. (*a*) D.G. Hall, R. Müller, and P. Deslongchamps. Tetrahedron Lett. **33**, 5221 (1992); (*b*) Tetrahedron Lett. **33**, 5217 (1992).
10. W.J. Wadsworth. Org. React. **25**, 73 (1977).
11. A.J. Mancuso, S.L. Huang, and D. Swern. J. Org. Chem. **43**, 2480 (1978).
12. T. Minawi, I. Niki, and T. Agawa. J. Org. Chem. **39**, 3236 (1974).
13. D.G. Hall, A.-S. Caillé, M. Drouin, S. Lamothe, R. Müller, and P. Deslongchamps. Synthesis. In press.
14. E.W. Collington and A.I. Meyers. J. Org. Chem. **36**, 3044 (1971).
15. D.B. Dess and J.C. Martin. J. Am. Chem. Soc. **113**, 7277 (1991).
16. P.E. Sonnet. Tetrahedron, **36**, 557 (1980).
17. E. Pretsch, J. Seibl, W. Simon, and T. Clerc. Tables of spectral data for structure determination of organic compounds. 2nd ed. Springer-Verlag, Berlin. 1989.
18. E.L. Eliel and S.H. Wilen. Stereochemistry of organic compounds. Wiley, New York. 1994. p. 621.
19. M.J.S. Dewar, E.G. Zoebish, E.F. Healy, and J.J.P. Stewart. J. Am. Chem. Soc. **107**, 3902 (1985).

Can. J. Chem. Downloaded from www.nrcresearchpress.com by 46.23.64.124 on 09/08/12
For personal use only.

Studies on the transannular Diels–Alder reaction of 15-membered macrocyclic trienes containing a *trans-trans* diene. Part II: Evidence for unsymmetrical transition states in the formation of A.B.C.[6.6.7] tricyclic products[1]

Dennis G. Hall, Renate Müller, and Pierre Deslongchamps

Abstract: In the preceding paper (Part I) we described the preparation of 10 model TTT and TTC cyclopentadecatrienes. Their conversion to A.B.C.[6.6.7] tricyclic products via a transannular Diels–Alder (TADA) reaction and the analysis of the resulting diastereoselection along with proofs of structures are described in the present article (Part II). The required temperature of reaction was significantly higher (~100°C) in comparison to that required for the 14-membered lower homologs, indicating that proximity effects are playing a key role in the TADA reaction. The presence of ester groups in the chain was found to favor either of the two possible transition states (*endo* or *exo*) on the basis of steric effects, thus controlling the TST/CSC ratio of tricycles from TTC macrocycles, and the TAC/CAT ratio from TTT macrocycles. A formyl substituent on the dienophile can further influence the diastereoselection through the hypothesis of unsymmetrical transition states and allowed, for the first time, the use of Lewis acids as catalysts in the TADA reaction. This investigation demonstrates a general methodology for the stereocontrolled synthesis of A.B.C.[6.6.7] tricycle structures related to several polycyclic natural products.

Key words: transannular, Diels–Alder, 15-membered ring, A.B.C.[6.6.7] tricycles, diterpene.

Résumé : Dans l'article précédent (Partie I), nous avons décrit la préparation de 10 cyclopentadécatrienes modèles de géométrie TTT et TTC. Leur conversion en produits tricycliques A.B.C.[6.6.7] via une réaction de Diels–Alder transannulaire (DATA) et l'analyse de la diastéréosélection résultante accompagnée des preuves de structure sont décrites dans l'article qui suit (Partie II). La température de réaction requise fut significativement plus élevée (~100°C) à comparer aux homologues inférieurs à 14 membres, indiquant que les effets de proximité jouent un rôle clé dans la réaction DATA. La présence de groupements ester sur la chaîne a permis de favoriser un ou l'autre des deux états de transition possibles (*endo* ou *exo*) par des effets stériques, contrôlant ainsi le ratio des tricycles TST/CSC à partir des macrocycles TTC, et le ratio TAC/CAT à partir des macrocycles TTT. Un substituant formyle sur le diénophile peut influencer davantage la diastéréosélection à travers l'hypothèse d'états de transition non-symétriques et a aussi permis, pour la première fois, l'utilisation d'acides de Lewis comme catalyseurs dans la réaction DATA. Cette étude démontre une méthodologie générale permettant de synthétiser de manière stéréocontrôlée des structures tricycliques A.B.C.[6.6.7] que l'on retrouve chez plusieurs produits naturels polycycliques.

Mots clés : transannulaire, Diels–Alder, cycle à 15 membres, tricycles A.B.C.[6.6.7], diterpène.

Introduction

In the preceding article (1), we reported the synthesis of 10 model 15-membered macrocyclic trienes **1–10** (cf. Tables 1 and 2), each containing a *trans-trans* diene and a *cis* or *trans* trisubstituted dienophile. In this paper (Part II), we wish to report our results on the investigation of the reaction conditions and the analysis of the stereochemical outcome of their thermal conversions to A.B.C.[6.6.7] tricyclic products through a transannular Diels–Alder (TADA) reaction. Such a general study, in which the geometry (*trans* or *cis*), the nature, and the position (pro-6.6 or pro-6.7) of a substituent on the dienophile are systematically varied, should enable a better understanding of the factors governing diastereoselection. In particular, the obtention of formyl-substituted macrocyclic substrates (**3, 5, 8, 10**) opens doors for effecting Lewis acid catalysis for the first time on transannular systems with the benefit of milder reaction conditions.

Results and discussion

Each model macrocyclic triene **1–10** can, in principle, yield two diastereomeric products via two possible boat-type transi-

Received March 20, 1995.

D.G. Hall, R. Müller, and P. Deslongchamps.[2] Laboratoire de synthèse organique, Département de chimie, Faculté des sciences, Université de Sherbrooke, Sherbrooke, QC J1K 2R1, Canada.

[1] Taken in part from D.G. Hall; Ph.D. Thesis, 1995.

[2] Author to whom correspondence may be addressed. Telephone: (819) 821-7002. Fax: (819) 821-7910. E-mail: dlnchamp@structure.chimie.usherb.ca

Can. J. Chem. Downloaded from www.nrcresearchpress.com by 80.90.12.36 on 09/08/12
For personal use only.

Table 1. TADA reactions of TTC 15-membered macrocyclic trienes.

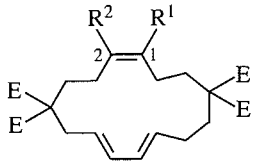

E = CO_2CH_3

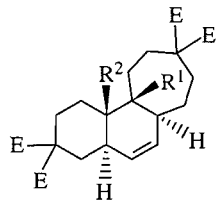

a: TST (*endo*)

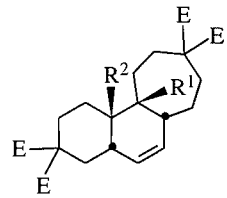

b: CSC (*exo*)

Entry		Macrocyclic substrate	Method[a]	Temp., Time	Yield[b]	Products[c] and ratios[d]	
	9	$R^1 = CH_2OMOM$, $R^2 = H$				**9a**	**9b**
1			Thermal	200°C, 3 h	88%	85:15	
	10	$R^1 = CHO$, $R^2 = H$				**10a**	**10b**
2			Thermal	140°C, 3 h	85%	100:0[f]	
3			$AlCl_3$ or $SnCl_4$	rt, 2 h	85%	100:0[f]	
4			$BF_3 \cdot OEt_2$, CH_2Cl_2	rt, 30 s		100:0[f]	
	6	$R^1 = H$, $R^2 = CH_3$				**6a**	**6b**
5			Thermal	200°C, 4 h	63%	86:14	
	7	$R^1 = H$, $R^2 = CH_2OMOM$				**7a**	**7b**
6			Thermal	200°C, 3 h	55%	90:10	
	8	$R^1 = H$, $R^2 = CHO$				**8a**	**8b**
7			Thermal	200°C, 7 h	60%	76:24	
8			Thermal	140°C, 3 h[e]		76:24	
9			$AlCl_3$ or $SnCl_4$	rt, 20 h	No reaction		
10			$SnCl_4$, C_6H_6	80°C, 2 h		87:13	
11			$BF_3 \cdot OEt_2$, CH_2Cl_2	rt, 2 h[e]		95:5	

[a]Thermal reactions were performed neat or in toluene into a dried Pyrex tube sealed under vacuum. Acid-catalyzed reactions used excess Lewis acids and could be accomplished either in CH_2Cl_2 or toluene.

[b]Total yields of isolated products.

[c]Diastereomeric pairs are all separable on silica gel except **9a/9b**, which were separated as their alcohol derivatives.

[d]Diastereomeric ratios were determined by ^1H nmr analysis of crude reaction mixtures.

[e]At this point, the reaction is 76% completed (entry 8); 48% (entry 11).

[f]Minor isomer could not be detected by ^1H nmr.

Scheme 1.

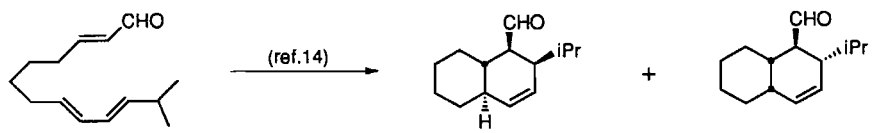

150°C	75	:	25
$AlEtCl_2$, 23°C	>98	:	2
$AlEtCl_2$, -78°C	>99	:	1

tion states, arising from either an *endo* or an *exo* approach. In the preceding paper of this series (Part I) it was shown that the ground state conformation of the diene moiety in our substrates is the *transoid* form. To collapse into tricycles, the *cisoid* form is required (2). This conformational factor, along with others such as steric and electronic effects stemming from the dienophile substituent, will be discussed herein. A special emphasis will be placed on a comparison with the IMDA reaction for which an excellent review article recently appeared (3). It should be stated, however, that the superior level of sophistication of the transannular variant (the intramolecular variant is limited to the formation of bicyclic systems) is associated with more parameters. For instance, two ring junctions (A.B.[6.6] and B.C.[6.7] are formed in a single operation instead of only one for the IMDA reaction. Also, whereas the IMDA literature is overflowing with examples in the decalin series (see example in Scheme 1), we are aware of only three cases (4) reporting the preparation of bicyclo-[6.7] systems (Scheme 2).

The discussion also includes the proof of structures for the various tricyclic compounds reported herein as well as a comparison with results previously obtained with 14-membered macrocyclic trienes.

TADA reaction of pro-6.7-substitued TTC macrocyclic substrates 9 and 10

Macrocyclic trienes **9** and **10** can give a *trans-syn-trans* (TST) tricycle via an *endo* approach and a *cis-syn-cis* (CSC) tricycle, this time formed from an *exo* approach[3] (Scheme 3). Upon heating at 200°C for 3.0 h in a sealed tube, MOMO-methyl-

[3] The *endo/exo* denomination employed herein is relative to the dienophile substituent.

Can. J. Chem. Downloaded from www.nrcresearchpress.com by 80.90.12.36 on 09/08/12
For personal use only.

Can. J. Chem, Downloaded from www.nrcresearchpress.com by 80.90.12.36 on 09/08/12
For personal use only.

Table 2. TADA reactions of TTT 15-membered macrocyclic trienes.

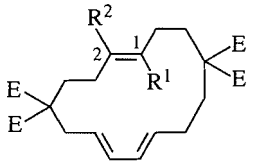

E = CO_2CH_3

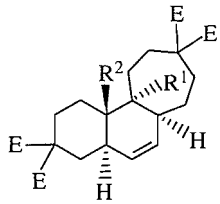

a: TAC

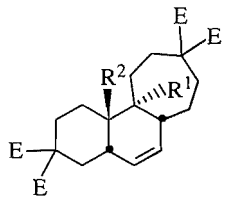

b: CAT

Entry		Macrocyclic substrate	Method[a]	Temp., Time	Yield[b]	Products[c] and ratios[d]	
	4	$R^1 = CH_2OMOM$, $R^2 = H$				**4a**	**4b**
1			Thermal	205°C, 6.5 h	62%	78:22	
	5	$R^1 = CHO$, $R^2 = H$				**5a**	**5b**
2			Thermal	320°C, 1.5 min		77:23[g]	
3			Thermal	150°C, 5.5 h		[g]	
4			$AlCl_3$ CH_2Cl_2	rt, 2 h	60%	84:16[g]	
5			$AlCl_3$ C_6H_6	rt, 1 h[e]		84:16	
	1	$R^1 = H$, $R^2 = CH_3$				**1a**	**1b**
6			Thermal	200°C, 4.5 h	63%	88:12	
	2	$R^1 = H$, $R^2 = CH_2OMOM$				**2a**	**2b**
7			Thermal	200°C, 3 h	61%	90:10	
	3	$R^1 = H$, $R^2 = CHO$				**3a**	**3b**
8			Thermal	130°C, 5 h[e]		100:0[f,g]	
9			Thermal	300°C, 3 min	90%	100:0[f,g]	
10			$AlCl_3$ C_6H_6	rt, 1.5 h	No reaction		
11			$SnCl_4$, C_6H_6	65°C, 4 h		[g]	

[a]Thermal reactions were performed neat or in toluene into a dried Pyrex tube sealed under vacuum. Acid-catalyzed reactions used excess Lewis acids and could be accomplished either in CH_2Cl_2 or toluene.

[b]Total yields of isolated products.

[c]Diastereomeric pairs are not separable on silica gel except **1a/1b**. Other pairs were separated as their alcohol derivatives.

[d]Diastereomeric ratios were determined by ^1H nmr analysis of crude reaction mixtures.

[e]At this point, the reaction is 85% completed for entry 5 and 40% for entry 8.

[f]Minor isomer could not be detected by ^1H nmr.

[g]Percentage of TDA products resulting from TTT→TTC in situ isomerization: entry 2: 40%; entry 3: >90%; entry 4: 10%; entry 8: 50%; entry 9: 25%; entry 11: 100%.

Scheme 2.

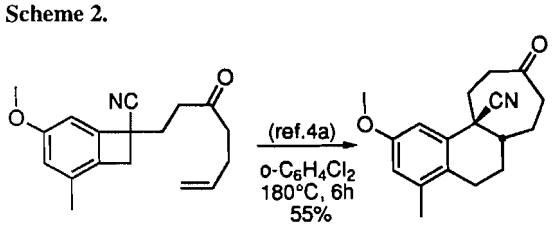

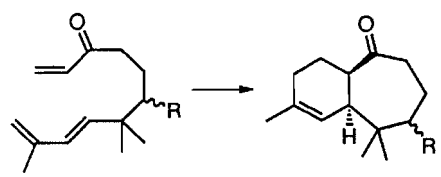

R = OPO(OEt)$_2$, 80°C, 18 h 90% (ref.4b)
R = H, 110°C, $AlCl_3$ 70% (ref.4c)

substituted macrocyclic triene **9** gave a high yield of an inseparable 85:15 mixture favoring TST tricycle **9a** over CSC **9b** (Table 1, entry 1). A comparison of the two transition states mentioned above reveals, in the CSC case, the presence of a

Scheme 3.

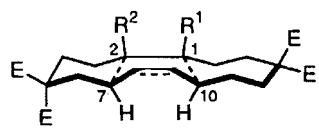

TST (*endo*) transition state

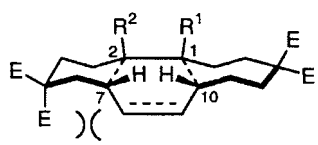

CSC (*exo*) transition state

severe 1,3-diaxial steric interaction between the pseudo-axial ester function of ring A in a chair conformation[4] and one of the sp^2 carbons (C7) of the diene. Such an interaction being absent in the TST transition state, the preferential formation of TST tricycle **9a** over CSC **9b** is readily explained. Due to the twist-

[4] In this case, with $R^2 = H$, a high-energy boat conformation in ring A could compete with this sterically hindered chair (see ref. 5).

Scheme 4.

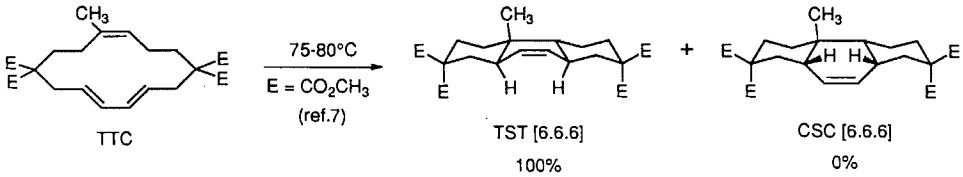

Scheme 5. Chemical derivatization for pro-6.7 substituted TST and CSC tricycles.

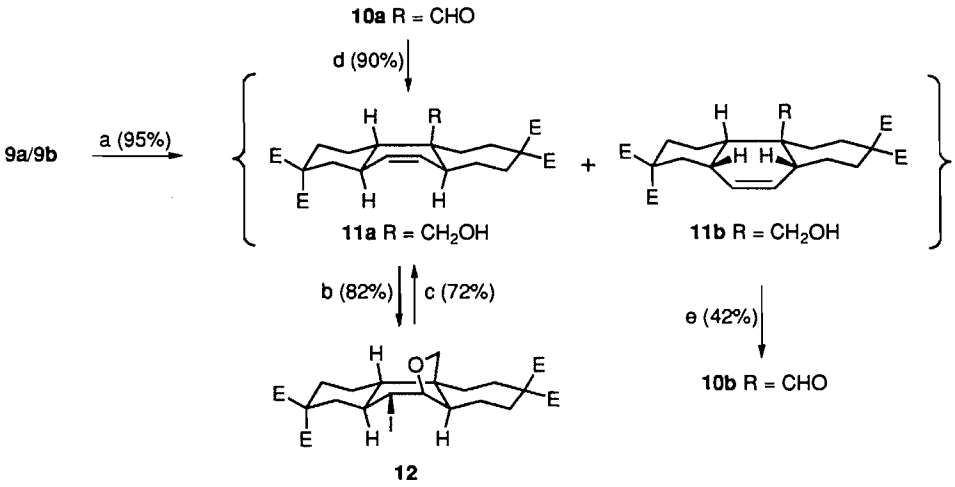

(a) conc. $HCl_{(aq.)}$ / H_2O / MeOH, 60-65°C, 5h. (b) $NaHCO_3$, I_2, THF, rt, 3h. (c) Zn, conc. $AcOH_{(aq.)}$, rt, 5h. (d) $NaBH_4$, THF / MeOH 1:1, 0°C, 30 min. (e) Dess-Martin periodinane, CH_2Cl_2, rt, 2h

chair conformation[5] of the seven-membered ring C being formed, it seems likely that the second malonate unit, on the basis of its steric interactions, will not help in discriminating between processes. This hypothesis is in agreement with a former observation from our laboratory concerning TTC 14-membered macrocycles (Scheme 4). In this example (7), two cooperative axial ester groups were necessary to prevent the formation of the CSC tricyclic product, indicating that only a single one is strongly involved in the present case. It is interesting to note the relatively lower reaction temperature (~80°C) needed in the latter example compared to that of **9**. Thus, an additional methylene group makes a significant difference, indicating that proximity and entropy effects play a very important role in the TADA reaction.

Following hydrolysis of the MOM ether of the mixture **9a/9b** (Scheme 5), the corresponding allylic alcohols TST **11a** and CSC **11b** could be separated with some difficulty by preparative thin-layer chromatography and individually characterized by standard means (ir, ^1H nmr, ^{13}C nmr, ms). Confirmation of the ring junction stereochemistry by nmr techniques was found impracticable for these compounds and for most others in this study. Key coupling constants could not be extracted from the complicated superposed multiplets observed in the ^1H nmr spectra. However, a more convenient way of effecting separation on a larger scale also offered a concomitant chemical proof of structure. Indeed, treatment of the **11a/11b** mixture under Bartlett's kinetic iodoetherification

Scheme 6.

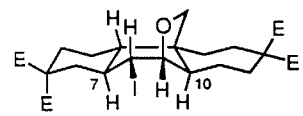

12

Approximate dihedral angles (ϕ) and observed coupling constants

ϕ H7CCH8 : 180° , J = 10.0 Hz
ϕ H8CCH9 : 90° , J = 0 Hz
ϕ H9CCH10 : 90° , J = 0 Hz

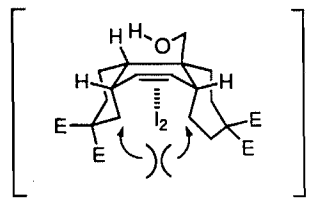

CSC **11b** iodoetherification transition state

conditions (8, 9) (Scheme 5) afforded TST iodoether **12** and unreacted CSC alcohol **11b**, very easily separable on silica gel. In fact, the alcohol and alkene functions of **11b** cannot be brought in close proximity for an iodine-mediated reaction, as strongly disfavored steric interactions would be created by the required conformational change (Scheme 6). On the other hand, iodoether **12**, which structure was confirmed by spectroscopic methods including ^1H nmr analysis (Scheme 6), could

[5] Cycloheptanes are more flexible than cyclohexanes. Conformational analysis of the former reveals the existence of more accessible conformations such as the twist-chair and chair, which readily interconvert (6).

Can. J. Chem. Downloaded from www.nrcresearchpress.com by 80.90.12.36 on 09/08/12
For personal use only.

Can. J. Chem. Downloaded from www.nrcresearchpress.com by 80.90.12.36 on 09/08/12
For personal use only.

be reconverted to the TST alcohol **11a** by treatment with zinc in acetic acid (Scheme 5).

The formyl macrocyclic analog **10** gave TST tricycle **10a** exclusively, under both thermal and Lewis acid-catalyzed conditions[6] (Table 1, entries 2–4).[7] It is noteworthy to mention the milder reaction conditions allowed in this reaction by the use of Lewis acids, with a temperature lowering of >100°C. The absence of any of the CSC diastereomer **10b** was confirmed by carrying out oxidation if CSC alcohol **11b** (Scheme 5). The corresponding ^{1}H nmr formyl peak of the putative aldehyde **10b** was clearly absent from crude spectra of thermolyzed **10** even after baseline amplification. Such a stereospecificity finds some precedent in the IMDA reaction of terminally activated decatrienes (Scheme 1), although in this example (14) reported by Roush et al., the thermal uncatalyzed reaction affords a rather modest selectivity (i.e., 75:25). The increase in selectivity observed on going from macrocycle **9** to activated analogue **10** can in principle be explained by the *endo* effect, which leads to a lower energy transition state presumably due to stabilizing secondary orbital interactions (2*a*). However, it was demonstrated decades ago that such an effect is weakly operative at temperatures higher than 75°C (15) although it is rather efficient at lower temperatures. In agreement with this, the *endo* effect is also known to have a reduced influence on the thermal IMDA reaction (3). Since TST tricycle **10a** is the exclusive product even at 150°C, a more viable explanation relies on the "concerted asynchronous transition state" hypothesis for unsymmetrically activated Diels–Alder substrates (3). Indeed, with R^1 = CHO as in **10**, the largest LUMO coefficient for acrolein-type dienophiles (16) lies at the β-site (C2), resulting at the transition state level in a short C2—C7 and a longer C1—C10 distance and indicating that the incipient bonding is more advanced in the former case (Scheme 3). Therefore, it follows that the importance of steric interactions in the vicinity of C2 and C7 must be emphasized,[8] including the key pseudo-1,3-diaxial interaction that is taking place in the CSC transition state as mentioned above. Consequently, as this steric interaction is magnified, the preclusion of the CSC tricycle **10b** is well understood when compared with the slight proportion of **9b** from macrocycle **9**. An alternative explanation, also relying on the crucial role of the short C2—C7 incipient bond, suggests that a *trans*-[6.6] ring junction will be strongly favored in such situations of decalin formation. This generalization has been drawn from the IMDA study of terminally activated decatrienes (3) (Scheme 1).

Tricyclic compound **10a** was chemically correlated to tricycle **9a** for structure confirmation by reduction with sodium borohydride, yielding alcohol **11a**, which was found spectroscopically identical to the alcohol obtained via hydrolysis of **9a**. Moreover, interesting arguments for the determination of the relative stereochemistry were deduced from the proton nmr analysis of tricycles **10a** and **10b** (the latter obtained from **9b** as in Scheme 5). Aside from its chemical correlation with **9a**, the *endo* (TSC) stereochemistry of **10a** was implied on the basis of a J_w coupling (1.0 Hz) between the aldehyde proton and the methine proton on the *trans* B.C.[6.7] ring junction.[9] A similar W spatial arrangement is indeed unattainable in **10b** and no coupling is actually observed.

TADA reaction of pro-6.6-substituted TTC macrocyclic substrates 6, 7, and 8

Like their regioisomers described in the previous section, TTC pro-6.6-substituted macrocyclic trienes **6, 7**, and **8** can give TST and CSC tricycles via transition states with dienophile substituents permuted from C1 to C2 (Scheme 3). Model macrocycle **6** having a methyl substituent on the dienophile was heated at 200°C for 4.0 h, giving an 86:14 mixture favoring TST tricycle **6a** over the CSC diastereomer **6b** in moderate yield (Table 1, entry 5). These TADA products were separated by preparative tlc and fully characterized by standard means. The major isomer was subjected to an alkene epoxidation procedure with trifluoroperacetic acid, leading to the formation of putative epoxide **13** (eq. [1], Scheme 7). The indicated oxirane stereochemistry is based on a presumed attack of the reagent from the less congested exocyclic face. This hypothesis, along with the TST relationship at ring junctions, is in line with the observed ^{1}H nmr coupling constants for HC7–HC8 and HC9–HC10 (9.0 Hz), which are characteristic of pseudo-diaxial arrangements.

The analogous macrocyclic triene **7**, bearing a $CH_3OCH_2OCH_2$- substituent, gave a similar ratio (90:10) of TST tricycle **7a** and CSC **7b** (Table 1, entry 6). The less polar TST product **7a** was isolated in pure form by preparative tlc, resulting in a modest yield of 55%. A substantial amount of a more polar fraction was found to contain one or more unknown macrocyclic by-products[10] as major components with a small proportion (ca. 15%) of CSC tricycle **7b**. The latter could not be formally identified from this mixture. However, its presence and proportion were assessed through a hydrolysis–oxidation sequence followed by comparison of ^{1}H nmr data of the resulting aldehyde mixture with those of pure **8b** originating from the TADA reaction of macrocycle **8** (vide infra). The proportion of **7b** in the original impure tlc fraction was then deduced and an approximate ratio with **7a** could be estimated. The predominance of TST tricyclic products **6a** and **7a** over their respective CSC diastereomers is readily explained using the same analysis as described for regioisomeric macrocycle **9** (see above). Indeed, a pseudo-diaxial steric interaction between an ester group of incipient ring A and sp^2 carbon 8 is still responsible for the superior energy of activation associated with the CSC transition state (Scheme 3). Compared to the case of model macrocycle **9**, inspection of molecular models shows that a permutation of the dienophile

[6] Excess acid was used since the malonate units of our model substrates can form strong chelates (10).

[7] Some exploratory experiments using "unclassical" reaction media were also tried. The use of 5 M $LiClO_4$ – Et_2O (11) for 48 h afforded only ~20% **10a**. Water–methanol 1:1 as a solvent was also shown to accelerate the transformation of **10** (80°C, 3 h, 60% conversion; 100°C, sealed tube, 3 h, 95% conversion). Unactivated macrocycle **6** (vide infra) was insensitive to the effect of hydroxyl-based solvents. These results are in opposition to Breslow's theory of hydrophobic acceleration (12) and point rather toward hydrogen-bonding effects (13) on the formyl group.

[8] We should be reminded here that the energy of nonbonding interactions developed between two sites is related to distance (r) by a factor of $1/r^6$ (17)!

[9] For other examples, see ref. 18. This observation is similar to the broadening effect of methyl signals in *trans* ring junctions of steroid derivatives (19).

[10] Upon heating at high temperatures, hypothetical side processes include transannular ene reactions and allylic MOM ether pyrolysis as a retro-ene reaction (20).

Scheme 7. Chemical derivatization for pro-6.6 substituted TST and CSC tricycles.

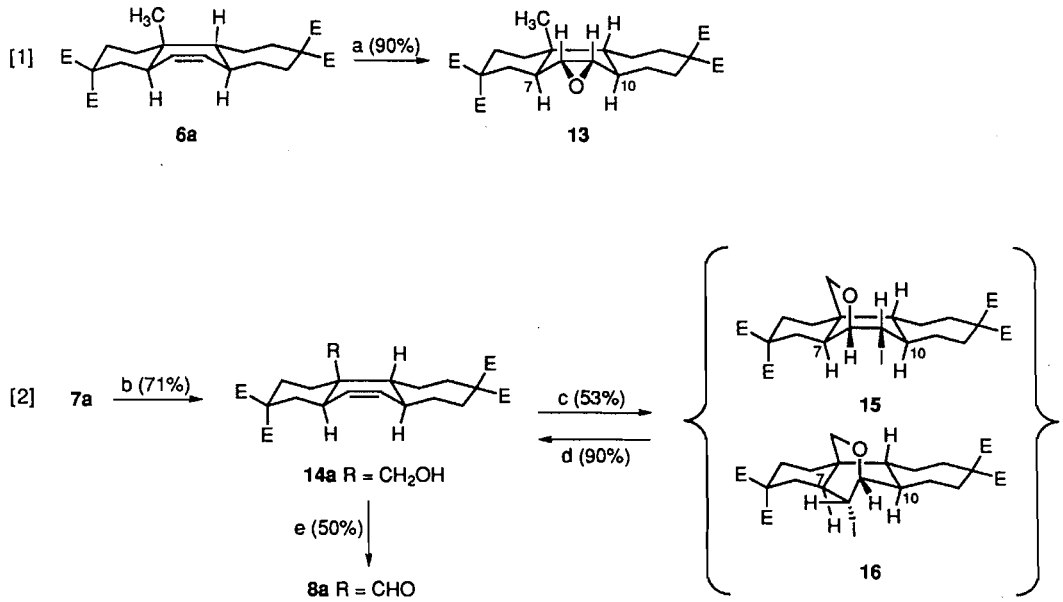

(a) NaH_2PO_4, CF_3CO_3H, $(ClCH_2)_2$, 0°C, 20 min. (b) conc. $HCl_{(aq.)}$ / H_2O / MeOH, 60-65°C, 12h.
(c) $NaHCO_3$, I_2, THF, rt, 2h. (d) Zn, conc. $AcOH_{(aq.)}$, rt, 2h. (e) NMO, TPAP, 4A m.s., CH_3CN, rt, 2h

substituent from C1 (pro-6.7) to C2 (pro-6.6) as in **6** and **7** should not affect the balance of steric interactions encountered in both transition states. Whether placed at C1 or C2, the substituent is not involved in any significant nonbonded interactions with the malonate moieties or any other group of rings A and C, hence explaining the comparable diastereoselection arising from macrocycles **9**, **6**, and **7**.

As for **9**, the *endo* (TST) stereochemistry of the major tricyclic product obtained from macrocycle **7** was confirmed by hydrolysis of **7a** and subjection of the resulting alcohol **14a** to conditions of iodoetherification (Scheme 7, eq. [2]). This could serve as well as a structure confirmation for **6a** since its ^1H nmr spectra is identical to those of **7a** and **14a** except for signals attributed to the C2 substituent. In contrast with **9a**, isomer **7a** led to the obtention of two inseparable cyclic iodoethers in a 4:3 ratio favoring the "normal" one (**15**) formed via a 5-membered ring closure at the proximal sp^2 carbon of **7a**. In this case, we believe that the minor iodoether **16** is observed because of the greater flexibility of the B.C.[6.7] ring junction in bringing the distal carbon (C9) close to the hydroxyl group, so that closure of the six-membered ring can take place. Compound **16** can adopt the stable conformation of a bicyclo[2.2.2] ring system and was readily differentiated from **15** on the basis of coupling constants from the C8 and C9 hydrogens (Scheme 7). The observed values are in agreement with the expected dihedral angles (ϕ) estimated by molecular model analysis.[11] Upon treatment in zinc – acetic acid suspension, the **15/16** mixture returned to the mother TST alcohol **7a** by reductive elimination.

[11] For **15**: ϕ H7CCH8 ~90°, J = 0 Hz; ϕ H8CCH9 ~90°, J = 0 Hz; ϕ H9CCH10 ~180°, J = 9.5 Hz. For **16**: ϕ H7CCH8 ~100°, J = 0 Hz; ϕ H8CCH9 ~30°, J = 2.5 Hz; ϕ H9CCH10 ~45°, J = 7.0 Hz.

Compared to macrocycle **10** and in contrast to the known behaviour of carbonyl-activated dienophiles, macrocycle **8** with an aldehyde function at the pro-6.6 position led to a decrease in *endo*-selectivity, giving a **8a/8b** ratio of 76:24 under thermal activation (Table 1, entries 7 and 8). This result is quite surprising on the basis of the aforementioned arguments according to which substrates **8** and **10** can be considered as sterically unbiased. However, the "asynchronous transition state" hypothesis still offers a satisfactory explanation. The shortest, and determining, incipient bond of unsymmetrical transition states arising from macrocycle **8** (Scheme 3; R^2 = CHO, R^1 = H) is now C1–C10, resulting in a situation the reverse of that encountered with macrocycle **10**. Therefore, it follows that the importance of steric interactions in the vicinity of C2 and C7 must be diminished, including the key pseudo-1,3-diaxial interaction that is taking place in the CSC transition state. As this steric interaction is weakened, the formation of a slightly greater proportion of CSC (*exo*) tricycle **8b** than of **6b** and **7b** is now clarified. This result is also a clear demonstration of the inhibition of *endo* stabilization at high temperatures.

It is known from the IMDA reaction (3) that the effect of Lewis acid catalysis is twofold: (*a*) secondary orbital interactions become substantially more important as a large increase in *endo* selectivity is generally observed; (*b*) the asynchronicity of bond formation is greatly enhanced. Both of these effects find their origin in the accentuation of the size difference already present between the LUMO coefficients on both the carbonyl and the olefin (16). The use of tin tetrachloride for activating the TADA reaction of macrocycle **8** led to a rise in *endo* selectivity with an **8a/8b** ratio of 87:13 obtained (entry 10). The intrinsically stronger Lewis acid (21), boron trifluoride etherate, allowed the reaction to proceed slowly at room temperature, with the associated advantage of a better dia-

Can. J. Chem. Downloaded from www.nrcresearchpress.com by 80.90.12.36 on 09/08/12
For personal use only.

Can. J. Chem. Downloaded from www.nrcresearchpress.com by 80.90.12.36 on 09/08/12
For personal use only.

stereomer bias standing at 95:5 (entry 11). Also, this result is still in line with a corresponding enforcement of *endo* stabilization through temperature lowering. Thus, the first of the two effects described above tends to overcome the latter since increased asynchronicity leading to a longer C2—C7 forming bond translates into a reduced ester–C8 interaction in the CSC transition state.

Also, the TADA reaction of macrocyclic triene **8** is significantly slower than that of **10**, as exemplified by entries 2 and 8 (thermal) and entries 3 and 4 and 9–11 (Lewis acid catalyzed). In particular, tin tetrachloride failed to cause any reaction of **8** at room temperature whereas **10** reacted completely in less than 2 h under the same conditions. Assuming that a six-membered ring closure is faster than that of a seven-membered ring at transition state level, this observation is also in line with the above theoretical arguments. Indeed, the TADA reaction of **10** gives rise to the six-membered ring A by closure at the most advanced bonding site (C2—C7) whereas the fastest developing bond of **8** (C1—C10) involves rather the disfavored seven-membered ring C closure. Clearly, only an asynchronous mechanism can account for such observations.[12]

As expected, the major TST (*endo*) product **8a** showed the doublet signal (J = 1.0 Hz) diagnostic of *trans* stereochemistry for the aldehyde ^{1}H nmr resonance whereas CSC aldehyde appeared as a singlet. Futhermore, tricycle **8a** was chemically correlated to **7a** by oxidation (22) of **14a** (Scheme 7). Finally and most importantly, the less favored CSC tricycle **8b** was heated at 210°C for 5 h and remained unchanged. This control experiment served in ascertaining the kinetic nature of the diastereomeric ratios resulting from the TADA reactions described in this article.

Scheme 8.

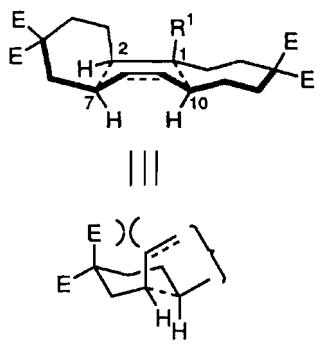

CAT (*endo*) transition state

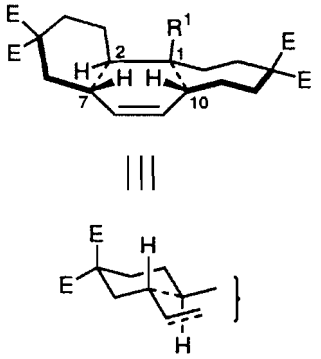

TAC (*exo*) transition state

TADA reaction of pro-6.7-substituted TTT macrocyclic substrates 4 and 5

In principle, macrocyclic trienes **4** and **5** can lead to a *cis-anti-trans* (CAT) tricycle via an *endo* approach and a *trans-anti-cis* (TAC) diastereomer from an *exo* approach (Scheme 8). Actually, the TAC tricycle **4a** was found to dominate over CAT **4b** by a 78:22 ratio in the thermal reaction of macrocycle **4** (Table 2, entry 1). In this case, the pseudo-1,3-diaxial interaction due to one of the ester functions of ring A is now present in the *endo* transition state (Scheme 8). The absence of a similar steric interaction in the *exo* transition state explains the preponderance of the corresponding TAC tricycle **4a**. The resulting tricycles **4a** and **4b** could not be separated on silica gel plates even with many attempts under various solvent systems. Hydrolysis of the MOM ether of the **4a/4b** mixture gave pure TAC tricyclic alcohol **17a** and pure CAT diastereomer **17b** (Scheme 9) after separation by preparative thin-layer chromatography. The major TAC tricyclic alcohol **17A** was oxidized with pyridinium chlorochromate (23) to give aldehyde **5a**. The proton nmr signal of the aldehyde hydrogen showed the expected singlet since no W arrangement is possible with the C10 methine hydrogen in this TAC stereochemistry.

The TTT formyl-substituted macrocyclic triene **5** gave a similar diastereomeric ratio of 77:23, again favoring TAC tricycle **5a** over CAT tricycle **5b** when heated at 320°C for 1.5 min (Table 1, entry 2). Unfortunately, the crude mixture was accompanied by ca. 40% of TST tricycle **10a**. The latter tricycle formed after in situ thermal isomerization of TTT macrocycle **5** to the TTC geometrical isomer **10**, as discussed thoroughly in the preceding paper (Part I). This process, which might also be promoted by the glass wall acidic sites, was even more important at lower temperatures for longer times (entry 3). However, the extent of this undesirable isomerization reaction could be limited by making use of Lewis acid catalysis at room temperature (entry 5). A **5a/5b** ratio of 84:16, close to the ratio observed in the uncatalyzed thermal reaction examined above, was obtained under aluminium trichloride catalysis. The decreased proportion of CAT tricycle **5b** can be attributed to the strengthening of the aforementioned 1,3-diaxial interaction present in the CAT transition state (Scheme 8), caused by the enhancement of asynchronicity induced by Lewis acid complexation. Again, contrary to **5a**, the possibility of having a W arrangement with C10—H made the minor tricyclic product **5b** show a typical doublet (J = 1.0 Hz) for the ^{1}H nmr signal of the aldehyde hydrogen.

TADA reaction of pro-6.6-substituted TTT macrocyclic substrates 1, 2, and 3

Macrocyclic trienes **1–3** can theoretically afford the TAC tricycle (*endo* approach) and the CAT diastereomeric tricycle (*exo* approach). Methyl-substituted marcocycle **1** and MOMO-methyl-substituted analog **2** both have moderate yields and similar diastereomeric ratios (~90:10) favoring TAC tricyclic products **1a** and **2a** over CAT tricycles **1b** and **2b** (Table 2, entries 6 and 7). Inspection of the CAT transition state (Scheme 10) reveals a severe 1,3-diaxial steric interaction

[12] The mechanistic consequences related to this phenomenon will be soon communicated as a detailed kinetic study.

Scheme 9. Chemical derivatization for pro-6.7 substituted TAC and CAT tricycles.

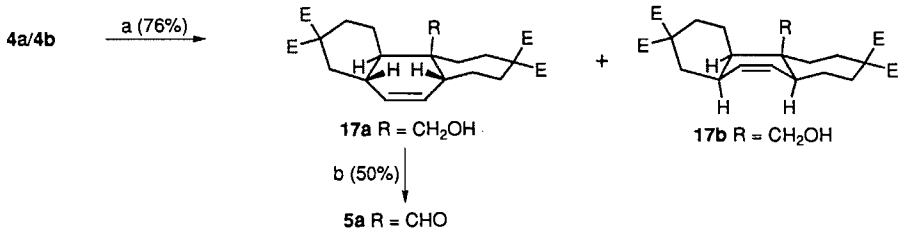

(a) conc. $HCl_{(aq.)}$ / H_2O / MeOH, 65-70°C, 2.5h. (b) NaOAc, PCC, 3A m.s., CH_2Cl_2, rt, 1h

Scheme 10.

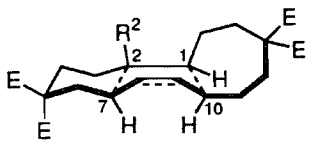

TAC (*endo*) transition state

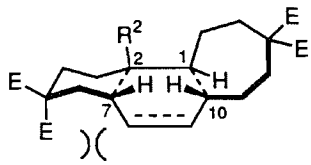

CAT (*exo*) transition state

between the pseudo-axial ester function of ring A in a chair conformation and a sp^2 carbon (C8) of ring B. This interaction being absent in the TAC transition state leading to **1a** and **2a**, the ratio in favor of these tricycles is readily understood. The second pair (**2a** and **2b**) was not separable on silica gel but recrystallization of the diastereomeric mixture afforded nice pure monocrystals of TAC tricycle **2a**, for which the stereochemistry was confirmed by X-ray diffraction analysis (24). Since ^1H nmr spectra of **1a** and **2a**, and **1b** and **2b**, were identical in all respects except for the C2 substituent, this proof of structure served as well for the methyl-substituted series. Moreover, the half-widths of the C2-methyl singlets of **6a** and **6b**, which measured, respectively, 2.0 and 1.0 Hz, are in line with an expected signal broadening due to long-range W coupling with H-C7 in such *trans*-decalin systems as TST **6a** (19). The **2a/2b** mixture was also characterized through hydrolysis of the MOM protecting group and facile separation of the corresponding alcohols **18a** and **18b** (Scheme 11).

As for its regioisomer **5**, enal inversion remained an unsolved problem for the TADA reaction of TTT formyl-substituted macrocyclic triene **3** (Table 2, entries 8–11). Although TAC tricycle **3a** was the exclusive TADA product from macrocycle **3**, it was also accompagnied by tricycles **8a** and **8b** originating from TTC macrocyclic triene **8** formed in situ. As for the TTC series, the Lewis acid catalyzed reaction (entries 10 and 11) was slower in the case of pro-6.6-activation than for **5** (entries 4 and 5), and the higher temperature required for the TADA reaction of **3** resulted in complete isomerization to **8** and isolation of its corresponding tricycles **8a** and **8b**. This unwanted competing process confers little synthetic potential upon the present example of TTT macrocycle **3**. However, its stereospecific conversion to TAC tricycle **3a** is doubtlessly valuable from a theoretical point of view. In analogy with the thermal TADA reaction of TTC macrocycle **8**, this result can also be rationalized with the asynchronous transition state hypothesis. Indeed, the presence of a formyl substituent (R^2) at the pro-6.6 position (Scheme 10) results in transition states having a short C1—C10 and a longer C2—C7 distance, a logical consequence of faster bonding development at the site bearing the larger β-LUMO coefficient. The magnitude of steric interactions around the short C1—C10 incipient bond is then raised, conferring upon the B.C.[6.7] ring junction a decisive role in transition state discrimination. When such a situation exists, as for **8**, an increased trend toward obtaining a *cis* B.C.[6.7] ring junction is observed.[13] Compared to unactivated macrocycles **1** and **2**, this elusive factor further favors the TAC transition state leading to **3a**. The absence of CAT tricycle **3b** in the crude nmr spectra was confirmed by its indirect synthesis, which was carried out through oxidation of **18b** with tetra-*n*-propylammonium perruthenate (TPAP) (22). Pure TAC tricycle **3a** was obtained in a similar fashion from alcohol **18a**. With the secured X-ray structure of **2a** in hand, these chemical derivatization efforts proved the reliability of our ^1H nmr argument concerning the multiplicity of aldehyde protons that was exploited throughout this study. A clear doublet (J = 1.5 Hz) was indeed observed for the aldehyde signal of **3a** whereas **3b** exhibited a sharp singlet.

Conclusion

In contrast to the 14-membered macrocyclic trienes, the 15-membered homologs described herein were isolable and showed that an additional methylene group makes a significant difference in reactivity, indicating that proximity effects play a key role in the TADA reaction. A systematic study of dienophile substituent effects enables us to answer questions about the factors governing the stereochemical outcome of the cycloaddition reaction. Thus, only one substituent, such as an ester, along the tethering chains is necessary to exert a strong stereodirecting effect and favor either of the two possible approaches (*endo* or *exo*). Moreover, it was found that a formyl substituent on the dienophile can alter the geometry of the transition state, thereby influencing the extent of steric interactions and thus leading to different diastereomeric excess compared to unactivated cases. These observations can be considered as additional evidence for the asynchronous transition state theory. In particular, Lewis acid catalyzed

[13] Owing to their superior conformational flexibility, bicyclo[6.7] systems do not seem to have a clear preference for a *trans* ring junction as in the more rigid decalin series.

Can. J. Chem. Downloaded from www.nrcresearchpress.com by 80.90.12.36 on 09/08/12
For personal use only.

Scheme 11. Chemical derivatization for pro-6.6 substituted TAC and CAT tricycles.

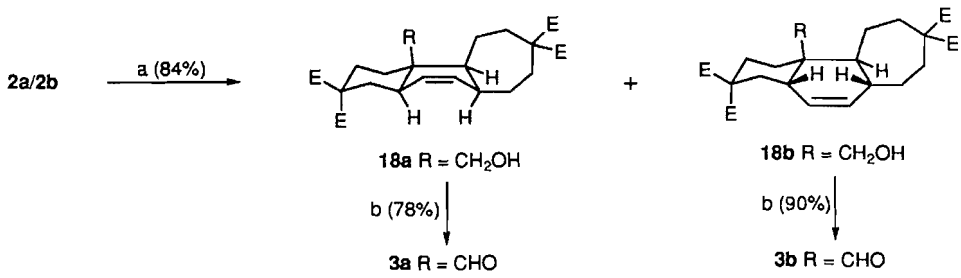

(a) conc.$HCl_{(aq.)}$ / H_2O / MeOH, 60-65°C, 12h. (b) NMO, TPAP, 4A m.s., CH_3CN, rt, 1h

Diels–Alder reactions were performed for the first time at the transannular level and were shown again to have a tremendous accelerating effect.

The work reported herein further extends the scope of the transannular Diels–Alder reaction for the stereoselective preparation of A.B.C.[6.6.7] tricyclic compounds. The power of this strategy, coupled with the ease with which rings can now be made, makes it very appealing for natural products syntheses. Such applications are presently underway in our laboratory.

Experimental section

General

The reader is referred to this section in the preceding paper (Part I). Lewis acids such as $SnCl_4$ and BF_3OEt_2 were purchased from Aldrich Chemical Co. and used without further purification. The diastereomer ratios were evaluated by measuring peak height and surface of representative signals on the ^1H nmr spectra of crude reaction mixtures.

Model procedures for the TADA reactions

A. Noncatalyzed thermal reactions in sealed tubes (ref. 25)

A clean Pyrex tube (20 cm long, exterior diameter 9 mm, interior diameter 5 mm; quartz was used for reactions with low boiling point solvents at T >250°C) was washed with ammonium hydroxyde, rinsed with distilled water, and oven and flame dried. The macrocyclic triene was added[14] and the tube was sealed under vacuum. For reactions using solvent, 0.5–1.0 mL were inserted and sometimes small quantities of a tertiary amine were added as an acid scavenger.[15] The tube was heated in a temperature-controlled oven for a given time and allowed to cool to room temperature, after which it was opened. The contents were transferred in a flask with diethyl ether and concentrated. The crude product was purified as indicated.

B. Lewis acid-catalyzed reactions

To a stirred solution of the formyl-substituted macrocyclic triene in a given anhydrous solvent at room temperature was added the Lewis acid (generally 3.0 equiv.). The mixture was stirred at the desired temperature for a given time and a solution of aqueous saturated sodium bicarbonate was added at room temperature (for small-scale reactions, a few drops may be added and the mixture directly purified by flash chromatography over a silica gel column). The mixture was extracted four times with diethyl ether or ethyl acetate and the combined organic layers were dried with anhydrous magnesium sulfate, filtered, and concentrated. The crude product was analyzed and purified as indicated.

TADA reaction of macrocycle ***9****: mixture of (7,2-*trans*-2,1-*syn*-1,10-*trans*)-1-(methoxymethoxy)methyl-5,5,13,13-tetrakis(methoxycarbonyl)-tricyclo[8.5.0.0^{2,7}]pentadec-8-ene* ***9a*** *and (7,2-*cis*-2,1-*syn*-1,10-*cis*)-1-(methoxymethoxy)methyl-5,5,13,13-tetrakis(methoxycarbonyl)-tricyclo[8.5.0.0^{2,7}]pentadec-8-ene* ***9b***

Following general procedure A, TTC macrocycle triene **9** (0.210 g, 0.41 mmol) was heated in toluene (1.0 mL) at 200°C for 3.0 h, yielding a crude mixture of tricyclic products **9a** and **9b** (0.22 g, quant., ratio: **9a**:**9b** = 85:15). Preparative thin-layer chromatography purification (20 cm × 20 cm, 4 plates, 0.05 cm thickness, 30% ethyl acetate in hexanes, three elutions) gave a pure mixture of **9a** and **9b** (0.184 g, 88%, viscous oil). These tricyclic products were found inseparable even under various solvent systems. They were individually characterized as their alcohol derivatives **11a** and **11b** (see below).

TST **9a**/CSC **9b**: ir (neat): 2980–2820, 1730 (br) cm^{-1}; ^1H nmr (300 MHz, $CDCl_3$) δ (ppm) (unless indicated, similar peaks arising from both diastereomers are superimposed and indistinguishable): 5.56 (1H, br d, *J* = 9.0 Hz, -*H*C=CH- **9a**), 5.51 (1H, br d, *J* = 9.0 Hz, -HC=C*H*- **9a**), 5.42 (1H, ddd, *J* 10.0 Hz, 2.5 Hz, 2.5 Hz, -*H*C=CH- **9b**), 5.28 (1H, br d, *J* = 10.0 Hz, -HC=C*H*- **9b**), 4.54 (2H, AB m, -OCH_2O-), 3.77 (3H, s, -CO_2CH_3 **9b**), 3.76 (3H, s, -CO_2CH_3 **9a**), 3.72 (1H, d, *J* = 10.0 Hz, -*H*CHOMOM **9b**), 3.72 (3H, s, -CO_2CH_3 **9a**), 3.70 (6H, s, -CO_2CH_3 **9a**), 3.69 (3H, s, -CO_2CH_3 **9b**), 3.68 (3H, s, -CO_2CH_3 **9b**), 3.67 (3H, s, -CO_2CH_3 **9b**), 3.58 (1H, d, *J* = 9.0 Hz, -HCHOMOM **9a**), 3.32 (3H, s, -OCH_3), 3.26 (1H, d, *J* = 10.0 Hz, -HC*H*OMOM **9b**), 3.12 (1H, d, *J* = 9.0 Hz, -HC*H*OMOM **9a**), 2.65–1.15 (17H, m, other -CH_2- and -CH- from both diastereomers); ms *m/e*: 495 (M^+-CH_3), 478 (M^+-CH_3OH), 435 ($M^+-CH_3OCH_2OH$). Exact Mass calcd. for $C_{25}H_{35}O_{10}$: 495.2230; found: 495.2211 ± 0.0014.

*(7,2-*trans*-2,1-*syn*-1,10-*trans*)-1-Hydroxymethyl-5,5,13,13-tetrakis(methoxycarbonyl)-tricyclo[8.5.0.0^{2,7}]pentadec-8-ene* ***11a*** *and (7,2-*cis*-2,1-*syn*-1,10-*cis*)-1-hydroxymethyl-5,5,13,13-tetrakis(methoxycarbonyl)-tricyclo[8.5.0.0^{2,7}] pentadec-8-ene* ***11b***

The above mixture of tricyclic methoxymethyl ethers **9a**/**9b**

[14] Dry dichloromethane can be used as a transfer solvent and evaporated under the positive pressure of a nitrogen stream; the tube is then vacuum pumped for >1 h.

[15] This practice did not have any effect on diastereoselectivity. Furthermore, radical inhibitors were found to be unnecessary.

Can. J. Chem. Downloaded from www.nrcresearchpress.com by 80.90.12.36 on 09/08/12
For personal use only.

Can. J. Chem. Downloaded from www.nrcresearchpress.com by 80.90.12.36 on 09/08/12
For personal use only.

(0.182 g, 0.36 mmol) was stirred 5.0 h at 60–65°C in the following solvent system: concentrated aqueous hydrochloric acid – water–methanol (0.5:1.0:8.5, 5.0 mL). The mixture was allowed to cool to room temperature and quenched with a solution of acqueous saturated sodium bicarbonate (20 mL). The resulting mixture was extracted with diethyl ether (3 × 15 mL) and ethyl acetate (2 × 10 mL). The combined organic phases were dried over anhydrous magnesium sulfate, filtered, and concentrated, giving a crude mixture of alcohol derivatives TST **11a** and CSC **11b** (0.158 g, 95%, ratio **11a**:**11b** = 85:15, white foamy solid). These diastereomers could hardly be separated on a small scale (10 mg/plate) using the following preparative tlc conditions: 20 cm × 20 cm plate, 0.05 cm thickness, 25% diethyl ether in benzene, four elutions. For larger quantities, the chemical procedure described below was found more convenient.

TST **11a** (less polar): ir (neat): 3550 (br), 2950, 1730 cm^{-1}; ^1H nmr (300 MHz, $CDCl_3$) δ (ppm): 5.56 (2H, narrow AB m, -HC═CH-), 3.75 (3H, s, $-CO_2CH_3$), 3.71 (3H, s, $-CO_2CH_3$), 3.69 (6H, s, 2 × $-CO_2CH_3$), 3.59 (1H, d, *J* = 10.5 Hz, -*H*CHOH), 3.40 (1H, d, *J* = 10.5 Hz, -HC*H*OH), 2.61 (1H, dd, *J* = 10.0 Hz, 2.0 Hz) and 2.45 (1H, m) and 2.30–2.25 (2H, m) and 2.12–1.95 (2H, m) and 1.90–1.60 (8H, m) and 1.48–1.17 (4H, m) (other $-CH_2-$ and -CH-, -OH); ^{13}C NMR (75 MHz, $CDCl_3$) δ (ppm): 173.31, 172.64 (2), 171.44, 134.79, 133.38, 67.05, 57.22, 55.04, 52.61, 52.51, 46.76, 44.65, 44.34, 37.25, 35.73, 33.39, 32.33, 28.47, 27.80, 26.41, 25.93; ms *m/e*: 448 (M^+-H_2O), 435 (M^+-OCH_3). Exact Mass calcd. for $C_{25}H_{35}O_9$: 448.2097; found: 448.2093 ± 0.0013.

CSC **11b** (more polar): ir (neat): 3545 (br), 2955, 1730 cm^{-1}; ^1H nmr (300 MHz, $CDCl_3$) δ (ppm): 5.43 (1H, ddd, *J* = 10.0 Hz, 2.5 Hz, 2.5 Hz, -*H*C═CH-), 5.29 (1H, br d, *J* = 10.0 Hz, -HC═C*H*), 3.78 (3H, s, $-CO_2CH_3$), 3.693 (3H, s, $-CO_2CH_3$), 3.684 (3H, s, $-CO_2CH_3$), 3.678 (3H, s, $-CO_2CH_3$), 3.47 (1H, d, *J* = 11.0 Hz, -*H*CHOH), 3.37 (1H, d, *J* = 11.0 Hz, -HC*H*OH), 2.62 (1H, br s) and 2.58–2.45 (2H, m) and 2.40 (1H, dm, *J* = 11.0 Hz) and 2.28 (1H, ddd, *J* = 14.0 Hz, 9.0 Hz, 2.0 Hz) and 2.13 (1H, dd, *J* = 14.0 Hz, 5.5 Hz), and 2.02–1.85 (2H, m) and 1.75–1.20 (10H, m) (other $-CH_2-$ and -CH-, -OH); ^{13}C nmr (75 MHz, $CDCl_3$) δ (ppm): 173.14 (2), 171.99, 171.44, 132.27, 127.08, 64.64, 58.33, 52.86, 52.59, 52.43, 52.07, 42.15, 37.63, 37.06, 35.13, 32.17, 31.46, 27.52, 26.92, 24.74, 19.33; ms *m/e*: 448 (M^+-H_2O), 435 (M^+-OCH_3). Exact Mass calcd. for $C_{24}H_{32}O_8$: 448.2097; found: 448.2093 ± 0.0013.

*Iodoether **12** and CSC alcohol **11b***

To a stirred solution of the above mixture of tricyclic alcohols **11a/11b** (0.155 g, 0.33 mmol, ratio: **11a:11b** = 85:15) in tetrahydrofuran (3.0 mL) were successively added powdered sodium bicarbonate (0.17 g, 2.0 mmol) and iodine (0.51 g, 2.0 mmol). The mixture was stirred 3.0 h at room temperature, after which diethyl ether (50 mL) and a saturated aqueous solution of sodium thiosulfate (50 mL) were added. The phases were separated after the organic layer had faded out and the aqueous layer was extracted with diethyl ether (3 × 25 mL). The combined organic layers were washed with brine, dried over anhydrous magnesium sulfate, filtered, and concentrated. The residue was purified by flash chromatography (30% ethyl acetate in hexanes), yielding unreacted CSC tricyclic alcohol **11b** (19.1 mg, 12%, clear oil and TST tetracyclic iodoether **12** (0.138 g, 70%, white powder). No traces of iodoether originating from alcohol **11b** were found whereas alcohol **11a** was totally consumed (combined yield: 82%, isolated ratio **12**:**11b** = 85:15).

12: tlc: uv visible; ir (neat): 2950, 2860, 1740, 1730, 1430 cm^{-1}; ^1H nmr (300 MHz, $CDCl_3$) δ (ppm): 4.36 (1H, s, -O-CH-), 3.80 (3H, s, $-CO_2CH_3$), 3.72 (6H, s, 2 × $-CO_2CH_3$), 3.71 (3H, s, $-CO_2CH_3$), 3.66 (1H, d, *J* = 7.5 Hz, -*H*CHO-), 3.63 (1H, d, *J* = 9.0 Hz, -HC-I), 3.43 (1H, d, *J* = 7.5 Hz, -HC*H*O-), 2.78 (1H, br d, *J* = 12.0 Hz, and 3.58–3.43 (2H,m) and 2.30–2.12 (3H, m) and 1.97–1.18 (11H, m) (other $-CH_2-$ and -CH-); ^1H nmr (300 MHz, C_6D_6) δ (ppm): 4.48 (1H, s, -O-CH-), 3.69 (1H, d, *J* = 10.0 Hz, -HC-I), 3.55 (1H, d, *J* = 8.0 Hz, -*H*CHO-), 3.39 (3H, s, $-CO_2CH_3$), 3.30 (3H, s, $-CO_2CH_3$), 3.28 (3H, s, $-CO_2CH_3$), 3.27 (3H, s, $-CO_2CH_3$), 3.11 (1H, d, *J* = 8.0 Hz, -HC*H*O-), 3.01 (1H, ddd, *J* = 13.0 Hz, 2.5 Hz, 2.5 Hz, C6-H eq.), 2.59 (1H, ddd, *J* = 10.0 Hz, 2.5 Hz, 2.5 Hz, C4-H eq.), 2.43 (1H, dd, *J* = 13.5 Hz, 7.0 Hz) and 2.25 (1H, dd, *J* = 15.0 Hz, 10.0 Hz), and 2.07 (1H, *J* = 11.5 Hz, 11.5 Hz, 2.0 Hz) and 1.97 (1H, dd, *J* = 15.0 Hz, 8.0 Hz) and 1.85– 1.68 (2H, m) and 1.62–1.40 (5H, m) and 1.34 (1H, dddd, *J* 15.0 Hz, 6.5 Hz, 2.0 Hz, 2.0 Hz) and 1.14 (1H, ddd, *J* = 16.0 Hz, 13.0 Hz, 2.0 Hz) and 1.08–0.93 (2H, m) (other $-CH_2-$ and -CH-); ^{13}C nmr (75 MHz, $CDCl_3$) δ (ppm): 172.56, 171.94 (2), 171.06, 90.19, 81.37, 58.09, 54.97, 52.80, 52.58, 52.43, 46.00, 44.02, 43.91, 39.11, 37.25, 33.83, 32.33, 28.85, 26.73, 25.83, 23.69; ^{13}C nmr (75 MHz, C_6D_6) δ (ppm): 172.33, 172.04, 171.20 (2), 90.68, 81.27, 58.16, 55.34, 53.06, 52.20 (2), 52.11 (2), 46.05, 44.26 (2), 40.36, 37.84, 33.76, 32.86, 29,33, 27.12, 26.06; ms *m/e*: 561 (M^+-CH_3O), 465 (M^+-I). Exact Mass calcd. for $C_{23}H_{30}O_8I$: 561.0987; found: 561.0983 ± 0.0017.

*TST alcohol **11a** via reductive elimination of **12***

To a stirred solution of iodoether **12** (67.1 mg, 0.113 mmol) in glacial acetic acid (3.0 mL) was added powdered zinc (75 mg, 1.13 mmol). The mixture was stirred for 5.0 h at room temperature, after which it was filtered through a cotton plug (rinsed with dichloromethane). The filtrate was neutralized with a saturated aqueous solution of sodium bicarbonate (~5 mL) and extracted with dichloromethane (4 × 10 mL). The combined organic layers were washed with brine (3 mL), dried over anhydrous magnesium sulfate, filtered, and concentrated. The residue was purified by flash chromatography (50% ethyl acetate in hexanes), affording TST tricyclic alcohol **11a** (38.0 mg, 72% clear oil). This material gave ^1H nmr spectral data identical to those of the same compound obtained from methoxymethyl ether **9a** (see above).

*TADA reaction of macrocycle **10:** (7,2-*trans*-2,1-*syn*-1,10-*trans*)-1-formyl-5,5,13,13-tetrakis(methoxycarbonyl)-tricyclo[8.5.0.$0^{2,7}$]pentadec-8-ene **10a***

To a solution of TTC pro-6.7 formyl-substituted macrocyclic triene **10** (62.0 mg, 0.13 mmol) in dichloromethane (2.0 mL) was added tin tetrachloride (0.40 mL, 0.40 mmol, 1.0 M in dichloromethane). The clear yellowish solution was stirred at room temperature for 2.0 h, after which it was quenched with a solution of saturated aqueous sodium bicarbonate (5 mL) and diluted with diethyl ether (15 mL). The aqueous phase was extracted with diethyl ether (5 × 10 mL) and the combined organic layers were dried over anhydrous magnesium sulfate, filtered, and concentrated. The residue was purified by flash chromatography (30% ethyl acetate in hexanes), yielding TST

Can. J. Chem. Downloaded from www.nrcresearchpress.com by 80.90.12.36 on 09/08/12
For personal use only.

tricyclic aldehyde **10a** (53.0 mg, 85%, clear oil) with no observed traces of CSC diastereomer **10b**; ir (neat): 2960, 2860, 1735 cm^{-1}; ^1H nmr (300 MHz, $CDCl_3$) δ (ppm): 9.34 (1H, br s, -CHO), 5.68 (2H, AB m, -CH=CH-), 3.77 (3H, s, $-CO_2CH_3$), 3.73 (3H, s, $-CO_2CH_3$), 3.70 (3H, s, $-CO_2CH_3$), 3.68 (3H, s, $-CO_2CH_3$), 2.67 (1H, ddd, J = 13.0 Hz, 3.0 Hz, 3.0 Hz) and 2.47 (1H, m) and 2.30 (1H, m) and 2.25–1.10 (14H, m) (other $-CH_2-$ and -CH-); ^1H nmr (250 MHz, C_6D_6) δ (ppm): 9.17 (1H, d, J = 1.0 Hz, -CHO), 5.46 (2H, narrow AB m, -CH=CH-), 3.28 (3H, s, $-CO_2CH_3$), 3.27 (3H, s, $-CO_2CH_3$), 3.26 (3H, s, $-CO_2CH_3$), 3.25 (3H, s, $-CO_2CH_3$), 2.80 (1H, ddd, J = 13.5 Hz, 3.0 Hz, 3.0 Hz) and 2.58–2.45 (2H, m) and 2.40–0.90 (14H, m) (other $-CH_2-$and -CH-); ^{13}C nmr (75 MHz, $CDCl_3$) δ (ppm): 202.35, 172.90, 172.43,172.25, 171.12, 134.55, 133.95, 56.59, 55.47, 54.67, 52.65 (br), 44.77, 41.73, 37.22, 34.50, 31.90, 29.35, 27.36, 26.49, 23.87; ms *m/e*: 464 (M^+), 435 (M^+-CHO). Exact Mass calcd. for $C_{24}H_{32}O_9$: 464.2046; found: 464.2054 ± 0.0014.

*(7,2-*cis*-2,1-*syn*-1,10-*cis*)-1-Formyl-5,5,13,13-tetrakis (methoxycarbonyl)-tricyclo[8.5.0.0^{2,7}]pentadec-8-ene* ***10b***

To a stirred solution of CSC tricyclic alcohol **11b** (19.0 mg, 0.041 mmol) in dichloromethane (1.0 mL) was added the Dess–Martin periodinane (21.0 mg, 0.049 mmol). The mixture was stirred for 2.0 h at room temperature, then diluted with diethyl ether (15 mL) and saturated aqueous sodium bicarbonate solution (5 mL). Pentahydrated sodium thiosulfate was added (90 mg, 0.37 mmol) and the two-phase mixture was vigorously stirred until the ethereal layer became clear (~15 min). The phases were then separated and the organic layer was washed with saturated aqueous sodium bicarbonate solution (3 mL) and water (3 mL). The residue was purified by flash chromatography (30% ethyl acetate in hexanes), yielding pure formyl-substituted CSC tricycle **10b** (8.0 mg, 42%, foamy solid); ir (neat): 2955, 2865, 2695, 1730 cm^{-1}; ^1H nmr (300 MHz, $CDCl_3$) δ (ppm): 9.28 (1H, s, -CHO), 5.52 (1H, ddd, J = 10.0 Hz, 3.5 Hz, 3.5 Hz, -*H*C=CH-), 5.23 (1H, br d, J = 10.0 Hz, -HC=C*H*), 3.77 (3H, s, $-CO_2CH_3$), 3.69 (3H, s, $-CO_2CH_3$), 3.68 (3H, s, $-CO_2CH_3$), 3.66 (3H, s, $-CO_2CH_3$), 2.63–2.51 (2H, m) and 2.45 (2H, dm, J = 12.5 Hz) and 2.32–2.03 (3H, m) and 1.89 (1H, m) and 1.77–1.20 (9H, m) (other $-CH_2-$ and -CH-); ^1H nmr (300 MHz, C_6D_6) δ (ppm): 8.94 (1H, s, -CHO), 5.41 (1H, ddd, J = 10.0 Hz, 3.0 Hz, -*H*C=CH-), 5.38 (1H, ddd, J 10.0 Hz, 3.0 Hz, 3.0 Hz, -HC=C*H*-), 3.34 (3H, s, $-CO_2CH_3$), 3.33 (3H, s, $-CO_2CH_3$), 3.24 (3H, s, $-CO_2CH_3$), 3.23 (3H, s, $-CO_2CH_3$), 2.80–0.80 (17H, m, other $-CH_2-$ and -CH-); ^{13}C nmr (75 MHz, $CDCl_3$) δ (ppm): 203.97, 172.68, 172.42, 171.75, 171.12, 132.17, 126.27, 58.09, 54.98, 52.73, 52.61, 52.18, 37.99, 37.25, 37.00, 34.82, 32.89, 31.72, 27.10, 26.99, 25.37, 18.65; ms *m/e*: 464 (M^+), 446 (M^+-H_2O), 435 (M^+-CHO). Exact Mass calcd. for $C_{24}H_{32}O_9$: 464.2046; found: 464.2052 ± 0.0014.

TST alcohol ***11a*** *via reduction of* ***10a***

To a stirred solution of TST tricyclic aldehyde **10a** (7.0 mg, 0.015 mmol) in 1:1 tetrahydrofuran/methanol (0.6 mL) cooled to 0°C was added sodium borohydride (~1 mg, ~0.025 mmol). The mixture was stirred 30 min at 0°C, after which it was quenched by addition of a saturated aqueous ammonium chloride solution (2 mL) and extracted with diethyl ether (4 × 10 mL). The combined organic layers were washed with brine (5 mL), dried with anhydrous magnesium sulfate, filtered, and concentrated. Purification of the residue by flash chromatography on a small column (diethyl ether) afforded pure alcohol derivativ **11a** (6.3 mg, 90%). This material was found identical by ^1H nmr analysis to the same compound obtained from methoxymethyl ether **9a** (see above).

TADA reaction of macrocycle ***6****: (7,2-*trans*-2,1-*syn*-1,10-*trans*)-2-methyl-5,5,13,13-tetrakis(methoxycarbonyl)-tricyclo[8.5.0.0^{2,7}]pentadec-8-ene* ***6a*** *and (7,2-*cis*-2,1-*syn*-1,10-*cis*)-2-methyl-5,5,13,13-tetrakis(methoxycarbonyl)-tricyclo[8.5.0.0^{2,7}]pentadec-8-ene* ***6b***

Following general procedure A, neat TTC macrocyclic triene **6** (15.9 mg, 0.035 mmol) was heated at 200°C for 4.0 h, yielding a crude mixture of tricyclic products **6a** and **6b** (14.1 mg, 89%, ratio: **6a:6b** = 84:16). Preparative thin-layer chromatography purification (20 cm × 20 cm, 0.05 cm thickness, 10% ethyl acetate in carbon tetrachloride, five elutions) gave pure **6a** (9.0 mg, 57%, foamy solid) and pure **6b** (1.0 mg, 6%, foamy solid).

TST **6a** (less polar): ir ($CHCl_3$): 3000–2820, 1725 cm^{-1}; ^1H nmr (250 MHz, $CDCl_3$) δ (ppm): 5.59 (1H, ddd, J = 9.0 Hz, 2.5 Hz, -*H*C=CH-), 5.43 (1H, ddd, J = 9.0 Hz, 3.0 Hz, 3.0 Hz, -HC=C*H*), 3.74 (3H, s, $-CO_2CH_3$), 3.710 (3H, s, $-CO_2CH_3$), 3.707 (3H, s, $-CO_2CH_3$), 3.698 (3H, s, $-CO_2CH_3$), 2.41–2.17 (4H, m) and 2.02–1.16 (12H, m) and 0.93 (1H, m) (other $-CH_2-$ and -CH-); 0.73 (3H, s, $-CH_3$; ^1H nmr (250 MHz, C_6D_6) δ (ppm): 5.51 (1H, br d, J = 9.0 Hz, -*H*C=CH-), 5.42 (1H, br d, J = 9.0 Hz, -HC=C*H*-), 3.35 (2H, s, $-CO_2CH_3$), 3.34 (3H, s, $-CO_2CH_3$), 3.292 (3H, s, $-CO_2CH_3$), 3.285 (3H, s, $-CO_2CH_3$), 2.65 (1H, m) and 2.57–2.40 (2H, m) and 2.35 (1H, dddd, J = 14.5 Hz, 4.5 Hz, 4.5 Hz, 4.5 Hz) and 2.10–1.95 (4H, m) and 1.87–1.55 (6H, m) and 1.41–1.25 (1H, m) and 1.21 (1H, ddd, J = 13.0 Hz, 3.5, 3.5 Hz) and 0.90 (1H, ddd, J = 12.5 Hz, 7.5 Hz, 3.5 Hz) (other $-CH_2-$ and -CH-), 0.70 (3H, s, $-CH_3$); ms *m/e*: 450 (M^+), 435 (M^+-CH_3), 418 (M^+-CH_3OH). Exact Mass calcd. for $C_{24}H_{34}O_8$: 450.2253; found: 450.2246 ± 0.0013.

CSC **6b** (more polar): ir ($CHCl_3$): 3000–2840, 1725 cm^{-1}; ^1H nmr (250 MHz, $CDCl_3$) δ (ppm): 5.50 (1H, br dt, J = 11.0 Hz, 3.0 Hz, -*H*C=CH-), 5.32 (1H, br d, J = 11.0 Hz, -HC=C*H*), 3.75 (3H, s, $-CO_2CH_3$), 3.68 (9H, s, 3 × $-CO_2CH_3$), 2.6–0.8 (17H, m, other $-CH_2-$ and -CH-), 1.00 (3H, s, $-CH_3$); ^1H nmr (250 MHz, C_6D_6) δ (ppm): 5.42 (2H, narrow m, -HC=CH-), 3.38 (3H, s, $-CO_2CH_3$), 3.36 (3H, s, $-CO_2CH_3$), 3.29 (3H, s, $-CO_2CH_3$), 3.25 (3H, s, $-CO_2CH_3$), 2.74–2.60 (4H, m) and 2.45 (2H, m) and 2.2–1.0 (11H, m) (other $-CH_2-$ and -CH-), 0.79 (3H, s, $-CH_3$); ms *m/e*: 450 (M^+), 435 (M^+-CH_3), 418 (M^+-CH_3OH). Exact Mass calcd. for $C_{24}H_{34}O_8$: 450.2253; found: 450.2246 ± 0.0013.

rac*(8S,9R)-(7,2-*trans*-2,1-*syn*-1,10-*trans*)-2-Methyl-8,9-oxyranyl-5,5,13,13-tetrakis(methoxycarbonyl)-tricyclo[8.5.0.0^{2,7}]pentadecane* ***13***

To a stirred solution of TST tricycle **6a** (2.1 mg, 0.0046 mmol) and sodium dihydrogen phosphate monohydrate (3.5 mg, 0.025 mmol) in 1,2-dichloroethane (1.0 mL) cooled to 0°C was added trifluoroperacetic acid (9.9 mL, 0.0093 mmol, 0.94 M in 1,2-dichloroethane). After 20 min, the solids were filtered off and the solvents were concentrated. The residue was purified by flash chromatography (30% ethyl acetate in hexanes), yielding epoxide derivative **13** (2.0 mg, 90%); ir

Can. J. Chem. Downloaded from www.nrcresearchpress.com by 80.90.12.36 on 09/08/12
For personal use only.

($CHCl_3$): 1725 cm^{-1}; ^1H nmr (250 MHz, $CDCl_3$) δ (ppm): 3.75 (3H, s, $-CO_2CH_3$), 3.71 (9H, s, 3 × $-CO_2CH_3$), 2.78 (1H, dd, J = 9.0 Hz, 4.5 Hz, -HC-O-), 2.74 (1H, dd, J = 9.0 Hz, 4.5 Hz, -O-CH-), 2.56 (1H, ddd, J = 13.5 Hz, 4.0 Hz, 2.0 Hz) and 2.47–1.05 (16H, m, other $-CH_2-$ and -CH-), 0.96 (3H, s, $-CH_3$); ms *m/e* 466 (M^+), 451 (M^+-CH_3), 448 (M^+-H_2O), 434 (M^+-CH_3OH).

*TADA reaction of macrocycle 7: (7,2-*trans*-2,1-*syn*-1,10-*trans*)-2-(methoxymethoxy)methyl-5,5,13,13-tetrakis(methoxycarbonyl)-tricyclo[8.5.0.0^{2,7}]pentadec-8-ene **7a** and (7,2-*cis*-2,1-*syn*-1,10-*cis*)-2-(methoxymethoxy)methyl-5,5,13,13-tetrakis(methoxycarbonyl)-tricyclo[8.5.0.0^{2,7}]pentadec-8-ene **7b***

Following general procedure A, TTC macrocyclic triene **7** (11.0 mg, 0.021 mmol) in toluene (1.0 mL) was heated at 200°C for 3.0 h, yielding a crude mixture (12.0 mg) of tricyclic products **7a** and **7b**, along with one or more unknown macrocycles. Preparative thin-layer chromatography purification (20 cm × 20 cm, 0.05 cm thickness, 30% ethyl acetate in hexanes, two elutions) gave pure TST tricycle **7a** (6.6 mg, 55%, clear oil) and a more polar fraction (4.5 mg) containing one or more unknown macrocycles and presumably a weak proportion of CSC tricycle **7b**, for which no signals could be formally assigned from the ^1H nmr analysis of the mixture. All attempts in separating the compounds of this second fraction on silica gel were unsuccessful. However, its presence and approximate proportion were confirmed through the following sequence of reactions. MOM ether hydrolysis was carried out on the impure fraction using the conditions previously described in this article. The resulting crude mixture of alcohols was oxidized under standard conditions using *n*-tetrapropylammonium perruthenate, giving a crude mixture of aldehydes (homogeneous spot by tlc). The ^1H nmr analysis of this material showed, upon integration, a ca 15% proportion of CSC tricycle **8b** (see below for its formation from **8** and spectral characteristics). If this proportion was kept constant during the aforementioned transformations, the polar fraction originating from thermolysis of **7** contained ~0.7 mg (4.5 mg × 15%) of CSC tricycle **7b**, resulting in a **7a/7b** ratio of about 90:10.

TST **7a** (less polar): ir (neat): 2950, 1730 cm^{-1}; ^1H nmr (300 MHz, $CDCl_3$) δ (ppm): 5.60 (1H, ddd, J = 9.0 Hz, 2.5 Hz, 2.5 Hz, -*H*C=CH-), 5.40 (1H, ddd, J = 9.0 Hz, 3.0 Hz, 3.0 Hz, -HC=C*H*), 4.56 (1H, d, J = 6.5 Hz, -O*H*CHO-), 4.52 (1H, d, J = 6.5 Hz, -OHC*H*O-), 3.75 (3H, s, $-CO_2CH_3$), 3.71 (9H, s, 3 × $-CO_2CH_3$), 3.58 (1H, d, J = 9.5 Hz, *H*CHO-MOM), 3.33 (3H, s, $-OCH_3$), 3.07 (1H, d, J = 9.5 Hz, -HC*H*OMOM), 2.42–2.19 (4H, m) and 2.06–1.50 (10H, m) and 1.47–1.20 (3H, m) (other $-CH_2-$ and -CH-); ^{13}C nmr (75 MHz, $CDCl_3$) δ (ppm): 173.29, 172.77, 172.66, 171.62, 135.20, 130.53, 96.99, 69.47, 56.63, 55.33, 54.87, 52.67, 52.60, 52.54, 52.33, 46.42, 41.19, 40.73, 36.14, 33.35, 32.43, 31.95, 31.62, 26.76, 26.02, 25.81; ms *m/e*: 478 (M^+-CH_3OH), 448 (M^+-MOMOH). Exact Mass calcd. for $C_{25}H_{34}O_9$: 478.2203; found: 478.2200 ± 0.0014.

*(7,2-trans-2,1-syn-1,10-trans)-2-Hydroxymethyl-5,5,13,13-(7,2-*trans*-2,1-*syn*-1,10-*trans*)-2-Hydroxymethyl-5,5,13,13-tetrakis(methoxycarbonyl)-tricyclo[8.5.0.0^{2,7}]pentadec-8-ene **14a***

The TST tricyclic methoxymethyl ether **7a** (9.0 mg, 0.018 mmol) was stirred at 60–65°C for 12 h in the following solvent system: concentrated aqueous hydrochloric acid – water – methanol (0.5:1.0:8.5, 2.0 mL). The mixture was allowed to warm to room temperature and then quenched with a solution of aqueous saturated sodium bicarbonate (3 mL). The resulting mixture was extracted with diethyl ether (2 × 5 mL) and ethyl acetate (2 × 5 mL). The combined organic phases were dried over anhydrous magnesium sulfate, filtered, and concentrated. Purification by preparative thin-layer chromatography (20 cm × 20 cm, 0.05 cm thickness, 40% ethyl acetate in hexanes) afforded alcohol derivative **14a** (5.8 mg, 71%, clear oil); ir (neat): 3550 (br), 2950, 1730 cm^{-1}; ^1H nmr (300 MHz, $CDCl_3$) δ (ppm): 5.61 (1H, ddd, J = 9.5 Hz, 2.0 Hz, 2.0 Hz, -*H*C=CH-), 5.47 (1H, ddd, J = 9.5 Hz, 2.5 Hz, 2.5 Hz, -HC=C*H*-), 3.76 (3H, s, $-CO_2CH_3$), 3.75 (3H, s, $-CO_2CH_3$), 3.72 (3H, s, $-CO_2CH_3$), 3.71 (3H, s, $-CO_2CH_3$), 3.65 (1H, d, J = 10.5 Hz, -*H*CHOH), 3.37 (1H, d, J = 10.5 Hz, -HC*H*OH), 2.48–2.18 (4H, m) and 2.08–1.00 (14H, m) (other $-CH_2$ and -CH, -OH); ms *m/e*: 448 (M^+-H_2O), 435 (M^+-OCH_3). Exact Mass calcd. for $C_{24}H_{32}O_8$: 448.2097; found: 448.2093 ± 0.0013.

*Mixture of iodoethers **15** and **16***

To a stirred solution of TST tricyclic alcohol **14a** (3.0 mg, 0.0064 mmol) in tetrahydrofuran (0.5 mL) at room temperature were successfully added sodium bicarbonate (3.2 mg, 0.038 mmol) and crystalline iodine (10.0 mg, 0.038 mmol). The mixture was stirred at room temperature for 2.0 h, after which it was diluted with diethyl ether (20 mL) and extracted with a saturated aqueous sodium thiosulfate solution (5 mL). The organic layer was washed twice with brine (3 mL), dried over anhydrous magnesium sulfate, filtered, and concentrated. Purification of the residue by preparative thin-layer chromatography (10 × 20 cm, 0.05 cm thickness, 40% ethyl acetate in hexanes) afforded a pure inseparable mixture of tetracyclic iodoethers **15** and **16** (2.0 mg, 53%, ratio by ^1H nmr: **15/16** = 4:3).

15/16: tlc: uv visible; ir (neat): 2950, 1735 cm^{-1}; ^1H nmr (300 MHz, $CDCl_3$) δ (ppm): 4.38 (1H, s, -OCH- **15**), 4.07 (1H, d, J = 9.0 Hz, -*H*CHO- **16**), 3.94 (1H, d, J = 8.0 Hz, -*H*CHO- **15**), 3.84 (1H, dd, J = 7.0 Hz, 2.5 Hz, -OCH- **16**), 3.80 (3H, s, $-CO_2CH_3$ **16**), 3.78 (3H, s, $-CO_2CH_3$ **15**), 3.77 (3H, s, $-CO_2CH_3$ **15**), 3.73 (3H, s, $-CO_2CH_3$ **15**), 3.724 (3H, s, $-CO_2CH_3$ **16**), 3.716 (3H, s, $-CO_2CH_3$ **16**), 3.71 (3H, s, $-CO_2CH_3$ **16**), 3.70 (3H, s, $-CO_2CH_3$ **15**), 3.68 (1H, d, J = 9.5 Hz, -HC-I **15**), 3.47 (1H, d, J = 2.5 Hz, -HC-I **16**), 3.33 (1H, d, J = 8.0 Hz, -HC*H*O- **15**), 3.22 (1H, d, J = 9.0 Hz, -HC*H*O- **16**), 2.71 (1H, ddd, J = 13.5 Hz, 5.0 Hz, 2.0 Hz, C7-H **16**) 2.48−0.92 (33H, m, other $-CH_2-$ and -CH- from **15** and **16**); ms *m/e*: 561 (M^+-CH_3O), 465 (M^+-I). Exact Mass calcd. for $C_{23}H_{30}O_8I$: 561.0985; found: 561.0977 ± 0.0017.

*TST alcohol **14a** via reductive elimination of **15/16***

To a solution of tetracyclic iodoether mixture **15/16** (~1.5 mg, 0.0025 mmol) in glacial acetic acid (0.5 mL) was added powdered zinc (~2 mg, 0.025 mmol). The suspension was vigorously stirred for 2.0 h at room temperature, after which it was filtered over a cotton plug (rinsed with dichloromethane). The filtrate was neutralized with a solution of saturated aqueous sodium bicarbonate (5 mL) and the aqueous phase was extracted with dichloromethane (4 × 5 mL). The combined organic layers were washed with brine (3 mL), dried over anhy-

Can. J. Chem. Downloaded from www.nrcresearchpress.com by 80.90.12.36 on 09/08/12
For personal use only.

drous magnesium sulfate, filtered, and concentrated to give pure TST tricyclic alcohol **14a** (~1.5 mg, >90%). This material gave ^{1}H nmr spectral data identical to those of the same compound obtained from methoxymethyl ether **7a** (see above).

*TADA reaction of macrocycle **8**: (7,2-*trans*-2,1-*syn*-1,10-*trans*)-2-formyl-5,5,13,13-tetrakis(methoxycarbonyl)-tricyclo[8.5.0.0^{2,7}]pentadec-8-ene **8a** and (7,2-*cis*-2,1-*syn*-1,10-*cis*)-2-formyl-5,5,13,13-tetrakis(methoxycarbonyl)-tricyclo[8.5.0.0^{2,7}]pentadec-8-ene **8b***

Following general procedure A, neat pro-6.6 formyl-substituted TTC macrocyclic triene **8** (12.0 mg, 0.026 mmol) was heated at 200°C for 7.0 h, yielding a crude mixture of tricyclic products **8a** and **8b** (11.0 mg, 92%, ratio by ^{1}H nmr: **8a**:**8b** = 76:24). Preparative thin-layer chromatography purification (20 cm × 20 cm, 0.1 thickness, 35% ethyl acetate in hexanes, three elutions) gave pure TST tricycle **8a** (5.5 mg, 46%, clear oil) and CSC tricyclic diastereomer **8b** (1.5 mg, 13%).

TST **8a** (less polar): ir (neat): 2970, 2870, 1735 (br) cm^{-1}; ^{1}H nmr (250 MHz, $CDCl_3$) δ (ppm): 9.37 (1H, s, -CHO), 5.75 (2H, narrow AB m (s), -HC=CH-), 3.76 (3H, s, -CO_2CH_3), 3.71 (6H, s, 2 × -CO_2CH_3), 3.69 (3H, s, -CO_2CH_3), 2.57 (1H, m) and 2.50–1.20 (16H, m) (other -CH_2- and -CH-); ^{1}H nmr (250 MHz, C_6D_6) δ (ppm): 9.26 (1H, d, *J* = 1.5 Hz, -CHO), 5.49 (1H, ddd, *J* = 10.0 Hz, 2.0 Hz, 2.0 Hz, -*H*C=CH-), 5.42 (1H, ddd, *J* = 10.0 Hz, 2.0 Hz, 2.0 Hz, -HC=C*H*-), 3.36 (3H, s, -CO_2CH_3), 3.32 (3H, s, -CO_2CH_3), 3.28 (3H, s, -CO_2CH_3), 3.23 (3H, s, -CO_2CH_3), 2.73 (1H, ddd, *J* = 13.0 Hz, 2.5 Hz, 2.5 Hz) and 2.59–2.39 (2H, m) and 2.38–1.10 (14H, m) (other -CH_2- and -CH-); ^{13}C nmr (75 MHz, $CDCl_3$) δ (ppm): 203.84, 172.76, 172.19, 171.95, 171.20, 137.30, 130.99, 56.51, 54.80, 54.48, 52.78 (2), 46.98, 42.13, 35.69, 32.55, 32.42, 32.19, 29.82, 28.03, 25.03, 23:98; ms *m/e*: 464 (M^+), 435 (M^+−CHO). Exact Mass calcd. for $C_{24}H_{32}O_9$: 464.2046; found: 464.2035 ± 0.0014.

TST **8b** (more polar): ir (neat): 2970, 2860, 1740 (br) cm^{-1}; ^{1}H nmr (250 MHz, $CDCl_3$) δ (ppm): 9.40 (1H, s, -CHO), 5.56 (1H, ddd, *J* = 10.0 Hz, 2.5 Hz, 2.5 Hz, -*H*C=CH-), 5.39 (1H, ddd, *J* = ddd, *J* = 10.0 Hz, 2.5 Hz, 2.5 Hz, -HC=C*H*-), 3.75 (3H, s, -CO_2CH_3), 3.69 (3H, s, -CO_2CH_3), 3.68 (3H, s, -CO_2CH_3), 3.66 (3H, s, -CO_2CH_3), 2.80–1.15 (17H, m, other -CH_2- and -CH-); ^{1}H nmr (250 MHz, C_6D_6) δ (ppm): 8.99 (1H, s, -CHO), 5,39 (1H, br d, *J* = 10.0 Hz, -*H*C=CH-), 5.30 (1H, br d, *J* = 10.0 Hz, -HC=C*H*-), 3.33 (3H, s, -CO_2CH_3), 3.28 (3H, s, -CO_2CH_3), 3.27 (3H, s, -CO_2CH_3), 3.17 (3H, s, -CO_2CH_3), 2.70–1.20 (17H, m, other -CH_2- and -CH-); ms *m/e*: 464 (M^+), 435 (M^+−CHO). Exact Mass calcd. for $C_{24}H_{32}O_9$: 464.2046; found: 464.2035 ± 0.0014.

*TST aldehyde **8a** via oxidation of **14a***

To a stirred solution of TST tricyclic alcohol **14a** (3.0 mg, 0.0064 mmol) in acetonitrile (0.3 mL) at room temperature were successively added molecular sieves (4Å, 5 mg), *N*-methylmorpholine oxide (1 mg, 0.0096 mmol), and tetra-*n*-propylammonium perruthenate (a few crystals, cat.) The resulting mixture was stirred for 2.0 h and then concentrated to dryness. The residue was filtered over a small column of silica gel (application with dichloromethane) under the conditions of flash chromatography purification (30% ethyl acetate in hexanes), yielding pure TST 2-formyl-substituted tricycle **8a** (1.5 mg, 50%, foamy oil). This aldehyde was found identical by ^{1}H nmr analysis to the one obtained from the TADA reaction of macrocycle **8** (see above).

*TADA reaction of macrocycle **4**: mixture of (7,2-*trans*-2,1-*anti*-1,10-*cis*)-1-(methoxymethoxy)methyl-5,5,13,13-tetrakis(methoxycarbonyl)-tricyclo[8.5.0.0^{2,7}]pentadec-8-ene **4a** and (7,2-*cis*-2,1-*anti*-1,10-*trans*)-1-(methoxymethoxy)methyl-5,5,13,13-tetrakis(methoxycarbonyl)-tricyclo[8.5.0.0^{2,7}]pentadec-8-ene **4b***

Following general procedure A, neat TTT macrocyclic triene **4** (33.0 mg, 0.065 mmol) was heated at 200°C for 6.5 h, yielding a crude mixture of tricyclic products **4a** and **4b** (32.0 mg, 98%, ratio by ^{1}H nmr: **4a**:**4b** = 78:22). Preparative thin-layer chromatography purification (20 cm × 20 cm, 0.05 cm thickness, 30% ethyl acetate in hexanes, two elutions) gave a pure mixture of **4a** and **4b** (20.5 mg, 62%, oil) along with another fraction containing starting macrocyclic triene **4** (1.9 mg, 6%). These tricyclic products were found inseparable even under various solvent systems. They were individually characterized as their alcohol derivatives **17a** and **17b** (see below).

TAC **4a**/CAT **4b**: ir (neat): 2950–2820, 1750, 1740 cm^{-1}; ^{1}H nmr (300 MHz, $CDCl_3$) δ (ppm): 5.47 (1H, ddd, *J* = 9.5 Hz, 2.5 Hz, 2.5 Hz, -*H*C=CH **4a**), 5.32 (1H, br d, *J* = 9.5 Hz, -HC=C*H* **4a**), 5.50–5.25 (2H, m, -*H*C=C*H* **4b**), 4.60–4.47 (4H, m, -OCH_2O- **4b/4a**), 3.74 (3H, s, -CO_2CH_3 **4a**), 3.73 (3H, s, -CO_2CH_3 **4a**), 3.70 (6H, s, 2 × -CO_2CH_3 **4b**), 3.69 (6H, s, 2 × -CO_2CH_3 **4b**), 3.68 (6H, s, 2 × -CO_2CH_3 **4b**), 3.52 (1H, d, *J* = 10.5 Hz, -*H*CHOMOM **4b**), 3.43 (1H, d, *J* = 10.5 Hz, -HC*H*OMOM **4b**), 3.41 (1H, d, *J* = 9.5 Hz, -*H*CHOMOM **4a**), 3.33 (3H, s, -OCH_3 **4b**), 3.30 (3H, s, -OCH_3 **4a**), 3.25 (1H, d, *J* = 9.5 Hz, -HC*H*OMOM **4a**), 2.55–1.10 (34H, m, other -CH_2- and -CH- **4b/4a**); ^{1}H nmr (300 MHz, C_6D_6) δ (ppm): 5.44 (1H, br ddd, *J* = 9.0 Hz, 2.5 Hz, 2.5 Hz, -*H*C=CH- **4b**), 5.31 (2H, s, -*H*C=C*H*- **4a**), 5.18 (1H, br ddd, *J* = 9.0 Hz, 2.5 Hz, 2.5 Hz, -HC=C*H*- **4b**), 4.47 (1H, d, *J* = 6.5 Hz, -O*H*CHO- **4b**), 4.45 (1H, d, *J* = 6.5 Hz, -OHC*H*O- **4b**), 4.38 (1H, d, *J* = 6.5 Hz, -O*H*CHO- **4a**), 4.33 (1H, d, *J* = 6.5 Hz, -OHC*H*O- **4a**), 3.64 (1H, d, *J* = 10.0 Hz, -*H*CHOMOM **4b**), 3.56 (1H, d, *J* = 10.0 Hz, -*H*CHOMOM **4a**), 3.52 (1H, d, *J* = 10.0 Hz, -HC*H*OMOM **4b**), 3.37 (3H, s, -CO_2CH_3 **4a**), 3.36 (6H, s, 2 × -CO_2CH_3 **4b**), 3.32 (3H, s, -CO_2CH_3 **4b**), 3.30 (6H, s, 2 × -CO_2CH_3 **4a**), 3.26 (6H, s, -CO_2CH_3 **4a** and -CO_2CH_3 **4b**), 3.24 (3H, s, -OCH_3 **4b**), 3.22 (1H, d, *J* = 10.0 Hz, -HC*H*OMOM **4a**), 3.15 (3H, s, -OCH_3 **4a**), 2.8–0.8 (34H, m, other -CH_2- and -CH- **4b/4a**); ^{13}C nmr (75 MHz, $CDCl_3$) δ (ppm) (peaks without an annotation belong to **4a**, remaining peaks from **4b** are indistinguishable from the baseline): 172.67, 171.48, 131.63 (**4b**), 131.46, 130.86 (**4b**), 128.82, 97.13 (**4b**), 96.71, 71.55, 57.71, 55.17, 52.68, 52.52, 49.08, 43.56, 40.16, 37.88, 34.35, 32.37, 31.71, 29.68, 27.52, 25.80, 22.43, and many other minor peaks tentatively ascribed to **4b**: ms *m/e*: 495 (M^+−CH_3), 478 (M^+−CH_3OH), 465 (M^+−MOM). Exact Mass calcd. for $C_{25}H_{34}O_9$: 478.2203; found: 478.2197 ± 0.0014.

*(7,2-*trans*-2,1-*anti*-1,10-*cis*)-1-Hydroxymethyl-5,5,13,13-tetrakis(methoxycarbonyl)-tricyclo[8.5.0.0^{2,7}]pentadec-8-ene **17a** and (7,2-*cis*-2,1-*anti*-1,10-*trans*)-1-hydroxy methyl-5,5,13,13-tetrakis(methocycarbonyl)-tricyclo[8.5.0.0^{2,7}]pentadec-8-ene **17b***

The above mixture of tricyclic products **4a/4b** (6.0 mg,

Can. J. Chem. Downloaded from www.nrcresearchpress.com by 80.90.12.36 on 09/08/12
For personal use only.

0.012 mmol) was stirred at 65–70°C for 2.5 h in the following solvent system: concentrated aqueous hydrochloric acid – water – methanol (1:1:8, 1.0 mL). The mixture was allowed to cool to room temperature and then quenched with a solution of aqueous saturated sodium bicarborate (3 mL). The resulting mixture was extracted with ethyl acetate (2 × 10 mL) and the combined organic phases were washed with aqueous saturated ammonium chloride (2 mL), dried over anhydrous magnesium sulfate, filtered, and concentrated. The crude product was purified by preparative thin-layer chromatography (10 cm × 20 cm, 0.05 cm thickness, 30% ethyl acetate in hexanes, two elutions) yielding pure TAC alcohol derivative **17a** (3.2 mg, 58%, oil) and the CAT diastereomer **17b** (~1 mg, 18%).

TAC **17a**: R_f = 0.22 (50% ethyl acetate in hexanes); ir (neat): 3450 (br), 2960–2830, 1730 cm^{-1}; ^1H nmr (300 MHz, $CDCl_3$) δ (ppm): 5.52 (1H, br dm, J = 10.0 Hz, -*H*C═CH-), 5.35 (1H, br d, J = 10.0 Hz, -HC═C*H*-), 3.74 (6H, s, 2 × -CO_2CH_3), 3.70 (3H, s, -CO_2CH_3), 3.69 (3H, s, -CO_2CH_3), 3.55 (1H, d, J = 11.0 Hz, -*H*CHOH), 3.46 (1H, d, J = 11.0 Hz, -HC*H*OH), 2.58–2.38 (2H, m) and 2.25–0.80 (16H, m) (other -CH_2- and -CH-, -OH); ^1H nmr (300 MHz, C_6D_6) δ (ppm): 5.30 (2H, narrow AB m, -HC═CH-), 3.36 (3H, s, -CO_2CH_3), 3.35 (3H, s, -CO_2CH_3), 3.31 (3H, s, -CO_2CH_3), 3.30 (1H, d, J = 10.5 Hz, -*H*CHOH), 3.26 (3H, s, -CO_2CH_3), 3.11 (1H, d, J = 10.5 Hz, -HC*H*OH), 2.75–2.55 (4H, m) and 2.33 (2H, m) and 2.12 (1H, br t, J = 11.0 Hz) and 2.05–1.20 (10H, m) and 1.16 (1H, td, J = 12.0 Hz, 4.5 Hz) (other -CH_2- and -CH-, -OH); ^{13}C nmr (75 MHz, $CDCl_3$) δ (ppm): 174.08, 173.71, 173.11, 131.62, 129.07, 66.46, 55.12, 52.68, 52.55, 43.26, 40.89, 37.93, 34.35, 32.37, 29.70, 27.68, 27.55, 25.96, 25.72, 22.87, 22.43; ms *m/e*: 466 (M^+), 448 (M^+-H_2O), 435 (M^+-OCH_3). Exact Mass calcd. for $C_{24}H_{34}O_9$: 466.2203; found: 466.2195 ± 0.0014.

CAT **17b**: R_f = 0.30 (50% ethyl acetate in hexanes); ir (neat): 3500 (br), 2950–2820, 1730 cm^{-1}; ^1H nmr (300 MHz, C_6D_6) δ (ppm): 5.43 (1H, br d, J = 10.5 Hz, -*H*C═CH-), 5.17 (1H, ddd, J = 10.5 Hz, 2.5 Hz, 2.5 Hz, -HC═C*H*-), 3.49 (1H, d, J = 11.0 Hz, -*H*CHOH), 3.36 (3H, s, -CO_2CH_3), 3.35 (3H, s, -CO_2CH_3), 3.32 (3H, s, -CO_2CH_3), 3.30 (3H, s, -CO_2CH_3), 3.26 (1H, d, J = 11.0 Hz, -HC*H*OH), 2.7–0.8 (18H, m, other -CH_2 and -CH-, -OH); ms *m/e*: 466 (M^+), 448 (M^+-H_2O), 435 (M^+-OCH_3). Exact Mass calcd. for $C_{24}H_{34}O_9$: 466.2203; found: 466.2195 ± 0.0014.

(7,2-trans-*2,1*-anti-*1,10*-cis*)-1-Formyl-5,5,13,13-tetrakis-(methoxycarbonyl)-tricyclo[8.5.0.0^{2,7}]pentadec-8-ene* ***5a***

To a stirred solution of TAC tricyclic alcohol **17a** (~2 mg, 0.004 mmol) in dichloromethane (0.5 mL) at room temperature were successively added powdered molecular sieves (3 Å, 1 mg), sodium acetate (2–3 crystals), and pyridinium chlorochromate (2.0 mg, 0.009 mmol). The mixture was stirred 1.0 h at room temperature, then diluted with ethyl acetate and filtered over a small Florisil column (rinsed with ethyl acetate). The filtrate was concentrated, yielding formyl-substituted TAC tricycle **5a** (<1 mg, ~50%, δ CHO: 9.41 ppm (1H, s)), identical with the **5a** originating from the reaction of macrocycle **5** described below.

TADA reaction of macrocycle ***5****: mixture of (7,2*-trans-*2,1*-anti-*1,10*-cis*)-1-formyl-5,5,13,13-tetrakis(methoxycarbonyl)-tricyclo[8.5.0.0^{2,7}]pentadec-8-ene* ***5a*** *and CAT* ***5b***

Following general procedure B, formyl-substituted macrocyclic triene **5** (5.0 mg, 0.011 mmol) in dichloromethane (0.5 mL) was treated with aluminium trichloride (excess, >3 equiv.) for 2.0 h at room temperature. The crude product (silica gel filtered, product ratio **5a**:**5b**:**5** = 6:1:1 with minor amounts of **10** and **10a** originating from isomerization of **5**) was purified by preparative thin-layer chromatography (8 cm × 20 cm, 0.05 cm thickness, 30% ethyl acetate in hexanes, two elutions), yielding an inseparable mixture of tricyclic products TAC **5a**/CAT **5b** (3.0 mg, ~60%, ratio **5a**:**5b** = 5.3:1) and a more polar band (uv–visible) containing unreacted **5** (1 mg, ~20%).

TAC **5a**/CAT **5b**: ir (neat): 2980–2820, 2740, 1730 cm^{-1}; ^1H nmr (300 MHz, $CDCl_3$) δ (ppm) (unless indicated, similar peaks arising from both diastereomers are superimposed and indistinguishable): 9.57 (1H, s, -CHO), 5.64 (1H, ddd, J = 10.0 Hz, 5.0 Hz, 2.5 Hz, -*H*C═CH-), 5.42 (1H, br d, J = 10.0 Hz, -HC═C*H*), 3.78 (3H, s, -CO_2CH_3 **5b**), 3.76 (3H, s, -CO_2CH_3 **5a**), 3.75 (3H, s, -CO_2CH_3 **5b**), 3.73 (3H, s, -CO_2CH_3 **5a**), 3.72 (3H, s, -CO_2CH_3 **5b**), 3.70 (3H, s, -CO_2CH_3 **5a**), 3.68 (3H, s, -CO_2CH_3 **5a**), 2.8–0.8 (17H, m, other -CH_2- and -CH- from both diastereomers); ^1H nmr (300 MHz, C_6D_6) δ (ppm): 9.81 (1H, d, J = 1.0 Hz, -CHO **5b**), 9.41 (1H, s, -CHO **5a**), 5.43 (1H, ddd, J = 10.0 Hz, 2.5 Hz, 2.5 Hz, -*H*C═CH- **5b**), 5.33 (1H, ddd, J = 10.0 Hz, 4.0 Hz, 2.0 Hz, -*H*C═CH- **5a**), 5.25 (1H, br d, J = 10.0 Hz, -HC═C*H*- **5a**), 5.22 (1H, dm, J = 10.0 Hz, HC═C*H*- **5b**), 3.35 (3H, s, -CO_2CH_3 **5a**), 3.330 (3H, s, -CO_2CH_3 **5b**), 3.327 (3H, s, -CO_2CH_3 **5b**), 3.28 (3H, s, -CO_2CH_3 **5a**), 3.270 (3H, s, -CO_2CH_3 **5a**), 3.264 (3H, s, -CO_2CH_3 **5b**), 3.25 (3H, s, -CO_2CH_3 **5b**), 3.23 (3H, s, -CO_2CH_3 **5b**), 2.7–0.9 (34H, m, other -CH_2- and -CH- from both diastereomers); ms *m/e*: 464 (M^+), 446 (M^+-H_2O), 435 (M^+-CHO). Exact Mass calcd. for $C_{24}H_{32}O_9$: 464.2046; found: 464.2052 ± 0.0014.

TADA reaction of macrocycle ***1****: (7,2*-trans-*2,1*-anti-*1,10*-cis*)-2-methyl-5,5,13,13-tetrakis(methoxycarbonyl)-tricyclo[8.5.0.0^{2,7}]pentadec-8-ene* ***1a*** *and (7,2*-cis-*2,1*-anti-*1,10*-trans*)-2-methyl-5,5,13,13-tetrakis(methoxycarbonyl)-tricyclo[8.5.0.0^{2,7}]pentadec-8-ene* ***1b***

Following general procedure A, neat TTT macrocyclic triene **1** (10.0 mg, 0.022 mmol) was heated at 200°C for 4.5 h, yielding a crude mixture of tricyclic products **1a** and **1b** (10 mg, ~100%, ratio: **1a**:**1b** = 88:12). Preparative thin-layer chromatography purification (20 cm × 20 cm, 0.05 cm thickness, 3% ethyl acetate in toluene, four elutions) gave pure **1a** (5.2 mg, 52%, foamy solid) and pure **1b** (1.1 mg, 11%, foamy solid).

TAC **1a** (less polar): ir ($CHCl_3$): 3000–2850, 1725 cm^{-1}; ^1H nmr (250 MHz, $CDCl_3$) δ (ppm): 5.56 (1H, br d, J = 11.0 Hz, -*H*C═CH-), 5.22 (1H, br d, J = 11.0 Hz, -HC═C*H*-), 3.75 (3H, s, -CO_2CH_3), 3.74 (3H, s, -CO_2CH_3), 3.70 (3H, s, -CO_2CH_3), 3.68 (3H, s, -CO_2CH_3), 2.6–1.7 (17H, m, other -CH_2- and -CH-), 0.69 (3H, s, CH_3); ^1H nmr (250 MHz, C_6D_6) δ (ppm): 5.38 (1H, br d, J = 10.0 Hz, -C*H*═CH-), 5.21 (1H, br d, J = 10.0 Hz, -CH═C*H*-), 3.39 (3H, s, -CO_2CH_3), 3.37 (3H, s, -CO_2CH_3), 3.29 (3H, s, -CO_2CH_3), 3.27 (3H, s, -CO_2CH_3), 2.73 (1H, m) and 2.62 (1H, ddd, J = 14.0 Hz, 9.5 Hz, 2.0 Hz) and 2.47 (1H, m) and 2.42 (1H, m), 2.25–2.05 (1H, m) and 2.06 (1H, m) and 1.98 (1H, m) and 1.97 (1H, m) and 1.92 (1H, td, J = 14.0 Hz, 4.5 Hz) and 1.87 (1H, dd, J = 14.5 Hz, 10.5 Hz) and 1.64 (1H, ddd, J = 14.5 Hz, 8.5 Hz, 6.0 Hz) and 1.45–1.08 (6H, m) (other -CH_2- and -CH), 0.70 (3H, s, $w_{1/2}$ = 2.0

Can. J. Chem. Downloaded from www.nrcresearchpress.com by 80.90.12.36 on 09/08/12
For personal use only.

Hz, $-CH_3$); ms *m/e*: 450 (M^+), 435 (M^+-CH_3), 419 (M^+-OCH_3). Exact Mass calcd. for $C_{24}H_{34}O_8$: 450.2253; found: 450.2246 ± 0.0013.

CAT **1b** (molar polar): ir ($CHCl_3$): 3000–2850, 1725 cm^{-1}; ^1H nmr (250 MHz, $CDCl_3$) δ (ppm): 5.52 (1H, ddd, J = 10.0 Hz, 5.0 Hz, 2.5 Hz, -*H*C=CH-), 5.34 (1H, br d, J = 10.0 Hz, -HC=C*H*-), 3.75 (3H, s, $-CO_2CH_3$), 3.73 (3H, s, $-CO_2CH_3$), 3.71 (3H, s, $-CO_2CH_3$), 3.70 (3H, s, $-CO_2CH_3$), 2.5–0.8 (17H, m, other $-CH_2$- and -CH-), 0.76 (3H, s, $-CH_3$); ^1H nmr (250 MHz, C_6D_6) δ (ppm): 5.54 (1H, m, -HC=CH-), 5.23 (1H, br d, J = 10.0 Hz, -HC=C*H*-), 3.37 (3H, s, $-CO_2CH_3$), 3.368 (3H, s, $-CO_2CH_3$), 3.32 (3H, s, $-CO_2CH_3$), 3.25 (3H, s, $-CO_2CH_3$), 2.7–0.8 (17H, m, other $-CH_2$- and -CH-), 0.75 (3H, s, $w_{1/2}$ = 1.0 Hz, $-CH_3$); ms *m/e*: 450 (M^+), 435 (M^+-CH_3), 418 (M^+-CH_3OH). Exact Mass calcd. for $C_{24}H_{34}O_8$: 450.2253; found: 450.2250 ± 0.0013.

TADA reaction of macrocycle **2**: *(7,2-*trans*-2,1-*anti*-1,10-*cis*)-2-(methoxymethoxy)methyl-5,5,13,13-tetrakis(methoxycarbonyl)-tricyclo[8.5.0.0^{2,7}]pentadec-8-ene* **2a** *and (7,2-*cis*-2,1-*anti*-1,10-*trans*)-2-(methoxymethoxy)methyl-5,5,13,13-tetrakis(methoxycarbonyl)-tricyclo[8.5.0.0^{2,7}]pentadec-8-ene* **2b**

Following general procedure A, neat TTT macrocyclic triene **2** (31.0 mg, 0.061 mmol) in toluene (1.0 mL) was heated at 200°C for 3.0 h, yielding a crude mixture of TAC tricyclic products **2a** and CAT **2b** (32.0 mg, quant., ratio: **2a**:**2b** = 90:10). Preparative thin-layer chromatography purification (20 cm × 20 cm, 2 plates, 0.05 cm thickness, 30% ethyl acetate in hexanes, two elutions) gave pure mixture **2a** and **2b** (19.0 mg, 61%, clear oil). These tricycles were found inseparable on silica gel even with many attempts under various solvent systems. However, a portion of pure mixture **2a/2b** could be recrystallized (dichloromethane–hexanes), affording nice pure crystals (mp 168–170°C) of TAC tricycle **2a** as thick prisms. A suitable crystal was analyzed by X-ray diffraction and confirmed the stereochemistry expected for **2a**. The mother liquor as concentrated and gave substantially enriched (>90%) CAT tricycle **2b**. These two diastereomeric tricycles were also more conveniently characterized in pure form as their alcohol derivatives **18a** and **18b** (see below).

TAC **2a**/CAT **2b** (pure mixture): ir (neat): 2950, 1730, 1440 cm^{-1}.

TAC **2a**: ^1H nmr (300 MHz, $CDCl_3$) δ (ppm): 5.56 (1H, ddd, J = 10.0 Hz, 3.0 Hz, 3.0 Hz, -*H*C=CH-), 5.19 (1H, ddd, J = 10.0 Hz, 2.0 Hz, 2.0 Hz, -HC=C*H*-), 4.52 (2H, narrow m, $-OCH_2O$-), 3.75 (3H, s, $-CO_2CH_3$), 3.71 (3H, s, $-CO_2CH_3$), 3.70 (3H, s, $-CO_2CH_3$), 3.68 (3H, s, $-CO_2CH_3$), 3.53 (1H, d, J = 10.5 Hz, -*H*CHOMOM), 3.47 (1H, d, J = 10.5 Hz, -HC*H*OMOM), 3.35 (3H, s, $-OCH_3$), 2.58 (1H, m) and 2.47–2.33 (2H, m) and 2.32–2.16 (4H, m) and 2.06–1.20 (9H, m) and 1.00 (1H, dt, J = 13.5 Hz, 3.5 Hz) (other $-CH_2$- and -CH-), ^{13}C nmr (75 MHz, $CDCl_3$) δ (ppm): 173.37, 172.62, 171.93, 171.58, 134.23, 127.02, 97.09, 65.24, 58.47, 55.50, 55.10, 52.51 (br), 52.18, 48.94, 40.91, 40.59, 37.68, 32.31, 30.21, 28.72, 27.60, 26.72, 22.19; ms *m/e*: 479 (M^+-OCH_3), 448 ($M^+-MOMOH$). Exact Mass calcd. for $C_{24}H_{32}O_8$: 448.2097; found: 448.2105 ± 0.0013.

CAT **2b** ^1H nmr (300 MHz, $CDCl_3$) δ (ppm): 5.52 (1H, m, -HC=CH-), 5.36 (1H, dd, J = 10.5 Hz, 1.5 Hz, -HC=CH-), 4.51 (2H, AB m, $-OCH_2O$-), 3.76 (3H, s, $-CO_2CH_3$), 3.724 (3H, s, $-CO_2CH_3$), 3.716 (3H, s, $-CO_2CH_3$), 3.710 (3H, s, $-CO_2CH_3$), 3.40 (1H, d, J = 9.5 Hz, -*H*CHOMOM), 3.30 (3H, s, $-OCH_3$), 3.25 (1H, d, J = 9.5 Hz, -HC*H*OMOM), 2.70–0.75 (17H, m, other $-CH_2$- and -CH-); ms *m/e*: 478 (M^+-HOCH_3), 448 ($M^+-MOMOH$). Exact Mass calcd. for $C_{24}H_{32}O_8$: 448.2097; found: 448.2105 ± 0.0013.

*(7,2-*trans*-2,1-*anti*-1,10-*cis*)-2-Hydroxymethyl-5,5,13,13-tetrakis(methoxycarbonyl)-tricyclo[8.5.0.0^{2,7}]pentadec-8-ene* **18a** *and (7,2-*cis*-2,1-*anti*-1,10-*trans*)-2-hydroxymethyl-5,5,13,13-tetrakis(methoxycarbonyl)-tricyclo[8.5.0.0^{2,7}]pentadec-8-ene* **18b**

The above mixture of tricyclic methoxymethyl ethers **2a/2b** (17.0 mg, 0.033 mmol) was stirred at 60–65°C for 12.0 h in the following solvent system: concentrated aqueous hydrochloric acid – water – methanol (0.5:1.0:8.5, 2.0 mL). The mixture was then allowed to warm to room temperature and quenched with a solution of aqueous saturated sodium bicarbonate (5 mL). The resulting mixture was extracted with diethyl ether (2 × 10 mL) and ethyl acetate (2 × 5 mL). The combined organic phases were dried over anhydrous magnesium sulfate and filtered on a medium fritted glass funnel covered with a 1 cm thick silica gel pad. Concentration of the filtrate left a crude mixture (1.50 mg, 94%) of alcohol derivatives TAC **18a** and CAT **18b**. A facile separation by preparative thin-layer chromatography (20 cm × 20 cm plate, 0.05 cm thickness, 50% ethyl acetate in hexanes, one elution) yielded pure TAC tricyclic alcohol **18a** (12.0 mg, 75%, clear oil) and CAT diastereomer **18b** (1.4 mg, 9%, clear oil).

TAC **18a** (less polar): ir (neat): 3555 (br), 2955, 2860, 1730 cm^{-1}; ^1H nmr (300 MHz, $CDCl_3$) δ (ppm): 5.57 (1H, ddd, J = 10.0 Hz, 3.0 Hz, 3.0 Hz, -*H*C=CH-), 5.22 (1H, ddd, J = 10.0 Hz, 2.0 Hz, 2.0 Hz, -HC=C*H*-), 3.78–3.65 (2H, m (2 hidden d), -*H*CHOH and -HC*H*OH), 3.74 (3H, s, $-CO_2CH_3$), 3.72 (3H, s, $-CO_2CH_3$), 3.69 (3H, s, $-CO_2CH_3$), 3.68 (3H, s, $-CO_2CH_3$), 2.58 (1H, m) and 2.46–1.60 (14H, m) and 1.56–1.43 (2H, m) and 1.02 (1H, dt, J = 13.5 Hz, 4.0 Hz) (other $-CH_2$- and -CH-, -OH); ^{13}C nmr (75 MHz, $CDCl_3$) δ (ppm): 173.30, 172.68, 172.25, 171.56, 134.43, 127.33, 59.58, 58.40, 55.16, 52.67, 52.51, 52.37, 48.75, 40.73, 40.57, 37.62, 37.50, 32.27, 30.34, 28.60, 27.80, 26.79, 22.13; ms *m/e*: 448 (M^+-H_2O), 435 (M^+-OCH_3). Exact Mass calcd. for $C_{24}H_{32}O_8$: 448.2097; found: 448.2088 ± 0.0013.

CAT **18b** (more polar): ir (neat): 3560 (br), 2950, 1730 cm^{-1}; ^1H nmr (300 MHz, $CDCl_3$) δ (ppm): 5.53 (1H, ddd, J = 11.0 Hz, 5.0 Hz, 2.5 Hz, -*H*C=CH-), 5.39 (1H, dd, J = 11.0 Hz, 1.0 Hz, -HC=C*H*-), 3.75 (3H, s, $-CO_2CH_3$), 3.72 (3H, s, $-CO_2CH_3$), 3.71 (3H, s, $-CO_2CH_3$), 3.70 (3H, s, $-CO_2CH_3$), 3.50 (1H, d, J = 11.0 Hz, -*H*CHOH), 3.44 (1H, d, J = 11.0 Hz, -HC*H*OH), 2.45–1.22 (17H, m, other $-CH_2$- and -CH-), 1.15 (1H, br, -OH); ms *m/e*: 448 (M^+-H_2O), 435 (M^+-OCH_3). Exact Mass calcd. for $C_{24}H_{32}O_8$: 448.2097; found: 448.2088 ± 0.0013.

*(7,2-*trans*-2,1-*anti*-1,10-*cis*)-2-Formyl-5,5,13,13-tetrakis-(methoxycarbonyl)-tricyclo[8.5.0.0^{2,7}]pentadec-8-ene* **3a**

To a stirred solution of TAC tricyclic alcohol **18a** (11.5 mg, 0.025 mmol) in acetonitrile (0.5 mL) at room temperature were successively added 4Å molecular sieves (15 mg), *N*-methyl morpholine (4.5 mg, 0.037 mmol), and tetra-*n*-propyl ammonium perruthenate (~0.5 mg (a few crystals), ~0.001

Can. J. Chem. Downloaded from www.nrcresearchpress.com by 80.90.12.36 on 09/08/12
For personal use only.

mmol). The resulting mixture was stirred at room temperature for 1.0 h, after which it was concentrated to dryness. The residue was purified by flash chromatography (15% ethyl acetate in hexanes, application with dichloromethane), yielding pure aldehyde derivative **3a** (9.0 mg, 78%, clear oil); ir (neat): 2955, 2860, 1730 cm^{-1}; ^1H nmr (300 MHz, $CDCl_3$) δ (ppm): 9.78 (1H, d, J = 1.0 Hz, -CHO), 5.78 (1H, ddd, J = 10.0 Hz, 3.0 Hz, 3.0 Hz, -*H*C=CH), 5.52 (1H, ddd, J = 10.0 Hz, 2.0 Hz, 2.0 Hz, -HC=C*H*), 3.74 (6H, s, 2 × $-CO_2CH_3$), 3.67 (6H, s, 2 × $-CO_2CH_3$), 2.60–0.80 (17H, m, other $-CH_2-$ and -CH-); ^1H nmr (300 MHz, C_6D_6) δ (ppm): 9.77 (1H, d, J = 1.5 Hz, -CHO), 5.35 (1H, ddd, J = 10.0 Hz, 3.0 Hz, 3.0 Hz, -*H*C=CH-), 5.21 (1H, ddd, J = 10.0 Hz, 2.0 Hz, 2.0 Hz, -HC=C*H*-), 3.40 (3H, s, $-CO_2CH_3$), 3.34 (3H, s, $-CO_2CH_3$), 3.28 (3H, s, $-CO_2CH_3$), 3.19 (3H, s, $-CO_2CH_3$), 2.72–2.41 (3H, m) and 2.27 (2H, m) and 1.99 (1H, m) and 1.90–1.57 (4H, m) and 1.48 (1H, dt, J = 14.0 Hz, 7.0 Hz) and 1.40–0.80 (6H, m) (other $-CH_2-$ and -CH-); ^{13}C nmr (75 MHz, $CDCl_3$) δ (ppm): 207.14, 173.05, 171.94, 171.55, 171.12, 134.73, 126.95, 58.15, 54.92, 52.68, 52.58, 51.50, 47.04, 39.95, 39.05, 36.81, 33.58, 28.85, 27.74, 27.54, 21.20; ms *m/e*: 464 (M^+), 446 (M^+-H_2O), 435 (M^+−CHO). Exact Mass calcd. for $C_{24}H_{32}O_9$: 464.2046; found: 464.2042 ± 0.0014.

*7,2-*cis*-2,1-*anti*-1,10-*trans*)-2-Formyl-5,5,13,13-tetrakis-(methoxycarbonyl)-tricyclo[8.5.0.0^{2,7}]pentadec-8-ene* ***3b***

To a stirred solution of CAT tricyclic alcohol **18b** (~1.5 mg, ~0.0032 mmol) in acetonitrile (0.25 mL) at room temperature were successively added 4 Å molecular sieves (3 mg), *N*-methyl morpholine (~1 mg, >0.005 mmol), and tetra-*n*-propyl ammonium perruthenate (a few crystals, catalytic). The resulting mixture was stirred at room temperature for 1.0 h, after which it was concentrated to dryness. The residue was purified by flash chromatography (25% ethyl acetate in hexanes, application with dichloromethane), yielding quite pure (~90%) aldehyde derivative **3b** (~0.7 mg, ~50%); ir (neat): 2925, 2845, 1725 cm^{-1}; ^1H nmr (300 MHz, $CDCl_3$) δ (ppm): 9.46 (1H, s, -CHO), 5.62 (1H, m, -*H*C=CH-), 5.45 (1H, dd, J = 11.0 Hz, 1.0 Hz, -HC=C*H*-), 3.76 (3H, s, $-CO_2CH_3$), 3.74 (3H, s, $-CO_2CH_3$), 3.72 (6H, s, 2×$-CO_2CH_3$), 2.50–0.80 (17H, m, other $-CH_2-$ and -CH-); ^1H nmr (300 MHz, C_6D_6) δ (ppm): 9.33 (1H, s, -CHO), 5.43 (1H, ddd, J = 10.5 Hz, 5.0 Hz, 2.0 Hz, -*H*C=CH), 5.16 (1H, dd, J = 10.5 Hz, 1.5 Hz, -HC=C*H*), 3.36 (3H, s, $-CO_2CH_3$), 3.31 (6H, s, 2 × $-CO_2CH_3$), 3.23 (3H, s, $-CO_2CH_3$), 2.70–0.80 (17H, m, other $-CH_2-$ and -CH-); ms *m/e*: 464 (M^+), 446 (M^+-H_2O), 435 (M^+−CHO). Exact Mass calcd. for $C_{24}H_{32}O_9$: 464.2046; found: 464.2042 ± 0.0014.

TADA reaction of macrocycle 3: TAC aldehyde ***3a***

Following general procedure A, neat pro-6.6 formyl-substituted TTT macrocyclic triene **3** (2.0 mg, 0.0043 mmol) was heated at 300°C for 3 min, yielding a crude mixture of tricyclic products **3a**, **8a**, and **8b** (1.8 mg, 90%, ratio: **3a**:**8a**:**8b** = 4.01:1.2:0.4).

Acknowledgements

This research was financially supported by the Natural Sciences and Engineering Research Council of Canada (NSERC, Ottawa) and by the "Ministère de l'Enseignement Supérieur et de la Science (Fonds FCAR, Québec)." D.G. Hall thanks NSERC for a 1967 Postgraduate Award. We wish to acknowledge the help of Mr. Guy Falardeau for an extensive nmr analysis of compound **12**.

References

1. D.G. Hall, R. Müller, and P. Deslongchamps. Can. J. Chem. **73**, 1675 (1995).
2. (*a*) J. Sauer and R. Sustmann. Angew. Chem. Int. Ed. Engl. **19**, 779 (1980); (*b*) F.A. Carey and R.J. Sundberg. *In* Advanced organic chemistry. 3rd ed. Plenum Press, New York. 1990. p. 288; (*c*) F. Fringuelli and A. Taticchi. *In* Dienes in the Diels–Alder reaction. Wiley, New York. 1990.
3. W.R. Roush. *In* Comprehensive organic synthesis. Vol. 4. *Edited by* B.M. Trost. Pergamon Press, Oxford. 1991. pp. 513–550.
4. (*a*) T. Kametani, T. Honda, Y. Shiratori, H. Matsumoto, and K. Fukumoto. J. Chem. Soc. Perkin Trans 1, 1386 (1981); (*b*) W. Oppolzer and R.L. Snowden. Helv. Chim. Acta, **64**, 2592 (1981); (*c*) E. Wenkert and K. Naemura. Synth. Commun. 45 (1973).
5. Y.L. Dory, C. Ouellet, S. Berthiaume, A. Favre, and P. Deslongchamps. Bull. Soc. Chim. Fr. **131**, 121 (1994).
6. E.L. Eliel and S.H. Wilen. *In* Stereochemistry of organic compounds. Wiley, New York. 1994. p. 762.
7. A. Ndibwami, S. Lamothe, P. Soucy, S. Goldstein, and P. Deslongchamps. Can. J. Chem. **71**, 714 (1993).
8. F.B. Gonzàlez and P.A. Bartlett. Org. Synth. **64**, 175 (1986).
9. M. Labelle, H.E. Morton, Y. Guindon, and J.P. Springer. J. Am. Chem. Soc. **110**, 4533 (1988).
10. A. Rauk, I.R. Hunt, and B.A. Keay. J. Org. Chem. **59**, 6806 (1994).
11. (*a*) P.A. Grieco. Aldrichimica Acta, **24**, 59 (1991); (*b*) P.A. Grieco, J.J. Nunes, and M.D. Gaul. J. Am. Chem. Soc. **112**, 4595 (1990).
12. R. Breslow. Acc. Chem. Res. **24**, 159 (1991).
13. (*a*) J.F. Blake, D. Lim, and W.L. Jorgensen. J. Org. Chem. **59**, 803 (1994); (*b*) W. Blokzijl and J.B.F.N. Engberts. J. Am. Chem. Soc. **114**, 5440 (1992).
14. W.R. Roush, A.P. Essenfeld, and J.S. Warmus. Tetrahedron Lett. **28**, 2447 (1987).
15. (*a*) J.R.L. Smith, R.O.C. Norman, and M.R. Stillings. Tetrahedron, **34**, 1381 (1978); (*b*) J. Sauer. Angew. Chem. Int. Ed. Engl. **6**, 16 (1967).
16. I. Fleming. *In* Frontier orbitals and organic chemical reactions. Wiley, New York. 1976. p. 163.
17. E.L. Eliel and S.H. Wilen. *In* Stereochemistry of organic compounds. Wiley, New York. 1994, p. 36.
18. S. Hasegawa and Y. Hirose. Phytochemistry, **24**, 2041 (1985).
19. (*a*) M. Barfield and B. Chakrabarti. Chem. Rev. **69**, 757 (1969); (*b*) L.M. Jackman and S. Sternhell. *In* Application of NMR spectroscopy in organic chemistry. 2nd ed. Pergamon Press, Oxford. 1969.
20. J. March. *In* Advanced organic chemistry. 4th ed. Wiley, New York. 1992. p. 1044.
21. P. Laszlo and M. Teston. J. Am. Chem. Soc. **112**, 8750 (1990).
22. S.V. Ley, J. Norman, W.P. Griffith, and S.P. Marsden. Synthesis, 639 (1994).
23. E.J. Corey and J.W. Suggs. Tetrahedron Lett. **16**, 2647 (1975).
24. A.G. Michel, D.G. Hall, and M. Drouin. Acta Crystallogr. Sect. C: Cryst. Struct. Commun. **C49**, 1830 (1993).
25. E. Ciganek. *In* Organic reactions. Vol. 32. *Edited by* W.G. Dauben. Wiley, New York. 1984. p. 96.

Raman and resonance-Raman spectra of polypyrrole with application to sensor – gas probe interactions

Stephen J. Vigmond, Vida Ghaemmaghami, and Michael Thompson

Abstract: Raman spectra of the oxidized and neutral forms of polypyrrole show a relative intensity shift from the high wave number region to the low wave number region as the source wavelength is increased from 514.5 to 1064 nm. Variations in band positions are also observed with changes in excitation source; particularly, two C=C stretches at 1500 and 1605 cm^{-1} can be observed with the neutral polymer but only a single band is observed at 1575 cm^{-1} when sources of higher energy are used. These changes arise from differences in the electronic states of the two forms that can greatly alter the intensities of the numerous bands. The oxidized and neutral forms of the polymer both act as electron acceptors towards the gas phase species tested here (toluene, water, methanol, and ammonia). The increased electron density induces an upward shift of the peaks at 915 and 1035 cm^{-1} of the neutral polymer and increases the relative intensity of the 1575 cm^{-1} peak of the oxidized polymer using 1064 and 514.5 nm sources, respectively.

Key words: polypyrrole, Raman spectroscopy, gas probe interactions.

Résumé : Lorsqu'on augmente la longueur d'onde de la source de 514,5 à 1064 nm, les spectres Raman des formes oxydées et neutres du polypyrrole présentent un déplacement de l'intensité relative de la région des nombres d'onde élevés à celle des nombres d'onde plus faibles. On a aussi observé des variations dans les positions des bandes avec des changements dans la source d'excitation; en particulier, on peut observer deux élongations C=C à 1500 et 1605 cm^{-1} avec le polymère neutre, mais on observe une seule bande à 1575 cm^{-1} lorsqu'on utilise des sources d'énergie plus élevée. Ces changements proviennent de différences dans les états électroniques des deux formes qui peuvent modifier considérablement les intensités des diverses bandes. Les formes oxydées et neutres du polymère agissent toutes les deux comme accepteurs d'électron par rapport aux espèces gazeuses étudiées ici (toluène, eau, méthanol et ammoniac). Lorsqu'on utilise respectivement des sources respectivement de 1064 et de 514,5 nm, l'augmentation de la densité électronique induit un déplacement vers des valeurs plus grandes des pics à 915 et 1035 cm^{-1} du polymère neutre et une augmentation de l'intensité relative du pic à 1575 cm^{-1} du polymère oxydé.

Mots clés : polypyrrole, spectroscopie Raman, étude des interactions gazeuses.

[Traduit par la rédaction]

Introduction

Although conducting polymers have been extensively studied over the past 15 years, there is still much to learn about these unique materials (1). The insolubility of many of these polymers limits the methods available for their analysis. Some of the more common techniques used to probe these materials include cyclic voltammetry (2), UV–visible (3), and IR (4) absorption spectroscopies, X-ray photoelectron spectroscopy (5), and ellipsometry (6). We have been investigating polypyrrole, one of the most stable conducting polymers, with respect to its potential role as a chemical sensor (7, 8). In its employment as a gas phase sensor, the resistance of the oxidized, conducting form is monitored (9–12). In the presence of various analytes, cationic sites along the polymer backbone become neutralized, either by electron donation to the polymer or by proton abstraction from the polymer (9), which decreases the measured conductivity. It is the nature of these interactions that we wish to examine.

Infrared and UV–visible spectroscopies have previously been used to study the interactions of selected vapors with polypyrrole. Several problems limit the utility of IR in this area; Ratcliffe (10) found polypyrrole to be too thin for analysis and Gustafsson et al. (9) reported that ammonia obscures the interesting features of the polypyrrole spectrum if the spectrum is collected during experimental exposure. From UV–visible spectroscopy and work function analysis, Topart and Josowicz (13) concluded that polypyrrole can be either an electron donor or acceptor, with its behavior being dependent upon the counteranion present.

The analysis of polypyrrole by Raman spectroscopy provides greater spectral information than UV–visible spectroscopy and may circumvent some of the difficulties associated with IR spectroscopy. The fact that Raman spectroscopy is based on scattering phenomena leads to the possibility of analysis of insoluble samples that require no sample preparation.

Received April 11, 1995.

S.J. Vigmond, V. Ghaemmaghami, and M. Thompson.[1]
Department of Chemistry, University of Toronto, 80 St. George Street, Toronto, ON M5S 1A1, Canada.

[1] Author to whom correspondence may be addressed. Telephone: (416) 978-3575. Fax: (416) 978-8775. E-mail: bgranozi@alchemy.chem.utoronto.ca

Can. J. Chem. Downloaded from www.nrcresearchpress.com by 80.90.12.36 on 09/08/12
For personal use only.

Can. J. Chem. Downloaded from www.nrcresearchpress.com by 80.90.12.36 on 09/08/12
For personal use only.

Table 1. UV–visible and Raman absorptions of polypyrrole.

Method	State of polypyrrole	Absorption	Assignment	Ref.
UV	Oxidized	490 nm	Valence to upper bipolaron band	16
		1000 nm (v. br)	Valence to lower bipolaron band	3
	Intermediate	550 nm	Lower to upper polaron band	3
	Neutral	420 nm	Valence to conduction band	17
Raman	Oxidized	1575 cm^{-1}	C=C str	18
		1420 cm^{-1}	C–N str	19
		1040 cm^{-1}	C–H def	18
		936 cm^{-1}	Ring def, asymm.	4
	Neutral	1562 cm^{-1}	C=C and inter-ring C–C str	14
		1526 cm^{-1}	N–C and C–C str	14
		1319 cm^{-1}	C–C str	14
		1044 cm^{-1}	C–H def	14
		998 cm^{-1}	Ring def, sym	14

Several Raman studies of polypyrrole have been published previously where the source used generally has a wavelength of 514.5 nm (14, 15). A list of generally accepted assignments is provided in Table 1. Recently, FT-Raman spectra of neutral and oxidized polypyrrole (with relatively large counterions) have been published (20). In addition, an FT-Raman study of a polypyrrole-polyester composite has been discussed (21). As the electronic states of polypyrrole are altered with an increase in the oxidation level of the polymer, through the formation of polaron and bipolaron structures, absorption maxima in the UV–visible region will shift (see Table 1). Typically, the electronic absorptions of conducting polymers shift toward the near-infrared region as the oxidation level is increased. Therefore, as noted for other conducting polymers (22, 23), Raman spectra of polypyrrole will be a function of the excitation wavelength resulting from resonance or near-resonance conditions that originate from the localized structures formed in the polymer. These effects, which may be related to the increasing double-bond character of the $C_{\alpha-\alpha'}$ and $C_{\beta-\beta}$ bonds but the decreasing electron density along $C_{\alpha-\beta}$ (24), will be manifested in shifts of the relative intensities of the absorption bands and their positions.

In the present work, Raman spectra of polypyrrole are collected using sources of 514.5, 568, 752, and 1064 nm, the latter being part of an FT-Raman system. While other studies have employed more than one source, this study utilizes, to our knowledge, the widest range of source wavelengths to date. The initial stage of this study is an analysis of the changes observed in the Raman spectra of both the oxidized and neutral forms of polypyrrole as the excitation wavelength and the type of instrument are varied. Perchlorate, a relatively small dopant, is used as the counterion. The shift in relative intensities in the spectra arising from changes in the source wavelengths allows some control over which segments of the polymer are being probed. The second part deals with the application of this methodology to the in situ analysis of gas phase interactions of polypyrrole. It is hoped that this methodology can specifically resolve the question of electron donation or acceptance in the presence of various analytes and, more generally, provide greater understanding of the types of molecular interactions that may occur. Most previous work in this field has concentrated on interactions with the oxidized polymer only. However, the oxidized form is mainly composed of neutral segments so their contribution to the ultimate behavior of a polypyrrole sensor needs to be considered also and this is possible using this spectroscopic technique. These results are put in context with complementary mass-based results from acoustic wave sensor work that we report in a companion paper (25). Here frequency decreases indicate the relative degrees of interaction between the analytes and polypyrrole. Furthermore, the shapes of the response curves provide information regarding changes in the viscoelastic properties of the polymer and also the net retention or loss of its solvation sheath.

Experimental section

Materials

Pyrrole was purchased from Aldrich (Milwaukee, Wis.) and distilled prior to use. Tetrabutylammonium perchlorate (TBAP), electrochemical grade, was supplied by Fluka (Switzerland) and used as received. All solvents, used both in the electrochemical procedures and to generate the vapors, were of reagent grade and procured from BDH (Toronto, Canada). Water was passed through a Corning column to remove organic compounds and was doubly distilled. Pure helium and ammonia-in-helium were purchased from Matheson.

Instrumentation

Gold-plated 9 MHz piezoelectric quartz crystals were obtained from International Crystal Manufacturing Company, Oklahoma. These crystals were utilized as working electrodes (0.25 cm^2 gold on each side) in the polymerization of pyrrole with a combined platinum wire and Ag/AgCl (3 M KCl) electrode from Metrohm as the counter and reference electrodes, respectively. Electrochemical oxidations and reductions were performed with a polarographic analyzer (model 473) from ECO Instruments (Cambridge, Mass.).

FT-Raman spectra were acquired with a Bomem Ramspec 150 spectophotometer employing a Quantronix Nd:YAG laser emitting at 1064 nm and an InGaAs detector. The incident laser power was adjusted such that the power reaching the detector was in the range of 0.20–0.25 W. Spectra were accumulated in a backscattering geometry with the resolution set at 4 cm^{-1}. One hundred scans were accumulated over approximately 10 min. Data collection and manipulation were performed with Bomem Easy (version 1.45) software. Spectral intensities were normalized against an instrument response curve.

Micro Raman spectra were measured with a triplemate spectrometer (model 1877D, Spex Industries Inc.), which incorporated a microscope (1482D Micromate; 40× for polymer analysis, 10× for gas probe experiments) that focused the incident radiation down to an approximately 10 μm spot. An argon ion visible laser and a near-infrared krypton laser were available as excitation sources. Laser power settings of 400 mW were found to provide power of 6–7 mW at the sample with the Micro system. The detectors used were an intensified linear diode array (model IRY/G from Princeton Instruments, Inc.) and a liquid-nitrogen-cooled charge-coupled device

Can. J. Chem. Downloaded from www.nrcresearchpress.com by 80.90.12.36 on 09/08/12
For personal use only.

Fig. 1. Schematic of cell employed in Raman gas-probe experiments.

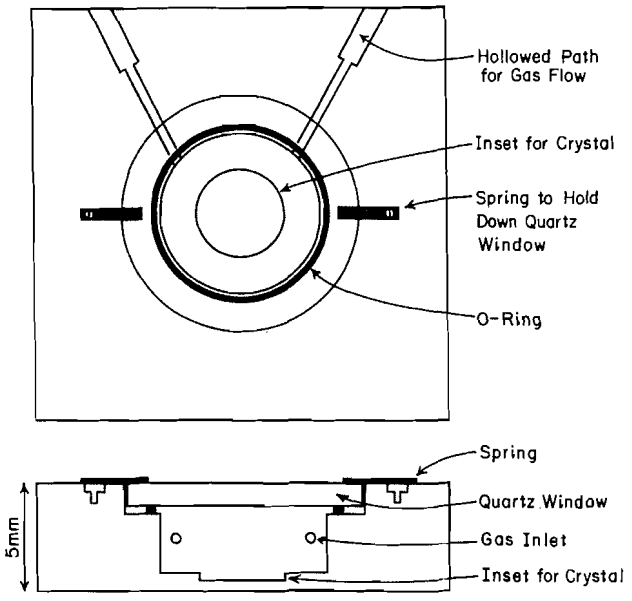

(CCD) detector (model LN/CCD from Princeton, Instruments, Inc.). Accumulation times of 3 min were typically employed for polymer analysis and 5 min for gas phase studies. The programs NSMA and CSMA (part of the ST-120 package from Princeton Instruments, Inc.) were used to control data acquisition with the diode array and CCD detectors, respectively. Conversion of diode numbers to wavenumbers was accomplished by running calibration spectra of neon at the settings used to collect the Raman scattering.

With both Raman systems, the samples for polymer analysis were mounted onto glass slides so that the source beam impinged directly onto the polymer. For the spectra relating to the gas phase analyses, the samples were enclosed in the cell shown schematically in Fig. 1. In this configuration, the excitation beam and the scattered light both have to pass through a 1-mm-thick window.

Procedures

Electrochemical polymerizations and oxidation state modifications were performed as described previously (7). Briefly, electrochemical procedures were performed in a cell that protected the electrical contacts of the piezoelectric crystal from the electrolyte solution. Electropolymerization was carried out in a solution of pyrrole and TBAP (both 0.1 M) in acetonitrile, after deoxygenation by bubbling nitrogen through the solution, at +1.0 V (vs. Ag/AgCl) for 1 min. Scanning electron micrographs indicate the films are approximately 0.3 μm thick (7). Oxidations (at +1.0 V) and reductions (at −1.5 V) of the as-prepared films were performed in 0.1 M TBAP, also after deoxygenation, for 10 min. Simultaneous measurements of the current indicated that this amount of time was sufficient to reach an equilibrium state.

For the gas phase experiments, helium flow rates were maintained at approximately 35 mL/min. Methanol, water, and toluene were introduced into the flow-through train by diverting the helium flow over a 50 mL reservoir of the appropriate solvent contained in a solvent trap (previously described in greater detail) (7). The concentrations of methanol, water, and toluene were determined by trapping the vapors from trial runs of approximately 1 h in a liquid nitrogen bath and found to be 95 ± 10, 15 ± 5, 10 ± 5 ppm, respectively. Ammonia was supplied as a mixture in helium and used without further dilution (2.09 ± 0.05%). After spectra were collected in the presence of the gaseous analytes, pure helium was reintroduced in order to observe the recovery of the system.

Table 2. Raman frequencies for oxidized and neutral polypyrrole films.

Excitation Wavelength (nm)	Frequencies (cm^{-1}) Oxidized	Neutral
514.5	1575(s)	1575(s)
		1420(w)
	1365(m, v, br)	1335(m)
	1245(w)	1245(w)
	1055(m)	1045(m)
	975(m)	990(m)
	935(m)	925(m)
568	1560(s)	
	1350(s, br)	
	1240(w)	
	1075(m)	
	1055(m)	
	965(m)	
	930(m)	
752	1590(s)	1605(w)
		1490(w)
	1370(m)	1400(w)
	1335(w)	1300(m)
	1235(m)	1235(m)
	1080(m)	
	1055(w)	1040(m)
	930(s)	920(s, sh)
1064	1580(s)	1605(w)
		1500(m)
	1370(m, br)	1405(w)
		1300(m)
	1230(m)	1215(m)
	1075(m, br)	1035(m, sh)
	930(s, sh)	915(s, sh)

Results and discussion

The reason for employing gold-coated piezoelectric crystals as the polymer substrate was to maintain our previous experimental conditions (25). Although we are not reporting any new microgravimetric results, this ensures the most relevant comparisons to previous results and also allows us to work with well-characterized samples. Raman spectra of as-prepared and neutral polypyrrole were recorded using 514.5, 752, and 1064 nm sources. A spectrum of the as-prepared polymer using a 568 nm source was also obtained. The spectra are presented in Figs. 2–5 and a summary of the band positions is provided in Table 2.

Can. J. Chem. Downloaded from www.nrcresearchpress.com by 80.90.12.36 on 09/08/12
For personal use only.

Fig. 2. Raman spectra of (*a*) as-prepared and (*b*) neutral polypyrrole with 514.5 nm source.

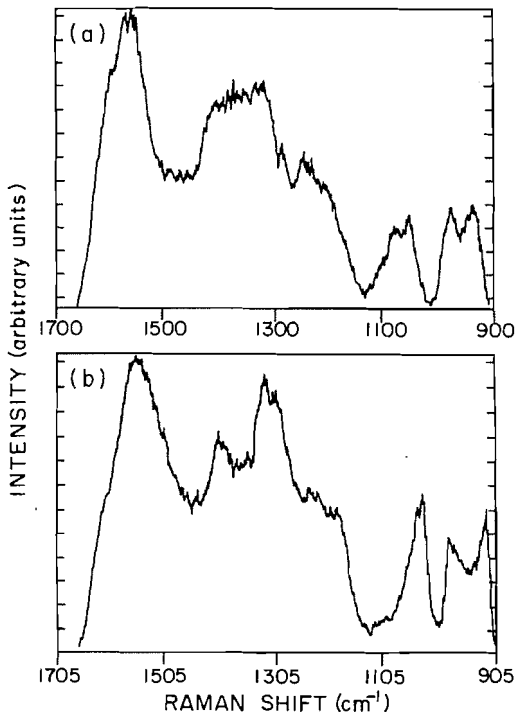

Fig. 3. Raman spectrum of as-prepared polypyrrole with 568 nm source.

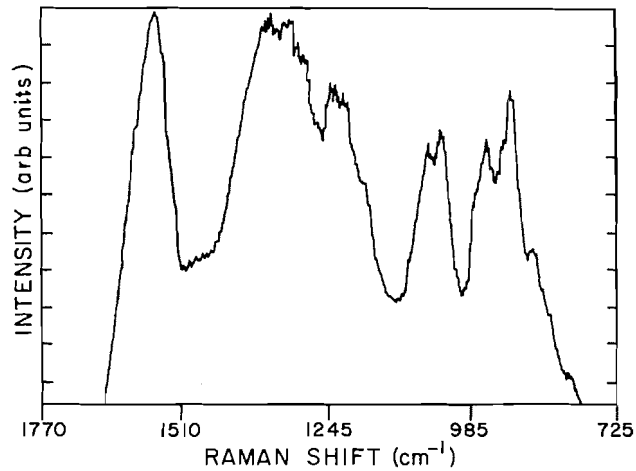

Fig. 4. Raman spectra of (*a*) as-prepared and (*b*) neutral polypyrrole with 752 nm source.

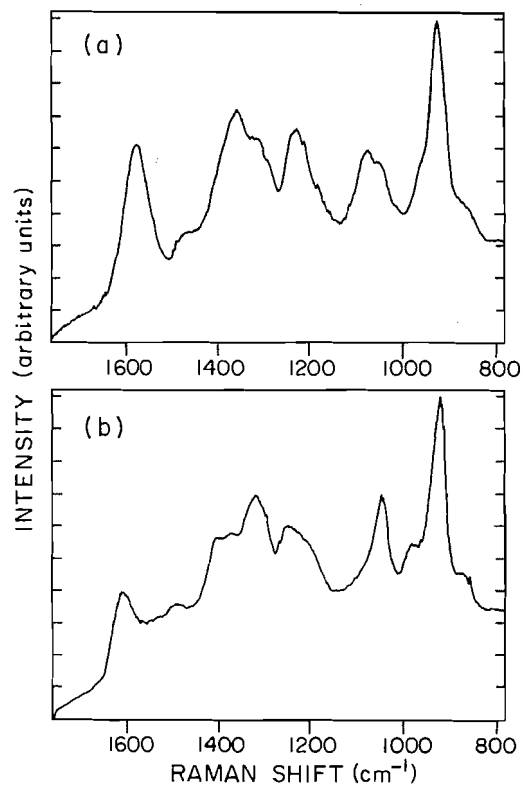

Wavelength dependence of intensities

The spectra clearly demonstrate the variation in relative intensities produced by altering the excitation wavelength. The spectra recorded with the 514.5 nm source (Fig. 2) agree with most other published spectra using sources of similar wavelength. Generally, spectra recorded with excitations of 514.5 nm or shorter are dominated by the C=C stretch near 1575 cm^{-1} for both the oxidized and neutral states. Choi and Tachikawa (18) attribute the strong signal to the fact that it arises from resonance Raman scattering. One advantage of the 488 nm source over the 514.5 nm source used in this study is that the shorter wavelength is closer to the valence-to-conduction and (or) upper-bipolaron bands of the polymer and, accordingly, this generates spectra with greater intensities (26). As the excitation wavelength becomes longer, there appears to be a gradual enhancement of the relative intensities of the bands at lower wave numbers. Even an increase to 530.9 nm is shown to produce a weaker C=C stretch compared to bands at 1414 and 1320 cm^{-1} for the as-prepared polymer (15).

The spectrum of the oxidized polymer using the 568 nm line (Fig. 3) shows a more even distribution of intensities across the entire range. This wavelength was selected in an effort to induce the SERS phenomenon. Thinner polymer samples were employed (20 s polymerizations corresponding to approximately 10^3 Å) and the underlying gold was roughened by slowly vapor-depositing 40 Å of gold on top (which had a UV-visible absorption maximum near 630 nm), but no enhancements could be detected. The lack of enhancement is likely associated with the thickness of the sample since the phenomenon decays as r^{-3} from the surface. Shorter polymerization times produce less uniform coatings so thinner coatings were not attempted. Virdee and Hester (15) failed to observe SERRS effects with gold electrodes that had been subjected to numerous oxidation–reduction cycles, but the films in this study were also relatively thick.

The spectra recorded with the 752 nm source (Fig. 4) begin to be dominated by bands in the lower wave number region and good resolution of the peaks is observed. The FT-Raman spectra (Fig. 5) are even more skewed in this direction. At this longer excitation wavelength, the intensity of the Raman signals from the neutral polypyrrole are quite weak above 1100 cm^{-1} so they appear noisy but the peaks below this are strong and sharp. The previously reported FT-spectra (20) are significantly broader in this region due to recording the spectra at a

Can. J. Chem. Downloaded from www.nrcresearchpress.com by 80.90.12.36 on 09/08/12
For personal use only.

Fig. 5. FT-Raman spectra of (*a*) as-prepared and (*b*) neutral polypyrrole with 1064 nm source.

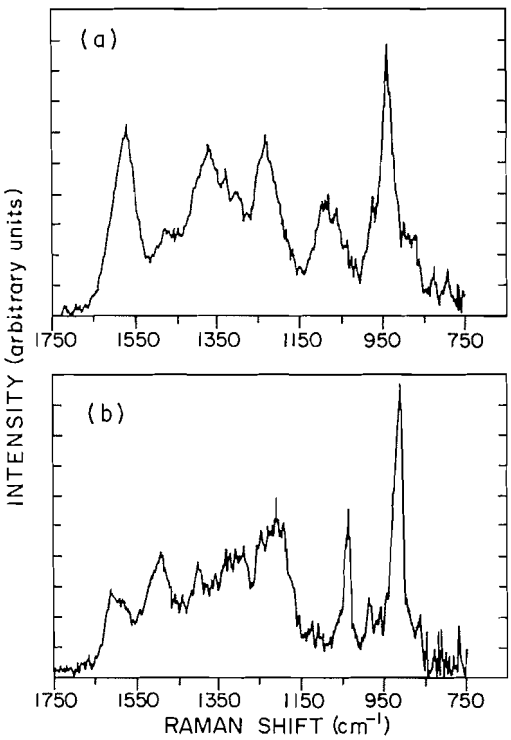

lower resolution and using larger counteranions that may have produced a greater degree of disorder in the polymer. The weaker spectrum from the neutral polymer is a result of the UV–visible absorbances discussed previously. Oxidized polypyrrole has a very broad absorbance above 1000 nm so that resonance conditions are possible with the 1064 nm source, but no such enhancement is possible with the neutral form.

Wavelength dependence of band positions

The broadness of the Raman bands makes it difficult to detect small shifts in the frequency with changes in the source excitation but some trends are evident (see Table 2). The C=C stretches appear at slightly higher wave numbers as the excitation wavelength is increased to 752 nm but the band of the oxidized polymer is lower in the FT-Raman spectrum. The C=C stretch of the neutral polymer produces a broad peak at 1575 cm^{-1} but generates two peaks with longer wavelength sources; while an intense, single peak is observed with the 514.5 nm source (and up to at least a 632 nm source (14, 24)), the other spectra show peaks at approximately 1500 cm^{-1} (although it is very weak in the 752 nm spectrum) and 1605 cm^{-1}. Jenden *et al.* (20) attribute the peak near 1500 cm^{-1} to some pyrrole rings adapting a *cis* geometry but peaks near 1500 and 1600 cm^{-1} are typical of C=C stretching bands in the spectra of 2,5-dialkylpyrrole derivatives so we consider the longer sources to be probing a nonconjugated component of the neutral polymer.

Therefore, the peak near 1575 cm^{-1} appears to be quite sensitive to the oxidation state of the polymer and the experimental conditions used to collect the spectrum. While we could not discern a frequency shift between the two states with the 514.5 nm source (see Table 2), in situ monitoring of the electrochemical cycling of the polymer with this source typically shows a 10 cm^{-1} decrease upon going from the oxidized form to the neutral form (15, 26). Burkowska and Jackowska (26) attribute the shift to the amount of charge on the polymer modulating the force constants of the pyrrole ring. Our spectra of these free-standing films do show that subsequent oxidations of as-prepared polypyrrole at +1.0 V or +1.4 V shift this band 10–15 cm^{-1} upwards with all sources used in this study, which may arise from the polymer being in a higher oxidation state or be an effect from the partial chlorination incurred upon oxidation.

The central region, from about 1200 to 1400 cm^{-1}, cannot be monitored as easily because the peaks are broad and tend to overlap. No wavelength dependence on excitation is detected in this region. The C–H deformations near 1050 cm^{-1} also remain consistent as the source is varied; the neutral spectra display a relatively sharp peak at 1040 cm^{-1} while the oxidized state has two almost equal and broader components at 1080 and 1055 cm^{-1}. The C–H out-of-plane deformations (900–1000 cm^{-1}) are very sensitive to the experimental conditions. While both polypyrrole states exhibit a pair of near-equal intensity peaks at approximately 930 and 980 cm^{-1} with the shorter wavelength sources, the two bands are nearly coincident with the 752 and 1064 nm sources (Figs. 4 and 5, respectively); in both cases the remaining peaks appear skewed to the high wave number side. From the spectra presented here and others published previously (14, 15), the higher peak is observed at progressively lower wave numbers as the excitation wavelength is increased while the lower wave number peak remains fixed at 930 cm^{-1} for the oxidized form and 915 cm^{-1} for the neutral state.

Furukawa et al. (14) have assigned the peaks at 930 and 1080 cm^{-1} to the bipolaron structure and those at 970 and 1050 cm^{-1} to the polaron structure, while the strong band at 1580 cm^{-1} is considered to be an overlap of the two oxidized structures. Although the 980 cm^{-1} peak coalesces into the lower one making relative intensities difficult to ascertain, the two peaks at 1080 and 1050 cm^{-1} remain clearly resolved and of constant relative intensity, indicating no wavelength preference between the two structures. This is not surprising as the absorption bands are similar for the cationic and dicationic species.

The spectra discussed to this point illustrate the sensitivity of the Raman technique to the structure of polypyrrole. The characteristic band positions observed in Figs. 2–5 clearly differentiate the oxidized and neutral forms as well as providing some discrimination between the polaron and bipolaron components, which arises from the changing charge densities along the polymer. They also show the advantage of using several sources to maximize the resolution of certain regions; with the 514.5 nm source, C–H out-of-plane deformations produce two peaks that are not resolved by the higher wavelength sources but the higher wavelength sources are able to separate two C=C stretches in the neutral polymer. Although Raman frequencies are not a function of the excitation source, the complex structure of polypyrrole allows resonance conditions of particular structures to become more dominant as the source is changed and cause certain bands to appear at slightly different frequencies. This phenomenon has previously been described in the analysis of several conducting polymers; it was attributed to the existence of several radical cation structures in polypyrrole (14), nonuniformly doped domains of

Can. J. Chem. Downloaded from www.nrcresearchpress.com by 80.90.12.36 on 09/08/12
For personal use only.

polyacetylene (23), and to the probing of different degrees of delocalization in polyfuran (22). A full analysis of the effects of the source wavelength permits us to more fully exploit the capabilities of Raman spectroscopy for studying the behavior of polypyrrole.

Practical considerations also affect the usefulness of the two Raman systems. The major advantages of the FT-Raman spectrometer are the inherent accuracy in determining the frequencies of the bands and the accumulation of the entire spectrum in a single run. Therefore, much smaller shifts may be measured more reliably with this spectrometer. The Spex Micro system can only monitor spectral regions of fixed ranges so several spectra may be required to obtain a complete spectrum at a desired resolution. Although each grating and filter setting requires a separate calibration, the microscope attachment provides more efficient collection of the Raman scattering, which reduces accumulation time. However, it is through this combination of instruments that the wide range of excitation sources is possible and able to provide a more thorough analysis of polypyrrole. The gas phase analyses therefore examined the extreme experimental conditions available (i.e., 514.5 and 1064 nm sources) in order to determine the type of information that may be acquired.

Gas phase studies with the 1064 nm source

The four probe gases (water, ammonia, methanol, and toluene) were found to have no effect on the relative intensities of any of the peaks with the 1064 nm source. However, while most of the peaks in the central region of the spectra are broad and their positions are difficult to assign accurately, the bands at 915 and 1035 cm^{-1} in the spectrum of neutral polypyrrole and 930 cm^{-1} in the oxidized spectrum are all quite sharp and show small shifts towards higher wave numbers in the presence of all the analytes tested. The most obvious increase occurs with the 915 cm^{-1} peak of the neutral polymer that typically shifts between two and three wave numbers for all of the analytes while the 1035 cm^{-1} peak increases between one and two wave numbers. The results from the as-prepared and further-oxidized samples are less consistent; the shifts are smaller and in some cases even decrease. The as-prepared polymer shows increases in the C–H bending band of approximately 1.5 and 1.0 cm^{-1} in the presence of water and toluene, respectively, but the other cases are less clear.

The 915–930 cm^{-1} peaks have been attributed to the pyrrole ring deformation and the 1035 cm^{-1} band to a C–H bend (14). The shift to higher wave numbers is consistent with the formation of hydrogen bonds to the pyrrole units. From semi-empirical calculations, Campos-Vallette et al. (27) have proposed that pyrrole forms N–H···π hydrogen-bonded complexes. This type of interaction would hinder the deformation vibrations and cause their upward shift. The fact that the neutral polymer exhibits larger shifts implies that this phenomenon occurs through the neutral rings in the polymer backbone. The weaker shifts observed with the oxidized polymers result from the fact that although this state is partially composed of neutral segments, it also contains a large number of cationic pyrrole units. The shift of the C–H band at the 1035 cm^{-1} band, with respect to the 915 cm^{-1} peak, is 90, 70, 70, and 30% (each approximately $\pm$10%) for toluene, ammonia, water, and methanol, respectively. Since electron donation to the pyrrole rings may occur through several modes, depending upon the analyte, such as an overlap of aromatic rings or hydrogen bonding with an -OH group, the various Raman bands of the pyrrole ring will be affected differently. At this point, the significantly lower relative shift of the 1035 cm^{-1} band induced by methanol cannot be explained.

Gas phase studies with the 514.5 nm source

The spectra from the 514.5 nm source are slightly broader, making the determination of frequency shifts even more difficult. From the superpositioning of spectra with and without the gas probe being present, small upwards shifts of the 915 cm^{-1} band may be observed in the presence of water and methanol. No shifts were observed in any of the experiments with toluene. With this source also, the shift is more predominant in the spectra of the neutral polymer. The software employed with the dispersive Raman spectrometer makes it more difficult to determine the size of the shifts but it is approximately the same as that observed with the FT-Raman system.

From the careful analysis of approximately 100 gas phase spectra, a relative intensity change is detected with the 514.5 nm source upon introduction of some of the gaseous probes. By overlaying the 1575 cm^{-1} peaks of the spectra from the polymer with and without the gas probe, a relative decrease in the rest of the spectrum is often found in the presence of the probe; this most plausibly indicates a relative increase of the 1575 cm^{-1} peak itself (Fig. 6). This is more pronounced in the spectra of the oxidized polymer. The relative increase of this band is likely the reverse scenario of the response phenomenon observed by Battisti and Aroca (28) upon adsorption of NO_x on Langmuir–Blodgett monolayers of phthalocyanine complexes. The electron-withdrawing capability of NO_x decreases the electron density of the pyrrole moieties in these complexes. An explanation lies in the loss of electronic density about the nuclei involved in the vibration with resulting change in the polarizability of the bonds and loss of scattering intensity. This is reflected in the relative intensity of a band at 1530 cm^{-1}, which is assigned to a stretching vibration with a strong contribution from the pyrrole structures present. An increase in the relative intensity of the 1575 cm^{-1} band, therefore, implies that water and methanol increase the electron density of the analogous stretch. Results with toluene are often ambiguous and may have required longer exposures to create more significant effects.

The combination of excitation wavelengths and equipment provides complementary information. The 1064 nm source generates the greatest relative intensity and sharpest peaks in the low wave number region. Hence, the neutral polymer shows the greatest sensitivity to the gas phase probes with this source. Because it is part of the FT-Raman system, it further provides the most accurate determination of the band positions. Conversely, the 514.5 nm source appears to enhance the high wave number region and allows the most sensitive detection of changes to the 1575 cm^{-1} peak. Therefore, by varying the source wavelength, changes in band position and relative intensities are independently monitored. Changes in vibrational frequency are typically a result of intermolecular interactions and the shift of the 915 cm^{-1} peak to higher wave numbers is consistent with the formation of hydrogen bonds to the neutral polymer, inhibiting the deformation vibrations. Variations of relative intensities usually indicate an electronic

Can. J. Chem. Downloaded from www.nrcresearchpress.com by 80.90.12.36 on 09/08/12
For personal use only.

Fig. 6. Superposition of as-prepared polypyrrole in (*i*) helium and with (*ii*) toluene in helium using gas-cell and 514.5 nm source.

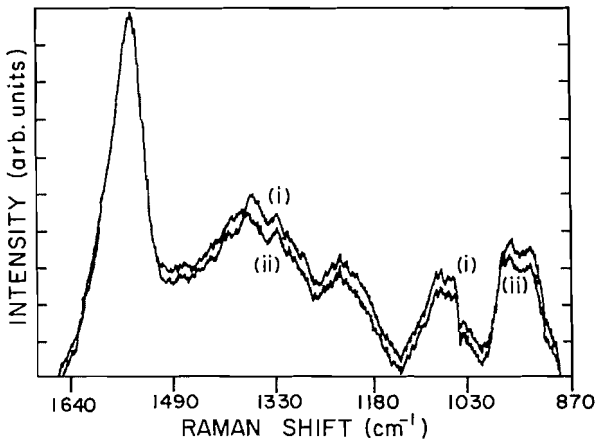

interaction and this is what is observed with the oxidized polymer. This suggests a different type of interaction, an electron donation through the cationic structures of the conducting polymer.

The magnitudes of the band shifts and enhancement are not very large but are reasonable for the low analyte levels being measured. The veracity of the effect is supported by the reproducibility of the phenomenon and the fact that the reversible nature of the interactions was detected in the cycle of pure He, gas-probe-in-He, and then the return to pure He. It is hoped that more polar probes will produce greater effects.

Comparison with microgravimetric analysis

Monitoring the gas phase interactions of polypyrrole with polymer-coated thickness–shear mode (TSM) piezoelectric crystals indicates two types of interactions, one through the neutral polymer and the other through the cationic (or dicationic) sites of the oxidized polymer. While the mass-based response to toluene is approximately two times greater with the neutral material than the oxidized polymer, hydrogen-bonding species such as water and methanol exhibit maximum degrees of interaction when the polymer is in an extreme oxidation state (i.e., after applying the most oxidizing or reducing potential). These observations are supported by the Raman results presented here. Again, two types of interaction are independently observed, one with the neutral polymer when the 1064 nm source is used and the other with the oxidized polymer using the 514.5 nm source.

Although both the neutral and oxidized states of polypyrrole act as electron acceptors, the two modes of interaction generate different spectral phenomena that appear to be determined by the oxidation state of the polymer. While water and methanol would be expected to interact through the -OH group with the neutral polymer, toluene must interact by another mode, perhaps by the overlap of the aromatic rings, yet the introduction of all species produces upward shifts of the 915 and 1035 cm^{-1} peaks. The response of the oxidized polymer also appears restricted; in this case only changes in relative intensities are observed, but a wider range of gas probes needs to be examined.

At least for the concentrations of the gas phase probes used in this study, there does not appear to be any spectral interference from the analytes. While this has been reported to be a limitation of analogous studies using IR spectroscopy, the Raman spectra presented here do not exhibit bands from the analytes themselves. On the other hand, the spectra yield no information about the importance of the role of polymer solvation as detected with the TSM piezoelectric crystals. The microgravimetric work suggests that in most cases a certain amount of analyte is retained upon return to pure helium and, in certain cases, an exchange between analyte and the original solvent (acetonitrile from the preparation of the polymer) occurs. The magnitude of these phenomena is a function of the oxidation state of the polymer and the relative strengths of the solvent and analyte interactions. The net retention of analyte is probably the reason for the incomplete recovery observed by Raman spectroscopy with both modes of interaction. However, as the upward shifts of the neutral polymer are quite small themselves and it is difficult to accurately quantify the relative intensity increases, no attempt was made to estimate the degree of retention.

Therefore, both the Raman spectra and the TSM piezoelectric sensors are useful techniques for the study of polypyrrole. Initially, TSM sensors appear to be far superior in their ability to provide quantitative data, but this must be tempered by the fact that the frequency shifts that are observed are also extremely sensitive to changes in the viscoelastic properties of the polymer that will occur from interactions with solvents. Caution must be exercised in their analysis. Therefore, several different techniques should be applied to the analysis of polypyrrole, and the sensitivity of Raman spectra to changes in the electronic states of conducting polymers makes it a powerful complementary method.

Conclusions

The electronic states of polypyrrole that are generated by the oxidation of the polymer are seen to couple with the experimental conditions used to obtain Raman spectra. Both relative intensities and band positions are functions of the excitation wavelength employed. This sensitivity towards the experimental conditions has been exploited to discriminate between interactions occurring with the neutral and oxidized segments of polypyrrole, which should help to better define their respective roles in the behavior of the conducting polymer. Information regarding the neutral polymer dominates the FT-Raman spectra while the behavior of the oxidized form dominates the spectra from the dispersive instrument with a source wavelength of 514.5 nm. Dispersive instruments are able to provide spectra with good resolution in a short time if restricted to small spectral windows, so improved sensitivity in detecting shifts of the 900–1100 cm^{-1} bands with the 514.5 nm source should be possible. Although only qualitative results have thus far been obtained with the gas phase probes, it was determined that both the neutral and oxidized components act as electron acceptors with the gas phase probes tested here, although probably by different mechanisms. A more complete correlation between the shifts and gas phase concentrations will follow and it will also be interesting to apply this methodology to cases where the polymer acts as an electron donor.

Acknowledgments

We are very grateful for support received from the Natural Sciences and Engineering Research Council of Canada. Also, assistance with experiments from X. Gu of the Ontario Laser and Lightwave Centre and G. Kovacs and C. Jennings of the Xerox Research Centre of Canada are gratefully acknowledged.

References

1. A.F. Diaz, K.K. Kanazawa, and G.P. Gardini. J. Chem. Soc. Chem. Commun. **635** (1979).
2. C.P. Andrieux, P. Audebert, P. Happiot, and J.-M. Saveant. J. Am. Chem. Soc. **112**, 2439 (1990).
3. Y. Son and K. Rajeshwar. J. Chem. Soc. Faraday Trans. **88**, 605 (1992).
4. M. Kofranek, T. Kovar, A. Karpfen, and H. Lischka. J. Chem. Phys. **96**, 4464 (1992).
5. J.G. Eaves, H.S. Munro, and D. Parker. Polym. Commun. **28**, 38 (1987).
6. S.J. Higgins and A. Hamnett. Electrochim. Acta, **36**, 2123 (1991).
7. S.J. Vigmond, K.M.R. Kallury, V. Ghaemmaghami, and M. Thompson. Talanta, **39**, 449 (1992).
8. S.J. Vigmond, K.M.R. Kallury, and M. Thompson. Anal. Chem. **64**, 2763 (1992).
9. G. Gustafsson, I. Lundström, B. Liedberg, C.R. Wu, O. Inganas, and O. Wennerstrom. Synth. Met. **31**, 163 (1989).
10. N.M. Ratcliffe. Anal. Chim. Acta, **239**, 257 (1990).
11. P.N. Bartlett and S.K. Ling-Chung. Sens. Actuators, **20**, 287 (1987).
12. J.M. Slater and E.J. Watt. Analyst, **116**, 1125 (1991).
13. P. Topart and M. Josowicz. J. Phys. Chem. **96**, 8662 (1992).
14. Y. Furukawa, S. Tazawa, Y. Fujii, and I. Harada. Synth. Met. **24**, 329 (1988).
15. H.R. Virdee and R.E. Hester. Croat. Chem. Acta, **61**, 357 (1988).
16. Y. Tesuka, J. Ohyama, T. Ishiii, and K. Aoki. Bull. Chem. Soc. Jpn. **64**, 2045 (1991).
17. D. Blackwood and M. Josowicz. J. Phys. Chem. **95**, 493 (1991).
18. C.S. Choi and H. Tachikawa. J. Am. Chem. Soc. **112**, 1757 (1990).
19. T. Inove, I. Hosoya, and T. Yamase. Chem. Lett. 563 (1987).
20. C.M. Jenden, R.G. Davidson, and T.G. Turner. Polymer, **34**, 1649 (1993).
21. J.J. Hearn, I.W. Fletcher, S.P. Church, and S.P. Armes. Polymer, **34**, 262 (1993).
22. V. Hernandez, F.J. Ramirez, G. Zotti, and J.T. Lopez Navarrete. Chem. Phys. Lett. **191**, 419 (1992).
23. Y. Furukawa, H. Ohta, A. Sakamoto, and A. Tasumi. Specrochim. Acta, **47A**, 1367 (1991).
24. C.J. Zhong, Z.Q. Tian, and Z.W. Tian. J. Phys. Chem. **94**, 2171 (1990).
25. Z. Deng, D.C. Stone, and M. Thompson. Can. J. Chem. **73**, 1427 (1995).
26. J. Bukowska and K. Jackowska. Synth. Met. **35**, 143 (1990).
27. M. Campos-Vallette, K.A. Figueroa, and C. Vargas. Spectrochim. Acta, **44A**, 601 (1988).
28. D. Battasti and R.J. Aroca. J. Am. Chem. Soc. **114**, 1201 (1992).

Can. J. Chem. Downloaded from www.nrcresearchpress.com by 80.90.12.36 on 09/08/12
For personal use only.

Anticipating molecular polarity 1: a back-of-the-envelope approach to topologically induced polarity in non-alternant monocycles

James Clayton Baum, Eric Donald Martin, Jack Leon Ginsburg, and Richard Francis Langler

Abstract: Perturbation theory is applied to fully π-bonded non-alternant monocycles at the Hückel level. An effective "back-of-the-envelope" approach is developed that permits one to anticipate Hückel charge patterns for these monocycles. Very little modification is required to alter the basic approach so that it will permit rapid anticipation of AM1-calculated charge patterns for such compounds.

Key words: hydrocarbon polarity, perturbation theory.

Résumé : On a appliqué la théorie perturbationnelle (au niveau de Hückel) à des monocycles complètement liés par des liaisons π non alternantes. On a développé une approche efficace «pouvant être effectuée sur le dos d'une enveloppe» qui permet d'anticiper les patrons de charge de Hückel de ces monocycles. Il suffit d'apporter des modifications mineures pour modifier l'approche de base et pour ainsi pouvoir arriver à une anticipation rapide des patrons de charge de tels composés, tels que calculés par AM1.

Mots clés : polarité de hydrocarbure, théorie perturbationnelle.

[Traduit par la rédaction]

Introduction

In an earlier study (1), we reached the conclusion that topologically induced polarity in some hydrocarbon ground states cannot be anticipated with aromaticity arguments. We have, therefore, sought to develop an approach that would be independent of aromaticity arguments. The present account describes a perturbational approach to anticipating topologically induced polarity in fully π-bonded non-alternant hydrocarbon monocycles (e.g., **1**).

Previous studies (1–3) have described non-alternant molecules with nonbonding electrons in their Lewis structures. This structural feature leads to extremes for hydrocarbon singlet-state polarity. We now examine fully π-bonded non-alternant monocycles.

Both π-ylides (e.g., **2**) and non-π-ylides (e.g., **3**) have nonbonding molecular orbitals (2) (NBMOs). The occupation or non-occupation of these NBMOs plays a pivotal role in determining their polarity. In graph-theoretical terms (4, 5), any fully π-bonded structure containing n carbon atoms must have at least one acyclic Sachs' graph s_n. Because non-alternant monocycles have no even-membered rings, there can be no cyclic Sachs' graphs s_n. Therefore, the constant term (a_n) in the characteristic polynomial cannot be zero. No fully π-bonded non-alternant hydrocarbon monocycle has an NBMO.

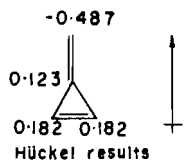

1

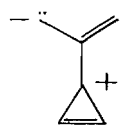

2

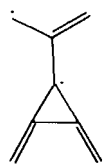

3

Methods

We now develop a method for deducing the nodal properties of the HOMOs and LUMOs of neutral even acyclic polyenes. If such an acyclic polyene has n carbon atoms, its HOMO will have (n/2)-1 nodes. *The HOMO nodal pattern may be rapidly generated by bringing together a set of ethylene HOMOs so that each contact point introduces a phase dislocation.*

Received May 16, 1995.

J.C. Baum and E.D. Martin. Department of Chemistry, Florida Institute of Chemistry, Melbourne, FL 32901, U.S.A.
J.L. Ginsburg. Department of Chemistry, St. Mary's University, Halifax, NS B3H 3C3, Canada.
R.F. Langler.[1] Department of Chemistry, Mount Allison University, Sackville, NB E0A 3C0, Canada.

[1] Author to whom correspondence may be addressed. Telephone and Fax: (506) 364-2361.

Can. J. Chem. Downloaded from www.nrcresearchpress.com by 46.23.64.124 on 09/08/12
For personal use only.

Can. J. Chem. Downloaded from www.nrcresearchpress.com by 46.23.64.124 on 09/08/12
For personal use only.

Scheme 1.

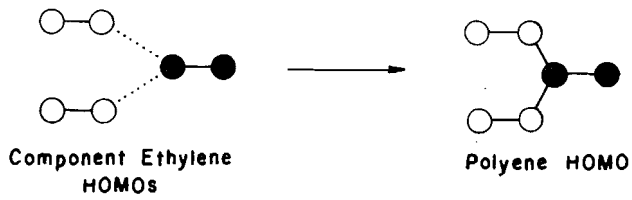

Every other atom in the polyene may be starred. From the Pairing Theorem (6), the LUMO's nodal properties may be deduced from those of the HOMO since the sign of each starred LUMO coefficient is reversed from that in the HOMO.

Scheme 2.

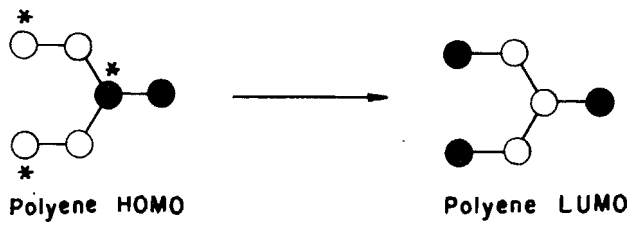

The nodal properties of the polyene LUMO may be deduced directly by bringing together a set of ethylene LUMOs so that each contact point introduces a bonding interaction.

Scheme 3.

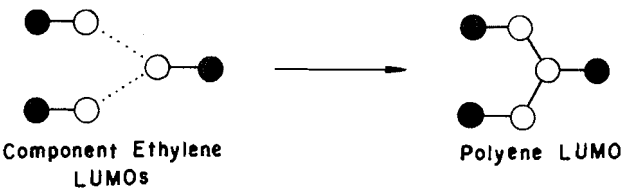

AM1 computations were done using the MOPAC 5 program (7).

Simple Hückel calculations were carried out in the usual way (assuming the orthogonality of adjacent p orbitals). Hückel calculations were also carried out in partially recombined fragments (bond integrals < β) in the same manner described previously (8) for pentadienyl and methine.

The orientations of dipole moments are indicated by arrows whose heads represents the *negative* end of the dipole.

Results and discussion

A. Anticipating polarization at the Hückel level

(i) Odd substituents

We applied a first-order perturbational analysis (9) to methylene cyclopropene **1**. First, envision two ethylene units "docking" to form methylene cyclopropene as shown in Scheme 4. The ethylene unit (C_1C_2) with two contact points will be called the "cap" and the ethylene unit (C_3C_4) with one contact point will be called the "stem."

Scheme 4.

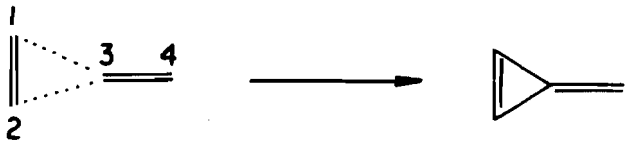

As the ethylene units dock, the stem and cap molecular orbitals mix. Table 1 presents the π-molecular orbitals (*i*) at the outset of this process, (*ii*) after docking (first-order molecular orbitals), and (*iii*) after docking (Hückel molecular orbitals for methylene cyclopropene **1**).

Table 1. Zeroth-order, first-order, and Hückel molecular orbitals for two ethylene units docking to form methylene cyclopropene (**1**) as depicted in Scheme 4.

Stage	Molecular orbitals
Zeroth order	ϕ_1: $0.500p_1 + 0.500p_2 + 0.500p_3 + 0.500p_4$
	ϕ_2: $0.500p_1 + 0.500p_2 - 0.500p_3 - 0.500p_4$
	ϕ_3: $0.707p_1 - 0.707p_2$
	ϕ_4: $0.707p_3 - 0.707p_4$
First order	ϕ_1: $0.471p_1 + 0.471p_2 + 0.707p_3 + 0.236p_4$
	ϕ_2: $0.471p_1 + 0.471p_2 - 0.236p_3 - 0.707p_4$
	ϕ_3: $0.707p_1 - 0.707p_2$
	ϕ_4: $0.371p_1 + 0.371p_2 - 0.632p_2 + 0.632p_4$
Methylene cyclopropene	ϕ_1: $0.522p_1 + 0.522p_2 + 0.611p_3 + 0.281p_4$
	ϕ_2: $0.368p_1 + 0.368p_2 - 0.253p_3 - 0.815p_4$
	ϕ_3: $0.707p_1 - 0.707p_2$
	ϕ_4: $0.302p_1 + 0.302p_2 - 0.749p_3 + 0.505p_4$

The polarization of the methylene cyclopropene **1** framework (Hückel level) can be deduced from ϕ_2 and ϕ_3 (see Table 1 and Scheme 4). ϕ_2 and ϕ_3 are "reverse polarizing," i.e., in ϕ_2 (occupied) the stem-derived portion has the largest coefficient(s) and in ϕ_3 (vacant) the cap-derived portion has the largest coefficient(s). Electron density is compartmentalized and the framework polarized so that the stem is electron-rich and the cap electron-deficient as shown in **1**.

Close examination of Hückel results for even non-alternant monocycles has led us to the following generalization. *The Polarity Postulate: polarity of the lowest-lying singlet state of any fully π-bonded even non-alternant hydrocarbon monocycle can be anticipated by inspection of a single pair of π-orbitals.*

The nodal properties of the polarizing orbitals (ϕ_2, ϕ_3 for methylene cyclopropene in Table 1) arise from a linear combination of the acyclic polyene frontier molecular orbitals (see the Methods section), i.e., $HOMO_{stem} - HOMO_{cap}$ leads to the nodal properties for the occupied polarizing orbital of the monocycle and $LUMO_{stem} + LUMO_{cap}$ leads to the nodal properties for the vacant polarizing orbital of the monocycle.

One of the polarizing orbitals for **1** (ϕ_3) is derived from a very weakly perturbed cap orbital. The weakness of the perturbation can be anticipated on the grounds that docking introduced two equal interactions, one bonding, one antibonding. Scheme 5 presents a generalized representation for the cap-weighted product orbital to cover those cases that lack symmetry and will then have small but non-zero stem coefficients in the final orbital.

The other polarizing orbital for **1** (ϕ_2) is derived from a strongly perturbed cap orbital. A strong perturbation is expected whenever *both* stem–cap interactions are bonding or *both* are antibonding. Not only does a strong perturbation pro-

Scheme 5.

duce a stem-weighted orbital but, for methylene cyclopropene (Table 1), a first-order perturbation introduces moderate mixing of ϕ_4 (zeroth order) with ϕ_2 (zeroth order). Thus, the stem-weighted orbital mixes $HOMO_{cap} - HOMO_{stem} + LUMO_{stem}$ with the greatest weight given to $HOMO_{stem}$, i.e., X > Y in Scheme 6.

Scheme 6.

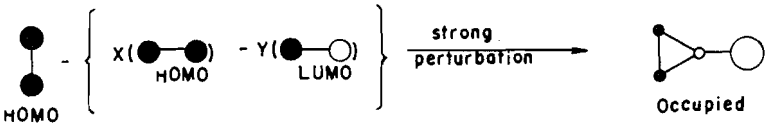

Application of this analysis leads to the following expectation for fulvene's stem-weighted polarizing orbital:

Scheme 7.

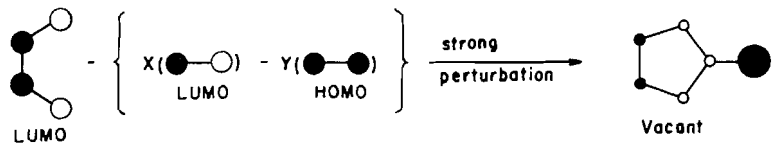

The relative magnitude of the coefficients in the stem-weighted polarizing orbital can be anticipated by mixing the stem frontier orbitals together with a weighting that favors the "primary" stem frontier orbital. In general, one can now expect that stem-weighted polarizing orbitals will have coefficients that alternate small, large, small, large ... over the stem portion of the orbital. Precisely this pattern emerges if one tracks the development of stem-weighted orbitals (at the Hückel level) as docking proceeds (see Scheme 8).

Scheme 8.

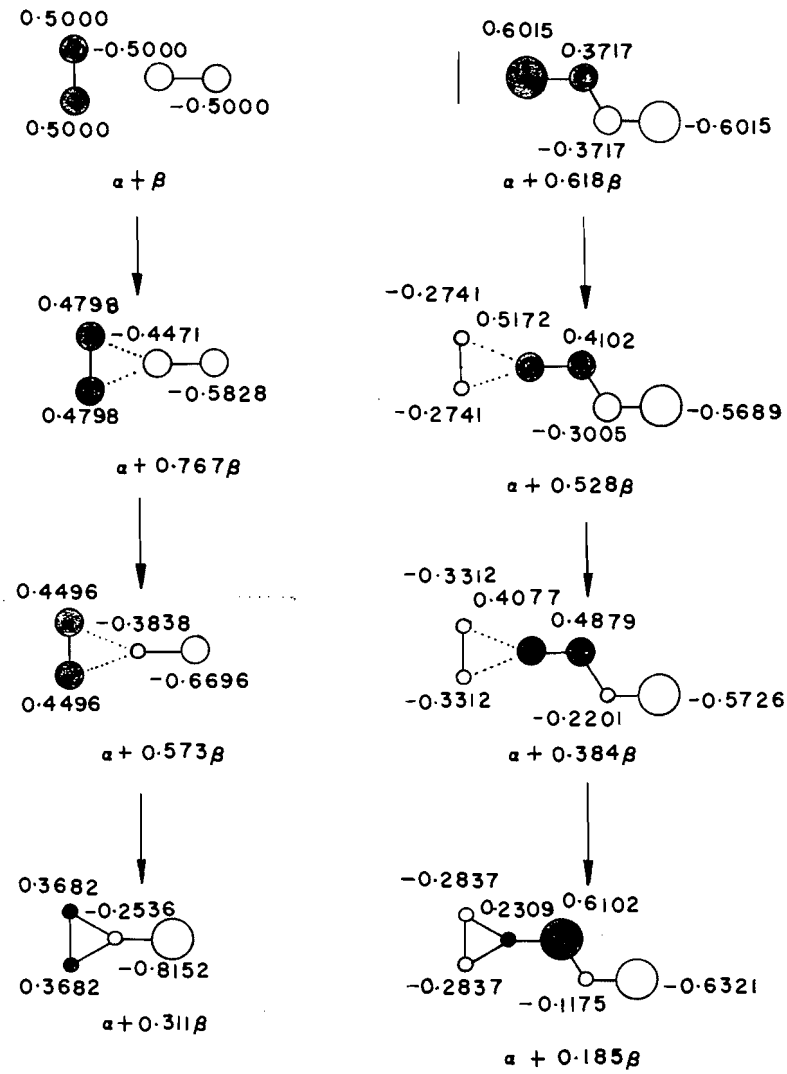

Can. J. Chem. Downloaded from www.nrcresearchpress.com by 46.23.64.124 on 09/08/12
For personal use only.

Can. J. Chem. Downloaded from www.nrcresearchpress.com by 46.23.64.124 on 09/08/12
For personal use only.

Dynamic polarity analyses: It is now clear that acyclic polyene frontier orbitals can be used to anticipate Hückel polarization for even non-alternant monocyclic singlets. Neither the relative magnitudes of the coefficients in the acyclic polyene frontier orbitals nor the nodal properties of the polarizing orbitals of the monocycle need be known. See Scheme 9 for a representative dynamic polarity analysis.

Scheme 9.

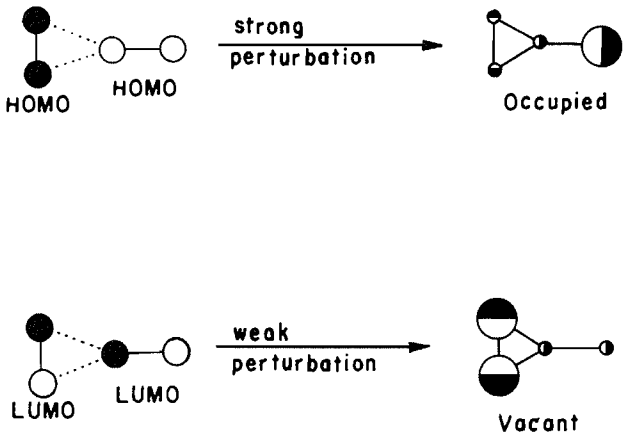

Deducing the polarity of a monocycle requires knowledge of both polarizing orbitals. If they are reverse-polarizing, the monocycle will have moderate polarity. The orientation of the dipole moment will be obvious from the forms of the polarizing orbitals. From Scheme 9, **1** is expected to have its dipole oriented as shown by the dipole arrow accompanying its structure.

Now consider the radialene **4**. Sequential disconnection of each odd substituent with subsequent docking as shown for methylene cyclopropene (Scheme 4) would lead to the conclusion that each exocyclic methylene in **4** has a large coefficient in the stem-weighted polarizing orbital. This analysis leads to the following generalization. *The Odd Substituent Rule: in the stem-weighted polarizing orbital of any fully π-bonded even non-alternant monocycle, all odd substituents are polarized in the same manner.*

Thus, the following dynamic polarity analysis is appropriate for the radialene **4**.

Scheme 10.

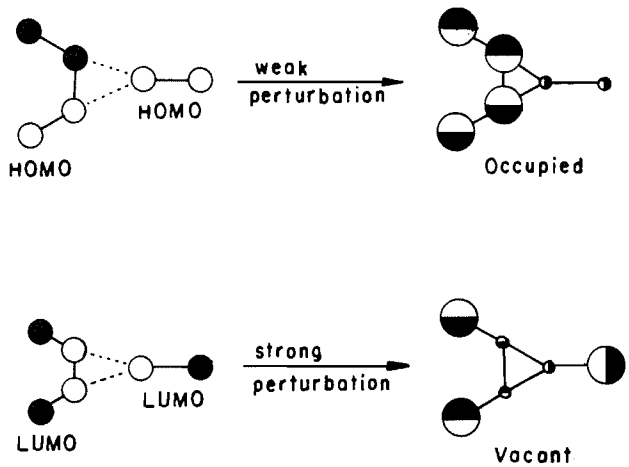

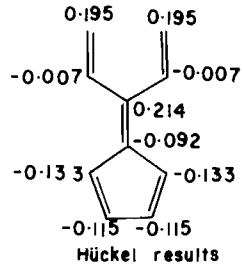

Because the polarizing orbitals for **4** have largest coefficients in common, the orbitals are *not* reverse-polarizing. Therefore, the radialene framework is not significantly polarized. An immediate consequence of the Odd Substituent Rule is that fully π-bonded non-alternant monocycles with one exocyclic double bond are moderately polarized while those with more than one exocyclic π-bond are nonpolar.

(ii) Even substituents

Consider the dynamic polarity analysis of the fulvene relative **5** presented in Scheme 11.

Scheme 11.

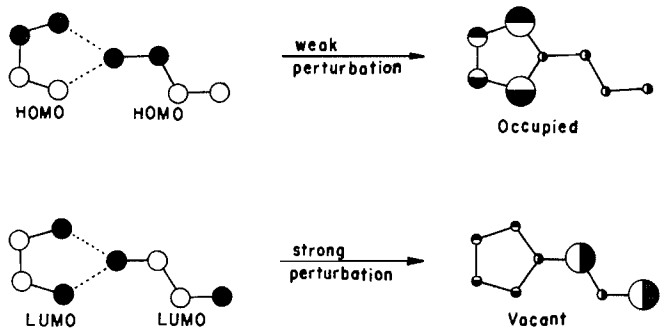

In general, the cap coefficients in the cap-weighted molecular orbital (MO) will be smaller than the large coefficients in the stem-weighted MO. All cap coefficients are large in the cap-weighted MO and only half of the stem-weighted coefficients are large in the stem-weighted MO. Consider the effect each type of site would have on a substituent were it to be appended to one of them. The stem atoms that have large coefficients in the stem-weighted polarizing orbital are strongly polarizing (active) and those with small coefficients are nonpolarizing (inactive). The cap atoms have moderate-sized coefficients in the cap-weighted MO and are therefore moderately polarizing (moderately active). The Hückel partial charges for some vinyl-substituted relatives of **5** are shown on **6**, **7**, and **8**. The foregoing discussion leads to the following generalization. *The Building Rule: if a polarized even non-*

Can. J. Chem. Downloaded from www.nrcresearchpress.com by 46.23.64.124 on 09/08/12
For personal use only.

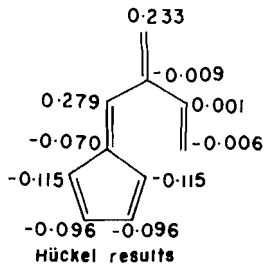

7

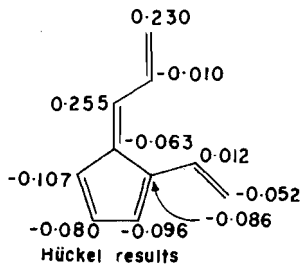

8

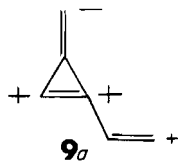

9*a*

alternant monocycle is modified by appending an even substituent to an inactive stem atom, the even substituent will not be polarized. An even substituent attached to any cap atom will be weakly polarized. An even substituent attached to an active stem atom will be strongly polarized.

B. Comparison of Hückel and AM1 results

A dynamic polarity analysis leads to the atomic charge distribution for the cap-substituted vinyl methylene cyclopropene shown on structure **9***a*. Hückel and AM1 calculated atomic charges are presented for several non-alternant monocycles as **9***b*, **9***c*, **10***a*, **10***b*, **11***a*, and **11***b*.

Quantitatively, AM1 results for lowest-lying singlet states indicate that fully π-bonded non-alternant monocycles have more weakly polarized frameworks than Hückel results suggest. If polarization is characterized by summing the partial positive charges accruing from the π-system alone, then Hückel polarization is typically about four times larger than AM1 polarization. Compare the Hückel results on **9***b* with the AM1 results on **9***c*.

Qualitatively, AM1 polarization of odd substituents is shorter range, fading faster as one moves through the substituent away from the ring (see **10***a* for Hückel results and **10***b* for AM1 results on the same structure). Even substituents appended to cap sites are always moderately polarized at the Hückel level. At the AM1 level, cap-appended even substituents are very weakly polarized except when attached to three-membered rings. AM1 support for the Building Rule as it applies to stem-appended even substituents is presented on structures **12** and **13**.

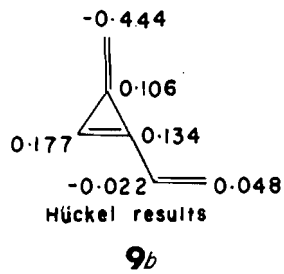

9*b*

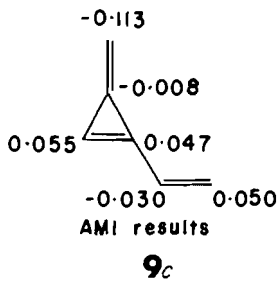

9*c*

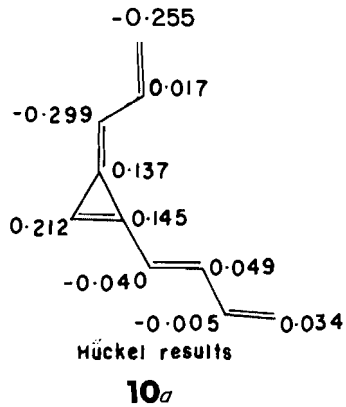

10*a*

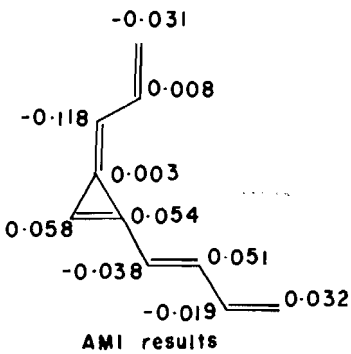

10*b*

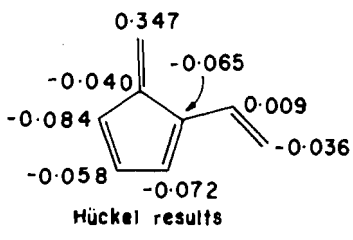

11*a*

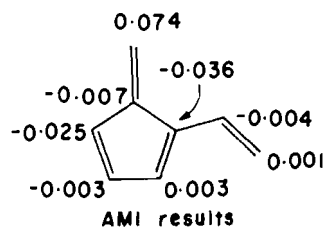

11*b*

C. Very rapid polarity analyses

From the generalizations presented heretofore, it is now possible to carry out extremely rapid "back-of-the-envelope" polarity analyses for non-alternant monocycles. First, if the fully π-bonded even non-alternant monocycle has more than one exocyclic double bond, it is not polarized (Odd Substituent Rule) and is of no interest. Second, for those structures having only one exocyclic double bond, partial charges (*c*) and (*c*′) will develop as shown on **A**. If the ring contains $4J + 3$ carbon atoms, *c* will be positive and *c*′ will be negative. If the ring contains $4J + 1$ carbon atoms, *c* will be negative and *c*′ will be positive. Polarity of even substituents is depicted on **A** (Building Rule).

While many of the compounds that we have examined computationally are not presently known, the three parent compounds have been prepared and their dipole moments

Table 2. Dynamic polarity analyses, expected charge patterns, and AMI atomic charges calculated from AMI π-electron population numbers.

Compound	Occupied orbital	Vacant orbital	Predicted charge pattern	AMI π-electron population numbers
1				
4				
9	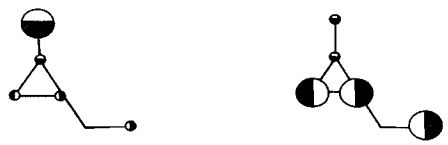			
14	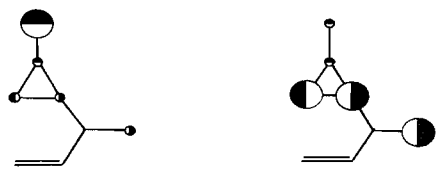			
15	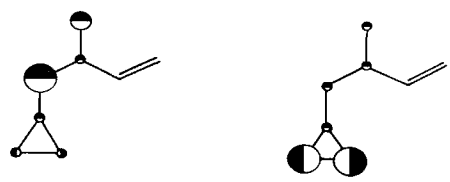			
16				
11	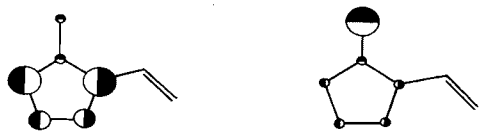			

Can. J. Chem. Downloaded from www.nrcresearchpress.com by 46.23.64.124 on 09/08/12
For personal use only.

Table 2. (*concluded*).

Compound	Occupied orbital	Vacant orbital	Predicted charge pattern	AMI π-electron population numbers
17	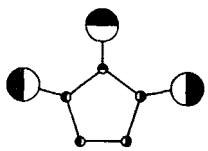	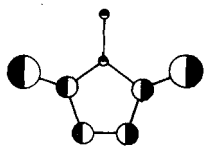	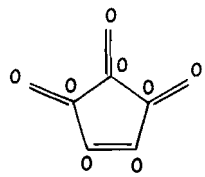	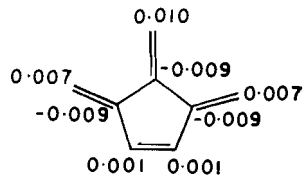
18	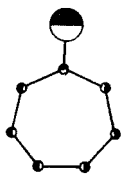	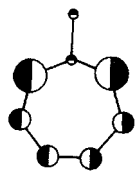	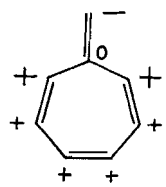	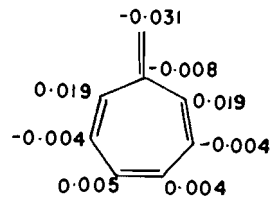
19	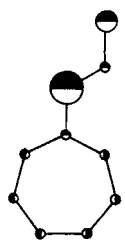	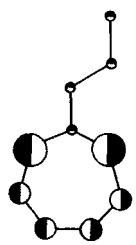	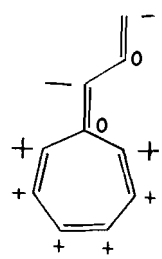	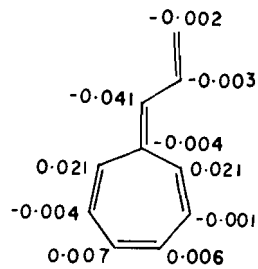
20	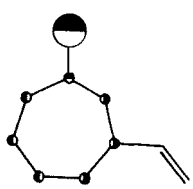	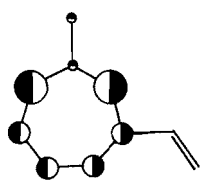	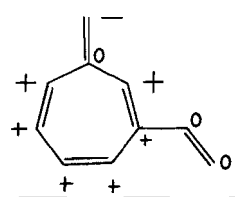	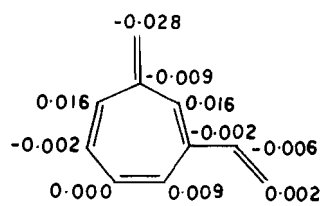

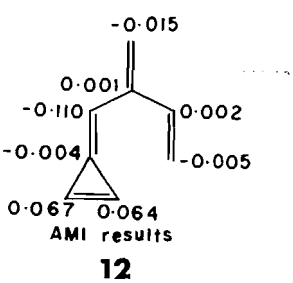

12

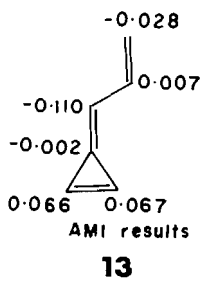

13

determined experimentally. Methylene cyclopropene has an AM1 dipole moment of 1.20 D and an experimental dipole moment (10) of 1.90 D. Fulvene has an AM1 dipole moment of 0.69 D and an experimental dipole moment (11) of 0.44 D. Heptafulvene has an AM1 dipole moment of 0.36 D and an experimental dipole moment (12) of 0.48 D.

Table 2 presents the relative magnitudes of the coefficients of the polarizing orbitals as deduced from dynamic polarity analyses, consequent charge patterns, and AM1-calculated

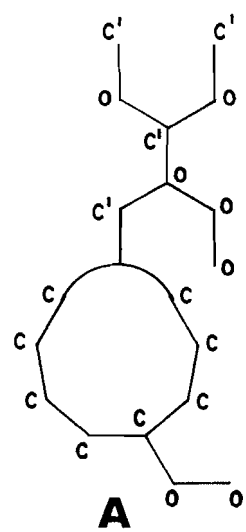

A

Can. J. Chem. Downloaded from www.nrcresearchpress.com by 46.23.64.124 on 09/08/12
For personal use only.

charge patterns for a modest selection of fully π-bonded non-alternant monocycles.

As might be expected from the ethylene LUMO coefficients, the cap atoms contained in polarized cyclopropenyl rings have similar AM1-calculated charge densities (see compounds **1** and **9** in Table 2). However, longer acyclic polyenes, e.g., butadiene, have frontier orbitals in which the coefficients of terminal carbon atoms are substantially larger than the coefficients for nonterminal carbon atoms. Thus, an examination of the HOMO of butadiene would lead to the expectation that the terminal cap atoms contained in polarized cyclopentadienyl rings should have much larger charges than nonterminal cap atoms. The AM1 results from compounds **11** and **16** in Table 2 offer support for such an expectation. Tabulated comparisons of dynamic polarity analyses and AM1 π-electron populations for an additional 42 non-alternant monocycles are available as supplementary material.[2]

Conclusions

Dynamic polarity analyses have been defined and developed for fully π-bonded non-alternant monocycles. They have led to a very rapid "back-of-the-envelope" scheme for qualitatively anticipating topologically induced polarity in such monocycles. These "back-of-the-envelope" predictions for charge patterns are in good agreement with AM1 molecular orbital computed polarities. This work provides an effective approach to predicting topologically induced polarity in non-alternant *bicycles* that will be described in due course.

[2] This material can be purchased from: The Depository of Unpublished Data, Document Delivery, CISTI, National Research Council Canada, Ottawa, Canada K1A OS2.

Acknowledgements

The authors gratefully acknowledge the use of computing facilities at both the Florida Institute of Technology and St. Mary's University.

References

1. R.F. Langler, J.L. Ginsburg, R. Snooks, and R.J. Boyd. J. Phys. Org. Chem. **4**, 566 (1991).
2. R.F. Langler and L. Precedo. Can. J. Chem. **68**, 939 (1990).
3. J.R. Dias. Tetrahedron Lett. **32**, 4659 (1991).
4. J.R. Dias. Molecular orbital calculations using chemical graph theory. Springer Verlag, Berlin. 1993.
5. N. Trinajstic. Chemical graph theory. Vol 1. CRC Press, Boca Raton, Fla. 1983. p. 50.
6. M.J.S. Dewar and R.C. Dougherty. The PMO theory of organic chemistry. Plenum Press, New York. 1975. p. 75.
7. J.P. Stewart. Program 455, Quantum Chemistry Program Exchange, Bloomington, Ind. 1991.
8. K.A. Durkin and R.F. Langler. J. Phys. Chem. **91**, 2422 (1987).
9. W.T. Borden. Modern molecular orbital theory for organic chemists. Prentice–Hall, Engelwood Cliffs, N.J. 1975.
10. T.D. Norden, S.W. Staley, W.H. Taylor, and M.D. Harmony. J. Am. Chem. Soc. **108**, 7912 (1986).
11. R.D. Brown, F.R. Burden, and J.E. Kent. J. Chem. Phys. **49**, 5542 (1968).
12. A. Bauder, C. Keller, and M. Neuenschwander. J. Mol. Spectrosc. **63**, 281 (1976).

Can. J. Chem. Downloaded from www.nrcresearchpress.com by 46.23.64.124 on 09/08/12
For personal use only.

Pyridine hydrobromide perbromide mediated regioselective heterocyclization of *ortho*-cyclohexenyl phenols[1]

Krishna C. Majumdar and Anup K. Kundu

Abstract: A number of 3,4-benzo-9-bromo-2-oxabicyclo[3.3.1]nonanes (**9***a–h*) are synthesized in almost quantitative yields by regioselective heterocyclization of *ortho*-cyclohexenyl phenols (**8***a–h*). The structures of 3,4-benzo-9-bromo-2-oxabicyclo[3.3.1]nonane **9** have been unambiguously settled by the synthesis of 9-chloromercuri-3,4-(4′-methoxybenzo)-2-oxabicyclo[3.3.1]nonane **13**, which has an X-ray determined structure, and by converting **13** to product **9***c* with bromine in sunlight in 45% yield. The 6-chloro-2-cyclohexenenyl phenol **8***i* and 2-cyclohexenyl-4-methyl phenol **8***j* failed to give any cyclic product but instead furnished the ring-brominated products **10***i* and **10***j*, respectively.

Key words: pyridine hydrobromide perbromide, regioselective heterocyclization, *ortho*-cyclohexenyl phenol, oxabicyclo[3.3.1]nonane, 6-*endo* trig.

Résumé : On a synthétisé un certain nombre de 3,4-benzo-9-bromo-2-oxabicyclo[3.3.1]nonanes (**9***a–h*) avec des rendements pratiquement quantitatifs en procédant à l'hétérocyclisation régiosélective d'*ortho*-cyclohexénylphénols (**8***a–h*). On a établi sans ambiguïté la structure du 3,4-benzo-9-bromo-2-oxabicyclo[3.3.1]nonane (**9**) en procédant à la synthèse du 9-chloromercuri-3,4-(4′-methoxybenzo)-2-oxabicyclo[3.3.1]nonane (**13**) dont on a déterminé la structure par diffraction des rayons X et que l'on a transformé en composé **9***c*, avec un rendement de 45%, par réaction du composé **13** avec du brome en présence de lumière solaire. Les 6-chloro-2-cyclohexénenylphénol (**8***i*) et 2-cyclohexényl-4-méthylphénol (**8***j*) ne donnent naissance à aucun produit cyclique; plutôt ils fournissent respectivement les produits bromés sur le cycle **10***i* et **10***j*.

Mots clés : perbromure du bromhydrate de pyridine, hétérocyclisation régiosélective, *ortho*-cyclohexénylphénol, oxabicyclo[3.3.1]nonane, cyclé 6-*endo*.

[Traduit par la rédaction]

Introduction

We recently reported (1) a one-step mercury(II) mediated regioselective heterocyclization of *ortho*-cyclohexenyl *N*-methylaniline **1** to 1-alkoxy *N*-methyl tetrahydrocarbazole **2** (Scheme 1). This was found to be much simpler than a three-step process we had reported earlier (2) for the cyclization of *ortho*-cyclohexenyl phenols. Our earlier method involved the regioselective cyclization of *ortho*-cyclohexenyl phenols **3** to chromans **6** in 50% overall yield in three steps (3), viz., (*i*) acetylation of the phenolic -OH, (*ii*) addition of bromine to the cyclohexenyl bond, and (*iii*) internal nucleophilic attack at the C3 carbon of the cyclohexenyl side chain in alcoholic potassium hydoxide (Scheme 2). It was necessary to deactivate the phenol ring towards electrophilic attack by acetylation to avoid any ring bromination and as a consequence three steps were necessary to complete the cyclization for the introduction of a bromine in the newly formed pyran ring (Scheme 2). Our recent work on the regioselective synthesis of a number of heterocycles (4) prompted us to search for a simple and efficient reagent for this heterocyclization. We have recently achieved a facile entry to this ring system **6** (5) with the use of a well-known brominating agent, pyridine hydrobromide perbromide, which we report here.

Scheme 1.

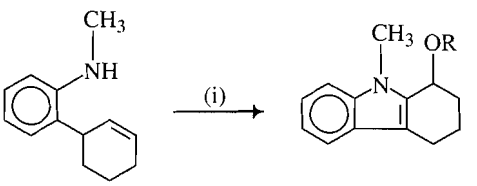

1 **2**

The starting materials *ortho*-cyclohexenyl phenols **8***a–j* were prepared (6) by the Claison rearrangement of 3-aryloxy cyclohexenes **7** (Scheme 3).

Received March 9, 1995.

This paper is dedicated to Professor B.S. Thyagarajan of the University of Texas at San Antonio, on the occasion of his 65th birth anniversary.

K.C. Majumdar[2] and A.K. Kundu. University of Kalyani, Kalyani-741235 W.B., India.

[1] For a preliminary report see ref. 14.
[2] Author to whom correspondence may be addressed.

Can. J. Chem. Downloaded from www.nrcresearchpress.com by 46.23.64.124 on 09/08/12
For personal use only.

Scheme 2.

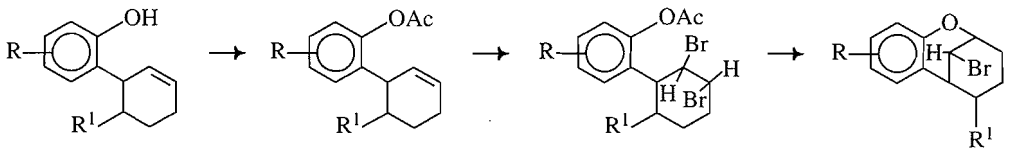

3 4 5 6

Scheme 3. Reagents: (i) $PhNEt_2/\Delta$.

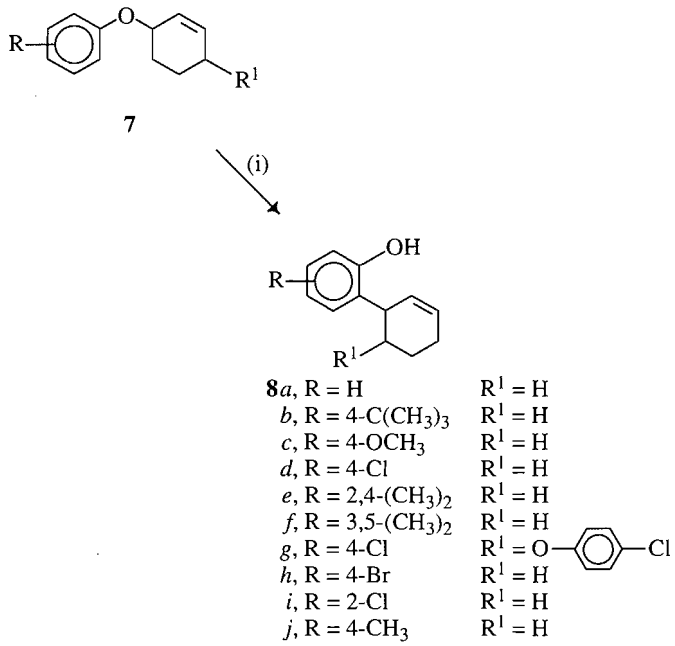

7

8*a*, R = H, R^1 = H
b, R = 4-$C(CH_3)_3$, R^1 = H
c, R = 4-OCH_3, R^1 = H
d, R = 4-Cl, R^1 = H
e, R = 2,4-$(CH_3)_2$, R^1 = H
f, R = 3,5-$(CH_3)_2$, R^1 = H
g, R = 4-Cl, R^1 = O-Ph-Cl
h, R = 4-Br, R^1 = H
i, R = 2-Cl, R^1 = H
j, R = 4-CH_3, R^1 = H

Results and discussion

ortho-Cyclohexenyl phenyl **8***a* was magnetically stirred with one equivalent of pyridine hydrobromide perbromide in dichloromethane at 0–5°C for 2 h. The reaction was monitored by tlc. A low-melting solid was obtained in 92% yield. Elemental analysis and spectral data indicated this to be 3,4-benzo-9-bromo-2-oxabicyclo[3.3.1]nonane **9***a*. Substrates **8***b–h* successfully underwent cyclization regioselectively to give 3,4-benzo-9-bromo-2-oxabicyclo[3.3.1]nonanes **9***b–h* in 90–96% (isolated) yields (Scheme 4). Altogether 10 different substrates were used for this study. Two substrates (**8***i* and **8***j*) did not give the cyclized product. 6-Chloro-2-cyclohexenyl phenol **8***i* and 2-cyclohexenyl-4-methyl phenol **8***j* furnished ring-brominated products, viz., 4-bromo-6-chloro-2-cyclohexenyl phenol **10***i* and 6-bromo-2-cyclohexenyl-4-methyl phenol **10***j*, respectively, instead of the cyclized product (Scheme 4). At present we do not know why **8***j* should not cyclize. Both 4-methoxy and 4-chloro (**8***c* and **8***d*) do and it is difficult to explain why the electronically intermediate and sterically identical **8***j* should not. The other case that does not cyclize, **8***i*, can perhaps be understood as a steric issue but here too the 2,4-dimethyl compound **8***e* does cyclize satisfactorily. This remains inexplicable.

The formation of product **9** may be explained by the formation of cyclic bromonium ion **11** followed by a 6-"*endo*" cyclization (7) to give **9** (Scheme 5). The cyclization of the proposed bromonium intermediate **11** is facile under such a mild condition perhaps due to favourable juxtaposition of the reacting functionalities to give a stable bicyclic product **9**. The reaction becomes faster in a mixture of solvents, viz., a 1:1 mixture of dichloromethane and methanol. The reaction is complete in 30–40 min instead of 2 h as was required in dichloromethane alone.

The alternative mode of cyclization by a 5-"*exo*"-trig to give **12** is discarded as the products obtained, **9**, remain unaffected when refluxed with potassium cyanide in acetone in presence of potassium iodide (8) or when refluxed with ethanolic potassium hydroxide (9) (12%) for 4 h. An unequivocal proof for the structure of product **9** is provided by means of a transformation route. Compound **8***c* was converted to **13**, the structure of which has been determined by X-ray (10). Compound **13** was then treated with bromine under sunlight to give the product **9***c* in 45% yield (Scheme 6).

The high-field (400 MHz) ^{1}H NMR spectrum of the compound **9***c* showed three lone protons: at δ 4.09–4.17 assignable to proton H_a, at δ 4.75–4.82 assignable to proton H_b, and at δ 3.53–3.59 assignable to proton H_c. The signal at δ 4.09–4.17 due to H_a appeared as a seven-line multiplet; however, careful expansion of the region showed eight lines (ddd, J = 6.86, 4.28, and 10.15 Hz). The signal at δ 4.75–4.82 due to H_b appeared as a triplet, which again on careful expansion appeared as a doublet of doublets with coupling constants J = 6.86 and 6.40 Hz. The signal at δ 3.53–3.59, which initially appeared as an AB quartet, again on careful expansion was found to be a doublet of triplets with coupling constants J = 6.80 and 6.40 Hz. The proton assignments were made from a 2D spectrum and proton decoupling experiments. A Dreiding model of compound **9** can be constructed by 1,3-fusion of the pyran ring in the half-chair conformation with the cyclohexane ring in the chair conformation (distorted) as shown in Fig. 1. However, the coupling constant of 10.15 Hz cannot be explained if the molecule **9***c* attains this conformation. The alternative model that can be constructed, again by 1,3-fusion of the pyran ring in the half-chair form with the cyclohexane ring in the boat (distorted) form, is shown in Fig. 2. The coupling constant J = 10.15 Hz can be explained if the molecule **9** attains this conformation. It may be noted that [3,3,1]bicyclononane is known to be in the chair-boat conformation (11). The 100 MHz ^{1}H NMR spectra of compounds **9***a*, *b*, *d–h* were then compared with the ^{1}H NMR (100 MHz) spectrum of compound **9***c* for which high-field ^{1}H NMR is available. The ^{1}H NMR pattern is found to be similar except for the aromatic region, due to ring substitution.

It is relevant to mention here that on treatment with pyridine hydrobromide perbromide under similar conditions 3-cyclohexenyl-4-hydroxy coumarin **14** afforded only the tribromo derivative **15** (4*b*), and 3-cyclopentenyl-4-hydroxy coumarin **16** furnished the linearly fused furochromone derivative **17** (12).

Pyridine hydrobromine perbromide is a mild reagent and

Can. J. Chem. Downloaded from www.nrcresearchpress.com by 46.23.64.124 on 09/08/12
For personal use only.

Scheme 4. Reagents: (i) $PyHBr_3/CH_2Cl_2$.

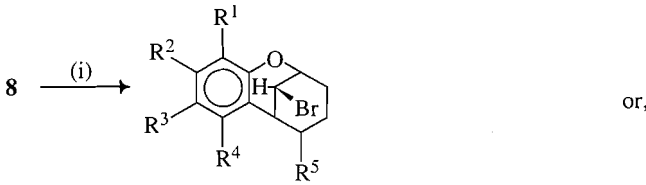

or,

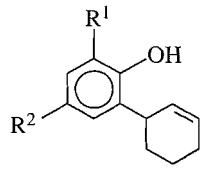

9*a*, $R^1 = R^2 = R^3 = R^4 = R^5 = H$
b, $R^1 = R^2 = R^4 = R^5 = H$, $R^3 = C(CH_3)_3$
c, $R^1 = R^2 = R^4 = R^5 = H$, $R^3 = OCH_3$
d, $R^1 = R^2 = R^4 = R^5 = H$, $R^3 = Cl$
e, $R^1 = R^3 = CH_3$, $R^2 = R^4 = R^5 = H$
f, $R^1 = R^3 = R^5 = H$, $R^2 = R^4 = CH_3$
g, $R^1 = R^2 = R^4 = H$, $R^3 = Cl$, $R^5 = O$— 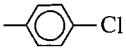
h, $R^1 = R^2 = R^4 = R^5 = H$, $R^3 = Br$

10*i*, $R^1 = Cl$
$R^2 = Br$
j, $R^1 = Br$
$R^2 = CH_3$

Scheme 5.

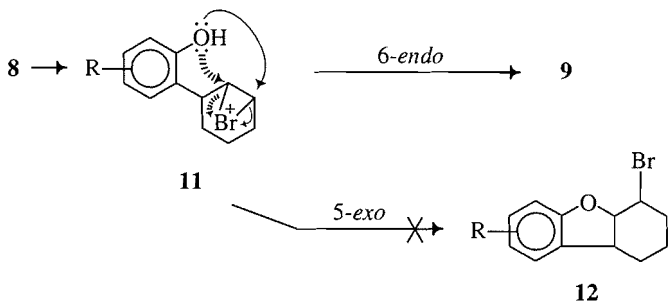

Scheme 6. Reagents: (i) Br_2-$CHCl_3/h\nu$.

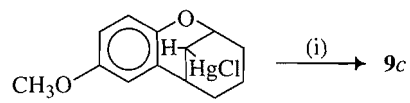

Scheme 7. Reagents: (i) $PyHBr_3/CH_2Cl_2$.

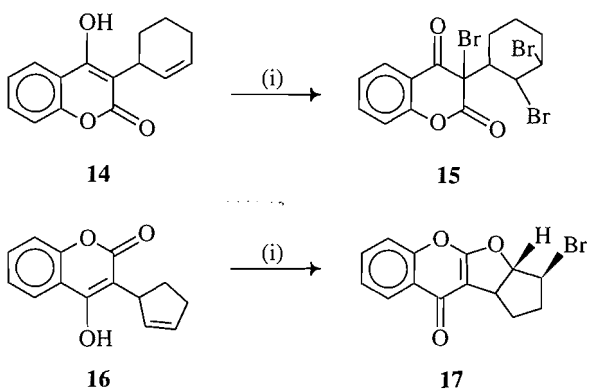

reacts at a low temperature. It is superior, as in most cases (except in case of **8***i* and **8***j*) it does not seem to affect the aromatic ring of the phenol due to rapid formation of bromonium ion and its cyclization before any ring bromination can take place. Thus deactivation by acetylation is not necessary and the additional base treatment (Step iii) is avoided. Pyridine hydrobromide perbromide had earlier been selectively used

Fig. 1.

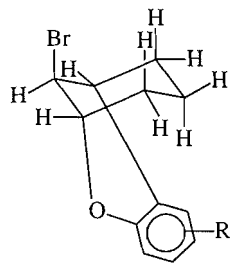

Fig. 2.

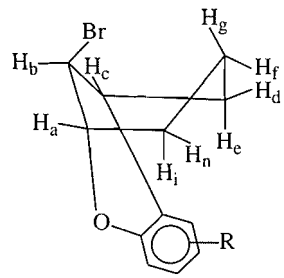

for nuclear bromination of phenols (13). Another method of entry to 3,4-benzo-9-bromo-2-oxabicylo[3.3.1]nonane of the type **9** may involve oxymercuration and replacement of the chloromercury group by bromine, which is a relatively low-yield (10) (overall) process. The methodology presented here is mild, chemoselective, and gives 3,4-benzo-9-bromo-2-oxabicyclo[3.3.1]nonanes in almost quantitative yields.

Experimental

Melting points were determined in a sulphuric acid bath and are uncorrected. UV absorption spectra were recorded in EtOH on a Hitachi 200-20 spectrophotometer (λ_{max} in nm) and IR spectra in KBr discs on a Perkin–Elmer 1330 apparatus (ν_{max} in cm^{-1}). ^1H NMR spectra were run in $CDCl_3$ with $SiMe_4$ as internal standard on a Jeol Fx-100 (100 MHz) instrument at the Indian Institute of Chemical Biology, Calcutta (chemical shifts in δ, ppm). Elemental analyses and mass spectra were recorded by RSIC (CDRI), Lucknow. Silica gel (60–120 mesh) was obtained from Qualigen and aluminium oxide (basic) from SRL. Extracts were dried over anhydrous sodium sulphate.

Can. J. Chem. Downloaded from www.nrcresearchpress.com by 46.23.64.124 on 09/08/12
For personal use only.

Can. J. Chem. Downloaded from www.nrcresearchpress.com by 46.23.64.124 on 09/08/12
For personal use only.

Preparation of compounds 7*a–j*

Compounds **7***a* (6), **7***c* (10), and **7***g* (2) were prepared according to published procedures.

General procedure for the preparation of compound **7**b, d–f, h–j

A mixture of phenol (0.02 mol), 3-bromocyclohexene (0.02 mol), and anhydrous K_2CO_2 (4 g) was refluxed in dry acetone (100 mL) on a water bath for 10 h. The reaction mixture was then cooled, filtered, and the solvent was removed. The residual mass was extracted with $CHCl_3$ (3 × 50 mL). The $CHCl_3$ extract was washed with potassium hydroxide solution (20%) to remove unreacted phenol, then with brine (3 × 50 mL), and dried (Na_2SO_4). The solvent was removed and the crude mass was chromatographed over aluminium oxide (basic, SRL) using petroleum ether (60–80°C) as eluant to give compounds **7***b*, **7***d–f*, **7***h–j*.

Compound **7**b*:* Viscous oil (89%), UV (EtOH), λ_{max}: 277 (log ϵ 3.10), 226 (log ϵ 3.83) nm; IR (KBr), ν_{max}: 3010, 2940, 1600, 1500, 1380, 1280, 1230, and 1160 cm^{-1}; ^1H NMR (100 MHz; $CDCl_3$–TMS), δ: 1.30 (s, 9H), 1.68–2.08 (m, 6H), 4.68–4.88 (bs, 1H), 5.84–6.08 (m, 2H), 6.80–6.96 (m, 2H), and 7.20–7.40 (m, 2H). Anal. calcd. for $C_{16}H_{22}O$: C 83.48, H 9.56%; found: C 83.25, H 9.45%.

Compound **7**d*:* Viscous oil (88%), UV (EtOH), λ_{max}: 283 (log ϵ 2.99), 230 (log ϵ 3.73) nm; IR (KBr), ν_{max}: 3120, 2936, 1594, 1488, 1235, and 1169 cm^{-1}; ^1H NMR (400 MHz; $CDCl_3$–TMS), δ: 1.50–2.20 (m, 6H), 4.74 (s, 1H), 5.80–5.88 (m, 1H), 5.94–6.01 (m, 1H), 6.80–6.88 (m, 2H), and 7.18–7.28 (m, 2H). Anal. calcd. for $C_{12}H_{13}ClO$: C 69.06, H 6.23%; found: C 69.12, H 6.05%.

Compound **7**e*:* Viscous oil (87%), UV (EtOH), λ_{max}: 279 (log ϵ 3.10), 226 (log ϵ 3.69) nm; IR (KBr), ν_{max}: 3010, 2920, 1600, 1480, 1380, 1240, 1210, and 1120 cm^{-1}; ^1H NMR (100 MHz; $CDCl_3$–TMS), δ: 1.60–2.12 (m, 6H), 2.20 (s, 3H), 2.28 (s, 3H), 4.64–4.92 (bs, 1H), 5.84–6.12 (m, 2H), and 6.72–7.16 (m, 3H). Anal. calcd. for $C_{14}H_{18}O$: C 83.17, H 8.91%; found: C 83.01, H 8.65%.

Compound **7**f*:* Viscous oil (85%), UV (EtOH), λ_{max}: 275 (log ϵ 3.44), 224 (log ϵ 3.70) nm; IR (KBr), ν_{max}: 3010, 2925, 1585, 1450, 1310, 1290, 1150, and 1060 cm^{-1}; ^1H NMR (100 MHz; $CDCl_3$–TMS), δ: 1.64–2.12 (m, 6H), 2.28 (s, 6H), 4.64–4.84 (bs, 1H), 5.84–6.00 (m, 2H), and 6.56 (s, 3H). Anal. calcd. for $C_{14}H_{18}O$: C 83.17, H 8.91%; found: C 83.47, H 9.12%.

Compound **7**h*:* Viscous oil (88%), UV (EtOH), λ_{max}: 208 (log ϵ 3.78), 229 (log ϵ 4.14), 282 (log ϵ 3.13) nm; IR (KBr), ν_{max}: 3120, 2940, 1590, 1490, 1410, 1290, 1245, and 1180 cm^{-1}; ^1H NMR (100 MHz; $CDCl_3$–TMS), δ: 1.54–2.38 (m, 6H), 4.58–4.86 (bs, 1H), 5.70–6.14 (m, 2H), 6.70–6.98 (m, 2H), and 7.28–7.66 (m, 2H). Anal. calcd. for $C_{12}H_{13}BrO$: C 56.91, H 5.13%; found: C 56.82, H 5.31%.

Compound **7**i*:* Viscous oil (82%), UV (EtOH), λ_{max}: 280 (log ϵ 2.63), 205 (log ϵ 3.64) nm; IR (KBr), ν_{max}: 3020, 2930, 1580, 1470, 1440, 1270, 1240, and 1050 cm^{-1}; ^1H NMR (100 MHz; $CDCl_3$–TMS), δ: 1.60–2.56 (m, 6H), 4.60–4.96 (m, 1H), 5.72–6.20 (m, 2H), and 6.76–7.60 (m, 4H). Anal. calcd. for $C_{12}H_{13}ClO$:C 69.06, H 6.23%; found: C 69.48, H 6.35%.

Compound **7**j*:* Viscous oil (90%), UV (EtOH), λ_{max}: 226 (log ϵ 3.77), 280 (log ϵ 2.89) nm; IR (KBr), ν_{max}: 3020, 2930, 1610, 1510, 1395, 1242, 1180, and 1038 cm^{-1}; ^1H NMR (100 MHz; $CDCl_3$–TMS), δ: 1.59–2.19 (m, 6H), 2.28 (s, 3H), 4.63–4.99 (bs, 1H), 5.75–6.15 (m, 2H), and 6.71–7.23 (m, 4H). Anal. calcd. for $C_{13}H_{16}O$:C 82.98, H 8.51%; found: C 82.80, H 8.32%.

Claisen rearrangement of compounds **7**a–j

Compounds **8***a* (6), **8***c* (10), and **8***g* (2) were prepared according to published procedure.

General procedure for the Claisen rearrangement of compounds **7***b*, d–f, h–j

Compound **7***b*, *d–f*, *h–j* (1 g) was refluxed in *N*,*N*-diethylaniline (5 mL) for 16 h. The reaction mixture was cooled and poured into ice-cold dilute (1:1) hydrochloric acid and extracted with $CHCl_3$. The extract was washed with dilute hydrochloric acid, brine, and water and dried (Na_2SO_4). Evaporation gave the crude product, which was chromatographed over aluminium oxide (basic, SRL). Elution of the column with benzene gave compounds **8***b*, *d–f*, *h–j*.

Compound **8**b*:* Gummy mass (87%), UV (EtOH), λ_{max}: 279 (log ϵ 3.50), 223 (log ϵ 3.95) nm; IR (KBr), ν_{max}: 3490, 3018, 2950, 1608, 1449, 1499, 1363, 1266, and 1092 cm^{-1}; ^1H NMR (100 MHz; $CDCl_3$–TMS), δ: 1.30 (s, 9H), 1.60–2.00 (m, 6H), 3.40–3.72 (bs, 1H), 5.28 (s, 1H), 5.76–6.20 (m, 2H), 6.68–6.84 (m, 1H), and 7.08–7.28 (m, 2H). Anal. calcd. for $C_{16}H_{22}O$: C 83.48, H 9.56%; found: C 83.78, H 9.77%.

Compound **8**d*:* Gummy mass (74%), UV (EtOH), λ_{max}: 284 (log ϵ 3.07), 228 (log ϵ 3.84) nm; IR (KBr), ν_{max}: 3400, 3000, 2910, 1580, 1410, 1260, 1210, 1160, and 1110 cm^{-1}; ^1H NMR (100 MHz; $CDCl_3$–TMS), δ: 1.60–2.00 (m, 6H), 3.44–3.68 (bs, 1H), 5.28 (s, 1H), 5.68–5.88 (m, 1H), 6.00–6.20 (m, 1H), 6.68–6.80 (m, 1H), and 7.00–7.20 (m, 2H). Anal. calcd. for $C_{12}H_{13}ClO$: C 69.06, H 6.23%; found: C 69.42, H 6.13%.

Compound **8**e*:* Gummy mass (75%), UV (EtOH), λ_{max}: 280 (log ϵ 3.19), 223 (log ϵ 3.72) nm; IR (KBr), ν_{max}: 3460, 3120, 2910, 1640, 1445, 1400, 1295, 1185, and 1035 cm^{-1}; ^1H NMR (100 MHz; $CDCl_3$–TMS), δ: 1.60–1.96 (m, 6H), 2.16 (s, 3H), 2.20 (s, 3H), 3.36–3.60 (bs, 1H), 5.24 (s, 1H), 5.72–6.16 (m, 2H), 6.76 (s, 1H), and 6.80 (s, 1H). Anal. calcd. for $C_{14}H_{18}O$: C 83.17, H 8.91%; found: C 83.29, H 8.74%.

Compound **8**f*:* Gummy mass (72%), UV (EtOH), λ_{max}: 282 (log ϵ 3.33), 223 (log ϵ 3.91) nm; IR (KBr), ν_{max}: 3464, 3014, 2926, 1621, 1572, 1455, 1283, 1212, 1170, and 1056 cm^{-1}; ^1H NMR (100 MHz; $CDCl_3$–TMS), δ: 1.62–2.04 (m, 6H), 2.22 (s, 3H), 2.26 (s, 3H), 3.60–3.84 (bs, 1H), 5.88–6.28 (m, 3H), and 6.56 (s, 2H). Anal. calcd. for $C_{14}H_{18}O$: C 83.17, H 8.91%; found: C 83.46, H 8.61%.

Compound **8**h*:* Viscous oil (75%), UV (EtOH), λ_{max}: 209 (log ϵ 3.96), 284 (log ϵ 3.27) nm; IR (KBr), ν_{max}: 3445, 3160, 1670, 1405, 1265, 1215, and 1105 cm^{-1}; ^1H NMR (100 MHz; $CDCl_3$–TMS), δ: 1.55–2.35 (m, 6H), 3.35–3.75 (m, 1H), 5.31 (s, 1H), 5.63–5.91 (m, 1H), 5.95–6.27 (m, 1H), and 6.55–7.24 (m, 3H). Anal. calcd. for $C_{12}H_{13}BrO$: C 56.91, H 5.13%; found: C 56.98, H 5.23%.

Compound **8**i*:* Gummy mass (87%), UV (EtOH), λ_{max}: 277 (log ϵ 2.65), 206 (log ϵ 3.92) nm; IR (KBr), ν_{max}: 3520, 3140, 2925, 1595, 1445, 1400, 1325, 1240, 1190, and 1070 cm^{-1}; ^1H NMR (100 MHz; $CDCl_3$–TMS), δ: 1.60–2.28 (m, 6H), 3.64–4.00 (m, 1H), 5.52–5.84 (m, 2H), 5.88–6.12 (m, 1H), 6.84 (t, J = 8 Hz, 1H), and 7.04–7.44 (m, 2H). Anal. calcd. for $C_{12}H_{13}ClO$: C 69.06, H 6.23%; found: C 69.53, H 6.39%.

Compound **8**j*:* Gummy mass (77%), UV (EtOH), λ_{max}: 282

Can. J. Chem. Downloaded from www.nrcresearchpress.com by 46.23.64.124 on 09/08/12
For personal use only.

(log ε 3.19), 222 (log ε 3.63) nm; IR (KBr), ν_{max}: 3430, 3010, 2910, 1690, 1610, 1570, 1480, 1440, 1400, 1250, and 1130 cm^{-1}; ^1H NMR (100 MHz; $CDCl_3$–TMS), δ: 1.60–2.16 (m, 6H), 2.24 (s, 3H), 3.36–3.72 (bs, 1H), 5.20 (s, 1H), 5.68–6.20 (m, 2H), and 6.72–7.12 (m, 3H). Anal. calcd. for $C_{13}H_{16}O$: C 82.98, H 8.51%; found: C 82.77, H 8.71%.

General procedure for the cyclization of compounds ***8***a–j

The brominating agent, solid pyridine hydrobromide perbromide (1 mmol), was added to a methylene chloride solution (20 mL) of the compounds ***8****a–j* (1 mmol). The reaction mixture was then stirred for 2 h on a magnetic stirrer at 0–5°C. After completion of the reaction (monitored by tlc), the mixture was washed with 5% $NaHCO_3$ solution (3 × 25 mL) and water (3 × 25 mL), and dried (Na_2SO_4). The residual mass, after removal of the solvent, was subjected to column chromatography over silica gel using petroleum ether (40–60°C) as eluant to give cyclization product ***9****a–h*, but two substrates (***8****i* and ***8****j*) did not give cyclized product. In these cases, ring-brominated products **10***i* and **10***j* were obtained. When the solvent was changed to a 1:1 mixture of dichloromethane and methanol the reaction was complete in 30–40 min.

Compound ***9***a*:* mp 38°C (92%), UV (EtOH), λ_{max}: 280 (log ε 3.54), 223 (log ε 3.77) nm; IR (KBr), ν_{max}: 3040, 2920, 1590, 1465, 1450, 1220, 1200, 1175, and 1105 cm^{-1}; ^1H NMR (100 MHz; $CDCl_3$–TMS), δ: 1.68–2.08 (m, 6H), 3.44–3.74 (dt ≈ q, J = 6.80, 6.40 Hz H_c), 4.08–4.28 (ddd, J = 10.15, 6.86, 4.28 Hz, H_a), 4.72–4.96 (dd ≈ t, J = 6.86, 6.40 Hz, H_b), and 6.80–7.36 (m, 4H); *m/z*: 252, 254 (M^+). Anal. calcd. for $C_{12}H_{13}BrO$: C 56.92, H 5.14%; found: C 57.13, H 5.26%.

Compound ***9***b*:* mp 68°C (93%), UV (EtOH), λ_{max}: 283 (log ε 3.44), 226 (log ε 3.75) nm; IR (KBr), ν_{max}: 3030, 2940, 1600, 1470, 1350, 1250, 1200, 1170, and 1110 cm^{-1}; ^1H NMR (100 MHz; $CDCl_3$–TMS), δ: 1.28 (s, 9H), 1.76–2.16 (m, 6H), 3.42–3.76 (dt ≈ q, J = 6.80, 6.40 Hz, H_c), 4.04–4.36 (ddd, J = 10.15, 6.86, 4.28 Hz, H_a), 4.68–4.94 (dd ≈ t, J = 6.86, 6.40 Hz, H_b), 6.72–6.88 (m, 1H), and 7.12–7.24 (m, 2H); *m/z*: 308, 310 (M^+). Anal. calcd. for $C_{16}H_{21}BrO$: C 62.14, H 6.80%; found: C 62.28, H 6.96%.

Compound ***9***c*:* mp 65°C (90%), UV (EtOH), λ_{max}: 298 (log ε 3.24), 224 (log ε 3.49) nm; IR (KBr), ν_{max}: 3000, 2920, 1600, 1470, 1350, 1250, 1190, 1170, and 1130 cm^{-1}; ^1H NMR (100 MHz; $CDCl_3$–TMS), δ: 1.60–2.28 (m, 6H), 3.60 (q, J = 6 Hz, 1H), 3.76 (s, 3H), 4.04–4.28 (m, 1H), 4.82 (t, J = 7 Hz, 1H), and 6.68–6.88 (m, 3H); ^1H NMR (400 MHz; $CDCl_3$–TMS), δ: 1.34–1.45 (m, H_g), 1.62–1.75 (m, H_i), 1.80–1.95 (m, H_e, H_d, H_f), 2.09–2.18 (m, H_h), 3.53–3.59 (dt ≈ q, J = 6.80, 6.40 Hz, H_c), 3.75 (s, 3H, -OCH_3), 4.09–4.17 (ddd, J = 10.15, 6.86, 4.28 Hz, H_a), 4.75–4.82 (dd ≈ t, J = 6.86, 6.40 Hz, H_b), 6.65–6.68 (dd, J = 8.2 Hz, 1H), 6.70 (d, J = 2 Hz, 1H), and 6.79 (d, J = 8 Hz, 1H). Anal. calcd. for $C_{13}H_{15}BrO_2$: C 55.12, H 5.30%; found: C 55.19, H 5.19%.

Compound ***9***d*:* Viscous oil (92%), UV (EtOH), λ_{max}: 289 (log ε 3.59), 230 (log ε 3.98) nm; IR (KBr), ν_{max}: 3020, 2920, 1620, 1590, 1470, 1455, 1360, 1260, 1225, 1200, 1180, and 1110 cm^{-1}; ^1H NMR (100 MHz; $CDCl_3$–TMS) δ: 1.68–2.28 (m, 6H), 3.42–3.76 (dt ≈ q, J = 6.80, 6.40 Hz, H_c), 4.04–4.28 (ddd, J = 10.15, 6.86, 4.28 Hz, H_a), 4.72–4.96 (dd ≈ t, J = 6.86, 6.40 Hz, H_b), and 6.68–7.40 (m, 3H). Anal. calcd. for $C_{12}H_{12}ClBrO$: C 50.09, H 4.17%; found: C 50.22, H 4.12%.

Compound ***9***e*:* mp 42°C (96%), UV (EtOH), λ_{max}: 285 (log ε 3.44), 223 (log ε 3.81) nm; IR (KBr), ν_{max}: 3000, 2920, 1600, 1560, 1460, 1420, 1365, 1190, and 1120 cm^{-1}; ^1H NMR (100 MHz; $CDCl_3$–TMS), δ: 1.60–2.06 (m, 6H), 2.20 (s, 3H), 2.24 (s, 3H), 3.40–3.74 (dt ≈ q, J = 6.80, 6.40 Hz, H_c), 4.04–4.28 (ddd, J = 10.15, 6.86, 4.28 Hz, H_a), 4.68–4.94 (dd ≈ t, J = 6.86, 6.40 Hz, H_b), and 6.72–6.92 (m, 2H); *m/z*: 280, 282 (M^+). Anal. calcd. for $C_{14}H_{17}BrO$:C 59.79, H 6.05%; found: C 59.88%, H, 5.93%.

Compound ***9***f*:* Viscous oil (93%), UV (EtOH), λ_{max}: 284 (log ε 3.50), 223 (log ε 3.93) nm; IR (KBr), ν_{max}: 3000, 2920, 1590, 1450, 1370, 1280, 1220, 1165, 1150, and 1120 cm^{-1}; ^1H NMR (100 MHz; $CDCl_3$–TMS), δ: 1.54–2.08 (m, 6H), 2.28 (s, 3H), 2.36 (s, 3H), 2.80–3.20 (dt ≈ q, J = 6.80, 6.40 Hz, H_c), 3.28–3.58 (ddd, J = 10.15, 6.86, 4.28 Hz, H_a), 4.62–4.80 (dd ≈ t, J = 6.86, 6.40 Hz, H_b), 6.50 (s, 1H), and 6.60 (s, 1H); *m/z*: 280, 282 (M^+). Anal. calcd. for $C_{14}H_{17}BrO$: C 59.79, H 6.05%; found: C 59.92, H 6.11%.

Compound ***9***g*:* Viscous oil (90%), UV (EtOH), λ_{max}: 288 (log ε 3.81), 228 (log ε 3.51) nm; IR (KBr), ν_{max}: 2940, 1590, 1480, 1460, 1230, 1170, and 1100 cm^{-1}; ^1H NMR (100 MHz; $CDCl_3$–TMS), δ: 1.72–2.24 (m, 4H), 4.00–4.36 (m, 2H), 4.68–5.12 (m, 2H), and 6.76–7.52 (m, 7H). Anal. calcd. for $C_{18}H_{15}Cl_2BrO_2$: C 52.17, H 3.62%; found: C 52.29, H 3.50%.

Compound ***9***h*:* Viscous oil (93%), UV (EtOH), λ_{max}: 209 (log ε 3.96), 280 (log ε 3.88) nm; IR (KBr), ν_{max}: 3140, 2940, 1600, 1560, 1405, 1325, 1225, 1112, and 1045 cm^{-1}; ^1H NMR (100 MHz; $CDCl_3$–TMS), δ: 1.72–2.40 (m, 6H), 3.40–3.74 (dt ≈ q, J = 6.80, 6.40 Hz, H_c), 4.00–4.32 (ddd, J = 10.15, 6.86, 4.28 Hz, H_a), 4.72–4.96 (dd ≈ t, J = 6.86, 6.40 Hz, H_b), and 6.80–7.24 (m, 3H). Anal. calcd. for $C_{12}H_{12}Br_2O$: C 43.37, H 3.61%; found: C 43.45, H 3.53%.

Compound ***10***i*:* mp 132°C (95%), UV (EtOH), λ_{max}: 284 (log ε 3.82), 222 (log ε 4.27) nm; IR (Nujol), ν_{max}: 3455, 3130, 1435, 1395, 1310, and 1150 cm^{-1}; ^1H NMR (400 MHz; $CDCl_3$–TMS), δ: 1.62–2.58 (m, 6H), 3.95–4.03 (m, 1H), 4.82–5.02 (m, 2H), 5.75 (s, 1H), 7.15 (bs, 1H), and 7.40 (bs, 1H). Anal. calcd. for $C_{12}H_{12}ClBrO$: C 50.09, H 4.17%; found: C 50.12, H 4.07%.

Compound ***10***j*:* mp 138°C (90%), UV (EtOH), λ_{max}: 223 (log ε 4.11), 284 (log ε 3.64) nm; IR (Nujol), ν_{max}: 3440, 3120, 1395, 1315, 1230, and 1150 cm^{-1}; ^1H NMR (100 MHz; $CDCl_3$–TMS), δ: 1.48–2.16 (m, 6H), 2.25 (s, 3H), 3.84–4.08 (m, 1H), 4.80–5.08 (m, 2H), 5.52 (s, 1H), 6.84 (s, 1H), and 7.16 (s, 1H). Anal. calcd. for $C_{13}H_{15}BrO$: C 58.42, H 5.61%; found: C 58.59, H 5.80%.

Chloromercuration of compound ***8***c

To a stirred solution of $HgCl_2$ (2 mmol) in water (12 mL) was added ***8****c* (2 mmol) and stirring was continued for 24 h at room temperature, during which time a heavy greyish oil settled down. The supernatant was decanted and a little methanol was added to the oil when a white precipitate was obtained. It was filtered, dried, and recrystallized from chloroform–methanol to obtain **13**. Yield 47%, mp 230°C.

Bromination of compound ***13***

The chloromercurated product **13** (0.4 g) was taken up in chloroform (20 mL) and warmed to 50°C. The solution was then exposed to direct sunlight and a solution of bromine (2 drops) in chloroform (10 mL) added to it with stirring. After the bromine was used up, the mixture was stirred for further a 45 min,

and then cooled in an ice–salt bath for 15 min. The precipitated mercuric bromide was filtered off and the solution was successively washed with saturated aqueous $NaHSO_3$ and salt water, and dried (Na_2SO_4). The solvent was removed to give a highly viscous liquid, which was purified by passing through a silica gel column and eluting the column with petroleum ether (60–80°C). The product was found to be identical with the product **9***c*, mp 64°C, yield (45%).

Attempted dehydrobromination of compound **9**c

A mixture of cyclized product **9***c* (50 mg) and potassium hydroxide (250 mg) in rectified spirit (2 mL) was refluxed on a water bath for 4 h. No change was observed as evidenced from the tlc of the reaction mixture and also from co-tlc with the starting material (**9***c*).

Attempted functionalization of compound **9**a

A mixture of the cyclized product **9***a* (60 mg), powdered potassium cyanide (90 mg), and 5% potassium iodide solution in acetone (2 mL) was stirred and heated under reflux for 12 h. No change was observed when examined by tlc.

Acknowledgment

We thank the C.S.I.R. (New Delhi) and the University of Kalyani for financial assistance. We are also grateful to Professor J.W. Lown of the University of Alberta, Edmonton, Canada, for the 400 MHz ^{1}H NMR and COSY spectra of compound **9***c* reported in this paper.

References

1. K.C. Majumdar, R.N. De, and S. Saha. Tetrahedron Lett. **31**, 1207 (1990).
2. K.C. Majumdar and B.K. Sen. Indian J. Chem. **22B**, 1184 (1983).
3. R. Gaertner. J. Am. Chem. Soc. **73**, 4400 (1951).
4. (*a*) K.C. Majumdar, A.T. Khan, A.K. Gupta, and K. Dey. Synth. Commun. **20**, 1249 (1990); (*b*) K.C. Majumdar, A.T. Khan, A.K. Gupta, A.K. Kundu, and P.K. Choudhury. Indian J. Chem. **31B**, 667 (1992); (*c*) K.C. Majumdar and P.K. Choudhury. Synth. Commun. **22**, 3013 (1992).
5. L.F. Fieser and M. Fieser. Reagents for organic synthesis. Vol. 1. Wiley, New York. 1967. p. 967.
6. Gy Frater and H. Schmid. Helv. Chim. Acta, **50**, 255 (1967).
7. K.C. Nicolaou, C.V.C. Prasad, P.K. Somers, and C.K. Hwang. J. Am. Chem. Soc. **111**, 5330 (1989).
8. R. Gaertner. J. Am. Chem. Soc. **74**, 5319 (1952).
9. S.K. Chattopadhyay, B.K. Sen, and K.C. Majumdar. Indian J. Chem. **25B**, 56 (1986).
10. T. Hosokawa, S. Miyagi, S. Murahashi, and A. Sonoda. J. Org. Chem. **43**, 719 (1978).
11. E.L. Eliel. Stereochemistry of carbon compounds. McGraw–Hill Book Company, Inc., New York. 1962. p. 296.
12. K.C. Majumdar, P.K. Choudhury, and M. Nethaji. Tetrahedron Lett. **35**, 5925 (1994).
13. (*a*) S. Kachigaeshi, T. Kakinami, H. Tokiyama, T. Hirakawa, and T. Okamoto. Chem. Lett. 627 (1987); (*b*) C. Djerassi and C.R. Scholz. J. Am. Chem. Soc. **70**, 417 (1948).
14. K.C. Majumdar and A.K. Kundu. Indian J. Chem. **32B**, 605 (1993).

Can. J. Chem. Downloaded from www.nrcresearchpress.com by 46.23.64.124 on 09/08/12
For personal use only.

COMMUNICATIONS

Liquid chromatographic analysis and isolation of diastereoisomers obtained by an aldolization reaction

Michel Lafosse, Philippe Morin, Christophe Anceau, Gérard Coudert, Gérald Guillaumet, and Michel Dreux

Abstract: A new route using an aldolization reaction has been investigated in order to synthesize a precursor of pilocarpin, an alkaloid having sympathomimetic properties. To study the stereoselectivity of this route and to propose a mechanism, liquid chromatography has been used to analyse and to isolate each diastereoisomer for a structural determination by NMR. To further investigate the reaction mechanism, seven different aldehydes (or ketones) were used in the aldolization reaction, producing seven different mixtures. This paper describes the improvement of LC conditions with diol- and amino-bonded silica and the nonaqueous mobile phases required for the isolation of each isomer.

Key words: diastereoisomers, pilocarpin precursor, normal phase liquid chromatography, diol- and amino-bonded silicas.

Résumé : On a étudié une nouvelle voie de synthèse, impliquant une aldolisation, d'un précurseur de la pilocarpine, un alcaloïde possédant des propriétés sympathomimétiques. Dans le but d'évaluer la stéréosélectivité de cette voie et d'en proposer un mécanisme, on a utilisé la chromatographie liquide pour analyser et pour isoler chacun des diastéréoisomères dont on a déterminé la structure par RMN. Afin d'étudier le mécanisme réactionnel plus à fond, on a utilisé sept aldéhydes (ou cétones) différents au cours de la réaction d'aldolisation; on a ainsi produit sept mélanges différents. Dans ce travail, on décrit les améliorations des conditions de CL avec des silices liées à des diols et des amines et les phases mobiles non aqueuses nécessaires pour isoler chacun des isomères.

Mots clés : diastéréoisomères, précurseur de la pilocarpine, chromatographie liquide en phase normale, silices liées à des diols et à des amines.

[Traduit par la rédaction]

The synthesis of pilocarpin, an alkaloid with parasympathomimetic properties, was undertaken starting from a retrosynthetic analysis, with the aim of separating this natural molecule into accessible substructures (Fig. 1). The current work concerns the aldolization reaction between a chiral lactone B having a substituent R^4 and an imidazolic aldehyde C in order to obtain the pilocarpin precursor A. Several assumptions can be made about this pilocarpin precursor. Firstly, since in the pilocarpin structure the chiral carbon C2 possesses a well-defined configuration (*S* configuration: see Fig. 1), in the pilocarpin precursor A certain asymmetric carbon atoms (C2, C4, and C6) should also have well-defined configurations. Secondly, carbon C4 should have an *S* configuration in order to direct the aldolization reaction towards a *trans* configuration of C2–C4 as proposed in Fig. 1. Lastly, as carbon C6 has lost its asymmetric character in pilocarpin (Fig. 1), in the precursor it should have an *R* or *S* configuration.

Thus, starting from a chiral lactone B in which the C4 possesses an *S* configuration, we wished to confirm that the aldolization reaction occurred on the least hindered side of the lactone B as predicted by results previously obtained by groups studying alkylation (1–6) or hydroxylation (7), which would have preferentially produced *trans* isomers 2*S* 4*S* 6*R* and (or) 2*S* 4*S* 6*S* (Fig. 1).

To demonstrate the stereoselectivity or nonstereoselectivity of the aldolization reaction and conclude that it can occur preferentially on one side of the lactone B, the composition of the mixture produced by this reaction must be determined by liquid chromatography (LC). Liquid chromatographic analy-

Received December 12, 1994.

Michel Lafosse,[1] Philippe Morin, Christophe Anceau, Gérard Coudert, Gérald Guillaumet, and Michel Dreux. Institut de chimie organique et analytique, Unité de recherche associée au Centre national de la recherche scientifique, n° 499, BP 6759, Université d'Orléans, F 45067 Orléans Cedex 2, France.

[1] Author to whom correspondence may be addressed. Telephone: 38.41.70.44. Fax: 38.41.72.81.

Can. J. Chem. Downloaded from www.nrcresearchpress.com by 46.23.64.124 on 09/08/12
For personal use only.

Fig. 1. Scheme of the retrosynthetic analysis of pilocarpin. A = pilocarpin precursor, B = chiral lactone, and C = imidazolic aldehyde. The aldolization reaction between a chiral lactone B and an imidazolic aldehyde C gives the pilocarpin precursor A.

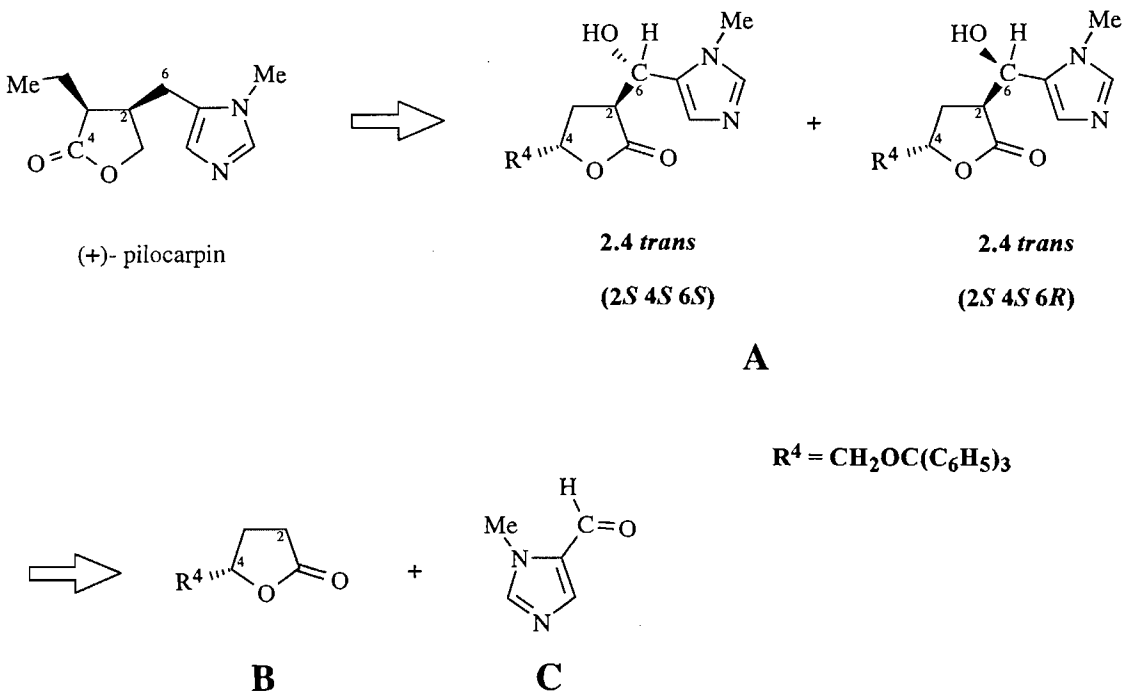

Fig. 2. Diastereoisomer nomenclature of the aldolization reaction products.

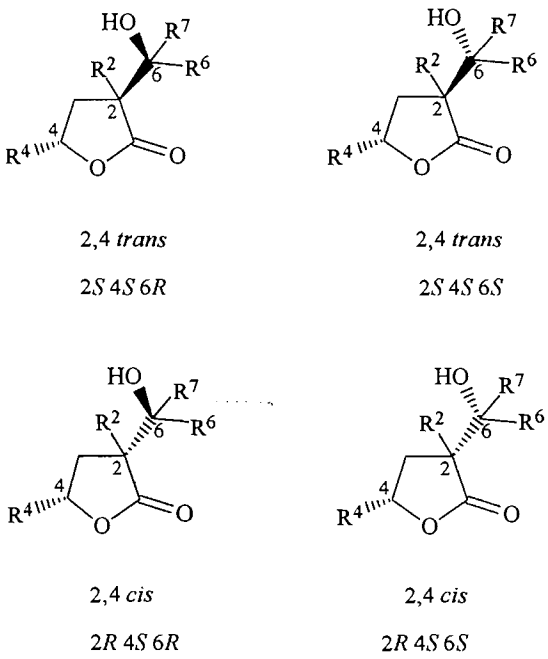

sis must be selective to separate the four diastereoisomers, i.e., one pair of *trans* isomers plus one pair of *cis* isomers (Fig. 2) if the reaction occurred on both sides of the lactone B. The aim of this work is to obtain the best LC conditions required to isolate each pure diastereoisomer in a quantity large enough to carry out its structural determination by ^1H and ^{13}C NMR.

To try to control the formation of *trans* isomers, a general study of the aldolization reaction was carried out using only one chiral lactone with two different substituents R^4 and diverse aldehydes or ketones C as shown in Table 1.

Experimental

Table 1 reports X1 as an isomer mixture containing the pilocarpin precursor A and the other mixtures X2, X3 ...U as instruments that highlight possible orientation effects in the aldolization reaction according to the protecting groups. Different reaction conditions were also tried out (temperature, solvent nature, reaction time ...) in order to determine any tendency towards the formation of single or pairs of compounds among the four diastereoisomers (8). The carbon configuration of different isomers obtained by LC was determined by ^1H and ^{13}C NMR (8, 9).

Chromatography was carried out using a Shimadzu LC 8A pump equipped with a model 7125 injection valve with a 1 mL loop (Rheodyne), a model SPD 6A UV spectrophotometer (Shimadzu) with a preparative cell, and a Shimadzu CR 3A calculator. The solvents were LC grade. In each case the injection solvent was mobile phase or, if the solubility was insufficient, mobile phase with a slightly higher percentage of the strongest solute solvent.

Since preliminary analytical tests by reversed phase LC were unable to show the presence of several diastereoisomers in the precursor compounds of the pilocarpin X1, only normal phase LC with silica and alkane–alcohol mixtures, as shown in the literature (10–13), was considered to separate the diastereoisomers. However, to avoid any difficulty arising from the inconsistency of the adsorbent activity of bare silica, polar-bonded silicas (diol, amino) were used. The following col-

Can. J. Chem. Downloaded from www.nrcresearchpress.com by 46.23.64.124 on 09/08/12
For personal use only.

Table 1. Isomer mixtures list.

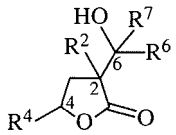

Isomer mixture	Carbon:	C2	C4	C6		C6
	Substituent:	R^2	R^4	R^6		R^7
X1		H	CH_2OTr^a			H
X2		H	CH_2OTr	C_6H_5		H
X3		H	CH_2OTr	CH_3		H
Y		CH_3	CH_2OTr	C_6H_5		H
Z1		H	CH_2OTr		$-(CH_2)_5-$	
Z2		H	CH_2OTr	C_6H_5		C_6H_5
U[b]		H	CH_3	C_6H_5		H

[a] $CH_2OTr = CH_2OC(C_6H_5)_3$

[b] The configuration of C4 is 4*R* and not 4*S*. Change in the R^4 nature justifies the change in the C4 configuration.

umns were used: from Merck, Lichrosorb Diol 7 μm, 250 × 9.4 mm; Lichrospher NH2 5 μm, 250 × 4 mm; and from the laboratoire de Chimie organique at the University of Bordeaux a diamino silica 10 μm, 250 × 4.6 mm (14).

For the capacity factor calculation, the dead volume was determined by UV signal created by an excess of one of the eluent constituents.

Results and discussion

1. Diol-bonded silica as stationary phase

Due to the decreasing efficiency when the amount of injected analyte increases, the selectivity must be enhanced.

As shown in Fig. 3, log *k'* varies linearly versus the percentage of hexane in the hexane–dichloromethane mixture as mobile phase. These curves are nearly parallel, which means that the selectivity between two compounds is nearly constant whatever the mobile phase composition. Mixture Z1 is well separated (Fig. 3c) whatever the dichloromethane content (in a similar manner to the mixture Z2) but the best choice for isolation of each isomer would appear to be the hexane–dichloromethane (50:50, v/v) eluent since (*i*) the analysis time is relatively short, (*ii*) resolution remains high ($R = 3.4$), (*iii*) solubility of the analyte mixture in the eluent is appreciable. So, 1 mL of mixture Z1 at 25 mg/L in a solvent having the same composition as the eluent could be directly chromatographed and yielded each pure isomer.

The diastereoisomers of mixture Y can also be obtained with the same eluent. In this case, obtaining three compounds instead of the four theoretically possible can be explained by kinetic and thermodynamic factors.

Concerning the mixture X2, the first two peaks are not separated on these systems (Fig. 3a), while the four peaks of the mixture X3 are well separated with hexane–dichloromethane

Fig. 3. Variation of the capacity factors *k'* of diastereoisomers as a function of the hexane content in the hexane–dichloromethane mobile phase. Column: Lichrosorb Diol 7 μm (250 × 9.4 mm). Solutes: (a) X2; (b) U; (c) Z1 (see Table 1).

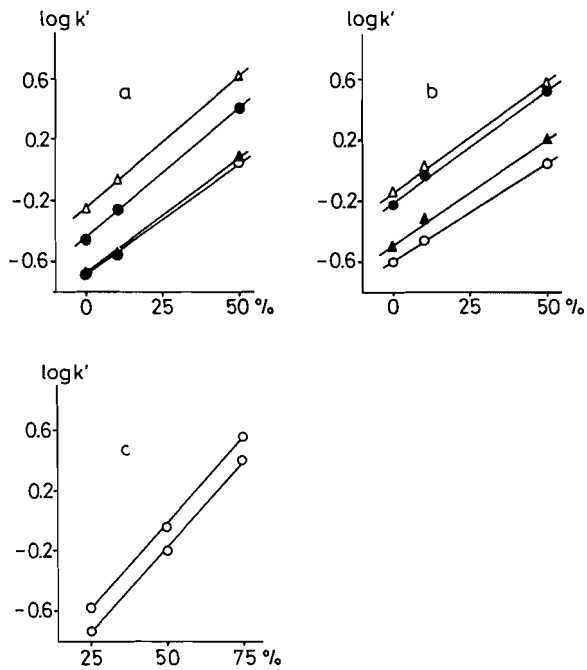

(50:50, v/v). Resolution between two successive peaks is, for the three pairs of isomers, respectively, $R_{1,2} = 2.6$, $R_{2,3} = 7$, and $R_{3,4} = 8.3$. Each isomer of the mixture U can be theoretically isolated (Fig. 3b) but synthetic impurities coelute either with the peak under poor eluent strength or with the first peak under a strong eluent, which requires a second purification in order

Can. J. Chem. Downloaded from www.nrcresearchpress.com by 46.23.64.124 on 09/08/12
For personal use only.

Table 2. Elution order and configuration of isomers. Stationary phase: Lichrosorb Diol. Mobile phase: hexane–dichloromethane (50:50, v/v).

	Elution order			
Mixture	1	2	3	4
X3	2*R* 4*S* 6*S*	2*S* 4*S* 6*R*	2*R* 4*S* 6*R*	2*S* 4*S* 6*S*
Y	2*R* 4*S* 6*S*	2*S* 4*S* 6*S*	2*R* 4*S* 6*R*	
Z1	2*S* 4*S* 6*R*	2*S* 4*S* 6*S*		
Z2	2*S* 4*S* 6*R*	2*S* 4*S* 6*S*		

Table 3. Variation of the capacity factor k' and selectivity α according to the nature and composition of eluents on a Lichrospher NH_2 5 μm (250 × 4 mm). Mobile phase: hexane–alcohol.

		Hexane–methanol (95:5)		Isomer	Hexane–ethanol (95:5)	
Mixture	Isomer	k'	α		k'	α
	2*S* 4*R* 6*S*	10.6		2*S* 4*R* 6*S*	2.2	
			1.13			1.06
	2*R* 4*R* 6*R*	12		2*R* 4*R* 6*R*	2.5	
U			1.10			1.25
	2*R* 4*R* 6*S*	13.2		2*S* 4*R* 6*R*	3.1	
			1.08			1.05
	2*S* 4*R* 6*R*	14.3		2*R* 4*R* 6*S*	3.3	

		Hexane–ethanol (98:2)		Isomer	Hexane–isopropanol (98:2)	
		k'	α		k'	α
	2*R* 4*S* 6*R*	8		2*R* 4*S* 6*R*	4.8	
			1.15			1.14
	2*S* 4*S* 6*S*	9.2		2*S* 4*S* 6*S*	5.5	
X2			1.17			1.16
	2*S* 4*S* 6*R*	10.8		2*S* 4*S* 6*R*	6.3	
			1.36			1.31
	2*R* 4*S* 6*S*	14.7		2*R* 4*S* 6*S*	8.3	

to obtain the individual diastereoisomer. As shown in Table 2, diol-bonded silica as stationary phase resolved only four mixtures (X3, Y, Z1, and Z2). Consequently, amino-bonded silica was used for the remaining three.

2. Amino-bonded silica as stationary phase

This more polar stationary phase requires a stronger organic modifier such as alcohol instead of dichloromethane. But the nature of the alcohol greatly influences retention, as shown in Table 3 and Fig. 4. Hexane modified by 5% ethanol was a stronger eluent than hexane with the same content of methanol. This behaviour is the reverse of that observed in the so-called eluotropic series of alumina or bare silica. It is also observed when comparing the influence of ethanol and isopropanol (Table 3). Moreover, the nature of the alcoholic modifier influences the selectivity. With hexane–ethanol (98:2, v/v) as eluent, selectivity and retention enabled sufficient resolution to obtain each of the four pure diastereoisomers X2 on an analytical column in semi-preparative amounts. The elution order of diastereoisomers X2 is the following: 2*R* 4*S* 6*R*, 2*S* 4*S* 6*S*, 2*S* 4*S* 6*R*, then 2*R* 4*S* 6*S*.

As regards the mixture U, impurities can coelute with one of the peaks whatever the mobile phase. This explains why another modifier was tried: tetrahydrofuran in a ternary eluent with hexane and dichloromethane. This solvent possesses a proton-acceptor character, which is not the case for dichloromethane (dipole–dipole interactions) and the alcohol (proton donor) (15), thus modifying the solvating power of the solute and its adsorption energy. Retention and especially selectivity are greatly improved and in the case of the U mixture enabled isolation of each pure diastereoisomer as shown in Fig. 4.

Concerning the pilocarpin precursor X1 mixture, any one of the previous systems is suitable. A comparison of different commercial aminopropyl-bonded phases (Lichrospher, Zorbax, and Erbasil) shows identical results in separation capabilities whatever the mobile phase composition. However, a diaminopropyl-bonded phase especially designed for hydro-

Can. J. Chem. Downloaded from www.nrcresearchpress.com by 46.23.64.124 on 09/08/12
For personal use only.

Fig. 4. Isocratic separation of the U diastereoisomers on amino-bonded silica (Lichrospher NH_2 5 μm, 250 × 4 mm) with a ternary eluent (hexane–dichloromethane–tetrahydrofuran, 60:40:1, v/v/v) at 2 mL min^{-1}. Solutes: (a) 2*S* 4*R* 6*R*; (b) 2*S* 4*R* 6*S*; (c) 2*R* 4*R* 6*R*; (d) 2*R* 4*R* 6*S*; i = impurity.

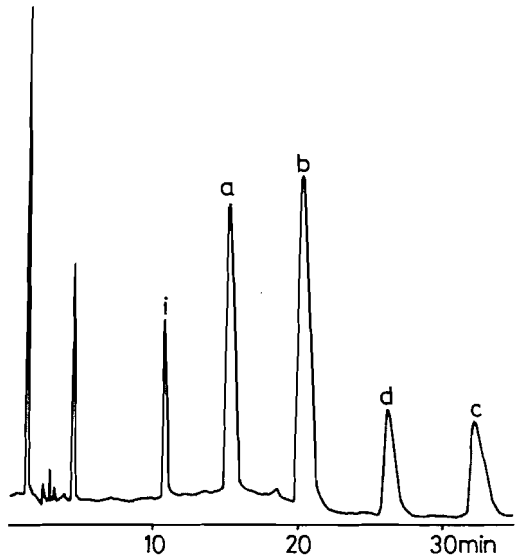

carbon analysis (16) exhibited better selectivity and resolution. This bonding is much more retentive than the commercial monoaminopropyl bonding and has allowed the use of higher percentages of dichloromethane in ternary eluent (hexane–dichloromethane–methanol, 49:49:2); consequently the solubility of the mixture X1 increases with an increase in dichloromethane content and allows the injection of considerable quantities of solute. The elution order of diastereoisomers is the following: 2*R* 4*S* 6*R*, 2*S* 4*S* 6*S*, 2*S* 4*S* 6*R*, then 2*R* 4*S* 6*S*.

So, LC with polar-bonded silicas (diol and amino) as stationary phase is highly flexible as it allows various mobile phases to be tried and has enabled us to separate and isolate different pure diastereoisomers formed during the aldolization reaction of a multistep analysis. The identification of each isomer by NMR (9) indicates that the reaction is not stereoselective whatever the reaction conditions or the aldolization reagent. These results are negative as regards our initial aim of synthesizing pilocarpin, but they allow us to propose a reaction mechanism (9).

Acknowledgements

The authors thank the Laboratoires Merck for the gift of an amino Lichrospher column and Professor G. Felix (University of Bordeaux) for the diamino column.

References

1. T. Tomioka, H. Mizagarchi, and K. Koga. Tetrahedron Lett. 4967 (1978).
2. S. Takano, N. Tamura, and K. Ogasawara. J. Chem. Soc. Chem. Commun. 1159 (1981).
3. S. Takano, K. Inomata, A. Karotaki, T. Ohkawa, and K. Ogasawara. J. Chem. Soc. Chem. Commun. 1720 (1987).
4. T. Tomioka, T. Ishigaro, and K. Koga. J. Chem. Soc. Chem. Commun. 652 (1979).
5. T. Tomioka and K. Koga. Tetrahedron Lett. 3313 (1979).
6. T. Tomioka, T. Ishigaro, and K. Koga. Tetrahedron Lett. 2973 (1980).
7. S. Hanessain, S.P. Sahoo, and P.J. Murray. Tetrahedron Lett. 5671 (1985).
8. C. Anceau. Ph.D. Thesis. University of Paris XI, France. 1991.
9. C. Anceau, G. Dauphin, G. Coudert, and G. Guillaumet. Bull. Soc. Chim. Fr. **131**, 291 (1994).
10. G.R. Padmanabhan, J. Fogel, J.A. Mollica, J.M. O'Connor, and R. Strusz. J. Liq. Chromatogr. **3**, 1079 (1980).
11. S. Barkan and I.W. Wainer. J. Chromatogr. **240**, 547 (1982).
12. J.M. Maitre, G. Boss, B. Testa, and K. Hostettmann. J. Chromatogr. **356**, 341 (1986).
13. X.L. Lu and S.K. Yang. Yaoxue Xuebao, **23**, 67 (1988).
14. A. Le Morzellec. Ph.D. Thesis. University of Bordeaux, France. 1989.
15. R. Rosset, M. Caude, and A. Jardy. Chromatographies en phases liquide et supercritique. 3rd ed. Masson, Paris. 1991. p. 48.
16. G. Felix, E. Thoumazeau, J.M. Colin, and G. Vion. J. Liq. Chromatogr. **10**, 2115 (1987).

Can. J. Chem. Downloaded from www.nrcresearchpress.com by 46.23.64.124 on 09/08/12
For personal use only.

A study of the vacuum pyrolysis of 4-diazo-3-isochromanone with HeI ultraviolet photoelectron spectroscopy

N.H. Werstiuk, J. Ma, C.D. Roy, A.J. Kresge, and E. Jefferson

Abstract: A newly developed ultraviolet photoelectron spectrometer – CO_2 laser instrument that utilizes a 50-W CW laser as a directed heat source was used to study the vacuum pyrolysis of 4-diazo-3-isochromanone (**1**). Analysis of the pyrolysate with ultraviolet photoelectron spectroscopy and photoionization mass spectrometry established that **1** undergoes a facile, unexpected pyrolysis at a laser power level of 26 W yielding N_2, CO, and benzocyclobutenone (**6**). A multistep mechanism beginning with the formation of 4-carbena-3-isochromanone (**2**), which rearranges to oxaketene **3**, can be written for the reaction. If **3** is an intermediate, it must be unusually thermally labile for it readily decarbonylates to 2-carbena-3,4-benzotetrahydrofuran (**4**). The ring opening of **4** into the *ortho*-quininoid ketene **5** and the cyclization of **5** into **6** are possible final steps in the conversion of **1** into **6**.

Key words: vacuum pyrolysis, 4-diazo-3-isochromanone, HeI ultraviolet photoelectron spectroscopy.

Résumé : On a utilisé un nouveau spectromètre photoélectronique ultraviolet – laser au CO_2, qui utilise un laser CW de 50 W comme source dirigée de chaleur, pour étudier la pyrolyse sous vide de la 4-diazo-3-isochromanone (**1**). L'analyse du pyrolysat par spectroscopie photoélectronique et par spectrométrie de masse avec photoionisation a permis d'établir que, sous l'influence d'une puissance laser de 26 W, **1** subit une pyrolyse facile et inattendue qui fournit du N_2, du CO et de la benzocyclobuténone (**6**). Pour cette réaction, on peut proposer un mécanisme en plusieurs étapes qui commence par la formation de la 4-carbéna-3-isochromanone (**2**) qui se réarrange en oxacétène, **3**. Si le composé **3** est un intermédiaire, il doit être exceptionnellement labile vis-à-vis de la chaleur parce qu'il donne facilement une réaction de décarboxylation conduisant au 2-carbéna-3,4-benzotétrahydrofurane (**4**). L'ouverture de cycle du composé **4** en cétène *ortho*-quinonoïde **5** et la cyclisation de cette dernière en **6** sont les étapes finales possibles pour la conversion de **1** en **6**.

Mots clés : pyrolyse sous vide, 4-diazo-3-isochromanone, spectroscopie photoélectronique ultraviolette.

[Traduit par la rédaction]

Can. J. Chem. Downloaded from www.nrcresearchpress.com by 46.23.64.124 on 09/08/12
For personal use only.

To facilitate the preparation and detection of highly reactive transients in the gas phase, we developed an ultraviolet photoelectron (pe) spectrometer – CW CO_2 laser apparatus and used it successfully to study the vacuum pyrolysis of 6,6-dihalobicyclo[3.1.0]hexanes (1) and 1,2,3-benzotriazines (2). To extend our research to other reactive species, we used this one-of-a-kind instrument to study the vacuum pyrolysis of 4-diazo-3-isochromanone (**1**). We undertook this study (*a*) because **1** is a potential source of two interesting transients, 4-carbena-3-isochromanone (**2**) and its Wolff rearrangement product (3) oxaketene **3**, and (*b*) because there is a lack of information on the vacuum pyrolysis of α-diazocarbonyl compounds in contrast to the substantial body of work documenting the photochemistry of this class of compounds (4–10). We expected that a pe spectroscopic study of **1** would yield information about the stability/reactivity of **2** and oxaketene **3** and provide fundamental information about their electronic structures and bonding. This communication documents the results of our study.

To obtain the pe spectrum of **1**,[2] a 10 mg sample was placed in a bottle-shaped quartz sample tube (1, 2) that was inserted into an electrically heated brass probe tip. Because the source pressure (5×10^{-4} Torr; Torr = 133.3 Pa) was low at ambient temperature, it was necessary to heat the sample tube to a temperature (48°C) slightly below its melting point (this yielded a suitable partial pressure of **1** and avoided the side reactions that occurred in the melt) and to use N_2 as a makeup gas to maintain the source pressure at 7×10^{-3} Torr. In keeping with the results of our previous study (2), this approach allowed us to obtain a spectrum of **1**. As seen in Fig. 1(*a*), the low-IE band of N_2 at 15.6 eV (11) dominates the spectrum of **1** acquired

Received July 14, 1995.

N.H. Werstiuk,[1] **J. Ma, and C.D. Roy.** Department of Chemistry, McMaster University, Hamilton, ON L8S 4M1, Canada.
A.J. Kresge and E. Jefferson. Department of Chemistry, University of Toronto, Toronto, ON M5S 1A1, Canada.

[1] Author to whom correspondence may be addressed. Telephone: (905) 525-9140. Fax: (905) 522-2509.

[2] The synthesis (by A.J.K. and E.J.) of **1**, a new compound (mp 48–49°C), was adapted from a procedure used for the synthesis of other α-diazocarbonyl compounds (14). Its spectroscopic properties (ir, nmr, and ms) were entirely in accord with the proposed structure.

Can. J. Chem. Downloaded from www.nrcresearchpress.com by 46.23.64.124 on 09/08/12
For personal use only.

Fig. 1. (*a*) HeI pe spectrum of **1** obtained at a probe temperature of 48°C with N_2 as a make-up gas; (*b*) spectrum of the pyrolysate of **1** obtained at a laser power level of 26 W with no makeup gas; (*c*) spectrum of the pyrolysate of **1** obtained at a laser power of 47 W; (*d*) spectrum of an authentic sample of benzocyclobutenone (**6**) obtained at ambient temperature with N_2 (15.6 eV) as the calibrant.

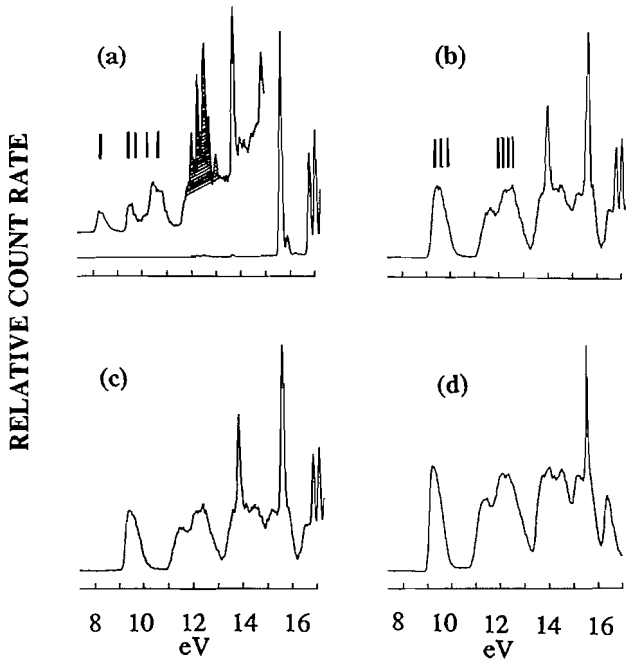

this way. Even so, a vertical expansion of the spectrum[3] between 7 and 14 eV revealed the low-IE bands of **1**. The vertical solid lines on this spectrum show the five lowest ionization energies (8.49, 9.70, 9.93, 10.38, and 10.87 eV) of compound **1** calculated with HAM/3 (12). The equilibrium geometry obtained at the HF/6–31G** level of theory with GAUSSIAN 92 (13) was used in the HAM/3 calculations.

When **1** was pyrolyzed by heating the tip of the sample tube (the hot zone (550 ± 50°C) was 1.5–2 mm in length) at a laser power level of 26 W (1, 2), a different pe spectrum (Fig. 1(*b*)) was obtained. No significant change was seen in the spectrum (Fig. 1(*c*)) when the pyrolysis was carried out at a laser power level of 47 W. While N_2 (identified by the band at 15.6 eV (11)) was expected, we were surprised to find CO (identified by the band at 14.0 eV (11)) as a major product of the reaction because *para*-substituted phenylketenes do not decarbonylate even at laser power levels greater than 40 W.[4] By comparing the calculational IEs (HAM/3//AM1) of possible products (carbene **2**, oxaketene **3**, carbene **4**, the *ortho*-quininoid ketene **5**, and benzocyclobutenone **6**) with the vertical IEs obtained from the pe spectrum of the pyrolysate, we concluded that the

Fig. 2. (*a*) Photoionization mass spectrum of benzocyclobutenone (**6**) obtained at ambient temperature; (*b*) photoionization mass spectrum of the pyrolysate of **1** obtained at a laser power of 26 W.

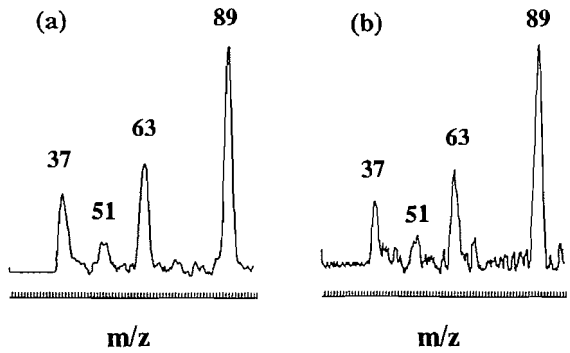

Scheme 1.

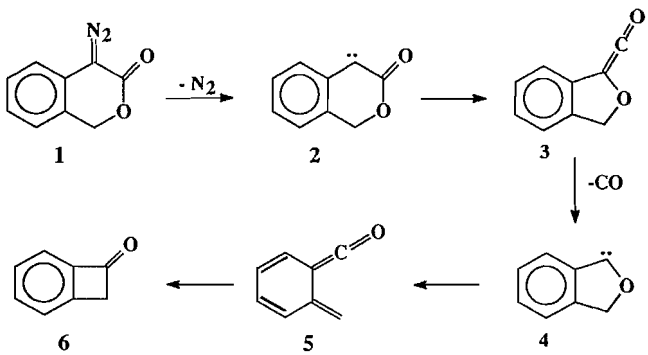

product probably was **6**. We prepared an authentic sample of **6** (16) and obtained its pe spectrum, which is displayed as Fig. 1(*d*). Aside from the peaks arising from CO and N_2, the pe spectra of the pyrolysate (Figs. 1(*b*) and 1(*c*): the vertical lines show the seven lowest IEs 9.64, 9.85, 10.05, 12.25, 12.32, 12.66, and 12.80 eV of **6** calculated with HAM/3//6–31G**)) are virtually identical to the pe spectrum of **6**. We also established that the authentic sample of benzocyclobutenone does not pyrolyze even at the maximum power level (60 W) of the laser. Additional support for **6** as the pyrolysis product was obtained by running the pe spectrometer in its photoionization mass spectrometer mode.[5] The mass spectra of the authentic sample of **6** acquired at ambient temperature and the pyrolysate obtained at a laser power of 26 W are displayed in Fig. 2 as (*a*) and (*b*), respectively. That the mass spectra are virtually identical (**6** does not exhibit a molecular ion under the experimental conditions used in this study) establishes that 4-diazo-3-isochromanone does, in fact, afford benzocyclobutenone in high yield. Even though the intermediates (4-carbena-3-isochromanone (**2**), oxaketene (**3**), 2-carbenatetrahydro-3,4-benzofuran (**4**), and the *ortho*-quininoid ketene (**5**)) shown in Scheme 1 were not detected by pe spectroscopy or mass spec-

[3] The cross-hatched peaks ranging between 12 and 13 eV arise from traces of O_2 (12.1–12.8 eV) and H_2O (12.6 eV) that are present in the source chamber. The band at 13.7 eV, which has a very low intensity relative to the band at 15.6 eV of N_2 in the unexpanded spectrum, arises from ionization by the 537.0 Å line (23.1 eV photons) known to have 2% the intensity of the 584.3 Å line (21.2 eV photons) of the HeI discharge (15).

[4] N.H. Werstiuk, J. Ma (McMaster University), and M. Liu (University of Prince Edward Island); work in progress.

[5] When the pe spectrometer was modified, an 200 amu quadrupole mass spectrometer was interfaced with the source chamber. The pes instrument is switched to the mass spectrometer mode simply by applying a +25 V potential to the upper element of an einzel lens to which a retard potential is applied in the pes mode. This positive potential nudges the ions generated by photoionization through the circular entrance slit of the quadrupole mass spectrometer located 2.5 cm above the upper element of the lens.

trometry, it represents a working hypothesis for the mechanism of the vacuum pyrolysis of **1**. If **3** is an intermediate in the pyrolysis reaction and the source of the CO, then **3** must be unusally thermally labile because *para*-substituted phenylketenes prepared from the corresponding diazoacetophenones by vacuum pyrolysis are stable even at laser power levels beyond 40 W.[4] The enhanced reactivity of **3** must be due largely to the methoxy group, which destabilizes the ketene and stabilizes the carbene. To define the role of **3** in the pyrolysis reaction will necessitate additional studies on its preparation and vacuum pyrolysis. Support that **5** could be an intermediate in the reaction is found in the work of Schiess and Heitzmann (17) who proposed that *ortho*-quininoid ketenes are intermediates in the pyrolytic conversion of *ortho*-alkyl-substituted aromatic acyl halides into benzocyclobutenones at 500–600°C. Whatever intermediates, **2**, **3**, **4**, and **5**, are involved in the pyrolysis of **1**, they must be very short-lived and thermally labile because the pyrolysis hot zone of our apparatus is only 2 mm in length (1, 2). This work also indicates that the preparative-scale vacuum pyrolysis of substituted 4-diazo-3-isochromanones might be a convenient alternate route to substituted benzocyclobutenones.

Acknowledgements

We thank the Natural Sciences and Engineering Research Council of Canada and the United States National Institutes of Health for financial support.

References

1. N.H. Werstiuk, C.D. Roy, and J. Ma. Can. J. Chem. **72**, 2537 (1994).
2. N.H. Werstiuk, C.D. Roy, and J. Ma. Can. J. Chem. **73**, 146 (1995).
3. L. Wolff. Justus Liebigs Ann. Chem. **394**, 23 (1912).
4. W. Kirmse. *In* Advances in carbene chemistry. Vol. 1. *Edited by* U.H. Brinker. JAI Press Inc., Greenwich, Conn. 1994. pp 39–42.
5. B.M. Trost and P.L Kinson. J. Am. Chem. Soc. **97**, 2438 (1975).
6. R.J. McMahon, O.L. Chapman, R.A. Hayes, T.C. Hess, and H.-P. Krimmer. J. Am. Chem. Soc. **107**, 7597 (1985).
7. A. Allen, A.J. Kresge, N.P. Schepp, and T.T. Tidwell. Can. J. Chem. **65**, 1719 (1987).
8. R.J. McMahon, C. J. Abelt, O.L. Chapman, J.W. Johnson, C.L Kreil, J-P. LeRoux, A.M. Mooring, and P.R. West. J. Am. Chem. Soc. **109**, 2456 (1987).
9. C. Bachman, T.Y. N'Guessan, F.Debû, M. Monnier, J. Pourcin, J-P. Aycard, and H. Bodot. J. Am. Chem. Soc. **112**, 7488 (1990).
10. J. Andraos and A.J. Kresge. J. Photochem. Photobiol. A: **57**, 165 (1991).
11. K. Kimura, S. Katsumata, Y. Achiba, T. Yamazaki, and S. Iwata. The handbook of HeI photoelectron spectra of organic molecules: ionization energies, ab initio assignments and valence electronic structure of 200 molecules. Japan Scientific Societies Press, Tokyo. 1981.
12. L. Asbrink, C. Fridh, and E. Lindholm. HAM/3. Quantum Chemistry Program Exchange (QCPE) Bull. **13**, 393 (1981).
13. M.J. Frisch, G.W. Trucks, M. Head-Gordon, P.M.W. Gill, M.W. Wong, J.B. Forseman, B.G. Johnson, H.B. Schlegel, M.A. Robb, E.S. Replogle, R. Gomperts, J.L. Andres, K. Raghavachari, J.S. Binkley, C. Gonzalez, R.L. Martin, D.J. Fox, D.J. Defrees, J. Baker, J.J.P. Stewart, and J.A. Pople. GAUSSIAN 92. Gaussian Inc. Pittsburgh, Pa. 1992.
14. J.S. Baum, D.A. Shook, and H.M.L. Davies. Synth. Commun. **17**, 1709 (1987).
15. J.W. Rabalais. *In* Principles of ultraviolet photoelectron spectroscopy. J. Wiley and Sons, New York. 1977. Chap. 2.
16. O. Abou-Teim, M.C. Goodland, and J.F. McOmie. J. Chem. Soc. Perkin Trans. 1, 2659 (1983).
17. P. Schiess and M. Heitzmann. Angew. Chem. Int. Ed. Engl. **16**, 469 (1977).

Can. J. Chem. Downloaded from www.nrcresearchpress.com by 46.23.64.124 on 09/08/12
For personal use only.

Micellar properties of two-headed surfactant systems: the disodium 1,2-alkanedisulfates

Ellen K. Comeau, Ellen J. Beck, Jennifer F. Caplan, Calvin V. Howley, and D. Gerrard Marangoni

Abstract: A family of two-headed surfactants, the disodium 1,2-alkanedisulfates, has been synthesized by the addition of chlorosulfonic acid to the corresponding 1,2-alkanediol. The ability of these salts to form micelles in aqueous solution is demonstrated from solution conductance measurements and counterion activity measurements of the sodium ion. The critical micelle concentrations (cmc's) and apparent degrees of counterion binding (β′ values) of these surfactants indicate that the addition of the second headgroup has a profound effect on the micelles formed by the disulfates when compared to their monosulfate analogues.

Key words: surfactants, synthesis, micellization, cmc values, counterion binding.

Résumé : On a synthétisé une famille d'agents de surface à deux têtes, les alcane-1,2-disulfates de disodium, par addition d'acide chlorosulfonique sur les alcane-1,2-diols correspondants. Faisant appel à des mesures de conductivité des solutions et d'activité du contre-ion sodium, on a démontré l'habilité de ces sels à former des micelles en solutions aqueuses. Les concentrations micellaires critiques (cmc) et les degrés apparents de liaison du contre-ion (valeurs β) de ces agents de surface indiquent que, par comparaison avec leurs analogues monosulfates, l'addition d'une deuxième tête a un effet important sur les micelles formées par les disulfates.

Mots clés : agents de surface, synthèse, micellisation, valeurs cmc, liaison de contre-ions.

[Traduit par la rédaction]

Introduction

The application of surfactant technology to a number of industrial and pharmaceutical processes is well known. Recent advances in the understanding of surfactant aggregation in concentrated systems (e.g., emulsions and microemulsions) have led to the use of surfactants in systems such as liquid developers in electronic printing, and in the production of thin insulators, sensors, and magnetic media (1). In view of the increasing and varied number of applications, it is somewhat surprising that the ionic surfactants usually used are long-chain hydrocarbons with typical head groups like sulfate, sulfonate, trimethylammonium, carboxylate, and phosphate, or nonionic surfactants (the alkyl (polyethylene oxide) family) or zwitterionic surfactants (e.g., the betaines). In fact, the bulk of the work in all areas of surfactant technology, including discussions about the driving forces for surfactant aggregation into simple micelles, has been limited to systems similar to those described above. A number of theories of micellization have been proposed (2–5) that describe reasonably the micellization of standard one-headed, one-tailed surfactants containing hydrocarbon, perfluorocarbon, and mixed hydrocarbon–fluorocarbon chains. Recently, the synthesis of novel surfactants, in particular surfactants possessing multiple or unusual headgroups, has been gaining attention in the literature (6–14). As an example, Jobe and Reinsborough (6) have studied the properties of micelles formed by disodium 4-alkyl-3-sulfonatosuccinates (i.e., cmc's, aggregation numbers, and degrees of counterion binding) as a function of the alkyl chain length, using a number of different techniques. These authors concluded that the addition of the second polar head group made it more difficult for the surfactant molecules to cluster together to form micelles; hence, these two-headed surfactants had relatively high cmc's and small aggregation numbers. The degrees of counterion binding appeared to be in the range most often quoted for single-headed surfactants of comparable chain length.

Bolaform surfactants, i.e., surfactants in which the head groups are at both ends of a nonpolar chain, represent another class of two-headed surfactants that has been examined recently in the literature (7–10). Bolaform surfactants differ from single-headed surfactants in that having the hydrophilic head group at both ends of the alkyl chain places significant restrictions on the orientation and packing of the monomers in the micelle. Bolaform surfactants have cmc's that are comparable to single-headed surfactants of half the alkyl chain length (7–10). The surface tension vs. log concentration curves for aqueous solutions of bolaform alkanedisulfates indicate that the cross-sectional area of bolaform sulfate surfactants is about twice as large as the singly charged analogue with the same alkyl chain length. Therefore, bolaform surfac-

Received March 14, 1995.

E.K. Comeau, E.J. Beck, J.F. Caplan, C.V. Howley, and D.G. Marangoni.[1] Department of Chemistry, St Francis Xavier University, P.O. Box 5000, Antigonish, NS B2G 2W5, Canada.

[1] Author to whom correspondence may be addressed. Telephone: (902) 867-2324. Fax: (902) 867-5153. E-mail: gmarango@juliet.stfx.ca

Can. J. Chem. Downloaded from www.nrcresearchpress.com by 80.90.12.36 on 09/08/12
For personal use only.

Can. J. Chem. Downloaded from www.nrcresearchpress.com by 80.90.12.36 on 09/08/12
For personal use only.

tants are proposed to adopt a loop-like configuration at the air–water interface.

It appears that the synthesis and characterization of surfactants having two or more headgroups on adjacent carbon atoms or branched groups at different points of attachment in the alkyl chain have been little investigated in the literature (11–14). We have synthesized a family of surfactants, the disodium 1,2-alkanedisulfates, of medium to long alkyl chain length, and characterized the micelles formed by these surfactants via conductance measurements, counterion activity measurements, and spectroscopic methods. We have compared the properties of the micelles formed by these surfactants to monosulfate surfactants having the same alkyl chain length. As expected, the addition of the second sulfate group affects greatly the properties of the alkanedisulfate micelles, when compared with the well-known alkanesulfate amphiphiles.

The disodium 1,2-alkanedisulfates were synthesized by reacting the corresponding 1,2-alkanediol (Aldrich Chemical Co.) with a 10% molar excess of chlorosulfonic acid in dichloromethane or diethyl ether cooled in an ice bath. The reaction mixture was diluted with an equal volume of cold ethanol or methanol, neutralized with 6 M NaOH, and brought to room temperature and stirred for 2–4 h. The surfactants crystallized from the solvent mixture and were filtered and recrystallized from ethanol or methanol, and washed with a cold methanol–water or ethanol–water mixture. Soxhlet extraction from dichloromethane or diethyl ether was used to rid the surfactant of residual diol. The overall yield of product was about 65–70%. The purified surfactants were characterized by NMR and FT-IR spectroscopy. The presence of residual chloride and sulfate ions in the final product was checked by capillary electrophoresis (Waters Quanta model 4000).

The cmc measurements and estimates of the degree of counterion binding for the disulfate surfactants were obtained via conductance measurements and counterion emf measurements. The conductance measurements were done on a YSI model 32 conductance bridge, using a YSI dip cell (cell constant = 1.0 cm^{-1}). Counterion emf measurements were obtained with a Corning combination sodium electrode connected to a Fisher Accumet pH meter. All measurements were done in a jacketed measuring cell maintained at 25.00 ± 0.02°C with a Haake 4000 temperature bath.

In Fig. 1, we present the FT-IR spectra for the C_{12} diol and the C_{12} disulfate, respectively. The infrared spectrum of the solid diol exhibits two peaks at about 3300 cm^{-1} that are absent in the spectrum of the disulfate surfactant. As well, we note the appearance of a large band in the fingerprint region at about 1200 cm^{-1} in the FT-IR spectrum of the disulfate amphiphile. These changes in the FT-IR spectrum are consistent with those observed when 1-dodecanol is converted to sodium dodecylsulfate (SDS), which is the monosulfate counterpart of this surfactant (15). Therefore, the addition of two sulfonate groups to the starting diol was successful. The presence of residual sodium chloride and sodium sulfate in the purified amphiphiles was confirmed by capillary electrophoresis. The amount of inorganic ion impurities present in the C_{16} disulfate is reduced greatly, but not eliminated completely, when the surfactants were washed with the methanol (ethanol) – water mixtures (Fig. 2). Since the properties of the micelles formed by disulfate surfactants would be affected by the presence of residual inorganic ions, we checked for the presence of chloride and sulfate in highly purified samples of SDS by capillary electrophoresis, and found chloride and sulfate ions present at the ppm level. Given that the aggregation numbers, β′ values, and enthalpy of micellization for our very pure SDS samples were in excellent agreement with the literature values, we feel that the presence of inorganic ions at the same level of concentration will also have a negligible effect on the properties of disulfate micelles. Finally, the amount of sulfate in the final product appears to be slightly larger than the concentration of chloride ion in the final product, which may be due to the well-known hydrolysis of sodium alkanesulfates in aqueous solution (16). It is possible that the rate of hydrolysis of disulfate surfactants is increased over the hydrolysis rate of the monosulfate amphiphiles, due to increased electrostatic interactions between adjacent charged headgroups. We are currently investigating the hydrolysis of a number of sulfate and disulfate surfactants via capillary electrophoresis as a function of pH and temperature in our laboratory.

The cmc values 1,2-alkanedisulfates, obtained from the breaks in the conductance versus concentration or counterion emf vs. log ($C_{surf,t}$) curves, are presented in Table 1 and plotted in Fig. 3 for carbon chain lengths of 10–16. The apparent degrees of counterion binding, the β′ values, obtained from the ratio of slopes method from the conductance or activity measurements, are also presented in Table 1. For comparison, the cmc values of the sodium alkanesulfates are also plotted in Fig. 3 (17–21). It is quite evident that the addition of the second negatively charged headgroup has a profound effect on the cmc values of the disodium 1,2-alkanedisulfates when compared with the sodium alkanesulfates possessing the same number of carbon atoms. Therefore, in agreement with the predictions of Shinoda et al. (17), the disulfate surfactants have higher critical micelle concentrations in water, reflecting a shift in the hydrophilic–lipophilic balance. We note that when we estimate the Gibbs energy of micelle formation, $\Delta_{mic}G^\circ \approx 2RT \ln X_{cmc}$, from the simple pseudo-phase separation model (i.e., ignoring the effects of the counterion dissociation), the difference in $\Delta_{mic}G^\circ$ between the alkanesulfates and the alkanedisulfates of the same alkyl chain length is constant at about 8.3 ± 0.8 kJ/mol (Fig. 4). In fact, the slope of the plot of $\Delta_{mic}G^\circ$ vs. the carbon chain length for the two surfactant families is the same within experimental error. This indicates that the Gibbs transfer energy for the CH_2 from the aqueous phase to the micellar phase is the same for both surfactant families (ca. −3.2 kJ/mol).

The apparent degrees of counterion binding, the β′ values, for disodium alkanedisulfates are lower than those of sodium alkanesulfates of comparable chain length. It should be mentioned, however, that when comparing values of the degree of counterion binding, one should compare values determined via the same method. Therefore, the β′ values that we reported for the sodium alkanesulfates are those obtained by the ratio of slopes method using conductance measurements (18–21). We see from Table 1 that the β′ values for the alkanedisulfates range from 0.26 for 1,2-SDecDS to 0.40 for 1,2-SHDS. The decrease in the β′ values for alkanedisulfate micelles over the alkanesulfate micelles indicates a significant reduction of the surface charge density of the micelle formed by the two-headed surfactants. We note, however, that the measurement of the β′ value via the ratio of slopes method assumes that the molar conductivity of the micelle is a simple function of the

Fig. 1. FT-IR spectra for (*a*) 1,2-dodecanediol and (*b*) disodium 1,2-dodecanedisulfate.

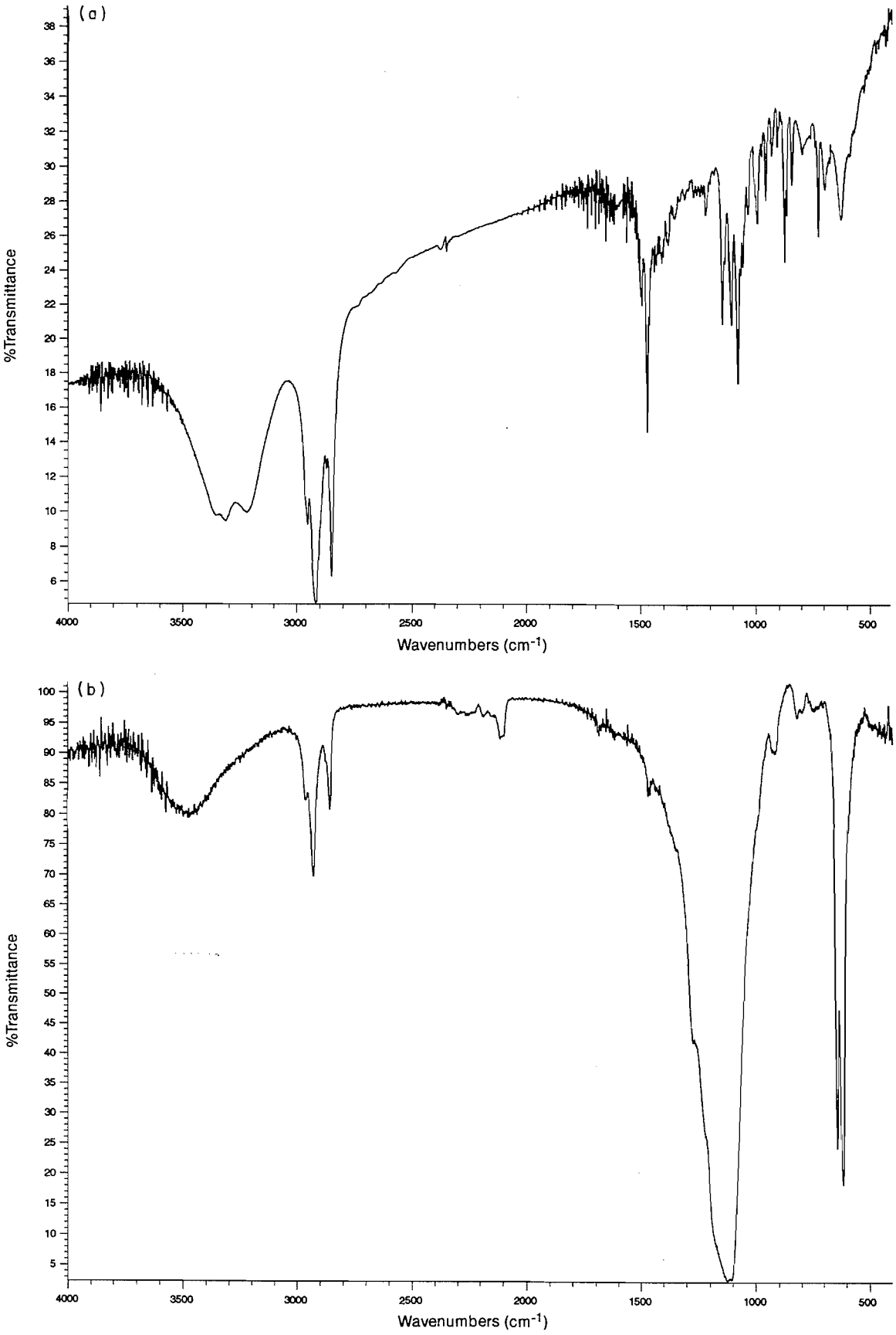

Can. J. Chem. Downloaded from www.nrcresearchpress.com by 80.90.12.36 on 09/08/12
For personal use only.

Can. J. Chem. Downloaded from www.nrcresearchpress.com by 80.90.12.36 on 09/08/12
For personal use only.

Fig. 2. (*a*) Ion chromatogram (via capillary electrophoresis) of crude 1,2-disodium hexadecanedisulfate. (*b*) Ion chromatogram of the same sample of 1,2-disodium hexadecanedisulfate after washing the product with a methanol–water mixture.

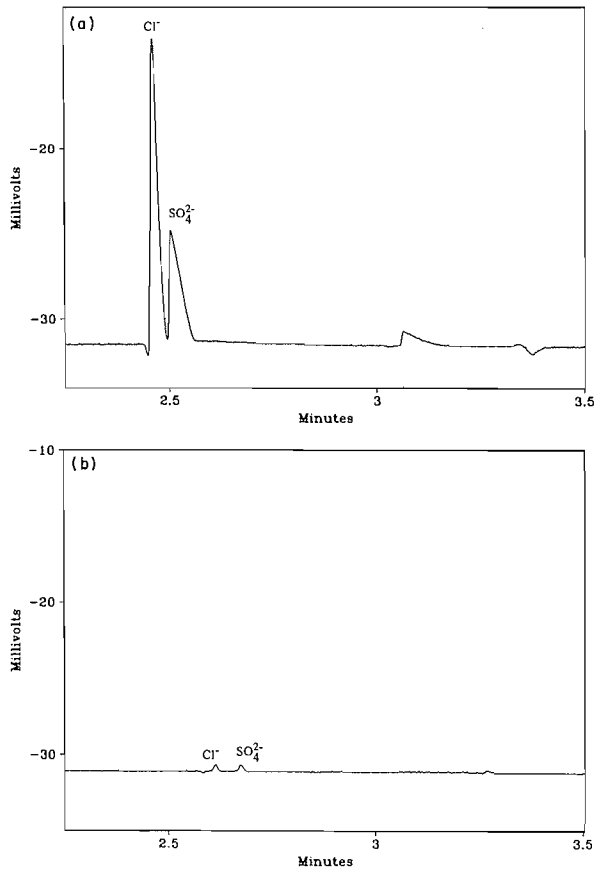

Fig. 3. Critical micelle concentration (cmc) values (± 0.3 mM, conductance measurements) for sodium alkanesulfate surfactants (●) and disodium 1,2-alkanedisulfate surfactants (▲) in water as a function of the alkyl chain length.

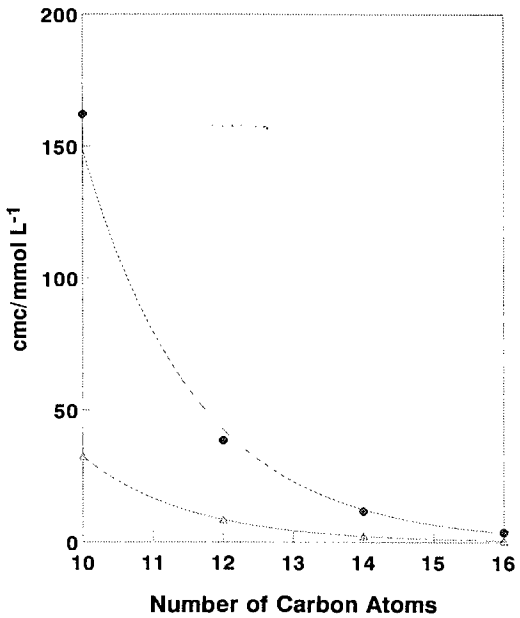

Fig. 4. The ln X_{cmc} values for sodium alkanesulfate surfactants (●) and disodium 1,2-alkanedisulfate surfactants (▲) as a function of the alkyl chain length.

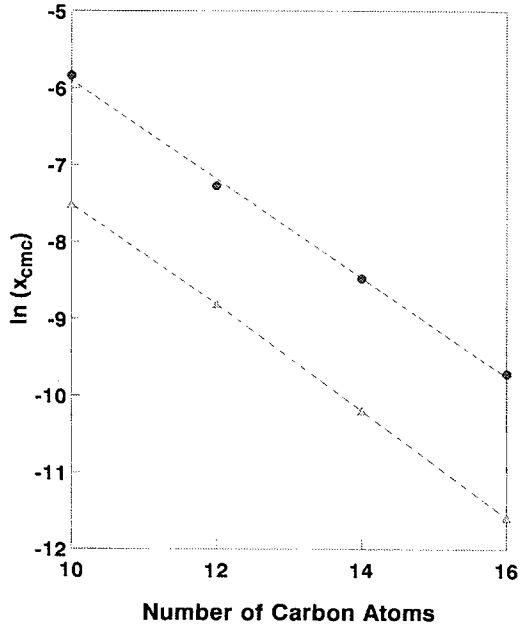

number of dissociated headgroups. Since micelles are compact, highly charged structures, the fraction of charge carried by the two-headed surfactant micelle may be significant, leading to low estimates of the degree of counterion binding. If the counterion binding estimates obtained in this fashion are indeed reasonable, the small β′ values for the disulfate surfactants compared to the monosulfate surfactants suggests that these micelles have much smaller aggregation numbers than the alkanesulfate surfactants of the same chain length. The surface charge density of the disulfate surfactants increases as the surfactant chain length increases, indicating that the aggregation number of disulfate micelles will increase with increasing chain length. The increase in the β′ values for the disulfate micelles with increasing surfactant chain length is comparable to the increase in the apparent counterion binding values observed for the sodium alkanesulfates as a function of the length of the amphiphile chain (Table 1).

In conclusion, cmc's and β′ values for a series of disulfated 1,2-alkanediols indicate that the addition of the second headgroup significantly changes the properties of the micelles formed by the two-headed surfactants, such as the cmc values and the β′ values. We expect that, due to the shift in the hydrophilic–lipophilic balance, other important properties of the surfactant and the micelles will be altered (e.g., surface-tension lowering (12), solubilization of co-surfactants, and aggregation numbers). Kooreman and Engberts (11) have demonstrated that two-headed sulfate surfactants are extremely stable towards precipitation by hard water ions (e.g., Ca^{2+}). All these properties will be the subject of future publications.

Acknowledgments

The financial support of the Natural Sciences and Engineering Research Council of Canada (NSERC) (research grant, D.G.M) and the St. F.X. University Council for Research is

Table 1. Critical micelle concentration (cmc) values (± 0.3 mM) and degrees of counterion binding (β′ ± 0.02) of disodium 1,2-alkanedisulfates and sodium alkanesulfates (17–21) as a function of the carbon chain length.

	Alkanedisulfates		Alkanesulfates	
Carbon chain length	cmc (mmol L^{-1})	β′	cmc (mmol L^{-1})	β′
10	162.2	0.26	32.5	0.53 (19)
12	38.5	0.30	8.36	0.63 (19)
14	11.6	0.36	2.20	0.53 (21)
16	3.76	0.40	0.57	0.50 (21)

greatly appreciated. E.J.B. wishes to acknowledge the grant of NSERC Undergraduate Summer Research Awards. C.V.H. and J.F.C. are grateful to St. F.X. University for financial support. The authors thank Truis Smith-Palmer at St. F.X. for her help with the capillary electrophoresis experiments. NMR spectra were obtained at the Atlantic Region Magnetic Resonance Centre (Dalhousie).

References

1. M.J. Rosen. *In* Surfactants in emerging technologies. *Edited by* M. J. Rosen. Surf. Sci. Ser. No. 26. Marcel Dekker, New York. 1986.
2. J.N Israelachvili, D.J Mitchell, and B.W Ninham. J. Chem. Soc. Faraday Trans. 2, **72**, 1525 (1976); J.N Israelachvili and H. Wennerström. Langmuir, **6**, 873 (1990).
3. F. Franks. *In* Water — a comprehensive treatise. Vol. 4. *Edited by* F. Franks. Plenum, New York. 1975. pp. 1–93.
4. B. Lindman and H. Wennerström. Top. Current Chem. **87**, 1 (1980).
5. C. Tanford. The hydrophobic effect: the formation of micelles and biological membranes. John Wiley, New York. 1973.
6. D.J. Jobe and V.C. Reinsborough. Aust. J. Chem. **34**, 320 (1984).
7. K. Ikeda, T. Nakasima, K. Esumi, and K. Meguro. Bull. Chem. Soc. Jpn. **62**, 578 (1989).
8. K. Tamaki, Y. Ohara, Y. Akimoto, and K. Koshishi. Bull. Chem. Soc. Jpn. **67**, 856 (1994).
9. K. Meguro, K. Ikeda, A. Otsuji, M. Taya, M. Yasuda, and K. Esumi. J. Colloid Interface Sci. **118**, 372 (1987).
10. M. Frindi, B. Michels, H. Levy, and R. Zana. Langmuir, **10**, 1140 (1994).
11. P.A. Kooreman and J.F.B.N. Engberts. Recl. Trav. Chim. Pays-Bas, **113**, 163 (1994).
12. A.A. El-Sawy, S.A. Essaway, M.M. El-Sukkary, and A.M.F. Eissa. Hung. J. Ind. Chem. **20**, 25 (1992).
13. B.J. Ravoo and J.F.B.N. Engberts. Langmuir, **10**, 1735 (1994).
14. Y.-P. Zhu, A. Masuyama, Y. Kobata, Y. Nakatsuji, M. Okahara, and M.J. Rosen. J. Colloid Interface Sci. **158**, 40 (1993).
15. Aldrich library of FT-IR spectra. Aldrich Chem. Co., Milwaukee, Wis.
16. J.L. Kurz. J. Phys. Chem. **66**, 2239 (1962).
17. K. Shinoda, T. Nakagawa, B. Tamamushi, and T. Isemura. *In* Colloidal surfactants. Academic Press, New York. 1963. p. 44.
18. S. Kaneshina, M. Tanaka, T. Tomida, and R. Maturra. J. Colloid Interface Sci **48**, 450 (1974).
19. E.D. Goddard and G.C. Benson. Can. J. Chem. **35**, 986 (1957).
20. P. Mukerjee and K.J. Mysels. Critical micelle concentrations for aqueous surfactant systems. US-NBS, No. 36. U.S. GPO, Washington, D.C. 1971.
21. H.J. Evans. J. Chem. Soc. 579 (1956).

Can. J. Chem. Downloaded from www.nrcresearchpress.com by 80.90.12.36 on 09/08/12
For personal use only.

Non-equilibrium particle morphology in dispersion-polymerized polystyrene particles[1]

Anthony J. Paine and Richard R. Shivers

Can. J. Chem. Downloaded from www.nrcresearchpress.com by 46.23.64.124 on 09/08/12
For personal use only.

Abstract: The interior particle morphology of dispersion-polymerized polystyrene particles was investigated by freeze fracture TEM (FFTEM) in order to compare the morphology of particles formed under two extreme mechanistic conditions: (*a*) particle growth by scavenging of dead polymer chains formed in solution (which gives rise to large particles of 5–10 μm) and (*b*) particle growth by oligomeric radical capture and polymerization inside the particle (giving rise to small particles of 1 μm or less). Although not generally recognized in the literature, ascribing mechanistic significance to an observed morphology requires a demonstration that the morphology is of the non-equilibrium type, i.e., the morphology depends upon how the particle was formed. An equilibrium morphology, by definition, must be independent of the particle formation route, and therefore carries no mechanistic information. In this case, large PS particles of 6.5 μm were found to have a nodular morphology that was unchanged on heating well above T_g, indicating an equilibrium structure (the nodularity of amorphous polymers is briefly rationalized by comparison with literature results over the past 20 years). On the other hand, small PS particles of 1.3 μm had a pronounced radial structure that could be converted into the nodular morphology by the same heat treatment, or by dissolving and precipitating from a suitable solvent combination. This means that the small particles have a non-equilibrium morphology, from which we may attempt to draw mechanistic inferences consistent with the suspected growth mechanism.

Key words: dispersion-polymerized polystyrene, non-equilibrium polystyrene particle morphology, freeze fracture transmission electron microscopy.

Résumé : On a étudié la morphologie de la particule intérieure d'une dispersion de particules de polystyrène (PS) par la technique de FFTEM dans le but de comparer la morphologie des particules formées sous deux conditions mécanistiques extrêmes : (*a*) croissance des particules par piégeage des chaînes mortes de polymère formées en solution (qui donnent lieu à de grosses particules de 5–10 μm) et (*b*) croissance des particules par une capture d'un radical oligomérique et une polymérisation à l'intérieur de la particule (donnant lieu à de petites particules de 1 μm ou moins). Même si ce fait n'est généralement pas reconnu dans la littérature, l'attribution d'une signification mécanistique à une morphologie observée nécessite une démonstration que la morphologie est d'un type non équilibré, c'est-à-dire que la morphologie dépend de la façon dont la particule s'est formée. Par définition, une morphologie d'équilibre doit être indépendante de la voie de formation de la particule; elle n'a donc aucune signification mécanistique. Dans ce cas, on a trouvé que de grosses particules de PS de 6,5 μm possèdent une morphologie nodulaire qui ne change pas par chauffage à des températures bien supérieures à la T_g; ceci suggère l'existence d'une structure en équilibre (on rationalise brièvement le caractère nodulaire de polymères amorphes par comparaison avec des résultats rapportés dans la littérature au cours des 20 dernières années). Par ailleurs, les petites particules de PS de 1,3 μm possèdent une structure radiale prononcée qui peut être transformée en morphologie nodulaire par le même traitement par la chaleur ou par dissolution et reprécipitation à partir d'une combinaison appropriée de solvants. Ces résultats signifient que les petites particules possèdent une morphologie qui n'est pas équilibrée et on peut essayer d'en tirer des conclusions mécanistiques en accord avec le mécanisme supposé de croissance.

Mots clés : polymérisation d'une dispersion de particules de polystyrène, morphologie d'un type non équilibré, FFTEM.

[Traduit par la rédaction]

Received September 9, 1994.

This paper is dedicated to Professor J.E. (Jim) Guillet in recognition of his contributions to Canadian chemistry.

Anthony J. Paine.[2] Xerox Research Centre of Canada, 2660 Speakman Drive, Mississauga, ON L5K 2L1, Canada.
Richard R. Shivers. Department of Zoology, University of Western Ontario, London, ON N6A 3K7, Canada.

[1] Presented, in part at IUPAC MACRO 90, Montreal, Canada, July 1990.
[2] Author to whom correspondence may be addressed. Telephone: (905) 823-7091. Fax: (905) 822-7022.

Can. J. Chem. Downloaded from www.nrcresearchpress.com by 46.23.64.124 on 09/08/12
For personal use only.

Introduction

Dispersion polymerization of styrene in polar solvents differs from other types of particle-forming polymerizations, such as suspension or emulsion polymerization. The initial reaction mixture, comprising styrene monomer, steric stabilizer polymer, initiator, and alcohol, is homogeneous. Typical steric stabilizers are alcohol-soluble homopolymers such as hydroxypropyl cellulose (HPC), poly(acrylic acid) (PAA), or poly(*N*-vinylpyrrolidone) (PVP), which graft to the polystyrene as it is formed, although block copolymers and macromers can also be used. Since the initial mixture is homogeneous, the polymerization begins as a solution polymerization. After a short period of time, the homogeneous solution becomes cloudy as the particles nucleate and subsequently grow. Under favourable circumstances, the final particles are monodisperse, in the size range of 1–15 μm.

These reactions have been investigated extensively within Xerox by Lok, Hair, Ober, Paine, and co-workers (1–7), and in the Lehigh University laboratories of Vanderhoff and El-Aasser (8, 9). Figure 1 summarizes the qualitative view of the mechanism of dispersion polymerization, as seen by Ober and Lok (1, 2). When polymerization is initiated, chains of homopolystyrene together with a small amount of graft are formed. The homopolymer is insoluble and precipitates from solution while the graft goes to the particle surface to develop a steric stabilizer layer. Once the particles are formed, the monomer partitions between the particle and continuous phases, and polymerization takes place in both phases, causing the particles to grow. At the end of the reaction the isolated and washed particles have grafted steric stabilizer exclusively on the particle surface. The evidence for this includes transmission electron microscopy (TEM) observation (4), fluorescence quenching studies (3), and X-ray photoelectron spectroscopy (XPS) (7).

An important mechanistic feature is that the balance between the amount of polymerization occurring inside the particles vs. that occurring in the continuous phase depends on the particle size (5, 6). The low-volume fraction of solids after nucleation tends to favour extensive initiation in the continuous phase, rather than in the nuclei. From a consideration of the diffusion constants and chemical kinetics, it can be shown that when the final particle size is large (on the order of 5–10 μm), there are relatively fewer particles, and polymer is primarily formed by termination in solution and accretion of dead polymer onto the nuclei. As a result, the observed molecular weights are low and comparable to those from solution polymerization. On the other hand, when the final particle size is small (on the order of 1 μm), there are many more growing nuclei, and they rapidly scavenge growing oligomer from the continuous phase before it can terminate, and this leads to polymerization inside the particle, with gel-effect-induced increases in the molecular weight. The mechanism for small-particle growth is very similar to that for emulsion polymerization, and leads to comparably high molecular weights.

We became interested in the morphology of dispersion-polymerized particles as a consequence of some earlier work done by one of us with Mitchell Winnik and co-workers on the nonaqueous dispersion polymerization of methyl methacrylate in hydrocarbon solvents (10). Several features of their system were dramatically different from ours. For example, fluorescence quenching studies led them to believe the particle

Fig. 1. Schematic of the mechanism of dispersion polymerization (from Ober and Lok (1, 2)).

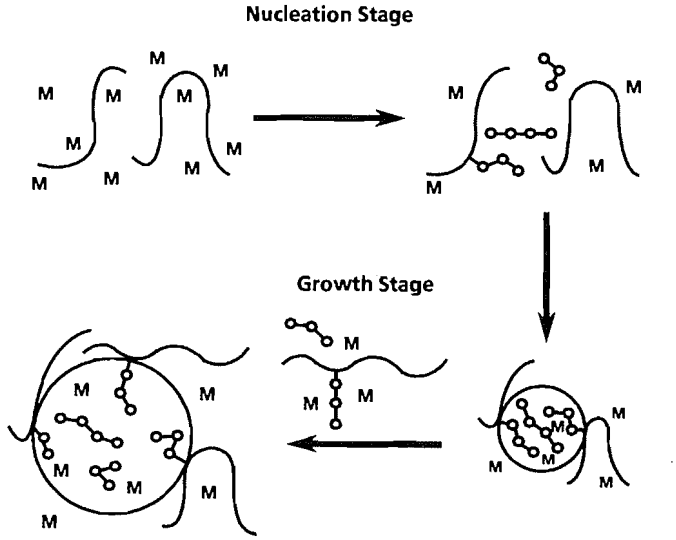

structure was of an interpenetrating network of stabilizer throughout the core, while similar measurements (3), together with TEM sectioning and staining results (4), indicated that the stabilizer on the particles that are the subject of this paper was almost exclusively on the surface. The prior authors applied freeze fracture TEM (FFTEM) to several colloidal particles and concluded that the observed structures implied something about the mechanisms of particle nucleation and growth (10, 11). Since our mechanistic study suggested small and large particles grew by different mechanisms, we were anxious to have a look at the freeze fracture morphologies of the polystyrene particles.

Although the explicit objective of the work with Winnik in ref. 10 was to use FFTEM "to obtain new information on the subjects of primary particle formation and monomer–polymer particle growth mechanisms," we were concerned about the morphology–mechanism connection. Although not recognized in that paper, or in the literature in general, ascribing mechanistic significance to an observed morphology requires a demonstration that the morphology is of the non-equilibrium type, i.e., that the morphology depends upon how the particle was formed. The prior work assumed the morphology was non-equilibrium. However, if their observed morphologies were of the equilibrium type (by definition, independent of the particle formation route), they could not possibly carry any mechanistic information.

Thus, the objectives of our study were twofold: (*i*) to compare the morphologies of dispersion-polymerized PS particles formed under the mechanistic extremes; and (*ii*) to critically evaluate whether the observed morphologies could have mechanistic significance.

Experimental section

Particle synthesis and characterization

The details of PVP-stabilized polystyrene particle synthesis were reported earlier (7, 12). Briefly, styrene, AIBN, PVP (mol. wt. 40 000), and optional costabilizer (Triton N-57 (nonylphenol poly(ethylene oxide) from Rohm and Haas) or Aerosol OT-100 (AOT; dioctyl sodium sulfosuccinate from

Can. J. Chem. Downloaded from www.nrcresearchpress.com by 46.23.64.124 on 09/08/12
For personal use only.

Table 1. Summary of the synthesis of large and small polystyrene particles by dispersion polymerization.[a]

	Large particles (M137)	Small particles (M87TP)
Synthetic conditions		
PVP (g)	31.3	1.25
Costabilizer (wt/g)	Triton N-57 (31.3)	AOT (0.340)
Solvent (vol/mL)	EtOH (1500.0)	EtOH (56.0)/H_2O (14.0)
Styrene (mL)	500.0	10.0
AIBN (wt% to monomer)	2%	1%
M_w (MWD)	53 500 (3.27)	391 000 (5.04)
Residual sytrene (ppm)	7300	430
Particle size (μm (GSD))	6.35 (1.03)	1.17 (1.16)
Heated sample no.	RS-6	RS-4
Particle size (μm (GSD))	6.3 (1.57)	1.4 (1.41)
Mass fraction original particles	60%	80%

[a]Particle size measurement (volume d_{50} and GSD $\equiv (d_{84}/d_{16})^{1/2}$) by Coulter Multisizer.

American Cyanamid)) were mixed in alcohol, then polymerized at 70°C for 24 h. The resulting latex particles were washed several times with ethanol, then with water, and were freeze-dried. Synthetic conditions, particle size, and molecular weight data are reported in Table 1. ^{13}C NMR indicated that the polymer was atactic in both cases (multiple peaks for the backbone CH_2 groups between 40 and 50 ppm).

Freeze fracture TEM procedure

The details of this procedure were published before in the work with Winnik and co-workers (10). Briefly, particles were suspended at approximately 1% loading in 30% glycerol – 0.1 M sodium cacodylate – 0.01% Triton X-100. A drop of this suspension was frozen in Freon-22 in liquid N_2, then fractured under vacuum at 77 K to give free break through the sample. The surface of the free break was coated with 1–2 nm Pt at a 45° shadowing angle; then 10–30 nm C at 90°. The replica-coated sample was thawed, rinsed in de-ionized water, then soaked 48 h in $CHCl_3$ to dissolve the polystyrene. The replicas were placed on copper TEM grids and examined with a Philips 201 EM. In these micrographs, the white areas correspond to shadows of rough features on the fracture surface that did not receive Pt. Approximately 50–100 micrographs were taken of each sample.

Heating experiment

The particles were suspended at 100 mg loading in 0.5 mL glycerol in a 10 mL test tube. The tubes were capped and placed into an oil bath at 245 ± 5°C for 2 min, then removed and allowed to cool slowly in air at room temperature. The samples were checked for particle coalescence by remeasuring particle size and GSD. The results posted in Table 1 show that fewer than half the original particles coalesced during this procedure.

Precipitation experiment

The procedure was similar to that already published (3, 4). The precipitation of these small particles was difficult because of the high ratio of the molecular weight of the polystyrene to the PVP stabilizer — about 10×, while the process works best at 0.3–3×. A solution of M87TP particles (1.0 g) in dioxane (20 mL) was stirred 3 h, then precipitated with MeOH (250 mL) added at 200 mL min^{-1} with a peristaltic pump. A large lump of coagulum was obtained with only some latex. The experiment was repeated with rapid MeOH addition with a squirt bottle with similar results. A third experiment (0.51 g in 20 mL THF precipitated with 250 mL MeOH added at 10 mL min^{-1}) eliminated the coagulum but gave a high yield of large flocs. The latexes from the three experiments were combined, filtered through a 74 μm filter, washed with MeOH (2 × 50 mL), then with water (2 × 50 mL), and freeze-dried to obtain precipitated particles (217 mg; 9% yield) with volume median diameter 4.6 μm and GSD = 2.7.

Results

The background to FFTEM and the artifact potential from plastic deformation are discussed in depth in the earlier papers with Winnik (10, 11), as well as basic textbooks (13–15) or review articles (16). Briefly, one observes brittle fracture through the centre of the particle, in addition to protrusions and extrusions caused by fractures at the particle surface – matrix interface. For the purposes of this discussion, we selected FFTEM micrographs where the fractures went through the interior of the particle. These were in the vast majority, and permit the discussion to focus on the interior morphology. Plastic deformation artifacts were largely absent.

This investigation focussed on two types of dispersion-polymerized particles: 6.35 μm, "large" particles of low molecular weight typical of considerable solution polymerization and accretion of dead polymer (M 137 in Table 1); and 1.17 μm, "small" particles of high molecular weight typical of extensive radical capture and gel-effect polymerization similar to emulsion polymerization (M87TP in Table 1). Figure 2 shows a typical micrograph from the fractured surface of the small particles. It is remarkably similar to Winnik's earlier samples of poly(methyl methacrylate) (PMMA) (10), and shows the same radial morphology, almost spherulitic. The shadowing shows a highly irregular surface, with some features as much as 100–600 nm high. The thin lines apparently radiating from the centre are typically 200 nm long, but only

Fig. 2. Typical FFTEM of small particles showing the radial structure.

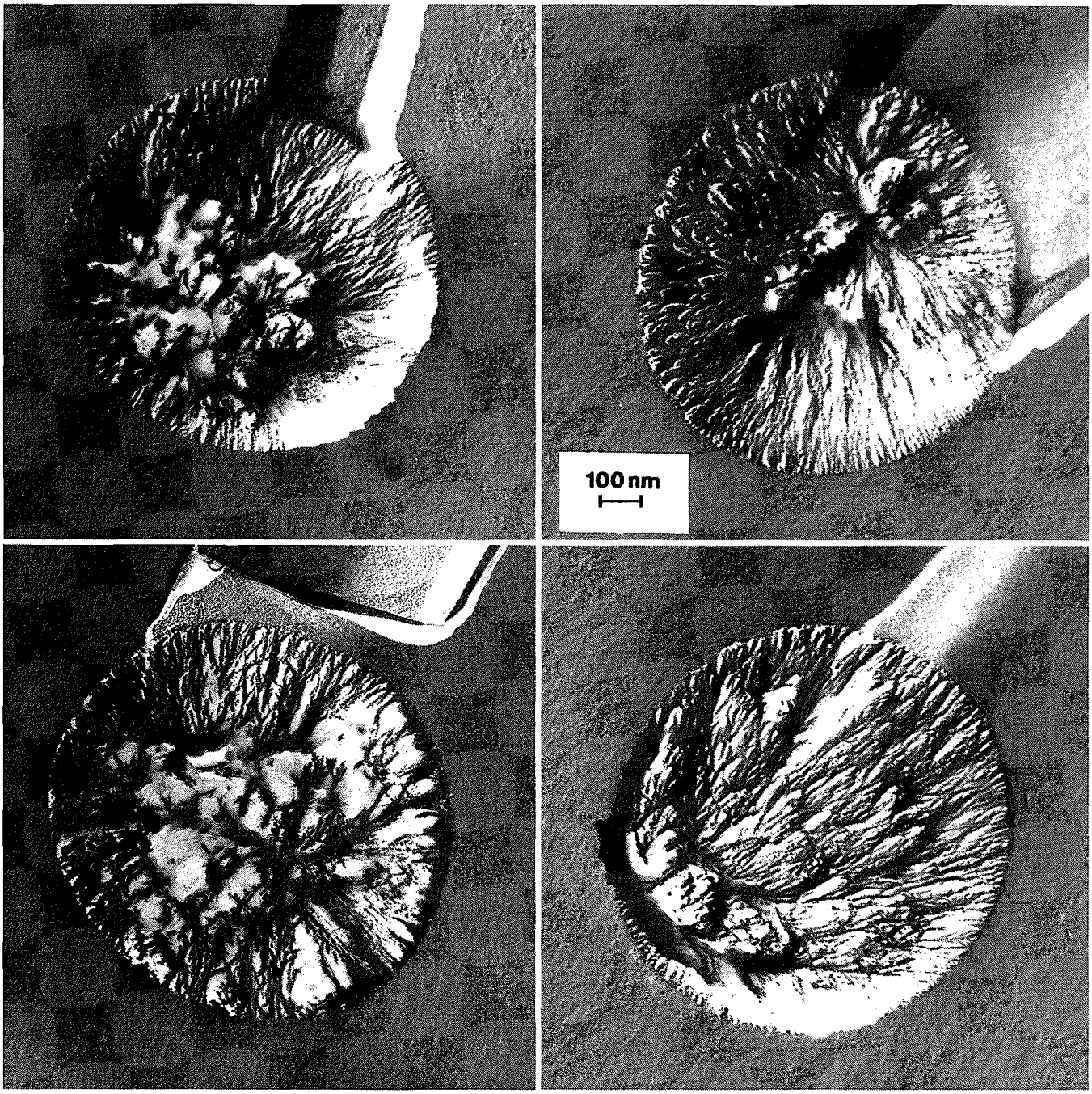

Can. J. Chem. Downloaded from www.nrcresearchpress.com by 46.23.64.124 on 09/08/12
For personal use only.

7–8 nm wide, and appear to be made up of little dots. It is not clear whether the dots represent real topology or are a decoration artifact of the platinum coating. However, it may be noteworthy that the width of the lines is comparable to the expected radius of gyration, around 7 nm for polymer of 400 000 molecular weight.

The centers of the small particles appear different from the exterior or shell portion, and appear nodular, like the bulk of the large particles (Fig. 3). The fracture of the larger particles reveals a much different morphology, which appears isotropically nodular. The size of these highly irregular nodules is around 20–60 nm, about 10–25× the radius of gyration of polystyrene of comparable molecular weight, and their size is relatively constant throughout the particles. Thus, in this case, the nodular dimensions do not reflect anticipated polymer dimensions in the amorphous particle. At the particle surface there is only subtle evidence for an intermittent 20–50 nm thick layer where the ruggedness dissipates. Presumably this is the surface graft region, though the visualization of the layer is far less effective than in our prior work where the particles were embedded in epoxy, sectioned, and then stained for TEM to reveal a well-defined surface layer of grafted stabilizer (4).

Thus, comparing Figs. 2 and 3, there is a major difference apparent in the interior morphology of the small and large particles. Both particles were composed of amorphous atactic polystyrene, though it might seem that either size or molecular

Fig. 3. Typical FFTEM of large particles showing the nodular structure.

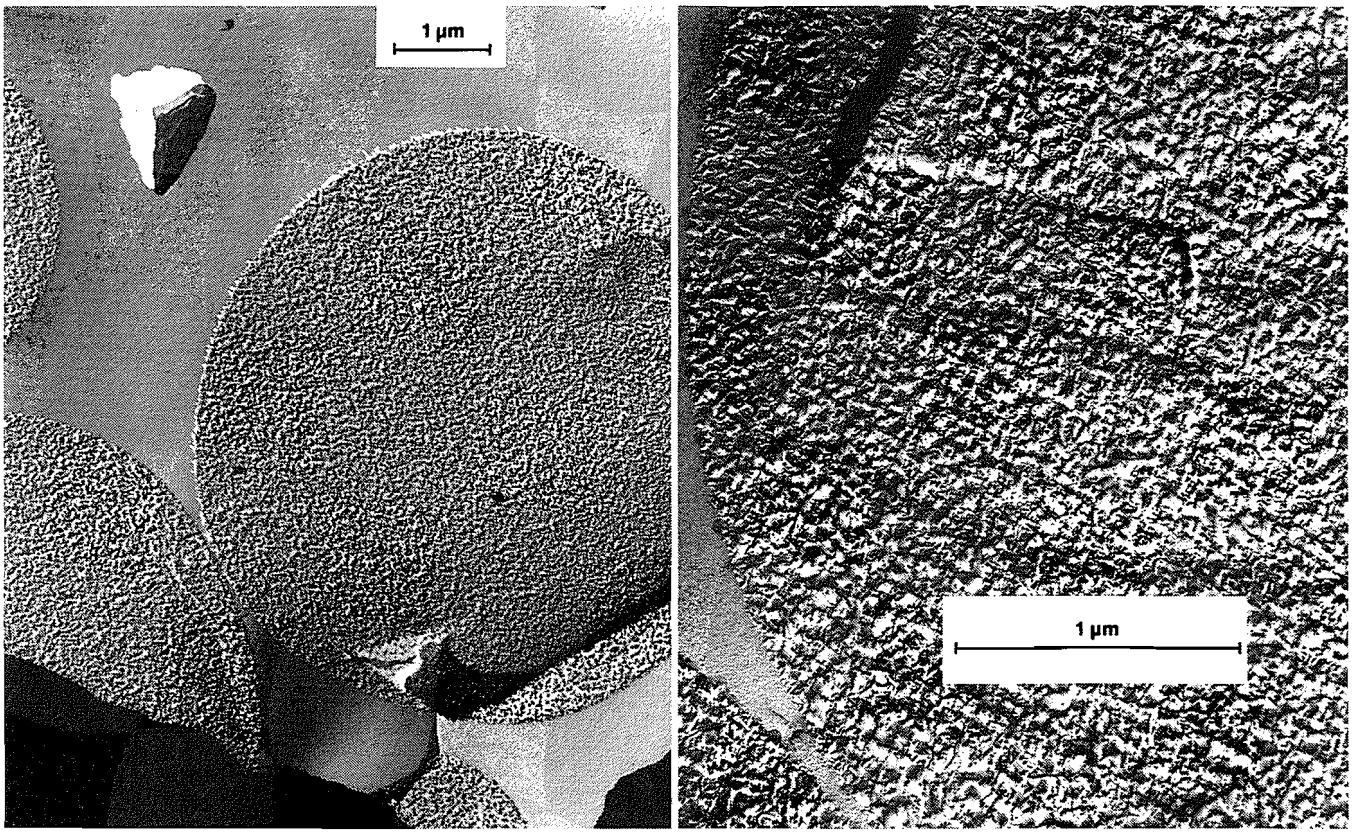

Can. J. Chem. Downloaded from www.nrcresearchpress.com by 46.23.64.124 on 09/08/12
For personal use only.

weight differences could be the main driver behind the morphological differences.

To evaluate the size and molecular weight effects, and to detect if either or both structures were equilibrium morphologies, the particles were heated well above the glass transition temperature T_g (~100°C) and close to the melting point T_m (~240°C) of polystyrene (17). By using a glycerol dispersion, conditions were found to minimize the amount of inter-particle coalescence, while maximizing the opportunity to rearrange into the lowest energy interior morphology.

As Fig. 4 shows, the large particles were mostly unaffected after heating. The nodule size appears to be about the same, or possibly larger, about 30–100 nm, suggesting that this is an equilibrium structure.

On the other hand, the small particles changed dramatically after heating, as shown in Fig. 5. Their radial structure was converted into the nodular form common for the large particles with a nodule size of about 30–100 nm, very similar to that of the larger particles with molecular weight seven times lower. The particle size is still ~1 μm, yet the morphology appears radically different from that of the original particles, so the morphological differences in these photographs are not a size-dependent artifact. Thus, the heating experiment suggests that (*i*) the nodular structure is thermodynamically preferred, and (*ii*) the small particles were initially formed in a non-equilibrium morphology somehow induced by their synthetic conditions.

It is also interesting to consider the results of precipitation on the non-equilibrium morphology. In earlier work it was noted that dispersion-polymerized particles may be dissolved in a solvent common for the polystyrene and surface graft, and then precipitated into a solvent that is poor for the polystyrene but good for the soluble chains on the graft, to produce new latex particles of very wide size distribution (3, 4, 7). Prior TEM and fluorescence-quenching experiments had suggested the surface stabilizer morphologies of native and precipitated particles were identical. In this particular case, the precipitation of the small particles was difficult because of the high ratio of MW_{PS}/MW_{PVP} (about 10, while the process works best at 0.3–3), with the result that coagulum accounted for 90% of the product. Nevertheless, the precipitated particles from three experiments were combined and subjected to FFTEM to compare the morphology.

Again, Fig. 6 shows that the primary morphology of the precipitated particles was of the nodular type, although some of the very tiny particles may be radial. This may hint at either an artifact or a size dependence to morphology at very small particle sizes. Nevertheless, it is certainly clear that 1 μm particles that were radial in their native state can be precipitated into the nodular morphology, and they account for most of the particulate mass after precipitation.

Discussion

The results show that there appear to be two particle morphologies in these dispersion-polymerized PS particles: nodular and radial. Small particles are formed in the non-equilibrium radial structure as synthesized, but this can be converted into the nodular structure, either by heating or precipitating the particles. Since the large particles have the same type of structure before and after heating, it follows that the nodular structure is the equilibrium structure. We now consider the consequences of the nodular and the radial structures.

Fig. 4. Typical FFTEM of large particles after heating. Note the retention of nodular structure.

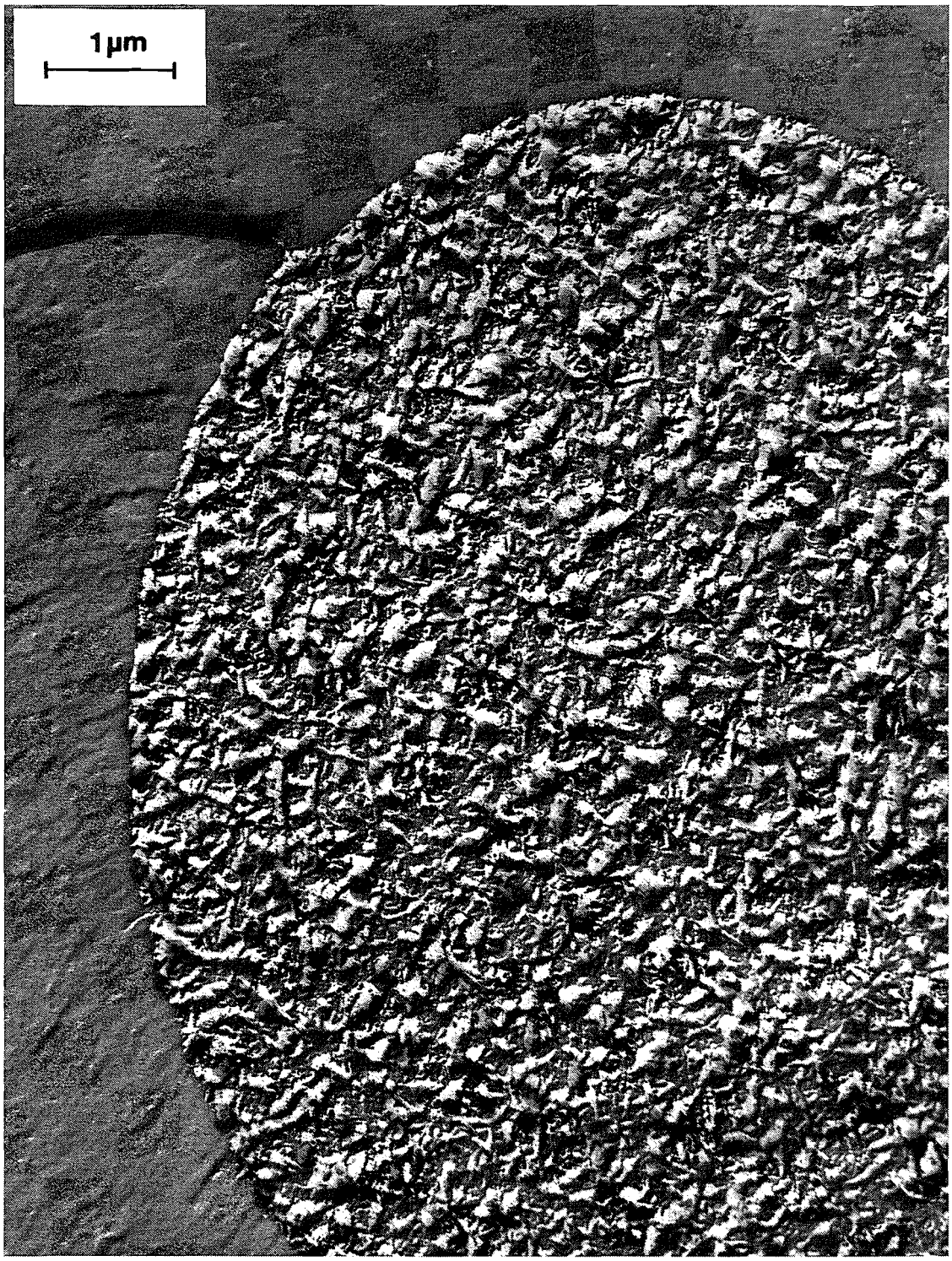

Can. J. Chem. Downloaded from www.nrcresearchpress.com by 46.23.64.124 on 09/08/12
For personal use only.

Nodular morphology of amorphous polystyrene

Since the nodular structure of the large particles is the equilibrium structure, we can garner no mechanistic information about the particle formation from it. In particular, it says nothing about any accretion mechanism for dead polymer, and nothing about the size of the species accreting onto the particle during its growth. For example, both Winnik (10) and Bassett (18) interpreted the presence of nodules, or a raspberry structure, to an accretion mechanism in particle formation. However, without separate evidence that the morphology was a non-equilibrium structure, their mechanistic inferences must be discounted. It is interesting that there have been a number of reports about nodular structures in amorphous polymers over the past 20 years, though the evidence for nodules in

Fig. 5. Typical FFTEM of small particles after heating. Contrast with Fig. 2 (radial structure).

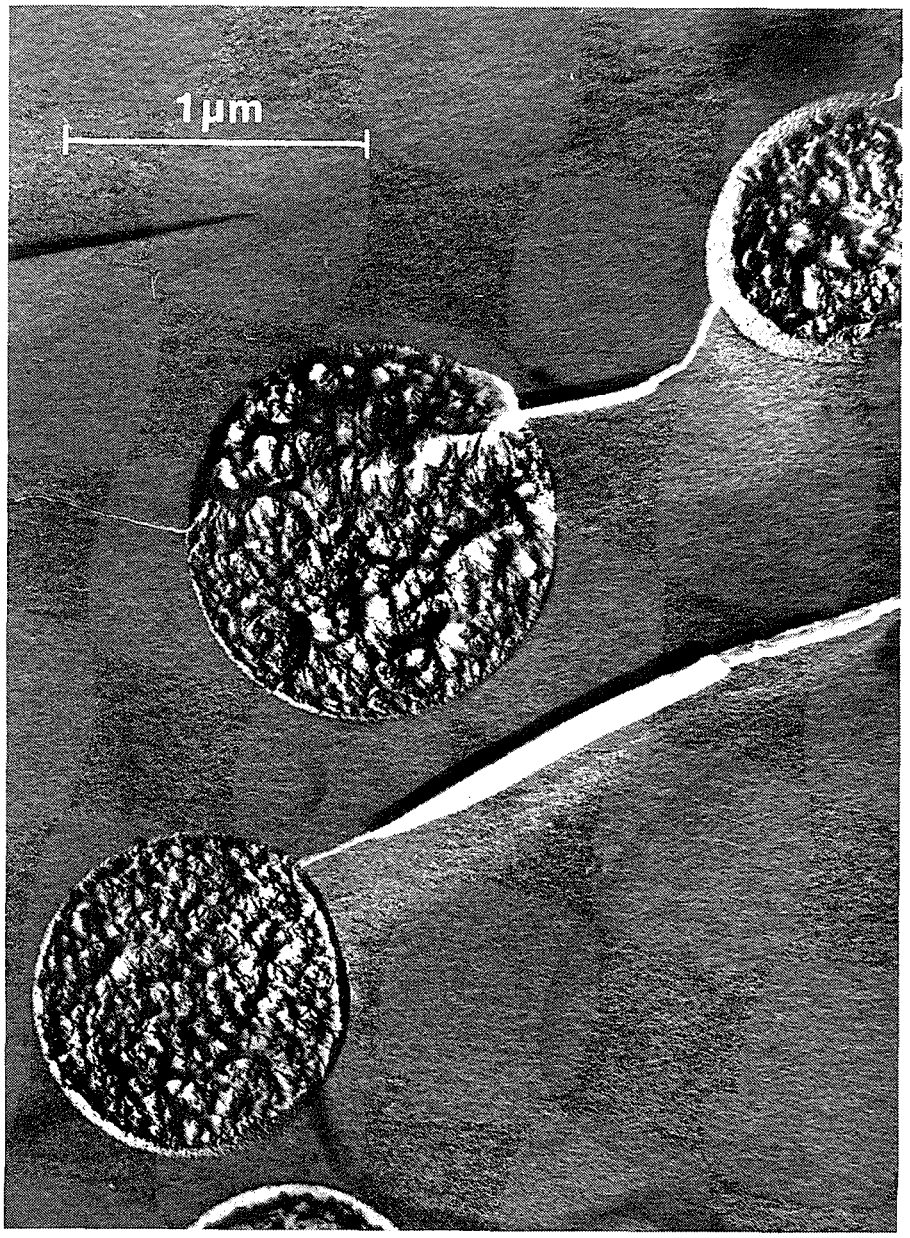

Can. J. Chem. Downloaded from www.nrcresearchpress.com by 46.23.64.124 on 09/08/12
For personal use only.

amorphous polystyrene has not been particularly strong (16, 19–23). The nodules were certainly evident in similar sectioned particles examined by regular TEM (4), where interior features on the order of 50–100 nm seemed to orient in lines parallel to the sectioning knife edge.

In traditional polymer morphology texts, most EM work on polymer fracture is generally at much lower resolution than that shown here (15). Even so, some of the published micrographs hint at a smaller level of structure than is generally discussed.

During the 1970s and early 1980s there was some controversy in the literature over microstructure in amorphous polymers, especially atactic polystyrene (23). Quenching of amorphous polymers (primarily poly(ethylene terephthalate) (PET), but also PS and poly(vinyl chloride)–solvent gels) gave rise to nodular structures of 4–13 nm in diameter and a diffuse electron diffraction ring, indicative of short-range order on this scale. Geil suggested that features less than 5 nm could be instrument artifacts (phase contrast effects that can arise when the replica is slightly out of focus) (16), but features larger than 8 nm were likely real. This caused Geil to conclude that Yeh's original observation (19) about atactic PS with 3.5 nm nodules could be ruled out. Irrespective of that controversy, the nodules observed here are in the 20–100 nm range, much too large to be phase contrast effects.

The nodules arise during either polymerization or cooling because polymer solidification at the glass transition temperature is not a true equilibrium process, unless the cooling rate is infinitely slow. Discontinuous changes in entropy and entropy production during solidification can give rise to dissipative structures like the nodules seen in these micrographs (24, 25). Thus, the nodule structure represents the non-equilibrium structures formed during the solidification process, not the polymerization process. Other symptoms of microstructure in

Fig. 6. Typical FFTEM of precipitated small particles.

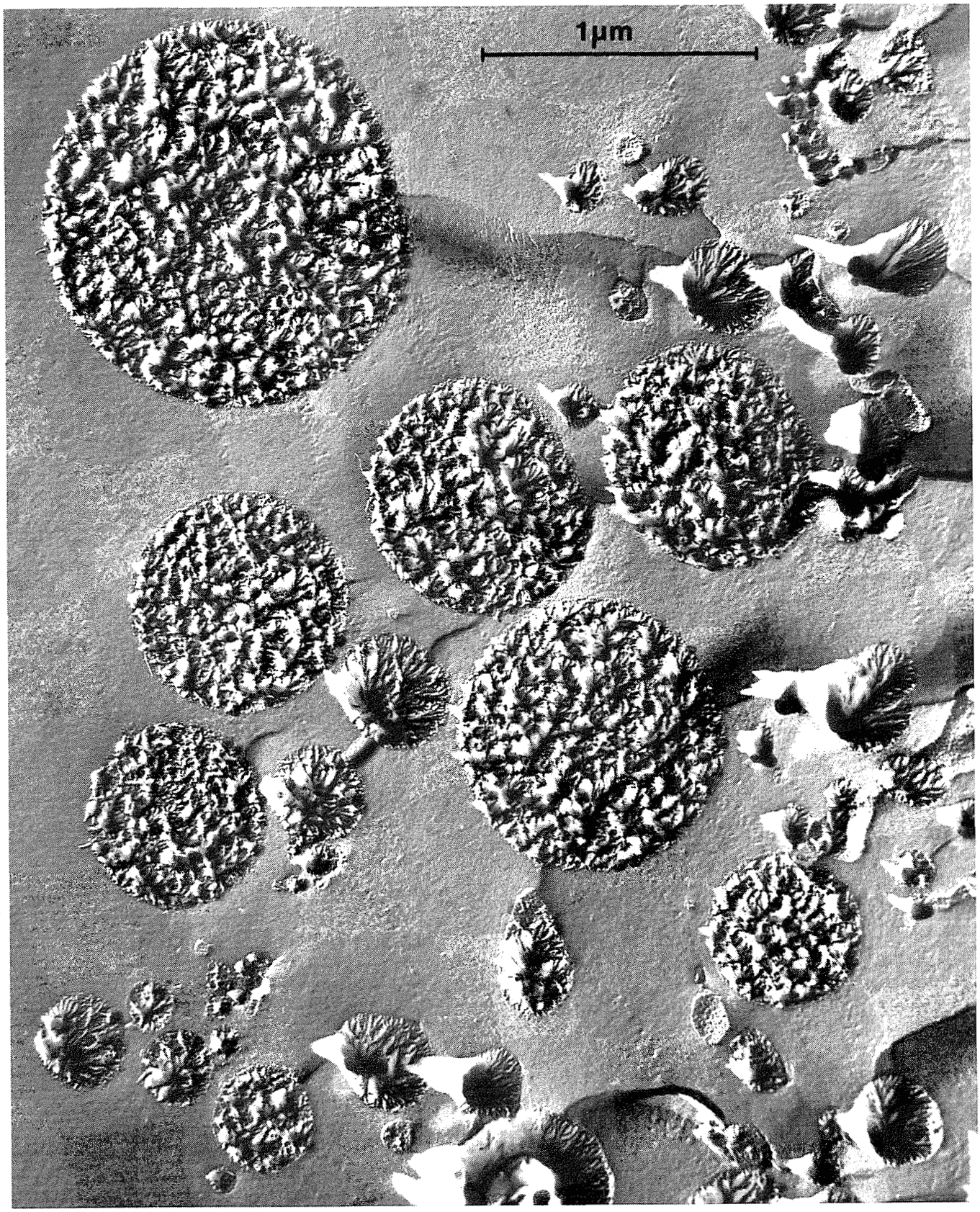

Can. J. Chem. Downloaded from www.nrcresearchpress.com by 46.23.64.124 on 09/08/12
For personal use only.

Fig. 7. Hypothetical cause of radial morphology in small PS particles.

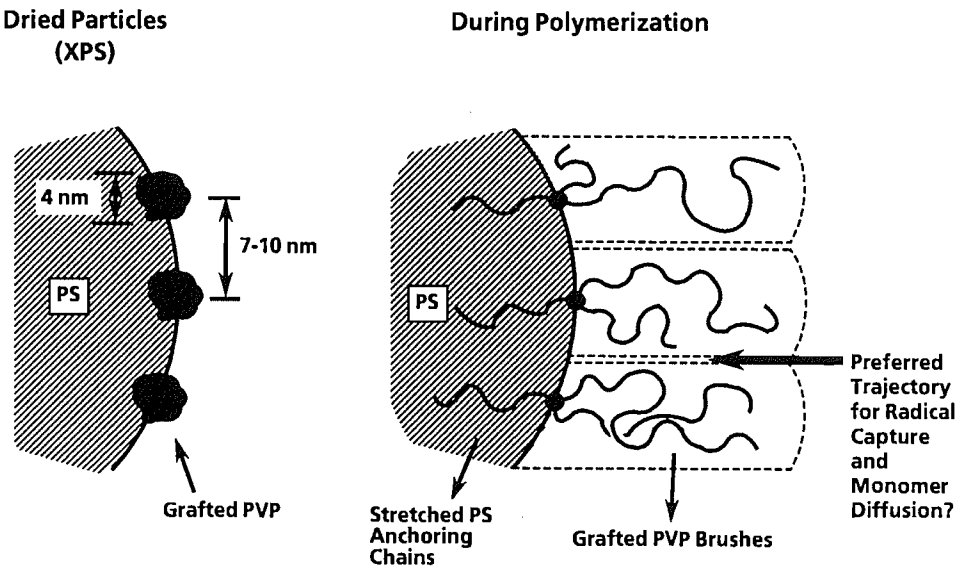

amorphous polymers include the well-known densification with time below T_g (26), which presumably reflects the gradual elimination of high-energy boundaries within the sample.

The effect of quenching rate on nodule size has been examined in the literature, but remains confusing. In the case of PET the nodules disappear at high quench rates (23). On the other hand, annealed PS had very fine, nearly invisible nodules, while quenched PS had larger nodules (20 nm) similar to those shown here (27). Correlation lengths of 50–70 nm were obtained by SAXS. In the present dispersion polymerization system the quench during synthesis is expected to occur slowly as the particles gradually consume plasticizing monomer. In the heating experiment, the quench was relatively slow: the tubes were allowed to cool undisturbed in air. Likewise, in the precipitation experiment, there may be sufficient plasticization by dioxane to permit a relatively slow quench.

Radial morphology of dispersion-polymerized polystyrene

To confirm the freeze fracture morphologies, it is quite challenging to find independent corroborative evidence for the morphological change observed in the small particles. Among techniques that might be applied are differential scanning calorimetry (DSC), rheology, NMR, small-angle X-ray scattering, neutron scattering, and accurate density measurement. By definition, the non-equilibrium structure should be a higher energy state than the equilibrium structure,so one might expect some exotherm corresponding to the rearrangement. However, if the rearrangement occurs at or above T_g, or even worse, above T_m, it may not be possible to measure a significant difference between first and second sweeps of the same sample.

The rheology of compressed disks of the particles showed no significant difference between the first and second sweeps, except around the T_g, and that might be due to the plasticization by residual monomer. Differences in morphology might express themselves through the density, and NMR could be a sensitive tool to measure this. However, significant effects would only be observed if a large fraction of the chains experience a local change upon going from one morphology to another. If the changes are at grain boundaries on the 20–100 nm scale, very little measurable difference is expected.

Small-angle X-ray scattering (21) and neutron scattering (28, 29) are possible probes for changes in the size of grains within the amorphous structure. Recently, Gilbert and coworkers carried out small-angle neutron scattering experiments to determine the extent of monomer/polymer spatial inhomogeneities in very small 100 nm emulsion-polymerized polystyrene latex particles (28). They found that surface-anchoring effects of the initiator sulfate groups caused the particles to adopt a core-shell morphology when the radius of gyration of the polymer was less than the particle radius.

It seems likely that during dispersion polymerization, the overall instantaneous monomer content inside the particles is relatively low (despite good thermodynamic driving force from water in the solvent), like the situation in emulsion polymerization. The gel effect suggests the particle interiors are quite viscous. With the dispersion-polymerized particles being very much larger than emulsion-polymerized particles, it is highly probable that the monomer is radially distributed with higher concentrations near the particle surface, where it can be polymerized by incoming captured oligomeric radicals.

In Fig. 7 we propose a possible relationship between the radial morphology and the mechanism of particle growth by radical capture. Previous surface analysis of these same particles in the dry state by X-ray photoelectron spectroscopy (XPS) and time-of-flight secondary ion mass spectrometry (TOF-SIMS) has led to the picture on the left-hand side of Fig. 7 (7). It appears that the collapsed but grafted PVP stabilizer chains occur in surface blobs of approximately 4 nm size, spaced some 7–10 nm apart on the dry particle surface. From this picture, we can infer that during polymerization the grafted chains were acting as stabilizers: random brushes in the compatible aqueous alcohol solvent. Since the radius of gyration of the PVP chains in methanol is about 14 nm (6), they are too close to form mushrooms, and likely prefer brush coils.

We hypothesize that perhaps the brush morphology of the

Can. J. Chem. Downloaded from www.nrcresearchpress.com by 46.23.64.124 on 09/08/12
For personal use only.

Can. J. Chem. Downloaded from www.nrcresearchpress.com by 46.23.64.124 on 09/08/12
For personal use only.

stabilizer chains in solution results in a preference for radical capture and monomer diffusion toward the particle in the channels between brushes, and away from anchor points. Such a preference might lead to preferred polymerization between anchor points. Since the particles grow with the constant reorganization of the graft to remain on the particle surface, it is also possible that the anchoring chains could become stretched as the growing particle boundary moves outward. Such stretching is more likely when the anchoring chains are of higher molecular weight (i.e., 400 K in the small particles vs. 54 K in the large) and have more entanglements. Perhaps these factors lead to a net orientation of the growing polymer perpendicular to the surface as is ultimately revealed in the FFTEM micrographs in Fig. 2.

It is interesting that the apparent width of the radial structures in Fig. 2 (7 nm) is about the same as the anchor point separation in Fig. 7, and about the same as the radius of gyration of PS of the high molecular weight. This hypothesis is also consistent with the observation of radial structures in emulsion-polymerized PMMA particles (10). In that case the anchoring points are the initiator sulfate groups, which also want to continually reorient to remain on the particle surface during growth. Since the anchoring chains in emulsion polymerization are also of high molecular weight, they may also stretch during growth, rather than remaining as random coils.

At the present time, we view this hypothesis as tentative. Further testing is not a trivial problem. It is not clear how X-ray or neutron scattering could resolve nodular from radial structures. Perhaps the most productive avenue would be to examine the FFTEM morphology of emulsion-polymerized particles from seeded reactions with different molecular weights controlled by chain transfer agent. Using seeded polymerizations should eliminate particle size effects, and the constant solvent (water) leaves only the molecular weight of the anchoring groups as the morphological variable.

Conclusions

The interior morphology of these dispersion-polymerized particles is fascinating, but there are few comparative data available on polymers made by other routes. It seems clear that the large particles are formed in an equilibrium nodular morphology, so the morphology cannot be used to infer anything about mechanism. Thus, there is less mechanistic information available from FFTEM than may have seemed the case to previous investigators (10, 11). On the other hand, the small dispersion-polymerized particles were formed in a radial non-equilibrium morphology that could be converted into the nodular morphology by either heating or precipitation. We have crudely speculated that this morphology might arise from the presence of anchored stabilizer chains on the particle surface that may serve to direct incoming monomer and oligomeric radicals into microscopically oriented channels. A similar mechanism may also prevail in emulsion polymerization. Thus, this work helps to clarify the mechanistic inferences available from FFTEM, and poses some challenging questions yet to be investigated.

Acknowledgements

We are indebted to Mr. J. McNulty for the particle syntheses, Dr. G. Hamer for NMR, and Mr. S. Drappel for DSC and rheological measurements.

References

1. C.K. Ober, K.P. Lok, and M.L. Hair. J. Polym. Sci. Polym. Lett. Ed. **23**, 103 (1985).
2. K.P. Lok and C.K. Ober. Can. J. Chem. **63**, 209 (1985).
3. F.M. Winnik and A.J. Paine. Langmuir, **5**, 903 (1989).
4. A.J. Paine, Y. Deslandes, P. Gerroir, and B. Henrissat. J. Colloid Interface Sci. **138**, 170 (1990).
5. A.J. Paine, W. Luymes, and J. McNulty. Macromolecules, **23**, 3104 (1990).
6. A.J. Paine. Macromolecules, **23**, 3109 (1990).
7. Y. Deslandes, D.F. Mitchell, and A.J. Paine. Langmuir, **9**, 1468 (1993).
8. C.M. Tseng, Y.Y. Lu, M.S. El-Aasser, and J.W. Vanderhoff. J. Polym. Sci. Part A: Polym. Chem. **24**, 2995 (1986).
9. Y.Y. Lu, M.S. El-Aasser, and J.W. Vanderhoff. J. Polym. Sci. Part B: Polym. Phys. **26**, 1187 (1988).
10. B. Disanayaka, C.-L. Zhao, M.A. Winnik, R. Shivers, and M.D. Croucher. Langmuir, **6**, 162 (1990).
11. M.A. Winnik, C.-L. Zhao, O. Shaffer, and R.R. Shivers. Langmuir, **9**, 2053 (1993).
12. A.J. Paine and J. McNulty. J. Polym. Sci.: Polym. Chem. Ed. **28**, 2569 (1990).
13. J.H.M. Willison and A.J. Rowe. *In* Practical methods in electron microscopy. Vol. 8. North Holland Publishers, Amsterdam. 1980.
14. D.G. Robinson, U. Ehlers, R. Herken, B. Herrmann, F. Mayer, and F.W. Schurmann. Methods for preparation for electron microscopy. Springer-Verlag, New York. 1987.
15. A.E. Woodward. Atlas of polymer morphology. Hanser Publishers, Munich. 1988.
16. P.H. Geil. Polym. Mater. Pap. Semin. Am. Soc. Met. 1975. pp. 119–174.
17. J. Bandrup and E.H. Immergut. Polymer handbook. 3rd ed. John Wiley and Sons, New York. 1989.
18. D.R. Basset. *In* Science and technology of polymer colloids. *Edited by* G.W. Poehlein, R.H. Ottewill, and J.W. Goodwin. NATO ASI Ser. E: **220** (1983).
19. G.S.Y. Yeh. J. Macromol. Sci. Phys. **B6**, 451 (1972).
20. G.S.Y. Yeh and S.L. Lambert. J. Macromol. Sci.-Phys. **B6**, 599 (1972).
21. P.H. Geil. J. Macromol. Sci.-Phys. **B12**, 173 (1976).
22. Y.C. Yang and P.H. Geil. J. Macromol. Sci.-Phys. **B22**, 463 (1983).
23. S. Lee, H. Miyaji, and P.H. Geil. J. Macromol. Sci.-Phys. **B22**, 489 (1983).
24. P. Glansdorff and I. Prigogine. Thermodynamic theory of structure, stability and fluctuations. Interscience, New York. 1971.
25. P.H. Lindenmeyer. J. Polym. Sci.: Polym. Phys. **17**, 1965 (1979).
26. R. Simha. Polym. Eng. Sci. **20**, 82 (1980).
27. Yu. S. Lipatov, V.V. Shilov, V.V. Tsukruk, O.A. Lokhonya, V.N. Bliznyuk, and Yu. P. Gomza. Dokl. Biochem. **270**, 912 (1983).
28. M.F. Mills, R.G. Gilbert, D.H. Napper, A.R. Rennie, and R.H. Ottewill. Macromolecules, **26**, 3553 (1983).
29. D. Beyer, W. Lebek, W.-D. Hergeth, and K. Schmutzler. Colloid Polym. Sci. **268**, 744 (1990).

Syntheses and interfacial characterization of graft copolymers from styrene and 2-hydroxyethyl methacrylate that comprise either trunks or branches

Hidekazu Yoshida, Shinichi Itsuno, and Koichi Ito

Abstract: Polystyrene (PS) and poly(2-hydroxyethyl methacrylate) (PHEMA) macromonomers with either *p*-vinylbenzyl or methacrylate end groups were prepared by living anionic polymerizations of styrene and 2-(trimethylsilyloxy)ethyl methacrylate, respectively, followed by appropriate end-capping. They were radically copolymerized with 2-hydroxyethyl methacrylate and styrene, respectively, to afford PS-*g*-PHEMA and PHEMA-*g*-PS, having PS trunks with PHEMA branches or the reverse architecture. ^{1}H NMR spectra of the graft copolymers in deuterated methanol showed their micelle formation with PS and PHEMA chains as the core and the shell, respectively. In chloroform the reverse micelles were observed. Contact angle measurements of water on the graft copolymer films revealed that PS chains were generally dominant on the free surface. The films either cast from methanol or after immersion into water, however, were apparently wettable, indicating dominant PHEMA chains on the surface.

Key words: styrene, 2-hydroxyethyl methacrylate, graft copolymer, micelle formation, wettability.

Résumé : On a préparé des macromonomères de polystyrène (PS) et de poly(méthacrylate de 2-hydroxyéthyle) (PHEMA) portant des groupes terminaux *p*-vinylbenzyle ou méthacrylate en procédant à des polymérisations anioniques vivantes respectivement du styrène et du méthacrylate de 2-(triméthylsilyoxy)éthyle, suivies d'une addition appropriée d'un groupe terminal. On les a ensuite copolymérisés d'une façon radicalaire avec du méthacrylate de 2-hydroxyéthyle et du styrène pour obtenir des PS-*g*-PHEMA et PHEMA-*g*-PS respectivement qui possèdent soit des troncs de PS avec des branches de PHEMA soit les architectures inverses. Les spectres RMN du ^{1}H des copolymères greffés déterminés dans le méthanol deutéré présentent des formations de micelles dans lesquelles les chaînes de PS forment le coeur et celles de PHEMA la périphérie. Dans le chloroforme, on observe les micelles inverses. Des mesures des angles de contact de l'eau avec les films de copolymères greffés révèlent que les chaînes de PS sont généralement dominantes sur la surface libre. Toutefois, les films obtenus à partir du méthanol, ou immédiatement après immersion dans l'eau, peuvent apparemment être mouillés; ceci indique que les chaînes PHEMA dominent à la surface.

Mots clés : styrène, méthacrylate de 2-hydroxyméthyle, copolymère greffé, formation de micelle, mouillage.

[Traduit par la rédaction]

Introduction

Current progress in macromonomer techniques has made it possible to prepare a variety of well-defined graft copolymers with relatively easy access (1). The technique is based on copolymerization between a given trunk-forming monomer (M_1) and a known, branch-forming macromonomer (M_2) as illustrated in Fig. 1. The trunk/branch composition can be essentially controlled by the feed ratio and the monomer reactivity ratio of M_1 under the usually employed condition of very high molar ratio of M_1 to M_2, i.e., $[M_1]/[M_2] \gg 1$, since the molecular weight of M_2 is usually very high compared with that of M_1. Thus the conventional copolymerization equation (Mayo–Lewis equation) can be approximated as follows.

$$[1] \quad \frac{d[M_1]}{d[M_2]} = \frac{1 + r_1[M_1]/[M_2]}{1 + r_2[M_2]/[M_1]} \cong r_1 \frac{[M_1]}{[M_2]}$$

where $r_1 = k_{11}/k_{12}$ and $r_2 = k_{22}/k_{21}$ are the monomer reactivity ratios of M_1 and M_2, respectively, and k_{ij} is the propagation rate constant of a propagating chain ending in M_i reacting with a monomer M_j, with i and $j = 1$ or 2.

A number of macromonomers and therefore a much greater number of graft copolymers have been synthesized. Among others, amphiphilic graft copolymers (2) have been our inter-

Received March 2, 1995.

This paper is dedicated to Professor J.E. (Jim) Guillet in recognition of his contributions to Canadian chemistry.

H. Yoshida, S. Itsuno, and K. Ito.[1] Department of Materials Science, Toyohashi University of Technology, Tempaku-cho, Toyohashi, 441 Japan.

[1] Author to whom correspondence may be addressed. Telephone: +81-532-47-0111. Fax: +81-532-48-5833.

Can. J. Chem. Downloaded from www.nrcresearchpress.com by 46.23.64.124 on 09/08/12
For personal use only.

Fig. 1. Preparation of a graft copolymer by the macromonomer technique.

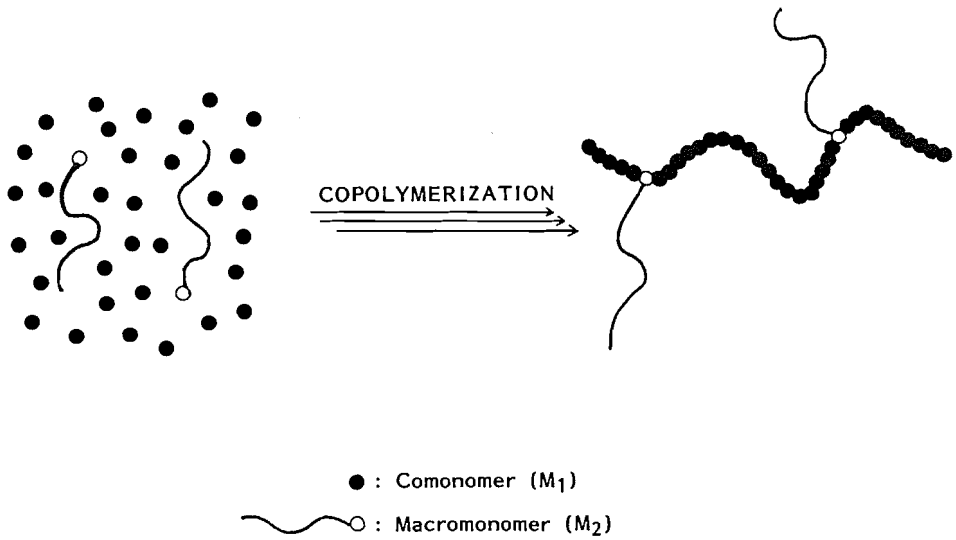

Can. J. Chem. Downloaded from www.nrcresearchpress.com by 46.23.64.124 on 09/08/12
For personal use only.

est because the hydrophilic and hydrophobic chains incorporated into either the trunk or the branch will segregate into the respective microdomains via microphase separation to exert interesting surface- or interface-active behavior. Previously, we reported a graft copolymer, PHEMA-*g*-PS, with poly(2-hydroxyethyl methacrylate) (PHEMA) as the trunk and polystyrene (PS) as the branch, prepared by copolymerization of 2-hydroxyethyl methacrylate (HEMA) and the PS macromonomer with a methacrylate end group (3). The same graft copolymer has been evaluated as a blood-compatible, self-reinforced hydrogel by Yamashita et al. (4). The corresponding block copolymer, PS-*b*-PHEMA, has been established as an excellent antithrombogenic material, most probably as a result of its microphase-separated surface structure (5). Related poly(α-methylstyrene)-*b*-PHEMA have been prepared and examined in terms of the surface properties (6).

Therefore we thought it fundamentally interesting and important to prepare PS-*g*-PHEMA, with PS as the trunk and PHEMA as the branch, in addition to PHEMA-*g*-PS, and to compare their interfacial properties as a function of the composition and the architecture. This paper describes in detail the syntheses of the corresponding PS and PHEMA macromonomers by use of the living anionic polymerization technique as given in Fig. 2, their radical copolymerization reactivities in the preparation of graft copolymers, and micelle formation and wettability of the graft copolymers obtained

Experimental

Materials

All reagents and solvents used for anionic polymerization and end-capping were purified by conventional procedures and finally distilled into ampoules fitted with breakable seals under a vacuum line (10^{-5} Torr; 1 Torr = 133.3 Pa). Styrene, ethylene oxide (EO), methacryloyl chloride (MAC), HEMA, 2,2′-azobisisobutyronitrile (AINBN), benzene, *p*-vinylbenzyl chloride (VBC), tetrahydrofuran (THF), and dimethylformamide (DMF) were purified as described previously (3, 7).

2-(Trimethylsilyloxy)ethyl methacrylate (TMSEMA) was prepared from HEMA and hexamethyldisilazane (8), and finally distilled from a yellow-colored solution containing triethylaluminum before polymerization. *p*-Vinylbenzyl bromide (VBB) was prepared from VBC by reacting with sodium bromide at 60°C for 2 days in benzene and water with tetrabutylammonium bromide as a phase transfer catalyst. Conversion of Cl to Br was 80%, as measured by ^{1}H NMR. The mixture was distilled over calcium hydride into an ampoule. 1,1-Diphenyl-3-methylpentyllithium (DPHLi) was prepared from *s*-butyllithium with 1,1-diphenylethylene in THF at room temperature. Lithium chloride (99.99%, Aldrich) was dried under vacuum at 130°C for 12 h and used as solution in THF.

Preparation of PS macromonomers

PS-VB (Fig. 2) was prepared by the method reported by Asami et al. (9). Living anionic polymerization of styrene with *s*-butyllithium (*s*BuLi) was conducted in benzene at 0°C for 1 h. The resulting red solution was diluted with more than 30 vol.% THF and then terminated by dropping into a THF solution containing excess VBC at 0°C and stirred for 24 h. The macromonomer was isolated by precipitation into methanol, purified by repeated reprecipitations from benzene into methanol, and freeze-dried from benzene. PS-MA was prepared by end-capping with EO, followed by termination with MAC, according to the procedure described before (3), and purified similarly.

The end-group functionality (*f*) of the PS macromonomers was determined as the extent of their incorporation in copolymerization with a large excess of methyl methacrylate (MMA), as evaluated by gel permeation chromatography (GPC) with a UV detector (10). Copolymerization was conducted with 0.1 g of each macromonomer with 1 g of MMA in THF with AIBN (1 wt.%) at 60°C for 3 days.

Preparation of PHEMA macromonomers

Living anionic polymerization of TMSEMA was conducted, as described by Hirao et al. (8), with DPHLi as an initiator in THF, containing excess lithium chloride in some cases, at −78 to −90°C for 30 min. PHEMA-VB was prepared by adding excess VBB–THF solution at −78°C, followed by stirring

Can. J. Chem. Downloaded from www.nrcresearchpress.com by 46.23.64.124 on 09/08/12
For personal use only.

Fig. 2. Preparation of PS and PHEMA macromonomers. DPH = 1,1-diphenyl-3-methylpentyl (diphenylhexyl), VBC = *p*-vinylbenzyl chloride, VBB = *p*-vinylbenzyl bromide, EO = ethylene oxide, MAC = methacryloyl chloride.

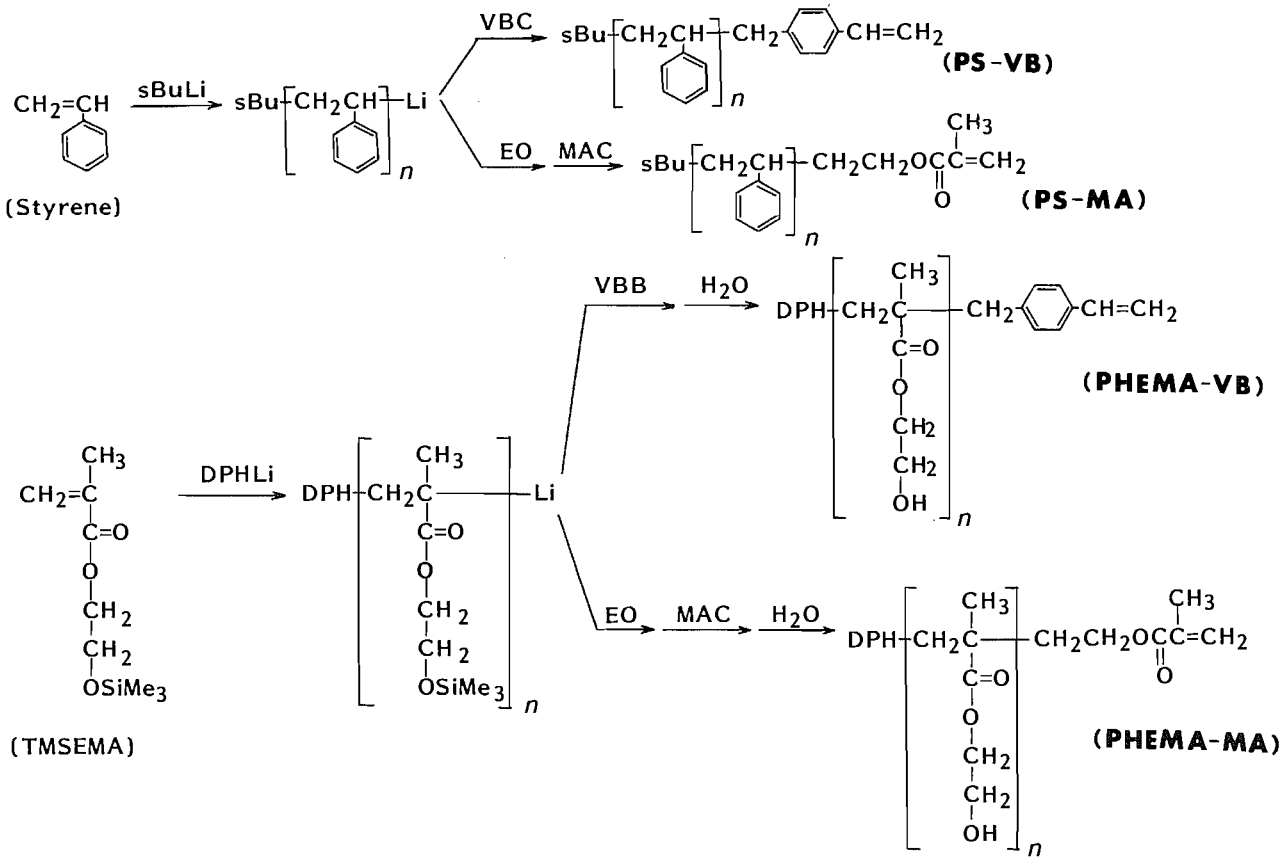

for 24 h. After addition of a few drops of 1.2 N aqueous HCl, the solution was evaporated to about one third volume and poured into water to precipitate PHEMA-VB. The macromonomer was reprecipitated three times from methanol into diethyl ether, and dried in vacuo.

PHEMA-MA was prepared by end-capping with EO and termination with MAC, as follows. Excess EO was added at −78°C to the living poly-TMSEMA solution obtained as above, the temperature was allowed to rise very slowly to 0°C over about 10 h, and then excess MAC–THF solution was added and stirred for 24 h at 0°C. The macromonomer was similarly isolated and purified. PHEMA macromonomers were partly benzoylated (8) to be soluble in THF as the eluent for characterization by GPC.

Copolymerization of macromonomers to prepare graft copolymers

Macromonomer and comonomer were weighed into an ampoule with AIBN (2 wt.% to the total monomer) and DMF (20 mL), and sealed after three to four cycles of freeze–thaw under liquid nitrogen. Copolymerization was carried out at 60°C. For evaluation of monomer reactivity ratios (r_1), the copolymerization was stopped before 10% conversion. Usually 5% conversion was attained in 1–3 h. The products were precipitated either into diethyl ether in the case of PS macromonomer or into methanol in the case of PHEMA macromonomer to remove the unreacted monomers.

For preparative isolation of graft copolymers, the copolymerization was conducted for a prolonged time (about 4 days) to 70–80% conversation. The resulting mixture was poured into water. The precipitated polymers were dried in vacuo, dissolved in THF, and repeatedly reprecipitated into methanol–hexane (7/3 v/v) to remove PHEMA macromonomer or homopolymer, and then into diethyl ether – hexane (3/1 v/v) to remove PS macromonomer or homopolymer. The purification was monitored by GPC and thin-layer chromatography (TLC).

Characterization methods

^{1}H NMR spectra were recorded on a JEOL 270 MHz spectrometer (JNM-GX-270), usually in eight scans with a pulse delay time of 30 s. GPC was carried out at 40°C on a JASCO Trirotar III equipped with RI (Shodex SE-11) or UV detector (Uvidec-100-III at 254 nm) with appropriate combination of columns (Shodex A-802 ~ 805). THF was used as an eluent at a flow rate of 1 mL/s and calibration was made with standard polystyrenes. TLC was taken on a silica gel plate with ethyl acetate and methanol as the eluents, which develop selectively the homopolymers, PS and PHEMA, respectively, but not the graft copolymers.

Contact angle of water on the air side of a polymer film was measured at 20°C by a CA-A type apparatus of Kyowa Kagaku Co., Ltd. Polymer films were prepared on clean glass slides by casting from ca. 5 wt.% solutions followed by slow evaporation of the solvent on standing overnight and were finally dried in vacuo at room temperature. A water droplet of

Can. J. Chem. Downloaded from www.nrcresearchpress.com by 46.23.64.124 on 09/08/12
For personal use only.

Fig. 3. ^{1}H NMR spectra of PHEMA macromonomers in CD_3OD. (*a*) PHEMA-VB-1; (*b*) PHEMA-MA-1. Hatched peaks are due to undeuterated solvent (CH_3OH).

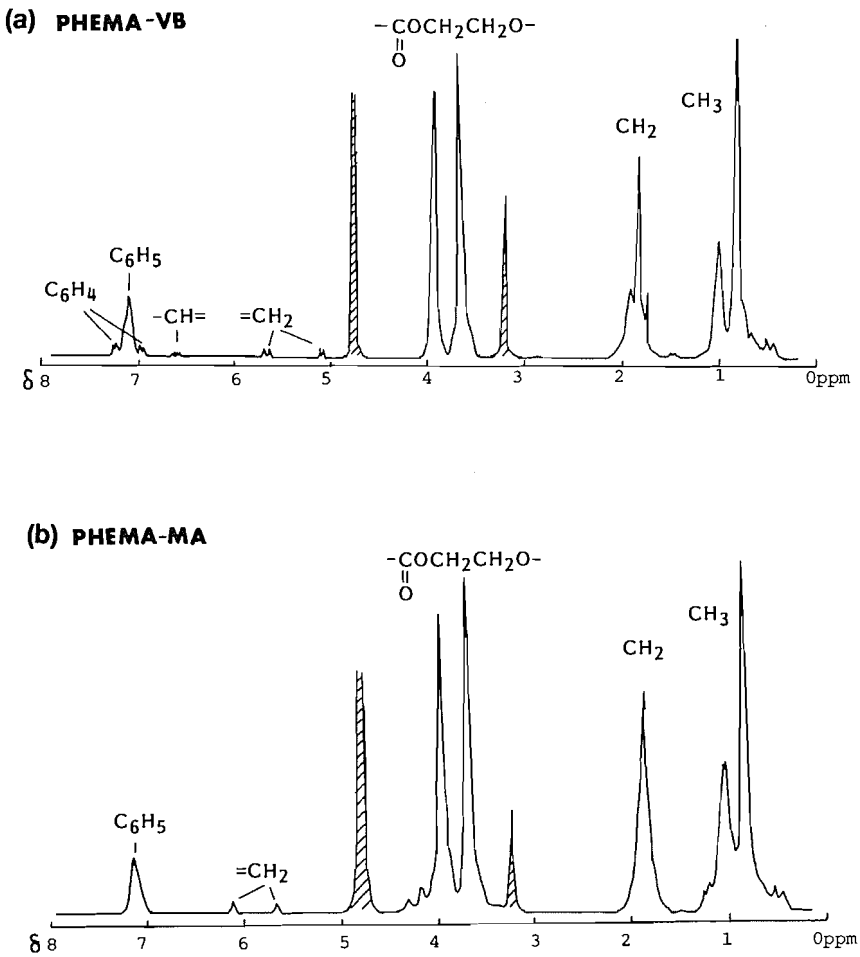

ca. 2 mm diameter was placed on the polymer film and the contact angle was measured in less than 1 min to avoid evaporation or expansion of the droplet. The contact angle was also measured on the film after immersion into water for a given time and immediate wiping off of the free water with a soft tissue.

Results and discussion

Preparation of macromonomers

PS-MA (3, 4, 11) and PS-VB (9) were prepared according to known methods as given in Fig. 2. PHEMA macromonomers were first prepared by living anionic polymerization of the trimethylsilyl-protected monomer (TMSEMA) (8), followed by end-capping with VBB or with EO and MAC. VBB was used instead of VBC because the former was reported to react satisfactorily with the living (meth)acrylate anions (12–14). Figure 3 shows typical ^{1}H NMR spectra.

The results of characterization of the macromonomers are summarized in Table 1. The yield was almost quantitative in each case and the molecular weight could be controlled by the ratio of the monomer to the initiator in feed as expected for the living polymerization. The molecular weight distribution was fairly sharp although, for PHEMA macromonomers, it was found that addition of excess lithium chloride was effective in improving the monodispersity, as reported by Teyssié and coworkers (15) for the anionic polymerization of (meth)acrylates. The advantage of the present method of preparation of PHEMA macromonomers over that of radical chain-transfer polymerization plus end-group transformation (16) is clear in the simplicity, and in the sharp molecular weight distribution attained.

The functionality of the end group (f), however, was not so quantitative but usually in the range of 70–90%. This result appears to come from unexpected terminations that occurred after complete conversion of the monomers between the living polymer anions and some impurities before or during the end-capping reactions, since the molecular weight distribution of the polymers remained, in all cases, fairly sharp. The macromonomers were used as such in the following by considering the functionality in calculating the feed composition.

Copolymerization of the macromonomers and preparation of graft copolymers

The PS and PHEMA macromonomers were copolymerized with HEMA and styrene, respectively, to low conversions to evaluate their copolymerization reactivities. A very large molar excess of the comonomer ($[M_1]/[M_2] > 100$) was used for application of the approximated relation, eq. [1]. The composition of the products after removal of the unreacted mac-

Can. J. Chem. Downloaded from www.nrcresearchpress.com by 46.23.64.124 on 09/08/12
For personal use only.

Table 1. Characterization of macromonomers.

Code	M_n[a]	M_w/M_n[b]	f[c]
PS-MA-1	2 900	1.07	90
PS-MA-2	12 400	1.22	85
PS-VB-1	2 500	1.04	84
PS-VB-2	9 200	1.14	92
PHEMA-MA-1	2 900	1.37	71
PHEMA-MA-2	3 900	1.32	77
PHEMA-MA-3[d]	8 700	1.12	72
PHEMA-MA-4[d]	14 200	1.06	45
PHEMA-VB-1	4 700	1.30	85
PHEMA-VB-2	11 000	1.32	78
PHEMA-VB-3[d]	3 200	1.12	75
PHEMA-VB-4[d]	3 700	1.06	91

[a]Number-average molecular weight determined by GPC for PS macromonomers and by ^{1}H NMR for PHEMA micromonomers (from the intensity ratio of the peaks due to ester CH_2 at δ 3.7–4.0 to phenyl C_6H_5 at δ 7.1, see Fig. 3).

[b]Ratio of weight-average to number-average molecular weights determined by GPC. PHEMA macromonomers were evaluated for the benzoylated products.

[c]Double-bond functionality in per cent determined by MMA copolymerization method for PS macromonomers and by ^{1}H NMR for PHEMA macromonomers (from the intensity ratio of the peaks due to double bond methylenes $=CH_2$ to phenyl C_6H_5, see Fig. 3).

[d]Polymerization of TMSEMA was carried out in the presence of lithium chloride (5–9 equiv. to the initiator, PPHLi).

Table 2. Copolymerization reactivity ratio, r_1 (in DMF, at 60°C).

M_1	M_2	M_n of M_2	r_1	$1/r_1$
HEMA	PS-MA-1	3100	1.84 ± 0.16	0.54
HEMA	PS-VB-1	3600	0.73 ± 0.01	1.37
Styrene	PHEMA-MA-1	2900	1.08 ± 0.08	0.93
Styrene	PHEMA-VB-4	3700	2.92 ± 0.16	0.34

romonomers was determined, as described previously (3), by ^{1}H NMR in a mixed solvent of $CDCl_3$ and CD_3OD (see Fig. 4 for an example). The corresponding monomer reactivity ratio (r_1) was obtained from at least three experiments in each system and found to be independent of the feed composition, as before (3, 7). The results are given in Table 2.

The result that r_1 was considerably higher than unity for the copolymerization of HEMA with PS-MA and that of styrene with PHEMA-VB, in spite of their similar structure in the polymerizing groups, indicates the reduced relative reactivity ($1/r_1 = k_{12}/k_{11}$) of the macromonomer (M_2) as compared to the low molecular weight analog (M_1). This tendency is also apparent in the results for the systems of HEMA with PS-VB and of styrene with PHEMA-MA, because the conventional copolymerization between styrenes and methacrylates is usually of more alternating tendency, with the reactivity ratios around 0.5 (17), as was found for the copolymerization of styrene and HEMA (4). These results support the previous notion (3, 7) that incompatibility between the macromonomer and the growing polymer backbone, i.e., between PS and PHEMA in the present case, appears to interfere thermodynamically with their mutual interpenetration, resulting in the apparently reduced reactivity of the macromonomers, as has been frequently referred to in copolymerization involving macromonomers (18, 19).

Also, interestingly, the values of the reactivity ratios in Table 2 indicate that the copolymerizations of HEMA with PS-VB and of styrene with PHEMA-MA will produce PHEMA-*g*-PS and PS-*g*-PHEMA, respectively, with more azeotropic or more homogeneous compositions than those from the other combinations, HEMA with PS-MA or styrene with PHEMA-VB. This is true at least under the condition where the approximation $[M_1]/[M_2] \gg 1$ holds in the monomer mixture.

The graft copolymers used for interfacial characterization as described below were prepared by prolonged copolymerization to much higher conversions (70–90%). They were, however, purified by repeated precipitations from THF into methanol–hexane and diethyl ether – hexane to remove PHEMA and PS homopolymers, respectively, probably together with any graft copolymers very rich in PHEMA and PS components. The purified graft copolymers were thus isolated to 10–30 wt.% yields. They were confirmed by GPC and TLC to be free of unreacted macromonomers and PHEMA or PS homopolymers. Their compositions were found by ^{1}H NMR to be very close to those in feed, irrespective of the combination of the macromonomer and comonomer, suggesting that the graft copolymers thus isolated are fairly homogeneous in composition.

Micelle formation of the graft copolymers as examined by ^{1}H NMR

As previously reported for PHEMA-*g*-PS copolymers (3), similar micelle formation was observed for the graft copolymers of reverse architecture, PS-*g*-PHEMA. Figure 4 shows the ^{1}H NMR spectra of the graft copolymers obtained by copolymerization of styrene and the macromonomer, PHEMA-MA-1 (M_n = 2900). The sample with PHEMA 62.1 wt.% was apparently soluble in CD_3OD to give a spectrum that showed clearly the peaks due to the PHEMA branches but few peaks due to the PS trunks. On addition of $CDCl_3$ (ca. 30 vol.%), the peaks due to the PS trunks also clearly appeared. This result indicates that the PS chains insoluble in methanol constitute a micelle core that behaves as a rigid "solid" to give peaks too broad to be observed. On the other hand, PHEMA chains are very soluble in methanol to give their own peaks, keeping the solution apparently clear by surrounding the insoluble PS cores. Chloroform, a good solvent for PS chains, destroys the micelle structure in cooperation with methanol, giving rise to a normal spectrum in the mixed solvent.

Exactly the reverse was observed with the sample with 19.8 wt.% PHEMA, which showed only those peaks due to PS trunks in $CDCl_3$, indicating micelle formation with PHEMA branches as the core surrounded by PS trunks. This micelle was destroyed on addition of CD_3OD to give a normal spectrum. These results clearly support micelle formation of the graft copolymers in a selective solvent, as illustrated in Fig. 5. On the other hand, a random copolymer prepared by copolymerization of styrene and HEMA was found to show a normal spectrum even in a single selective solvent (3), indicating that the statistical distribution of styrene and HEMA units with very short sequence lengths prevents micelle formation.

Can. J. Chem. Downloaded from www.nrcresearchpress.com by 46.23.64.124 on 09/08/12
For personal use only.

Fig. 4. ^{1}H NMR spectra of graft copolymers. (*a*) PS-*g*-PHEMA (62.1 wt.% HEMA) in CD_3OD and in CD_3OD–$CDCl_3$ (7/3 v/v); (*b*) PS-*g*-PHEMA (19.8 wt.% HEMA) in $CDCl_3$ and in $CDCl_3$–CD_3OD (7/3 v/v). Hatched peaks are due to undeuterated solvents ($CHCl_3$, CH_3OH).

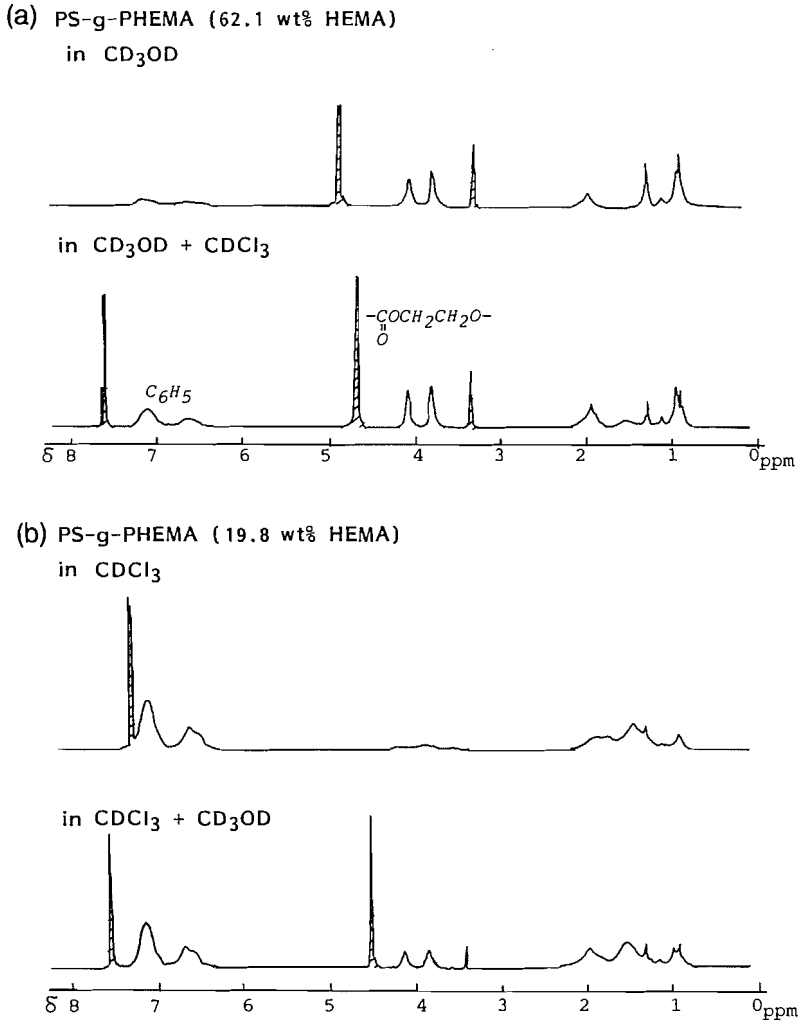

Wettability of graft copolymer films

Surface properties of the graft copolymers were evaluated most conveniently by the measurement of the contact angle of water on polymer films cast from appropriate solvents. Figure 6 shows the effect of the casting solvent on the wettability of the graft copolymers as a function of the composition. As expected, the films cast from DMF and chloroform, which are common and PS-selective solvents, respectively, were found to be nonwettable just like polystyrene, almost independently of the composition and the architecture of the graft copolymers. Thus the PS chains, which have lower surface energy than the PHEMA chains, generally prefer to be exposed to the free surface.

The films cast from methanol, a PHEMA-selective solvent, however, were found to be wettable just like PHEMA homopolymer, again independently of the composition. In accord with the ^{1}H NMR measurement in CD_3OD, the PHEMA chains comprising the micelle shells prefer to selectively cover the surface of the as-cast films. After baking at 150°C, a higher temperature than both T_g's of PS and PHEMA, however, they became nonwettable like polystyrene, as expected thermodynamically as a result of the rearrangement of the surface morphology.

The above observations for the graft copolymers are quite different from those of the random copolymers of styrene and HEMA, which showed, either before or after baking of the films, a smooth change in cos θ with composition (3), indicating the importance of microphase separation of the hydrophobic (PS) and hydrophilic (PHEMA) chains in exerting their interfacial activities. As to the effect of the architecture of the graft copolymers, PS-*g*-PHEMA appeared to be a little more wettable than PHEMA-*g*-PS, as in Fig. 6. The former was also found to be soluble in methanol over a wider composition, even to as low as 30 wt.% PHEMA. Thus the solubility as well as the surface property of a graft copolymer, with a given composition and molecular weight, appear to be more readily controlled by the branches than by the trunks. This may be expected from a geometrical consideration, since the branches may more easily constitute the micelle shells, extending their chains into a medium, than do the trunks, as in Fig. 5.

The usual preference of the PS chains on the film surface, as described above, is also violated when the films are allowed

Can. J. Chem. Downloaded from www.nrcresearchpress.com by 46.23.64.124 on 09/08/12
For personal use only.

Fig. 5. Schematic illustration of micelle formation of PS-*g*-PHEMA in selective solvents and its destruction in a common solvent. Solid and broken lines indicate trunk (PS) and branch (PHEMA) chains, respectively.

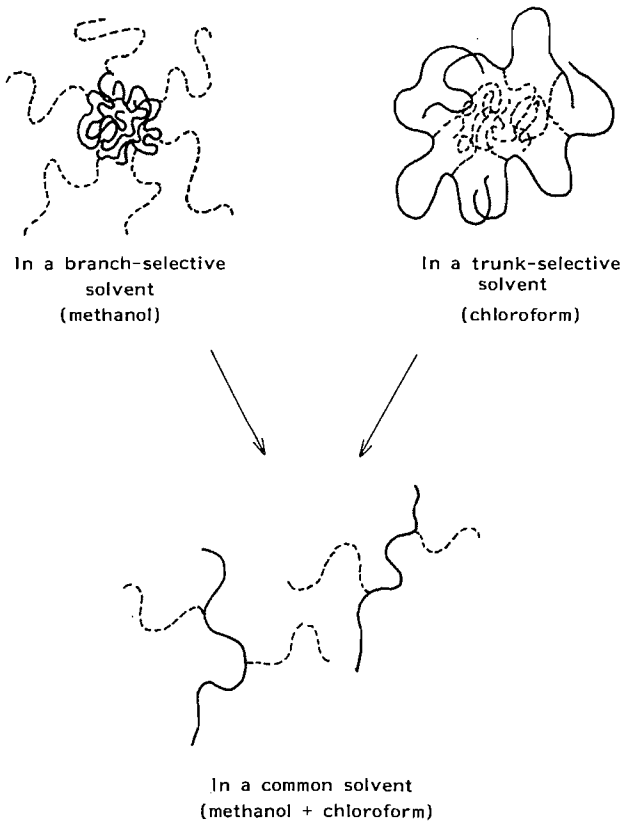

Fig. 6. Contact angle of water on films of PS-*g*-PHEMA (open symbols) and PHEMA-*g*-PS (solid symbols) cast from methanol (□, ■), DMF (○, ●), and chloroform (△, ▲). M_n's of the branches (macromonomers) are in the range of 2500–4700.

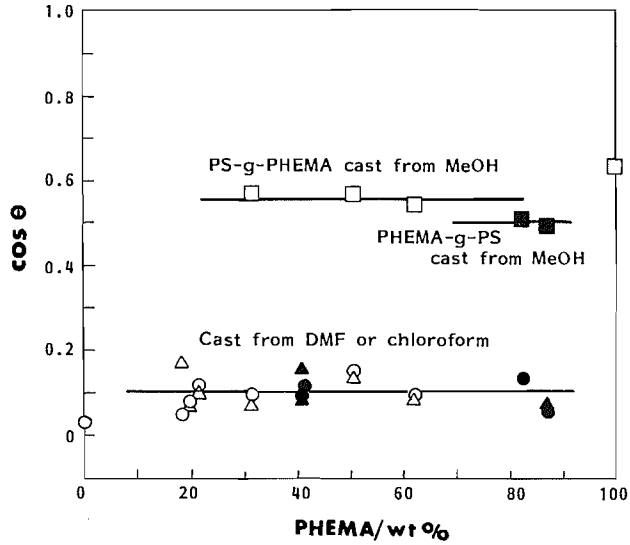

Fig. 7. Change of contact angle of water on graft copolymer films by immersion into water. (*a*) PS-*g*-PHEMA (PS/PHEMA =1/1 w/w); (*b*) PHEMA-q-PS (PHEMA/PS = 1/1 w/w), prepared with M_n of the branches (macromonomers) as indicated.

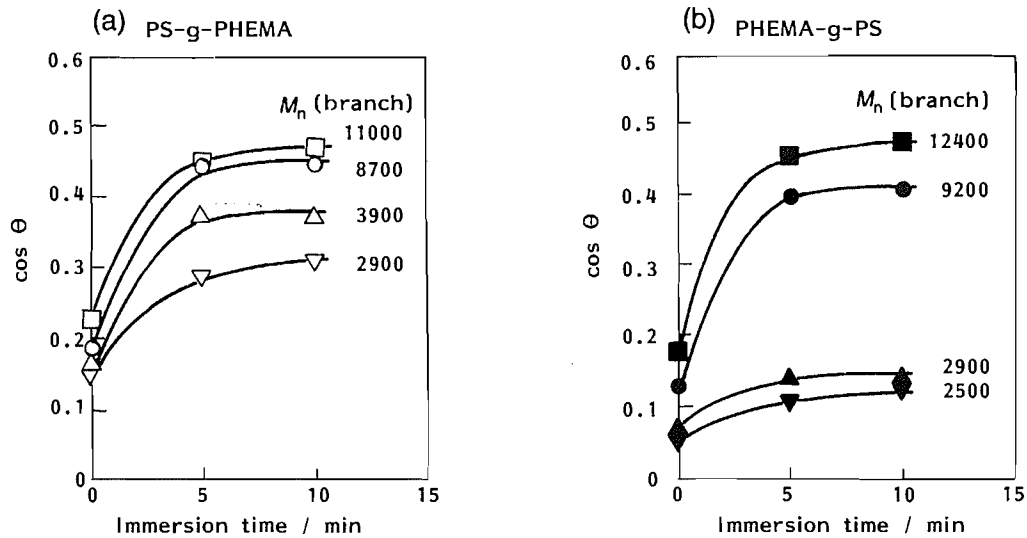

contact with a medium that is selective to PHEMA chains. Figure 7 shows the change in the contact angle on graft copolymer films by immersion into water, indicating clearly the rearrangement of the surface from PS-dominant (nonwettable) to PHEMA-dominant (wettable), particularly for graft copolymers with branches of higher M_n. It also appears that PS-*g*-PHEMA changes a little more rapidly to a more wettable level than its counterpart, PHEMA-*g*-PS, when compared at lower

M_n of the branches. The change of the surface composition and properties of these amphiphilic graft as well as block copolymers, depending on the environment, particularly in contact with water, appears to be an important factor in their usefulness as biocompatible materials (4, 5, 20).

Acknowledgments

This work was undertaken as part of the project, "Syntheses of well-controlled amphiphilic block and graft copolymers and their application to antithrombogenic material," presided over by Prof. S. Nakahama, Tokyo Institute of Technology, and supported by 17th Nissan Science Foundation. Helpful discussions with Prof. S. Nakahama, Dr. A. Hirao, Tokyo Institute of Technology, and Prof. T. Okano, Tokyo Women's Medical College, are gratefully acknowledged.

References

1. (*a*) Y. Yamashita (*Editor*). Chemistry and industry of macromonomers. Hüthig & Wepf, Basel. 1993; (*b*) K. Ito. Nippon Gomu Kyokaishi, **65**, 553 (1993); (*c*) Y. Kawakami. Prog. Polym. Sci. **19**, 203 (1994).
2. K. Ito. Hyomen, **28**, 739 (1990).
3. K. Ito, Y. Masuda, T. Shintani, T. Kitano, and Y. Yamashita. Polym. J. **15**, 443 (1983).
4. S. Yamashita, K. Shibatani, K. Takakura, and K. Imai. Kobunshi Ronbunshu, **39**, 187 (1982).
5. (*a*) T. Okano. Cell Technol. **8**, 199 (1989); (*b*) T. Okano, K. Suzuki, N. Yui, Y. Sakurai, and S. Nakahama. J. Biomed. Mater. Res. **27**, 1519 (1993).
6. S.K. Kang and M.S. Jhon. J. Colloid Interface Sci. **144**, 390 (1991).
7. (*a*) K. Ito, H. Tsuchida, T. Kitano, E. Yamada, and T. Matsumoto. Polym. J. **17**, 827 (1985); (*b*) K. Ito, K. Tanaka, H. Tanaka, G. Imai, S. Kawaguchi, and S. Itsuno. Macromolecules, **24**, 2348 (1991).
8. A. Hirao, H. Kato, K. Yamaguchi, and S. Nakahama. Macromolecules, **19**, 1294 (1986).
9. R. Asami, M. Takaki, and H. Hanahata. Macromolecules, **16**, 628 (1983).
10. M. Takaki, R. Asami, S. Tanaka, H. Hayashi, T.E. Hogen-Esch. Macromolecules, **19**, 2900 (1986).
11. G.O. Schulz and R. Milkovich. J. Appl. Polym. Sci. **27**, 4773 (1982).
12. B.C. Anderson, G.D. Andrews, P. Arthur, Jr., H.W. Jacobson, L.R. Melby, A.J. Playtin, and W.M. Sharkey. Macromolecules, **14**, 1597 (1981).
13. P. Lutz, P. Masson, G. Beinert, and P. Rempp. Polym. Bull. **12**, 79 (1984).
14. K. Antoin, J.-P. Lamps, P. Rempp, and Y. Gnanou. Polymer, **31**, 967 (1990).
15. S.K. Varshney, J.P. Hautekeer, R. Fayt, R. Jérôme, and Ph. Teyssié. Macromolecules, **23**, 2618 (1990).
16. Y. Kawakami, K. Inagaki, Y. Yamashita, and L.J. Mathias. J. Polym. Sci.: Polym. Lett. Ed. **19**, 629 (1981).
17. G. Odian. *In* Principles of polymerization. 3rd ed. Wiley & Sons, New York. 1991. Chap. 6.
18. Y. Tsukahara, N. Hayashi, X.-L. Jiang, and Y. Yamashita. Polym. J. **21**, 377 (1989).
19. G.F. Meijs and E. Rizzardo. J. Macromol. Sci. Rev. Macromol. Chem. Phys. **C30**, 305 (1990).
20. H. Mori, A. Hirao, S. Nakahama, and K. Senshu. Macromolecules, **27**, 4093 (1994).

Can. J. Chem. Downloaded from www.nrcresearchpress.com by 46.23.64.124 on 09/08/12
For personal use only.

The role of polymer flexibility on the interaction with surfactant micelles: poly(vinyl alcohol) and sodium dodecyl sulphate aqueous micelle interactions studied by dynamic fluorescence quenching

Jan van Stam, Nadine Wittouck, Mats Almgren, Frans C. De Schryver, and Maria da Graça Miguel

Abstract: The interactions between poly(vinyl alcohol) and the surfactant sodium dodecyl sulphate in aqueous solutions have been investigated by means of static and dynamic fluorescence measurements. By static fluorescence measurements the onset of interaction, the critical aggregation concentration, is determined to be 6.5 mM at 20°C and 7.0 mM at 40°C. By dynamic fluorescence measurements without added quencher the influence on the lifetime of the fluorescent probe, pyrene, by the presence of the polymer is investigated. From measurements with an added quencher, dimethylbenzophenone, the surfactant aggregation numbers of the micellar aggregates formed upon interaction between the surfactant and the polymer and the quenching rate constant are obtained. At the two polymer concentrations, i.e., 0.2% and 2.0%, the surfactant aggregation numbers at low surfactant concentration are very small, but increase rapidly with increasing surfactant concentration. Comparisons are made with results from a system where poly(ethylene oxide) instead of poly(vinyl alcohol) is the polymer.

Key words: dynamic fluorescence quenching, polymer–surfactant interactions, aggregation numbers.

Résumé : Faisant appel à des mesures de fluorescence statique et dynamique, on a examiné les interactions entre l'alcool polyvinylique et l'agent tensioactif dodécylsulfate de sodium, en solutions aqueuses. Sur la base de mesures de fluorescence statique, on a déterminé qu'au début des interactions, la concentration critique d'agrégation est égale à 6,5 mM à 20°C et à 7,0 mM à 40°C. Utilisant des mesures de fluorescence dynamique sans addition de désactivant, on a étudié l'influence du polymère sur le temps de vie de la sonde fluorescente, pyrène. Sur la base de mesures effectuées en présence de diméthylbenzophénone agissant comme désactivant, on a pu déterminer la constante de vitesse de désactivation et les nombres d'agrégation de l'agent tensioactif des agrégats micellaires formés lors de l'interaction entre l'agent tensioactif et le polymère. Aux deux concentrations du polymère, à savoir 0,2 et 2,0%, on réalise que les nombres d'agrégation de l'agent de surface sont très faibles à la faible concentration de l'agent tensioactif, mais qu'ils augmentent rapidement avec une augmentation de la concentration de l'agent tensioactif. On fait des comparaisons avec les résultats obtenus avec un système dans lequel le polymère est du poly(oxyde d'éthylène) au lieu de l'alcool polyvinylique.

Can. J. Chem. Downloaded from www.nrcresearchpress.com by 46.23.64.124 on 09/08/12
For personal use only.

Received February 21, 1995.

This paper is dedicated to Professor J.E. (Jim) Guillet in recognition of his contributions to Canadian chemistry.

J. van Stam. Laboratorium of Molecular Dynamics and Spectroscopy, Department of Chemistry, Katholieke Universiteit Leuven, Celestijnenlaan 200F, B-3001 Heverlee, Belgium, and Department of Physical Chemistry, University of Uppsala, POB 532, S-751 21 Uppsala, Sweden. Present address: Katholieke Universiteit Leuven.
N. Wittouck and F.C. De Schryver.[1] Laboratorium of Molecular Dynamics and Spectroscopy, Department of Chemistry, Katholieke Universiteit Leuven, Celestijnenlaan 200F, B-3001 Heverlee, Belgium.
M. Almgren. Department of Physical Chemistry, University of Uppsala, POB 532, S-751 21 Uppsala, Sweden.
M.d.G. Miguel. Departamento de Química, Universidade de Coimbra, 3049 Coimbra, Portugal.

[1] Author to whom correspondence may be addressed, at Katholieke Universiteit Leuven, Departement Scheikunde, Laboratorium Moleculaire Dynamica en Spectroscopie, Celestijnenlaan 200F, B-3001 Heverlee (Leuven), Belgium. Telephone: +32 - 16 - 32 74 05. Telefax: +32 - 16 - 32 79 89. E-mail: frans.deschryver@chem.kuleven.ac.be

Mots clés : désactivation dynamique de la fluorescence, interactions polymère – agent tensioactif, nombres d'agrégation.

[Traduit par la rédaction]

Can. J. Chem. Downloaded from www.nrcresearchpress.com by 46.23.64.124 on 09/08/12
For personal use only.

1. Introduction

The presence of a nonionic polymer in aqueous solutions of ionic surfactants causes changes in the physical properties of the micellar aggregates formed by the surfactant (1, 2). Such systems are of interest from a fundamental as well as from an applied point of view, polymer–surfactant solutions are for instance used in paints, pharmaceutical drugs, and in systems for enhanced oil recovery.

Among anionic surfactant – polymer systems, sodium dodecyl sulphate (SDS) – poly(ethylene oxide) (PEO) is one of the most studied, both by classical and modern methods (1–20). The system SDS – poly(vinyl alcohol) (PVA), on the other hand, has been studied mainly by classical methods (11, 21–25). These report a behaviour quite similar to that found in the SDS – PEO system, e.g., an onset of interaction below the critical micelle concentration (cmc) and about the same degree of solubilization of hydrophobic species (22*a*, 23). It is also evident that SDS and PVA interact with each other, as solubility and surface tension differ from polymer-free SDS solutions.

In previous reports, the use of the dynamic fluorescence quenching method (DFQ) on the SDS–PEO system (10, 19, 20) was reported. In salt-free systems (10, 19) it was found that the onset of interaction occurred at a concentration lower than the cmc, this concentration referred to as the critical aggregation concentration (cac). Presence of salt (20) lowered the cac due to screening of the electrostatic repulsion between the surfactant headgroups. Further, it was found that at the cac the aggregation number of the micellar-like aggregates formed by the surfactant molecules with the interacting polymer exposed an aggregation number much lower than that found for ordinary SDS micelles, approximately 30[2] as compared to 60. Except for the highest salt concentration, increasing the SDS concentration led to an increase of the aggregation number up to a limiting value, slightly lower than the aggregation number for ordinary micelles. This was explained by a model in which the polymer chain can interact with a certain number of aggregates, depending on the polymer chain length (19). At low polymer concentrations, this number will be reached at the cac, whereas at high polymer concentrations the initial number of aggregates will be lower than at the saturation limit. Upon addition of surfactant there is, initially, primarily an increase in the number of aggregates. As the saturation limit is approached it is mainly the already formed aggregates that grow, possibly in competition with formation of ordinary micelles.

The theories proposed for the interaction between an ionic surfactant and a nonionic polymer (26, 27) point in the same direction as the experimental results, e.g., interaction starts at a cac lower than the cmc and the aggregates formed have a micelle-like structure but with lower aggregation number. The aggregation numbers found, however, in the SDS–PEO system are lower than predicted by theory, and the increase of the aggregation number in this system when more surfactant is added is not explained.

In studies of the interaction between polyelectrolytes and micelles of opposite charge (28, 29), it was found that a flexible polyelectrolyte induced the same lowering of the aggregation number (28) as was found in the SDS–PEO system, while a more rigid polyelectrolyte left the micellar aggregation numbers more or less unchanged (29). It was to investigate whether such a dependence on the polymer flexibility also holds for uncharged systems that we have chosen to study the interaction between SDS and PVA.

In this study, results from static and dynamic fluorescence measurements are reported. From static measurements the cac is obtained. From dynamic fluorescence measurements without added quencher the decay time, τ_0, of the excited probe, pyrene, is obtained, while measurements with dimethylbenzophenone as added fluorescence quencher give the aggregation numbers of the surfactant aggregates and the quenching rate constant k_q.

2. Experimental section

2.1 Materials

Poly(vinyl alcohol) (PVA), 100% hydrolyzed, was from Merck (average molecular weight 115 000) and was used as supplied; c^* was determined as 1.3% w/v (Dr. Fang Liqi, private communication), which means that a 0.2% solution is dilute and a 2% solution is semi-dilute. Pyrene (Aldrich) and dimethylbenzophenone (DMBP) (Aldrich 99%) were recrystallized twice from ethanol. Sodium dodecyl sulphate (SDS) was from BDH, specially pure. Conductivity measurements gave a cmc in accordance with literature (≈8 mM) so no further purification of SDS was done. All solutions were prepared with distilled water. Measurements were performed at two temperatures, 20°C and 40°C. At these two temperatures SDS micelles have approximately the same aggregation number, i.e., 55–65 (19).

The preparation of samples for fluorescence measurements was described earlier (28). The pyrene concentration was kept low enough ($<10^{-5}$ M) to prevent excimer formation. The DMBP concentration was chosen to be less than one DMBP molecule per aggregate.

2.2 Methods

Static fluorescence measurements were used to determine the onset of surfactant aggregation and were carried out on a SPEX Fluorolog 1680 combined with a SPEX spectroscopy laboratory coordinator DM1B. The cell-holder was connected to a standard water-bath. All slits were 0.5 mm.

The ratio between the third and the first vibronic peaks (the III/I ratio) in the pyrene steady-state fluorescence spectrum depends on the polarity of the pyrene microenvironment (30). This can be used to probe surfactant aggregation, as pyrene will be almost exclusively dissolved in the less polar surfactant aggregates as they are formed. We have choosen to set cac

[2] The aggregation number at 9 mM total SDS concentration at 20°C and 0.2% PEO reported in ref. 19 is 26 but should be 34.

Can. J. Chem. Downloaded from www.nrcresearchpress.com by 46.23.64.124 on 09/08/12
For personal use only.

equal to the inflection point (the second derivative of a fitted polynomial of order 3 was used to determine the inflection point) obtained when the III/I values are plotted against the SDS concentration.

Dynamic fluorescence decay data were collected with the single photon counting technique. The setup is described elsewhere (28).

3. Theory and data analysis

3.1 Theory

Dynamic fluorescence quenching in microheterogeneous solutions has been well described in the literature (31–38). Under the conditions that the excitation pulse is narrow compared to the fluorescence decay time and no migration of probe or quencher occurs within the time-resolution of the experiment, the interpretation with the Infelta–Tachiya model (39, 40) in a generalized version (41–43) is straightforward.

The fluorescence decay is described (39, 40) by

$$[1] \quad F(t) = A_1 \exp[-A_2 t - A_3\{1-\exp(-A_4 t)\}]$$

where the parameters have the following meaning under the circumstances stated above:

A_1 is the fluorescence intensity at time $t = 0$, i.e., $F(0)$.

A_2 is the decay rate at long times. If there is no exchange of probe or quencher between the micellar phase and the bulk, A_2 will equal the unquenched decay rate k_0, or, equivalently, $1/A_2$ will equal the decay time τ_0 – leading to parallel decays at long times in the logarithmic representation for a set of experiments differing only in quencher concentrations.

A_3 is the average number of quencher molecules per aggregate. With a known amount of bound surfactant molecules and the distribution of quencher between micelles and the bulk phase, the average surfactant aggregation number, $\langle a \rangle$, can be calculated from

$$[2] \quad \langle a \rangle = A_3 S_m / Q_m$$

where S_m is the concentration of bound surfactant (the total surfactant concentration minus the cac or the cmc) and Q_m the concentration of bound quencher (the total quencher concentration minus the amount dissolved in the aqueous sub-phase).

A_4 equals the first-order quenching rate constant k_q for one quencher.

The fluorescence decay time in absence of added quencher, τ_0, was determined in separate experiments. From measurements with added quencher A_2 (eq. [1]) was determined, and the difference between $1/A_2$ and τ_0 is a measure of the condition that the probe and quencher are stationary during the time-window of the experiments. If this difference is close to zero, the quencher does not migrate between micelles or between micelles and the bulk phase. The probe, pyrene, does certainly not migrate under the present conditions, but the quencher, DMBP, has some solubility in the aqueous bulk phase (Dr. Jan Alsins, private communication). It turned out, however, that also the quencher remained in its micelle during the time-window of the measurement.

Nevertheless, the solubility of DMBP in water requires special treatment in order to determine an accurate value of Q_m for use in eqs. [2] and [6], see below.

To determine the distribution constants, K_D, for the distribution of DMBP between the aqueous bulk and the surfactant aggregates,

$$[3] \quad K_D = Q_m/(Q_{aq} S_m)$$

the concentration of DMBP at saturation was determined by absorption measurements (20, 44) for different SDS–PVA solutions at both temperatures. The distribution constant obtained is then used for the determination of Q_m by

$$[4] \quad Q_m = Q_t S_m K_D/(S_m K_D + 1)$$

where Q_t is the total quencher concentration.

The aggregation numbers obtained by eq. [2] should be treated as quencher-averaged aggregation numbers, $\langle a \rangle_q$ (45–47). The $\langle a \rangle_q$ is an apparent property, dependent on Q_m. The weight-averaged aggregation number, $\langle a \rangle_w$, is obtained by extrapolation to zero quencher concentration (45, 46) according to:

$$[5] \quad \langle a \rangle_q = \langle a \rangle_w - 1/2\sigma^2\eta + 1/6\kappa\eta^2 - \ldots$$

where σ^2 is the variance and κ gives the skewness of the size distribution of the system. η is given by

$$[6] \quad \eta = Q_m/S_m$$

It should also be noted here that the solutions were not deoxygenated, which means that the fluorescence decay was quenched by dissolved oxygen. From the measurements it was found that the presence of oxygen only affects the decay time and does not influence the use of eq. [1].

3.2 Data analysis

The computer programs (48) used for estimation of the natural lifetime and the parameters A_1–A_4 in eq. [1] are mainly based on the programs by Löfroth (49). The fitting parameters were obtained by minimizing the global reduced χ_ν^2:

$$[7] \quad \chi_\nu^2 = \left[\sum_{\forall x}\sum_{\forall y} \omega_{xy}(h_{xy}^{obs} - h_{xy}^{calc})^2\right]/\nu$$

where x sums over all experiments and y over the appropriate channels for each experiment. h denotes the observed and calculated fluorescence decay histogram value, respectively, ω is the statistical weight (a Poisson distribution is assumed), and ν represents the degrees of freedom for the entire data surface. The models were fitted under the global analysis approach (49, 50). The fit was considered to be good if $\chi_\nu^2 \leq 1.25$.

4. Results and discussion

4.1 Critical aggregation concentration

The pyrene III/I ratios were obtained from static fluorescence measurements, Fig. 1. At low SDS concentrations, the value is about 0.65, slightly higher than generally expected for pyrene dissolved in water, i.e., 0.55–0.60 (30). The difference is probably due to the presence of PVA, but does not influence the use of the method. This conclusion was further supported by the fact that the decay time for pyrene in aqueous PVA solu-

Can. J. Chem. Downloaded from www.nrcresearchpress.com by 46.23.64.124 on 09/08/12
For personal use only.

Fig. 1. Pyrene III/I vibronic peak ratios from static fluorescence measurements in 0.1% PVA at 20°C (open symbols) and at 40°C (filled symbols). Measurements in 0.2% PVA and 2% PVA showed the same behaviour.

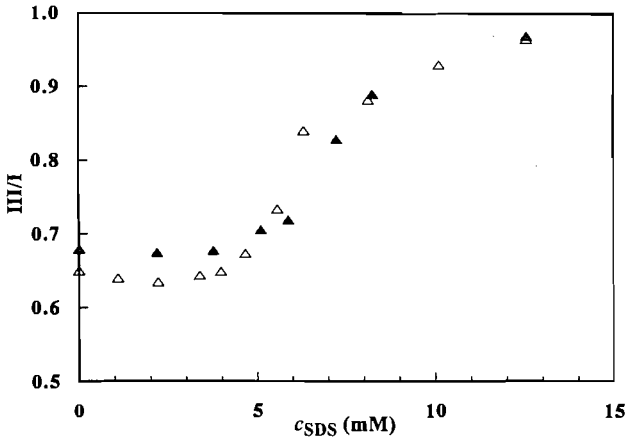

Fig. 2. DMBP distribution constants, k_D, at different SDS concentrations in 0.2% PVA (open symbols) and 2% PVA (filled symbols); circles at 20°C and squares at 40°C. Inserted lines serve as guides for the eye.

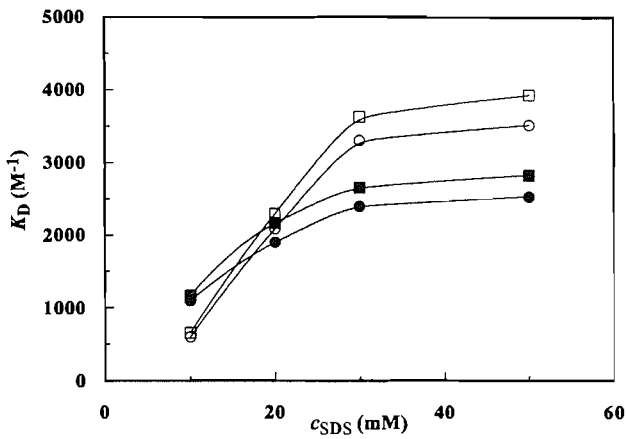

tion was equal to the decay time for pyrene dissolved in pure water. When surfactant aggregation starts, pyrene will be almost exclusively found in the surfactant aggregates, exposing the pyrene molecules to a less polar environment. Consequently, the III/I ratio will show an increase at this point, which was found at a SDS concentration around 5 mM, Fig. 1. The III/I ratio continues to increase up to a limiting value of approximately 0.92, or what is found in pure SDS micelles (30). The steep increase in III/I shows that the aggregation process is highly cooperative in nature, as is ordinary micelle formation. A closer examination of the III/I ratio as a function of SDS concentration yields a cac value of 6.5 mM at 20°C, while it is 7.0 mM at 40°C. The cac in a salt-free SDS–PEO system was found to be 5.5 mM (20)[3] for PEO at 25°C with molecular weights lower than 250 000. Thus, the interaction starts at about the same cac in the present system.

4.2 DMBP distribution between the aqueous and aggregate sub-phases

The K_D values determined at 20°C and 40°C are shown graphically in Fig. 2. The values at the lowest surfactant concentration are the most uncertain: the crossover below 20 mM SDS is an effect of this uncertainty. Nevertheless, the K_D values were used as determined.

The K_D in the present system (approximately 2000 M^{-1} for 20 mM SDS at both PVA concentrations and at both temperatures) is intermediate as compared to the value in polymer-free 20 mM SDS solution, with $K_D \approx 2900\ M^{-1}$ and $\approx 1950\ M^{-1}$ at 20°C and 40°C, respectively (Dr. Jan Alsins, private communication), and the SDS–PEO system, where K_D is $\approx 1600\ M^{-1}$ in 0.2% PEO and $\approx 1900\ M^{-1}$ in 2.0% PEO at both temperatures and 20 mM SDS. This leads to a picture in which the SDS micelle is less altered in size and (or) structure in the SDS–PVA system than in the SDS–PEO system.

Combining eqs. [2] and [4] gives

$$[8] \quad \langle a \rangle = A_3[S_m/Q_t + 1/(Q_t K_D)]$$

from which it follows that an overestimation of K_D leads to an underestimated aggregation number (the product $Q_t K_D$ is, for ordinary micellar solutions in the order of unity).

The aggreation numbers in ref. 19 are in error since K_D-values for pure SDS micelles were used. A recalculation using the correct K_D-values gave small changes of the aggregation numbers at all SDS concentrations except those close to the cac.[2] The overall picture, however, does not change from that given in ref. 19. In all comparisons with the SDS–PEO system, the recalculated aggregation numbers are used.

The water solubility of DMBP also raises the question of whether it affects the photophysical deactivation of the excited probe via quencher migration from the bulk into the surfactant aggregate. Such an effect, if present, should be most pronounced at SDS concentrations close to the cac. At the cac the concentration of aggregates is, roughly, 10^{-4} M, leading to a DMBP bulk-concentration, Q_{aq}, of about 10^{-5} M (assuming one quencher per aggregate on average and 10% dissolved in the aqueous bulk). For a diffusion-limited process one can set the second-order rate constant for migration from the bulk into the aggregates, k_+, to be in the order of $5 \times 10^9\ s^{-1}$ (34), giving the product $k_+ Q_{aq}$ to be about $5 \times 10^4\ s^{-1}$, which should be compared with $k_0\ (=1/\tau_0)$, approximately $4 \times 10^6\ s^{-1}$ in this system, see Table 1. Thus, the effect of quencher migration is only 1% or less of the natural deactivation rate, which is negligible.

4.3 Pyrene fluorescence decay time

The numerical results from the fitting of eq. [1] to the fluorescence decay data and subsequent treatment are compiled in Tables 1 and 2. The pyrene fluorescence decay time, τ_0, Fig. 3, decreases with increasing SDS concentration at the low PVA concentration. If compared with the decay times found in 0.2% PEO (19), one finds an almost identical behaviour at both temperatures and 0.2% PVA concentration. This results in the same picture as proposed earlier (19), with the polymer in close contact with the aggregates causing a steric shielding against penetration, and subsequent quenching, by bulk-dissolved oxygen. As the surfactant concentration increases, this shielding effect decreases due to lower polymer-to-surfactant ratios, and the lifetimes come closer to those found in polymer-free systems.

At 2% polymer concentration, the lifetimes are longer in the SDS–PVA system at the lowest SDS concentration. At this

[3] Also, J. van Stam and C. Lindblad. Unpublished results.

Can. J. Chem. Downloaded from www.nrcresearchpress.com by 46.23.64.124 on 09/08/12
For personal use only.

Table 1. Pyrene fluorescence decay times, weight-average aggregation numbers, and quenching rate constants at 20°C obtained by dynamic fluorescence measurements. In pure SDS micellar solutions, not deoxygenated, the pyrene decay time is approximately 180 ns at 20°C, the SDS aggregation number approximately 55–65, and the DMBP quenching rate constant approximately 5×10^7 s^{-1}.

$[SDS]_{tot}$ (mM)	R_b	τ_0 (ns)	$\langle a \rangle_w$	$k_q \times 10^{-7}$ (s^{-1})
0.2% PVA				
9	0.053	245.0	38.8	2.8
10	0.075	237.4	44.4	2.8
15	0.185	211.2	49.1	2.9
40	0.749	206.6	59.1	3.2
50	0.956	189.6	59.5	3.4
60	1.174	197.3	61.4	3.1
2.0 % PVA				
10	0.008	235.7	20.7	2.7
15	0.020	229.6	34.9	2.7
30	0.054	224.1	44.4	2.6
40	0.079	215.9	46.4	2.5
50	0.100	220.8	49.2	2.4
60	0.123	215.9	49.9	2.4
100	0.214	211.8	54.4	2.3

Table 2. Pyrene fluorescence decay times, weight-average aggregation numbers, and quenching rate constants at 40°C obtained by dynamic fluorescence measurements. In pure SDS micellar solutions, not deoxygenated, the pyrene decay time is approximately 135 ns at 40°C, the SDS aggregation number approximately 55–65, and the DMBP quenching rate constant approximately 8×10^7 s^{-1}.

$[SDS]_{tot}$ (mM)	R_b	τ_0 (ns)	$\langle a \rangle_w$	$k_q \times 10^{-7}$ (s^{-1})
0.2% PVA				
9	0.043	166.2	25.2	6.1
10	0.065	167.2	31.3	6.0
15	0.174	181.6	35.2	5.7
40	0.739	155.8	45.7	6.1
50	0.946	153.8	48.1	6.2
60	1.164	156.5	59.4	6.2
2.0 % PVA				
10	0.008	191.3	18.9	6.1
15	0.019	181.8	30.1	6.1
30	0.053	172.8	41.2	5.7
40	0.078	172.0	42.4	5.4
50	0.099	174.5	50.8	5.5
60	0.122	163.5	51.6	5.4
100	0.213	161.4	54.7	5.3

higher polymer concentration the lifetimes do not reach values close to the lifetimes in polymer-free solutions within the concentration range studied. This is due to the much lower ratios of bound surfactant to polymer monomer unit (denoted R_b) in these systems. Increasing the surfactant concentration to raise this ratio will also lead to a higher ionic strength, which would influence both the shape and the size of the micellar aggregates.

Fig. 3. Pyrene fluorescence decay times in PVA solutions (filled symbols) and PEO solutions (open symbols) at 0.2% (circles) and 2.0% (squares) polymer concentration as a function of the ratio R_b (see text for details) at two temperatures: (*a*) 20°C and (*b*) 40°C. Data for the SDS–PEO system are from ref. 19.

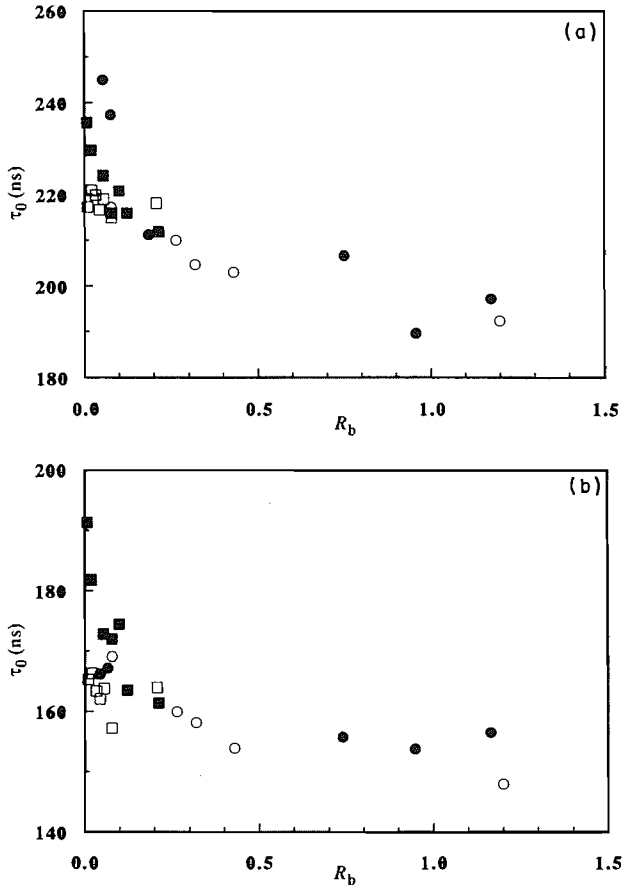

4.4 Surfactant aggregation numbers

For determination of the surfactant aggregation numbers, dynamic fluorescence quenching measurements were performed. The fluorescence decays, two typical examples of which are shown in Fig. 4, show well-developed exponential decays at long times. The parallel tails assure that any probe and (or) quencher migration is negligible on this time scale. The determined weight-average aggregation numbers, obtained by the use of eq. [5], are represented graphically in Fig. 5, together with the recalculated (see above) aggregation numbers from ref. 19 for SDS–PEO.

At 0.2% PVA the aggregation numbers as a function of the SDS concentration are initially very small, but increase steeply with increasing surfactant concentration. This aggregation behaviour resembles that of the SDS–PEO system, where a marked decrease in aggregation numbers, by a factor of 2 of those for the ordinary micelles, was found at low surfactant concentrations (19). The aggregation numbers increase more quickly, however, in the present system, Fig. 5.

Can. J. Chem. Downloaded from www.nrcresearchpress.com by 46.23.64.124 on 09/08/12
For personal use only.

Fig. 4. The logarithm of the fluorescence intensity versus time from dynamic fluorescence quenching measurements at two temperatures: (*a*) 20°C and (*b*) 40°C. The total SDS concentration is 15 mM and the PVA concentration 0.2%. The DMBP concentrations (total concentration) are from top to bottom: 0, 0.043, 0.085, and 0.126 mM, respectively.

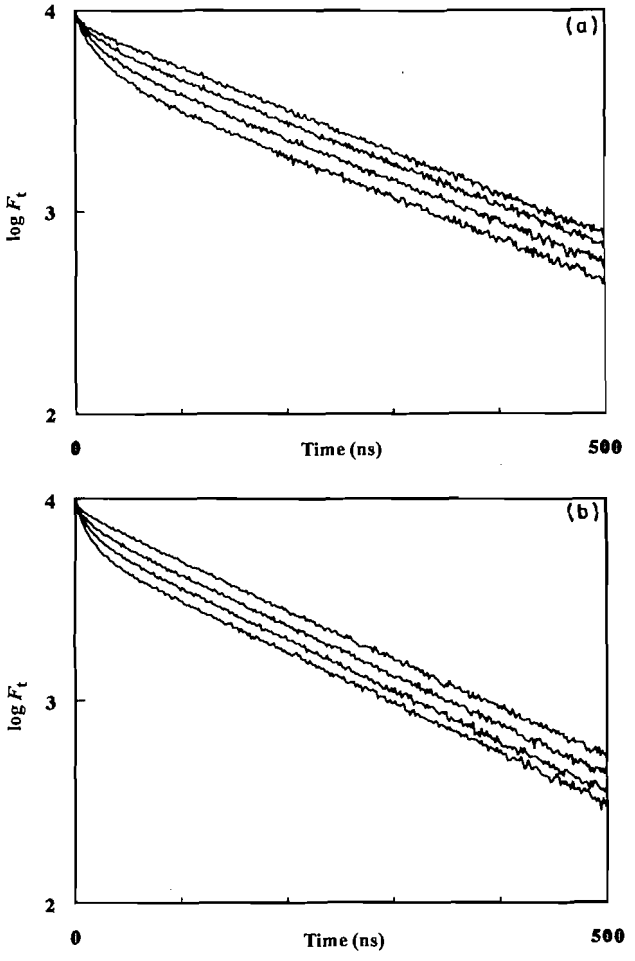

Fig. 5. SDS weight-averaged aggregation numbers for PVA solutions (filled symbols) and PEO solutions (open symbols) at 0.2% (circles) and 2.0% (squares) polymer concentration as a function of the ratio R_b (see text for details) at two temperatures: (*a*) 20°C and (*b*) 40°C. Data for the SDS–PEO system are from ref. 19. The aggregation number for SDS micelles is about 55–65 in this concentration range.

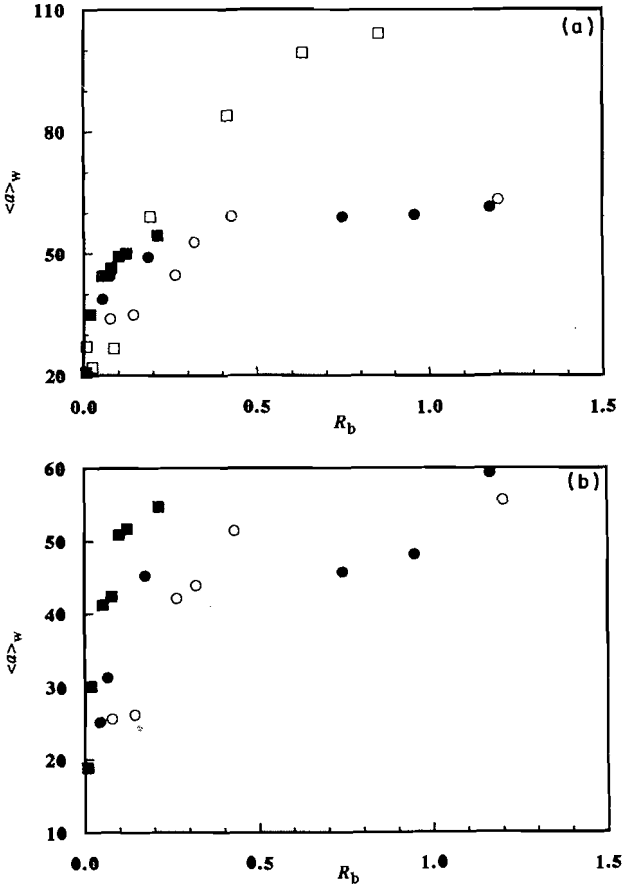

At 2% PVA, the picture is very much the same as for 0.2% PVA. At this higher polymer concentration the surfactant aggregation numbers are also smaller than those for ordinary SDS micelles. Comparing the two surfactant–polymer systems at 2% polymer concentration, one finds that with PVA as polymer approximately 50 mM ($R_b \approx 0.10$) SDS is needed to reach about the same aggregation number as in polymer-free SDS solutions, whereas approximately 100 mM SDS is needed when PEO is the polymer (19). This could be interpreted as a difference in the interaction capability of the two polymers, i.e., that the formation of free aqueous micelles, not interacting with the polymer, starts at a lower R_b when PVA is the polymer. The aggregation numbers determined will in such a case be a weighted average of the aggregation numbers of the aqueous micelle and the aggregate interacting with the polymer (19).

The reason for these differences may be due to the different hydrophobicity of the two polymers. Another parameter of importance is the polymer flexibility: wrapping around small aggregates would be less favourable for a polymer with lower flexibility. In two earlier communications it was found that a stiff polyelectrolyte left the aggregation numbers more or less unaffected (28), while a flexible one caused a decrease in the aggregation numbers (29). In fact, the unperturbed end-to-end distance, $r_0/M^{0.5}$ (r_0 is calculated from the unperturbed mean-square end-to-end distance $\langle r^2 \rangle_0$ and M is the polymer molecular weight), independent of molecular weight, is 0.95 nm for PVA and 0.75 nm for PEO in water (51), showing, along with other macromolecular parameters, that PVA is less flexible than PEO. Furthermore, in a study of the interaction between the cationic surfactant cetyltrimethylammonium chloride (CTAC) and poly(vinyl alcohol-*co*-vinyl acetate) (PVA-Ac), it was concluded that the aggregation numbers were significantly lowered by the presence of the polymer (52). The value of $r_0/M^{0.5}$ for poly(vinyl acetate) (PVAc) is about 0.70 nm (51) and the copolymer PVA-Ac could be expected to be intermediate in flexibility between PVA and PVAc.

Assuming the flexibility to be an important parameter for interactions between an uncharged polymer and SDS micellar aggregates justifies the following description of the SDS–PVA system:

At 0.2% PVA, the polymer interacts with the SDS micelle to form small aggregates at low surfactant concentrations.

Can. J. Chem. Downloaded from www.nrcresearchpress.com by 46.23.64.124 on 09/08/12
For personal use only.

Fig. 6. First-order quenching rate constant k_q for PVA solutions (filled symbols) and PEO solutions (open symbols) at 0.2% (circles) and 2.0% (squares) polymer concentration as a function of the weight-averaged aggregation number $\langle a \rangle_w$ at two temperatures: (*a*) 20°C and (*b*) 40°C. Data for the SDS–PEO system are from ref. 19.

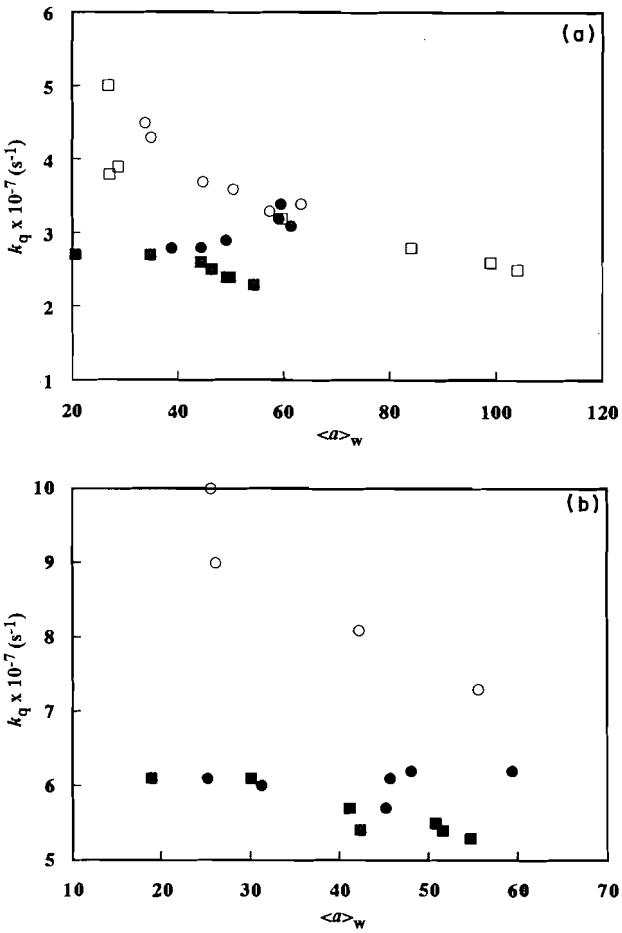

These aggregates grow rapidly when the SDS concentration is increased, possibly due to formation of aqueous SDS micelles not interacting with PVA. The more flexible PEO can wrap around the surfactant aggregate in a more efficient way, and the increase in aggregation number is delayed, as compared to the SDS–PVA system. At higher R_b-values, the two polymers impose the same effect on the SDS aggregation numbers, independent of temperature.

At 2.0% PVA, the results are more or less identical with those obtained at the lower polymer concentration: with increasing surfactant concentration the surfactant aggregation numbers rapidly increase.

4.5 Quenching rate constants

Some reports have paid attention to the fluorescence quenching rate in surfactant–polymer systems (10*a*, 19, 20, 28, 29). The quenching rate constant, k_q, is thought to be inversely proportional to the micellar or aggregate volume, or, equally, to the aggregation number – predicted by theory (53) and experimentally found in systems with small, spherical, micelles, even if in some it has been found to depend on $V^{-1.2}$ (31).

Surprisingly, this does not hold in many surfactant–polymer systems (10*a*, 19, 20, 28, 29). The quenching rate changes much less than the aggregation number, as is also found in the present system, see Fig. 6. There is a slowing down of the quenching rate with increasing aggregation number, but not at all to the extent expected should it be inversely proportional to the aggregation number. Furthermore, k_q is lower in surfactant–polymer systems than in the corresponding surfactant systems. In a discussion of pyrene excimer formation in the SDS–PEO system, Zana et al. (10*a*) proposed a specific interaction between pyrene and PEO. The generality of the effect seems to rule out this proposal, however, and a change in the "microviscosity" due to more rigid packing in the surfactant–polymer aggregate (20) seems to be a more general explanation. This increased viscosity would affect the translational diffusion of the probe and quencher molecules within the aggregates.

In the SDS–PEO system at 20°C, the quenching rate constant is more or less independent of the polymer concentration. The values of k_q at 0.2% PVA fits well into this picture, whereas the quenching rate is significantly lower at the higher PVA concentration. At 40°C this effect is even more pronounced, also at the lower PVA concentration the quenching rate is slowed down with respect to the SDS–PEO system. A reasonable explanation is the small but significant difference in θ temperature between PVA and PEO: in water the θ temperature is about 10°C lower for the former polymer (51). Thus, raising the temperature from 20 to 40°C will change the flexibility and (or) hydrophilicity of PVA as compared to PEO to such an extent that there will be a measurable difference in the quenching rate constant values.

5. Conclusions

The presence of PVA influences the SDS aqueous micellar aggregates and dynamics. The interaction starts at both temperatures at a critical aggregation concentration below the cmc, 6.5 mM at 20°C and 7 mM at 40°C. At 0.2% PVA, the polymer shields the excited probe from oxygen quenching, due to penetration by bulk-dissolved oxygen molecules, to the same extent as does PEO. The aggregation numbers are affected in the same way by the two polymers at the lowest SDS concentrations, but increase more steeply with increasing surfactant concentration when PVA is the polymer due to the less flexible PVA chain as compared to the PEO chain. At 2.0% PVA, the SDS micellar aggregation numbers at low SDS concentrations are also much lower than those found for free SDS micelles and are comparable to those at 0.2% PVA. Increasing the SDS concentration increases the surfactant aggregation numbers rapidly. The results concerning the aggregation numbers are in qualitative accordance with those found in a similar study of the system CTAC–PVA-Ac (52). The small difference in θ temperature in water between PVA and PEO induces a significant difference in the quenching rate constant values: PVA, having a lower θ temperature, affects the micelles more than PEO, leading to a slowing down of the translational diffusion of the dissolved quencher and a lower value for the quenching rate constant.

Acknowledgements

J.v.S. is a post-doctoral fellow at the Katholieke Universiteit Leuven. J.v.S. thanks the Swedish Natural Science Research

Council (NFR) for a postdoctoral grant through the European Human Capital and Mobility Scheme. N.W. thanks I.W.O.N.L. (Belgium) and K.U. Leuven for financial support. M.A. thanks The Swedish National Board for Industrial and Technical Development (NUTEK) for support. F.D.S. acknowledges financial support through IUAP-III-040 and IUAP-II-16. M.M. thanks The Swedish Institute for a grant making a visit at Uppsala University possible. We are grateful to the help from Ms Anna Lindahl, Ms Charlotta Naeslund, and Ms Hanna Söderholm in performing the absorption measurements when determining the quencher distribution constants. We want to thank Professor Wyn Brown for fruitful discussions and Professor Emad Mukhtar for skillful maintenance of the laser systems.

References

1. E.D. Goddard. Colloids Surf. **19**, 255 (1986).
2. B. Lindman and K. Thalberg. *In* Interactions of surfactants with polymers and proteins. *Edited by* E.D. Goddard and K.P. Ananthapadmanabhan. CRC Press, Boca Raton, Fla. 1993. Chap. 5.
3. (*a*) M.N. Jones. J. Colloid Interface Sci. **23**, 36 (1967); (*b*) J. Colloid Interface Sci. **26**, 532 (1968).
4. M.J. Schwuger. J. Colloid Interface Sci. **43**, 491 (1972).
5. (*a*) K. Shirahama and N. Ide. J. Colloid Interface Sci. **54**, 450 (1976) (*b*) K. Shirahama, M. Tohdo, and M. Muruhashi. J. Colloid Interface Sci. **86**, 282 (1982).
6. Y. Moroi, H. Akisada, M. Saito, and R Matuura. J. Colloid Interface Sci. **61**, 233 (1977).
7. (*a*) B. Cabane. J. Phys. Chem. **81**, 1639 (1977); (*b*) B. Cabane and R. Duplessix. J. Phys. **43**, 1529 (1982); (*c*) Colloids Surf. **13**, 19 (1985); (*d*) J. Phys. **48**, 651 (1987).
8. D.M. Bloor and E. Wyn-Jones. J. Chem. Soc. Faraday Trans. 2, **78**, 657 (1982).
9. (*a*) N. Turro, B. Baretz, and P.-L. Kuo. Macromolecules, **17**, 1321 (1984); (*b*) P.-L- Kuo, M. Okamoto, and N. Turro. J. Phys. Chem. **91**, 2934 (1987).
10. (*a*) R. Zana, P. Lianos, and J. Lang. J. Phys. Chem. **89**, 41 (1985); (*b*) *In* Microdomains in polymer solutions. *Edited by* P. Dubin. Plenum Press, New York and London. 1985. pp. 357–368.
11. T. Gilyani and E. Wolfram. *In* Microdomains in polymer solutions. *Edited by* P. Dubin. Plenum Press, New York and London. 1985. pp. 383–405.
12. J. Francois and J. Dayantis. Eur. Polym. J. **21**, 165 (1985).
13. (*a*) E. Lissi and E. Abuin. J. Colloid Interface Sci. **105**, 1 (1985); (*b*) F. Quina, E. Abuin, and E. Lissi. Macromolecules, **25**, 5173 (1990).
14. (*a*) F.M. Witte and J. Engberts. J. Org. Chem. **52**, 4767 (1987); (*b*) J. Brackman and J. Engberts. J. Colloid Interface Sci. **132**, 250 (1989); (*c*) J. Brackman. Langmuir, **7**, 469 (1991).
15. R. Ramachandaran and G.J. Kennedy. Colloids Surf. **54**, 261 (1991).
16. Z. Gao, R.E. Wasylishen, and J. Kwak. J. Phys. Chem. **95**, 462 (1991).
17. P. Dubin, J.H. Gruber, J. Xia, and H. Zhang. J. Colloid Interface Sci. **148**, 35 (1992).
18. C. Maltesh and P. Somasundaram. Langmuir, **8**, 1926 (1992).
19. J. van Stam, M. Almgren, and C. Lindblad. Prog. Colloid Polym. Sci. **84**, 13 (1991).
20. J. van Stam, W. Brown, J. Fundin, M. Almgren, and C. Lindblad. *In* Colloid–polymer interactions. *Edited by* P.L. Dubin and P. Tong. ACS Symp. Ser. **532**, 194 (1993).
21. T. Isemura and A. Imanishi. J. Polym. Sci. **33**, 337 (1958).
22. (*a*) S. Saito. J. Colloid Interface Sci. **24**, 227 (1967); (*b*) S. Saito, T. Tuniguchi, and K. Kitamura. J. Colloid Interface Sci. **37**, 154 (1971).
23. H. Arai and S. Horin. J. Colloid Interface Sci. **30**, 372 (1969).
24. K.E. Lewis and C.P. Robinson. J. Colloid Interface Sci. **32**, 539 (1970).
25. B.J. Birch, D.E. Clarke, R.S. Lee, and J. Oakes. Anal. Chim. Acta, **70**, 417 (1974).
26. R. Nagarajan. Colloids Surf. **13**, 1 (1985).
27. E. Ruckenstein, G. Huber, and H. Hoffman. Langmuir, **3**, 382 (1987).
28. M. Almgren, P. Hansson, E. Mukhtar, and J. van Stam. Langmuir, **8**, 2405 (1992).
29. K. Thalberg, J. van Stam, C. Lindblad, M. Almgren, and B. Lindman. J. Phys. Chem. **95**, 8977 (1991).
30. K. Kalyanasundaram and J.K. Thomas. J. Am. Chem. Soc. **99**, 2039 (1977).
31. M. Almgren. *In* Kinetics and catalysis in microheterogenous systems. *Edited by* M. Grätzel and M. Kalyanasundaram. Marcel Dekker, New York. 1991. p. 63.
32. R. Zana. *In* Surfactants in solution. Vol. 22. *Edited by* R. Zana. Marcel Dekker, New York and Basel. 1987. pp. 241–292.
33. M. Almgren. Adv. Colloid Interface Sci. **41**, 9 (1992).
34. E. Roelants and F.C. De Schryver. Langmuir, **3**, 209 (1987).
35. N. Boens, A. Malliaris, M. Van der Auweraer, H. Luo, and F.C. De Schryver. Chem. Phys. **121**, 199 (1988).
36. M. Van der Auweraer, E. Roelants, A. Verbeeck, and F.C. De Schryver. *In* Surfactants in solution. Vol. 7. *Edited by* K.L. Mittal. Plenum Press, New York. 1989. p. 141.
37. M. Gehlen and F.C. De Schryver. Chem. Rev. **93**, 199 (1993).
38. F.C. De Schryver, N. Boens, M. Van der Auweraer, L. Viaene, S. Reekmans, B. Hermans, J. van Stam, M. Gehlen, H. Berghmans, M. Berghmans, and M. Ameloot. Pure Appl. Chem. **67**, 157 (1995).
39. (*a*) P.P. Infelta, M. Grätzel, and J.K. Thomas. J. Phys. Chem. **78**, 190 (1974); (*b*) P.P. Infelta and M. Grätzel. J. Phys. Chem. **78**, 5280 (1983).
40. (*a*) M. Tachiya. Chem. Phys. Lett. **33**, 289 (1975); (*b*) J. Chem. Phys. **76**, 340 (1982); (*c*) J. Chem. Phys. **78**, 5282 (1983).
41. M. Almgren, J.-E. Löfroth, and J. van Stam. J. Phys. Chem. **90**, 4431 (1986).
42. M. Gehlen, M. Van der Auweraer, and F.C. De Schryver. Photochem. Photobiol. **54**, 613 (1991).
43. M. Gehlen, M. Van der Auweraer, and F.C. De Schryver. Langmuir, **8**, 64 (1992).
44. M. Almgren and J. Alsins. Prog. Colloid Polym. Sci. **74**, 55 (1987).
45. M. Almgren and J.-E. Löfroth. J. Chem. Phys. **76**, 2734 (1982).
46. G.G. Warr and F. Grieser. J. Chem. Soc. Faraday Trans. 1, **82**, 1813 (1986).
47. (*a*) M. Almgren, J. Alsins, E. Mukhtar, and J. van Stam. J. Phys. Chem. **92**, 4479 (1988); (*b*) *In* Reactions in compartmentalized liquids. *Edited by* W. Knoche and R. Schomäcker. Springer-Verlag, Berlin and Heidelberg. 1989. pp. 61–68.
48. J. van Stam and B. Medhage. Finn. Chem. Lett. **15**, 67 (1988).
49. (*a*) J.-E. Löfroth. Eur. Biophys. J. **13**, 45 (1985); (*b*) Anal. Instrum. **14**, 403 (1985).
50. (*a*) J.R. Knutson, J.M. Beechem, and L. Brand. Chem. Phys. Lett. **102**, 501 (1983); (*b*) J.M. Beechem, M. Ameloot, and L. Brand. Anal. Instrum. **14**, 379 (1985).
51. J. Brandrup and E.H. Immergut *(Editors)*. Polymer handbook. 3rd ed. John Wiley & Sons, New York. 1989.
52. S. Reekmans, M. Gehlen, F.C. De Schryver, N. Boens, and M. Van der Auweraer. Macromolecules, **26**, 687 (1993).
53. (*a*) J. Dederen, M. Van der Auweraer, and F.C. De Schryver. Chem. Phys. Lett. **68**, 451 (1979); (*b*) M. Van der Auweraer, J. Dederen, E. Geladé, and F.C. De Schryver. J. Chem. Phys. **74**, 1140 (1981).

Can. J. Chem. Downloaded from www.nrcresearchpress.com by 46.23.64.124 on 09/08/12
For personal use only.

Azo polymers for reversible optical storage. 8. The effect of polarity of the azobenzene groups

Mei-Sing Ho, A. Natansohn, C. Barrett, and P. Rochon

Abstract: Poly[4′-[[(2-methacryloyloxy)ethyl]ethylamino]azobenzene] (pMAEA) was prepared. Its reversible optical storage properties were studied and compared with the properties of previously reported poly[4-(2-methacryloyloxy)ethylazobenzene] (pMEA) and poly[4-nitrophenyl-4′-[[2-(methacryloyloxy)ethyl]ethylamino]phenyldiazene] (pDR1M). The effect of the dipole moment of the azobenzene moiety on the optical storage properties was studied by comparing the photochemically induced birefringence "writing" and "relaxation" behaviors. The writing and relaxation rates are both in the order pDR1M > pMAEA > pMEA. In addition, pDR1M, which contains donor/acceptor substituents in the azobenzene side chain, exhibits the highest saturation level of optically induced birefringence. The fraction of birefringence conserved after relaxation is lowest for pMEA, which has no donor/acceptor substituents in the azobenzene side chain, and highest for pDR1M.

Key words: polymers, azobenzene type, birefringence, photochemically induced orientation, reversible optical storage.

Résumé : On a preparé le poly[4′-[[(2-méthacryloyloxy)éthyl]éthylamino]azobenzène] (pMAEA). On a étudié ses propriétés d'emmagasinage optique réversible et on les a comparées avec celles des poly[4-(2-méthacryloyloxy)éthylazobenzène] (pMEA) et poly[4-nitrophényl-4′-[[2-(méthacryloyloxy)éthyl]éthylamino]-phényldiazène] (pDR1M). On a étudié l'effet du moment dipolaire de la portion azobenzène sur les propriétés d'emmagasinage optique en comparant les comportements à l'«écriture» et à la «relaxation» de la biréfringence photochimiquement induite. Les vitesses dans les modes écriture et relaxation sont dans chaque cas dans l'ordre pDR1M > pMAEA > pMEA. De plus, le pDR1M, qui contient des substituants donneur/accepteur dans la chaîne latérale, présente le niveau de saturation de biréfringence optiquement induite le plus élevé. La fraction de la biréfringence qui est conservée après relaxation est le plus élevé avec le pDR1M et le plus faible avec le pMEA qui ne porte pas de substituants donneur/accepteur dans la chaîne latérale de l'azobenzène.

Mots clés : polymères, type azobenzène, biréfringence, orientation photochimiquement induite, emmagasinage optique réversible.

[Traduit par la rédaction]

Introduction

Azo polymers are attracting much attention because of their potential use in various optical applications (1). In previous publications, we have demonstrated that stable birefringence can be optically induced in amorphous polymer thin films (2–7). The mechanism postulated for optically induced birefringence is related to the *trans–cis–trans* isomerization of the azobenzene group. A series of *trans–cis–trans* isomerization cycles is accompanied by the movement of the rigid azo groups and eventually creates an excess of azo groups oriented perpendicular to the laser polarization direction. This dichroism produces a measurable birefringence. Circularly polarized light restores the initial disordered state of the azo groups. According to Rau (8), azo compounds can be divided into three classes: azobenzene type, aminoazobenzene type, and pseudo-stibene type. Azobenzenes with electron donor and electron acceptor substituents (pseudo-stilbene type) and aminoazobenzene-type molecules isomerize from the *cis* configuration back to the *trans* configuration very quickly at room temperature. However, the thermal *cis–trans* isomerization in azobenzene-type molecules is relatively slow, and it is even possible to isolate the *cis* isomer.

We are studying various aspects of the mechanism for the optically induced supramolecular organization and structure–properties relationship of the polymers. However, our previous studies have only focused on azo polymers with the pseudo-stilbenes (2–6) and azobenzene (7) type side chain. To have a better understanding of the mechanism and the requirements for achieving optically induced supramolecular orientation, it is important to explore the optical properties of polymers with the aminoazobenzene-type side chain. This paper presents the synthesis of an azo polymer that contains an

Received February 27, 1995.

This paper is dedicated to Professor J.E. (Jim) Guillet in recognition of his contributions to Canadian chemistry.

M.-S. Ho and A. Natansohn.[1] Department of Chemistry, Queen's University, Kingston, ON K7L 3N6, Canada.
C. Barrett, and P. Rochon. Department of Physics, Royal Military College, Kingston, ON K7K 5L0, Canada.

[1] Author to whom correspondence may be addressed. Telephone: (613) 545-2008. Fax: (613) 545-6669. E-mail: natansoh@qucdn.queensu.ca

Can. J. Chem. Downloaded from www.nrcresearchpress.com by 46.23.64.124 on 09/08/12
For personal use only.

Can. J. Chem. Downloaded from www.nrcresearchpress.com by 46.23.64.124 on 09/08/12
For personal use only.

Chart 1.

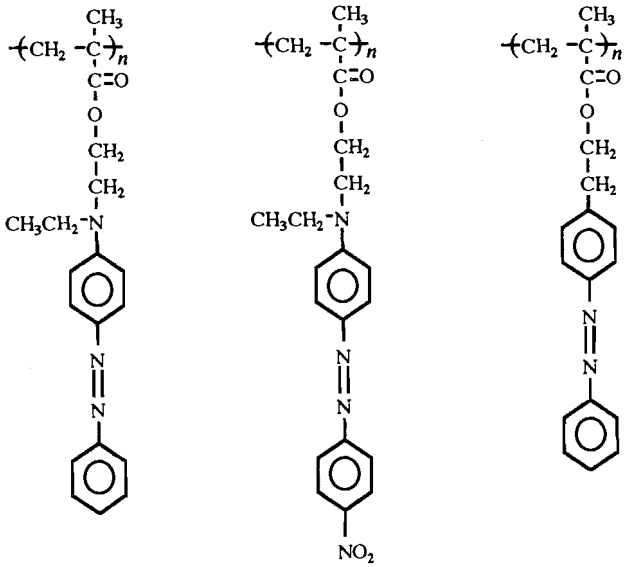

pMAEA pDR1M pMEA

aminoazobenzene-type group in the side chain. In addition, its optical properties are compared with two structurally similar azo polymers, pMEA (7) and pDR1M (9). The molecular structures of the three polymers compared are presented in Chart 1.

Experimental

The proton spectra were recorded on a Bruker AC-F 200 NMR spectrometer. UV absorption spectra were obtained from a Hewlett Packard 8452A diode array spectrophotometer. The molecular weight was obtained from a Waters Associates liquid chromatograph equipped with μ-Styragel columns and a R401 differential refractometer. The glass transition temperature (T_g) was obtained with a Mettler TA 3000 thermal analysis system equipped with a TC10A TA processor and a DSC30 head.

Monomer

4′-[[(2-Methacryloyloxy)ethyl]ethylamino]azobenzene (MAEA)

The monomer was prepared according to the synthetic scheme shown in Scheme 1. 4′-[[(2-Methacryloyloxy)ethyl]-ethylamino]azobenzene was obtained by reacting the corresponding alcohol with methacryloyl chloride. The 4′-[2-(hydroxy)ethyl)ethylamino]azobenzene was prepared by coupling the diazonium salt of aniline with 2-(*N*-ethylanilino)ethanol and the procedure is as follows.

Aniline (2.4 g, 0.025 mol) was dissolved in a solution of concentrated HCl (10 mL) in water (50 mL). The mixture was cooled in an ice bath until the temperature was below 4°C. Then a solution containing sodium nitrite (1.9 g, 0.027 mol) in water (20 mL) was added slowly to the aniline solution. The mixture was allowed to stir in the ice bath for 15 min. The resultant solution, which contained the diazonium salt, was added to a solution of 2-(*N*-ethylanilino)ethanol (4.2 g, 0.025 mol) in glacial acetic acid (10 mL) and water (20 mL). The mixture was stirred for 5 min in the ice bath and aqueous

Scheme 1.

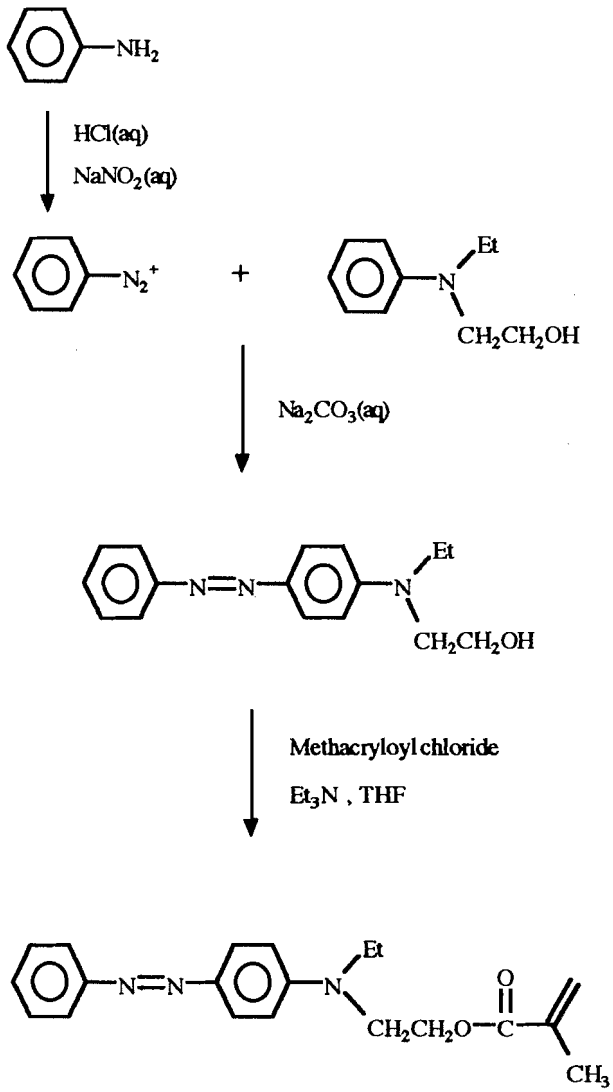

sodium carbonate solution was added to adjust the pH to ~6. The solid was filtered and air dried. The solid was recrystallized from ethanol–water mixture (3/2 by volume). Yield 4.5 g of 4′-[2-(hydroxy)ethyl)ethylamino]azobenzene (68%): mp 119–120°C. ^{1}H NMR($CDCL_3$), δ: 1.24(3H), 1.76(1H), 3.50(2H), 3.60(2H), 3.88(2H), 6.80(2H), 7.50(3H), 7.88(4H). Anal. calcd. for $C_{16}H_{19}N_3O$: C 71.35, H 7.11, N 15.60; found: C 71.53, H 7.29, N 15.58.

A solution of 4′-[2-(hydroxy)ethyl)ethylamino]azobenzene (5.4 g, 0.020 mol) and triethylamine (3.0 mL) was dissolved in THF (80 mL). The solution was kept in an ice bath for 10 min. A solution of distilled methacryloyl chloride (2.3 mL, 0.022 mol) in THF (20 mL) was added slowly to the above mixture. After the addition of methacryloyl chloride, the resultant mixture was stirred at room temperature overnight. The solvent was removed by rotary evaporation and the residue was washed with a solution of sodium carbonate (1.6 g) in water (100 mL). The product was extracted with diethyl ether and the solution was washed with water and dried over anhydrous sodium sulphate. The solvent was removed by rotary evaporation and the residue was purified by column chromatography

Can. J. Chem. Downloaded from www.nrcresearchpress.com by 46.23.64.124 on 09/08/12
For personal use only.

Fig. 1. UV–vis spectra of pMEA, pDR1M, and pMAEA polymer films.

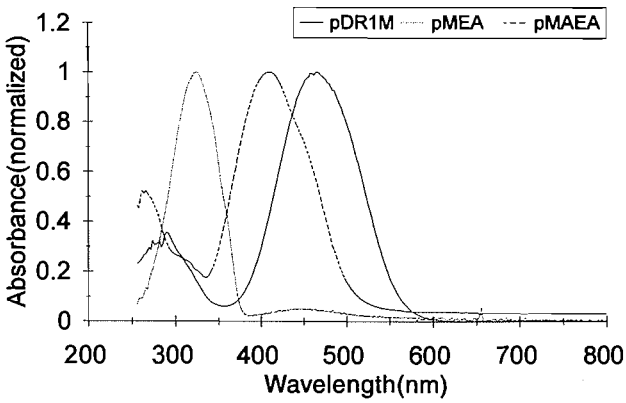

over silica gel and eluented with chloroform. Yield 5.0 g (74%) of 4′-[[(2-methacryloyloxy)ethyl]ethylamino]azobenzene as a red viscous liquid. ^{1}H NMR($CDCl_3$), δ: 1.24(3H), 1.95(3H), 3.55(2H), 3.72(2H), 4.38(2H), 5.60(1H), 6.12(1H), 6.80(2H), 7.50(3H), 7.88(4H). Anal. calcd. for $C_{20}H_{23}N_3O_2$: C 71.19, H 6.87, N 12.45; found: C 70.76, H 6.97, N 12.14.

Polymer

The polymerization of MAEA was carried out in dry toluene with 1% weight 2,2'-azobisisobutyronitrile (AIBN) as initiator. The monomer was allowed to polymerize under argon at 60°C for 2 days. The polymerization was stopped by pouring the reaction mixture into methanol. The polymer was redissolved in THF, precipitated again in methanol, and finally dried under vacuum. The yield was 60% and the polymer had a weight-average molecular weight of 41 000 (relative to polystyrene). From the DSC, the glass transition temperature was found to be 104°C for pMAEA. The preparations of pMEA (7) and pDR1M (9) have been reported previously.

Polymer films and optical studies

Thin films of the polymers were obtained by dissolving the polymers in THF and spin-coating onto clean glass slides. The films were allowed to dry and were subsequently heated above the T_g of the polymers. Relatively homogeneous thin films from 100 to 400 nm thickness were obtained by this procedure. Film thickness was determined by interferometry. Detailed procedures for the measurement of the optically induced birefringence (2–6) and thermal *cis–trans* isomerization rate (10) have been described previously.

Results and discussion

The UV–vis spectra for pMAEA, pDR1M, and pMEA films are shown in Fig. 1. The maximum absorbances (λ_{max}) are 410, 458, and 324 nm for pMAEA, pDR1M, and pMEA, respectively. The UV–vis spectrum of pMEA exhibits a high-intensity band in the UV region and the low-intensity band in the visible region corresponds to the absorption band of the cis isomer. These bands are characteristic for the "azobenzene" type in Rau's classification (8). The UV–vis spectra of pMAEA and pDR1M exhibit high-intensity bands in the visible region, which is characteristic for the "aminoazobenzene" and "pseudo-stilbene" types (8). In addition, the λ_{max} of the polymers suggests that the dipole moments of the *trans* isomers are in the order pDR1M > pMAEA > pMEA. The absorptivity values for pMEA, pMAEA, and pDR1M at 514 nm are 5.8×10^2 cm^{-1}, 3.5×10^3 cm^{-1} and 3.6×10^4 cm^{-1} respectively.

Fig. 2. Write–erase profile of optically induced and erased birefringence of pMAEA with laser beam at 488 nm. Time = 0 s: linearly polarized laser ON; time = 20 s: laser OFF; time = 45 s: circularly polarized laser ON.

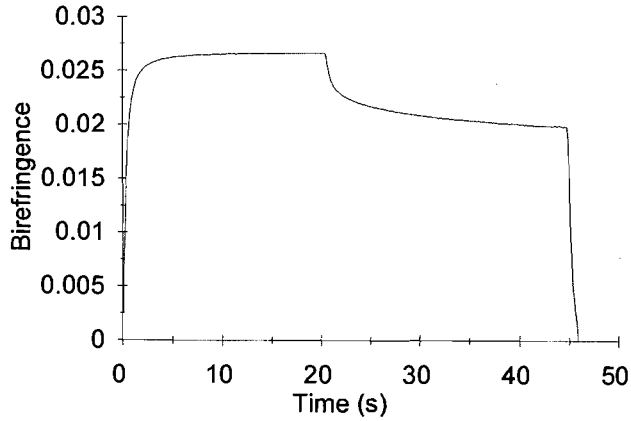

For the sake of consistency, a writing laser beam with a wavelength of 514 nm (0.7 W/cm^2) was used to induce birefringence in all the polymer films. Figure 2 shows a typical sequence of inducing and erasing birefringence for pMAEA. Birefringence is induced to a saturated level by a linearly polarized laser beam, and relaxation occurs when the laser beam is turned off at 20 s. As the circularly polarized laser beam is turned on at 45 s, the induced birefringence is "erased." Both pMEA (7) and pDR1M (9) exhibit similar write–erase profiles. The saturation levels of birefringence for pMEA, pMAEA, and pDR1M are 0.012, 0.026, and 0.103, respectively. This result suggests that the saturation level of birefringence follows the order of strength of the dipole moment of the azo group in the polymer. However, it has been observed that a polymer with nitrophenylazocarbazole in the side chain[2] exhibits a saturation level of birefringence as high as 0.09, although its λ_{max} (428 nm) is quite similar to pMAEA. This suggests that not only the dipole moment of the side group but also the presence of the nitro group may be important to achieve high induced birefringence. Since the maximum obtainable birefringence should depend on the interaction between the oriented dipoles (11), the presence of a lateral dipole can stabilize the local orientational ordering induced by the polarized laser beam. In fact, the presence of a terminal nitro group in liquid crystals was found to enhance the layered smectic phase (12).

The growth and relaxation of the optically induced birefringence can be quite well described by the biexponential functions [1] and [2], respectively. In fact, eq. [1] and [2] were found to give good fits to the growth and relaxation of the optically induced birefringence in other polymer systems (9).[2] To study the structural effect on the optical properties, data from the growth and relaxation of the optically induced birefringence were analyzed by eqs. [1] and [2], respectively. The fitting parameters obtained are summarized in Table 1.

[2] M.S. Ho, J. Paterson, C. Barrett, A. Natansohn, and P. Rochon. To be published.

Table 1. Parameters obtained by fitting the birefringence growth curves and decay curves to eqs. [1] and [2], respectively. Experiments were performed at room temperature.

Parameter	pMEA	pMAEA	pDR1M
k_a (s^{-1})	1.45 ± 0.01	3.10 ± 0.01	4.45 ± 0.02
k_b (s^{-1})	0.26 ± 0.01	0.54 ± 0.01	0.58 ± 0.01
$A \times (10^3)$	11.3 ± 0.1	22.3 ± 0.1	91.5 ± 0.2
$B \times (10^3)$	1.18 ± 0.07	4.20 ± 0.07	12.4 ± 0.2
A_n[a]	0.905	0.841	0.881
B_n[b]	0.095	0.159	0.119
k_c (s^{-1})	0.70 ± 0.01	1.68 ± 0.03	1.90 ± 0.09
k_d (s^{-1})	0.037 ± 0.001	0.095 ± 0.002	0.113 ± 0.004
$C \times 10^3$	2.35 ± 0.02	3.70 ± 0.03	7.53 ± 0.18
$D \times 10^3$	1.86 ± 0.01	3.46 ± 0.02	7.85 ± 0.08
$E \times 10^3$	8.41 ± 0.01	19.6 ± 0.1	84.1 ± 0.1
C_n[b]	0.186	0.138	0.08
D_n[b]	0.147	0.130	0.08
E_n[b]	0.667	0.732	0.84
α (cm^{-1})[c]	5.8×10^2	3.5×10^3	3.6×10^4
k_i (s^{-1})[d]	$(1.9 \times 10^{-4}) \pm (3 \times 10^{-5})$	0.53 ± 0.03	0.22 ± 0.01

[a] $A_n = A/(A + B)$; $B_n = B/(A + B)$.
[b] $C_n = C/(C + D + E)$; $D_n = D/(C + D + E)$; $E_n = E/(C + D + E)$.
[c] Absorptivity at 514 nm.
[d] Thermal *cis–trans* isomerization rate.

$$[1] \quad y = A(1 - \exp(-k_a t)) + B(1 - \exp(-k_b t))$$

$$[2] \quad y = C \exp(-k_c t) + D \exp(-k_d t) + E$$

The writing process involves an initial "fast" response mode and a "slow" response mode. The fast process is associated with the *trans–cis–trans* isomerization rates, with quantum yields, and with the local mobility of the azo group. Therefore, the fast process is controlled by the size of the azo group, the free volume around it, and the strength of the coupling interaction between the azo group and the polymer backbone. The slow process should be associated with the coupling interaction between the azo group and the polymer segments and with the mobility of the polymer segments. The parameter A in eq. [1] represents the contribution of the fast growth component with rate constant k_a. The parameter B represents the contribution of the slow growth component with rate constant k_b. Similarly, the relaxation process can be described by a "fast" mode and a "slow" mode, which are represented by the terms $C \exp(-k_c t)$ and $D \exp(-k_d t)$, respectively, in eq. [2]. In addition, the parameter E represents the induced birefringence conserved after relaxation.

Growth of the optically induced birefringence

Since k_a and k_b in Table 1 represent the rate constants for the fast and slow response modes, it is clear that pMEA has a slower writing response to the writing laser beam than pMAEA and pDR1M. For all three polymers, the parameter A indicates that the fast response mode contribution, which is related to the isomerization and reorientation of the chromophores, is the major component of the optically induced birefringence. The probability of an optical transition from *trans*-azobenzene to *cis*-azobenzene is proportional to $|\mu \cdot \boldsymbol{E}|^2$, where μ is the transition dipole moment and $\boldsymbol{E}$ is the electric field of the laser beam (13). Since the optically induced birefringence is created from the *trans–cis–trans* isomerization and reorientation of the azo moieties, it is expected that the rate of inducing birefringence will depend on the isomerization rate. For the same electric field, azo moieties with larger dipole moments would have a faster *trans–cis* isomerization rate and hence a faster rate of inducing birefringence. In addition, *trans–cis* isomerization rates also depend on the energy absorbed by the polymer film at the irradiation wavelength. The absorptivity of pMEA films at 514 nm is much lower than that of pDR1M and pMAEA, and most of the energy is absorbed by the *cis* isomers. Therefore, the *trans–cis* isomerization rate will be much lower in pMEA than in pDR1M and pMAEA. In spite of the low absorption at 514 nm, using a laser at this wavelength can photochemically activate the *cis–trans* isomerization, which otherwise would be very slow thermally (14) (see also Table 1). Therefore, pMEA can still give a reasonably fast response under these experimental conditions. Although the *trans–cis* and *cis–trans* isomerizations are both photochemically activated at the irradiating wavelength, a slower writing response for pMAEA than for pDR1M is observed. This discrepancy probably comes from the fact that pDR1M has a higher absorptivity and a larger dipole moment than pMAEA. As well as the rate of isomerization, the rate of inducing birefringence should also depend on the molecular associations among the chromophores. The molecular associations should be, in principle, more pronounced for polymers with stronger polar groups. For pDR1M, the donor/acceptor arrangement provides a large dipole, and the intra-chain and inter-chain interactions among these dipoles can create a local ordering that contributes to the observed induced birefringence.

Since it is proposed that the slow component in the writing process is related to the overall motion of the polymer matrix,

Can. J. Chem. Downloaded from www.nrcresearchpress.com by 46.23.64.124 on 09/08/12
For personal use only.

Can. J. Chem. Downloaded from www.nrcresearchpress.com by 46.23.64.124 on 09/08/12
For personal use only.

Table 2. The weight-average molecular weight (M_w), polydispersity index (M_w/M_n), and glass transition temperatures (T_g) of the polymers investigated.

Polymer	M_w	M_w/M_n	T_g (°C)
pMEA	70 000	2.2	80
pMAEA	41 000	2.2	104
pDR1M	9 000	1.8	116

its magnitude should be affected by the molecular weight and glass transition temperature of the polymer sample. It is expected that the higher the molecular weight and the glass transition temperature of a polymer, the more difficult such motions are. Among the three polymers, pMEA exhibits the lowest glass transition temperature and highest molecular weight (Table 2). Although k_b is not solely determined by the molecular weight, it appears that the high molecular weight of pMEA could be the reason for it having the smallest k_b among the three polymers studied. In spite of having the highest glass transition temperature, pDR1M exhibits the largest k_b. This result suggests that the low molecular weight of pDR1M would facilitate the mobility of the polymer matrix.

Relaxation of the induced birefringence

As shown in Table 1, the relaxation rates (k_c and k_d) also follow the order pDR1M > pMAEA > pMEA. Although the thermal *cis–trans* isomerization is expected to be involved in the relaxation processes, the relaxation rates are much faster than the thermal *cis–trans* isomerization rate for pMEA ($k_i = 1.9 \times 10^{-4}$ s^{-1}) (14). Therefore, the contribution of thermal *cis–trans* isomerization to the relaxation processes should be insignificant for pMEA; in this case the dipole reorientation and the relaxation of the polymer segments would be the major constituents in the relaxation processes. The situation is very different for pDR1M and pMAEA, since both polymers exhibit fast thermal *cis–trans* isomerization rates (Table 1), which would have a significant effect on the observed relaxation rates. In addition to the contribution from thermal *cis–trans* isomerization, one should also consider the effect of molecular association during the dipole reorientation. The effect of molecular association should be more pronounced for the azo group with a stronger dipole. Therefore, the effect of molecular association might account for the difference between the relaxation rates (k_c and k_d) of pMAEA and pDR1M. Similar to the writing process, the slow component in the relaxation process is also related to the overall mobility of the polymer matrix. As pointed out in the previous section, the overall mobility of the polymer matrix would be affected by the glass transition temperature and molecular weight of the polymer. The higher the molecular weight and glass transition temperature of a polymer, the more difficult such motions are. As shown in Table 1, pMEA, which exhibits the lowest glass transition temperature and highest molecular weight, has the smallest k_d among the three polymers. On the other hand, pDR1M, which exhibits the highest glass transition temperature and lowest molecular weight, has the largest k_d. This result agrees with the previous suggestion that the low molecular weight of pDR1M facilitates an increased mobility of the polymer matrix.

The parameter E in eq. [2] is time independent, thus it represents the birefringence conserved in the polymer film after relaxation. It is interesting to note that the fraction of induced birefringence remaining after relaxation is different for every polymer. The fractions of birefringence remaining after relaxation are 0.67, 0.73, and 0.84 for pMEA, pMAEA, and pDR1M, respectively. This result agrees with the suggestion that dipolar interactions are important in stabilizing the local ordering, as discussed in previous section. In addition, the fraction of birefringence remaining increases with the increase in glass transition temperature of the polymer. This observation is reasonable because the orientational ordering conserved in the polymer will depend on the difference between the operating temperature and the glass transition temperature.

Conclusion

The saturated levels of birefringence were found to increase with the increase in dipole moment of the azo moiety in the azo polymers. In addition, the fraction of birefringence conserved after relaxation also follows the same trend as the dipole moment and glass transition temperature. The writing and relaxation behaviors were found to be related to the dipole moment of the azo moiety, the glass transition temperature, and the molecular weight of the polymer. From a practical point of view, the azo moiety with donor/acceptor arrangement (pseudo-stilbene-type azobenzene) gives the best optical properties. The pseudo-stilbene-type azobenzene offers the advantages of fast *trans–cis–trans* isomerization and strong dipolar interactions, which are important for the optically induced ordering and stability.

Acknowledgment

Funding from the Office of Naval Research (U.S), the Natural Sciences and Engineering Research Council of Canada, and the Department of National Defense Canada is gratefully acknowledged.

References

1. S. Xie, A. Natansohn, and P. Rochon. Chem. Mater. **5**, 403 (1993).
2. P. Rochon, J. Gosselin, A. Natansohn, and S. Xie. Appl. Phys. Lett. **60**, 4 (1992).
3. A. Natansohn, P. Rochon, J. Gosselin, and S. Xie. Macromolecules, **25**, 2268 (1992).
4. A. Natansohn, S. Xie, and P. Rochon. Macromolecules, **25**, 5531 (1992).
5. P. Rochon, D. Bissonnette, A. Natansohn, and S. Xie. Appl. Opt. **32**, 7277 (1993).
6. A. Natansohn, P. Rochon, M. Pezolet, P. Audet, D. Brown, and S. To. Macromolecules, **27**, 2580 (1994).
7. A. Natansohn, P. Rochon, M.S. Ho, and C. Barrett. Macromolecules, **28**, 4179 (1995).
8. H. Rau. *In* Photochemistry and photophysics. Vol. II. *Edited by* J.F. Rabek. CRC Press, Boca Raton, Fla. 1990. Vol. II. pp. 119–141.
9. M.S. Ho, A. Natansohn, and P. Rochon. Macromolecules. In press.
10. C. Barrett, A. Natansohn, and P. Rochon. Macromolecules, **27**, 4781 (1994).
11. D. Brown, A. Natansohn, and P. Rochon. Macromolecules. In press.

12. M.S. Ho, B.M. Fung, and J.P. Bayle. Mol. Cryst. Liq. Cryst. **225**, 383 (1993).
13. U. Wiesner, M. Antonietti, C. Boeffel, and H.W. Spiess. Makromol. Chem. **191**, 2133 (1990).
14. C. Barrett, A. Natansohn, and P. Rochon. Chem. Mater. **7**, 899 (1995).

Can. J. Chem. Downloaded from www.nrcresearchpress.com by 46.23.64.124 on 09/08/12
For personal use only.

Reactive collisions in quadrupole cells. 6. H/D exchange reactions of protonated alkylbenzenes with D_2O, CH_3OD, and C_2H_5OD[1]

Jinsong Ni and Alex. G. Harrison

Can. J. Chem. Downloaded from www.nrcresearchpress.com by 46.23.64.124 on 09/08/12
For personal use only.

Abstract: The H/D exchange reactions occurring on collision of protonated alkylbenzenes with C_2H_5OD, CH_3OD, and D_2O at low collision energies in the quadrupole collision cell of a hybrid tandem mass spectrometer have been studied for 22 alkylbenzenes. The exchange reactions with D_2O are much less efficient than the exchange reactions with C_2H_5OD or CH_3OD; this difference is rationalized on energetics grounds. The H/D exchange of the protonated alkylbenzenes with C_2H_5OD or CH_3OD leads, typically, to 40–70% deuterium incorporation in the protonated alkylbenzene and, for most cases, to significant ion signals corresponding to exchange of the added hydrogen and the aromatic hydrogens. Thus, the method is a feasible approach to counting the number of aromatic hydrogens in alkylbenzenes. The extent of exchange decreases with increasing size of the alkyl group in monoalkylbenzenes for reasons that are not readily understood.

Key words: protonated alkylbenzenes, H/D exchange, reactive collisions.

Résumé : On a étudié les réactions d'échange H/D qui se produisent par collision d'alkylbenzènes protonés avec du C_2H_5OD, CH_3OD et D_2O, à de faibles énergies de collision dans la cellule de collision quadripolaire d'un spectromètre de masse hybride à tandem. Les réactions d'échange avec le D_2O sont beaucoup moins efficaces que les réactions d'échange avec le C_2H_5OH ou le CH_3OD; on rationalise cette différence sur la base des énergies. L'échange H/D des alkylbenzènes protonés avec le C_2H_5OD ou le CH_3OD conduit d'une façon typique à une incorporation de 40 à 70% de deutérium et, dans la plupart des cas, à des signaux ioniques significatifs correspondants à l'échange de l'hydrogène additionné et les hydrogènes aromatiques. Ainsi, il est possible d'utiliser cette méthode pour compter le nombre d'hydrogènes aromatiques dans les alkylbenzènes. Pour des raisons qui ne sont pas bien comprises, le taux d'échange diminue avec une augmentation de la grosseur du groupe alkyle des monoalkylbenzènes.

Mots clés : alkylbenzènes protonés, échange H/D, collisions réactives.

[Traduit par la rédaction]

Introduction

The exchange of hydrogen for deuterium in organic molecules has been widely used in structural studies by mass spectrometry (1, 2) and in mechanistic studies in gas-phase ion chemistry (3). This exchange has frequently been carried out in solution prior to admission of the sample or in the inlet system when the sample and a deuterium-containing reagent are mixed. Soon after the development of chemical ionization (CI) (4) it was clearly shown (5, 6) that H/D exchange reactions can occur in the ion source of the mass spectrometer under CI conditions. The simplest of these exchange processes involves the exchange of all the labile hydrogens in a molecule using a deuterated reagent gas such as D_2O, CH_3OD, or ND_3 (5–14). It also has been shown that protonated aromatic hydrocarbons exchange the aromatic hydrogens when D_2O, CH_3OD, or C_2H_5OD are used as chemical ionization reagents (15–19) and such exchange reactions have been developed into a method for identifying alkyl aromatic isomers (18, 19).

More recently, there has been an interest in separating the ionization event from the isotopic exchange event using tandem mass spectrometry. In this approach ions produced by any ionization means are mass-selected and react with a deuterium-containing reagent gas at low collision energies in a suitable gas-phase collision cell. Using a triple quadrupole mass spectrometer, Ranasinghe et al. (20) showed that the number of active hydrogens in a variety of aromatic compounds could be determined from the mass shift that occurred when the protonated species, formed by CI, was allowed to collide with ND_3 at low collision energies in the quadrupole collision cell. Dookeran and Harrison (21) have carried out a more detailed study of the H/D exchange reactions of protonated aromatic amines with ND_3 in the quadrupole collision

Received February 17, 1995.

This paper is dedicated to Professor J.E. (Jim) Guillet in recognition of his contributions to Canadian chemistry.

J. Ni[2] **and A.G. Harrison.**[3] Department of Chemistry, University of Toronto, Toronto, ON M5S 1A1, Canada.

[1] Taken, in part, from the Ph.D. Thesis of J. Ni, University of Toronto, 1994.

[2] Present Address: Department of Medicinal Chemistry, University of Utah, Salt Lake City, Utah.

[3] Telephone: (416) 978-3577. Fax: (416) 978-8775.

Can. J. Chem. Downloaded from www.nrcresearchpress.com by 46.23.64.124 on 09/08/12
For personal use only.

cell of a hybrid tandem BEqQ (see experimental section) mass spectrometer. The H/D exchange reactions of protonated peptides with ND_3 at low collision energies in the collision cell of a tandem four-sector mass spectrometer have been studied by Cheng and Fenselau (22) while the exchange reactions of protonated peptides with CD_3OD have been investigated by Gard et al. (23) using ion cyclotron resonance (ICR) techniques. The H/D exchange reactions of protonated amino acids and peptides with ND_3 in the quadrupole collision cell of a hybrid tandem mass spectrometer also have been studied (24). Nourse et al. (25) have obtained some distinction among methylguanine isomers from the rate and extent of H/D exchange of mass-selected MH^+ ions with D_2O in a Fourier transform mass spectrometer. In the negative ion mode, Ni and Harrison (26) have shown that the number of enolic hydrogens in enolate ions can be counted from the H/D exchange of the enolate ions with CH_3OD or C_2H_5OD in the quadrupole collision cell of a tandem hybrid BEqQ mass spectrometer. Chan and Enke (27) have shown that the $[M - H]^-$ ions of the three dichlorobenzenes give distinctive H/D exchange patterns on reaction with D_2O or ND_3 in the collision cell of a triple quadrupole mass spectrometer.

Of particular relevance to the present work is the report by Stone (28) of a study of the H/D exchange reactions of protonated aromatic hydrocarbons with D_2O and CD_3OD in the quadrupole collision cell of a triple quadrupole mass spectrometer. In general, rather little exchange was observed, suggesting that the tandem mass spectrometric approach was clearly inferior to the chemical ionization approach (19, 20) to counting hydrogens in aromatic hydrocarbons. The present study presents a detailed study of the H/D exchange reactions of protonated aromatic hydrocarbons with D_2O, CH_3OD, and C_2H_5OD and presents a more optimistic evaluation of the tandem mass spectrometric approach to counting the aromatic hydrogens in alkylbenzenes.

Experimental

All experimental work was carried out using a VG Analytical ZAB-2FQ hybrid BEqQ mass spectrometer, which has been described in detail previously (29). Briefly, this instrument is a reversed-geometry (BE) double-focussing mass spectrometer that is followed by a deceleration lens system, an r.f.-only quadrupole collision cell (q), and a quadrupole mass analyzer (Q). The appropriate MH^+ ions were mass-selected by the BE double-focussing mass spectrometer at 6 keV ion energy, decelerated to a kinetic energy of 3 eV (laboratory scale), and introduced into the quadrupole collision cell, which contained C_2H_5OD, CH_3OD, or D_2O at an indicated pressure of 3×10^{-5} Torr (1 Torr = 133.3 Pa) as read by the ionization gauge attached to the pumping line leading from the quadrupole stage. It is estimated that the actual pressure in the collision cell is 100–1000 times the indicated pressure. The reaction products were analyzed by the final quadrupole mass spectrometer; the resulting mass spectra were accumulated on a multi-channel analyzer with, typically, 25–50 2-s scans being accumulated.

The incident ion kinetic energy and the pressure of reactant gas in the collision cell are the two major parameters that determine the extent of H/D exchange. Earlier studies (21, 24, 26) have shown that incident ion energies in the range of 1–5 eV (laboratory scale) give a reasonable extent of exchange with higher ion energies affording better sensitivity because of greater transmission of the incident ion beam; the present experiments were carried out at 3 eV incident ion energy. The method used to establish this ion energy in a reproducible fashion has been presented in detail previously (21, 26). The rate of H/D exchange of the protonated alkylbenzenes was found to be comparable to that of the enolate ions studied previously (26) with the result that we used the maximum indicated pressures (3×10^{-5} Torr) of deuterated reagent gas that were attainable with the existing experimental configuration. This pressure is about a factor of 10 higher than was used for the exchange of the labile hydrogens of protonated aromatic amines (21) or protonated amino acids (24) with ND_3. Since the ionization cross section is expected to be greatest for C_2H_5OD and least for D_2O (30), the use of the same indicated pressure means that the actual collision cell pressure was least for the alcohol and greatest for D_2O; despite the higher D_2O pressure the exchange with D_2O was the least efficient, as discussed below.

The MH^+ ions of the alkylbenzenes were produced by Brønsted acid chemical ionization using CH_4 as the reagent gas. The EI/CI source was operated in the CI mode at 200°C and an ionizing electron energy of 100 eV. The alkylbenzenes were introduced through a heated inlet system while the CH_4 was introduced through the CI reagent gas inlet. All chemicals were obtained from Aldrich Chemical Co. and were used as received. The listed isotopic purities of the deuterium-containing reagents were D_2O (99.9 at.% D), CH_3OD (99.5 at.% D), and C_2H_5OD (99.5 at.% D).

Results and discussion

The results obtained for the exchange of 22 protonated alkylbenzenes with C_2H_5OD, CH_3OD, and D_2O are presented in Tables 1–3. The final column of each table records the extent of exchange expressed as the percent deuterium incorporation (% D.I.) defined as

$$[1] \quad \%\ \text{D.I.} = \left(\sum_{r=0}^{n-1} r I_r / n \sum_{r=0}^{n-1} I_r \right) \times 100$$

where n is the number of peaks in the cluster (including the unexchanged MH^+ ion) and I_r is the relative intensity for the peak containing r deuterium atoms. The relative ion signals were reproducible to within 10% from day to day.

With either C_2H_5OD or CH_3OD as exchange gas, the extent of exchange was sufficient that, in most cases, one observed an appreciable ion signal corresponding to exchange of the hydrogen added in the ionization step plus all the hydrogens bonded to the aromatic ring. The extent of exchange with D_2O was considerably less; the reasons for this will be discussed below. For the protonated C_4-alkylbenzenes reacting with C_2H_5OD, peaks were observed that suggest exchange of more hydrogens than the aromatic hydrogens and the hydrogen added in the ionization step. Thus, for the protonated diethylbenzenes and methylpropylbenzene, where one would expect $d_5[MH]^+$ as the most highly exchanged ion signal, weak signals were observed that corresponded, nominally, to ions containing six, seven, and eight deuteriums. These appear to be the cluster ions $(C_2H_5OD)_2(C_2H_5OH)H^+$, $(C_2H_5OD)_3H^+$, and

Can. J. Chem. Downloaded from www.nrcresearchpress.com by 46.23.64.124 on 09/08/12
For personal use only.

Table 1. H/D exchange of protonated alkylbenzenes with C_2H_5OD.

Compound	$d_x[MH]^+$ (% of base peak)									
	d_0	d_1	d_2	d_3	d_4	d_5	d_6	d_7	d_8	%D.I.
Toluene	4	19	47	79	95	100	52	1	2	65
o-Xylene	14	13	42	91	100	25				56
m-Xylene	12	13	48	98	100	24				62
p-Xylene	17	18	49	98	100	24				61
Ethylbenzene	28	35	55	83	100	72	36	4	6	56
1,2,3-Trimethylbenzene	32	37	71	100	71					61
1,2,4-Trimethylbenzene	30	35	69	100	71					62
Mesitylene	19	30	67	100	77					66
n-Propylbenzene	94	56	84	100	100	32	10	6	8	40
o-Methylethylbenzene	24	20	52	100	99	20				58
m-Methylethylbenzene	23	19	49	96	100	21				59
p-Methylethylbenzene	17	16	48	97	100	22				61
i-Propylbenzene	24	100	36	11	5	3	1			23
1,2,3,4-Tetramethylbenzene	53	78	100	53						51
1,2,3,5-Tetramethylbenzene	56	78	100	54						51
o-Diethylbenzene	28	62	91	100	53	10	8	12	7	47
m-Diethylbenzene	46	59	84	100	55	11	9	15	9	45
p-Diethylbenzene	89	56	85	100	56	11	9	13	9	41
p-Methylpropylbenzene	100	45	50	42	16	3	3	5	3	27
n-Butylbenzene	51	100	68	25	10	7	13	17	10	28
s-Butylbenzene	63	100	39	20	11	5	8	9	6	24
i-Butylbenzene	52	100	51	28	15	2	7	8	4	26

Table 2. H/D exchange of protonated alkylbenzenes with CH_3OD.

Compound	$d_x[MH]^+$ (% of base peak)							
	d_0	d_1	d_2	d_3	d_4	d_5	d_6	%D.I.
Toluene	1	4	11	35	78	100	58	75
o-Xylene	4	14	47	100	99	25		63
m-Xylene	16	14	49	100	93	22		60
p-Xylene	20	15	47	100	99	25		61
Ethylbenzene	25	17	26	61	100	99	52	64
1,2,3-Trimethylbenzene	25	23	59	100	76			66
1,2,4-Trimethylbenzene	26	22	59	100	75			66
Mesitylene	22	23	60	100	75			66
n-Propylbenzene	58	33	63	100	96	32	19	46
o-Methylethylbenzene	44	14	38	91	100	23		57
m-Methylethylbenzene	23	13	38	91	100	23		61
p-Methylethylbenzene	30	14	38	91	100	24		60
i-Propylbenzene	100	16	22	48	53	17	5	34
1,2,3,4-Tetramethylbenzene	58	44	100	97				60
1,2,3,5-Tetramethylbenzene	43	45	100	97				63
o-Diethylbenzene	41	23	57	100	87	21		54
m-Diethylbenzene	35	15	38	88	100	24		58
p-Diethylbenzene	49	16	38	88	100	25		56
p-Methylpropylbenzene	100	19	26	51	51	14		38
n-Butylbenzene	100	21	16	22	24	24	15	32
s-Butylbenzene	100	22	15	18	14	9	6	22
i-Butylbenzene	100	23	14	17	15	16	11	26

Table 3. H/D exchange of protonated alkylbenzenes with D_2O.

Compound	$d_x[MH]^+$ (% of base peak)							
	d_0	d_1	d_2	d_3	d_4	d_5	d_6	%D.I.
Toluene	45	100	99	62	21	7	1	30
o-Xylene	47	100	92	58	20	4		41
m-Xylene	79	100	91	55	19	4		39
p-Xylene	97	100	81	46	14	2		27
Ethylbenzene	53	100	66	39	16	5		26
1,2,3-Trimethylbenzene	100	87	55	24	6			27
1,2,4-Trimethylbenzene	100	84	51	23	5			26
Mesitylene	100	74	41	17	4			24
n-Propylbenzene	100	78	38	20	7	2		17
o-Methylethylbenzene	100	90	57	25	8			22
m-Methylethylbenzene	83	100	69	32	9			25
p-Methylethylbenzene	100	96	64	31	9			24
i-Propylbenzene	86	100	33	16	8	3		18
1,2,3,4-Tetramethylbenzene	100	59	24	7				22
1,2,3,5-Tetramethylbenzene	100	49	19	5				20
o-Diethylbenzene	100	54	26	9	3			15
m-Diethylbenzene	100	87	49	20	6			21
p-Diethylbenzene	100	65	45	18	4			19
p-Methylpropylbenzene	100	47	23	9	4			15
n-Butylbenzene	100	76	26	11	5			14
s-Butylbenzene	100	53	17	7	4			11
i-Butylbenzene	100	65	23	10	5			13

$(C_2H_5OD)_3D^+$, arising either by endothermic proton transfer to C_2H_5OD followed by exchange and clustering at the pressures existing in the collision cell or by the reaction sequence

[2] $ArH^+ + ROD \rightarrow Ar \text{ --- } H^+O(D)R$

[3] $Ar \text{ --- } H^+O(D)R + ROD \rightarrow Ar + (ROD)_2H^+$

followed by further clustering. Both reactions [2] and [3] are likely to be exothermic. For the protonated butylbenzenes it is not clear whether the apparent $d_6[MH]^+$ ion signal is a totally exchanged aromatic species or is an ethanol cluster ion; consequently, this ion signal was not included in the evaluation of the % D.I. values. Similar weak interference ions (not included in the table) were observed in the reaction of protonated toluene with CH_3OD and corresponded to $(CH_3OD)_3H^+$ and $(CH_3OD)_3D^+$ (these species are isobaric with $d_7[MH]^+$ and $d_8[MH]^+$). Such cluster ions were generally observed for both the alcohol systems but only in a limited number of cases do they create uncertainty as to the number of exchangeable hydrogens. As Hawthorne and Miller (18) have noted in CI studies, the use of CH_3OD as the exchange gas gives lower mass cluster ions and affords fewer interferences. Unexpectedly, weak signals corresponding, nominally, to $d_7[MH]^+$ and $d_8[MH]^+$ also were observed in the exchange of the MH^+ ion of toluene, ethylbenzene, and *n*-propylbenzene with C_2H_5OD. The origin of these ion signals is not clear.

The extent of exchange we have observed is considerably greater than that reported by Stone (28). For the reaction of protonated toluene, the protonated xylenes, and protonated mesitylene with CD_3OD, Stone's results correspond to percent deuterium incorporations in the range 6–14% while we observe 60–70% deuterium incorporation on reaction of the protonated species with CH_3OD. Stone also reported that protonated i-propylbenzene was unreactive with CD_3OD while we observe 34% deuterium incorporation on reaction with CH_3OD. With D_2O as the collision gas, Stone's data give 2–4% deuterium incorporation in the protonated xylenes compared to the present values of 30–40%. Since the extent of exchange depends on a number of parameters such as pressure and incident ion energy, the exact origin of these differences is difficult to establish. Stone's results were reported for a nominal collision energy of 0 eV, however, he later noted (private communication, 1993) that it was necessary to apply a bias of +10 V to the quadrupole collision cell to reduce the primary ion beam intensity to zero, indicating that the incident ion energy in the "0" eV collisions was higher than supposed. It has been shown in this laboratory (24, 26) that the extent of deuterium incorporation decreases markedly with increasing incident ion energy and it is likely that the differences between the present data and those of Stone (28) arise, in part, from differences in the incident ion energy.

Hawthorne and Miller (18) have reported a detailed study of the exchange reactions of alkylbenzenes with CH_3OD under chemical ionization (CI) conditions and it is of interest to compare the present results with their data. In their study the MD^+ ion is formed in the initial ionization step and it is this species that subsequently undergoes gas-phase H/D exchange reactions with CH_3OD. From their data one can calculate the percent deuterium incorporation in the MD^+ ion. These % D.I. figures are comparable to ours with two exceptions. Hawthorne and Miller (18) reported that *meta*-substituted alkylbenzenes showed distinctly less exchange than the *ortho* or *para* isomers. Thus, from their data one obtains the following

Can. J. Chem. Downloaded from www.nrcresearchpress.com by 46.23.64.124 on 09/08/12
For personal use only.

Can. J. Chem. Downloaded from www.nrcresearchpress.com by 46.23.64.124 on 09/08/12
For personal use only.

% D.I. values: *o*-xylene (73), *m*-xylene (58), *p*-xylene (75), 1,2,3-trimethylbenzene (57), 1,2,4-trimethylbenzene (60), mesitylene (29). In contrast, we observe similar extents of exchange for the three xylenes and for the three trimethylbenzenes not only with CH_3OD reagent gas but also with C_2H_5OD and with D_2O as reagent gases.

On the other hand we do observe a significant decrease in the extent of H/D exchange for monoalkylbenzenes as the size of the alkyl group increases. Thus, with C_2H_5OD as the reagent gas, we observe 65% D.I. for protonated toluene, 56% D.I. for protonated ethylbenzene, 40% D.I. for protonated *n*-propylbenzene, 23% D.I. for protonated i-propylbenzene and 24–28% D.I. for the protonated butylbenzenes. A similar decrease with increasing alkyl group size also is observed when CH_3OD is the reagent gas. Such a decrease of extent of exchange with increasing alkyl group size was not observed by Hawthorne and Miller (18) using CH_3OD CI. In their work *n*-hexyl and *n*-pentyl benzene showed similar extents of exchange as the propyl benzenes and all showed a greater extent of exchange than ethylbenzene. The effect of the alkyl group size in the present work is not a mass effect since the protonated trimethylbenzenes and protonated methylethylbenzenes show considerably higher % D.I. values than do the protonated propyl benzenes, while the protonated tetramethylbenzenes and diethylbenzenes show a much greater extent of exchange than do the protonated butylbenzenes. (It might be noted, in passing, that the exchange reactions of protonated *tert*-butylbenzene could not be studied because of the low intensity of MH^+ in the CH_4 CI mass spectrum (31).

There is substantial evidence (17, 32, 33) that H/D exchange occurs by the general mechanism shown in Scheme 1 for a

Scheme 1.

$$MH_n^+ + DOR \rightarrow MH_n^+ \cdots DOR \rightarrow MH_{n-1} \cdots HDOR^+$$

$$\downarrow$$

$$MH_{n-1}D^+ + HOR \leftarrow MH_{n-1}D^+ \cdots HOR$$

species with *n* interchangeable hydrogens interacting with ROD. An essential requirement is that proton transfer from MH_n^+ to ROD be endothermic, otherwise simple proton transfer will occur. A plausible potential energy surface for exchange is shown in Fig. 1. The energy of the intermediate $[MH_{n-1} \cdots HDOR^+]$, relative to the separated species MH_{n-1} + $RODH^+$, is determined by the strength of the ion/neutral interaction. If this interaction energy is less than the difference in the energy between MH_{n-1} + $RODH^+$ and MH_n^+ + ROD, which is given by the difference in proton affinities of MH_{n-1} and ROD, the intermediate $[MH_{n-1} \cdots HDOR^+]$ will not be accessible for thermal energy reactants and H/D exchange will not occur. Table 4 lists the proton affinities of C_2H_5OH, CH_3OH, H_2O, and those alkylbenzenes for which proton affinities have been recorded (34). As these data show, proton transfer from a protonated alkylbenzene to H_2O (D_2O) is 23 kcal mol^{-1} (toluene) to 34 kcal mol^{-1} (mesitylene) endothermic. Since the bonding energy in the $[MH_{n-1} \cdots HD_2O^+]$ complex is likely to be less than 20 kcal mol^{-1}, it is not surprising that H/D exchange of protonated alkylbenzenes with D_2O is inefficient. Only reactants with excess energy should be able to surmount the central energy barrier. On the other hand, proton transfer from protonated alkylbenzenes to CH_3OH (CH_3OD) is 8–19 kcal mol^{-1} endothermic and to C_2H_5OH (C_2H_5OD) is 2–12 kcal mol^{-1} endothermic. Thus, for these systems, the $[MH_{n-1} \cdots HDOR^+]$ complex should be accessible and H/D exchange should occur relatively efficiently.

Fig. 1. Schematic potential energy surface for H/D exchange between MH_n^+ and ROD.

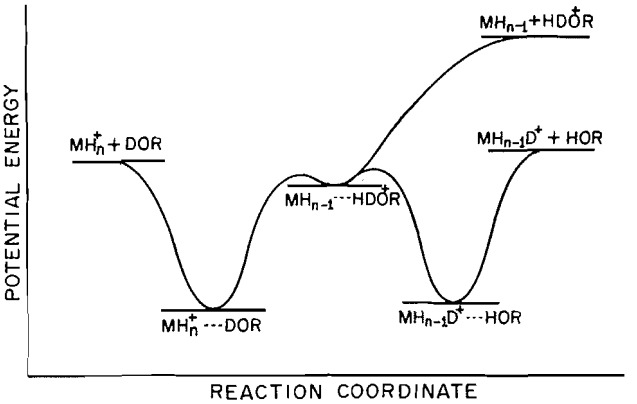

Table 4. Some proton affinities (kcal mol^{-1}).

Compound	Proton affinity[a]
Water	167
Methanol	182
Ethanol	188
Toluene	190
Ethylbenzene	192
n-Propylbenzene	192
i-Propylbenzene	192
n-Butylbenzene	192
o-Xylene	193
m-Xylene	196
p-Xylene	192
Mesitylene	201

[a]From ref. 34.

The energetics argument cannot rationalize the relatively poorer exchange of the larger monalkylbenzenes. However, to exchange all aromatic hydrogens it is necessary that all ring positions be sampled, either by a hydrogen ring walk (35) in the protonated species or by interaction of the $HDOR^+$ moiety in the intermediate complex with all different positions of the aromatic ring. Although it is known (35) that hydrogen randomization by the ring walk mechanism is relatively facile for protonated benzene, toluene, and the xylenes, it is possible that hydrogen randomization becomes less facile as the size of the alkyl group increases. This could arise if the charge site is localized through ion – induced dipole interactions with the more readily polarized larger alkyl groups. It is not clear why similar effects of alkyl group size were not observed by Hawthorne and Miller.

Acknowledgements

The authors are indebted to the Natural Sciences and Engineering Research Council of Canada for financial support and to Professor J.A. Stone for helpful discussions.

References

1. K. Biemann. Mass spectrometry: organic chemical applications. McGraw–Hill, New York. 1962. Chap. 5.

2. H. Budzikiewicz, C. Djerassi, and D.H. Williams. Structure elucidation of natural products by mass spectrometry. Vol. 1. Holden Day, San Francisco, Calif. 1964. Chap. 2.
3. J.L. Holmes. *In* Mass spectrometry. *Edited by* A. Maccoll. Int. Rev. Sci. Phys. Chem., Ser. Two, Butterworth, London. 1975–1976.
4. M.S.B. Munson and F.H. Field. J. Am. Chem. Soc. **88**, 2621 (1966).
5. D.F. Hunt, C.N. McEwen, and R.A. Upham. Tetrahedron Lett. 4539 (1971).
6. D.F. Hunt, C.N. McEwen, and R.A. Upham. Anal. Chem. **44**, 1292 (1972).
7. W. Blum, E. Schrumpf, J.G. Liehr, and W. Richter. Tetrahedron Lett. 565 (1975).
8. Y.Y. Lin and L.L. Smith. Biomed. Mass Spectrom. **6**, 15 (1979).
9. M.V. Buchanan. Anal. Chem. **54**, 570 (1982).
10. M.V. Buchanan. Anal. Chem. **56**, 546 (1984).
11. K.P. Madhusudanan, K. Sachdev, D.A. Harrison, and D.K. Kulshreshtha. Int. J. Mass Spectrom. Ion Phys. **62**, 289 (1984).
12. R.-H. Liu, L.A. Low, F.P. Smith, E.G. Piotrowski, and A.-F. Hsu. Org. Mass Spectrom. **20**, 511 (1985).
13. D.J. Miller and S.B. Hawthorne. Fuel, **68**, 105 (1989).
14. A. Guarini, G. Guglielmetti, N. Andriollo, and M. Vincenti. Anal. Chem. **64**, 204 (1992).
15. B.S. Freiser, R.L. Woodlin, and J.L. Beauchamp. J. Am. Chem. Soc. **97**, 6895 (1975).
16. D.P. Martinson and S.E. Buttrill. Org. Mass Spectrom. **11**, 762 (1976).
17. D.F. Hunt and S.K. Sethi. J. Am. Chem. Soc. **102**, 6953 (1980).
18. S.B. Hawthorne and D.J. Miller. Anal. Chem. **57**, 694 (1985).
19. D.J. Miller and S.B. Hawthorne. *In* Novel techniques in fossil fuel mass spectrometry. ASTM STP 1019. *Edited by* T.R. Ashe and K.W. Wood. Am. Soc. Testing Materials, Philadelphia, Pa. 1989.
20. A. Ranasinghe, R.G. Cooks, and S.K. Sethi. Org. Mass Spectrom. **27**, 77 (1992).
21. N.N. Dookeran and A.G. Harrison. J. Am. Soc. Mass Spectrom. **6**, 19 (1995).
22. X. Cheng and C. Fenselau. Int. J. Mass Spectrom. Ion Processes, **122**, 109 (1992).
23. E. Gard, M.K. Green, J. Bregar, and C.B. Lebrilla. J. Am. Soc. Mass Spectrom. **5**, 623 (1994).
24. N.N. Dookeran and A.G. Harrison. J. Mass Spectrom. **30**, 666 (1995).
25. B.D. Nourse, R.L. Hettich, and M.V. Buchanan. J. Am. Soc. Mass Spectrom. **4**, 109 (1993).
26. J. Ni and A.G. Harrison. J. Am. Soc. Mass Spectrom. **3**, 853 (1992).
27. S. Chan and C.G. Enke. J. Am. Soc. Mass Spectrom. **5**, 282 (1994).
28. J.A. Stone. Org. Mass Spectrom. **28**, 1119 (1993).
29. A.G. Harrison, R.S. Mercer, E.J. Reiner, A.B. Young, R.K. Boyd, R.E. March, and C.J. Porter. Int. J. Mass Spectrom. Ion Processes, **74**, 13 (1986).
30. A.G. Harrison, E.G. Jones, S.K. Gupta, and G.P. Nagy. Can. J. Chem. **44**, 1967 (1966).
31. J.A. Herman and A.G. Harrison. Org. Mass Spectrom. **16**, 423 (1981).
32. J.I. Brauman. *In* Kinetics of ion molecule reactions. *Edited by* P. Ausloos. Plenum Press, New York. 1979.
33. A.G. Harrison. Chemical ionization mass spectrometry. 2nd. ed. CRC Press, Inc., Boca Raton, Fla. 1992.
34. S.G. Lias, J.L. Liebman, and R.D. Levin. J. Phys. Chem. Ref. Data, **13**, 695 (1984).
35. D. Kuck. Mass Spectrom. Rev. **9**, 583 (1990).

Can. J. Chem. Downloaded from www.nrcresearchpress.com by 46.23.64.124 on 09/08/12
For personal use only.

The reaction of some *endo*-5-acetyl norborn-2-enes with benzene thiol: a thermally induced non-allylic [1,3]-acetyl shift, as anticipated by a photochemical precedent

Johannes Leitich, Ingeborg Heise, and Kurt Schaffner

Can. J. Chem. Downloaded from www.nrcresearchpress.com by 46.23.64.124 on 09/08/12
For personal use only.

Abstract: The thermal reaction of benzene thiol with *rac*-1-(4a*S**,5*R**,8*S**,8a*R**-5,8-methano-1,2,3,4,4a,5,8,8a-octahydro-4a-naphthyl)ethanone (**10***b*), an *endo*-5-acetylnorborn-2-ene with a particularly close distance between one olefinic carbon and the keto carbon, and with its 8a*S** epimer **10***a*, has been investigated. Besides the conventional unrearranged adducts **16***a*, *b* and **17***a*, *b* of the thiol to the C=C bonds of **10***a*, *b*, an adduct **18** was formed from **10***b* that involved a [1,3]-acetyl shift; no other products were formed. The dependence of adduct ratios on thiol concentration is consistent with two competing reactions of an intermediate radical **14***b* formed by addition of thiyl radical to the C=C bond of **10***b*, namely, abstraction of hydrogen from thiol (which is the conventional reaction path) vs. intramolecular attack of the radical on the keto group inducing the [1,3] shift of the latter. This shift constitutes an intramolecular variety of the known alkyl transposition reaction of ketones initiated by a reversible attack of an alkyl radical on a keto carbonyl group to generate an intermediate *tert*-alkoxyl radical; however, it is very much faster than the intermolecular reaction and corresponds to an effective molarity between 10^7 and 10^{10}. These findings have a bearing on the mechanism of photorearrangements homologous to the ODPM (oxa-di-π-methane) photorearrangement, such as ODPE (oxa-di-π-ethane) and higher homologues, in that they support a two-step mechanism involving this type of acyl shift.

Key words: oxadi-π-methane photorearrangement; oxadi-π-ethane photorearrangement; acetyl shift, non-allylic [1,3]; thiol, addition to C=C bonds; norbornenes.

Résumé : On a étudié la réaction thermique du benzènethiol avec le *rac*-1-(4a*S**,5*R**,8*S**,8a*R**-5,8-méthano-1,2,3,4,4a,5,8,8a-octahydro-4a-naphtyl)éthanone (**10***b*), un *endo*-5-acétylnorborn-2-ène comportant une distance particulièrement courte entre le carbone oléfinique et le carbone cétonique, ainsi qu'avec son épimère 8a*S**, **10***a*. En plus des adduits conventionnels non réarrangés (**16***a* et *b* et **17***a* et *b*) du thiol sur les doubles liaisons C=C des produits **10***a* et *b*, il se forme un adduit **18** à partir du produit **10***b* qui implique un déplacement [1,3] d'acétyle; il ne se forme aucun autre produit. La relation entre les rapports d'adduits et la concentration en thiol est en accord avec l'existence de deux réactions en compétition d'un intermédiaire radicalaire **14***b* qui se formerait par l'addition du radical thiyle sur la double liaison C=C du composé **10***b*, à savoir l'enlèvement d'un hydrogène à partir du thiol (qui est le chemin réactionnel normal) vs. une attaque intramoléculaire du radical sur le groupe cétonique induisant un déplacement [1,3] de ce dernier. Ce déplacement constitue une variété intramoléculaire de la réaction de transposition connue des groupes alkyles des cétones initiées par une attaque réversible d'un radical alkyle sur un groupe carbonyle d'une cétone pour générer un intermédiaire radicalaire *tert*-alkoxyle; toutefois, il est beaucoup plus rapide que celui de la réaction intermoléculaire et il correspond à une molarité effective intermédiaire entre 10^7 et 10^{10}. Puisqu'ils offrent un support pour un mécanisme à deux étapes impliquant ce type de déplacements de groupes acyles, les résultats obtenus ont une relation avec le mécanisme des photoréarrangements homologues du photoréarrangement ODPM (oxa-di-π-méthane), comme les réarrangements ODPE (oxa-di-π-éthane) et ceux de leurs homologues supérieurs.

Mots clés : photoréarrangement oxadi-π-méthane, photoréarrangement oxadi-π-éthane, déplacement non allylique [1,3] d'acétyle, addition de thiol sur des liaisons C=C, norbornènes.

[Traduit par la rédaction]

Received March 31, 1995.

This paper is dedicated to Professor J.E. (Jim) Guillet in recognition of his contributions to Canadian chemistry.

J. Leitich, I. Heise, and K. Schaffner.[1] Max-Planck-Institut für Strahlenchemie, Postfach 101365, D-45413 Mülheim an der Ruhr, Germany.

[1] Author to whom correspondence may be addressed. Telephone: +49 208 306 3612. Fax: +49 208 306 3952.

Can. J. Chem. Downloaded from www.nrcresearchpress.com by 46.23.64.124 on 09/08/12
For personal use only.

Scheme 1.

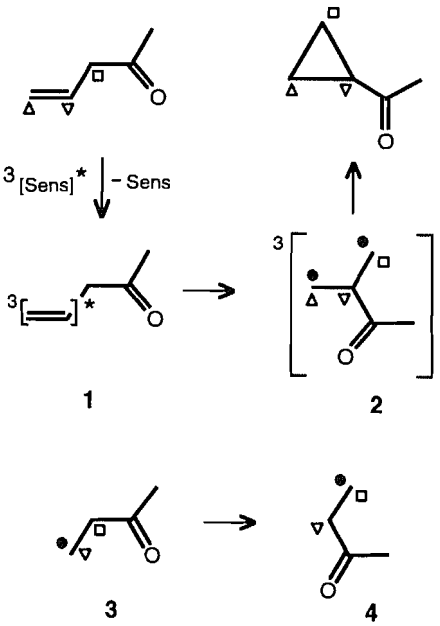

Background: ODPM- and free-radical-induced [1,2]-acyl shifts

The rearrangement of many β,γ-unsaturated ketones to give, via [1,2]-migration of an acyl (i.e., alkylketo) moiety, α-cyclopropyl ketones ("oxa-di-π-methane" (ODPM) rearrangement, Scheme 1) is a well-known photoreaction (for reviews, see ref. 1). It is most frequently encountered in triplet sensitization, and in the context of the present work we shall refer to the triplet-sensitized reaction only. Evidence has been obtained for a reactive state **1** that is characterized by $^3(\pi, \pi^*)$ excitation residing predominantly in the olefinic moiety of the unsaturated ketone (2). Stereochemical evidence suggests the intermediacy of the triplet 1,3-diradical **2** (3). In the case of systems with isolated olefinic double bonds, the ODPM rearrangement has been found to be efficient only when the olefinic double bond is part of a ring that constrains the double bond into planarity and thus prevents it from adopting, in its $^3(\pi, \pi^*)$ state, the energetically more favourable and, presumably, shorter lived perpendicular conformation (1).

Recently, Caldwell et al. presented evidence that perpendicular $^3(\pi, \pi^*)$ states of some typical olefins are quite accurately described as 1,2-diradicals (4), in view of both their heats of formation (4*a*) and of their reactivity (4*b*). If an olefinic double bond formed part of a ring that constrained it into planarity, the heat of formation of its triplet state was found to be higher than expected for a 1,2-diradical by several kcal/mol (4*a*) and its reactions faster by one order of magnitude or more (for simplicity, we shall call this difference the "non-perpendicularity effect"), but qualitatively its reactivity still resembled that of a (bi)radical (4*b*). This immediately links the [1,2]-acyl migration step **1** → **2** (ODPM) to the well-known [1,2]-acyl migration **3** → **4**, which is observed in monoradicals derived from dialkyl ketones and for which, in two cases, first-order rate constants and Arrhenius parameters have been measured (5). The step **1** → **2** can thus be viewed as being essentially a migration **3** → **4** with its rate being strongly enhanced by the non-perpendicularity effect.

Norborn-2-en-5-one (**6**) may serve as an example for which both bonds of [1,2]-acyl shifts have been described (Scheme 2). Firstly, **6** gives ODPM efficiently (6). Secondly, the free radical **7** formed by addition of benzene thiyl radical to the C=C bond of **6** gives the free-radical-induced [1,2]-acyl shift. Thiols are known to add across C=C bonds via a free-radical chain mechanism involving reversible addition of a thiyl radical to the C=C bond to give a carbon-centered radical that subsequently abstracts hydrogen from thiol to give the final addition product, thereby regenerating the thiyl radical (7, 8). Thus, norbornene with benzene thiol (PhSH) reacts exothermally after an induction period to form exclusively the *exo* adduct **5** (8, 9). In the case of **6**, reaction with benzene thiol gives, besides the two regioisomeric unrearranged *exo* adducts analogous to **5**, the rearranged adduct **9**, which clearly results from the intermediate **7** by a [1,2]-acyl shift to give **8** before hydrogen abstraction. As the product ratios are independent of thiol concentration (0.1–4.5 M), the establishment of an equilibrium between **7** and **8** before hydrogen abstraction has been inferred (10).

Introduction

We recently described norbornene systems undergoing "oxa-di-π-ethane" (ODPE) photorearrangements (11). These are homologous to the ODPM photorearrangements. They are encountered with γ,δ- rather than β,γ-unsaturated ketones, and they undergo a [1,3]- rather than a [1,2]-acyl migration, leading ultimately to α-cyclobutyl rather than to α-cyclopropyl ketones (**10** → **12**, Scheme 3). The excited state characteristics of the ODPE also resemble those of the ODPM rearrangements in that ODPE occurs preferentially on triplet sensitization of the olefinic double bond, whereas the excitation of the carbonyl group by direct irradiation tends to give rise to a different photochemistry. This led us to conjecture a mechanism of the triplet-sensitized ODPE, shown in Scheme 3, analogous to that of the ODPM rearrangement shown in Scheme 1, and hence led us to formulate the rearrangement step ^{3}**10*** → **11**.

If this conjecture is correct, the monoradical **14** (Scheme 4) formed by addition of benzene thiyl radical to **10** might be expected to show a hitherto unobserved thermal nonallylic [1,3]-acyl migration, for reasons outlined above and in full analogy to the case of **6**. To test this, we chose two substrates, **10***a* and **10***b*, which differ in the stereochemistry of the fusion of a cyclohexane to the norbornene skeleton. Both substrates give ODPE, but **10***b* does so much more efficiently than **10***a* (11). The presumed reason for this is a twofold effect of the *trans* ring fusion in **10***b*: firstly, it exerts an extra strain that is relieved on acetyl migration, and secondly, it places the acetyl group closer to the C=C bond. Thus, the distance between the carbonyl C-atom to which it forms the new bond is 2.8 Å for **10***a* (according to models (12, 13)) but only 2.59 Å for **10***b* (by X-ray crystallography; R. Goddard and C. Krüger, personal communication). In either case, *a* or *b*, the thiol-induced acetyl migration would be anticipated to be much slower than the ODPE-induced migration because the latter would be accelerated by the non-perpendicularity effect.

Results and discussion

Heating a 1:1 molar mixture of **10***a* and benzene thiol, either neat or 0.2 M in acetonitrile and at complete or partial conver-

Can. J. Chem. Downloaded from www.nrcresearchpress.com by 46.23.64.124 on 09/08/12
For personal use only.

Scheme 2.

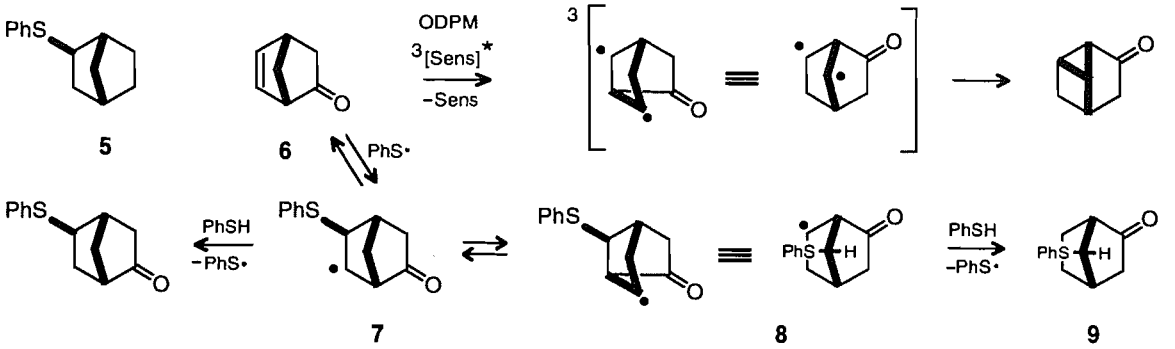

Scheme 3.

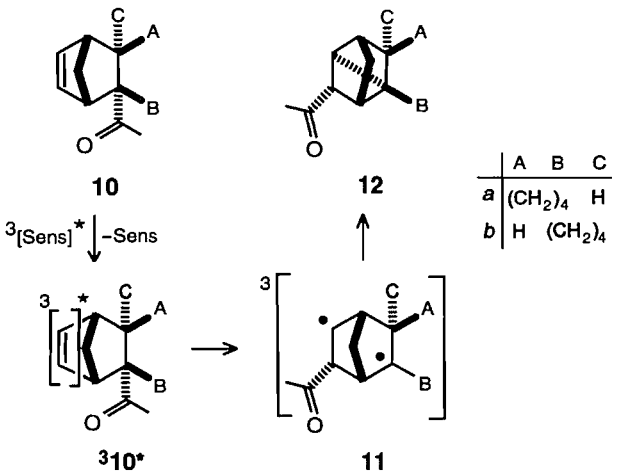

Scheme 4.

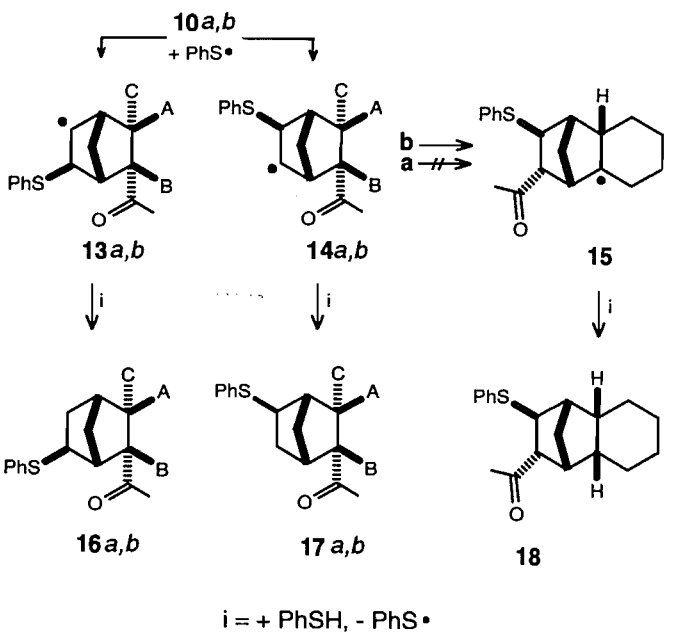

sion, gave a 1:2 mixture of the two unrearranged *exo* addition products **16***a* and **17***a* and no indication of acetyl migration (Scheme 4). With **10***b*, however, a rearranged addition product of structure **18** was obtained, as well as a mixture of the two

Scheme 5.

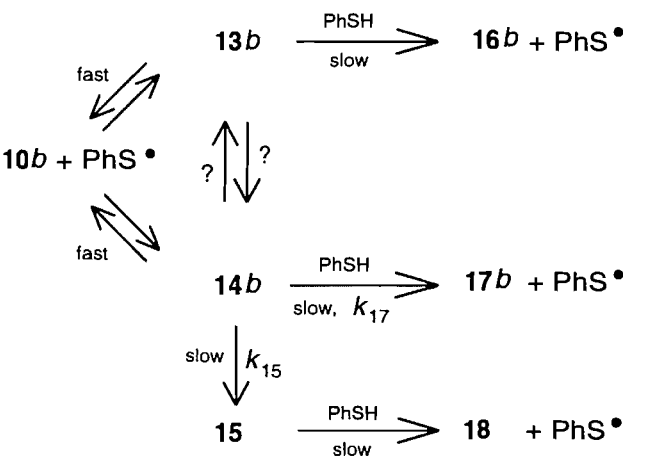

unrearranged *exo* addition products **16***b* and **17***b*. **18** obviously arose from **14***b* via the anticipated [1,3]-acetyl migration to give the radical **15**, which then abstracted hydrogen from benzene thiol on the *exo* side of the norbornane moiety. The product ratio [**17***b*]/[**18**] varied proportionally to [PhSH] and thus covered a range of 0.1–0.8 (see Table 1). The product ratio [**16***b*]/[**17***b*], on the other hand, did not change significantly with [PhSH] under the same conditions and amounted to 1.97 ± 0.27 (95% probability level). These findings are consistent with a reaction scheme (Scheme 5) that features: (*a*) a competition between the rearrangement **14***b* → **15** and the reaction of **14***b* with PhSH to give **17***b*; (*b*) a fast equilibration between radicals **13***b* and **14***b* before further reaction, probably by fast addition/elimination of PhS˙ (7, 8), although a direct interconversion **13***b* ⇆ **14***b* cannot be ruled out. The irreversibility of the rearrangement **14***b* → **15**, which contrasts to the reversibility **7** ⇆ **8**, is in line with the strain release on going from **14***b* to **15**, and the difference in the rearrangement propensity between *a* and *b* conforms with the relative ODPE behaviour of **10***a* vs. **10***b*.

As can be derived from Scheme 5, the value of 0.28 ± 0.06 M^{-1} for [**17***b*][**18**]$^{-1}$[PhSH]$_{av}^{-1}$ at 60°C (95% probability level; Table 1) can be equated to the ratio of the rate constants, k_{17}/k_{15}, of the two competing reactions of **14***b*. Assuming k_{17} to be equal to the rate constant for hydrogen abstraction from PhSH by isopropyl radical at 60°C, 1.4 × 10^8 M^{-1} s^{-1} (14), one obtains an estimate for k_{15} at 60°C of 5 × 10^8 s^{-1}. The analogous rate constant for **14***a* is estimated at <10^7 s^{-1}. If the first-order decay constant of ^{3}**10***b** to give **10***b* were tentatively

Table 1. Analytical runs: product ratios obtained from 0.105 mmol **10***b* with varied concentrations of benzene thiol in CD_3CN, 2 h at 60°C.

$[PhSH]_0$[a] M	Conversion of **10***b*, %	$[PhSH]_{av}$[b] M	$\frac{[17b]}{[18]}$	$\frac{[17b]}{[18][PhSH]_{av}}$	$\frac{[16b]}{[17b]}$
0.357	48.6	0.309	0.093	0.302	2.14
0.498	72.4	0.428	0.134	0.313	1.97
0.498	53.9	0.446	0.131	0.294	2.00
1.04	75.0	0.962	0.244	0.254	2.03
1.77	59.3	1.71	0.439	0.257	1.96
3.27	44.3	3.23	0.880	0.273	1.91
3.27	47.0	3.23	0.793	0.246	1.78
				0.277 ± 0.064[c]	1.97 ± 0.27[c]

[a]Initial concentration.
[b]Concentration average over the reaction time.
[c]Probability level = 95%.

taken to be similar to that of its parent olefin, norbornene, i.e. $(250\ ns)^{-1} = 4 \times 10^6\ s^{-1}$ (15), the value for k_{15} of $5 \times 10^8\ s^{-1}$ could indeed have predicted the highly efficient ODPE rearrangement of ^{3}**10***b** via the mechanism of Scheme 3, even without invoking the acceleration by the non-perpendicularity effect.

One conceivable mechanism for the rearrangement **14***b* → **15** would involve elimination of acetyl radical from **14***b* with simultaneous ring closure to form a cyclopropane, followed by ring-opening attack of the acetyl radical on the cyclopropane, to give **15**. To check this possibility, we studied the behaviour of quadricyclane (tetracyclo[3.2.0.$0^{2,7}$.$0^{4,6}$]heptane, a model compound for the putative cyclopropane intermediate) towards acetyl radical generated from acetaldehyde in a radical chain reaction (16). For conditions under which norbornene cleanly added acetaldehyde in such a radical chain reaction to give *exo*-2-acetyl norbornane (as described previously in ref. 17), quadricyclane remained unchanged. Hence, any reaction of acetyl radical with quadricyclane must be much slower than diffusion controlled. Since our putative cyclopropane intermediate would liberate less strain energy on ring opening than would quadricyclane and hence would be expected to react even less readily with acetyl radical than the latter, this finding effectively rules out the envisaged mechanism for the rearrangement **14***b* → **15** as the reaction products comprise only **16***b*, **17***b*, and **18** but no acetyl-free compound. For the ODPE rearrangement **10** → **12**, also, such a mechanism can be excluded since it would be expected to lead preferentially not to **12** but instead to an isomer of **12** containing a cyclopropane ring. As a consequence, there remains no reasonable mechanism for the rearrangement **14***b* → **15** other than via the bridged structure **19** (Scheme 6; R = PhS); analogously, ^{3}**10***b** → **11***b* must proceed via **19** (R = ·). Thus, the rearrangement **14***b* → **15** is an intramolecular variety of the known free-radical alkyl displacement reaction of ketones (18) of which Scheme 6 shows one example (19).

The rate constant of ca. $5 \times 10^8\ s^{-1}$ at 60°C for **14***b* → **15**, however, is much higher than that of the reaction shown in Scheme 6, $\log_{10}(kMs) = (7.5 \pm 0.5) - (11\ 500 \pm 1100)/4.576T$ (19), which corresponds to a pseudo-first-order rate constant in acetone at 60°C of 0.6–180 s^{-1}. Hence, the effective concentration of **14***b* amounts to an impressive 10^7–10^{10} M. This again emphasizes the importance of a short distance between the bond-forming carbon atoms and (or) of molecular strain acting as a driving force. The role of **19** as an intermediate or a transition state parallels that of **20** (rather than an acyl radical – olefin geminate pair) in the [1,2]-acyl shifts (5*b*) and in the ODPM rearrangements (1). Moreover, one may anticipate [1,*n*]-acyl shifts with $n > 3$ via species homologous to **19** provided the conditions of close distance plus favourable relative orbital orientation plus favourable thermodynamics be fulfilled. Indeed, one case of an "oxa-di-π-propane" photorearrangement, homologous to both ODPM and ODPE and featuring a [1,4]-acyl shift, was described as early as 1977 (20). Molecular models of the unsaturated ketone giving this rearrangement confirm the close distance and favourable orbital orientation between the carbonyl C-atom and the olefinic C-atom to which it forms the new bond; they bring to light a prohibitively unfavourable and inflexible relative orientation (pointing away from each other) of those two orbitals that are to form the second new C—C bond. This argues against the concerted mechanism suggested by Hayakawa et al. (20) but is perfectly in line with a two-step mechanism analogous to Schemes 1 and 3.

Scheme 6.

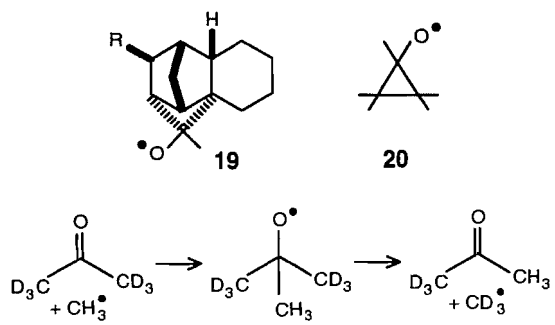

Elucidation of molecular structures

Of each new compound, the following NMR spectra were obtained: 400 MHz ^{1}H, 100 MHz ^{13}C (Broad Band decoupled

Can. J. Chem. Downloaded from www.nrcresearchpress.com by 46.23.64.124 on 09/08/12
For personal use only.

Can. J. Chem. Downloaded from www.nrcresearchpress.com by 46.23.64.124 on 09/08/12
For personal use only.

(BB) and Distortionless Enhancement by Polarization Transfer (DEPT)), and $^1H/^{13}C$ Correlation Spectroscopy (CH-COSY). Moreover, $^1H/^1H$ spin–spin decoupling and $^1H/^1H$ NOE (Nuclear Overhauser Effect) experiments were carried out whenever instructive. These NMR spectroscopic data, together with IR, UV, the analytical data, and base-catalyzed H/D exchange experiments, sufficed to derived the complete molecular structures of all new compounds independently of each other. This includes also the compounds mentioned below. The structural work was facilitated by the following empirically established NMR assignments (13, 21): Firstly, one particular NMR pattern common to all new compounds, namely, a CH_2 group showing a geminal $J_{H,H}$ value of 8.5–10.5 Hz, each of the two hydrogen atoms being further coupled weakly (1.4–1.8 Hz) to two methine hydrogen atoms that show a mutual coupling of 1.1–1.7 Hz. This feature is characteristic of the bridge $-CH_a.CH_2.CH_b-$ in norborn(a,e)nes. Secondly, values of 2–5 Hz and 0–1 Hz, respectively, which are characteristic for $^3J_{HH}$ of norborn(a,e)ne bridgehead protons with norborn(a,e)ne *exo* and *endo* protons, respectively. Thirdly, a characteristic long-range coupling of 1.5–3.5 Hz between norborn(a,e)ne *endo* protons and the one norborn(a,e)ne methano-bridge proton that is *anti* relative to them.

The following chemical transformations starting from **18** bear out the molecular structure of **18** as derived spectroscopically.

With stoichiometric amounts of strong base, **18** readily eliminated benzene thiol to give **21** (Scheme 7). This reaction occurred even with the traces of alkali present in commercial silica gel. With less than stoichiometric amounts of strong base, the remaining excess of **18** was recovered unchanged. In contrast to benzene thiol, sodium benzene thiolate in methanol left **10***b* unchanged. The latter two facts preclude the possibility of a catalytic conversion of **10***b* to **21** with benzene thiol plus base.

Compound **21** was also not entirely stable to alkali, but it added methanol under the influence of catalytic amounts of sodium methoxide to give at first a 7:3 equilibrium mixture of **21** and **24**. Much more slowly under the same conditions, this mixture changed into a 7:3:3 equilibrium mixture of **21**, **24**, and **25** (^1H NMR analysis). The latter mixture was also obtained starting from pure **25**. The formation of these secondary products in the preparation of **21** from **18** was avoided by the use of an excess of silver oxide as the base.

Both **23** (obtained by irradiation of **12***b* (11)) and **21** cleanly gave the same product, **22**, on catalytic hydrogenation. Catalytic amounts of sodium methoxide in methanol epimerized **22** to 98% **26**.

In perdeuterio methanol as a solvent, catalytic amounts of sodium methoxide exchanged the α-carbonyl *exo* methine protons of **22** and **24** for deuterons within minutes, whereas the exchange of the corresponding *endo* methine protons of **25** and **26** required many hours. In the case of compound **18**, benzene thiol elimination was even faster than proton exchange, which means that in alkaline media every enolate anion formed eliminated thiolate much faster than it was reprotonated.

Scheme 7.

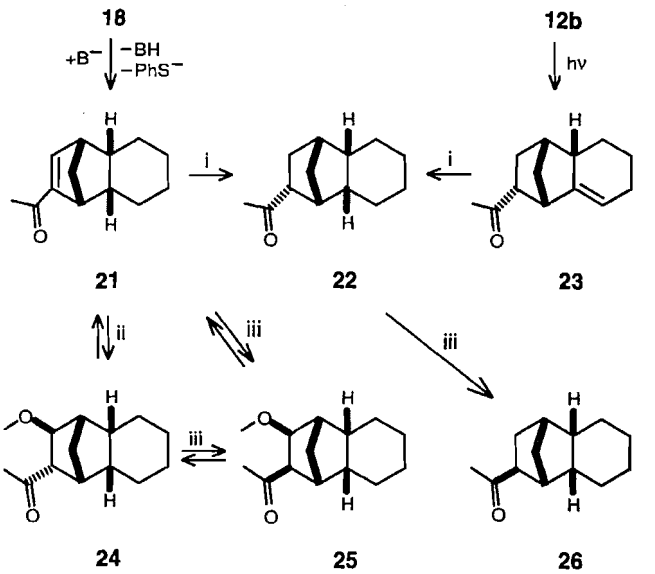

i = H_2/ Pd
ii = CH_3ONa / CH_3OH, fast
iii = CH_3ONa / CH_3OH, slow

Experimental

Instrumentation, general methods, and materials. General remarks

For NMR spectroscopy, the instruments and software were obtained from Bruker GmbH: for quantitative analyses of product mixtures, WH-270; all other measurements on AM-400. All spectra are in $CDCl_3$. In the following, δ values are given relative to internal tetramethylsilane (TMS) and apparent coupling constants are in Hz. "α" and "β" subscripts to H-atoms refer to *syn* and *anti* arrangements, respectively, relative to the norbornane methano bridge, in compliance with existing rules for nomenclature. This bridge is assigned the position number 9. The subscripts "a" and "b" of its H-atoms refer to *anti* and *syn* arrangements, respectively, relative to the unbridged cyclohexane ring. NOE enhancements are not mentioned if found between geminal or strongly coupled vicinal protons. UV spectra (in *n*-hexane) were recorded on an Omega-10 spectrophotometer (Bruins Instruments, Munich). IR spectra were obtained on a Perkin–Elmer 580 spectrophotometer. Electron impact mass spectra were obtained on a Finnigan MAT 8200 instrument using 70 eV electrons. Melting points were determined on a Kofler hot stage and are uncorrected. Elemental analyses were performed by H. Kolbe (formerly: Dornis u. Kolbe), Mülheim a.d. Ruhr. C, H, and S (where applicable) analyses were obtained for all new compounds; the maximum deviation was 0.26%, the average deviation was 0.11%.

Preparative chromatographic separations were carried out over silica gel 0.04–0.063 mm (Merck) with *n*-pentane, followed by *n*-pentane + 1% ether as the eluent. All solvents were technical grade and were redistilled before use. Benzene thiol was a commercial product whose purity, in particular the absence of diphenyl disulfide, was checked by ^1H NMR.

rac-*1-(1*R*,3*S*,4*R*,4a*S*,8a*R*-1,4-Methano-3-phenylthio-decahydro-4a-naphthyl)ethanone (**16**a) and* rac-*1-(1*S*,2*R*,4*S*,4a*R*,8a*R*-1,4-methano-2-phenylthio-decahydro-4a-naphthyl)ethanone (**17**a)*

A mixture of 200 mg (1.05 mmol) **10***a* (11) and 150 mg (1.36

Can. J. Chem. Downloaded from www.nrcresearchpress.com by 46.23.64.124 on 09/08/12
For personal use only.

mmol) benzene thiol was heated at 90°C for 22 h. Chromatography over 70 g absorbent eluted crystalline fractions, 23 mg diphenyl disulfide (mp 52–58°C), 90 mg (28.5%) **16***a*, and 177 mg (56%) **17***a*, in this order.

16*a*: mp 72–73°C (from pentane at −23°C). UV, λ_{max} (log ε): 259 (3.67), 282 (sh), 294 nm (sh). IR (KBr): 1692 cm^{-1}. ^1H NMR: 7.38 (bd; 8 Hz; 2 phenyl *o*-H), 7.2–7.3 (m; 3 phenyl H), 2.88 (ddd; 8.2, 4.2, 2.2 Hz; 3-H), 2.23 (ddd; 12.5, 6.0, 1.6 Hz; 8a-H), 2.11 (q; 3 × 1.4 Hz; 4-H), 1.94 (dq; 4.6, 3 × 1.5 Hz; 1-H), 1.75–1.85 (m; *endo*-2-H, 2 9-H), 1.78 (s; CH_3), 1.5–1.65 (m; 1 CH_2), 1.41–1.49 (m; 3 methylene H), 1.38 (ddd; 13.0, 4.6, 4.2 Hz; *exo*-2-H), 1.20 (m; 1 methylene H), 0.95–1.08 m; 2 methylene H). NOE enhancements: 1-H/8a-H, *endo*-2-H/8a-H, 3-H/4-H, 3-H/8a-H, 3-H/phenyl *o*-H, 4-H/phenyl *o*-H, 4-H/methyl-H, phenyl *o*-H/methyl-H. ^{13}C NMR: 212.5 (C═O), 136.0 (quat. phenyl C), 132.3 (2 phenyl *o*-C), 128.8 (2 phenyl *m*-C), 127.1 (phenyl *p*-C), 61.4 (C-4a), 51.5 (C-4), 47.0 (C-3), 43.3 (C-1), 40.5 (C-8a), 38.0 (C-2), 32.3 (C-9), 26.0 (methyl-C), 25.9, 24.0, 17.8, 16.8 (C-5 through C-8). MS, *m/e*: 300 (10%, M^+), 191 (54%), 176 (100%), 43 (97%).

17*a*: mp 117–118°C (from diethyl ether – pentane at −23°C). UV, λ_{max} (log ε): 257.4 (3.96), 276 (sh), 284 (sh), 294 nm (sh). IR (KBr): 1695 cm^{-1}. ^1H NMR: 7.25 (m; 4 phenyl H), 7.14 (m; phenyl *p*-H), 3.19 (ddd: 8.2, 4.8, 1.8 Hz; 2-H), 2.33 (ddd; 12.7, 5.7, 1.7 Hz; 8a-H), 2.22 (dq; 4.2, 3 × 1.5 Hz; 4-H), 2.11 (s; CH_3), 1.94 (q; 3 × 1.5 Hz; 1-H), 1.85 (ddq; 10.5, 2.6, 3 × 1.5 Hz; 9-H_b), 1.69 (dq; 10.5, 3 × 1.5 Hz; 9-H_a), 1.68 and 1.65 (m; 2 5-H), 1.62 (ddd; 13.8, 8.2, 2.6 Hz; *endo*-3-H), 1.41–1.55 (m; 3 methylene H), 1.34 (ddd; 13.8, 4.8, 4.2 Hz; *exo*-3-H), 1.21, 1.10, 1.04 (m; 3 methylene H). NOE enhancements: 1-H/2-H, 1-H/8a-H, 1-H/phenyl *o*-H, 2-H/8a-H, 2-H/phenyl *o*-H, *endo*-3-H/4-H, 4-H/methyl-H, 5-H/methyl-H, 8-H_α/9-H_b. ^{13}C NMR: 212.2 (C═O), 137.0 (quat. phenyl C), 129.0 (2 phenyl C), 128.7 (2 phenyl C), 125.6 (phenyl *p*-C), 60.6 (C-4a), 49.0 (C-1), 46.8 (C-2), 45.7 (C-4), 40.6 (C-8a), 34.6 (C-3), 32.7 (C-9), 26.1 (methyl-C), 25.7, 23.9, 17.8, 16.9 (C-5 through C-8). MS, *m/e*: 300 (36%, M^+), 191 (63%), 43 (100%).

rac-*1-(1*R**,3*S**,4*R**,4a*S**,8a*S**-1,4-Methano-3-phenylthiodecahydro-4a-naphthyl)ethanone (**16**b) and* rac-*1-(1*S**,2*R**,4*S**,4a*R**,8a*S**-1,4-methano-2-phenylthiodecahydro-4a-naphthyl)ethanone (**17**b)*

10*b* (200 mg, 1.05 mmol) (11) and benzene thiol (127 mg, 1.15 mmol) were mixed at room temperature, whereupon the mixture warmed spontaneously. After 24 h at room temperature, chromatography over 150 g absorbent eluted 15 mg unidentified material, 147 mg (46.5%) **16***b*, 26 mg mixture, 65 mg (20.6%) **17***b*, 10 mg mixture, and 78 mg of a mixture of **18** and **21** in comparable amounts, in this order.

16*b*: mp 40–42°C (from pentane at −23°C). UV, λ_{max} (log ε): 258.5 (3.70), 282 nm (sh). IR (KBr): 1699 cm^{-1}. ^1H NMR: 7.33 (bd; 7 Hz; 2 phenyl *o*-H), 7.25 (m; 2 phenyl *m*-H), 7.19 (m; phenyl *p*-H), 3.03 (ddd; 7.8, 2.7, 2.1 Hz; 3-H), 2.54 (dtd; 13.0, 2 × 11.3, 4.5 Hz; 8-H_β), 2.21 (m, *b* = 8 Hz, 1-H and 4-H), 2.12 (ddd; 13.7, 7.8, 2.4 Hz; *endo*-2-H), 2.06 (bd; 10.0 Hz; 9-H_a), 1.96 (ddd; 13.0, 4.3, 2.4 Hz; 5-H_β), 1.89 (s; CH_3), 1.69 (dddt; 13.0, 4.5, 4.3, 2 × 2.3 Hz; 7-H_β), 1.61 (dtt; 13.3, 2 × 4.0, 2 × 2.4 Hz; 6-H_α), 1.57 (dd; 11.3, 3.0 Hz; 8a-H), 1.51 (td; 2 × 13.0, 4.0 Hz; 5-H_α), 1.43 (dddt; 10.0, 2.4, 2.1, 2 × 1.8 Hz; 9-H_b), 1.38 (m; 8-H_α), 1.30 (m; 7-H_α), 1.30 (ddt; 13.7, 4.0, 2 × 2.7 Hz; *exo*-2-H), 1.10 (qt; 3 × 13.3, 2 × 4.3 Hz; 6-H_β). NOE enhancements: 1-H/*endo*-2-H, *endo*-2-H/8-H_β, 3-H/4-H, 3-H/methyl-H, 3-H/phenyl *o*-H, 4-H/methyl-H. ^{13}C NMR: 212.0 (C═O), 136.5 (quat. phenyl C), 131.3 (2 phenyl *o*-C), 128.9 (2 phenyl *m*-C), 126.8 (phenyl *p*-C), 57.7 (C-4a), 56.6 (C-8a), 49.5 (C-3), 48.2 (C-4), 41.8 (C-1), 37.9 (C-9), 36.0 (C-5), 30.5 (C-2), 28.5 (methyl C), 27.3 (C-7), 23.9 (C-6), 22.7 (C-8). MS, *m/e*: 300 (28%, M^+), 191 (100%), 43 (83%).

17*b* mp 112–113°C (from diethyl ether – pentane at −23°C). UV, λ_{max} (log ε): 257.5 (4.02), 276 (sh), 284 (sh), 294 nm (sh). IR (KBr): 1702 cm^{-1}. ^1H NMR: 7.23 (m; 4 phenyl H), 7.11 (m; phenyl *p*-H), 3.60 (ddd; 7.3, 6.5, 1.7 Hz; 2-H), 2.65 (dtd; 13.0, 2 × 11.0, 4.7 Hz, 8-H_β), 2.33 (bs, *b* = 8 Hz; 4-H), 2.22 (bs, *b* = 7 Hz; 1-H), 2.07 (ddd; 13.0, 4.7, 2.0 Hz; 5-H_β), 2.06 (s; CH_3), 1.74 (dtt; 13.0, 2 × 4.5, 2 × 2.5 Hz; 7-H_β), 1.70 (ddd; 13.5, 7.3, 3.5 Hz; *endo*-3-H), 1.65 (bd; 10.0 Hz; 9-H_a), 1.65 (m; 6-H_α), 1.62 (ddd; 13.0, 2.8, 2.1 Hz; 8a-H), 1.53 (td; 2 × 13.0, 4.0 Hz; 5-H_α), 1.49 (ddtd; 10.0, 3.5, 2 × 1.9, 1.7 Hz; 9-H_b), 1.47 (m; 8-H_α), 1.36 (m; 7-H_α), 1.29 (ddd; 13.5, 6.5, 3.6 Hz; *exo*-3-H), 1.16 (qt; 3 × 13.3, 2 × 4.7 Hz; 6-H_β). NOE enhancements: 1-H/2-H, 1-H/phenyl *o*-H, 2-H/8-H_β, 2-H/phenyl *o*-H, *endo*-3-H/4-H, 4-H/methyl-H, 6-H_β/8-H_β, 6-H_β/methyl-H. ^{13}C NMR: 211.8 (C═O), 137.7 (quat. phenyl C), 128.7 (2 phenyl C), 128.0 (2 phenyl C), 125.2 (phenyl *p*-C), 56.7 (C-8a), 56.5 (C-4a), 48.6 (C-1), 42.9 (C-4), 39.5 (C-2), 38.7 (C-9), 38.2 (C-3), 35.8 (C-5), 28.6 methyl-C), 27.2 (C-7), 24.0 (C-6), 22.5 (C-8). MS, *m/e*: 300 (64%, M^+), 191 (44%), 147 (47%), 43 (100%).

rac-*1-(1*R**,2*R**,3*S**,4*S**,4a*R**,8a*S**-1,4-Methano-3-phenylthiodecahydro-2-naphthyl)ethanone (**18**)*

To a solution of 1100 mg (5.78 mmol) **10***b* (11) in 25 mL acetonitrile at room temperature was added 830 mg (7.53 mmol) benzene thiol under stirring. After stirring 2 h at 60°C the solvent was evaporated and the residue dissolved in a small amount of diethyl ether – pentane. At −23°C this solution deposited 1060 mg (61%) colourless crystals. After recrystallization from *n*-pentane at −70°C, 956 mg (55%), mp 56–58°C. UV, λ_{max} (log ε): 258.5 (3.85), 284 (sh), 294 nm (sh). IR (KBr): 1705 cm^{-1}. ^1H NMR: 7.33 (bd; 8 Hz; 2 phenyl *o*-H), 7.24 (bt; 8.0, 7.3 Hz; 2 phenyl *m*-H), 7.13 (bt; 2 × 7.3 Hz; phenyl *p*-H), 4.16 (dd; 5.9, 2.2 Hz; 3-H), 2.81 (ddq; 4.1, 2.8, 3 × 1.7 Hz; 1-H), 2.51 (dd; 5.9, 4.1 Hz; exchangeable by D; 2-H), 2.28 (dq; 2.8, 3 × 1.7 Hz; 4-H), 2.17 (s; CH_3), 1.88 (dt; 9.8, 2 × 1.7 Hz; 9-H_a), 1.88 (m; 4a-H and 8a-H), 1.64 (m; 1 methylene H), 1.57 (m; 1 methylene H), 1.50 (m; 5-H_β), 1.49 (ddt; 9.8, 2.2, 2 × 1.7 Hz; 9-H_b), 1.29 (m; 1 methylene H), 1.25 (m; 5-H_α), 1.22 (m; 8-H_α), 1.14 (m; 1 methylene H), 1.02 (tdd; 2 × 13.0, 11.5, 4.2 Hz; 8-H_β). NOE enhancements: 2-H/9-H_a, 2-H/methyl-H, 2-H/phenyl *o*-H, 3-H/4-H, 3-H/5-H_β, 3-H/8-H_β, 3-H/phenyl *o*-H, 4-H/phenyl *o*-H. ^{13}C NMR: 207.6 (C═O), 136.9 (quat. phenyl C), 129.1 (2 phenyl *o*-C), 128.7 (2 phenyl *m*-C), 125.7 (phenyl *p*-C), 62.6 (C-2), 48.2 (C-4), 45.6 (C-1), 41.4 (C-3), 39.8 (C-9), 39.7 and 39.6 (C-4a and C-8a), 28.8 (methyl-C), 21.2 (C-8), 20.4 and 19.9 (C-6 and C-7), 18.9 (C-5). MS, *m/e*: 300 (49%, M^+), 218 (20%), 191 (35%), 43 (100%).

rac-*1-(1*R**,4*S**,4a*S**,8a*S**-1,4-Methano-1,4,4a,5,6,7,8,8a-octahydro-2-naphthyl)ethanone (**21**)*

A solution of 140 mg (0.46 mmol) **18** in 21 mL methanol was

Can. J. Chem. Downloaded from www.nrcresearchpress.com by 46.23.64.124 on 09/08/12
For personal use only.

stirred with 70 mg (0.60 milliequivalents) of dry silver oxide at room temperature for 2 h. After dilution with diethyl ether, filtration, and evaporation of solvent the residue was dissolved in *n*-pentane and the solution was cleared by filtration. At −23°C the solution deposited crystals, 43.8 mg (49%), mp 32–34°C. The mother liquor contained 15.7 mg of material, which was discarded. UV, λ_{max} (log ε): 243 (3.95), 330 (1.60), 343 (sh), 359 (sh), 376 nm (sh). IR (KBr): 1658, 1581 cm^{-1}. ^1H NMR: 6.96 (ddd; 3.4, 1.0, 0.9 Hz; 3-H), 3.21 (ddddd; 3.7, 1.9, 1.8, 1.4, 1.0 Hz; 1-H), 2.92 (ddddd; 3.7, 3.4, 1.9, 1.8, 1.4 Hz; 4-H), 2.24 (s; CH_3), 2.05 (dddd; 12.0, 10.0, 5.0, 3.7 Hz; 4a-H), 2.01 (dddd; 12.0, 10.0, 5.0, 3.7 Hz; 8a-H), 1.53 (dt; 8.5, 2 × 1.8 Hz; 9-H_a), 1.53 (m; 6-H_β and 7-H_β), 1.48 (m; 5-H_α), 1.45 (m; 8-H_α), 1.35 (dtd; 8.5, 2 × 1.4, 0.9 Hz; 9-H_b), 1.28 (m; 6-H_α and 7-H_α), 0.67 (tdd; 2 × 13.0, 12.0, 4.7 Hz; 5-H_β), 0.45 (tdd; 2 × 13.0, 12.0, 4.7 Hz; 8-H_β). ^{13}C NMR: 195.6 (C═O), 150.3 (C-2), 148.2 (C-3), 48.8 (C-9), 48.6 (C-4), 45.5 (C-1), 38.9 (C-4a), 38.1 (C-8a), 25.6 (methyl C), 23.9 (C-5), 23.7 (C-8), 20.3 and 20.0 (C-6 and C-7). MS, *m/e*: 190 (19%, M^+), 109 (91%), 43 (100%).

rac-*1-(1*R*,2*R*,4*R*,4a*S*,8a*S*-1,4-Methanodecahydro-2-naphthyl)ethanone (22)*

(*a*) A solution of 170.4 mg (0.90 mmol) **21** in 13 mL ethanol, containing 10 mg of 10% Pd on charcoal (Fluka), was hydrogenated at ambient temperature and pressure. After 30 min 22.9 mL H_2 had been absorbed (required: 21.8 mL) and hydrogen absorption ceased. Filtration and evaporation left 162 mg (94%) residue, pure **22** according to ^1H NMR. The solution in pentane deposited 138 mg (80%), mp 43–44°C. UV, λ_{max} (log ε): 228 (1.82), 258 (1.48), 278 (1.43), 287 (sh), 295 (sh), 304 (sh), 313 nm (sh). IR (KBr): 1697 cm^{-1}. ^1H NMR: 2.72 (ddtd; 4.0, 3,8, 2 × 1.6, 1.1 Hz; 1-H), 2.58 (ddd; 11.1, 5.8, 3.8 Hz; exchangeable by D; 2-H), 2.16 (ddtd; 5.0, 4.4, 2 × 1.6, 1.1 Hz; 4-H), 2.15 (s; CH_3), 2.15 (ddd; 13.0, 5.8, 2.0 Hz; *endo*-3-H), 1.81 (tdd; 2 × 12.0, 4.8, 4.0 Hz; 8a-H), 1.76 (tt; 2 × 12.0, 2 × 4.4 Hz; 4a-H), 1.51 (ddt; 9.2, 2.0, 2 × 1.6 Hz; 9-H_b), 1.48 (dt; 9.2, 2 × 1.6 Hz; 9-H_a), 1.34 (ddd; 13.0, 11.1, 5.0 Hz; *exo*-3-H), 1.62/1.25, 1.57/1.12, 1.40/1.18, 1.20/0.97 (all m; 4 CH_2). NOE enhancements: 1-H/methyl-H, 2-H/9-H_a. ^{13}C NMR: 211.0 (C═O), 55.5 (C-2), 45.3 (C-1), 42.2 (C-9), 41.5 (C-4), 40.2 (C-8a), 39.8 (C-4a), 29.0 (methyl C), 22.3 (C-3), 21.8, 20.7, 20.0, 19.4 (C-5 through C-8). MS, *m/e*: 192 (6%, M^+), 177 (63%), 67 (79%), 43 (100%). (*b*) From **23** in complete analogy to above.

rac-*1-(1*R*,2*S*,3*S*,4*S*,4a*R*,8a*S*-1,4-Methano-3-methoxydecahydro-2-naphthyl)ethanone (24)*

A solution of 610 mg (2.03 mmol) **18** and 126 mg (3.15 mmol) sodium hydroxide in 16 mL methanol was left at room temperature for 45 min. Addition of water and diethyl ether, extraction of the aqueous phase with three further portions of ether, washing the ether layers with water, drying them over anhydrous magnesium sulfate, and evaporation of the ether left 414 mg residue, which was chromatographed over 320 g adsorbent to elute 27 mg unidentified, 223 mg (57.7%) **21** (pure according to ^1H NMR; after crystallization from pentane at −23°C, 170 mg (44%), mp 32–34°C), 23 mg unidentified, 125.5 mg (27.8%) **24** (pure according to ^1H NMR; after crystallization from pentane at −70°C and collecting the crystals by inverse filtration in the cold, 99 mg (21.9%)), and 11 mg unidentified material, in this order.

24: mp 12–14°C. UV, λ_{max} (log ε): 244 (1.79), 278 (1.36), 284 (sh), 293 (sh), 304.5 (sh), 315 nm (sh). IR (KBr): 1703 cm^{-1}. ^1H NMR: 4.08 (dd; 3.6, 1.8 Hz; 3-H), 3.22 (s; OCH_3), 2.75 (ddddd; 4.1, 3.5, 1.6, 1.5, 1.4 Hz; 1-H), 2.39 (dd; 4.1, 3.6 Hz; exchangeable by D; 2-H), 2.29 (dddd; 4.0, 1.6, 1.5, 1.4 Hz; 4-H), 2.17 (s; CCH_3), 1.81 (m; 4a-H), 1.78 (m; 8a-H), 1.70 (dt; 9.5, 2 × 1.6 Hz; 9-H_a), 1.60/1.22 and 1.53/1.11 (4 m; 6-CH_2 and 7-CH_2), 1.37 (ddt; 9.5, 1.8, 2 × 1.4 Hz; 9-H_b), 1.30 (m; 5-H), 1.20 (m; 5-H), 1.18 (m; 8-H_α), 0.87 (tdd; 2 × 13.0, 12.4, 4.8 Hz; 8-H_β). NOE enhancements: 1-H/acetyl-H, 2-H/9-H_a, 2-H/acetyl-H, 3-H/4-H, 3-H/5-H_β, 3-H/methoxyl-H, 4-H/methoxyl-H. ^{13}C NMR: 209.1 (C═O), 76.8 (C-3), 64.6 (C-2), 56.2 (OCH_3), 45.8 (C-4), 44.4 (C-1), 39.4 (C-8a), 39.0 (C-9), 37.7 (C-4a), 29.0 (CCH_3), 21.4 (C-8), 20.4, 20.2 (C-6 and C-7), 19.0 (C-5). MS, *m/e*: 222 (16%, M^+), 190 (15%), 140 (89%), 43 (100%).

rac-*1-(1*R*,2R*,3*S*,4*S*,4a*R*,8a*S*-1,4-Methano-3-methoxydecahydro-2-naphthyl)ethanone (25)*

18 (600 mg, 2 mmol) was added to a solution of 600 mg (15 mmol) NaOH in 40 mL methanol. After 24 h at room temperature the mixture was poured into 350 mL water. This mixture was extracted with five 100-mL portions of diethyl ether. The ether layers were washed with water and dried over anhydrous magnesium sulfate. After evaporation of the ether the residue was distilled (Kugelrohr, 0.1 Torr (1 Torr = 133.3 Pa), bath temperature 120°C) to give 380 mg distillate, which was chromatographed over 140 g absorbent to elute 4 mg diphenyl disulfide, 14 mg unidentified, 149 mg (39%) **21** (pure according to ^1H NMR; 82 mg, mp 33–34°C, after crystallization from pentane at −22°C), 13 mg unidentified, 113 mg (25%) **25** (pure according to ^1H NMR; 88 mg (20%) after crystallization from pentane at −22°C), 29 mg (6.5%) mixture **24** + **25** (85:15), and 12 mg unidentified material, in this order.

25: mp 52–53°C. UV, λ_{max} (log ε): 227 (1.93), 277 nm (1.45). IR (KBr): 1705 cm^{-1}. ^1H NMR: 3.91 (ddd; 7.6, 1.5, 1.0 Hz; 3-H), 3.22 (s; OCH_3), 2.98 (dd; 7.6, 2.2 Hz; exchangeable by D; 2-H), 2.34 (ddt; 4.5, 1.8, 2 × 1.5 Hz; 1-H), 2.30 (dddt; 3.2, 1.8, 2 × 1.5, 1.0 Hz; 4-H), 2.09 (s; CCH_3), 1.79 (tt; 2 × 11.5, 2 × 4.5 Hz; 8a-H), 1.77 (dt; 9.8, 2 × 1.8 Hz; 9-H_a), 1.76 (tdd; 2 × 11.5, 5.5, 3.2 Hz; 4a-H), 1.63/1.27 (each a m of 2 H; 2 CH_2), 1.24 (ddt; 9.8, 2.2, 3 × 1.5 Hz; 9-H_b), 1.27/1.20 (2 m; 1 CH_2), 1.20/1.15 (2 m; 1 CH_2). NOE enhancements: 1-H/2-H, 2-H/8-H_β, 2-H/acetyl-H, 3-H/4-H, 3-H/5-H_β, 3-H/methoxyl-H, 4-H/methoxyl-H, acetyl-H/methoxyl-H. ^{13}C NMR: 207.6 (C═O), 81.1 (C-3), 57.2 (OCH_3), 53.8 (C-2), 43.2 (C-4), 41.0 (C-1), 38.9 (C-4a), 36.3 (C-8a), 35.7 (C-9), 31.3 (CCH_3), 20.3, 20.1, 19.9, 19.7 (C-5 through C-8). MS, *m/e*: 222 (8%, M^+), 140 (61%), 43 (100%).

rac-*1-(1*R*,2*S*,4*R*,4a*S*,8a*S*-1,4-Methanodecahydro-2-naphthyl)ethanone (26)*

A solution of 120 mg (62.5 mmol) **22** and 13 mg (24 mmol) sodium methoxide in 4 mL methanol was left at room temperature for 5 days. After addition of water the mixture was extracted five times with diethyl ether. The combined ether layers, after washing with water, drying over anhydrous magnesium sulfate, and evaporation of the solvent, left 121 mg residue, composed, except for traces of ether, of 98% **26** and 2% **22** (^1H NMR analysis). The solution of the residue in *n*-pentane at −70°C deposited a solid, which was collected by

Can. J. Chem. Downloaded from www.nrcresearchpress.com by 46.23.64.124 on 09/08/12
For personal use only.

inverse filtration. It became liquid at room temperature and was distilled (Kugelrohr, 0.1 Torr, bath temperature 80°C) to give 88.6 mg (74%) **26** as a colourless liquid. UV, λ_{max} (log ϵ): 282 (1.50), 291 (sh), 301 (sh), 314 nm (sh). IR (KBr): 1708 cm^{-1}. ^1H NMR: 2.67 (ddd; 8.9, 5.6, 1.2 Hz; exchangeable by D; 2-H), 2.31 (dddd; 4.2, 1.7, 1.5, 1.0 Hz; 1-H), 2.13 (tddd; 2 × 4.2, 1.7, 1.5, 1.0 Hz; 4-H), 2.09 (s; CH_3), 1.80 (tdd; 2 × 11.8, 5.8, 4.2 Hz; 8a-H), 1.69 (tddd; 2 × 11.8, 5.7, 4.2, 1.3 Hz; 4a-H), 1.66 (dddd; 13.0, 5.6, 4.2, 1.3 Hz; *exo*-3-H), 1.57 (ddd; 13.0, 8.9, 2.4 Hz; *endo*-3-H), 1.26 (dt; 9.7, 2 × 1.7 Hz; 9-H_a), 1.22 (dddt; 9.7, 2.4, 2 × 1.5, 1.2 Hz; 9-H_b), ca. 1.65 (5-H_α and 8-H_α), 1.30 (5-H_β and 8-H_β), ca. 1.30 and ca. 1.23 (each 2 H; 6-H and 7-H). NOE enhancements: 1-H/2-H, 1-H/methyl-H, 2-H/8-H_β, 2-H/methyl-H, *endo*-3-H/5-H_β. ^{13}C NMR: 210.5 (C=O), 48.1 (C-2), 44.3 (C-1), 40.6 (C-4), 39.3 (C-8a), 38.0 (C-4a), 37.1 (C-9), 28.6 (methyl-C), 25.4 (C-3), 20.24, 20.22, 20.20, 20.0 (C-5 through C-8). MS, *m/e*: 192 (7%, M^+), 174 (7%), 149 (100%), 67 (99%), 43 (46%).

Product ratios: from weighed amounts of reactants were determined by ^1H NMR, in situ in most cases; e.g., from **10***a* and benzene thiol in CD_3CN; from **18**, **21**, **24**, or **25** with sodium methoxide in CD_3OD.

*Analytical runs with **10**b and varied concentrations of benzene thiol*

For each run, 20 mg (0.105 mmol) **10***b* was placed in an NMR tube. This NMR tube was then equipped with a "Quickfit" glass head that allowed the following operations: Evacuation and filling of the NMR tube with Ar, addition by syringes of a measured volume of acetonitrile-d_3 followed by a measured volume of benzene thiol, and capping the tube, all under a steady slow stream of Ar. The NMR tubes thus prepared (sample volumes ca. 0.5 mL) were heated at 60°C for 2 h and then analyzed by ^1H NMR spectroscopy. The analysis was facilitated by the perfectly isolated signals at δ = 5.98 (**10***b*, 2 H), 4.10 (**18**), 3.94 (-SH), 3.49 (**17***b*), and 3.03 (**16***b*). No compounds besides these five and, in two cases, some diphenyl disulfide (δ = 7.5) were found to be present in any significant amount. Conversions of **10***b* varied (44–75%) since the radical chain reaction depends on adventitious catalysis for its start; this should, however, not affect the product ratios. $[PhSH]_0$ values, i.e., the concentrations of benzene thiol at the beginning of the reaction, were calculated from the volumes of benzene thiol added and its density (1.078 at 20°C); they were checked by ^1H NMR. In the first run, which featured the smallest volume of added PhSH of all runs, a discrepancy was noted and the NMR-based value was preferred over the volume-based one. In the calculations of $[\mathbf{17}b][\mathbf{18}]^{-1}[PhSH]_{av}^{-1}$ (= k_{17}/k_{15}) values (see Scheme 5 and Table 1, fifth column), average benzene thiol concentrations $[PhSH]_{av}$ were used that took into account the consumption of PhSH during reaction. Average values and their confidence limits were obtained from the fifth and sixth columns, respectively, of Table 1.

Free-radical chain addition experiments with aldehydes

Experiments were performed as described in the literature (16, 17) except that di-*tert*-butyl hyponitrite (DBH; 1,2-di-*tert*-butoxydiazene) (22) was used as the free-radical starter since it decomposes at somewhat lower temperature (23) than the commonly used starters (AIBN, diacyl peroxides), which is convenient when working with acetaldehyde (bp 21°C). Sodium hyponitrile was prepared via diazotation of hydroxylamine (24) and converted to silver hyponitrite by combining its aqueous solution with that of silver nitrate and collecting the precipitate; the silver hyponitrite was converted to DBH as described (22). Three vials, each containing a homogeneous mixture of 1 g acetaldehyde, 0.5 g substrate, and 50 mg DBH, degassed and under 1 atm of Ar (1 atm = 101.3 kPa), were left standing together at 20°C. The substrate was norbornene in the first, quadricyclane (purchased from Aldrich, pure according to ^1H NMR) in the second, and a 1:1 mixture of norbornene and quadricyclane in the third vial. After 93 h, in each case the norbornene was quantitatively converted to *exo*-2-acetyl-norbornane (17), identified by ^1H NMR comparison with an authentic sample prepared from 2-acetyl-5-norbornene, *endo,exo* mixture from Aldrich, via catalytic hydrogenation of the *exo* isomer; the quadricyclane, however, had remained entirely unchanged in each case (^1H NMR analysis). A similar reactivity difference was observed at 45°C using pivalaldehyde in place of acetaldehyde.

References

1. (*a*) M. Demuth. Org. Photochem. **11**, 37 (1991); (*b*) D.I. Schuster. *In* Rearrangements in ground and excited states. Vol. 3. *Edited by* P. de Mayo. Academic Press, New York. 1980. pp. 232–279.
2. (*a*) D.E. Sadler, J. Wendler, G. Olbrich, and K. Schaffner. J. Am. Chem. Soc. **106**, 2064 (1984); (*b*) H.U. Gonzenbach, I.M. Tegmo-Larsson, J.P. Grosclaude, and K. Schaffner. Helv. Chim. Acta, **60**, 1091 (1077).
3. (*a*) S. Domb and K. Schaffner. Helv. Chim. Acta, **53**, 677 (1970); (*b*) B. Winter and K. Schaffner. J. Am. Chem. Soc. **98**, 2022 (1976); (*c*) W.G. Dauben, G. Lodder, and J.D. Robbins. J. Am. Chem. Soc. **98**, 3030 (1976).
4. (*a*) T. Ni, R.A. Caldwell, and L.A. Melton. J. Am. Chem. Soc. **111**, 457 (1989); (*b*) R.A. Caldwell and L. Zhou. J. Am. Chem. Soc. **116**, 2271 (1994); (*c*) R.A. Caldwell, J.F. Diaz, D.C. Hrncir, and D.J. Unett. J. Am. Chem. Soc. **116**, 8138 (1994).
5. (*a*) S. Wollowitz and J. Halpern. J. Am. Chem. Soc. **110**, 3112 (1988); (*b*) D.A. Lindsay, J. Lusztyk, and K.U. Ingold. J. Am. Chem. Soc. **106**, 7087 (1984).
6. (*a*) J. Ipaktschi. Tetrahedron Lett. 2153 (1969); (*b*) M.A. Schexnayder and P.S. Engel. Tetrahedron Lett. 1153 (1975).
7. W.A. Pryor. *In* Mechanisms of sulfur reactions. McGraw–Hill, New York. 1962. pp. 75–93.
8. G.D. Brindell and S.J. Cristol. *In* Organic sulfur compounds. Vol. 1. *Edited by* N. Kharash. Pergamon Press, Oxford. 1961. pp. 121–133.
9. D.I. Davies, L.T. Parfitt, C.K. Alden, and J.A. Claisse. J. Chem. Soc. C, 1585 (1969), and references cited.
10. D.I. Davies, D.J.A. Pearce, and E.C. Dart. J. Chem. Soc. Perkin Trans. 1, 433 (1973).
11. J. Leitich and K. Schaffner. Angew. Chem. Int. Ed. Engl. **32**, 441 (1993).
12. C.R. Castro, R. Dutler, A. Rauk, and H. Wieser. J. Mol. Struct. (Theochem), **152**, 241 (1987).
13. R.J. Abraham and J. Fisher. Magn. Reson. Chem. **23**, 856 (1985).
14. J.A. Franz, B.A. Bushaw, and M.S. Alnajjar. J. Am. Chem. Soc. **111**, 268 (1989).
15. (*a*) K. Nakabayashi, S. Toki, and S. Takamuku. Chem. Lett. 1889 (1986); (*b*) A.J.G. Barwise, A.A. Gorman, and M.A.J. Rodgers. Chem. Phys. Lett. **38**, 313 (1976).
16. M.S. Kharash, W.H. Urry, and B.M. Kuderna. J. Org. Chem. **14**, 248 (1949).

17. H. Stockmann. J. Org. Chem. **29**, 245 (1964).
18. L. Batt. *In* Chemical kinetics of small organic radicals. Vol. 3. *Edited by* Z.B. Alfassi. CRC Press, Boca Raton, Fla. 1988. pp. 31–40.
19. H. Knoll, G. Richter, and R. Schliebs. Int. J. Chem. Kinet. **12**, 623 (1980).
20. K. Hayakawa, H. Schmid, and G. Frater. Helv. Chim. Acta, **60**, 561 (1977).
21. (*a*) J.C. Davis and T.V. van Auken. J. Am. Chem. Soc. **87**, 3900 (1965); (*b*) E.I. Snyder and B. Franzus. J. Am. Chem. Soc. **86**, 1166 (1964); (*c*) P. Laszlo and P.v.R Schleyer. J. Am. Chem. Soc. **86**, 1171 (1964); (*d*) J. Am. Chem. Soc. **85**, 2709 (1963).
22. H. Kiefer and T.G. Traylor. Tetrahedron Lett. 6163 (1966).
23. R.C. Neuman and R.J. Bussey. J. Am. Chem. Soc. **92**, 2440 (1969).
24. A.W. Scott. J. Am. Chem. Soc. **49**, 986 (1927).

Can. J. Chem. Downloaded from www.nrcresearchpress.com by 46.23.64.124 on 09/08/12
For personal use only.

β-Trichlorosilylstyrene oligomers[1]

Michael A. Brook, Thomas Sebastian, Peter Hülser, Ralf Jüschke, Stefan Wenzel, Jennifer A. Townsend, and Patricia R. Falletta

Abstract: Under cationic conditions using triflic acid as the initiator, it is possible to oligomerize β-trichlorosilylstyrene **2** to low molecular weight oligomers **14** with a maximum degree of polymerization of about 9. Termination of the process was shown to occur by an intramolecular Friedel–Crafts reaction, leading to highly functionalized, indane-terminated oligomers **9**, **12**, etc. At lower temperatures, the reaction is diastereoselective. The oligomerization process was shown to require electron-withdrawing groups on silicon; the replacement of Cl spectator ligands with alkoxy or alkyl groups led to protiodesilylation. The mechanism for formation of the indane-terminated oligomers is discussed.

Key words: cationic polymerization, β-silylstyrene, stereoselective oligomerization, indene termination.

Résumé : Sous des conditions cationiques utilisant de l'acide triflique comme initiateur, il est possible de provoquer une oligomérisation du β-trichlorosilylstyrène, **2**, en oligomères **14** de bas poids moléculaire et comportant un degré maximal de polymérisation d'environ 9. On a montré que le processus de terminaison se produit par une réaction de Friedel–Crafts intramoléculaire conduisant à des oligomères **9**, **12**, etc. se terminant par des indanes hautement fonctionnalisés. À des températures plus basses, la réaction est diastéréosélective. On a montré que le processus d'oligomérisation nécessite la présence de groupes électroattracteurs sur le silicium; le remplacement des coordinateurs Cl agissant comme spectateurs par des groupes alkoxyles ou alkyles conduit à une protiodésilylation. On discute du mécanisme de formation des oligomères se terminant par un indane.

Mots clés : polymérisation cationique, β-silylstyrène, oligomérisation stéréosélective, terminaison par un indène.

[Traduit par le rédaction]

Introduction

Silicones possess very different properties from carbon-based polymers. Typically, they have very low glass transition temperatures (1), are relatively bioinert,[4] hydrophobic (2), and thermally stable. The presence of silicon in an organic polymer conveys some of these special properties to the composite material. Its incorporation into the polymer chain may be done in a variety of ways, including the formation of block copolymers of silicones and polyolefins under anionic (3) or other conditions (4), the use of a silicon-functionalized monomer in which the silicon is distal from the reactive site (e.g., *p*-$Me_3SiC_6H_4CH{=}CH_2$), by post polymerization grafting of a silicon-containing group (5),[5] or, inefficiently, by the direct polymerization of vinylsilanes (6). In most cases, advantage is taken of the fact that reactions at silicon tend to take place under ionic conditions. Thus, any radical processes used for polymerization do not affect the silicon moiety and ionic processes used to modify the silicon do not affect the polymer.[6]

We have been interested for some time in the addition of electrophiles to vinylsilanes. During the course of a study in which the addition of electrophiles to silicon-substituted styrenes was examined, we discovered that the nature of the groups on silicon dramatically affected the reactivity of the molecules (8). For example, although the addition of Friedel–

Received April 10, 1995.

This paper is dedicated to Professor J.E. (Jim) Guillet in recognition of his contributions to Canadian chemistry.[2]

M.A. Brook,[3] **T. Sebastian, P. Hülser, R. Jüschke, S. Wenzel, J.A. Townsend, and P.R. Falletta.** Department of Chemistry, McMaster University, 1280 Main St. W., Hamilton, ON L8S 4M1, Canada.

[1] Part of the M.Sc. thesis of T.S.

[2] It is a tremendous pleasure to dedicate this paper to Jim Guillet. While an undergraduate, his teaching sparked my interest in polymers. He fostered that interest through his fascinating research activities and was tremendously supportive in my early efforts in polymer chemistry for all of which I am deeply grateful.

[3] Author to whom correspondence may be addressed. Natural Sciences and Engineering Research Council University Research Fellow, 1985–1995. Telephone: (905) 525-9140, ext. 23483. FAX (905) 522-2509. E-mail: mabrook@mcmaster.ca

[4] This statement has become quite controversial given the current legal situation for manufacturers of silicone breast prostheses. A variety of detrimental aspects of silicones, particularly in their effect on the immune system, have been suggested. Nonetheless, comparable bioinertness has not been observed with other man-made polymers, and silicones remain constituents of pharmaceutical preparations, medical devices (non-implanted), etc.

[5] The introduction of silicon into polymers more commonly involved the radically induced grafting of the above monomers onto an existing polymer chain: Neste Öy produces a "moisture cure" polyethylene in this manner.

[6] It should, however, be noted that alkylsilyl groups (which lead to the first three properties outlined above) can participate in radical reactions via α-SiCH abstraction. These reactions are much less efficient than radical propagation of olefins. Functionalized silicon groups, in which Cl or OR groups are bound to silicon, readily react with water or nucleophiles. See ref. 7.

Can. J. Chem. Downloaded from www.nrcresearchpress.com by 46.23.64.124 on 09/08/12
For personal use only.

Scheme 1.

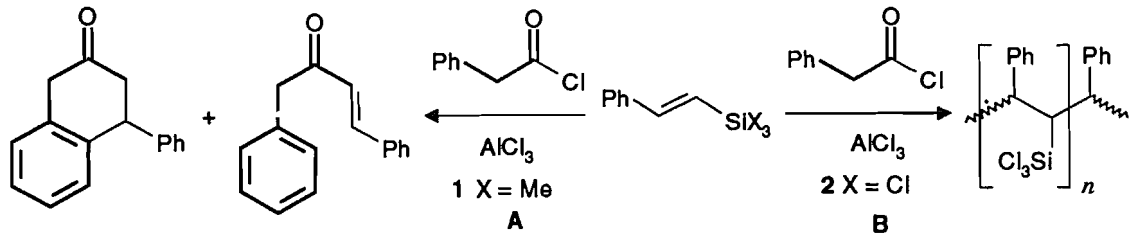

Scheme 2.

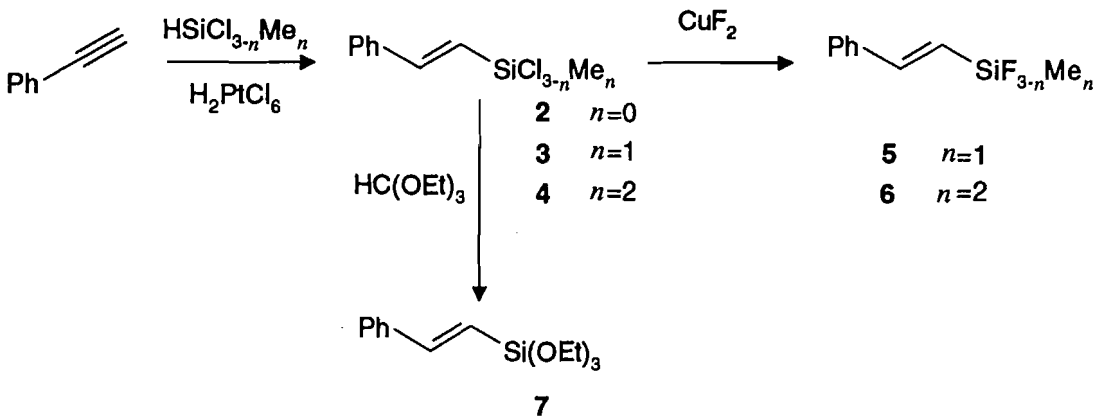

Crafts acylating agents to trimethylsilylstyrene **1** led to the mixture of addition and elimination products (Scheme 1A)(9, 10), addition of the same electrophile to the trichlorosilyl derivative **2** led to addition products (11) accompanied by a higher molecular weight material that was extremely difficult to characterize (Scheme 1B); elimination products were not observed.

Few polymers are based upon vinylsilanes. Although trichloro-, trimethyl-, and trimethoxyvinylsilane may be radically polymerized to give polymers (6), more highly substituted polymer chains have not been produced by the direct polymerization of vinylsilanes. One notable exception is the work of Weber and Chan who demonstrated that silylated butadienes can be polymerized (12). The difficulty in preparing highly substituted polymers is, of course, a problem that is not limited to vinylsilanes: the polymerization of 1,2-disubstituted olefins is normally difficult.

We have discovered that under cationic conditions, using triflic acid as the cationic initiator, it is possible to cleanly oligomerize β-trichlorosilylstyrene **2** (13). The mechanism of polymer formation and the properties of the resultant silicon-containing oligomers are described in the following sections.

Results and discussion

Preparation

As with many vinylsilanes, the preparative route of choice is hydrosilation of a precursor alkyne. This process, typically catalyzed with transition metal complexes (14), especially those derived from Pt (H_2PtCl_6, Speier's catalyst (15), and $Pt_2(H_2C{=}CHSiMe_2OSiMe_2CH{=}CH_2)_4$, Karstedt's catalyst (16)), is remarkably efficient and highly regio- and stereoselective. The hydrosilation of phenylacetylene with $HSiCl_3$ in the presence of H_2PtCl_6 (17) led to the production of **2** in 95% isolated yield after distillation (Scheme 2). Similarly, using $HSiMe_nCl_{3-n}$ (n = 1, 2) in the presence of H_2PtCl_6, **3** and **4** were cleanly prepared. Fluoro compounds **5** and **6** were synthesized by halide exchange of **2** and **3**, respectively, using CuF_2 (17). The completely methylated compound **1** was prepared by reaction of **2** with MeLi or MeMgBr. The ethoxylated compound **7** was prepared by the reaction of **2** with $HC(OEt)_3$ (18). The materials were purified by distillation.

Oligomerization

It is not possible to polymerize vinylchlorosilanes anionically: initiators such as n-BuLi preferentially react at silicon in an S_N2 fashion (this fact was used to prepare moisture-stable analogues, see below). To establish if **2** would polymerize under radical conditions, it was reacted with di-*tert*-butyl peroxide above the initiator decomposition temperature. It is not surprising that only unreacted starting materials were recovered; as noted above, the radical polymerization of 1,2-disubstituted olefins is generally quite difficult.

Having established that the higher molecular weight materials produced from the electrophilic addition of acylium ions to the styrylsilanes (Scheme 1) were not the result of radical reactions, an attempt was made to establish reproducible cationic conditions under which higher molecular weight materials could be prepared and to determine their structures.

Initiators for cationic polymerization are typically proton sources in which the counterion is non-nucleophilic (19). These can be classified into three groups: carbocationic initiators such as Meerwein's salts, stable cations ($Ph_3C^+X^-$), or Friedel–Crafts acylation reagents; Lewis acids contaminated with traces of water or alcohol (co-catalysts) that form a Brønsted acid in situ; or protonic acids. Initially, the first class of initiators was examined. However, the reaction of **2** with

Can. J. Chem. Downloaded from www.nrcresearchpress.com by 46.23.64.124 on 09/08/12
For personal use only.

Scheme 3.

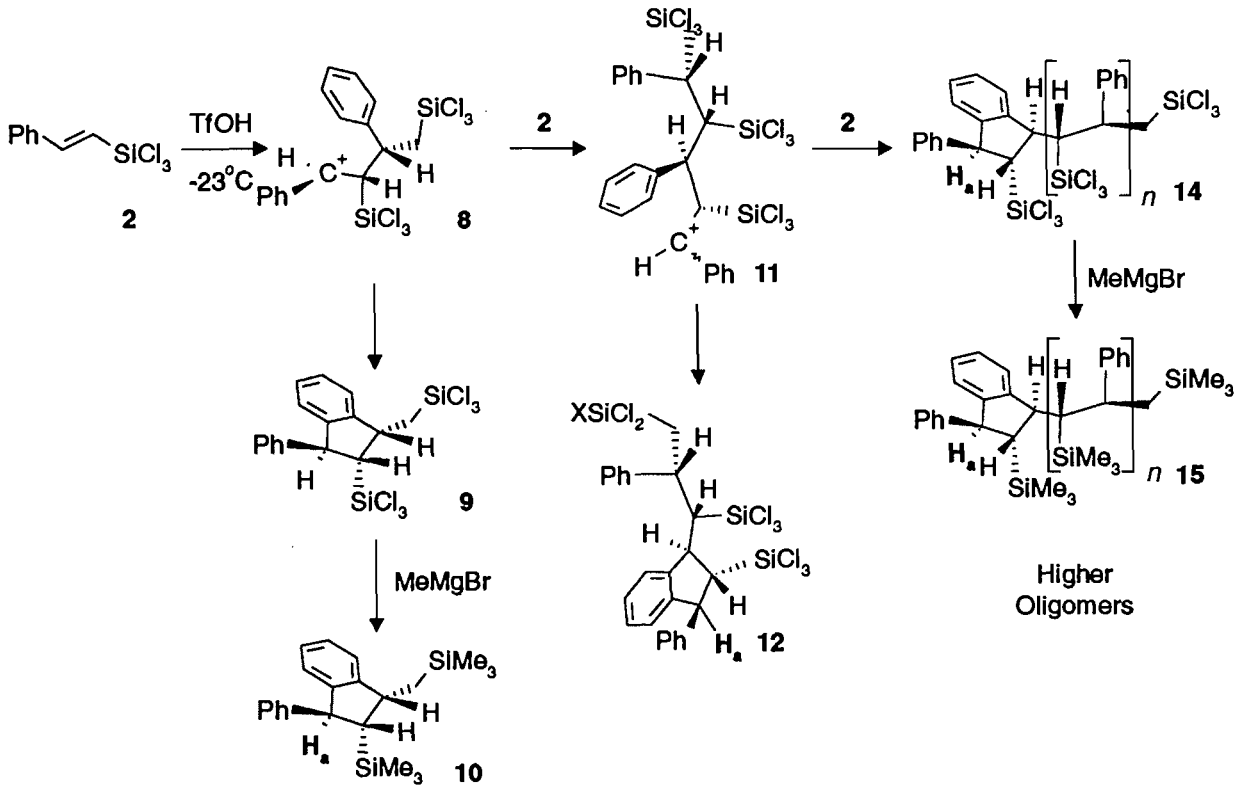

$Ph_3C^+BF_4^-$ or CH_3COCl–$AlCl_3$ as initiators[7] led to recovered starting materials or, in the latter case depending on the reaction conditions, an intractable tar. While it proved possible to produce oligomeric mixtures with the second class of initiators including $BF_3{\cdot}Et_2O$, $AlCl_3$, $ZnCl_2$, or $TiCl_4$, with water, EtOH, or MeOH as co-catalysts, these reactions were completely irreproducible. A systematic evaluation of the reaction parameters failed to provide a set of reaction conditions that would always lead to oligomers. The structure of these oligomeric materials was not examined in detail.

The use of strong acids including $HSbCl_6$, H_3PO_4, HBF_4, and HSO_3CF_3 (trifluoromethanesulfonic acid, triflic acid, TfOH) led to oligomeric materials **14** (Scheme 3). Oligomerization was favoured by the stronger acids: weaker acids with more nucleophilic counterions led to other processes including elimination at carbon and nucleophilic substitution at silicon. The only electrophile with which oligomerization was observed reproducibly was triflic acid.

Because of the instability to hydrolysis of the oligomeric products, the reaction mixture was converted to an air-stable mixture by reaction with MeLi or MeMgBr. Separation by flash chromatography and analysis by mass spectrometry allowed confirmation of the molecular weight dispersity of the reaction. The highest oligomer that could be clearly detected was a nonamer. Using GPC calibrated with polystyrene standards, the degree of polymerization of the reaction was shown to be very low (DP ca. 3, M_n 1000), although with rather large error bars given the low molecular weight of the compounds present.

[7] Elizabeth Jefferson and Michael A. Brook, unpublished results.

Solvent effects

Cationic polymerization clearly involves the intermediacy of at least a highly polarized or ionic species. Thus, the reaction outcome should be dependent upon solvent polarity. To examine this question, the reaction was attempted in a series of solvents (Table 1) of differing polarity varying from pentane (Table 3) to acetonitrile; the use of hydroxylic solvents is precluded because they lead to the exchange of functional groups on silicon. The catalyst used for initiation, triflic acid, is not very soluble in the less polar solvents examined (pentane, $HCCl_3$, and H_2CCl_2), and this was also a contributing factor to the reaction outcome. In the event, only in the chlorinated hydrocarbons was it possible to achieve acceptable, reproducible yields of oligomers. In polar solvents, huge amounts of catalyst were required to take the reaction to reasonable degrees of conversion; acetone and DMSO led to polymerization of acetone and of the chlorosilanes (20, 21), respectively.

Concentration effects

Acid and monomer concentration

Oligomerization only occurred with very high concentrations of monomer and, indeed, of initiator. At <5 mol% ratio of TfOH, conversion was incomplete (Table 1).[8] Thus, between 5 and 10 mol% of initiator was added. In the same way that hydroxylic solvents can lead to nucleophilic substitution at silicon (22), we believe that exchange of triflate and chloride can occur at silicon. The impact of such an exchange is the effec-

[8] These reactions were typically run with a saturated solution of triflic acid.

Can. J. Chem. Downloaded from www.nrcresearchpress.com by 46.23.64.124 on 09/08/12
For personal use only.

Can. J. Chem. Downloaded from www.nrcresearchpress.com by 46.23.64.124 on 09/08/12
For personal use only.

Table 1. Product distribution in the oligomerization of **2** as a function of reaction solvent

Solvent[a]	Mol% TfOH	Product ratios (Scheme 3, Scheme 5) **2**:**9**+**16**+other dimers:**12**+**24**+other trimers
$CHCl_3$	2.8	21:34:45
$CHCl_3$	5	0:50:15
CH_2Cl_2	2.8	7:71:22
CH_2Cl_2:DMF 20:1	18	75:25:0
Acetone	225	decomposition[b]
CH_3CN	320	4:56:40
CH_3CN:DMF 10:1	19	7:40:54
DMSO	235	decomposition[c]
DMF	430	40:40:20

[a]All reactions performed at [**2**] = 4.2 M in the solvent specified.
[b]Polyaldol condensation of acetone was the outcome of this reaction.
[c]Conversion to silicones occurred (20, 21).

Scheme 4.

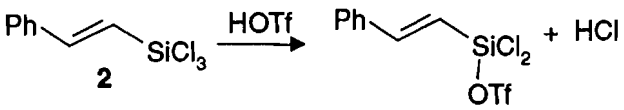

Table 2. Relation of degree of polymerization to monomer concentration.

Monomer concentration [**2**]	Reaction time (h)	Dimers (%)	Trimers (%)	Higher oligomers (%)
8.43 mM	48	96		
42.15 mM	4	80	14	
4.2 M	2	50	15	30
Bulk	2	50	15	30

tive removal of acid catalyst from the system. Although the proton concentration is not affected by ligand exchange at silicon, the protons are less reactive; dry HCl bubbled into $CHCl_3$ was not an effective catalyst for the oligomerization of **2**. A large amount of catalyst, when compared to conventional cationic polymerization, was thus required to force the reaction to completion. Any exchange of groups should also have an effect on the rate of polymerization of the styrene, although this has not been established.

In spite of the use of relatively high acid levels, at low monomer concentrations (below 10 mM [**2**] in $HCCl_3$), little reaction was observed; primarily starting materials were recovered at reaction temperatures varying from −60°C to 60°C. The range of concentrations between 8 mM and neat **2** was examined. The molecular weight distributions over this range are given in Table 2.

At the lower concentration range, unless an unduly long reaction time was permitted (≥2 days), a great deal of unreacted starting material accompanied dimer and trimer formation (10). Above a monomer concentration of 4.2 M, higher oligomers accompanied the lower molecular weight species. However, even when the reaction was run neat, higher oligomers remained minor products and the dimer and trimer dominated the reaction mixture. An attempt was made to increase the molecular weight by metering in monomer using a syringe pump during the reaction in order to maximize monomer concentration throughout the reaction. This effort, however, also led primarily to the preparation of low molecular weight materials. Similarly, lowering the reaction temperature, which commonly leads to higher molecular weights in cationic polymerization (19), gave essentially the same molecular weight distribution: at −60°C only a small increase in the trimer/dimer ratio was noted.

Fig. 1. ORTEP representation of **10**, the dimer of **2**.

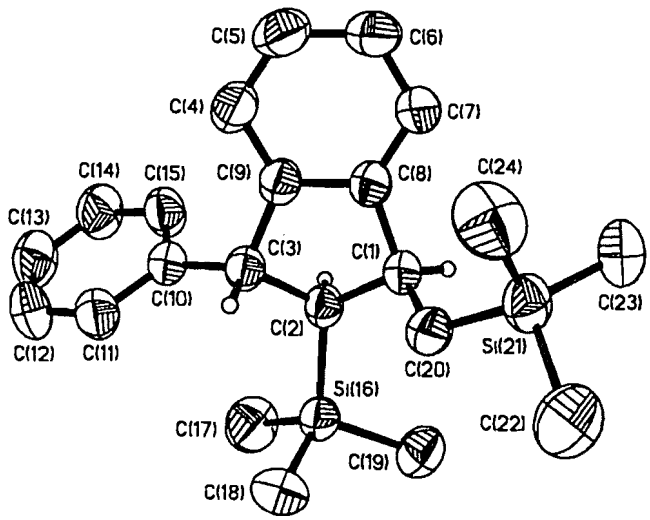

Product structure and stereochemistry: temperature effects

Although the molecular weight distribution of the oligomer was not found to be highly temperature dependent, the stereochemistry of the products was. Thus, at low temperature only one dimeric product **9** was isolated. It was possible to determine the crystal structure of the methylated dimer **10** prepared from **2**, which showed the presence of an indane group (the ORTEP picture is shown in Fig. 1 (10)). The permethylated trimer **13** (from **12**) was similarly a single compound containing the indane structure although the relative

Can. J. Chem. Downloaded from www.nrcresearchpress.com by 46.23.64.124 on 09/08/12
For personal use only.

Scheme 5.

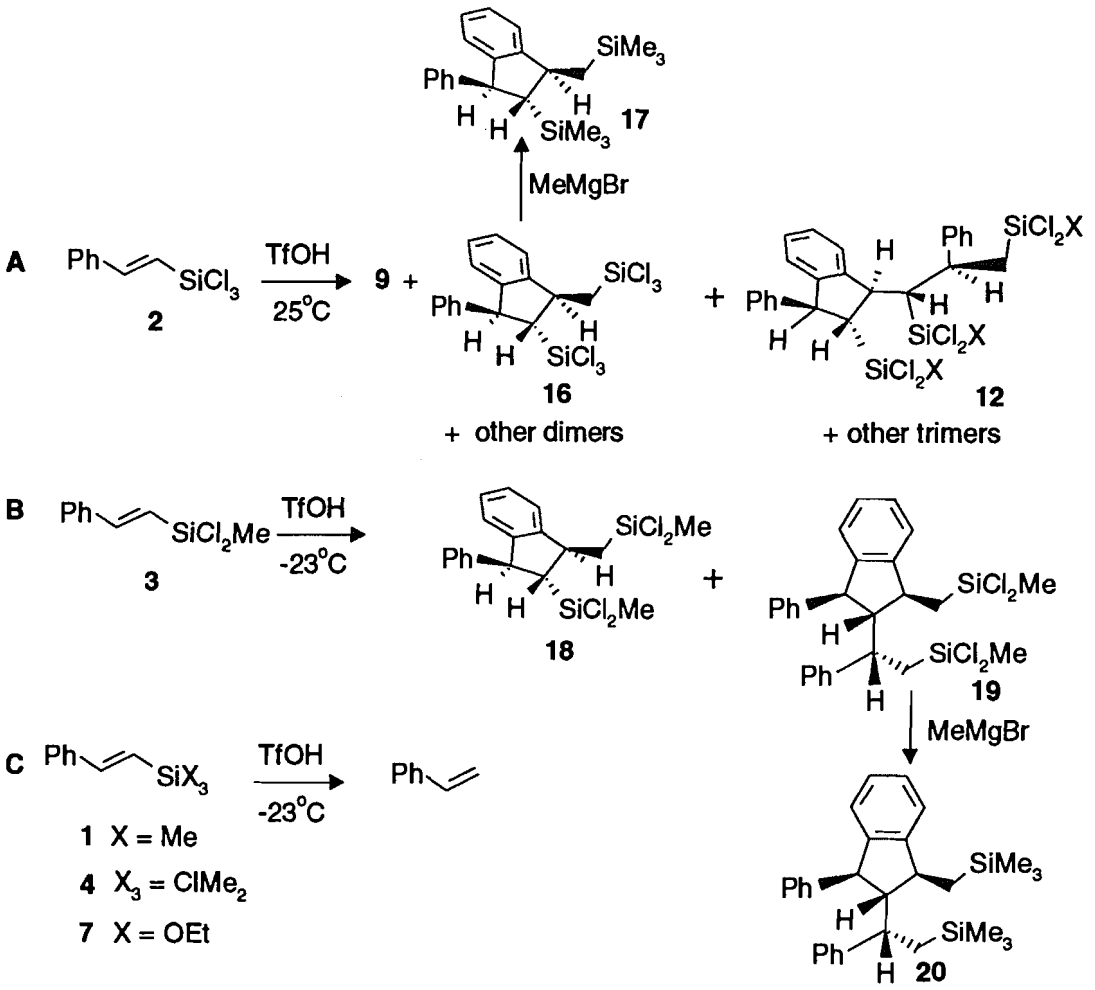

stereochemistry of this species was not unambiguously determined. The remaining higher molecular weight isomers were similarly terminated by indanes as clearly determined by the NMR signal for the doubly benzylic proton on the ring.

Performing the reaction at room temperature led to a deterioration of the stereochemical integrity; in addition to the dimeric product **9**, the isomer **18** and one other was produced. Similarly, several isomeric trimers including **12** were observed at higher temperatures (Scheme 5).

Effect of Ligands on Silicon

The degree to which oligomerization took place was highly dependent on the groups on silicon. As the number of Cl groups was reduced and replaced with methyl groups, the degree of protiodesilylation increased. This process, leading to styrene, could be seen from ^{1}H NMR studies of the reaction as it progressed and through the polystyrene that was isolated at the end of the reaction. Thus, with **2** or **5** protiodesilylation was not observed. However, with **3** or **6** ca. 35% protiodesilylation occurred, giving a dimer **18**, a desilylated trimer **19**, and styrene (Scheme 5B); with **4** or **1** (23) the products of the reaction did not contain silicon. Similarly, the exchange of one heteroatom Cl for another, for example, the replacement of $SiCl_3$ in **2** with $Si(OEt)_3$ **7** (18), led exclusively to protiodesilylation (Scheme 5C).

Table 3. Stereoselectivity as a function of reaction temperature and silyl group.[a]

Compound	Solvent	Temperature (°C)	Dimers **9**:**16**:other dimers	Trimers **12**:**19**
2	$CDCl_3$	−55	46:4:0	
2	$CDCl_3$	−23	40:6:0	
2	$CDCl_3$	0	19:9:0	
2	$CDCl_3$	25	11:5:2	
2	Pentane	−23	12:6:0	
2	Pentane	0	12:6:0	
2	Neat	0	18:5:4	
3	$CDCl_3$	−23	0:7:0	0:25
5[b]	$CDCl_3$	0	12:5:0	
6[b]	$CDCl_3$	0	0:6:0	0:16

[a]Recovered starting material and higher oligomers account for the remaining product, total = 100%.

[b]The product stereochemistry is that shown for dimers **9**, **18** and trimer **19** in Scheme 5, but with the silyl groups SiF_3 and $SiMeF_2$, respectively.

Mechanism

The mechanism of the oligomerization of **2** and related derivatives is presumably simple electrophilic addition. Electrophilic addition to vinylsilanes usually occurs more efficiently than to normal olefins. The presence of the silyl group nor-

Scheme 6.

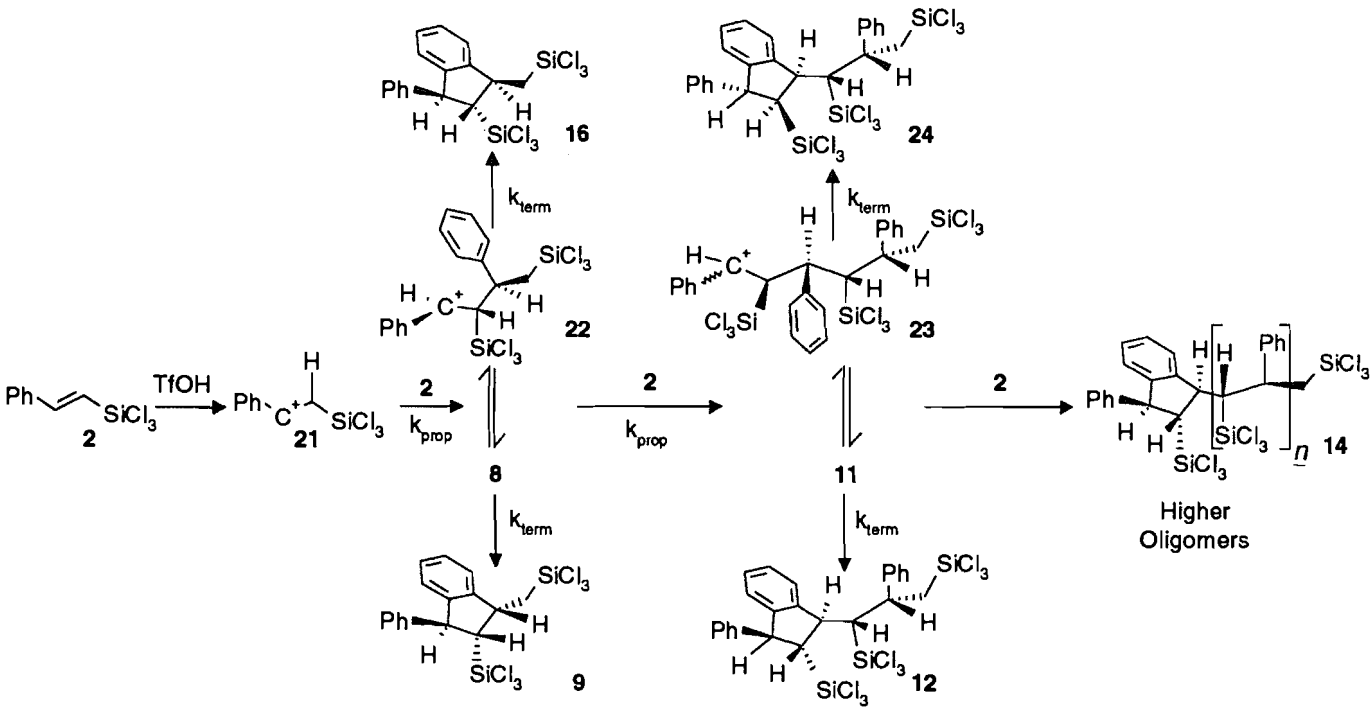

mally activates the double bond inductively. In addition, the intermediate cation **21**, formed by the protonation of **2** (Scheme 6), is stabilized through the β-effect by the silyl group (hyperconjugative stabilization of the cation by the Si—C σ-bond (8, 24)); the aryl group provides the most important stabilizing effect. If the β-effect is large (8), the cation will be better stabilized ($SiMe_3$, $SiMe_2Cl$, $Si(OMe)_3$) but will simultaneously be more susceptible to nucleophilic attack giving styrene (Scheme 5C)(23). With a less susceptible leaving group ($SiCl_3$, $SiCl_2Me$) protiodesilylation is avoided and **21** dimerizes to **8** or **22**. This process can be repeated, leading to higher oligomers, or termination can occur *via* an intramolecular Friedel–Crafts reaction, leading to indane-terminated species **14** (25). At low temperature, the stereochemistry of this closure involves attack of the phenyl group on the face of the cation opposite to the face bearing the silicon group (e.g., the dimer cation **8**→**9** and **23**→**24**). At higher temperatures, any stabilization of the cation by the silyl group (β-effect) is overshadowed by rotation and several isomers are produced.

The molecular weight distribution of the oligomerization will reflect the relative rates of the unimolecular termination and the bimolecular propagation reactions k_{term}/k_{prop} (19). As described above, all attempts to favour the bimolecular process by temperature control or control of monomer concentration were relatively unsuccessful; the highest molecular weight oligomer observed was a nonamer. This suggests that the lifetimes of the cations **8** and higher homologues are very low; unless the concentration of monomer **2** is high, deprotonation (**21**→**2**) or Friedel–Crafts termination (**8**→**9**) predominate (Scheme 6).

Utilization of the oligomers

Chlorosilanes are remarkably reactive species. The exposure of these functional groups to almost any nucleophile including hydroxylic species (water, alcohols, acids), amines, carbanions (RMgBr, RLi) etc., leads to substitution reactions at silicon. Indeed, it is this reactivity that is utilized to prepare silicone polymers (1).

The oligomers **14** (Scheme 3) have several special properties. In addition to their diastereoselective synthesis, the materials possess a high degree of functionality on a short chain and are liquids soluble in most solvents (with the exception of water). As with most trifunctional silanes ($RSiCl_3$), hydrolysis of **14** led to a rigid silsesquioxane (Scheme 7A). Films made by the hydrolysis of **14** were very brittle. However, the high degree of functionality on such a short chain might make **14** a useful crosslinking agent for polymers terminated with a functional group that will react with chlorosilanes. Polymers that appear to be suitable include living anionic polymers (26), polyethylene glycols, hydroxy-terminated silicones, etc. (Scheme 7B). Our efforts in these areas will be reported in due course.[9]

Experimental section

Apparatus, materials, and methods

The continuous wave ^1H NMR spectra were recorded on a Varian EM-390 (90 MHz) spectrometer and the Fourier spectra on a Bruker AM-500 (500 MHz) spectrometer or a Bruker AC-200 (200 MHz) spectrometer. ^{13}C (75.6 MHz) and ^{29}Si NMR (59.6 MHz) were performed on a Bruker AC-300 (at 300 MHz for protons). Chemical shifts are reported with respect to tetramethylsilane as standard, set to 0 ppm. Coupling constants (*J*) are recorded in hertz (Hz). The abbrevia-

[9] J. Jiang, M.A. Brook, and J. M. Dickson. Manuscript in preparation.

Can. J. Chem. Downloaded from www.nrcresearchpress.com by 46.23.64.124 on 09/08/12
For personal use only.

Scheme 7.

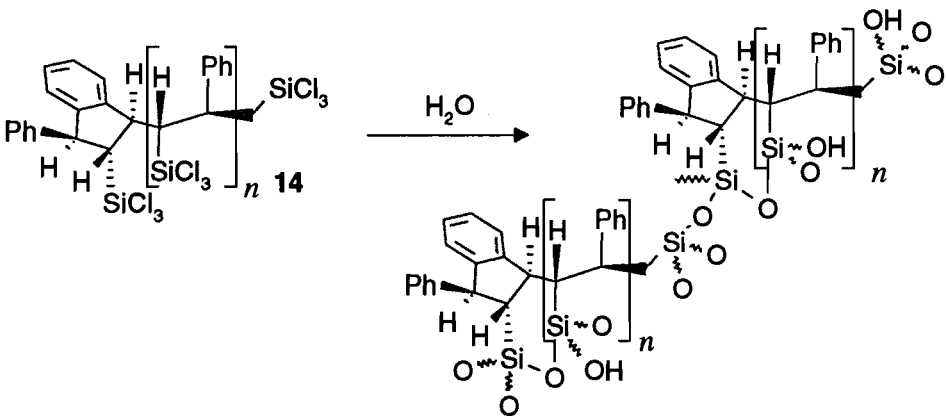

tions s = singlet, d = doublet, t = triplet, dd = doublet of doublets, m = multiplet, etc., are used in reporting the spectra.

Electron impact (EI) and chemical ionization (CI, NH_3) mass spectra were recorded at 70 eV with a source temperature of ca. 200°C on a VG analytical ZAB-E mass spectrometer equipped with a VG 11-250 data system. High-resolution mass spectral (HRMS) data were obtained with the VG-ZAB-E instrument by the EI method. Infrared spectra were run on a Perkin Elmer 283 spectrometer and Fourier spectra on a BIO RAD FTS-40 spectrometer, as neat films.

X-ray diffraction data for compound **10** were collected at room temperature on a Nicolet R3/m diffractometer with a Mo tube. The full experimental details have been reported elsewhere (10).

The copolymers were analyzed for the molecular weight distribution using a Waters gel permeation chromatograph equipped with a Waters 410 differential refractive index detector and a Foxboro Miran 1A variable wavelength IR detector to monitor the silicone distribution in copolymers. Narrow molecular weight silicone standards from Scientific Polymer Products (Ontario, N.Y.) were used for calibration of the chromatographic system.

All solvents were thoroughly dried before use. Dichloromethane was distilled over P_2O_5. Diethyl ether, THF, and hexane were distilled over Na–benzophenone. NEt_3 was dried by refluxing with NaOH and distilling over BaO.

Due to the tendency of halo groups on silicon to hydrolyze easily (**CAUTION: hydrolysis leads to production of HCl**), all reactions were carried out in dry apparatus under a nitrogen atmosphere with the use of septa and syringes for the transfer of reagents.

Preparation of 2–7

The hydrosilation of phenylacetylene to give **2–4** (8, 17), the conversion of **2**→**1** and **2**→**7** using MeMgBr (13, 17) and $HC(OEt)_3$ (18), respectively, and the preparation of the fluoro compounds using CuF_2 have also been reported (**2**→**5** and **3**→**6** (8)).

Attempted radical polymerization of 2

To **2** (2.0 g, 8.4 mmol) was added di-*tert*-butylperoxide (2.0 mg, 0.014 mmol, 0.1 wt.%) and the mixture was refluxed for 16 h at 140°C under a N_2 atmosphere. ^1H NMR clearly showed only starting material present in the reaction mixture.

General procedure 1: oligomerization of 2 with triflic acid as catalyst

To a solution of **2** (2.68 g, 11.3 mmol) in $CHCl_3$ (2.5 mL, frequently $CDCl_3$ was used, giving similar results, to facilitate NMR examination of the reaction) cooled to −23°C under a N_2 atmosphere was added triflic acid (0.1 mL, 1.13 mmol, 0.1 wt.%). The solution immediately turned dark red-orange and became viscous. After stirring for 2–4 h, the solution was allowed to warm to room temperature. The solvent could be removed under vacuum to give a quantitative mixture of oligomers. IR (KBr) ν: 3060, 3020, 2900, 1590, 1480, 1440, 1270, 1230, 1175, 1015, 725 cm^{-1}; ^1H NMR ($CDCl_3$, 200 MHz) δ: 1.6–2.7 (5H, m, backbone H's), 3.9–4.8 (<1H, doubly benzylic H_a, see Scheme 6), 7.2 (12 H, m).

General procedure 2: methylation of the oligomers

To facilitate structural characterization, the oligomeric residue (1 g) was diluted with ether (10 mL) cooled to 0°C and an excess of MeMgBr added (10 mL, 2.5 M in Et_2O). The mixture was allowed to warm to room temperature overnight, was quenched with water (20 mL), extracted with ether (3 × 20 mL), and the combined organic fractions dried over $MgSO_4$. The solvents were removed under reduced pressure to give a colourless oil (0.7 g, 93%). GPC (against polystyrene standards): M_n = 425. The compounds were separated (1.4 g) using flash chromatography with hexane as eluent. The major fractions R_f 0.37, 0.23, and 0.17 were isolated.

10: 0.70 g (50%); mp 75°C; IR (KBr pellet) ν: 3070, 3020, 2950, 2900, 1600, 1490, 1470, 1450, 1410, 1250, 1150, 1025, 990, 935, 850, 750, 690, 640 cm^{-1}; ^1H NMR ($CDCl_3$, 500 MHz) δ: −0.10 (s, 9 H), 0.04 (s, 9 H), 0.91 (dd, 1 H, J = 11.9, 14.2 Hz), 1.02 (dd, 1 H, J = 2.9, 14.2 Hz), 1.89 (dd, 1 H, J = 6.5, 11.5 Hz), 3.52 (ddd, 1 H, J = 2.9, 6.5, 11.9 Hz), 4.39 (d, 1 H, J = 11.5 Hz), 6.76–7.30 (m, 9 H); ^{13}C NMR ($CDCl_3$, 63.9 MHz) δ: −0.83, −0.27, 21.65, 43.13, 49.08, 51.52, 123.40, 124.59, 125.51, 126.09, 126.39, 128.27, 128.90, 144.73, 148.82, 150.20; ^{29}Si NMR ($CDCl_3$ 49.7 MHz) δ: −0.71, 0.27; HRMS (high resolution, EI, *m/z*), calcd. for M^+: 353.2043; found; 352.2030. Combustion analysis, calcd. for $C_{22}H_{32}Si_2$: C 74.93, H 9.15; found: C 74.83, H 9.27.

13 (contaminated with tetramer): 0.20 g (15%); IR (neat) ν: 3060, 3020, 2950, 2900, 1600, 1490, 1450, 1250, 1165, 855, 825, 750 cm^{-1}; ^1H NMR ($CDCl_3$, 500 MHz) δ: −0.23–0.04 (m, 27H), 0.82–1.04 (m, 2H), 1.30–1.47 (m, 1H), 1.82–1.89

Can. J. Chem. Downloaded from www.nrcresearchpress.com by 46.23.64.124 on 09/08/12
For personal use only.

Can. J. Chem. Downloaded from www.nrcresearchpress.com by 46.23.64.124 on 09/08/12
For personal use only.

(m, 1H), 3.41–3.53 (m, 1H), 4.03–4.12 (m, 1H), 4.30–4.38 (m, 1H), 7.0–7.32 (m, 14H); ^{13}C NMR ($CDCl_3$, 75.6 MHz) δ: −1.89–0.99 (m), 14.08, 21–24 (m), 42–52 (m), 123–129 (m), 142–147 (m); ^{29}Si NMR ($CDCl_3$, 59.6 MHz) δ: −0.84–0.59 (m); MS (EI) *m/z*: 704 (M^+, tetramer, (1), 672 (1), 617 (1), 570 (1), 555 (1), 528 (M^+, trimer, 100), 513 (51), 441 (64), 351 (39), 274 (70), 249 (94), 177 (100).

Higher oligomers: 0.4 g (30%); ^1H NMR, ^{13}C NMR, and ^{29}Si NMR were used in conjunction with mass spectroscopy to confirm that this fraction also contained indane-terminated oligomers. Based on the integration of the backbone protons (<3 ppm in ^1H NMR) to the doubly benzylic proton (3–4 ppm), the oligomers in this fraction are estimated to be 4–9 monomer units in length as confirmed by the mass spectrum. ^1H NMR ($CDCl_3$, 200 MHz) δ: 0.90 (m), 0.9–2.0 (m), 3.2–3.6 (m), 3.9 (m), 4.5 (m), 7.1 (m); ^{13}C NMR ($CDCl_3$, 75.6 MHz) δ: −1.2–1.0 (m), 22–34 (m), 42–52 (m), 122–129 (m), 144–149 (m); ^{29}Si NMR ($CDCl_3$, 59.6 MHz) δ: 0.00 (m), 16.9 (m); MS (EI) *m/z*: 1511 (9mer $M^+ - 73(SiMe_3)$), 1335 (8mer $M^+ - 73$), 1159 (7mer $M^+ - 73$), 983 (6mer $M^+ - 73$), 807 (5mer $M^+ - 73$).

Oligomerization of 3 with triflic acid as catalyst

Procedure 1 as above: **3** (2.45 g, 11.3 mmol); triflic acid (0.1 mL, 1.13 mmol, 0.1 wt.%). ^1H NMR ($CDCl_3$, 200 MHz) δ: 0.3 (s); 0.65 (s), 0.7–4.5 (m), 7.4 (m).

Methylation of the oligomers

Procedure 2 as above: oligomeric residue (1 g); MeMgBr added (10 mL, 2.5 M in Et_2O). Yield 0.75 g (92%). ^1H NMR ($CDCl_3$, 200 MHz) δ: 0.1–0.6 (m); 1.3–1.6 (m), 2.6 (m), 3.8 (d, J = 8 Hz), 7.5 (m).

The compounds were separated (1.4 g) using flash chromatography with hexane as eluent. The major fractions R_f 0.37, 0.35, and 0.16 were isolated.

17: 0.32 g, 40%; mp 66°C; IR (KBr pellet) *v*: 3070, 3030, 2960, 2890, 1600, 1495, 1470, 1450, 1405, 1250, 1165, 1130, 1030, 1010, 875, 865, 830, 750, 700, 685 cm^{-1}; ^1H NMR ($CDCl_3$, 500 MHz) δ: −0.02 (s, 9 H), 0.04 (s, 9 H),1.13 (dd, 1 H, J = 6.6, 15.2 Hz), 1.17 (dd, 1 H, J = 5.2, 15.2 Hz), 1.57 (t, 1 H, J = 8.5 Hz), 3.35 (dd, 1 H, J = 5.2, 6.6 Hz), 4.20 (d, 1 H, J = 8.5 Hz), 6.81–7.30 (m, 9 H); ^{13}C NMR ($CDCl_3$, 63.9 MHz) δ: −1.82, 0.29, 25.00, 42.57, 44.98, 53.08, 123.47, 124.73, 126.08, 126.22, 126.49, 128.27, 128.54, 146.62, 146.82, 150.01; ^{29}Si NMR ($CDCl_3$ 49.7 MHz) δ: −0.29, 2.64; MS (high resolution, EI, *m/z*): calcd. for M+ 353.2043; found: 352.2039. Combustion analysis, calcd. for $C_{22}H_{32}Si_2$: C 74.93, H 9.15, found: C 74.83, H 9.27.

20: 0.15 g, 20%; IR (KBr pellet) *v*: 3060, 3030, 2950, 2920, 2900, 2860, 1600, 1490, 1450, 1415, 1240, 850, 830, 745, 695 cm^{-1}; ^1H NMR ($CDCl_3$, 500 MHz) δ: −0.28 (s, 9 H), 0.09 (s, 9 H), 0.82 (d, 2 H, J = 6.7 Hz), 1.04 (dd, 1 H, J = 12.1, 14.7 Hz), 1.10 (dd, 1 H, J = 3.3, 14.7 Hz), 2.47 (dt, 1 H, J = 3.6, 5.3 Hz), 2.88 (ddd, 1 H, J = 3.2, 7.1, 11.2 Hz), 3.10 (dt, 1 H, J = 5.5, 6.2 Hz), 4.27 (d, 1 H, J = 5.3 Hz), 6.90–7.27 (m, 14 H); ^{13}C NMR ($CDCl_3$, 63.9 MHz) δ: −1.03, −0.09, 20.50, 25.52, 45.23, 46.45, 54.20, 65.89, 123.90, 125.40, 125.76, 126.22, 126.36, 126.74, 128.19, 128.38, 128.98, 144.95, 146.83, 149.09; ^{29}Si NMR ($CDCl_3$ 49.7 MHz) δ: −0.37, 0.73; HRMS (EI, *m/z*): calcd. for $M^+ - CH_3$: 441.2434; found: 441.2389. Combustion analysis, calcd. for $C_{30}H_{40}Si_2$: C 78.88, H 8.83, found: C 79.28, H 9.03.

The third fraction also comprised higher, indane-terminated oligomers.

Oligomerization of 4–7 with triflic acid as catalyst

Procedure 1 as above: e.g., **7** (4.0 mL, 19.6 mmol); $CDCl_3$ (4 mL); triflic acid (0.3 mL, 3.4 mmol). The residue in all three cases comprised unreacted starting materials, styrene, and polystyrene.

Controlling the oligomerization reaction

Acid concentration (Table 1)

Following General Procedure 1, the sensitivity of the reaction to the acid concentration was examined. The reaction with **2** (2.68 g, 11.3 mmol) was repeated with 10 mol%, 7 mol%, 5 mol%, 4 mol%, and 2 mol% triflic acid. Below 5 mol%, a significant amount of unreacted starting material was observed (>50%). This is attributed to loss of the triflic acid via nucleophilic exchange with Cl at silicon. HCl was shown to be ineffective as a catalyst for the oligomerization of **2**. At 5 mol% triflic acid or higher, the molecular weight distributions, as described above, were identical within experimental error.

Monomer concentration (Table 2)

The oligomerization was run at four different monomer concentrations. General Procedure 1 was followed with two exceptions, the triflic acid was used at 24 mol%; the amount of $CDCl_3$ controlled the monomer concentration (**2** (0.1 g, 0.422 mmol), triflic acid (0.01 mL, 0.1 mmol)) varied from 8.43 mM, 42.15 mM, 4.2 M, and bulk polymerization. The results are incorporated in Table 2. If shorter reaction times were used at the lowest concentration, the dimer was accompanied by unreacted **2**, the concentration of which decreased with increasing reaction time.

Temperature effects (Table 3)

The reaction (General Procedure 1) was examined at several temperatures from −55°C to 25°C. To shorten chain lengths and facilitate characterization of the stereochemical identity of the products much higher initiator concentrations were used (10–20 mol%). The yields reported below (Table 3) were calculated following isolation of the products by flash chromatography. The main change in the product distribution was the deterioration of stereochemical control as the temperature was increased (Table 3). The most convenient temperature that led to high levels of stereocontrol and acceptable conversion rates was −23°C.

Solvent effects (Table 1)

Using General Procedure 1, the oligomerization of **2** was repeated in a series of solvents. The product distributions and yields are shown in Table 1. It was necessary to use huge excesses of triflic acid in some cases to produce polymer; presumably, salting out of the acid reduced its concentration and its acidity was lower in the most polar medium. Methylene chloride and chloroform were judged to be the best solvents for this conversion.

Acknowledgements

We gratefully acknowledge financial support of this work

from the following sources: the Natural Sciences and Engineering Research Council of Canada, the Ontario Centre for Materials Research (OCMR), the Deutscher Akademischer Austauschdienst (a McMaster University – Universität Duisburg exchange scholarship to P.H., R.J., and S.W), the McMaster Institute for Polymer Production Technology (a summer research scholarship to J.A.T.), and Employment and Immigration Canada (a SEED grant to P.R.F.). We note, in particular, that Professor Jim Guillet was instrumental in providing us with a small envelope of OCMR money when we really needed it. We thank Colin Fyfe (University of British Columbia) for helpful discussions and for his encouragement to pursue these oligomeric materials.

References

1. W. Noll. Chemistry and technology of silicones. Academic, New York and London. 1968.
2. A. Tomanek. Silicones and industry. Hanser Verlag–Wacker Chemie GmbH, Munich. 1991.
3. H. Iwata and S. Isozaki. J. Appl. Polym. Sci. **49**, 1041 (1993); T. Kasemura, C. Komatu, H. Nishihara, S. Takahashi, Y. Oshibe, H. Ohmura, and T. Yamamoto. J. Adhes. **47**, 17 (1994).
4. A. Harashima. Dow Corning Toray Silicone Co., Ltd., Japan. Eur. Pat. EP 568102, Chem. Abstr. **120**, 325 824 (1993); A. Bachari, G. Belorgey, G. Helary, and G. Sauvet. Macromol. Chem. Phys. **196**, 411 (1995).
5. C. Bergstrom, A. Jafs, S. Jakobsson, I. Seppa, and M.L. Markkula. Öy Neste, Finland; Öy Kwh Plast. Eur. Pat. EP 484093, Chem. Abstr. **117**, 214 084 (1992).
6. R.M. Pike and D.L. Bailey. J. Polym. Sci. **22**, 55 (1956); K. Hayakawa, K. Kawase, H. Tamakita, and T. Yumoto. J. Polym. Sci. Polym. Chem. **19**, 3145 (1981); Y. Iwakura, F. Toda, and K. Hattori. J. Poly. Sci. Part A-1, **6**, 1633 (1068).
7. E.W. Colvin. Silicon in organic synthesis. Butterworths, London. 1981; W.P. Weber. Silicon reagents for organic synthesis. Springer, Berlin. 1983; I. Fleming. *In* Comprehensive organic chemistry. Vol. 3. *Edited by* D. Neville Jones. Pergamon, Oxford. 1979. Chap. 13.
8. M.A. Brook and A. Neuy. J. Org. Chem. **55**, 3609 (1990); M.A. Brook, M.A. Hadi, and A. Neuy. J. Chem. Soc. Chem. Commun. 957 (1989).
9. I. Fleming and A. Pearce. J. Chem. Soc. Perkin Trans. 1, 2485 (1980).
10. M.A. Brook, C. Henry, E. Jefferson, R. Jüschke, T. Sebastian, M. Tomaszewski, and S. Wenzel. Bull. Soc. Chim. Fr. In press.
11. C. Henry and M.A. Brook. Tetrahedron, **50**, 11379 (1994); Inorg. Chim. Acta, **220**, 145 (1994); M.A. Brook, C. Henry, R. Jüschke, and P. Modi. Synlett, **2**, 97 (1993).
12. X. Zhang, Q. Zhou, W.P. Weber, R.F. Horvath, T.-H. Chan, and G. Manuel. Adv. Chem. Ser. **224**, 679 (1990); X. Zhang, Q. Zhou, W.P. Weber, R.F. Horvath, T.H. Chan, and G. Manuel. Macromolecules, **21**, 1563 (1988); L. Wang, C.X. Liao, and W.P. Weber. J. Polym. Sci. Part A: Polym. Chem. **31**, 1789 (1993); H.S.J. Lee and W.P. Weber. Polym. Prepr. (Am. Chem. Soc., Div. Polym. Chem.), **31**, 424 (1990).
13. M.A. Brook, P. Modi, and J. M. Dickson. Macromolecules, **26**, 2624 (1993); M.A. Brook, P. Hülser, and T. Sebastian. Macromolecules, **22**, 3814 (1989).
14. I. Ojima. *In* The chemistry of organic silicon compounds. Vol. 1, *Edited by* S. Patai and Z. Rappoport. Wiley, Chichester, England. 1989. Chap. 25, pp. 1479–1526.
15. J.L. Speier. Adv. Organomet. Chem. **17**, 407 (1979).
16. B.D. Karstedt. U.S. Patent 3,775,452, (1973).
17. K. Tamao, J. Yoshida, H. Yamamoto, T. Kakui, H. Matsumoto, M. Takahashi, A. Kurita, M. Murata, and M. Kumada. Organometallics, **1**, 355 (1982); K. Tamao, M. Akita, and M. Kumada. J. Organomet. Chem. **254**, 13 (1983).
18. L.M. Shorr. J. Am. Chem. Soc. **76**, 1390 (1954).
19. H.R. Allcock and F. W. Lampe. Contemporary polymer chemistry, 2nd ed. Prentice Hall, Englewood Cliffs, N.J. 1990.
20. C. Le Roux, H. Yang, S. Wenzel, and M.A. Brook. Submitted for publication.
21. H. Fritsche, U. Hasserodt, and F. Korte. Chem. Ber. **97**, 1988 (1964); K. Naumann, G. Zon, and K. Mislow. J. Am. Chem. Soc. **91**, 2788 (1969); L. Horner and W.D. Balzer. Tetrahedron Lett. 1157 (1965); T.H. Chan, A. Melnyk, and D.N. Harpp. Tetrahedron Lett. 201 (1969); M.F. Lappert and J.K. Smith. J. Chem. Soc. 3225 (1961).
22. C. Eaborn. Organosilicon chemistry. Butterworths, London. 1960.
23. K.E. Koenig and W.P. Weber. J. Am. Chem. Soc. **95**, 3416 (1973).
24. A.R. Bassindale, and P.G. Taylor. *In* The chemistry of organic silicon compounds. *Edited by* S. Patai and Z. Rappoport. Wiley, Chichester, England. 1989. Chap. 14, pp. 893–963; J.B. Lambert. Tetrahedron, **46**, 2677 (1990); A.W.P. Jarvie. Organomet. Chem. Rev. Sect. A: **6**, 153 (1970); J.B. Lambert, G. Wang, R.B. Finzel, and D.H.Teramura. J. Am.Chem. Soc. **109**, 7838 (1987); J.B. Lambert and R.B. Finzel. J. Am. Chem. Soc. **104**, 2020 (1982); J.B. Lambert, and G.-T. Wang. J. Phys. Org. Chem. **1**, 169 (1988); J.B. Lambert and E.C. Chelius. J. Am. Chem. Soc. **112**, 8120 (1990); S.G. Weirschke, J. Chandrasekhar, and W.L. Jorgensen. J. Am. Chem. Soc. **107**, 1496 (1985).
25. M. Moreau, K. Matyjaszewski, and P. Sigwalt. Macromolecules, **20**, 1456 (1987); T. Higashimura, M. Hiza, and H. Hasegawa. Macromolecules, **12**, 217 (1979); Macromolecules, **12**, 1058 (1979); T. Kunitake, and K. Takarabe. Macromolecules, **12**, 1061 (1979); M. Hiza, H. Hasegawa, and T. Higashimura. Polymer J. **12**, 379 (1980).
26. T. Shiraki and M. Karaushi. Jpn. Kokai Tokkyo Koho, Japanese Patent 05306313 A2 931119 Heisei, 1993; S. Cheng and H. Zhu. Yingyong Huaxue, **9**, 13 (1992); H.L. Hsieh and A.G. Kitchen. ACS Symp. Ser. **212**, 291 (1983); T. Masuda, Y. Ohta, and S. Onogi. Polym. Prepr. (Am. Chem. Soc., Div. Polym. Chem.), **12**, 346 (1971).

Can. J. Chem. Downloaded from www.nrcresearchpress.com by 46.23.64.124 on 09/08/12
For personal use only.

Redox reactions of 3,5-di-*tert*-butyl-1,2-benzoquinone. Implications for reversal of paper yellowing

S.V. Jovanovic, K. Kónya, and J.C. Scaiano

Can. J. Chem. Downloaded from www.nrcresearchpress.com by 46.23.64.124 on 09/08/12
For personal use only.

Abstract: One- and two-electron transfer reactions of 3,5-di-*tert*-butylcatechol and the corresponding quinone were studied by fast kinetic spectroscopy coupled with laser photolysis and pulse radiolysis, and by cyclic voltammetry in aqueous solutions. Photoionization of catechol yields the same semiquinone radical as the formate-radical-induced quinone reduction in the pulse radiolysis experiment. The neutral semiquinone radical deprotonates at $pK_r = 6.0 \pm 0.1$, as deduced from the pH induced changes in the radical spectra. The two-electron reduction potentials of quinone and catechol were measured by cyclic voltammetry in aqueous solutions containing 25% methanol in the pH range 3–14. The pH dependence has two linear parts with slopes of 0.056 and 0.03 V/pH, intersecting at $pK_a = 10.0$. This is in excellent agreement with $pK_a = 10.05 \pm 0.05$ obtained spectrophotometrically. The reduction potential of 3,5-di-*tert*-butyl quinone, $E_7 = 0.01 \pm 0.04$ V, was obtained from the one-electron transfer equilibrium of the quinone with the oxygen/superoxide redox couple by pulse radiolysis. The rate constant of the reaction of quinone with the superoxide radical, $k = 1.2 \times 10^9$ M^{-1} s^{-1}, is higher than those of the superoxide reduction by catechols and phenols (typically $\sim 10^5$ M^{-1} s^{-1}); thus, lignin *o*-quinones could be efficient scavengers of superoxide under the conditions relevant for the photo-induced yellowing of lignin-rich paper. The reaction with $O_2^{\cdot-}$ effectively bleaches yellow quinone and generates metastable furanone, which hydrolyses to muconic acid, thus completely eliminating yellow quinone. 3,5-Di-*tert*-butylquinone also undergoes rapid bleaching with ascorbate, $k = 600 \pm 100$ M^{-1} s^{-1}, in methanol. The reaction has a 1:1 stoichiometry and leads to complete reduction of quinone to catechol with concomitant oxidation of ascorbate to dehydroascorbate. This unusual selectivity and the fact that the reaction of the milder oxidant 3,5-di-*tert*-butylquinone is an order of magnitude faster than that of stronger oxidant *p*-benzoquinone ($k = 60 \pm 10$ M^{-1} s^{-1}) suggest that a nucleophilic attack of quinone at the ascorbate double bond initiates the reaction.

Key words: superoxide, lignin, photochemistry, quinone.

Résumé : Faisant appel à voltampérométrie cyclique et à la spectroscopie cinétique rapide couplée à photolyse laser et à la radiolyse pulsée, on a étudié les réactions de transfert d'un et de deux électrons du 3,5-di-*tert*-butylcatéchol et la quinone correspondante, en solutions aqueses. La photoionisation du catéchol fournit le même radical semiquinone que celui produit lors de la réduction radicalaire de la quinone induite par le formiate dans l'expérience de radiolyse pulsée. Sur la base des changements induits de pH dans le spectre radicalaire, le radical semiquinone neutre se déprotone à un $pK_r = 6{,}0 \pm 0{,}1$. On a utilisé la voltampérométrie cyclique pour mesurer les potentiels de réduction à deux electrons quinone/catéchol en solutions aqueuses contenant 25% de méthanol, à des pH allant de 3 à 14. La relation avec le pH présente deux parties linéaires avec des pentes de 0,056 et 0,03 V/pH, avec ordonnée à l'origine de $pK_a = 10{,}0$. Cette valeur est en bon accord avec le $pK_a = 10{,}05 \pm 0{,}05$ obtenu spectrophotographiquement. On a obtenu le potentiel de réduction de la 3,5-di-*tert*-butylquinone, $E_7 = 0{,}01 \pm 0{,}04$ V, à partir de l'équilibre de transfert monoélectronique de la quinone avec le couple redox oxygène/superoxyde par radiolyse pulsée. La constante de vitesse de la réaction de la quinone avec le radical superoxyde, $k = 1{,}2 \times 10^9$ M^{-1} s^{-1}, est plus élevée que celles obtenues pour la réduction des catéchols et de phénols par le superoxyde (d'une façon typique $\sim 10^5$ M^{-1} s^{-1}); le *o*-quinones de la lignine pourraient donc être des pièges efficaces du superoxyde dans des conditions prévalent lors du jaunissement photoinduit du papier riche en lignine. La réaction du $O_2^{\cdot-}$ blanchit efficacement la quinone jaune et génère une furanone métastable qui s'hydrolyse en acide muconique en éliminant complètement le jaune de la quinone. La 3,5-di-*tert*-butylquinone subit aussi un blanchiment avec l'ascorbate dans le méthanol, $k = 600 \pm 100$ M^{-1} s^{-1}. La stoechiométrie de la réaction est 1 : 1 et elle conduit à une réduction complète de la quinone en catéchol avec une oxydation concomitante de l'ascorbate en déhydroascorbate. Cette sélectivité inhabituelle et le fait que la

Received March 15, 1995.

This paper is dedicated to Professor J.E. (Jim) Guillet in recognition of his contributions to Canadian chemistry.

S.V. Jovanovic, K. Kónya, and J.C. Scaiano.[1] Department of Chemistry, University of Ottawa, Ottawa, ON K1N 6N5, Canada.

[1] Author to whom correspondence may be addressed. Telephone: (613) 562–5896. Fax: (613) 562–5170.

réaction de l'oxydant plus doux 3,5-di-*tert*-butylquinone soit un ordre de grandeur plus rapide que celle de l'oxydant plus puissant *p*-quinone ($k = 60 \pm 10$ M^{-1} s^{-1}) suggère qu'une attaque nucléophile de la quinone au niveau de la double liaison de l'ascorbate initie la réaction.

Mots clés : superoxyde, lignine, photochimie, quinone.

[Traduit par la rédaction]

Introduction

Light-induced changes in thermomechanical and chemical pulps are initiated by the excitation of lignin chromophores, whose content may be as high as 23% in bleached pulp (1, 2). Subsequent reactions of excited chromophores lead to the formation of free radicals of phenoxyl, phenacyl, and peroxyl type and, probably, of singlet oxygen. These unstable species undergo complex reactions leaving behind non-radical products, the major classes being quinones, phenol dimers and oligomers, and organic peroxides and hydroperoxides (1). It is noteworthy that most of these "stable" products are extremely photochemically and chemically reactive. For example, organic peroxides and hydroperoxides can be cleaved photochemically or thermally to yield alkoxyl radicals, which could initiate further radical processes, resulting in increased brightness – reversion products. Of particular interest are the formation and the fate of yellow quinones, since they are believed to account for most of the photogenerated yellow color of the pulp.

Quinones may be formed in the oxidation reactions of the *o*-methoxyphenoxyl radicals followed by hydrolysis of the incipient arylmethoxide cation (3, 4). Major methoxyphenols in lignin are 2–methoxy- (vanillin-type) and 2,6-dimethoxyphenol (syringyl-type) (2). The corresponding *ortho*-quinones are unstable in protic solvents, which led us to model their redox properties using more stable 3,5-di-*tert*-butyl-1,2-benzoquinone. It is noteworthy that *o*-quinones are also produced by action of dioxygenase on catechols, which are chromophores in a variety of important biomolecules, such as epinephrine, dihydroxyphenylalanine (DOPA), DOPamine, quercetin, and rutin, and which prompted extensive research of their oxidation (5–10).

Photooxidation of 3,5-di-*tert*-butylcatechol, upon direct excitation (at 280 nm), or via a sensitizer (Rose Bengal), yields a mixture of products (6), among which yellow quinone and colorless 3,5-di-*tert*-butyl-5-(carboxymethyl)-2-furanone were identified by IR and NMR spectroscopy. These results were later revised (5), and an endoperoxide was identified as a major product of singlet oxygen reaction with the catechin derivative. Quinone and 3,5-di-*tert*-butyl-5-(carboxymethyl)-2-furanone (7) were the main products of oxidation of 3,5-di-*tert*-butylcatechol by the superoxide radical in tetrahydrofuran solutions. The formation of furanone from quinone was also demonstrated (7), which led to the conclusion that the superoxide radical reacted with both catechol and quinone, yielding the same semiquinone radical. The semiquinone radical was postulated (7) to react with another superoxide radical to form the furanone. It should be emphasized that the superoxide reaction effectively "bleaches" yellow quinone to a practically non-oxidizable metastable furanone (yields muconic acid upon hydrolysis), which is of interest for the reversal of paper yellowing. The above superoxide reactions are, in fact, one-electron transfer processes, the reaction with catechol being the reduction (superoxide→hydrogen peroxide) and that with quinone the oxidation of the superoxide radical (superoxide→oxygen). However, the kinetics and energetics of these electron transfer processes have yet to be established. We believe that the knowledge of redox characteristics of catechols is important not only for the improvement of the bleaching and yellowing inhibition strategies, since both quinones and catechols are abundant in thermomechanical pulp, but also for the understanding of the mechanisms of action of dioxygenases, where the establishment of the redox equilibria of various oxy species may play a role.

Ascorbate has been proposed as an inhibitor of photoyellowing of thermomechanical pulp (TMP), on the basis of its excellent radical-scavenging properties (1). However, ascorbate has also been shown to react thermally with *p*-quinones (11). It is, therefore, conceivable that it may also react with *o*-quinones (12), converting them to less colored products, thus effectively bleaching the pulp. Although the intermediacy of semiquinone radicals has been demonstrated in the *p*-quinone–ascorbate system (11), actual kinetic data for this two-electron reduction of quinone have not been reported. To establish fully the role of ascorbate in the reversal of yellowing, it is desirable to understand the kinetics and mechanism of the *o*-quinone reduction.

In this study, the redox and acid–base properties of 3,5-di-*tert*-butyl-semiquinone radicals have been studied by laser flash photolysis and pulse radiolysis. The one-electron reduction potential of quinone was determined by pulse radiolysis, whereas the two-electron reduction potential was measured by cyclic voltammetry in aqueous solutions (containing 25% methanol to dissolve the quinone). The redox properties of the quinone are consistent with the rapid oxidation of superoxide. The reaction with ascorbate was studied by UV–VIS and NMR spectroscopy. The implications of these results for the reversal of yellowing of lignin-rich TMP are discussed.

Materials and methods

All chemicals used in this study were of the highest purity commercially available. 3,5-Di-*tert*-butylcatechol, 3,5-di-*tert*-butyl-1,2-benzoquinone, ascorbate, and CD_3OD were Aldrich products; methanol and 2-propanol were Omnisolv grade from BDH; KCl and phosphate buffer were from Fisher or Merck. Water was purified through a Millipore MilliQ system, to a resistance better than 18 MΩ/cm. Solutions were freshly prepared before each experiment. The pH of the solutions was adjusted with NaOH (Merck or Fisher) and $HClO_4$ (Merck or Fisher). The solutions were saturated with high purity gases, N_2, N_2O, O_2, and N_2O:O_2 = 4:1 prior to the experiment.

Laser flash photolysis was performed on a system similar to that described in previous publications (13, 14) . A solution was made to flow from a container through a 7×7 mm^2 Suprasil cell, where it was photolyzed by pulses from a Lumonics EX-510 excimer laser (Kr/F_2/He, 248 nm, ~5 ns). The signal from the photomultiplier was initially captured by a Tektronix

Can. J. Chem. Downloaded from www.nrcresearchpress.com by 46.23.64.124 on 09/08/12
For personal use only.

Can. J. Chem. Downloaded from www.nrcresearchpress.com by 46.23.64.124 on 09/08/12
For personal use only.

2440 digital oscilloscope interfaced to a Macintosh IIcx computer, which was used for data acquisition and processing. Software for the laser system was written in the LabVIEW Version 2.2 programming environment from National Instruments.

For pulse radiolysis studies (15), we used the 3.0 MeV Van-de-Graaff pulse radiolysis facility at the Max-Planck-Institute für Strahlenchemie, Mülheim, Germany. Absorbed doses were ~20 Gy/pulse for the spectra determination, and ~2–3 Gy/pulse for the kinetic measurements, as determined by thiocyanate dosimetry.

Cyclic voltammetry was performed in the standard electrochemical cell, with glassy carbon as the working electrode, platinum mesh as a counter, and saturated calomel as the reference electrode, controlled from an EG&G Princeton VersaStat potentiostat. To avoid rapid autooxidation of catechol in an oxygen atmosphere, a buffered aqueous solution containing 25% v/v methanol without redox-active solutes was first purged with N_2 for ~20 min. Then catechol and quinone were injected (typically 0.25–1 mL in 82 mL total volume) as concentrated methanol solutions to achieve the desired concentrations in the buffered aqueous–methanol mixture.

The reactions of ascorbate with quinones were monitored by UV–VIS spectroscopy. The methanol solutions of ascorbate and quinone were mixed in a 10×10 mm^2 Suprasil quartz cell and quickly placed in the spectrophotometer. The *p*-benzoquinone–ascorbate reaction was monitored at 320 nm, where pseudo-first-order kinetics were observed for 1 mM *p*-benzoquinone and 0.01–0.25 mM ascorbate. The *o*-quinone (3,5-di-*tert*-butyl-1,2-benzoquinone)–ascorbate reaction was monitored at 400 nm. Pseudo-first-order kinetics could not be achieved under normal experimental conditions, so second-order kinetics were used. The concentrations of quinone and ascorbate were kept equal, and varied over the range 0.3–1.5 mM, and the second-order rate was obtained by extrapolation to the initial absorbance of the solution corrected for dilution due to the mixing of solutes. The identity of the products was investigated by NMR spectroscopy. The ^{13}C NMR spectra were recorded on a Varian Gemini 200 NMR spectrometer in deuterated methanol and D_2O solutions.

Results and discussion

Generation of semiquinone radicals

Semiquinone radicals may in principle be generated from 3,5-di-*tert*-butylcatechol or the corresponding quinone by the following methods: (*a*) by photoionization or chemionization (one-electron oxidation by strong transient oxidants, such as $Br_2^{\bullet-}$, and $^{\bullet}N_3$, radicals) of catechol; (*b*) H-atom abstraction from catechol by alkoxyl or peroxyl radicals generated by photochemical or radiation chemical methods, such as the *tert*-butoxyl radical; (*c*) via the excited triplet state of quinone, which has an n,π^* configuration, and is capable of H-atom abstraction from suitable H-atom donors; and (*d*) one-electron reduction of quinone by strong transient reductants, such as $CO_2^{\bullet-}$, $(CH_3)_2C^{\bullet}OH$.

One-electron oxidation of catechol with strong transient oxidants, although probably fast, $k \sim 10^9$ M^{-1} s^{-1}, might lead to the formation of adducts, as demonstrated (16) in the case of $Br_2^{\bullet-}$ reaction with phloroglucinol. The excited triplet state of 3,5-di-*tert*-butyl-1,2–benzoquinone undergoes rapid ($k \sim 10^6$ M^{-1} s^{-1}) intramolecular deactivation (17), which effectively competes with any intermolecular H-atom transfer and thus limits the use of this method for the generation of semiquinone radicals. Consequently, we used the 248 nm laser photoionization of catechol and the reduction of quinone with the formate radical anion, $CO_2^{\bullet-}$, to generate the semiquinone radicals.

Direct laser photoionization at 248 nm yields the semiquinone radical cation and an electron, eq. [1]. Similar to other semiquinone radicals (18), the radical cation rapidly loses a proton ($pK_r < 2$) to become the neutral radical in the pH range 2–14.

[1] 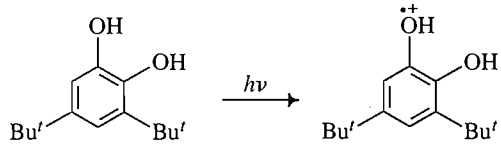

[2] 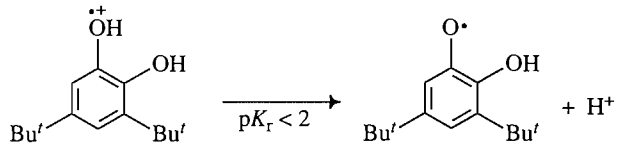

The quantum yield of photoionization, $\Phi = 0.26 \pm 0.03$, was determined in aqueous solutions at pH 9 ([3,5-di-*tert*-butylcatechol] = 0.3 mM), against the yield of electron in an N_2-saturated aqueous solution of KI ($\Phi = 0.29$) (19). The dependence of the transient optical density at 650 nm (solvated electron) vs. laser power was linear, indicating that the photoionization of 3,5-di-*tert*-butylcatechol is a monophotonic process at this wavelength. Solvated electron is easily scavenged with 2-chloroethanol, which enables the investigation of the spectral, acid–base, and redox properties of semiquinone radicals. The spectrum of the semiquinone radical is presented in Fig. 1.

The formate radical was generated by the pulse radiolysis of an N_2O-saturated aqueous solution of 0.1 M sodium formate and 0.1 mM quinone by the following sequence of reactions (20):

[3] $$H_2O \rightsquigarrow e_{aq}^-, {}^{\bullet}OH, H, H_3O^+, \ldots$$

[4] $$e_{aq}^- + N_2O + H_2O \longrightarrow {}^{\bullet}OH + OH^- + N_2$$
$$k = 9 \times 10^9 \text{ M}^{-1} \text{ s}^{-1}$$

[5] $$^{\bullet}OH + HCOO^- \longrightarrow H_2O + CO_2^{\bullet-}$$
$$k = 2.5 \times 10^9 \text{ M}^{-1} \text{ s}^{-1}$$

[6] $$H + HCOO^- \longrightarrow H_2 + CO_2^{\bullet-}$$
$$k \sim 2 \times 10^8 \text{ M}^{-1} \text{ s}^{-1}$$

The formate radical is a strong reductant, $E_7 = -2.0$ V (21), and rapidly reduces *o*-quinone.

Depending on the pH of the solution, the semiquinone radical anion formed in reaction (7) may be protonated to the neutral semiquinone radical (vide infra). The absorption spectrum of the semiquinone radical anion obtained upon $CO_2^{\bullet-}$ reaction with quinone is also presented in Fig. 1.

It is obvious from Fig. 1 that both photochemical and radiation chemical methods yield the same semiquinone radical, as expected. The noticeable difference exists in the 370–420

Can. J. Chem. Downloaded from www.nrcresearchpress.com by 46.23.64.124 on 09/08/12
For personal use only.

Fig. 1. Absorption spectra of the semiquinone radical anion, obtained by laser photolysis of 0.21 mM 3,5-di-*tert*-butylcatechol in N_2-saturated aqueous solution at pH 7, 20°C, containing 1% 2-chloroethanol to scavenge solvated electrons (–□–) normalized to A_{310} in the pulse radiolysis experiment; and pulse radiolysis of an N_2O-saturated aqueous solution of 35 mM NaOOCH and 0.07 mM 3,5-di-*tert*-butyl-1,2-benzoquinone at pH 7, 20°C (–○–).

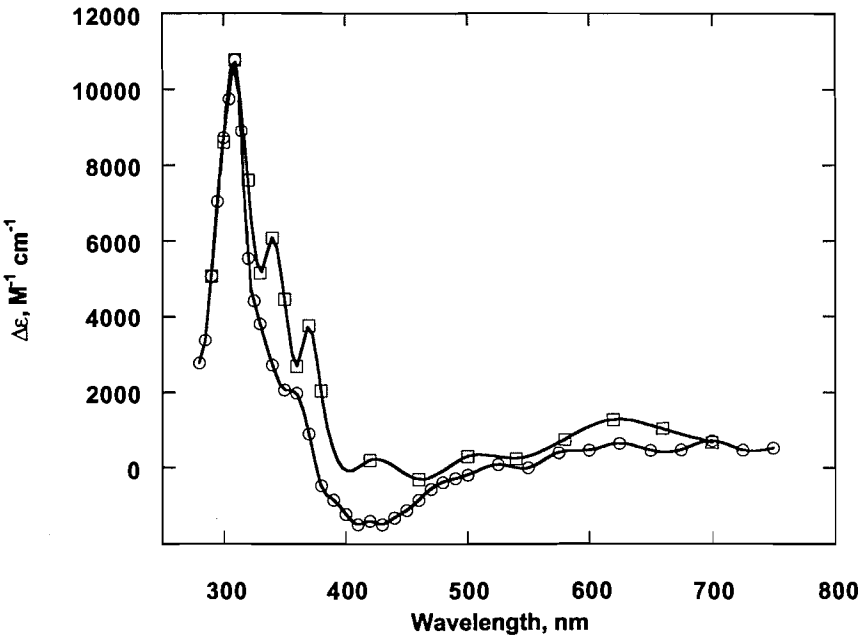

[7] $CO_2^{\bullet-}$ + 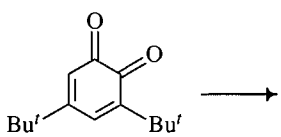 → 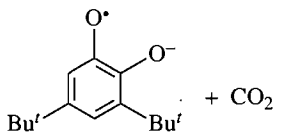 + CO_2

$k = 1.5 \times 10^9\ M^{-1}\ s^{-1}$

nm region, where the negative absorbance in the radiation chemical experiment occurs as a consequence of the bleaching of the parent quinone. The presence of the weak 650 nm band in the spectrum is expected for the *o*-semiquinone radical (22).

The neutral semiquinone radical undergoes deprotonation in neutral and alkaline media, as derived from the pH-dependent spectral changes, Fig. 2.

[8] 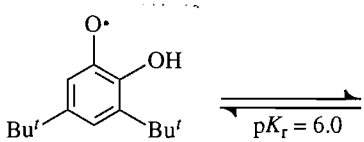 $pK_r = 6.0$ 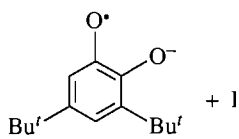 + H

The pK_r of the semiquinone radical anion (6.0 ± 0.1) is 4 pH units lower than that of parent catechol (pK_a = 10.05 ± 0.05, determined spectrophotometrically), which is similar to the data previously reported for a series of substituted hydroquinones and corresponding semiquinone radicals (10, 18). Such change in the acidity probably originates from the aromaticity of the semiquinone radical, which facilitates proton loss.

Redox potential of catechol/quinone redox pair

3,5-Di-*tert*-butylcatechol, QH_2, and the corresponding quinone, Q, may exhibit the following acid–base and electron-transfer equilibria in aqueous solutions,

[9] $^{-}Q^{\bullet} + e^- + 2H^+ \longrightarrow QH_2$

[10] $QH_2 \rightleftharpoons QH^- + H^+$ ($pK_a = 10.05$)

[11] $Q + e^- \longrightarrow {}^{-}Q^{\bullet}$

[12] $QH_2 + Q \longrightarrow 2\dot{Q}H$

[8] $^{-}Q^{\bullet} + H^+ \rightleftharpoons {}^{\bullet}QH$ ($pK_a = 6.0$)

Consequently, in the cyclic voltammetry of aqueous solutions the cathodic process is the one-electron reduction of quinone, whereas the anodic process corresponds to the oxidation of catechol. Both processes yield short-lived semiquinone radicals, which are in equilibrium with the parent catechol and quinone. The voltammograms of catechol–quinone mixtures were recorded in aqueous solutions (containing 25% methanol) at various pH in the range from 2 to 14. The standard electrode potential for the two-electron reduction of quinone was measured as a function of the concentrations of catechol and quinone (0.5–2 mM), and calculated according to the Nernst expression (23).

Can. J. Chem. Downloaded from www.nrcresearchpress.com by 46.23.64.124 on 09/08/12
For personal use only.

Fig. 2. The absorption spectra of the neutral (■) and anion (●) semiquinone radical obtained by pulse radiolysis of an N_2O-saturated aqueous solution of 35 mM NaOOCH and 0.07 mM 3,5-di-*tert*-butyl-1,2-benzoquinone at pH 3 and 7, respectively. The titration curve of the change of absorbance at 310 nm with the pH is shown as an inset.

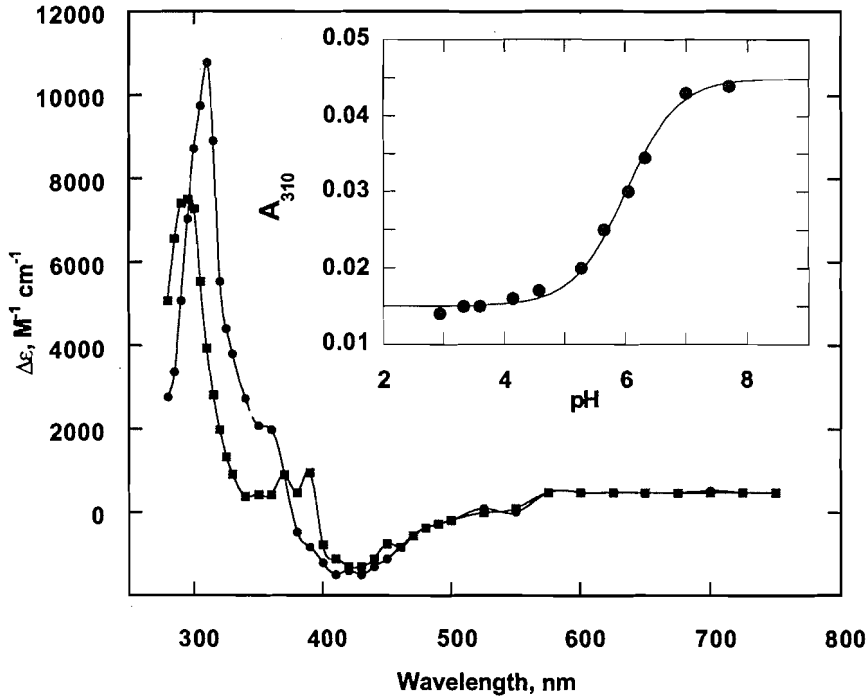

Fig. 3. Two-electron reduction potentials of 3,5-di-*tert*-butyl-1,2-benzoquinone measured at various pH values. Solid lines are best fits to the experimental data.

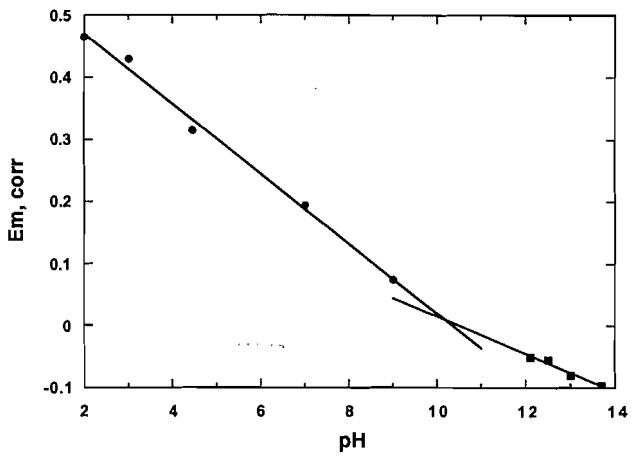

The half-cell reaction is

[13] $Q + 2e + 2H^+ \rightarrow QH_2$

which leads to the following expression for the pH dependence of the reduction potential (24),

[14] $E_m{}^i = E^0(Q/QH_2) + 0.03 \log\{f_Q(a^2H^+/f_{QH_2} + a_H + K_a/f_{QH^-}\}$

where $E_m{}^i$ and $E^0(Q/QH_2)$ represent the standard reduction potentials at pH = i and 0, respectively, and activity coefficients, f_i, are the function of the ionic strength of the solution (21). K_a is the thermodynamic dissociation constant of catechol. The pH dependence of the two-electron reduction potential of 3,5-di-*tert*-butyl-1,2-benzoquinone in 25% methanol – water at 20°C is presented in Fig. 3.

The pH dependence of the reduction potential is consistent with two linear regions with slopes equal to 0.056 and 0.03 V/pH, which means that the half-cell reactions involve QH_2 and QH^- in the respective pH range. The thermodynamic dissociation constant, $pK_a = 10.0$, may be derived from the intersection of the linear segments, in excellent agreement with $pK_a = 10.05 \pm 0.05$, determined spectrophotometrically.

$E^0(Q/QH_2) = 0.58$ V is obtained by extrapolation of the 0.056 V/pH portion of the pH dependence to pH = 0. This value is approximately equal to the standard potential, provided that the activity coefficients of quinone and catechol are equal at pH = 0 (which is a reasonable assumption at 0.1 M ionic strength). $E^0(Q/QH_2) = 0.58$ V is 0.12 V lower than 0.699 V (21) for the 1,4-benzoquinone/hydroquinone couple (which must be lower than the standard potential of the *o*-quinone/catechol couple (10, 18)), as expected from favorable electron-donating properties of the *tert*-butyl group.

The one-electron oxidation potential of 3,5-di-*tert*-butyl-1,2-benzoquinone was also determined by pulse radiolysis of aqueous solutions against the oxygen/superoxide redox couple. At pH 7, the superoxide radical was generated by the formate system (20), and was found to rapidly transfer an electron to quinone to form the semiquinone radical anion, as illustrated in the following reaction,

[15] 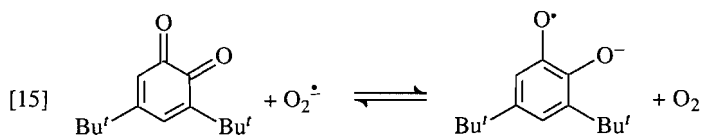

$k_f = (1.2 \pm 0.12) \times 10^9\ M^{-1}\ s^{-1}$ $K_{kin} = 400 \pm 120$; $K_{abs} = 620 \pm 60$
$k_r = (3 \pm 1) \times 10^6\ M^{-1}\ s^{-1}$

Can. J. Chem. Downloaded from www.nrcresearchpress.com by 46.23.64.124 on 09/08/12
For personal use only.

Table 1. Electron-transfer reactions of various substituted quinones with oxygen/superoxide redox couple in homogeneous aqueous solutions at 25°C.[a]

Radical from	E_7, V	pK_r[b]	k, M^{-1} s^{-1}	
			$O_2^{\cdot-} + Q$	$Q^{\cdot-} + O_2$
2,6-Dichloro-*p*-benzoquinone	n.m.	<3.0	3.0×10^9	$<10^6$
p-Benzoquinone	0.078	4.0	7.6×10^8	$<10^6$
3,5-Di-*tert*-butyl-*o*-benzoquinone[c]	0.010	6.0	1.2×10^9	3×10^6
2,5-Dimethyl-*p*-benzoquinone	−0.043	4.3	3.4×10^8	5×10^6
2,3-Dimethoxy-5-methyl-*p*-benzoquinone	−0.051	3.9	4.6×10^8	8×10^6
2,6-Dimethyl-*p*-benzoquinone	−0.055	4.7	2.9×10^8	6×10^6
Oxygen	−0.15	4.8		
Duroquinone	−0.260	5.9	8.0×10^6	2×10^8

[a]The rate constants taken from ref. 35 and reduction potentials from ref. 21.
[b]S.V. Jovanovic. Unpublished data.
[c]This study.

where K_{kin} and K_{abs} are the equilibrium constants determined from kinetic and spectroscopic studies, respectively.

The establishment of the electron transfer equilibrium between the quinone/semiquinone radical and oxygen/superoxide redox couples was monitored at 310 nm, where the difference in extinction coefficients of the semiquinone and superoxide radicals is optimal. The equilibrium constant from equilibrium absorbances, K_{abs}, was derived from the influence of the ratio of concentrations of quinone and oxygen (introduced to the solution as a N_2O:O_2 mixture) on the absorbance at 310 nm. The concentrations of quinone and oxygen were varied from 0.006 to 0.03 mM and from 0.026 to 1.3 mM, respectively. Since both quinone radical anion ($2k \sim 1 \times 10^8$ M^{-1} s^{-1}) and superoxide radical ($2k \sim 1 \times 10^8$ M^{-1} s^{-1}) at ~0.2 mM (1.4 Gy/pulse) do not decay appreciably over the time necessary for the establishment of the redox equilibrium (≤100 μs), the pseudo-first-order rates can be determined with sufficient accuracy. These data are used to evaluate the kinetic parameters of the redox equilibrium.

The redox potential difference between the oxygen/superoxide and quinone/semiquinone redox couples derived from the measured equilibrium constant using the Nernst equation yields $\Delta E = 0.16$ V. Since the reduction potential of oxygen is $E_7 = -0.15$ V (21), the reduction potential of quinone at pH 7 is $E_7(Q/^{\cdot-}Q^{\cdot}) = -0.15 + 0.16 = 0.01 \pm 0.04$ V.

With this value and $E_7(Q/QH_2) = 0.195$ V from cyclic voltammetry, we calculate the one-electron reduction potential of the 3,5-di-*tert*-butylcatechol radicals, $E_7(Q^{\cdot-}, 2H^+/QH_2) = 0.38$ V, and the semiquinone formation constant, $\log K_{f,7} = -6.16$ (see, for example ref. 21). The calculated reduction potential of the catechol radicals is in good agreement with the value of 0.34 V predicted from the Brown substituent constants (25–27). Such low reduction potential means that electron-rich methoxy- and methyl-substituted catechols are very sensitive to oxidation, which converts them to colored quinones.

The redox properties of 3,5-di-*tert*-butylquinone favor its reaction with the superoxide radical over the pH range 3–14, which is of significance for the bleaching and yellowing of pulp.[2] The superoxide radical may be generated either thermally from hydrogen peroxide (28, 29) in the peroxide bleaching, or photochemically from singlet oxygen (30–33) in the course of photoyellowing of pulp. Assuming that substituent effects in the catechol derivatives are similar to those in the hydroquinone derivatives, i.e., that the electron-rich substituents make both reduction potential of catechol radical and oxidation potential of quinone more negative, it may be concluded that all lignin-derived *o*-quinones (such as 3-methoxy-1,2-benzoquinone) are expected to be rapidly oxidized by the superoxide radical (see Table 1). On the basis of close to diffusion-controlled rate constants, the reactions of the superoxide radicals with quinones are by far the most efficient route for superoxide disappearance in a system devoid of substantial concentrations of transition metal ions.

[2] Because $pK_a = 4.8$ (27) for the protonation of $O_2^{\cdot-}$ to $HO_2^{\cdot}$, the reactions in acidic media, pH < 4, where $HO_2^{\cdot}$ predominates, may be considerably slower than those in neutral and alkaline media.

Two-electron reduction of quinone by ascorbate

Mixing methanol solutions of ascorbate and 3,5-di-*tert*-butyl-1,2-benzoquinone results in rapid disappearance of the yellow color, which provides a convenient method for monitoring the reaction.

[16] 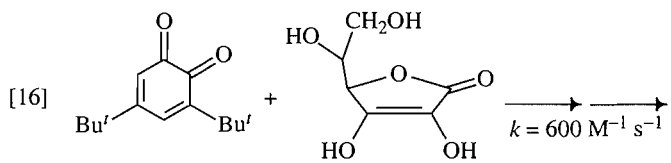

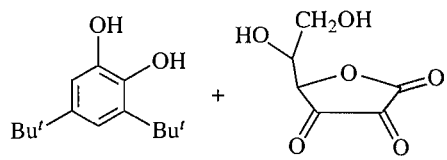

The reaction rate constant was derived from the second-order kinetics for various initial concentrations of the quinone and ascorbate as $k = 600 \pm 100$ M^{-1} s^{-1}. The stoichiometry of this reaction appears to be 1:1, as deduced from the variation of the concentrations of both reactants and the measurements of the residual absorbance at 400 nm (data not shown). The identity of the products of the reaction was verified by ^{13}C NMR spectroscopy in CD_3OD. The NMR spectra of reactants and products of the above reaction are presented in Fig. 4.

Can. J. Chem. Downloaded from www.nrcresearchpress.com by 46.23.64.124 on 09/08/12
For personal use only.

Fig. 4. ^{13}C NMR spectra of methanol-d_4 solutions containing the products of the reaction of 1 M 3,5-di-*tert*-butyl-1,2-benzoquinone and 1 M ascorbate; 1 M 3,5-di-*tert*-butyl catechol; and 1 M dehydroascorbate (in D_2O).

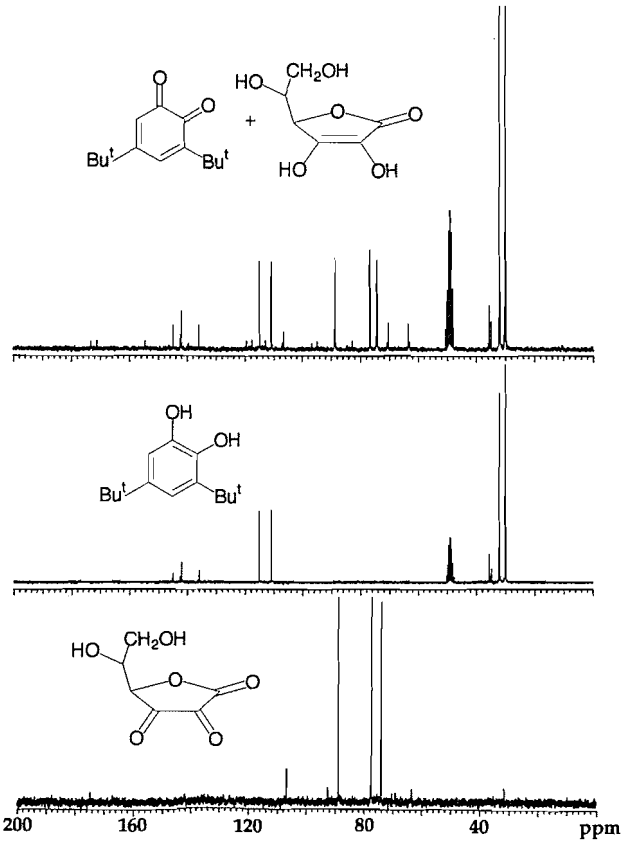

The products of the two-electron reduction of 3,5-di-*tert*-butyl-1,2-benzoquinone by ascorbate are indeed catechol and dehydroascorbate, as may be seen from Fig. 4. Consequently, one mole of the quinone reacts with one mole of ascorbate to produce one mole each of catechol and oxidized ascorbate. This is surprising, considering the reported intermediate formation of free radicals, namely semiquinone and ascorbate radicals, whose reactions must produce a more complicated mixture of products. In an attempt to rationalize these results we investigated the reaction of ascorbate with 1,4-benzoquinone. This reaction was previously shown (11) to involve the intermediacy of semiquinone radicals, and constitutes the two-electron reduction of the quinone to hydroquinone:

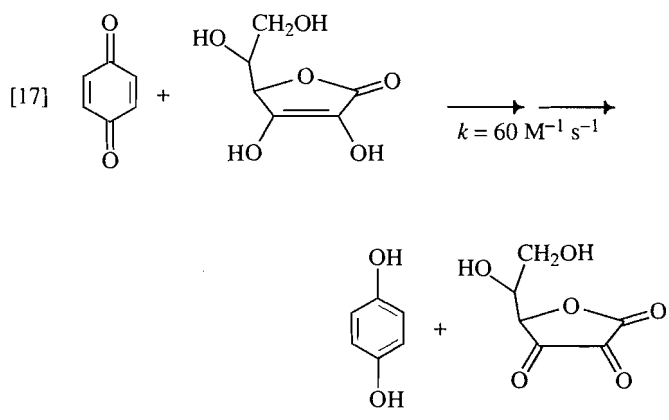

Fig. 5. ^{13}C NMR spectra of methanol-d_4 solutions containing the products of the reaction of 1 M 1,4-benzoquinone and 1 M ascorbate; 1 M hydroquinone; and 1 M dehydroascorbate (in D_2O).

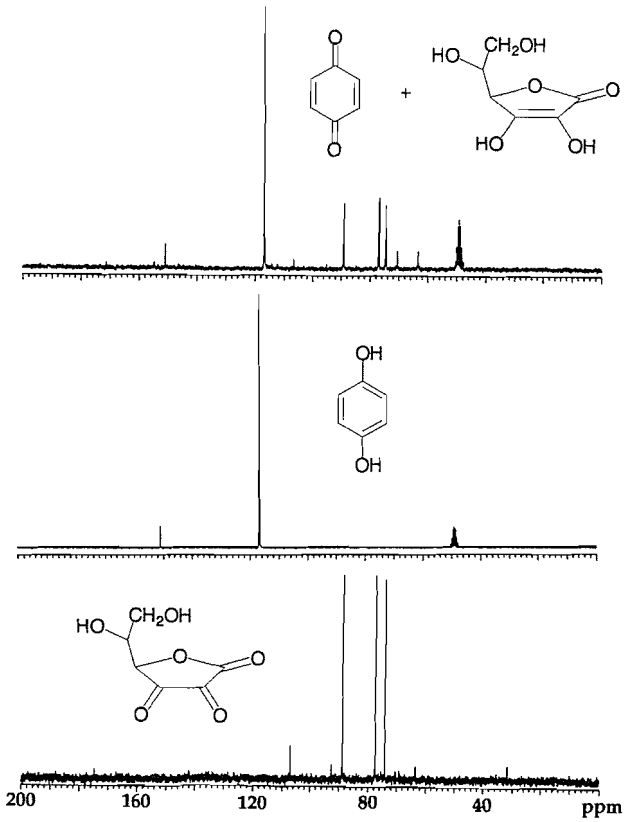

We studied the reaction of *p*-benzoquinone and ascorbate in methanol solutions. Similar to the reaction with *o*-quinone, the final products are fully reduced quinone, hydroquinone, and dehydroascorbate (also confirmed by NMR spectroscopy, see Fig. 5). However, the reaction rate constant is found to be an order of magnitude slower than that with *o*-quinone, $k = 60 \pm 10\ M^{-1}\ s^{-1}$ compared to $600\ M^{-1}\ s^{-1}$. This difference in the rates of the reactions is in contrast the redox properties of the quinones. Namely, *p*-quinone is, by 0.12 V, a stronger oxidant than *o*-quinone, which means that the electron transfer involving *p*-quinone is more exothermic and thus expected to be faster.

Conclusions

o-Semiquinone radical may be produced either by photoionization of 3,5-di-*tert*-butylcatechol or by the reduction of the quinone induced by the radiolytically generated formate radical. $pK_a = 6.0$ is determined from the pH-dependent changes in the semiquinone radical spectra.

The two-electron reduction potential of quinone, $E^{0'} = 0.58$ V, is lower than $E^{0'} = 0.699$ V of the unsubstituted 1,4-benzoquinone (which must be lower than that of *o*-quinone) (10, 18), a consequence of the substituent effect of electron-donating *tert*-butyl groups. Similar two-electron reduction potentials are also expected for other *o*-quinones substituted by electron-rich substituents (for example, $\sigma^+[ortho(OCH_3)] = -0.67$, $\sigma^+[ortho(CH_3)] = -0.27$, should be compared with

$2\sigma^+[meta(C(CH_3)_3)] = -0.14$) (26). The one-electron reduction potential of 3,5-di-*tert*-butyl-1,2–benzoquinone determined by pulse radiolysis at pH 7, $E_7 = 0.01 \pm 0.04$ V, enables calculation of the reduction potential of the corresponding catechol radicals, $E_7 = 0.38$ V, which is lower than $E_7 = 0.53$ V of unsubstituted catechol. Low reduction potential of the catechol radicals, in general (see also refs. (10, 18, 25, 34) means that they are highly sensitive to oxidation.

3,5-di-*tert*-butyl-1,2-benzoquinone and various electron-rich methoxy- and methyl-*o*-quinones appear to be moderately strong oxidants, capable of oxidizing the superoxide radical at any pH. The oxidation of the superoxide radical by the quinones is a very efficient route for the superoxide decay. Since this reaction was shown (7, 9) to decompose yellow quinone to colorless and photoinactive products, it is of relevance for the reversal of photoyellowing of lignin-rich pulp.

Two-electron reduction of the quinones by ascorbate is an efficient bleaching reaction, since it yields colorless products, hydroquinone and dehydroascorbate. This reaction occurs spontaneously in the dark and may contribute to the potential use of ascorbate in the protection of pulp from photo-induced yellowing. However, it should be noted that dihydroxybenzenes are highly oxidizable substrates, whose oxidation ultimately leads to the production of yellow products (quinones and (or) phenol dimers and oligomers). Therefore, in the use of ascorbate as an inhibitor, the reduction of various quinones actually wastes ascorbate, thus diminishing its efficacy.

Acknowledgment

This work was supported by the Natural Sciences and Engineering Research Council of Canada and the Canadian Network of Centers of Excellence through the Mechanical and Thermomechanical Wood Pulps Network. We are grateful to Prof. Steen Steenken of the Max-Planck-Institute für Strahlenchemie who kindly provided access to the pulse radiolysis equipment. The assistance of Ms. Rada Simpraga in cyclic voltammetry experiments is gratefully acknowledged. J. C. S. is supported by a Killam Fellowship awarded by the Canada Council.

References

1. G.J. Leary. J. Pulp Pap. Sci. **20**, J154 (1994).
2. C. Heitner and J.C. Scaiano. Photochemistry of lignocellulosic materials. ACS Symp. Ser. **531**, 1993.
3. D. Hawley and R.N. Adams. J. Electroanal. Chem. **8**, 163 (1964).
4. L. Zhang and G. Gellerstedt. Acta Chem. Scand. **48**, 490 (1994).
5. F. Jensen and C.S. Foote. Photochem. Photobiol. **46**, 325 (1987).
6. T. Matsuura, A. Nishinaga, N. Yoshimura, T. Arai, K. Omura, H. Matsushima, S. Kato, and I. Saiyo. Tetrahedron Lett. **21**, 1673 (1969).
7. Y. Moro-oka and C.S. Foote. J. Am. Chem. Soc. **98**, 1510 (1976).
8. H. Nohl, W. Jordan, and R.J. Youngman. Adv. Free Radical Biol. Med. **2**, 211 (1986).
9. D.T. Sawyer, T.S. Calderwood, C.L. Johlman, and C.L. Wilkins. J. Org. Chem. **50**, 1409 (1985).
10. S. Steenken and P. Neta. J. Phys. Chem. **86**, 3661 (1982).
11. R. Pethig, P.R.C. Gascoyne, J.A. McLaughlin, and A. Szent-Gyorgyi. Proc. Natl. Acad. Sci. U.S.A. **80**, 129 (1983).
12. Y. Hasebe, Y. Tanaka, and S. Uchiyama. Anal. Lett. **27**, 41 (1994).
13. J.C. Scaiano. J. Am. Chem. Soc. **102**, 7747 (1980).
14. J.C. Scaiano, M. Tanner, and D. Weir. J. Am. Chem. Soc. **107**, 4396 (1985).
15. V. Jagannadham and S. Steenken. J. Am. Chem. Soc. **106**, 6542 (1984).
16. D. Wang, I. Gyorgy, K. Hildenbrand, and C. von Sonntag. J. Chem. Soc. Perkin Trans. 2, 46 (1994).
17. B. Alkenings, H. Bettermann, I. Dasting, and H.-J. Schroers. Spectrochim. Acta, **49A**, 315 (1993).
18. S. Steenken and P. Neta. J. Phys. Chem. **83**, 1134 (1979).
19. J. Calvert and J. N. Pitts, Jr. Photochemistry. J. Wiley and Sons, London. 1966 .
20. C. von Sonntag. The chemical basis of radiation biology. Taylor and Francis, London. 1987 .
21. P. Wardman. J. Phys. Chem. Ref. Data, **18**, 1637 (1989).
22. A.B. Berinstein, M.K. Whittlesey, and J.C. Scaiano. *In* Photochemistry of lignocellulosic materials. *Edited by* Heitner and Scaiano. American Chemical Society, Washington, D. C. 1993. p. 111.
23. G. Kortum. Treatise on electrochemistry. Elsevier Publishing Company, Amsterdam. 1965.
24. W.M. Clark. Oxidation–reduction potentials of organic systems. The Williams and Wilkins Comp., Baltimore. 1960 .
25. S.V. Jovanovic, M. Tosic, and M.G. Simic. J. Phys. Chem. **95**, 10824 (1991).
26. C. Hansch, A. Leo, and R.W. Taft. Chem. Rev. **91**, 165 (1991).
27. J. Lind, X. Shen, T.E. Eriksen, and G.J. Merenyi. J. Am. Chem. Soc. **112**, 479 (1990).
28. J. Gierer. Holzforschung, **44**, 395 (1990).
29. J. Gierer. Holzforschung, **44**, 387 (1990).
30. A.A. Gorman, I.R. Gould, I. Hamblett, and M.C. Standen. J. Am. Chem. Soc. **106**, 6956 (1984).
31. N. Houba-Herin, C.M. Calberg-Bacq, J. Piette, and A. Van de Vorst. Photochem. Photobiol. **36**, 297 (1982).
32. M. Luiz, M.I. Gutierez, G. Bocco, and N.A. Garcia. Can. J. Chem. **71**, 1247 (1993).
33. I. Saito, T. Matsuura, and K. Inoue, J. Am. Chem. Soc. **105**, 3200 (1983).
34. S. V. Jovanovic, S. Steenken, M. Tosic, B. Marjanovic, and M. G. Simic. J. Am. Chem. Soc. **116**, 4846 (1994).
35. B.H.J. Bielski, D.E. Cabelli, R.L. Arudi, and A.B. Ross. J. Phys. Chem. Ref. Data, **14**, 1041 (1985).

Can. J. Chem. Downloaded from www.nrcresearchpress.com by 46.23.64.124 on 09/08/12
For personal use only.

Optical properties of side-chain liquid crystal copolymers of monosubstituted cholesteryl itaconate and a non-chiral mesogen

J.M.G. Cowie and H.W. Hunter

Can. J. Chem. Downloaded from www.nrcresearchpress.com by 46.23.64.124 on 09/08/12
For personal use only.

Abstract: New mono- and disubstituted cholesteryl derivatives of itaconic acid have been prepared and their thermotropic liquid crystalline behaviour examined. The monosubstituted derivative has been homopolymerized, and also copolymerized with a non-chiral mesogen 4-cyanophenyl-4′-(6-acryloyl oxyhexyloxy) benzoate. Examination of the series of copolymers prepared, using differential scanning calorimetry and hot-stage polarizing microscopy, showed that when the content of the cholesteryl itaconate was high, both a smectic-A phase (S_A) and a cholesteric phase (N*) were present. It was found that the S_A phase could be eliminated by lowering the content of the cholesteryl itaconate in the copolymers, giving samples that displayed only the N* phase over a much wider temperature range. The samples in the N* phase also exhibited selective reflection of visible light that changed from short to long wavelengths as the samples were cooled from the isotropic melt. These colours can be locked into the glassy state of the polymer by quenching below the glass transition temperature, but only if the S_A phase is absent. It was also noted that at high contents of the cholesteryl itaconate the selective reflection appears to occur in the ultraviolet region.

Key words: itaconic acid, copolymers, liquid crystalline polymers, cholesteric phases, selective reflection.

Résumé : On a préparé de nouveaux itaconates de mono- et di-cholestéryle et on a examiné leur comportement comme cristaux liquides thermotropes. On a homopolymérisé l'ester monosubstitué et on l'a aussi copolymérisé avec un mésogène non chiral, le 4′-(6-acryloyloxyhexyloxy)benzoate de 4-cyanophényle. L'examen de la série des copolymères qui ont été préparés en faisant appel à la calorimétrie à balayage différentiel et à la microscopie à plaque chauffante polarisante a permis de montrer que le contenu en itaconate de cholestéryle est élevé et que l'on retrouve une phase smectique-A (S_A) ainsi qu'une phase cholestérique (N*). On a trouvé que la phase S_A peut être éliminée en abaissant le contenu de l'itaconate de cholestéryle dans les échantillons donnant des copolymères qui ne présentent que la phase N* sur une plage plus étendue de température. Les échantillons dans la phase N* présentent aussi une réflexion sélective de la lumière visible qui passe des longueurs d'onde courtes à élevées lorsque les échantillons sont refroidis à partir du produit fondu isotrope. Ces couleurs peuvent être figées dans l'état vitreux du polymère par une trempe à une température inférieure à celle de la transition de la vitre; cette possibilité n'existe que si la phase S_A est présente. On a aussi noté que, si la quantité d'itaconate de cholestéryle est élevée, la réflexion sélective semble se produire dans la région ultraviolette.

Mots clés : acide itaconique, copolymère, polymères cristallines liquides, phases cholestériques, réflexion sélective.

[Traduit par la rédaction]

Introduction

Interest in chiral side-chain liquid crystal polymers has grown rapidly in recent years because of their potential in emerging optical technologies. Many exhibit piezo and pyroelectric effects, some are ferroelectric, and others are capable of selective reflection of electromagnetic radiation, particularly in the visible region (1–4). This latter property can be a function of both structure and temperature and in our own work we have used copolymerization as an additional means of fine tuning this behaviour (5–7). While these previous studies have used the strategy of introducing a chiral centre in the spacer between the mesogen and the chain backbone, this synthetic approach can be simplified by using instead the cholesteryl unit as a natural chiral mesogen and synthesizing monomers with this as a pendant side chain. While this structure tends to be susceptible to oxidative degradation and it is not the ideal unit to use for practical applications, examination of such systems can assist in our understanding of the relationships between copolymer constitution and the resulting optical properties.

Received March 15, 1995.

This paper is dedicated to Professor J.E. (Jim) Guillet in recognition of his contributions to Canadian chemistry.

J.M.G. Cowie[1] and H.W. Hunter. Department of Chemistry, Heriot-Watt University, Edinburgh EH14 4AS, Scotland.

[1] Author to whom correspondence may be addressed. Telephone: 44-131-451-3106. Fax: 44-131-451-3180.

Can. J. Chem. Downloaded from www.nrcresearchpress.com by 46.23.64.124 on 09/08/12
For personal use only.

Freidzon et al. (8) have observed differences in behaviour when the cholesteryl group is attached to acrylate and methacrylate units. Here we have selected the analogue, itaconic acid, as one monomer unit because it has the additional flexibility of having two functional sites for modification, if that is deemed necessary for further property modification. Both mono- and disubstituted cholesteryl itaconate ester monomers have been synthesized, but only the monosubstituted derivative proved amenable to polymerization reactions. These are structures **1** and **2**, shown below, and the monomer selected for the copolymerization reaction is 4-cyanophenyl-4′-(6-acryloxyhexyloxy) benzoate **3**, which is mesogenic but non-chiral.

Monomer structures

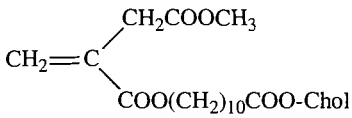

1

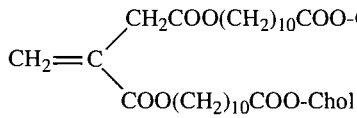

2

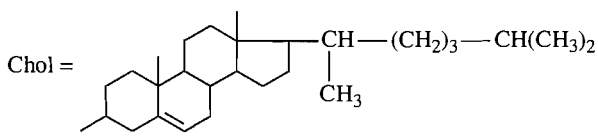

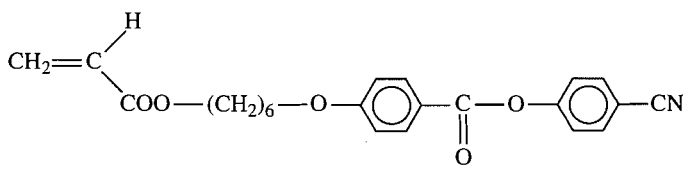

3

Experimental section

Monomer synthesis

The precursor to the preparation of both mono- and disubstituted cholesteryl itaconates was cholesteryl-11-bromo undecanoate, which was synthesized following a route similar to that proposed by Freidzon et al. (9).

Cholesteryl-11-bromo undecanoate

Redistilled and dried triethylamine (4.05 g, 0.04 mol) was added to a solution of cholesterol (11.6 g, 0.03 mol) in anhydrous benzene (150 mL) and the mixture vigorously stirred whilst 10-bromo undecanoyl chloride (11.35 g, 0.04 mol) was added slowly dropwise, at room temperature. The resultant pink-coloured solution was stirred for a further 2 h and then the benzene removed in vacuo. Diethyl ether (200 mL) was added to the mixture along with water (100 mL), the layers were separated, and the organic phase was washed with two further portions of water (2 × 50 mL). The dried ($MgSO_4$) organic phase was reduced to about one quarter of its original volume and poured into a large excess of methanol to precipitate the product which was then collected by filtration. After washing with methanol the product, was dried and analysed for purity by tlc. No further purification was needed. Yield: 14.6 g, 77%; mp 104–106°C (lit. (9) mp 105°C).

1-[1-[Cholesteryloxy)carbonyl]-10-decanyl]-2-methylene-4-methyl butane-1,4-dioate 1

Monomethyl itaconate (6.34 g, 4.4 mmol) from the esterification of methanol with itaconic acid in the presence of acetyl chloride was dissolved in anhydrous methanol (15 mL) and cesium hydroxide (6.74 g, 4.4 mmol) was added. After complete dissolution the methanol was evaporated to give the cesium salt of monomethyl itaconate. Anhydrous DMF (120 mL) was added and the mixture stirred at 50°C for 2 h in the presence of hydroquinone (ca. 0.5 g). Cholesteryl-11-bromo undecanoate (7 g, 1.1 mmol) was then added and the mixture stirred for a further 24 h under nitrogen at 50°C. After cooling, DMF was coevaporated with xylene in vacuo and the residue dissolved in chloroform (200 mL). After washing with water (50 mL) the organic layer was washed with saturated sodium bicarbonate (2 × 50 mL) and then with water (50 mL). The chloroform layer was dried ($MgSO_4$), evaporated, and subjected to column chromatography using silica gel. The bromide starting material was eluted with toluene (R_f = 0.88, toluene) and the desired mixed ester was eluted with a 20% chloroform in toluene mixture (R_f = 0.22, toluene). Yield: 2.27, 74%; mp 14–17°C; ^1H nmr, δ ppm ($CDCl_3$; 90 MHz): 0.5–3.25 (m, 63H) cholesteryl R-H, undecyl $R(CH_2)_8$-COO-, vinyl -CH_2CO_2-; 3.7 (s, 3H) RCO_2CH_3; 4.13 (t, 2H) R-CH_2OCO-; 4.6 (m, 1H); 3α-H; 5.34 (m, 1H) cholesteryl 6-H (olefinic); 5.8 (s, 1H) vinylic H, *trans* to carbonyl; 6.3 (s, 1H) vinylic H, *cis* to carbonyl. Anal. calcd. for $C_{44}H_{72}O_6$ (696 $gmol^{-1}$): C 75.79, H 10.33; found: 76.19, H 10.81%.

Di-[1{(cholesteryloxy)carbonyl}-10-decanyl]-2-methylene butane 1,4-dioate 2

Anhydrous dicesium itaconate (2.6 g, 6.6 mmol) was prepared by dissolving relative amounts of itaconic acid and cesium hydroxide in methanol and evaporating to dryness. (Care must be taken at this point to ensure that the hygroscopic salt remains dry, as this affects the final yield.) The salt was added

Can. J. Chem. Downloaded from www.nrcresearchpress.com by 46.23.64.124 on 09/08/12
For personal use only.

to a solution of cholesteryl-11-bromo undecanoate (9.5 g, 15 mmol) in dry DMF (100 mL) and the heterogeneous mixture stirred at ca. 70°C for 24 h under a blanket of nitrogen. It is important to keep the reaction temperature at 70°C or below to avoid isomerization of the itaconate ester into the citraconate ester. On cooling the reaction mixture, DMF was coevaporated in vacuo with xylene. Chloroform (250 mL) and water (50 mL) were added and the mixture shaken. The organic layer was washed with a further portion of water (50 mL) followed by saturated sodium bicarbonate solution (2 × 50 mL), and finally with water (50 mL). The dried ($MgSO_4$) organic layer was evaporated in vacuo and the crude product purified by column chromatography using silica gel. Unreacted bromide was eluted with toluene ($R_f = 0.88$, toluene) and the desired diester eluted with a 10% chloroform in toluene mixture ($R_f = 0.46$, toluene). Yield: 5.1 g, 63%; mp 38–40°C; ir: $\bar{\nu}$(thin film): 2850, 1720, 1660, 1470, 1395, 1180 cm^{-1}; ^1H nmr, δ ppm ($CDCl_3$; 80 MHz): 0.5–3.25 (m, 124H) cholesteryl R-H, undecyl $R(CH_2)_8COO$-, vinyl-CH_2CO_2-; 4.15 (t, 4H) RCH_2OCO; 4.6 (m, 2H) 3α-H; 5.34 (m, 2H) cholesteryl 6-H (olefinic); 5.8 (s, 1H) vinylic H *trans* to carbonyl; 6.32 (s, 1H) vinylic H *cis* to carbonyl. Anal. calcd. for $C_{81}H_{134}O_8$ (1234 $gmol^{-1}$): C 78.78, H 10.86; found: C 79.98, H 10.96%.

The comonomer 4-cyanophenyl-4′-(6-acryloyloxyhexyloxy) benzoate was prepared using a general procedure outlined by Portugall et al. (10) that was modified in the following three stages.

4-(6-Hydroxyhexyloxy)benzoic acid

4-Hydroxybenzoic acid (25.5 g, 0.185 mol) was dissolved in a mixture of ethanol (65 mL), water (28 mL), potassium hydroxide (27.75 g, 0.49 mol) and a pinch of potassium iodide. 1-Chloro-6-hydroxyhexane (23 g, 0.168 mol), was then added slowly, dropwise, and the mixture refluxed for 20 h. After cooling the mixture, the ethanol was evaporated in vacuo and the residue dissolved in water (200 mL). This aqueous solution was washed with diethyl ether (3 × 50 mL), then adjusted to pH 2 with 2 N HCl and the resultant precipitate collected by filtration. After washing with water and drying, the product was recrystallized from ethanol. Yield: 21.6 g, 54%; mp 139–142°C (lit. (10) mp 139°C).

4-(6-Acryloyloxyhexyloxy) benzoic acid

The alcohol prepared as above (21.6 g, 0.09 mol) was esterified azeotropically with freshly distilled acrylic acid (26 g, 0.36 mol) in benzene (300 mL) using *p*-toluene sulphonic acid (6 g, 0.03 mol) as the catalyst and hydroquinone (2 g, 0.018 mol) as the polymerization inhibitor. Reflux was continued for a further 20 h. On cooling, the reaction mixture was diluted with diethyl ether (1000 mL) and washed carefully with warm water until no more acrylic acid was detected. The organic layer was dried ($MgSO_4$), evaporated, and the crude product recrystallized from isopropanol to afford the liquid crystalline benzoic acid derivative. Yield: 17.6 g, 67%; k $\xrightarrow{86°C}$ N $\xrightarrow{90°C}$ I. Anal. calcd. for $C_{16}H_{20}O_5$ (292 $gmol^{-1}$): C 65.75, H 6.84; found: C 66.22, H 6.99%.

4-Cyanophenyl-4′-(6-acryloyloxyhexyloxy)benzoate 3

The target monomer was prepared by firstly converting the acid into the corresponding acid chloride, then condensing this with *p*-cyanophenol. The acid (17.32 g, 0.059 mol) was stirred with thionyl chloride (35.7 g, 0.3 mol) in the presence of DMF (2 drops) and 2,6-di-*tert*-butyl-4-methyl phenol (4.4 g, 0.02 mol). After ca. 25 min, by which time solution was achieved, the excess thionyl chloride was removed by rotary evaporation and high vacuum (1–2 h). The acid chloride residue was dissolved in anhydrous chloroform (30 mL), then added slowly dropwise into a stirred solution of *p*-cyanophenol (7.03 g, 0.059 mol) and triethylamine (6.07 g, 0.06 mol) in chloroform (20 mL) at 0°C. After the addition the mixture was stirred at room temperature for 24 h and then chloroform (200 mL) added. This solution was washed with water (50 mL) followed by 2 N sodium hydroxide solution (3 × 50 mL) and water (2 × 50 mL). The organic layer was dried ($MgSO_4$), evaporated, then subjected to flash chromatography, using dichloromethane as both the solvent and the eluant. The monomer was finally recrystallized from isopropanol and shown to be pure by tlc. Yield: 16 g, 69%; mp 72–75°C (lit. (10) mp 72°C); ^1H nmr, δ ppm ($CDCl_3$; 90 MHz); 1.2–2.1 (m, 8H) $R(CH_2)_4R$; 4.01–4.13 (overlapping t's, 2 × 2H) $ArOCH_2R$ and RCH_2OCO; 5.63–6.5 (m, 3H) vinylic H; 6.78–8.2 (4 × d, 8H) Ar-H. Anal. calcd. for $C_{23}H_{23}NO_5$ (393 $gmol^{-1}$): C 70.23, H 5.85, N 3.56; found: C 71.15, H 5.97, N 3.61%.

Characterization of liquid crystal behaviour

A hot-stage polarizing microscope was used to identify the mesophases in the samples and the temperature range of stability. Transitions were also located by differential scanning calorimetry (DSC) and the instrument used was a Perkin Elmer DSC2 at a scanning rate of 20°C min^{-1}. Glass transition temperatures (T_g) were recorded as the onset of the baseline shift that occurs during this transition and the mesophase transitions were detected from the presence of small endothermic peaks during the heating cycle or exothermic peaks on cooling.

Copolymerizations

Reactions were carried out under vacuum, using benzene as solvent at a temperature of 60°C, in the presence of the radical initiator 2,2′-azo bisisobutyronitrile (0.5 mol%). For copolymerizations the reaction conversion was restricted to ≤15% to minimize composition drift and the copolymers were isolated by precipitation in methanol, ethanol, or ether. Samples were purified by repeated dissolution–precipitation, then dried in vacuo. Copolymer compositions proved difficult to determine with any accuracy and so the trends in behaviour are expressed in terms of the molar feed composition of the monosubstituted itaconate monomer, f_1.

Characterization

Molar masses were measured either by membrane osmometry (Knauer) or by vapour pressure osmometry (Hewlett–Packard 302b).

Results and discussion

The cholesteryl derivatives of itaconic acid **1** and **2** are new compounds, both of which were found to exhibit liquid crystal phases, and their mesogenic characteristics can be compared with other cholesteryl acrylates and methacrylates that have been reported elsewhere (8). The monosubstituted monomer **1** displayed both a smectic A (S_A) phase and a cholesteric phase

Table 1. Comparison of the phase transition temperatures for cholesteryl containing monomers of the general structure

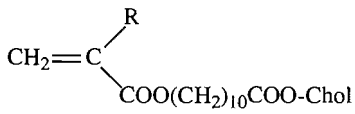

R	Meosphase temperature ranges
H[a]	$k_I \xrightarrow{28} k_{II} \xrightarrow{51} S \xrightarrow{54} N^* \xrightarrow{73} I$
CH_3[a]	$k \xrightarrow{55} S \xrightarrow{58} N^* \xrightarrow{62} I$
CH_2COOCH_3	$k \xrightarrow{16} S_A \xrightarrow{42} N^* \xrightarrow{54} I$
$CH_2COO(CH_2)_{10}COOChol$	$k \xrightarrow{39} S_A \xrightarrow{65} N^* \xrightarrow{72} I$

k = crystal; I = isotropic liquid
[a]Data from ref. 8.

(N*) in common with the acrylic analogues, and the transition temperatures for each can be compared with reference to Table 1.

While the phases observed are similar in all cases, the temperature at which each appears depends strongly on the substituent on the α-carbon atom. Freidzon et al. (8) reported two crystal phases for the acrylate derivative that then passed into a brief smectic phase (51–54°C), before the appearance of the N* phase as the temperature was raised. For the methacrylate derivative the melting temperature T_m was higher but the clearing temperature T_I was lower, giving a restricted liquid crystal range of only 7°C in total. The itaconate derivatives both exhibited much wider temperature ranges for the liquid crystal phases. Monomer **1** had the lowest T_m, but the S_A phase is now extended over a 26°C range, although T_I is again the lowest in the series. The increased size of the -(-CH_2CO_2-CH_3) side group in **1** appears to destabilize the crystalline order but enhanced the formation of a smectic phase. Monomer **2** also exhibited an extended S_A phase that was stable over 26°C but the added bulk of the second side-chain raises both T_m and T_I, with a concomitant reduction in the range for the N* phase. In both cases the itaconate derivatives have extended S_A phases that appear to be a consequence of the bulky substituents on the α-carbon atom.

Homopolymerization

The polymerization of **1** was successful but high molar mass material was difficult to obtain, with typical values of M_n lying around 10^4. Attempts to polymerize **2**, however, were totally unsuccessful and, although conditions were varied, no polymer was formed using radical initiators. Itaconic acid derivatives (11) are known to be more difficult to polymerize than their acrylate or methacrylate counterparts, and it would appear that the steric restrictions imposed by the disubstituted derivative are too great to allow polymer formation.

The polymer (**P1**) of monomer **1** was also found to be a thermotropic liquid crystalline material and passes through the following sequence of phase changes where "g" represents the glassy state:

$$g \xrightarrow{-35°C} k \xrightarrow{41°C} S_A \xrightarrow{52°C} N^* \xrightarrow{64°C} I$$

The DSC trace, shown in Fig. 1, indicates that the sample

Fig. 1. DSC trace for polymer of monomer **1**.

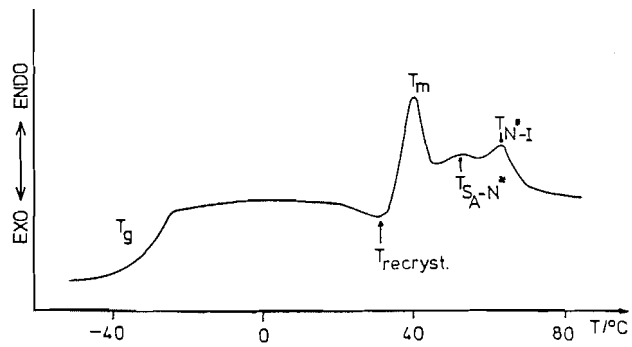

undergoes a cold crystallization followed rapidly by melting at T_m = 41°C, which is much higher than the parent monomer **1**. There are also increases in the $T_{S_A-N^*}$ and T_{N^*-I} transition temperatures for the polymer, which is typical when mesogens are incorporated into a polymer chain and the motional modes are now more restricted.

Liquid crystal textures

Liquid crystal polymers with chiral mesogenic groups, either in the main chain or, more commonly as with the samples reported here, in the side chain, display a cholesteric (or chiral nematic) phase that has special optical properties. The directors of the nematic layers tend to be displaced by a few degrees from those in the adjacent layers, such that they trace out a supermolecular helical structure, formed by the directors twisting regularly about an axis perpendicular to the layers. This chiral perturbation minimizes the energy of the stacked array with each molecule skewed at an average angle $\pm\theta$ with respect to its neighbours above and below. These helical aggregates have dimensions of the order of visible light and exhibit remarkable circular dichroism effects, being able to reflect circularly polarized light of wave length λ_R, selectively. This wavelength is proportional to the pitch p of the helical structure in the liquid crystal phase, i.e.,

$$[1] \quad \lambda_R = \tilde{n}\mathbf{p}$$

where $\tilde{n}$ is the average refractive index of the cholesteric phase.

Can. J. Chem. Downloaded from www.nrcresearchpress.com by 46.23.64.124 on 09/08/12
For personal use only.

Fig. 2. Photomicrographs of the focal-conic fanned texture of the smectic A phase for monomer **1** (top) and polymer **P1** (bottom). Magnification × 200.

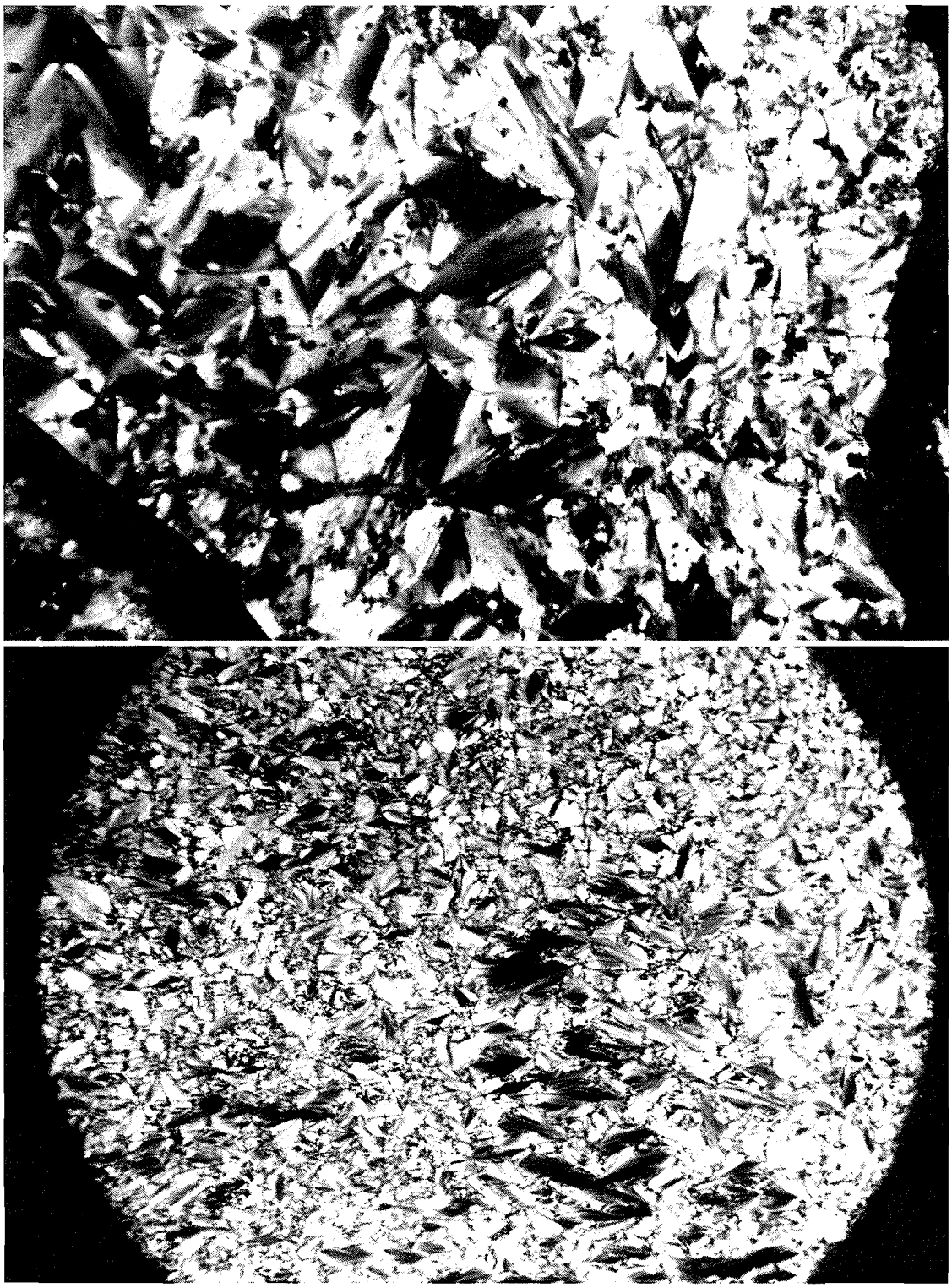

Can. J. Chem. Downloaded from www.nrcresearchpress.com by 46.23.64.124 on 09/08/12
For personal use only.

Examination of the itaconate monomers and polymer, using a hot-stage microscope, showed that on cooling from the isotropic melt all the samples formed a grey-coloured homogeneous planar texture with oily streaks, spontaneously. This is typical of the Granjean texture exhibited by most cholesteric phases and is formed more rapidly in the monomers than the polymer because of the lower viscosity of the former.

On cooling further, selective reflection of visible light was observed with the colours appearing first as blue and changing through the spectrum to red as the transition from the cholesteric to the smectic phase was approached. At this point the planar texture was rapidly transformed into the focal-conic fanned texture typical of a smectic A phase, as shown in Fig. 2.

As the pitch of the helical structure formed can be varied by

Can. J. Chem. Downloaded from www.nrcresearchpress.com by 46.23.64.124 on 09/08/12
For personal use only.

Table 2. Phase transition temperatures for copolymers of monomers **1** and **3**.

Sample number	f_1	T_g/°C	Tm/°C	T_{S-N^*}/°C	T_{N^*-I}/°C
P3	0.00	37	—	—	126
4a	0.10	26	—	—	94
4b	0.25	28	—	—	120
4c	0.50	19	—	—	115
4d	0.75	7	—	69	80
P1	1.00	−35	41	52	64

Fig. 3. Phase transition temperatures plotted as a function of monomer **1** in the copolymerization feed f_1 for copolymers of **1** and **3**. (Δ) Glass transition; (□) melting temperature; (+) transition from S_A to N^* phase; (○) clearing temperature.

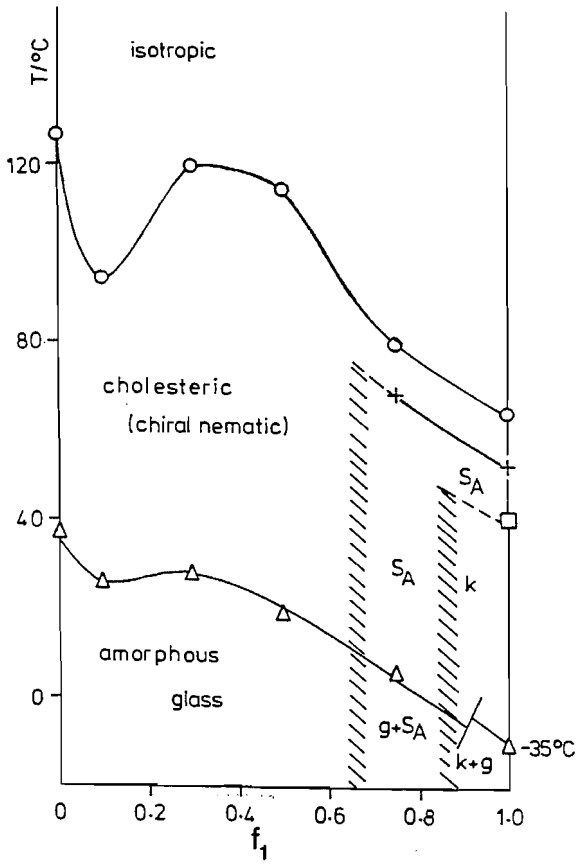

altering the temperature, the value of λ_R can also be changed. In the case of the systems studied here, the colour changes indicate that the helix pitch is short at temperatures just below the clearing temperature (characterized by the blue reflection, although the suggestion is that the samples may reflect in the UV initially) and progressively lengthens or unwinds as the temperature drops until it becomes very long and the molecules pass into the more ordered smectic phase.

Copolymers of 1 and 3

We have shown previously (5–7) that copolymerization of a chiral mesogen with a non-chiral mesogen can alter (*a*) the number of liquid crystal phases observed, (*b*) the temperature range over which the liquid crystal phases are stable, and (*c*) can effect some control over the wavelength of the selective reflection. For example, it has been observed (12) that the pitch of the helix in an N* phase is a function of the mole fraction of chiral units X* in the copolymer, i.e.,

$$[2] \quad \lambda_R \alpha {}^{1}/_{X^*}$$

These phenomena were examined here by preparing copolymers of the cholesteric monomer **1** with the non-chiral monomer **3**. Details of the samples and their transition temperatures are given in Table 2. The temperature stability ranges are better represented diagrammatically and are shown plotted as a function of the mole fraction of **1** in the copolymerization feed f_1, in Fig. 3.

The copolymerization reactions were much more facile than the homopolymerization of **1** and average values of M_n for the copolymers were found to be in the region of (2–6) × 10^4. All exhibited glass transition temperatures, T_g, ranging from below to above ambient, indicating that the samples were amorphous with no evidence of the crystallinity observed in the homopolymer **P1**.

Another general observation is that copolymers with lower concentrations of the chiral monomer incorporated in the chain do not display a smectic phase. This is a distinct advantage as it is now possible to freeze a particular reflection colour into the polymer glass, by quenching the copolymer rapidly from the appropriate temperatures in the N* phase. This is not possible, or is extremely difficult, to do if there is an intervening smectic phase, as there is a tendency for the helical structure to unwind rapidly at the transition point between the N* and S_A phases during the cooling cycle.

The samples were examined in some detail using DSC and the hot-stage polarizing microscope. Copolymers **4a** and **4b** with low concentrations of **1** in the chain exhibited only the N* phase. On cooling from the isotropic melt both formed pale blue, homogeneous, planar textures with white oily streaks, characteristic of the cholesteric phase. Slow cooling of sample **4a** gave reflected colour changes in the sequence:

95°C/blue → 64°C/yellow → 40°C/orange

Sample **4b** showed a similar trend but in a different temperature range:

82°C/blue → 68°C/green → 50°C/yellow → 25°C/red-orange

As the alignment of the samples, on cooling from the isotropic

melt, is not perfect, the colours are "grainy," because they are a diffuse mixture of slightly different wavelengths centred on the main reflected wavelength that dominates the sample colour. This is caused by the tilting of the helical aggregates away from the ideal planar state.

The colour changes were found to be reversible on heating and the sequences indicate that the helical structure is unwinding as the temperature is lowered. This is the normally observed trend for both main-chain (13) and side-chain (14) polymers, but the opposite temperature dependence has been known to occur (8). This can be explained by postulating that the temperature dependence of the pitch of the helix is a consequence of two opposing effects. As the temperature rises the system expands and the pitch length increases, but this is offset by an increase in the displacement angle θ between the directors, which leads to a reduction in the pitch (15). In the systems discussed here the latter appears to dominate.

With a further increase in the cholesteric monomer content of the polymer the behaviour of the samples changes. Sample **4c** still exhibits only the one liquid crystal phase, N*, but on cooling from the melt an imperfect grey/blue planar texture was formed that was improved only after annealing the sample for 12 h. The selective reflection was now quite indistinct and was no longer a vivid blue. It was likely that λ_R was now partially displaced into the ultraviolet region and further slow cooling was needed to initiate a change to a pale blue reflection that remained stable until room temperature was reached.

When the content of **1** in the feed exceeded 0.5 mol fraction as for sample **4d**, the smectic-A phase reappeared, which restricted the N* phase to about 11°C. A grey-coloured planar texture formed spontaneously on cooling from above T_I and remained unchanged on further cooling until the N*–S_A transition was approached. Here the so-called pretransitional phenomenon (16) was observed, which is manifest as a rapid series of colour changes through the visible spectrum as the helix unwinds, followed by the transformation into the typical fanned focal-conic texture of the S_A phase. A similar phenomenon was observed on cooling the polymer **P1**.

The relationship expressed in eq. [2] was confirmed by the observations made on these copolymer samples. In the temperature range 60–70°C, for example, the selective reflection colours for **4a**, **4b** and **4c** were green, yellow, and blue, respectively, indicating a move to shorter wavelengths as the content of **1** in the copolymer increased. Thus a greater preponderance of the cholesteric units leads to a shortening of the pitch length of the helical structure in the N* phase with a possible move of the λ_R into the ultraviolet region. Unfortunately, the increased content of **1** also leads to the formation of a smectic phase, which would make it difficult to lock the UV reflecting phase into these polymer glasses.

Acknowledgements

The authors wish to thank DSM for financial support (H.W.H.) during the course of this investigation.

References

1. G.H. Heilmeier, L.A. Zanonic, and L.A. Barton. Appl. Phys. (Paris) Lett. **13**, 46 (1968).
2. G.W. Gray. J. Phys. (Paris), **36**, 337 (1975).
3. M. Schadt and W. Helfrich. Appl. Phys. Lett. **18**, 127 (1971).
4. R.B. Meyer, L. Liebert, L. Strzelecki, and P. Keller. J. Phys. (Paris) Lett. **36**, L69 (1975).
5. J.M.G. Cowie and H.W. Hunter. Makromol. Chem. **191**, 1393 (1990).
6. J.M.G. Cowie and H.W. Hunter. Makromol. Chem. **192**, 143 (1991).
7. J.M.G. Cowie and H.W. Hunter. J. Polym. Sci. Part A: Polym. Chem. **31**, 1179 (1993).
8. Ya. S. Freidzon, V.P. Shibaev, A.V. Kharitonov, and N.A. Platé. *In* Liquid crystal polymers. *Edited by* N.A. Platé. Plenum Press, New York. 1993. p. 227.
9. Ya. S. Freidzon, A.V. Kharitonov, V.P. Shibaev, and N.A. Platé. Mol. Cryst. Liq. Cryst. **88**, 87 (1982).
10. M. Portugall, H. Ringsdorf, and R. Zentel. Makromol. Chem. **183**, 2311 (1982).
11. J.M.G. Cowie, S.A.E. Henshall, I.J. McEwen, and J. Velickovic. Polymer, **18**, 612 (1977).
12. H. Finkelmann and G. Rehage. Makromol. Chem. Rapid Commun. **3**, 859 (1982).
13. J.M.G. Cowie and H.H. Wu. Makromol. Chem. **189**, 1511 (1988).
14. N.A. Platé and V.P. Shibaev. *In* Comb shaped polymers and liquid crystals. Plenum Press, New York. 1987.
15. P.N. Keating. Mol. Cryst. Liq. Cryst. **8**, 315 (1969).
16. H. Finkelmann and G. Rehage. Adv. Polym. Sci. **60/61**, 99 (1984).

Can. J. Chem. Downloaded from www.nrcresearchpress.com by 46.23.64.124 on 09/08/12
For personal use only.

A stabilized and persistent tetraketene: 1,4-bis(1′,4′-dioxo-3′-trimethylsilyl-2′-buta-1′,3′-dienyl)benzene

Ronghua Liu and Thomas T. Tidwell

Abstract: Reaction of 1,4-bis(trimethylsilylethynyl)benzene with CCl_3COCl and Zn gave 1,4-bis(4′,4′-dichloro-2′-trimethylsilyl-3′-oxo-1′-cyclobutenyl)benzene (**7**), which reacted with concentrated H_2SO_4 at 87°C to give 1,4-bis(2′-trimethylsilyl-3′,4′-dioxo-1′-cyclobutenyl)benzene (**8**). Photolysis of **8** in $CDCl_3$ with 350 nm light gave the bisketene **9**, which on further photolysis formed the title tetraketene **10**, as identified by its spectral properties. Upon heating of **10** the successive closure of the two bisketene moieties, first to give the mono(cyclobutenedione) **9** and then to reform **8** in a slower step, was observed by NMR and UV spectroscopy. Reaction of **10** with MeOH gave the tetraester **11**, which was assigned the *erythro* configuration at each of the succinate moieties.

Key words: ketenes, photolysis, cyclobutenediones, esterification, silicon.

Résumé : La réaction du 1,4-bis(triméthylsilyléthynyl)benzène avec le CCl_3COCl et le Zn conduit au 1,4-bis(4′,4′-dichloro-2′-triméthylsilyl-3′-oxo-1′-cyclobuténynl)benzène (**7**) qui réagit avec du H_2SO_4 à 87°C, pour fournir du 1,4-bis(2′-triméthylsilyl-3′,4′-dioxo-1′-cyclobuténynl)benzène (**8**). La photolyse du composé **8**, dans du $CDCl_3$ à 350 nm, fournit le biscétène **9** qui par photolyse ultérieure forme le tétracétène **10** mentionné dans le titre qui a été identifié par ses propriétés spectrales. Lors du chauffage du composé **10** on a pu observer les cyclisations successives des deux portions biscéténiques qui conduisent en premier lieu à la mono(cyclobutènedione) **9** et qui redonnent le composé **8** lors d'une réaction plus lente. La réaction du composé **10** avec de l'alcool méthylique conduit au tétraester **11** auquel on a attribué la configuration *érythro* pour chacune des portions succinates.

Mots clés : cétènes, photolyse, cyclobutènediones, estérification, silicium.

[Traduit par la rédaction]

Introduction

Ketenes have been actively studied for 90 years (1), and the first bisketene, carbon suboxide (O=C=C=C=O), was reported in 1906 (2*a*). Because of their interesting and potentially useful polyfunctionality, the chemistry of carbon suboxide (2) and other bisketenes (1*e*, 3–5) has been of continued interest. In particular, the potential utility of these materials as polymer intermediates has been widely recognized (4*e*, *f*).

Recently we reported (6) that a variety of long-lived 1,2-bisketenes **1** substituted with stabilizing (7) trialkylsilyl groups (Me_3Si, *t*-$BuMe_2Si$, i-Pr_3Si) may be prepared from photolysis or thermolysis of the corresponding cyclobutenediones (**2**), as shown in eq. [1]. When these bisketenes have two trialkylsilyl substituents they are thermodynamically stable relative to the cyclobutenedione precursors (6*a*, *b*), but in examples substituted with one Me_3Si group and either Ph (**3**) or Me the bisketene is rather long lived at room temperature, but reverts to the more stable cyclobutenedione at measurable rates at higher temperatures (6*c*, *d*).

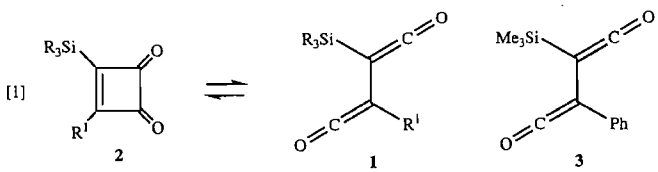

Bisketenes in which the ketenyl groups are nonadjacent have been prepared and directly observed in only a few cases (1*e*, 4*a*, *b*). 1,2-Bisketenes without stabilizing silyl substituents were previously generated as intermediates that could be detected at low temperatures, or trapped by various reagents (5). Polyketenes may have been generated (8) by photolysis of polycyclobutenediones in a matrix at 30 K, as in the reaction of **4** to give an IR band at 2115 cm^{-1}, possibly due to hexaketene **5** (eq. [2]). Further photolysis led to decarbonylation and possible formation of cyclooctadecanonyne (C_{18}). We now report the preparation and reactivity of a longlived tetraketene stabilized by Me_3Si groups.

Results and discussion

The reaction of trimethylsilylacetylene with 1,4-diiodobenzene in the presence of palladium acetate, copper(I) iodide, and triphenylphosphine gave 1,4-bis(trimethylsilylethy-

Received April 10, 1995.

This paper is dedicated to Professor J.E. (Jim) Guillet in recognition of his contributions to Canadian chemistry.

R. Liu and T.T. Tidwell.[1] Department of Chemistry, University of Toronto, Toronto, ON M5S 1A1, Canada.

[1] Author to whom correspondence may be addressed. Fax: (416) 287-7204. E-mail: tidwell@lake.scar.utoronto.ca

Can. J. Chem. Downloaded from www.nrcresearchpress.com by 46.23.64.124 on 09/08/12
For personal use only.

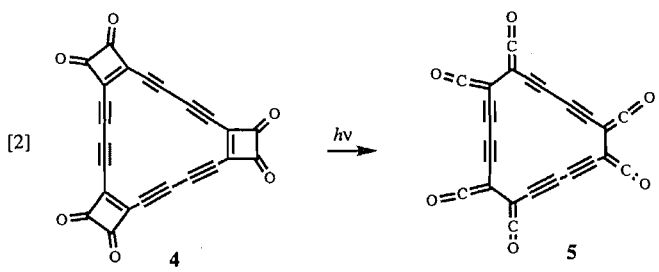

nyl)benzene **6** in 88% yield. This reaction is analogous to a reported preparation of **6** using $Pd(PPh_3)_2Cl_2$ (9*a*). The reaction of **6** with dichloroketene generated from trichloroacetyl chloride and zinc dust, activated by ultrasonic irradiation (9*c*), gave the bis(oxocyclobutenyl)benzene **7** (eq. [3]), together with minor amounts of products of chlorine migration. Reaction of **7** with concentrated H_2SO_4 at 87°C followed by hydrolysis gave the tetraketone **8** (eq. [4]). The structures of **7** and **8** were easily assigned from their characteristic spectral properties, especially their ^1H NMR spectra, which showed only single Me_3Si and aryl resonances for each.

Upon heating of **8** to 100°C in $CDCl_3$ no significant change could be detected in the ^1H NMR spectrum. However, upon photolysis with 350 nm light for 5 min at 25°C there was a color change to a deeper yellow, and the ^1H NMR spectrum indicated the presence of three components assigned (vide infra) as residual tetraketone **8**, the bisketene **9**, and the tetraketene **10**, in a relative ratio of 30:30:40. Upon further photolysis for 1 h the signals due to **8** and **9** each decreased to less than 5% of the total, and 90% of the signals present were assigned to the tetraketene **10**. Upon further photolysis for an additional 15 h further signals appeared, assigned to formation of the alkyne **6** to the extent of about 5%. These photochemical changes correspond to those observed in the photochemical ring opening of the cyclobutenedione **2** (R_3Si = Me_3Si, R^1 = Ph) to form the bisketene **3** (6*c*, *d*), and so the process is assigned as initial photolysis of tetraketone **8** to form the bisketene **9**, which on further photolysis forms the tetraketene structure **10** (eq. [5]). Other evidence for the structure of **10**

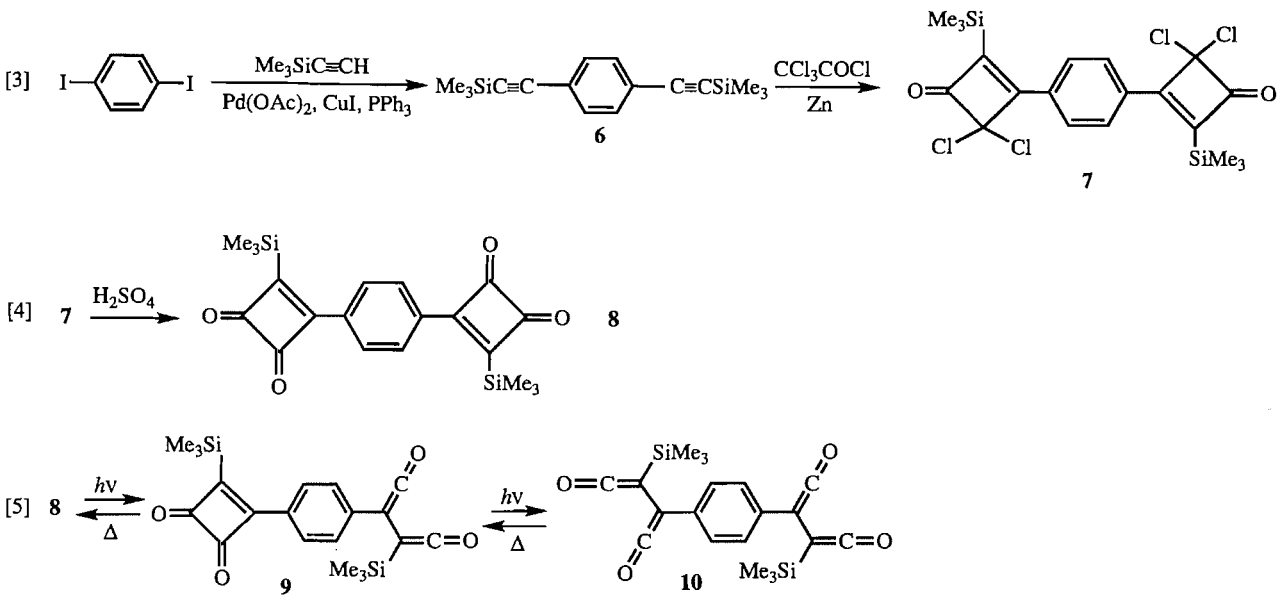

includes the ketenyl IR band observed at 2086 cm^{-1}, which is comparable to that at 2084 cm^{-1} for bisketene **3** (6*c*, *d*), and the very distinctive signals in the ^{13}C NMR spectrum at δ 6.9 and 32.8 for the Me_3Si and aryl-substituted ketenyl carbons, as compared to the values for the corresponding carbons of **3** at δ 7.9 and 33.5, respectively.

Upon heating, the reversion of **10** to **8** could be observed by monitoring the disappearance of the UV absorption of **10** at 280 nm, and the increase in absorption at 320 nm. Two separate processes were observed, and these are attributed to the initial conversion of **10** to **9**, and then a slower conversion of **9** to **8**. Upon heating the solution of **10** in $CDCl_3$ for 10 min at 100°C, the signals due to **10** completely disappeared, and the spectra of **9** could be observed, together with those of **8**, in a ratio of 55:45. Spectral features assigned to **9** include the ketenyl IR band at 2101 cm^{-1}, ^1H NMR absorption of the ketenyl and cyclobutenyl $(CH_3)_3Si$ groups at δ 0.24 and 0.47, respectively, and signals for nonequivalent pairs of protons on the aromatic ring at 7.26 and 7.94 (each doublet, J = 8.4 Hz). The kinetics of the thermal conversion of **10** to **9** and then to **8** are under investigation as part of a study of the effect of aryl substituents on the rates of bisketene ring closures.[2]

The appreciable kinetic stability at room temperature of the bisketene **9** and the tetraketene **10** are indicative of significant barriers for the ring closure. Analogous behavior has been previously found experimentally for **3** (6*c*, *d*), and quantitative agreement has been found (6*e*) between the experimental barrier for ring opening of **2** (R = Me, R^1 = Me_3Si) and the theoretically calculated barrier for **2** (R = H, R^1 = SiH_3).

Excess methanol was added, at −78°C, to a solution of the tetraketene **10** generated by photolysis of **8**, and the solution was kept at 0°C for 10 h. By this time the tetraketene had disappeared, and signals attributed to a mixture of the stereomeric tetraesters **11** were observed. The mixture was purified by flash chromatography, and the product had NMR, IR, and mass spectral properties consistent with those expected for **11**.

[2] R. Liu, work in progress.

Can. J. Chem. Downloaded from www.nrcresearchpress.com by 46.23.64.124 on 09/08/12
For personal use only.

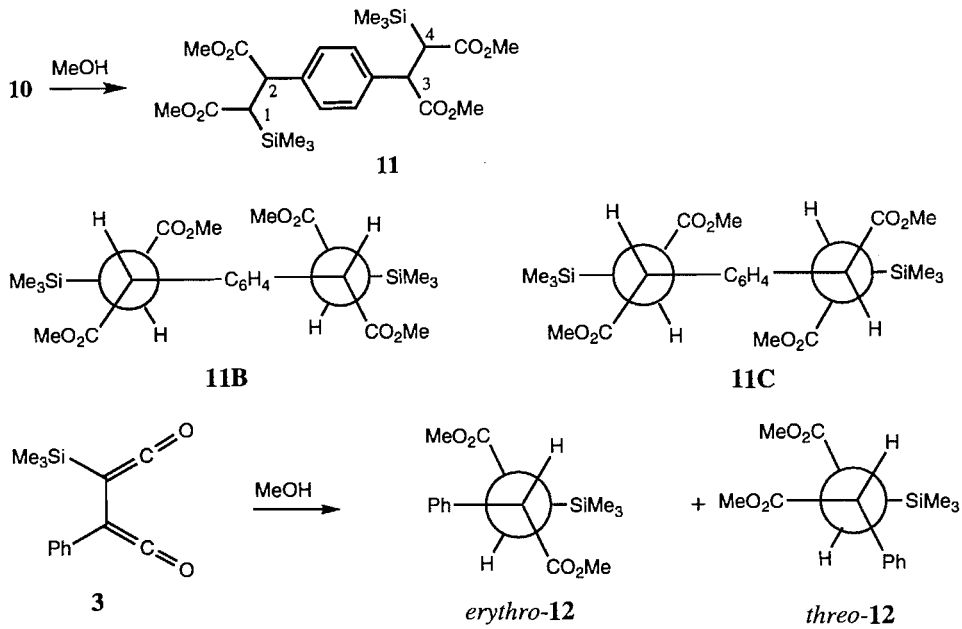

There are six possible diastereoisomers of **11**, but the ^1H and ^{13}C NMR spectra indicated that a single diastereomer predominated, and the spectra resembled those of the isomer of **12** from the reaction of **3** with MeOH, which has been assigned the *erythro* structure (6*d*). On this basis the structure of the major isomer of **11** is also assigned as being one of the two *erythro*, *erythro* diastereomeric structures of **11**, either the achiral **11B**, or the chiral **11C**, or a mixture of the two, which would be expected to have very similar chromatographic and spectral properties.

The structure assigned (6*d*) as the *erythro* isomer of **12** showed, in the ^1H NMR spectrum ($CDCl_3$), δ: 0.13 (Me_3Si), 3.10 (d, J = 12.4 Hz, C*H*TMS), 3.38 and 3.62 (each OCH_3), 4.02 (d, J = 12.4 Hz, C*H*Ph), and 7.24–7.34 (br s, Ph), while the structure assigned as the *threo* isomer gave an ^1H NMR spectrum ($CDCl_3$), δ: −0.21 (Me_3Si), 2.96 (d, J = 12.4 Hz, C*H*TMS), 3.60 and 3.69 (each OCH_3), 4.09 (d, J = 12.4 Hz, C*H*Ph), and 7.31 (br s, Ph). The major peaks for **11** were δ: 0.11 (Me_3Si), 3.04 (d, J = 12.4 Hz, C*H*TMS), 3.33 and 3.62 (each OCH_3), 4.00 (d, J = 12.4 Hz, C*H*Ph), and 7.27 (s, C_6H_4), and these are in close agreement with the structure assigned as *erythro*-**12**, but not *threo*-**12**.

The six diastereomers of **11** and the respective absolute configurations of the carbons 1–4 are **A** (*R, R, R, R/S, S, S, S*), **B** (*R, S, R, S*; achiral), **C** (*R, S, S, R/S, R, R, S*), **D** (*R, R, R, S/S, S, S, R*), **E** (*R, R, S, S*; achiral), and **F** (*R, S, R, R/S, R, S, S*), and of these **B** and **C** each have two *erythro* side chains.

In the reaction of **3** with MeOH there was a 2/1 preference for the formation of the isomer assigned the *erythro* structure **12** as opposed to the *threo* structure **12**. Experiments are in progress to determine whether this product mixture represents an equilibrium mixture of these two structures.

In summary, photolysis of **8** produces the bisketene **9**, which upon further photolysis forms the tetraketene **10**. Both **9** and **10** are long lived at room temperature and can be directly observed by IR, NMR, and UV spectroscopy. The thermal conversion of **10** to **9**, which then forms **8** in a slower step, is also observable, and reaction of **10** with MeOH leads to the tetraester **11**. The further chemistry of these unique polyfunctional intermediates is being actively explored.

Experimental

General procedures

Most of the reagents and solvents were obtained from Aldrich or BDH. Ether was distilled from sodium–benzophenone. All reactions were carried out in oven-dried glassware and $CDCl_3$, used as a reaction solvent, was dried over 4A molecular sieves. NMR spectra were measured using Varian Germini 200 and XL-400 spectrometers. Infrared spectra were measured using Nicolet DX FT-IR and Perkin–Elmer 882 instruments. Mass spectra were obtained on a VG 70-2505 instrument by Dr. A. Young. The sonicator was a Branson model 1200. The UV absorption data were obtained using a Varian 210 instrument. Photolyses were carried out with a Rayonet RPR-100 photoreactor.

1,4-Bis(trimethylsilylethynyl)benzene (6)

To a 500 mL three-neck flask equipped with a Dry Ice condenser was added successively 250 mL triethylamine, 1,4-diiodobenzene (20.0 g, 0.061 mol), triphenylphosphine (0.65 g, 2.48 mmol), cuprous iodide (0.24 g, 1.26 mmol), (trimethylsilyl)acetylene (14.7 g, 0.15 mol), and palladium(II) acetate (0.32 g, 1.42 mmol), and the reaction mixture was stirred at room temperature for 4 h under nitrogen and then the solvent was removed using the rotary evaporator. The residue was recrystallized from hexanes to afford colorless crystals of **6** (14.5 g, 0.054 mol, 88%), with spectra and melting point consistent with the literature (9*a*).

1,4-Bis(4′,4′-dichloro-2′-trimethylsilyl-3′-oxo-1′-cyclobutenyl) benzene (7)

To a dry, 100 mL round-bottom flask under nitrogen was added zinc dust (13.0, g, 0.2 mol), **6** (2.0 g, 7.4 mmol), and 60 mL anhydrous ether. The flask was then partially submerged

Can. J. Chem. Downloaded from www.nrcresearchpress.com by 46.23.64.124 on 09/08/12
For personal use only.

Can. J. Chem. Downloaded from www.nrcresearchpress.com by 46.23.64.124 on 09/08/12
For personal use only.

in a sonicator water bath, trichloroacetyl chloride (21.9 g, 0.116 mol) dissolved in 12 mL anhydrous ether was added dropwise over 0.5 h, and the reaction mixture was left under sonication for another 2 h. The product was filtered through Celite to remove unreacted zinc, the Celite was washed with ether, and the solvent was evaporated from the filtrate. The residue was separated by flash chromatography, with elution by 2/3 dichloromethane and hexanes, to give a light yellow solid (1.95 g, 3.96 mmol, 52%), which by ^{1}H NMR was a mixture of **7** and a small amount of an isomeric product of chlorine migration. Pure **7** was obtained by recrystallization from ethyl acetate and hexanes; mp 181.0–182.0°C; IR ($CDCl_3$): 1799 (C=O), 1620 (C=C), 1550 cm^{-1}; ^{1}H NMR ($CDCl_3$), δ: 0.43 (s, 18H, Me_3Si), δ: 8.08 (s, 4H, Ar), ^{13}C NMR ($CDCl_3$), δ: −1.6, 125.6, 130.4 132.0, 157.6, 178.4, 182.3; EIMS, *m/z*: 496, 494, 492, 490 (M^+, 27), 449 (M^+ − CO, CH_3, 15), 149 (M^+ − 4Cl, 2CO, 2TMS, 38); 73 (Me_3Si^+, 100); HRMS, *m/z*, calcd. for $C_{20}H_{22}Cl_4O_2Si_2$: 489.9912; found: 489.9924.

1,4-Bis(2′-trimethylsilyl-3′,4′-dioxo-1′-cyclobutenyl)-benzene (8)

Crude **7** (0.31 g, 0.62 mmol) was dissolved in 10 mL chloroform in a 50 mL round-bottom flask, 10 mL concentrated sulfuric acid was added with magnetic stirring, and the mixture was heated at 87°C for 0.5 h. The reaction mixture was added to 100 mL of ice–water mixture, extracted three times with 20-mL portions of ether, the extracts were washed with three 40-mL portions of water and dried over anhydrous magnesium sulfate, and the solvents were evaporated to give 0.28 g crude tetraketone **8**. Purification by flash chromatography eluted with 30% dichloromethane in hexanes gave pure tetraketone **8** (66 mg, 0.17 mmol, 28%) as a yellow solid, mp 203.0 – 203.5°C; IR ($CDCl_3$): 1732 (s, C=O), 1776 (w, C=O), 1488 (m, C=C) cm^{-1}; UV, λ_{max} (acetonitrile): 320 nm; ^{1}H NMR ($CDCl_3$), δ: 0.50 (s, 18, Me_3Si), 8.10 (s, 4, Ar); ^{13}C NMR ($CDCl_3$), δ: −1.8, 129.8, 132.7, 197.0, 197.5, 199.9, 205.6; EIMS *m/z*: 382 (M^+, 25), 326 (M^+ −2CO, 28), 293 (M^+ − TMS, O, 33); 73 (100, Me_3Si^+); HRMS, *m/z* calcd. for $C_{20}H_{22}O_4Si_2$: 382.1057; found: 382.1047.

1,4-Bis(1′,4′-dioxo-3′-trimethylsilyl-2′-buta-1′,3′-dienyl)benzene (10)

A solution of **8** (0.010 g, 0.03 mmol) in 0.8 mL $CDCl_3$ in an NMR tube was degassed for 15 min, then sealed and photolyzed at 350 nm for 5 min at 25°C. The ^{1}H NMR spectrum revealed the presence of residual **8**, the bisketene **9** (vide infra), and the tetraketene **10** in a relative ratio of 30:30:40. Upon further photolysis for 1 h, the signals due to **8** and **9** each decreased to less than 5% of the total, and 90% of the signals present were assigned to the tetraketene **10**, as identified by its spectral properties: IR ($CDCl_3$): 2086 (C=C=O) cm^{-1}; UV, λ_{max} : 280 nm; ^{1}H NMR ($CDCl_3$), δ: 0.20 (s, 18, Me_3Si), 7.05 (s, 4, Ar); ^{13}C NMR ($CDCl_3$ at −30°C), δ: −0.8, 6.9, 32.8, 124.2, 127.7, 178.0, 203.0. Upon further photolysis the amount of **10** in the sample decreased, and the ^{1}H NMR signal of the alkyne **6** increased.

1-(1′,4′-Dioxo-3′-trimethylsilyl-2′-buta-1′,3′-dienyl)-4-(2′-trimethylsilyl-3′,4′-dioxo-1′-cyclobutenyl)benzene (9)

The sample of **10** obtained above was heated for 10 min at 100°C. The ^{1}H NMR spectrum revealed the absence of **10**, and the presence of **8** and **9** in a ratio of 45:55. The structure of **9** was assigned based on its mode of formation and spectral properties: IR ($CDCl_3$); 2101 cm^{-1}; ^{1}H NMR ($CDCl_3$), δ: 0.24 (s, 9, Me_3Si), 0.47 (s, 9, Me_3Si), 7.26 and 7.94 (each d, 2, J = 8.4 Hz, C_6H_4). Upon further heating for 20 min there was almost complete reformation of **8**, as indicated by ^{1}H NMR.

Reaction of tetraketene 10 with methanol to form esters (11)

Tetraketone **8** (25 mg, 0.065 mmol) in 0.5 mL $CDCl_3$ was photolyzed under 350 nm for 35 min, and then 72 μL (excess) anhydrous methanol was added at −78°C. The NMR tube then was warmed to room temperature and left overnight at 0°C. After purification by radial chromatography using 30/70 ethyl acetate/hexanes, the product was shown by ^{1}H NMR to be a mixture of tetraester stereoisomers. The major isomer gave IR ($CDCl_3$): 1756, 1734 (C=O) cm^{-1}; ^{1}H NMR ($CDCl_3$), δ: 0.11 (s, 18, Me_3Si), 3.04 (d, 2, J = 12.4 Hz, C*H*TMS), 3.33 and 3.62 (each s, 6, OCH_3), 4.00 (d, 2, J = 12.4 Hz, C*H*Ph), 7.27 (s, 4, Ar); ^{13}C NMR ($CDCl_3$), δ: 2.12, 41.36, 49.40, 50.83, 52.18, 128.08, 138.07, 173.14, 173.16; EIMS, *m/z*: 510 (2, M^+), 495 (67, M^+ − CH_3), 451 (100, M^+ −CO_2Me); HRMS, *m/z* calcd. for $C_{24}H_{38}O_8Si_2$: 510.2105; found: 510.2094.

Acknowledgement

Financial support by the Natural Sciences and Engineering Research Council of Canada, and the Ontario Centre for Materials Research, is gratefully acknowledged.

References

1. (*a*) H. Staudinger. Chem. Ber. **38**, 1735 (1905); (*b*) D. Borrmann. Methoden der Organischen Chemie. Vol. 7. Part 4, Thieme Verlag, Stuttgart. 1968; (*c*) S. Patai (*Editor*). The chemistry of ketenes, allenes and related compounds. Wiley, New York. 1980; (*d*) E. Schaumann and S. Scheiblich. *In* Methoden der Organischen Chemie. Vol. E15. Part 3. Thieme Verlag, Stuttgart. 1993. Chaps. 4, 6, 8; (*e*) T.T. Tidwell. Ketenes. John Wiley, New York. 1995.
2. (*a*) O. Diels and B. Wolf. Chem. Ber. **39**, 689 (1906); (*b*) H. Staudinger and S. Bereza. Chem. Ber. **41**, 4461 (1908); (*c*) H. Ulrich. Cycloaddition reactions of heterocumulenes. Academic Press, New York. 1967. Chap. 3, pp. 110–121; (*d*) T. Kappe and E. Ziegler. Angew. Chem. Int. Ed. Engl. **13**, 491 (1974); (*e*) T. Kappe. *In* Methoden der Organischen Chemie. Vol. 15E. Thieme Verlog, Stuttgart. 1993.
3. (*a*) H. Staudinger and K. Clar. Chem. Ber. **44**, 1623 (1911); (*b*) H. Staudinger and W. Kreis. Helv. Chim. Acta, **6**, 321 (1923); (*c*) H. Staudinger. Die Ketene. Ferdinand Enke, Stuttgart. 1912. p. 19; (*d*) E. Wedekind, M. Miller, and C. Weinard. J. Prakt. Chem. **109**, 161 (1925).
4. (*a*) W.R. Hatchard and A.K. Schneider. J. Am. Chem. Soc. **79**, 6261 (1957); (*b*) A.T. Blomquist and Y.C. Meinwald. J. Am. Chem. Soc. **79**, 2021 (1957); (*c*) A.T. Blomquist and R.D. Spencer. J. Am. Chem. Soc. **70**, 30 (1948); (*d*) P.E. Eaton and B.D. Leipzig. J. Am. Chem. Soc. **105**, 1656 (1983); (*e*) P. Zarras and O. Vogl. Prog. Polym. Sci. **16**, 173 (1991); (*f*) A.T. Blomquist. U.S. Patent 3,002,024. 1961; Chem. Abstr. **56**, 8657b (1962).
5. (*a*) G. Maier, H.P. Reisenauer, and T. Sayrac. Chem Ber. **115**, 2192 (1982); (*b*) M. Kasai, M. Oda, and Y. Kitahara. Chem. Lett. 217 (1978); (*c*) R. Hochstrasser and J. Wirz. Angew. Chem. Int. Ed. Engl. **28**, 181 (1989); (*d*) H. Tomioka, H. Fukao,

and Y. Izawa. Bull. Chem. Soc. Jpn. **51**, 540 (1978); (*e*) R.D. Miller and S. Kirchmeyer. J. Org. Chem. **58**, 90 (1993); (*f*) N. Obata and T. Takizawa. Bull. Chem. Soc. Jpn. **50**, 2017 (1977); (*g*) H.A. Staab and J. Ipaktschi. Chem. Ber. **101**, 1457 (1968); (*h*) D.R. Boate, L.J. Johnson, P.C. Kwong, E. Lee-Ruff, and J.C. Scaiano. J. Am. Chem. Soc. **112**, 8858 (1990); (*i*) T. Mosandl and C. Wentrup. J. Org. Chem. **58**, 747 (1993); (*j*) C.F. Jewell, Jr., L.S. Liebeskind, and M. Williamson. J. Am. Chem. Soc. **107**, 6715 (1985).

6. (*a*) A.D. Allen, J. Ma, M.A. McAllister, T.T. Tidwell, and D.-c. Zhao. Acc. Chem. Res. **28**, 265 (1995); (*b*) D.-c. Zhao, A.D. Allen, and T.T. Tidwell. J. Am. Chem. Soc. **115**, 10 097 (1993); (*c*) A.D. Allen, W.-Y. Lai, J. Ma, and T.T. Tidwell. J. Am. Chem. Soc. **116**, 2625 (1994); (*d*) A.D. Allen, R. Ji, W.-Y. Lai, J. Ma, and T.T. Tidwell. Heteroat. Chem. **5**, 235 (1994); (*e*) M.A. McAllister and T.T. Tidwell. J. Am. Chem. Soc. **116**, 7233 (1994); (*f*) N.H. Werstiuk, J. Ma, M.A. McAllister, T.T. Tidwell, and D.-c. Zhao. J. Chem. Soc. Faraday Trans. **90**, 3383 (1994); (*g*) A.D. Allen, J.D. Colomvakos, W.-Y. Lai, R. Liu, J. Ma, T.T. Tidwell, and D.-c. Zhao. Pure Appl. Chem. **67**, 777 (1995).
7. (*a*) L. Gong, M.A. McAllister, and T.T. Tidwell. J. Am. Chem Soc. **113**, 6021 (1991); (*b*) A.D. Allen and T.T. Tidwell. Tetrahedron Lett. **32**, 847 (1991); (*c*) M.A. McAllister and T.T. Tidwell. J. Org. Chem. **59**, 4506 (1994); (*d*) R.A. Ruden. J. Org. Chem. **39**, 3607 (1974); (*e*) R.L. Danheiser and H. Sard. J. Org. Chem. **45**, 4810 (1980); (*f*) L.L. Shchukovskaya, R.I. Pal'chik, and A.N. Lazarev. Dokl. Akad. Nauk SSSR, **164**, 357 (1965); (*g*) Y. Kita, J. Sekihachi, Y. Hayashi, Y. Da, M. Yamamoto, and S. Akai. J. Org. Chem. **55**, 1108 (1990).
8. (*a*) Y. Rubin, S.S. Lin, C.B. Knobler, J. Anthony, A.M. Boldi, and F. Diederich. J. Am. Chem. Soc. **113**, 6943 (1991); (*b*) F. Diederich and Y. Rubin. Angew. Chem. Int. Ed. Engl. **31**, 1101 (1992); (*c*) F. Diederich, Y. Rubin, O.L. Chapman, and N.S. Goroff. Helv. Chim. Acta, **77**, 1441 (1994).
9. (*a*) S. Takahashi, Y. Kuroyama, K. Sonogashira, and N. Hagihara. Synthesis, 627 (1980); (*b*) Y. Stenstrøm. Synth. Commun. **22**, 2801 (1992); (*c*) G. Mehta and H.S.P. Rao. Synth. Commun. **15**, 991 (1985); (*d*) L.R. Krepski and A. Hassner. J. Org. Chem. **43**, 2879 (1978).

Can. J. Chem. Downloaded from www.nrcresearchpress.com by 46.23.64.124 on 09/08/12
For personal use only.

Fluorescence energy transfer studies in a cross-linked polyurethane network

Jie Yang and Mitchell A. Winnik

Abstract: A series of cross-linked polyurethane samples, labeled with dyes suitable for fluorescence energy transfer experiments, were prepared (donor, phenanthrene; acceptor, anthracene). Fluorescence decay profiles for these samples were measured as a function of acceptor concentration. These decays obey Förster nonradiative energy transfer kinetics, with an energy transfer critical distance (R_0) of 26.7 Å. Fluorescence intensities, calculated from the decays by integrating the decay profiles, also fit the Perrin model, with a quenching radius (R_s) of 25.6 Å. The fluorescence decay profiles were further examined with a distribution analysis method, which also revealed uniformly distributed donors and acceptors in the polymer matrices.

Key words: fluorescence quenching, fluorescence decay, phenanthrene, anthracene, polyurethane.

Résumé : Nous avons préparé une série d'échantillons de polyuréthanes réticulés, marqués de colorants appropriés pour des expériences de transfert d'énergie de fluorescence (donneur : phénanthrène; accepteur : anthracène). Nous avons mesuré les profils de décroissance de la fluorescence en fonction de la concentration d'accepteur. Ces décroissances obéissent à une cinétique de transfert d'énergie non radiative de Förster avec une distance critique de transfert d'énergie (R_0) de 26,7 Å. Les intensités de fluorescence, calculées à partir des décroissances par une intégration des profils de décroissance, s'ajustent aussi au modèle de Perrin, avec un rayon de désactivation (R_s) de 25,6 Å. On a aussi examiné les profils de décroissance à l'aide d'une méthode d'analyse statistique qui a aussi révélé que la distribution des donneurs et des accepteurs est uniforme dans les matrices de polymères.

Mots clés : désactivation de la fluorescence, décroissance de la fluorescence, phénanthrène, anthracène, polyuréthane.

[Traduit par la rédaction]

Introduction

Fluorescence energy transfer is being used increasingly in polymer science, to study various polymer properties (1), such as polymer conformation (2), diffusion (3), and morphology (4). To use this method, polymers are usually labeled with fluorescent dyes, among which the phenanthrene–anthracene pair (Phe, energy transfer donor; An, energy transfer acceptor) have often been employed (2*c*, 3*a*, 4*d*). In both simple and cross-linked polymer films, energy transfer from phenanthrene (donor) to anthracene (acceptor) should occur by the dipole coupling (Förster) mechanism. Direct nonradiative energy transfer (DET) by the Förster mechanism leads to nonexponential fluorescence decay curves (5). The shape of the curve depends upon the detailed description of the donor–acceptor (Phe/An) pair distribution. In films that are not cross-linked, one anticipates a uniform distribution of donors and acceptors. However, for labeled polymers of high molecular weight, the "correlation hole" can perturb the dye distribution (6). Therefore, in cross-linked polymer films, one has to exercise special care to establish whether the cross-linking chemistry perturbs that distribution. Here we examine cross-linked polyurethane films containing covalently bound Phe and An in the polymer backbone. Through careful fluorescence decay measurements, we establish that there is in fact a uniform distribution of donors and acceptors in the system.

In a system with uniformly distributed donors and acceptors in three dimensions, the donor fluorescence intensity decay $I_D(t)$ is described by eq. [1], where τ_0 is the donor fluorescence lifetime in the absence of acceptors, and P is proportional to the acceptor (quencher) concentration [Q] (5, 7):

$$[1] \quad I_D(t) = A \exp\left[-\frac{t}{\tau_0} P\left(\frac{t}{\tau_0}\right)^{0.5}\right]$$

$$[2] \quad P = \gamma \times \frac{4\pi^{3/2} N R_0^3 [Q]}{3000}$$

In eq. [2], γ is an orientation factor, N is Avogadro's number, and R_0 is the Förster critical radius for energy transfer.

The Perrin model (8) is a related but simplified model, which also describes static quenching between randomly distributed and immobile fluorophores and quenchers that are accidentally in proximity. In this model, one presumes that there is instantaneous quenching of an excited donor (D*) by a

Received January 31, 1995.

This paper is dedicated to Professor J.E. (Jim) Guillet in recognition of his contributions to Canadian chemistry, and for many years of assistance and advice.

J. Yang and M.A. Winnik.[1] Department of Chemistry and Erindale College, University of Toronto, Toronto, ON M5S 1A1, Canada.

[1] Author to whom correspondence may be addressed: Telephone : (416) 978–6495. Fax: (416) 978–0541. E-mail: mwinnik@alchemy.chem.utoronto.ca

Can. J. Chem. Downloaded from www.nrcresearchpress.com by 46.23.64.124 on 09/08/12
For personal use only.

Table 1. Polyurethane sample compositions.

Sample	Polytetramethylene glycol **5** (mg)	Triisocyanate **4** (mg)	Phe-diol **3** (mg)	An-diol **6** (mg)	An/Phe Ratio
PU0	1500	575	0.8	0	0
PU1	1500	575	0.8	0.8	1
PU3	1500	575	0.8	2.4	3
PU6	1500	575	0.8	4.8	6
PU9	1500	575	0.8	7.2	9
PU12	1500	575	0.8	9.6	12

Note: Stock solutions were prepared by dissolving Phe-diol and An-diol in poly(tetramethylene glycol), in order to avoid weighing small amount of fluorescent dyes; see the experimental section for details.

Scheme 1. Synthesis of phenanthrene-diol **3**.

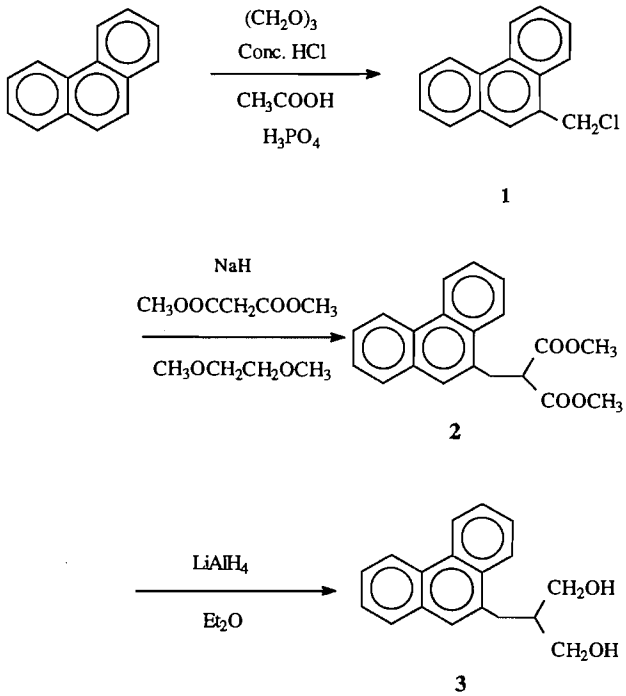

Scheme 2. Preparation of crosslinked polyurethane network labeled with energy transfer donor (Phe) and acceptor (An).

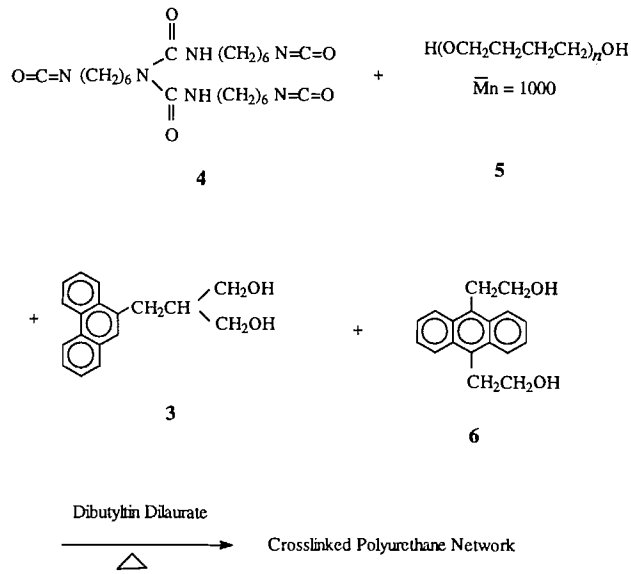

quencher (Q) if this quencher is inside a spherical volume V centered on D*, and there is no quenching when the quencher is outside of this volume. From data plotted according to this model, eq. [3], one can obtain R_s, the radius of the quenching sphere.

$$[3] \quad \ln \frac{F_0}{F} = V[Q] = \frac{4}{3}\pi R_s^3[Q]$$

Here F is the fluorescence intensity in the presence of quenchers, and F_0 is that when [Q] = 0. As originally proposed, the Perrin model predicts that $\tau = \tau_0$ for Q outside of V and $\tau = 0$ for Q inside V.

In this paper, we wish to report the synthesis of a new fluorescent label molecule (phenanthrene-diol **3**, Scheme 1), the preparation of cross-linked polyurethane networks labeled with both phenanthrene and anthracene chromophores (Scheme 2), and the study of fluorescence energy transfer for the above polyurethane samples by fluorescence decay measurements (9).

Results and discussion

1. Polyurethane sample preparation

To prepare labeled polyurethane samples, diol derivatives of the donor and acceptor dyes are needed. The anthracene-diol derivative **6** has been reported previously in the literature. We developed a rather straightforward synthesis of the phenanthrene-diol derivative **3** by the route shown in Scheme 1. These two dyes were then introduced as co-reactants in the polyurethane synthesis.

The cross-linked polyurethane network was formed between a polymer-diol **5** (polytetramethylene glycol) and the triisocyanate **4** (Desmurdo N-100) as shown in Scheme 2. A series of polyurethane samples (PU0 – PU12) were prepared with different anthracene acceptor (**6**) concentrations, while the phenanthrene donor (**3**) concentration was kept constant. The compositions are given in Table 1.

Can. J. Chem. Downloaded from www.nrcresearchpress.com by 46.23.64.124 on 09/08/12
For personal use only.

Can. J. Chem. Downloaded from www.nrcresearchpress.com by 46.23.64.124 on 09/08/12
For personal use only.

Fig. 1. UV absorption spectrum for sample PU1.

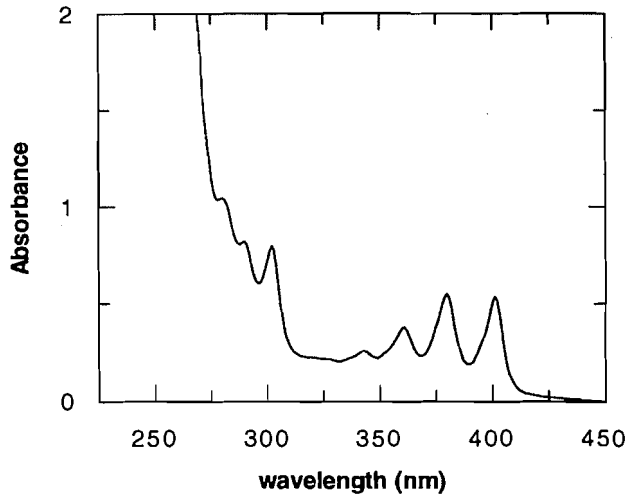

Fig. 2. Fluorescence emission spectrum for sample PU0 (λ_{ex} = 300 nm).

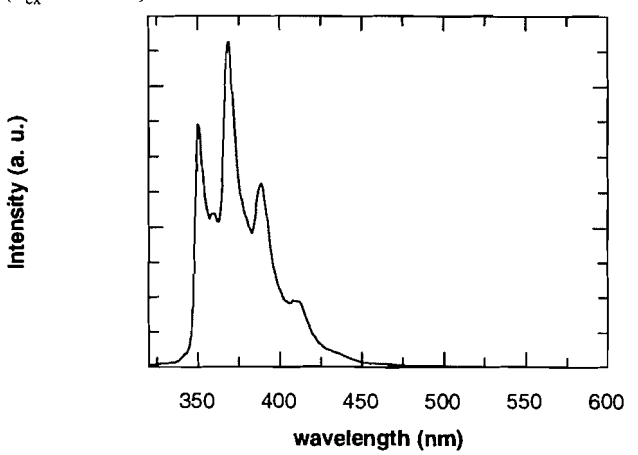

2. Sample characterization

During the preparation of polyurethane samples, an FT-IR spectrometer was used to monitor the monomer **4** consumption at 2270 cm^{-1}. This band disappeared completely after 48 h under the experimental conditions. The above prepared samples were also characterized by UV, fluorescence emission, and fluorescence excitation spectroscopies. The UV absorption spectrum for sample PU1 (An/Phe = 1) is shown in Fig. 1. One can see the characteristic band of phenanthrene at 300 nm, and the typical four vibronic bands for anthracene at 340, 360, 380, and 400 nm, respectively. The fluorescence emission spectrum for sample PU0 (labeled with Phe only) is shown in Fig. 2, which is a typical phenanthrene fluorescence spectrum.

Two fluorescence spectra for sample PU1 (An/Phe = 1) are shown in Fig. 3. This sample is labeled with equal amounts of Phe and An. Excitation of the sample at 360 nm (λ_{ex}) leads to An emission only (Fig. 3*a*), whereas excitation at λ_{ex} = 300 nm gives results in fluorescence from both Phe and An (Fig. 3*b*). One can also see that the Phe emission intensity is very weak, while that from An is strong. This indicates significant fluorescence energy transfer from Phe to An in the sample. The fluorescence excitation spectrum (λ_{em} = 500 nm) for PU1 in Fig. 4 corresponds to the UV absorption bands for anthracene and phenanthrene in the sample.

Fig. 3. Emission spectra for sample PU1: (*a*) λ_{ex} = 360 nm; (*b*) λ_{ex} = 300 nm.

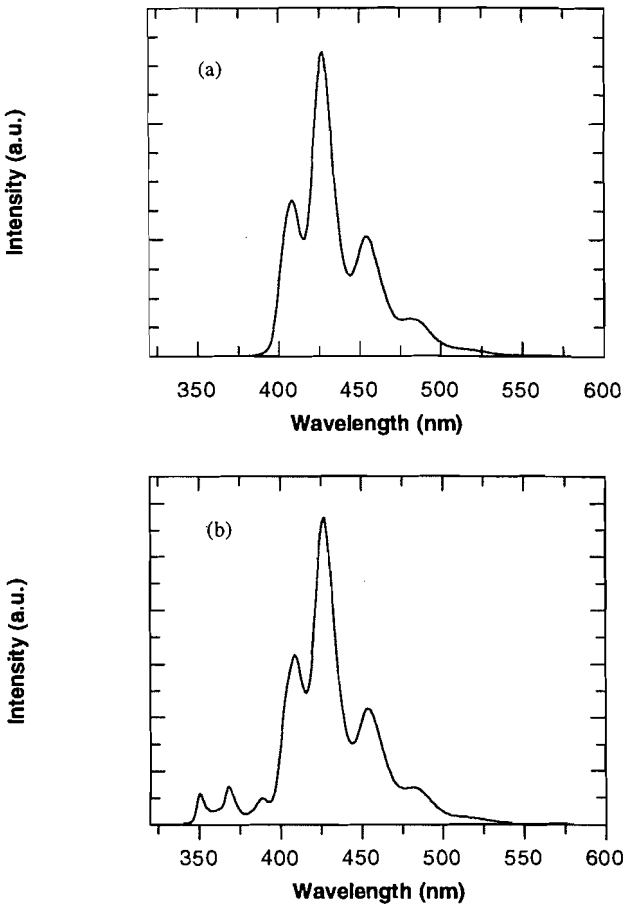

Fig. 4. Excitation spectrum for PU1 (λ_{em} = 500 nm).

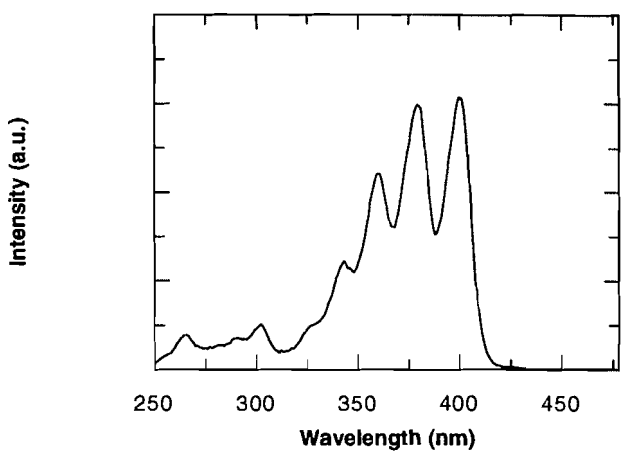

3. Fluorescence decay studies

For each polyurethane sample, fluorescence decay profiles of the energy donor (Phe) were measured using the Time Correlated Single Photon Counting technique. Samples were excited at 300 nm (λ_{ex}), and the fluorescence emission was detected at 366 nm (λ_{em}). Sample PU0 (labeled with only Phe) gives a single exponential decay of the phenanthrene fluorescence (cf. Fig. 5), with a lifetime of 49.7 ns (χ^2 = 1.04).

Can. J. Chem. Downloaded from www.nrcresearchpress.com by 46.23.64.124 on 09/08/12
For personal use only.

Fig. 5. Fluorescence decay for sample PU0 and the weighted residuals, for an exponential fit ($\tau_0 = 49.7$ ns, $\chi^2 = 1.04$).

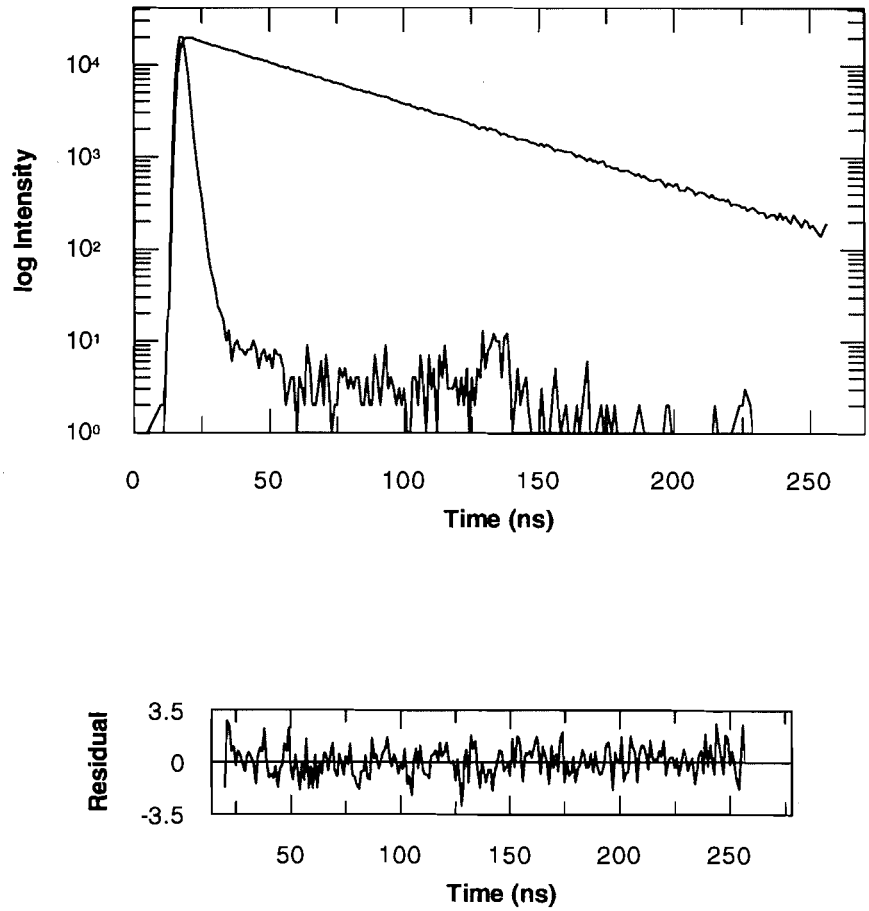

Fig. 6. Fluorescence decay curves for polyurethane samples (from top to bottom: PU0, PU1, PU3, PU6, PU9, PU12).

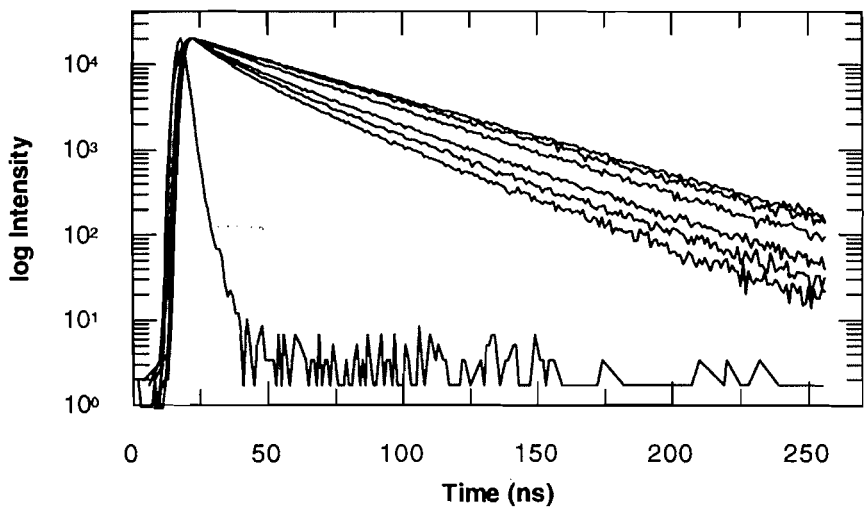

The introduction of acceptors (An) into samples PU1 – PU12 enhances the phenanthrene fluorescence decay rate and makes the decay nonexponential (Fig. 6). With the increase of anthracene concentration, one can see that the curvature of the decay curves increases and that the area under a decay curve decreases. We used the two related models, the Förster energy transfer model and the Perrin static quenching model, to analyze these decay curves. The Förster model is concerned with the shape of the decay curves, and the Perrin model is related to the area under each decay curve.

(a) Data fitting with the Förster energy transfer equation

In the polyurethane samples, the quenching of Phe fluorescence is expected to follow the direct nonradiative energy

Can. J. Chem. Downloaded from www.nrcresearchpress.com by 46.23.64.124 on 09/08/12
For personal use only.

Table 2. Förster equation fitting of phenanthrene fluorescence decays for polyurethane samples.

Sample	10^3 [An] (M)	P	τ_0 (fixed)	χ^2
PU0	0	0.00189	49.7	1.01
PU1	1.50	0.118	49.7	1.12
PU3	4.51	0.327	49.7	1.31
PU6	9.02	0.674	49.7	1.04
PU9	13.5	1.01	49.7	1.35
PU12	18.0	1.29	49.7	1.58

Fig. 7. Weighted residuals from Förster equation fits to the decays shown in Fig. 6.

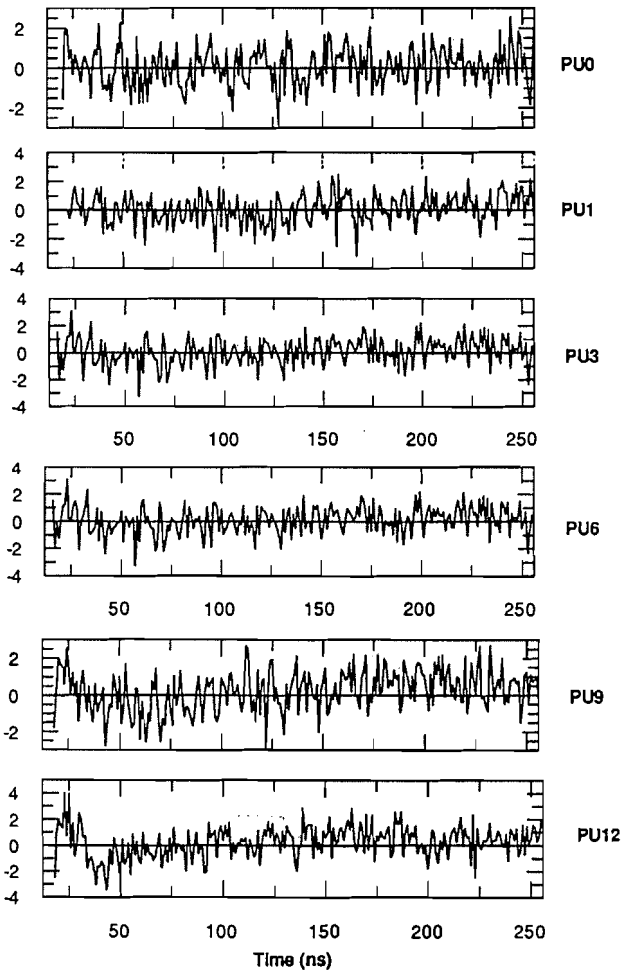

transfer (DET) mechanism proposed by Förster, in which the Phe fluorescence intensity is described by eq. [1]. The donor fluorescence decay profiles from the samples (Fig. 6) were fitted to eq. [1]. The fitting results are listed in Table 2 and the residuals are given in Fig. 7. Note that this is a two-parameter fit to the data since τ_0 is known independently.

The decay profiles fit well to eq. [1] for samples PU0 – PU6, with acceptable χ^2 and evenly distributed residuals. However,

Fig. 8. Plot of P vs. anthracene concentration for polyurethane samples.

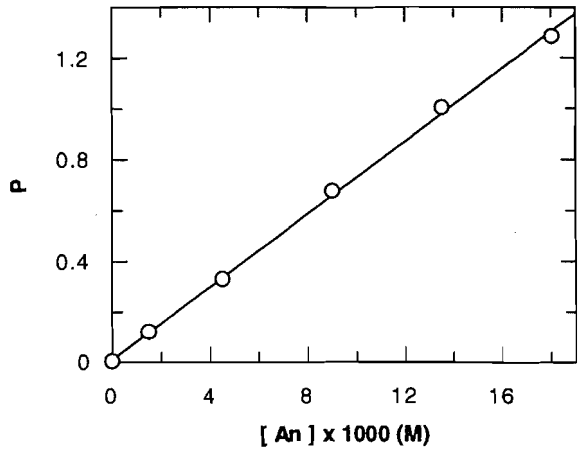

the χ^2 values for PU9 (1.35) and PU12 (1.58) are a little high, and the plot of weighted residuals indicates that the largest deviations occur at early times in the decay. These two samples, consisting of high concentrations of An (acceptor), require longer times to collect the Phe fluorescence data compared with the rest of the polyurethane samples, and this would allow more drift in the lamp profile, which often leads to deviations in the fit at early times of the decay. Overall, the data fitting is reasonably good.

According to the Förster mechanism (5), the parameter P should be linear with the acceptor concentration [An] (cf. eq. [2]). We plot P against [An] in Fig. 8 and obtain a straight line with a slope of 72.4 M^{-1}. This slope contains the Förster energy transfer critical radius R_0, which can be calculated from eq. [2] (5, 7). In a rigid polymer film, the orientation factor $\gamma = 0.8452$ (7), and the critical radius R_0 was calculated to be 26.7 Å. This calculated critical radius R_0 is very close to the R_0 reported for the Phe/An pair in several cases (24.1 Å (4*d*), 25.2 Å (10), and 25.5 Å (11)). From the above analysis, we conclude that nonradiative energy transfer in the polyurethane network obeys the Förster dipole–dipole interaction mechanism (5), which also implies that the fluorescent labels Phe and An are randomly distributed in the cross-linked polyurethane network.

The issue of uniform donor and acceptor distribution in the matrix can be examined more deeply through a *distribution analysis* of the fluorescence decay profiles. The Förster expression (eq. [1]) is derived through an integration over an assumed uniform donor–acceptor distribution. The fluorescence decays previously analyzed in terms of the Förster expression were reanalyzed using the exponential series method (12). In this approach, one fits the decay to a large number of evenly spaced exponential terms and optimizes their coefficients. This approach is often very powerful at identifying multiple distributions of donor decay rates within a sample (3*c*).

Results are shown in Fig. 9. In each case our sample is characterized by an unimodal distribution of acceptors surrounding excited donors. As the acceptor concentration increases, the distribution shifts to the right. The mean acceptor concen-

Can. J. Chem. Downloaded from www.nrcresearchpress.com by 46.23.64.124 on 09/08/12
For personal use only.

Fig. 9. Acceptor distributions for polyurethane samples. The graph plots relative number of donors undergoing energy transfer on the *y*-axis vs. the number density of acceptors at a distance r/R_0 from the donor. From top to bottom: PU1, PU3, PU6, PU9, PU12. The shaded areas are not normalized.

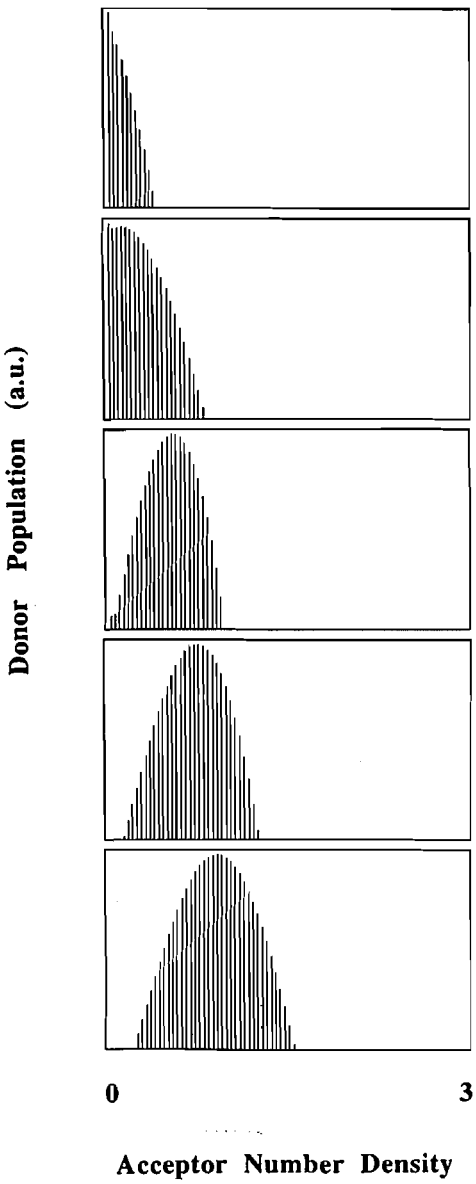

tration calculated from these distributions corresponds to that of the sample itself.

(b) Data fitting with the Perrin model

In fitting the data to the Perrin model (eq. [3]), one needs to know the fluorescence intensities F_0 and F. It is normally very difficult to obtain absolute fluorescence intensities from measurements on film samples by steady-state fluorescence spectroscopy. An alternative is to integrate the normalized intensity decay curves (13, 14), since the fluorescence quantum yield is given by

$$[4] \quad \Phi_f = k_f \int_0^\infty I_D(t)dt$$

Fig. 10. Plot of ln (F_0/F) vs. anthracene concentration for polyurethane samples

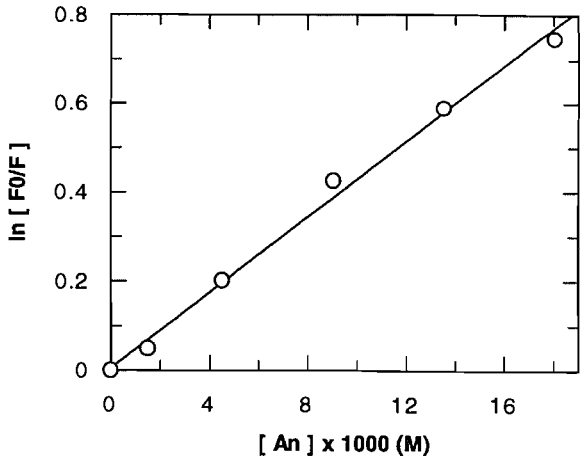

where k_f is the radiative rate coefficient for the fluorophore, and Φ_f refers to the fluorescence quantum yield. Thus:

$$[5] \quad \frac{F_0}{F} = \frac{\Phi_f^0}{\Phi_f} = \frac{\int_0^\infty I_D{}^0(t)dt}{\int_0^\infty I_D(t)dt}$$

In our calculations, we fit each decay curve into the sum of two exponential decay terms, and F is giving by eq. [6]. In Fig. 10 we see that the plot of ln (F_0/F) vs. [An] yields a linear fit, with a slope of 42.7 M^{-1}. The Perrin quenching sphere radius R_s was calculated, from eq. [3], to be 25.6 Å.

$$[6] \quad F = \int_0^\infty I_D(t)\,dt = \int_0^\infty (A_1 \exp(-t/\tau_1) + A_2 \exp(-t/\tau_2))dt = A_1\tau_1 + A_2\tau_2$$

Conclusion

In cross-linked polyurethane networks, the fluorescence of covalently bound phenanthrene is quenched by the bound anthracene groups. By analyzing the phenanthrene fluorescence intensity decay profiles, we found that the fluorescence quenching obeys Förster energy transfer kinetics, with R_0 = 26.7 Å. This establishes that these donor and acceptor groups are randomly distributed in the polymer matrix and that the cross-linking chemistry does not perturb their distribution. The fluorescence intensities, obtained by integrating the area under each decay curve, also fit the Perrin model, with a quenching radius R_s of 25.6 Å. The similarity of the two R values serves as a reminder of the similarity of the two models in the case of randomly distributed donor and acceptor pairs in rigid media.

Experimental section

Synthesis of 9-chloromethylphenanthrene (1)

A reported procedure (15) was followed to synthesize compound **1**. A mixture of phenanthrene (35.7 g, 0.20 mol), paraformaldehyde (11 g, 0.37 mol), glacial acetic acid (36 ml), 12 N HCl (110 mL), and 85% phosphoric acid (16.5 mL) was stirred vigorously in a 500 mL round-bottom flask fitted with a reflux condenser. The reaction temperature was controlled at

Can. J. Chem. Downloaded from www.nrcresearchpress.com by 46.23.64.124 on 09/08/12
For personal use only.

85°C for 52 h. This reaction mixture was then poured over 200 mL of crushed ice, and extracted with 3 x 200 mL of diethyl ether. The combined organic layer was washed with water until neutral, dried over magnesium sulfate, and the solvent was removed *in vacuo* to leave 40 g of dark paste. Column chromatography was carried out three times on this dark paste (with pure hexanes as the eluting solvent). 9–Chloromethylphenanthrene (35.0 g, yield 77%) was isolated, with a melting point of 101–102°C (lit. (15) mp 101–102°C). ^{1}H NMR ($CDCl_3$, 200 MHz, δ ppm): 8.55–8.80 (m, 2H, Ar-H), 8.1–8.3 (m, 1H, Ar-H), 7.5–7.95 (m, 6H, Ar-H), 5.05 (s, 2H, CH_2). Mass (*m/e*, peak intensity in parentheses): 228 (M^+ + 2, 14), 226 (M^+, 38), 192 (28), 191 (100), 190 (15), 189 (38).

Synthesis of dimethyl 2-(9-Phenanthrylmethyl) malonate (2)

To a 3–neck, 500 mL round-bottom flask (under nitrogen) was added 2.08 g of NaH (50% content, 43.4 mmol) and 150 mL of dimethoxyethane (dried and distilled over $LiAlH_4$). Dimethyl malonate (5.63 g, 43.4 mmol, Aldrich) in 30 mL of dimethoxyethane was added dropwise. After 15 min, 9–chloromethylphenanthrene (7.0 g, 31 mmol) in 20 mL of dimethoxyethane was added over 10 min. and the resulting solution was heated to 60°C for 4 h. The reaction mixture was then washed with water, extracted with diethyl ether (3 × 80 mL), and the combined organic layer was dried over magnesium sulfate. After evaporating the solvent *in vacuo*, the oily residue **2** (10 g) was obtained, which was used directly in the next step without further purification.

Synthesis of 2-(9-phenanthrylmethyl)-1,3-propanediol (3)

The above 10 g of oily residue **2** was dissolved in 200 mL of anhydrous diethyl ether in a 500 mL round bottom flask. Excess of $LiAlH_4$ (1.5 g) was added to the solution, and the resulting mixture was refluxed for 5 h. Ethanol (20 mL) was cautiously added to the reaction mixture, followed by 150 mL of water. This mixture was extracted with diethyl ether (3 × 100 mL). The combined organic layer was dried over magnesium sulfate, and the solvent was evaporated *in vacuo*. The residue was column chromatographed (20% acetone in hexanes, v/v). 2-(9-Phenanthrylmethyl)-1,3-propanediol (**3**) was isolated in 52% yield (4.3 g, mp 145–146°C). ^{1}H NMR (DMSO-d_6, 200 MHz, δ ppm): 8.7–8.9 (m, 2H, Ar-H), 8.2–8.3 (m, 1H, Ar-H), 7.8–8.0 (m, 1H, Ar-H), 7.5–7.7 (m, 5H, Ar-H), 4.6 (t, 2H, 2OH), 3.4–3.6 (m, 4H, $2OCH_2$), 3.3–3.4 (m, 1H, CH), 3.05–3.15 (d, 2H, CH_2). ^{13}C NMR and APT (DMSO-d_6, 50 MHz, δ ppm):135.47, 131.54, 131.18, 130.55, 129.41, 128.16, 127.48, 127.09, 127.03, 126.65, 126.44, 125.15, 123.67, 122.93, 61.73 (OCH_2), 44.41 (CH), 31.72 (CH_2). Mass (*m/e*, peak intensity in parentheses): 267 (M^+ + 1, 15), 266 (M^+, 53), 217 (41), 192 (100), 191 (99).High resolution mass calculated for $C_{18}H_{18}O_2$: 266.1307, found: 266.1311 .

Synthesis of 9,10-anthracenediethanol (6) (ref. 16)

9,10–Dibromoanthracene (10 g, 30 mmol, Aldrich) and anhydrous diethyl ether (180 mL) were added into a 250 mL, 3–neck round-bottom flask. This mixture was stirred under nitrogen, and cooled to 5°C (ice-water bath). *n*-BuLi (7.5 mL, 75 mmol, 10.0 M hexane solution, Aldrich) was added with a syringe over a period of 10 min and stirred for another 20 min. An excess of ethylene oxide (6.0 g, 136 mmol, Fisher) was added over 10 min. This solution was stirred at 5°C for 1 h, and was allowed to warm up to room temperature. It was then poured over crushed ice (100 mL), and extracted with diethyl ether (100 ml) and chloroform (3 × 100 mL). The combined organic solvents were dried over magnesium sulfate and evaporated *in vacuo*. 9,10–Anthracenediethanol (5.35 g, yield 67%) was obtained after a column chromatograph (30% acetone in hexanes, v/v); mp 224–225°C (lit. (16) mp 221–225°C). ^{1}H NMR (DMSO-d_6, 200 MHz, δ ppm): 8.3–8.5 (m, 4H, Ar-H), 7.5–7.7 (m, 4H, Ar-H), 4.9 (m, 2H, 2OH), 3.8 (m, 8H, $4CH_2$). ^{13}C NMR (DMSO-d_6, 50 MHz, δ ppm): 130.43, 129.81, 125.42 (2C), 62.04 (OCH_2), 31.82 (CH_2). Mass (*m/e*, peak intensity in parentheses): 267 (M^+ + 1, 16), 266 (M^+, 56), 235 (59), 217 (28), 205 (100), 191 (47).

Example of polyurethane sample preparation: PU6 film preparation

(*a*) Stock solution A(6): To a 50 mL Erlenmeyer flask was added polytetramethylene glycol (7.5 g, M_n = 1000, Teracol 1000, Dupont), phenanthrene-diol **3** (4.0 mg), and anthracenediol **6** (24.0 mg). This mixture was then heated to 90°C under nitrogen with stirring to dissolve the two solid diols. This mixture was kept at room temperature in the dark as stock solution A(6).

(*b*) Film casting: Stock solution A(6) (1500 mg) and triisocyanate **4** (Desmurdo N-100, 575 mg, Miles Chem. Co.) were added to a small test tube with stirring. This mixture was subsequently warmed up to 50°C to make a homogeneous solution. Dibutyltin dilaurate (1 μL, Polysciences Inc.) was added afterwards. The resulting viscous liquid was cast onto the surface of quartz plates (1 × 10 × 25 mm). These samples were kept under nitrogen at room temperature for at least 48 h before any testing. The triisocyanate **4** was completely polymerized after 48 h, as was monitored by FT-IR at the wave number of 2270 cm^{-1}.

UV and fluorescence measurements

The UV absorption spectrum was measured with a Perkin–Elmer Lambda 6 spectrometer. Fluorescence spectra were measured with a SPEX Fluorolog 2 instrument equipped with a DMA 3000 data system. Fluorescence decay profiles were measured by the time-correlated single photon counting technique (9) as described previously (3*a*). The excitation wavelength was 300 nm, the emission wavelength was 366 nm, and 20 000 counts were collected in the maximum channel.

Acknowledgments

The authors thank 3M and 3M Canada Inc. for their support of this research.

References

1. H. Morawetz. Science, **240**, 172 (1988).
2. (*a*) L. Stryer. Annu. Rev. Biochem. **47**, 819 (1978), (*b*) E. Haas. *In* Photophysical and photochemical tools in polymer science. *Edited by* M.A. Winnik. NATO ASI Ser. C: **182**; Reidel, Dordrecht, The Netherlands. 1985. pp. 325–350; (*c*) D. Ng and J.E. Guillet. Macromolecules, **15**, 724 (1982); **15**, 728 (1982) (*d*) G. Liu, J.E. Guillet, E.T.B. Al-Takrity, A.D. Jenkins, and D.R.M. Walton. Macromolecules, **23**, 1393 (1990); (*e*) B.

Pispisa, M. Venanzi, A. Palleschi, and G. Zanotti. Macromolecules, **27**, 7800 (1994).
3. (*a*) Y. Wang and M.A. Winnik. J. Phys. Chem. **97**, 2507 (1993); (*b*) Macromolecules, **26**, 3147 (1993); (*c*) Y.S. Liu, L. Li, S. Ni, and M.A. Winnik. Chem. Phys. **177**, 579 (1993); (*d*) A. Dhinojwala and J.M. Torkelson. Macromolecules, **27**, 4817 (1994); (*e*) G. Liu, J.E. Guillet, E.T.B. Al-Takrity, A.D. Jenkins, and D.R.M. Walton. Macromolecules, **23**, 4164 (1990).
4. (*a*) J.M. Drake, J. Klafter, and P. Levitz. Science **251**, 1574 (1991); (*b*) F. Mikes, H. Morawetz, and K.S. Dennis. Macromolecules, **17**, 60 (1984); (*c*) Y. Wang and H. Morawetz. Macromolecules, **23**, 1753 (1990); (*d*) S. Ni, P. Zhang, Y. Wang, and M.A. Winnik. Macromolecules, **27**, 5742 (1994).
5. (*a*) T. Förster. Discuss. Faraday Soc. **27**, 7 (1959); (*b*) J.B. Birks. Photophysics of aromatic molecules. Wiley–Interscience, New York. 1970.
6. A.S. Mendelsohn, M.O. de la Cruz, and J.M. Torkelson. Macromolecules, **26**, 6789 (1993).
7. J. Baumann and M.D. Fayer. J. Chem. Phys. **85**, 4087 (1986).
8. F. Perrin. C. R. Hebd. Seances Acad. Sci. **178**, 1978 (1924).
9. D.V. O'Connor and D. Phillips. Time-correlated single photon counting. Academic Press, London. 1984.
10. Y. Wang, C. Zhao, and M.A. Winnik. J. Chem. Phys. **95**, 2143 (1991).
11. I.B. Berlman. Energy transfer parameters of aromatic compounds. Academic Press, New York. 1973.
12. (*a*) Y. S. Liu and W.R. Ware. J. Phys. Chem. **97**, 5980 (1993); (*b*) Y.S. Liu, P. de Mayo, and W.R. Ware. J. Phys. Chem. **97**, 5987 (1993); **97**, 5995 (1993).
13. M. Inokuti and F. Hirayama. J. Chem. Phys. **43**, 1978 (1965).
14. K.B. Eisenthal and S. Siegel. J. Chem. Phys. **41**, 652 (1964).
15. F. Fernandez, G. Gomez, C. Lopez, and A. Santos. Synthesis, 802 (1988).
16. D.F. Evans and M.W. Upton. J. Chem. Soc. Dalton Trans. 1141 (1985).

Can. J. Chem. Downloaded from www.nrcresearchpress.com by 46.23.64.124 on 09/08/12
For personal use only.

Activation barriers for oxygen diffusion in polystyrene and polycarbonate glasses: effects of codissolved argon, helium, and nitrogen

Bojie Wang and Peter R. Ogilby

Can. J. Chem. Downloaded from www.nrcresearchpress.com by 46.23.64.124 on 09/08/12
For personal use only.

Abstract: A recently developed spectroscopic technique was used to determine oxygen diffusion coefficients as a function of temperature for polystyrene and polycarbonate films. Data were recorded at total pressures <300 Torr over the temperature range 5–45°C under conditions in which argon, helium, and nitrogen, respectively, were copenetrants. In all cases, the presence of the additional gas caused an increase in the oxygen diffusion coefficient. Arrhenius plots of the data yield (*a*) a diffusion activation barrier, E_{act}, and (*b*) a diffusion coefficient, D_0, that represents the condition of "barrier-free" gas transport for the temperature domain over which the Arrhenius plot is linear. For all cases examined in both polystyrene and polycarbonate, D_0 increased with an increase in the partial pressure of added gas. In polystyrene, the presence of an additional gas did not change E_{act}. In polycarbonate, E_{act} obtained in the presence of helium and argon likewise did not differ from that obtained in the absence of the copenetrant. When nitrogen was the added gas, however, a larger value of E_{act} was obtained. This latter observation is interpreted to reflect the plasticization of polycarbonate by nitrogen. E_{act} and D_0 data are discussed within the context of a model that distinguishes between dynamic and static elements of free volume in the polymer matrix.

Key words: oxygen diffusion, polystyrene, polycarbonate, activation barrier.

Résumé : On a utilisé une technique spectroscopique développée récemment pour déterminer les coefficients de diffusion de l'oxygène, en fonction de la température, dans des films de polystyrène et de polycarbonate. On a enregistré les données à des pressions totales inférieures à 300 Torr, à des températures allant de 5 à 45°C, dans des conditions telles que l'argon, l'hélium et l'azote sont respectivement des copénétrants. Dans tous les cas, la présence de gaz additionnel provoque une augmentation du coefficient de diffusion de l'oxygène. Les courbes d'Arrhenius des données permettent d'obtenir (*a*) une barrière d'activation à la diffusion, E_{act}, et (*b*) un coefficient de diffusion, D_0, qui représente la condition de transport du gaz « sans barrière » pour le domaine de température pour lequel la courbe d'Arrhenius est linéaire. Pour tous les cas examinés tant dans le polystyrène que le polycarbonate, la valeur de D_0 augmente avec une augmentation de la pression partielle du gaz additionné. Dans le polystyrène, la présence d'un gaz additionnel ne provoque pas de changement dans la valeur de E_{act}. Dans le polycarbonate, les valeurs de E_{act} obtenues en présence d'hélium et d'argon ne diffèrent pas de celles obtenues en l'absence de copénétrant. Toutefois, lorsqu'on ajoute de l'azote comme copénétrant, on obtient une valeur plus élevée pour E_{act}. On interprète cette dernière observation comme un reflet de la plasticisation du polycarbonate par l'azote. On discute des données de E_{act} et de D_0 dans le contexte d'un modèle qui permet de distinguer entre les éléments dynamiques et statiques du volume libre dans la matrice de polymère.

Mots clés : diffusion de l'oxygène, polystyrène, polycarbonate, barrière d'activation.

[Traduit par la rédaction]

Introduction

Studies of oxygen diffusion in amorphous organic polymer glasses are important from fundamental and practical perspectives. For those interested in polymer photophysics and photochemistry, such studies are useful because oxygen is an efficient quencher of excited electronic states (1–6). Studies of oxygen diffusion should also be useful for those interested in packaging materials, protective coatings, polymer oxidative degradation, and membranes for gas separation. With respect to the latter, the effect that other gases may have on the oxygen diffusion coefficient is certainly very important.

We recently developed a spectroscopic technique to quantify oxygen diffusion coefficients for polymer films (7). In this method, oxygen *sorption* into the film is followed by monitoring the 1270 nm phosphorescence of singlet oxygen [$O_2(a^1\Delta_g)$

Received March 30, 1995.

This paper is dedicated to Professor J.E. (Jim) Guillet in recognition of his contributions to Canadian chemistry.

B. Wang and P.R. Ogilby.[1] Department of Chemistry, University of New Mexico, Albuquerque, NM 87131, U.S.A.

[1] Author to whom correspondence may be addressed. Telephone: (505) 277-6655. Fax: (505) 277-2609.

Can. J. Chem. Downloaded from www.nrcresearchpress.com by 46.23.64.124 on 09/08/12
For personal use only.

$\rightarrow O_2(X^3\Sigma_g^-)]$. Singlet oxygen is produced from ground state oxygen by energy transfer from a photosensitizer dissolved in the polymer. The experiment is performed under conditions in which only one sensitizer state (invariably the triplet) is the singlet oxygen precursor.

$$[1]\quad \text{Sens} \xrightarrow{h\nu} \text{Sens}^* \xrightarrow{O_2(X^3\Sigma_g^-)} O_2(a^1\Delta_g) + \text{Sens}$$

Thus, upon exposure of a polymer film to oxygen, the intensity of singlet oxygen phosphorescence increases as the concentration of $O_2(X^3\Sigma_g^-)$ in the film increases. Although the proportionality constant that relates the photosensitized $O_2(a^1\Delta_g)$ phosphorescence intensity to the amount of sorbed oxygen can be determined in independent control experiments, it is not necessary with this technique to explicitly know the solubility of oxygen in the polymer. Data obtained behave according to eq. [2], in which the amount of $O_2(X^3\Sigma_g^-)$ that has entered the film at time $t(M_t)$, normalized by the amount at time = ∞ (M_∞), is expressed as a function of the film thickness ι and the diffusion coefficient D (7,8).

$$[2]\quad \frac{M_t}{M_\infty} = 1 - \sum_{n=0}^{\infty} \frac{8}{(2n+1)^2\pi^2} \exp\left(\frac{-D(2n+1)^2\pi^2 t}{4\iota^2}\right)$$

For films cast onto an oxygen-impermeable substrate, ι is the distance from the front to back surface of the film. For free-standing films, ι is the distance from the film center to a surface. Diffusion coefficients obtained from iterative fits of the data to eq. [2] are independent of (*a*) the film thickness over the range ~15–90 μm, and (*b*) the concentration of the singlet oxygen sensitizer over the range ~$(0.1–1.5) \times 10^{-3}$ M. Furthermore, diffusion coefficients obtained from free-standing films are identical to those recorded from films cast onto a substrate.

We recently used this technique to determine oxygen diffusion coefficients as a function of temperature in polystyrene and polycarbonate films (8). Over comparatively large temperature ranges, the diffusion coefficient behaved according to eq. [3], and we were able to obtain values of E_{act} and D_0 for films under a number of different conditions.

$$[3]\quad D = D_0 \exp(-E_{act}/RT)$$

We discovered that when nitrogen gas is a copenetrant, values of D, D_0 and E_{act} for oxygen diffusion can differ from those obtained in the absence of nitrogen (8). In an attempt to find the origin of this interesting phenomenon, we extended our work to include a study of the effects of helium and argon on D, D_0 and E_{act} for oxygen diffusion. The results of this latter study are presented and discussed in the current paper.

Experimental section

The methods by which we prepare polymer films and quantify oxygen diffusion coefficients have been previously described in detail (7, 8). Briefly, polycarbonate films were prepared by first dissolving the polymer and the sensitizer in CH_2Cl_2 to yield a homogenous mixture. The CH_2Cl_2 was then removed, and the resultant solid pressed between heated platens. Samples prepared for this study were heated at 250°C for 7 min under vacuum and in the absence of an applied load. A 1 metric ton load was then applied and maintained for 3 min on the 250°C sample. Resultant films were removed from the heated press and equilibrated with the ambient atmosphere. Data were recorded from free-standing films. Although attempts were made to prepare polycarbonate films from CH_2Cl_2 solutions by spin-casting, the samples thus obtained were not of the same high optical quality as those obtained by heated pressing (i.e., the cast films were cloudy). Polystyrene films were prepared from benzene solutions by spin-casting onto quartz substrates. Film thicknesses were determined from absorption spectra using the Beer–Lambert law (7). Unless indicated otherwise, all of the experiments were performed under conditions in which the degassed polymer sample was abruptly exposed to an ambient atmosphere containing (*a*) 30 Torr of oxygen (1 Torr = 133.3 Pa), and (*b*) the copenetrant gas at a partial pressure that ranged from 50 to 500 Torr.

Polystyrene (Aldrich) had an average molecular weight of 280 000. Poly(bisphenol A carbonate) (Polysciences, Inc.) had an average molecular weight of 34 000. Helium and argon (Spectra Gases,Inc.) were 99.999% pure. Nitrogen and oxygen (Argyle Medical Supply, Inc.) were 99.95% pure. The singlet oxygen photosensitizer, *meso*-tetraphenylporphine (Porphyrin Products, Inc.) was used as received.

Results

1. Isothermal data

(a) Polystyrene

Oxygen sorption was monitored subsequent to exposure of a degassed 18 μm thick 25°C polystyrene sample to an ambient atmosphere containing only 30 Torr of oxygen. The oxygen diffusion coefficient obtained under these conditions ($(2.0 \pm 0.2) \times 10^{-7}$ cm^2/s) was the same, within experimental error, as that obtained in our earlier studies ($(2.3 \pm 0.3) \times 10^{-7}$ cm^2/s) (7, 8). The same sample was then exposed to an ambient atmosphere containing (*a*) 30 Torr of oxygen, and (*b*) helium, nitrogen, and argon, respectively, at a partial pressure that ranged from 50 to 500 Torr. Oxygen diffusion coefficients D obtained under these conditions are listed in Table 1. For data recorded with added nitrogen, values of D obtained in the present study are slightly larger than those obtained in our earlier work (Table 1) (8). Nevertheless, both nitrogen data sets have common features that are also found with the helium and argon data: (*a*) values of D increase with an increase in the partial pressure of added gas over the range ~30–300 Torr, and (*b*) above ~300 Torr of added gas, further increases in D do not occur with an increase in the partial pressure of added gas. Subsequent to recording the data listed in Table 1, we again recorded a diffusion coefficient of $(2.0 \pm 0.2) \times 10^{-7}$ cm^2/s upon exposure of the same sample to an atmosphere containing only 30 Torr of oxygen.

(b) Polycarbonate

Oxygen sorption was monitored subsequent to exposure of a degassed 50 μm thick 25°C polycarbonate sample to an ambient atmosphere containing only 30 Torr of oxygen. The oxygen diffusion coefficient obtained under these conditions ($(7.0 \pm 0.7) \times 10^{-8}$ cm^2/s) was slightly larger than, but nevertheless similar to, that obtained in our earlier studies ($(5.5 \pm 0.5) \times 10^{-8}$ cm^2/s) (7, 8). The same sample was then exposed to an

Can. J. Chem. Downloaded from www.nrcresearchpress.com by 46.23.64.124 on 09/08/12
For personal use only.

Table 1. Oxygen diffusion coefficients (D) for 25°C polystyrene under various partial pressures P of added gas.[a]

	$D(\times 10^7)$			
P (Torr)	Nitrogen[b]	Nitrogen	Helium	Argon
0	2.3	2.0	2.0	2.0
30	3.0			
50		3.7	4.0	4.0
100		4.7	4.7	5.4
110	3.6			
200		6.5	6.5	6.8
290	3.8			
300		7.7	7.7	8.2
350	3.8			
400		7.7	7.7	8.2
500		7.7	7.7	8.2

[a]The data were recorded at an oxygen partial pressure of 30 Torr. Values of D have the units cm^2/s. Errors on D are ±10% of the value indicated.

[b]From ref. 8.

Table 2. Oxygen diffusion coefficients (D) for 25°C polycarbonate under various partial pressures of added gas.[a]

	$D(\times 10^7)$			
P (Torr)	Nitrogen[b]	Nitrogen	Helium	Argon
0	0.55	0.70	0.70	0.70
44	0.67			
50		1.3	1.4	1.3
100		1.9	1.9	1.9
130	0.68			
200	0.68	2.4	2.6	2.6
300	0.68	3.1	3.1	3.2
400		3.0	3.3	3.7
500		3.1	3.4	3.7

[a]The data were recorded at an oxygen partial pressure of 30 Torr. Values of D have the units cm^2/s. Errors on D are ±10% of the value indicated.

[b]From ref. 8.

ambient atmosphere containing (*a*) 30 Torr of oxygen, and (*b*) helium, nitrogen, and argon, respectively, at a partial pressure that ranged from 50 to 500 Torr. Oxygen diffusion coefficients obtained under these conditions are listed in Table 2. For data recorded with added nitrogen, values of D obtained in the present study are larger than those obtained in our earlier work (Table 2) (8). As with the polystyrene data discussed above, both nitrogen data sets nevertheless have common features that are also found with the helium and argon data: values of D (*a*) increase with an increase in the partial pressure of added gas, and (*b*) reach a threshold above which further increases in D do not occur with an increase in the partial pressure of added gas. Data from the system in which helium is the added gas are shown in Fig. 1. Subsequent to recording the data listed in Table 2, we again recorded a diffusion coefficient of $(7.0 \pm 0.7) \times 10^{-8}$ cm^2/s upon exposure of the same sample to an atmosphere containing only 30 Torr of oxygen.

Fig. 1. Plot of the oxygen diffusion coefficient as a function of the partial pressure of helium added to the atmosphere surrounding a polycarbonate sample. The data are listed in Table 2. The solid line is a cubic spline fit to the data.

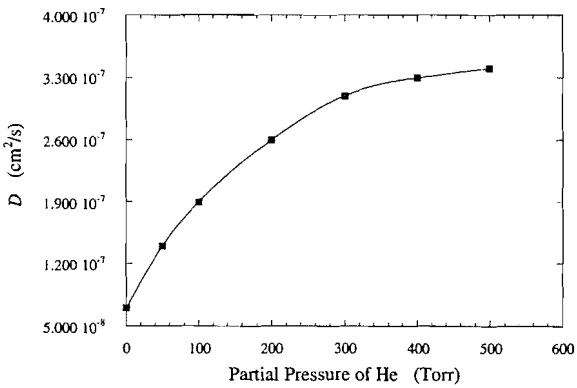

2. Effect of temperature on D

Polymer samples used for the isothermal studies discussed above were not used in the temperature-dependent studies. Rather, fresh samples were prepared. For a given material, all data listed in Tables 3 and 4 were obtained from the same sample. After recording the temperature-dependent data for each of the three copenetrants, we ascertained that D(25°C) for the additive-free material was identical to that initially measured.

(a) Polystyrene

Oxygen sorption was monitored as a function of temperature subsequent to exposure of a 20 μm thick degassed polystyrene sample to an ambient atmosphere containing only 30 Torr of oxygen. The oxygen diffusion coefficient obtained under these conditions at 25°C ($(2.0 \pm 0.2) \times 10^{-7}$ cm^2/s) was the same as that obtained in the isothermal study. Diffusion coefficients recorded at other temperatures were identical to those obtained in our earlier study (Table 3) (8). The sample was then exposed to an ambient atmosphere containing (*a*) 30 Torr of oxygen, and (*b*) helium, nitrogen, and argon, respectively, at partial pressures of both 50 and 100 Torr. Oxygen diffusion coefficients D obtained under these conditions as a function of temperature are listed in Table 3. Plots of ln D *vs.* $1/T$ for these data are shown in Figs. 2–4. The data indicate that, in all cases examined, E_{act} was independent of (*a*) the added copenetrant, and (*b*) the pressure of the ambient atmosphere surrounding the sample. Although D_0 was similarly independent of whether the added copenetrant was He, Ar, or N_2, D_0 did depend on the pressure of the system; as the ambient pressure was increased, D_0 increased.

(b) Polycarbonate

Oxygen sorption was monitored as a function of temperature subsequent to exposure of a 50 μm thick degassed polycarbonate sample to an ambient atmosphere containing only 30 Torr of oxygen. Over the temperature range studied, the oxygen diffusion coefficients obtained in the present study were slightly larger than those obtained in our earlier work (Table 4) (8). Plots of ln D vs. $1/T$ for these two data sets are shown in Fig. 5. The current data yield an E_{act} for oxygen diffusion that is identical to that obtained in our earlier study, and a D_0 value

Table 3. Oxygen diffusion coefficients (D) for polystyrene.

	$D(\times 10^7)$[a]						
T(°C)	No added gas[b]	100 Torr He	50 Torr He	100 Torr Ar	50 Torr Ar	100 Torr N_2	50 Torr N_2
−5	0.5						
5		2.0	1.5		1.7	2.0	1.6
10	0.9	2.5	2.1	2.7	2.0	2.6	2.1
15	1.1	3.2	2.6	3.7	2.6	3.4	2.6
20	1.4			4.8	3.1	4.1	3.1
21		4.4	3.5	5.3	3.7		
25	2.0	4.7	4.0	5.6	4.0	5.0	4.0
30	2.4	6.2	4.7	6.4	4.3	6.2	4.6
35	3.0	7.2	5.5	8.4	6.1		
40	3.4				7.0		
45	4.4						
50	4.9						
55	5.9						
60	6.5						
65	7.6						
E_{act}:[c]	29.9 ± 0.7[e]	30.7 ± 0.8	30.2 ± 1.4	31 ± 2	29.7 ± 1.3	31.2 ± 0.8	29.5 ± 1.0
D_0:[d]	0.032 ± 0.002[e]	0.117 ± 0.019	0.076 ± 0.017	0.15 ± 0.07	0.063 ± 0.016	0.16 ± 0.05	0.06 ± 0.02

[a]Units for D are cm^2/s.
[b]Abbreviated list of data in ref 8.
[c]Units are kJ/mol. Errors on E_{act} and D_0 are the standard deviation obtained from the linear least-squares analyses.
[d]Units are cm^2/s.
[e]Calculated from full data set in ref 8.

Table 4. Oxygen diffusion coefficients (D) for polycarbonate.

	$D(\times 10^8)$[a]							
T(°C)	No added gas[b]	No added gas[c]	100 Torr He	50 Torr He	100 Torr Ar	50 Torr Ar	100 Torr N_2	50 Torr N_2
0	0.92							
5	1.7							
10	2.2							
15	2.8	3.3	8.5	6.4	8.8	6.9	8.7	5.9
20	3.1	4.6	12.3	8.5	12.0	10.1	12.0	7.6
25	5.4	5.8	16.1	11.5	17.4	13.1	17.7	11.0
30		7.8	23.1	16.0	24.1	16.1	23.0	15.8
35	8.4	9.9	29.2	20.9	26.5	20.7	29.8	22.2
40	11	12.6	35.0	27.0	35.9	27.0	41.0	28.1
45	14	17.0	47.0	33.5	46.3	33.5	54.0	33.8
50	17							
55	22							
60	28							
65	32							
70	43							
75	46							
E_{act}:[d]	40.2 ± 0.7	40.7 ± 0.7	42.7 ± 1.4	42.9 ± 0.8	41.4 ± 2.0	39.1 ± 0.9	46.1 ± 1.0	46.7 ± 1.7
D_0:[e]	0.5 ± 0.2	0.8 ± 0.9	4.8 ± 1.7	3.9 ± 0.9	3.0 ± 1.9	1 ± 3	19.8 ± 2.4	16.6 ± 4.0

[a]Units for D are cm^2/s.
[b]Reference 8.
[c]This study.
[d]Units are kJ/mol. Errors on E_{act} and D_0 are the standard deviation obtained from the linear least-squares analyses.
[e]Units are cm^2/s.

Can. J. Chem. Downloaded from www.nrcresearchpress.com by 46.23.64.124 on 09/08/12
For personal use only.

Can. J. Chem. Downloaded from www.nrcresearchpress.com by 46.23.64.124 on 09/08/12
For personal use only.

Fig. 2. Plots of ln D vs. $1/T$ for oxygen diffusion coefficients, D, determined in polystyrene. Data shown as filled squares were recorded under conditions in which the polymer film was exposed to an ambient atmosphere containing only 30 Torr of oxygen. The solid line through these data is a linear least-squares fit to data recorded over a wider temperature range than that shown here (see Table 3 and ref. 8). Data recorded under conditions in which the ambient atmosphere contained 100 (●) and 50 (□) Torr, respectively, of nitrogen in addition to 30 Torr of oxygen are also shown. Solid lines are linear least-squares fits to the data.

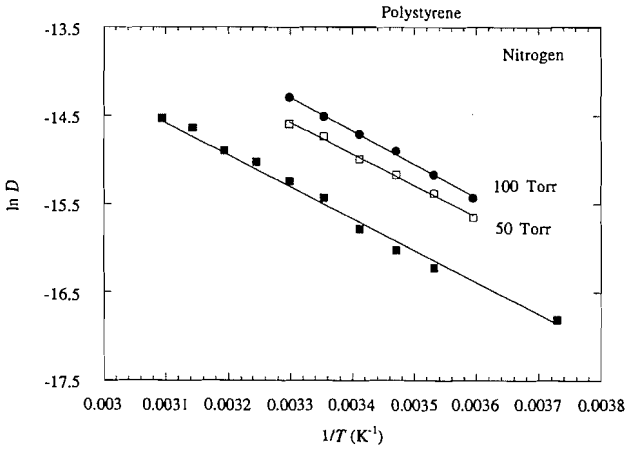

Fig. 3. Plots of ln D vs. $1/T$ for oxygen diffusion coefficients, D, determined in polystyrene. Data were recorded under conditions in which the ambient atmosphere contained 100 (□) and 50 (◆) Torr, respectively, of argon in addition to 30 Torr of oxygen. Solid lines are linear least-square fits to the data. The linear least-squares fit for data recorded under conditions in which the polymer film was exposed to an ambient atmosphere containing only 30 Torr of oxygen (see Fig. 2) is also shown.

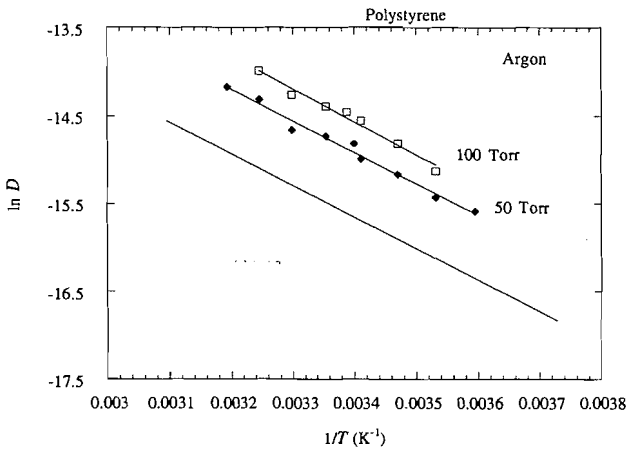

that is only slightly larger than that obtained earlier (the comparatively large error bars on D_0 in the present study reflect the small number of points in the ln D vs. $1/T$ plot).

The sample was then exposed to an ambient atmosphere containing (*a*) 30 Torr of oxygen, and (*b*) helium, nitrogen, and argon, respectively, at partial pressures of both 50 and 100 Torr. Oxygen diffusion coefficients D obtained under these conditions as a function of temperature are listed in Table 4. Plots of ln D *vs.* $1/T$ for these data are shown in Figs. 6–8. The data

Fig. 4. Plots of ln D vs. $1/T$ for oxygen diffusion coefficients, D, determined in polystyrene. Data were recorded under conditions in which the ambient atmosphere contained 100 (□) and 50 (◆) Torr, respectively, of helium in addition to 30 Torr of oxygen. Solid lines are linear-least squares fits to the data. The linear least-squares fit for data recorded under conditions in which the polymer film was exposed to an ambient atmosphere containing only 30 Torr of oxygen (see Fig. 2) is also shown.

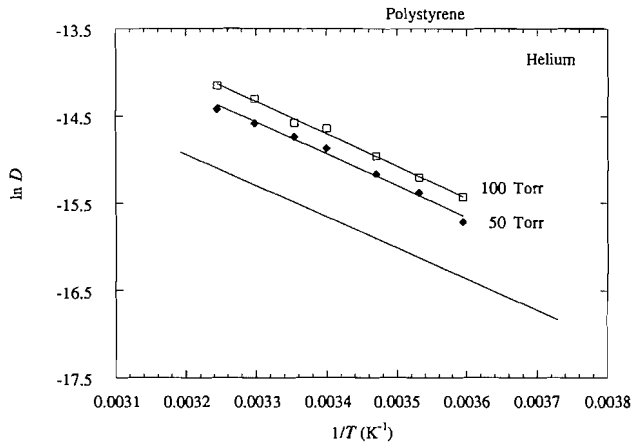

Fig. 5. Plots of ln D vs. $1/T$ for oxygen diffusion coefficients, D, determined in polycarbonate. Data were recorded under conditions in which the ambient atmosphere contained only 30 Torr of oxygen. Solid lines are linear least-squares fits to the data. Data shown as open squares were recorded in our earlier study (Table 4 and ref. 8).

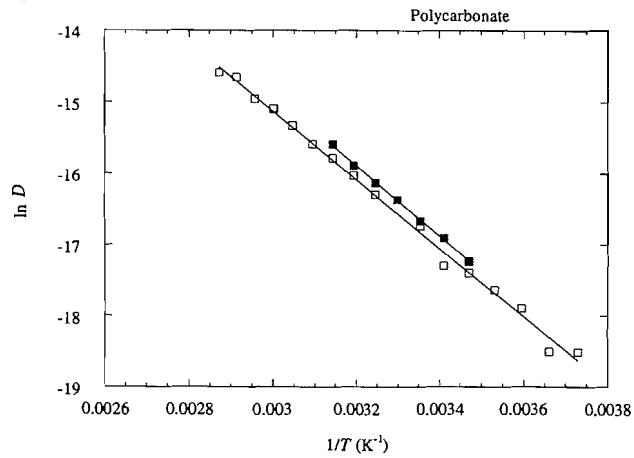

shown indicate that, with one exception, the general effects of an added gas on E_{act} and D_0 that were observed with polystyrene also apply to polycarbonate. Specifically, an increase in the pressure of added gas results principally in an increase in D_0. Furthermore, in comparison to the unperturbed system, the addition of either helium or argon does not significantly change E_{act}. When nitrogen is the added copenetrant, however, a larger value of E_{act} is obtained. This increase in the slope of the ln D vs. $1/T$ plot, in turn, results in a comparatively large value of D_0.

Can. J. Chem. Downloaded from www.nrcresearchpress.com by 46.23.64.124 on 09/08/12
For personal use only.

Fig. 6. Plots of ln D vs. $1/T$ for oxygen diffusion coefficients, D, determined in polycarbonate. Data were recorded under conditions in which the ambient atmosphere contained 100 (■) and 50 (□) Torr, respectively, of nitrogen in addition to 30 Torr of oxygen. Solid lines are linear least-squares fits to the data. Data recorded under conditions in which the polymer film was exposed to an ambient atmosphere containing only 30 Torr of oxygen (see Fig. 5) are also shown.

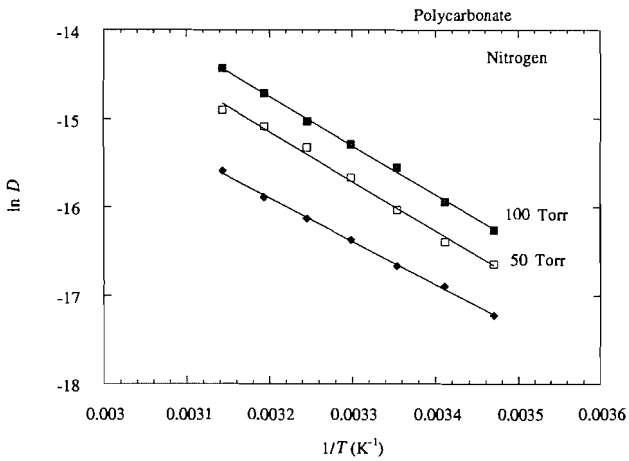

Fig. 7. Plots of ln D vs. $1/T$ for oxygen diffusion coefficients, D, determined in polycarbonate. Data were recorded under conditions in which the ambient atmosphere contained 100 (■) and 50 (□) Torr, respectively, of argon in addition to 30 Torr of oxygen. Solid lines are linear least-squares fits to the data. Data recorded under conditions in which the polymer film was exposed to an ambient atmosphere containing only 30 Torr of oxygen (see Fig. 5) are also shown.

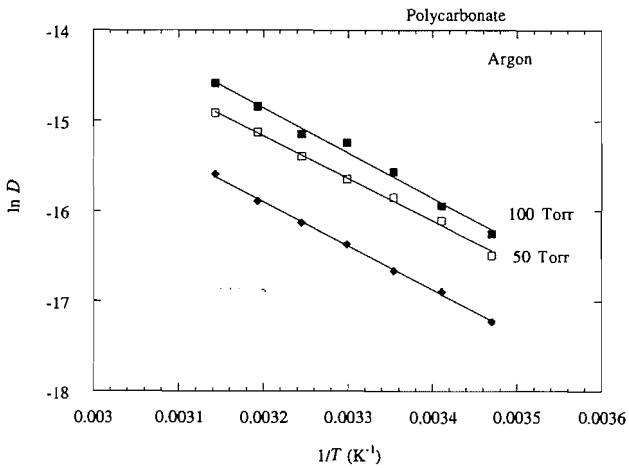

Discussion

1. General background on gas diffusion

Models based on the concept of "free volume" have thus far proven effective in understanding gas mobility in glassy polymers (9–16). From this perspective, gas diffusion is perceived to depend on the presence of spaces in the polymer matrix through which the diffusing molecule can move. We can expand this concept by recognizing that, over a specific temperature range and in a given period of time, these spaces will

Fig. 8. Plots of ln D vs. $1/T$ for oxygen diffusion coefficients, D, determined in polycarbonate. Data were recorded under conditions in which the ambient atmosphere contained 100 (■) and 50 (□) Torr, respectively, of helium in addition to 30 Torr of oxygen. Solid lines are linear least-squares fits to the data. Data recorded under conditions in which the polymer film was exposed to an ambient atmosphere containing only 30 Torr of oxygen (see Fig. 5) are also shown.

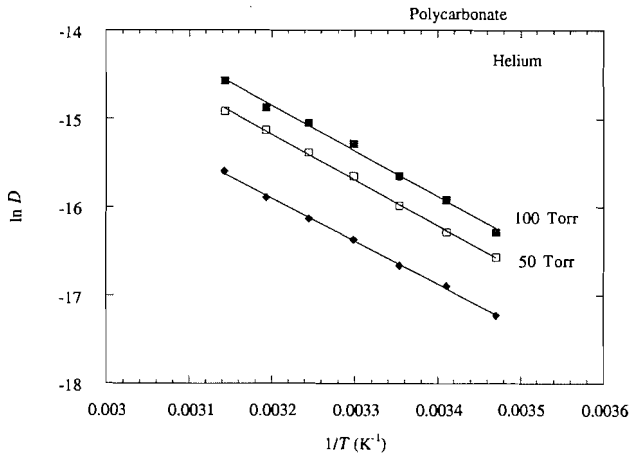

be either dynamic or static (8). The former derive from ephemeral cavities created by thermally accessible conformational changes and segmental motions of the macromolecule. In defining a static cavity, we envision spaces in the matrix whose volume is essentially independent of the thermally accessible motions of the macromolecule. When summed over the entire polymer sample, these dynamic and static spaces define an overall free volume characteristic of a particular material at a given temperature.

The notion that a dissolved gas molecule can exist within a cavity in the polymer matrix is a defining feature of the dual-mode sorption model (17–19). In liquids, gas sorption behaves according to Henry's law, in which the mole fraction of a dissolved gas depends linearly on the partial pressure of that gas in the atmosphere surrounding the sample. In amorphous glasses, however, isothermal gas sorption does not often behave according to Henry's law, and a second pressure-dependent term is commonly added to the Henry's law term to account for this deviation. This "Langmuir" term is included to describe a proposed population of gas molecules sorbed in the matrix cavities of the glass. Although exchange between the Henry domain of molecularly dissolved gas and the Langmuir domain of encapsulated gas is proposed to be facile, separate Langmuir (D^L) and Henry (D^H) diffusion coefficients can nevertheless be defined.

The molecular events that define static and dynamic cavities, and hence that control gas diffusion, are thermally activated. Specifically, over limited temperature ranges, the diffusion coefficient D behaves according to eq. [3] (2, 3, 8, 9, 15, 20), which is analogous to the Arrhenius equation. The exponential term thus represents the fraction of diffusing molecules able to surmount a diffusion activation barrier E_{act} at the temperature T. The magnitude of this exponential term ranges from 1.0 at large T to 0 at low T. The activation barrier E_{act} is believed to derive principally from characteristic motions of the macromolecule in a given temperature domain,

Can. J. Chem. Downloaded from www.nrcresearchpress.com by 46.23.64.124 on 09/08/12
For personal use only.

and is thus likely to manifest events that define the dynamic free volume of a material. If ln D varies linearly with $1/T$ over a given temperature range, it is typically concluded that the type of polymer motions and interactions that control gas mobility do not change within this temperature domain (E_{act} is obtained from the slope in a plot of ln D vs. $1/T$). Activation barriers for oxygen diffusion can be compared to barriers for macromolecular motion independently obtained from temperature-dependent NMR or dielectric/mechanical relaxation studies (3, 8).

In a plot of ln D vs. $1/T$, D_0 is obtained by extrapolating to $1/T = 0$. At such infinitely high temperatures, gas transport can be considered "barrier-free" (i.e., $\exp(-E_{act}/RT) = 1.0$). This condition corresponds to an 'imaginary' state of the material because the polymer will clearly not remain an amorphous glass at these temperatures. We simply envision a state of the polymer under conditions where all the diffusing molecules are able to surmount the activation barrier E_{act} characteristic of a given temperature domain. From this perspective, D_0 can be considered to reflect the static free volume of the matrix for the temperature domain defined by the ln D vs. $1/T$ plot.

Elements that define a given D_0 and E_{act} clearly pertain only to a specific temperature domain. Successive increases in E_{act} and D_0 for successively higher temperature domains reflect, in part, polymer motions that incorporate increasingly larger segments of the macromolecule. The increase in the number and kind of accessible polymer motions with temperature is often manifested by noticeable morphological changes in the polymer (e.g., glass to rubber transition).

The incorporation of a low molecular weight solute in a solid polymer often perturbs molecular phenomena that influence gas diffusion (8, 13, 19–21). This perturbation may involve (*a*) a filling of voids in the matrix, and (or) (*b*) a change in the intra- and inter-molecular interactions of the macromolecule that influence specific polymer motions. The additive may act either to facilitate or inhibit gas diffusion relative to diffusion in the unperturbed, additive-free material. The addition of these low molecular weight solutes to the polymer is also often manifested in other properties of the material. For example, some additives, called plasticizers, can facilitate motion of larger macromolecular segments and make a rigid polymer more flexible (i.e., the plasticizer lowers T_g). This increase in segmental motion would be reflected in larger values of E_{act} and D_0. Conversely, an antiplasticizer hinders certain motions of the polymer, and is thus expected to yield both a more rigid material and smaller values of E_{act} and D_0. Note that, for a plasticized material in which values of E_{act} and D_0 are larger than E_{act} and D_0 in the unperturbed, additive-free material, plots of ln D vs. $1/T$ for plasticized and additive-free samples may intersect. Thus, at a given temperature, the oxygen diffusion coefficient D for the plasticized polymer can be *smaller* than that found in the additive-free polymer (8). This point is illustrated in Fig. 9.

When transition state theory is applied to the problem of gas diffusion, the terms in eq. [3] take on additional meaning (9). E_{act} will correspond to an activation enthalpy $\Delta H^{\ddagger}$ for diffusion. D_0 will be a function of the activation entropy $\Delta S^{\ddagger}$ for diffusion and a term λ that defines the distance between equilibrium positions for the diffusing molecule in the matrix (eq. [4]).

Fig. 9. Illustration of a phenomenon that can be observed upon the addition of a plasticizer to a given material. Examples of data that behave in this fashion are given in ref. 8.

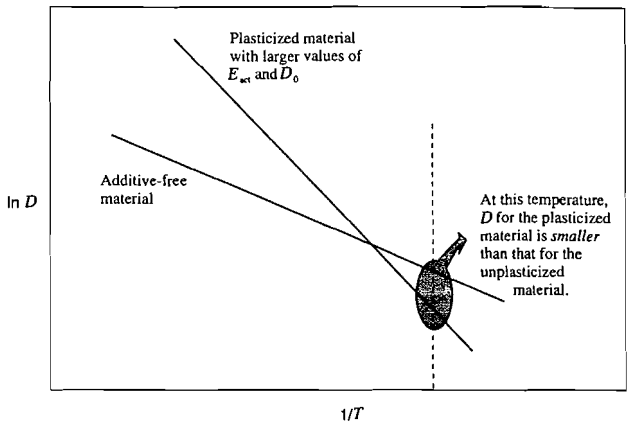

$$[4] \quad D_0 = \exp \lambda^2 \frac{kT}{h} \exp(\Delta S^{\ddagger}/R)$$

The dependence of D_0 on temperature in eq. [4], however, indicates that transition state theory may not provide a totally accurate model with which the data can be interpreted; plots of ln D vs. $1/T$ are indeed reasonably linear over temperature ranges that can be as large as 80–100°C.

2. The copenetrants nitrogen, helium, and argon

Size

Published data on covalent radii indicate that He, Ar, and N_2 increase in size with the relative ratios of approximately 1:2:3, respectively (22–24). The covalent radius of oxygen does not differ significantly from that of nitrogen.

Diffusion coefficients

Data recorded in 35°C polycarbonate indicate that diffusion coefficients for N_2, Ar, O_2, and He increase with the relative ratios 1:1.8:3.1:360, respectively (25, 26). In 35°C polystyrene, diffusion coefficients for N_2, O_2, and He increase with the relative ratios 1:3.3:312 (14). These data indicate that, upon exposure of a degassed film to a mixture of oxygen and helium, the rate of oxygen incorporation into the film will be significantly slower than the rate of helium incorporation. At the other limit, upon exposure of a degassed film to a mixture of oxygen and nitrogen, oxygen will "precede" nitrogen into the film. Nitrogen will nevertheless be present in the film, particularly near the film surface, while oxygen is still being incorporated from the atmosphere.

3. Effect of added gas on oxygen solubilities

In our experiment, when the polymer sample has reached equilibrium with the ambient atmosphere, the intensity of the singlet oxygen signal will be proportional to the solubility of oxygen in that material. In all experiments, we found that in the presence of added He, Ar, and N_2, the singlet oxygen intensity at equilibrium was ~5–10% larger than that in the absence of the added gas. This systematic change barely exceeds our limits of error in monitoring the singlet oxygen

Can. J. Chem. Downloaded from www.nrcresearchpress.com by 46.23.64.124 on 09/08/12
For personal use only.

intensity. Such a change may indeed derive from an additive-dependent increase in the solubility of oxygen. Although unlikely, we nevertheless cannot presently exclude the possibility that the added gas may increase the rate constant for singlet oxygen phosphorescence, thus giving the appearance of an increase in the amount of oxygen dissolved in the polymer (27, 28). We nevertheless suggest that, under our conditions, additive-dependent changes in the solubility of oxygen are not pronounced. With reference to the discussion in Sect. 5 below, the data certainly do not indicate a copenetrant-induced decrease in the oxygen solubility.

4. Isothermal data

(a) Polystyrene

In the absence of an added copenetrant, the oxygen diffusion coefficient we obtain in 25°C polystyrene agrees with (*a*) our earlier data (8), and (*b*) data published by other investigators (2, 29–31). For diffusion coefficients recorded with nitrogen as a copenetrant, differences between the pressure dependence of our present data and the pressure dependence of data in our previous study (8) likely derive from differences in the respective samples. For example, these polystyrene films were prepared by spin-casting, and differences in the rate of solvent evaporation may have yielded subtle differences in the free volume of the resultant films.

(b) Polycarbonate

In the absence of an added copenetrant, the 25°C diffusion coefficient we obtain in this study ($(7.0 \pm 0.7) \times 10^{-8}$ cm^2/s) is approximately a factor of two larger than that of Muruganandam et al. (25); using Arrhenius parameters reported by the latter, we calculate a value for D(25°C) of 3.9×10^{-8} cm^2/s. For diffusion coefficients recorded with nitrogen as a copenetrant, our present pressure-dependent data are also larger than those recorded in our previous study (8). As with the data recorded in polystyrene, these differences likely derive from differences in the preparation of the respective samples. In this case, our films were prepared by hot-pressing material that had previously been dissolved in CH_2Cl_2 (see Experimental section). Thus, differences in (*a*) the amount of residual CH_2Cl_2 remaining in the material at the time of pressing, and (or) (*b*) the temperature history of the samples may have yielded differences in the free volume of the respective films.

For all data in polystyrene and polycarbonate, values of D (*a*) increased with an increase in the partial pressure of added gas, and (*b*) reached a threshold above which further increases in D did not occur with an increase in the partial pressure of added gas. Within the errors of our measurement, values of D were independent of the specific copenetrant added to the ambient atmosphere. On the basis of the latter observation, these data thus appear to simply reflect a pressure effect on the oxygen diffusion coefficient.

Oxygen diffusion coefficients in polycarbonate and poly(methylmethacrylate) [PMMA] have been observed to increase with an increase in the ambient pressure of oxygen over the range ~50–1000 Torr (32). Similarly, CO_2 diffusion coefficients in PMMA and PMMA blends depend on the CO_2 pressure to which the polymer sample is exposed (33). In the latter experiment, which was performed over the range 1–25 atm (1 atm = 101.3 kPa), pressure-dependent changes in the diffusion coefficient reflect plasicization of the polymer by CO_2. Indeed, plasticization of polymers by high pressures (>1 atm) of CO_2, Ar, and N_2 is a documented phenomenon (34, 35). On the basis of our temperature-dependent data (vide infra), however, we suggest that, with the possible exception of nitrogen added to polycarbonate, the dependence of D on the pressure of added gas shown in Tables 1 and 2 and Fig. 1 does not reflect polymer plasticization.

5. Effect of temperature on D. Values of D_0 and E_{act}

For a given material, temperature-dependent data for each of the three copenetrants were recorded using the same film. Thus, reported values of D_0 and E_{act} do not reflect differences in sample preparation.

(a) Polystyrene

Published data obtained from NMR and mechanical/dielectric relaxation measurements indicate that rotation of the pendant phenyl group in polystyrene is the principal chracteristic motion of the macromolecule in the temperature range −5–85°C (36, 37). Reported values for the activation energy of this process are ~38 kJ/mol (36, 37). The similarity between this value and the E_{act} values obtained for oxygen diffusion (Table 3) indicate that, at these temperatures, phenyl group rotation may create the dynamic cavities in polystyrene that control oxygen transport. In 1974, Guillet and co-workers likewise suggested that the rotation of the pendant phenyl group likely influences oxygen diffusion (3).

The data in Table 3 and Figs. 2–4 indicate that addition of the copenetrant does not affect E_{act}. This general phenomenon was also noted by Barker in the analogous study of the oxygen pressure dependence on oxygen diffusion in PMMA and polycarbonate (32). We conclude from our E_{act} data that, in this temperature domain and at these pressures, added He, Ar, and N_2 do not inflence the motions of polystyrene that define the dynamic free volume. We have indicated that plasticizers can facilitate the motion of different and (or) comparatively larger segments of the macromolecule. Such changes are invariably manifested by an increase in E_{act} (8). It thus appears that under these conditions in polystyrene, He, Ar, and N_2 do not act as a plasticizer.

Addition of the copenetrant, however, influences D_0; D_0 increases with an increase in the pressure of added gas. This same phenomenon was likewise reflected in Barker's ln D vs. $1/T$ plots as the oxygen pressure was increased in PMMA and polycarbonate (32). An interpretation of these D_0 data should also address the isothermal pressure dependence of D shown in Tables 1 and 2 and Fig. 1. (Because E_{act} is independent of pressure, pressure-dependent changes in D reflect changes in D_0.)

From the perspective of transition state theory, the added gas may exert its effect on D_0 via changes in λ and (or) $\Delta S^{\ddagger}$ (eq. [4]). With respect to the latter, the presence of the copenetrant in the cavity through which oxygen is moving is likely to increase the available degrees of freedom, and as a result cause an increase in the activation entropy for diffusion. For a given polymer and copenetrant, the increase in D_0 with an increase in copenetrant pressure corresponds to a $\Delta S^{\ddagger}$ value that becomes increasingly positive. Thus, with an increase in copenetrant pressure, the data reflect a transition state for oxygen propagation that becomes increasingly disordered. It is somewhat more complicated, however, to understand how

Can. J. Chem. Downloaded from www.nrcresearchpress.com by 46.23.64.124 on 09/08/12
For personal use only.

increases in copenetrant pressure above a threshold of ~200–300 Torr must correspond to a lack of change in $\Delta S^{\ddagger}$.

The copenetrant may also fill voids and thus cause an increase in λ, the "jump distance" between equilibrium oxygen positions in the matrix. However, we again return to the data in Fig. 1 and Tables 1 and 2 and find it difficult to rationalize how an increase in the copenetrant pressure above a threshold of ~200–300 Torr must correspond to a lack of change in λ. These points, coupled with the expected temperature dependence of D_0 shown in eq. [4], indicate that transition state theory is not likely to be an appropriate perspective for the interpretation of our data.

We now consider whether or not our data reflect features of the dual-mode sorption model as described by Koros (17). From this perspective, the copenetrant and oxygen would compete for "Langmuir cavities" in the polymer. In experiments such as ours in which the oxygen partial pressure is held constant and the polymer is not plasticized by the copenetrant, we would expect (*a*) a decrease in the number of oxygen molecules in the Langmuir domain as the added-gas partial pressure is increased, and (*b*) no change in the number of oxygen molecules dissolved in the Henry domain. Thus, as discussed by Koros, displacement of oxygen from the Langmuir domain by added copenetrant should result in a *decrease* in the overall solubility of oxygen in the polymer. This expectation is not supported by our data (vide supra, Sect. 3).

From the perspective of the dual-mode sorption model, overlooking expected changes in oxygen solubility, the observed increase in D with an increase in the copenetrant pressure could reflect displacement of oxygen by the copenetrant from Langmuir sites that hinder the net propagation of oxygen.[2] This interpretation presumes a distribution of Langmuir sites, some of which bind or trap oxygen more effectively than others. An attractive feature of this model is that, under conditions in which the polymer is not plasticized, such traps would eventually all be filled by the copenetrant, thus causing no further changes in D with an increase in copenetrant pressure (Fig. 1 and Tables 1 and 2).

Finally, we have indicated that an increase in D_0 may be interpreted to reflect an increase in the so-called static component of free volume. Thus, our data may reflect an internal pressure-induced expansion of cavities in the polymer that does not substantially perturb the segmental motions that define E_{act}. At these comparatively low pressures, such an expansion would be opposed by a matrix-dependent restoring force that, in turn, could yield data such as those shown in Tables 1 and 2 and Fig. 1. Furthermore, such a pressure-induced increase in static free volume might also result in a slight increase in the solubility of oxygen in the polymer. Solubility data discussed in Sect. 3 are not inconsistent with this expectation. Certainly, additional experiments need to be performed to further test this hypothesis.

(b) Polycarbonate

As discussed with respect to our isothermal data, the differences between our present results and those recorded in our earlier study likely derive from differences in the respective samples. It is interesting to note, particularly in light of the discussion above on pressure-dependent changes in D_0, that plots of ln D vs. $1/T$ generated from different samples yield the same E_{act} but different D_0 values (Fig. 5).

Published data obtained from NMR and mechanical/dielectric relaxation measurements indicate that rotation of the phenyl group in the polycarbonate backbone, along with attendant local segmental conformational changes, is the principal characteristic motion of the macromolecule in the temperature range −5–75°C (2, 36, 38–40). The similarity between reported values for the activation energy of this process (~38–50 kJ/mol) (2, 36, 38–40) and the E_{act} values obtained for oxygen diffusion (Table 4) indicate that, at these temperatures, this motion may create the dynamic cavities in polycarbonate that control oxygen transport.

With respect to the effects of added He and Ar, the discussion above for polystyrene is equally applicable for the polycarbonate data. In particular, the E_{act} data indicate that He and Ar do not act as plasticizers. Data recorded when nitrogen is the copenetrant, however, indicate otherwise. Values of E_{act} obtained at both 100 and 50 Torr of added nitrogen are ~5 kJ/mol larger than values of E_{act} obtained under the other conditions (Table 4). The change in slope of the ln D vs. $1/T$ plot that yields a larger E_{act} also yields larger D_0 values. Thus, in this case, the data are consistent with the added gas acting as a plasticizer.

Conclusions

Over the temperature range ~5–45°C, oxygen diffusion coefficients D for polystyrene and polycarbonate films increase upon the addition of He, Ar, or N_2 as copenetrants. Except for the case of added nitrogen in polycarbonate, this increase in D does not derive from a change in the activation barrier for diffusion. Rather, the increase in D reflects an increase in the parameter D_0, which is the pre-exponential factor in an Arrhenius treatment. These data may reflect a copenetrant pressure-dependent (*a*) expansion of the cavities in the matrix that make up the so-called static free volume, and (or) (*b*) displacement of oxygen from Langmuir "trap" sites that hinder the propagation of oxygen through the matrix.

In polycarbonate, the data indicate that nitrogen acts as a plasticizer. In this case, the added gas causes an increase in both E_{act} and D_0 for oxygen diffusion. These changes are interpreted to reflect nitrogen-dependent increases in the segmental motions that define both dynamic and static elements of free volume in the macromolecule.

Acknowledgments

This work was supported by the National Science Foundation under grant CHE-9402145. The authors thank E. A. Walters and R. A. Assink for helpful discussions.

References

1. J.E. Guillet. Polymer photophysics and photochemistry. Cambridge University Press, Cambridge. 1985.
2. J.E. Guillet and M. Andrews. Macromolecules, **25**, 2752 (1992).
3. A.C. Somersall, E. Dan, and J.E. Guillet. Macromolecules, **7**, 233 (1974).

[2] We thank a referee for this interpretation.

4. A. Gilbert and J. Baggott. Essentials of molecular photochemistry. CRC Press, Boca Raton, Fla. 1991.
5. K.-K. Iu and P.R. Ogilby. J. Phys. Chem. **92**, 4662 (1988)
6. R.D. Scurlock, D.O. Mártire, P.R. Ogilby, V.L. Taylor, and R. L. Clough. Macromolecules, **27**, 4787 (1994).
7. Y. Gao and P.R. Ogilby. Macromolecules, **25**, 4962 (1992).
8. Y. Gao, A.M. Baca, B. Wang, and P.R. Ogilby. Macromolecules, **27**, 7041 (1994).
9. S. Glasstone, K.J. Laidler, and H. Eyring. The theory of rate processes. McGraw-Hill, New York. 1941.
10. M.H. Cohen and D. Turnbull. J. Chem. Phys. **31**, 1164 (1959).
11. C.A. Kumins and T.K. Kwei. *In* Diffusion in polymers. *Edited by* J. Crank and G.S. Park. Academic Press, London. 1968. p. 107.
12. C.E. Rogers. *In* Polymer permeability. *Edited by* J. Comyn. Elsevier, London. 1985. p. 11.
13. Y. Maeda and D.R. Paul. J. Polym. Sci. Part B: Polym. Phys. **25**, 1005 (1987).
14. A.C. Puleo, N. Muruganandam, and D.R. Paul. J. Polym. Sci. Part B: Polym. Phys. **27**, 2385 (1989).
15. J.S. Vrentas and J.L. Duda. J. Polym. Sci. Polym. Phys. Ed. **15**, 403 (1977).
16. S.A. Stern and S. Trohalaki. ACS Symp. Ser. **423**, 22 (1990).
17. W.J. Koros. J. Polym. Sci. Polym. Phys. Ed. **18**, 981 (1980).
18. D.R. Paul. Ber. Bunsen-Ges. Phys. Chem. **83**, 294 (1979).
19. S. Zhou and S.A. Stern. J. Polym. Sci. Part B: Polym. Phys. **27**, 205 (1989).
20. V. Stannett. *In* Diffusion in polymers. *Edited by* J. Crank and G.S. Park. Academic Press, London. 1968. p. 41.
21. Y. Maeda and D.R. Paul. J. Membrane Sci. **30**, 1 (1987).
22. J.E. Huheey. Inorganic chemistry. Harper and Row, New York. 1983.
23. M. Karplus and R.N. Porter. Atoms and molecules. W. A. Benjamin, Menlo Park, Calif. 1970.
24. J.C. Bailar, T. Moeller, J. Kleinberg, C.O. Guss, M.E. Castellion, and C. Metz. Chemistry. Academic Press, New York. 1984.
25. N. Muruganandam, W.J. Koros, and D.R. Paul. J. Polym. Sci. Part B: Polym. Phys. **25**, 1999 (1987).
26. W.J. Koros, A.H. Chan, and D. R. Paul. J. Membrane Sci. **2**, 165 (1977).
27. R.D. Scurlock and P.R. Ogilby. J. Phys. Chem. **91**, 4599 (1987).
28. R.D. Scurlock, S. Nonell, S.E. Braslavsky, and P.R. Ogilby. J. Phys. Chem. **99**, 3521 (1995).
29. D.Y. Chu, J.K. Thomas, and J. Kuczynski. Macromolecules, **21**, 2094 (1988).
30. M. Nowakowska, J. Najbar, and B. Waligora. Eur. Polym. J. **12**, 387 (1976).
31. H.-J. Timpe, B. Basse, F.W. Muller, and C. Muller. Eur. Polym. J. **23**, 967 (1987).
32. R.E. Barker. J. Polym. Sci. **58**, 553 (1962).
33. J.S. Chiou and D.R. Paul. J. Appl. Polym. Sci. **32**, 2897 (1986).
34. R.A. Assink. J. Polym. Sci. Polym. Phys. Ed. **12**, 2281 (1974).
35. W.-C. V. Wang, E.J. Kramer, and W.H. Sachse. J. Polym. Sci. Polym. Phys. Ed. **20**, 1371 (1982).
36. O. Yano and Y. Wada. J. Polym. Sci. Part A-2: **9**, 669 (1971).
37. T.M. Connor. J. Polym. Sci. Part A-2: **8**, 191 (1970).
38. P.M. Henrichs and V.A. Nicely. Macromolecules, **24**, 2506 (1991).
39. J.H. Walton, M.J. Lizak, M.S. Conradi, T. Gullion, and J. Schaefer. Macromolecules, **23**, 416 (1990).
40. A.K. Roy, A.A. Jones, and P.T. Inglefield. Macromolecules, **19**, 1356 (1986).

Can. J. Chem. Downloaded from www.nrcresearchpress.com by 46.23.64.124 on 09/08/12
For personal use only.

Photodegradation mechanism of phenyl isopropenyl ketone – methyl methacrylate copolymers in the solid phase and their performance as a deep UV resist

Kazuyuki Sugita, Tomohito Ishida, Masahito Kushida, Kieko Harada, Kyoichi Saito, and Nobuo Ueno

Can. J. Chem. Downloaded from www.nrcresearchpress.com by 46.23.64.124 on 09/08/12
For personal use only.

Abstract: Phenyl isopropenyl ketone (PIPK) copolymer films were irradiated with a low-pressure mercury lamp, and benzoyl side-chain cleavage and main-chain scission at various temperatures were followed by UV spectral changes and gel permeation chromatography, respectively. Quantum yields of both reactions and the ratio of the latter to the former reaction increased markedly above their glass transition temperatures. The main-chain scission continued to proceed by irradiation even after the side chain ceased to split. These experimental results suggest a new reaction mechanism of photosplitting of the methyl methacrylate ester side chain on the carbon adjacent to the C=C bond followed by β-scission, in addition to the known benzoyl side-chain cleavage followed by β-scission or C=C bond formation. The enhanced quantum yield for the main-chain scission of the PIPK copolymer at 130°C realized sensitivity of 100 mJ/cm^2 as a DUV resist, which was 1200 times as high as that of poly(methyl methacrylate) exposed at room temperature and developed under similar conditions.

Key words: Norrish type I cleavage, β-scission of main chain, temperature dependence, photosplitting of ester side chain, conjugated polymer radical.

Résumé : On a irradié des films de copolymère de phényl(isopropényl)cétone (PIPK) à l'aide d'une lampe au mercure à basse pression et on a observé le clivage de la chaîne latérale benzoyle ainsi que la scission de la chaîne principale, à diverses températures, en faisant appel respectivement aux changements des spectres UV et à la chromatographie par perméation de gel. Les rendements quantiques des deux réactions ainsi que les rapports de la dernière réaction par rapport à la première augmentent d'une façon marquée au-dessus de leur température de transition vitreuse. Sous l'influence de l'irradiation, la scission de la chaîne principale se produit encore même lorsque la chaîne latérale a cessé de se cliver. Ces résultats expérimentaux suggèrent que, en plus du mécanisme connu impliquant un clivage de la chaîne latérale benzoyle, suivi d'une scission-β ou de la formation d'une liaison C=C, il existe un nouveau mécanisme réactionnel pour la réaction de photoclivage de la chaîne latérale du méthacrylate de méthyle; il implique le carbone adjacent de la liaison C=C et il est suivi par une scission-β. Le rendement quantique plus élevé pour la scission de la chaîne principale du copolymère PIPK, à 130°C, a permis d'atteindre une sensibilité de 100 mJ/cm^2 comme résistante DUV; cette valeur est 1200 fois plus élevée que celle du poly(méthacrylate de méthyle) exposé à la température ambiante et développé dans des conditions semblables.

Mots clés : clivage Norrish de type I, scission-β de la chaîne principale, relation avec la température, photoclivage de la chaîne latérale ester, radical polymère conjugé.

[Traduit par la rédaction]

Introduction

The continuing increase in the packaging density and shrinkage of the pattern size of electronic devices requires advanced resists that are sensitive to radiation in the deep ultraviolet (DUV, λ = 180–300 nm) region. Isopropenyl ketone polymers represent an important class of positive DUV resists based on main-chain scission. Poly(methyl isopropenyl ketone) (PMIPK) is a commercially available resist, but the sensitivity is not high enough (140 mJ/cm^2 as reported by Nakane et al. (1) and 1000 mJ/cm^2 by Nate and Kobayashi (2)). MacDonald et al. (3) found that the quantum yield of main-chain scission at 313 nm in films of poly(*tert*-butyl isopropenyl ketone) (PTBIPK) is 12 times higher than that of PMIPK, but the high molecular weight polymer was not obtained for investigating the lithographic characteristics.

Another attempt at developing excellent DUV resists

Received March 24, 1995.

This paper is dedicated to Professor J.E. (Jim) Guillet in recognition of his contributions to Canadian chemistry.

K. Sugita,[1] T. Ishida, M. Kushida, K. Harada, K. Saito, and N. Ueno. Department of Specialty Materials, Chiba University, Yayoi-cho, Inage-ku, Chiba, 263 Japan.

[1] Author to whom correspondence may be addressed. Telephone: +81-43-290-3437. Fax: +81-43-290-3039.

Fig. 1. Degradation scheme of PMMA–PIPK: (*a*) photolysis by Norrish Type I, (*b*) β-scission, (*c*, *d*) hydrogen abstraction, (*e*) auto-oxidation, (*f*) thermal decomposition, and (*g*) photolysis of MMA ester side chain on the carbon adjacent to the C=C bond.

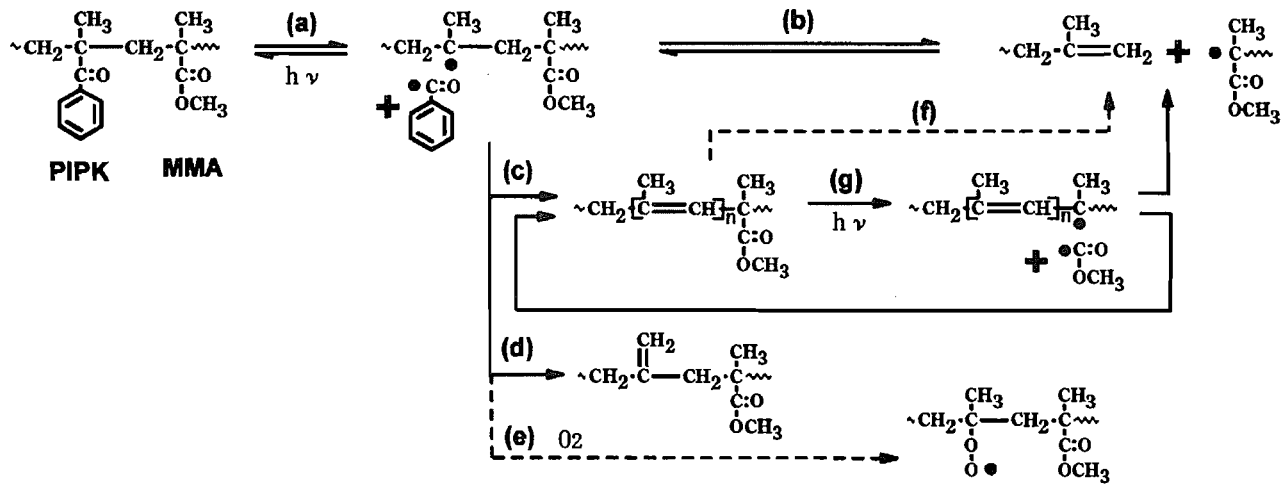

sought to enhance the sensitivity of poly(methyl methacrylate) (PMMA) (700 mJ/cm^2 reported by Lin (4) and 11 000 mJ/cm^2 by Nate et al. (2)) by copolymerizing radiation-active monomers with methyl methacrylate (MMA). Incorporation of 16 mol% of 3-oximino-2-butanone methacrylate (5) and 3 mol% of indenone (6) results in 30 and 35 times increase in the sensitivity, respectively. The benzoyl chromophore of the phenyl isopropenyl ketone (PIPK) unit is highly sensitive to DUV light, and its copolymer with MMA (the copolymer is hereafter designated as PMMA–PIPK) has been reported to be 110 (28 mol% of PIPK) and 350–800 times (6–35 mol% of PIPK) as sensitive as PMMA when irradiated with a Xe–Hg lamp (2) and 254 nm light (7), respectively. In addition, bleaching of the resist film was also observed during DUV irradiation (7), which is preferable for efficient light penetration through the entire film thickness and formation of resist patterns with a steep profile (8).

Photochemistry, as well as photophysics, of solid ketone polymers is well documented in the extensive reviews by Guillet (9, 10): the Norrish type I reaction, the Norrish type II reaction, photoreduction of the carbonyl group, and the formation of cyclobutanol. For polymers with a γ-hydrogen at the carbonyl group (e.g., poly(styrene-*co*-phenyl vinyl ketone) (PS–PVK) and poly(methyl methacrylate-*co*-methyl vinyl ketone) (PMMA–MVK) (11)) where the Norrish type II mechanism is possible, a large increase in the quantum yield of chain scission by the type II mechanism, Φ_{II}, is observed at and above the glass transition temperature, T_g, because this reaction requires a large amount of free volume for the six-membered intermediate. The generality of this effect suggests that even in the solid phase above T_g the conformational freedom of large segments of the polymer chain is comparable to that in solution, and consequently one should expect equivalent chemical reactivity.

On the other hand, methyl isopropenyl ketone (MIPK) copolymers with ethylene or styrene (PE–MIPK or PS–MIPK) degrade mainly by the type I mechanism (12). Cleavage produces a small methyl radical and a polymer radical, and the former has a greater probability of escaping the polymer cage. There is a small but continuous increase in the quantum yield of chain scission, Φ_I, with a temperature increase, but no discontinuous change is observed in the region of T_g, since the process requires a very small volume of activation in order to occur.

PIPK does not homopolymerize by radical polymerization, and the PIPK unit exists in between two MMA units in the copolymer chain (13, 14). PMMA–PIPK, which has no γ-hydrogen, is reported to degrade exclusively by the Norrish type I mechanism involving cleavage of the larger benzoyl moiety, followed by β-scission of the main chain (15, 16) (Fig. 1, a and b). Therefore the bleaching can be ascribed to the hypochromic effect caused by the cleavage and to partial escape of the benzoyl moiety from the polymer matrix. Photosplitting of the ester side chains of PMMA generates polymer radicals, the structure of which is the same as those from PMMA–PIPK involving the benzoyl side-chain cleavage. β-Scission proceeds from only 2.6% of the polymer radicals and most of the radicals form C=C bonds in the main chain or the side chain (17) (Fig. 1, c (n = 1) and d). The fate of the C=C bond still remains to be clarified.

One objective of this paper is to study the temperature dependence of the type I reaction involving benzoyl side-chain cleavage and of the succeeding main-chain scission in the case of PMMA–PIPK. The other is to elucidate the photodegradation mechanism of a promising DUV resist, PMMA–PIPK, and, at the same time, the PMMA standard resist.

Experimental

Materials

PIPK was prepared from propiophenone by the Mannich reaction followed by deamination, and copolymerized with MMA by suspension or bulk polymerization with 2,2′-azobis(isobutyronitrile) (AIBN) as an initiator as described in the previous papers (7, 18). The copolymer was reprecipitated from the benzene–methanol system. The PIPK content in the copolymer was estimated from the absorbance at 280 nm due to n–π^* transition in the UV spectrum in $CHCl_3$, assuming the molar absorptivity was equal to that of propiophenone (7, 14). The content was confirmed further by ^{1}H NMR. Molecular weights were determined by gel permeation chromatography (GPC) in toluene using a Waters type 410 chromatogram

Can. J. Chem. Downloaded from www.nrcresearchpress.com by 46.23.64.124 on 09/08/12
For personal use only.

Table 1. Summary of polymer data.

Polymer abbrev.	Method of polymerization	PIPK content (mol%)	M_n	M_w	M_w/M_n	T_g (°C)
PMMA–PIPK 06a	Suspension	5.8	22 000	46 000	2.1	101
PMMA–PIPK 06b	Suspension	6.1	50 900	124 000	2.4	
PMMA–PIPK 35	Bulk	35.0	9 000	15 000	1.7	87
PMMA	Suspension	0	91 300	219 000	2.4	105

Can. J. Chem. Downloaded from www.nrcresearchpress.com by 46.23.64.124 on 09/08/12
For personal use only.

Fig. 2. Schematic diagram of irradiation apparatus with (*a*) 8 W and (*b*) 15 W mercury lamps.

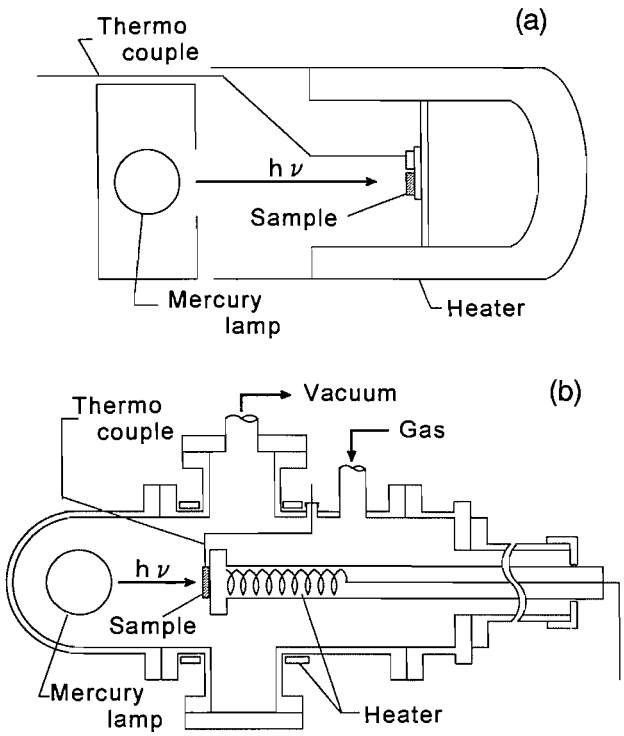

equipped with a Ultrastyryl Gel Linear 10674 column and an RI detector. Polymer data are summarized in Table 1.

Polymer film preparation

PMMA–PIPK and PMMA films were prepared by spin-coating from toluene solutions onto quartz or glass plates, and prebaked in an air-circulating oven at 140°C for 30 min. They were used for UV spectral and resist performance measurements, respectively. Polymer samples for GPC measurements were scratched from the glass plates after irradiation. Polymer films of as similar thickness as possible (500–750 nm) were used for each series of experiments.

DUV irradiation

Low-pressure mercury lamps of 8 W and 15 W without filters were used as the light source, which mainly emits DUV light of wavelength 254 nm. Irradiation in air was performed in the apparatus shown in Fig. 2*a*, while the effects of irradiation atmosphere were studied by using the chamber in Fig. 2*b*. In both cases the sample temperature was monitored with a thermocouple that was fixed on the sample holder. Incident light intensity, I_0, was measured to be 0.11–0.28 mW/cm^2 for PMMA–PIPK or 2.87 mW/cm^2 for PMMA (Apparatus a) and 0.83 mW/cm^2 for PMMA–PIPK (Apparatus b) with an Eppley air-type thermopile.

Measurement of benzoyl group removal

Concentration of remaining benzoyl groups was calculated from the absorbance at 242 nm, and the number of absorbed photons from the absorbance at 254 nm in the UV spectra, where the ε_{242} and ε_{254} values used were 12 700 and 7 600, respectively.

Measurement of main-chain scission

The molecular weights were measured for PMMA–PIPK before and after DUV irradiation at various temperatures using GPC. The number of moles of the main-chain scission, S_n, and quantum yield for main-chain scission, Φ_{cs} (=Φ_I), are calculated by the following equation:

$$\Phi_{cs} = S_n/I_{abs} = (M_{n0}/M_n - 1)m/M_{n0}/I_{abs}$$

where, M_{n0} and M_n are number-averaged molecular weights before and after DUV irradiation, respectively, m is a sample mass, and I_{abs} is the number of moles of photons (in einstein) absorbed by the polymer sample.

Resist performance

A polymer film was irradiated with 254 nm DUV light, developed in methyl isobutyl ketone (MIBK) without agitation at 23°C for 180 s, and rinsed with isopropanol (IPA) for 20 s. These developing conditions were selected to keep thickness reduction of the resist film in the unexposed area smaller than 10% of the initial thickness of the PMMA – PIPK 06b film.

The developed depth, which was the difference in film thickness between the exposed and the unexposed areas, was measured with an interference microscope after evaporating aluminum onto the surface of the specimen. The remaining resist thickness was obtained by reducing the measured depth from the thickness in the unexposed area, normalized to the initial thickness, and plotting against the logarithm of a varying radiation energy (dose) to give the characteristic lithographic curve. The sensitivity was defined as the minimum incident dose (in mJ/cm^2) required for complete removal of the resist film. The contrast, γ, was obtained as the slope of the linear part of the characteristic curve.

Can. J. Chem. Downloaded from www.nrcresearchpress.com by 46.23.64.124 on 09/08/12
For personal use only.

Fig. 3. UV spectra of 750 nm-thick PMMA–PIPK 06a films before and after irradiation (*a*) at 30°C and (*b*) at 130°C.

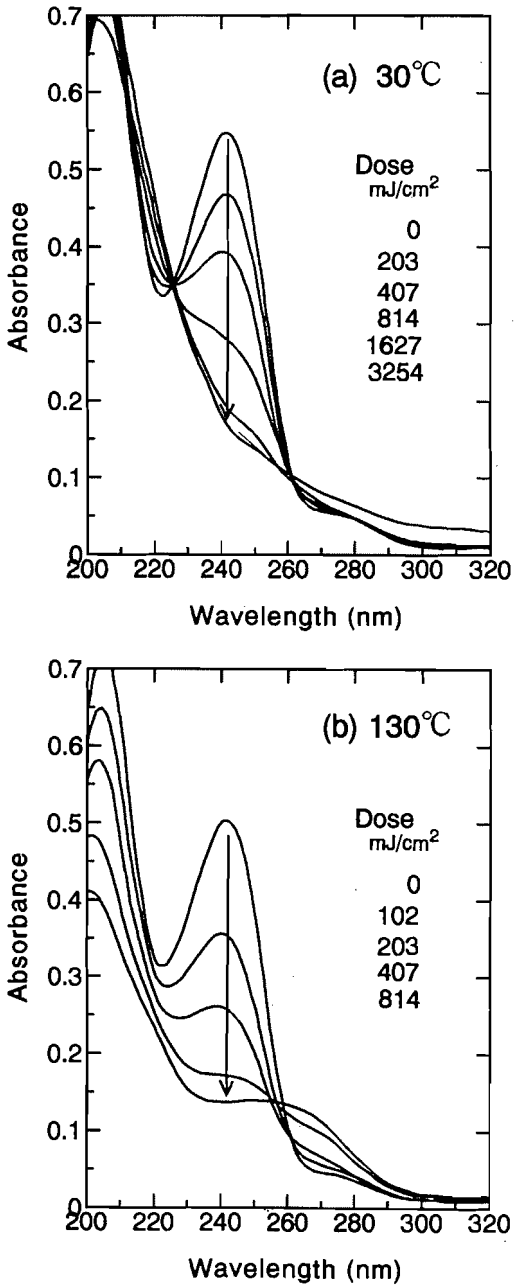

Results and discussion

I-1 Temperature dependence of benzoyl group removal

UV spectral changes were measured for PMMA–PIPK 06a after DUV irradiation at 30°C and 130°C, and are shown in Figs. 3*a* and 3*b*, respectively. PMMA has a weak absorption below 260 nm, which is negligible compared with that of PIPK copolymers (7). The absorption band at 242 nm decreased as the irradiation dose increased, and the copolymer films showed good bleaching characteristics. This is ascribed to cleavage of the benzoyl groups from the PIPK side chain by the Norrish Type I pathway (Fig. 1, a), and, perhaps, to the escape of some of the benzoyl groups from the polymer matrix, as no isosbestic point is observed in Fig. 3*b*. Naito et al. detected the benzoyl moieties as benzaldehyde, with a high yield in DUV photolysis of PMMA–PIPK in dioxane solutions (15). UV absorption remaining after the band at 242 nm ceased to decrease by DUV irradiation was considered to be due to the photoproducts formed by the benzoyl group removal, and calculation of the quantum yield was performed by subtracting the residual UV absorption.

Fig. 4. Temperature dependence of quantum yield for (*a*) benzoyl group removal and (*b*) main-chain scission of PMMA–PIPK 06a films (-●- and -○-) and PMMA–PIPK 35 films (-▲- and -△-).

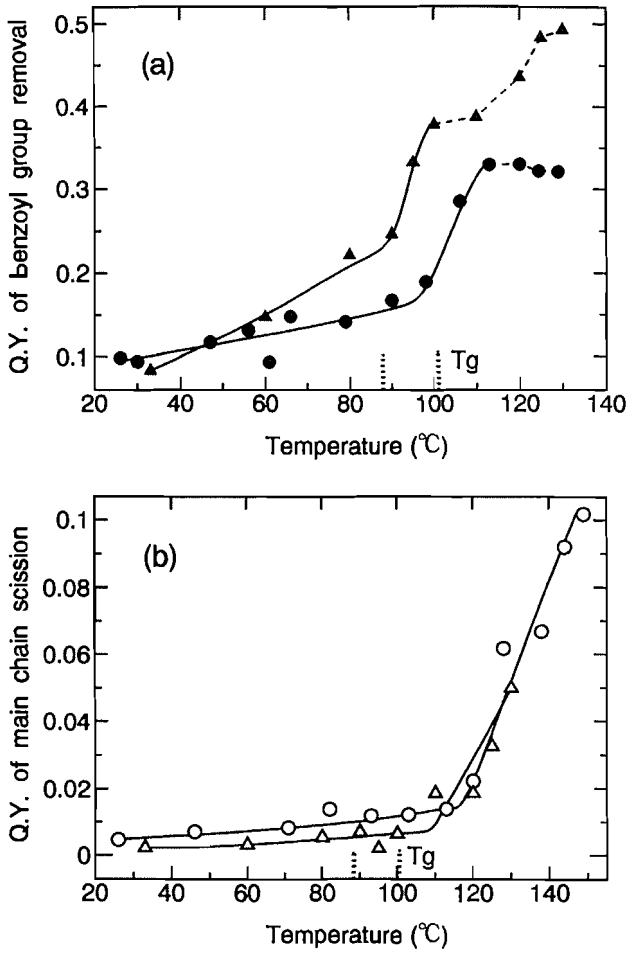

Quantum yields for the benzoyl group removal were calculated for PMMA–PIPKs 06a and 35 irradiated at various temperatures. They are plotted in Fig. 4*a* as a function of the irradiation temperature. The quantum yield increased abruptly above each T_g of the PMMA–PIPKs, as is observed with the quantum yield for main chain scission of PMMA–MVK by the type II mechanism, Φ_{II} (11). The increase was considered to be caused by a free volume increase above T_g, allowing the benzoyl radical to escape from the side-chain cage, and suppressing the back reaction: the benzoyl radical can be recombined with the polymer radical to again form the PIPK side chain. The activation energies below T_g for PMMA–PIPKs 06a and 35 were found to be 3.9 and 9.0 kJ/mol, respectively, which are a little smaller than the value of 12.5 kJ/mol for PMMA–MVK to form the six-membered intermediate by crankshaft motion of the main chain (11). A similar tempera-

Can. J. Chem. Downloaded from www.nrcresearchpress.com by 46.23.64.124 on 09/08/12
For personal use only.

ture dependence of quantum yield on T_g and other secondary transitions was not found in Norrish type I cleavage of PE–MIPK and PS–MIPK, where smaller CO, $CH_3^{\cdot}$, and $CH_3CO^{\cdot}$ escape with great efficiency through polymeric glassy matrices (12). The dependence was observed in quenching of excited benzophenone in solid PMMA matrix, in which the quenching rate of phosphorescence was controlled by diffusion of benzophenone molecules (19). The activation energy for the carbonyl loss of PS–MIPK is calculated from the data in ref. 12 to be 5.5 kJ/mol between 64 and 104°C, and that for the benzophenone diffusion is reported to be 40 kJ/mol (19). The former is comparable to, but the latter is much larger than, that for benzoyl group removal in the case of PMMA–PIPK.

I-2 Temperature dependence of main-chain scission

The polymer radical, which is generated by Norrish type I cleavage, undergoes β-scission of the main chain to reduce the molecular weight (Fig. 1, b) (15). Since Norrish type II elimination scarcely occurs with the ketone polymer that has no γ-hydrogen at the carbonyl group (16), the decrease in the molecular weight is primarily brought about by β-scission through the type I mechanism. Quantum yield for main-chain scission was calculated from the GPC measurement on PMMA–PIPKs 06a and 35 irradiated at various temperatures. They are plotted in Fig. 4*b* as a function of the irradiation temperature. The quantum yield increased markedly at a certain temperature about 20°C higher than each T_g of the PMMA–PIPKs. The increase in the quantum yield was ascribed to a free volume increase, which was necessary for the polymer fragment generated by β-scission to escape from the cage and for suppression of recombination between the fragments to reunite the main chain. Activation energies below and above the critical temperature were 5.9 and 41 kJ/mol for PMMA–PIPK 06a, respectively. As mentioned in Sect. I-1, PS–MIPK degrades mainly by the type I mechanism. The quantum yield for the main-chain scission as well as the loss of carbonyl function does not show a discontinuous change in the region of T_g (12). However, a similar temperature dependence of quantum yield and similar values of activation energy for PMMA–PIPK have been reported, with chain scission and cross-linking between polymer radicals influenced by segment motion of poly(vinyl acetate) (20).

I-3 Correlation between benzoyl group removal and main-chain scission

Benzoyl group removal and main-chain scission in PMMA–PIPK 06a are plotted as a function of absorbed photon in Figs. 5*a* and 5*b*, respectively. When the slope in Fig. 5*b* is compared with that of the initial linear part of the corresponding curve in Fig. 5*a*, it is found that main-chain scission occurs from only 2.5% and 10% of the polymer radicals generated by benzoyl side-chain cleavage at 30°C and 130°C, respectively. The former value, 2.5%, is quite similar to the value of 2.6% observed with main-chain scission of PMMA after the ester side-chain removal (17). Compared with this, the ratio of 10% indicates much enhanced efficiency of main-chain scission at 130°C. As Fig. 5*b* indicates, main-chain scission continues to proceed even after benzoyl group removal reaches a saturated value (see dotted arrows in Fig. 5a), which suggests the possibility of other degradation mechanisms for PMMA–PIPK than the Norrish type I cleavage followed by β-scission (Fig. 1, a and b).

Fig. 5. Photolyses of (*a*) side chain and (*b*) main chain of PMMA–PIPK 06a irradiated at 30°C (-●- and -○-) or 130°C (-■- and -□-) in air.

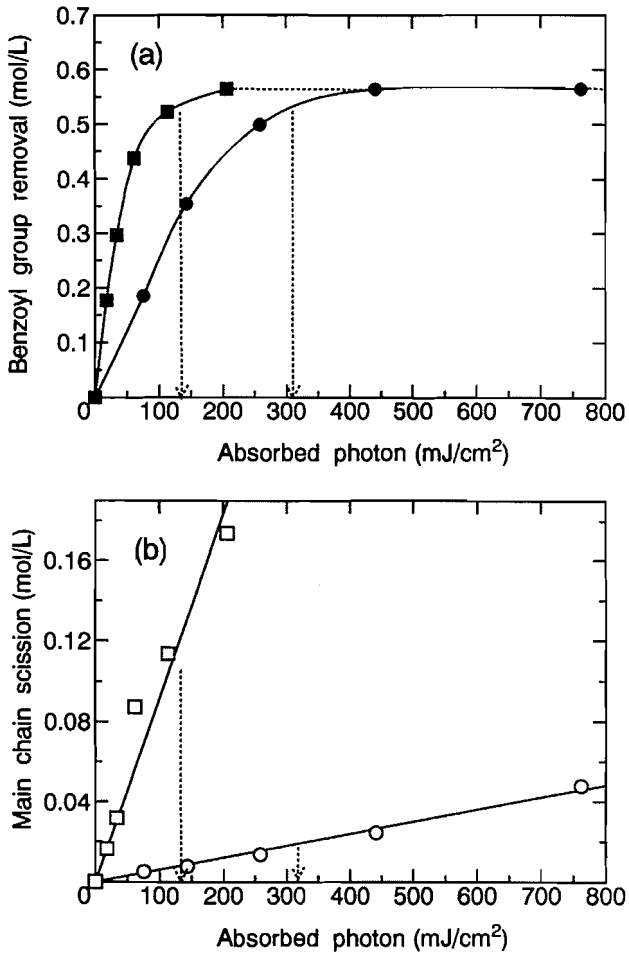

When PMMA–PIPK is irradiated with 254 nm light, the primary photochemical event is exclusively Norrish type I cleavage of the ketone side chain to form the polymer radical (15, 16). Then, some polymer radicals may undergo β-scission of the main chain, but others may form C=C bonds in the main chain (Fig. 1, c) or in the side chain by hydrogen abstraction (Fig. 1, d) (17), start auto-oxidation with addition of O_2 (Fig. 1, e), or be converted to stable polymer radicals or unstable intermediates from which main-chain scission can occur by post-exposure heating (Fig. 1, f). The probability of main-chain scission via Fig. 1, e and f mechanisms will be discussed next in Sects. I-4 and I-5.

I-4 Influence of ambient atmosphere on main-chain scission

PMMA–PIPK 06b was irradiated at 30°C or 130°C in different atmospheres: O_2, air, and N_2. Benzoyl group removal and main-chain scission are plotted as a function of absorbed photon in Figs. 6*a* and 6*b*, respectively. These figures are quite similar to Figs. 5*a* and 5*b*, regardless of different ambient atmospheres during DUV irradiation.

No increase in main-chain scission at 130°C in O_2 compared with that in air shows negligible contribution of auto-oxidation, which would be initiated by addition of O_2 to the

Can. J. Chem. Downloaded from www.nrcresearchpress.com by 46.23.64.124 on 09/08/12
For personal use only.

Fig. 6. Atmospheric influence on photolyses of (*a*) side chain and (*b*) main chain of PMMA–PIPK 06b irradiated at 30°C or 130°C. ○: in air, △: in O_2, and □: in N_2.

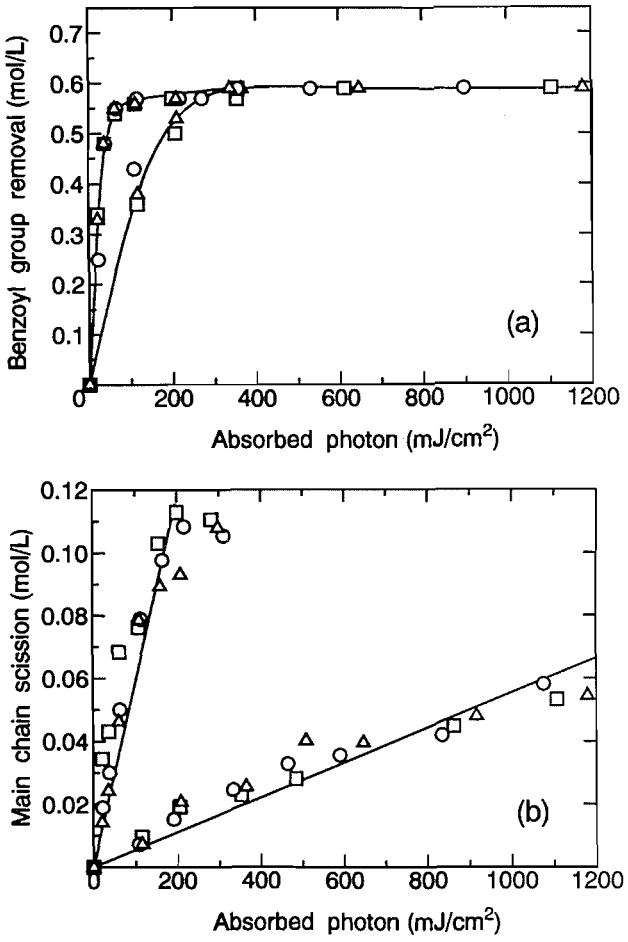

polymer radical (Fig. 1, e). No increase in main-chain scission at 30°C in N_2 compared with that in air suggests no detectable quenching of the polymer radical by O_2. These results indicate that ambient atmosphere hardly influences degradation, including auto-oxidation, of PMMA–PIPK in the solid phase, probably due to slow diffusion of the O_2 molecule into the polymer film, as was reported by Kato et al. in a comparison of the photolysis of copolymers of MMA with MIPK in solution and in the solid phase (21, 22).

I-5 Effect of post-exposure heating on main-chain scission

PMMA–PIPK 06b was irradiated at 30°C or 130°C and then heated at 130°C for a period equal to the irradiation. The results are shown in Fig. 7. Heating at 130°C after irradiation at 30°C or 130°C had no effect on further scission of the main chain. Heating at 130°C without irradiation also had no effect. These experiments reveal that although some stable polymer radicals and thermally unstable intermediates may remain in the polymer matrix, the quantities are too small to influence the degradation scheme.

I-6 Photolysis of PMMA at an elevated temperature

Main-chain scission was measured on a PMMA film of the same thickness and had been irradiated or heated under the

Fig. 7. Influence of heating at 130°C on main-chain scission of PMMA- PIPK 06b after irradiation at 30°C (●: with and ○: without heating) or 130°C (■: with and □: without heating). ◆: heated at 130°C without irradiation.

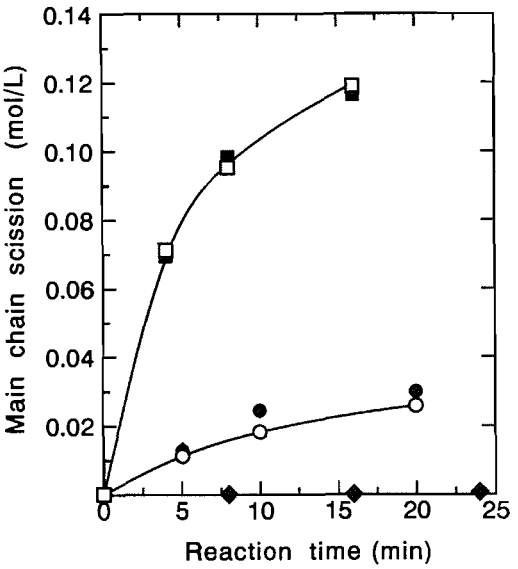

Fig. 8. Main-chain photolyses of PMMA films irradiated at 30°C (○) and 130°C (□). ◆: heated at 130°C without irradiation. (- - -) and (– – –): photolyses for PMMA–PIPK 06b at 30°C and 130°C, respectively.

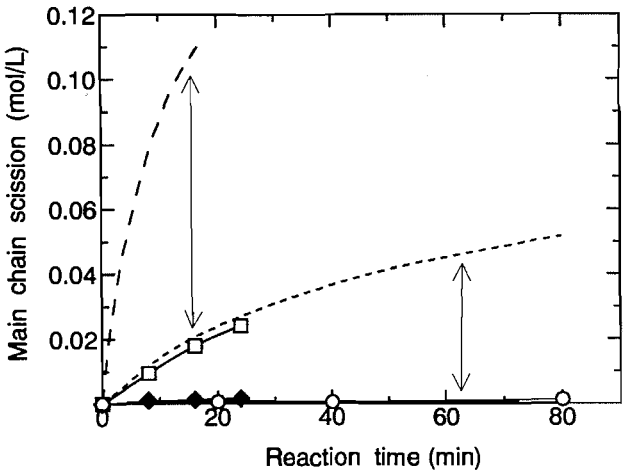

same conditions as a PMMA–PIPK 06b film. The number of main-chain scissions is plotted against irradiation or heating time in Fig. 8. The dashed and broken lines indicate the plots for photolyses of PMMA–PIPK 06b at 30°C and 130°C, respectively. Photolysis of PMMA at 30°C and thermolysis at 130°C were negligibly slow, compared with photolysis of PMMA–PIPK at 30°C. However, PMMA was found to degrade at about 25% of the photolysis rate of PMMA–PIPK 06b by DUV irradiation at 130°C, which is above its T_g.

I-7 Degradation mechanism of PMMA–PIPK and PMMA

Based on the results observed in Sects. I-1–I-6 in addition to those reported in refs. 15, 16, 17, 21, and 22, the primary photochemical event for PMMA–PIPK is Norrish type I cleavage of the phenyl ketone side chain to generate the polymer radical

Fig. 9. Characteristic lithographic curves for PMMA–PIPK films irradiated at 30°C (○) and 130°C (●) and for PMMA irradiated at 30°C (■), developed with MIBK for 180 s. The PMMA film was also developed with MIBK for 90 s (□).

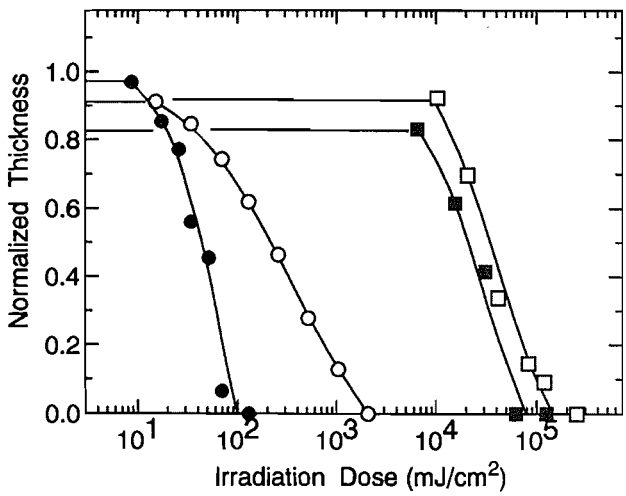

(Fig. 1, a). Then, a small number of the polymer radicals contribute to molecular weight decrease through β-scission (Fig. 1, b), but most of them are stabilized to form C=C bonds by hydrogen abstraction (Fig. 1, c and d).

Since the contributions of auto-oxidation of the polymer radical (Fig. 1, e) and thermal decomposition of stable radicals or unstable intermediates derived from the polymer radical (Fig. 1, f) were found to be small, main-chain scission by DUV irradiation after the benzoyl side chain ceased to split cannot be explained by the known mechanisms of Fig. 1, a–f. The MMA ester side chain on the carbon adjacent to the C=C bond can split to form conjugated polymer radicals (Fig. 1, g) by DUV irradiation more easily than can the intrinsic PMMA ester side chain. Some of the conjugated radicals will contribute to main-chain scission, but others will be stabilized again by further hydrogen abstraction from the main chain or the side chain. UV absorption at 242 nm due to the photoproducts discussed in Sect. I-1 can be ascribed to these conjugated C=C bonds, which were formed by successive photo-splitting of ester groups and hydrogen abstraction (Fig. 1, c ($n \geq 2$)). All these degradation mechanisms except the initial type I cleavage of benzoyl groups hold valid also for PMMA, because the polymer radicals are of exactly the same structure for both PMMA–PIPK and PMMA. The primary photoprocess, which is cleavage of ester groups in the case of PMMA, occurs less readily than that with PMMA–PIPK, but it is likely to be accelerated above the T_g.

II. Resist performance

Characteristic lithographic curves were obtained with polymer films of PMMA–PIPK 06b of ca. 750 nm thickness exposed at 30°C and 130°C, and are shown in Fig. 9. The sensitivity was 1600 and 100 mJ/cm^2, and the contrast was 0.6 and 1.3 at 30°C and 130°C, respectively. In Fig. 4*b*, quantum yields of main-chain scission at 30°C and at 130°C are 0.0029 and 0.036, respectively. The difference in sensitivity is a little larger than that of the quantum yield.

The contrast at 130°C was improved compared with that at 30°C, but little difference of M_w/M_n was observed, by GPC, between PMMA–PIPKs exposed with DUV light of radiation energy at each sensitivity dose at 30°C and at 130°C. In addition to the partial escape of split benzoyl groups observed in the UV spectra with no isosbestic point in Fig. 3*b*, thickness reduction (self-development) was actually detected to be 90 nm during DUV irradiation of 450 mJ/cm^2 at 130°C. Therefore, it is likely that gaseous photoproducts as well as main-chain scission enhanced the dissolution rate of the resist film in the exposed area, and the contrast at 130°C was higher than that at 30°C .

Characteristic curves of PMMA were also obtained with films exposed at 30°C and developed with MIBK for 180 s (the same conditions as for PMMA–PIPK) or developed with MIBK for 90 s (the same conditions as in the previous paper (2), which give a similar ratio of thickness reduction in the unexposed area by wet development). The sensitivities of PMMA–PIPK 06b at 30°C and 130°C were 75 and 1200 times as high as that of PMMA exposed at room temperature and developed under similar conditions. The sensitivity enhancement is ascribed to both efficient absorption of DUV light and high quantum yield for main-chain scission, especially highly effective photosplitting of the benzoyl side chain by the Norrish type I mechanism.

The findings in this study are applicable to actual lithography in the following three patterns:

1. Exposure at a higher temperature than T_g, rather than post-exposure bake, is effective for the increase in quantum yield for main-chain scission. In this case development at a lower temperature than T_g is necessary for preventing the latent image from being smeared.

2. Lowering the T_g of the resist film by incorporation of, or formulation with, plasticizing units will increase the quantum yield. This methodology has already been partially adopted in the molecular design of FBM, poly(1,1,1,2,3,3–hexafluorobutyl methacrylate) (T_g = 50°C) (23).

3. Incorporation of an appropriate substituent on the phenyl ring of PIPK will increase the absorption of DUV radiation and (or) the quantum yield for main-chain scission, and hence the sensitivity. This study will be reported in another contribution by some of the present authors (24).

Conclusion

Temperature dependence of benzoyl side-chain cleavage and main-chain scission of PMMA–PIPK irradiated with DUV light showed a large and discontinuous increase in the quantum yields of the type I mechanism in the region of T_g. The correlation between cleavage and scission revealed a new reaction mechanism of photosplitting of the MMA ester side chain on the carbon adjacent to the C=C bond. This mechanism also holds valid for PMMA.

Efficient DUV absorption and high quantum yield for main-chain scission above T_g realized a sensitivity of 100 mJ/cm^2 for PMMA–PIPK as a DUV resist.

References

1. Y. Nakane, T. Tsumori, and T. Mifune. Semicond. Int. **2**, 45 (1979).
2. K. Nate and T. Kobayashi. J. Electrochem. Soc. **128**, 1394 (1981).
3. S.A. MacDonald, H. Ito, C.G. Willson, J.W. Moore, H.M. Gharapetian, and J.E. Guillet. ACS Symp. Ser. **266**, 179 (1984).

Can. J. Chem. Downloaded from www.nrcresearchpress.com by 46.23.64.124 on 09/08/12
For personal use only.

4. B.J. Lin. J. Vac. Sci. Technol. **12**, 1317 (1975).
5. C.W. Wilkins, Jr., E. Reichmanis, and E.A. Chandross. J. Electrochem. Soc. **127**, 2510 (1980).
6. R.L. Hartless and E.A. Chandross. J. Vac. Sci. Technol. **19**, 1333 (1981).
7. K. Sugita, N. Ueno, K. Harada, M. Kushida, Y. Suzuki, Y. Takeuchi, and J.E. Guillet. Polym. J. **25**, 1059 (1993).
8. C.G. Willson. ACS Symp. Ser. **219**, 145 (1983).
9. J.E. Guillet. Polymer photophysics and photochemistry. Cambridge Univ. Press, Cambridge, U.K. 1985. pp. 261–294.
10. J.E. Guillet. *In* Advances in photochemistry. Vol. 14. *Edited by* D.H. Volman, G.S. Hammond, and K. Gollnick. John Wiley & Sons, New York. 1988. pp. 91–133.
11. E. Dans and J.E. Guillet. Macromolecules, **6**, 230 (1973).
12. J.E. Guillet, S.K. Li, and H.C. Ng. ACS Symp. Ser. **266**, 165 (1984).
13. J.E. Mulvaney, J.G. Dillen, and J.L. Laverty. J. Polym. Sci. Polym. Chem. Ed. **6**, 1841 (1968).
14. R. Roussel, M. Galin, and J.C. Galin. J. Macromol. Sci. Chem. **A10**, 1485 (1976).
15. I. Naito, K. Tashiro, and A. Kinoshita. J. Photochem. **23**, 73 (1983).
16. S.G. Bond and J.R. Ebdon. Polymer, **35**, 451 (1994).
17. J.O. Choi, J.A. Moore, J.C. Corelli, J.P. Silverman, and H. Bakhru. J. Vac. Sci. Technol. B: **6**, 2286 (1988).
18. K. Sugita, T. Kilp, and J.E. Guillet. J. Polym. Sci. Polym. Chem. Ed. **14**, 1901 (1976).
19. K. Horie, K. Morishita, and I. Mita. Macromolecules, **17**, 1746 (1984).
20. G. Geuskens, M. Borsu, and C. David. Eur. Polym. J. **8**, 1347 (1972).
21. M. Kato and M. Yamazaki. Makromol. Chem. **177**, 3455 (1976).
22. M. Kato and Y. Yoneshige. Makromol. Chem. **164**, 159 (1973).
23. M. Kakuchi, S. Sugawara, K. Murase, and K. Matsuyama. J. Electrochem. Soc. **124**, 1648 (1977).
24. Y. Takeuchi, J.E. Guillet, K. Sugita, N. Ueno, K. Harada, and Y. Suzuki. J. Polym. Sci. Polymer Chem. Ed. Submitted.

Can. J. Chem. Downloaded from www.nrcresearchpress.com by 46.23.64.124 on 09/08/12
For personal use only.

Photomodulation of the hydrophilic properties of acrylic polymers containing side-chain azobenzene chromophores

Nicola Tirelli, Angelina Altomare, Francesco Ciardelli, and Roberto Solaro

Abstract: Partially hydrophilic polymers have been prepared by free-radical copolymerization of *trans*-4-acryloyloxyazobenzene with *N-tert*-butylacrylamide and *N*-isopropylacrylamide. A turbidimetric method has been adapted to investigate the dependence of the polymer hydrophilic–hydrophobic balance on chemical composition and extent of photoisomerization of side-chain azobenzene chromophores. Irradiation at 366 nm of polymer suspension in THF–water induces the isomerization of azobenzene groups from the planar apolar *trans* form to the nonplanar polar *cis* form. Correspondingly, the solution turbidity is appreciably modified. Experimental results are discussed in terms of polymer structural parameters. Suspension stability and the possibility of carrying out photochemical cycles have been also investigated.

Key words: photochromic polymers, photoresponsive polymer, photomodulation of polymer properties, azobenzene-containing polymers, acryloyloxyazobenzene, *N-tert*-butylacrylamide.

Résumé : On a préparé des polymères partiellement hydrophiles par copolymérisation radicalaire du *trans*-4-acryloxyazobenzène avec les *N-tert*-butylacrylamide et *N*-isopropylacrylamide. On a adapté une méthode turbidimétrique pour étudier la dépendance de la balance hydrophile–hydrophobe sur la composition chimique et le degré de photoisomérisation de la chaîne latérale des chromophores azobenzènes. L'irradiation, à 360 nm, d'une suspension de polymère dans un mélange THF–eau induit une isomérisation des groupes azobenzènes de la forme *trans*, plane et apolaire, vers la forme *cis*, non planaire et polaire. D'une façon correspondante, la turbidité de la solution est modifiée d'une façon appréciable. On discute des résultats expérimentaux en fonction des paramètres structuraux du polymère. On a étudié la stabilité de la suspension et la possibilité d'effectuer des cycles photochimiques.

Mots clés : polymères photochromes, polymère photorépondant, photomodulation des propriétés d'un polymère, polymères contenant de l'azobenzène, acryloxyazobenzène, *N-tert*-butylacrylamide.

[Traduit par la rédaction]

Introduction

In recent years increasing attention has been focused on polymeric systems and gels based on *N*-alkylacrylamide, for their well-known properties of thermoreversible swelling or collapse, and for their possible application as drug release systems, chemo-mechanical transducers, sensors, and selective pumps (1–5). Polymer gelation can also be controlled by parameters other than temperature, e.g., pH, ionic strength, and solvent composition (6–8). However, only a few attempts to achieve a *photochemical* control of this transition have been reported so far (9–11).

For some time our research group has been investigating the preparation and the photochromic characterization of synthetic polymers having a hydrocarbon backbone and bearing photoactive moieties, mainly azobenzene groups, in the side chains (12–19). Until now, however, this research has been mainly focused on hydrophobic systems.

In the present paper we report on the results obtained in an investigation of the photomodulation of the hydrophilic–hydrophobic balance of radical copolymers of a photochromic monomer, *trans*-4-acryloyloxyazobenzene (**AAB**), with a hydrophilic monomer, N-*tert*-butylacrylamide (**NTBA**). For comparison, copolymers of **AAB** with *N*-isopropylacrylamide (**NIPA**) have been also studied. Modulation of polymer solubility parameters was carried out by reversible photochemical control of phase segregation.

The choice of the azobenzene chromophore as photochromic group has been suggested because of its stability and the

Received March 10, 1995.

This paper is dedicated to Professor J.E. (Jim) Guillet in recognition of his contribution to Canadian chemistry.

Nicola Tirelli, Angelina Altomare, and Roberto Solaro. Department of Chemistry and Industrial Chemistry, University of Pisa, via Risorgimento 35, 56126 Pisa, Italy.
Francesco Ciardelli.[1] Department of Chemistry and Industrial Chemistry, University of Pisa, via Risorgimento 35, 56126 Pisa, Italy, and Centro Macromolecole Stereordinate Otticamente Attive, University of Pisa, Italy.

[1] Author to whom correspondence may be addressed. Telephone: 50-918229. Fax: 50-918260.

Can. J. Chem. Downloaded from www.nrcresearchpress.com by 46.23.64.124 on 09/08/12
For personal use only.

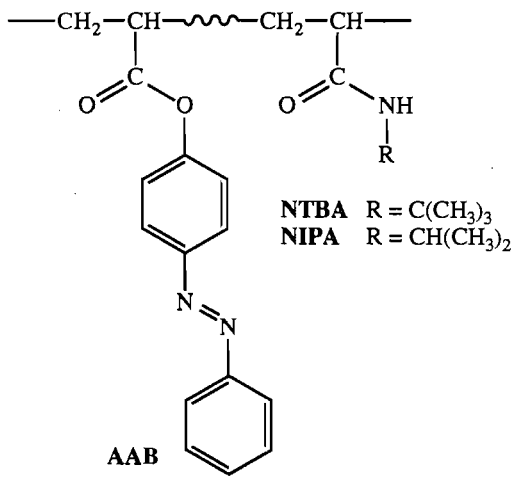

photoreversibilty of the *trans→cis* isomerization process. Moreover, only the photoinduced change of side-chain polarity can affect polymer solubility. On the contrary, triphenylmethane and spiropyran derivatives are less stable and the charge photogeneration induced by light irradiation gives rise to a significant increase of ionic strength.

Experimental

Polymer synthesis and characterization has been reported in a previous paper (17).

Spectrograde anhydrous THF (Erba) and bidistilled water were used as solvents. UV measurements were performed at 25°C in THF–H_2O in solvent mixtures by a Jasco Uvidec 510 spectrophotometer connected to a microcomputer for automatic collection and processing of experimental data. Microscopy analyses were performed by a Polyvar optical microscope equipped with polarizing filters and a photographic apparatus.

Phase segregation experiments were carried out by repeated additions of a small amount (10–50 μL) of water to a stirred polymer solution in THF while recording the 380 nm optical density. Each addition was limited so as to induce a variation of absorbance lower than 0.04. Subsequent additions were delayed until photometric stabilization.

Photoisomerization experiments were carried out on polymer solutions or suspensions, by using the following experimental setup: the emission from a 150 W high-pressure Hg/Xe lamp, filtered by a 366 nm or 440 nm interference filter (Balzer) having ±5 nm bandwidth, was guided by a 3 mm × 50 cm quartz fibre on top of a magnetically stirred 10 mm quartz cell placed within the UV spectrophotometer. Isomerization kinetics were monitored by measuring the 320 nm absorbance or 380 nm scattering every 5–10 s. About 1000–1500 data points were collected for each photoisomerization experiment.

Results and discussion

Copolymers of acryloyloxyazobenzene (**AAB**) with *N-tert*-butylacrylamide (**NTBA**) and with *N*-isopropylacrylamide (**NIPA**) were prepared by free-radical polymerization in benzene, as reported elsewhere (17). For comparison the corresponding homopolymers were also synthesized. Data relevant to chemical composition and molecular weight of the investigated samples are summarized in Table 1.

Table 1. Characterization of copolymers of 4-acryloyloxyazobenzene (**AAB**) with *N-tert*-butylacrylamide (**NTBA**) and *N*-isopropylacrylamide (**NIPA**).

Sample	Comonomer (type)	**AAB**[a] (mol%)	$\overline{M}_n$[b]	$\overline{M}_w/\overline{M}_n$[b]
pAAB	—	100	3 800	1.5
ABBA1	**NTBA**	74.1	4 700	2.0
ABBA2	**NTBA**	57.0	6 500	1.5
ABBA3	**NTBA**	33.2	10 100	1.6
ABBA4	**NTBA**	12.9	15 500	1.7
pNTBA	**NTBA**	0	14 800	2.0
ABPA1	**NIPA**	71.6	8 200	1.3
ABPA2	**NIPA**	52.5	7 500	1.6
ABPA3	**NIPA**	28.6	11 600	1.5
ABPA4	**NIPA**	13.7	11 500	1.7
pNIPA	**NIPA**	0	16 100	1.7

[a]Evaluated by ^{1}H NMR.
[b]Evaluated by GPC in THF.

The reactivity ratios obtained for the investigated systems (respectively, $r_{AAB} = 0.66$ and $r_{NIPA} = 0.57$; $r_{AAB} = 0.91$ and $r_{NTBA} = 0.53$) indicate some tendency to an alternating enchainment of monomeric units ($r_{AAB} \times r_{NIPA} = 0.38$; $r_{AAB} \times r_{NTBA} = 0.49$).

On irradiation at 366 nm, corresponding to the $\pi \rightarrow \pi^*$ electronic transition, the intensity of the 320 nm absorbance of copolymer solution in THF shows an exponential decay, and a plot of $\log(A_0 - A_\infty)/(A_t - A_\infty)$, where A_0, A_t, and A_∞ are, respectively, the absorbance at time 0, t, and at the photostationary state, exhibits a linear dependence upon irradiation time, in accordance with the occurrence of a first-order kinetics ($k_i \approx 4\times10^{-4}$ s^{-1}). The occurrence, in the UV spectra of the solutions, of two distinct isosbestic points at about 280 and 380 nm indicates that only two absorbing species, namely, the *trans* and *cis* isomers, are present and that no side reaction occurs. The *trans→cis* photoisomerization process can be reversed either thermally ($k_t \approx 5\times10^{-6}$ s^{-1} at 25°C) or by irradiation at 440 nm ($k'_i \approx 1\times10^{-2}$ s^{-1}), corresponding to the $n \rightarrow \pi^*$ electronic transition.

Polymer precipitation

Hydrophilicity of polymer samples can be ranked by measuring either the precipitation temperature in a given water – organic solvent mixture or the solvent composition at a definite temperature. Both methods decrease the thermodynamic strength of the solvent, thus reducing the solvation of polymer macromolecules. This decrease causes the system to cross binodal or spinodal lines in the phase diagram (20, 21) and formation of metastable polymer solutions or phase separation of polymeric materials is observed. However, to evaluate the possible effect of *trans–cis* photoisomerization, it was necessary that the thermal back-isomerization rate did not change too much in different runs. As a consequence, the temperature was kept constant at 25°C while changing the solvent composition.

Experimentally, the 380 nm absorbance of polymer solutions in THF was monitored while adding increasing amounts of water. The 380 nm wavelength was selected, as neither

Can. J. Chem. Downloaded from www.nrcresearchpress.com by 46.23.64.124 on 09/08/12
For personal use only.

Can. J. Chem. Downloaded from www.nrcresearchpress.com by 46.23.64.124 on 09/08/12
For personal use only.

Table 2. Dependence of the solvent composition at the inflection point and at the end point on the chemical composition of **AAB/NTBA** copolymers.

AAB content (mol%)	Water/THF ratio (vol/vol) at the inflection point		Light scattering at the end point	
	Non-irradiated	Irradiated[a]	Non-irradiated	Irradiated[a]
100	0.59	0.56	1.43	0.84
74.1	0.58	0.57	1.75	1.19
57.0	0.66	0.63	1.63	1.00
33.2	0.63	0.51	1.18	0.70
12.9	0.55	0.51	n.d.	n.d.
0	0.54	0.54	0.47	0.47

[a]At the photostationary state under irradiation at 366 nm.

Fig. 1. Dependence of 380 nm light scattering on solvent composition (sample pAAB, $c = 0.147$ g/L) at 25°C. ○, experimental data; ●, data corrected for dilution.

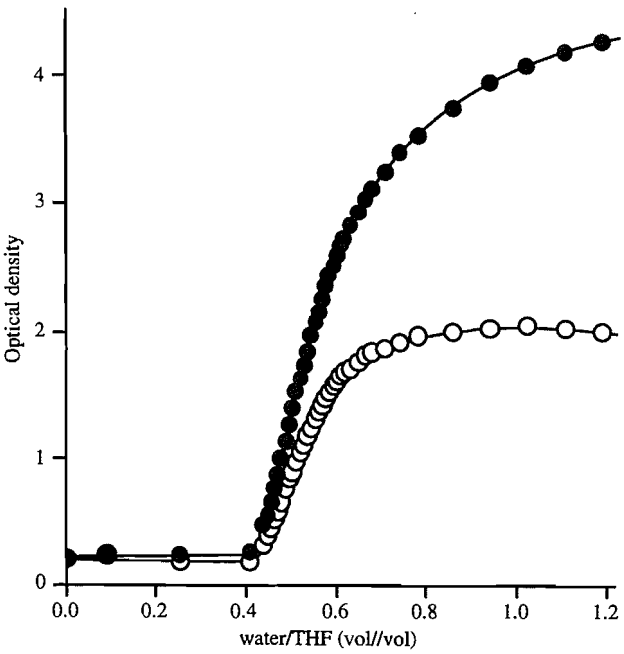

Fig. 2. UV spectra of **AAB/NTBA** copolymer (sample AABA3) at 25°C in water–THF solution at different water contents.

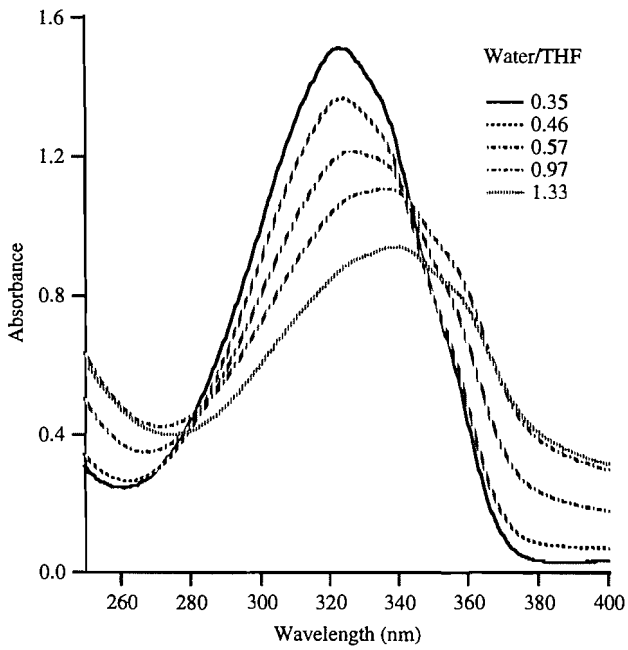

trans- nor *cis*-azobenzene have an appreciable absorption at this wavelength. The recorded variation of the 380 nm absorption could therefore be attributed almost exclusively to the light scattering of the precipitated polymer.

Optical microscopy examination of suspensions gave evidence that polymer microparticles were highly swollen and allowed us to associate the observed increase of light scattering on water addition during the precipitation process to an increase of their average size.

Polymer suspensions thus obtained were characterized by a rather low stability and, on stirring, the spherical polymer microparticles gave rise to multinuclear aggregates. However, addition of 1.0 g/L of sodium dodecylsulfate to polymer solutions noticeably improved the stability of suspensions whose 380 nm scattering remained almost constant over at least 20 h.

For each polymer sample, experiments were carried out using polymer solutions having concentrations between 0.02 and 0.2 g/L. The inflection point of the titration curves and light scattering at complete precipitation, averaged over at least three runs, were recorded as a measure of polymer hydrophilicity (Table 2). To better display the inflection point, measured absorbance values were corrected for the increasing dilution due to water addition (Fig. 1). However, values reported in Table 2 and subsequent figures use uncorrected experimental data.

During the precipitation process, a shift of the maximum of the $\pi \rightarrow \pi^*$ absorption band from 320 to 350 nm was recorded. This effect is too large to be attributed solely to a solvent effect and seems to arise from a modification of the relative intensity of the different components of the band (Fig. 2). However, no sound explanation can be put forward at present.

The starting concentration of polymer solution significantly affected not only the final light scattering but also the position of the inflection point, for polymer samples both in the all-*trans* configuration and at the photostationary state under irradiation at 366 nm (Table 3). This result is not unexpected; in fact, it is known that a larger decrease of the thermodynamic

Table 3. Influence of polymer concentration (sample ABBA2) on the 380 nm light scattering and solvent composition at the inflection point.

Non-irradiated sample			Irradiated sample[a]		
Conc. (g/L)	Absorbance	Water/THF vol. ratio	Conc. (g/L)	Absorbance	Water/THF vol. ratio
0.04	0.30	0.69	0.04	0.19	0.72
0.06	0.41	0.64	0.08	0.25	0.66
0.07	0.47	0.63	0.19	0.67	0.57
0.17	0.97	0.52	0.37	1.08	0.53
0.36	1.16	0.44	0.83	1.13	0.49

[a]At the photostationary state under irradiation at 366 nm.

Fig. 3. Dependence of the water/THF ratio at the inflection point on the composition of **AAB/NTBA** (-●-) and **AAB/NIPA** (-■-) copolymers (c = 0.1 g/L) at 25°C.

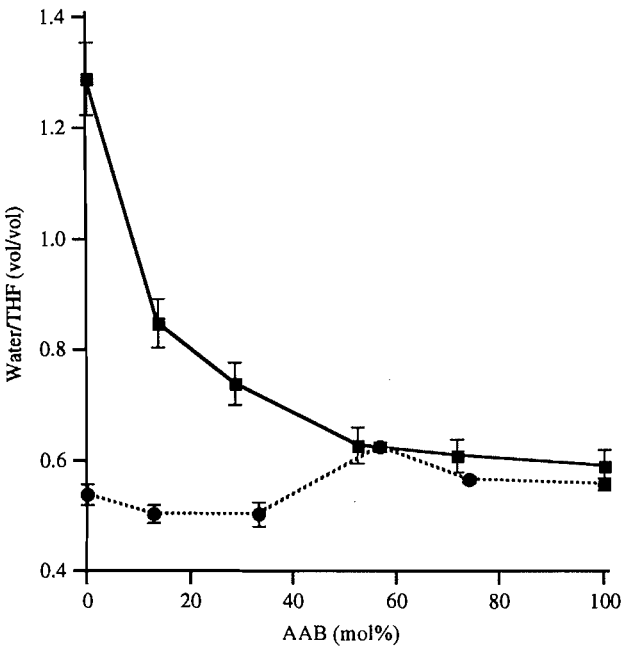

Fig. 4. Dependence of the water/THF ratio at the inflection point on the composition of **AAB/NTBA** copolymers (c = 0.1 g/L) in the all-*trans* configuration (-●-) and at the photostationary state under irradiation at 366 nm (-○-) at 25°C.

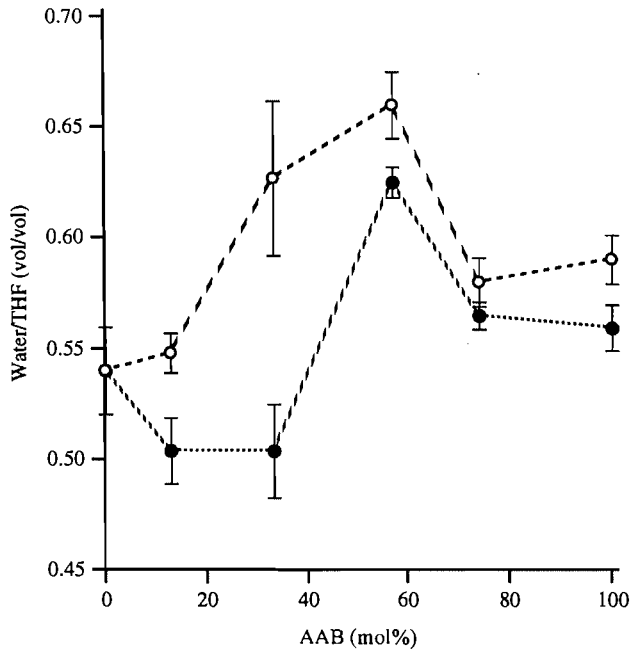

solvent strength is required in order to make more dilute polymer solutions cross binodal and spinodal lines (20). Comparison of the solvent composition at the inflection point for different *trans*-**AAB/NTBA** copolymer samples showed that the water/THF ratio increased from 0.60 to 0.65 on increasing the **NTBA** content from 0 to about 40% and then decreased to about 0.54 (Fig. 3).

On the basis of the expected different hydrophobicity of **AAB** units as compared to **NTBA** units, one should anticipate a monotonic dependence of the amount of water required for polymer precipitation on the chemical composition of the copolymers. The observed trend highlights the complexity of the precipitation process, which is influenced not only by the hydrophilic–hydrophobic balance, but also by molecular weight ($\overline{M}_n$), the polydispersity index ($\overline{M}_w/\overline{M}_n$), and polymer conformation. In particular, it seems reasonable to attribute the observed behavior to the concurrent variation of copolymer hydrophilicity and molecular weight (Table 1) and to some specific interaction between monomeric units.

However, the range of water content at the inflection point spanned by different polymer samples is quite small, indicating that the **AAB** and **NTBA** monomeric units are characterized by rather similar hydrophobicity, thus allowing other minor factors to manifest their effect. To verify this point, copolymers of **AAB** with **NIPA**, a monomer significantly more hydrophilic than **NTBA**, were investigated under the same experimental conditions. As expected, a monotonic increase from 0.6 to 1.7 of the water/THF ratio at the inflection point was observed as the content of **NIPA** units changed from 0 to 100% (Fig. 3).

Photomodulation of polymer suspension properties

Slow addition of water to polymer solutions at the photostationary state under irradiation at 366 nm induced polymer coacervation, analogous to that observed for polymer samples containing azobenzene chromophores in the all-*trans* configuration.

Independent of polymer chemical composition, the inflection point in the precipitation plots of polymer samples having a large content of *cis*-**AAB** units occurred at a larger water/

Can. J. Chem. Downloaded from www.nrcresearchpress.com by 46.23.64.124 on 09/08/12
For personal use only.

Can. J. Chem. Downloaded from www.nrcresearchpress.com by 46.23.64.124 on 09/08/12
For personal use only.

Fig. 5. Dependence of the 380 nm light scattering at the end point on polymer concentration (sample ABBA3) at 25°C: non-irradiated (-●-), and at the photostationary state under irradiation at 366 nm (-○-).

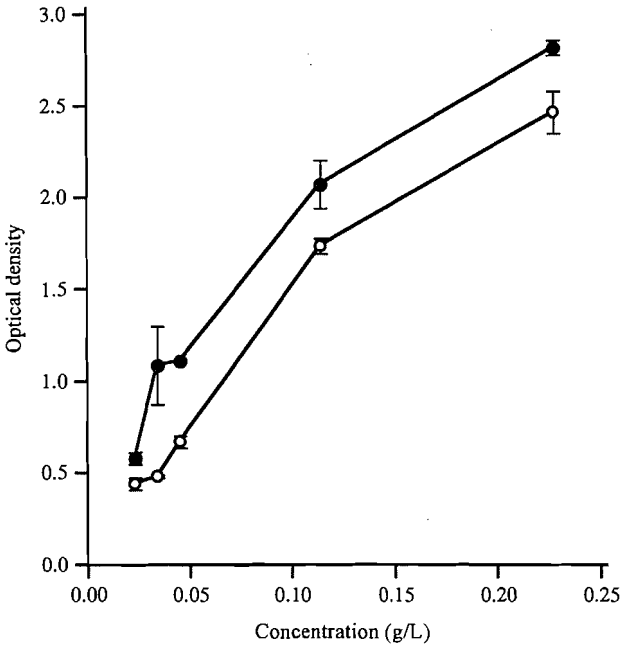

Fig. 6. Dependence of 380 nm light scattering at the end point on the composition of **AAB/NTBA** copolymers (c = 0.069 g/L) at 25°C: non-irradiated (-□-), precipitated at the photostationary state (-●-), and irradiated at 366 nm after precipitation (-○-).

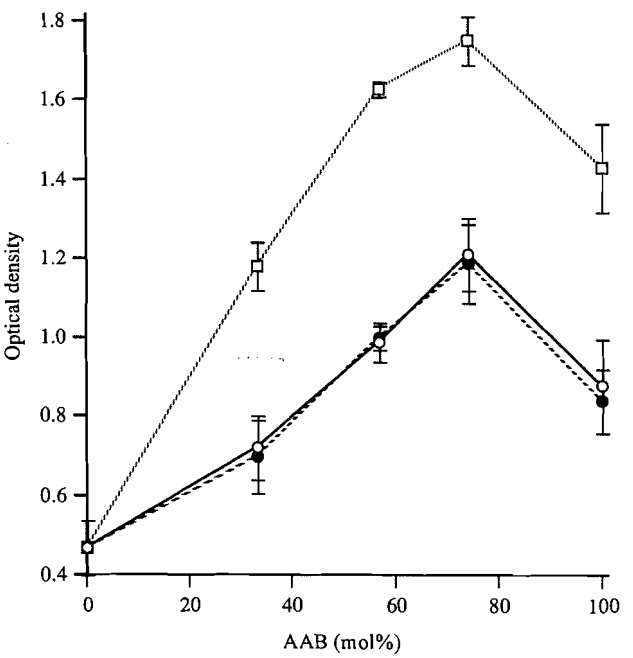

THF ratio than the corresponding all-*trans* samples (Fig. 4). By selecting a suitable solvent composition, photodissolution–photoprecipitation cycles could be effected by successive irradiation at 366 and 440 nm. Taking into account that no modification of polymer molecular weight, polydispersity index, and content and distribution of monomeric co-units occurs on irradiation, the observed trend must be attributed to a variation of the overall polymer hydrophilicity, due to the increasing content of more polar *cis*-chromophores.

Fig. 7. Variation of the light scattering at 380 nm of a polymer suspension by cycling irradiation at 366 and 440 nm (sample ABBA1, c = 0.069 g/L in water–THF at 25°C).

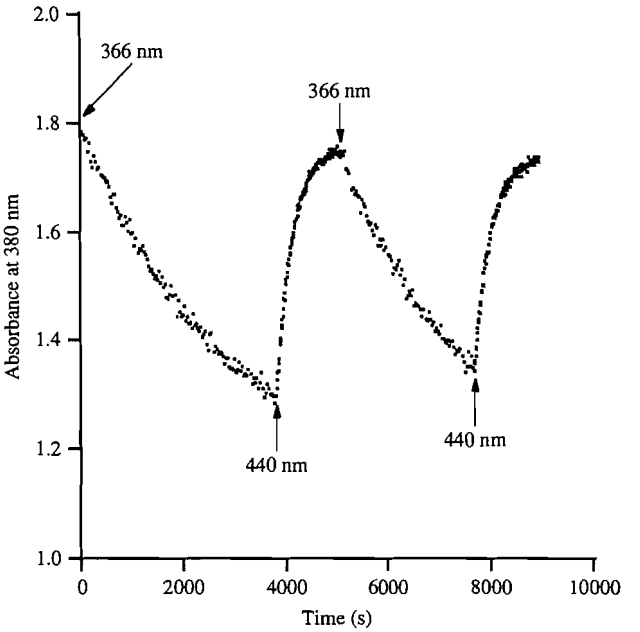

It was observed that in all cases the light scattering of polymer suspensions at the photostationary state was lower than that of the corresponding non-irradiated samples. To avoid possible interference by a partial photodissolution process, the scattering of polymer solutions having different concentrations (Fig. 5) or content of **AAB** units (Fig. 6) was recorded at a water/THF ratio of 1.2, well beyond the end point of both *trans* and *cis* forms. Optical microscopy analysis of polymer suspensions seems to indicate that this effect arises from a decrease of the average size of polymer microparticles, due to their lower extent of swelling. A variation of the particle refraction index cannot, however, be ruled out.

Identical values of light scattering were recorded either by precipitation of solutions at the photostationary state or by irradiation at 366 nm of all-*trans* polymer suspensions (Fig. 6). Photoisomerization of polymer suspensions exhibited first-order kinetics, having rate constants of the same order of magnitude as those measured in solution. This result seems to confirm a significant swelling of polymer particles.

The light scattering of polymer suspensions can be repeatedly cycled between two extreme values by alternate irradiation at 366 and 440 nm (Fig. 7). The different absorbance levels reached during the cyclic switching process depend on the different irradiation times used in the four cycles reported and to some extent on the limited stability of the investigated polymer suspension. This demonstrates the possibility of reversibly photomodulating the scattering of copolymer suspensions, which, at least in principle, could be used as optical switches.

Concluding remarks

Investigation of the precipitation of partially hydrophilic copolymers of acryloyloxyazobenzene with *N-tert*-butylacrylamide by water addition to THF solutions has shown that several structural parameters can contribute to the overall hydrophilic–hydrophobic balance due to the very similar hydrophobicity of the two comonomers. Indeed, in copolymers of **AAB** with *N*-isopropylacrylamide, a more hydrophilic comonomer, only the chemical composition affected the water/THF ratio necessary for polymer precipitation.

Irradiation of polymer suspensions at 366 and 440 nm has demonstrated the possibility of photomodulating both the solubility of polymer samples and the light scattering of polymer suspensions. This last phenomenon is rather large, a 30–50% variation of the 380 nm absorbance being observed. Some information on the photomodulation of polymer solubility is available in the literature (11, 22–25), whereas, to the best of our knowledge, this is the first report on the photomodulation of the light scattering of photochromic polymer suspensions.

In principle, photomodulation of the light scattering of suitable polymer suspensions could be used for the fabrication of optical switches. However, the limited stability of suspensions may prevent their practical application. The possibility of photomodulating the swelling of cross-linked polymers, which are inherently stable, is at present under investigation.

References

1. M. Heskins and J.E. Guillet. J. Macromol. Sci. Chem. **2**, 1441 (1968).
2. M. Ilavsky. Macromolecules, **15**, 782 (1982).
3. Y. Hirokawa and T. Tanaka. J. Chem. Phys. **81**, 6379 (1984).
4. A.S. Hoffman, A. Afrassabi, and L.C. Dong. J. Controlled Release, **4**, 213 (1986).
5. H.G. Schild. Prog. Polym. Sci. **17**, 163 (1992).
6. R.A. Siegel and B.A. Firestone. Macromolecules, **21**, 3254 (1988).
7. H.G. Schild and D.A. Tirrell. J. Phys. Chem. **94**, 4352 (1990).
8. H.G. Schild and D.A. Tirrell. Macromolecules, **24**, 948 (1991).
9. D. Kungwatchakun and M. Irie. Makromol. Chem. Rapid Commun. **9**, 243 (1988).
10. A. Mamada, T. Tanaka, D. Kungwatchakun, and M. Irie. Macromolecules, **23**, 1517 (1990).
11. M. Irie. Adv. Polym. Sci. **110**, 49 (1993).
12. F. Ciardelli. M. Aglietto, C. Carlini, E. Chiellini, and R. Solaro. Pure Appl. Chem. **54**, 521 (1982).
13. F. Ciardelli, C. Carlini, R. Solaro, A. Altomare, O. Pieroni, J.L. Houben, and A. Fissi. Pure Appl. Chem. **56**, 329 (1984).
14. A. Altomare, C. Carlini, F. Ciardelli, R. Solaro, and N. Rosato. J. Polym. Sci. Polym. Chem. Ed. **22**, 1267 (1984).
15. A. Altomare, F. Ciardelli, R. Lima, and R. Solaro. Polym. Adv. Technol. **2**, 3 (1991).
16. A. Altomare, F. Ciardelli, R. Lima, and R. Solaro. Chirality, **3**, 292 (1991).
17. A. Altomare, F. Ciardelli, R. Solaro, and N. Tirelli. Macromol. Chem. Phys. In press.
18. L. Angiolini, D. Caretti, C. Carlini, A. Altomare, and R. Solaro. J. Polym. Sci. Part A: Polym. Chem. **32**, 2849 (1994).
19. F. Ciardelli, O. Pieroni, A. Fissi, A. Altomare, R. Solaro, and N. Tirelli. Polym. Adv. Technol. **6**, 32 (1995).
20. A.Y. Grosberg and D.V. Kuznetsov. Macromolecules, **26**, 4249 (1993).
21. M. Doi and S.F. Edwards. The theory of polymer dynamics. *Edited by* M. Doi and S.F. Edwards. Clarendon Press, Oxford. 1986, p. 140.
22. O. Pieroni, A. Fissi, J.L. Houben, and F. Ciardelli. J. Am. Chem. Soc. **107**, 2990 (1985).
23. A. Fissi and O. Pieroni. Macromolecules, **22**, 1115 (1989).
24. M. Irie and D. Kunwatchakun. Macromolecules, **19**, 2476 (1986).
25. M. Irie and R. Iga. Macromolecules, **19**, 2480 (1986).

Can. J. Chem. Downloaded from www.nrcresearchpress.com by 46.23.64.124 on 09/08/12
For personal use only.

Solvent clustering, polar network density, and thermodynamic interactions in coordination polymers: an inverse gas chromatography study of metal-ion-containing polyesters of poly(diethylene glycol-*co*-succinic acid)

G. Julius Vancso and Zhanjie Tan

Can. J. Chem. Downloaded from www.nrcresearchpress.com by 46.23.64.124 on 09/08/12
For personal use only.

Abstract: The spatial distribution of toluene and THF in the polyester poly(diethylene glycol-*co*-succinic acid) and its Mg^{2+}-containing "telechelic" derivative was described by Kirkwood–Buff–Zimm (KBZ) cluster integrals. The values of KBZ integrals as a function of the volume fraction of solvent in the polymer–solvent systems were obtained from finite concentration inverse gas chromatography measurements utilizing the elution-on-a-plateau technique. The results show that toluene has a higher self-affinity to form clusters in the pure polyester than THF, which is more homogeneously distributed in the polymer. Data for preferential solvation indicate that a segregation of parts of the polymer chains is present in the toluene–polyester system. When metal ions are introduced, the self-affinity of the solvent molecules to gather increases, whereas solvent clusters of toluene form in the free volume, and the gathering of the THF is likely to take place close to the metal ions. Based on the electron donacity values of the various donor groups present in the metal-ion-containing polymer it was assumed that THF in the Mg^{2+}-containing polyester will be bound to the central metal ion while the apolar toluene will participate in the solvation of the apolar parts of the polymer and will be "repelled" from the ion-containing regions. The concentration of these ionic centres, which act as effective cross-links in the coordination polymer, was determined from measurements of thermodynamic activity. A comparison of the experimental and estimated effective cross-link density values indicates a nearly atomic dispersion of Mg^{2+} in the metal-ion-containing polyesters.

Key words: inverse gas chromatography, cluster integrals, solvent partition in polymers, metal-ion-containing polyesters, Flory–Huggins interaction parameter.

Résumé : Utilisant les intégrales d'agrégats de Kirkwood–Buff–Zimm (KBZ), on a décrit la distribution spatiale du toluène et du THF dans le polyester, poly(diéthylène glycol-*co*-acid succinique), et dans son dérivé «téléchélique» contenant du Mg^{2+}. Utilisant la technique d'élution sur un plateau lors de mesures de chromatographie en phase gazeuse inversée, à concentration définie, on a obtenu les valeurs des intégrales de KBZ en fonction de la fraction volumique du solvant dans les systèmes polymère–solvant. Les résultats montrent que le toluène possède une autoaffinité à former des agrégats qui est plus grande dans le polyester pur que celle du THF qui est distribué d'une façon plus homogène dans le polymère. Les données relatives à la solvatation préférentielle indiquent qu'il existe une ségrégation de parties des chaînes de polymère dans le système toluène–polyester. Quand on introduit des ions metalliques, l'autoaffinté des molécules de solvant augmente, alors que les agrégats de solvant du toluène se forment dans le volume libre, et l'agrégation du THF se produit probablement près des ion métalliques. Sur la base des valuers exprimant la facilité à donner des électrons des divers groupes donneurs présents dans le polymère contenant l'ion métallique, on a fait l'hypothèse que le THF présent dans le polyester contenant du Mg^{2+} se lie à l'ion métallique central alors que le toluène qui est apolaire participe à la solvation

Received April 24, 1995.

This paper is dedicated to Professor J.E. (Jim) Guillet in recognition of his contributions to Canadian chemistry.

G.J. Vancso[1] and Z. Tan. Department of Chemistry, University of Toronto, 80 St. George Street, Toronto, ON M5S 1A1, Canada.

[1] Author to whom correspondence may be addressed. Present address: University of Twente, Faculty of Chemical Technology, P.O. Box 217, NL-7500 AE Enschede, The Netherlands. Fax: +31 (0)53-4893823.

des parties apolaires du polymère et se trouve repousser des régions contenant les ions. Se basant sur des mesures de l'activité thermodynamique, on a déterminé la concentration de ces centres ioniques qui agissent comme agents réticulants effectifs dans le polymère de coordination. Une comparaison des valeurs expérimentales et évaluées de la densité de réticulation effective indique la présence d'une dispersion pratiquement atomique du Mg^{2+} dans les polyesters contenant des ions métalliques.

Mots clés : chromatographie en phase gazeuse inverse, intégrales d'agrégats, partition de solvants dans les polymères, polyesters contenant des ions métalliques, paramètre d'interaction de Flory–Huggins.

[Traduit par la rédaction]

Introduction

Novel, high-value-added engineering polymers with targeted properties can either be synthesized from different monomers in various polymerization reactions, or be prepared by chemical or physcial modification of existing polymers. Ionomeric polymers are a good example of chemical modification. A commercially important class of ionomers are ethylene copolymers containing acrylic or methacrylic acid comonomer neutralized by a metal salt (acetate or oxide of Zn, Na, Mg, etc.) (1, 2). The ionic groups act as thermally reversible cross-links. In these polymers, microphase separation, which results in the formation of clusters of the nonpolar hydrocarbon parts of the polymer and the ionic metal carboxylates, can occur (3). The onset of cluster formation may depend on ion concentration; however, this idea is not universally accepted (4). The restricted mobility model of Eisenberg et al. (5) is useful to explain dynamic mechanical and thermal properties of ionomers containing ionic multiplets.

To understand and control structure–property relations of ion-containing coordination polymers, the spatial distribution of the various constituents must be known. One method that could be used to study short-range order in ion-containing coordination polymers is offered by the use of inverse gas chromatography (IGC) (6, 7). The use of IGC for the study of polymers was pioneered, for the most part, by Guillet and coworkers (6–8). The adjective "inverse" indicates that the point of interest is the stationary phase in the chromatographic column that includes the "unknown" sample.

In an IGC experiment a chromatographic column is packed with the polymer sample, which is either in the form of small pieces (with the longest dimension being less than ca. 50 μm) of the polymer sample mixed with chromatographic support or as a thin film coated onto the support. A molecular probe, e.g., solvent vapor, carried by an inert gas, is injected into the column and the retention time of the probe is measured. The retention of the probe in the column is a result of gas–bulk interactions between the molecular probe and the polymer. These interactions include predominantly either absorption or adsorption or both, depending on the experimental conditions. In the limit of decreasing probe concentration, infinite dilution of the probe in the polymer can be approached. Infinite dilution IGC has been used to study a wide range of structural and thermodynamic properties of polymers and polymer–solvent systems. These include determination of degree of crystallinity (9), cross-link density of insoluble networks (10), glass transition and melting temperature (11), thermal transition temperatures of insoluble liquid-crystalline polymers (12), activity coefficients and enthalpies of solution (6), solvent diffusion coefficients (6), surface area measurements (13), etc. The particular advantage of IGC is that it can be used to obtain molecular characteristics of nonsoluble polymers. A sorption equilibrium can also be established in an IGC experiment at a given volume fraction of the probe in the polymer. In this case, the vapor pressure of the probe in the carrier gas is controlled by a saturator condenser at the "inlet" side of the column. The column is purged by a mixture of the carrier gas and the vapor of the probe, which has a vapor pressure adjusted to the value required. This process results in a sorption equilibrium with a constant probe concentration in the polymeric stationary phase. This "plateau" concentration of the probe in the polymer can be perturbed by injecting a small amount of the same solvent probe (elution-on-a-plataeu). This experiment gives information about structure and thermodynamics of the polymer studied at finite (low) concentrations of the probe. The physical basis for "finite concentration" IGC (FCIGC) was developed by Conder and Purnell (14) and was soon adapted by Brockmeier et al. to study polymers (15). In this work we will be concerned with absorption of the molecular probe. In this case the retention volume is independent of the amount of probe injected.

In preliminary studies, we used FCIGC to study the partition of solvent molecules and clustering of polymer segments and solvent molecules in the polymer matrix in various amorphous polymers (16, 17). To quantitatively characterize spatial short-range order we developed an approach to use FCIGC data to obtain cluster integrals and mean cluster size. This work reports results regarding clustering of solvents, network density, and thermodynamic interactions in metal-ion-containing coordination polyesters and their neutral counterparts.

Aliphatic polyesters containing carboxylic chain ends can be modified by introducing oxides of bivalent metals (e.g., MgO, ZnO) that form complexes with functional ~COOH end groups (18, 19). Such metal-ion-containing coordination polyesters represent a special case of ion-containing polymers that has found numerous applications. Physical properties of coordination polyesters, such as glass transition temperature (T_g) (20, 21), melt viscosity (18*b*), and crystalline morphology (18*c*), can be altered in a controlled fashion. For example, the T_g of the metal-ion-containing polyester poly(diethylene glycol-*co*-succinic acid) (PDEG–SA) rises with increasing amount of the metal ions and tends to a constant value that corresponds to the T_g of the polymer with infinitely high molar mass. Further, the heat capacity change measured at T_g decreases and the melt viscosity increases with increasing complex concentration. These results were interpreted by assuming that a dynamic ionic-polar network had formed with the complexes and that, as a result, the chain mobility became restricted and the specific free volume decreased. It was postulated that, depending on the

Can. J. Chem. Downloaded from www.nrcresearchpress.com by 46.23.64.124 on 09/08/12
For personal use only.

stoichiometry, the following dominating complex species can form (18, 21):

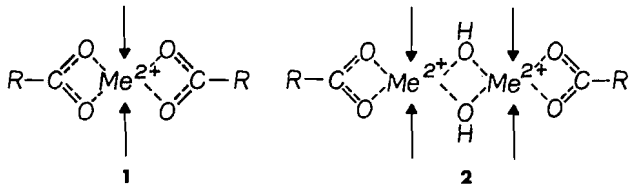

1 2

The arrows in **1** and **2** correspond to empty coordination sites, and can act as "polar cross-linking" sites for different ligands on the neighboring polyester chains (such as donor oxygen atoms of alcoholic OH, COOH, and ester groups) to coordinate the metal ions. Structure **1** is predominant at 0.5 mol MeO/COOH, while **2** dominates at around 1.0 mol MeO/COOH.

In this work our attention focused on the different thermodynamic interactions between polymer–solvent probe and polymer–polymer molecules in a pure polyester of PDEG–SA and its coordination complex formed in reactions with MgO. Also discussed are the Hildebrand solubility parameter for the pure and metal-ion-containing polyesters, preferential solvation and spatial distribution of toluene and tetrahydrofuran (THF) in the polymer, and the average degree of ionic cross-link density in the coordination polyesters.

Experimental

The synthesis and characterization of PDEG–SA and the preparation of the complex with MgO is described in ref. 21. The number-average molar mass of the polymer used in this study was 1060 g/mol, and the polymer contained statistically equal amounts of COOH and OH chain-terminal groups. DEG–SA with Mg^{2+} was obtained by mixing the polymer with MgO at a molar ratio of 0.8 MgO/COOH. The solvent probes used in IGC experiments were analytical grade purchased from Aldrich. All solvents were dried with molecular sieves.

The IGC apparatus was set up exactly as described by Price and Guillet (7). The chromatographic support was Chromosorb G with 60–80 mesh size, dimethyldichlorosilane-treated, acid-washed product from Chromatographic Specialties. Other details of the instrument and the experimental procedures are described in ref. 10.

Infinite dilution IGC

The values of the effective Flory–Huggins χ parameters for solvent probe–polymer interactions were determined from IGC experiments using eq. [45] from ref. 6*a* for 10 different solvent probes at 80°C. Then the expression on the left of eq. [1] was plotted as a function of the known solubility parameter δ_1 of the solvent probes used (22) (the so-called Guillet plot). This yielded a linear relationship with a slope of $2\delta_2/RT$, where δ_2 is the solubility parameter of the polymer sample, V_1 is the molar volume (which we use to approximate the partial molar volume) of the probe, and χ_s is the entropy contribution to χ:

$$[1] \qquad \frac{\delta_1^2}{RT} - \frac{\chi}{V_1} = \frac{2\delta_2}{RT}\delta_1 - \left(\frac{\delta_2^2}{RT} + \frac{\chi_s}{V_1}\right)$$

Cluster integrals from finite concentration IGC

In this section we briefly discuss the definition and physical interpretation of cluster integrals and their determination from FCIGC. A detailed description of this approach is the subject of another paper.[2]

The spatial distribution of solvent molecules in a polymer matrix or the distribution of polymer segments can be described by fluctuations in the corresponding values of the particle number densities. Local deviations from the mean particle number density values can be expressed by G_{ij} Kirkwood–Buff–Zimm (KBZ) integrals (23, 24). In the polymer–solvent system the particle number density of the species "j" ($j = 1$ for solvent, $j = 2$ for polymer segment) is defined by $\rho_j = N_j/V$ with N_j particles in the subsystem with a volume V. The value of the product $\rho_j G_{ij}$ describes the excess (or deficiency) in the average number of j molecules, surrounding a typical molecule of the sort "i" relative to the overall number density of j for the entire system. "Typical" in this context refers to average for i taken over the entire system. The tendency of particles of type j to gather around i-type particles (or particle affinity as it is often referred to), can be described by the value of G_{ij}. To normalize for molecular size effects, it is convenient to introduce the ratio $G_{ij}/\bar{V}_j$ where $\bar{V}_j$ is the partial molar volume of particles j (25, 26). The value of $G_{ij}/\bar{V}_j$ can also be used to characterize preferred spatial gathering of solvent or polymer segments around the specified "partner." At a given volume fraction of the species i, an increase of the value of $G_{ii}/\bar{V}_i$ corresponds to a greater tendency of the i species to form self-clusters. Preferential solvation of i around j can be given by $(G_{ij} - G_{jj})/\bar{V}_j$. A positive value of this expression means favored preferential solvation of j around i (24).

Different experimental techniques, including scattering experiments and thermodynamic measurements, allow us to determine cluster integrals. An excellent example for the thermodynamic approach is given by Ben-Naim (27) who used partial molar volumes, isothermal compressibilities, and partial vapor pressures to obtain $G_{ij}/\bar{V}_j$ values in the water–ethanol system. Scattering experiments were employed by Benoit et al., for example, to study concentration fluctuations in polymer solutions and polymer blends (28).

We used finite concentration IGC to obtain cluster integrals in polymer–solvent systems. Preliminary work has been reported (16, 17), while details of the approach will be described elsewhere.[2]

To obtain the values of the KBZ cluster integrals we first determined the value of the effective Flory–Huggins interaction parameter and its dependence on the volume fraction of the solvent v_1:

$$[2] \qquad \chi = \chi^{\infty} + \beta v_1$$

In eq. [2] we assume a linear dependence of χ on v_1.

In finite concentration IGC experiments, the concentration dependence of the χ parameter is determined by utilizing the elution-on-a-plateau technique. The net retention volume at different concentrations of the solvent probe must be mea-

[2] Z. Tan and G.J. Vancso. Manuscript in preparation.

Can. J. Chem. Downloaded from www.nrcresearchpress.com by 46.23.64.124 on 09/08/12
For personal use only.

Fig. 1. Plot of $jV_N(c)/[w_p\{1-\psi(c)\}]$ vs. concentration of solvent probe in the mobile phase, c, for the pure polyester PDEG–SA and its metal-ion-containing derivative (see eq. [3] in the text). The data at c = 0 were obtained by infinite dilution IGC.

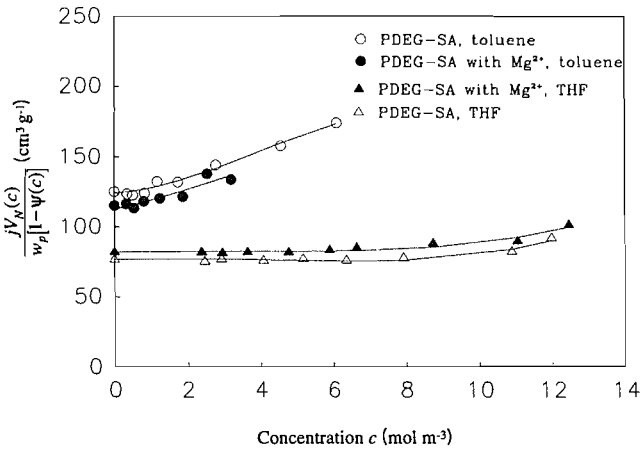

sured to obtain the volume fraction of the solvent v_1 in the polymer–solvent system.

The concentration of the solvent probe q (number of moles of solvent in 1 g of polymer) in the polymer can be expressed by using the Conder–Purnell treatment (9) with the following expression:

$$[3] \qquad q(c) = (1/w_p)\int_0^c jV_N(c')/[1-\psi(c')]dc'$$

where w_p is the mass of the polymer in the column, c is the concentration of the probe in the mobile phase, j is a correcting factor that accounts for the nonideality and compressibility of the gas phase (there is a pressure gradient along the column), and ψ is the corrected mole fraction of the solvent in the mobile phase (10*b*). Figure 1 shows the reduced retention volume (the function to be integrated in eq. [3]) measured for the polyester samples with and without Mg^{2+} as a function of the concentration of the solvent probes (toluene and THF). The weight fraction of the probe can be obtained from the q value determined from eq. [3]:

$$[4] \qquad w_1 = qM_1/(1+qM_1)$$

where M_1 is the molar mass of the solvent probe. The volume fraction of the probe can be obtained with the density values of the solvent and polymer if one assumes volume additivity during mixing:

$$[5] \qquad v_1 = \frac{w_1/\rho_s}{w_1/\rho_s + (1-w_1)/\rho_p}$$

In eq. [5] ρ_s and ρ_p are the mass density of the solvent and polymer, respectively. In other words, by using eq. [5] we assume that the values of the partial molar volumes in the polymer–solvent system are equal to the corresponding values of the molar volumes in the pure states.

For binary gaseous mixtures (e.g., for the mixture of the vapor of the solvent probe and the carrier gas) the fugacity of the components can be expressed by a virial series. We calculated the thermodynamic activity of the solvent a_1 from the fugacity of the probe f_1, which is controlled by the experiment. The concentration dependence of the χ parameter was then obtained from eq. [6]:

$$[6] \qquad \ln a_1 = \ln(1-v_2) + [1-(1/r)]v_2 + \chi v_2^2$$

where r is a parameter related to the ratio of the partial molar volumes of the polymer $\bar{V}_2$ vs. the solvent $\bar{V}_1$, $r = \bar{V}_2/\bar{V}_1$. For binary systems, the volume fraction of the polymer v_2 is related to the volume fraction of the solvent via $v_2 = 1 - v_1$. The cluster integral can then be obtained by the following equations using the abbreviation $S(0)$ defined as

$$[7] \qquad S(0) = [(1/v_1) + (1/rv_2) - (2\chi^{\infty} + 2\beta - 3v_2\beta)]^{-1}$$

$$[8] \qquad G_{11}/\bar{V}_1 = (1/v_1)[(S(0)/v_1) - 1]$$

$$[9] \qquad \frac{G_{21}-G_{11}}{\bar{V}_1} = \frac{1}{v_1}\left[1 - S(0)\left(\frac{1}{v_1}+\frac{1}{v_2}\right)\right]$$

In eq. [7] $S(0)$ is the scattering structure factor of the system at the limit of zero scattering angle and is related to the concentration–concentration fluctuation (25, 26).

Determination of cross-link density by finite concentration IGC

For cross-linked systems the thermodynamic activity a_1 can be written as

$$[10] \qquad \ln a_1 = \ln(1-v_2) + [1-(1/r)]v_2 + \chi v_2^2 + \rho_p \bar{V}_1 \gamma_e [v_2^{1/3} - (2v_2/\Lambda)]$$

In eq. [10] γ_e is the effective cross-link density and Λ is the functionality of the network (10). The effective cross-link density γ_e is defined as the number of moles of elastically effective cross-linked chains per gram of polymer sample (29).

A comparison of eqs. [6] and [10] shows that the difference between linear polymers and cross-linked systems is described by the fourth term on the right-hand side of eq. [10]. This term, introduced by Flory and Rehner (30), takes into account the change in the free energy due to elastic contributions of the deformed network swollen by the solvent probe. With the χ parameter obtained from FCIGC experiments, we estimated the effective cross-link density of the polar-ionic network of the metal-ion-containing coordination polyesters. Toluene was used as solvent probe in these experiments.

Results and discussion

To study the possible change in the cohesive energy density as a result of complex formation of Mg^{2+} ions with the polymer, infinite dilution IGC experiments were performed.

The Guillet plot of infinite dilution IGC data as described earlier was used to obtain the solubility parameter of the polyester PDEG–SA with and without the carboxylate complexes. The plots of $[(\delta_1^2/RT) - (\chi/V_1)]$ vs. δ_1 for 10 different solvents obtained at 80°C are shown in Fig. 2. The solvents used (listed in increasing order of their Hildebrand solubility parameter δ_1) were *n*-hexane, *n*-octane, cyclohexane, ethyl acetate, toluene, benzene, acetone, propanol, ethanol, and methanol. The value of δ_2 was 10.3 $(\text{cal cm}^{-3})^{1/2}$ within

Can. J. Chem. Downloaded from www.nrcresearchpress.com by 46.23.64.124 on 09/08/12
For personal use only.

Can. J. Chem. Downloaded from www.nrcresearchpress.com by 46.23.64.124 on 09/08/12
For personal use only.

Fig. 2. Guillet plot of the pure polyester PDEG–SA and its Mg^{2+}-containing derivative as a function of the solubility parameters of the solvents used in infinite dilution IGC.

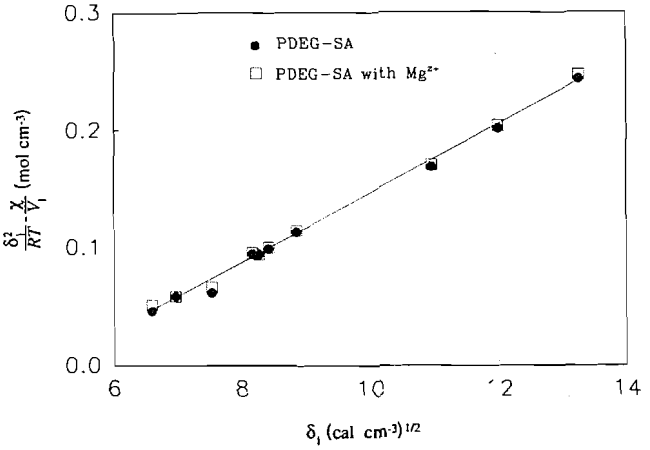

Fig. 3. The effective Flory–Huggins interaction parameter χ vs. the volume fraction of the solvent probes.

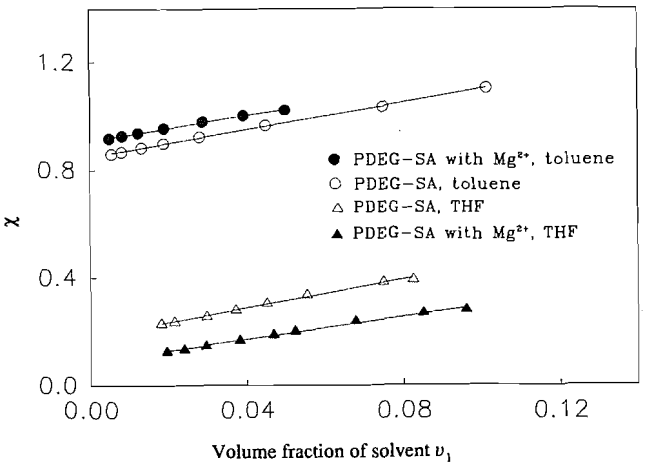

the experimental error of ca. ±0.5 (cal $cm^{-3})^{1/2}$ for both the pure PDEG–SA and the Mg^{2+}-ion-containing coordination polyester. Thus, for the ion concentration utilized in this work, no difference was obtained by infinite dilution IGC for the probe-averaged value of δ_2 between the pure and the Mg^{2+}-containing polymers. It is interesting to mention that pressure–volume–temperature (PVT) phase diagrams can also be used to obtain solubility parameter data (31). PVT experiments were performed on the polymers discussed in this study. Numerical fits of PVT data (32) yielded δ_2 = 15.0 (cal $cm^{-3})^{1/2}$ for the pure DEG–SA and δ_2 = 15.5 (cal $cm^{-3})^{1/2}$ for the metal-ion-containing polymer. This small increase in the solubility parameter, obtained in PVT experiments, only slightly exceeded the estimated error of PVT data, which was ca. ±0.2 (cal $cm^{-3})^{1/2}$. The deviation between IGC and PVT results, however, is far beyond the experimental error. One possible explanation for the unrealistically high δ_2 values obtained in PVT experiments is that the polyester decomposed during the pressurization (pressures up to 200 MPa and temperatures up to 100°C) in the PVT sample cell, which was filled with Hg. This might result in an increase of the absolute value of δ_2 (e.g., δ_2 for ethylene glycol is 14.6 (cal $cm^{-3})^{1/2}$ (33)).

Figure 3 shows the concentration dependence of the χ parameter for the pure polyester DEG–SA with toluene and with THF as well as for the metal-ion-containing polymer with the same two solvents. The corresponding IGC experiments were performed at 75°C. The value of χ is lower for DEG–SA with the polar THF than for the polymer with toluene. This is what one would expect as it is well known that THF is the better solvent for DEG–SA.

For the more polar solvent THF the value of χ becomes smaller if ions are introduced into the polymer. This trend is opposite for the polyester with the significantly less polar toluene, i.e., in this case the χ parameter increases when complexes are formed. Generally, an increase in the χ value corresponds to a poorer solvent–polymer affinity. For the ion-containing polyesters the ligands coordinated to the central metal ion of the complex include ~OH and ester carbonyl groups. These can be replaced by a ligand group with a higher donor strength, such as THF, which results in a strong interaction between the solvent probe and the sample and thus contributes to a decrease in the χ value of THF with the metal-ion-containing polymer.

The strength of coordinate bonds ($-\Delta H$) can be expressed by the "*E* and *C* equation," as follows:

$$[11] \qquad -\Delta H = E_A E_B + C_A C_B$$

where ΔH is the enthalpy of adduct formation, the subscript A refers to acid and B to base, *E* is an empirical parameter related to the tendency of the given species to form electrostatic bonding, and *C* describes the tendency to undergo covalent bonding (34). A quantitative comparison using Table 1 of ref. (34) shows that the expected $-\Delta H$ value of THF is higher than that of representative esters ($CH_3COOC_2H_5$), ketones ($(CH_3)_2CO$), or ethers ($(C_2H_5)_2O$). Thus, the polar solvent THF in the metal-ion-containing polyester will be bound to the central metal ion, while the apolar solvent will participate in the solvation of the apolar parts of the macromolecules and will be "repelled" from the ion-containing regions.

Let us assume that at high temperatures (e.g., 75°C) the association of the ligands having low donor strengths with the metal ions becomes weak. The role of Mg^{2+} would then be to connect only neighboring chains and thus it would increase the effective molar mass (i.e., there are not multifunctional cross-links present). If this metal-ion-containing polymer is cooled to, for example, 40°C, a network can form at the lower temperature with a functionality Λ in eq. [10] greater than 2 (e.g., Λ = 4). By using eq. [10] and calculating the activity difference, $\Delta \ln a_1$, for the two temperatures, the increase of the γ_e value upon cooling can be obtained from the following formula:

$$[12] \qquad \Delta \ln a_1 = \Delta \ln a_{1,L} + \rho_p(T_2)\bar{V}_1(T_2)\gamma_e[v_2^{1/3} - (2v_2/\Lambda)]$$

where $\Delta \ln a_{1,L}$ refers to the difference in the thermodynamic activity for the linear polymer going from T_2 = 75°C to T_2 = 40°C. This approximation yielded γ_e = 9.0 (±1.0) × 10^{-4} mol g^{-1} for the effective cross-link density of the ion-containing polymer with Λ = 4. By assuming that each metal ion acts as a junction point, the calculated γ_e value is 15.1 ×

Fig. 4. The value of the reduced self-cluster integral $G_{11}/\bar{V}_1$ of the solvents toluene and THF (see eq. [8] in the text) as a function of the volume fraction of the solvent probes.

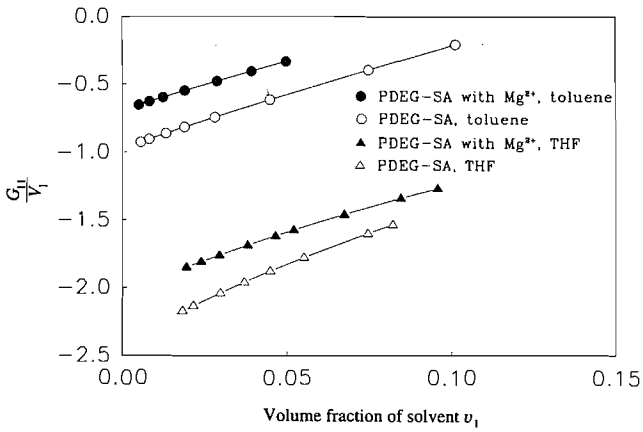

Fig. 5. The value of $(G_{21} - G_{11})/\bar{V}_1$ (preferential solvation, see eq. [9] in the text) as a function of the volume fraction of the solvent probes.

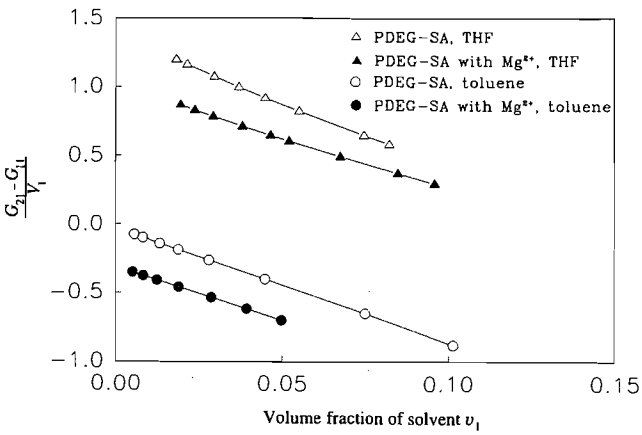

10^{-4} mol g^{-1} for $\Lambda = 4$. A comparison of the experimental and calculated γ_e values gives a strong indication for a nearly atomic dispersion of Mg^{2+} in the metal-ion-containing polymers, that is, it means that the existence of Mg^{2+} clusters with a large number of ions is unlikely in the polyester studied.

The values of the reduced cluster integrals $G_{11}/\bar{V}_1$ and $(G_{21} - G_{11})/\bar{V}_1$ were calculated as a function of the volume fraction of the solvent, as described earlier in the paper. Data obtained for solvent clusters $G_{11}/\bar{V}_1$ are shown in Fig. 4 while results for the combination of the cluster integrals $(G_{21} - G_{11})/\bar{V}_1$ are depicted in Fig. 5.

The value of the solvent self-cluster integral for both the pure polyester and the metal-ion-containing polyester $G_{11}/\bar{V}_1$ is greater for toluene than for THF. This corresponds to a higher self-affinity of toluene molecules to form self-clusters than is the case with THF, which is more homogeneously distributed in the polymer. The preferential solvation of the polymer by the solvent is characterized by $(G_{21} - G_{11})/\bar{V}_1$. As can be seen in Fig. 5, the value of this combination of cluster integrals is higher, and positive, for THF compared with the case for toluene. The positive $(G_{21} - G_{11})/\bar{V}_1$ value for the THF–polyester systems corresponds to stronger specific interaction between the solvent and the polymer than that between the solvent–solvent molecules. The negative $(G_{21} - G_{11})/\bar{V}_1$ values for the toluene-containing polyester systems along with the high $G_{11}/\bar{V}_1$ values correspond to preferential gathering of solvent molecules in the free volume available in the polymer. In the polymer samples probed with toluene, the negative $(G_{21} - G_{11})/\bar{V}_1$ values also indicate that a segregation of the macromolecules is present in the toluene–polyester systems. The value of $G_{11}/\bar{V}_1$ is higher for the ion-containing polyesters than for the neutral polymer for both solvent probes. This corresponds to an increased self-affinity of the solvent molecules to gather when metal ions are introduced. For the apolar toluene this gathering is likely to occur in the free volume (negative $(G_{21} - G_{11})/\bar{V}_1$ values, see Fig. 5). The gathering of THF is likely to take place close to the metal ions. (The corresponding $(G_{21} - G_{11})/\bar{V}_1$ values are positive.)

It is interesting to point out the relative change of the values of $G_{11}/\bar{V}_1$ and the Flory–Huggins χ parameter for the pure polyesters and the polyesters with metal ions. The results shown in Fig. 3 clearly indicate that the value of the χ parameter increases for the polyester–toluene systems when Mg^{2+}-containing complexes are present, while it decreases for the polyester with THF when the metal ions are introduced. On the other hand, $G_{11}/\bar{V}_1$ values show an increase for the metal-ion-containing polymer compared with the pure polyester for both toluene and THF. This trend might seem surprising at first glance. In fact, a detailed analysis of the $G_{11}/\bar{V}_1$ values shows that the differences in the slopes of the χ parameter values as a function of the solvent probe concentration are responsible for this effect. An increase in the χ parameter value at zero solvent concentration (χ^∞ in eq. [2]) with unchanged slope of the χ vs. concentration curve (the value of β in eq. [2]) makes the $G_{11}/\bar{V}_1$ values larger. An increase in the slope β, however, has the opposite effect, that is, it corresponds to a decrease in the value of $G_{11}/\bar{V}_1$ at an unchanged χ^∞ value. As can be seen in Fig. 3, the value of the slope of the χ vs. concentration plots for the pure polyester with THF is significantly higher than the slopes of the three other straight lines. This larger slope value is then the reason for the increase in the $G_{11}/\bar{V}_1$ values of the Mg^{2+}-ion-containing polyester system with THF as solvent probe in spite of the decrease of the corresponding χ^∞ values.

It can be shown (35) that the mean cluster size (MCS) of a solvent cluster is given by:

$$[13] \qquad \text{MCS} = (v_1 G_{11}/\bar{V}_1) + 1$$

The value of MCS (which describes the average number of molecules in a cluster) as a function of solvent probe concentration can be calculated from the concentration dependence of the χ parameter (eq. [2]) by a linear fit to the χ values determined from IGC (see Fig. 3). The χ^∞ and β values in eq. [2] can be used to calculate $G_{11}/\bar{V}_1$, which allows a direct determination of the MCS with the corresponding v_1 values.

Corresponding MCS curves for the polymer systems studied in this work are shown in Fig. 6. The value of the expected mean cluster size for a predominantly entropy-driven solution process with preferential solvent would result in MCS $\cong$ 1, showing that no significant gathering of solvent molecules takes place. Such behavior was observed for

Can. J. Chem. Downloaded from www.nrcresearchpress.com by 46.23.64.124 on 09/08/12
For personal use only.

Can. J. Chem. Downloaded from www.nrcresearchpress.com by 46.23.64.124 on 09/08/12
For personal use only.

Fig. 6. The mean cluster size, MCS (see eq. [13] in the text), of the solvents toluene and THF, calculated from the concentration dependence of the effective Flory–Huggins interaction parameter χ as a function of the volume fraction of the solvent probes.

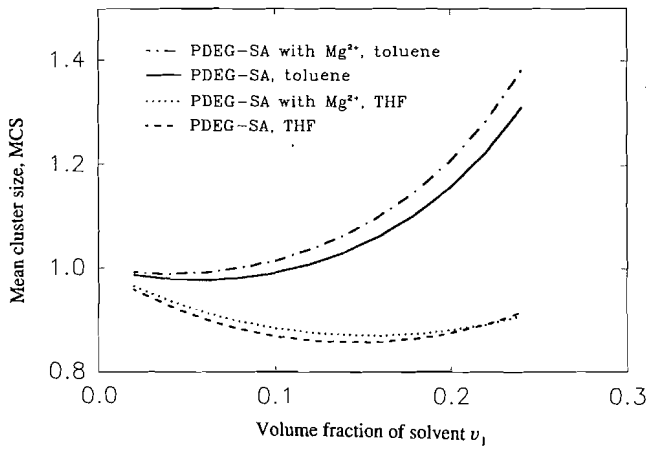

the THF–polyester systems, while the toluene–polyester mixtures showed a significant increase of MCS of solvents with increasing toluene concentration (see Fig. 6). This is a result of the congregation of the absorbed solvent molecules in the free volume of the polymer matrix. For such systems, with increasing values of the Flory–Huggins χ parameter, the mean solvent cluster size progressively increases and can tend to infinity if phase separation occurs.

In conclusion, inverse gas chromatography, utilizing the technique of elution-on-a-plateau, was used to study solvent clustering and partition in polyesters of poly(diethylene glycol-*co*-succinic acid) and their complexes with metal ions. IGC allowed us to obtain specific and detailed information concerning spatial distribution of solvents and the thermodynamics of the polyesters and their coordination polymers with Mg^{2+} using a good and a less good solvent.

Acknowledgements

The authors would like to thank Professor J.E. Guillet for directing their interest to inverse gas chromatography studies of polymers. Grateful thanks are due to Ms. Susan Arbuckle for her help with the write-up of this paper. The work was financially supported by the Natural Sciences and Engineering Research Council of Canada, and by the Ontario Centre for Materials Research. G.J.V. would like to take this opportunity to express his sincere appreciation to Professor James Guillet for all of the enlightening discussions, stimulating joint work in many areas of polymer science, collegiality, and last but not least friendship, which made working as a member of the faculty of the Chemistry Department in Toronto a great pleasure. I will miss you, Jim, in my new job! Thank you.

References

1. A. Eisenberg and M. King. Ion-containing polymers. Academic Press, New York. 1977.
2. L. Holliday. Ionic polymers. Applied Science, London. 1975.
3. S. Bonotto and E.F. Bonner. Macromolecules, **1**, 510 (1968).
4. J. Greener, J.R. Gillmor, and R.C. Daly. Macromolecules, **26**, 6416 (1993).
5. A. Eisenberg, B. Hird, and R.B. Moore. Macromolecules, **23**, 4098 (1990).
6. (*a*) J.E.G. Lipson and J.E. Guillet. *In* Developments in polymer characterization. Vol. 3. *Edited by* J.V. Dawkins. Applied Science, Barking. 1982; (*b*) J.-M. Braun and J.E. Guillet. Adv. Polym. Sci. **21**, 107 (1976).
7. G.J. Price and J.E. Guillet. J. Macromol. Sci. Pure Appl. Chem. **A23**, 1487 (1986).
8. O. Smidsrod and J.E. Guillet. Macromolecules, **2**, 272 (1969).
9. (*a*) J.-M. Braun and J.E. Guillet. J. Polym. Sci. Polym. Chem. Ed. **13**, 1119 (1975); (*b*) A.N. Stein and J.E. Guillet. Macromolecules, **3**, 102 (1970); (*c*) D.G. Gray and J.E. Guillet. Macromolecules, **4**, 129 (1971).
10. (*a*) G.J. Price, K.S. Siow, and J.E. Guillet. Macromolecules, **22**, 3116 (1989); (*b*) Z. Tan, R. Jaeger, and G.J. Vancso. Polymer, **35**, 3231 (1994).
11. V.R. Alishoev, V.G. Berezkin, and Y.V. Melnikova. Russ. J. Phys. Chem. **39**, 105 (1965).
12. M. Romansky and J.E. Guillet. Polymer, **35**, 584 (1994).
13. D.G. Gray and J.E. Guillet. Macromolecules, **5**, 316 (1972).
14. (*a*) J.R. Conder and J.H. Purnell. Trans. Faraday Soc. **64**, 1505 (1968); (*b*) Trans. Faraday Soc. **64**, 3100 (1968); (*c*) Trans. Faraday Soc. **65**, 824 (1969); (*d*) Trans. Faraday Soc. **65**, 829 (1969); (*e*) J.R. Conder and C.L. Yong. Physico-chemical measurement by gas chromatography. Wiley, New York. 1979.
15. (*a*) N.F. Brockmeier, R.W. McCoy, and J.A. Meyer. Macromolecules, **5**, 130 (1972); (*b*) Macromolecules, **5**, 464 (1972); (*c*) Macromolecules, **6**, 176 (1973).
16. Z. Tan and G.J. Vancso. Polym. Mater. Sci. Eng. **70**, 411 (1994).
17. G.J. Vancso, Z. Tan, and I. Vancso-Szmercsanyi. Polym. Mater. Sci. Eng. **70**, 409 (1994).
18. (*a*) I. Vancso-Szmercsanyi. Kunststoffe, **60**, 1066 (1970); (*b*) I. Vancso-Szmercsanyi and Z. Szekely-Pecsi. J. Polym. Sci. Polym. Chem. Ed. **21**, 1901 (1983); (*c*) Z. Szekely-Pecsi, I. Vancso-Szmercsanyi, F. Czer, J. Varga, and K. Belinda. J. Polym. Sci. Polym. Phys. Ed. **19**, 703 (1981).
19. I. Vancso-Szmercsanyi and P. Hischberg. Acta Chim. Acad. Sci. Hung. **83**, 79 (1974).
20. I. Vancso-Szmercsanyi, B. White, and G.J. Vancso. J. Appl. Polym. Sci. Appl. Polym. Symp. **51**, 241 (1992).
21. B. White, G. Liu, I. Vancso-Szmercsanyi, and G.J. Vancso. Polym. Bull. **28**, 95 (1992).
22. G. DiPaola-Baranyi and J.E. Guillet. Macromolecules, **11**, 228 (1978).
23. (*a*) J.G. Kirkwood and F.P. Buff. J. Chem. Phys. **19**, 774 (1951); (*b*) B.H. Zimm. J. Chem. Phys. **21**, 934 (1953).
24. E. Matteoli and G.A. Mansoori (*Editors*). Advances in thermodynamics. Vol. 2. Fluctuation theory of mixtures. Taylor and Francis, New York. 1990.
25. A. Horta. Macromolecules, **25**, 5651 (1992).
26. A. Horta. Macromolecules, **25**, 5655 (1992).
27. A. Ben-Naim. J. Chem. Phys. **67**, 4884 (1977).
28. H. Benoit, M. Benmouna, and W. Wu. Macromolecules, **23**, 1511 (1990).
29. J.E. Mark and B. Erman. Rubberlike elasticity: A molecular primer. Wiley, New York. 1988.
30. P.J. Flory and J. Rehner. J. Chem. Phys. **11**, 521 (1943).
31. R. Simha and T. Somcynsky. Macromolecules, **2**, 342 (1969).
32. E. Luchelli, I. Tomka, G. Vancso, and P. Yeh. Polym. Bull. **20**, 569 (1988).
33. J. Brandrup and E.H. Immergut (*Editors*). Polymer handbook. Wiley, New York. 1989. Chap. 7.
34. R.S. Drago. Coord. Chem. Rev. **33**, 251 (1980).
35. (*a*) H.W. Starkweather. J. Polym. Sci. Polym. Lett. **1**, 133 (1963); (*b*) *In* Structure–solubility relationships in polymers. *Edited by* F.W. Harris and R.B. Seymour. Academic Press, New York. 1977.

The effect of transformation products of the antioxidant BHT on the initial stages of thermo- and photo-oxidation of LDPE

J. Kovářová, J. Rotschová, O. Brede, and M. Burgers

Can. J. Chem. Downloaded from www.nrcresearchpress.com by 46.23.64.124 on 09/08/12
For personal use only.

Abstract: The effect of individual transformation products of 2,6-di-*tert*-butyl-4–methylphenol (**1**, BHT), namely, 2,6-di-*tert*-butyl-4-hydroxy-2,5-cyclohexadienone (**3**), 2,6-di-*tert*-butyl-1,4-benzoquinone (**4**), and 3,5,3′,5′-tetra-*tert*-butylstilbenequinone (**5**), in the course of thermal- and photo-degradation of LDPE has been examined. Oxidative DSC studies combined with oxygen uptake measurements, IR spectroscopy data, and embrittlement tests proved to be sufficiently sensitive to detect differences in the stability of the above-mentioned samples. A comparative study revealed a pronounced stabilizing effect of **5** in LDPE thermooxidation at moderate temperatures (90–100°C). The stabilizing action of BHT is due in part at least to its coloured transformation product.

Key words: LDPE, thermooxidation, photooxidation, transformation products of phenolic antioxidants.

Résumé : On a étudié l'effet des produits individuels de transformation du 2,6-di-*tert*-butyl-4-méthylphénol (**1**, BHT), soit les 2,6-di-*tert*-butyl-4-hydroxycyclohexa-2,5-diénone (**3**), 2,6-di-*tert*-butyl-1,4-benzoquinone (**4**) et 3,5,3′,5′-tétra-*tert*-butylstilbènequinone (**5**), sur le cours des dégradations thermiques et photochimiques du LDPE. Des études oxydantes de DSC combinés à des mesures d'absorption d'oxygène, à des données de spectroscopie et à des tests de fragilisation se sont avérées suffisamment sensibles pour détecter des différences de stabilité dans les échantillons mentionnés plus haut. Une étude comparative a permis de mettre en évidence un effet stabilisant important du produit **5** sur la thermooxydation du LDPE à des témperatures modérées (90 à 100°C). L'action stabilisante du BHT est due en partie à son produit de transformation coloré.

Mots clés : LDPE, thermooxydation, photooxydation, produits de transformation d'antioxydants phénoliques.

[Traduit par la rédaction]

Introduction

The use of sterically hindered phenols such as 2,6-di-*tert*-butyl-6-methylphenol (BHT, **1**) and octadecyl-3-(3′,5′-di-*tert*-butyl-4′-hydroxyphenyl)propionate (Irganox 1076, **2**) to protect polymers against oxidative degradation is well established. Under atmospheric conditions, they are known to interfere with the chain-propagating step of the polymer oxidation mechanism (postulated originally for hydrocarbons by Bolland and Gee (1, 2)) as they react with the chain-carrying $R^{\bullet}$, $RO^{\bullet}$, and $RO_2^{\bullet}$ radicals; for example,

$$ArOH + RO_2^{\bullet} \rightarrow ArO^{\bullet} + RO_2H$$

Received June 6, 1995.

This paper is dedicated to Professor J.E. (Jim) Guillet in recognition of his contributions to Canadian chemistry.

J. Kovářová[1] **and J. Rotschová.** Institute of Macromolecular Chemistry, Academy of Sciences of the Czech Republic, 162 06 Prague 6, Czech Republic.
O. Brede and M. Burgers. Max-Planck-Society, Time-Resolved Spectroscopy Group at the University of Leipzig, Permoserstr. 15, D-04303 Leipzig, Germany.

[1] Author to whom correspondence may be addressed. Telephone: +42 (2) 360 341-9. Fax: +42(2) 367 981. E-mail: kovarova@imc.cas.cz

The resulting, relatively stable radicals $ArO^{\bullet}$ either mesomerize and dimerize, disproportionate, or scavenge other peroxy radicals to form numerous nonradical transformation products (3, 4).

The antioxidant BHT has been used for many years to stabilize polyolefins and polystyrenes during processing, but because of its high volatility is not suitable for long-term ageing stability. However, BHT and its mechanism of activity have been studied extensively (5, 6) as a model for other phenolic stabilizers. Various BHT transformation products resulting from phenoxyl radical decay have been isolated and identified; these are typically unsaturated systems such as the cyclohexadienone (**3**), the benzoquinone (**4**), and stilbenequinone (**5**) (Scheme 1). The last compound is highly coloured ($\varepsilon = 1.1 \times 10^5\ M^{-1}\ cm^{-1}$ at $\lambda = 452$ nm) due to the large number of conjugated double bonds, and is mostly responsible for the yellowing of polymers stabilized with BHT.

Several antioxidant transformation products are reported to have some stabilizing properties. Henman (7) showed that di-*tert*-butylbenzoquinone (**4**) and tetra-*tert*-butylstilbenequinone (**5**) were more effective melt stabilizers for polypropylene than BHT itself, and both compounds were found to retard the oxidation of tetralin and polypropylene (8, 9). A stabilizing effect of both compounds was also found in the thermooxidation and photooxidation of high-impact polystyrene (10). On the other hand Klemchuk and Horng (11) reported that **4** and **5** retained no stabilizing activity in polypropylene oven-aged at 150°C.

Can. J. Chem. Downloaded from www.nrcresearchpress.com by 46.23.64.124 on 09/08/12
For personal use only.

Scheme 1. Structures of phenolic antioxidants and transformation products.

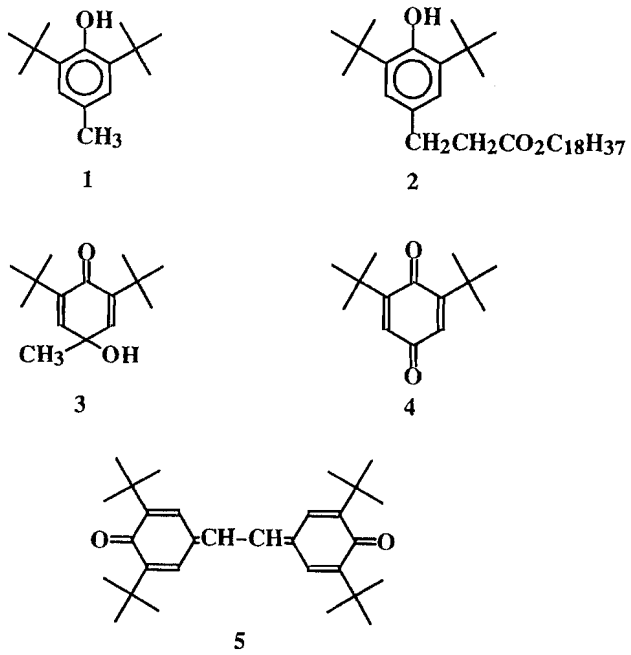

Since relatively little is known about the chemical reactivity and antioxidant mechanism of these compounds, a study was undertaken in which several of the known transformation products of BHT were investigated on their own. To this end, two main approaches were followed: (i) steady-state ageing experiments involving samples of polyethylene doped with the pure transformation products, to determine if stabilization occurs and under what conditions; and (ii) time-resolved experiments using electron pulse radiolysis and laser flash photolysis, to study the elementary reactions of the pure compounds both in nonpolar liquids (as a model for polymers) and in molten polyethylene.

A preliminary report about time-resolved experiments made with the stilbenequinone compound has been given by Brede et al. (12). In the present paper, the results from steady-state ageing experiments are presented.

Results and discussion

Environmental degradation limits the lifetime of articles made from polyolefins. These lifetimes are generally too long to be determined in tests performed under environmental (mild) conditions. As a result, most investigations into the degradation of polyolefins are done under accelerated conditions. Since the degradation mechanism highly depends on the experimental conditions and test methods used, a combination of methods was applied in our degradation study of LDPE containing the additives depicted in Scheme 1.

Thermooxidation

The results of oxygen absorption measurements of doped LDPE samples at a temperature of 180°C are shown in Fig. 1 and Table 1. All samples containing the transformation products **3–5** were comparable to the blank LDPE without additives or rather showed a slight pro-oxidative effect. They retained none of the stabilizing activity of the hindered phenol. Similar results were reported by Klemchuk and Horng (11) for polypropylene oxidation in the presence of stilbene-quinone at 150°C.

Table 1. Oxidation of doped LDPE: the induction periods (IP) from the oxygen absorption measurements in the melt at 180°C; embrittlement times ET_T and ET_P, i.e., ageing up to failure on manual bending of strips at 100°C for the thermooxidation and 40°C for the photooxidation (λ_{max} = 350 nm), respectively. Melting points of virgin LDPE strips (Tm_V) and strips embrittled at 100°C (Tm_E), measured by DSC under N_2 (heating rate 10°C/min)

Additive	IP (min)	ET_T (days)	ET_P (days)	Tm_V (°C)	Tm_E (°C)
-	100	27	160	109.4	113.6
1	180	119	160	109.8	113.3
2	735	>360	160	110.1	112.0
3	80	16	160	110.0	113.1
4	80	33	160	110.3	111.5
5[a]	70	54	160	109.6	111.3
5[b]	70	179	>180	110.3	111.7

[a]Concentration 5×10^{-4} M.
[b]Concentration 5×10^{-3} M.

Even BHT, one of the strongest processing stabilizers, under these experimental conditions (polymer melt at 180°C, pure O_2 atmosphere) represents a relatively weak antioxidant. On the other hand, the oxygen uptake in the presence of Irganox 1076, which is used industrially and was placed in our study as a reference compound, showed a distinct induction period (IP).

In the oxygen uptake method, which is the most direct way to study polymer oxidation, the assumption is implicitly made that the drop of the pressure in a closed system corresponds quantitatively to the consumption of oxygen. The possible formation of gaseous degradation products or volatilization of additives at high temperatures might, however, influence the pressure drop and cause an error in the calculated oxygen uptake value. It is also generally accepted that an ageing test done at temperatures above the melting point of the polymer does not correspond to what is happening in the solid state (13) and has only limited predictive value for the lifetime of an article or for the ranking of stabilizers at service temperatures.

The thermooxidative stability of LDPE films was tested in an air oven at 90°C. The chemical changes accompanying polymer degradation were monitored by means of IR spectroscopy. The course of carbonyl group formation (characterized as the carbonyl index $CI = A_{1720}/A_{720}$) during oven ageing of the doped LDPE films is shown in Fig. 2. In this study, the raw carbonyl index is used as a measure of the extent of degradation and no explicit information is given concerning the composition (i.e., the relative amount of ketones, acids, esters, etc.) contributing to the broad IR absorption band of carbonyls in LDPE-oxidized samples. For detailed information on chemical changes occurring in PE degradation see refs. (14–16). Although such a simple procedure neglects the complex structure of the carbonyl region it nevertheless gives compar-

Fig. 1. Oxygen uptake in the high-temperature oxidation of LDPE doped with compounds **1–5** (OH-CHD = **3**, BQ = **4**, SQ = **5**); sample size 40 mg. For the number codes of the additives see the Experimental.

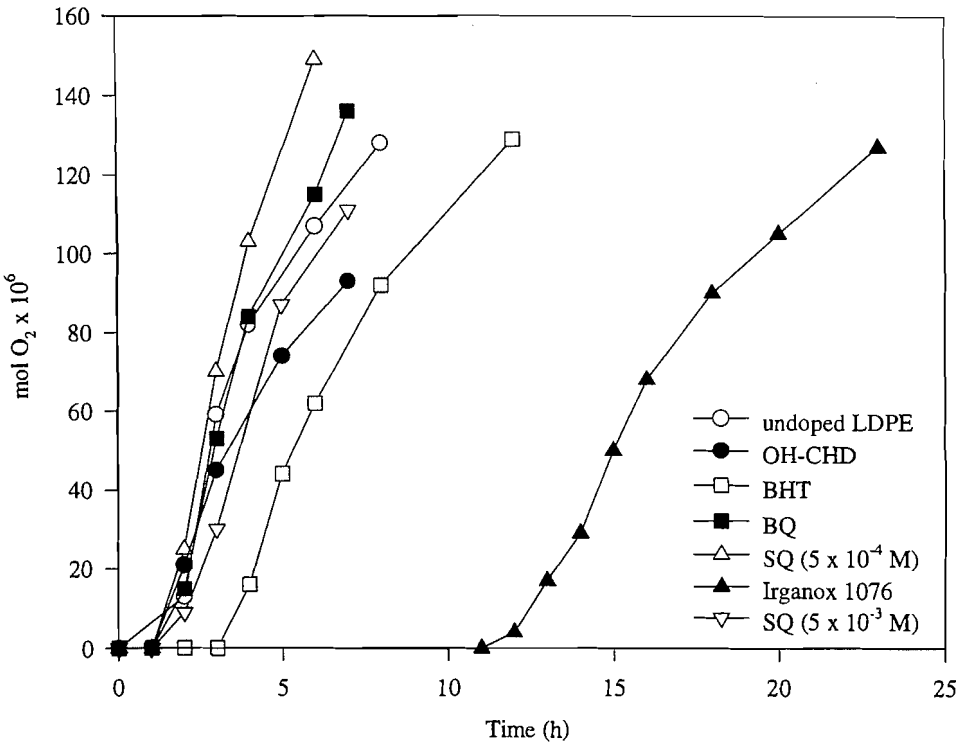

ative information about the effect of individual additives **1–5** on the course of LDPE degradation.

The results in Fig. 2 indicate an almost identical pattern of changes in both the pure LDPE and LDPE doped with BHT (IP = 7 days); the hydroxycyclohexadienone **3** shows in this group of samples a slightly pro-oxidative effect. The low stabilizing activity of BHT is explained by its high volatility and, consequently, its physical loss from the oven-aged polymer at 90°C. The compatibility of additives with LDPE is generally poorer than for other polyolefins (4). The presence of the benzoquinone (**4**) on the other hand retards the carbonyl formation in LDPE for up to 65 days, while the stilbene-quinone (**5**) completely inhibits chemical changes in LDPE. It is evident that the observed concentration-dependent antioxidant activity of **5** compares well with that of the most effective stabilizer, the commercial Irganox 1076. In the case of **5** the H-donor antioxidant mechanism, characteristic for phenols, is hardly applicable. The oxidation chain-carrying ROO• radicals can possibly add to the system of conjugated double bonds in the stilbene-quinone, in analogy with the scheme proposed by Boozer and Hammond (17) for other conjugated systems.

The chain-breaking acceptor mechanism, in which the chain-carrying radical adds to the inhibitor, is often envisaged for the transformation products of phenols that have a structure of conjugated dienones (i.e., quinone methides, stilbene-quinones, and benzoquinones). The radicals involved in this reaction type are alkyl radicals, which are not particularly effective in hydrogen abstraction from the inhibitor. In the presence of a sufficient amount of oxygen, as in our experiments, these reactions are not very important because the alkyl radicals are transformed very rapidly into peroxy radicals. Only under conditions of oxygen starvation, for example in an extruder, their importance increases and they may even become dominant (4).

Photooxidation

The increase in carbonyl index (CI) was also taken as an indication of the extent of photooxidative degradation in LDPE films. Figure 3 shows the results for doped films after exposure to a light source having its peak emission at 350 nm. In practically all the samples here a gradual and equal increase of CI from the beginning of and throughout the exposure is seen. Only in the case of the stilbene-quinone (**5**) at a higher concentration (5×10^{-3} M) a certain protection (even a slight IP) in the early stages of LDPE photooxidation was observed. Presumably, this effect can be attributed to the filter effect of the highly coloured compound **5** and its subsequent chemical conversion to colorless species, since a bleaching of the sample was observed. Similar behaviour has already been reported for the photooxidation of HIPS (10) containing **5**. Generally, highly conjugated discoloring antioxidant transformation products, and the stilbene-quinone in particular, are very sensitive to UV light and undergo reduction in color during exposure to UV radiation (11), but the reactions involved are not yet known.

In contrast to the thermooxidation results (Fig. 2), none of the antioxidants and BHT transformation products **3–5** acts as effective photostabilizer or as photooinitiator.

Can. J. Chem. Downloaded from www.nrcresearchpress.com by 46.23.64.124 on 09/08/12
For personal use only.

Fig. 2. Development of carbonyl absorbance (CI = 1720/720 cm^{-1}) in the thermooxidation of LDPE films at 90°C.

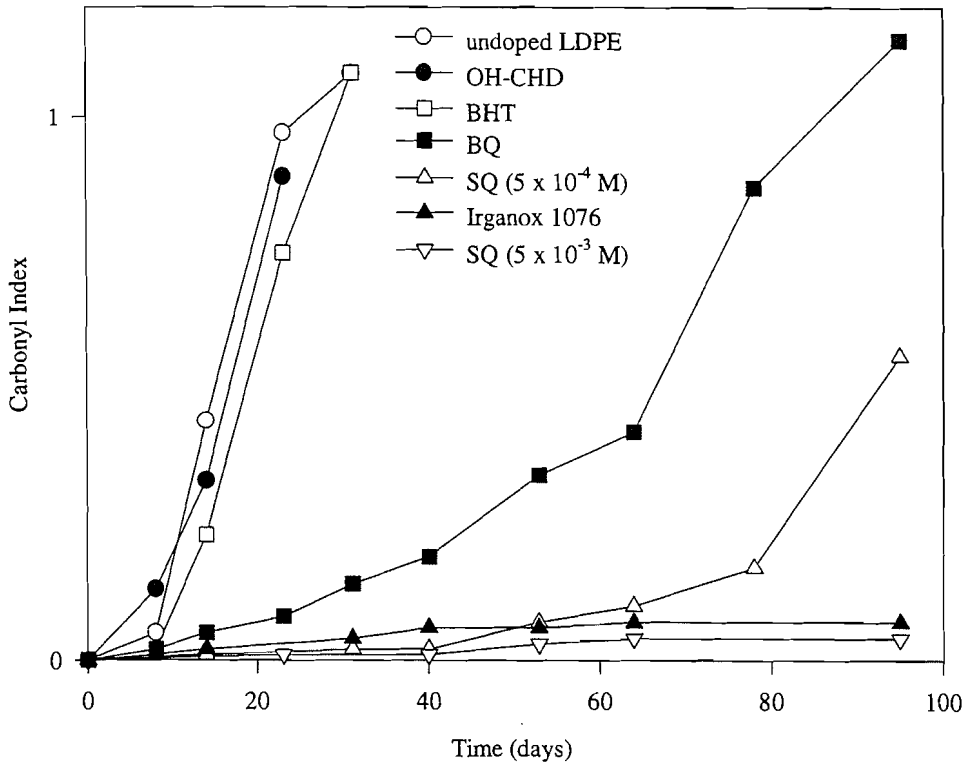

Can. J. Chem. Downloaded from www.nrcresearchpress.com by 46.23.64.124 on 09/08/12
For personal use only.

While IR measurements provide evidence for the nature and extent of chemical changes occurring during photo- or thermooxidation of LDPE films, they do not provide direct evidence concerning the accompanying changes in the mechanical and thermal properties of the polymer.

Embrittlement tests

The effect of additives **1–5** on changes in the mechanical characteristics of oxidized LDPE was examined. Table 1 depicts the results of the completed embrittlement tests: times to embrittlement (on manual bending at a bending angle 90°) for thermooxidized (ET_T) or photooxidized (ET_P) polymer strips were evaluated. The results in both cases correlate well with the results from the IR measurements. The additives used had no effect on photooxidative changes in LDPE as all UV-irradiated samples failed in the same time interval (after 160 days); the only exception, as before, was the sample with stilbene-quinone (5×10^{-3} M) (Table 1).

In contrast to the photooxidation results, embrittlement times (ET_T) for thermooxidized LDPE strips differ significantly due to the nature of the additives present (Table 1); the pronounced stabilizing ability of **5** and **2**, as in the oven-ageing experiments, was confirmed. However, BHT showed a much better performance than before. The influence of sample thickness seems to be operative as a possible explanation for the difference in stabilizing behaviour of BHT. Even at lower temperatures the physical loss of BHT from LDPE film samples is reported to be very high (4). Additional pressing in the case of preparing 0.1 mm thick films for the oven-ageing study (as compared to strips for embrittlement tests) has certainly also contributed to the volatilization of BHT and thus to its apparent very low antioxidative activity in the oven-aged sample.

This statement is also supported by the results from DSC measurements in air (Table 2). When comparing the additive stabilities of the virgin LDPE strips and films, a certain decrease in the onset temperature of oxidation (T_0) is evident for all additives, but for BHT the effect is greatest. Thus for the efficiency evaluation rating of individual additives the results from the embrittlement test give a more realistic picture.

The temperature T_0 at which the oxidation exotherm first deviates from the baseline has frequently been employed to evaluate the stability of various polymers and to quantify the performance of antioxidants (18–21).

Reviewing the results in Table 2, all virgin additive-containing samples exhibit higher T_0 than pure LDPE and thus display a certain stabilizing or inhibiting effect on polymer autoxidation. This effect is, however, rather small for **3** and **4**; BHT and stilbene-quinone show a more pronounced and comparable influence on T_0, while **2** is again by far the most effective additive. The results in Table 3 reveal clearly a temperature dependence of the inhibiting efficiency of **5**.

In most cases the T_0 values for the doped LDPE samples embrittled in the 100°C thermooxidation approach the T_0 value of the undoped polymer. A shift in the opposite direction was, however, observed for stilbene-quinone (at 5×10^{-3} M) and

Fig. 3. Development of carbonyl absorbance (CI = 1720/720 cm^{-1}) in the photooxidation of LDPE films.

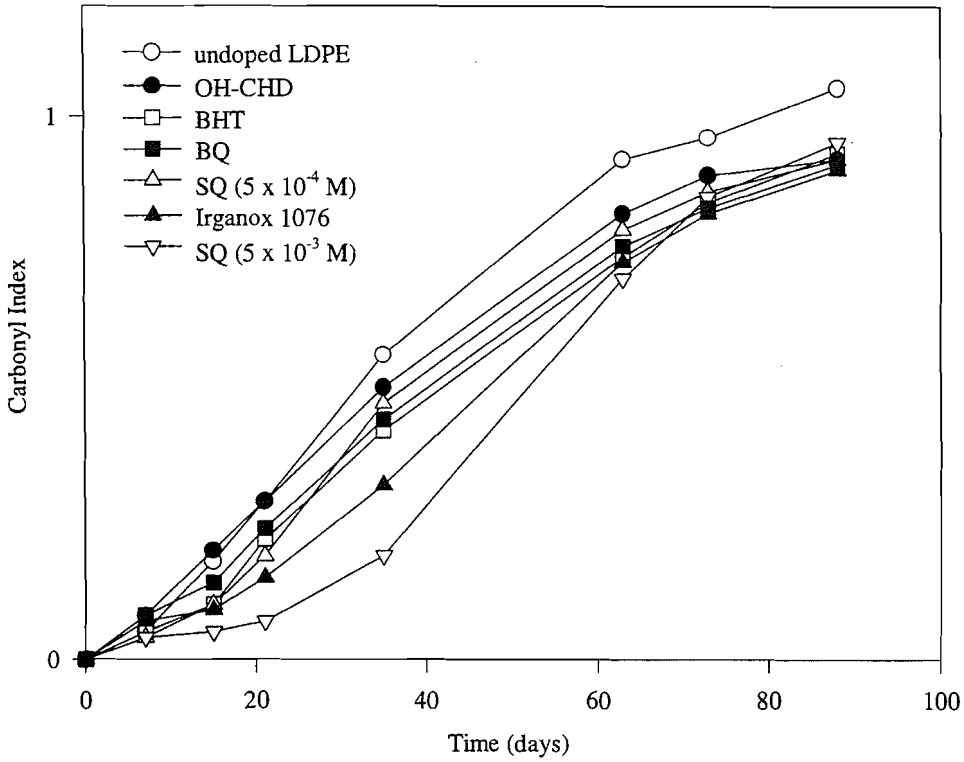

Table 2. Oxidation characteristics of LDPE samples measured by DSC under air

	Virgin samples		Embrittled strips	
Additive	T_o strips (°C)	T_o films (°C)	T_o thermo (°C)	T_o photo (°C)
—	160.1	158.1	159.1	167.1
1	198.5	180.8	169.5	174.0
2	228.5	223.8	(231.0)[c]	177.0
3	171.2	170.6	162.5	172.3
4	177.0	174.5	159.0	175.0
5[a]	180.0	175.5	159.0	168.0
5[b]	196.2	193.6	204.1	—

[a,b]See Table 1.
[c]Only one strip out of five broke down.

Table 3. Oxidation characteristics of LDPE strips measured by isothermal DSC

Sample	T (°C)	OIT (min)	τ_{max} (min)
1	180	28	55
2	180	716	948
5[b]	180	45	82
1	170	47	100
4	170	7	43
5[a]	170	5	40
5[b]	170	87	150
5[b]	160	224	378

[a,b]See Table 1, τ_{max} represents time of the oxidation exotherm peak.

Irganox 1076 (Table 2); they both exhibit T_o values even higher than in the respective virgin samples. This finding would suggest that another mechanism than the purely oxidative one can also contribute to the mechanical failure (embrittlement) of the sample. The increased melting points (T_m) of the embrittled samples (Table 1) can serve as an indication for morphology changes taking place during the degradation of LDPE.

Summarizing the results for the influence of individual additives **1**–**5** on the oxidative degradation of LDPE, some points should be mentioned:

Different test methods require different preparation conditions (i.e., films, strips, etc.) and the thermal history may, as in the case of BHT in our study, influence the sample oxidative stability by lowering the additive content in relation to its volatility. Then, conclusions based on the results of single test method could prove to be erroneous.

Since stilbene-quinone itself is a thermally stable compound (mp 312°C), its low stabilizing activity at high temperature must be ascribed to other effects than to its thermal decomposition. The change of the degradation mechanism due to the increase of the temperature well above the LDPE melt-

Can. J. Chem. Downloaded from www.nrcresearchpress.com by 46.23.64.124 on 09/08/12
For personal use only.

Can. J. Chem. Downloaded from www.nrcresearchpress.com by 46.23.64.124 on 09/08/12
For personal use only.

ing temperature might be one of the reasons for the observed inactivity of **5**. Similarly, hindered amine stabilizers were reported to be effective in polyolefins at temperatures below 100°C while they lost the activity at higher temperatures (around 150°C) (22).

As well as the suggested temperature dependence of the LDPE degradation mechanism, a relative drop of the additive concentration is also to be taken into account when the melting temperature of the semicrystalline polymer is reached. The additive is then homogeneously distributed in the entire melt at a relatively lower concentration than in the solid polymer where the additive is restricted to only the amorphous phase. Thus, the lower concentration may not be sufficient to inhibit the high-temperature degradation processes of the LDPE melt. This hypothesis is further supported by the results in Tables 2 and 3, which clearly reveal a strong concentration dependence of the inhibiting efficiency of **5**.

Of the transformation products studied, stilbene-quinone shows an undisputable stabilizing effect in the thermooxidation of LDPE at moderate temperatures, while at high temperatures and in irradiated samples it is practically inactive.

From the DSC measurements under nitrogen, changes in the phase behaviour taking place during the degradation of the doped LDPE samples are indicated. A detailed study of this phenomenon is under way and will be discussed in detail later on.

Experimental

Materials

The following stabilizers and their transformation products were used: 2,6-di-*tert*-butyl-4-methylphenol (**1**, mp 67°C); octadecyl-3-(3′,5′-di-*tert*-butyl-4′-hydroxyphenyl)propionate (**2**, Irganox 1076, Ciba-Geigy AG, mp 49–50°C); 2,6–di- *tert*-butyl-4-methyl-4-hydroxy-2,5–cyclohexadiene-1-one (**3**, mp 111–112°C) (23); 2,6-di-*tert*-butyl-1,4-benzoquinone (**4**, Fluka AG, mp 63,5°C); 3,5,3′,5′-tetra-*tert*-butyl-stilbene-4,4′-quinone (**5**, mp 312°C) (24).

The additives were melt-blended at 150°C with an unstabilized LDPE (Leuna, AL 21FA, density 0.919, MI 436 K/5 kp = 0.32/10 min). The concentration was 10^{-2} M (mol/kg of polymer) for each additive except **5**, for which 5×10^{-4} and 5×10^{-3} M were used.

Plates 3 mm thick were then compression moulded at 170°C. From these plates strips for the embrittlement tests and films for IR measurements were cut and pressed, respectively.

Methods and measurements

Oxygen uptake experiments were conducted with 40 mg LDPE samples in closed glass vessels under pure oxygen at atmospheric pressure. The oxygen uptake was monitored with a mercury pressure device (25), while the temperature was kept at 180 ± 1°C using an oil block. The induction period (IP) was determined graphically on the plot of oxygen consumption versus time (25).

Polymer films (ca. 0.1 mm thick) were mounted in slide holders and either oven-aged in air at 90°C or photooxidized at 40°C using an Osram L 20 W/73 fluorescent tube with a wavelength range 315–405 nm (λ_{max} = 350 nm) and constant light intensity.

Polymer strips (50 × 3 × 1.7 mm) in glass tubes were placed in a thermostated block and thermooxidized at 100 ± 0.5°C, or directly mounted in the holders of the photooxidation box. The embrittlement tests were performed at room temperature by pulling the strips out of the tube up to one third of their length, and manually bending at a 90° angle over the tube's edge. For these strips (five of each sample) the times to embrittlement were found to have good reproducibility. A similar procedure was also reported by Gugumus (4).

The effect of exposure time on the development of functional groups in the thermo- and photooxidized films was determined by IR spectroscopy on a Perkin Elmer 577 spectrophotometer. An increase of the carbonyl concentration was evaluated as the ratio of the carbonyl group absorbance (A_{1720}) to that of the standard band absorbance (A_{720}), and is defined as the carbonyl index CI (A_{1720}/A_{720}).

The melting and crystallization behavior of LDPE samples was analyzed by differential scanning calorimetry with a Perkin Elmer DSC 7, calibrated with indium prior to use. The thermal transitions in N_2 (30mL/min) were recorded at a heating rate of 10°C/min. DSC in air was used to study the effect of BHT transformation products on the oxidative stability of LDPE. Both the isothermal and the dynamic mode (heating rate 3°C/min) were used to determine the performance of these compounds. A constant flow of air 50 mL/min was kept during the measurements. In the dynamic experiments the temperature T_o for the start of an exothermal reaction is determined, and is referred to as the onset oxidation temperature. The average of two determinations was taken as T_o for the sample. From isothermal DSC runs, performed at 180, 170, and 160°C, the oxidation induction time (OIT) for the onset of the oxidation exotherm was noted.

References

1. J.L. Bolland and G. Gee. Trans Faraday Soc. **42**, 236 (1946).
2. J.L. Bolland. Trans. Faraday Soc. **44**, 669 (1948).
3. J. Pospíšil. Adv. Polym. Sci. **36**, 69 (1980).
4. F. Gugumus. *In* Plastics additives. *Edited by* R. Gächter and H. Müller. Hanser Publishers, Munich, Vienna, New York. 1990. pp.1–100.
5. J. Pospíšil. Polym. Degrad. Stab. **40**, 217 (1993).
6. G. Scott. *In* Atmospheric oxidation and antioxidants. Vol. I. *Edited by* G. Scott. Elsevier Science Publishers, Amsterdam. 1993. p.121.
7. T.J. Henman. *In* Developments in polymer stabilization. Vol. I. *Edited by* G. Scott. Applied Science Publishers, London. 1979. p. 39.
8. I. Buben and J. Pospíšil. Collect. Czech. Chem. Commun. **40**, 987 (1975).
9. I. Buben and J. Pospíšil. J. Polym. Sci. **57**, 261 (1976).
10. J. Virt, L. Rosík, J. Kovářová, and J. Pospíšil. Eur. Polym. J. **16**, 247 (1980).
11. P.P. Klemchuk and Paul-Li Horng. Polym. Degrad. Stab. **34**, 333 (1991).
12. O. Brede, M. Burgers, J. Kovářová, and I. Kúdelka. Radiat. Phys. Chem. In press.
13. N.C. Billingham, D.C. Bott, and A.S. Manke. Dev. Polym. Degrad. **3**, 63 (1981).
14. J.H. Adams. J. Polym. Sci. A-1: **8**, 1077 (1970); **8**, 1269 (1970).
15. F. Gugumus. Polym. Degrad. Stab. **27**, 19 (1990).
16. J. Lacoste and D.J. Carlsson. J. Polym. Sci. Part A: Polym. Chem. **30**, 493 (1992).
17. C.E. Boozer and G.S. Hammond. J. Am. Chem. Soc. **76**, 3861 (1954).

18. K. Karlsson, C. Assargren, and U.W. Gedde. Polym. Test. **9**, 421 (1990).
19. L.J. Taylor and J. Tobias. J. Appl. Polym. Sci. **26**, 2917 (1981).
20. M. Day, J.D. Cooney, C. Klein, and J.L. Fox. J. Therm. Anal. **41**, 225 (1994).
21. J. Kovářová, L. Rosík, and J. Pospíšil. Polym. Mater. Sci. Eng. **58**, 215 (1988).
22. P. Gijsman. Polym. Degrad. Stab. **43,** 171 (1994).
23. M.S. Kharash and B.S. Joshi. J. Org. Chem. **22**, 1439 (1957).
24. C.D. Cook. J. Org. Chem. **18**, 261 (1953).
25. R. Peter, E. Mäder, M. Rätzsch, J. Kovářová, J. Rotschová, and J. Pospíšil. Angew. Makromol. Chem. **184**, 167 (1991).

Can. J. Chem. Downloaded from www.nrcresearchpress.com by 46.23.64.124 on 09/08/12
For personal use only.

Conformational dependence of electronic spectra and zero-field splitting parameters in 2-naphthylphenylcarbene

Olivier Parisel, Gaston Berthier, and Eva Migirdicyan

Abstract: Quantum mechanical calculations using ab initio and semi-empirical methods have been carried out for elucidating the electronic structure and geometry of 2-naphthylphenylcarbene conformers. The *Z/cis* conformer has the lowest ground state triplet energy, the lowest triplet–triplet (T_0–T_1) transition energy, as well as the largest zero-field splitting parameter *D*. A clear-cut relationship between the *D* value and the geometry is pointed out.

Key words: carbenes, conformational isomerism, triplet–triplet transitions, CS-INDO/CI calculations, ZFS *D* parameters.

Résumé : Dans le but d'étudier la structure électronique et la géométrie du 2-naphtylphényle carbène, des calculs de chimie quantique (ab initio et semi-empiriques) ont été réalisés sur différents conformères de ce carbène. Le calcul montre que c'est le conformère *Z/cis* qui présente l'énergie minimale dans son état triplet fondamental, l'énergie de transition triplet–triplet (T_0–T_1) la plus faible ainsi que la valeur la plus élevée du paramètre *D* de séparation des sous-niveaux triplets en champ nul. Une relation simple reliant *D* et la géométrie est mise en évidence.

Mots clés : carbènes, isomérie conformationnelle, transitions triplet–triplet, calculs CS-INDO/CI, paramètres *D* de ZFS.

Can. J. Chem. Downloaded from www.nrcresearchpress.com by 46.23.64.124 on 09/08/12
For personal use only.

Introduction

The geometry of carbenes has long been a source of concern for spectroscopists as well as for quantum chemists. For many years, the structure of methylene (CH_2) in its triplet ground state was a matter of debate (1). While Foster and Boys (2) predicted a bent equilibrium geometry, Herzberg (3) concluded that the molecule was linear on the basis of his pioneering studies of the electronic spectrum of CH_2. This spectrum was subsequently reinterpreted by Herzberg and Johns (4) in terms of a bent structure of the methylene molecule. The EPR experiments of Wasserman, Yager, and Kuck (5) established that the structure of CH_2 in a Xe matrix at 4.2 K is bent with a bond angle of 136°. Finally, Bunker et al. (6) found that, in the gas phase, the equilibrium bond angle of CH_2 is 134.037° ± 0.045°. This value determined from the IR laser magnetic resonance spectra is in excellent agreement with the ab initio prediction of McLaughlin, Bender, and Schaefer (1, 7) of 134° ± 2° for the equilibrium bond angle of CH_2.

Received April 24, 1995.

This paper is dedicated to Professor J.E. (Jim) Guillet in recognition of his contributions to Canadian chemistry.

Olivier Parisel and Gaston Berthier. École Normale Supérieure, Laboratoire de radioastronomie millimétrique, 24, rue Lhomond, 75231 Paris Cédex 05, France.
Eva Migirdicyan.[1] Laboratoire de photophysique moléculaire du Centre national de la recherche scientifique, Bâtiment 213, Université Paris-Sud, 91405 Orsay Cédex, France.

[1] Author to whom correspondence may be addressed.

Diphenylcarbene (DPC), like methylene, has a bent triplet ground state that can be either planar or nonplanar according to the mutual orientation of the two phenyl rings. In previous reports (8, 9), it was shown that two distinct fluorescence spectra are emitted from DPC in an *n*-hexane Shpolskii matrix over the temperature range between 4.2 and 77 K: a sharp fluorescence with an origin band at 502.8 nm and a broad blue-shifted fluorescence with λ_{max} = 482 nm. The two fluorescence spectra were attributed to two different conformations of DPC trapped in this Shpolskii matrix. The low-energy sharp fluorescence was attributed to a DPC molecule with a geometry similar to that of dibenzocycloheptadienylidene (DBC), the carbene with the ethano bridge, since DPC and DBC both have their fluorescence origins at 502.8 nm. In this geometry,

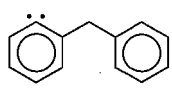

DPC

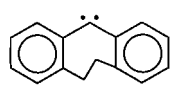

DBC

the two aromatic rings of DPC are not too far from being coplanar. The broad blue-shifted fluorescence was attributed to a nonplanar DPC conformer in which the carbenic bond angle is 140° and the dihedral angles between each benzene ring and the average plane are close to 30°. This geometry corresponds to that determined by Anderson and Kohler (10), who used the ENDOR technique for DPC in benzophenone. This implies that DPC has nearly the same geometry in *n*-hexane and in benzophenone, which is consistent with the fact

Can. J. Chem. Downloaded from www.nrcresearchpress.com by 46.23.64.124 on 09/08/12
For personal use only.

that the broad fluorescence with λ_{max} = 482 nm observed in *n*-hexane is very similar to the broad structureless phonon band with λ_{max} = 476 nm observed in benzophenone (11).

A detailed CS-INDO/CI investigation was performed for three different geometries of DPC including both the above-mentioned structures (9). This theoretical approach is based on a carefully designed multireference perturbation and uses a semi-empirical valence-Hamiltonian specifically developed and parametrized for conformational and spectroscopic problems.

The aim of the present work is to extend the CS-INDO/Cl predictions to the conformers of a larger carbene, the 2-naphthylphenylcarbene (2-NPC). EPR experiments (12) performed with 2-NPC in a 2-methyltetrahydrofuran matrix at 77 K indicate that this carbene has a triplet ground state T_0 like methyl-

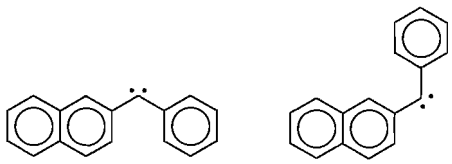

E/trans 2-NPC *Z/cis* 2-NPC

ene and DPC. In addition, 2-NPC in this glassy matrix at 77 K can exist in two different conformations, *syn* and *anti*, which have different zero-field splitting (ZFS) parameters in the T_0 ground state. Such a conformational isomerism was first observed in EPR experiments for 1- and 2-naphthylcarbenes (13) and the measured *D* values were assigned to specific conformers on the basis of calculations involving the relationship established between the ZFS parameters *D* and π spin densities in the frame of the point-spin model (14, 15).

The fluorescence spectra of 2-NPC in *n*-hexane and *n*-heptane Shpolskii matrices at 4.2 K are composed of several quasi line spectra with origins shifted by 30–300 cm^{-1} from each other (16). Furthermore, the fluorescence and EPR spectra reveal that there is a light-induced transformation of the conformer emitting at 600.5 nm into the one emitting at 589.5 nm in the *n*-heptane matrix. Based on preliminary estimates of the ZFS parameter *D* (12), these spectra have been attributed to the planar *E/trans* (*syn*) and *Z/cis* (*anti*) conformers of 2-NPC, each one being trapped in several different sites of the matrix (16). To check these interpretations on a theoretical basis, the transition energies and the ZFS parameters *D* of 2-NPC in several geometries have been calculated.

Computational techniques

To determine the low-energy triplet and singlet states of the *E/trans* and *Z/cis* conformers of 2-NPC, we performed CS-INDO (Conformational Spectra – Intermediate Neglect of Differential Overlap) quantum mechanical calculations similar to those we successfully applied to DPC. As proven by a large number of applications in the field of photochemistry (17), this method is especially convenient for dealing with problems of conformations of conjugated molecules in their ground states as well as in their excited states. The CI treatment itself is performed using the CIPSI (Configuration Interaction by Perturbative Selected Iterations) procedure, which is a multireference second-order perturbation method involving a variational subspace *S* constructed in an iterative way (18); the selection threshold of the configurations included in subspace *S* according to their first-order contributions in the total wave functions of the different states is about $\eta \approx 0.08$. The starting molecular orbitals were obtained through an open-shell self-consistent field (SCF) treatment of the triplet ground state of DPC, performed using the restricted Hartree–Fock procedure proposed by Nesbet (19).

The parameters required by CS-INDO were taken from our earlier studies on conjugated molecules involving similar (second-order perturbation) CI treatments (20) and were used without any special adjustment for carbenic systems. They are the screening factors $k_{\sigma\sigma}$ (= 1.0), $k\sigma\pi$ (= 0.75), $k_{\pi\pi}$ (= 0.6) determining the values of the resonance integrals in a hybridized valence basis set; in addition, there are *n*-type screening parameters (for the selection criterion of these parameters, see ref. 21) for the electrons originating from the carbenic atom C1, for which we took an sp^3-type hybridization similar to an oxygen atom in a C-O-C group (i.e., $k_{n\sigma} = 0.8$, $k_{nn} = 0.74$, $k_{n\pi} = 0.68$). Note that, in this representation, the atomic functions describing the two unpaired electrons on C1 are the minus (π type) and plus (σ type) combinations of the two sp^3-type orbitals pointing in the plane orthogonal to the C2C1C3 plane; the conventional description in terms of *n* and π_0 orbitals can be restored by simply going back from the hybridized orbital basis to the (s, p_x, p_y, p_z) primitive basis set. The one-center integrals γ_{AA} were given the standard values γ_{HH} = 12.85 eV and γ_{CC} = 10.93 eV, and the two-center integrals γ_{AB} were computed by the Ohno–Klopman formula, a very suitable recipe for CI treatments including polyexcited configurations (22). It has been shown, in particular, that combining polyexcited CI treatments with Ohno–Klopman Coulomb integrals provides good predictions of the triplet state energies (22, 23). All the computations were carried out with our CS-INDO-CIPSI program running on an IBM RISC-SYSTEM/6000 workstation.

As geometry input data, we used idealized bond lengths and bond angles R_{CC} = 1.4 Å, R_{CH} = 1.1 Å, and CCC = HCC = 120°, except for the angle parameters involving the carbenic atom.

(*i*) In a first treatment, planar conformations were assumed for both the *E/trans* and *Z/cis* conformers with an apex angle α equal to 150° taken from the EPR experiments on DPC (24).

(*ii*) A second series of calculations was carried out using partially optimized geometries derived from ab initio ROHF/3-21G treatments. The nonfrozen parameters were the apex angle α and both the dihedral angles Φ_1 (out-of-plane torsion centered on the carbenic atom for the phenyl group) and Φ_2 (rotation angle of the phenyl around the C1C3 bond).

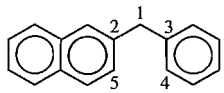

α = (2 1 3)
Φ_1 = (3 1 2 5)
Φ_2 = (4 3 1 2)

(*iii*) Five different geometries were determined for the following fixed values of Φ_1: 0°, 45°, 90°, 135°, and 180°, while allowing α and Φ_2 to vary during the optimization procedure.

(*iv*) A final optimization was performed with α, Φ_1, and Φ_2 varying simultaneously.

The optimized geometries obtained as described above were then used to compute the corresponding vertical transition energies.

The *D* values were determined by the method described in ref. 9 but using integrals $D_{\sigma\pi}^{CC}$ adjusted on the experimental *D* parameter of the DPC molecule (D_{exp} = 0.4050 cm^{-1} (25) and *d* = 0.965 Å). In the present calculations, all the one- and two-center terms have been taken into account.

Can. J. Chem. Downloaded from www.nrcresearchpress.com by 46.23.64.124 on 09/08/12
For personal use only.

Table 1. ROHF/3-21G optimized structures of 2-NPC in the ground state and the corresponding energies.

	Φ_1[a]	Φ_2[a]	α[a]	Energy (au)
E/trans	0	0	149.05	−647.025 221
	30.77	30.63	135.24	−647.033 220
	45	20.12	134.68	−647.032 976
	90	1.19	133.57	−647.031 422
	135	−19.33	135.18	−647.033 090
	153.17	−33.45	135.56	−647.033 507
Z/cis	180	0	148.91	−647.025 513

[a]All values in degrees, see text for definitions.

Table 2. CS-INDO/CIPSI transition energies (eV) for the planar conformers of 2-NPC.

		E/trans		*Z/cis*			
State		Singlet state	Triplet state	Singlet state	Triplet state	Orbital occupancy in the main configuration	Transition
T_0	$^3A''$		0		0	$^3(n\pi_0)$	
S_1	$^1A''$	0.58		0.58		$^1(n\pi_0)$	
S_2	$^1A'$	1.05		0.98		π_0^2	$n \rightarrow \pi_0$
S_3	$^1A'$	1.75		1.54		n^2	$\pi_0 \rightarrow n$
S_4	$^1A''$	1.94		1.97		$^1(n\pi^*) + {}^1(n\pi)$	$\pi_0 \rightarrow \pi^*$
T_1	$^3A''$		1.96		1.98	$^3(n\pi^*) + {}^3(n\pi)$	$\pi_0 \rightarrow \pi^* + (\pi \rightarrow n)$
T_2	$^3A''$		2.67		2.70	$^3(n\pi^*) + {}^3(n\pi)$	$\pi_0 \rightarrow \pi^* + (\pi \rightarrow n)$
S_5	$^1A''$	2.68		2.70		$^1(n\pi^*) + {}^1(n\pi)$	

Table 3. CS-INDO/CIPSI transition energies for nonplanar conformers of 2-NPC as a function of the Φ_1 deformation angle (values in eV).

	Φ_1[a]				
State	30.77°	45°	90°	135°	153.17°
T_0	—	—	—	—	—
S_1	0.50	0.60	0.62	0.56	0.53
S_2	0.81	0.90	0.69	0.87	0.79
S_3	1.73	1.48	1.48	1.40	1.68
S_4	1.89	1.97	2.11	1.94	1.91
T_1	2.05	2.10	2.11	2.08	2.01
T_2	2.66	2.71	2.57	2.68	2.62
T_3	2.90	3.32	3.53	3.43	2.84

[a]See text for definition.

Results and discussion

1. Ground state energetics

The optimized geometries have been collected in Table 1 together with their corresponding energy: the departure from planarity results in the decrease of the apex angle α from about 150° in planar forms to about 135° in the nonplanar ones. The conformers corresponding to the lowest energies are obtained for Φ_1 = 30.77° or Φ_1 = 153.17°, which gives an overall molecular structure more or less similar to that determined by ENDOR experiments in the case of DPC (10). Between these two conformers, the pseudo-*Z/cis* (Φ_1 = 153.17°) conformer lies 63 cm^{-1} below the pseudo-*E/trans* one (Φ_1 = 30.77°) when using the ROHF/3-21G level of calculation.

The energy barriers for the conversion of these forms into each other are 395 cm^{-1} (pseudo *E/trans* → pseudo *Z/cis*) and 458 cm^{-1} (pseudo *Z/cis* → pseudo *E/trans*). Our previous experimental results (16) indicated that, in the *n*-heptane Shpolskii matrix, the species fluorescing at 589.5 nm converts thermally at 90 K (corresponding to 60 cm^{-1}) into the species fluorescing at 600.5 nm. Therefore, the actual energy barrier should be smaller than our theoretical SCF value. Increasing the accuracy of the calculated energy barrier would require the consideration of correlation effects and possible matrix effects. Furthermore, the zero-point energy correction for the Φ_1 = 90° conformer is expected to be smaller than the corresponding one in pseudo-planar conformers as a consequence of the lack of conjugation between the two aromatic cycles: this results in a decrease of the energy barrier height.

Nevertheless, these experimental results, coupled to our predictions on absolute energies, suggest that the species emitting at 600.5 nm in the *n*-heptane matrix (and at 600.1 nm in the *n*-hexane matrix) is the pseudo-*Z/cis* conformer while the one emitting at 589.5 nm in the *n*-heptane matrix (and at 588.8 nm in the *n*-hexane matrix) is the pseudo-*E/trans* one.

2. Transition energies of the conformers

The CS-INDO/CIPSI transition energies are listed in Table 2 for the planar conformers and in Table 3 for the nonplanar

Fig. 1. Adiabatic correlation diagram from the planar *E/trans* conformer to the *Z/cis* conformer through nonplanar forms.

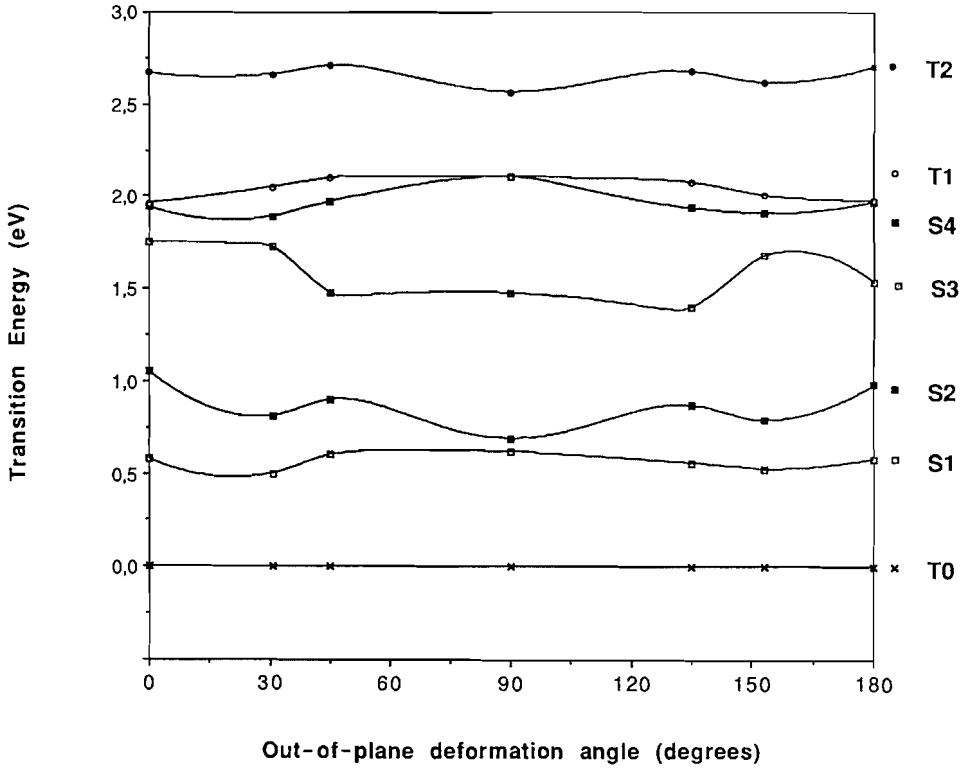

ones. The T_0–T_1 transition energies compare favorably with the previous experimental results (16). The comparison between theoretical predictions and experimental results enables us to propose the following assignment:

pseudo-*E/trans*, Φ_1 = 30.77°, $(T_0–T_1)_{calcd}$ = 2.05 eV, $(T_0–T_1)_{exp}$ = 2.11 eV;

pseudo-*Z/cis*, Φ_1 = 153.17°, $(T_0–T_1)_{calcd}$ = 2.01 eV, $(T_0–T_1)_{exp}$ = 2.06 eV.

This assignment is consistent with the ground state energetics discussed above.

The correlation diagram from the planar *E/trans* conformer to the *Z/cis* conformer through nonplanar forms is presented in Fig. 1.

The T_0–T_1 transition energies of 1.96 and 1.98 eV calculated for the planar 2-NPC conformers are lower than the corresponding energy of 2.62 eV computed for the planar (C_{2v}) DPC (9), in good agreement with the expected energy shift for more extended conjugated systems. This indicates that the CS-INDO parameters can be transferred from a medium-size molecule, like DPC, to larger compounds.

When aromatic molecules present sparsely spaced electronic levels of a given multiplicity, the vibrational structures of their emission and absorption, or excitation, spectra generally show mirror-image symmetry. In contrast, when the molecules present two close-lying electronic states of different symmetry, the latter can interact vibronically through an inducing mode of appropriate symmetry. In such a case, the vibronic levels of one manifold will be mixed with levels of appropriate symmetry of the other manifold, resulting in level shifts and intensity redistribution. In the case of 2-NPC, the second excited triplet state T_2 is separated from the T_1 state by 0.71 eV (5727 cm^{-1}) for the pseudo-*E/trans* conformer and by 0.72 eV (5808 cm^{-1}) for the pseudo-*Z/cis* conformer. This large separation explains why the quasi line fluorescence spectra of both conformers exhibit mirror-image symmetry with the corresponding excitation spectra, as far as vibrational frequencies up to 1700 cm^{-1} are concerned (16). Such a mirror-image symmetry does not exist for DPC (see Fig. 4 in ref. 9) where the corresponding T_1–T_2 separation is about 0.03 eV (~240 cm^{-1}).

3. ZFS parameter *D*

The computed values for the ZFS parameter $D(T_0)$ in the ground state T_0 and $D(T_1)$ in the first excited state T_1 of 2-NPC in various geometries are gathered in Table 4. It should be noticed that our evaluation of the ZFS parameters assumes that the principal axes of the *D* tensor for the *E/trans* and *Z/cis* 2-NPC conformers in their T_0 state are approximately the same as in DPC and that they are not changed when passing from T_0 to T_1 (25). These *D* values were obtained by considering only the first-order contributions due to the spin–spin interaction between the two unpaired electrons.

Table 4 reveals that the largest $D(T_0)$ values are obtained for the planar conformers of 2-NPC: the $D(T_0)$ and $D(T_1)$ values decrease upon out-of-plane torsion with respect to the Φ_1 dihedral angle. For both states, the minimum is reached at Φ_1 = 90°. In this geometry, the π_0 orbital on the carbenic center remains conjugated with the phenyl ring while the *n* orbital now conjugates with the naphthyl group, unlike the planar conformers for which no conjugation at all occurs between the *n* orbital and the π system of the rings. As a consequence of this increased delocalization effect, the average separation

Can. J. Chem. Downloaded from www.nrcresearchpress.com by 46.23.64.124 on 09/08/12
For personal use only.

Table 4. Zero-field splitting parameters D for the T_0 and T_1 states as a function of the out-of-plane deviation Φ_1[a].

Φ_1	$D(T_0)$[b]	$D(T_1)$[b]
0 (*E/trans*)	0.4103	0.0744
30.77	0.3405	0.0619
45	0.3399	0.0578
90	0.2760	0.0537
135	0.3444	0.0582
153.17	0.3461	0.0633
180 (*Z/cis*)	0.4147	0.0756

[a]See text for definitions. All D values are in cm^{-1}.

[b]Only the main configuration of the CI wave function has been retained in the evaluation of the D parameters.

between the π_0 and n unpaired electrons increases, leading to a smaller $D(T_0)$ value.

Furthermore, it is noteworthy that the D values may be fitted with respect to Φ_1 according to eq. [1]:

$$[1] \quad D(T_i) = a_i + b_i \cos^2 \Phi_1 \qquad i = 0, 1$$

For the ground state T_0, $a_0 = 0.272$ cm^{-1} and $b_0 = 0.126$ cm^{-1} with a correlation coefficient $r_0 = 0.92$. For the excited state T_1, $a_1 = 0.0497$ cm^{-1} and $b_1 = 0.0215$ cm^{-1} with a correlation coefficient $r_1 = 0.90$.

Such an equation has to be compared to the Heller–McConnell formula (26), which gives a relationship between carbon spin densities of radicals and EPR coupling constants.

A further refinement in this fitting would include the role of the Φ_2 and α angles. In addition, it might be necessary to use a set of two equations, instead of eq. [1], in order to account for the asymmetry of the molecule, as suggested by Douady et al. (27) for the β hydrogen hyperfine coupling constants. Such a discussion is, however, beyond the scope of this paper. We just want to emphasize that such a relationship could contribute to the determination of the structure of diarylcarbenes when their ZFS parameters are known.

In Table 4, the $D(T_0)$ values are always higher for the *Z/cis* and pseudo-*Z/cis* ($\Phi_1 \geq 90°$) conformers than for the *E/trans* and pseudo-*E/trans* ones ($\Phi_1 \leq 90°$). As a consequence, we assign the compound having the largest experimental $D(T_0)$ value (12, 16) to the pseudo-*Z/cis* conformer of 2-NPC. This attribution is consistent with the fact reported in ref. 16 that the conformer with the largest $D(T_0)$ value fluoresces at the highest wavelength, in agreement with our results on transition energies (see sect. 2). Although the difference between the $D(T_0)$ values of the *Z/cis* (or pseudo-*Z/cis*) and the *E/trans* (or pseudo-*E/trans*) conformers of 2-NPC is small (but significant), this attribution is opposite to the one previously presented in ref. 12 that was based on an erroneous comparison of spin densities, but is consistent with the revised analysis presented in ref. 28.

The electronic structure of the excited T_1 state involves the promotion of the unpaired electron from the π_0 orbital to a π^* orbital. As in the case of DPC (9), this π^* orbital has only a minor contribution from the carbenic $2p\pi$ atomic orbital. Thus the excitation results in a delocalization of the unpaired electron on the rings and in a lack of corresponding spin density on the carbenic center, while retaining the spin density originating from the n unpaired electron. As a consequence, the average separation between the two unpaired electrons is increased relative to the T_0 ground state: the ZFS parameter $D(T_1)$ is then expected to decrease relative to $D(T_0)$, which is in agreement with the values presented in Table 4. However, the electronic distributions are very different in the T_0 and T_1 states, so that our assumption of taking the same principal axes, and consequently the same ordering of the three sublevels $|x\rangle$, $|y\rangle$, and $|z\rangle$, in both states may be questionable. In addition, the contribution of the second-order spin-orbit coupling between singlet and triplet states should be considered. As seen in Table 2, the spin-orbit interaction is likely to particularly affect the $D(T_1)$ value because of the very small separation between the S_4 and T_1 states: ΔE $(S_4–T_1) = 81$ cm^{-1}. Furthermore, this coupling could also induce energy shifts capable of disturbing the ordering of the T_1 sublevels.

Conclusion

In this contribution, three different calculations involving absolute energies, transition energies, and ZFS D parameters have been performed using three different methods for different conformers of the 2-NPC molecule.

Due to the very small differences in the calculated values between the pseudo-*E/trans* and pseudo-*Z/cis* conformers, it might be risky to draw unambiguous conclusions. However, these three different calculations lead to a series of converging results, consistent with the experimental data (16), but in disagreement with the assignment reported in refs. 12 and 16 that has now been found to be erroneous (28): the conformer emitting at 600.5 nm and at 600.1 nm (respectively, in the n-heptane and in the n-hexane matrices) would likely be the pseudo-*Z/cis* conformer with $\Phi_1 \approx 153°$ while the one fluorescing at 589.5 nm and at 588.8 nm (respectively, in the n-heptane and in the n-hexane matrices) would be the pseudo-*E/trans* conformer with $\Phi_1 \approx 31°$. In addition, our calculated D values have demonstrated their dependence on $\cos^2 \Phi_1$, thus establishing a clear-cut relationship between the ZFS parameters and the geometries of diarylcarbenes.

Acknowledgments

The authors are indebted to Drs A. Després (Orsay), Y. Ellinger (Paris), and M.S. Platz (Columbus, Ohio) for helpful comments and enlightening discussions.

References

1. H.F. Schaefer. Science, **231**, 1100 (1986), and references therein.
2. J.M. Foster and S.F. Boys. Rev. Mod. Phys. **32**, 305 (1960).
3. G. Herzberg. Proc. R. Soc. London, Ser. A: **262**, 291 (1961).
4. G. Herzberg and J.W.C. Johns. J. Chem. Phys. **54**, 2276 (1971).
5. E. Wasserman, W.A. Yager, and V.J. Kuck. Chem. Phys. Lett. **7**, 409 (1970).
6. P.R. Bunker, P. Jensen, W.P. Kraemer, and R. Beardsworth. J. Chem. Phys. **85**, 3724 (1986).

Can. J. Chem. Downloaded from www.nrcresearchpress.com by 46.23.64.124 on 09/08/12
For personal use only.

7. D.R. McLaughlin, C.F. Bender, and H.F. Schaefer. Theor. Chim. Acta, **25**, 352 (1972).
8. K.W. Haider, M.S. Platz, A. Després, V. Lejeune, and E. Migirdicyan. J. Phys. Chem. **94**, 142 (1990).
9. A. Després, V. Lejeune, E. Migirdicyan, A. Admasu, M.S. Platz, G. Berthier, O. Parisel, J.P. Flament, I. Baraldi, and F. Momicchioli. J. Phys. Chem. **97**, 13358 (1993).
10. R.J.M. Anderson and B.E. Kohler. J. Chem. Phys. **65**, 2451 (1976).
11. R.J.M. Anderson, B.E. Kohler, and J.M. Stevenson. J. Chem. Phys. **71**, 1559 (1979).
12. V. Maloney and M.S. Platz. J. Phys. Org. Chem. **3**, 135 (1990).
13. A.M. Trozzolo, E. Wasserman, and W.A. Yager. J. Am. Chem. Soc. **87**, 129 (1965).
14. R.S. Hutton and H.D. Roth. J. Am. Chem. Soc. **104**, 7395 (1982).
15. H.D. Roth and R.S. Hutton. Tetrahedron, **41**, 1567 (1985).
16. B. Kozankiewicz, A. Després, V. Lejeune, E. Migirdicyan, D. Olson, J. Michalak, and M.S. Platz. J. Phys. Chem. **98**, 10419 (1994).
17. U. Mazzucato and F. Momicchioli. Chem. Rev. **91**, 1679 (1991).
18. B. Huron, J.P. Malrieu, and P. Rancurel. J. Chem. Phys. **58**, 5745 (1973).
19. R.K. Nesbet. Rev. Mod. Phys. **35**, 552 (1963).
20. F. Momicchioli, I. Baraldi, and G. Berthier. Chem. Phys. **123**, 103 (1988).
21. I. Baraldi, A. Carnevali, F. Momicchioli, and G. Ponterini. Spectrochim. Acta, **49A**, 471 (1993).
22. F. Momicchioli, I. Baraldi, and M.C. Bruni. Chem. Phys. **70**, 161 (1982); **82**, 229 (1983).
23. P. Swiderek and G. Hohlneicher. J. Mol. Struct. (Theochem), **262**, 187 (1992).
24. A.M. Trozzolo, E. Wasserman, and W.A. Yager. J. Chim. Phys. 1663 (1964).
25. R.W. Brandon, G.L. Closs, and C.A. Hutchison, Jr. J. Chem. Phys. **37**, 1878 (1962).
26. C. Heller and H.M. McConnell. J. Chem. Phys. **32**, 1535 (1960).
27. J. Douady, Y. Ellinger, A. Rassat, R. Subra, and G. Berthier. Mol. Phys. **3**, 217 (1967).
28. H.D. Roth and M.S. Platz. J. Phys. Org. Chem. In press.

Can. J. Chem. Downloaded from www.nrcresearchpress.com by 46.23.64.124 on 09/08/12
For personal use only.

Protected building blocks for luminescent and redox-active dendritic metal complexes. Excited state properties and electrochemical behavior

Alberto Juris, Margherita Venturi, Luca Pontoni, Immaculada Resino Resino, Vincenzo Balzani, Scolastica Serroni, Sebastiano Campagna, and Gianfranco Denti

Abstract: The mononuclear complexes $[Ru(2,3\text{-}Medpp)_3]^{5+}$, $[Ru(2,3\text{-}Medpp)_2(bpy)]^{4+}$, and $[Ru(2,3\text{-}Medpp)(bpy)_2]^{3+}$ and the dinuclear complex $[(2,3\text{-}Medpp)_2Ru(\mu\text{-}2,3\text{-}dpp)Ru(2,3\text{-}Medpp)_2]^{8+}$ (bpy = 2,2′-bipyridine; 2,3-dpp = 2,3-bis(2-pyridyl)pyrazine; 2,3-Medpp$^+$ = monomethylated 2,3-bis(2-pyridyl)pyrazine) have been synthesized. Their absorption spectra, luminescence properties, and electrochemical behavior have been investigated and compared with those of the mononuclear $[Ru(bpy)_3]^{2+}$, $[Ru(2,3\text{-}dpp)_3]^{2+}$, $[Ru(2,3\text{-}dpp)_2(bpy)]^{2+}$, and $[Ru(2,3\text{-}dpp)(bpy)_2]^{2+}$ and the dinuclear $[(bpy)_2Ru(\mu\text{-}2,3\text{-}dpp)Ru(bpy)_2]^{4+}$ parent compounds. The complexes examined are fundamental units in the synthesis of polynuclear metal complexes of dendrimeric structure and nanometer size.

Key words: luminescence, ruthenium complexes, dendrimers, electrochemistry, photochemistry.

Résumé : On a synthétisé les complexes mononucléaires $[Ru(2,3\text{-}Medpp)_3]^{5+}$, $[Ru(2,3\text{-}Medpp)_2(bpy)]^{4+}$ et $[Ru(2,3\text{-}Medpp)(bpy)_2]^{3+}$ et le complexe dinucléaire $[(2,3\text{-}Medpp)_2Ru(\mu\text{-}2,3\text{-}dpp)Ru(2,3\text{-}Medpp)_2]^{8+}$ (bpy = 2,2′-bipyridine; 2,3-dpp = 2,3-bis(2-pyridyl)pyrazine; 2,3-Medpp$^+$ = 2,3-bis(2-pyridyl)pyrazine monométhylé). On a examiné leurs spectres d'absorption, leurs propriétés de luminescence et leurs comportements électrochimiques et on les a comparés aux propriétés correspondantes des complexes parents mononucléaires $[Ru(bpy)_3]^{2+}$, $[Ru(2,3\text{-}dpp)_3]^{2+}$, $[Ru(2,3\text{-}dpp)_2(bpy)]^{2+}$ et $[Ru(2,3\text{-}dpp)(bpy)_2]^{2+}$ et dinucléaire $[(bpy)_2Ru(\mu\text{-}2,3\text{-}dpp)Ru(bpy)_2]^{4+}$. Les complexes étudiés sont les unités fondamentales dans la synthèse de complexes métalliques polynucléaires de structure dendrimérique et de grosseur du nanomètre.

Mots clés: luminescence, complexes du ruthénium, dendrimères, électrochimie, photochimie.

[Traduit par la rédaction]

Introduction

Much attention is currently devoted to the preparation of tree-like structures, also called arborols or dendrimers (1). Particularly interesting are dendrimers that incorporate in their building blocks specific "pieces of information" such as the capability to absorb and emit visible light and to reversibly exchange electrons. Such species could find applications as components in molecular electronics (2) and as photochemical molecular devices (3) for solar energy conversion and information storage (4). Ideal components to build up dendrimers of this type are transition metal complexes (5). In the last few years we have used Ru(II) and Os(II) as metals, 2,3- and 2,5-bis(2-pyridyl)pyrazine (2,3-dpp and 2,5-dpp) as bridging ligands, and 2,2′-bipyridine (bpy) and 2,2′-biquinoline (biq) as terminal ligands and we have developed a synthetic strategy to prepare luminescent and redox-active polynuclear metal complexes of dendrimeric structure, where the desired metals and ligands can be placed in specific sites of the supramolecular structure (6). Species containing 4 (7), 6 (8), 7 (9), 10 (10), 13 (11), and 22 (12) metal-based units have been obtained. Dendrimers containing metal atoms have also been reported by other groups (13).

We report here the synthesis and discuss the absorption spectra, the luminescence properties, and the electrochemical behavior of mono- and dinuclear Ru(II) complexes that contain the 2,3-Medpp$^+$ ligand. In this ligand one of the two chelating sites is temporarily blocked by the presence of a methyl group. For this reason one can refer to 2,3-Medpp$^+$ as a "protected" counterpart of the "deprotected" bis-chelating 2,3-dpp. The novel complexes described in this paper, which

Received April 21, 1995.

This paper is dedicated to Professor J.E. (Jim) Guillet in recognition of his contributions to Canadian chemistry.

A. Juris, M. Venturi, L. Pontoni, I. R. Resino, and V. Balzani.[1] Dipartimento di Chimica "G. Ciamician," Università di Bologna, via Selmi 2, 40126 Bologna, Italy.
S. Serroni and S. Campagna. Dipartimento di Chimica Inorganica, Analitica e Struttura Molecolare, Università di Messina, via Sperone 31, 98166 Messina, Italy.
G. Denti. Laboratorio di Chimica Inorganica, Istituto di Chimica Agraria, Università di Pisa, via S. Michele degli Scalzi 2, 54126 Pisa, Italy.

[1] Author to whom correspondence may be addressed. Telephone: 51-259560. Fax: 51-259456. E-mail: photochem@ciam01.ciam.unibo.it

Can. J. Chem. Downloaded from www.nrcresearchpress.com by 46.23.64.124 on 09/08/12
For personal use only.

Fig. 1. Structural formulas, labels, and schematic representation of the ligands and complexes investigated.

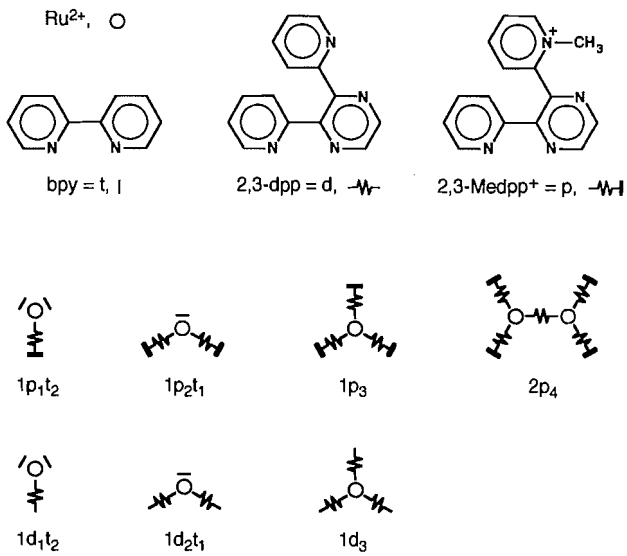

can be viewed as fundamental units of some of our dendrimers, and other related compounds are schematized in Fig. 1. In that figure and throughout the text each compound is designated by a label where the first number indicates the nuclearity, the letters indicate the type (and its lower index the number) of peripheral ligands: deprotected 2,3-dpp ligands (d), protected 2,3-Medpp$^+$ ligands (p), or terminal monochelating ligands (t). Finally, the "prime" notation indicates the presence of labile ligands (Cl^-).

Experimental section

Materials and methods

The preparation of the precursor compounds 2,3-Medpp$^+$ (**p**) (12), $[Ru(2,3\text{-}Medpp)_2Cl_2]^{2+}$ (**1'p$_2$**) (12), and $[Ru(bpy)_2Cl_2]\cdot 2H_2O$ (**1't$_2$**) (14), and of compounds $[Ru(2,3\text{-}dpp)(bpy)_2]^{2+}$ (**1d$_1$t$_2$**) (7*b*), $[Ru(2,3\text{-}dpp)_2(bpy)]^{2+}$ (**1d$_2$t$_1$**) (7*b*), and $[Ru(2,3\text{-}dpp)_3]^{2+}$ (**1d$_3$**) (15) has been previously reported.

Equipment

Absorption spectra were obtained at room temperature by means of a Perkin–Elmer λ-6 spectrophotometer. Luminescence spectra were obtained with a Perkin–Elmer LS-50 spectrofluorimeter. Emission quantum yields were measured at room temperature (20°C) with the optically dilute method (16), calibrating the spectrofluorimeter with a standard lamp. $[Ru(bpy)_3]^{2+}$ in aerated aqueous solution was used as a quantum yield standard, assuming a value of 0.028 (17). Emission lifetimes were measured with an Edinburgh 199 single-photon counting device. Electrochemical measurements were carried out in argon-purged acetonitrile solution at room temperature with a PAR 273 multipurpose apparatus interfaced to a PC. The working electrode was a Pt microelectrode or a glassy carbon (8 mm^2, Amel) electrode. The counter electrode was a Pt wire, and the reference electrode was a SCE separated with a fine glass frit. The concentration of the complexes was 5×10^{-4} M. Tetrabutylammonium hexafluorophosphate (0.05 M) was added as supporting electrolyte. Cyclic voltammograms were obtained at sweep rates of 20, 50, 100, and 200 mV/s. For reversible processes, half-wave potentials (vs. SCE) were calculated as an average of the cathodic and anodic peaks. The criteria for reversibility were the separation between cathodic and anodic peaks, the close-to-unity ratio of the intensities of the cathodic and anodic currents, and the constancy of the peak potential on changing scan rate. For irreversible processes, the potential values were evaluated from differential pulse voltammetry (DPV) peaks. The number of exchanged electrons was measured with DPV experiments performed with a scan rate of 20 mV/s, a pulse height of 30 mV, and a duration of 40 ms. The procedure for the calibration of the number of electrons corresponding to the various redox waves has been described in detail (10*b*). Experimental errors in the reported data are as follows: absorption maxima, 2 nm; emission maxima, 5 nm; emission lifetimes, 10%; emission quantum yields, 20%; redox potentials, 20 mV. As far as molar absorption coefficients are concerned, the uncertainty in their absolute values is ~10% because of the very dilute solutions used (10^{-5}–10^{-4} M).

Synthesis of the new complexes

*$[Ru(2,3\text{-}Medpp)(bpy)_2](PF_6)_3$ (**1p$_1$t$_2$**)*

Solid $AgNO_3$ (65 mg, 0.384 mmol) was added to a solution of $[Ru(bpy)_2Cl_2]\cdot 2H_2O$ (100 mg, 0.192 mmol) in 1:2 (v/v) H_2O/EtOH (11 mL). The resulting suspension immediately changed color from deep red to orange, with precipitation of AgCl. After 1 h stirring at room temperature, 2,3-Medpp$^+$ (76 mg, 0.192 mmol) was added and the mixture was refluxed for 18 h. After removal of AgCl by repeated centrifugation, the solution was concentrated to 2/3 of its volume. An excess of NH_4PF_6 was added to the mother liquor and the dark red solid so obtained was filtered out. The product was then purified by recrystallization from CH_3CN–EtOH (yield 71%).

*$[Ru(2,3\text{-}Medpp)_2(bpy)](PF_6)_4$ (**1p$_2$t$_1$**)*

Solid $AgNO_3$ (11 mg, 0.062 mmol) was added to a suspension of $[Ru(2,3\text{-}Medpp)_2Cl_2](PF_6)_2$ (20 mg, 0.021 mmol) in 1:2 (v/v) H_2O/EtOH (15 mL). After 2 h stirring at room temperature, bpy (5 mg, 0.032 mmol) was added and the mixture was refluxed for 16 h. After removal of AgCl by repeated centrifugation, the solution was filtered. An excess of NH_4PF_6 was added to the mother liquor and the orange solid so obtained was filtered out. The product was washed repeatedly with diethyl ether to eliminate the excess of the ligand. The compound was dissolved in the minimum volume of CH_3CN and the solution was purified by flash chromatography on Sephadex G-10 and concentrated to a volume of about 2 mL. Addition of 12 mL of diethyl ether caused the precipitation of an orange compound that was separated by filtration (yield 77%).

*$[Ru(2,3\text{-}Medpp)_3](PF_6)_5$ (**1p$_3$**)*

Solid $AgNO_3$ (9.5 mg, 0.055 mmol) was added to a suspension of $[Ru(2,3\text{-}Medpp)_2Cl_2](PF_6)_2$ (26 mg, 0.027 mmol) in 1:2 (v/v) H_2O/EtOH (10 mL) . After stirring for 2 h at room temperature, 2,3-Medpp$^+$ (11 mg, 0.027 mmol) was added and the mixture was refluxed for 6 days, the progress of the reaction being followed by TLC. After removal of AgCl by repeated centrifugation, the solution was filtered, an excess of NH_4PF_6 was added, and the solution was rotary evaporated to dryness. The compound was dissolved in the minimum volume of

Can. J. Chem. Downloaded from www.nrcresearchpress.com by 46.23.64.124 on 09/08/12
For personal use only.

Can. J. Chem. Downloaded from www.nrcresearchpress.com by 46.23.64.124 on 09/08/12
For personal use only.

Fig. 2. Procedure for the synthesis of the luminescent and redox-active dendritic metal complexes. For labels of the complexes, see text and Fig. 1.

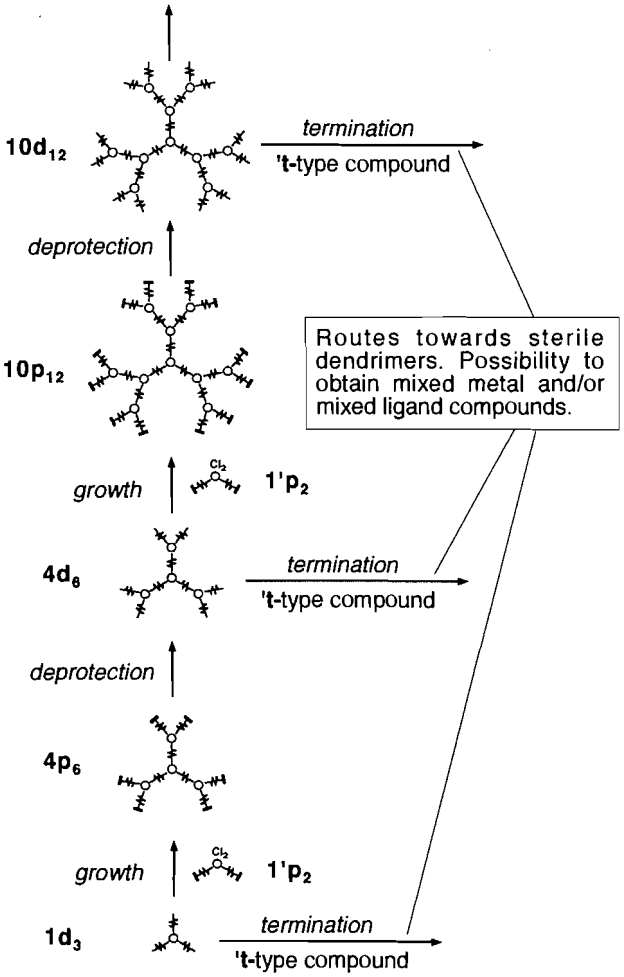

CH_3CN and the solution was purified by flash chromatography on Sephadex G-10 (1 cm × 20 cm). The first (brown-orange) eluted band contained the required complex. After concentration the product was precipitated by addition of diethyl ether (yield 25%).

*[(2,3-Medpp)$_2$Ru(μ-2,3-dpp)Ru(2,3-Medpp)$_2$](PF$_6$)$_8$ (**2p$_4$**)*
Solid $AgNO_3$ (15 mg, 0.088 mmol) was added to a suspension of [Ru(2,3-Medpp)$_2$Cl$_2$](PF$_6$)$_2$ (42 mg, 0.044 mmol) in 1:2 (v/v) H_2O/EtOH (10 mL) . After stirring for 1 h at room temperature, 2,3-dpp (5 mg, 0.022 mmol) was added and the mixture was refluxed for 15 h, the progress of the reaction being followed by TLC and absorption spectra. After removal of AgCl by repeated centrifugation, the solution was filtered and an excess of NH_4PF_6 was added. The orange solid was filtered and washed with ethanol and diethyl ether. The compound was then dissolved in acetonitrile and after addition of ethanol the solution was concentrated. The precipitate so obtained was filtered and washed with diethyl ether (yield 62%).

Elemental analyses of all the new compounds were consistent with the given formulation.

Results and discussion

The divergent synthetic approach developed to construct our dendrimers is illustrated in Fig. 2. The two key compounds for this synthesis are the [Ru(2,3-dpp)$_3$]$^{2+}$ (**1d$_3$**) and [Ru(2,3-Medpp)$_2$Cl$_2$]$^{2+}$ (**1'p$_2$**) mononuclear species. Reaction of the "complex ligand" **1d$_3$** with the "complex metal" **1'p$_2$** in a 1:3 molecular ratio leads to the tetranuclear complex **4p$_6$** (first generation of our dendrimers), which in its periphery contains six protected chelating sites. Demethylation of **4p$_6$** yields the tetranuclear complex **4d$_6$**, which can play the role of complex ligand. Reaction of **4d$_6$** with the complex metal **1'p$_2$** in 1:6 molecular ratio leads to the decanuclear compound **10p$_{12}$** (second generation of our dendrimers). Deprotection of **10p$_{12}$** leads to the decanuclear complex ligand **10d$_{12}$**, which contains 12 vacant chelating sites. The divergent iterative synthesis has been carried out up to this stage (6*d*). In principle, iteration of this procedure can lead to further generations, but difficulties are expected due to the increasing number of reaction sites (1). The reaction of the complex ligand deprotected species (**d**-family) with complex metal building blocks ('**t**-family, e.g., **1't$_2$**) yields coordinatively saturated (sterile) dendrimers (termination steps, Fig. 2).

As one can see, this synthetic procedure is based on protection–deprotection steps that involve methylation and demethylation of peripheral chelating sites. The study of the properties of methylated building blocks is therefore essential to better characterize the dendrimers.

There are also other important reasons to investigate the excited state and electrochemical properties of the novel complexes. In dendrimer terminology, **1d$_3$** is the core of a tri-dendron (three-branched structure). It could be interesting to develop di-dendron and mono-dendron structures (Fig. 3). In our systems, the cores of such structures are the mononuclear complexes **1d$_2$t$_1$** and **1d$_1$t$_2$**. Another interesting structure is that of a bis di-dendron having as a core the **2d$_4$** (which can be obtained by demethylation of **2p$_4$**). The excited state and electrochemical properties of the core units in such structures cannot be inferred by the properties of the **1d$_2$t$_1$**, **1d$_1$t$_2$**, and **2d$_4$** complexes because the properties of the 2,3-dpp bridging ligand change strongly on coordination of a second metal unit. The methylated **1p$_1$t$_2$**, **1p$_2$t$_1$**, and **2p$_4$** species, which have been investigated in this paper, can be considered much better models for such cores.

Electrochemical behavior

Previous investigations of the free 2,3-dpp and bpy ligands (18) and of their complexes (5–12) have shown that (*i*) the 2,3-dpp ligand is reduced at less negative potentials than bpy; (*ii*) in the complexes, oxidation is metal centered and reduction is ligand centered; (*iii*) metal coordination moves the reduction potentials of the ligands to much less negative values; (*iv*) when 2,3-dpp plays the role of a bridge between two metal ions, its reduction potentials move further towards less negative values.

On the basis of the above results one can expect that (*a*) the reduction potential of 2,3-Medpp$^+$ is less negative than that of 2,3-dpp since methylation is in some way similar to metal coordination; (*b*) when 2,3-dpp is methylated on one side and coordinated to a metal ion on the other side, its behavior should be somewhat similar to that exhibited by bridged 2,3-

Table 1. Electrochemical results in argon-purged acetonitrile solution at room temperature.[a]

Compound	E_{ox}	E_{red}							
$[Ru(bpy)_3]^{2+}$ [b]	+1.29	−1.33	−1.52	−1.78					
p		−0.76[c]	−1.16	−1.57					
d[d]		−1.93	−2.55	−2.74					
$\mathbf{1p_1t_2}$	+1.47	−0.72[c]	−0.90	−1.03	−1.16	−1.51	−1.72		
$\mathbf{1d_1t_2}$[d,e]	+1.31	−1.04	−1.43	−1.64					
$\mathbf{1p_2t_1}$	+1.66	−0.67[c]	−0.78[c]	−0.92	−1.03	−1.19	−1.34	−1.48	−1.73[f]
$\mathbf{1d_2t_1}$[d,e]	+1.46	−0.99	−1.17	−1.58					
$\mathbf{1p_3}$	+1.77	−0.63[c]	−0.80[c,g]	−0.95	−1.06	−1.16	−1.44[f]		
$\mathbf{1d_3}$[d]	+1.60	−0.94	−1.08	−1.32					
$\mathbf{2p_4}$	+1.82	−0.64[c]	−0.78[c,g]	−0.92[c]	−1.03[c]	−1.12	−1.21	−1.46[f]	

[a]Potentials in volts vs. SCE; unless otherwise noted, the waves are reversible and monoelectronic; for irreversible waves the potential is evaluated from the DPV peaks.
[b]This work, in agreement with literature data (5*a*).
[c]Irreversible wave.
[d]E_{red} taken from ref. 18 (only the data relevant for this paper are reported).
[e]E_{ox} values taken from ref. 20.
[f]Multielectronic wave.
[g]Bielectronic wave.

Fig. 3. Schematic representation of dendrimers based on tri- (a), di- (b), mono- (c), and bis di-dendron (d) cores.

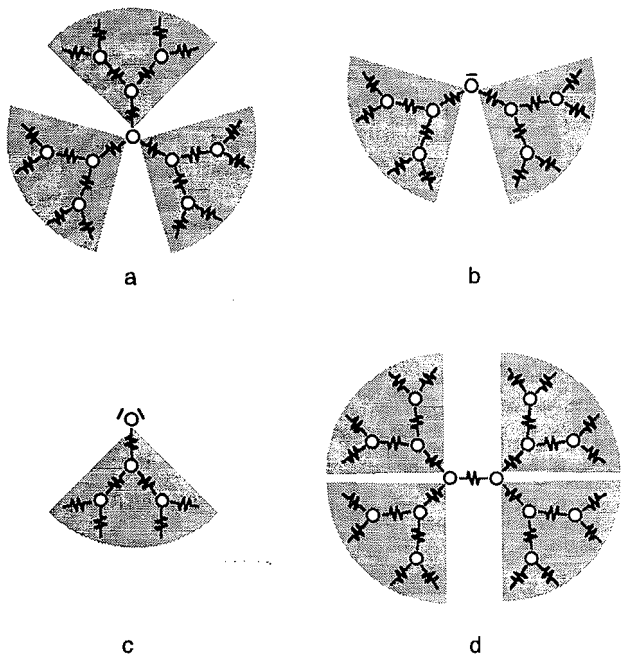

dpp in polynuclear metal complexes; however, the methylated and metal-coordinated sites are not equivalent.

The results obtained are gathered in Table 1 and displayed in graphical form in Fig. 4. To facilitate the discussion, previously reported data for compounds of related families are also shown.

Electrochemical oxidation

All the oxidation processes are reversible with ΔE ca. 60 mV. The data reported in Table 1 and Fig. 4 show that on replacing bpy of $[Ru(bpy)_3]^{2+}$ with 2,3-dpp or 2,3-Medpp$^+$, a progressive increase in the potential at which the metal is oxidized occurs. It can also be noted that the displacement caused by 2,3-Medpp$^+$ is larger than that caused by 2,3-dpp. These results can be rationalized by considering that the electron donor power decreases in the series bpy > 2,3-dpp > 2,3-Medpp$^+$. For the dinuclear complex $\mathbf{2p_4}$, one could expect either simultaneous or successive oxidation of the two metal centers, depending on the degree of metal–metal interaction. The observed oxidation wave is monoelectronic, close to the upper limit of the potential window in the solvent used. This suggests that there is a noticeable metal–metal interaction and that the second oxidation process cannot be seen because of experimental limitations.

Electrochemical reduction

Most of the reduction processes exhibit an irreversible character in cyclic voltammetry (CV). The following discussion will therefore be limited to a few considerations based on the observed sequences of the differential pulse voltammetry peaks (Table 1 and Fig. 4).

First of all, one can notice that upon methylation the first three reduction waves of 2,3-dpp are displaced to less negative potentials by as much as 1.1–1.4 V. Metal coordination on 2,3-dpp has a similar, but smaller, effect. Metal coordination on 2,3-Medpp$^+$ has, apparently, an even smaller effect, suggesting that reduction occurs on the methylated pyridine.

From Fig. 4 it is clear that the first reduction process of $\mathbf{1p_1t_2}$ concerns the 2,3-Medpp$^+$ ligand, most likely on the methylated pyridine (see above). The second and third reduction processes occur in the potential range for which 2,3-dpp is reduced in $\mathbf{1d_1t_2}$ (18). Since in $\mathbf{1d_1t_2}$ bpy reduction occurs at more negative potentials (18), the second and third reduction processes of $\mathbf{1p_1t_2}$ can be assigned to the 2,3-Medpp$^+$ ligand. Comparison with the second and third reduction waves of free 2,3-Medpp$^+$ shows that the third wave is much more affected by metal coordination than the second one. Therefore one can conclude that the third reduction process involves the metal-coordinated site more directly. Whereas the fourth reduction wave of $\mathbf{1p_1t_2}$ is difficult to assign, the fifth and the sixth can be attributed to bpy reduction.

Can. J. Chem. Downloaded from www.nrcresearchpress.com by 46.23.64.124 on 09/08/12
For personal use only.

Fig. 4. Schematic comparison of the redox potentials for the new compounds and related parent species (see also Table 1). The greyed circles represent multielectronic processes. Notice that the reductions of **d** occur outside the potential range shown in this figure. For the labels of the compounds, see text and Fig. 1.

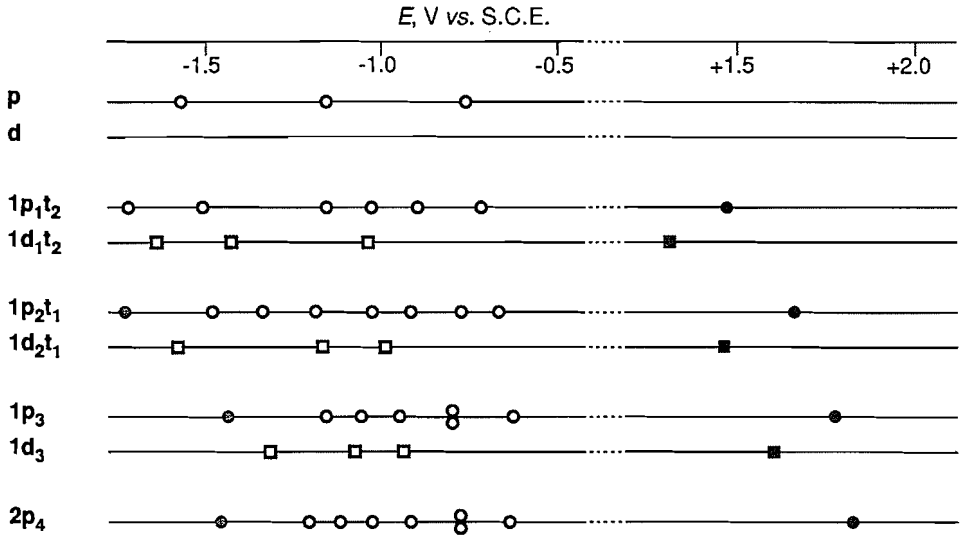

For $\mathbf{1p_2t_1}$, where two 2,3-Medpp$^+$ ligands are present, one could assign the first two processes to successive reduction of the two methylated sites. This would imply some interaction between the methylated pyridine moieties. According to this hypothesis the first wave moves slightly to less negative potentials compared with $\mathbf{1p_1t_2}$ because replacement of bpy by 2,3-Medpp$^+$ makes the metal ion more positive. The smaller separation between the two reduction waves compared with $\mathbf{1d_2t_1}$ (18) can be accounted for by the increased distance between the two reduced sites. An alternative interpretation will be given after discussion of $\mathbf{1p_3}$.

For $\mathbf{1p_3}$ the results show that there is a first, monoelectronic, process followed by a two-electron process. An attempt to assign these reduction processes can be based on the following considerations. The metal-coordinated site of 2,3-dpp in $\mathbf{1d_1t_2}$ is 300 mV more difficult to reduce than the methylated site of 2,3-Medpp$^+$ in $\mathbf{1p_1t_2}$ (Table 1). In the latter complex, however, the metal-coordinated site of 2,3-Medpp$^+$, because of its positive charge, is certainly easier to reduce than the metal-coordinated site of 2,3-dpp of the former complex. Furthermore, the difference in the reduction potential between the methylated and metal-coordinated site of 2,3-Medpp$^+$ is expected to decrease substantially along the series $\mathbf{1p_1t_2}$, $\mathbf{1p_2t_1}$, $\mathbf{1p_3}$ because of the increase in the positive charge on the metal, as shown by the parallel displacement to more positive potentials of the (metal-centered) oxidation wave (Table 1, Fig. 4). Therefore in $\mathbf{1p_3}$ the reduction orbitals of the methylated and metal-coordinated sites are likely very close in energy and their relative position can change upon addition of electrons. It should also be noted that for reasons of distance the interaction between the metal-coordinated sites is much stronger than the interaction between the methylated sites. In the light of the above considerations, the reduction pattern of $\mathbf{1p_3}$ could be interpreted as follows. The first reduction process may concern an orbital of the metal-coordinated sites. The second electron would then enter a methylated site, but its presence raises the energy of the orbitals of the metal-coordinated sites, while it does not practically affect the energy of the two other methylated sites. In other words, for the two-electron reduced species the lowest energy orbitals could be those of the three (weakly interacting) methylated sites. As a consequence, the third methylated site would also become available for reduction at the same potential as the second one, accounting for the observed reduction pattern.

Within this scheme, the first two reduction waves of $\mathbf{1p_2t_1}$ can be assigned to a metal-coordinated site and a methylated site, respectively, with a subsequent electron rearrangement to give a species where the two methylated sites are reduced.

The above discussion suggests that detailed assignment of reduction waves occurring at more negative potentials of $\mathbf{1p_2t_1}$ and $\mathbf{1p_3}$ is difficult because several reduction orbitals of different localization, whose energy ordering can change on successive addition of electrons, are present.

The behavior of the dinuclear $\mathbf{2p_4}$ complex is similar to that of $\mathbf{1p_3}$, with the additional complication that two, nonequivalent chelating sites (of bridging and methylated ligands) are present. A tentative interpretation of the first four reduction waves can be given along the same guidelines followed for $\mathbf{1p_3}$. The first reduction process could involve an orbital of the bridging ligand more localized on one of the two metal ions. This would increase in energy the reduction orbitals of the confining methylated sites, leaving unperturbed the energy of the reduction orbitals of the two methylated sites belonging to the other moiety of the complex. The second and third reduction processes could thus involve the latter (non-interacting) sites. The fourth process would then concern a methylated site of the moiety of the reduced metal-coordinated sites. This would probably change the orbital energy ordering, leading to a species where the four electrons are localized on the four methylated sites.

Excited state properties

The absorption and luminescence spectra of compounds $\mathbf{1p_1t_2}$, $\mathbf{1p_2t_1}$, $\mathbf{1p_3}$, and $\mathbf{2p_4}$ are shown in Figs. 5 and 6, respectively. Table 2 shows the wavelengths of the lowest energy absorption maxima, the wavelengths of the maxima of the lumines-

Can. J. Chem. Downloaded from www.nrcresearchpress.com by 46.23.64.124 on 09/08/12
For personal use only.

Can. J. Chem. Downloaded from www.nrcresearchpress.com by 46.23.64.124 on 09/08/12
For personal use only.

Fig. 5. Absorption spectra of the new complexes in acetonitrile solution at room temperature. For abbreviations, see text and Fig. 1.

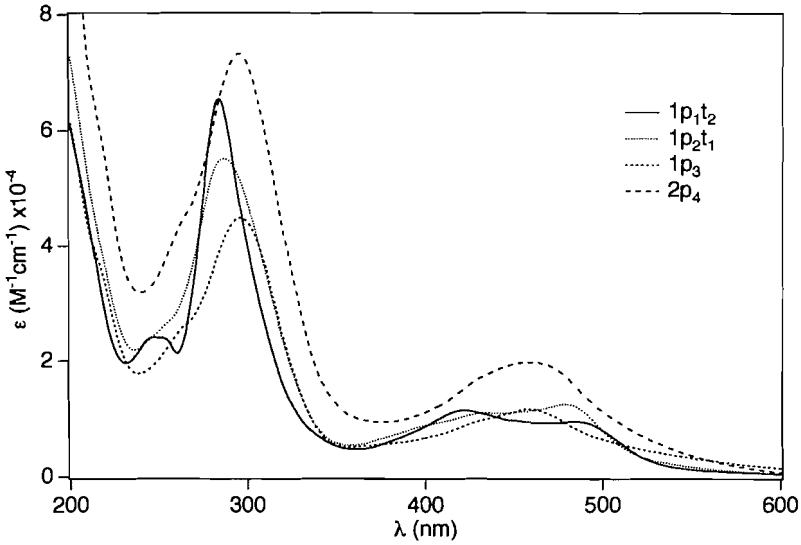

Fig. 6. Luminescence spectra (uncorrected) of the new complexes in acetonitrile fluid solution at room temperature (top) and in MeOH/EtOH 4:1 (v/v) rigid matrix at 77 K (bottom). For abbreviations, see text and Fig. 1.

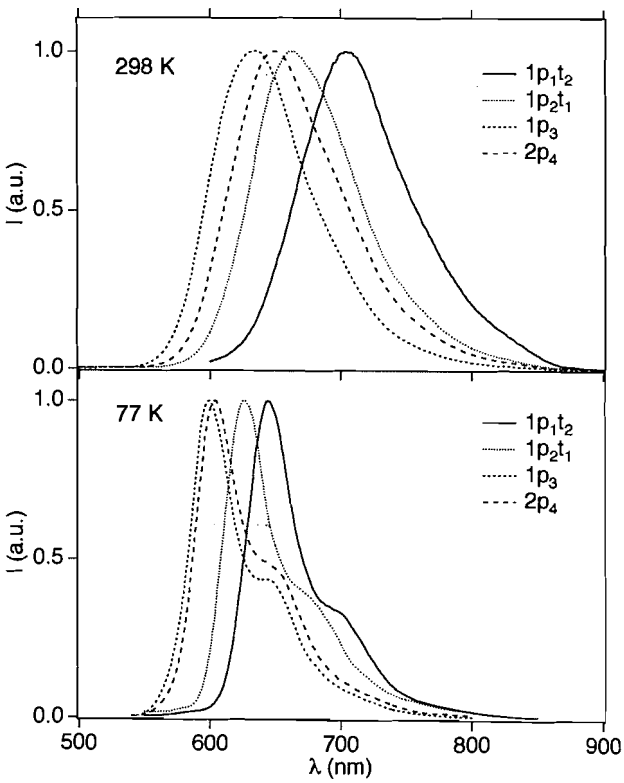

cence bands at 298 and 77 K, the lifetimes of the luminescent excited states at 298 and 77 K, and the luminescence quantum yields at 298 K. The corresponding data for related complexes ($[Ru(bpy)_3]^{2+}$, corresponding mononuclear d-family compounds, and $[(bpy)_2Ru(\mu\text{-}2,3\text{-}dpp)Ru(bpy)_2]^{4+}$ (**2t$_4$**)) are also shown for comparison purposes.

It is well known (5) that in Ru(II)–polypyridine complexes the absorption bands in the visible region are due to spin-allowed transitions from a metal-centered orbital (t_{2g} in octahedral symmetry) to a ligand-centered orbital (π^*). Such transitions are usually called MLCT (metal-to-ligand charge transfer). It is also known that the luminescent excited state is the lowest lying, formally triplet MLCT level, ^{3}MLCT.

It is convenient to compare and discuss the properties of the mononuclear compounds investigated starting from the $[Ru(bpy)_3]^{2+}$ parent complex and observing the effect obtained when one or more bpy ligands are replaced by 2,3-dpp or 2,3-Medpp$^+$ ligands.

Let us first recall the properties of the **1d$_1$t$_2$**, **1d$_2$t$_1$**, and **1d$_3$** complexes. As we have seen above, 2,3-dpp is a worse electron donor and a better electron acceptor than bpy. In particular, its lowest energy π^* orbital lies below that of bpy (6). As a consequence, in **1d$_1$t$_2$** the lowest energy MLCT excited state involves the 2,3-dpp ligand and lies at lower energy than the lowest MLCT level of $[Ru(bpy)_3]^{2+}$. Therefore, the absorption and emission bands of **1d$_1$t$_2$** are red-shifted compared with those of $[Ru(bpy)_3]^{2+}$ (Table 1). Passing to **1d$_2$t$_1$**, and **1d$_3$**, the lowest energy π^* orbital remains that of 2,3-dpp, but the energy of the t_{2g} metal orbital decreases because 2,3-dpp is a worse electron donor than bpy, as also shown by the potentials for the metal oxidation. For this reason, both the absorption and emission maxima move progressively to the blue along the **1d$_1$t$_2$**, **1d$_2$t$_1$**, and **1d$_3$** series. In the last compound, however, the bands are still red shifted compared with $[Ru(bpy)_3]^{2+}$, indicating that the stabilization of the π^* orbital in passing from bpy to 2,3-dpp is not compensated by the corresponding stabilization of the t_{2g} metal orbitals.

Methylation of 2,3-dpp stabilizes the π^* ligand orbital and at the same time reduces the electron-donor power. Therefore in the mixed-ligand **1p$_1$t$_2$** complex the lowest energy MLCT transition involves the 2,3-Medpp$^+$ ligand and the corresponding absorption and emission bands are red shifted with respect to both $[Ru(bpy)_3]^{2+}$ and **1d$_1$t$_2$** (Table 1). On passing to **1p$_2$t$_1$**, and **1p$_3$**, the bands move to the blue for the same reason discussed above.

Comparison between the **1d$_1$t$_2$**, **1d$_2$t$_1$**, and **1d$_3$** compounds

Table 2. Spectroscopic and photophysical data.[a]

	Absorption[b] 298 K λ_{max}, nm (ε, M^{-1} cm^{-1})	Luminescence 298 K λ_{max},[d] nm	τ,[e] ns	Φ_{em}[e]	77 K[c] λ_{max},[d] nm	τ, μs
$[Ru(bpy)_3]^{2+}$[f]	451 (13 000)	630	890[g]	0.059[g]	587	4.8
$\mathbf{1p_1t_2}$	485 (9 550)	735	240	0.011	649	3.4
$\mathbf{1p_2t_1}$	480 (12 500)	690	570	0.028	627	4.5
$\mathbf{1p_3}$	458 (11 700)	652	760[h]	0.018	600	5.7
$\mathbf{1d_1t_2}$[i]	475 sh (11 500)	691	380	0.023	628	4.2
$\mathbf{1d_2t_1}$[j]	465 (13 600)	670	253[k]		622	
$\mathbf{1d_3}$[l]	455 (13 000)	650	190[h]	0.013	600	5.1
$\mathbf{2p_4}$	457 (19 900)	668	870	0.033	607	5.5
$\mathbf{2t_4}$[i]	527 (24 200)	802	125	0.003	709	2.0

[a]In acetonitrile solution, unless otherwise noted.
[b]Lowest energy absorption band.
[c]In 4:1 MeOH/EtOH matrix.
[d]Corrected emission maxima.
[e]Deaerated solution, unless otherwise noted.
[f]This work, unless otherwise noted, in agreement with literature data (5*a*).
[g]From ref. 21.
[h]This is not strictly a single exponential decay.
[i]From ref. 7*b*.
[j]From ref. 20.
[k]Aerated solution.
[l]For previously reported data see ref. 15.

and the corresponding methylated species $\mathbf{1p_1t_2}$, $\mathbf{1p_2t_1}$, and $\mathbf{1p_3}$ shows that the bands of $\mathbf{1p_1t_2}$, are strongly red shifted compared with those of $\mathbf{1d_1t_2}$, and that such a shift decreases (especially as far as the emission bands are concerned) for the second members of the two series and becomes almost negligible for the third members. This behavior is due to the fact that replacing the "ancillary" ligands affects the energy of the t_{2g} metal orbitals more effectively with 2,3-Medpp$^+$ than with 2,3-dpp.

We have seen above that in the mononuclear species replacement of bpy with 2,3-Medpp$^+$ causes a decrease in the energy of the lowest excited state. It is interesting to notice that the opposite effect occurs for the dinuclear species. This different behavior originates from the fact that in $\mathbf{2t_4}$ and $\mathbf{2p_4}$ there is a 2,3-dpp ligand that bridges two metal ions (μ-2,3-dpp). It is well known that coordination to two metal ions lowers considerably the energy of the π^* orbital of 2,3-dpp (6–12), so that the lowest excited state of $\mathbf{2t_4}$ involves charge transfer from the t_{2g} metal orbital to the π^* orbital of the bridging ligand. This, coupled with the presence of strong electron-donating ancillary bpy ligands, accounts for the very low energy of the absorption and emission bands in $\mathbf{2t_4}$. When bpy is replaced by the weaker electron donor 2,3-Medpp$^+$ (i.e., in $\mathbf{2p_4}$), the Ru → μ-2,3-dpp CT transition is displaced to higher energy. The Ru → μ-2,3-dpp level could even move above the Ru → 2,3-Medpp$^+$ level, which in $\mathbf{2p_4}$ is expected to lie at higher energy than in $\mathbf{1p_2t_1}$: the electrochemical results, however, show that the LUMO is centered on μ-2,3-dpp, so that also the luminescent level should involve the bridging ligand.

The data collected in Table 2 show that the luminescence efficiencies and lifetimes for the methylated complexes are in the range expected for Ru(II)–polypyridine complexes. In particular, the excited state lifetimes of $\mathbf{1p_3}$ and $\mathbf{2p_4}$ are very close to that exhibited by $[Ru(bpy)_3]^{2+}$. More generally, within the family of mononuclear methylated compounds one can observe a decrease of the excited state lifetime (both at 77 and 298 K) along the series $\mathbf{1p_3} > \mathbf{1p_2t_1} > \mathbf{1p_1t_2}$. One can notice that the excited state energy also decreases along the series.

It is well known (5) that the ^{3}MLCT luminescent level of Ru(II)–polypyridine complexes can undergo nonradiative deactivation through two different routes: (*i*) direct decay to the ground state, whose rate increases with decreasing energy of the ^{3}MLCT level (energy-gap rule (19)); (*ii*) thermally activated crossing to an upper lying, triplet metal-centered level, ^{3}MC, which is strongly distorted compared to the ground state geometry and therefore undergoes fast deactivation to the ground state. At low temperature (77 K) the second route is certainly frozen so that one expects the rate of radiationless decay to increase with decreasing energy of the ^{3}MLCT level. Using the Φ_{em} and τ values at 298 K (Table 2) it is possible to calculate the radiative (k_r) rate constant by eq. [1].

$$[1] \quad k_r = \Phi_{em}/\tau$$

The nonradiative rate constant (k_{nr}) value at 77 K has been evaluated by eq. [2] using the τ value at 77 K, and with the usual approximation that the k_r value is independent of temperature.

$$[2] \quad k_{nr} = 1/\tau - k_r$$

Figure 7 presents the plot of log k_{nr} vs. emission energy at 77

Can. J. Chem. Downloaded from www.nrcresearchpress.com by 46.23.64.124 on 09/08/12
For personal use only.

Fig. 7. Plot of log k_{nr} vs. emission energy for the complexes studied. Data refer to 77 K photophysical properties.

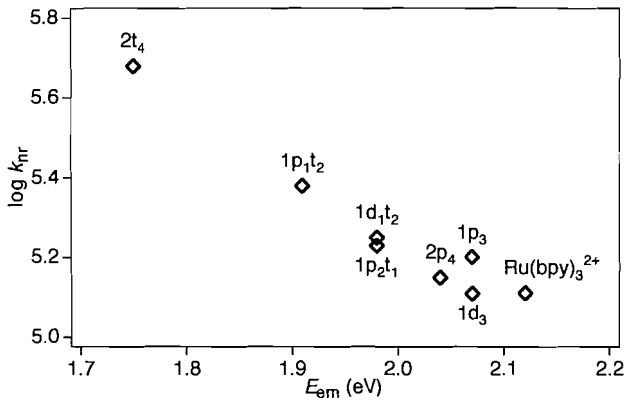

K, showing that the energy-gap rule is satisfactorily obeyed at low temperature. At room temperature route (*ii*) also becomes important. Quantitative assessments of the relative importance of routes (*i*) and (*ii*) at room temperature are difficult to discuss, since the energy of the upper-lying ^{3}MC state is also expected to change.

Acknowledgements

We wish to thank L. Minghetti, M. Minghetti, and L. Ventura for technical assistance. This work was supported by the Consiglio Nazionale delle Ricerche (Progetto Strategico Tecnologie Chimiche Innovative) and the Ministero dell'Università e della Ricerca Scientifica e Tecnologica. S.S. would like to thank CNR for the grant No. 201.03.20. I.R.R. was Erasmus Exchange Student, from Barcelona University, for the academic year 1993–1994.

References

1. (*a*) D.A. Tomalia, A.M. Naylor, and W.A. Goddard III. Angew. Chem. Int. Ed. Engl. **29**, 138 (1990); (*b*) G.R. Newkome, C.N. Moorefield, and G.R. Baker. Aldrichimica Acta, **25**, 31 (1992); (*c*) D.A. Tomalia and H.D. Durst. Top. Curr. Chem. **165**, 193 (1993); (*d*) J.M.J. Fréchet. Science, **263**, 1710 (1994); (*e*) R.F. Service. Science, **267**, 458 (1995); (*f*) G. Denti, S. Campagna, and V. Balzani. *In* Mesomolecules: from molecules to materials. *Edited by* D. Mendenhall, A. Greenberg, and J. Liebman. Chapman and Hall, New York. 1995. p. 69.
2. F.L. Carter, R.E. Siatkowski, and H. Wohltjen (*Editors*). Molecular electronic devices. North-Holland, Amsterdam. 1988.
3. V. Balzani, L. Moggi, and F. Scandola. *In* Supramolecular photochemistry. *Edited by* V. Balzani. Reidel, Dordrecht, The Netherlands. 1987. p. 1.
4. (*a*) J.-M. Lehn. Angew. Chem. Int. Ed. Engl. **29**, 1304 (1990); (*b*) V. Balzani and F. Scandola. Supramolecular photochemistry. Horwood, Chichester, U.K. 1991; (*c*) B. O'Regan and M. Graetzel. Nature, **353**, 737 (1991).
5. (*a*) A. Juris, V. Balzani, F. Barigelletti, S. Campagna, P. Belser, and A. von Zelewsky. Coord. Chem. Rev. **84**, 85 (1988); (*b*) T.J. Meyer. Acc. Chem. Res. **22**, 163 (1989); (*c*) F. Scandola, M.T. Indelli, C. Chiorboli, and C.A. Bignozzi. Top. Curr. Chem. **158**, 73 (1990); (*d*) K. Kalyanasundaram. Photochemistry of polypyridine and porphyrin complexes. Academic Press, London. 1991.
6. (*a*) G. Denti, S. Serroni, S. Campagna, A. Juris, M. Ciano, and V. Balzani. *In* Perspectives in coordination chemistry. *Edited by* A.F. Williams, C. Floriani, and A.E. Merbach. VCH, Basel. 1992. p. 153; (*b*) G. Denti, S. Serroni, S. Campagna, A. Juris, and V. Balzani. Mol. Cryst. Liquid Cryst. **234**, 79 (1993); (*c*) V. Balzani, S. Campagna, G. Denti, A. Juris, S. Serroni, and M. Venturi. Coord. Chem. Rev. **132**, 1 (1994); (*d*) S. Campagna, G. Denti, S. Serroni, A. Juris, M. Venturi, V. Ricevuto, and V. Balzani. Chem. Eur. J. **1**, 211 (1995).
7. (*a*) S. Campagna, G. Denti, L. Sabatino, S. Serroni, M. Ciano, and V. Balzani. J. Chem. Soc. Chem. Commun. 1500 (1989); (*b*) G. Denti, S. Campagna, L. Sabatino, S. Serroni, M. Ciano, and V. Balzani. Inorg. Chem. **29**, 4750 (1990); (*c*) G. Denti, S. Serroni, S. Campagna, V. Ricevuto, and V. Balzani. Inorg. Chim. Acta, **182**, 127 (1991); (*d*) G. Denti, S. Serroni, S. Campagna, V. Ricevuto, and V. Balzani. Coord. Chem. Rev. **111**, 227 (1991).
8. (*a*) S. Campagna, G. Denti, S. Serroni, M. Ciano, and V. Balzani. Inorg. Chem. **30**, 3728 (1991); (*b*) G. Denti, S. Serroni, S. Campagna, V. Ricevuto, A. Juris, and V. Balzani. Inorg. Chim. Acta, **198–200**, 507 (1992).
9. G. Denti, S. Campagna, L. Sabatino, S. Serroni, M. Ciano, and V. Balzani. Inorg. Chim. Acta, **176**, 175 (1991).
10. (*a*) S. Serroni, G. Denti, S. Campagna, M. Ciano, and V. Balzani. J. Chem. Soc. Chem. Commun. 944 (1991); (*b*) G. Denti, S. Campagna, S. Serroni, M. Ciano, and V. Balzani. J. Am. Chem. Soc. **114**, 2944 (1992).
11. S. Campagna, G. Denti, S. Serroni, M. Ciano, A. Juris, and V. Balzani. Inorg. Chem. **31**, 2982 (1992).
12. S. Serroni, G. Denti, S. Campagna, A. Juris, M. Ciano, and V. Balzani. Angew. Chem. Int. Ed. Engl. **31**, 1493 (1992).
13. (*a*) G.R. Newkome, F. Cardullo, E.C. Constable, C.N. Moorefield, and A.M.W. Cargill Thompson. J. Chem. Soc. Chem. Commun. 925 (1993); (*b*) Y.-H. Liao and J.R. Moss. J. Chem. Soc. Chem. Commun. 1774 (1993); (*c*) S. Achar and R.J. Puddephatt. Angew. Chem. Int. Ed. Engl. **33**, 847 (1994).
14. B.P. Sullivan, D.J. Salmon, and T.J. Meyer. Inorg. Chem. **17**, 3334 (1978).
15. K.J. Brewer, W.R. Murphy, Jr., S.R. Spurlin, and J.D. Petersen. Inorg. Chem. **25**, 882 (1986).
16. J.N. Demas and G.A. Crosby. J. Phys. Chem. **75**, 991 (1971).
17. K. Nakamaru. Bull. Chem. Soc. Jpn. **55**, 2697 (1982).
18. S. Roffia, M. Marcaccio, C. Paradisi, F. Paolucci, V. Balzani, G. Denti, S. Serroni, and S. Campagna. Inorg. Chem. **32**, 3003 (1993).
19. J.V. Caspar and T.J. Meyer. J. Am. Chem. Soc. **105**, 5583 (1983).
20. G. Denti, S. Campagna, L. Sabatino, S. Serroni, M. Ciano, and V. Balzani. *In* Photochemical conversion and storage of solar energy. *Edited by* E. Pelizzetti and M. Schiavello. Kluwer, Dordrecht, The Netherlands. 1991. p. 27.
21. K. Nakamaru. Bull. Chem. Soc. Jpn. **55**, 1639 (1982).

Can. J. Chem. Downloaded from www.nrcresearchpress.com by 46.23.64.124 on 09/08/12
For personal use only.

Investigation of mesophase transitions in liquid crystals using inverse gas chromatography

Gareth J. Price and Ian M. Shillcock

Abstract: Inverse Gas Chromatography, IGC, has been used to study phase transitions in three low molar mass liquid crystals and one side-chain liquid crystalline polymer. This extension of previous work has shown that transitions between all of the various mesophases can be detected and their temperatures measured with an accuracy and precision comparable to that of more conventional techniques. For one of the compounds, 4,4′-(*n*-hexyloxy)cyanobiphenyl, the kinetics of solidification from the supercooled nematic phase have been measured. The process took place in two stages which could be interpreted in terms of a modified version of the Avrami model of polymer crystallization. An explanation of the results is that the solid support is providing a large number of nucleation sites for the initial part of the solidification, which is completed in a slow, diffusion-limited process. However, further work is required to confirm this mechanism.

Key words: inverse gas chromatography (IGC), liquid crystals, mesophase transitions, activity coefficients, retention volumes.

Résumé : On a utilisé la chromatographie en phase gazeuse inverse (IGC) pour étudier les transitions de phase de trois cristaux liquides de faibles masses molaires et d'un polymère cristal-liquide avec chaîne latérale. Cette extension du travail précédent a permis de démontrer que l'on peut détecter toutes les transitions entre les diverses mésophases et de mesurer leurs températures avec une exactitude et une précision comparables à celles des techniques plus conventionnelles. Pour l'un des composés, le 4,4′-(*n*-hexyloxy)cyanobiphényle, on a mesuré la cinétique de la solidification à partir de la phase nématique surrefroidie. Le processus se produit en deux étapes que l'on peut interpréter en fonction d'une version modifiée du modèle d'Avrami de la cristallisation d'un polymère. On peut expliquer les résultats en supposant que le support solide fournit un grand nombre de sites de nucléation pour la partie initiale de la solidification que est complétée par un processus lent, à diffusion limitée. Toutefois, des travaux ultérieurs seront nécessaires pour confirmer ce mécanisme.

Mots clés : chromatographie gazeuse inverse (IGC), cristaux liquides, coefficients d'activité, volumes de rétention.

[Traduit par la rédaction]

Introduction

The use of Inverse Gas Chromatography, IGC, for characterizing structure and interactions in involatile materials was pioneered by Guillet and co-workers in the late 1960s and early 1970s (1–3). The alternative term "molecular probe experiment" (4) more accurately describes the technique. A volatile compound introduced into the carrier gas is used to "probe" the properties of an involatile material packed into the chromatography column. Since its introduction, a large number of materials have been studied by IGC although perhaps the major class has been polymers (5). The basis of the method is the recording, under accurately controlled conditions, of the specific retention volume, $V°_g$, the volume of carrier gas at S.T.P. needed to elute a probe molecule from the column per gram of stationary phase (6). Isothermal operation allows determination of thermodynamic parameters such as activity coefficients and interaction parameters (7–10) in bulk polymers or blends and investigation of the chemical nature of polymeric surfaces (11, 12). The temperature variation of retention, plotted in the form shown schematically in Fig. 1, allows measurement of a range of structural transitions (13–16).

At low temperatures, the probe can only interact with the surface of the glassy polymer (3–5). In general, the retention volume decreases with rising temperature. However, as the temperature passes through the glass transition temperature, T_g, the probe can enter the structure of amorphous regions of the rubbery polymer leading to a deviation from linearity of the retention diagram. The retention volume now rises until all of the amorphous region can be probed and the plot returns to linearity. Crystalline regions of the polymer are impermeable to the probe so that, when melting occurs, the amount of amorphous material and hence the retention volume increases leading to a second transition in the diagram. Above the maximum temperature at which crystalline polymer exists, i.e., the melt-

Received April 10, 1995.

This paper is dedicated to Professor J.E. (Jim) Guillet in recognition of his contributions to Canadian chemistry.

G.J. Price[1] and I.M. Shillcock. School of Chemistry, University of Bath, Claverton Down, Bath, BA2 7AY, U.K.

[1] Author to whom correspondence may be addressed. Telephone: +44 1225 826504. Fax: +44 1225 826231. E-mail: G.J.Price@uk.ac.bath

Can. J. Chem. Downloaded from www.nrcresearchpress.com by 46.23.64.124 on 09/08/12
For personal use only.

Can. J. Chem. Downloaded from www.nrcresearchpress.com by 46.23.64.124 on 09/08/12
For personal use only.

Fig. 1. Schematic retention diagram for a semicrystalline polymer.

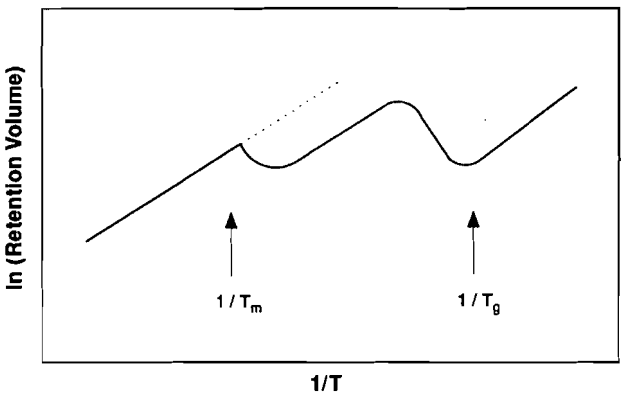

ing temperature, T_m, the plot returns to linearity and equilibrium bulk sorption measurements can be made. In some cases, other transitions such as side-group rotations have been associated (14) with other deviations from linearity in the plots.

The difference between the retention volume in the semicrystalline region and that at the same temperature extrapolated from the totally amorphous region (shown by the broken line in Fig. 1) can be used to investigate the amount of crystalline material in polymers. It follows that

$$[1] \quad \text{Crystalline fraction} = \left(1 - \frac{V°_g(\text{experimental})}{V°_g(\text{extrapolated})}\right)$$

This approach has been used to estimate both the degree of crystallinity (3, 4, 15, 16) and, by following retention as a function of time, the rate of crystallization (17) in polymers. The IGC method has the advantage over, for example, density measurements that no properties of the 100% crystalline material are needed. The usual method of interpreting polymer crystallization (18) relies on the Avrami method (19, 20), which relates the volume fraction of crystalline material, V_c to the time, t, by:

$$[2] \quad (1 - V_c) = \exp -(K t^n)$$

where K is effectively a rate constant for the crystallization and the exponent n is an integer representing (21) the sum of the number of dimensions in which crystal growth takes place (1 for rods, 2 for discs, and 3 for spherulites) and the order of the time dependence of the nucleation (0 for instantaneous nucleation and 1 for sporadic growth where the number of nucleation sites varies linearly with time). Hence, n is typically 4 for an ideal spherulitic crystal growth. However, this model is recognised to be somewhat idealized and, in reality, several crystallization mechanisms often operate concurrently leading to the measurement of fractional exponents.

Liquid crystals, and in particular liquid crystal polymers, LCPs, are becoming increasingly important in a number of technologies (22). Liquid crystalline stationary phases are finding increasing use in analytical GC where they allow the separation of closely related isomers (23) on the basis of their molecular shapes. The thermodynamic properties of a small number of these materials have been studied using IGC (24–29). Romansky and Guillet (30) have also studied main-chain liquid crystal polymers and Laub and co-workers (31) have investigated some of the thermodynamic properties of side-chain LCPs from the point of view of their use as analytical stationary phases.

Despite the work described above, there has not been, to our knowledge, a systematic and comprehensive study of the use of IGC to investigate a range of the properties of liquid crystals. The present authors illustrated the potential of IGC for studying these materials in a preliminary study of the transition temperatures in one low molecular weight and one polymeric cyanobiphenyl (32). In this paper, that study is extended to a wider range of mesophase types. In addition, the methods used to investigate crystallinity in polymers have been applied to one of the liquid crystals in order to measure the rate of transition from the mesophase to the solid crystal phase.

Experimental

Differential scanning calorimetry

To give a comparison with the IGC results, the transition temperatures were also measured using a DuPont 9900 calorimeter employing an indium control for calibration. As usual, a small variation of the results obtained at different heating rates was noticed and, to allow accurate values to be recorded in a convenient time, a heating or cooling rate of 5°C min^{-1} was employed. Cycling was commenced at room temperature and the temperature raised to well above the highest transition before cooling at 5°C min^{-1}. Duplicate runs were performed in all cases.

Inverse gas chromatography

Chromatographic measurements were performed on a modified Pye Unicam 204 chromatograph fitted with FID detection and modified by the addition of fittings that allowed the pressure at the inlet to the column to be measured using a mercury manometer. The apparatus conformed in terms of temperature and flow rate stability to the accepted requirements for this type of work.[2] Nitrogen was used as the carrier gas at flow rates between 20 and 80 cm^3 min^{-1}, measured using a soap bubble flow meter. The probe molecules, detailed below, were of analytical grade or better and were obtained from commercial sources. Their retention times were determined by injecting approximately 0.01–0.05 μL from a syringe and recording to ±0.01 min with a Spectra-Physics SP4270 integrator. The mean of at least three readings agreeing to within experimental uncertainty was recorded. No dependence on the amount of probe injected was noted for any system reported here. The column temperature was measured to ±0.1°C using a thermocouple attached to the column that had been calibrated against a Tinsley Type 5840 platinum resistance thermometer. The temperature variation through the oven was less than 0.2°C.

Column preparation

Three low molecular weight liquid crystals were studied along with a side-chain polysiloxane containing a cyanobiphenyl mesogen. They were chosen to demonstrate the applicability of our methods to a number of different mesophases including nematic (N), smectic-A (S_A), smectic-C (S_C), and cholesteric (C) as well as the isotropic (I) and solid crystalline (K) phases.

[2] A.E. Bolivari, T.C. Ward, P.A. Koning, and D.P. Sheehy. See ref. 2, p. 12.

Can. J. Chem. Downloaded from www.nrcresearchpress.com by 46.23.64.124 on 09/08/12
For personal use only.

Fig. 2. Structures and expected phase transition of the liquid crystal stationary phases (temperatures in °C).

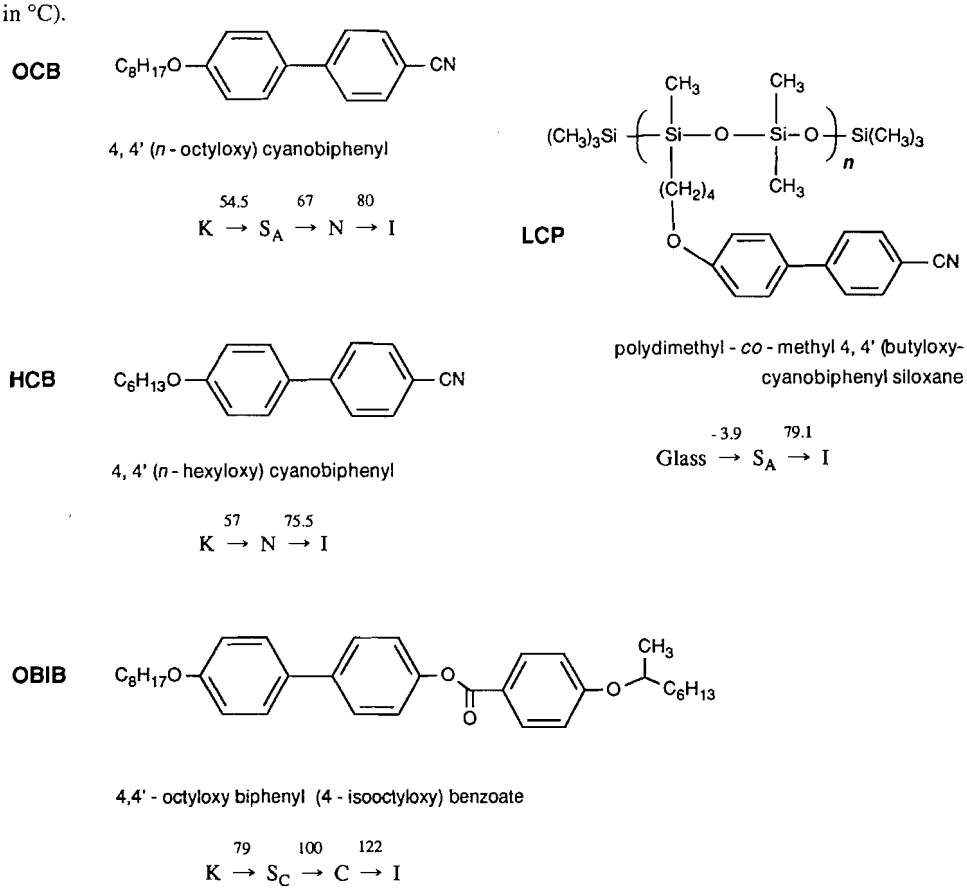

The structures, along with the manufacturer's reported phase transitions, are shown in Fig. 2. The acronyms which will be used for each of the LCs used are also shown.

The stationary phases were prepared in the usual way by coating the support from a solution of the LC in the minimum amount of chloroform required to completely cover the required mass of solid support. The support (Chromosorb P of 100–120 mesh size) was added to the solution and the chloroform removed slowly under constant agitation in a rotary evaporator. The resulting stationary phase was dried under vacuum to constant weight and a known amount packed into 1/4 in. o.d. copper tubing. The exact amount of liquid crystal on the column was determined by calcination or, for LCP, by exhaustive soxhlet extraction. Loadings in the range of 8–16% by weight were used. Within this range, no significant variation of retention with loading was observed.

Results and discussion

Differential scanning calorimetry

To validate the IGC results, the mesophase transition temperatures were first measured using the conventional technique of DSC. The results are shown in Fig. 3 and the transition temperatures and associated enthalpy changes are listed in Table 1, which shows the average of at least two cycles.

The results show satisfactory agreement with the manufacturer's values with agreement to within ±1°C apart from the polymer LC that would be expected to show larger batch-to-batch variation than the low molar mass versions. As expected, the largest energy changes were associated with the transition to or from the solid crystalline (K) phase since this involved the major realignment on a molecular scale. The transitions at the clearing point (i.e., into the isotropic phase) are also clearly shown but with much lower energy changes associated with the smaller degree of molecular ordering or disordering involved. It is significant that the $S_A \rightarrow N$ transition in OCB was barely discernable while that for $S_C \rightarrow C$ in OBIB was larger than that at the clearing temperature. A considerable hysteresis was observed, particularly around the melting (K) temperature. The shapes of the peaks suggest that this is not solely due to kinetic factors in the calorimetry but indicate a significant degree of supercooling.

The chromatographic measurements described below were performed on liquid crystals coated onto a solid support. It has previously been suggested (33, 34) that the support might alter phase transitions in the thin films of material present on coated supports so that it was important to ensure that this was not the case in our systems. DSC measurements were therefore performed on samples of the coated stationary phases used in the IGC work to evaluate any such effects. The results are shown in Table 2 and show no significant difference from the bulk, unsupported materials except for the supercooling effects in the $N \rightarrow K$ transition measured on cooling the HCB sample, with the transition being depressed by some 3°C. The original behaviour is restored after storage so that it is reasonable to assume that there is a small kinetic effect but no significant

Fig. 3. DSC thermograms for liquid crystals. (*a*) HCB; (*b*) OCB; (*c*) LCP; (*d*) OBIB.

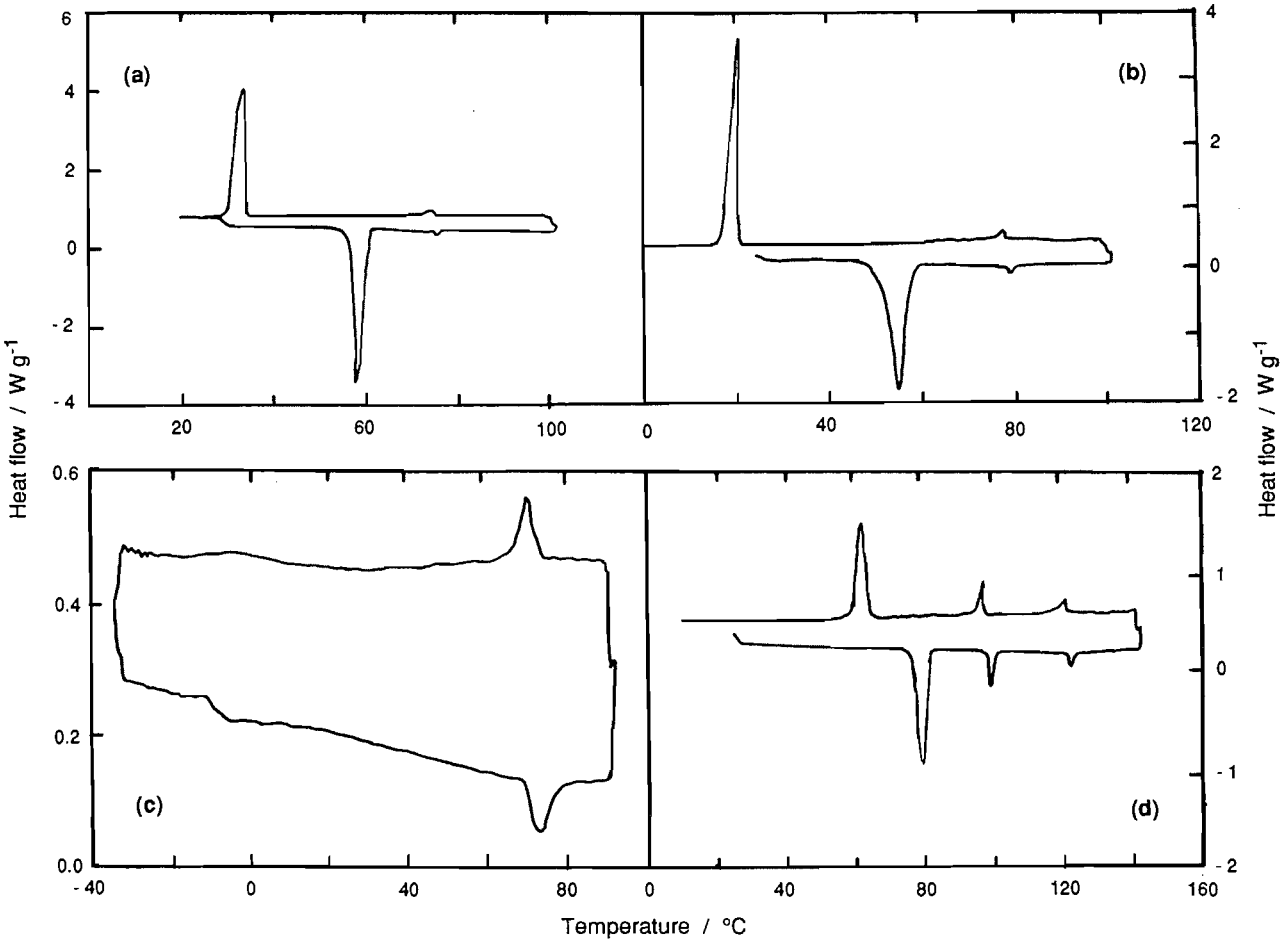

alteration of the mesophase properties by coating onto the support. This is also supported by the results for OCB and LCP.

Inverse gas chromatography

As noted above, the primary measurement (6) in IGC is $V°_g$, given by:

$$[3] \quad V°_g = F(t_r - t_m)/w$$

where t_r and t_m are the retention times of the solvent and an inert marker, respectively, w is the weight of polymer on the column, and F is the flow rate of carrier gas, corrected to S.T.P. The flow rate is calculated from:

$$[4] \quad F = F' \left(\frac{273.2}{T_f}\right)\left(\frac{P_0}{760}\right)\left(\frac{P_0 - P_w}{P_0}\right)\left(\frac{3[(P_i/P_0)^2 - 1]}{2[(P_i/P_0)^3 - 1]}\right)$$

where F' is the flow rate measured at a flowmeter temperature T_f and atmospheric pressure P_0 (measured in Torr; 1 Torr = 133.3 Pa). Thus, the first three terms of eq. [4] represent F' corrected to S.T.P., while the last two account, respectively, for the vapour pressure of water in the flow meter, P_w, and the compressibility of the gas as it passes through the column, P_i being the pressure at the column inlet.

Retention diagrams were recorded for a range of hydrocarbon probes in each of the LCs and examples are shown in Figs. 4–7. For clarity, only a selection of the results is shown. More polar probes such as chloroform are good solvents for the LCs and Braun and Guillet (35) demonstrated that these give less clear transitions in polymer phases due to strong interactions below T_g.

Each of the diagrams displays the same general form as in Fig. 1 and clearly shows the melting transitions in the results recorded on heating the samples. The inter-mesophase transitions are less clear, as would be expected since the differences are due to relatively minor structural changes in the stationary phase compared to the melting. However, it is notable that all of the various mesophase transitions in the accessible temperature range could be seen in the retention diagrams whereas, as noted above, the $S_A \rightarrow N$ transition in OCB could not be detected in the DSC thermograms. It can also be seen in the retention diagrams that, in general, aromatic probes gave much larger increases in $V°_g$ on passing through the transitions, particularly those from the K phase. The increase in $V°_g$ is related to probe interaction with the LC surface below the melting temperature and to probe solubility above it. Related work (36) has shown that the aromatic probes are better solvents for the LCs than aliphatic species.

Figures 4 and 5 clearly show that OCB and HCB form stable, supercooled solids on cooling below the melting point. The large change of retention that occurs on melting is not seen on freezing. However, a small change of retention vol-

Can. J. Chem. Downloaded from www.nrcresearchpress.com by 46.23.64.124 on 09/08/12
For personal use only.

Can. J. Chem. Downloaded from www.nrcresearchpress.com by 46.23.64.124 on 09/08/12
For personal use only.

Table 1. Mesophase transitions measured by DSC.

		Heating[a]		Cooling[b]	Manuf.[c]
		Temp. (°C)	Enthalpy (kJ mol^{-1})	Temp. (°C)	Temp. (°C)
HCB	K → N	58.6 ± 1.3	32.3 ± 1.4	34.0 ± 0.5	57
	N → I	75.4 ± 0.3	0.54 ± 0.1	74.3 ± 0.2	75.5
OCB	K → S_A	55.4 ± 0.5	29.9 ± 1.2	22.4 ± 0.4	54.5
	S_A → N	66.1 ± 0.3	0.03 ± 0.01		67
	N → I	79.6 ± 0.3	0.93 ± 0.2	77.5 ± 0.2	80
OBIB	K → S_C	78.8 ± 0.2	20.3 ± 0.1	62.8 ± 0.1	79
	S_C → C	99.4 ± 0.4	2.74 ± 0.2	97.3 ± 0.2	100
	C → I	122.1 ± 0.4	1.18 ± 0.2	120.6 ± 0.1	122
LCP	G → S_A	−6.8 ± 1.4		−13.4 ± 1.2	−3.9
	S_A → I	73.2 ± 0.9	1.82 ± 0.2	69.7 ± 0.1	79.1

[a]Measured on the heating cycle.
[b]Measured on the cooling cycle.
[c]Values measured by hot-stage microscopy and reported in manufacturer's literature.

Table 2. Comparison of results for bulk and supported HCB.

		Bulk LC		Supported LC	
		Temperature (°C)	Enthalpy (kJ mol^{-1})	Temperature (°C)	Enthalpy (kJ mol^{-1})
HCB	K → N	58.6 ± 1.3	32.3 ± 1.4	57.4 ± 0.6	28.7 ± 2.4
	N → I	75.4 ± 0.3	0.54 ± 0.1	76.1 ± 0.4	0.46 ± 0.2
	I → N	74.3 ± 0.2	0.66 ± 0.1	74.7 ± 0.4	0.51 ± 0.1
	N → K	34.0 ± 0.5	23.8 ± 1.0	30.9 ± 0.6	18.0 ± 1.4
OCB	K → S_A	53.4 ± 0.4		53.1 ± 0.8	
	N → I	78.1 ± 0.6		79.1 ± 0.6	
LCP	S_A → I	71.1 ± 1.2		71.0 ± 1.1	

Fig. 4. Retention diagram for probes in HCB. × *n*-hexane; ● benzene; ▼ *n*-nonane; ◆ cyclohexane; + *o*-xylene; —— indicates results on heating, ----- indicates results on cooling.

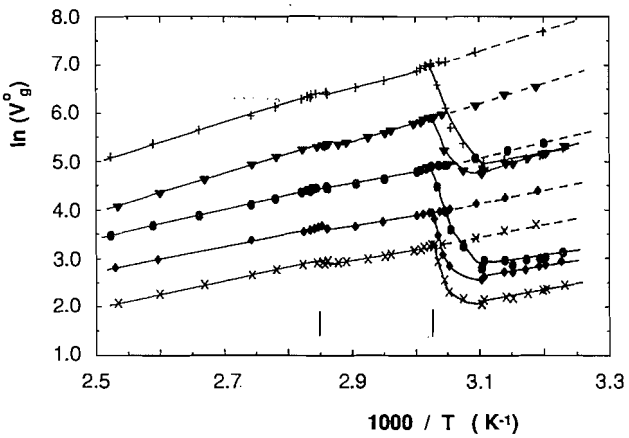

Fig. 5. Retention diagram for probes in OCB. × *n*-hexane; ● benzene; ▼ *n*-nonane; ◆ cyclohexane; + *o*-xylene; —— indicates results on heating, ----- indicates results on cooling.

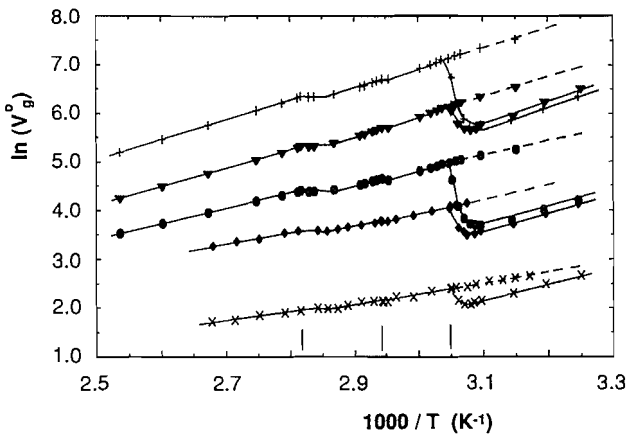

ume does occur, shown as N → N′ and S_A → S_A′ in the tables, the prime ′ indicating a supercooled phase. Below this temperature, the linear region of the retention diagram extends well below the equilibrium freezing point. Retention volumes measured in this region remained constant for several days. With OBIB, similar hysteresis was seen but the supercooled phase was only stable for a few degrees below the melting point.

By analogy with crystallization studies in polymers, the transitions were recorded at the highest temperature at which the lower phase exists. These measurements are more clearly

Can. J. Chem. Downloaded from www.nrcresearchpress.com by 46.23.64.124 on 09/08/12
For personal use only.

Fig. 6. Retention diagram for probes in OBIB. × *n*-octane; ■ *n*-nonane; ◆ benzene; ▼ *o*-xylene; —— indicates results on heating, ----- indicates results on cooling.

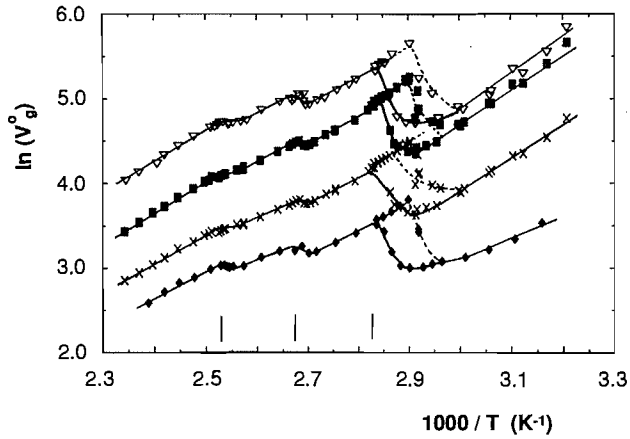

Fig. 7. Retention diagram for probes in LCP. × *n*-hexane; ● benzene; ▼ *n*-nonane; ◆ cyclohexane; + *o*-xylene; —— indicates results on heating, ----- indicates results on cooling.

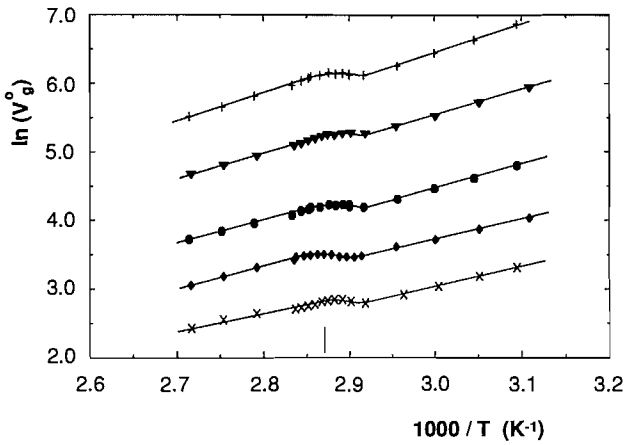

Fig. 8. Expanded retention diagram for *n*-hexane and benzene in OCB. × *n*-hexane; ● benzene; —— indicates results on heating, ----- indicates results on cooling.

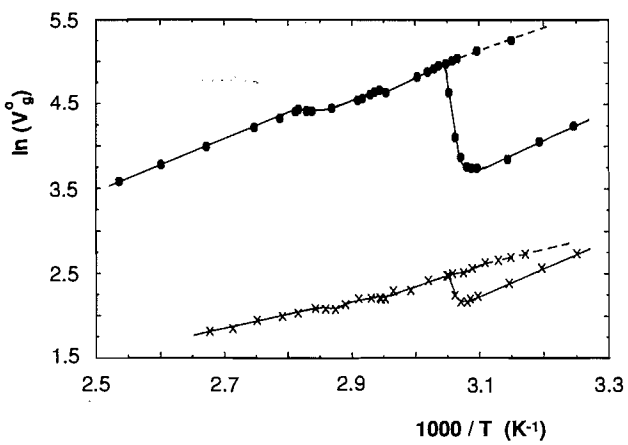

seen in the enlarged diagram for benzene and *n*-hexane in OCB shown in Fig. 8. The transition temperatures measured for all probes studied are shown in Tables 3–6. Note that the apparatus used was not capable of sub-ambient work so that T_g for LCP could not be measured.

Table 3. Mesophase transition temperatures (°C) for HCB measured by IGC.

Probe	N → I	N → N′	K → N
n-Pentane	76.9 ± 0.6	57.6 ± 0.4	57.5 ± 0.5
n-Hexane	76.6 ± 0.6	57.6 ± 0.7	57.3 ± 0.2
n-Heptane	76.5 ± 0.7	57.4 ± 0.5	57.2 ± 0.1
n-Octane	76.0 ± 0.4	57.6 ± 0.7	57.0 ± 0.3
n-Nonane	75.7 ± 0.5	58.0 ± 0.7	57.3 ± 0.5
Benzene	77.0 ± 0.6	57.7 ± 0.6	57.4 ± 0.9
Toluene	76.8 ± 0.4	57.1 ± 0.4	57.2 ± 0.2
Ethyl benzene	76.9 ± 0.6	57.6 ± 0.4	57.5 ± 0.5
o-Xylene	76.7 ± 0.6	57.3 ± 0.8	57.1 ± 0.3
m-Xylene	76.9 ± 0.6	57.8 ± 0.7	56.9 ± 0.5
p-Xylene	77.0 ± 0.5	57.6 ± 0.7	57.2 ± 0.2
Cyclohexane	76.9 ± 0.6	57.5 ± 0.4	57.1 ± 0.2
Average	76.7 ± 0.7	57.6 ± 0.5	57.2 ± 0.4

Despite the differences in the degree of change in the retention diagrams, there was no significant probe-to-probe variation in the measured transition temperatures so that it is clear that the probes were not influencing and distorting the structural transitions. Under the conditions used in this work, the probe is at infinite dilution so that it would not be expected to influence the stationary phase. The lack of probe sample size effects would appear to confirm this.

Comparison of the average values shown in Tables 3–6 with the DSC results in Tables 1 and 2 shows excellent agreement to within 1°C. The change in $V°_g$ for LCP takes place over a range of 3–4°C, which is rather wider than seen for the low molar mass LCs, presumably due to the polydispersity of the polymer LC. The precision of the IGC technique is therefore comparable with that of, for example, DSC or polarized microscopy. Clearly, while not as convenient as DSC merely to measure the transition temperatures, IGC could be valuable since a number of other parameters (32, 36) can be measured in the same experiment, amongst which are thermodynamic properties such as activity coefficients that yield information on the interactions between the components in the system. It has previously been shown that deviations occur at the phase transitions in plots of activity coefficient (or their logarithm) versus reciprocal temperature. These results in our systems will be discussed elsewhere (36) but this treatment did not significantly increase the precision of the measurements.

Measurement of crystallization kinetics

The observation of metastable, supercooled phases described above led us to consider the use of IGC to investigate the kinetics of the crystallization to the solid crystal phase. In each of OCB and OBIB, the conversion from supercooled to crystal solid was too rapid to be measured conveniently with our current apparatus. Hence, HCB was used to investigate our method.

For these experiments, the column oven was held for some time in the nematic phase so that a consistent equilibrium value of $V°_g$ was measured. The temperature was then reduced

Can. J. Chem. Downloaded from www.nrcresearchpress.com by 46.23.64.124 on 09/08/12
For personal use only.

Table 4. Mesophase transition temperatures (°C) for OCB measured by IGC.

Probe	N → I	$S_A \rightarrow N$	$S_A \rightarrow S'_A$	K → N
n-Pentane	80.0 ± 0.6	66.4 ± 0.1	53.6 ± 0.4	55.1 ± 0.5
n-Hexane	80.5 ± 0.7	66.4 ± 0.1	53.6 ± 0.4	55.1 ± 0.5
n-Heptane	30.5 ± 0.7	66.4 ± 0.1	53.6 ± 0.4	55.3 ± 0.3
n-Octane	80.0 ± 0.8	66.4 ± 0.1	53.6 ± 0.3	55.1 ± 0.5
n-Nonane	80.7 ± 0.6	66.5 ± 0.4	53.2 ± 0.7	54.8 ± 0.2
2-Methyl hexane	80.5 ± 0.7	66.5 ± 0.2	53.4 ± 0.5	55.3 ± 0.5
3-Methyl hexane	80.5 ± 0.7	66.5 ± 0.2	53.4 ± 0.5	55.1 ± 0.5
2,3-Dimethylpentane	80.5 ± 0.7	66.4 ± 0.1	53.4 ± 0.5	55.5 ± 0.5
2,4-Dimethylpentane	80.5 ± 0.7	66.4 ± 0.1	53.4 ± 0.5	55.0 ± 0.4
2,2,3-Trimethylbutane	80.5 ± 0.7	66.5 ± 0.4	53.4 ± 0.5	54.9 ± 0.6
Cyclohexane	81.1 ± 0.6	66.7 ± 0.1	53.6 ± 0.3	55.3 ± 0.4
Benzene	81.2 ± 0.4	66.4 ± 0.5	53.5 ± 0.5	54.8 ± 0.2
Toluene	81.0 ± 0.4	66.4 ± 0.4	53.5 ± 0.5	54.7 ± 0.3
Ethyl benzene	81.2 ± 0.8	66.5 ± 0.5	53.2 ± 0.7	55.0 ± 0.4
o-Xylene	80.8 ± 0.5	66.5 ± 0.6	53.5 ± 0.5	55.0 ± 0.4
m-Xylene	80.2 ± 0.6	66.5 ± 0.4	53.3 ± 0.5	55.1 ± 0.5
p-Xylene	81.0 ± 0.6	66.5 ± 0.4	53.3 ± 0.6	54.8 ± 0.2
Average	80.7 ± 0.6	66.5 ± 0.2	53.4 ± 0.3	55.1 ± 0.4

Table 5. Mesophase transition temperatures (°C) for OBIB measured by IGC.

Probe	C → I	$S_C \rightarrow C$	K → S_C
n-Octane	122.5 ± 0.5	99.3 ± 0.5	77.2 ± 0.3
n-Nonane	122.1 ± 0.7	99.3 ± 0.5	77.1 ± 0.4
n-Decane	121.3 ± 0.5	99.3 ± 0.5	77.1 ± 0.4
Benzene	121.6 ± 0.5	99.1 ± 0.9	78.3 ± 0.2
Toluene	122.0 ± 0.7	99.3 ± 1.0	78.0 ± 0.5
Ethyl benzene	121.6 ± 0.5	99.6 ± 0.7	77.2 ± 0.1
o-Xylene	121.8 ± 0.6	99.7 ± 0.4	77.5 ± 0.4
m-Xylene	121.6 ± 0.5	99.7 ± 0.4	77.4 ± 0.3
p-Xylene	121.6 ± 0.5	99.6 ± 0.4	77.4 ± 0.3
Average	121.8 ± 0.6	99.4 ± 0.3	77.5 ± 0.6

Fig. 9. Specific retention volumes for solidification HCB at 38.5°C. × *n*-pentane; ■ *n*-hexane; + *n*-heptane; ◆ benzene; ▼ toluene.

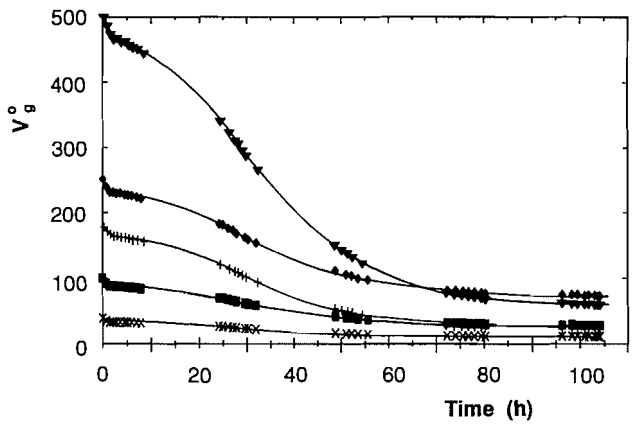

as rapidly as possible to below the transition temperature and values of V°_g recorded isothermally as a function of time. A plot of the results for the retention of five probes in HCB at 38.5°C is shown in Fig. 9. Several distinct regions can be seen in the curves. After an initial rapid fall in V°_g associated with the equilibration to the lower temperature, the values settled into two distinct regions. The first involved approximately 30–35% of the mass of the HCB and occupied around 8–10 h, after which the remainder of the compound crystallized at a rate that slowed as complete crystallization is approached.

If the values of V°_g at the start, at time t, and at the end of the crystallization process are denoted by $V^\circ_g(0)$, $V^\circ_g(t)$, and $V^\circ_g(\infty)$ respectively, the mass fraction of crystallinity, W_c, at time t is

$$[5] \quad W_c = \frac{V^\circ_g(t) - V^\circ_g(0)}{V^\circ_g(\infty) - V^\circ_g(0)}$$

The results obtained using *n*-heptane as the probe at four different temperatures are shown in Fig. 10. As expected, the solidification process proceeded faster at higher temperatures although there was no significant difference between the results at 43.6°C and those at 38.5°C. The two-stage nature of the solidification is particularly evident in these plots. The probe-to-probe reproducibility is excellent as shown by the results for five probes at 38.5°C shown in Fig. 11, all of which agree to well within experimental uncertainty.

The degree of crystallinity can be used in eq. [2] to calculate the Avrami parameters. Formally, the Avrami treatment refers to the volume fraction of crystallinity whereas IGC yields mass fraction values. However, the difference in density between the two phases will be small (36) so that the approximation has been made that the values will be equivalent. Modification and rearrangement of eq. [2] leads to:

$$[6] \quad \ln(\ln(1 - W_c)) = \ln K + n \ln t$$

Can. J. Chem. Downloaded from www.nrcresearchpress.com by 46.23.64.124 on 09/08/12
For personal use only.

Table 6. Mesophase transition temperatures (°C) for LCP measured by IGC.

Probe	$S_A \rightarrow I$	Probe	$S_A \rightarrow I$
n-Pentane	74.3 ± 0.5	*o*-Xylene	74.3 ± 0.8
n-Hexane	73.2 ± 0.6	*m*-Xylene	75.2 ± 0.7
n-Heptane	73.5 ± 0.8	*p*-Xylene	73.9 ± 1.0
n-Octane	73.0 ± 0.5	2-Methyl hexane	75.8 ± 0.5
n-Nonane	72.8 ± 0.6	3-Methyl hexane	75.5 ± 1.0
Cyclohexane	75.5 ± 0.7	2,3-Dimethylpentane	74.7 ± 0.6
Benzene	73.8 ± 0.8	2,4-Dimethylpentane	75.2 ± 0.4
Toluene	74.0 ± 0.6	2,2,3-Trimethylbutane	76.0 ± 0.7
Ethyl benzene	74.0 ± 0.7		
		Average	74.4 ± 1.6

Fig. 10. Degree of crystallization of HCB measured using *n*-heptane as probe. × 48.7°C; ◆ 46.6°C; + 43.6°C; ■ 38.5°C.

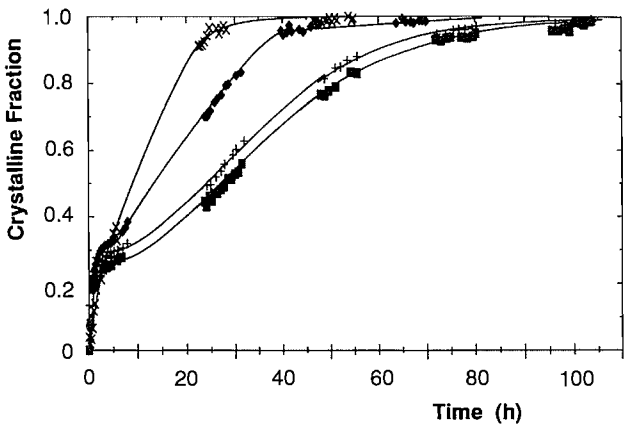

Fig. 11. Degree of crystallization of HCB at 38.5°C. × *n*-pentane; ■ *n*-hexane; + *n*-heptane; ◆ benzene; ▼ toluene.

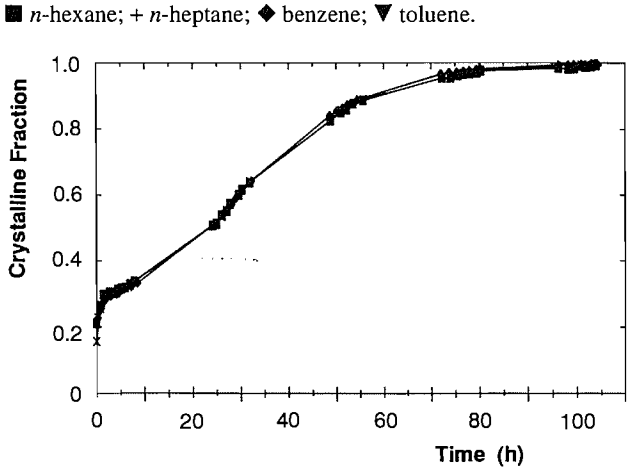

so that K and n can be measured from a suitable plot of the data. The plot of the results for *n*-heptane retention is shown in Fig. 12. While there was significant scatter in some of the results, particularly at early times, some general trends emerge. The data were particularly imprecise as the sample approached total crystallinity so that these data were not included in the analysis.

The two regions of crystallization can clearly be seen in the

Fig. 12. Avrami plot for crystallization of HCB. × 48.7°C; ◆ 46.6°C; + 43.6°C; ■ 38.5°C.

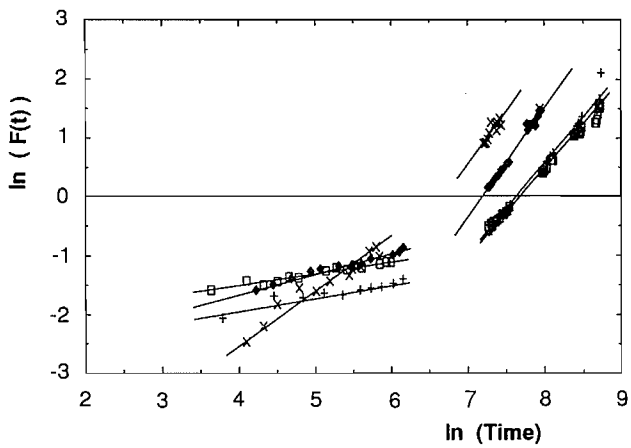

plot with the initial, faster crystallization being complete in approximately 10 h. The results recorded at 48.7°C have a different form from the other three temperatures, although it should be pointed out that there are relatively few data points at longer times due to the higher rate of the process. The reason for this is not clear, as it seems to be sufficiently far away from the equilibrium N → K transition temperature (~57°C) that thermal effects should not be important, but may be related to its proximity to the stable supercooled region. The plots at the other three temperatures showed very similar characteristics. The Avrami constants were calculated by performing a least-squares fit to the results in each of the two regions, the values being shown in Table 7.

The process in Region 1 is several orders of magnitude faster than that in Region 2 as shown by the K_1 and K_2 values, although it should be noted that the units will differ depending on the value of n. There is no clear trend of K_1 or K_2 values with the temperature. It should be noted that K_2 carries a large uncertainty due to the extrapolation of a steep portion of the graph and depends critically on the value of n_2. The values of the exponent, n, are very low compared with previous studies of bulk LCs. For example, Price and co-workers obtained a value of $n = 4$ for the transition to solid of several cholesteryl esters (37–39) while n was found to be 2 for the other transitions. The growth rate of crystalline spherulites was also found to be independent of temperature. Jabarin and Stein (40),

Table 7. Avrami constants for N′ → K transition of HCB.

Temperature (°C)	Region 1[a]		Region 2[a]	
	n_1	K_1/min^{-n}	n_2	K_2/min^{-n}
48.7 ± 0.3	0.80	3.7×10^{-3}	1.7	1.2×10^{-5}
46.6 ± 0.3	0.33	5.3×10^{-2}	1.9	7.0×10^{-7}
43.6 ± 0.4	0.21	9.8×10^{-2}	1.4	2.1×10^{-5}
38.5 ± 0.4	0.22	6.0×10^{-2}	1.6	3.8×10^{-6}

[a]The division between region 1 and region 2 is taken at ln (t/h) = 7.

using light scattering, measured n to be 3 for the I → C transition in cholesteryl myristate, suggesting that the growth involved disk-shaped spherulites. It should also be noted that while the crystallization of most polymers gives n values of 3–4, in a few examples, such as poly(*trans*-butene) and PTFE, results as low as 0.2 have been reported (41). The solidification of some thermotropic copolyesters (42) yielded values from 0.2 to 0.8.

There are two major differences between the current work and previous studies. Firstly, the transition being studied here is from a supercooled, and therefore more viscous, mesophase. Secondly, the HCB is spread as a thin film onto a solid support, which may place restrictions on the spherulite growth.

Chang and Wunderlich (42, 43) suggested that in similar situations, low values of n, even approaching zero, could be obtained. For example, crystallization from a viscous medium where mobility is restricted, described as a "cold crystallization," would restrict the rate of crystallite growth. Also, a situation where a large number of nucleation sites existed originally but decreased with time would add a negative time exponent, denoted a, further reducing n. Another factor is that if the solidification is dominated by a diffusion process, this would involve a t^m dependence of the crystal growth rate where m would normally be 0.5. These factors led Chang and Wunderlich to recast the Avrami equation [6] as:

$$[7] \quad \ln(\ln(1 - W_c)) = \ln K^* + \{n(1 - m) - a\} \ln t$$

Hence, our IGC results can be interpreted in these terms. The solid support would provide a relatively large number of nucleation sites for the early stages of the solidification, at which growth would be restricted due to viscosity and steric factors. The number of sites would reduce as the crystallites coalesced during growth. After this initial stage, crystallization continues in a more conventional 2- or 3-dimensional growth that is diffusion limited (i.e., $n = 3$ or 4). It is tempting to explain the two-stage process in terms of a nucleated solidification onto the support followed by a more conventional "freezing" of the remaining material. Preliminary calculations (36) suggest that the 30–35% of HCB involved in the primary crystallization is approximately that needed to coat the support. However, at this stage, this explanation is rather speculative and more work is necessary to fully elucidate the mechanism of the solidification. However, it is clear that IGC has a significant role to play in this type of work, particularly in systems where the transitions are relatively slow.

Conclusions

It has been shown that IGC can be used to measure the temperatures of a range of mesophase transitions in liquid crystals. It can be applied to a wide range of materials, both low molar mass and polymeric. The accuracy and precision are comparable with other techniques although IGC is slower and less convenient solely to measure the transition temperatures. This disadvantage is outweighed by the ability to measure other data such as thermodynamic activity coefficients and interaction parameters. This work has also demonstrated the potential of IGC as a method of following the kinetics of solidification in suitable mesogenic systems.

Acknowledgements

We are grateful to the Science and Engineering Research Council for the award of a research studentship (to I.M.S.) and particularly to Merck Ltd for providing the liquid crystals used in this work. On a more personal note, I would like to thank Jim Guillet for a stimulating two years spent in his laboratory and for the inspiration needed when starting out on a research career. I am more grateful than I can say!

References

1. O. Smidsrød and J.E. Guillet. Macromolecules, **2**, 272 (1969).
2. A. Lavoie and J.E. Guillet. Macromolecules, **2**, 443 (1969).
3. J.E. Guillet and A.N. Stein. Macromolecules, **3**, 102 (1970).
4. D.G. Gray and J.E. Guillet. Macromolecules, **4**, 129 (1971).
5. D.R. Lloyd, T.C. Ward, and H.P. Schreiber (*Editors*). Inverse gas chromatography: characterization of polymers and other materials. A.C.S., Washington. 1989.
6. J.R. Conder and C.L. Young. Physicochemical measurement by gas chromatography. J. Wiley and Sons, Chichester. 1979.
7. D.D. Patterson, Y.B. Tewari, H.P. Schreiber, and J.E. Guillet. Macromolecules, **4**, 356 (1971).
8. G.J. Price and J.E. Guillet. J. Solution Chem. **16**, 605 (1987).
9. M.M. Tian and P. Munk. J. Chem. Eng. Data, **39**, 742 (1994).
10. P. Sakellariou, M.H. Abraham, and G.S. Whiting. Colloid Polym. Sci. **272**, 872 (1994).
11. F. Champagne, J.F. Li, H.P. Schreiber, and G. DiPaola-Baranyi. J. Appl. Polym. Sci. **54**, 743 (1994).
12. P. Mukhopadhay and H.P. Schreiber. Macromolecules, **26**, 6391 (1993).
13. J.E. Guillet, M. Romansky, G.J. Price, and R. van der Mark. *In* Inverse gas chromatography: characterization of polymers and other materials. *Edited by* D.R. Lloyd, T.C. Ward, and H.P. Schreiber. A.C.S., Washington. 1989. p. 20.
14. J.M. Braun and J.E. Guillet. J. Polym. Sci. Polym. Chem. **13**, 1119 (1975).
15. W. Orts, M. Romansky, and J.E. Guillet. Macromolecules, **25**, 949 (1992).
16. M. Cortezar, J.J. Iruin, and J.I. Eguizabal. Polym. Bull. **29**, 415 (1992).
17. A.N.Stein, D.G. Gray, and J.E. Guillet. Br. Polym. J. **3**, 175 (1971).
18. B. Wunderlich. Macromolecular physics, crystal nucleation, growth, annealing. Academic Press, New York. 1976.
19. M. Avrami. J. Chem. Phys. **7**, 1103 (1939).
20. M. Avrami. J. Chem. Phys. **8**, 212 (1940).
21. M. Alger. Polymer science dictionary. Elsevier, New York. 1990.
22. P.J. Collings. Liquid crystals: nature's delicate phase of matter. Adam Hilger, Bristol. 1990.
23. Z. Witkiewicz. J. Chromatogr. **251**, 311 (1982).
24. S. Ghodbane, G.A. Oweimreen, and D.E. Martire. J. Chromatogr. **556**, 317 (1991).

Can. J. Chem. Downloaded from www.nrcresearchpress.com by 46.23.64.124 on 09/08/12
For personal use only.

25. D.E. Martire, P.A. Blasco, P.F. Carone, L.C. Chow, and H. Vincini. J. Phys. Chem. **72**, 3489 (1968).
26. H-J. Moegel, G. Kraus, and M. Novak. J. Chromatogr. **324**, 29 (1985).
27. J. Coca, I. Medina, and S.H. Langer. Chromatographia, **25**, 825 (1988).
28. G.A. Oweimreen. Mol. Cryst. Liq. Cryst. **68**, 257 (1980).
29. G.A. Oweimreen and A-K.I. Shihab. J. Chem. Eng. Data, **266**, 39 (1994).
30. M. Romansky and J.E. Guillet. Polymer, **35**, 584 (1994).
31. G.M. Janini, R.J. Laub, J.H. Purnell, and O.S. Tyagi. *In* Side chain liquid crystal polymers. *Edited by* C.B. McArdle. Blackie, Glasgow. 1989. p. 395.
32. G.J. Price and I.M. Shillcock. Polymer, **34**, 89 (1993).
33. J.E. Haky and G. Muschik. J. Chromatogr. **238**, 367 (1982).
34. W. Marcinciak and Z. Witkiewicz. J. Chromatogr. **207**, 333 (1981).
35. J.M. Braun and J.E. Guillet. Macromolecules, **9**, 340 (1976).
36. G.J. Price and I.M. Shillcock. Manuscripts in preparation.
37. F.P. Price and A.K. Fritzsche. J. Phys. Chem. **77**, 396 (1973).
38. F.P. Price and J.H. Wendorff. J. Phys. Chem. **75**, 2839 (1971).
39. F.P. Price and J.H. Wendorff. J. Phys. Chem. **75**, 2849 (1971).
40. S.A. Jabarin and R.S. Stein. J. Phys. Chem. **77**, 409 (1973).
41. J. Grebowicz, S.Z.D. Chang, and B. Wunderlich. J. Polym. Sci. Polym. Phys. **24**, 675 (1986).
42. S.Z.D. Chang. Macromolecules, **21**, 2475 (1988).
43. S.Z.D. Chang and B. Wunderlich. Macromolecules, **21**, 3327 (1988).

Can. J. Chem. Downloaded from www.nrcresearchpress.com by 46.23.64.124 on 09/08/12
For personal use only.

Solid-state photochemistry of π-conjugated poly(3-alkylthiophenes)

Mohamed S.A. Abdou and Steven Holdcroft

Abstract: Films of poly(3-alkylthiophenes) undergo simultaneous photobleaching, cross-linking, and chain scission when irradiated in air with UV or visible light. The quantum yields of the latter two processes were determined using Chalesby–Pinner theory. Under the irradiation conditions employed the cross-linking density is ~4.5 times greater than the fracture density (chain scission). This corroborates the observation that poly(3-alkylthiophenes) are negative-type photoresists. Although the quantum yield of cross-linking is relatively low, the polymer maintains a relatively high degree of π-conjugation following irradiation. The mechanism of cross-linking and insolubilization proceeds via a classical photooxidation route that is initiated by photolysis of residual iron impurities. Photobleaching involves photosensitization, and reaction of singlet oxygen. $^1O_2$ undergoes a 1,4 Diels–Alder addition to thienyl units which results in a loss of π-conjugation, a blue shift in the absorption spectrum of the polymer, and a decrease in the optical density. Photobleaching, cross-linking, and chain scission are considerably reduced in the absence of oxygen.

Key words: photochemistry, polymers, thin films, degradation, cross-linking.

Résumé : Lorsqu'on les soumet à une irradiation UV ou visible dans l'air, les films de poly(3-alkylthiophènes) subissent des photoblanchiments, des réticulations et des scissions de chaînes simultanés. Utilisant la théorie de Chalesby–Pinner, on a déterminé les rendements quantiques des deux derniers processus. Dans les conditions d'irradiation employées, la densité de la réticulation est environ 4,5 fois plus grande que la densité de fracture (scission des chaînes). Ces résultats corroborent l'observation que les poly (3-alkylthiophènes) sont des photorésistances de type négatif. Même si le rendement quantique de la réticulation est relativement bas, le polymère maintient un degré relativement élevé de conjugaison π après l'irradiation. Le mécanisme de réticulation et d'insolubilisation procède par le biais d'une photooxydation classique qui est initiée par la photolyse d'impuretés ferriques résiduelles. Le photoblanchiment implique une photosensibilitation et la réaction d'un oxygène singulet. Le $^1O_2$ subit une addition-1,4 de Diels–Alder sur les unités thiényles qui provoquent une perte de conjugaison π, un déplacement vers le bleu dans le spectre d'absorption du polymère et une diminution de la densité optique. Les réactions de photoblanchiment, réticulation et scission de chaîne sont fortement réduites en l'absence d'oxygène.

Mots clés : photochimie, polymères, films minces, dégradation, réticulation.

[Traduit par la rédaction]

Introduction

The effect of light on π-conjugated polymers plays an important role when they are utilized in specialized technical innovations such as optoelectronic devices, photoconduction (1), electroluminescence (2, 3), photovoltaics (4), and photolithography of semiconducting and electronically conducting polymer *wires* in the design of integrated circuitry and device fabrication (5–8). However, few studies probe the chemical reactions that result from the interaction of light with π-conjugated polymers. Studies of the photochemistry of π-conjugated polymers are thus necessary in order to understand the effect of light on these materials and to improve their properties.

Polyacetylene (PA) was one of the first conjugated organic polymers to undergo photochemical study. It was found that irradiation of the soluble Durham precursor to PA leads to photobleaching and insolubilization of the material (9, 10). The mechanism of photobleaching was explained by invoking reactions of singlet oxygen with the polymer. The origin of singlet oxygen was not discussed.

Photochemically induced insolubilization of another conjugated polymer, poly(*p*-phenylene sulfide) (PPS), has also been examined as a means to photoimage conjugated polymers (11). The technique uses a photooxidant and is based on the solubility difference between exposed (photooxidized) and unexposed (neutral) polymer. A soluble sulfur-phenylated PPS derivative can be employed for this application so that the photoacid generator, a triaryl sulfonium salt, is chemically bound to the polymer backbone (12). A detailed photochemical study of PPS has been performed using oligomers of phenylene sulfide and their halogenated derivatives (13). PPS is photodegraded by UV–VIS light. The reported mechanism of

Received April 11, 1995.

This paper is dedicated to Professor J.E. (Jim) Guillet in recognition of his contributions to Canadian chemistry.

Mohamed S.A. Abdou and Steven Holdcroft.[1] Department of Chemistry, Simon Fraser University, Burnaby, BC V5A 1S6, Canada.

[1] Author to whom correspondence may be addressed. Telephone: (604) 291-3345. Fax: (604) 291-3765.

Can. J. Chem. Downloaded from www.nrcresearchpress.com by 46.23.64.124 on 09/08/12
For personal use only.

Can. J. Chem. Downloaded from www.nrcresearchpress.com by 46.23.64.124 on 09/08/12
For personal use only.

photodegradation involves homolytic cleavage of the C—S bond via the singlet state to produce thiophenoxy radicals.

Photochemical reactions of precursors to π-conjugated poly(*p*-phenylene vinylenes) (PPV) have been investigated (14). Precursors derived from 1,4-bis(tetrahydrothiophenium salts) of benzene and its 2,5-derivatives are soluble in organic solvents. Photochemical elimination converts the insulating, soluble, precursor into the insoluble π-conjugated polymer. However, irradiation was performed with a 514 nm Ar^+ laser source, a wavelength at which the polymer films have very low absorption coefficients, and thus no elimination occurs upon direct photolysis even with high exposure doses (~350 W/cm^2). Photosensitizers such as azo-sulfonic dyes enhance the efficiency of photoelimination. Irradiation of the PPV precursor with 488 nm and 254 nm light, wavelengths at which the polymer precursor is highly absorbing, failed to completely convert the precursor to a fully conjugated polymer. Prolonged irradiation resulted in degradation products such as carbonyl and hydroxyl groups (15, 16).

Polyaniline (PANI) has also been subject to photochemical investigation for applications in photolithography (17,18). To date, lithography of such polymers has not been the result of photochemical reaction of PANI but rather photodoping reactions using photoacid generators, e.g., triphenyl sulfonium salts (12, 17). Photogenerated acids are effective dopants (oxidants) of the polymer. Photolithography is achieved because of the differential solubility between the doped and neutral polymer. Other methods used for photoimaging PANI include the reduction of doped polymer films containing semiconductor microparticulates and laser-induced electropolymerization (19, 20). The photochemistry of PANI in its various forms has been studied, e.g., leucoemeraldine, emeraldine base, and emeraldine salt forms (21). Exposure to light degrades the polymer, as manifested by the formation of carbonyl groups and a blue shift in the interband (π–π*) transition. Both of these observations indicate disruption of the conjugated system. The extent of degradation depends on the oxidation state of the material and the wavelength of excitation. The rate decreases with an increase in the doping level of the polymer.

Photolithography of polypyrrole (PPy) has been investigated in a similar manner to PANI, and includes photoelectrochemical polymerization of pyrrole on semiconductor electrodes (21), and photosensitized polymerization using sensitizers and sacrificial oxidizing agents (22). Laser ablation has also been used to image PPy but the technique damages the polymer surrounding the irradiated spot, thus producing patterns of low resolution (23).

Another important class of conjugated polymer are the poly(3-alkylthiophenes) (P3ATs). We have been investigating these systems in order to understand their photochemical degradation, offer rationale strategies for enhancing photostability, and design conjugated materials that act as both photoresists and electronic conductors (5–8, 24). Poly(3-hexylthiophene) degrades in nonaqueous solvents containing dissolved molecular oxygen when irradiated with UV or visible light. Degradation takes the form of both reduced π-conjugation and chain scission. The former manifests itself as photobleaching and is largely the product of photosensitization and reaction of singlet oxygen. Chain scission occurs via the classical route of photooxidation where scission is initiated by photolysis of trace amounts of transition metal salts.

Fig. 1. Chemical structure of poly(3-alkylthiophenes).

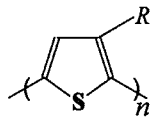

R = *hexyl*

The photochemistry of aqueous solutions of water-soluble derivatives of P3ATs containing alkanesulfonate substituents has also been investigated (8). Aqueous solutions of these polymers exhibit a substantial increase in photostability because the lifetime of the reactive intermediate, singlet oxygen, is much lower in aqueous solution.

We have previously shown that films of poly(3-alkylthiophenes) undergo cross-linking, and thus become insoluble in organic solvents when irradiated with UV-VIS light (6*b*). These characteristics make poly(3-alkylthiophenes) interesting candidates for photoresist technology since polymer films can be readily spin-cast onto solid substrates, irradiated through a photomask, and unexposed polymer removed by dissolution to provide a negative photoimage. Oxidation of the cross-linked polymer results in an electronically conducting pattern. In contrast to conventional photolithography, the soluble π-conjugated polymer acts as both the photoresist and the precursor to an electronically conducting pattern. In this paper, we wish to provide the photochemical details of the mechanisms of photo-oxidation, photocross-linking, and insolubilization of this class of polymer in the solid state (Fig. 1).

Experimental

Polymer synthesis

Poly(3-hexylthiophene) (P3HT) was prepared by oxidative coupling using $FeCl_3$ (25). The iron content of the polymer was determined by standard acid digestion procedures followed by atomic absorption analysis (24). The identity of the iron impurities was determined using Mössbauer spectroscopy (24). P3HT containing 1.3 wt.% iron was employed in this study. The molecular weight of the polymer was determined using gel permeation chromatography (26). The polymer possessed a number average molecular weight, M_n, of 10 000 and molecular weight distribution of ~3. The polymer also possessed an HT:HH ratio of 80:20 as determined by ^{1}H NMR (27). Polymer solutions were prepared by dissolving an appropriate amount of solid polymer in toluene, followed by filtration through a 0.2 μm filter to remove insoluble residues. Polymer films were prepared by spin casting. Thin films of polymer (0.1–0.25 μm) were spin-cast (2000–5000 rpm for 30 s) onto glass or quartz slides from dilute solutions of the polymer dissolved in toluene (10 mg/mL). Films were prebaked at 120°C for 30 min. The thicknesses of the polymer films were measured using a profilometer (Tencor Instruments, Alpha-Step 200).

Photolyses

The illumination source was a 150 W mercury lamp (Illumination Industries Ltd.). Irradiation was carried out using a 300 nm cut-off filter unless stated otherwise. The wavelength of irradiation was selected using an appropriate 10 nm bandwidth interference filter or cutoff filters. The temperature of the cell was maintained at 25°C using a cooling block and a circulating water bath. Photolysis was performed in ambient air,

Can. J. Chem. Downloaded from www.nrcresearchpress.com by 46.23.64.124 on 09/08/12
For personal use only.

unless otherwise stated. The intensity of incident light at 435 nm was 1.39 mW/cm^2 as measured by radiometer/photometer (International Light, model L 1350).

Sol fraction (ref. 28)

Thin films of polymer (100 nm) were spin-cast onto quartz slides from dilute solutions of the polymer in toluene (10 mg/mL). After drying, the polymer films were exposed through the quartz. Back-side exposure was performed for evaluation of resist parameters. After irradiation, the soluble fraction was extracted by solvent development using chloroform. The sol fraction, S, was determined by measuring the optical density, OD, of the soluble polymer fraction following irradiation and development. The solubility of the polymer (sol fraction, S) was determined using the following equation (28, 29):

$$[1] \quad S + S^{1/2} = \frac{p_o}{q_o} + \frac{1}{q_o \overline{P}_n} \frac{1}{r}$$

where p_o and q_o represent the fracture and cross-linking densities per unit radiation dose, $\overline{P}_n$ is the number average degree of polymerization, and r is the absorbed irradiation dose. The ratio p_o/q_o indicates the relative amount of scission to cross-linking as a function of irradiation.

Lithographic parameters and quantum yield (ref. 30)

Lithographic parameters were determined from gel dose curves constructed by plotting the residual thickness of the polymer film after solvent development as a function of the energy absorbed by the polymer. The contrast of the photoresist, γ_n, is defined as the rate of insolubilization (or the rate of cross-linking) at a constant input energy. It is calculated using the equation:

$$[2] \quad \gamma_n = \frac{1}{\log D_g^0 - \log D_g^i} = \left[\log \frac{D_g^0}{D_g^i} \right]^{-1}$$

For negative photoresists, D^ig is the minimum radiation dose required to induce a reaction such that an insoluble gel (residue) of polymer remains after development. The sensitivity of the resist is signified by the exposure dose required to yield a particular response in the resist polymer after development. It is most commonly defined as the dose required to leave 50% of the original thickness. D^0g is the dose required to produce 100% gel formation of the original film and was determined by extrapolation of the linear portion of the sensitivity plot to a dose value equivalent to original film thickness, l_o.

The relationship between the quantum yield of cross-linking, Φ_x, and gel dose, r_{gel} is given by

$$[3] \quad r_{gel} = \frac{\rho}{2 \times 2.303 \, M_w \varepsilon M \Phi_x}$$

where ρ is density, M_w is the weight average molecular weight, ε is the extinction coefficient of the chromophore, and M is its molarity in the solid film.

Instrumentation

FTIR spectra were recorded on a Bomem Michelson FTIR (120 series). The polymer samples were prepared by solvent evaporation in the form of thin polymer films on KBr discs. UV–VIS spectra were recorded on a Perkin Elmer Lambda 3A. Measurements were conducted at 25°C. Thin polymer films were prepared by spin coating of polymer solutions onto quartz slides. ^{13}C magic angle spinning/cross polarization (MAS/CP) NMR spectra were obtained using a TT-14 spectrometer modified for solid-state NMR studies. Differential scanning calorimetry (DSC) measurements were performed using a Perkin–Elmer DSC 7 calorimeter. The temperature was scanned over 380°C from −30°C with a heating rate of 5.0°C/min.

Fig. 2. Solubility curve of P3HT following irradiation with 435 nm light.

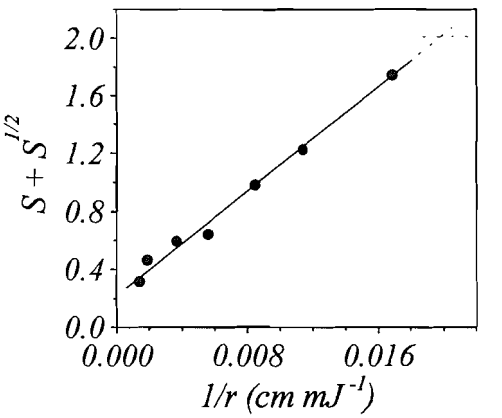

Results and discussion

Sol–gel properties of poly(3-alkylthiophenes)

Figure 2 shows a solubility plot of poly(3-hexylthiophene) films following irradiation with 435 nm light under ambient conditions. This graph was constructed by plotting the soluble fraction $S + S^{1/2}$ of P3HT films as a function of $1/r$ according to eq. [1]. The intercept of the linear plot at infinite exposure dose provides the ratio of photochain scission to photocross-linking, p_o/q_o. A value of 0.23 was calculated that indicates thin films of P3HT undergo simultaneous cross-linking and chain scission. From this, the crosslinking density, q_o, was found to be ~4.5 times greater than the fracture density, p_o. The energy required for incipient gelation of the polymer, r_{gel}, calculated from extrapolation of the linear plot to a sol fraction $S + S^{1/2} = 2$, was 49 mJ/cm^2, or 1.78×10^{-7} einstein/cm^2. Using eq. [3], the quantum yield of cross-linking, Φ_x, at 435 nm was calculated to be 2.37×10^{-3} mol/einstein^{-1}. Using the ratio p_o/q_o, the quantum yield of main-chain scission, Φ_s, was estimated to be 5.45×10^{-4} mol/einstein. Main-chain scission was indeed observed experimentally as evidenced by a decrease in M_n of the soluble extractable component of the polymer following irradiation and development.

The fact that cross-linking and insolubilization were observed meant the polymer was a suitable candidate for photolithography. The lithographic parameters of P3HT at 435 nm were determined from a sensitivity curve shown in Fig. 3 that was constructed by plotting the remaining thickness of polymer films after solvent development, l/l_o, against exposure dose. The gel content (film thickness) increased with

Can. J. Chem. Downloaded from www.nrcresearchpress.com by 46.23.64.124 on 09/08/12
For personal use only.

Fig. 3. Sensitivity plot of P3HT using 435 nm light.

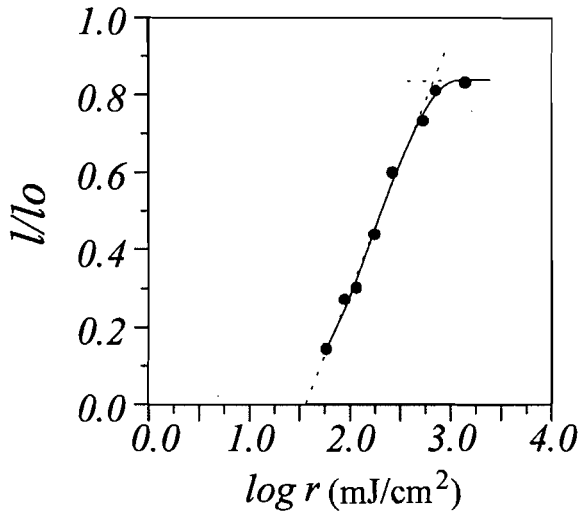

increasing exposure dose until the thickness remaining was similar to the original film thickness. The values of gel dose, r_{gel} (or D_g^i), sensitivity, $D_g^{0.5}$, and contrast, γ, were calculated to be 38, 190 mJ/cm^2, and 0.8, respectively. The gel dose values determined from both the solubility and sensitivity curves are in agreement to within ~25%.

In a previous study, lithographic parameters were investigated using much higher intensity laser light (442 nm He–Cd laser) (6). Lithographic parameters were similarly determined from gel dose curves constructed by plotting the residual thickness of the polymer image deposited on a substrate after solvent development as a function of the exposure dose. The dose of incipient gelation, D_g^i, was found to be 7.7 mJ/cm^2, the sensitivity at 50% gel formation, $D_g^{0.5}$, was 61 mJ/cm^2, and the contrast, γ_n, was 0.7. The discrepancy between values obtained by laser lithography (Cd–He laser irradiation) and conventional photolithography (Hg lamp irradiation) is due to the difference in irradiation intensity.

The effect of irradiation on the conjugation length and conductivity of P3HT was investigated. The change in π-conjugation can be monitored qualitatively by observing the change of optical density of the film with irradiation. Prolonged irradiation of thin films of P3HT at 435 nm in ambient air causes the optical density of the film to decrease. Figure 4 shows a plot of optical density of the polymer film (at λ = 500 nm) against the irradiation dose.

Neutral, undoped polymer film has a strong absorption band at 500 nm, indicating a significant degree of π-conjugation along the polymer backbone. The electronic transition of solid polymer films correlates to an effective conjugation length of ~6 thiophene units (31, 32). Figure 4 shows that the effective conjugation length of the polymer does not change appreciably for irradiation doses <300 mJ/cm^2; above this value the π-conjugation system was visibly disrupted (photobleaching). Photochemical insolubilization requires considerably less energy dosage than 300 mJ/cm^2; thus polymers can be rendered insoluble while maintaining extensive conjugation.

FTIR measurements on thin solid polymer films were used to determine which photochemical processes lead to an insoluble product. Figure 5 shows FTIR spectra of thin films of the

Fig. 4. Relative optical density (λ = 500 nm) of P3HT films versus irradiation dose (irradiation wavelength = 435 nm).

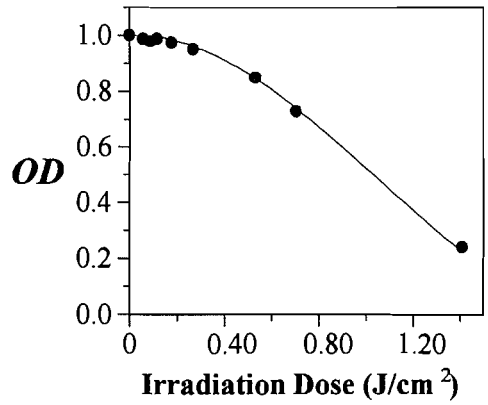

Fig. 5. FTIR spectra of P3HT films before and after 12 h irradiation. Irradiation in air with a polychromatic light (>300 nm).

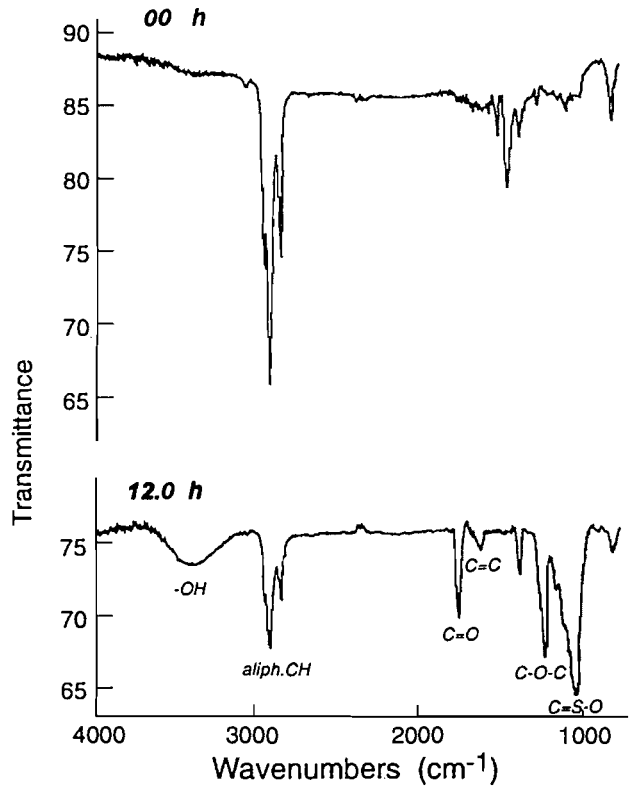

polymer before and after irradiation in air using polychromatic light (>300 nm). The following new IR bands appear in the spectra following irradiation: 3400, 1743, 1610, 1230, and 1045 cm^{-1}. The band at 2962 cm^{-1}, due to C–H stretching in the alkyl chain, decreases with exposure time. Prolonged exposure causes this band to disappear completely. The bands at 1743, 1610, and 1045 cm^{-1} were previously assigned to C=O, C=C, and C=S$^+$-O$^-$ residues and result from a 1,4 Diels–Alder addition of photosensitized singlet oxygen to thienyl moieties in the main chain (5, 24). Kinetic studies (Fig. 6) establish that these absorption bands evolve immediately upon irradiation and that all three bands increase in intensity at

Can. J. Chem. Downloaded from www.nrcresearchpress.com by 46.23.64.124 on 09/08/12
For personal use only.

Fig. 6. Time-dependent evolution of functional groups during irradiation. Data obtained from FTIR spectra (see text for details). Irradiation of P3HT in air with polychromatic light (>300 nm).

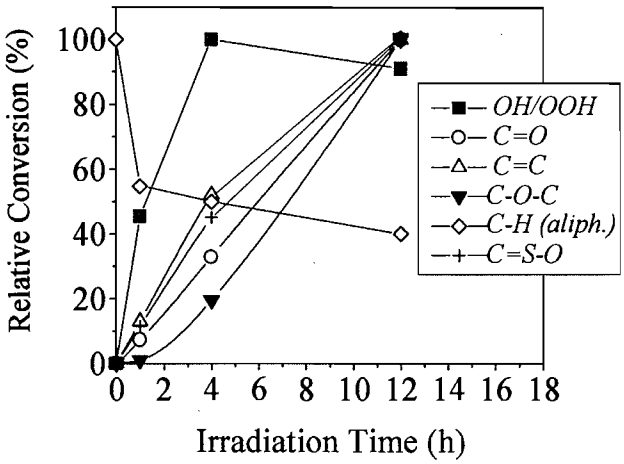

relatively the same rate. This indicates they are products of a common reaction pathway.

Assignment of the IR bands at 3400 cm^{-1} (-OH), and 1230 cm^{-1} (C-O-C, ether linkage) is made by invoking a mechanism of oxidative degradation and cross-linking of the alkyl side chain in analogy to that observed in the photooxidation of polyolefins (33). The mechanism of photooxidation of polyolefins, and presumably of alkyl side chains, begins with an initiation step in which an impurity, usually a transition metal ion, photosensitizes the generation of reactive free radicals. Potential photoinitiators of this process for films of P3HT are residual ferric salts that originate from the ferric chloride used in the polymerization of hexylthiophene. Extensive purification does not remove trace ferric salts. Even polymers purified by repeated recrystallization contain trace iron salts (>0.05 wt.%) (24).

Solid-state NMR was used to provide further information on the chemical changes in the polymer following irradiation. Figure 7 shows the ^{13}C spectra of P3HT before and after irradiation. Noteworthy is the formation of C-O and C=O functionalities as indicated by the NMR signals at ~70 and ~220 ppm, respectively. This was accompanied by a decrease in the carbon signals due to both the alkyl side chains (14–30 ppm) and the thienyl moieties (120–140 ppm). The changes in the NMR spectra of the photolyzed polymers are consistent with assignments made using FTIR data.

In studies of the photochemistry of the polymers in solution, it was found that irradiation causes both photobleaching and chain scission (5, 24). The former involves photosensitization, and reaction of singlet oxygen, while the latter followed a classical photooxidation route. Given this, it is probable that the photobleaching and cross-linking observed for films of P3HT also proceed via two independent reaction pathways. To test this hypothesis, singlet oxygen was generated ex situ, and its effect on cross-linking and photobleaching was examined. The hypochlorite – hydrogen peroxide system was chosen to generate singlet oxygen ($^1O_2$) for these studies since it does not contaminate the test sample with impurities (24). Reaction of thin films of P3HT (~100 nm) with singlet oxygen was monitored over a period of 20 h. The optical density of the film at

Fig. 7. MAS/CP ^{13}C NMR spectra of P3HT: (*a*) pristine polymer, (*b*) after 48 h irradiation. Irradiation in air with a polychromatic light (>300 nm).

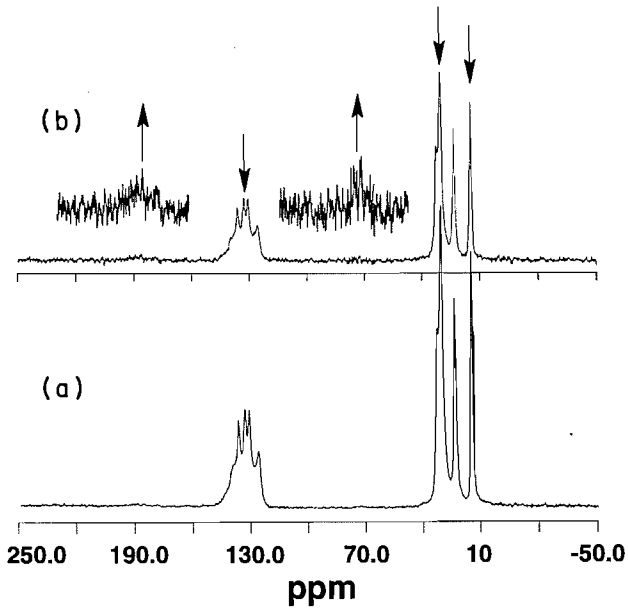

500 nm decreased by ~ 20% but the polymer remained soluble. It is noteworthy that, in contrast to this, virtually no change in optical density was observed when the minimum irradiation dose was used to photocross-link the polymer. Thus, photobleaching appears to involve $^1O_2$ whereas cross-linking does not.

FTIR analysis of the polymer following exposure to $^1O_2$ showed strong signals due to sulfine (1090–1020 cm^{-1}), keto (1730 cm^{-1}), and olefinic (1650 cm^{-1}) residues. Notably, no hydroxyl or ether functionalities were observed. Reaction products are consistent with reported mechanisms observed for the reaction of $^1O_2$ with small-molecule thienyls (34, 35) and longer chain thienyls (5, 24). In this mechanism, shown in Scheme 1, $^1O_2$ undergoes a 1,4 Diels–Alder addition with thienyl units. Endoperoxide residues **2** may be envisaged as intermediates in the formation of the sulfine. However, their formation as primary oxygenation products can only be inferred from the photochemical products because endoperoxides derived from heterocyclic 1,4-dienes are generally unstable at room temperature (36) and decompose to form either the sulfine **3** or the *trans*-diketone **4**.

The dominant reaction leading to polymer photobleaching involves photosensitization, and reaction, of singlet oxygen. Photosensitization of singlet oxygen is often the result of triplet–triplet annihilation (Scheme 2).

Singlet oxygen generation via triplet states of polythiophene ($^3P^*$) appears unlikely, given the recent phosphorescence and transient spectroscopic data, which indicate a very low quantum yield ($<10^{-6}$) for triplet formation (37, 38)[2]. An alternative explanation for photosensitization of singlet oxygen is based on dissociation of an excited state charge transfer complex. Recently, it was demonstrated that photogeneration of singlet oxygen in solid films of polystyrene can

[2] Also, B. Xu and S. Holdcroft. Unpublished results.

Can. J. Chem. Downloaded from www.nrcresearchpress.com by 46.23.64.124 on 09/08/12
For personal use only.

Scheme 1.

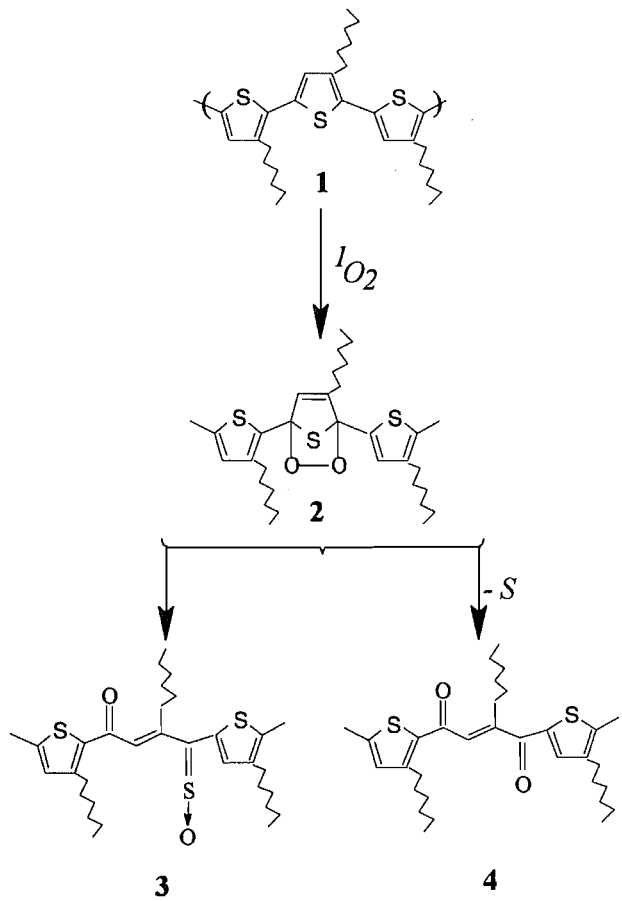

Scheme 2.

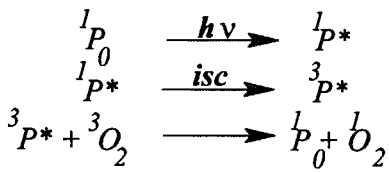

result from irradiation of oxygen–polystyrene charge transfer complexes (39). A similar mechanism can be anticipated for P3ATs. Indeed, the existence of a charge transfer complex formation between oxygen and P3ATs has been recently confirmed using optical and electron spin resonance spectroscopies, and electrical measurements (40). The following is a possible mechanism that describes the photosensitization process (Scheme 3) (41).

In this mechanism, the ground state P3HT·O_2 charge transfer complex (CTC) is a triplet due to multiplicity multiplication of the singlet ground state of P3HT and the triplet nature of molecular oxygen. Excitation of the P3HT·O_2 complex yields a triplet excited state that is close in energy to the excited singlet state (41). Dissociation of the latter is believed to yield singlet oxygen. The formation of $^1O_2$ from ^{3}CTC* is improbable because it is spin forbidden. Further photophysical studies are necessary to clarify this mechanism.

Photoinduced cross-linking appears to involve photooxidation of polymers and is rationalized in terms of a free-radical chain reaction comprising initiation, propagation, and termination steps. It is well documented that photooxidation reactions of saturated polymers such as polyethylene are initiated by photolysis of residual metal catalyst. In the case of P3ATs prepared by oxidative coupling using $FeCl_3$ the impurities are residual ferric salts (24, 42). We have previously shown that interaction of these impurities leads to chain scission in solution (24). The impurities were shown to be octahedral Fe(III) hydroxychloro complexes ($[Fe(H_2O)_4(OH)_2]X$) where X is a chloride or hydroxyl ion. These salts have broad electronic absorptions that extend from the UV to the visible region of the spectrum (~250–450 nm) (43). $Fe^{3+}\cdot X^-$ undergoes photoreduction to yield iron(II) and a free radical X$^\bullet$ according to eq. [4]:

Scheme 3.

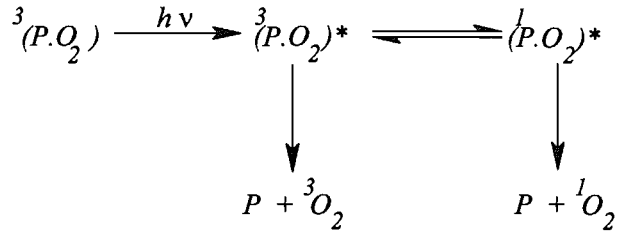

[4] $Fe^{3+}\cdot X^- \xrightarrow{h\nu} [Fe^{2+}X^\bullet] \rightarrow Fe^{2+} + X^\bullet$

The resulting radicals (X$^\bullet$) are sufficiently reactive to abstract hydrogen atoms from most hydrocarbons (RH), thus initiating photodegradation reactions (eq. [5]).

[5] $RH + X^\bullet \rightarrow R^\bullet + HX$

The primary point of H-abstraction from P3HT is the α-carbon atom of the alkyl group due to the lower dissociation energy of the α-C—H bond (44). Abstraction of an H-atom is presumably followed by the addition of oxygen to the polymer-bound radical and the formation of hydroperoxide. The rate of reaction of oxygen with free radicals is known to be diffusion controlled (45). Cleavage of the peroxide by the absorption of light, or by reaction with Fe(II) species, produces alkoxy radicals that can couple with polymer-bound radicals to form ether linkages (Scheme 4). OH radicals are produced in subsequent reactions. These propagate the photoxidation process by participating in additional H-atom abstraction reactions.

FTIR analyses of photolyzed P3HT is consistent with the proposed mechanisms and reveals the formation of ether groups (see Fig. 5). A kinetic study of the evolution of 3400 (-OH/-OOH) and 1230 (C-O-C) cm^{-1} bands (Fig. 6) further supports the proposed mechanism. The IR band at 3400 cm^{-1} reaches steady state after only a relatively short period of irradiation (<4 h). This implies that the rate of formation of these residues is equal to their rate of depletion. This is consistent with initial formation of hydroperoxide and its subsequent photolysis to form alkoxy radicals and OH. An induction period (~2 h) is observed for the formation of the ether band at 1230 cm^{-1}. The ether band then evolves continuously with irradiation and does not reach a steady state value even after 12 h of photolysis. This indicates that formation of the ether

Can. J. Chem. Downloaded from www.nrcresearchpress.com by 46.23.64.124 on 09/08/12
For personal use only.

Scheme 4.

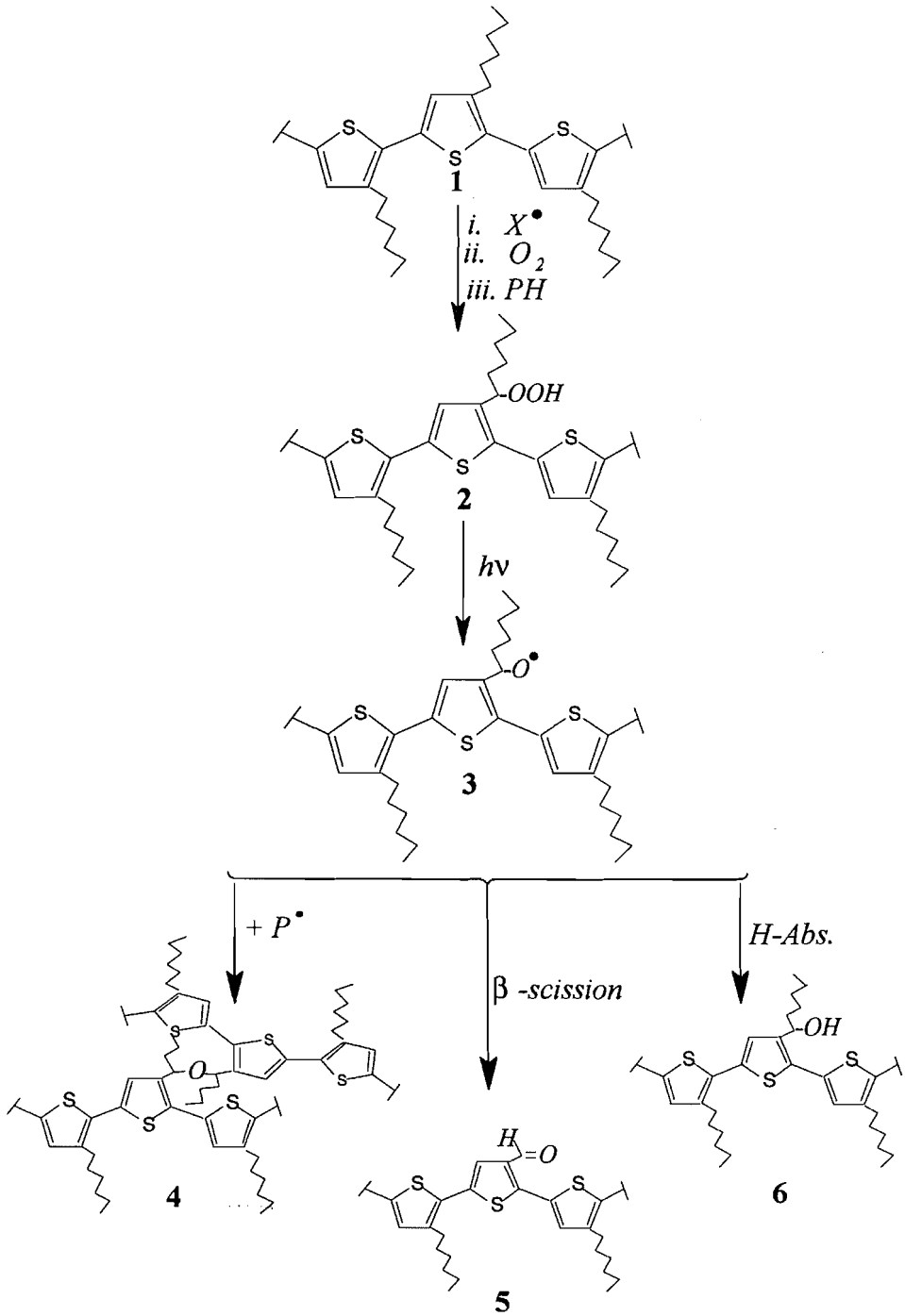

group is the result of a secondary photochemical reaction. This is consistent with the hypothesis that ether linkages form via the free-radical chain reaction.

When thin P3HT films were irradiated in an argon atmosphere, the films remained soluble in toluene and changes in the IR spectra were negligible, even after 24 h of photolysis.

The photochemical mechanism proposed for photooxidation of P3HT involves participation of the alkyl substituents. In the absence of the alkyl side chain one can anticipate that the photochemical properties of polythiophenes will be different. Parallel studies with side-chain-free α-hexathiophene and poly(thiophene) reveal the absence of photooxidation under the same experimental conditions used for P3HT, thus corroborating the hypothesis that alkyl side chains are involved in the photooxidation process. Photobleaching was still observed for these systems, however, since photosensitization and reaction of singlet oxygen are independent of the presence or absence of the alkyl side chain.

The thermal stability of P3ATs was investigated using differential scanning calorimetry (DSC) and FTIR spectroscopy.

Can. J. Chem. Downloaded from www.nrcresearchpress.com by 46.23.64.124 on 09/08/12
For personal use only.

The DSC thermogram of P3HT under N_2 exhibited endothermic transitions at 55°C and 170°C. These transitions are assigned to T_g and T_m, respectively, and are consistent with thermal studies using dynamic mechanical analysis (46, 47) P3ATs underwent thermal decomposition in air at ~250°C. Under an inert atmosphere, the polymer was thermally stable up to 350°C. FTIR was used to provide insight into the mechanism of this process. Films of the polymer heated in vacuo at 200°C for 15 h remained completely soluble in organic solvents and FTIR spectra of the polymer before and after thermal treatment were identical. When polymer films were heated under identical conditions but in the presence of an oxygen atmosphere, the films were rendered insoluble. Films heated in oxygen exhibited almost identical FTIR spectra to those produced by irradiation of poly(3-hexylthiophene) in oxygen, i.e., a decrease in the intensity of the bands at ~2900 cm^{-1} (C-H) and an increase in the bands at 3400 (-OH) and 1230 cm^{-1} (C-O-C) were observed. However, the band at 1045 cm^{-1} due to sulfine ($C{=}S^{+}\text{-}O^{-}$) was absent in the thermally treated sample. This is not surprising since the sulfine residue, a photochemically generated product, arises from singlet oxygen formation. Indeed, photolysis of the thermally treated sample in oxygen generated the sulfine residue. It is evident that the reaction pathway involving singlet oxygen generation and Diels–Alder addition is not required for insolubilization of the polymer. The similarity of the thermal and photochemical products of poly(3-hexylthiophene) in the presence of oxygen implies similar chemical routes. It is well known from studies of polyolefins that thermal treatment in the presence of oxygen results in a free-radical chain reaction initiated by H-abstraction, followed by formation of hydroperoxide, peroxide bond cleavage, and cross-linking via ether bond formation (48). The same chemical events occur in the photooxidative process, the difference being that in one case the initial H-abstraction is thermally driven, while in the other it is photochemically driven.

Conclusions

Films of poly(3-alkylthiophenes) (P3ATs) undergo simultaneous cross-linking and chain scission when irradiated in air with UV or visible light. The mechanism of cross-linking and insolubilization proceeds via free-radical chain reactions that appear to be initiated by photolysis of residual iron impurities. The mechanisms of photocross-linking and insolubilization of poly(3-hexylthiophenes) described in this work are believed applicable to poly(3-alkylthiophenes) in general. It appears that cross-linking requires an α-CH_2 in the 3-position and would preclude poly(3-alkoxythiophenes) from exhibiting cross-linking. However, photobleaching might still occur for these polymers since this occurs via photosensitization and reaction of singlet oxygen.

Poly(3-alkylthiophenes) are thermally stable up to 350°C under inert atmosphere. In air, the material degrades at temperatures above 250°C. Degradation takes the form of autooxidation, which is initiated by residual metal impurities.

Acknowledgements

Financial support of this work by the Natural Sciences and Engineering Research Council of Canada is gratefully acknowledged.

References

1. N.T. Binh, M. Gailberger, and H. Bassler. Synth. Met. **47**, 77 (1992).
2. R.H. Friend, D.D.C. Bradley, and P.D. Townsend. J. Phys. D: Appl. Phys. **20**, 1367 (1987).
3. B. Xu and S. Holdcroft. Thin Solid Films, **242**, 174 (1994).
4. M.J. Sailor, E.J. Ginsburg, C.B. Gorman, A. Kumar, R.H. Grubbs, and N.S. Lewis. Science, **249**, 1146 (1990).
5. S. Holdcroft. Macromolecules, **24**, 4834 (1991).
6. M.S.A. Abdou, M.I. Arroyo, G. Diaz-Quijada, and S. Holdcroft. Chem. Mater. **3**, 1003 (1991); (*b*) M.S.A. Abdou, Z.W. Xie, A. Leung, and S. Holdcroft. Synth. Met. **52**, 159 (1992).
7. M.S.A. Abdou, Z.W. Xie, J. Lowe, and S. Holdcroft. Proc. SPIE—Int. Soc. Opt. Eng. **2195**, 756 (1994).
8. M.I. Arroyo, G. Diaz-Quijada, M.S.A. Abdou, and S. Holdcroft. Macromolecules, **28**, 975 (1995).
9. P.C. Allen, D.C. Bott, C.S. Brown, L.M. Connors, S. Gray, N.S. Walker, P.I. Clemonson, and W.J. Feast. Electronic properties of conjugated polymers III. *Edited by* H. Kuzmany, M. Mehring, and S. Roth. Springer-Verlag, Berlin. 1989.
10. P.I. Clemonson, W.J. Feast, M.M. Ahmad, P.C. Allen, D.C. Bott, C.S. Brown, and L.M. Connors. Polymer, **32**, 356 (1992).
11. B.M. Novak, E. Hagen, A. Viswanathan, and L. Magde. Polym. Prepr. (Am. Chem. Soc. Wiv. Polym. Chem.), **31**, 482 (1990).
12. J.V. Crivello and L.H.W. Lam. J. Polym. Sci. Polym. Chem. Ed. **18**, 2677 (1980).
13. P.K. Das, P.J. DesLauriers, D.R. Fahey, F.K. Wood, and F.J. Cornforth. Macromolecules, **26**, 5024 (1993).
14. A.T. Filho and R. Lenz. J. Polym. Sci. Polym. Phys. **31**, 959 (1993).
15. M. Onoda, H. Nakayama, and K. Yoshino. IEEE Trans. Electr. Insul. **27**, 636 (1992).
16. J. Bullot, B. Dulieu, and S. Lafrant. Synth. Met. **61**, 211 (1993).
17. M. Angelopoulos, J.M. Shaw, W.-S. Huang, and R.D. Karplan. Mol. Cryst. Liq. Cryst. **189**, 221 (1990).
18. M. Angelopoulos, J.M. Shaw, K-L. Lee, W-S. Huang, M-A. Lecorre, and M. Tissier. Polym. Eng. Sci. **32**, 1535 (1992).
19. J.Y. Jin, N. Teramae, and H. Haraguchi. Chem. Lett. 101 (1993).
20. S. Kuwabata, N. Takahashi, S. Hirao, and H. Yoneyama. Chem. Mater. **5**, 437 (1993).
21. M. Okano, K. Itoh, A. Fujishima, and K. Honda. J. Electrochem. Soc. **134**, 837 (1987).
22. H. Segawa, T. Shimidzu, and K. Honda. J. Chem. Soc. Chem. Commun. 132 (1989).
23. L.S. Van Dyke, C.J. Brumlik, C.R. Martin, Z. Yu, and G.J. Collins. Synth. Met. **52**, 299 (1993).
24. M.S.A. Abdou and S. Holdcroft. Macromolecules, **26**, 2954 (1993).
25. R. Sugimoto, S. Takeda, H.G. Gu, and K. Yoshino. Chem. Express, **1**, 635 (1986).
26. S. Holdcroft. J. Polym. Sci. Polym. Phys. **29**, 1585 (1991).
27. H. Mao, B. Xu, and S. Holdcroft. Macromolecules, **26**, 1163 (1993).
28. A. Charlesby and S.H. Pinner. Proc. R. Soc. London, Ser. A: **249**, 367 (1958).
29. C. David, W. Demarteau, and G. Geuskenes. Polymer, **8**, 497 (1967).
30. L.F. Thompson, C.G. Wilson, and M.J. Bowden. (*Editors*). ACS Symp. Ser. 219, American Chemical Society, Washington, D.C. 1983.
31. J.L. Bredas, R. Silbey, D.S. Boudreaux, and R.R. Chance. J. Am. Chem. Soc. **105**, 6555 (1983).
32. J.C. Scott, P. Pfluger, M.T. Krounbi, and G.B. Street. J. Chem. Phys. **78**, 3212 (1983).

33. J.E. Guillet. Polymer photophysics and photochemistry. Cambridge University Press, New York. 1985.
34. C.N. Skold and R.H. Schlessinger. Tetrahedron. Lett. 791 (1970).
35. H.H. Wasserman and W. Strehlow. Tetrahedron. Lett. 795 (1970).
36. K. Gollnick. *In* Singlet oxygen—reaction with organic compounds and polymers. *Edited by* B. Ranby and L.F. Rabek. John Wiley, New York. 1978.
37. B. Xu and S. Holdcroft. J. Am. Chem. Soc. **115**, 8447 (1993).
38. V. Wintgens, P. Valat, and F. Garnier. J. Phys. Chem. **98**, 228 (1994).
39. H.C. Beachell and S.P. Nemphos. J. Polym. Sci. **21**, 113 (1956).
40. M.S.A. Abdou, F. Orfino, Z.W. Xie, M.J. Deen, and S. Holdcroft. Chem. Mater. **6**, 838 (1994).
41. J.B. Birks. Photophysics of aromatic molecules. Wiley, London. 1970.
42. M.S.A. Abdou, X. Lu, Z.W. Xie, F. Orfino, M.J. Deen, and S. Holdcroft. Chem. Mater. **7**, 631 (1995).
43. N. Uri. Chem. Rev. **52**, 357 (1952).
44. B. Ranby and J.F. Rabek. Photodegradation, photooxidation and photostabilization of polymers. John Wiley, London. 1975.
45. K.U. Ingold. Acc. Chem. Res. **2**, 1 (1969).
46. S-A. Chen and J-M. Ni. Macromolecules, **25**, 6081 (1992).
47. W-P. Hsu, K. Levon, K-S. Ho, A.S. Myerson, and T.K. Kwei. Macromolecules, **26**, 1323 (1993).
48. L. Reich and S.S. Stivala. Autoxidation of hydrocarbons and polyolefins. Marcel Dekker, Inc., New York. 1969.

Can. J. Chem. Downloaded from www.nrcresearchpress.com by 46.23.64.124 on 09/08/12
For personal use only.

Unusually strong emission from an exciplex formed between benzenoid solvents and dibenzoylmethanatoboron difluoride. Formation of a triplex

Pierre Valat, Véronique Wintgens, Yuan L. Chow, and Jean Kossanyi

Can. J. Chem. Downloaded from www.nrcresearchpress.com by 46.23.64.124 on 09/08/12
For personal use only.

Abstract: Benzene derivatives give, in cyclohexane solution, a strongly emitting (Φ_f up to 0.8) excited complex with dibenzoylmethanatoboron difluoride ($DBMBF_2$). The rate constant k_{ex} for the complex formation varies between 3.5×10^9 and 2.6×10^{10} M^{-1} s^{-1} depending on the benzene derivative, and the complex emission can already be detected at very low concentrations of the aromatics. This behaviour is different from that found in acetonitrile where the $DBMBF_2$ emission disappeared completely before the new emission of the complex could be detected. The position of the complex emission and its lifetime depend upon the redox potential of the aromatics: the lower the latter, the longer the lifetime and the more the emission is red-shifted. The monotonous increase of the lifetime and of the fluorescence quantum yield of the emission with the concentration of the aromatics has been interpreted on the basis of an equilibrium between the exciplex and excited $DBMBF_2$. The equilibrium constant varies with the electron-donating property of the aromatics, from 2.7 for benzene to 560 M^{-1} for isodurene. A decrease in the excited complex lifetime or in its fluorescence quantum yield is observed in some cases when the aromatics concentration is close to that of the pure solvent. Such behaviour is believed to arise from a new equilibrium resulting from the interaction of the exciplex with a second molecule of the aromatics to form triplex species. A detailed kinetic study has been undertaken in case of *p*-xylene, and the rate constants of all the processes involved in the double equilibrium have been determined. No basic difference is observed in the rate constant for exciplex formation when a single or double equilibrium is assumed; on the other hand, large discrepancies are found in the exciplex deactivation processes, specially for the back reaction from the exciplex to excited $DBMBF_2$. The equilibrium constants between $DBMBF_2$ and the exciplex, on one hand, and between the latter and the triplex are 56.6 and 0.68 M^{-1}, respectively, when the concentration of *p*-xylene in cyclohexane is 3.3 M.

Key words: fluorescence, exciplex, triplex, dibenzoylmethanatoboron difluoride, kinetics.

Résumé : En solution dans le cyclohexane, les dérivés du benzène donnent un complexe excité fortement émissif (jusqu'à $\Phi_f = 0.8$) avec le difluorure de dibenzoylmethanatobore ($DBMBF_2$). Cette émission de fluorescence est déjà détectable aux faibles concentrations en dérivé du benzène. Ce comportement se distingue de celui observé dans l'acétonitrile où l'émission de $DBMBF_2$ disparait complètement avant que n'apparaisse celle de l'exciplexe. La constante de vitesse de formation de l'exciplexe varie entre $3{,}5 \times 10^9$ et $2{,}6 \times 10^{10}$ M^{-1} s^{-1} suivant l'aromatique. Dans le cyclohexane, le complexe émet à une longueur d'onde d'autant plus grande et sa durée de vie est d'autant plus élevée que le potentiel redox de l'aromatique est faible. L'augmentation régulière de la durée de vie et du rendement quantique de fluorescence de l'exciplexe résulte d'un équilibre entre le $DBMBF_2$ excité et l'exciplexe. La constante de cet équilibre varie de 2,7 à 560 M^{-1}; elle est d'autant plus élevée que le caractère électrodonneur de l'aromatique est grand. Une diminution de la durée de vie, ou du rendement quantique de fluorescence du complexe excité est observée avec certains aromatiques pour des concentrations très élevées. Ce phénomène a été expliqué par l'établissement d'un second équilibre formant un triplexe excité et mettant en jeu deux molécules du dérivé benzénique pour une de $DBMBF_2$. Une étude cinétique détaillée a été

Received June 2, 1995.

This paper is dedicated to Professor J.E. (Jim) Guillet in recognition of his contributions to Canadian chemistry.

P. Valat, V. Wintgens, Y.L. Chow,[1] and J. Kossanyi.[2] Laboratoire des matériaux moléculaires, Centre national de la recherche scientifique, 2–8, rue Henry Dunant, 94320-Thiais, France.

[1] Visiting Professor from Department of Chemistry, Simon Fraser University, Burnaby, British Columbia, Canada.
[2] Author to whom correspondence may be addressed. Telephone: (1) 49 78 12 43. Fax: (1) 49 78 13 23.

entreprise dans le cas du *p*-xylène et les constantes de vitesse de tous les processus mis en jeu dans le double équilibre ont pu être calculées. On ne trouve pas de différence fondamentale dans la valeur de la constante de formation de l'exciplexe suivant le traitement à un ou à deux équilibres. En revanche, les constantes de vitesse des processus qui désactivent l'exciplexe intermédiaire, en particulier le retour à $DBMBF_2$ excité, diffèrent fortement suivant le traitement. Les constantes d'équilibre, entre $DBMBF_2$ et l'exciplexe d'une part, et entre ce dernier et le triplexe sont respectivement de 56,6 et 0,68 M^{-1} lorsque la concentration en *p*-xylène est 3,3 M.

Mots clés : fluorescence, exciplexe, triplexe, difluorure de dibenzoylméthanatobore, cinétique.

Can. J. Chem. Downloaded from www.nrcresearchpress.com by 46.23.64.124 on 09/08/12
For personal use only.

Introduction

Electron transfer constitutes an important chemical process because of its extensions in chemistry and biology. The quenching of the fluorescence of molecules by electron-withdrawing or electron-donating species is well established (1, 2). In some cases this quenching is accompanied by a weak and broad emission at wavelengths longer than the quenched fluorescence (3–5). The influence of the solvent on the course of the electron or charge transfer process has been intensively studied in both its theoretical (6–10) and experimental (11–14) aspects. Ultrafast (up to 10^{13} s^{-1}) electron transfer has been shown to occur between excited dyes and weakly polar electron-donating solvent molecules (15).

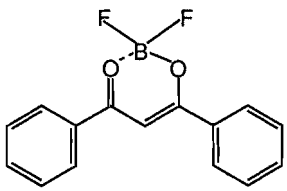

Dibenzoylmethanatoboron difluoride

Dibenzoylmethanatoboron difluoride ($DBMBF_2$) exhibits very different photoreaction and photophysical patterns in alkylbenzenes from those in acetonitrile or dichloromethane as solvents (16). $DBMBF_2$ fluoresces with moderate efficiency ($\Phi_f = 0.1$) in acetonitrile solution and its fluorescence has been found (17) to be quenched by alkylbenzenes, presumably through an exciplex formation. In acetonitrile, the quenching by toluene and *p*-xylene as a function of solvent fractions is unusual in that the quenching is straightforward at low concentrations of the quencher, but a strong, broad, structureless and red-shifted fluorescence, attributed to an exciplex, emerges at high mole fractions (>3 mol L^{-1} for toluene and >6 mol L^{-1} for *p*-xylene) of the aromatics, with a lifetime that increases with the proportion of the aromatics in the solvent mixture. In the quenching by benzene, the exciplex begins to emit with a lifetime that increases systematically with the benzene concentration, even at low concentration of the quencher.

A behaviour similar to that observed with benzene in acetonitrile is found with all the benzene derivatives studied (toluene, *m*-xylene, *p*-xylene, mesitylene, and isodurene) when cyclohexane is used as solvent. Then, the exciplex fluorescence quantum yield increases rapidly from $\Phi_f = 0.046$ in cyclohexane to become higher than 0.5 in all cases except isodurene. It is the aim of the present article to introduce a new series of strongly emitting excited complexes and, more specifically, to rationalize the evolution in lifetime and fluorescence quantum yield of the $DBMBF_2$ exciplex as the concentration of the benzene derivative is increased.

Experimental

The UV–visible absorption spectra were obtained using a Varian–Cary model 219 apparatus. Fluorescence spectra were recorded with a SLM 8000C spectrofluorimeter equipped with a spectral correction unit by excitation at 389 nm. Fluorescence quantum yields were determined in pure cyclohexane solution, as well as in mixtures with benzene, toluene, *m*-xylene, *p*-xylene, mesitylene, and isodurene. A 10^{-4} mol L^{-1} solution of 5,6,8,9-tetrahydro-7-phenyldibenzo[*c*,*h*]xanthylium perchlorate in dichloromethane solution ($\Phi_f = 0.95$) was taken as secondary actinometer (18). The absolute fluorescence quantum yields are given with less than 10% error but their values relative to each other are estimated with less than 3% error.

Singlet lifetimes longer than 0.8 ns were measured with a frequency-tripled pulsed YAG laser (from B.M. Industries) of 30 ps fwhm. The light was focused through a cylindrical lens onto the sample placed in front of a photodiode. The output from the photodiode was fed into a Tektronix 7912 AD digitized oscilloscope and the data stored in an Apple II+ microcomputer were analyzed directly at any wavelength and compared to several kinetic treatments: mono-exponential with or without a residue, bi-exponential, combination of first and second order decays, ... The final curves were displayed on a Hewlett–Packard model 7470A graphic plotter. For lifetimes higher than 1 ns, the fitting of the curves was obtained with $\sum(y_i - y_{exp})^2$ smaller than 5×10^{-4}. For lifetimes lower than 2 ns, the fluorescence decay is measured with ca. 6% or less error, while for lifetimes higher than 4 ns the decay can be evaluated with less than 3% error. For shorter lived fluorescent species (<800 ps), the same laser was used with a TSN 506 streak-camera having ca. 10 ps time resolution. The fluorescence was focused through an optical coupling on the slit of the streak-camera and the data were transferred to a multichannel analyzer that permitted the accumulation of several decay measurements. In this way, lifetimes of 60 ps (±10%) or more could be handled as described for the data stored in the digitized oscilloscope.

The triplet signal and lifetime were determined using a frequency-doubled pulsed ruby laser (347.5 nm) from JK Laser following the experimental protocol already described (19).

Dibenzoylmethanatoboron difluoride ($DBMBF_2$) was prepared according to known procedures (16). Benzene (Aldrich, spectroscopic grade), toluene (Aldrich, ACS reagent), *m*-xylene (Aldrich, anhydrous), *p*-xylene (Aldrich, HPLC grade), mesitylene (Aldrich, 99% pure), and isodurene (Aldrich, 95+) were used as received.

Fig. 1. Fluorescence emission of the exciplex formed by addition of benzene to the cyclohexane solution of $DBMBF_2$. Benzene concentration (mol L^{-1}): (1) 0; (3) 0.27 M; (5) 0.88 M; (7) 1.68 M; (9) 2.92 M; (11) 4.64 M; (13) 5.78 M; (15) 7.52 M; (17) 9.40 M; (19) pure benzene. Inset: residual $DBMBF_2$ fluorescence spectra obtained by subtraction of the exciplex emission from the total luminescence at the following benzene concentrations (mol L^{-1}, from the upper to the lower curve): (1) 0; (5) 0.88 M; (7) 1.58 M; (9) 2.92 M; (11) 4.65 M; (13) 5.78 M; (14) 6.63 M.

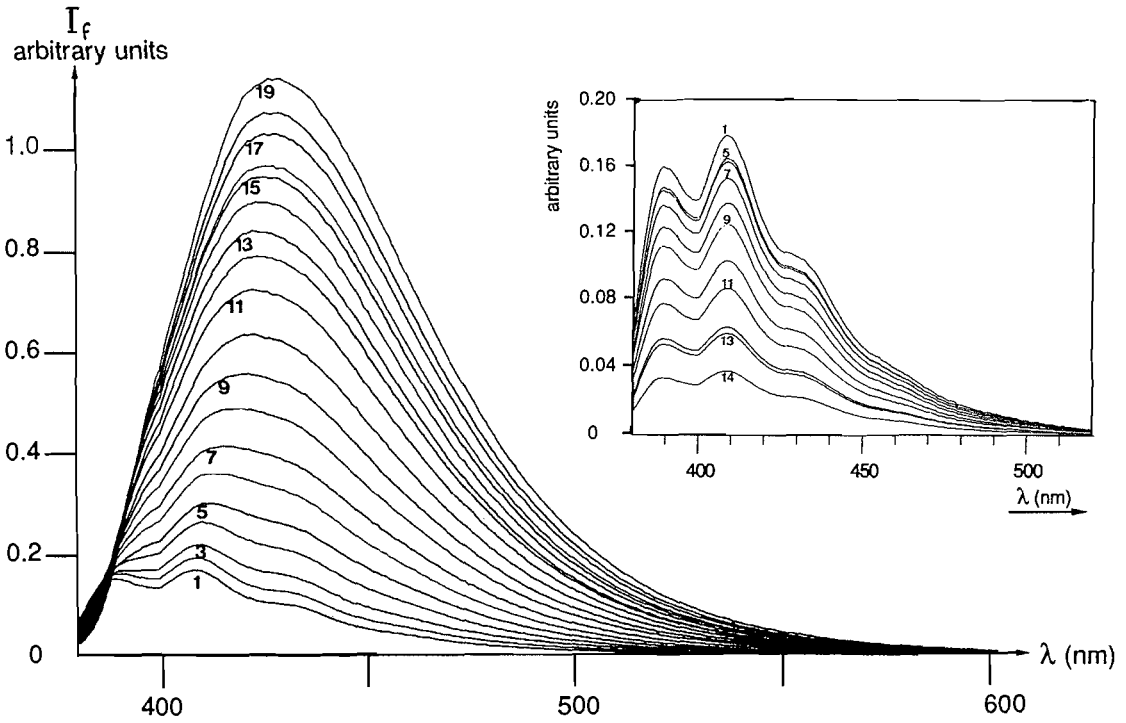

Results and discussion

$DBMBF_2$ absorption and emission

The $DBMBF_2$ absorption band in the aromatic solvents was found identical in overall profile to that of $DBMBF_2$ absorption in cyclohexane but its position (maximum at 368 nm) is slightly red-shifted.

In cyclohexane solution, $DBMBF_2$ showed a fluorescence spectrum with maxima at 389, 409, and 432 nm. Its fluorescence quantum yield, Φ_f^{A0}, in the absence of aromatic quencher in cyclohexane solution and at room temperature (22 ± 1°C), equals 0.046 and its lifetime is 0.14 ns.

Flash photolysis of $DBMBF_2$ in cyclohexane solution gave an O_2 sensitive *T–T* absorption showing a maximum at 740 nm and a triplet yield Φ_T of the order of 0.01. In the absence of O_2, the triplet lifetime is 17.5 μs. The singlet to triplet intersystem crossing could be regarded as a negligible process in the deactivation of singlet excited $DBMBF_2$ to its ground state. Thus, in cyclohexane solution, the radiative and the nonradiative decays are the main deactivation processes of the $DBMBF_2$ singlet excited state. The corresponding rate constants, k_f^A and k_{nrA}, are easily deduced: $k_f^A = \Phi_f^{A0}/\tau_A^0 = 3.3 \times 10^8\ s^{-1}$ and $k_{nrA} = (1 - \Phi_f^{A0} - \Phi_T)/\tau_A^0 = 6.8\ 10^9\ s^{-1}$, respectively.

Quenching of $DBMBF_2$ fluorescence by the aromatics

Addition at room temperature (22 ± 1°C) of small amounts of the benzene derivatives to the cyclohexane solution of $DBMBF_2$ (at a concentration of ca. 3×10^{-5} mol L^{-1}) first modifies slightly the shape of the fluorescence spectrum by changing the relative intensities of the three peaks while the total fluorescence intensity is increased (Fig. 1). Further additions of the aromatics suppress the vibrational structure of the fluorescence, which changes into a new broad emission with a maximum shifted progressively from ca. 420 nm to 427 nm for benzene, 444 nm for toluene, 460 nm for *m*-xylene, 470 nm for *p*-xylene, 472 nm for mesitylene, and to 497 nm for isodurene.

The exciplex emission can be fully characterized in the solutions of pure benzene derivatives. Except with isodurene, the measurement of the quenching process by the aromatics is made difficult because of the overlap of $DBMBF_2$ fluorescence with the exciplex emission. The fluorescence spectra of the exciplexes obtained in the pure benzene derivatives have been taken as reference spectra to isolate the $DBMBF_2$ residual emission profile from the recorded total emission spectra by using the mathematical treatment already described (17). This technique introduces a small error as a result of a small bathochromic shift of the total emission profile at high aromatics concentrations. The quenching of $DBMBF_2$ fluorescence by benzene under steady state conditions is shown in Fig. 1 as an example. Having extracted the residual $DBMBF_2$ fluorescence spectra at various concentrations of the benzene derivative (inset of Fig. 1), the results have been used to evaluate the Stern–Volmer quenching rate constant K_{SV} from the plot of the ratio of the fluorescence in the absence (Φ_f^{A0}) and in the presence (Φ_f^A) of

Can. J. Chem. Downloaded from www.nrcresearchpress.com by 46.23.64.124 on 09/08/12
For personal use only.

Can. J. Chem. Downloaded from www.nrcresearchpress.com by 46.23.64.124 on 09/08/12
For personal use only.

Fig. 2. Stern–Volmer plot of the quenching of $DBMBF_2$ fluorescence in cyclohexane solution ([D] in mol L^{-1}): (*a*) by benzene (△ △ △) and toluene (* * *); (*b*) by *m*-xylene (o o o), *p*-xylene (▲ ▲ ▲), mesitylene (× × ×), and isodurene (+ + +).

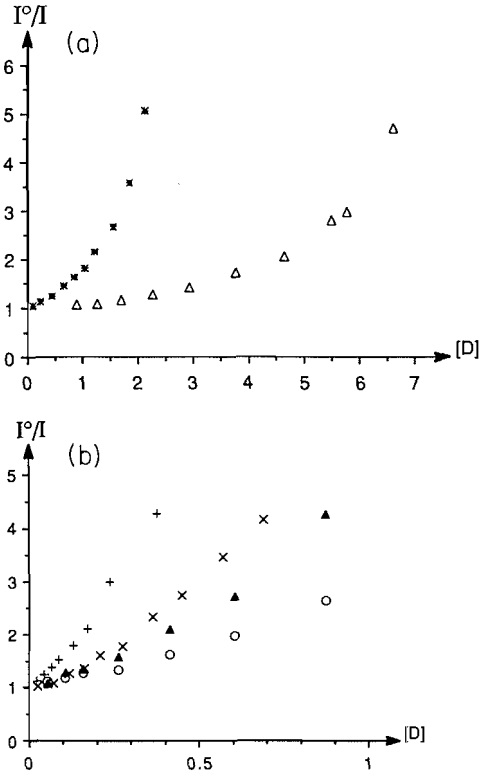

quencher vs. the concentration of the quencher. In all cases, the quenching does not give a straight line but shows (Fig. 2) an upward curvature, which occurs already at moderate concentrations of the quencher (ca. 1.5 mol L^{-1} for benzene, 1.0 mol L^{-1} for toluene, 0.5 mol L^{-1} for *m*- and *p*-xylene, 0.4 mol L^{-1} for mesitylene, and 0.2 mol L^{-1} for isodurene) and which, in the absence of any other process, could correspond to a static quenching. The curvature is more pronounced when the electron-donating properties of the aromatics increase (the oxidation potentials versus SCE are 2.38, 2.28, 1.88, 1.77, 1.80, and 1.73 V for benzene (20), toluene (20), *m*-xylene (20, 21), *p*-xylene (21), mesitylene (21), and isodurene (20), respectively). However, no ground state association could be detected in the absorption spectra of the mixture of the two compounds. An attempt to fit the data obtained on the basis of a double equilibrium, one to form a ground state charge transfer complex between $DBMBF_2$ and *p*-xylene and the other between excited $DBMBF_2$ and the exciplex, led to the conclusion that if such a ground state equilibrium does occur, its constant K_0 is lower than 10^{-3}. Evaluation of the K_{SV} constant has been carried out by fitting the experimental data of $\Phi_f^{A^0}/\Phi_f^A$ with a third-degree polynomial of the type $\Phi_f^{A^0}/\Phi_f^A = 1 + ax + bx^2 + cx^3$. The values obtained (Table I) show a monotonous increase of K_{SV} with the electron-donating character of the aromatics (from 0.1 M^{-1} for benzene to 3.4 M^{-1} for isodurene).

Fig. 3. Decay of the full fluorescence of excited $DBMBF_2$ in the presence of 3.27 mol L^{-1} of *p*-xylene in cyclohexane solution (5 ns per division).

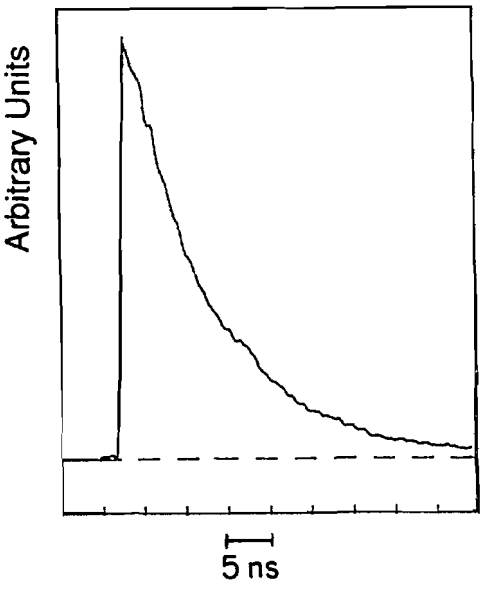

Exciplex formation

Addition of the methyl-substituted benzene derivatives to a solution of $DBMBF_2$ in both polar and nonpolar solvents decreases the $DBMBF_2$ fluorescence intensity around 390 and 410 nm and gives rise to a new broad emission at longer wavelengths (from 430 to 495 nm, depending on the aromatics) that decays monoexponentially when analyzed in the nanosecond time range (Fig. 3). This emission increases and is steadily red-shifted as the concentration of the benzene derivative is increased, in agreement with an exciplex formation. The quenching of the singlet excited state of $DBMBF_2$ by 1,3-cyclohexadiene (E_{ox} = 1.58 V/SCE (22)) was reported earlier (23). The transformation of the latter into its radical cation by electron transfer to $DBMBF_2$ has already been reported (23) although no exciplex fluorescence could be observed.[3] Quenching of the fluorescence of $DBMBF_2$ by 1,4-cyclohexadiene (E_{ox} = 1.90 V/SCE (24)), 1,3-cyclooctadiene (E_{ox} = 1.89 V/SCE (25)), and 1-methylcyclohexene (E_{ox} = 1.77 V/SCE (26)) is also observed but, again, no exciplex emission could be detected. On the other hand, pyridine (E_{ox} = 2.12 V/SCE (24)) gives rise to a new emission around 418 nm. Thus, it seems likely that the aromatic π-electron system is needed for the quencher to give a fluorescent exciplex with $DBMBF_2$.

Stabilization of the exciplex, as the number of methyl substituents on the benzene ring increases, can be interpreted in terms of the lowering of the exciplex energy, which is visualized by the red shift of the exciplex emission as the oxidation potential of the aromatics decreases. A concomitant increase of the lifetime of the exciplexes from 2 ns with benzene all the way up to 22.9 ns with isodurene corroborates this stabilization.

Both the exciplex lifetime and fluorescence quantum yield increase progressively as the concentration of the aromatics increases. Such behaviour suggests that the exciplex is

[3] C.I. Johansson, unpublished results (Simon Fraser University).

formed reversibly and can be analyzed within the framework of Scheme 1:

Scheme 1.

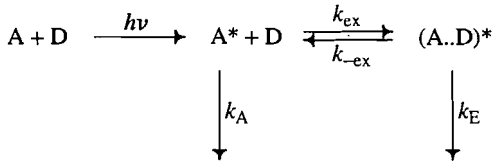

where $k_A = k_f^A + k_{nrA}$ and $k_E = k_f^{ex} + k_{nrE}$. A and D represent $DBMBF_2$ and the benzene derivative, respectively. k_f^A and k_{nrA} are the radiative and nonradiative rate constants of excited $DBMBF_2$ in cyclohexane (in the absence of aromatic donor), k_f^{ex} and k_{nrE} being the corresponding rate constants for the $DBMBF_2$ exciplex (A..D)* at the concentration [D] of the aromatics, respectively.

$\tau_A^0 = (k_A)^{-1} = (k_f^A + k_{nrA})^{-1}$ corresponds to the lifetime of A* in the absence of D, while $\tau_{ex} = (k_E + k_{-ex})^{-1}$ is the lifetime of the exciplex at concentration [D] of the aromatic donor. The latter expression is valid because τ_A^0 is small compared to τ_{ex} and, therefore, the dissociation from (A..D)* to A* must be slow enough to be neglected. If the reverse is fast under the condition $\tau_A^0 \gg \tau_{ex}$, then τ_{ex} of the exciplex would be equal to τ_A^0 of $DBMBF_2$.

The decays measured on the ns time scale are all found to be first order at both the short and long wavelengths. However, in the short-wavelength range, where $DBMBF_2$ emits, the decay is found to be second order when analyzing on the picosecond time scale but, 0.42 ns after the laser pulse (after three lifetimes of $DBMBF_2$ fluorescence in the absence of any aromatics), the $DBMBF_2$ emission intensity has decreased by a factor of 20 to become negligible. When the aromatics are present, this intensity is even more reduced after the same time interval due to the quenching process and, even when the two emissions do not overlap, $DBMBF_2$ fluorescence decays in the ns range because of its equilibrium with the exciplex.

Application of the steady state assumption to A* and to (A..D)* under continuous irradiation conditions of the cyclohexane solution of A + D leads to the following expressions for $DBMBF_2$ (Φ_f^A) and exciplex (Φ_f^E) fluorescence quantum yields:

$$[1] \quad \frac{I^0}{[A^*]} = k_A + \frac{k_{ex}k_E[D]}{k_{-ex} + k_E}$$

$$[2] \quad \Phi_f^A = \frac{k_f^A}{k_A + \dfrac{k_{ex}k_E[D]}{k_{-ex} + k_E}}$$

$$[3] \quad \Phi_f^E = \frac{k_f^{ex}k_{ex}[D]}{k_{-ex} + k_E} \times \frac{1}{k_A + \dfrac{k_{ex}k_E[D]}{k_{-ex} + k_E}}$$

Combining expressions [2] and [3] gives

$$[4] \quad \frac{\Phi_f^E}{\Phi_f^A} = \frac{k_f^{ex}k_{ex}[D]}{k_f^A(k_{-ex} + k_E)} = \frac{k_f^{ex}}{k_f^A} k_{ex}\tau_{ex}[D]$$

while relation (2) leads to

$$[5] \quad \frac{\Phi_f^{A0}}{\Phi_f^A} - 1 = \frac{k_{ex}k_E[D]}{k_A(k_{-ex} + k_E)} = K_{SV}[D]$$

Φ_f^{A0}, the fluorescence quantum yield of $DBMBF_2$ in the absence of the aromatic donor D, is measured easily; $(k_A)^{-1}$, which corresponds to the lifetime of $DBMBF_2$ in cyclohexane in the absence of benzene derivative, is known; $(k_{-ex} + k_E)^{-1}$, the lifetime of the exciplex at the concentration [D] of the aromatics, can be measured.

In the pure aromatics solution, the exciplex fluorescence quantum yield is high (see Table 1) and its lifetime τ_{ex} increases with the number of methyl substituents on the benzene ring: e.g., 2.0 ns in benzene, 4.0 ns in toluene, 8.2 ns in *m*-xylene, 14.4 ns in *p*-xylene, 13.6 ns in mesitylene, and 22.9 ns in isodurene. At the same time, the emission maximum undergoes a bathochromic shift increasing with the reduction potential of the donor (see Table 1). The plot of the fluorescence quantum yield versus the concentration of the aromatics shows that all the curves appear (Fig. 4) to have two slopes and to asymptotically approach their maxima at lower concentration with more substituted benzene, and even with benzene, although less pronounced with the latter. The quantum yield even decreases slightly above a certain concentration of the aromatics, as observed for *m*- and *p*-xylene as well as for isodurene. The same phenomenon is also observed when plotting the exciplex lifetime as a function of the aromatics concentration (Fig. 5). But it is only in the case of isodurene that the lifetime of the exciplex reaches a maximum and then decreases. Such behaviour, which may involve an additional deactivation pathway for the exciplex due to the increased benzene derivative concentration, will be discussed later.

As far as we are aware, there exist only few examples in the literature (27) describing exciplex fluorescence quantum yield enhancement of more than one order of magnitude (up to 0.8) with respect to that of the parent compound itself. A red shift by more than 100 nm (>5100 cm^{-1}) of the exciplex emission with respect to the position of the $DBMBF_2$ absorption maximum makes these exciplexes interesting as potential laser dyes.

When plotting the reciprocal of the exciplex fluorescence quantum yield versus the reciprocal of the aromatics concentration (eq. [6]), one can (*i*) get the maximum value reached by this quantum yield when the concentration of the aromatics is infinitive; (*ii*) deduce the ratio k_E/k_f^{ex} from the intercept of the plot:

$$[6] \quad \frac{1}{\Phi_f^{ex}} = \frac{k_E}{k_f^{ex}} + \frac{1}{k_f^{ex}k_{ex}\tau_A^0\tau_{ex}[D]}$$

We already pointed out (vide supra) that the increase of the exciplex (A..D)* lifetime with the concentration of the aromatic (Scheme 1) arises from its equilibrium with the starting excited $DBMBF_2$ (A*). This equilibrium must be strongly displaced toward the exciplex in the pure aromatics and, under such conditions, the quantum yield Φ_{-ex} of the back reaction (A..D)* → A* could be neglected with respect to the quantum yield Φ_E of the intrinsic deactivation of the exciplex, i.e., $k_{-ex} \ll k_E$. This hypothesis agrees with the high values of the exciplex fluorescence quantum yields obtained for all the benzene derivatives studied except isodurene.

Since $\Phi_E = \Phi_{ex}k_E\tau_{ex}$ and $\Phi_f^{ex} = \Phi_{ex}k_f^{ex}\tau_{ex}$, relation [6] indicates that the intercept of the plot of $1/\Phi_f^{ex}$ vs 1/[D] corresponds also to the ratio Φ_E/Φ_f^{ex} at infinite dilution. However,

Can. J. Chem. Downloaded from www.nrcresearchpress.com by 46.23.64.124 on 09/08/12
For personal use only.

Can. J. Chem. Downloaded from www.nrcresearchpress.com by 46.23.64.124 on 09/08/12
For personal use only.

Table 1. Quantum yields (±3%), lifetimes (±3%), and kinetics data (±6%) for the exciplex formed between $DBMBF_2$ and the benzene derivatives on the basis of a simple equilibrium.

	Compound					
	Benzene	Toluene	*m*-Xylene	*p*-Xylene	Mesitylene	Isodurene
$(\lambda_f)_{max}$ (nm)[a]	427	444	460	470	472	497
Maximum moles per litre	11.2	9.41	8.16	8.11	7.20	6.63
K_{SV} (L mol^{-1})[b]	0.1	0.4	1.4	1.9	1.4	3.4
At infinite dilution[c]						
$(\tau_{ex})_\infty$ (ns)	1.97	3.97	8.16	14.4	13.57	21.3
$(k_E/k_f^{ex})_\infty$[d]	1.2	0.9	1.2	1.1	1.3	3.9
$(\Phi_f^{ex})_\infty$	0.85	?	0.82	0.88	0.58	0.14
$(k_f^{ex})_\infty \times 10^{-7}$ s^{-1} [e]	43	?	10.0	6.1	4.27	0.66
$(k_E)_\infty \times 10^{-7}$ s^{-1}	50.3	?	12.2	7.2	7.3	4.7
$(k_{nrE})_\infty \times 10^{-7}$ s^{-1} [f]	7.3	?	2.2	1.10	3.03	4.04
$(\Phi_{nrE})_\infty$	0.15	?	0.18	0.12	0.42	0.86
At maximum values[g]						
$(\tau_{ex})_{max}$ (ns)	1.97	3.97	8.16	14.4	13.57	22.9
$(\Phi_f^{ex})_{max}$	0.44	0.68	0.54	0.63	0.55	0.13
$(k_E/k_f^{ex})_{max}$[d]	1.17	1.16	1.53	1.38	1.75	7.89
$(k_f^{ex})_{max} \times 10^{-7}$ s^{-1} [e]	22	17	6.6	4.3	4.05	0.55
$(k_E)_{max} \times 10^{-7}$ s^{-1}	26.7	19.7	10.1	5.9	7.1	4.3
$(k_{nrE})_{max} \times 10^{-7}$ s^{-1} [f]	4.7	2.7	4.1	1.6	3.0	3.7
$(\Phi_{nrE})_{max}$	0.09	0.11	0.33	0.23	0.41	0.84
$(\Phi_{ex})_{max}$[h]	0.53	0.79	0.87	0.86	0.96	0.97

[a]Maximum of the fluorescence emission of the complex in the pure aromatics.
[b]Stern–Volmer constant obtained from relation [5] at low concentration of D.
[c]The values with the subscript ∞ are determined in pure aromatic solution.
[d]From the intercept of the plot of $1/\Phi_f^{ex}$ versus 1/[D].
[e]Calculated by using the relation $k_f^{ex} = \Phi_f^{ex}/\tau_{ex}$.
[f]$(k_{nrE}) = (k_E) - (k_f^{ex})$
[g]Data with subscript "max" are obtained from the maximum values of Φ_f^{ex} and τ_{ex}.
[h]Calculated using expression [7].

Fig. 4. Variation of the global fluorescence quantum yield Φ_f as a function of the benzene derivative concentration ([D], mol L^{-1}): (△ △ △) benzene; (∗ ∗ ∗) toluene; (○ ○ ○) *m*-xylene; (▲ ▲ ▲) *p*-xylene; (× × ×) mesitylene.

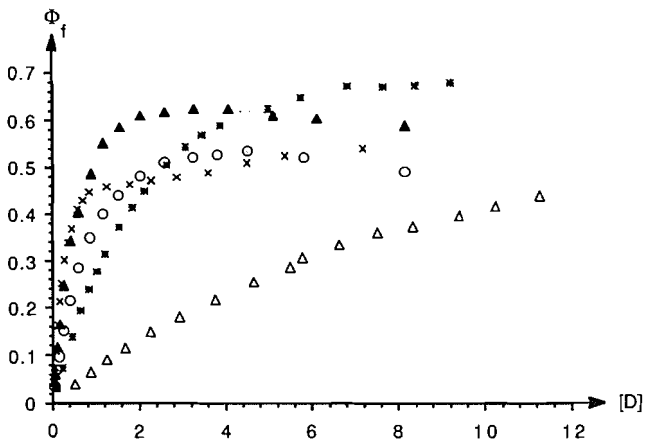

Fig. 5. Variation of the lifetime τ_f (in nanoseconds) of the excited species in cyclohexane solution as a function of the benzene derivative concentration (in mol L^{-1}): (△ △ △) benzene; (∗ ∗ ∗) toluene; (○ ○ ○) *m*-xylene; (▲ ▲ ▲) *p*-xylene; (+ + +) isodurene.

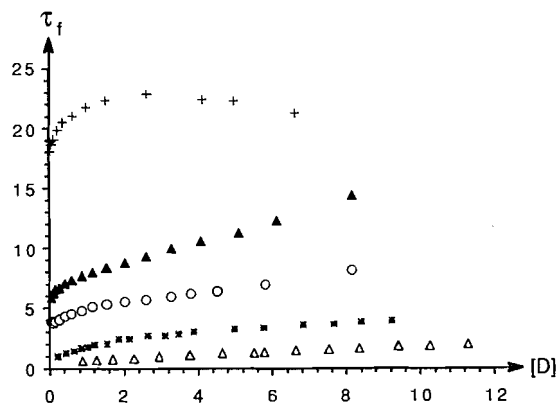

there is one ambiguity in this plot because the maximum value that the concentration of the aromatics can take is when it constitutes the solvent itself: 11.2 M for benzene, 9.4 M for toluene, 8.2 M for *m*-xylene, 8.1 M for *p*-xylene, 7.2 M for mesitylene, and 6.6 M for isodurene. Because of this ambiguity, two values of the Φ_E/Φ_f^{ex} ratio have been evaluated (see Table 1). One, $(1/\Phi_f^{ex})_\infty$, corresponds to the intercept of the plot, which is obtained using only values of Φ_f^{ex} at low concentrations of the aromatics, thus eliminating any additional processes occurring at high concentrations. The other,

Table 2. Kinetics data for the equilibrium between excited $DBMBF_2$ and its exciplex formed with benzene derivatives on the basis of a simple equilibrium.

	Aromatics					
	Benzene	Toluene	*m*-Xylene	*p*-Xylene	Mesitylene	Isodurene
K_{SV} (L mol^{-1})[a]	0.1	0.4	1.4	1.9	1.4	3.4
$k_E \times 10^{-7}$ s^{-1} [b]	26.7	19.7	10.1	5.9	7.1	4.3
$k_{ex} \times 10^{-9}$ M^{-1} s^{-1}	3.5	9.2	15.0	23.0	25.0	26.0
$k_{-ex} \times 10^{-7}$ s^{-1}	104	44	19	4.1	9.6	0.3
K_1 (L mol^{-1})[c]	2.7	14	51	230	140	560

[a]Stern–Volmer constant.
[b]Using the values deduced for the maximum values of Φ_f^{ex} and τ_{ex}.
[c]Equilibrium constant calculated with relation [9].

$(1/\Phi_f^{ex})_{max}$, is based on the fact that the concentration of the quencher cannot be higher than the number of moles of the quencher contained in 1 L of solution; putting the different values of [D]max and the experimental values obtained for $(\tau_{ex})_{max}$ in eq. [6] gives the $(\Phi_f^{ex})_{max}$ values shown in Table 1.

As the intercept corresponds to the Φ_E/Φ_f^{ex} ratio, knowledge of $(\Phi_f^{ex})_{max}$ allows determination of Φ_E (the sum of the intrinsic radiative and nonradiative quantum yields of the exciplex) and of $(\Phi_{nrE})_{max}$. The deactivation rate constants of the exciplex, k_f^{ex} and k_{nrE}, can easily be obtained since the lifetime of the exciplex in the pure benzene derivatives is known, and since the quantum yield Φ_{-ex} for the return of the exciplex to excited $DBMBF_2$ can be ignored.

The calculations were performed using two sets of data. One is deduced from the plot of $1/\Phi_f^{ex}$ versus 1/[D] according to relation [6] while the other set uses the maximum values measured for the exciplex lifetime $(\tau_{ex})_{max}$ and for the fluorescence quantum yield $(\Phi_f^{ex})_{max}$.

The quantum yield for exciplex formation Φ_{ex} can be calculated from the expression $\Phi_f^{ex} = \Phi_{ex} k_f^{ex} \tau_{ex}$ as long as τ_{ex}, Φ_f^{ex}, and k_f^{ex} are known.

Table 1 gives the values of τ_{ex}, Φ_f^{ex}, Φ_{nrE}, and Φ_{ex} calculated in both cases, and of the rate constants k_f^{ex}, k_E, and k_{nrE}.

Once τ_{ex} and Φ_f^{ex} are known, the rate constant for exciplex formation k_{ex} can be obtained from expression [7], which is deduced from eq. [6].

$$[7] \quad k_{ex} = \frac{1}{k_f^{ex} \tau_A^0 \tau_{ex} [D] \left(\frac{1}{\Phi_f^{ex}} - \frac{k_E}{k_f^{ex}} \right)}$$

This has been done at low concentrations (<1 M) of the aromatic donor since k_f^{ex}, τ_A^0, and k_E are already known, while Φ_f^{ex} and τ_{ex} were measured for various concentrations of the aromatics [D].

Toluene is an exception in the series since the plot of $1/\Phi_f^{ex}$ versus 1/[D] gives an intercept smaller than unity, which is meaningless. Therefore the ratio (k_E/k_f^{ex}) used to determine k_{ex} for toluene is the one calculated for $1/\Phi_f^{ex}$ at the concentration of pure toluene, 9.4 mol L^{-1}.

The data given in Table 2 for k_{ex} correspond to the average of the different k_{ex} values determined according to relation [7] for all concentrations <1 M of the aromatics. It can be seen that the value of k_{ex} measured by this method increases regularly with the electron-donating property of the aromatics to become larger than the diffusion rate constant k_{diff} of cyclohexane ($k_{diff} = 6.7 \times 10^9$ L mol^{-1} s^{-1}) for all the aromatics except benzene and toluene. However, with the proportion of the aromatics increasing in the reaction mixture, k_{diff} also increases slightly since it is larger (28) for the aromatics (at least for benzene, $k_{diff} = 1.0 \times 10^{10}$ L mol^{-1} s^{-1}, and for toluene $k_{diff} = 1.1 \times 10^{10}$ L mol^{-1} s^{-1}) than for cyclohexane. So, although the values obtained for k_{ex} must be regarded as an estimate, their increase with the electron-donating properties of the aromatics is a good indication that the process involves the formation of a charged species. That k_{ex} is found to be larger than the diffusion rate constant is evidence of the surrounding of $DBMBF_2$ by several molecules of the benzene derivative at high concentration (>1 M) and, therefore, the involvement of a static quenching process. As already stated, no equilibrium between the two entities and a charge transfer complex seems to be operating in the ground state.

The rate constant k_{-ex} for the back reaction from the exciplex to excited $DBMBF_2$ can be deduced from the rearrangement of the Stern–Volmer constant K_{SV} given in relation [5]:

$$[8] \quad k_{-ex} = k_E \left(\frac{k_{ex} \tau_A^0}{K_{SV}} - 1 \right)$$

The values deduced from this expression can be found in Table 2. They show for all the aromatics used, with the exception of benzene, that the rate constant of the back reaction from the exciplex to the parent excited $DBMBF_2$ is always smaller than that of the complex formation. This also means that the value of the equilibrium constant K_1 existing between (A* + D) and (A..D)* must be important. This constant K_1 as formulated by relation [9] now becomes accessible since the three rate constants k_{ex}, k_{-ex}, and k_E have been calculated.

$$[9] \quad K_1 = \frac{[(A..D)^*]}{[A^*][D]} = \frac{k_{ex}}{k_{-ex} + k_E}$$

The equilibrium constant values obtained for benzene and its five derivatives can be found in Table 2. As can be seen, only with benzene is this constant small due to a non-negligible back reaction from the exciplex to excited $DBMBF_2$.

The value obtained for K_1 increases with the number of

Can. J. Chem. Downloaded from www.nrcresearchpress.com by 46.23.64.124 on 09/08/12
For personal use only.

methyl substituents bound to the aromatics. This behaviour was expected from the steady state fluorescence-quenching experiments; effectively, high concentrations of the aromatics were needed in the case of benzene and toluene, corresponding to the smallest quenching rate constants of the series of compounds, while the quenching already occurred at low concentrations of the good electron-donating aromatics.

Double equilibrium. Triplex formation

To a first approximation, the equilibrium between A* and (A..D)*, proposed to explain the increase in lifetime of the exciplex as the concentration of the aromatics is increased, is valid for benzene and toluene since the plot of $1/\Phi_f^{ex}$ versus 1/[D] gives almost straight lines. However, for toluene, we already noted that the intercept of this plot has a meaningless value lower than unity.

On the other hand, the plot of the fluorescence quantum yield as a function of the concentration of the aromatics shows curves with at least two slopes, and this is visible even for benzene (Fig. 4). Also, the fluorescence quantum yield of the exciplex, obtained with the xylenes, mesitylene, and isodurene, increases with the proportions of the aromatics in the solvent mixture, reaches a maximum value for a certain concentration of the aromatics, and decreases or remains approximately constant at high concentrations of the aromatics. Similar behaviour was previously found in acetonitrile solution for the exciplex given by $DBMBF_2$ with toluene and *p*-xylene (17). This behaviour could have been taken as an indication that the stabilization of the exciplex depends upon the polarity of the solvent (17). However, here, the dielectric constant of the solvent varies very little between cyclohexane (ε = 2.023) and the aromatics (29): ε = 2.284 for benzene, 2.379 for toluene, 2.374 for *m*-xylene, 2.270 for *p*-xylene, and 2.279 for mesitylene. Furthermore, since the ε values for *p*-xylene and mesitylene are closer to that of cyclohexane than the ε value of benzene, the effect should be more important with benzene than with *p*-xylene. This is not the case, and the formation of the exciplex increases monotonously with the concentration of benzene. Furthermore, the effect should be most pronounced with toluene and with *m*-xylene since they have the highest ε values of the aromatics investigated. Again, this is not the case. Therefore, a solvent effect cannot be a plausible explanation for the observed concentration effect.

An alternative possibility to explain the evolution of the exciplex observed at high concentrations of the benzene derivatives would be the formation of a triplex (and (or) a multiplex) in which two (or more) aromatic donor molecules are associated with $DBMBF_2$. However, since the excited species decays monoexponentially, the triplex (and (or) multiplex) must not only emit in the same region as the exciplex but must also be in equilibrium with the exciplex and have a fluorescence quantum yield different from that of the exciplex. Scheme 2 illustrates such a double equilibrium involving an exciplex and a triplex (or multiplex):

Scheme 2.

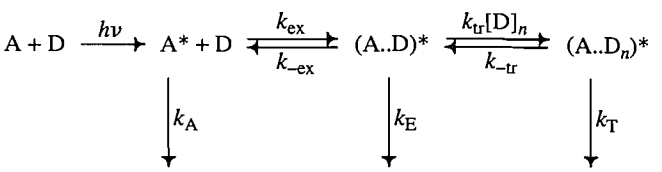

k_A and k_E have the same meaning as in Scheme 1; $k_T = k_f^{tr} + k_{nrT}$ represents the intrinsic deactivation rate constant of the triplex (or multiplex) in the absence of back reaction from (A..D_n)* to (A..D)*.

With the hypothesis of a triplex species (n = 2), the regular increase of both Φ_f^{ex} and τ_{ex}, to reach their maximum values in the pure aromatics, means that the triplex has a higher fluorescence quantum yield and a longer lifetime than the exciplex itself (this is observed with benzene, toluene, and mesitylene).

On the other hand, when both the quantum yield and the lifetime of the fluorescence first increase but then decrease at high concentration of the aromatics, as is the particular case with isodurene, two hypotheses can be put forward: (*i*) either the triplex is in equilibrium with the exciplex but has a lower fluorescence efficiency and a shorter lifetime than the exciplex, or (*ii*) the formation of the triplex is less efficient than that of the exciplex and is irreversible.

A third case is found here, with the *m*- and *p*-xylenes, where the lifetime of the complex increases continuously with the concentration of the aromatics while its fluorescence quantum yield first increases and then begins to decrease at high concentrations of the aromatics. Such behaviour can be taken as an indication that the triplex has a longer lifetime but a lower fluorescence quantum yield than the exciplex.

Figures 4 and 5 present the evolution of the fluorescence quantum yield and of the fluorescence lifetime, respectively, as a function of the concentration of the benzene derivatives. They illustrate well the three cases described above.

Yet, the decrease of the lifetime and (or) of the fluorescence quantum yield at high concentrations of the aromatics could be interpreted in terms of quenching of the exciplex by the aromatics and could correspond to triplex formation. Then, both the lifetime and the quantum yield of the exciplex fluorescence should decrease, as found with isodurene. However, such a process cannot be operating with the xylenes since their fluorescence lifetime increases continuously with the concentration of the aromatics. For all the aromatics studied here, the polarity of the solvent mixtures remains practically constant; consequently, no shift of the exciplex emission should occur even at high concentrations of the aromatics if the process involved was a simple quenching of the exciplex. This is not the case, as shown in Fig. 6 with a 13 nm bathochromic shift at high concentrations of *p*-xylene. Similarly, a 10 and 24 nm red shift is observed in the high concentration ranges for mesitylene and isodurene, respectively.

Triplex formation with *p*-xylene

The triplex approach has been undertaken in the case of *p*-xylene because of the high fluorescence quantum yield and the long lifetime observed for the excited complex at the various concentrations in *p*-xylene.

Application of the steady state assumption to A*, (A..D)*, and (A..D_2)* under continuous irradiation of the cyclohexane

Can. J. Chem. Downloaded from www.nrcresearchpress.com by 46.23.64.124 on 09/08/12
For personal use only.

Fig. 6. Fluorescence emission of the exciplex formed by addition of *p*-xylene to the cyclohexane solution of $DBMBF_2$. *p*-xylene concentration (mol L^{-1}): (1) 0; (3) 0.11 M; (5) 0.26 M; (7) 0.61 M; (9) 1.17 M; (11) 2.04 M; (13) 3.27 M; (15) 5.11 M; (17) pure *p*-xylene.

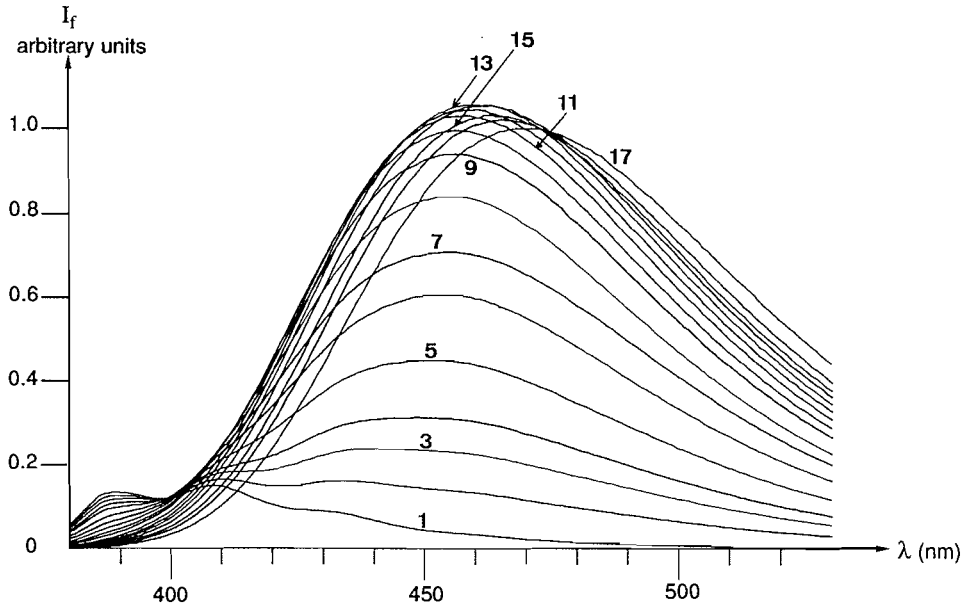

solution of A + D leads to new expressions of the quantum yields as a function of the concentration of D. Thus the Stern–Volmer expression is changed into:

$$\frac{\Phi_f^{A^0}}{\Phi_f^A} - 1 = k_{ex}\tau_A^0[D]\left\{\frac{1}{\tau_E^0\left[(k_{-ex}+k_E)+\dfrac{k_{tr}k_T[D]}{k_{-tr}+k_T}\right]} + \frac{k_{tr}k_T[D]}{(k_{-ex}+k_E)(k_{-tr}+k_T)+k_{tr}k_T[D]}\right\}$$

Incorporation of the equilibrium constant K_2 between the exciplex (A..D)* and the triplex (A..D_2)* species

$$[10]\quad K_2 = \frac{[(A..D)^*]}{[(A..D)^*][D]} = \frac{k_{tr}}{k_{-tr}+k_T}$$

in the above Stern–Volmer expression leads to:

$$[11]\quad \frac{\Phi_f^{A^0}}{\Phi_f^A} = 1 + \frac{k_{ex}\tau_A^0[D]}{\tau_E^0[(k_{-ex}+k_E)+K_2k_T[D]]} + \frac{k_{ex}k_{tr}\tau_A^0[D]^2}{(k_{-ex}+k_E)\left(1+\dfrac{k_{-tr}}{k_T}\right)+k_{tr}[D]}$$

That relation [11] reduces to expression [5] in the absence of triplex formation is readily verified.

Equation [11] can be changed into:

$$[12]\quad \frac{\Phi_f^{A^0}}{\Phi_f^A} = 1 + k_{ex}\tau_A^0[D] - \frac{k_{ex}k_{-ex}[D]}{k_Ak_TK_2\left[\dfrac{k_{-ex}+k_E}{k_TK_2}+[D]\right]}$$

which is of the following form:

$$\frac{\Phi_f^{A^0}}{\Phi_f^A} = 1 + a[D] - \frac{b[D]}{c+[D]}$$

and which can be fitted with the different values of Φ_f^A to obtain the parameter $a = k_{ex}\tau_A^0$, thus permitting the evaluation of k_{ex}. This fit of the Φ_f^A data to expression [12] gives the value 3.9 L mol^{-1} for the $k_{ex}\tau_A^0$ product. Since $\tau_A^0 = 0.14 \times 10^{-9}$ s,

Can. J. Chem. Downloaded from www.nrcresearchpress.com by 46.23.64.124 on 09/08/12
For personal use only.

the rate constant for exciplex formation is $k_{ex} = 27.9 \times 10^9$ L mol^{-1} s^{-1}, a value that is 20% higher than that (23.0×10^9 L mol^{-1} s^{-1}) calculated with the hypothesis of a single equilibrium between A* and (A..D)*.

The expression for $1/\Phi_f^{ex}$, used formerly in the case of a simple equilibrium between A* and (A..D)*, can be reformulated by including the second equilibrium constant K_2 between (A..D)* and (A..D_2)* given by relation [10]. This leads to:

$$[13] \quad \frac{1}{\Phi_f^{ex}} = \frac{k_E}{k_f^{ex}} + \frac{K_2 k_T [D]}{k_f^{ex}} + \frac{K_2 k_T}{k_f^{ex} k_{ex} \tau_A^0} + \frac{k_{-ex} + k_E}{k_f^{ex} k_{ex} \tau_A^0 [D]}$$

As expected, expression [13] is reduced to relation [6] in the absence of the second equilibrium. It can be written in the new form:

$$[14] \quad \frac{1}{\Phi_f^{ex}} = \frac{\frac{K_2 k_T}{k_f^{ex}}[D]^2 + \left(\frac{k_E}{k_f^{ex}} + \frac{k_A K_2 k_T}{k_f^{ex} k_{ex}}\right)[D] + \frac{k_A(k_{-ex} + k_E)}{k_f^{ex} k_{ex}}}{[D]}$$

To evaluate the fluorescence data of both the exciplex and the triplex, we need the expression for the quantum yield of the triplex emission. This is obtained by application of the steady state principle to the reactions of Scheme 2:

$$[15] \quad \frac{1}{\Phi_f^{tr}} = \frac{\frac{k_T}{k_f^{tr}}[D]^2 + \left(\frac{k_E}{k_f^{tr} K_2} + \frac{k_A k_T}{k_f^{tr} k_{ex}}\right)[D] + \frac{k_A(k_{-ex} + k_E)}{k_f^{tr} k_{ex} K_2}}{[D]^2}$$

For simplification, we shall abbreviate the following rate constant expressions: k_T/k_f^{tr} by $X(1)$; $k_T K_2$ by 10^8 $X(2)$; $(k_{-ex} + k_E)$ by 10^8 $X(3)$; k_E/k_f^{ex} by $X(4)$; k_f^{ex} by $10^8 X(5)$; and assign to $k_A/k_{ex} = X(6)$ the reciprocal of the value (3.9 L $\times$ mol^{-1}) obtained from the Stern–Volmer plot.

Relations [14] and [15] can be transformed into eqs. [16] and [17], respectively:

$$[16] \quad \frac{1}{\Phi_f^{ex}} = \frac{\frac{X(2)}{X(5)}[D]^2 + \left(X(4) + \frac{X(2)X(6)}{X(5)}\right)[D] + \frac{X(3)X(6)}{X(5)}}{[D]}$$

and

$$[17] \quad \frac{1}{\Phi_f^{tr}} = \frac{X(1)[D]^2 + \left(X(1)X(6) + \frac{X(1)X(4)X(5)}{X(2)}\right)[D] + \frac{X(3)X(6)}{X(5)}}{[D]^2}$$

The fitting of the curve of the reciprocal of the global fluorescence quantum yield $1/(\Phi_f^{ex} + \Phi_f^{tr})$ vs. the reciprocal of the *p*-xylene concentration has been carried out (Fig. 7) using the Levenberg–Margnardt algorithm given in the IGOR Pro program from Watermetrics. The best fit is obtained for the following values: $X(1) = 2.04$, $X(2) = 0.4$, $X(3) = 3.62$, $X(4) = 1.015$, and $X(5) = 1.18$.

The ratio $k_T/k_f^{tr} = X(1) = 2.04$ is the reciprocal of the triplex intrinsic fluorescence quantum yield in the absence of back reaction to the exciplex. This gives $(\Phi_f^{tr})_0 = 0.49$. Similarly, $k_E/k_f^{ex} = X(4)$ is the reciprocal of the exciplex intrinsic fluorescence quantum yield with no other deactivation than fluorescence and nonradiative decay. Thus, $(\Phi_f^{ex})_0 = 0.98$. The fluorescence rate constant of the exciplex, $k_f^{ex} = 1.18 \times 10^8$ s^{-1}, the intrinsic deactivation process of the exciplex, $k_E = 1.20 \times 10^8$ s^{-1}, and the rate constant for the back reaction from the exciplex to excited $DBMBF_2$, $k_{-ex} = 2.42 \times 10^8$ s^{-1}, are deduced from the values obtained for $X(3)$, $X(4)$, and $(X5)$. The nonradiative deactivation rate constant of the exciplex, $k_{nrE} = 2 \times 10^6$ s^{-1}, and the intrinsic lifetime of the exciplex, $\tau_{ex}^0 = 1/k_E = 8.3$ ns, are easily deduced from the above data.

In pure *p*-xylene solution, the fluorescence quantum yield of the excited complex and its lifetime are 0.59 and 14.4 ns, respectively. Yet, the value obtained from the fit of the curve for the intrinsic fluorescence quantum yield of the triplex is 0.49, that is ca. 20% lower than the measured value. Therefore, even in pure *p*-xylene solution the triplex does revert in part to the exciplex, which fluoresces with an efficiency twice as high as that of the triplex. Consequently, the lifetime of the pure triplex must be higher than the 14.4 ns found in pure *p*-xylene. We have arbitrarily multiplied the measured lifetime by 1.2 and taken $\tau_{tr}^0 = 17$ ns.

Then, $k_T = \frac{1}{\tau_{tr}^0} = 5.9 \times 10^7$ s^{-1} and the value of K_2 is deduced from $X(2) = k_T K_2 = 0.4 \times 10^8$ M^{-1}s^{-1}. This gives $K_2 = 0.68$ M^{-1}. k_f^{tr} is obtained from $X(1)$: $k_f^{tr} = 2.9 \times 10^7$ s^{-1} and this permits the evaluation of $k_{nrT} = 3.0 \times 10^7$ s^{-1} since $k_{nrT} = k_T - k_f^{tr}$.

Access to the constants of the remaining two reactions, the forward and the backward triplex formation from the exciplex, is more complex. They could be reached by neglecting the back reaction from the exciplex to excited $DBMBF_2$, at high *p*-xylene concentrations. This hypothesis is quite reasonable when comparing the rate constant for exciplex formation (27.9×10^9 M^{-1} s^{-1}) with that for the reverse reaction (2.42×10^8 s^{-1}). Then, the only equilibrium to be considered at high *p*-xylene concentrations is the one between the exciplex and the triplex. On this basis, the kinetic treatment used in other cases (30, 31)

Can. J. Chem. Downloaded from www.nrcresearchpress.com by 46.23.64.124 on 09/08/12
For personal use only.

Can. J. Chem. Downloaded from www.nrcresearchpress.com by 46.23.64.124 on 09/08/12
For personal use only.

can be applied here. If the exciplex and the triplex have different decays ($\tau_{ex} = 1/\lambda_1$, and $\tau_{tr} = 1/\lambda_2$), they can be described as

$$\lambda_1, \lambda_2 = \frac{1}{2}\left\{(k_{tr}[D] + k_E + k_{-tr} + k_T \pm \sqrt{(k_{tr}[D] + k_E - k_{-tr} - k_T)^2 + 4k_{tr}k_{-tr}[D]}\right\}$$

Since the intrinsic lifetime of the triplex is longer than that of the exciplex, and because the two species are in equilibrium, the λ value to be considered is the one having the minus sign before the square root. Then, the relation to be used (after remodeling the expression under the square root) is

$$\frac{1}{\tau_{tr}} = \lambda_2 = \frac{1}{2}\left\{k_{tr}[D] + k_E + k_{-tr} + k_T - \sqrt{(k_{tr}[D] + k_{-tr})^2 + 2(k_{tr}[D] - k_{-tr})(k_E - k_T) + (k_E - k_T)^2}\right\}$$

For a 3.27 M concentration in *p*-xylene, the lifetime of the excited species is 10.0 ns and the overall fluorescence quantum yield is 0.63. At this concentration, the [triplex]/[exciplex] ratio deduced from relation [10] is 4.1; this means that, under steady state conditions, there is 20% of exciplex for 80% of triplex in the cyclohexane solution that is 3.27 M in *p*-xylene (in pure *p*-xylene, the exciplex represents only 9% and the triplex 91% of the excited species).

The importance of triplex formation implies that k_{tr} [D] is much greater than $(k_{-ex} + k_E) = 3.62 \times 10^8$ s^{-1}. So, since $(k_{tr}[D] + k_{-tr})^2$ is larger than $(k_{-ex} + k_E)^2$, which is equal to 13×10^{16} s^{-2}, it is at least 36 times more important than $(k_E - k_T)^2 = 3.6 \times 10^{14}$ s^{-2}. Consequently, the last factor under the square-root sign in the expression for λ_2 can be neglected in favor of the first factor and, therefore, λ_2 is reduced to

$$[18] \quad \frac{2}{\tau_{tr}} = 2\lambda_2 = k_{tr}[D] + k_{-tr} + k_E + k_T - (k_{tr}[D] + k_{-tr})\sqrt{1 + \frac{2(k_{tr}[D] - k_{-tr})(k_E - k_T)}{(k_{tr}[D] + k_{-tr})^2}}$$

The lifetime of the excited species is known at the different concentrations of *p*-xylene. The other constants k_E and k_T having already been calculated, k_{tr} and k_{-tr} become the only unknown parameters in expression [18]. Similarly, formula [10] gives another relation between the same two rate constants since K_2 and k_T are known. The two expressions [10] and [18] lead to the values $k_{tr} = 2.1 \times 10^9$ M^{-1} s^{-1} and $k_{-tr} = 1.55 \times 10^9$ s^{-1} for the triplex formation rate constant and for that of the reverse reaction, respectively.

Scheme 3 can now summarize the different kinetic data for the double equilibrium between excited $DBMBF_2$, the exciplex (A..D)*, and triplex (A..D_2)* species formed with *p*-xylene in cyclohexane solution:

Scheme 3.

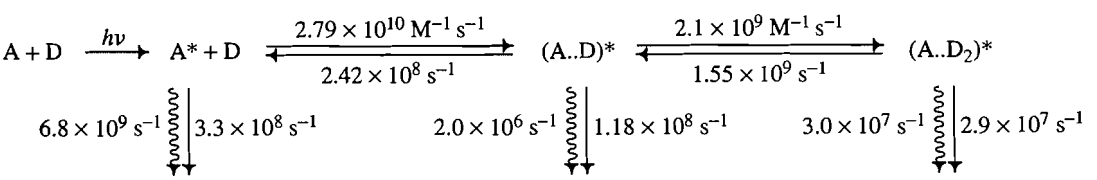

Fig. 7. Plot of the reciprocal of the global fluorescence quantum yield versus the reciprocal of *p*-xylene concentration in cyclohexane solution (× × ×). The points (····) represent the best fit of the calculated curve compared to the experimental values.

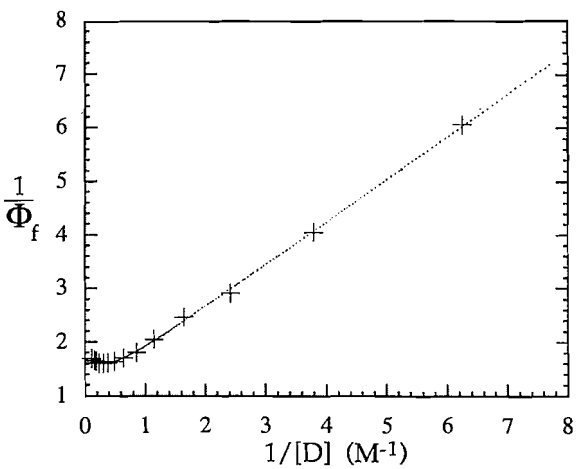

The constant K_1 of the first equilibrium between excited $DBMBF_2$ and the exciplex (A..D)* is

$$[19] \quad K_1 = \frac{[(A..D)^*]}{[A^*][D]} = \frac{k_{ex}}{k_E + k_{-ex} + k_T K_2 [D]}$$

Since k_E, k_{ex}, k_{-ex}, k_T, and K_2 have been calculated in the case of *p*-xylene, the equilibrium constant K_1 becomes accessible. At the concentration 3.27 M in *p*-xylene, K_1 = 56.6 M^{-1}. This value is four times lower than the value (Table 2) obtained when considering a single equilibrium process. Furthermore, the maximum value that can be reached by K_1, at low concentration of *p*-xylene, is of the order of 77 M^{-1}, a value that is still three times lower than that given on the basis of a single equilibrium.

Comparison of the two treatments, the one limited to the exciplex only, and the other that takes into account the formation of the triplex species, shows, in the case of *p*-xylene, that no important difference between the two approaches is reflected in the rate constant for the exciplex formation (2.79 instead of 2.3×10^{10} L mol^{-1} s^{-1}). However, involvement of the triplex species strongly modifies the rate

constant for the back reaction of the exciplex to $DBMBF_2$ (by a factor of 37) and the exciplex fluorescence rate constant only slightly (by a factor of 2).

Indeed, the different possibilities discussed above can explain the various evolutions observed in the lifetime and the fluorescence quantum yield of all the excited species studied. However, they do not completely explain the changes observed from one complex to the other. The increase in the excited species lifetime could be related to the increased electron-donating properties of the aromatics, but the results obtained with isodurene are puzzling since its lifetime, although the longest, as expected, decreases above a certain isodurene concentration (perhaps by formation of a multiplex). On the other hand, the fluorescence quantum yield of the excited species decreases above a certain concentration of the aromatics with the two xylenes and with isodurene but not with mesitylene. Such a difference cannot be related to the reduction potential of the aromatics but possibly to the steric hindrance introduced by the methyl groups in the formation of the complex.[4]

Conclusion

$DBMBF_2$ has been shown to give rise to a series of strongly fluorescent excited complexes with one or two molecules of benzene derivatives. The lifetime and the fluorescence quantum yield of the excited species increase monotonously with the concentration of the benzene derivative, but several of them reach a maximum value that decreases in the high concentration range of the aromatics. The two excited complexes are formed in a double equilibrium with the starting excited $DBMBF_2$. All the rate constants involved in this double equilibrium have been evaluated for the complex given with *p*-xylene.

References

1. M. Julliard. *In* Photoinduced electron transfer. Part B. *Edited by* M.A. Fox and M. Chanon. Elsevier, Amsterdam. 1988. p. 216.
2. S. Kebarle and S. Chowhurry. Chem. Rev. **87**, 513 (1987).
3. J.R. Gould, S. Farid, and R.H. Young. J. Photochem. Photobiol. A: **65**, 133 (1992).
4. A. Weller. Pure Appl. Chem. **16**, 115 (1968).
5. H. Beens, K. Knibbe, and A. Weller. J. Chem. Phys. **47**, 1183 (1967).
6. I. Rips, J. Klafter, and J. Jortner. J. Chem. Phys. **94**, 8557 (1990).
7. D.F. Calef. *In* Photoinduced electron transfer. Part A. *Edited by* M.A. Fox and M. Chanon. Elsevier, Amsterdam. 1988. p. 362.
8. W. Nadler and R.A. Marcus. J. Chem. Phys. **86**, 3906 (1987).
9. H. Sumi and R.A. Marcus. J. Chem. Phys. **84**, 4894 (1986).
10. L.D. Zusmann. Chem. Phys. **49**, 295 (1980).
11. H. Kandori, K. Kemnitz, and K. Yoshihara. J. Chem. Phys. **96**, 8042 (1992).
12. G.C. Walker, E. Åkerson, A.E. Johnson, N.E. Levinger, and P. Barbara. J. Phys. Chem. **96**, 3728 (1992).
13. P. Suppan. Top. Curr. Chem. **163**, 95 (1992).
14. E.M. Kosower and D. Huppert. Annu. Rev. Phys. Chem. **91**, 127 (1987).
15. K. Yoshihara, A. Yartsev, Y. Najasawa, H. Kandori, A. Douhal, and K. Kemnitz. Pure Appl. Chem. **63**, 1671 (1993).
16. (*a*) Y.L. Chow and X.E. Cheng. J. Chem. Soc. Chem. Commum. 1043 (1990); (*b*) Can. J. Chem. **69**, 1331 (1991); **69**, 1575 (1991).
17. Y.L. Chow, S.S. Wang, Z.L. Liu, V. Wintgens, P. Valat, and J. Kossanyi. New J. Chem. **18**, 923 (1994).
18. (*a*) S. Tripathi, M. Simalty, J. Pouliquen, and J. Kossanyi. Bull. Soc. Chim. Fr. 600 (1986); (*b*) M.C. Gazeau, M. Simalty, P. Valat, V. Wintgens, J. Kossanyi, D. Doizi, G. Salvetat, J. Jaraudias, B. Perly, J. Vian, and J.-L. Peglion. J. Phys. Org. Chem. In press.
19. P. Valat, S. Tripathi, V. Wintgens, and J. Kossanyi. New J. Chem. **14**, 825 (1990).
20. W.C. Neikam and M.M. Desmond. J. Am. Chem. Soc. **86**, 4811 (1964).
21. E.S. Pysh and N.C. Yang. J. Am. Chem. Soc. **85**, 2124 (1963).
22. R. Breslow and R.W. Johnson. Tetrahedron Lett. 3443 (1975).
23. Y.L. Chow and X.X. Ouyang. Can. J. Chem. **69**, 423 (1991).
24. L.L. Miller, G.D. Nordblom, and E.A. Mayeda. J. Org. Chem. **37**, 916 (1972).
25. S.L.P. Chang and D. Schuster. J. Phys. Chem. **91**, 3644 (1987).
26. J. Mattay, J. Gersdorf, and K. Buchkremer. Chem. Ber. **120**, 307 (1987).
27. (*a*) F. Fages, J.-P. Desvergnes, H. Bouas-Laurent, P. Marsau, J.-M. Lehn, F. Kotzyba-Hibert, A.-M. Albrecht-Gary, and M. Al-Joubbeh. J. Am. Chem. Soc. **111**, 8672 (1989); (*b*) F. Fages, J.-P. Desvergnes, and H. Bouas-Laurent. J. Am. Chem. Soc. **111**, 96 (1989).
28. S.L. Murov. Handbook of Photochemistry, 2nd ed. Marcel Dekker Inc., New York, 1993. p. 208.
29. R.C. Weast (*Editor*). Handbook of chemistry and physics. 61st ed. CRC Press, Boca Raton, Fla 1980. p. E-57.
30. M.C.C. de Lange, D. Thorn Leeson, K.A.B. Van Kuijk, A.H. Huizer, and C.A.G.O. Varma. Chem. Phys. **174**, 425 (1993)
31. F. Lahmadi, P. Valat, and J. Kossanyi. New. J. Chem. **19**, 965 (1995).

[4] Further work on this subject is in progress.

Can. J. Chem. Downloaded from www.nrcresearchpress.com by 46.23.64.124 on 09/08/12
For personal use only.

Synthesis and characterization of a series of poly(α,ω-alkyldiynes) and copoly(α,ω-alkyldiynes)

J.C. Kennedy, J.R. MacCallum, and D.H. MacKerron

Abstract: A series of poly(α,ω-alkyldiynes) and copoly(α,ω-alkyldiynes) were synthesized by catalytic Glaser coupling reactions. Two routes were investigated and developed. These routes were chosen in anticipation that high molar mass, linear and polydisperse, polymers would be achieved. GPC (gel permeation chromatography) curves revealed that this was possible for the majority of polymers synthesized by the first route. However, a wide range of molar masses were obtained by the second route with a significant low molar mass tail present in almost all GPC curves. Very low M_n (number average molar mass) values by GPC gave correspondingly very high M_n values by end-group analysis (EGA). Hence, it was proposed that the low molar mass tail was a consequence of cyclic structures. From these results and observations a mechanism for the polymerization of the α,ω-alkyldiynes was proposed.

Key words: poly(α,ω-alkyldiynes), Glaser coupling, molar mass.

Résumé : On a synthétisé une série de poly(α,ω-alkyldiynes) et de copoly(α,ω-alkyldiynes) par les réactions de couplage catalytique de Glaser. On a étudié et développé deux voies. Ces voies ont été choisies dans le but d'obtenir des polymères linéaires et polydispersés de poids moléculaires élevés. Des courbes de chromatographie par perméation de gel (GPC) ont révélé que ceci est possible pour la majorité des polymères synthétisés par la première voie. Toutefois, la seconde voie a conduit à de grandes variations dans les poids moléculaires et, dans chaque cas, les courbes de GPC ont toutes présentées des traînées avec des quantités importantes de produits de faibles poids moléculaires. Des valeurs très faibles de M_n (valeur moyenne de la masse molaire) par GPC fournissent des valeurs correspondantes élevées de M_n par l'analyse des groupes terminaux (EGA). On suggère donc que les traînées de faible poids moléculaire sont une conséquence de structures cycliques. Sur la base de ces résultats et de l'ensemble des observations, on propose un mécanisme pour la polymérisation des α,ω-alkyldiynes.

Mots clés : poly(α,ω-alkyldiynes), couplage de Glaser, masses molaires.

[Traduit par la rédaction]

Introduction

It has been shown by several workers that α,ω-alkyldiynes can be polymerized through an oxidative "Glaser" coupling reaction catalysed by a complex of a copper salt and *N,N,N′,N′*-tetramethylethylenediamine (TMEDA) (1–6).

This reaction of α,ω-alkyldiynes was first performed by Hay (1) in 1967 when 1,6-heptadiyne, 1,7-octadiyne, and 1,8-nonadiyne were polymerized. Hay's reaction system consisted of 2 g (0.02 mol) Cu(I)Cl, 7 g (0.058 mol) TMEDA, 135 mL pyridine, and 0.05 mol of α,ω-alkyldiyne monomer (a 1:29 molar ratio of Cu(I)Cl to TMEDA was used). The number average molar masses were low, as polymer precipitation was a problem.

To achieve higher molar mass polymers Hay's system was modified by White in 1971 (2). The pyridine solvent used in Hay's system was replaced by 1,2-dichlorobenzene and the catalyst concentration lowered. Previously Hay (1) had employed high catalyst concentrations to achieve rapid polymerization rates before polymer had the chance to precipitate out of solution. With precipitation no longer a problem, catalyst concentrations could be considerably lower with low copper salt concentrations making purification easier. The reaction system employed by White was 0.150 g (0.0015 mol) Cu(1)Cl, 0.23 mL (0.0015 mol) TMEDA, 1.7 mL pyridine in 48 mL 1,2-dichlorobenzene; to this was added 0.0396 mol α,ω-alkyldiyne in 10 mL 1,2-dichlorobenzene (a 1:1 molar ratio of Cu(I)Cl:TMEDA was used). Also, since high monomer concentrations were employed it would seem less likely that the α,ω-alkyldiynes would cyclize on polymerization (7).

In 1989, Butera et al. (3,4) synthesized poly(α,ω-alkyldiynes) using a polymerization procedure based upon that of White's. However, Butera incorporated a polymerization delay time: the reaction was allowed to proceed overnight at

Received March 15, 1995.

This paper is dedicated to Professor J.E. (Jim) Guillet in recognition of his contributions to Canadian chemistry.

J.C. Kennedy. North East Wales Institute, Multidisciplinary Research and Innovation Centre, Kelsterton Road, Connah's Quay, Deeside, North Wales, CH5 4BR U.K.
J.R. MacCallum.[1] School of Chemistry, University of St. Andrews, St. Andrews, Fife, KY16 9ST, U.K.
D.H. MacKerron. I.C.I. Chemicals and Polymers, Wilton Materials Centre, P.O. Box 90, Middlesbrough, Cleveland, TS68JE, U.K.

[1] Author to whom correspondence may be addressed. (Telephone: (44) 1334-462546. Fax: (44) 1334-462030.

Can. J. Chem. Downloaded from www.nrcresearchpress.com by 46.23.64.124 on 09/08/12
For personal use only.

Can. J. Chem. Downloaded from www.nrcresearchpress.com by 46.23.64.124 on 09/08/12
For personal use only.

room temperature before the final polymerization temperature was set, then the contents were left to polymerize for the desired time. Butera's system had the added advantage over White's system in that the polymerization delay time had better control over the polydispersity (PDI) of the poly(α,ω-alkyldiynes) formed. Gel permeation chromatography (GPC) traces of the poly(α,ω-alkyldiynes) gave almost ideal polydisperse curves (theoretically, polydispersity being 2). With almost ideal PDI at high molar masses it will be very unlikely that cyclic structures (7) will have formed and the polymer will comprise a distribution of linear molar masses.

A similar approach to the methods adopted above was carried out by Kevelam et al. (5) in 1975. The reaction system chosen for the polymerization work consisted of 0.25 g (1.28×10^{-3} mol) Cu(I)Cl, 0.64 mol of TMEDA, 80 mL pyridine, and 0.0216 mol of 1,8–nonadiyne (a 1:50 molar ratio of Cu(I)Cl to TMEDA was used). The contents were polymerized at 26°C for several hours with low M_n values being obtained by vapour pressure osmometry.

There are several reasons why the molar mass of the poly(1,8-nonadiyne) synthesized by Kevelam was low:

(*i*) polymerisation temperature — higher temperatures are required; (*ii*) solvent — pyridine solvent was used, 1,2-dichlorobenzene is a far superior solvent; (*iii*) cyclic oligomers — the system used by is dilute; therefore there is a tendency for the polymers to cyclize (7); (*iv*) concentration — using a more concentrated system will promote higher molar mass.

An improvement in the polymerization procedure of Kevelam was reported by Knol et al. (6) in 1984. Initially Knol followed the same procedure adopted by Kevelam, but the solvent pyridine was replaced by 1,2-dichlorobenzene. This modified procedure doubled the M_n values obtained by vapour pressure osmometry. Knol further optimized the polymerization conditions by increasing the temperature of polymerization and changing the concentration (a more dilute solution was used). Knol claimed that molar masses (M_n), measured by membrane osmometry, were as high as 20 000. However, with the exclusion of molar mass distribution curves by GPC it is not possible to predict whether cyclic or oligomeric structures form during the polymerization reaction.

Three main differences exist between the polymerization systems optimized by Butera (3,4) and Knol (6). These are (*i*) polymerization delay time — in Butera's route a polymerization delay time was included in the syntheses of the polymers whereas in Knol's route this was excluded and the flask contents were polymerized immediately; (*ii*) copper(I) chloride:TMEDA — in Butera's route the copper(I) chloride:TMEDA ration is 1:1 whereas in Knol's route the copper(I) chloride:TMEDA ratio is 1:50; (*iii*) solvent system — in Butera's route the 1,2-dichlorobenzene: pyridine solvent system is used whereas in Knol's route 1,2-dichlorobenzene solvent is used exclusively.

For the purpose of this study these two routes optimized by Butera and Knol were selected and developed even further for polymerization and copolymerization of a series of α,ω-alkyldiynes.

Butera's route was further developed by varying the polymerization temperature from 60 to 80°C and increasing the time of polymerization by 1. The concentration of the α,ω-alkyldiyne(s) in the polymerization medium was not increased, as polymer precipitation became a major problem. In this study this route will be referred to as *polymerization Route A*.

Knol's route was further developed by varying the polymerization temperature from 40 to 80°C, varying the polymerization time from 6 to 15 h, and increasing the α,ω-alkyldiyne(s) concentration in the polymerization from 0.011 mol dm^{-3} to 0.4 mol dm^{-3}. In this study this route will be referred to as *polymerization Route B*.

The work described in this paper concerns the molar mass characteristics of these polymers. The molar mass characteristics of the polymers synthesized by polymerization Routes A and B are studied by gel permeation chromatography (GPC), end-group analysis (EGA), and ^1H nmr spectroscopy. This gives an indication whether polydisperse linear polymers can by synthesized by both polymerization Routes A and B. From these results a mechanism for the polymerization of α,ω-alkyldiynes for both routes A and B is proposed.

Experimental procedures

Materials

The monomers 1,7-octadiyne, 1,8-nonadiyne, 1,9-decadiyne, 1,10-undecadiyne, and 1,11-dodecadiyne were synthesized from sodium acetylide and the respective α,ω-dibromoalkane by following a literature procedure (8) and were distilled once more prior to use. All other reagents and solvents (Aldrich, high purity) were purified an distilled before use. All glassware was thoroughly dried at 120°C before use.

Synthesis of poly(α,ω-alkyldiynes) and copoly(α,ω-alkyldiynes)

Polymerization, Route A

To a 50 mL wide-mouthed Erlenmeyer flask, equipped with a magnetic stirrer, an oxygen inlet tube, and a thermometer, 20 mL 1,2-dichlorobenzene, 0.71 mL (8.8 mmol) pyridine, 0.096 mL (0.625 mmol) TMEDA, and 0.0625 g (0.625 mmol) copper(I) chloride were added, producing a light green solution. Oxygen was then bubbled through the stirring solution for 40 min (the solution turned dark green shortly after oxygen flow was started). A solution of 0.0165 mol of the chosen α,ω-alkyldiyne(s) in 4 mL of 1,2-dichlorobenzene was then slowly added to the stirring reaction mixture. The reaction was allowed to proceed overnight (with continuous oxygen flow), after which time a milky green suspension was formed. The flask was then placed in an oil bath at temperatures ranging from 70 to 90°C. Upon placing the flask into the oil bath the reaction mixture turned clear and was dark green in colour. The reaction was allowed to polymerize at the desired temperature for 5 h (*an hour more than the polymerization time adopted by Butera et al.* (3, 4). After this time, the flask was removed from the oil bath and allowed to cool (with stirring) for 15 min. The mixture was then added dropwise to a stirred solution of 5 mL concentrated HCl in 250 mL methanol. The resultant precipitate was allowed to stir for 15 min in the methanol–HCl mixture. The precipitate was then dried over a Büchner funnel (with aspiration) and subsequently dissolved in 100 mL of dichloromethane. The polymer was reprecipitated four times, twice in methanol–HCl, then twice in pure methanol, to obtain a white semicrystalline product. The polymer was dried over a Büchner funnel (with aspiration), then

Can. J. Chem. Downloaded from www.nrcresearchpress.com by 46.23.64.124 on 09/08/12
For personal use only.

under vacuum at room temperature, and its yield recorded. The polymer was then dissolved in dichloromethane, the solution was filtered using Hyflo-Supercel filtering agent to give a clear solution. The polymer was stored in dichloromethane as a 1% weight/volume solution (the polymer was filtered to remove any low molar mass species that may affect the polydispersity of the polymers and stored in dilute solution because of its photoreactivity in the solid state). A small quantity of this purified polymer was evaporated, dried under vacuum, and then dissolved in deuterochloroform for ^{1}H nmr – end-group analysis (EGA) studies.

Polymerization, Route B

To a 25 mL wide-mouthed Erlenmeyer flask, stirred in an oil bath (temperatures ranging from 70 to 90°C) equipped with a magnetic stirrer, an oxygen inlet tube, and a thermometer were added 10 mL 1,2-dichlorobenzene and 3.8 mL (25 mmol) TMEDA. Once the desired temperature of the solution was reached 0.05 g (0.5 mmol) of copper(I) chloride was added. Oxygen was then bubbled through the stirring solution for 40 min (the solution turned dark green shortly after oxygen flow was started). A solution of 7.45 mmol of the chosen α,ω-alkyldiyne(s) in 5 mL of 1,2-dichlorobenzene was added to the stirring reaction mixture. The reaction mixture was left to polymerize at the desired temperature for the chosen length of time. Then, the flask was removed from the oil bath and allowed to cool (with stirring for 15 min).

Note: The remainder of this procedure is the same as Route A, the only difference being the quantities of acid and solvents used in the work-up. In Route B 2 mL concentrated HCl, 100 mL methanol, and 50 mL of dichloromethane were used.

Molar mass characterization techniques

Gel permeation chromatography (GPC)

Molar mass averages were obtained by using GPC. The GPC analyses were carried out using a MC/GPC/3 series chromatograph (equipped with a Shodex mixed gel column capable of wide molar mass range resolution), using a refractive index detector and chloroform as solvent (1 mL/min at 24°C). All molar masses are reported with respect to polystyrene standards.

End-group analysis (EGA) by ^{1}H nmr spectroscopy

Number average molar masses (M_n) were obtained by using EGA. All ^{1}H nmr spectra were recorded at 300 MHz on a Brüker AM-300 spectrometer. EGA is limited to linear polymers and the sensitivity of this method decreases rapidly as the chain length increases and the number of end groups drops (i.e., a practical upper limit will restrict what M_n values can be measured). EGA assigns an absolute M_n value for the polymer molar mass, unlike GPC, which assigns an M_n value for the polymer molar mass relative to polystyrene standards.

A typical EGA calculation for the polymer poly(1,10-undecadiyne) is now given. This polymer was synthesized by polymerization route A. The polydispersity index (PDI) of the polymer was almost ideal (i.e., M_w/M_n = 2.09) and the M_n value is high enough to assume a distribution of linear molar masses.

In Fig. 1 the ^{1}H nmr spectrum of 1,10-undecadiyne is shown. The spectrum reveals three peaks: (a) δH = 1.35 ppm

Fig. 1. The ^{1}H nmr spectrum of 1,10-undecadiyne.

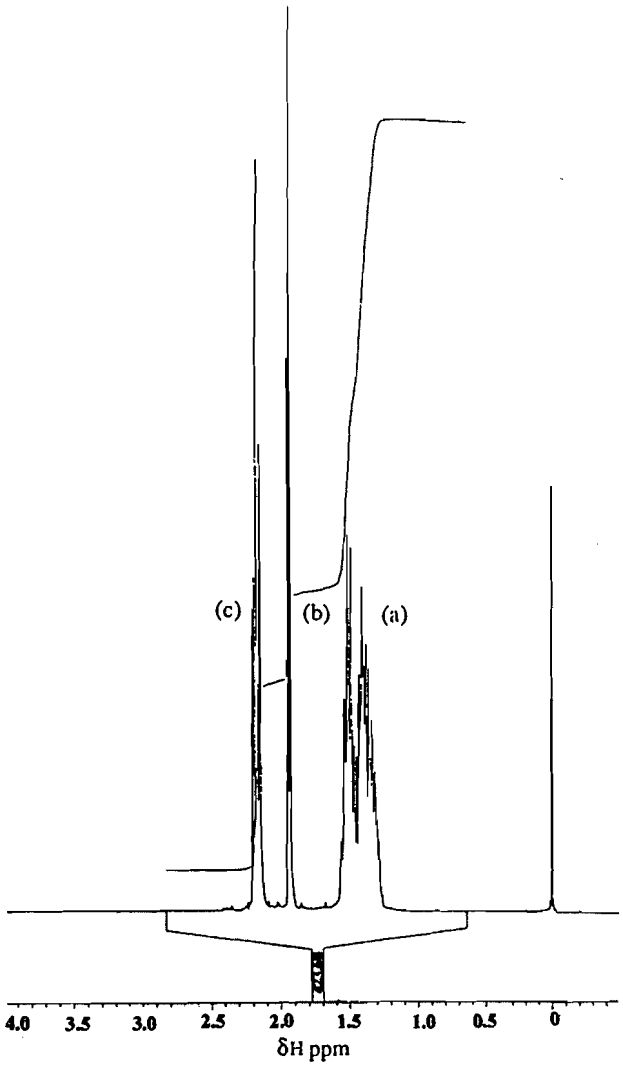

(multiplet) — represents ten methylene protons in the middle of the monomer chain; (b) δH = 1.94 ppm (triplet) — represents two terminal alkyne protons at either end of the monomer chain; (c) δH = 2.15 ppm (multiplet) — represents four methylene protons attached to the two terminal alkyne groups. That is, for 1,10-undecadiyne:

$$\underset{(b)}{HC{\equiv}C\text{-}}\underset{(c)}{H_2C\text{-}}\underset{(a)}{(CH_2)_5\text{-}}\underset{(c)}{CH_2\text{-}}\underset{(b)}{C{=}CH}$$

When the monomer is oxidatively polymerized to give a linear structure the signal for the two terminal alkyne end groups (b) at δH = 1.94 ppm decreases in intensity with respect to the two signals (a) and (c) for the methylene protons in the polymer chain. As the molar mass of the polymer increases the signal (b) decreases in intensity. Therefore at high molar masses the signal (b) is broad and indistinguishable with respect to signals (a) and (c) in the ^{1}H nmr spectrum.

This can be shown in Fig. 2 in the ^{1}H nmr spectrum of poly(1,10-undecadiyne). In the ^{1}H nmr spectrum of poly(1,10-undecadiyne) the triplet signal for the two terminal alkyne groups is barely recognizable; therefore integration of the sig-

Can. J. Chem. Downloaded from www.nrcresearchpress.com by 46.23.64.124 on 09/08/12
For personal use only.

Fig. 2. The ^{1}H nmr spectrum of poly(1,10-undecadiyne).

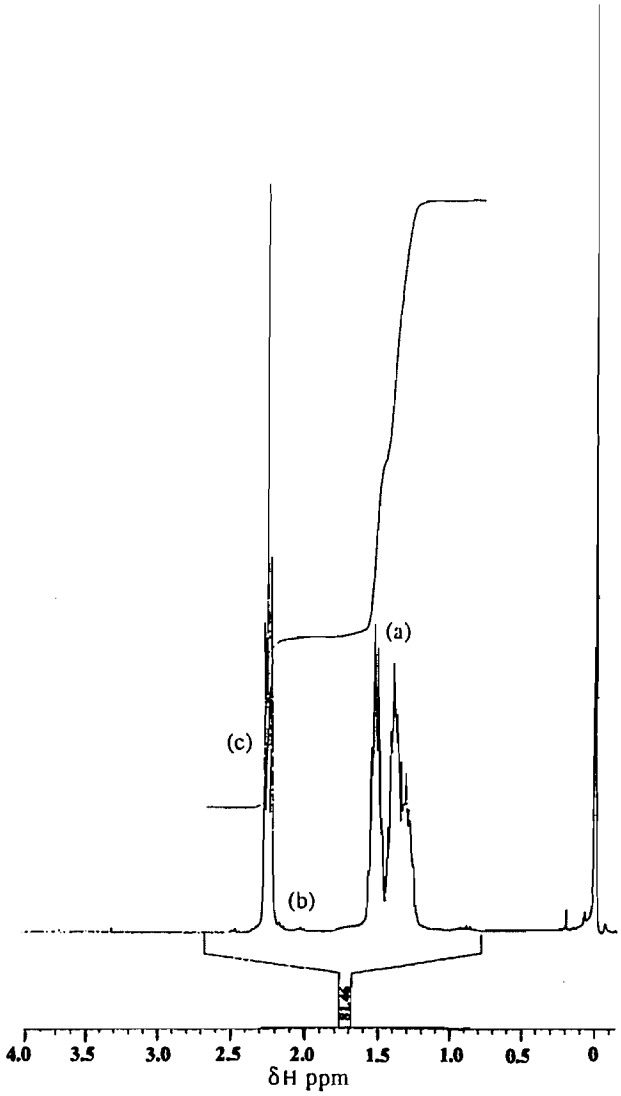

nal is not possible. To obtain an M_n value for this polymer, expansion of this peak with respect to either signal (a) or signal (c) is necessary. In all end-group analysis calculations signal (b) was expanded with respect to signal (a).

This was done by expanding the triplet peak (b) for the two terminal alkyne protons by a factor of 8 with respect to the multiplet peak (a) for the $(CH_2)_5$ protons (which occur along the main chain of the linear polymer) so the areas of both peaks can be compared. This is shown in Fig. 3.

To obtain a value for M_n the areas of the peaks were cut out, weighed, and the following series of arithmetical calculations were performed;

$$H(C{\equiv}C\text{-}H_2C\text{-}\underline{CH_2CH_2CH_2CH_2CH_2}\text{-}CH_2\text{-}C{\equiv}C)_nH$$

(b) (c) (a) (c) (b)

1. Mass of the multiplet peak (a) for $(CH_2)_5$ protons
2. Mass of the triplet peak (b) for two terminal alkyne protons

Fig. 3. Expansion of triplet signal for two terminal alkyne groups (b) by a factor of 8 with respect to the $(CH_2)_5$ protons (a) that occur along the length of the linear polymer chain.

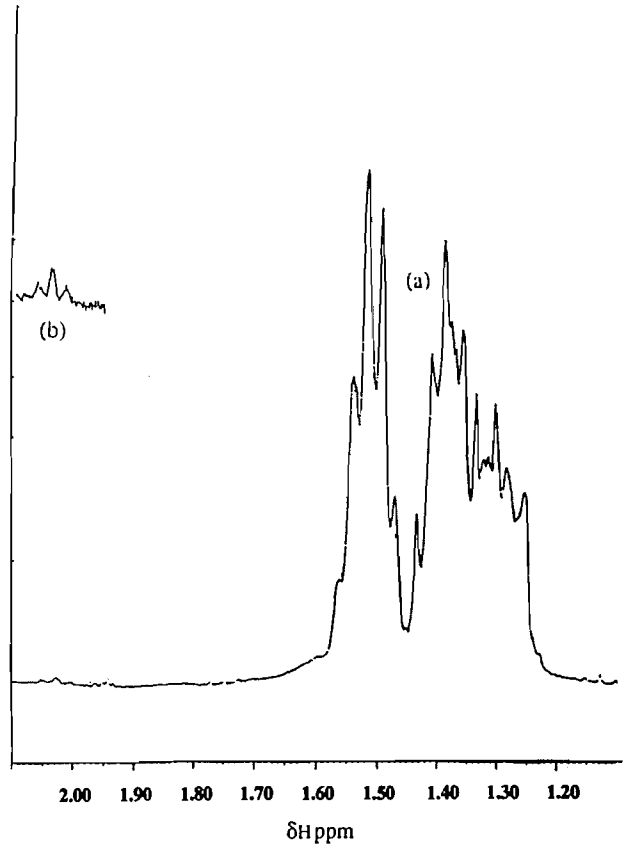

There are ten protons that occur along the main chain of the linear polymer and two terminal alkyne protons at either end of the polymer chain.

To obtain a value for the number of repeat units (n) in the polymer chain, the mass of the multiplet peak (a) for the $(CH_2)_5$ protons must be divided by 5 to give the mass of $-CH_2-$ in the main chain of the linear polymer. The mass of the triplet peak (b) for the terminal alkynes must be divided by 8 to give the mass of HC≡C at either end of the linear polymer chain.

The number of repeat units (n) can be obtained by the following expression:

$$\frac{\text{mass of -CH- in the main chain of the linear polymer}}{\text{mass of HC≡C at either end of the linear polymer chain}}$$

The number of repeat units n is then multiplied by the relative molar mass (r.m.m.) of the repeat unit of poly(1,10-undecadiyne), giving the M_n of the poly(1,10-undecadiyne):

$$M_n = n \times \text{r.m.m.}$$

Errors are bound to arise in the EGA calculation and these include the following.

(*i*) Judgement of where the baseline should be set for the multiplet peak of the methylene protons (when it is cut out) requires consistency.

(*ii*) Also in some cases the triplet peak was poorly resolved. The sensitivity of EGA decreases rapidly as the chain length

Table 1. Polymers synthesized by Route A.

Polymer	Temperature of polymerization (°C)	Time of polymerization (h)	Yield (%)
(A1) poly(1,7-octadiyne)	65	5	87
(A2) poly(1,8-nonadiyne)	65	5	91
(A3) poly(1,9-decadiyne)	60	5	93
(A4) poly(1,9-decadiyne)	80	5	89
(A5) poly(1,9-decadiyne)	65	5	91
(A6) 50:50 poly(1,8-non):poly(1,9-dec)	65	5	87
(A7) poly(1,10-undecadiyne)	65	5	88
(A8) 50:50 poly(1,9-dec):poly(1,10-undec)	65	5	90
(A9) poly(1,11-dodecadiyne)	65	5	85

Table 2. Polymers synthesized by Route B.

Polymer	Temperature of polymerization (°C)	Time of polymerization (h)	Yield (%)
(B1) poly(1,8-nonadiyne)	60	6	84
(B2) poly(1,8-nonadiyne)	60	8	89
(B3) poly(1,9-decadyne)	80	6	86
(B4) poly(1,9-decadiyne)	80	10	85
(B5) poly(1,9-decadiyne)	40	15	89
(B6) poly(1,9-decadiyne)	60	15	91
(B7) poly(1,9-decadiyne)	80	15	90
(B8) poly(1,11-dodecadiyne)	80	8	83
(B9) 50:50 poly(1,9-dec):poly(1,10-undec)	60	8	88
(B10) 80:20 poly(1,9-dec):poly(1,11-dodec)	60	8	85

Can. J. Chem. Downloaded from www.nrcresearchpress.com by 46.23.64.124 on 09/08/12
For personal use only.

increases because the number of end groups drops. Therefore cutting out this peak is difficult and requires careful work with no guarantee of an accurate result for M_n.

However, EGA does have an obvious advantage over GPC (when studying a distribution of linear molar masses exclusively) in that an absolute value is obtained by EGA, whereas in GPCD a value relative to a polystyrene standard is obtained.

Results and discussion

Molar mass results

Polymerization conditions and yields for a range of polymers are shown in Tables 1 and 2.

For the polymers synthesized by **Route A** all polymers, except for poly(1,7-octadiyne), were very soluble in chloroform, dichloromethane, and tetrahydrofuran at room temperature. 1,2-Dichlorobenzene and 1,2-dichloroethane will also dissolve the polymers, but not as readily as the above solvents. Poly(1,7-octadiyne) was insoluble in a range of solvents at room temperature and at elevated temperatures. However, it was sparingly soluble in 1,2-dichlorobenzene at elevated temperatures.

For the polymers synthesized by **Route B** all polymers, except for poly(1,11-dodecadiyne), were very soluble in chloroform, dichloromethane, and tetrahydrofuran at room temperature. 1,2-Dichlorobenzene and 1,2-dichloroethane also dissolve the polymers, but not as readily as the above solvents. Poly(1,11-dodecadiyne) was very soluble in chloroform and methylene chloride at room temperature, but insoluble in tetrahydrofuran at room temperature and only sparingly soluble in 1,2-dichlorobenzene at room temperature.

It was noted that the polymers stored in methylene chloride solution synthesized from **Route B** gave a coloured solution (i.e., yellow/orange/brown) whereas those synthesized from **Route A** were clear when stored in methylene chloride solution.

The molar mass values of the polymers studied by EGA and GPC for both polymerization routes A and B are presented in Tables 3 and 4, respectively.

One GPC curve from polymerization Route A and the majority of the GPC curves from polymerization Route B have a significant low molar mass tail present. It is proposed that this low molar mass tail is not only the consequence of linear oligomeric structures but also low molar mass cyclics formed during the course of the polymerization.

All GPC curves from polymerization Route A, with the exception of polymer A2, poly(1,8-nonadiyne), polymerized for 5 h at 65°C, were Gaussian in shape at high molar masses. The GPC curve for A2 was non-Gaussian in shape with a combination of low and high molar masses, i.e., a large distribution of molar masses with PDI as high as 6.37 (see Table 3). The M_n value obtained by EGA was 15 000 whereas the M_n value obtained by GPC was 5 890. This strongly favours the proposal that low molar mass cyclics contribute to the low molar mass tail. The high value for M_n by EGA suggests that the calculation overestimates the number of methylene pro-

Table 3. Molar mass values of polymers synthesized by Route A.

Polymer	M_n (EGA)	M_n (GPC)	M_w (GPC)	PDI (GPC)
(A2) poly(1,8-nonadiyne)	15 000	5 890	37 500	6.37
(A3) poly(1,9-decadiyne)	13 625	20 900	46 500	2.22
(A4) poly(1,9-decadiyne)	12 380	19 600	45 600	2.33
(A5) poly(1,9-decadiyne)	10 520	29 300	180 000	6.14
(A6) 50:50 poly(1,8-non):poly(1,9-dec)	15 757	24 100	73 900	3.07
(A7) poly(1,10-undecadiyne)	19 600	28 300	59 200	2.09
(A8) 50:50 poly(1,9-dec):poly(1,10-undec)	14 362	28 300	59 600	2.11
(A9) poly(1,11-dodecadiyne)	12 454	14 100	32 100	2.28

N.B. Refer to Table 1 for polymerization temperature, time, and yield.

Table 4. Molar mass values of polymers synthesized by Route B.

Polymer	M_n (EGA)	M_n (GPC)	M_w (GPC)	PDI (GPC)
(B1) poly(1,8-nonadiyne)	12 320	12 536	58 742	4.69
(B2) poly(1,8-nonadiyne)	8 544	8 460	48 100	5.69
(B3) poly(1,9-decadiyne)	11 000	9 621	40 604	4.22
(B4) poly(1,9-decadiyne)	10 006	7 660	24 802	3.24
(B5) poly(1,9-decadiyne)	13 788	15 770	64 400	3.86
(B6) poly(1,9-decadiyne)	17 563	3 266	5 435	1.66
(B7) poly(1,9-decadiyne)	10 290	9 379	36 421	3.88
(B8) poly(1,11-dodecadiyne)	12 418	6 998	25 160	3.60
(B9) 50:50 poly(1,9-dec):poly(1,10-undec)	14 453	17 290	49 299	2.85
(B10) 80:20 poly(1,9dec):poly(1,11-dodec)	10 043	5 900	12 703	2.15

N.B. Refer to Table 2 for polymerization temperature, time, and yield.

tons contributing to the M_n value. *When cyclic structures are present the calculations will involve methylene protons from the linear chains and also methylene protons from the cyclic structures. Therefore these methylene protons will be compared with the terminal protons from the linear chains exclusively as the cyclic structures do not possess end-group protons. Hence an exaggerated M_n value will be obtained by EGA.*

In the majority of cases from polymerization Route B, GPC curves are non-Gaussian in shape with the presence of a low molar mass tail.

PDI values of 4.69 and 5.69 for polymers B1 and B2, respectively, were obtained and results for M_n by EGA and GPC for the individual polymers were comparable. However, polymer B1 produces a higher M_n polymer, indicating that the shorter polymerization time produces higher M_n polymer.

PDI values of 4.22 and 3.24 for polymers B3 and B4, respectively, were obtained. The results for M_n by EGA and GPC or polymer B3 were comparable with values of 11 000 and 9 621. However, results for M_n by EGA and GPC for polymer B4 were not as comparable, values of 10 006 and 7 660 being recorded. Polymer B3 produces a marginally higher M_n polymer, again indicating that the shorter polymerization time produces higher M_n polymer.

For polymer B5, a PDI value of 3.86 was obtained and a high M_n value of 16 700 was obtained by GPC. This high M_n value of GPC gives a fair comparison with the M_n value of 13 788 obtained by EGA. The GPC curve for polymer B6 was Gaussian in shape but comprised low molar masses. A PDI value of 1.66 was obtained and an M_n value of 3 266 was obtained by GPC. However, the very low M_n value of 3 266 obtained by GPC contrasts with the high M_n value of 17 563 measured by EGA (see Table 4). *This strongly suggests that a high percentage of low molar mass cyclics were formed during the course of the polymerization.*

From the results by EGA and GPC the following conclusions are drawn for poly(1,9-decadiyne) polymerized for 15 h:

(*i*) Low polymerization temperatures (40°C) — produces high M_n values with a small percentage of low molar mass material.

(*ii*) Intermediate polymerization temperatures (60°C) — produces very low M_n values by GPC but correspondingly very high M_n values by EGA, suggesting that a high percentage of low molar mass cyclics are formed during the polymerization.

(*iii*) High polymerization temperatures (80°C) — produces intermediate M_n values with a broad distribution of molar masses.

For B8, a PDI value of 3.60 was obtained and an M_n value of 6 988 was obtained by GPC. However, this low value of 6 988 obtained by GPC compares with the M_n value of 12 418 by EGA. This also suggests that a high percentage of low molar mass cyclics are formed during the course of the polymerization.

For B9, a PDI value of 2.85 was obtained and an M_n value of 17 290 was obtained by GPC. This high M_n value compares with an M_n value of 14 453 by EGA.

For B10, a PDI value of 2.15 was obtained and an M_n value

Can. J. Chem. Downloaded from www.nrcresearchpress.com by 46.23.64.124 on 09/08/12
For personal use only.

Can. J. Chem. Downloaded from www.nrcresearchpress.com by 46.23.64.124 on 09/08/12
For personal use only.

of 5 900 was obtained by GPC. This M_n value of 5 900 obtained by GPC compares with the correspondingly high M_n value of 10 043 measured by EGA. Again, this suggests that a high percentage of low molar mass cyclics are formed during the course of the polymerization.

Polymers synthesized by both polymerization routes A and B produces similar material at high molar masses. This was evident after curve idealization work was performed on the majority of polymers produced by polymerization route B and the one polymer from polymerization Route A. Molar mass distribution curves were idealized to represent a Gaussian shape at higher molar masses by outlining a curve inside the authentic GPC molar mass distribution curve and hence eliminating the low molar mass tail. The details of the curve idealization work can be found elsewhere (9).

The next section of this paper discusses the consequence of the low molar mass tail with reference to the cyclization of α,ω-alkyldiynes.

Cyclization of α,ω-alkyldiynes

It is proposed that the low molar mass tail that is present in the GPC curve for poly(1,8-nonadiyne) from polymerization route A and the majority of GPC curves from polymerization route B are not only a consequence of oligomeric linear-type structures, but also of low molar mass cyclic structures formed during the course of the polymerization.

Cyclic structures are greatly favoured using homogeneous, nonaqueous, mildly basic conditions (10). The effect of dilution has not been properly evaluated although it is anticipated that the smaller the concentration of the α,ω-alkyldiyne, the less tendency there will be to form linear oligomeric or polymeric structures.

Previous oxidative coupling work on α,ω-alkyldiynes that cyclize

(A) Using cupric acetate – pyridine system: High-dilution systems will yield increased proportions of the smaller cyclic hydrocarbons (7). Concentrations of ~0.0035 mol dm^{-3} used for tetradeca-1,13-diyne ($HC{\equiv}C\text{-}(CH_2)_{10}\text{-}C{\equiv}CH$) yields cyclic monomer and dimer in 17 and 30% yield, respectively, the yields being improved when the dilution is higher.

Moderate concentration systems yield increased proportions of the higher cyclic hydrocarbons (10, 11). Concentrations of ~0.0075–0.13 mol dm^{-3} were used for monomers of the series $HC{\equiv}C\text{-}(CH_2)_n\text{-}C{\equiv}CH$ (where n = 2–6). On oxidative coupling, cyclic trimers, tetramers, pentamers, hexamers, and heptamers were formed.

(B) Using cuprous chloride (Cu(I)Cl) and oxidant (12–15): High-concentration systems yield predominantly linear dimers and tetramers but in some instances cyclic dimers were formed. Concentrations of ~0.7–1.25 mol dm^{-3} were used for monomers of the series $HC{\equiv}C\text{-}(CH_2)_n\text{-}C{\equiv}CH$ (where n = 2–6). On oxidative coupling it was found that, as well as linear dimers and tetramers being formed, cyclic dimers were formed in the case of 1,6-heptadiyne, 1,7-octadiyne, and 1,8-nonadiyne, but not in the case of 1,5-hexadiyne and 1,9-decadiyne.

From the above observations it is evident that cyclization can occur in both dilute and concentrated medium for (A). It can also occur in a highly concentrated medium for (B) with the α,ω-alkyldiyne monomers 1,6-heptadiyne, 1,7-octadiyne, and 1,8-nonadiyne.

Oxidative coupling work on α,ω-alkyldiynes investigated in this study

In this study polymerization routes A and B both involve cuprous chloride – TMEDA and an oxidant; therefore comparison can be made with (*B*) in previous oxidative coupling work on α,ω-alkyldiynes that cyclize.

As a basis for polymerization, route A, work was carried out with reference to Butera's system (4). In the original study by Butera the α,ω-alkyldiyne concentration employed was 0.665 mol dm^{-3}. There were no reports of a low molar mass tail in the GPC curves for poly(1,6-heptadiyne), poly(1,8-nonadiyne), and poly(1,11-dodecadiyne).

The same α,ω-alkyldiyne concentration of 0.665 mol dm^{-3} was employed for polymerization route A in this present study, with a low molar mass tail being evident in the GPC curve of poly(1,8-nonadiyne).

As a basis for polymerization route B, work was carried out with reference to the systems of Kevelam (5) and Knol (6). In the original study by Kevelam et al. the 1,8-nonadiyne concentration employed was 0.27 mol dm^{-3}. This was modified by Knol et al. with the 1,8-nonadiyne concentration decreased to 0.102 mol dm^{-3}. In both studies no GPC was performed and, therefore, no low molar mass tail could be observed.

In this study the α,ω-alkyldiyne concentration was increased to 0.4 mol dm^{-3} for polymerization route B, with a low molar mass tail being evident for the majority of polymers in their GPC curve.

The two concentrations of 0.665 mol dm^{-3} and 0.40 mol dm^{-3} employed for the α,ω-alkyldiynes in polymerization routes A and B, respectively, lie close to the values employed for the concentration of the α,ω-alkyldiynes for (*B*) in previous oxidative coupling work on α,ω-alkyldiynes that cyclize (i.e., 0.7–1.25 mol dm^{-3}) (12–15).

Reasoning that favours cyclic structures of α,ω-alkyldiynes contributing to the low molar mass tail includes the following.

(*i*) Values of M_n by EGA that are very high compared with their corresponding M_n value by GPC.

(*ii*) In the GPC curves the low molar mass tail elution peak values are ~1200, which can correspond to cyclic pentamer, hexamer, and heptamer as the elution values of the α,ω-alkyldiyne monomers are ~200.

(*iii*) Mildly basic conditions promote cyclization (10). In polymerization route B, the coordinating ligand TMEDA is present in excess.

(*iv*) Moderate concentrations employed with the cupric acetate – pyridine system (~0.075–0.13 mol dm^{-3}) produced higher cyclics, i.e., trimers, tetramers, pentamers, hexamers, and heptamers of the α,ω-alkyldiynes 1,6-heptadiyne, 1,7-octadiyne, 1,8-nonadiyne, and 1,9-decadiyne (10,11). Although in this study systems involved cuprous chloride – TMEDA and oxidant the concentrations employed were also moderate, i.e., 0.665 mol dm^{-3} and 0.4 mol dm^{-3} for polymerization routes A and B, respectively. Therefore it was possible that higher cyclics mentioned above may have formed.

To fully establish whether low molar mass cyclic structures are present, further examination is necessary. If facilities were available a useful analytical tool for analysing fractions of eluant coming off the GPC column would be preparative GPC. An example of this technique was described by Dodgson et al. (16), who separated broad fractions of cyclic and linear poly(dimethylsiloxanes). Although preparative GPC was not

Can. J. Chem. Downloaded from www.nrcresearchpress.com by 46.23.64.124 on 09/08/12
For personal use only.

available, attempts to isolate the cyclic structures by mass spectroscopy were carried out; these were unsuccessful and therefore inconclusive.

However, on the basis of points (*i*) – (*iv*) above, there is evidence that strongly favours the presence of low molar mass cyclic structures in the low molar mass tail of the GPC curves.

Mechanism of oxidative coupling of polymerization routes A and B

From previous studies on the mechanism for the oxidative coupling of reaction of α,ω-alkyldiynes several points were concluded:

(*i*) The cupric ion (copper II) is the actual oxidant (7, 17, 18)

$$2RC{\equiv}CH+Cu^{2+} \rightarrow RC{\equiv}C\text{-}C{\equiv}CR + 2H^{+} + Cu(I)$$

The Cu(I) can then oxidize back to Cu(II) for further coupling.

$$2Cu(I) + 0.5O_2 + H_2O \rightarrow 2Cu(II) + OH^{-}$$

(*ii*) Under acidic conditions the reaction rate increases with increasing Cu(I) concentration (7, 17, 18).

(*iii*) The greater the acidity of the terminal alkyne the faster the reaction rate (7, 18).

(*iv*) The reaction is second order with respect to the concentration of the alkyne (17, 18).

(*v*) A bridged dimeric structure was isolated for the catalyst complex, confirmed by X-ray diffraction studies, and consistent with detailed mechanistic studies (5, 7, 17–19).

(*vi*) Increasing the basicity of ligand, i.e., TMEDA > TEA > py, and the ligand concentration increases the reaction rate (5, 20).

(*vii*) On increasing the polymerization temperature from 26 to 65°C (i.e., Kevelam's (5) and Knol's (6) work) and decreasing the concentration of the α,ω-alkyldiyne, a corresponding increase in reaction rate and molar mass were achieved.

In this present study involving oxidative polymerization routes A and B further observations were made:

(*i*) For Route A: on increasing the polymerization temperature from 60 to 80°C an optimum polymerization temperature of 65°C was established for poly(1,9-decadiyne). An M_n value of 29 300 was achieved.

(*ii*) For Route B: on increasing the polymerization temperature from 40 to 80°C for poly(1,9-decadiyne) the M_n values go through a minimum.

(*iii*) For Route B: on increasing the time for polymerization for both monomers 1,8-nonadiyne and 1,9-decadiyne there is a corresponding decrease in molar mass (M_n).

As previously mentioned, there are three main differences between polymerization routes A and B:

1. Polymerization delay time
2. Cu(I)Cl:TMEDA ratio
3. Solvent system employed

In polymerization route A the Cu(I)Cl:TMEDA ratio is 1:1 with pyridine controlling the basicity of the reaction medium. In polymerization route B the Cu(I)Cl:TMEDA ratio is 1:50 with no pyridine solvent present, therefore the excess TMEDA controls the basicity of the reaction medium. In route A the pyridine solvent is present in 13 molar equivalents more than the Cu(I)Cl and TMEDA molar equivalents. In route B the TMEDA is in excess by 49 molar equivalents. Kevelam has shown that the reaction rate for oxidative coupling increases with increasing ligand concentration and increased basicity of ligand (5). Pyridine has a pK_b of 8.75 (21) and TMEDA has a pK_b of 4.9 (22). Therefore, since TMEDA is present in 3–4 times greater amount than pyridine and it is more basic than pyridine, the rate of oxidative coupling for polymerization route B will be faster than for polymerization route A. The solubility of the bridged dimeric catalytic complex decreases with increasing TMEDA concentration, causing a maximum reaction rate (5). Also, the more basic the ligand, the more it will facilitate the entrance of the acetylenic end group in the bridged dimeric catalytic complex.

However, more importantly, since there is a greater concentration of base in polymerization route B, it is conceivable that the two end-group protons could be removed from an α,ω-alkyldiyne monomer, dimer, trimer, tetramer, pentamer, etc., giving a doubly negatively charged terminal diacetylene, i.e., for the case of the α,ω-alkyldiyne monomer.

When there is a high concentration of these doubly negatively charged terminal diacetylenes present there is a high probability that two of these will coordinate like bidentate ligands to the bridged dimeric catalytic complex; then, on intramolecular oxidative coupling, a cyclized product will form. However, as the reaction proceeds to higher molar mass polymer, cyclization will be less of a problem as linear polymerization is more sterically favourable (23).

A mechanism for the polymerization of the α,ω-alkyldiynes to give both linear and cyclic structures now shown.

Then the catalytic complex reforms:

$$2\ CuCl + 2\ TMEDA + 0.5\ O_2 + H_2O \rightleftharpoons [Complex]$$

This structure can continue to polymerize linearly or to cyclize.

The above mechanism can also be explained for both linear and cyclic routes by way of kinetic expressions (L = ligand, M = monomer, B = base, D = dimer, CD = cyclic dimer).

Linear route

[1] $Cu(I) + L \rightarrow [Cu(I)L]$

[2] $[Cu(I)L] + 0.5\ O_2 + H_2O \rightleftharpoons [Cu_2(II)L_2O_2H_2]^{2+} = [Complex]$

[3] $M + B \rightleftharpoons M^{-} + BH^{+}$

[4] $M^{-} + [Complex] \rightleftharpoons [M{\cdot}Complex] = OH^{-}$

[5] $[M{\cdot}Complex] + [M] \rightleftharpoons [M_2{\cdot}Complex] + OH^{-}$

[6] $[M_2{\cdot}Complex] \rightarrow D + 2[Cu(I)L]$

Then the catalytic complex reforms, i.e.:

$$2[Cu(I)L] + 0.5\ O_2 + H_2O \rightarrow [Complex]$$

and steps [3]–[6] repeat themselves.

Cyclic route

Steps [1] and [2] as above. Then

Can. J. Chem. Downloaded from www.nrcresearchpress.com by 46.23.64.124 on 09/08/12
For personal use only.

Mechanism

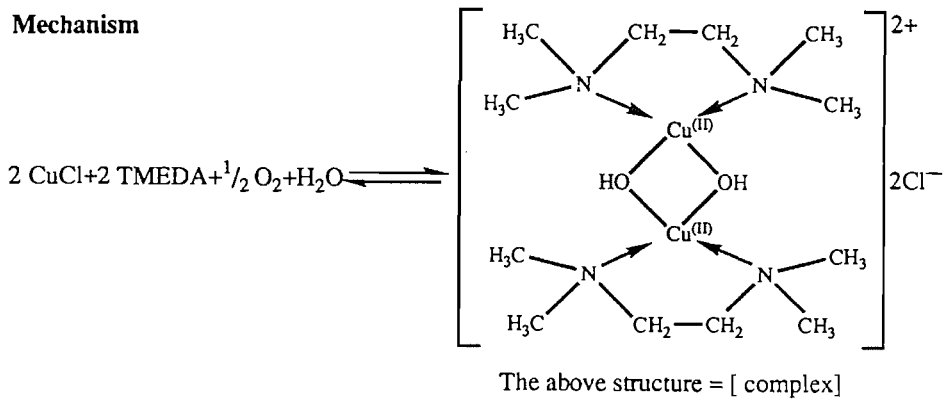

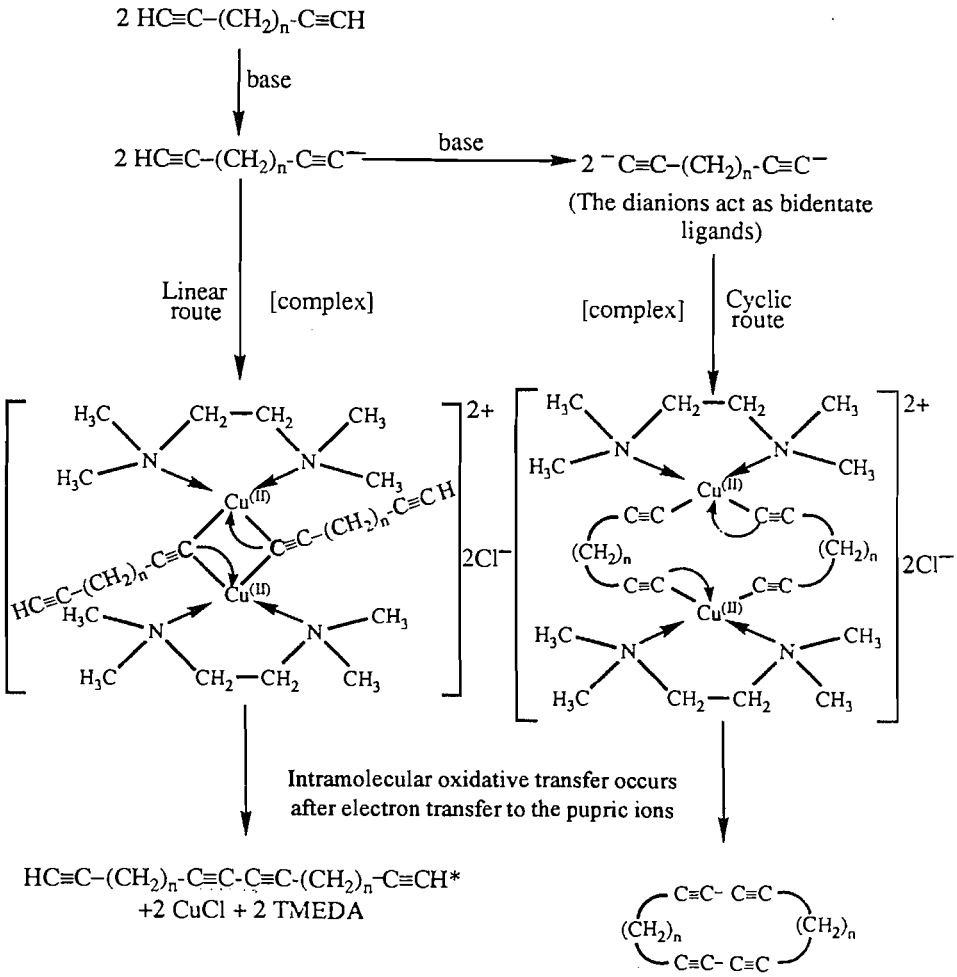

$M + 2B \rightleftharpoons M^{2-} + 2BH^+$
$M^{2-} + [Complex] \rightleftharpoons [M{\cdot}Complex] + OH^-$
$[M{\cdot}Complex] + [M^{2-}] \rightleftharpoons [M_2{\cdot}Complex] + OH^-$
$[M_2{\cdot}Complex] \rightarrow CD + 2[Cu(I)L]$

Then the catalytic complex reforms as above.

Acknowledgement

The partial support of this work by I.C.I. Chemicals and Polymers, Wilton Materials Centre, is gratefully acknowledged.

References

1. A.S. Hay. U.S. Patent 3300456 (1967).
2. D.M. White. Polym. Prepr. (Am. Chem. Soc. Div. Polym. Chem), **12**, 155 (1971).
3. R.J. Butera and J.B. Lando. J. Polym. Sci. Polym. Phys. Ed. **27**, 2451 (1989).
4. R.J. Butera, B. Simic-Glavaski, and J.B. Lando. Macromolecules, **23**, 199 (1990).
5. H.J. Kevelam, K.P. de Jong, H.C. Meinders, and G. Challa. Makromol. Chem. **176**, 1369 (1975).
6. K. Knol, L.W. van Horssen, G. Challa, and E.E. Havinga. Polym. Commun. **26**, 71 (1985).
7. G. Eglinton and A.R. Galbraith. J. Chem. Soc. 889 (1959).
8. L. Brandsma. Preparative acetylenic chemistry. Elsevier Publishing Company, Amsterdam. 1971. pp. 19, 20, 22, and 50.

9. J.C. Kennedy. Ph.D. Thesis, University of St. Andrews. 1992.
10. G. Eglinton and W. McCrae. Adv. Org. Chem. **4**, 225 (1963).
11. F. Sondheimer, Y. Amiel, and R. Wolovsky. J. Am. Chem. Soc. **81**, 4600 (1959).
12. F. Sondheimer, Y. Amiel. J. Am. Chem. Soc. **79**, 5817 (1957).
13. F. Sondheimer and Y. Amiel. J. Am. Chem. Soc. **78**, 4178 (1956).
14. Y. Amiel, F. Sondheimer, and R. Wolovsky. Proc. Chem. Soc. London, 22 (1957).
15. F. Sondheimer, Y. Amiel, and R. Wolovsky J. Am. Chem. Soc. **79**, 6263 (1957).
16. K. Dodgson, D. Sympson, and J.A. Semlyen. Polymer, **19**, 1285 (1978).
17. W.G. Nigh. *In* Oxidation in organic chemistry. Part B. *Edited by* W.S. Trahanovsky. Academic Press, New York. 1973. pp. 1–31.
18. T.F. Rutledge. Acetylenic compounds. Reinhold, New York. 1968. Chap. 6.
19. H.C. Meinders, R. van Bolhuis, and G. Challa. J. Mol. Catal. **5**, 225 (1979).
20. A.S. Hay. J. Org. Chem. **27**, 3320 (1962).
21. R.C. Weast (*Editor*). Handbook of chemistry and physics. 64th ed. The Chemical Rubber Co., Ohio. 1983–1984. p. D165.
22. T.E. Mead. J. Phys. Chem. **66**, 2149 (1962).
23. W. Baker, J.F.W. McOmie, and W.D. Ollis. J. Chem. Soc. 200 (1951).

Can. J. Chem. Downloaded from www.nrcresearchpress.com by 46.23.64.124 on 09/08/12
For personal use only.

Photo-initiated and thermal curing of epoxides by the use of photo-base generators bearing acyloxyimino groups

Ken-ichi Ito, Yoshitaka Shigeru, Yu-uichi Kawata, Katsuhiko Ito, and Masahiro Tsunooka

Abstract: The formation of amines by the photolysis of *O*-acyloximes derived from acetophenone oxime, benzophenone oxime, fluorenone oxime, and 2-acetonaphthone oxime and the curing of epoxides by the resulting amines were investigated. The quantum yields of their photolysis at 366 nm in polystyrene films depend on their structures, and those for bifunctional ones bearing phenyl or naphthyl moieties were found to be very high, at 0.88 and 0.76, respectively. The yields of the resulting amines in polymer matrices were higher than those in solution. The yields for *O*-acyloximes bearing a naphthyl moiety were ca. 90% and higher than for those bearing a phenyl moiety. Although the resulting amines were efficient photo-cross-linkers for poly(glycidyl methacrylate), they were not effective for curing of epoxy resins (oligomers). On the other hand, polymer amines with a glass transition temperature lower than room temperature, which were obtained by the photolysis of copolymers bearing acyloxyimino groups, were found to be effective photo-cross-linkers for the epoxy resins.

Key words: photo-base generator, acyloxyimino group, photo-initiated and thermal curing, poly(glycidyl methacrylate), epoxy resin.

Résumé : On a étudié la formation d'amines par la photolyse d'*O*-acyloximes dérivées des oximes de l'acétophénone, de la benzophénone, de la fluorénone et de l'acéto-2-naphtone et la réaction des amines qui en résultent avec les époxydes. Les rendements quantiques de leurs photolyses à 366 nm, dans des films de polystyrène, dépendent de leurs structures; on a trouvé que ceux des composés bifonctionnels avec des portions phényle ou naphtyle sont très élevés, soit respectivement 0,88 et 0,76. Les rendements des amines qui en résultent dans les matrices de polymère sont plus elevés que ceux en solution. Les rendements pour les *O*-acyloximes portant un groupe naphtyle sont plus élevés (environ 90%) que ceux des acyloximes portant un groupe phényle. Même si les amines qui en résultent sont des photoréticuleurs efficaces pour le poly(méthacrylate de glycidyle), ils ne sont pas efficaces pour la cuisson des résines époxy (oligomères). Par ailleurs, on a trouvé que les amines polymériques, qui se forment par photolyse de copolymères portant des groupes acyloxyimino et qui présentent une température de transition vitreuse inférieure à la température ambiante, sont des photoréticuleurs efficaces pour les résines époxy.

Mots clés : générateur de photobase, groupe acyloxyimino, photoinitiation et cuisson thermique, poly(méthacrylate de glycidyle), résine époxy.

[Traduit par la rédaction]

Introduction

A large number of photo-acid generators such as aromatic diazonium salts and aromatic iodonium salts have been developed and their wide use in the fields of photo-curable coatings (1) and chemically amplified photo-resists (2) investigated. Similarly, although photo-base generators are expected to be promising as photo-cross-linkers for epoxides, used without worrying about corrosive trouble derived from photo-generated acids, only a few articles were published before 1990 concerning photo-base generators and their applications. Kutal and Willson reported that the photolysis of a cobalt–ammine complex led to the formation of ammonia, which induced the cross-linking of a glycidyl methacrylate – ethyl acrylate copolymer upon heating (3). Winkle and Graziano utilized an amine generated by photolysis of an *o*-nitrobenzyl carbamate in a positive photoresist (4). We had also reported that in the photolysis of copolymers of *O*-acryloyl acetophenone oxime (AAPO) with styrene, pendant acyloxyimino (AOI) groups led to pendant amino groups in a good yield (5). Recently, studies on photo-base generators such as *o*-nitrobenzyl carbamates (6) and α,α-dimethyl-3,5-dimethoxybenzyl carbam-

Received April 30, 1995.

This paper is dedicated to Professor J.E. (Jim) Guillet in recognition of his contributions to Canadian chemistry.

K. Ito. Central Laboratory, Rengo Co. Ltd., 1-86, Ohhiraki, 4-chome, Fukushima-ku, Osaka 553, Japan.
Y. Shigeru, Y. Kawata, K. Ito, and M. Tsunooka.[1] Department of Applied Chemistry, College of Engineering, University of Osaka Prefecture, 1-1, Gakuen-cho, Sakai, Osaka 593, Japan.

[1] Author to whom correspondence may be addressed. Telephone: 81-722-52-1161, ext. 2314. Fax: 81-722-59-3340.

Can. J. Chem. Downloaded from www.nrcresearchpress.com by 46.23.64.124 on 09/08/12
For personal use only.

Fig. 1. Structures and abbreviations of *O*-acyloximes.

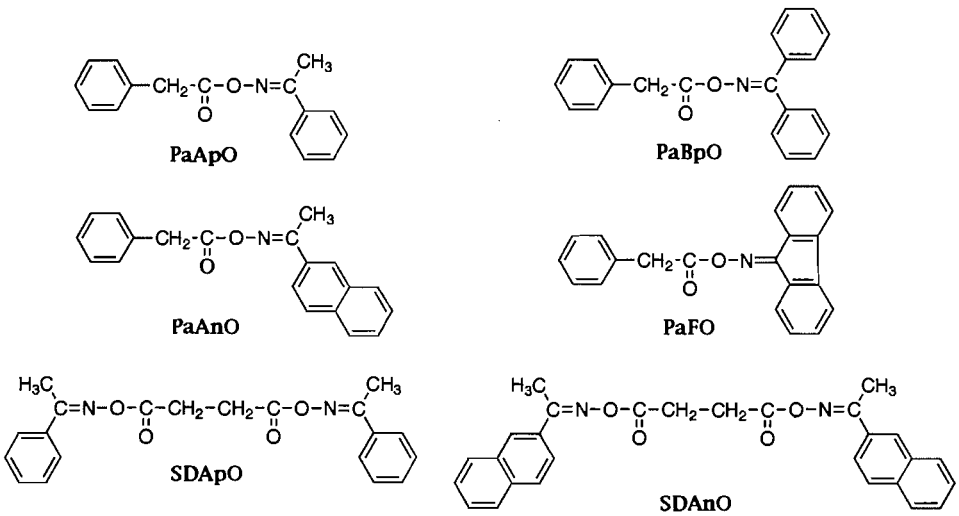

Fig. 2. Structures and abbreviations of copolymers bearing AOI groups.

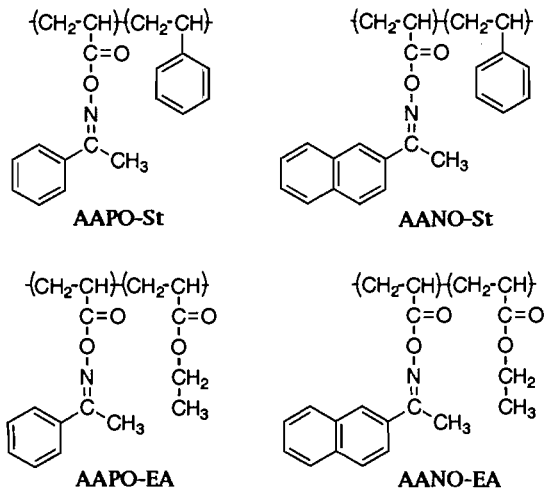

ates (7) have been reported and their utility is gradually being recognized. In particular, applications to microlithography, that is, chemically amplified photo-resists using photo-base generators, have been developed in analogy with those using photo-acid generators. For example, Leung et al. reported the decarboxylation of pendant carboxylic acid groups using photo-generated amines as catalysts (8), and Fréchet et al. (9) and Mckean et al. (10) also used photo-generated amines as catalysts for imidization of polyamic esters. In addition, for application to UV curing, Nishikubo and co-workers (11) utilized amines generated by the photolysis of blocked amines as cross-linkers of epoxy resins or polyurethane oligomers.

In previous articles, we reported that the yields of amines formed by the photolysis of some *O*-acyloximes in polystyrene (PSt) films depended on their structures (12), and these amines were efficient cross-linkers for poly(glycidyl methacrylate) (PGMA) films, but not for epoxy resins (13). In this article, we report various features of *O*-acyloximes as photo-base generators and their applications to photo-initiated and thermal curing of epoxides.

Experimental

Materials

Monofunctional *O*-acyloximes, i.e., *O*-phenylacetyl acetophenone oxime (PaApO), *O*-phenylacetyl 2-acetonaphthone oxime (PaAnO), *O*-phenylacetyl benzophenone oxime (PaBpO), and *O*-phenylacetyl fluorenone oxime (PaFO), and bifunctional *O*-acyloximes, i.e., *O,O′*-succinyl diacetophenone oxime (SDApO) and *O,O′*-succinyl di-2-acetonaphthone oxime (SDAnO), were prepared by a method similar to that described in a previous article (12). Their structures and characteristics are shown in Fig. 1 and Table 1, respectively.

O-Acryloyl acetophenone oxime (AAPO) and *O*-acryloyl 2-acetonaphthone oxime (AANO) were prepared by reaction of the corresponding oximes with acryloyl chloride by a method similar to that described in a previous article (14). Styrene (St) and ethyl acrylate (EA) were purified by distillation under reduced pressure. Copolymers of AAPO or AANO with St or EA were prepared by radical copolymerization in benzene using α,α′-azobisisobutyronitrile (AIBN) as initiator under vacuum at 60°C (5). In the case of the copolymer of molecular weight below 10 000, 0.2 mol% lauryl mercaptan as chain transfer agent was added in the benzene solution. The structures and abbreviations of the copolymers are shown in Fig. 2. The contents of monomeric AAPO and AANO in the copolymers were determined by their elemental analysis carried out on a Yanaco MT-3 CHN corder. Their molecular weights were determined by using GPC (JASCO) in comparison with those of polystyrene standards. Their glass transition temperatures (T_g's) were determined by using DSC (Rigaku DSC 8230). Table 2 shows the polymerization conditions and the characteristics of the copolymers.

Poly(glycidyl methacrylate) ($\overline{M}_n$ = 117 000) was prepared by solution polymerization in benzene using AIBN as initiator under vacuum at 60°C and was purified by reprecipitation of PGMA in tetrahydrofuran (THF) with methanol. Commercial epoxy resins, EPOLIGHT 100MF (trimethylol propane triglycidyl ether, epoxy equivalent: 140) (TMPGE) and EOCN 104S (*o*-cresol novolac epoxy resin, epoxy equivalent: 215) (EOCN) were provided by Kyoueisha Yusi Kagaku Kogyo

Can. J. Chem. Downloaded from www.nrcresearchpress.com by 46.23.64.124 on 09/08/12
For personal use only.

Table 1. Preparation and characteristics of *O*-acyloximes.

O-Acyloxime	Yield (%)	Melting point (°C)	IR[a] (cm^{-1})	UV[d] λ_{max} (nm)	UV[d] ε (L mol^{-1} cm^{-1})	Elemental analysis (%)
PaApO ($C_{16}H_{15}O_2N$)	36.0	42–43.5	1770[b]	245	14 200	Found: C 76.13, H 6.02, N 5.60 Calcd: C 75.87, H 5.97, N 5.53
PaAnO ($C_{20}H_{17}O_2N$)	57.8	85–87	1770[b]	247	22 500	Found: C 79.19, H 5.65, N 4.62 Calcd: C 79.54, H 5.64, N 4.56
PaBpO ($C_{21}H_{17}O_2N$)	68.0	81–82	1770[b]	253	16 600	Found: C 80.50, H 5.40, N 4.40 Calcd: C 80.00, H 5.43, N 4.44
PaFO ($C_{20}H_{17}O_2N$)	85.2	128–132	1775[b]	255	59 400	Found: C 81.02, H 4.63, N 4.43 Calcd: C 80.50, H 4.82, N 4.47
SDApO ($C_{20}H_{20}O_4N_2$)	79.1	155–158	1760[c]	245	27 900	Found: C 67.92, H 5.64, N 8.01 Calcd: C 68.17, H 5.72, N 7.95
SDAnO ($C_{28}H_{24}O_4N_2$)	72.0	208–210	1760[c]	247	40 000	Found: C 74.02, H 5.34, N 6.07 Calcd: C 74.34, H 5.31, N 6.19

[a]Absorbance due to carbonyl group.
[b]In CCl_4.
[c]In $CHCl_3$.
[d]In tetrahydrofuran.

Table 2. Preparation[a] and characteristics of copolymers bearing AOI groups.

Copolymer	Content of AAPO[b] or AANO[c] (mol%) In feed	In copolymer	P.T.[d] (h)	Conversion (%)	$M_n/10^4$	M_w/M_n	T_g (°C)
AAPO(33)–EA[e]	30	33	2.0	26.1	9.2	1.80	5.1
AAPO(26)–EA	25	28	7.0	29.6	0.52	1.88	0.8
AANO(32)–EA	30	32	13.5	45.1	9.0	2.17	37.4
AAPO(34)–St[f]	33	34	7.5	40.2	8.5	1.96	93.3
AAPO(29)–St	33	29	14.0	37.7	0.33	2.44	70.2

[a]Initiator: 0.4 wt.% α,α′-azobisisobutyronitrile to monomer; polymerization temperature: 60°C.
[b]*O*-Acryloyl acetophenone oxime.
[c]*O*-Acryloyl 2-acetonaphthone oxime.
[d]Polymerization time.
[e]Ethyl acrylate.
[f]Styrene.

Fig. 3. Structures and abbreviations of epoxy resins.

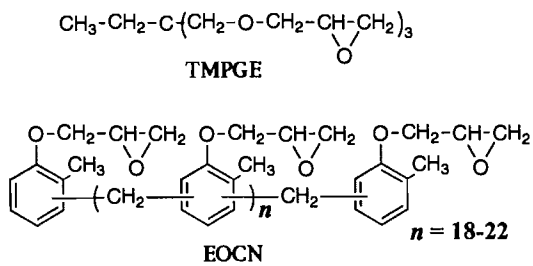

Co. Ltd. The structures and the degree of polymerization of epoxy resins are shown in Fig. 3.

Reagent grade benzophenone (BP) was recrystallized from ethanol. Tetrahydrofuran (Reagent grade) was distilled prior to use. 3,5-Dinitrobenzoyl chloride (Tokyo Kasei Co., HPLC labeling grade, mp 67–69°C) (DNBC) was used without further purification. Polystyrene (Katayama Kagaku Kogyo Co., $\overline{M}_n$ = 113 000) was purified by reprecipitation of PSt in THF with methanol. Poly(methyl acrylate) ($\overline{M}_n$ = 129 000) (PMA) was prepared and purified in a similar manner to PGMA.

Photo-irradiation and quantitative analysis of amines or amino groups

The determination of the yield of amines for *O*-acyloximes in polymer films was carried out by a method similar to that described in a previous article (12). That is, polymer films (35–45 μm thick) with 5 wt.% *O*-acyloxime and 10 wt.% BP as sensitizer to the polymer were prepared by casting THF solutions of the polymer and additives on a Petri dish. In the

Can. J. Chem. Downloaded from www.nrcresearchpress.com by 46.23.64.124 on 09/08/12
For personal use only.

Can. J. Chem. Downloaded from www.nrcresearchpress.com by 46.23.64.124 on 09/08/12
For personal use only.

case of PSt films, they were taken out of the Petri dish after standing overnight in the dark at room temperature and dried under reduced pressure (3 Torr; 1 Torr = 133.3 Pa) overnight at room temperature. These films were irradiated with a high-pressure mercury lamp (Sen Tokusyu Kogen, HL-100, 100 W) without a filter at a distance of 10 cm at room temperature under N_2 for 1 h to photolyze the *O*-acyloximes completely. On the other hand, PMA films were irradiated on a Petri dish in a similar manner as described above because they were too soft to take out of the Petri dish, their T_g being below room temperature. The intensity of the incident light was 4.10 mW/cm^2 at 366 nm. A water-vapor treatment was carried out to completely hydrolyze the photolysates formed by the photolysis of *O*-acyloximes in the irradiated film. That is, the irradiated film was allowed to stand for 10 min in a glass chamber with saturated water vapour at 25°C. Then the polymer films (40–50 mg) were dissolved in THF (2 mL). After the amines in the solution were converted into *N*-3,5-dinitrobenzoylamines (DNBAs) by the reaction with DNBC, the amount of DNBAs in the solution was determined on a HPLC equipped with a UV detector (JASCO 970-UV).

Quantitative analysis of the amines formed in solution was carried out as follows. A benzene solution (3 mL) of an *O*-acyloxime (0.1 mol/L) containing BP (0.1 mol/L) in a quartz cell (1 × 1 × 5 cm) was irradiated under N_2 for 1 h, in a similar manner as described above. After the irradiated benzene solution (0.5 mL) was diluted with THF (19.5 mL), DNBC (ca. 20 mg) was added to a portion (2 mL) of the solution. The very small amount of water in the THF was enough to hydrolyze the photolysates formed by the photolysis of *O*-acyloximes. The amount of amines in the solution was determined on the HPLC in a manner similar to that described above.

Determination of the yield of amino groups for copolymers bearing AOI groups was carried out by a method similar to that described in a previous article (5). That is, the films of copolymers with 10 wt.% BP (ca. 20 μm thick) were irradiated without a filter, in a manner similar to that described above, to photolyze the AOI groups completely; this was confirmed by the disappearance of the absorption of AOI groups at 1760 cm^{-1} in the IR spectrum. After the water-vapour treatment, the irradiated film was dissolved in THF, and the resulting polymer in THF was purified by reprecipitation with methanol 3 times. Then the polymer was dried under reduced pressure (3 Torr) overnight at room temperature. The nitrogen content of the polymer was determined by elemental analysis. The yield of amino groups was calculated from the nitrogen content.

Quantum yield of photolysis of *O*-acyloximes in a polymer matrix

The PSt films (ca. 45 μm thick) containing 5 wt.% *O*-acyloximes and a given amount of BP were irradiated with 366 nm light by use of the high-pressure mercury lamp combined with a filter (Toshiba UV-D1B) at room temperature in air in a similar manner to that described above. The degree of decomposition of the *O*-acyloximes was determined by following the changes in absorbance, at about 1750 cm^{-1}, due to the AOI groups in their IR spectra, which were measured on a IR spectrometer (JASCO IR-810). The quantum yield of photolysis of *O*-acyloximes in PSt films with 366 nm light (ϕ_{366}) was determined as moles of decomposed *O*-acyloximes divided by einsteins of light absorbed by the film (eq. [1]).

$$[1] \quad \phi_{366} = \Delta m/\Delta I_{abs} = \Delta m/[I_0(1 - 10^{-A})tS]$$

where Δm: moles of decomposed *O*-acyloximes (mol); ΔI_{abs}: einsteins of light absorbed by the film (einstein); I_0: intensity of light at 366 nm (einstein cm^{-2} s^{-1}); A: absorbance of the film at 366 nm; S: irradiated area of the film (cm^2); and t: irradiation time (s).

The intensity of the irradiating light was determined by potassium ferrioxalate actinometry (15).

Photo-chemical insolubilization of PGMA films with *O*-acyloximes

The PGMA films (ca. 35 μm thick) with a given mol% *O*-acyloxime and 10 wt.% BP prepared by the casting method were irradiated in a similar manner as that described above, in air for 1 h, followed by the water-vapor treatment. Then the films were heated at 80°C for 1 h on a hot plate. The films (ca. 0.05 g) were immersed in THF (5 mL) for 1 d at room temperature; then the insoluble fractions were separated by centrifugation. The supernatant liquid was next removed and THF (5 mL) was added for washing the insoluble fraction, and the insoluble fraction was again separated by centrifugation. This series of washing operations with THF was repeated 3 times, the supernatants were removed, and then methanol (5 mL) was added for washing the insoluble fraction. This insoluble fraction was separated by centrifugation. After most of the solvent was removed by an aspirator, the insoluble fraction was dried under reduced pressure (3 Torr) at room temperature overnight, and its dry weight determined (13).

Photo-chemical insolubilization of the films composed of copolymers bearing AOI groups and epoxy resins

Thin films (ca. 0.15 μm thick) containing a given amount of copolymers bearing AOI groups an epoxy resin, and BP were prepared by casting their THF solutions onto a quartz plate. Each film was irradiated on the quartz plate with the high-pressure mercury lamp at a distance of 7 cm, at room temperature in air, for a given time. Then the irradiated film was heated at a given temperature for a given time. In this case, the water-vapor treatment was not carried out because the insoluble fraction of the film was not changed by this treatment. After the film was immersed in THF for 10 min at room temperature, it was dried under hot air for a few minutes. The insoluble fractions were determined from the difference in thickness of the films before and after the immersion. The thickness of the films was determined by two-beam interferometry with an interference microscope (Nikon OPTIPHOT).

Results and Discussion

Amine formation by the photolysis of *O*-acyloximes

In a previous article (12), we reported that amines are formed in the photolysis of *O*-acyloximes in PSt films as shown in Scheme 1. That is, benzophenone (BP) absorbs UV light and the energy of the excited BP is transferred to the *O*-acyloximes. The decomposition of the excited *O*-acyloxime (**1**) leads to the formation of an alkyl radical (**2**), an imino radical (**3**), and carbon dioxide. Then an azomethine (**4**) is formed by the recombination of 2 and 3, and finally an amine (**5**) and a

Scheme 1.

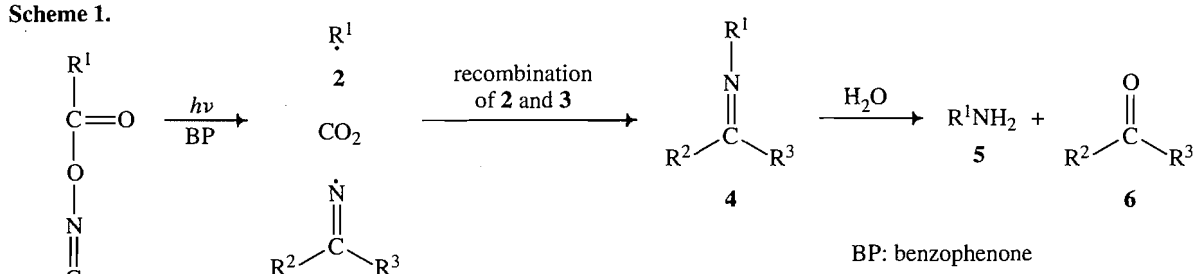

ketone (**6**) are generated by the hydrolysis of **4**. Most of the intermediary azomethines are considered to be easily hydrolyzed by water vapor in air during irradiation since PGMA films (even ca. 35 μm thick) containing *O*-acyloximes and BP were insolubilized appreciably by heating after irradiation under air without a water-vapor treatment (16). Besides, although imines and azines are obtained from **3** as described in the previous article (12), the yield of the azines was very low and the yield of the imines depended on the structure of the *O*-acyloximes.

Table 3 gives quantum yields of photolysis at 366 nm (ϕ_{366}) for *O*-acyloximes in the presence of 10 wt.% BP. The ϕ_{366} for PaAnO was highest among the monofunctional *O*-acyloximes, at 0.58, and that for PaFO was lowest, at 0.06. Although the triplet energies of the *O*-acyloximes are deduced to be close to triplet energies of the original ketones (17), it is difficult to clarify the relation between the triplet energies and the ϕ_{366} values for each at present. The ϕ_{366} for PaAnO was hardly altered by the change in amount of BP as sensitizer in the range of 5–15 wt.%. This result shows that the decomposition rate is proportional to the amount of BP over this range, and that the efficiency of decomposition based on absorbed light intensity is the same. Interestingly, the ϕ_{366} for the bifunctional *O*-acyloximes, i.e., SDApO and SDAnO, was higher than for the monofunctional *O*-acyloximes. Similar results were observed for the ϕ_{366} of pendant acyloxyimino (AOI) groups in polymers (Table 3).

Table 4 shows the yields of amines based on decomposed *O*-acyloximes. The yields of amines for PaApO and PaAnO in the PSt films were 72% and 89%, respectively, which were ca. 30% higher than those in benzene solutions. This result shows that the recombination of imino and alkyl radicals occurs more effectively in a polymer matrix than in solution. As described in a previous article (12), it is deduced that the movement of *O*-acyloximes is restricted by the PSt main chains since the glass transition temperature (T_g) of PSt containing 5 wt.% *O*-acyloximes and 10 wt.% BP is 54°C, and higher than room temperature. This result suggests that the increase in the yield is due to a cage effect of the polymer matrix.

On the other hand, the yields for PaApO and PaAnO in PMA films were lower than those in PSt films. Since the segment motions in the main chains in the PMA (T_g = 7°C) occur at room temperature, it is deduced that the PMA matrix is not effective for the formation of amine precursors.

The yields of amines for PaAnO and SDAnO in PSt films were ca. 20% higher than those for PaApO and SDApO, respectively. This result suggests that the bulkiness of a naphthyl moiety in PaAnO and SDAnO was advantageous to the formation of amine precursors. Similarly, the yield of amine for PaBpO was high, as well as that for PaAnO or SDAnO. This seems to be due to the bulkiness of AOI groups bearing two phenyl moieties. These results suggest that the bulkiness of the AOI group is important for efficient formation of the amine precursors.

The formation of polymer amines was also similarly investigated. Figure 4 shows the relationship between the yield of amino groups and the content of AAPO or AANO in the copolymers. The results for AAPO copolymers are taken from a previous article (5). In Fig. 4, yields of amino groups for AANO–St's were almost the same as those for AAPO–St's at any content of AANO. This result was different from the result for *O*-acyloximes described above. It seems that, judging from the T_g's of the copolymers, the motions of pendant AOI groups are restricted more strongly by the main chains of the copolymers at room temperature, and that the yields for the two copolymers are almost the same. Here, since an increase in the contents of AANO in the copolymers leads to an

Table 3. Apparent quantum yields of photolysis at 366 nm (ϕ_{366}) for *O*-acyloximes in polystyrene films.

Compound	BP content (wt.%)	ϕ_{366}
PaApO	10	0.41
PaAnO	5	0.59
	10	0.58
	15	0.54
PaBpO	10	0.35
PaFO	10	0.06
SDApO	10	0.88
SDAnO	10	0.76
AAPO(26.3)–St	10	0.70

Table 4. Yields of amines in photolysis of *O*-acyloximes under N_2.

		Yield (%)		
		Solid phase		
O-Acyloxime	Resulting amine	PSt	PMA	Liquid phase
PaApO	Benzylamine	72	40	43
PaAnO	Benzylamine	89	73	57
PaBpO	Benzylamine	89	—	—
SDApO	Ethylenediamine	68	—	—
SDAnO	Ethylenediamine	90	—	—

Can. J. Chem. Downloaded from www.nrcresearchpress.com by 46.23.64.124 on 09/08/12
For personal use only.

Can. J. Chem. Downloaded from www.nrcresearchpress.com by 46.23.64.124 on 09/08/12
For personal use only.

Fig. 4. Relationship between contents of AAPO or AANO in copolymers and yields of amino groups: (○, ●) AAPO–St, (△, ▲) AANO–St.

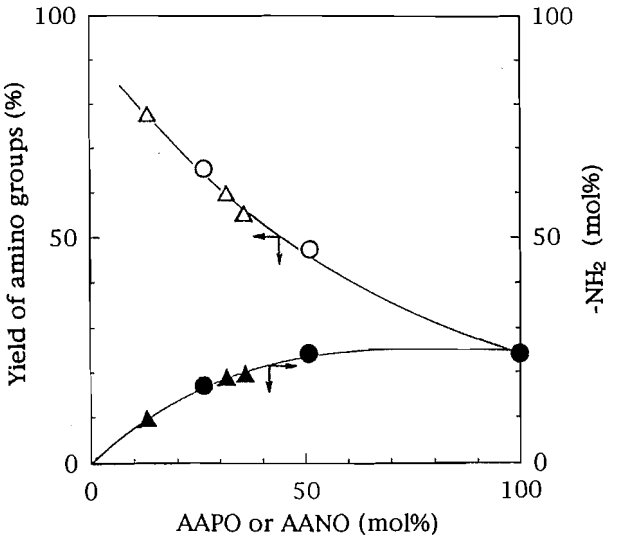

Table 5. Insolubilization[a] of PGMA films with *O*-acyloximes and BP by UV irradiation.

O-Acyloxime	Content (mol%)	Insoluble fraction (%)
PaApO	0.3	41
	0.6	62
PaAnO	0.3	49
	0.6	70
SDApO	0.15	75
	0.3	85
SDAnO	0.15	79
	0.3	96

[a]Irradiated for 1 h and then heated at 80°C for 1 h after water-vapor treatment at 25°C for 10 min.

increase in their T_g's, the effect of T_g on the yield was not considered.

Photo-chemical insolubilization of PGMA film with *O*-acyloximes

Table 5 shows the results of insolubilization of PGMA films containing *O*-acyloximes and BP by UV irradiation. The films were irradiated for 1 h in air and then heated at 80°C for 1 h after water-vapor treatment. No insolubilization of the films occurred by the water-vapor treatment and (or) by heating without irradiation. From the results for insoluble fractions of the films, PaAnO was more active than PaApO and a similar relation was observed for bifunctional *O*-acyloximes. However, the bifunctional *O*-acyloximes, SDApO and SDAnO, were more active than the monofunctional ones, PaApO and PaAnO. In Table 4, the yield of benzylamine for PaAnO is higher than that for PaApO. Thus, the order of activity of the monfunctional *O*-acyloximes as photo-cross-linkers is understood to be due to the difference in the yields of amines. Although there is no difference in the yields of amines between monofunctional and bifunctional oximes with the same AOI groups, bifunctional oximes were much more active as photo-cross-linkers than the monfunctional ones. Ethylenediamine and benzylamine are obtained in the photolysis of bi- and monofunctional *O*-acyloximes, respectively. Although the difference in their basicity should be considered, bifunctionality of the resulting amine is thought to be beneficial for cross-linking.

While these results show that the *O*-acyloximes acted as photo-cross-linkers of PGMA, these amines were not efficient cross-linkers for trifunctional epoxy resins such as TMPGE, as described in a previous article (13). We later investigated thermal curing of epoxy resins by polymer amines formed by the photolysis of copolymers bearing AOI groups.

Photo-chemical insolubilization of AAPO copolymer films with TMPGE as a cross-linker

Figure 5 shows the effect of irradiation time and heating temperature on photo-cross-linking of AAPO(34)–St or AAPO(33)–EA films. On heating at 150°C after irradiation, both films were insolubilized rapidly at almost the same rate With lowering of the heating temperature, the insolubilization rate of AAPO(34)–St films fell significantly, while that of AAPO(33)–EA films did so only slightly. To clarify the difference in the photo-cross-linking behavior of these copolymers, effects of miscibility of TMPGE and BP with the copolymers and of the T_g's of the copolymers on the photo-cross-linking were investigated. The miscibility of the copolymers with TMPGE and BP was satisfactory, because only one T_g was observed for each film composed of AAPO–St or AAPO–EA, BP, and TMPGE. The T_g's of AAPO(34)–St and AAPO(33)–EA with 10 wt.% TMPGE and 10 wt.% BP were 68.3 and −11.8°C, respectively.

Figure 6 shows Arrhenius plots of the photo-cross-linking of AAPO(34)–St and AAPO(33)–EA films. The photo-cross-linking rate (κ) was determined as a reciprocal of the time required for insolubilization of 50% of the copolymer film in Fig. 5. The apparent activation energies (E_{act}) of insolubilization for AAPO(34)–St and AAPO(33)–EA films that were calculated from the plot were 64.3 and 21.3 kJ/mol, respectively. The cause of the lowering in E_{act} for AAPO(33)–EA is thought to be due to the difference in energy required for the segmental motion of AAPO(33)–EA, because miscibility of TMPGE with both polymers was good and the T_g of AAPO(33)–EA was considerably lower than that of AAPO(34)–St.

Figure 7 shows the effects of the molecular weights of AAPO copolymer and the heating temperature after irradiation on insoluble fractions of AAPO copolymer films. The films were heated at a given temperature for 10 min after irradiation for 10 min in air.

All AAPO films were cross-linked effectively by TMPGE on heating at 150°C after irradiation, while the proportion of the insoluble fractions was very different at lower temperatures. Insolubilization of AAPO(33)–EA (T_g = 5.1°C, $\overline{M}_n$ = 92 000) films occurred at room temperature and the insoluble fraction of the film reached ca. 50%, while heating at temperatures over 70°C was required for insolubilization of AAPO(34)–St (T_g = 93.3°C, $\overline{M}_n$ = 85 000) films. Since the T_g of AAPO(33)–EA is lower than room temperature, it is deduced that the reaction of amino groups in the copolymer with epoxy groups occurs efficiently at room temperature. Although the T_g's of AAPO(26)–EA (T_g = 0.8°C, $\overline{M}_n$ = 5200)

Fig. 5. Effect of irradiation time and heating temperature on photo-cross-linking[a] of AAPO(34)–St films (*a*) and AAPO(33)–EA films (*b*) with 10 wt.% BP and 10 wt.% TMPGE (ca. 0.15 μm thick): (■) 60°C, (□) 80°C, (●) 100°C, (○) 150°C.
[a]After irradiation in air, heated for 5 min.

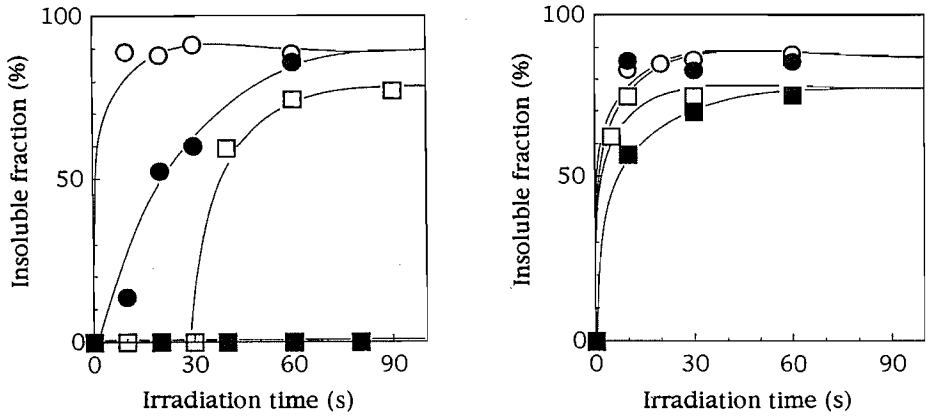

Fig. 6. Arrhenius plot of photo-cross-linking of copolymer films (ca. 0.15 μm thick) with 10 wt.% BP and 10 wt.% TMPGE: (○) AAPO(34)–St, (▲) AAPO(33)–EA. κ: Photo-cross-linking rate at 50% of insoluble fraction of copolymer films.

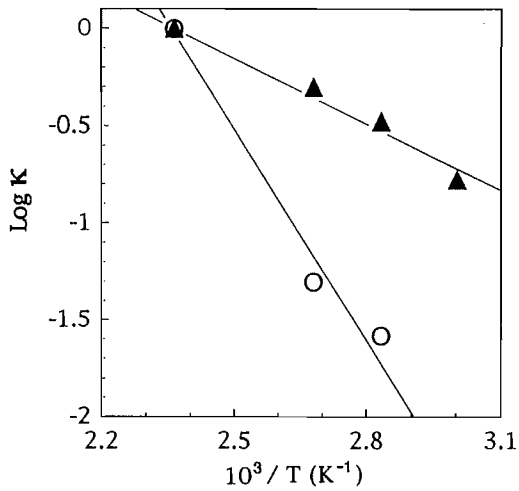

Fig. 7. Effects of molecular weights of AAPO copolymers and heating temperature on insoluble fraction[a] of AAPO copolymer films (ca. 0.15 μm thick): with 10 wt.% BP and 10 wt.% TMPGE: (○) AAPO(33)–EA (M_n = 92 000, T_g = 5.1°C), (●) AAPO(26)–EA (M_n = 5200, T_g = 0.8°C), (□) AAPO(34)–St (M_n = 85 000, T_g = 93.3°C), (■) AAPO(29)–St (M_n = 3300, T_g = 70.2°C).
[a]After irradiation for 10 min in air, heated for 10 min.

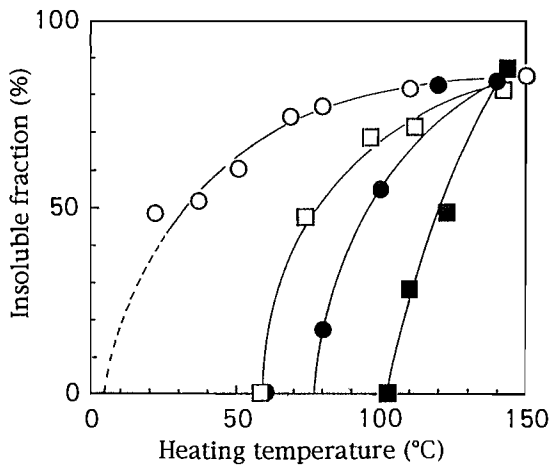

and AAPO(29)–St (T_g = 70.2°C, $\overline{M}_n$ = 3300) were lower than those of the corresponding copolymers, which had higher molecular weights, the higher temperature for insolubilization of the former two copolymers was needed. It is deduced that the lowering of molecular weights of the copolymers affects the insolubilization more strongly than the lowering of T_g.

Photo-chemical insolubilization of epoxy resin films by use of AAPO or AANO copolymers as photo-cross-linkers

Table 6 shows relations between the ratio of TMPGE and AAPO copolymers in the films and the insoluble fractions. The films were heated at 100°C for 5 min after irradiation for 10 min in air. The insoluble fractions for any copolymer except AAPO(29)–St were highest at 10 wt.% TMPGE. At this wt.%, insoluble fractions for both AAPO(33)–EA and AAPO(34)–St, which had higher molecular weights, were ca. 90%.

The insoluble fractions were lowered with an increase in content of TMPGE. In the case of AAPO copolymers, which had lower molecular weights, the insoluble fractions were lower than those for the copolymers that had higher molecular weights. Especially, AAPO(29)–St films were not insolubilized at any ratio. These results show that AAPO copolymers do not work as photo-cross-linkers for TMPGE at low content.

Table 7 shows the effect on the insoluble fractions of the weight ratio of an epoxy resin with a higher molecular weight, EOCN, to the copolymers. Since only one T_g was observed in any ratio of EOCN and copolymer and the T_g varied with the ratio as shown in Table 8, it is thought that the miscibilities of EOCN with the copolymers were also good. The films were heated at 100°C for 5 min after irradiation for 10 min in air. The insoluble fractions for AAPO(33)–EA and AANO(32)–EA were ca. 80% at any ratio except AANO(32)–EA with 80 wt.% EOCN. This result was very different from the results in

Can. J. Chem. Downloaded from www.nrcresearchpress.com by 46.23.64.124 on 09/08/12
For personal use only.

Table 6. Effect on the insoluble fractions of the ratio of TMPGE and AAPO copolymer in films with 10 wt.% BP.[a]

Epoxide/copolymer (wt%)	Insoluble fraction (%) AAPO(33)–EA ($\bar{M}_n$ = 92 000) (T_g = 5.1°C)	AAPO(26)–EA ($\bar{M}_n$ = 5200) (T_g = 0.8°C)	AAPO(34)–St ($\bar{M}_n$ = 85 000) (T_g = 93.3°C)	AAPO(29)–St ($\bar{M}_n$ = 3300) (T_g = 70.2°C)
0/100	0	0	0	0
10/90	89	65	88	0
20/80	79	56	74	0
30/70	71	49	53	0
40/60	54	32	29	0
50/50	41	0	0	0
60/40	36	0	0	0
70/30	29	0	0	0
80/20	0	0	0	0
90/10	0	0	0	0
100/0	0	0	0	0

[a]After irradiation for 10 min in air, heated at 100°C for 5 min.

Table 7. Effect on the insoluble fractions of the ratio of EOCN and copolymer bearing AOI groups in films with 10 wt.% BP.[a]

Epoxide/copolymer (wt%)	Insoluble fraction (%) AAPO(33)–EA ($\bar{M}_n$ = 92 000) (T_g = 5.1°C)	AANO(32)–EA ($\bar{M}_n$ = 90 000) (T_g = 37.4°C)	AAPO(34)–St ($\bar{M}_n$ = 85 000) (T_g = 93.3°C)
20/80	82	82	75
40/60	84	81	—
50/50	82	79	62
60/40	83	—	60
80/20	80	69	53

[a]After irradiation for 10 min in air, heated at 100°C for 5 min.

Table 8. Effect on the T_g of the ratio of EOCN and copolymer bearing AOI groups.

Epoxide/copolymer (wt.%)	T_g (°C) AAPO(33)–EA	AANO(32)–EA	AAPO(34)–St
0/100	5.1	37.4	93.3
20/80	2.1	13.2	39.8
50/50	−3.3	5.1	19.0
80/20	−8.2	−3.0	6.9
100/0	−9.6	−9.6	−9.6

Table 6. Although the films of AAPO(34)–St were also insolubilized even at lower content of the copolymer, the proportion of insoluble fractions of AAPO(34)–St was lower than that of AAPO(33)–EA or AANO(32)–EA. It is thought that the T_g's of their copolymers played an important role in the insolubilization. These results suggest that copolymers bearing AOI groups can be used as effective photo-cross-linkers for epoxy resins by choosing an appropriate combination of epoxy resin and copolymers.

Conclusions

1. The use of *O*-acyloximes and copolymers bearing AOI

Can. J. Chem. Downloaded from www.nrcresearchpress.com by 46.23.64.124 on 09/08/12
For personal use only.

groups as photo-base generators was verified. This could be applied to photo-initiated curing of epoxides.

2. The yields of amine for *O*-acyloximes bearing a bulky moiety such as a naphthyl group were found to reach ca. 90% in PSt films under N_2.

3. It was found that the T_g of copolymers bearing AOI groups played a very important role in the curing of epoxides when the copolymers were used as photo-cross-linkers.

Acknowledgement

We appreciate gift samples of epoxy resins from Kyoueisha Yusi Kagaku Kogyo Co. Ltd.

References

1. J.V. Crivello. CHEMTECH, 624 (1980).
2. J.M.J. Fréchet. Pure Appl. Chem. **64**, 1239 (1992).
3. C. Kutal and C.G. Willson. J. Electrochem. Soc. **134**, 2280 (1987).
4. M.R. Winkle and K.A. Graziano. J. Photopolym. Sci. Technol. **3**, 419 (1990).
5. K.H. Song, M. Tsunooka, and M. Tanaka. J. Photochem. Photobiol. A: **44**, 197 (1988).
6. J.F. Cameron and J.M.J. Fréchet. J. Am. Chem. Soc. **113**, 4303 (1991).
7. J.F. Cameron and J.M.J. Fréchet. J. Photochem. Photobiol. A: **59**, 105 (1991).
8. M. Leung, J.M.J. Fréchet, J.F. Cameron, and C.G. Willson. Polym. Mater. Sci. Eng. **68**, 30 (1993).
9. J.M.J. Fréchet, J.F. Cameron, C.M. Chung, S.A. Haque, and C.G. Willson. Polymer Bull. **30**, 369 (1993).
10. D.R. Mckean, G.M. Walraff, W. Volksen, N.P. Hacker, M.I. Sanchez, and J.W. Labadie. Polym. Mater. Sci. Eng. **66**, 237 (1992).
11. E. Takehara, A. Kameyama, and T. Nishikubo. Polym. J. **25**, 421 (1993).
12. K. Ito, M. Nishimura, M. Sashio, and M. Tsunooka, J. Polym. Sci. Part A: Polym. Chem. **32**, 2177 (1994).
13. K. Ito, M. Nishimura, M. Sashio, and M. Tsunooka. J. Polym. Sci. Part A: Polym. Chem. **32**, 1793 (1994).
14. M. Tsunooka, S. Imono, K. Nakayama, H. Kuwabara, and M. Tanaka. J. Polym. Sci. Polym. Chem. Ed. **24**, 317 (1986).
15. S.L. Murov. *In* Handbook of photochemistry. Dekker, New York. 1973. p. 119.
16. K. Ito, M. Nishimura, M. Sashio, and M. Tsunooka. Chem. Lett. 1153 (1992).
17. H. Sakuragi, S. Ishikawa, T. Nishimura, M. Yoshida, N. Inamoto, and K. Tokumaru. Bull, Chem. Soc. Jpn. **49**, 1949 (1976).

Can. J. Chem. Downloaded from www.nrcresearchpress.com by 46.23.64.124 on 09/08/12
For personal use only.

Chemically modified pullulans II. New hydrophobically substituted derivatives

G. Mocanu, A. Carpov, S. Chapelle, L. Merle, and G. Muller

Abstract: New hydrophobically substituted pullulans were synthesized, such as (*i*) neutral derivatives obtained by direct esterification of pullulan with adenine and thymine butyric acid and (*ii*) ionic derivatives obtained by amidation of carboxymethyl pullulan with aromatic amines (aminopyrene and adenine). Rheological measurements in dilute solutions allowed us to test the influence of the hydrophobic aromatic substituents and of the ionicity of the parent support on the nature of the hydrophobic associations in dilute solutions. The rheological studies on the pullulan derivatives revealed mainly intramolecular hydrophobic associations for both ionic and non-ionic derivatives, suggesting a more compact conformation than that of the precursor.

Key words : hydrophobically modified pullulans, esterification, amidation, condensed aromatic ring, size exclusion chromatography, multi-angle laser light scattering.

Resumé : On a synthétisé de nouveaux pullulanes substitués d'une façon hydrophobe, tels que les dérivés neutres obtenus par estérification directe du pullulane avec l'acide butyrique de l'adénine et de la thymine ainsi que les dérivés ioniques obtenus par amidation du carboxyméthylpullulane avec des amines aromatiques (aminopyrène et adénine). Des mesures rhéologiques en solutions diluées ont permis de vérifier l'influence des substituants aromatiques hydrophobes et du caractère ionique du support parent sur la nature des associations hydrophobes en solutions diluées. Les études rhéologiques sur les dérivés du pullulane ont mis en évidence l'existence d'associations principalement hydrophobes intramoléculaires pour les dérivés aussi bien ioniques que non ioniques; ceci suggère que la conformation est beaucoup plus compacte que celle du précurseur.

Mots clés : pullulanes hydrophobiquement modifiés, estérification, amidation, noyau aromatique condensé, chromatographie par exclusion stérique, diffusion de la lumière laser à angles multiples.

[Traduit par la rédaction]

Introduction

Pullulan is a neutral water-soluble exopolysaccharide with a linear flexible macromolecular chain, formed mainly by α-1,6-linked maltotriose sequences containing α-1,4-linked D-glucose units (pannose) in a 2:1 ratio.

The reactivity of its alcohol groups permits the obtention of a large variety of pullulan derivatives, such as etherified (1), esterified with aliphatic or aromatic acids (2, 3), cationized (5), sulfoalkylated (6), or sulfated (6) pullulans.

Recently, many studies have been devoted to hydrophobically modified water-soluble synthetic polymers (7–9) and natural polysaccharides (10–12). Special concern for such materials may be explained by their interesting properties, leading to their use as tensioactive agents (13), associative thickeners, and support for enzyme immobilization (13) in biotechnology and medicine (14). Hydrophobically modified pullulans have been much less studied. Sunamoto and co-workers have reported the synthesis and properties of palmitoyl (15) and cholesteryl (16) modified pullulan derivatives and their use as host for protein guests (16, 17).

The present paper reports the synthesis, in organic medium, of new hydrophobically modified pullulan derivatives: i.e., non-ionic by esterification with adenine and thymine *n*-butyric acid in the presence of dicyclohexylcarbodiimide, and ionic by amidation of carboxymethyl pullulan with aromatic amines (aminopyrene or adenine).

The choice of nucleic bases and of aminopyrene was made for two reasons: (*i*) introduction of a hydrophobic moiety on the polysaccharide chain, (*ii*) utilization as fluorescent labels for further photophysical measurements.

The rheological behaviour of these derivatives was studied for comparative determination, as a first approach, of the nature of the hydrophobic associations of derivatives of a same precursor.

Received April 10, 1995.

This paper is dedicated to Professor J.E. (Jim) Guillet in recognition of his contributions to Canadian chemistry.

A. Carpov and G. Mocanu. "Petru Poni" Institute of Macromolecular Chemistry, 6600 Iasi, Romania.
S. Chapelle. Laboratoire de RMN, DO Unité de recherche associée n° 464, 76821 Mont-Saint-Aignan Cedex, France.
L. Merle and G. Muller.[1] Polymères, biopolymères, membranes, Unité de recherche associée n° 500 du Centre national de la recherche scientifique, UFR des sciences, Université de Rouen, 76821 Mont-Saint-Aignan Cedex, France.

[1] Author to whom correspondence may be addressed. Telephone: 33 35 14 60 00. Fax: 33 35 14 67 04.

Experimental section

Materials

Pullulan Pi 20 (Pu) was purchased from Hayashibara Chemical Laboratory (Okoyama, Japan). Adenine, thymine, 1-aminopyrene, 4-chlorobutyric acid ethyl ester, and *N,N'*-

Can. J. Chem. Downloaded from www.nrcresearchpress.com by 46.23.64.124 on 09/08/12
For personal use only.

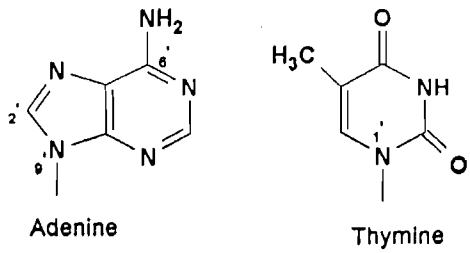

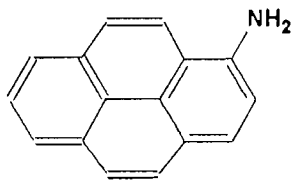

dicyclohexylcarbodiimide (DDCI) are commercial products from Aldrich.

Dimethylformamide and dimethyl sulfoxide (Prolabo) were freshly distilled on CaH_2 under argon.

Carboxymethyl pullulan (CMPNa), with a degree of substitution DS = 0.88, was a laboratory sample synthesized in Romania according to the procedure reported in a patent (18) and recently characterized (19).

Synthesis of intermediate products

Ethyl-2 (adenine-9-yl) butyrate and its acid (ABA), and ethyl thymine-1-yl butyrate and its acid (TBA) were synthesized following the method described by Overberger and Morishima (20) for propionic adenine derivatives. Thymine-1–yl butyric acid (TBA) was obtained by methanolic alkaline hydrolysis. This milder hydrolysis was preferred to the acidic one (5 N HCl), which leads to complex degradation products.

The purity was checked by ^1H NMR in DMSO-d_6; ABA: aliphatic (CH_2), 4.2 ppm; Ad-NH_2: 7.35 ppm (2H), H_2-H_8Ad: 8.25 ppm, 2H; TBA: CH_3: 1.75 ppm, aliphatic (CH_2): 3.25–4.20 ppm; T-H_2: 7.5 ppm; and mass spectroscopy analysis (in glycerol matrix: ABA, *m/z*, $[MH]^+$: 222; TBA, *m/z*, $[MH]^+$: 213.

Synthesis of pullulan esters

Pullulan adenine-9-yl butyric acid ester (PAE)

Pu (1 g, 6.17 mM) and 0.02 g of *N,N*-dimethylamino pyridine (DMPA) were dissolved in 10 mL of dry DMSO, at room temperature. Separately, 0.681 g (3.08 mM) of ABA was dissolved in 10 mL of DMSO together with 0.634 g (3.08 mM) of *N,N'*-dicyclohexylcarbodiimide, the mixture was stirred for 30 min at room temperature, and then added to the pullulan solution. The reaction was run for 48 h at room temperature under stirring. Then the polymer was precipitated three times by pouring the water solution into ethyl alcohol, was washed with warm alcohol to extract the last traces of adenine physically included in the polymer, and finally the clear aqueous solution was freeze-dried (recovery: 90% of pullulan derivative). Any free adenine can be detected, by checking by UV (TLC eluant: dichloromethane:methanol, 92:8).

The pullulan-containing thymine (PTE) derivatives were obtained in the same way. Table 1 summarizes the different samples obtained.

Table 1. Adenine and thymine ester pullalan derivatives.

Sample	Reagent	Molar ratio reagent per glucose unit	% Content per mole by UV
G3	Adenine-9-butyric acid	0.5/1	4.57
G4	Adenine-9-butyric acid	0.75/1	5.8
G5	Adenine-9-butyric acid	1.2/1	7.05
G6	Thymine-1-yl butyric acid	0.5/1	4.57
G7	Thymine-1-yl butyric acid	0.5/1	4.57

Table 2. Carboxymethyl pullulan containing an amide group.

Sample	Reagent	Molar ratio reagent per glucose unit	% Content per mole	
			by UV	Conductimetry
G9	1-Aminopyrene	0.2/1	4.57	2.05
G10	Adenine	0.4/1	3.4	5.8

Synthesis of pullulans containing amide groups (aminopyrene and adenine)

With 1-aminopyrene (or with adenine): to 1 g (4.71 mM) of CMP (as COOH) (with DS = 0.88) dissolved in 10 mL of dry DMSO was added 0.19 g (0.92 mM) of DDCI under stirring during 30 min. Then, 0.2 g (0.92 mM) of aminopyrene and 0.02 g of DMPA in 10 mL of DMSO were added to the carbodimide preactivated CMP (as COOH), and stirred at room temperature during 48 h. The polymer (sodium salt) was purified as above, neutralized, then dialyzed against water and freeze-dried. Any free aminopyrene can be detected.

Methods

The adenine and thymine contents of the pullulan esters were determined by UV analysis of their aqueous solutions, taking as model samples the butyric esters (ε = 13 900 and 11 600 L mol^{-1} cm^{-1} at 260 and 267 nm, respectively, for N_9-adenine and N_1-thymine *n*-butyl ethyl esters). The results are listed in Table 1.

The degrees of substitution (DS) of the hydrophobic moiety of the carboxymethyl pullulan were established by conductimetric titration in an excess of acid, following the method of Eyler et al. (21) as the difference between the DS of precursor and that of the modified polymer, in good accord with the results obtained from UV analysis for aminopyrene and adenine derivatives, thus confirming the accuracy of the conductimetric method. The contents of CMP are presented in Table 2.

Rheological measurements were performed in dilute solutions with a low-shear 30 Contraves rheometer. Size Exclusion Chromatography (SEC) curves were obtained as described in ref. 19.

NMR spectra were recorded at 323 K, on a Brucker ARX 400 spectrometer equipped with a multinuclear 5 mm probe.

Can. J. Chem. Downloaded from www.nrcresearchpress.com by 46.23.64.124 on 09/08/12
For personal use only.

Scheme 1.

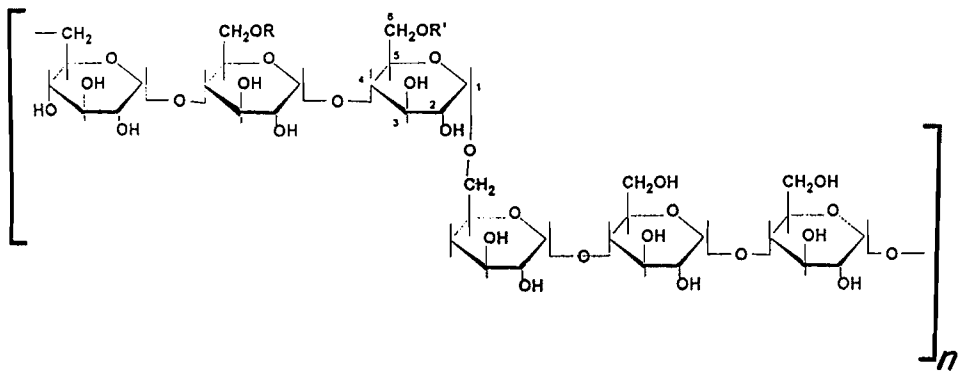

R = R′ = H: pullulan
Ester pullulan derivatives (R = H)
R′ = -$COCH_2CH_2CH_2$-N_9 Ad (PAE) or -$COCH_2CH_2CH_2$-N_1 T (PTE)
adenine-9-yl *n*-butyric or thymine-1-yl *n*-butyric ester pullulans

Carboxymethyl-pullulan amides
R = -CH_2COONa or R′ = -CH_2CONHR'' (R″ = 1-aminopyrene or N_6-adenine)

The ^{13}C frequency was 100.62 MHz. An aqueous solution of 2,2,3,3-tetrahydroxide-3–trimethyl silyl propionate (TMSP) was taken as chemical shift reference. Spectra were broad-band decoupled and obtained with nuclear Overhauser enhancement. Sample concentrations were ~20% in D_2O.

Results and discussion

The structures of the synthesized hydrophobically substituted derivatives are presented in Scheme 1.

As seen from the data presented in Table 1, the percentage of the esterification reaction (in the presence of DDCI), due to the weak acidity of ABA or TBA, remains low enough, as less than 10% of the amount of reagent was used.

Because of its low nucleophilicity, the *exo* amino group of adenine is usually attacked only by reactive acid chloride or anhydride. The adenine was grafted to the CMP by the Ad_6NH_2 group, through the anhydride intermediate of CMP (usual mechanism of DDCI), in spite of the very low p*K* value of adenine. Nevertheless, the reaction of amidation is nearly quantitative (Table 2).

Figures 1(*a*) and 1(*b*) show the ^{13}C NMR of CMP and the modified adenine CMP spectrum. The CMP spectrum was assigned on the basis of the known pullulan ^{13}C NMR data (21). The main difference between both spectra is the appearance of a new signal around 80 ppm corresponding to the deshielding of C_6(1-6) by the amide substitution and the broadening of the signals due to the C_6(1-6) (61.5 ppm) and C_4(1-4) (77.1 ppm) non-substituted carbon atoms; this broadening was attributed to an equilibrium between several conformers.

The spectrum of adenine CMP is similar to that of CMP, except that two small new peaks are detected: one at 185.7 ppm corresponding to an amide carbonyl group and the second at 154.5 ppm assigned to the $C_{2'}$ of adenine. The presence of these two peaks bears evidence that CMP was modified via the NH_2 of the adenine. The relative ratio of the amide and the carboxymethyl group peaks was around 3%, in agreement with UV data (although no quantitative inverse gating procedure was used). Let us mention also the presence of six well-resolved α-C_1 anomeric peaks due to the nonequivalence of the six α-glucose units; the quaternary carbon atoms of adenine do not appear.

The plot of reduced viscosity against the concentration of pullulan precursor is compared to those of its nucleic base esters, in dilute 0.1 N NaCl solutions (Fig. 2). The intrinsic viscosities [η] decrease when the content of hydrophobic substituent increases. The change in viscosities can be attributed to the intramolecular interaction. Indeed, we verified that no degradation occurred due to the action of the carbodimide or to the presence of the acid group of the reagents, as checked on pullulan treated either with DCCI or ABA alone. As the [η] values obtained are of the same order as those for the pullulan precursor, it may be assumed that no degradation takes place on the polymeric chain during the reaction. Thus, the polymer coil contraction detected by the viscosimetry change can be attributed to hydrophobic association.

Generally, the introduction of hydrophobic groups will affect the intrinsic viscosity and the Huggins constant *k′* in the classical relation:

$$\eta_{red} = [\eta] + k'[\eta]^2 c$$

For a random coil polymer, a common value of 0.3–0.8 is found for *k′* and values larger than 0.8 indicate association. From data reported in Table 3, it is clear that *k′* is only slightly changed for both modified pullulan derivatives. On the other hand, the viscosity was found to decrease strongly in the case of adenine-containing pullulan, from $[\eta]_0$ = 66 for pullulan itself to 33.5, to 25.5, to 12.5 mL g^{-1} with ABA content increasing from 4.07 to 7.05% (Table 3), in contrast with the value of the intrinsic viscosities of the PTE derivatives (0.98 and 2.19%), which remain very similar to that of the precursor. This viscosity change is correlated with the hydrophobic character of the grafted moiety, which is more pronounced for the adenine group than for the thymine group.

Can. J. Chem. Downloaded from www.nrcresearchpress.com by 46.23.64.124 on 09/08/12
For personal use only.

Fig. 1. ^{13}C NMR spectra of (*a*) CMP sodium salt modified with adenine at N^6 (~3%) (36 000 scans); (*b*) expanded carbonyl region, compared to (*c*) CMP (DS ~0.88) (20 200 scans), in D_2O, at 100.62 MHz.

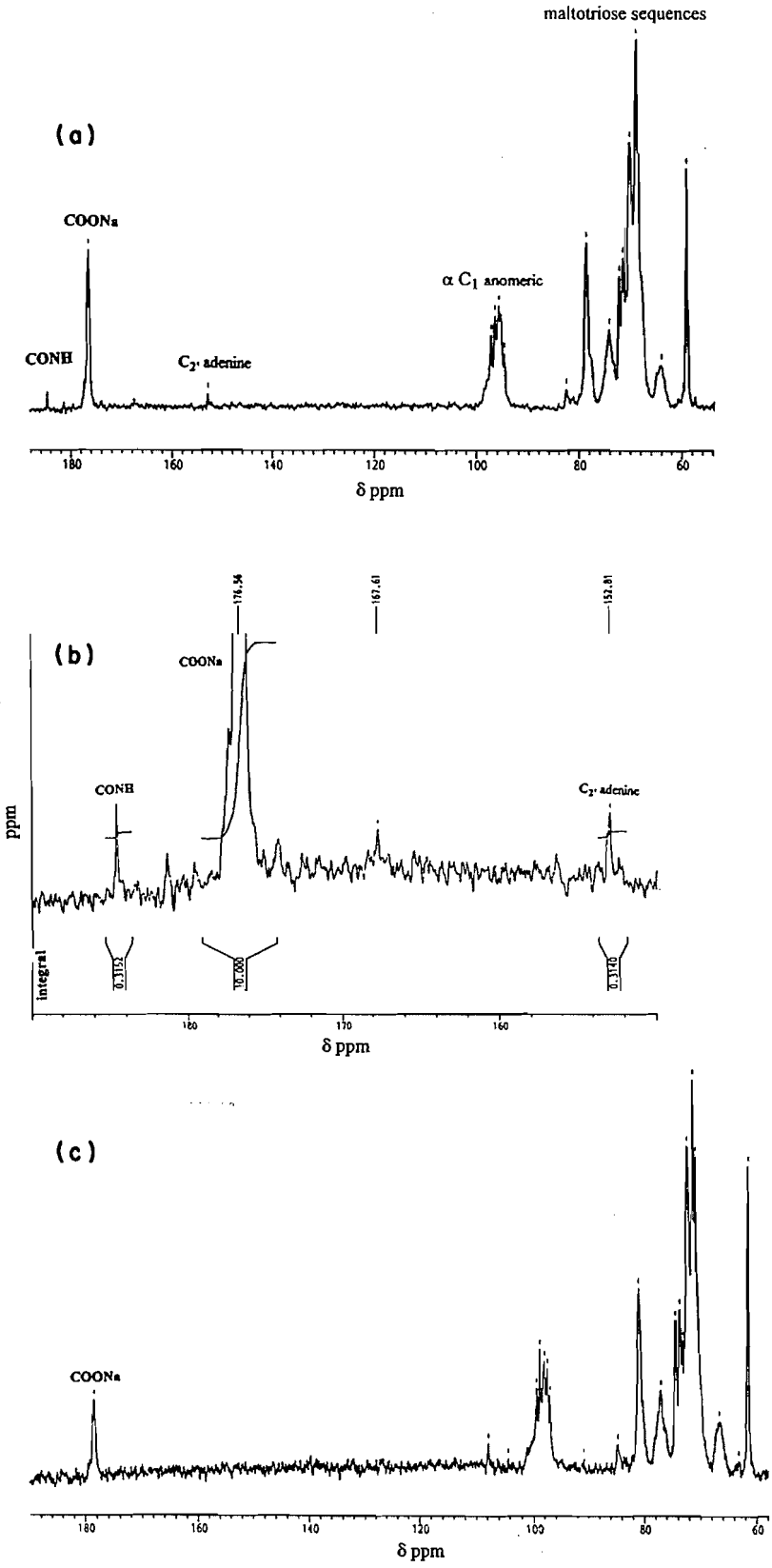

Can. J. Chem. Downloaded from www.nrcresearchpress.com by 46.23.64.124 on 09/08/12
For personal use only.

Fig. 2. Reduced viscosity versus concentration (g L^{-1}) of pullulan precursor compared to its nucleic base ester derivatives in 0.1 N NaCl: 1, pullulan; 2, modified with ABA: (a) 4.57% (G_3), (b) 5.8% (G_4), (c) 7.05% (G_5); 3, modified with TBA: (a′) 0.98% (G_6), (b′) 2.19% (G_7); 4, 1:1 mixture of G_4 and G_7.

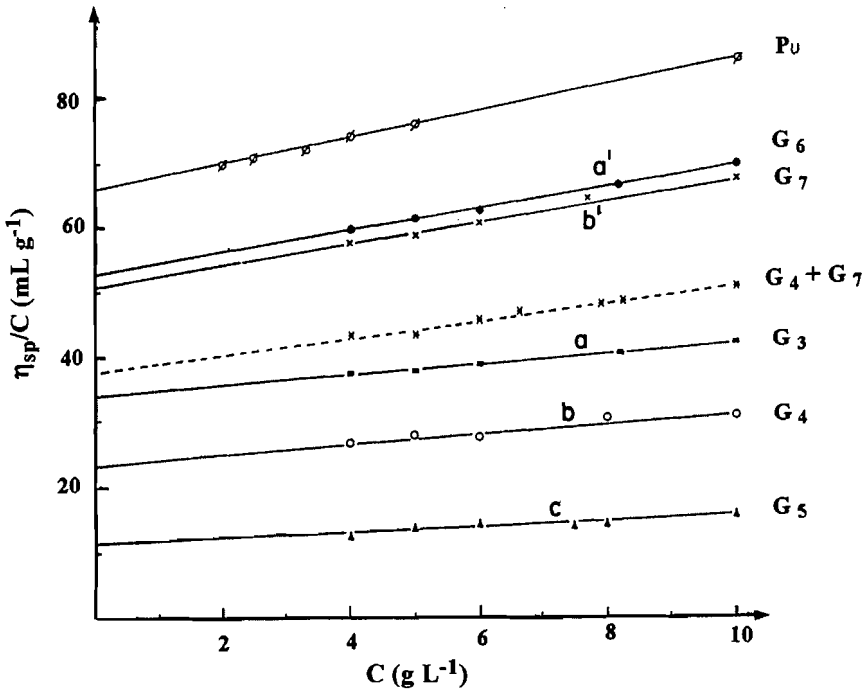

Table 3. Intrinsic viscosity and Huggins constants of modified pullulans.

Sample	% Molar content	$[\eta]_0$	k'
Pu	—	66	0.46
G3	4.07	33.5	0.75
G4	5.8	25.5	0.77
G5	7.05	12.5	0.60
G6	0.98	52.5	0.61
G7	2.19	50.5	0.66
G6 + G7	7.99	37.5	0.89
CMP	—	190	0.10
G9(pyr)	2.0	94.3	0.62
G10(ad)	3.4	87.14	0.38

As is well known, adenine and thymine derivatives in solution form a hydrogen bond association, if they are in opposition to each other; however, the amino group of the adenine or the carbonyl group of the thymine can also associate with the hydroxyl group of the sugar moiety. Consequently, if these last interactions take place in a solution of a 1:1 mixture of adenine- and thymine-substituted pullulan solutions, it is possible to have a decrease in $[\eta]$, corresponding to intramolecular association, and an increase in k', the Huggins constant. Plotting the reduced viscosity of a solution of a 1:1 mixture of samples G4 (adenine – butyric acid ester) and G7 (thymine – butyric acid ester) pullulan derivatives versus concentration gave an average $[\eta]$ value that lies between those for the viscosity of the two separate polymer solutions (Fig. 2). These results suggest that the hydrophobic associations are preponderant or stronger than the possible association by hydrogen bonds, even in a solution of polymers containing both adenine and thymine units, probably at too low a content. (Note, however, that if the substitution is more than 5–6%, the modified polysaccharides are not soluble in water.)

In Table 3 are presented the $[\eta]$ values and k' Huggins constants for the pullulan precursor and its derivatives.

Light scattering measurements performed on sample G4 (pullulan – adenine butyric acid ester, 5.8%) showed a M_W value higher than that of its pullulan precursor ($M_W \sim 3.5 \times 10^5$) and a second virial coefficient A_2 with a negative value ($A_2 \sim -3.7 \times 10^{-3}$ mL mol g^{-2}), which may be attributed to formation of self-aggregates. Later, the same measurement performed after 2 weeks on the same solution showed significant changes of M_W and A_2. This observation suggests the occurrence of an undesirable hydrolysis reaction of ester linkages (as already mentioned for other polysaccharides modified by an ester group), with formation of the parent acid, which in turn can accelerate the degradation of the polysaccharide chain.

Figure 3(*a*) presents the plots of reduced viscosity versus concentration in a dilute concentration of carboxymethyl pullulan and its two amide derivatives (Table 3). As can be seen, the aminopyrene and adenine-CMP derivatives present a similar decrease in $[\eta]$ value, which can be attributed to similar hydrophobic intramolecular interactions of the pyrene (G9) or

Can. J. Chem. Downloaded from www.nrcresearchpress.com by 46.23.64.124 on 09/08/12
For personal use only.

Fig. 3. (*a*) Reduced viscosity versus concentration (g L^{-1}) of CMP derivatives, in 0.1 N NaCl: 1, CMP-pullulan; 2, modified (a) with 1-aminopyrene: 1.92% (G_{10}), (b) with adenine: 3.1% (G_9); (*b*) reduced viscosity for G_9 and G_{10} in the semi-dilute concentration domain.

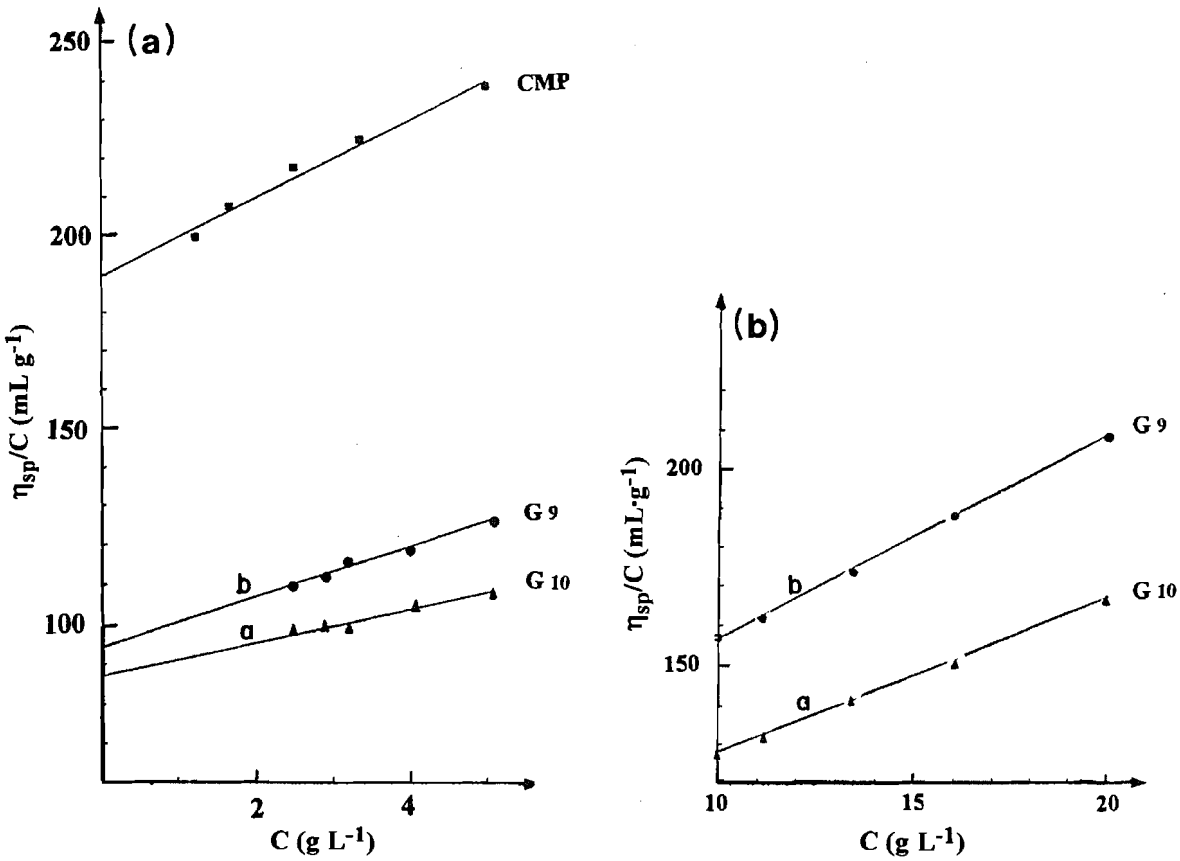

the adenine group (G10). The plots of $[\eta]/c$ versus c remain linear, even in the semi-dilute domain, probably due partly to the high flexibility of the pullulan skeleton but also to the condensed structure of the grafted molecule, both factors favouring the predominance of intramolecular associations. Indeed, for pullulan modified with a linear alkyl chain, we observed the formation of intermolecular hydrophobic associations[2] in the semi-dilute concentration range above approximatively 3.5 g L^{-1}. The great difference between the intrinsic viscosity at the same ionic strength (0.1 N NaCl) between the pullulan and its carboxymethyl derivatives (from $[\eta]_0$ = 66 to 190 mL g^{-1}) is probably the consequence of two additive factors, namely, an electrostatic effect due to the presence of unscreened carboxylic groups at the ionic strength used and a greater rigidity of the polysaccharide chain as a result of the introduction of the carboxymethyl group.

From Size Exclusion Chromatography (SEC) coupled to a multi-angle laser detector as described in ref. 19 (for the experimental procedure and equations used), there has been clear evidence that both CM-aminopyrene and -adenine (G9 and G10) are heterogeneous mixtures of two kinds of polymer populations, corresponding to the large first peak at $M_W \sim 1.3 \times 10^5$, approximately the molecular weight of the CMP precursor (exclusion volume ~29.54 mL), and to the second peak (about 10%) (exclusion volume ~36.54 mL), with a much larger molecular weight ($M_W \sim 1.4 \times 10^6$) (Fig. 4(*b*)), corresponding probably to the aggregate polysaccharide molecule, through the interaction of the bulky hydrophobic pyrene group. (π–π^* interaction). Figure 4(*a*) shows the normal profile of CMP modified by the aminopyrene detected classically (exclusion volume ~34 mL). These aggregates have a more compact conformation than the CMP precursor, which explains the inversion of the exclusion volumes in SEC as already mentioned for self-aggregated polymers like xanthane (22), or for globular proteins.

Conclusions

This paper reports some preliminary results on new hydrophobically modified pullulan derivatives. The aim of this work was to point out the influence of the nature of the hydrophobic aromatic substituent and of the ionicity of the parent precursor on the nature of the associations in the dilute concentration range. The reported data indicate that the introduction of aromatic hydrophobic substituents mainly induce *intramolecular associations* in ionic or non-ionic dilute polymer solutions. This is probably a consequence of the bulkiness of aromatic substituents such as pyrene that favours the establishment of intramolecular associations even in the semi-dilute domain of concentration. The presence of a long spacer chain would seem favourable for the formation of intermolecular interactions, as has been reported with other systems.

[2] G. Mocanu, personal communication.

Can. J. Chem. Downloaded from www.nrcresearchpress.com by 46.23.64.124 on 09/08/12
For personal use only.

Fig. 4. SEC multi-angle laser light scattering of CMP aminopyrene (~2%) in 0.1 N $LiNO_3$; (*a*) normal view from the refractive index detector; (*b*) view at 44.5° scattering angle.

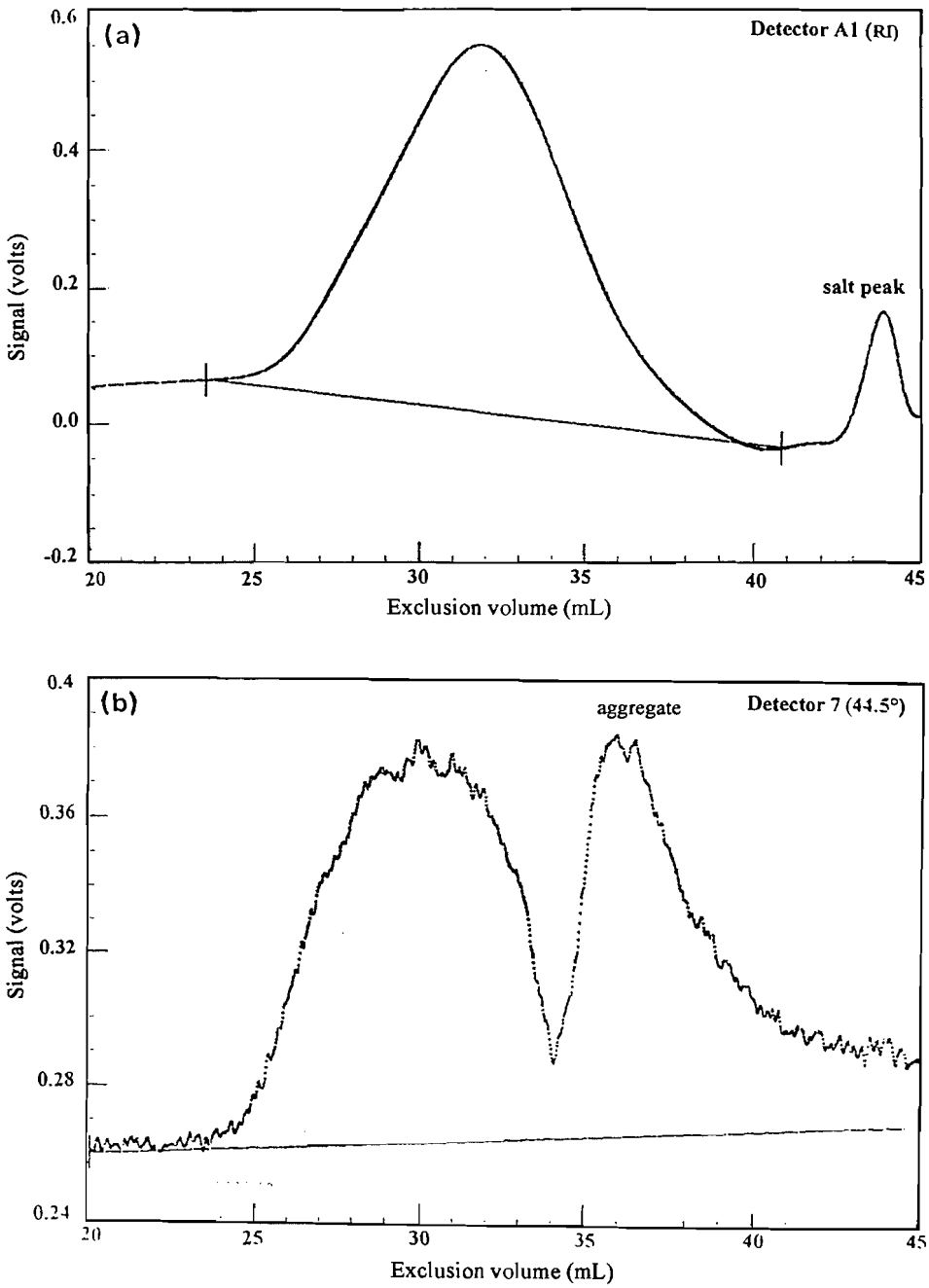

Can. J. Chem. Downloaded from www.nrcresearchpress.com by 46.23.64.124 on 09/08/12
For personal use only.

Acknowledgement

We cordially thank Dr. L. Picton for the GPC measurement on a SEC (MALLS) Wyatt on line, using ASTRA v-30 software.

References

1. F. Fujita, K. Fukami, and M. Fujimoto. Ger. Patent 2.749.744 (1978).
2. H. Hijiya, and M. Shiosaka. Jap. Kohaï 74.83.779 (1974).
3. H. Hijiya, and M. Shiosaka. Ger. Patent 2.362.985 (1974).
4. J. Onishi. Jap. Kokaï 60. 156.702 (1985).
5. A. Carpov, G. Mocanu, D. Mihai, and R. Ghiocel. Rom. Patent 85.860 (1984).
6. A. Carpov, G. Mocanu, and D. Mihai. Rom. Patent 88.034 (1984).
7. J. Duhamel, A. Yekde, Y.Z. Hu, and M.A. Winnick. Macromolecules, **4**, 7024 (1992).
8. A.S. Ezzell, C.E. Hoyle, D. Creed, and C. McCornick. Macromolecules, **25**, 1887 (1992).
9. A.S. Ezzell and C. McCornick. Macromolecules, **25**, 1881 (1992).
10. L.M. Landoll. J. Polym. Sci. Polym. Chem. Ed. **20**, 443 (1982).
11. R. Tanaka. Carbohydr. Polym. **12**, 443 (1990).

12. H.J. Dualeh and C.A. Steiner. Macromolecules, **23**, 251 (1990).
13. M. Sandberg, P. Lundahl, E. Greijer, and M. Belew. Biochim. Biophys. Acta, **924**, 185 (1987).
14. A. Carlson, T. Soto, and J. Sunamoto. Bull. Chem. Soc. Jpn. **62**, 791 (1989).
15. M. Tokada, T. Yuzurike, K. Katayame, K. Iwamoto, and J. Sunamoto. Biochem. Biophys. Acta, **802**, 237 (1984).
16. K. Akiyoshi, S. Yamaguchi, and J. Sunamoto. Chem. Lett. 1263 (1991).
17. T. Nishikawa, K. Akiyoshi, and J. Sunamoto. Macromolecules, **27**, 7654 (1994).
18. British Patent 1.419.482 (1975).
19. L. Picton, G. Mocanu, D. Mihai, A. Carpov, and G. Muller. Carbohydr. Polym. In press.
20. C.G. Overberger and Y. Morishima. J. Polym. Sci. Polym. Chem. Ed. **18**, 1247 (1980).
21. R.W. Eyler, E.D. Klug, and F. Diephuis. Anal. Chem. **119**, 24 (1947).
22. G. Muller, I. Capron, and M. Grisel. Int. J. Polym. Anal. Charact. In press.

Can. J. Chem. Downloaded from www.nrcresearchpress.com by 46.23.64.124 on 09/08/12
For personal use only.

New amphiphilic copolymers derived from hydrophobically modified vinyl saccharides

Joachim Klein, Markwart Kunz, and Lutz Guderjahn

Abstract: The synthesis and characterization of new amphiphilic copolymers derived from copolymerization of hydrophobically modified so-called vinyl saccharides with 1-vinyl-2-pyrrolidone are described. The vinyl saccharides were prepared in a two-step synthesis. In the first step hydrophobically modified saccharide derivatives were synthesized without protecting procedures by direct reductive amination of the reducing keto-disaccharide isomaltulose (Palatinose®) with *n*-dodecylamine. In the second step the resulting *N*-dodecylaminopolyols were coupled with allyl glycidyl ether to give polymerizable amphiphilic vinyl saccharides. The copolymerizations with 1-vinyl-2-pyrrolidone were performed as free radical aqueous solution polymerizations. The characterization of the copolymers was carried out by measuring the viscosity and light scattering in water as well as in trichloromethane, in addition to surface tension measurements and solubilization studies. The solution properties of the copolymers in water and trichloromethane differ remarkably. While the values for the intrinsic viscosities in both solvents are comparable, the weight-average molecular weights in water are much higher than those in trichloromethane, indicating the formation of aggregates in aqueous solution. The vinyl pyrrolidone copolymers are also very surface active, lowering the surface tension of water to as low as 30 mN/m. The combination of measurements of surface tensions and solubilization studies indicates that their hydrophobic association behaviour is formally comparable to those of low molecular weight surfactants.

Key words: vinyl saccharides, isomaltulose, hydrophobic association, amphiphilic polymers.

Résumé : On décrit la synthèse et la caractérisation de nouveaux copolymères amphiphiles dérivés d'une copolymérisation de la 1-vinyl-2-pyrrolidone avec des soit disant saccharides vinyliques modifiés d'une façon hydrophobe. Les saccharides vinyliques ont été préparés par une synthèse en deux étapes. Dans la première étape, on a synthétisé les dérivés saccharidiques modifiés d'une façon hydrophobe, sans procédures de protection, en procédant à une amination réductrice du céto-disaccharide réducteur isomaltulose (Palatinose®) avec de la *n*-dodécylamine. Dans la deuxième étape, on a procédé au couplage des *N*-dodécylpolyols ainsi obtenus avec de l'oxyde d'allyle et de glycidyle qui a conduit aux saccharides vinyliques amphiphiles. On a effectué les copolymérisations avec la 1-vinyl-2-pyrrolidone sous la forme de polymérisations radicalaires en solutions aqueuses. La caractérisation des copolymères a été effectuée par la mesure de leur viscosité et de leur diffusion de la lumière en solution dans l'eau ainsi que dans le trichlorométhane; on a aussi fait appel à leurs tensions superficielles et à des études de solubilisation. Les propriétés des copolymères en solution dans l'eau sont très différentes de celles dans le trichlorométhane. Alors que les valeurs des viscosités intrinsèques sont comparables dans les deux solvants, les poids moléculaires moyens dans l'eau sont beaucoup plus élevés que ceux dans le trichlorométhane; ceci indique qu'il y a formation d'agrégats en solution aqueuse. Les copolymères de la vinylpyrrolidone ont une grande influence sur les propriétés de surface; elles diminuent la tension superficielle de l'eau jusqu'à des valeurs aussi basses que 30 mN/m. La combinaison des mesures de tensions de surface et des études de solubilisation indique que leurs comportements d'association hydrophobe sont formellement comparables à ceux d'agents de surface de faibles poids moléculaires.

Mots clés : saccharides vinyliques, isomaltulose, association hydrophobe, polymère amphiphiles.

[Traduit par la rédaction)

Received May 10, 1995.

This paper is dedicated to Professor J.E. (Jim) Guillet in recognition of his contributions to Canadian chemistry.

J. Klein.[1] Lehrstuhl für Makromolekulare Chemie, Department of Chemistry, Technical University of Braunschweig, Pockelsstr. 14, D-38106 Braunschweig, Federal Republic of Germany.
M. Kunz and L. Guderjahn. Zentralabteilung für Forschung, Entwicklung und Services, Südzucker AG Mannheim/Ochsenfurt, Wormserstr. 11, D-67283 Obrigheim/Pfalz, Federal Republic of Germany.

[1] Author to whom correspondence may be addressed.

Can. J. Chem. Downloaded from www.nrcresearchpress.com by 46.23.64.124 on 09/08/12
For personal use only.

Scheme 1. Reductive amination of isomaltulose with *n*-dodecylamine. "Z" = mixture of three amphiphilic saccharide derivatives.

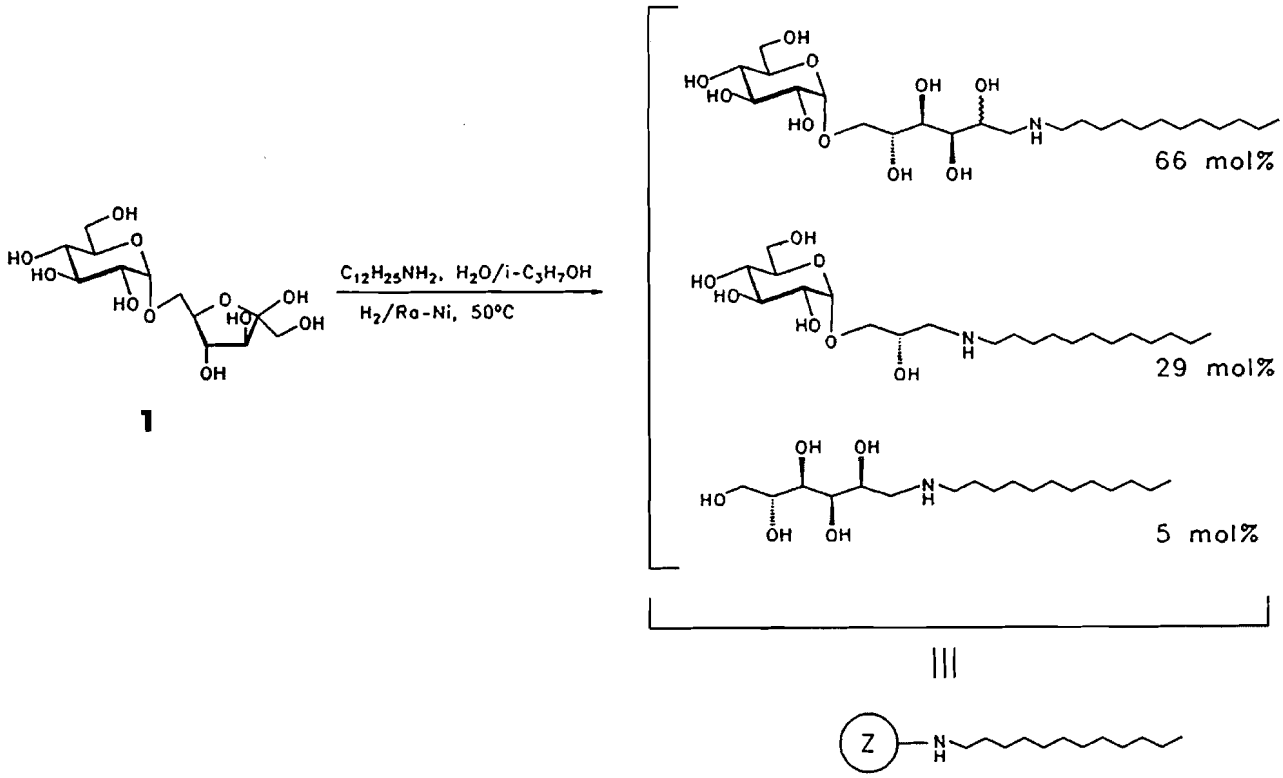

1

2

Introduction

Hydrophobically modified water-soluble polymers, so-called polymeric surfactants, are a particularly interesting class of water-soluble macromolecules. The first report on such polymers was the synthesis of hydrophobically modified poly(vinylpyridine)s (so-called "polysoaps") by Strauss et al. (1, 2).

Recently, interest in hydrophobically modified water-soluble polymers, for both fundamental research and technical application, has increased significantly. Therefore, a wide range of these polymers with various structural concepts and different synthesis approaches have been produced and investigated (3–6).

A rather interesting approach is the synthesis of carbohydrate based amphiphilic polymers, which can be produced by a three-step synthesis, starting from the reductive amination of a reducing carbohydrate, coupling the resulting amino sugar with a polymerizable compound, and finally polymerizing the vinyl saccharide (7).[2]

This paper describes the synthesis of one of these types of amphiphilic polymers, derived from copolymerization of a hydrophobically modified vinyl saccharide and 1-vinyl-2-pyrrolidone, and includes a study of the solution properties in water and trichloromethane, respectively.

Results and discussion

Synthesis of the copolymers

The preparation of vinyl saccharides requires strictly monofunctionalized carbohydrate derivatives. This can be achieved either by the laborious way via protected sugars (8) or by the much easier way, through the reductive amination of reducing carbohydrates (9).

The reductive amination is a two-step reaction; in the first step the aminating agent is added to the reducing saccharide forming "Schiff bases" or osylamines, followed by a heterogeneously catalyzed hydrogenation. Hydrazine and ammonia as aminating agents generally lead to primary aminopolyols, while with alkyl amines secondary aminopolyols are formed (7).

Meanwhile, extensive studies have been done concerning the application of different mono- and disaccharides and varying the aminating agents (10). Due to its stability and selectivity, the reducing keto-disaccharide isomaltulose (6-*O*-(α-D-glucopyranosyl)-D-fructose, Palatinose®)[3] is generally a very interesting starting compound for the synthesis of monoaminopolyols (10). Therefore, isomaltulose was selected as the carbohydrate compound and, in order to produce amphiphilic saccharide derivatives, *n*-dodecylamine was chosen as the aminating agent.[4]

To ensure the preparation of an *n*-dodecylamine-free product suitable for technical applications, without the need for laborious purification steps, amination with *n*-dodecylamine was carried out with a triple molar excess of the saccharide. Normally, for amination with hydrazine or ammonia a large excess of the aminating agent is used.[5] The excess sugar alco-

[2] Generally, saccharide derivatives bearing a polymerizable C=C double bond are called "vinyl saccharides" (see also ref. 9).

[3] Registered trademark of Südzucker AG, Mannheim/Ochsenfurt, FRG.

[4] The mixture of the three carbohydrate compounds from Scheme 1 is described as "Z" in the following schemes.

[5] M. Kunz and S. Rieger. Unpublished results.

Can. J. Chem. Downloaded from www.nrcresearchpress.com by 46.23.64.124 on 09/08/12
For personal use only.

Scheme 2. Reaction of **2** with allyl glycidyl ether.

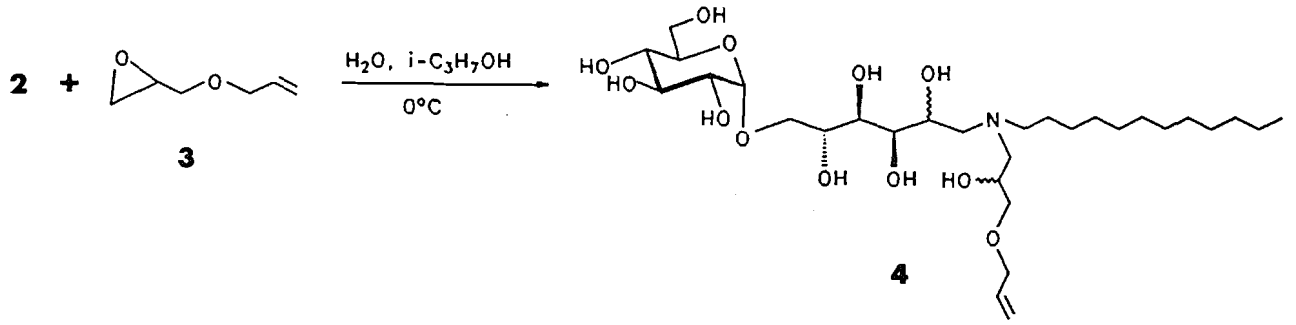

Scheme 3. Copolymerization of **4** with 1-vinyl-2-pyrrolidone.

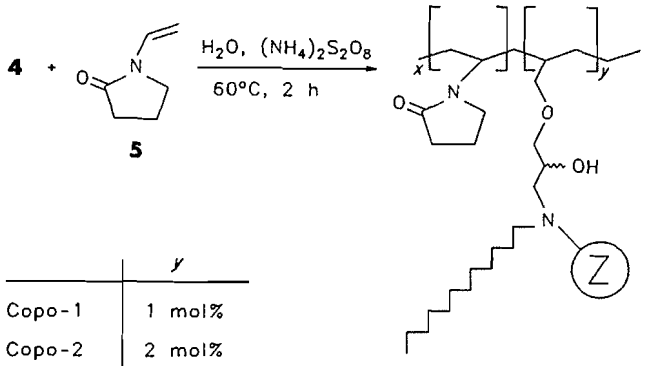

	y
Copo-1	1 mol%
Copo-2	2 mol%
Copo-3	3 mol%

hols resulting from hydrogenation of isomaltulose could be removed easily by passing the raw product through a cation exchange column loaded with NH_4^+ ions (11).

As the ^{13}C NMR and mass spectra show, the resulting product is a mixture of three *N*-dodecylaminopolyols resulting from rearrangement or cleavage of isomaltulose. The amounts of the three *N*-dodecylaminopolyols could be determined by HPLC analysis (12). Since it was not possible to separate the three amphiphilic carbohydrates in larger amounts, and the ratio of the different *N*-dodecylaminopolyols was known, the mixture of the reaction was considered to be applicable for a derivatization with allyl glycidyl ether.

Further details concerning the reaction of isomaltulose with *n*-alkyl amines in the presence of Raney nickel will be presented shortly.[6]

Studies about the surface activity of *N*-alkylaminopolyols showed these compounds to be very effective surfactants (13).

The addition of epoxides to amines to form aminocarbinols is a technically widely used method, for example, for the production of fatty amine ethoxylate surfactants (14), and it is suitable for the preparation of vinyl saccharides (11).

The reaction of *N*-dodecylaminopolyols with allyl glycidyl ether was performed with a triple excess of the epoxide component to ensure the complete consumption of the saccharide component. The copolymerizations of **4** with 1-vinyl-2-pyrrolidone were carried out with small molar amounts (1–3%) of the vinyl saccharides. The polymerization reactions were terminated after short reaction times in order to prepare copolymers with randomly distributed monomers (yields 10–20%, cf. Table 3). The structural properties of the three *N*-dodecylaminopolyol-based vinyl saccharides being similar, their polymerization behaviour was assumed to be similar too.

To obtain reliable results from the characterization of the copolymers, it was essential to quantitatively remove residual amphiphilic vinyl saccharide monomers. Therefore, the copolymers were purified by repeated precipitation from cold acetone–methanol mixture and dialysis of the resulting aqueous solutions against deionized water, for several weeks. No signals of any possible residual monomers could be detected in the ^1H NMR spectra.

Solution properties of amphiphilic copolymers

The copolymers derived from amphiphilic vinyl saccharides are, analogously to the corresponding homopolymer poly(vinylpyrrolidone) (PVP), soluble in water as well as in trichloromethane, so that the solution properties of these polymers could be investigated in both solvents.

The values of the intrinsic viscosities [η] of the copolymers in both solvents are rather similar; this is comparable to nonmodified PVP. In the observed concentration range, from 0.1 to 1% (w/w), a linear correlation between η_{sp}/c values and solution concentration could be determined.

The results from light-scattering measurements of the copolymer solutions in both solvents are significantly different. In trichloromethane the apparent weight-average molecular weights ($M_W^{app}(CHCl_3)$) range from about 1.9×10^5 (Copo-2) to 2.9×10^5 g/mol (Copo-1) (cf. Fig. 1*c*). In water the molecular weights ($M_W^{app}(H_2O)$) could be determined to be in the range of $(4.8–11.3) \times 10^6$ g/mol (cf. Figs. 1*a*, 1*b*). Analogous measurements of the corresponding PVP solutions showed only slight differences between both solvents.

The second virial coefficients A_2 are in the range from 5.1 to 17.1 bar cm^6 g^{-2} in water and from 5.4 to 11.7 bar cm^6 g^{-2} in trichloromethane. The corresponding *z*-average of radii of gyration $\langle R_G^2 \rangle_z^{1/2}$ ranges from 120 to 267 nm in water and from 46 to 81 nm in trichloromethane.

The amount of incorporated amphiphilic saccharide units influences the shape of the solvated macromolecules in aqueous solution. The Zimm plots indicate the transition from a rodlike polymer shape (cf. Fig. 1*a*: Copo-1, curvature for $c = 0$ convex downwards) to a more spherical type (cf. Fig. 1*b*: Copo-3, curvature for $c = 0$ convex upwards) with increasing amount of amphiphilic saccharides (15, 16).

Furthermore, compared to nonmodified PVP, the copolymers have very effective surfactant properties, lowering the surface tension of water to less than 30 mN/m, although only small molar amounts of amphiphilic vinyl saccharides were used. The shape of the σ vs. log *c* isotherms of the copolymers

[6] M. Kunz and M. Schüttenhelm. Manuscript in preparation.

Can. J. Chem. Downloaded from www.nrcresearchpress.com by 46.23.64.124 on 09/08/12
For personal use only.

Can. J. Chem. Downloaded from www.nrcresearchpress.com by 46.23.64.124 on 09/08/12
For personal use only.

Table 1. Results from light scattering and viscometry in water and trichloromethane at 25°C.

	Copo-1		Copo-2		Copo-3	
Parameter	H_2O	$CHCl_3$	H_2O	$CHCl_3$	H_2O	$CHCl_3$
$[\eta]$ (cm^3/g)	67	55	49	42	41	38
k_H (--)	0.50	0.33	0.60	0.40	0.64	0.27
η (1%, w/w) (mPa s)	1.75	0.63	1.45	0.57	1.33	0.54
dn/dc (cm^3/g)	0.170	0.088	0.175	0.084	0.171	0.080
M_w^{app}(g/mol $\times 10^{-5}$)	47.7	2.88	59.3	1.88	113.1	1.96

$[\eta]$: intrinsic viscosity; k_H: Huggins constant; dn/dc: refractive index increment; M_w^{app}: apparent weight-average molecular weight.

is comparable to that of low molecular weight surfactants (e.g., the monomer unit **4**). The surface tensions reach a constant minimum value at a concentration characteristic of the copolymers, which is similar to the critical micelle concentration, (cmc) of low molecular weight surfactants (17) (cf. Fig. 2*a*). To compare the surface activity of the copolymers with each other as well as with the corresponding vinyl saccharide monomer **4**, it is useful to consider the surface tensions as a function of the concentration of incorporated amphiphilic monomers in the copolymers. In this case, the minimum surface tensions as well as the cmc's of the monomer and the copolymers are nearly equal (cf. Fig. 2*b*).

To obtain additional information concerning the solution properties of the copolymers in water and the question of the existence of a cmc for these polymeric amphiphiles, the solubilization behaviour of eosine in aqueous solution was investigated (18).

Extinctions of the eosine solutions were determined at 515 and 536 nm at various copolymer concentrations. At definite copolymer concentrations, which correlate with the cmc's found by measurement of surface tensions, characteristic changes of slopes of the extinction curves could be observed, indicating the transition from a hydrophilic to a hydrophobic environment of the eosine molecules and offering strong evidence for hydrophobic association (19) (cf. Fig. 3).

Conclusions

It is well known that hydrophobically modified water-soluble polymers associate in aqueous media via their hydrophobic groups (3–6). The properties of such polymers are mainly defined by the number of incorporated hydrophobic groups per molecule.

The solution properties of the vinyl pyrrolidone copolymers of this work can be explained by assuming the formation of aggregates in water via hydrophobic association. The light-scattering studies show that the polymer coils are not associated in trichloromethane. The ratio of the molecular weights determined in water and trichloromethane is therefore a number expressing the average degree of hydrophobic association.

Extensive studies on the surface activity of polymeric surfactants are remarkably rare. Discussions about whether there is a critical concentration of such polymers in water indicating the beginning of the formation of aggregates, similar to the cmc of low molecular weight surfactants, are contradictory (3–6, 18, 20).

Our measurements of surface tensions and solubilization studies show that the aggregation process in water is a function of the number of hydrophobic groups being solvated. This behaviour is therefore comparable to low molecular weight surfactants. The concentration could analogously be described as the "critical aggregation concentration" (cac).

Light-scattering and viscometric studies of the polymer solutions were performed at concentrations higher than the cac, so that these properties of the aggregates were definitely

Fig. 1. (*a*) Zimm plot of Copo-1 in water at 25°C. (*b*) Zimm plot of Copo-3 in water at 25°C. (*c*) Zimm plot of Copo-1 in trichloromethane at 25°C.

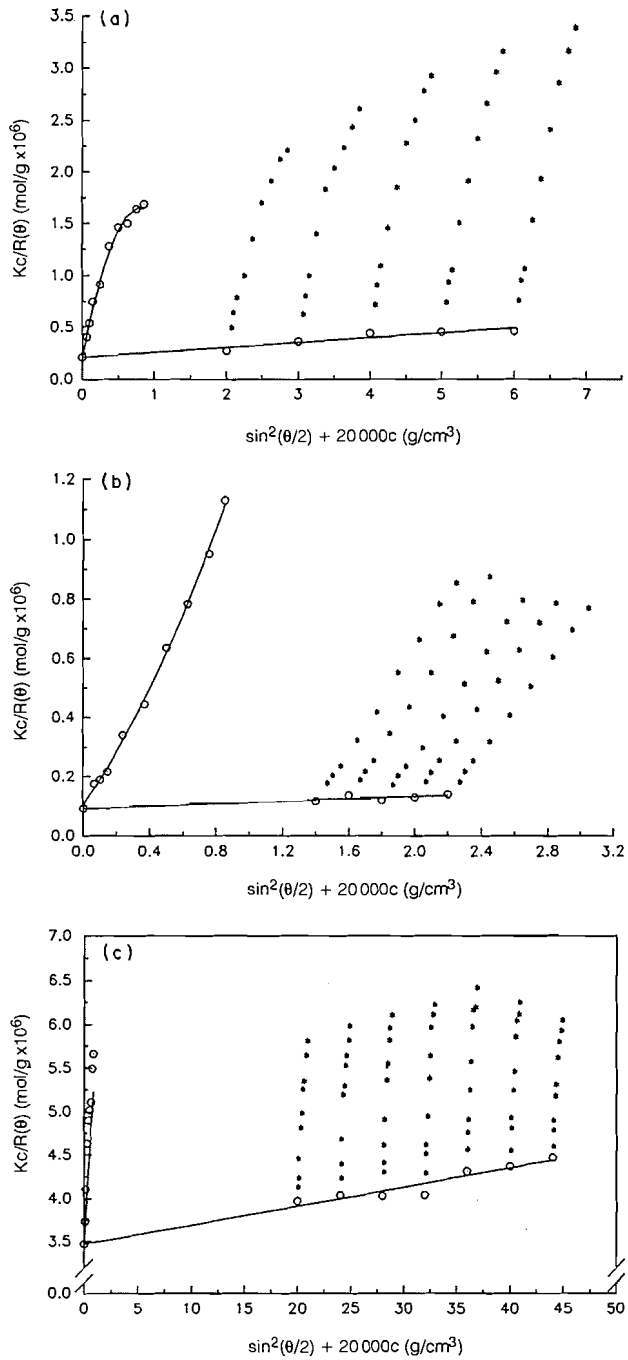

Can. J. Chem. Downloaded from www.nrcresearchpress.com by 46.23.64.124 on 09/08/12
For personal use only.

Fig. 2. Surface tensions of Copo-1 – Copo-3, **4**, and polyvinylpyrrolidone (PVP) in water at 25°C as a function of (*a*) polymer concentration; (*b*) concentration of amphiphilic saccharide units.

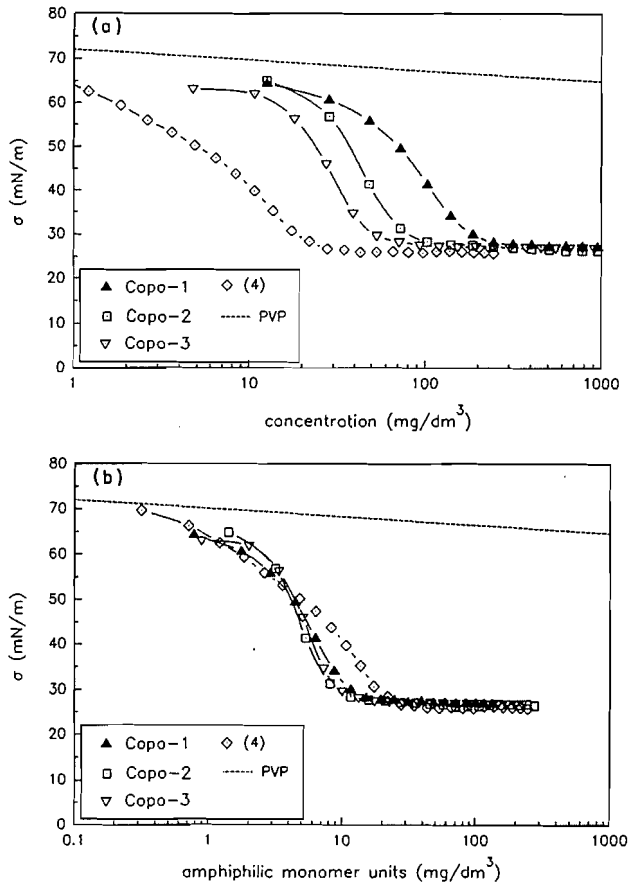

Fig. 3. Solubilization studies of Copo-1 with eosine at 25°C.

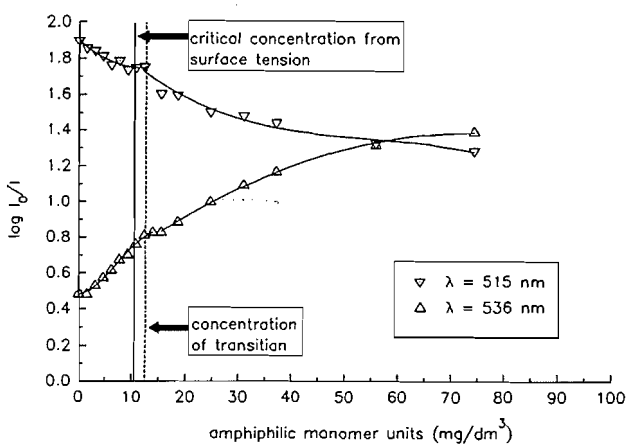

determined. The results from light-scattering measurements in water correlate with results from the determination of surface tensions and solubilization, showing the formation of large aggregates. Viscometry only shows a slight increase of the size of solvated coils, which could be explained by assuming that light scattering is a method more affected by the formation of a small number of large aggregates than viscometry (21).

Table 2. Results of measurements of surface tensions and solubilization of eosine.

Parameter	Copo-1	Copo-2	Copo-3	Surfactant monomer (**4**)[a]
"cmc" (surf.-act.[b]) (mg monomer[c]/dm³)	11	9	9	25
"cmc" (surf.-act.[b]) (mg copolymer/dm³)	180	80	50	25
σ_{min} (mN/m)	28	28	29	26
"cmc" (solub.[c]) (mg monomer[d])/dm³)	12–16	11–17	9–18	30–40
"cmc" (solub.[c]) (mg copolymer/dm³)	200–250	100–150	50–100	30–40

[a]**4** is the abbreviation for the surfactant vinyl saccharide monomer (cf. Scheme 2).
[b]Determined by measurements of surface activity.
[c]Determined by solubilization of eosine (yellow).
[d]According to average weight percent of **4** in the copolymers.

A particular structural feature of amphiphilic vinyl saccharide based systems is the sterically ambitious saccharide unit, which is closely positioned to the hydrophobic alkyl chain (cf. Scheme 3). The formation of "micellar structures" at low polymer concentrations could therefore be affected, resulting in the need for a minimum number of hydrophobic groups to form aggregates, which are determinable by the applied methods. At low concentrations the polymer molecules might preferably be adsorbed at the surface, lowering the surface tension of water significantly. The amphiphilic saccharide units must be concentrated at the surface and the vinyl pyrrolidone units connecting the hydrophobic groups must be turned away to form flexible loops. This behaviour might be responsible for the high surface activity with small molar amounts of hydrophobic groups.

As well, the average number of hydrophobic per polymer molecule in the amphiphilic copolymers N is in the range between $N=25$ (Copo-1) and $N=47$ (Copo-3), which is too small for the formation of intramolecular aggregates. For the average number of low molecular weight surfactant molecules forming micellar structures (e.g., fatty alcohol ethoxylates) N is in the range between $N=100$ (*n*-octyl) and $N=400$ (*n*-dodecyl) (22). The type of micellar structure discussed here therefore requires a larger number of macromolecules, which is confirmed by the results of light-scattering and solubilization studies.

Further statements concerning these aspects, however, will require more detailed investigations of a larger compositional and molecular weight spectrum of these amphiphilic polymers.

Experimental part

Mixture of 1-deoxy-1-*N*-dodecyl-6-*O*-(α-D-glucopyranosyl)-D-mannit resp. -sorbit, 1-deoxy-1-*N*-dodecyl-3-*O*-(α-D-glucopyranosyl)-L-glycerol, and 1-deoxy-1-*N*-dodecyl-D-sorbit (2)

Isomaltulose monohydrate (Südzucker AG, Mannheim/Ochsenfurt, Germany) (1.39 mol, 500 g) was dispersed in 1600

Table 3. Details of the preparation of amphiphilic copolymers by solution copolymerization in water.

Copolymer	(4)[a] (mol%)	VP[b] (mol/L)	(4)[a] (mol/L)	React. Init.[c] (mol/L)	React. stemp. (°C)	React. time (h)	Yield (%)
Copo-1	1	2.57	2.86×10^{-2}	1.30×10^{-3}	60	2	12
Copo-2	2	2.57	5.14×10^{-2}	1.30×10^{-3}	60	2	17
Copo-3	3	2.06	6.86×10^{-2}	1.06×10^{-3}	60	2	11

[a]**4** is the abbreviation for the surfactant vinyl saccharide monomer (cf. Scheme 2).
[b]VP: 1-vinyl-2-pyrrolidone.
[c]Initiator: $(NH_4)_2S_2O_8$.

Can. J. Chem. Downloaded from www.nrcresearchpress.com by 46.23.64.124 on 09/08/12
For personal use only.

mL of a mixture of distilled water and propanol-2 (30/70, v/v) and cooled down to 10°C. Under vigorous stirring, *n*-dodecylamine (Fluka, Neu-Ulm, FRG) (0.461 mol, 86 g), dissolved in 400 mL of a mixture of distilled water and propanol-2 (30/70, v/v) was added slowly. The mixture was stirred for 14 h and filled into a 5 L high-pressure autoclave together with aqueous Raney Nickel suspension (Merck, Darmstadt, FRG) (120 g). The mixture was hydrogenated for 24 h at 50°C, 200 bar (1 bar = 100 kPa), and 1000 rpm. The autoclave was depressurized and the mixture diluted with propanol-2 (500 mL). The catalyst was removed by filtration and the filtrate was passed through a glass column, packed with cation exchanger (IR 120, 20–50 mesh, NH_4^+ form) in order to remove hydrogenation products of **1**. After washing the column bed with 2 L of distilled water, the *N*-dodecylaminopolyols (**2**) were eluted by a mixture of 10% aqueous ammonia and propanol-2 (50/50, v/v). The eluent was removed in vacuo and the product isolated by freeze-drying. Yield: 75% (referred to *n*-dodecylamine) ^{13}C-NMR (75.5 MHz, D_2O/propanol-2-d_8 (70/30, v/v), δ: 14.49 (C-12″), 23.28 (C-11″), 26.75–32.61 (C-10″–C-2″), 48.74 (C-1″), 50.58 (C-1), 61.46 (C-6′), 69.44 (C-6), 69.73–73.95 (C-2–C-5, C-2′–C-5″), 98.99, 99.24 (C-1′). Mass spectra (FAB pos., 3-nitrobenzylalcohol), *m/e*(%): 534 (26, $(M + Na)^+$), 512 (100, $(M + H)^+$), 422 (26, $(GPG + H)^+$), 350 (40, $(M - C_6H_{10}O_5 + H)^+$), 260 (44, $(M - C_6H_{10}O_5 + H)^+$).

Mixture of 1-deoxy-1-*N*-dodecyl-1-*N*-(2-hydroxy-4-oxa-6-heptenyl)-6-*O*-(α-D-glucopyranosyl)-D-mannit resp. -sorbit, 1-deoxy-1-*N*-dodecyl-1-*N*-(2-hydroxy-4-oxa-6-heptenyl)-3-*O*-(α-D-glucopyranosyl)-L-glycerol, and 1-deoxy-1-*N*-dodecyl-1-*N*-(2-hydroxy-4-oxa-6-heptenyl)-D-sorbit (4)

2 (0.03 mol, 15 g) was dispersed in propanol-2 and the suspension cooled down to 0°C. Allyl glycidyl ether (**3**) (Fluka, Neu-Ulm, FRG) (0.09 mol, 10.3 g) was added slowly under vigorous stirring. While being stirred, the mixture was warmed up to room temperature over a period of 14 h. Excess **3** was removed in vacuo, the crude product dissolved in propanol-2, and recrystallized from acetone/diethyl ether (30/70, v/v). Yield: 88%. ^{13}C NMR (100.6 MHz, D_2O/propanol-2-d_8, (70/30, v/v)), δ: 15.72 (C-12″); 24.47 (C-11″); 27.93–33.79 (C-10″–C-2″); 57.38–59.97 (C-1, C-1″, C-7); 62.84 (C-6′); 71.16 (C-6); 69.73–75.35 (C-2–C-5, C-2–C-5′, C-8); 74.95, 74.44 (C-9, C-10), 100.34 (C-1′), 118.93 (C-12); 136.59 (C-11). Mass spectra (FAB neg., glycerol), m/e(%): 625 (37, $(M)^-$), 624 (100, $(M - H)^-$), 510 (20, $M - C_6H_{10}O_2 - H)^-$), 462 (22, $M - C_6H_{10}O_5 - H)^-$).

Synthesis of copolymers

The copolymerizations were carried out in aqueous media employing $(NH_4)_2S_2O_8$ as initiator. The monomers **4** and **5** were dissolved in doubly distilled, filtered, and degassed water and placed in a steel cyclinder under nitrogen atmosphere. Initiator was added as an aqueous solution and the polymerization procedure started by raising the temperature to 60°C. The reactions were stopped after 2 h by purging air through the mixture and pouring the solutions into a large amount of cool acetone/methanol (50/50, v/v). The precipitated polymers were dissolved in water, the precipitation repeated five times, and the polymer solutions dialyzed in special tubes (Reichelt-Chemie-Technik, Heidelberg, Germany, cutoff: 10 000 D) against distilled water for 3 weeks. Finally, the polymers were isolated by freeze-drying.

Characterization of the polymers

Viscometry

Measurements were carried out in doubly distilled water and trichloromethane, respectively, at 25°C in a Ubbelohde capillary viscometer (Schott, Mainz, Germany) and a rotational viscometer (Low Shear LS 100, Contraves, Zürich, Switzerland) at shear rates between 1×10^{-3} and 1 s^{-1}).

Light-scattering measurements

These measurements were performed in doubly distilled water and trichloromethane, respectively, at 25°C employing a wide-angle photo-gonio-diffusometer (model 42 000 "SOFICA," Le Mesnil-Saint Denis, France) with a vertically polarized incident beam of $\lambda_0 = 632.8$ nm from a He-Ne laser at 9 angles between 30° and 135°.

Before measuring, the solutions were carefully filtered through membranes (polycarbonate membranes (Nuclepore, Pleasanton, Calif., U.S.A.) for aqueous solutions and cellulose membranes (Sartorius, Göttingen, Germany) for trichloromethane solutions, respectively). The concentration ranges chosen were fitted to the maximum of the signal intensity.

The refractive index measurements were carried out with a Brice–Phoenix differential refractometer (BP-2000 V, Virtis Co., New York, U.S.A.) at $\lambda = 632.8$ nm and 25°C.

Surface tensions

The measurements of surface tension were carried out at 25°C with an automatic processor–tensiometer (K 12C, Krüss GmbH, Hamburg, Germany) using a platinum plate according to *Wilhelmy* (23). The measurements were stopped, when the

standard deviation(s) of 10 values of surface tension, s_{max}, were 0.01 or lower. The interval between two measurements was 10 min.

Solubilization

The solubilization properties of the amphiphilic copolymers in water were determined by treating aqueous solutions of eosin (yellow) (1×10^{-5} mol/L) with various concentrations of the copolymers (**5**) and measuring the UV absorbance of the solutions at 25°C and $\lambda = 515$ nm and 536 nm, respectively, with a UV photometer (Uvikon 930, Kontron Instruments, Eching, Germany).

References

1. U.P. Strauss and E.G. Jackson. J. Polym. Sci. **6**, 649 (1951).
2. U.P. Strauss and N.L. Gershfield. J. Phys. Chem **58**, 747 (1954).
3. P. Anton, P. Köberle, and A. Laschewsky. Makromol. Chem. **194**, 1 (1994).
4. T.K. Wang, I. Iliopoulos, and R. Audebert. *In* Water-soluble polymers. *Edited by* S.W. Shalaby, C.L. McCormick, and G.B. Butler. ACS Symp. Ser. **467**, Am. Chem. Soc., Washington, D.C. 1991.
5. L.M. Landoll. J. Polym. Sci. Poly. Chem. Ed. **20**, 443 (1982).
6. A. Rauscher, H. Hoffmann, H. Rehage, and J. Fock. Tenside Surfactants, Deterg. **29**, 2 (1992).
7. J. Klein, M. Kunz, and J. Kowalczyk. Makromol. Chem. **191**, 517 (1990).
8. J. Klein and K. Blumenberg. Makromol. Chem. **189**, 805 (1988).
9. J. Klein and D. Herzog. Makromol. Chem. **188**, 1217 (1987).
10. M. Kunz. *In* Carbohydrates as organic raw materials. *Edited by* F.W. Lichtenthaler. VCH, Weinheim. 1991.
11. L. Guderjahn. Doctoral dissertation, Technical University of Braunschweig (1995).
12. M. Schüttenhelm. Doctoral dissertation, Technical University of Braunschweig (1995).
13. L. Guderjahn, M. Kunz, and M. Schüttenhelm. Tenside Surfactants, Deterg. **31**, 146 (1994).
14. K. Kosswig. *In* Ullmann's Encyclopedia of Industrial Chemistry. Vol. A 25. *Edited by* B. Elvers, S. Hawkins, and W. Russey. VCH, Weinheim. 1994.
15. H. Benoit and P. Doty. J. Phys. Chem. **57**, 958 (1953).
16. W. Burchard. Physikalisch-Chemische Eigenschaften von Polysacchariden. *In* Polysaccharide. *Edited by* G. Franz. Springer, Berlin. 1991.
17. D. Myers. Surfactant science and technology. 2nd ed. Verlag Chemie, Weinheim. 1992. 188ff.
18. M.L. Corrins, H.B. Klevens, and W.D. Harkins. J. Chem. Phys. **14**, 216 (1946); **14**, 480 (1946).
19. H. Finkelmann and E. Jahns. *In* Polymer association structures — microemulsions and liquid crystals. *Edited by* M. A. El-Nokaly. ACS Symp. Ser., **384**, Am. Chem. Soc., Washington D.C. 1989.
20. Yu. V. Tanchuk and G.S. Pop. Colloid J. USSR, **40**, 1024 (1978).
21. W. M. Kulicke (Hrsg.). Fließverhalten von Stoffen und Stoffgemischen. Hüthig & Wepf-Verlag, Basel. 1986. 188ff.
22. Y. Morishima, T. Kobayashi, and S. Nozakura. Polym. J. (Tokyo), **21**, 267 (1989).
23. L. Wilhelmy. Ann. Phys. **119**, 177 (1863).

Can. J. Chem. Downloaded from www.nrcresearchpress.com by 46.23.64.124 on 09/08/12
For personal use only.

Spectral properties of ionic derivatives of pyrene and their aggregates with anionic surfactant and polyelectrolyte

Pavol Hrdlovič, Lubica Horinová, and Štefan Chmela

Abstract: A multifunctional probe based on pyrene, the chloride of the 2,2,6,6-tetramethyl-4-hydroxypiperidinium ester of 4-(1-pyrene)butyric acid, at a concentration of 5×10^{-5} mol dm^{-3} exhibits excimer-like green emission with the maximum at 480 nm in the presence of sodium dodecylsulfate below its critical micelle concentration. A similar effect has been observed for this probe in the presence of the sodium salt of polyacrylic acid in the same concentration range. 1-Pyrenemethylammonium chloride exhibits a broad green excimer-like emission for sodium dodecylsulfate but not for the sodium salt of polyacrylic acid. The quenching constants of the monomeric and excimer-like emissions were determined for acrylamide, 1-oxo-2,2,6,6-tetramethyl-4-hydroxypiperidine, potassium iodide, and copper(II) sulfate, representing neutral, ionic, and free-radical types of quenchers. The rate constants of quenching for N-oxyl radicals indicate that the monomeric emission from both water-soluble probes is diffusion controlled. For other types of quenchers the rate constant of bimolecular quenching is lower. The quenching of the excimer-like emission of an aggregate of the chloride of the 2,2,6,6-tetramethyl-4-hydroxypiperidinium ester of 4-(1-pyrene)butyric acid is less efficient than in the case of 1-pyrenemethylammonium chloride, which indicates a more packed structure of the former aggregate.

Key words: pyrene, ionic derivative, emission, micelle, aggregation, quenching.

Résumé : La sonde multifonctionnelle basée sur le pyrène, le chlorure de l'ester 2,2,6,6-tétraméthyl-4-hydroxypipéridinium de l'acide 4-(1-pyrène)butyrique, à des concentrations de 5×10^{-5} mol dm^{-3}, en présence de dodécylsulfate de sodium à une concentration inférieure à sa concentration micellaire critique, présente une émission verte, semblable à celle d'un excimère, avec un maximum à 480 nm. On a observé un effet semblable avec cette sonde, en présence du sel de sodium de l'acide polyacrylique, à des concentrations semblables. Avec le dodécylsulfate de sodium, le chlorure de 1-pyrèneméthylammonium présente une émission verte large, semblable à celle d'un excimère; il ne la présente pas avec le sel de sodium de l'acide polyacrylique. On a déterminé les constantes de désactivation des émissions de type monomères ou excimères pour l'acrylamide, la 1-oxo-2,2,6,6-tétraméthyl-4-hydroxypipéride, l'iodure de potassium et le sulfate de cuivre(II) qui représentent des désactiveurs de type ionique, neutre et radicalaires. Les constantes de vitesses pour la désactivation des radicaux N-oxyles indiquent que l'émission monomérique provenant des deux sondes solubles dans l'eau sont contrôlées par la diffusion. Pour d'autres types de désactiveurs, la constante de vitesse de la désactivation est plus faible. La désactivation de l'émission semblable à celle d'un excimère d'un agrégat du chlorure de l'ester 2,2,6,6-tétraméthyl-4-hydroxypipéridinium de l'acide 4-(1-pyrène)butyrique est moins efficace que dans le cas du chlorure de 1-pyrèneméthylammonium; ceci indique que la structure du premier agrégat est plus compacte.

Mots clés : pyrène, dérivés ioniques, émission, micelle, agrégation, désactivation.

[Traduit par la rédaction]

Introduction

Fluorescence of hydrophobic, hydrophilic, and amphiphilic probes is widely used for characterization of either a homogeneous or heterogeneous surrounding (1–4). It is advantageous that these probes contain the pyrene moiety as the reporting chromophore (5).

Recently, it was observed that some ionic pyrene derivatives aggregate in the presence of polyelectrolytes and ionic surfactants in concentrations below the critical micelle concentration (cmc) (6–11). The formation of aggregates was observed for sodium salts of 1-pyrenesulfonic and 4-(1-pyrene)butyric acids with cetyltrimethylammonium chloride, 1-pyrenebutyltrimethylammonium chloride with the sodium salt of dodecylsulfate, and certain polyelectrolytes. Absorption, emission, lifetime measurements, and quenching indicate that these aggregates are ground-state complexes (6–11) arising from the ionic and hydrophobic interactions of the above molecules.

In this paper we describe the spectral properties of multifunctional probes derived from pyrene. Besides pyrene as a

Received May 5, 1995.

This paper is dedicated to Professor J.E. (Jim) Guillet in recognition of his contributions to Canadian chemistry.

P. Hrdlovič,[1] L. Horinová, and Š. Chmela. Institute of Polymers, Slovak Academy of Sciences, 842 36 Bratislava, Dúbravská cesta 9, Slovak Republic.

[1] Author to whom correspondence may be addressed. Telephone: 0042 7 373448. Fax: 0042 7 375923. E-mail: upolhrdl@savba.savba.sk

Can. J. Chem. Downloaded from www.nrcresearchpress.com by 46.23.64.124 on 09/08/12
For personal use only.

Can. J. Chem. Downloaded from www.nrcresearchpress.com by 46.23.64.124 on 09/08/12
For personal use only.

Chart 1. Structures of the fluorescence probes.

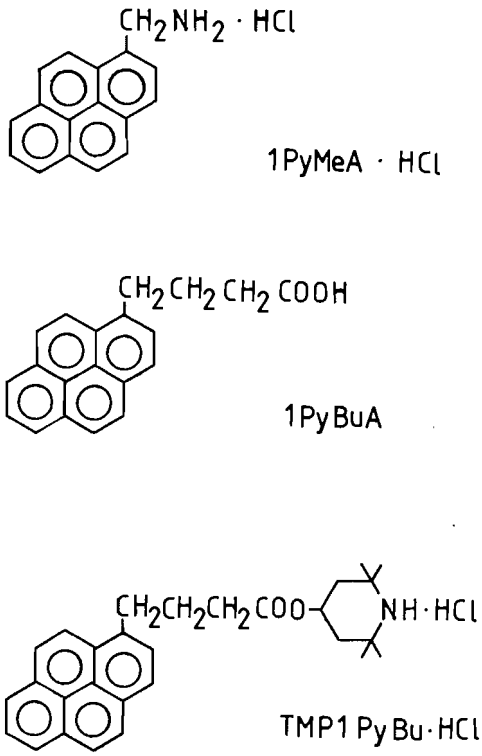

chromophore, the probes contain an additional functionality, a sterically hindered amine, which may enter neutralization and oxidation reactions.

The chloride of this probe, at higher concentration in ethanol, exhibits bathochromically shifted emission. In water solution, it exhibits even more bathochromically shifted emission, which appears at low concentration of the probe and in the presence of ionic surfactant or polyelectrolyte.

This paper is aimed at the more detailed characterization of this probe. A comparison of its behaviour with less sterically hindered ammonium chlorides was also made.

Experimental

The structures of the fluorescence probes used in this paper are shown in Chart 1.

The 2,2,6,6-tetramethyl-4-hydroxypiperidinium ester of 4-(1-pyrene)butyric acid (TMP1Py Bu) was prepared by reesterification of the methyl ester of 4-(1-pyrene)butyric acid (mp 43–45°C) with 2,2,6,6-tetramethyl-4-hydroxypiperidine. The reesterification catalyst tetrabutylorthotitanate was added to the stirred solution of reagents after clearing, and the solution was heated under reflux. Viscous liquid was isolated as the product. Attempts to crystallize it from ethanol, *n*-heptane, and diethyl ether were unsuccessful. The absorption spectrum of the product was identical with that of 4-(1-pyrene)butyric acid in ethanol: λ_{max} (ε): 243 nm (4.76), 276 nm (4.60), 342 nm (4.52). Its fluorescence spectrum in ethanol was identical with that of the sodium salt of the parent acid in water: λ_{max}: 377, 398, and 418 nm. ^{1}H NMR, $CDCl_3$, δ: 1.15–1.30 (2H, multiplet, CH_2, 3 + 5 axial H of piperidine ring), 1.15 (6H, singlet, CH_3, 2 + 6 axial H), 1.24 (6H, singlet, CH_3, 2 + 6 equatorial H), 1.87–2.06 (2H, multiplet, CH_2, 3 + 5 equatorial H of piperidine ring), 2.19 (2H, quintet, CH_2, middle group in propylene chain), 2.41 (2H, triplet, CH_2, at pyrene ring), 2.80 (1H, broad singlet, >NH), 3.35 (2H, triplet, CH_2CO-O), 5.15 (1H, multiplet, >CH of piperidine ring), 7.6–8.3 (9H, multiplet, pyrene).

The 2,2,6,6-tetramethyl-4-hydroxypiperidinium ester of 4-(1-pyrene)butyric acid was dissolved in diethyl ether and precipitated with methanol saturated by HCl. The white powder of the chloride of the ester (TMP1PyBu·HCl) was filtered, washed, and dried. It exhibits a rather broad range of mp, 220–230°C. The melting is accompanied by decomposition. The absorption and emission spectra of TMP1PyBu·HCl were the same as those of the parent amine.

4-(1-Pyrene)butyric acid (1PyBuA) was a commercial product (Aldrich-Chemie Steinheim, F.R.G.). For the synthesis of TMP1PyBu·HCl, 4-(1-pyrene)butyric acid was prepared by addition of succinic acid anhydride to pyrene (12) followed by the reduction of 3–(1–pyrenoyl)propanoic acid (13).

1-Pyrenemethylammonium chloride (1PyMeA·HCl) was a commercial product (Aldrich-Chemie, Steinheim, F.R.G.).

1-Oxo-2,2,6,6-tetramethyl-4-hydroxypiperidine (TMPNO) was prepared by standard oxidation of the parent amine (Chemko Strážske, n.e., Slovakia) with *m*-chloroperbenzoic acid.

Sodium dodecylsulfate (SDS), product of Merck (Darmstadt, F.R.G), was used without any further purification. The sodium salt of poly(acrylic acid) (PAANa) DEGAPAS 4104W was the product of Degussa AG (Hanau, F.R.G.).

All other chemicals and solvents were commercial products of Lachema Ltd., Brno, Czech Republic.

Absorption spectra were recorded on SPECORD UV–VIS and M-40 (C. Zeiss, Jena, F.R.G.) spectrometers. Emission spectra were taken on a Perkin–Elmer MPF-4 spectrometer (Perkin–Elmer, Norfolk, Conn., U.S.A.), which was connected through the interface and A/D converter to a microcomputer (14) for data collection, processing, and plotting on an XY 4110 plotter (Laboratorní přístroje, Prague, Czech Republic). The fluorescence lifetime measurements were performed on a LIF 200 (Laser Technik Berlin GmbH., Berlin, F.R.G.), which operates as a stroboscope. The output signal was digitized and transferred to the microcomputer (15). In most cases the decay curves were evaluated by a simple phase-plane method assuming monoexponential decay (16). If the agreement between experimental and calculated curves was not satisfactory, i.e., the standard deviation $G^{1/2} = ((I_{exp} - I_{cal})^2)^{1/2}$ was larger than 5%, the modified method of nonlinear regression by Marquardt (17) was used. When the fluorescence lifetime was substantially longer than 0.5 ns, which corresponds to the half-width of the nitrogen laser pulse, the simple method without deconvolution for fitting of the decay curve to the mono- or biexponential curve was applied (18).

^{1}H NMR spectra were measured on a 300 MHz AM-300 instrument (Bruker, F.R.G.).

Results and discussion

The multifunctional probe combines in one molecule the luminescence properties of the pyrene chromophore with the properties of a sterically hindered amine, which exhibits an acid–base or oxidation–reduction functionality. Such a probe, in which hydrophobic and hydrophilic parts are combined, is also soluble in a larger range of solvents. As the maximum solubility of the TMP1PyBu·HCl probe in water is 0.001 mol

Can. J. Chem. Downloaded from www.nrcresearchpress.com by 46.23.64.124 on 09/08/12
For personal use only.

Fig. 1. Emission spectrum of TMP1PyBu·HCl in ethanol at the concentration (1) 4×10^{-5} mol dm^{-3}; (2) 4×10^{-4} mol dm^{-3}; (3) 4×10^{-3} mol dm^{-3}.

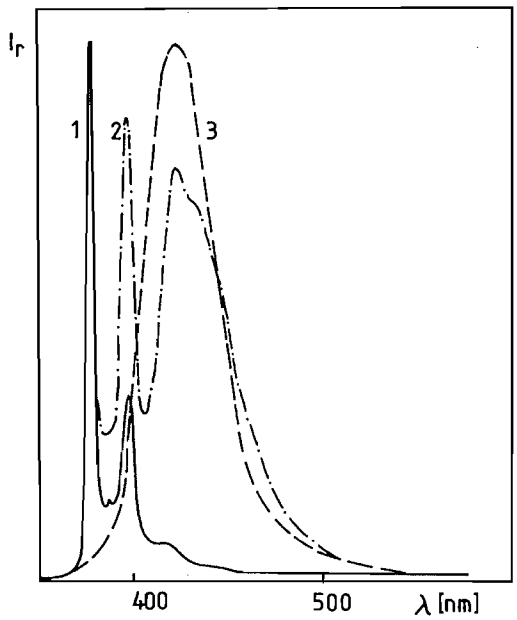

Fig. 2. Emission spectrum of potassium salt of 1PyBuA at the concentration (1) 10^{-4} mol dm^{-3}; (2) 10^{-3} mol dm^{-3}; (3) 10^{-2} mol dm^{-3}.

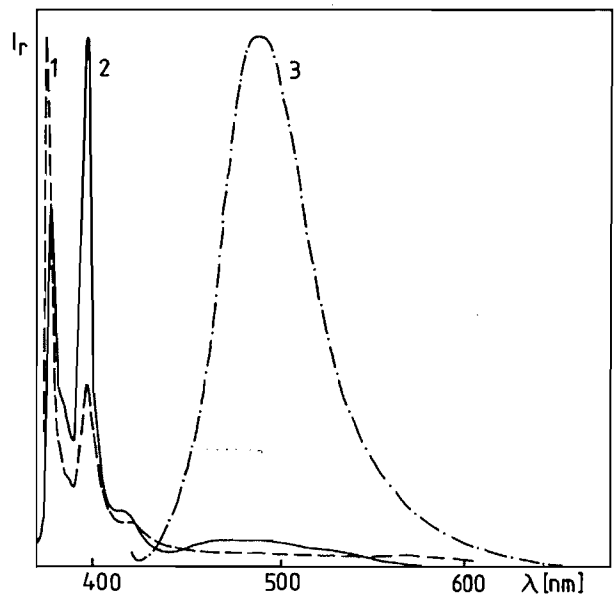

dm^{-3}, the concentration dependence of the fluorescence spectra was investigated in ethanol, which is a protic and polar solvent having properties similar to water.

The emission spectra of unsubstituted 1PyBuA, 1PyMeA·HCl, and TMP1PyBu·HCl are bathochromically shifted when the concentration increases from 10^{-5} up to 4×10^{-3} mol dm^{-3} (Fig. 1). The vibrationally resolved monomer emission with a narrow maximum at 377 nm is transformed gradually to a broad excimer emission, which was observed at 440 nm for TMP1PyBu·HCl and at 480 nm for 1PyMeA·HCl. Formation of excimers appears to be a diffusion-controlled process occurring at concentrations above 10^{-4} mol dm^{-3}. No excimer formation due to increased concentration could be observed under the limited solubility of the above chlorides in water.

Fig. 3. Dependence of relative quantum yield of excimer emission on the concentration of 1PyBuA in ethanol (○), of its potassium salt (Δ), and of TMP1PyBu·HCl in ethanol (x).

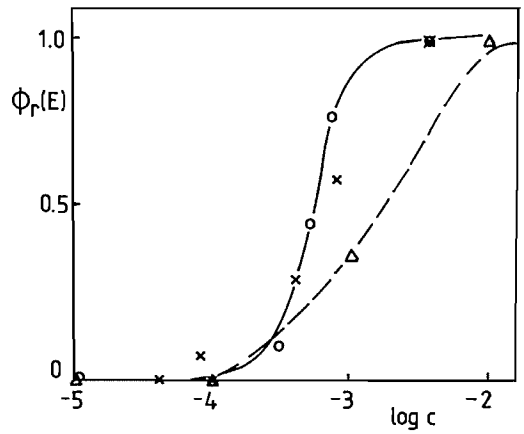

The potassium salt of 4-(1-pyrene)butyric acid, which is sufficiently soluble in water, forms the excimer at higher concentrations (Fig. 2). The excimer is characterized by a broad peak with a maximum at 480 nm. This maximum is bathochromically shifted by about 20 nm in comparison with the broad emission of TMP1PyBu·HCl in ethanol. On the other hand, the shift of monomer fluorescence in comparison with the excimer-like emission is more than 110 nm (3205 cm^{-1}). The dependence of the ratio of monomer to excimer-like emission is characterized by a sigmoidal course (Fig. 3). Anions of 4-(1-pyrene)butyric acid in water give less steep plots of the ratio of monomer to excimer-like emission than the chlorides in ethanol. Thus it appears that the ionic repulsion of chlorides in ethanol is weaker than the repulsion of anions of 4-(1-pyrene)butyric acid.

It has recently been observed that the aggregation of some ionic derivatives of pyrene at a low concentration (10^{-5}–10^{-4} mol dm^{-3}) occurs in the presence of ionic surfactants below, or approximately at, the critical micelle concentration. Under these conditions, the dynamic formation of excimers is excluded. The aggregation manifests itself by a red-shifted excimer-like emission at 480 nm. This phenomenon had not previously been observed for chlorides of amines. The positive charge on the TMP1PyBu·HCl molecule is more sterically shielded than in other cationic pyrene probes (6, 8) and on 1PyMeA·HCl it is less shielded. The interaction of the above-mentioned probes with SDS in the concentration range 10^{-5}–10^{-2} mol dm^{-3} was therefore investigated.

As seen from Fig. 4, TMP1PyBu·HCl at the concentration 5×10^{-5} mol dm^{-3} in water solution exhibits monomer fluorescence with a well-resolved vibrational structure dominated by a narrow band at 377 nm. This emission is identical with that of the potassium salt of 1PyBuA. The fluorescence lifetime is 117 ns and its decay corresponds excellently to a monoexponential decay. Addition of anionic surfactant SDS at a concentration above 10^{-4} mol dm^{-3} distinctly changes the spectrum. In the concentration range from 10^{-4} to 10^{-2} mol dm^{-3} a broad

Can. J. Chem. Downloaded from www.nrcresearchpress.com by 46.23.64.124 on 09/08/12
For personal use only.

Fig. 4. Emission spectrum of TMP1PyBu·HCl (1) at the concentration 5×10^{-5} mol dm^{-3}; (2) in the presence of SDS (5×10^{-3} mol dm^{-3}).

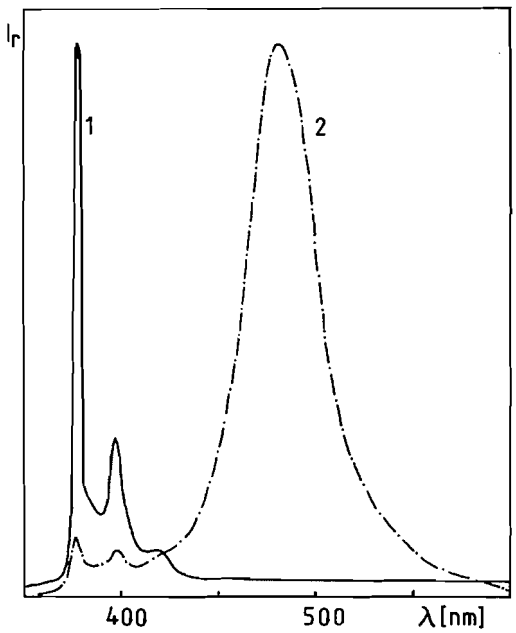

Fig. 5. Emission spectrum of TMP1PyBu·HCl (5×10^{-5} mol dm^{-3}) in the presence of SDS (1) 5×10^{-3} mol dm^{-3}; (2) 9×10^{-2} mol dm^{-3}.

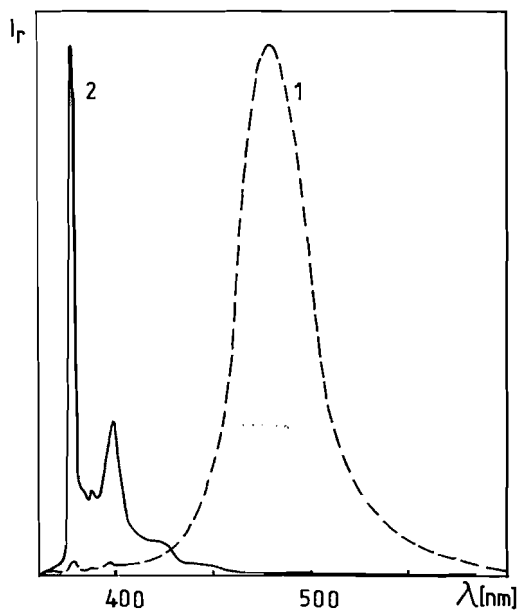

emission without any vibrational structure was observed at 480 nm. Its lifetime is 44 ns. It is shorter than the lifetime of monomer emission. The decay curve of this excimer-like emission does not fit monoexponential decay as well as does the decay curve of monomer emission. The largest deviation from monoexponential decay was observed at the beginning of the process. The excimer-like emission is reduced and monomer emission reappears (Fig. 5) above the cmc (8×10^{-3} mol dm^{-3}). The intensity of monomer fluorescence is slightly lower and its lifetime is slightly shorter.

Fig. 6. Emission spectrum of 1PyMeA·HCl at the concentration 5×10^{-5}mol dm^{-3} at (1) in the presence of 10^{-2} mol dm^{-3} SDS and (2) 5×10^{-3} mol dm^{-3}.

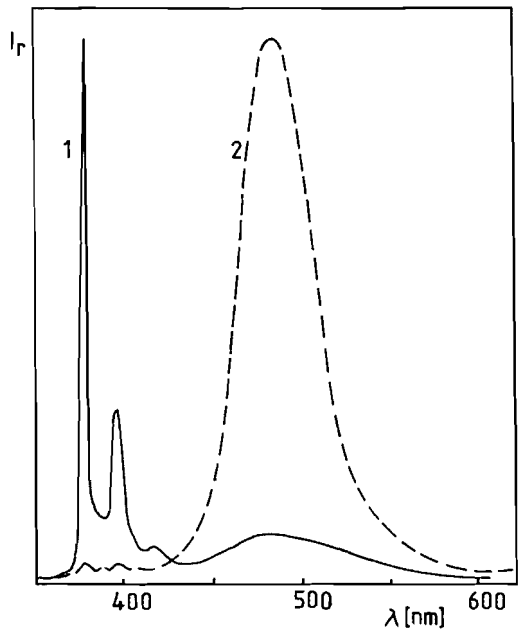

Fig. 7. Absorption spectrum of TMP1PyBu·HCl (1.25×10^{-4} mol dm^{-3}, cuvette thickness 0.1 cm) (1) in water and (2) in the presence of SDS (5×10^{-3} mol dm^{-3}).

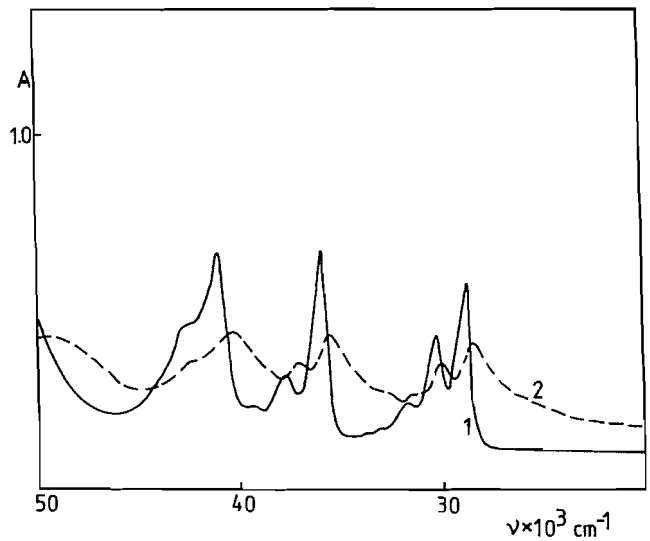

The same effect caused by addition of surfactant was observed for 1PyMeA·HCl. The excimer-like emission (Fig. 6) was observed in a narrower concentration range. The lifetime of monomer fluorescence at a concentration of 5×10^{-5} mol dm^{-3} is slightly longer than in the case of TMP1PyBu·HCl (around 130 ns) and again fits excellently to the monoexponential decay. The lifetime of excimer-like emission is 45 ns, which is the same value as for the emission originating from the aggregate based on TMP1PyBu·HCl with SDS.

The absorption spectra of the aggregate based on TMP1PyBu·HCl with SDS are more diffuse than those with 1PyMeA·HCl. (Fig. 7).

Can. J. Chem. Downloaded from www.nrcresearchpress.com by 46.23.64.124 on 09/08/12
For personal use only.

Fig. 8. Emission spectrum of TMP1PyBu·HCl (5×10^{-5} mol dm^{-3}) in water in the presence of PAANa (1) 10^{-3} mol dm^{-3}; (2) 5×10^{-3} mol dm^{-3}.

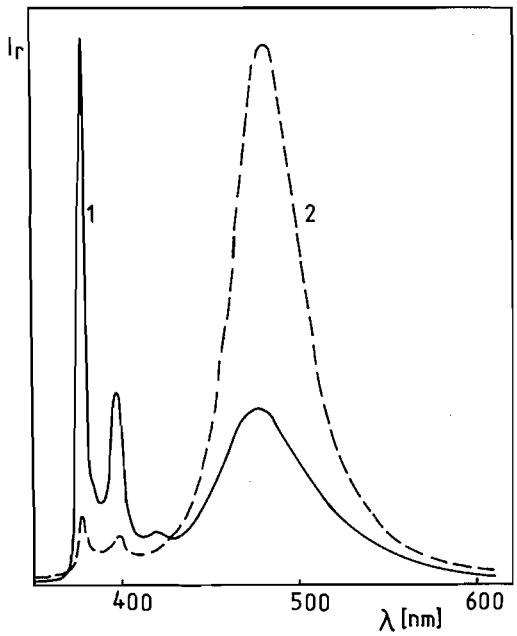

Fig. 9. Dependence of the ratio $I_E//I_M$ for TMP1PyBu·HCl on the concentration of SDS (o) and PAANa (x) and for 1PyMeA on the concentration of SDS (□).

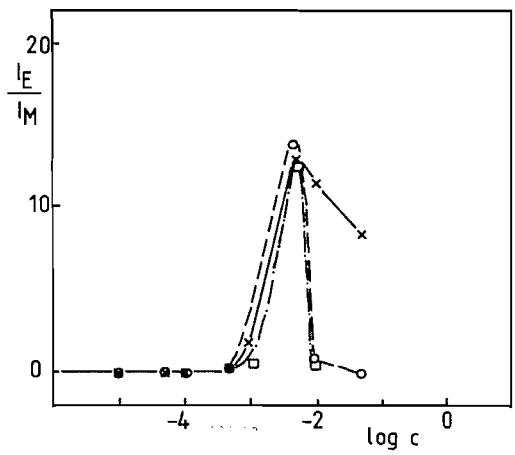

These observations indicate that the excimer-like emission stems from the stable ground-state aggregate (6, 8) formed by two molecules of TMP1PyBu·HCl with the pyrene chromophore in a sandwich-like arrangement and several molecules of surfactants. The hydrophilic anionic part of the surfactant interacts with the cationic part of TMP1PyBu·HCl or 1PyMeA·HCl and the hydrophobic parts, long alkyl chains, stabilize the aggregate. The positive charges are probably on opposite sides.

When the concentration of SDS is higher than the cmc, the aggregates begin to disintegrate. The hydrophobic interactions in the core of a pure SDS micelle repulse the probe in the water phase and the monomer emission reappears. This means that the hydrophobic interactions of the surfactants disturb the fine balance between the hydrophobic interaction of the pyrene

Fig. 10. Stern–Volmer dependence for quenching of TMP1PyBu·HCl emission by free radical 1-oxo-2,2,6,6-tetramethyl-4-hydroxypiperidine (1) at 377 nm and (2) at 480 nm in the presence of SDS (5×10^{-3} mol dm^{-3}).

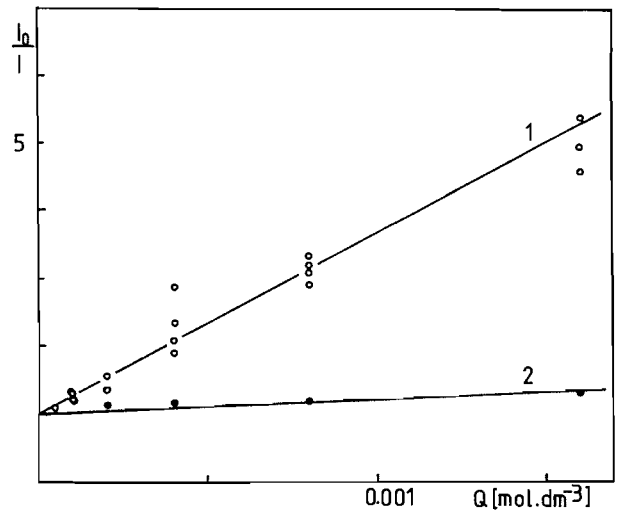

chromophores and ionic interactions between probe and surfactants.

Similar aggregation effects have been observed between ionic pyrene derivatives and polyelectrolytes (7, 9–11). We have observed, for example, an excimer-like emission for TMP1PyBu·HCl at a concentration of 5×10^{-5} mol dm^{-3} in the presence of PAANa at a concentration above 10^{-3} mol dm^{-3} of AANa structural units (Fig. 8). The mean lifetime of this emission is around 53 ns and the kinetics is better fitted by biexponential than monoexponential decay. It involves a fast decay, $\tau_1 = 13.7$ ns (50%), and a slow decay, $\tau_2 = 62.3$ ns (50%). On the other hand, 1PyMeA exhibits only monomer fluorescence in the same concentration range. The kinetics in the presence of PAANa corresponds to biexponential decay with $\tau_1 = 14.5$ ns (58%) for fast and $\tau_2 = 107.5$ ns (42%) for the slow part with a mean lifetime 92.7 ns.

As shown in Fig. 9, the concentration range for formation of aggregates based on both probes is rather narrow.

The most effective quencher for monomer and excimer emission of both probes is a free radical, 1-oxo-2,2,6,6-tetramethyl-4-hydroxypiperidine (Table 1). The solubility of this free radical in water is sufficient for this type of quenching experiment. The rate constant of quenching of the monomer fluorescence of TMP1PyBu·HCl is about 2.3×10^{10} dm^3 mol^{-1} s^{-1} assuming a lifetime of 117 ns. This indicates that quenching is controlled by diffusion. Quenching of the excimer-like emission of TMMP1PyBu·HCl by a free radical is six times less efficient (Fig. 10). Moreover, quenching of the excimer-like emission of aggregates TMP1PyBu·HCl/PAANa is even less efficient although it is slightly longer-lived.

On the other hand, monomer and excimer-like emissions of 1PyMeA·HCl are quenched in both cases by diffusion-controlled rates. An electron-donating quencher such as acrylamide is quite efficient for the monomer fluorescence of TMP1PyBu·HCl but completely inefficient for the excimer-like emission.

Ions such as I^- or the cation Cu^{2+} are quenchers of the monomer and excimer-like emission of TMP1PyBu·HCl but they are

Can. J. Chem. Downloaded from www.nrcresearchpress.com by 46.23.64.124 on 09/08/12
For personal use only.

Table 1. Quenching of monomer and excimer emission of ionic probes of pyrene.

Quencher	λ^a (nm)	K_{sv} ($dm^3\ mol^{-1}$)	$k_q \times 10^{10}$ ($dm^3\ mol^{-1}\ s^{-1}$)
TMP1PyBu·HCl			
1-Oxo-2,2,6,6-tetramethyl-	377	2700	2.30
4-hydroxypiperidine	480(SDS)	185	0.42
	480(PAANa)	60	0.14
Acrylamide	377	930	0.80
	480(SDS)	0	0
KJ	377	260	0.22
	480(SDS)	32[b]	0.07
$CuSO_4$	377	1250	1.07
	480(SDS)	93	0.21
1PyMeA·HCl			
1-Oxo-2,2,6,6-tetramethyl-	377	1670	1.28
4-hydroxypiperidine	480(SDS)	560	1.24

[a]Wavelength at which K_{sv} was determined.

[b]The value of K_{sv} was determined immediately after addition of quencher. After longer standing at laboratory temperature the white voluminous precipitate starts to fall out.

Fig. 11. Dependence of the ratio I_E/I_M for the aggregate of TMP1PyBu·HCl at the concentration of PAANa 5×10^{-3} mol dm^{-3} (⊗) and 5×10^{-2} mol dm^{-3} (○) on time, and total dependence of I_T for the same aggregate at 5×10^{-3} mol dm^{-3} (□) and 5×10^{-2} mol dm^{-3} (■) on time.

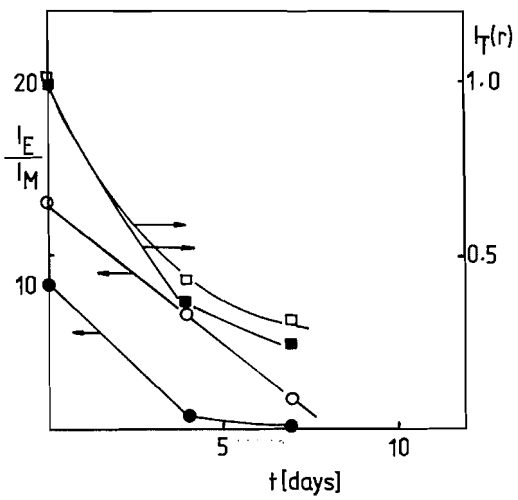

less efficient than N-oxyl radical. Both quenchers are about 10 times more efficient at quenching monomer emission than the excimer-like emission. Although quenching data in these micellar systems may involve considerable error, we should expect that quenching of monomer fluorescence with the I^- anion is more efficient than with the Cu^{2+} cation because TMP1PyBu·HCl has a positive charge. Consequently, K_{sv} for quenching with I^- should be higher than that with Cu^{2+}. In fact, quenching with copper(II) ions is even more efficient. This indicates that the charge of TMP1PyBu·HCl is well shielded from the pyrene chromophore where the fluorescence originates.

In the case of the aggregate TMP1PyBu·HCl/SDS, all types of quenchers are less efficient. This might be explained by the fact that quenchers must overcome a hydrophobic barrier formed by alkyl chains of the anionic surfactants. The least effective quencher in this intrusion seems to be neutral acrylamide. The aggregate with PAANa is even less efficiently quenched.

The aggregate 1PyMeA·HCl/SDS seems to be less packed since monomer and excimer-like emission are quenched by a diffusion-controlled rate.

The charges on aggregates of all types are compensated and therefore both ionic quenchers should be equally effective. Copper(II) is, however, more efficient.

Generally, the aggregates exhibit a low stability. As shown in Fig. 11, the ratio I_E/I_M decreases with time as well as the total emission. After some time a voluminous precipitate begins to form. Addition of I^- anion accelerates this process. Therefore, the quantitative data may include some error because all the factors influencing precipitation are not known. The clear solution after precipitation exhibits only monomer fluorescence of lower intensity.

In conclusion, one can say that the chlorides of pyrene amino derivatives exhibit the same aggregation phenomena as those with alkylammonium functional groups. It has been clearly established that the probe TMP1PyBu·HCl yields more packed aggregates than 1PyMeA·HCl.

Acknowledgement

The authors thank the Grant Agency of the Slovak Republic for support through grant No. 2/1014/94.

References

1. K. Kalyanasundaram. Photochemistry in microheterogeneous systems. Academic Press, New York. 1987.
2. A. Malliaris. Adv. Colloid Interface Sci. **27**, 153 (1987).
3. A. Malliaris. Int. Rev. Phys. Chem. **7**, 95 (1988).
4. S. Reekmans and F.C. DeSchryver. Frontiers in supramolecular organic chemistry and photochemistry. *Edited by* H.J. Schneider and H. Durr. VCH, Weinheim. 1991. p. 287.
5. F.M. Winnik. Chem. Rev. **93**, 587 (1993).

6. W.G. Herkstroeter, P.A. Martic, S.E. Harbunon, J.L.R. Williams, and S. Farid. J. Polym. Sci. Polym. Chem. Ed. **21**, 2473 (1983).
7. H.G.O. Becker, R. Schülz, M.G. Kuzmin, N.A. Sadovsky, and I.V. Soboleva. J. Prakt. Chem. **329**, 87 (1987).
8. S.G. Bertolotti, O.E. Zimerman, J.J. Cosa, and C.M. Previtali. J. Lumin. **55**, 105 (1993).
9. M. Tiera, M.G. Neumann, S.G. Bertolotti, and C.M. Previtali. J. Macromol. Sci. Chem. **A29**, 689 (1992).
10. M.Y. Tiera, M.G. Neumann, S.G. Bertolotti, and C.H. Previtoli. J. Macromol. Sci. Chem. **A31**, 439 (1994).
11. O.E. Zimerman, J.J. Cosa, and C.M. Previtali. J. Macromol. Sci. Chem. **A31**, 859 (1994).
12. E. Buchta and P. Vincke. Chem. Ber. **98**, 208 (1965).
13. J.W. Cook and C.L. Hewet. J. Chem. Soc. 398 (1933).
14. G. Moyze, J. Mlýnek, D. Jurčák, and P. Hrdlovič. Chem. Listy, **86**, 57 (1992).
15. D. Jurčák, J. Mlýnek, G. Moyze, and P. Hrdlovič. Chem. Listy, **83**, 531 (1989).
16. J.N. Demas and A.W. Adamson. J. Chem. Phys. **57**, 2463 (1971).
17. D.V. O'Connor and D. Phillips. Time correlated single photon counting. Academic Press, London. 1984. p. 231.
18. F. Hrnčírik. Chem. Prum. **31/56**, 594 (1981).

Can. J. Chem. Downloaded from www.nrcresearchpress.com by 46.23.64.124 on 09/08/12
For personal use only.

Fluorescence spectroscopy of mechanical pulps III: Effect of chlorite delignification

Jennifer A. Olmstead, Jian H. Zhu, and Derek G. Gray

Abstract: Many paper and wood samples fluoresce, but the sources of the emission are not well understood. Fluorescence excitation and emission spectra of paper sheets prepared from thermomechanical pulp (TMP) and bleached chemithermomechanical pulp (BCTMP) showed that the emission from the BCTMP was significantly higher than that from the TMP. Removing almost all of the lignin from both pulps by means of an acid chlorite treatment did not reduce the fluorescence significantly. By means of an approximate correction for changes in sheet reflectivity caused by the chlorite treatment, the fluorescence intensity was found to increase with lignin removal. Clearly, fluorescence is not simply related to lignin content.

Key words: wood pulp, lignin, cellulose, fluorescence spectra, acid chlorite delignification.

Résumé : Plusieurs échantillons de bois et de papier donnent lieu à de la fluorescence, mais les sources de ces émissions ne sont pas bien comprises. Les spectres d'excitation et d'émission de fluorescence de feuilles de papiers préparés à partir de pâte thermomécanique (TMP) et de pâte chimithermomécanique blanchie (BCTMP) ont permis de démontrer que l'émission à partir d'une pâte BCTMP est beaucoup plus importante que celle provenant d'une pâte TMP. L'enlèvement de pratiquement toute la lignine à partir des deux pâtes, par un traitement avec un chlorite acide, ne réduit pas la fluorescence d'une façon significative. En introduisant une correction approximative pour les changements de réflectivité causés par le traitement au chlorite, on a trouvé que l'intensité de la fluorescence augmente avec l'enlèvement de la lignine. Il est évident que la fluorescence n'est pas simplement reliée au contenu en lignine.

Mots clés : pâte de papier, lignine, cellulose, spectre de fluorescence, délignification par du chlorite acide.

[Traduit par la rédaction]

1. Introduction

Fluorescence emission has been observed from a wide variety of pulps (1, 2) and lignin components (3, 4). Reductive treatments with compounds such as sodium borohydride result in an apparent increase in fluorescence intensity and a blue shift in emission, whereas oxidative reactions under irradiation with ultraviolet light or treatment with sodium periodate produce decreases and red shifts in emission. Davidson et al. (5) suggested that blue shifts produced in bleached or reduced papers were due to the formation of new products that fluoresce in this shorter wavelength region. Generally, the fluorescence of pulps had been attributed solely to lignin, possibly phenylcoumaran and coniferyl alcohol structures. However, our previous results (6) suggested that cellulose contributes significantly to the fluorescence emission of mechanical pulps, and that lignin or some lignin components must act as an absorbing screen or fluorescence quencher in addition to being a source of fluorescence emission. The results from quantum yield studies of mechanical pulps and cellulose also indicate that fluorescence emission under ultraviolet excitation is decreased in the presence of lignin ($\phi_f = 0.11$ for cellulose vs. $\phi_f = 0.015$ and 0.051 for TMP and peroxide-bleached TMP, respectively) (7).

Recently, Castellan et al. (8, 9) contested these conclusions. Using fluorescent lifetime measurements and fluorescence microscopy, they found that the fluorescence from cellulose sheets and from borohydride-reduced wood sections both underwent bi-exponential decay, but with radically different lifetimes (8), and that fluorescence emission from stone groundwood was stronger than that from cellulose (9). Furthermore, stone groundwood and cellulose behave differently when radiated sequentially with UV and visible light. They also investigated a number of model compounds absorbed on cellulose, and found fluorescence emission maxima of 360 nm for coniferyl alcohol compounds and 400 nm for biphenyl structures. Based on these observed differences between pure cellulose and lignin-containing samples, they concluded that fluorescence of wood sections and papers made from mechanical pulps originated from lignin and not cellulose.

Our original conclusions were that fluorescence of mechanical pulps originates primarily with some (as yet unidentified) source associated with the cellulose, and that screening groups

Received March 13, 1995.

This paper is dedicated to Professor J.E. (Jim) Guillet in recognition of his contributions to Canadian chemistry.

J.A. Olmstead, J.H. Zhu, and D.G. Gray.[1] Paprican and Department of Chemistry, Pulp and Paper Research Centre, McGill University, 3420 University St., Montréal, QC H3A 2A7, Canada.

[1] Author to whom correspondence may be addressed. Telephone: (514) 398-6182. Fax: (514) 398-8254. E-mail: dggray@pulpaper.mcgill.ca

Can. J. Chem. Downloaded from www.nrcresearchpress.com by 46.23.64.124 on 09/08/12
For personal use only.

Fig. 1. Fluorescence spectra for TMP (solid lines) and BCTMP (dotted lines). Excitation spectra are observed at 420 and 480 nm; emission spectra are generated with an excitation wavelength of 320 nm.

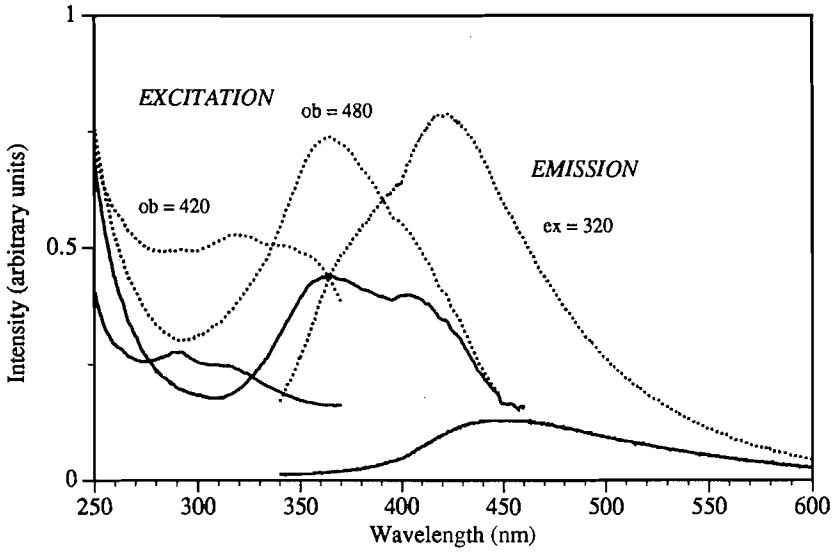

in lignin tend to absorb this emission. While this may be oversimplified and naive, it does account for many of our observations, and those reported in the literature. In fact, the results reported by Castellan et al. (9) contain elements that support our conclusions: the fact that fluorescence emission of wood sections increased upon borohydride treatment indicates that carbonyl groups present in the sections were screening or otherwise quenching emission. Based on our hypothesis, removal of lignin from a mechanical pulp might result in an increase in fluorescence emission: essentially the chromophore screen affecting the fluorescence would disappear.

To try and distinguish between the possible sources of fluorescence, we here report some further experiments, where we measure the changes in fluorescence from mechanical pulps after acid chlorite delignification. If our hypothesis is correct, removal of the lignin by this selective procedure (10) should increase the fluorescence. Conversely, if lignin is the sole source of the fluorescence, then its removal should lead to the disappearance of the fluorescence.

2. Experimental section

Mechanical pulps used in this study were a black spruce (*picea mariana*) thermomechanical pulp (TMP) and a mixed hardwood peroxide-bleached chemithermomechanical pulp (BCTMP). Pulp samples were subjected to acidic sodium chlorite delignification (11). Lignin contents of all pulps (Klason and acid-soluble lignin) were determined using standard methods (11). Less than 0.1% Klason and 1.5% acid soluble lignin was detected after the chlorite treatment.

Thin sheets (~12 g/m^2) were made from delignified TMP and BCTMP, as well as from the untreated pulps, using the method of Schmidt and Heitner (12). Fluorescence measurements were carried out for all samples using a Spex Fluorolog spectrofluorometer, as previously described (6). Three fluorescence spectra were measured for each pulp: two excitation spectra with observation at 420 and 480 nm, and an emission spectrum with excitation at 320 nm. Each fluorescence spectrum shown in this paper has been averaged over five sets of spectral data taken at different locations on a sheet. UV–visible reflectance and absorption spectra were obtained for the same sheets using a Pye–Unicam PU-3300 spectrophotometer fitted with an integrating sphere, according to Schmidt and Heitner (12).

For comparison, fluorescence spectra were also measured for a delignified pulp to which milled wood lignin had been added. Milled wood lignin was isolated from unbleached softwood using the methods of Brownell (13) and Björkman (14). A dioxane solution of this lignin (0.4%) was added dropwise to delignified unbleached TMP; fluorescence spectra of this sample were measured before and after addition of the lignin, once the dioxane had evaporated. The sheet was left in the sample holder throughout this part of the experiment, to eliminate artifacts caused by variable scattering.

3. Results and discussion

3.1. Comparison of untreated pulps

Fluorescence spectra and reflectance spectra of TMP and BCTMP are presented in Figs. 1 and 2, respectively. A number of differences are evident, which may largely be attributed to bleaching and sulphonation that destroy screening groups (6).

The reflectance of BCTMP is higher over the 300–600 nm range. Accordingly, the absorption coefficient is lower, indicating that fewer absorbing groups in general are present in the BCTMP. The absorption present at 360 nm for TMP disappears in the BCTMP absorption spectrum: Schmidt and Heitner (15) have attributed changes in this region to quinones and coniferaldehyde groups that are consumed in bleaching and sulphonation reactions.

Fluorescence emission observed from BCTMP is higher than from TMP in all spectra obtained (Fig. 1). Excitation and emission spectra both vary with the observation/excitation wavelength. Emission spectra measured with excitation at 320

Can. J. Chem. Downloaded from www.nrcresearchpress.com by 46.23.64.124 on 09/08/12
For personal use only.

Can. J. Chem. Downloaded from www.nrcresearchpress.com by 46.23.64.124 on 09/08/12
For personal use only.

nm clearly demonstrate the impact of the screening groups in lignin on observed emission. Bleaching and sulphonation reactions both act to decrease the chromophore content of pulps, affecting primarily quinones and coniferaldehyde structures (15). Removal of screening groups, particularly in the 350–500 nm range, increases the amount of observed emission in this region. The same basic principle may help to explain the increase in fluorescence emission of pulps upon borohydride reduction as reported by others (8, 9).

Removal of screening groups via bleaching and sulphonation affects excitation spectra in two ways. Decreasing the screen at the observation wavelength allows for increased apparent emission (as for emission spectra). The removal of screening groups in the excitation range also results in increased emission, since the fluorophores are able to absorb a greater proportion of the incident light. In TMP, at least two broad peaks are visible in the excitation spectrum for emission at 420 nm (wavelength associated mainly with cellulose emission): these occur at 290 and 320 nm. These maxima are both present in the corresponding excitation spectra of BCTMP. Excitation spectra measured with an observation wavelength of 480 nm contain contributions from both cellulose and lignin. Both maxima, at 360 and 410 nm, undergo an increase upon bleaching and sulphonation, due to the reasons outlined above. The relative intensity of the peaks changes as well: in TMP, the maxima are of nearly equal intensity, whereas the peak at 360 nm dominates the spectrum of CTMP.

3.2. Effect of chlorite delignification

If lignin is the sole source of fluorescence from mechanical pulps, then delignification, which removes lignin, should produce decreases in fluorescence emission. Acid chlorite treatment of the TMP and CTMP samples removes almost all of the lignin, but the fluorescence signals remain almost constant, or even increase. At the same time, the absorption of the sheets decreases, and the reflectance increases. The emission properties of both pulps (from different sources, under radically different treatments) undergo similar changes during delignification, indicating that these changes are not isolated artifacts.

Absorption and reflectance spectra of untreated and delignified samples are shown in Fig. 2. An increase in reflectance was observed for both pulps upon delignification. Differences in the absorption spectra indicate that several lignin chromophores disappear when lignin is removed. Fewer chromophores are present in the BCTMP before delignification, which would account for the smaller decrease in absorption. Differences in reflectance and absorption spectra in the 350–400 nm region may be attributed to bleaching and (or) sulphonation reactions, which remove coniferaldehyde and other lignin aromatic carbonyl groups that screen emission. The decrease in absorption in the 250–350 nm region must arise from a decrease in aromatic rings (280 nm) and residual carbonyl groups (320 nm) as the lignin is removed.

These changes in reflectance and absorption will change the intensity of light striking the fluorophores in the sheet. To compare intensities of fluorescence before and after delignification, this effect should be considered. A rigorous consideration of the interactions between scattering, absorption, and fluorescence in highly scattering media such as paper is very complex. However, the following approximate approach may be used to correct for the change in reflectance, based on a

Fig. 2. (*a*) Reflectance and (*b*) absorption spectra of pulps before (thick lines) and after delignification (thin lines). Spectra of TMP are solid lines, BCTMP are broken lines. Difference spectra are calculated as (treated) − (untreated), so positive values represent gains, negative values represent losses due to delignification.

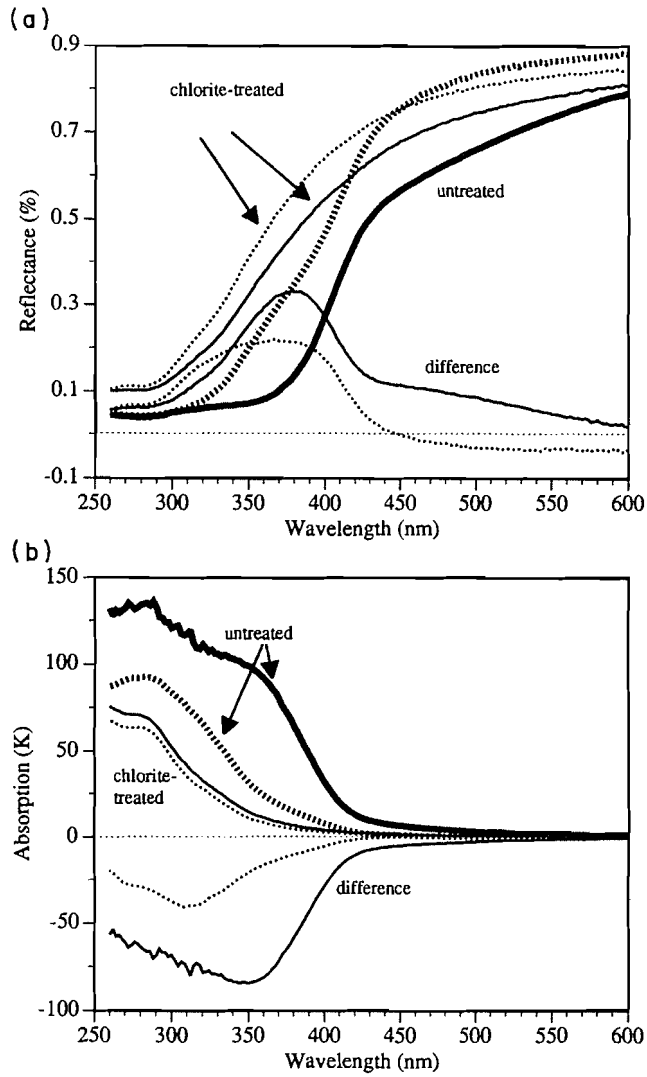

method to estimate the fluorescence quantum yields of pulp handsheets (7).

The total fluorescence of the system, I_f, is related to the amount of absorbed light I_{ab} and the quantum yield Φ_f as $I_f = \Phi_f I_{ab}$. The observed fluorescence i_f is a fraction of this,

$$[1] \quad i_f = \alpha I_f = \alpha \Phi_f I_{ab}$$

If we assign the constant terms to a single variable, $\alpha\Phi_f = c$. Then $i_f = cI_{ab}$ and $i_f = c(I_{in} - I_{sc})$ where I_{in} is incident intensity and I_{sc} is the intensity of scattered radiation. Thus,

$$[2] \quad i_f = cI_{in}\left(1 - \frac{I_{sc}}{I_{in}}\right)$$

or

Fig. 3. Fluorescence spectra for (*a*) TMP and (*b*) BCTMP sheets. Solid lines: before chlorite treatment; broken lines: after chlorite treatment to remove lignin. Spectra of chlorite-treated pulps have been corrected for differences in sheet reflectance using eq. [5]. Excitation spectra were observed at 420 and 480 nm; emission spectra were generated by excitation with 320 nm light.

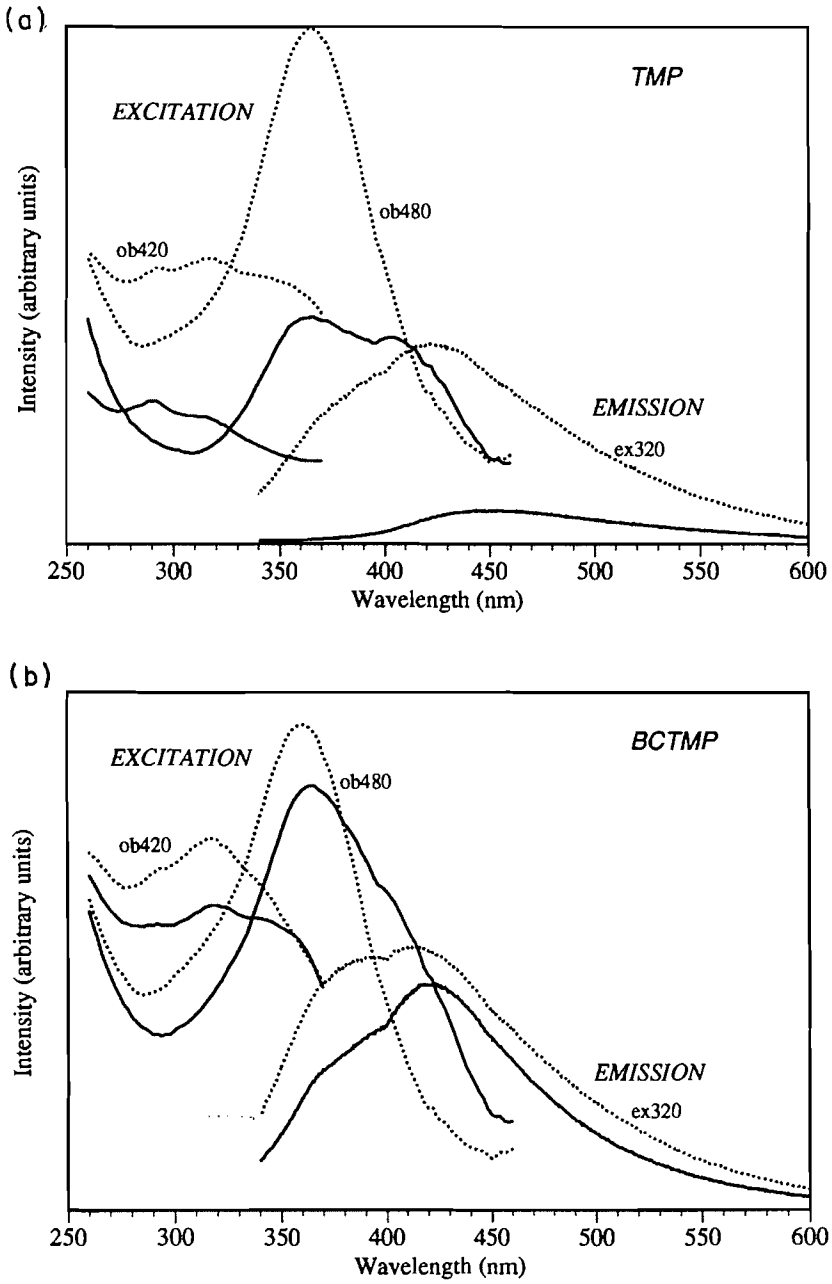

[3] $i_f = cI_{in}(1 - R_\infty)$

R_∞ is a measurable quantity. It is the proportion of incident light reflected from an optically thick sample, i.e., $R_\infty = I_{sc}I_{in}/I_{in}$. R_∞ changes with chlorite treatment. The "corrected" fluorescence, or the fluorescence that would have been observed if R_∞ had not changed with chlorite treatment, can be expressed as

[4] $i_f^{cor} = cI_{in}(1 - R_\infty^0)$

where R_∞^0 is the reflectance of the original untreated sample. The corrected spectrum is related to the measured spectrum by combining eqs. [3] and [4], and rearranging:

[5] $$i_f^{cor} = \frac{(1 - R_\infty^0)}{(1 - R_\infty)} i_f$$

Fluorescence spectra for TMP and BCTMP before and after chlorite delignification are shown in Fig. 3. Clearly, the delignification shows an increase in fluorescence. However, the

Can. J. Chem. Downloaded from www.nrcresearchpress.com by 46.23.64.124 on 09/08/12
For personal use only.

Fig. 4. Fluorescence spectra of delignified TMP before (solid lines) and after (broken lines) loading with milled wood lignin. Fluorescence spectra of a milled-wood lignin – dioxane solution are also shown (thin dotted lines), and are scaled for comparison.

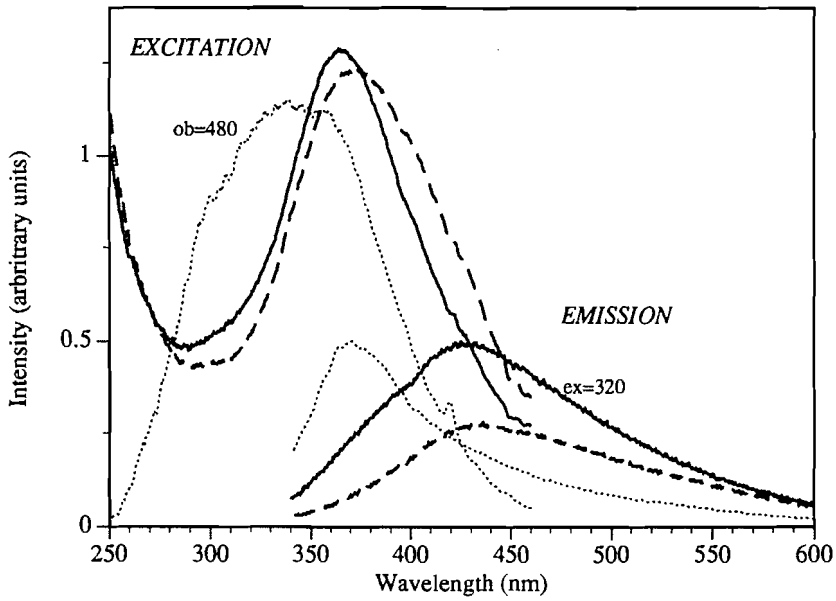

disappearance of some spectral features, most notably a peak in the excitation spectrum at 410 nm (observed at 480 nm), indicates that lignin does make a minor contribution to the total fluorescence emission of mechanical pulps.

3.3. Fluorescence upon addition of milled wood lignin

Since removal of lignin from mechanical pulps causes an apparent increase in emission under excitation at 320 nm, addition of lignin to a delignified pulp should produce the opposite effect. In fact, this is the case, as may be seen in Fig. 4. The fluorescence emission spectrum of chlorite-treated TMP (λ_{ex} = 320 nm) undergoes a decrease when milled wood lignin is added to the sheet. Decreases at 320 and 350 nm and an increase at 415 nm may be observed in the excitation spectrum upon addition of lignin. Most of the changes may again be attributed to absorption of lignin, particularly at emission wavelengths below 430 nm. These changes closely mirror the changes seen during delignification, and provide further evidence as to the role of lignin in mechanical pulp fluorescence. The similarity of the changes seen during delignification and addition of lignin also indicates that the fluorescence properties of pulps are not overly dependent on formal lignin–cellulose bonds present in mechanical pulps: rather, lignin and cellulose act independently.

Concluding remarks

The physical processes involved in fluorescence from scattering media such as paper are complex, and eq. [5] may be an oversimplification. Nevertheless, the basic emission spectra for excitation at 320 nm show no decrease in fluorescence intensity when the lignin content of the TMP and BCTMP pulps was reduced from >25% to <2%. Furthermore, when dioxane lignin was added to the sheets, the fluorescence intensity increased. Thus a primary role of lignin in the photochemistry of mechanical pulps is the screening or quenching of fluorescence; the source of the fluorescence remains an open question.

Acknowledgments

We thank Nazeer Muradali (Paprican) for technical assistance and Dr. John Schmidt (Paprican) for use of the UV–visible spectrophotometer. Samples of milled wood lignin were supplied by Dr. Jiashu Wang (McGill University). This research was supported by the Government of Canada through the Network of Centres of Excellence Mechanical Pulps Network.

References

1. (*a*) H. Tylli, I. Forsskahl, and C. Olkkonen. J. Photochem. Photobiol. A: **67**, 117 (1992); (*b*) Proc. 7th Int. Symp. on Wood and Pulping Chemistry, Beijing, China, 1993. CTAPI. p. 458.
2. (*a*) M. Beyer, D. Steger, and K. Fischer. J. Photochem. Photobiol. A: **76**, 217 (1993); (*b*) H. Choudhury, S. Collins, and R.S. Davidson. J. Photochem. Photobiol. A: **69**, 109 (1992).
3. K. Lundquist, B. Josefsson, and G. Nyquist. Holzforschung, **32**, 27 (1978).
4. A. Castellan, A. Nourmamode, C. Noutary, C. Belin, and P. Fornier de Violet. J. Wood Chem. Technol. **12**, 19 (1992)
5. R.S. Davidson, L.A. Dunn, A. Castellan, and A. Nourmamode. J. Photochem. Photobiol. A: **58**, 349 (1991).
6. J.A. Olmstead and D.G. Gray. J. Photochem. Photobiol. A: **73**, 59 (1993).
7. J.H. Zhu and D.G. Gray. J. Photochem. Photobiol. A: **73**, 67 (1993).
8. A. Castellan and R.S. Davidson. J. Photochem. Photobiol. A: **78**, 275 (1994).
9. (*a*) A. Castellan, H. Choudhury, R.S. Davidson, and S. Grelier. J. Photochem. Photobiol. A: **81**, 117 (1994); (*b*) J. Photochem. Photobiol. A: **81**, 123 (1994).
10. L.E. Wise, M. Murphy, and A.A. D'Addieco. Paper Trade J. **122**, 35 (1946).
11. B.L. Browning. Methods of wood chemistry. Interscience Publishers, New York. 1967.
12. J.A. Schmidt and C. Heitner. TAPPI, **76**, 117 (1993).
13. H.H. Brownell. TAPPI, **48**, 513 (1965).
14. A. Björkman. Sven. Papperstidn. **59**, 447 (1956).
15. J.A. Schmidt and C. Heitner. J. Wood Chem. Technol. **15**, 223 (1995).

Can. J. Chem. Downloaded from www.nrcresearchpress.com by 46.23.64.124 on 09/08/12
For personal use only.

Role of the reaction parameters in the direct synthesis of aromatic polyamides

Alberto Mariani, Sabina L.E. Mazzanti, and Saverio Russo

Abstract: A thorough study, devoted to analyzing the role of various reaction parameters in the direct synthesis of poly(*p*-phenylene terephthalamide) and poly(*p*-benzamide), activated by triphenyl phosphite, is described. The effects of temperature, salt type and concentration, amount of triphenyl phosphite and its stepwise introduction, as well as monomer and reagent concentrations, are considered. The inherent viscosity values of the above aromatic polyamides are higher than those reported in the literature for analogous syntheses and are comparable to the values of typical samples obtained by the acyl chloride routes.

Key words: poly(*p*-benzamide), poly(*p*-phenylene terephthalamide), triphenylphosphite, direct synthesis, aromatic polyamides.

Résumé : On décrit une étude complète orientée vers l'analyse du rôle de divers paramètres réactionnels dans la synthèse directe du poly(téréphtalamide de *p*-phénylène) et du poly(*p*-benzamide), activée par le phosphite de triphényle. On a considéré l'effet de la température, du type de sel et de sa concentration, de la quantité de phosphite de triphényle et de son introduction par étape ainsi que des concentrations de monomère et de réactifs. Les valeurs de la viscosité inhérente des polyamides aromatiques mentionnés plus hauts sont plus élevées que celles rapportées dans la littérature pour des synthèses analogues et elles sont comparables aux valeurs d'échantillons typiques obtenus par des voies impliquant les chlorures d'acyles.

Mots clés : poly(*p*-benzamide), poly(téréphtalamide de *p*-phénylène), phosphite de triphényle, synthèse directe, polyamides aromatiques.

[Traduit par la rédaction]

Introduction

In 1974, Yamazaki et al. (1) performed the direct synthesis of aromatic polyamides employing triphenyl phosphite (TPP) as activator. Only low molecular weight *para*-oriented polyamides were obtained with their original method.

In 1982 Higashi et al. (2) found a great improvement of the inherent viscosity (η_{inh}) value of poly(*p*-phenylene terephthalamide) (PPD-T) by adding to the solvent medium a salt mixture composed of $CaCl_2$ and LiCl, instead of LiCl alone, as previously suggested by Yamazaki et al. (3). However, their attempts to also use the double salt system in the synthesis of poly(*p*-benzamide) (PBA) did not provide any η_{inh} improvement. Later on, Preston and co-workers (4, 5) found that the optimum temperature for the direct synthesis of both polymers is 115°C.

Recently we reported that, when very accurate purification procedures are used, the inherent viscosities of PPD-T and PBA can reach rather high values (6). In the case of PPD-T, the η_{inh} value obtained in our laboratory is very close to that of the same polymer synthesized by using terephthaloyl chloride, which is used in all industrial recipes instead of the corresponding diacid.

In the present paper we report a systematic study of the role of several reaction parameters in order to evaluate the best experimental conditions for the direct synthesis of PPD-T and PBA, taken as examples for AA–BB and A–B polyamides, respectively.

In particular, we studied the effect of temperature, salt type and concentration, amount of TPP and its stepwise introduction, under both Yamazaki and Higashi conditions. With the above terms, we designate a reaction medium based on *N*-methyl pyrrolidone (NMP), pyridine (Py), and triphenyl phosphite (TPP), plus lithium chloride or lithium and calcium chlorides, respectively. Within each system, component (including monomer or reactants) concentrations can largely be varied. The slight discrepancy between the optimum η_{inh} values quoted in the present paper (see later) and those found previously (6) is due to minor differences in the purification procedures and polymerization setups.

Experimental section

(a) Materials

NMP (Aldrich) was refluxed under vacuum in the presence of CaH_2 for 8 h and distilled under the same conditions. Then it was refluxed under vacuum in the presence of P_2O_5 for 6 h and dis-

Received March 21, 1995.

This paper is dedicated to Professor J.E. (Jim) Guillet in recognition of his contributions to Canadian chemistry.

A. Mariani and S.L.E. Mazzanti. Dipartimento di Chimica, Università, via Vienna 2, 07100 Sassari, Italy.
S. Russo.[1] Istituto di Chimica Industriale, Università, corso Europa 30, 16132 Genoa, Italy, and IMAG CNR, via De Marini 6, 16149 Genoa, Italy.

[1] Author to whom correspondence may be addressed at: Istituto di Chimica Industriale, Università, corso Europa 30, 16132 Genoa, Italy. Telephone: +39-10-3538555. Fax: +39-10-3538323. E-mail: RUSSO@CISI.UNIGE.IT

Can. J. Chem. Downloaded from www.nrcresearchpress.com by 46.23.64.124 on 09/08/12
For personal use only.

Can. J. Chem. Downloaded from www.nrcresearchpress.com by 46.23.64.124 on 09/08/12
For personal use only.

tilled; the treatment was repeated twice. Py (Aldrich) was refluxed under an inert atmosphere in the presence of sodium hydroxide for 6 h and distilled; the treatment was repeated three times. LiCl (Carlo Erba) and $CaCl_2$ (Fluka) were dried for 24 h at 340°C under vacuum. TPP (Aldrich) was purified by fractional distillation under vacuum. The procedure was repeated three times. Diphenyl phosphite (DPP), Aldrich, was purified by fractional distillation under vacuum. The procedure was repeated three times. *p*-Phenylenediamine (PPD), Fluka, was purified by sublimation at reduced pressure. The procedure was repeated three times. Terephthalic acid (TA), Amoco, was dried for 24 h at 80°C under vacuum. *p*-Aminobenzoic acid (pABA), Aldrich, was dried for 24 h at 100°C under vacuum.

(b) Procedure

1. Synthesis of PBA in a solvent medium containing LiCl (so-called Yamazaki conditions)

In a typical run, by operating in a dry-box under inert atmosphere, 10 mL of NMP, 3.3 mL of Py, 1.37 g of pABA, 1.70 mL of TPP, and 0.5 g of LiCl were added to a 50 mL three-neck flask, fitted with an inlet and an outlet for inert gas (in most cases argon) and a magnetic stirrer. Oxygen traces were preliminarily removed from the components mentioned above by several cycles of vacuum and argon. The vessel was placed in a thermostatically controlled oil bath at 115°C. The reaction mixture became a clear gel within 0.5 h. After 4 h of reaction, the polymer obtained was ground in a blender in the presence of methanol. The reaction product was washed with boiling methanol and dried in a vacuum oven for 18 h at 80°C. Polymer yield was determined gravimetrically.

2. Synthesis of PBA in a solvent medium containing LiCl and $CaCl_2$ (so-called Higashi conditions)

NMP (25 mL), Py (5 mL), pABA (1.13 g), TPP (1.30 mL), $CaCl_2$ (1.5 g), and LiCl (0.5 g) were added to the above reaction vessel as described. All polymerization procedures and the operations on the resultant polymer were as mentioned in point 1.

3. Synthesis of PPD-T in a solvent medium containing LiCl (Yamazaki conditions)

In a typical run, 9 mL of NMP, 6 mL of Py, 0.3068 g of TA, 0.1997 g of PPD, 1.11 mL of TPP, and 0.4 g of LiCl were added to the above reaction vessel as described. All polymerization procedures and the operations on the resultant polymer were as mentioned in point 1.

4. Synthesis of PPD-T in a solvent medium containing LiCl and $CaCl_2$ (Higashi conditions)

In a typical run, 12.5 mL of NMP, 2.5 mL of Py, 0.2077 g of TA, 0.1352 g of PPD, 0.72 mL of TPP, 0.75 g of $CaCl_2$, and 0.25 g of LiCl were added to the above reaction vessel as described. All polymerization procedures and the operations on the resultant polymers were as mentioned in point 1 above.

(c) Polymer characterization

Viscosities, expressed as η_{inh}, of polymer solutions (at the concentration of 0.1 g/dL) were determined in 96% H_2SO_4 at 25°C using a Ubbelhode-type viscometer.

Results and discussion

In a recent paper (6) we reported on the critical relevance of high purification methods joined with very accurate polymerization procedures in order to obtain high molecular weight aromatic polyamides. In the present work, a systematic evaluation of various reaction parameters (see below) for both Higashi and Yamazaki conditions is explored, taking into account the aforementioned importance of high purification levels for all reaction components.

Namely, we studied the influence of variables such as TPP/monomer (or reactant) molar ratio, salt type and concentration, reaction temperature, and mode of TPP addition to the reacting mixture, in terms of both polymer yields (which were almost always quantitative) and polymer molecular weights (MW). The latter are hereafter reported in terms of inherent viscosities, i.e., true experimental values, instead of MW data calculated from still controversial [η]–M relationships (7, 8).

The aromatic polyamides considered are PBA and PPD-T.

Table 1. Effect of [TPP]/[pABA] ratio in the synthesis of PBA (Yamazaki conditions).[a]

Sample	[TPP]/[pABA]	η_{inh} (dL/g)
0.34	0.4	0.31
0.13	0.6	2.00
0.20	0.8	1.80
0.15	1.0	1.26

[a]Experimental conditions: [pABA] = 0.75 mol/L; NMP/Py = 3 (v/v); 3.7% LiCl (w/v); T = 115°C.

Table 2. Effect of [TPP]/[pABA] ratio in the synthesis of PBA (Higashi conditions).[a]

Sample	[TPP]/[pABA]	η_{inh} (dL/g)
0.21	0.4	0.10
0.18	0.6	1.53
0.19	0.8	1.38
0.12	1.0	1.40

[a]Experimental conditions: [pABA] = 0.27 mol/L; NMP/Py = 5 (v/v); 1.7% LiCl (w/v); 5.0% $CaCl_2$ (w/v); T = 115°C.

(a) Effect of the [TPP]/[monomer] or [TPP]/[reactant] ratio

1. [TPP]/[pABA]

We studied the synthesis of PBA prepared under Yamazaki or Higashi conditions and found that the best molar ratio for the synthesis of high molecular weight PBA was, in every case, [TPP]/[pABA] = 0.6. Thus, in Tables 1 (Yamazaki conditions) and 2 (Higashi conditions) are listed the η_{inh} values of PBA synthesized using different ratios of [TPP]/[pABA] (from 0.4 to 1.0). As shown in the tables, the inherent viscosity values decrease rapidly when [TPP]/[pABA] < 0.6, whereas such values for the two systems seems less prone to change at higher ratios.

2. [TPP]/[TA]

Table 3 lists the inherent viscosities of PPD-T synthesized under Yamazaki conditions, varying the molar ratio from 1.3 to 2.3 (a ratio of 2 refers to stoichiometric conditions). As we

Table 3. Effect of [TPP]/[TA] ratio in the synthesis of PPD-T (Yamazaki conditions).[a]

Sample	[TPP]/[TA]	η_{inh} (dL/g)
0.32	1.3	0.24
0.28	1.7	0.36
0.27	2.0	0.31
0.29	2.3	0.38

[a]Experimental conditions: [TA] = [PPD] = 0.125 mol/L; NMP/Py = 1.5 (v/v); 2.7% LiCl (w/v); T = 115°C.

Table 4. Effect of [TPP]/[TA] ratio in the synthesis of PPD-T (Higashi conditions).[a]

Sample	[TPP]/[TA]	η_{inh} (dL/g)
0.44	2.0	6.84
0.42	2.2	8.15
0.43	2.4	6.89

[a]Experimental conditions: [TA] = [PPD] = 0.083 mol/L; NMP/Py = 5 (v/v); 1.7% LiCl (w/v); 5.0% $CaCl_2$ (w/v); T = 115°C.

can see, the [TPP]/[reactant] ratio in this system seems to be less critical than in the PBA synthesis. Moreover, the inherent viscosity values of the resultant polymers are very low. This is probably due to polymer precipitation during the reaction, which thereafter proceeds in a heterogeneous phase.

The situation is sharply different for polymerization under Higashi conditions, with a total reagent concentration of 0.166 mol/L (Table 4) being used. In these experiments, no precipitation of the polymer is observed and a complete gelation of the reacting mixture appears to take place. Under these conditions, the growth of the polymer chains is surely more extensive than in the previous system.

(b) Effect of salt type and concentration

1. PBA

The types of salt dissolved in the reaction medium and the concentration of salts have been studied in detail. LiCl and $CaCl_2$ have been used alone or mixed together. Table 5, which is based on a [TPP]/[pABA] ratio = 0.6, gives the η_{inh} data obtained using different concentrations of salts.

The values obtained under experimental conditions indicated under footnote *a* are related to a monomer concentration of 0.75 mol/L. The maximum value obtained (η_{inh} = 2.15 dL/g) is higher than the best literature value (5) (η_{inh} = 1.8 dL/g), most probably because of a better purification of reagents and solvents. As can be seen from the table, the highest η_{inh} value for this relatively high monomer concentration corresponds to the synthesis where the largest total salt concentration has been used.

The values obtained under experimental conditions indicated under footnote *b* are related to a lower monomer concentration of 0.27 mol/L. It can be seen that the sample 0.18 has the lowest inherent viscosity. It may therefore be concluded that, in this system, $CaCl_2$ has a negative effect. The highest η_{inh} value (2.19 dL/g) has been obtained when a high salt concentration in the reaction medium, based on LiCl only, has been used.

It is known (3) that the main effect of salts dissolved in the solvent mixture is to increase the solubility of rigid polymer chains, allowing the synthesis to be carried out in a homogeneous phase. We may infer that a high salt concentration has a marked positive effect for systems leading to a high polymer concentration. On the other hand, when the polymer concentration is relatively low, the solubility problems for polyamides are less important, with a scant effect linked to the increase of salt concentration, in particular if $CaCl_2$ is present in the reaction mixture.

2. PPD-T

The nature of the salt is the most important parameter in the synthesis of this polymer. Our study has been focused on a [TPP]/[TA] ratio = 2.

The data obtained from experiments carried out under conditions indicated by footnote *a* in Table 6 are related to some syntheses carried out using a total reagent concentration of 0.25 mol/L. It is clear that the mixed salt system is the worst. In general, the η_{inh} values are very low and there are no big differences among the three values. This result is probably due to polymer precipitation during the synthesis, which makes further polymer growth unfavorable. In the same table, the data obtained from experiments carried out under conditions indicated by footnote *b* are related to syntheses performed at a total reagent concentration equal to 0.166 mol/L. By comparing these latter values with the previous ones, the importance of working with a lower reactant concentration in order to avoid polymer precipitation during the synthesis is clearly evident.

(c) Temperature effect

1. PBA

All above syntheses were made at 115°C, i.e., at the best conditions suggested in the literature (5). We considered it relevant to also check this assumption for the experimental conditions leading to the optimum data of our experiments. Table 7 gives the inherent viscosities of PBA synthesized under the best conditions previously quoted (Table 6), using reaction temperatures in the range of 105 to 120°C. Our data confirm the presence of a maximum value for the reaction at 115°C with η_{inh} = 2.19, as compared to 1.8 dL/g, quoted in the literature (5).

2. PPD-T

Table 8 refers to temperature effects on some syntheses made under Yamazaki conditions at [TPP]/[TA] ratio = 2.0. It is evident that this system is not very sensitive to the variation of temperature. The inherent viscosity values are rather low and almost constant.

More significant in this respect is the Higashi system. The data reported in Table 9 refer to syntheses made at a [TPP]/[TA] ratio of 2.2, which represents the best ratio found for these experimental conditions. The highest value is obtained at 115°C and is equal to 8.15 dL/g, much higher than the best literature value of 6.2 dL/g (5).

It is relevant to observe that the Higashi system is more sensitive to temperature variations than the Yamazaki system. It can also be seen that a dramatic decrease of η_{inh} occurs when

Can. J. Chem. Downloaded from www.nrcresearchpress.com by 46.23.64.124 on 09/08/12
For personal use only.

Can. J. Chem. Downloaded from www.nrcresearchpress.com by 46.23.64.124 on 09/08/12
For personal use only.

Table 5. Effect of salt type and concentration in the synthesis of PBA.

Sample	LiCl (%; w/v)	$CaCl_2$ (%; w/v)	LiCl + $CaCl_2$ (%; w/v)	η_{inh} (dL/g)
0.13[a]	3.7	0.0	3.7	2.00
0.22[a]	3.7	11.3	15.0	2.15
0.24[a]	0.9	2.8	3.7	0.85
0.18[b]	1.6	4.8	6.4	1.53
0.28[b]	1.4	0.0	1.4	1.82
0.29[b]	6.7	0.0	6.7	2.19

[a]Experimental conditions: [pABA] = 0.75 mol/L; NMP/Py = 3 (v/v); [TPP]/[pABA] = 0.6; T = 115°C.
[b]Experimental conditions: [pABA] = 0.27 mol/L; NMP/Py = 5 (v/v); [TPP]/[pABA] = 0.6; T = 115°C.

Table 6. Effect of salt type and concentration in the synthesis of PPD-T.

Sample	LiCl (%; w/v)	$CaCl_2$ (%; w/v)	LiCl + $CaCl_2$ (%; w/v)	η_{inh} (dL/g)
0.33[a]	2.7	0.0	2.7	0.32
0.30[a]	0.7	2.0	2.7	0.21
0.52[a]	0.0	3.5	3.5	0.24
0.51[b]	5.5	0.0	5.5	1.22
0.31[b]	6.7	0.0	6.7	1.16
0.34[b]	0.0	6.7	6.7	1.26
0.44[b]	1.7	5.0	6.7	6.84

[a]Experimental conditions: [TA] = [PPD] = 0.125 mol/L; NMP/Py = 1.5 (v/v); [TPP]/[TA] = 2.0; T = 115°C.
[b]Experimental conditions: [TA] = [PPD] = 0.083 mol/L; NMP/Py = 5 (v/v); [TPP]/[TA] = 2.0; T = 115°C.

Table 7. Temperature effect in the synthesis of PBA (Yamazaki conditions).[a]

Sample	Temperature (°C)	η_{inh} (dL/g)
0.35	105	1.70
0.44	110	1.66
0.29	115	2.19
0.43	120	1.53

[a]Experimental conditions: [pABA] = 0.27 mol/L; NMP/Py = 5 (v/v); [TPP]/[pABA] = 0.6; 6.7% LiCl (w/v).

Table 8. Temperature effect in the synthesis of PPD-T (Yamazaki conditions).[a]

Sample	Temperature (°C)	η_{inh} (dL/g)
0.53	100	0.28
0.38	110	0.36
0.27	115	0.31
0.37	120	0.37

[a]Experimental conditions: [TA] = [PPD] = 0.125 mol/L; NMP/Py = 1.5 (v/v); [TPP]/[TA] = 2.0; 2.7% LiCl (w/v).

Table 9. Temperature effect in the synthesis of PPD-T (Higashi conditions).[a]

Sample	Temperature (°C)	η_{inh} (dL/g)
0.49	107	7.71
0.42	115	8.15
0.48	122	6.27

[a]Experimental conditions: [TA] = [PPD] = 0.083 mol/L; NMP/Py = 5 (v/v); [TPP]/[TA] = 2.2; 1.7% LiCl (w/v); 5.0% $CaCl_2$ (w/v).

the temperature is increased above the optimum value of 115°C.

(d) Mode of TPP addition

1. PBA

In 1984 Preston and co-workers (5) noticed that a direct synthesis of PBA from the dimer of the pABA, instead of the monomer itself, made it possible to obtain a polymer with a higher inherent viscosity. By this method, PBA with η_{inh} = 4.6 dL/g, as compared to the value of 1.8 dL/g for the polymer synthesized directly from pABA, was obtained and represents the highest value reached so far by the direct synthesis activated with TPP. In our opinion, an alternative and simpler route could produce

Table 10. Effect of TPP stepwise addition in the synthesis of PBA (Yamazaki conditions).[a]

Sample	[TPP]/[pABA]	η_{inh} (dL/g)	Increment (%)
0.13	0.6	2.00	—
0.16[b]	0.6	2.25	13
0.15	1.0	1.26	—
0.17[b]	1.0	2.07	64

[a]Experimental conditions: [pABA] = 0.75 mol/L; NMP/Py = 3 (v/v); 3.7% LiCl (w/v); T = 115°C.
[b]The same as above; stepwise addition of TPP.

Table 11. Effect of TPP stepwise addition in the synthesis of PBA (Higashi conditions).[a]

Sample	[TPP]/[pABA]	η_{inh} (dL/g)	Increment (%)
0.18	0.6	1.53	—
0.37[b]	0.6	1.96	28
0.12	1.0	1.40	—
0.36[b]	1.0	1.77	26

[a]Experimental conditions: [pABA] = 0.27 mol/L; NMP/Py = 5 (v/v); 1.7% LiCl (w/v); 5.0% $CaCl_2$ (w/v); T = 115°C.
[b]The same as above; stepwise addition of TPP.

relatively larger (as compared to the usual procedures) amounts of dimer in situ, by using a stepwise addition of TPP, thus initially activating only part of the carboxylic groups.

In Table 10, data concerning four syntheses made under Yamazaki conditions at a pABA concentration of 0.75 mol/L and two different [TPP]/[pABA] ratios are reported. Relevant improvements of η_{inh}, when TPP is added stepwise, were obtained.

The same conclusion can be reached from the data of Table 11, which refers to four syntheses performed using the more dilute pABA concentration of 0.27 mol/L under Higashi conditions. Also for this system a good improvement of inherent viscosity was found.

On this basis, a comparison between our highest η_{inh} value (sample 0.29 in Table 7), reached using a monomer concentration of 0.27 mol/L and 6.7% LiCl, and the corresponding η_{inh} value obtained from a synthesis made under the same conditions but with stepwise TPP addition, shows that under the latter conditions a further increase of η_{inh} (from 2.19 to 2.35 dL/g) was found. The above value is, probably, the highest η_{inh} obtained so far, when a direct synthesis from pABA is employed.

2. PPD-T

In contrast to PBA, the literature does not report, for the PPD-T synthesis, any improvement for the reaction made starting from the "dimer" (9). Similarly, in our stepwise procedure, no increase of η_{inh} was found.

(e) Use of DPP

As previously indicated, the best [TPP]/[pABA] ratio is 0.6, a rather unusual value if we consider that each TPP molecule activates a carboxylic function, allowing it to react with the amino group. It can be reasonably assumed that DPP, formed as by-product during the reaction, is also able to activate the acidic group. Two attempts of PBA synthesis using DPP instead of TPP, for two different [phosphite]/[pABA] ratios were successful, although they gave rather low η_{inh} values, and fully justify our assumption. Thus, DPP can be considered to promote the reaction between the acid and the amino functions, although with lower efficiency. This may also be due to the presence of high concentrations of phenol not easily removed in our DPP. Phenol may be responsible, in our opinion, for the rather low η_{inh} values obtained ($\leq$0.2 dL/g). Direct evidence of its role was demonstrated by its addition in equimolar amount to the monomer in a typical synthesis of PBA by TPP. The η_{inh} of PBA was lowered from 2.0 to 0.06 dL/g. Literature data on polyamidohydrazides synthesized in the presence of DPP, on the contrary, reveal that the latter is a better reagent than TPP (10).

Conclusions

Direct synthesis appears a very easy and useful method for obtaining, on a laboratory scale, aromatic polyamides characterized by a large range of inherent viscosity values, which depend on the experimental conditions, thoroughly studied in the present work, chosen for their synthesis.

In addition, accurate purification procedures and proper choice of the reaction conditions make it possible to reach quite high polymer molecular weights, close to those obtained by acyl chloride routes.

Advantages of direct synthesis are the ease to carrying it out, the use of relatively stable diacids instead of moisture-

Can. J. Chem. Downloaded from www.nrcresearchpress.com by 46.23.64.124 on 09/08/12
For personal use only.

and temperature-sensitive compounds, such as acyl chlorides, and also the simplicity and low cost of the experimental equipment.

On the contrary, the high concentration of TPP required, as well as the problems connected with its removal from the polyamide, may represent a relevant disadvantage.

Further improvement of the reaction can be envisioned by continually removing the phenol formed as by-product. As a consequence, it would be possible to shift the equilibrium more and more towards the products and avoid the possibility of the phenol reacting with the growing polymer chains.

Acknowledgment

This work was partially supported by Ministero dell'Universitá della Ricerca Scientifica (MURST) and Consiglio Nazionale delle Ricerche (CNR) funds.

References

1. N. Yamazaki, F. Higashi, and J. Kawabata. J. Polym. Sci. Polym. Chem. Ed. **12,** 2149 (1974).
2. F. Higashi, S.-I. Ogata, and Y. Aoki. J. Polym. Sci. Polym. Chem. Ed. **20,** 2081 (1982).
3. N. Yamazaki, N. Matsumoto, and F. Higashi. J. Polym. Sci. Polym. Chem. Ed. **13,** 1373 (1975).
4. W.R. Krigbaum, R. Kotek, Y. Mihara, and J. Preston. J. Polym. Sci. Polym. Chem. Ed. **22,** 4045 (1984).
5. W.R. Krigbaum, R. Kotek, Y. Mihara, and J. Preston. J. Polym. Sci. Polym. Chem. Ed. **23,** 1907 (1985).
6. S. Russo, A. Mariani, V.N. Ignatov, and I.I. Ponomarev. Macromolecules, **26,** 4984 (1993).
7. M. Arpin, and C. Strazielle. Polymer, **18,** 591 (1977).
8. V.N. Tsvetkov, I.N. Shtennikova, T.V. Peker, G.I. Kudriavtsev, A.V. Volokhina, and V.D. Kalmykova. Eur. Polym. J. **13**, 455 (1977).
9. W.R. Krigbaum and R. Kotek. J. Polym. Sci. Polym. Chem. Ed. **22,** 873 (1984).
10. F. Higashi and M. Ishikawa. J. Polym. Sci. Polym. Chem. Ed. **18,** 2905 (1980).

Can. J. Chem. Downloaded from www.nrcresearchpress.com by 46.23.64.124 on 09/08/12
For personal use only.

Mechanical behaviour of polymer mixtures in the phase separation region

V.N. Kuleznev and L.B. Kandyrin

Abstract: The liquid–liquid phase transition triggered by changes in the composition of polymer mixtures in solution or melt is often accompanied by "critical" opalescence, which signals the appearance of a microemulsion in the mixture. The viscosity of the polymer mixture in this region is characterized by a sharp minimum, observed, as a rule, over an extremely narrow range of concentration. Depending on the concentration of the solution, the type of polymer, and the solvent, the viscosity may decrease by a factor of 8–10. On transition from micro- to macro-separation, viscosity rapidly increases back to the original level. Changes in the composition of the mixture can alter the concentration at which phase separation occurs, but the minimum in viscosity invariably corresponds to the moment of phase separation. The critical opalescence region represents the formation of phase particles up to 80–100 nm in size, and this corresponds to the point of viscosity drop. This effect is due to the appearance of thermodynamically stable microemulsions in the polymer mixture, in the region between the binodal and the spinodal in the phase diagram. These emulsions are characterized by lower molecular interaction of incompatible polymers in the highly developed interfacial layer. Extremal changes at the point of phase separation are also observed for other mechanical characteristics of polymer mixtures in solutions or melts, for example, G' and G'' dynamic moduli or complex viscosity η^*.

Key words: polyblends, critical phenomena, viscosity, emulsions, phase separation.

Résumé : Les transitions de phase liquide–liquide provoquées par des changements dans la composition de mélanges de polymères fondus ou en solution sont souvent accompagnées par une opalescence critique qui signale l'apparition d'une microémulsion dans le mélange. La viscosité du mélange de polymère dans cette région est caractérisée par un minimum pointu généralement observé sur une bande extrêmement étroite de concentration. Suivant la concentration de la solution, le type de polymère et le solvant, la viscosité peut diminuer par un facteur allant de 8 à 10. Lors de la transition de la microséparation en macroséparation, la viscosité augmente rapidement pour revenir au niveau original. Des changements dans la composition du mélange peuvent affecter la concentration à laquelle la séparation de phase se produit; toutefois, le minimum de viscosité correspond invariablement au moment de la séparation de phase. La région de l'opalescence critique représente la formation d'une phase de particules dont la grosseur varie de 80 à 100 nm et elle correspond au point de diminution de la viscosité. Cet effet est dû à l'apparition, dans le mélange de polymère, de microémulsions thermodynamiquement stables dans la région entre le binodal et de spinodale du diagramme de phase. Ces émulsions sont caractérisées par une interaction moléculaire plus faible des polymères incompatibles dans la couche interfaciale hautement développée. On a aussi observé des changements extrêmes à ce point de la séparation de phase pour d'autres caractéristiques mécaniques de mélanges de polymères fondus ou en solution, par exemple, pour les modules dynamiques G' et G'' et pour la viscosité complexe η^*.

Mots clés : mélanges complexes, phénomène critique, viscosité, émulsions, séparation de phase.

[Traduit par la rédaction]

During a stay of V. Kuleznev in the laboratory of Jim Guillet in 1965–1966, the idea arose of investigating the influence of butadiene–styrene block copolymers on the compatibility of polystyrene and polybutadiene (PS–PB) in appropriate solvents. Although the work was not concluded, two important experimental facts emerged. The first was that the block copolymers increased the concentration of PS–PB where phase separation occurred, that is, improved the compatibility of these polymers in the solution. The second was that solutions of the block copolymers with sufficiently high molecular weights were turbid and opalescent themselves. This second observation led us to the possibility of employing internal block segregation in block copolymers to form stable microemulsions. Further development of this idea in our laboratory in Moscow demonstrated the possibility of forming stable microemulsions in polymer–polymer mixtures when the stability was provided by "thermodynamics" and not by chemical bonds between the segregated macromolecules.

This paper considers the rheological properties of these unique systems, and is published with deep gratitude to Pro-

Received February 15, 1995.

This paper is dedicated to Professor J.E. (Jim) Guillet in recognition of his contributions to Canadian chemistry.

V.N. Kuleznev[1] and L.B. Kandyrin. M.V. Lomonossov Institute of Fine Chemical Technology, 86 Vernadsky Prosp., Moscow 117571, Russia.

[1] Author to whom correspondence may be addressed. Fax: 7-095-333-3362.

Can. J. Chem. Downloaded from www.nrcresearchpress.com by 46.23.64.124 on 09/08/12
For personal use only.

Can. J. Chem. Downloaded from www.nrcresearchpress.com by 46.23.64.124 on 09/08/12
For personal use only.

Fig. 1. Phase diagram with region of existence of one-phase stable (1), metastable (2), labile (3), and thermodynamically stable disperse systems (4). Data from ref. 28. I, binodal; II, spinodal.

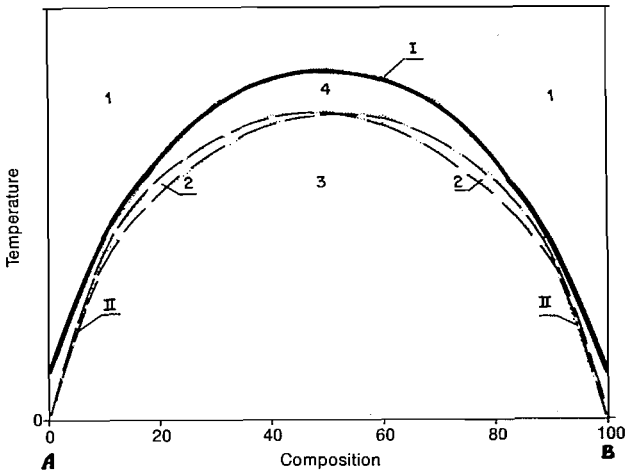

fessor Jim Guillet for providing the opportunity for repeatedly working together.

Binary polymer mixtures in solution, melt, or the solid state may be one- or two-phased depending on the temperature, concentration, or composition of the mixture. The binodal that Gibbs described as the boundary of the absolute phase stability (Fig. 1) acts as a barrier between the one- and two-phase regions in the phase diagram. In the immediate vicinity of the binodal, homophasal statistical fluctuations appear in the one-phase system, with their composition and density different from the average (1). When passing through the binodal, the values of these homophasal fluctuations rise to such an extent that they can viewed as seeds of a new phase, i.e., a heterophasal state. This state is maintained up to the spinodal, which Gibbs described as the boundary of the absolute phase instability. Following the transition over the spinodal, two macrophases emerge in the system, taking in some cases a substantial period of time to evolve, particularly if the viscosity of the system is high.

The region bordering the spinodal on the side of either the one-phase or two-phase system is characterized by lower thermodynamic stability. Progressive large-scale fluctuations create a specific granular structure throughout the system. Externally this is indicated by the appearance of critical opalescence. This was first described by Smoluchowski (2), and later quantitatively described for single-component systems by Ornstein and Zernicke (3) and for bi-component systems by Debye (4, 5). The phase separation of mixtures of low molecular weight liguids, as well as polymer–solvent mixtures, occurs sharply due to comparatively high interfacial tension, since the range of critical opalescence is very narrow. On the other hand, the range of large-scale fluctuations is considerably wider for the phase separation of polymer–polymer or polymer–polymer–solvent mixtures. This makes it possible to carry out a detailed study of the physical properties of these systems. Such studies are of considerable interest, since the appearance of large-scale fluctuations near the critical point is accompanied by extreme changes in certain physical properties such as compressibility, thermal expansion, and heat capacity even for mixtures of low molecular weight liquids (6–10). Regrettably, the mechanical properties of polymer mixtures in the critical region have not yet been thoroughly investigated. This is probably due to the fact that the low mutual solubility of most polymers results in a critical point (transition over the binodal) with a concentration of a given component being less than 1%. In consequence there is only a low probability of detection of anomalies caused by changes in the mechanical properties of the polymer mixtures. The results of some investigations have demonstrated that the concentration (or temperature) dependence of the viscosity becomes nonmonotonical at the phase transition point, with an uneven decrease in the viscosity (11–16).

The objective of the experiments described in this paper was to study peculiar changes in the rheological properties of polymer mixtures in solution and in the melt, in the critical area where the mixture goes from the one-phase to the two-phase condition.

Experimental section

The following polymers, all of industrial grade, were employed: polyisoprene (PI-1), Cariflex-JR 500, mol. wt. 9×10^5; polystyrene (PS-1), block polymerized, mol. wt. 2.8×10^5; polymethacrylate (PMMA), suspension polymerized, mol. wt. 2.4×10^5; and their solutions in benzene, decahydronaphthalene, toluene, and other solvents. To study the influence caused by the width of molecular weight distribution, we also analyzed mixtures of polyisoprene (PI-2) and polystyrene (PS-2), each with a narrow MWD (M_w/M_n = 1.05), and their solutions in α-methylnaphthalene.

Polymer mixtures in solution were obtained by mixing equiconcentrated solutions of each polymer in a common solvent. In the case of melt studies, samples were prepared by pressing films obtained from polymer mixtures in a common solvent, followed by evaporation of the solvent in vacuo at a suitable temperature.

One-phase solutions of the polymers were highly stable. Separating solutions of polymer mixtures were thoroughly stirred so as to be homogenized prior to measurement. Time-intensive measurements were conducted, for solutions only, in high-boiling solvents. Good reproducibility was observed in all experiments.

The turbidities of one- and two-phase solutions and films were measured with a photoelectric double-beam turbidmeter with light filters having different pass bands. The known relationship between turbidity and the wavelength of the passing light (17) was used to calculate the size and number of dispersed particles in the sample. The viscosity at a steady flow was measured by a rotation viscosimeter with coaxial cylinders, with various rotation speeds of the inner cylinder.

Dynamical mechanical characteristics of the polymer mixture solutions (G', G'', η^*) were measured by a low-amplitude mechanical spectrometer with coaxial cylinders in the 10^{-2}–10^3 s^{-1} frequency range.

The viscosity of the polymer mixtures in the absence of solvent was measured with a capillary viscosimeter at 170 ± 0.2°C.

Results

The most simple case in studying the phase transition region of solutions of polymer mixtures involves an examination of

Can. J. Chem. Downloaded from www.nrcresearchpress.com by 46.23.64.124 on 09/08/12
For personal use only.

Fig. 2. Concentration dependence of turbidity D (1), viscosity lg η (2), and lower layer volume V (3) for benzene solutions of PI-1–PS-1 mixture (3:7).

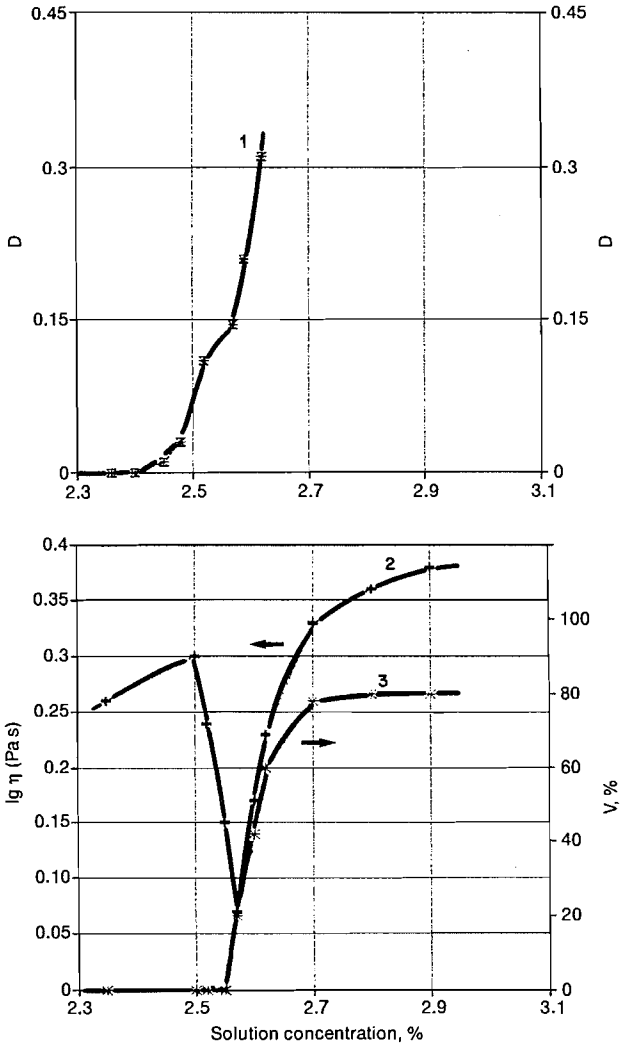

the relationship between properties and concentration in the interval that contains the phase separation point. Depending on the concentration of the solution, the ratio of polymers therein, the temperature, and the nature of the polymers and their molecular weight distribution, the position of the phase separation point can shift substantially. Figure 2 illustrates the dependence on concentration of viscosity and turbidity for a solution of PI-1 and PS-1 (3:7 mixture) in benzene. The same figure presents the concentration dependence of the volume of the lower layer (PS) in the separated two-phase mixture. A higher concentration of the solution raises the turbidity near the point of separation. The "critical" opalescence appearing in the solution indicates the formation of concentration and composition fluctuations. This state usually precedes macroseparation of the system. The plateau in the concentration dependence of the turbidity prior to separation can be more or less pronounced, but further increases in solution concentration lead to a sharp increase in turbidity due to macroseparation. It should be mentioned that the plateau representing critical opalescence can be reached from two regions, a dilute one-phase solution or a concentrated two-phase solution. The

Fig. 3. Dependence of viscosity of toluene solutions of PI-1–PS-1 mixture (1:1) on reciprocal value of their concentration. Figures near curves represent logarithms of shear stress used to determine viscosity (Pa).

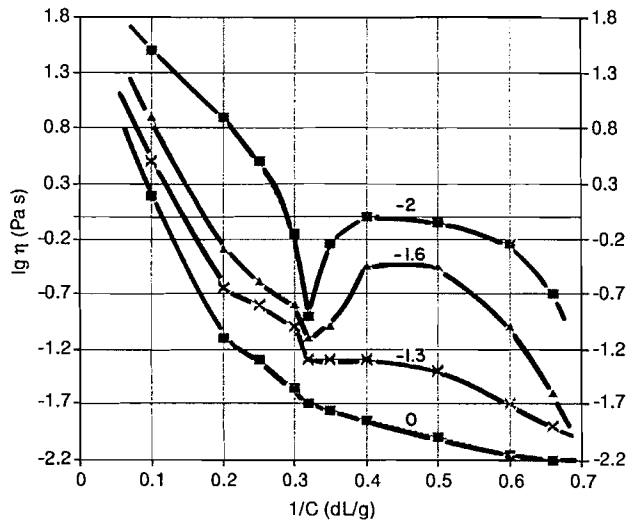

intensity of critical opalescence (solution turbidity) remains the same and does not change with time. This indicates that the solution structure is in an equilibrium state in the area of critical opalescence.

Analysis of the changes in viscosity near the phase transition point is of considerable interest. With increasing concentration below this point the viscosity increases as expected, but when the region of "critical" opalescence is reached, there is a dramatic decrease. Depending on the concentration of the solution, the type of polymer, and the solvent, the viscosity can drop by a factor of 7–10. This occurs over a very narrow range in concentration in the immediate vicinity of the phase separation point. At the appearance of the first signs of macroseparation, i.e., the appearance of a second macrolayer in the solution, the viscosity then rapidly increases again, returning to a value close to the original. Altering the ratio of polymers in the mixture, or employing a different solvent, changes the concentration at which phase separation occurs. However, the minimum in viscosity invariably coincides with the region of phase separation. An increase in the shear stress (at which the viscosity of the solution is measured) reduces the effect of the diminishing viscosity. At certain, sufficiently high, levels of shear stress, this effect for practical purposes does not occur. Comparing changes in viscosity in the region of phase separation with the reciprocal value of the concentration of the solution results in a dependence (Fig. 3) that resembles to a certain extent the van der Waals isotherm for a real gas. Increases in shear stress can in this case be compared to an increase in temperature, since both factors act to destroy association of like macromolecules in the mixture of incompatible polymers. In other words, the two factors tend to homogenize the system.

The phase separation point can be approached at constant concentration of the mixture by changing the ratio of the polymers in the solution, as illustrated in Fig. 4. In this case also, the critical opalescence appears when approaching points of phase separation, indicating pre-separation fluctuations. The appearance of critical opalescence is also accompanied by a

Can. J. Chem. Downloaded from www.nrcresearchpress.com by 46.23.64.124 on 09/08/12
For personal use only.

Fig. 4. Dependence of viscosity lg η (1) and turbidity D (2) of toluene solutions of PI-1–PS-1 mixtures on the ratio of polymer components in the mixture. Solution concentration 2.5%.

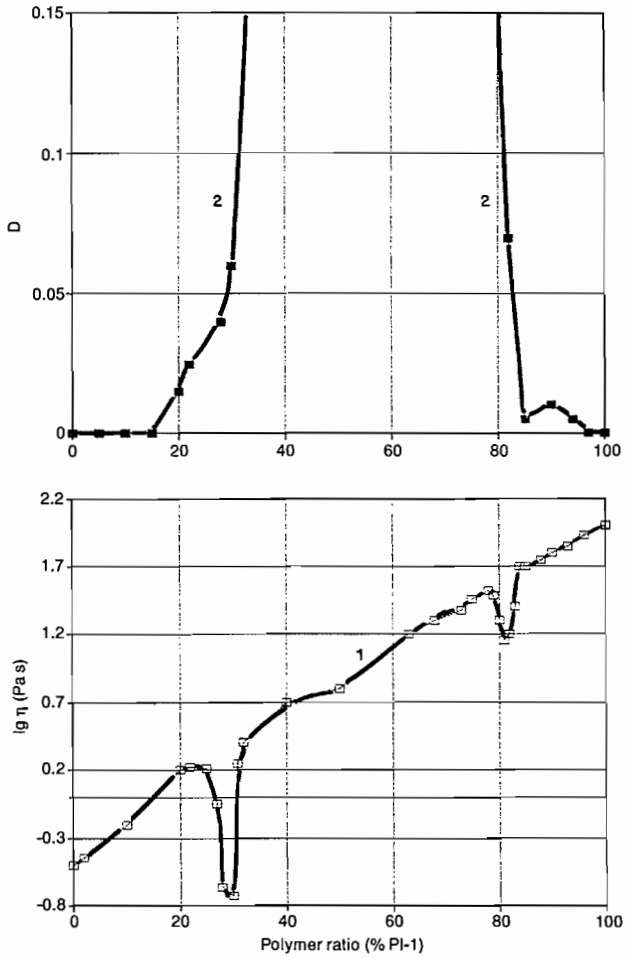

Fig. 5. Dependence of loss modulus G'' on polymer ratio of the mixture of PI-1 and PS-1 solutions in decahydronaphthalene (2), and of the mixture of PI-2 and PS-2 solutions in α-methylnaphthalene (1).

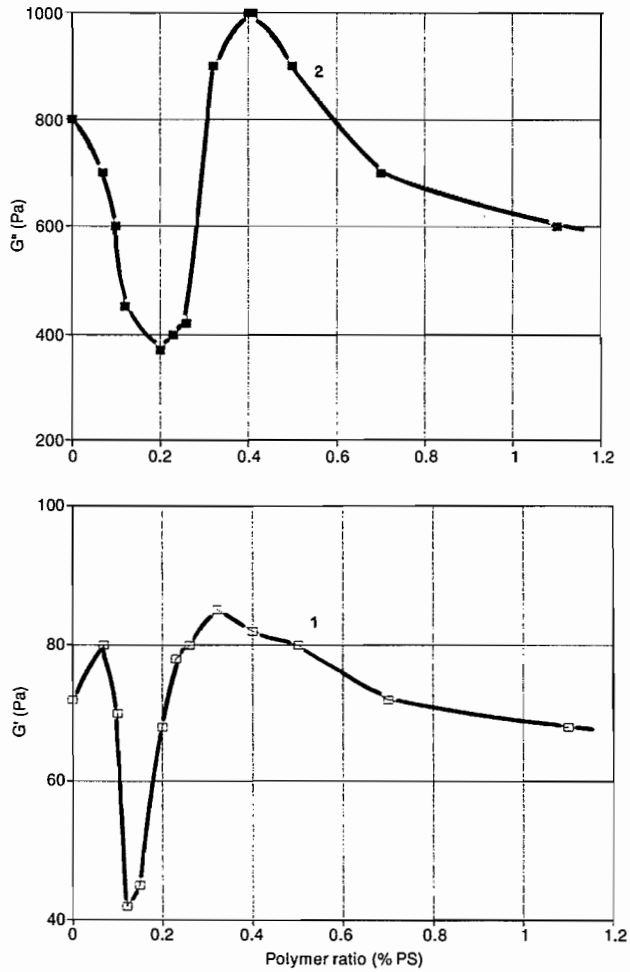

sharp drop in viscosity. It can be noted that the concentration of the solution for the system shown in Fig. 4 is relatively low. The mutual solubility of the components of this system is relatively high, so that a considerable amount of polymer can be added before reaching the separation points. Increasing the concentration of the solution causes the phase separation points to move closer to the Y-axes. In the absence of solvent the solubility of one polymer in another, which corresponds to the points of phase separation, is below 1%.

Extremal changes when reaching the phase separation point occur not only in the viscosity, but also in other mechanical characteristics of mixed polymer solutions. Figure 5 shows the dependence on concentration of the dynamic loss modulus G'', as determined with a low-amplitude mechanical spectrometer for concentrated solutions of PI-1:PS-1 mixtures in decahydronaphthalene. The position of the minimum in G'' corresponds exactly to the region of critical opalescence. To determine the role played by the width of the MWD, we measured the dependence of G'' on polymer ratio for a solution of mixtures of two monodisperse polymers PI-2 and PS-2 in α-methylnaphthalene (curve 1 of Fig. 5). In this case also there was good correspondence between the position of the G'' minimum and the critical opalescence. It can be noted that for the monodisperse mixture, the region that contains the G'' minimum is narrower than that of the mixture of polydisperse polymers. This is understandable, since the mutual polymer solubility depends on the molecular mass. The existence of low molecular weight fractions in polydisperse samples, with a higher mutual solubility than that of high molecular weight fractions, serves to extend the range of concentration that corresponds to the separation region.

A study of the optical characteristics of solutions of the polymer mixtures at different wavelengths of transmitted light, the so-called turbidity spectrum technique (17), made it possible to calculate the sizes and numbers of particles in the disperse phase of the investigated solutions, both in the region of critical opalescence, and probably in the two-phase region. It was found that the region of critical opalescence corresponds to the formation of a maximum number of particles with a size of 80–100 nm (Fig. 6). Further increases in concentration (or changes in composition) that result in rapid phase separation lead to a rapid increase in the sizes of the disperse particles, to 400–500 nm. At the same time, their number decreases proportionally. The total interfacial surface of the system, which is maximum in the region of critical opalescence, is reduced just as quickly. The system becomes unsta-

Can. J. Chem. Downloaded from www.nrcresearchpress.com by 46.23.64.124 on 09/08/12
For personal use only.

Fig. 6. Dependence of the size (1) and number (2) of particles of disperse phase in solutions of mixed PB-1 and PS-1 in toluene on the ratio of polymers in the mixture. Solution concentration 5%.

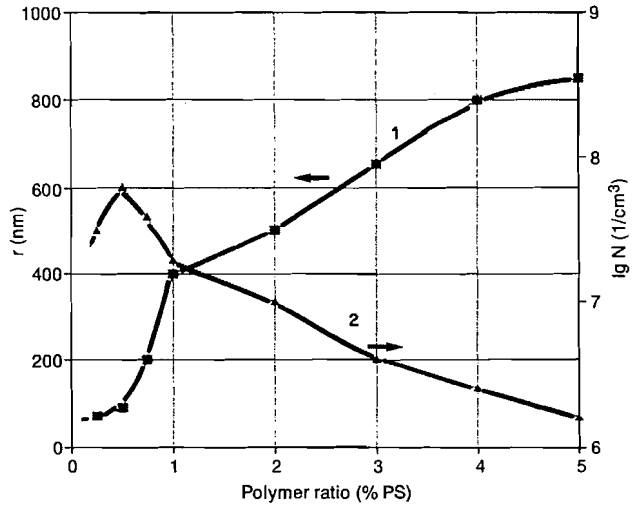

ble, and is separated into two phases with a minimal interfacial surface.

The rapid drop in viscosity in the critical region of phase separation is characteristic not only of polymer mixtures in solution, but also of polymer mixtures in the absence of solvent. In this case, the experimental detection of the effect becomes difficult due to the low mutual solubilities of polymers of high molecular weight at attainable temperatures. Figure 7 illustrates the dependence of turbidity of PS–PMMA films on PMMA content. Film turbidity was determined at temperatures similar to those employed for the determination of rheological properties, 170±0.2°C. As seen in Fig. 7, the range of concentration of PMMA that corresponds to the onset of film turbidity also corresponds to a viscosity drop. Analogous effects were also observed in the study of the rheological properties of the other pairs of polymers in solution or in the melt.

Discussion

To explain the results obtained in this study, it is advisable to discuss the phase structure of mixtures. A two-component mixture is known to exist in both a one-phase state and a two-phase state. The number of phases corresponding to a given composition of the mixture and temperature is determined, according to Gibbs, by binodal and spinodal positions. The region between the binodal and the spinodal is called the metastable region, and corresponds to a situation where the one-phase structure of the system is stable in relation to small changes in thermodynamic parameters but if unstable when nuclei of the second phase appear. Gibbs proposed treating the work needed for the appearance of the critical seed element of the new phase as a measure of the stability of the metastable state. Volmer and Rehbinder showed that is the interfacial tension of the system is sufficiently low, the spontaneous appearance of thermodynamically stable emulsions becomes possible (18, 19). The stability of such emulsions is associated with the excess entropy, and consequently free energy, released by the participation in the Brownian movement of the particles formed in the emulsion (20, 21).

Fig. 7. Dependence of the size (1), number (2) of particles, and viscosity (3) of mixed PS-1–PMMA melt on mixture composition.

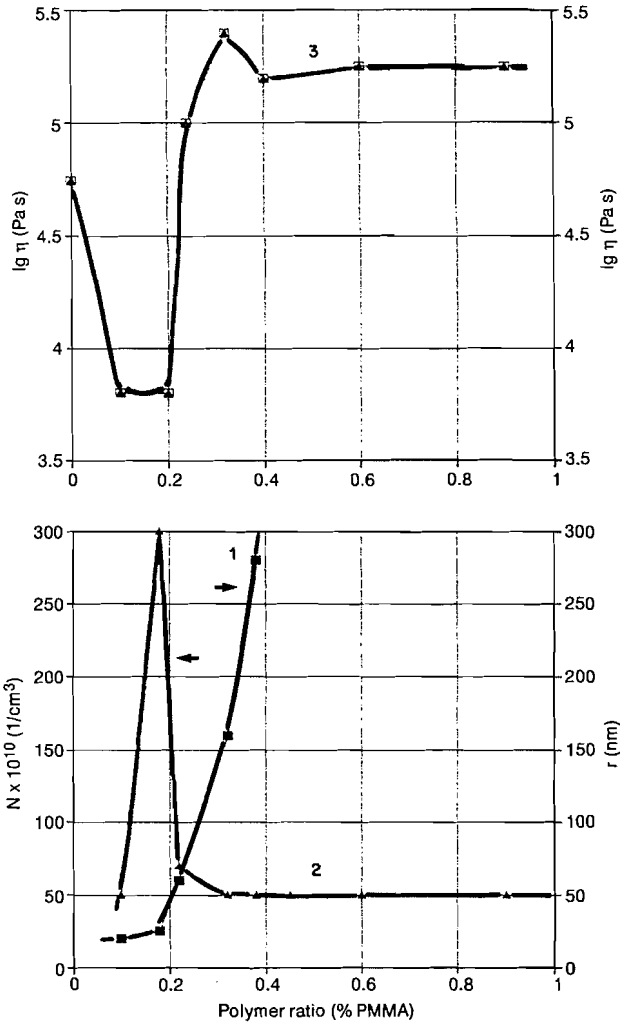

Interfacial tension in the polymer–polymer system is very low, especially in the region of formation of the new phase (22). In consequence, there is a high probability of spontaneous formation of emulsions in mixed polymer solutions near the critical point. The experimental detection of critical opalescence in solutions of polymer mixtures (Figs. 2, 4) and melts, together with estimated sizes and numbers of particles in such emulsions (Figs. 6, 7) verifies the above proposition. These emulsions are likely to be in an equilibrium state, since the system fully maintains its structure, in a solution with sufficiently low viscosity, for a year or more. Moreover, the particle sizes in a disperse emulsion, as well as the number of particles, are not altered by moderate heating and cooling. Solutions of polymer mixtures of moderate concentration exhibit little change in the concentration of phase separation on changing the temperature. In consequence, emulsion stability is maintained with increasing temperature (in the absence of diffusion complications) in high molecular weight viscous liquids, and this can be taken as a sign that the system is in an equilibrium state.

The sharp viscosity drop observed in the region of the existence of critical emulsion can be explained as follows. The

interfacial layer that appears on phase separation contains large volumes of substances belonging to both phases. This is because the thickness of the layer and the interfacial surface area, governed by the small sizes and large numbers of particles in the region of phase separation, are great. Insignificant molecular interaction of incompatible polymers in the interfacial layer leads to a decrease in the cohesion energy density of the mixture as a whole (23), which is equivalent to an increase in the concentration of the free volume inside the interfacial layer (24, 25). Such a system should possess low viscosity. Since the appearance of spontaneously formed highly disperse emulsions is characteristic only of a narrow concentration range near the phase separation point, the concentration range showing the drop in viscosity is also narrow. A small increase in concentration of the solution, or a slight alteration in the composition of the mixture, can push the system beyond the limit of emulsion stability. This causes an instant phase separation of the system, an abrupt drop of interfacial area by 2–3 decimal orders, and an immediate growth of viscosity.

Changes in viscosity on appearance of a new phase, or even a simple restructuring of the supermolecular structure, are a common characteristic for even the most diverse systems. Thus in dilute solutions of PS–PMMA mixtures, increasing the concentration of the solution results in a transition from a structure with isolated coils to a structure characterized by dynamic contacts and interpenetration of coils (critical concentration c_1 according to Doty and Steiner (26)). For this polymer mixture in the solution, a slight, but fully reproducible, minimum in the viscosity was observed exactly at the c_1 point (27). Even in a dilute solution of block copolymer, a minimum in viscosity was observed at the moment of transition from a structure of mixed blocks to a structure of segregated blocks, caused by changing temperature (28, 29).

In conclusion, it can be noted that the uneven distribution of free volume in the system near the critical region in, for example, melted polymer mixtures can be maintained at a lower temperature of the mixtures, even below the glass transition point, where the molecular mobility is limited and the system is no longer in an equilibrium state. Such a system can also have anomalous characteristics when its structure remains similar to that of the "critical" emulsion.

References

1. Ya.I. Frenkel. Kinetic theory of liquids (*in Russian*). Nauka Publ., Leningrad. 1975.
2. M. Smoluchowski. Ann. Phys. **25**, 205 (1908).
3. Z.S. Ornstein and F. Zernicke. Phys. Z. **19**, 761 (1926).
4. P. Debye. Electromagnetic Scattering. M. Keller, New York. 1963. p. 185.
5. P. Debye, D. Woermann, and B. Chu. J. Polym. Sci. A-1, **1**, 256 (1963).
6. A.E. Sheidlin. Experimental investigation of high-parameter water and water vapour thermal capacity (*in Russian*). Teploenergetica Publ., Moscow. 1954. p. 11–14.
7. H.I. Amerkhanov and A.M. Karimov. Dokl. Akad. Nauk SSSR, **113**, 368 (1957).
8. V.K. Semenchenko and E.L. Zorin. Dokl. Akad. Nauk SSSR, **120**, 245 (1960).
9. A.A. Tagyer, V.E. Dreval, and K.G. Habarova. Vysokomol. Soedin. **6**, 1593 (1964).
10. P. Debye. J. Chem. Phys. **31**, 680, (1959).
11. V.N. Kuleznev, L.B. Kandyrin, L.S. Krochina, and E.F. Bukanova. Kolloidn. Zh. **33**, 539 (1971).
12. V.N. Kuleznev, A.E. Chalykh, V.D. Klykova, and L.V. Vershinin. Kolloidn. Zh. **47**, 30 (1985); L.V. Vershinin, V.D. Klykova, V.N. Kuleznev, and L.B. Kandyrin. Kollodn. Zh. **44**, 318 (1982).
13. V.N. Kuleznev. Kolloidn. Zh. **49**, 881 (1987).
14. V.N. Kuleznev and V.D. Klykova. Macromol. Chem. Macromol Symp. **38**, 31 (1990).
15. T. Miura and H. Tanaka. 4th SPSJ Int. Polym. Conf. New Developments in Polymer Science and Technology. Yokohama, Japan. Nov. 29 – Dec. 3 1992. Prepr. Tokyo, 1992.
16. S. Shimada, K. Kasima, I. Hori, and H. Kashiwabara. Macromolecules, **23**, 3769 (1990).
17. V.N. Klenin, C.Yu. Shegolev, and V.N. Lavrushin. Characteristic functions of light scattering in disperse systems (*in Russian*). Saratov Univ. Publ., Saratov. 1977. p. 176.
18. M. Volmer. Z. Phys. Chem. **125**, 151 (1927).
19. P.A. Rehbinder. Kolloidn. Zh. **20**, 527 (1958).
20. E.D. Shukin and P.A. Rehbinder. Kolloidn. Zh. **20**, 645 (1957).
21. E.D. Shukin, A.V. Pertsov, and E.A. Amelina. Colloid chemistry (*in Russian*). Univ. Publ., Moscow. 1982. p. 217.
22. J. Joanny and F. Leiblier. J. Phys. Chem. **39**, 951 (1978).
23. V.N. Kuleznev, B.A. Dogadkin, and V.D. Klykova. Kolloidn. Zh. **30**, 255 (1968).
24. V.N. Kuleznev, L.B. Kandyrin, and V.D. Klykova. Kolloidn. Zh. **34**, 231 (1972).
25. Yu. S. Lipatov. Interphase phenomena in polymers (*Russ.*). Naukova Dumka Publ., Kiev. 1980. p. 256.
26. F. Doty and R. Steiner. J. Polym. Sci. **5**, 383 (1950).
27. L.H. Cragg and C.C. Bigelow. J. Polym. Sci. **24**, 429 (1957); A. Dondos, P. Rempf, and H. Benoit. Polymer, **13**, 97 (1972).
28. N.P. Fedoseeva, V.M. Kuchumova, L.A. Kochanova, and E.D. Shukin. Kolloidn. Zh. **40**, 946 (1978).
29. D.F. Siqueira, S.P. Nunes, and B.A. Wolf. Macromolecules, **27**, 1045 (1994).

Can. J. Chem. Downloaded from www.nrcresearchpress.com by 46.23.64.124 on 09/08/12
For personal use only.

Sequence specificities for lysozyme depolymerization of partially *N*-acetylated chitosans

Bjørn T. Stokke, Kjell M. Vårum, Hilde K. Holme, Ragnhild J.N. Hjerde, and Olav Smidsrød

Can. J. Chem. Downloaded from www.nrcresearchpress.com by 46.23.64.124 on 09/08/12
For personal use only.

Abstract: The influence of sugar residue sequence in partially *N*-acetylated chitosans on relative hydrolysis rate catalyzed by lysozyme was studied. The relative rates were modelled assuming an Arrhenius-type relation for the relative rate constants. The apparent activation energy was assumed to consist of additive contributions from GlcN or GlcNAc residues within the polymer chain interacting with sites A–F of the active cleft of lysozyme. This model accounted well for the relative hydrolysis rates reported for well-defined oligomers. Calculated and experimental data for the dependence of the initial relative hydrolysis rates on fraction of acetylated units, F_A, showed an $F_A^{3,6}$ dependence. A fully water-soluble highly *N*-acetylated chitosan with F_A = 0.68 was depolymerized using lysozyme for further testing of the model. Analyses of the ^{13}C nuclear magnetic resonance spectra of the diad sequences at the new reducing and nonreducing ends formed by lysozyme showed that this enzymatic depolymerization was dominated by chitosan sequences presenting GlcNAc residues to sites C, D, and E of the active cleft. In contrast, there was no selectivity between GlcNAc and GlcN residues interacting with site F. These selectivities were confirmed by the calculated contributions to the apparent activation energy of these sites. The experimentally determined depletion in the diad and triad frequencies of GlcNAc during the course of lysozyme hydrolysis was in good agreement with the model calculations.

Key words: lysozyme, chitosan, chitin, sequence specificity, subsite model.

Résumé : On a étudié l'influence de la séquence des résidus de sucre, dans des chitosanes partiellement *N*-acétylés, sur le vitesses relatives d'hydrolyse par le lysozyme. On a fait un modèle des vitesses relatives en supposant qu'on peut leur appliquer une relation du type d'Arrhenius. On a supposé que l'énergie d'activation apparente est formée de contributions additives des résidus GlcN ou GlcNAc présents dans la chaïne de polymère avec les sites A à F de la cavité du lysozyme. Ce modèle a permis d'expliquer les vitesses d'hydrolyse relatives rapportées pour des oligomères bien définis. Les données calculées et expérimentales concernant la dépendance des vitesses d'hydrolyse relatives initiales sur la fraction d'unités acétylées, F_A, présentent une dépendance $F_A^{3,6}$. Dans le but de vérifier plus à fond le modèle et utilisant le lysozyme, on a dépolymérisé un chitosane *N*-acétylé, complètement soluble dans l'eau et de F_A = 0,68. Des analyses par de la résonance magnétique nucléaire ^{13}C des séquences de diades aux extrémités réductrices et non réductrices formées par le lysozyme ont montré que cette dépolymérisation enzymatique est dominée par des séquences de chitosane présentant des résidus GlcNAc aux sites C, D et E de la cavité active. Par opposition, aucune sélectivité a pu être observée entre les résidus GlcNAc et GlcN qui interagissent avec le site F. On a confirmé ces sélectivités par les contributions calculées à l'énergie apparente d'activation de ces sites. La diminution déterminée expérimentalement dans les fréquences des diades et triades du GlcNAc durant l'hydrolyse par le lysozyme est en bon accord avec les calculs faite avec les modèles.

Mots clés : lysozyme, chitosane, chitine, spécificité séquentielle, modèle d'un sous site.

[Traduit par la rédaction]

Received April 10, 1995.

This paper is dedicated to Professor J.E. (Jim) Guillet in recognition of his contributions to Canadian chemistry.

B.T. Stokke.[1] Norwegian Biopolymer Laboratory, Department of Physics, NTH, University of Trondheim, N-7034 Trondheim, Norway. **K.M. Vårum, H.K. Holme, R.J.N. Hjerde, and O. Smidsrød.** Norwegian Biopolymer Laboratory, Department of Biotechnology, NTH, University of Trondheim, N-7034 Trondheim, Norway.

[1] Author to whom correspondence may be addressed. Telephone: +47 73 59 34 34. Fax: +47 73 59 36 28. E-mail: bstokke@phys.unit.no

Fig. 1. Schematic illustration of a chitosan segment interacting with the six sites of the active cleft of lysozyme. The arrow between sites D and E depicts the localization of the bond being hydrolysed.

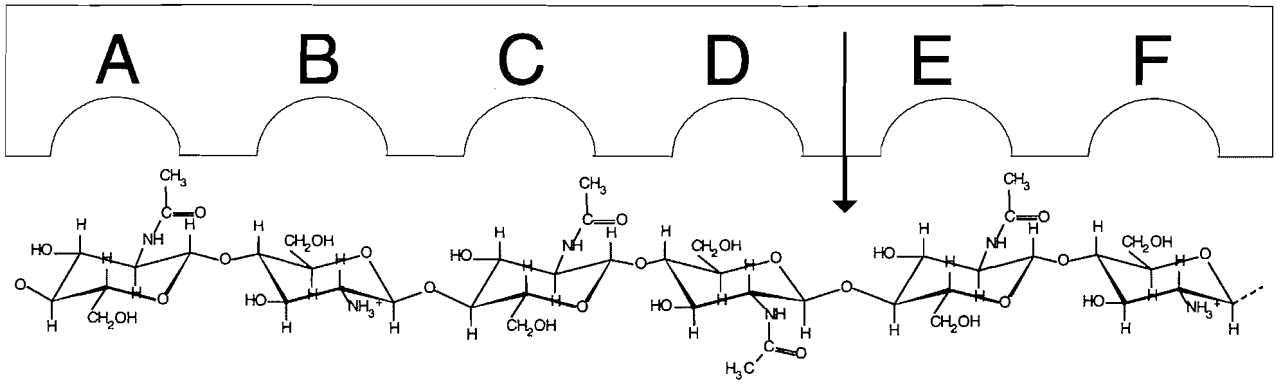

→4)-β-D-GlcNAc-(1→4)-β-D-GlcN-(1→4)-β-D-GlcNAc-(1→4)-β-D-GlcNAc-(1→4)-β-D-GlcNAc-(1→4)-β-D-GlcN-(1→

Introduction

Development and the use of biodegradable polymers require knowledge about the mechanisms of action of enzymes on polymer substrates. Heteropolysaccharides constitute a highly complex field when considered as substrates for polymer-modifying or -cleaving enzymes. Their heterogeneity in chain length, sequence distribution, and the possibility of single-chain and multiple- or multichain enzyme attacks make such a basic enzyme concept as molar substrate concentration difficult to apply. Still, some specificity must be present in the recognition process between the polymeric substrate and the active cleft of the enzyme. This paper considers the influence of the sequential distribution in partially *N*-acetylated chitosans on their enzymatic depolymerization by lysozyme. The primary objective is to explore the influence of sequence distribution on the relative hydrolysis rates, and changes in fractional occurrence of the possible diad and triad combinations due to depolymerization.

Chitosans are made from chitin by *N*-deacetylation under homogeneous or heterogeneous conditions. The resulting polysaccharide consists of 2–acetamido-2–deoxy-β-D-glucopyranose (GlcNAc; **A** unit) and 2–amino-2–deoxy-β-D-glucopyranose (GlcN; **D** unit) connected by (1→4) linkages. It has previously been shown that the sequential arrangement of **A** and **D** residues in the polymer chain is governed by Bernoullian statistics for a range of samples with fraction of acetylated residues, F_A, from 0.01 to 0.5 (1, 2). Lysozyme (EC 3.2.1.17) hydrolyses the β-(1→4) glycosidic linkage in chitin. Depolymerization of chitosans by lysozyme has been studied by various groups because of the large interest in biomedical applications of this polysaccharide. Hirano et al. (3) reported that optimum degradation rates were achieved for chitosans having an F_A of 0.8. However, these data could be difficult to interpret because of differences in solubility as a function of F_A for the chitosans used in that study (4, 5). Nordtveit et al. (4) reported that the initial depolymerization rate of partially *N*-acetylated chitosans catalyzed by lysozyme increases in proportion to F_A raised to the 3.6 power ($F_A^{3.6}$). The interpretation of these observations was made by considering the relative susceptibility of the 64 possible hexamers acting as substrates in a Michaelis–Menten analysis of lysozyme, combined with their relative fraction occurring at different F_A. Furthermore, the rate dependence on substrate and enzyme concentrations followed a Michaelis–Menten type of kinetics.

In this study, a molecular model for quantitative prediction of relative hydrolysis rates by lysozyme for chitosans having different F_A is developed. The model adopted shares many of the features employed in the subsite models of α-amylases acting on linear substrates of the homopolysaccharide α−(1→4)-glucopyranose (6, 7). A crucial difference when comparing lysozyme action on chitosans with α-amylases on amylose-type substrates is the information that can be obtained by studying the depolymerization products. For the binary heteropolysaccharide chitosan, analysis of newly formed end groups and their adjacent neighbours may provide information about subsite specificity that may not be obtained for a hompolysaccharide. As an integrated part of our strategy, we therefore analysed new reducing and nonreducing ends of the lysozyme-depolymerized chitosan using nmr methods.

Molecular model for lysozyme depolymerization of chitosans

The aims of the model were to quantitatively predict relative initial hydrolysis rates for lysozyme-catalyzed depolymerization of chitosans spanning a range of F_A, and to study potential changes in polysaccharide sequence information as a function of degree of depolymerization. The active cleft of lysozyme recognizes six hexose residues at subsites designated A–F. The glycosidic linkage being hydrolysed is located between the sugar residues interacting at sites D and E (Fig. 1). Amano and Ito (8) reported that the relative hydrolysis rates for partially *N*-acetylated oligomers derived from chitosan depend strongly on the acetylation pattern of the oligomers. They also report, by studying the products formed from various oligomers, that more than one binding mode to the active cleft can result in hydrolysis. Their data therefore suggest that the acetylation pattern in chitosan polymers may influence the relative susceptibilities for hydrolysis of the glycosidic linkages within the polymer.

Lysozyme hydrolysis of chitooligomers occurs either by direct hydrolysis of 1:1 substrate-to-enzyme complexes, or 2:1 substrate-to-enzyme complexes, with the relative importance depending on the concentration ratios and degree of polymerization (9, 10). Furthermore, the transglycosylation

Can. J. Chem. Downloaded from www.nrcresearchpress.com by 46.23.64.124 on 09/08/12
For personal use only.

Table 1. Productive binding modes of GlcN (**D**) and GlcNAc (**A**) to the active cleft of lysozyme and associated contribution to apparent activation energy, E_a.[a]

	Interaction subsites in the active cleft of lysozyme					
Residue type	A	B	C	D	E	F
GlcNAc (**A**)	ΔE_A^A	ΔE_B^A	ΔE_C^A	ΔE_D^A	ΔE_E^A	ΔE_F^A
GlcN (**D**)	ΔE_A^D	ΔE_B^D	ΔE_C^D	ΔE_D^D	ΔE_E^D	ΔE_F^D
Parameter set I		−2.00	−1.49	7.80	−0.25	−1.07
(kcal mol^{-1})			4.49	8.85	5.71	−1.16
Parameter set II	−3.0	−2.00	−1.49	7.80	−0.25	−1.07
(kcal mol^{-1})	0	0	4.49	8.85	5.71	−1.16
Parameter set III	−1.5	−2.00	−1.49	7.80	−0.25	−1.07
(kcal mol^{-1})	0	0	4.49	8.85	5.71	−1.16
Parameter set IV	−1.5	−2.00	−1.49	7.80	−0.25	−1.07
(kcal mol^{-1})	0	0	4.49	10.85	5.71	−1.16

[a]The numerical constant k (eq. [2]) was estimated to be 12 544.

Can. J. Chem. Downloaded from www.nrcresearchpress.com by 46.23.64.124 on 09/08/12
For personal use only.

pathway becomes increasingly important relative to the hydration and release of degraded products as the molar concentration of nonreducing ends increases (9, 10). In the following it was assumed that lysozyme hydrolysis data used in the model was governed by random, multiple attack of lysozyme, and that the 2:1 substrate-to-enzyme pathway and the transglycosylation were negligible. Omitting the transglycosylation was justified by working with substrate concentrations lower than about 2×10^{-3} M in aqueous solvents, where the hydration and release of products dominate (9). Disregarding the pathway involving 2:1 substrate-to-enzyme complexes was valid at least in the case of polymeric substrates, but also the experimental data reported by Amano and Ito (8) do not appear to involve significant amounts of 2:1 complexes. This indicates that the parameters for the model to be estimated from hydrolysis rates of various chitooligomers, and from the experiments carried out on higher molecular weight material, correspond with respect to the dominating hydrolysis pathways.

The steady-state Michaelis–Menten enzyme kinetics equations for the 64 possible types of hexasaccharides were deduced by Nordtveit et al. (4):

$$[1] \quad V_{tot} = \frac{\Sigma f_i V_f^i}{1 + K_S/[S]}$$

In eq. [1], V_{tot} is the total hydrolysis rate, the summation is over all possible hexasaccharides, f_i and V_f^i are the fraction of hexasaccharide i and associated maximum hydrolysis rate, respectively. K_S is the dissociation constant for all substrate types, and [S] is the total molar substrate concentration. Equation [1] was derived by assuming the dissociation constants for all substrate types were equal. This assumption was based on the experimental finding that the net hydrolysis rate showed a characteristic levelling off as a function of [S] at the same [S] for different F_A (4). The relative rate for lysozyme hydrolysis of chitosans with increasing F_A can then be calculated using eq. [1], provided that all f_i at a given F_A, and their associated V_f^i and K_S, are given. The fractions f_i were calculated using Bernoullian sequence statistics. Substrate saturation was assumed in the calculation, i.e., $K_S/[S] << 1$ in eq. [1].

The hydrolysis rates, V_f^i, for the 64 hexasaccharides were calculated by applying an activation energy, $E_{a(i)}$, to describe the rate-limiting step of the hydrolysis:

$$[2] \quad V_f^i = k \exp(-E_{a(i)}/RT)$$

where k is a constant, R is the molar gas constant, and T the absolute temperature. It was furthermore assumed that the influence of the hexasaccharide acetylation sequence can be represented by additive contributions arising from each of the **A** or **D** residues within a given oligosaccharide interacting with the subsites A–F in the active cleft of lysozyme. Thus, a contribution ΔE_S^T to $E_{a(i)}$ is assigned to each site S, S = A, B, C, D, E, and F, for interaction with residue of type T, T = **A** or **D**, to the apparent activation energy (Table 1). As an example, consider the hexassacharide **ADAAAD** perfectly aligned in the active cleft of lysozyme (Fig. 1). The hydrolysis rate for this hexasaccharide can then be written:

$$[3] \quad V_f^{ADAAAD} = k \exp[-(\Delta E_A^A + \Delta E_B^D + \Delta E_C^A + \Delta E_D^A + \Delta E_E^A + \Delta E_F^D)/RT]$$

It is sufficient to consider only the hexasaccharides for the initial hydrolysis of high molecular weight polymers. But the same formalism was also applied to oligomers not saturating all sites of the active cleft of lysozyme. If the selected bond between the D and E sites indicated unoccupied sites in the active cleft, these were neglected. This description of the relative hydrolysis rates was also limited to oligosaccharides spanning the D–E sites. Oligosaccharides smaller than hexasaccharides were treated by only considering binding modes that span the D–E sites in lysozyme, and that vacant sites did not contribute to the apparant activation energy. In the present description, differences in relative hydrolysis rates arising

Can. J. Chem. Downloaded from www.nrcresearchpress.com by 46.23.64.124 on 09/08/12
For personal use only.

both from the (microscopic) Michaelis–Menten constants and from the catalytic activities (corresponding to the acceleration factor used by Allen (6)) for different types of chitosan sequences are treated in one term. The motivation for not distinguishing these two possibilities is that binding data for various chitosan sequences have only been determined for a limited number of partly *N*-acetylated trisaccharides (11).

Estimates of values for the various ΔE_S^T were obtained by employing the experimental data reported for relative hydrolysis rates of various tri- and tetrasaccharides (8). These provided 13 equations analogous to eq. [3] for the relative hydrolysis rates with a total of 9 unknowns, ΔE_S^T for T=**A** and **D** and S=C–F, and T=**A** and S=B. These 9 parameters were estimated by minimalization of the sum of the square of residuals between theoretical and reported hydrolysis rates using a Simplex algorithm (12). The equations for the theoretical hydrolysis rates for the various chitooligomers were analogous to eq. [3]. The chitooligomers having more than one productive binding mode were represented by summation over the binding modes, yielding a nonlinear set of equations. Each of the 9 estimated parameters therefore represents a *mean* for the observed hydrolysis rates that includes a given parameter. Estimates for the remaining three contributions to $E_{a(i)}$ were obtained by using the reported relative hydrolysis rates of fully acetylated oligosaccharides to ΔE_A^A (9). Experimental data that can be used to estimate ΔE_A^D and ΔE_B^D are not known, and they were assumed not to influence the relative hydrolysis rates. An estimate of the numerical constant k (eq. [2]) was obtained by assuming a total activation energy of 3 kcal mol^{-1} for the fully acetylated pentamer (9). Note that the *relative* hydrolysis rates V_f^i, however, are independent of this numerical value.

Changes in sequence composition during lysozyme hydrolysis of partially *N*-acetylated chitosans were calculated using a Monte Carlo procedure. First, an ensemble of monodisperse model chitosans with a user selectable F_A and degree of polymerization, DP, was constructed. The sequences of **A** and **D** units in the chains were generated assuming a Bernoullian sequence statistic for the two residues, as previously shown experimentally (1, 2). Furthermore, the lysozyme depolymerization of the reconstructed ensemble was modelled by selecting a linkage at random in a polymer chain for each cycle in the computational procedure. The cycle number was proportional to reaction time with an unknown proportionality constant. Correlation between calculated and experimental data was therefore based on average degree of polymerization to circumvent this limitation.

The selected linkage was assumed to be the one hydrolysed and the adjoining four residues towards the nonreducing end and two residues towards the reducing end were inspected to assign the appropriate hydrolysis rate. No change was introduced to the ensemble if the selected linkage had previously been hydrolysed. The selected linkage was hydrolysed with a relative probability proportional to the relative hydrolysis rate determined by the composition of the hexasaccharide, or shorter oligosaccharide, interacting with the active cleft of lysozyme (eq. [2]). In addition to the relative hydrolysis rates needed for the 64 hexasaccharides, the hydrolysis rates for oligomers with fewer than six residues appearing as a result of multiple cleavages in the same polymer chain, that is, penta-, tetra-, and trisaccharides, were assigned in the same way. These oligomers were assigned with two binding modes spanning the hydrolysis site of the active cleft in lysozyme. Using this approach, a large number of relative hydrolysis constants was needed; these, however, could be reduced to the 12 contributions to the activation energy as described above. The calculated degradation products were characterized with respect to sequential distribution of the ensemble, distribution of degree of polymerization, and chemical composition of free mono-, di-, tri-, and tetrasaccharides.

Materials and methods

Chitosan

Chitin was isolated from shrimp shells. Chitosan was prepared by homogeneous *N*-deacetylation of chitin (13). The chitosan was converted into the chloride salt (chitosan-HCl), filtered and lyophilized. The fraction of *N*-acetylated units was determined by high-field proton nmr spectroscopy (1) to be 68% (F_A = 0.68). The intrinsic viscosity, [η], was determined to 800 mL/g as previously described (14). The number-average molecular weight M_n was estimated from the Mark–Houwink–Sakurada equation (15) as 1.7×10^5 g mol^{-1}.

A lower molecular weight chitosan used for lysozyme depolymerization studies was prepared by depolymerization of chitosan by nitrous acid as previously described (5). The chitosan (F_A = 0.68, M_n = 1.7×10^5 g mol^{-1}) was degraded by 30 mg $NaNO_2$/g chitosan, yielding a sample with intrinsic viscosity of 44 mL/g.

Lysozyme degradation of chitosan

The depolymerized chitosan was used as a substrate for the lysozyme hydrolysis studies. Solutions of chitosan (30 mg) in distilled water (13 mL) were prepared, solid NaCl was added to an ionic strength of 0.05 M, and the pH was adjusted to 4.5. Lysozyme from chicken egg white (Sigma L-6876) was used without further purification. The chitosan–lysozyme solutions were incubated at room temperature for 2 h, lysozyme was (partially) denatured by boiling for 1 h, and the pH subsequently adjusted to 6.5. Lysozyme was still active after this treatment, and in order to fully deactivate the enzyme, 0.3 mL of a mixture of a protease stock solution (3.0 mg α-chymotrypsin (EC 3.4.21.1, Sigma C-4129, type 2), 3.0 mg trypsin (EC 3.4.21.4, Sigma T-8253, type 3 from bovine pancreas), and 3.0 mg NaCl in 2.0 mL distilled water at pH 6.5) was added. The lysozyme–chitosan solutions were incubated for 10 min, the pH was adjusted to 4.5 with HCl, and the solution was lyophilized. Increasing degrees of depolymerization were obtained by employing increasing amounts of lysozyme (1.5, 3.75, and 7.5 mg lysozyme per 30 mg chitosan), corresponding to molar ratios of hexasaccharide units to enzyme of 230, 93, and 46, respectively.

Nuclear magnetic resonance spectroscopy

The number-average degree of polymerization (DP_n) of the lysozyme-degraded chitosans was determined by high-field proton nmr spectroscopy using a JEOL EX-400 (399.65 MHz) spectrometer as previously described (16). The fraction of acetylated units and the diad and triad frequencies were determined by ^{13}C nmr spectroscopy employing a Bruker AM-500 (125.76 MHz) spectrometer (2). The interpretations of the spectra were based on the assignments of carbon resonances

Table 2. Relative chitooligosaccharide hydrolysis rates.

Compound[a]	Relative rate[b]	Binding mode[c] A B C D E F	Calculated relative rate, eq. [2][d] Set I	Set II	Set III	Set IV
AAA	1.0	**A-A-A**	0.66	0.66	0.66	0.66
		A-A-A	0.34	0.34	0.34	0.34
AAD	0.0	**A-A-D**	0.00	0.00	0.00	0.00
	0.4	**A-A-D**	0.38	0.39	0.39	0.39
DAA	0.0	**D-A-A**	0.00	0.00	0.00	0.00
	0.0	**D-A-A**	0.06	0.06	0.06	0.06
AAAA	21	**A-A-A-A**	16.88	16.88	16.88	16.88
		A-A-A-A	3.78	3.78	3.78	3.78
		A-A-A-A	0.34	0.34	0.34	0.34
AAAD	0.0	**A-A-A-D**	0.00	0.00	0.00	0.00
	4.7	**A-A-A-D**	4.36	4.36	4.36	4.36
		A-A-A-D	0.34	0.34	0.34	0.34
ADAA	0.0	**A-D-A-A**	0.00	0.00	0.00	0.00
	0.7	**A-D-A-A**	0.69	0.69	0.69	0.03
	0.0	**A-D-A-A**	0.00	0.00	0.00	0.00
ADAD	0.0	**A-D-A-D**	0.00	0.00	0.00	0.00
	0.8	**A-D-A-D**	0.80	0.80	0.80	0.03
	0.0	**A-D-A-D**	0.00	0.00	0.00	0.00
AAAAA		**A-A-A-A-A**		2195.	192.5	192.5
		A-A-A-A-A		96.4	96.5	96.5
AAAAAA		**A-A-A-A-A-A**		12539	1100.	1100.

[a]The notation designates the chitooligosaccharides without any linkage illustrations, as used by Amano and Ito (8).

[b]The experimental data for relative hydrolysis rates are those reported (8) in the binding modes specified in their Table 3. The lysozyme hydrolyses were carried out at T = 37°C, 0.04 M ammonium acetate, pH 5.25.

[c]The notation designates the chitooligosaccharides with linkage illustrations in their apparent productive binding modes.

[d]The calculated values were based on the parameter values listed in Table 1.

in the trimer **A-A-A** ($(GlcNAc)_3$ (17)), the trimer **D-D-D** ($(GlcN)_3$ and higher GlcN oligomers (18)), and our previous assignments of ^{13}C nmr spectra (2). Absolute values of ^{13}C chemical shift values are difficult to compare, as the shift values are given relative to different standards and temperatures. However, *relative* shift differences between carbons can be directly compared. The chemical shifts, δ of the resonances for the new nonreducing and reducing ends were assigned based on the similarity of difference in δ of the resonances in central and terminal units of the **A-A-A** and **D-D-D** trisaccharides and that observed. Details of this analysis will be given elsewhere (19).

Results and discussion

Model parameters.

The estimated subsite contributions to the activation energy (E_a) for the relative lysozyme hydrolysis rates of chitooligomers are listed in Table 1. Parameter set I contains the nine estimated values obtained from the oligomer data (8) as explained above. The values range from -2 kcal mol^{-1} for presenting **A** residues to site B, to 8.85 kcal mol^{-1} for presenting **D** residues to site D. The sum of the contributions to E_a from the fully acetylated pentamer spanning subsites B–F was set to 3 kcal mol^{-1} (9), yielding k = 12 544. It should be noted that it is a prerequisite in the model that the chitooligomers should interact with both subsites D and E for the approach to be valid. The interpretation of a negative contribution to E_a in the present model implies that the hydrolysis rate increases when that site is occupied. The parameter values show strong preference for **A** relative to **D** residues in subsites C and E. The relative rate of hydrolysis for chitooligomers presenting **A** residues relative to **D** residues to site D is calculated to 5.6, whereas there is hardly any selectivity in the F-site. Note that these parameter values were derived without any assumptions about relative contributions to the hydrolysis rate arising from different binding modes of a given chitooligosaccharide. The contributions to E_a for the fully acetylated hexamer are negative for interactions at all sites except D, which corresponds to the trend observed for the binding energies to these sites (9).

In Table 2, the calculated rate constants for the chitooligosaccharides are compared with the reported experimental relative hydrolysis rates (8) to test the quality of the best fit. The agreement between the calculated relative hydrolysis rates (eq. [2]) using the estimated contributions to E_a and the experimentally determined relative rates is excellent. The largest deviation is 0.06 for the **DAA** in the DEF binding mode. The selected number of figures included in Table 2 for the relative rates is intended only to show the precision in the fit of the model to the observations, and not to reflect the num-

Can. J. Chem. Downloaded from www.nrcresearchpress.com by 46.23.64.124 on 09/08/12
For personal use only.

Table 3. The ^{13}C nmr chemical shift assignments[a] in D_2O at 90°C (pD 4) for lysozyme depolymerized chitosan oligomers.

	Carbon			
Sequence[b]	C1	C3	C4	C5
-A-**A** (α)	92.9	71.9	82.4	(72.6)
-A-**A** (β)	97.4	75.0	82.0	77.2
-**A**-A-	103.6			
-A-**A**-		74.7	82.0	77.2
-**D**-D-	100.0			
-D-**D**-		72.6	79.8	77.3
A-A- (nonreducing)		76.1	(72.6)	78.5
A-D- (nonreducing)		76.0	(72.6)	78.5

[a]Chemical shifts given relative to the resonance of sodium 3-(trimethylsilyl)propionate-d_4.

[b]Underlined residue depicts the one being considered, others indicate neighbours in the chain segment depicted with the reducing end to the right. Glycosidic linkages are indicated with a short line and its absence refers specifically to reducing or nonreducing ends. The notation assumes the nonreducing end to the left, and the reducing end to the right.

Can. J. Chem. Downloaded from www.nrcresearchpress.com by 46.23.64.124 on 09/08/12
For personal use only.

ber of significant figures. The data (Table 2) also illustrate the approach adopted for the chitooligosaccharides where the net relative rate for more than one productive binding mode was determined experimentally. The net rate was assumed to be equal to the sum of the different binding modes. The estimated values of ΔE_S^T allow direct calculation of the relative rates for different binding modes without any further assumptions. A further aspect of the model is that the relative hydrolysis rates for chitooligosaccharides other than those used in the experimental studies can be predicted.

The good agreement between the experimentally determined relative hydrolysis rates and the best fit of the model shows the quality of the noncooperative additive model. Typical for many recognition processes, e.g., chain pairing or formation of α-helical structures, are their cooperative nature, i.e., that a given state is not independent of other states. Likewise, it could be expected, in the current model, that contributions ΔE_S^T may depend on the type of residue that is interacting in the neighbouring sites. An extension to a cooperative model would be at the expense of an increasing number of parameters. The good agreement between the best fit of the model data and the experimentally determined parameters (Table 2) indicates that it is not necessary to extend the model to include nearest neighbour effects.

The parameter set II (Table 1) is completed for the contributions not directly calculable from the experimental data (8). The values of ΔE_A^A were selected to nearly reproduce the reported increase in relative hydrolysis rates from fully acetylated pentamer to hexamer. The experimental values, however, dictate that the most favorable contribution to E_a arises from interaction in the A-site, and an additional value for this parameter was therefore also selected (Table 1, set III) for further testing. The parameter values for ΔE_A^D and ΔE_B^D were set to zero as a first approximation, since experimental data have not been reported. Parameter set IV was derived from set III by adding 2 kcal mol^{-1} to ΔE_D^D. This is based on the results from the nmr analysis of the new reducing ends introduced by lysozyme hydrolysis of partially *N*-acetylated chitosans (see below) that showed a stronger preference for **A** units relative to **D** units interacting at site D compared to the data of Amano and Ito (8). The fit to the observed relative hydrolysis rate deviates therefore for the **A-D-A-A** and **A-D-A-D** tetrasaccharides using parameter set IV compared to the other parameter sets (Table 2).

Nuclear magnetic resonance spectroscopy

The 125 MHz proton decoupled ^{13}C nmr spectra of the chitosan substrate (F_A = 0.68, DP_n = 30) and the same chitosan extensively hydrolysed (DP_n = 7) by lysozyme are shown in Fig. 2. The selection of the relatively high F_A, intermediate DP_n, substrate for these studies was based on increased sensitivity towards changes in diad and triad frequencies with increasing F_A, and the possibility of determining DP_n directly from the number of reducing ends and of characterizing the diad and triad frequencies of the substrate without depolymerization. From the ^1H nmr spectra of the lysozyme-degraded chitosan (data not shown), it was found that the new reducing ends were exclusively from **A** units, as previously reported for lysozyme hydrolysis of a more deacetylated chitosan sample (16). This interpretation confirms the strong preference for **A** units interacting at site D for hydrolysis to occur. The lysozyme hydrolysis of the partially *N*-acetylated chitosan introduces new reducing and nonreducing end signals, as clearly seen in Fig. 2. Assignments of these end signals were much simplified by the fact that the new reducing ends were exclusively from **A** units (19).

The chemical shift assignments of the spectra are shown in Table 3. The resonances of the α- and β-anomers of C1 are seen at 92.9 and 97.4 ppm, respectively, which represent upfield shifts of 6.2 and 10.7 ppm from the **AA** diad (103.6 ppm). The absence of sequence splitting in the resonances of the α- and β-anomers of C1 suggests that the preceding unit of the reducing **A** units may not be dependent on the composition

Can. J. Chem. Downloaded from www.nrcresearchpress.com by 46.23.64.124 on 09/08/12
For personal use only.

Fig. 2. The ^{13}C nmr spectrum (125 MHz) of a solution of chitosan used as substrate for lysozyme hydrolysis, $DP_n = 30$ (*a*), and a lysozyme-hydrolysed sample with $DP_n = 7$ (*b*), in D_2O at $T = 90°C$.

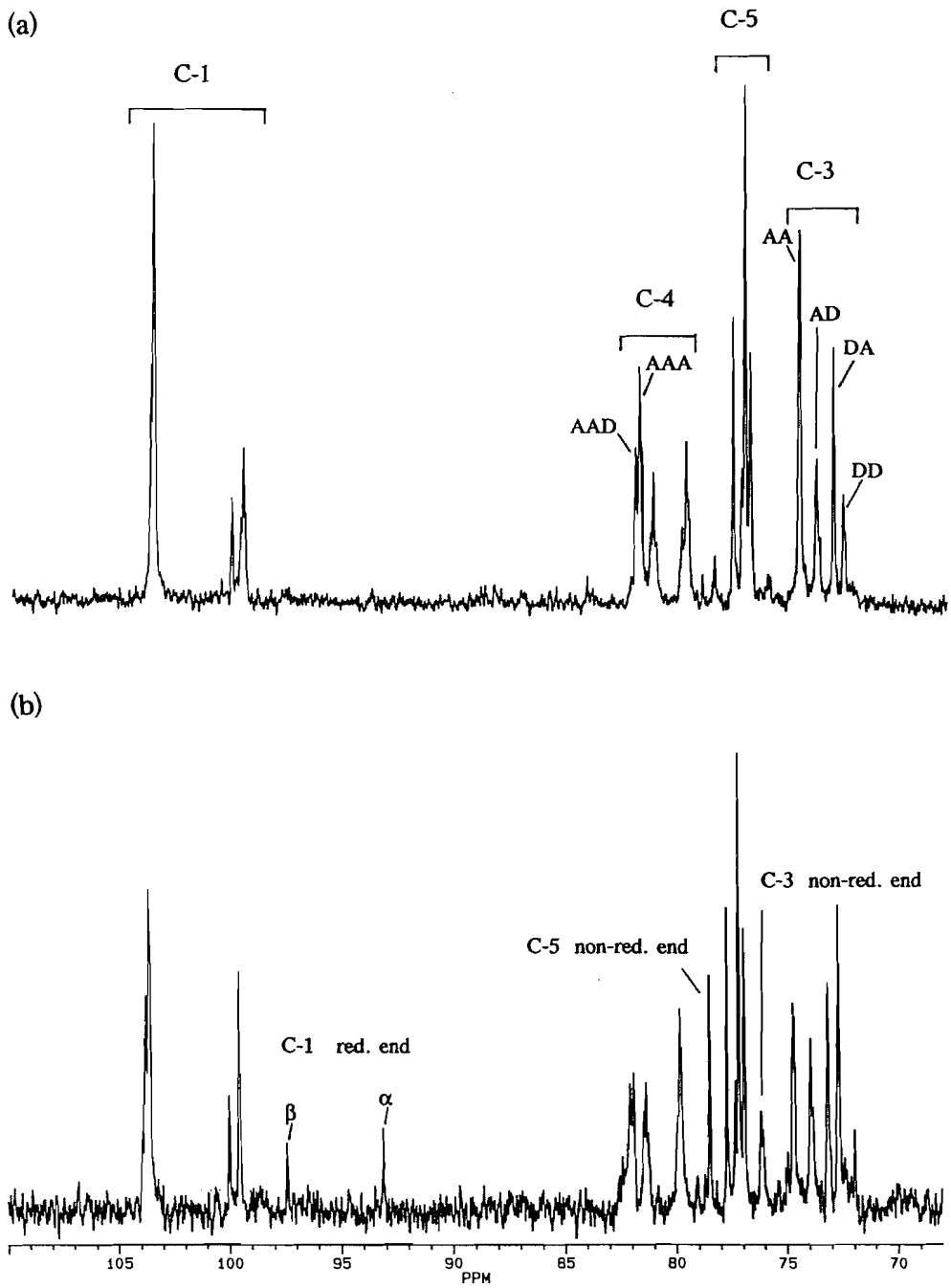

of the chitosan, i.e., the reducing end is exclusively -**A**-**A** or -**D**-**A**. If this neighbouring unit is an **A**, it implies preference for **A** units interacting at site C of lysozyme for the hydrolysis. This is consistent with the data from hydrolysis of oligomers (8) and is also seen in the estimated parameter values (Table 1). However, the possibility that the C1 anomers are insensitive to the neigbouring unit cannot be excluded. Note also the absence of reducing end resonances from **D** units in the area for these resonances (18), in agreement with the proton nmr spectra (16). However, the C1 resonances were not used for quantification of diad frequencies, because the **AA** and **AD** diads were poorly resolved, and the nonreducing ends were not resolved from the diads.

The finding that F_A was constant during lysozyme depolymerization of the chitosan samples (Table 4) indicates that α-chymotrypsin used to deactivate lysozyme (see Materials and methods) did not hydrolyze the -NH-CO-CH_3 linkage in the chitosan. The observed changes in the diad and triad frequencies arise therefore from differences in hydrolysis rates of the chitooligomers and not from depletion of acetylated units.

Detailed assignments of the diad frequencies and the reducing or nonreducing ends were performed on C3, C4, and C5.

Table 4. Composition and diad and triad frequencies in chitooligomers obtained by lysozyme depolymerization from C3 and C4 resonances determined by ^{13}C nmr spectroscopy.

		F_A	F_{AA}		F_{DA}	F_{AD}	F_{DD}	F_{AAA}	F_{AAD}
DP_n	Resonance:	C3	C3	C4	C3	C3	C3	C4	C4
30[a]		0.68	0.440	0.448	0.230	0.212	0.118	0.306	0.142
			0.449[b]		0.221[b]	0.221[b]	0.109[b]	0.301[b]	0.148[b]
20		0.70	0.486	0.461	0.214	0.182	0.118	0.256	0.205
15		0.68	0.419	0.433	0.251	0.201	0.129	0.235	0.198
7		0.68	0.416	0.397	0.254	0.228	0.102	0.179	0.218

[a]Substrate for lysozyme hydrolysis prepared by nitrite degradation of the high M_n sample.
[b]Calculated assuming Bernoullian sequence distribution and experimentally determined F_A.

These were carried out to get information on the specificity of the individual sites on lysozyme towards the **A** and **D** units, and to obtain experimental data from diad and triad frequencies that could be compared to the calculated data. The nmr data detailing the analysis of nearest neighbour composition to the new nonreducing and reducing ends will be reported separately (19), but key features relevant for comparison with the calculations are given here. Note that the resonance at ~82 ppm is the **AA** diad from C4, which is further split into two resonance lines, identified with the triads **AAA** (at the lowest ppm value) and **AAD** (2). The **AAA** triad clearly decreases in intensity relative to **AAD** as lysozyme hydrolyses the chitosan (Fig. 2).

The absence of sequence splitting in the resonances of the α- and β-anomers of C3, as for C1, again suggests that the preceding unit of the reducing **A** units is independent of the composition of the chitosan, i.e., site C on lysozyme must bind an **A** unit for hydrolysis to occur. The resonance at ~76 ppm from C3 at the nonreducing end is split into two resonance lines, indicating that this carbon is sensitive to the nearest neighbour, which can be either an **A** or a **D** unit. The intensities of the two resonance lines at 76.1 and 76.0 ppm were found to be identical to the fraction of **A** and **D** units in the chitosan. These two resonances were identified as **AA** (at the higher ppm value) and **AD** (at the lower ppm value) in a separate experiment where a partially *N*-acetylated chitosan with $F_A = 0.5$ was degraded with lysozyme and the two resonances were found to be identical in intensity (data not shown). Because the **A** and **D** units are randomly distributed along the chain and the neighbouring unit to the nonreducing end associates with subsite F for the hydrolysis to occur, these data show that there is no selectivity for **A** or **D** units at site F on lysozyme degrading partially *N*-acetylated chitosans. That the calculated contributions from **A** and **D** units to E_a (Table 1) show no strong preference for either type of residue is in line with this data. The nmr data thus support the model adopted in describing the relative hydrolysis rates. Previous studies of lysozyme-catalyzed transglycosylation reaction at subsites E and F have shown that there is a strong preference for GlcNAc (**A**) at subsite E through its 2-acetamido group while this group is not involved in interactions at subsite F (20), according to our results.

Comparison of observed and calculated relation between initial hydrolysis rates and F_A

Figure 3 shows the calculated initial hydrolysis rate for chitosans having F_A = 0.05–0.7 for the parameter sets II–IV. Sub-

Fig. 3. Calculated relative hydrolysis rates for chitosans versus degree of acetylation, F_A, using parameter set II (———), set III (— — —), and set IV (- - - -) compared with the experimentally determined initial hydrolysis rates (○, (ref. 4)). The units for relative rates are those for the oligosaccharides in the case of the calculated curves (Table 2), and are normalized to a relative rate set to 1 for $F_A = 0.12$ for the experimental data.

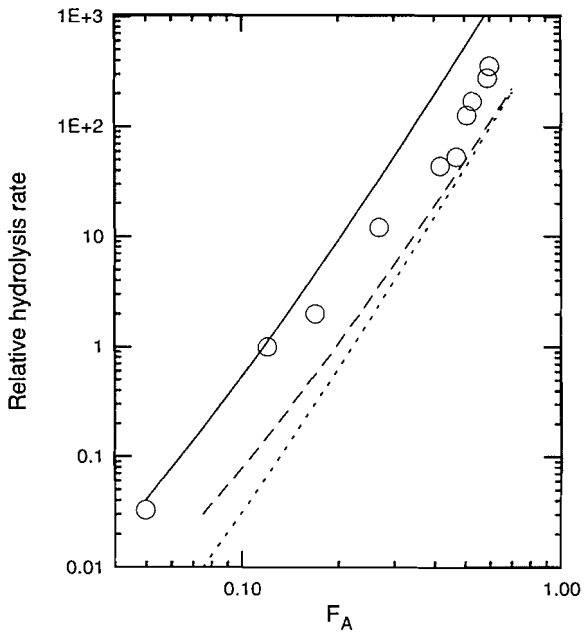

strate saturation was further assumed for all 64 hexamers, i.e., $K_S/[S] << 1$ in eq. [1]. These model data were compared with the experimental data for the initial hydrolysis rates reported by Nordtveit et al. (4). The experimentally determined initial hydrolysis rates were reported to depend on F_A raised to the 3.6 power ($F_A^{3.6}$). The calculations show that the relative initial hydrolysis rates versus F_A depend on the parameter set, i.e., on the hydrolysis rate increase of fully acetylated oligomers from tetramers to hexamers. On the other hand, the calculations also show that the relative dependence on F_A is not sensitive to this increase. The reason for this is the relatively small fraction of fully acetylated pentamer or higher oligomer sequences. The results from the nmr data, indicating no selectivity between **A** and **D** units interacting with site F, suggest that the relative hydrolysis rate at the maximum should

Can. J. Chem. Downloaded from www.nrcresearchpress.com by 46.23.64.124 on 09/08/12
For personal use only.

Can. J. Chem. Downloaded from www.nrcresearchpress.com by 46.23.64.124 on 09/08/12
For personal use only.

depend on F_A raised to the fifth power (F_A^5) and not the sixth power (F_A^6). Increasing the selectivity for **A** units relative to **D** units in site D (parameter set III compared to IV) yields a stronger dependence on F_A for the lower F_A values (less than about 0.15).

The experimentally determined initial rates show an excellent fit to the calculations when only the dependence on F_A is considered, and the experimental data appear to be more in line with calculations based on parameter sets II and III than on IV. However, since the comparison is based on relative rates, further comparison based on absolute rates is required to discriminate between different parameter sets. Direct comparisons between absolute rates are also difficult because the solution conditions for lysozyme hydrolysis of the chitooligomers, $T = 37°C$, 0.04 M ammonium acetate, pH 5.25 (8), differ from those used for lysozyme hydrolysis of chitosan, T = 20°C, 0.1 M KCl, pH 4.5 (4). This does not invalidate the present calculations discussing relative effects of F_A because the relative dependence of initial hydrolysis rate on F_A has been found to be largely independent of solution ionic strengths and pH (21).

The present model for lysozyme action on chitosans also reproduces the nonlinear time course of lysozyme hydrolysis of partially *N*-acetylated chitosans (data not shown). This is in line with the experimental data (4) and illustrates that lysozyme preferentially hydrolyses the fully acetylated sequences in the polymeric chain.

Comparison of calculated and observed changes in chitosan sequence information

A further interesting aspect of lysozyme hydrolysis of chitosans is the potential change in sequential distribution in the polymeric chain. Since the relative hydrolysis rates show a strong preference for cleavage of the fully acetylated sequences, concomitant decrease in fractions of **AA** diads, F_{AA}, and **AAA** triads, F_{AAA}, is expected as the degradation continues. The Monte Carlo calculations of lysozyme hydrolysis of partially *N*-acetylated chitosans predict changes in the relative amounts of the diads and triads. In particular, the F_{AA} and F_{AAA} are predicted to decrease.

Removal of a diad occurs by direct cleavage of the glycosidic linkage. As an example, consider the tetrameric sequence consisting of four **A** units (-$\mathbf{A_1}$-$\mathbf{A_2}$-$\mathbf{A_3}$-$\mathbf{A_4}$-) numbered 1–4 to illustrate the three diad frequencies in this tetramer sequence ($\mathbf{A_1A_2}$, $\mathbf{A_2A_3}$, and $\mathbf{A_3A_4}$). Cleavage of the glycosidic linkage between $\mathbf{A_2}$ and $\mathbf{A_3}$ removes one of the three diads ($\mathbf{A_2A_3}$). Since this cleavage leads to new nonreducing and reducing ends, it must be taken into account in analysis of the sequence information from the nmr spectra. Since it is likely that the C3 and C4 carbon resonances, which were used to determined the diad frequencies, are most influenced by the preceding residue in the chain (2), we need to consider the three diads $\mathbf{A_1\underline{A}_2}$, $\mathbf{A_2\underline{A}_3}$, and $\mathbf{A_3\underline{A}_4}$, where the underlining means the unit from which the resonance originates. By cleaving the glycosidic linkage between $\mathbf{A_2}$ and $\mathbf{A_3}$, the three diads $\mathbf{A_1\underline{A}_2}$ (with $\mathbf{A_2}$ at the reducing end), $\mathbf{\underline{A}_3A_4}$ (with $\mathbf{A_3}$ at the nonreducing end), and $\mathbf{A_3\underline{A}_4}$ (with $\mathbf{A_3}$ at the nonreducing end) are observed in the nmr spectrum. Either the reducing **or** the nonreducing end should be included in the **AA** diad for correspondence with the calculations. This becomes increasingly more important the lower the DP_n, as is the case for the lysozyme-hydrolysed chitooligomers. Concerning C3, both the reducing and the nonreducing ends are shifted out of the **AA** diad, while for C4 only the β-reducing end is contained in the **AA** diad. The diad frequencies as a function of lysozyme degradation using C3 and C4 have been corrected, and are shown in Table 4.

Fig. 4. Experimentally determined change in fraction of diad frequency F_{AA} (*a*) and triad frequency F_{AAA} (*b*) due to lysozyme depolymerization of a chitosan substrate with $DP_n = 30$, $F_A = 0.68$. Monte Carlo simulated changes in the corresponding diad and triad using parameter set II (———), set III (— — —), and set IV (- - - -) using an ensemble of 1000 chains. Note that increasing extents of lysozyme hydrolysis yielding decreasing DP_n correspond to moving from the right to the left on the *x*-scale.

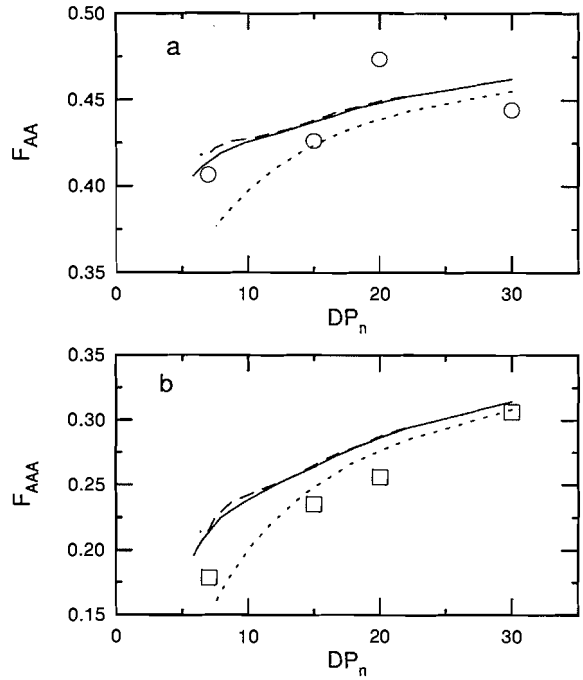

Comparison of the observed changes in the F_{AA} diads as a result of lysozyme degradation with those calculated using the Monte Carlo approach (Fig. 4*a*) shows that there is good agreement between the relative reduction in this diad fraction betweeen the experiments and the model. Analogously, there is good agreement between the experimentally determined reduction of F_{AAA} and the calculated values (Fig. 4*b*). The predicted decrease in both F_{AA} and F_{AAA} is larger at a given DP_n for parameter set IV than for sets II and III. This is as expected since parameter set IV implies a stronger preference for **A** units at site D. The experimental uncertainty does not, however, allow preference for either parameter set as the best fit.

Conclusions

This is the first study of the lysozyme specificity for GlcN (**D**) and GlcNAc (**A**) at the six possible subsites in the active cleft using a combination of nmr and modelling techniques. This allows us to relate the hydrolysis rates at the polymer level to those for chitooligomers. A molecular model for considering chemical heterogeneity in polysaccharides when they act as enzymatic substrates is proposed. It is assumed that the relative hydrolysis rate for the rate-limiting step in the reaction

can be described by an activation energy. The activation energy was further assumed to consist of additive contributions specific for the type of substrate residue interacting at a given subsite in the active cleft of the enzyme. These contributions reveal selectivities between **A** and **D** residues in sites C–F that were found to be consistent with the terminal sequences for both the reducing and nonreducing ends introduced by lysozyme, as determined by nmr spectroscopy. Using the calculated relative hydrolysis rates for the possible hexasaccharides, good agreement was found between experimental data for initial hydrolysis rates for polymeric chitosan substrates with F_A from 0.04 to 0.60. It was further found that preferential hydrolysis of fully acetylated sequences in a polymeric chitosan substrate yielded depletion of the F_{AA} diad and the F_{AAA} triad that was in quantitative agreement with that predicted using a Monte Carlo calculation. In summary, this study shows that the preferential lysozyme hydrolyses reported for oligomeric substrates are preserved for the polymeric substrate. The general approach of using an activation energy to account for different sequences interacting with the subsites of the enzyme could also be explored for other types of enzymes working on *co*-polymeric substrates. Alginate M- and G-lyase depolymerizing alginates (22–24), β-D-mannanase hydrolysing galactomannan (25), and chitinase/chitosanase depolymerizing chitosan (26) are all examples in this respect.

Acknowledgements

The authors are indebted to M.Sc. Are Kristiansen and Eng. A. Østensen for recording the ^{1}H nmr and ^{13}C nmr spectra, respectively. This work is supported by The Norwegian Research Council (Grants BT 23484, 104966/110, and 107484/410) and Pronova Biopolymer a.s. (Drammen, Norway).

References

1. K.M. Vårum, M.W. Anthonsen, H. Grasdalen, and O. Smidsrød. Carbohydr. Res. **211**, 17 (1991).
2. K.M. Vårum, M.W. Anthonsen, H. Grasdalen, and O. Smidsrød. Carbohydr. Res. **217**, 19 (1991).
3. S. Hirano, H. Tsuchida, and N. Nagao. Biomaterials, **10**, 574 (1989).
4. R.J. Nordtveit, K.M. Vårum, and O. Smidsrød. Carbohydr. Polym. **23**, 253 (1994).
5. K.M. Vårum, M.H. Ottøy, and O. Smidsrød. Carbohydr. Polym. **25**, 65 (1994).
6. J.D. Allen. Methods Enzymol. **64**, 248 (1980)
7. E.A. MacGregor, A.W. MacGregor, L.J. Macri, and J.E. Morgan. Carbohydr. Res. **257**, 249 (1994).
8. K.-I. Amano and E. Ito. Eur. J. Biochem. **85**, 97 (1978).
9. J.A. Rupley and V. Gates. Proc. Natl. Acad. Sci. U.S.A. **57**, 496 (1967).
10. A. Masaki, T. Fukamizo, A. Otakara, T. Torikata, K. Hayashi, and T. Imoto. J. Biochem. (Tokyo), **90**, 1167 (1981).
11. T. Fukamizo, Y. Ikeda, T. Ohkawa, and S. Goto. Eur. J. Biochem. **210**, 351 (1992).
12. M.S. Caceci and W.P. Cacheris. Byte, 340 (May) (1984).
13. T. Sannan, K. Kurita, K. Ogura, and Y. Iwakura. Polymer, **19**, 458 (1978).
14. K. I. Draget, K.M. Vårum, E. Moen, H. Gynnild, and O. Smidsrød. Biomaterials, **13**, 635 (1992).
15. M.W. Anthonsen, K.M. Vårum, and O.Smidsrød. Carbohydr. Polym. **22**, 193 (1993).
16. K. Ishiguro, N. Yoshie, M. Sakurai, and Y. Inoue. Carbohydr. Res. **237**, 333 (1992).
17. J. Boyd, R. Porteous, and N. Soffe. Carbohydr. Res. **139**, 35 (1985).
18. A. Domard and N. Cartier. Int. J. Biol. Macromol. **11**, 297 (1989).
19. K.M. Vårum, H. K. Holme, M. Izume, B.T. Stokke, and O. Smidsrød. Submitted.
20. J.J. Pollock and N. Sharon. Biochemistry, **9**, 3913 (1970).
21. R.J.Nordtveit, K.M.Vårum, and O. Smidsrød. Carbohydr. Polym. In press.
22. K. Østgaard, B.T. Stokke, and B. Larsen. Carbohydr. Res. **260**, 83 (1994).
23. K. Østgaard. Carbohydr. Polym. **19**, 51 (1992).
24. P. Gacesa. Int. J. Biochem. **24**, 545 (1992).
25. B.V. McCleary, A.H. Clark, I.C.M. Dea, and D.A. Rees. Carbohydr. Res. **139**, 237 (1985).
26. M. Izume, S. Nagae, H. Kawagishi, M. Mitsutomi, and A. Ohtakara. Biosci. Biotech. Biochem, **56**, 448 (1992).

Can. J. Chem. Downloaded from www.nrcresearchpress.com by 46.23.64.124 on 09/08/12
For personal use only.

Luminescence studies of hydrophobically modified, water-soluble polymers. I. Fluorescence anisotropy and spectroscopic investigations of the conformational behaviour of copolymers of acrylic acid and styrene or methyl methacrylate

J.R. Ebdon, B.J. Hunt, D.M. Lucas, I. Soutar, L. Swanson, and A.R. Lane

Abstract: Fluorescence spectroscopy and anisotropy measurements have been used to study a series of styrene – acrylic acid, STY–AA, and methyl methacrylate – acrylic acid, MMA–AA, copolymers in dilute methanolic and aqueous solutions. Copolymerization of either STY or MMA with AA has little effect upon the rate of intramolecular segmental motion in methanol solutions. In aqueous media, intramolecular hydrophobic aggregation occurs and restricts the macromolecular dynamics to an extent dependent upon pH, nature of the comonomer, and copolymer composition. The hydrophobic domains formed in these copolymer systems can solubilize organic guests. In this respect, STY is a more powerful modifier of AA-based polymer behaviours than is MMA. In general, the hydrophobic modification increases the solubilization power of the resultant polymer. Furthermore, the copolymers retain their solubilization capacities to higher values of pH the more hydrophobic the comonomer and the greater its content in the copolymer. The interiors of the hydrophobic aggregates reduce the mobilities of occluded guests: the microviscosities of the domain interiors depend upon the nature of the hydrophobe, pH, and copolymer composition.

Key words: fluorescence, anisotropy, water-soluble polymers, acrylic acid, hydrophobic modification.

Résumé : On a utilisé des mesures d'anisotropie et de spectroscopie de fluorescence pour étudier une série de copolymères de styrène – acide acrylique, STY–AA, et de méthacrylate de méthyle – acide acrylique, MMA–AA, en solutions diluées dans le méthanol et dans l'eau. La copolymérisation du STY ou du MMA avec l'AA n'a que de faibles effets sur la vitesse du mouvement segmental intramoléculaire, en solutions méthanoliques. En milieu aqueux, il se produit une agrégation hydrophobe intramoléculaire et elle restreint la dynamique macromoléculaire qui dépend, jusqu'à un certain point, sur la nature du comonomère et de la composition du copolymère. Les domaines hydrophobes qui se forment dans ces systèmes de copolymères peuvent solubiliser des hôtes organiques. À ce point de vue le STY est un modificateur plus puissant des comportements des polymères basés sur le AA que ceux basés sur le MMA. En général, la modification hydrophobe augmente le pouvoir de solubilisation du polymère qui en résulte. De plus, plus le comonomère est hydrophobe et plus il contient de copolymère, plus les copolymères conservent leurs propriétés de solubilisation à des valeurs élevées de pH. Les intérieurs des agrégats hydrophobes réduisent les mobilités des hôtes occlus : les microviscosités des domaines intérieurs dépendent de la nature de l'hydrophobe, du pH et de la composition en copolymère.

Mots clés : fluorescence, anisotropie, polymères solubles en milieu aqueux, acide acrylique, modification hydrophobe.

[Traduit par la rédaction]

Received April 30, 1995.

This paper is dedicated to Professor J.E. (Jim) Guillet in recognition of his contributions to Canadian chemistry.

J.R. Ebdon, B.J. Hunt, D.M. Lucas, I. Soutar,[1] **and L. Swanson.** The Polymer Centre, School of Physics and Chemistry, Lancaster University, Lancaster LA1 4YA, U.K.
A.R. Lane. Royal Mail Research Centre, Wheatstone Road, Dorcan, Swindon SN3 4RD, U.K.

[1] Author to whom correspondence may be addressed. Telephone: +44-1524-593655. Fax: +44-1524-844037.

Can. J. Chem. Downloaded from www.nrcresearchpress.com by 46.23.64.124 on 09/08/12
For personal use only.

Can. J. Chem. Downloaded from www.nrcresearchpress.com by 46.23.64.124 on 09/08/12
For personal use only.

Introduction

Water-soluble and water-swellable polymers constitute an important class of materials that finds application in a diverse range of technologies including those concerned with the production of agrochemicals, adhesives, coatings, enhancers for oil recovery, foodstuffs, personal care products, superabsorbants, inks, and coding systems. Consequently, a significant amount of effort has been expended, in recent years, in attempts to better understand the factors that govern the physical behaviour of macromolecules in aqueous media. (For recent overviews, see, for example, refs. 1 and 2).

Certain water-soluble polymers and their hydrophobically modified forms have the ability to solubilize species that would otherwise be sparingly soluble in water. When the hydrophobic pockets formed by such molecules are composed of a significant amount of aromatic material, the polymers have the potential for performance of photochemistry upon occluded guests, which is considerably enhanced by energy transfer from the host macromolecule. The field of "energy-harvesting" water-soluble polymers has been pioneered by Guillet and his co-workers. Guillet has coined the terms "antenna effect" and "photozyme" to describe the energy-channeling process and the "light-harvesting" polymers, respectively.

In the first published example (3) of the antenna effect in aqueous media, it was shown that the transfer of energy from naphthyl species to terminal anthryl groups in an acrylic acid – 1-naphthylmethyl methacrylate copolymer was much more efficient in alkaline aqueous solution than in organic solvents. It was proposed that the hydrophobic naphthyl derivatives formed aggregates in the aqueous medium, thereby enhancing the energy transfer process (3). This report was followed by a series of papers on the antenna effect, initiated in 1982 (4). These seminal publications illustrate the importance of the antenna effect upon the photophysics and photochemistries that occur within the close confines of the hydrophobic domains, which can be created in aqueous polymer solutions. The photocatalytic activity of photozyme systems has been amply illustrated (5–11). The field of photon-harvesting polymers has been the subject of an excellent review (12).

Luminescence spectroscopy has featured prominently in studies of the physical behaviour of water-soluble polymers: techniques employed include those of fluorescence quenching (e.g., refs. 13–20), energy transfer (e.g., refs. 3, 4, 12, 21–23), excimer formation (e.g., refs. 24–32), phosphorescence (19, 33–35), and fluorescence anisotropy (e.g., refs. 13, 36–43). Time-resolved anisotropy measurements, TRAMS, involving labelled polymers, are particularly useful in the study of the conformational behaviour of polymers since they allow direct examination of the segmental dynamics of the macromolecule. (See, for example, refs. 44–46 and references therein.) However, relatively few studies involving TRAMS have been reported on water-soluble polymers (13, 37–43).

In the current article, we report on fluorescence anisotropy studies (both time-resolved and steady state) on the effects of hydrophobic modification (through copolymerization) upon the conformational behaviour of acrylic acid-based polyelectrolytes. The investigations have involved the use of both fluorescent labels and probes. The resultant data are of relevance to considerations of the development of novel polymeric solubilizing media, including photozymes.

Experimental

Materials

Methyl methacrylate (Aldrich) and styrene were freed of inhibitor using 10% NaOH, washed with distilled water until the washings were neutral to litmus, dried (molecular sieve), and distilled under high vacuum. Acrylic and methacrylic acids (Aldrich) were prepolymerized using uv irradiation and fractionally distilled under high vacuum, immediately prior to use. Acenaphthylene (Aldrich, 99%) was purified by multiple recrystallization from ethanol, followed by sublimation under high vacuum. 1-Vinyl naphthalene was synthesized from 1-acetonaphthone (Aldrich) by reduction ($NaBH_4$) to the carbinol followed by dehydration ($KHSO_4$). The monomer was purified by fractional vacuum distillation.

Polymers of acrylic acid (AA) and copolymers of AA with styrene (STY) or methyl methacrylate (MMA) were formed by free radical solution (50 wt.% toluene) polymerization under high vacuum at 60°C using 2,2′-azobisisobutyronitrile (AIBN) as initiator. Polymerizations leading to labelled macromolecules contained 0.5 mol% luminescent monomer (acenaphthylene, ACE, or 1-vinylnaphthalene, VN) in the feed. Polymers were purified by multiple precipitation: at acrylic acid contents $\geq$70 mol% in feed, methanol was used as solvent, diethyl ether as precipitant. At lesser acrylic acid contents, tetrahydrofuran was the solvent with 40/60 petroleum ether as precipitant.

Samples of poly(methacrylic acid), PMAA, were prepared by free radical polymerization in benzene (80 wt.%) at 60°C and purified by multiple precipitation (methanol into diethyl ether).

Instrumentation

Steady state luminescence spectra were recorded using a Perkin–Elmer LS50 spectrometer. Time-resolved fluorescence measurements were made using the technique of time-correlated, single-photon counting (TCSPC). Fluorescence "lifetimes" were determined from decay profiles recorded on an Edinburgh Instruments 199 spectrometer using a thyratron-gated flashlamp (with either H_2 or D_2 as discharge medium). A fast photomultiplier tube (Philips XP2020Q) was used to detect fluorescence, producing an instrument response function of ca. 1.0–1.2 ns (FWHM) dependent, inter alia, upon discharge medium. Corroborative lifetime data were determined by analysis of decay curves recorded in magic angle (54.7° with respect to the plane of vertically polarized excitation) observations of emissions produced using synchrotron radiation (from the Synchrotron Radiation Source, SRS, EPSRC Daresbury Laboratory, Warrington, U.K.). Fluorescence detection at the SRS employed a Philips XP4278b photomultiplier, resulting in an instrument response function of <330 ps (FWHM). Details of the SRS have been previously published (see, for example, refs. 43, 46, 47).

Molar masses and the polydispersities of their distributions were estimated using aqueous size exclusion chromatography (SEC). The SEC system employed incorporated the following components: a Waters Associates model 6000 pump, a Rheodyne injector, and Waters Associates Ultrahydrogel mixed gel (2 × 30 cm) columns. A sample concentration of 0.1% w/v with an injection volume of 100 μL and a flow rate of 0.8 cm^3 s^{-1} was employed for all samples. Data acquisitions and sub-

Can. J. Chem. Downloaded from www.nrcresearchpress.com by 46.23.64.124 on 09/08/12
For personal use only.

Table 1. Polymer characteristics.

Polymer	$\overline{M}_n$/kg mol^{-1}	D
PAA[a]	172	3.2
PMAA	150	1.9
PAA-ACE[b]	108	2.8
PAA-VN	164	1.8
MMA(20)–AA[c]	123	3.6
MMA(29)–AA	50	3.3
MMA(38)–AA	97	7.5
MMA(50)–AA	66	4.1
MMA(34)–AA-ACE[d]	127	6.1
MAA(54)–AA-ACE	66	3.0
MMA(45)–AA-VN	83	5.0
STY(27)–AA	61	2.7
STY(44)–AA	13	3.3
STY(27)–AA-ACE	27	3.0
STY(39)–AA-ACE	54	5.6
STY(33)–AA-VN	50	2.8
STY(44)–AA-VN	32	2.6

[a]AA = acrylic acid; MAA = methacrylic acid; PAA = homopolymer of acrylic acid.

[b]ACE = acenaphthylene; VN = 1-vinylnaphthalene; PAA-ACE = acenaphthylene labelled poly(acrylic acid).

[c]MMA = methyl methacrylate; STY = styrene; MMA(20)–AA = methyl methacrylate – acrylic acid copolymer, containing 20 mol% MMA.

[d]MMA(34)–AA-ACE = acenaphthylene labelled methyl methacrylate – acrylic acid copolymer containing 34 mol% MMA.

sequent analyses were performed using a Polymer laboratories PL data station with associated software. Narrow distribution poly(ethylene oxide) standards were used for column calibration in all instances.

Copolymer compositions were determined from ^{1}H nmr using a JEOL FX-100 spectrometer.

Results and discussion

Polymer characterization

Apparent molar mass data and composition information are listed in Table 1, where D (= $\overline{M}_w/\overline{M}_n$) is the polydispersity.

Aqueous SEC analyses of polymers are prone to distortion of the resultant chromatograms from the elution profiles that would be obtained on the basis of a "pure size exclusion mechanism" through the intervention of interactions between the eluting solute and the gel employed. Polyelectrolyte-gel adsorption can be reduced, in general, by addition of a low molar mass electrolyte to the eluant (see, for example, ref. 48). However, use of 0.1M $NaNO_3$(aq) solution did not effect elution of any of the polymer samples within the range of calibration volumes established using the PEO standards.

Following trials involving a variety of elution media, an elution mixture comprising a solution of $NaNO_3$ (0.1 M) in an aqueous mixture containing 20 wt.% acetonitrile, was used: this eluant produced SEC responses of "normal" elution profile for all polymer samples analysed. However, since the hydrophobically modified forms of the polymers have the greatest potential for interaction with the surfaces within the pores of the gel, the molar mass data must be regarded with caution. The data listed in Table 1 indicate that the *apparent* molar mass of the various polyacids studied in this work decreases, in general, as the intramacromolecular concentration of hydrophobic modifier increases. In addition, the apparent drift to lower molar mass with high hydrophobe content is more evident in the AA copolymers containing styrene as the "modifying comonomer."

Neither observation is unexpected: the more hydrophobic the polymer, the greater will be its tendency to interact with the separating gel. Consequently, the distribution of eluting solutes will be displaced to larger elution volumes and, thence, to lower apparent molar masses. In turn, the molar mass data, recorded in Table 1, must be regarded as approximating to representations of the true distribution of molar masses. The "apparent" values of molar mass listed in Table 1 have to be regarded as lower limits to their "true" values. Within this context, we shall discuss the photophysical and solubilization properties of these systems on the assumption that we are dealing with high molar mass polyacids, whose properties are independent of molar mass.

Time-resolved anisotropy measurements (TRAMS) upon labelled polyacids

TRAMS experiments upon macromolecules bearing luminescent labels are, arguably, *the* most powerful of all the fluorescence methods used in interrogation of the conformational behaviour of polyelectrolytes. TRAMS data report upon the reorientational characteristics of the label, which, in turn, reflect restrictions imposed upon polymer chain mobility as hydrophobically modifying comonomers are added to the water-soluble macromolecule. At low intramolecular concentrations of hydrophobically modifying comonomer, steric constraints upon local segmental mobility will dominate the observed changes in segmental dynamics, which, in turn, should parallel those apparent in solvents other than water. At higher hydrophobic contents, intramolecular aggregation involving the hydrophobic species will occur, resulting in additional restrictions upon segmental mobility. As is demonstrated below, the creation of intramolecular hydrophobic domains in dilute aqueous polymer solutions is the dominant influence in determining the dynamic behaviour of such systems.

The TRAMS experiment, in studies of macromolecular dynamics, employs polarized light to photoselectively excite those labels whose transition vectors for absorption are preferentially aligned, at the moment of absorption, parallel to the (vertical) plane of polarization of the incident radiation. (The probability of absorption falls off as $\cos^2\theta$ where θ is the angle between the molecule's transition vector and the plane of polarization of the excitation.) This creates the necessary anisotropy within an otherwise randomly oriented distribution of chromophores. The extent to which this anisotropy is retained in the fluorescence emitted at any time, t, following excitation, depends upon the extent of chromophore reorientation during this period and is reflected in the difference of the intensities of emission observed in planes parallel ($I_\parallel$) and perpendicular ($I_\perp$) to that of the incoming excitation. Information regarding rotational motion of a fluorescent label (and, thence, regarding the relaxation behaviour of the macromolecule to which it is affixed) may be obtained by analysis of the *observed*, time-dependent anisotropy, $R(t)$, given by

$$[1] \quad R(t) = \frac{I_{\parallel}(t) - I_{\perp}(t)}{I_{\parallel}(t) + 2I_{\perp}(t)} = \frac{D(t)}{S(t)}$$

In the simplest of situations, that of a spherical rotor, the true time dependence, $r(t)$, of the emission anisotropy would be described by a simple exponential function, i.e.,

$$[2] \quad r(t) = r_0 \exp(-t/\tau_c)$$

where τ_c is the parameter of (most) interest, being the rotational correlation time for the motion. r_0 is the intrinsic anisotropy, a fundamental spectroscopic characteristic of the chromophore (related, inter alia, to the relative configuration of the transition vectors for absorption and emission, respectively).

Recovery of relaxation data is not as straightforward as is the case for fluorescence data alone. The severity of the problem depends upon the relative rates of decay of the luminescence and its anisotropy and their relationship to the time scale upon which the pulse from the excitation source distorts the observed decay profiles.

In the case of fluorescence decay data, information regarding the relaxation of the distribution of excited states responsible for the emission can be recovered, in a reasonably direct fashion, in an iterative reconvolution procedure in which the instrument response function (the *observed* excitation profile) is convoluted with a mathematical model (appropriate to "expectation") of the fluorescence response and the resultant "fit" is optimized in comparison with the observed fluorescence profile. In the TRAMS experiment, the finite width of the excitation pulse will distort each of the observed fluorescences, $I_{\parallel}(t)$ and $I_{\perp}(t)$. However, although either of these fluorescence responses (containing information regarding both electronic and reorientational relaxation) is amenable to the "deconvolution" procedure described above, the combination function, $R(t)$, can *not* be treated in this "simple" fashion. Other approaches must be adopted in instances where it is anticipated that failure to deconvolute the anisotropy data might lead to evolution of misleading information regarding the reorientational relaxation process under investigation. Such will always be the case in analysing anisotropy data accrued in the earlier stages of the observed fluorescence responses where the influence of the excitation pulse is significant. The time range over which such distortions of $R(t)$ are apparent will, naturally, depend upon the excitation source and the detection system employed, as revealed in the instrument response function. Under the conditions employed in the current study (cf. "Experimental" above) the instrument response function generated by the SRS exhibits an instrument response function of FWHM <300 ps.

Procedures for ensuring reliable retrieval of rotational relaxation data from TRAMS experiments have been discussed elsewhere (for example, see refs. 45 and 46). In the current study, $R(t)$ has been analysed directly (i.e., without any attempt to account for data distortion by the excitation pulse) and the resultant correlation times, τ_c, compared to those evolved in both impulse reconvolution, IR (49, 50), and autoreconvolution, AR (46, 51), analyses. Each of the latter (IR and AR) forms of approach seeks to "deconvolute" the $R(t)$ data and thereby provides a check upon the reliability of direct analysis of $R(t)$ (46).

A problem that accompanies direct analysis of $R(t)$ is the fact that it is not possible to establish a value for r_0. Consequently, the time from which analysis of $R(t)$ should be initiated is uncertain. As in previous TRAMS studies of polymer relaxation in which we have employed (43, 46) such direct analyses, fitting $R(t)$ has been initiated from a decay channel in which the apparent anisotropy, R, has attained a value corresponding to that "expected" for the chromophore involved, on the basis of both steady-state ("Perrin-plot") (e.g., see ref. 44) and TRAMS (43, 46) studies of the relaxation behaviour of polymers bearing the same labels. This is clearly unsatisfactory in the absence of means of testing the reliability of the direct analysis approach (such as those afforded by the IR (49, 50) and AR (46, 51) approaches). As we have observed previously (46), direct analysis of $R(t)$ data in the absence of such safeguards can be misleading: in particular, the decay of $R(t)$ can appear to be more complex than that of the true anisotropy, $r(t)$. In studies of labelled macromolecules, direct analyses of $R(t)$ can, in turn, appear to imply that a more complex model than is justified should be employed to characterize the polymer relaxation behaviour.

Table 2. Correlation times for segmental motion of hydrophobically modified polymers containing varying amounts of acrylic acid, in methanol, as recovered by DA, IR, and AR analyses.

Polymer	τ_c(DA)/ns	τ_c(IR)/ns	τ_c(AR)/ns
STY(27)–AA-ACE	2.4	2.3	2.0
STY(39)–AA-ACE	2.8	2.9	3.0
STY(33)–AA-VN	1.9	1.8	1.6
STY(44)–AA-VN	2.2	2.1	1.9
MMA(45)–AA-VN	1.5	1.4	1.4

Segmental dynamics of the hydrophobically modified forms of PAA in methanol

Table 2 lists rotational correlation times, obtained using the various analytical approaches and modelling the anisotropy using a function of the form

$$[3] \quad r(t) = r_0 \exp(-t/\tau_c) + r_\infty$$

The anisotropy decays were, in each case, well described by this model function. Furthermore, the resultant values of r_∞, applied as a freely varying parameter, lay close to zero, as is to be expected for rotational relaxation of a chromophore that is not confined within a restricted geometry.

In consideration of these data, it is apparent that

(*i*) the segmental dynamics of the macromolecules depend upon the nature and quantity of the copolymerized hydrophobically modifying monomer. Incorporation of 45 mol% MMA produces a polyelectrolyte with a correlation time for reorientation of its VN label of 1.4 (±0.1) ns, which is similar in magnitude to that of PAA–VN itself (τ_c = 1.2 (±0.1) ns (46)). Incorporation of styrene into the polymer, on the other hand, produces a less flexible polyacid: the greater the styrene content of the copolymer, the longer is the associated correlation time.

In good organic solvents of similar viscosity, the room temperature segmental dynamics of polystyrene and poly(methyl methacrylate) are characterized by correlation times that are both similar to one another (see, for example, ref. 52) and slightly greater than that of PAA in methanol (46). Consequently, as is

Can. J. Chem. Downloaded from www.nrcresearchpress.com by 46.23.64.124 on 09/08/12
For personal use only.

Can. J. Chem. Downloaded from www.nrcresearchpress.com by 46.23.64.124 on 09/08/12
For personal use only.

observed in the case of MMA, incorporation of either styrene or MMA in copolymers with AA would not be expected, on steric grounds, to alter the rate of segmental motion to any marked extent. It may then be that the effects induced by the less polar comonomer, styrene, are the results of intramolecular interactions between styryl residues and (or) blocks of styryl species within the polyacid coil. Such effects are enhanced in aqueous media (see below) under conditions in which aggregation occurs to form intramolecular hydrophobic domains.

(*ii*) The values obtained for τ_c at a given styrene content show a dependence upon the label employed: those for ACE-labelled polymers are greater than those of the VN-labelled species. In general, ACE and VN labels produce equivalent information in fluorescence anisotropy determinations of macromolecular relaxation times in dilute fluid solutions. Under certain conditions, notably when segmental motion of the macromolecule becomes hindered, the labels appear to relax at different rates. A recent example of this effect is to be found in a report of TRAMS investigations of the conformational behaviour of PMAA (42): at low pH the relaxation data characteristic of the reorientational motions of the ACE and VN labels are not comparable. A likely explanation is that additional depolarization of the fluorescence from VN occurs as a result of rotation of the label independent of that of the polymer chain. It is possible that a similar effect is being observed in the current work: the motion of the VN might enjoy a degree of decoupling from that of the polymer segments as the motion of the latter becomes more restricted due to interactions between the styryl residues. The effect has also been observed in TRAMS studies of PMAA in methanol using VN and ACE labels (46).

Segmental dynamics of the hydrophobically modified forms of PAA in aqueous media

TRAMS studies of the ACE and VN amphiphilic polyelectrolytes reveal that the relaxation behaviour of these hydrophobically modified polymers is complex. Modelling of $r(t)$ by the functional form represented in eq. [3], although providing fits in DA and IR analyses that could be deemed statistically adequate, resulted in a finite value for r_∞. This gives cause for concern, since there is no reason to suppose that the relaxation of any of these macromolecules in dilute fluid solution *should* be characterized by a residual anisotropy. Furthermore, values of r_0 obtained by IR analysis were less than those expected for ACE or VN labels on the basis of previous TRAMS studies on other macromolecules. In addition, AR analyses indicated that modelling of $r(t)$ by a single exponential function was less than statistically adequate (an observation consistent with the fact that IR analyses in which r_∞, in eq. [3], was fixed at zero did not result in adequate fitting to the data).

These features of the analyses of the TRAMS data are similar to those which we have reported (42) in studying the conformational behaviour of PMAA in acid media. However, in contrast to the latter system, adoption of a dual exponential decay function for $r(t)$ of the form

$$[4] \quad r(t) = A_1 \exp(-t/\tau_{c1}) + A_2 \exp(-t/\tau_{c2}) + r_\infty$$

did not result in "best fits" to the current data in which freely varied r_∞ values converged to negligible proportions. Clearly, the relaxation behaviours of the hydrophobically modified polyacids are at least as complex as that of PMAA.

Fig. 1. Correlation times for intramolecular segmental motion of ACE-labelled PAA and a series of hydrophobically modified AA copolymers. (▽) STY(39)–AA-ACE; (●) STY(27)–AA-ACE; (□) MMA(34)–AA-ACE; (○) PAA-ACE.

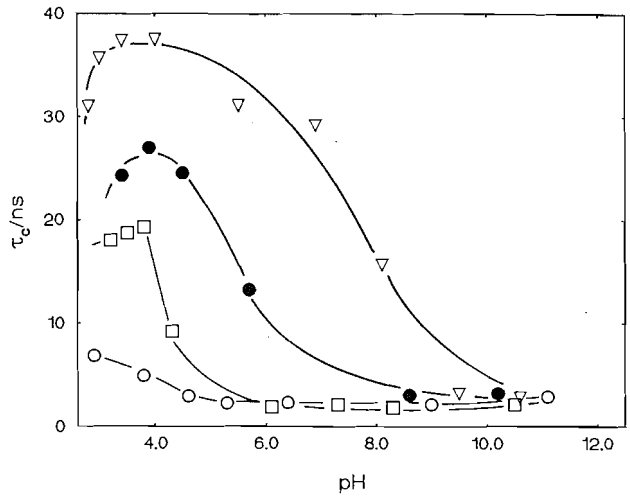

Fig. 2. Correlation times for intramolecular segmental motion of VN-labelled PAA and a series of hydrophobically modified AA copolymers. (□) STY(44)–AA-VN; (▽) STY(33)–AA-VN; (●) MMA(45)–AA-VN; (○) PAA-VN.

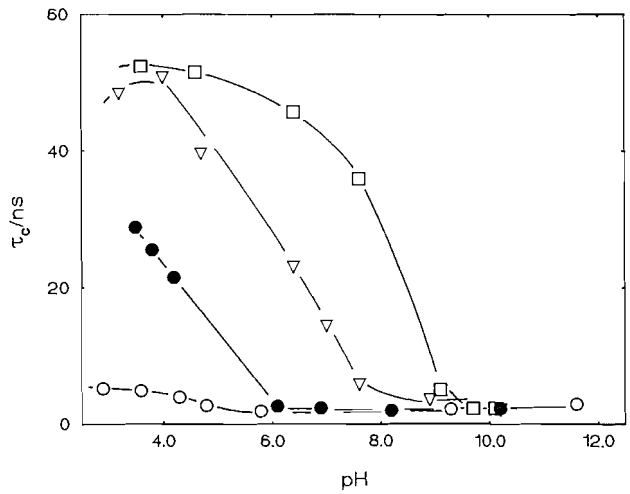

It is likely that the relaxations of each of these hydrophobically modified species are characterized by a broad distribution of relaxation times. TRAMS studies of these and other modified systems continue. However, for the current purposes of examining the effects of incorporation of a modifying comonomer upon the inherent pH-dependent conformational behaviour of the polyacid, single exponential analyses, using eq. [3], suffice in providing a characteristic "average correlation time" for the chain dynamics of a given copolymer at a particular pH. The resultant data are shown in Figs. 1 and 2.

Reference to Figs. 1 and 2 reveals that (*i*) neutralization of PAA is accompanied by a conformational transition in which the segmental mobility of the polyelectrolyte increases over a pH range (from ca. pH 3 to pH 5) such that τ_c decreases from ca. 6 ns for the polyacid to ca 2 ns for the polysalt; and (*ii*) introduction of a hydrophobically modifying comonomer such as MMA or styrene has a marked effect upon the segmental mobility of the acidic forms of the resultant polyelectro-

Can. J. Chem. Downloaded from www.nrcresearchpress.com by 46.23.64.124 on 09/08/12
For personal use only.

lytes: τ_c increases by factors of between ca. 3 and 4 (dependent upon pH and copolymer content) upon incorporation of MMA and between ca. 4 and 9 (again dependent upon pH and degree of hydrophobe loading) for the styrene-containing copolyacids. The magnitude of the effects of the copolymerized hydrophobic species is much greater than would be predicted solely on the grounds of steric constraints upon intramacromolecular mobility (as discussed above) and considerably exceeds those induced by the same amounts of hydrophobic comonomer upon the chain dynamics of the same polyacids when dispersed in dilute methanolic solutions.

In contrast, the presence of the hydrophobic units incorporated in the polymers by copolymerization of MMA or styrene has only a moderate influence upon the intramolecular dynamics of the fully neutralized forms of the modified polyacids: the copolysalts exhibit segmental relaxation rates similar both to one another and to those of the copolymers when dispersed in methanol.

(*iii*) Incorporation of a hydrophobic monomer has a pronounced effect, dependent upon both the polarity of the modifying comonomer and the content of the copolyacid, on the conformational behaviour of the polyelectrolyte. In general, the pH range over which the transition in segmental relaxation dynamics between the acidic form of the water-soluble copolymer and its completely neutralized analogue occurs is both broadened and shifted to higher values of pH. These effects are the result of the formation of hydrophobic domains formed by intramolecular aggregation of the hydrophobic repeat units that result from copolymerization of either MMA or styrene with AA. At lower values of pH, the influence of these intramacromolecular aggregates completely dominates the dynamic aspects of the behaviour of the copolymers in dilute aqueous solutions as is apparent by comparison with the conformational behaviour of PAA itself or, indeed, with the relaxation characteristics of the copolymers in methanol. In the latter solvent, as discussed above, MMA-modified copolymers exhibit segmental relaxations that differ little in rate from those of PAA, whilst those of the styrene-based systems might exhibit relatively minor effects resultant upon aggregation of the copolymerized styryl residues in the macromolecules. Our proposal that the significant differences between the dynamic behaviour of the hydrophobically modified polyacids in aqueous acidic media and that in methanol are the result of domain formation is supported by studies of the solubilization of guest molecules, as discussed below.

(*iv*) The segmental relaxation data of the hydrophobically modified forms of PAA show an *apparent* label dependence in acidic media. In both the styrene and MMA-modified systems there is the implication that, for a given hydrophobe content and a given pH, the apparent rate of segmental relaxation of the hydrophobically modified polyelectrolyte is dependent upon the label (ACE vs. VN) employed. Given the differences between the nature of the way in which each label is attached to the macromolecule, differences in fluorescence anisotropy might be expected. However, the observed trends in τ_c are opposite to those of "intuitive reasoning" based upon the premise that the VN label might experience subsidiary rotational mobility as a result of motion about the bond of attachment to the polymer chain: for a given type of hydrophobic modifier, at a common copolymer content, it would appear that the VN label produces τ_c values for reorientational relaxation that exceed those of the ACE label at similar extents of neutralization of the polyacid. However, it is likely that these trends (which are opposite to those observed in the behaviour of the hydrophobically modified polyelectrolytes in methanol (as described above) *and* PMAA in aqueous media (42)) are artifacts that derive from the complexity of the time dependence of the decay of $r(t)$ and the simplicity of the current "single exponential" approach to analysis of the TRAMS data.

Application of eq. [3] in modelling the anisotropy decay via a single exponential function results, as discussed above, in an average correlation time that we hope is representative of the distribution of reorientational processes of the label, which reduce the relaxation of emission anisotropy to zero. This procedure seems justified, to some extent, by the self-consistent trends that emerge in the τ_c data, for a given label, as both the pH of the medium and the composition of the copolymers are varied. However, fitting to eq. [3] disguises the complexity of the anisotropy relaxation since the longer rotational processes are reflected in the presence of an apparent residual anisotropy, r_∞. Consequently, since the VN label has the potential for loss of anisotropy through motion independent of the polymer chain, which is not enjoyed by the ACE moiety, consistency between the τ_c values obtained using the two different labels should not (necessarily) be expected. In other words, although τ_c will increase as the overall distribution of relaxation processes shifts to longer times, the mode in which τ_c and r_∞ combine to reflect such shifts will not be the same for each label. Allied to this effect is the observation that, in general, direct analysis of the raw anisotropy function (from a point in the decay at which the perturbing influence of the excitation pulse is negligible) tend to produce similar estimates for τ_c (and r_∞) as those furnished by the IR method, in the case of the ACE-labelled copolymers. The VN-labelled species, in contrast, produced marked differences, in some instances, between the τ_c values estimated using the DA and IR methods. (The τ_c data shown in Fig. 2 are those recovered by the IR method of analysis.)

Solubilization studies using luminescent probe molecules

The dramatic changes in τ_c induced by hydrophobic modification, as revealed in TRAMS experiments and described above, are consistent with the supposition that the hydrophobic components of the resultant polyelectrolytes form aggregates within the macromolecular coil. The creation of hydrophobic domains can be tested using luminescent probes since these domains act as solubilizing pockets for organic guests. Furthermore, the photophysical characteristics of the occluded guests can yield information regarding the nature of their host matrix. In the current work, three luminescent guests; pyrene, 9-methylanthracene, and perylene, have been used to probe the interiors of the hydrophobic cavities formed in the styrene- and MMA-modified AA polymers.

Pyrene

Pyrene is one of the most widely used fluorescent probes. Photophysical applications involving pyrene in the study of aqueous polymer solutions and in other organized media have formed the basis of a recent excellent review (29). The fluorescence spectrum of a pyrene probe offers a simple and convenient means of sensing the molecule's local environment (53, 54). In particular, the ratio of the intensities of two specific

Can. J. Chem. Downloaded from www.nrcresearchpress.com by 46.23.64.124 on 09/08/12
For personal use only.

Fig. 3. I_3/I_1 ratios from the fluorescence spectra of pyrene (10^{-6} M) dispersed in various AA-based polymers (10^{-2} wt.%). (○) STY(44)–AA; (□) STY(27)–AA; (▽) MMA(38)–AA; (●) PAA-VN.

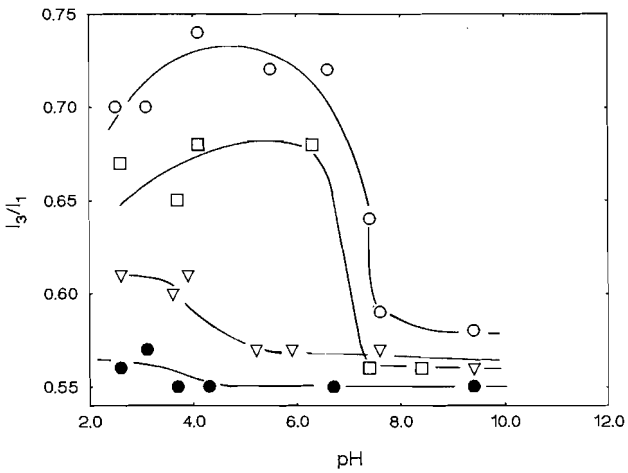

vibronic bands (the I_3/I_1 ratio) within the emission spectrum provides a measure of the polarity of the medium in which the pyrene is dissolved (54). This ratio is plotted in Fig. 3 as a function of pH, for pyrene dispersed in dilute (10^{-2} wt.%) solutions of PAA and various hydrophobically modified polyacids. It should be noted that at a pyrene concentration of 10^{-6} M there is no evidence in the fluorescence spectrum for excimer formation in any of the systems studied (including pure water). With reference to Fig. 3, it is apparent that

(*i*) the I_3/I_1 ratio for the PAA solution is virtually independent of pH. If the pyrene is solubilized at all by the polymer, it experiences a microenvironment that is very similar to that of water itself.

(*ii*) Hydrophobic modification using styrene leads to the generation, at lower pH values, of hydrophobic domains capable of solubilizing pyrene. The hydrophobicity of these domains is considerably enhanced compared to that of PAA itself. Indeed, the I_3/I_1 ratio attained for pyrene solubilized in the polyacid form of the STY(44)–AA copolymer indicates that the solubilization sites afforded to the probe are similar in polarity to those found in certain micellar systems (54). Even at high pH (>8.0) the copolymer creates a microenvironment for the pyrene of lesser polarity than that of the aqueous phase.

(*iii*) The hydrophobicity of the microenvironment afforded to the solubilized guest depends upon the nature of the modifying comonomer. The domains created in MMA–AA copolymers are more polar than those in STY–AA species of a similar (overall) composition.

(*iv*) For a given hydrophobic modifier, the hydrophobicity of the solubilizing domains is dependent upon the composition of the copolymer.

(*v*) The polarity of the microenvironment sensed by the dispersed probe depends upon the pH of the system. The dependence of I_3/I_1 upon pH constitutes a kind of "photophysical titration curve" that allows the effects of neutralization, upon the nature of the intramolecular solubilizing cavities formed in the various polymers, to be examined. The curves reflect the trends apparent in the pH dependencies of the relaxation characteristics of the various polymers (themselves determined

Fig. 4. Excitation spectra for pyrene (10^{-6} M; λ_a = 380 nm) dispersed in STY(44)–AA at various values of pH.

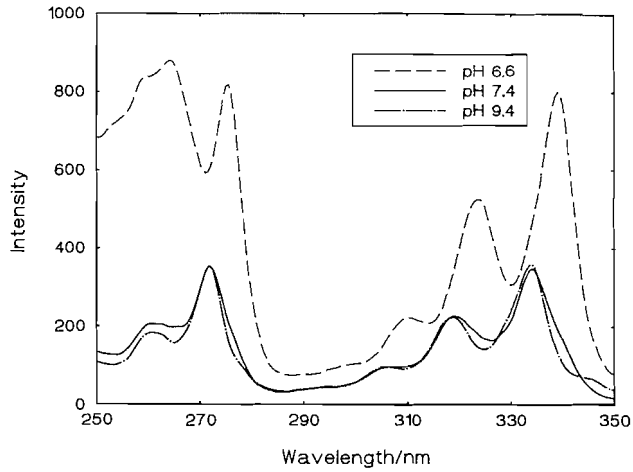

largely by the existence, or otherwise, of intramolecular aggregation). Again, it can be seen that hydrophobic modification shifts the range in pH, over which the change in the conformational behaviour of the polyacid becomes apparent, to higher pH. The greater the mole fraction of hydrophobic comonomer incorporated into the polymer, the greater the shift.

Solubilization of pyrene in the styrene–AA copolymers results in other changes in the probe's spectral characteristics that can be used to detect the presence of intramolecular aggregates. Upon occlusion in a styrene-rich "pocket," both the excitation and emission spectra of the pyrene become red-shifted. The effect is shown, for excitation, in Fig. 4. At low pH (below that of the conformational transition of the copolyacid) the excitation spectra of the solubilized probe exhibit a 0–0 vibronic band for the ($S_1 \leftarrow S_0$) transition that is centred at about 338 nm. At pH values greater than ca. 7 for the STY(44)–AA copolymer, the position of this band moves to higher energy, becoming centred at ca. 333 nm. Similar red shifts in excitation spectra are observed when excimer formation, involving "preassociated" pyrenes, occurs (for example, see ref. 29 and references therein). However, under the conditions employed in the current work, there was no spectral evidence (whether steady state or time-resolved) for excimer formation between the pyrene probes. In this instance, the spectral shifts merely reflect the location of the pyrenes in a solvating medium that consists, largely, of styryl residues. This observation is supported by the facts that

(*i*) similar shifts are induced in the spectra of pyrene when dispersed in toluene as opposed to water.

(*ii*) When the number of solubilizing sites is decreased (by reducing the STY(44)–AA concentration, from 10^{-2} to 10^{-3} wt.%) the pyrene becomes distributed more equally between the aqueous and polymer domains. The effects on the resultant excitation spectra are shown in Fig. 4: at low to intermediate pH, the 0–0 vibronic band peaks at 338 nm but contains a shoulder at 333 nm resultant upon a contribution to the overall spectrum from pyrene molecules dissolved in the bulk aqueous medium and (or) more polar regions within the polymer coils.

(*iii*) In these more dilute (10^{-3} wt.%) polymer solutions, selection of excitation wavelengths in the blue and red edges of the broadened and partially split vibronic bands, respectively, produces emission spectra that differ in I_3/I_1 ratio: the spectrum

Can. J. Chem. Downloaded from www.nrcresearchpress.com by 46.23.64.124 on 09/08/12
For personal use only.

Table 3. Fluorescence decay parameters resultant upon dual exponential fitting to the time-resolved fluorescence of pyrene (10^{-6} M) dispersed in various AA-based polymer systems (10^{-2} wt.%) at various values of pH.

Polymer	pH	τ_1/ns[a]	τ_2/ns	χ^2	$\langle\tau\rangle$/ns
PAA	3.1	—	132	1.6	132
MMA(38)–AA	3.9	274 (0.58)	118	1.0	209
	5.2	200 (0.37)	114	1.3	146
	5.9	—	130	1.6	130
STY(27)–AA	4.1	324 (0.85)	125	1.1	295
	6.3	306 (0.70)	122	1.1	250
	7.4	153 (0.25)	122	1.0	132
STY(44)–AA	4.1	312 (0.96)	67	1.1	301
	5.5	317 (0.96)	64	1.1	307
	6.6	317 (0.89)	104	1.0	294
	7.4	273 (0.52)	111	1.2	195
	10.1	—	127	1.3	127
pyrene/H_2O		—	130	1.4	130

[a]Figures in parentheses show fractional contribution to overall fluorescence.

produced by excitation into the red edge of a vibronic band (e.g., at 340 nm) has a higher I_3/I_1 ratio than that resultant upon excitation into a blue edge (e.g., at 318 nm). This implies that the distribution of pyrenes excited at 340 nm experiences, on average, a more hydrophobic set of microenvironments than those enjoyed by the excited states created in absorption at 318 nm. The photoselectivity of different distributions of pyrene molecules, within the overall probe population, through variation of excitation wavelength is further demonstrated by the excited state lifetime data discussed below.

The singlet excited state lifetime of pyrene is sensitive to the polarity of its surroundings (55). This effect has been used, for example, in pyrene probe studies of the conformational behaviour of poly(methacrylic acid) (14, 15, 18, 56). In a similar fashion, the fluorescence lifetime can be used to detect the existence of solubilizing cavities within the hydrophobically modified AA copolymers. Representative data are shown in Table 3 for 10^{-6} M pyrene dispersed in 10^{-2} wt.% solutions of various AA-based systems.

With reference to Table 3, it can be noted that

(*i*) the lifetime of pyrene dispersed in the PAA solution, even at low pH, is identical (within experimental error) to that in water (130 ± 5 ns). This supports the conclusions based upon trends in I_3/I_1 ratio that the PAA (if it has *any* solubilization capacity for pyrene, at this concentration) presents the probe with a solvent environment similar to that of the bulk aqueous phase.

(*ii*) At pH values below the conformational transition (as revealed in TRAMS experiments) for each particular macromolecule, the decays of the fluorescence from the pyrene probe become too complex for adequate description in terms of a single exponential function. At pH values higher than that of the conformational transition, the fluorescence decays become simpler and are characterized by a single lifetime of the order of 130 ns. These data are consistent with our belief that, during the conformational transition, the intramolecular hydrophobic aggregates, which characterize the acid form of the polymer, disintegrate. The pyrene is then ejected into the aqueous phase as the polymer loses its capacity for solubilization.

Table 4. Fluorescence decay parameters resultant upon triple exponential fitting to the time-resolved fluorescence of pyrene (10^{-6} M) dispersed in STY(44)–AA (10^{-3} wt.%) at various values of pH.

pH	λ_e/nm	τ_1/ns[a]	τ_2/ns[a]	τ_3/ns	$\langle\tau\rangle$/ns
3.5	318	322 (0.52)	131 (0.44)	26	228
	340	306 (0.68)	117 (0.29)	20	244
6.0	318	321 (0.50)	127 (0.48)	28	223
	340	320 (0.63)	122 (0.35)	16	245
7.2	318	341 (0.39)	133 (0.59)	29	210
	340	354 (0.48)	133 (0.49)	21	236

[a]Figures in parentheses show fractional contribution to overall fluorescence.

(*iii*) The complexities of the fluorescence decays of the pyrene guest, observed at low pH, typify the photophysical behaviour of excited state species, whether probes (14, 15, 18, 19, 56) or labels (15), when enclosed within the hydrophobic domains of water-soluble polymers. Dual exponential analyses of the fluorescence decays obtained from pyrene dispersed in the hydrophobically modified copolyacids result in fits to the observed emissions that are justified on statistical grounds. In most cases, this procedure leads to evolution of a component of the pyrene emission with a lifetime that is close to that obtained for the probe in water or in polymeric dispersion, at high pH. In addition, a longer-lived component is also obtained. It is tempting, following the approach of Thomas and co-workers (14, 15, 18, 56) to ascribe these components to populations of pyrene chromophores solubilized in polar environments (or in the bulk aqueous phase itself) and in hydrophobic domains, respectively. However, as we have discussed previously (19), it is probably an oversimplification to assume that these two populations are sufficiently distinct, within the overall distribution of dispersed probes, to be resolved by such an analysis. It is more likely that the double exponential fitting procedure merely serves to parameterize, in a statistically adequate fashion, the fluorescences emanating from a broad, heterogeneous range of environments. However, these twin parameters, τ_1 and τ_2, and their relative contributions to the overall fluorescence (listed in Table 3) can be used as indicators of the ranges in pH over which hydrophobic domains are generated within the coils of polyelectrolytes. Alternatively, the average fluorescence lifetime, $\langle\tau\rangle$, derived using eq. [5], can be used as a monitor for the regions of pH in which intramolecular aggregates of hydrophobic components of the AA copolymers are present.

$$[5] \quad \langle\tau\rangle = \frac{\sum a_i\tau_i^2}{\sum a_i\tau_i}$$

In eq. [5], τ_i represents the "lifetime" parameters evolved in multiexponential fitting according to eq. [6], where a_i represents the various pre-exponential terms and B is a "background" parameter:

$$[6] \quad i(t) = B + \sum_i a_i \exp(-t/\tau_i)$$

Can. J. Chem. Downloaded from www.nrcresearchpress.com by 46.23.64.124 on 09/08/12
For personal use only.

Clearly, had data been collected at more frequent intervals in pH, a plot of $\langle\tau\rangle$ against pH would have furnished a complementary (but more onerous in construction) "titration curve" to that afforded by I_3/I_1 ratios.

The lifetime data of Table 3 reveal that the copolymer MMA(38)–AA sustains occlusion of pyrene guests at low pH. The pH range over which solubilization is effected, however, is less than that maintained in either STY(27)–AA or STY(44)–AA. These observations are consistent with the findings based upon I_3/I_1 ratios, discussed above.

As the concentration of the AA copolymer is reduced, the number of solubilizing domains available to the probe also decreases. Studies of the fluorescence spectra of the overall pyrene probe distribution revealed (vide supra) a dependence upon excitation wavelength in the more dilute solutions of the copolymeric hosts. These observations are substantiated by time-resolved fluorescence measurements, as discussed below.

When pyrene (10^{-6} M) is dispersed in solutions of STY(44)–AA at a copolymer concentration of 10^{-3} wt.%, the decay data become more complex (in that they require a minimum of three exponential terms to be applied in the model fitting function (eq. [6])) than in dispersions that are an order of magnitude more concentrated. The data from triple exponential fitting of the pyrene fluorescences are listed in Table 4. A dependence upon polymer concentration (by comparison with the data in Table 3), pH, and excitation wavelength is apparent.

The reconvolution analyses consistently retrieve a lifetime component of between ca. 115 and 135 ns. This is, perhaps, not unexpected in these dilute systems since, as argued above, it might be expected that these dispersions will contain a fair proportion of pyrene molecules that are located within the bulk aqueous phase and (or) the more polar interiors of the polymer coil. In this respect, the time-resolved data corroborate those derived from the spectroscopic investigations. Moreover, the proportion of emission associated with this component of the overall fluorescence intensity, increases (*a*) as the pH of the solution increases and (*b*) as the excitation wavelength is changed from 340 nm to 318 nm. (As the excitation and emission spectra indicate (vide supra), excitation at 318 nm preferentially excites pyrene molecules located within the more polar regions of the dispersion. On the other hand, 340 nm radiation, accesses probes located within the more hydrophobic domains). The average lifetime, $\langle\tau\rangle$, also reflects this excitation wavelength dependence.

It is not anticipated that the triple exponential fits accomplish more than mere parameterization of the observed decay profiles: the three resultant "lifetimes" will have little *physical* significance. However, recovery of *one* component of lifetime close to that of pyrene in water may not be entirely fortuitous since a significant population of the pyrenes will be located in aqueous microenvironments. The two parameters recovered would, in combination with this component, serve to characterize the broad distribution of chromophoric environments to be found in these heterogenous systems.

Fluorescence anisotropy measurements, using probe molecules, can be used to investigate the local viscosity that they sense when solubilized in water-soluble polymers (see, for example, ref. 13 and references therein). Values of the reciprocal anisotropy of the steady state fluorescence of pyrene, dispersed in various AA-based matrices, are listed in Table 5. Also included, for comparison, are values of the anisotropy of this probe dispersed in poly(methacrylic acid), PMAA, at low pH. Under these conditions, PMAA is said to "hypercoil" (see, for example, refs. 13 and 42 and references therein). Consequently, the much-studied PMAA system provides a useful reference point for comparison of the emission anisotropies obtained in the hydrophobically modified AA macromolecules.

Table 5. Fluorescence anisotropy data for pyrene dispersed (10^{-6} M) in a variety of polyacids (10^{-2} wt.%).

Polymer	pH	r^{-1}	τ_c/ns[a]	τ_c/ns[b]
PAA	3.4	>150	<25	—
PMAA	3.7	100	55	75
	4.4	93	60	85
MMA(38)–AA	3.4	49	140	—
	5,0	>150	<25	—
STY(27)–AA	4.4	37	220	—
	5.0	69	90	110
STY(44)–AA	3.7	25	510	800
	4,1	28	385	520
	6.2	47.5	150	105

[a]Estimated from steady-state data using eq. [7] and $r_0^{-1} = 15$ (see text).
[b]Estimated from TRAMS data via IR analysis (see text).

The steady-state r^{-1} values provide a means of identifying the conditions under which the pyrene probe is, or is not, solubilized by the various polyacids. For example, the fluorescence from the pyrene probe dispersed in PAA at low pH and in MMA(38)–AA at pH 5 is completely (within the accuracy of the experiment) depolarized. This observation is consistent with the I_3/I_1 and fluorescence lifetime data, which indicate that the probe is solubilized to a minimal extent in these media (vide supra). In contrast, at the lower pH value of 3.4, emission from the probe dispersed in MMA(38)–AA exhibits a finite value of r^{-1}. It is interesting that, at this pH, the emission of the pyrene probe, solubilized by this copolymer, is more polarized than that of pyrene solubilized in the PMAA hypercoil.

In the STY–AA systems, the probe's fluorescence is more anisotropic than in any of the other systems. Furthermore, as the pH is increased the fluorescence becomes more depolarized. The pH value at which marked increases in r^{-1} occur in these systems depends upon the styrene content of the copolymer: at high pH the emission becomes completely depolarized. However, at pH values of 5 and 6.2 for the STY(27)–AA and STY(44)–AA systems, respectively, the fluorescence of the pyrene guest exhibits a lesser degree of anisotropy than that obtained in either system, at lower pH. Since both I_3/I_1 and τ data indicate that pyrene is still solubilized at these higher pH values, the r^{-1} data imply that neutralization of the AA derivatives in the copolymers results in a partial expansion of the hydrophobic domains *prior* to the disaggregation that occurs at higher pH (which, in turn, results in complete loss of solubilization capacity for pyrene).

The r^{-1} data are not strictly comparable: r^{-1} depends upon the mobility of the solubilized probe on the time scale imposed by its excited state lifetime. This is expressed by the Perrin equation, as

$$[7] \quad r^{-1} = r_0^{-1}\,(1 + \langle\tau\rangle/\tau_c)$$

Can. J. Chem. Downloaded from www.nrcresearchpress.com by 46.23.64.124 on 09/08/12
For personal use only.

Table 6. Fluorescence decay parameters for 9-methylanthracene recovered using single or double exponential models for $i(t)$.

Solution	τ_1/ns (±0.1)	τ_1/ns (±0.2)
Cyclohexane	4.3	—
H_2O	11.0	—
PAA (pH = 3.4)	10.9	—
PMAA (pH = 3.5)	13.8 (0.47)[a]	10.6
(pH = 5.3)	12.6 (0.8)	8.9
MMA(38)–AA (pH = 3.4)	12.2 (0.92)	5.9
STY(44)–AA (pH = 3.9)	15.1 (0.73)	9.0
(pH = 5.0)	15.2 (0.70)	8.1
(pH = 6.4)	15.3 (0.73)	8.7
(pH = 7.5)	12.0 (0.84)	7.1
(pH = 8.4)	10.9	
(pH = 10.2)	10.9	

[a]Figures in parentheses represent fractional contribution to the total fluorescence.

However, since $\langle\tau\rangle$ for pyrene in the PMAA and the STY–AA systems (at all pH values listed in Table 5) and MMA(38)–AA at pH 3.4 is ca. 300 ns, the r^{-1} data do reflect restrictions that the media impose on the probe's rotational mobility. A more valid comparison of relative mobilities of the probe under the varying conditions employed in this study, would be afforded by examination of the relevant τ_c data. In principle, these can be obtained using eq. [7] *provided* that the intrinsic anisotropy, r_0, is known for the probe, in the medium of interest. Unfortunately, conventional approaches (see, for example, ref. 44) to the determination of r_0 in steady state measurements are not applicable in this instance. (Addition of organic quenchers, to reduce $\langle\tau\rangle$, for example, would disrupt the hydrophobic domains under investigation.)

τ_c data can be obtained using TRAMS (as described above for labelled polymer samples). With appropriate "deconvolution," using the IR approach, estimates of r_0 are also furnished in such experiments. Unfortunately, the period of the electron storage ring, at the SRS Daresbury, is too short to allow TRAMS experiments to be performed upon excited states as long lived as that of pyrene. Lower repetition rates than that of the SRS must be employed. Pulsed laser sources have been used to effect in studies of water-soluble polymers bearing pyrenyl labels (57). In this context, the high stability of the laser source allows data collection to high signal-to-noise ratios, despite the relatively long accumulation times required. Pulsed flashlamps are much more limited, in this respect. Nevertheless, we have performed a limited number of TRAMS experiments, within the current investigation, using a thyratron-gated flashlamp employing D_2 as discharge medium (D_2 produces a more intense excitation flash than H_2). Figure 5 shows typical decay data for pyrene solubilized in STY(44)–AA at pH = 4.0. The data provide a good graphic illustration of the effects of the restrictions imposed upon the rotational tumbling of the pyrene constrained within the hydrophobic cavities of this polymer: covergence of the fluorescence intensity components, $I_\parallel$ and $I_\perp$, requires several hundred nanoseconds to accomplish.

The resultant data were analysed by the IR method, using a single exponential model for $r(t)$. The resultant τ_c values are listed in Table 5. The IR analyses of the various systems resulted in a consistent estimate for r_0^{-1} of 15.5 (± 0.5). This value was used in eq. [7] to estimate τ_c for each of the systems studied using steady state anisotropy determinations. The resultant data are also listed in Table 5. It can be seen that

(*i*) reasonable agreement is achieved between the relaxation data obtained in steady state and time-resolved experiments, given the limitations of the approaches adopted. (The application of a single exponential analytical procedure, for the modelling of $r(t)$, is likely to be an oversimplification, considering the complexities of the polymer dispersions under investigation. However, adoption of a more sophisticated model for the TRAMS data was not considered to be warranted under the resolution obtained using flashlamp excitation.)

(*ii*) The trends apparent in the τ_c values corroborate the observations made earlier on the basis of the steady state r^{-1} data:

(*a*) at low pH, each of the hydrophobically modified systems presents the pyrene guest with an environment that is more restrictive to motion, than that which exists in the hypercoiled form of PMAA. (Caution must be exercised here: a hydrophobic guest has the potential to influence the cavity in which is is occluded. There is spectral evidence[2] that the guest can alter the nature of its solubilizing pocket. It has also been reported that 9-methylanthracene induces production of a proportion of hydrophobic domains in PMAA that is not present in the unperturbed hypercoil (13).)

(*b*) The cavity/pyrene guest combination restricts the rotational freedom of the probe at low pH, to an extent that depends upon the nature of the hydrophobic modifier (i.e., MMA vs. styrene) and the copolymer composition.

(*c*) At pH values less than those associated with loss of solubilization capacity, the STY–AA systems seem to experience a relaxation of the restrictions to rotation of the guest, compared to those imposed in highly acidic media.

9-Methylanthracene

9-Methylanthracene has been a fluorescent reporter upon the conformational behavior of PMAA in aqueous media (13, 39, 58, 59). In particular, it has been reported that the fluorescence characteristics of this probe are sensitive to the viscosity of its microenvironment (60). In pure solvents, the fluorescence decays of 9-methylanthracene are monoexponential and their rates decrease with increasing viscosity (13). However, when solubilized in PMAA the decays become biexponential: it has been reported (13, 39) that a longer-lived component (of lifetime ca. 13 ns) is accompanied, in PMAA solution, by a shorter component of τ around 5–7 ns (dependent upon the tacticity of the PMAA).

Incorporation of 9-methyanthracene (10^{-5} M) into solutions of PMAA and hydrophobically modified forms of AA results in red shifts of both its excitation and emission spectra. The extent of the shift is dependent upon the polymer. Solubilization of the probe in STY(44)–AA at low pH, for example, results in a larger displacement of the spectra to lower energy than when the probe is incorporated in the PMAA hypercoil. The shifts might reflect differences in microviscosity and (or) hydrophobicity of the coil interiors.

Table 6 lists fluorescence liftetime data for the 9-methylanthracene probe dispersed in a variety of solvent media. In

[2] I. Soutar and L. Swanson. Unpublished data.

Can. J. Chem. Downloaded from www.nrcresearchpress.com by 46.23.64.124 on 09/08/12
For personal use only.

Fig. 5. $I_{\parallel}$ (upper curve) and $I_{\perp}$ decay curves (λ_a = 380 nm), following vertically polarized excitation (λ_e = 340 nm) of pyrene (10^{-6} M) dispersed in STY(44)–AA (10^{-2} wt.%) at pH = 4.0 and 298 K.

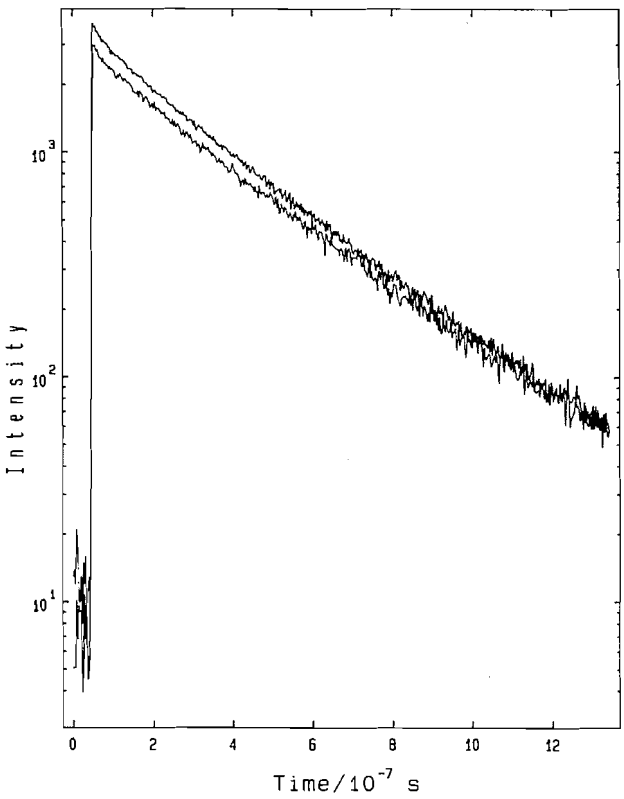

accord with previous observations (13, 39) the fluorescence decays become nonexponential when the probe is dispersed in aqueous solutions of polymers. In such systems, double-exponential models of the true decay (of the form of eq. [6], with i = 2) provide statistically adequate fits to the observed fluorescence profile.

The lifetime obtained for 9-methylanthracene in cyclohexane aggrees well with that reported by other workers (13, 39). Comparison of that of 11 ns, obtained in an aqueous medium (saturated solution at 298 K), with those reported by Snare et al. (39) in a variety of solvents over a range of viscosities, reveals that the lifetime of the solute is not determined by solvent viscosity alone.

In PMAA solution, recovery of a lifetime component of ca. 13 ns is consistent with earlier reports (13, 39). However, the lifetime of the second component is somewhat greater than that previously reported (13, 39). (It should be noted that the technique of time-correlated single-photon counting is not particularly well adapted to the recovery of two closely matched decay parameters. However, recovery of a component of magnitude similar to that of the probe in water gives confidence in the dual exponential fitting procedure (deemed both necessary and adequate on the grounds of "goodness of fit").)

The complexities of the fluorescence decays, obtained in the two copolymer systems studied, confirm the existence of solubilizing domains in these species at low pH. The STY(44)–AA system was studied over a range of pH values and the data clearly indicate the extended range of pH over which solubilization of the probe is effected. In this respect, the data support the findings of TRAMS upon the labelled copolymers indicating that this hydrophobically modified polymer does not fully uncoil until a pH of about 8 is attained. At higher values of pH, the fluorescence decay of the probe is monoexponential, showing that it has been ejected into the aqueous phase. In a similar fashion, the simplicity of decay of the probe's fluorescence, characterized by a lifetime of 10.9 (±0.1) ns, confirms that, in the presence of PAA, the probe experiences an environment similar to that of the bulk aqueous phase.

Steady-state fluorescence anisotropy studies of 9-methylanthracene solubilized in PMAA and STY(44)–AA at low pH, provide information that broadly supports our findings, using pyrene as a probe, regarding the relative microviscosities of the two systems. Fluorescence from the probe, solubilized in STY(44)–AA at pH = 4.2, is less depolarized (r^{-1} = 17.4) than that obtained in PMAA at pH = 3.4 (r^{-1} = 20.5). Using $\langle\tau\rangle$ values (based on eq. [5]) and an r_0^{-1} of 10.22 (based upon an estimate of the intrinsic polarization quoted for 9-methylanthracene frozen in a methylcyclohexane low-temperature glass (61)) we arrive at correlation times of ca. 19 and 12 ns, respectively. These data again suggest that rotation of the probe is more restricted in the hydrophobically modified copolymer than in the PMAA hypercoil. (Of interest in this context, it can be noted that Snare et al. (39) have shown that the time-resolved fluorescence anisotropy of 9-methylanthracene solubilized in PMAA may be resolved into two components (of 33 and 11 ns, respectively). The steady-state estimate of τ_c for the same probe in PMAA gives a value that is very close to that of the shorter of the two τ_c values recovered in TRAMS (39).)

Marked differences are apparent in the values of τ_c that result from anisotropy measurements of solubilized 9-methylanthracene and pyrene. These emphasize the fact that measurements of the rotational mobility of a given probe reflect both its intrinsic molar volume *and* the effects that it might induce by "drawing a cloak" of solvating species about itself as it enters the hydrophobic domains within the polymer coils. These observations are further substantiated by luminescence measurements upon solubilized perylene as described below.

Perylene

Fluorescence experiments involving both pyrene and 9-methylanthracene are complicated by the fact that both probes have significant solubility in water (62). Perylene, on the other hand, is soluble only to the extent of about 10^{-9} M in water (62). Consequently, its presence as a solubilized guest in a hydrophobic cavity can be detected, very simply, by the dramatic increase in its fluorescence intensity when compared to that of a saturated solution in water alone. For example, when dispersed in 10^{-2} wt.% solutions of STY(44)–AA at a nominal concentration of 10^{-5} M, solubilization of the probe occurs at pH values of less than ca. 7.5, as indicated by the concomitant appearance of discernible fluorescence.

As a consequence of its short-lived excited state (perylene solubilized in STY(44)–AA, for example, has a fluorescence lifetime of about 6 ns) perylene is not particularly well suited to anisotropy probing of media of very high viscosity. In STY(44)–AA the value of r^{-1}, observed in steady-state experiments, is 4.0. The value of r_0^{-1} for perylene is quoted as being of the order of 2.8 (63). Incorporation of these estimates into eq. [7] yields an estimate of 14 ns for τ_c. This value (subject to some

Can. J. Chem. Downloaded from www.nrcresearchpress.com by 46.23.64.124 on 09/08/12
For personal use only.

error, due to the assumptions involved) is very similar to that obtained from solubilization of 9-methylanthracene, under similar conditions, and suggests that the interiors of the hydrophobic domains produced in such copolymers are highly viscous.

Conclusions

1. Hydrophobic modification via copolymerization alters the conformational behaviour of polyacrylic acid: (*i*) in acid media, hydrophobic domains, which do not exist in PAA itself, are formed in MMA–AA and STY–AA copolymers; (*ii*) aggregation between hydrophobic components of the modified polyacids can, dependent upon hydrophobe and copolymer composition, markedly affect the segmental dynamics of the macromolecule; (*iii*) the creation of hydrophobic aggregates opposes the Coulombic forces of repulsion between the carboxylate anions formed during neutralization of the polyacid. The net effect is to shift, to higher values, the pH range over which chain expansion occurs, producing the more flexible open coil associated with the polysalt.

2. The hydrophobic domains formed in the AA-based copolymers can solubilize organic guests. It is apparent that (*i*) the microviscosity of the domain interiors is much greater than that of water; (*ii*) the hydrophobicity and microviscosity of the domain interiors depend upon both the nature of the modifying monomer and the composition of the copolymer; (*iii*) dependent upon the nature of the modifying comonomer and the copolymer composition, the hydrophobic aggregates disintegrate at higher pH and the solubilization capacity of the polymer, for organic guests, is lost; (*iv*) at intermediate pH values, such that guest solubilization can still be effected, the hydrophobic pockets of the polymeric host seem to exert lesser constraints upon probe motion than is the case at lower pH values.

Acknowledgements

The authors take pleasure in acknowledging financial support from the Science and Engineering Research Council (SERC) (now the Engineering and Physical Sciences Research Council (EPSRC)) (equipment, CASE studentship (to D.L.), and beamtime at the SRS), the Leverhulme Trust (research fellowship to L.S.), and the Royal Mail Research Centre (Swindon) (equipment and CASE support).

References

1. J.E. Glass (*Editor*). Polymers in aqueous media: performance through association. ACS Adv. Chem. Ser. **223**. ACS, Washington, D.C. 1989.
2. S.W. Shalaby, C.L. McCormick, and G.B. Butler (*Editors*). Water-soluble polymers: synthesis, solution properties and applications. ACS Symp. Ser. **467**. ACS, Washington, D.C. 1991.
3. D.A. Holden, W.A. Rendall, and J.E. Guillet. Ann. N.Y. Acad. Sci. **366**, 11 (1981).
4. D. Ng and J.E. Guillet. Macromolecules, **15**, 724 (1982).
5. M. Nowakowska, B. White, and J.E. Guillet. Macromolecules, **21**, 3430 (1988).
6. M. Nowakowska, B. White, and J.E. Guillet. Macromolecules, **22**, 2317 (1989).
7. B. White, M. Nowakowska, and J.E. Guillet. J. Photochem. Photobiol. **50**, 147 (1989).
8. M. Nowakowska and J.E. Guillet. Chem. Br. 327 (1991).
9. M. Nowakowska, E. Sustar, and J.E. Guillet. J. Am. Chem. Soc. **113**, 253 (1991).
10. E. Sustar, M. Nowakowska, and J.E. Guillet. J. Photochem. Photobiol. **63**, 357 (1992).
11. M. Nowakowska, H. Bakhtiyari, E. Osselton, M.R. Steel, and J.E. Guillet. J. Photochem. Photobiol. **64**, 329 (1992).
12. S.E. Webber. Chem Rev. **90**, 1469 (1990).
13. K.P. Ghiggino and K.L. Tan. *In* Polymer photophysics. *Edited by* D. Phillips. Chapman and Hall, London. 1985. Chap. 7.
14. T.S. Chen and J.K. Thomas. J. Polym. Sci. Polym. Chem. Ed. **17**, 1003 (1979).
15. D.Y. Chu and J.K. Thomas. Macromolecules, **17**, 2142 (1984).
16. J.A. Delaire, M.A.J. Rogers, and S.E. Webber. J. Phys. Chem. **88**, 6219 (1984).
17. K.S. Arora and N.J. Turro. J. Polym. Sci. Polym. Chem. Ed. **25**, 259 (1987).
18. A.F. Olea and J.K. Thomas. Macromolecules, **22**, 1165 (1989).
19. I. Soutar and L. Swanson. Eur. Polym. J. **29**, 371 (1993).
20. P. Pascal, J. Duhamel, Y. Wang, M.A. Winnik, X.X. Zhu, P. Macdonald, D.H. Napper, and R.G. Gilbert. Polymer, **34**, 1134 (1993).
21. I. Nataga and H. Morawetz. Macromolecules, **14**, 87 (1981).
22. F.M. Winnik. Polymer, **31**, 2125 (1990).
23. H. Ringsdorf, J. Simon, and F.M. Winnik. Macromolecules, **25**, 5353 (1992).
24. F.M. Winnik, M.A. Winnik, H. Ringsdorf, and J. Venzmer. J. Phys. Chem. **95**, 2583 (1991).
25. N.J. Turro and K.S. Arora. Polymer, **27**, 783 (1986).
26. H. Ringsdorf, J. Venzmer, and F.M. Winnik. Macromolecules, **24**, 1678 (1991).
27. B. Bednar, Z. Li, Y. Huang, L.C.P. Chang, and H. Morawetz. Macromolecules, **18**, 1829 (1985).
28. H.T. Oyama, W.T. Tang, and C.W. Frank. Macromolecules, **20**, 474 (1987).
29. F.M. Winnik. Chem. Rev. **93**, 587 (1993).
30. Y. Morishima, T. Kobayashi, S. Nozakura, and S.E. Webber. Macromolecules, **20**, 807 (1987).
31. C.L. McCormick, C.E. Hoyle, and M.D. Clark. Macromolecules, **23**, 3124 (1990).
32. C.L. McCormick, C.E. Hoyle, and M.D. Clark. Macromolecules, **24**, 2397 (1991).
33. I. Soutar and L. Swanson. Polym. Commun. **32**, 264 (1991).
34. N.J. Turro, G. Caminati, and J. Kim. Macromolecules, **24**, 4054 (1991).
35. N.J. Turro, J. Kim, and G. Caminati. Macromolecules, **26**, 1930 (1993).
36. E.V. Anufrieva and Yu. Ya. Gotlib. Adv. Polym. Sci. **40**, 1 (1981).
37. J.J. Heyward and K.P. Ghiggino. Macromolecules, **23**, 5170 (1990).
38. B. Bednar, J. Trnena, P. Svoboda, S. Vajda, V. Fidler, and K. Prochazka. Macromolecules, **24**, 2054 (1991).
39. M.J. Snare, K.L. Tan, and F.E. Treloar. J. Macromol. Sci. Chem. **17**, 189 (1982).
40. I. Soutar and L. Swanson. Macromolecules, **23**, 5170 (1990).
41. I. Soutar and L. Swanson. Polymer, **35**, 1942 (1994).
42. I. Soutar and L. Swanson. Macromolecules, **27**, 4304 (1994).
43. J.R. Ebdon, D.M. Lucas, I. Soutar, and L. Swanson. Macromol. Symp. **79**, 167 (1994).
44. I. Soutar. Polym. Int. **26**, 35 (1991).
45. I. Soutar. Makromol. Chem. Macromol. Symp. **53**, 393 (1992).
46. I. Soutar, L. Swanson, R.E. Imhof, and G. Rumbles. Macromolecules, **25**, 4399 (1992).
47. The SRS. EPSRC Daresbury Laboratory, Warrington. 1991.
48. Y. Kato. *In* Size exclusion chromatography. *Edited by* B.J. Hunt and S.R. Holding. Backie, Glasgow. 1989. Chap. 7.
49. P. Wahl. Chem. Phys. **7**, 210 (1975).
50. M.D. Berkeley, A.A. Kowalczyk, and L. Brand. J. Chem. Phys. **75**, 3581 (1981).

51. A.J. Marsh, G. Rumbles, I. Soutar, and L. Swanson. Chem. Phys. Lett. **31**, 195 (1992).
52. I. Soutar. *In* Developments in polymer photochemistry. Vol. 2. *Edited by* N.S. Allen. Applied Science, Barking. 1982. Chap. 4.
53. A. Nakajima. Bull. Chem. Soc. Jpn. **44**, 3237 (1971).
54. K. Kalayanasunderam and J.K. Thomas. J. Am. Chem. Soc. **99**, 2039 (19770.
55. J.B. Birks. Photophysics of aromatic molecules. Wiley-Interscience, London. 1970.
56. D. Chu and J.K. Thomas. J. Am. Chem. Soc. **108**, 6270 (1986).
57. I. Soutar, L. Swanson, S.J.L. Wallace, K.P. Ghiggino, D.J. Haines, and T.A. Smith. *In* Multi-dimensional NMR, FT/IR/Raman and fluorescence spectroscopy in polymer analysis. *Edited by* M.W. Urban and T.A. Provder. ACS Symp. Ser. **598**, 363 (1995).
58. F.E. Treloar. Chem. Scr. **10**, 216 (1976).
59. K.L. Tan and F.E. Treloar. Chem. Phys. Lett. **73**, 1103 (1979).
60. U.E. Blatt, F.E. Treloar, K.P. Ghiggino, and R. Gilbert. J. Phys. Chem. **85**, 2810 (1981).
61. K.C. Dowling and J.K. Thomas. Macromolecules, **23**, 1059 (1990).
62. R.S. Pearlman, S.H. Yalkowsky, and S. Banerjee. J. Phys. Chem. Ref. Data, **13**, 555 (1984).
63. J.R. Lakowicz. Principles of fluorescence spectroscopy. Plenum Press, New York. 1983.

Can. J. Chem. Downloaded from www.nrcresearchpress.com by 46.23.64.124 on 09/08/12
For personal use only.

Chain exchange kinetics of diblock copolymer micelles studied by nonradiative energy transfer. 1. Experimental design and theory

Guojun Liu

Can. J. Chem. Downloaded from www.nrcresearchpress.com by 46.23.64.124 on 09/08/12
For personal use only.

Abstract: A fluorescence experiment involving mixing donor-labeled micelles with acceptor-labeled unimers has been designed and a kinetic scheme for describing such an experiment has been proposed. An approximate analytical solution was found for the decrease in the donor fluorescence intensity at time t after sample mixing relative to that at time zero, $I(t)/I(0)$. Treating the data of this decrease in donor fluorescence intensity as a function of time using the derived equation allows the simultaneous determination of the rate constant k_n for unimer incorporation into micelles and the quenching efficiency φ of donor fluorescence by an acceptor in a micelle.

Key words: polymer micelles, dynamics, chain exchange, energy transfer.

Résumé : On a mis au point une expérience de fluorescence impliquant le mélange des micelles contenant un donneur marqué avec des unimères accepteurs marqués et on propose un schéma cinétique pour décrire une telle expérience. On a trouvé une solution analytique approximative pour expliquer la diminution de l'intensité de la fluorescence du donneur à un temps t relatif au temps zéro, $I(t)/I(0)$, du mélange de l'échantillon. Le traitement des données relatives à la diminution de l'intensité de la fluorescence du donneur en fonction du temps en faisant appel à l'équation dérivée permet de déterminer simultanément la constante de vitesse, k_n, pour l'incorporation de l'unimère dans les micelles et pour l'efficacité d'extinction, φ, de la fluorescence d'un donneur par un accepteur dans une micelle.

Mots clés : micelles de polymère, dynamique, échange de chaîne, transfert d'énergie.

[Traduit par la rédaction]

1. Introduction

Due to their potential medical and pharmaceutical applications, block copolymer micelles have attracted much attention in the past decade (1–4). Significant progress has been made in the theoretical (5–12) and experimental (13–19) understanding of the equilibrium properties, such as the size and aggregation number, of micelles. The study of micelle chain exchange dynamics has, however, been relatively rare from either a theoretical (20, 21) or experimental (22–26) point of view.

In a micellar system, chain exchange between a pool of unimers and micelles, the breakdown of larger micelles into smaller ones (fission), and the formation of larger micelles from smaller ones (fusion) may all occur simultaneously (1). Of all the processes, chain exchange, in which a unimer chain U is either dissociated from a micelle M_n with n chains or added to a micelle M_{n-1} with $n-1$ chains, is the most fundamental:

$$[1] \qquad M_n \underset{k_n}{\overset{k_{-n}}{\rightleftharpoons}} M_{n-1} + U$$

where k_n and k_{-n} are the rate constants for chain incorporation into and dissociation from a micelle, respectively. Rate constants k_n and k_{-n} are related, at equilibrium, by

$$[2] \qquad K_n[M_{n-1}][U] = k_{-n}[M_n]$$

where [U] and $[M_n]$ denote the concentrations of U and M_n, respectively.

Halperin and Alexander (20) have recently argued that the chain exchange process is much faster than the micelle fusion and fission processes. The slower fusion rate can be understood as due to the strong repulsion between the coronas of two micelles approaching one another. The fission rate is lower because the simultaneous disentanglement of a few chains or more from the core of a micelle is kinetically unfavorable. Based on the assumption that only one chain is either incorporated into or dissociated from a micelle at a time, Halperin and Alexander derived scaling relations between k_{-n} and polymer structural parameters such as the length of each block of a diblock copolymer.

Due to the dominance of the chain exchange process

Received May 2, 1995.

This paper is dedicated to Professor J.E. (Jim) Guillet in recognition of his contributions to Canadian chemistry.

G. Liu.[1] Department of Chemistry, the University of Calgary, 2500 University Drive, NW, Calgary, AB T2N 1N4, Canada

[1] Telephone: (403) 220-5341. Fax: (403) 289-9488.

Can. J. Chem. Downloaded from www.nrcresearchpress.com by 46.23.64.124 on 09/08/12
For personal use only.

in block copolymer micelles, the Aniansson and Wall (A–W) (27) analysis of micelle dynamics, originally developed for small-molecule surfactant micelles, should apply. The A–W theory was formulated to describe a typical perturbation and relaxation experiment. In such an experiment, a miceller system at equilibrium is suddenly subjected to a minor perturbation such as a jump in temperature or pressure. Due to the change in external conditions, the concentration of unimers or micelles or their equivalents should relax after the initial perturbation, according to the A–W theory, to their new equilibrium values with two relaxation times τ_1 and τ_2. In the short-time domain characterized by τ_1, the total number of micelles would remain unchanged while the mass concentrations of micelles and unimers, in terms of grams per litre of solution, adjust so that they attain approximately their equilibrium values. In the second stage characterized by τ_2, micelle disintegration and formation take place. This is accompanied by either growth or reduction in micelle sizes. The A–W theory has been very successful as it relates τ_1 and τ_2 to k_{-n} and to characteristic micellar parameters such as the average aggregation number $\bar{n}$ and the variance σ in $\bar{n}$.

The relaxation kinetics of diblock copolymer micelles studied so far have been found to follow a two-stage mechanism in agreement with the A–W theory. Rate constants such as K_{-n} for diblock micelles have, however, not been reported. The difficulty has been in establishing the equivalence between the experimentally determined τ_1 and τ_2 and those discussed by A–W, owing to complications from the techniques used for monitoring the relaxation of a micellar system.

Light scattering has, for example, been the most popular technique for monitoring micelle relaxation kinetics but the validity of such a usage is questionable. To see the significance of such an experiment, we will first simplify the expression for the scattered light intensity $i_\theta(t)$ by making some assumptions. We assume that the micellar particles are sufficiently small or the scattered light intensity is detected at a small enough angle θ so that the scattering function $P(\theta)$ is approximately 1 (28). We further assume that the micelle solution is dilute, and interparticle interference negligible. Under these conditions, we have

$$[3] \qquad i_\theta(t) \propto \bar{M}_w c_m$$

where $\bar{M}_w$ and c_m are the weight-average molar mass and the mass concentration of micelles, respectively. In the time domain immediately after a perturbation, the number of micelles, according to the A–W analysis, is approximately constant. Any increase in c_m would naturally also lead to an increase in $\bar{M}_w$ of micelles. Thus, $i_\theta(t)$ in this region does not increase linearly but, rather, quadratically with c_m, a situation not addressed by Aniansson and Wall.

In the time domain when micelle size redistribution dominates, c_m is more or less constant but $\bar{M}_w$ varies. Thus, the use of light scattering, in this time domain, is in agreement with the spirit of the Aniansson and Wall discussion. The quadratic c_m dependence in the short-time domain can be accounted for if the initial process is well resolved or decoupled from the micelle size redistribution process characterized by τ_2. In reality, the two processes are coupled. Due to the coupling of these two processes and the different connotations of the scattered light intensity $i_\theta(t)$ in the two regimes, the analysis of $i_\theta(t)$ using

$$[4] \qquad i_\theta(t) = \sum_{i=1}^{2} a_i \exp(-t/\tau_i)$$

where a_i are the amplitude coefficients, will not yield τ_1 and τ_2 values that are the same as the concentration relaxation times for unimers or micelles.

In addition to the aforementioned complication, most of the previous studies were plagued by the use of large perturbations. The use of large perturbations, such as the sudden change in solvent composition (2) or temperature (23) to cause micelle formation from a solution with no micelles, or vice versa, makes the experimental detection of the relaxation process easier but the A–W theory inapplicable.

Fluorescence techniques are ideal for studying chain exchange dynamics as they are sensitive to minor changes in the properties of a system if an experiment is well designed. Wang et al. (24) and Procházka et al. (25) for example, labeled identical diblock copolymers with fluorescence donors and acceptors and prepared micelles from differently labeled chains, respectively. Micelles containing differently labeled chains were then mixed. Due to chain exchange after mixing, donors residing in the same micelles as acceptors may transfer electronic excitation energy to acceptors, via the dipole–dipole energy transfer mechanism (29). Energy transfer decreases the fluorescence intensity of the donor but increases that of the acceptor, although the donor is selectively excited in the process. The beauty about the experiments of Wang et al. and Procházka et al. was that they were carried out near equilibrium conditions, if the donor- and acceptor-labeled chains could be viewed as identical.

The experimental data of Wang et al. and Procházka et al., i.e., the variation in the fluorescence intensity $I(t)$ of the donor as a function of time, have been fitted with a sum of two exponential terms. The difficulty there again lies in relating the τ_1 and τ_2 values recovered to k_{-n}. In this case, $I(t)$ is, by no means, a linear function of a concentration parameter such as the number of acceptor-labeled chains entering a micelle consisting primarily of donor-labeled chains. Instead, $I(t)$ is a complex function of the efficiency of energy migration among donor groups, the number and locations of donors and acceptors in a micelle, and the rate constant for energy transfer, etc. It is not surprising that when attempted by Wang et al., only numerical expressions were found between $I(t)$ and k_{-n}, and the numerical solutions did not explain the experimental data well.

In this paper, I will describe the proper design of the experiment involving mixing donor- and acceptor-labeled chains to enable the unambiguous analysis of fluorescence data to yield rate constant k_n. In Sect. 2, the experimental design and the kinetic model for the experiment will be described, and the approximate solutions for some important equations will be presented. In Sect. 3, errors that may be introduced due to the treatment of experimental data with approximate analytical solutions found in Sect. 2 will be estimated for commonly encountered experimental conditions. Some conclusions will be drawn in Sect. 4.

Can. J. Chem. Downloaded from www.nrcresearchpress.com by 46.23.64.124 on 09/08/12
For personal use only.

2. Experimental design and theory

Experimental design

I will use fluorene- and pyrene-labeled polystyrene (PS) and poly(2-hydroxylethyl methacrylate) (PHEMA) block copolymers, i.e., PS-*b*-PHEMA-Fl(y), PS-*Py*-PHEMA-Fl(y), which have been synthesized and are currently being studied in my laboratory (30),[2] to illustrate the essential features of such an experiment:

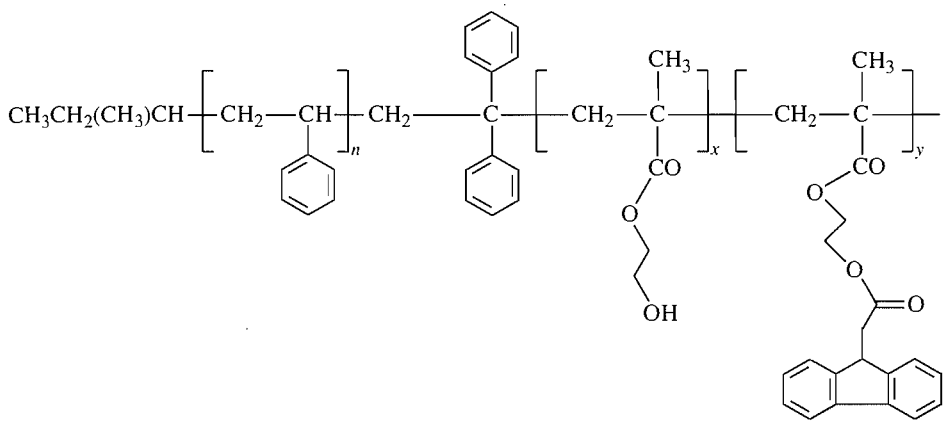

PS-*b*-PHEMA-Fl(y)

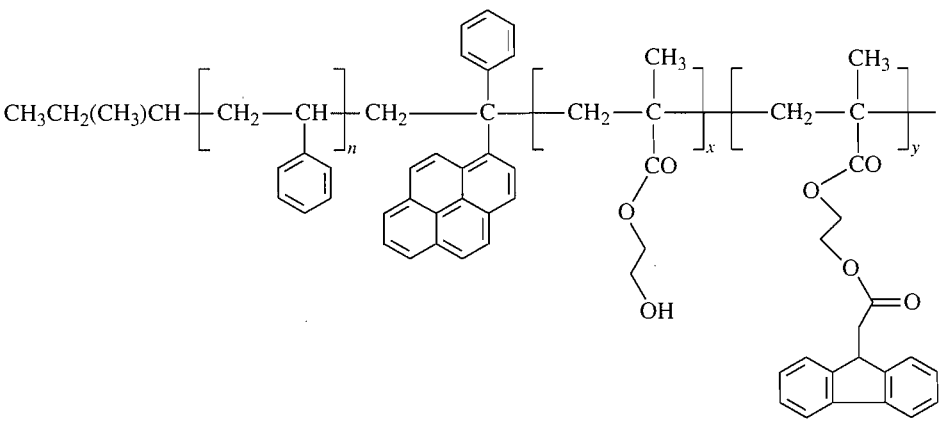

PS-*Py*-PHEMA-Fl(y)

The PHEMA blocks of these polymers are labeled by fluorene at a density y typically less than 10% as denoted by the "Fl(y)" suffix. The PS-*Py*-PHEMA polymer is labeled to minimize the structural differences between it and PS-*b*-PHEMA-Fl(y).

A micelle solution will be prepared first from PS-*b*-PHEMA-Fl(y) in a THF-cyclohexane mixture that is selectively poor for the PHEMA block. The molar micelle concentration c_M^0 is tuned using:

$$[5] \qquad c_M^0 = \frac{c - c^*}{\bar{n}}$$

to be close to the critical micelle concentration c^*. In eq. [5], $\bar{n}$ denotes the average micelle aggregation number and c the polymer concentration.

Then, an equal volume of a PS-*Py*-PHEMA-Fl(y) sample at a polymer concentration c_{Py}^0, which is below c^*, e.g. $c_{Py}^0 \approx 0.50c^*$ or $c_{Py}^0 \approx 0.50c_M^0$, is added to the PS-*b*-PHEMA-Fl(y) micelle solution. After mixing, the decrease in the fluorescence intensity of the donor and the increase in that of the acceptor as a function of time will be monitored while exciting the donor group selectively.

Analysis of the experiment

Three important features of the experiment described above are discussed here. First, a unimer solution of PS-*Py*-PHEMA-Fl(y) instead of its micelle solution is mixed with a micelle solution of PS-*b*-PHEMA-Fl(y). This will greatly simplify the kinetic description. Immediately after the mixing, unimer concentration [U] is diluted by a factor of 0.75, since [U] = $0.50c^*$ for the PS-*Py*-PHEMA-Fl(y) solution and [U] = c^* for the PS-*b*-PHEMA-Fl(y) micelle solution. Due to the relatively large negative deviation of [U] from c^*, the system will respond rapidly by dissociating some unimers from the existing micelles until the total unimer concentration is again approximately c^*. This initial adjusting period, characterized by τ_I, is short (20).

After τ_I, the average size of the micelles in the system is

[2] Studies of chain exchange kinetics are currently being performed.

Can. J. Chem. Downloaded from www.nrcresearchpress.com by 46.23.64.124 on 09/08/12
For personal use only.

smaller than their equilibrium size. Micelle size redistribution takes place. In this process, a small number of micelles will disintegrate and the majority will increase their size. It is the kinetics of chain exchange in this long-time domain, between PS-*b*-PHEMA-Fl(y) chains, associated mostly with micelles, and PS-*Py*-PHEMA-Fl(y) chains, existing almost exclusively as unimers, that is the focus of discussion here. Due to the assumption that acceptor-labeled chains initially only exist as unimers, the kinetic scheme here is much simpler than for the case when two micellar solutions are mixed, as one does not need to keep track of micelles consisting dominantly of donor- and acceptor-labeled chains, respectively.

Then, the concentration of PS-*Py*-PHEMA-Fl(y) is lower than c_M^0, e.g., $c_{Py}^0 \approx 0.50c_M^0$. This ensures a low probability of each micelle having more than one quencher. As will be seen later, this condition again greatly simplifies the derivation of the mathematical expressions for the donor and acceptor fluorescene intensities as a function of time.

Thirdly, I have chosen fluorene as the energy donor and pyrene as the acceptor or quencher because fluorene transfer energy to pyrene with a critical energy transfer distance of ~32 Å (31). Also, efficient energy migration among different fluorene groups is possible in a micellar core because the critical energy transfer distance between two fluorene groups is ~22 Å (31). Energy migration increases the effective radius of fluorene fluorescence quenching by pyrene, which ensures that a single pyrene group inside a micelle core will lead to the effective quenching of the fluorescence of fluorene. With the use of fluorene and pyrene, we have determined a quenching efficiency of ~15% for the incorporation of one PS-*Py*-PHEMA-Fl(y) chain into a micelle of PS-*b*-PHEMA-Fl(y), where both samples have 3% of fluorene labeling and an equal number of styrene and HEMA units (i.e., 100), respectively. The average aggregation number for such a micelle has been determined to be around 63 and the hydrodynamic radius to be some 140 Å (30).

General kinetic model

In my treatment, the fastest occurring unimer exchange process is assumed to be mainly responsible for the incorporation of PS-*Py*-PHEMA-Fl(y) into PS-*b*-PHEMA-Fl(y) micelles.

$$[6] \qquad M_n + U \underset{k_{-(n+1)}}{\overset{k_{(n+1)}}{\rightleftharpoons}} M_{n+1}$$

$$[7] \qquad M_n \underset{k_n}{\overset{k_{-n}}{\rightleftharpoons}} M_{n-1} + U$$

$$[8] \qquad M_nPy_i + \wedge\wedge\wedge\wedge\wedge\wedge\wedge Py \underset{[(i+1)/(n+i+1)]k_{-n}}{\overset{k_n}{\rightleftharpoons}} M_nPy_{i+1}$$

where $i = 0, 1, \ldots, m-1$.

In the above equations, U and $\wedge\wedge\wedge\wedge\wedge\wedge\wedge Py$ represent PS-*b*-PHEMA-Fl(y) and PS-*Py*-PHEMA-Fl(y) unimers, respectively; M_n denotes a micelle with n PS-*b*-PHEMA-Fl(y) chains; m stands for the maximal number of PS-*Py*-PHEMA-Fl(y) chains that a micelle can take up. The factor $(i+1)/(n+i+1)$ before k_{-n} in eq. [8] accounts for the fact that every unimer chain, either U or $\wedge\wedge\wedge\wedge\wedge\wedge\wedge Py$, has an equal chance to exit a micelle and that there are only $(i+1)$ $\wedge\wedge\wedge\wedge\wedge\wedge\wedge Py$ out of a total of $(n+i+1)$ chains in a micelle M_nPy_{i+1}.

Since eqs. [6] and [7] do not involve $\wedge\wedge\wedge\wedge\wedge\wedge\wedge Py$ and will not affect the fluorescence properties of the system, I will not consider them any further. I have also assumed that the k_n for PS-*b*-PHEMA-Fl(y) and PS-*Py*-PHEMA-Fl(y) addition to a micelle is the same. So are their k_{-n} values. The last assumption may be validated by synthesizing PS-*b*-PHEMA-Fl(y) and PS-*Py*-PHEMA-Fl(y) polymers with everything identical except the difference in the pyrene label.

From eq. [8] we have the following equations for describing the change in the concentration of micelles of n unimers containing i PS-*Py*-PHEMA-Fl(y) chains:

$$[9] \qquad \frac{d[M_nPy_i]}{dt} = k_n[\sim\sim Py][M_nPy_{i-1}] - \frac{i}{n+i}k_{-n}[M_nPy_i] - k_n[M_nPy_i][\sim\sim Py] + \frac{i+1}{n+i+1}k_{-n}[M_nPy_{i+1}]$$

$$i = 0, 1, 2, \ldots, m$$

In using eq. [9] for $d[M_nPy_0]/dt$ or $d[M_n]/dt$, one should remember $[M_nPy_{-1}] = 0$. For $d[M_nPy_m]/dt$, one resorts to the assumption that a micelle with $(m+1)\wedge\wedge\wedge\wedge\wedge\wedge\wedge Py$ groups does not form.

In using the same rate constant k_n for PS-*Py*-PHEMA-Fl(y) incorporation into a micelle regardless of the i value, I have implicitly assumed that m is small compared to n and the presence of a few PS-*Py*-PHEMA-Fl(y) chains will not significantly perturb the property of a micelle.

Equation [9] is general and applies to micelles of all sizes or of different n. If assuming that n has a very sharp distribution around the average aggregation number $\bar{n}$ and the n independence of k_n and k_{-n}, an approximation used in all previous studies (1, 27), the kinetic equations for the concentrations, $[MPy_i]$, of micelles with i PS-*Py*-PHEMA-Fl(y) chains, i.e., $\sum_n[M_nPy_i]$, are

$$[10] \qquad \frac{d[MPy_i]}{dt} = k_n[\sim\sim Py][MPy_{i-1}] - \frac{i}{\bar{n}+i}k_{-n}[MPy_i] - k_n[MPy_i][\sim\sim Py] + \frac{i+1}{\bar{n}+i+1}k_{-n}[MPy_{i+1}] \qquad i = 0, 1, 2, \ldots, m$$

Again, one is cautioned that $[MPy_{-1}] = 0$ and $[MPy_{m+1}] = 0$ when using eq. [10] for finding $d[M]/dt$ and $d[MPy_m]/dt$, where [M] is the concentration of micelles containing no pyrene at time t.

Due to the nonlinearity of the series of equations denoted by eq. [10], they generally do not give exact analytical solutions for $m > 1$. They can, however, be easily solved numerically.

Kinetic model for the low c_{Py}^0/c_M^0 case

Since c_{Py}^0 has been assumed to be low relative to c_M^0, the probability for the incorporation of two or more PS-*Py*-PHEMA-Fl(y) chains into the same micelle is low and we can use eq. [10] by setting $m = 1$:

$$[11] \qquad \frac{d[MPy]}{dt} = k_n[M][\sim\sim\sim Py] - \frac{1}{\bar{n}+1}k_{-n}[MPy]$$

Can. J. Chem. Downloaded from www.nrcresearchpress.com by 46.23.64.124 on 09/08/12
For personal use only.

To simplify notation, let:

[12] $x = [\text{MPy}]$

Due to the assumption of no moe than one acceptor per micelle,

[13] $[\text{M}] = c_{\text{M}}^0 - x$

and the concentration of $\wedge\wedge\wedge\wedge\wedge\wedge Py$, [$\sim\sim\sim$ Py], is related to x by

[14] $[\sim\sim\sim \text{Py}] = c_y^0 - x$

where c_y^0 is the initial PS-Py-PHEMA-Fl(y) concentration. Since $\bar{n}$ is typically larger than 50, the second term on the right-hand side of eq. [11] is assumed to be negligible. Inserting eqs. [13] and [14] and neglecting the second term, eq. [11] becomes

[15] $$\frac{dx}{dt} = k_n(c_{\text{M}}^0 - x)(c_y^0 - x)$$

The solution for x from eq. [15] can be found in most physical chemistry textbooks to be

[16] $$x = \frac{c_y^0(1 - e^{-kt})}{1 - \frac{c_y^0}{c_{\text{M}}^0} e^{-kt}}$$

where

[17] $k = (c_{\text{M}}^0 - c_y^0)k_n$

Equation [17] gives $x = 0$ at $t = 0$ and $x = c_y^0$ as $t \rightarrow \infty$. These results are reasonable and suggest the validity of the equation.

Decrease in normalized donor fluorescence intensity as a function of time

Due to the low concentration of polymers existing as unimers, light is mainly absorbed by fluorene dispersed inside the micellar cores and I assume that light is emitted from fluorene or pyrene associated with micelles only. If the efficiency of fluorene fluorescence quenching by a PS-*Py*-PHEMA-Fl(y) chain in a micelle is φ, the fluorescence intensity $I(t)$ of the donor at time t normalized relative to that $I(0)$ at time $t = 0$ should be:

[18] $$\frac{I(t)}{I(0)} = \frac{c_{\text{M}}^0 - \varphi x}{c_{\text{M}}^0}$$

Inserting eq. [16] and simplifying gives:

[19] $$\frac{I(t)}{I(0)} = 1 - \varphi \frac{c_y^0 - c_y^0 e^{-kt}}{c_{\text{M}}^0 - c_y^0 e^{-kt}}$$

At $t = 0$, eq. [19] gives $I(t)/I(0) = 1$. Extrapolating to infinitely long times, $I(t)/I(0) \rightarrow 1 - \varphi(c_y^0/c_{\text{M}}^0)$. These predictions are intuitively reasonable, suggesting the validity of eq. [19].

Increase in the acceptor fluorescence intensity

After solution mixing, the acceptor fluroescence intensity increases with time. This increase is proportional to the magnitude of x:

[20] $$I_{\text{Py}}(t) \propto \frac{c_y^0(1 - e^{-kt})}{1 - \frac{c_y^0}{c_{\text{M}}^0} e^{-kt}}$$

Fig. 1. Decrease (top graph) in donor fluorescence intensity and increase (bottom graph) in acceptor fluorescence intensity as a function of time after sample mixing. Curves generated from eqs. [24] and [25], respectively, using $k_n = 1.00 \times 10^4$ (M^{-1} s^{-1}), $c_{\text{M}}^0 = 10^{-6}$ M, and $\varphi = 0.400$.

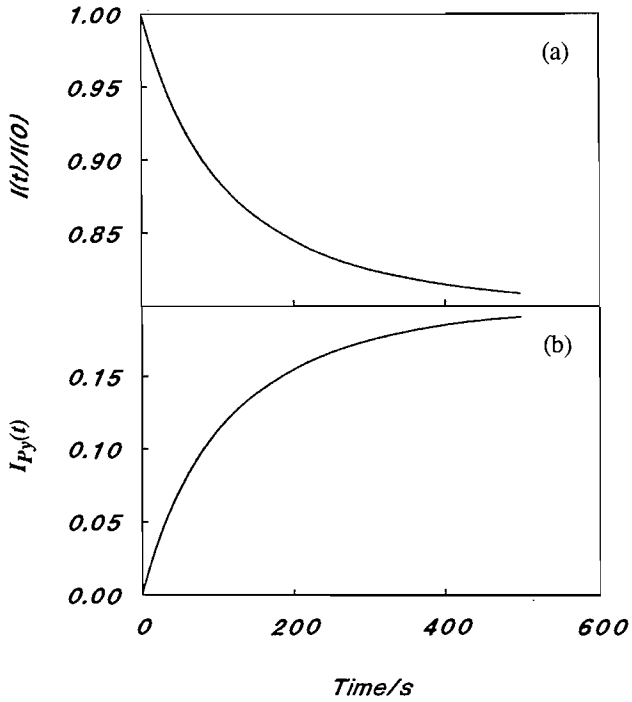

3. Discussion

Equations [19] and [20]

Illustrated in Fig. 1 are solutions for eqs. [19] and [20] using the following parameters: $c_y^0 = 5 \times 10^{-7}$ M, $c_{\text{M}}^0 = 1 \times 10^{-6}$ M, $\varphi = 0.40$, and $k_n = 10^4$ M^{-1} s^{-1}. These curves look very similar in shape to those obtained experimentally by Wang et al. (24) and Procházka et al. (25) and suggest that our theoretical results agree with experimental results, at least qualitatively. We will report the treatment of our own experimental results elsewhere (30).

Both the increase in the fluorescence intensity of the acceptor and the decrease in that of the donor with time can be fitted using eqs. [20] and [19], respectively, to obtain k and thus k_n. The decrease in the fluorescence intensity of the donor with time is, however, richer in information as it can be fitted using eq. [19] to obtain both k_n and φ. Therefore, in this paper I emphasize the treatment of donor decay data.

Accuracy of the no more than one acceptor in one micelle approximation

In my derivation so far, I have assumed each micelle can, at most, contain one acceptor due to the low c_y^0/c_{M}^0 value. In reality, the equilibrium distribution of acceptors inside mi-

Can. J. Chem. Downloaded from www.nrcresearchpress.com by 46.23.64.124 on 09/08/12
For personal use only.

Table 1. Variation of $P(i)$ with $\langle s \rangle$ as calculated from the Poisson distribution and from solving eqs. [12]–[14] at $t = 1000$ s setting $m = 10$. The following parameters: $k_n = 1.00 \times 10^4$ (M^{-1} s^{-1}), $k_{-n} = 10^{-2}$ (s^{-1}), $c_M^0 = 10^{-6}$ M, and $\bar{n} = 100$, were used for solving eqs. [12]–[14].

	$\langle s \rangle$					
	0.100		0.500		0.900	
	Poisson	Our approach	Poisson	Our approrach	Poisson	Our approach
$P(0)$	0.905	0.906	0.607	0.604	0.407	0.387
$P(1)$	0.090	0.089	0.303	0.311	0.365	0.398
$P(2)$	0.009	0.004	0.076	0.073	0.165	0.164
$P(3)$	0.000	0.000	0.013	0.011	0.049	0.042
$P(4)$	0.000	0.000	0.002	0.001	0.011	0.008

celles obeys the Poisson distribution. Letting $c_y^0/c_M^0 = \langle s \rangle$, the probability $P(i)$ for a micelle to contain i acceptors is given by:

$$[21] \qquad P(i) = \frac{\langle s \rangle^i}{i!} \exp(-\langle s \rangle)$$

The variation of $P(i)$ with $\langle s \rangle$ for the $\langle s \rangle$ values of 0.100, 0.500, and 0.900 is tabulated in Table 1. Even when $\langle s \rangle$ = 0.50, the probability of finding two or more acceptors in a single micelle is already quite significant. This affects the φ and k_n results recovered by fitting donor fluorescence intensity decay curves using eq. [19]. The error introduced due to the use of eq. [19] for treating experimental data will be examined in this subsection.

The series of equations denoted by eq. [10] can be solved numerically for $[MPy_i]$, the concentrations of micelles with different numbers, i, of acceptors. From known $[MPy_i]$, the relative donor fluorescence intensity at time t can be calculated using:

$$[22] \qquad \frac{I(t)}{I(0)} = 1 - \sum_{i=1}^{\infty} \varphi(i) \frac{[MPy_i]}{c_M^0}$$

where $\varphi(i)$ is the efficiency of donor fluorescence quenching by i acceptor groups residing in a micelle. Due to the small $m/\bar{n}$ ratio, I assume that the rate constant $k_q(i)$ of fluorene fluorescence quenching by pyrene increases with the number i of quenchers in a micelle following:

$$[23] \qquad k_q(i) = ik_q(1)$$

where $k_q(1)$ is the rate constant of fluorescence quenching by one quencher in a micelle.
$\varphi(i)$ is defined by

$$[24] \qquad \varphi(i) = \frac{ik_q}{ik_q + 1/\tau_0}$$

where τ_0 is the lifetime of fluorene in the absence of fluorescence quenching by pyrene. For a given $\varphi(1)$ not equal to 1, any other $\varphi(i)$ can be calculated using:

$$[25] \qquad \varphi(i) = \frac{i\varphi(1)/[1 - \varphi(1)]}{i\varphi(1)/[1 - \varphi(1)] + 1}$$

The relative donor fluorescence intensity at time t calculated using eq. [22] and $[MPy_i]$ solved from eq. [10] is the accurate result. The strategy here is to generate donor decay curves from this approach and then to fit the decay curves using eq. [19] to see how the recovered k_n and φ values deviate from k_n and $\varphi(1)$, input to estimate the error involved with the use of eq. [19].

Fig. 2. Variation in $[MPy_i]$ where $i = 0, 1, \ldots, 4$ (from top down as i increases) as a function of time after solution mixing. Curves generated from simultaneous differential equations [12]–[14] by setting $m = 4$, $k_n = 1.00 \times 10^4$ (M^{-1} s^{-1}), $k_{-n} = 10^{-2}$ (s^{-1}), $c_M^0 = 10^{-6}$ M, $c_y^0 = 0.500 \times 10^{-6}$ M, $\bar{n} = 100$, and $\varphi = 0.150$.

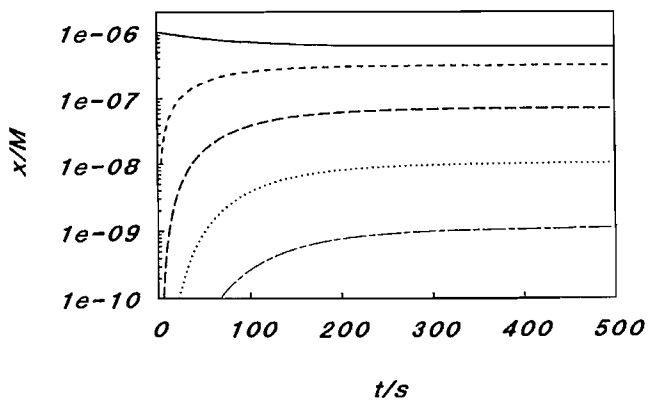

The set of curves in Fig. 2 illustrate how $[MPy_i]$, where $i = 0$, 1, 2, 3, and 4, vary with time after sample mixing. The curves were generated using $k_n = 1.00 \times 10^4$ M, $k_{-n} = 10^{-2}$ M, $c_M^0 = 10^{-6}$ M, $c_y^0 = 0.500 \times 10^{-6}$ M, and $\bar{n} = 100$. Initially, only MPy are formed in significant amounts. As time progresses, MPy_2, MPy_3, and then MPy_4 begin to form. At long times, the concentration of each species no longer changes significantly with time, indicating the establishment of acceptor distribution equilibrium. All these behaviors are intuitively expected and thus suggest the validity of our approach.

At sufficiently long times, the solution of eq. [10] gives the equilibrium concentrations of micelles containing varying numbers of PS-*Py*-PHEMA-Fl(y) chains. For a micellar system with $k_n = 1.00 \times 10^4$ M, $k_{-n} = 10^{-2}$ M, $c_M^0 = 10^{-6}$ M, and $\bar{n} = 100$ and varying c_y^0, I have solved $[MPy_i]$

Can. J. Chem. Downloaded from www.nrcresearchpress.com by 46.23.64.124 on 09/08/12
For personal use only.

Fig. 3. Comparison of the transient donor intensity decay curve (—) generated using simultaneous differential equations [12]–[14] and eq. [27] with that (- - -) generated using eq. [24]. The shared parameters are $k_n = 1.00\times10^4$ (M^{-1} s^{-1}), $c_M^0 = 10^{-6}$ M, $c_y^0 = 0.500\times10^{-6}$ M, and $\varphi = 0.150$. The solution of the simultaneous differential equations also required the use of $\bar{n} = 100$, and $k_{-n} = 10^{-2}$ (s^{-1}). Also illustrated is the best fit (···) to (—) by eq. [24].

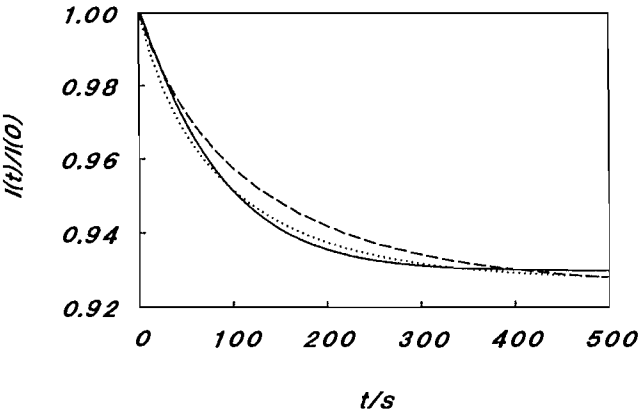

where $i = 0, 1, \ldots,$ and 4 at time $t = 10^3$ s, a sufficiently long time, and used them for calculating $P(i)$ from

$$[26] \qquad P(i) = \frac{[MPy_i]}{\sum_{i=0}^{4}[MPy_i]}$$

The $P(i)$ values calculated are tabulated in Table 1 for comparison with those calculated from the Poisson distribution given by eq. [21]. The superb agreement between these two approaches, particularly at low $\langle s\rangle$ values, confirms the validity of our solutions.

Illustrated in Fig. 3 is the comparison between a transient donor fluorescence intensity decay curve generated using the accurate approach described above from eq. [22] and that generated from eq. [19]. The curves were constructed using $k_n = 1.00 \times 10^4$ M, $c_M^0 = 10^{-6}$ M, $c_y^0 = 0.500 \times 10^{-6}$ M, and $\varphi(1) = 0.150$ in common. The construction of the decay curve from the more accurate approach also used $k_{-n} = 10^{-2}$ M and $\bar{n} = 100$. The $\bar{n}$ value of 100 is typical. The k_n value of 10^{-2} M was calculated from eq. [2] by assuming that $[M_{n-1}] \approx [M_n]$ and $[U] = 10^{-6}$ M. At $\langle s\rangle = 0.500$, substantial differences between results from the two approaches already exist.

At short times, the agreement between the two approaches is good. The slightly lower values of $I(t)/I(0)$ calculated from eq. [19] are due to neglecting, in the approximate approach, the dissociation of PS-*Py*-PHEMA-Fl(y) chains from micelles once they are incorporated into micelles. At intermediate times, the more accurate approach leads to lower $I(t)/I(0)$ values, because the formation of micelles with more than one PS-*Py*-PHEMA-Fl(y) chain is now substantial and these processes lead to the more rapid incorporation of PS-*Py*-PHEMA-Fl(y) chains and thus the more rapid decrease in $I(t)/I(0)$. At long times when the equilibrium quencher distribution is approximately established, lower quenching is obtained again from the more accurate approach. This is because $\varphi(i) < i\varphi(1)$ holds for all $i > 1$ according to eq. [25] and the uniform distribution of quenchers in micelles would lead to more quenching than is the case when quenchers are concentrated in relatively fewer micelles.

Table 2. Errors in recovered φ and k_n due to the use of eq. [24]. Also examined is the effect of $\varphi(1)$ input on the recovered φ and k_n values. Donor fluorescence intensity decay data were generated using eqs. [12]–[14] and [27] by setting $m = 10$, $k_n = 1.00 \times 10^4$ (M^{-1} s^{-1}), $k_{-n} = 10^2$ (s^{-1}), $c_M^0 = 10^{-6}$ M, and $\bar{n} = 100$.

s	φ	$k_n \times 10^{-4}$ (M^{-1} s^{-1})
$\varphi(1) = 0.150$		
0.100	0.147	1.07
0.300	0.145	1.22
0.500	0.146	1.39
0.700	0.147	1.53
0.900	0.152	1.57
$\varphi(1) = 0.300$		
0.100	0.291	1.08
0.500	0.278	1.43
0.900	0.281	1.70
$\varphi(1) = 0.500$		
0.100	0.481	1.08
0.500	0.442	1.49
0.900	0.430	1.84

Also illustrated in Fig. 3 is the best fit to the accurate curve by eq. [19]. The best fit was obtained by minimizing the following function:

$$[27] \qquad \chi^2 = \frac{1}{N}\sum_{i=1}^{N}\frac{[y_{cal}(i) - y_{sim}(i)]^2}{y_{sim}(i)}$$

where N, equal to 250 in this case, is the total number of data points fitted; $y_{sim}(i)$ and $y_{cal}(i)$ are the simulated donor intensity from the more accurate approach and data at time t_i calculated using eq. [19], respectively.

The error involved with the use of eq. [19] for fitting data calculated from the more accurate approach at different $\langle s\rangle$ and $\varphi(1)$ values can be seen from Table 2. As $\langle s\rangle$ increases, the assumption of no more than one quencher per micelle becomes increasingly invalid and it is expected that the error in k_n and φ values recovered will increase.

As input $\varphi(1)$ increases, φ recovered deviates more negatively from $\varphi(1)$. This is reasonable considering that $\varphi(i)$ becomes increasingly smaller than $i\varphi(1)$ for $i > 1$ as $\varphi(1)$ increases. If $\varphi(i)$ values are less than $i\varphi(1)$, it is expected that the quenching efficiency in a system where quenchers are distributed among different micelles according to the Poisson distribution is lower than in a system in which quenchers are uniformly distributed.

Effect of experimental errors on the recovered k_n and φ values

It is assumed, from now on, that all experimental data will be treated using eq. [19] because the error involved with its use can be estimated using Table 2 for cases when $\langle s\rangle \leq 0.900$.

Can. J. Chem. Downloaded from www.nrcresearchpress.com by 46.23.64.124 on 09/08/12
For personal use only.

Fig. 4. Best fit (—) by eq. [24] to donor fluorescence intensity decay data (○) at a noise level $er\% = 1\%$. The noise-added data were derived from the curve in Fig. 1*a*.

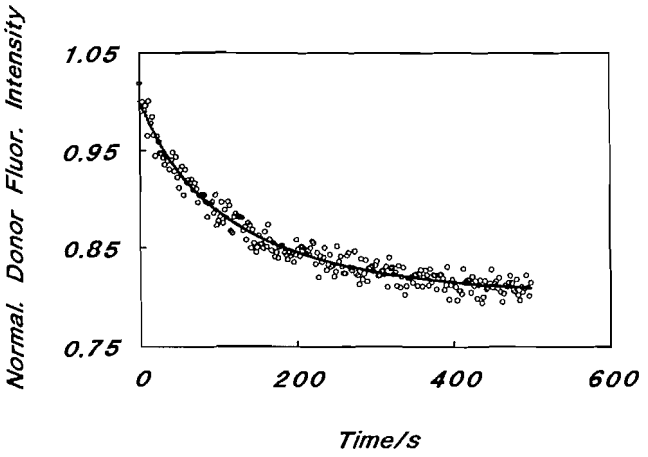

What are to be examined next are the errors introduced to recovered k_n and φ values due to experimental uncertainties in c_M^0 and c_y^0 values and the statistical error in donor intensity decay data.

To simulate experimental donor fluorescence intensity data, noise has been added to the donor intensity decay curve shown in Fig. 1 using the following formula

$$[28] \qquad \frac{I(t)}{I(0)} = \frac{I(t)}{I(0)}[1 + er\% \times r(t)]$$

where $er\%$ is the average percentage error in the $I(t)/I(0)$ data and $r(t)$ are random numbers generated by an IMSL subroutine supported on our university computer system. The $r(t)$ values obey a Gaussian distribution with a zero mean and a variance of 1. After noise addition with $er\% = 1\%$, the donor decy curves of Fig. 1*a* are now illustrated in Fig. 4 by 250 data points represented by ○'s.

Noise-added curves were fitted using eq. [19] by minimizing χ^2 as defined by eq. [27]. The solid curve in Fig. 4 represents the best fit to the scattered data. Tabulated in the first three rows of Table 3 are φ and k_n values obtained by fitting donor fluorescence intensity decay curves at different noise levels. As noise level or $er\%$ increased, errors in recovered φ and k_n values increased and the errors seem to be smaller than $er\%$ in each case. Actual fluorescence intensity fluctuation should be less than ±1%. The error in recovered φ and k_n values due to fluorescence intensity fluctuation should be negligible.

The error in c_M^0 derives mainly from the uncertainty in the determination of $\bar{n}$. Assuming that a ±5% error is associated with the true c_M^0 values of 1.00×10^{-6} M, the error in recovered φ and k_n due to the wrongly input c_M^0 values of 0.95×10^{-6} and 1.05×10^{-6} M can be seen in Table 3. The relative error in recovered φ and k_n values is comparable with that in c_M^0.

The error in c_y^0 mainly derives from the uncertainty in the determination of the molar mass of PS-*Py*-PHEMA-Fl(y). The deviation in the c_y^0 values determined from the true value of 0.500 caused errors mostly in the recovered φ value. That a positive error in c_y^0 leads to a negative error in φ is expected,

Table 3. Effect on the recovered φ and k_n values of uncertainties in c_M^0 values and statistical errors in donor fluorescence intensity decay data. The true values should be 0.400 and 1.00×10^4 M^{-1} s^{-1}, respectively.

Source of error	φ	$k_n \times 10^{-4}$ (M^{-1} s^{-1})
er (%)		
1.000	0.3984	1.007
2.000	0.3970	1.017
3.000	0.3956	1.030
$c_M^0 \times 10^6$/M		
0.950	0.3803	1.064
1.050	0.4167	0.955
$c_y^0 \times 10^6$/M		
0.48	0.4140	1.003
0.52	0.3840	1.010

as the experimental degree of fluorescence quenching, approximately equal to $\varphi c_y^0/c_M^0$, should not vary with the erroneous assignment of c_y^0.

Other concerns

Other concerns about the validity of our kinetic scheme include the use of a single rate constant k_n for chain incorporation and of a single rate constant k_q for fluorescence quenching. The incorporation of a PS-*Py*-PHEMA-Fl(y) chain into a micelle is a complex process. The chain first of all has to encounter a micelle, squeeze through the corona layer to touch the core, and then the PHEMA block has to creep into the core. Of the three processes, the creeping of the PHEMA block into the core is the likely rate-determining step and k_n would be a measure of how fast this process occurs, as argued by Halperin and Alexander (20).

The quenching of fluorene fluorescence by a pyrene group in a micelle needs to be described by a few rate constants as shown previously by the author (32). After fluorene excitation, energy will be passed around among different fluorene groups due to energy migration until it finally arrives at the pyrene site and gets trapped. The rate constant of fluorescence quenching would depend on where in the core of a micelle, relative to the position of the pyrene trap, a fluorene group is initially excited by light absorption. The quenching rate constant would be larger if the initially excited fluorene group is closer to the pyrene. When we assume a single rate constant, i.e., $k_q(1)$, for fluorescence quenching, we are assuming the use of an average value.

4. Summary

A fluorescence experiment involving mixing donor-labeled micelles with acceptor-labeled unimers has been designed and a kinetic scheme describing such an experiment has been proposed. In the approximate form of this scheme, the concentration of acceptor-labeled unimers has been assumed to be low so that the probability for having micelles with more than one acceptor is negligible. Based on this assumption,

approximate analytical solutions were found for the decrease in the donor fluorescence intensity and the increase in the acceptor fluorescence intensity as a function of time after sample mixing. Treating the decrease in donor fluorescence intensity as a function of time using the derived equation allows the simultaneous determination of the rate constant k_n for unimer incorporation into micelles and the quenching efficiency φ of donor fluorescence by an acceptor in a micelle. Errors in k_n and φ determined due to the assumption of no more than one acceptor per micelle have been estimated for frequently encountered experimental situations by comparing donor fluorescence intensity decay data calculated from our approximate approach and those from a more accurate model. Also examined are possible errors in the determined k_n and φ values due to experimental uncertainties in the micellar concentration c_M^0 and acceptor-labeled chain concentration c_Y^0.

The described experiment is easy to carry out. If successful, it will be the first determination of k_n values for diblock micelles.

Acknowledgment

The Natural Sciences and Engineering Research Council of Canada is thanked for covering publication and computation costs, and the University of Calgary is acknowledged for use of its computational facilities.

References

1. R.J. Hunter. Foundations of colloid science. Clarendon Press, Oxford. 1986.
2. Z. Tuzar and P. Kratochvil. Surf. Colloid. Sci. **15**, 1 (1992).
3. A. Halperin, M. Tirrell, and T.P. Lodge. Adv. Polym. Sci. **100**, 31 (1992).
4. A.P. Gast. *In* Scientific methods for the study of polymer colloids and their applications. *Edited by* F. Candau and R.H. Ottewill. Kluwer Academic Publishers, Amsterdam. 1990.
5. M. Daoud and J.P. Cotton. J. Phys. **43**, 531 (1982).
6. L. Leibler, H. Orland, and J.C. Wheeler. J. Chem. Phys. **79**, 3550 (1983).
7. A. Halperin. Macromolecules, **20**, 2943 (1987).
8. G.S. Grest, K. Kremer, and T.A. Witten. Macromolecules, **20**, 1376 (1987).
9. M.R. Munch and A.P. Gast. Macromolecules, **21**, 1360 (1988).
10. N.P. Balsara, M. Tirrell, and T.P. Lodge. Macromolecules, **24**, 1975 (1991).
11. Z. Gao and A. Eisenberg. Macromolecules, **26**, 7353 (1993).
12. D. Izzo and C.M. Marques. Macromolecules, **26**, 7189 (1993).
13. M.D. Major, J.M. Torkelson, and A.M. Brearley. Macromolecules, **23**, 1700 (1990).
14. M. Wilhelm, C.-L. Zhao, Y. Wang, R. Xu, M.A. Winnik, J.-L. Mura, G. Riess, and M.D. Croucher. Macromolecules, **24**, 1033 (1991).
15. I. Astafieva, X.F. Zhong, and A. Eisenberg. Macromolecules, **26**, 7339 (1993).
16. Z. Gao, S.K. Varshney, S. Wong, and A. Eisenberg. Macromolecules, **27**, 7923 (1994).
17. D. Kiserow, K. Prochazka, C. Ramireddy, Z. Tuzar, P. Munk, and S.E. Webber. Macromolecules, **25**, 461 (1992).
18. A. Qin, M. Tian, C. Ramireddy, S.E. Webber, P. Munk, and Z. Tuzar. Macromolecules, **27**, 120 (1994).
19. P. Alexandridis, J.F. Holzwarth, and T.A. Hatton. Macromolecules, **27**, 2414 (1994).
20. A. Halperin and S. Alexander. Macromolecules, **22**, 2403 (1989).
21. A. Johner and J.-F. Joanny. Macromolecules, **23**, 5299 (1990).
22. M. Tian, A. Qin, C. Ramireddy, S.E. Webber, P. Munk, Z. Tuzar, and K. Procházka. Langmuir **9**, 1741 (1993).
23. C. Honda, Y. Hasegawa, R. Hirunuma, and T. Nose. Macromolecules, **27**, 7660 (1994).
24. Y. Wang, C.M. Kausch, M. Chu, R.P. Quirk, and W.L. Mattice. Macromolecules, **28**, 904 (1995).
25. K. Procházka, B. Bednár, E. Mukhtar, P. Svoboda, J. Trnëná, and M. Almgren. J. Phys. Chem. **95**, 4563 (1991).
26. B. Bednár, K. Edwards, M. Almegren, S. Tormod, and Z. Tuzar. Makromol. Chem. Rapid Commun. **9**, 785 (1988).
27. (*a*) E.A.G. Aniansson and S.N. Wall. J. Phys. Chem. **78**, 1024 (1974); (*b*) J. Phys. Chem. **79**, 986 (1975); (*c*) E.A.G. Aniansson, S.N. Wall, M. Almgren, H. Hoffman, I. Kielmann, W. Ulbricht, R. Zana, J. Lang, and C. Tondre. J. Phys. Chem. **80**, 905 (1976).
28. R.J. Young and P.A. Lovell. Introduction to polymers. 2nd ed. Chapman & Hall, London. 1991.
29. Th. Förster. *In* Modern quantum chemistry. *Edited by* O. Sinanöglu. Academic Press, New York. 1965.
30. G. Liu, C.K. Smith, N. Hu, and J. Tao. Macromolecules. Submitted.
31. I.B. Berlman. Energy transfer parameters of aromatic compounds. Academic Press, New York. 1973.
32. G. Liu. J. Phys. Chem. **99**, 5465 (1995).

Can. J. Chem. Downloaded from www.nrcresearchpress.com by 46.23.64.124 on 09/08/12
For personal use only.

Mechanism of acid-catalyzed photoaddition of methanol to 3-alkyl-2-cyclohexenones

David I. Schuster, Jie-Min Yang, Jan Woning, Timothy A. Rhodes, and Anton W. Jensen

Can. J. Chem. Downloaded from www.nrcresearchpress.com by 46.23.64.124 on 09/08/12
For personal use only.

Abstract: Contrary to a previous report, it is concluded that formation of methanol adducts to 3-methyl-2-cyclohexenones and of deconjugated enones on irradiation of the enones in acidified solutions proceeds via protonation of the intermediate enone π,π^* triplet excited state and not by protonation of a relatively long-lived ground state *trans*-cyclohexenone. A rate constant for protonation of the triplet state of 3-methyl-2-cyclohexenone by sulfuric acid of 1.7×10^9 M^{-1} s^{-1} was determined by laser flash photolysis in ethyl acetate. Based on quantum efficiencies of product formation, a rate constant of ca. 10^8 M^{-1} s^{-1} was estimated for protonation of the enone triplet by acetic acid, which is too small to cause measurable reduction in the triplet state lifetime in the mM concentration range used in the preparative studies. The intermediate carbocation can be trapped by methanol, or revert to starting enone or the exocyclic deconjugated enone by loss of a proton. Since products revert to starting materials in an acid-catalyzed process, there is an acid concentration at which the yields of products are optimal. This concentration is ca. 6 mM for acetic acid, but is only 0.1 mM for *p*-toluenesulfonic or sulfuric acids. Product formation could be quenched using 1-methylnaphthalene and cyclopentene as triplet quenchers; in the latter case, formation of [2 + 2] photoadducts was observed to compete with formation of methanol adducts. Quenching rate constants were determined by laser flash studies.

Key words: laser flash photolysis, kinetic absorption spectroscopy (KAS), photoacoustic calorimetry (PAC), protonation of triplet states, *trans*-cyclohexenones.

Résumé : Contrairement à ce qui a été publié antérieurement, on montre que la formation d'adduits du méthanol avec les 3-méthylcyclohexén-2-ones et les énones déconjuguées, par irradiation des énones en solutions acidifiées, ne se produisent pas par le biais d'une protonation de l'état fondamental de la *trans*-cyclohexénone qui possède une durée de vie relativement longue. Faisant appel à la photolyse laser éclair dans l'acétate d'éthyle, on a déterminé que la constante de vitesse de protonation de l'état triplet de la 3-méthylcyclohexén-2-one, par de l'acide sulfurique, est de $1{,}7 \times 10^9$ M^{-1} s^{-1}. En se basant sur les efficacités quantiques de formation du produit, on a évalué que la constante de vitesse pour la protonation du triplet de l'énone par l'acide acétique est d'environ 10^8 M^{-1} s^{-1} qui est beaucoup trop faible pour provoquer une réduction mesurable du temps de vie de l'état triplet dans la zone de concentration (mM) utilisé dans les études préparatives. On peut piéger le carbocation intermédiaire par le méthanol ou le laisser retourner à l'énone de départ ou à l'énone exocyclique déconjuguée par perte d'un proton. Puisque les produits retournent aux produits de départ dans un processus acidocatalysé, il existe une concentration d'acide à laquelle les rendements en produits sont optimaux. Cette concentration est d'environ 6 mM pour l'acide acétique, mais elle n'est que de 0,1 mM pour les acides sulfurique et *p*-toluènesulfonique. La formation de produit peut être désactivée par l'utilisation du 1-méthylnaphtalène ou du cyclopentène comme désactivants des triplets; dans le dernier cas, on a observé la formation de photoadduits [2 + 2] qui sont en compétition avec la formation d'adduits du méthanol. On a déterminé les constantes de vitesse de désactivation à l'aide d'études au laser éclair.

Mots clés : photolyse laser éclair, spectroscopie d'absorption cinétique, calorimétrie photoacoustique, protonation des états triplets, *trans*-cyclohexénones.

[Traduit par la rédaction]

Received April 10, 1995.

This paper is dedicated to Professor J.E. (Jim) Guillet in recognition of his contributions to Canadian chemistry.

D.I. Schuster,[1] J.-M. Yang, J. Woning, T.A. Rhodes, and A.W. Jensen. New York University, Faculty of Arts and Sciences, Department of Chemistry, New York, NY 10003, U.S.A.

[1] Author to whom correspondence may be addressed. Telephone: (212) 998-8447. Fax: (212) 260-7905. E-mail: schustrd@is2.nyu.edu

Scheme 1.

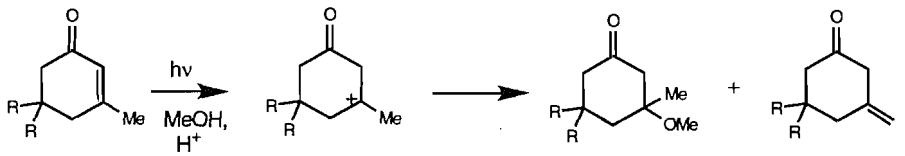

1*a*, R = Me **2***a*, R = Me **3***a*, R = Me **4***a*, R = Me
1*b*, R = H **2***b*, R = H **3***b*, R = H **4***b*, R = H

Scheme 2.

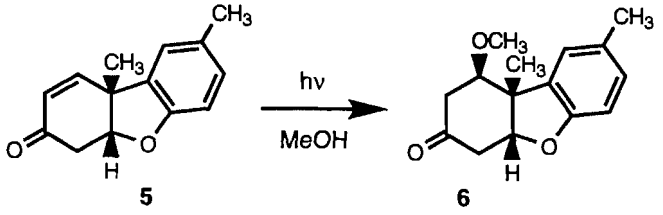

5 **6**

Introduction

It was reported by Rudolph and Weedon (1) that small amounts of acetic acid catalyze the photochemical addition of methanol to isophorone (**1***a*) in benzene or ethyl acetate solvents (see Scheme 1). The limiting quantum yield of this reaction (ϕ ca. 0.04) was reached at ca. 0.004 M acetic acid. The reaction is accompanied by deconjugation to enone **4***a*. Quenching of the reaction by isoprene (a common triplet quencher) gave a linear Stern–Volmer plot, implicating the T_1 state of **1***a* as the reactive intermediate. Formation of neither **3***a* nor **4***a* proceeds efficiently in the absence of acetic acid, or in neat methanol. The mechanism therefore appears to involve interaction of acetic acid with either the T_1 state of **1***a* or a subsequent intermediate to give carbocation **2***a* (or its enol tautomer), which then either deprotonates to give **4***a* or is trapped by methanol to give adduct **3***a*.

Based on an estimated triplet lifetime of 10 ns for **1***a*, Rudolph and Weedon (1) ruled out direct trapping of the triplet by 0.004 M acetic acid, since they estimated that a protonation rate constant of ca. 10^{12} M^{-1} s^{-1} was required, which would be higher than the diffusion-controlled rate. By analogy with the proposed mechanism for acid-catalyzed photochemical reactions of cyclohexenes (2), it was suggested that the reaction intermediate trapped by acetic acid was a ground state *trans* isomer of **1***a* with an estimated lifetime of 1 μs. Although *trans*-cyclohexenones have never been directly observed to date (3), stereochemical data consistent with the intermediacy of a *trans*-cyclic enone have been reported for the photochemical addition of methanol to Pummerer's ketone **5** (a 2-cyclohexenone) (Scheme 2) and for the photochemical addition of nucleophiles to 2-cycloheptenones and 2-cyclooctenones (4, 5). Based on kinetic data, Schuster et al. suggested that photochemical [2 + 2] cycloadditions of 2-cyclohexenones to alkenes might occur in some cases via transient twisted ground state *trans*-2-cyclohexenones (6). In response to the report by Rudolph and Weedon, we now report the results of steady-state and nanosecond flash photolysis studies of isophorone (**1***a*) and 3-methyl-2-cyclohexenone (**1***b*) in neutral and acidic media (7).

Fig. 1. Relative yield of methanol adduct of Pummerer's ketone (compound **6**) in benzene containing 10% methanol as a function of acetic acid concentration.

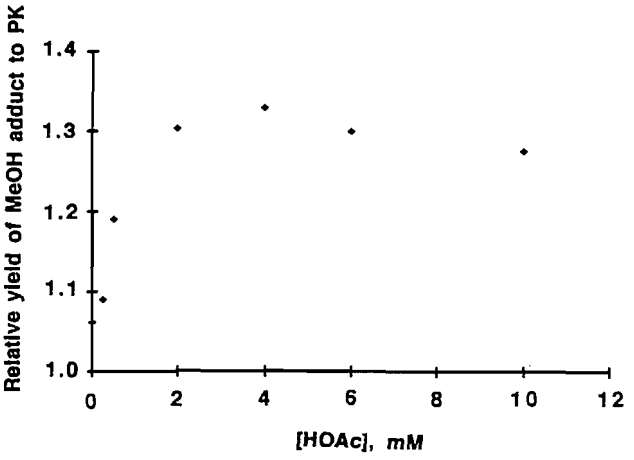

Results and discussion

A. Continuous irradiations

We first wanted to establish whether Pummerer's ketone (PK, **5**) behaved in a manner similar to that reported by Rudolph and Weedon for isophorone (1). Indeed, irradiation of PK in benzene containing 10% methanol and varying amounts of acetic acid led to a methanol adduct, according to GC–MS analysis, presumably the adduct **6** previously described by Hart and co-workers (4). As shown in Fig. 1, the yield of this adduct peaked at about 4 mM HOAc, consistent with the findings for isophorone (1). Having established this similarity in photochemical behavior, we decided to focus our studies on 3-methyl-2-cyclohexenone (**1***b*), which has been the subject of numerous mechanistic investigations in our laboratory (3, 6, 8–10).

Continuous irradiation of **1***b* in 90:10 ethyl acetate – methanol containing up to 0.008 M acetic acid gave **3***b* and **4***b*. These compounds were characterized by ^{1}H NMR spectroscopy and GC–MS (see Experimental for details). A plot of the yield of these products vs. the concentration of acetic acid is shown in Fig. 2. Analogous to the behavior of isophorone **1***a* and PK (see above), the yields of **3***b* and **4***b* level off at acetic acid concentrations above ca. 0.006 M. This behavior is probably due to the thermal instability of these products, which both undergo acid-catalyzed reversion to the starting material **1***b*. Upon irradiation of **1***b* in ethyl acetate – methanol containing a stronger acid, *p*-toluenesulfonic or sulfuric acid, **3***b* and **4***b* were again obtained, but in this case their yields sharply declined at acid concentrations above 10^{-4} M (Fig. 3).

Can. J. Chem. Downloaded from www.nrcresearchpress.com by 46.23.64.124 on 09/08/12
For personal use only.

Can. J. Chem. Downloaded from www.nrcresearchpress.com by 46.23.64.124 on 09/08/12
For personal use only.

Fig. 2. Relative yields of methanol adduct of 3-methylcyclohexenone (compound **3***b*,◆) and deconjugated enone (**4***b*,▲) in ethyl acetate containing 10% methanol as a function of acetic acid concentration.

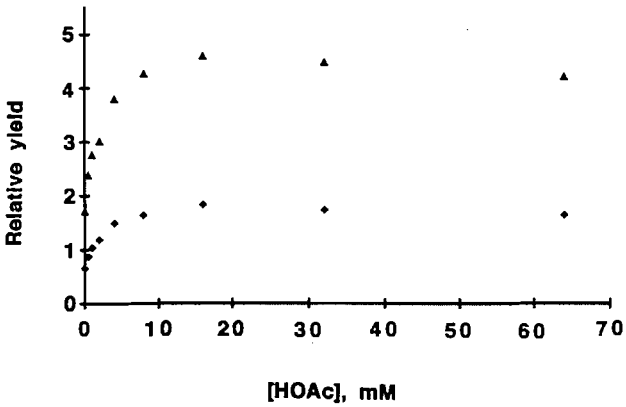

Fig. 3. (*a*) Relative yields of compound **3***b* as a function of the concentration of *p*-toluenesulfonic acid in ethyl acetate solvent. (*b*) Same as (*a*) but using sulfuric acid in place of *p*-toluenesulfonic acid.

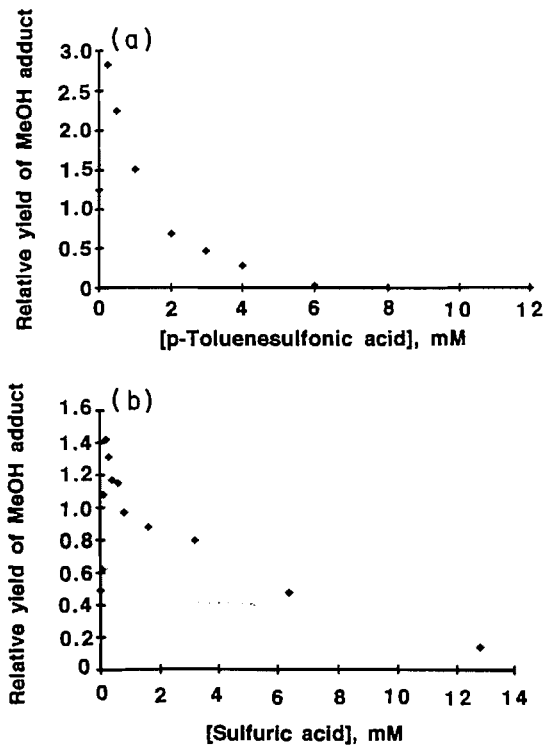

Although linear Stern–Volmer plots were obtained for quenching of both products by the triplet quencher 1-methylnaphthalene (1-MeNA), quantitative data in this system were not very reproducible, probably because of competitive light absorption by the quencher at the concentrations required for these experiments (up to 0.3 M) using broad spectral sources. Better data were obtained under similar reaction conditions using cyclopentene as the triplet quencher. In this case, a reduction in the yields of products **3***b* and **4***b* was observed concomitant with an increase in yields of the well-known [2+2] cycloadducts **7** (see Fig. 4). It is well established (8) that

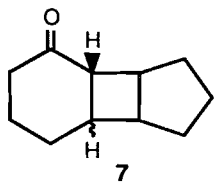

7

photocycloaddition of enones to alkenes occurs via enone triplet excited states. Thus, the steady-state behavior of **1***b* in acidic methanol, which clearly occurs via triplet states of the enone, closely resembles that previously reported (1) for isophorone (**1***a*).

B. Laser flash photolysis — kinetic absorption spectroscopy

Using both nanosecond kinetic absorption spectroscopy (KAS) (8, 11) and time-resolved photoacoustic calorimetry (PAC) (9), the triplet lifetime of isophorone (**1***a*) in acetonitrile was found to be 79 ns, much higher than previously assumed (1). Thus, direct protonation of triplet excited states of **1***a* by acids is more likely than previously concluded (1). In principle, if the second-order rate constant for protonation of the triplet is sufficiently large, the enone triplet lifetime should decrease as a function of increasing acid concentration. We elected to use enone **1***b*, which, as shown above, behaves similarly to enone **1***a* under the photochemical reaction conditions.

For the laser flash (KAS) studies, **1***b* was excited with a 10 ns pulse of a YAG (355 nm) or nitrogen laser (337 nm). Following excitation, the triplet lifetime (τ_T) was determined from the decay of the transient absorption at 280 nm (8, 11). The values for τ_T measured under different conditions were 78 ± 2 ns in benzene containing up to 2×10^{-3} M HOAc; 73 ± 2 ns in neat EtOAc; 79 ± 2 ns in EtOAc–MeOH 90:10 containing up to 2×10^{-3} M HOAc; and 95 ± 3 ns in MeOH containing up to 7×10^{-3} M HOAc (the indicated errors reflect the 90% confidence limit). (Values of τ_T for enones are consistently higher in methanol than in nonpolar and aprotic polar solvents (3)). Thus, τ_T appears to be independent of the acetic acid concentration within experimental error. However, when acetic acid was replaced by sulfuric acid, direct quenching of the triplet of enone **1***b* in ethyl acetate was observed. From the Stern–Volmer plot shown in Fig. 5, a rate constant of 1.7×10^9 M^{-1} s^{-1} for protonation of the triplet of **1***b* was obtained using eq. [1]. This value can then be used to calculate the quantum yield

$$[1] \quad 1/\tau_{obs} = 1/\tau_0 + k_a[H^+]$$

$$[2] \quad \phi_a = k_a\tau_T[H^+]$$

of protonation of the triplet (ϕ_a) using eq. [2]. Thus, at a sulfuric acid concentration of 10^{-3} M, where τ_T was determined to be 58 ns, ϕ_a is ~0.1. This is slightly greater than the quantum yield of product formation (ϕ = 0.04), suggesting that deprotonation of carbocation **2**b to regenerate the starting material competes with formation of **3***b* and **4***b*.

Based on our value of τ_T for isophorone (**1***a*), the quantum yield reported (1) for formation of photoproducts **3***a* and **4***a* from **1***a* at 4×10^{-3} M acetic acid would require a rate constant k_a for protonation of the enone triplet by acetic acid of ca. 10^8

Fig. 4. (*a*) and (*b*) Relative yields of **3***b* and the *cis*- and *trans*-fused isomers of **7** upon irradiation of **1***b* in ethyl acetate containing 10% methanol and 10 mM acetic acid, as a function of the concentration of added cyclopentene. (*c*) and (*d*) Stern–Volmer plots of the ratio of the yields of **3***b* and **4***b* in the absence and presence of cyclopentene as a function of cyclopentene concentration.

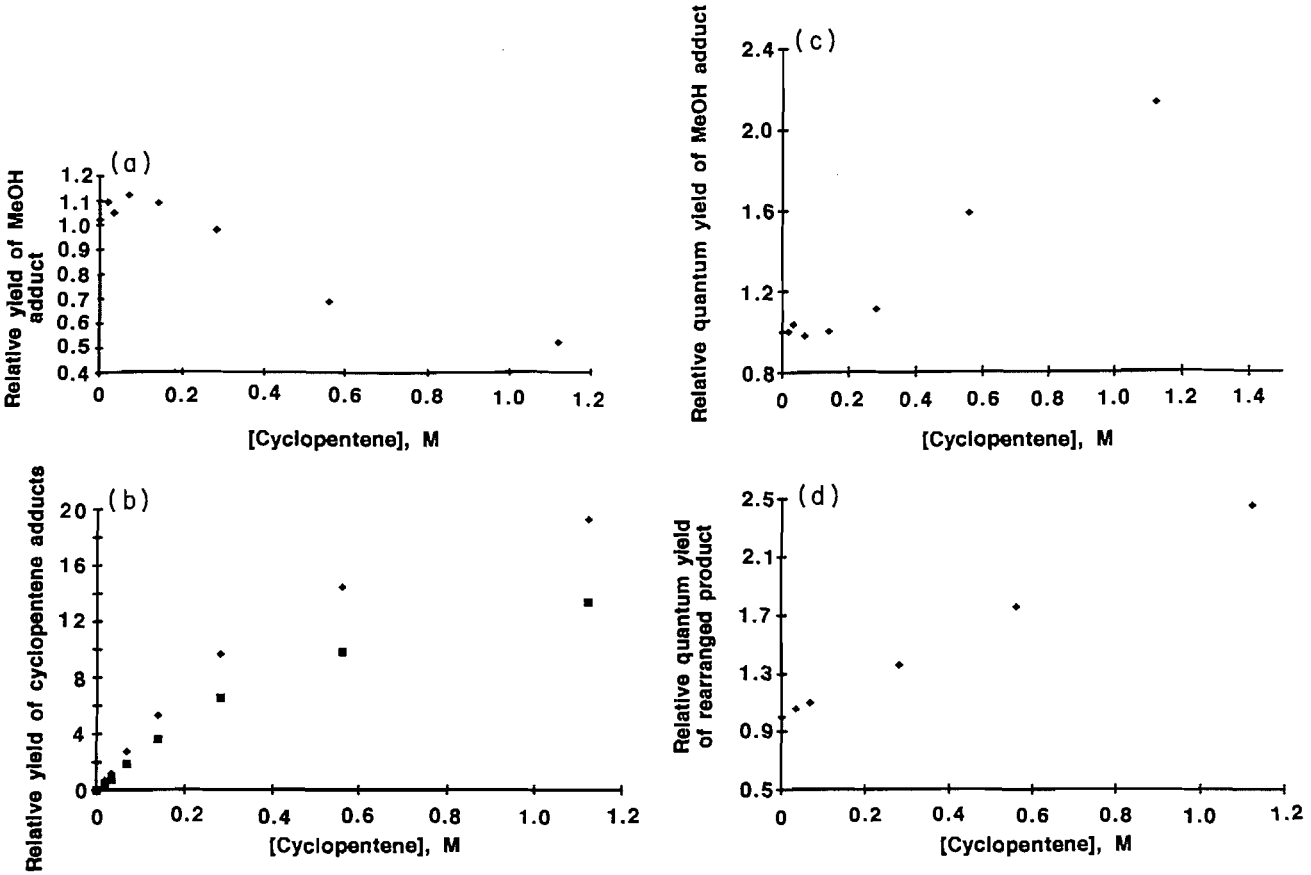

Fig. 5. Inverse triplet lifetime (in s^{-1}) of **1***b* in ethyl acetate as a function of sulfuric acid concentration.

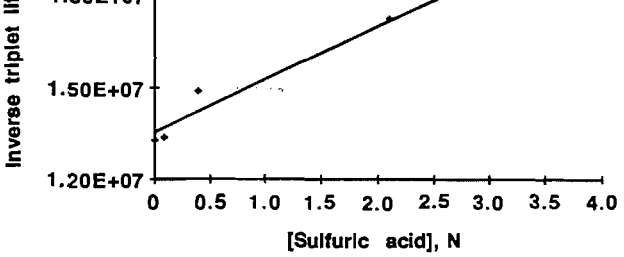

M^{-1} s^{-1} rather than the previous estimate (1) of 10^{12} M^{-1} s^{-1}. This lower value of k_a is realistic given that HOAc is a much weaker acid than H_2SO_4. Using eq. [1] it can be calculated that the reduction in τ_T for **1***b* would be too small to be detected by KAS over the HOAc concentration range (up to 7 mM) utilized in these studies, in accord with our observations.

Rudolph and Weedon (1) reported that the Stern–Volmer slope $k_q\tau_T$ for quenching of deconjugation of **1***a* by isoprene in benzene solvent was 60 M^{-1}, which is consistent with quenching of a triplet state of lifetime about 80 ns since rate constants for triplet energy transfer to acyclic 1,3-dienes in related systems are typically about 10^8 M^{-1} s^{-1} (8). Rudolph and Weedon (1) also showed a plot of the inverse quantum yield for deconjugation of **1***a* in benzene vs. the inverse concentration of acetic acid. Based on the slope and intercept of this plot, assuming a linear correlation, they concluded that the enone triplet state could not be the species undergoing protonation. In addition to their erroneous assumption regarding the rate of decay of the enone triplet, the significant deviation of their data from the assumed straight-line correlation at high acid concentrations was ignored. Given the kinetic and thermodynamic instability of the deconjugation product **4***b* observed in the present study (see Experimental), the validity of the quantum yield data reported for formation of **4***a* in acidic solution as well as the derived kinetic parameters (1) are open to question. In any event, the inconsistency between the kinetic data of Rudolph and Weedon (1) and the results of the present study need to be resolved.

As a check of the steady-state quenching studies discussed earlier, rate constants for quenching of triplet states of **1***b* by both 1-MeNA and cyclopentene were directly measured. Stern–Volmer plots of $(\tau_T)^{-1}$ vs. quencher concentrations in ethyl acetate (in the absence of methanol or acetic acid) afford quenching rate constants of 4.5×10^9 M^{-1} s^{-1} and 5.6×10^6 M^{-1} s^{-1}, respectively (see Figs. 6 and 7). The latter value is within a factor of 3 of that (1.6×10^7 M^{-1} s^{-1}) calculated from

Can. J. Chem. Downloaded from www.nrcresearchpress.com by 46.23.64.124 on 09/08/12
For personal use only.

Can. J. Chem. Downloaded from www.nrcresearchpress.com by 46.23.64.124 on 09/08/12
For personal use only.

Fig. 6. Inverse triplet lifetime (in s^{-1}) of **1***b* in ethyl acetate in the absence of methanol and acetic acid as a function of 1-methylnaphthalene concentration.

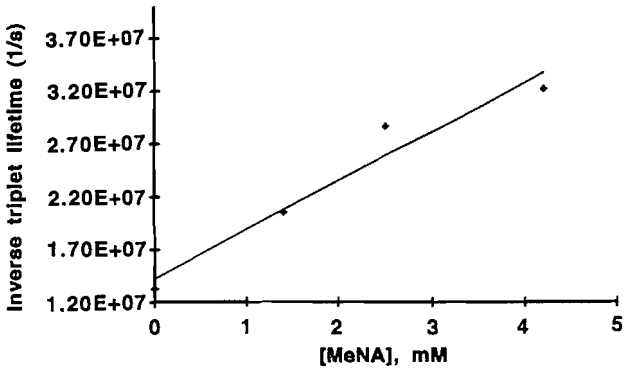

Fig. 7. Same as Fig. 6, but using cyclopentene as the triplet quencher.

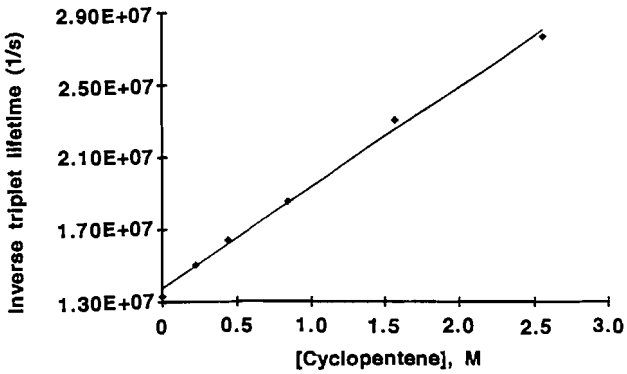

the slope (1.29 M^{-1}) of the steady-state Stern–Volmer plot in Fig. 4*b* under the reaction conditions, assuming a triplet lifetime of 80 ns. However, quenching of product formation by 1-MeNA is not nearly as efficient as expected from the diffusion-controlled triplet quenching rate constant measured by flash photolysis. A likely explanation is that under the steady-state reaction conditions, where 1-MeNA is competing with the enone for light with a broad spectral distribution generated from the Hanovia or Rayonet lamps (see Experimental), 1-MeNA may be acting as both a singlet sensitizer and a triplet quencher. This is not unreasonable since the singlet excited state lifetime of 1-MeNA is nearly 100 ns in polar solvents (12) and diffusion-controlled singlet energy transfer to **1***b* at a concentration of 0.07 M should be an efficient process.

Conclusions

Based on both steady-state and flash kinetic data, we conclude that it is highly probable that the species actually undergoing protonation in these reactions is the enone triplet excited state and not a ground state *trans*-cyclohexenone. The enone triplet in these systems is sufficiently long lived that direct quenching by acids to give the carbocations **2** is a kinetically viable process. Whether protonation of the triplet may be adiabatically reversible under these conditions remains in question. As far as the intermediacy of *trans*-cyclohexenones is concerned, we have repeatedly failed to detect such species on laser flash photolysis of a large number of cyclohexenones (8). Furthermore, PAC data (7, 9) for isophorone, 3-methyl-2-cyclohexenone, and other 2-cyclohexenones rigorously exclude the formation of a high-energy ground state intermediate with a lifetime in the microsecond range and measurable (>0.05) quantum efficiency. That is, intersystem crossing and radiationless decay of the enone triplet accounts for essentially all (>98%) of the energy of the absorbed photon. Substantial heat discrepancies are seen only in cases where bona fide strained ground state *trans* isomers are formed, as with 1-acetylcyclohexene (13). As noted earlier, some inconsistencies between our present data and the earlier report by Rudolph and Weedon (1) remain to be resolved. Theoretical calculations by Johnson[2] indicate that *trans*-2-cyclohexenones indeed appear to lie in a potential minimum on the 2-cyclohexenone ground state energy surface. However, under ambient conditions, the lifetimes of such species are expected to be extremely short, probably on the order of nanoseconds or even less. Thus, we conclude that *trans*-cyclohexenones are not likely intermediates in the photoreactions of cyclohexenones under the acidic conditions described in this paper and in the earlier study (1), and that the only hope of observing such species spectroscopically is by generating them in particularly favorable systems at very low temperatures.

Experimental

A. Laser flash photolysis

General sample preparation

Commercially available 3-methyl-2-cyclohexenone, cyclopentene, and 1-methylnaphthalene were purified by careful distillation. All the solvents employed were either HPLC grade or spectrograde. Sample solutions were prepared by weighing the enone in volumetric flasks followed by addition of the proper amount of other chemicals such as methanol or acetic acid into the flask and adding the solvent to the mark. A pipet was used to transfer solutions to the reaction cells. The optical density of the solutions studied ranged from 0.5 to 1.0 at the excitation wavelength. All samples were purged with either argon or oxygen-free nitrogen for at least 10 min prior to the experiments. Quenchers (either neat or in solution) were added using a microlitre syringe. At Columbia University, data was obtained by averaging 10–30 laser pulses in each measurement depending on the signal-to-noise ratio. At the National Research Council in Ottawa, data from 30–200 laser pulses were averaged.

Apparatus and procedures

The nanosecond laser flash photolysis configurations at Columbia University and at the National Research Council of Canada are very similar, but differ in details such as the type of laser used and in the arrangement of the exciting and analyzing beams. In experiments carried out at Columbia University (14), a Quanta Ray Q-switched Nd-YAG laser was used. After pulse selection, amplification, and frequency conversion, pulses of duration of ca. 6 ns and energies of 2–5 mJ/pulse, which varied less than 10% in intensity at 355 nm, were provided. The exciting and analyzing beams were oriented at

[2] R. Johnson, University of New Hampshire, private communication of unpublished results.

Can. J. Chem. Downloaded from www.nrcresearchpress.com by 46.23.64.124 on 09/08/12
For personal use only.

right angles (crossed-beam arrangement). The analyzing light source was a 150 W xenon lamp (Oriel). The samples (2 mL) were contained in Super cells with a 10 mm optical path.

At the NRC in Ottawa (15), a Molectron UV-24 nitrogen laser, providing pulses of 8–10 ns and energies up to 10 mJ at 337.1 nm, was employed. A crossed-beam arrangement with an angle of 15° was used throughout. The use of this small angle configuration considerably decreases the volume irradiated and is more convenient for lower energy lasers (16). A pulsed 200 W xenon lamp was employed in the monitoring system and a high-intensity B & L monochromator and an RCA-4840 photomultiplier tube were used at the detection end. The photomultiplier response was fed to a 7A16A plug-in used in a R7912-Tektronix transient digitizer that contains a 4K local memory in which each trace was stored. The samples (1 mL) were contained in Suprasil cells made of 7 × 3 mm rectangular tubing (Vitro Dynamics). The temperature of the cell was controlled by a constant-temperature nitrogen flow and was measured with a copper–constantan thermocouple.

At both laboratories, the lifetime of the optically detected transient is determined from the slope of a plot of ln (I/I_0) as a function of time. Although the data collection and analysis were controlled by the computer using programs developed individually in each lab, the baseline and region of the trace to be analyzed is determined manually by the operator. The error in the triplet lifetimes evaluated by the present analyzing method is estimated to be ±10%.

B. Steady-state photolyses

All preparative reactions were done using a Rayonet 350 nm Srinivasan–Griffin photochemical reactor, which has a broad range from 300 to 400 nm, with a maximum at 350 nm, a Hanovia 550 W high-pressure mercury arc lamp, or a Hanovia 450 W medium-pressure mercury arc lamp. The latter two required a water-cooled jacket and the samples were suspended in Pyrex test tubes outside the immersion well. All three reactors were equipped with a merry-go-round rotating turntable for even irradiation of each sample. Samples in Pyrex tubes that filter out light below 280 nm were purged with argon for 10 min prior to irradiation. All reactions were monitored by capillary GC analysis, using either a Hewlett–Packard model 5890 gas chromatograph equipped with a Hewlett–Packard 3396A integrator or a Hewlett–Packard 5710A gas chromatograph equipped with an 18740B capillary column control, 5702A oven temperature programmer, and a 3390A integrator. The same type of capillary column (Alltech, 30 m × 0.25 mm Heliflex, RSL-150) was used throughout. *n*-Dodecane was used as the internal standard. The major products formed in the reaction were analyzed by GC–MS, using a Hewlett–Packard model 5992 GC–MS system equipped with a Hewlett–Packard 20 m × 0.25 mm cross-linked methyl silicone capillary column. Ultraviolet absorption spectra were obtained with a Cary 210 double-beam spectrophotometer.

Preparative cycloaddition of methanol to Pummerer's ketone **5**

Pummerer's ketone (PK) was synthesized and purified as described in the literature (4). A series of benzene solutions containing 0.145 M PK and 10% MeOH and various concentrations of acetic acid were prepared. The final concentrations of acetic acid were 0.0, 0.25, 0.50, 1.00, 2.00, 4.00, 6.00, and 10.00 mM. These solutions in Pyrex tubes were purged with argon for 10 min and irradiated with a Hanovia 450 W lamp for 45 h. One new product was formed in the reaction, which was confirmed by GC–MS to be the PK–methanol adduct. The mass spectrum of the adduct, *m/z* (relative intensity), was 246 (42.7) M^+, 160 (14.9), 159 (79.9), 147 (11.4), 146 (100), 145 (49.0), 115 (15.5), 91 (10.0).

*Optimization of photoaddition of methanol to 3-methyl-2-cyclohexenone (**1**b)*

This experiment was carried out in ethyl acetate solvent with a series of solutions containing 0.145M **1***b*, 10% methanol, and acetic acid concentrations of 0.00, 2.00, 4.00, 8.00, 16.00, 32.00, and 64.00 mM, respectively. The samples were purged with argon for 10 min and then irradiated for 24 h. Several new species appeared on GC analysis, which corresponded to compounds **3***b*, **4***b*, and trace amounts of 3-methyl-3-cyclohexenone (**8**) and enone photodimers. The mass spectra of each component, *m/z* (rel. intensity), were as follows: **3***b*: 142 (10.2) M^+, 110 (11.8), 85 (83.1), 72 (40.6), 54 (100), 42 (86.0); **4***b*: 110 (20.2) M^+, 82 (100), 54 (35.2), 41 (14.5); **8**: 110 (10.3), 82 (20.1), 55 (25.0), 43 (100.0). Similar results were obtained when benzene was employed as the solvent. When sulfuric acid or *p*-toluenesulfonic acid was used as the catalyst, the acid concentrations in the tubes were 0.0, 0.025, 0.05, 0.1, 0.2, 0.4, 0.8, 1.6, 3.2, 6.4, and 12.8 mN, respectively. The results otherwise were similar to those obtained using acetic acid as the catalyst.

*Preparative scale irradiation of 3-methyl-2-cyclohexenone (**1**b) in methanol*

To 335 μL (4.5 mmol) of **1***b* in a 35 mL Pyrex test tube were added 3.1 mL MeOH, 28 mL EtOAc, and lastly 17 μL of HOAc. The final concentrations of **1***b* and HOAc were 0.14 M and 0.01 M, respectively. Each solution was then sealed with a rubber septum and purged with argon for 30 min. Each sample was then irradiated with a 450 W medium-pressure Hg arc lamp fitted with a water-cooled jacket at a distance of about 1 cm from the jacket for 18 h. GC–MS analysis of the irradiated mixture indicated conversion to two major photoproducts. The crude mixture was then washed ($NaHCO_3$, water, and brine), dried over anhydrous $MgSO_4$, gravity filtered, and concentrated in vacuo. When washings were not performed and the sample was concentrated immediately after irradiation, the deconjugated product **4***b* decomposed. The crude ^1H NMR spectrum (200 MHz, $CDCl_3$) of the washed photoproduct indicated the presence of some unreacted **1***b* along with methanol adduct **3***b* ((s, 3.15 ppm, 3H, $-OCH_3$; m, 1.5–2.6 ppm, $-CH_2-$; s, 1.21 ppm, 3H, $-CH_3$), lit. NMR in CCl_4 (17) (s, 3.00 ppm, 3H, $-OCH_3$; m, 1.5–2.5 ppm, 8H, $-CH_2-$; s, 1.15, 3H, $-CH_3$)) and deconjugated product **4***b* (m, 4.77 ppm, 1H, vinyl H, J = ~1 Hz; m, 4.69 ppm, 1H, vinyl H, J = ~1 Hz; d, 3.08 ppm, 2H, allylic H α to the carbonyl, J = 1.14 Hz; m, 1.5–2.5 ppm, $-CH_2-$). Attempts to purify previously uncharacterized **4***b* were not successful since **4***b* slowly decomposed on distillation (55°C, 1.5 Torr; 1 Torr = 133.3 Pa), and completely decomposed on chromatography on silica (1:1 pentane:EtOAc) or activated basic Brockmann 1 alumina (EtOAc). As **4***b* decomposed, the ratio between the ^1H NMR peaks at 4.69 and 4.77 to the allylic proton α to the carbonyl (3.08) remained constant.

Quenching of the photoaddition of methanol to 3-methyl-2-cyclohexenone by cyclopentene

Cyclopentene was added using a microlitre syringe to solutions containing 0.145 M **1***b*, 10% MeOH, and 10 mM HOAc, to give final cyclopentene concentrations of 0.00, 0.020, 0.035, 0.070, 0.14, 0.28, 0.56, and 1.12 M, respectively. The solutions were purged with argon for 10 min, then irradiated through Pyrex using a 350 nm Rayonet Lamp for 17 h, and were then analyzed directly using capillary GC.

Quenching of the photoaddition of methanol to 3-methylcyclohexenone by 1-methylnaphthalene

Benzene solutions were prepared containing 0.07 M **1***b*, 10% MeOH, 10 mM HOAc, and *n*-dodecane as an internal standard for GC analyses. Varying amounts of 1-methylnaphthalene were added to give final concentrations of 0.020, 0.035, 0.070, 0.14, and 0.28 M, respectively. The solutions in Pyrex tubes were purged with argon, irradiated for 20 h using a 550 W Hanovia lamp, and then analyzed for products **3***b* and **4***b* using capillary GC.

Acknowledgments

This work was supported in part by grants CHE-890009 and CHE-9400666 from the National Science Foundation of the United States. We also thank Dr. J. C. Scaiano at the National Research Council of Canada in Ottawa and Professor Nicholas J. Turro of Columbia University for allowing us to use their nanosecond laser flash equipment, and for their invaluable assistance in these experiments. We also thank Dr. Monica Barra at the NRC for her help with the laser flash studies. We finally thank George Lem for helpful suggestions in the course of preparation of this manuscript.

References

1. A. Rudolph and A.C. Weedon. J. Am. Chem. Soc. **111**, 8756 (1989).
2. R. Bonneau, J. Joussot-Dubien, L. Salem, and A. Yarwood. J. Am. Chem. Soc. **98**, 4329 (1976).
3. D.I. Schuster. *In* The chemistry of enones. Part 2. *Edited by* S. Patai and Z. Rappoport. John Wiley and Sons, Ltd., Chichester, U.K. 1989. pp. 623–756.
4. E. Dunkelblum, H. Hart, and M. Jeffares. J. Org. Chem. **43**, 3409 (1973).
5. H. Hart and E. Dunkelblum. J. Am. Chem. Soc. **100**, 541 (1978).
6. D.I. Schuster, P.B. Brown, L.J. Capponi, C.A. Rhodes, J.C. Scaiano, P.C. Tucker, and D. Weir. J. Am. Chem. Soc. **109**, 2533 (1987).
7. Presented at the 201st National Meeting of the American Chemical Society, Atlanta, Ga. April 14–19, 1991. Abstract ORGN 303.
8. D.I. Schuster, D.A. Dunn, G.E. Heibel, P.B. Brown, J.M. Rao, J. Woning, and R. Bonneau. J. Am. Chem. Soc. **113**, 6245 (1991).
9. D.I. Schuster, G.E. Heibel, R.A. Caldwell, and W. Tang. Photochem. Photobiol. **52**, 645 (1990).
10. D.I. Schuster, G.E. Heibel, and J. Woning. Angew. Chem. Int. Ed. Engl. **30**, 1345 (1991).
11. R. Bonneau. J. Am. Chem. Soc. **102**, 3816 (1980).
12. J.C. Scaiano (*Editor*). Handbook of organic photochemistry. Vol. I. CRC Press, Inc., Boca Raton, Fla. 1989. p. 409.
13. R. Bonneau and P. Fornier de Violet. C.R. Seances Acad. Sci. Ser. 3: **284**, 631 (1977).
14. G.E. Heibel. Ph. D. Dissertation, New York University, 1990.
15. J.C. Scaiano. J. Am. Chem. Soc. **102**, 7747 (1980).
16. R.D. Small, Jr. and J.C. Scaiano. J. Phys. Chem. **81**, 828 (1977).
17. T. Sato, S. Yoshiie, T. Imamura, K. Hasegawa, M. Miyahara, S. Yamamura, and O. Ito. Bull. Chem. Soc. Jpn. **50**, 2714 (1977)

Can. J. Chem. Downloaded from www.nrcresearchpress.com by 46.23.64.124 on 09/08/12
For personal use only.

Studies of the inhibition of autooxidation of polypropylene with 4,4′-bis(2,6-di-*tert*-butylphenol)

E.L. Shanina, G.E. Zaikov, and N.A. Mukmeneva

Abstract: The kinetics of 4,4′-bis(2,6-di-*tert*-butylphenol) (BP) consumption in the oxidation of polypropylene (PP) at 130°C in air has been studied. It is shown that 3,3′,5,5′-tetra-*tert*-butyl-4,4′-diphenoquinone (DPQ) is the main product of conversion of the starting BP. An effect of synergism has been revealed on studying stabilization of PP with BP–DPQ mixtures. The antioxidative activity of BP was compared with that of some other stabilizers.

Key words: polypropylene oxidation, antioxidative activity, 4,4′-bis(2,6-di-*tert*-butylphenol), 3,3′,5,5′-tetra-*tert*-butyl-4,4′-diphenoquinone.

Résumé : On a étudié la cinétique de la consommation du 4,4′-bis(2,6-di-*tert*-butylphénol) (BP) lors de l'oxydation du polypropylène (PP) à 130°C, dans l'air. On montre que le produit principal de la conversion du BP de départ est la 3,3′,5,5′-tétra-*tert*-butyl-4,4′-diphénoquinone (DPQ). On a mis en évidence un effet de synergie lors de l'étude sur la stabilisation du PP par des mélanges de BP-DPQ. On a comparé l'activité antioxydante du BP avec celles d'autres stabilisants.

Mots clés : oxydation du polypropylène, activité antioxydante, 4,4′-bis(2,6-di-*tert*-butylphénol), 3,3′5,5′-tétra-*tert*-butyl-4,4′-diphénoquinone.

[Traduit par la rédaction]

Introduction

In spite of the fact that many new antioxidants and even whole classes of novel compounds with antioxidant activity have been developed, the sterically hindered phenols are still of practical and scientific interest. The careful study of the properties and behavior of such phenols in oxidizable systems suggests that the potential of these compounds is still far from exhausted and further research in this direction promises new prospects. In this connection, it is 4,4′-bis(2,6-di-*tert*-butylphenol) (bisphenol-1, BP-1) that seems to be one of the most promising inhibitors in the class of sterically hindered phenols. Some peculiarities of the inhibition of the autooxidation of solid state isotactic polypropylene (PP) with this particular bisphenol are considered in this work.

Experimental

Thoroughly purified isotactic Moplen grade PP with intrinsic viscosity 1.53 dL/g (decalin, 135°C) and crystallinity of 60% was used in the form of a finely dispersed powder with a particle size $\leq 5 \times 10^{-3}$ cm. Octadecyl 3,5-di-*tert*-butyl-4-hydroxyphenolpropionate (phenol-1) and 2,6-di-*tert*-buty-4-methylphenol (Hinmont, phenol-2) were used as inhibitors without further purification. The initiator, dimethylacetylene carbinol (DAC) was purified by recrystallization from heptane and ethanol. Cumene was purified as described previously (1). Samples of polymer were oxidized at 130°C in air under conditions that excluded the loss of additives due to evaporation. The inhibitor content in the polymer was calculated after its extraction from PP with chlorobenzene and subsequent determination of the induction period for oxidation of the cumene–initiator–inhibitor extract mixture. The procedures for preparing the oxidizing samples, measuring the induction period for oxidation of the polymer in the solid state, and determining the inhibitor concentration were reported in detail previously (2, 3). The concentration of 3,3′,5,5′-tetra-*tert*-butyl-4,4′-diphenoquinone (diphenoquinone, DPQ) in PP was determined spectrophotometrically with a Specord UV–vis instrument after extracting the DPQ from the polymer with heptane. In preliminary tests the DPQ was shown to be the only conversion product of the starting bisphenol-1 that absorbs in the visible region of the spectrum, with an extinction coefficient equal to 8.3×10^4 L mol^{-1} cm^{-1} (heptane, $\lambda = 422$ nm).

The DPQ used was prepared according to the literature procedure (4) by oxidizing 2,6-di-*tert*-butylphenol with molecular oxygen in the presence of the pyridine–CuCl catalytic system. The starting bisphenol-1 was synthesized by the oxidative dehydrogenation of 2,6-di-*tert*-butylphenol with PDQ in the presence of an alkaline catalyst (5).

Received March 1, 1995.

This paper is dedicated to Professor J.E. (Jim) Guillet in recognition of his contribution to Canadian chemistry.

E.L. Shanina and G.E. Zaikov.[1] Institute of Chemical Physics, The Russian Academy of Sciences, 2B Vorobyevskoye Chaussee, Moscow 117 334, Russia.
N.A. Mukmeneva. Kazan State Technological University, 68 Karl Marx Street, Kazan 420 015, Tatarstan, Russia.

[1] Author to whom correspondence may be addressed. Fax: 7-095 938 2156. E-mail: chembio@glas.apc.org

Can. J. Chem. Downloaded from www.nrcresearchpress.com by 46.23.64.124 on 09/08/12
For personal use only.

Can. J. Chem. Downloaded from www.nrcresearchpress.com by 46.23.64.124 on 09/08/12
For personal use only.

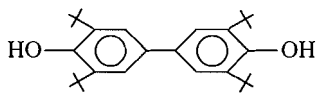

Bisphenol-1 (BP-1)

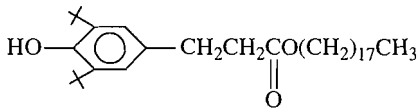

Phenol-1

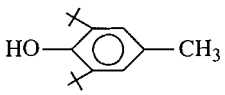

Phenol-2

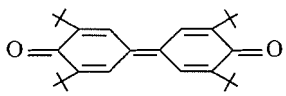

Diphenoquinone (DPQ)

X = *tert*-butyl-$C(CH_3)_3$

Results and discussions

Bisphenol-1 inhibits oxidation of cumene at 60°C, with the inhibition coefficient (f) dependent upon the initiation rate W_{in} as shown below:

$W_{in} \times 10^6$ mol L^{-1} s^{-1}	1.8	0.14	0.17
f	1.8	2.1	2.8

Some of the values exceed those usual for inhibitors of this type. The value of 2 implies ease of quinoid structure formation. The experimental f values under the conditions of the initiated oxidation can be explained by a number of factors. Thus, a hydroxybiphenyloxy radical (**1**) arising from a reaction of bisphenol-1 with a peroxy radical $RO_2^{\bullet}$ may then react with another peroxy radical $RO_2^{\bullet}$ to give either diphenoquinone or the corresponding quinophenol (**2**); the formation of the latter may be accompanied by an enhancement of the inhibition coefficient f.

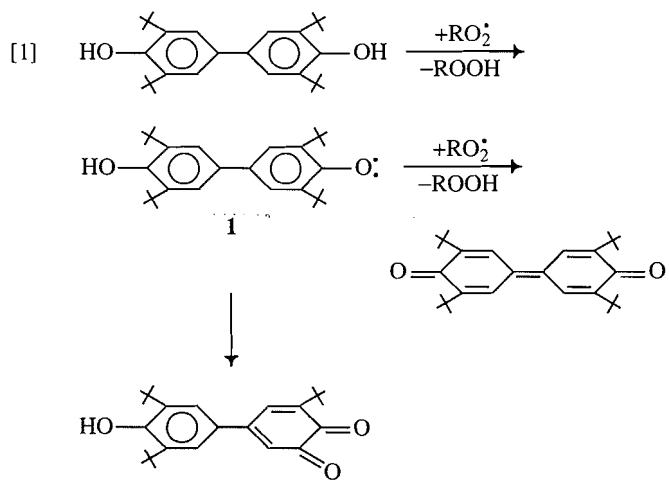

2

At high initiation rates, however, the inhibition coefficient f may be diminished owing to a reaction of hydroxybiphenyloxy radical with oxygen.

The consumption of bisphenol-1 in the course of oxidation of PP is shown in Fig. 1. The kinetic curve obtained cannot, however, be defined by a simple kinetic equation although, by analogy with other sterically hindered phenols, one can suppose that the initial rate of bisphenol-1 consumption (3.6×10^{-8} mol kg^{-1} s^{-1}) characterizes the rate of its oxidation with atmospheric oxygen (2). Bisphenol-1 is shown to be easily oxidized in air. Even thoroughly purified samples of it may contain a small admixture of diphenoquinone, e.g., up to 0.0015% in BP-1 used in this work, according to spectral data. Though one could assume that such an easily oxidizable inhibitor as bisphenol-1 does not possess a high antioxidative activity, a simple comparison of the gross index, the induction period, for oxidation of PP per se and its mixtures with three different additives (bisphenol-1, phenol-1, and phenol-2) disproves this assumption. At the same initial concentration bisphenol-1 appears to be at least as effective as phenols 1 and

Fig. 1. The kinetics of bisphenol-1 consumption (•) and diphenoquinone accumulation (○) in oxidizing polypropylene (130°C in air).

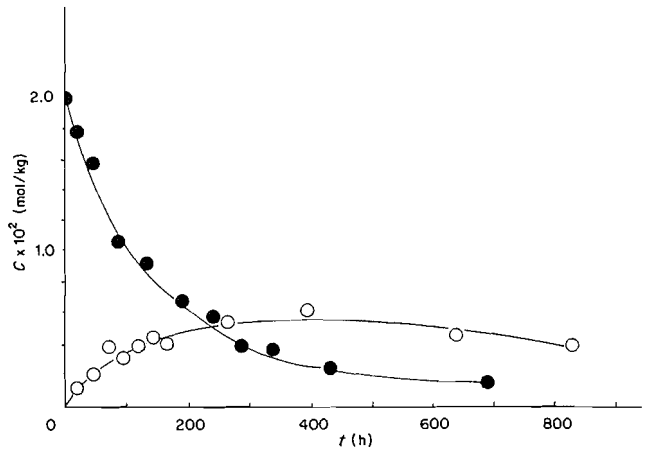

Table 1. The antioxidative efficiency of phenolic inhibitors in the oxidizing solid state of PP (130°C).[a]

Inhibitor (In)	[In] × 10^4 mol/kg	Induction period (h)
Bisphenol-1	5.0	170
Phenol-1	5.0	90[b]
Phenol-2	5.0	90[b]
Bisphenol-1	2.0	20
Phenol-1	2.0	18
—	—	0.5

[a]The phenols used under the conditions of the initiated oxidation (cumene–DAC–phenol–chlorobenzene) differ in value of the stoichiometric initiation coefficient f. However, so long as the f values are unknown, due to the more complex kinetics of the process under the conditions of autooxidation, samples were taken with the same concentration of an inhibitor.

[b]It is of interest to note that under the conditions of the runs described, in which the inhibitor volatility is of no importance, the efficiencies of phenols 1 and 2 are identical.

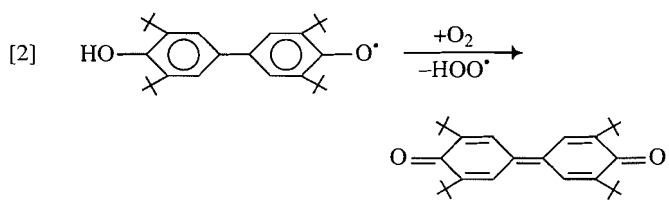

Can. J. Chem. Downloaded from www.nrcresearchpress.com by 46.23.64.124 on 09/08/12
For personal use only.

2, respectively (Table 1). In Fig. 1 there is also shown the change in diphenoquinone concentration, the main conversion product in the course of the bisphenol-1 consumption. For example, the initial rate of diphenoquinone accumulation is 1.6×10^{-8} mol kg^{-1} s^{-1}, which is more than twice as small as the rate of bisphenol-1 consumption. It seems quite probable that several processes may contribute to the formation of diphenoquinone.

1. A reaction ([1]) of the hydroxybiphenyloxy radicals with peroxy radicals

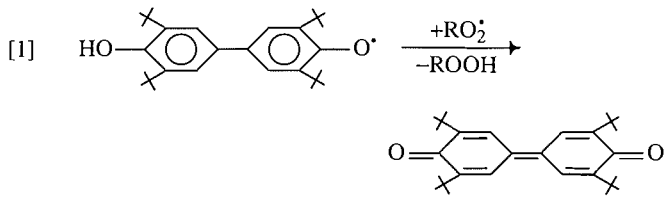

2. A reaction ([2]) of the hydroxybiphenyloxy radicals with atmospheric oxygen

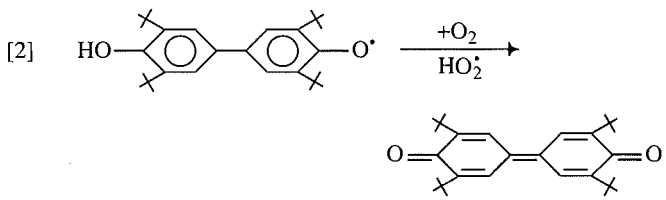

3. A reaction ([3]) of disproportionation of the hydroxybiphenyloxy radicals

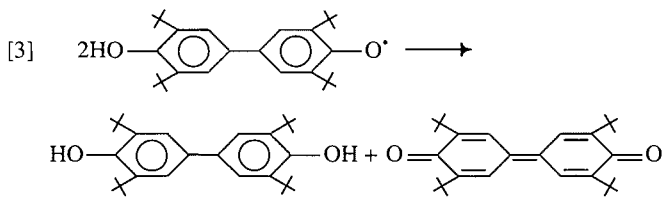

Whereas in the liquid phase the rate constant of this reaction is $\sim 10^6$ L mol^{-1} s^{-1} (6), in the solid state there is a possible leveling of the rate constants and this reaction can play a significant role.

4. Various reactions of quinolide peroxide decomposition

However, the corresponding curve in Fig. 1 shows clearly that diphenoquinone is not only accumulating, but also is consumed in the process of the inhibited oxidation of the polymer, thus appearing as an active intermediate. So the data obtained have led to the necessity of a more detailed study of the role of diphenoquinone in the process of PP oxidation inhibited by bisphenol-1. With this aim in view, a series of tests were carried out to determine the induction periods for the oxidation of PP samples that contain both bisphenol-1 and diphenoquinone in various ratios, with the total concentration being constant. The results are summarized in Table 2.

As apparent from these data, under the conditions of PP autooxidation at 130°C, diphenoquinone acts in fact as an inhibitor, though it is much less effective than bisphenol-1. However, the inhibiting activity of quinones is known to manifest itself, as a rule, under conditions of oxygen deficiency. Hence, insofar as the ratio of concentrations of alkyl and peroxide macroradicals in the oxidizing solid polymer is higher than that, for example, in the liquid phase, the induction period in the tests in which diphenoquinone was added may have been caused by its reaction with alkyl radicals. The bisphenol-1–diphenoquinone mixtures, in which the content of the former exceeds 50%, are protecting the polymer more effectively than bisphenol-1 itself.

Table 2. The antioxidative efficiency of the BP–DPQ mixtures in the process of PP autooxidation.

[BP] × 10^4 mol/kg	[DPQ] × 10^4 mol/kg	Induction period (h)
5.0	—	155
4.0	1.0	220
3.0	2.0	270
2.0	3.0	50
1.0	4.0	25
—	5.0	10

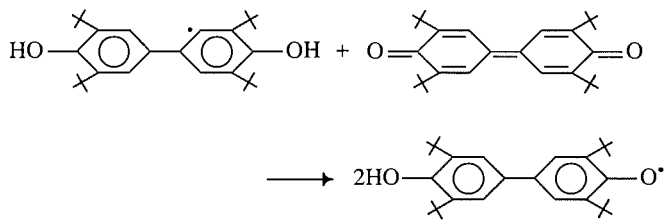

The observed synergism of action of the bisphenol-1–diphenoquinone mixtures may be caused by reaction between the components to produce the hydroxybiphenyloxy radicals. In any case, the synergism of the phenol–quinone mixture in the liquid phase has been interpreted in the same way (7). In terms of the formal kinetics, the above-mentioned reaction between bisphenol-1 and diphenoquinone will not necessarily result in an increase in the antioxidative activity of the mixture, since, instead of a molecule of bisphenol-1 capable of terminating two kinetic chains, there are formed two hydroxybiphenyloxy radicals, each of which is capable of terminating one kinetic chain. However, under the conditions of the autooxidation process, when the initiation rates are low, some side reactions with the participation of both bisphenol-1 and the hydroxybiphenyloxy radicals may also occur along with the "classical" reactions of the inhibited oxidation, thus decreasing values of the stoichiometric inhibition coefficient f. Besides, a certain gain in the antioxidative efficiency can also be attained owing to the possible formation of the additional oxyradicals from the hydroxy groups of various monophenols arising in the process of the inhibited oxidation.

One more mechanism is reported in the literature that seems to be suitable for interpreting the observed syneristic effect, namely, the formation of phenoxyl radicals from reaction of a quinone with hydroperoxide radicals (8). The latter are believed to be generated from hydrogen peroxide derived in its turn by splitting off the hydroperoxide groups from the oxidized polymer. The alternation of a reaction of a hydroperoxide radical with quinone (Q), leading to the formation of a phenoxyl radical (PhO·), and a reaction of the latter with an

alkylperoxide radical ($RO_2^{\bullet}$)of the substrate creates an effect of repeated termination of kinetic oxidation chains:

$$HO_2^{\bullet} \xrightarrow{Q} PhO^{\bullet} \xrightarrow{RO_2^{\bullet}} Q \xrightarrow{HO_2^{\bullet}} PhO^{\bullet} \quad \text{etc.}$$

As a matter of fact, under the conditions of experiments carried out in this work, the polymer is practically not oxidized, and therefore the content of hydrogen peroxide is very low. In this case, however, a reaction [2] of oxidation of the hydroxy-

[2] 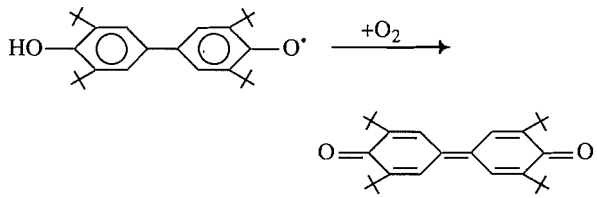

biphenyloxy radicals could serve as an alternative source of the hydroperoxy radicals $HO_2^{\bullet}$

Since this reaction is reversible, at high concentrations of diphenoquinone the equilibrium can be shifted toward the formation of the hydroxybiphenyloxy radicals.

The experimental data obtained appear to be insufficient to solve the problem of the mechanism responsible for the synergistic effect in the PP–bisphenol-1–diphenoquinone system. It should, however, be noted that although reactions which can in principle occur in the autooxidizing polymer, a phenolic inhibition system, have been explored fairly well, a kinetic characterization of the process for individual specific systems appears to present great difficulty. In addition to a large number of reactions with the participation of both the inhibitor and the radical thereof, the situation is complicated by the formation of active molecular conversion products from the initial bisphenol-1. Among them there can be compounds with prooxidative activity (e.g., quinolide peroxides) and the so-called secondary inhibitors of oxidation (e.g., new binuclear phenols, quinones, active radicals thereof, etc.).

The complicated mechanism of the process of inhibited autooxidation of polymers makes it practically impossible to compare the activity of the antioxidant using only one parameter, for example, oxidation with atmospheric oxygen. The PP–bisphenol-1 system gives clear proof of the fact that the easy oxidizability of the inhibitor, decreasing its efficiency, can be compensated for by formation of a new active product, diphenoquinone. The synergistic effect of the mixture of diphenoquinone and the starting bisphenol-1 substantially increases the protection of the polymer against oxidation, producing under the above-mentioned experimental conditions a better result than that obtained with such a widely used inhibitor as phenol-2.

It was also of interest to compare the antioxidative activity of bisphenol-1 with that of structurally similar bisphenol-2 and bisphenol-3. Under the conditions of oxidation at 130°C, the values of the induction period found for the samples containing bisphenol-1, bisphenol-2, or bisphenol-3 appeared to be 100, 45, and 20 h, respectively. Though efficiency of an inhibitor depends upon many factors, it is the synergistic effect of the bisphenol-1–diphenoquinone system that plays the most important role in the case of bisphenol-1. As regards bisphenol-2, it seems possible that a cycle of processes, including formation and conversion of galvinoxyl radical **3**, can occur. In the case of bisphenol-3, an intermediate formation of stilbene quinone **4**, possessing a weak antioxidative activity (9), should also not be discounted.

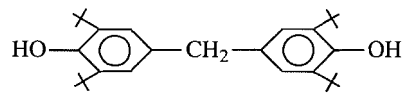

Bisphenol-2

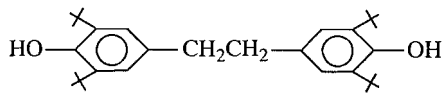

Bisphenol-3

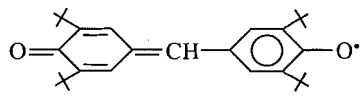

3

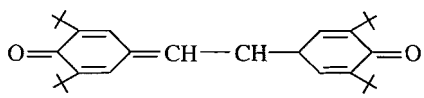

4

References

1. V.A. Belyakov, R.F. Vasil'ev, and G.F. Fedorova. Khim. Vyso. Energ. **12**, 247 (1978).
2. E.L. Shanina, V.A. Roginsky, and V.B. Miller. Vysokomol. Soed. Ser. A, **18**, 1160 (1975).
3. E.L. Shanina, V.A. Roginsky, and G.E. Zaikov. Vysokomol. Soed. Ser. A, **28**, 1971 (1986).
4. V.V. Karpov, M.L. Khidekel, L.V. Gorbunova, and G.A. Razuvaev. Izv. Akad. Nauk SSSR, Ser. Khim. **9**, 1717 (1964).
5. E.F. Zaweski. U.S. Patent 3,562,338; Ref. Zh. Khim. (20) (1971), Ref. No. N 195 (H 195); Brit. Pat. 1,133,405, Nov. 13, 1968; Chem. Abstr. **70**(7), 28.628e (1969).
6. V.A. Roginsky. Phenol antioxidants: reactivity and effectiveness (In Russian). Nauka, Moscow. 1988. p. 95.
7. L.I. Mazaletskaya, G.V. Karpukhina, G.A. Lazarev, et al. Izv. Akad. Nauk SSSR, Ser. Khim. **5**, 1188 (1989).
8. E.T. Denisov. Oxidation and destruction of the carbochained polymers (in Russian). Khimia, Leningrad. 1990. p. 241.
9. E.L. Shanina, V.A. Belyakov, and G.E. Zaikov. Polym. Degrad. Stab. **27**, 309 (1990).

Can. J. Chem. Downloaded from www.nrcresearchpress.com by 46.23.64.124 on 09/08/12
For personal use only.

Energy migration and transfer in styrene-containing polymers with inhibited excimer formation

Kenneth P. Ghiggino, David J. Haines, Trevor A. Smith, and Gerard J. Wilson

Abstract: Steady-state and time-resolved fluorescence spectroscopic techniques have been used to examine energy transfer and the migration of photoexcitation energy in styrene-containing polymer systems in which excimer formation is inhibited. In particular, copolymers of styrene and *p-tert*-butyl styrene with acenaphthylene (ACE) acceptor chromophores have been studied. Energy transfer efficiencies between styrene moieties and ACE chromophores incorporated as in-chain traps have been determined and are higher than predicted for a single-step Förster dipole–dipole energy transfer process. The results are discussed with reference to the possible mechanisms for excitation energy transport in these polymers.

Key words: polystyrene fluorescence, energy migration, energy transfer, excimer.

Résumé : On a utilisé les techniques de spectroscopie de fluorescence à l'état stationnaire et à résolution temporelle pour examiner le transfert d'énergie et la migration de l'énergie de photoexcitation dans des systèmes de polymères contenant du styrène dans lesquels la formation de l'excimère est inhibée. On a étudié en particulier des copolymères du styrène et du *p-tert*-butylstyrène avec de l'acénaphtylène (ACE) comme accepteur de chromophores. On a déterminé les efficacités du transfert d'énergie entre des portions styrène et des chromophores ACE incorporés sous la forme de pièges insérés dans la chaîne et elles sont plus élevées que celles prédites pour un processus de transfert d'énergie dipôle–dipôle de Förster en une seule étape. On discute des résultats en faisant référence aux mécanismes possibles pour le transport de l'énergie d'excitation dans ces polymères.

Mots clés : polystyrène, fluorescence, migration d'énergie, transfert d'énergie, excimère.

[Traduit par la rédaction]

Introduction

The close proximity of chromophores along a polymer chain is conducive to the process of migration and trapping of photoexcitation energy. Ng and Guillet (1) and others realized that polymers could act as "antenna" to relocate energy efficiently away from the initial site of light absorption to "trap" moieties where useful sensitized chemistry could occur. The effective absorption cross section of the trap moiety could thus be enhanced considerably. The goal of developing such "light-harvesting" polymers, which can mimic the processes in the photosynthetic apparatus or may be exploited in polymer photodegradation and (or) protection applications, has provided a considerable impetus for polymer photochemistry and photophysics over the past decade (2, 3).

There is now substantial experimental evidence for energy migration and energy transfer occurring in vinyl aromatic polymer systems obtained largely from fluorescence measurements (4). These experiments usually involve the observation of luminescence from a trap following excitation of the polymer chromophores. Alternatively, energy migration among randomly oriented chromophores has been shown to lead to depolarization of the polymer fluorescence following excitation by polarized light. These experiments have been discussed in detail elsewhere. (3, 5, 6) A considerable challenge in polymer photochemistry is to understand the mechanisms by which energy transfer and trapping occur. In a recent paper the possible pathways for energy transport in polymers were discussed from a theoretical viewpoint (7).

Besides energy migration and trapping, there are numerous other factors that can help determine the fate of excitation energy residing in vinyl aromatic polymers following irradiation with light. One such factor is excited-state dimer (excimer) formation, which is a further consequence of the close proximity of the chromophores along the polymer backbone. The formation of excimers is usually undesirable in light-harvesting systems since these species can trap the migrating exciton, thus terminating the energy migration process and

Received May 9, 1995.

This paper is dedicated to Professor J.E. (Jim) Guillet in recognition of his contributions to Canadian chemistry.

K.P. Ghiggino,[1] T.A. Smith, and D.J. Haines. Photophysics Laboratory, School of Chemistry, University of Melbourne, Parkville, Victoria, Australia, 3052.
G.J. Wilson. Commonwealth Scientific and Industrial Research Organization, Division of Chemicals and Polymers, Clayton, Victoria, Australia, 3168.

[1] Author to whom correspondence may be addressed. Telephone: +61-3-344-7031. Fax: +61-3-347-5180.

Can. J. Chem. Downloaded from www.nrcresearchpress.com by 46.23.64.124 on 09/08/12
For personal use only.

Can. J. Chem. Downloaded from www.nrcresearchpress.com by 46.23.64.124 on 09/08/12
For personal use only.

thereby reducing the efficiency of relocation of the excitation energy to the desired site (8). The kinetic behaviour of excimer formation has also proven difficult to model even in comparatively simple systems such as bichromophoric ("model") molecules (9). The additional complexity contributed by the occurrence of excimer formation to the time-resolved fluorescence behaviour observed from polymers has also retarded progress in attempts to elucidate the mechanism and rate of the energy migration/transfer processes in such systems. It is therefore desirable to exclude or at least minimize excimer formation in such studies.

In this work we report experimental studies of energy migration and trapping in polymers containing *p-tert*-butylstyrene in which excimer formation has been inhibited significantly.

Experimental section

Acenaphthene and acenaphthylene (Aldrich) were purified by multiple recrystallization from methanol. Styrene was vacuum distilled prior to use. *para-tert*-Butyl styrene monomer and the corresponding homopolymer (PTBS) were synthesized by Mr Ludger Pille (University of Melbourne). All solvents used for spectroscopic work were free of fluorescent impurities in the spectral regions of interest. Copolymers of styrene and acenaphthylene (PS–ACE) and *p-tert*-butylstyrene and acenaphthylene (PTBS–ACE) were both prepared by free radical copolymerization (using AIBN initiator) under dry nitrogen at 60°C in tetrahydrofuran and heptane solvents, respectively.

Copolymer compositions were determined by absorption spectroscopy and molecular weights were measured by gel permeation chromatography and light scattering. All spectroscopic measurements were made at room temperature in either dichloromethane (DCM) or dichloroethane (DCE). Polymer solutions were prepared to optical densities of 0.3 or less at 262 nm and degassed via multiple freeze–pump–thaw cycles. The polymer concentration is less than 2.5 μM and interchain interactions during the excited state lifetimes in these systems (<20 ns) can be neglected.

Absorption and fluorescence spectra were recorded using a Hitachi model 150-20 spectrophotometer and a Hitachi model F-4010 fluorimeter, respectively. Molecular weights were determined using a Waters GPC system equipped with microstyrogel columns and calibrated with PS standards. Light scattering was performed using a Wyatt Technology Corporation Dawn-F laser photometer. Fluorescence decay measurements were obtained using the time-correlated single-photon counting technique as described previously (3). The frequency-doubled output of a cavity-dumped Spectra Physics model 3500 dye laser (rhodamine 110 dye) pumped synchronously by a mode-locked Spectra Physics model 2030 argon ion laser was used as the excitation source (instrument response ≈ 80 ps FWHM).

Results and discussion

In previous work on synthetic aromatic polymer systems the amount of excimer formation has been controlled to some extent by (*i*) changing the tacticity of the polymer (10–12), (*ii*) randomly copolymerizing inert "spacer" groups into the polymer (13), (*iii*) preparing copolymers with alternating inert groups (14), (*iv*) sterically hindering excimer formation by attaching bulky groups to the chromophore (15), and (*v*) using chromophores in which excimer formation is inhibited for other reasons (1, 16, 17). The latter two methods are preferred as the other approaches are expected to adversely affect the efficiency of energy migration by increasing the interchromophore separation. We report here recent results obtained using method (*iv*) for styrene-containing polymers.

Fig. 1. UV absorption spectra and steady-state fluorescence spectra (λ_{ex} = 260 nm) of PTBS (thick line) and PS (thin line) at 20°C in dilute, degassed dichloroethane.

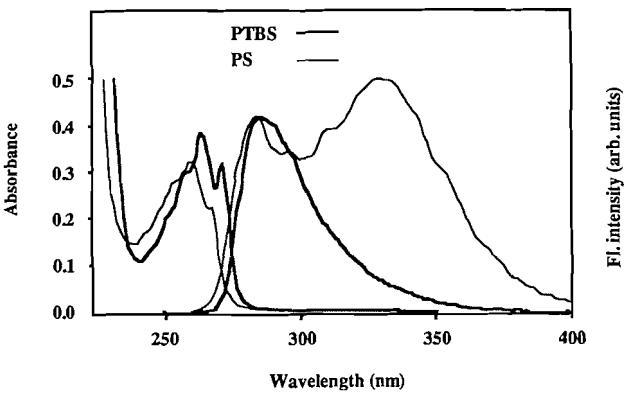

The photophysical behaviour of polystyrene has been studied in detail by numerous authors; however, there is still some debate regarding the occurrence and extent of energy migration in this polymer (18, 19). Furthermore, if energy migration does occur in this polymer, contradictions exist in the literature as to the mechanism (resonance or exchange) by which it occurs (18, 20). Excimer fluorescence is readily observable in PS at room temperature and the complexity introduced by excimer formation may be a factor contributing to the apparent confusion relating to the question of energy migration in PS. In an effort to study energy transfer and migration in styrene-containing polymers without the complication of excimer formation, we have examined polymers containing the *p-tert*-butylstyrene (TBS) group in which excimer formation between adjacent chromophores is hindered by the steric constraints of the bulky *tert*-butyl groups on the chromophores, while maintaining the close average interchromophore separation required for facile energy migration assuming a dipole–dipole mechanism.

The absorption and fluorescence spectra of the poly(*p-tert*-butylstyrene) homopolymer (PTBS) and poly(styrene) (PS) in dilute degassed solutions of 1,2-dichloroethane are given in Fig. 1. The absence of a clear emission band at 330 nm in the case of PTBS indicates that excimer formation has been efficiently suppressed as compared with PS. It is assumed that the bulky *tert*-butyl groups do not allow the close approach of the chromophoric units to form the usual planar "sandwich" excimer configuration in which the rings are typically 3–3.5 Å apart (21).

Having demonstrated that there are few, if any, excimer sites present in this polymer, polymers containing the TBS and energy acceptor groups would appear to be suitable candidates for the investigation of energy migration. To this end polymers containing styrene or TBS along with the acenaphthyl chromophore were synthesized and characterized as described in the Experimental section. The physical properties of the

Can. J. Chem. Downloaded from www.nrcresearchpress.com by 46.23.64.124 on 09/08/12
For personal use only.

Table 1. Physical properties of copolymers.

Copolymer	M_n	S:ACE	M_w	R_g (nm)	$V_h \times 10^{22}$ (dm^3)
PS–ACE	29 200	64 : 1	45 300	7[a]	7.5
PTBS–ACE	88 100	203 : 1	160 000	10 ± 3[b]	21.4

Abbreviations: S:ACE = styrene:acenaphthylene ratio calculated using M_n (the number average molecular weight). R_g = radius of gyration. V_h = hydrodynamic volume.

[a]Calculated using classical Flory theory (35). Mark–Houwink parameters: $K_w = 21.0 \times 10^{-3}$ cm^3 g^{-1} and $a = 0.66$ for atactic PS in dichloroethane at 25°C (36).

[b]Measured using light scattering (37).

Fig. 2. Emission (λ_{ex} = 262 nm) and fluorescence excitation spectra (λ_{obs} = 350 nm) of PS–ACE at 20°C in dilute, degassed dichloroethane solution. The normalized absorption spectrum of PACE (light line) is included for reference.

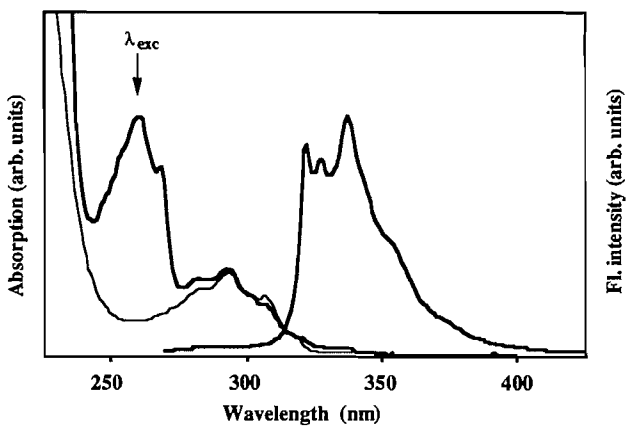

polymers used are collected in Table 1. The ratios of donor (styrene or *tert*-butylstyrene) to acceptor (acenaphthylene) chromophore in the copolymers were determined by absorption spectroscopy using poly(acenaphthylene) (PACE) as a reference compound. This also permitted determination of the relative absorptions due to each species at a given wavelength.

The hydrodynamic volume (V_h) of a single polymer coil can be calculated using the radius of gyration (R_g) and eq. [1] assuming a random coil, where ξ is a numerical factor (assumed to be 0.8).

$$[1] \quad V_h = \frac{4}{3}\pi\xi^3 R_g^3$$

The emission and fluorescence excitation spectra of radically prepared PS–ACE copolymer are shown in Fig. 2 from which it is clear that excitation of the styrene (donor) chromophores results in a fluorescence spectrum that is dominated by acenaphthylene (trap) emission.

It is possible to calculate the theoretical transfer efficiency from a styrene or *tert*–butylstyrene donor to an acenaphthylene acceptor (Eff_{th}) assuming electronic energy transfer occurs via a single-step Förster-type mechanism (22, 23), eq. [2].

$$[2] \quad Eff_{th} = \pi^{1/2}\gamma \exp(\gamma^2)[1-\mathrm{erf}(\gamma)]$$

where $\gamma = C/C_0$, C is the effective acceptor concentration within the volume of the polymer coil, and C_0 is the Förster critical transfer concentration given by eq. [3].

$$[3] \quad C_0 = \frac{3000}{2\pi^{3/2}NR_0^3} \qquad (\mathrm{mol\ dm^{-3}})$$

In eq. [3] N is Avogadro's number and R_0 (cm) is the Förster critical transfer distance, the donor–acceptor separation at which there is equal probability of excitation transfer and spontaneous deactivation. The expression for R_0 is given by eq. [4].

$$[4] \quad R_0^6 = \frac{9000\ln(10)\kappa^2\Phi_d}{128\pi^5 n^4 N}\int_0 \frac{F_d(\bar{\nu})\varepsilon_a(\bar{\nu})}{\bar{\nu}^4}\,d\bar{\nu} \qquad (\mathrm{cm^6})$$

Here, κ^2 is an orientation factor that, for a random distribution of transition dipoles, has a value of 2/3, Φ_d is the quantum yield of fluorescence from the donor in the absence of acceptor, n is the refractive index of the solvent, and the integral term, designated J, is a measure of the degree of spectral overlap between the absorption spectrum of the acceptor ($\varepsilon_a(\bar{\nu})$ is the extinction coefficient of the acceptor at wavenumber, $\bar{\nu}$), and the unit area normalized fluorescence emission spectrum of the donor, $F_d(\bar{\nu})$.

Figures 3 and 4 show the overlap of the donor emission and acceptor absorption spectra for PS–PS and PTBS–PTBS self-transfer, and PS–ACE and PTBS–ACE energy transfer. The resultant values for spectral overlap integral term, J, along with the corresponding R_0 and C_0 values are given in Table 2.

From the data presented in Table 2, a beneficial effect of *tert*-butyl substitution, from the point of view of dipole–dipole energy transfer, is the almost doubling of the R_0 value for self-transfer in PTBS compared with PS. This is due to the fourfold increase in the Φ_{fl} (PTBS = 0.12, PS = 0.03) and the absence of much long-wavelength emission in PTBS compared with PS. It has been suggested (24) that using an R_0 calculated from PS is inappropriate because of the presence of excimers acting as traps, and that the R_0 for PS should be close to that for isopropylbenzene (6.47 Å) (25). This being the case, the R_0 for PTBS calculated in this work still indicates that self-transfer should be more prevalent in this polymer than in PS.

It is instructive at this point to compare the R_0 values calculated from the photophysical properties of the chromophores with the actual average interchromophore separation. A value of 6.63 Å has been determined for the latter from X-ray analysis of crystalline isotactic PS (26), while MM2 minimization of a *trans-gauche* diad in PTBS suggests an interchromophore separation of 6.6 Å. Using 6.6 Å as a typical interchromophore separation for these polymers and assuming a random distribution of transition dipoles, it can be seen by inspection of eq. [5] describing the rate of donor–acceptor transfer, that for R_0 = 6.47 Å, the rate of self-transfer in PS via a resonance mecha-

Can. J. Chem. Downloaded from www.nrcresearchpress.com by 46.23.64.124 on 09/08/12
For personal use only.

Fig. 3. Overlap of absorption and emission spectra for self-transfer in PS (upper) and PTBS (lower), respectively.

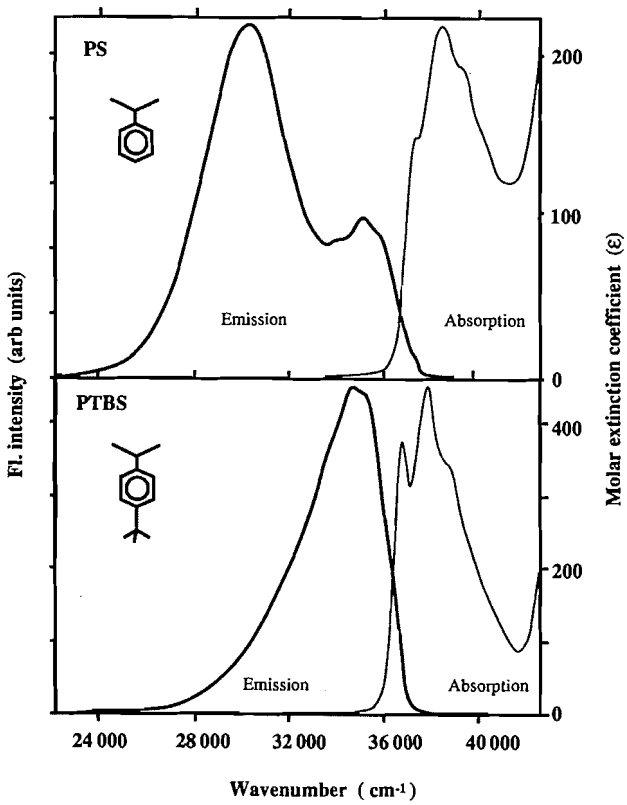

Fig. 4. Overlap of acenaphthene absorption spectrum and the PS (upper) and PTBS (lower) emission spectra, respectively.

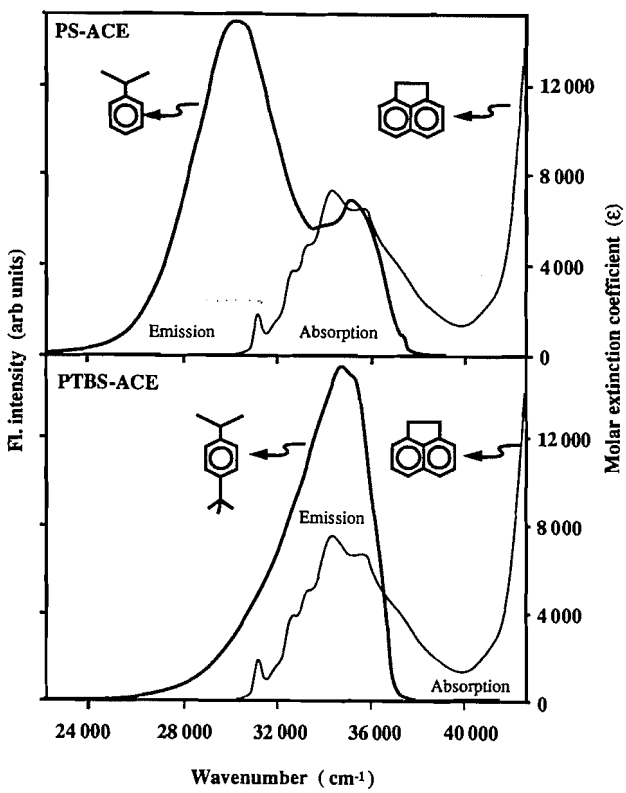

nism must be quite close to the fluorescence rate of the unquenched donor ($1/\tau_D$), with the rate being slightly greater for PTBS self-transfer.

$$[5] \quad k_{DA}(R) = \frac{3\kappa^2}{2\tau_D}\left(\frac{R_0}{R}\right)^6$$

In eq. [5] τ_D is the donor lifetime in the absence of energy transfer, R is the intermolecular separation, and the other terms have been defined previously. Using ethylbenzene (τ_D = 13 ns) (27) as a model compound for PS results in a Förster transfer rate of 7×10^7 s^{-1} (or ~14 ns per hop). In the case of PTBS a model compound is not yet available but, using a donor lifetime of 10 ns estimated from the homopolymer decay, a rate of 2×10^8 s^{-1} (~5 ns per hop) is obtained. It should be emphasized that these hopping rates will depend strongly on the dynamic interchromophore separations, which can be smaller and larger than those determined from energy-minimized and crystal structures. Nevertheless the above considerations suggest that singlet energy migration would not be expected to be facile in these polymers if the transfer is via a series of Förster hops. At the typical interchromophore separations in these systems (~ 5–7 Å) it is possible that orbital overlap effects (e.g., exchange interactions) are important. Using Monte Carlo simulations, Blonski and Sienicki (20) have suggested that exchange interactions are responsible for the energy migration process in PS. Recent work in this laboratory has shown that a combination of Coulombic (dipole–dipole) and exchange interactions can lead to a rate of energy transfer substantially higher than that expected by a purely dipole–dipole mechanism (28). In addition, the possibilities of overlap-dependent energy transfer induced by superexchange interactions through the polymer backbone connecting the chromophores has recently been proposed (7).

We now turn our attention to the steady-state sensitization results. It is clear from eq. [2] that calculation of the theoretical transfer efficiency requires knowledge of the effective local acceptor concentration (C_{eff}) in the polymer volume. The average number of acceptor molecules per chain can be determined by a combination of absorption and molecular weight measurements and C_{eff} is then obtained from the the number of acceptor molecules per chain and the hydrodynamic volume (V_h; see Table 1).

Table 3 lists the relevant energy transfer data for the PS–ACE and PTBS–ACE systems, including the effective acceptor concentration (C_{eff}), the critical transfer concentration (C_0) (see Table 2), the theoretical transfer efficiency (Eff_{Th}) (calculated using eq. [2]), and the experimentally determined transfer efficiency (Eff_{Exp}).

The efficiency of acenaphthylene sensitization was determined from comparison of excitation and absorption spectra as described elsewhere (29). This method does not require evaluation of the fluorescence quantum yield of the donor or acceptor. The fluorescence and fluorescence excitation spectra for a PS–ACE sample with absorbances at 262 nm (PS and ACE excited) and 295 nm (ACE only excited) of 0.268 and 0.096, respectively, are shown in Fig. 2. For 262 nm excitation (donor region) the intensity of ACE emission expected for 0% energy transfer is evaluated from the fraction of light absorbed by the ACE at 262 nm and the emission yield determined by exciting ACE alone at 295 nm. The intensity of ACE emission expected

Can. J. Chem. Downloaded from www.nrcresearchpress.com by 46.23.64.124 on 09/08/12
For personal use only.

Table 2. Photophysical parameters for energy transfer within the polymers and copolymers used.

Polymer	Φ_d	$J \times 10^{17}$ (M^{-1} cm^3)	R_0(Å)	C_0(M)
PS	0.030[a]	0.122	4.17[c]	6.17
PTBS	0.126[b]	0.871	7.34	1.13
PS–ACE	0.030	0.147	13.6	0.178
PTBS–ACE	0.126	0.333	19.8	0.058

[a]Berlman (38).
[b]Calculated relative to the quantum yield of PS.
[c]Based on data for PS (see also discussion in text).

Table 3. Relevant energy transfer data for the copolymers examined in this study.

Copolymer	C_{eff}(M)	C_0(M)	γ	Eff_{Th}(%)	Eff_{Exp}(%)
PS-ACE	0.010	0.178	0.056	9	31
PTBS–ACE	0.003	0.058	0.057	10 ± 5	21

for 100% energy transfer from the donor to the acceptor is determined by assuming all light absorbed by the polymer at 262 nm is emitted from the acceptor. Comparison of the actual intensity measured with that expected for 0% and 100% energy transfer enabled extraction of the experimental transfer efficiency. These values are also listed in Table 3 along with the corresponding single-step theoretical transfer efficiencies.

From the data presented in Table 3 it is apparent that for both PS–ACE and PTBS–ACE the experimentally determined energy transfer efficiency far exceeds that calculated assuming a single-step Förster-type mechanism. This suggests that photon-harvesting effects are indeed operating. However, as discussed above, it is unlikely that energy migration is occurring via a purely Coulombic dipole–dipole mechanism.

For PTBS–ACE the donor:acceptor ratio is approximately 203:1 and this gives rise to an observed energy transfer efficiency to the ACE trap of 21%. For PS–ACE the ratio is only 64:1, i.e., the excitation has to travel only about one third as far before it encounters a trap, yet the energy transfer efficiency in PS–ACE has increased to only 31%. This result is not too surprising when one considers that there are approximately seven to nine excimer-forming sites at room temperature in a polymer chain of this length (30, 31) as well as the four to five ACE traps per PS chain. While excimers may be able to participate in energy transfer to ACE, they will also limit the energy migration length and provide additional deactivation pathways for excitation energy in the polymer thus decreasing the overall transfer efficiency.

Time-resolved data show that in all cases the fluorescence decay from the monomer emission region cannot be described adequately by a single exponential decay function. Whilst this is not unusual for homopolymers with excimer-forming sites such as PS, the reasons for the observed non-exponentiality of the PTBS homopolymer fluorescence decay (Fig. 5) are not clear. Monte Carlo calculations have shown that the presence of any energy trapping site will introduce non-exponentiality to fluorescence decays (3), which may indicate that excimer formation might not be completely inhibited within this polymer. However, for the copolymers the dominant cause of the observed non-exponentiality is almost certainly the presence

Fig. 5. Fluorescence decays of PTBS homopolymer (upper trace) and PTBS–ACE (lower trace) following excitation at 273 nm.

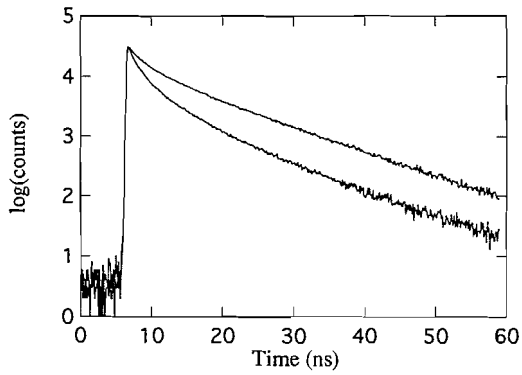

of the ACE trap. One noteworthy feature of the time-resolved data from the PS–ACE and PTBS–ACE polymers is the absence of any rise time of the trap fluorescence observable within the time resolution of our detection system (≈80 ps). Attempts to recover the experimentally observed trap rise time using numerical simulation of single-step time-dependent Förster theory have, to date, been unsuccessful. In all cases the predicted trap rise time is at least an order of magnitude slower than that observed experimentally. We take this as further evidence that, in addition to single-step, dipole–dipole energy transfer, mechanisms may be operative that enhance the rate of energy trapping in these polymers. Previous estimations of the singlet energy migration coefficient in polystyrene of about 10^{-8} m^2/s^{-1} from trapping and quenching data are also consistent with high migration efficiencies (32, 33).

Time-resolved fluorescence anisotropy measurements have the most potential to yield quantitative information with respect to the existence and rate of excitation transport (34). Such measurements on the polymers under discussion in this paper are currently in progress but the results will be reported elsewhere.

Conclusions

In the work reported here the formation of excimers in sty-

rene-based polymers has been restricted by attaching a *tert*-butyl group at the *para* position. Qualitative considerations on the basis of donor:trap ratios indicate that the efficiency of energy transfer to an acenaphthylene trap incorporated onto the polymer chain is greater in PTBS–ACE than in PS–ACE where the competition from excimers hinders energy migration. The observed efficiency is greater than can be rationalized in terms of a single-step Förster transfer from excited donor to acenaphthylene acceptor, providing evidence for down-chain energy migration. Consideration of the parameters involved in self-transfer via a series of dipole–dipole hops and the rapid (undetectable) rise times observed for the acceptor suggest Förster transfer is not the dominant process for energy migration in these polymers and other mechanisms enhancing energy transfer are operative.

Acknowledgments

Financial support for this work from the Australian Research Council (ARC) is acknowledged. D.J.H. acknowledges the financial support of a University of Melbourne Postgraduate Scholarship (MUPS).

References

1. D. Ng and J.E. Guillet. Macromolecules, **15**, 724 (1982).
2. J. Guillet. Polymer photophysics and photochemistry. Cambridge University Press, Cambridge. 1985.
3. K.P. Ghiggino and T.A. Smith. Prog. React. Kinet. **18**, 375 (1993).
4. S.E. Webber. Chem. Rev. **90**, 1469 (1990).
5. R.F. Ried and I. Soutar. J. Polym. Sci. Polym. Phys. Ed. **16**, 231 (1978).
6. A.D. Stein, K.A. Peterson, and M.D. Fayer. J. Chem. Phys. **92**, 5622 (1990).
7. G.D. Scholes and K.P. Ghiggino. J. Photochem. Photobiol. A: **80**, 355 (1994).
8. Y. Morishima, Y. Tominaga, S. Nomura, and M. Kamachi. J. Phys. Chem. **96**, 1990 (1992).
9. T.A. Smith, D.A. Shipp, G.D. Scholes, and K.P. Ghiggino. J. Photochem. Photobiol. A: **80**, 177 (1994).
10. H. Boudevsha and C. Brutchkov. Makromol. Chem. **180**, 1113 (1979).
11. C. David, N. Putman de Lavarielle, and G. Geuskens. Eur. Polym. J. **10**, 617 (1974).
12. T. Ishii, T. Handa, and S. Matsunaga. J. Polym. Sci. Polym. Phys. Ed. **17**, 811 (1979).
13. R.A. Anderson, R.F. Reid, and I. Soutar. Eur. Polym. J. **16**, 945 (1979).
14. D. Phillips, A.J. Roberts, and I. Soutar. J. Polym. Sci. Polym. Lett. Ed. **18**, 123 (1980).
15. T. Nakahira, T. Sakuma, S. Iwabuchi, and K. Kojima. J. Polym. Sci. Polym. Phys. Ed. **20**, 1863 (1982).
16. S. Ito, K. Yamashita, M. Yamamoto, and Y. Nishijima. Chem. Phys. Lett. **117**, 171 (1985).
17. S. Ohmori, S. Ito, and M. Yamamoto. Ber. Bunsen-Ges. Phys. Chem. **93**, 815 (1989).
18. K. Sienicki. Macromolecules, **23**, 5025 (1990).
19. C.F.C. Porter and D. Phillips. Eur. Polym. J. **30**, 189 (1994).
20. S. Blonski and K. Sienicki. Macromolecules, **19**, 2936 (1986).
21. W. Klöpffer (*Editor*). Organic molecular photophysics. Vol. 1. Wiley, London. 1973.
22. T. Förster. Z. Naturforsch. A: Astrophys. Phys. Phys. Chem. **4A**, 321 (1949).
23. T. Förster. Discuss. Faraday Soc. **27**, 7 (1959).
24. R. Gelles and C.W. Frank. Macromolecules, **15**, 747 (1982).
25. I.B. Berlman. Energy transfer parameters of aromatic compounds. Academic Press, New York. 1973.
26. G. Natta. Makromol. Chem. **35**, 94 (1960).
27. F. Heisel and G. Laustriat. J. Chim. Phys. **66**, 1881 (1969).
28. G.D. Scholes, A.H.A. Clayton, and K.P. Ghiggino. J. Chem. Phys. **97**, 7405 (1992).
29. F. Bai, C.-H. Chang, and S.E. Webber. Macromolecules, **19**, 2484 (1986).
30. P.D. Fitzgibbon and C.W. Frank. Macromolecules, **15**, 733 (1982).
31. R. Gelles and C.W. Frank. Macromolecules, **15**, 741 (1982).
32. K. Sienicki and C. Bojarski. Polym. Photochem. **6**, 205 (1985).
33. K. Sienicki and C. Bojarski. Macromolecules, **18**, 2714 (1985).
34. C.R. Gochanour, H.C. Andersen, and M.D. Fayer. J. Chem. Phys. **70**, 4254 (1979).
35. P.J. Flory. Statistical mechanics of chain molecules. John Wiley & Sons, New York. 1969.
36. J. Brandup and E.H. Immergut (*Editors*). Polymer handbook. 2nd ed. Wiley, New York. 1975.
37. Z. Küçükyavuz and S. Küçükyavuz. Eur. Polym. J. **14**, 867 (1978).
38. I.B. Berlman. Handbook of fluorescence spectra of aromatic molecules. 2nd ed. Academic Press, New York. 1971.

Can. J. Chem. Downloaded from www.nrcresearchpress.com by 46.23.64.124 on 09/08/12
For personal use only.

Luminescence measurements of oxygen permeation and oxygen diffusion in thin polymer films

Ahmad Yekta, Zahra Masoumi, and Mitchell A. Winnik

Abstract: A new method is developed for analyzing the diffusion of oxygen in thin polymer films via fluorescence quenching measurements. We begin by reviewing previous methods, all of which involve approximations, for the measurement of permeability and diffusion coefficient by luminescence quenching; their shortcomings are clarified. An exact analytic theory is developed that successfully couples Fick's laws of diffusion to the Stern–Volmer equation of intensity quenching. Various modes of experimentation with polymeric films are considered. The equations we derive make the unexpected prediction that the rate of emission intensity decay when O_2 diffuses into a polymer film is much faster than the rate of emission intensity enhancement when O_2 diffuses out of the same film, even when the molecular diffusivity remains unchanged. Experiments show that this is indeed the observed behaviour.

Key words: diffusion coefficient, oxygen permeability, polymers, quenching, luminescence quenching, Fick's laws, Stern–Volmer equation.

Résumé : Faisant appel à des mesures de décroissance de la fluorescence, on a mis au point une nouvelle méthode pour analyser la diffusion de l'oxygène dans des films minces de polymère. On passe en revue les méthodes décrites antérieurement pour la mesure de la perméabilité et du coefficient de diffusion par décroissance de la luminescence; toutes ces méthodes impliquent des approximations et on a clarifié leurs limitations. On a mis au point une théorie analytique exacte qui relie avec succès les lois de diffusion de Fick avec l'équation de Stern–Volmer de la décroissance de l'intensité. On considère divers modes d'expérimentation avec des films polymériques. Les équations que l'on a dérivées permettent de faire la prédiction inattendue que la vitesse de décroissance de l'intensité de l'émission, lorsque du O_2 diffuse dans un film de polymère, est beaucoup plus rapide que la vitesse d'augmentation de l'intensité de l'émission lorsque le O_2 diffuse du même film, même lorsque la diffusivité moléculaire demeure la même. Les expériences montrent que le comportement observé correspond à cette prédiction.

Mots clés : coefficient de diffusion, perméabilité à l'oxygène, polymères, décroissance, décroissance de la luminescence, lois de Fick, équation de Stern–Volmer.

[Traduit par la réduction]

Introduction

Oxygen diffusivity in polymers is most commonly determined by measuring the rate of oxygen permeation across a membrane. One exposes one side of the polymer film to oxygen at time zero and measures the flux of oxygen across the film as a function of time. Knowing the dimensions of the film and the partial pressure of oxygen on the high-pressure side, one can calculate the diffusion coefficient and the permeability from the flux (1). The diffusion coefficient D_{O_2} is determined from the kinetics of the approach of the O_2 flux to its steady-state value, and at steady state, the flux measures the permeability P_{O_2}, which is equal to the product of the oxygen solubility in the film (S_{O_2}) and D_{O_2}.

It is not always convenient to determine D_{O_2} and S_{O_2} in this way, particularly where it is difficult to prepare free-standing films. Because oxygen is such a powerful quencher of fluorescence and phosphorescence, there is a natural attraction to using this property to determine these values. Unfortunately, the approaches that satisfy diffusion equations in a rigorous way have been cumbersome from the point of view of experimental detail. On the other hand, experiments that are easy to carry out do not conform to geometries where it has been possible to evaluate rigorously the coupling between the diffusion equation and the luminescence quenching kinetics.

This is a topic that has long been of interest to J. E. Guillet. He has worked in the area and has published two key reviews on this topic (2, 3). Here we would like to present a rigorous theoretical solution to the simplest way of measuring oxygen diffusion in polymer thin films by luminescence quenching. We believe that it is fitting that we publish this work in a journal issue dedicated to Professor Guillet.

Received March 30, 1995.

This paper is dedicated to Professor J.E. (Jim) Guillet in recognition of his contributions to Canadian chemistry.

A. Yekta, Z. Masoumi, and M.A. Winnik.[1] Department of Chemistry and Erindale College, University of Toronto, Toronto, ON M5S 1A1, Canada.

[1] Author to whom correspondence may be addressed. Telephone: (416) 978-8545. Fax: (416) 978-0541. E-mail: mwinnik@alchemy.chem.utoronto.ca

Can. J. Chem. Downloaded from www.nrcresearchpress.com by 46.23.64.124 on 09/08/12
For personal use only.

Can. J. Chem. Downloaded from www.nrcresearchpress.com by 46.23.64.124 on 09/08/12
For personal use only.

From a historical point of view, one of the first approaches to measuring luminescence quenching in polymers involved a polymer rod of large diameter (i.e., cm) containing a uniform distribution of dye molecules (4, 5). All oxygen is removed from the rod under vacuum, rendering the entire rod brightly fluorescent or phosphorescent. At $t = 0$, the rod is exposed to air and illuminated at one end. As O_2 penetrates into the rod, it quenches emission from nearby dye molecules, forming a dark cylindrical shell at the periphery of the rod. The thickness of this dark shell grows with increasing diffusion time. One lays a ruler across the end of the rod and tries to measure the thickness of the bright circle and dark outer ring as a function of time. Because diffusion occurs on the scale of centimeters, the experiment takes a long time (weeks to months). Measuring the appropriate distances accurately is not easy, and the analysis ignores oxygen diffusion into the rod ends.

Another approach due to Cox also looks at large samples (6). Here one constructs a square cell with centimeter-scale height. The cell is filled with a polymer containing the dye and all oxygen is removed. Cox irradiated a thin (1 mm) middle cross section of the cell, and then allowed oxygen to diffuse into the cell from the top. As the oxygen concentration profile propagates through the illuminated middle slice, the emission intensity is quenched. Note that because of the experimental design, with the plane of the slice perpendicular to the propagation direction of the O_2 profile, there will at all times be a nearly uniform O_2 concentration in the plane of the illumination. There are a number of technical difficulties involved with this experiment, particularly ones of alignment of the illuminated plane, focus of the collection optics, and the long time scale of the experiment. Nevertheless, for this geometry as well as the cylindrical geometry described above, rigorous application of Fick's laws of diffusion is possible.

From the point of experimental ease, what one would like to be able to do is to spread a thin film (1–100 μm) containing the dye on a flat substrate, and mount it in a fluorescence spectrometer in a cell with a controlled atmosphere. At $t = 0$, one could pass air or oxygen into the cell and measure the time profile of the decay of the emission intensity (on the order of minutes), or flush nitrogen into the cell containing air and observe the growing-in of the emission intensity as oxygen diffuses out of the film. From an analytical point of view one would like to have a relationship that connects the measurable intensity-versus-time profiles to the diffusivity of the penetrating quencher.

The Guillet group was one of the first to report experiments involving oxygen diffusion into dye-doped polymer films (7, 8). They calculated diffusion coefficients from their data, but in their data analysis they made simplifying assumptions about the connection between the oxygen diffusion and the extent of luminescence quenching in the film. They used Fick's laws to calculate the amount of oxygen that had entered into the film at time t, but to calculate the amount of quenching they assumed that this amount could be treated as an effective average uniform concentration over the sample thickness. This neglects the details of the concentration profile of quencher in the film and introduces an error into the calculated diffusion coefficient value.

We have been able to derive an exact expression relating the concentration profile to the fluorescence quenching. The equations we derive make the unexpected prediction that the rate of emission intensity decay when O_2 diffuses into a thin polymer film is much faster than the rate of emission intensity increase when O_2 diffuses out of the same film. Experiments show that this is indeed the observed behavior. Values of D_{O_2} and P_{O_2}can now be obtained with accuracy and with excellent precision.

Experimental

Fluorescence measurements employed a SPEX Fluorolog 2 with a DM3000 data system, operated in the time-base mode. Polymer films were prepared by either casting onto quartz plates or onto a Teflon surface. In the latter case, the films could be peeled off after drying to yield free-standing films. The film was then mounted in a sample chamber (3 cm^3) through which various gases could be passed at a controlled rate. The cell and the details of polymer film preparation will be described in more detail in a future publication. The flow rates were about 150 cm^3/s so that the gas in the chamber could be replaced every 20 ms. The polymers, silicone resin solutions EXP-36-X20 and GP-197, were obtained from Genesee Polymers, Flint, Mich. The dye, platinum octaethylporphine (Porphyrin Products, Logan, Utah), was dissolved in 1,1,1-trichloroethane (Caledon) to give a 100 ppm stock solution. An aliquot of the dye solution was added to that of the resin so that the dye concentration in the dry resin would be ca. 10 ppm. Samples were excited at 534 nm, and emission was monitored at 646 nm.

Computer programs for simulation and data analysis were written in Quick-basic. The summation expressing $\rho(x, t)$ (cf. eq. [9]) converges rapidly except for very short times. Even for times as short as $Dt/L^2 = 0.001$, 60 summation terms are sufficient to give an accuracy better than 1 in 10^6. The integration in eq. [9] was performed by dividing the range into 100 segments and employing the Simpson algorithm. Data fits were performed by inputting the experimental value of B and adjusting D/L^2 as a parameter, requiring that the half-way points (between maximum and minimum intensities) of theory and experiment overlap. More sophisticated analysis requiring minimization of χ^2 criteria can be performed, but will not be considered here.

Previous analyses of oxygen quenching in thin films

Equilibrium state measurements

Experiments have been reported in which the oxygen concentration in the film has been allowed to come to equilibrium. Under these circumstances, the quencher concentration should be macroscopically uniform throughout the sample, at its equilibrium solubility limit, Q_{eq}. Within the context of the underlying assumptions, this type of experiment yields the quencher permeability in the matrix. One typically measures the fluorescence or phosphorescence intensity of the polymer film in the absence of oxygen (I^0), and compares it to the corresponding intensity after equilibration (I_{eq}) with an external atmosphere containing oxygen with a partial pressure of p_Q. To analyze the data one assumes a Stern–Volmer (SV) type of relation, eq [1], where k_q represents the bimolecular rate constant of quenching, modeled after kinetics of quenching in fluid media, and τ^0 is the unquenched fluorescence or phosphorescence lifetime.

Can. J. Chem. Downloaded from www.nrcresearchpress.com by 46.23.64.124 on 09/08/12
For personal use only.

$$[1a]\quad \frac{\tau^0}{\langle\tau_{eq}\rangle} = \frac{I^0}{I_{eq}} = 1 + k_q\tau^0 Q_{eq}$$

One feature of these experiments that remains unresolved is that while the unquenched decay profile of the dye is often exponential, and thus characterized by a well-defined τ^0 value, these decays become non-exponential when oxygen is present (9–11). The Stern–Volmer equation is derived from assumptions that lead to the prediction that $I^0/I_{eq} = \tau^0/\tau_{eq}$. Since the decay in the presence of quencher is not exponential, this poses a problem in the assumption of SV kinetics since τ_{eq} is not defined. One can either ignore the problem by examining intensities only, or sidestep the issue by replacing τ_{eq} with its mean value $\langle\tau_{eq}\rangle$ calculated from the decay profile. While the former approach is more common, when decay profiles are measured, one often finds that $I^0/I_{eq} = \tau^0/\langle\tau_{eq}\rangle$. That is, for low concentrations of Q_{eq}, the SV relation [1] is usually obeyed, even when the sample shows nonexponential decays of luminescence.

For oxygen, in terms of its external partial pressure p_Q, the equilibrium solubility Q_{eq} is proportional to p_Q (Henry's law) in the range of low to moderate pressures (1), i.e. $Q_{eq} = Sp_Q$, where S is the Henry's law constant of the gas solubility.[2] In this case eq. [1*a*] reduces to

$$[1b]\quad \frac{\tau^0}{\langle\tau_{eq}\rangle} = \frac{I^0}{I_{eq}} = 1 + (k_q\tau^0 S)\,p_Q$$

By varying the external pressure of the gas, and each time allowing for equilibration, one obtains a linear plot of eq. [1*b*]. From the slope and the knowledge of τ^0 one then calculates the product k_qS.

The rate coefficient k_q is related to the diffusivity of the quencher. For fluid media,

$$[2]\quad k_q = \alpha k_{diff}$$

where α is the probability of quenching in an encounter complex of the excited state/quencher, and k_{diff} is the diffusion-controlled rate constant of the formation of the encounter pair. The diffusional encounter theory of Smoluchowski (3, 12) provides a direct proportionality relation between k_{diff} and the diffusion coefficient D.

$$[3]\quad k_{diff} = 4\pi\sigma N_A D$$

where σ is the diameter of the encounter complex (about 10 Å), and N_A is Avogadro's number. Substitution in eq. [1*b*] yields

$$[4]\quad \frac{\tau^0}{\langle\tau_{eq}\rangle} = \frac{I^0}{I_{eq}} = 1 + (4\pi\sigma N_A\alpha\tau^0)(D\,S)p_Q$$

where the product (DS) equals the permeability (P) of the quencher. Thus following the above assumptions equilibrium state measurements allow for the determination of the permeability of oxygen in polymeric samples.

There are three types of uncertainties in this kind of analysis. The first is the questionable applicability of the kinetics of fluid media to rigid polymeric media with possible domains of microscopic inhomogeneities. Second is the magnitude of σ in eq. [3], and the last concerns the magnitude of α in eq. [2]. In principle these parameters should be determined independently, but in fact their values remain ambiguous. For example, while some authors (13, 14) have assumed α to be unity, Guillet and Andrews (8) argue that for phosphorescence quenching by O_2 (a ground state triplet), spin statistics imply that α is at most 1/9, and probably less because of electronic overlap considerations.

Jones (13) studied O_2 quenching of the phosphorescence lifetime of naphthalene solubilized in poly(methyl methacrylate) (PMMA) and fitted the data to eq. [4]. With the assumption that $\alpha = 1$, $\sigma = 10$ Å, the authors calculate for the oxygen permeability at room temperature, $P = (1.1 \pm 0.2) \times 10^{-17}$ $cm^2 \cdot s^{-1}$ $(mole/cm^3) \cdot (mm\ Hg)^{-1}$. This can be converted to the usual units[2] $P_{O_2} = 1.8 \times 10^{-15}$, which compares unfavourably with the two reported classical measurement (15, 16) values of 2.9×10^{-14}, and 1.2×10^{-14} (34°C), respectively. Only with the Guillet presumption of $\alpha = 1/9$ do we get an acceptable agreement with the classical measurements.

For oxygen in polystyrene we can compare data of steady-state fluorescence quenching from the studies of Nowakowska et al. (14). These workers measured I^0/I_{eq} as a function of oxygen pressure for the three different fluorescent probes, naphthalene, triphenylene, and perylene, solubilized in polystyrene. Here the excited states are singlet and their $\alpha = 1$, $\sigma =$ 11 Å assumption is more reasonable. From their data for the plot of eq. [3] we calculate[2] oxygen permeabilities in polystyrene of 3.8×10^{-13}, 3.7×10^{-13}, and 6.3×10^{-13}, respectively, for the three dyes. These values can be compared with the classically measured (15) value of 1.9×10^{-13}.

Transient measurements

Guillet (2, 3, 7, 8) and co-workers and MacCallum and Rudkin (17) extended this kind of analysis to transient measurements on thin polymer films. In these experiments, they measured the rate of decrease of luminescence intensity from the dye-doped film following exposure of the film to oxygen. The challenge in these experiments is to relate the decrease in emission intensity to the Fickian diffusion of oxygen into the film. In their analysis, these workers invoked two types of simplifying assumptions. First, they used the sample-width-averaged, time-dependent concentration of oxygen in the sample to relate $I(t)$ to the quencher concentration. Second, they employed asymptotic solutions to diffusion equations, which could be evaluated analytically. Thus to analyze their data, Guillet and Andrews used the long-time behavior ($t \to \infty$) of the Fick's law solution for the mean oxygen concentration (8), whereas MacCallum and Rudkin (17) used the corresponding short-time ($t \to 0$) behaviour (see Appendix A).

A novel advance in the area of transient measurements of

---

[2] The units for S are usually expressed as cm^3 (gas at STP)/cm^3 polymer/Pa of the external pressure. On this basis, permeability would have units of

$$P = \frac{(\text{quantity of permeant}) \cdot (\text{film thickness})}{(\text{film area}) \cdot (\text{time}) \cdot (\text{pressure drop across the film})}$$

$$= \frac{cm^3(\text{gas at STP})\ cm}{cm^2 \cdot s \cdot Pa} = DS$$

Can. J. Chem. Downloaded from www.nrcresearchpress.com by 46.23.64.124 on 09/08/12
For personal use only.

oxygen diffusion was made when Gao, Ogilby and co-workers (18, 19) developed a technique for directly monitoring the O_2 uptake. In this technique, as the external pressure of O_2 evolves, one irradiates (visible light) the polymer film containing a sensitizer dye. Simultaneously, one observes the near-infrared (1270 nm) phosphorescence of excited singlet molecular oxygen, which is generated when ground state O_2 (a triplet state) interacts with the excited dye. For sufficiently low concentrations of dissolved O_2, the intensity of the 1270 nm signal is linearly proportional to the total O_2 uptake of the sample, and can be related to the diffusivity via a Fick's law solution of the total uptake. This technique is promising and we believe that the data analysis can be extended to regimes of higher oxygen pressure by taking an approach very similar to the one being developed in this writing.

Our major contribution in this paper is to extend these works by providing an exact derivation of the expected behaviour of $I(t)$ for all time t, and employing numerical methods, both to simulate and to analyze real experimental data. While the older experiments dealt with only one experimental situation, a thin polymer film on a solid substrate exposed at $t = 0$ to oxygen, there are in fact four different types of experiments that one can carry out. These provide four different sets of boundary conditions for solutions to the diffusion equations and thus four independent ways of evaluating the connection between experiment and data analysis. For oxygen diffusion *into* a sample, one can examine both substrate-supported and free-standing films (in-diffusion from both sides). For oxygen diffusion out of a sample (I increases from I_{eq} to I^0), one also can compare free standing and substrate-supported films.

Although the present model deals with situations where the lumophore is imbedded in the polymer film, thereby limiting application to optically transparent films, luminescence methodology can also be applied to nontransparent films. Lu and Weiss (20) have recently shown that one can extend the experiments for cases in which it is difficult to observe fluorescence from the film itself. In a modification of the Lu–Weiss approach, the nontransparent film containing the quencher is immersed in a transparent liquid containing the fluorophore. As the quencher diffuses out of the film, it quenches fluorescence emanating from the solution.

Transient measurements of oxygen diffusion

Assumptions of the model

The most convenient shape of a polymeric sample for diffusion studies is that of a thin film that can be modeled by a rectangular sheet of *uniform* thickness L, and infinite extension (relative to L). The mathematical description of diffusion normal to the plane of the film is that of one-dimensional diffusion. We assume that the *immobile* luminescent dye is *uniformly* distributed throughout the film. The samples are illuminated continuously with excitation light of constant intensity. The experiments involve quenchers diffusing into (or out of) the sample, with a concurrent decrease (or increase) of the detected luminescence intensity, $I(t)$. For simplicity we consider cases where the quencher concentration (Q) changes between the values of zero and Q_{eq} (equilibrium solubility of the penetrant), corresponding to the measurable intensities I^0 and I_{eq}, respectively. The required change is brought about by an abrupt variation of the external concentration (or pressure) of the quencher between zero and some required external equilibrium value. During the time the sample evolves from one equilibrium state to another, the quencher concentration at various depths in the film changes with time with a concentration profile expressed by $Q(x, t)$ while, over this time, the external quencher concentration is kept constant (i.e., in contact with a large reservoir).

At any time t, the instantaneous elemental luminescence intensity ($\delta I(x, t)$) emanating from an infinitesimally thin layer of the sample, between x and $x + dx$, is given by a Stern–Volmer (SV) type relation

$$[5a] \quad \frac{\delta I^0}{\delta I(x, t)} = 1 + AQ(x, t); \qquad \delta I^0 = I^0 dx$$

$$[5b] \quad \delta I(x, t) = \frac{I^0 dx}{1 + AQ(x, t)}$$

where $Q(x, t)$ is the quencher concentration at position x and time t; I^0 is the observable total luminescence intensity of the sample in the absence of quenchers, and the proportionality constant A^{-1} can be identified as the equilibrated quencher concentration ($Q_{1/2}$) capable of reducing I^0 to $I^0/2$. The elemental intensities cannot be measured. What is measured is the sum total of the elemental intensities. It follows that when the emission intensity is compared between the two equilibrium states of the sample, one has

$$[6] \quad \frac{I^0}{I_{eq}} = 1 + AQ_{eq}$$

which can be used to substantiate the validity of eq. [6]. Equation [6] and [1] are functionally equivalent and we can identify the constant A as $k_q\tau^0$. Such equivalence is, however, not necessary because no mechanistic relation is being assumed.

There are a number of technical issues that need to be satisfied in this type of experiment. First, it is important that the optical density (OD) of the sample at the wavelength of excitation be small (OD < 0.1) and that the film be transparent. These conditions imply that the excitation light will penetrate into the film with nearly uniform intensity. Second, the lifetime (τ^0) of the excited lumophore (in the absence of quenchers) should be at least two orders of magnitude shorter than the time scale of quencher diffusion across the film thickness. That is,

$$[7] \quad \tau^0 < 10^{-2} (L^2/D)$$

An order of magnitude estimate of the value of L^2/D can be obtained from the time that is taken for the signal to reach halfway between I^0, and I_{eq} in an experiment where the quencher *diffuses out* of the film. Under these conditions, although the evolving system is not at a true steady state, at any point in the sample, the excited-state concentration can be evaluated through the application of (pseudo) steady-state approximations that lead to SV-type equations. This condition is easily satisfied for a variety of systems.

Finally, the film thickness L must be sufficiently small that

Can. J. Chem. Downloaded from www.nrcresearchpress.com by 46.23.64.124 on 09/08/12
For personal use only.

the optical detection system picks up elements of intensity from all points along the excitation path in the sample with an equal weight. In practice, most samples will have (and should have) $L < 1$ mm. Therefore, this requirement is satisfied by all commercial luminescence instrumentation systems having a light-collecting element more than 10 cm away from the sample. One way to check that this condition is satisfied is to see whether the observed $I(t)$ time profiles are identical when viewed from the front face and from the back side of the excitation area. This assumption may not be valid, for instance, if an optical fiber close to the sample is used to pick up the emission.

Development of the model

We assume that Fick's laws of diffusion apply, and that D is a constant throughout the sample. Thus

$$[8a] \quad \frac{\partial Q(x,t)}{\partial t} = D\frac{\partial^2 Q(x,t)}{\partial x^2}$$

For simplicity of notation, we define a dimensionless concentration profile and obtain

$$[8b] \quad \rho(x,t) \equiv Q(x,t)/Q_{eq}$$

$$[8c] \quad \frac{\partial \rho(x,t)}{\partial t} = D\frac{\partial^2 \rho(x,t)}{\partial x^2}$$

The boundary conditions for solving eq. [8] are described later. The observable intensity is related to the solution of eq. [8] by summing the elemental intensities defined in eq. [5*b*]. From the these requirements, it follows that

$$[9a] \quad I(t) = \frac{I^0}{L}\int_0^L \frac{dx}{1 + B\rho(x,t)}$$

$$[9b] \quad B \equiv AQ_{eq} = \left(\frac{I^0}{I_{eq}} - 1\right)$$

The analytical behaviour of $I(t)$ is not trivial and in fact we shall show surprising differences between diffuse-in and diffuse-out experiments. Note that the rate of intensity decay depends upon Q_{eq}, a feature not taken into account in previous analyses of this type of experiment. The direct measurement of the equilibrium penetrant solubility is, however, not necessary. The constant B in eq. [9*a*] is related to the measurable intensity ratio I^0/I_{eq} as indicated in eq. [9*b*], and serves as an input parameter for the data analysis procedure. One then has to evaluate numerically the integral in eq. [9*a*], employing $\rho(x, t)$ obtained as a solution to eq. [8*c*], to obtain the best value of D/L^2 as a fitting parameter.

We draw attention to the fact that B is a parameter expressing the sensitivity of the system to quenching (quenching efficiency) that is independent of the sample size. For the samples we have encountered, values of B range between 0.1 and several hundreds, depending on the type of polymer in use and also on the oxygen pressure applied. In practice, values of B lower than 0.5 are not desirable because the overall signal variation will approach the instrumental noise level, while very high values of B imply there may be little signal to measure when the system approaches saturation with the quencher. In theory, however, one has a good control over the value of B. On the basis of our earlier discussions we can identify B with $k_q\tau^0 Q_{eq}$, which is roughly proportional to the diffusion coefficient D. While the value of k_q is determined by the size of the diffusing quencher and the type of polymeric matrix involved, can be varied greatly by going from fluorescent to phosphorescent probes. Also, the value of quencher solubility Q_{eq} can be easily controlled by varying the external pressure (concentration) of the equilibrating quencher. Further discussion on the properties of $I(t)$ are given after we consider the various possible types of experimentation.

There are four distinct experiments that one can carry out to obtain independent measures of oxygen diffusion D_{O_2} in a polymer film, that correspond to four different boundary conditions for solving eq. [8]. One pair of experiments refers to a polymer film mounted on an impermeable substrate (e.g., quartz) so that oxygen diffusion can occur across only one film surface. For a free-standing film, the second pair of experiments involves oxygen diffusion across both surfaces. Within each sample geometry, one can follow the increase in $I(t)$ as oxygen diffuses into the film, or one can follow the increase in $I(t)$ as oxygen diffuses out of the film. In Figs. 1*a* and 1*b* we show the two sample geometries, where the penetrant in Fig. 1*a* has started to diffuse into a film previously devoid of Q from one side of exposure. Figure 1*b* depicts the case for two sides of exposure. The excitation light enters the film along the x axis. Regions of lower quencher concentration will yield higher emission intensities.

For evaluation of the diffusion equation, we set one face of exposure at $x = 0$. If the sample has two faces of exposure, these are located at $x = 0$, and $x = L$. The boundary conditions needed for the solution of $\rho(x, t)$ from eq. [8*c*] are determined by the direction of net quencher flow, and the number of exposed sample faces. The information needed is the initially uniform concentration in the sample, $\rho(x, 0)$, the concentration of quencher dissolved at the surface(s) of exposure, and the locus x^* of zero flux in the sample. That is,

$$[10] \quad D\left.\frac{\partial \rho(x,t)}{\partial x}\right]_{x=x^*} = 0$$

In analysis of diffusion problems, one commonly assumes that the infinitesimally thin layer at the exposed surface achieves its equilibrium concentration of sorbant Q_{eq} instantaneously. Therefore $\rho(x, t)$ at the exposed face is equal to unity as soon as the surface partial pressure of oxygen p_{O_2} has a finite non zero value, as for "diffuse-in" experiments, and $\rho(x, t)$ at the exposed face is equal to zero when $p_{O_2} = 0$, as for "diffuse-out" experiments. Table 1 summarizes the boundary conditions for the four possible modes of experimentation, along with the corresponding solutions to eq. [8*c*].

The solutions to $\rho(x, t)$ can be found by reference to texts (21) dealing with the mathematics of diffusion, and are given in Table 1 in terms of the family of terms in the expression [11]

$$[11] \quad F(x,t,L) = \frac{4}{\pi}\sum_{n=\text{odd}}^{\infty}\frac{1}{n}\exp\{-n^2\pi^2 Dt/L^2\}\sin(n\pi x/L)$$

Can. J. Chem. Downloaded from www.nrcresearchpress.com by 46.23.64.124 on 09/08/12
For personal use only.

Table 1. Boundary conditions and functional forms for the solutions of eq. [8], $\rho(x, t)$, for the two different pairs of experiments.

	Diffuse-out experiments		Diffuse-in experiments	
	$x = 0$ face	$x = 0, L$ faces	$x = 0, L$ faces	$x = 0$ face
$\rho(x, 0)$	1	1	0	0
ρ(exposure, t)	0	0	1	1
Zero flux, $x^* =$	L	$L/2$	$L/2$	L
$\rho(x, t)$	$F(x, t, 2L)$	Eq. (11), $F(x, t, L)$	$1 - F(x, t, L)$	$1 - F(x, t, 2L)$

Fig. 1. Schematic representation of quencher Q in in-diffusion experiments where the film sample is either supported on a substrate with only one face of exposure (*a*), or free standing and with two faces of exposure (*b*). Excitation light enters the sample along the x axis. The degree of shading represents the quencher concentration profile, while the degree of whiteness at various values of x represents the relative luminescence intensity emanating from those points.

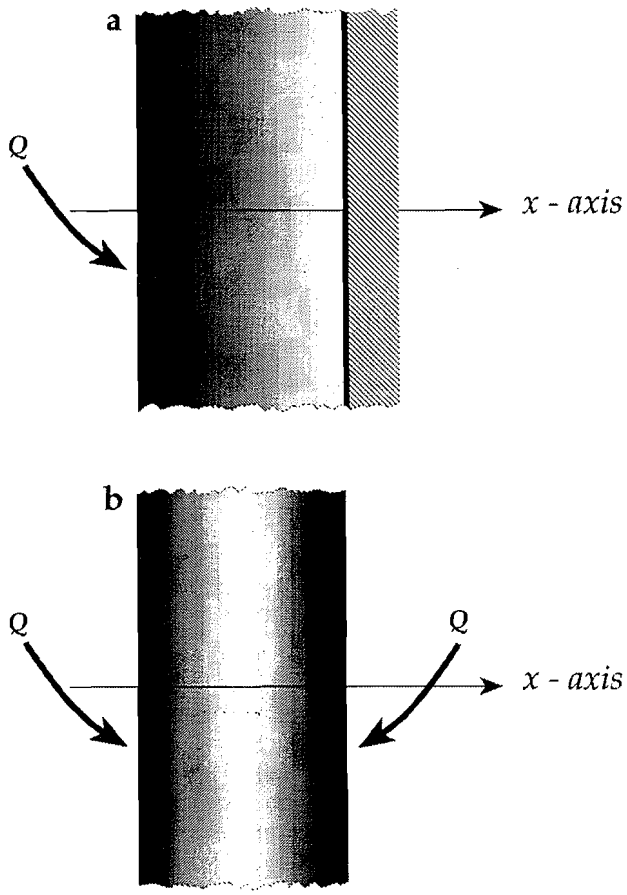

Concentration profiles calculated in this way for diffuse-out experiments are shown in Fig. 2 for various values of reduced time Dt/L^2. Two features of these profiles are noteworthy. First, for a given direction of net flow, a sample of thickness L with one side of exposure shows an evolution of the concentration profile that is identical to that of a sample of thickness $2L$ with two sides of exposure. That is, for the evolution of $Q(x, t)$, doubling the number of exposure sides is equivalent to halving the film thickness. It is important to recognize, however, that because of the way $Q(x, t)$ enters into eq. [9], this statement is *not* true for the evolution of the $I(t)$ time profiles.

Fig. 2. Calculated relative concentration profiles from films initially equilibrated with O_2, and then p_{O_2} is reduced to zero at $t = 0$: (*a*) one side of exposure, (*b*) two sides of exposure. Calculations employ $\rho(x, t)$ functions defined in Table 1. Adjacent to each profile is a number indicating the reduced diffusion time as the ratio Dt/L^2. Corresponding in-diffusion profiles can be calculated from the relation $\rho_{in}(x, t) = [1 - \rho_{out}(x, t)]$.

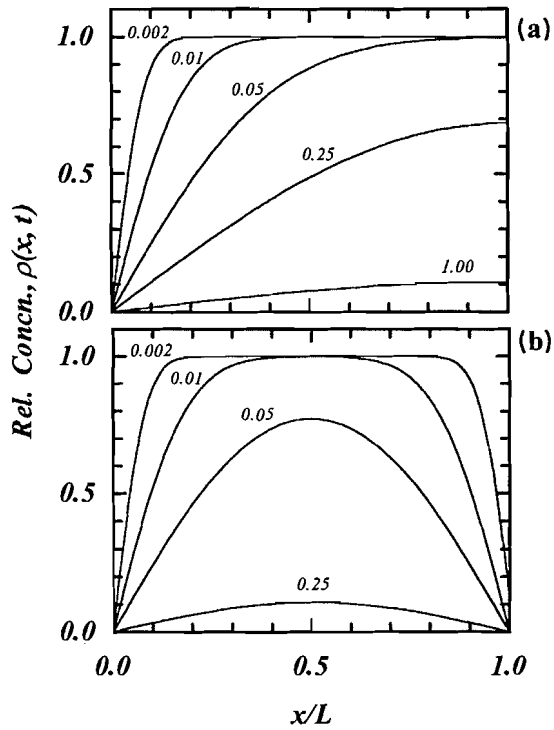

Second, as seen in Table 1, for a fixed sample thickness and exposure side, the concentration profiles of the in-flow and out-flow experiments are related by the simple expression that they add up to Q_{eq}. However, as we shall see, depending on the quenching efficiency (value of B in eq. [9*b*]), the time profiles $I(t)$ can be drastically different. This will have important implications in the design of experiments and analysis of the data.

Simulated luminescence data

In a typical experiment, a polymer film is mounted in the sample chamber of a fluorescence spectrometer in a cell that allows control of the surrounding atmosphere. One flushes the

Can. J. Chem. Downloaded from www.nrcresearchpress.com by 46.23.64.124 on 09/08/12
For personal use only.

Fig. 3. Simulated (eq. [9], Table 1) luminescence intensity vs. time transient profiles for a sample film of thickness L and quenching sensitivity $I^0/I_{eq} = 4$ ($B = 3$); (*a*) exposure on one side, (*b*) exposure on two sides. Rising transients correspond to out-diffusion experiments where the sample is initially equilibrated with some external partial pressure of O_2, p_{O_2}, and at time $t = 0$ the system is flushed with N_2. Decaying transients correspond to in-diffusion experiments where the sample is free of any dissolved oxygen, and at time $t = 0$ the system is flushed with an excess of gas of external partial pressure of O_2, p_{O_2}. Notice that the absolute magnitude of the initial slopes for the decaying transients are larger by about $(I^0/I_{eq})^2 \approx 16$ times, when compared to the rising transients.

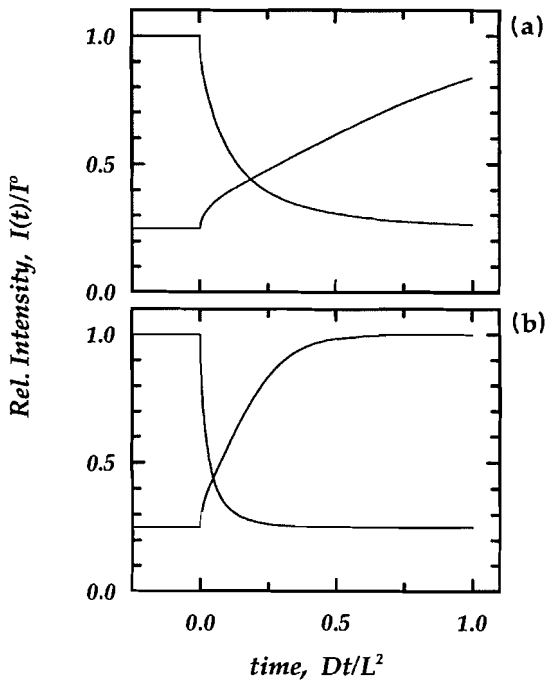

cell with a gas like nitrogen or argon until oxygen has been removed completely from the film, and the emission intensity holds steady at its most intense value. At this point, one has $Q = 0$, inside and outside of the sample, and $I = I^0$. At time zero, the sample is at once exposed to a *fixed* external partial pressure of oxygen. In the sample, $Q(x, t)$ increases to its final uniform equilibrium value, Q_{eq}, and concurrently the measured intensity drops to its final value I_{eq}. One now has one data set to be analyzed. The same sample is now ready for an out-diffusion experiment. That is, the external concentration (pressure) of oxygen is at once brought to zero (e.g., flushing with N_2). There is a net diffusion of quenchers out of the sample, until $Q = 0$ everywhere in the sample. The measured intensity increases concurrently from I_{eq} to I^0. Furthermore, the final intensity values are the same, whether one has one or two sides of the film exposed to the outside atmosphere, since Q_{eq} is the same in both experiments. All simulations satisfy the expression $I^0/I_{eq} = 1 + AQ_{eq}$, which is, of course, a consequence of our assumption of the SV quenching relation.

Examples of these experiments, employing simulated data according to eq. [9], are shown in Fig. 3*a* for a single exposure face, whereas Fig. 3*b* describes the system with two exposure faces. In this simulation the value of the intensity ratio I_{eq}/I^0 is arbitrarily chosen to be 0.25 ($B = 3$). Examples for other

Fig. 4. The same simulated out-diffusion experiment as in Fig. 3, but examined on a longer time scale.

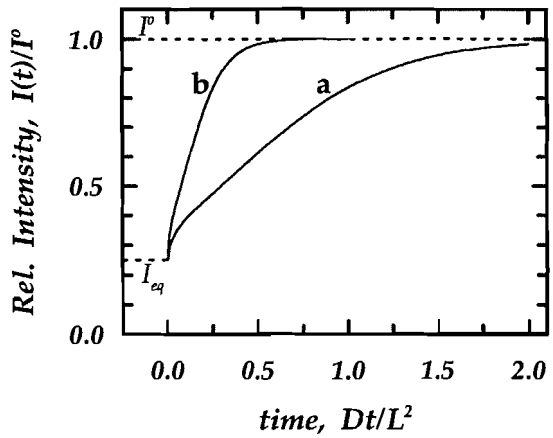

choices of B will be given when we compare theory with experimental data. Figure 4 shows the quencher out-diffusion simulations of Fig. 3 on a longer time scale. It is clear that equilibrium is approached more rapidly for two-face exposure than for diffusion across a single film surface. Significantly, in both examples we see that the time profiles for the in-diffusion experiment are very different than those for the out-diffusion experiment. They have different shapes, and they seem to require different amounts of time to come to equilibrium. Note that there is no difference in the diffusion coefficient of the penetrant into and out of the film. Rather, this result indicates that the oxygen concentration profile couples to the emission quenching process in very different ways in the two experiments.

Previous considerations of transient oxygen-quenching experiments treated the quencher concentration at time t as being uniformly distributed in the film. Such models fail to predict the difference between experiments in which the quencher diffuses into the film and those in which it diffuses out of the film. There are other differences as well between the exact analysis presented here and those involving asymptotic solutions to the diffusion equation. In Fig. 5 we compare the analysis of simulated data for two cases in which oxygen is allowed to diffuse into a luminescent polymer film. In the first case, at equilibrium, $I_{eq}/I^0 = 0.67$, whereas in the second case, $I_{eq}/I^0 = 0.25$. Analysis of the data according to the MacCallum expression (eq. [A3], Appendix) generates the two dotted lines, which lie significantly below the solid lines representing the exact solution to the quenching data. The shape of the Guillet expression (eq. [A4]) has no dependence on I_{eq}/I^0, and for both experiments yields the broken line in Fig. 5. The simplifying assumptions made in both of these analyses of the quenching-coupled-to-diffusion experiment, unfortunately, lead to significant errors.

Experimental data

In Fig. 6, we show plots of experimental data for oxygen diffusion into an uncured silicone epoxy resin film, 745 μm thick, containing 50 ppm platinum octaethylporphine as the luminescent dye. Two pairs of curves are displayed. One shows a rapid decrease in emission intensity after exposure of the deoxygenated film to air at 1.0 atm (101.3 kPa). The sec-

Can. J. Chem. Downloaded from www.nrcresearchpress.com by 46.23.64.124 on 09/08/12
For personal use only.

Fig. 5. Comparison of results obtained by fitting simulated data to eqs. [A3] and [A4] with those obtained using eq. [9]. Solid lines refer to the exact calculations (eq. [9]) of $I(t)/I^0$ for I_{eq}/I^0 equal to 0.67 and 0.25. Dotted traces refer to the same data analyzed according to the MacCallum formulation (eq. [A3]) The broken line refers to the data as analyzed with the Guillet formulation (eq. [A4]) where the transient decay shape has no dependence on the value of I_{eq}.

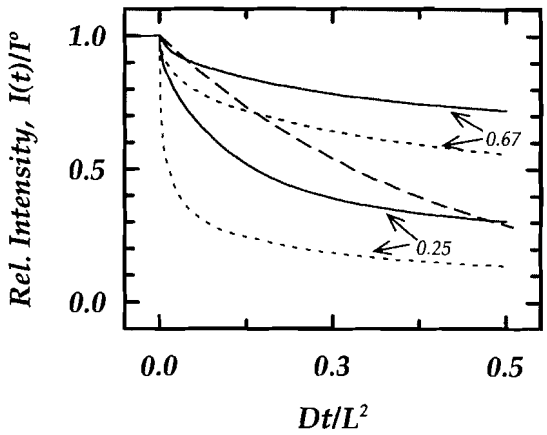

Fig. 6. Analysis of experimental data for a film (L = 745 μm) of Genesee silicone epoxy resin EXP-36-X20 containing 50 ppm of platinum octaethylporphine (λ_{ex} = 534 nm, λ_{em} = 646 nm). The solid lines represent experimental data. In the out-diffusion experiment, the sample, initially equilibrated with air, is at once flushed with N_2. Following the leveling off of the rising transient, I^0/I_{eq} = 9.15. In the in-diffusion experiment, the sample initially equilibrated with N_2 is at once flushed with air. Here I^0/I_{eq} = 9.76. Broken lines refer to theoretical fits of the data, using eq. [9] and Table 1, with $D = 1.0 \times 10^{-5}$ cm^2 s^{-1} (rising transient), and $D = 1.2 \times 10^{-5}$ cm^2 s^{-1} (decaying transient). The inset displays details of the transients on a shorter time scale.

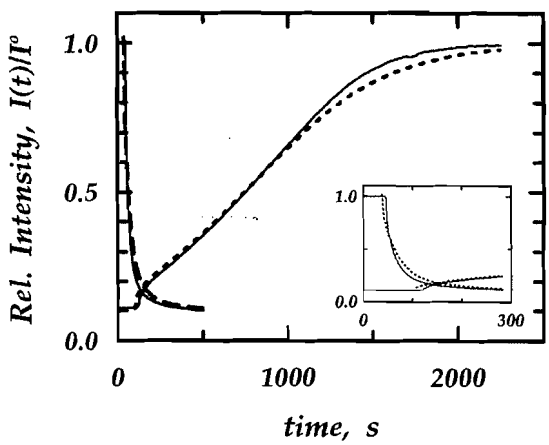

ond curve shows the much slower increase in the emission intensity following complete removal of oxygen from the external atmosphere. The dashed lines in Fig. 6 represent the best theoretical fits to the data employing eq. [9]. For the rising transient, we obtained a value of $D_{O_2} = 1.0 \times 10^{-5}$ cm^2 s^{-1}, whereas for the decaying transient, the best-fit value is $D_{O_2} = 1.2 \times 10^{-5}$ cm^2 s^{-1}. The insert shows the comparison between

Fig. 7. Analysis out-diffusion experimental data for two different films of Genesee silicone resin GP-197 containing 150 ppm of platinum octaethylporphine (λ_{ex} = 534 nm, λ_{em} = 646 nm). The solid lines represent experimental data. Curve (*a*) refers to a film of L = 80 μm supported on a glass substrate. Curve (*b*) refers to a free-standing film with two sides of exposure and L = 112 μm. Broken lines refer to theoretical fits obtained using eq. [9] and Table 1, for (*a*) with $D = 6.0 \times 10^{-7}$ cm^2 s^{-1} and I^0/I_{eq} = 4.20; and for (*b*) with $D = 5.4 \times 10^{-7}$ cm^2 s^{-1} and I^0/I_{eq} = 4.34.

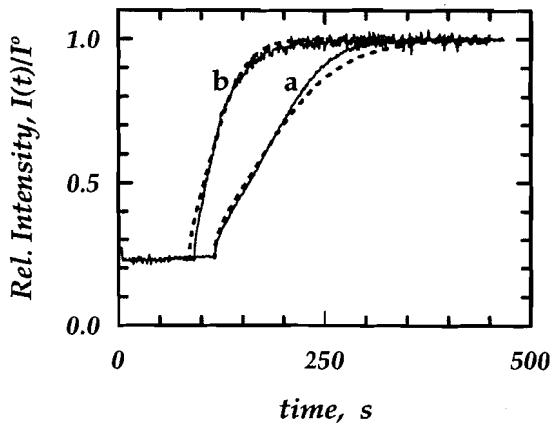

the experimental and best-fit (theoretical) data on an expanded time scale.

A second experiment is shown in Fig. 7 for a different silicone resin. Here we compare diffusion-out experiments for a substrate-supported film (a) of thickness L = 80 μm with (b) a free-standing film of thickness L = 112 μm. Fits to the data yield $D_{O_2} = 6.0 \times 10^{-7}$ cm^2 s^{-1} for the former case and $D_{O_2} = 5.4 \times 10^{-7}$ cm^2 s^{-1} for the latter. While there are small deviations between the experimental and fitted data, which may be related to non-uniformity of film thickness, the fit is on the whole very good and, most important, it accommodates and confirms the most surprising feature of the model, namely, that the rate of intensity decay for diffusion of oxygen into the sample is more rapid than the rate of intensity growth for oxygen diffusion out of the film.

Conclusion

Luminescence quenching experiments employing a fluorescence spectrometer operated in the time base mode with steady illumination of a sample can provide precise values (±10–15%) of the diffusion constant for oxygen into and out of thin polymer films, provided that the data are analyzed by taking into account the time evolution of the concentration profile of oxygen as a quencher in the system. The model predicts, and experiments show, that the rate of intensity decrease is much faster for oxygen diffusing into the film than the rate of intensity increase for oxygen diffusion out of the film.

Acknowledgments

The authors thank the De Havilland Co., the Ontario Centre for Materials Research, the Natural Sciences and Engineering Research Council of Canada, and the Province of Ontario of their support of this work.

Can. J. Chem. Downloaded from www.nrcresearchpress.com by 46.23.64.124 on 09/08/12
For personal use only.

References

1. W.-Y. Wen. Chem. Soc. Rev. **22**, 117 (1993).
2. J. E. Guillet. *In* Photophysical and photochemical tools in polymer science. *Edited by* M. A. Winnik. Kluwer, Dordrecht. 1986. pp. 467–494.
3. J. E. Guillet. Polymer photophysics and photochemistry. Cambridge University Press, New York. 1987. pp. 52–70.
4. E. I. Hormats and I. C. Unterleitner. J. Phys. Chem. **69**, 3677 (1965).
5. G. Shaw. Trans. Faraday Soc. **63**, 2181 (1967).
6. M. E. Cox and B. Dunn. J. Polym. Sci. Part A: Polym. Chem. **24**, 621 (1986).
7. A. C. Somersall, E. Dan, and J. E. Guillet. Macromolecules, **7**, 233 (1974).
8. J. E. Guillet and M. Andrews. Macromolecules, **25**, 2752 (1992).
9. K. Horie. *In* Photophysics of polymers. *Edited by* J. M. Torkelson. ACS Symp. Ser. 358, ACS, Washington, D. C. 1987.
10. L. A. Sacksteder, J. N. Demas, and B. A. DeGraff. Anal. Chem. **65**, 3480 (1993).
11. H. N. McMurray and P. Douglas. Presented at the XVIth International Conference on Photochemistry. Vancouver, Canada. August 1–6, 1993.
12. M. Smoluchowski. J. Phys. Chem. **92**, 129 (1917).
13. P. F. Jones. J. Polym. Sci. Part B: Polym. Lett. **6**, 487 (1968).
14. P. F. Nowakowska, J. Najbar, and B. Waligora. Eur. Polym. J. **12**, 387 (1976).
15. J. Brandrup and E. H. Immergut (*Editors*). Polymer handbook. 3rd ed. John Wiley, New York. 1989.
16. K. Higashide, K. Omata, Y. Nozawa, and H. Yoshioka. J. Polym. Sci. Chem. Ed. **15**, 2019 (1977).
17. J. R. MacCallum and A. L. Rudkin. Eur. Polym. J. **14**, 655 (1978).
18. Y. Gao and P. R. Ogilby. Macromolecules, **25**, 4962 (1992).
19. Y. Gao, A. M Baca, B. Wang, and P. R. Ogilby. Macromolecules, **27**, 7041 (1994).
20. L. Lu and R. G. Weiss. Macromolecules, **27**, 219 (1994).
21. J. Crank and G. S. Park. Diffusion in polymers. Academic Press, London. 1968.

Appendix A

Previous analyses of the transient in-diffusion of oxygen experiment invoke the assumption that at every instant of time the observed luminescence intensity $I(t)$ is related to the mean concentration of quencher $\langle Q_q(t)\rangle$ through a SV-type of relation. Therefore, for quencher in-diffusion through one face of exposure, one would have

$$[A1] \quad \frac{I^0}{I(t)} = 1 + A\langle Q(t)\rangle$$

where A is some proportionality constant. The mean concentration of quencher $\langle Q_q(t)\rangle$ is found from a Fick's law solution of the system for the quencher concentration profiles $Q(x, t)$ and is given by

$$[A2] \quad \langle Q_q(t)\rangle = \frac{1}{L}\int_0^L Q(x,t)\,dx = Q_{eq}\left[1 - \frac{8}{\pi^2}\sum_{n=\text{odd}}^{\infty}\frac{1}{n^2}\exp\{-n^2\pi^2 Dt/4L^2\}\right]$$

For very short times $\langle Q_q(t)\rangle$ approximates as $4(Dt/\pi L^2)^{1/2}$, while for longer times only the first exponential term of eq. [A2] is needed. Such considerations lead to the suggestions

$$[A3] \quad I(t)_{t\to 0} = \frac{I^0}{1 + \frac{4B}{\pi^{1/2}}(Dt/L^2)^{1/2}}$$

$$[A4] \quad I(t)_{t\to 0} \sim \exp(-Dt/4L^2)$$

where the constant B is defined by eq. [9*b*].

Pyrene-labeled amphiphilic poly-(*N*-isopropylacrylamides) prepared by using a lipophilic radical initiator: synthesis, solution properties in water, and interactions with liposomes

Françoise M. Winnik, Alexander Adronov, and Hiromi Kitano

Can. J. Chem. Downloaded from www.nrcresearchpress.com by 46.23.64.124 on 09/08/12
For personal use only.

Abstract: Fluorescently labeled amphiphilic poly-(*N*-isopropylacrylamides) (PNIPAM) substituted with a *N*-[4-(1-pyrenyl)butyl]-*N*-*n*-octadecyl group at the chain end were prepared by free-radical polymerization in dioxane of *N*-isopropylacrylamide (NIPAM) using 4,4′-azobis{4-cyano-*N*,*N*-[4-(1-pyrenyl)butyl]-*n*-octadecyl}pentanamide as the initiator. The solution properties of the polymers in water were studied as a function of polymer concentration and temperature. Quasi-elastic light-scattering measurements and fluorescence experiments monitoring the pyrene excimer and pyrene monomer emissions revealed the presence of multimolecular polymeric micelles below the lower critical solution temperature (LCST) of PNIPAM. These underwent partial, reversible reorganization as they were heated above the LCST. The interactions of the pyrene-labeled amphiphilic PNIPAM with dimyristoylphosphatidylcholine (DMPC) liposomes have been examined in water at 25°C. From fluorescence experiments it was established that the polymeric micelles are disrupted irreversibly upon contact with the liposomes. The anchoring of the polymer chains occurs by insertion of their hydrophobic tail within the phospholipidic bilayer, as evidenced from a large decrease of the pyrene excimer emission relative to pyrene monomer emission. The copolymers remained anchored within the bilayer as the temperature of the copolymer–liposome suspension was raised above the LCST of PNIPAM.

Key words: liposome, poly-(*N*-isopropylacrylamide), fluorescence, micelles.

Résumé : On a préparé des poly-(*N*-isopropylacrylamides) (PNIPAM) amphiphiles, substitués par un groupe *N*-[4-(1-pyrényl)butyl]-*N*-*n*-octadécyle au bout de la chaîne et marqués pour la fluorescence, en effectuant une polymérisation radicalaire, dans le dioxane, du *N*-isopropylacrylamide (NIPAM) à l'aide du 4,4′-azobis{4-cyano-*N*,*N*-[4-(1-pyrényl)butyl]-*n*-octadécyl}pentanamide comme initiateur. On a étudié les propriétés des polymères en solution en fonction de la concentration du polymère et de la température. Des mesures de diffusion quasi-élastique de la lumière et de fluorescence impliquant l'examen de l'évolution des émissions de l'excimère du pyrène et du pyrène monomère ont permis de mettre en évidence la présence de micelles polymériques multimoléculaires à des températures inférieures à la température critique la plus basse de la solution (LCST) de PNIPAM. Lorsqu'on les chauffe au-dessus de la LCST, ces micelles subissent des réorganisations partielles et réversibles. Opérant dans l'eau, à 25°C, on a étudié les interactions du PNIPAM amphiphile marqué au pyrène avec les liposomes dimyristoylphosphatidylcholine (DMPC). Sur la base des expériences de fluorescence, on a établi que les micelles polymériques sont détruites au contact des liposomes. L'ancrage des chaînes de polymère se produit par une insertion de leur queue hydrophobe dans la bicouche phospholipidique, cette conclusion est basée sur une diminution importante de l'émission de l'excimère du pyrène par rapport à l'émission du monomère du pyrène. Les copolymères restent ancrés dans la bicouche même lorsqu'on augmente la température de la suspension copolymère–liposome au-dessus de la LCST du PNIPAM.

Mots clés : liposome, poly-(*N*-isopropylacrylamide), fluorescence, micelles.

[Traduit par la rédaction]

Received April 27, 1995.

This paper is dedicated to Professor J.E. (Jim) Guillet in recognition of his contributions to Canadian chemistry.

F.M. Winnik[1] **and A. Adronov.** Department of Chemistry, McMaster University, 1280 Main St W., Hamilton, ON L8S 4M1, Canada.
H. Kitano. Department of Chemical and Biochemical Engineering, Toyoma University, Toyoma, 390 Japan.

[1] Author to whom correspondence may be addressed. Telephone: (905) 525-9140, ext. 23497. Fax: (905) 522-2509.

Can. J. Chem. Downloaded from www.nrcresearchpress.com by 46.23.64.124 on 09/08/12
For personal use only.

Introduction

A drug may appear extremely promising on the basis of testing protocols carried out in vitro; however, its effectiveness in vivo is often stifled by the complex nature of living organisms. The main problems involved in the effective administration of highly potent drugs can be summarized in two points: drugs are rapidly cleared from the blood system, hence they do not have a sufficiently long residence time to act on target tissues, and many drugs are toxic not only to malignant cells but also to healthy cells in the body. Such unfavorable circumstances may be alleviated significantly through the use of drug delivery systems. These are composite materials in which a drug is integrated within another phase that, ideally, carries the drug to a specific, targeted site within the body and also controls the rate of drug release. Liposomes, which consist of a spherical bilayer membrane capturing a pool of water in their center, have attracted considerable interest as delivery systems. The practical value of liposomes derives from two unique properties: (*i*) their ability to entrap either water-soluble materials in the internal water reservoir or liposoluble compounds in their lipid bilayer; and (*ii*) their compatibility with natural membranes, making them safe for medical applications.

Even with the advantages of facile production, biocompatibility, and capacity to encapsulate a wide variety of molecules, early liposome-based drug delivery systems performed rather poorly. The problems were traced primarily to the rapid uptake of the liposomes in the reticulo-endothelial system (RES). Liposomes in the blood stream are quickly labeled by opsonins present in blood plasma. These proteins are part of the defense mechanism signalling to phagocytes the presence in the blood of foreign substances (1). Adsorption of opsonins on the surface of liposomes triggers their removal from the blood and a subsequent increase of their concentration in the RES. It was quickly recognized that surface modification of the liposomes that would mimic the surfaces of cells would prevent the immune system from attacking liposomes, hence increasing their residence time in blood. Allen and Chong discovered that surface sialic acid, in the form of gangliosides, serves as an effective surface modifier, inducing significant prolongation of the liposome circulation half-life (2). Sterically stabilized liposomes (S-liposomes) are now produced industrially under the trade name "Stealth Liposomes" and are employed in drug delivery systems targeted at tumor cells. In this case the stabilization of the liposomes is achieved by incorporation of polyethylene glycol derivatives within the outer liposome surface. The current understanding of the reason behind the increased half-life of S-liposomes is the inhibition of opsonization by plasma proteins due to the presence of polyethylene glycol chains anchored on the outer liposome surface.

While polyethylene glycol coated liposomes have been especially successful in improving the performance of liposome-based drug delivery systems (3, 4), other polymer coatings have been investigated and have met with some level of success. Sunamoto et al. pioneered the use of polysaccharide derivatives, such as amylopectin and mannan (5). They showed that coating the outer surface of liposomes with polysaccharides produced vesicles that are much more stable, not only under laboratory conditions, but also in vivo (6). A range of biocompatible synthetic polymers, either neutral or charged, have also been studied with regard to their role in imparting structural stability to liposomes (7). Several recent studies have demonstrated that the polymer coatings may not only play a passive protective role, but may in fact participate in the drug release process by responding to some external stimulus (8). We (9–11) and others (12, 13) have explored the use of hydrophobically modified poly-(*N*-isopropylacrylamides) (HM-PNIPAM) as liposome stabilizers. The polymers employed consist of a neutral hydrophilic chain made up of *N*-isopropylacrylamide units to which were attached at random a few octadecyl chains (9, 12) or phosphatidylethanolamine moieties (13). The alkyl substituents are known to interact strongly with lipid bilayers (14) and thus can serve as anchors for the polymer onto the liposomes. PNIPAM is very soluble in cold water, but its solution undergoes phase separation as it is warmed up past a critical temperature (32°C), the lower critical solution temperature or LCST (15, 16). Detailed investigations of this phase transition have established that at the LCST the PNIPAM chains undergo a collapse from hydrated extended coils to hydrophobic globules, which aggregate and form a separate phase (17). This temperature sensitivity of the polymer chain was used to simulate the dynamics of cell membranes, by anchoring the polymer onto liposomes and subjecting the systems to repeated heating-cooling cycles in temperature domains including the polymer LCST (9–11).

We observed recently that certain PNIPAM grafted surfaces resist protein adsorption in physiological environment (18), via a mechanism akin to that put forward to account for the protective effect of polyethylene glycol chains. Thus we set about to investigate the preparation of PNIPAM-stabilized liposomes and to test their effectiveness in drug delivery systems capable of preventing the adsorption of opsonins. We chose to employ HM-PNIPAM in which the octadecyl chains are incorporated as end groups, rather than as grafts randomly distributed along the polymer chain. This strategy should permit a finer control over the PNIPAM chain density on the liposome outer surface. The interactions between liposomes and the HM-PNIPAM were established by monitoring the photophysical properties of fluorescently labeled polymers in which a pyrenyl group was incorporated as part of the hydrophobic end moiety. The polymers were obtained by free-radical polymerization of *N*-isopropylacrylamide using a pyrenyl-substituted lipophilic initiator. The synthesis, characterization, and solution properties of the polymers are presented here. Special emphasis will be given to results obtained from fluorescence techniques. Evidence is given for the formation of polymeric micelles in aqueous solutions below and above the lower critical temperature. We then report a series of spectroscopic measurements aimed at assessing the interactions of dimyristoylphosphatidylcholine (DMPC) liposomes and the pyrene end-labeled polymers. The effect of polymer concentration, relative to liposome concentration, and the influence of changes in solution temperature are examined in detail.

Experimental

Materials and instrumentation

Water was deionized with a Barnstead NANOpure water purification system. Reagent grade solvents were used in all

Fig. 1. Synthetic scheme for the preparation of the polymerization initiator Py-ODA (**3**); (a): $CHCl_3$–THF.

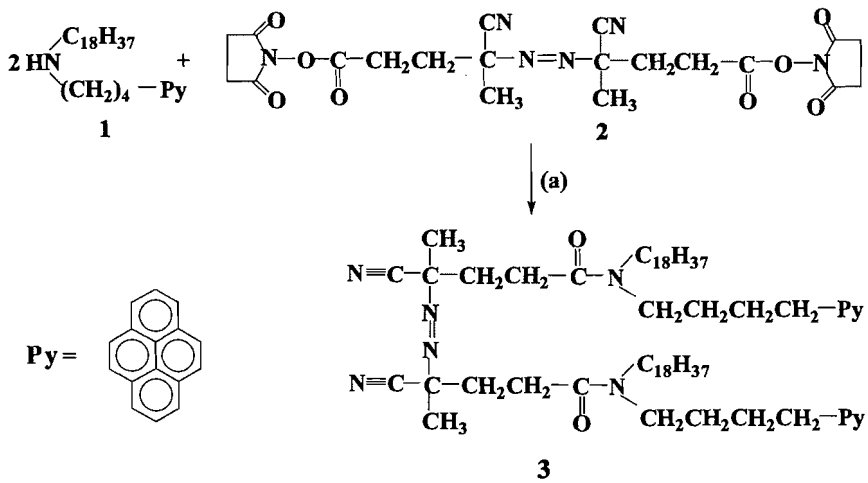

Can. J. Chem. Downloaded from www.nrcresearchpress.com by 46.23.64.124 on 09/08/12
For personal use only.

syntheses. Dioxane was purified by distillation from sodium under nitrogen. *N*-isopropylacrylamide (NIPAM, Eastman Kodak Chemicals) was purified by recrystallization from toluene/hexane 10/1 v/v. Dimyristoylphosphatidylcholine (DMPC, 99%, synthetic grade) was purchased from Sigma Chemicals. 4-(1-Pyrene)butyric acid was obtained from Aldrich Chemical Co. Stearylamine and carbonyldiimidazole were obtained from Wako Chemicals. Disuccinimidyl 4,4′-azobis(cyanovaleric acid) (**2**, Fig. 1) was prepared as described previously (19). Proton NMR spectra were recorded for $CDCl_3$ solutions of the polymers at ambient temperature on a Bruker 200 MHz spectrometer. Gel permeation chromatography (GPC) was performed with a Waters 590 programmable HPLC system equipped with a Waters 410 differential refractometer and three Ultrastyragel polystyrene columns (eluent: THF, flow rate: 1.0 mL min^{-1}). The weight and number average molecular weights were determined from a calibration curve established with polystyrene standards. Thin-layer chromatography (TLC) was performed with silica gel coated glass plates obtained from Whatman. UV spectra were measured using a Hewlett Packard 8452A photodiode array spectrometer equipped with a Hewlett Packard 89090A temperature controller and operated under the HP ChemStation Windows-based software. Steady-state fluorescence spectra were recorded on a SPEX Fluorolog 212 spectrometer operated by the DM3000F data system. Temperature control of the samples was achieved using a water-jacketed cell holder connected to a Neslab circulating bath. The temperature of the sample fluid was measured with a thermocouple immersed in a water-filled cuvette placed in one of the four cell holders. Liposome and polymeric micelle sizes were determined by quasi-elastic light-scattering (QELS) measurements at a fixed 90° scattering angle with a NICOMP 370 Submicron Particle Sizer or a Brookhaven Instrument Corp. model BI-9000AT correlator equipped with a Lexel (25 mW) argon ion laser operating at 514.5 nm. Data analysis was performed with the software provided by the manufacturers. Liposomes were obtained by extrusion using a LiposoFast Large system (Avestin Inc. Ottawa, Canada) connected to a nitrogen cylinder.

Syntheses

N-*[4-(1-Pyrenyl)butyl]*-N-n-*octadecylamine* ***1***

4-(1-Pyrenyl)butyric acid (4.31 g, 15 mmol), stearylamine (4.58 g, 17 mmol), and carbonyldiimidazole (2.98 g, 18.4 mmol) were dissolved in an anhydrous mixture of THF/DMF (1:1 v:v, 20 mL) at room temperature. The mixture was stirred overnight. The solvent was evaporated, yielding an oily residue. This was triturated vigorously with MeOH. A brown-colored paste was obtained (6.02 g, 11.1 mmol). A solution of this paste in dry THF (100 mL) was poured in a three-necked flask equipped with a condenser. $LiAlH_4$ (6.32 g, 166 mmol) was added slowly. The reaction mixture was stirred at 50°C overnight. After dropwise addition of water (10 mL) the precipitate was treated with THF and diethyl ether to extract the desired product. Evaporation of the combined extracts yielded *N*-[4-(1-pyrenyl)butyl]-*N*-*n*-octadecylamine (14.34 g, 74.8%) as a light-brown solid.

*4,4′-Azobis{4-cyano-*N,N-*[4-(1-pyrenyl)butyl]*-n-*octadecyl]-pentanamide (PyODA)* ***3*** *(Fig. 1)*

A solution of disuccinimidyl 4,4′-bis(4-cyanovalerate) (**2**, 1.59 g, 3.35 mmol) in THF (20 mL) was added to a solution of *N*-[4-(1-pyrenyl)butyl]-*N*-*n*-octadecylamine (**1**, 3.52 g, 6.7 mmol) in chloroform (40 mL). The mixture was stirred at room temperature overnight. The solvent was evaporated in vacuo at room temperature, yielding an oily material. The residue was dissolved in chloroform (50 mL). It was washed twice with a 5% sodium bicarbonate solution (50 mL) and twice with water (50 mL). The organic phase was dried with anhydrous Na_2SO_4, filtered, and evaporated. The product was purified by chromatography on silica gel eluted with ethanol. A final precipitation from acetonitrile yielded the initiator PyODA **3** (530 mg, 0.41 mmol, 12.2% yield relative to disuccinimidyl 4,4′-bis(4-cyanovalerate)); IR: 3041 (C-H aromatic), 2926, 2854 (ν_{as} and ν_s CH_2), 2239 (-CN stretching), 1627 (C=O stretching, tertiary amide), 1605, 1491 (aromatic), 1460 ($\delta_s$aliphatic CH_2) cm^{-1}.

b-*PNIPAM-(C_{18}Py)/530 (Fig. 2)*

NIPAM (4.42 mmol, 0.5 g) and PyODA (0.03 mmol, 40 mg)

Fig. 2. Chemical structures of the polymers described in this study.

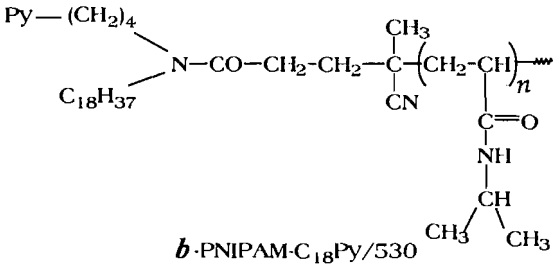

b-PNIPAM-C_{18}Py/530

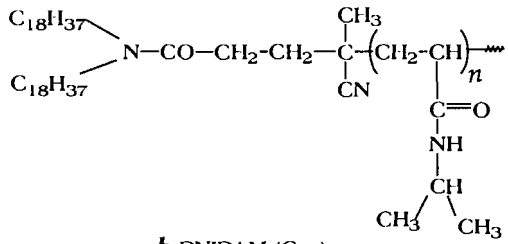

b-PNIPAM-$(C_{18})_2$

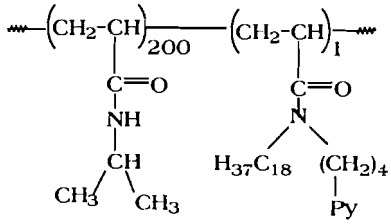

b-PNIPAM-C_{18}Py/200

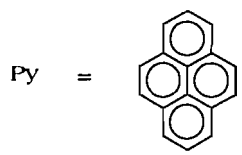

were dissolved in dioxane (5 mL). The solution was degassed by bubbling N_2 for 10 min. It was heated to 70°C for 17 h. The polymer was recovered by precipitation in hexane (50 mL). It was dissolved in THF (1 mL) and reprecipitated into diethyl ether (200 mL). The polymer was separated by filtration and dried in vacuo at 40°C for 24 h (320 mg).

b-*PNIPAM-(C_{18}Py)/910 (Fig. 2)*

This polymer was prepared by the same procedure, starting with NIPAM (0.026 mol, 3.0 g) and PyODA (0.13 mmol, 170 mg) and yielding 2.72 g of purified polymer.

Cloud point measurements

Cloud points were determined by spectrophotometric detection of the changes in turbidity (λ = 390 nm) of aqueous polymer solutions (0.26 g L^{-1}) heated at a constant rate (0.2°C min^{-1}) in a magnetically stirred UV cell. The value reported is the temperature at which turbidity of the solution appears upon heating.

Fluorescence measurements

Slit widths were set at 1 nm for both excitation and emission monochromators. For the emission spectra the excitation wavelength was set at 346 nm and the emission range was 370–600 nm. Excitation scans were measured between 280 and 360 nm with emission being monitored at 378 and 472 nm. Excitation spectra were measured in the ratio mode, while emission spectra were not corrected. The excimer-to-monomer emission intensity (I_E/I_M) ratios were calculated by taking the ratio of the emission intensity at 472 nm to the half-sum of the emission intensities at 398 and 378 nm after subtraction of the excimer contribution. For the studies at different temperatures, measurements were repeated until no change in consecutive spectra was observed, to ensure that an equilibrium had been reached. Time-based fluorescence scans were performed with excitation at 346 nm and emission at 378 nm to monitor the increase in monomer emission over a period of 3–5 h.

Solutions for spectroscopic analysis

Polymer solutions in water were prepared at room temperature from an aqueous concentrated stock solution of polymer. The stock solution (6.0 g L^{-1}) was diluted in water to the desired concentration (usually 0.26 g L^{-1}). In the preparation of polymer–liposome mixtures, the stock polymer solution was added to a freshly prepared liposome suspension to gain the desired polymer concentration (0.26 g L^{-1}). The liposome concentration was only slightly lowered, since a very small volume of the concentrated polymer stock was required to reach the proper concentration, e.g., the phospholipid concentration changed from 1.0 to 0.96 g L^{-1}. Polymer–liposome mixtures were allowed to equilibrate for 3–4 h prior to measurements, unless otherwise specified. Solutions in methanol were degassed by vigorous bubbling with solvent-saturated argon for 1 min prior to fluorescence analysis. Aqueous solutions were not degassed.

Liposome preparation

DMPC (approximately 10 mg) was weighed out in a vial and dissolved in a minimal amount of chloroform. The chloroform was evaporated, with a stream of nitrogen, in such a way as to form a thin film of phospholipid on the walls of the vial. The vial was evaporated further under vacuum (water aspirator) for 2 h at room temperature. Deionized water was added to the vial, causing the phospholipid film to disperse in the water. This suspension was subjected to 10 consecutive freeze–thaw cycles. The resulting suspension was passed 15 times through a polycarbonate membrane, 0.1 μm pore size, housed in a Liposofast Large apparatus. Nitrogen (20–60 psi; 1 psi = 6.9 kPa) was used to force the suspension through the membrane. The diameters of the liposomes obtained ranged from 140 to 160 nm. All liposome suspensions were stored under refrigeration and used within a day after preparation.

Results and discussion

Synthesis and characterization of the copolymers

The polymerizations were accomplished in dioxane solutions, starting with two different molar ratios of *N*-isopropylacryl-

Can. J. Chem. Downloaded from www.nrcresearchpress.com by 46.23.64.124 on 09/08/12
For personal use only.

Table 1. Physical properties of the polymers.

Polymer	NIPAM:C_{18}:Py	DP[a]	M_n[b]	M_w[b]	M_w/M_n[b]	Ref.
b-PNIPAM-C_{18}Py/530	530:1:1	530	22 600	62 300	2.76	This work
b-PNIPAM-C_{18}Py/910	910:1:1	910	29 000	67 700	2.29	This work
b-PNIPAM-$(C_{18})_2$/280	280:1:0	280	25 000	78 000	3.14	22
b-PNIPAM-$(C_{18})_2$/540	540:1:0	540	20 000	74 000	3.33	22
PNIPAM-C_{18}Py/200	200:1:1	200	23 000	38 000	1.66	20

[a]Determined by UV (see text).
[b]Obtained by GPC (relative to polystyrene standards).

Table 2. Properties of the polymers in water.

Polymer	LCST, °C	*d*,[a] nm	Polydispersity[b]	I_E/I_M 25°C	I_E/I_M 40°C	Ref.
b-PNIPAM-C_{18}Py/530	32.2	41 ± 1	0.16 ± 0.01	2.20	0.80	This work
b-PNIPAM-C_{18}Py/910	32.1	45 ± 2	0.17 ± 0.01			This work
b-PNIPAM-$(C_{18})_2$/280	31.5	73 ± 6	0.16 ± 0.01	—	—	22
b-PNIPAM-$(C_{18})_2$/540	32	72 ± 5	0.12 ± 0.02	—	—	22
PNIPAM-C_{18}Py/200	30.6	38 ± 1	0.23 ± 0.01	1.20	0.45	20

[a]Effective diameter, measured at 25°C.
[b]Polydispersity = μ_2/Γ, where Γ and μ_2 are the first two moments of the measured distribution.

amide and initiator, PyODA, leading to two polymer samples with slightly different physical properties (Table 1). Several precipitations with THF (solvent) – diethyl ether (non-solvent) were performed to purify the polymers. The absence of low molecular weight fluorescent impurities was ascertained by TLC analysis using 254 and 340 nm illumination to detect the pyrene chromophore. Of particular importance to the experiments described here is the absence of low molecular weight pyrene derivatives, since they may affect the spectroscopic measurements aimed at characterizing the polymer properties. Polymers with reasonably high molecular weights and broad molecular weight distributions were obtained in all cases. The average numbers of monomer units per pyrene end group were determined by UV analysis of polymer solutions in methanol, using *N*-[4-(1-pyrenyl)butyl]-*N*-*n*-octadecylacrylamide (ε_{341} (MeOH) = 34 900) (20), as model compound. Numbers of NIPAM units per pyrenyl group of 530 and 910 were calculated for polymers prepared with initial monomer/initiator ratios of 147 and 200, respectively. Consistent with our previous nomenclature we designate these polymers as *b*-PNIPAM-C_{18}Py/530 and *b*-PNIPAM-C_{18}Py/910 (Fig. 2). The number of monomer units per polymer end group was confirmed by an analysis of the ^{1}H NMR spectroscopy. The ratio of isopropyl to C_{18} groups was calculated from the area of the singlet at 3.97 ppm, due to the resonance of the isopropylidene proton of the monomer unit and the area of the triplet centered at 0.85 ppm, attributed to the resonance of the terminal methyl protons of the octadecyl chain. The number of monomer units per polymer end group calculated from either NMR or UV data should correspond to the degree of polymerization of the polymers, assuming that termination occurred by disproportionation and chain transfer (21). From the data presented it is not possible to assert that some polymers do not carry pyrenyl groups at both chain ends. The assumption that substitution occurred at only one end of each macromolecule is based on mechanistic considerations and on supportive evidence from an earlier investigation of NIPAM polymerization initiated with the dioctadecyl analogue of PyODA (22).

Properties of the copolymers in water. Evidence for micelle formation

The polymers were soluble in water at or below room temperature. Optically clear aqueous solutions of polymer concentrations as high as 6.0 g L^{-1} were prepared with no difficulty. As expected, the aqueous solutions became turbid when heated, signaling the occurrence of a lower critical solution temperature (LCST). This temperature (32.2 °C) is identical to that of PNIPAM (15) (Table 2). This may seem surprising, since as a rule the LCST of a polymer in water decreases with increasing hydrophobicity (23). This trend was observed in a previous study of the block copolymers *b*-PNIPAM-$(C_{18})_2$/280 and *b*-PNIPAM-$(C_{18})_2$/540 (20) (Table 2). It suggests that the hydrophobic substituents are not exposed to water, but rather form a micellar structure protected from water by the PNIPAM chains and therefore do not make a hydrophobic contribution to the LCST.

The formation of such micellar structures in aqueous solutions of *b*-PNIPAM-C_{18}Py/530 was confirmed by quasi-elastic light-scattering measurements (QELS). The experiments were carried out at a fixed angle (90°) with solutions (0.3 g L^{-1}) of the copolymers kept at 25°C. Strong signals were detected, indicating the presence of polymeric micelles, in contrast to the case of homopolymer (PNIPAM) solutions, which gave no detectable response. The sizes of the polymeric

Can. J. Chem. Downloaded from www.nrcresearchpress.com by 46.23.64.124 on 09/08/12
For personal use only.

Can. J. Chem. Downloaded from www.nrcresearchpress.com by 46.23.64.124 on 09/08/12
For personal use only.

micelles are reported as effective diameter, d, determined by a cumulant analysis of the data (Table 2). From the calculated polydispersity values it is apparent that there is a broad distribution of micelle sizes. The sizes were insensitive to changes in temperature below the LCST (32.2°C). At 35°C, intermicellar aggregation took place, as indicated by an increase in the average diameter of the polymeric micelles from 44 nm at 25°C to 70 nm at 35°C. These larger polymeric micelles were stable for several hours at 35°C, implying that no further aggregation took place. Upon cooling below the LCST the solutions recovered their optical clarity. QELS measurements on these solutions revealed the presence of micelles of the same average size as those observed in the solutions before the heating–cooling cycle. The formation of the polymeric micelles and their microscopic structure are dictated by the action of two competing forces: (*a*) the hydrophobic forces (for reviews, see ref. 24) on the alkyl-pyrenyl groups in water that sequester them in the aggregate center and (*b*) the excluded volume repulsion between the polymers that limits the aggregate size. The balance of these two forces is expected to depend not only on the molecular architecture of the copolymers but also on the application of external stimuli, such as changes in temperature and in solvent composition. Micellar structures exist in water and also in water–alcohol mixtures within a narrow composition range.[2] Polymeric micelles do not form in methanol or in tetrahydrofuran. In these solvents no signal was detected by QELS analysis of polymer solutions ranging in concentration from 1 g L^{-1} to 6 g L^{-1}.

Characterization of the hydrophobic clusters by fluorescence spectroscopy

Emission spectra of the polymer *b*-PNIPAM-C_{18}Py/530 in water and in methanol are shown in Fig. 3. The emission of the polymer in water is dominated by a broad signal centered at 472 nm attributed to pyrene excimers (intensity I_E). The much weaker contribution of isolated excited pyrene ("monomer" emission, intensity I_M) is also detected, with the [0,0] band located at 378 nm. In a methanolic solution the polymer exhibits a much stronger emission due to excited isolated pyrene chromophores. The excimer emission, while still detectable, is very weak (I_E/I_M = 0.15). The contrast of the two spectra provides vivid evidence of the differences in the microstructure of the aqueous and the methanolic polymer solutions. The fact that pyrene excimer emission is very strong from aqueous polymer solutions implies that the pyrene groups are in close spatial proximity, incorporated within hydrophobic clusters. In methanol the polymer chains are isolated from each other and free to diffuse. Pyrene excimer emission can occur when a pyrene chromophore in its excited state comes into close proximity of a ground-state pyrene. Since each polymer chain carries only one chromophore, intrapolymeric excimer formation is precluded. As a consequence, the excimer contribution is much weaker than in the related case of the randomly substituted copolymer PNIPAM-C_{18}/200 (20), where excimer formation can take place by interaction of pyrenes attached to the same macromolecule.

Concentration studies confirm this description and emphasize the differences between the polymeric solutions in the two solvents. The ratio I_E/I_M measured from methanolic solutions

[2] F.M. Winnik. Unpublished results.

Fig. 3. Fluorescence spectra of pyrene-labeled poly(*N*-isopropylacrylamide) (*b*-PNIPAM-C_{18}Py/530, 0.26 g L^{-1}) (*a*) in water and (*b*) in methanol. Excitation wavelength: 346 nm.

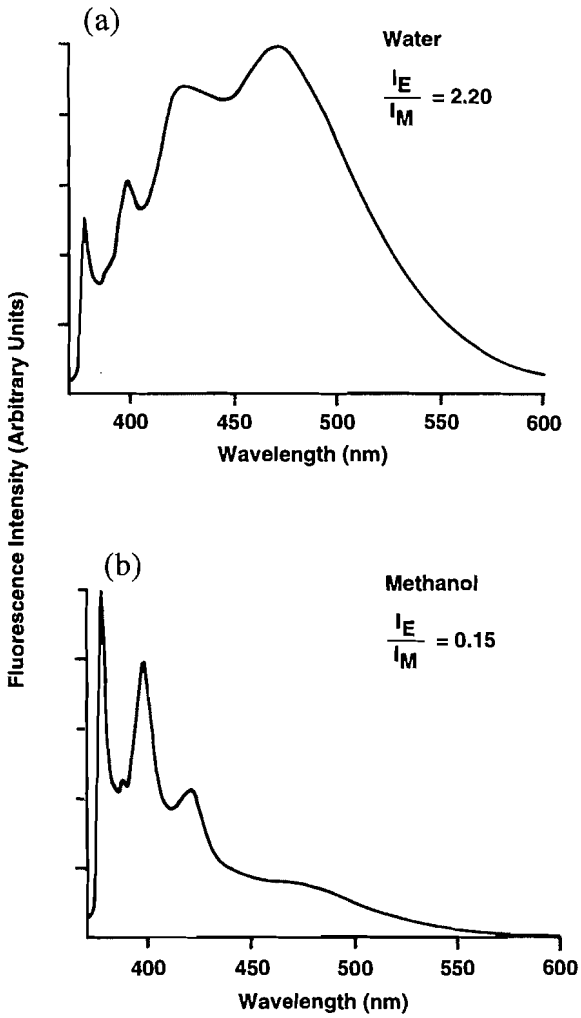

decreases with polymer concentration. Only pyrene monomer emission is observed when the polymer concentration is 0.03 g L^{-1} or lower. The ratio I_E/I_M measured from aqueous solutions was insensitive to changes in polymer concentrations ranging from 0.03 to 2 g L^{-1}, implying that the hydrophobic aggregates form at polymer concentrations as low as 0.03 g L^{-1}, the limit of detection of our instrument. An interesting spectroscopic point needs to be clarified. It concerns the exact nature of the pyrene excimer: is it a diffusion-controlled dynamic excimer, or does it originate from preformed ground-state pyrene aggregates, a frequent occurrence in aqueous solutions of pyrene-labeled polymers (25)? A comparison of the UV absorption spectra and of the excitation spectra monitored for the excimer and monomer emissions points to the existence of ground-state pyrene aggregates. The following observations in particular are significant: (*i*) the excitation spectra for the monomer and excimer emissions from aqueous polymer solutions are clearly different. The general features of the spectra are similar, but the former is blue-shifted by 2 nm; (*ii*) the widths of the bands in the two spectra differ, with extensive band broadening in the case of the spectrum monitored for the excimer; (*iii*) the UV spectra of the polymer in water have

Table 3. Spectrophysical parameters measured in solutions of PNIPAM-C_{18}Py/530.

	Fluorescence spectrum (25°C)		Fluorescence spectrum (35°C)		UV absorption spectrum	
Parameter	H_2O	MeOH	H_2O	MeOH	H_2O	MeOH
P_M[a]	2.01	3.04	2.24	2.94		
λ_M[b], nm	343	340.5	343.5	340.5		
P_E[a]	1.90		1.85			
λ_E[b], nm	345		344.5			
$\Delta\lambda$[c], nm	2		1.0			
P_A[d]					1.86	3.14
λ_{max}, nm					346	342

[a] P_M, P_E: peak-to-valley ratios for the (0,0) transition in the excitation spectra viewed at the monomer emission (378 nm) and at the excimer emission (472 nm), respectively.

[b] λ_M, λ_E: wavelength corresponding to the maximum in the excitation spectra monitored for the monomer and the excimer, respectively;

[c] $\Delta\lambda = \lambda_E - \lambda_M$.

[d] P_A: peak-to-valley ratio for the (0,0) transition in the ^1L_a band.

Fig. 4. Fluorescence spectra of *b*-PNIPAM-C_{18}Py/530 (0.26 g L^{-1}) measured at several temperatures between 15 and 40°C. Excitation wavelength: 346 nm.

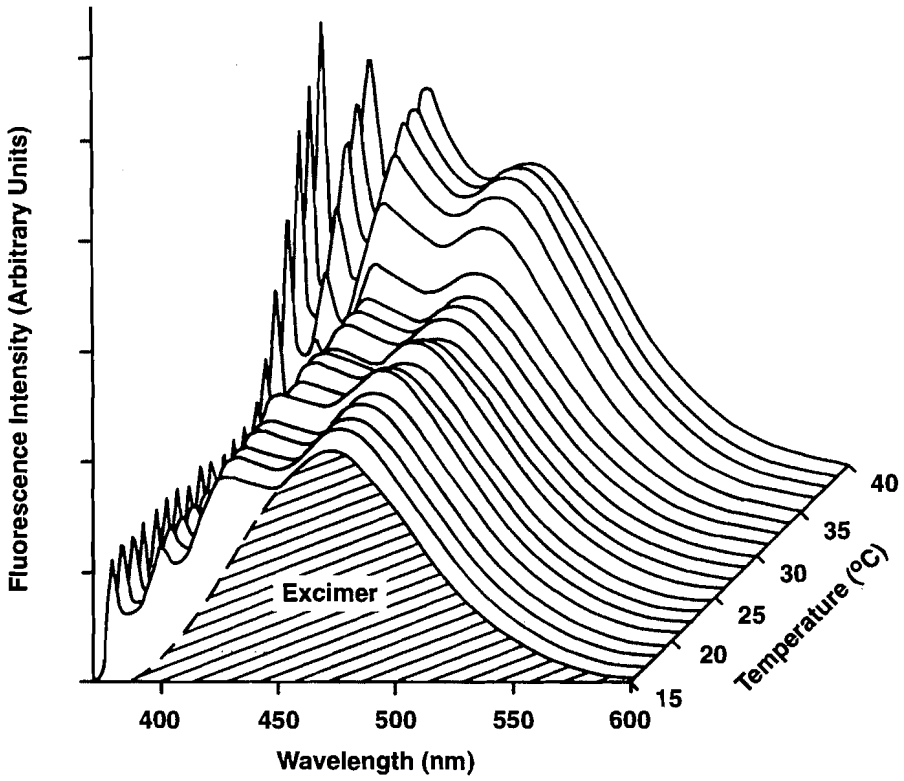

maxima at 346 nm, compared to 342 nm in methanol; and (*iv*) the UV spectra of the polymer in water exhibit a hypochromic effect accompanied by peak broadening. Relative measures of these effects are given by the peak-to-valley ratios P_M and P_E for the (0,0) transition in the excitation spectra viewed at the monomer emission and at the excimer emission, respectively, and $\Delta\lambda = \lambda_{max}$(excimer) $- \lambda_{max}$(monomer) (Table 3). This question will be addressed in more detail by carrying out time-dependent fluorescence measurements.

When a solution of *b*-PNIPAM-C_{18}Py/530 in water was heated from 15 to 45°C, several spectroscopic events occurred (Fig. 4). The ratio I_E/I_M increased slightly to reach a maximum value of 2.20 at 30°C. Then it decreased sharply to reach a value of 0.75 at 45°C. The midpoint of the transition was 32°C (Fig. 5). These changes were reversible: upon cooling of the solution, the ratio I_E/I_M increased to reach a value slightly higher than the value recorded before the heating–cooling cycle. A hysteresis in the temperature profile was observed, indicating that the time scale of polymer reorganization is rather long and that equilibrium was not achieved in scans performed at an approximate cooling or heating rate of 0.5°C min^{-1}. The initial I_E/I_M ratio was recovered when solutions car-

Can. J. Chem. Downloaded from www.nrcresearchpress.com by 46.23.64.124 on 09/08/12
For personal use only.

Can. J. Chem. Downloaded from www.nrcresearchpress.com by 46.23.64.124 on 09/08/12
For personal use only.

Fig. 5. Plot of the excimer-to-monomer emission intensity ratio (I_E/I_M) as a function of temperature for an aqueous solution of *b*-PNIPAM-C_{18}Py/530 (0.26 g L^{-1}) measured while heating the solution.

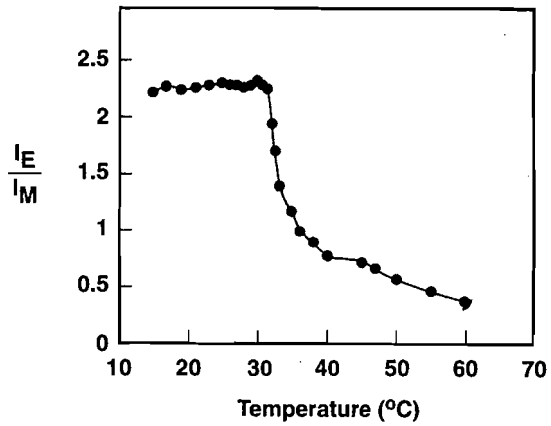

Fig. 6. Chemical structure of dimyristoylphosphatidyl choline (DMPC).

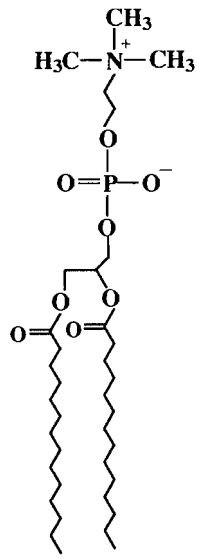

Dimyristoylphosphatidylcholine (DMPC)

ried through one heating–cooling cycle were kept at room temperature for 24 h. The decrease of I_E/I_M observed for *b*-PNIPAM-C_{18}Py/530 solutions above the LCST reflects a strong enhancement of the pyrene monomer, rather than a decrease in the pyrene excimer emission (see Fig. 4). This increase in total emission intensity is indicative of the occurrence of a significant level of pyrene self-quenching in cold solutions.

From the changes with temperature of the pyrene emission we conclude that at the LCST the morphology of the original polymeric micelles is disrupted to a small but significant extent. The temperature-induced collapse of the PNIPAM chains triggers a reorganization of the hydrophobic core such that a large fraction of the thermodynamically unstable pyrene aggregates falls apart. The original micelles conserve the over-

Fig. 7. Fluorescence spectra of *b*-PNIPAM-C_{18}Py/530 (0.26 g L^{-1}) (*a*) in water and (*b*) in the presence of DMPC liposomes; temperature 25°C; equilibrium time: 3 h; excitation wavelength: 346 nm.

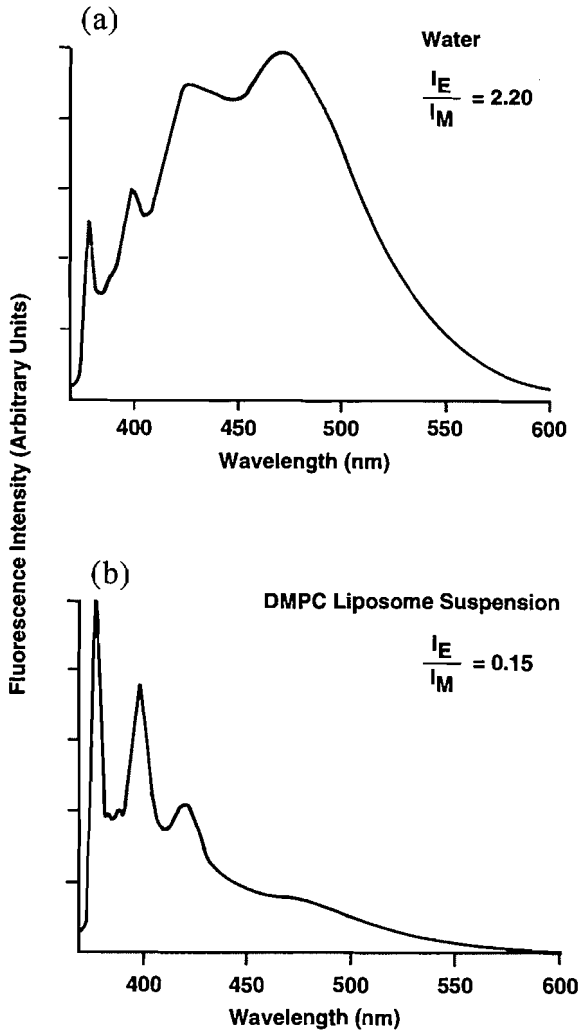

all morphology they adopted in the solutions below the LCST, as indicated by QELS measurements. Viewed at the molecular level this phase separation process differs in several key aspects from that occurring in solutions of the randomly alkylated amphiphilic polymers. In solutions of these polymers phase separation results in a disruption of the hydrophobic clusters formed below the LCST and a more isotropic distribution of the pyrenyl-octadecyl chains within the polymer-rich phase (20).

Interaction of the polymers and liposomes

Dimyristoylphosphatidylcholine (DMPC) (Fig. 6) liposomes were prepared by dispersion of the phospholipid in water and subsequent extrusion of the suspension through a polycarbonate membrane of 0.1 μm average pore size. Under these conditions unilamellar vesicles form predominantly (26, 27). The liposome diameters, measured by QELS, ranged from 140 to 160 nm in all the preparations. The structure and fluidity of lipidic bilayers exhibit a well-documented temperature dependence (28). Below a characteristic temperature, T_C, the phase transition temperature, the lipo-

Fig. 8. Fluorescence spectra of *b*-PNIPAM-C_{18}Py/530 (0.26 g L^{-1}) in the presence of DMPC liposomes measured at several temperatures between 15 and 40°C. Excitation wavelength: 346 nm.

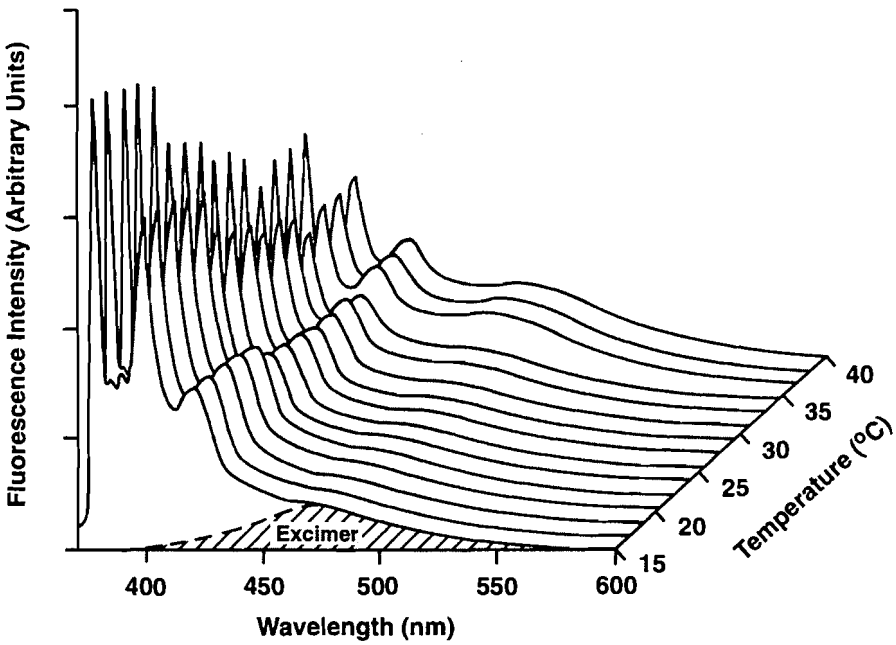

some bilayer exists in the solid-analogous phase in which the alkyl groups are crystallized in an all-*trans* configuration. As the temperature is raised above the T_C the bilayer passes from this tightly ordered "solid" phase to a liquid-crystal phase, where freedom of motion of individual chains is higher. The alkyl groups are able to adopt conformations other than the all-*trans* configuration and to undergo rotational movements. This tends to create void volumes and to allow lateral diffusion within the plane of the membrane. The phase transition temperature of DMPC liposomes, 23°C (29), is such that the experiments carried out at room temperature and above monitor the interactions of the polymers and a fluid membrane.

Another important consideration in the design of the experiments has to do with the relative concentrations of polymers and liposomes in the samples under study. Most experiments described here were performed with a lipid concentration of 1 g L^{-1} and a polymer concentration of 0.26 g L^{-1}. Under these conditions, assuming that all the liposomes are unilamellar and that each liposome (diameter: 150 nm) contains about 182 000 phospholipids (30), there are approximately 260 polymer chains for each liposome.

The addition of a solution of *b*-PNIPAM-Py-C_{18}/530 to DMPC liposomes triggered remarkable changes in the emission of the labeled polymer (Fig. 7). Most noticeable was a sharp decrease in the pyrene excimer emission, relative to pyrene monomer emission. The ratio I_E/I_M dropped from a value of 2.20 for the polymer in water to ca. 0.15 in the presence of liposomes. The spectral changes, however, were not instantaneous. The equilibration time required was found to be on the order of 3–5 h, depending on the relative concentrations of polymer and liposomes. This was observed from time-based fluorescence scans that monitored the increase in monomer emission as a function of time. The decrease in pyrene excimer emission is diagnostic of the disruption of the hydrophobic clusters into which the pyrene groups were accommodated in close proximity within the polymeric micelles formed by the HM-PNIPAM in water. In the system liposome–HM-PNIPAM the pyrene emission originates primarily from pyrenes unable to get into close proximity. This observation is taken as a strong indication of the insertion of the hydrophobic polymer tail of *b*-PNIPAM-C_{18}Py/530 within the lipid bilayer, thus generating "stabilized liposomes" (Fig. 9).

Next we monitored the effects of changes in temperature on the stability of the polymer–liposome association. As the temperature of a liposome–polymer suspension in water was increased above LCST, it was found that the I_E/I_M ratio increased marginally, from 0.2 to ca. 0.4. This small change reflects an increase of the excimer emission intensity at the expense of pyrene monomer emission (Fig. 8). Several possible explanations for this increase exist. It is likely that as the polymer chains collapse at the LCST, some chains are pulled away from the lipidic bilayer due to steric factors. They may then aggregate into polymeric micelles in the surrounding solvent. There was no visual indication of macroscopic polymeric aggregation. However, on the basis of the evidence gathered to date, some degree of disintegration of the liposome–polymer system cannot be dismissed. Another interpretation of the increase in pyrene excimer emission is that, during the process of contraction, several polymer chains become tangled and pull the pyrenes closer together, with concomitant increase in excimer emission. This mechanism was proposed to account for the increase in excimer emission intensity observed in the case of the interaction of DMPC liposomes with the randomly grafted polymer PNIPAM-C_{18}Py/200, the "molecular accordion" (9).

Can. J. Chem. Downloaded from www.nrcresearchpress.com by 46.23.64.124 on 09/08/12
For personal use only.

Can. J. Chem. Downloaded from www.nrcresearchpress.com by 46.23.64.124 on 09/08/12
For personal use only.

Fig. 9. Schematic representation of the conformational changes involved as *b*-PNIPAM-C_{18}Py/530 polymeric micelles enter in contact with an aqueous suspension of DMPC liposomes.

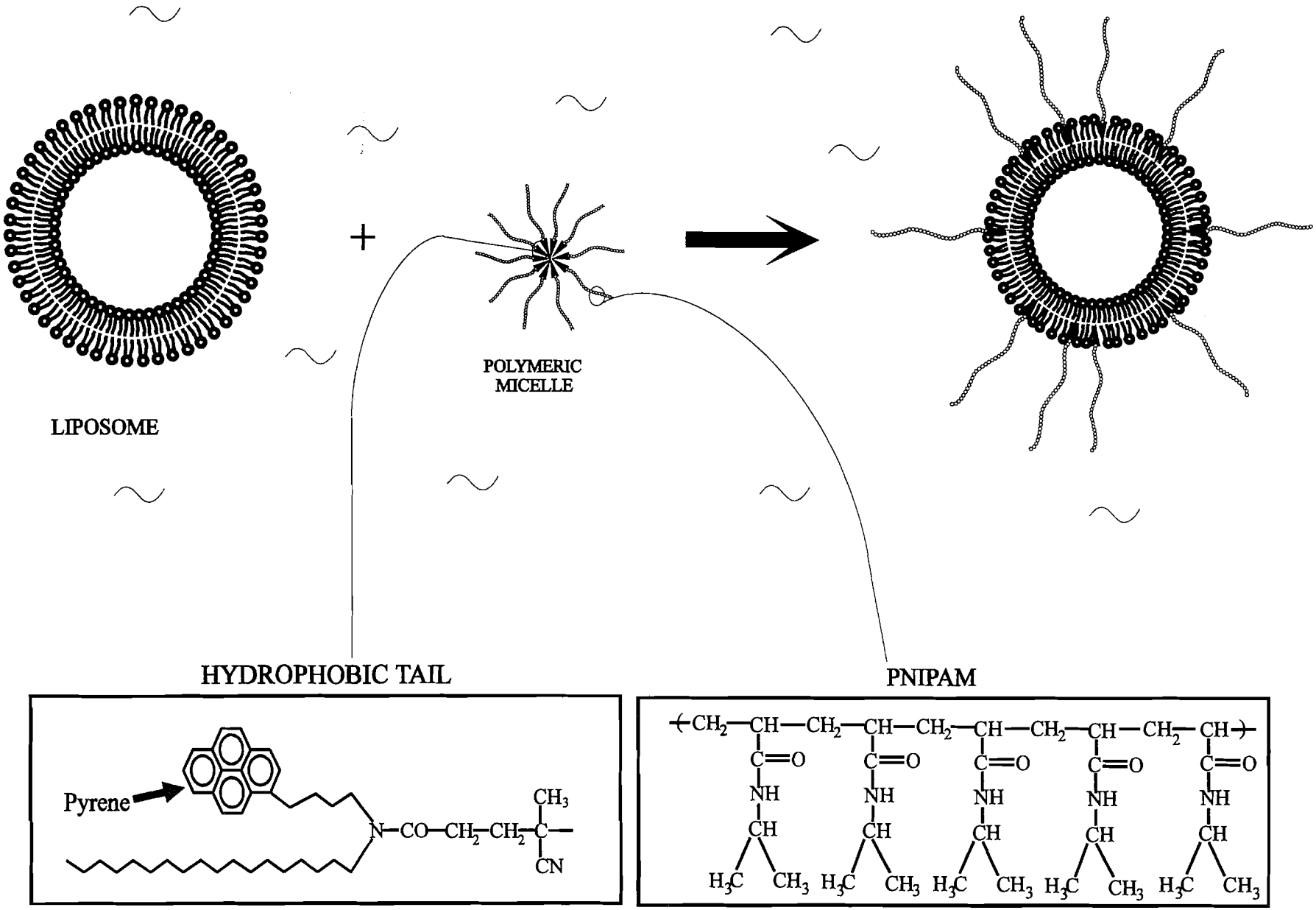

Can. J. Chem. Downloaded from www.nrcresearchpress.com by 46.23.64.124 on 09/08/12
For personal use only.

Conclusions

Pyrene end-labeled poly-(*N*-isopropylacrylamides) prepared with the lipophilic initiator PyODA form micelles in water, with a hydrophobic core consisting of octadecyl chains and pyrene groups and a loose corona of solvated PNIPAM chains. The pyrene groups in the core are placed in close proximity, as evidenced by the strong contribution of pyrene excimers to the total pyrene emission and implied by the significant quenching of the pyrene emission. When placed in contact with liposomes, the polymeric micelles are disrupted irreversibly. The polymer chains reorganize on the liposome surface in a slow process that results in a separation of the octadecyl–pyrenyl groups previously held in close contact within the core of the micelles. The hydrophobic tails of the polymers insert themselves within the fluid lipidic bilayer, creating "stabilized liposomes" consisting of vesicles decorated with hydrated PNIPAM chains extending in the aqueous environment. The effectiveness of the PNIPAM chains in preventing protein adsorption will be studied next, with the design of novel drug release systems as an ultimate objective.

Acknowledgments

F.M.W. and A. A. thank the Natural Sciences and Engineering Research Council of Canada for financial support, Mr. A. Davidson and Ms. L. Lee for their assistance in the preparation of polymer samples, and Mr. H. Ketelson for performing light-scattering measurements.

It is a pleasure for us to dedicate this publication to Professor Jim Guillet. Indeed the 1968 article in the Journal of Macromolecular Science (ref. 15 of this manuscript), authored by Heskins and Guillet, is quoted in nearly every paper dealing with poly-(*N*-isopropylacrylamide). But even more to the credit of Jim Guillet, it is his enthusiasm and his willingness to share his experience with PNIPAM that has triggered many a scientist to employ the unusual properties of PNIPAM in "intelligent devices." Thank you, Jim.

References

1. I. Rott, J. Brostoff, and D. Male. *In* Immunology. 3rd ed. Mosby, St. Louis, Mo. 1993. Chap. 1.
2. T.M. Allen and A. Chonn. FEBS Lett. **223**, 42 (1987).
3. A.L. Klibanov, K. Murayama, A.M. Beckerleg, V.P. Torchilin, and L. Huang. FEBS Lett. **268**, 235 (1990); Biochim. Biophys. Acta, **1062**, 142 (1991).
4. A. Gabizon, D.C. Price, J. Huberty, R.S. Bresalier, and D. Papahadjopoulos. Cancer Res. **50**, 6371 (1990); A. Gabizon, R. Catane, B. Uziely, B. Kaufman, T. Safra, R. Cohen, F. Martin, A. Huang, and Y. Barenholz. Cancer Res. **54**, 987 (1994).
5. J. Sunamoto, T. Sato, H. Taguchi, and H. Hamazaki. Macromolecules, **25**, 5667 (1992); J. Sunamoto. J. Colloid Interface Sci. **145**, 502 (1991); J. Sunamoto, T. Sato, M. Hirota, K. Fukushima, K. Hiratano, and K. Hara. Biochim. Biophys. Acta, **898**, 323 (1987).
6. J. Sunamoto, K. Iwamoto, M. Takada, T. Yuzuriha, and K. Katayama. Polym. Sci. Technol. (Plenum), **23**, 157 (1983).
7. M.Y. Özden and V.N. Hasirci. British Polym. J. **23**, 229 (1990); and references therein; K. Ishihara and N. Nakabayashi. J. Polym. Sci.: Polym. Chem. **29**, 831 (1991).
8. J.L. Thomas, H. You, and D.A. Tirrell. J. Am. Chem. Soc. **117**, 2949 (1995); and references therein; H. Ringsdorf, J. Schlarb, and J. Venzmer. Angew. Chem. Int. Ed. Engl. **127**, 113 (1988).
9. H. Ringsdorf, J. Venzmer, and F.M. Winnik. Angew. Chem. Int. Ed. Engl. **30**, 315 (1991).
10. H. Ringsdorf, J. Simon, and F.M. Winnik. *In* Colloid–polymer interactions, particulate, amphiphilic, and biological surfaces. ACS Symp. Ser. **532**, American Chemical Society, Washington D.C. 1993. Chap. 17.
11. H. Ringsdorf, E. Sackmann, J. Simon, and F.M. Winnik. Biochim. Biophys. Acta, **1153**, 335 (1993).
12. K. Kono, H. Hayashi, and T. Takagishi. J. Controlled Release, **30**, 69 (1994).
13. X. S. Wu, A. S. Hoffman, and P. Yager. Polymer, **33**, 4659 (1992).
14. C. Tanford. *In* The hydrophobic effect: formation of micelles and biological membranes. John Wiley & Sons, New York. 1980.
15. M. Heskins and J.E. Guillet. J. Macromol. Sci. Chem. **A2**, 1441 (1968).
16. H.G. Schild. Prog. Polym. Sci. **17**, 163 (1992).
17. Th. Binkert, J. Oberreich, M. Meeves, R. Nyffenegger, and J. Ricka. Macromolecules, **24**, 5806 (1991); S. Fujishige, K. Kubota, and I. Ando. J. Phys. Chem. **93**, 3311 (1989); I. Yamamoto, K. Iwasaki, and S. Hirotsu. J. Phys. Soc. Jpn. **58**, 210 (1989).
18. T. Bohanon, G. Elender, W. Knoll, P. Köberle, J.-S. Lee, A. Offenhäusser, H. Ringsdorf, E. Sackmann, J. Simon, G. Tovar, and F.M. Winnik. J. Am. Chem. Soc. Submitted.
19. H. Kitano, Y. Akatsuka, and N. Ise. Macromolecules, **24**, 42 (1991).
20. H. Ringsdorf, J. Venzmer, and F.M. Winnik. Macromolecules, **24**, 1678 (1991).
21. P.J. Flory. *In* Principles of polymer chemistry. Cornell University Press, Ithaca, N.Y. 1953. Chap. 4.
22. F.M. Winnik, A.R. Davidson, G.K. Hamer, and H. Kitano. Macromolecules, **25**, 1876 (1992).
23. L.D. Taylor and L.D. Cerankowski. J. Polym. Sci: Polym. Chem. Ed. **13**, 2551 (1975).
24. A. Ben-Naim. *In* Hydrophobic interactions. Plenum Press, New York. 1980.
25. F.M. Winnik. Chem. Rev. **93**, 587 (1993).
26. R.R.C. New (*Editor*). Liposomes, a practical approach. Oxford University Press, Oxford, England. 1990.
27. F. Olson, C.A. Hunt, F.C. Szoka, W. Vail, E. Mayhew, and D. Paphadjopoulos. Biochim. Biophys. Acta, **601**, 559 (1980); L. D. Mayer, M.J. Hope, and P.R. Cullis. Biochim. Biophys. Acta, **858**, 161 (1986).
28. D. Chapman. Q. Rev. Biophys. **8**, 185 (1975).
29. S. Mabrey and J.M. Sturtevant. Proc. Natl. Acad. Sci. U.S.A. **73**, 3862 (1976).
30. C. Huang and T. Mason. Proc. Natl. Acad. Sci. U.S.A. **75**, 308 (1978).

Photophysical studies of hydrophobically functionalized polyionene systems in aqueous solutions

P. Uznanski, J. Pecherz, and M. Kryszewski

Can. J. Chem. Downloaded from www.nrcresearchpress.com by 46.23.64.124 on 09/08/12
For personal use only.

Abstract: Complexes of polyionene and anionic dyes and surfactant were prepared by exchange reaction of counterions in the parent polymer. Fluorescence studies were conducted to observe some characteristic behaviour of these complexes in water. Polyionenes with aromatic hydrocarbons adopt an open conformation and there is no evidence for interpolymer interactions. On the contrary, polyionenes with long aliphatic counterions easily form microdomains in aqueous solution due to hydrophobic interaction as evidenced by an increase in excimer emission. Microdomains have an interpolymer nature, as confirmed by measurements of energy transfer from naphthalene to pyrene moieties. Polyionenes with SDS counterions interact with external surfactant molecules and form polymer–surfactant aggregates. Electrostatic repulsions between aggregates dominate on hydrophobic interaction between polymer chains and are responsible for conformational changes.

Key words: hydrophobically modified polymers, surfactants, complexation, fluorescence, nonradiative energy transfer.

Résumé : On a préparé des complexes de polyionènes, de colorants anioniques et d'agents de surface en procédant à l'échange de contre-ions dans le polymère fondamental. On a effectué des études de fluorescence pour observer quelques-uns des comportements caractéristiques de ces complexes dans l'eau. Les polyionènes, avec les hydrocarbures aromatiques, adoptent une conformation ouverte et on n'a pas relevé des données pouvant suggérer l'existence d'interactions interpolymères. Tel qu'on a pu le mettre en évidence par une augmentation de l'émission excimère, les polyionènes et les contre-ions aliphatiques longs, en solutions aqueuses, donnent au contraire facilement lieu à la formation de microdomaines à cause de l'interaction hydrophobe. Tel que confirmé par des mesures de transfert d'énergie des portions naphtalènes aux portions pyrènes, les microdomaines ont une nature interpolymérique. Les polyionènes et les contre-ions SDS interagissent avec des molécules externes d'agent de surface et ils forment des agrégats polymère – agents de surface. Les répulsions électrostatiques entre les agrégats dominent l'interaction hydrophobe entre les chaînes de polymères et elles sont responsables des changements conformationnels.

Mots clés : polymères hydrophobiquement modifiés, agents de surface, complexation, fluorescence, transfert non radiatif d'énergie.

[Traduit par la rédaction]

Introduction

The importance of aqueous systems composed of water-soluble polymers and low molecular weight surfactants for technological applications has encouraged the synthesis of new types of hydrophobically modified polymers. Hydrophobic functionalization is usually achieved by introducing aliphatic or condensed hydrocarbon residues of different length or size to given parts of a macromolecule to enhance the strength of polymer–surfactant interactions. Attention has been attracted to neutral water-soluble polymers such as poly(ethylene oxide) (1) or poly(acrylamide)s (2, 3) and to polyelectrolytes, i.e., charged polymers showing amphiphilic properties (4, 5).

Hydrophobically modified water-soluble synthetic polyelectrolytes bearing charges on their side groups, such as polycarboxylic acid (4), poly(sodium acrylate)s (6), cellulose derivatives (7), or poly(*N*-vinylpyridinium bromide) (8) and related polymers have been the systems more recently investigated, mainly by fluorescence techniques. Up to this time, however, little work has been done in the field of aliphatic ionenes in solution, this being one of the simplest ion-containing polymers (9). To this class of polycations belong polymers with ammonium or sulfonium groups in the main chain. Solid state ionenes with low charge density, i.e., with long alkylene chain length in the repeat unit, can form high quality amorphous solids, so their bulk properties have been the subject of

Received April 21, 1995

This paper is dedicated to Professor J.E. (Jim) Guillet in recognition of his contributions to Canadian chemistry.

P. Uznanski,[1] J. Pecherz, and M. Kryszewski. Centre of Molecular and Macromolecular Studies, Polish Academy of Sciences 90-363 Lodz, Sienkiewicza 112, Poland.

[1] Author to whom correspondence may be addressed. Telephone: 48-42-87-57-61. Fax: 48-42-84-71-13.

Scheme 1. Structures of the complexes of polyionene and anionic low molecular weight counterions.

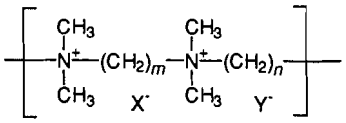

Polycation - I (m = 10, n = 10)

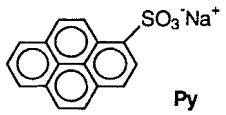

Py

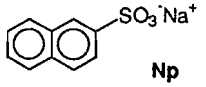

Np

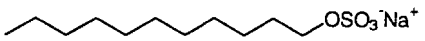

SDS

detailed studies (10). By the proper choice of low molecular weight counterions, which balance the charges on the N^+ or S^+ cation, one can tailor the thermal, optical, electrical, and related properties of solid polyionenes. On the other hand, the conformation of polyionenes in solution can be controlled by different charge density on the polymer chain or by counterions of different hydrophobicity. The preparation of starting polyionene followed by the exchange of bromide anions is an easy procedure and provides a convenient way to prepare a broad class of ionenes with different aggregation properties.

We recently reported preliminary investigations on polyionene, of the general chemical formula presented in Scheme 1, having the spiropyrane group as counterion (11). The results indicated that such solution properties of the photochrome–ionene complex as the kinetics of photochromic reaction were affected by the hydrophobic part of the polymer and a Coulombic interaction with quaternary ammonium ions. The present paper is devoted to further study of polyionene systems in water solution complexed with salts of pyrene and naphthalene chromophores and with anionic surfactant. For such "hydrophobically functionalized Coulombic composites," characteristic of various hydrophobicities, the polymer chain conformation in water was modified to influence the photophysical properties of these systems. The hydrophobic nature of ionenes was investigated by means of spectrofluorometry using the fluorescence properties of the pyrene counterions. This label is commonly used for the study of microheterogeneous systems (4, 5). Our results show that the photophysical properties of pyrene related to the conformational behaviour of polyionene in solution are complex and depend strongly on the hydrophobic nature of the counterions. The structure–property relationship of polyionene solutions indicates that the system investigated, characterized by relatively low ion concentration, could be considered as ionomers rather than as polyelectrolyte (12).

Experimental

The parent polyionene (Scheme 1) having relatively high molecular weight (200 repeating units in the main chain structure) was synthesized by reacting alkenediamines with dibromoalkanes following the Menschutkin reaction and procedures

Table 1. The investigated molecular composites of polyionene and chromophore–surfactant complexes.

Counterion X^- 10%	Counterion Y^- 90%	Abbreviation
$PySO_3^-$	BF_4^-	I–Py
NSO_3^-	BF_4^-	I–N
$PySO_3^-$	SDS	I–Py–SDS
NSO_3^-	SDS	I–N–SDS
$PySO_3^-$	NSO_3^-I–Py–N	

that have been described by Rembaum et al. (13). It has uniform distribution of the length of the alkylene units between the N^+ atoms (m = 10, n = 10). 1-Pyrenesulfonic acid (Py), 1-naphthalenesulfonic acid (N) prepared as the sodium salt, and sodium dodecyl sulfate (SDS) were commercial products of fluorescence grade from Aldrich and were used as received. The exchange of bromide counterions in the parent polycation with anionic fluorophores, surfactant, and with tetrafluoroborates (to lower hygroscopicity of the solid samples) was carried out in water at 30°C by the same method as reported previously (13,14). Thus integral-type complexes, i.e., with cationic sites on the main chain of polyionene and $PySO_3^-$, NSO_3^-, SDS, or BF_4^- residues of well-defined composition, were obtained. Low molar concentration of the ionic group (below 9%) along the aliphatic chain of the polyionene and large size of counterions lead to its low solubility in water solution.

The polycations investigated are presented, with their abbreviations, in Scheme 1 and in Table 1. The content of aromatic anion in the polyionene was 10 mol% with respect to the N^+-charged groups. Thus the chromophore loadings on the copolymer could be considered as high. The complementary concentrations of SDS, NSO_3^-, or BF_4^- ions were 90 mol%. The polyionenes were dissolved in dipolar aprotic solvents of high polarity, e.g., DMF or DMSO. For all measurements we used triply distilled ion-exchanged water.

All polymers obtained were poorly soluble in water but polyionenes with an anionic surfactant displayed the highest solubility. In our experiments a small volume of concentrated solution of polyionene complexes in *N,N*-dimethylformamide (DMF), generally 1×10^{-1} M, was added to the water solution. The mixture was shaken and degassed by bubbling with nitrogen for 10 min. The fluorescence properties of the samples showed no time-dependent changes during the measurements. In all sample solutions, the polyionene concentration was 3×10^{-4} M of monomer units.

Photostationary fluorescence and excitation spectra were measured with a Perkin–Elmer LS-50 luminescence spectrometer equipped with the front face accessory. The excitation wavelengths were 280 and 340 nm for naphthalene and pyrene, respectively. All the measurements were carried out at room temperature in a quartz cell of 2 mm thickness.

Results and discussion

Fluorescence of pyrene is widely used for the polarity study of microheterogeneous systems. It readily forms excimers and is an energy acceptor via nonradiative energy transfer (NRET) from the naphthalene or fluorene chromophore; thus one could expect to detect its emission behavior depending on the nature

Can. J. Chem. Downloaded from www.nrcresearchpress.com by 46.23.64.124 on 09/08/12
For personal use only.

Can. J. Chem. Downloaded from www.nrcresearchpress.com by 46.23.64.124 on 09/08/12
For personal use only.

Fig. 1. Plot of I_3/I_1 for $PySO_3Na$ emission as a function of water content in various DMF– H_2O mixtures.

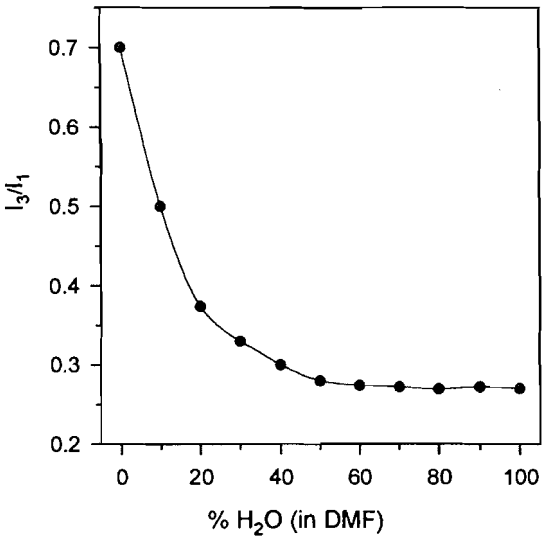

of the local environment (4, 5). The steady-state emission spectrum of pyrene provides three parameters, the ratio, I_3/I_1, of the intensities of the third to first vibronic bands, and the ratio, I_E/I_M, of the excimer emission relative to the monomer emission. The changes in the ratios I_E/I_M and I_3/I_1 are then used to determine the critical aggregation concentration (cac) or to detect the presence of hydrophobic microdomains for the polymers in solution (4).

In unsubstituted pyrene, a polarity-dependent emission band is correlated with vibronic coupling. The intermolecular processes responsible for vibronic coupling are solvent dipole – solute induced dipole moment interactions that distort nuclear vibrations of b_{3g} symmetry (15). Usually, for unsymmetrically substituted pyrene, the immediate environment has little influence on vibronic coupling since the substituent itself breaks the vibronic symmetry. In the case of noncomplexed $PySO_3Na$ chromophore, the fluorescence spectrum depends markedly on solvent polarity. In Fig. 1 we plotted values of I_3/I_1 as a function of water content in binary mixtures of DMF and H_2O. On going from neat DMF ($\varepsilon = 37.6$) to pure water ($\varepsilon = 80.4$) the values change from 0.7 to as low as 0.27. The same dependence with an identical plot of I_3/I_1 vs. $\%H_2O$ content was obtained for I–Py samples. When the ionic surfactant SDS is added to the water solution of $PySO_3Na$ no changes occur either in the monomeric or the excimeric part of the emission. The fluorescence independence of SDS concentration was observed over the range from 10^{-5} to 5×10^{-2} M, i.e., well below the critical micelle concentration (cmc) of SDS. This means that nonbonded dyes are not sequestered by the hydrophobic core of the micelles, probably because of its good solubility in water.

Figure 2 compares the fluorescence spectra of I–Py–SDS and I–Py in aqueous solution at room temperature. The fluorescence spectra depend on the polyionene composition. No changes were observed in the monomer part of the pyrene emission spectrum for either sample while for the copolymer with SDS counterions, as well as a strong monomer fluorescence I_M, a characteristic structureless excimer emission band I_E appears, with a maximum at about 480 nm.

Fig. 2. Normalized fluorescence spectra of I–Py (broken line) and I–Py–SDS (solid line) in water.

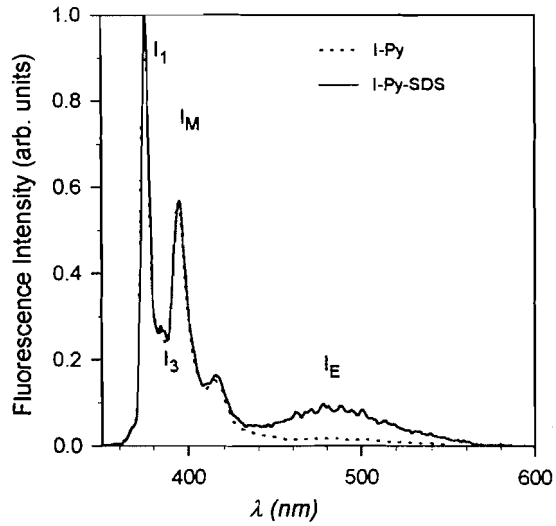

Fig. 3. Excimer-to-monomer intensity ratio I_E/I_M and the ratio of vibronic band intensities I_3/I_1 for pyrene in water solution at different polyionene concentrations.

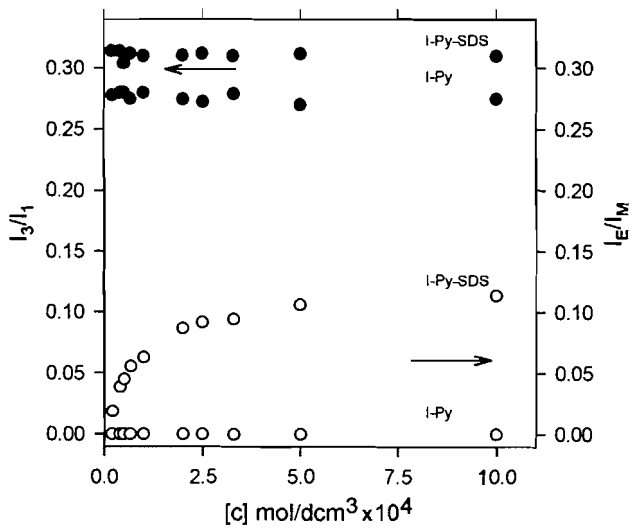

Figure 3 presents the plots of the ratios I_3/I_1 and I_E/I_M as a function of I–Py–SDS concentration in water solution. For comparison on the same plot, we show the fluorescence parameters of I–Py samples. The values of both parameters are constant upon increasing polyionene concentration: I_3/I_1 achieved the value of 0.27 while excimer emission was not detected in the range of concentration examined. In the case of I–Py–SDS samples, the ratio I_3/I_1 of pyrene fluorescence was estimated to be 0.31 and also shows fixed values vs. concentration. On the other hand, values of the excimer-to-monomer intensity ratio I_E/I_M increase continuously until a certain critical concentration equal to 3×10^{-4} M is reached and then they remain constant upon further increase of the I–Py–SDS concentration. This type of behaviour is connected with excimer formation and suggests its interchain origin. For I–Py the content of the hydrophobic pyrene units, although high (9 mol%), is not sufficient to form hydrophobic aggregates in aqueous solution.

Can. J. Chem. Downloaded from www.nrcresearchpress.com by 46.23.64.124 on 09/08/12
For personal use only.

Fig. 4. Steady-state fluorescence emission spectra of polyionenes excited at 290 nm in aqueous solution: (*a*) I–N–Py; (*b*) mixture of I–N and I–Py; (*c*) mixture of I–N–SDS and I–Py–SDS.

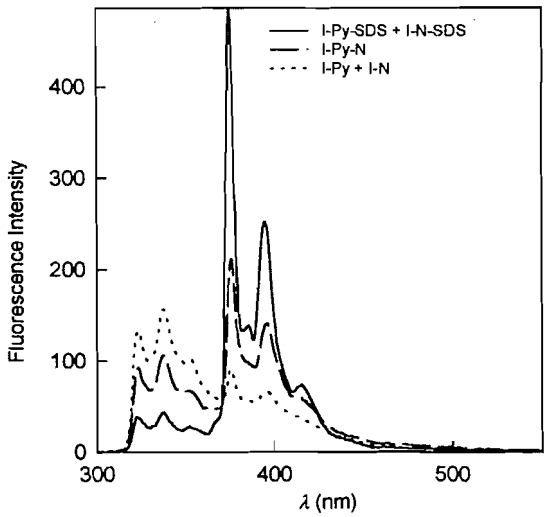

The established values of vibronic band intensities I_3/I_1 for both ionenes are understandable because the pyrene residue is confined to strong Coulombic interaction from charged N^+ groups on the polymer chain and the presence of hydrophobic domains has little influence on I_3/I_1 behaviour in water solution. The solvation of salt groups was found to be dependent on the dielectric constant (ε) of the solvent: dipolar molecules of DMF solvate SO_3^- ions in another way than do H_2O molecules. For higher ε (in water) the Coulombic interaction between ions is reduced and the effect of vibronic coupling on the vibronic structure of the emission band is influenced mainly by substituent interactions and not by solvent molecules as is normally observed.

Both polyionenes were poorly soluble in water; however, I-Py gives a transparent solution whereas the I–Py–SDS sample is turbid. This suggests that the differences in photophysical behaviour of I–Py and I–Py–SDS could arise from different polymer conformations. The question is whether polyionene forms aggregates because of self-organization of the hydrophobic groups and whether the hydrophobic aggregation has an intramolecular or intermolecular character. Comparative studies can provide some evidence of fluorescence on the association of I–Py–SDS polyionene with additional surfactant molecules, and from the nonradiative energy transfer (NRET) phenomena between naphthalene and pyrene groups in polyionenes of different counterion composition: singly labelled (I–Py, I–N, I–Py–SDS, I–N–SDS) and doubly labelled (I–Py–N).

The efficiency of NRET between donor (naphthalene) and acceptor (pyrene) depends on their separation distance and their relative orientation. NRET is particularly useful for estimation of polymer chain dimensions in solution or distances between macromolecules smaller than 100 Å. In the glassy state I–Py–N shows an efficient "antenna" effect in the energy transfer from naphthalene to pyrene groups (14). For such high efficiency to be possible, most of the $PySO_3^-$ groups must exist

Fig. 5. Fluorescence spectra of I–Py–SDS in the presence of varying concentrations of SDS.

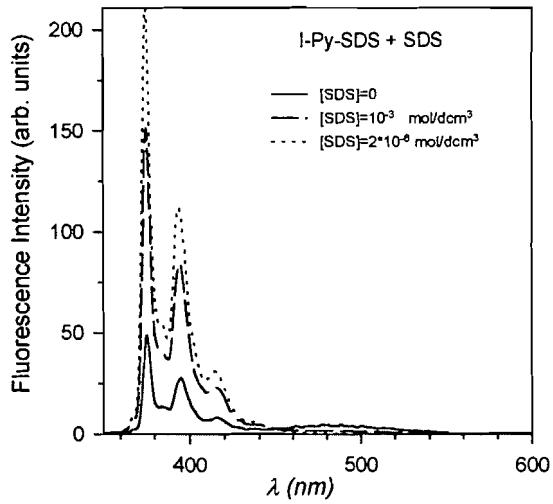

within a distance from the NSO_3^- groups of less than the Förster radius R_0 (28.64 Å), defined as a distance at which there is a 0.5 probability for the NRET mechanism of deactivation of the donor excited state (16). Figure 4 shows the structured fluorescence spectra of pyrene and naphthalene on excitation of the naphthalene chromophores at 290 nm for ionenes with different counterions. All the observed emission spectra show pyrene fluorescence; however, in aqueous solution the extent of energy transfer is much lower than for the glassy state, where the NRET is complete. This emission is also lower than the fluorescence intensity observed on direct excitation of the Py moieties. For the mixture of singly labelled polyionenes with naphthalene (I–N) and pyrene residues (I–Py), naphthalene predominates in the steady-state emission spectra, which implies that the mean interpolymer distances must be larger than R_0 and the chains do not form aggregates. It is evident from Fig. 5 that the presence of SDS counterions on the polyionene chain enhances energy transfer efficiency, resulting in a change in polymer aggregation. Moreover, the observed lack of an excimer band can be exclusively accounted for by the interpolymer association of I–Py–SDS and I–N–SDS.

Further evidence for formation of polyionene complexes can be derived from the interaction of I–Py–SDS with additional surfactant molecules. Figure 5 compares fluorescence spectra of I–Py–SDS in the presence of varying concentrations of SDS. The intensity of excimer emission decreases progressively with increasing [SDS], while monomer emission increases. Simultaneously with the fluorescence changes, one can observe a decrease of apparent light scattering from the samples. The aqueous solution of I–Py–SDS is turbid. In composition with additional SDS molecules at low surfactant concentration (below cmc) the sample becomes less turbid. Then, above the cmc it is completely transparent. Thus the suppression of the excimer emission may be attributed to compartmentalization of the $PySO_3^-$ counterions by external SDS molecules and changes in polymer chain conformation due to the formation of polyionene–surfactant complexes. A schematic representation of the micellization of I–Py–SDS

Fig. 6. Proposed conformation of I–Py–SDS in aqueous solution and an illustration of a local aggregate structure of I–Py–SDS and SDS. Solid lines and filled circles represent polyionene with N^+ ions, open circles represent polar heads in $PySO_3^-$ counterion and in SDS surfactant.

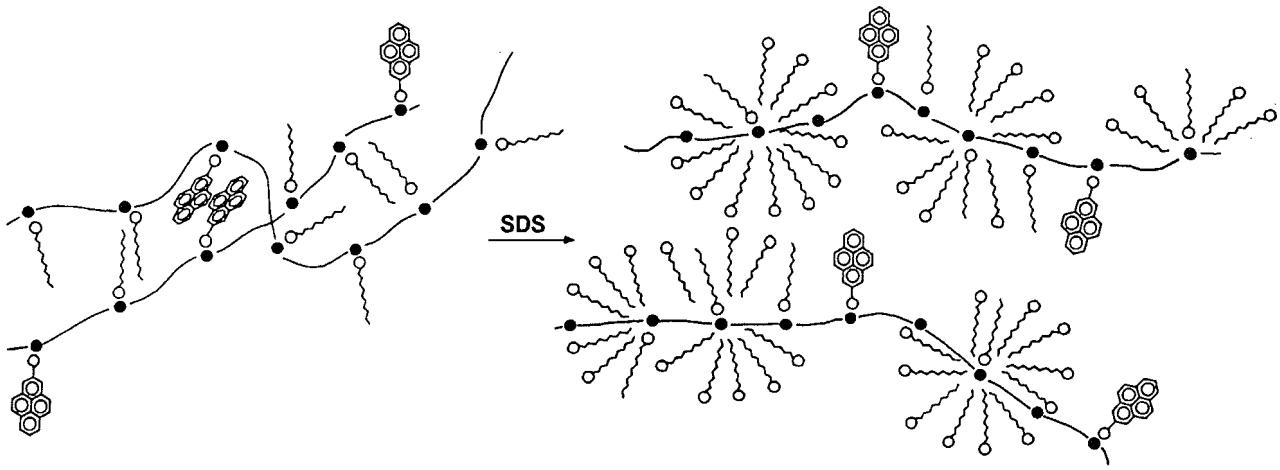

induced by the addition of SDS to the solution is shown in Fig. 6.

In the polyionene aggregate several SDS and $PySO_3^-$ groups (from different chains) participate in the complexes. Addition of external SDS surfactant molecules leads to rearrangement of the coil structure. They bind by hydrophobic interaction to SDS counterions in I–Py–SDS chains. We rather excluded the possibility that they can be attracted by Coulombic interaction to N^+-charged groups in the vicinity of $PySO_3^-$, SDS, or BF_4^- counterions. An increase in SDS concentration above the cmc leads to changes in polyionene coil structure: the chains are more separated from each other and more expanded due to repulsive interactions between SDS micelles bound to the polyionene chain, as illustrated in Fig. 6. On this basis, we consider that polyionene complexes with excess surfactant are not compact. The behaviour in water solution of I–Py–SDS exhibits a more pronounced tendency to interchain aggregation. Separation of pyrene groups by SDS micelles is expected to be the mechanism responsible for increasing monomer fluorescence intensity. Adsorption of anionic surfactant on hydrophobically modified ionenes leads to decreasing excimer formation due to the expansion and (or) separation of the polymer chains: greater concentration of SDS increases hydrophobic interactions between nonpolar fragments of polyionene chains and the surfactant counterions and enhances the repulsive forces between SDS micelles. For I–Py samples the changes in fluorescence spectra are small and even at higher SDS concentration the fluorescence remains unchanged.

Conclusions

In the study presented, we have hydrophobically modified ionene polymers in a way other than through formation of covalent bonds. Polyionenes with pyrene and naphthalene counterions are not able to form stable aggregates in aqueous solution even at relatively high molar concentration, contrary to polyelectrolytes with long aliphatic counterions. This confirms that the hydrophobicity of alkanes is much stronger than that of aromatic hydrocarbons (4). Hydrophobic domains are efficiently formed for I–Py–SDS samples and have an interpolymer nature, as evidenced by measurements of the extent of energy transfer from naphthalene to pyrene in mixtures of polyionenes of different composition. I–Py accepts an extended conformation whereas I–Py–SDS is in a coiled interpolymer conformation as demonstrated by polyionene interactions with external surfactant molecules. The interaction of I–Py–SDS with excess of surfactant leads to formation of polymer–surfactant aggregates. SDS counterions facilitate association of excess surfactant with the ionene chain. It was found that the conformation of I–Py–SDS/SDS is more open than in the case of I–Py or I–Py/SDS systems. The difference is considered to derive from the nature of the interaction between aromatic and aliphatic hydrocarbons.

It is hoped that further studies with polycations of different charge density in the main chain may elucidate the relationship between the structure of polyionene complexes and their association properties in water.

References

1. Y.-Z. Hu, Ch.-L. Zhao, M. A. Winnik, and P. R. Sundararajan. Langmuir, **6**, 880 (1990).
2. F.M. Winnik, H. Ringsdorf, and J. Venzmer. Langmuir, **7**, 912 (1991).
3. H.G. Schild and D.A. Tirrel. Macromolecules, **25**, 4553 (1992).
4. Y. Morishima. Prog. Polym. Sci., **15**, 949 (1990).
5. F. M. Winnik. Chem. Rev., **93**, 587 (1993).
6. B. Magny, I. Iliopoulos, R. Audebert, L. Piculell, and B. Lindman. Prog. Colloid Polym. Sci. **89**, 118 (1992).
7. F. Guillemet and L. Piculell. J. Phys. Chem. **99**, 9201 (1995).
8. K.N. Bakeev, E.A. Ponomarenko, T. V. Shishkanova, D.A. Tirrell, A.B. Zezin, and V.A. Kabanov. Macromolecules, **28**, 2886 (1995).
9. K. Abe, M. Koide, and E. Tsuchida. J. Polym. Sci. Polym. Chem. Ed. **15**, 2469 (1977); E.A. Bekturov, R.E. Khamzamulina, G. Reinisch, W. Jaegger, and Z.K. Belgibaeva. Acta Polym. **35**, 521 (1984); Y. Suzuki and S. Tazuke. Macromolecules, **13**, 25 (1980); **14**, 1742 (1981); Makromol. Chem. **185**, 521 (1984).

Can. J. Chem. Downloaded from www.nrcresearchpress.com by 46.23.64.124 on 09/08/12
For personal use only.

10. T. Tsutsui, R. Tanaka, and T. Tanaka. J. Polym. Sci. Polym. Lett. Ed. **14**, 2259 (1976); L. Dominquez, W. H. Meyer, and G. Wegner. Makromol. Chem. Rapid Commun. **8**, 151 (1987); M. Kryszewski and J. Pecherz. Polym. Adv. Technol. **5**, 146 (1993).
11. P. Uznanski, J. Pecherz, and M. Kryszewski. Mol. Cryst. Liq. Cryst. **246**, 351 (1994).
12. H. Morawetz. Acc. Chem. Res. **27**, 174 (1994).
13. A. Rembaum, W. Baumgartner, and A. Eisenberg. J. Polym. Sci. Part B: Polym. Lett. **6**, 159 (1968).
14. W.H. Meyer, J. Pecherz, A. Mathy, and G. Wegner. Adv. Mater. **30**, 153 (1991).
15. D.S. Kaprovich and G.J. Blanchard. J. Phys. Chem. **99**, 3951 (1995).
16. D.A. Holden and J.E. Guillet. Macromolecules, **13**, 289 (1980).

Can. J. Chem. Downloaded from www.nrcresearchpress.com by 46.23.64.124 on 09/08/12
For personal use only.

Photochemistry of nonconjugated diketones: internal self-quenching and energy transfer

Peter J. Wagner and Harlan W. Frerking, Jr.

Abstract: The triplet state behavior of nine α,ω-dibenzoylalkanes indicates the occurrence of a rapid quenching interaction between the two carbonyl groups. This quenching is fastest ($k = 3 \times 10^7$ s^{-1}) in dibenzoylbutane, is slightly slower ($\sim 10^7$ s^{-1}) in dibenzoylethane, dibenzoylpentane, and 2,2-dibenzoylpropane, but is absent in 1,3-dibenzoylpropane. It also occurs in several "mixed" 1,4-diaroylbutanes incorporating *p*-ethylbenzoyl or *p*-methoxybenzoyl chromophores This internal self-quenching is interpreted as the intramolecular counterpart of the well-known bimolecular self-quenching of aryl ketones, although no exact mechanism can be proposed. Such internal quenching does not occur as rapidly, if at all, in three "turned around" diketones: δ-(*p*-acetylphenyl)valerophenone, δ-(*p*-acetylphenoxy)valerophenone, and γ-(*p*-acetylphenoxy)butyrophenone. This fact, together with the varying rates of internal self-quenching in the dibenzoylalkanes, indicates the necessity for a very specific and close orientation of the two carbonyl groups for self-quenching. In the mixed diketones containing a *p*-alkylbenzoyl group, triplet excitation appears to be fully equilibrated between the two chromophores. However, in those containing a *p*-methoxybenzoyl group, excitation does not fully equilibrate before triplet decay, as evidenced by different quenching efficiencies for products from the two carbonyls. Analysis indicates intramolecular energy transfer rate constants $\leq 10^8$ s^{-1}. These are sufficiently lower than in other bichromophoric systems to suggest relatively slow energy hopping in the polymers of phenyl vinyl ketone.

Key words: nonconjugated diketones, dibenzoylalkanes, self-quenching, energy transfer, triplet ketones.

Résumé : Le comportement de l'état triplet de neuf α,ω-dibenzoylalcanes indique qu'il se produit une rapide interaction de désactivation entre les deux groupes carbonyles. Cette désactivation se fait le plus rapidement ($k = 3 \times 10^7$ s^{-1}) dans le dibenzoylbutane; elle est légèrement plus lente ($\sim 10^7$ s^{-1}) dans les dibenzoyléthane, dibenzoylpentane et 2,2-dibenzoylpropane, mais elle est totalement absente dans le 1,3-dibenzoylpropane. Elle se produit aussi dans plusieurs 1,4-diaroylbutanes « mixtes » qui incorporent les chromophores *p*-éthylbenzoyle ou *p*-méthoxybenzoyle. On interprète cette autodésactivation interne comme la contrepartie intramoléculaire de l'autodésactivation bimoléculaire bien connue des arylcétones, même si aucun mécanisme exact a été proposé. Si elles se produisent, de telles désactivations internes ne se produisent pas non plus rapidement dans les trois dicétones « qui sont retournées » : δ-(*p*-acétylphényl)valérophénone, δ-(*p*-acétylphénoxy)valérophénone et γ-(*p*-acétylphénoxy)butyrophénone. Ce fait, pris avec les vitesses variables de l'autodésactivation interne dans les dibenzoylalcanes, indique qu'il est nécessaire d'avoir une orientation spécifique et rapprochée des deux groupes carbonyles pour obtenir de l'autodésactivation. Dans les cas des dicétones mixtes contenant un groupe *p*-alkylbenzoyle, il semble que l'excitation triplet est complètement équilibrée entre les deux chromophores. Toutefois, dans celles qui contiennent un groupe *p*-méthoxybenzoyle, il semble, sur la base des efficacités de désactivation différentes pour les produits des deux carbonyles, que l'excitation ne s'équilibre pas avant la décroissance du triplet. Une analyse indique que les constantes de vitesse pour le transfert intramoléculaire de l'énergie sont $\leq 10^8$ s^{-1}. Ces valeurs sont suffisamment plus faibles que celles dans les systèmes bichromophores pour suggérer que, dans les polymères de la phényl vinyl cétone, le transfert d'énergie par sauts est relativement lent.

Mots clés : dicétones non conjuguées, dibenzoylalcanes, autodésactivation, transfert d'énergie, cétones triplets.

[Traduit par la rédaction]

Received August 10, 1995.

This paper is dedicated to Professor J.E. (Jim) Guillet in recognition of his contributions to Canadian chemistry.

P.J. Wagner[1] and H.W. Frerking, Jr.[2] Chemistry Department, Michigan State University, East Lansing, MI 48824, U.S.A.

[1] Author to whom correspondence may be addressed. Telephone: (517) 355-9715, ext. 132. Fax: (517) 353-1793. E-mail: wagner@cemvax.cem.msu.edu

[2] This paper is based on the Ph. D. Thesis of Harlan W. Frerking, Jr., Michigan State University, 1978.

Can. J. Chem. Downloaded from www.nrcresearchpress.com by 46.23.64.124 on 09/08/12
For personal use only.

Can. J. Chem. Downloaded from www.nrcresearchpress.com by 46.23.64.124 on 09/08/12
For personal use only.

Introduction

Two decades ago, when we published a systematic study of the Norrish type II photoreactions of γ- and δ-substituted alkyl phenyl ketones (1), we noted that 1,4-dibenzoylbutane reacts in only half the quantum yield observed for similar monoketones (2). Later it became apparent that triplet aryl ketones undergo often efficient self-quenching by their ground state molecules (3, 4). Therefore it seemed likely that dibenzoylbutane undergoes the same reaction in an internal fashion. More recently, however, several studies on 1,3-dibenzoylpropanes (5, 6) and on poly(phenyl vinyl ketone) (7–9) suggest that no such internal self-quenching occurs in the triplet states of these molecules and that triplet energy transfer between equivalent chromophores is very efficient. Singer et al. have discussed several geometric approaches that might lead to self-quenching (4). Because of our interest in intramolecular energy transfer in ketones (10) and diketones (11), we decided to investigate the behavior of several dibenzoylalkanes to verify the difference between dibenzoylpropane and -butane and to better define the geometric requirements for self-quenching. In the process we were led to delve more completely into the kinetics of reversible triplet energy transfer (12), a topic that will be addressed briefly in this paper and more thoroughly in a forthcoming paper.

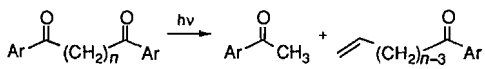

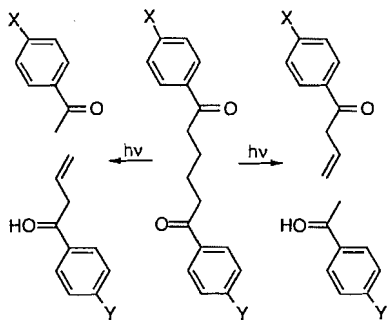

Experimental section

Materials

Solvents

Benzene and pyridine were purified as in earlier work. Ethanol and dioxane were purified as recommended by Riddick (13). Methylcyclohexane (Eastman) was stirred with sulfuric acid until further portions remained colorless, then washed, dried, and distilled. Cyclohexane (Matheson, Coleman, and Bell, spectrograde) was recrystallized twice from itself. 2-Methyltetrahydrofuran was purified by the procedure of Gordon and Ford (14). Gold label Aldrich 2-methylbutane was used as received.

Internal standards

Tetradecane, hexadecane, and octadecane were all available from earlier studies. Di-*n*-ethyl and di-*n*-butyl phthalate were used as received from Aldrich. Di-*n*-propyl phthalate was prepared by treatment of phthalic anhydride with 1-propanol and distillation, bp 128°C (1.2 Torr; 1 Torr = 133.3 Pa).

Quenchers

trans-Stilbene was used as received from J.T. Baker. *cis*-1,3-Pentadiene (Chemical Samples Co.) was used as received. 2,5-Dimethyl-2,4-hexadiene (Chemical Samples Co.) was allowed to sublime in the refrigerator.

Ketones

Acetophenone, valerophenone, *p*-methoxyacetophenone, and *p*-methoxyvalerophenone were all available from earlier studies.

The following ketones were all synthesized. Their melting points (uncorrected) were measured on a Thomas–Hoover Unimelt capillary apparatus. IR spectra were recorded on a Perkin–Elmer 237B; UV, in benzene on a Cary 17 spectrometer, ^{1}H NMR, in $CDCl_3$ on a Varian T-60 or Gemini 300; ^{13}C NMR, in $CDCl_3$ on a Varian CFT-20; mass spectra, at 70 eV on a Hitachi RMU-6. All products were checked for purity by GC analysis and by the lack of extraneous peaks in their NMR spectra.

2,2-Dimethyl-1,3-diphenylpropan-1,3-dione was prepared by Smedley's procedure (15) in 25% yield. Dimethylmalonic acid (Aldrich, 25 g) was treated with excess thionyl chloride. The crude acid chloride was then treated with excess benzene and $AlCl_3$. After normal work-up the crude diketone was recrystallized from ethanol to yield white crystals, mp (dec.) 97.2°C (lit. (15) mp 99°C); IR ($CHCl_3$): 1670 cm^{-1}; UV λ_{max} (n,π^*): 320 nm; ^{1}H NMR δ: 1.6 (s, 6H), 7.30 (tt, 4H, J = 7, 2 Hz), 7.41 (tt, 2H, J = 7, 2 Hz), 7.82 (dd, 4H, J = 7 Hz); ^{13}C NMR δ: 25.14, 59.32, 128.36, 128.95, 132.69, 200.01; MS *m/z*: 252, 147, 105 (base), 77.

1,4-Diphenylbutane-1,4-dione was prepared by Becker's procedure of irradiating acetophenone (450 mL) with phenol and silica gel (16). After three recrystallizations from ethanol the dione was isolated in 5% yield as white crystals, mp 145°C (lit. (16) mp 144–145°C; IR ($CHCl_3$): 1690 cm^{-1}; UV λ_{max} (n,π^*): 313 nm; ^{1}H NMR δ: 3.39 (s, 4H, CH_2), 7.43 (tt, 4H, J = 7.0, 2.0 Hz), 7.54 (tt, 2H, J = 7.0, 2.0 Hz), 8.02 (dd, 4H, J = 7, 2 Hz); ^{13}C NMR δ: 32.4, 127.9, 128.4, 132.9, 136.7, 198.4; MS *m/z*: 238, 220, 133, 105 (base), 77.

1,5-Diphenylpentane-1,5-dione was prepared by Friedel–Crafts acylation of benzene with glutaryl chloride and aluminum chloride. It was purified by six recrystallizations from ethanol–water as white crystals, mp 64.2°C (lit. (17) mp 66.7°C, (6) mp 65°C); IR ($CHCl_3$) 1690 cm^{-1}; UV λ_{max} (n,π^*): 317 nm; ^{1}H NMR δ: 2.15 (quin, 2H, J = 7 Hz), 3.00 (t, 4H, J = 7 Hz), 7.43 (tt, 4H, J = 7.0, 2.0 Hz), 7.54 (tt, 2H, J = 7.0, 2.0 Hz), 7.92 (dd, 4H, J = 7, 2 Hz); ^{13}C NMR δ: 18.45, 37.2, 127.7, 128.2, 132.7, 136.6, 199.4; MS *m/z*: 252, 147, 133, 120, 105 (base), 77.

1,6-Diphenylhexane-1,6-dione was prepared by the Friedel–Crafts acylation of benzene with adipoyl chloride. It was purified by four recrystallizations from ethanol–water as white crystals, mp 106°C (lit. (18) mp 106–108°C); IR ($CHCl_3$): 1690 cm^{-1}; UV λ_{max} (n,π^*): 319 nm; ^{1}H NMR δ: 1.80 (tt, 4H, J = 7, 3 Hz), 2.95 (t, 4H, J = 7 Hz), 7.43 (tt, 4H, J = 7, 2 Hz), 7.54 (tt, 2H, J = 7, 2 Hz), 7.92 (dd, 4H, J = 7, 2 Hz); ^{13}C NMR δ: 23.5, 38.0, 127.6, 128,2, 132.5, 136.6, 199.45; MS *m/z*: 266, 248, 147, 146, 120, 105, 77 (base).

1,7-Diphenylheptane-1,7-dione was prepared by Friedel–Crafts acylation of benzene with pimeloyl chloride. It was purified by five recrystallizations from ethanol–water as white

Can. J. Chem. Downloaded from www.nrcresearchpress.com by 46.23.64.124 on 09/08/12
For personal use only.

crystals, mp 65.5–66°C (lit. (18) mp 67–68°C); IR ($CHCl_3$): 1690 cm^{-1}; UV λ_{max} (n,π^*): 318 nm; ^1H NMR δ: 1.70 (quin, 2H, J = 7 Hz), (tt, 4H, J = 7, 6 Hz), 2.95 (t, 4H, J = 6 Hz), 7.43 (tt, 4H, J = 7, 2 Hz), 7.54 (tt, 2H, J = 7, 2 Hz), 7.92 (dd, 4H, J = 7, 2 Hz); ^{13}C NMR δ: 23.5, 28.4, 37.7, 127.45, 128.0, 132.3, 136.4, 199.4; MS *m/z*: 280, 175, 161, 160, 146, 133, 120 (base), 105, 77.

*1,6-Bis-(*p*-ethylphenyl)hexane-1,6-dione*: Ethylbenzene was acylated with adipoyl chloride and $AlCl_3$. Normal work-up gave crude product in 25% yield. Two recrystallizations from ethanol–water gave white crystals, mp 96.2°C; IR ($CHCl_3$): 1685 cm^{-1}; UV λ_{max} (n,π^*): 318 nm; ^1H NMR δ: 1.22 (t, 6H, J = 7.6 Hz), 1.80 (tt, 4H, J = 7, 3 Hz), 2.70 (quart, 4H, J = 7.6 Hz), 2.99 (tt, 4H, J = 7, 3 Hz), 7.18 (d, 4H, J = 8 Hz), 7.82 (d, 4H, J = 8 Hz); ^{13}C NMR δ: 14.7, 23.7, 28.5, 37.9, 127.6, 127.85, 134.4, 149.3, 199.1; MS *m/z*: 322, 174, 161, 148, 145, 133 (base), 105.

*1,6-Bis-(*p*-methoxyphenyl)hexane-1,6-dione*: Adiponitrile (5.4 g) was added dropwise over 0.5 h to a 50 mL ether solution of the Grignard reagent prepared from 41 g *p*-bromoanisole and 4.8 g magnesium. Another 50 mL ether was added and the solution was refluxed for 4 h. The cooled solution was added slowly to excess HCl and ice. The resulting precipitate was not soluble in dilute aqueous HCl or in chloroform. After being heated, the aqueous portion provided very little product. The original precipitate was treated with hot 5 N HCl for 2 h. The cooled heterogeneous mixture was extracted with chloroform, with most of the remaining solid dissolving. Normal work-up provided 12 g of tan solid. Recrystallization from ethanol provided white crystals, mp 141.5–142.5°C; IR (KBr): 3000, 2951, 2938, 1671, 1599, 1254, 1169, 972, 833, 605 cm^{-1}; ^1H NMR ($CDCl_3$) δ: 1.78 (tt, 4H, J = 7, 3 Hz), 2.95 (tt, 4H, J = 7, 3 Hz), 6.90 (d, 4H, J = 9 Hz), 7.91 (d, 4H, J = 9 Hz); ^{13}C NMR ($CDCl_3$) δ: 24.26, 38.05, 55.51, 113.64, 130.01, 130.26, 163.31, 198.65; MS *m/z*: 326, 176, 150, 135 (base).

*1-Phenyl-6-(*p*-methoxyphenyl)hexane-1,6-dione*: Reaction of phenyl magnesium bromide with γ-chlorobutyronitrile afforded γ-chlorobutyrophenone (1). Its ethylene glycol ketal was prepared in routine fashion. The ketal was added dropwise over 15 min to a stirred solution of 1.4 g NaCN in 10 mL DMSO held at 90–95°C during the addition. The solution was then heated for 6 h at 125°C. The cooled solution was added to 50 mL of dilute aqueous $NaHCO_3$. Extraction into ether and solvent evaporation left 5 g (82%) of crude cyanoketal. This was added to the Grignard reagent prepared from 17 g *p*-bromoanisole in 30 mL ether. After 1 h reflux, the cooled solution was added to excess HCl–ice. The resulting aqueous layer was washed with ether, then heated on a steam bath. A solid separated; the entire mixture was extracted with chloroform. Normal work-up gave 2 g of off-white solid (30%). Recrystallization from hexane, then from methanol–hexane, gave white crystals, mp 111–112.5°C; IR (KBr): 1680, 1669, 1601, 1254, 1160, 1170 cm^{-1}; ^1H NMR (CDCl3) δ: 1.81 (tt, 4H, J = 7, 3 Hz), 2.96 (tt, 2H, J = 7, 3 Hz), 3.01 (tt, 2H, J = 7, 3 Hz), 6.91 (d, 2H, J = 8.9 Hz), 7.43 (t, 2H, J = 7 Hz), 7.53 (tt, 1H, J = 7, 2 Hz), 7.92 (d, 2H, J = 8.9 Hz), 7.935 (dd, 2H, J = 7 Hz); ^{13}C NMR ($CDCl_3$) δ: 23.84, 24.00, 37.93, 38.30, 55.33, 113.57, 127.90, 128.46, 129.92, 130.17, 132.84, 136.83, 163.25, 198.47, 199.92; MS *m/z*: 296, 176, 150, 146, 135 (base), 105.

Methyl 5-benzoylpentanoate was prepared by Friedel–Crafts acylation of benzene with the acid chloride of adipic acid monomethyl ester (prepared from adipic acid monomethyl ester by treatment with excess thionyl chloride), as described by Kemppainen (19). IR (neat): 1750, 1690, 1600, 1450 cm^{-1}; ^1H NMR (CCl_4) δ: 1.60 (m, 4H), 2.20 (t, 2H, J = 6 Hz), 2.75 (t, 2H, J = 6 Hz), 3.40 (s, 3H) 7.25 (t, 2H, J = 7 Hz), 7.45 (tt, 1H, J = 7, 2 Hz), 7.85 (dd, 2H, J = 7, 2 Hz).

*1-Phenyl-6-(*p*-ethylphenyl)hexane-1,6-dione*: Methyl 5-benzoylpentanoate was hydrolyzed with aqueous sodium hydroxide. The resulting acid was recrystallized once from ethanol–water and then treated with excess thionyl chloride at room temperature for 2 h. The crude acid chloride so obtained (9 g) was dissolved in 15 mL CH_2Cl_2 and added dropwise to 16.5 g $AlCl_3$ in 20 mL CH_2Cl_2 at 0°C; 5 g ethylbenzene was then added. The mixture was stirred at room temperature for 2.5 h and then poured onto 200 g of ice. Normal work-up furnished 8.8 g (75%) of brown solid. Recrystallization from ethanol–water gave white crystals, mp 77.5–78°C. IR (CCl_4): 1690, 1605 cm^{-1}; UV λ_{max} (n,π^*): 317 nm; ^1H NMR (CCl_4) δ: 1.20 (t, 3H, J = 7 Hz), 1.75 (m, 4H), 2.65 (quin, 2H, J = 7 Hz), 2.85 (m, 4H), 7.28 (d, 2H, J = 8 Hz), 7.43 (tt, 2H, J = 7, 2 Hz), 7.54 (tt, 1H, J = 7, 2 Hz), 7.82 (d, 2H, J = 8 Hz), 7.94 (dd, 2H, J = 7, 2 Hz); MS *m/z*: 294, 276, 174, 148, 146, 133 (base),105.

1,5-Diphenylpentan-1-one was prepared in 23% yield by the general procedure of Stork and Dowd (20). The cyclohexylimine of acetophenone was treated with ethyl magnesium bromide in THF and then with 3-bromo-1-phenylpropane (Aldrich). After normal work-up the crude oil was vacuum distilled and the fraction boiling between 133 and 142°C (0.025 Torr) collected. It was recrystallized six times from ethanol–water as white crystals, mp 44.5°C (lit. (21) mp 47°C); IR (CCl_4): 1695, 1450 cm^{-1}; UV λ_{max} (n,π^*): 319 nm; ^1H NMR δ: 1.65 (m, 4H), 2.73 (t, 2H, J = 6 Hz), 2.90 (t, 2H, J = 6 Hz), 7.15 (m, 5H), 7.43 (tt, 2H, J = 7, 2 Hz), 7.53 (tt, 1H, J = 7, 2 Hz), 7.94 (dd, 2H, J = 7, 2 Hz); ^{13}C NMR δ: 23.7, 30.75, 35.5, 38.0, 125.4, 127.7, 128.2, 132.5, 136.8, 141.9, 199.7; MS *m/z*: 238, 148, 133, 120, 118, 117, 105 (base), 91, 77.

*1-Phenyl-5-(*p*-acetylphenyl)pentan-1-one*: Acetyl chloride (3.6 g) was mixed with 15.2 g $AlCl_3$ in 35 mL methylene chloride at 0°C; 9.0 g of 1,5–diphenylpentan-1-one in 10 mL CH_2Cl_2 was added dropwise; the mixture was stirred at room temperature for 2 h. Normal work-up provided 10.4 g (94%) of crude solid. Four recrystallizations from methanol–water gave white crystals, mp 64.5°C; IR ($CHCl_3$): 1695, 1610 cm^{-1}; UV λ_{max} (n,π^*): 317 nm; ^1H NMR δ: 1.75 (m, 4H), 2.56 (s, 3H), 2.73 (t, 2H, J = 7 Hz), 3.00 (t, 2H, J = 7 Hz), 7.28 (d, 2H, J = 8 Hz), 7.43 (tt, 2H, J = 7, 2 Hz), 7.53 (tt, 1H, J = 7, 2 Hz), 7.87 (d, 2H, J = 8 Hz), 7.94 (dd, 2H, J = 7, 2 Hz); ^{13}C NMR δ: 23.55, 26.1, 30.3, 35.44, 37.9, 127.6, 128.2, 132.6, 134.8, 136.7, 147.7, 199.5; MS *m/z*: 280, 162, 160 (base), 133, 120, 105.

*1-Phenyl-5-(*p*-valerylphenyl)pentan-1-one* was prepared as was the *p*-acetyl compound except that valeryl chloride was used. Crude product was recrystallized five times from methanol to give white crystals, mp 60.2°C; IR (CCl_4): 1695, 1610 cm^{-1}; UV λ_{max} (n,π^*): 320 nm; ^1H NMR δ: 1.0 (t, 3H, J = 7

Can. J. Chem. Downloaded from www.nrcresearchpress.com by 46.23.64.124 on 09/08/12
For personal use only.

Hz), 1.7 (m, 8H), 2.75 (t, 2H, J = 7 Hz), 3.00 (t, 2H, J = 7 Hz), 7.18 (d, 2H, J = 8 Hz), 7.43 (tt, 2H, J = 7, 2 Hz), 7.55 (tt, 1H, J = 7, 2 Hz), 7.82 (d, 2H, J = 8 Hz), 7.94 (dd, 2H, J = 7, 2 Hz); ^{13}C NMR δ: 13.7, 22.2, 23.6, 26.4, 30.4, 35.5, 37.95, 127.8, 128.0, 128.3, 132.7, 134.8, 136.8, 147.5, 199.7, 199.8; MS *m/z*: 322, 280, 265 (base), 202, 167, 161, 160, 147, 133, 131, 120, 105.

4-Phenoxy-1-phenylbutane-1-one was prepared by a procedure similar to that described by Kalir and Balderman (22). *O*-(Tetrahydropyran-2-yl)mandelonitrile was treated with sodium hydride in DMSO under nitrogen; 1-bromo-3-phenoxypropane was added and the mixture stirred for 1 day and then acidified. Normal extraction and work-up provided pale yellow crystals in 97% yield. Three recrystallizations from ethanol gave white crystals, mp 62°C (lit. (1) mp 62.5–63.5°C); IR ($CHCl_3$): 1695, 1603 cm^{-1}; UV λ_{max} (n,π^*): 316 nm; ^{1}H NMR δ: 2.25 (tt, 2H, J = 7, 6 Hz), 3.15 (t, 2H, J = 7 Hz), 4.05 (t, 2H, J = 6 Hz), 7.0 (dd, 2H, J = 9, 2 Hz), 7.43 (tt, 2H, J = 7, 2 Hz), 7.54 (tt, 1H, J = 7, 2 Hz), 7.92 (dd, 2H, J = 7. 2 Hz); ^{13}C NMR δ: 23.5, 34.6, 66.5, 114.2, 120.4, 127.7, 128.2, 1219.1, 132.7, 136.6, 158.6, 199.1; MS *m/z*: 240, 147 (base), 120, 105.

*4-(*p*-Acetylphenoxy)-1-phenylbutan-1-one* was prepared by Friedel–Crafts acetylation of 4-phenoxybutyrophenone; white crystals were obtained after work-up and recrystallization from ethanol, mp 92°C; IR ($CHCl_3$): 1690, 1605 cm^{-1}; UV λ_{max} (n,π^*): 316 nm; ^{1}H NMR δ: 2.25 (tt, 2H, J = 6, 7 Hz), 2.40 (s, 3H), 3.19 (t, 2H, J = 7 Hz), 4.11 (t, 2H, J = 6 Hz), 6.89 (d, 2H, J = 9 Hz), 7.43 (tt, 2H, J = 7, 2 Hz), 7.54 (tt, 1H, J = 7, 2 Hz), 7.89 (d, 2H, J = 9 Hz), 7.96 (dd, 2H, J = 7, 2 Hz); ^{13}C NMR δ: 23.5, 26.1, 34.5, 67.1, 114.0, 127.8, 128.5, 130.2, 130.4, 133.0, 135.6, 162.7, 196.5, 199.0; MS *m/z*: 282, 163, 147 (base), 120, 105.

*4-(*p*-Valerylphenoxy)-1-phenylbutan-1-one* was prepared in 87% yield by the same procedure as followed for the *p*-acetyl homologue above, except for the use of valeryl chloride. It was purified by two recrystallizations from ethanol as white crystals, mp 116°C. IR ($CHCl_3$): 1690, 1603 cm^{-1}; UV λ_{max} (n,π^*): 316 nm ; ^{1}H NMR δ: 1.00 (t, 3H, J = 7 Hz), 1.6 (m, 4H), 2.25 (tt, 2H, J = 7, 6 Hz), 2.85 (t, 2H, J = 7 Hz), 3.15 (t, 2H, J = 7 Hz), 4.10 (t, 2H, J = 6 Hz), 6.85 (d, 2H, J = 4 Hz), 7.35 (m, 3H), 7.85 (d, 2H, J = 9 Hz), 7.96 (dd, 2H, J = 7, 2 Hz); ^{13}C NMR δ: 13.7, 22.3, 23.4, 26.5, 34.5, 37.8, 67.0, 113.9, 127.8, 128.4, 130.1, 132.9, 136.7, 162.4, 198.9, 199.05; MS *m/z*: 324, 282, 267, 205, 177, 148 (base), 121, 120, 105.

*4-(*p*-Cyanophenoxy)-1-phenylbutan-1-one* was prepared by S_N2 displacement on γ-iodobutyrophenone. Benzene was acylated with 35 g 4-chlorobutyryl chloride and 36 g $AlCl_3$ and furnished a 95% yield of crude 4-chloro-1-phenylbutan-1-one. Distillation provided a 70% yield of pure ketone, bp 100–103°C at 0.55 Torr (lit. (23) bp 126–129°C at 5 Torr); IR (neat): 1690, 1600 cm^{-1}; ^{1}H NMR (CCl_4) δ: 2.15 (quin, 2H, J = 7 Hz), 3.05 (t, 2H, J = 7 Hz), 3.55 (t, 2H, J = 7 Hz), 7.43 (tt, 2H, J = 7, 2 Hz), 7.54 (tt, 1H, J = 7, 2 Hz), 7.92 (dd, 2H, J = 7, 2 Hz).

A mixture of 43 g chloroketone and 75 g sodium iodide in 500 mL 2-butanone was refluxed for 2 h. After the solvent was removed, the resulting sludge was taken up in a mixture of 500 mL ether and 500 mL water. The ether layer was separated, washed, and distilled, leaving 51 g (78%) of crude 4-iodoketone as an oil. IR (neat): 1690, 1230, 745, 695 cm^{-1}; ^{1}H NMR δ: 2.2 (m, 2H), 3.0 (t, 2H, J = 3 Hz), 3.3 (t, 2H), 7.35 (m, 3H), 7.85 (m, 2H). The 4-iodo-1-phenylbutan-1-one was converted to its ethylene glycol ketal by reflux in a Dean–Stark apparatus. Normal work-up provided a 93% yield of ketal as an oil: ^{1}H NMR δ: 1.9 (t, 2H), 3.0–4.0 (m, 8H), 7.25 (m, 5H).

To 300 mL of DMSO containing 4.6 g sodium under nitrogen, 23.8 g 4-cyanophenol in 300 mL DMSO was added dropwise; the resulting mixture was stirred until all the sodium had dissolved. The iodoketone ketal (54 g) in 300 mL DMSO was then added dropwise over 6 h and let stir another 24 h. The mixture was heated to 60°C for 1 h. Water was added to the cooled mixture, which was then extracted with four 500 mL portions of ether. Normal work-up and solvent removal left 33 g (73%) of a light brown solid. Two recrystallizations from ethanol gave 4-(*p*-cyanophenoxy)-1-phenylbutan-1-one as white crystals, mp 117°C. IR ($CHCl_3$): 2210, 1690, 1515, 1260, 1175 cm^{-1}; UV λ_{max} (n,π^*): 316 nm; ^{1}H NMR δ: 2.2 (quin, 2H, J = 3 Hz), 3.15 (t, 2H, J = 3 Hz), 4.05 (t, 2H, J = 3 Hz), 6.85 (d, 2H, J = 9 Hz), 7.43 (tt, 2H, J = 7, 2 Hz), 7.54 (tt, 1H, J = 7, 2 Hz), 7.75 (d, 2H, J = 9 Hz), 7.96 (dd, 2H, J = 7, 2 Hz); ^{13}C NMR δ: 23.2, 34.25, 67.1, 103.6, 114.9, 118.9, 127.7, 128.3, 132.9, 133.6, 136.5, 161.9, 198.8; MS *m/z*: 265, 147 (base), 120, 105, 77.

5–Phenoxy-1-phenylpentan-1-one: This ketone was prepared by two methods. The first involved treatment of 5-iodo-1-phenylpentan-1-one with the sodium salt of phenol. Normal work-up gave a complex mixture from which 12 g of desired product (21%) was isolated by chromatography through 3 lb alumina. The eluting solvent was continuously varied from hexane to ethyl acetate, with chloroform providing the product fraction. The ketone was also prepared in 39% yield from 25 g *O*-(tetrahydropyran-2–yl)mandelonitrile and 25 g 1-bromo-4-phenoxybutane by the procedure described above for the 4-phenoxy ketone. In both cases, three recrystallizations from ethanol provided white crystals, mp 68.7–69.0°C; IR ($CHCl_3$): 1690, 1603 cm^{-1}; UV λ_{max} (n,π^*): 318 nm; ^{1}H NMR δ: 1.95 (m, 4H), 3.0 (t, 2H, J = 7 Hz), 3.95 (t, 2H, J = 6 Hz), 6.85 (d, 2H, J = 9 Hz), 7.20 (m, 5H), 7.85 (dd, 2H, J = 7, 2 Hz); ^{13}C NMR δ: 20.7, 28.6, 37.9, 67.3, 114.3, 120.4, 127.8, 128.4, 129.2, 132.7, 136.8, 158.8, 199.6; MS *m/z*: 254, 161, 131, 105 (base), 94, 91, 77.

*5-(*p*-Acetylphenoxy)-1-phenylpentan-1-one*: A 5 g portion of the above ketone was subjected to Friedel–Crafts acetylation as described above for the analogous butanone. Recrystallization from ethanol gave white crystals, mp 125.2–125.5°C. IR ($CHCl_3$): 1685, 1603, 1175 cm^{-1}; UV λ_{max} (n,π^*): 317 nm; ^{1}H NMR δ: 1.9 (m, 4H), 2.50 (s, 3H), 3.11 (t, 2H, J = 7 Hz), 4.11 (t, 2H, J = 6 Hz), 6.89 (d, 2H, J = 9 Hz), 7.43 (tt, 2H, J = 7, 2 Hz), 7.54 (tt, 1H, J = 7, 2 Hz), 7.89 (d, 2H, J = 9 Hz), 7.96 (dd, 2H, J = 7, 2 Hz); ^{13}C NMR 20.6, 26.05, 28.4, 37.7, 67.7, 113.9, 127.8, 128.4, 130.05, 130.4, 132.8, 136.7, 162.7, 196.5, 199.5; MS *m/z*: 296, 161 (base), 149, 120, 105, 77.

*5-(*p*-Valerylphenoxy)-1-phenylpentan-1-one* was prepared in 82% yield from 5 g 1,5-diphenyl-1-pentanone by the Friedel–Crafts reaction just described for the acetyl derivative. Recrystallization from ethanol provided white crystals, mp 111.7–112.0°C; IR ($CHCl_3$): 1690, 1600, 1515, 1175 cm^{-1}; UV λ_{max} 317 nm; ^{1}H NMR δ: 1.0 (t, 3H, J = 3 Hz), 1.2–2.0 (m, 8H), 3.11 (t, 2H, J = 7 Hz), 4.20 (t, 2H, J = 6 Hz), 6.95 (d, 2H, J = 9 Hz), 7.43 (tt, 2H, J = 7, 2 Hz), 7.54 (tt, 1H, J = 7, 2 Hz),

Can. J. Chem. Downloaded from www.nrcresearchpress.com by 46.23.64.124 on 09/08/12
For personal use only.

7.85 (d, 2H, J = 9 Hz), 7.96 (dd, 2H, J = 7, 2 Hz); ^{13}C NMR δ: 13.77, 20.61, 22.33, 26.59, 28.48, 37.80, 67.69, 113.84, 128.37, 129.94, 130.06, 132.79, 136.75, 162.53, 199.02, 199.63; MS *m/z*: 338, 296, 281, 177, 162, 161 (base), 147, 121, 120, 105.

*5-(*p*-Cyanophenoxy)-1-phenylpentan-1-one* was prepared in 70% yield from 11 g of 5-iodo-1-phenylpentan-1-one and 9.1 g 4-cyanophenol as described above for the homologous butanone. Six recrystallizations from ethanol gave white crystals, mp 96.2–96.5°C; IR: 2215, 1690, 1605, 1175 cm^{-1}; UV λ_{max} (n,π^*): 318 nm; ^{1}H NMR δ: 1.9 (m, 4H), 3.05 (t, 2H, J = 7 Hz), 4.0 (t, 2H, J = 6 Hz), 6.95 (d, 2H, J = 9 Hz), 7.43 (tt, 2H, J = 7, 2 Hz), 7.54 (tt, 1H, J = 7, 2 Hz), 7.75 (d, 2H, J = 9 Hz), 7.96 (dd, 2H, J = 7, 2 Hz)); ^{13}C NMR δ: 20.5, 28.3, 37.7, 103.6, 115.0, 127.75, 128.1, 128.4, 132.8, 133.7, 136.7, 162.05, 199.4; MS *m/z*: 279, 162, 161 (base) 143, 133, 132, 120, 119, 105 (base), 102.

p-*Ethylvalerophenone*: Friedel–Crafts acylation of ethylbenzene with valeryl chloride gave an oil that was purified by repeated vacuum distillation, bp 93°C (0.35 Torr) (lit. (24) bp 169–171°C at 32 Torr). GC analysis indicated 99.15% *para* isomer, 0.84% *ortho* isomer, and 0.01% unknown impurity. IR (neat): 1690, 1605 cm^{-1}; UV λ_{max} (n,π^*): 309 nm; ^{1}H NMR δ: 1.10 (t, 3H, J = 7 Hz), 1.25 (t, 3H, J = 7 Hz), 1.4–1.7 (m, 4H), 2.65 (quart, 2H, J = 7 Hz), 2.65 (t, 2H, J = 7 Hz), 7.28 (d, 2H, J = 8 Hz), 7.87 (d, 2H, J = 8 Hz); ^{13}C NMR δ: 13.6, 14.85, 22.2, 26.35, 28.6, 37.9, 127.7, 128.0, 134.6, 149.4, 199.8; MS *m/z*: 190, 161, 148, 133 (base), 105.

p-*Ethylacetophenone*: Friedel–Crafts acetylation of excess ethylbenzene gave a liquid, bp 50.5–51°C (0.1 Torr) (lit. (25) bp 125°C at 20 Torr). GC analysis indicated 0.85% *ortho* isomer. IR (neat): 1690,1605 cm^{-1}; UV λ_{max} (n,π^*): 309 nm; ^{1}H NMR (CCl_4) δ: 1.25 (t, 3H, J = 7 Hz), 2.45 (s, 3H), 2.65 (quart, 2H, J = 7 Hz), 7.10 (d, 2H, J = 8 Hz), 7.70 (d, 2H, J = 8 Hz); MS *m/z*: 148, 133 (base), 105.

Procedures

Product identification

Acetophenone and its *p*-ethyl and *p*-methoxy derivatives were identified by their characteristic GC retention times. The same was true for propene, which produces a sharp peak well before the solvents. It could be analyzed quantitatively by keeping the samples in an ice bath before analysis; its peak intensity was calibrated for Stern–Volmer plots by equating its yield to that of the nonvolatile acetophenone. The several ω-(*p*-acetylphenyl) diketones were themselves products from the *p*-valerylphenyl diketones. The various vinyl ketone products also formed by type II photoelimination were apparent in GC peaks comparable in size to those of the acetophenones, although their structures were not routinely verified. Likewise, in all cases small GC peaks were observed with retention times, relative to starting diketone, characteristic of cyclobutanols.

Product formation from the diketones was determined by a representative analysis of just one, 5-(*p*-acetylphenyl)-1-phenylpentan-1-one. A 2 g sample in 450 mL benzene under nitrogen was irradiated in an immersion well with a quartz-filtered 450-W Hanovia mercury arc. After 6 h no diketone was detectable by HPLC. Removal of solvent left 2 g of oil, which was dissolved in a few mL of hexane and chromatographed through 65 g of Mallinkrodt Silicar CC-7 silica gel. The column was eluted with hexane mixed with increasing proportions of methylene chloride and then with increasing proportions of ethyl acetate. Acetophenone and *p*-allylacetophenone eluted in the range 40:60 to 80:20 CH_2Cl_2:hexane; their structures were determined by comparison to authentic samples. The fraction eluting at 20:80 ethyl acetate:CH_2Cl_2 was found to be a single compound assigned as *cis*-1-phenyl-2-(*p*-acetylphenyl)methylcyclobutanol. Evaporation of solvent left 0.21 g of oil: IR ($CHCl_3$): 3580, 3475, 1690, 1605, 1275, 1185 cm^{-1}; UV λ_{max} (CH_2Cl_2): 254 nm (ε = 15 000); ^{1}H NMR δ: 1.5 (m, 1H), 2.0 (m, 2H), 2.2 (d, 1H, J = 2 Hz), 2.4 (s, 3H), 2.95 (m, 4H), 7.15 (m, 3H), 7.65 (m, 2H); MS *m/z*: 280, 252, 237, 161, 145, 134, 122, 121 (base), 120, 107, 106, 105. Earlier and later fractions contained another 0.08 g. The fractions that eluted at 40% ethyl acetate yielded 0.074 g analyzed as 93% of one compound; it was assigned as the *trans* cyclobutanol; IR ($CHCl_3$): 3580, 3450, 1690, 1605, 1275, 1185 cm^{-1}; UV λ_{max} (CH_2Cl_2): 254 nm (ε = 9500); ^{1}H NMR δ: 1.2–3.0 (m, 11H), 6.8–7.75 (m, 9H); MS *m/z*: 280, 252, 237, 161, 145, 134, 120 (base), 115, 105. Another 0.14 g was contained in earlier fractions.

Spectroscopy

Phosphorescence spectra were taken on a Perkin–Elmer MPF-44A spectrophotometer equipped with a differential corrected spectrum unit and a Hitachi phosphorescence accessory. Samples, typically 10^{-3}–10^{-4} M in 5 mm quartz tubes, were held in a quartz Dewar containing liquid nitrogen.

Steady state photokinetics

As in previous work (1), samples were prepared in volumetric glassware; 2.8 mL aliquots were transferred into constricted 13 × 100 mm Pyrex or Kimax culture tubes, which were then subjected to three freeze–pump–thaw cycles at high vacuum before being sealed. All samples in a given experiment were irradiated in parallel on a "merry-go-round" apparatus (26) set in a room temperature water bath. Light was provided by a 450-W Hanovia mercury arc housed in an immersion well inside a Vycor vessel containing a basic solution 0.002 M in potassium chromate to isolate the 313 nm emission band. Samples were analyzed either by GC or HPLC, with response factors for products and standards calibrated with authentic samples. Both long-chain alkanes and long-chain alkyl benzoates were used as internal standards.

Results

The dibenzoylalkanes shown in Scheme 1, with from one to five intervening carbons, were prepared by standard methods. Dibenzoylmethane could not be studied because of the preponderance of the enol form, so 2,2-dibenzoylpropane **2,2Bz$_2$Pr** was studied instead. Neither this compound nor 1,2-dibenzoylethane **12Bz$_2$Et** underwent any measurable photodegradation after prolonged irradiation. Both diketones did sensitize the *cis–trans* isomerization of 1,3-pentadiene and of stilbene. Figure 1 shows the sensitization plots obtained, from which $k_q\tau$ and Φ_{isc} values were extracted (27). The Φ_{isc} values for a few other ketones were obtained by measuring the

Can. J. Chem. Downloaded from www.nrcresearchpress.com by 46.23.64.124 on 09/08/12
For personal use only.

Scheme 1.

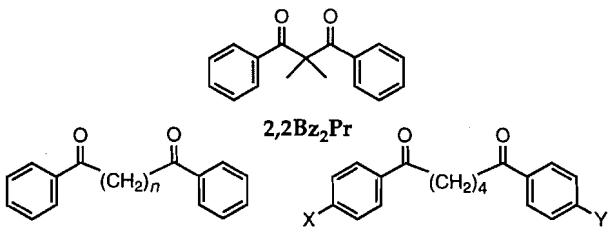

1,2Bz$_2$Et	$n = 2$	**1Bz4EtBzBu**	X = H ; Y = Et
1,3Bz$_2$Pr	$n = 3$	**1,4EtBz$_2$Bu**	X = Y = Et
1,4Bz$_2$Bu	$n = 4$	**1Bz4AnBu**	X = H ; Y = OMe
1,5Bz$_2$Pn	$n = 5$	**1,4An$_2$Bu**	X = Y = OMe

Fig. 1. Double reciprocal plots for (●) *trans*→*cis* isomerization of stilbene sensitized by **2,2BzPr** (bottom *x*, left *y* axis) and (■) *cis*–*trans* isomerization of 1,3-pentadiene sensitized by **1,2BzEt** (top *x*, right *y* axis).

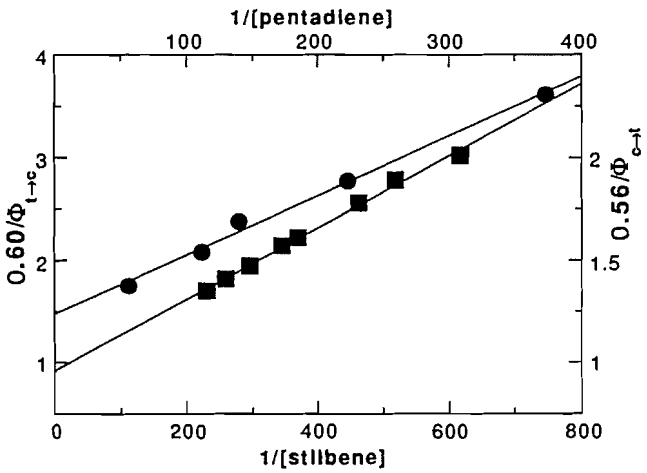

Fig. 2. Dependence of quantum yields for acetophenone formation from **1,3Bz$_2$Pr** on conversion: (▲) in benzene; (●) in benzene with 4.5 M dioxane; (○) reciprocal plot of data in 4.5 M dioxane (right *y* axis).

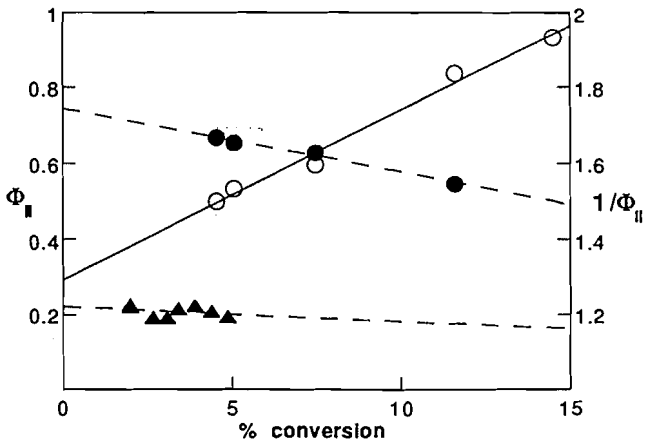

extent of isomerization of a single high concentration of pentadiene.

Dibenzoylpropane, -butane, and -pentane all undergo Norrish type II photoelimination. Quantum yields of acetophenone formation were determined for degassed benzene solutions containing 0.01 M diketone and various concentrations of dioxane. Comparable valerophenone solutions were irradiated simultaneously as actinometers (28). The values so measured were reproducible within ±5%. For the first two diketones quantum yields reached maximum levels at 4–5 M dioxane; but for **1,5Bz$_2$Pn** they get even higher in *tert*-butyl alcohol. The maximum and minimum values are recorded in Table 1. Benzoylalkenes accompany the acetophenone; they were not measured directly, but peaks of the appropriate size and retention time were noted during GC analysis. In the case of dibenzoylpropane **1,3Bz$_2$Pr**, the coproduct is phenyl vinyl ketone, an excellent triplet quencher (9). Acetophenone quantum yields decreased with increasing conversion as shown in Fig. 2 (28). Table 2 contains the values extrapolated to zero conversion, as determined from plots of reciprocal quantum yields, one of which is included in Fig. 2. Diketone disappearance quantum yields were also measured in pure benzene, in the presence of 4.5 M dioxane or 1 M pyridine, and in *tert*-butyl alcohol. In most cases disappearance yields were 15 ± 5% higher than acetophenone yields (29). GC peaks corresponding to the expected minor cyclobutanol coproducts were observed but not measured quantitatively except for dibenzoylbutane **1,4Bz$_2$Bu**, where $\Phi_{CB} = 0.05$ in benzene, and for dibenzoylpentane **1,5Bz$_2$Pn**, where $\Phi_{CB} = 0.14$ in *tert*-butyl alcohol. The chemical yields of cyclobutanol were in the 10 ± 5% range for the other diketones studied.

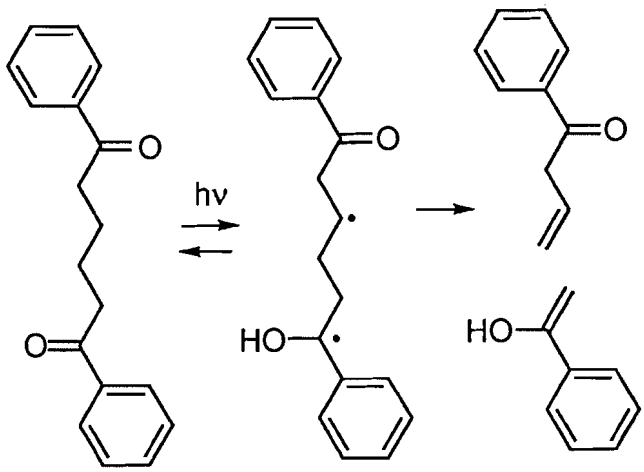

Triplet lifetimes were measured by standard quenching techniques. Degassed benzene solutions containing 0.01 M diketone and varying concentrations of 2,5-dimethyl-2,4-hexadiene were irradiated to ~5% conversion. Stern–Volmer plots were linear with the slopes listed as $k_q\tau$ values in Table 1. The value for dibenzoylpropane was corrected upward for product quenching from the data in Fig. 2, by multiplying the observed slope by Φ^{0conv}/Φ_{obs} as described earlier (28).

The same measurements were performed on two groups of unsymmetric diketones: diaroylbutanes with different *para* substituents; and ones in which one benzoyl group is turned around. Scheme 2 depicts these compounds and their abbreviations. Proper interpretation of their behavior necessitated study of the *p,p'*-disubstituted 1,4-dibenzoylbutanes shown in Scheme 1 and the model monoketones shown in Scheme 2. Table 2 lists steady state quantum yields and $k_q\tau$ values, some of which were reported much earlier (1). As with the symmetric diketones, acetophenones were the major products

Can. J. Chem. Downloaded from www.nrcresearchpress.com by 46.23.64.124 on 09/08/12
For personal use only.

Table 1. Steady state photokinetic parameters for α,ω-dibenzoylalkanes.

Ketone	Φ_{II} [a]	Φ_{II}^{max} [b]	Φ_{dis} [a]	Φ_{II}^{max} [b]	Φ_{isc} [c]	$k_q\tau(M^{-1})$
2,2Bz$_2$Pr	0	0	0	0	0.70	488[c]
1,2Bz$_2$Et	0	0	0	0	1.0	300 ± 3[c]
1,3Bz$_2$Pr	0.22[d]	0.77[d]	0.27[d]	1.0[d]	1.02	154 ± 1[d]
1,4Bz$_2$Bu	0.42	0.54	0.45	0.59	1.02	80 ± 2.4
1,5Bz$_2$Pn	0.37	0.76[e]	0.39	0.92[e]		45 ± 1.4
1,4EtBz$_2$Bu	0.27	0.28	0.30		1.06	371 ± 10
1,4An$_2$Bu[f]	0.04	0.06[g]				10 000

[a]In benzene.
[b]4 M dioxane added.
[c]By sensitization.
[d]Extrapolated to zero conversion.
[e]In *tert*-butyl alcohol.
[f]Values from ref. 11.
[g]Pyridine added.

Table 2. Steady state photokinetic parameters for unsymmetric diketones.

Ketone	Φ_{II} [a]	Φ_{II}^{max} [b]	Φ_{dis} [a]	Φ_{II}^{max} [b]	Φ_{isc} [c]	$k_q\tau(M^{-1})$
1Bz4(EtBz)Bu (Bz)	0.26	0.36	0.42			149
1Bz4(EtBz)Bu (EtBz)	0.072	0.11				165
1Bz4AnBu (Bz)[d]	0.20					240
1Bz4AnBu (An)[d]	0.01					370
δ(4AcPh)VP (Bz)	0.30	0.51	0.39	0.59	1.03	177
δ(4VaPh)VP (Bz)	0.21	0.34		0.65	1.04	100
δ(4VaPh)VP (Tol)	0.12	0.23				93
γ(4AcPhO)BP (Bz)	0.29	0.53				552
γ(4VaPhO)BP (Bz)	0.33	0.49				349
γ(4VaPhO)BP (An)	0.039	0.065				438
δ(4AcPhO)VP (Bz)	0.34	0.42				2010
δ(4VaPhO)VP (Bz)	0.21	0.31				1130
δ(4VaPhO)VP (An)	0.075	0.16				1580

[a]In benzene.
[b]4 M dioxane added.
[c]By sensitization.
[d]Reference 11.

Scheme 2.

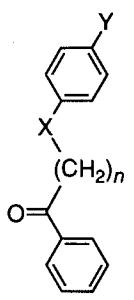

	n	X	Y
δPhVP	3	CH_2	H
δAcPhVP	3	CH_2	COMe
δVaPhVP	3	CH_2	COBu
γPhOBP	3	O	H
γCNPhOBP	3	O	CN
γAcPhOBP	3	O	COMe
γVaPhOBP	3	O	COBu
δPhOVP	4	O	H
δCNPhOVP	4	O	CN
δAcPhOVP	4	O	COMe
δVaPhOVP	4	O	COBu

pEtVP X = Et; Y = Me
pMeOVP X = OMe; Y = Me
γEstBP X = H; Y = CO_2Me
δEstVP X = H; Y = CH_2CO_2Me

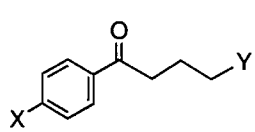

measured, although cyclobutanols were also observed. For the δ-substituted valerophenones, especially **δPhVP** and **δPhOVP**, some δ-hydrogen abstraction would be expected to compete (30). Additional product peaks in the GC suggested the formation of cyclopentanols in low yields. In the case of

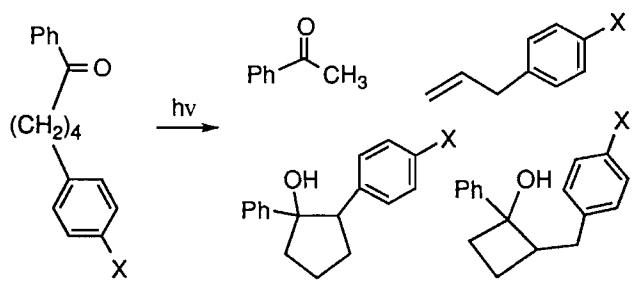

δ-(*p*-valerylphenyl)valerophenone **γVaPhVP** and γ- and δ-(*p*-valerylphenoxy)butyro- and valerophenones **γVaPhOBP**

Table 3. Spectroscopic data for diketones and model monoketones.

Compound	γ_{max}, n,π^*[a] (nm)	ε(313 nm)[a] ($[M]^{-1}$ cm^{-1})	phos 0–0 band (E_T)[b] (nm)	(kcal/mol)
2,2Bz$_2$Pr	320	215	394	(72.6)
1,2Bz$_2$Et	313	129	384	(74.5)
1,3Bz$_2$Pr	317	100	386	(74.1)
1,4Bz$_2$Bu	319	110	385	(74.3)
1,5Bz$_2$Pn	318	110	384	(74.5)
PhCOBu (VP)	320	47	385	(74.3)
1,4EtBz$_2$Bu	318	157	393	(72.7)
pEtVP	309	76	392	(72.9)
1Bz4EtBzBu	317	145	392	(72.7)
1,4An$_2$Bu	314	300	397	(72.0)
pMeOVP	313	147	397	(72.0)
δValPhVP	320	128	392	(72.9)
γValPhOBP	316	211	401	(71.3)
δValPhOVP	317	224	400	(71.5)

[a]In benzene at room temperature.
[b]In 2-methyltetrahydrofuran at 77 K.

and **δVaPhOVP**, type II reaction of the valeryl group was detected both by appearance of the homologous acetylketones and by measurement of propene formation. Triplet lifetimes of the different δ-phenoxyvalerophenones were confirmed by flash kinetics. For the *p*-methoxybenzoyl groups of **δAcPhOVP** and **δVaPhOVP**, these were 500 and 450 ns, respectively.

Spectroscopy

UV spectra of the various diketones were measured in benzene; phosphorescence spectra, in 2-methyltetrahydrofuran at 77 K. Table 3 contains all the relevant data, including extinction coefficients at 313 nm, where the compounds were irradiated. **1,3Bz$_2$Pr**, **1,4Bz$_2$Bu**, and **1,5Bz$_2$Pn** behave just like valerophenone in absorption. Their emission spectra nearly duplicate the characteristic n,π^* spectrum of valerophenone, with 0–0 bands at 385 ± 1 nm (74.3 kcal/mol). **1,2Bz$_2$Et** and **2,2Bz$_2$Pr** show the same emission spectra but have larger extinction coefficients at 313 nm, respectively. Likewise, **1,4EtBz$_2$Bu** and **1,4An$_2$Bu** mimic the behavior of *p*-ethyl- and *p*-methoxyvalerophenone in both absorption and emission, the latter occurring at lower energy and showing broader structure, as expected for systems with π,π^* lowest triplets. The various ω-substituted alkanophenone model monoketones have spectra like that of valerophenone.

Discussion

The diketones that we have studied are divided into symmetric and unsymmetric categories because intramolecular energy transfer affects the kinetics for the two quite differently. Each symmetric diketone has two identical chromophores, either of which can be excited with equal probability. After excitation of one of the carbonyls, energy transfer will eventually equilibrate the excitation such that each carbonyl is excited for exactly half the time on a given molecule. In contrast, the absorption ratio for the unsymmetric diketones with two different chromophores need not be 50:50 and can vary with wavelength. Since the two chromophores have different triplet energies, rates of internal energy transfer are not equal and define a distribution of interconverting triplets that begins equal to the ratio of extinction coefficients and rapidly establishes an equilibrium that is not 50:50. Inasmuch as triplet excitation equilibrates between the two chromophores before significant decay occurs, both chromophores will show the same equilibrium lifetime, as defined by eq. [1], where $1/\tau^0$ represents the sum of all unimolecular and pseudo-first-order decay rate constants for a given carbonyl triplet *exclusive of its rate of energy transfer to the other* and the χ's reflect the fractional population of triplet excitation on each chromophore (27). In that case the same triplet lifetime is measured no matter which chromophore is monitored for both steady state Stern-Volmer quenching studies and direct flash kinetic detection of triplet decay. If the two chromophores are not completely equilibrated, because natural decay is competitive with energy transfer, then the kinetics become complicated; Stern–Volmer plots diverge and curve in opposite directions (27). This situation is discussed more fully below.

$$[1] \quad 1/\tau_{eq} = \chi_{Bz}/\tau^0_{Bz} + \chi_{RBz}/\tau^0_{RBz}$$

For the symmetric diketones, separate τ's and χ's cannot be distinguished, since energy transfer is degenerate. The unexcited benzoyl group effectively behaves merely as an electron-withdrawing substituent in its effect on the reactivity of the excited benzoyl. For the unsymmetric diketones, the apparent rate constants for excited state decay of each chromophore are different from those intrinsic to the chromophore, depending also on rate constants for triplet energy transfer and relative extinction coefficients β.

Derivation of triplet decay rate constants

Tables 4 and 5 contain rate constants for hydrogen abstraction and radiationless decay of all the monoketones and symmetric diketones studied; Table 6 contains apparent rate constants for the unsymmetric diketones. These are all derived from the

Can. J. Chem. Downloaded from www.nrcresearchpress.com by 46.23.64.124 on 09/08/12
For personal use only.

Can. J. Chem. Downloaded from www.nrcresearchpress.com by 46.23.64.124 on 09/08/12
For personal use only.

Table 4. Photokinetic parameters for triplet decay of model ketones.

Ketone	Φ_{II}[a]	Φ_{II}^{max}[b]	Φ_{dis}[a]	Φ_{dis}^{max}[b]	$k_q\tau$ (M^{-1})	$1/\tau$ (10^7 s^{-1})	$k_{\gamma\text{-H}}$[c] (10^7 s^{-1})	k_d[d] (10^7 s^{-1})
PhCOBu[e]	0.33	0.85	0.40	1	40	15	15	0
γ-EstBP	0.50[e]	0.58	0.51[e]	0.60	490[e]	1.2	1.2	0
δ-EstVP[e]	0.61	0.72	0.79	1	131 ± 3	4.6	4.6	0
pEtVP	0.27	0.54		0.63	253 ± 22	2.4	1.6	0.8
pMeOVP[f]	0.14	0.22		0.26	2200	0.27	0.07	0.20
δPhVP	0.30	0.64		~1	42 ± 2	14	11	3
γPhOBP[e]	0.32	0.66		~0.73	23	26	19	7
γ(CNPhO)BP	0.38	0.53		~0.6	81 ± 2	7.5	4.5	3.0
δPhOVP	0.43	0.70		~1	193 ± 6	3.1	2.4	0.7
δ(CNPhO)VP	0.40	0.56		~1	404 ± 9	1.5	0.9	0.6

[a]In benzene.
[b]In *tert*-butyl alcohol.
[c]Φ_{dis}^{max}/τ.
[d]$1/\tau - k_H$.
[e]Reference 1.
[f]Reference 33.

Table 5. Triplet decay rate constants (units of 10^7 s^{-1}) for symmetric α,ω-diketones.

Ketone	$1/\tau$[a]	$k_{\gamma\text{-H}}$[b]	Expected $k_{\gamma\text{-H}}$	k_d[c]	Expected k_d	k_{sq}
1,1Bz$_2$Pr	1.2	0	0	1.2	0	1.2
1,2Bz$_2$Et	2.0	0	0	1.7	0	1.7
1,3Bz$_2$Pr	3.8	3.8	?	0	0	0
1,4Bz$_2$Bu	7.4	4.4	4.5	3.0	0	3.0
1,5Bz$_2$Pn	13.2	12.0	8	1.2	0	1.2
1,4EtBz$_2$Bu	1.5	0.48	0.4	1.0	0.1	0.9
1,4An$_2$Bu	0.60	0.04	0.03	0.54	0.2	0.34

[a]Based on $k_q = 6 \times 10^9$ M^{-1} s^{-1}.
[b]Φ_{dis}^{max}/τ.
[c]$1/\tau - k_{\gamma\text{-H}}$.

Table 6. Triplet decay rate constants (units of 10^7 s^{-1}) for unsymmetric diketones.

Ketone	$1/\tau$[a]	$k_{\gamma\text{-H}}$[b]	Model $k_{\gamma\text{-H}}$	k_d[c]	Model k_d	k_{sq}
1Bz4EtBzBu (Bz)	4.0	1.7	4.5	2.3	0	2.3
1Bz4EtBzBu (EtBz)	3.6	0.43	0.4	3.2	0.8	
1Bz4AnBu (Bz)	2.5	0.50	4.5	2.0	0	1.3
1Bz4AnBu (An)	1.7	0.018	0.03	1.5	0.2	
δ(4AcPh)VP (Bz)	3.5	2.0	~6[d]	1.5	3	0
δ(4VaPh)VP (Bz)	5.9	2.3	~6[d]	3.6	3	0
δ(4VaPh)VP (EtBz)	6.2	1.6	1.6	4.6	0.8	
γ(4AcPhO)BP (Bz)	1.0	0.72	4.5	0.23	3	0
γ(4VaPhO)BP (Bz)	1.7	1.0	4.5	0.7	3	0
γ(4VaPhO)BP (An)	1.3	0.10	0.07	1.2	0.2	
δ(4AcPhO)VP (Bz)	0.30	0.15	0.9	0.15	0.6	0
δ(4VaPhO)VP (Bz)	0.53	0.19	0.9	0.34	0.6	0
δ(4VaPhO)VP (An)	0.38	0.07	0.07	0.21	0.2	

[a]Based on $k_q = 6 \times 10^9$ M^{-1} s^{-1}.
[b]Φ_{dis}^{max}/τ.
[c]$1/\tau - k_{\gamma\text{-H}}$.
[d]Estimated.

Can. J. Chem. Downloaded from www.nrcresearchpress.com by 46.23.64.124 on 09/08/12
For personal use only.

reciprocal triplet lifetimes contained in the $k_q\tau$ values, with k_q equaling 6×10^9 M^{-1} s^{-1} in benzene (31). Rate constants $k_{\gamma-H}$ for γ-hydrogen abstraction equal Φ^{max}/τ, where Φ^{max} is either the maximum quantum yield for acetophenone formation in Lewis base solvents, multiplied by 1.1 to take into account cyclobutanol formation, or the maximum disappearance quantum yield. For most of the model phenyl ketones this value is 1 and no other triplet decay occurs (1). For *para*-substituted phenyl ketones, however, π,π* triplets usually lie below the reactive *n*,π* triplets (32); this situation reduces reactivity sufficiently that some quenching by solvent or impurities occurs, such that $1/\tau > k_{\gamma-H}$ (33). Such is the case for the *p*-alkyl and *p*-alkoxy ketone chromophores that occur in many of the diketones in Tables 4 and 5; we lump all decay other than γ-hydrogen abstraction into k_d by equating it to $1/\tau - k_{\gamma-H}$.

To detect any internal self-quenching, we must properly dissect these k_d values into competing chemical and physical decay modes. It is well established that both Norrish type I cleavage and bimolecular hydrogen abstraction are too slow to compete with γ-hydrogen abstraction in such triplet alkanophenones (34). Only three other forms of triplet decay normally need be considered:

(*i*) Quenching by benzene is known to involve charge transfer (4, 35) and has an observed rate of $(1–10) \times 10^5$ s^{-1} (4). This process is competitive only for very long-lived triplets and may contribute to k_d for *p*-alkoxyphenyl ketones (33).

(*ii*) Bimolecular rate constants for self-quenching by ground state ketone have been measured in the $10^6–10^8$ M^{-1} s^{-1} range (4). For the *p*-alkoxyphenyl ketones at ketone concentrations 0.01–0.1 M, this process would have a rate of $10^6–10^7$ s^{-1} (36).

(*iii*) For the δ-phenylvalerophenones, significant δ-hydrogen abstraction should compete, on the order of 15–20%. The normal 20/1 γ/δ rate ratio is lowered by inductive deactivation of the γ-hydrogens (1) and by conjugative activation of the δ-hydrogens, as occurs with δ-alkoxy groups (30). The same effect probably occurs to a lesser extent in the δ-phenoxyvalerophenones.

The k_H value calculated for **δPhVP** just from type II products leaves a k_d value that undoubtedly represents entirely δ-hydrogen abstraction. This fact cannot be gleaned just from product yields, since the 1,5-biradicals produced by δ-hydrogen abstraction seem to cyclize very inefficiently (30). Thus there is no reason to suggest the occurrence of internal self-quenching by the δ-phenyl group, such as is very rapid ($k \sim 10^9$ s^{-1}) with β-phenyl ketones (37). We have verified independently that γ-phenylbutyrophenone undergoes γ-hydrogen abstraction in 100% quantum efficiency.[3] This finding limits the rate of internal quenching by a γ-phenyl to $<5 \times 10^7$ s^{-1} and suggests an even lower rate for a δ-phenyl.

Rate constants for γ-hydrogen abstraction in symmetric diketones

We are the third group to measure the triplet lifetime of **13Bz$_2$Pr** by steady state Stern–Volmer quenching with similar results, the other groups reporting $k_q\tau$ values ~180 M^{-1} (5, 6). Scaiano's group also did a laser flash measurement by sensitizing formation of triplet naphthalene and obtained a value of 260 M^{-1} (6). Thus $1/\tau$ values have ranged from 2.3×10 to 4.0×10^7 s^{-1}, with different measures being taken to correct for quenching by acrylophenone product. We have measured a 100% quantum yield for product formation from **13Bz$_2$Pr**, and Scaiano's group has reported a comparably high value for the homolog 1,3–dibenzoylbutane (6). Consequently γ-hydrogen abstraction is concluded to represent the entirety of triplet decay. The monoketone model, **γEstBP**, has a considerably longer triplet lifetime. As we pointed out originally (1), the ester function appears to deactivate γ C—H bonds inductively without providing much conjugative activation. It appears that the benzoyl group does provide enough conjugative stabilization of the developing γ-radical site to increase the inductively depressed rate of reaction some 3-fold. It is important to point out here that the conversion dependence of quantum yields for **13Bz$_2$Pr** is relatively small compared to that of **γEstBP** (28). This fact corroborates the shorter triplet lifetime of the diketone relative to the ketoester.

Table 5 contains "expected" $k_{\gamma-H}$ values based on the well-known (1) large inductive effects of γ and δ substituents. Table 4 summarizes the kinetic behavior of those model monoketones needed to predict the behavior of individual ketone units in these diketones. The excellent Hammett correlation of such substituent effects on triplet reactivity (1) allows calculation of "expected" rate constants for new compounds; those for the diaroylbutanes and **15Bz$_2$Pn** were calculated by using the same σ_I value for benzoyl as for other carbonyl groups, 0.30, and the measured ρ_δ and ρ values of −1.85 and −0.76, respectively. The close agreement between expected and measured $k_{\gamma-H}$ values provides a good test for the accuracy of values based on quantum yields.

Self quenching in the α,ω-diaroylalkanes

As Tables 4 and 5 indicate, none of the dibenzoylalkanes is expected to undergo any physical decay, whereas the bisethyl- and -dimethoxybenzoylalkanes should undergo some slow physical decay, probably bimolecular quenching. However, except for **1,3Bz$_2$Pr**, all of these diaroylalkanes have k_d values $\geq 10^7$ s^{-1}. Since all other modes of decay have been ruled out, we must conclude that they all undergo internal self-quenching, the intramolecular equivalent of the bimolecular self-quenching known for phenyl ketones. We emphasize that our conclusion of significant self-quenching for the diaroylbutanes is based on low quantum yield measurements that have been reproduced by three separate students (2, 11) and thus seem reliable.

The observed order of k_{sq} values is unusual, with perhaps the most intriguing question being why no internal quenching occurs in triplet **1,3Bz$_2$Pr**. Apart from imposing a mechanistic puzzle, this result is very important in terms of the work on energy transfer in polymers based on phenyl vinyl ketone. The many examples of highly efficient energy transfer to trapping agents in these polymers could not exist if 1,3-dibenzoylalkane subunits underwent rapid self-quenching.

We shall discuss possible mechanisms for this quenching effect after we have analyzed the behavior of the unsymmetric diketones. These were chosen for study only after we were convinced that the symmetric diketones undergo significant internal quenching. An obvious structural parameter that can be modified is the orientation between the benzoyl groups allowed by the tether connecting them. Thus the γ- and δ-acylphenyl and -acylphenoxy ketones have one of the two

[3] P.J. Wagner and B. Giri, unpublished results.

Can. J. Chem. Downloaded from www.nrcresearchpress.com by 46.23.64.124 on 09/08/12
For personal use only.

Fig. 3. Stern–Volmer plots for quenching by 2,5-dimethyl-2,4-hexadiene of acetophenone formation from (■) **1,4Bz$_2$Bu** and from (○) **1Bz4EtBzBu**; and of *p*-ethylacetophenone formation from (□) **1,4EtBz$_2$Bu** and from (●) **1Bz4EtBzBu**.

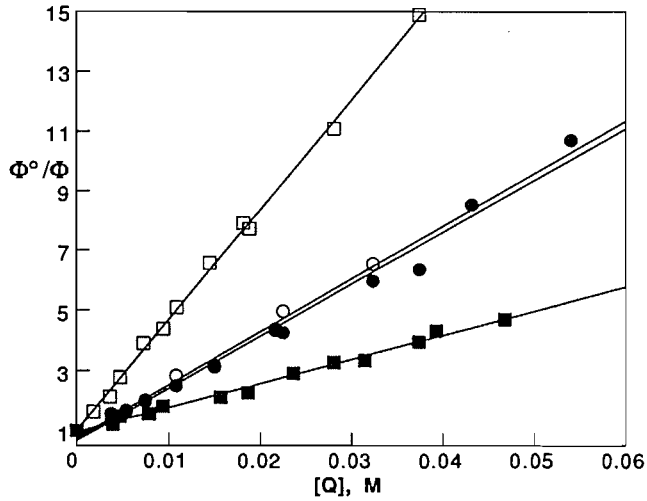

Fig. 4. Stern–Volmer plots for quenching by 2,5-dimethyl-2,4-hexadiene of acetophenone formation from (■) **δPhVP**, (●) **δ(VaPh)VP**, and (▲) **δ(AcPh)VP**; (□) of *p*-ethylacetophenone formation from **pEtVP**; and (○) of propene formation from **δ(VaPh)VP**.

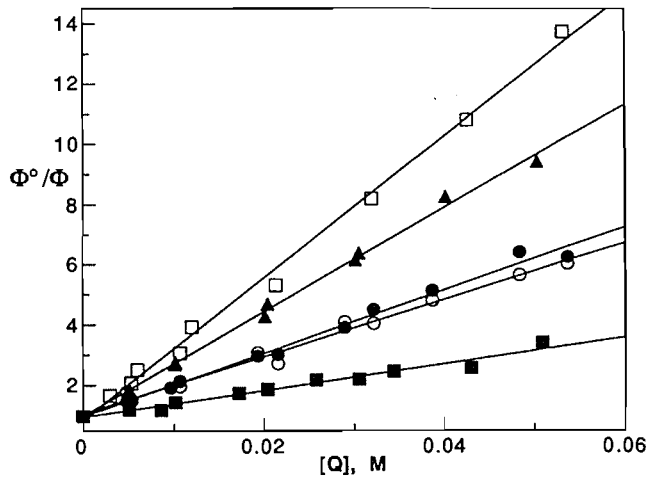

benzoyl groups turned around so that it must orient itself differently in relation to the other benzoyl group when the tether coils enough for them to interact.

Rate constants for γ-hydrogen abstraction in unsymmetric diketones

All of the diketones in Table 6 have one benzoyl group and either a *p*-alkylbenzoyl group or a *p*-alkoxybenzoyl group. In all cases the energy of the benzoyl n,π^* triplet is higher than that of the π,π^* triplet of the *p*-substituted benzoyl group. Therefore the equilibrium distribution of excitation favors the substituted benzoyl groups, leaving $\chi_{Bz} < 0.5$. The table lists "model" rather than "expected" k_H and k_d values, since all observed rate constants are altered by internal energy transfer. Equation [2], a corollary of eq. [1], describes the observed rate constant for reaction when triplet excitation is equilibrated between two nonequivalent chromophores. The observed rate constant is the normal (model) rate constant for a chromophore weighted by the fractional distribution of excitation on that chromophore. Thus k_H/k_{model} should equal χ for each chromophore, although the measurements are more precise for the benzoyl group. Interestingly, k_H and k_{model} are nearly equal for reaction of the substituted benzoyl chromophore in each diketone, reflecting the fact that most of the excitation resides on that chromophore.

$$[2] \quad k_H^{obs} = \chi_{Bz} k_{model}$$

Figures 3 and 4 display the quenching plots for the two diketones with one *p*-alkylbenzoyl chromophore. For **1Bz4EtBzBu**, acetophenone and *p*-ethylacetophenone formation are quenched with the same efficiency. Likewise, for **δVaPhVP**, acetophenone and propene are quenched with equal efficiency. In each diketone the two chromophores have identical triplet lifetimes, so excitation equilibrates between them before they decay. These equilibrium lifetimes are intermediate between those of the monoketone models. Figure 4 also shows the behavior of **δAcPhVP**. Reaction of its benzoyl group is quenched more readily than is the case for the valeryl homolog, which has a shorter overall lifetime because of reaction by the valeryl group.

The k_H/k_{model} value for **1Bz4EtBzBu** suggests a χ_{Bz} value of 3/8. This value means that the lowest triplets of the two chromophores are very close in energy, so that transfer of triplet excitation has nearly the same rate in both directions. No direct model for the δ-(*p*-acylphenyl)valerophenones was studied, but a model k_H value of half that for **δPhVP** itself was estimated based on the effects of a cyano group on **δPhOVP**; this value is consistent with a χ_{Bz} value of 3/8. No appreciable physical decay occurs in the monoketone models for **1Bz4EtBzBu**, which itself shows a significant k_d value that we ascribe to self-quenching, just as in **1,4Bz$_2$Bu**. In contrast, the two δ-(*p*-acylphenyl)valerophenones have k_d values comparable to those for **δPhVP**, which is attributed in all three to δ-hydrogen abstraction. There is no need to invoke any internal self-quenching.

The same conclusion about self-quenching can be drawn from the kinetics of the other three diketones, none of which appear to have fully equilibrated triplets. Equation [5] below describes how the quantum yield of acetophenone formation and thus the observed k_H value depends on both kinetics and relative absorption (β's) in such cases. For **1Bz4AnBu**, k_d is much larger than any physical decay rates of the model monoketones, so self-quenching is indicated. The turned-around analogs all have k_d values no larger than the monoketone models and are concluded not to undergo any internal self-quenching. In these ketones the k_H/k_{model} values suggest χ_{Bz} values of 0.1, which translates into a 9/1 ratio for energy transfer rates.

Scheme 3 shows why the χ_{Bz} values for the diketones are larger than would be anticipated from the χ^{n,π^*} values of the model *p*-substituted monoketones, which are 0.12 and 0.01 for *p*-alkyl and *p*-methoxy, respectively (33). Electron-donating groups raise n,π^* energies as well as lower π,π^* energies, so the energy gap ΔE_{ex} between the lowest triplets of two chromophores is lower than the $n,\pi^* - \pi,\pi^*$ energy gap ΔE_{in} in the *p*-substituted chromophore (11).

Can. J. Chem. Downloaded from www.nrcresearchpress.com by 46.23.64.124 on 09/08/12
For personal use only.

Scheme 3.

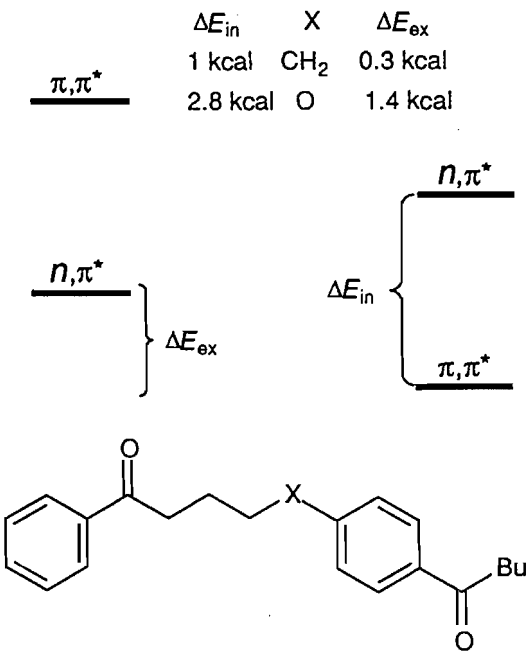

Structural dependence of k_{sq}

The rate constants for this internal self-quenching show three distinct variations:

1. Only the α,ω-diaroylalkanes display this form of internal quenching. Since the π systems of the turned-around diketones are as close to each other as they are in the α,ω-diaroylalkanes, we conclude that close contact between the carbonyl groups is required.

2. In the 1,4-diaroylbutanes, k_{sq} decreases as the π,π* triplet becomes lower in energy than the *n*,π* triplet. This behavior parallels the corresponding drops in observed rate constants for *n*,π* reactions (33, 38) and strongly suggests that the self-quenching involves mainly the *n*,π* triplet. This conclusion reinforces the first one. The relative ordering is opposite to that reported for bimolecular self quenching, where the order is π,π* *p*-methoxyacetophenone (36) > *n*,π* benzophenone (4). It already has been concluded that bimolecular self-quenching can occur by more than one mechanism (5). Apparently the tether prevents the two benzoyl groups from attaining whatever orientation favors rapid quenching of π,π* triplets.

3. In the α,ω-diaroylalkanes, the fastest rate occurs for a four-carbon tether, which is not unusual in organic chemistry, but the lack of reaction for the three-atom tether is surprising. Apparently a very specific orientation of the two carbonyls is required for this quenching interaction, one that is not possible with the three-atom tether and that becomes less likely for tethers longer than four atoms. At this point we cannot suggest a more exact description of the interaction, except that it must provide a path for radiationless decay. The most likely possibilities are some form of excimer interaction or a chemical reaction such as revertible radical addition. Since internal excimer formation is usually favored by three-carbon tethers and since it has been shown that rates for hydrogen abstraction in 2,4-dibenzoylpentanes are very sensitive to conformation (5), a radical reaction-like process may seem favored, although radical additions to carbonyls work well for three-atom tethers (39).

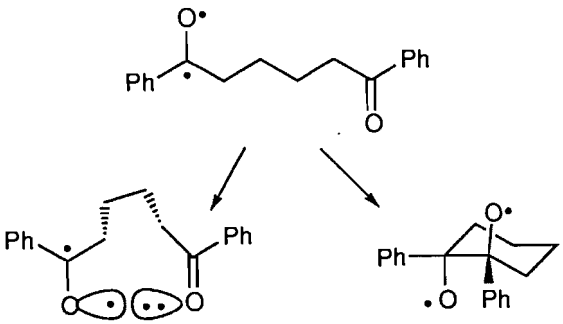

Fig. 5. Stern–Volmer plots for quenching by 2,5-dimethyl-2,4-hexadiene of acetophenone formation from (- - -) **γPhOBP**, (■) **γ(CNPhO)BP**, (▲) **δ(AcPhO)BP**, and (○) **γ(VaPhO)BP**; (. . . .) of *p*-methoxyacetophenone formation from **pMeOVP**; and (●) of propene formation from **γ(VaPhO)BP**.

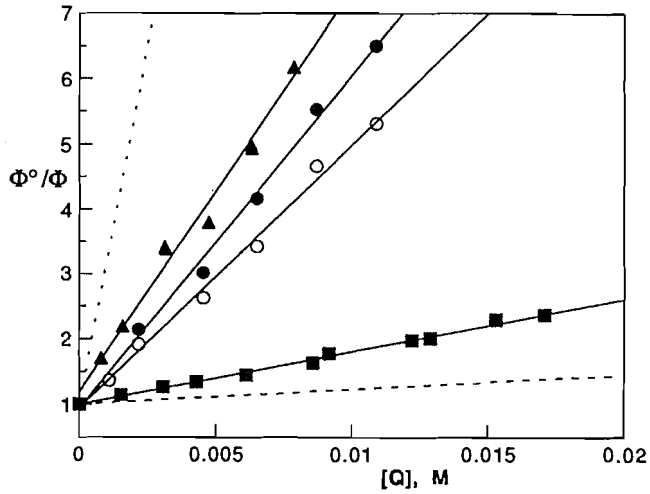

4. The electronic spectra of the 1,1- and 1,2-dibenzoylalkanes, especially the former, with its nonunity intersystem crossing yield, suggest some direct mixing of the chromophores. Their relatively high k_{sq} values may indicate a mechanism different from that in **1,4Bz$_2$Bu**.

Rates of intramolecular energy transfer

When we first studied **1Bz4AnBu** and noted similar $k_q\tau$ values for quenching reaction from both chromophores (11), we treated the system as if it were fully equilibrated, even though the two $k_q\tau$ values differed by more than normal experimental error. Figure 5 shows the quenching behavior for the various γ-(acylphenoxy)butyrophenones and their models. Acetophenone and propene are formed from the two different chromophores of **γVaPhOBP** and are not quenched with the same efficiency. Plots of **δVaPhOVP** and its models look very similar. Having now found two more examples of diketones in which the benzoyl and alkoxybenzoyl chromophores are not quenched equally, we can analyze all three cases with the complete equation that describes quenching of two partially equilibrating chromophores. Scheme 4 displays the reactions that determine the extent of excitation interconversion in one representative diketone. Equations [3] and [4] describe how quantum yields and Stern–Volmer plots depend on the various kinetic parameters (27). Equation [3] is given in two forms: the general one where subscripts u and r distinguish the unre-

Can. J. Chem. Downloaded from www.nrcresearchpress.com by 46.23.64.124 on 09/08/12
For personal use only.

Scheme 4.

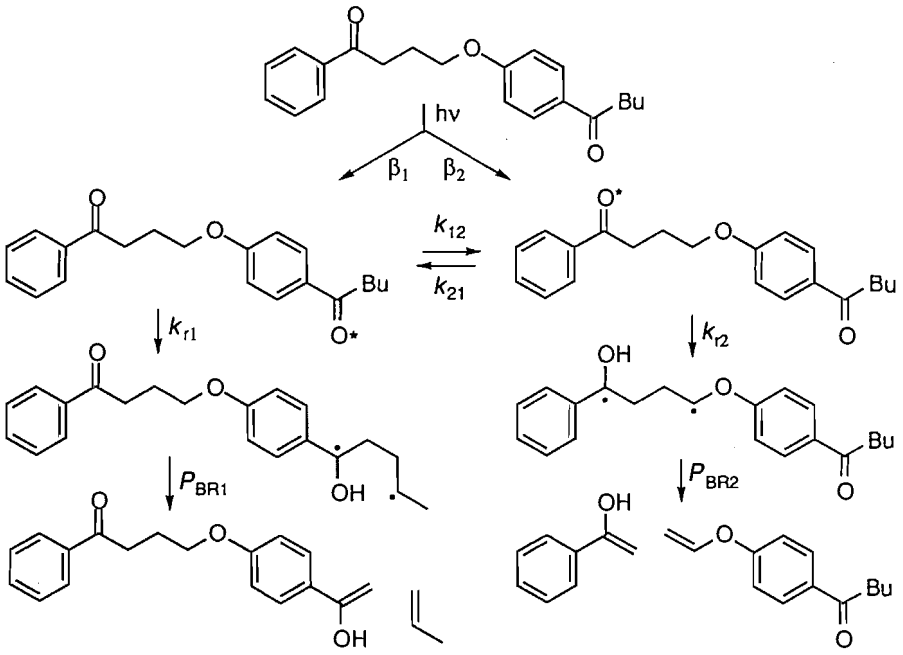

acting and reacting chromophores, and one specific to acetophenone formation from the benzoyl chromophore. In Eq. [4] the numerator is basically the product of two Stern–Volmer expressions divided by D, which equals 1 when no state interconversion occurs and approaches zero as equilibration becomes complete. The denominator, which handles quenching of interconversion and includes the fraction of light β absorbed by each chromophore, differs for products formed from each state. The β's are determined by the extinction coefficients of the two chromophores: $\beta_1 = 1 - \beta_2 = \varepsilon_1/(\varepsilon_1 + \varepsilon_2)$. All the rate constants except for k_{12} and k_{21} can be estimated closely from the kinetics of the model monoketones or symmetric diketones. The τ values are dominated by k_r (= $k_{\gamma\text{-H}}$) and k_{12} or k_{21} values in these diketones, where physical decay reactions are slow. The χ_{Bz} values gleaned from quantum yields furnish the k_{21}/k_{12} values, which are 5/3 and 9/1.

[3] $$\Phi_r = P_{BR}k_r\tau_r(\beta_r + \beta_u k_{ur}\tau_u)D^{-1}$$
$$\Phi_{AP} = P_{BR}k_H\tau_{Bz}[\beta_{Bz} + \beta_{RBz}k_{12}\tau_{RBz}]/(1 - k_{12}\tau_{RBz}k_{21}\tau_{Bz})$$

[4] $$\Phi^0/\Phi = \frac{1 + (k_q\tau_1 + k_q\tau_2)[Q]D^{-1} + k_q^2\tau_1\tau_2[Q]^2D^{-1}}{1 + \beta_r k_q\tau_u[Q](\beta_r + \beta_u k_{ur}\tau_u)^{-1}}$$

[5] $$D = 1 - k_{12}\tau_1\, k_{21}\tau_2$$

Figures 6 and 7 show the best fit of the data for two of the diketones to eqs. [3] and [4]. The benzoyl chromophore is always state 2; the *p*-alkoxybenzoyl, state 1; $1/\tau_r = 1/\tau_r^0 + k_{ru}$; $1/\tau_u = 1/\tau_u^0 + k_{ur}$.

For **1Bz4AnBu**, the following values were used: $k_q = 6 \times 10^9$ for each state; $1/\tau_2' = 7 \times 10^7$; $1/\tau_1' = 1 \times 10^7$; $P_{BR2}k_{r2} = 3 \times 10^7$; $P_{BR1}k_{r1} = 2 \times 10^5$; $\beta_2 = 0.3$; $\beta_1 = 0.7$; $k_{21} = 1 \times 10^8$; $k_{12} = 2 \times 10^7$. With these parameters, $D = 0.61$, and the predicted quantum yield ratio of 0.21/0.01 matches that actually measured. The dotted and dashed lines in Figs. [6] and [7] represent 5-fold changes in the energy transfer rate constants

Fig. 6. Stern–Volmer quenching of **1Bz4AnBu** by 2,5-dimethyl-2,4-hexadiene: (□) acetophenone formation; (■) *p*-methoxyacetophenone formation. Calculated plots: (——) $k_{21} = 1 \times 10^8$ s^{-1}; (— — —) $k_{21} = 5 \times 10^8$ s^{-1}; (- - - -) $k_{21} = 2 \times 10^7$ s^{-1}.

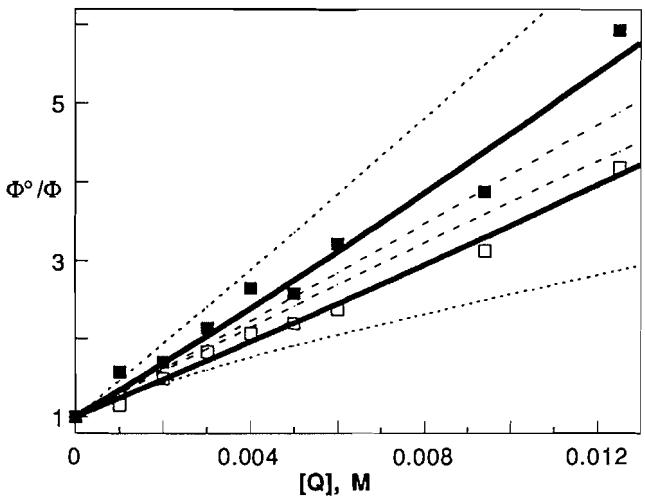

and show just how sensitive such plots are to these values. Thus the not-quite-equal slopes for the experimental data indicate two triplets that are about 2/3 equilibrated. Decreasing D to 0.2 (90% interconversion) brings the two plots within experimental error of each other, whereas increasing it to 0.98 (15% interconversion) causes the plots to diverge sharply.

For **δVaPhOVP**, the following values predict the experimental data in Fig. 7: $k_q = 6 \times 10^9$ for each state; $1/\tau_2' = 2 \times 10^7$; $1/\tau_1' = 3 \times 10^6$; $P_{BR2}k_{r2} = 1 \times 10^7$; $P_{BR1}k_{r1} = 2 \times 10^5$; $\beta_2 = 0.25$; $\beta_1 = 0.75$; $k_{21} = 7 \times 10^7$; $k_{12} = 7 \times 10^6$. With these parameters, $D = 0.46$, which represents 70% interconversion, and the quantum yield ratio is 0.22/0.08, the same as that measured. The 450 ns triplet lifetime measured by flash kinetics corrob-

Can. J. Chem. Downloaded from www.nrcresearchpress.com by 46.23.64.124 on 09/08/12
For personal use only.

Fig. 7. Stern–Volmer plots for quenching of **δVaPhOVP** by 2,5-dimethyl-2,4-hexadiene: (○) acetophenone formation; (●) propene formation. (——) $k_{21} = 7 \times 10^7$ s^{-1}; (— — —) $k_{21} = 3.4 \times 10^8$ s^{-1}; (- - - -) $k_{21} = 1.4 \times 10^7$ s^{-1}.

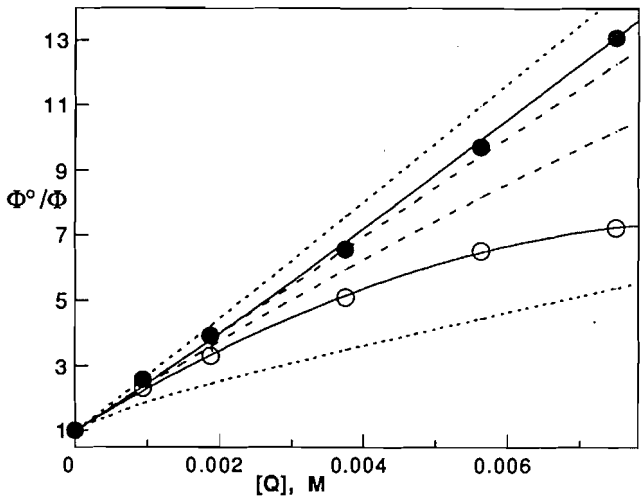

Fig. 8. Calculated Stern–Volmer plots for quenching of acetophenone (bottom 3) and propiophenone (top 3) formation from 1,3-dibenzoylbutane in benzene. (——) plots reported in ref. 6, $k_{21} = 3 \times 10^7$ s^{-1}, $D = 0.98$; (— — —) $k_{21} = 1.5 \times 10^8$ s^{-1}, $D = 0.81$; (- - - -) $k_{21} = 6 \times 10^6$ s^{-1}, $D = 0.998$.

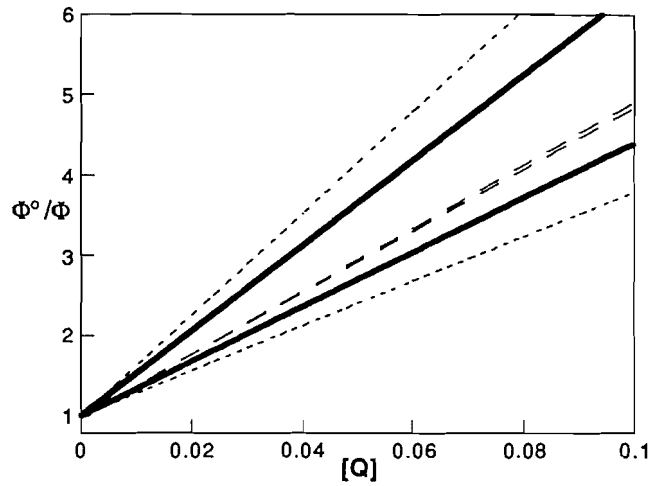

orates the conclusion that near-equilibrium conditions obtain. Again, the calculated plots for faster and slower energy transfer rates indicate how little leeway there is in estimating such rate constants from the experimental data.

The rate constants for exothermic energy transfer from benzoyl to alkoxybenzoyl group near 10^8 s^{-1} are only 1/10 the $\sim 10^9$ M^{-1} s^{-1} value for bimolecular energy transfer between phenyl alkyl ketones (28, 40). This amounts to an unusually low effective molarity of only 0.1 M for two "reactants" separated by a flexible four-atom link. A similar analysis of **γVaPhOBP** provides a set of energy transfer rate constants five times larger than those for **δVaPhOVP**, exactly the kind of distance dependence on energy transfer that one would expect (10, 12, 41). Moreover, it appears that the turned-around diketone with four atoms between the benzoyl group and the alkoxybenzoyl benzene ring undergoes energy transfer somewhat faster than the 1-benzoyl-4-anisyl system. Both comparisons reinforce the notion that the α,ω-dibenzoyl structure can inhibit formation of the best orientation for orbital overlap of the two benzoyl groups.

Postscript

The relatively low rate constants for $n,\pi^* \rightarrow n,\pi^*$ triplet energy transfer are well established (42). Therefore we must emphasize that the exothermic rate constants that we have estimated represent $n,\pi^* \rightarrow \pi,\pi^*$ energy transfer, which usually is faster (43).The conclusion that energy transfer in these diketones is relatively slow reopens the question as to its rapidity in 1,3-dibenzoylpropane structures. As just mentioned, we would normally expect that shortening the connecting tether by one carbon would increase energy transfer rate constants 5- to 10-fold. That would leave a rate constant of no more than 10^9 s^{-1} in **1,3Bz$_2$Pr**. However, we wonder whether the conformational constraints that reverse the normal rate ratio for self-quenching may also apply to energy transfer. In their study of 1,3-dibenzoylbutane, Scaiano and co-workers found unequal $k_q\tau$ values for quenching of acetophenone and propiophenone formation in benzene (6). Assuming internal energy transfer so rapid as to assure equilibration, they speculated at length about a cause for the difference without posing a solid explanation. We have made a much fuller study of the quenching of unsymmetric diketones that will soon be published and we find that solvent changes can greatly affect the degree of curvature and divergence shown in plots such as Figs. 5–7. Consequently we offer Fig. 8 as a *possible* explanation for the behavior of the 1,3–dibenzoylbutane. If energy transfer is much slower than assumed, just as is self-quenching, then the decay rate constants expected for this compound would predict that the two Stern–Volmer plots diverge exactly as was observed. (The analysis assumes that a-alkylation slightly enhances extinction coefficients, as Lewis has reported (40), and also raises the triplet energy slightly.) We do not at this point maintain this suggestion as fact, just as an interesting possibility, and offer it to emphasize how many factors must be balanced in a thorough analysis of the quenching behavior of bichromophoric systems. In particular, it is important to note that internal energy transfer rates of only 10^8 s^{-1} would be sufficient to make the system behave as though it were fully equilibrated. Therefore the observation of the same $k_{q\tau}$ values for the two chromophores in such diketones (6) cannot be used as evidence for energy transfer rates any faster than 10^8 s^{-1} in 1,3-dibenzoyl units of either diketones or polymers.

Acknowledgment

This work was supported by continuing grants from the National Science Foundation. We thank Dr. Anna Gudmundsdottir for measuring some NMR spectra to update those originally taken on low-resolution machines.

This paper is submitted in recognition of Professor James Guillet's singular fusion of photochemical and polymer research, in which he has applied photochemical knowledge to fashion useful polymeric materials and fashioned unique polymer structures to develop new photochemical knowledge and methodology.

References

1. P.J. Wagner and A.E. Kemppainen. J. Am. Chem. Soc. **94**, 7495 (1972).
2. P.J. Wagner. Acc. Chem. Res. **4**, 168 (1971).
3. D.I. Schuster and T.M. Weil. J. Am. Chem. Soc. **95**, 4091 (1973).
4. L.A. Singer, R.E. Brown, and G.A. Davis. J. Am. Chem. Soc. **95**, 8639 (1973); M.W. Wolf, R.E. Brown, and L.A. Singer. J. Am. Chem. Soc. **99**, 526 (1977)..
5. R. Salvin, J. Maybeck, and J. Faure. J. Photochem. **6**, 9 (1976); R. Salvin and J. Maybeck. J. Photochem. **7**, 411 (1977).
6. J.P. Bays, M.V. Encinas, R.D. Small, Jr., and J.C. Scaiano. J. Am. Chem. Soc. **102**, 727(1980).
7. C. David, W. Demarteau, and G. Geuskens. Polymer, **9**, 497 (1967).
8. F.J. Golemba and J.E. Guillet. Macromolecules, **7**, 212 (1972); A.C. Somersall, E. Dan, and J.E. Guillet. Macromolecules, **7**, 233 (1974).
9. M.V. Encinas, K. Funabashi, and J.C. Scaiano. Macromolecules, **12**, 1167 (1979); P.K. Das, M.V. Encinas, and J.C. Scaiano. J. Photochem. **12**, 357 (1980); J.C. Scaiano and J.C. Selwyn. Macromolecules, **14**, 1723 (1981).
10. P.J. Wagner and G.M. El-Taliawi. J. Am. Chem. Soc. **114**, 8325 (1992).
11. P.J. Wagner and T. Nakahira. J. Am. Chem. Soc. **95**, 8474 (1973).
12. P.J. Wagner, B.P. Giri, H.W. Frerking, Jr., and J. DeFrancesco. J. Am. Chem. Soc. **114**, 8326 (1992).
13. J.A. Riddick. *In* Techniques of organic chemistry. Vol. 2. 2nd ed. *Edited by* A. Weisberger. Wiley, New York. 1970.
14. A.J. Gordon and R.A. Ford. The chemist's companion. Wiley, New York. 1972. p. 436.
15. I. Smedley. J. Chem. Soc. **48**, 1484 (1901).
16. H.-D. Becker. J. Org. Chem. **32**, 2140 (1967).
17. H.B. Henbest, E.P.H. Jones, and I.M.S. Wells. J. Chem. Soc. 2696 (1949).
18. F.S. Kipping and W.H. Perkin, Jr. J. Chem. Soc. **55**, 330 (1889).
19. A.E. Kemppainen. Ph. D. Thesis, Michigan State University, 1971.
20. G. Stork and S.R. Dowd. J. Am. Chem. Soc. **85**, 2178 (1963).
21. H. Staudinger. Makromol. Chem. **4**, 289 (1963).
22. A. Kalir and D. Balderman. Synthesis, 358 (1973).
23. J.W. Wilt and J.W. Hill. J. Org. Chem. **26**, 3523 (1961); T.L. Cairns and B.E. Englund. J. Org. Chem. **21**, 140 (1956).
24. L.E. Kaschtanov. Zh. Obshch. Khim. **2**, 515 (1932).
25. S.F. Birch, R.A. Dean, F.A. Fidler, and R.A. Lowry. J. Am. Chem. Soc. **71**, 1362 (1949).
26. F.G. Moses, R.S.H. Liu, and B.M. Monroe. Mol. Photochem. **1**, 245 (1969).
27. P.J. Wagner. *In* Creation and detection of the excited state. *Edited by* A.A. Lamola. Wiley, New York. 1971, p. 174; *In* Handbook of organic photochemistry. Vol. II. *Edited by* J.C. Scaiano. CRC Press, Boca Raton, Fla. 1989, p. 251.
28. P.J. Wagner, I.E. Kochevar, and A.E. Kemppainen. J. Am. Chem. Soc. **94**, 7489 (1972).
29. P.J. Wagner, P.A. Kelso, A.E. Kemppainen, J.M. McGrath, H.N. Schott, and R.G. Zepp. J. Am. Chem. Soc. **94**, 7506 (1972).
30. P.J. Wagner, P.A. Kelso, A.E. Kemppainen, and R.G. Zepp. J. Am. Chem. Soc. **94**, 7500 (1972).
31. J.C. Scaiano, W.J. Leigh, M.A. Meador, and P.J. Wagner. J. Am. Chem. Soc. **107**, 5806 (1985).
32. N.C. Yang, D.S. McClure, S.L. Murov, J.J. Houser, and R. Dusenbery. J. Am. Chem. Soc. **89**, 5466 (1967).
33. P.J. Wagner, A.E. Kemppainen, and H.N. Schott. J. Am. Chem. Soc. **95**, 5604 (1973).
34. P.J. Wagner. Top. Curr. Chem. **66**, 1 (1976).
35. P.J. Wagner, R.J. Truman, A.E. Puchalski, and R. Wake. J. Am. Chem. Soc. **108**, 7727 (1986).
36. O.L. Chapman and G. Wampfler. J. Am. Chem. Soc. **91**, 5390 (1969).
37. P.J. Wagner, P.A. Kelso, A.E. Kemppainen, A. Haug, and D.R. Graber. Mol. Photochem. **2**, 81 (1970); J.C. Netto-Ferreira, W.J. Leigh, and J.C. Scaiano. J. Am. Chem. Soc. **107**, 2617 (1985).
38. M. Berger, E. McAlpine, and C. Steel. J. Am. Chem. Soc. **100**, 5147 (1978); M.V. Encina, E.A. Lissi, E. Lemp, A. Zanocco, and J.C. Scaiano. J. Am. Chem. Soc., **105**, 1856 (1983).
39. R. Walton and B. Fraser-Reid. J. Am. Chem. Soc. **113**, 5791 (1991).
40. F.D. Lewis, R.W. Johnson, and D.E. Johnson. J. Am. Chem. Soc. **96**, 6090 (1974); M.V. Encinas and J.C. Scaiano. Chem. Phys. Lett. **63**, 305 (1979); J. Am. Chem. Soc. **101**, 727 (1979).
41. D.O. Cowan and A.A. Baum. J. Am. Chem. Soc. **93**, 1153 (1971); P.J. Wagner and B.J. Scheve. J. Am. Chem. Soc. **101**, 378 (1979).
42. P. Lechtken and N.J. Turro. Angew. Chem. Int. Ed. Engl. **12**, 314 (1973).
43. M.F. Mirbach, V. Ramamurthy, M.J. Mirbach, N.J. Turro, and P.J. Wagner. Nouv. J. Chim. **4**, 471 (1980).

Can. J. Chem. Downloaded from www.nrcresearchpress.com by 46.23.64.124 on 09/08/12
For personal use only.

Solvent effect on the photophysics of bisphenol-A-based polycarbonate and diphenylcarbonate

Charles E. Hoyle, Isaac B. Rufus, and Himanshu Shah

Abstract: Polycarbonate and diphenylcarbonate exhibit an anomalous fluorescence emission with peak maximum around 350 nm in polar solvents that may be attributed to the association of diarylcarbonate moieties in a polar solvent cage. The red-shifted emission is attributed to intermolecular interactions in polar solvents and intramolecular interactions in polycarbonate. The photophysical behavior of polycarbonate and diphenylcarbonate is different from that of 1,3-diphenylpropane where a red-shifted emission is due to excimers formed by phenyl groups separated by three carbon atoms and is independent of the polarity of the solvent.

Key words: diphenylcarbonate, polycarbonate, aggregates, photophysics.

Résumé : Le polycarbonate et le carbone de phényle présentent tous les deux une émission de fluorescence anormale, avec un maximum autour de 350 nm dans des solvants polaires, qui peut être attribuée à l'association des portions de carbonate de diaryle dans une cage de solvant polaire. On attribue le déplacement vers le rouge de l'émission à des interactions intramoléculaires dans les solvants polaires et à des interactions intramoléculaires dans le polycarbonate. Le comportement photophysique du polycarbonate et du carbonate de diphényle est différent de celui du 1,3-diphénylpropane pour lequel le déplacement de l'émission vers le rouge est causé par les excimères formés par les groupes phényles séparés par trois atomes de carbone et il est indépendant de la polarité du solvant.

Mots clés : carbonate de diphényle, polycarbonate, agrégats, photophysique.

[Traduit par la rédaction]

1. Introduction

Polycarbonate has many attributes that contribute to its use in a variety of applications. Unfortunately, it degrades upon exposure to sunlight, necessitating an understanding of polycarbonate photochemistry and photophysics. Even though the photodegradation of polycarbonate has been studied for several decades, there are few papers (1–3) on the photophysics of polycarbonate and corresponding models, none of which reports on solvent effects. In contrast, there are numerous reports on the effects of solvent polarity on the photophysical behavior of polystyrene (4, 5), and Hirayama (5) reported that the intramolecular excimers of 1,3-diphenyl alkanes, which are models for the polystyrene repeat unit, are not influenced by solvent polarity.

1,3-Diaryl systems containing hetero atoms like O, N, and S are of particular interest for photophysical studies since they occur as repeat units in important polymers, i.e., polycarbonate. There is a question of whether 1,3-diphenyl systems with hetero atoms will behave in a manner similar to that of 1,3-diphenyl alkanes. It has previously been reported that both 1,3-diphenylcarbonate (DPC) and polycarbonate exhibit primarily monomer emission with a peak maximum around 300 nm (3, 6–8) in a relatively nonpolar solvent such as dichloromethane. In this paper, we report on the effect of solvent polarity on the photophysical behavior of DPC and polycarbonate, both of which contain 1,3-diaryl repeat units separated by a bridging system with hetero atoms incorporated.

Received May 1, 1995.

This paper is dedicated to Professor J.E. (Jim) Guillet in recognition of his contributions to Canadian chemistry.

C. E. Hoyle,[1] I.B. Rufus, and H. Shah.
Department of Polymer Science, University of Southern Mississippi, Hattiesburg, MS-39406-0076, U.S.A.

[1] Author to whom correspondence may be addressed. Telephone: (601) 266-4868. Fax: (601) 266-5504.

2. Experimental details

Diphenylcarbonate (99%, Aldrich) was sublimed three times. Phenylbenzoate (99%, Aldrich), phenylacetate (99%, Aldrich), 1,3-diphenyl acetone (99%, Aldrich), ethylene glycol (spectrophotometric grade, 99+%, Aldrich), and 1,3-diphenylpropane (TCI, 99%) were used as received. Spectrophotometric grade dichloromethane, methanol, acetonitrile, cyclohexane, 1,4-dioxane, dichloroethane, tetrahydrofuran, isopropanol, and isobutanol were used as received from Burdick and Jackson. The polycarbonate sample, Lexan-140, was received from GE plastics and used after two reprecipitations.

UV-visible absorption spectra were obtained on a Perkin–Elmer Lambda-6 spectrophotometer and fluorescence spectral measurements were made on a SPEX Fluorolog-2 spectrophotometer. Fluorescence emission spectra were recorded without emission correction unless otherwise mentioned. Fluorescence lifetime measurements were measured with time-correlated single-photon counting instruments from Photochemical Research Associates and Edinburgh Analytical Instruments.

Can. J. Chem. Downloaded from www.nrcresearchpress.com by 46.23.64.124 on 09/08/12
For personal use only.

Can. J. Chem. Downloaded from www.nrcresearchpress.com by 46.23.64.124 on 09/08/12
For personal use only.

Fig. 1. UV absorption spectra of DPC (2×10^{-3} M): (a) in cyclohexane, (b) acetonitrile, (c) dichloromethane, and (d) methanol.

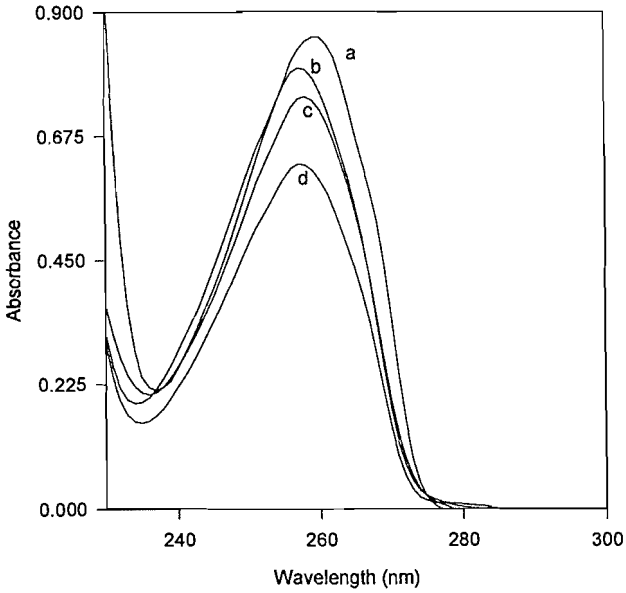

Fig. 2. Fluorescence emission spectra of DPC (5×10^{-3} M): (a) in methanol, (b) methanol evaporated and the DPC residue redissolved in dichloromethane, (c) dichloromethane evaporated from (b) and residue redissolved in methanol, and (d) dichloromethane. $\lambda_{EX} = 270$ nm.

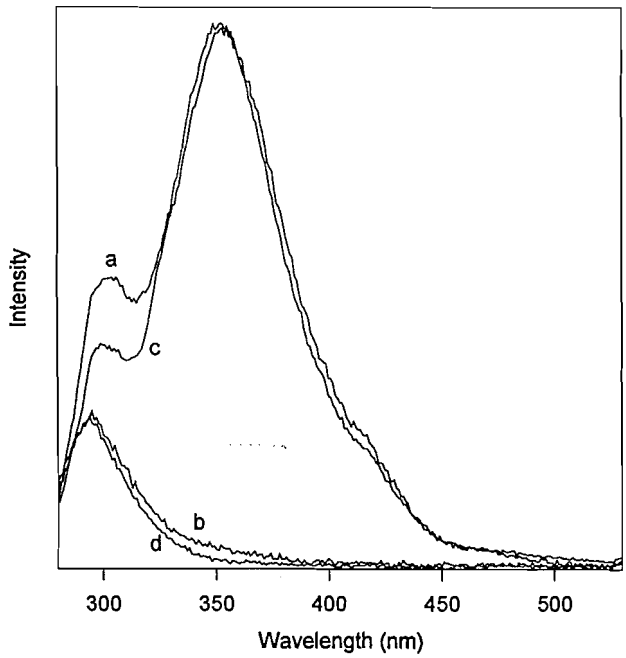

3. Results and discussion

3.1 Photophysics of DPC

The polarity of the solvent has only a very modest hypsochromic effect on the UV absorption spectral maximum of DPC (Fig. 1), suggesting that the spectrum with peak maximum around ~257 nm is due to a π,π^* transition. In addition to the shift of the peak absorption maximum to slightly higher energies in polar solvents, there is a very weak absorption band in polar solvents, at wavelengths greater than 280 nm extending to around 300 – 310 nm. Surprisingly, the fluorescence spectrum of DPC is quite different in polar and nonpolar solvents as can be seen by comparing the results in Fig. 2 in methanol and dichloromethane. In methanol, DPC shows a bimodal spectrum with two emission peaks, one at 300 nm and another at 350 nm, when excited at 270 nm (Fig. 2a). In the relatively (compared to methanol) nonpolar solvent dichloromethane, DPC has only one emission peak with a maximum at 300 nm (Fig. 2d). To show that no reaction occurs between methanol and DPC, the solvent from the methanol solution was evaporated and the DPC residue redissolved in dichloromethane. The fluorescence spectrum of DPC redissolved in dichloromethane exhibits only one emission peak at 300 nm (Fig. 2b), indicating that the 350 nm emission peak is not due to a chemical reaction between methanol and DPC, a photochemical reaction product produced in the fluorimeter, or an impurity. To further illustrate this point, dichloromethane from the redissolved solution of DPC was evaporated and the residue redissolved in methanol a second time. Again the fluorescence spectrum of the solution of DPC in methanol (Fig. 2c) is identical to the fluorescence emission spectrum of the fresh solution of DPC in methanol (Fig. 2a), confirming that the 350 nm emission is not from an impurity. We have found in general that, in polar solvents, DPC exhibits a 350 nm emission in addition to the 300 nm emission (Table 1), while in relatively nonpolar solvents like cyclohexane and tetrahydrofuran, DPC exhibits only one emission band with peak maximum around 300 nm (Table 1). (It should be noted that a hydrolysis product of DPC and hence a suspect impurity, phenol, does not show any fluorescence emission peak at 350 nm in any of the polar solvents in Table 1.) While in methanol the I_{350}/I_{300} ratio decreases with a decrease in the concentration of DPC (Fig. 3), concentrated solutions of DPC in dichloromethane, DPC in a PMMA matrix (up to 30 wt.% loading), and DPC crystals do

Table 1. UV-absorption maxima and fluorescence emission maxima of diphenylcarbonate in different solvents.

Solvents	λ_{max}/nm[a]	Fluorescence emission maxima[b] (λ_{Ex} = 270 nm) I	II	Solvent dielectric constant
Cyclohexane	259	294	—	2.02
n-Hexane	259	293	—	1.88
1,4-Dioxane	259	296	—	2.25
Dichloromethane	258	294	—	8.93
Tetrahydrofuran	258	294	—	7.58
Dichloroethane	259	300	—	10.36
Methanol	257	302	350	32.70
Isopropanol	—	299	353	19.92
Isobutanol	—	294	352	16.68
Acetonitrile	257	299	342	37.50
ACN:H_2O 1:1	257	299	353	~58.80
Ethylene glycol	—	302	350	37.70
30% DPC/PMMA	258	295	—	—
DPC crystals	—	293	—	—

[a]λ_{max} reported for 2×10^{-3} M DPC solutions.
[b]Emission maxima from uncorrected fluorescence spectra.

Can. J. Chem. Downloaded from www.nrcresearchpress.com by 46.23.64.124 on 09/08/12
For personal use only.

Fig. 3. Fluorescence emission spectra of DPC in methanol as a function of concentration: (a) 5×10^{-3} M ($I_{350}/I_{300} = 1.46$), (b) 2×10^{-3} M ($I_{350}/I_{300} = 0.86$), and (c) 5×10^{-4} M ($I_{350}/I_{300} = 0.34$). $\lambda_{EX} = 270$ nm.

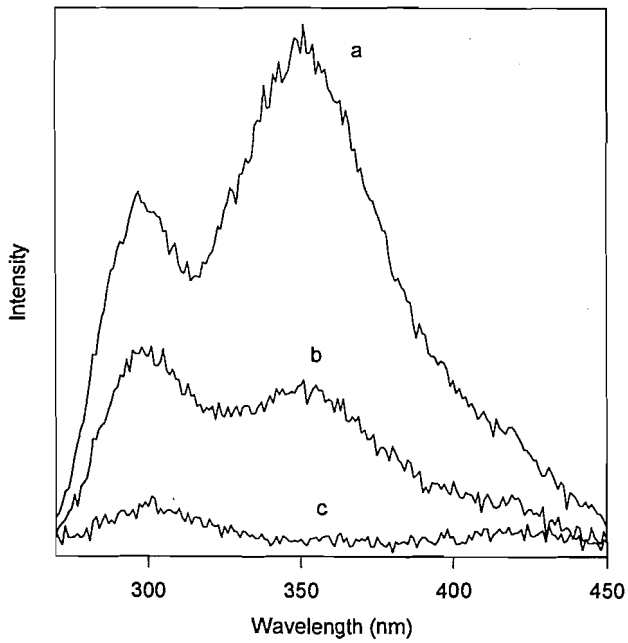

Fig. 4. Fluorescence excitation spectra of DPC (2×10^{-3} M) in methanol: (a) $\lambda_{EM} = 300$ nm and (b) $\lambda_{EM} = 350$ nm.

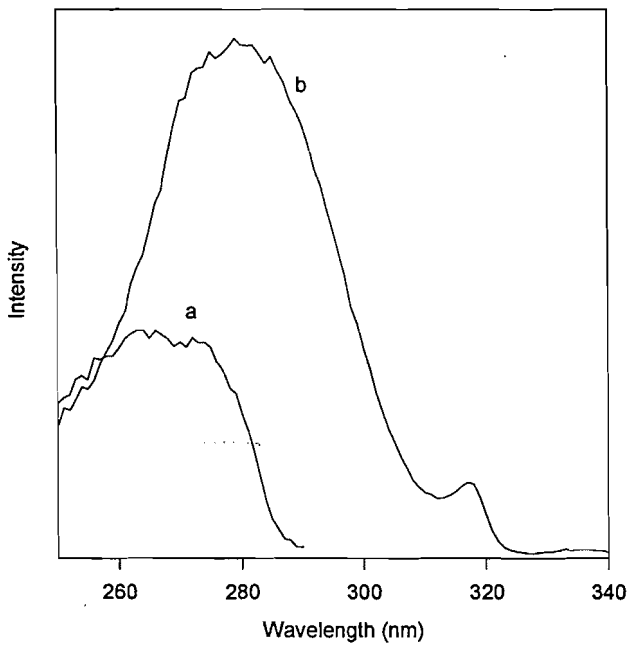

not exhibit any fluorescence with an emission peak around 350 nm, but exhibit only the normal emission (peak maximum near 300 nm) from the excited singlet state. The above observations suggest that the 350 nm emission arises from intermolecular interactions between diphenylcarbonate molecules in polar solvents and is not the result of an intramolecular interaction. The excitation scan for the 300 nm emission peak in methanol (Fig. 4a) is essentially identical to the UV absorption spectrum

Fig. 5. Fluorescence emission spectra of DPC (5×10^{-3} M): (a) in cyclohexane and (b) in methanol. $\lambda_{EX} = 290$ nm.

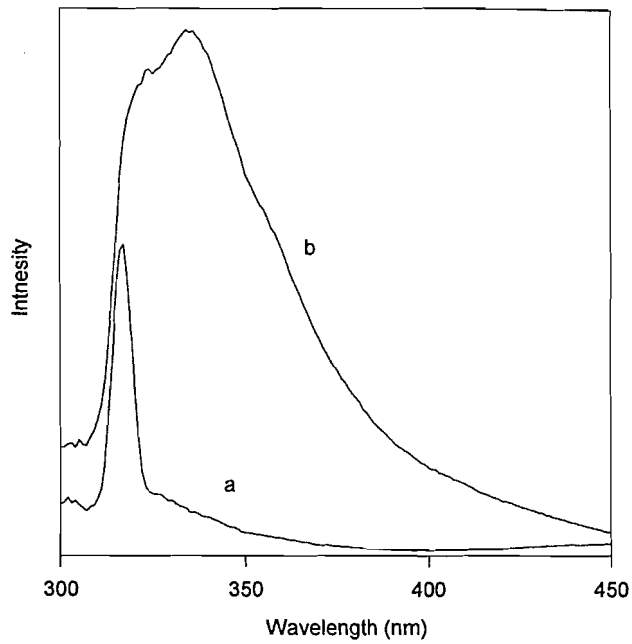

of DPC, indicating that the 300 nm emission arises from direct excitation of DPC. The excitation scan for the 350 nm emission peak (Fig. 4b) is shifted to lower energy than that for the 300 nm emission peak, indicating that the 350 nm emission may be due to some type of solvent-induced aggregate formation. When excited at shorter wavelengths where excitation of single chromophores no doubt occurs, the 350 nm emission may be due to preformed excimers or excited aggregates.

When DPC in polar solvents is excited at 290 nm, a fluorescence emission peak is observed at 350 nm (e.g., Fig. 5) that is not observed in nonpolar solvents, providing additional support that DPC may form aggregates in polar solvents. Since polar solvents form strong solvent cages (9), it is not totally unexpected that DPC might easily aggregate in such polar solvents. Addition of 1% (v/v) water to anhydrous acetonitrile (~0.001 wt.% water) does not increase the intensity of the 350 nm emission peak significantly (figure not shown), suggesting that the 350 nm fluorescence emission peak of DPC observed in polar solvents is probably not due to the presence of large amounts of water in these solvents. However, we cannot totally rule out the role of trace amounts of water in contributing to the red-shifted emission found in polar solvents since there was a trace amount of water present initially even in the purported anhydrous acetonitrile.

For comparison with DPC, we consider 1,3-diphenylpropane, which exhibits fluorescence with emission peak maxima at 300 and 350 nm in dichloromethane (Fig. 6) as reported by Hirayama (5). We have confirmed the report by Hirayama (5) that the fluorescence spectrum of 1,3-diphenylpropane is independent of the chromophore concentration and the solvent polarity (Fig. 6), i.e., the 350 nm peak is observed in both polar and nonpolar solvents. The excitation scans for 1,3-diphenylpropane of the 300 and 350 nm emission peaks are identical in polar and nonpolar solvents (Fig. 7). These obser-

Can. J. Chem. Downloaded from www.nrcresearchpress.com by 46.23.64.124 on 09/08/12
For personal use only.

Fig. 6. Fluorescence emission spectra of 1,3-diphenylpropane: (a) 5×10^{-3} M in dichloromethane ($I_{340}/I_{295} = 2.75$), (b) 5×10^{-4} M in dichloromethane ($I_{340}/I_{295} = 2.72$), and (c) 5×10^{-4} M in methanol. $\lambda_{EX} = 260$ nm.

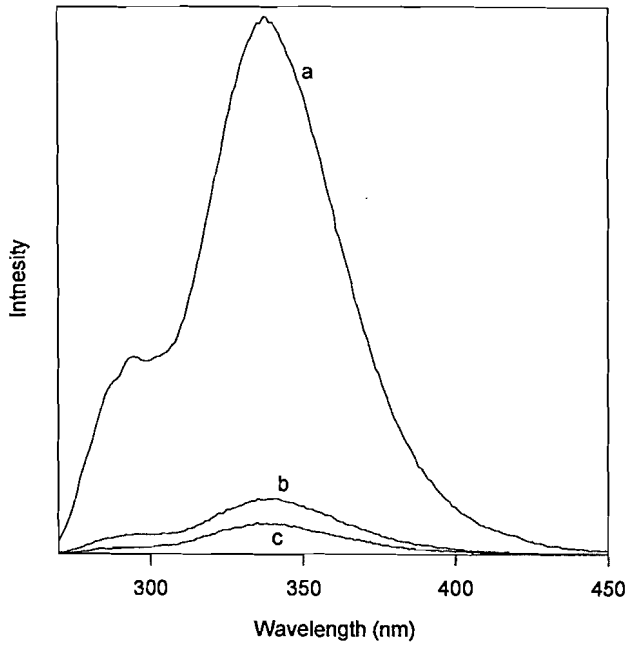

Fig. 7. Fluorescence excitation spectra of 1,3-diphenylpropane (5×10^{-4} M): (a) in methanol ($\lambda_{EM} = 300$ nm), (b) in dichloromethane ($\lambda_{EM} = 300$ nm), (c) in methanol ($\lambda_{EM} = 350$ nm), and (d) in dichloromethane ($\lambda_{EM} = 350$ nm).

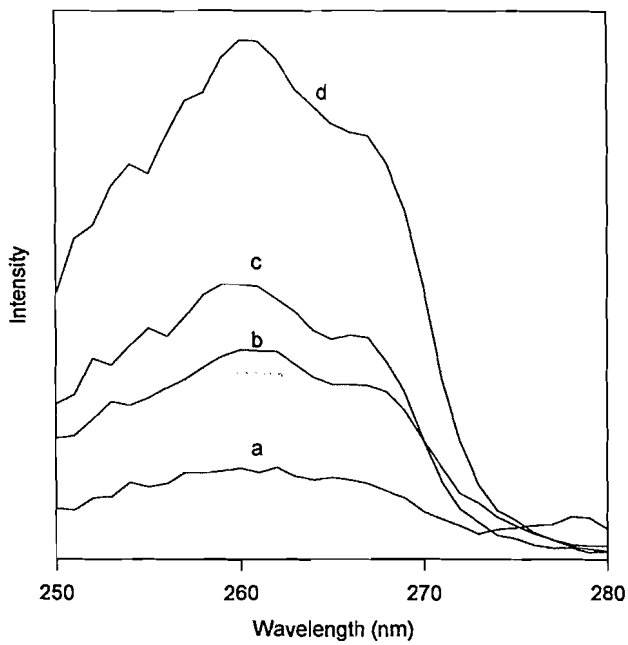

vations suggest that 1,3-diphenylpropane forms an intramolecular excimer in both nonpolar and polar solvents, but that little or no aggregation occurs, whereas DPC probably forms some type of fluorescent aggregates at higher concentrations in polar solvents.

In addition to the results for 1,3-diphenylpropane, we found that 1,3-diphenylacetone does not show any solvent-dependent fluorescence emission, but rather exhibits two emission peaks, one at 300 nm and another at 340 nm, which are not affected by concentration or by the polarity of the solvent. Apparently the polarity of the solvent plays an important role only when the carbonyl group is connected to the phenyl groups via oxygen.

Table 2. Fluorescence lifetime data on DPC.

Solvent	λ_{EX}/nm	λ_{EM}/nm	τ_1/ns	τ_2/ns
Cyclohexane	260	290	1.78	—
Methanol	260	290	0.96	3.40
Methanol	260	340	0.42	3.80

Fig. 8. Fluorescence excitation and emission spectra of phenylacetate: (a) 1×10^{-2} M in cyclohexane ($\lambda_{EX} = 260$ nm), (b) 1×10^{-3} M in acetonitrile ($\lambda_{EX} = 260$ nm), (c) 1×10^{-3} M in acetonitrile ($\lambda_{EM} = 300$ nm), and (d) 1×10^{-3} M in acetonitrile ($\lambda_{EM} = 350$ nm).

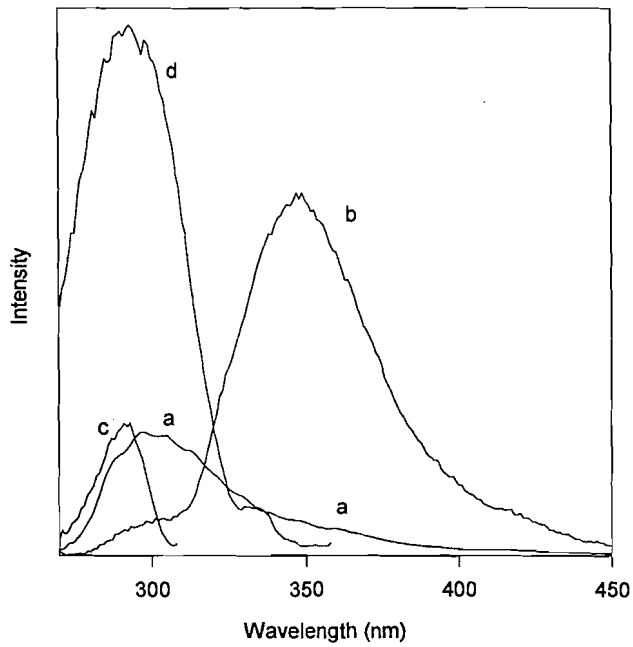

Fluorescence lifetime studies (Table 2) show that the decay curve of the unassociated DPC (in cyclohexane) is single exponential with a lifetime of 1.78 ns. In methanol, the decay of fluorescence at 290 nm can be described by the sum of two exponential functions with 35% contribution from a longer lived component (3.40 ns) and 65% contribution from a short-lived component (0.96 ns). When the fluorescence decay is monitored at 340 nm, the fraction (87%) of the longer lived component (3.80 ns) is higher than that (13%) of the short-lived component (0.42 ns). Although no conclusive assignments can be made, the long-lived component may be from a preformed excimer or aggregate and the shorter lived component from a single excited monomer species. The decrease in lifetime of the purported monomer emission (compared to cyclohexane) in methanol could be a solvent polarity effect, self-quenching, or a combination of both.

Phenylacetate behaves quite similarly to DPC. In cyclohexane, phenylacetate exhibits only one fluorescence emission peak at 300 nm (Fig. 8a), whereas in acetonitrile phenylacetate

Can. J. Chem. Downloaded from www.nrcresearchpress.com by 46.23.64.124 on 09/08/12
For personal use only.

Fig. 9. Fluorescence emission spectra of phenylacetate as a function of concentration in acetonitrile: (a) 1×10^{-4} M ($I_{360}/I_{300} = 1.9$), (b) 5×10^{-4} M ($I_{360}/I_{300} = 3.7$), and (c) 1×10^{-3} M ($I_{360}/I_{300} = 14.8$). $\lambda_{EX} = 280$ nm.

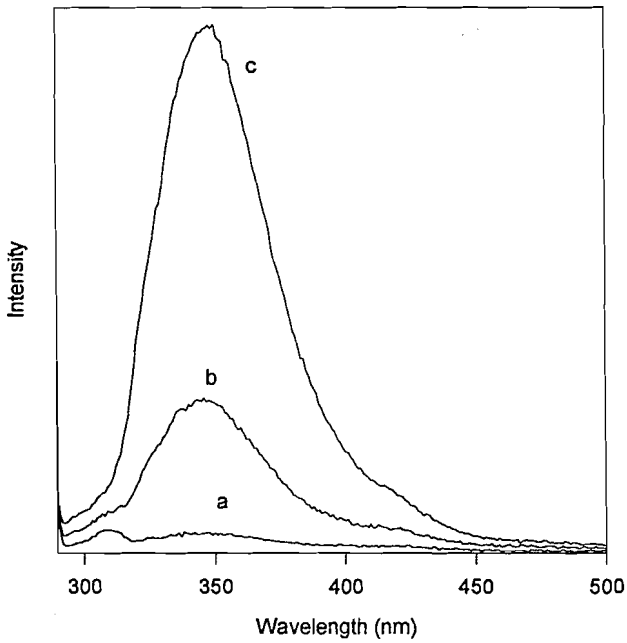

Fig. 10. Fluorescence emission spectra of polycarbonate (0.1 mg/mL): (a) in a mixture of 25% methanol and 75% dichloromethane, (b) solvent mixture evaporated from (a) and the residue redissolved in dichloromethane, and (c) in fresh dichloromethane. $\lambda_{EX} = 270$ nm.

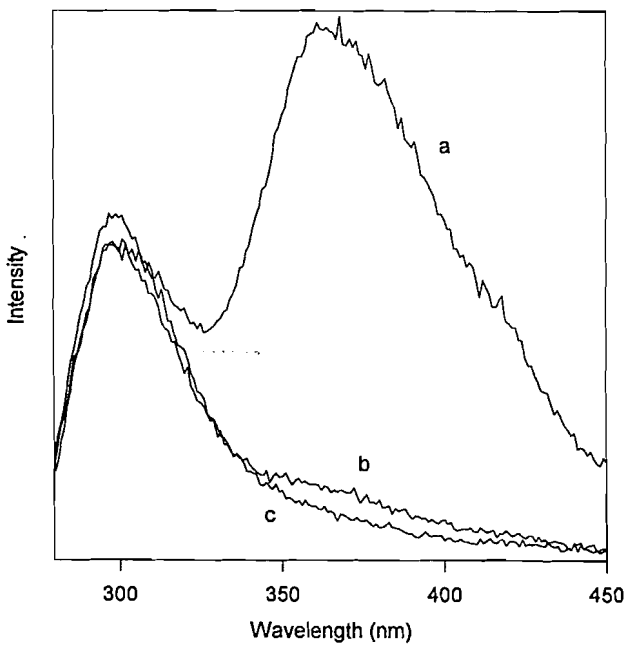

has a strong fluorescence with emission peak at 350 nm and a weak emission with peak maximum around 300 nm (Fig. 8b). This corroborates our previous observation that the 350 nm emission observed in the case of DPC is not due to a 1,3 intramolecular interaction. As observed for DPC, the excitation scan of the 350 nm fluorescence emission peak of phenylacetate is also red-shifted compared to that of the 300 nm fluorescence emission peak (Fig. 8 c and d), indicating that the 350 nm emission peak may well be from an aggregate when excited at longer wavelengths. In addition, the ratio of the intensity of the 350 nm peak to that of the 300 nm emission peak appears to decrease with decrease in concentration (difficult to assess absolutely due to low intensity of emission with peak maximum at ~300 nm), suggesting that for phenylacetate the 350 nm emission is also due to intermolecular association in polar solvents (Fig. 9).

Fig. 11. Fluorescence emission spectra of polycarbonate (0.1 mg/mL): (a) in dichloromethane, (b) in 25% acetonitrile and 75% dichloromethane mixture, and (c) in 50% acetonitrile and 50% dichloromethane mixture. $\lambda_{EX} = 265$ nm.

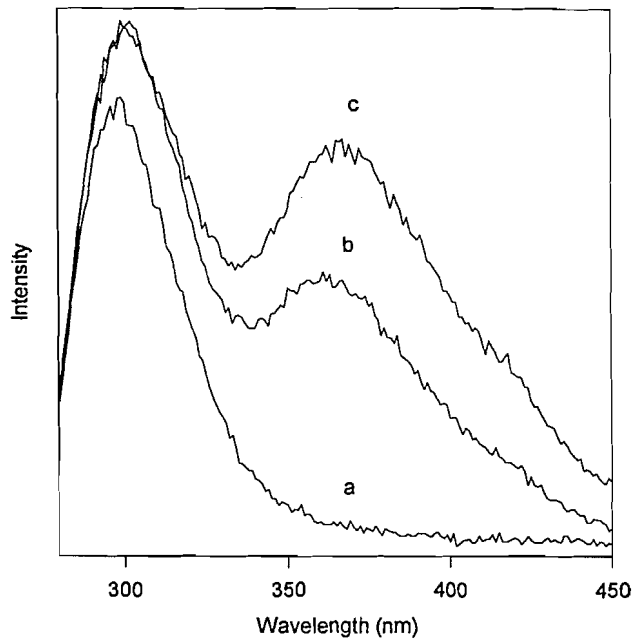

3.2 Photophysics of polycarbonate

Having analyzed the fluorescence of DPC, which is a model for the repeat units of polycarbonate, we next extend our study to polycarbonate. In addition to polarity effects, in the case of polycarbonate the solubility parameter must also be considered, i.e., dichloromethane is a good solvent for polycarbonate, while methanol and acetonitrile are non-solvents for polycarbonate. Mixtures of dichloromethane and methanol and dichloromethane and acetonitrile are thus relatively poor solvents for polycarbonate. In a mixture of dichloromethane(75%, v/v) and methanol (25%, v/v), polycarbonate exhibits two emission peaks, one at 300 nm and another at 360 nm upon excitation at 270 nm (Fig. 10a). When the methanol and dichloromethane mixture was evaporated and the residue (polycarbonate) redissolved in dichloromethane, the resultant fluorescence spectra showed only one emission peak around 300 nm (Fig. 10b), essentially that observed for the fresh sample (Fig. 10c). These results clearly show that the 360 nm emission is not due to a reaction product or an impurity. In a mixture of dichloromethane and acetonitrile, polycarbonate also exhibits an emission with peak maximum around 360 nm in addition to the regular emission at 300 nm (Fig. 11). The intensity of the 360 nm emission peak increases as the fraction of acetonitrile

Can. J. Chem. Downloaded from www.nrcresearchpress.com by 46.23.64.124 on 09/08/12
For personal use only.

Fig. 12. Fluorescence excitation spectra of polycarbonate (0.1 mg/mL) in a mixture of 25% acetonitrile and 75% dichloromethane: (a) λ_{EM} = 305 nm and (b) λ_{EM} = 365 nm.

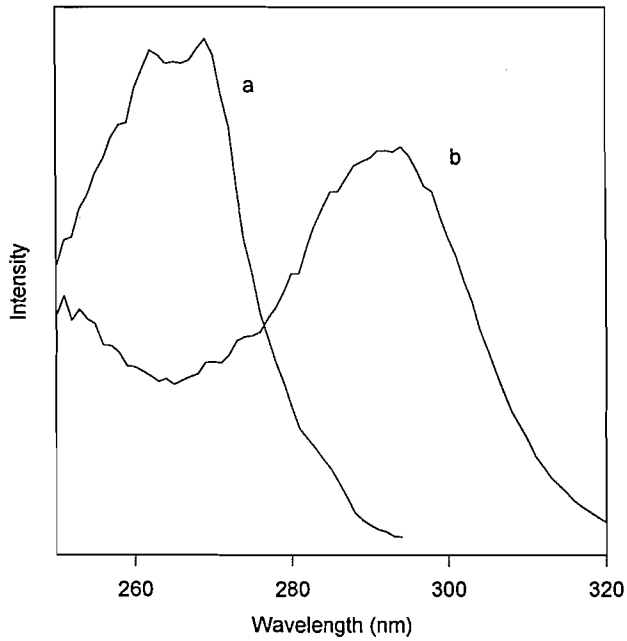

Fig. 13. Fluorescence emission spectra (emission corrected) of polycarbonate (0.1 mg/mL): (a) in dichloromethane (solubility parameter of 9.7 $(cal/cc)^{1/2}$), (b) in a mixture of 53% cyclohexane and 47% dichloromethane (solubility parameter of 8.4 $(cal/cc)^{1/2}$), and (c) in a mixture of 27% methanol and 73% dichloromethane (solubility parameter of 11.0 $(cal/cc)^{1/2}$). λ_{EX} = 270 nm.

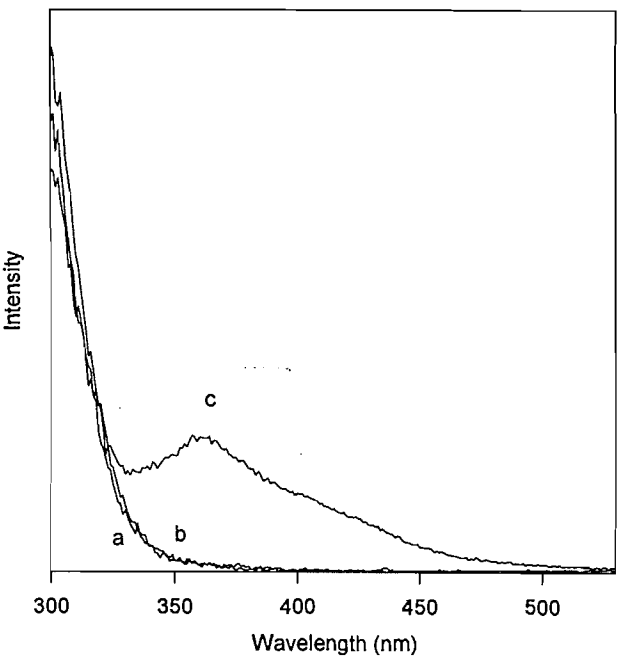

increases in the dichloromethane–acetonitrile mixture (Fig. 11). Likewise, in a dichloromethane–methanol mixture, as the fraction of methanol increases, the intensity of the 360 nm emission peak also increases (not shown). The excitation scan of the 360 nm emission peak extends to longer wavelengths compared to that recorded for the 300 nm emission peak of polycarbonate

Fig. 14. Fluorescence emission spectra of polycarbonate (0.1 mg/mL/75% dichloroethane and 25% methanol mixture) as a function of temperature: (a) 4°C, (b) 24°C, and (c) 60°C. λ_{EX} = 260 nm.

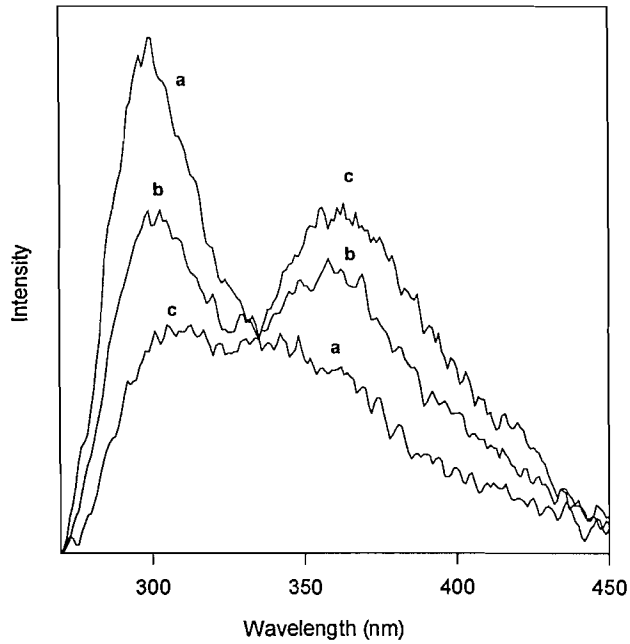

in both mixtures of dichloromethane and acetonitrile (Fig. 12) and dichloromethane and methanol (not shown), indicating that the 360 nm emission, at least when excited above 280 nm, probably results from an aggregate absorption. In contrast to these observations, when a polycarbonate solution in pure dichloromethane is excited at 290 nm, no red-shifted fluorescence emission peak can be observed.

To check whether the 360 nm emission of polycarbonate is dependent on the thermodynamic quality (good/poor) of the solvent, or simply the solvent polarity as was found for the model DPC, fluorescence spectra of a given concentration of polycarbonate were recorded as a function of the solubility parameter of the solvent mixture comprised of dichloromethane and either a nonpolar poor solvent or a polar poor solvent. When the solubility parameter of the solvent (9.7 for dichloromethane) is decreased by 1.3 units (i.e., 47% dichloromethane plus 53% cyclohexane) the fluorescence emission spectrum of polycarbonate does not change (Fig. 13). However, when the solubility parameter of the solvent is increased by 1.3 units (i.e., 27% methanol plus 73% dichloromethane) the emission with peak maximum at 360 nm is observed (Fig. 13c). These observations indicate that the 360 nm emission is independent of the thermodynamic goodness/poorness of the solvent, but highly dependent upon the polarity of the solvent.

3.3 Effect of temperature on the fluorescence spectra of polycarbonate in a mixture of dichloroethane and methanol

Normally the intensity of the fluorescence emission peak of aggregates (dimers) decreases with an increase in temperature as a result of dissociation at higher temperatures (10). In the present case, the I_{360}/I_{300} ratio increases as the temperature is increased (Fig. 14). The effects of variation of temperature are reversible (figures not shown). We cannot explain the origin

Fig. 15. Fluorescence emission spectra of polycarbonate in a mixture of 27% methanol and 73% dichloromethane as a function of concentration: (a) 0.10 mg/mL (I_{360}/I_{301} = 1.35), (b) 0.05 mg/mL (I_{360}/I_{301} = 1.48), and (c) 0.02 mg/mL(I_{360}/I_{301} = 1.30). λ_{EX} = 270 nm.

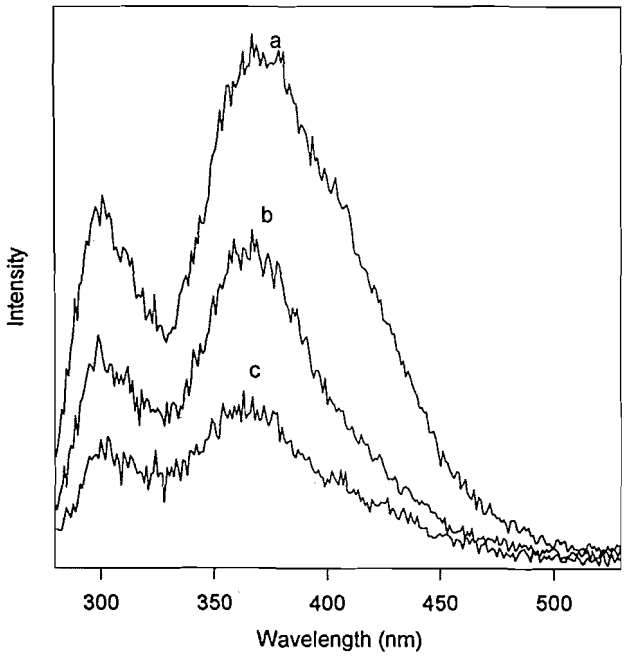

of the temperature effect in Fig. 14 at present. However, we note that such a temperature effect has also been observed for poly(ethylene terephthalate) (11–15), another main-chain polymer.

3.4 Effect of concentration on the ratio of the emission intensity at 360 nm to that at 300 nm (I_{360}/I_{300}) for polycarbonate in methanol–dichloromethane solvent mixtures

As suggested previously, the red-shifted emission with peak maximum at 350 nm emission peak in the case of DPC arises from intermolecular interactions in polar solvent cages. In the case of polycarbonate, the I_{360}/I_{300} ratio decreases negligibly upon dilution (Fig. 15). Apparently the 360 nm emission (peak maximum) of polycarbonate in a mixture of dichloromethane and methanol is due to intramolecular aggregation (at least when excited at longer wavelengths) in a strong polar solvent cage. This is in contrast to the 350 nm emission (peak maximum) in the case of DPC and phenylacetate that results primarily from an intermolecular process in each case.

4. Conclusions

A polar solvent induced red-shifted fluorescence emission from polycarbonate, DPC, and phenylacetate has been identified. In the case of DPC and phenylacetate it is suggested that the red-shifted emission results mainly from intermolecular aggregation, while in the case of polycarbonate it is largely due to intramolecular aggregation within a strong polar solvent cage. Diphenylcarbonate, phenylacetate, and polycarbonate behave much differently than other 1,3 systems such as 1,3-diphenylpropane and polystyrene, which exhibit intramolecular excimer formations and are not influenced greatly by solvent polarity.

Acknowledgement

We thank Ciba-Additives (Ciba-Geigy Corporation) for their financial support of this work. We also thank A. Factor (G.E. Plastics) for the polycarbonate sample.

References

1. J.S. Humphrey, Jr., A.R. Shultz, and D.D.G. Jaquiss. Macromolecules, **6**, 305 (1973).
2. A. Gupta, R. Liang, J. Moacanin, R. Goldbeck, and D. Kliger. Macromolecules, **13**, 262 (1980).
3. S. Pankasem, J. Kuczynski, and K. Thomas. Macromolecules, **27**, 3773 (1994).
4. R.M. Masegosa, I.H. Fuente, I.F. dePierola, and A. Horta. Polymer, **28**, 231 (1987).
5. F. Hirayama. J. Chem. Phys. **42**, 3163 (1965).
6. C.E. Hoyle, H. Shah, and G.L. Nelson. J. Polym. Sci. Part A: Polym. Chem. **30**, 1525 (1990).
7. M. H. Chipalkatti and J. Kaski. Polym. Mater. Sci. Eng. **64**, 131 (1991).
8. D.S. Weiss, H. Yang, P.M. Thompson, and D.A. Chen. Polym. Prepr. **33**, 891 (1992).
9. C.E. Kalmus and M. Hercules. J. Am. Chem. Soc. **96**, 449, (1974).
10. M. Irie, T. Kamijo, M. Alkawa, T. Takemura, K. Hayashi, and H. Baha. J. Phys. Chem. **81**, 1571 (1977).
11. M.F. Sonnenschein and C.M. Roland. Polymer, **31**, 2023 (1990).
12. D.J. Hemker, C.W. Frank and J.W. Thomas, Polymer, **29**, 437 (1988).
13. J.R. MacCallum. *In* Photophysics of polymers. *Edited by* C.E. Hoyle and J.M. Torkelson. American Chemical Society, Washington, D.C. 1987.
14. F. Mendicuti, B. Patel, V.N. Vellarkad, and W.L. Mattice. Polymer, **29**, 1669 (1989).
15. M. Hennecke, K. Kurz, and J. Fuhrmann. Polymer, **30**, 1072 (1989).

Can. J. Chem. Downloaded from www.nrcresearchpress.com by 46.23.64.124 on 09/08/12
For personal use only.

The synthesis and polymerization behaviour of silicon-bridged [1]- and [2]ferrocenophanes with sterically demanding trimethylsilyl substituents attached to the cyclopentadienyl rings

Timothy J. Peckham, Daniel A. Foucher, Alan J. Lough, and Ian Manners

Can. J. Chem. Downloaded from www.nrcresearchpress.com by 46.23.64.124 on 09/08/12
For personal use only.

Abstract: The silicon-bridged [1]ferrocenophane Fe(η-$C_5H_3SiMe_3)_2(SiMe_2)$ (**5**) was synthesized via the reaction of Li_2[Fe(η-$C_5H_3SiMe_3)_2$]·tmeda (tmeda = tetramethylethylenediamine) with Me_2SiCl_2 in hexanes. The disilane-bridged [2]ferrocenophane Fe(η-$C_5H_3SiMe_3)_2(Si_2Me_4)$ (**7**) was prepared using a similar route from the disilane $ClMe_2SiSiMe_2Cl$. Despite the presence of sterically demanding $SiMe_3$ substituents on the cyclopentadienyl rings, compound **5** was found to undergo thermal ring-opening polymerization at 170°C to produce very soluble, high molecular weight poly(ferrocenylsilane) **6** with $M_w = 1.4 \times 10^5$, $M_n = 8.4 \times 10^4$. However, the [2]ferrocenophane **7** was found to be resistant to thermal ring-opening polymerization even at 350°C and decomposed above 380°C. A single-crystal X-ray diffraction study of **7** revealed that the steric interactions between the bulky $SiMe_3$ groups are relieved by a significant twisting of the disilane bridge with respect to the plane defined by the centroids of the cyclopentadienyl ligands and the metal atom. The angle between the planes of the cyclopentadienyl rings in **7** was found to be 5.4(6)°, slightly greater than that in the non-silylated analogue Fe(η-$C_5H_4)_2(Si_2Me_4)$ (**4***a*) (4.19(2)°), and dramatically less than the corresponding tilt angle of the strained, polymerizable, silicon-bridged [1]ferrocenophane Fe(η-$C_5H_4)_2(SiMe_2)$ (**1**) (20.8(5)°). The length of the Si—Si bond in **7** (2.342(3) Å) was found to be close to the sum of the covalent radii (2.34 Å). Crystals of **7** are monoclinic, space group *C*2/*c*, with $a = 23.689(3)$ Å, $b = 11.174(1)$ Å, $c = 31.027(3)$ Å, $\beta = 109.16(1)°$, $V = 7758(2)$ Å^3, and $Z = 12$.

Key words: ring-opening polymerization, ferrocenophane, organometallic polymers.

Résumé : On a synthétisé le [1]ferrocénophane ponté par un silicium, Fe(η-$C_5H_3SiMe_3)_2(SiMe_2)$ (**5**), par une réaction du Li_2[Fe(η-$C_5H_3SiMe_3)_2$]·tmeda (tmeda = tétraméthyléthylènediamine) avec du Me_2SiCl_2 dans de l'hexane. On a préparé le [2]ferrocénophane ponté par deux silanes, Fe(η-$C_5H_3SiMe_3)_2(Si_2Me_4)$ (**7**), faisant appel à une voie semblable à partir du disilane $ClMe_2SiSiMe_2Cl$. Malgré la présence sur les noyaux cyclopentadiényles de substituants $SiMe_3$ ayant une demande stérique importante, on a trouvé que le composé **5** subit une polymérisation thermique par ouverture de cycle à 170°C qui conduit au poly(ferrocénylsilane) **6** très soluble et de poids moléculaire élevé avec $M_w = 1{,}4 \times 10^5$, $M_n = 8{,}4 \times 10^4$. Toutefois, on a trouvé que le [2]ferrocénophane **7** est résistant à une polymérisation thermique par ouverture de cycle, même à 350°C, et qu'il se décompose à 380°C. Une étude de diffraction des rayons X par un cristal unique du composé **7** montre que les interactions stériques entre les groupes $SiMe_3$ stériquement encombrants sont apaisées par une déformation importante du pont disilane par rapport au plan défini par les centroïdes des coordinats cyclopentadiényles et de l'atome de métal. On a trouvé que l'angle entre les plans des noyaux cyclopentadiényles du composé **7** est de 5,4(6)°, ce qui est légèrement supérieur à la valeur de 4,19(2)° observée dans l'analogue non silylé Fe(η-$C_5H_4)_2(Si_2Me_4)$ (**4***a*) et de beaucoup inférieure à celle observée (20,8(5)°) dans [1]ferrocénophane ponté par un silicium, polymérisable et tendu Fe(η-$C_5H_4)_2(SiMe_2)$ (**1**). On a trouvé que la longueur de la liaison Si—Si dans le composé **7** (2,342(3) Å) se rapproche de la somme de rayons covalents (2,34 Å). Les cristaux du composé **7**

Received April 13, 1995.

This paper is dedicated to Professor J.E. (Jim) Guillet in recognition of his contributions to Canadian chemistry.

T.J. Peckham, D.A. Foucher, A.J. Lough, and I. Manners.[1] Department of Chemistry, University of Toronto, 80 St. George St., Toronto, ON, M5S 1A1, Canada.

[1] Author to whom correspondence may be addressed. Telephone: (416) 978–6157. Fax: (416) 978–8775.

sont monocliniques, groupe d'espace $C2/c$, avec $a = 23{,}689(3)$, $b = 11{,}174(1)$ et $c = 31{,}027(3)$ Å, $\beta = 109{,}16(1)°$, $V = 7758(2)$ Å^3, et $Z = 12$.

Mots clés : polymérisation par ouverture de cycle, ferrocénophane, polymères organométalliques.

[Traduit par la rédaction]

High polymers in which transition metals are incorporated directly into the main chain are attractive synthetic targets due to their unusual physical and chemical properties. Such materials are expected to possess an interesting and potentially useful range of electronic, magnetic, and optical characteristics that are not readily achieved using traditional organic polymers (1–4). However, for the most part, progress in this area has been limited by the synthetic challenge of obtaining high molecular weight, well-defined polymers (4).

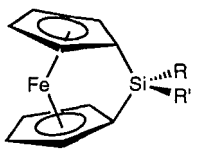

1

R, R' = H, alkyl, aryl

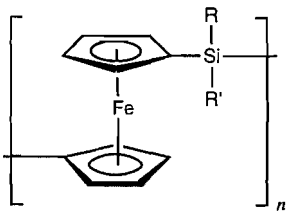

2

R, R' = H, alkyl, aryl

In 1992, we reported the synthesis of soluble, high molecular weight poly(ferrocenylsilanes) (**2**) via the thermal ring-opening polymerization (ROP) of silicon-bridged [1]ferrocenophanes (**1**) (5). More recently, we have demonstrated that living ROP can also be achieved in solution at room temperature in the presence of anionic initiators (6). This has provided access to poly(ferrocenylsilanes) with controlled molecular weights as well as to block copolymers (7). In addition, random copolymers are accessible via thermal copolymerization of different monomers (8). We have also shown that ROP is catalyzed in solution by certain transition metal complexes (9) and that the ROP route can be extended to other strained [*n*]metallocenophanes; thus, polymers such as poly(ferrocenylgermanes) and poly(ferrocenylethylenes) have been prepared from germanium-bridged [1]ferrocenophanes and hydrocarbon-bridged [2]ferrocenophanes, respectively (10–17). Crystallographic studies have revealed that these polymerizable monomers possess ring-tilted structures in which the planes of the cyclopentadienyl ligands are tilted by angles of up to 31° (17). By contrast, in ferrocene the cyclopentadienyl rings are planar. The apparent strain in these highly ring-tilted molecules is believed to provide the driving force for their facile thermal ROP.

Although the ROP strategy has been successfully applied to [2]metallocenophanes **3***a*–**3***c* with a hydrocarbon bridge, the analogues **4***a* and **4***b* with a disilane bridge possess only modest tilt angles (**4***a*, 4.19(2)°; **4***b*, 7.8(5)°) and are resistant to ROP, presumably as a result of their significantly less strained structures (13, 18).

The rationale behind the work described in this paper was as follows. Firstly, it is known that the presence of sterically demanding substituents generally hinders the formation of high molecular weight polymers via ROP. For example, Compton and Rauchfuss have reported that the desulfurization of [3]trithiaferrocenophanes with phosphines yields polymers with ferrocene and disulfido units in the backbone (19). The molecular weights of the polymers formed when an *n*-butyl substituent is present on the cyclopentadienyl rings (M_n = ca. 100 000) are much higher than when bulkier *tert*-butyl substituents are attached (M_n = ca. 3000). It was therefore of interest

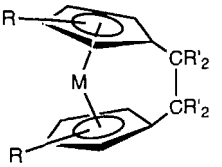

3*a* M = Fe, R = H, R' = H
3*b* M = Fe, R = Me, R' = H
3*c* M = Ru, R = H, R' = H
3*d* M = Fe, R = H, R' = Me

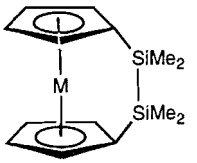

4*a* M = Fe
4*b* M = Ru

to examine if significantly lower molecular weight products would be generated by the ROP of [1]ferrocenophanes incorporating bulky substituents. Isolation of low molecular weight poly(ferrocenylsilanes) would allow end-group analysis and might yield useful information on the thermal ROP mechanism. Secondly, we felt that polymerization of disilane-bridged [2]ferrocenophanes might even be facilitated if sterically demanding substituents, such as trimethylsilyl groups, were present on the cyclopentadienyl rings. Thus, the preference for these bulky substituents to minimize steric interactions with one another might provide an additional driving force for ROP. Thirdly, we have previously shown that a *trans* zigzag conformation is likely for the high polymer **2** (R = R' = Me) in ordered regions in the solid state (20). The presence of bulky trimethylsilyl substituents might be expected to impart unusual conformational properties to the macromolecules both in the solid state and solution which would influence the interactions between the transition metal centers that dominate the electrochemical behaviour (4).

In this paper, we describe our studies on the influence of trimethylsilyl groups on the thermal polymerization behaviour of silicon-bridged [1]- and [2]ferrocenophanes.

Results and discussion

Synthesis of the bis(trimethylsilyl)-substituted, silicon-bridged [1]ferrocenophane 5

The dilithiation of bis(trimethylsilyl)ferrocene was previously shown to be regio- and stereoselective by Silver and coworkers (21). Thus, reaction of this species with *n*BuLi·tmeda

Can. J. Chem. Downloaded from www.nrcresearchpress.com by 46.23.64.124 on 09/08/12
For personal use only.

Can. J. Chem. Downloaded from www.nrcresearchpress.com by 46.23.64.124 on 09/08/12
For personal use only.

(tmeda = tetramethylethylenediamine) followed by Ph_2PCl yielded 1,1′-bis(diphenylphosphino)-3,3′-bis(trimethylsilyl)-ferrocene. This regio- and stereoselectivity was viewed to be attractive as the formation of more well-defined ferrocenophane monomers and corresponding polymers rather than mixtures of isomers would be anticipated.

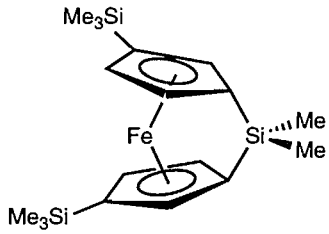

5

The silicon-bridged [1]ferrocenophane **5** was prepared via the reaction of the dilithium salt $Li_2[Fe(\eta\text{-}C_5H_3SiMe_3)_2]\cdot$tmeda with dichlorodimethylsilane (22). The synthesis and isolation of the dilithium salt was achieved by reacting dilithioferrocene with 2 equivalents of chlorotrimethylsilane, purification of the bis(trimethylsilyl)ferrocene by vacuum distillation, deprotonation of the product with 2 equivalents of *n*-BuLi in the presence of tmeda, followed by recrystallization from hexanes at −78°C. The final product (**5**) was purified by vacuum distillation (80°C, 0.005 Torr; 1 Torr = 133.3 Pa) as a red-orange liquid.

The purified silicon-bridged [1]ferrocenophane **5** was characterized by ^1H, ^{13}C, and ^{29}Si NMR as well as by mass spectrometry, and the data were consistent with the assigned 1,1′-3,3′-substituted structure. In particular, the ^{13}C NMR chemical shift of the ipso carbons of the cyclopentadienyl groups attached to the $SiMe_2$ bridge (36.9 ppm) showed the characteristic upfield shift compared to the other cyclopentadienyl carbons (22). This upfield shift is a well-established trend for strained, ring-tilted main group element-bridged [1]ferrocenophanes and is probably indicative of increased sp^3 character for the ipso carbon bonded to the bridging silicon in comparison with ipso carbons in unbridged, substituted ferrocenes (22, 23). Interestingly, all the other cyclopentadienyl ^{13}C NMR resonances are located further downfield than the resonances reported for other symmetrically substituted, silicon-bridged [1]ferrocenophanes (e.g., **1**). The ^1H NMR revealed two pseudo quartets and a pseudo triplet in the cyclopentadienyl region, characteristic of an $A_2B_2C_2$ spin system. The ^{29}Si NMR spectrum of **5** showed two singlet resonances at −3.3 and −5.4 ppm, of relative intensity 1:2, which were assigned to the $SiMe_2$ bridge and the two equivalent trimethylsilyl groups, respectively. The mass spectrum of **5** showed a molecular ion at *m/e* 386 as the most abundant peak.

Thermal ROP of the bis(trimethylsilyl)-substituted, silicon-bridged [1]ferrocenophane 5

When **5** was heated in an evacuated Pyrex tube for 3 h at 170°C the tube contents became more viscous and then immobile. The poly(ferrocenylsilane) **6**, a red-orange powder, was isolated by dissolution in THF followed by precipitation into methanol. GPC analysis revealed that the polymer was of high molecular weight (M_w = 140 000) with a relatively narrow weight distribution (M_w/M_n = 1.7). The results of multinuclear NMR studies were consistent with the assigned structure. A single, broad ^1H NMR resonance was found in the cyclopentadienyl region. In addition, broad resonances for the protons from the bridging $SiMe_2$ and pendant $SiMe_3$ groups were observed. The ^{29}Si NMR spectrum for **6** revealed two broad resonances (−5.9 ppm, $SiMe_2$; −2.5 ppm, $SiMe_3$) that are found upfield with respect to the monomer **5**. The ^{13}C NMR resonance attributable to the (C_{ipso}−$SiMe_2$) ipso carbons was shifted to a more conventional region associated with cyclopentadienyl carbons in unbridged, substituted ferrocenes compared to that in **5**. This indicated that the strain of the ring-tilted monomer **5** was relieved by ROP to yield polymer **6** in which the cyclopentadienyl ligands were approximately parallel. The polymer formed air-stable, amber, free-standing, brittle films, which were cast from a solution of **6** in toluene via slow solvent evaporation. The polymer was shown to be extremely soluble, even in nonpolar solvents such as hexanes.

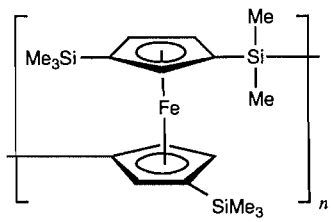

6

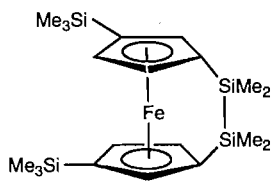

7

Synthesis of the bis(trimethylsilyl)-substituted, disilane-bridged [2]ferrocenophane 7

The disilane-bridged [2]ferrocenophane **7** was synthesized in a similar manner to the [1]ferrocenophane **5** by employing 1,2-dichloro-1,1,2,2-tetramethyldisilane in the place of dichlorodimethylsilane. Compound **7** was isolated by vacuum distillation (120°C, 0.05 Torr) as reddish-orange crystals of low melting point. Multinuclear NMR studies were consistent with the assigned structure. The ^{29}Si NMR spectrum revealed two resonances: one corresponding to the $SiMe_3$ substitutents (−9.7 ppm) and the other to the bridging $SiMe_2$ groups (−4.0 ppm). In sharp contrast to **5**, the ^{13}C NMR resonances associated with the cyclopentadienyl carbons bonded to the bridging disilane unit occur at 76.0 ppm. This is consistent with a much less tilted and strained structure for **7** than is the case for **5**. One interesting feature of the ^1H NMR of **7** was the presence of *three* resonances in the region for methyl groups bonded to silicon. The resonance at 0.28 ppm (singlet, 18H) was attributed to the protons in the two $SiMe_3$ groups. The other two resonances (multiplets at 0.45 ppm and 0.25 ppm, 6H for each) were assigned to inequivalent methyl groups bonded to the bridging silicons. In addition, two resonances were detected in the methyl region of the ^{13}C NMR spectrum of **7**. This situation was in contrast with that for the [1]ferrocenophane **5** where the methyl substituents at the bridging silicon atom were found to be equivalent. To examine in detail the effects the bulky $SiMe_3$ groups would have on the structure of the disilane-bridged [2]ferrocenophane ***4a*** (13), compound **7** was studied by single-crystal X-ray diffraction.

X-ray structure of 7

Reddish-orange, X-ray diffraction-quality crystals of **7** were isolated from a vacuum distillation. Figure 1 shows two alternative views of **7** (molecule B) A summary of cell constants and data collection parameters is included in Table 1 and the

Can. J. Chem. Downloaded from www.nrcresearchpress.com by 46.23.64.124 on 09/08/12
For personal use only.

Fig. 1. (*a*) Molecular structure of **7** (molecule B) (vibrational ellipsoids at the 25% probability level). (*b*) Alternate view of **7** (vibrational ellipsoids at the 25% probability level).

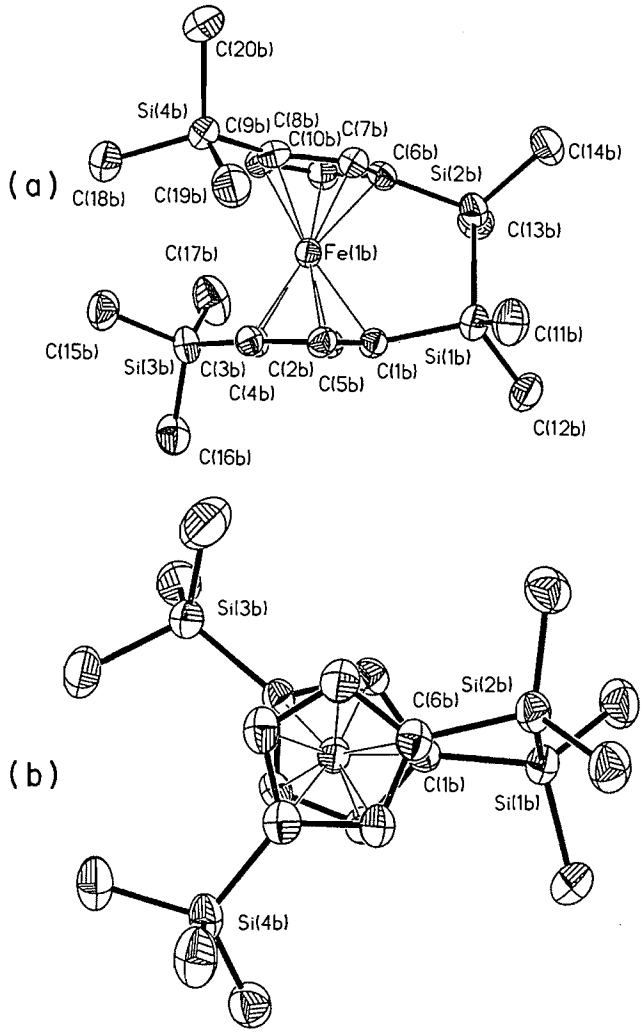

fractional coordinates and important bond lengths and angles are listed in Tables 2 and 3. A summary of important structural features is presented in Table 4. Compound **7** crystallizes in space group *C*2/*c* with $Z = 12$. Hence there are two independent molecules in the structure. One of these molecules (molecule A) has twofold crystallographic symmetry with the Fe atom on a special position. The presence of a C2 axis leads to the inequivalent methyl groups on the bridging silicon atoms. All bond lengths and angles quoted within the text for **7** are for molecule B. Molecules A and B were not found to possess significantly different geometrical parameters with the exception of the C(ipso)-Si-Si-C(ipso) torsion angle.

A comparison of the structural features of **7** with those of the strained monomer **1** (13) and the relatively strain-free species **4***a* (13) is informative and suggests that **7** is relatively unstrained. The dihedral angle between the planes of the cyclopentadienyl rings is 5.9(6)°, only slightly greater than for **4***a* (4.19(2)°) and is dramatically smaller than for **1** (20.8(5)°). Also, the angle β between the plane of the cyclopentadienyl rings and the bridging silicon – ipso carbon bond is 12.6(4)°

Table 1. Summary of crystal data and intensity collection parameters.

	7
Empirical formula	$C_{20}H_{36}FeSi_4$
M_r	444.7
Crystal classification	Monoclinic
Space group	*C*2/*c*
a, Å	23.689(3)
b, Å	11.174(1)
c, Å	31.027(3)
β, deg	109.16(1)
V, Å^3	7758(2)
Z	12
D_{calc}, g cm^{-3}	1.142
μ(Mo, Kα), cm^{-1}	7.71
F(000)	2856
ω-scan width, deg	0.37 + 0.68 tan θ
Range 2θ collected, deg	4.1–52.0
Total no. of reflections	8246
No. of unique reflections	7605
R_{int}	0.024
No. of observed data used ($I > 3\ \sigma(I)$)	2694
Weighting *g*	0.0006
R	0.0399
R_w	0.0460
GOF	1.17
(Δ/σ)max in last cycle	0.01
No. of parameters refined	340
Δρ(max) in final *F* map, e Å^{-3}	0.58

compared to 10.8(3)° for **4***a*. The corresponding value in **1** is much greater (37.0(6)°) and suggests significantly less strain in both **7** and **4***a*. The twist angle for **7** (22.9(8)°) is significantly greater than in **4***a* (8.4(4)°) and is attributable to the unfavourable steric interactions between the two $SiMe_3$ groups. The twist angle for **4***a* is comparable to the corresponding angle in **3***d* (24) (8.9(13)°) whereas virtually no twisting occurs with the disilane-bridged [2]ruthenocenophane **4***b* (18) (0.2(5)°). The twisting of the bridge in **7** as well as the bulkiness of the $SiMe_3$ groups, also results in a significantly increased staggering of the cyclopentadienyl rings such that the stagger angle of 17.7(8)° is much greater than those found in either **4***a* (6.0(1)°) or **4***b* (rings are virtually eclipsed, 0.6(7)°). The larger Ru atom of **4***b* leads to an elongated Si—Si bond (2.370(2) Å) in comparison to **7** where the Si—Si bond length (2.349(3) Å) is similar to that found for **4***a* (2.3535(9) Å) and is close to the average for a typical Si—Si bond length (2.34 Å).

Thermal polymerization behaviour of the bis(trimethylsilyl)-substituted, disilane-bridged [2]ferrocenophane 7

In contrast to the [1]ferrocenophane **5**, when the [2]ferrocenophane **7** was heated in a sealed, evacuated tube at 350°C for 24 h, no increase in melt viscosity was observed. Furthermore, analysis of the contents of the tube by ^{1}H NMR revealed only the presence of **7** and no high molecular weight material ($M_w >$ 1000) was detected by GPC. Similarly, a sample of compound **7** was heated from 380 to 420°C over a span of about 2 h and

Can. J. Chem. Downloaded from www.nrcresearchpress.com by 46.23.64.124 on 09/08/12
For personal use only.

Table 2. Atomic coordinates and equivalent isotropic displacement coefficients ($Å^2$) for **7**.

Atom	*x*	*y*	*z*	*U*(eq)[a]
Fe(1a)	0.500	0.1079(1)	0.2500	0.046(1)
Si(1a)	0.5498(1)	−0.1688(1)	0.2737(1)	0.054(1)
Si(2a)	0.5099(1)	0.2970(1)	0.3442(1)	0.082(1)
C(1a)	0.5625(2)	−0.0073(5)	0.2910(2)	0.053(3)
C(2a)	0.5314(2)	0.0552(5)	0.3168(2)	0.057(3)
C(3a)	0.5391(3)	0.1819(5)	0.3140(2)	0.060(3)
C(4a)	0.5762(2)	0.1962(5)	0.2858(2)	0.064(3)
C(5a)	0.5900(2)	0.0826(5)	0.2723(2)	0.057(3)
C(6a)	0.5642(3)	−0.2617(5)	0.3264(2)	0.080(3)
C(7a)	0.6010(3)	−0.2142(5)	0.2419(2)	0.079(3)
C(8a)	0.4452(3)	0.2366(6)	0.3580(3)	0.116(4)
C(9a)	0.4855(4)	0.4332(5)	0.3093(3)	0.126(5)
C(10a)	0.5722(3)	0.3342(7)	0.3972(2)	0.129(5)
Fe(1b)	0.1769(1)	0.1682(1)	0.0961(1)	0.055(1)
Si(1b)	0.2136(1)	−0.1140(2)	0.0926(1)	0.070(1)
Si(2b)	0.2560(1)	0.0040(2)	0.0486(1)	0.074(1)
Si(3b)	0.0230(1)	0.2458(2)	0.0559(1)	0.077(1)
Si(4b)	0.2518(1)	0.3942(2)	0.1732(1)	0.078(1)
C(1b)	0.1574(3)	−0.0087(5)	0.1015(2)	0.057(3)
C(2b)	0.1098(3)	0.0504(5)	0.0672(2)	0.062(3)
C(3b)	0.0867(3)	0.1484(5)	0.0860(2)	0.061(3)
C(4b)	0.1206(3)	0.1479(5)	0.1334(2)	0.060(3)
C(5b)	0.1632(3)	0.0538(5)	0.1432(2)	0.059(3)
C(6b)	0.2441(3)	0.1576(6)	0.0684(2)	0.065(3)
C(7b)	0.2664(3)	0.1979(6)	0.1144(2)	0.068(3)
C(8b)	0.2371(3)	0.3071(6)	0.1201(2)	0.071(3)
C(9b)	0.1957(3)	0.3327(6)	0.0752(3)	0.075(3)
C(10b)	0.2003(3)	0.2443(6)	0.0443(2)	0.075(3)
C(11b)	0.2678(3)	−0.1509(6)	0.1498(2)	0.099(4)
C(12b)	0.1779(3)	−0.2555(5)	0.0655(2)	0.098(4)
C(13b)	0.2129(3)	−0.0098(7)	−0.0137(2)	0.101(4)
C(14b)	0.3375(3)	−0.0222(6)	0.0593(3)	0.104(4)
C(15b)	0.0268(3)	0.3873(6)	0.0869(2)	0.107(4)
C(16b)	−0.0471(3)	0.1670(6)	0.0540(2)	0.106(4)
C(17b)	0.0219(3)	0.2753(8)	−0.0019(2)	0.152(5)
C(18b)	0.1872(3)	0.4911(6)	0.1706(3)	0.103(4)
C(19b)	0.2681(3)	0.2917(6)	0.2226(2)	0.096(4)
C(20b)	0.3178(3)	0.4922(6)	0.1793(3)	0.120(4)

[a]Equivalent isotropic *U* defined as one third of the trace of the orthogonalized U_{ij} tensor.

another sample heated at about 160°C over a span of 20 h in the presence of the anionic initiator, potassium trimethylsilanoate, $K[OSiMe_3]$.[2] In both cases, no oligomeric or polymeric material could be detected by either GPC or mass spectrometry. ^1H NMR for the sample heated in the presence of $K[OSiMe_3]$ revealed only the presence of unreacted **7** whereas ^1H NMR of the sample heated over the range from 380 to 420°C showed both the presence of unreacted **7** and very broad resonances in both the cyclopentadienyl region and the SiMe region that were assigned to unidentified decomposition products.

Summary

The introduction of sterically demanding trimethylsilyl substituents to the cyclopentadienyl rings does not significantly affect the polymerizability of silicon-bridged [1]ferrocenophanes. A high molecular weight poly(ferrocenylsilane) was still formed via the ROP of **5** at elevated temperatures. The presence of these bulky ligands has some significant effects on the structure of disilane-bridged [2]ferrocenophanes with an increase in both the tilt angle and the degree of twisting of the disilane bridge. However, these distortions were found to be insufficient to allow ROP, and **7** was found to be stable to 380°C.

We are now studying in detail the properties of the poly(ferrocenylsilane) **6** and related polymers with bulky side groups. Our results will be reported in the near future.

Experimental section

All chemicals unless otherwise noted were purchased from

[2] Anionic ROP has been shown to occur for a number of silicon-containing ring systems. See, for example: refs. 6 and 25.

Table 3. (*a*) Bond lengths (Å) and (*b*) selected angles (deg) for **7**.

(*a*)

Fe(1a)—C(3a)	2.069(5)	Fe(1a)—C(2a)	2.045(5)
Fe(1a)—C(1a)	2.057(5)	Fe(1a)—C(5a)	2.033(5)
Fe(1a)—C(4a)	2.037(5)	Si(1a)—C(1a)	1.878(6)
Si(1a)—C(6a)	1.872(6)	Si(1a)—C(7a)	1.868(7)
Si(1a)—Si(1i)	2.334(8)	Si(2a)—C(9a)	1.847(7)
Si(2a)—C(10a)	1.860(6)	C(3a)—C(2a)	1.434(8)
C(3a)—C(4a)	1.438(10)	C(2a)—C(1a)	1.434(9)
C(1a)—C(5a)	1.420(9)	C(5a)—C(4a)	1.409(8)
Fe(1b)—C(1b)	2.050(6)	Fe(1b)—C(2b)	2.034(6)
Fe(1b)—C(3b)	2.068(6)	Fe(1b)—C(4b)	2.046(7)
Fe(1b)—C(5b)	2.047(6)	Fe(1b)—C(6b)	2.046(6)
Fe(1b)—C(7b)	2.034(6)	Fe(1b)—C(8b)	2.072(6)
Fe(1b)—C(9b)	2.046(7)	Fe(1b)—C(10b)	2.050(8)
Si(1b)—Si(2b)	2.340(3)	Si(1b)—C(1b)	1.863(7)
Si(1b)—C(11b)	1.862(6)	Si(1b)—C(12b)	1.860(6)
Si(2b)—C(6b)	1.876(7)	Si(2b)—C(13b)	1.873(6)
Si(2b)—C(14b)	1.870(6)	Si(3b)—C(3b)	1.846(6)
Si(3b)—C(15b)	1.838(7)	Si(3b)—C(16b)	1.863(7)
Si(3b)—C(17b)	1.815(8)	Si(4b)—C(8b)	1.846(7)
Si(4b)—C(18b)	1.855(7)	Si(4b)—C(19b)	1.849(7)
Si(4b)—C(20b)	1.866(7)	C(1b)—C(2b)	1.434(7)
C(1b)—C(5b)	1.436(9)	C(2b)—C(3b)	1.429(9)
C(3b)—C(4b)	1.427(8)	C(4b)—C(5b)	1.421(8)
C(6b)—C(7b)	1.422(9)	C(6b)—C(10b)	1.438(9)
C(7b)—C(8b)	1.443(9)	C(8b)—C(9b)	1.445(9)
C(9b)—C(10b)	1.405(10)		

(*b*)

C(1a)—Si(1a)—C(6a)	108.5(3)	C(1a)—Si(1a)—C(9)	109.9(3)
C(6a)—Si(1a)—C(7a)	110.3(3)	C(1a)—Si(1a)—Si(1i)	102.4(2)
C(6a)—Si(1a)—Si(1i)	114.1(2)	C(7a)—Si(1a)—Si(1i)	111.3(2)
C(3a)—Si(2a)—C(8a)	109.7(3)	C(3a)—Si(2a)—C(9a)	111.9(3)
C(8a)—Si(2a)—C(9a)	108.2(4)	C(3a)—Si(2a)—C(10a)	106.4(3)
C(8a)—Si(2a)—C(10a)	110.8(4)	C(9a)—Si(2a)—C(10a)	109.8(3)
Fe(1a)—C(3a)—Si(2a)	129.8(3)	Fe(1a)—C(3a)—C(2a)	68.7(3)
Si(2a)—C(3a)—C(2a)	125.5(3)	Fe(1a)—C(3a)—C(4a)	68.3(3)
Si(2a)—C(3a)—C(4a)	129.3(4)	C(2a)—C(3a)—C(4a)	105.1(5)
Fe(1a)—C(2a)—C(3a)	70.5(3)	Fe(1a)—C(2a)—C(1a)	70.0(3)
C(3a)—C(2a)—C(1a)	110.5(5)	Fe(1a)—C(1a)—Si(1a)	114.1(2)
Fe(1a)—C(1a)—C(2a)	69.1(3)	Si(1a)—C(1a)—C(2a)	124.2(4)
Fe(1a)—C(1a)—C(5a)	68.8(3)	Si(1a)—C(1a)—C(5a)	128.0(5)
C(2a)—C(1a)—C(5a)	105.8(5)	Fe(1a)—C(5a)—C(1a)	70.6(3)
Fe(1a)—C(5a)—C(4a)	69.9(3)	C(1a)—C(5a)—C(4a)	109.4(6)
C(3a)—C(4a)—C(5a)	109.2(5)	C(1b)—Fe(1b)—C(2b)	41.1(2)
C(1b)—Fe(1b)—C(3b)	70.1(2)	C(2b)—Fe(1b)—C(3b)	40.8(3)
C(1b)—Fe(1b)—C(4b)	68.9(3)	C(2b)—Fe(1b)—C(4b)	67.4(3)
C(3b)—Fe(1b)—C(4b)	40.6(2)	C(1b)—Fe(1b)—C(5b)	41.0(3)
C(2b)—Fe(1b)—C(5b)	68.0(2)	C(3b)—Fe(1b)—C(5b)	69.1(2)
C(4b)—Fe(1b)—C(5b)	40.6(2)	C(1b)—Fe(1b)—C(6b)	101.9(3)
C(2b)—Fe(1b)—C(6b)	112.4(3)	C(3b)—Fe(1b)—C(6b)	146.9(2)
C(4b)—Fe(1b)—C(6b)	166.7(2)	C(5b)—Fe(1b)—C(6b)	126.3(2)
C(1b)—Fe(1b)—C(7b)	112.2(2)	C(2b)—Fe(1b)—C(7b)	145.3(3)
C(3b)—Fe(1b)—C(7b)	172.2(3)	C(4b)—Fe(1b)—C(7b)	132.4(3)
C(5b)—Fe(1b)—C(7b)	107.4(2)	C(6b)—Fe(1b)—C(7b)	40.8(3)
C(1b)—Fe(1b)—C(8b)	147.1(2)	C(2b)—Fe(1b)—C(8b)	171.7(2)

Can. J. Chem. Downloaded from www.nrcresearchpress.com by 46.23.64.124 on 09/08/12
For personal use only.

Table 3 (*concluded*).

C(3b)—Fe(1b)—C(8b)	133.6(3)	C(4b)—Fe(1b)—C(8b)	112.3(3)
C(5b)—Fe(1b)—C(8b)	117.6(2)	C(6b)—Fe(1b)—C(8b)	69.9(3)
C(7b)—Fe(1b)—C(8b)	41.1(3)	C(1b)—Fe(1b)—C(9b)	166.1(3)
C(2b)—Fe(1b)—C(9b)	131.5(2)	C(3b)—Fe(1b)—C(9b)	111.7(3)
C(4b)—Fe(1b)—C(9b)	122.0(2)	C(5b)—Fe(1b)—C(9b)	152.9(3)
C(6b)—Fe(1b)—C(9b)	68.8(3)	C(7b)—Fe(1b)—C(9b)	68.1(3)
C(8b)—Fe(1b)—C(9b)	41.1(2)	C(1b)—Fe(1b)—C(10b)	126.2(3)
C(2b)—Fe(1b)—C(10b)	107.2(3)	C(3b)—Fe(1b)—C(10b)	117.1(2)
C(4b)—Fe(1b)—C(10b)	152.1(2)	C(5b)—Fe(1b)—C(10b)	165.1(3)
C(6b)—Fe(1b)—C(10b)	41.1(3)	C(7b)—Fe(1b)—C(10b)	68.0(3)
C(8b)—Fe(1b)—C(10b)	69.0(3)	C(9b)—Fe(1b)—C(10b)	40.1(3)
Si(2b)—Si(1b)—C(1b)	101.2(2)	Si(2b)—Si(1b)—C(11b)	112.6(2)
C(1b)—Si(1b)—C(11b)	107.6(3)	Si(2b)—Si(1b)—C(12b)	115.6(3)
C(1b)—Si(1b)—C(12b)	111.3(3)	C(11b)—Si(1b)—C(12b)	108.2(3)
Si(1b)—Si(2b)—C(6b)	100.6(3)	Si(1b)—Si(2b)—C(13b)	111.2(2)
C(6b)—Si(2b)—C(13b)	108.9(3)	Si(1b)—Si(2b)—C(14b)	115.0(3)
C(6b)—Si(2b)—C(14b)	110.0(3)	C(13b)—Si(2b)—C(14b)	110.6(3)
C(3b)—Si(3b)—C(15b)	110.6(3)	C(3b)—Si(3b)—C(16b)	108.0(3)
C(15b)—Si(3b)—C(16b)	108.2(3)	C(3b)—Si(3b)—C(17b)	110.5(4)
C(15b)—Si(3b)—C(17b)	110.1(4)	C(16b)—Si(3b)—C(17b)	109.4(3)
C(8b)—Si(4b)—C(18b)	110.9(3)	C(8b)—Si(4b)—C(19b)	109.9(3)
C(18b)—Si(4b)—C(19b)	110.1(4)	C(8b)—Si(4b)—C(20b)	107.8(4)
C(18b)—Si(4b)—C(20b)	108.3(3)	C(19b)—Si(4b)—C(20b)	109.9(3)
Fe(1b)—C(1b)—Si(1b)	113.9(3)	Fe(1b)—C(1b)—C(2b)	68.8(3)
Si(1b)—C(1b)—C(2b)	127.4(5)	Fe(1b)—C(1b)—C(5b)	69.3(3)
Si(1b)—C(1b)—C(5b)	125.3(4)	C(2b)—C(1b)—C(5b)	105.3(3)
Fe(1b)—C(2b)—C(1b)	70.1(3)	Fe(1b)—C(2b)—C(3b)	70.9(3)
C(1b)—C(2b)—C(3b)	111.4(5)	Fe(1b)—C(3b)—Si(3b)	130.3(3)
Fe(1b)—C(3b)—C(2b)	68.3(3)	Si(3b)—C(3b)—C(2b)	127.2(4)
Fe(1b)—C(3b)—C(4b)	68.9(3)	Si(3b)—C(3b)—C(4b)	127.8(5)
C(2b)—C(3b)—C(4b)	104.8(5)	Fe(1b)—C(4b)—C(3b)	70.5(4)
Fe(1b)—C(4b)—C(5b)	69.7(4)	C(3b)—C(4b)—C(5b)	110.1(5)
Fe(1b)—C(5b)—C(1b)	69.6(4)	Fe(1b)—C(5b)—C(4b)	69.6(4)
C(1b)—C(5b)—C(4b)	108.4(5)	Fe(1b)—C(6b)—Si(2b)	114.4(3)
Fe(1b)—C(6b)—C(7b)	69.2(4)	Si(2b)—C(6b)—C(7b)	124.9(5)
Fe(1b)—C(6b)—C(10b)	69.6(4)	Si(2b)—C(6b)—C(10b)	127.3(5)
C(7b)—C(6b)—C(10b)	106.1(6)	Fe(1b)—C(7b)—C(6b)	70.0(4)
Fe(1b)—C(7b)—C(8b)	70.8(4)	C(6b)—C(7b)—C(8b)	110.8(5)
Fe(1b)—C(8b)—Si(4b)	128.4(4)	Fe(1b)—C(8b)—C(7b)	68.0(3)
Si(4b)—C(8b)—C(7b)	126.7(5)	Fe(1b)—C(8b)—C(9b)	68.5(4)
Si(4b)—C(8b)—C(9b)	128.8(5)	C(7b)—C(8b)—C(9b)	104.5(6)
Fe(1b)—C(9b)—C(8b)	70.4(4)	Fe(1b)—C(9b)—C(10b)	70.1(4)
C(8b)—C(9b)—C(10b)	109.0(6)	Fe(1b)—C(10b)—C(6b)	69.3(4)
Fe(1b)—C(10b)—C(9b)	69.8(4)	C(6b)—C(10b)—C(9b)	108.7(5)

Symmetry code: *i* 1 − *x*, 0.5 − *x*.

Can. J. Chem. Downloaded from www.nrcresearchpress.com by 46.23.64.124 on 09/08/12
For personal use only.

Aldrich Chemicals Co. 1,2-Dichloro-1,1,2,2,-tetramethyldisilane (26) and dilithioferrocene (27) were synthesized using literature methods. All silanes were distilled and stored under nitrogen. Ferrocene was purified via Soxhlet extraction using hexanes. All syntheses were carried out under an atmosphere of prepurified nitrogen using either standard Schlenk techniques or an inert-atmosphere drybox (Vacuum Atmospheres). Solvents used in these syntheses were dried by standard methods, distilled, and stored under nitrogen.

The 200 or 400 MHz ^{1}H NMR spectra were recorded on a Varian Gemini 200 and a Varian XL 400 spectrometer, respectively. The 100.5 MHz ^{13}C NMR and 79.5 MHz ^{29}Si NMR spectra were recorded on the Varian XL 400 spectrometer. The ^{29}Si NMR data were acquired in a proton-decoupled mode using a DEPT pulse sequence with $^{2}J_{Si-H} = 6.7$ Hz. The ^{13}C NMR data were acquired in a proton-decoupled mode using an APT pulse sequence. Mass spectra were obtained with the use of a VG 70-250S mass spectrometer operating in an electron impact (EI) mode. Elemental analyses were performed by the Canadian Microanalytical Service Ltd., Delta, B.C.

Molecular weights were estimated by gel permeation chromatography (GPC) using a Waters Associates liquid chromatograph equipped with a 510 HPLC pump, U6K injector, ultrastyragel columns with a pore size between 10^3 to 10^5

Can. J. Chem. Downloaded from www.nrcresearchpress.com by 46.23.64.124 on 09/08/12
For personal use only.

Table 4. Selected structural data for [1]- and [2]metallocenophanes.

	1	3*d*	4*a*	7[d]	4*b*
Si—Si distance Å			2.3535(9)	2.334(3) 2.349(3)	2.370(2)
Fe displacement,[a] Å	0.2164(11)	0.432(12)	0.027(3)	0.069(5) 0.071(5)	0.092(6)
Ring tilt, α, deg	20.8(5)	23(1)	4.19(2)	4.8(6) 5.9(6)	7.8(5)
β,[b] deg	37.0(6)	10.8(10)	10.8(3)	12.7(4) 12.0(4) 12.6(4)	12.4(3)
Twist,[c] deg		8.9(13)	8.4(4)	18.3(8) 22.9(8)	0.2(5)
Cp-Fe-Cp, δ, deg	167.74(8)	163.4(6)	176.48(3)	175.2(3) 175.1(3)	174.2(2)
Reference	13	24	13	This work	18

[a]The displacement of the iron atom from the line joining the two centroids of the cyclopentadienyl rings.

[b]The angle(s) between the planes of the cyclopentadienyl ligands and the C(Cp)—E bonds (where E = bridging atom).

[c]The angle(s) between the plane defined by the centroids of the cyclopentadienyl ligands and the metal atom and the E—E bond (where E = bridging atom).

[d]The first line represents the value for molecule A and the second line is for molecule B.

Fig. 2. Distortions in metallocenophanes defining angles α, β, and δ.

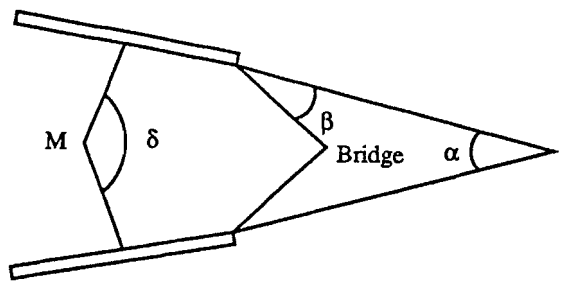

Angstroms, and a Waters 410 differential refractometer. A flow rate of 1.0 mL/min was used and samples were dissolved in a solution of 0.1% tetra-*n*-butylammonium bromide in THF. Polystyrene standards were used for calibration purposes.

Synthesis of dilithio-1,1′-bis(trimethylsilyl)-ferrocene·tmeda

The synthesis of dilithio-1,1′-bis(trimethylsilyl)ferrocene was a modification of a literature method (21, 28).

Dilithioferrocene·tmeda (25.0 g, 79.6 mmol) was suspended in 180 mL of freshly distilled diethyl ether. Chlorotrimethylsilane (20.1 mL, 159.2 mmol) was added dropwise to the above solution with stirring at 0°C using an ice–water bath. The reaction mixture was allowed to warm up to room temperature and stir overnight. Unreacted dilithioferrocene was separated from the reaction mixture by cannulation of the solution through a filter frit. The solvent was removed under high vacuum before subliming to remove any ferrocene. The resultant bright red oil was further purified by distillation under high vacuum (80°C, 0.05 Torr). Yield of 1, 1′-bis(trimethylsilyl)ferrocene: 19.8 g (75%).

The distilled 1,1′-bis(trimethylsilyl)ferrocene was then dissolved in 100 mL of freshly distilled hexanes. Butyllithium in hexanes (75 mL, 120 mmol) and TMEDA (14.0 mL, 120 mmol) were added dropwise to the solution at room temperature with stirring. The solution was allowed to warm up to room temperature and stirred overnight. The product was precipitated from hexanes at −78°C as a reddish-orange solid that was isolated by cannulation of the suspension onto a filter frit at −78°C. Yield (based on 1,1′-bis(trimethylsilyl)ferrocene): 7.1 g (26%).

Synthesis of 1,1′-bis(trimethylsilyl)-ferrocendiyldimethylsilane (5)

Dilithio-1,1′-bis(trimethylsilyl)ferrocene·tmeda (2.00 g, 4.37 mmol) was suspended in 100 mL of freshly distilled hexanes and cooled down to −78°C. To this stirred suspension was added 0.6 mL (4.95 mmol) of freshly distilled dichlorodimethylsilane. The mixture was allowed to warm up to room temperature and stir overnight. This solution was filtered through a filter frit and the solvent removed under high vacuum. The moisture-sensitive product was then isolated as a red-orange liquid by high-vacuum distillation (88°C, 0.005 Torr). Yield: 0.95 g (56%). For **5**: ^{29}Si NMR (C_6D_6) δ: −3.3 (s, $SiMe_2$, 1Si), −5.4 (s, $SiMe_3$, 2Si) ppm; ^{13}C NMR (C_6D_6) δ: 82.9 (η-C_5H_3), 82.7 (η-C_5H_3, C-$SiMe_3$), 80.4 (η-C_5H_3), 77.4 (η-C_5H_3), 36.9 (η-C_5H_3, C-Si), 0.34 (-$SiMe_3$), −3.0 (-$SiMe_2$) ppm; ^{1}H NMR (C_6D_6) δ: 4.39 (m, 2H, Cp), 4.13 (m, 2H, Cp), 4.03 (m, 2H, Cp), 0.40 (s, 6H, $SiMe_2$), 0.24 (s, 18H, $SiMe_3$) ppm; MS (EI, 70 eV) *m/z* (%): 386 (100, M^+), 371 (26, $M^+ - CH_3$), 357 (5, $M^+ - CH_3 - CH_2$).

Thermal ring-opening polymerization of 5

A 0.35 g (0.91 mmol) sample of **5** was sealed in an evacuated Pyrex glass tube and heated at 170°C for 3 h. The resultant polymer **6** was dissolved in THF and precipitated dropwise into methanol. The polymer was isolated as a red-orange powder. Yield: 0.19 g (54%). For **6**: ^{29}Si NMR (C_6D_6) δ: −5.9 (br

Can. J. Chem. Downloaded from www.nrcresearchpress.com by 46.23.64.124 on 09/08/12
For personal use only.

s, $SiMe_2$, 1Si), −2.5 (s, $SiMe_3$, 2Si) ppm; ^{13}C NMR (C_6D_6) δ: 79.5 (Cp), 77.0 (Cp), 76.2 (Cp), 76.2 (br s, Cp, C-Si), 74.7 (Cp), 1.1 (-$SiMe_3$), 0.25 (-$SiMe_2$) ppm; ^1H NMR (C_6D_6) δ: 4.30 (br s, 6H, Cp), 0.75 (br s, 6H, $SiMe_2$), 0.32 (br s, 18H, $SiMe_3$) ppm. Anal. calcd.: C 55.9, H 7.8; found: C 55.2, H 7.6. GPC: $M_w = 1.4 \times 10^5$, $M_n = 8.4 \times 10^4$, polydispersity (M_w/M_n) = 1.7.

Synthesis of 1,1′-bis(trimethylsilyl)ferrocendiyl-(1,1,2,2)-tetramethyldisilane (7)

Dilithio-1,1′-bis(trimethylsilyl)ferrocene·tmeda (1.65 g, 3.60 mmol) was dissolved in 80 mL of freshly distilled hexanes and cooled to −78°C in a Dry Ice – acetone slurry. 1,2-Dichloro-1,1,2,2-tetramethyldisilane (0.7 mL, 3.74 mmol) was added dropwise with stirring. The reaction mixture was allowed to warm up to room temperature and stir overnight. The solution was then filtered through a filter frit and the solvent removed under high vacuum. The product **7** was isolated as a red-orange liquid by high-vacuum distillation (120°C, 0.05 Torr). Yield: 0.75 g (47%). For **7**: ^{29}Si NMR ($CDCl_3$) δ: −4.0 ($SiMe_2$), −9.7 ($SiMe_3$) ppm; ^{13}C NMR ($CDCl_3$) δ: 78.3 (Cp), 77.4 (Cp), 76.8 (ipso C, -$SiMe_3$), 76.0 (ipso C, -$SiMe_2$-), 75.4 (Cp), 0.1 ($SiMe_3$), −0.1 ($SiMe_2$), −3.8 ($SiMe_2$) ppm; ^1H NMR ($CDCl_3$) δ: 4.6 (m, 2H, Cp), 4.5 (m, 2H, Cp), 4.0 (m, 2H, Cp), 0.45 (s, 6H, -$SiMe_2$-), 0.28 (s, 18H, $SiMe_3$-), 0.25 (s, 6H, -$SiMe_2$-) ppm; MS (EI, 70 meV) *m/z* (rel. intensity): 444 (100, M^+), 429 (18, M^+ − Me), 386 (6, M^+ − $SiMe_2$), 371 (15, M^+ − $SiMe_3$). Anal. calcd.: C 54.1, H 8.1; found: C 53.8, H 8.2.

Attempted thermal ROP of 7

A 0.10 g (0.22 mmol) sample of **7** was sealed in an evacuated Pyrex glass tube and heated at 350°C for 24 h. A second sample (0.22 g, 0.50 mmol) was sealed in an evacuated Pyrex glass tube and heated (*i*) at 380°C for 30 min, (*ii*) at 390°C for 30 min, (*iii*) at 400°C for 30 min, (*iv*) at 410°C for 30 min and (*v*) at 420°C for 30 min. A third sample (0.30 g, 0.68 mmol) was sealed in an evacuated Pyrex glass tube in the presence of a trace amount of K[$OSiMe_3$] and heated at 140°C for 2 h, at 160°C for 14 h, and then at 180°C for 2 h. All samples were dissolved in THF and precipitated dropwise into methanol. Subsequent analysis of the first two samples revealed only **7** (^1H NMR) and small molecules (GPC). The third sample was a dark reddish-brown viscous liquid that was mostly soluble in THF (the insoluble product was a black precipitate). Analysis by ^1H NMR showed only **7** and unidentified products (broad resonances from 4.0 to 4.4 ppm (cyclopentadienyl region) and from 0.0 to 0.4 ppm (Si-Me region)). Analysis by GPC and mass spectrometry revealed only small molecules.

X-ray structure determination technique

Intensity data were collected on an Enraf–Nonius CAD4 diffractometer at low temperature (185 K) using graphite monochromated Mo Kα radiation, λ = 0.710 73 Å. The ω-scan technique was used with variable scan speeds. The intensities of three standard reflections, which were measured every 2 h, indicated no decay. The data were corrected for Lorentz and polarization effects and also for absorption (using ψ-scan data). The structures were solved by direct methods (29). Non-hydrogen atoms were refined with anisotropic thermal parameters by full-matrix least squares to minimize $\Sigma w(F_o - F_o)^2$, where $w^{-1} = \sigma_2(F_o) + g(F_o)^2$. The hydrogen atoms were included in calculated positions with C—H = 0.96 Å. Crystal data, data collection, and least-squares parameters are listed in Table 1.[3] All calculations were performed and structural diagrams created using SHELXTL PC (29) on a 486 personal computer.

Acknowledgement

We thank the Natural Sciences and Engineering Research Council of Canada (NSERC) Operating Grants Program for financial support of this work. We also thank the University of Toronto for an Open Fellowship for T.J.P. I. M. thanks the Alfred P. Sloan Foundation for a Research Fellowship (1994–1996). We are also grateful to Nick Plavac for obtaining the ^{29}Si NMR spectra.

References

1. (*a*) C.U. Pittman, Jr., C.E. Carraher Jr., and J.R. Reynolds. Encyclopedia of polymer science and engineering. Vol. 10. *Edited by* H.F. Mark, N.M. Bikales, C.G. Overberger, and G. Menges. Wiley, New York. 1989. p. 541; (*b*) J.E. Sheats, C.E. Carraher, Jr., C.U. Pittman, Jr., M. Zeldin, and B. Currell. Inorganic and metal-containing polymeric materials. Plenum, New York. 1989; (*c*) K.E. Gonsalves and M.D. Rausch. Inorganic and organometallic polymers. ACS Symp. Ser. **360**. American Chemical Society, Washington, D.C. 1988; (*d*) H. R. Allcock. Adv. Mater. **6**, 106 (1994).
2. (*a*) H.B. Fyfe, M. Melkuz, D. Zargarian, N.J. Taylor, and T.B. Marder. J. Chem. Soc. Chem. Commun. 188 (1991); (*b*) M.E. Wright and M.S. Sigman. Macromolecules, **25**, 6055 (1992); (*c*) S.J. Davies, B.F.G. Johnson, M.S. Khan, and J. Lewis. J. Chem. Soc. Chem. Commun. 187 (1991); (*d*) S.C. Tenhaeff and D.R. Tyler. J. Chem. Soc. Chem. Commun. 1459 (1989); (*e*) I. Manners. Annu. Rep. Prog. Chem. A: Inorg. Chem. **88**, 77 (1991); (*f*) E.W. Neuse and L. Bednarik. Macromolecules, **12**, 187 (1979); (*g*) K.C. Sturge, A.D. Hunter, R. McDonald, and B.D. Santarsiero. Organometallics, **11**, 3056 (1992); (*h*) K. Gonsalves, L. Zhan-ru, and M.D. Rausch. J. Am. Chem. Soc. **106**, 3862 (1984); (*i*) T.J. Katz, A. Sudhakar, M.F. Teasley, A.M. Gilbert, W.E. Geiger, M.P. Robben, M. Wuensch, and M.D. Ward. J. Am. Chem. Soc. **115**, 3182 (1993); (*j*) H.M. Nugent and M. Rosenblum. J. Am. Chem. Soc. **115**, 3848 (1993); (*k*) W.J. Patterson, S.P. McManus, and C.U. Pittman. J. Polym. Sci.: Poly. Chem. Ed. **12**, 837 (1974).
3. P.F. Brandt and T.B. Rauchfuss. J. Am. Chem. Soc. **114**, 1926 (1992).
4. I. Manners. Adv. Organomet. Chem. **37**, 131 (1995).
5. D.A. Foucher, B. Tang, and I. Manners. J. Am. Chem. Soc. **114**, 6246 (1992).
6. R. Rulkens, A.J. Lough, and I. Manners. J. Am. Chem. Soc. **116**, 797 (1994).

[3] Tables of complete bond lengths and angles, anisotropic thermal parameters, and hydrogen atom coordinates, and figures showing the molecular structure of **7**, have been deposited as supplementary material and can be purchased from: The Depository of Unpublished Data, Document Delivery, CISTI, National Research Council of Canada, Ottawa, Canada K1A 0S2. This material, with the exception of the anisotropic thermal parameters, has also been deposited with the Cambridge Crystallographic Data Centre, and can be obtained on request from The Director, Cambridge Crystallographic Data Centre, University Chemical Laboratory, 12 Union Road, Cambridge, CB2 1EZ, U.K. Structure factor amplitudes are no longer being deposited and may be obtained directly from the author.

7. R. Rulkens, Y. Ni, and I. Manners. J. Am. Chem. Soc. **116**, 12121 (1994).
8. (*a*) E. Fossum, K. Matyjaszewski, R. Rulkens, and I. Manners. Macromolecules, **28**, 401 (1995) (*b*) J.K. Pudelski, R. Rulkens, D.A. Foucher, A.J. Lough, P.M. MacDonald, and I. Manners. Macromolecules, **28**, 7301 (1995).
9. Y. Ni, R. Rulkens, J.K. Pudelski, and I. Manners. Makromol. Chem. Rapid Commun. **16**, 637 (1995).
10. D.A. Foucher and I. Manners. Makromol. Chem. Rapid Commun. **14**, 63 (1993).
11. D.A. Foucher, R. Ziembinski, B.Z. Tang, P.M. Macdonald, J. Massey, R. Jaeger, G.V. Vancso, and I. Manners. Macromolecules, **26**, 2878 (1993).
12. D.A. Foucher, C.H. Honeyman, J.M. Nelson, B. Tang, and I. Manners. Angew. Chem., Int. Ed. Engl. **32**, 1709 (1993).
13. W. Finckh, B.-Z. Tang, D.F. Foucher, D.B. Zamble, R. Ziembinski, A. Lough, and I. Manners. Organometallics, **12**, 823 (1993).
14. D.A. Foucher, R. Ziembinski, R. Petersen, J. Pudelski, M. Edwards, Y. Ni, J. Massey, C.R. Jaeger, G.J. Vancso, and I. Manners. Macromolecules, **27**, 3992 (1994).
15. D.A. Foucher, M. Edwards, R.A. Burrow, A.J. Lough, and I. Manners. Organometallics, **13**, 4959 (1994).
16. J.K. Pudelski, D.A. Foucher, C.H. Honeyman, A.J. Lough, I. Manners, S. Barlow, and D. O'Hare. Organometallics, **14**, 2470 (1995).
17. J. Pudelski, D.P. Gates, R. Rulkens, A. Lough, and I. Manners. Angew. Chem. Int. Ed. Engl. **34**, 1506 (1995).
18. J.M. Nelson, A.J. Lough, and I. Manners. Organometallics, **13**, 3703 (1994).
19. D.L. Compton and T.B. Rauchfuss. Organometallics, **13**, 4367 (1994).
20. J. Rasburn, R.J. Petersen, T. Jahr, R. Rulkens, I. Manners, and G.J. Vancso. Chem. Mater. **7**, 871 (1995).
21. R.A. Brown, A. Houlton, R.M.G. Roberts, J. Silver, and C.S. Frompton. Polyhedron, **11**, 2611 (1992).
22. A.G. Osborne, R.H. Whiteley, and R.E. Meads. J. Organomet. Chem. **193**, 345 (1980).
23. D. Seyferth and H.P. Withers. J. Organomet. Chem. **185**, C1 (1980).
24. M. Burke-Laing and K.N. Trueblood. Acta Crystallogr. **19**, 373 (1965).
25. M. Cypryk, M. Gupta, and K. Matyjaszewski. J. Am. Chem. Soc. **113**, 1046 (1991).
26. H. Sakurai, K. Tominaga, T. Wantanabe, and M. Kumada. Tetrahedron Lett. 5493 (1966).
27. J.J. Bishop, A. Davison, M.L. Katcher, D.W. Lichtenberg, R.E. Merrill, and J.C. Smart. J. Organomet. Chem. **27**, 241 (1971).
28. M.D. Rausch and D.J. Ciapenelli. J. Organomet. Chem. **10**, 127 (1967).
29. G.M. Sheldrick. SHELXTL-PC, Siemens Analytical X-ray Instruments Inc., Madison, Wis. 1990.

Can. J. Chem. Downloaded from www.nrcresearchpress.com by 46.23.64.124 on 09/08/12
For personal use only.

Radical-induced degradation of a lignin model compound. Decomposition of 1-phenyl-2-phenoxyethanol[1]

Y. Huang, D. Pagé, D.D.M. Wayner, and P. Mulder

Abstract: Reaction of 1-phenyl-2-phenoxyethanol (**1**) with thermally or photochemically generated *tert*-butoxyl radicals leads, via the intermediate ketyl radical, to the formation of the corresponding ketone, α-phenoxyacetophenone (**4**), as the only product at low conversion under an inert atmosphere. An approximately twofold increase in the product yield is observed when the reactions are carried out under oxygen. Under the photochemical conditions it is shown that **4** is the primary product and that acetophenone and phenol are formed as a result of secondary photolysis of **4**. These data suggest that the rate constant for fragmentation of the ketyl radical derived from **1** is on the order of 10 s^{-1} at 298 K and contradict a report in the literature that suggests a rate constant of $>10^6$ s^{-1}. The relevance of this study to the photodegradation of lignin and consequent photoyellowing is discussed and a revised mechanism for the photoyellowing of pulp is proposed.

Key words: ketyl radical, photochemical degradation, thermal degradation, lignin.

Résumé : Lorsqu'on effectue la réaction du 1-phényl-2-phénoxyéthanol (**1**) avec des radicaus *tert*-butoxyles générés thermiquement ou photochimiquement à de faibles taux de conversion, sous une atmosphère inerte, le seul produit à se former, par le biais du radical cétyle intermédiaire, est la cétone correspondante, α-phénoxy-acétophénone (**4**). Lorsqu'on effectue la réaction sous une atmosphère d'oxygène, le rendement en produit est approximativement doublé. Dans des conditions photochimiques, il a été démontré que **4** est le produit primaire et que de l'acétophénone et du phénol se forment par le biais d'une photolyse secondaire de **4**. Ces données suggèrent que la constante de vitesse de fragmentation du radical cétyle dérivé de **1** est de l'ordre de 10 s^{-1}, à 298 K, et elles sont en contradiction avec des données de la littérature qui suggèrent que la constante de vitesse est $>10^6$ s^{-1}. On discute de l'intérêt de cette étude pour la photodégradation de la lignine et jaunissement photochimique qui en découle et on propose un mécanisme révisé pour jaunissement de la pulpe.

Mots clés : radical cétyle, dégradation photochimique, dégradation thérmique, lignine.

[Traduit par la rédaction]

Introduction

The chemical and photochemical processes leading to the yellowing of mechanical pulps have been the subject of numerous investigations (1–3). In general, it is agreed that phenoxyl radicals generated from the degradation of lignin are important intermediates whose subsequent oxidation leads to the formation of products that absorb well into the visible. Several photochemical routes to phenoxyl radicals have been proposed (Scheme 1). While much attention had been given to paths A and B, Schmidt and Heitner (4) showed that the extent of yellowing was far greater than expected on the basis of the quantities of ketone and phenolic residues in lignin-rich papers. They proposed that up to 70% of the photogenerated chromophores were generated via path C in which ketyl radicals, generated from β-guaiacoxybenzyl alcohols, underwent fragmentation to give the phenoxyl radical directly and a substituted acetophenone (via the initally formed enol).

While the formation and reactivity of phenoxyl radicals in the lignin matrix is not well understood, a number of photochemical studies (5–12) using model compounds in solution or adsorbed on solid supports have provided some insights into the factors influencing all of the proposed mechanisms. In one of these studies (7) it was suggested that the fragmentation of 1-phenyl-2-phenoxyethanol-1-yl radical (**1**˙) formed from the reaction of photogenerated *tert*-butoxyl radicals with 1-phenyl-2-phenoxyethanol (**1**, eqs. [1], [2]) undergoes rapid fragmentation to yield phenoxyl radical and acetophenone (**2**, eq. [3]) thus giving kinetic support to the ketyl radical mechanism (path C). To better understand the dynamics of the formation and reaction of **1**˙, we have studied the radical-induced thermal and photochemical decomposition of **1** in acetonitrile and benzene. The thermal and photochemical experiments are similar in that *tert*-butoxyl radicals are the abstracting species.

Received April 11, 1995.

This paper is dedicated to Professor J.E. (Jim) Guillet in recognition of his contributions to Canadian chemistry.

Y. Huang, D. Pagé, and D.D.M. Wayner.[2] Steacie Institute for Molecular Sciences, National Research Council of Canada, Ottawa, ON K1A 0R6, Canada.
P. Mulder.[2] Center for Chemistry and the Environment, Leiden Institute of Chemistry, Gorlaeus Laboratories, 2300 RA Leiden, The Netherlands.

[1] Issued as NRCC No. 39077.
[2] Authors to whom correspondence may be addressed. Telephone (D.D.M.W.): (613) 954–5242.

Can. J. Chem. Downloaded from www.nrcresearchpress.com by 46.23.64.124 on 09/08/12
For personal use only.

Scheme 1. Mechanism of photoyellowing of mechanical pulps.

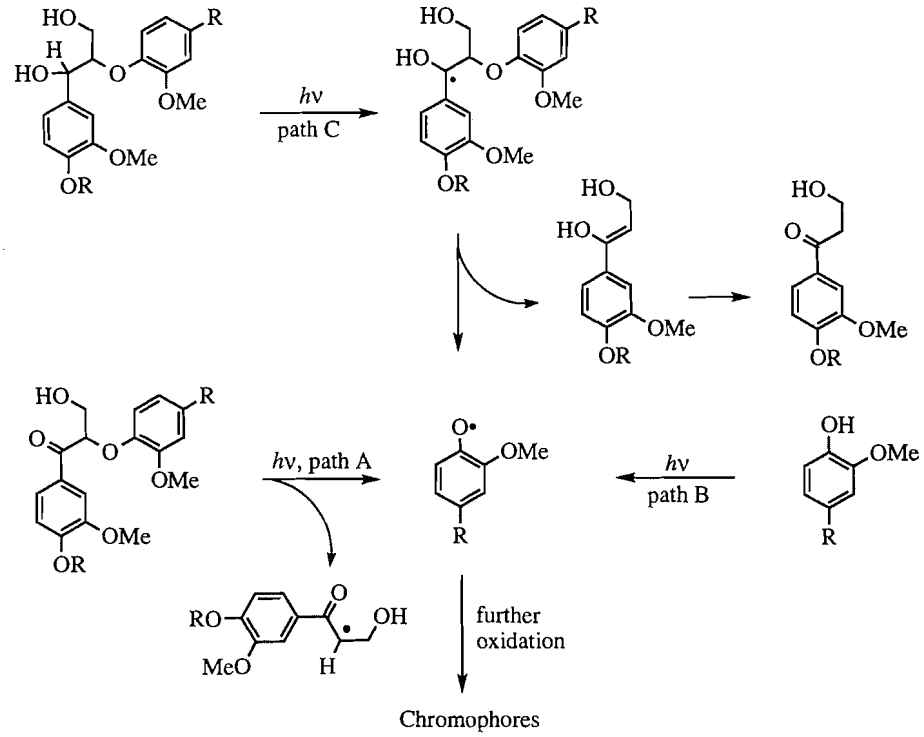

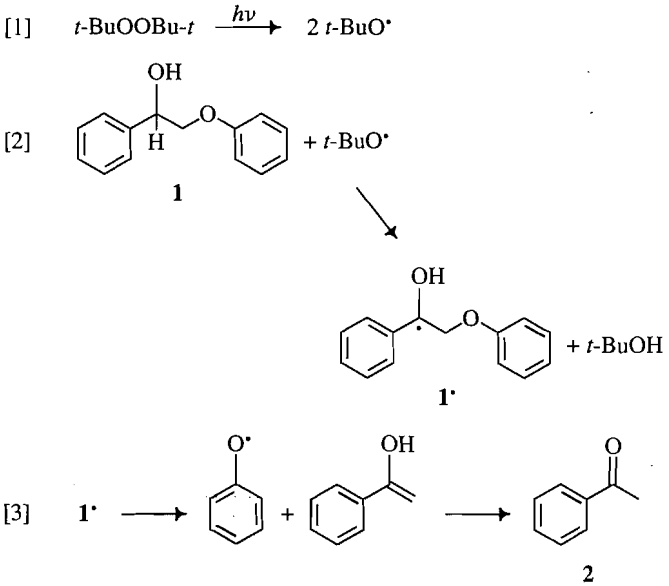

Results

Thermal decomposition of 1 in the presence of di-*tert*-butylhyponitrite (BONNOB)

In BONNOB–acetonitrile (10 mol%), the decomposition of 1-phenyl-2-phenoxyethanol (**1**, 0.2 M)) at 60°C for 5 h (ca. 5 half-lives) yields only one product, α-phenoxyacetophenone (**4**, see Table 1) in approximately 6% yield (ca. 34% based on BONNOB after taking into account the expected cage effect of 12% (13)). In the presence of oxygen, the yield of **4** is higher (about 17%, 97% based on BONNOB). No acetophenone or phenol was formed. At higher stoichiometric ratios of BONNOB (50 mol%) under argon, the yield of **4** increased to 18% (20% based on BONNOB). At higher conversion, under oxygen, the mass balance was lower and a yield of **4** of 27% (32% based on BONNOB) was obtained.

Products obtained at 120°C using di-*tert*-butyl peroxide as initiator are shown in Table 2. In this case **4**, acetophenone (**2**), and phenol (**3**) are formed as products (the yields of **2** and **3** are

Table 1. HPLC product yields from the thermal decomposition of BONNOB in the presence of **1**.[a]

Run	BONNOB (mol%)	Atmosphere	Product yield (%) 1	2	4
1	10	Ar	91.3	nd	6.3
2	10	O_2	80.3	nd	16.8
3	50	Ar	80.2	nd	18.0
4	50	O_2	65.0	nd	27.5

[a]Average of two determinations. At 60°C for 5 h. nd = not detected.

Table 2. HPLC product yields from the thermal decomposition of DTBP in the presence of **1**.[a]

Run	DTBP (mol%)	Product yield (%) 1	2,3	4
1	0	99.4	nd	nd
2	10	26.7	14.0[b]	12.5

[a]Average of two determinations. In acetonitrile at 120°C for 5 h in a sealed ampule. Freeze–pump–thaw degassed. nd = not detected.
[b]The yields of **2** and **3** were the same.

Can. J. Chem. Downloaded from www.nrcresearchpress.com by 46.23.64.124 on 09/08/12
For personal use only.

Can. J. Chem. Downloaded from www.nrcresearchpress.com by 46.23.64.124 on 09/08/12
For personal use only.

Table 3. HPLC product yields from the photochemical decomposition of DTBP/Benzene (2:1) in the presence of **1**.[a]

			Product yield (%)			
Run	Mode	Atmosphere	**1**	**2**	**3**	**4**
1	Direct	Ar	57.6	3.6	3.1	30.8
2	Direct	O_2	40.9	1.9	2.6	38.6
3	Sensitized	Ar	58.7	3.9	3.1	26.3
4	Sensitized	O_2	44.6	2.2	1.9	35.5

[a]Average of two determinations. Irradiation at 350 nm in a Rayonet® reactor at 30°C for 4 h. Conversions were too low when 10 or 50 mol% DTBP were used. Similar results obtained by HPLC and GC analysis.

Table 4. HPLC product yields from the photochemical decomposition of DTBP/acetonitrile (1:2) in the presence of **1**.[a]

			Product yield (%)			
Run	Mode	Atmosphere	**1**	**2**	**3**	**4**
1	Direct	Ar	60.2	0.8	1.0	26.1
2	Direct	O_2	44.7	nd	nd	36.5
3	Sensitized	Ar	62.8	0.6	0.8	23.5
4	Sensitized	O_2	52.2	nd	nd	25.4

[a]Average of two determinations. Irradiation at 350 nm in a Rayonet® reactor at 30°C for 4 h. Conversions were too low when 10 or 50 mol% DTBP were used. Similar results obtained by HPLC and GC analysis. nd = not detected.

Table 5. HPLC product yields from the photochemical decomposition **4**.[a]

			Product yield (%)			
Run	Solvent	λ, nm (*t*, h)	**2**	**3**	**4**	**5**
1	Benzene	350(4)	1.1	2.9	89.9	nd
2		300(2)	1.6	4.0	85.5	Trace
3	Acetonitrile	350(4)	Trace	Trace	94.6	nd
4		300(4)	nd	nd	90.1	nd
5		300(18)	1.2	6.5	57.6	~2.4
6	+ PhSH[b]	300(4)	6.8	6.3	84.7	Trace

[a]Average of two determinations. Conversions were too low when 10 or 50 mol% DTBP were used. Similar results obtained by HPLC and GC analysis. nd = not detected.
[b]0.025 M.

equal). In these high-temperature experiments the mass balances were poor and account for only about half of the total mass. The remainder of the mass appears to be an intractable tar. At this temperature, in the absence of di-*tert*-butyl peroxide, the starting compound is stable for the duration of the experiment (Table 2, entry 1).

Photochemical decomposition of 1 in the presence of di-*tert*-butylperoxide (DTBP)

These irradiations were carried out as described by Scaiano et al. (7). A solution of DTBP/benzene (2:1) containing **1** was irradiated for 4 h at 350 nm (Rayonet reactor, 30°C) to give a light yellow solution. The results are shown in Table 3. α-Phenoxyacetophenone (**4**) was formed as the predominant product with yields of 31% under argon (entry 1) and 39% under oxygen (entry 2). Small amounts of acetophenone and phenol were produced under both argon and oxygen. Triplet sensitization by anthracene gave similar results (entries 3 and 4). Although the energy transfer to DTBP is slow (14), absorption by anthracene prevents secondary photolysis of the primary products. The mass balance obtained under argon was generally better than that obtained under oxygen (the solutions under oxygen also were more highly coloured). Similar experiments carried out in acetonitrile are shown in Table 4 and are essentially the same as those obtained using benzene.

Compound **4** was irradiated in both benzene and acetonitrile, under argon, to determine its stability under our conditions. These results are summarized in Table 5. In benzene, after 4 h irradiation at 350 nm, acetophenone (**2**) and phenol (**3**) were formed with yields of 1.1% and 2.9%, respectively. However, at 300 nm, a small amount of new product was observed by GC–MS and HPLC, which corresponds in mass to the dimer (**5**) that is formed, presumably, by dimerization of the phenacyl radical. In acetonitrile, **4** appears to be photostable after irradiation for 4 h with only a trace of the dimer observed. After prolonged irradiation (18 h) some acetophenone and phenol were observed. Addition of thiophenol to the irradiation mixture (as a hydrogen atom donor) suppresses the dimer formation and improves the yield of acetophenone. These results are consistent with previously reported photochemical behaviour of **4** (15).

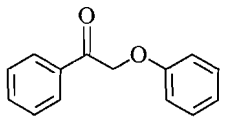

4

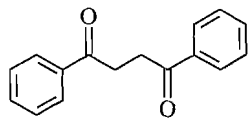

5

Laser flash photolysis

The rate constant for reaction of *tert*-butoxyl radicals with **1** was reported to be 2×10^6 M^{-1} s^{-1} using a benzhydrol probe method in benzene (7). We have determined a rate constant for reaction of the cumyloxyl radical of 1.5×10^6 M^{-1} s^{-1} using direct detection of the decay of the cumyloxyl radical, generated from photolysis of dicumyl peroxide as described by Avila, Lusztyk, and Ingold (16). In our experiments, the plot of the experimental first-order rate constant versus the concentration of **1** had a downward curvature at high concentration of **1**. The slope of this line at low concentrations (<0.3 M) was equal to the rate constant for the bimolecular hydrogen atom abstraction. At high concentrations, the limiting slope is about one third that at low concentration. Nevertheless, the agreement between the two sets of results is considered to be adequate. Spectroscopic results indicated a long-lived residual signal with shoulders at ca. 440 and 400 nm and an apparent maximum near 330 nm, after the cumyloxyl radical had completely disappeared. The residual signal between 350 and 500 nm was found to be completely quenched in the presence of oxygen.

Can. J. Chem. Downloaded from www.nrcresearchpress.com by 46.23.64.124 on 09/08/12
For personal use only.

Fig. 1. Transient absorption spectrum recorded 6 μs following 308 nm laser excitation of a solution containing **1** (0.5 M) and di-*tert*-butyl peroxide (0.2 M) in acetonitrile solution under argon (●) and under oxygen (■). The inset shows the temporal evolution of the signal at 440 nm under argon and under oxygen (same symbols), which has been tentatively assigned to the ketyl radical derived from **1**.

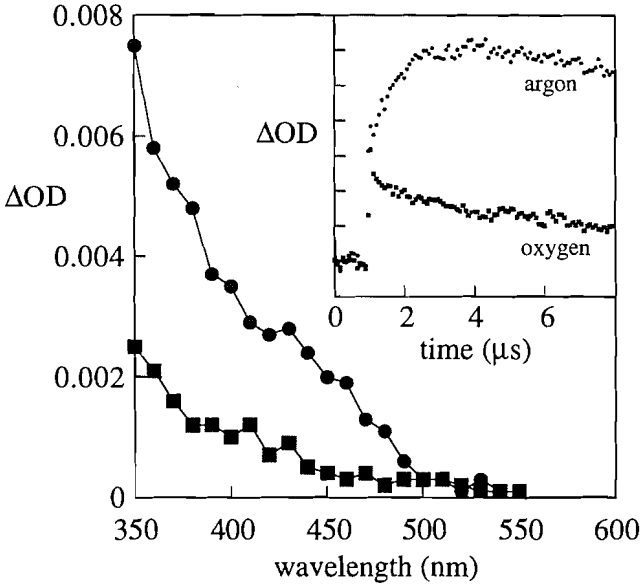

Irradiation of DTBP in acetonitrile (308 nm) in the presence of **1** gave a similar residual spectrum, in this case unobscured by the competitive absorption of the alkoxyl radical (Fig. 1). A clear growth of the signal at 440 nm was now observed and, as in the previous case, the residual spectrum was completely quenched by oxygen (see inset, Fig. 1). An absorption previously assigned to phenoxyl radical (7) was not observed. The long-lived signal at 440 nm has been tentatively assigned to the ketyl radical derived from **1** (see below).

ESR measurements

Several attempts were made to record the ESR spectrum of **1**˙. A mixture containing 0.1 M **1** in DTBP/benzene (9:1 v/v) was photolyzed in a 6 mm diameter quartz tube in an ESR cavity. A weak spectrum, which was clearly a mixture of radicals, was obtained from which definitive identification of **1**˙ was not possible. The use of partially deuterated **1** ($PhCHOHCD_2OPh$) resulted in a similar mixture of radicals without affecting the overall spectral width (which implies that abstraction from the methylene does not contribute significantly to the observed spectrum). Under the same conditions, using 1-phenylethanol instead of **1**, the corresponding ketyl radical spectrum was clearly evident as the major contributor to the spectrum.

Discussion

Thermochemical considerations

Estimation of the thermochemistry of reaction [3] provides a reasonable starting point to understanding the kinetics. The fragmentation of a similar radical, 2-phenoxy-1-phenylpropyl (reaction [4]), has been reported by Franz and co-workers (17). The corresponding rate constant was shown to follow a temperature dependence given by $\log (k_4) = 13.4 - 18/2.303RT$ (in kcal mol^{-1}), leading to $k_4 = 3$, 39, and 2460 s^{-1} at 30, 60 and 120°C, respectively. Since the overall enthalpy change, $\Delta H°_4$, is 12 kcal mol^{-1}, an activation energy of ca. 6 kcal mol^{-1} for the addition of phenoxyl radical to β-methylstyrene was derived.

[4] $PhC\dot{H}(Me)OPh \rightarrow PhCH{=}CHMe + PhO\cdot$

To use the data for reaction [4] to assess ΔH_3, the effect on the thermochemistry upon removal of the β-methyl group and replacement of the benzylic hydrogen by a hydroxyl group must be estimated. According to standard group additivity rules $\Delta\Delta H°_f(PhC(H_2)CH_3 \rightarrow PhC(H)(OH)CH_3)$ can be evaluated to be −41 kcal mol^{-1}, leading to a value of $\Delta H°_f$ (**1**) of −39 kcal mol^{-1}. The strength of the benzylic C—H bond is lowered as a result of the additional stabilization by the OH group. Although the amount of experimental data is limited, a difference of 7 kcal mol^{-1} for the C—H bond in CH_3CH_2–H and $CH_3CH(OH)$-H represents an upper limit leading to a value of $\Delta H°_f(PhC\dot{}(OH)CH_2OPh)$ of −12 kcal mol^{-1}. In reaction [3] the enol of acetophenone is formed. Using a group increment derived from group additivities and experimental data (18, 19) $\Delta\Delta H°_f(CH_3C(H){=}CH_2 \rightarrow CH_3C(OH){=}CH_2) =$ −47 kcal mol^{-1}, a value of $\Delta H°_f(PHC(OH){=}CH_2)$ of −12 kcal mol^{-1} is obtained. Thus, a value of ΔH_3 of 12 kcal mol^{-1} is obtained and (assuming $\log A = 13.4$ and $E_a = \Delta H + 6$ kcal mol^{-1} (17)) rate contants at 30, 60, and 120°C of 2.6, 38, and 2400 s^{-1}, respectively, are predicted.

Alternatively, $\Delta H°_f(PhCH_2CH_2OPh)$ can be estimated from group additivities to be 2 kcal mol^{-1} and the C—H bond energy to be ca. 86 kcal mol^{-1} (20); a value of $\Delta H°_f(PhC\dot{H}CH_2OPh) = 36$ kcal mol^{-1} is obtained. An assessment of the effect of the hydroxyl group can be made since it is possible to quantify the thermochemisty of reactions [5] and [6] using known bond energies (21) and heats of formation of enols (18, 19) to give $\Delta H_5 = 3.0$ and $\Delta H_6 = 3.2$ kcal mol^{-1}. This demonstrates that the hydroxyl group has a negligible effect on the thermochemistry. Therefore, it is expected that the thermochemistry of fragmentation of 2-phenoxy-1-phenylethyl radical, reaction [7], should be the same as reaction [3], leading to $\Delta H_3 = 11$ kcal mol^{-1}. Thus, two independent thermochemical assessments of reaction [3] give the same result.

[5]

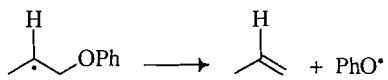

$\Delta H°_f$/kcal mol^{-1} 13.2 4.8 11.4

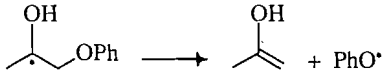

[6] $\Delta H°_f$/kcal mol^{-1} −31.8 −40 11.4

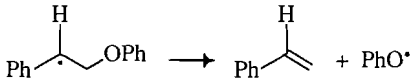

[7] $\Delta H°_f$/kcal mol^{-1} 35.8 35.3 11.4

It is important to comment on the selectivity of reaction [2] especially in light of the inability to observe **1**˙ by ESR spec-

Can. J. Chem. Downloaded from www.nrcresearchpress.com by 46.23.64.124 on 09/08/12
For personal use only.

troscopy. The observed rate constant, k_2, of 1.5×10^6 M^{-1} s^{-1} in DTBP/benzene (1:9, v/v) represents the sum of the reactivities at all sites. The extent to which abstraction from the methylene contributes can be estimated by the reactivity of the *tert*-butoxyl radical towards 2,3-dihydro-1,4-benzodioxane, which was measured to be 3.3×10^5 M^{-1} s^{-1} (per molecule) in DTBP/benzene (1:2, v/v). Since the solvent effect on the rate constants is small, the contribution to the overall rate constant from methylene abstraction should be ca. 1.7×10^5 M^{-1} s^{-1} (ca. 10% of the overall reaction). However, one should keep in mind that the radicals (or mixture of radicals) observed by ESR spectroscopy are not necessarily those generated most efficiently but those that are most persistent (22). Since the rate constants were determined at 20°C and since the selectivity is expected to be temperature dependent, the contribution from methylene abstraction should increase to ca. 15% at 60°C and 25% at 120°C. In addition to only moderate selectivity in reaction [2], radical generation by secondary photolysis of products as described above also is likely to contribute to the complex ESR spectrum observed.

The data present above are not consistent with the rapid ($>10^6$ s^{-1}) fragmentation of **1**˙ as reported by Scaiano et al. (7), who also used reaction [2] as a source of the radical. The approximate twofold increase in the yield of the ketone **4** upon introduction of oxygen is consistent with a mechanism in which direct reaction with oxygen (reaction [8]) competes with the bimolecular disproportionation of **1**˙ to give one equivalent of **1** and one of **4** (reaction [9]). In the presence of oxygen all of the ketyl radicals are trapped by reaction [8] and subsequently tranformed into **4**. The slightly higher than twofold increase in the yield of **4** in the presence of oxygen may be indicative of a small amount of autoxidation under oxygen (presumably via the hydroperoxyl radical). Given that the average steady state concentration of radicals under these conditions at 60°C is on the order of 10^{-8} M, and assuming a value of $2k_9$ of 5×10^9 M^{-1} s^{-1} (23), an upper limit of $k_3 < 0.1k_9$ of only 6 s^{-1} for reaction [3] at 60°C is obtained.[3] Since the rate constant is expected to decrease by about a factor of 10 at room temperature, an upper limit for k_3 of only ca. 1 s^{-1} is derived. This value is consistent with the thermochemical estimates described above, which can only be expected to have order of magnitude precision.

[8] 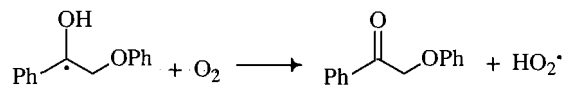

[9] $$2\,\mathbf{1}^{\cdot} \longrightarrow \mathbf{1} + \mathbf{4}$$

An interesting aspect of the reactivity of **1**˙ is the apparent lack of combination of ketyl radicals to form a pinacol. There is considerable literature concerning combination versus disproportionation of alkyl and benzylic radicals (24). In these cases combination is often preferred even though the products tend to be sterically hindered. On the other hand, Fischer and co-workers studied the self-reaction of 2-propanol-2-yl and concluded from CIDNP polarization patterns that 80% of the ketyl radical reacted by disproportionation while only 20% reacted by combination (23). Thus, it is difficult to predict a priori the fraction of combination. However, it has been pointed out[4] that the concentration of oxygen in argon-saturated solutions may be has high as 10^{-7} M. Since the average radical concentrations are on the order of 10^{-8} M, it is likely that the disproportionation between two ketyl radicals will not occur and that the apparent disproportionation is mediated by oxygen (eqs. [8] and [10]). Given this possibility and assuming $k_{10} = 5 \times 10^9$ M^{-1} s^{-1}, the upper limit for reaction [3] should be raised to $k_3 < 0.1k_8[O_2] = 50$ s^{-1} at 60°C, which is more in line with the thermochemical prediction of 38 s^{-1} at this temperature. This slightly revised mechanism would also explain the absence of pinacol in all of these reactions.

[10] $$\mathbf{1}^{\cdot} + HO_2^{\cdot} \rightarrow \mathbf{1} + O_2$$

At higher temperatures there is evidence for the fragmentation and chain decomposition of **1** via reactions [3] and [11]. At 120°C the half-life of DTBP is some 15 h yet after only 5 h a significant fraction of the starting material has reacted and, for the first time, acetophenone and phenol are observed. The increased importance of reaction [3] at the higher temperature simply reflects the fact that the disproportionation is nearly activationless.

[11] $$PhO^{\cdot} + \mathbf{1} \rightarrow PhOH + \mathbf{1}^{\cdot}$$

The observation of **4** from the photo-induced decomposition had not been previously reported (7). However, in light of the data above, it is clear that **4** is, indeed, the primary photoproduct and the acetophenone and phenol are formed in these reactions as a result of secondary photolysis. Our proposed mechanism also is consistent with the observed kinetics and spectra from laser flash photolysis. Although too weak to make an unequivocal assignment, it is likely that the long-lived, broad transient observed between 350 and 500 nm that is quenched by oxygen is actually the ketyl radical, **1**˙ (Fig. 1).

Given the sluggishness of reaction [3] it may be necessary to modify the current mechanism for photoyellowing of pulp. An alternative is presented in Scheme 2 in which both the unimolecular fragmentation of the ketyl radical and its reaction with oxygen may occur. Although the fragmentation of the ketyl radicals from lignin itself is expected to be faster, under conditions in a rigid matrix where reaction [3] can be reversible, reaction of the radical with oxygen may play an important role. This reaction, in which the acetophenone moiety is generated by autoxidation of the benzylic alcohol groups, leads to a greater fraction of the photoyellowing occurring via Path A. The revised mechanism in Scheme 2 is consistent with the observation of Schmidt and Heitner (3) that the carbonyl content of the pulp increases upon irradiation. It also is consistent with the general conclusion that these groups are the major source of long-wavelength chromophores in pulp (4). A consequence of this mechanism is that it may be practical to consider inhibitors of photoyellowing based on the trapping and (or) repair of ketyl radicals generated in environments inaccessible to oxygen. Studies of the thermal decomposition of other model compounds more structurally relevant to lignin are underway.

[3] The factor of 0.1 represents the detection limit of the HPLC analysis. If reaction [3] were faster, we would expect to detect both acetophenone and phenol.

[4] J.C. Scaiano, private communication.

Scheme 2. Revised mechanism for photoyellowing of mechanical pulps.

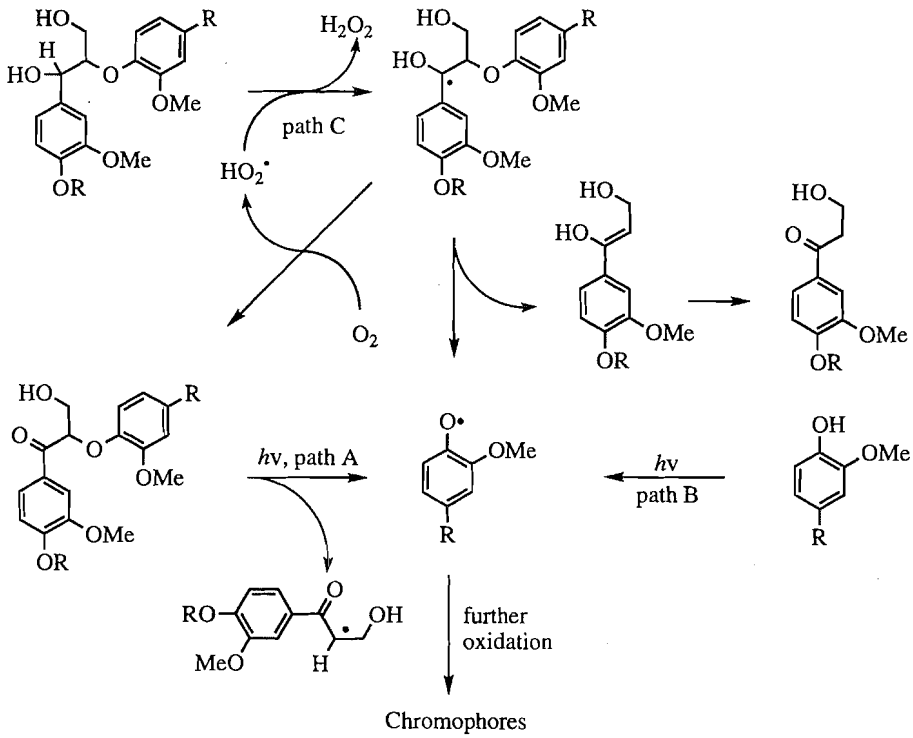

Experimental

Chemicals

Acetonitrile was distilled before use. Di-*tert*-butyl peroxide was purified on an alumina column. Di-*tert*-butyl hyponitrite was prepared as described by Mendenhall (25). Other chemicals were used as received.

α-Phenoxyacetophenone was prepared by reaction of phenol (1.2 equiv.), potassium carbonate (1.2 equiv.), and 2-bromoacetophenone (1.0 equiv.) in dry acetone at room temperature (about 20 h). The product was recrystallized twice from ethanol.

1-Phenyl-2-phenoxyethanol was prepared by reduction of α-phenoxyacetophenone with $LiAlH_4$ (1.1 equiv.) in anhydrous ether. The solution was refluxed for 1 h and then quenched with a saturated NH_4Cl solution. The product was recrystallized twice from pentane.

Deuterated 1-phenyl-2-phenoxyethanol (**1**-d_2) was prepared from the α-phenoxyacetophenone-d_2, which was, itself, prepared by reaction of α-phenoxyacetophenone with potassium hydroxide and D_2O in 1,4-dioxane. The detailed procedure is given in ref. 6. ^1H NMR analysis indicated that 95% of α-protons of the α-phenoxyacetophenone had been exchanged.

Thermal decomposition of 1-phenyl-2-phenoxyethanol

The reaction mixture contained 1.0 mL acetonitrile with 50 mg of **1** and 20 mg (50 mol%) or 4 mg (10 mol%) of di-*tert*-butyl hyponitrite. The solutions were purged with argon or oxygen for 15 min and were then heated in a constant-temperature bath (60 ± 0.5°C) for 5 h. The resulting solution was quantitatively analyzed by HPLC using benzophenone as an internal standard. For the reactions under oxygen, oxygen was continuously passed over the solution during the reaction. Reactions carried out at 120°C were performed in Pyrex tubes containing 0.5 mL of solution (25 mg of **1** and 3.5 mg (10 mol%) of di-*tert*-butyl peroxide) and were degassed and sealed under vacuum with three freeze–pump–thaw cycles. The products were quantified by HPLC using an internal standard (benzophenone) and calibration curves based on authentic samples of reactants and products.

Photochemical degradations

Irradiations were performed in a Rayonet® reactor with 12-RPR-3000 or 12-RPR-3500 lamps. A 1.0 mL solution containing 50 mg of **1** or **4** and any other additives were syringed into 7 mm × 7mm laser tubes. The solutions were purged with argon or oxygen for 15 min before irradiation.

Laser Flash Photolysis

This instrument has been described in detail elsewhere (26). Nanosecond transient absorption spectra were obtained using a flow system to ensure the presence of unphotolyzed substrate for each laser pulse. Rate constants were obtained using static 7 × 7 mm^2 quartz cells. A Lumonics model EX530 eximer laser (308 nm; ≤40 mJ/pulse; ≈8 ns/pulse) was used as the laser excitation source.

Acknowledgements

The authors thank the Network of Centres of Excellence for Mechanical and Chemimechanical Wood Pulps for financial support and Drs. J.C. Scaiano, L.J. Johnston, and N.P. Schepp for helpful discussions. One of us (P.M.) acknowledges the Leiden Institute of Chemistry for enabling his sabbatical leave at the National Research Council of Canada.

Can. J. Chem. Downloaded from www.nrcresearchpress.com by 46.23.64.124 on 09/08/12
For personal use only.

References

1. J. Gierer and S.Y. Lin. Sven. Papperstidn. **75**, 233 (1972).
2. G.J. Leary. TAPPI, **51**, 257 (1968).
3. J.A. Schmidt and C. Heitner. J. Wood Chem. Technol. **11**, 397 (1991).
4. J.A. Schmidt and C. Heitner. J. Wood. Chem. Technol. **13**, 309 (1993).
5. J.C. Netto-Ferreira, I.G.J. Avellar, and J.C. Scaiano. J. Org. Chem. **55**, 89 (1990).
6. J.C. Netto-Ferreira and J.C. Scaiano. Tetrahedron Lett. **30**, 443 (1989).
7. J.C. Scaiano, J.C. Netto-Ferreira, and V. Wintgens. J. Photochem. Photobiol. **59**, 265 (1991).
8. J.A. Schmidt, A.B. Berinstain, F. De Rege, C. Heitner, L.J. Johnston, and J.C. Scaiano. Can. J. Chem. **69**, 104 (1991).
9. L. Hurrel, L.J. Johnston, N. Mathivanan, and D. Vong. Can. J. Chem. **71**, 1340 (1993).
10. J.C. Scaiano, M.K. Whittlesey, A.B. Berinstain, P.R.L. Malenfant, and R.H. Schuler. Chem. Mater. **6**, 836 (1994).
11. J.K.S. Wan, M. Yat Tse, and M.C. Depew. Res. Chem. Intermed. **17**, 59 (1992).
12. I.A. Shkrob, M.C. Depew, and J.K.S. Wan. Res. Chem. Intermed. **17**, 271 (1992).
13. H. Kiefer and T.G. Traylor. J. Am. Chem. Soc. **89**, 6667 (1967).
14. J.C. Scaiano and G.G. Wubbels. J. Am. Chem. Soc. **103**, 640 (1981).
15. J.C. Scaiano and J.C. Netto-Ferreira. J. Photochem. **32**, 253 (1986).
16. D. Avila, J. Lusztyk, and K.U. Ingold. J. Am. Chem. Soc. **114**, 6576 (1992).
17. J.T. Autrey, M.S. Alnajjar, D.A. Nelson, and J.A. Franz. J. Org. Chem. **56**, 2197 (1991).
18. A.J. Kresge and N.P. Schepp. J. Chem. Soc. Chem. Commun. 1548 (1989).
19. Y. Chiang, A.J. Kresge, and N.P. Schepp. J. Am. Chem. Soc. **111**, 3977 (1989).
20. S.E. Stein, J.M. Rukkers, and R.L. Brown. NIST Structures and Properties Data Base, Version 2.0, National Institute of Standards and Technology, Gaithersburg, Md. 1994.
21. D. F. McMillen and D. M. Golden. Annu. Rev. Phys. Chem. **33**, 493 (1982).
22. D. Griller and K.U. Ingold. Acc. Chem. Res. **8**, 13 (1976).
23. B. Blank, A. Henne, G.P. Laroff, and H. Fischer. Pure Appl. Chem. **41**, 475 (1975).
24. H. Fischer and H. Paul. Acc. Chem. Res. **20**, 200 (1987).
25. G.D. Mendenhall. Tetrahedron Lett. **24**, 451 (1985).
26. S. Kazanis, A. Asarani, and L.J. Johnston. J. Phys. Chem. **95**, 4430 (1991).

Can. J. Chem. Downloaded from www.nrcresearchpress.com by 46.23.64.124 on 09/08/12
For personal use only.

Effect of the degree of neutralization on the micellization of block ionomers

Karine Khougaz, Diep Nguyen, Claudine E. Williams, and Adi Eisenberg

Can. J. Chem. Downloaded from www.nrcresearchpress.com by 46.23.64.124 on 09/08/12
For personal use only.

Abstract: The effect of neutralization on the micellization of polystyrene-*b*-poly(acrylic acid) (PS-*b*-PAA) was investigated by static light scattering (SLS) and small-angle X-ray scattering (SAXS). The block copolymers, present initially in single chain form in either dioxane or benzene–methanol (90/10 (v/v)), were neutralized to different degrees by the addition of cesium hydroxide dissolved in methanol. The solutions were simultaneously monitored by SLS. It was found that micelle formation began near 5% neutralization. The normalized scattered light intensity at 90° (I_{90}/c) increased dramatically in the neutralization range between ca. 10 and 60%. For neutralization degrees between 60 and ca. 100%, I_{90}/c did not change significantly with a further increase in the percent of neutralization. In the second part of the study, two block copolymers, PS(600)-*b*-PAA(34) and PS(600)-*b*-PAA(45) (the number of monomer units is given in parentheses), were prepared from benzene–methanol (90/10 (v/v)) with different degrees of neutralization: 5, 25, 60, 100, and 150%. The resulting solutions were freeze-dried and the dried samples were redissolved in toluene. These samples were investigated by SLS and SAXS. By SLS, the aggregation numbers (f) were found to be the same between 5 and 60% neutralization. An increase in f was observed in going from 60 to 100%; i.e., f increased from 82 to 92 for PS(600)-*b*-PAA(34), and from 79 to 110 for PS(600)-*b*-PAA(45). The f values for the two block copolymers at 150% neutralization were found to be the same as those for 100% neutralization. The core radii values (R_{core}) were measured for the neutralized PS(600)-*b*-PAA(45) samples at 0.05 g/mL in toluene by SAXS. The R_{core} values increased from 5 to 60% neutralization, remained constant from 60 to 100%, and increased again in the range from 100 to 150%. The results are explained by dynamic considerations. For low percent neutralization, between 5 and 60%, the micelles and single chains are proposed to be in a dynamic equilibrium state. For higher percent neutralization, between 60 and 100%, the dynamics are probably much slower.

Key words: block copolymers, micelles, ionomers, light scattering, small angle X-ray scattering (or SAXS).

Résumé : Faisant appel à la diffusion statique de la lumière (SLS) et la diffusion des rayons X à petit angle (SAXS), on a étudié l'effet de la neutralisation sur la micellisation du polystyrène-*b*-poly(acide acrylique) (PS-*b*-PAA). Les copolymères à blocs, qui sont présents initialement sous la forme d'une chaîne simple dans le dioxane ou dans un mélange benzène–méthanol (90/10 (v/v)), se neutralisent à des degrés divers par l'addition d'hydroxyde de césium dissous dans le méthanol. On a examiné les solutions simultanément par SLS. On a trouvé que la formation de micelles commence près d'environ 5% de neutralisation. L'intensité normalisée de la lumière diffusée à 90° (I_{90}/c) augmente d'une façon dramatique dans la plage de neutralisation allant d'environ 10 à 60%. Pour des degrés de neutralisation variant de 60 à environ 100%, le I_{90}/c ne varie pas beaucoup avec les augmentations du pourcentage de neutralisation. Dans la deuxième partie de cette étude, on a préparé deux copolymères à bloc PS(600)-*b*-PAA(34) et PS(600)-*b*-PAA(45) (le nombre d'unités de monomères est donné entre parenthèse), à partir de solutions dans un mélange benzène–méthanol (90/10 (v/v)) et avec des degrés de neutralisations de 5, 25, 60, 100 et 150%. On a séché les solutions obtenues à froid et on a redissous les échantillons secs dans du toluène. On a étudié ces échantillons par SLS et par SAXS. Par SLS, on a trouvé que les nombres d'agrégation (f) sont les mêmes pour des neutralisations allant de 5 à 60%. On a observé une augmentation dans la valeur de f en passant de 60 à 100%, c'est-à-dire que la valeur de f est passée de 82 à 92 pour le PS(600)-*b*-PAA(34), et de 79 à 110 pour le PS(600)-*b*-PAA(45). Dans le cas de chacun des copolymères à bloc, on a trouvé que la valeur de f est la même à 150% de neutralisation qu'à 100%. Utilisant le SAXS, on a mesuré les valeurs des rayons de coeur (R_{core}) d'échantillons de PS(600)-*b*-PAA(45) à 0,05 g/mL, dans le

Received May 16, 1995.

This paper is dedicated to Professor J.E. (Jim) Guillet in recognition of his contributions to Canadian chemistry.

K. Khougaz, D. Nguyen,[1] **and A. Eisenberg.**[2] Department of Chemistry, McGill University, 801 Sherbrooke Street West, Montréal, QC H3A 2K6, Canada.
C.E. Williams. Laboratoire pour l'Utilisation du Rayonnement Électromagnétique (LURE), Université Paris-Sud, 91405 Orsay Cedex, France.

[1] Present address: Brookhaven National Laboratory, HFBR, Upton, NY 11973, U.S.A.
[2] Author to whom correspondence may be addressed. Telephone: (514) 398-6934. Fax: (514) 398-3797.

toluène. Ces valeurs augmentent pour des degrés de neutralisation allant de 5 à 60% et elles demeurent constantes de 60 à 100%; elles augmentent de nouveau de 100 à 150%. On explique les résultats par des considérations dynamiques. À des pourcentages de neutralisation faibles (de 5 à 60%), on suggère que les micelles et les chaînes isolées sont dans un état d'équilibre dynamique. À un degré plus élevé de neutralisation (de 60 à 100%), les dynamiques sont probablement beaucoup plus lentes.

Mots clés : copolymères à bloc, micelles, ionomères, diffusion de la lumière, diffusion des rayons à petit angle (SAXS).

[Traduit par la rédaction]

1. Introduction

Block copolymers tend to form micellar structures when dissolved in a solvent that is selective for one of the blocks. Increasing interest has focused on the formation and characterization of these micelles, and the phenomenon has been reviewed (1–5). Recently, considerable research has been performed on nonionic block copolymers that micellize in aqueous media (6–12) or in organic solvents (13–17). Research on the micellization of ionic block copolymers, as compared to that on nonionic block copolymers, is more scarce. Ionic block copolymers, due to their amphiphilic nature, are able to form either polyelectrolyte or ionomer micelles, depending on the nature of the solvent. For instance, in an aqueous environment, polyelectrolyte micelles are formed with a hydrophobic core and a charged ionic corona. Several studies have focused on the characterization of these micelles (4, 18–20). In organic solvents, ionomer micelles are formed with an ionic core and a nonionic corona. The latter micelle structure will be the focus of the present paper.

The association of block ionomers composed of lightly sulfonated polystyrene-*b*-poly(*tert*-butylstyrene) (PS-*b*-P*t*-BS) copolymers has been investigated in polar (21, 22) and nonpolar solvents (23). In polar solvents it was found that the sulfonated block copolymers formed micelles with a charged sulfonated polystyrene corona surrounding an insoluble P*t*-BS core at room temperature (21, 22). At higher temperatures it was found that charged monomolecular micelles were present (21). The aggregation behavior of the block copolymer with 2.3 mol% sulfonation was also investigated in cumene. In this solvent, reverse micelles, in which the sulfonated PS formed the micelle cores were observed. It was found by static and dynamic light scattering (SLS, DLS) that single chains and reverse aggregates coexisted (23). Due to the polydispersity in the degree of sulfonation, the aggregates were found to be formed by copolymer chains of higher ionic contents. This result was similar to that obtained from the aggregation of polystyrene-*b*-poly(metal methylacrylate) (PS-*b*-PMtMA) (24).

Block ionomer micelles that are composed of a nonionic corona of polystyrene and an ionic core of either neutralized poly(methacrylic acid) or poly(acrylic acid), or quaternized poly(4-vinylpyridine), have been extensively studied in this laboratory by several techniques (24–32).[3] It was shown that block ionomer micelles composed of PS-*b*-PMtMA form very stable micelles (24). A systematic study investigated the dependence of the block copolymer composition on the micellar characteristics by size exclusion chromatography (SEC) (24), DLS (25), and viscometry (25). The method of micelle preparation was found to significantly influence the micelle characteristics (25). For instance, the neutralization medium had an effect on the hydrodynamic radius (R_h) of the micelles. The block copolymer neutralized in benzene–methanol was found to have a larger R_h than that in dioxane. It should be noted that both solvents dissolved the acid copolymer as single chains. Also, it was found that neutralized samples that were recovered by freeze-drying and redissolved had a larger aggregation number (f) and R_h than those that were formed directly upon neutralization (25).

Block copolymers of polystyrene-*b*-poly(sodium acrylate) (PS-*b*-PANa) were also investigated by SEC, and it was found that micellization can occur for ionic block lengths as short as three units (26). The critical micelle concentration (cmc) values for a series of PS(660)-*b*-PANa(x), where x ranged from 2.6 to 14 units, were determined by SLS. The cmc values for these micelles were found to be of the order of 10^{-8} M (27). The analysis of the cmc by SLS was based on a recent micellization model that accounts for the polydispersity of the insoluble block length (28). In a study by ^{2}H NMR, the dynamics of PS chains in micelle corona for reverse ionomer micelles were investigated (29). The PS segments near the core were observed to have a restricted mobility compared to those further from the core or to single chains in solution.

The micellization of block ionomer micelles has also been investigated by small-angle X-ray scattering (SAXS) in the solid state and in solution (30–32).[3] An increasing degree of organization in solutions of reverse micelles, formed by polystyrene-*b*-poly(cesium methacrylate) (PS-*b*-PMACs) and polystyrene-*b*-poly(cesium acrylate) (PS-*b*-PACs) in toluene, was observed in the concentration range of 0.01 to 0.1 g/mL.[3] The core radii (R_{core}), calculated aggregation numbers, and surface areas per chain for the reverse ionomer micelles were also fitted to the predictions of the star model (30, 31). It was also found that the ionic core radii of several ionomer micelles were the same in the solid state as in solution (toluene).[3] This result showed that, once micellization occurs, the morphology of the micelles in solution is retained upon solvent evaporation. Also, the micelle cores of the reverse ionomers in toluene would be expected to be solvent free. The chain extension of the block forming the core was also investigated in the solid state (30). The effect of the ionic chain polydispersity on the size of the spherical ionic microdomains was examined for polystyrene-*b*-poly(4-vinylpyridinium methyl iodide) (PS-*b*-P4VPMeI) and PS-*b*-PACs (32). It was found that the polydispersity effect depended on the conditions of sample preparation.

The purpose of the present paper is to investigate the effect of different degrees of neutralization on the micellar properties of polystyrene-*b*-poly(acrylic acid). The samples were measured by using two complementary scattering techniques,

[3] Also, D. Nguyen, C.E. Williams, and A. Eisenberg. To be published.

Can. J. Chem. Downloaded from www.nrcresearchpress.com by 46.23.64.124 on 09/08/12
For personal use only.

Can. J. Chem. Downloaded from www.nrcresearchpress.com by 46.23.64.124 on 09/08/12
For personal use only.

static light scattering and small-angle X-ray scattering. Information on the weight average molecular weight, radius of gyration, second virial coefficient, and core radius was obtained by these two methods in combination. This paper will first discuss the neutralization of the acid copolymer with cesium hydroxide as a function of the solvent and the ionic block length. The results on samples prepared with different degrees of neutralization as investigated by SLS and SAXS will then be presented and discussed.

2. Experimental

Materials

The block copolymers, polystyrene-*b*-poly(acrylic acid), were prepared by sequential anionic polymerization; the details are given in ref. 26. For convenience, a summary of the synthesis will be given here. The copolymers were synthesized by sequential anionic copolymerization of the styrene monomer followed by *tert*-butyl acrylate. The initiator was the reaction product of *sec*-butyllithium with a few drops of α-methylstyrene. The polymerization was carried out in tetrahydrofuran (THF) at −78°C under an atmosphere of nitrogen. The apparatus employed for the polymerization allowed the withdrawal of the reaction mixture in the course of the synthesis. Therefore, for a given constant polystyrene block length, a series of diblocks was obtained with poly(*tert*-butyl acrylate) segments of different lengths. Aliquots of the reaction mixtures were withdrawn for characterization after the polystyrene block was formed and every time following addition of the second monomer. Polystyrene-*b*-poly(acrylic acid) (PS-*b*-PAA) was obtained by acid-catalyzed hydrolysis of the *tert*-butyl acrylate segments in toluene at 80°C using *p*-toluenesulfonic acid as the catalyst. The PS-*b*-PAA was recovered and purified by repeated precipitation in cold methanol. The samples were then dried in a vacuum oven at 50°C for 48 h. The composition of the copolymers was determined by either FT-IR using copolymers in the ester form or by titration of the acid. The molecular weight of the polystyrene block was determined with a precision of ±5% by size exclusion chromatography in THF using narrow molecular weight polystyrene standards. The polydispersity index of the PS block was 1.10.

For neutralization of PS-*b*-PAA, a known amount of the dried copolymer was dissolved in benzene–methanol (90/10 (v/v)) at a concentration of 2% (w/w). The acid samples were neutralized by dropwise addition of CsOH in methanol to the solutions. For two block copolymers, PS(600)-*b*-PAA(34) and PS(600)-*b*-PAA(45), samples with different degrees of neutralization were prepared, i.e., 5, 25, 60, 100, and 150%, by addition of different amounts of CsOH–methanol. The solutions were stirred for 1–2 h, and the diblock ionomers were recovered by freeze-drying. The samples were then further dried at 60°C for 48 h under vacuum. Abbreviations are used to indicate the copolymer composition; for example, PS(600)-*b*-PACs(34) represents a polystyrene chain of 600 units joined to a poly(cesium acrylate) chain of 34 units; PAA denotes poly(acrylic acid).

Sample preparation for SLS

Three PS-*b*-PAA block copolymers, PS(600)-*b*-PAA(45), PS(600)-*b*-PAA(34), and PS(600)-*b*-PAA(13), were prepared by dissolving the copolymer either in dioxane or in a benzene–methanol mixture (90/10 (v/v)). The initial concentrations of the solutions depended on the block copolymer composition, and they ranged from ca. 2.5×10^{-3} to 6×10^{-3} g/g. The solvent and polymer solutions were filtered through 0.2 and 0.45 μm PTFE filters, respectively, into scintillation vials, which were used for the light scattering measurements. Titration curves were obtained by adding dropwise a predetermined amount of CsOH–methanol to the PS-*b*-PAA block copolymer solutions. The concentration of CsOH used was 1.0, 0.44, and 0.18 M for PAA block lengths of 45, 34, and 13 units, respectively. The amounts of CsOH–methanol added did not represent a significant volume as compared to the total volume of the solution. For instance, to achieve 100% degree of neutralization of PS(600)-*b*-PAA(45) in dioxane (10 mL), 144 μL of CsOH–methanol was required. This amount of CsOH–methanol represents ca. 1.4% of the total volume. It should be noted that these values are given for illustrative purposes only, since the actual solution volume is changing during the course of the measurement, as will be explained below. After each addition of CsOH–methanol, the solutions were stirred for ca. 10 min and the scattered light intensity was measured five times; the average value was used. Typical average percent error in the scattered intensity at 90° was ca. 3%. For higher degrees of neutralization, the scattered intensity increased above the detection limit of the detectors, and thus the polymer solutions were diluted by the addition of solvent. For the two samples PS(600)-*b*-PAA(45) and PS(600)-*b*-PAA(34), which were prepared with specific degrees of neutralization (5, 25, 60, 100, 150%), the weight average molecular weight (M_w), radius of gyration (R_g), and second virial coefficient (A_2) were determined by constructing a Zimm plot. A minimum of four concentrations were used for each Zimm plot analysis.

Static light-scattering and specific refractive index increment (d*n*/d*c*) measurement

Light-scattering experiments were performed using a DAWN-F multiangle laser photometer (Wyatt Technology, Santa Barbara, Calif.) at 25°C, which operates at 15 angles, from 26° to 137°, and is equipped with a He-Ne laser (632.8 nm). Data acquisition and analysis utilized the DawnF and SkorF softwares, respectively. Zimm plots were processed with Aurora software. The specific refractive index increments (d*n*/d*c*) were determined using the Wyatt/Optilab 903 interferometric refractometer and accompanying software (Dndc 2.01) at a wavelength of 630 nm. The cell constant was determined by calibration with different concentrations of sodium chloride (99.999%, Aldrich) solutions. Eight to ten concentrations were measured for each d*n*/d*c* determination. The d*n*/d*c* values were obtained from the slope of a plot of refractive index versus polymer concentration. The d*n*/d*c* values for PS-*b*-PAA and PS-*b*-PACs were found to be 0.110 mL/g, which is the same as the literature values for polystyrene in toluene (33). It should be noted that, in general, for block copolymers with different refractive indices, an apparent weight average molecular weight ($M_{w,app}$) is obtained by SLS (34). However, in the present case, $M_{w,app}$ is close to the true M_w values since the refractive index increments of the block copolymers and of the soluble block in toluene were the same. This result is probably due to the small weight fraction of the insoluble block.

Can. J. Chem. Downloaded from www.nrcresearchpress.com by 46.23.64.124 on 09/08/12
For personal use only.

Sample preparation for SAXS

Micellar solutions were obtained by dissolving the freeze-dried powder in toluene at a concentration of 5% (0.05 g/mL). For the SAXS experiment, the solution was enclosed in a 1.5 mm thick cell with Kapton® windows. The SAXS measurements were carried out at room temperature.

SAXS measurement

The small-angle X-ray scattering experiments were performed at the D22 station of the LURE-DCI synchrotron radiation source (Orsay, France). A description of the spectrometer has been published elsewhere (35) It is a specialized spectrometer equipped with double crystal, fixed exit, monochromator providing a beam of a narrow energy range tunable from 4 to 15 keV (3–0.8 Å). The size of the beam at the sample was about 1 mm^2. The scattered X-rays were detected with a Xe-CO_2 gas-filled, one-dimensional position sensitive detector with a resolution of 217 μm. Samples were studied in the angular q range from 0.006 $Å^{-1}$ to 0.30 $Å^{-1}$ ($q = 4\pi \sin\theta / \lambda$, where θ is one half the scattering angle, and λ is the X-ray wavelength). The resulting scattering intensities were corrected for the incident beam decay, sample thickness, and transmission. The background scattering from the solvent was also subtracted. The q resolution is of the order of 0.003 $Å^{-1}$.

3. Results and discussion

The Results and discussion section is divided into three parts. In the first part, the effect of neutralization on the micellization of PS-*b*-PAA is discussed qualitatively. Neutralization was followed in two different solvents, dioxane and a benzene–methanol mixture for three different block copolymers. The aim was to examine the effect that increasing degree of neutralization has on the solvent quality for the block copolymer, in particular for the block forming the micelle core. In the second and third parts, more quantitative results are presented that were obtained by SLS and SAXS, respectively. The samples investigated were prepared with specific degrees of neutralization and measured in toluene, which is a nonsolvent for PAA and PACs.

3.1. Titration of PS-*b*-PAA with CsOH–MeOH

Figure 1 summarizes some of the results obtained in this study for the titration of PS(600)-*b*-PAA(45) as well as the results for this sample with different degrees of neutralization. The aggregation numbers (f) (Fig. 1*a*) and core radii (R_{core}) (Fig. 1*b*) will be discussed in Sects. 3.2 and 3.3. First, a typical titration curve obtained for PS(600)-*b*-PAA(45) dissolved in dioxane, which is given in Fig. 1*b*, will be addressed. For this sample, the scattered intensity at 90° was normalized to the polymer concentration and measured as a function of the percent neutralization of the PAA chains with CsOH–methanol. It should be noted that PS-*b*-PAA in dioxane is present as single chains, since the solvent is good for both blocks. However, upon neutralization, the solubility of the partially neutralized PAA block decreases, and thus the chains associate to form the micelle core.

It is interesting to establish at which percent neutralization of the PAA chains micellization starts from a solution of single chains. This value can be determined by examining the inset of Fig. 1*b*, which shows the normalized scattered intensity (I_{90}/c) as a function of the percent neutralization near the origin of the plot. It was found that I_{90}/c was constant below ca. 5% neutralization, after which the value began to increase. Thus, micellization occurred in the block copolymer when ca. 2 of the 45 PAA units per chain (i.e., ca. 5%) were converted to the salt form.

Fig. 1. Summary of results for PS(600)-*b*-PAA(45) as a function of percent neutralization; (*a*) aggregation numbers (f) for freeze-dried samples measured in toluene; (*b*) core radii (R_{core}) for freeze-dried samples measured in toluene (▲) and scattered light intensity at 90° normalized to polymer concentration (I_{90}/c) as a function of the percent neutralization with CsOH–methanol measured in dioxane (○). The inset shows I_{90}/c for low percent of neutralization. The lines are shown as a guide for the eye.

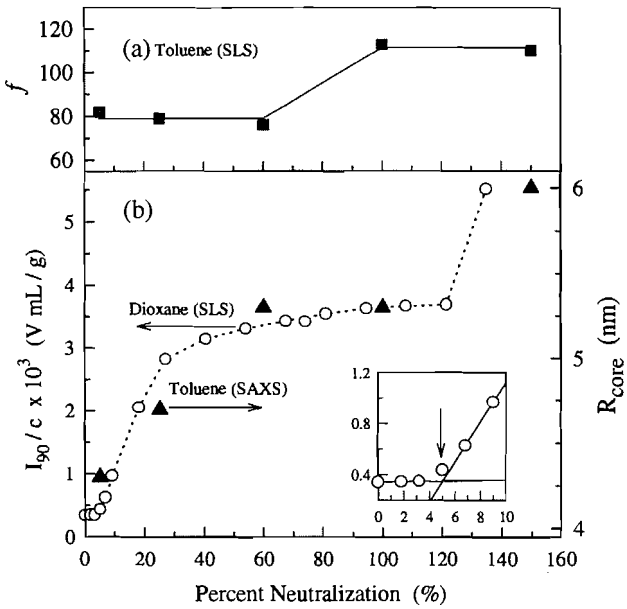

Fig. 2. Scattered light intensity at 90° normalized to polymer concentration (I_{90}/c) as a function of the percent neutralization with CsOH–methanol in benzene–methanol (90/10 (v/v)) for PS(600)-*b*-PAA(34) (●) and PS(600)-*b*-PAA(13) (▲). The lines are shown as a guide for the eye.

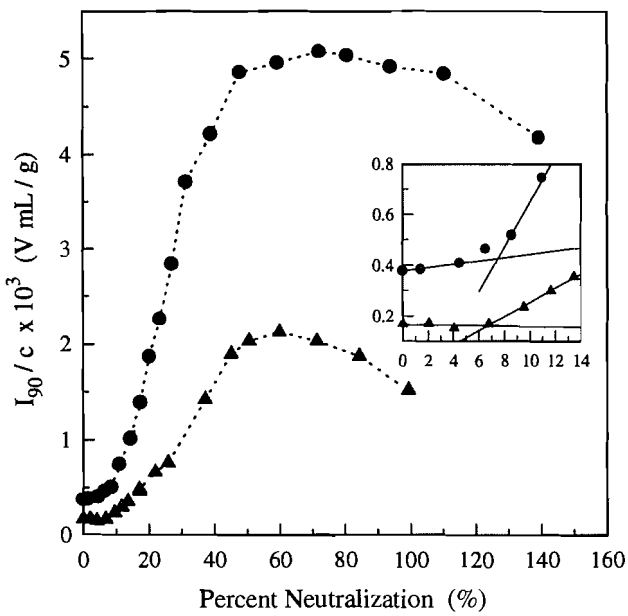

Can. J. Chem. Downloaded from www.nrcresearchpress.com by 46.23.64.124 on 09/08/12
For personal use only.

A similar titration was performed for PS(600)-*b*-PAA(13) and PS(600)-*b*-PAA(34) in benzene–methanol (90/10 (v/v)), with the results shown in Fig. 2. In this solvent mixture, the block copolymers are also initially present as single chains. The titration curve will be discussed in greater detail later in this section. It should be noted that the first increase in I_{90}/c also occurred at low degrees of neutralization for both block copolymers, specifically at ca. 7% (see inset of Fig. 2). This value was found to be independent of the PAA block length.

Once micellization has begun, it is of interest to examine the effects of further addition of CsOH–methanol on I_{90}/c. For PS(600)-*b*-PAA(45) in dioxane (Fig. 1*b*), it was observed that above 5%, I_{90}/c increased rapidly with increasing degree of neutralization. For instance, between 10 and 60% neutralization, the normalized scattered intensity increased by a factor of ca. 6. A further increase in the degree of neutralization resulted in a less dramatic increase in the scattered intensity. For instance, from 60 to 100% neutralization, the scattered intensity increased by only 10%. However, at 135% neutralization, I_{90}/c increased significantly. This latter increase may arise from the solubilization of the excess neutralizing agent, CsOH, in the micelle core, and will be discussed in Sect. 3.3.

The shape of the titration curve can give information on the solvent environment for the block copolymer with increasing degree of neutralization. First, it should be noted that for low degrees of neutralization, the micelle cores are expected to be swollen with dioxane and methanol. This occurs because the core is composed of PAA chains that are only partially neutralized. The dioxane and methanol would preferentially solvate the unneutralized sections of the PAA block while the block copolymer is in the micellar form. However, as the percent neutralization increases, the high ionic content of the core is expected to create an unfavorable environment for dioxane and methanol. As a result, these solvents would be expelled progressively from the micelle core. Consequently, it can be suggested that the micelle cores are more swollen at low degrees of neutralization than those at higher degrees.

For low degrees of neutralization, the cmc values would be expected to decrease with increasing neutralization. This aspect can be understood because increasing the degree of neutralization results in an increase in the number of ionic groups per chain, and the association of ionic chains would be expected to be stronger than that of acid chains. Also, as a result of the increase in the number or concentration of ionic groups, the solvent quality for the core decreases. Therefore, micelles would form at a lower concentration. Since the cmc decreases, the increase in I_{90}/c at low degrees of neutralization can be attributed, in part, to an increase in the number of the micelles.

To relate I_{90}/c to the weight average molecular weight (M_w) of the particles, M_w was evaluated for PS(600)-*b*-PAA(45) in dioxane for two degrees of neutralization, 7 and 50%. These measurements were performed by taking the samples that had been measured for the titration curve (Fig. 1*b*) and diluting them with dioxane to obtain different concentrations. The results for these samples at different concentrations were represented as Zimm plots. The M_w values for the 7 and 50% neutralized samples were determined to be 1.6×10^5 and 9.3×10^5 g/mol, respectively. Thus, M_w increases by a factor of ca. 6 in this neutralization range.

The effect of using benzene–methanol (90/10 (v/v)) as the solvent medium for the neutralization process was investigated. As noted previously, for this solvent composition, the acid block copolymer is present as single chains, since benzene and methanol are good solvents for the PS and the PAA blocks, respectively. Thus, at low degrees of neutralization it would be expected that methanol would solvate the unneutralized sections of the PAA block, in the same manner as dioxane and methanol discussed previously. Figure 2 illustrates the results obtained for two block copolymers, PS(600)-*b*-PAA(34) and PS(600)-*b*-PAA(13). The shape of the titration curve was similar to that of PS(600)-*b*-PAA(45) dissolved in dioxane (Fig. 1*b*). However, for higher degrees of neutralization, i.e., above ca. 100% for PS(600)-*b*-PAA(34) and above ca. 80% for PS(600)-*b*-PAA(13), further increase in the percent neutralization resulted in a slight decrease of I_{90}/c. At this point, the reason for the slight decrease is not fully understood.

3.2. SLS results on freeze-dried samples

To relate the normalized scattered intensities as a function of the percent neutralization to the actual changes in the micelle aggregation numbers and sizes, samples for PS(600)-*b*-PAA(34) and PS(600)-*b*-PAA(45) with different degrees of neutralization, i.e., 5, 25, 60, 100, and 150%, were prepared and investigated. The PS-*b*-PAA copolymers were dissolved in benzene–methanol (90/10 (v/v)) and CsOH–methanol was added dropwise in order to obtain micelles that have a low polydispersity in core sizes. The neutralized samples, which were recovered by freeze-drying, consisted of micellar structures that were simply redissolved in toluene, a selective solvent for PS, and then characterized by SLS and SAXS. Thus, complications arising from the penetration of solvent in the micelle core are avoided.

The results for the SLS measurements of the copolymers dissolved in toluene are given in Table 1. The aggregation numbers (f) were determined from the ratio of M_w of the micelles to that of a single chain. It should be recalled that the acid form of the block copolymer aggregates in toluene. It was found for PS(600)-*b*-PAA(34) that the aggregation numbers (f) increased from 63 to 80, in going from 0% to 5% neutralization. Thus, the incorporation of just a few ionic groups along the PAA chain affects the micellization significantly. The aggregation numbers for 5, 25, and 60% neutralization were essentially constant at a value of ca. 82 ± 3. A significant increase in f was observed between 60 and 100% neutralization, i.e., from 81 to 92. The same trends in f were observed for PS(600)-*b*-PAA(45). For instance, f was ca. 79 ± 2 for the samples at 5, 25, and 60%, and f increased from 76 to 110 between 60 and 100%. Also, the f values for both copolymer samples were measured for 150% neutralization and were found to be the same as those for 100% neutralization. This result shows that there is no effect on f for neutralization levels above the stoichiometric amount. The results for PS(600)-*b*-PAA(45) are illustrated in Fig. 1*a*.

The trends in the aggregation numbers with increasing percent neutralization can be examined by speculating on the dynamics of the block copolymer in the neutralization medium. The aggregation numbers fall into three regions, depending on the percent neutralization, i.e., between 5 and 60%, between 60 and 100%, and between 100 and 150% (Fig. 1*a*). The region between 5 and 60% will be considered first. In the previous section, it was suggested that, for low degrees of neutralization, the single chains and micelles were in a

Table 1. Results for different percent neutralization for PS-*b*-PAA in toluene.

Percent neutralization (%)	$M_w \times 10^{-6}$ (g mol^{-1})	f	R_g (nm)	$A_2 \times 10^5$ (mL mol g^{-2})	R_{core} (nm)
PS(600)-*b*-PAA(34)					
0	4.1	63	27	1.4	
5	5.1	80	26	1.0	
25	5.6	85	25	1.8	
60	5.5	81	26	1.4	
100	6.4	92	34	1.8	
150	6.5	93	29	1.3	
PS(600)-*b*-PAA(45)					
5	5.4	82	24	0.67	4.3
25	5.3	79	24	0.35	4.7
60	5.3	76	24	0.94	5.3
100	8.1	110	31	0.68	5.3
150	7.9	110	29	0.42	6.0

dynamic equilibrium state due to the solubilization of solvent in the micelle cores. As a result, micelle formation was expected to occur under equilibrium conditions. In this study, the aggregation numbers of the micelles recovered by freeze-drying from this dynamic state were found to be independent of the degree of neutralization. The freeze-dried samples, which were redissolved in toluene, would be expected to exist in a much less mobile state than those in benzene–methanol. This can be anticipated, since toluene is a nonsolvent for the PAA block, and thus the micelle cores would not be swollen with solvent in contrast to the situation with methanol. Therefore, significant rearrangement of the micelles in the toluene solutions would not occur.

The dynamics of the system for the second region, ranging from 60 to 100%, are believed to be considerably reduced compared to those for the lower degrees of neutralization. This can be understood by considering that an increase in the degree of neutralization of the core-forming block reduces its solubility, resulting in micelle formation. As a result of the decreased solubility, the unfavorable solvent is progressively expelled from the core. This process increases the glass transition temperature (T_g) of the core, resulting in a decreased mobility in the core. In fact, when the temperature of measurement is below the T_g, the micelle core can be considered as "frozen." As a result of some or all of these factors, the aggregation numbers for the redissolved freeze-dried samples were found to increase with increasing percent neutralization between 60 and 100%.

In the third region, for degrees of neutralization between 100 and 150%, the aggregation numbers were the same as those at 100%. This result was expected, since a further increase in the neutralization above 100% would not change the ionic nature of the block copolymers appreciably.

The radius of gyration (R_g) and second virial coefficient (A_2) values determined by SLS for PS(600)-*b*-PAA(34) and PS(600)-*b*-PAA(45) are given in Table 1. For both block copolymers, it was found that the R_g values were essentially constant for the neutralization range of 0–60%, and increased slightly for the samples at 100 and 150% neutralization. For instance, for PS(600)-*b*-PAA(34), the average R_g value for the samples at 0–60% neutralization was 26 ± 1 nm, and that for PS(600)-*b*-PAA(45) for the samples at 5–60% was 24 nm. For 100 and 150% neutralization, the R_g values for both samples were only slightly higher than those at lower degrees of neutralization, with a value of ca. 30 nm. The A_2 values did not exhibit any specific trends with the percent neutralization.

3.3. SAXS results on freeze-dried samples

The core sizes for the neutralized PS(600)-*b*-PAA(45) samples were measured by SAXS. In general, for an assembly of scattering particles, the scattered intensity (I(q)) is the product of the particle shape factor (P(q)) and the structure factor (S(q)), which characterize the spatial correlation of the scatterers (36, 37). Since it is a product of two functions, it is often difficult to separate one from the other experimentally. In the present system, since the sizes of the spheres are so much smaller than the characteristic distances between them, and since the contrast between the two media is substantial, the attribution is unambiguous.

The SAXS profiles showed a pronounced shape factor peak for samples at and above 5% neutralization. However, for the acid diblock, PS(600)-*b*-PAA(45), no shape factor features were observed due to the low contrast between the PAA and PS blocks. From the position of the minima of the shape factor, one can calculate the radius of the cores (R_{core}). A detailed description of the data analysis has been published elsewhere (31).

The core radii were found to increase with increasing percent neutralization from 5% to 60%; they remained constant from 60% to 100% neutralization and increased at 150% neutralization. The R_{core} values are summarized in Table 1. The trends in R_{core} with increasing degree of neutralization were similar to those of the I_{90}/c values for PS(600)-*b*-PAA(45) in dioxane. The results are compared in Fig. 1*b*. From the R_{core} values, it can be suggested that micelles begin to form between 0 and 5% neutralization, and that the cores continue to grow in size until 60% of the acid is neutralized. The initial growth in R_{core} accompanies the replacement of the protons in the acid diblock by the Cs^+ ions, which are larger in size than the protons. The fact that R_{core} remained constant between 60 and 100% neutralization suggests that a preferred core size for the micelle has been attained. At 150% neutralization, the

Can. J. Chem. Downloaded from www.nrcresearchpress.com by 46.23.64.124 on 09/08/12
For personal use only.

extra neutralizing agent enters the core in which the medium is already highly polar, thus increasing the core size. The solubilization of the excess cesium hydroxide in the micelle cores was also found to occur in PS(600)-*b*-PAA(45) neutralized in dioxane (Fig. 1*b*). The solubilization of excess neutralizing agent in or near the ionic cores has also been suggested for many random (38) and telechelics ionomers (39).

4. Summary

It was found that when single chains of PS-*b*-PAA were neutralized, they started to form micelles near 5% neutralization. The onset of micellization was almost identical for samples having a PS length of 600 units and PAA lengths of 45, 34, and 13 units. It was found that I_{90}/c increased for the block copolymers significantly in the range of 10–60% neutralization. For neutralization levels between 60 and 100%, the normalized scattered intensity did not change significantly with a further increase in the degree of neutralization. For higher degrees of neutralization the solvent media were found to affect the I_{90}/c values, with an increase for dioxane, but a decrease for benzene–methanol solvents.

The block copolymers PS(600)-*b*-PAA(34) and PS(600)-*b*-PAA(45) neutralized with different degrees in benzene–methanol (90/10 (v/v)), freeze-dried, and redissolved in toluene were studied by SLS and SAXS. The results fell into three regions, depending on the percent neutralization. In the first region, for degrees of neutralization between 5 and 60%, the micelle cores were expected to be swollen with solvent during the neutralization in benzene–methanol, and the association that occurs would likely be dynamic. It was found that the f values were constant, and the aggregation numbers did not depend on the percent of neutralization. The R_{core} values in this range increased due to the replacement of the protons with the Cs^+ ions, which are larger in size. In the second region, for degrees of neutralization between 60 to 100%, dynamics are expected to be much slower. In that range, the f values were found to increase with increasing percent neutralization and the R_{core} was found to be constant. The two results would suggest that the density of the micelle core increases in this range. Finally, at degrees of neutralization between 100 and 150%, the f values were constant, showing no further dependence of the aggregation on the percent of neutralization. On the other hand, R_{core} increased due to the solubilization of the excess neutralizing agent into the ionic cores.

Acknowledgments

The authors would like to thank Dr. Sunil K. Varshney who synthesized the block copolymers in connection with another project as well as Dr. Joon-Seop Kim and Mr. Matthew Moffitt for very useful discussions. This work was supported by the Natural Sciences and Engineering Research Council of Canada (NSERC) and le Fonds pour la Formation de Chercheurs et l'Aide à la Recherche (FCAR). K.K. and D.N. are grateful for scholarship funding provided from NSERC and FCAR.

References

1. J. Selb and Y. Gallot. *In* Polymeric amines and ammonium salts. *Edited by* E.J. Goethals. Pergamon Press, New York. 1980. pp. 205–218.
2. C. Price. *In* Development in block copolymers. Vol. 1. *Edited by* I. Goodman. Elsevier Applied Science, London. 1982. pp. 39–80.
3. G. Riess, G. Hurtrez, and P. Bahadur. Encyclopedia of polymer science and engineering. Vol 2. *Edited by* J. Kroschwitz, H.F. Mark, N.M. Bikales, C.G. Overberger, and G. Menges. Wiley, New York. 1985. pp. 324–434.
4. J. Selb and Y. Gallot. *In* Development in block copolymers. Vol. 2. *Edited by* I. Goodman. Elsevier Applied Science, London. 1985. pp. 27–96.
5. Z. Tuzar and P. Kratochvíl. *In* Surface and colloid science. Vol. 1. *Edited by* E. Matijevic. Plenum Press, New York. 1993. pp. 1–83.
6. G. Kwon, M. Naito, M. Yokoyama, T. Okano, Y. Sakurai, and K. Kataoka. Langmuir, **9**, 945 (1993).
7. C.V. Nicholas, Y.-Z. Luo, N.-J. Deng, D. Attwood, J.H. Collett, C. Price, and C. Booth. Polymer, **34**, 138 (1993).
8. F. Caldérara, Z. Hruska, G. Hurtrez, J.-P. Lerch, T. Nugay, and G. Riess. Macromolecules, **27**, 1210 (1994).
9. Z. Zhou and B. Chu. Macromolecules, **27**, 2025 (1994).
10. Z. Yang, S. Pickard, N.-J. Deng, R.J. Barlow, D. Attwood, and C. Booth. Macromolecules, **27**, 2371 (1994).
11. A.V. Kabanov, I.R. Nazarova, I. Astafieva, E.V. Batrakova, V.Y. Alakhov, A.A. Yaroslavov, and V.A. Kabanov. Macromolecules, **28**, 2303 (1995).
12. T. Nivaggioli, P. Alexandridis, T.A. Hatton, A. Yekta, and M.A. Winnik. Langmuir, **11**, 730 (1995).
13. D. Kiserow, J. Chan, C. Ramireddy, P. Munk, and S.E. Webber. Macromolecules, **25**, 5338 (1992).
14. M. Antonietti, S. Heinz, M. Schmidt, and C. Rosenauer. Macromolecules, **27**, 3276 (1994).
15. D.F. Siqueira, S.P. Nunes, and B.A. Wolf. Macromolecules, **27**, 4561 (1994).
16. H.I. Unal, C. Price, P.M. Budd, and R.H. Mobbs. Eur. Polym. J. **30**, 1037 (1994).
17. M. Villacampa, J.R. Quintana, R. Salazar, and I. Katime. Macromolecules, **28**, 1025 (1995).
18. Y. Morishima, Y. Itoh, T. Hashimoto, and S.-I. Nozakura. J. Polym. Sci. Polym. Chem. Ed. **20**, 2007 (1982).
19. (*a*) T. Cao, P. Munk, C. Ramireddy, Z. Tuzar, and S.E. Webber. Macromolecules, **24**, 6300 (1991); (*b*) D. Kiserov, K. Prochazka, C. Ramireddy, Z. Tuzar, P. Munk, and S.E. Webber. Macromolecules, **25**, 461 (1992).
20. I. Astafieva, X.F. Zhong, and A. Eisenberg. Macromolecules, **26**, 7339 (1993).
21. C.L. Phoon, J.S. Higgins, W. Burchard, and D.G. Peiffer. Macromol. Rep. **A29**, 179 (1992)
22. Z. Zhou, B. Chu, G. Wu, and D.G. Peiffer. Macromolecules, **26**, 2968 (1993).
23. Z. Zhou, D.G. Peiffer, and B. Chu. Macromolecules, **27**, 1428 (1994).
24. A. Desjardins and A. Eisenberg. Macromolecules, **24**, 5779 (1991).
25. A. Desjardins, T.G.M. van de Ven, and A. Eisenberg. Macromolecules, **25**, 2412 (1992).
26. X.F. Zhong, S.K. Varshney, and A. Eisenberg. Macromolecules, **25**, 7160 (1992).
27. K. Khougaz, Z. Gao, and A. Eisenberg. Macromolecules, **27**, 6341 (1994).
28. Z. Gao and A. Eisenberg. Macromolecules, **26**, 7353 (1993).
29. Z. Gao, X.F. Zhong, and A. Eisenberg. Macromolecules, **27**, 794 (1994).
30. D. Nguyen, S.K. Varshney, C.E. Williams, and A. Eisenberg. Macromolecules, **27**, 5086 (1994).
31. D. Nguyen, C.E. Williams, and A. Eisenberg. Macromolecules, **27**, 5090 (1994).

Can. J. Chem. Downloaded from www.nrcresearchpress.com by 46.23.64.124 on 09/08/12
For personal use only.

32. D. Nguyen, X.F. Zhong, C.E. Williams, and A. Eisenberg. Macromolecules, **27**, 5173 (1994).
33. J. Brandup and E.H. Immergut (*Editors*). Polymer handbook. 3rd ed. John Wiley and Sons, New York. 1989.
34. H. Benoit and D. Froelich. *In* Light scattering from polymer solutions. *Edited by* M.B. Huglin. Academic Press, New York. 1972. Chap. 11.
35. J.M. Dubuisson, J.M. Dauvergne, C. Depautex, P. Vachette, and C.E. Williams. Nucl. Instrum. Methods. Phys. Res. Sect. A: **246**, 636 (1986).
36. C.E. Williams. *In* Neutron, X-ray and light scattering: introduction to an investigative tool for colloidal and polymeric systems. *Edited by* P. Lindner and Th. Zemb. North-Holland, Amsterdam. 1991. p.101.
37. C.E. Williams. *In* Neutron and synchrotron radiation for condensed matter studies I. *Edited by* J. Baruchel, J.-L. Hodeau, M.S. Lehmann, J.-R. Regnard, and C. Schlenker. Springer-Verlag, Berlin. 1993. Chap. 10.
38. J.-S. Kim and A. Eisenberg. J. Polym. Sci. Part B: Polym. Phys. **33**, 197 (1995), and references therein.
39. S. Bagrodia, M.R. Tant, G.L. Wilkes, and J.P. Kennedy. Polymer, **28**, 2207 (1987).

Can. J. Chem. Downloaded from www.nrcresearchpress.com by 46.23.64.124 on 09/08/12
For personal use only.

Cocrystallization in random copolymers of poly(β-hydroxybutyrate-*co*-β-hydroxyvalerate) and its effect on crystalline morphology

William J. Orts, David L. VanderHart, Terry L. Bluhm, and Robert H. Marchessault

Can. J. Chem. Downloaded from www.nrcresearchpress.com by 46.23.64.124 on 09/08/12
For personal use only.

Abstract: Small-angle X-ray scattering (SAXS) and solid state CPMAS ^{13}C NMR were used to describe the crystalline morphology of a series of bacterially produced poly(β-hydroxybutyrate-*co*-β-hydroxyvalerate) copolymers containing random distributions of 3-hydroxybutyrate (3HB) and 3-hydroxyvalerate (3HV). Modeling of SAXS results showed that the morphology of this isodimorphic system is better described by two phases, crystalline and amorphous, having defects within each domain. This is in contrast to a model with a large interfacial region between phases. For the 3HV composition range 0–27 mol%, the polymer crystallizes in a poly(β-hydroxybutyrate)-type crystalline lattice. Solid state NMR results showed that there is significant incorporation of the 3HV minor component into the poly(β-hydroxybutyrate) crystalline phase over this composition range . The ratio of the 3HV content in the crystalline phase relative to the overall 3HV content is not linear, but increases with increasing 3HV. For the 21 and 27% 3HV samples, the 3HV content in the crystalline phase is as much as 2/3 of the overall 3HV content. Inclusion of 3HV is correlated to an increase in crystalline disorder (as measured by SAXS), implying that it is easier to accommodate the bulkier 3HV comonomer into a crystalline region that already contains defects.

Key words: bacterial polyesters, poly(3-hydroxyalkanates), small-angle X-ray scattering, solid state NMR, cocrystallization.

Résumé : On a utilisé la diffraction des rayons X à de petits angles (SAXS) et la RMN du ^{13}C CPMAS à l'état solide pour décrire la morphologie cristalline d'une série de copolymères poly(β-hydroxybutyrate-*co*-β-hydroxyvalérate) produits par une voie bactérienne et contenant des distributions au hasard de 3-hydroxybutyrate (3HB) et de 3-hydroxyvalérate (3HV). Un modelage des résultats SAXS a montré que la meilleure façon de décrire la morphologie de ce système isodimorphique est à l'aide de deux phases, l'une cristalline et l'autre amorphe, ayant des défauts dans chaque domaine. Pour une composition de 3HV allant de 0 à 27 mol%, le polymère cristallise dans une réseau cristallin du type poly(β-hydroxybutyrate). Les résultats de la RMN à l'état solide ont montré que, sur cette plage de composition, il se produit une incorporation importante du composant mineur du 3HV dans la phase cristalline du poly(β-hydroxybutyrate). Le rapport de la quantité de 3HV contenue dans la phase cristalline par rapport à la quantité totale de 3HV n'est pas linéaire; il augmente avec une augmentation du 3HV. Pour les échantillons contenant 21 et 27% de 3HV, la quantité de 3HV contenue dans la phase cristalline représente pratiquement les 2/3 de la quantité totale de 3HV. Il existe une corrélation entre l'inclusion du 3HV et l'augmentation du désordre cristallin (tel que mesuré par SAXS); ceci implique qu'il est plus facile d'accommoder le gros comonomère 3HV dans une région cristalline qui contient déjà des défauts.

Mots clés : polyesters bacteriens, poly(3-hydroxyalcanoates), diffusion rayons-X aux petits angles, RMN de l'état solide, cocristallisation.

[Traduit par la rédaction]

Received May 3, 1995.

This paper is dedicated to Professor J.E. (Jim) Guillet in recognition of his contributions to Canadian chemistry.

W.J. Orts.[1,2] Reactor Radiation Division, National Institute of Standards and Technology, Gaithersburg, MD 20899, U.S.A.
D.L. VanderHart. Polymers Division, National Institute of Standards and Technology, Gaithersburg, MD 20899, U.S.A.
T.L. Bluhm. Xerox Corporation, 800 Philips Road, Webster, NY 14580, U.S.A.
R.H. Marchessault. Department of Chemistry, McGill University, 3420 University St., Montreal, QC H3A 2A7, Canada.

[1] Author to whom correspondence may be addressed. Telephone: (301) 975–4507. Fax: (301) 921-9847. E-mail: orts@rrdstrad.nist.gov
[2] Part of this paper is taken from the Ph.D. thesis of W.J. Orts, Chemistry Department, University of Toronto, 1991.

Can. J. Chem. Downloaded from www.nrcresearchpress.com by 46.23.64.124 on 09/08/12
For personal use only.

Introduction

Poly(β-hydroxybutyrate), PHB, and its random copolymers with 3-hydroxyvalerate, P(3HB-*co*-3HV) are bacterially produced biodegradable thermoplastics (1–3). They have found a market niche as biodegradable packaging materials and surgical implants due, in part, to properties imparted by their unique crystallization behaviour (4, 5). PHB is a highly stereoregular polymer that crystallizes rapidly into large crystallites (6). Consequently, the homopolymer tends to have problems with embrittlement and aging. Random copolymers of P(3HB-*co*-3HV) exhibit significant improvements in mechanical and thermal properties (2) due to their "less perfect" crystalline morphology . Even though P(3HB-*co*-3HV) random copolymers have the same high crystallinity as the PHB homopolymers, they exhibit greater ductility and lower melting temperatures than PHB.

In general, the crystalline morphology of random copolymers lies between two extremes represented by (*i*) complete exclusion of the noncrystallizable "other" comonomer from the crystalline phase (7) and (*ii*) uniform inclusion of both comonomers (8). P(3HB-*co*-3HV) are remarkable in that they are isodimorphic; i.e., both the 3HV and 3HB comonomers are included in the crystalline phases (5). Thus, the crystalline morphology is clearly not described by the exclusion model, a conclusion that was drawn from observations that both the PHB and PHV homopolymers crystallize in similar 2_1 helix structures, that the degree of crystallinity for the P(3HB-*co*-3HV) copolymers remains high (>60%) over the full copolymer composition range, and that the X-ray and electron diffraction patterns of the 3HB- or 3HV-rich copolymers vary little with copolymer composition.

There is increasing evidence, however, that the cocrystallization of both comonomers is not uniform, and that there is selective partitioning of comonomers between crystalline and amorphous phases (4, 9–11). Partitioning must alter the dynamics of crystallization, with ramifications such as altering the number of defects in the crystalline phase, and changing the crystalline domain sizes. Changes in the crystalline morphology are likely to change end-use properties such as film ductility and susceptibility to biodegradation.

In this report we relate the degree of cocrystallization to the crystalline morphology of random copolymers of P(3HB-*co*-3HV) for compositions of 0–27% 3HV. Over this composition range, P(3HB-*co*-3HV) crystallizes in a PHB-type crystal lattice. This means we will be looking at the inclusion of the bulkier 3HV group into the PHB-type crystal lattice. Partitioning of comonomers will be quantified using solid state ^{13}C NMR, while the crystalline morphology will be described using results from X-ray scattering.

Experimental

Samples of P(3HB-*co*-3HV) were produced by pilot-scale batch fermentations of *Alcaligenes eutrophus* and kindly provided by Imperial Chemical Industries (ICI), U.K.[3] Molecular weights of these isotactic random copolymers ranged from 200 to 400k. The as-received samples had been originally precipitated from chloroform solution using methanol, which effectively "erased" the thermal history. For studies on the effect of crystallization temperature, samples were melt-pressed at 10°C above their melting temperature using a Carver press at 17.2 MPa for 4 min in a nitrogen environment. Immediately following pressing, samples were quenched in liquid nitrogen and immediately placed in a vacuum oven at a specific crystallization temperature, T_c. Samples were maintained at T_c until they reached an equilibrium degree of crystallinity as measured by wide angle X-ray diffraction. Equilibrium crystallinity was 60–65% for all samples studied, although achieving this took as long as 500 h for the 17 and 21% 3HV samples. Differential scanning calorimetry data were recorded using a Perkin–Elmer DSC-2C.

X-ray measurements were made on a Phillips powder diffractometer model PW 1710 equipped with a pulse height analyzer using nickel-filtered Cu K_α radiation ($\lambda = 1.54$ Å) passed through a graphite monochromator. The degree of crystallinity was calculated from wide-angle diffracted intensity (2θ = 10°–40°) using Ruland's method (12). The amorphous scattering component was estimated by measuring the scattering curve from a 21% 3HV sample immediately after quenching in liquid nitrogen. Small-angle X-ray scattering (SAXS) data were collected using a Kratky camera mounted on the same X-ray source, and using a proportional counter 20 cm from the source. Slit-smearing and Lorentz factor corrections (12) were made by multiplying the observed intensity, I, by the scattering vector, $s = 2 \sin \theta/\lambda$.

The NMR spectrometer used for ^{13}C spectroscopy is noncommercial and operates at 2.35 T (25.193 MHz for ^{13}C nuclei). Cross polarization (CP) techniques along with high power decoupling and magic angle spinning (MAS) were combined (13) to produce CPMAS spectra. The nutation frequencies corresponding to the rf field strengths were 66 and 69 kHz for carbons and protons, respectively.

The ^{13}C NMR technique isolates the spectra corresponding to the crystalline and amorphous phases of each sample, as described previously (9, 14). It is based on a simple model that the solid is made up of two phases, crystalline and amorphous, a model that will be tested by the SAXS measurements. In brief, the ^{13}C NMR method consists of taking spectra at different proton spin locking (SL) times prior to cross polarization. During SL, relaxation of polarization takes place more rapidly in the amorphous phase than in the crystalline region due to the greater mobility of carbons in the amorphous phase. Consequently, as the spin lock time increases, the fraction of the total spectral intensity arising from the crystalline regions will increase. By varying the spin lock time, one can recognize the spectral features of the crystalline and amorphous phases, respectively, and isolate the spectra corresponding to each of the two phases. These spectra are isolated by taking linear combinations of experimental spectra acquired with two different SL times. The criteria for isolation of the linear combination spectrum of the crystalline region is that no region of negative intensity is allowed. This approach is successful when net proton polarization gradients are insignificant on distance scales of the monomers and when the time scale of spin diffusion averaging over the domain size of each phase exceeds the time scale of the shorter $T_{1\rho}{}^H$, the rotating frame relaxation time. These conditions have been met for the

[3] Certain commercial material and equipment are identified in this paper in order to specify adequately the experimental procedure. This in no way implies endorsement or recommendation by the National Institute of Standards and Technology.

Fig. 1. Schematic representations and corresponding density profiles of two models of the lamellar morphology of semicrystalline random copolymers. In (*a*), the sharp boundary model, interfaces between domains are sharp with defects or density fluctuations within both domains (defects are represented by circles). In the three-phase diffuse boundary model (*b*) there is a significant interfacial region with an increasing number of defects away from the crystalline core.

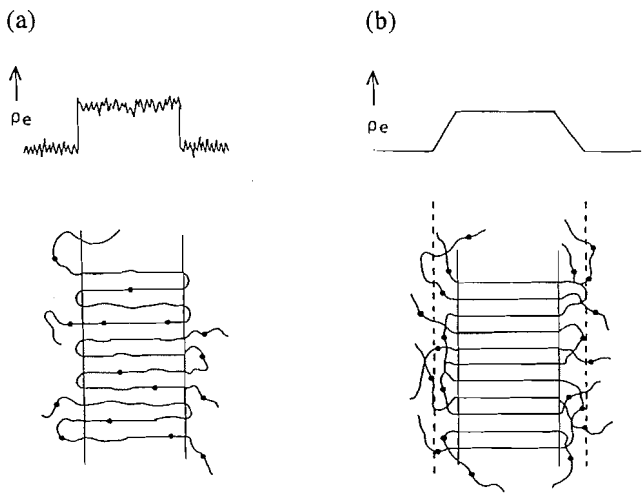

P(3HB-*co*-3HV) samples used in this study (14) since the crystalline and amorphous domains are large relative to the monomer size. Moreover, since the shorter $T_{1\rho}{}^{H}$ is approximately 6 ms for these samples, spin diffusion rates imply that overall repeat distances should exceed 6 nm for the experiment to work. In our samples, overall repeat distances were in the range 8–20 nm.

Results and discussion

Small-angle X-ray scattering

It is generally accepted that homopolymers crystallize from the melt into some form of chain-folded lamellar morphology. For random copolymers, this morphology varies not only with the crystallization and annealing conditions, but also with the copolymer composition and the degree of partitioning. Thus, before quantifying the extent of partitioning and discussing its effect on the semicrystalline morphology of melt-crystallized P(3HB-*co*-3HV) random copolymers, we will first use SAXS to determine if a two-phase lamellar model is appropriate to describe this system.

The X-ray scattering intensity from a semicrystalline polymer depends on the electron density differences between domains. Figure 1 is a schematic representation of two models that can be used to describe inclusion of defects into a lamellar crystal along with their respective electron density profiles. In the sharp boundary model (Fig. 1*a*), defects are uniformly spread over two distinct domains, with the corresponding electron density profiles changing sharply at the phase boundary. In the diffuse boundary model, three domains are present: a crystalline and amorphous phase, and a third interfacial region consisting of an increasing number of defects nearer the amorphous domain boundary. The corresponding electron density model is assumed uniform in the crystalline and amorphous phases with a linear density variation in the interfacial region.

The two models outlined in Fig. 1 can be distinguished using SAXS by considering deviations to Porod's law. According to Porod behaviour (15, 16), the *slit-smeared* intensity, I, from an ideal two-phase system with sharp boundaries varies at intermediate angles with the scattering vector s ($s = 2 \sin \theta/\lambda$ such that $I \propto I/s^3$. Ruland (15) and Vonk (16) have shown that deviations from ideal Porod-type behaviour for lamellar structures alter this behaviour such that

$$[1] \quad Is^3 = K_s + \Phi s^3$$

for the sharp boundary model and

$$[2] \quad Is^3 = K_s + \Phi s^2$$

for the (three-phase) diffuse interface model, where K_s is proportional to the electron density difference between phases and Φ is an indication of the interface thickness in eq. [2] and of the density fluctuations within phases in eq. [1]. Accordingly, the diffuse boundary model can be distinguished from the sharp boundary model by plotting Is^3 versus either s^2 or s^3, which should be linear for the appropriate model.

In Fig. 2 the slit-smeared intensity obtained for the 21% 3HV copolymer sample quench-crystallized at 60°C is multiplied by s^3 and plotted against s^3 (Fig. 2*a*) and s^2 (Fig. 2*b*). In Fig. 2*b*, the diffuse boundary model is shown to be clearly inappropriate, not only due to the relative nonlinearity of the data in the Porod region, but also due to the physically unrealistic negative y-axis intercept derived from the best fit through the data. In contrast, when the data are plotted according to the sharp boundary model (Fig. 2*a*; eq. [1]), there is a clear linearity of the data and physically reasonable intercepts.

There is a systematic trend in the shape of the intensity curves with respect to the copolymer composition. In Fig. 3 the slit-smeared intensity data obtained from a series of copolymer samples differing in 3HV composition are plotted according to eq. [1] (samples were crystallized at 60°C from a quenched state). With increasing copolymer composition there is a corresponding increase in the slope, Φ, and a decrease in the intercept, K_s. Noting that K_s is proportional to the density differences between phases and that Φ reflects the fluctuations within a phase (15, 16), the trend in Fig. 3 can be interpreted as an increase in disorder within one or both phases of the sample and a decrease in density difference between phases as the 3HV content increases. Mitomo et al. (17) reported that the total (macroscopic) density of P(3HB-*co*-3HV) copolymers decreases with increasing 3HV content. Their reported explanation, that density decreases due to a decrease in the degree of crystallinity, is at odds with the wide-angle X-ray diffraction evidence showing crystallinity consistently >60% over the 0–21% 3HV composition range. An alternative explanation for the trend in Fig. 3 consistent with high crystallinity is that, with increasing overall 3HV composition, comonomers of 3HV are included increasingly more in the PHB-type crystal. Increased cocrystallization of the energetically less favourable comonomer in the lattice causes defects in the crystalline phase and lowers the apparent overall density. In this picture the increase in Φ is primarily due to a greater number of defects (or density fluctuations) in the crystalline phase rather than in the noncrystalline phase. To investigate this further we sought to quantify the degree of

Can. J. Chem. Downloaded from www.nrcresearchpress.com by 46.23.64.124 on 09/08/12
For personal use only.

Can. J. Chem. Downloaded from www.nrcresearchpress.com by 46.23.64.124 on 09/08/12
For personal use only.

Fig. 2. The observed slit-smeared SAXS data obtained from the 21% 3HV sample of P(3HB-*co*-3HV) random copolymers plotted according to (*a*) the sharp boundary model and (*b*) the diffuse boundary model. The failure of the diffuse boundary model to describe the data is indicated by nonlinearity in the high angle "Porod region" of the data (which is data at angles higher than the one marked with an arrow) and by the physically unrealistic negative *y*-intercept. The sharp boundary model corresponds to a better description of the SAXS data.

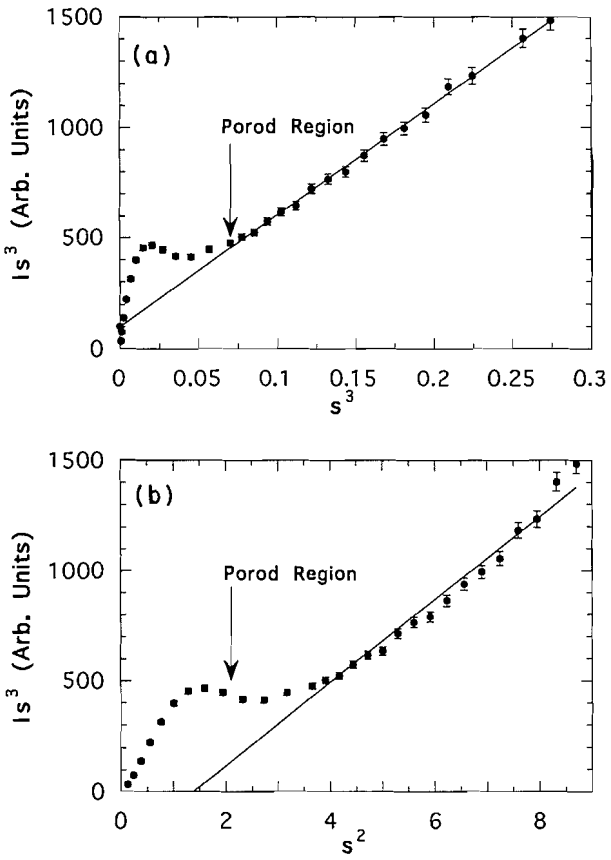

cocrystallization (i.e., the mole fraction of 3HV groups in the PHB-type crystalline phase) and thus correlate the degree of cocrystallization with the relative crystalline disorder.

NMR analysis

The NMR method is exemplified by the spectra from the 21% 3HV as-received sample shown in Fig. 4. Spectrum 4A is the experimental CPMAS spectrum taken with 1 μs SL and 0.7 ms CP time. Since this spectrum is similar to previously published CPMAS data (5, 10, 11), the assignment of carbon resonances from Bluhm et al. (5) were used and are included in the figure. Spectrum 4B is an experimental spectrum taken at the longer SL time of 15 ms, but using the same CP time. To generate the spectra 4C and 4D, representing the crystalline and noncrystalline phases, respectively, we generated linear combinations of spectra 4A and 4B. The details of generating the crystalline and amorphous spectra have been outlined in a previous paper (9, 14). Separation of spectra is based on differences in molecular mobility between the crystalline and amorphous phases in these samples, which means relaxation takes place more rapidly in the amorphous domain than in the crystalline phase.

Fig. 3. The measured slit-smeared SAXS data from samples of P(3HB-*co*-3HV) of compositions 0, 4, 8, 17, and 21% 3HV plotted according to the sharp boundary model. The clear increase of the slope as a function of 3HV composition is indicative of a greater number of fluctuations or defects within the crystalline and amorphous phases. We attribute increased fluctuations to an increase in the number of defects in the crystalline phase as a result of cocrystallization.

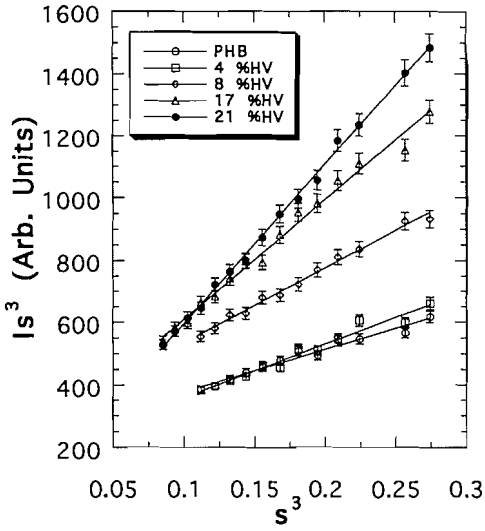

Another assertion that allows a separation of crystalline and amorphous spectra is that, due to spin diffusion, the proton polarization level for a minority species, like 3HV, in the crystalline phase will be very similar to that of its neighbouring 3HB crystalline comonomer. Spectra 4C and 4D are produced by assuming (*i*) that the sharper features at a given resonance correspond to the crystalline phase and (*ii*) that the polarization of an amorphous entity will relax more rapidly during SL than a corresponding crystalline group. For P(3HB-*co*-3HV) there is no ambiguity in separating the crystalline and amorphous spectral features since the linewidths of the carbons in the crystalline phase are quite narrow and there are clear changes in relative peak heights between crystalline and amorphous features at different SL times. Scaling in Fig. 4 is chosen so that A or B is the sum of C and D. As a final check, the apparent crystallinity of this sample is 0.60 according to the NMR analysis, which is very consistent with the measured X-ray crystallinities.

The degree of cocrystallization was readily calculated from spectrum 4C by integrating the two OCH peaks, V3 and B3, after lineshape deconvolution. Cocrystallization was quite considerable; for the sample with an overall 3HV mole fraction of 0.21 the 3HV mole fraction in the crystalline phase proved to be 0.119 ± 0.011. Using the method illustrated in Fig. 4, we generated crystalline spectra for five other P(3HB-*co*-3HV) samples: 0, 4, 8, 17, and 27% 3HV. The results derived from these spectra are plotted in Fig. 5, a plot of the measured composition of 3HV in the crystalline region as a function of the total 3HV composition.

Several conclusions can be drawn from the results in Fig. 5. First, a significant number of 3HV residues are included in the crystalline phase for each of the samples. The partitioning of the 3HV comonomers, however, is not linear. Any linear fit to

Can. J. Chem. Downloaded from www.nrcresearchpress.com by 46.23.64.124 on 09/08/12
For personal use only.

Fig. 4. The 25MHz CPMAS solid state ^{13}C NMR spectra associated with the 21% 3HV sample. Spectra A and B are experimental data with 1 μs SL and 15 ms SL times, respectively, but a common cross polarization process after spin locking. Spectra C and D correspond to the crystalline and noncrystalline phases, respectively. These latter spectra are different linear combinations of spectra A and B. The sum of C and D is exactly spectrum A. The resonance assignments of the 3HB and 3HV comonomers are represented in the spectra as indicated by the B and V labels, respectively.

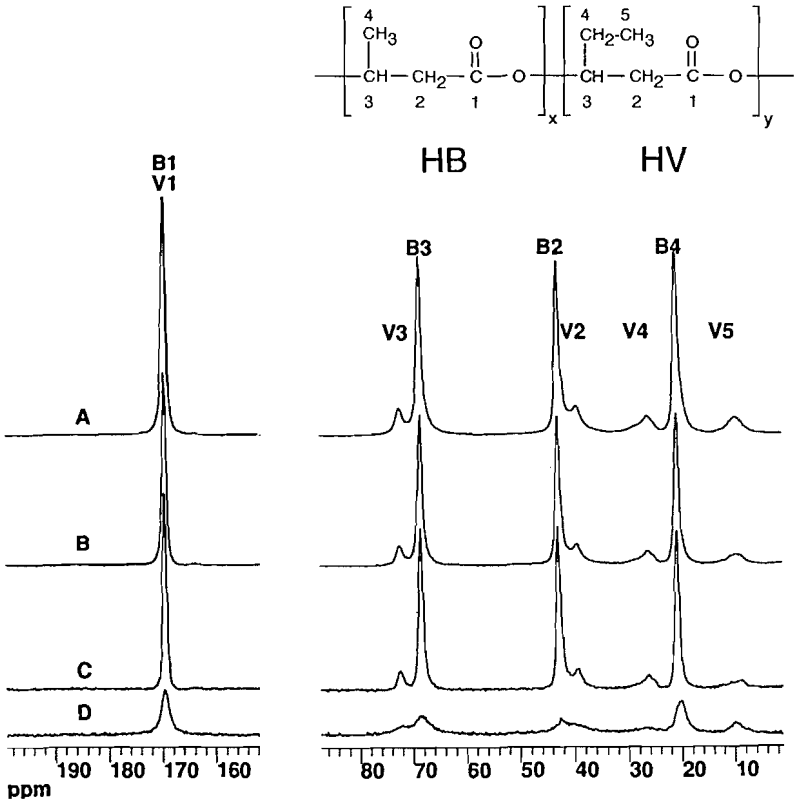

Fig. 5. A plot of the mol% 3HV in the crystalline phase (circles; using the first *y*-axis) as a function of the overall 3HV content. The best-fit curve is quadratic in the overall 3HV content, and is strictly an empirical fit. The disorder parameter derived from SAXS (open diamonds; second *y*-axis) has been normalized to map onto the same *y*-axis and shows the correlation between the inclusion of 3HV comonomers and the relative disorder in the sample.

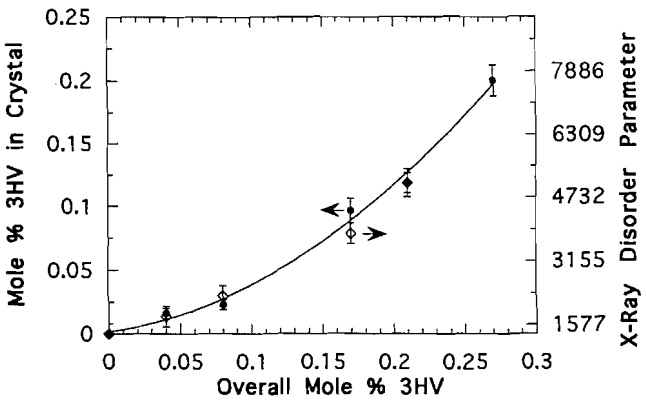

these data would fall outside of experimental error. Instead of linear partitioning, there is a greater tendency to exclude 3HV at low overall 3HV content. For example, for the 4% 3HV sample, the ratio of included 3HV to total 3HV content is less than 0.4. In contrast, for the 21 and 27% samples, the ratio of included to overall 3HV content is ~2/3. The curve in Fig. 5 is an empirical best-fit quadratic in the overall mol% 3HV, which is constrained to pass through the origin and is included to "guide the eye." (This is not necessarily the true functional form of this relationship.) Finally, there is a correlation between the disorder parameter measured by X-ray (Φ from eq. [1]) and the degree of cocrystallization. The disorder parameter, after appropriate normalization onto the *y*-axis, has also been plotted in Fig. 5 as a function of 3HV. The functional form of Φ corresponds to the results from NMR. Clearly, as the relative number of defects in the crystalline phase increases there is a greater tendency to include the larger 3HV residues. This is reasonable considering that it should be easier to add the excess volume of the 3HV group into an already imperfect lattice. At low 3HV compositions, cocrystallization would mean inclusion into a relatively defect-free lattice, which appears to be less favourable.

Can. J. Chem. Downloaded from www.nrcresearchpress.com by 46.23.64.124 on 09/08/12
For personal use only.

The NMR results presented here are similar in a general sense to previous solid state NMR studies on P(3HB-*co*-3HV) cocrystallization (10, 11). Both previous studies, which were based on lineshape deconvolution, also reported significant inclusion of 3HV in the PHB-type lattice. In the present NMR study, which we feel is based on fewer assumptions than the two previous studies, we calculate a higher degree of cocrystallization. For example, Kamiya et al. (10) saw no 3HV incorporation until the 3HV content was above 18 mol%.

It could be argued that the differences between the previously reported degrees of partitioning and our present results are due to thermal history. To test this we determined the degree of partitioning for a 27% 3HV sample before and after annealing at 84°C for 18 h. The measured 3HV content in the crystalline phase decreased only marginally from 0.200 to 0.184. In a more extensive test, the crystalline order was measured for a wide range of samples using the SAXS disorder parameter (Φ from eq. [1]) at crystallization temperatures ranging from 30 to 120°C (data not shown). In general, there was little significant change in relative order for a given copolymer sample as a function of T_c. There was, however, some increase in order for the 17% and 21% 3HV samples crystallized within 5°C of their respective melting temperatures. At first glance it is reasonable to assume that the degree of cocrystallization for random copolymers will decrease for crystallization nearer the melting temperature. The argument would be that partitioning is governed by the kinetics of crystallization. The decrease in the rate of crystallization obtained nearer the melting temperature allows more time to exclude the energetically less favoured stems with higher 3HV content from the crystalline phase, resulting in fewer defects.

It is interesting to speculate, however, on why varying the thermal history does not have a more profound effect on the measured degree of cocrystallization (or the disorder parameter). First, the picture of crystallization described in the previous paragraph is simplistic in that it ignores chain connectivity and entropic issues. If we use the argument that annealing "pushes" portions of a crystalline stem rich in defects out of the crystalline phase, it must push that group toward the interface between the crystalline and amorphous phases. This interface, however, is already crowded, considering that this is a region where density considerations cause many chains to fold tightly on themselves (18). Such crowding must prevent any significant buildup of the relatively bulkier 3HV groups in this interfacial area. Another argument that counters the idea that annealing "irons out" defects is the previously reported (19, 20) observation that, at a given crystallization temperature, the crystalline stem length (or lamellar long period) increases with increasing 3HV content. For example, at a constant crystallization temperature of 115°C, the long period measured by SAXS for the 21% 3HV copolymer (with a melting temperature of 118°C) is 22 nm, whereas for PHB (with a melting temperature of 180°C) the long period is 11.4 nm. Presumably, the long period increases with 3HV due to a smaller undercooling, i.e., the T_c is closer to the melting temperature. With increasing crystalline stem length, there is a greater probability that the average composition in the crystalline phase is closer to the overall 3HV composition. Finally, with crystallinities of $\geq$60%, with crystalline stem lengths of more than 10 nm (encompassing more than 40 monomers within each stem), and with sharp boundaries between phases, it is hard to imagine from statistics alone any two-phase crystalline structure without significant cocrystallization.

Summary

This study has shown that the morphology of melt-crystallized P(3HB-*co*-3HV) random copolymers is well described by a two-phase model consisting of two distinct domains (crystalline and amorphous) with density fluctuations or "defects" within each domain. Based on a two-phase model, CPMAS ^{13}C NMR has been used to quantify the degree of cocrystallization of 3HV in the PHB-type crystal structure. For samples with a 3HV composition in the range 0–27%, a significant fraction of 3HV residues are incorporated into the crystalline phase, especially for samples richer in defects. For the 21 and 27% 3HV samples, the 3HV content in the crystalline phase reaches 2/3 of the overall 3HV content. The ratio of the 3HV content in the crystalline phase relative to the overall 3HV content increases with increasing 3HV, and is correlated to an increase in crystalline disorder (as measured by SAXS). This supports arguments that inclusion of the "other" comonomer is accompanied by formation of a defect in the crystal, and that it is easier to accommodate a defect in a crystal structure already containing defects. Finally, based on the length of crystalline stems in the lamellar domain, the high degree of crystallinity (>60%), and on the limitations of chain connectivity during crystallization, one can argue that thermal history has a limited affect on the extent of cocrystallization for P(3HB-*co*-3HV).

Acknowledgements

W.J.O. and R.H.M. welcome this opportunity to recognize James Guillet for his visionary role in the field of degradable plastics. He has been a role model of one who balances scientific creativity with practical results. W.J.O. also thanks the National Science Foundation (USA) for financial support under agreement number DMR-9122444.

References

1. E.A. Dawes. *In* Microbial energetics. Blackie, Glasgow, U.K. 1986.
2. P.A. Holmes, L.F. Wright, and S.H. Collins. Eur. Pat. Appl. **0 052 459** (1982); Eur. Pat. Appl. **0 069 497** (1983).
3. Y. Doi, A. Tamaki, M. Kunioka, and K. Soga. Appl. Microbiol. Biotechnol. **28**, 330 (1988).
4. M. Sanchez Cuesta, J. Martinez-Salazar, P.A. Barker, and P.J. Barham. J. Mater. Sci. **27**, 5335 (1992).
5. T.L. Bluhm, G.K. Hamer, R.H. Marchessault, C.A. Fyfe, and R.P. Veregin Macromolecules, **19**, 2861 (1986).
6. P.J Barham, A. Keller, E.L. Otun, and P.A. Holmes. J. Mater. Sci. **19**, 2781 (1984).
7. P.J. Flory. Trans. Faraday Soc. **51**, 848 (1955).
8. I.C. Sanchez and R.K. Eby. Macromolecules, **8**, 638 (1975); G.D. Gaddy and R.K. Eby. Polym. Commun. **31**, 298 (1990).
9. D.L. VanderHart, W.J. Orts, and R.H. Marchessault. Macromolecules. **28**, 6394 (1995).
10. N. Kamiya, M. Sakurai, Y. Inoue, and R. Chujo. Macromolecules, **24**, 3888 (1991).
11. N. Yoshie, M. Sakurai, Y. Inoue, and R. Chujo. Macromolecules, **25**, 2048 (1992).
12. W. Ruland. Acta. Crystallogr. **14**, 1180 (1961); L.E. Alexander. *In* X-ray diffraction methods in polymer science. Wiley, New York. 1969.

13. J. Schaefer, E.O. Stejksel, and R. Buchdahl. Macromolecules, **8**, 291 (1975).
14. D.L. VanderHart and E. Perez. Macromolecules. **19**, 1902 (1986).
15. W. Ruland. J. Appl. Crystallogr. **4**, 70 (1971).
16. C.G. Vonk. J. Appl. Crystallogr. **11**, 541 (1978).
17. H. Mitomo, P.J. Barham, and A. Keller. Polym. J. Tokyo, **19**, 1241 (1987).
18. E.A. DiMarzio and C.M. Guttman. Polymer, **21**, 733 (1980).
19. W.J. Orts, R.H. Marchessault, and T.L. Bluhm. Macromolecules, **24**, 6435 (1991).
20. W.J. Orts, M. Romansky, and J.E. Guillet. Macromolecules, **25**, 949 (1992).

Can. J. Chem. Downloaded from www.nrcresearchpress.com by 46.23.64.124 on 09/08/12
For personal use only.

Arene-functionalized polyisocyanides: photophysics of well-defined homopolymers and block copolymers for efficient light harvesting

Bo Hong and Marye Anne Fox

Can. J. Chem. Downloaded from www.nrcresearchpress.com by 46.23.64.124 on 09/08/12
For personal use only.

Abstract: Steady-state and time-resolved fluorescence spectroscopy of the homopolymers and di- and triblock copolymers of 2-naphthylethylisocyanide (**7**), 9-anthrylethylisocyanide (**10**), and 2-phenanthrylethylisocyanide (**11**) exhibit emission from the isolated chromophores, i.e., naphthyl, anthryl, or phenanthryl, upon excitation at 284 or 354 nm. The absence of excimer emission in the fluorescence spectra of all these homopolymers is indicative of a rigid polymeric backbone. Fluorescence quenching in diblock copolymers containing a dimethylaniline donor block and a naphthalene or anthracene acceptor block takes place through directional energy migration to the acceptor–quencher interface. The migrating excited state is then quenched at the interface either by photoinduced electron transfer in the anthracene–dimethylaniline diblock copolymer or by exciplex formation in the naphthalene–dimethylaniline diblock copolymer. Upon incorporation of an intervening block derived from pentamethylphenylethylisocyanide **8**, exciplex formation is suppressed in the related triblock copolymer. Transient absorption spectra of this family of di- and triblock copolymers reveal the formation of radical ion pairs, with a lifetime of 1.1 μs in the anthracene–dimethylaniline diblock copolymer.

Key words: electron transfer, energy migration, excimer emission, polyisocyanides, block copolymers.

Résumé : La spectroscopie de fluorescence en état stationnaire et résolue dans le temps, appliquée aux homopolymères et aux copolymères à deux et à trois blocs des isocyanures de 2-naphtyléthyle (**7**), de 9-anthryléthyle (**10**) et de 2-phénanthryléthyle (**11**) présente des émissions provenant des chromophores isolées, c'est-à-dire du naphtyle, de l'anthryle ou du phénanthryle lorsqu'on les excite à 284 ou à 354 nm. L'absence d'une émission de l'excimère dans les spectres de fluorescence de chacun de ces homopolymères indique que le squelette est rigide. La dégénérescence de la fluorescence dans les copolymères à deux blocs, contenant un bloc donneur diméthylaniline et un bloc accepteur naphtalène ou anthracène, se produit par une migration directionnelle de l'énergie à l'interface accepteur–désactiveur. L'état excité qui migre est alors désactivé à l'interface par un transfert d'électron photoinduit dans le copolymère à deux blocs anthracène–diméthylaniline ou par la formation du exciplexe dans le copolymère à deux blocs naphtalène–diméthylaniline. Lors de l'incorporation d'un bloc intermédiaire dérivé de l'isocyanure de pentaméthylphényléthyle, **8**, la formation de l'exciplexe est supprimée dans le copolymère à trois blocs apparenté. Les spectres d'absorption des espèces transitoires de cette famille de copolymères à deux et à trois blocs révèlent qu'il y a formation de paires d'ions radicaux dont le temps de vie est 1,1 μs dans le copolymère à deux blocs anthracène–diméthylaniline.

Mots clés : transfert d'électron, migration d'énergie, émission de l'excimère, polyisocyanures, copolymères à blocs.

[Traduit par la rédaction]

Introduction

The construction of synthetic chromophore- and quencher-labeled polymers for highly efficient light harvesting remains an elusive, but important, goal (1–4). When such polymers incorporate an energetically graded series of photosensitizers or redox relays, unidirectional electron transfer and (or) energy migration over extended distances can be achieved (1, 3). These systems must include: (*i*) synthetic control of the orientation and spacing of the absorbers, relays, and quenchers; (*ii*) a means of identifying the mode and rate of energy and electron transfer within a homopolymeric block (through-space or through-bond); (*iii*) a means of optimizing energy or electron transfer across the interface between blocks; (*iv*) a mechanism for the prevention of energy-wasting back electron transfer and its consequent charge recombination; and (*v*)

Received May 5, 1995.

This paper is dedicated to Professor J.E. (Jim) Guillet in recognition of his contributions to Canadian chemistry.

B. Hong and M.A. Fox.[1] Department of Chemistry and Biochemistry, University of Texas at Austin, Austin, TX 78712, U.S.A.

[1] Author to whom correspondence may be addressed. Telephone: (512) 471-1811. Fax: (512) 471-7791. E-mail: MAFOX@mail.utexas.edu

Synthesis of cyclic and acyclic imides, sulfonimides, and *N*-carbobenzyloxyamides by ketene trapping

David I. MaGee, Mahesh Ramaseshan, and James D. Leach

Abstract: A convenient and general method for the synthesis of cyclic and acyclic imides, sulfonimides, and *N*-benzyloxycarbonyl amides via the inter- and intramolecular trapping of ketenes has been developed. Heating the corresponding amido, sulfonamido, and carbamamido ethyl ethynyl ethers at 150°C for 3 h produced the desired compounds in good to excellent yields.

Key words: ketenes, imides, sulfonimides, *N*-benzyloxycarbonyl amides.

Résumé : On a mis au point une méthode générale et appropriée de synthèse d'imides cycliques et aliphatiques, de sulfonimides et d'amides de *N*-benzoyloxycarbonyles qui fait appel à un piégeage inter- et intramoléculaire de cétènes. Si l'on chauffe les oxydes d'éthynyle et d'amido-, de sulfamido- et carbamidoéthyles à 150°C, pendant 3 h, on obtient les produits désirés avec des rendements qui varient de bons à excellents.

Mots clés : cétènes, imides, sulfonimides, amides de *N*-benzoyloxycarbonyles.

[Traduit par la rédaction]

Introduction

Cyclic imides and their N-derivatives are an important class of compounds found in interesting natural products such as Showdomycin (1), Sesbanimides (2, 3), bengamides and isobengamides (4), as well as in many interesting unnatural products (4). Cyclic imides have also gained attractive use as intermediates for the synthesis of alkaloids (5–7) and other natural products (8, 9).

In recent years the use and synthesis of imides have received considerable attention (10, 11), however, most studies have been limited to succinimide- and phthalimide-derived compounds. Recently we demonstrated the synthetic utility of the intramolecular trapping of *in situ* generated ketenes as a general method for the efficient formation of lactones (12) and lactams (13). Encouraged by these results, we envisaged the possible utility of this method for the construction of cyclic and acyclic imides, sulfonimides, and *N*-alkoxycarbonyl amides, Scheme 1. Ficini (14) and later Arens and co-workers (15, 16) showed that heating ethyl alkynyl ethers at temperatures above 120°C caused them to undergo a retro-ene reaction to generate a ketene and ethylene, with the ketene being trapped with various added amine and alcohol nucleophiles. Surprisingly, the only related examples we could find of a ketene being trapped with nitrogen nucleophiles other than amines were by Dunbar and White (17) and Rice et al. (18); however, in both studies only ketene itself was used, and with a limited number of amide nucleophiles. Endeavors to utilize our methodology for the synthesis of cyclic and acyclic imides as well as sulfonimides and *N*-benzyloxycarbonyl amides are described herein.

Scheme 1

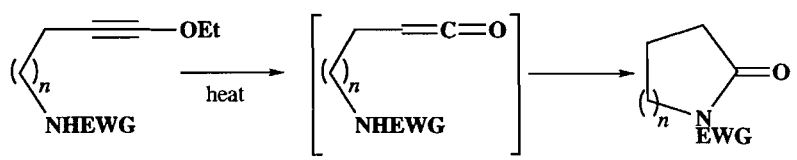

Received April 11, 1995.

D.I. MaGee,[1] M. Ramaseshan, and J.D. Leach. Department of Chemistry, Bag Service No. 45222, University of New Brunswick, Fredericton, NB E3B 6E2, Canada.

[1] Author to whom correspondence may be addressed. Fax (506) 453-4981. E-mail: DMaGee@unb.ca

Can. J. Chem. Downloaded from www.nrcresearchpress.com by 46.23.64.124 on 09/08/12
For personal use only.

Can. J. Chem. Downloaded from www.nrcresearchpress.com by 46.23.64.124 on 09/08/12
For personal use only.

Scheme 2

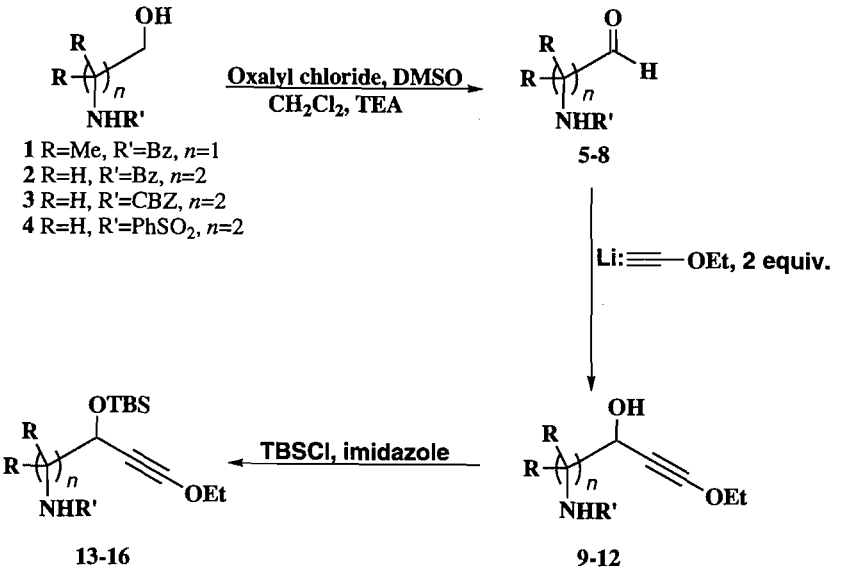

Scheme 3

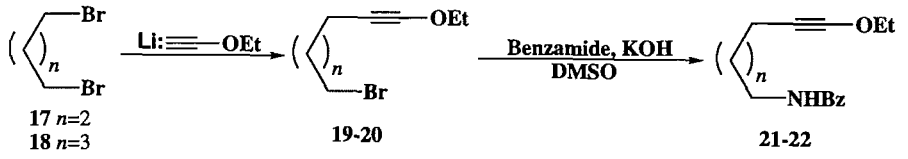

Scheme 4

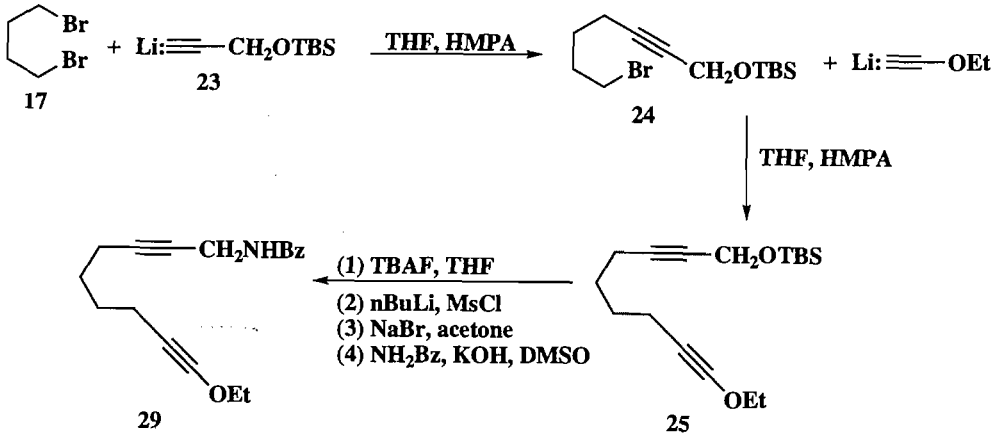

Scheme 5

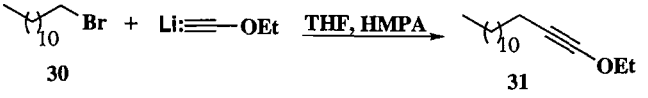

Results and discussion

The cyclization precursors shown in Table 1 were prepared according to standard procedures and, except for entries 8 and 9, are outlined in schemes 2 and 3. Alkynyl ether **29** (13) was constructed according to the following protocol: (*i*) treatment of 1-*tert*-butyldimethylsiloxy-2-propynyl lithium (19) with 2 equivalents of 1,4-dibromobutane (THF, HMPA, room temperature (RT), 86%); (*ii*) substitution of the bromide with 1.2 equivalents of 1-ethoxy ethynyl lithium (THF, HMPA, 0°C–

Can. J. Chem. Downloaded from www.nrcresearchpress.com by 46.23.64.124 on 09/08/12
For personal use only.

Table 1. Ketene cyclizations with electron-deficient nitrogen nucleophiles

Entry	Substrate	Product[a]	%Yield[b]
1	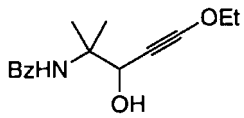 **9**	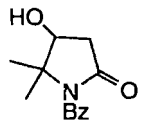 **32**	86
2	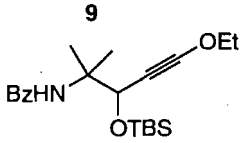 **13**	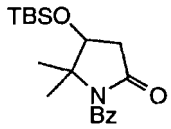 **33**	75
3	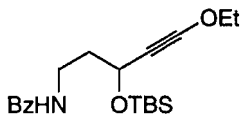 **14**	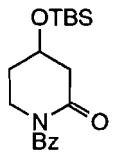 **34**	79
4	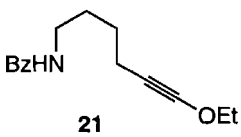 **21**	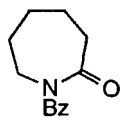 **35**	68
5	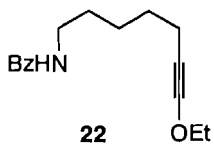 **22**	**36**	58
6	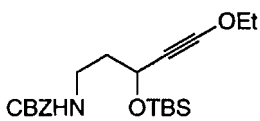 **15**	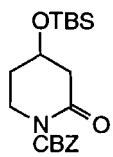 **37**	81
7	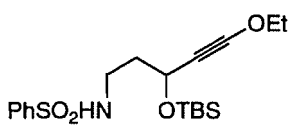 **16**	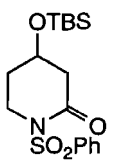 **38**	76
8	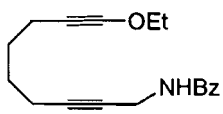 **29**	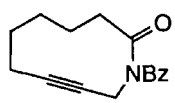 **39**	0
9	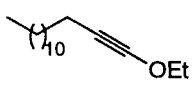 **31**	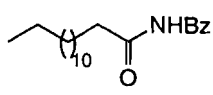 **40**	95

[a]All compounds gave satisfactory ^{1}H and ^{13}C NMR, IR, and HRMS.
[b]All yields are isolated and are unoptimized.

Can. J. Chem. Downloaded from www.nrcresearchpress.com by 46.23.64.124 on 09/08/12
For personal use only.

Scheme 6

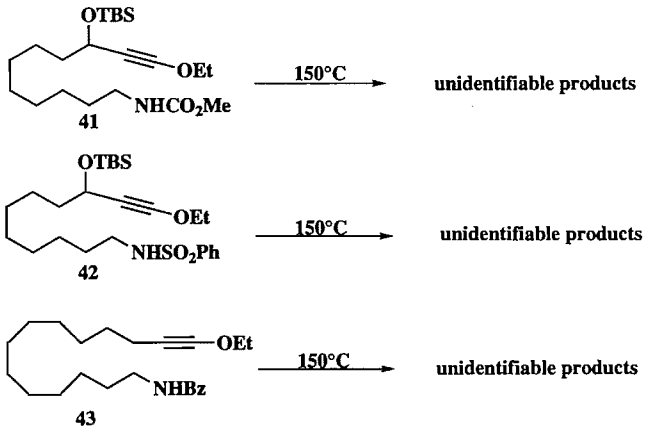

RT, 82%) (20); (*iii*) deprotection of the silyl ether (TBAF, THF, 92%) (21); (*iv*) mesylation (*n*BuLi, MsCl, THF, 86%); (*v*) bromide formation (NaBr, acetone, 77%); and (*vi*) displacement of the halide with benzamide (KOH, DMSO, 94%) (22), Scheme 4.

Compound **31** was generated in a straightforward manner by alkylation of 1-bromododecane with 1-ethoxy ethynyl lithium (THF, HMPA, 95%), Scheme 5. **Note:** *All of the alkynyl ether compounds are extremely acid and thermally labile, and in our hands decompose readily on standing at room temperature over a period of a few days. Once prepared they should be used immediately, or they can be stored for 2–3 weeks with no significant decomposition in benzene under* N_2 *at* $-10°C$.

Each of the alkynyl ether substrates was then heated at 150°C in refluxing xylenes for 3 h to effect cyclization, except entry 9 where the alkynyl ether was refluxed for 3 h in the presence of 2 equivalents of benzamide, Table 1.

Several points are worth noting about Table 1. First, *sterically hindered or unhindered amides cyclize to give the imide products in good to excellent yields. Five- to eight-membered rings are formed with equal ease* (entries 1–5); of particular note is entry 5 where a fully saturated eight-membered ring is generated. This contrasts with the difficulties encountered by other cyclization methods in related systems (23, 24). Ether protecting groups are unaffected by the reaction conditions (TBS in entries 2, 3, 6, and 7, and MOM (25)), and in one case regiospecific cyclization was accomplished in the presence of a free alcohol (entry 1). Poor nitrogen nucleophiles such as sulfonamides and carbamates also undergo the cyclization with proficiency equal to their amide analogues (entries 6 and 7). Unsymmetrical acyclic imides can be formed easily and efficiently (entry 9).

Efforts to extend this methodology to include substrates that would produce larger than eight-membered rings met with no success. For instance, when alkynyl ether **29** was subjected to our cyclization protocol only unidentifiable products were obtained (entry 8). Attempts to effect successful cyclization using high-dilution syringe pump addition with or without 10 equivalents of tri-*n*-butylamine (12) also proved fruitless.

The reasons for this failure are not readily apparent; however, it could be due to the reduced nucleophilicity of the nitrogen and the increased entropic and enthalpic factors associated with constructing these rings that chemistry other than the desired cyclization occurs. For example in entry 8, if the competition between O- and N-cyclization becomes important due to ease and rate of cyclization, then production of the undesired 12-membered imino ether heterocycle would predominate. The formation of this type of product under the reaction conditions could then very easily result in other unwanted chemistry.

To explore whether this was in fact the problem, three other substrates were examined, Scheme 6. It was expected that carbamate **41** and sulfonamide **42** should not suffer this difficulty, so that cyclization may proceed normally. In amide **43** it was felt that on going to a larger ring system the propensity for O- versus N-cyclization should be more or less identical so the normal cyclization product should reappear, albeit in diminished yields compared to our previous examples. However, when compounds **41**–**43** were heated to 150°C in xylenes for 3 h, myriad unidentifiable products were obtained in each case. The reason for this still eludes us; clearly, all the factors that prevent efficient cyclization in these systems are not yet known.

In summary, we have demonstrated the feasibility of utilizing in situ generated ketenes for the construction of acyclic imides as well as small and medium ring imides, sulfonimides, and *N*-carbobenzyloxyamides. Studies designed to utilize this methodology for the synthesis of biologically important natural products as well as to investigate the chemistry of these compounds are now in progress.

Experimental

All commercial reagents were purchased from Aldrich Chemicals (Milwaukee) and used without any further purification. Reaction solvents were dried according to established procedures (26). All reactions were performed in oven-dried glassware (120°C) under an inert atmosphere of nitrogen unless otherwise stated. Reaction temperatures refer to external baths. Alcohols **1** (27), **2** (28), **3** (29), and **4** (30) were prepared and used according to literature procedures.

Column chromatography was carried out according to the procedure of Still et al (31) using Merck silica gel (230–400 mesh). Thin-layer chromatographic analyses were performed on Merck F_{254} 0.25 mm plates. Infrared (IR) spectra were recorded on a Bruker IFS25 FTIR and are reported in wave numbers (cm^{-1}). Mass spectra were recorded on a Kratos MS50TC and were recorded in FAB or high-resolution EI modes. All ^1H nuclear magnetic resonance (NMR) spectra were recorded on an XL200 (200 MHz) spectrometer with chemical shifts reported in ppm (δ) with tetramethylsilane as an internal standard. Coupling constants (*J*) are reported in Hz. All ^{13}C nuclear magnetic resonance spectra were recorded on a Unity 400 (400 MHz) spectrometer.

General procedure for the preparation of aldehydes 5–8

The preparation of N-*(1,1-dimethyl-2-oxoethyl)benzamide* **5** *is representative*

Oxalyl chloride (0.85 mL, 9.74 mmol) and CH_2Cl_2 (20 mL) were placed in a 100 mL RBF cooled to −78°C followed by dropwise addition of DMSO (1.7 mL , 24.35 mmol). After 30 min, alcohol **1** (27) (1.25 g, 6.49 mmol) in CH_2Cl_2 (10 mL) was added, followed 1 h later by triethylamine (5.1 mL, 36.34

Can. J. Chem. Downloaded from www.nrcresearchpress.com by 46.23.64.124 on 09/08/12
For personal use only.

mmol). The cold bath was removed and the slurry was allowed to warm to room temperature. Dilution with CH_2Cl_2 (20 mL), washing with H_2O (3 × 30 mL), drying ($MgSO_4$), and evaporation of solvent gave a yellow oil. The oil was purified by silica gel chromatography (2:1 hexane – ethyl acetate) to furnish aldehyde **5** (32) as a chromatographically pure colourless oil (950 mg, 77%). IR ($CHCl_3$): 3295 (br), 3263 (br), 1732 (st), 1626 (st), 1527 (m). ^{1}H NMR ($CDCl_3$): 9.48 (s, 1H), 7.76–7.42 (m, 5H), 6.78 (s, 1H), 1.50 (s, 6H).

N-*(3-Oxopropyl)benzamide* ***6***: IR ($CHCl_3$): 3500 (m), 2900(st), 2850 (st), 1720 (st), 1650 (st), 1520 (w). ^{1}H NMR ($CDCl_3$): 9.84 (s, 1H), 7.76–7.74 (m, 5H), 6.82 (s, 1H), 3.75 (q, 2H, J = 5.7), 2.85 (t, 2H, J = 5.7). ^{13}C NMR ($CDCl_3$): 201.7 (1C), 167.4 (1C), 134.2 (1C), 131.6 (1C), 128.3 (2C), 126.9 (2C), 43.8 (1C), 33.4 (1C). HRMS (m^+/z) found: 177.0775; calcd.: 177.0789).

3-(Benzyloxycarbonylamino)propionaldehyde **7** *(33)*: IR ($CHCl_3$): 3313 (br), 3299 (br), 3278 (br), 3217 (br), 1716 (st), 1652 (st). ^{1}H NMR ($CDCl_3$): 9.80 (s, 1H), 7.34 (m, 5H), 5.08 (s, 2H), 3.48 (q, 2H, J = 6.0), 2.77 (t, 2H, J = 6.0). ^{13}C NMR ($CDCl_3$): 201.1 (1C), 156.2 (1C), 136.3 (1C), 128.4 (2C), 128.0 (2C), 127.9 (1C), 66.6 (1C), 43.9 (1C), 34.4 (1C). HRMS (m^+/z) found: 277.0891; calcd.: 277.0895.

N-*(3-Oxopropyl)benzene sulfonamide* ***8***: IR ($CHCl_3$): 3306 (br), 3299 (br), 3287 (br), 3217 (br), 1716 (st), 1343 (st). ^{1}H NMR ($CDCl_3$): 9.72 (s, 1H), 7.87–7.52 (m, 5H), 3.21 (t, 2H, J = 6.0), 2.74 (t, 2H, J = 6.0). ^{13}C NMR ($CDCl_3$): 200.8 (1C), 139.6 (1C), 132.7 (1C), 129.1 (2C), 126.9 (2C), 43.5 (1C), 36.7 (1C). HRMS (m^+/z – CO) found: 185.0518; calcd.: 185.05113.

Preparation of *N*-(4-ethoxy-2-hydroxy-1,1-dimethylbut-3-ynyl)benzamide 9

Ethyl ethynyl ether (0.98 mL, 10 mmol) and THF (10 mL) were placed in a 50 mL RBF. The solution was cooled to 0°C and, after addition of *n*-BuLi (3.71 mL, 9.4 mmol), was stirred for 30 min; then aldehyde **5** (900 mg, 4.7 mmol) was syringed into the solution in one portion. After 1 h the reaction was quenched with pH 10 NH_4Cl (10 mL), extracted into Et_2O (20 mL), dried (K_2CO_3), and the solvent evaporated in vacuo. The crude product was purified by silica gel chromatography (3:1 hexane – ethyl acetate) to provide **9** as a chromatographically pure colourless oil (965 mg, 79%). IR ($CHCl_3$): 3406 (br), 3388 (br), 3287 (br), 2985 (st), 2260 (st), 1654 (st). ^{1}H NMR ($CDCl_3$): 7.66–7.36 (m, 5H), 6.23 (s, 1H), 4.36 (s, 1H), 4.0 (q, 2H, J = 7.0), 1.50 (s, 6H), 1.23 (t, 3H, J = 7.0). ^{13}C NMR ($CDCl_3$): 168.5 (1C), 134.9 (1C), 131.5 (1C), 128.5 (2C), 126.9 (2C), 94.0 (1C), 74.5 (1C), 69.9 (1C), 59.0 (1C), 36.9 (1C), 25.0 (1C), 23.3 (1C), 14.2 (1C). FABMS (NOBA): (m^+ + H) 262 (100).

Preparation of *N*-(5-ethoxy-3-hydroxypent-4-ynyl)-benzamide 10

To a 10 mL RBF cooled to −78°C were successively added ethyl ethynyl ether (0.25 mL, 1.29 mmol), THF (2 mL), and *n*-BuLi (0.27 mL, 0.68 mmol). After 10 min, aldehyde **6** (60 mg, 0.34 mmol) in THF (3 mL) was added and the solution was stirred at this temperature for 30 min. Following quenching with pH 10 NH_4Cl (10 mL), the solution was diluted with Et_2O (10 mL), the layers separated, the organic phase dried (K_2CO_3), and the solvent evaporated in vacuo. The reddish brown crude product **10** (67 mg, 80%) was used directly in the next reaction without further purification. IR ($CDCl_3$): 3381 (br), 3368 (br), 2980 (st), 2270 (st), 1651 (st), 1537 (st). ^{1}H NMR ($CDCl_3$): 7.78–7.46 (m, 5H), 7.10 (s, 1H), 4.63 (m, 1H), 4.08 (q, 2H, J = 7.0), 3.85 (m, 2H), 1.97 (m, 2H), 1.37 (t, 2H, J = 7.0). ^{13}C NMR ($CDCl_3$): 167.8 (1C), 134.4 (1C), 131.4 (1C), 128.5 (2C), 126.9 (2C), 94.2 (1C), 74.7 (1C), 61.0 (1C), 38.7 (1C), 37.6 (1C), 37.0 (1C), 14.3 (1C). FABMS (NOBA): (m^+ + H) 248 (40).

Preparation of 5-(benzyloxycarbonylamino)-1-ethoxypent-1-yne-3-ol 11

Ethyl ethynyl ether (0.68 mL, 7.0 mmol) in THF (5 mL) was placed in a 50 mL RBF. The solution was cooled to −78°C, *n*-BuLi (4.3 mL, 6.9 mmol) was added, and, after stirring for 10 min, aldehyde **7** (650 mg, 3.14 mmol) in THF (5 mL) was syringed in. Stirring of the mixture was continued for an additional 30 min before quenching with 10 mL of pH 10 NH_4Cl solution. The product was extracted into Et_2O (20 mL) and dried (K_2CO_3), the solvent was evaporated in vacuo, and the brown oil was purified by silica gel chromatography (1:1 hexane – ethyl acetate) to give **11** as a chromatographically pure colourless oil (530 mg, 61%). IR ($CHCl_3$): 3305 (st), 3299 (br), 3278 (br), 2260 (st), 1658 (st), 1435 (w). ^{1}H NMR ($CDCl_3$): 7.34 (m, 5H), 5.09 (s, 2H), 4.23 (m, 1H), 4.09 (q, 2H, J = 7.0), 3.74 (m, 2H), 1.84 (m, 2H), 1.34 (t, 3H, J = 7.0). ^{13}C NMR ($CDCl_3$): 156.8 (1C), 136.5 (1C), 128.5 (2C), 128.3 (1C), 128.1 (2C), 94.0 (1C), 74.7 (1C), 66.7 (1C), 60.4 (1C), 38.9 (1C), 38.2 (1C), 37.7 (1C), 14.3 (1C). FABMS (NOBA): (m^+ + H) 278 (15).

Preparation of *N*-(5-ethoxy-3-hydroxypent-4-ynyl)-benzene sulfonamide 12

A 25 mL RBF was cooled to −78°C and THF (5 mL), ethyl ethynyl ether (0.49 mL, 5.0 mmol), and *n*-BuLi (3.0 mL, 4.5 mmol) were successively added. After 30 min aldehyde **8** (442 mg, 2.08 mmol) in THF (3 mL) was added and the solution was stirred at this temperature for 30 min before warming to room temperature and quenching with pH 10 NH_4Cl (10 mL). Extraction with Et_2O (20 mL), drying (K_2CO_3), evaporation of the solvent, and purification of the crude oil by SiO_2 chromatography (2:1 hexane – ethyl acetate) gave alcohol **12** as a chromatographically pure colourless oil (296 mg, 50%). IR ($CHCl_3$): 3331 (br), 3305 (br), 3287 (br), 2264 (st), 1345 (st), 1163 (w). ^{1}H NMR ($CDCl_3$): 7.87–7.51 (m, 5H), 5.32 (s, 1H), 4.66 (t, 1H, J = 5.0), 4.06 (q, 2H, J = 7.0), 3.27 (m, 2H), 1.74 (m, 2H), 1.31 (t, 3H, J = 7.0). ^{13}C NMR ($CDCl_3$): 139.9 (1C), 132.5 (1C), 129.1 (2C), 127.0 (2C), 94.5 (1C), 74.8 (1C), 61.2 (1C), 40.4 (1C), 38.4 (1C), 36.9 (1C), 14.3 (1C). FABMS (NOBA): (m^+) 283 (6).

Preparation of *N*-(2-*tert*-butyldimethylsiloxy-4-ethoxy-1,1-dimethylbut-3-ynyl)benzamide 13

Alcohol **9** (56 mg, 0.21 mmol), CH_2Cl_2 (5 mL), imidazole (16 mg, 0.23 mmol), and *tert*-butyldimethylsilyl chloride (35 mg, 0.23 mmol) were placed in a 10 mL RBF. The reaction mixture was stirred at room temperature for 12 h, the solids were filtered off, and the filtrate was evaporated in vacuo. Purification by silica gel chromatography (5:1 hexane – ethyl acetate)

Can. J. Chem. Downloaded from www.nrcresearchpress.com by 46.23.64.124 on 09/08/12
For personal use only.

generated TBS ether **13** as a chromatographically pure colourless oil (75 mg, 93%). IR ($CHCl_3$): 2985 (st), 2260 (st), 1654 (st), 1435 (w). ^1H NMR ($CDCl_3$): 7.60–7.25 (m, 5H), 6.28 (s, 1H), 4.41 (s, 1H), 4.02 (q, 2H, J = 7.1), 1.53 (s, 6H), 1.25 (t, 3H, J = 7.1), 0.88 (s, 9H), 0.08 (s, 6H). ^{13}C NMR ($CDCl_3$): 167.0 (1C), 136.0 (1C), 131.0 (1C), 128.4 (2C), 126.7 (2C), 94.4 (1C), 74.4 (1C), 69.1 (1C), 58.1 (1C), 37.1 (1C), 25.8 (1C), 22.9 (1C), 22.3 (1C), 18.1 (1C), 14.4 (1C), −3.8 (1C), −4.2 (1C). FABMS (NOBA): (m^+ + H) 376 (22).

Preparation of *N*-(3-*tert*-butyldimethylsiloxy-5-ethoxypent-4-ynyl)benzamide 14

Alcohol **10** (67 mg, 0.27 mmol), THF (5 mL), imidazole (19.4 mg, 0.28 mmol), and *tert*-butyldimethylsilyl chloride (43 mg, 0.28 mmol) were placed in a 10 mL RBF. The reaction mixture was stirred at room temperature for 12 h, the solids were filtered off, and the filtrate was evaporated in vacuo. Purification by silica gel chromatography (3:1 hexane – ethyl acetate) generated TBS ether **14** as a chromatographically pure colourless oil (60 mg, 62%). IR ($CHCl_3$): 3350 (st), 2900 (st), 2260 (st), 1725 (st), 1650 (st). ^1H NMR ($CDCl_3$): 7.76–7.38 (m, 5H), 4.68 (m, 2H), 4.07 (q, 2H, J = 7.0), 3.66 (q, 2H, J = 6.1), 1.93 (m, 2H), 1.37 (t, 2H, J = 7.0), 0.87 (s, 9H), 0.07 (s, 6H). ^{13}C NMR ($CDCl_3$): 167.4 (1C), 135.0 (1C), 131.1 (1C), 128.4 (2C), 126.9 (2C), 94.2 (1C), 74.5 (1C), 62.7 (1C), 38.7 (1C), 37.4 (1C), 37.1 (1C), 25.9 (3C), 18.2 (1C), 14.4 (1C). FABMS (NOBA): (m^+ + H) 362 (18).

Preparation of 5-(benzyloxycarbonylamino)-3-*tert*-butyldimethylsiloxy-1-ethoxypent-1-yne 15

To a 10 mL RBF containing alcohol **11** (522 mg, 1.89 mmol) and THF (5 mL) were added *tert*-butyldimethylsilyl chloride (422 mg, 2.8 mmol) and imidazole (204 mg, 3.0 mmol). After stirring at room temperature for 12 h the solids were filtered off and the filtrate was evaporated in vacuo. Purification by silica gel chromatography (8:1 hexane – ethyl acetate) gave **15** as a chromatographically pure colourless oil (610 mg, 83%). IR (neat): 2956 (m), 2857 (m), 2264 (st), 1730 (st), 1696 (st). ^1H NMR ($CDCl_3$): 7.31 (m, 5H), 5.40 (bs, 1H), 5.12 (s, 2H), 4.54 (t, 1H, J = 4.8), 4.06 (q, 2H, J = 7.0), 3.39 (m, 2H), 1.82 (m, 2H), 1.32 (t, 3H, J = 7.0), 0.87 (s, 9H), 0.14 (s, 3H), 0.10 (s, 3H). ^{13}C NMR ($CDCl_3$): 156.3 (1C), 136.8 (1C), 128.4 (2C), 127.9 (2C), 127.2 (1C), 93.9 (1C), 74.4 (1C), 66.4 (1C), 62.1 (1C), 39.0 (1C), 38.2 (1C), 38.1 (1C), 25.8 (1C), 18.1 (1C), 14.4 (1C), −4.8 (1C), −5.2 (1C). FABMS (NOBA): (m^+ + H) 392 (19).

Preparation of *N*-(3-*tert*-butyldimethylsiloxy-5-ethoxypent-4-ynyl)benzene sulfonamide 16

Alcohol **12** (235 mg, 0.83 mmol), THF (6 mL), *tert*- butyldimethylsilyl chloride (188 mg, 1.25 mmol), and imidazole (102 mg, 1.5 mmol) were placed in a 25 mL RBF. The reaction mixture was stirred for 12 h at room temperature, the solids were filtered off, and the filtrate was evaporated in vacuo. Purification of the crude product by silica gel chromatography (3:1 hexane – ethyl acetate) gave sulfonamide **16** as a pure colourless oil (85 mg, 26%). IR ($CHCl_3$): 3320 (br), 3285 (br), 2957 (br), 2895 (br), 2263 (st), 1344 (st), 1160 (st). ^1H NMR ($CDCl_3$): 7.87–7.54 (m, 5H), 5.48 (s, 1H), 4.55 (t, 1H, J = 5.0), 4.0 (q, 2H, J = 7.0), 3.21 (m, 2H), 1.72 (m, 2H), 1.31 (t, 3H, J = 7.0), 0.87 (s, 9H), 0.06 (s, 6H). ^{13}C NMR ($CDCl_3$): 135.0 (1C), 131.1 (1C), 128.4 (2C), 126.9 (2C), 94.2 (1C), 74.5 (1C), 62.7 (1C), 38.9 (1C), 37.4 (1C), 37.1 (1C), 25.9 (3C), 18.2 (1C), 14.4 (1C), −4.6 (1C), −5.1(1C). FABMS (NOBA): (m^+ + H) 398 (21).

Preparation of 6-bromo-1-ethoxyhex-1-yne 19

To a 25 mL RBF cooled to 0°C were successively added diethylamine (0.29 mL, 2.8 mmol), THF (5 mL), and *n*-BuLi (1.7 mL, 2.8 mmol). After 15 min chloroacetaldehyde diethyl acetal (0.14 mL, 0.93 mmol) was added, followed 2 h later by 1,4-dibromobutane (200 mg, 0.93 mmol) in HMPA (6 mL). After agitating the reaction mixture at 0°C for 2 h and at room temperature for 12 h it was quenched with pH 10 NH_4Cl (10 mL), diluted with Et_2O (20 mL), and washed with H_2O (2 × 20 mL). The organic phase was separated, dried (K_2CO_3), evaporated in vacuo, and the crude product was purified by silica gel chromatography (50:1 hexane – ethyl acetate) to produce bromide **19** as a chromatographically pure colourless oil (150 mg, 79%). IR ($CHCl_3$): 2983 (st), 2856 (st), 2268 (st), 1320 (st). ^1H NMR ($CDCl_3$): 4.0 (q, 2H, J = 7.0), 3.45 (t, 2H, J = 6.7), 2.11 (m, 2H), 1.47 (m, 4H), 1.34 (t, 3H, J = 7.0). ^{13}C NMR ($CDCl_3$): 89.8 (1C), 73.9 (1C), 36.5 (1C), 33.5 (1C), 31.7 (1C), 28.0 (1C), 16.5 (1C), 14.4 (1C).

Preparation of 7-bromo-1-ethoxyhept-1-yne 20

A 100 mL RBF was cooled to 0°C and successively charged with diethylamine (1.4 mL, 13.5 mmol), THF (10 mL), and *n*-BuLi (8.4 mL, 13.5 mmol); the mixture was stirred for 30 min, and then treated with chloroacetaldehyde diethyl acetal (0.65 mL, 4.35 mmol). After 2 h 1,5-dibromopentane (0.6 mL, 4.35 mmol) in HMPA (10 mL) was added and stirring was continued at 0°C for 2 h and at room temperature for 12 h. Quenching with pH 10 NH_4Cl (10 mL), dilution with Et_2O (20 mL), washing with H_2O (2 × 20 mL), drying (K_2CO_3), and evaporation of the solvent in vacuo gave a dark oil. The crude product was purified on silica gel chromatography (50:1 hexane – ethyl acetate) to give bromide **20** as a chromatographically pure colourless oil (800 mg, 84%). IR ($CHCl_3$): 2981 (st), 2856 (st), 2270 (st), 1423 (w). ^1H NMR ($CDCl_3$): 4.0 (q, 2H, J = 7.0), 3.51 (t, 2H, J = 6.8), 2.11 (m, 2H), 1.47 (m, 6H), 1.34 (t, 3H, J = 7.0). ^{13}C NMR ($CDCl_3$): 89.5 (1C), 73.9 (1C), 45.0 (1C), 36.9 (1C), 32.2 (1C), 28.9 (1C), 26.0 (1C), 17.1 (1C), 14.3 (1C).

Preparation of *N*-(6-ethoxyhex-5-ynyl)benzamide 21

DMSO (2 mL) and powdered KOH (123 mg, 2.2 mmol) were placed in a 10 mL RBF. After 10 min benzamide (242 mg, 2 mmol) and bromide **19** (111 mg, 0.55 mmol) were added and stirring was continued for 30 min. The reaction mixture was poured into H_2O (10 mL) and extracted with CH_2Cl_2 (3 × 5 mL). The combined organic extracts were washed with H_2O (3 × 10 mL), dried (K_2CO_3), and the solvent was evaporated in vacuo. Purification by silica gel chromatography (2:1 hexane – ethyl acetate) furnished amide **21** (90 mg, 67%) as a chromatographically pure pale yellow oil. IR (neat): 3390 (m), 2912 (st), 2270 (st), 1648 (st), 1450 (m). ^1H NMR ($CDCl_3$): 7.78–7.45 (m, 5H), 6.31 (s, 1H), 4.03 (q, 2H, J = 7.0), 3.45 (q, 2H, J = 6.6), 2.19 (t, 2H, J = 6.1), 1.72–1.58 (m, 4H), 1.37 (t, 3H, J = 7.0). ^{13}C NMR ($CDCl_3$): 167.5 (1C), 134.8 (1C), 131.3 (1C), 128.5 (2C), 126.8 (2C), 89.7 (1C), 73.9 (1C), 39.6 (1C), 36.7 (1C), 28.7 (1C), 27.0 (1C), 17.0 (1C), 14.4 (1C). FABMS (glycerol): (m^+ + H) 246 (84).

Can. J. Chem. Downloaded from www.nrcresearchpress.com by 46.23.64.124 on 09/08/12
For personal use only.

Preparation of *N*-(7-ethoxyhept-6-ynyl)benzamide 22

Powdered KOH (1.54 g, 27.6 mmol) and DMSO (15 mL) were stirred for 15 min in a 50 mL RBF, then benzamide (2.6 g, 21.5 mmol) followed by bromide **20** (1 g, 4.6 mmol) in 5 mL of DMSO were added and stirring was continued for 30 min. The solution was poured into H_2O (20 mL) and extracted with CH_2Cl_2 (3 × 10 mL). The combined organic extracts were washed with H_2O (3 × 10 mL), dried (K_2CO_3), and the solvent was evaporated. Purification by silica gel chromatography (2:1 hexane – ethyl acetate) gave amide **22** as a chromatographically pure colourless oil (950 mg, 80%). IR ($CHCl_3$): 3340 (m), 2933 (st), 2264 (st), 1651 (st), 1430 (st), 1287 (st). ^{1}H NMR ($CDCl_3$): 7.78–7.45 (m, 5H), 6.12 (s, 1H), 4.0 (q, 2H, J = 7.0), 3.46 (q, 2H, J = 6.5), 2.13 (m, 2H), 1.49 (m, 6H), 1.34 (t, 3H, J = 7.0). ^{13}C NMR ($CDCl_3$): 167.5 (1C), 134.7 (1C), 131.2 (1C), 128.4 (2C), 126.8 (2C), 89.5 (1C), 73.8 (1C), 39.9 (1C), 36.9 (1C), 29.2 (1C), 29.1 (1C), 26.0 (1C), 17.0 (1C), 14.3 (1C). FABMS (NOBA): (m^+) 259 (100).

Preparation of 1-ethoxytetradec-1-yne 31

A 25 mL RBF was charged with ethyl alkynyl ether (0.1 mL, 0.45 mmol) and THF (5 mL), cooled to −78°C and *n*BuLi (0.16 mL, 0.4 mmol) was added dropwise to the mixture. After stirring for 30 min 1-bromododecane **30** (100 mg, 0.4 mmol) in THF (2 mL) and HMPA (5 mL) were added, the cold bath was removed, and the reaction mixture stirred at room temperature overnight, diluted with Et_2O (30 mL), and quenched with pH 10 NH_4Cl (10 mL). The ether layer was separated, washed with H_2O (2 × 20 mL), brine (2 × 20 mL), dried (K_2CO_3), and then evaporated. The oily residue was purified by silica gel chromatography (60:1 hexane – ethyl acetate) to furnish **31** as a chromatographically pure colourless oil (53 mg, 55%). IR ($CHCl_3$): 2960 (st), 2926 (br), 2260 (st), 1453 (m), 1103 (m). ^{1}H NMR ($CDCl_3$): 4.02 (q, 2H, J = 7.1), 3.41 (t, 2H, J = 6.8), 2.11 (p, 2H, J = 6.7), 1.88 (p, 2H, J = 6.6), 1.34 (t, 3H, J = 7.1), 1.53–1.21 (m, 14H). ^{13}C NMR ($CDCl_3$): 89.3 (1C), 73.8 (1C), 37.4 (1C), 31.9 (1C), 29.8 (1C), 29.7 (1C), 29.6 (2C), 29.6 (1C), 29.4 (1C), 29.2 (1C), 28.8 (1C), 22.7 (1C), 17.2 (1C), 14.4 (1C), 14.1 (1C). FABMS (NOBA): ($2m^+$ + H) 477 (100), (m^+ + H) 237 (10).

Preparation of 1-benzoyl-5,5-dimethyl-4-hydroxylpyrrolidin-2-one 32

To refluxing (150°C) xylenes (15 mL) in a base-washed 100 mL RBF was added amide **9** (25 mg, 0.096 mmol) in xylenes (5 mL) dropwise over 10 min. The solution was kept at reflux for 3 h, cooled to room temperature, and the solvent was evaporated in vacuo. Purification by silica gel chromatography (2:1 hexane – ethyl acetate) furnished imide **32** as a chromatographically pure colourless oil (20 mg, 86%). IR ($CHCl_3$): 3499 (br), 3485 (br), 3444 (br), 1698 (m), 1661 (m), 1651 (m), 1315 (m). ^{1}H NMR ($CDCl_3$): 7.68–7.25 (m, 5H), 4.03 (dd, 1H, J = 3.1, 6.0), 2.86 (dd,1H, J = 6.0, 18.4), 2.45 (dd, 1H, J = 3.1, 18.4), 1.50 (s, 3H), 1.49 (s, 3H). ^{13}C NMR ($CDCl_3$): 173.6 (1C), 171.9 (1C), 136.1 (1C), 132.3 (1C), 128.9 (2C), 128.1 (2C), 73.2 (1C), 66.7 (1C), 39.5 (1C), 24.6 (1C), 19.6 (1C). HRMS (m^+/z) found: 233.1053; calcd.: 233.1052.

Preparation of 1-benzoyl-3-(*tert*-butyldimethylsiloxy)-5,5-dimethylpyrrolidin-2-one 33

To refluxing (150°C) xylenes (15 mL) in a base-washed 100 mL RBF was added amide **13** (25 mg, 0.096 mmol) in xylenes (5 mL) dropwise over 10 min. The solution was kept at reflux for 3 h, cooled to room temperature, and the solvent was evaporated in vacuo. The residue was purified by silica gel chromatography (2:1 hexane – ethyl acetate) to furnish imide **33** as a chromatographically pure colourless oil (20 mg, 75%). IR ($CHCl_3$): 2954 (m), 2929 (m), 1742 (st), 1681 (st), 1145 (st). ^{1}H NMR ($CDCl_3$): 7.62–7.38 (m, 5H), 4.00 (dd, 1H, J = 4.6, 5.1), 2.82 (dd, 1H, J = 5.1, 17.6), 2.45 (dd, 1H, J = 4.6, 17.6), 1.51 (s, 3H), 1.48 (s, 3H), 0.93 (s, 9H), 0.11 (s, 6H). ^{13}C NMR ($CDCl_3$): 173.3 (1C), 171.9 (1C), 135.7 (1C), 132.2 (1C), 128.9 (2C), 128.1 (2C), 73.9 (1C), 67.2 (1C), 40.2 (1C), 25.7 (3C), 24.7 (1C), 20.1 (1C), 18.0 (1C), −4.6 (1C), −5.0 (1C). HRMS (m^+/z − $C(CH_3)_3$) found: 290.1219; calcd.: 290.1213.

Preparation of 1-benzoyl-4-(*tert*-butyldimethylsiloxy)-piperidin-2-one 34

A base-washed 100 mL RBF containing xylenes (50 mL) was brought to reflux (150°C) and amide **14** (100 mg, 0.28 mmol) in xylenes (10 mL) was added dropwise over 10 min. After complete addition and heating for 2 h, the mixture was cooled to room temperature, and the solvent evaporated in vacuo. Purification by silica gel chromatography (5:1 hexane – ethyl acetate) generated imide **34** as a chromatographically pure pale white waxy solid (73 mg, 79%). IR ($CHCl_3$): 2956 (st), 2929 (st), 1694 (st), 1667 (st), 1471 (m). ^{1}H NMR ($CDCl_3$): 7.58–7.40 (m, 5H), 4.33 (m, 1H), 3.78 (m, 2H), 2.74 (dd, 1H, J = 4.1, 16.4), 2.59 (dd, 1H, J = 4.8, 16.4), 2.10 (m, 2H), 0.90 (s, 9H), 0.01 (s, 6H). ^{13}C NMR ($CDCl_3$): 174.2 (1C), 172.1 (1C), 136.1 (1C), 131.5 (1C), 128.1 (2C), 128.0 (2C), 65.5 (1C), 43.8 (1C), 41.5 (1C), 31.1 (1C), 25.7 (3C), 18.0 (1C), 0.01 (2C). HRMS (m^+/z − $C(CH_3)_3$) found: 276.1062; calcd.: 276.1056.

Preparation of 1-benzoylazepan-2-one 35

A base-washed 50 mL RBF was charged with xylenes (20 mL) and brought to reflux (150°C). To this solution was added amide **21** (30 mg, 0.12 mmol) in xylenes (5 mL) dropwise over 10 min and, after complete addition the solution was heated for an additional 2 h. Upon cooling to room temperature and evaporation of solvent the residue was purified by silica gel chromatography (3:1 hexane – ethyl acetate) to produce imide **35** as a chromatographically pure colourless oil (17.8 mg, 68%). IR ($CHCl_3$): 2929 (m), 2800 (w), 1699 (st), 1694 (st), 1674 (st), 1440 (m). ^{1}H NMR ($CDCl_3$): 7.51 (m, 5H), 3.97 (m, 2H), 2.70 (m, 2H), 1.83 (m, 6H). ^{13}C NMR ($CDCl_3$): 177.5 (1C), 174.1 (1C), 136.6 (1C), 131.3 (1C), 128.1 (2C), 127.7 (2C), 45.2 (1C), 38.9 (1C), 29.7 (1C), 29.2 (1C), 23.8 (1C). HRMS (m^+/z) found: 217.1097; calcd.: 217.1103.

Preparation of 1-benzoylazocan-2-one 36

A 50 mL RBF charged with xylenes (20 mL) was brought to reflux (150°C) and amide **22** (50 mg, 0.19 mmol) in xylenes (5 mL) was added dropwise over 10 min. Following complete addition, the solution was refluxed for 3 h, cooled to room temperature, and the solvent was evaporated. The residue was purified by silica gel chromatography (2:1 hexane – ethyl acetate) to furnish imide **36** as a chromatographically pure colourless oil (25.7 mg, 58%). IR ($CHCl_3$): 2924 (m), 2760 (w), 1694 (st), 1668 (st), 1440 (m). ^{1}H NMR ($CDCl_3$): 7.48 (m, 5H), 3.98

Can. J. Chem. Downloaded from www.nrcresearchpress.com by 46.23.64.124 on 09/08/12
For personal use only.

(dd, 2H, J = 5.8, 6.0), 2.65 (dd, 2H, J = 5.9, 6.6), 1.90–1.61 (m, 8H). ^{13}C NMR ($CDCl_3$): 178.8 (1C), 174.1 (1C), 136.4 (1C), 131.1 (1C), 128.0 (2C), 127.7 (2C), 44.8 (1C), 35.8 (1C), 30.5 (1C), 28.9 (1C), 26.2 (1C), 23.7 (6C). HRMS (m^+/z) found: 231.1259; calcd.: 231.1260.

Preparation of 1-(benzyloxycarbonyl)-4-(*tert*-butyldimethylsiloxy)-piperidin-2-one 37

A base-washed 100 mL RBF containing xylenes (20 mL) was brought to reflux (150°C) and carbamate **15** (25 mg, 0.064 mmol) in xylenes (5 mL) was added dropwise over 10 min. After complete addition the reaction mixture was refluxed for 3 h, cooled to room temperature, the solvent evaporated, and the crude product purified by silica gel chromatography (7:1 hexane – ethyl acetate) to furnish **37** as a chromatographically pure pale yellow oil (20.2 mg, 87%). IR ($CHCl_3$): 2956 (st), 2928 (st), 2856 (m), 1777 (m), 1716 (st), 1471 (m). ^{1}H NMR ($CDCl_3$): 7.34 (m, 5H), 5.21 (s, 2H), 4.12 (m, 1H), 3.67 (t, 2H, J = 5.4), 2.57 (dd, 1H, J = 4.0, 17.4), 2.45 (dd, 1H, J = 4.2, 17.3), 1.83 (m, 2H), 0.80 (s, 9H), 0.071 (s, 6H). ^{13}C NMR ($CDCl_3$): 169.6 (1C), 154.1 (1C), 135.4 (1C), 128.5 (2C), 128.3 (1C), 128.0 (2C), 68.5 (1C), 64.8 (1C), 44.3 (1C), 42.2 (1C), 31.2 (1C), 25.7 (3C), 18.0 (1C), 1.0 (2C). HRMS (m^+/z – $C(CH_3)_3$) found: 306.1170; calcd.: 306.1162.

Preparation of 1-(benzenesulfonyl)-4-(*tert*-butyldimethylsiloxy)-piperidin-2-one 38

A 100 mL RBF containing xylenes (25 mL) was brought to reflux (150°C) and sulfonamide **16** (40 mg, 0.10 mmol) in xylenes (5 mL) was added dropwise over 10 min. After 3 h the reaction mixture was cooled to room temperature, the solvent evaporated, and the residue purified by silica gel chromatography (2:1 hexane – ethyl acetate) to furnish sulfonimide **38** as a chromatographically pure colourless oil (28.3 mg, 76%). IR ($CHCl_3$): 2957 (st), 2903 (w), 2856 (m), 1683 (st), 1344 (m). ^{1}H NMR ($CDCl_3$): 8.02–7.57 (m, 5H), 4.12 (m, 1H), 4.06 (m, 2H), 2.54 (dd, 1H, J = 3.8, 17.3), 2.44 (dd, 1H, J = 4.1, 17.2), 1.97 (m, 2H), 0.78 (s, 9H), 0.026 (s, 6H). ^{13}C NMR ($CDCl_3$): 168.9 (1C), 138.9 (1C), 133.6 (1C), 128.6 (2C), 128.4 (2C), 64.1 (1C), 43.2 (1C), 42.4 (1C), 30.9 (1C), 25.6 (3C), 17.8 (1C), 1.0 (2C). HRMS (m^+/z – $C(CH_3)_3$) found: 312.0713; calcd.: 312.0727.

Preparation of *N*-tetradecanoylbenzamide 40

A 100 mL RBF containing xylenes (25 mL) and benzamide (80 mg, 0.66 mmol) was brought to reflux (150°C) and alkynyl ether **31** (78 mg, 0.33 mmol) in xylenes (5 mL) was added dropwise over 25 min. The solution was refluxed for 3 h, cooled to room temperature, the solvent evaporated, and the residue purified by silica gel chromatography (2:1 hexane – ethyl acetate) to furnish imide **40** as a chromatographically pure colorless oil (104 mg, 95%). IR ($CHCl_3$): 3405 (w), 3394 (w), 2953 (s), 2916 (s), 1699 (m), 1677 (s), 1470 (m). ^{1}H NMR ($CDCl_3$): 8.60 (s, 1H), 7.83 (m, 2H), 7.54 (m, 3H), 3.00 (t, 2H, J = 7.2), 1.72–1.35 (m, 25H). ^{13}C NMR ($CDCl_3$): 176.0 (1C), 165.3 (1C), 133.2 (1C), 132.9 (1C), 129.0 (2C), 127.5 (2C), 37.5 (1C), 31.9 (1C), 29.7 (2C), 29.6 (1C), 29.6 (1C), 29.5 (1C), 29.4 (1C), 29.3 (1C), 29.2 (1C), 24.1 (1C), 22.7 (1C), 14.1 (1C). HRMS (m^+/z) found: 331.2502; calcd.: 331.2512.

Acknowledgments

Financial support from the Natural Sciences and Engineering Research Council of Canada and the University of New Brunswick is gratefully acknowledged. The authors wish to thank the reviewers of this manuscript for some helpful suggestions.

References

1. J.G. Buchanan. *In* Progress in the chemistry of organic natural products. Vol. 44. *Edited by* W. Hertz, H. Griselach, and G.W. Kirby. Springer Verlag, Vienna. 1983. p. 243.
2. R.G. Powell, C.-R. Smith, Jr., D. Weisleder, G.K. Matsumoto, J. Clardy, and J. Kozolowski. J. Am. Chem. Soc. **105**, 3739 (1983).
3. M. Adamczeski, E.Quiñoá, and P. Crews. J. Am. Chem. Soc. **111**, 647 (1989).
4. P.A. Evans and A.B. Holmes. Tetrahedron, **47**, 9131 (1991).
5. D.A. Burnett, J.-K. Choi, D.J. Hart, and Y.-M. Tsai. J. Am. Chem. Soc. **106**, 8201 (1984).
6. D. J. Hart and Y.-M. Tsai. J. Am. Chem. Soc. **106**, 8209 (1984).
7. H. Hiemstra, M.H.-Ah. Sho, R.J. Vijn, and N. Speckamp. J. Org. Chem. **50**, 4014 (1985).
8. R.W. King. Tetrahedron Lett. **22**, 2837 (1981).
9. A.R. Battersby, S.P.D. Turner, M.H. Block, Z.-C. Sheng, and S.C. Zimmerman. J. Chem. Soc. Perkin Trans. 1, 1577 (1988).
10. H. Yu. Ph.D. Thesis, University of New Brunswick, 1992.
11. W. Flitsh and S.R. Schindler. Synthesis, 685 (1975).
12. L. Liang, M. Ramaseshan, and D.I. MaGee. Tetrahedron, **49**, 2159 (1993).
13. D.I. MaGee and M. Ramaseshan. Synlett, 743 (1994).
14. J. Ficini. Bull. Soc. Chim. Fr. 1367 (1954).
15. J.C.W. Postma and J.F. Arens. Recl. Trav. Chem. Pays-Bas, **75**, 1377 (1956).
16. J. Nieunwenhuis and J.F. Arens. Recl. Trav. Chem. Pays-Bas, **77**, 761 (1958).
17. R.E. Dunbar and G.C. White. J. Org. Chem. **23**, 915 (1958).
18. F.O. Rice, J. Greenburg, C.E. Waters, and R.E. Vollrath. J. Am. Chem. Soc. **56**, 1760 (1934).
19. Li Liang. M.Sc. Thesis, University of New Brunswick, 1992.
20. S. Raucher and B.L. Bray. J. Org. Chem. **52**, 2332 (1987).
21. E.J. Corey and A. Venkateswarlu. J. Am. Chem. Soc. **94**, 6190 (1972).
22. R.W. Johnstone and M.E. Rose. Tetrahedron, **35**, 2169 (1979).
23. J. Diamond, W.F. Bruce, C. Gochman, and F.T. Tyson. J. Org. Chem. **25**, 65 (1960).
24. M.E. Garst, J.N. Bonfiglio, and J. Marks. J. Org. Chem. **47**, 1494 (1982).
25. M. Ramaseshan. Ph.D. Thesis, University of New Brunswick, 1995.
26. D.D. Perrin and W.L.F. Armarego. Purification of laboratory chemicals. 3rd ed. Pergamon Press, Toronto. 1988.
27. A. Levy and M. Litt. J. Polym. Sci. Part A-1: **6**, 57 (1968).
28. T.-L. Ho. Synth. Commun. **7**, 393 (1977).
29. T. Taguchi and T. Mukaiyama. Chem. Lett. 1 (1973).
30. M. Zaoral, J. Kolc, F. Korenczki, V.P. Cherneckii, and F. Sorm. Collect. Czech. Chem. Commun. **32**, 843 (1967).
31. W.C. Still, M. Kahn, and A. Mitra. J. Org. Chem. **43**, 2923 (1978).
32. A. Kampf and E. Dimant. Carbohydr. Res. **21**, 1 (1972).
33. J. Boukouvalas, B.T. Golding, R.W. McCabe, W. Richard, and P.K. Slaich. Angew. Chem. Int. Ed. Engl. **22**, 618 (1983).

Unusual polyketides from the wood-decay fungus *Sistotrema raduloides*

Albert K. Amegadzie, William A. Ayer, and Lynne Sigler

Abstract: The metabolites of the wood rot decay fungus *Sistotrema raduloides* (P. Karst) Donk have been investigated and a new type of norpentaketide has been discovered. The compounds sistodiolynne (**1**), sistolynone (**5**), and sistopyrone (**6**) represent new carbon skeletons among natural products. The compounds are very unstable and readily polymerize in the presence of air to give black insoluble material. It has been shown by ^{13}C NMR labelling experiments that they arise from five acetate units, and that a methyl carbon of one of the acetate units is lost during the biosynthesis. The structures were determined by spectroscopy methods, mainly NMR, and the absolute configuration of sistodiolynne was established by circular dichroism methods.

Key words: fungal metabolites, *Sistotrema raduloides*, norpentaketides, biosynthetic studies, polyacetylenes.

Résumé : On a étudié les métabolites du champignon *Sistotrema raduloides* (P. Karst) Donk de la pourriture du bois et on a découvert un nouveau type de norpentacétide. Les composés sistodiolynne (**1**), sistolynone (**5**) et sistopyrone (**6**) correspondent à de nouveaux squellettes carbonés des produits naturels. Les composés sont très instables et ils se polymérisent facilement en présence d'air pour donner des matériaux noirs qui sont insolubles. On a montré par des expériences de marquage en RMN du ^{13}C qu'ils proviennent de cinq unités acétates et qu'un carbone de méthyle de l'une des unités acétates est perdue au cours de la biosynthèse. On a déterminé les structures par des méthodes spectroscopiques, principalement la RMN, et on a déterminé la configuration absolue de la sistodiolynne par des méthodes de dichroïsme circulaire.

Mots clés : métabolites de champignons, *Sistotrema raduloides*, norpentacétides, études biosynthétiques, polyacétylènes.

[Traduit par la rédaction]

Introduction

The wood-decay fungus *Sistotrema raduloides* (P. Karst) Donk was recovered from indoor air during a study to evaluate building air quality of a museum in San Juan, Puerto Rico.[2] A member of the Corticiaceae (Basidiomycotina) having a widespread distribution in temperate areas, *S. raduloides* is known to cause white rot decay of both angiospermous and gymnospermous wood (1). On agar media of various kinds, the Puerto Rican isolate[3] was observed to form flaky carbonaceous deposits especially when the mycelium came into contact with glass surfaces. In this study we examined the metabolites produced when the fungus is grown in liquid still culture on Sabouraud dextrose medium. The metabolites proved to be very sensitive to air, forming an insoluble black polymer when exposed to the atmosphere in the absence of solvent. The structures of three of the air-sensitive metabolites are described, and the biosynthetic pathway by which they may be produced from acetate units is discussed.

Received July 4, 1995.

A.K. Amegadzie and W.A. Ayer.[1] Department of Chemistry, University of Alberta, Edmonton, AB T6G 2G2, Canada.
L. Sigler. University of Alberta Microfungus Herbarium, Devonian Botanic Garden, Edmonton, AB T6G 2E1, Canada.

[1] Author to whom correspondence may be addressed. Telephone: (403) 492-5476. Fax: (403) 492-8231

[2] The fungus is further described in the Experimental.

[3] We thank Dr. B. Bolanos, School of Medicine, University of Puerto Rico, San Juan, for bringing the isolate to our attention.

Results and discussion

Sistotrema raduloides was grown in still culture on Sabouraud dextrose broth at room temperature for 5 weeks. The mycelium was then separated from the culture broth by filtration and the filtrate was concentrated and extracted, first with CH_2Cl_2, then with ethyl acetate. In the initial experiment, the extracts were dried (Na_2SO_4) and concentrated to dryness under reduced pressure to give brown oils. On standing open to the atmosphere, the oils rapidly (ca. 2 min) solidified to a black amorphous solid. This material could not be dissolved in organic solvents or water. In subsequent experiments, the crude extracts were not concentrated to dryness but were kept as much as possible in a small volume of the extracting solvent under an inert atmosphere.

Sistodiolynne (**1**) was purified by preparative TLC. To

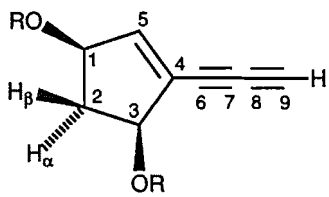

1 R = H
1a R = Ac

avoid polymerization the compound was eluted directly from the plate with acetone-d_6 and the solution was used for NMR measurements. The HREIMS was obtained by placing a drop

Can. J. Chem. Downloaded from www.nrcresearchpress.com by 46.23.64.124 on 09/08/12
For personal use only.

Table 1. ^{1}H NMR and ^{13}C NMR data for **1** and **1***a*.

	1	**1***a*	**1**	
Atom	δ, multi., *J*(Hz)	δ, multi., *J*(Hz)	Atom	δ_C, multi.
H-1α	4.62, bdd	5.60, m	C-1	76.1, d
H-2α	2.74, ddd, 13.5, 7.0, 7.0	2.95, ddd, 14.6, 6.7, 6.7	C-2	44.7, t
H-2β	1.50, ddd, 13.5, 6.2, 6.2	1.75, ddd, 14.6, 4.2, 4.2	C-3	73.4, d
H-3α	4.55, m	5.60, m	C-4	129.8, s
H-5	6.30, dd, 2.0, 1.0	6.44, bdd, 2.2	C-5	146.7, d
H-9	3.30, s	2.50, s	C-6	76.9, s
OH-1β	4.70, d, 6.5		C-7	72.0, s
OH-3β	4.48, d, 6.5		C-8	68.4, s
OH-1			C-9	74.1, d
-$COCH_3$		2.08, 2.02 (singlets)		

of the solution directly on the probe and determining the spectrum immediately. The spectrum indicates a molecular formula $C_9H_8O_2$. Peaks at $M^+ - 1$ and $M^+ - 18$ indicate the presence of hydroxyl group(s). The FTIR spectrum (thin film after evaporation of solvent) shows broad hydroxyl absorption centered around 3500 cm^{-1}, with a sharp absorption band protruding at 3287 cm^{-1}. This latter absorption, coupled with absorption at 2230 and 2050 cm^{-1}, is indicative of a terminal and a non-terminal alkyne (2). The ^{13}C NMR spectrum shows four signals in the *sp* carbon region, at 76.9, 74.1, 72.0, and 68.4, consistent with the presence of two triple bonds. A *J*-compensated APT spectrum revealed that the carbon at δ 74.1 carries a hydrogen. The UV spectrum shows absorption bands at 252 and 310 nm, the latter the more intense. This is consistent with the presence of a conjugated endiyne (ref. 2, pp. 3–21).

The ^{1}H NMR spectrum shows signals for all eight hydrogens (Table 1) and the ^{13}C NMR shows the nine carbons (Table 1). The sole methylene carbon, located at δ 44.7, was shown in an HETCOR (3) experiment to correlate to the protons at 2.74 (ddd, J = 13.5, 7.0, 7.0) and 1.50 (ddd, J = 13.5, 6.0, 6.0). These protons are coupled to the protons at δ 4.62 and 4.55, which are attached to the carbons at δ 73.4 and 76.1, respectively. This results in the sequencing of carbons 1, 2, and 3, with the hydroxyl groups assigned as *cis* because of the large chemical shift between the protons of the methylene group. It has been shown that in such *cis* 4-cyclopenten-1,3-diols, the hydrogen *syn* to the hydroxyl groups is upfield of the *anti* proton (4, 5). In confirmation of this, nOe enhancements of H-1α (7.5%) and H-3α (7.5%) were observed when the H-2α signal is irradiated, and no enhancement was seen when H-2β is irradiated. The HMBC spectrum shows that the alkenic hydrogen is correlated with the other alkenic carbon and with the alkynic carbon at δ 76.9, confirming that the trisubstituted double bond is in conjugation with the carbon–carbon triple bonds, as implied by the UV spectrum. Correlated of the alkynic H (δ 3.30) with this same carbon (δ 76.9) as well as with C-8 (δ 68.4) completes the connectivity of the endiyne system. The HMBC correlations are shown in Fig. 1. Since sistodiolynne must be monocyclic, structure **1** is assigned.

Acetylation of sistodiolynne (**1**) provided the diacetyl derivative **1***a* as an unstable oil. The HREIMS confirmed the molecular formula and, as shown in Table 1, the ^{1}H NMR spectrum is in good agreement with structure **1***a*.

Fig. 1. Significant HMBC correlations of sistodiolynne (**1**).

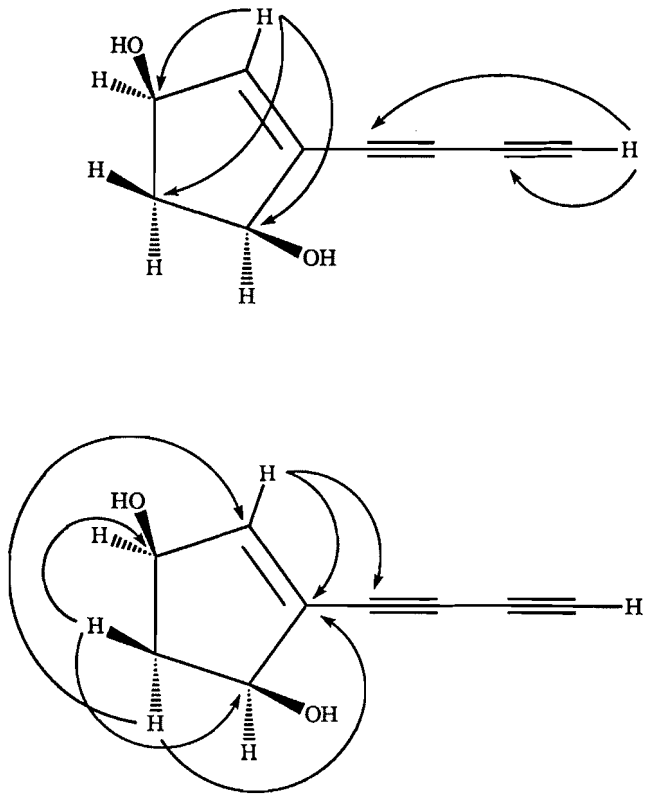

Catalytic hydrogenation (Pd–C, EtOAc) of sistodiolynne (**1**) provides a mixture of the saturated stereoisomers **2** and **3** that proved to be much more stable than sistodiolynne. However, they could not be separated by chromatography, but the derived di-*p*-bromobenzoates **2***a* and **3***a* were separable by preparative TLC. The isomer **2***a* was the major component

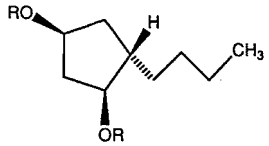

2 R = H
2a R = *p*-BrC_6H_4CO

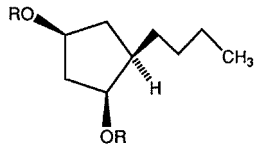

3 R = H
3a R = *p*-BrC_6H_4CO

Can. J. Chem. Downloaded from www.nrcresearchpress.com by 46.23.64.124 on 09/08/12
For personal use only.

Can. J. Chem. Downloaded from www.nrcresearchpress.com by 46.23.64.124 on 09/08/12
For personal use only.

(perhaps due to coordination of the catalyst with the hydroxyl groups), although **3***a* crystallized more readily. The HREIMS of **2***a* and **3***a* are very similar with each showing a molecular ion at *m/z* 522 ($C_{23}H_{24}O_4Br_2$). Loss of two molecules of *p*-bromobenzoic acid gives rise to a base peak at *m/z* 122 (C_9H_{14}). The ^{1}H NMR spectra of **2***a* and **3***a* are also very similar (see Experimental). The methylene hydrogens at C-2 and C-5 were identified by their different *geminal* couplings and by the ^{1}H–^{1}H COSY spectrum of **3***a*. The ^{13}C NMR (APT) spectra each show three methine carbons, two of which are oxygenated, five methylene carbons, and one methyl carbon. The complete ^{13}C NMR signal assignments were made by comparing the results of an HMQC experiment with the ^{13}C NMR spectra of **2***a* and **3***a* obtained during the ^{13}C-labelling experiments described later.

The stereochemistry of the butyl group in **2***a* and **3***a* is assigned on the basis of the chemical shift difference of H-3 in **2***a* and **3***a*. An alkyl group *vicinal* to the carbinyl proton is expected to make an upfield shift if it is *syn* to the carbinyl proton relative to when it is *anti* (6). In addition, irradiation of H-5α (δ 2.6) in **3***a* causes enhancement of H-1α (12%) and H-4 (14%). Similarly, irradiation of H-4 enhances the signal for H-3α by 15%.

The circular dichroism (CD) spectrum of **3***a* shows the first Cotton effect (negative) at 251 nm and the second (positive) at 231 nm. If we assume that the cyclopentane ring exists predominantly in the envelope conformation with the large butyl group in the equatorial lip position as depicted in **4**, a negative

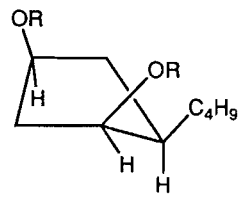

4 R = *p*-BrC_6H_4CO

chirality (7) exists between the chromophoric groups and the absolute configuration is as depicted in the structural formulae. MM2 calculations indicate that the conformation shown in **4** is the energy minimum (8).

Sistolynone (**5**) was isolated as an unstable oil by preparative TLC. The compound was washed from the adsorbent with deuterated chloroform and was not evaporated to dryness in order to prevent decomposition. This compound was less polar (higher R_f) than sistodiolynne (**1**). The molecular formula

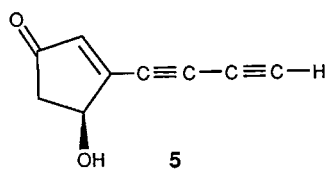

5

$C_9H_6O_2$ was determined by HREIMS, which indicated a molecular ion peak at *m/z* 146. The peak at *m/z* 118 represents loss of CO, suggesting the presence of a carbonyl group. A strong absorption band at 1710 cm^{-1} in the IR spectrum and a signal in the ^{13}C NMR (APT) spectrum at δ 204.4 confirm the presence of a ketonic carbonyl functionality. The position of this signal suggests an α,β-unsaturated five-membered ring ketone (9). The band at 3389 cm^{-1} is strong evidence for a hydroxyl group, and bands at 3284 and 2204 cm^{-1} indicate a terminal alkyne group.

A singlet at δ 2.9 in the ^{1}H NMR spectrum was easily recognized as the CH of a terminal alkyne. A methylene pair is evident from signals at δ 2.8 and 2.4 (J_{gem} = 18.6 Hz), the chemical shifts and the magnitude of the coupling constant suggesting that they are attached to the carbon α to the carbonyl group. The proton signal at δ 5.0 (dddd, J = 6.5, 5.0, 2.5, 1.0 Hz) is vicinally coupled to this methylene pair by 6.5 and 2.5 Hz and by 5.0 and 1.0 Hz to protons at δ 2.3 and 6.4, respectively. The signal at δ 2.3 disappears when D_2O is added to the sample, indicating that it is a hydroxyl hydrogen. The ^{13}C NMR spectrum is very straightforward and contains nine signals, three of which appear in the region of C≡C at δ 89.8, 68.2, and 66.8. This suggests the presence of a dialkyne system by analogy to the spectra observed for **1**. The terminal alkyne CH at δ 78.3 was distinguished from the rest of the signals by a *J*-compensated APT spectrum.

Based on all the spectral data discussed above, structure **5** is proposed for sistolynone. The small quantity of sistolynone obtained precluded other correlation experiments and derivatization.

Sistopyrone (**6**) also was obtained as an unstable oil by preparative TLC. The HREIMS spectrum displays a molecular ion peak at *m/z* 148, establishing $C_9H_8O_2$ as the molecular formula. The strong absorption at 1725 cm^{-1} in the FTIR spectrum suggests a carbonyl group. The ^{1}H NMR spectrum displays a total of six signals, three of which appear in the olefinic region between δ 7.41 and 6.18. The proton at δ 6.18 (H-3, ddd, J = 2.0, 1.0, 1.0 Hz) is coupled to protons at 7.41 (H-6, dd, J = 5.2, 1.0 Hz), 6.12 (H-5, dd, J = 5.2, 1.0 Hz), and 3.12 (2H, H-7, dtd, J = 7.0, 2.9, 1.0 Hz). The chemical shifts and coupling constants displayed by these olefinic protons, in addition to signals at δ 162.2 (s), 156.8 (s), 150.7 (d), 113.7 (d), and 108.0 (d) in the ^{13}C NMR spectrum, suggest a pyrone ring substituted at the 4-position (10, 11). HMQC correlations confirm the assignments for the partial structure mentioned above.

Infrared bands at 1955 and 853 cm^{-1} are indicative of an allene group (-HC=C=CH_2) (12). Signals at δ 209.7 (s), 85.5 (d), and 76.3 (t) are consistent with this functionality (12). The remaining signals in the ^{1}H NMR spectrum are a one-proton signal at δ 5.15 (qn, J = 7.0 Hz) and a two-proton signal at δ 4.79 (dt, J = 6.7, 2.9 Hz). Decoupling experiments provide confir-

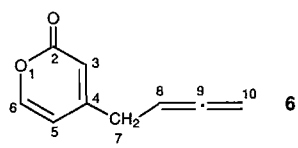

6

matory information concerning the allene group. In particular, the irradiation of the signal at δ 3.12 (dtd, 7.0, 2.9, 1.0 Hz) results in the collapse of signals at δ 6.18, 5.15, and 4.79. The signal at δ 5.15 becomes a triplet with J = 6.7 Hz, coupling only to the signal at δ 4.79. It became evident at this point that the signal at δ 5.15 is in fact an overlapping pair of triplets rather than a quintet. Structure **6** is consistent with these data. Lack of material precluded further experimentation.

Biosynthesis

The metabolites of *S. raduloides* represent a new structural

Can. J. Chem. Downloaded from www.nrcresearchpress.com by 46.23.64.124 on 09/08/12
For personal use only.

Fig. 2. Acetate labelling patterns in sistodiolynne (**1**).

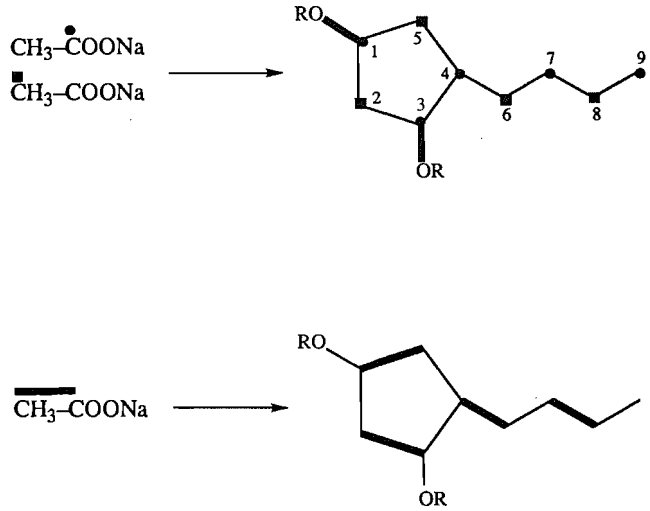

type of natural product. We have been unable to locate a compound in the literature with this carbon skeleton. The unbranched nature of the carbon skeletons in sistodiolynne (**1**) and sistolynone (**5**), along with the endiyne unit, suggest a polyketide origin. Liquid cultures of the fungus were grown in the presence of [1-^{13}C], [2-^{13}C], and [1,2-$^{13}C_2$] sodium acetate. Since the compounds are unstable, the labelled metabolites were reduced and transformed to the *p*-bromobenzoates in order to study the incorporation pattern. In the case of both di-*p*-bromoacetates, carbons 1, 3, 4, 7, and 9 were enhanced in the [1-^{13}C]acetate experiment and carbons 2, 5, 6, and 8 in the [2-^{13}C] case (illustrated in Fig. 2 for compound **1**). In the case of the C-1 labelling, the signals for C-3 and C-4 show some coupling, indicating that a significant number of molecules incorporating two labelled acetate units were present. In the case of the [1,2-C_2] acetate, C-9 appeared as an enhanced singlet, while all the other signals appeared as doublets. This implies that the compounds are norpentaketides, in which the methyl carbon of one of the acetate units has been lost (see Fig. 2). A 2D-INADEQUATE experiment on **2***a* obtained from the [1,2-$^{13}C_2$]acetate confirmed the spin-coupled carbons and firmly identified the carbon pairs as: C-1, C-5; C-2, C-3; C-4, C-6; and C-7, C-8 (see Experimental).

Most natural polyacetylenes are acetate derived, many by degradation of oleic acid (14). Loss of the terminal methyl via the sequence -CH_3 → CH_2OH → -CHO → -COOH and decarboxylation to yield the terminal acetylene is well documented (2, 14). One possible pathway is illustrated in Scheme 1 in which we use the carboxyl labelled case for illustrative purposes. The intermediate **7** may be derived from five acetate units or by degradation of oleic acid. Ring closure, adjustment of the oxidation level, and loss of the terminal methyl via oxidation and decarboxylation leads to sistodiolynne (**1**). An alternative scheme

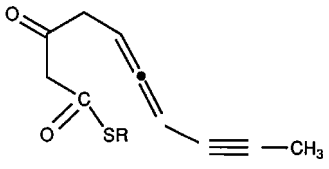

8

involving contraction of a six-membered ring derived from the tautomeric (with **7**) allene **8** is discussed in ref. 15.

The ^{13}C-labelling pattern established for sistopyrone is shown in Fig. 3 and suggests that it is derived by oxidative ring expansion of the sistodiolynne skeleton. Scheme 2 depicts a possible biogenetic pathway from sistolynone (**5**) to sistopyrone involving a Baeyer–Villager oxidation, dehydration, adjustment of side-chain oxidation level, and tautomerization to the allene. Again we choose the [1-^{13}C]acetate labelled case for illustrative purposes. As in the case of sistodiolynne, the signals for C-3 and C-4 appear as doublets, flanking a central singlet, indicating that these two carbons arise from acetate carbonyls.

The insoluble black polymeric material resulting when the crude extracts were exposed to oxygen was subjected to combustion analysis and shows an approximate empirical formula C_3H_2O that is not consistent with any of the individual compounds isolated, but suggestive of a general oxidative polymerization. We conclude that the graphite-like particles observed on solid agar media result from polymerization of the polyacetylenes produced by the fungus. The polymer was not investigated further. The instability of the compounds also precluded any investigation of biological activity.

Experimental

General methods

HREIMS were recorded on a Kratos AEI MS-50 mass spectrometer. FTIR spectra were recorded on a Nicolet 7199 FTIR and Nicolet MX-1 FTIR. NMR (^{1}H and ^{13}C) were obtained on a Varian Unity-500 spectrometer and Bruker WH-300, WM-360, and WH-400 spectrometers. NOE experiments were determined in the difference mode. The following 2D experiments, COSY, HMQC, and HMBC, were obtained on a Varian Unity-500 spectrometer. INADEQUATE was performed using a Bruker WH-300 spectromter. UV spectra were determined on a Hewlett Packard 8450A diode array spectrophotometer. Optical rotations were determined using a Perkin Elmer 241 polarimeter. Circular dichroism (CD) spectra were measured using a Jasco SS-20-2 spectropolarimeter. Preparative thin-layer chromatography (PTLC) was performed on E. Merck precoated 20 × 20 glass plates of silica gel 60 F-254. Hexanes refer to light petroleum (bp 60–68°C). All solvents were distilled prior to use.

Description of the fungus

In culture, *Sistotrema raduloides* (UAMH 7326) is moderately slow growing, reaching the edge of the petri dish in 4 or 5 weeks. It forms a dense, moderately thick, felty mat of mycelium. On 2% malt extract agar, UAMH 7326 developed a lattice-like network of reddish brown hyphal tufts that was associated with droplets of clear or amber liquid. On malt and other media such as cornmeal agar, the isolate formed yellowish to reddish brown sclerotia. Microscopic features of the fungus were observed in slide culture preparations in which the fungus is inoculated onto a block of cereal agar placed between two sterile glass coverslips. Microscopic preparations are made when the mycelium of the fungus grows onto the glass surfaces (16). Flaky black deposits were noticed on the glass coverslips and on the surface of colonies grown on various media when growth was examined under a dissecting microscope. These deposits were detected easily in UAMH 7326, but observed sparsely only in two of five other isolates of *S. raduloides*.

Microscopically, the isolate from air samples in Puerto Rico

Can. J. Chem. Downloaded from www.nrcresearchpress.com by 46.23.64.124 on 09/08/12
For personal use only.

Scheme 1.

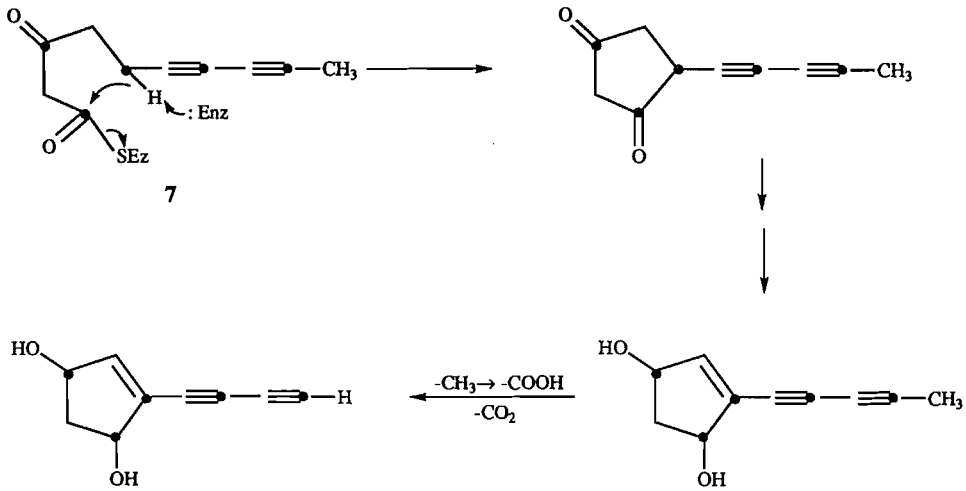

Scheme 2.

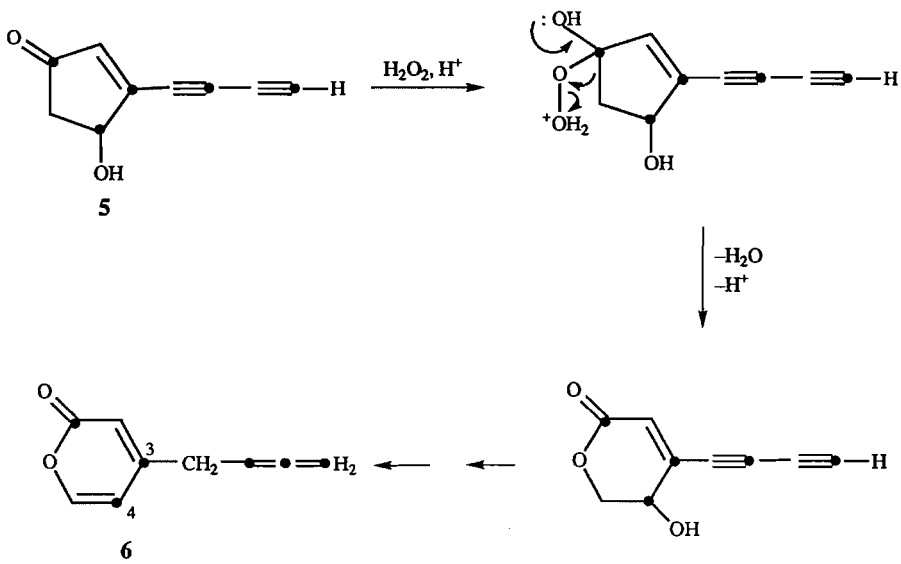

Fig. 3. Acetate labelling patterns in sistopyrone (**6**).

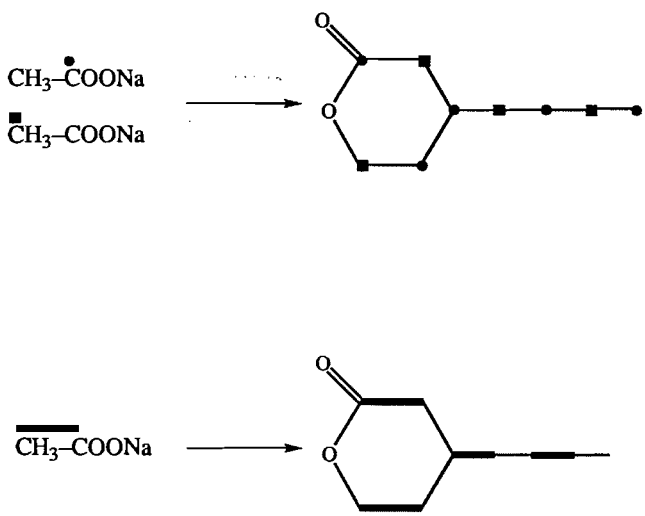

resembled other isolates of *S. raduloides* in forming conidia and yellowish-brown sclerotia having short spinelike appendages, but it lacked clamp connections. A characteristic feature of *S. raduloides*, as noted by others (1, 17, 18), is the formation of hyaline, thin-walled, pyriform (tear-drop) or obovate (egg-shaped) conidia having a flat basal scar. A single conidium forms at the end of a lateral branch and this branch proliferates sympodially to form additional short, blunt, branches, each of which forms a conidium. The entire structure may be simple with two to six conidia or the conidiophore may proliferate to form a small cluster of conidia. Detachment of the mature conidium leaves a truncate scar.

Where a fungus has more than one distinctive stage in its life cycle, it has been common practice to name both states. The solitary blastic conidia borne sympodially on blunt denticles are unusual among the Corticiaceae but this asexual stage has not previously been connected to a genus of Hyphomycetes. *Dexhowardia* Taylor (19) was described for a single species *Dexhowardia tetraspora* Taylor for a fungus suspected to have basidiomycetous affinity, and which lacked

Can. J. Chem. Downloaded from www.nrcresearchpress.com by 46.23.64.124 on 09/08/12
For personal use only.

clamp connections, and formed conidia on blunt denticles in the manner of *S. raduloides*. A further report on the biology of *S. raduloides* and its possible connection with *Dexhowardia* will be submitted to a mycological journal by L.S.

Growth of *Sistotrema raduloides* and isolation of the metabolites

Sistotrema raduloides strain UAMH 7326 was grown on Sabouraud dextrose agar (20 g/L) and the mycelial suspension was used to inoculate five 4-L Erlenmeyer flasks, each containing 2 L of Sabouraud dextrose broth (15 g in 1 L of redistilled water). The cultures were grown as still cultures at room temperature for 5 weeks. The culture broth was separated from the mycelium by filtration and the volume reduced under vacuum to ca. 400 mL. The concentrated broth was first extracted with methylene chloride and then with ethyl acetate. The organic layers were dried separately with anhydrous sodium sulphate, filtered, and concentrated to small volume under reduced pressure. Polymerization occurred if the solvent was completely removed. The methylene chloride extract was separated by preparative TLC and gave compounds **1**, **5**, and **6**. The ethyl acetate extract gave mainly compound **1**.

Labelling experiments

Liquid cultures were prepared as described above. A solution of [1-^{13}C] sodium acetate (5 mL, 0.2 mol/L) was added under sterile conditions 3 days after inoculation of the fungus. Four further additions were made at 2 day intervals, and the culture was allowed to grow for 5 weeks. The same procedure was followed using [2-^{13}C] sodium acetate and [1,2-^{13}C] sodium acetate. The isolation procedure was the same as described above.

*Sistodiolynne (**1**)*

(−)1*R*,3*S*-4-Butadiynyl-4-cyclopentene-1,3-diol, **1**, was isolated as an unstable colorless oil; TLC: R_f 0.18 (CH_2Cl_2:CH_3OH, 19:1); UV (MeOH): 310, 252 nm; FTIR ($CDCl_3$, cast): 3544 (br, OH), 3287 (≡C-H), 2230 (C≡C) cm^{-1}; ^{1}H NMR (acetone-d_6) δ: 6.30 (1H, dd, J = 2.0, 1.0 Hz, H-5), 4.70 (1H, d, J = 6.5 Hz, OH-1β), 4.62 (1H, bdd, H-1α), 4.55 (1H, m, H-3α), 4.48 (1H, d, J = 6.5 Hz, OH-3β), 3.30 (1H, s, H-9), 2.74 (1H, ddd, J = 13.4, 7.0, 7.0 Hz, H-2α), 1.50 (1H, ddd, J = 13.5, 6.2, 6.2 Hz, H-2β); ^{13}C NMR (acetone-d_6) δ: 146.7 (C-5, d), 129.8 (C-4, s), 76.9 (C-6, s), 76.1 (C-1, d), 74.1 (C-9, d), 73.4 (C-3, d), 72.0 (C-7, s), 68.4 (C-8, s), 44.7 (C-2, t); HREIMS (probe 100°C), *m/z* calcd. for $C_9H_8O_2$ (M^+): 148.0509; found: 148.0524, 147 ($C_9H_7O_2$, 25%), 130 (C_9H_6O, 10%), 119 (C_8H_7O, 49%), 102 (C_8H_6, 62%), 76 (C_6H_4, 89%), 74 (C_6H_2, 53%).

*O,O-Diacetylsistodiolynne (**1**a)*

Treatment of sistodiolynne (3–4 mg, estimated) in CH_2Cl_2 with acetic anhydride (0.2 mL) and pyridine (1.0 mL) for 12 h, followed by removal of the solvents under vacuum, gave an oil, which was purified by preparative TLC using 5% MeOH in CH_2Cl_2 and was eluted from the plate with deuterated chloroform; TLC: R_f 0.72; FTIR ($CDCl_3$, cast): 3251 (≡C-H), 1737)-COO-) cm^{-1}; ^{1}H NMR ($CDCl_3$) δ: 6.44 (1H, bd, J = 2.2 Hz, H-5), 5.60 (2H, m, H-1α3α), 2.95 (1H, ddd, J = 14.6m 6.7, 6.7 Hz, H-2α), 2.50 (1H, s, H-9), 2.08 (3H, s, OAc), 2.02 (3H, s, OAc), 1.75 (1H, ddd, J = 14.6, 4.2, 4.2 Hz, H-2β); HREIMS (probe 100°C) *m/z* calcd. for $C_{13}H_{12}O_4$ (M^+): 232.0736; found: 232.0730, (5%), 172 ($C_{11}H_8O_2$, 11%), 130 (C_9H_6O, 100%), 102 (C_8H_6, 34%).

Reduction and *p*-bromobenzoylation of sistodiolynne (**1**)

Catalytic hydrogenation (Pd–C, EtOAc, 40 psi (1 psi = 6.9 kPa)) of **1** provided a mixture of the saturated isomers (**2***a* and **3***b*), which were not separable by TLC. The mixture was treated with *p*-Br-BzCl (40 mg) and pyridine (2 mL) in CH_2Cl_2 with stirring at room temperature for 24 h. The resulting mixture was concentrated under vacuum to dryness. Separation of the di-*p*-bromobenzoate derivatives (**2***a* and **3***a*) was achieved by preparative TLC (5% EtOAc in hexanes, developed several times).

*Compound **2**a*

(−)1*S*,3*S*-Di-*p*-bromobenzoyloxy-4*S*-butylcyclopentane, **2***a*, was isolated as a yellowish sticky solid that could not be crystallized. TLC: R_f 0.31 (hexane:EtOAc, 9:1); FTIR (CH_2Cl_2, cast), 2957, 2955 (C-H), 1717 (-COO-) cm^{-1}; ^{1}H NMR ($CDCl_3$) δ: 7.9 (4H, m), 7.5 (4H, m), 5.4 (1H, m), 5.1 (1H, ddd, J = 7.2, 4.4, 3.8 Hz), 2.6 (1H, ddd, J = 15.5, 7.5, 7.2 Hz), 2.5 (1H, m), 2.3 (1H, dddd, J = 14.0, 7.6, 2.1, 2.1 Hz), 2.1 (1H, bd, J = 15.5 Hz), 1.7 (1H, ddd, J = 14.0, 9.3, 5.8 Hz), 1.6–1.3 (6H, m), 0.9 (3H, t, J = 6.7 Hz); ^{13}C NMR ($CDCl_3$) δ: 165.6 (2C, s), 131.7 (4C, d), 131.1 (4C, d), 129.3 (2C, s), 128.1 (2C, s), 80.5 (C-3, d), 75.6 (C-1, d), 44.0 (C-4, d), 38.9 (C-2, t), 37.5 (C-5, t), 33.1 (C-6, t), 30.1 (C-7, t), 22.8 (C-8, t), 14.0 (C-9, q); HMQC (125, 500 MHz) δ: 80.5 ⇔ 5.1; 75.6 ⇔ 5.4; 44.0 ⇔ 2.5; 38.9 ⇔ 2.6, 2.1; 37.5 ⇔ 2.3, 1.7; 33.1 ⇔ 1.6, 1.3; 30.1 ⇔ 1.3; 22.8 ⇔ 1.3; 14.0 ⇔ 0.9; HREIMS (probe 150°), *m/z* calcd. for $C_{23}H_{24}O_4{}^{79}Br^{81}Br$ (M^+ + 2): 524.0021; found: 524.0001 (2%), 522 (M^+, $C_{23}H_{24}O_4{}^{79}Br_2$, 1%), 322 ($C_{16}H_{19}O_2{}^{79}Br$, 3%), 122 ($C_9H_{14}$, 100%), 80 ($C_6H_8$, 48%).

*Compound **3**a*

(−)1*S*,3*S*-Di-*p*-bromobenzoyloxy-4*R*-butylcyclopentane, **3***a*, was recrystallized from hexane to give fine white needles, mp 110–111°C; TLC: R_f 0.27 (hexane:EtOAc, 9:1); $[\alpha]_D{}^{24}$ −14 (*c* 0.004, hexanes); CD, $\Delta\epsilon_{241}$: −3.6 (*c* 8.8 × 10^{-4}, hexanes); FTIR (CH_2Cl_2 cast) similar to **2***a*; ^{1}H NMR ($CDCl_3$) δ: 7.9 (2H, J = 9.0 Hz), 7.8 (2H, d, J = 9.0 Hz), 7.6 (2H, J = 9.0 Hz), 7.5 (2H, J = 9.0 Hz), 5.5 (1H, dddd, J = 10.0, 7.5, 5.0, 2.5 Hz), 5.4 (1H, bdd, J = 5.0, 4.1 Hz), 2.6 (1H, ddd, J = 13.7, 7.5, 7.0 Hz), 2.4 (1H, ddd, J = 15.5, 8.0, 5.0 Hz), 2.2 (1H, bd, J = 15.5 Hz), 2.0–2.1 (1H, m), 1.8 (1H, ddd, J = 13.7, 10.0, 5.2 Hz), 1.6–1.3 (6H, m), 0.9 (3H, m); ^{1}H–^{1}H COSY ($CDCl_3$) δ: 5.5 (H-1α) ⇒ 2.6 (H-5α), 2.4 (H-2α), 2.2 (H-2β), 1.8 (H-5β); 5.4 (H-3α) ⇒ 2.4 (H-2α), 2.2 (H-2β), 2.1 (H-4α); 2.6 (H-5α) ⇒ 5.5 (H-1α), 2.1 (H-4α), 1.8 (H-5β); 2.4 (H-2α) ⇒ 5.5 (H-1α), 5.4 (H-3α), 2.2 (H-2β); 2.2 (H-2β) ⇒ 5.5 (H-1α), 5.4 (H-3α), 2.4 (H-2α), 1.8 (H-5β); 2.1 (H-4α) ⇒ 5.4 (H-3O), 2.6 (H-5α), 1.8 (H-5β), 1.6–1.3 (H-6); 1.8 (H-5β) ⇒ 5.5 (H-1α), 2.6 (H-5α), 2.1 (H-4α); 1.6 (H-6α) ⇒ 2.1 (H-4α), 1.3 (H-6β), 1.5–1.3 (H-6, 7); differential nOe: H-4α to H-3α 15%, H-2α 10%, H-5α 7%, H-6α 7%; H-5α to H-5β 34%, H-4α 14%, H-1α 12%; ^{13}C NMR ($CDCl_3$) δ: 165.5 (1C, s), 165.4 (1C, s), 131.8 (2C, d), 131.6 (2C, d), 131.1 (2C, d), 131.0 (2C, d), 129.5 (1C, s), 129.3 (1C, s), 128.1 (2C, s), 76.8 (C-3, d), 75.0 (C-1, d), 43.6 (C-4, d), 39.8 (C-2, t), 37.7 (C-5, t), 30.4 (C-7, t), 29.1 (C-6, t), 22.8 (C-8, t), 14.0 (C-9, q), HMQC (125, 500 MHz) δ: 76.8 ⇔ 5.4; 75.0 ⇔ 5.5; 43.6 ⇔ 2.1; 39.8 ⇔ 2.4, 2.2; 37.7 ⇔

Can. J. Chem. Downloaded from www.nrcresearchpress.com by 46.23.64.124 on 09/08/12
For personal use only.

2.6, 1.8; 29.1 ⇔ 1.5; 22.8 ⇔ 1.3; 14.0 ⇔ 0.9; HREIMS (probe 150°C) similar to **3***a*.

*Sistolynone (**4**)*

Butadiynyl-4-hydroxyl-2-cyclopenten-1-one, **4**, was isolated as an unstable oil. TLC: R_f 0.33 (CH_2Cl_2:CH_3OH, 19:1); FTIR ($CDCl_3$ cast): 3387 (O-H), 3284 (≡C-H), 2204 (C≡C), 1710, 1683 (α,β-unsaturated carbonyl) cm^{-1}; ^1H NMR ($CDCl_3$) δ: 6.45 (1H, d, J = 1.0 Hz, H-2), 5.00 (1H, dddd, J = 6.5, 5.0, 2.5, 1.0 Hz, H-4), 2.90 (1H, s, H-10), 2.85 (1H, dd, J = 18.6, 6.5 Hz, H-5α), 2.40 (1H, dd, J = 18.6, 2.5 Hz, H-5β), 2.30 (OH, d, J = 5.0 Hz); ^{13}C NMR ($CDCl_3$) δ: 204.4 (C-1, s), 154.7 (C-3, s), 139.3 (C-2, d), 89.9 (C-7, s), 78.3 (C-9, d), 72.1 (C-4, d), 68.2 (C-6, s), 66.8 (C-8, s), 44.0 (C-5, t); HREIMS (probe 100°C), *m/z* calcd. for $C_9H_6O_2$ (M^+): 146.0368; found: 146.0363 (51%), 118 (C_8H_6O, (C_8H_6O, 31%), 74 (C_6H_2, 100%).

*Sistopyrone (**5**)*

(2,3-Butadienyl)pyran-2-one, **5**, was obtained in deuterated chloroform as an oil after preparative TLC, R_f 0.73 (CH_3OH, 19:1); FTIR, $CDCl_3$, cast): 1955 (C=C=C), 1725, 1651, 1637, 853 (=CH_2) cm^{-1}; ^1H NMR ($CDCl_3$) δ: 7.41 (1H, dd, J = 5.2, 1.0 Hz, H-6), 6.18 (1H, ddd, J = 2.0, 1.0, 1.0 Hz, H-3), 6.12 (1H, dd, J = 5.2, 2.0 Hz, H-5), 5.15 (1H, tt, J = 7.0, 6.7 Hz, H-8), 4.79 (2H, dt, J = 6.7, 2.9 Hz, H-10)), 3.12 (2H, dtd, J = 7.0, 2.9, 1.0 Hz, H-7); homonuclear decoupling (irradiation ⇒ effect): δ 6.18 ⇒ 7.41 (dd to d, J = 5.2 Hz), 6.12 (dd to d, J = 5.2 Hz), 3.12 (dtd to dt, J = 7.0, 2.9 Hz); δ 4.79 ⇒ 5.15 (tt to t, J = 7.0 Hz), 3.12 (dtd to dd, J = 7.0, 1.0 Hz); δ 3.12 ⇒ 6.18 (ddd to dd, J = 2.0, 1.0 Hz), 5.15 (tt to t, J = 6.7 Hz), 4.79 (dt to d, J = 6.7 Hz); ^{13}C NMR ($CDCl_3$) δ: 209.7 (C-9, s), 162.2 (C-2, s), 156.8 (C-4, s), 150.7 (C-6, d), 113.7 (C-3, d), 108.0 (C-5, d), 85.5 (C-8, d), 76.3 (C-10, t), 34.3 (C-7, t); HMQC (125, 500 MHz) δ: 113.7 ⇔ 6.18; 108.0 ⇔ 6.12; 76.3 ⇔ 4.79; 34.3 ⇔ 3.12; HREIMS (probe 100°C), *m/z* calcd. for $C_9H_8O_2$: 148.0524 (M^+); found: 148.0522 (8%), 120 (C_8H_8O, 75%), 91 (C_7H_7, 100%), 65 (C_5H_5, 23%), 39 (C_3H_3, 34%).

^{13}C-Labelled metabolites

[1,2-$^{13}C_2$]-Acetate labelled metabolites

*[1,2-$^{13}C_2$]-Di-p-bromobenzoate derivative (**2**a)*: ^{13}C NMR (CD_2Cl_2, 100 MHz) spin-coupled carbons: δ 80.9 (C-3, d, $J_{3,2}$ = 37.6 Hz), 76.1 (C-1, d, $J_{1,5}$ = 36.0 Hz), 44.3 (C-4, D, $J_{4,6}$ = 35.6 Hz), 39.3 (C-2, d, $J_{2,3}$ = 37.6 Hz), 37.8 (C-5, d, $J_{5,1}$ = 36.0 Hz), 33.5 (C-6, d, $J_{6,4}$ = 35.7 Hz), 30.5 (C-7, d, $J_{7,8}$ = 34.5 Hz), 23.1 (C-8, d, $J_{8,7}$ = 34.5 Hz); singlet carbon: 14.0 (C-9); INADEQUATE ($CDCl_2$, 75 MHz) cross peaks (two double quantum); δ: 80.9 (C-3) ⇔ 39.3 (C-2); 76.1 (C-1) ⇔ 37.8 (C-5); 44.3 (C-4) ⇔ 33.5 (C-6); 30.5 (C-7) ⇔ 23.1 (C-8).

*[1,2-$^{13}C_2$]-Sistopyrone (**5**)*: ^{13}C NMR ($CDCl_3$) spin-coupled carbons: δ209.7 (C-9, d, $J_{8,7}$ = 102.1 Hz), 162.2 (C-2, d, $J_{1,2}$ = 74.1 Hz), 156.8 (C-4, d, $J_{3,6}$ = 42.1 Hz), 150.7 (C-6, d, $J_{5,4}$ = 70.4 Hz), 113.7 (C-3, d, $J_{2,1}$ = 74.1 Hz), 108.0 (C-5, d, $J_{4,5}$ = 70.5 Hz), 85.5 (C-8, d, $J_{7,8}$ = 102.1 Hz), 34.3 (C-7, d, $J_{6,3}$ = 42.1 Hz); singlet carbon: 76.3 (C-10).

[1-^{13}C]-Acetate labelled metabolites

*[1-^{13}C]-Di-p-bromobenzoate derivative (**2**a)*: ^{13}C NMR (CD_2Cl_2) enhanced signals: δ 80.5 (C-3), 76.7 (C-1), 44.0 (C-4), 30.1 (C-7), 14.0 (C-9); natural abundance signals: δ 38.9 (C-2), 37.5 (C-5), 33.1 (C-6), 22.8 (C-8).

*[1-^{13}C]-Sistopyrone (**5**)*: ^{13}C NMR ($CDCl_3$) enhanced signals: δ 162.2 (C-1), 156.8 (C-3), 108.8 (C-4), 85.5 (C-7), 76.3 (C-9); natural abundance signals: δ 209.7 (C-8), 150.7 (C-5), 113.7 (C-2), 34.3 (C-6).

[2-^{13}C]-acetate labelled metabolites

*[2,^{13}C]-di-p-Bromobenzoate derivative (**2**a)*: ^{13}C NMR (CD_2Cl_2) enhanced signals: δ 38.9 (C-2), 37.5 (C-5), 33.1 (C-6), 22.8 (C-8); natural abundance signals: δ 80.5 (C-3), 76.7 (C-1), 44.0 (C-4), 30.1 (C-7), 14.0 (C-9).

*[2-^{13}C]-Sistopyrone (**5**)*: ^{13}C NMR ($CDCl_3$) enhanced signals: δ 209.7 (C-9), 150.7 (C-6), 113.7 (C-3), 34.3 (C-7); natural abundance signals: δ 162.2 (C-2), 156.8 (C-4), 108.8 (C-5), 85.5 (C-8), 76.3 (C-10).

Acknowledgements

We thank the Natural Sciences and Engineering Research Council of Canada for financial support, and Prof. D.D. Tanner for assistance in the MM2 calculation of compound **2***a*.

References

1. K. Nakasone. Cultural studies and identification of wood-inhabiting Corticiaceae and selected Hymenomycetes from North America. Mycologia Memoir No. 15, J. Cramer, Berlin. 1990. pp. 298–300.
2. F. Bohlman, T. Burkhardt, and C. Zdero. Naturally occurring acetylenes. Academic Press, London. 1973. p. 22.
3. A. Bax and G. Morris. J. Magn. Reson. **42**, 501 (1981).
4. F.G. Cocu, T. Posternak, and L.B. Wolczunowicz. Helv. Chim. Acta, **53**, 739 (1970).
5. B.M. Trost and T.R. Verhoeven. J. Am. Chem. Soc. **102**, 4730 (1980).
6. M. Antewais and D. Danneels. Org. Magn. Reson. **7**, 345 (1975).
7. N. Harade and K. Nakanishi. Circular dichroic spectroscopy—exciton coupling in organic stereochemistry. University Science Books, Mill Valley, Calif. 1983. pp. 10 and 11.
8. G. Chang, W.C. Guida, and W.C. Still. J. Am. Chem. Soc. **111**, 4379 (1989).
9. S.P. Tanis, E.D. Robinson, M.C. McMills, and W. Watt. J. Am. Chem. Soc. **114**, 8349 (1992).
10. W.H. Pirkle and M.J. Dines. J. Heterocycl. Chem. **6**, 1 (1969).
11. W.V. Turner and W.H. Pirkle. J. Org. Chem. **39**, 1935 (1974).
12. S.R. Landor. The chemistry of allenes. Academic Press, Toronto. 1982. p. 780.
13. A. Bax, R. Freeman, and S.P. Kempsell. J. Am. Chem. Soc. **102**, 4829 (1980).
14. J. Mann. Secondary metabolism. 2nd ed. Clarendon Press, Oxford. 1987. pp. 38–42.
15. A.K. Amegadzie. M.Sc. Thesis. University of Alberta, Edmonton. 1995. pp. 28–30.
16. L. Sigler. Clinical microbiology procedures handbook *Edited by* M. McGinnis. American Society for Microbiology, Washington, D.C. 1992. pp. 6.12.1–6.12.4.
17. M.B. Maxwell. Can. J. Bot. **32**, 259 (1954).
18. J.A. Stalpers. Stud. Mycol. **16**, 1 (1978).
19. J.J. Taylor. Mycopathol. Mycol. Appl. **40**, 305 (1970).

Optical absorption spectra of solvated electrons in 1-butylamine–water mixed solvents

Yixing Zhao and Gordon R. Freeman

Abstract: The optical absorption spectra of e_s^- in 1-butylamine–water mixed solvents increase smoothly in energy and intensity as the water content is increased, with the exception of a small decrease in intensity on going from 95 to 100 mol% water. At 298 K the value of $G\epsilon_{max}$ increases from 1.42×10^{-21} m^2/16 aJ (8.6×10^3 e_s^- L/100 eV mol cm) in pure 1-butylamine to 8.3×10^{-21} m^2/16 aJ (50×10^3 e_s^- L/100 eV mol cm) in pure water, and the value of E_{Amax} increases from 115 zJ (0.72 eV) to 278 zJ (1.74 eV). In the pure amine, if $G(e_s^-) = 0.27$, then $\epsilon_{max} = 5.3 \times 10^{-21}$ m^2/e_s^- (3200 m^2/mol). The solvent composition dependences of $G\epsilon_{max}$ and E_{Amax} indicate little selective solvation of e_s^- by water; this might be due to relatively "ideal" mixing of water and amine in the binary solvents. The temperature coefficient $-dE_{Amax}/dT = 0.43$ zJ/K in pure 1-butylamine, 0.47 in pure water, and has a minimum of 0.27 in the 50:50 mixture.

Key words: 1-butylamine–water mixed solvents, optical absorption spectra, solvated electron, temperature dependence.

Résumé : Dans des solvants mixtes 1-butylamine–eau, les spectres d'absorption optique des e_s^- augmentent en façon monotone, tant en énergie qu'en intensité, avec une augmentation de la quantité d'eau, à l'exception d'une légère diminution en passant de 95 à 100% d'eau. À 298 K, la valeur du $G\epsilon_{max}$ augmente de $1{,}42 \times 10^{-21}$ m^2/16 aJ ($8{,}6 \times 10^3$ e_s^- L/100 eV mol cm) dans la 1-butylamine pure à $8{,}3 \times 10^{-21}$ m^2/16 aJ (50×10^3 e_s^- L/100 eV mol cm) dans l'eau pure et les valeurs de E_{Amax} augmentent de 115 zJ (0,72 eV) à 278 zJ (1,74 eV). Dans l'amine pure, si $G(e_s^-) = 0{,}27$, alors $\epsilon_{max} = 5{,}3 \times 10^{-21}$ m^2/e_s^- (3200 m^2/mol). Les dépendances de $G\epsilon_{max}$ et de E_{Amax} avec la composition du solvant indiquent qu'il se produit très peu de solvatation spécifique des e_s^- par l'eau; ceci peut être causé par le mélange relativement «idéal» de l'eau et de l'amine dans les solvants binaires. Le coefficient de température $-dE_{Amax}/dT = 0{,}43$ zJ/K dans la 1-butylamine pure, 0,47 dans l'eau pure et elle passe par un minimum de 0,27 à un mélange 50 : 50.

Mots clés : solvants mixtes 1-butylamine–eau, spectres d'absorption optique, électron solvaté, dépendance sur la température.

[Traduit par la rédaction]

Introduction

An excess electron in a polar liquid can occupy a localized state as a result of its interaction with a certain number of neighboring molecules of the solvent. When this interaction leads to a thermally relaxed state of the electron with respect to the medium, the electron is called a solvated electron, e_s^- (1, 2).

The energy levels of e_s^-, as reflected by the energy of the optical absorption maximum E_{Amax}, are determined as much by details of the liquid structure as by the dielectric constant or the molecular dipole moment (3–5). The solvated electron in water has an intense optical absorption band in the visible region, with a peak at 715 nm, which corresponds to E_{Amax} = 277 zJ (6),[2] and $G\epsilon_{max} = 8.3 \times 10^{-21}$ m^2/16 aJ (5.0×10^4 e_s^- L/100 eV mol cm) (7, 8) at 298 K.

The values of E_{Amax} are similar in pure *n*-alcohols and water (9–11). However, there is a marked dependence of E_{Amax} on the composition of alcohol–water mixed solvents (10). The values of E_{Amax} in amines are much smaller than that in water (4, 12). It is therefore interesting to discover the composition dependence of e_s^- spectra in 1-butylamine–water mixed solvents. Data are reported in this paper.

Experimental

Materials

1-Butylamine (Fluka, >98%) was treated for 24 h with potassium and sodium alloy under UHP argon (99.999%, Liquid Carbonic Canada Ltd.) at 330 K, to remove electron scavengers. Fractional distillation was as reported in ref. 13; spectroscopic analysis was not done. The water content, measured by Karl–Fisher titration, was 0.09 mol%. The solvated electron half-life of pure 1-butylamine after a 100 ns pulse of 340 fJ (2.1 MeV) electrons (4 J/kg) at 298 K was about 4 μs. The

Received May 9, 1995.

Y. Zhao and G.R. Freeman.[1] Chemistry Department, University of Alberta, Edmonton, AB T6G 2G2, Canada.

[1] Author to whom correspondence may be addressed. Telephone: (403) 492-3468. Fax: (403) 492-8231. E-mail: knp@dept.chem.ualberta.ca

[2] In SI: a = atto = 10^{-18}, z = zepto = 10^{-21}, y = yocto = 20^{-24}.

Can. J. Chem. Downloaded from www.nrcresearchpress.com by 46.23.64.124 on 09/08/12
For personal use only.

Can. J. Chem. Downloaded from www.nrcresearchpress.com by 46.23.64.124 on 09/08/12
For personal use only.

Table 1. Parameters of solvated electron spectra in 1-butylamine–water at 298 K.

Water mol%	d^a (kg/m^3)	η^a (mPa s)	$G\varepsilon_{max}$ 10^{-21} (m^2/16 aJ)^b	E_{Amax} (zJ)	$W_{1/2}$ (zJ)	E_r (zJ)	E_b (zJ)	W_b/W_r	$-dE_{Amax}/dT$ (zJ/K)
0	737	0.50	1.42	115	149^c	102^c	215	2.31^c	0.43
10	748	0.59	1.58	143	219^d	108^d	303	2.81^d	0.36
30	770	0.88	2.26	189	178	137	314	2.36	0.30
50	801	1.45	3.72	214	164	155	319	1.77	0.27
70	844	2.21	5.01	248	147	183	330	1.26	0.30
90	925	2.14	7.03	273	134	215	349	1.31	0.41
95			8.60	275	133	219	352	1.38	0.44
99			8.65	277	135	221	356	1.41	0.46
100	997	0.89	8.30	278	139	223	362	1.53	0.47

[a]Reference 16.
[b]1(e_s^- L/100 eV mol cm) = 1.66×10^{-25} (m^2/16 aJ) in SI.
[c]At 225 K, near the fp 224 K.
[d]At 226 K.

Fig. 1. Optical spectra of solvated electrons in 1-butylamine–water mixed solvents at 298 K. Mol% water: ●, 100; ○, 90; ■, 70; □, 50; ▲, 30; △, 10; ×, 0. 100 zJ = 0.624 eV.

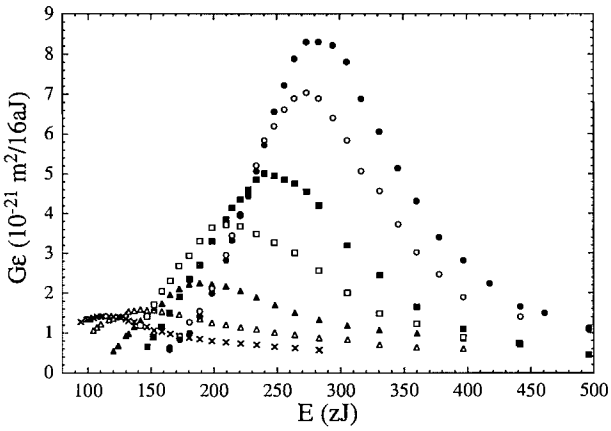

purification of water and the half-life of solvated electrons in water were as in ref. 14.

Techniques

The optical system, irradiation facilities, the silicon detector for wavelengths <1050 nm (14), the dosimetry (10), and the calculation of $G\epsilon_{max}$ (15) were described in the references cited. Bauch and Lomb monochromator gratings 1350 (No. 33-86-02) for 400–800 nm, 1350 (No. 33-86-03) for 700–1200 nm, and high-intensity monochromator (No. 33-86-78) for 1100–2600 nm were used in the measurements. Corning filters were placed in front of the monochromator to eliminate higher order light interference: CS 4-97 for 400–500 nm, CS 3-72 for 500–650 nm, CS 2-58 for 650–1050 nm, LL-1000 for 1050–1800 nm, and RL-1500 for 1800–2600 nm.

For the measurement of absorbance at wavelengths >1050 nm, an InSb infrared detector (model I935-IS) was used and is sensitive from 1050 to 2600 nm. The 3–97% response time of the detector, amplifier, and transient digitizer (Tekronix R7912) was 35 ns. The signal-to-noise ratio of the differential amplifier (Tektronix 7A13) was increased by using the 5 MHz filter, which gave a system response time of 96 ns.

Sample preparation was similar to that reported in ref. 14. Spectrosil optical cells were used: 10 mm pathlength for pure water to 70 mol% water, and 5 mm path for 50 mol% water to pure 1-butylamine.

Briefly, each 100 ns pulse of 340 fJ (2.1 MeV) electrons delivered about 4 Gy to the sample.

Physical properties

The normal freezing point of 1-butylamine is 224 K, and the normal boiling point is 351 K. The liquid is completely miscible with water.

The optical absorption spectra were measured at the following compsitions in mol% water: 0.0, 10.0, 30.0, 50.0, 70.0, 90.0, 95.0, 99.0 and 100.0. The densities and viscosities of the mixed solvent (16), except for 95.0 and 99.0 mol% water, are listed in Table 1. The relative permittivity of water at 298 K is 78.4 (17), and that of 1-butylamine is 4.78 (18).

Results and discussion

Absorbance and shape of e_s^- optical spectra at 298 K: solvent dependence

The optical spectra of e_s^- in 1-butylamine–water mixed solvents at 298 K are shown in Fig. 1. The spectra have no fine structure.

As the amount of water is increased in 1-butylamine the optical absorption band changes (Figs. 1–3, Table 1): (*i*) E_{Amax} increases; (*ii*) $G\epsilon_{max}$ increases; (*iii*) the band becomes narrower ($W_{1/2}$ decreases), except at >90 mol% water where the band broadens slightly.

The shift of E_{Amax} with water content in 1-butylamine (Fig. 2) is much closer to linear than is that in 1- or *tert*-butyl alcohol–water mixed solvents (Fig. 2 and ref. 10). This indicates that the amine–water solvents are less structured than are alcohol–water solvents. The spectra in 1-butanol–water and *tert*-butanol–water shift greatly with the addition of 10 mol% of water to the alcohol, which indicates that 10 mol% of water in the alcohols produces a particular structure (molecular packing) that affects the electron trap. This type of structure evidently does not occur in 1-butylamine–water mixed solvents. Hydrogen bonds in RNH_2 are weaker than those in ROH,

Can. J. Chem. Downloaded from www.nrcresearchpress.com by 46.23.64.124 on 09/08/12
For personal use only.

Fig. 2. Composition dependence of E_{Amax} and other parameters for mixed solvents at 298 K. ●, E_{Amax} in 1-butylamine–water mixtures; ○, E_{Amax} in *tert*-butanol–water mixtures (10); □, E_{Amax} in 1-butanol–water mixtures (10); ×, densities of 1-butylamine–water mixtures (16); +, viscosities of 1-butylamine–water mixtures (16); ---, viscosities of *tert*-butanol–water mixtures (21).

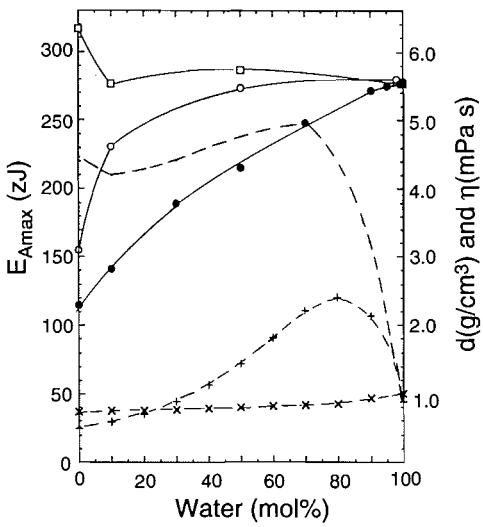

Fig. 3. Composition dependence of E_b (△), E_r (●), $G\epsilon_{max} \times 30$ (×), $W_{1/2}$ (○), and $W_b/W_r \times 50$ (■) in 1-butylamine–water mixtures at 298 K. *indicates the value at 225 K for pure 1-butylamine and 226 K for 90 mol% 1-butylamine. 16 aJ = 100 eV.

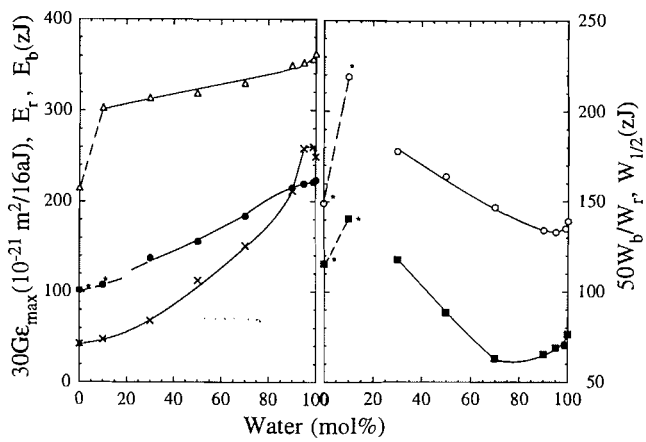

because the dipole moment of N–H is smaller than that of O–H (19), so the former liquids are less ordered (20).

The change of viscosity with water content in *t*-BuOH (ref. 21 and broken curve in Fig. 2) also indicates that a particular liquid structure exists at 10 mol% water, whereas there is no evidence for such a structure near 10 mol% water in 1-butylamine (+ curve in Fig. 2).

In view of the greater polarity of water than of 1-butylamine, one might have expected electrons to be more selectively solvated by water than is indicated by the gradual increases of E_{Amax} and $G\epsilon_{max}$ with water content (Figs. 2 and

Table 2. Half-life of solvated electron in 1-butylamine–water mixtures at 298 K.

	Water (mol %)																			
	0		10			30		50	70		90		95		99		100	
λ(nm)	$t_{1/2}$ (μs)	Tail (μs)[a]	$t_{1/2}$ (μs)	Tail (μs)[a]	$t_{1/2}$ (μs)	Tail (μs)[a]	$t_{1/2}$ (μs)[a]	$t_{1/2}$ (μs)	$t_{1/2}$ (μs)		$t_{1/2}$ (μs)		$t_{1/2}$ (μs)		$t_{1/2}$ (μs)		$t_{1/2}$ (μs)[b]	
700	4	>100	4	>100	1	>100	0.5	2	5		8		15		4			
800	3	>100	3	>100	1	>100	0.4	2	5		8		17		3			
1000	3	None	3	None	1	None	0.4	2	4		8		16		4			
1200	3	None	3	None	1	None	0.5											
1400	3	None	3	None	1	None												

[a]This long-lived absorption is negligible at λ > 1000 nm, and at any λ in solvents containing ≥50% water (Fig. 4).
[b]$t_{1/2}$ in pure water is >10 μs, but decreases with increasing pulse dose.

Can. J. Chem. Downloaded from www.nrcresearchpress.com by 46.23.64.124 on 09/08/12
For personal use only.

Fig. 4. The temperature effect on e_s^- optical spectra in pure 1-butylamine and the amine-rich mixtures with water. Pure 1-butylamine: ▲, 225.3 K; □, 236.3 K; ■, 247.7 K; ○, 271.0 K; ●, 298.7 K. 10 mol% water: ▲, 226.7 K; ■, 248.2 K; ○, 270.7 K; ●, 298.6 K. 30 mol% water: ▲, 228.5 K; △, 262.0 K; ●, 298.6 K. 50 mol% water: ▲, 230.0 K; ○, 262.8 K; ●, 298.8 K. Unidentified absorption tail with half-life longer than 100 μs: only the highest (+) and lowest (×) temperatures are shown for clarity.

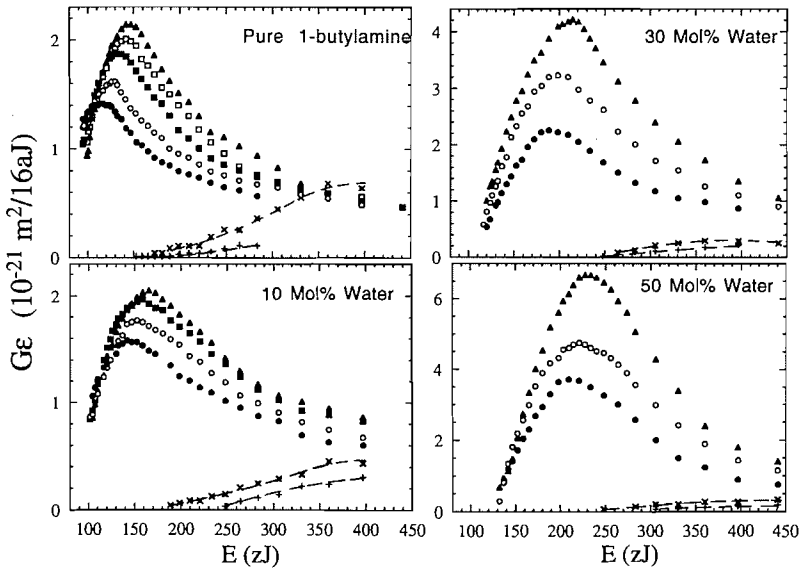

Fig. 5. Temperature dependence of E_{Amax} in 1-butylamine–water mixtures. The symbols are the same as those in Fig. 1, and +, 99 mol% water; ◇, 95 mol% water.

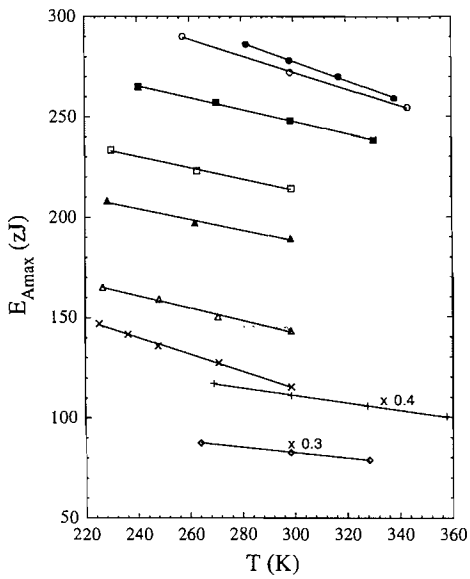

Fig. 6. Temperature coefficient ($-dE_{Amax}/dT$) (●) and viscosity (×) (16) in 1-butylamine–water mixtures. 1 zJ/K = 6.2 meV/K.

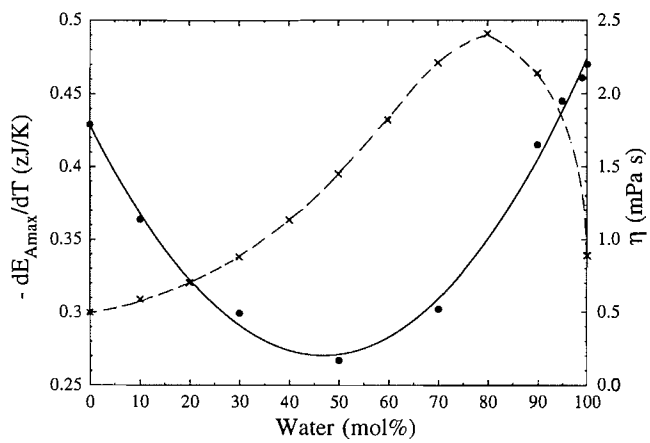

3). Many years ago we began the study of electron spectra and reactivities in alcohol–water mixed solvents expecting to find subtle changes and, instead, found large, structured changes. We have now begun the study of electron behavior in amine–water solvents, and expected much larger solvent-composition effects than we have observed. It seems that water and 1-butylamine form relatively ideal solutions; this might be related to the fact that 1-butylamine and water are completely miscible, whereas 1-butyl alcohol and water are not.

However, the effect of solvent composition on e_s^- may not be as ideal as it appears in the change of E_{Amax}. The half-life of e_s^- changes markedly with the composition of 1-butylamine–water mixtures (Table 2). As water is added to 1-butylamine, $t_{1/2}$ changes from 3 μs in pure butylamine to the minimum value of 0.5 μs in 50 mol% butylamine; then, when the 1-butylamine is decreased to 1 mol%, $t_{1/2}$ reaches the maximum value of 16 μs, a bit higher than that in pure water. This

incidates that the solvent structure in the region of 50 mol% 1-butylamine is different from those of the two extremities.

The value of $G\epsilon_{max}$ increases at 298 K from 1.42×10^{-21} m^2/16 aJ (8.6×10^3 e_s^- L/100 eV mol cm) in pure 1-butylamine to 8.3×10^{-21} m^2/16 aJ (50×10^3 e_s^- L/100 eV mol cm) in pure water (Table 1). The value in water agrees with that previously reported (6, 8).

The yield $G(e_s^-)$ in water at 298 K is 2.7 ent/16 aJ (6), and $\epsilon_{max} = 3.1 \times 10^{-21}$ m^2/e_s^- (1860 m^2/mol). In 1-butylamine at room temperature $G(e_s^-) = 0.27$ (22), which indicates $\epsilon_{max} = 5.3 \times 10^{-21}$ m^2/e_s^- (3200 m^2/mol).

The observed e_s^- are free ions. The low yield of e_s^- in 1-butylamine compared to that in water correlates (23, 24) with the lower value of the dielectric permittivity in the former than in the latter, 4.78 (18) and 78.4 (17), respectively.

Composition dependence of E_r, E_b, $W_{1/2}$, and asymmetry W_b/W_r at 298 K

Several parameters are used to describe the characteristics of the optical spectrum of e_s^-. E_r and E_b are the energies on the low-energy (red) and high-energy (blue) sides of the band at half the maximum absorbance. The width of the band at half height $W_{1/2}$ is divided at E_{Amax} into W_b (high-energy side) and W_r (low-energy side). The asymmetry of the band is represented by W_b/W_r. In Fig. 3 the values of E_r, E_b, $W_{1/2}$, and W_b/W_r are plotted against composition of 1-butylamine–water mixtures at 298 K. The values of E_r could only be obtained in pure butylamine and 10 mol% water near their freezing points, around 225 K.

The value of E_r (Fig. 3) increases smoothly from 1-butylamine to water, similar to the change of E_{Amax} (Fig. 2). However, there is a big jump in E_b from pure butylamine to 10 mol% water, and then E_b increases gently as more water is added.

The optical absorption at λ <1000 nm (E >200 zJ) had a long-lived tail that extended more than 100 μs (Fig. 4 and Table 2). The long-lived entity has not been identified. The absorbance due to e_s^- is taken as the portion above the long-lived tail. The tail decreases with increase of water content and increase of temperature (Fig. 4). The unidentified entity is only stable at low temperature and in an adequate amine environment.

The band asymmetry W_b/W_r increases from 2.3 in pure 1-butylamine to 2.8 in 10 mol% water, then decreases as more water is added, reaching a minimum of 1.26 at 70 mol%, and then increases slightly to 1.53 in pure water (Table 1 and Fig. 3). Thus the solvent composition has a more complex influence on the band asymmetry than on E_{Amax}.

Temperature effect on the optical spectra of e_s^-

Figure 4 shows the optical spectra of e_s^- in pure 1-butylamine to 50 mol% water at different temperatures. As the temperature is decreased the values of $G\epsilon_{max}$ and E_{Amax} increase.

The temperature coefficient of E_{Amax} has a minimum in 50 mol% water (Figs. 5 and 6). The e_s^- half-life also has a minimum at 50 mol% water (Table 2). These facts are probably related to the solvent structure, but we have no specific suggestion to offer.

Acknowledgments

We thank the Natural Sciences and Engineering Research Council of Canada for financial assistance, and the personnel of the Radiation Research Center for maintaining the accelerator and the electronic equipment.

References

1. R.F. Gould (*Editor*). Adv. Chem. Ser. **50**, 1965.
2. G.R. Freeman. *In* Kinetics of nonhomogeneous processes. *Edited by* G.R. Freeman. Wiley, New York. 1987. Chap. 2.
3. G.R. Freeman. J. Phys. Chem. **77**, 7 (1973).
4. F.Y. Jou and G.R. Freeman. Can. J. Chem. **60**, 1809 (1982).
5. J. Jay-Gerin and C. Ferradini. *In* Excess electrons in dielectric media. *Edited by* C. Ferradini and J. Jay-Gerin. CRC Press, London. 1991. Chap. 8.
6. E.J. Hart and M. Anbar. The hydrated electron. Wiley-Interscience, New York. 1970.
7. B.D. Michael, E.J. Hart, and K.H. Schmidt. J. Phys. Chem. **75**, 2798 (1971).
8. F.Y. Jou and G.R. Freeman. J. Phys. Chem. **83**, 2383 (1979).
9. F.Y. Jou and G.R. Freeman. Can. J. Chem. **57**, 591 (1979).
10. A.D. Leu, K.N. Jha, and G.R. Freeman. Can. J. Chem. **60**, 2342 (1982).
11. F.Y. Jou and G.R. Freeman. J. Phys. Chem. **88**, 3900 (1984).
12. J.F. Gavlas, F.Y. Jou, and L.M. Dorfman. J. Phys. Chem. **78**, 2631 (1974).
13. Y. Zhao and G.R. Freeman. Can. J. Chem. **73**, 392 (1995).
14. R. Chen, Y. Avotinsh, and G.R. Freeman. Can. J. Chem. **72**, 1083 (1994).
15. F.Y. Jou and G.R. Freeman. J. Phys. Chem. **85**, 629 (1981).
16. M.-J. Lee, S.-M. Hwang, and Y.-C. Kuo. J. Chem. Eng. Data, **38**, 577 (1993).
17. R.C. Weast (*Editor*). Handbook of chemistry and physics. 70th ed. CRC Press, Boca Raton, Fla. 1979. p. E-61.
18. Y.Y. Akhadov. Dielectric properties of binary solutions. Pergamon, Oxford. 1980. p. 144.
19. C.D. Gutsche and D.J. Pasto. Fundamentals of organic chemistry. Prentice-Hall, Englewood Cliffs, N.J. 1975. p. 132.
20. R.J. Fessenden and J.S. Fessenden. Organic chemistry. Willard Grant Press, Boston, Mass. 1979. p. 24.
21. P.C. Senanyake and G.R. Freeman. Can. J. Chem. **65**, 2441 (1987).
22. A.V. Vannikov, E.I. Mal'tzev, V.I. Zolotarevsky, and A.V. Rudnev. Int. J. Radiat. Phys. Chem. **4**, 135 (1972).
23. G.R. Freeman and J.M. Fayadh. J. Chem. Phys. **43**, 86 (1965).
24. W.A. Seddon, J.W. Fletcher, F.C. Sopchyshyn, and J. Jevcak. Can. J. Chem. **52**, 3269 (1974).

Can. J. Chem. Downloaded from www.nrcresearchpress.com by 46.23.64.124 on 09/08/12
For personal use only.

Unusual behavior of the conductivity of $LiNO_3$ in *tert*-butanol: ion clustering or ion-pair aggregation

Yixing Zhao and Gordon R. Freeman

Can. J. Chem. Downloaded from www.nrcresearchpress.com by 46.23.64.124 on 09/08/12
For personal use only.

Abstract: The electrical conductance of $LiNO_3$ in *tert*-butanol–water mixed solvents changes gradually from "normal" in pure water to "abnormal" in pure *tert*-butanol. In water the measured specific conductance increases with increase of temperature, and in *tert*-butanol the conductance *decreases* with increase of temperature. In pure *tert*-butanol, the electrical conductances of NH_4ClO_4 and $LiClO_4$ increase with the salt concentration and temperature at lower temperatures, but decrease at higher temperatures. The molar conductivity $\Lambda_0(10^{-4}$ S m^2 mol$^{-1})$ in *tert*-butanol at 300 K is 5.0 for NH_4ClO_4 and 4.0 for $LiClO_4$. Both activation energies E_{Λ_0} are 17 kJ mol^{-1}, which gives an unusual correlation between Λ_0 and viscosity η(mPa s): $\Lambda_0 \propto \eta^{-0.4}$. The values of Λ_0 for NH_4NO_3 and $LiNO_3$ in *tert*-butanol could not be measured, because ion aggregation is significant even at the lowest concentrations required to obtain conductances sufficiently above that of the solvent. The measured temperature coefficient of $LiNO_3$ conductance in *tert*-butanol is negative. Ion clustering of nitrate salts is attributed to poor solvation of the planar NO_3^- ions by the globular *tert*-butanol molecules. Ion aggregation in *tert*-butanol increases with increasing T, due to the relatively rapid decrease of the value of ϵT. Corrections are listed for reaction kinetics parameters for nitrate salts in pure *tert*-butanol solvent reported in Can. J. Chem. **73**, 392 (1995).

Key words: *tert*-butanol, ion-pair aggregation, lithium nitrate, electrical conductance, solvent effects.

Résumé : Dans des solvants mixtes *tert*-butanol–eau, la conductivité électrique du $LiNO_3$ passe graduellement de «normale» dans l'eau à «anormale» dans le *tert*-butanol pur. Dans l'eau, la conductivité spécifique mesurée augmente avec une augmentation de la température alors que, dans le *tert*-butanol, la conductivité *diminue* avec une augmentation de la température. Dans le *tert*-butanol, aux basses températures, les conductivités électriques du NH_4ClO_4 et du $LiClO_4$ augmentent avec une augmentation de la concentration et de la température alors que, à des températures plus élevées, elles diminuent. La conductivité molaire, $\Lambda_0(10^{-4}$ S m^2 mol$^{-1})$, dans le *tert*-butanol, à 300 K, est égale à 5,0 pour le NH_4ClO_4 et à 4,0 pour le $LiClO_4$. Les deux énergies d'activation, E_{Λ_0}, sont égales à 17 kJ mol^{-1}; ceci conduit à une corrélation inhabituelle entre Λ_0 et la viscosité, η (mPa s): $\Lambda_0 \propto \eta^{-0,4}$. Il n'a pas été possible de mesurer les valeurs de Λ_0 pour le NH_4NO_3 et le $LiNO_3$ dans le *tert*-butanol parce que l'agrégation des ions est suffisamment importante, même aux plus faibles concentrations requises pour obtenir des conductivités qui soient suffisamment plus élevées que celle du solvant. Le coefficient de température mesuré pour la conductivité du $LiNO_3$ dans le *tert*-butanol est négatif. On attribue la formation d'agrégats ioniques dans les sels nitriques à une mauvaise solvatation des ions NO_3^- planaires par les molécules globulaires de *tert*-butanol. L'agrégation dans le *tert*-butanol augmente avec une augmentation de la température et ceci est causé par la diminution relativement rapide de la valeur ϵT. On présente une liste de corrections pour les paramètres cinétiques de réactions des nitrates, dans le *tert*-butanol pur agissant comme solvant, qui ont été rapportés dans la Can. J. Chem. **73**, 392 (1995).

Mots clés : *tert*-butanol, agrégation des paires des ions, $LiNO_3$, conductivité électrique, effets de solvant.

[Traduit par la rédaction]

Introduction

The molar electric conductivity of an electrolyte solution decreases as the concentration of electrolyte is increased. The decrease in dilute solutions in hydroxylic solvents is attributed to the ionic atmosphere effect (1, 2) or the formation of ion pairs (3, 4). The formation of ion pairs Li_s^+, $NO_{3,s}^-$, where the subscript s represents "solvated," in different alcohols has been reported for pure propanols (5), 2-butanol (4), 1-hexanol, 1-octanol, and 1-decanol (6). However, there has been no report about the molar conductivity of lithium nitrate in *tert*-butanol. In connection with the study of the reactivity of solvated electrons e_s^- with nitrate ions (7), the electric conductances of lithium nitrate, ammonium nitrate, lithium perchlorate, and ammonium perchlorate were measured in the whole range of *tert*-butanol–water mixtures.

Received June 9, 1995.

Y. Zhao and G.R. Freeman.[1] Chemistry Department, University of Alberta, Edmonton, AB T6G 2G2, Canada.

[1] Author to whom correspondence may be addressed. Telephone: (403) 492-3468. Fax: (403) 492-8231. E-mail: knp@dept.chem.ualberta.ca

Fig. 1. Dependence of specific conductance of $LiNO_3$ on concentration in water–*tert*-butanol mixtures (100–70 mol% water) at different temperatures: ●, 278 K; ○, 283 K; ■, 298 K; □, 313 K; ▲, 328 K; △, 343 K.

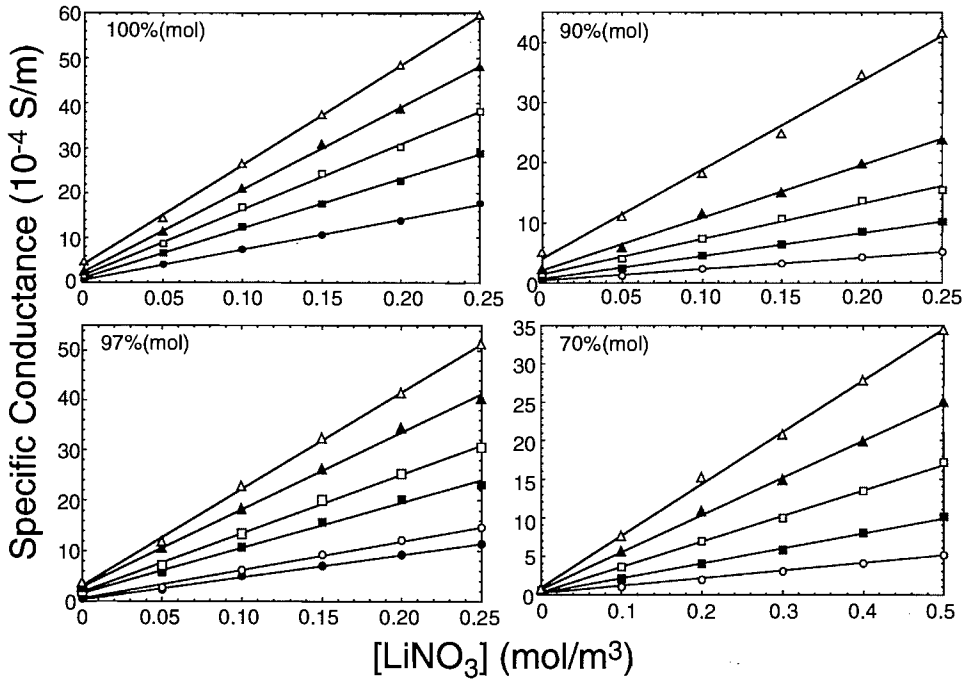

Fig. 2. Dependence of specific conductance of $LiNO_3$ on concentration in water–*tert*-butanol mixtures (50–0 mol% water) at different temperatures. Symbols as in Fig. 1, and ×, 308 K; +, 318 K.

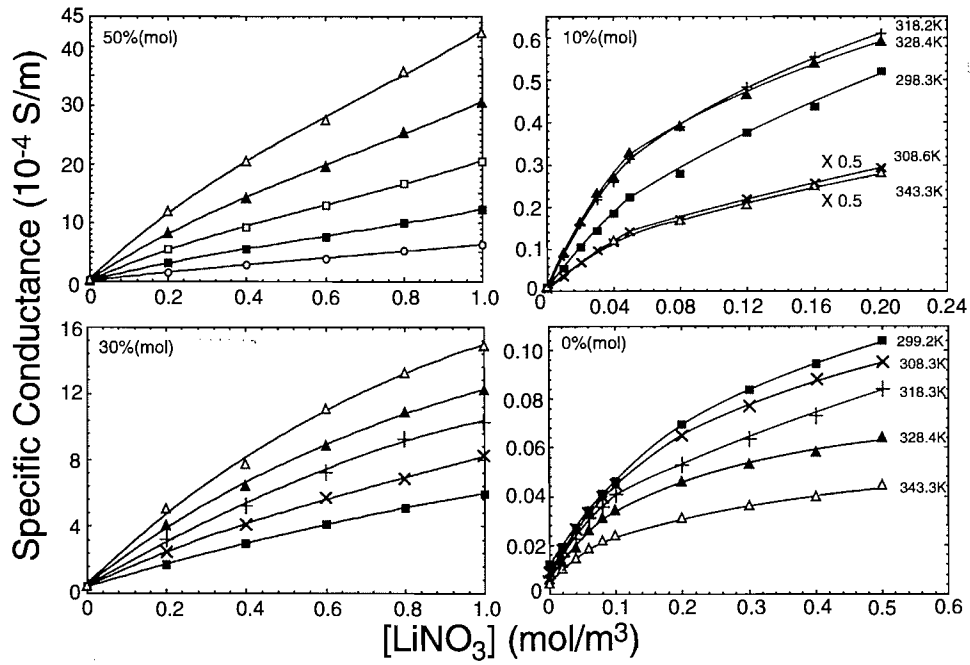

Unusual behavior was found for lithium nitrate in pure *tert*-butanol. It appears to be related to the aggregation of ion pairs found for lithium salts in aprotic solvents (8, 9). The conductance data are presented in this paper.

Experimental

The conductance measurement technique was the same as that reported in ref. 10, except that for the measurements of the

Can. J. Chem. Downloaded from www.nrcresearchpress.com by 46.23.64.124 on 09/08/12
For personal use only.

Can. J. Chem. Downloaded from www.nrcresearchpress.com by 46.23.64.124 on 09/08/12
For personal use only.

Fig. 3. Dependence of specific conductance of NH_4ClO_4, $LiClO_4$, NH_4NO_3, and $LiNO_3$ on concentration in pure *tert*-butanol at different temperatures. Symbols as in Figs. 1 and 2. Some conductances are multiplied by 0.5 to separate the curves.

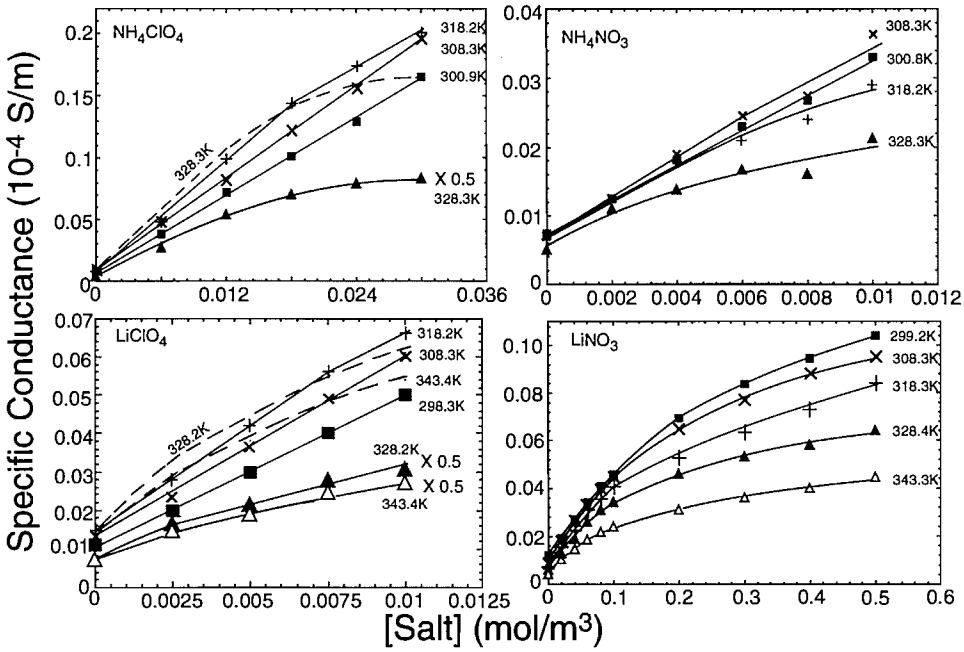

Fig. 4. Arrhenius plots of Λ_0 or initial slopes of salts in *tert*-butanol, and of fluidity ($1/\eta$) of *tert*-butanol: △, NH_4ClO_4; ▲, $LiClO_4$; ○, NH_4NO_3; ●, $LiNO_3$; ×, $1/\eta$, ref. 11.

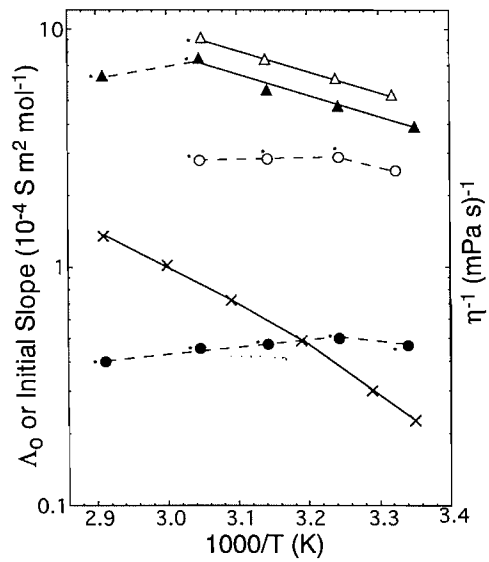

four salts in 10 mol% water and in pure *tert*-butanol, a freshly made solution was used for each temperature to minimize the formation of impurities during heating.

Results and discussion

Conductance of $LiNO_3$: "normal" in water, "abnormal" in *tert*-butanol

The dependences of specific conductance on the concentration of $LiNO_3$ in water – *tert*-butanol mixed solvents at different temperatures are plotted in Figs. 1 and 2. In 100–70 mol% water solvents the conductance increases linearly with the increase of $LiNO_3$ concentration over the range used (Fig. 1). However, as the water content of the solvent is further decreased, the conductance becomes sublinear with concentration (Fig. 2). In 100–30 mol% water the conductance increases monotonically with temperature. However, in 10 mol% water the conductance *decreases* at $T > 320$ K (Fig. 2). In pure *tert*-butanol, as the temperature is increased the conductance decreases monotonically (Fig. 2).

Figures 1 and 2 show the gradual transition of conductance behavior of $LiNO_3$ as the *tert*-butanol content of the solvent is increased. When the lines are gently sublinear, we used initial slopes of the curves to estimate the limiting molar conductivity Λ_0. For severely bent curves the values estimated in this way are too small to be Λ_0.

Comparison of molar conductivities of salts in *tert*-butanol

The measured specific conductances of four salts in *tert*-butanol are shown in Fig. 3. We see again the change from "normal" to "abnormal" behavior. For NH_4ClO_4 and $LiClO_4$, the specific conductance increases linearly with increase of concentration at temperatures around 300 K. However, as the temperature is increased the lines become sublinear, and the specific conductance *decreases* at higher temperatures. This behavior is more marked for the NH_4NO_3 solution. The concentration and temperature at which the line becomes sublinear decrease from NH_4ClO_4 to $LiClO_4$ to NH_4NO_3 (Fig. 3). The conductance of $LiNO_3$ in *tert*-butanol is so low that we could not measure it at the low concentrations used for the other salts. At the higher concentrations used (Fig. 3), the conductance at a given concentration decreases monotonically with increasing temperature.

Can. J. Chem. Downloaded from www.nrcresearchpress.com by 46.23.64.124 on 09/08/12
For personal use only.

Table 1. Arrhenius activation energies of viscosities and conductances of salts in some solvents at 298 K.

Solvent	Salt	Λ_0 (10^{-4} S m^2 mol^{-1})	E_{Λ_0} (kJ mol^{-1})	η (mPa s)	E_η (kJ mol^{-1})	$E_{\Lambda_0}/E_\eta = n$
Water[a]	NH_4ClO_4	140, 141[e]	16	0.89	16	1.0
	NH_4NO_3	145[e]				
	$LiClO_4$	106[e]				
	$LiNO_3$	108, 110[e]	15			0.9
1-PrOH[b]	$LiNO_3$	20	16	2.0	18	0.9
2-PrOH[b]	$LiNO_3$	20	22	2.0	22	1.0
1-BuOH[c]	NH_4NO_3	14	20	2.60	19	1.1
	$LiNO_3$	13	18			0.9
2-BuOH[d]	$Cu(ClO_4)_2$	19	23	3.05	26	0.9
	$LiNO_3$	(7)[f]	18			(0.7)[f]
iso-BuOH[a]	$Cu(ClO_4)_2$	19	25	3.40	24	1.0
	$LiNO_3$	9	19			0.8
t-BuOH[g]	NH_4ClO_4	5.0	17	4.5[h]	31[h]	0.55
	$LiClO_4$	4.0	17			0.55

[a]Reference 12.
[b]Reference 13.
[c]Reference 10.
[d]Reference 4.
[e]Reference 1.
[f]Probably low.
[g]Present work.
[h]Reference 11.

Table 2. Physical properties of salts at 298 K.

	Crystal form[a]	Density (kg m^{-3})[a]	Molar mass (kg mol^{-1})[a]	Molar density (mol m^{-3})	Molar density ratio[c]	Lattice energy (kJ mol^{-1})[d]	Λ (300 K)[e] (10^{-4} S m^2 mol^{-1})
NH_4ClO_4	Rhomb[b]	1950	0.117	16 700	0.48	580	5.0
$LiClO_4$	?	2428	0.106	22 900	0.66	723	4.0
NH_4NO_3	Rhomb[b]	1725	0.080	21 600	0.63	676	2.4
$LiNO_3$	Trigonal	2380	0.069	34 500	1.00	848	0.5

[a]Reference 14*a*.
[b]Orthorhombic or rhombic; NH_4NO_3 is monoclinic at T >305.3 K.
[c]Based on $LiNO_3$.
[d]Reference 14*b*.
[e]In *tert*-butanol, from "initial slopes" of the plots in Fig. 4. The values for the nitrates are not Λ_0.

Figure 4 shows the Arrhenius plots of Λ_0 (for straight lines) and initial slopes (for curves, marked*) in *tert*-butanol. A linear Arrhenius plot is obtained for NH_4ClO_4 in the temperature range measured. However, it would likely be bent at higher temperatures. The ionic atmosphere effect calculated from the Debye–Hückel equation (1) is negligible at these concentrations (3% at the highest concentration used). For $LiClO_4$ the line bends at 328 K, and for NH_4NO_3 it seems to have bent at about 300 K. The Arrhenius activation energies obtained at lower temperatures for NH_4ClO_4 and $LiClO_4$ (Fig. 4) are 17 kJ mol^{-1}. The mean Arrhenius activation energy of fluidity ($1/\eta$) of *tert*-butanol (11) below 318 K (Fig. 4) is 38 kJ mol^{-1}. This indicates that the correlation between molar conductivities of the two salts and the viscosity η of pure *tert*-butanol is $\Lambda_0 \propto \eta^{-n}$, with $n \approx 0.4$, which is unusual and does not follow Walden's rule, $n = 1$ (1). The conductances of many salts (Table 1) in water (12) and pure 1- and 2-propanol solvents (13), and in 1- (10), iso- (12), and 2-butanol (4) approximately follow Walden's rule. However, for $LiNO_3$ in iso- (12) and 2-butanol (4), they deviate significantly from Walden's rule, with n = 0.7–0.8. More study is needed to understand the behavior of salt conduction in these solvents.

For NH_4NO_3, the apparent activation energy calculated from 300 to 308 K is 14 kJ mol^{-1}, and is nearly zero between 308 and 328 K (Fig. 4). This seems to indicate that clusters of nitrate and ammonium ions form in *tert*-butanol solvent at higher temperatures.

For $LiNO_3$, the Arrhenius plot has a negative slope at T >308 K (Fig. 4). The value of the initial conductance slope at 299 K (Fig. 3) is 0.5×10^{-4} S m^2 mol^{-1}, which is much lower than the molar conductivities of the other three salts at the same temperature (Table 2). We conclude that Li^+ and NO_3^- ions have a strong tendency to form multi-ion clusters in *tert*-butanol.

Can. J. Chem. Downloaded from www.nrcresearchpress.com by 46.23.64.124 on 09/08/12
For personal use only.

Fig. 5. Temperature dependence of ϵT of some solvents, normalized to the values at 298 K (ref. 16): □, water; ■, ethanol; ×, 1-propanol; ●, *tert*-butanol; ○, 10 mol% water in *tert*-butanol; △, 30 mol% water in *tert*-butanol.

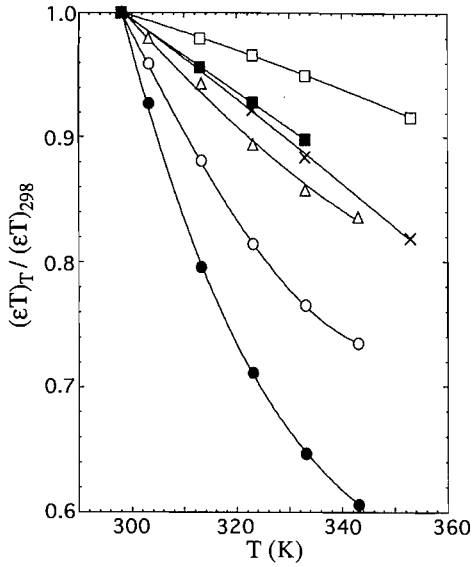

Comparing the molar conductivities with physical parameters (14) of the four salts (Table 2), the conductivities correlate inversely with the molar density and lattice energy of the crystalline salts. The molar density and lattice energy reflect the ability of the ions to pack together. NH_4ClO_4 has the lowest molar density and lattice energy, and the highest molar conductivity (Table 2). The values for $LiClO_4$ and NH_4NO_3 are in the middle (but their relative order is reversed). $LiNO_3$ has the highest molar density and lattice energy, and the lowest molar conductivity. $LiNO_3$ is the smallest molecule, with ionic radii (15) $R_{Li^+} = 74$ pm and $R_{NO_3^-} = 189$ pm; NH_4ClO_4 is the largest molecule, with ionic radii (15) $R_{NH_4^+} = 146$ pm and $R_{ClO_4^-} = 200$ pm.

The approximate inverse relationships between the molar conductivity and the molar density and lattice energy of the salts indicate the extent of formation of ion clusters in *tert*-butanol. The *tert*-butanol molecules are globular; the planar NO_3^- ions would fit less well than the globular ClO_4^- ions into the liquid structure, so NO_3^- might be less tightly solvated than is ClO_4^- in *tert*-butanol. The solvent has a low relative permittivity ($\epsilon = 12.4$ at 298 K) (16), so the Coulombic attraction between oppositely charged ions is greater than in solvents with higher permittivities. These factors might explain the reversal of the electrolyte conductivity/crystal lattice energy orders of $LiClO_4$ and NH_4NO_3. We attribute the low observed conductivity of $LiNO_3$ solutions to the formation of ion clusters, mainly larger than pairs.

In aprotic solvents such as tetrahydrofuran, diethyl ether, pyridine, and diethyl carbonate, the salts LiNCS and LiBr form ion pairs that can agglomerate (8, 9). For example, the following species have been detected by various spectroscopic methods (8, 9):

[1] $Li_s^+ + NCS_s^- \rightleftharpoons LiNCS_s$

[2] $2\,LiNCS_s \rightleftharpoons (LiNCS)_{2,s}$

Table 3. Λ_0[a] of salts in *tert*-butanol at different temperatures.

	Λ_0 (300 K)	Λ_0 (308 K)	E_{Λ_0} (kJ mol^{-1})
NH_4ClO_4[b]	5.0	6.0	17
$LiClO_4$[b]	4.0	4.6	17
NH_4NO_3[c]	~5		
$LiNO_3$[c]	~4		

[a] 10^{-4} S m^2 mol^{-1}.
[b] Measured values.
[c] Estimated values, see text.

[3] $2\,(LiNCS)_{2,s} \rightleftharpoons (LiNCS)_{4,s}$

The trimer $(LiNCS)_{3,s}$ was not detected. The tetramer has a cubane-like structure. The species LiNCS is strongly polar, but the dimer and tetramer are nonpolar. The pairing and agglomeration reactions are entropy driven; each step involves partial desolvation of the species (9).

We suggest that, while *tert*-butanol is a protic solvent, the globular alkyl group hinders it from efficiently solvating Li^+ and NO_3^- ions.

The reason for the unusual temperature dependence of salt conductance in *tert*-butanol is that the product of the relative permittivity and temperature ϵT *decreases* rapidly as the temperature is increased. Ion association constants vary inversely as the product ϵT (17).

The value of ϵT for hydroxylic solvents decreases with increasing T, but the relative decrease is much faster for *tert*-butanol than for water and other simple alcohols (Fig. 5). Values (16) of ϵT normalized to that at 298 K are plotted in Fig. 5 for water, ethanol, 1-propanol, and *tert*-butanol, as well as for 10% and 30% water in *tert*-butanol. The behavior of ϵT for the 30 mol% water solvent is close to that of 1-propanol, and the conductance behavior of $LiNO_3$ in this mixed solvent is not excessively abnormal (Fig. 2).

Estimate of Λ_0 for $(NH_{4,s}^+ + NO_{3,s}^-)$ and $(Li_s^+ + NO_{3,s}^-)$ in *tert*-butanol

The initial slope method and attempts to fit the data to the Debye–Onsager (1, 2) and ion association (3, 4) models gave unreasonably low values of Λ_0 for the two nitrate salts. More complex models (18) have too many adjustable parameters for our purpose.

We suspect that the planar NO_3^- ions are not well solvated by the globular *tert*-butanol molecules, and that this makes the nitrate salts susceptible to ion clustering, or aggregation of ion pairs as in aprotic solvents (9). However, for the analysis of reaction rate constants (7) we need values of Λ_0. An indirect method of estimation has therefore been used.

The ratio of Λ_0 values for $NH_4ClO_4/LiClO_4$ equals 1.3 in both water and *tert*-butanol (Table 1). In water the values of Λ_0 for the two ammonium salts are equal, and those of the two lithium salts are equal (Table 1), so the same is assumed to be true in *tert*-butanol. We thereby arrive at the Λ_0 values listed in Table 3.

Corrections to parameter values in ref. 7

The values of some of the kinetics parameters estimated for

Table 4. Corrected parameter values for pure *tert*-butanol solvent in ref. 7.

Parameter	Location[a]	$LiNO_3$		NH_4NO_3	
		Old	New	Old	New
Λ_0 (10^{-4} S m^2 mol^{-1})	T2, F8	1.9	4	2.4	5
r_d (nm)	F9	0.97	0.46	0.78	0.37
κR_r	F10	13	6		
κ	T4	6.1	3		

[a]T, Table; F, Figure.

tert-butanol solvents were out of line with those for the water–alcohol mixed solvents (ref. 7: Tables 2 and 4, Figs. 8, 9, and 10). The corrected values of Λ_0 bring the other parameters into line. The old and corrected values of the parameters are listed in Table 4.

Acknowledgements

We thank the Natural Sciences and Engineering Research Council of Canada for financial assistance, and the personnel of the Radiation Research Center for maintaining the electronic equipment.

References

1. P.W. Atkins. Physical chemistry. 4th ed. Freeman, New York. 1990. Chap. 25 and p. 963.
2. R. Chen and G.R. Freeman. J. Phys. Chem. **96**, 7107 (1992).
3. J.E. Gordon. The organic chemistry of electrolyte solutions. Wiley, New York. 1975. p. 385
4. S.A. Peiris and G.R. Freeman. Can. J. Chem. **69**, 884 (1991).
5. S.A. Peiris and G.R. Freeman. Can. J. Chem. **68**, 940 (1990).
6. R. Chen and G.R. Freeman. J. Phys. Chem. **99**, 4970 (1995).
7. Y. Zhao and G.R. Freeman. Can. J. Chem. **73**, 392 (1995).
8. M. Chabanel and Z. Wang. Can. J. Chem. **62**, 2320 (1984).
9. M. Chabanel. Pure Appl. Chem. **62**, 35 (1990).
10. R. Chen and G.R. Freeman. Can. J. Chem. **71**, 1303 (1993).
11. P.C. Senanayake, N. Gee, and G.R. Freeman. Can. J. Chem. **65**, 2441 (1987).
12. R. Chen, Y. Avotinsh, and G.R. Freeman. Can. J. Chem. **72**, 1083 (1994).
13. T.B. Kang and G.R. Freeman. Can. J. Chem. **71**, 1297 (1993).
14. R.C. Weast (*Editor*). Handbook of chemistry and physics. 70th ed. CRC Press, Boca Raton, Fla. 1974; (*a*) pp. B-93–132; (*b*) pp. D-89–103.
15. D.A. Johnson. Some thermodynamic aspects of inorganic chemistry. 2nd ed. Cambridge University Press, Cambridge. 1982. pp. 46–49.
16. Y.Y. Akhadov. Dielectric properties of binary solutions. Pergamon Press, New York. 1980. pp. 277, 282, 456.
17. H.S. Harned and B.B. Owen. The physical chemistry of electrolytic solutions. 3rd ed. Reinhold, New York. 1958. p. 291.
18. J.-C. Justice. *In* Comprehensive treatise of electrochemistry. Vol. 5. *Edited by* B.E. Conway, J. O'M. Bockris, and E. Yeager. Plenum, New York. 1983. pp. 311–314.

Can. J. Chem. Downloaded from www.nrcresearchpress.com by 46.23.64.124 on 09/08/12
For personal use only.

Radiolysis studies on the corrosion inhibitors 1-hexyn-3-ol, cinnamonitrile, and 1,3-diethyl-2-thiourea

A.J. Elliot, M.P. Chenier, and D.C. Ouellette

Abstract: In this publication we report: (*i*) the rate constants for reaction of the hydrated electron with 1-hexyn-3-ol ($(8.6 \pm 0.3) \times 10^8$ dm^3 mol^{-1} s^{-1} at 18°C), cinnamonitrile ($(2.3 \pm 0.2) \times 10^{10}$ dm^3 mol^{-1} s^{-1} at 20°C), and 1,3-diethyl-2-thiourea ($(3.5 \pm 0.3) \times 10^8$ dm^3 mol^{-1} s^{-1} at 22°C). For cinnamonitrile and diethylthiourea, the temperature dependence up to 200°C and 150°C, respectively, is also reported; (*ii*) the rate constants for the reaction of the hydroxyl radical with 1-hexyn-3-ol ($(5.5 \pm 0.5) \times 10^9$ dm^3 mol^{-1} s^{-1} at 20°C), cinnamonitrile ($(9.2 \pm 0.3) \times 10^9$ dm^3 mol^{-1} s^{-1} at 21°C), and diethylthiourea ($(8.0 \pm 0.8) \times 10^8$ dm^3 mol^{-1} s^{-1} at 22°C). For cinnamonitrile, the temperature dependence up to 200°C is also reported; (*iii*) the rate constant for the hydrogen atom reacting with 1-hexyn-3-ol ($(4.3 \pm 0.4) \times 10^9$ dm^3 mol^{-1} s^{-1} at 20°C).

Key words: radiolysis, corrosion inhibitors, rate constants.

Résumé : Dans ce travail, on rapporte : (*i*) les constantes de vitesse des réactions de l'électron hydraté avec l'hex-1-hexyn-3-ol ($(8,6 \pm 0,3) \times 10^8$ dm^3 mol^{-1} s^{-1} à 18°C), le cinnamonitrile ($(2,3 \pm 0,2) \times 10^{10}$ dm^3 mol^{-1} s^{-1}, à 20°C) et avec la 1,3-diéthyl-2-thiourée ($(3,5 \pm 0,3) \times 10^8$ dm^3 mol^{-1} s^{-1}, à 22°C). Pour le cinnamonitrile et pour la diéthylthiourée, on a aussi déterminé la dépendance des vitesses de réaction sur la température jusqu'à 200°C et 150°C, respectivement; (*ii*) les constantes de vitesse de la réaction du radical hydroxyle avec l'hex-1-yn-3-ol ($(5,5 \pm 0,5) \times 10^9$ dm^3 mol^{-1} s^{-1}, à 20°C), le cinnamonitrile ($(9,2 \pm 0,3) \times 10^9$ dm^3 mol^{-1} s^{-1}, à 21°C), et avec la 1,3-diéthyl-2-thiourée ($(8,0 \pm 0,8) \times 10^8$ dm^3 mol^{-1} s^{-1}, à 22°C). Pour le cinnamonitrile, on a aussi déterminé la dépendance de la vitesse de la réaction avec la température jusqu'à 200°C; (*iii*) la constante de la vitesse de réaction de l'atome d'hydrogène avec l'hex-1-yn-3-ol ($(4,3 \pm 0,4) \times 10^9$ dm^3 mol^{-1} s^{-1}, à 20°C).

Mots clés : radiolyse, inhibiteurs de corrosion, constantes de vitesse.

[Traduit par la rédaction]

Introduction

Radioisotopes, such as ^{60}Co, are incorporated in the iron oxide surface of the carbon-steel pipework of the primary heat transport system in a nuclear reactor, and the ensuing radiation fields are of concern during maintenance procedures (1). Decontamination solutions are used to dissolve the iron oxide layer by solubilizing the iron (e.g., as an ethylenediamine tetraacetic acid (EDTA) complex); the radioisotopes are also released at this stage (2). In the case of the CAN-DECON™ process, the decontamination formulation developed by AECL, the EDTA is then regenerated by removing the iron on an ion-exchange column. However, this ion-exchange resin, which also absorbs the radioisotopes released during the oxide dissolution, has to be disposed of following the decontamination. One means of minimizing the generation of ion-exchange waste is to add a corrosion inhibitor to the decontamination formulation in order to minimize the corrosion of the bare carbon-steel pipework exposed after the oxide has been removed. This corrosion, while generally not important from a plant integrity viewpoint, does generate extra soluble iron, which in turn generates more ion-exchange waste. Over the years, there has been an emphasis on finding corrosion inhibitors that are halide and sulphur free to minimize corrosion to I-600 and I-800 alloys during subsequent reactor operations by residues containing chlorine or sulphur.

Based on general radiation chemistry experience, the corrosion inhibitors screened thus far for potential use in decontamination formulations should be degraded preferentially to the organic acids. During a full system decontamination, dose rates in the range of 200–1200 Gy h^{-1} are expected, depending on the time after reactor shutdown, and whether the reactor is fuelled or defuelled. A study of the radiolytic degradation of selected inhibitors has been undertaken to predict their radiolytic degradation during a reactor decontamination. In this publication, some aspects are described of the radiation chemistry of three corrosion inhibitors: 1-hexyn-3-ol, cinnamonitrile, and 1,3-diethyl-2-thiourea.

Received July 11, 1995.

A.J. Elliot,[1] M.P. Chenier, and D.C. Ouellette. Reactor Chemistry Branch, Chalk River Laboratories, Chalk River, ON K0J 1J0, Canada.

[1] Author to whom correspondence may be addressed. (Telephone: (613) 584-8811, ext. 3188. Fax: (613) 584-4445.

Can. J. Chem. Downloaded from www.nrcresearchpress.com by 46.23.64.124 on 09/08/12
For personal use only.

Can. J. Chem. Downloaded from www.nrcresearchpress.com by 46.23.64.124 on 09/08/12
For personal use only.

Experimental

All chemicals were used as supplied. The inhibitors studied, with their sources are 1-hexyn-3-ol (Alfa Products), cinnamonitrile (Aldrich), and 1,3-diethyl-2-thiourea (Fisher Scientific). The other chemicals were AR grade or better. All solutions were prepared in high-purity water that had been distilled once, passed through a Millipore Milli-Q system, and then redistilled from alkaline permanganate. In most of the experiments reported here, the solutions were saturated with the appropriate gas by the syringe-bubbler technique; for some of the γ-radiolysis experiments, the solutions were degassed by freeze–pump–thaw cycles on a vacuum line and then sealed in Pyrex ampoules.

The experimental arrangements for the pulse radiolysis studies have been described in earlier publications (3, 4). A 0.5 μs pulse length was used for these experiments and the dosimeter was an oxygen-saturated KSCN solution (0.01 mol dm^{-3}) where the $G\epsilon_{475}$ value of 2.39×10^{-4} was used. G is defined as the number of species formed per 100 eV (1 eV is equivalent to 1.602×10^{-19} J) and the molar extinction coefficient, ϵ_{475}, is expressed in units of $dm^3\ mol^{-1}\ cm^{-1}$. Where required, density corrections were made for dosimetry.

For all steady-state radiolysis studies, the solutions were irradiated at room temperature in a GAMMACELL at a dose rate of about 1.2 Gy s^{-1}. The dose rate was determined by the Fricke dosimeter (5).

Results and discussion

Radiolysis studies of 1-hexyn-3-ol

The rate constants of the reactions of the hydrated electron, hydroxyl radical, and hydrogen atom with 1-hexyl-3-ol were measured using pulse radiolysis techniques. As 1-hexyn-3-ol is quite volatile and is partially stripped from solution during bubbling, even when the gas is passed through a prebubbler filled with the same solution, its concentration was determined by measuring its absorbance at 237 nm using ϵ_{237} of 445 $dm^3\ mol^{-1}\ cm^{-1}$.

Only weak optical transients were observed in the 350–720 nm range when deoxygenated 10^{-3} mol dm^{-3} 1-hexyn-3-ol solutions were pulse irradiated. This is consistent with the observations of Anderson and Schulte-Frohlinde (6), who studied acetylene solutions using pulse radiolysis; the only significant absorption they observed was in the 200–320 nm range.

The rate constant of $(8.6 \pm 0.3) \times 10^8$ $dm^3\ mol^{-1}\ s^{-1}$ (18°C) was measured for the reaction of the hydrated electron (e_{aq}^-) with 1-hexyn-3-ol (reaction [1]) from the first-order decay of the hydrated electron, as monitored by its absorption at 720 nm in deoxygenated solutions containing 6.8×10^{-4} mol dm^{-3} and 1.6×10^{-3} mol dm^{-3} 1-hexyn-3-ol:

[1] $e_{aq}^- + CH{\equiv}C\text{-}CHOH\text{-}(CH_2)_2\text{-}CH_3 \rightarrow (CH{\equiv}C\text{-}CHOH\text{-}(CH_2)_2\text{-}CH_3)^-$

The rate constant of $(5.5 \pm 0.5) \times 10^9$ $dm^3\ mol^{-1}\ s^{-1}$ (20°C) for the reaction of the hydroxyl radical with 1-hexyn-3-ol (reaction [2]) was measured by competition kinetics in both aerated and N_2O-saturated solutions (natural pH) containing $(1–8) \times 10^{-3}$ mol dm^{-3} KSCN and $(0–2) \times 10^{-3}$ mol dm^{-3} 1-hexyn-3-ol:

[2] $OH + CH{\equiv}C\text{-}CHOH\text{-}(CH_2)_2\text{-}CH_3 \rightarrow$ products

The competition was followed by measuring the absorbance of $(SCN)_2^-$ at 475 nm; the rate constant for reaction [3] was taken to be 1.1×10^{10} $dm^3\ mol^{-1}\ s^{-1}$ (7):

[3] $OH + SCN^- (+SCN^-) \rightarrow (SCN)_2^- + OH^-$

In the N_2O-saturated solutions, corrections were made for the scavenging of the hydrated electron by 1-hexyn-3-ol (reaction [1]) in competition with reaction [4]:

[4] $e_{aq}^- + N_2O (+H_2O) \rightarrow OH + OH^- + N_2$

$k_4 = 9.1 \times 10^9$ $dm^3\ mol^{-1}\ s^{-1}$ (ref. 7)

The rate constant for the reaction of hydrogen atoms with 1-hexyn-3-ol (reaction [5]) was measured to be $(4.3 \pm 0.4) \times 10^9$ $dm^3\ mol^{-1}\ s^{-1}$ at 20°C by competition kinetics in deoxygenated 5×10^{-4} mol dm^{-3} ferricyanide ion (pH 1.8) solutions containing $(0–4.9) \times 10^{-4}$ mol dm^{-3} 1-hexyn-3-ol. The competition was monitored by the depletion of the ferricyanide ion absorption at 420 nm, assuming that the rate constant for hydrogen atoms reacting with ferricyanide ion (reaction [6]) was 5.8×10^9 $dm^3\ mol^{-1}\ s^{-1}$ (8):

[5] $H + CH{\equiv}C\text{-}CHOH\text{-}(CH_2)_2\text{-}CH_3 \rightarrow$ products

[6] $H + Fe(CN)_6^{3-} \rightarrow Fe(CN)_6^{4-}$

On a longer time scale, after reactions [5] and [6] were complete, further ferricyanide ion was reduced to ferrocyanide ion by the free radical products formed from reaction of the hydroxyl radical and hydrogen atom. A rate constant of 1.7×10^8 $dm^3\ mol^{-1}\ s^{-1}$ was measured for this reduction. While this rate constant is about an order of magnitude slower than that normally associated with the reduction of ferricyanide by simple α-hydroxy radicals as derived from 2-propanol, etc., it is still much faster than that of a β-hydroxy radical (e.g., $^{\bullet}CH_2CH_2OH$) (9). This suggests that the radicals are probably α-hydroxy radicals, a point that will be returned to later.

It is interesting to compare the rate constant for reaction of the hydrated electron with 1-hexyn-3-ol, $CH{\equiv}C\text{-}CHOH\text{-}(CH_2)_2\text{-}CH_3$ (8.6×10^8 $dm^3\ mol^{-1}\ s^{-1}$) to that of the electron reaction with acetylene, $CH{\equiv}CH$ (2.0×10^7 $dm^3\ mol^{-1}\ s^{-1}$) (6), and with propargyl alcohol, $CH{\equiv}C\text{-}CH_2OH$, of 2.1×10^8 $dm^3\ mol^{-1}\ s^{-1}$ (10). Substitution of the acetylene group greatly affects the rate of reaction towards the hydrated electron. However, there is no significant difference between the reaction rates of the hydroxyl radical and hydrogen atom with acetylene, 4.5×10^9 and 2.3×10^9 $dm^3\ mol^{-1}\ s^{-1}$ (6), respectively, and those with 1-hexyn-3-ol.

Some γ-radiolysis studies of 1-hexyn-3-ol were made to measure the loss of starting material. N_2O-saturated and deoxygenated solutions containing 10^{-3} mol dm^{-3} 1-hexyn-3-ol at natural pH were γ-irradiated and analyzed using UV spectroscopy. The UV spectrum of 1-hexyn-3-ol has a single absorption at 235 nm associated with an electronic transition in the acetylene group. As such, this method of analysis reflects only what has happened to this acetylene group; reactions occurring at the other end of the molecule are not monitored.

In deoxygenated solutions, G(acetylene loss) of ca. 50 was measured. This high G-value was confirmed by high-pressure

Can. J. Chem. Downloaded from www.nrcresearchpress.com by 46.23.64.124 on 09/08/12
For personal use only.

Fig. 1. The spectra calculated (see text) for the transient formed from cinnamonitrile by reaction of the hydrated electron (◆), the hydroxyl radical (▲), and the hydrogen atom (○). Dose per pulse was about 5 Gy.

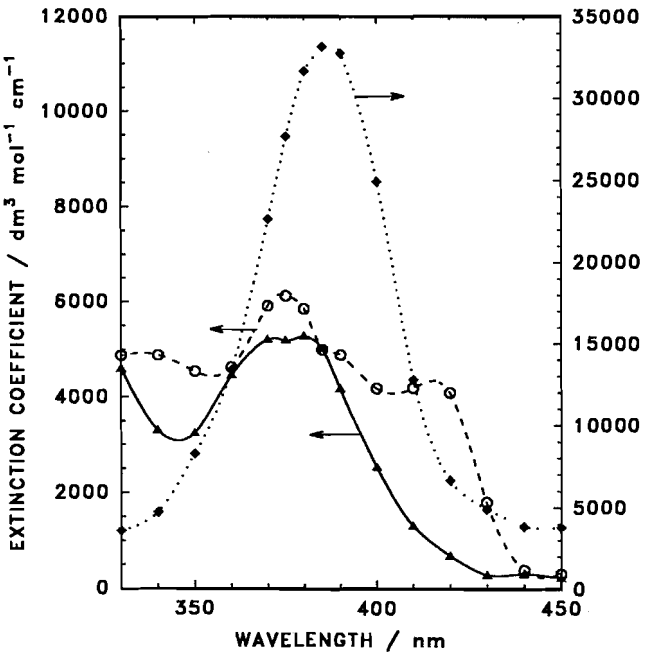

liquid chromatography; analysis of two samples gave *G*-values of the loss of 1-hexyn-3-ol of 40 and 100. For N_2O-saturated solutions, *G*(acetylene loss) was near 20. A deoxygenated solution at pH 2.6 was also studied and *G*(acetylene loss) was ca. 14.

The above results indicate that the hydrated electron reacts with the acetylene group (reaction [1]) to form a radical anion, which initiates a small chain polymerization reaction. The hydroxyl radical and the hydrogen atom also appear to initiate small chain reactions. Both presumably can add to the acetylene group; however, both can also abstract the hydrogen at carbon-3 (reaction [7]) to form an α-hydroxy radical:

[7] $OH,H + CH{\equiv}C\text{-}CHOH\text{-}(CH_2)_2\text{-}CH_3 \rightarrow CH{\equiv}C\text{-}\dot{C}OH\text{-}(CH_2)_2\text{-}CH_3 + H_2O, H_2$

Evidence for reaction [7] comes from pulse radiolysis experiments, where the *G*-value for ferricyanide reduction in pH 1.8 solutions from the radicals formed in reactions [2] and [5] was about 70% of the yield of hydroxyl and hydrogen atoms. Addition of the hydroxyl radical or the hydrogen atom to the acetylene triple bond will produce a β- or γ-hydroxy radical, either of which are anticipated to be much poorer reducing agents for ferricyanide.

Radiolysis studies of cinnamonitrile

As will be described later, the rate constants for the reaction of the hydrated electron (reaction [8]) and the hydroxyl radical (reaction [9]) with cinnamonitrile are $(2.3 \pm 0.2) \times 10^{10}$(20°C) and $(9.2 \pm 0.3) \times 10^9$ dm^3 mol^{-1} s^{-1} (21°C), respectively. To determine the absorption characteristics of the transients formed from reaction of the hydrated electron, the hydroxyl radical, and the hydrogen atom with cinnamonitrile, the spectra were recorded from a helium-purged 10^{-3} mol dm^{-3} cinnamonitrile solution at pH ~9 (10^{-3} mol dm^{-3} borate) and at pH 1 (0.1 mol dm^{-3} $HClO_4$), and from a N_2O-saturated 10^{-4} mol dm^{-3} cinnamonitrile solution at pH ~9 (10^{-3} mol dm^{-3} borate). The spectra of the transient species are shown in Fig. 1. The extinction coefficients were calculated from the $G\epsilon$ values observed by assuming a *G*(H) of 0.55 (5) and a *G*(OH) of 5.6 in the N_2O-saturated solution (taken from Fig. 4 in ref. 11 and adjusting the result by 1.06 to allow for the difference in $G\epsilon$ used for dosimetry in the two laboratories), a *G*(OH) of 2.72, a *G*(H) of 0.55, and a $G(e_{aq}^-)$ of 2.76 in the helium-saturated solution at pH ~9 (12), and a *G*(OH) of 2.81 and *G*(H) of 3.55 in 0.1 mol dm^{-3} $HClO_4$ (5).

The spectrum of the electron adduct has a maximum extinction coefficient of 33 300 dm^3 mol^{-1} cm^{-1} near 385 nm. The extinction coefficient of the radical anion formed in eq. [8] is similar in magnitude to that of cinnamamide (13) and cinnamic acid (14).

[8] $e_{eq}^- + C_6H_5\text{-}CH{=}CH\text{-}CN \rightarrow (C_6H_5\text{-}CH{=}CH\text{-}CN)^{\cdot -}$

The latter two radical anions undergo acid–base equilibria: cinnamamide (pK_a = 7.2) (13) and cinnamic acid (pK_a = 5.6 and 11.6) (14). Although no pH studies were done in this study, the extinction coefficients at natural pH and at pH~9 were the same, within experimental error, suggesting that the radical anion probably does not have a pK_a near pH 9. This radical anion decayed by first-order kinetics with a rate constant of 1.3×10^5 s^{-1} (24°C) in solutions at natural pH and with a rate constant of 1.8×10^5 s^{-1} (24°C) in solutions buffered with 10^{-3} mol dm^{-3} borate. The transient species formed from reaction of the hydroxyl radical (reaction [9]) did not decay significantly in the time period of the decay of the radical anion.

[9*a*] $OH + C_6H_5\text{-}CH{=}CH\text{-}CN \rightarrow (HO\text{-}C_6H_4)\text{-}CH{=}CH\text{-}CN$

[9*b*] $OH + C_6H_5\text{-}CH{=}CH\text{-}CN \rightarrow C_6H_5\text{-}\dot{C}H\text{-}CHOH\text{-}CN$

The spectrum arising from the reaction of the hydroxyl radical has a maximum extinction coefficient of 5200 dm^3 mol^{-1} cm^{-1} near 375 nm. The hydroxyl radical can react either with the aromatic ring of cinnamonitrile to form cyclohexadienyl radicals (reaction [9*a*]) or with the olefinic group (reaction [9*b*]). The peak observed at 375 nm arises primarily from the cyclohexadienyl radicals; the benzyl radical formed in reaction [9*b*] absorbs near 310–330 nm (15), but we did not record the spectrum in the region. The spectrum of the species formed from the hydroxyl radical reaction is very similar to that observed by Bobrowski and Raghaven (15) for cinnamic acid, suggesting that only 30% of the hydroxyl radicals are reacting by reaction [9*a*] to form the cyclohexadienyl radical.

The spectrum from the transients arising from reaction of the hydrogen atom has a maximum extinction coefficient of 6100 dm^3 mol^{-1} cm^{-1} near 375 nm, and also has a shoulder at 425 nm. This can be interpreted as arising from a mixture of benzyl and cyclohexadienyl radicals that are produced from the hydrogen atom reacting with the ring and the side chain (15). This spectrum is similar in shape, but is slightly more intense than that observed for reaction of the hydrogen atom with cinnamic acid (15).

Can. J. Chem. Downloaded from www.nrcresearchpress.com by 46.23.64.124 on 09/08/12
For personal use only.

Fig. 2. The first-order rate constant for the reaction of the hydrated electron with cinnamonitrile as a function of temperature.

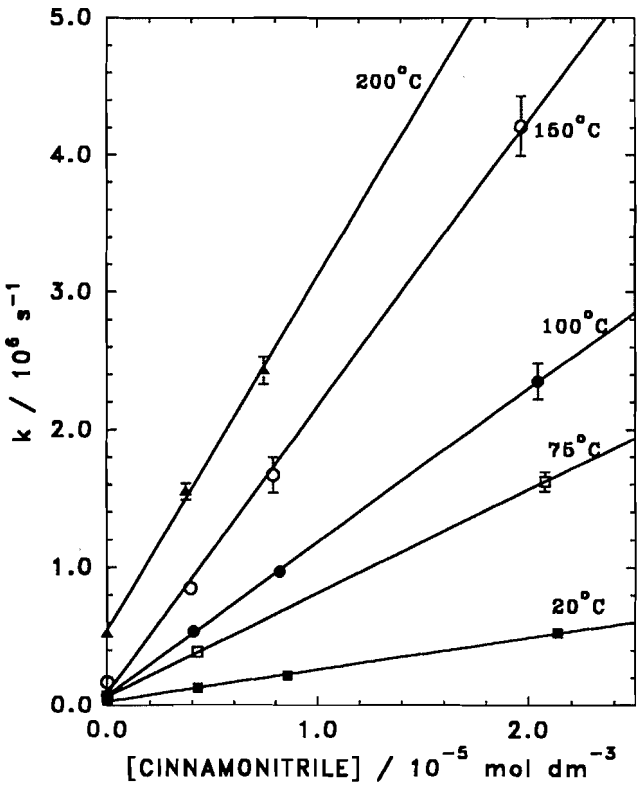

Thermal decomposition studies carried out by us in aqueous solutions indicated that cinnamonitrile was relatively stable at 200°C; i.e., only 10% decomposed in 45 min. This encouraged us to study the rate constant for reaction of the hydrated electron and the hydroxyl radical with cinnamonitrile as a function of temperature. Figure 2 shows the first-order rate constants for decay of the hydrated electron (measured at λ_{max}) as a function of the cinnamonitrile concentration for temperatures up to 200°C. These helium-saturated solutions were buffered with 10^{-3} mol dm^{-3} borate ions. The rate constants for reaction [8] are summarized by the Arrhenius plot in Fig. 3. The room temperature value is near to that expected for a diffusion-controlled reaction, and the line through the date is an Arrhenius fit with an activation energy of 16.1 kJ mol^{-1}. For a truly diffusion-controlled reaction, an activation energy nearer ~20 kJ mol^{-1} would be expected, based on the Smoluchowski equation (16):

$$k_{diff} = 4\pi\,(D_e + D_c)(r_e + r_c)\,N_0\,1000\ \text{dm}^3\ \text{mol}^{-1}\ \text{s}^{-1}$$

where D_e and D_c are the diffusion coefficients and r_e and r_c are the reaction radii for the hydrated electron and cinnamonitrile, respectively. At room temperature, D_e is probably 5 to 10 times larger than D_c (17); furthermore, the temperature dependence of D_e (E_a = 20.75 kJ mol^{-1} (18)) is greater than D_c, which probably has the same dependence as self-diffusion in water (E_a = 15–16 kJ mol^{-1} (17)). As can be seen, the temperature dependence of the reaction is dominated by the diffusion of the hydrated electron in water.

Fig. 3. An Arrhenius plot of the rate constant for reaction of the hydrated electron with cinnamonitrile (○) and diethythiourea (■) and the rate constants observed for the reaction of the hydroxyl radical with cinnamonitrile at 4.5×10^{-5} mol dm^{-3} (◇), 5.3×10^{-5} mol dm^{-3} (▽), and 7.8×10^{-5} mol dm^{-3} (△). All solution were buffered with 10^{-3} mol dm^{-3} borate buffer. The broken lines are the Arrhenius fits to the data.

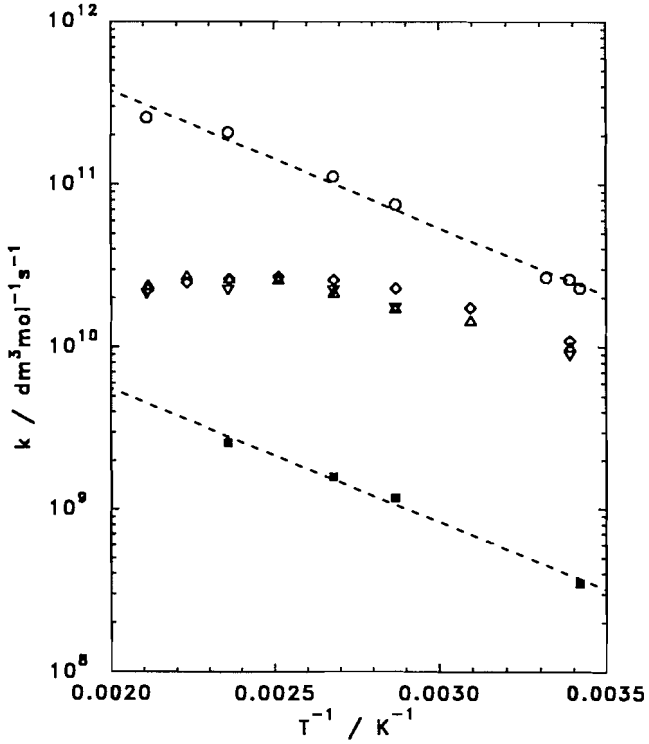

The rate constant for the reaction of the hydroxyl radical with cinnamonitrile was measured by following the first-order buildup of the absorption at 380 nm in N_2O-saturated solutions. Where appropriate, corrections for the decay of the species formed had to be made using the kinetic package FACSIMILE (19). These results are summarized in Fig. 3. While the rate constant observed at 21°C, $(9.2 \pm 0.3) \times 10^9$ dm^3 mol^{-1} s^{-1}, is close to that expected for diffusion control at room temperature, the temperature dependence of the rate constant is considerably less than that expected for diffusion control; obviously, the reaction is being controlled by the activation energy associated with the individual steps in the overall chemical reaction. Similar temperature dependences for reaction of hydroxyl radicals with aromatic compounds have recently been reported and discussed (20).

Only a few γ-radiolysis studies were undertaken . The *G*-value for cyanide ion formation was measured to be 0.10 ± 0.01 and 0.20 ± 0.02, respectively, for helium- and N_2O-saturated solutions containing 4×10^{-4} mol dm^{-3} cinnamonitrile. This suggests that cyanide is a minor product formed by the reaction of the hydroxyl radical. Based on the loss of the cinnamonitrile absorption at 275 nm, the *G*-values for cinnamonitrile loss measured in a 4×10^{-4} mol dm^{-3} cinnamonitrile solutions saturated with helium at natural pH and at pH 2 were the same, namely 4.4 ± 0.1; for a N_2O-saturated solution it was 4.0 and for a O_2-saturated solution it was 2.0. This is consistent with the efficient reactions of the hydrated electron,

Can. J. Chem. Downloaded from www.nrcresearchpress.com by 46.23.64.124 on 09/08/12
For personal use only.

Fig. 4. The spectra observed after pulsing a N_2O-saturated 2×10^{-3} mol dm^{-3} diethylthiourea solution (■) at pH 9, a helium-saturated 2×10^{-2} mol dm^{-3} diethylthiourea solution (▲) at pH 9, and a helium-saturated 2×10^{-2} mol dm^{-3} diethylthiourea solution (□) at pH 1. The dose per pulse was about 6 Gy. The dotted spectrum is the N_2O-saturated 2×10^{-3} mol dm^{-3} diethylthiourea solution scaled by 2.72/5.6 (see text).

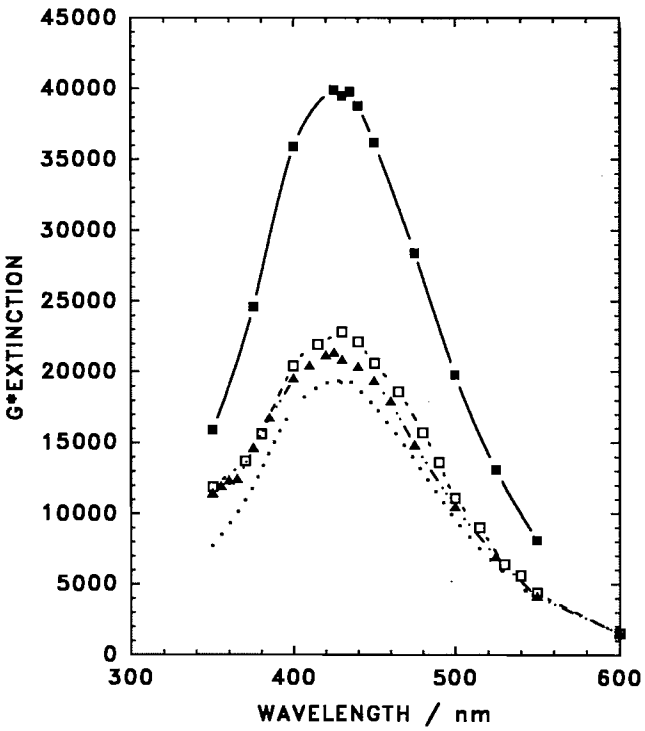

hydroxyl radical, and hydrogen atom with cinnamonitrile, but it also indicates that no chain reaction was initiated and that the superoxide ion, O_2^-, does not react significantly with cinnamonitrile.

Radiolysis studies of diethylthiourea

Figure 4 shows the spectra obtained from a pulse-irradiated, N_2O-saturated 2×10^{-3} mol dm^{-3} diethylthiourea solution (10^{-3} mol dm^{-3} borate buffer), a helium-saturated 2×10^{-2} mol dm^{-3} diethylthiourea solution (10^{-3} mol dm^{-3} borate buffer), and a helium-saturated 2×10^{-2} mol dm^{-3} diethylthiourea solution (pH 1 with $HClO_4$). The dotted line in Fig. 4 is the spectrum of the hydroxyl radical induced transient in a helium-saturated solution (assuming $G(OH) = 2.72$), calculated from the spectrum for a N_2O-saturated solution ($G(OH) = 5.6$). The difference between the dotted spectrum and the two spectra from helium-saturated solutions represents the spectra from the transient products of the reaction of the hydrated electron and hydrogen with diethylthiourea. As can be seen, the transients formed from the hydrated electron and the hydrogen atom only absorb slightly in the wavelength range studied. This is consistent with the recent publication by Dey et al. (21). The hydroxyl radical induced spectrum has a maximum extinction coefficient of 7100 dm^3 mol^{-1} cm^{-1} near 425 nm. The rate constant for the reaction of the hydroxyl radical with diethylthiourea was found to be $(8.0 \pm 0.8) \times 10^8$ dm^3 mol^{-1} s^{-1} at 22°C, measured from the buildup of the absorption at 425 nm. While the rate constant is in agreement with that reported recently (21), our extinction coefficient is 25% higher. This rate constant is comparible to that of the ketone analogue, diethylketone (7).

Tests on the thermal stability of aqueous solutions of diethylthiourea indicate that about 20% of the diethylthiourea decomposes at 180°C in about 10 min. Much faster decompositions were observed at 200°C. The rate of reaction of the hydrated electron with diethylthiourea (reaction [10]) was followed up to 150°C, and the results are summarized in Fig. 3.

[10] $e_{aq}^- + (C_2H_5NH)_2C{=}S \rightarrow ((C_2H_5NH)_2C{=}S)^{\cdot -}$

The rate constant at 22°C is $(3.5 \pm 0.3) \times 10^8$ dm^3 mol^{-1} s^{-1}, about two orders of magnitude below that expected if the reaction was diffusion controlled. Interestingly, the activation energy for the reaction (15.8 kJ mol^{-1}) is similar to that for the hydrated electron reaction with cinnamonitrile, as seen in Fig. 3. This rate is about an order of magnitude less than that for thiourea, suggesting that there may be some steric hinderance by the ethyl groups for the reaction with the hydrated electron in diethyl thiourea. The value of 5×10^8 dm^3 mol^{-1} s^{-1} reported in ref. 21 for k_{10} is slightly higher than that reported here.

The rate of reaction of the hydroxyl radical could not be measured at higher temperatures, because the product(s) formed decayed far too rapidly to estimate the first-order build-up rate constant.

Some preliminary steady-state γ-radiolysis studies were undertaken to measure the loss of diethylthiourea; however, monitoring its absorption near 240 nm was not practical, as it appeared that products were formed that absorbed in the same spectral region. All that could be said is that the G(diethylthiourea loss) was >0.6 and >0.9, respectively, for N_2O- and helium-saturated solutions containing 10^{-5} mol dm^{-3} diethylthiourea at natural pH. These low G-values may also be, in part, a result of products being formed from diethylthiourea that are more reactive towards the hydrated electron and hydroxyl radical than the parent compound.

Conclusions

The rate data collected in this paper support the concept that, in general, corrosion inhibitors react rapidly with the free radical species formed in the radiolysis of water. When corrosion inhibitors are used in reactor decontamination formulations, they will generally be depleted preferentially compared to the organic acids. In any full-system field application of the decontamination formulation, the operators will have to be prepared to add more inhibitors as they are radiolytically destroyed.

Acknowledgements

The authors would like to thank Dr G.V. Buxton, University of Leeds, for helpful discussions. This work was funded by the CANDU Owners Group under WPIR-15-6811.

References

1. D.H. Lister. Water Chemistry II, British Nuclear Energy Society, London. 1980 p. 139.

2. D.G. Miller and R.A. Speranzini. Nucl. Eng. Int. **40**(10), 28 (1995).
3. A.J. Elliot and D.R. McCracken. Radiat. Phys. Chem. **33**, 69 (1989).
4. A.J. Elliot, M.P. Chenier, and D.C. Ouellette. J. Chem. Soc. Faraday Trans. **89**, 119 (1993).
5. J.W.T. Spinks and R.J. Woods. An introduction to radiation chemistry. 2nd ed. John Wiley & Sons, New York. 1976.
6. R.F. Anderson and D. Schulte-Frohlinde. J. Phys. Chem. **82**, 22 (1978).
7. G.V. Buxton, C.L. Greenstock, W.P. Helman, and A.B. Ross. J. Phys. Chem. Ref. Data, **17**, 513 (1988).
8. A.J. Elliot, Radiat. Phys. Chem. **34**, 753 (1989).
9. G.E. Adams and R.L. Willson. Trans. Faraday. Soc. **65**, 2981 (1969).
10. A.M. Afanassiev, K. Okazaki, and G.R. Freeman. Can. J. Chem. **57**, 839 (1979).
11. R.H. Schuler, A.L. Hartzell, and B. Behar. J. Phys. Chem. **85**, 192 (1981).
12. Z.D. Draganic and I.G. Draganic. J. Phys. Chem. **77**, 765 (1973).
13. V. Madhavan, N.N. Lichtin, and E. Hayon. J. Am. Chem. Soc. **97**, 2989 (1975).
14. V. Madhavan, N.N. Lichtin, and E. Hayon. J. Org. Chem. **41**, 2320 (1976).
15. K. Bobrowski and N.V. Raghavan. J. Phys. Chem. **86**, 4432 (1982).
16. A.M. North. The collision theory of chemical reactions in liquids. Methuen, London. 1964.
17. A.J. Elliot, D.R. McCracken, G.V. Buxton, and N.D. Wood. J. Chem. Soc. Faraday Trans. **86**, 1539 (1990).
18. K.H. Schmidt, P. Han, and D.M. Bartels. J. Phys. Chem. **96**, 199 (1992); **99**, 10530 (1995).
19. A.R. Curtis and W.P. Sweetenham. Harwell Research Report AERE-R 12805, 1988.
20. L. Ashton, G.V. Buxton, and C.R. Stuart. J. Chem. Soc. Faraday Trans. **91**, 1631 (1995).
21. G.R. Dey, D.B. Naik, K. Kishore, and P.N. Moorthy. J. Chem. Soc. Perkin Trans. 2, 1625 (1994).

Can. J. Chem. Downloaded from www.nrcresearchpress.com by 46.23.64.124 on 09/08/12
For personal use only.

Comportement photochimique du 4-nitrosophénol en solution aqueuse

Jean-François Pilichowski, Pierre Boule et Jean-Philippe Billard

Résumé : En milieu acide (pH ≈ 1) le 4-nitrosophénol irradié entre 296 et 366 nm se transforme majoritairement (75–80%) en benzoquinone. Le rendement quantique de cette réaction dépend de la longueur d'onde : il est environ 6 fois plus élevé à 365 nm qu'à $\lambda \leq 313$ nm. Ce phénomène est attribué à un équilibre tautomérique entre les formes nitroso et quinone monooxime, la première étant photochimiquement beaucoup plus réactive que la seconde. Dans l'eau distillée non tamponnée (pH = 5–6), il apparaît une espèce intermédiaire qui présente en CLHP un temps de rétention voisin de celui de la benzoquinone et dont le maximum d'absorption est situé à 235 nm. La transformation de cet intermédiaire est accélérée en milieu acide.

Mots clés : photochimie, 4-nitrosophénol, effet de longueur d'onde.

Abstract: In acidic medium (pH ≈ 1) 4-nitrosophenol irradiated in the range 296–366 nm is mainly transformed into benzoquinone (75–80%). The quantum yield of this reaction is wavelength dependent: it is about 6 times higher at 365 nm than at $\lambda \leq 313$ nm. This phenomenon is attributed to an equilibrium between two tautomeric forms, nitroso and quinone monooxime, the former being much more photoreactive than the latter. In unbuffered aqueous solution (pH = 5–6) the formation of an intermediate is observed. Its HPLC retention time is just a little shorter than that of benzoquinone and the maximum of its absorption band is located at 235 nm. The rate of transformation of this intermediate increases with decreasing pH.

Key words: photochemistry, 4-nitrosophenol, wavelength effect.

Introduction

Les nitrosophénols sont des composés dont le comportement photochimique a été très peu étudié. Le 4-nitrosophénol en particulier peut pourtant apparaître, en solution aqueuse, soit dans la photolyse du 4-nitrophénol (1), soit par excitation des ions nitrate (2, 3) ou nitrite en présence de phénol (3). À forte concentration en ions nitrite, la réaction devient même spécifique. Le but de ce travail est d'une part, de déterminer l'influence de différents paramètres (pH, longueur d'onde, oxygénation) sur la vitesse de phototransformation du 4-nitrosophénol et d'autre part, d'analyser les produits formés dans le but de prévoir le devenir de ce composé dans l'environnement.

Partie expérimentale

Le 4-nitrosophénol commercial (Aldrich) a été purifié par cristallisation fractionnée dans un mélange hexane–éther. Une chromatographie de contrôle (gel de silice sur couche mince) a permis de s'assurer de la pureté du produit. L'analyse CLHP et la RMN du proton ont confirmé l'efficacité de cette purification. La *p*-benzoquinone, Merck *for synthesis*, a été purifiée par sublimation. Elle a été obtenue sous forme de cristaux jaune clair.

Reçu le 19 mai 1995.

J.-F. Pilichowski, P. Boule[1] et J.-P. Billard. Laboratoire de photochimie moléculaire et macromoléculaire (Unité de recherche associée au Centre national de la recherche scientifique, n° 433), Université Blaise Pascal (Clermont-Ferrand), F - 63177 Aubière Cedex, France.

[1] Auteur à qui la correspondance doit être adressée. Téléphone : (33) 73 40 71 76. Télécopieur : (33) 73 40 77 00.

Les spectres UV–visible ont été enregistrés sur Cary 118 ou Cary 3 (Varian).

L'irradiation monochromatique des solutions a été réalisée grâce à un monochromateur Bausch et Lomb équipé d'une lampe à vapeur de mercure très haute pression de type HBO 200 W ou USH 200 DP.

Les intensités de lumière ont été évaluées par actinométrie chimique au ferrioxalate de potassium ou à l'Aberchrome 540 (en n'utilisant qu'une fois les solutions) (4).

Les solutions ont été analysées par CLHP sur colonne inverse C_{18} 250 mm × 4 mm en utilisant des mélanges eau–méthanol comme éluant.

Résultats

Propriétés spectrophotométriques du 4-nitrosophénol

Le spectre UV–visible du 4-nitrosophénol en solution aqueuse, dont les caractéristiques sont données dans le tableau 1, permet d'évaluer son pK_a à 6,2 (figure 1). Ce résultat est en bon accord avec les valeurs données dans la littérature, 6,2 (7) et 6,5 (8). On peut noter que le 4-nitrosophénol est plus acide que le 4-nitrophénol ($pK_a \approx 7$ à 25°C (9)).

Tautomérie

En faisant réagir l'acide nitreux sur le phénol, on obtient de façon très majoritaire le 4-nitrosophénol (**I**). Par action de l'hydroxylamine sur la *p*-benzoquinone, il se forme de la *p*-quinone monooxime (**II**). Dans certaines conditions expérimentales, ces deux produits peuvent être obtenus, séparément, sous forme cristalline (6). Par contre, en solution, chacune des espèces évolue vers un mélange unique qui correspond à une tautomérie :

Can. J. Chem. Downloaded from www.nrcresearchpress.com by 46.23.64.124 on 09/08/12
For personal use only.

Can. J. Chem. Downloaded from www.nrcresearchpress.com by 46.23.64.124 on 09/08/12
For personal use only.

Fig. 1. (*a*) Spectre UV–visible d'une solution aqueuse de 4-nitrosophénol ($4{,}4 \times 10^{-4}$ mol L^{-1}) à différents pH. (*b*) Détermination du pK_a (≈23°C).

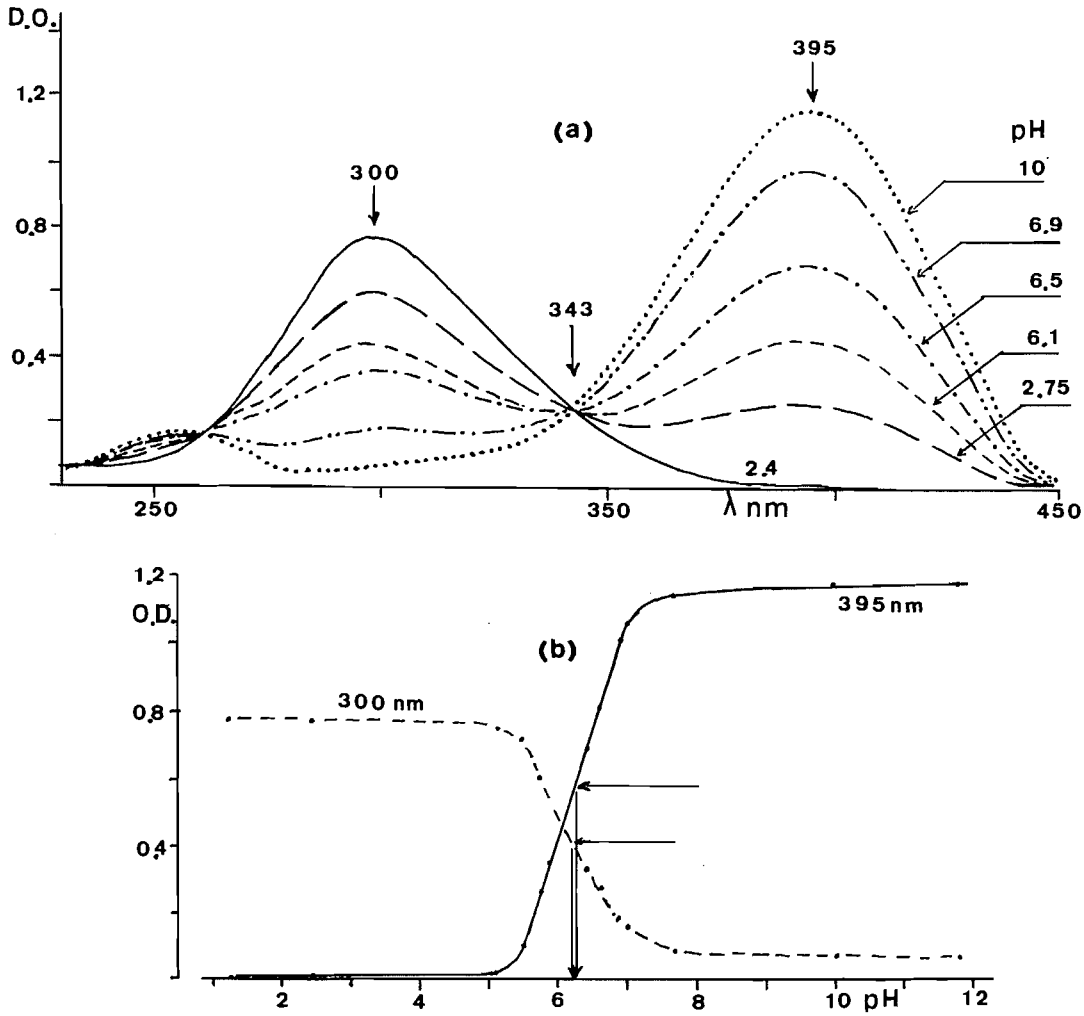

Tableau 1. Maximums d'absorption et coefficients d'extinction molaire du 4-nitrosophénol en solution aqueuse.

	Forme neutre	Forme anionique	
λ max (nm) :	300	256	395
ε (mol^{-1} L cm^{-1}) :	17 200 ± 800[a]	3500 ± 100[a]	26 400 ± 800[a]
	9375[b]		2500[b]
	18 200[c]	3800[c]	29 500[c]

[a]Ce travail (chaque valeur correspond à la moyenne de 5 mesures).
[b]Référence 5.
[c]Référence 6.

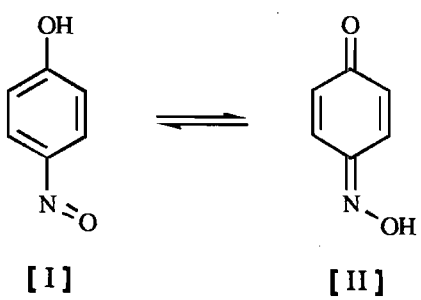

[I] [II]

Une analyse par RMN, dans des conditions rigoureusement anhydres, a permis d'observer expérimentalement cet équilibre dans différents solvants (10).

[II] / [I] = 83/17 dans le dioxanne, l'éthanol, l'éther

[II] / [I] = 75/25 dans l'acétone

Par contre, à notre connaissance, il n'existe pas de données relatives aux solutions aqueuses, mais on peut supposer un comportement analogue en solution acide. En milieu basique, par contre, chacune des deux formes conduit aux formes déprotonées, mésomères d'une espèce unique.

Fig. 2. Evolution du spectre UV d'une solution aérée 10^{-3} mol L^{-1} de 4-nitrosophénol irradiée à 365 nm à pH = 1 (épaisseur 1 mm). (———) $t = 0$; (—— ——) $t = 15$ min; (—·—·—) $t = 30$ min; (· · · · · ·) $t = 45$ min.

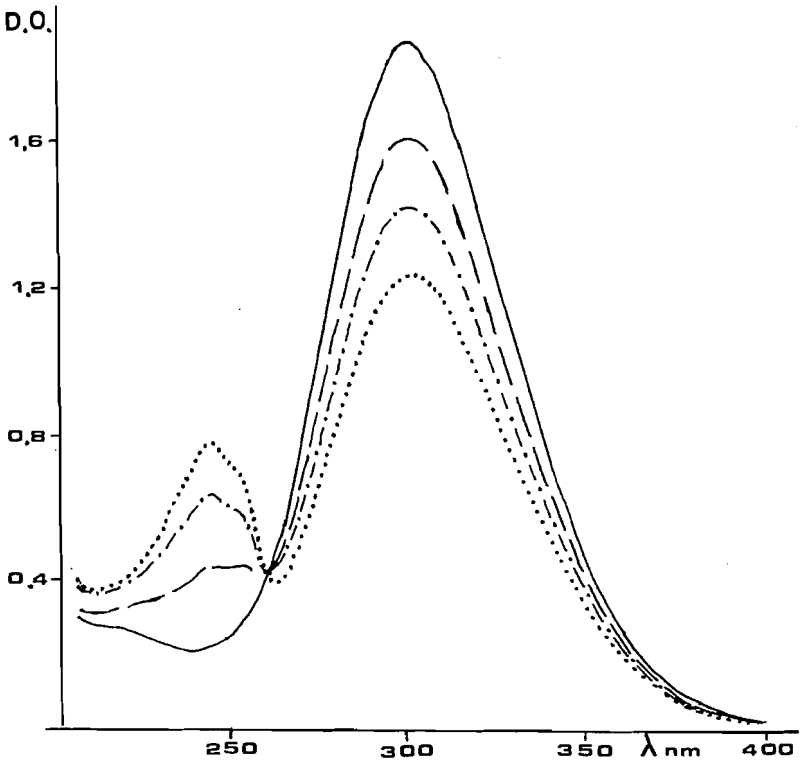

Tableau 2. Rendement quantique de phototransformation du 4-nitrosophénol (10^{-3} mol L^{-1}) dans la zone de pH = 0,8–3, évalué par CLHP.

λ nm	ϕ disp ($\times 10^4$)
296	7 ± 0,5
305	6 ± 0,5
313	7 ± 0,5
334	16 ± 2
365	42 ± 3

Évolution photochimique

Des solutions acides (pH de l'ordre de 1) ou basiques (pH > 9) aérées ou désoxygénées de concentration comprise entre 10^{-4} et 10^{-3} mol L^{-1} ont été irradiées à différentes longueurs d'onde. Il a été vérifié préalablement que ces solutions sont stables pendant plusieurs jours, en absence de lumière.

En solution basique, l'évolution photochimique à 365 nm est extrêmement lente. Le rendement quantique de disparition peut être estimé inférieur à 10^{-6}. Par contre, l'évolution en milieu acide peut être suivie par spectrophotométrie UV et par chromatographie CLHP. Quelle que soit la longueur d'onde d'irradiation (313, 334 ou 365 nm) d'une solution aérée 10^{-3} mol L^{-1}, on constate la formation très largement majoritaire d'un produit qui a été identifié à la *p*-benzoquinone grâce à son spectre UV (figure 2) et à son temps de rétention en CLHP. La *p*-benzoquinone représente environ 75–80% de la transformation. La formation d'une très faible quantité de 4-nitrophénol a également été observée lors d'irradiations longues (>50% de disparition).

L'oxygène n'a pas d'influence appréciable sur la vitesse de transformation, ni sur la formation de la benzoquinone. Il en est de même de l'addition de faibles quantités (≤5%) de méthanol à la solution. Par contre, le rendement quantique de la réaction dépend beaucoup de la longueur d'onde, comme cela apparaît dans le tableau 2 : il est environ 6 fois plus élevé à 365 nm qu'à $\lambda \leq 313$ nm.

En milieu faiblement acide (solution aqueuse non tamponnée; pH ≈ 5), il apparaît initialement un composé intermédiaire (X) dont le maximum d'absorption est situé à 235 nm (figure 4) et dont le temps de rétention en CLHP est légèrement plus faible que celui de la benzoquinone BQ (figure 3). Ce composé disparaît avec formation de benzoquinone (figure 3), la vitesse de transformation augmentant avec la diminution du pH. À température ambiante, la durée de cette transformation varie de 1 à 2 min à pH = 1, jusqu'à plusieurs heures en milieu neutre.

Après irradiation d'une solution dégazée, jusqu'à un avancement de l'ordre de 50%, la formation d'azote a pu être mise en évidence par spectrométrie de masse de la phase gazeuse. Une légère augmentation de pression a aussi pu être observée (en plaçant le réacteur dans un mélange glace–eau pour fixer la pression de vapeur d'eau).

Discussion

Effet de longueur d'onde

Les différentes longueurs d'onde utilisées correspondent apparemment à la même bande d'absorption dont la maximum

Can. J. Chem. Downloaded from www.nrcresearchpress.com by 46.23.64.124 on 09/08/12
For personal use only.

Fig. 3. Chromatogramme CLHP d'une solution non tamponnée de 4-nitrosophénol 10^{-3} M irradiée à 365 nm. Eluant MeOH/H_2O 40:60; détection à 270 nm. BQ : *p*-benzoquinone, X : intermédiaire. (*a*) Quelques minutes après l'irradiation; (*b*) environ 15 min plus tard; (*c*) après 4 h.

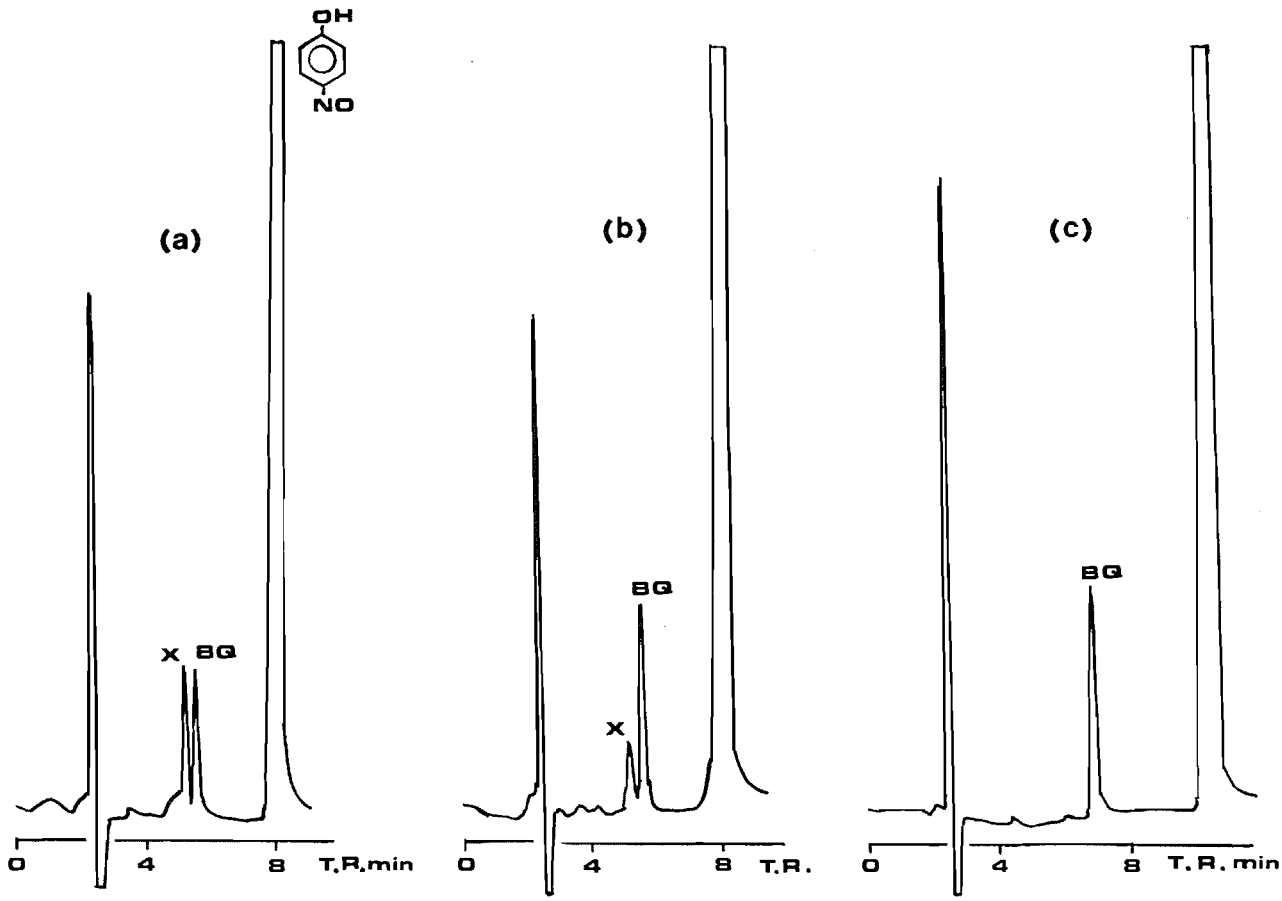

Fig. 4. Spectre UV obtenu sur un détecteur à barrette de diodes du produit X qui se forme avant la *p*-benzoquinone.

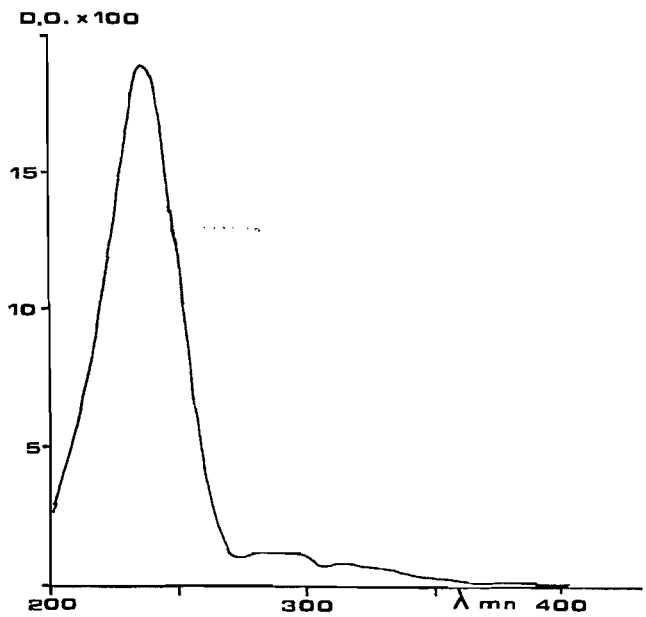

est situé à 300 nm. Le fait que le rendement quantique de la phototransformation décroisse avec la longueur d'onde entre 365 et 313 nm peut être attribué à l'existence de l'équilibre tautomérique signalé, la forme absorbant à plus grande longueur d'onde étant beaucoup plus réactive que l'autre. La bande d'absorption observée correspondrait alors à la superposition des bandes de chacun des deux tautomères. N'ayant pas directement accès aux propriétés spectrophotométriques des deux formes, nous nous sommes reportés aux données de la littérature relatives à des composés comparables sur le plan structural. Les spectres UV–visible du *p*-nitrosoanisole et de la *p*-benzoquinone monooxime méthyl éther présentent des maximums situés respectivement à 333 et 313 nm, avec des coefficients d'extinction molaires voisins (11). Par analogie, on peut supposer que la forme nitroso du 4-nitrosophénol absorbe à plus grande longueur d'onde que la forme quinone-oxime (environ entre 315 et 400 nm). La photoréactivité de la première serait donc 6–7 fois plus élevée que celle de la deuxième. Un phénomène analogue a été signalé dans le cas du 3-chloro-4-nitrosophénol (12).

Mécanisme de la réaction

Le temps de rétention CLHP et le spectre UV de l'intermédiaire mis en jeu lors de la photolyse du 4-nitrosophénol permettent de penser qu'il s'agit d'une espèce de structure voisine de la benzoquinone, cet intermédiaire se transformant rapidement en benzoquinone en milieu acide. Cette réaction pourrait être expliquée par la formation intermédiaire de 4-hydroxyamino-2,5-cyclohexadiénone qui proviendrait de l'hydrolyse de la forme quinonoxime. Cependant, ce mécanisme est incompatible avec l'effet de longueur d'onde observé. Par contre, le passage par une forme oxaziridine a

Can. J. Chem. Downloaded from www.nrcresearchpress.com by 46.23.64.124 on 09/08/12
For personal use only.

déjà été signalé dans la photolyse des nitrones (13, 14), des aldoximes et cétoximes (13, 15). Par analogie avec le mécanisme suggéré par Isawa et al. (14), la formation d'oxaziridine peut être expliquée par une polarisation de la liaison N—O à l'état excité. On peut donc proposer le mécanisme suivant :

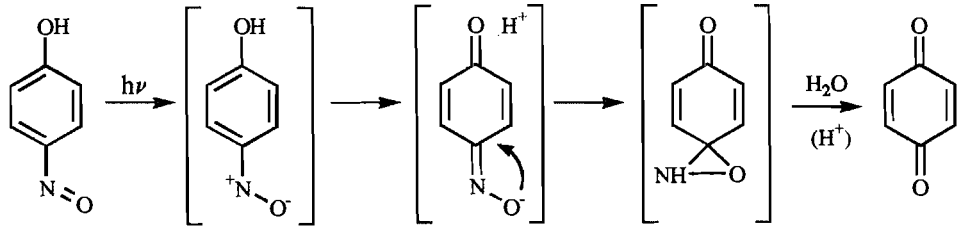

La formation d'azote ne peut se produire que dans une étape ultérieure. Elle pourrait, par exemple, faire intervenir la formation d'un dérivé de l'hydroxylamine, difficile à mettre en évidence.

Remerciements

Les auteurs remercient J.L. Philippart pour les mesures de spectrométrie de masse de la phase gazeuse.

Bibliographie

1. A. Alif, P. Boule et J. Lemaire. Chemosphere, **16**, 2213 (1987).
2. R. Niessen, D. Lenoir et P. Boule. Chemosphere, **17**, 1977 (1988).
3. F. Machado et P. Boule. J. Photochem. Photobiol. A: **86**, 73 (1995).
4. P. Boule et J.F. Pilichowski. J. Photochem. Photobiol. A: **71**, 51 (1993).
5. H.H. Hodgson. J. Chem. Soc. 520 (1937).
6. J.T. Hays, E.H. Butts et H.L. Young. J. Org. Chem. **32**, 153 (1967), et références citées.
7. K.M. Ibne-Rasa. J. Am. Chem. Soc. **84**, 4962 (1962).
8. The Merck Index. 10th ed. Merck & Co., Inc., Rahway, N.J. 1983. p. 952.
9. Beilstein's Handbuch der Organischen Chemie. **6**, 226 (1923).
10. H. Uffman. Tetrahedron Lett. **38**, 4631 (1966).
11. L.C. Anderson et M.B. Geiger. J. Am. Chem. Soc. **54**, 3065 (1932).
12. A. Kraaijeveld et E. Havinga. Recl. Trav. Chim. Pays-Bas, **73**, 537 (1954).
13. G.G. Spence, E.C. Taylor et O. Buchardt. Chem. Rev. **70**, 231 (1970).
14. H. Isawa, P. de Mayo et T. Tabala. Can. J. Chem. **47**, 51 (1969).
15. T. Oine et T. Mukai. Tetrahedron Lett. 157 (1969).

Can. J. Chem. Downloaded from www.nrcresearchpress.com by 46.23.64.124 on 09/08/12
For personal use only.

Protonation of porphocyanine — a new expanded tetrapyrrolic macrocycle

Lily Yun Xie and David Dolphin

Abstract: The porphocyanine nucleus contains six nitrogen atoms, four of which are theoretically capable of accepting a proton in acidic solution. However, only the monoprotonated and diprotonated forms have been observed. These two forms were characterized by their visible and fluorescence spectra. pK_a values of 6.0 ± 0.1 and 4.4 ± 0.1 were determined by spectrophotometric titration. The monoprotonated monocationic form can be observed in methanol.

Key words: porphocyanine, protonation, octaethylporphocyanine, octaethylporphyrin.

Résumé : Le noyau porphocyanine contient six atomes d'azote, dont quatre sont en théorie capables d'accepter un proton d'une solution acide. Toutefois, on n'a observé que les formes mono- et diprotonées. On a caractérisé ces deux formes par leurs spectres visible et de fluorescence. Faisant appel à un titrage spectrophotométrique, on a déterminé que les valeurs de pK_a sont respectivement de 6,0 ± 0,1 et 4,4 ± 0,1. On peut observer la forme monocationique monoprotonée dans le méthanol.

Mots clés : porphocyanine, protonation, octaéthylporphocyanine, octaéthylporphyrine.

[Traduit par la rédaction]

Can. J. Chem. Downloaded from www.nrcresearchpress.com by 46.23.64.124 on 09/08/12
For personal use only.

We recently communicated the synthesis and characterization of a new class of tetrapyrrolic macrocycles, porphocyanines **1** (1–3), and showed that these compounds were capable of catalyzing the photosensitized oxidation of cholesterol (3). They are potential photosensitizers for photodynamic therapy for cancer treatment because they offer long-wavelength absorption between 795 and 810 nm in their free base form, which would in principle confer superior tissue penetration to visible light than is the case with existing drugs. It is important to know the nature of the ionic species of a photosensitizer in solution as a function of pH (4), since it is known that the longest wavelength absorption and fluorescence emission are affected by protonation of the porphocyanine nucleus, which contains four potential sites for protonation. Furthermore, protonation of porphocyanine might effect biodistribution of the photosensitizer in vivo (4–7) Finally, the pK_a data of porphocyanines are valuable in understanding the reactivity and aromaticity of this new macrocycle.

It is of interest to compare the protonation properties of the porphocyanine with those of porphyrin (**2**), azaporphyrin (**3**), sapphyrin (**4**), and phthalocyanine (**5**). Several techniques have been used in the measurement of pK_a values of porphyrins and related compounds taking account of their poor solubility in water, i.e., potentiometric titration in glacial acetic acid, and spectrophotometric titration in nitrobenzene and in aqueous detergent solutions (7–9). The pK_a value of sapphyrin was, however, recently estimated using a spectrophotometric method in a biphasic system (10).

Received June 16, 1995.

L.Y. Xie and D. Dolphin.[1] Department of Chemistry, University of British Columbia, 2036 Main Mall, Vancouver, BC V6T 1Z1, Canada.

[1] Author to whom correspondence may be addressed. Telephone: (604) 822-4571.

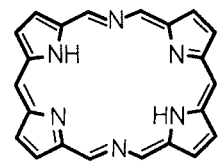

1

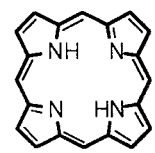

2

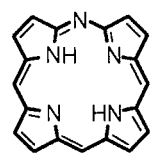

3

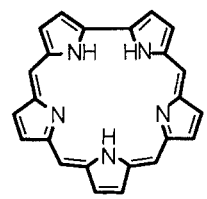

4

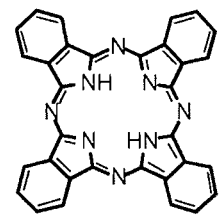

5

Experimental

Octaethylporphocyanine (H_2P) was prepared according to the procedure described previously (1) and was dissolved in dichloromethane. The absorbance changes at specific wavelengths were monitored upon mixing a CH_2Cl_2 solution of octaethylporphocyanine (3.5×10^{-4} M) and a pH-adjusted aqueous NaCl solution ($[Cl^-]_{total}$ = 0.1 M). Electronic spectra were recorded on a Hewlett–Packard 8452A diode array spectrophotometer. The pH values were recorded on a Fisher Accumet pH meter model 210 with a glass combination electrode (Fisher Scientific). The pH meter was calibrated at 25°C with standard buffer solutions for pH 4.00 and 7.00 prior to the pH measurements. Fluorescence emission spectra were measured on an Aminco Bowman Series 2 luminescence spectrometer using a flash lamp as the excitation source. Solutions of porphocyanine were handled under dim light to avoid photodegradation.

Can. J. Chem. Downloaded from www.nrcresearchpress.com by 46.23.64.124 on 09/08/12
For personal use only.

Results and discussion

Because of the poor water solubility of octaethylporphocyanine, we attempted to solubilize the material in 2.5% sodium dodecyl sulphate (SDS) solution in order to obtain the pK_a values in a solvent system that simulates the experimental conditions used in our photodynamic bioassay experiments (liposomal formulations). The solubility of octaethylporphocyanine can be enhanced by addition of 0.1 N HCl solution but, unfortunately, the amount of octaethylporphocyanine that went into the detergent solution was still insufficient to allow a meaningful analysis of the spectral changes in the regions of interest. Moreover, octaethylporphocyanine was found to behave differently in 2.5% SDS solution and organic solvents. In SDS solution only the dication was observed between pH 2 and 5 and, as the pH increased, the 748 nm band (of the dication) decreased and eventually disappeared with no formation of new bands. That is, neither the monocation nor free base were observed in SDS solution even though octaethylporphocyanine exhibits very distinct absorption bands for both the dication and free base in dichloromethane, with their longest wavelength bands appearing more than 50 nm apart. Thus we employed a biphasic spectrophotometric titration method previously used for estimating the pK_a's of sapphyrin **4** (10).

In the aqueous dichloromethane system, octaethylporphocyanine was well behaved as a function of $[H^+]$. At low pH (below 4), two isosbestic points were observed at 729 and 754 nm in the 720–820 nm region (Fig. 1), indicating that within this pH range only two species, dication and monocation, are dominant. At high pH (above 6), two isosbestic points were also obtained, at 732 and 778 nm (Fig. 2), indicating that within this pH range only monocation and free base are present in significant concentrations. The fluorescence emission spectra of the different forms of octaethylporphocyanine were recorded; three species fluoresce, at 751, 764, and 802 nm, respectively. At low pH, only two peaks (751 and 764 nm) were observed in the fluorescence emission spectrum, consistent with the isosbestic points seen in the optical absorption spectrum (Fig. 1), whereas at high pH, two peaks (764 and 802 nm) were observed, consistent with the isosbestic points in Fig. 2. It was clear that throughout the titration there were only three species, free base, monocation, and dication, present in solution. Two equivalents of HCl will protonate the free base to give the spectrum of the dication, which remains the same upon addition of further equivalents of acids (eqs. [1] and [2]).

$$[1]\quad H_2P + H^+ \overset{K_3}{\longleftrightarrow} H_3P^+$$

$$[2]\quad H_3P^+ + H^+ \overset{K_4}{\longleftrightarrow} H_4P^{2+}$$

The dication spectrum remains unchanged even in the concentrated H_2SO_4. It is well known in the literature that the protonation of phthalocyanine (**5**) occurs at the methine azo groups rather than in the centre of the molecule (11). Very little is known about the protonation behavior of azaporphyrins (**3**) (see ref. 11, p. 75, and ref. 12). However, it was shown previously that protonation of the internal nitrogen in azaetioporphyrin preceded the protonation of the methine bridging nitrogen that had an estimated pK value of ca. −3.3 (13). Despite the fact that porphocyanine contains two imine linkages in the macrocycle, we believe that it behaves more like azaporphyrin than phthalocyanine. Protonations of porphocyanine have thus been assigned to the inner pyrrolinene nitrogens (Scheme 1) and further protonation of imine nitrogen was not observed even in concentrated sulphuric acid. The

Fig. 1. Absorption spectra of octaethylporphocyanine in dichloromethane equilibrated with 0.1 M NaCl solutions from pH 3.9 to 2.3 at 22°C. Two isosbestic points at 729 and 754 nm were observed.

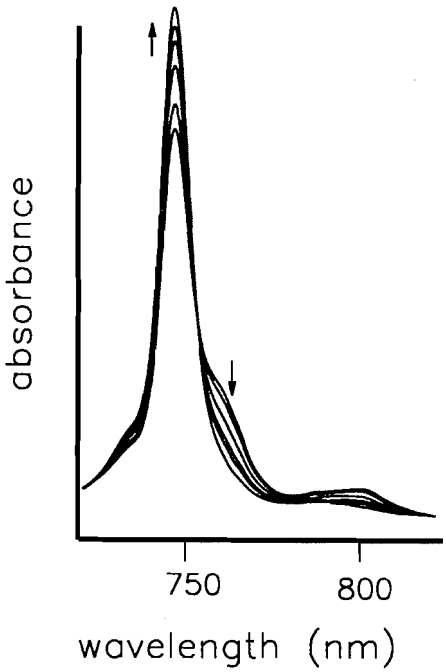

Fig. 2. Absorption spectra of octaethylporphocyanine in dichloromethane equilibrated with 0.1 M NaCl solutions from pH 7.2 to 5.4 at 22°C. Two isosbestic points at 732 and 778 nm were observed.

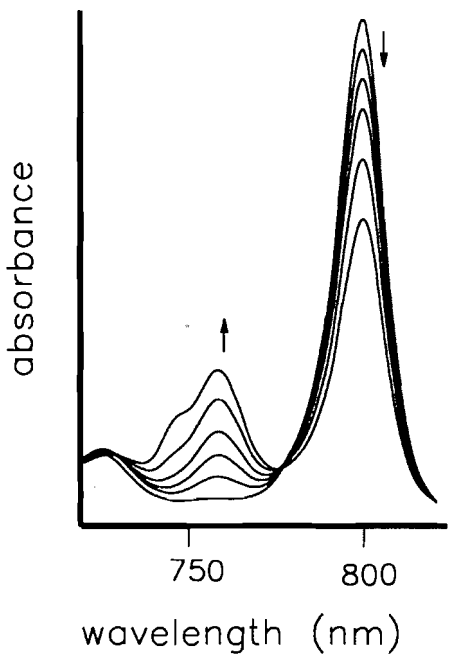

Scheme 1.

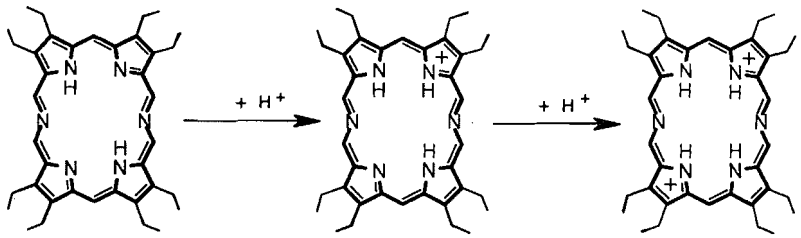

weak basicity of the imine nitrogens was also reflected in the inability of these atoms to coordinate with zinc (1).

Using the absorbance changes at high pH at 798 nm from Fig. 2, K_3 could be obtained from the following eq. [3] (14)

$$[3] \quad \frac{1}{A_0 - A} = \frac{K_3}{A_0 - A_1} \cdot \frac{1}{[H^+]} + \frac{1}{A_0 - A_1}$$

where A_0 and A_1 are the absorbances of the pure free base and pure monocation of the octaethylporphocyanine at 798 nm, and A is that of a mixture of monocation and free base at this specific wavelength. The data for the pH values and absorbances necessary for the calculation of K_3 are given in Table 1. The value of K_3 was calculated from the linear relationship between $1/(A_0 - A)$ and $1/[H^+]$ to be approximately $(1.1 \pm 0.1) \times 10^{-6}$, corresponding to a pK_3 of 6.0 ± 0.1 (Fig. 3). The absorbance and $[H^+]$ relationship for the calculation of K_4 can be easily derived as follows:[2]

$$[4] \quad \frac{1}{A_\infty - A} = \frac{[H^+]}{(A_\infty - A_2)K_4} + \frac{1}{A_\infty - A_2}$$

where A_∞ and A_2 are the absorbances of the dication and monocation forms of octaethylporphocyanine at 748 nm, and A is that of a mixture of monocation and dication at this specific wavelength. Using the absorbance changes from Fig. 1 at low pH at 748 nm (Table 2), K_4 can be obtained from the linear relationship between $1/(A_\infty - A)$ and $[H^+]$ (Fig. 4) according to eq. [4]. K_4 was found to be $\sim(4.2 \pm 0.1) \times 10^{-5}$, corresponding to a pK_4 of 4.4 ± 0.1.

A distribution diagram was calculated based on the pK values determined here (Fig. 5). It is clear that the concentration of free base is insignificant below pH 4.0 and that the concentration of dication is negligible above pH 6. Thus the spectrum of monocation in dichloromethane was obtained by subtracting the spectrum of free base from the actual spectrum at pH 6.1. The longest visible absorptions for the three individual species appear distinctly at 748, 760, and 798 nm, respectively. This calculated spectrum of the monocation was found to be the same as the spectrum obtained in methanol. Normally porphyrins form dications on treatment with acids and the intermediate monocationic species are rarely present by

[2] Since $A_2 = \varepsilon_{H_3P^+}cl$, $A_\infty = \varepsilon_{H_4P^{2+}}cl$, and $A = \varepsilon_{H_3P^+}[H_3P^+]l + \varepsilon_{H_4P^{2+}}[H_4P^{2+}]l$, where $c = [H_3P^+] + [H_4P^{2+}]$, it is readily shown from eq. [2] that

$$\frac{A - A_2}{A_\infty - A} = \frac{[H_4P^{2+}]}{[H_3P^+]} = \frac{[H^+]}{K_4}$$

Therefore,

$$\frac{A_\infty - A_2}{A_\infty - A} = \frac{[H^+]}{K_4} + 1$$

Rearranging this equation affords eq. [4].

Table 1. Change of absorbances as a function of $[H^+]$ for pH 6.10–7.20 at 798 nm in CH_2Cl_2–H_2O at 22°C.

A_{798}	$1/(A_0 - A)_{798}$	pH	$1/[H^+]$
0.923	22.2	7.20	1.58×10^7
0.851	8.55	6.75	5.62×10^6
0.791	5.65	6.50	3.16×10^6
0.691	3.61	6.25	1.78×10^6
0.571	2.52	6.10	1.26×10^6

Note: $(A_0)_{798} = 0.968$.

Table 2. Change of absorbances as a function of $[H^+]$ for pH 3.15–3.90 at 748 nm in CH_2Cl_2–H_2O at 22°C.

A_{748}	$1/(A_\infty - A)_{748}$	pH	$[H^+]$
1.00	14.3	3.15	7.08×10^{-4}
0.973	10.3	3.30	5.01×10^{-4}
0.919	6.62	3.50	3.16×10^{-4}
0.837	4.29	3.70	2.00×10^{-4}
0.788	3.55	3.90	1.26×10^{-4}

Note: $(A_\infty)_{748} = 1.07$.

Fig. 3. Plot of $1/(A_0 - A)_{798}$ vs. $1/[H^+]$ from the data in Table 1 to determine the K_3 from eq. [3].

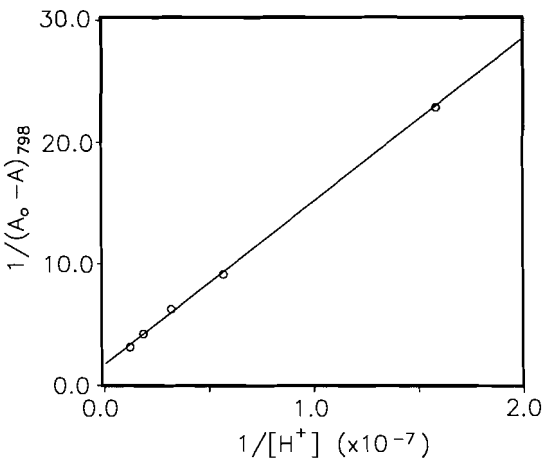

Can. J. Chem. Downloaded from www.nrcresearchpress.com by 46.23.64.124 on 09/08/12
For personal use only.

Can. J. Chem. Downloaded from www.nrcresearchpress.com by 46.23.64.124 on 09/08/12
For personal use only.

Fig. 4. Plot of $1/(A_\infty - A)_{748}$ vs. $[H^+]$ from the data in Table 2 to determine the K_4 from eq. [4].

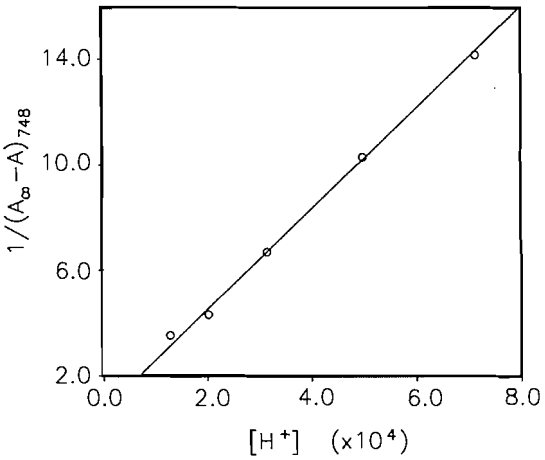

Fig. 5. Distribution diagram of the ionic species of octaethylporphocyanine in solution as a function of pH.

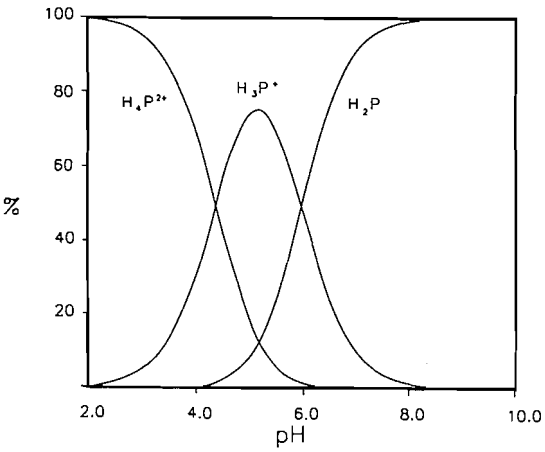

themselves either in solution or the solid state. A crystal structure of octaethylporphyrin monocation (15) and spectral investigation of this monocationic species (16) and that of a tetraphenylporphyrin derivative (17) are among the few such examples in the literature. The fact that octaethylporphocyanine exists as a monocation in a polar organic solvent like methanol indicates that the stability of the monocationic form may result from a nondistorted structure. Distortion of monocationic forms in both tetraphenylporphyrin and octaalkylporphyrin may explain why monocations are rarely observed. In the case of porphyrins the second protonation is normally easier than the first, and only under special conditions can the monocations be observed (8, 18). Porphocyanine, on the other hand, does not seem to need to distort to accommodate a proton, as is seen in the X-ray crystal structure of the zinc derivative where two protons are easily accommodated by two adjacent pyrroles without any distortion from planarity (1). This could, at least in part, be attributed to the observation of a single monocationic species in methanol. It is worth noting that in methanol, addition of HCl led to the formation of dication but addition of NaOH bleached the compound. Thus the free base spectra in methanol was obtained in the presence of

Fig. 6. Optical spectra of porphocyanine in methanol in the presence of triethylamine (-···-), in the presence of HCl (—), and in neat methanol (---).

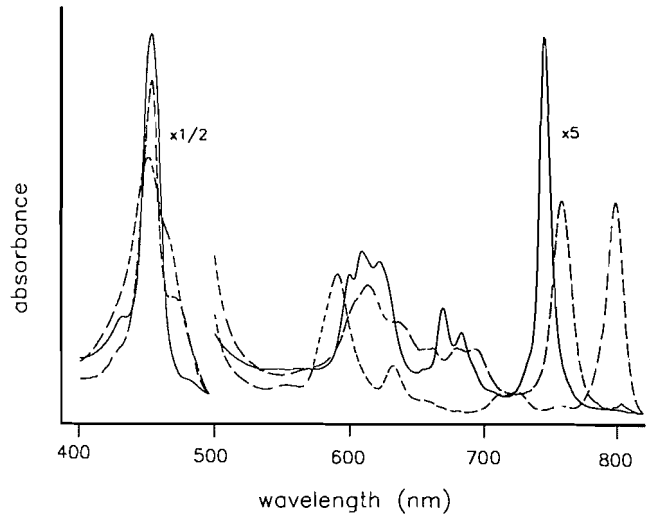

triethylamine. In acetic acid, octaethylporphocyanine is present as the dication whereas octaethylporphyrin exists as the monocationic form (13). The optical spectra of free base, monocation, and dication of octaethylporphocyanine in methanol are presented in Fig. 6.

The pK_3 and pK_4 values of octaethylporphyrin were determined to be 6.1 and 4.6 in nitrobenzene–$HClO_4$ (19). It is difficult to make a comparison between data determined by different methods; however, we tentatively draw the conclusion that the protonation behavior of porphocyanine is similar to that of porphyrins, with pK_3 and pK_4 differing by about two pK units. We feel that the only proper comparison can be made between porphyocyanine **1** and sapphyin **4** where pK_a values were measured under similar conditions. Octaethylporphocyanine is much less basic than 3,8,12,13,17,22-hexaethyl-2,7,18,23-tetramethylsapphyrin with pK_3 and pK_4 values of 9.5 and 3.5 (10). Attempts by us to determine the pK's of octaethylporphyrin in the same biphasic solvent system were unsuccessful.

Acknowledgment

We thank the Natural Sciences and Engineering Research Council of Canada for financial support.

References

1. D. Dolphin, S.J. Rettig, H. Tang, T. Wijesekera, and L.Y. Xie. J. Am. Chem. Soc. **115**, 9301 (1993).
2. L.Y. Xie and D. Dolphin. J. Chem. Soc. Chem. Commun. 1475 (1994).
3. R.W. Boyle, L.Y. Xie, and D. Dolphin. Tetrahedron Lett. **35**, 5377 (1994).
4. R.H. Pottier, J.P. Laplante, Y-F.A. Chow, and J.C. Kennedy. Can. J. Chem. **63**, 1463 (1985).
5. R.H. Pottier, J.C. Kennedy, Y.F.A. Chow, and F. Cheung. Can. J. Spectrosc. **33**, 57 (1988).
6. D. Brault, C.Vever-Bizet, and T.L. Doan. Biochim. Biophys. Acta, **857**, 238 (1986).
7. M. Smith. *In* Porphyrins and metalloporphyrins. *Edited by* K.M. Smith. Elsevier, Amsterdam. 1975. p.1.

8. N. Phillips. Rev. Pure Appl. Chem. **10**, 35 (1960).
9. S. Arnoff. J. Phys. Chem. **62**, 428 (1958).
10. Furuta, M.J. Cyr, and J.L. Sessler. J. Am. Chem. Soc. **113**, 6677 (1991).
11. B.D. Berezin. Coordination compounds of porphyrins and phthalocyanines. *Translated by* V.G. Vopian. John Wiley & Sons, Chichester. 1981. p.66.
12. O.V. Malkova, V.G. Andrianov, V.G. Berezin, and N.V. Chizhova. Zh. Org. Khim. **26**, 2440 (1990); Chem. Abstr. **115**, 182918 (1990).
13. R. Grigg, R.J. Hamilton, M.L. Jozefowicz, C.H. Rochester, R.J. Terrell, and H. Wickwar. J. Chem. Soc. Perkin Trans. 2, 407 (1973).
14. N. Kobayashi, M. Fujihira, T. Osa, and T. Kuwana. Bull. Chem. Soc. Jpn. **53**, 2195 (1980).
15. N. Hirayama, A. Takenaka, Y. Sasada, E. Watanabe, H. Ogoshi, and Z. Yoshida. J. Chem. Soc. Chem. Commun. 330 (1974).
16. H. Ogoshi, E. Watanabe, and Z. Yoshida. Tetrahedron, **29**, 3241 (1973).
17. O. Almarsson, A. Blaskó, and T.C. Bruice. Tetrahedron, **49**, 10239 (1993).
18. P. Hambright. *In* Porphyrins and metalloporphyrins. *Edited by* K.M. Smith. Elsevier, Amsterdam. 1975. p. 233.
19. L.Z. Gong. Gaodeng Xuexiao Huaxue Xuebao, **6**, 131 (1985).

Can. J. Chem. Downloaded from www.nrcresearchpress.com by 46.23.64.124 on 09/08/12
For personal use only.

Iron porphyrin catalyzed oxidation of lignin model compounds: oxidation of phenylpropane and phenylpropene model compounds

Futong Cui and David Dolphin

Abstract: The oxidation of 1-(4-ethoxy-3-methoxyphenyl)propane (**2**) and 1-(4-ethoxy-3-methoxyphenyl)propene (**3**) by *meso*-tetra(2,6-dichloro-3-sulphonatophenyl)porphyrin iron chloride (TDCSPPFeCl, **1**) and *tert*-butylhydroperoxide (*t*-BuOOH) are discussed. In addition to a C_α-hydroxylation product, demethoxylation and direct aromatic ring cleavage products were found in the oxidation of **2**. When **3** was oxidized by **1** and *t*-BuOOH in aqueous acetonitrile, an acetonitrile-incorporated product was found. A mechanism for the oxidation of **3** is proposed.

Key words: lignin, ligninase, iron porphyrin, model, degradation.

Résumé : On discute de l'oxydation du 1-(4-éthoxy-3-méthoxyphényl)propane (**2**) et du 1-(4-éthoxy-3-méthoxyphényl)propène (**3**) par du chlorure de *meso*-tétra(2,6-dichloro-3-sulfatophényl)porphyrine fer (**1**) et l'hydroperoxyde de *tert*-butyle (*t*-BuOOH). En plus d'un produit d'hydroxylation en C_α, l'oxydation du produit **2** a conduit à des produits de déméthoxylation et de clivage direct du noyau aromatique. Lors de l'oxydation du composé **3** par le composé **1** et le *t*-BuOOH, en solution aqueuse d'acétonitrile, on a observé la formation d'un produit incorporant de l'acétonitrile. On propose un mécanisme pour l'oxydation du produit **3**.

Mots clés: lignine, ligninase, porphyrine fer, modèle, dégradation.

[Traduit par la rédaction]

Introduction

Lignin is an aromatic, heterogeneous biopolymer composed of phenylpropanoid units, which are interconnected by C—C and C—O bonds. It occurs widely in plants in the form of lignocellulose (the complex of lignin and cellulose and hemicelluloses), the predominant land-produced biomass. Lignin is among the most persistent carbon–oxygen polymers in nature. Because of the close association of lignin and cellulose, lignin acts as a barrier to the biodegradation of lignocellulose. Lignin-degrading enzymes, lignin peroxidases (1, 2) and Mn(II)-dependent peroxidases (3), have been isolated from the most studied lignin-degrading white rot fungus, Basidiomyce *Phanerochaete chrysosporium*. Lignin peroxidases have been shown capable of catalyzing a variety of degradations and transformations of lignin model compounds (4), including C_α—C_β cleavage of β-O-4 and β-1 dimers (1, 2), β-O-4 cleavage of β-O-4 dimers (5), C_α oxidation (6) and benzylic methylene hydroxylation (7) (C_α hydroxylation), C_α—C_β double bond hydroxylation (2), and aromatic ring cleavage of veratryl alcohol (8) and β-O-4 dimers (9). Iron porphyrins have been used as lignin peroxidase models and shown able to catalyze C_α—C_β cleavage

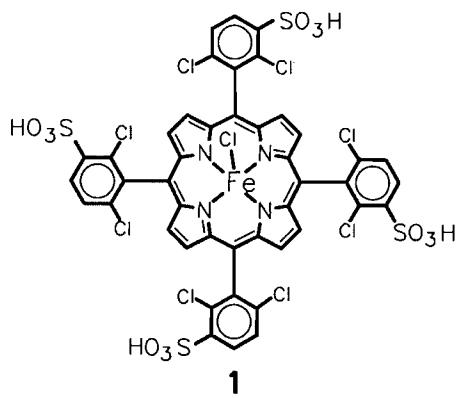

1

(10–14), C_α oxidation (10, 12, 13), and aromatic ring cleavage reactions (15). We report in this paper the C_α hydroxylation of the phenylpropane model compound, the C_α—C_β double bond hydroxylation (glycol formation) of the phenylpropene model compound, along with other reactions of the two model compounds catalyzed by *meso*-tetra-(2,6-dichloro-3–sulfonatophenyl)porphyrin iron chloride (**1**, TDCSPPFeCl). Related water-soluble metalloporphyrins have also been used by Labat and Meunier (16).

Received November 8, 1994.[1]

F. Cui[2] and D. Dolphin.[3] Department of Chemistry, The University of British Columbia, 2036 Main Mall, Vancouver, BC V6T 1Z1, Canada.

[1] Revision received September 12, 1995.

[2] Present address: Forintek Canada Corp., Vancouver, BC V6T 1W5.

[3] Author to whom correspondence may be addressed. Telephone: (604) 822–4571. Fax: (604) 822–9678. E-mail: david@dolphin.chem.ubc.ca

Can. J. Chem. Downloaded from www.nrcresearchpress.com by 46.23.64.124 on 09/08/12
For personal use only.

Can. J. Chem. Downloaded from www.nrcresearchpress.com by 46.23.64.124 on 09/08/12
For personal use only.

Scheme 1.

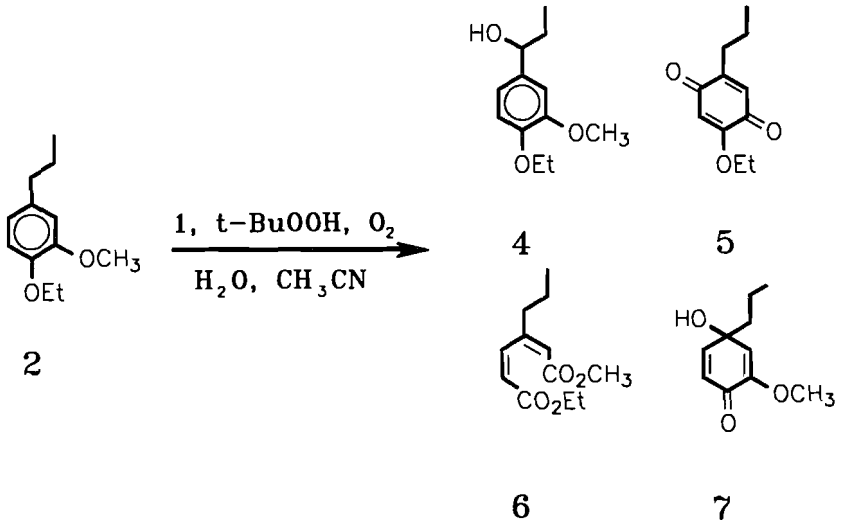

2 4 5 6 7

Results and discussion

Tien and Kirk (7) first found that lignin peroxidase catalyzed the hydroxylation of the benzylic methylene group of 2-(3,4-dimethoxyphenyl)ethanol to give 3,4-dimethoxyphenylglycol, which was then further oxidized at the C_α position. Renganathan et al. (17, 18) also reported the C_α hydroxylation of 4-ethoxy-3-methoxyphenylpropane by lignin peroxidase. In addition to the C_α hydroxylation product (**4**) found earlier (17, 18), oxidation of 1-(4-ethoxy-3-methoxyphenyl)propane (**2**) by TDCSPPFeCl and *t*-BuOOH in air at room temperature also gave **5**, **6**, and **7** as major products (Scheme 1). Small amounts of other unidentified products were found by TLC and GC analysis.

The formation of 2-ethoxy-5-propyl-2,5-cyclohexadien-1,4-dione (**5**) is not unexpected since a similar product, 2-hydroxymethyl-5-methoxy-2,5-cyclohexadien-1,4-dione, was found during the oxidation of veratryl alcohol by both lignin peroxidase (19) and by iron porphyrins (14).

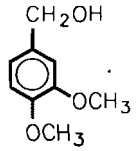

veratryl alcohol

A muconate was first found in the oxidation of a β-O-4 dimer by lignin peroxidase (20). Direct ring cleavage products from the oxidation of veratryl acetate (14) and from veratryl methyl ether (21) have also been reported. The formation of **6** shows that ring cleavage is also an important reaction of the substituted phenylpropane substructure (**8**) of lignin. Phenyl–alkyl cleavage has been found in the oxidation of veratryl alcohol and derivatives by lignin peroxidase (19, 21–23) and by biomimetic systems (14). A mechanism for the phenyl–alkyl cleavage of phenolic model compounds has been proposed (24) as shown in Scheme 2. Formation of **10** results from two one-electron oxidations of **8**. Oxidation of **2** (Scheme 3) gave compound **7**, which is an analog of intermediate **10**, and the characterization of **10** supports the proposed cleavage mechanism (24). Phenyl–alkyl cleavage of **7** did not occur because of the absence of a hydroxy group at the C_α position.

Scheme 2.

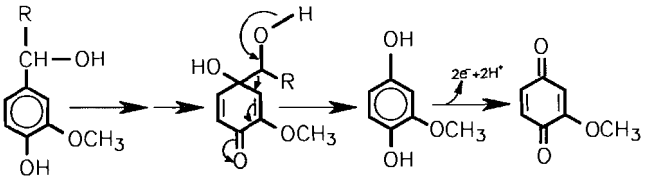

9 10

The alkoxy-substituted phenylpropane substructure (**8**) has been suggested as a chain terminus of lignin (25). The relation between C_α hydroxylation of this substructure and lignin biodegradation has not been established (7, 17, 18). Leisola et al. (19, 23) have suggested a pathway of lignin biodegradation that involves the release of low molecular weight quinones and ring cleavage products from the chain terminii of lignin. The quinones and ring cleavage products so released are finally metabolized to carbon dioxide by the fungus, *P. chrysosporium* (23). According to Leisola's hypothesis (19, 23), demethoxylation and aromatic ring cleavage of **2** to give **5** and

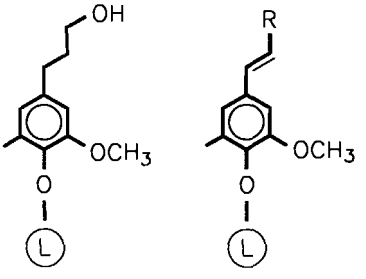

8 **11**

R=CH_2OH or CHO

6 are more important degradative reactions for lignin biodegradation than the C_α hydroxylation. It is possible that the C_α hydroxylation product **4** or its C_α-carbonyl analog cannot be metabolized directly, since it has been demonstrated that veratryl alcohol and its C_α oxidation product (veratraldehyde) are not directly metabolized (23).

Scheme 3.

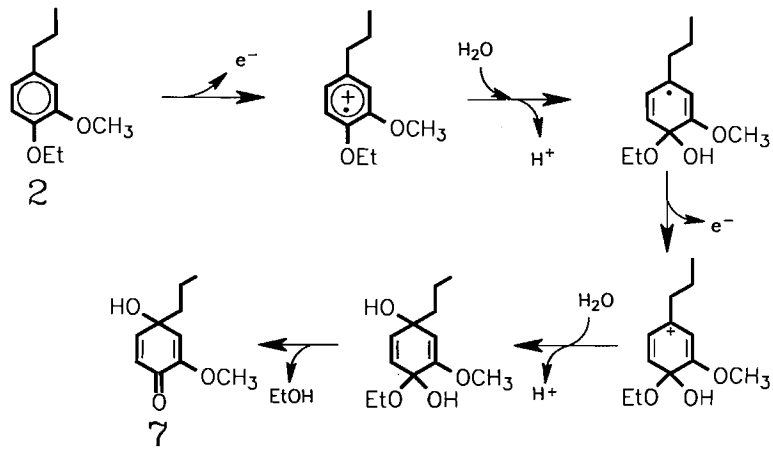

Scheme 4.

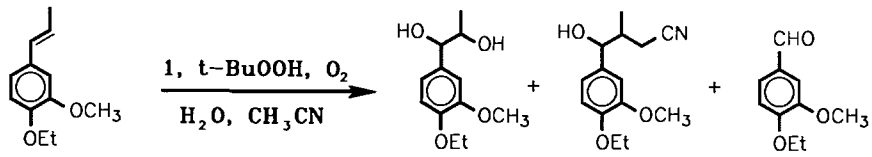

Alkoxy-substituted phenylpropene substructures (**11**) are also found in the lignin chain terminii (25). Diol formation was reported to be the first step in the biodegradation by *P. chrysosporium* culture of lignin model compounds containing this substructure (26–29). 1-(4-Ethoxy-3-methoxyphenyl)propene (**3**) has been used as a model compound for this substructure of lignin. Lignin peroxidase (2, 17, 30) was shown to be able to catalyze the hydroxylation of **3** to give 1-(4-ethoxy-3-methoxyphenyl)-1,2-propanediol (**12**). The oxygen of the 2-hydroxy group of **12** was later shown to be from molecular oxygen (31). TDCSPPFeCl (1) was found to closely mimic lignin peroxidase in the oxidation of **3**. When **3** was oxidized by TDCSPPFeCl and *t*-BuOOH in aqueous acetonitrile in air, 4-ethoxy-3-methoxybenzaldehyde, the diol **12**, and the solvent-incorporated product 4-hydroxy-4-(4-ethoxy-3-methoxyphenyl)-3-methylbutyronitrile (**13**) were obtained (Scheme 4).

Cytochromes P-450 (32), which are monooxygenases and function by activating molecular oxygen, are able to catalyze diol formation from alkenes via an epoxide intermediate. Lignin peroxidases are peroxidases (7, 17, 33–35) having peroxidase and haloperoxidase activity (36). No monooxygenase activity of lignin peroxidase has been reported so far. Because of the great chemical diversity of lignin structure, diol formation from lignin via an epoxide intermediate is unlikely since the substrate needs to approach the active site of cytochromes P-450 closely for direct oxygen atom transfer and epoxide formation to occur. The ability of the ligninolytic culture of *P. chrysosporium* to metabolize lindane (1,2,3,4,5,6-hexachlorocyclohexane) to carbon dioxide (37) suggests the presence of enzymic activity other than that of peroxidases, though it is still not clear which enzyme(s) is responsible for lindane degradation.

While no direct evidence is available to exclude the epoxide pathway of diol formation, the formation of **13** from the oxidation of **3** certainly suggests radical formation as at least one of the pathways. Scheme 5 illustrates a pathway for the formation of **12** and **13**. One-electron oxidation of **3** gives the cation radical. Attack at the cation radical by water gives the C_β-centred radical, coupling of which with oxygen or a further one-electron oxidation followed by reaction with water gives the diol **12**. Coupling of the C_β-centred radical with acetonitrile radical gives **13**. In addition, when **3** was oxidized under oxygen (bubbling oxygen through the reaction mixture), little **13** was detected, probably because of the competitive coupling of molecular oxygen with the C_β-centred radical.

In conclusion, although **8** and **11** substructures might be present in lignin in small amounts, we believe that the reactions of the phenylpropane and phenylpropene model compounds described above are important for lignin biodegradation since the two substructures are mostly located at the chain terminal from where lignin biodegradation most probably begins.

Experimental

NMR spectra were recorded on a Varian XL 300 or a Bruker WH 400 spectrometer using tetramethylsilane as an internal standard. Low-resolution mass spectra (LRMS) were recorded on an AEI MS9 spectrometer and high-resolution mass spectra (HRMS) were recorded on a KRATOS MS50 spectrometer. An HP 5890A gas chromatograph equipped with a 25 m HP17 capillary column was used for the GC analyses. Product yield was calculated based on GC peak area percentage of the total product peak area. Delsi Nermag R10–10C/Kratos MS80RFA instruments were used for the GCMS analyses. Infrared spectra were obtained on a Perkin–Elmer 1710 Fourier transform spectrometer. Preparative thin-layer chromatography (TLC) was performed on a model 7924T chromatotron (Harrison

Can. J. Chem. Downloaded from www.nrcresearchpress.com by 46.23.64.124 on 09/08/12
For personal use only.

Scheme 5.

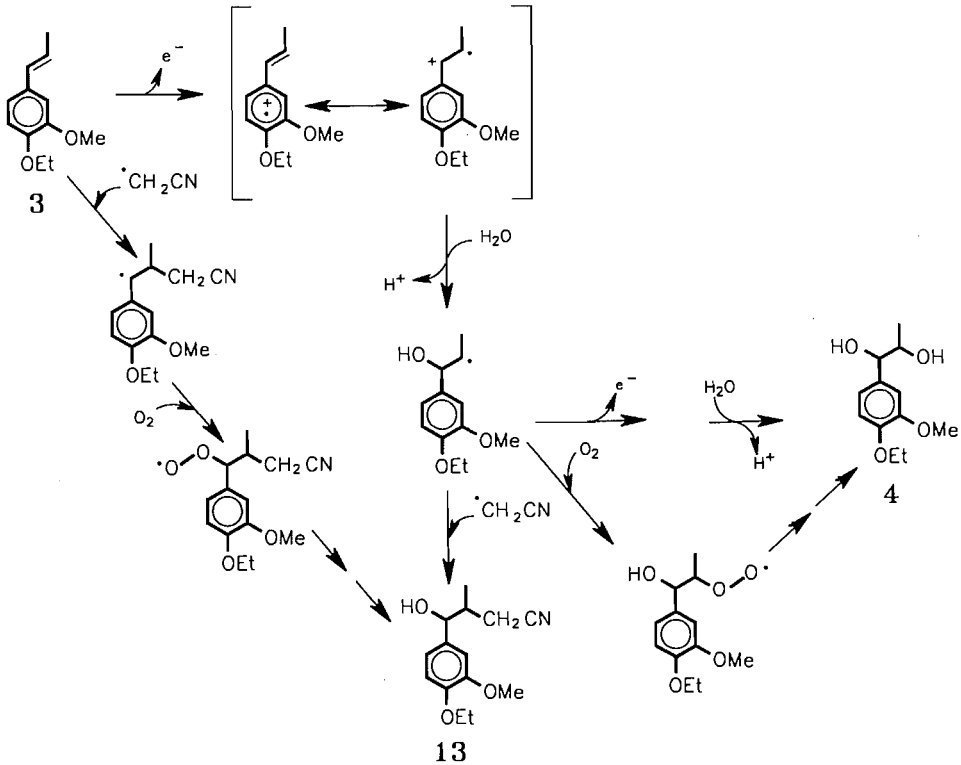

Research) using silica gel 60 PF_{254} as absorbent. Merck precoated silica gel 60 PF_{254} TLC plate (0.2 mm) was used for analytical purposes. *t*-BuOOH, eugenol, and isoeugenol were from Aldrich.

Syntheses of model compounds

Compound **2** and **3** were synthesized following reported procedures (38, 39).

Oxidation of 1-(4-ethoxy-3-methoxyphenyl)propane (2) and 1-(4-ethoxy-3-methoxyphenyl)propane (3)

Compound **2** (0.25 mmol) was reacted with *t*-BuOOH (1.25 mmol) and TDCSPPFeCl (0.5 μmol in 500 μL of water) in 20 mL of 1:1 acetonitrile/pH 3 phosphate buffer (0.1 M) at room temperature in air for 3 h. Unreacted *t*-BuOOH was decomposed by adding solid potassium iodide. The solution was then extracted with ethyl acetate (3 × 10 mL). The iodine in the extract was removed by washing with aqueous sodium thiosulphate. The organic extract was dried over sodium sulphate, filtered, and evaporated. One fifth of the residue was acetylated with excess acetic anhydride/pyridine (1:1) and analyzed by GC and GCMS. The rest was separated on a chromatotron as previously described (16). Compounds **5**, **6**, and **7** were obtained in 23, 18, and 20% yields, respectively.

The oxidation of **3** was carried out in the same manner as for **2**, except that the reaction time was 2 h, to give 4-ethoxy-3-methoxybenzaldehyde (20%), **12** (33%), and **13** (18%). When the reaction was carried out for 3 h or longer, 4-ethoxy-3-methoxybenzaldehyde was the major product.

1-(4-Ethoxy-3-methoxyphenyl)propanol (**4**) was obtained in a 20% yield and identified as its acetate; MS: 252, 192, 131, 164, 163, 149, 133, 131, 107, 103, 91, 79, 77.

2-Ethoxy-5-propyl-2,5-cyclohexadien-1,4-dione (**5**): ^{1}H NMR ($CDCl_3$) δ: 0.97 (3H, t, J = 8 Hz), 1.47 (3H, t, J = 7 Hz), 1.51–1.57 (2H, m), 2.41 (2H, m), 4.01 (2H, q, J = 7 Hz), 5.90 (1H, s), 6.49 (1H, s, br). MS *m/z* (%): 194 (4.0), 179 (3.7), 167 (4.1), 166 (5.1), 165 (8.4), 151 (34.8), 150 (23.7), 149 (32.6), 69 (100.0), 67 (22.3), 57 (25.6), 55 (23.4), 53 (28.0), 44 (20.6), 43 (34.4), 41 (30.0). Exact Mass calcd. for $C_{11}H_{14}O_3$: 194.0939; found (HRMS): 194.0934.

Compound **6**: ^{1}H NMR ($CDCl_3$) δ: 0.3 (3H, t, J = 7 Hz), 1.26 (3H, t, J = 7 Hz), 1.44–1.57 (2H, m), 2.39 (2H, t, J = 7 Hz), 3.67 (3H, s), 4.34 (2H, q, J = 7 Hz), 5.76 (1H, s, br), 5.88 (1H, d, J = 12 Hz), 7.05 (1H, dd, J_1 = 12 Hz, J_2 = 1–2 Hz). MS *m/z* (%): 226 (2.74), 211 (1.10), 195 (4.73), 194 (2.27), 181 (9.78), 167 (71.67), 153 (100.0), 149 (10.12), 139 (75.41). Exact Mass calcd. for $C_{12}H_{18}O_4$: 226.1200; found (HRMS): 226.1204.

4-Hydroxy-2-methoxy-4-propyl-2,5-cyclohexadien-1-one (**7**) (40): FTIR (KBr pellet) (cm^{-1}): 3436, 1672, 1645, 1214. ^{1}H NMR ($CDCl_3$) δ: 0.94 (3H, t, J = 8 Hz), 1.26–1.36 (2H, m), 1.76–1.81 (2H, m), 1.92 (1H, s, exchangeable), 3.69 (3H, s), 5.72 (1H, d, J = 2–3 Hz), 6.20 (1H, d, J = 10 Hz), 6.83 (1H, dd, J_1 = 2–3 Hz, J_2 = 10 Hz). MS *m/z* (%): 182 (13.9), 166 (21.8), 140 (22.8), 139 (100.0), 111 (39.3), 94 (29.41), 93 (33.3), 81 (26.7), 79 (32.0), 77 (46.0), 69 (88.0), 68 (29.3), 67 (25.5), 66 (28.9), 65 (68.4), 55 (85.5), 53 (53.4), 52 (26.6), 51 (47.6). Exact Mass calcd. for $C_{10}H_{14}O_3$: 182.0939; found (HRMS): 182.0942.

1-(4-Ethoxy-3-methoxyphenyl)-1,2-propandiol (**12**) (30) (isolated as its diacetate): ^{1}H NMR ($CDCl_3$) δ: 1.08 (3H, d, J = 7 Hz), 1.45 (3H, t, J = 7 Hz), 2.05 (3H, s), 2.07 (3H, s), 3.89 (3H,

Can. J. Chem. Downloaded from www.nrcresearchpress.com by 46.23.64.124 on 09/08/12
For personal use only.

s), 4.10 (2H, q, $J = 7$ Hz), 5.23–5.29 (1H, m), 5.71 (1H, d, $J =$ 8 Hz), 6.82–6.91 (3H, m). MS *m/z* (%): 310 (8.0), 266 (3.0), 250 (9.0), 223 (7.5), 208 (15.4), 182 (11.3), 181 (100.0), 151 (19.6), 125 (10.1), 43 (41.6). Exact Mass calcd. for $C_{16}H_{22}O_6$: 310.1414; found (HRMS): 310.1416.

4-Hydroxy-4-(4-ethoxy-3-methoxyphenyl)-3-methylbutyronitrile (**13**) (identified as its acetate): ^{1}H NMR ($CDCl_3$) δ: 1.00 (3H, d, $J = 7$ Hz), 1.45 (3H, t, $J = 8$ Hz), 2.10 (3H, s), 2.30–2.40 (2H, m), 2.46–2.53 (1H, m), 3.89 (3H, s), 4.10 (2H, q, $J = 8$ Hz), 5.51 and 5.60 (1H, two doublets in a ratio of 7:2, $J = 8$ Hz), 6.80–6.84 (3H, m). MS *m/z* (%): 291 (10.1), 232 (3.4), 223 (3.6), 204 (1.4), 203 (1.8), 182 (10.6), 181 (100.0), 164 (3.7), 153 (14.5), 86 (17.3), 84 (27.4), 43 (35.3). Exact Mass calcd. for $C_{16}H_{21}O_4N$: 291.1465; found (HRMS): 291.1471.

Acknowledgements

This work was supported by the Natural Sciences and Engineering Research Council of Canada. We also wish to thank one of the referees, who suggested a modification to the mechanism in Scheme 5.

References

1. M. Tien and T.K. Kirk. Science, **221**, 661 (1983).
2. J.K. Glenn, M.A. Morgan, M.B. Mayfield, M. Kuwahara, and M.H. Gold. Biochem. Biophys. Res. Commun. **114**, 1077 (1983).
3. M. Kuwahara, J.K. Glenn, M.A. Morgan, and M.H. Gold. FEBS Lett. **169**, 247 (1984).
4. T.K. Kirk and R.L. Farrell. Annu. Rev. Microbiol. **41**, 465 (1987).
5. T. Umezawa and T. Higuchi. Agric. Biol. Chem. **48**, 1917 (1984).
6. T.K. Kirk, M. Tien, P.J. Kersten, M.D. Mozuch, and B. Kalyanaraman. Biochem. J. **236**, 279 (1986).
7. M. Tien and T.K. Kirk. Proc. Natl. Acad. Sci. U.S.A. **81**, 2280 (1984).
8. M.S.A. Leisola, B. Schmidt, V. Thanei-Wyss, and A. Fiechter. FEBS Lett. **189**, 267 (1985).
9. T. Umezawa, M. Shimada, T. Higuchi, and K. Kusai. FEBS Lett. **205**, 287 (1986).
10. M. Shimada, T. Habe, T. Umezawa, and T. Higuchi. Biochem. Biophys. Res. Commun. **122**, 1247 (1984).
11. T. Habe, M. Shimada, T. Okamoto, B. Panijpan, and T. Higuchi. J. Chem. Soc. Chem. Commun. 1324 (1985).
12. T. Habe, M. Shimada, and T. Higuchi. Mokuzai Gakkaishi, **31**, 54 (1985).
13. M. Shimada, T. Habe, T. Higuchi, T. Okamoto, and B. Panijpan. Holzforschung, **41**, 277 (1987).
14. F. Cui and D. Dolphin. Can J. Chem. **70**, 2314 (1992).
15. M. Shimada, T. Hattori, T. Umezawa, T. Higuchi, and T. Okamoto. Colloq. INRA (Lignin Enzymic Microb. Degrad. Symp. Int.), **40**, 151 (1987).
16. G.L. Labat and B. Meunier. New J. Chem. **13**, 801 (1989); J. Org. Chem. **54**, 5008 (1989).
17. V. Renganathan, K. Miki, and M.H. Gold. Arch. Biochem. Biophys. **241**, 304 (1985).
18. V. Renganathan, K. Miki, and M.H. Gold. Arch. Biochem. Biophys. **246**, 155 (1986).
19. M.S.A. Leisola, S.D. Haemmerli, J.D.G. Smit, J. Troller, R. Waldner, H.E. Schoemaker, and H. Schmidt. Colloq. INRA (Lignin Enzymic Microb. Degrad. Symp. Int.), **40**, 81 (1987).
20. T. Umezawa and T. Higuchi. FEBS Lett. **182**, 257 (1985).
21. H.W.H. Schmidt, S.D. Haemmerli, H.E. Schoemaker, and M.S.A. Leisola. Biochemistry, **28**, 1776 (1989).
22. S.D. Haemmerli, H.E. Schoemaker, H.W.H. Schmidt, and M.S.A. Leisola. FEBS Lett. **220**, 149 (1987).
23. M.S.A. Leisola, S.D. Haemmerli, R. Waldner, H.E. Schoemaker, H.W.H. Schmidt, and A. Fiechter. Cellulol. Chem. Technol. **22**, 267 (1988).
24. H. Numba, F. Nakatsubo, and T. Higuchi. Wood Res. **69**, 52 (1986).
25. A. Sakakibara. *In* Recent advances in lignin biodegradation research. *Edited by* T. Higuchi, H.-M. Chang, and T.K. Kirk. Uni Publishers, Tokyo. 1983. pp. 12–33.
26. T. Umezawa, F. Nakatsubo, and T. Higuchi. Agric. Biol. Chem. **47**, 2677 (1983).
27. T. Higuchi. Wood Res. **67**, 47 (1981).
28. T. Katagama and T. Higuchi. Abstr. 25th Symp. Lignin Chem. Fukuoko, Japan, 1980. pp. 5–8.
29. F. Nakatsubo, T.K. Kirk, M. Shimada, and T. Higuchi. Arch. Microbiol. **128**, 416 (1981).
30. M.H. Gold, M. Kuwahara, A.A. Chiu, and J.K. Glenn. Arch. Biochem. Biophys. **234**, 353 (1984).
31. L.A. Anderson, V. Renganathan, A.A. Chiu, T.M. Loehr, and M.H. Gold. J. Biol. Chem. **260**, 6080 (1985).
32. B.W. Griffin, J.A. Peterson, and R.W. Estabrook. *In* The porphyrins. Vol. VII. *Edited by* D. Dolphin. Academic Press, New York. 1979. pp. 333–375.
33. D. Kuila, M. Tien, J.A. Fee, and M.R. Ondrias. Biochemistry, **24**, 3394 (1985).
34. V. Renganathan and M.H. Gold. Biochemistry, **25**, 1626 (1986).
35. L.A. Anderson, V. Renganathan, T.M. Loehr, and M.H. Gold. Biochemistry, **26**, 2258 (1987).
36. V. Renganathan, K. Miki, and M.H. Gold. Biochemistry, **26**, 5127 (1987).
37. J.A. Bumpus, M. Tien, D. Wright, and S.D. Aust. Science, **228**, 434 (1985).
38. A.P. Khrimian, A.B. DeMilo, R.M. Waters, R.T. Cunningham, and B.A. Leonhardt. J. Chem. Ecol. **19**, 2935 (1993).
39. A. Enoki, G.P. Guldshy, and M.H. Gold. Arch. Microbiol. **129**, 141 (1981).
40. H.H. Nimz and G. Turznik. Cellul. Chem. Technol. **14**, 727 (1980).

Can. J. Chem. Downloaded from www.nrcresearchpress.com by 46.23.64.124 on 09/08/12
For personal use only.

The photochemical nucleophile–olefin combination, aromatic substitution (photo-NOCAS) reaction. Part 10: intramolecular reactions involving alk-4-enols and 1,4-dicyanobenzene[1]

Kimberly A. McManus and Donald R. Arnold

Can. J. Chem. Downloaded from www.nrcresearchpress.com by 46.23.64.124 on 09/08/12
For personal use only.

Abstract: Our study of the photochemical nucleophile–olefin combination, aromatic substitution (photo-NOCAS) reaction has been extended to include alk-4-enols. Irradiation of acetonitrile solutions of the alk-4-enols, 6-methyl-5-hepten-2-ol (**16**) and 5-methyl-5-hexen-2-ol (**17**), and the aromatic, 1,4-dicyanobenzene (**1**), leads to cyclized 1:1 (alk-4-enol:aromatic) adducts. The addition of biphenyl (**5**) to the irradiation mixture, serving as a codonor, increases the yields and the efficiency of formation of the adducts. The structures assigned to the products, *trans*-2-(isopropyl 4-cyanophenyl)-5-methyltetrahydrofuran (**18**, 29%) and *cis*-2-(isopropyl 4-cyanophenyl)-5-methyltetrahydrofuran (**19**, 24%) from **16** (reaction [5]), and *r*-2-(methyl 4-cyanophenyl)-2,*t*-5-dimethyltetrahydrofuran (**20**, 13%), *r*-2-(methyl 4-cyanophenyl)-2,*c*-5-dimethyltetrahydrofuran (**21**, 7%), *r*-3-(4-cyanophenyl)-3,*t*-6-dimethyltetrahydropyran (**22**, 11%), and *r*-3-(4-cyanophenyl)-3,*c*-6-dimethyltetrahydropyran (**23**, 2%), from **17** (reaction [6]), rests mainly upon analysis of the ^{1}H and ^{13}C nuclear magnetic resonance spectra. The structures of **19**, **22**, and **23** were firmly established by X-ray crystallography. The observed ratio of regioisomers indicates a strong preference for 1,5-*exo-trig*, relative to 1,6-*endo-trig*, cyclization of the intermediate alk-4-enol radical cation. The mechanistic implication of these results is discussed.

Key words: photoinduced electron transfer, radical ions, cyclization of radical cations, intramolecular reactions of radical cations.

Résumé : Notre étude de la réaction de substitution aromatique avec combinaison de nucléophile et d'oléfine a été étendue de façon à inclure les alc-4-énols. L'irradiation de solutions dans l'acétonitrile des alc-4-énols, 6-méthylhept-5-én-2-ol (**16**) et 5-méthylhept-5-én-2-ol (**17**), et du 1,4-dicyanobenzène (**1**) conduit à des adduits 1 : 1 cyclisés (alc-4-énol : aromatique). L'addition de biphényle (**5**, qui agit comme codonneur) au milieu d'irradiation augmente les rendements et l'efficacité de la formation des adduits. Les structures ont été principalement assignées sur la base de l'analyse de leurs spectres RMN du ^{1}H et du ^{13}C : *trans*-2-(isopropyl 4-cyanophényl)-5-méthyltétrahydrofurane (**18**, 29%) et *cis*-2-(isopropyl 4-cyanophényl)-5-méthyl-tétrahydrofurane (**19**, 24%) (à partir du produit **16**, réaction [5]) et *r*-2-(méthyl 4-cyanophényl)-2,*t*-5-diméthyltétrahydrofurane (**20**, 13%), *r*-2-(méthyl 4-cyanophényl)-2,*c*-5-diméthyltétrahydrofurane (**21**, 7%), *r*-3-(4-cyanophényl)-3,*t*-6-diméthyltétrahydrofurane (**22**, 11%), *r*-3-(4-cyanophényl)-3,*c*-6-diméthyltétrahydrofurane (**23**, 2%) (à partir du produit **17**, réaction [6]). Les structures des composés **19**, **22** et **23** ont été confirmées par diffraction des rayons X. Les rapports de régioisomères observés indiquent que, pour la cyclisation du cation radical alc-4-énol intermédiaire, il existe une forte préférence pour une cyclisation 1,5-*exo-trig* par rapport à une cyclisation 1,6-*endo-trig*. On discute des implications mécanistiques de ces résultats.

Mots clés : transfert d'électron photoinduit, ions radicaux, cyclisation de cations radicaux, réactions intramoléculaires de cations radicaux.

[Traduit par la rédaction]

Received June 20, 1995.

K.A. McManus and D.R. Arnold.[2] Department of Chemistry, Dalhousie University, Halifax, NS B3H 4J3, Canada.

[1] This is also Part 37 of the series Radical Ions in Photochemistry; see refs. 1 and 2 for preceding parts of these series.

[2] Author to whom correspondence may be addressed. Telephone: (902) 494-3714. Fax: (902) 494-1310. E-mail: arnold@chem1.chem.dal.ca

Can. J. Chem. Downloaded from www.nrcresearchpress.com by 46.23.64.124 on 09/08/12
For personal use only.

Scheme 1

Mechanism for formation of photo–NOCAS products.

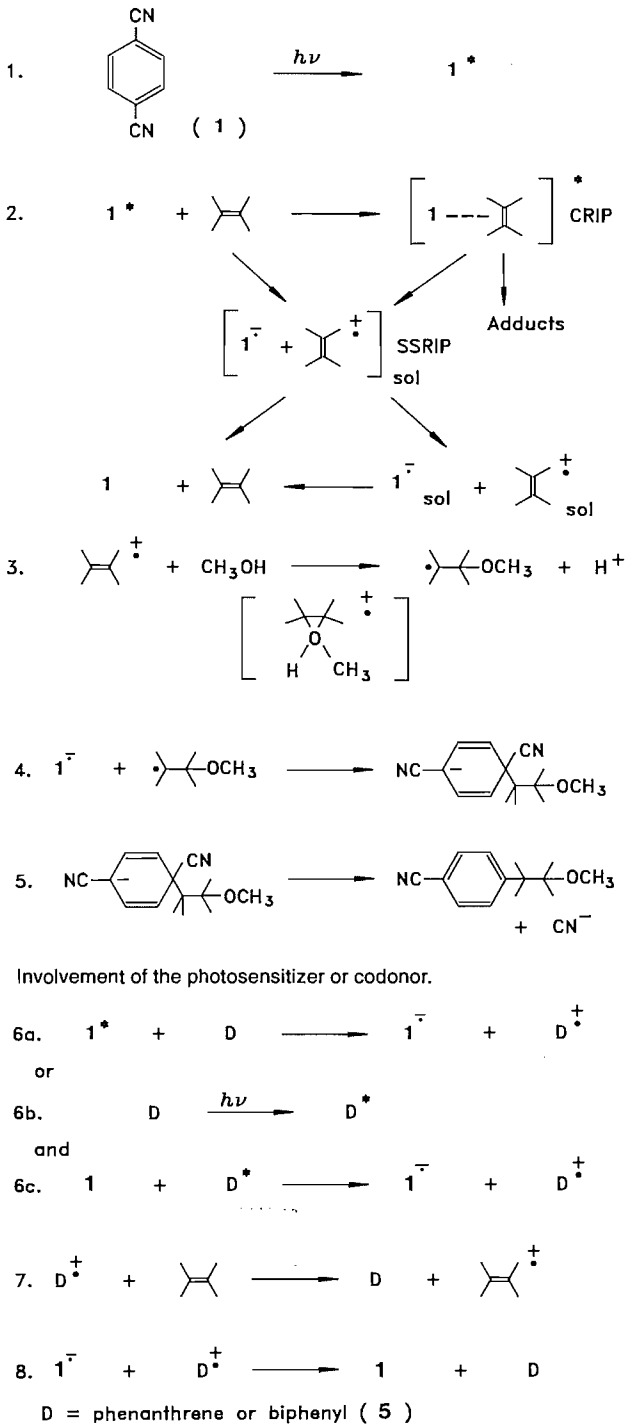

Involvement of the photosensitizer or codonor.

Introduction

Initial studies of the photochemical nucleophile–olefin combination, aromatic substitution (photo-NOCAS) reaction involved the combination of a nucleophile (usually an alcohol), simple mono-olefins, and an electron-withdrawing substituted aromatic (1, 3). One of the first examples combined methanol, 2-methylpropene (**2**), and 1,4-dicyanobenzene (**1**) (reaction [1]) (3). Subsequent studies have confirmed the proposed mechanism (Scheme 1). Firstly, photoinduced single electron transfer occurs from the olefin to the singlet excited state of **1** (Scheme 1, steps 1 and 2) (1, 3). The resulting olefin radical cation is then attacked by the nucleophile (methanol) to give the β-alkoxy alkyl radical (step 3). This radical couples with the 1,4-dicyanobenzene radical anion ($\mathbf{1}^{-\cdot}$) at an *ipso* position (step 4), followed by loss of cyanide ion and rearomatization (step 5). Addition of a codonor, biphenyl (**5**), to the photo-NOCAS reaction has been shown to increase the efficiency of product formation (Scheme 1, steps 6 and 7) (1, 3). This increase in efficiency is thought to be due to a smaller energy of reorganization for the biphenyl (**5**) – 1,4-dicyanobenzene (**1**) radical-ion pair than for the olefin – 1,4-dicyanobenzene (**1**) radical-ion pair, resulting in an increase in the efficiency of solvent separation of the radical ions from the initially formed geminate radical-ion pair (SSRIP) (3). Subsequent studies have therefore generally included biphenyl (**5**), serving as a codonor, along with the nucleophile, the olefin, and the aromatic.

A variety of substituted olefins have been examined and the regio- and stereoselectivity of the reaction have been established. From the first examples, the regiochemistry of the reaction has been described as *anti*-Markovnikov. That is, the nucleophile (methanol) becomes attached to the olefinic double bond at the least substituted carbon. Results reported here, for the archetypical example of a trisubstituted olefin, 2-methyl-2-butene (**6**), are consistent with this generalization (reaction [2]).

Recently, the scope of this study was extended to include dienes, both conjugated and nonconjugated (1). Nonconjugated 1,5- and 1,6-dienes have been shown to undergo intramolecular cyclization at the radical cation stage, before reaction with the nucleophile, to yield products resulting from substitution of the aromatic with a saturated six- and (or) seven-membered ring (reactions [3] and [4]). The observation of these diene-cyclized products stimulated this study, to further extend the reaction to alk-4-enols. Intramolecular addition could occur, formation of the alkenol radical cation followed by attack of the hydroxyl group, to yield 1,5-*exo-trig* and (or) 1,6-*endo-trig* cyclized product(s).

Rules for cyclization of the common intermediates (carbocations, carbanions, and radicals) are already well understood (4, 5). From the results of the photo-NOCAS reaction involving the cyclization of the unconjugated dienes and the cyclization of the alk-4-enols we can now begin to define rules for cyclization of radical cations.

Results

An acetonitrile–methanol (3:1) solution of 2-methyl-2-butene (**6**), 1,4-dicyanobenzene (**1**), and biphenyl (**5**) was irradiated (reaction [2]). Progress of the reaction was monitored by capillary column gas chromatography with a flame ionization detector (gc/fid). The first indication of the structure of the products was obtained from a gas chromatograph equipped with a mass selective detector (gc/ms). Products were isolated by medium-pressure liquid column chromatography (mplc) on silica gel. Yields were based upon the amount of 1,4-dicyanobenzene (**1**) consumed; the olefin was present in excess. Two 1:1:1 (nucleophile:olefin:aromatic) photo-NOCAS adducts (**7** and **8**) were obtained in high yield (70%

Can. J. Chem. Downloaded from www.nrcresearchpress.com by 46.23.64.124 on 09/08/12
For personal use only.

Reaction [1] (3a,b)

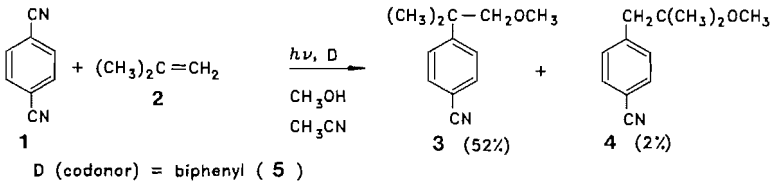

D (codonor) = biphenyl (5)

Reaction [2]

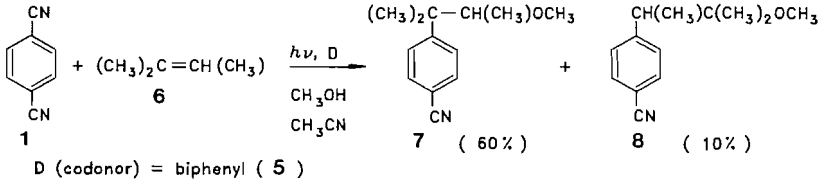

D (codonor) = biphenyl (5)

Reaction [3] (1c)

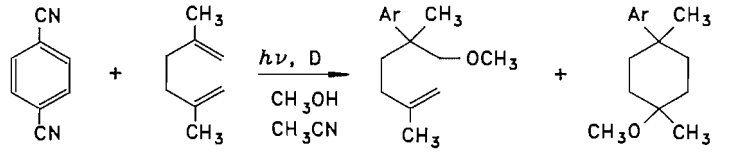

D = biphenyl (5)
Ar = 4-cyanophenyl

trans (4%)
and
cis (9%)

Reaction [4] (1d)

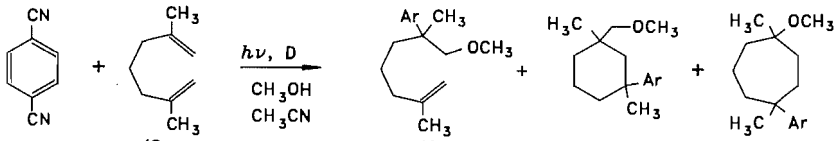

D = biphenyl (5)
Ar = 4-cyanophenyl

(5%)

cis (12%)
trans (11%)

cis (12%)
trans (10%)

isolated). The mass spectrum of the major adduct (**7**, 87%) has the base peak at 59 *m/z* (C_3H_7O) and the second largest peak at 145 *m/z* (cyanophenylpropyl). For the minor adduct (**8**, 13%), analogous fragments occur at 73 *m/z* (C_4H_9O) and 130 *m/z* (cyanophenylethyl). The ratio of products was determined from the integrated peak area in the gc/fid of the reaction mixture. The adducts were isolated by medium-pressure liquid column chromatography (mplc) and the ratio of the isolated products is in good agreement with the gc/fid results. The structural assignments rest firmly upon an analysis of the ^1H and ^{13}C nmr spectra.

The alk-4-enols chosen for study were (±) 6-methyl-5-hepten-2-ol (**16**) and (±) 5-methyl-5-hexen-2-ol (**17**). When acetonitrile solutions of the alk-4-enol, 1,4-dicyanobenzene (**1**), and biphenyl (**5**) were irradiated with a medium-pressure mercury vapour lamp through Pyrex, the products were cyclized 1:1 (alk-4-enol:**1**) photo-NOCAS adducts. Structural assignments were based primarily upon detailed analysis of ^1H and ^{13}C nmr spectra and, for three of the products (**19**, **22**, and **23**), structures were firmly established by X-ray crystallography.[3]

Irradiation of an acetonitrile solution of 6-methyl-5-hepten-2-ol (**16**), 1,4-dicyanobenzene (**1**), and biphenyl (**5**) gave *trans*-2-(isopropyl 4-cyanophenyl)-5-methyltetrahydrofuran (**18**, 29%) and *cis*-2-(isopropyl 4-cyanophenyl)-5-methyltetrahydrofuran (**19**, 24%) (reaction [5]). Both **18** and **19** result from intramolecular 1,5-*exo-trig* cyclization; no product indicative of 1,6-*endo-trig* cyclization was detected.

[3] Data for **22** and **23** may be purchased from: The Depository of Unpublished Data, Document Delivery, CISTI, National Research Council Canada, Ottawa, Canada K1A 0R6. Details of data collection, structural analysis and refinement, and tables of interatomic distances and bond angles have also been deposited with the Cambridge Crystallographic Data Centre and may be obtained on request from the Director, Cambridge Crystallographic Data Centre, University Chemical Laboratory, 12 Union Road, Cambridge, CB2 1EZ, U.K.

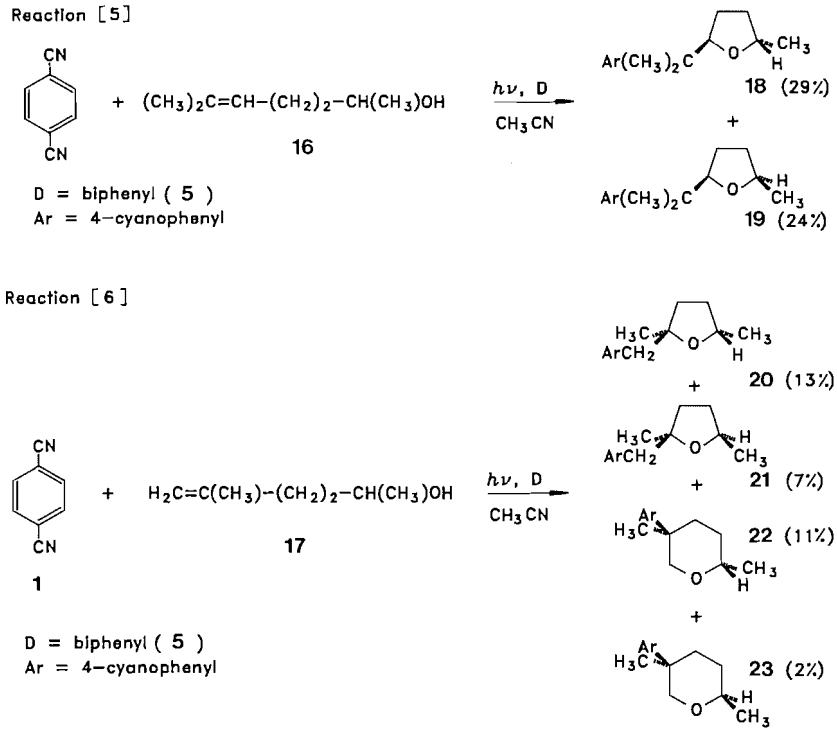

Four photo-NOCAS adducts resulted from irradiation of an acetonitrile solution of 5-methyl-5-hexen-2-ol (**17**), 1,4-dicyanobenzene (**1**), and biphenyl (**5**). The structures and yields of these products were: *r*-2-(methyl 4-cyanophenyl)-2,*t*-5-dimethyltetrahydrofuran (**20**, 13%), *r*-2-(methyl 4-cyanophenyl)-2,*c*-5-dimethyltetrahydrofuran (**21**, 7%), *r*-3-(4-cyanophenyl)-3,*t*-6-dimethyltetrahydropyran (**22**, 11%), and *r*-3-(4-cyanophenyl)-3,*c*-6-dimethyltetrahydropyran (**23**, 2%) (reaction [6]). Compounds **20** and **21** result from 1,5-*exo-trig* cyclization; their combined yield makes this the major (60%) mode of cyclization. Compounds **22** and **23** result from 1,6-*endo-trig* cyclization.

Structural assignments

The initial structural assignments for **7** and **8**, based upon the fragmentation pattern in their mass spectra, were confirmed by ^{1}H and ^{13}C nmr spectroscopy. Adduct **7** was identified as the *anti*-Markovnikov product, 2-(4-cyanophenyl)-3-methoxy-2-methylbutane. The aliphatic region of the ^{1}H nmr spectrum shows a doublet (0.92 ppm) corresponding to a methyl group adjacent to a methine group. The proton of the methine group produces a quartet (3.30 ppm). This low-field quartet is indicative of a methine group adjacent to an oxygen. Protons adjacent to oxygen generally occur at lower field (3.2–3.7 ppm) than those adjacent to the 4-cyanophenyl group (2.4–3.0 ppm) (1, 3). A singlet (3.24 ppm) represents the methoxy methyl group and the typical AA′XX′ pattern in the aromatic region of the ^{1}H nmr spectrum is indicative of the 4-cyanophenyl group. Further support for the *anti*-Markovnikov orientation was provided by the ^{13}C nmr spectrum. A singlet (43.10 ppm) representing an aryl-substituted quaternary carbon is observed, along with a doublet (84.28 ppm) indicating a methine carbon bonded to a methoxy group.

Compound **8** was identified as the Markovnikov product, 3-(4-cyanophenyl)-2-methoxy-2-methylbutane. Compound **8** shows characteristic patterns similar to those of **7**. A distinctive feature in the ^{1}H nmr spectra is the appearance of a quartet (2.90 ppm) at higher field for **8**, as opposed to the quartet (3.30 ppm) at lower field for **7**, indicating the methine group is aryl substituted (**8**) rather than methoxy substituted (**7**). In the ^{13}C nmr spectrum, there is a doublet (48.96 ppm) at higher field for **8**, as opposed to the doublet (84.28 ppm) at lower field that appears in the spectrum of **7**. Again, this supports a methine group aryl substituted in **8** rather than methoxy substituted as in **7**.

Compound **19** was identified as *cis*-2-(isopropyl 4-cyanophenyl)-5-methyltetrahydrofuran. The presence of three methyl groups, one of which is adjacent to a methine, is indicated by two singlets and a doublet (J = 6.1 Hz) in the aliphatic region of the ^{1}H nmr spectrum. A high-field multiplet represents the four hydrogens of the methylene groups on the tetrahydrofuran ring. A low-field multiplet at 3.91 ppm shows a methine group, adjacent to an oxygen, and substituted with an alkyl-aryl group. Another low-field multiplet appears at 3.92 ppm with one of its couplings being 6.1 Hz. This represents the methine group, adjacent to an oxygen, and substituted by a methyl group. An AA′XX′ pattern in the aromatic region is indicative of a 4-cyanophenyl group. The ^{13}C nmr spectrum of **19** indicates a quaternary carbon, substituted by two methyl groups and an aryl group (41.53 ppm), and two doublets (75.53 and 86.50 ppm) for two methine groups bonded to oxygen. The *cis* configuration, as well as the overall structure of **19**, was firmly established by X-ray diffraction of a single crystal (Fig. 1).

Compound **18** was identified as *trans*-2-(isopropyl 4-cyanophenyl)-5-methyltetrahydrofuran, the configurational isomer of **19**. The mass spectrum and the ^{1}H and ^{13}C nmr spectra of **18** are very similar to those of the *cis* isomer.

Adduct **20** was identified as *r*-2-(methyl 4-cyanophenyl)-2,*t*-5-dimethyltetrahydrofuran. The ^{1}H nmr spectrum exhibits

Can. J. Chem. Downloaded from www.nrcresearchpress.com by 46.23.64.124 on 09/08/12
For personal use only.

Fig. 1. X-ray structure for *cis*-2-(isopropyl 4-cyanophenyl)-5-methyltetrahydrofuran (**19**); details in the experimental section.

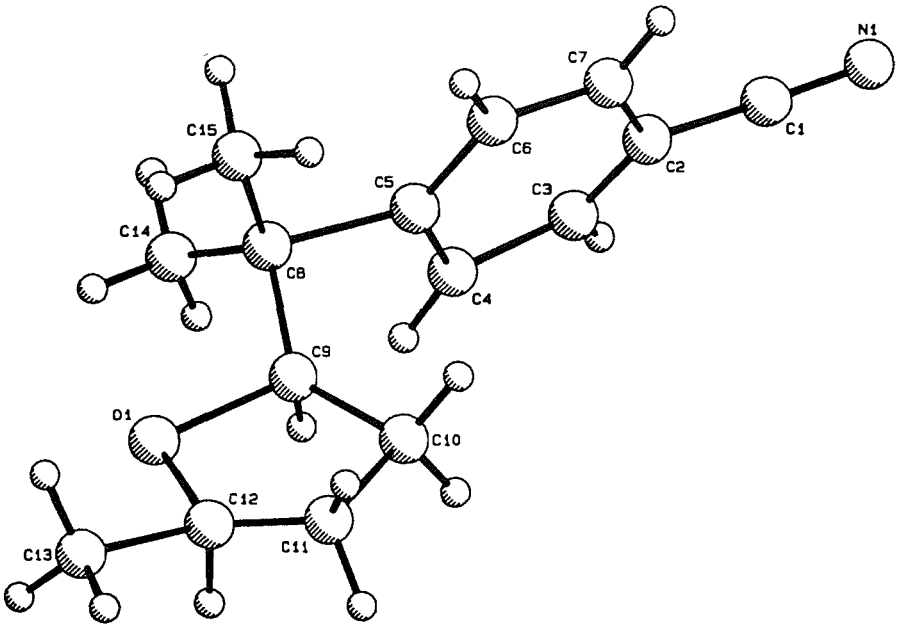

a singlet and a doublet (J = 6.1 Hz) in the aliphatic region, indicative of two methyl groups, one of which is adjacent to a methine group. Two high-field multiplets represent two methylene groups of the tetrahydrofuran ring. Two lower field doublets (2.79 and 2.86 ppm, J = 13.3 Hz) represent the methylene group substituted with the aryl group. At 3.90 ppm, another multiplet appears with one of its couplings being J = 6.1 Hz. This represents the methine group adjacent to an oxygen and substituted by a methyl group. An AA′XX′ pattern in the aromatic region is indicative of the 4-cyanophenyl group. The ^{13}C nmr spectrum of **20** indicates a methylene group (46.92 ppm) substituted by an aryl group and a doublet and a singlet (75.27 and 82.42 ppm, respectively) indicate a methine group and a quaternary carbon bonded to oxygen. The *cis* configuration of the methyl groups, as well as the overall structure of **20**, was established by the observed nuclear Overhauser enhancement (NOE). When the low-field multiplet (3.90 ppm) due to the proton adjacent to the oxygen was irradiated, a strong NOE was observed in the signal due to the protons in the aromatic region. No NOE was observed in the signal due to the methylene protons (2.79 and 2.86 ppm). This is consistent with the assigned structure since the methine proton is significantly closer to the aromatic protons (AA′) than to the methylene group.

Compound **21**, *r*-2-(methyl 4-cyanophenyl)-2,*c*-5-dimethyltetrahydrofuran, was identified as the configurational isomer of **20**. The ^1H and ^{13}C nmr spectra are very similar to those of **20**. The NOE experiment, irradiation of the low-field (4.06 ppm) multiplet due to the methine group, showed no enhancement in the signals due to the aromatic protons or to the methylene group (2.78 and 2.86 ppm).

Compound **23** was identified as *r*-3-(4-cyanophenyl)-3,*c*-6-dimethyltetrahydropyran. The ^1H nmr spectrum exhibits a singlet and a doublet (J = 6.1 Hz) in the aliphatic region, indicative of two methyl groups, one of which is adjacent to a methine group. Four high-field multiplets represent the two adjacent methylene groups on the tetrahydropyran ring. A low-field doublet (3.43 ppm, J = 12.2 Hz) and a low-field doublet of doublets (4.33 ppm, J = 12.2 Hz, J = 3.0 Hz) represent the methylene group adjacent to the oxygen and the stereogenic carbon, aryl and methyl substituted. Another multiplet appears at 3.47 ppm, exhibiting a coupling of J = 6.1 Hz. This represents the methine group adjacent to the oxygen and substituted by a methyl group. The AA′BB′ pattern in the aromatic region is indicative of the 4-cyanophenyl group. The ^{13}C nmr spectrum of **23** indicates a quaternary carbon substituted by an aryl group (38.04 ppm) and a doublet and a triplet (74.19 and 75.22 ppm, respectively) for methine and methylene groups bonded to oxygen. The quaternary aryl carbon, cyano substituted, was observed at 109.47 ppm, a cyano group at 119.16 ppm, two types of CH groups in the aromatic region (128.10 and 131.98 ppm), and the quaternary aryl carbon, alkyl substituted, as a singlet at 152.37 ppm. The *trans* configuration of methyl groups, as well as the overall structure of **23**, was firmly established by X-ray crystallography (Fig. 2). In the crystal, the aryl group attached to C-3 is axial and the methyl group attached to C-6 is equatorial. Molecular mechanics calculations (MMX) also indicate that this conformer is more stable (15 kJ/mol) than the alternative chair conformer with both methyl groups axial.

Compound **22**, *r*-3-(4-cyanophenyl)-3,*t*-6-dimethyltetrahydropyran, is the configurational isomer of **23**. The ^1H and ^{13}C nmr spectra of **22** are very similar to those of **23**; in this case the protons of the 4-cyanophenyl group show up as a distinct AA′XX′ pattern in the ^1H nmr spectrum. The overall structure of **22** was further confirmed by X-ray analysis (Fig. 3). In the crystal of this isomer, both the aryl group attached to C-3 and the methyl group attached to C-6 are equatorial. Again, molecular mechanics calculations (MMX) indicate that this conformer is more stable (6.2 kJ/mol) than the alternative chair conformer.

Can. J. Chem. Downloaded from www.nrcresearchpress.com by 46.23.64.124 on 09/08/12
For personal use only.

Can. J. Chem. Downloaded from www.nrcresearchpress.com by 46.23.64.124 on 09/08/12
For personal use only.

Fig. 2. X-ray structure for *r*-3-(4-cyanophenyl)-3, *c*-6-dimethyltetrahydropyran (**23**) (see footnote 3).

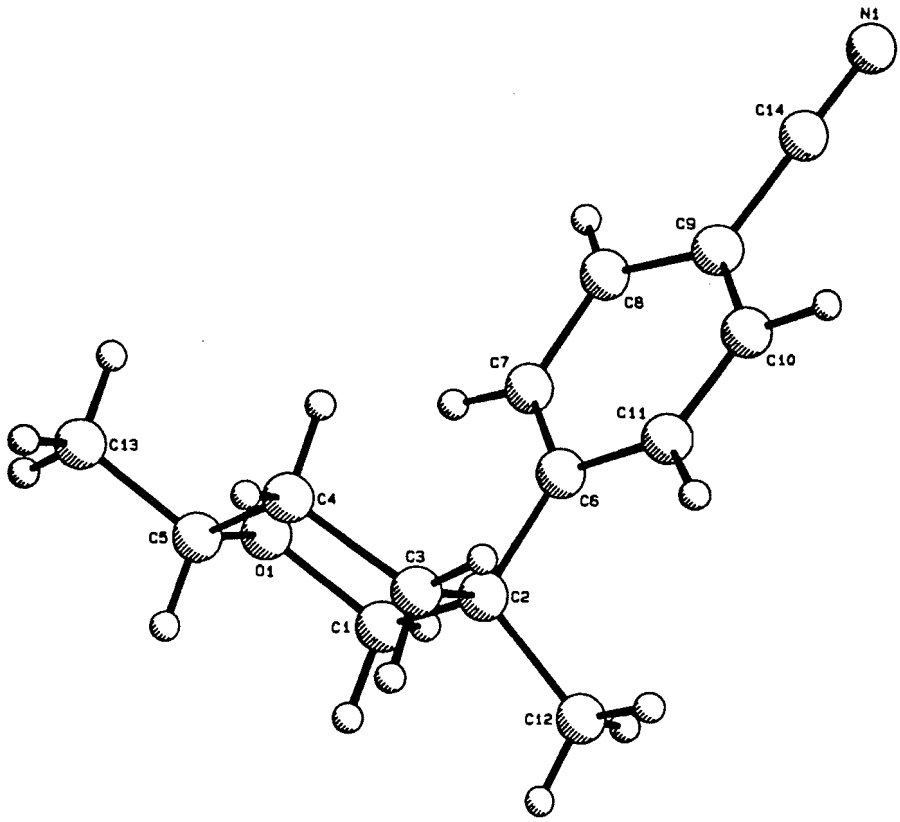

Table 1. The oxidation potentials of the alkenes and the calculated free energy change (ΔG_{et}) for the electron transfer process from the alkene to the electronic excited singlet state of the acceptor, 1,4-dicyanobenzene (**1**).

Alkene	$E_{1/2}^{ox}$ (V)[a]	ΔG_{et} (kJ/mol)[b]
2-Methyl-2-butene (**6**)	2.03	−57.8
6-Methyl-5-hepten-2-ol (**16**)	2.00	−60.7
5-Methyl-5-hexen-2-ol (**17**)	2.40	−22.1

[a]Oxidation potentials were measured at a platinum electrode relative to the saturated calomel electrode (SCE) using tetraethylammonium perchlorate (0.1 M TEAP) as the electrolyte in acetonitrile. The anodic waves were irreversible; the half-wave potentials were estimated by subtracting 0.028 V from the peak potentials (7).

[b]Based upon the Weller equation (6); $E_{0,0}$(**1**) 408.4 kJ/mol, $E_{1/2}^{red}$(**1**) −1.66 V, the Coulombic attraction term was taken to be 5.4 kJ/mol (*3a*).

Discussion

The initial steps in the proposed mechanism for the photo-NOCAS reaction involve excitation of the electron acceptor, 1,4-dicyanobenzene (**1**), followed by single electron transfer from the donor, the alkene (Scheme 1, steps 1 and 2). The ΔG_{et} for this process, calculated by the Weller equation (ref. 6):

$$\Delta G_{et} = F[E_{1/2}^{ox}(D) - E_{1/2}^{red}(A) - e/\varepsilon\alpha] - E_{0,0}(A)$$

is exergonic by more than 20 kJ/mol for each of the alk-4-enols studied (**16** and **17**) (Table 1); thus, this electron transfer process is expected to occur at the diffusion-controlled rate (6).

Photo-NOCAS adducts were formed upon irradiation of acetonitrile solutions of **1** and the alk-4-enols **16** and **17**; however, addition of a codonor, biphenyl (**5**), to the irradiation mixtures increases the efficiency of the reactions and the yields of adducts (Scheme 1, steps 6–8) (1).

The regiochemistry of the reaction is determined by initial attack of the nucleophile upon the radical cation of the olefin (Scheme 1, step 3) (1, 3). The selectivity of the intermolecular reaction is well established. The ratio of adducts obtained from 2-methylpropene (**2**) (reaction [1]) illustrates a preference (26:1) for nucleophilic attack at the primary carbon relative to attack at the tertiary carbon. The ratio of products from 2-methyl-2-butene (**6**) is 6:1 in favour of attack at the secondary relative to the tertiary carbon (reaction [2]). The same selectivity (6:1) was observed previously for the reaction involving 1-methylcyclohexene (3).

The intramolecular reaction of 6-methyl-5-hepten-2-ol (**16**) demonstrates a clear preference for 1,5-*exo-trig* relative to 1,6-*endo-trig* cyclization; no product having a tetrahydropyran ring was detected (reaction [5]). This preference for 1,5-*exo-trig* cyclization is even more evident in the reactivity of 5-methyl-5-hexen-2-ol (**17**) (reaction [6]). The normal intermolecular preference for nucleophilic attack at the primary over tertiary carbon (26:1) is now dominated by the preference (1.5:1) for 1,5-*exo-trig* over 1,6-*endo-trig* cyclization.

Reaction of the nucleophile (methanol) with the alkene radical cation is clearly more complex than illustrated in Scheme 1, step 3. The initial formation of an encounter complex may

Can. J. Chem. Downloaded from www.nrcresearchpress.com by 46.23.64.124 on 09/08/12
For personal use only.

Fig. 3. X-ray structure for *r*-3-(4-cyanophenyl)-3, *t*-6-dimethyltetrahydropyran (**22**) (see footnote 3).

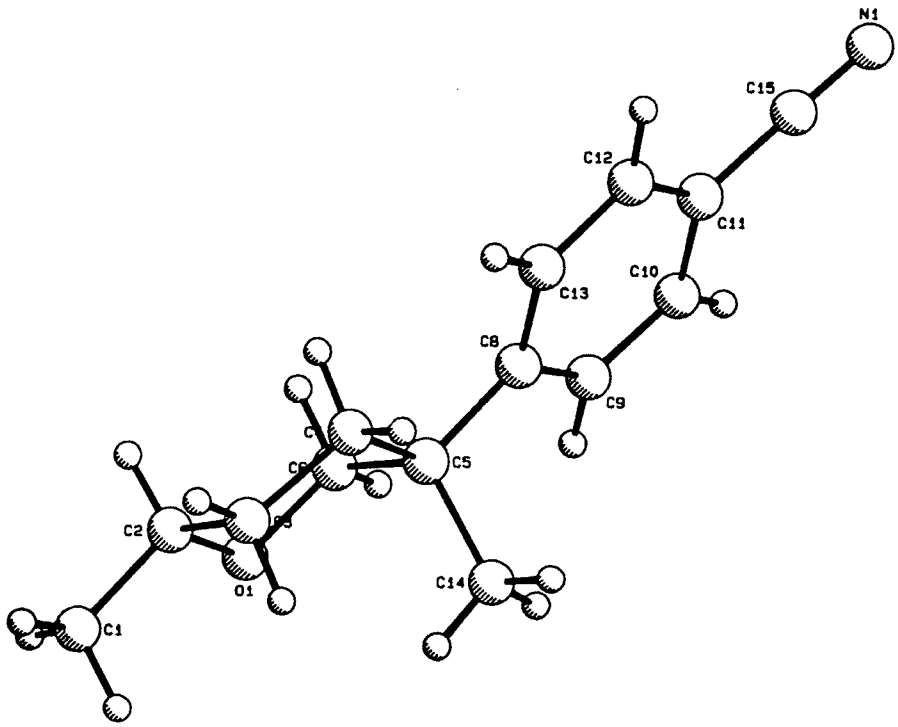

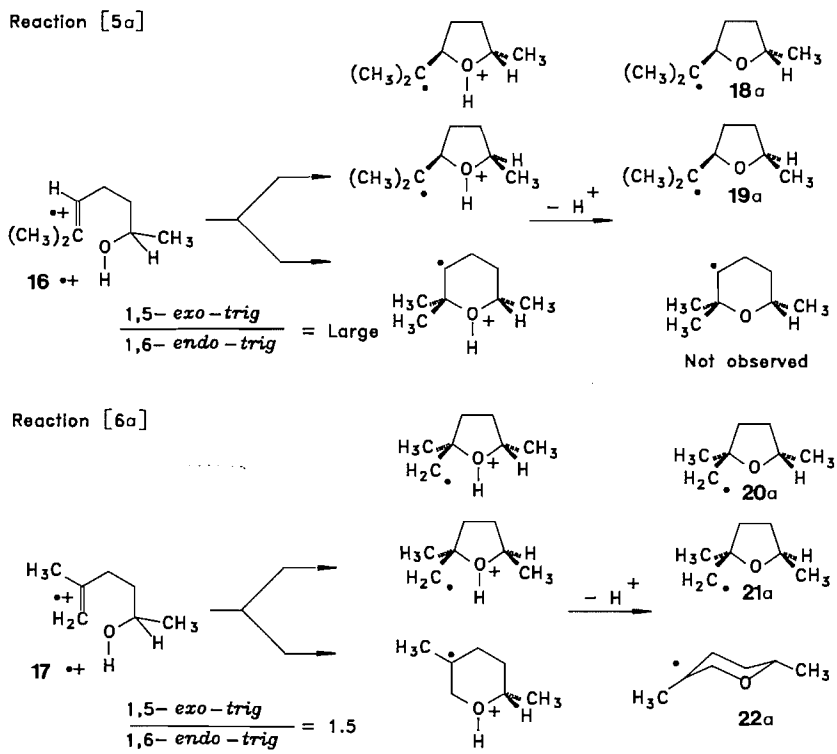

be followed by formation of a bridged radical cation intermediate, which proceeds on to distonic radical cations with alternative carbon–oxygen bond formation. Deprotonation from the oxygen of the distonic radical cations gives the alternative β-alkoxy radicals (reactions [5*a*] and [6*a*]). Presumably, all of the steps preceding formation of the β-alkoxy radicals are reversible. There is no reason, a priori, to presume that the primary β-alkoxy radical intermediates leading to the major products, the tetrahydrofurans (**20**, **21**), are more stable than the tertiary β-alkoxy radical leading to the tetrahydropyrans (**22**, **23**). This deduction is supported by the results of calculations (molecular mechanics (MMX) and semi-empirical

Table 2. Calculated and observed differences in energy (kJ/mol) between the intermediates **21***a*, **20***a*, and **22***a*.

Radical	AM1	MMX	Product ratio	ΔG = (obs.)[a]
Furan *trans* (**21***a*)	−135.18	65.73		
ΔG (kJ/mol)	0.09	4.69	**20/21** = 1.9	1.46
Furan *cis* (**20***a*)	−135.27	61.04		
ΔG (kJ/mol)	65.35	22.59	**20+21/22+23** = 1.5	1.00
Pyran (**22***a*)	−200.62	38.45		

[a]The calculated difference in activation energy (kJ/mol) derived from the observed product ratio.

(AM1)) that indicate that the tertiary β-alkoxy radical (**22***a*) is, in fact, significantly more stable than the primary β-alkoxy radicals (**20***a* and **21***a*) (Table 2). The observed product ratios from the intramolecular cyclizations lead to the conclusion that the regiochemistry is kinetically, not thermodynamically, controlled.

The ratio of stereoisomers obtained is also of interest. The stereochemistry of the tetrahydrofurans (**20** and **21**) is determined during the cyclization step (Scheme 1, step 3, reaction [6*a*]). The ratio of these products follows the relative energy of the intermediate radicals (**20***a* and **21***a*) (Table 2). Since formation of the intermediate radicals is not reversible, it is interesting to note that the ratio of the rates of formation of these intermediates parallels their relative thermodynamic stability.

The stereochemistry of the tetrahydropyrans (**22** and **23**) is determined during the coupling of the dimethyltetrahydropyranyl radical (**22***a*) with the 1,4-dicyanobenzene radical-anion (**1**$^{-\bullet}$) (Scheme 1, step 4). The product ratio indicates a distinct preference (**22/23** = 5.5) for radical–radical-anion coupling from the equatorial position of the pseudo-chair conformation of the radical, with the 2-methyl group in the equatorial position (**22***a*). The calculations (AM1) indicate the radical centre is essentially planar (dihedral angle = 178°). This is consistent with expectations based on the reactivity of alkyl-substituted cyclohexyl radicals (8). Diastereofacial selectivity is dependent upon the size of the reactant (**1**$^{-\bullet}$); equatorial attack is preferred with more bulky reactants. Furthermore, the axial methyl at C-3 of a tetrahydropyran is less hindered than an axial methyl on cyclohexane.

The first set of general rules for predicting the relative facility of ring forming reactions was adumbrated by J.E. Baldwin (4). The rules pertaining to the cyclization of radical intermediates were greatly expanded by Beckwith et al. (5). Several examples of the cyclization of alkenols, involving a wide variety of mechanisms, have been reported (9–26). There are, however, few reported examples of cyclization involving the alkenol radical cation, generated by photoinduced single electron transfer, and these examples have been limited to 1,1-diaryl substituted alkenes (9, 10). With these 1,1-diaryl alkenes, examples of cyclization proceeding 1,5-*exo*-, 1,6-*exo*-, and 1,7-*exo-trig* were observed; however, in all of these cases the regiochemistry of the reaction is dominated by preferred formation of the significantly more stable bis-benzylic radical. Furthermore, the intermediate β-alkoxy bis-benzylic radical is generally reduced, by back electron transfer from the acceptor radical anion, and the resulting anion is protonated; photo-NOCAS products were not observed (9, 10).

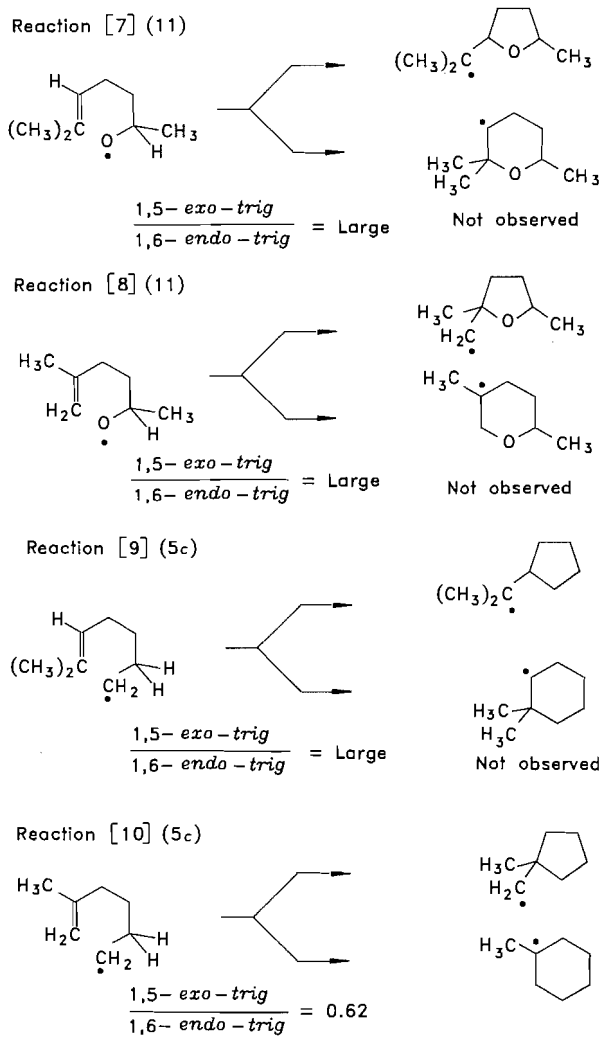

The preference for cyclization by the 1,5-*exo-trig* pathway, observed in reactions [5] and [6], is consistent with the previous explanation based upon **approach vector analysis** (4). The favoured transition state incorporates the oxygen and the alkene carbon atoms at the vertices of an obtuse triangle orthogonal to the nodal plane of the π-system. There is convincing evidence that the alkene radical cation maintains the planar structure of the alkene (27). At the transition state, the positive charge will be largely associated with the oxygen, and attached atoms, while the spin density will be borne by the carbon(s), and attached atoms, of the alkene. The structure of the transition state, for the cyclization of the alkenol radical cation, will be similar to that for the cyclization of an alkoxy radical and alkyl radical and it is interesting to compare/contrast these reactions (reactions [7] and [8] (11), and [9] and [10] (5*c*)).

The alkoxy radicals were generated by photolysis of the nitrites (11). In both cases (reactions [7] and [8]) cyclization occurs exclusively by the 1,5-*exo-trig* mode (ca. 60% yield of tetrahydrofuran products); no products resulting from 1,6-*endo-trig* cyclization were observed.

The alkyl radicals were generated by treatment of the halo compounds with Bu_3SnH (reactions [9] and [10]) (5*c*). The cyclization of the 6-methyl-5-heptenyl radical is essentially regiospecific, 1,5-*exo-trig* (reaction [9]). Cyclization of the 5-

Can. J. Chem. Downloaded from www.nrcresearchpress.com by 46.23.64.124 on 09/08/12
For personal use only.

Can. J. Chem. Downloaded from www.nrcresearchpress.com by 46.23.64.124 on 09/08/12
For personal use only.

methyl-5-hexenyl radical is not regiospecific; both 1,5-*exo-trig* and 1,6-*endo-trig* cyclization occur; in fact, 1,6-*endo-trig* is favoured.

The explanation given for the differences in reactivity between the alkoxy and alkyl radical cyclization (reactions [8] and [10]) is based upon differences in C—O versus C—C bond lengths. The shorter C—O bond lengths enhance the regiospecificity (and rate) of cyclization of the alkoxy radical (*5a*). The regiochemistry of the cyclization of the 5-methyl-5-hexen-2-ol radical cation ($\mathbf{17}^{+\bullet}$), to give the distonic radical cations (reaction [6a]), more closely resembles the alkyl radical than the alkoxy radical cyclizations, even though the same radicals (**20***a*, **21***a*) are ultimately formed. The same explanation can be applied; the C—O bonds of the intermediate distonic radical cations are longer that the C—O bonds of an ether. Consequently, the tether is long enough to allow 1,6-*endo-trig* cyclization (reaction [6]).

These reactions, cyclization of radical cation intermediates, will have synthetic utility.

Experimental

General information

The ^{1}H and ^{13}C nmr spectra were obtained from a Bruker 250 MSL spectrometer. Spectra were recorded in parts per million and frequencies are relative to tetramethylsilane. Infrared spectra (ir) were recorded on a Nicolet 205 FTIR or on an air-purged Perkin–Elmer 180 grating IR spectrometer and frequencies are reported in wave numbers (cm^{-1}). Elemental analyses were performed by Canadian Microanalytical Service Ltd., B.C. Melting points were determined using a Cybron Corporation Thermolyne apparatus with a digital thermocouple and are corrected. Progress of the reactions was followed by gas chromatography using a Hewlett–Packard (HP) 5890 gas chromatograph with a DB-1701 fused silica WCOT column (20 m × 0.25 mm, 0.4-μm film thickness) and a flame ionization detector (gc/fid). An HP 3392A integrator was interfaced with the gc/fid to obtain peak areas. An HP 5890 gas chromatograph with a 5% phenyl methyl silicone fused silica WCOT column (25 m × 0.20 mm, 0.33-μm film thickness) interfaced with an HP 5970 mass selective detector (gc/ms) was also used for product analyses. Mass spectra are reported as *m/z* (relative intensity). Separation of product mixtures was generally carried out using preparative medium-pressure liquid chromatography (mplc), a 2.5 cm × 1 m column packed with thin-layer chromatography (tlc) grade silica gel (without binder) (cat. no. 7747 Merck) at a pressure of 15 psi using helium (1 psi = 6.9 kPa). Connected to the mplc was a UV spectrophotometer – fraction collector that collects ca. 10 mL fractions.

Materials

Acetonitrile (Fisher ACS grade) was distilled twice, first from sodium hydride and then from phosphorus pentoxide. It was then passed through a column of basic alumina, refluxed over calcium hydride for 24 h (under a nitrogen atmosphere), fractionally distilled (under nitrogen), and stored over molecular sieves (3 Å) (*28a*). Methanol was distilled from magnesium turnings and then stored over molecular sieves (4 Å). 1,4-Dicyanobenzene (**1**) (Aldrich) was purified by treatment with Norite in methylene chloride, followed by recrystallization from 95% ethanol. Tetraethylammonium perchlorate (TEAP) (Aldrich) was recrystallized three times from water and then dried in a vacuum oven for 15 h, 70°C, 0.25 Torr (1 Torr = 133.3 Pa). (±) 6-Methyl-5-hepten-2-ol, 99% (**16**) and (±) 5-methyl-5-hexen-2-one, 99% (**17**) were obtained from the Aldrich Chemical Co. Sodium borohydride, reagent grade, was obtained from Caledon Laboratory Ltd. Biphenyl (**5**) (Eastman Kodak Co.) was recrystallized from methanol.

Irradiations

Irradiations were generally carried out on solutions of acetonitrile with 1,4-dicyanobenzene (**1**), the alk-4-enol, and biphenyl (**5**), a codonor. Solutions were irradiated in either 2 cm i.d. Pyrex tubes or 5 mm Pyrex nmr tubes, which were degassed by nitrogen ebullition. These samples were irradiated at 10°C using a CGE 1-kW or a Hanovia 450-W medium-pressure mercury vapour lamp contained in a water-cooled quartz immersion well.

Electrochemical measurements

Cyclic voltammetry was used to obtain the oxidation potential of the alk-4-enols. The apparatus has been described (*28b*). The working electrode was a platinum sphere (1 mm diameter) and the counter electrode was a platinum wire. The reference electrode was a saturated calomel electrode (sce), which was connected to the solution (TEAP 0.1 M, acetonitrile) through a Luggin capillary. The alk-4-enols were purified by prep/gc using a 0.95 cm × 350 cm aluminum column packed with 40% SE-30 on Chromosorb W 60/80 NAW. The alk-4-enol concentration was ca. 0.005 M. Since the anodic wave was irreversible, the half-wave potential was taken as 0.028 V before the anodic peak potential (7).

Formation of the methanol, 2-methyl-2-butene (6), 1,4-dicyanobenzene (1) photo-NOCAS adducts 7 and 8: reaction [2]

A solution of 2-methyl-2-butene (**6**) (2.7 g, 4.1 mL, 0.038 mol), 1,4-dicyanobenzene (**1**) (2.5 g, 0.019 mol), and biphenyl (**5**) (1.6 g, 0.010 mol) in acetonitrile–methanol (3:1, 160 mL) was degassed by nitrogen ebullition for 5 min and irradiated for 24 h using a 1-kW lamp at 10°C. The solvent was removed to yield a crude photolysate. **1** was totally consumed in the reaction. The crude photolysate was separated by chromatography (mplc) using a linear solvent gradient (hexanes – 5% diethyl ether, 95% hexanes). Products eluted in the order **7**, then **8**.

2-(4-Cyanophenyl)-3-methoxy-2-methylbutane (7)

The yield of **7** was 60%: infrared (Nicolet 205) ν: 2978(s), 2934(s), 2883(m), 2822(m), 2228(s), 1607(m), 1506(w), 1466(m), 1398(w), 1372(m), 1193(w), 1162(w), 1111(s), 1096(s), 1026(w), 840(s); ^{1}H nmr (250.13 MHz, $CDCl_3$) δ_{TMS}: 0.92 (d, 3H, $^3J_{3-4}$ = 6.1 Hz, CH_3 (4-H)), 1.31 (s, 3H, CH_3), 1.33 (s, 3H, CH_3), 3.24 (s, 3H, OCH_3), 3.30 (q, 1H, $^3J_{3-4}$ = 6.1 Hz, OCH (3-H)), 7.50 (d, 2H, $^3J_{2'-3'}$ = 8.5 Hz, $^3J_{5'-6'}$ = 8.5 Hz, H's adjacent to alkyl-substituted aryl carbon (2′-H, 6′-H)), 7.58 (d, 2H, $^3J_{2'-3'}$ = 8.5 Hz, $^3J_{5'-6'}$ = 8.5 Hz, H's adjacent to cyano-substituted aryl carbon (3′-H, 5′-H)); ^{13}C nmr (62.90 MHz, $CDCl_3$) δ: 13.72 (q), 24.14 (q), 24.55 (q), 43.10 (s, quaternary carbon, aryl substituted), 57.59 (q, OCH_3), 84.28 (d, OCH),

Can. J. Chem. Downloaded from www.nrcresearchpress.com by 46.23.64.124 on 09/08/12
For personal use only.

109.50 (s, quaternary aryl carbon, cyano substituted), 119.15 (s, CN), 127.68 (d, aromatic CH adjacent to alkyl-substituted aryl carbon), 131.57 (d, aromatic CH adjacent to cyano-substituted aryl carbon), 153.45 (s, quaternary aryl carbon, alkyl substituted); *ms m/z*: 51(2), 59(100), 60(3), 77(2), 89(2), 103(2), 115(2), 116(6), 130(5), 144(2), 145(7). Anal. calcd. for $C_{13}H_{17}NO$: C 76.81, H 8.43, N 6.89; found: C 77.12, H 8.47, N 7.15.

*3-(4-Cyanophenyl)-2-methoxy-2-methylbutane (**8**)*

The yield of **8** was 10%: infrared (Nicolet 205) ν: 2979(s), 2940(s), 2905(m), 2828(w), 2228(s), 1607(m), 1504(w), 1463(m), 1414(w), 1372(m), 1233(w), 1209(w), 1185(m), 1150(m), 1080(s), 1048(w), 840(m); ^{1}H nmr (250.13 MHz, $CDCl_3$) δ_{TMS}: 1.05 (s, 3H, CH_3), 1.09 (s, 3H, CH_3), 1.30 (d, 3H, $^3J_{3-4}$ = 7.0 Hz, CH_3 (4-H)), 2.90 (q, 1H, $^3J_{3-4}$ = 7.0 Hz, methine, aryl substituted (3-H)), 3.20 (s, 3H, OCH_3), 7.37 (d, 2H, $^3J_{2'-3'}$ = 8.4 Hz, $^3J_{5'-6'}$ = 8.4 Hz, H's adjacent to alkyl-substituted aryl carbon (2′-H, 6′-H)), 7.55 (d, 2H, $^3J_{2'-3'}$ = 8.4 Hz, $^3J_{5'-6'}$ = 8.4 Hz, H's adjacent to cyano-substituted aryl carbon (3′-H, 5′-H)); ^{13}C nmr (62.90 MHz, $CDCl_3$) δ: 15.48 (q), 22.70 (q, 2 CH_3), 48.96 (d, CH, aryl substituted), 49.20 (q, OCH_3), 76.33 (s, quaternary carbon adjacent to oxygen), 109.85 (s, quaternary aryl carbon, cyano substituted), 119.18 (s, CN), 130.04 (d, aromatic CH adjacent to alkyl-substituted aryl carbon), 131.42 (d, aromatic CH adjacent to cyano-substituted aryl carbon), 150.09 (s, quaternary aryl carbon, alkyl substituted); ms *m/z*: 51(2), 55(2), 59(5), 73(100), 74(5), 77(4), 102(2), 103(5), 116(5), 129(3), 130(8), 156(2), 188(2). Anal. calcd. for $C_{13}H_{17}NO$: C 76.81, H 8.43, N 6.89; found: C 76.47, H 8.40, N 7.07.

Formation of the 6-methyl-5-hepten-2-ol (16) and 1,4-dicyanobenzene (1) photo-NOCAS adducts 18 and 19: reaction [5]

A solution of 6-methyl-5-hepten-2-ol (**16**) (4.1 g, 4.9 mL, 0.032 mol), 1,4-dicyanobenzene (**1**) (2.1 g, 0.016 mol), and biphenyl (**5**) (2.5 g, 0.016 mol) in 160 mL of acetonitrile was degassed with nitrogen and irradiated for 117 h using a 450-W lamp. The crude photolysate was separated by chromatography (mplc) using a linear solvent gradient of hexanes – 1% ethyl acetate, 99% hexanes. Products were eluted in the order **18**, then **19**.

trans-*2-(Isopropyl 4-cyanophenyl)-5-methyltetrahydrofuran (**18**)*

The yield of **18** was 29%; infrared (PE-180) ν: 2971(s), 2931(m), 2871(m), 2231(s), 1601(m), 1501(m), 1456(w), 1401(w), 1071(s), 1001(m), 976(m), 851(w), 816(s); ^{1}H nmr (250.13 MHz, $CDCl_3$) δ_{TMS}: 1.18 (d, 3H, $^3J_{5-6}$ = 6.1 Hz, CH_3 (6-H)), 1.32 (s, 3H, CH_3), 1.36 (s, 3H, CH_3), 1.37 (m, 2H, H's on methylene groups of ring (3- or 4-H)), 1.77 (m, 2H, H's on methylene groups of ring (3- or 4-H)), 3.81 (m, 1H, $^3J_{4-5}$ = 6.0 Hz, $^3J_{4-5}$ = 6.0 Hz, $^3J_{5-6}$ = 6.1 Hz, H on methine group, methyl substituted (5-H)), 4.08 (m, 1H, $^3J_{2-3}$ = 6.4 Hz, $^3J_{2-3}$ = 8.5 Hz, H on methine group, alkyl-aryl substituted (2-H)), 7.54 (d, 2H, $^3J_{2'-3'}$ = 8.9 Hz, $^3J_{5'-6'}$ = 8.9 Hz, H's adjacent to alkyl-substituted aryl carbon (2′-H, 6′-H)), 7.59 (d, 2H, $^3J_{2'-3'}$ = 8.9 Hz, $^3J_{5'-6'}$ = 8.9 Hz, H's adjacent to cyano-substituted aryl carbon (3′-H, 5′-H)); ^{13}C nmr (62.90 MHz, $CDCl_3$) δ: 21.15 (q), 24.81 (q), 24.99 (q), 28.21 (t), 34.12 (t), 42.20 (s, quaternary carbon, methyl and aryl substituted), 76.02 (d, CH adjacent to oxygen), 86.20 (d, CH adjacent to oxygen), 109.64 (s, quaternary aryl carbon, cyano substituted), 119.21 (s, CN), 128.01 (d, aromatic CH adjacent to alkyl-substituted aryl carbon), 131.56 (d, aromatic CH adjacent to cyano-substituted aryl carbon), 152.63 (s, quaternary carbon, alkyl substituted); ms *m/z*: 55(4), 57(17), 67(19), 77(4), 85(100), 86(5), 115(5), 116(19), 128(4), 130(11), 142(5), 144(10), 145(11), 157(5). Anal. calcd. for $C_{15}H_{19}NO$: C 78.56, H 8.35, N 6.11; found: C 78.20, H 7.89, N 6.12. (The elemental analysis was obtained on a 50/50 mixture of isomers **18** and **19**).

cis-*2-(Isopropyl 4-cyanophenyl)-5-methyltetrahydrofuran (**19**)*

The yield of **19** was 24%; infrared (PE-180) ν: 2971(s), 2931(m), 2871(m), 2231(s), 1611(m), 1512(m), 1461(m), 1401(m), 1381(m), 1091(s), 1011(m), 821(s); ^{1}H nmr (250.13 MHz, $CDCl_3$) δ_{TMS}: 1.11 (d, 3H, $^3J_{5-6}$ = 6.1 Hz, CH_3 (6-H)), 1.32 (s, 3H, CH_3), 1.33 (s, 3H, CH_3), 1.40–1.90 (m, 4H, H's on methylene groups of ring (3- or 4-H)), 3.91 (m, 1H, $^3J_{2-3}$ = 7.4 Hz, $^3J_{2-3}$ = 7.4 Hz, H on methine group, alkyl-aryl substituted (2-H)), 3.92 (m, 1H, $^3J_{4-5}$ = 5.8 Hz, $^3J_{4-5}$ = 6.4 Hz, $^3J_{5-6}$ = 6.1 Hz, H on methine group, methyl substituted (5-H)), 7.54 (d, 2H, $^3J_{2'-3'}$ = 8.9 Hz, $^3J_{5'-6'}$ = 8.9 Hz, H's adjacent to alkyl-substituted aryl carbon (2′-H, 6′-H)), 7.59 (d, 2H, $^3J_{2'-3}$ = 8.9 Hz, $^3J_{5'-6'}$ = 8.9 Hz, H's adjacent to cyano-substituted aryl carbon (3′-H, 5′-H)); ^{13}C nmr (62.90 MHz, $CDCl_3$) δ: 20.87 (q), 24.68 (q), 24.93 (q), 27.01 (t), 32.90 (t), 41.53 (s, quaternary carbon, methyl and aryl substituted), 75.53 (d, CH adjacent to oxygen), 86.50 (d, CH adjacent to oxygen), 109.66 (s, quaternary aryl carbon, cyano substituted), 119.16 (s, CN), 128.03 (d, aromatic CH adjacent to alkyl-substituted aryl carbon), 131.45 (d, aromatic CH adjacent to cyano-substituted aryl carbon), 152.64 (s, quaternary carbon, alkyl substituted); ms *m/z*: 57(15), 67(15), 85(100), 86(4), 103(3), 104(3), 115(4), 116(16), 130(8), 142(6), 143(2), 144(8), 145(8), 157(3), 200(2). Anal. calcd. for $C_{15}H_{19}NO$: C 78.56, H 8.35, N 6.11; found: C 78.20, H 7.89, N 6.12. (The elemental analysis was obtained on a 50/50 mixture of isomers **18** and **19**). X-ray data: the crystals are monoclinic, space group $P2_1/a$, Z = 4, a = 10.908 (3) Å, b = 7.761 (3) Å, c = 15.708 (3) Å, β = 97.05 (1)°, P_c = 1.154 g/cm^3, μ = 0.669 cm^{-1}, λ = 0.70926 Å. Data are insufficient (only 264 reflections above $I > 1\sigma$); however, the model obtained after isotropic refinement is consistent with the assigned structure (**19**) (Fig. 1).

Preparation of 5-methyl-5-hexen-2-ol (17)

5-Methyl-5-hexen-2-one (6.7 g, 0.06 mol) was dissolved in 50 mL of 95% ethanol and the solution was stirred while sodium borohydride (1.0 g, 0.03 mol) was added slowly. The reaction mixture was left to stir overnight. The mixture was extracted with dichloromethane and the extract was dried over magnesium sulphate. The mixture was filtered and the solvent was removed on a rotary evaporator. The residue was distilled at atmospheric pressure to yield 4.6 g (67%) of the alcohol **17** (bp 156–157°C). The ^{1}H nmr spectrum was similar to that reported in the literature (22, 29). ^{1}H nmr (250.13 MHz, $CDCl_3$) δ_{TMS}: 1.20 (d, 3H, $^3J_{1-2}$ = 6.1 Hz, CH_3 (1-H)), 1.59 (m, 2H, CH_2), 1.74 (s, 3H, CH_3), 1.75 (br s, 1H, OH), 2.10 (m, 2H, CH_2), 3.80 (m, 1H, $^3J_{1-2}$ = 6.1 Hz, H on methine group,

Can. J. Chem. Downloaded from www.nrcresearchpress.com by 46.23.64.124 on 09/08/12
For personal use only.

hydroxyl substituted (2-H)), 4.72 (br s, 2H, vinyl methylene); ^{13}C nmr (62.90 MHz, $CDCl_3$) δ: 22.44 (q), 23.46 (q), 34.14 (t), 37.02 (t), 67.93 (d), 110.05 (t, vinyl methylene), 145.81 (s, vinyl quaternary carbon).

Formation of the 5-methyl-5-hexen-2-ol (17) and 1,4-dicyanobenzene (1) photo-NOCAS adducts 20–23: reaction [6]

A solution of 5-methyl-5-hexen-2-ol (**17**) (2.1 g, 0.018 mol), 1,4-dicyanobenzene (**1**) (1.0 g, 0.0078 mol), and biphenyl (**5**) (1.2 g, 0.0078 mol), in 80 mL of acetonitrile was degassed with nitrogen and irradiated for 139 h using a 1-kW lamp. The crude photolysate was separated by chromatography (mplc) using a linear solvent gradient of hexanes – 10% diethyl ether, 90% hexanes. Products were eluted in the order **23**, **20**, and **21** (together), then **22**. Separation of **20** and **21** was achieved by rechromatographing the mixture, using a linear solvent gradient of hexanes – 1% diethyl ether, 99% hexanes.

r-*2-(Methyl 4-cyanophenyl)-2,*t-*5-dimethyltetrahydrofuran (20)*

The yield of **20** was 13%: the melting point was 42–43°C; infrared (PE-180) ν: 2970(s), 2930(m), 2871(m), 2227(s), 1608(m), 1506(w), 1454(m), 1415(w), 1379(m), 1175(w), 1086(s), 960(w), 853(w); ^{1}H nmr (250.13 MHz, $CDCl_3$) δ_{TMS}: 1.18 (s, 3H, CH_3), 1.22 (d, 3H, $^3J_{5-6}$ = 6.1 Hz, CH_3 (6-H)), 1.56 (m, 1H, H on methylene groups of ring (3- or 4-H)), 1.70–1.95 (m, 3H, H's on methylene groups of ring (3- or 4-H)), 2.79 (d, 1H, $^3J_{1-1'}$ = 13.3 Hz, H on methylene group, aryl substituted (1-H)), 2.86 (d, 1H, $^3J_{1-1'}$ = 13.3 Hz, H on methylene group, aryl substituted (1′-H)), 3.92 (m, 1H, $^3J_{5-6}$ = 6.1 Hz, H on methine group, methyl substituted (5-H)), 7.34 (d, 2H, $^3J_{2'-3'}$ = 8.4 Hz, $^3J_{5'-6'}$ = 8.4 Hz, H's adjacent to alkyl-substituted aryl carbon (2′-H, 6′-H)), 7.56 (d, 2H, $^3J_{2'-3'}$ = 8.4 Hz, $^3J_{5'-6'}$ = 8.4 Hz, H's adjacent to cyano-substituted aryl carbon (3′-H, 5′-H)); ^{1}H NOE: Irradiation of the methine group at 3.90 ppm produced a NOE at 7.34–7.56 ppm. No enhancement was observed in the signal due to the methylene group 2.79 and 2.86 ppm ; ^{13}C nmr (62.90 MHz, $CDCl_3$) δ: 21.69 (q), 27.95 (q), 33.45 (t), 37.02 (t), 46.92 (t, CH_2, aryl substituted), 75.27 (d, CH adjacent to oxygen), 82.42 (s, quaternary carbon adjacent to oxygen), 109.84 (s, quaternary aryl carbon, cyano substituted), 119.09 (s, CN), 131.16 (d, aromatic CH adjacent to alkyl-substituted aryl carbon), 131.55 (d, aromatic CH adjacent to cyano-substituted aryl carbon), 144.22 (s, quaternary carbon, alkyl substituted); ms *m/z*: 51(4), 53(4), 56(5), 63(6), 89(19), 90(6), 99(100), 100(6), 116(25), 117(19), 173(5). Anal. calcd. for $C_{14}H_{17}NO$: C 78.10, H 7.96, N 6.51; found: C 77.90, H 7.94, N 6.52. (The elemental analysis was obtained using a 50/50 mixture of isomers **20** and **21**.)

r-*2-(Methyl 4-cyanophenyl)-2,*c-*5-dimethyltetrahydrofuran (21)*

The yield of **21** was 7%; infrared (PE-180) ν: 2969(s), 2928(m), 2871(m), 2227(s), 1608(m), 1507(w), 1455(m), 1414(w), 1374(m), 1243(w), 1176(w), 1117(m), 1089 (s), 962(w), 953(w), 885(w), 848(w), 824(w); ^{1}H nmr (250.13 MHz, $CDCl_3$) δ_{TMS}: 1.14 (d, 3H, $^3J_{5-6}$ = 6.1 Hz, CH_3 (6-H)), 1.19 (s, 3H, CH_3), 1.02–1.27 (m, 1H, H on methylene groups of ring (3- or 4-H)), 1.62–1.96 (m, 3H, H's on methylene groups of ring (3- or 4-H)), 2.78 (d, 1H, $^3J_{1-1'}$ = 13.4 Hz, H on methylene group, aryl substituted (1-H)), 2.86 (d, 1H, $^3J_{1-1'}$ = 13.4 Hz, H on methylene group, aryl substituted (1′-H)), 4.06 (m, 1H, $^3J_{5-6}$ = 6.1 Hz, H on methine group, methyl substituted (5-H)), 7.36 (d, 2H, $^3J_{2'-3'}$ = 8.2 Hz, $^3J_{5'-6'}$ = 8.2 Hz, H's adjacent to alkyl-substituted aryl carbon (2′-H, 6′-H)), 7.56 (d, 2H, $^3J_{2'-3'}$ = 8.2 Hz, $^3J_{5'-6'}$ = 8.2 Hz, H's adjacent to cyano substituted aryl carbon (3′-H, 5′-H)); ^{1}H NOE: Irradiation of the methine group at 4.06 ppm produced no NOE at 7.36–7.56 ppm or at 2.78 and 2.86 ppm; ^{13}C nmr (62.90 MHz, $CDCl_3$) δ: 21.18 (q), 27.22 (q), 33.69 (t), 36.84 (t), 48.07 (t, CH_2, aryl substituted), 74.77 (d, CH adjacent to oxygen), 82.46 (s, quaternary carbon adjacent to oxygen), 109.98 (s, quaternary aryl carbon, cyano substituted), 119.22 (s, CN), 131.45 (d, aromatic CH adjacent to alkyl-substituted aryl carbon), 131.47 (d, aromatic CH adjacent to cyano-substituted aryl carbon), 144.16 (s, quaternary carbon, alkyl substituted); ms *m/z*: 51(4), 53(4), 55(13), 56(6), 63(7), 89(15), 99(100), 100(7), 115(4), 116(29), 117(18), 156(4), 160(4), 173(6). Anal. calcd. for $C_{14}H_{17}NO$: C 78.10, H 7.96, N 6.51; found: C 77.90, H 7.94, N 6.52. (The elemental analysis was obtained using a 50/50 mixture of **20** and **21**.)

r-*3-(4-Cyanophenyl)-3,*t-*6-dimethyltetrahydropyran (22)*

The yield of **22** was 11%: the melting point was 67–68°C; infrared (PE-180) ν: 2970(s), 2933(s), 2855(m), 2228(s), 1608(m), 1508(m), 1466(w), 1459(w), 1448(w), 1383(m), 1097(s), 1058(m), 834(m); ^{1}H nmr (250.13 MHz, $CDCl_3$) δ_{TMS}: 1.27 (d, 3H, $^3J_{6-7}$ = 6.1 Hz, CH_3 (7-H)), 1.41 (s, 3H, CH_3), 1.60–1.69 (m, 1H, $^3J_{5ax-6ax}$ = 12.9 Hz, H's on methylene group (5-H)), 1.82–1.94 (m, 2H, H's on methylene group (4-H)), 3.41 (m, 1H, $^3J_{5ax-6ax}$ = 12.9 Hz, $^3J_{6ax-7}$ = 6.1 Hz, axial H on methylene group adjacent to the oxygen (6ax-H)), 3.55 (d, 1H, $^2J_{2ax-2eq}$ = 11.1 Hz, H on methylene group adjacent to the oxygen (2-H)), 3.85 (d, 1H, $^2J_{2ax-2eq}$ = 11.1 Hz, H on methylene group adjacent to the oxygen (2-H)), 7.42 (d, 2H, $^3J_{2'-3'}$ = 8.7 Hz, $^3J_{5'-6'}$ = 8.7 Hz, H's adjacent to alkyl-substituted aryl carbon (2′-H, 6′-H)), 7.62 (d, 2H, $^3J_{2'-3'}$ = 8.7 Hz, $^3J_{5'-6'}$ = 8.7 Hz, H's adjacent to cyano-substituted aryl carbon (3′-H, 5′-H)); ^{13}C nmr (62.90 MHz, $CDCl_3$) δ: 21.65 (q), 23.14 (q), 29.63 (t), 34.88 (t), 37.18 (s, quaternary carbon, aryl substituted), 74.04 (d, methine group adjacent to oxygen), 75.94 (t, methylene group adjacent to oxygen), 110.05 (s, quaternary aryl carbon, cyano substituted), 118.90 (s, CN), 126.25 (d, aromatic CH adjacent to alkyl-substituted aryl carbon), 132.20 (d, aromatic CH adjacent to cyano-substituted aryl carbon), 153.38 (s, quaternary carbon, alkyl substituted); ms *m/z*: 51(4), 55(5), 59(6), 77(5), 89(5), 97(5), 101(5), 103(5), 112(23), 115(10), 116(20), 128(9), 129(4), 140(4), 142(19), 143(100), 144(12), 156(6). X-ray structure, see Fig. 2.

r-*3-(4-Cyanophenyl)-3,*c-*6-dimethyltetrahydropyran (23)*

The yield of **23** was 2%: the melting point was 42–43°C; infrared (PE-180) ν: 2968(s), 2933(s), 2852(m), 2228(s), 1608(m), 1505(m), 1455(m), 1384(m), 1097(s), 1067(m), 1021(w), 868(w), 838(m), 737(w); ^{1}H nmr (250.13 MHz, $CDCl_3$) δ_{TMS}: 1.08 (s, 3H, CH_3), 1.09 (d, 3H, $^3J_{6-7}$ = 6.1 Hz, CH_3 (7-H)), 0.90-1.20 (m, 1H, $^2J_{5ax-5eq}$ = 13.4 Hz, $^3J_{4ax-5ax}$ = 13.4 Hz, axial H on methylene group (5ax-H)), 1.41 (m, 1H, $^2J_{5ax-5eq}$ = 13.4 Hz, equatorial H on methylene group (5eq-

H)), 1.70 (m, 1H, $^2J_{4ax-4eq}$ = 13.4 Hz, $^3J_{4ax-5ax}$ = 13.4 Hz, axial H on methylene group (4ax-H)), 2.16 (m, 1H, $^2J_{4ax-4eq}$ = 13.4 Hz, $^3J_{2eq-4eq}$ = 3.0 Hz, equatorial H on methylene group (4eq-H)), 3.43 (d, 1H, $^2J_{2ax-2eq}$ = 12.2 Hz, axial H on methylene group (2ax-H)), 3.47 (m, 1H, $^3J_{6-7}$ = 6.1 Hz, axial H adjacent to the oxygen (6ax-H)), 4.33 (dd, 1H, $^2J_{2ax-2eq}$ = 12.2 Hz, $^3J_{2eq-4eq}$ = 3.0 Hz, equatorial H on methylene group (2eq-H)), 7.61 (s, 4H, aromatic H's (2′-,3′-,5′-,6′-H)); ^{13}C nmr (62.90 MHz, $CDCl_3$) δ: 21.65 (q), 27.84 (q), 30.03 (t), 37.58 (t), 38.04 (s, quaternary carbon, aryl substituted), 74.19 (d, methine group adjacent to oxygen), 75.22 (t, methylene group adjacent to oxygen), 109.47 (s, quaternary aryl carbon, cyano substituted), 119.16 (s, CN), 128.10 (d, aromatic CH adjacent to alkyl-substituted aryl carbon), 131.98 (d, aromatic CH adjacent to cyano-substituted aryl carbon), 152.37 (s, quaternary carbon, alkyl substituted); ms *m/z*: 72(12), 77(5), 89(5), 101(5), 103(5), 115(10), 116(19), 128(8), 129(4), 140(5), 142(19), 143(100), 144(12), 156(6), 215(6). X-ray structure, see Fig. 3.

Acknowledgements

This work was supported by the Natural Sciences and Engineering Research Council of Canada. Preliminary experiments on 6-methyl-5-hepten-2-ol (**16**) were carried out by K. McMahon. We thank Dr. D.L. Hooper at the Atlantic Regional Magnetic Resonance Centre at Dalhousie University for the high-field nmr spectra and for help in the preparation of the manuscript. We are grateful to Dr. T.S. Cameron at Dalhousie for the X-ray analysis of **19**, **22**, and **23**.

References

1. (*a*) K.A. McManus and D.R. Arnold. Can. J. Chem. **72**, 2291 (1994); (*b*) D.R. Arnold, X. Du, and H.J.P. de Lijser. Can. J. Chem. **73**, 522 (1995); (*c*) D.R. Arnold, K.A. McManus, and X. Du. Can. J. Chem. **72**, 415 (1994); (*d*) D.A. Connor, D.R. Arnold, P.K. Bakshi, and T.S. Cameron. Can. J. Chem. **73**, 762 (1995).
2. (*a*) D.R. Arnold, X. Du, and J. Chen. Can. J. Chem. **73**, 307 (1995); (*b*) A.L. Perrott and D.R. Arnold. Can. J. Chem. **70**, 272 (1992); (*c*) R. Popielarz and D.R. Arnold. J. Am. Chem. Soc. **112**, 3068 (1990).
3. (*a*) R.M. Borg, D.R. Arnold, and T.S. Cameron. Can. J. Chem. **62**, 1785 (1984); (*b*) D.R. Arnold and M.S. Snow. Can. J. Chem. **66**, 3012 (1988); (*c*) D.R. Arnold and X. Du. Can. J. Chem. **72**, 403 (1994).
4. (*a*) J.E. Baldwin. J. Chem. Soc. Chem. Commun. 734 (1976); (*b*) J. Chem. Soc. Chem. Commun. 738 (1976).
5. (*a*) A.L.J. Beckwith. Tetrahedron, **37**, 3073 (1981); (*b*) A.L.J. Beckwith and C.H. Schiesser. Tetrahedron, **41**, 3925 (1985); (*c*) A.L.J. Beckwith, I.A. Blair, and G. Phillipou. Tetrahedron Lett. 2251 (1974); (*d*) A.L.J. Beckwith, C.J. Easton, and A.K. Serelis. J. Chem. Soc. Chem. Commun. 482 (1980); (*e*) A.L.J. Beckwith, T. Lawrence, and A.K. Serelis. J. Chem. Soc. Chem. Commun. 484 (1980); (*f*) A.L.J. Beckwith and T. Lawrence. J. Chem. Soc. Perkin Trans. 2, 1535 (1979); (*g*) A.L.J. Beckwith, G. Phillipou, and A.K. Serelis. Tetrahedron Lett. **22**, 2811 (1981); (*h*) A.L.J. Beckwith and G. Moad. J. Chem. Soc. Chem. Commun. 472 (1974).
6. D. Rehm and A. Weller. Isr. J. Chem. **8**, 259 (1970).
7. (*a*) R.S. Nicholson and I. Shain. Anal. Chem. **36**, 706 (1964); (*b*) Anal. Chem. **37**, 178 (1965).
8. W. Damm, B. Giese, J. Hartung, T. Hasskerl, K.N. Houk. O. Huter, and H. Zipse. J. Am. Chem. Soc. **114**, 4067 (1992).
9. Z.Q. Jiang and C.S. Foote. Tetrahedron Lett. **24**, 461 (1983).
10. K. Mizuno, T. Tamai, T. Nishiyama, K. Tani, M. Sawasaki, and Y. Otsuji. Angew. Chem. Int. Ed. Engl. **33**, 2113 (1994).
11. (*a*) M.-P. Bertrand and J.-M. Surzur. Bull. Soc. Chim. Fr. 2393 (1973); (*b*) J.-M. Surzur, M.-P. Bertrand, and R. Nouguier. Tetrahedron Lett. 4197 (1969).
12. G.L. Edwards and K.A. Walker. Tetrahedron Lett. **33**, 1779 (1992).
13. R.D. Rychnovsky and P.A. Bartlett. J. Am. Chem. Soc. **103**, 3963 (1981).
14. (*a*) R.M. Kennedy and S. Tang. Tetrahedron Lett. **33**, 3729 (1992); (*b*) S. Tang and R.M. Kennedy. Tetrahedron Lett. **33**, 5299 (1992).
15. S. Murata and T. Suzuki. Tetrahedron Lett. **28**, 4297 (1987).
16. S.M. Tuladhar and A.G. Fallis. Tetrahedron Lett. **28**, 523 (1987).
17. (*a*) M.L. Mihailovic, D. Marinkovic, S. Konstantinovic, and Z. Bugarcic. J. Serb. Chem. Soc. **51**, 1 (1986); (*b*) M.L. Mihailovic and D. Marinkovic. Croat. Chem. Acta, 59, 109 (1986); (*c*) M.L. Mihailovic, S. Konstantinovic, and R. Vukicevic. J. Serb. Chem. Soc. **52**, 175 (1987); (*d*) Z. Bugarcic, S. Konstantinovic, and M.L. Mihailovic. J. Serb. Chem. Soc. **52**, 725 (1987); (*e*) M.L. Mihailovic, Z. Petrovic, A. Teodorovic, S.Konstantinovic, and V. Andrejevic. C.R. Acad. Sci. Ser. 2, **308**, 29 (1989); (*f*) S. Konstantinovic, Z. Bugarcic, S. Milosavljevic, G. Schroth, and M.L. Mihailovic. Liebigs Ann. Chem. 261 (1992); (*g*) M.L. Mihailovic, R. Vukicevic, S. Konstantinovic, S. Milosavljevic, and G. Schroth. Liebigs Ann. Chem. 305 (1992).
18. E. Montaudon, X. Lubeigt, and B. Maillard. J. Chem. Soc. Perkin Trans. 1, 1531 (1991).
19. (*a*) M.J. Davies and B.C. Gilbert. J. Chem. Res. (S), 162 (1985); (*b*) B.C. Gilbert, R.G.G. Holmes, H.A.H. Laue, and R.O.C. Norman. J. Chem. Soc. Perkin Trans. 2, 1047 (1976).
20. A. Goosen, C.W. McCleland, and F.C. Rinaldi. J. Chem. Soc. Perkin Trans. 2, 279 (1993).
21. R.D. Rieke and N.A. Moore. Tetrahedron Lett. 2035 (1969).
22. G. Carr and D. Whittaker. J. Chem. Soc. Perkin Trans. 2, 359 (1989).
23. P.J. Kropp and H.J. Krauss. J. Am. Chem. Soc. **91**, 7466 (1969).
24. (*a*) K. Mori and P. Puapoomchareon. Liebigs Ann. Chem. 271 (1987); (*b*) Liebigs Ann. Chem. 1261 (1989).
25. M.A. Miranda and R. Tormos. J. Org. Chem. **58**, 3304 (1993).
26. Z. Cekovic and T. Srnic. Tetrahedron Lett. 561 (1976).
27. (*a*) X. Du, D.R. Arnold, R.J. Boyd, and Z. Shi. Can. J. Chem. **69**, 1365 (1991); (*b*) T. Clark and S.F. Nelsen. J. Am. Chem. Soc. **110**, 868 (1988); (*c*) J. Fujisawa, S. Sato, K. Shimokoshi, and T. Shida. J. Phys. Chem. **89**, 5481 (1985).
28. (*a*) A. Okamoto, M.S. Snow, and D.R. Arnold. Tetrahedron, **42**, 6175 (1986); (*b*) D.R. Arnold and D.D.M. Wayner. Can. J. Chem. **64**, 100 (1986).
29. R.A. LaForge, C.R. Whitehead, R.B. Keller, and C.E. Hummel. J. Org. Chem. **17**, 457 (1952).

Can. J. Chem. Downloaded from www.nrcresearchpress.com by 46.23.64.124 on 09/08/12
For personal use only.

Proton dissociation of aqueous organic acids studied by multivariate chemometrics

Roberto Aruga

Abstract: Thermodynamic data of proton dissociation of 75 organic acids belonging to four classes (protonated amines, aliphatic carboxylic acids, benzoic acids, phenols) have been processed by multivariate chemometric techniques. The variables consist of conventional thermodynamic quantities (Gibbs function, enthalpy, entropy) and of partial components of these quantities (internal and external, electrostatic and nonelectrostatic components). The above data refer to the aqueous medium, at 25°C and $I = 0$ mol dm^{-3}. The Gibbs function of deprotonation in the gas phase and the Hammett σ constant have also been considered. Multivariate techniques include Principal Component Analysis, Factor Analysis, and feature selection. Factor Analysis and related concepts have proved to be useful in defining the causes of differences in acid strengths and their respective importance.

Key words: acid dissociation data, chemometrics of; chemometrics of acid dissociation data; factor analysis of acid dissociation data; principal component analysis of acid dissociation data; thermodynamics of acid dissociation.

Résumé : On a examiné les données thermodynamiques de la dissociation protonique de 75 acides organiques appartenant à quatre classes (les amines protonées, les acides carboxyliques aliphatiques, les acides benzoïques et les phénols) à l'aide de techniques chimiométriques à plusieurs variables. Les variables incluent les quantités thermodynamiques conventionnelles (fonction de Gibbs, enthalpie et entropie) et les composantes partielles de ces quantités (composantes internes et externes, électrostatiques et non électrostatiques). Les données ci-dessus se réfèrent à un milieu aqueux, à 25°C et $I = 0$ mol dm^{-3}. On a aussi considéré la fonction de Gibbs de la déprotonation en phase gazeuse et la constante σ de Hammett. Les techniques à variables multiples comprennent l'analyse des composantes principales, l'analyse factorielle et la caractéristique de sélection. L'analyse factorielle et les concepts apparentés se sont avérés utiles pour définir les causes des différences dans les forces des acides et leurs importances respectives.

Mots clés : chimiométrie, données de dissociation acide, analyse factorielle, analyse des composantes principales, thermodynamique de la dissociation acide.

[Traduit par la rédaction]

Introduction

The study of the causes of differences in acid strengths in aqueous solution has passed through various stages in the last decades.

The traditional concept, according to which differences in acid strengths are mainly attributable to molecular properties of acids (e.g., polarization of the O—H bond, electronic structure of the anion, etc.) began to be criticized around 1960, when, as well as pK_a data, accurate values of enthalpy and entropy of deprotonation in aqueous solution were supplied by direct calorimetric techniques (1, 2). On the basis of calorimetric results, the importance of environmental effects (i.e., solute–solvent and solvent–solvent interactions) was pointed out.

Later, these studies were mainly carried on in the direction of a splitting up of conventional thermodynamic quantities into partial components, each of them being related to particular (e.g., molecular or environmental) effects.

The studies of Hepler and co-workers (3, 4) should be cited first in this field. Two components of thermodynamic quantities, one called internal, the other external, were proposed by Hepler, with reference to a proton exchange reaction between an aromatic substituted acid and the corresponding unsubstituted acid.

Nancollas, on the other hand (5), on the basis of previous studies of Gurney (6), proposed a splitting up of conventional thermodynamic quantities into an electrostatic (or long-range) and a nonelectrostatic (or short-range) contribution. These studies, on the whole, helped to clarify further particular questions related to proton–ligand and metal–ligand equilibria in solution.

Considering now the number of conventional (or global) and partial thermodynamic quantities available, it should be of

Received June 13, 1995.

R. Aruga.[1] Department of Analytical Chemistry, University of Turin, via Giuria 5, 10125 Turin, Italy.

[1] Telephone: 011-670.76.49. Fax: 011-670.76.15.

Can. J. Chem. Downloaded from www.nrcresearchpress.com by 46.23.64.124 on 09/08/12
For personal use only.

Can. J. Chem. Downloaded from www.nrcresearchpress.com by 46.23.64.124 on 09/08/12
For personal use only.

interest to study the processes of proton dissociation[2] in solution in a more general way, by using simultaneously all the above-cited parameters and the information content of each of them.

A problem of this kind, involving the simultaneous treatment of many variables, can be handled in a suitable way by the use of multivariate statistical techniques. Although these techniques have frequently been applied to analytical chemical data in recent years (e.g., to clinical and food data), and also to data of preparative and pharmaceutical organic chemistry, they have seldom been used for problems related to solution equilibria (7–9). Indeed, the methods of data interpretation normally used in the field of thermodynamics of solution equilibria consist, in general, of an univariate examination of tables of experimental results, and of a visual inspection of bidimensional (i.e., two-variable) plots. Obviously, in the presence of a considerable number of variables and objects (the latter are the acids, in this case) a univariate examination of the data becomes difficult and may lead to predominantly qualitative and rather uncertain conclusions.

Another problem concerns the actual reliability and usefulness of partial components of the thermodynamic quantities, especially the above-cited electrostatic and nonelectrostatic contributions. Chemometric techniques (and, in particular, feature selection methods) could be useful in clarifying these points.

On the basis of the above considerations, thermodynamic data of proton dissociation of 75 organic acids have been processed, in this work, by multivariate chemometric techniques. The acids belong to the following four categories: protonated amines, aliphatic carboxylic acids, benzoic acids, and phenols. Sets from 7 to 10 thermodynamic variables have been considered, the Hammett σ constant included (for a description of all the variables see the following section).

It must be noted that other thermodynamic variables that are coming into use (e.g., molar volume variation, molar compressibility, expansibility, specific heat variation, etc.) do not yet provide a sufficient number of accurate experimental data to justify their inclusion in this study.

Experimental data and parameters

The 75 acids studied here belong to the following four classes: protonated amines (symbol: A; 26 species investigated), aliphatic carboxylic acids (symbol: C; 10 species); benzoic acids (symbol: B; 19 species); phenols (symbol: P; 20 species). All the acid species are synthetically collected in the following list. *Class A*: ammonia, amines: methyl, ethyl, *n*-propyl, i-propyl, i-butyl, *sec*-butyl, *tert*-butyl, cyclohexyl, dimethyl, diethyl, di-*n*-propyl, di-i-propyl, di-*n*-butyl, di-*sec*-butyl, trimethyl, triethyl, tri-*n*-propyl; pyrrolidine, pyrrolidine-1-methyl; piperidine, piperidine-1-methyl; morpholine; piperazine; aniline; pyridine. *Class C*: formic acid; acetic acid; substituted acetic acids: fluoro, difluoro, trifluoro, bromo, chloro, dichloro; propanoic acid; butanoic acid. *Class B*: benzoic acid; substituted benzoic acids: 3-fluoro, 2-chloro, 3-chloro, 4-chloro, 3-hydroxy, 2-methoxy, 3-methoxy, 4-methoxy, 2-methyl, 3-methyl, 4-methyl, 3-cyano, 4-cyano, 2-amino, 3-amino, 4-amino, 3-nitro, 4-nitro. *Class P*: phenol; substituted phenols: 2-fluoro, 3-fluoro, 4-fluoro, 2-chloro, 3-chloro, 3-hydroxy, 2-methoxy, 3-methoxy, 4-methoxy, 4-formyl (CHO), 2-methyl, 3-methyl, 4-methyl, 2-cyano, 3-cyano, 4-cyano, 2-nitro, 3-nitro, 4-nitro.

In some instances the acid species are indicated one by one by means of a symbol (e.g., in Fig. 1). Each individual symbol consists of the symbol of the corresponding class followed by the serial number in the class, in accord with the above list. For example: symbol A2 indicates methylamine.

Among the variables considered here, there are, first, the usual three fundamental quantities of proton dissociation: ΔG^0, ΔH^0, ΔS^0. Entropy was obtained by: $\Delta G^0 = \Delta H^0 - T\Delta S^0$. As regards enthalpy, taking into account the generally greater accuracy of direct calorimetric values in comparison with those obtained from the variation of the equilibrium constant with temperature (10), calorimetric ΔH^0 values were preferred. For 10 acids only, because calorimetric data were unavailable, enthalpy values determined from the variation of equilibrium constants with temperature were used. The latter values have been considered reliable, as they refer to sufficiently wide temperature ranges.

The values of the above parameters were taken from the literature (11); some calorimetric enthalpy values for phenols obtained previously in this laboratory (12) were also taken into account. The parameters always refer to the aqueous medium, at $T = 25°C$ and $I = 0$ mol dm^{-3}. In only two cases ΔG^0 and ΔH^0 had to be corrected to $I = 0$. The Gibbs function was corrected by Davies' equation:

$$[1] \quad -\log \gamma_i = Az_i^2[I^{1/2}/(1 + I^{1/2}) - 0.2\, I]$$

where γ_i is the activity coefficient of the ith ionic species, A is 0.509 for water at 25°C, z_i is the ionic charge, and I the ionic strength.

The enthalpy values were corrected to $I = 0$ mol dm^{-3} by using (13, 14):

$$[2] \quad \Delta H_I^0 = \Delta H_{I'}^0 + RT^2 \Sigma \nu_i \partial(\ln \gamma_i)/\partial T$$

$$[3] \quad \Sigma \nu_i \partial(\ln \gamma_i)/\partial T = -3/2[(1/D)(\partial D/\partial T) + 1/T]$$

where ν_i is the number of moles of the species i, and D is the dielectric constant of the solvent. The values of R, D, and $\partial D/\partial T$ are those reported by Harned and Owen (15).

Electrostatic and nonelectrostatic contributions of Gibbs function and enthalpy have also been considered (ΔG_{el}, ΔG_{non}, ΔH_{el}, ΔH_{non}, respectively). A short account of their significance is given here; fuller details and the equations for their calculation have been reported and discussed previously (16–18). The electrostatic contribution represents long-range electrostatic interactions, which are affected by the dielectric nature of the solvent and by the temperature. Therefore, this part is determined by solute–solute electrostatic bonds and by long-range solute–solvent interactions. The nonelectrostatic contribution is determined by all the short-range factors, independent of dielectric constant and temperature. Thus it is mainly determined by solute–solute covalent bonds and by

[2] As some acids considered here (i.e., protonated amines) dissociate without giving rise to new ionic charges (nonionogenic decomposition), the more general term "acid dissociation" (or "proton dissociation") has been preferred in this text to the term "acid ionization."

Can. J. Chem. Downloaded from www.nrcresearchpress.com by 46.23.64.124 on 09/08/12
For personal use only.

Table 1. Thermodynamic quantities for proton dissociations of acids at 25°C (11, 21).[a]

Variable	Symbol	Mean	Standard dev.	Mean	Standard dev.
		Class A[b]		**Class C**	
$-\Delta G^0$	*G*	−57.5	9.4	−16.9	9.0
$-\Delta H^0$	*H*	−49.9	10.3	1.8	2.8
ΔS^0	*S*	−26	22	−63	31
$-\Delta G_{el}$	*GE*	−12.5	4.6	−20.4	6.6
$-\Delta G_{non}$	*GN*	−45.0	9.6	3.5	3.4
$-\Delta H_{el}$	*HE*	5.1	1.9	8.3	2.7
$-\Delta G^0_{gas}$	*GG*	−914	29	−1370	37
		Class B		**Class P**	
$-\Delta G^0$	*G*	−22.8	2.7	−51.1	6.4
$-\Delta H^0$	*H*	−0.5	3.7	−21.6	2.5
ΔS^0	*S*	−75	12	−99	15
$-\Delta G_{el}$	*GE*	−23.0	2.5	−28.1	3.1
$-\Delta G_{non}$	*GN*	0.2	3.0	−23.0	3.5
$-\Delta H_{el}$	*HE*	9.3	1.0	11.4	1.2
$-\Delta G^0_{gas}$	*GG*	−1370	18	−1390	32
$-\Delta H_{int}$	*HI*	1.1	2.6	5.5	6.2
$-\Delta H_{ext}$	*HX*	−1.1	3.4	−3.9	4.1

[a]Gibbs functions and enthalpies are expressed in kJ mol^{-1}; entropies in J K^{-1} mol^{-1}; variables *HI* and *HX* refer to exchange reaction [4].

[b]A: protonated amines; C: aliphatic carboxylic acids; B: benzoic acids; P: phenols.

Table 2. Values of the Hammett σ constants used for substituted benzoic acids and phenols (20).

2-F	1.20	4-CH_3	−0.17
3-F	0.34	2-CN	1.20
4-F	0.06	3-CN	0.56
2-Cl	0.40	4-CN	0.66
3-Cl	0.37	2-NH_2	−0.17
4-Cl	0.23	3-NH_2	−0.16
3-OH	0.12	4-NH_2	−0.66
2-OCH_3	0.60	2-NO_2	2.00
3-OCH_3	0.12	3-NO_2	0.71
4-OCH_3	−0.27	4-NO_2	0.78
2-CH_3	−0.12	4-CHO	0.42
3-CH_3	−0.07		

solute–solvent contact interactions (i.e., solvation interactions) (16). The nonelectrostatic part includes also the so-called cratic (or translational) contribution (6, 19). The cratic part of the Gibbs function is equal to $nRT \ln M_S$, where n is the number of moles of the reagents minus the moles of the products, R is the gas constant, T is the absolute temperature and M_S is the concentration of the solvent in mol dm^{-3}. Therefore, the cratic contribution (which is an entropy contribution) is constant for all the equilibria studied here and does not affect the differences and correlations between the above thermodynamic quantities. Moreover, taking into account that the difference between ΔG_{non} and ΔH_{non} is constant, as it is equal to the cratic part (18, 19), the following three quantities have been considered in this study: ΔG_{el}, ΔG_{non}, and ΔH_{el}. They were calculated by means of equations published previously (17, 18).

Enthalpy of proton dissociation in aqueous solution, following the treatment of Hepler (3, 4), can also be considered in terms of "internal" and "external" (or environmental) contributions. The former are related to intrinsic effects, i.e., to different conformations between the acid molecule and its anion. The latter are related to interactions between solute particles and the surrounding medium and to other external effects. Calculation of internal and external contributions is possible for symmetrical (or exchange) reactions of the following type:

[4] $HS + R^- \rightleftarrows S^- + HR$

where HR is an acid taken as reference, and HS is the corresponding substituted acid, with a structure similar to HR. For this kind of symmetrical reaction the following may be written: $\Delta H^0_{sym} = \Delta H_{int} + \Delta H_{ext}$. The enthalpy for reaction [4] is obtainable from the corresponding quantities of proton dissociation: $\Delta H^0_{sym} = \Delta H^0(HS) - \Delta H^0(HR)$. Moreover, it may be demonstrated (4) that: $\Delta H_{int} = \Delta H^0_{sym} - \beta \Delta S^0_{sym}$. Knowing the quantities for reaction [4], this relation allows one to obtain, with sufficient accuracy, both the internal and external enthalpy contributions. Numerous correlations from experimental data, for phenols and other aromatic acids at 25°C, are consistent with $\beta = 280$ K (4).

In accord with the above considerations, values of ΔH_{int} and ΔH_{ext} were obtained only for aromatic acids B and P. For

Can. J. Chem. Downloaded from www.nrcresearchpress.com by 46.23.64.124 on 09/08/12
For personal use only.

the same classes the values of the Hammett σ constant for each substituent (20) were also considered.

With the aim of a more complete investigation of deprotonation processes, the Gibbs function values of proton dissociation in the gas phase were also considered for all the acids. The values were taken from the review of Ritchie (21) and refer to 25°C.

In conclusion, the variables considered here are the following (the symbol used for each of them in the Discussion and in the figures is also indicated). For classes A, C, B, P (75 acids): the usual set of three conventional thermodynamic quantities of proton dissociation ($-\Delta G^0$, $-\Delta H^0$, ΔS^0; symbols: *G*, *H*, *S*, respectively); electrostatic and nonelectrostatic contributions ($-\Delta G_{el}$, $-\Delta G_{non}$, $-\Delta H_{el}$; symbols: *GE*, *GN*, *HE*); Gibbs function of proton dissociation in the gas phase ($-\Delta G^0_{gas}$; symbol: *GG*). For classes B and P (39 acids), in addition to the seven variables of the preceding list: internal and external contributions of enthalpy ($-\Delta H_{int}$, $-\Delta H_{ext}$; symbols: *HI*, *HX*); Hammett σ constant (symbol: *HM*). All the variables refer to 25°C and, for the aqueous phase, to $I = 0$ mol dm^{-3}. The sign has been fixed so that the more favourable a parameter is to proton dissociation, the more positive it is, and vice versa. The values of the thermodynamic variables have been arbitrarily collected in Table 1, and appear as the mean and the standard deviation for each class. Hammett σ constants are listed in Table 2.

Statistical treatment of the data

A preliminary step of the treatment consisted of the normalization (or standardization) of the raw data, to avoid misclassification due to the different order of magnitude and range of variation of the variables. Autoscaling, or t-transform, was used for this purpose. The values of each variable, after this scaling procedure, are characterized by zero as the mean value and by unit variance (22).

As they are coming into widespread use, only a brief account will be given of the chemometric techniques used here, together with references to specific works for fuller details. The programs contained in the statistical package PARVUS (23) were used in the calculations.

Principal Component Analysis (PCA), from an *n*-dimensional space corresponding to *n* measured variables, displays objects in a reduced space by finding a direction (first principal component, or first eigenvector) that best preserves the original variance. This corresponds to calculating a new variable as a weighted linear combination of the original ones. A second eigenvector is then chosen among all directions orthogonal to the first, so that maximum preservation of the residual variance can be obtained, and so on. Just two (or three) principal components are sufficient, in some cases, for a projection of the original hyperspace on to two (or three) dimensions, without excessive loss of information (22). This fact makes it possible to represent objects (acids in this case) and the corresponding homogeneous categories by means of only one diagram (namely, the diagram of the scores of objects on principal components). It must be stressed that the above-defined principal components have only a mathematical (and not physical) significance, as they only identify directions of largest dispersion of the data. The program EIGEN obtains the above new variables from the matrix of covariances and calculates eigenvectors by the method of Malinowski (24).

Factor Analysis (FA) was performed by a previous evaluation of principal components and by their rotation, in order to find the directions of variance corresponding to significant physical factors. The rotation was carried out by the Varimax method (Eigenvalue Weighted Varimax). The number of significant factors was found by two methods, i.e., by the average variance method and by double cross validation (24). The significant physical factors determined by Factor Analysis should be considered as a set of a few causes that explains the whole set of experimental variables. A corresponding group of experimental variables is associated with each factor. The variables of each group are collected with the factor representing them and, of course, they are correlated with each other. The correlation of a certain factor with each experimental variable is expressed by the loading. Therefore the matrix of loadings, which is obtained by Factor Analysis, allows one to determine the group of experimental variables best correlated with each single factor and, in consequence, to point out the nature of the factor itself. The importance of each factor is expressed in terms of the corresponding fraction of the total variance.

Selection of variables was also carried out. It gives a sequence of variables on the basis of their information content (i.e., on the basis of their ability to discriminate objects belonging to different classes). The method used here classifies variables on the basis of the corresponding Fisher weight (or F-ratio) (25). The value of the Fisher weight for each variable is the average of the values of all possible pairs of categories into which the objects have been subdivided.

Discussion

A Principal Component Analysis (PCA) was carried out, first, on the four classes of acids and on the corresponding seven variables (matrix 75 × 7; see Experimental data and parameters).

PCA identifies two principal components strongly prevailing over the others as regards the information content. They represent 98.6% of the total variance. The third principal component has a variance of only 0.1, i.e., much less than 1, which is the variance of the autoscaled original variables. This means, in the first place, that bidimensional representations of the scores of objects (i.e., acids) on the two first principal components represent a good approximation to the actual disposition in the seven original dimensions (see the preceding section). Secondly, it can be concluded that the global structure of the data is determined by two physical factors. The scores of the 75 acids on the first two eigenvectors are represented in Fig. 1.

Three fairly sharp clusters of acids appear in the figure: a first for class A, a second for P, with an evident linear structure, and a third deriving from classes C and B superimposed. The association between C and B leads one to conclude that, from a thermodynamic point of view, the common carboxylic nature of these acids prevails over the aliphatic and aromatic nature. It is worth mentioning, as regards class A, the lonely position (and then a different thermodynamic behaviour) of A25 and A26 (aniline and pyridine, respectively) in comparison with other members of the class.

The problem of correlations between variables was then investigated; it allows one to study the general physical factors

Can. J. Chem. Downloaded from www.nrcresearchpress.com by 46.23.64.124 on 09/08/12
For personal use only.

Fig. 1. Representation of 75 acids of 4 chemical classes (A = protonated amines; C = aliphatic carboxylic acids; B = benzoic acids; P = phenols) on the two first eigenvectors (98.6% of the total variance). For the symbols of each acid species see Experimental data and parameters.

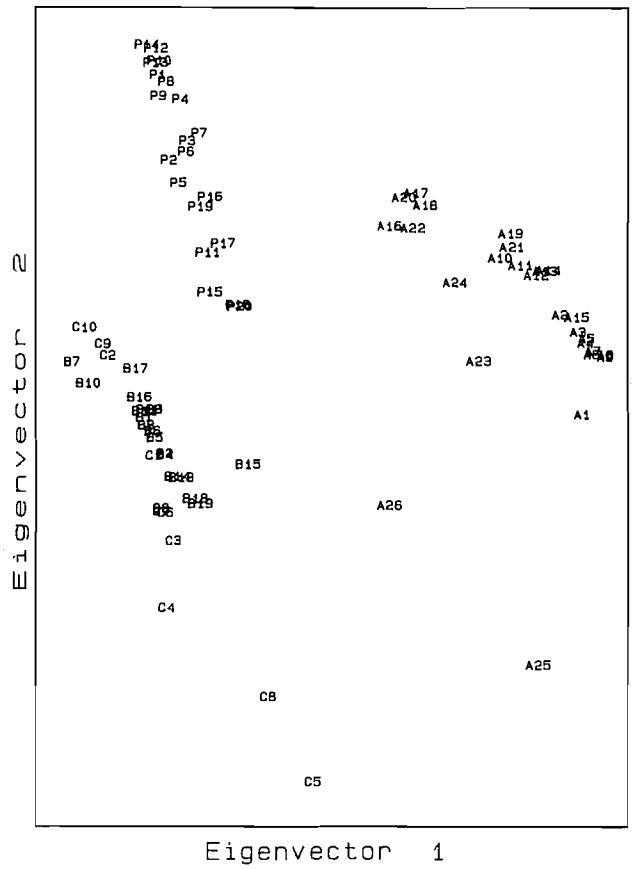

Table 3. Loadings of seven original variables on two significant factors (*F*1, *F*2), after rotation by Varimax.

Variable	*F*1	*F*2
G[a]	0.03	0.99
H	−0.43	0.90
S	0.98	−0.18
GE	0.98	−0.18
GN	−0.32	0.94
HE	−0.98	0.18
GG	0.75	−0.60

[a]For the significance of the symbols see Experimental data and parameters or Table 1.

that determine differences in acid strengths. For this purpose, a Factor Analysis was carried out on the same autoscaled matrix (75 × 7), together with an examination of the correlation coefficient matrix. Considering that there are two significant factors present (see above), the values of the loadings of the seven variables on the factors, after Variamax rotation, are reported in Table 3.

Fig. 2. Representation of the scores of 75 acids belonging to four (A, C, B, P) and of the loadings of seven thermodynamic variables on the axes of two Varimax-rotated factors (varivectors).

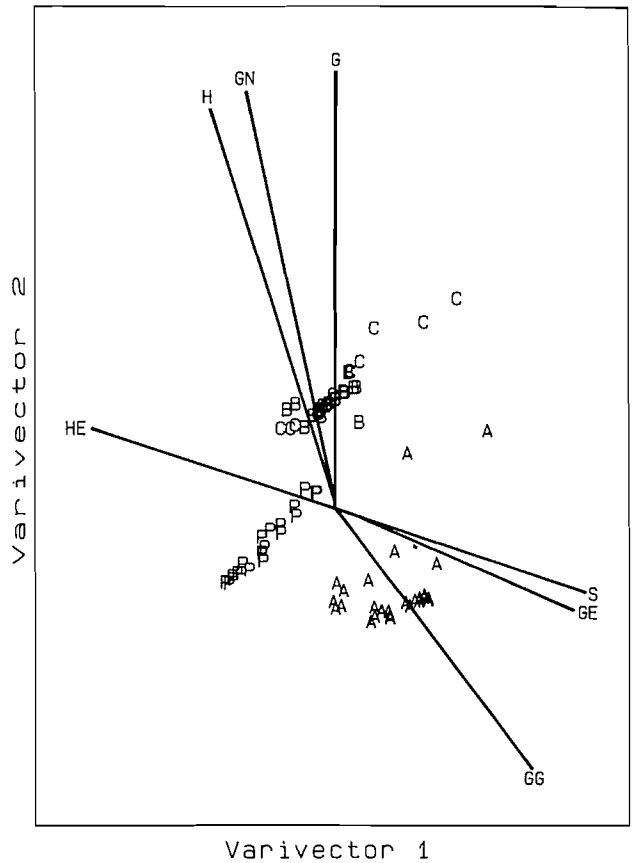

The loading values show a high correlation of *S*, *GE*, and *HE* with factor *F*1 (correlation is negative for *HE*), and of *G*, *H*, *GN* with *F*2. Considering the nature of the correlated variables, the former factor can be defined as "electrostatic," the latter as "nonelectrostatic." They account for 73% and 25% of the total variance, respectively. The angle between the two rotated eigenvectors is 61°, in accordance with a partial correlation between factors. The corresponding correlation coefficient matrix (Table 4) confirms the presence of the same clusters of mutually correlated variables.

An evident representation of these clusters of mutually correlated variables is given by the loadings in Fig. 2 (parallel or antiparallel loadings indicate a positive or negative correlation; orthogonal loadings a lack of correlation).

Anticorrelation between *S* and *HE* can be justified by taking into account that the aqueous solvent structuring process caused by an ionogenic proton dissociation (*S* unfavourable) gives rise to an electrostatic bond formation between the solvent molecules (*HE* favourable).

Correlations between variables were also studied for classes B and P only (39 acids), in order that all 10 variables could be included in the data treatment (see Table 1). A Principal Component Analysis carried out on the autoscaled (39 × 10) matrix shows that the three first eigenvectors account for 96.7% of the total variance (59.4%, 31.2%, and 6.1%, respectively). As concerns a possible presence of a third significant factor, the average variance method does not give, in this instance, as

Table 4. Correlation coefficient matrix of seven variables, referred to 75 acids.

	G	*H*	*S*	*GE*	*GN*	*HE*	*GG*
G	1.00	0.89	−0.15	−0.15	0.93	0.15	−0.57
H	0.89	1.00	−0.59	−0.59	0.99	0.59	−0.85
S	−0.15	−0.59	1.00	1.00	−0.49	−1.00	0.83
GE	−0.15	−0.59	1.00	1.00	−0.49	−1.00	0.83
GN	0.93	0.99	−0.49	−0.49	1.00	0.49	−0.80
HE	0.15	0.59	−1.00	−1.00	0.49	1.00	−0.83
GG	−0.57	−0.85	0.83	0.83	−0.80	−0.83	1.00

Table 5. Loadings of 10 variables on three significant factors (*F*1, *F*2, *F*3), after rotation by Varimax.

Variable	*F*1	*F*2	*F*3
G	0.49	0.87	−0.06
H	0.25	0.95	−0.16
S	0.86	0.48	0.16
GE	0.86	0.48	0.17
GN	0.34	0.93	−0.12
HE	−0.86	−0.48	−0.17
GG	0.68	0.42	0.50
HI	0.18	−0.17	0.92
HX	−0.63	0.42	−0.64
HM	0.10	−0.01	0.94

clear an indication as in the previous case. Several tests were therefore carried out with the method of double cross validation, using different numbers of random and diagonal cancellation groups. This test shows the presence of three significant factors at 95% confidence level. A subsequent Varimax rotation of the three eigenvectors gives the loadings of the 10 variables collated in Table 5.

The values in this table confirm the presence of two factors (electrostatic and nonelectrostatic, respectively) that have already been pointed out on the (75 × 7) matrix. They appear to be correlated with the same groups of variables as before. These factors, for the sake of brevity, can be indicated as F_{el} and F_{non}. The third factor (*F*3) appears highly and positively correlated with variable *HI* and with the Hammett σ constant (*HM*). Therefore *F*3 may represent the causes related to "internal" molecular effects, which depend on different electronic structures between an acid and its conjugate base and on other electronic effects. In the same manner, the correlation coefficient matrix (Table 6) shows a fairly high and positive correlation ($r = 0.80$) between *HI* and *HM*.

Therefore the internal contribution of enthalpy proves to be in agreement with the nature previously attributed to it (3). Considering now that Nancollas's nonelectrostatic contribution includes all effects the nature of which is not electrostatic or long-range, the internal contribution proposed by Hepler is likely to represent a part of the former. In other words, the two treatments appear to be complementary, in the sense that Hepler's concept of the internal part of enthalpy, being very specific, allows one to study the corresponding factor that otherwise could remain undefined. It must be noted, on the contrary, that the external contribution of enthalpy (*HX*), as it includes all the effects alien to *HI*, appears to be neither very specific nor significant.

Simultaneous examination of the scores of acids and of the loadings of variables on the factors was also done. The more positive the score of an acid species on the direction of a variable loading, the more favourable is that variable to the dissociation of the acid, and vice versa. The processing of the (75 × 7) matrix, which refers to the four classes of acids and to seven variables, is reported here by way of example. The corresponding scores and loadings on the two significant factors defined above are represented in Fig. 2.

As regards the direction of variance of F_{el}, which coincides with the direction of the loadings of *S*, *GE*, and *HE*, it can be noted that class A lies in a more favourable position than the other classes, with reference to *S* and *GE* (i.e., it has more positive scores on F_{el}), while the contrary occurs on *HE*. This can be easily justified by taking into account the explanation of the anticorrelation between *S* and *HE* reported above, and considering also that proton dissociation is not ionogenic for class A, while it is ionogenic for the other classes.

Class A, moreover, shows stronger acidity than the other classes in the gas phase (variable *GG* more favourable, i.e., more positive scores of class A on variable *GG*; Fig. 2). Considering the fairly high positive correlation of *GG* with *S* (Fig. 2 and Table 4) and of *GG* with the electrostatic factor (Table 3), the conclusion can be drawn that the stronger acidity of class A in the gas phase is mainly due to factor F_{el}. Since among the general effects related to F_{el} (see above) only solute–solute electrostatic interactions exist in the gase phase, it can be concluded that these interactions are responsible for the stronger acidity of class A in the gas phase. In this case, too, the nature of the proton dissociation process (ionogenic for C, B, P, nonionogenic for A) plays a leading role.

On the other hand, Fig. 2 shows that the order of acid strength of class A and of the other classes is reversed in the aqueous phase. In fact, considering that variable *G* is the fundamental measure of aqueous acid strength, class A shows in Fig. 2 a less favourable position on the direction of the loading of variable *G* in comparison with the other classes (this fact is also pointed out by the anticorrelation between *G* and *GG*: $r = -0.51$, see Table 4). As variable *G* is strongly correlated with F_{non} (see Table 3, where F_{non} is indicated as F_2), it could be concluded that the different series of acidities in water in comparison with those in the gas phase is caused by the solvent, which acts through a short-range nonelectrostatic factor (F_{non}), and not through a long-range factor. This con-

Can. J. Chem. Downloaded from www.nrcresearchpress.com by 46.23.64.124 on 09/08/12
For personal use only.

Table 6. Correlation coefficient matrix of 10 variables, referred to the acids of classes B and P.

	G	*H*	*S*	*GE*	*GN*	*HE*	*GG*	*HI*	*HX*	*HM*
G	1.00	0.96	0.83	0.83	0.98	−0.83	0.66	−0.10	0.09	−0.0
H	0.96	1.00	0.65	0.65	0.99	−0.65	0.49	−0.25	0.34	−0.1
S	0.83	0.65	1.00	1.00	0.72	−1.00	0.84	0.21	−0.45	0.2
GE	0.83	0.65	1.00	1.00	0.72	−1.00	0.85	0.22	−0.45	0.2
GN	0.98	0.99	0.72	0.72	1.00	−0.72	0.55	−0.20	0.26	−0.1
HE	−0.83	−0.65	−1.00	−1.00	−0.72	1.00	−0.85	−0.22	0.45	−0.2
GG	0.66	0.49	0.84	0.85	0.55	−0.85	1.00	0.54	−0.57	0.4
HI	−0.10	−0.25	0.21	0.22	−0.20	−0.22	0.54	1.00	−0.79	0.8
HX	0.09	0.34	−0.45	−0.45	0.26	0.45	−0.57	−0.79	1.00	−0.6
HM	−0.02	−0.15	0.26	0.26	−0.10	−0.26	0.47	0.80	−0.67	1.0

Table 7. Fisher weights of seven variables for three classes of acids: A, P, (C + B).

Variable	Fisher weight
GG	92.2
GN	29.6
H	27.8
G	14.8
GE	3.9
HE	3.9
S	3.9

firms the leading role of solvation in determining different series of acid strengths in the aqueous phase in comparison with the gas phase.

The lonely position pointed out for pyridine and aniline in comparison with the other amines (see above) is attributable to a more favourable value of variable *G* (Fig. 2), i.e., to a greater acid strength. This fact is obviously related to the aromatic nature of pyridine and aniline.

Data-processing procedures similar to those reported in the preceding discussion have also been carried out on every single class. Although this kind of investigation can be useful in the study of the thermodynamic behaviour of each class of acids and of each acid within the class, for the sake of brevity some of the conclusions obtained for class P only are reported here.

The cluster of class P shows a linear structure in Fig. 1. The significance of such a structure is more precisely defined by the following results, referring to 10 variables: (*i*) all the possible pairs between the 10 variables show significant linear correlation at 95% level of confidence; (*ii*) Factor Analysis identifies one significant factor only, accounting for 90% of the total variance. Consequently, the three general acidity factors indicated above come together into a unique factor, through which all the variables concordantly determine different acidities for phenols. As concerns the other classes (A, C, B), Factor Analysis indicates the presence of at least a second significant direction of variance (i.e., two factors at least), in agreement with a less linear structure of the corresponding clusters (Fig. 1).

It can now be noted, from a general point of view, that the problem investigated in the preceding discussion (i.e., the causes of *differences* in acid strengths) is distinct from the problem of the causes that determine the proton dissociation of a certain acid, or of a class of acids. The latter point can be cleared up in a simple way by means of a comparison between two components of the Gibbs function, for example, between the enthalpy and entropy contributions, or between *GE* and *GN* (see Table 1).

Finally, the discriminating ability of variables has been evaluated, by means of Fisher weight calculations. On the basis of the clusters of Fig. 1, three classes have been considered, namely: A, P, (C + D), and the group of the first seven variables of Table 1. The following sequence of variables, in order of decreasing discriminating ability, was obtained:

[5] $GG >> GN > H > G >> GE, HE, S$

It can be observed, first, that variable *GG* shows the highest discriminating ability, while the differentiation of acidities in water (variable *G*) is much less. Therefore these results seem to confirm the presence of a "levelling" effect exerted by the aqueous solvent, as was suggested previously (21). Electrostatic contributions (*GE*, *HE*) and the variable correlated to them (*S*) show the lowest discriminating ability. It is also worth mentioning that the highest discriminant ability among the variables referring to the aqueous medium is shown by a partial component (*GN*); its discriminating ability is then greater than that of conventional quantities (*G*, *H*, *S*). This fact points out the usefulness of the partial components of thermodynamic quantities proposed by Nancollas.

Conclusions

The well-known benefits of multivariate versus traditional methods are also confirmed in the case of thermodynamic data of proton dissociation, as regards both an immediate data representation and interpretation, and the attainment of certain conclusions not easily obtainable in any other way.

Among the latter conclusions, those obtained by means of Factor Analysis seem worth mentioning. Factor Analysis points out, on the basis of 10 experimental variables, three causes of different aqueous acid strength. These causes, ordered on the basis of decreasing importance (i.e., of decreasing percent variance) are the following. 1. A main factor (59.4% of the total variance), correlated with *S*, *GE*, *HE*, of electrostatic, long-range nature. 2. A factor correlated with *GN*, *G*, *H*, of nonelectrostatic, short-range nature (31.2% of

Can. J. Chem. Downloaded from www.nrcresearchpress.com by 46.23.64.124 on 09/08/12
For personal use only.

the total variance). 3. A minor factor (6.1%) correlated with *HI* and *HM*, of internal electronic nature.

On the other hand, the following facts are also pointed out in the Discussion: (*i*) variable *G* (which is connected with pK_H, and then represents the fundamental measure of aqueous acid strength) is correlated with nonelectrostatic factor F_{non}; (*ii*) feature selection (see relation [5]) attributes to the three nonelectrostatic variables a discriminating ability greater than that of electrostatic variables; in other words, relation [5] could be synthetically indicated as: $F_{non} > F_{el}$. Therefore, on the basis of the latter points, factor F_{non} appears to be the most important in determining different acid strengths in aqueous medium. This seems to contradict the results of Factor Analysis. Factor Analysis, indeed, gives a simple explanation of this fact. More precisely, it can be seen in Fig. 2 (or in Table 4) that variables *G*, *H*, *GN* are positively and mutually correlated while, within the electrostatic factor, *HE* is strongly anticorrelated with *S* and *GE*. It can then be concluded that the differences in aqueous acid strength observed by the experimenter are mainly caused by the nonelectrostatic, short-range factor, and Factor Analysis shows that this is due to a simple counterbalancing effect between *S* and *HE* that makes less important the actual influence of the long-range factor.

The concept of factor also permits one to show that the greater acidity in the gas phase of protonated amines as compared with the other classes is attributable to their respective nonionogenic and ionogenic nature, which acts through the long-range factor, while, on the other hand, the reverse order of acidities in water is due to solvation effects (short-range factor).

References

1. L.G. Hepler and W.F. O'Hara. J. Phys. Chem. **65**, 811 (1961).
2. L.P. Fernandez and L.G. Hepler. J. Am. Chem. Soc. **81**, 1783 (1959).
3. L.G. Hepler. J. Am. Chem. Soc. **85**, 3089 (1963).
4. J.W. Larson and L.G. Hepler. *In* Solute–solvent interactions. Vol. 1. *Edited by* J.F. Coetzee and C.D. Ritchie. Dekker, New York. 1969. Chap. 1.
5. G.H. Nancollas. Interactions in electrolyte solutions. Elsevier, Amsterdam. 1966.
6. R.W. Gurney. Ionic processes in solution. McGraw–Hill, New York. 1953.
7. S.D. Brown, T.B. Blank, S.T. Sum, and L.G. Weyer. Anal. Chem. **66**, 315R (1994).
8. S.D. Brown, R.S. Bear, and T.B. Blank. Anal. Chem. **64**, 22R (1992).
9. R. Aruga. J. Chim. Phys. **89**, 1853 (1992).
10. R. Aruga. J. Chem. Soc. Dalton. Trans. 2971 (1988).
11. J.J. Christensen, L.D. Hansen, and R.M. Izatt. Handbook of proton ionization heats and related thermodynamic quantities. Wiley, New York. 1976.
12. R. Aruga. Bull. Soc. Chim. Fr. I-293 (1984).
13. J.M. Austin, R.A. Matheson, and H.N. Parton. *In* The structure of electrolyte solutions. *Edited by* W.J. Hamer. Wiley, New York. 1959. pp. 370, 375.
14. R. Aruga. Inorg. Chem. **17**, 2503 (1978).
15. H.S. Harned and B.B. Owen. The physical chemistry of electrolytic solutions. Reinhold, New York. 1950. p. 116.
16. G.H. Nancollas. Q. Rev. Chem. Soc. **14**, 402 (1960).
17. S. Murakami and T. Yoshino. J. Inorg. Nucl. Chem. **43**, 2065 (1981).
18. R. Aruga. Can. J. Chem. **64**, 780, 785 (1986).
19. R. Aruga. Educ. Chem. **26**, 108 (1989).
20. C. Hansch and A. Leo. Substituent constants for correlation analysis in chemistry and biology. Wiley, New York. 1979.
21. C.D. Ritchie. *In* Solute–solvent interactions. Vol. 2. *Edited by* J.F. Coetzee and C.D. Ritchie. Dekker, New York. 1976. Chap. 12.
22. D.L. Massart and L. Kaufman. The interpretation of analytical chemical data by the use of cluster analysis. Wiley, New York. 1983.
23. M. Forina, R. Leardi, C. Armanino, and S. Lanteri. PARVUS. Elsevier, Amsterdam. 1988.
24. E.R. Malinowski. Factor Analysis in chemistry. Wiley, New York. 1991.
25. L. Kryger. Talanta, **28**, 871 (1981).

Can. J. Chem. Downloaded from www.nrcresearchpress.com by 46.23.64.124 on 09/08/12
For personal use only.

Photochemistry of *N*-(pyrimidin-2-one-4-yl)pyridinium derivatives. The ring contraction of pyrimidinone into imidazolinone

Grażyna Wenska, Bohdan Skalski, Stefan Paszyc, and Zofia Gdaniec

Abstract: Photochemical reactions ($\lambda > 300$ nm) of *N*-(1-methylpyrimidin-2-one)- and *N*-(1,5-dimethylpyrimidin-2-one)pyridinium chlorides were studied in deoxygenated aqueous solution at various pH's. Only the former compound was found to be reactive under these conditions to give pyrimidine ring contraction photoproducts 1-methyl-4-imidazolin-2-one and 1-methyl-4-imidazolin-2-one-5-carboxyaldehyde, with pH-dependent chemical yields. The photochemical pyrimidine ring contraction reaction does not occur for other photochemically reactive pyrimidin-2-ones bearing 3-methylimidazolium-1,1,2,4-triazol-1-yl, or imidazol-1-yl as substituents at the C-4 position. The suggested mechanism of the reaction involves the addition of water to the pyrimidinone part of the *N*-(1-methylpyrimidin-2-one)pyridinium salt in the excited triplet state as the primary photochemical step. Addition of alcohol to the pyridinium ring was found to be the major reaction under irradiation of *N*-(1-methylpyrimidin-2-one-4-yl)pyridinium chloride in methanol.

Key words: photochemistry, *N*-(pyrimidin-2-one-4-yl)pyridinium compounds, pyrimidine ring contraction, 1-substituted-4-imidazolin-2-ones, 4-imidazolin-2-one-5-carboxyaldehydes.

Résumé : Opérant à divers pH, dans des solutions désoxygénées, on a étudié les réactions photochimiques ($\lambda >$ 300 nm) des chlorures de *N*-(1-méthylpyrimidin-2-one)- et de *N*-(1,5-diméthylpyrimidin-2-one)pyridinium. On a trouvé que, dans ces conditions, le premier composé est le seul à fournir des photoproduits résultant d'une contraction du noyau pyrimidine, soit la 1-méthyl-4-imidazolin-2-one et le 1-méthyl-4-imidazolin-2-one 5-carboxyaldéhyde avec des rendements qui varient avec le pH. La réaction photochimique de contraction du noyau pyrimidine ne se produit pas avec les autres pyrimidin-2-ones photochimiquement réactives portant des substituants 3-méthylimidazolium-1,1,2,4-triazol-1-yle ou imidazol-1-yle en position C-4. Le mécanisme suggéré pour la réaction implique que, dans l'étape photochimique primaire, il y a addition d'eau à la portion pyrimidinone du sel *N*-(1-méthylpyrimidin-2-one)pyridinium dans l'état excité triplet. Lors de l'irradiation du chlorure de *N*-(1-méthylpyrimidin-2-one-4-yl)pyridinium dans le méthanol, on observe que l'addition d'alcool est la réaction principale.

Mots clés : photochimie, composés *N*-(pyrimidin-2-one-4-yl)pyridinium, contraction du noyau pyrimidine, 4-imidazolin-2-ones substituées en position 1, 4-imidazolin-2-one-5-carboxaldéhydes.

[Traduit par la rédaction)

Introduction

Common purine and pyrimidine nucleosides such as guanosine, inosine, thymidine, and uridine can be easily and efficiently converted to the corresponding, fluorescent *N*-(purin-6-yl)- and *N*-(pyrimidin-2-one-4-yl)pyridinium chlorides (1). Some of these derivatives can be incorporated into synthetic oligodeoxynucleotides and used for further, postsynthetic modifications (2, 3). Both purinyl- and pyrimidynyl-pyridinium compounds exhibit significant absorption in the near-UV region ($\lambda > 300$ nm) where common nucleic acid bases are transparent (4) and thus provide the opportunity for their selective excitation in oligonucleotide chains. The photophysical and photochemical properties of *N*-(purin-6-yl)pyridinium salts have been studied extensively over the last several years (5, 6). Some of them were shown to be useful as fluorescent markers in nucleic acids (2, 7) or as efficient acceptors in photochemically induced electron transfer processes (6, 8). In contrast to the purine derivatives, the pyrimidinyl-pyridinium salts have received little attention so far. As a continuation of our interest in this group of modified nucleobases we reported previously on the photophysical properties of pyridinium salts derived from uridine and thymidine (9). It was shown that the lowest energy electronic transition in these compounds is

Received June 1, 1995.

This paper is dedicated to Professor David Shugar on the occasion of his 80th birthday.

G. Wenska,[1] **B. Skalski,**[1] **and S. Paszyc.** Faculty of Chemistry, A. Mickiewicz University, Grunwaldzka 6, 60 780 Poznań, Poland.

Z. Gdaniec. Institute of Bioorganic Chemistry, Polish Academy of Sciences, Poznań, Poland.

[1] Authors to whom correspondence may be addressed.

Can. J. Chem. Downloaded from www.nrcresearchpress.com by 46.23.64.124 on 09/08/12
For personal use only.

Can. J. Chem. Downloaded from www.nrcresearchpress.com by 46.23.64.124 on 09/08/12
For personal use only.

Fig. 1. Changes in the UV spectra of an aqueous solution of **1***a* during irradiation with near-UV light (λ > 300 nm).

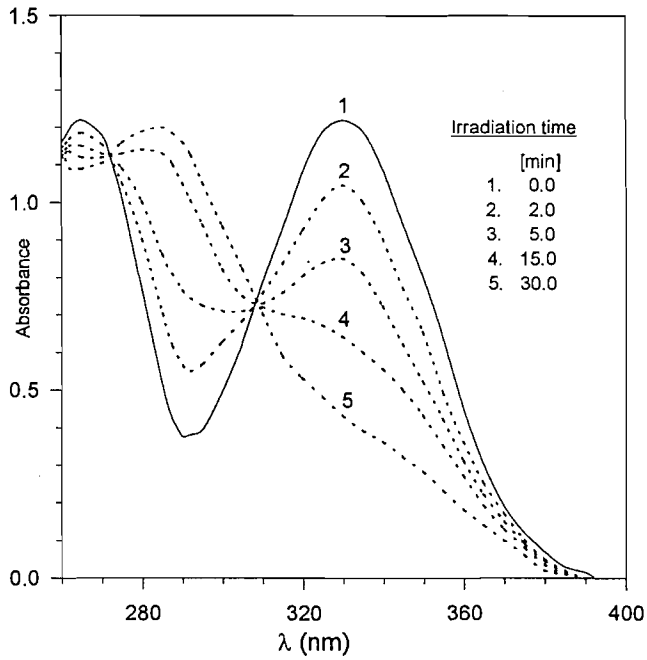

Fig. 2. HPLC of an irradiated solution of **1***a*.

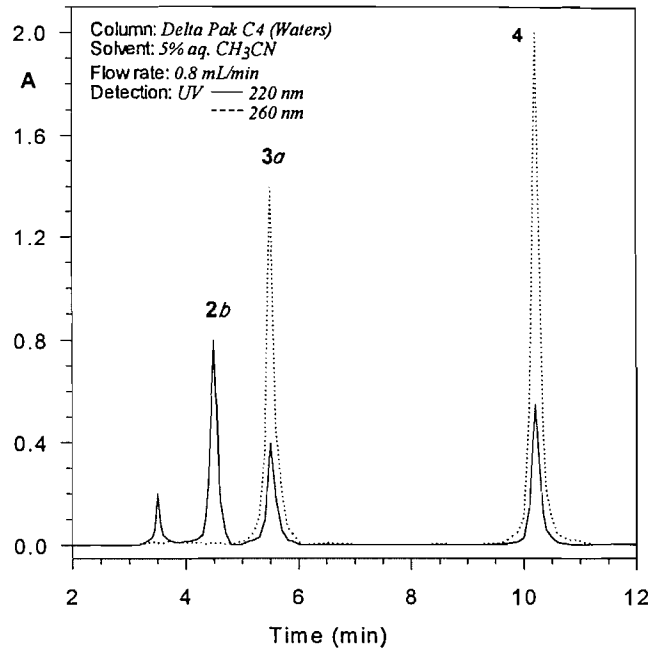

Scheme 1.

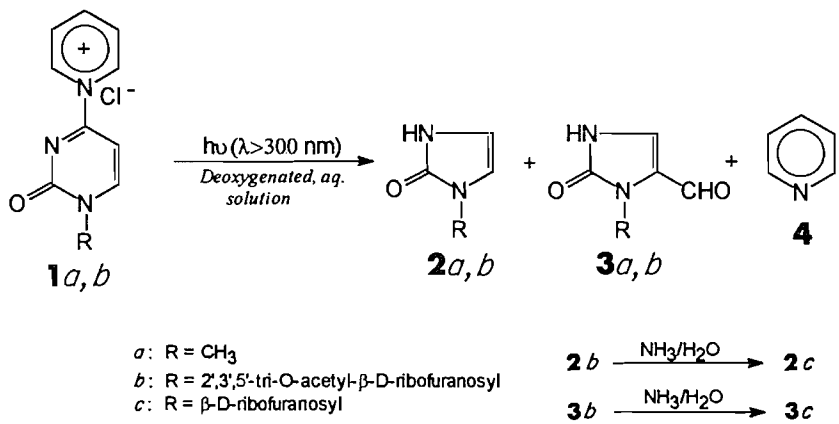

associated with a significant charge shift from the pyrimidinyl to the pyridinium moiety, and that the short-lived excited singlet state is deactivated mainly via a nonradiative process.

In the present work we report on the photochemical reactivity of pyridinium salts **1***a*,*b* derived from 1-methyluracil and tri-*O*-acetyluridine as well as structurally related compounds bearing heterocyclic substituents other than pyridine at the C-4 position of the pyrimidine ring.

Results and discussion

Photochemistry of 1*a*,*b* in aqueous solutions

An aqueous solution of **1***a* was irradiated with near-UV light (λ > 300 nm) in the absence of oxygen. As seen in Fig. 1, irradiation results in a gradual disappearance of the absorption band with a maximum at λ = 330 nm, characteristic of *N*-(pyrimidin-2-one-4-yl)pyridinium cations (9), with concomitant formation of a new absorption band at λ = 280 nm. HPLC analysis of the irradiated solution (Fig. 2) revealed the presence of three main photoproducts: **2***a*, **3***a*, and **4**, besides the unreacted starting material. Photoproduct **4** was identified as pyridine whereas the structures of **2***a* and **3***a* were assigned as 1-methyl-4-imidazolin-2-one and 1-methyl-4-imidazolin-2-one-5-carboxyaldehyde, respectively (Scheme 1), based on their spectral and elemental analysis data (vide infra). The chemical yields of the imidazolinone photoproducts depend on the pH of the irradiated solutions (cf. Table 1). The aldehyde **3***a* is the major product when irradiation is performed in water (pH 6.5) and the ratio **3***a*/**2***a* increases significantly when the irradiation of **1***a* is performed in slightly basic solution (0.002 M sodium bicarbonate, pH ~8.2). Because of the chemical instability of pyrimidynyl-pyridinium salts at pH > 9 (due to base-induced pyridinium ring opening (1)), the irradiation of **1***a* was not carried out in more basic solution. Prolonged irradiation of **1***a* reduces the yield of **3***a* (Table 1). In a separate experiment it was found that **3***a* undergoes slow degradation under irradiation with Pyrex filtered light; however, **2***a* was not found among the photoproducts.

In the case of pyridinium salt **1***b* derived from 2',3',5'-tri-*O*-acetyluridine, which is less resistant towards bases than **1***a*,

Can. J. Chem. Downloaded from www.nrcresearchpress.com by 46.23.64.124 on 09/08/12
For personal use only.

Table 1. Chemical yields (%) of photoproducts **2–4**.[a]

Irradiated compound	Solvent (pH)	Conversion (%)	2	3	4
1*a*	0.002 M $HClO_4$ (2.6)	69	*a*: 42	*a*: 20	95
1*a*	Water (6.5)	80	*a*: 20	*a*: 43	100
1*a*	Phosphate buffer (6.5)	86	*a*: 25	*a*: 31	100
1*a*	0.002 M $NaHCO_3$ (8.2)	60	*a*: trace	*a*: 71	70
1*b*	Water (6.5)	61	*b*: 38	*b*: 34	100
1*b*	0.002 M $NaHCO_3$ (8.2)	90	*b*: trace	*b*: 59	65

[a]The yields are determined by HPLC and are given relative to the amount of **1** that reacted.

Scheme 2.

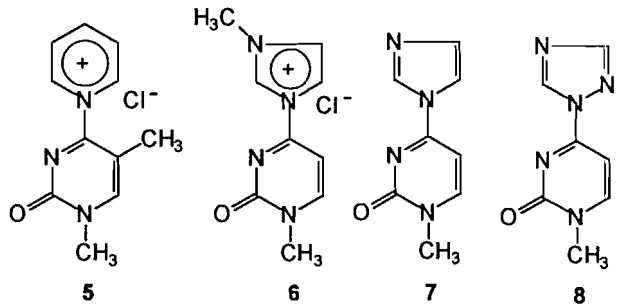

irradiation was performed in aqueous solution at pH 6.5. The expected photoproducts **2***b* and **3***b* were obtained in moderate yields (Scheme 1, Table 1). During the work-up of the irradiated solution of **1***b* in a preparative scale experiment, both photoproducts, **2***b* and **3***b*, were found to undergo partial deacetylation. Therefore they were fully deprotected and characterized as **2***c* and **3***c* (cf. Scheme 1 and Experimental).

The susceptibility to photochemical ring contraction has also been tested for the structurally related *N*-(1,5-dimethylpyrimidin-2-one-4-yl)pyridinium chloride, **5**, and compounds **6**, **7**, and **8** (Scheme 2) bearing 3-methylimidazolium-1, imidazol-1-yl, and 1,2,4-triazol-1-yl substituents at the C-4 position of the pyrimidine ring, respectively. Under the irradiation conditions used for the transformation of **1***a*, compound **5** appeared to be photochemically stable and the estimated quantum yield of its disappearance did not exceed 10^{-4}, whereas in the case of photochemically reactive **6**, **7**, and **8**, no appropriate ring contraction products (**2***a* and **3***a*) could be detected (HPLC) in photolyzed solutions.

The mechanism of the photochemical ring contraction of **1***a,b* is not yet completely clear, but we propose that the addition of a water molecule to the pyrimidinone part of the molecule in the excited triplet state is the primary photochemical event and is followed by a dark transformation of the resulting, unstable, intermediate into **2***a,b* and **3***a,b*. The following observations support the above suggestion.

(*i*) Pyridinium salts **1***a,b* are essentially stable ($\varphi < 10^{-4}$) during irradiation in dry acetonitrile under otherwise identical conditions.

Fig. 3. Stern–Volmer plot for quenching of the photochemical reaction of **1***a* by NaBr.

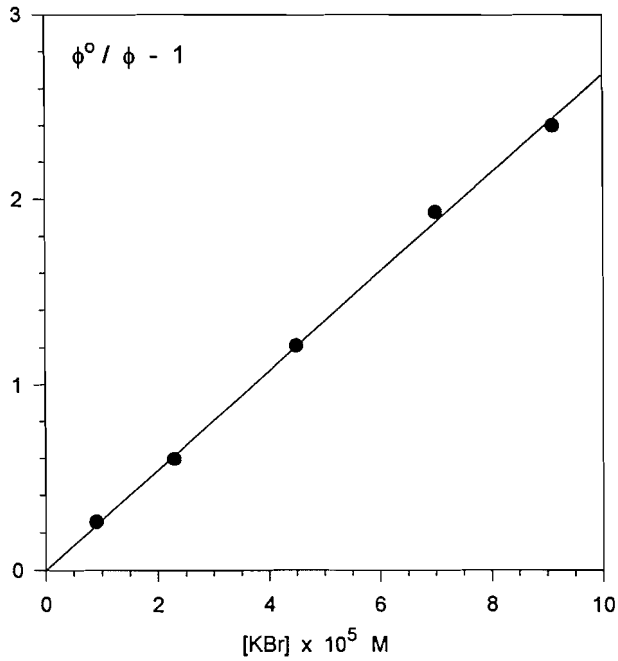

(*ii*) The photochemical reaction of **1***a* in water is quenched efficiently by bromide ions. Figure 3 shows the relevant Stern–Volmer plot. From the slope of this plot ($K_{sv} = k_q\tau$ = 26 600 $dm^3\ mol^{-1}$) an approximate value of 2.6×10^{-5} s for the lifetime of the reactive species is obtained, assuming $k_q \approx k_{diff} \approx 10^{10}\ dm^3\ mol^{-1}\ s^{-1}$. This value is three orders of magnitude greater than the lifetime of the excited singlet state of **1***a* ($\tau = 0.8$ ns (9)), indicating the involvement of an excited triplet state in the photochemical reaction. The lifetimes of triplet excited pyridinium cations in the purine series have been reported to be in the microsecond region (8).

(*iii*) The quantum yield of disappearance of **1***a* remains constant ($\varphi = 0.05 \pm 0.01$) over the entire pH range studied (pH

Table 2. ^{1}H NMR[a] spectral assignments of photoproducts **3***a*, **3***c*, and **2***c*.

Proton	**3***a*	**3***c*	**2***c*
H-5	—	—	6.63 (d, $J_{4,5}$ = 3.1 Hz)
Formyl H	9.18 (s)	9.16 (s)	—
H-4	7.56 (s)	7.68 (s)	6.50 (d)
N-CH_3	3.42 (s)	—	—
Ribose H-1′	—	6.15 (d, $J_{1',2'}$ = 6.0 Hz)	5.56 (d, $J_{1',2'}$ = 6.0 Hz)
H-2′	—	4.30 (dd, $J_{2',3'}$ = 5.0 Hz)	4.21 (m)
H-3′	—	4.78 (t, $J_{3',4'}$ = 5.1 Hz)	4.37 (m)
H-4′	—	4.00 (m, $J_{4',5'}$ = 5.6 Hz)	4.05 (m)
H-5′, H—5′	—	3.83–3.67 (m)	3.69 (m)

[a]Spectra measured in D_2O.

Table 3. ^{13}C NMR[a] spectral assignments of photoproducts **3***a*, **3***c*, and **2***c*.

Carbon	**3***a*	**3***c*	**2***c*
C-2	155.6	155.0	155.0
C-4	129.3	132.1	111.1
C-5	125.6	124.3	109.9
Formyl C	181.5	180.4	—
CH_3	29.7	—	—
C-1′	—	88.2	86.4
C-2′	—	71.9	73.7
C-3′	—	70.7	71.1
C-4′	—	84.9	85.1
C-5′	—	62.5	62.2

[a]Spectra measured in D_2O.

2.0–8.5) whereas, as mentioned above (cf. Table 1), the relative amounts of **2***a* and **3***a* are pH dependent. This suggests that the formation of these two photoproducts occurs via pH-controlled transformations of a common, thermally unstable, intermediate formed by the initial photoaddition of water to **1***a*.

Examples of photochemically induced transformations of pyrimidines into imidazoles have been reported (10–13). Pyrimidine 1-oxides give low yields of 5-acetyl imidazoles (10) via oxazirines. 5-Diazouracil undergoes ring contraction to 4-imidazoline-2-one-carboxylate via a carbene-type intermediate upon irradiation in methanol saturated with HCl (11, 12). The synthetic procedures leading to imidazolin-2-one-4- and 5-carboxylic acids and carboxylates have been reported (12, 14); however, to our knowledge, the synthesis of aldehydes **3***a,b* has not been previously described.

Identification of photoproducts 2*a,c* and 3*a,c*

The structure of photoproduct **2***a* was established mainly on the basis of its ^{1}H NMR spectrum and an elemental analysis, and was confirmed by comparison of its spectral data and chromatographic (HPLC) mobility with those of an authentic sample synthesized according to a known procedure (15). The ^{1}H NMR spectrum of **2***a* measured in D_2O shows two doublets at 6.51 and 6.38 ppm (J = 3.1 Hz) corresponding to HC=CH protons of the imidazole ring. Two sets of signals having similar chemical shifts and coupling constants appear in the spectrum of **2***c*, which is the nucleoside analog of **2***a*. The remaining resonances in the ^{1}H NMR spectrum of **2***c* correspond to ribose protons. The ^{1}H and ^{13}C NMR signals of **2***c*, as well as those of other photoproducts, were assigned based on chemical shift arguments and by analysis of homo (^{1}H–^{1}H) and hetero (^{1}H–^{13}C) two-dimensional COSY spectra. These assignments are presented in Tables 2 and 3. Contrary to aldehydes **3***a,c* but in agreement with the proposed structures, imidazolin-2-ones **2***a,c* do not show UV absorptions at λ > 240 nm.

The proposed structures of photoproducts **3***a* and **3***c* are consistent with both their ^{1}H and ^{13}C NMR spectra. The ^{1}H NMR spectrum of **3***a* consists of two singlets at 9.18 and 7.56 ppm corresponding to CHO and H-4 protons, respectively, and one singlet at 3.42 ppm, corresponding to NCH_3 protons (Scheme 2, Table 2). An unequivocal assignment of the site of attachment of the formyl group was deduced from the results of a long-range ^{1}H–^{13}C heteronuclear chemical shift correlation experiment. In the 2-D spectrum both quaternary carbon atoms (δ = 155.6 ppm and δ = 125.6 ppm) show cross peaks with N-CH_3 protons. This observation clearly points to the 5-carboxyaldehyde, **3***a*, and excludes the isomeric 1-methyl-4-imidazolin-2-one-4-carboxyaldehyde structure. As might be expected, the UV absorption spectra of **3***a* and **3***c* are pH dependent owing to their ground state prototropic equilibria (cf. Fig. 4). The relevant ground state ionization constants, pK, obtained from the spectrophotometric titration curves are equal to 9.3 and 8.8 for **3***a* and **3***c*, respectively. Upon prolonged storage in the presence of atmospheric oxygen in aqueous solution, **3***a* undergoes a slow oxidation to 1-methyl-4-imidazolin-2-one-5-carboxylic acid, which has been identified by comparison (HPLC and UV spectra) with an authentic sample prepared by condensation of *N*-methylurea with tartaric acid in fuming sulfuric acid (14). It has been shown that the UV spectra are of diagnostic value in distinguishing between the isomeric imidazolin-2-ones having carboxylic substituents located at the C-4 or C-5 positions of the imidazole ring (14).

It is interesting to note that a positional isomer of **3***c* having an aldehyde function at C-4 is an aglycone of the naturally occurring antibiotic nikkomycin X (16).

The photochemistry of 1*a* in methanol

The addition of a solvent molecule is the main reaction during the irradiation (λ > 300 nm) of **1***a* in deoxygenated methanol.

Can. J. Chem. Downloaded from www.nrcresearchpress.com by 46.23.64.124 on 09/08/12
For personal use only.

Can. J. Chem. Downloaded from www.nrcresearchpress.com by 46.23.64.124 on 09/08/12
For personal use only.

Fig. 4. The pH dependence of the UV absorption spectrum and the relevant spectrophotometric titration curve for the ground state prototropic equilibrium of **3***a*.

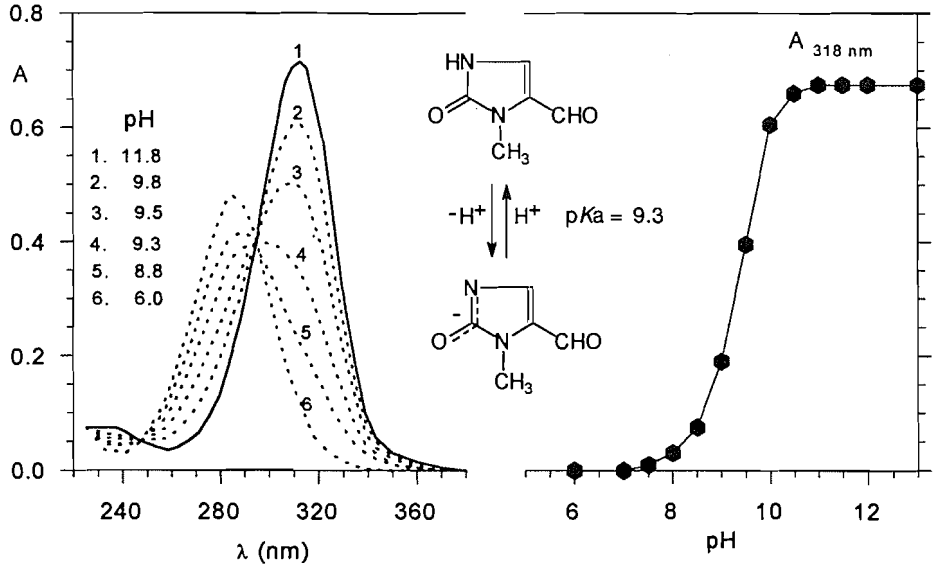

Scheme 3.

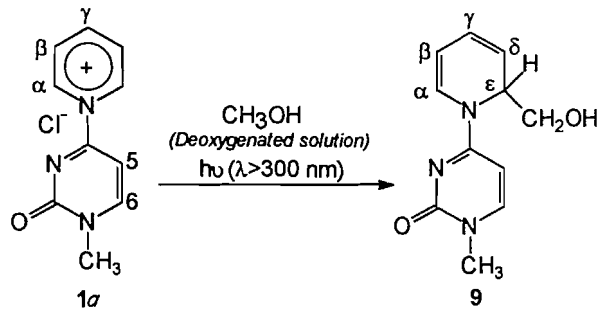

The addition occurs at the C-α position of the pyridinium residue leading to the dihydropyridine-type adduct **9** (Scheme 3). The quantum yield for conversion of substrate is 0.01. The mechanism of the reaction is most likely similar to that previously reported for the photochemical addition of electron donors such as alcohols, ethers, and amines to various *N*-alkyl-, *N*-alkenyl-, and *N*-heteroaromatic-pyridinium salts (17). The respective dihydropyridine-type photoadducts are formed by the initial electron transfer from the donor to the excited pyridinium salts, followed by coupling of the resulting radicals (17).

Identification of photoproduct 9

As is characteristic of the dihydropyridine structure, photoproduct **9** exhibits an intense absorption in the UV spectrum with a maximum at 335 nm (18). In the ^{1}H NMR spectrum of **9** recorded at room temperature, pyridine α and ε protons give rise to very broad signals at 6.51 and 5.67 ppm, respectively (Scheme 3, and Experimental). Lowering the temperature to 253 K results in sharpening of the signals and reveals their multiplet structure. This behaviour of the ^{1}H NMR spectrum is due to hindered rotation around the inter-ring bond caused by the presence of the *ortho* hydroxymethylene group in photoadduct **9**.

Experimental

General

^{1}H and ^{13}C NMR

Varian Unity 300 (300 MHz for ^{1}H); solvents: D_2O or $CDCl_3$ with dioxane or TMS as an internal reference, respectively; all chemical shifts converted to TMS scale (dioxane ^{1}H δ = 3.71 ppm; dioxane ^{13}C δ = 67.4 ppm).

UV

Perkin–Elmer Lambda-17 spectrophotometer.

Elemental analysis

Perkin–Elmer 2400 CHN analyzer.

Thin-layer chromatography (TLC)

Silica gel 60 F_{254} plates (Merck); solvent systems: A: $CHCl_3$–CH_3OH (5:1; v/v); B: $CHCl_3$–CH_3OH (10:1; v/v).

HPLC

Waters 600E; detection: Waters 991 photodiode-array UV–VIS detector; columns: Nova Pak C-18, 8 × 100 mm and Delta Pak C-4, 4.9 × 250 mm (analytical) and Nova Pak C-18, 25 × 100 mm (semipreparative); mobile phases: A: water; B: 50% acetonitrile, 50% water; C: 0.1 M ammonium acetate; D: 50% 0.1 M ammonium acetate, 50% acetonitrile.

Pyridinium salts **1***a, b* and **5**, and 4-substituted pyrimidin-2-ones **6–8** were synthesized as described previously (1*b, d*). 1-Methyl-4-imidazolin-2-one (15) and 1-methyl-4-imidazolin-2-one-5-carboxylic acid (14) were synthesized according to published procedures.

Analytical scale irradiations

The samples of aqueous solutions ($c = 1.6 \times 10^{-3}$ M) of **1***a, b* and **5–8** were placed in a 1 cm path length cell, deoxygenated, and irradiated on an optical bench with a high-pressure mercury lamp (HBO 200, Narva) through a Pyrex filter. Progress

Can. J. Chem. Downloaded from www.nrcresearchpress.com by 46.23.64.124 on 09/08/12
For personal use only.

of the reaction was monitored by UV spectroscopy and HPLC. The analytical HPLC was performed on a C-18 column eluted with 100%A (6 min) – 90%C/10%D (1 min) – 50%C/50%D (4 min) in the case of **1***a*, and a C-4 column eluted isocratically with a mixture of 70%C/30%D in the case of **1***b*. The results of chromatographic analyses obtained for the irradiations of **1***a, b* in aqueous solutions are collected in Table 1. The reaction quantum yields, φ, were measured for 313 nm excitation (Zeiss interference filter) using 2-hexanone as an actinometer (19).

General procedure for preparative irradiations

A concentrated aqueous solution (20 mL) containing 3.2 mmol of **1***a, b* was added to 2000 mL of the appropriate solvent (water, 0.002 M sodium bicarbonate, or methanol). Portions (60 mL) of the solutions ($c = 1.6 \times 10^{-3}$ M) were irradiated under an argon atmosphere with an immersion high-pressure mercury lamp (Original Hanau) through a Pyrex filter. The photolyzed solutions were collected and concentrated under reduced pressure. Irradiations were continued up to ca. 70% conversion of the substrate. Chemical yields of the photoproducts are given relative to the amount of substrate that reacted.

Isolation of photoproducts 2*a* and 3*a*

Photoproduct **2***a* was isolated from the irradiated aqueous solution of **1***a* by preparative HPLC (90%A/10%B). Fractions containing **2***a* were evaporated to give 37 mg of colourless solid (17% yield). UV (H_2O), λ_{max}: <220 nm. The ^{1}H NMR spectrum of the photoproduct is in agreement with that reported for 1-methyl-4-imidazolin-2-one (15).

Preparative scale synthesis of **3***a* was performed by irradiation of **1***a* in 0.002 M aqueous sodium bicarbonate. The desired photoproduct was separated from the irradiated mixture by preparative TLC using solvent system A and then subjected to further purification by means of preparative HPLC (90%A/10%B). Evaporation of the solvent gave 155 mg of colorless solid (55% yield). UV (H_2O), λ_{max} (nm) (ε (M^{-1}, cm^{-1})): 286.5 (13 300), (pH 1) 287 (13 600), (pH 12) 312.5 (20 300). ^{1}H and ^{13}C NMR data: Tables 2 and 3. Anal. calcd. for $C_5H_6N_2O_2$: C 47.62, N 22.21, H 4.79; found: C 47.01, N 22.09, H 4.71.

Isolation of photoproducts 2*c* and 3*c*

Leaving the irradiated solutions of **1***c* for several days at room temperature resulted in a partial deacetylation of photoproducts **2***b* and **3***b*, as indicated by HPLC and ^{1}H NMR analyses. Treatment of the mixture with diluted aqueous ammonia over 24 h at room temperature gave the fully deprotected nucleosides **2***c* and **3***c*, which were separated by preparative HPLC (0.005 M aqueous $HClO_4$). The appropriate fractions were collected, neutralized with Dowex-1 resin (HCO_3^-), and evaporated to dryness to give **2***c* (135 mg, 28% yield) and **3***c* (164 mg, 30% yield) as white powders.

2*c*: UV (H_2O), λ_{max}: <220 nm. ^{1}H and ^{13}C NMR data: Tables 2 and 3. Anal. calcd. for $C_8H_{12}N_2O_5$: C 44.45, H 5.59, N 12.96; found: C 44.37, H 5.54, N 12.87.

3*c*: UV (H_2O), λ_{max} (nm) (ε (M^{-1}, cm^{-1})): 283 (13 000), (pH 1) 283 (13 000), (pH 12) 311.5 (21 000). ^{1}H and ^{13}C NMR data: Tables 2 and 3. Anal. calcd. for $C_9H_{12}N_2O_6$: C 44.27, H 4.95, N 11.47; found: C 44.03, H 4.85, N 11.35.

Isolation of photoproduct 9

HPLC analysis (conditions as for irradiation of **1***a* in water) of the methanolic solution of **1***a* irradiated to 68% conversion revealed the presence of only one major photoproduct. Preparative TLC of the concentrated, irradiated solution using solvent system B followed by further purification on HPLC (75%A/25%B) gave an analytically pure sample (83 mg) of **9**, a white solid. Yield: 17% on the isolated product (50%–HPLC). UV (H_2O), λ_{max} (nm) (ε (M^{-1}, cm^{-1})): 283 (4060), 335 (13 900). ^{1}H NMR ($CDCl_3$, 293 K) δ ppm: 7.41 (d, J = 7.3 Hz, 1, H-6), 6.51 (br s, 1, H-α), 6.08 (dd, 1, H-γ), 6.01 (d, J = 7.3 Hz, H-5), 5.67 (br s, 1, H-ε), 5.61 (m, 1, H-δ), 5.51 (m, 1, H-β), 3.71–3.66 (m, 2, CH_2), 3.48 (br s, 1, OH), 3.48 (s, 3, N-CH_3). ^{1}H NMR ($CDCl_3$, 253 K) δ ppm: 7.47 (d, J = 7.3 Hz, 1, H-6), 6.49 (d, J = 7.47 Hz, 1, H-α), 6.10 (dd, 1, H-γ), 6.03 (d, J = 7.3 Hz, H-5), 5.73 (m, 1, H-ε), 5.62 (m, 1, H-δ), 5.56 (m, 1, H-β), 3.84 (s br, 1, OH), 3.71 (m, 2, CH_2) , 3.50 (s, 3, N-CH_3). ^{13}C NMR ($CDCl_3$, 293 K) δ ppm: 163.23 (C-4), 156.15 (C-2), 146.92 (C-6), 123.98 (C-α), 123.06 (C-γ), 121.12 (C-δ), 109.00 (C-β), 92.19 (C-5), 63.64 (CH_2), 54.16 (C-ε), 37.93 (N-CH_3). Anal. calcd. for $C_{11}H_{13}N_3O_2$: C 60.26, H 5.98, N 19.16; found: C 60.08, H 5.90, N 19.07.

Acknowledgements

This work was supported by the Polish Research Committee (grant PB 1031/9202).

References

1. (*a*) R.W. Adamiak, E. Biala, and B. Skalski. Nucleic Acids Res. **13**, 2989 (1985); (*b*) R.W. Adamiak, E. Biala, Z. Gdaniec, S. Mielewczyk, and B. Skalski. Chem. Scr. **26**, 3 (1986); (*c*) R. Fathi, B. Goswami, P.-P. Kung, B.L. Gaffney, and R.A. Jones. Tetrahedron Lett. **31**, 319 (1990); (*d*) G. Wenska, B. Skalski, and Z. Gdaniec. Can. J. Chem. **70**, 856 (1992).
2. H. Gao, R. Fathi, B.L. Gaffney, B. Goswami, P.-P. Kung, Y. Rhee, R. Jin, and R.A. Jones. J. Org. Chem. **57**, 6954 (1992).
3. A. Burdzy, B. Skalski, E. Biala, and R.W. Adamiak. Nucleosides Nucleotides. In press.
4. J.Cadet and P.Vigny. *In* Bioorganic photochemistry. Vol. 1. *Edited by* H. Morrison. J. Wiley & Sons, New York. 1990. pp. 1–272.
5. (*a*) B. Skalski, J. Bartoszewicz, S. Paszyc, Z. Gdaniec, and R.W. Adamiak. Tetrahedron, **43**, 3955 (1987); (*b*) B. Skalski, R.P. Steer, and R.E. Verrall. J. Am. Chem. Soc. **110**, 2055 (1988); (*c*) B. Skalski, S. Paszyc, R.W. Adamiak, R.P. Steer, and R.E. Verrall. Can. J. Chem. **68**, 2164 (1990); (*d*) G. Wenska, B. Skalski, S. Paszyc, S. Wnuk, and R.W. Adamiak. J. Fluoresc. **4**, 283 (1994).
6. B. Skalski, R.P. Steer, and R.E. Verrall. J. Am. Chem. Soc. **113**, 1756 (1991).
7. S. Mielewczyk, G. Dominiak, Z. Gdaniec, E. Krzymanska-Olejnik, R.W. Adamiak, and B. Skalski. Nucleosides Nucleotides, **10**, 263 (1991).
8. B. Marciniak, G.L. Hug, J. Rozwadowski, and K. Bobrowski. J. Am. Chem. Soc. **117**, 127 (1995).
9. G. Wenska, B. Skalski, J. Koput, and S. Paszyc. J. Photochem. Photobiol. A: **88**, 117 (1995).
10. M.R. Grimmett. *In* Comprehensive heterocyclic chemistry. Vol. 5. *Edited by* A.R. Katritzky and C.W. Reese. Pergamon Press, New York. 1984. p. 495.
11. B. Stanovnik, M. Tišler, and E. Voncina. Heterocycles, **12**, 761 (1979).

12. W. Klötzer, G. Dörler, B. Stanovnik, and M. Tišler. Heterocycles, **22**, 1763 (1984).
13. R.E. Van der Stoel, H.C. van der Plas, and H. Jongejan. Recl. Trav. Chim. Pays- Bas, **102**, 364 (1983).
14. B.A. Otter, E.A. Falco, and J.J. Fox. J. Org. Chem. **33**, 3593 (1968).
15. N.J. Leonard and D.F. Wiemer. J. Am. Chem. Soc. **98**, 8218 (1976).
16. H. Hagenmaier, A. Keckeisen, H. Zähner, and W.A. König. Liebigs Ann. Chem. 1494 (1979).
17. P.S. Mariano. Tetrahedron, **23**, 3845 (1983), and references cited therein.
18. T.J. Van Bergen and R.M. Kellogg. J. Am. Chem. Soc. **94**, 8451 (1972).
19. S.L. Murov. Handbook of photochemistry. Marcel Dekker, New York. 1983. p. 126.

Can. J. Chem. Downloaded from www.nrcresearchpress.com by 46.23.64.124 on 09/08/12
For personal use only.

Synthesis of steroidal [4,6-*b*,*c*]-benzothiazepines, a new class of aromatase inhibitor

Herbert L. Holland, Sudalaiyandi Kumaresan, and Gingipalli Lakshmaiah

Abstract: Several steroidal [4,6-*b*,*c*]benzothiazepines have been prepared via base-catalyzed Michael addition of 2-aminothiophenol to 3β,17β-diacetoxyandrost-4-en-6-one. The product of this reaction has the 4β,5α stereochemistry, but cyclizes to a benzothiazepine with the steroidal 4β,5β configuration, confirmed by X-ray crystallographic analysis. 2-Aminothiophenol reacts with 3β,17β-diacetoxyandrost-4-en-6-one under acidic conditions to give a steroidal 6-spiro-benzothiazole. An androst-4-ene-3,17-dione-based [4,6]benzothiazepine has been shown to be a moderate competitive inhibitor of the human placental aromatase enzyme with $IC_{50} = 42.3$ μM.

Key words: steroid, aromatase, benzothiazepine.

Résumé : On a préparé plusieurs [4,6-*b*,*c*]benzothiazépines stéroïdales par le biais d'une addition du 2-aminothiophénol sur la 3β,17β-diacétoxyandrost-4-én-6-one. Le produit possède une stéréochimie 4β,5α, mais il se cyclise en une benzothiazépine de configuration stéroïdale 4β,5β qui a été confirmée par diffraction des rayons X. Dans des conditions acides, le 2-aminothiophénol réagit avec la 3β,17β-diacétoxyandrost-4-én-6-one pour donner un 6-spiro-benzothiazole. Il a été démontré qu'une [4,6]benzothiazépine basée sur une androst-4-én-3,17-dione est un inhibiteur modérément compétitif de l'enzyme aromatase du placenta humain; $IC_{50} = 42,3$ μM.

Mots clés : stéroïde, aromatase, benzothiazépine.

[Traduit par la rédaction]

The enzyme aromatase (estrogen synthetase), responsible for the production of the estrogen hormones in human females, is currently of interest in view of its role as a possible regulator in the etiology of breast cancer (1). Of the many steroids that have been examined for their potential as aromatase inhibitors (1), two of the most potent are the 4-enol **1** (2) and the 6-oxime **2** (3, 4). These observations, together with a demonstration of the importance of the Δ^4-3-keto unit and substitution at C-4 and C-6 in the development of efficient steroidal aromatase inhibitors (4, 5), suggested that a steroid such as **3**, carrying the [4,6]benzothiazepine unit, might function as an efficient aromatase inhibitor.

The reactions between 2-aminothiophenol and 3β-acetoxy-Δ^4-6-ketosteroids with the stigmastane (6) and cholestane (7) skeletons (Scheme 1) have been reported to produce the corresponding 4α-substituted-5α-steroids, **4**. We have applied this reaction to the synthesis of **3** as outlined in Scheme 2, starting from 3β,17β-diacetoxyandrost-4-en-6-one (**5**), whose preparation we have previously described (3). When performed under acid-catalyzed conditions as described (6), addition of

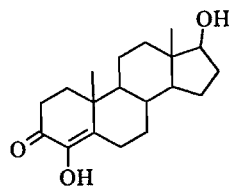

1

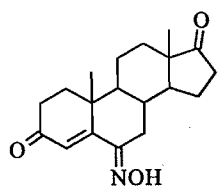

2

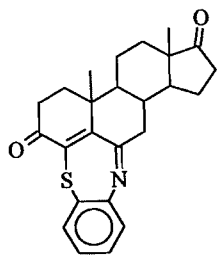

3

2-aminothiophenol to the ketone **5** gave only the spiro(benzothiazole) steroid **6** in 68% isolated yield. We were not able to isolate the expected product, benzothiazepine **8**, from this reaction. The structure of **6** follows from spectral data reported in the Experimental section and in Table 1, the significant nmr resonances being those associated with carbons 4–6. The configuration of **6** at C-6 has not been determined.

Reaction between ketone **5** and 2-aminothiophenol occurred to give the Michael addition product, 5α steroid **7**, in 87% yield

Received July 18, 1995.

H.L. Holland,[1] S. Kumaresan, and G. Lakshmaiah.
Department of Chemistry, Brock University, St. Catharines, ON L2S 3A1, Canada.

[1] Author to whom correspondence may be addressed.
Telephone: (905) 688-5550, ext. 3403.
E-mail: holland@chemiris.labs.brocku.ca

Can. J. Chem. Downloaded from www.nrcresearchpress.com by 46.23.64.124 on 09/08/12
For personal use only.

Can. J. Chem. Downloaded from www.nrcresearchpress.com by 46.23.64.124 on 09/08/12
For personal use only.

Scheme 1.

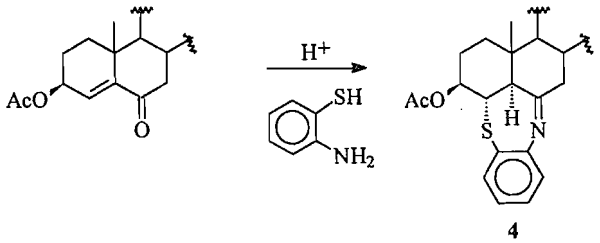

Scheme 2.

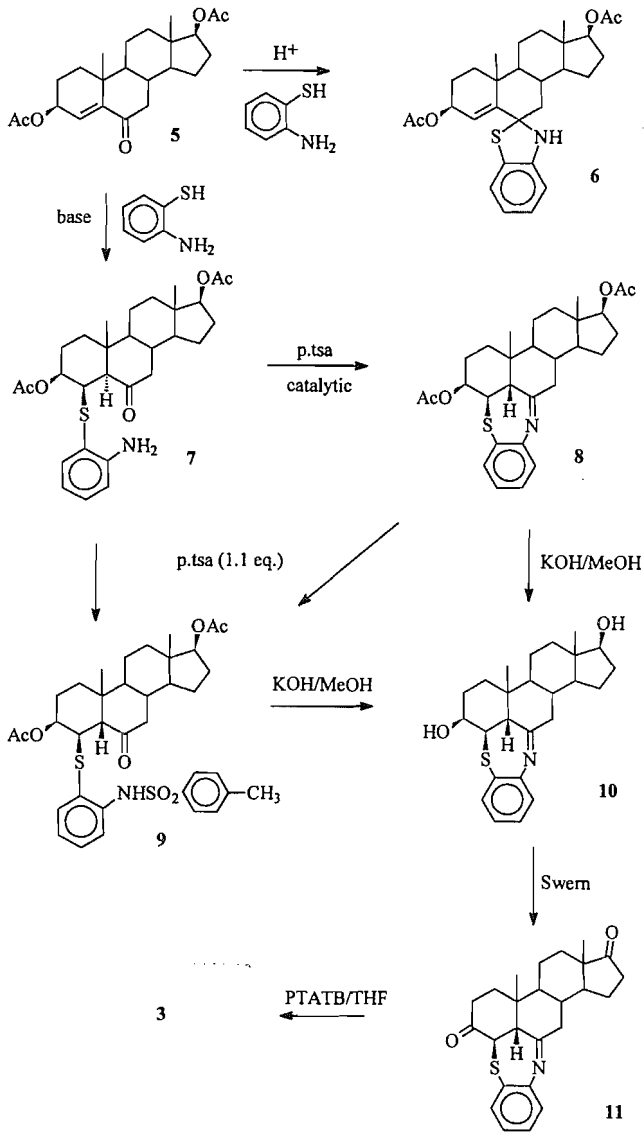

when carried out using basic catalysis. The stereochemistry of **7** at C-4, together with that of the AB ring junction, was confirmed as follows. That **7** is a 5α steroid follows clearly from its ^{13}C nmr spectrum (Table 1), with shifts for C-9 and C-19 being diagnostic of this stereochemistry (8, 9). The 4β configuration is then indicated by the ^{13}C resonance position of C-2, which shows a γ-*gauche* upfield shift of −3.5 ppm from the position of C-2 in corresponding C-4-unsubstituted steroids (9); the C-19 resonance position (3.6 ppm downfield from that of corresponding C-4-unsubstituted steroids (9)); and the appearance of the C-4 hydrogen resonance at δ 4.06 ppm as narrow doublet of doublets (J = 3.8 and 3.2 Hz), indicating the presence of only axial–equatorial couplings to hydrogens at C-3 and C-5. Michael addition to **5** from the axial (4β) side is predictable on stereoelectronic grounds (10) and is in accord with literature precedent (11): the 4α stereochemistry assigned earlier to similar products was based on "expectation" and is not substantiated by spectral data (7).

The addition product **7** is converted in high yield (91%) to the benzothiazepine **8** on treatment with a catalytic amount of *p*-toluenesulfonic (p.tsa) acid in refluxing benzene. It is clear from nmr analysis that **8**, and the subsequently derived intermediates **9–11**, possess the 5β configuration. This conclusion follows from the ^{13}C nmr data presented in Table 1, particularly the characteristic shifts for C-9 and C-19 (9), and the observation that the C-4 hydrogen resonance now appears at δ 4.01 ppm as a doublet of doublets with J = 12.9 and 2.5 Hz (in **8**, for example) caused by diaxial, and axial–equatorial couplings to hydrogens at C-5 and C-3, respectively. Proton nmr resonances at C-3, -4, and -5 were assigned in compounds **7–11** by ^1H–^1H COSY experiments, and the associated carbon resonances then assigned by SFORD spectra. In view of its unusual origin, this stereochemical analysis was confirmed by X-ray structure determination of the hydrolysis product, diol **10**, which is presented in Fig. 1.[2]

The formation of benzothiazepine **8** with 4β, 5β stereochemistry is at variance with the results of Mushfiq et al. depicted in Scheme 1 (6, 7), but their reported proton nmr data (6), in particular the assignment of the C-4 hydrogen at δ 2.8 ppm, do not support either their proposed structure or its 4α,5α stereochemistry. Condensation of **7** to a product with 5β stereochemistry is apparently thermodynamically driven. MM2 energy calculations on minimized structures using the Alchemy© or Hyperchem© modelling programmes indicate that **8** is more stable than the corresponding 5α isomer by 15.0 kcal/mol, the difference being associated entirely with angle and torsion strain. This assumption is strengthened by the isolation of the 5β sulfonamide **9** on treatment of **7** with larger amounts of p.tsa; this latter product was also obtained from **8** on further acid treatment, suggesting that formation of **9** from **7** proceeds via the benzothiazepine **8**. A possible route for the conversion of **8** to **9** in the presence of a larger amount of p.tsa may involve the acid-catalyzed addition of p.tsa across the C=N bond, followed by ring opening and O to N migration of the *p*-toluenesulfonyl group.

The diol **10**, obtained by hydrolysis of **8** or from cyclization of **9** under basic conditions, was converted in 90% yield by low-temperature Swern oxidation to the dione **11**. The latter then afforded benzothiazepine **3** on treatment with phenyl trimethyl ammonium tribromide. The target steroid **3** had an IC_{50} value of 42.3 μM when tested against human placental aromatase using 2.5 μM testosterone as substrate,[3] making it a moderately effective inhibitor of this enzyme. In spite of the importance of substitution at C-6 in the design of effective aromatase inhibitor (4), the recent suggestion (5) that the

[2] This analysis was carried out by Professor Ling-Kang Liu of the Institute of Chemistry, Academia Sinica, Taiwan.

[3] This assay was carried out by Drs. V.C.O. Njar and P. Dorfmüller, Department of Pharmaceutical Chemistry, Universität des Saarlandes, Germany.

Can. J. Chem. Downloaded from www.nrcresearchpress.com by 46.23.64.124 on 09/08/12
For personal use only.

Table 1. The ^{13}C nmr resonance positions of **3** and **5–11**.[a]

Carbon	3	5	6	7	8	9	10	11
1	36.7*	34.8	37.8	37.2	28.6	28.0	27.2	34.6*
2	33.8	23.2*	23.4*	23.2*	23.3*	22.9*	26.0	35.7*
3	192.6	69.2	70.6	75.8	72.7	72.4	70.2	204.5
4	135.3	129.0	108.9	43.8	57.6	49.9	61.6	63.6
5	159.0	147.8	144.4	60.2	48.2	56.7	48.4	53.0
6	169.9	201.6	78.8	207.7	178.3	196.2	179.2	174.5
7	45.0	45.7	48.5	46.1	39.4	35.7	39.7	37.6
8	34.1	34.0	31.6	35.6	35.1	35.2	35.2	35.3
9	52.8	51.1	53.5	54.0	41.0	39.9	41.0	43.7
10	43.0	38.3	37.4	40.4	37.8	39.4	39.0	38.7
11	20.7	20.3	20.3	20.3	20.7	20.6	20.7	20.5
12	31.1	36.4	36.5	36.3	36.7	36.2	36.5	31.3
13	47.7	42.7	42.6	42.6	42.9	43.0	43.2	47.7
14	51.3	51.1	49.8	51.1	51.3	50.2	51.6	51.6
15	21.7	24.1*	24.2*	23.2*	24.3*	24.8*	23.2	21.6
16	35.7*	27.4	27.4	27.4	27.6	27.4	30.6	35.7
17	219.1	82.2	82.4	82.2	82.4	81.9	81.6	219.4
18	13.7	12.0	12.1	12.0	12.1	12.0	11.1	13.7
19	17.8	19.6	21.3	16.6	24.3	24.5	24.2	22.7

[a]Chemical shifts marked with an asterisk may be interchanged in vertical columns.

Fig. 1. ORTEP structure of diol **10**.

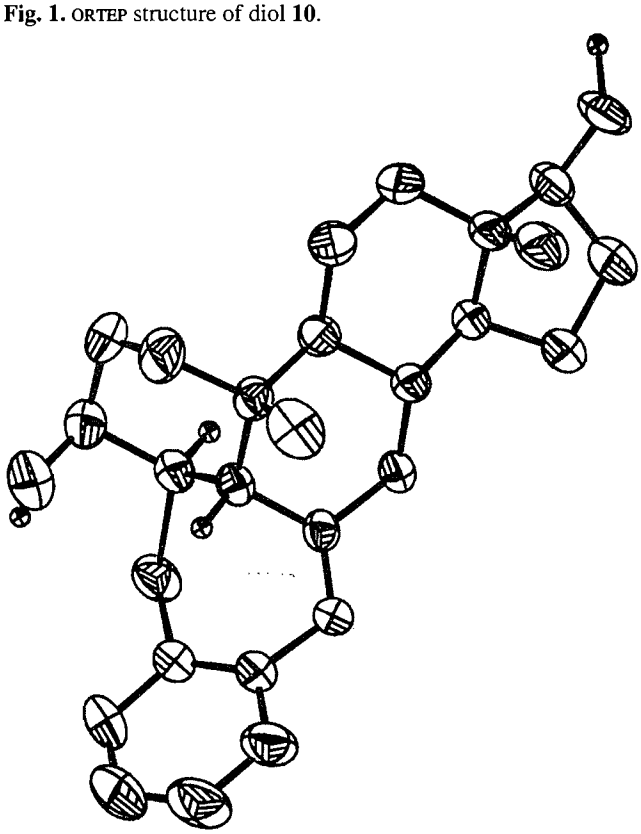

enzyme's active site possesses limited accessible volume in the C-6 region may account for the lack of high inhibitory activity of benzothiazepine **3**.

Experimental

Apparatus, materials, and methods

Melting points were determined on a Kofler heating stage. The nmr spectra were recorded at 200 MHz (routine ^1H) or 50 MHz (routine ^{13}C) with a Bruker AC200 spectrometer using $CDCl_3$ as solvent and $CHCl_3$ or TMS as internal standard. Proton signals were assigned from ^1H–^1H COSY data and carbon signals from a combination of JMOD and SFORD spectra. Mass spectra were obtained with a Kratos 1S instrument operating in EI mode. Thin-layer chromatography was performed on Merck silica gel 60F-254 and flash column chromatography used silica gel, 230–400 mesh. Microanalyses were performed by Guelph Chemical Laboratories, Guelph, Ontario.

X-ray structure determination was carried out with a 0.64 × 0.39 × 0.51 mm crystal on a Nonius diffractometer using the θ/2θ scan mode. Crystal data: $C_{25}H_{33}NO_2S$; FW 411.60; orthorhombic $P2_12_12_1$, a = 12.1438(13), b = 13.2605(19), c = 13.9445(12) Å, V = 2245.5(4) Å^3, Z = 4, ρ_c 1.218 g cm^{-3}, μ = 0.16 mm^{-1} (20°C, MoKα_1, λ = 0.70930 Å), $2\theta_{max}$ = 44.9°; 1688 unique reflections were obtained and the last least-squares cycle was calculated with 62 atoms, 263 parameters, and 1460 observed reflection ($I > 2\sigma_I$) out of 1688 total reflections; R = 0.036, R_w = 0.037. Details of the X-ray measurements and tables of data have been deposited as supplementary material.[4]

2-[6-Spiro-(3β,17β-diacetoxyandrost-4-enyl)]-4,5-benzo-2[*H*]-thiazole, 6

A mixture of androst-4-ene-3β,17β-diol-6-one diacetate (**5**)

[4] Tables of bond lengths and angles, torsion angles, atomic parameters and thermal parameters, together with ORTEP structures, may be purchased from: The Depository of Unpublished Data, Document Delivery, CISTI, National Research Council Canada, Ottawa, Canada K1A 0R6. Tables of bond lengths and angles, atomic parameters, and the ORTEP structures have also been deposited with the Cambridge Crystallographic Data Centre, and can be obtained on request from The Director, Cambridge Crystallographic Data Centre, University Chemical Laboratory, 12 Union Road, Cambridge, CB2 1EZ, U.K.

Can. J. Chem. Downloaded from www.nrcresearchpress.com by 46.23.64.124 on 09/08/12
For personal use only.

(3) (1.164 g, 0.3 mmol), 2-aminothiophenol (0.414 g, 3.3 mmol), dry methanol (8 mL), and 2 drops of concentrated HCl was refluxed under an argon atmosphere for 90 min. The mixture was then cooled in ice, and the precipitated solid collected by filtration and washed with cold methanol (2 mL). The resulting colourless solid (1.01 g) was crystallized from methanol–chloroform to yield **6**, mp 178–179°C; ^{1}H nmr included signals at δ: 0.85 (3H, s, 18-H), 1.27 (3H, s, 19-H), 2.03 (6H, s, OAc), 2.51 (1H, dd, J = 2.5, 12 Hz, 7-H), 3.88 (1H, s, exchanges D_2O, NH), 4.57 (1H, t, J = 8.8 Hz, 17-H), 5.34 (1H, d of t, J = 2.5, 9 Hz, 3-H), 6.15 (1H, s, 4-H), and 6.57–6.96 (4H, m, Ar-H) ppm; ms *m/z*(%): 495 (M^+, 7), 435(100), 420(42), 346(5), 241(27). Anal. calcd. for $C_{29}H_{37}NO_4S$: C 70.27, H 7.52, N 2.83, S 6.47%; found: C 70.04, H 7.92, N 3.11, S 6.44%.

3β,17β-Diacetoxy-4β-(2-aminothiophenyl)-5α-androstan-6-one, 7

Androst-4-ene-3β,17β-diol-6-one diacetate (**5**) (3) (0.582 g, 1.5 mmol) was added to a solution of 2-aminothiophenol (0.207 g, 1.66 mmol) in dry methanol in which a catalytic amount of sodium had been dissolved. The resulting mixture was refluxed under argon for 90 min, cooled in ice, and the precipitated solid was collected by filtration, washed with cold methanol, and crystallized from methanol–chloroform to give **7** (0.675 g, 87%), mp 190°C (sharp); ^{1}H nmr included signals at δ: 0.80 (3H, s, 18-H), 1.07 (3H, s, 19-H), 1.51 (3H, s, OAc), 2.05 (3H, s, OAc), 4.05 (1H, dd, J = 3.8, 3.2 Hz, 4-H), 4.6–4.8 (2H, m, 3- and 17-H), 5.30 (2H, s, exchanges D_2O, NH_2), 6.60 (2H, m, Ar-H), 7.04 (1H, t, Ar-H), and 7.54 (1H, d, Ar-H) ppm; ms *m/z*(%) 513(M^+, 2.5), 435(3.5), 388(7.5), 346(100), 328(17), 313(57). Anal. calcd. for $C_{29}H_{39}NO_5S$: C 67.81, H 7.65, N 2.73, S 6.24%; found: C 67.42, H 7.78, N 3.24, S 6.52%.

2′3′-Dihydro-3β,17β-diacetoxy-5β-androstano[4β,6-*b*,*c*]-1′,5′-benzothiazepine, 8

A solution of **7** (0.400 g, 0.78 mmol) and a catalytic amount of *p*-toluene sulfonic acid in dry benzene (30 mL) was refluxed for 3 h using a Dean–Stark trap. The solution was then cooled, ether (50 mL) added, and the solution was washed with water, followed by saturated aqueous sodium bicarbonate, water, and then dried over magnesium sulfate. Evaporation afforded a yellow solid that was crystallized from benzene–hexane to give 0.350 g (91%) of colourless **8**, mp 270°C (sharp); ^{1}H nmr included signals at δ: 0.81 and 0.83 (each 3H, s, 18- and 19-H), 2.0 and 2.05 (each 3H, s, OAc), 4.02 (1H, dd, J = 2.5, 12.9 Hz, 4-H), 4.65 (1H, t, J = 8.5 Hz, 17-H), 5.1 (1H, br s, 3-H), 7.0–7.4 (4H, m, Ar-H) ppm; ms *m/z*(%): 495(M^+, 100), 435(7.5), 215(43). Anal. calcd. for $C_{29}H_{37}NO_4S$: C 70.27, H 7.52, N 2.83, S 6.47%; found: C 69.74, H 7.83, N 2.97, S 6.48%.

3β,17β-Diacetoxy-4β-(2-[*p*-tolylsulfonylamino]thiophenyl)-5β-androstan-6-one, 9

(a) From 3β,17β-diacetoxy-4β-(2-aminothiophenyl)-5α-androstan-6-one (7)

A mixture of the adduct **7** (0.400 g, 0.78 mmol), *p*-toluenesulfonic acid monohydrate (0.163 g, 0.86 mmol), and benzene (25 mL) was refluxed in a Dean–Stark apparatus for 2.5 h. Chloroform (20 mL) was then added, and the resulting solution was washed with water, aqueous sodium bicarbonate, dried, and evaporated to give 0.300 g (58%) of **9**, crystallized from chloroform – petroleum ether, mp 243°C (sharp); ^{1}H nmr included signals at δ: 0.77 and 0.87 (each 3H, s, 18- and 19-H), 1.94 and 2.06 (each 3H, s, OAc), 2.36 (3H, s, Ar-CH_3), 3.70 (1H, dd, J = 2.6, 12.6 Hz, 5-H), 4.35 (1H, dd, J = 2.6, 12.6 Hz, 4-H), 4.56 (1H, t, J = 8.8 Hz, 17-H), 5.10 (1H, br s, 3-H), and 7.16–7.96 (8H, m, Ar-H) ppm; ms *m/z*(%): 495 (M − p.tsa, 100), 453(3.5), 435(10). Anal. calcd. for $C_{36}H_{45}NO_7S_2$: C 64.74, H 6.79, N 2.10, S 9.60%; found: C 64.63, H 6.99, N 2.19, S 9.76%.

(b) From 2′,3′-dihydro-3β,17β-diacetoxy-5β-androstano[4β,6-b,c]-1′,5′-benzothiazepine (8)

A mixture of the benzothiazepine **8** (0.040 g, 0.06 mmol), *p*-toluenesulfonic acid monohydrate (0.017 g, 0.09 mmol), and dry benzene was refluxed for 2.5 h. Chloroform (10 mL) was then added, and the solution was washed with water, aqueous sodium bicarbonate, dried, and evaporated to give **9** (0.040 g), identical in all respects with the sample prepared in (*a*).

2′,3′-Dihydro-3β,17β-dihydroxy-5β-androstano[4β,6-*b*,*c*]-1′,5′-benzothiazepine, 10

(a) From 2′,3′-dihydro-3β,17β-diacetoxy-5β-androstano[4β,6-b,c]-1′,5′-benzothiazepine (8)

A solution of the diacetate **8** (0.100 g, 0.15 mmol) in dry methanol (3 mL) containing KOH (0.100 g) was stirred at room temperature for 24 h. The solvent was removed by evaporation, ice-water (5 mL) was added to the residue, and the mixture stirred for 10 min. The resulting solid was collected by filtration and dried to yield 0.076 g (92%) of **10**, crystallized from methanol–chloroform, mp 262–264°C; ^{1}H nmr included signals at δ 0.77 and 0.80 (each 3H, s, 18- and 19-H), 3.70 (1H, t, 17-H), 3.86 (1H, br s, 3-H), 4.07 (1H, dd, J = 2.5, 12.6 Hz, 4-H), and 7.03–7.55 (4H, m, Ar-H) ppm; ms *m/z*(%): 411 (M^+, 100), 258(16), 162(15), 149(23). Anal. calcd. for $C_{25}H_{33}NO_2S$: C 72.95, H 8.08, N 3.40%; found: C 72.84, H 7.94, N 3.44%.

(b) From 3β,17β-Diacetoxy-4β-(2-[p-tolylsulfonyl-amino]thiophenyl)-5β-androstan-6-one (9)

Treatment of **9** (1.00 g) by the procedure described in (*a*) resulted in the formation of 0.59 g (96%) of **10**, identical in all respects with the sample described above.

2′,3′-Dihydro-3,17-diketo-5β-androstano[4β,6-*b*,*c*]-1′,5′-benzothiazepine, 11

A solution of dimethyl sulfoxide (18 mg) in dichloromethane (0.5 mL) was added dropwise at −65°C under an argon atmosphere to a solution of oxalyl chloride (13.5 mg) in dichloromethane (0.30 mL), and the resulting mixture stirred for 10 min at that temperature. A suspension of the diol **10** (20 mg, 0.05 mmol) in dichloromethane was then added over a period of 10 min; the mixture was stirred for 1 h at −65°C and then quenched by the addition of triethylamine (49.2 mg). The solution was allowed to reach room temperature, water (2 mL) was added, and the mixture was then extracted with dichloromethane. The extract was washed with water followed by saturated NaCl, dried, and evaporated to give a residue that on chromatography (hexane–acetone, eluting with 12% acetone

in hexane) gave the title product (18 mg, 90%), mp 231–233°C; ^{1}H nmr included signals at δ: 0.87 and 0.95 (each 3H, s, 18- and 19-H), 4.45 (1H, d, J = 14 Hz, 4-H), and 7.0–7.62 (4H, m, Ar-H) ppm; ms *m/z*(%): 407 (M^+, 34), 373(36), 358(52), 299(35), 243(35), 215(100). Anal. calcd. for $C_{25}H_{29}NO_2S$: C 73.67, H 7.17, N 3.44%; found: C 73.78, H 7.23, N 3.44%.

3,17-Diketo-androsteno[4,6-*b*,*c*]-1′,5′-benzothiazepine, 3

A solution of phenyl trimethyl ammonium tribromide (73 mg, 0.194 mmol) in dry THF (1.5 mL) was added at −2°C to a stirred solution of the diketone **11** (80 mg, 0.196 mmol) in dry THF over a period of 10 min, and the mixture stirred at this temperature for 2 h. The mixture was then extracted into dichloromethane, and the extract was washed with water followed by saturated NaCl, dried, and evaporated. The residue was chromatographed using hexane–acetone, the product (45 mg, 57%) being eluted with 10% acetone – hexane, mp 242–244°C; ^{1}H nmr included signals at δ: 0.95 (6H, s, 18- and 19-H) and 7.03–7.45 (4H, m, Ar-H) ppm; ms *m/z*(%): 405 (M^+, 10), 373(68), 358(100), 344(12), 316(16). Anal. calcd. for $C_{25}H_{27}NO_2S$: C 74.04, H 6.71, N 3.45%; found: C 74.03, H 6.64, N 3.43%.

Acknowledgements

We are grateful to Professor Ling-Kang Liu of the Institute of Chemistry, Academia Sinica, Taiwan, for carrying out the X-ray structure determination, and to Drs. V.C.O. Njar and P. Dorfmüller of the Department of Pharmaceutical Chemistry, Universität des Saarlandes, Germany, for the aromatase enzyme inhibition study. We are also grateful to Mr. T. Jones (Brock University) for assistance with the acquisition of spectral data. Financial support was provided by the Natural Sciences and Engineering Research Council of Canada.

References

1. L. Tan. Front. Biotransform. **6**, 63 (1992).
2. A.M.H. Brodie, W.M. Garratt, J.R. Hendrickson, C.-H. Tsai-Morris, P.A. Marcotte, and C.H. Robinson. Steroids, **38**, 393 (1981).
3. H.L. Holland, S. Kumaresan, L. Tan, and V.C.O. Njar. J. Chem. Soc. Perkin Trans. 1, 585 (1992).
4. L. Tan and P. Rousseau. Biochem. Biophys. Res. Commun. **147**, 1259 (1987); M. Gervais and L. Tan. Anticancer Res. **13**, 383 (1993).
5. M. Numazawa and M. Oshibe. J. Med. Chem. **37**, 1312 (1994).
6. M. Mushfiq and G. Mudgal. J. Ind. Chem. Soc. **69**, 784 (1992).
7. M. Mushfiq and N. Iqbal. J. Chem. Res. (S), 274 (1987).
8. H.L. Holland and E.M. Thomas. Can. J. Chem. **57**, 3069 (1979).
9. J.W. Blunt and J.B. Stothers. Org. Magn. Reson. **9**, 439 (1977).
10. D.N. Kirk and M.P. Hartshorn. Steroid reaction mechanisms. Elsevier, London. 1968. p. 193.
11. H. Mori. Chem. Pharm. Bull. **12**, 1224 (1964).

Can. J. Chem. Downloaded from www.nrcresearchpress.com by 46.23.64.124 on 09/08/12
For personal use only.

Synthesis of the carbocyclic analog of uridine 5′-(α-D-galactopyranosyl diphosphate) (UDP-Gal) as an inhibitor of β(1 → 4)-galactosyltransferase

Hideya Yuasa, Monica M. Palcic, and Ole Hindsgaul

Abstract: Uridine 5′-(5a-carba-α-D-galactopyranosyl diphosphate), the carbocyclic analog of UDP-galactose where the ring oxygen of the galactose residue is replaced by a methylene group, was chemically synthesized as a potential inhibitor of galactosyltransferases. It was found to be a competitive inhibitor of UDP-galactose:*N*-acetylglucosamine β(1 → 4)-galactosyltransferase from bovine milk (EC 2.4.1.22) with a K_i value of 58 μM, similar to the K_m value for UDP-galactose (25 μM).

Key words: carbocycles, UDP-5a-carbagalactose, galactosyltransferase, glycosyltransferase inhibitor.

Résumé : La 5′-(5a-carba-α-D-galactopyranosyl diphosphate) uridine, l'analogue carbocyclique de la UDP-galactose dans laquelle l'atome d'oxygène du résidu galactose a été remplacé par un groupe méthylène, a été synthétisée chimiquement comme un inhibiteur potentiel des galactosyltransférases. On a trouvé qu'elle est un inhibiteur compétitif de la UDP-galactose : *N*-acétylglucosamine β(1 → 4)-galactosyltransférase du lait bovin (EC 2.4.1.22) avec une valeur K_i de 58 μM, semblable à la valeur K_m de la UDP-galactose (25 μM).

Mots clés : carboxycles, UDP-5a-carbagalactose, galactosyltransférase, inhibiteur de glycosyltransférase.

[Traduit par la rédaction]

Introduction

Galactosyltransferases (Gal-T) catalyze the transfer of galactose from uridine 5′-diphosphate galactose (UDP-Gal, **1**) to growing oligosaccharide chains. Recent studies have revealed that a number of diseases are accompanied by structural changes of cell surface glycoconjugates; some of these structural changes are due to a change in Gal-T activity (1). For example, the down-regulation of Gal-T has been observed in multiple myeloma (2) and rheumatoid arthritis (3), while the up-regulation has been suggested for some liver diseases (4) and for Burkitt's lymphoma (5). Inhibitors of Gal-T could be important research tools since they might be able to regulate Gal-T activity, thereby clarifying the role of this enzyme in aberrant glycosylation. In the long term, small-molecule glycosyltransferase inhibitors may serve as drugs because they may be able to alter cell-surface glycosylation by decreasing galactosylation.

The unreactive sugar nucleotide analogs **2** (6) and **3** (7), which differ from UDP-Gal (**1**) in the diphosphate portion, have been synthesized previously and their K_i values were estimated to be 97 and 165 μM, respectively. The K_i (32 μM) of UDP is reported to be considerably lower (8), suggesting that an intact diphosphate grouping is preferred for binding. We therefore decided to synthesize the carbocyclic analog **4** of UDP-Gal, an analog expected to be unreactive while retaining an unmodified diphosphate linkage. The analog **4** might also be an inhibitor of UDP-Gal binding proteins such as the UDP-Gal transporter protein. A mutant of a cancer cell line lacking UDP-Gal transport protein does not metastasize (9).

During the course of this study, Toyokuni's group reported the synthesis of the carbocylic analog of guanosine 5′-(β-L-fucopyranosyl diphosphate) (GDP-Fuc) as an inhibitor of fucosyltransferases (FucT) and showed that the inhibitor binds to FucT comparably to GDP-Fuc (10). Here we report the synthesis of **4** and its inhibitory effect toward β(1 → 4)-Gal-T.

Results and discussion

Although two groups have reported the syntheses of 5a-carba-α-D-galactopyranose (11), the procedures used appeared cumbersome in view of the selective protection of hydroxyls required for UDP incorporation at OH-1. We therefore decided to employ the Ferrier reaction in the key step as has been frequently used in the synthesis of carbocycles (for example, see ref. 12). Initial attempts to use the Ferrier reaction for the synthesis of methyl 2,3,4-tri-*O*-acetyl-6-deoxy-α-L-*arabino*-hex-5-enopyranoside resulted in decomposition, so we elected to use benzyl groups for hydroxyl protection. Methyl 2,3,4-tri-*O*-benzyl-β-D-galactopyranoside **5** (13), obtainable in three steps from methyl β-D-galactopyranoside, was the starting material (Scheme 1).

Received August 1, 1995.

H. Yuasa,[1] M.M. Palcic, and O. Hindsgaul.[2] Department of Chemistry, University of Alberta, Edmonton, AB T6G 2G2, Canada.

[1] Present address: Department of Life Science, Faculty of Bioscience and Biotechnology, Tokyo Institute of Technology, Nagatsuta, Midori-ku, Yokohama 226, Japan.

[2] Author to whom correspondence may be addressed. Telephone: (403) 492-4171. Fax: (403) 492-7705. E-mail: Ole.Hindsgaul@Ualberta. Ca.

Can. J. Chem. Downloaded from www.nrcresearchpress.com by 46.23.64.124 on 09/08/12
For personal use only.

Can. J. Chem. Downloaded from www.nrcresearchpress.com by 46.23.64.124 on 09/08/12
For personal use only.

Scheme 1.

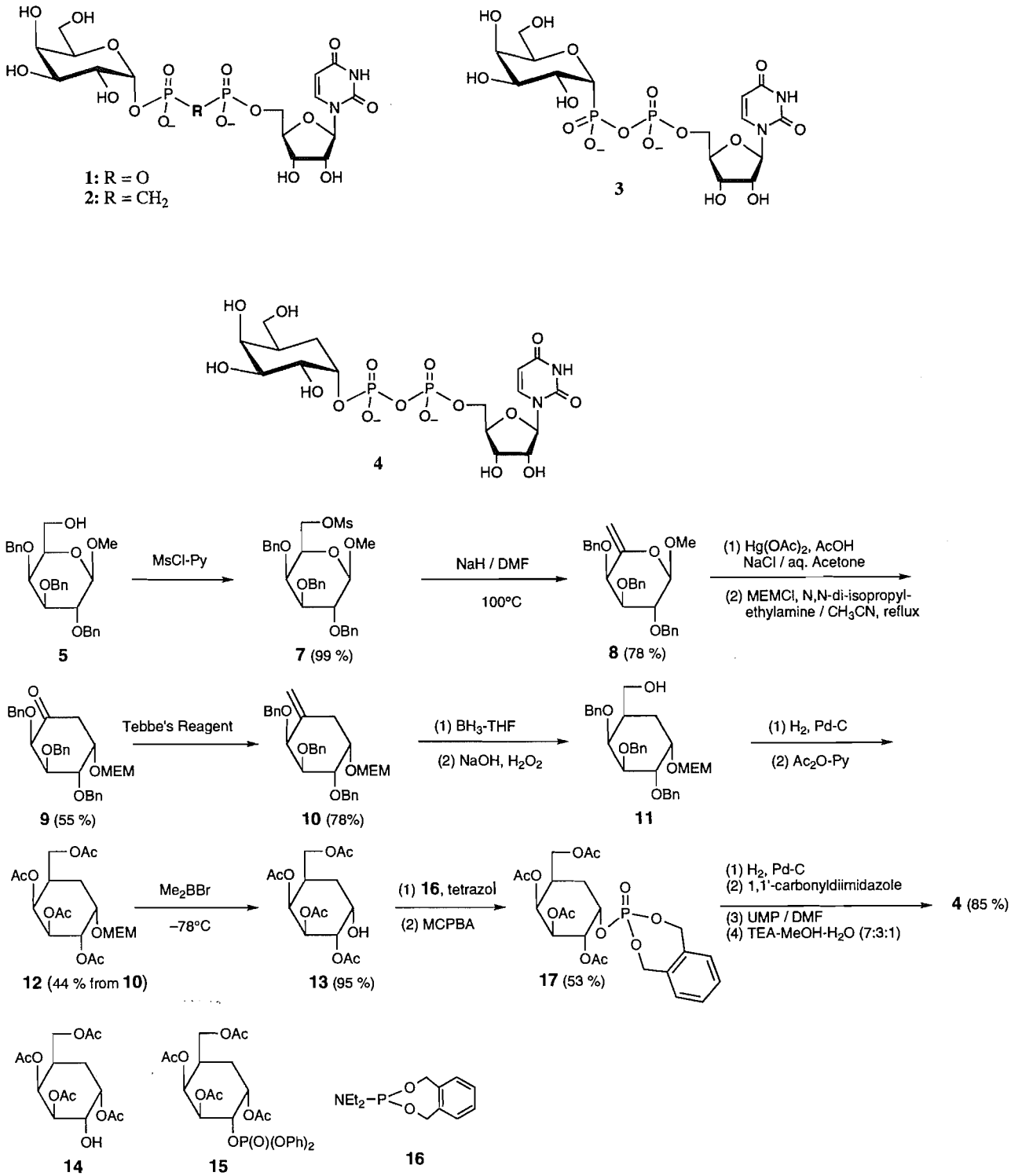

Attempts to introduce reactive leaving groups such as iodide and trifluoromethanesulfonate, for the purpose of producing alkene **8**, resulted instead in cyclization between O-3 and C-6 to give the 3,6-anhydro-sugar **6**, presumably through the mechanism shown in Scheme 2. The mesylate **7**, however, was readily prepared and reacted smoothly with sodium hydride to give **8**.

Application of the Ferrier reaction to **8** was successful and protection of the resultant hydroxyl group as the methoxyethoxymethyl (MEM) ether afforded the cyclohexanone **9**. Conversion of the carbonyl group of **9** into the required exocyclic methylene group was achieved with Tebbe's reagent (14) to give the methylenecyclohexane **10**. Attempted Wittig reaction of **9** with methylenetriphenylphosphorane gave only decomposition products.

The hydroboration of **10** gave a complex mixture contain-

Can. J. Chem. Downloaded from www.nrcresearchpress.com by 46.23.64.124 on 09/08/12
For personal use only.

Scheme 2.

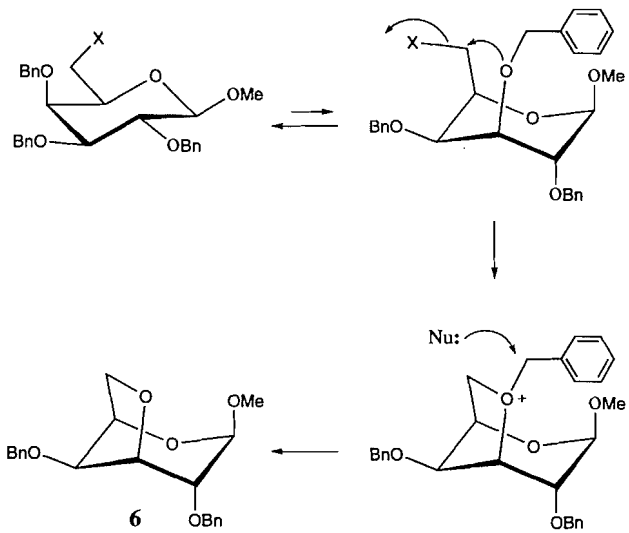

ing **11**, which was converted to **12** by hydrogenation (H_2, Pd/C) and acetylation. The coupling constants of the ring protons of **12** ($J_{1,2}$ 3.0, $J_{2,3}$ 11.0, $J_{3,4}$ 3.0, $J_{4,5}$ ~0 Hz) are consistent with the $^4C_1$ conformation. The C-5 epimer would not be expected to adopt this $^4C_1$ conformation. Common reagents used for deprotection of the MEM group in **12**, e.g., $ZnBr_2$ and $TiCl_4$, were unsuccessful, but dimethylboron bromide, developed by Guindon et al. (15), gave a high yield of the deprotected alcohol **13**.

Phosphorylation of the hydroxyl group in **13** was first attempted using diphenylphosphorochloridate and *n*-butyllithium. However, migration of the acetyl group from O-2 to O-1 was the major reaction yielding **14** (12%) and the 2-O-phosphorylated compound **15** (51%). Even pyridine as a solvent was sufficient to cause this migration so a milder method of phosphorylation was required. We therefore employed phosphitylation (16) with 2-dimethylamino-5,6-benzo-1,3-dioxa-2-phosphepane **16** followed by oxidation with *m*-chloroperoxybenzoic acid (MCPBA) to give the desired phosphate **17**. Removal of the benzyl esters of the phosphate by hydrogenation, activation with 1,1′-carbonyldiimidazole, coupling with uridine monophosphate (UMP), and de-O-acetylation then yielded the title compound **4**, which was purified by ion-exchange chromatography.

The K_i value of **4** toward UDP-galactose:N-acetylglucosamine β(1 → 4)-galactosyltransferase from bovine milk (EC 2.4.1.22) was determined to be 58 μM using a previously reported radiochemical "Sep-Pak" assay (17) with 8-methoxycarbonyloctyl 2-acetamido-2-deoxy-β-D-glucopyranoside as the acceptor. This value is essentially the same as the K_m value determined for UDP-Gal (25 μM) under the same experimental conditions, and the same as the K_i value for UDP-5′-thiogalactose (ref. 18, and unpublished data). To confirm that transfer of "carba-Gal" did not occur, a preparative synthesis was attempted using 20 units of Gal-T, 4.4 mg of compound **4**, and 1.6 mg of acceptor for 5 days at room temperature. No product formation was detected by ^1H NMR spectroscopy. Compound **4** was assumed to be stable under these conditions since UDP-Gal has been successfully used in such long incubations, but this issue was not specifically addressed in this work. Certainly, it is stable in the shorter incubations or unusual kinetic behaviour would have been observed. Under these conditions, less than 1 min would be required for complete galactosylation using the natural donor, UDP-Gal. From these results, the conclusions are that the ring oxygen of galactose is not essential for recognition of UDP-Gal by the enzyme but is essential for transfer to occur. This is consistent with the generally accepted mechanism for glycosyl transfer that involves an oxocarbonium ion-like transition state (19).

Experimental

All solvents and reagents used were reagent grade and, in cases where further purification was required, standard procedures (20) were followed. All solid reactants for moisture-sensitive reactions were dried overnight over phosphorus pentoxide under high vacuum prior to use. Solution transfers where anhydrous conditions were required were done under dry nitrogen using syringes. Molecular sieves were purchased from BDH chemicals. Thin-layer chromatograms (TLC) were performed on precoated silica gel 60-F254 plates (E. Merck, Darmstadt) and visualized by quenching of fluorescence and (or) by charring after spraying with 5% sulfuric acid in ethanol. For silica gel chromatography 40–63 μm (400–230 mesh) silica gel 60 (E. Merck No. 9385) and distilled solvents were used, and the ratio of silica gel to compound was in the range 50:1–100:1. Water was evaporated under the vacuum of an oil pump using a rotary evaporator equipped with a condenser containing acetone and Dry Ice. Organic solvents were removed on a rotary evaporator under the vacuum of a water aspirator with bath temperatures of 40°C or lower. Elemental analyses were performed by the Analytical Service Laboratory of the Chemistry Department.

Proton nuclear magnetic resonance (^1H NMR) spectra were recorded at 300 MHz (Bruker AM-300) with internal tetramethylsilane (δ 0 in $CDCl_3$) or external acetone (δ 2.225 in D_2O) at ambient temperature. Carbon-13 nuclear magnetic resonance (^{13}C NMR) spectra were recorded at 75 MHz (Bruker AM-300) with either internal tetramethylsilane (δ 0 in $CDCl_3$) or external 1,4-dioxane (δ 67.4 in D_2O) as the reference standard. Phosphorus-31 nuclear magnetic resonance (^{31}P NMR) spectra were recorded at 108 MHz (Bruker AM-200) with external H_3PO_4 (85%) (δ 0 in D_2O) as the reference standard. The chemical shifts at lower field, relative to external H_3PO_4, are expressed as positive numbers while those at higher field are expressed as negative numbers. Optical rotations were determined on a Perkin–Elmer 241 polarimeter in a 1 dm cell at ambient temperature (23 ± 1°C).

Methyl 2,3,4-tri-*O*-benzyl-6-*O*-methanesulfonyl-β-D-galactopyranoside (7)

A solution of methyl 2,3,4-tri-*O*-benzyl-β-D-galactopyranoside (**5**, 0.488 g, 1.05 mmol) and methanesulfonyl chloride (0.12 mL, 1.55 mmol) in pyridine (10 mL) was kept at room temperature for 2.5 h. Water was added to the reaction mixture, which was then extracted with CH_2Cl_2. The organic layer was washed with aqueous $NaHCO_3$ and concentrated. The residue was chromatographed on silica gel (hexane – ethyl acetate 3:1) to give **7** (0.563 g, 99%) as a white solid: $[\alpha]_D$ −14.2 (*c* 1.5, $CHCl_3$); R_f 0.38 (2:1 hexane – ethyl acetate). ^1H NMR ($CDCl_3$) δ: 7.4–7.25 (m, 15H, Ar), 5.00, 4.62 (each d, 2H, J_{gem} 11.5 Hz, $PhCH_2$), 4.90, 4.75 (each d, 2H, J_{gem} 11.0 Hz,

Can. J. Chem. Downloaded from www.nrcresearchpress.com by 46.23.64.124 on 09/08/12
For personal use only.

$PhCH_2$), 4.86, 4.74 (each d, 2H, J_{gem} 12.0 Hz, $PhCH_2$), 4.33 (dd, 1H, $J_{5,6a}$ 7.0, $J_{6a,6b}$ 10.8 Hz, H-6a), 4.29 (d, 1H, $J_{1,2}$ 7.5 Hz, H-1), 4.06 (dd, 1H, $J_{5,6b}$ 5.3 Hz, H-6b), 3.82 (dd, 1H, $J_{2,3}$ 9.5 Hz, H-2), (m, 1H, H-4), 3.65 (ddd, H-1, $J_{4,5}$ 1.0 Hz, H-5), 3.55 (d, 1H, $J_{3,4}$ 3.0 Hz, H-3), 3.55 (s, 3H, OCH_3), 2.93 (s, 3H, SO_2CH_3). Anal. calcd. for $C_{29}H_{34}O_8S$: C 64.19, H 6.32, S 5.91; found: C 63.97, H 6.30, S 6.27.

Methyl 2,3,4-tri-*O*-benzyl-6-deoxy-α-L-*arabino*-hex-5-enopyranoside (8)

A mixture of **7** (0.362 g, 0.667 mmol) and 50% NaH (75 mg, 1.6 mmol, from which the oil was removed by washing with hexane prior to use) in DMF (8 mL) was stirred for 2 h at 100°C. After cooling, ice-water was added and the mixture was extracted with Et_2O. The organic layer was dried over $MgSO_4$ and concentrated. The residue was chromatographed on silica gel (hexane – ethyl acetate 13:1) to give **8** (0.232 g, 78%) as a syrup: $[\alpha]_D$ −9.0 (*c* 2.0, $CHCl_3$); R_f 0.33 (10:1 hexane – ethyl acetate). ^1H NMR ($CDCl_3$) δ: 7.45–7.25 (m, 15H, Ar), 4.85–4.75 (m, 4H, 2 × $PhCH_2$), 4.62 (s, 2H, $PhCH_2$), 4.46, 4.44 (each d, 2H, J_{gem} 6.0 Hz, C=CH_2), 4.43 (d, 1H, $J_{1,2}$ 7.0 Hz, H-1), 4.02 (d, 1H, $J_{3,4}$ 3.2 Hz, H-4), 3.99 (dd, 1H, $J_{2,3}$ 9.5 Hz, H-2), 3.62 (s, 3H, OCH_3), 3.56 (dd, 1H, H-3). Anal. calcd. for $C_{28}H_{30}$plain$6O_5$: C 75.31, H 6.77; found: C 75.12, H 6.82.

(2*R*)-2,3/4,5-2,3,4-Tribenzyloxy-5-methoxyethoxymethoxycyclohexanone (9)

Enolate **8** (0.591 g, 1.32 mmol) and mercury(II) acetate (0.758 g, 2.38 mmol) were heated to reflux in 40% aqueous acetone (28 mL) containing acetic acid (1%) for 1 h. NaCl (0.758 g, 13 mmol) was added, and the mixture was heated for a further 20 min. After cooling, the mixture was concentrated, and the residue was partitioned between CH_2Cl_2 and water. The organic layer was dried over $MgSO_4$ and concentrated. The residue was chromatographed on silica gel (hexane – acetyl acetate 5:2) to give a mixture of (2*R*)-2,3/4,5-2,3,4-tribenzyloxy-5-hydroxycyclohexanone and unknown compounds as a syrup (0.615 g). A mixture of this syrup, 2-methoxyethoxymethyl chloride (0.78 mL, 6.83 mmol), and *N*,*N*-diisopropylethylamine (1.10 mL, 7.85 mmol) in CH_3CN (12 mL) was refluxed for 2 h. The mixture was concentrated and chromatographed on silica gel (hexane – ethyl acetate 3:1–5:2) to give **9** (0.376 g, 55%; R_f 0.39, 2:1 *n*-hexane – ethyl acetate) as a syrup and a mixture of unknown compounds (87 mg; R_f 0.29, the same solvent as above).

9: $[\alpha]_D$ +59.8 (*c* 1.2, $CHCl_3$); ^1H NMR ($CDCl_3$) δ: 7.4–7.15 (m, 15H, Ar), 4.83, 4.42 (each d, 2H, J_{gem} 12.5 Hz, $PhCH_2$), 4.75, 4.55 (each d, 2H, J_{gem} 12.5 Hz, $PhCH_2$), 4.72, 4.54 (each d, 2H, J_{gem} 12.0 Hz, $PhCH_2$), 4.71 (s, 2H, OCH_2O), 4.37 (dd, 1H, $J_{2,3}$ 3.0, $J_{2.6a}$ 0.5 Hz, H-2), 4.27 (ddd, 1H, $J_{4,5}$ 3.0, $J_{5,6a}$ 10.0, $J_{5.6b}$ 6.0 Hz, H-5), 3.99 (dd, 1H, $J_{3,4}$ 5.0 Hz, H-3), 3.95 (ddd, 1H, $J_{4,6b}$ 1.0 Hz, H-4), 3.69–3.64, 3.54–3.49 (each m, 4H, OCH_2CH_2O), 3.37 (s, 3H, OCH_3), 2.80 (ddd, 1H, $J_{6a,6b}$ 13.2 Hz, H-6a), 2.73 (ddd, 1H, H-6b); ^{13}C NMR δ: 204.6 (C-1), 138.1, 137.9, 128.4, 128.3, 127.9, 127.8, 127.7 (Ar), 94.6 (OCH_2O), 81.5, 77.9, 76.9, 73.8 (C-2, C-3, C-4, C-5), 73.5, 72.6, 71.7 ($PhCH_2$), 67.2 (OCH_2), 59.1 (OCH_3), 42.6 (C-6). Anal. calcd. for $C_{31}H_{36}O_7$: C 71.52, H 6.97; found: C 71.52, H 6.94.

(1*S*)-1,2/3,4-2,3,4-Tribenzyloxy-1-methoxyethoxymethoxy-5-methylenecyclohexane (10)

To a stirred solution of **9** (0.749 g, 1.44 mmol) in toluene–THF (9/3 mL/mL) containing pyridine (7 μL) was slowly added a 2 M solution of Tebbe's reagent ($Cp_2TiCH_2AlClMe_2$) in toluene (3.08 mL, 6.16 mmol) at −40°C. After stirring for 0.5 h at −40°C, the temperature was slowly increased to room temperature over 1.5 h. After addition of 0.3 M NaOH (0.1 mL) (gas was evolved), Et_2O and $MgSO_4$ were added to the reaction mixture. Insoluble material was removed by filtration with Celite and the filtrate was concentrated. The residue was chromatographed on silica gel (hexane – ethyl acetate 5:2) to give **10** (0.585 g, 78%) as a syrup: $[\alpha]_D$ +5.5 (*c* 1.5, $CHCl_3$); R_f 0.53 (2:1 *n*-hexane – ethyl acetate). ^1H NMR ($CDCl_3$) δ: 7.4–7.25 (m, 15H, Ar), 5.03 (d, 2H, C=CH_2), 4.81–4.34 (m, 8H, 3 × $PhCH_2$ and OCH_2O), 4.12 (m, 2H, H-1 and H-4), 3.98 (dd, 1H, $J_{1,2}$ 3.0, $J_{2,3}$ 9.0 Hz, H-2), 3.83 (dd, 1H, $J_{3,4}$ 3.5 Hz, H-3), 3.70, 3.50 (each m, 4H, OCH_2CH_2O), 3.38 (s, 3H, OCH_3), 2.5–2.35 (m, 2H, H-6a and H-6b), ^{13}C NMR δ: 141.2 (C-5), 139.0, 138.5 (C=CH_2 and Ar), 128.3, 128.2, 127.8, 127.7, 127.4, 127.3 (Ar), 94.8 (OCH_2O), 78.9, 78.7, 73.6 (C-1, C-2, C-3, C-4), 73.3, 72.6, 71.7 ($PhCH_2$), 69.7, 66.9 (OCH_2CH_2O), 59.0 (OCH_3), 33.9 (C-6). Anal. calcd. for $C_{32}H_{38}O_6$: C 74.11, H 7.38; found: C 73.72, H 7.49.

(1*S*)-1,2/3,5-2,3,4-Tribenzyloxy-5-hydroxymethyl-1-methoxyethoxymethoxycyclohexane (11)

To a stirred solution of **10** (1.205 g, 2.32 mmol) in THF (23 mL) was slowly added a 1 M solution of BH_3–THF complex (2.63 mL) at 0°C. The reaction mixture was allowed to warm to 20°C and stirred for 17 h. EtOH (4.8 mL) was added to the mixture at 0°C followed by 3 M NaOH (8.1 mL) and 30% H_2O_2 (4.8 mL) and the mixture was stirred for 5 h at room temperature. After addition of 1 M NaOH, the mixture was extracted three times with Et_2O. The combined organic layers were concentrated and the residue chromatographed on silica gel (hexane – ethyl acetate 1:1) to give **11**, contaminated with unknown impurities (0.940 g; R_f 0.25, 1:1 hexane – ethyl acetate), as a syrup, which was used for the next reaction without further purification.

(1*S*)-1,2/3,4,5-2,3,4-Triacetoxy-5-acetoxymethyl-1-methoxyethoxymethoxycyclohexane (12)

Syrupy **11** (0.94 g), described above, in MeOH (50 mL) was stirred under H_2 (1 atm = 101.3 kPa) in the presence of 5% Pd/C (0.882 g) for 5 h at room temperature, then filtered, and concentrated. The residue was chromatographed on silica gel (CH_2Cl_2–MeOH 8:1). The fractions containing the major product (R_f 0.22, 8:1 CH_2Cl_2–MeOH) were collected and concentrated to give a white solid (0.350 g), which was acetylated with acetic anhydride (3 mL) and pyridine (3 mL). The product obtained after evaporation and aqueous extraction was chromatographed on silica gel (hexane – ethyl acetate 1:1) to give **12** (0.444 g, 44% from **10**) as a syrup: $[\alpha]_D$ +38.9 (*c* 1.1, $CHCl_3$); R_f 0.27 (1:1 hexane – ethyl acetate). ^1H NMR ($CDCl_3$) δ: 5.54 (bs, 1H, H-4), 5.30 (dd, 1H, $J_{2,3}$ 11.0, $J_{3,4}$ 3.0 Hz, H-3), 5.14 (dd, 1H, $J_{1,2}$ 3.0 Hz, H-2), 4.78, 4.74 (each d, 2H, J_{gem} 7.5 Hz, OCH_2O), 4.22 (m, 1H, H-1), 3.96 (dd, 1H, J_{gem} 11.0, J_{vic} 9.5 Hz, C*H*HOAc), 3.87 (dd, 1H, J_{vic} 6.0 Hz, CH*H*OAc), 3.72, 3.54 (each m, 4H, OCH_2CH_2O), 3.38 (s, 3H, OCH_3), 2.51 (m, 1H, H-5), 2.10, 2.06, 2.04, 1.98 (each s, each 3H, OAc), 1.85 (ddt, 1H, $J_{5,6e}$ 3.8, $J_{4,6e}$ 1.5, $J_{6a,6e}$ 1.40 Hz, H-6e), 1.63 (m, 1H, H-6a). Anal. calcd. for $C_{19}H_{30}O_{11}$: C 52.53, H 6.96; found: C 52.45, H 7.04.

Can. J. Chem. Downloaded from www.nrcresearchpress.com by 46.23.64.124 on 09/08/12
For personal use only.

(1*S*)-1,2/3,4,5-2,3,4-Triacetoxy-5-acetoxymethyl-1-hydroxycyclohexane (13)

To a stirred solution of **12** (0.165 g, 0.38 mmol) in CH_2Cl_2 (5 mL) was added bromo dimethylborane (0.13 mL, 1.33 mmol) at −78°C. After 1 h, the mixture was diluted with CH_2Cl_2, washed with aqueous $NaHCO_3$, and concentrated. The residue was chromatographed on silica gel (hexane – ethyl acetate 1:1) to give **13** (0.125 g, 95%) as a syrup: $[\alpha]_D$ +35.3 (*c* 0.8, $CHCl_3$); R_f 0.5 (1:2 benzene – acetate). ^1H NMR ($CDCl_3$) δ: 5.54 (bs, 1H, H-4), 5.31 (dd, 1H, $J_{2,3}$ 10.5, $J_{3,4}$ 3.0 Hz, H-3), 5.19 (dd, 1H, $J_{1,2}$ 3.0 Hz, H-2), 4.26 (m, 1H, H-1), 3.98 (dd, 1H, J_{gem} 11.0, J_{vic} 9.0 Hz, C*H*HOAc), 3.87 (dd, 1H, J_{vic} 6.0 Hz, CH*H*OAc), 2.60 (m, 1H, H-5), 2.11 (s, 6H, 2 × Ac), 2.04, 1.99 (each s, each 3H, Ac), 1.83 (ddt, 1H, $J_{5,6e} = J_{6e,1}$ 4.0, $J_{4,6e}$ 1.5, $J_{6a,6b}$ 14.0 Hz, H-6e), 1.70 (m, 1H, H-6a). Anal. calcd. for $C_{15}H_{22}O_9$: 52.02, H 6.40; found: C 51.83, H 6.62.

(1*S*)-1,2/3,4,5-2,3,4-Triacetoxy-5-acetoxymethyl-1-(2-oxo-5,6-benzo-1,3,2-dioxaphosphep-2-yloxy)-cyclohexane (17)

To a solution of **13** (165 mg, 0.476 mmol) and tetrazole (107 mg, 1.53 mmol) in CH_2Cl_2 (3 mL) was added 2-dimethylamino-5,6-benzo-1,3-dioxa-2-phosphepane **15** (180 mg, 0.752 mmol) and the mixture was stirred at room temperature for 2 h. The reaction mixture was then cooled to −40°C and the solution of MCPBA (208 mg) in CH_2Cl_2 (3 mL) was added. The stirring was continued for 10 min at −40°C and for another 40 min at 0°C. The reaction mixture was diluted with CH_2Cl_2 and washed consecutively with aqueous $NaHSO_4$ and aqueous $NaHCO_3$. The organic layer was dried over $MgSO_4$ and concentrated. The residue was chromatographed on silica gel (hexane – ethyl acetate 1:2) to give **17** (147 mg, 53%) as a foam: $[\alpha]_D$ +53.6 (*c* 0.8, $CHCl_3$); R_f 0.17 (1:2 hexane – ethyl acetate). ^1H NMR ($CDCl_3$) δ: 7.4–7.25 (m, 4H, Ar), 5.57 (m, 1H, H-4), 5.4–5.1 (m, 7H, H-2, H-3, 2 × $ArCH_2$), 4.00 (dd, 1H, J_{gem} 11.5, J_{vic} 9.5 Hz, C*H*HOAc), 3.88 (dd, 1H, J_{vic} 6.0 Hz, CH*H*OAc), 2.12 (s, 6H, 2 × Ac), 2.06, 2.01 (each s, each 3H, Ac), 1.81 (m, 1H, H-6a), 1.62 (m, 1H, H-6b); ^{13}C NMR δ: 170.7, 170.3, 170.2, 170.0 ($COCH_3$), 135.0, 134.9, 129.2, 128.8, 128.75 (Ar), 74.7 (d, $J_{C\text{-}1,P}$ 5.3 Hz, C-1), 69.5, (d, $J_{C\text{-}2,P}$ 3.8 Hz, C-2), 69.2, 68.1 (C-3, C-4), 68.6, 68.5 (2 × $ArCH_2$), 62.7 (CH_2OAc), 32.7 (C-5), 28.0 (C-6), 20.9, 20.7 ($COCH_3$); ^{31}P NMR δ: −0.15. Anal. calcd. for $C_{23}H_{29}O_{12}P$: C 52.28, H 5.53; found: 52.16, H 5.62.

Uridine 5′-(5a-carba-α-D-galactopyranosyl diphosphate) (4)

A solution of **17** (54 mg, 0.102 mmol) in MeOH (4 mL) was stirred under H_2 (1 atm) in the presence of 5% Pd/C (24 mg) for 2 h at room temperature, then filtered and concentrated to give a syrup (R_f 0.70, 60:35:1 dichloromethane–methanol–water), which was dissolved in dry acetone (2 mL) and 1,1′-carbonyldiimidazole (50 mg, 0.246 mmol) was added. The mixture was stirred for 18 h at room temperature. When the reaction was complete, as monitored by TLC (the imidazolide has R_f 0.25, 3:1 $CHCl_3$–MeOH), MeOH (5 μL) was added and stirring continued for a further 20 min. The mixture was concentrated and dried over phosphorus pentoxide in vacuo for 6 h. Meanwhile, uridine 5′-monophosphate disodium salt (74 mg, 0.20 mmol) was passed slowly through a column of Dowex 50 × 8 (H^+) resin and the column was thoroughly washed with water. The eluate was concentrated and trioctylamine (94 μL, 2.15 mmol) was added. The mixture was coevaporated three times with DMF and a solution of the imidazolide in DMF (2.5 mL) was added. The mixture was stirred for 18 h at room temperature and monitored by TLC (the pyrophosphate coupling product has R_f 0.17, 60:40:3 CH_2Cl_2–MeOH–water). The solvent was evaporated and MeOH (3.5 mL), water (1.5 mL), and triethylamine (0.5 mL) were added. After 7 h, the reaction mixture was slowly passed through a column of Dowex 1 × 2-200 (3 × 12 cm, HCO_3^-) and the column was washed with 40 mM ammonium bicarbonate. The product was then eluted using a linear gradient from 40 to 700 mM ammonium bicarbonate (1.1 L) at 23°C. The column was at 23°C at a flow rate of 1.6 mL/min. Each fraction (12 mL) was monitored by UV absorption at 280 nm. Fractions of the product were pooled and concentrated. The residue was dissolved into water and remaining ammonium bicarbonate was removed by adding Dowex 50 × 8 (H^+) until the pH became less than 7.0 (CO_2 gas was evolved). After removing the resin by filtration, the filtrate was concentrated to 5 mL, passed through a Millex-SR 2 μM filter, and lyophilized to give **4** (49 mg, 85%) as a white solid: R_f 0.33 (7:3:1 i-propanol–water – conc. ammonium hydroxide). ^1H NMR (D_2O) δ: 7.97 (d, 1H, $J_{5,6}$ 8.3 Hz, H-6), 5.99 (d, 1H, $J_{1',2'}$ 3.0 Hz, H-1′), 5.98 (d, 1H, H-5), 4.62 (m, 1H, H-1″), 4.09 (m, 1H, H-4″), 3.78 (dd, 1H, $J_{2'',3''}$ 10.5, $J_{3'',4''}$ 3.0 Hz, H-3″), 3.68 (dt, $J_{1'',2''} = J_{2'',P}$ 3.0 Hz, H-2″), 3.62 (dd, 1H, $J_{5'',6a''}$ 8.0, $J_{6a'',6b''}$ 11.5 Hz, H-6a″), 3.52 (d, 1H, $J_{5'',6b''}$ 6.5 Hz, H-6b″), 2.14 (m, 1H, H-5″), 1.94, 1.55 (each m, 2H, ring methylene); ^{13}C NMR δ: 167.1 (C-4), 152.7 (C-2), 142.5 (C-6), 103.5 (C-5), 89.3 (C-1′), 84.1 (d, $J_{C\text{-}4',P}$ 8.4 Hz, C-4′), 76.5 (d, $J_{C\text{-}1'',P}$ 5.5 Hz, C-1″), 74.6, 72.4, 70.6, 70.5 (C-2′, C-3′, C-3″, C-4″), 65.7 (d, $J_{C\text{-}5',P}$ 5.5 Hz, C-5′), 63.2 (C-6″), 37.1 (C-5″), 27.7 (ring methylene of carbagalactose); ^{31}P NMR δ: −10.8 (d, $J_{P,P}$ 20.6 Hz, P attached to uridine), −11.2 (d, P attached to carbagalactose).

Inhibitory assay

Bovine milk β(1 → 4) galactosyltransferase was isolated by chromatography on UDP-hexanolamine and α-lactalbumin Sepharose (21, 22). Kinetic studies were carried out, as previously described (17), in 0.5 mL plastic microcentrifuge tubes that contained 420 μM 8-methoxycarbonyloctyl 2-acetamido-2-deoxy-β-D-glucopyranoside acceptor, 76 000 dpm of UDP-6[^{3}H] Gal, 0.01–1.1 mM UDP-Gal, 0.5 micro-units of enzyme, 250 mM NaCl, 8 mM $MnCl_2$, and 80 mM sodium cacodylate buffer, pH 7.5, in a total volume of 55 μL. After incubation for 20 min at 37°C, the samples were diluted to 500 μL with water and applied to C-18 reverse-phase cartridges. The cartridges were washed with 50–70 mL of water to removed unreacted donor and then the radiolabelled product eluted with 5 mL of methanol into 20 mL plastic scintillation vials. Ecolite (+) cocktail (10 mL) was added to the vials and the amount of product formed was quantitated by counting in a Beckman LS 1801 scintillation counter. Data were analyzed using nonlinear regression analysis of the Michaelis–Menten equation with Sigma Plot to give a K_m for the donor UDP-Gal of 25 μM under these conditions. The K_i for compound **3** was estimated by carrying out kinetic measurements with same range of donor concentrations with 100 μM of **3** added to all of the assay mixtures. Compound **3** was a competitive inhibitor of the galactosyltransferase with a K_i of 58 μM using the equa-

tion $K_m(app) = K_m(1 + [I]/[K_i]$ where $K_m = K_m$ for UDP-Gal, $K_m(app)$ is the K_m in the presence of inhibitor, and [I] is the inhibitor concentration (100 μMm).

No product was formed in incubations that contained 20 units of galactosyltransferase in 1.0 mL of 100 mM sodium cacodylate buffer, pH 7.5, 4.4 mg of compound **3**, and 1.6 mg of 8-methoxycarbonyl octyl 2-acetamido-2-deoxy-β-D-glucopyranoside acceptor after 5 days of reaction at ambient temperature. Only unreacted acceptor was re-isolated on Sep Pak cartridges as evidenced by ^{1}H NMR spectroscopy.

Acknowledgements

This work was supported by grants to both O.H. and M.M.P. from the Natural Sciences and Engineering Research Council of Canada. Thanks also to Ms. H. Li for the isolation of the galactosyltransferase and to Dr. K. Stangier for the kinetic evaluations.

References

1. A. Varki. Glycobiology, **3**, 97 (1993).
2. T. Nishiura, S. Fujii, Y. Kanayama, A. Nishikawa, Y. Tomiyama, M. Iida, T. Karasuno, H. Nakao, T. Yonezawa, N. Taniguchi, and S. Tarui. Cancer Res. **50**, 5345 (1990).
3. K. Furukawa, K. Matsuta, F. Takeuchi, E. Kosuge, T. Miyamoto, and A. Kobata. Int. Immunol. **2**, 105 (1990).
4. Y.S. Kim, J. Perdomo, J.S. Whitehead, and K.J. Curtis. J. Clin. Invest. **51**, 2033 (1972).
5. E. Nudelman, R. Kannagi, S. Hakomori, M. Parsons, M. Lipinski, J. Wiels, M. Fellous, and T. Tursz. Science, **220**, 509 (1983).
6. M.M. Vaghefi, R.J. Bernacki, W.J. Hennen, and R.K. Robins. J. Med. Chem. **30**, 1391 (1987).
7. M.M. Vaghefi, R.J. Bernacki, N.K. Dalley, B.E. Wilson, and R.K. Robins. J. Med. Chem. **30**, 1383 (1987).
8. J.T. Powell and K. Brew. Biochemistry, **15**, 3499 (1976).
9. J.W. Dennis, S. Laferté, C. Waghorne, M.L. Breitman, and R.S. Kerbel. Science, **236**, 582 (1987).
10. S. Cai, M.R. Stroud, S. Hakomori, and T. Toyokuni. J. Org. Chem. **57**, 6693 (1992).
11. H. Paulsen, W. von Deyn, and W. Röben. Liebigs Ann. Chem. 433 (1984); S. Ogawa, Y. Iwasawa, and T. Suami. Chem. Lett. 355 (1984).
12. R.J. Ferrier and S. Middleton. Chem. Rev. **93**, 2779 (1993); R. Blattner, R.J. Ferrer, and S.R. Haines. J. Chem. Soc. Perkin Trans. 1, 2413 (1985).
13. P.A.J. Gorin. Carbohydr. Res. **101**, 13 (1982).
14. F.N. Tebbe, G.W. Parshall, and G.S. Reddy. J. Am. Chem. Soc. **100**, 3611 (1978); S.H. Pine, G.S. Shen, and H. Hoang. Synthesis, 165 (1991).
15. Y. Guindon, C. Yoakim, and H.E. Morton. J. Org. Chem. **49**, 3912 (1984).
16. Y. Watanabe, Y. Komoda, K. Ebisuya, and S. Ozaki. Tetrahedron Lett. **31**, 255 (1990).
17. M.M. Palcic, L.D. Heerze, M. Pierce, and O. Hindsgaul. Glycoconjugate J. **5**, 49 (1988).
18. H. Yuasa, O. Hindsgaul, and M.M. Palcic. J. Am. Chem. Soc. **114**, 5891 (1992).
19. C.-H. Wong, R.L. Halcomb, Y. Ichikawa, and T. Kajimoto. Angew. Chem. Int. Ed. Engl. **34**, 521 (1995).
20. D.D. Perrin, W.L. Armarego, and D.R. Perrin. Purification of laboratory compounds. 2nd ed. Pergamon Press, London. 1980.
21. R. Baker, K.W. Olsen, J.H. Shaper, and R.L. Hill. J. Biol. Chem. **247**, 7135 (1972).
22. I.P. Trayer and R.L. Hill. J. Biol. Chem. **246**, 6666 (1973).

Can. J. Chem. Downloaded from www.nrcresearchpress.com by 46.23.64.124 on 09/08/12
For personal use only.

A deuterium NMR study of guest molecular dynamics of acetone in two organic inclusion compounds

Paul S. Sidhu, Jason Bell, Glenn H. Penner, and Kenneth R. Jeffrey

Abstract: Deuterium nuclear magnetic resonance (NMR) spectra and spin-lattice relaxation times (T_1) are used to investigate the dynamics of the guest molecule, acetone, in tris(5-acetyl-3-thienyl)methane (TATM) and cyclotriveratrylene (CTV) inclusion compounds. ^{13}C CPMAS powder NMR spectra were obtained for each clathrate, to verify inclusion. In acetone: TATM, the guest molecule is undergoing twofold reorientation about the CO bond, exchanging the two methyl groups. An activation energy of 20.8 (±1.4) kJ/mol, for the two-site jump motion, was found, independently, from deuterium NMR spectra and T_1 measurements. Acetone in CTV performs the same type of motion as acetone in TATM. Activation energies of 25.0 (±3.2) kJ/mol and 24.1 (±0.5) kJ/mol were determined using the same two techniques. In both inclusion compounds, the rate of methyl rotation within the acetone molecule is greater than 10^8 Hz even at the lowest temperature measured (84 K). Analytical expressions for the spin-lattice relaxation time (T_1), for a twofold jump, were derived. Calculated values of the effective quadrupolar coupling constant and T_{1min} for the guests agree very well with the experimental data. The 84 K spectrum of acetone:TATM unexpectedly shows some asymmetry, the origin of which is discussed. Finally, these two clathrates are compared to the recently examined acetone:tri-*ortho*-thymotide inclusion compound.

Key words: inclusion compounds, deuterium NMR, solid state NMR spectroscopy, molecular dynamics.

Résumé : On a utilisé les spectres de résonance magnétique nucléaire (RMN) et les temps de relaxation spin-réseau (T_1) du deutérium pour étudier la dynamique de la molécule invitée, l'acétone, dans les composés d'inclusion tris(5-acétyl-3-thiényl)méthane (TATM) et du cyclotrivératrylène (CTV). On a déterminé les spectres RMN CPMAS du ^{13}C de chacun des clathrates pour s'assurer de l'inclusion. Dans l'acétone : TATM, la molécule incluse subit une réorientation binaire autour de la liaison CO qui permet d'échanger les deux groupes méthyles. On a déterminé de façons indépendantes, par les spectres RMN du deutérium ainsi que par les mesures de T_1, que l'énergie d'activation est égale à 20,8 (±1,4) kJ mol^{-1} pour le mouvement de saut des deux sites. L'acétone dans le CTV est soumise au même type de mouvement que l'acétone dans le TATM. Les énergies d'activation mesurées par les deux techniques sont respectivement de 25,0 (±3,2) kJ mol^{-1} et de 24,1 (±0,5) kJ mol^{-1}. Dans les deux composés d'inclusion, la vitesse de rotation du groupe méthyle de la molécule d'acétone dépasse les 10^8 Hz, même pour la température de mesure la plus basse (84 K). On a dérivé les expressions analytiques du temps de relaxation spin-réseau (T_1) de l'échange binaire. Les valeurs calculées pour la constante de couplage quadripolaire effective et pour le T_{1min} pour les invitées sont en bon accord avec les valeurs expérimentales. Il est surprenant que le spectre de l'acétone : TATM, à 84 K, présente une certaine symétrie dont on discute l'origine. Enfin, on compare ces deux clathrates au produit d'inclusion acétone : tri-*ortho*-thymotide qui a été examiné récemment.

Mots clés : composés d'inclusion, RMN du deutérium, spectroscopie RMN à l'état solide, dynamique moléculaire.

[Traduit par la rédaction]

Introduction

In recent years, deuterium NMR spectroscopy has emerged as a very important technique for the study of anisotropic molecular motion in solids (1–3). Motion with reorientational rates in the range of 10^3–10^8 Hz may be examined by an analysis of the ^2H NMR powder lineshape (4). For faster

Received July 14, 1995.

P.S. Sidhu, J. Bell,[1] and G.H. Penner.[2] Guelph–Waterloo Centre for Graduate Work in Chemistry, Department of Chemistry and Biochemistry, University of Guelph, Guelph, ON N1G 2W1, Canada.

K.R. Jeffrey. Guelph–Waterloo Program for Graduate Work in Physics, Department of Physics, University of Guelph, Guelph, ON N1G 2W1, Canada.

[1] NSERC undergraduate research participant.

[2] Author to whom correspondence may be addressed. Telephone: (519) 824-4120. Fax: (519) 766-1499. E-mail: gpenner@uoguelph.ca

Can. J. Chem. Downloaded from www.nrcresearchpress.com by 46.23.64.124 on 09/08/12
For personal use only.

Can. J. Chem. Downloaded from www.nrcresearchpress.com by 46.23.64.124 on 09/08/12
For personal use only.

motions, an analysis of the deuterium spin-lattice relaxation time as a function of temperature may be used to extract quantitative information regarding the molecular motion (5). Deuterium NMR spectroscopy has developed into an excellent probe for the study of dynamic processes (6–8), because of the development of computer programs (9–12) capable of simulating deuterium NMR spectra as a function of reorientational rate, molecular geometry, and dynamic model, along with the availability of selectively deuterated molecules (13).

It is generally known that in many inclusion compounds, the relatively weak van der Waals interaction between host and guest affords the enclathrated moiety a large degree of motional freedom (14). Determination of the dynamics of a guest molecule provides insight into the guest–host interaction (15–18). For example, the potential for free rotation is undoubtedly hindered in inclusion compounds where the guest–host interaction involves hydrogen bonds. In addition, X-ray crystallographic data can assist in providing insight into the shape and size of the cavity formed by the host (19–22). We have chosen to study the dynamics of acetone enclathrated by two hosts, tris(5-acetyl-3-thienyl)methane, and cyclotriveratrylene. Both compounds are known to form inclusion compounds with a wide variety of fairly small guest molecules (23, 24).

Tris(5-acetyl-3-thienyl)methane (TATM), **1**, was first synthesized by Yakubov et al., in 1973, from 2-acetyl thiophene and chloroform in the presence of excess aluminum chloride. It was also noted that TATM forms inclusion compounds on recrystallization from various solvents (25).

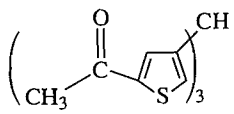

1

In 1977, Bin Din and Meth Cohn found that TATM forms 2:1 host:guest clathrates with a wide variety of organic compounds (23). The guest molecules reside in cavities formed by the TATM molecules. Furthermore, their study, at least to that point in time, failed to reveal a solvent that was not incorporated. Although the pure host compound melts at about 55°C, TATM inclusion compounds generally melt at temperatures above 100°C.

Recently, four crystal structures of TATM with various guests have been reported (26–29). In the presence of guest molecules, the TATM molecules generally form a triclinic lattice in which there is only one guest molecule per unit cell. In addition, the inability to precisely identify the positions of the guest's atom led to the conclusion that the guest molecules are disordered (30). Hydrogen bonds are absent in the ethanol:TATM inclusion compound. Finally, the TATM molecules were seen to form cavities of different sizes and shapes, depending on the guest molecule (26–29).

Turning our attention to cyclotriveratrylene (CTV), **2**, this compound was first obtained in 1915 by reaction between formaldehyde and veratrole (31) and was originally considered to be a cyclic hexamer (32). However, it was later shown by various experiments (33–35) to be a trimer $(C_9H_{12}O_2)_3$ possessing a rigid crown C_{3v} conformation (36).

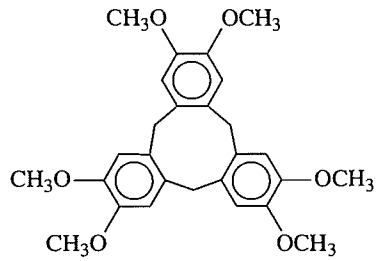

2

Inclusion compounds of cyclotriveratrylene were first reported in 1931 (37), but were studied in greater detail by Caglioti et al. some 25 years later (24). The crystal structure of the CTV:benzene:water inclusion compound shows that the CTV molecules form channels by stacking on top of one another, with the two guests residing in the channels surrounded by four stacks of CTV molecules. The water molecules form hydrogen bonds with the methoxy oxygen atoms of the host (38). An attempt to form a CTV:toluene clathrate gave water as the only guest with a CTV:H_2O ratio of about 1:0.16. A combined crystal structure and IR study was interpreted as indicating weak hydrogen bonding between water and the methoxy oxygens of CTV (39). As pointed out by Burlinson and Ripmeester, the ability of CTV to form inclusion compounds often depends critically on the presence or absence of water (40). Zhang and Atwood exploited this to prepare crystals of pure CTV (41). One common feature of these studies is that the CTV molecules stack along the crystallographic *b*-axis, and that the *b*-axis value changes little from guest to guest whereas the *a* and *c* axes depend strongly on the size of the guest molecule. An exception to this is the recent structure of $(C_{60})_{1.5}$(CTV)$(\text{toluene})_{0.5}$ where the C_{60} and CTV molecules form a ball and socket structure, nearly doubling the *b*-axis value (42).

Theoretical background

Solid state deuterium NMR spectroscopy is one of the principal techniques used to study guest motion in inclusion compounds. Deuterium is a quadrupolar nucleus and, as such, the interaction between the quadrupole moment of the nucleus and the electric field gradient of the surrounding charge distribution gives rise to a quadrupolar coupling, which is the major perturbation on the nuclear Zeeman interaction. In organic compounds, the electric field gradient arises primarily from the electronic structure of the C—D bond. In solution, rapid isotropic tumbling averages the quadrupolar coupling to zero, but in powders it gives rise to very broad spectra, yielding a superposition of signals for each possible orientation of the C—D bond with respect to the applied magnetic field. For a spin = 1 nucleus, there are two NMR transitions, resulting in a symmetric powder pattern spectrum.

There are two quantities that may be defined to describe the appearance of a ^2H NMR powder spectrum. The quadrupolar coupling constant characterizes the width.

$$[1] \qquad \chi = 2/3\,\Delta\nu_{zz}$$

Can. J. Chem. Downloaded from www.nrcresearchpress.com by 46.23.64.124 on 09/08/12
For personal use only.

Fig. 1. Three (spin = 1) NMR powder pattern spectra. (a) $\eta = 0$; (b) $\eta = 0.5$; (c) $\eta = 1.0$.

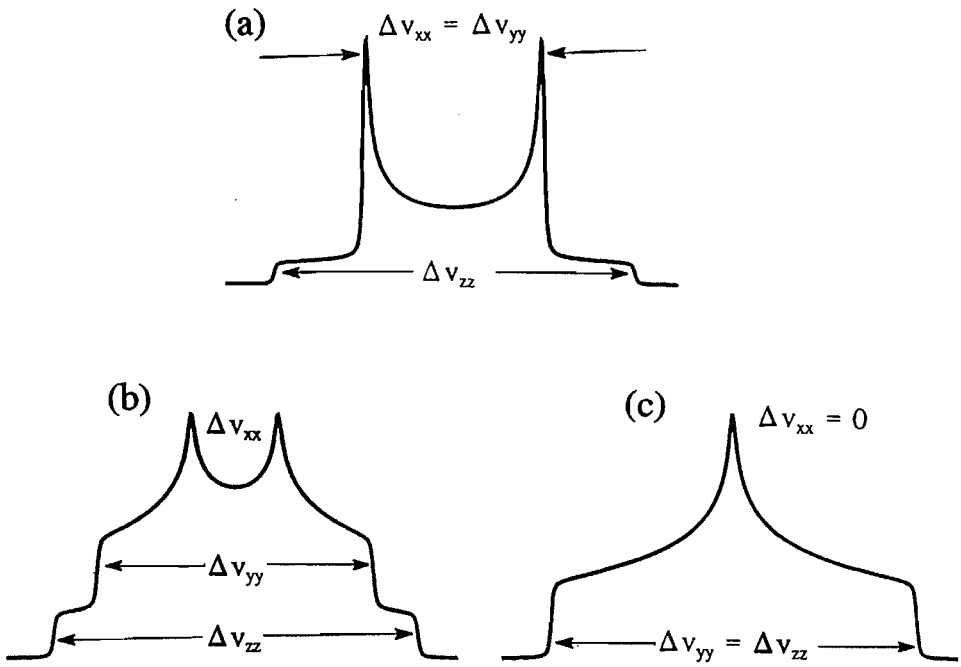

The asymmetry parameter defines the shape.

$$[2] \qquad \eta = \frac{\Delta\nu_{yy} - \Delta\nu_{xx}}{\Delta\nu_{zz}}$$

$\Delta\nu_{xx}$, $\Delta\nu_{yy}$, and $\Delta\nu_{zz}$ are the three splittings observed in a deuterium powder pattern spectrum (see Fig. 1).

Molecular motion has two general effects on the shape of the deuterium powder pattern. It narrows the powder signal, and may change the signal shape. In the case of ^2H quadrupolar coupling, reorientational rates of less than 10^3 Hz have no averaging effect, while motions with rates greater than 10^8 Hz are in the fast rate limit.

The simplest type of motion involves exchange of a deuterium nucleus between three or more equivalent sites. In the fast rate limit, the asymmetry parameter averages to zero, and the spectrum is compressed by a factor of $1/2(3\cos^2\theta - 1)$, where θ is the angle between the X—D bond and the rotation axis. In between the two extremes, a slow evolution of the spectrum from one form to the other is observed. Examples include three-site exchange of the deuterons in a methyl group ($\theta = 70.5°$) and in-plane six-site exchange of the deuterons on a benzene ring ($\theta = 90°$).

An example of asymmetric motion is exchange of a deuteron between only two equivalent sites. When $k > 10^8$ Hz, a non-zero asymmetry parameter is observed. An example is the two-site exchange of the *ortho* and *meta* deuterons of a monosubstituted benzene ring ($\theta = 60°$). The asymmetry parameter η and the quadrupolar coupling constant χ in the averaged spectrum depend on the angle θ for the motion involved (43).

Enclathrated guest molecules often undergo a precessional type of motion, which can be thought of as rotation of the principal symmetry axis on a cone that may have a circular or elliptical shape. This type of motion has a very small activation energy, and is usually only encountered in the fast rate limit at working temperatures. The motion can most simply be broken down into two components: precession on a circular cone and a two-site libration (44).

A further complicating factor in considering the motion of guest molecules is the possibility of unequal populations of the sites taken up by the exchanging deuterium nucleus. Since this leads to more or less preferred orientations for the guest, it introduces asymmetry into the powder spectrum. The justification for unequal populations can be either a non-uniform guest–host interaction, or a situation in which a rotation axis is not a symmetry axis.

Experimental

TATM was prepared according to the method of Yakubov et al. (25). 2-Acetyl thiophene and chloroform (6.2 equivalents) were refluxed for 24 h, in the presence of excess aluminum chloride (2.5 equivalents). After refluxing, 10% HCl was added to dissolve remaining $AlCl_3$. The TATM was then extracted with chloroform, and the organic phase was washed with saturated NaCl aqueous solution. The organic phase was then dried and filtered, and excess $CHCl_3$ was removed by rotary evaporation. The resulting plaque was recrystallized from ethanol. Finally, heating under vacuum for 12 h at 130°C removed enclathrated ethanol. The resulting solid was ground to yield an orange powder that had a broad melting point range of 52°–58°C. The purity was confirmed by solution NMR.

Cyclotriveratrylene was prepared according to the method of Oliverio and Casinovi (45). Cold (5°C) 70% H_2SO_4 (125 mL) was added to cold veratrole (1,2-dimethoxybenzene) (35 g), and the mixture was then cooled to 5°C. Over approximately 90 min, 10 g of 37% formaldehyde was added without letting the temperature rise above 10°C. This mixture was stirred for 0.5 h at 5°C, then finally poured onto 40 g of crushed ice. On standing overnight, a white solid sepa-

Can. J. Chem. Downloaded from www.nrcresearchpress.com by 46.23.64.124 on 09/08/12
For personal use only.

rated from solution. The resulting mixture was extracted into diethyl ether. There were three layers; the middle one contained crude product. The top two layers were decanted off and filtered. The crude product was then recrystallized from ethanol (1–1.5 L). A pink-grey solid (4.4 g), with melting point 226–227°C was obtained. The purity was verified by solution NMR.

The inclusion compounds were prepared by dissolving approximately 200 mg of host solid in 2–3 mL perdeuterated acetone (Aldrich), followed by slow evaporation. Verification of inclusion was done by acquiring ^{13}C CPMAS powder spectra of isotopically normal inclusion compounds. To determine guest:host stoichiometry, integrals of the peaks in the ^{1}H solution NMR spectra of the unenriched clathrate dissolved in $CDCl_3$ were determined. These spectra also showed that no water was present in either of the two isotopically enriched samples. Powder samples were packed in 5 mm o.d. NMR tubes that had been cut to lengths of 2–3 cm.

Deuterium NMR spectra were obtained at 44.7 MHz on a home-built spectrometer using the quadrupolar echo pulse sequence (46): $(\pi/2)_x$–τ_Q–$(\pi/2)_y$–τ_Q–acquire. The length of the $\pi/2$ pulse was approximately 3.5 μs. At each temperature, the echo signals were collected using a τ_Q value of 50 μs. The echo signals were Fourier transformed to obtain the deuterium NMR spectra. The temperature was controlled by flowing nitrogen gas through liquid nitrogen and then through the sample chamber, in combination with an electric heater and a thermocouple. The temperature was stable to within ±0.5 K during the course of each measurement.

The deuterium T_1 data were acquired using an inversion–recovery pulse sequence modified for quadrupolar nuclei: $(\pi)_x$–τ–$(\pi/2)_{\pm x}$–τ_Q–$(\pi/2)_y$–τ_Q–acquire. Typically, 12 values of τ were used to determine T_1 at each temperature. The pulse spacing, τ_Q, for the T_1 determination was 50 μs. The time between repetitions of the pulse sequence was always greater than $5T_1$. The data were fit using a nonlinear least-squares algorithm employing an exponential fitting function to obtain the relevant relaxation time parameters. The amplitude of the signal at each pulse spacing was determined from the echo integral.

^{13}C CPMAS NMR spectra were recorded on a Bruker ASX 200 spectrometer at a frequency of 50.3 MHz. The ^{13}C $\pi/2$ pulses were 4.0 μs, and cross-polarization times of 3 ms were used. Typically 100–150 transients were accumulated, and the recycle delay was 5 s. The samples were spun at 5 kHz, using a 5 mm Bruker MAS probe. The chemical shifts were referenced to the low-frequency signal of adamantane (29.5 ppm) and, following acquisition, an exponential apodization of 10 Hz was applied before the Fourier transform.

Lineshape simulations of quadrupolar echo spectra were carried out by standard methods using the program MXQET (9). Simulated spectra were visually matched to experimental lineshapes. Analysis of the T_1 data was done using the BPP spectral density function (47). The T_1 data were fit to equations of the following type (using K, τ_∞ and E_a as fitting parameters):

$$[3] \qquad \frac{1}{T_1} = K\left[\frac{\tau_c}{1+\omega_0^2\tau_c^2} + \frac{4\tau_c}{1+4\omega_0^2\tau_c^2}\right]$$

$$[4] \qquad \tau_c = \tau_\infty \exp(-E_a/RT)$$

In these equations, τ_c is interpreted as the correlation time for the motion, τ_∞ is the correlation time at infinite temperature, and ω_0 is the Larmor precession frequency. K is a constant that depends on the static quadrupolar coupling constant and the mode of molecular reorientation, while E_a is the activation energy for the motion of interest.

Results and discussion

Acetone in TATM

The ^{13}C CPMAS spectrum of the acetone:TATM inclusion compound is presented in Fig. 2. The signals were assigned using ^{13}C chemical shift correlation tables (48). The acetone CH_3 signal is located at 29.2 ppm, while the carbonyl peak appears at 202.6 ppm. The multiplicity of the TATM carbons is two, one strong and one weak signal for each carbon. This may originate from the fact that in the four crystal structures done on TATM inclusion compounds (26–29), two of the three thienyl rings of each TATM molecule participate in forming the cavity in which the guest resides, while the third thienyl ring does not. Thus, the two thienyl rings forming the cavity give rise to the strong signals, while the corresponding weak signals, of approximately 50% intensity, arise from the nonparticipating TATM thienyl ring. This is supported by the observation that the methane CH carbon gives only one signal, as there is only one methane carbon in each TATM molecule.

The deuterium NMR powder spectra of acetone-d_6 in the TATM inclusion compound are presented in Fig. 3, along with simulations. The acetone:TATM complex is characterized by a rapid rate ($k > 10^8$ Hz) of methyl rotation at all temperatures studied (142–273 K), because of its very low activation energy (2–5 kJ/mol) (49–51) and the fact that the 142 K spectrum is narrowed by at least a factor of three over the static spectrum. On top of this motion, there is exchange of the two methyl groups about the CO bond, the molecular C_2 axis. The rate of this motion is in the intermediate exchange region in the temperature range studied. Changes in the rate of this motion give rise to changes in the shape of the experimentally observed spectra. By fitting the simulations to their corresponding experimental spectra, it was possible to extract rates for the exchange between methyl groups as a function of temperature (see Fig. 3). A plot of ln k vs. $1000/T$ (k = rate of motion) gave an activation energy of 20.8 (±1.4) kJ/mol for methyl group exchange (see Fig. 4). In addition, in the simulations, it was necessary to employ a CD_3-C-CD_3 bond angle of 123° (±2°) to make a match to the experimental spectra. From microwave data, the angle in the gas phase is 116° (52, 53).

The profile of ^{2}H spin-lattice relaxation times for acetone:TATM, as a function of temperature, is presented in Fig. 5. Changes in T_1 in this temperature range result from changes in the rate of the above-mentioned twofold flips. By fitting the experimental data to eqs. [3] and [4], an activation energy of 20.8 (±0.5) kJ/mol for the C_2 exchange was determined. Note that this is the same value deduced from our spectral simulations. The constant K (see eq. [3]) was found to be 3.3×10^9 s^{-2}, and τ_∞ was determined as 2.03×10^{-13} s. Using these values of τ_∞ and E_a in eq. [4] and the fact that the jump rate $k = (2\tau_c)^{-1}$ for the twofold reorientation, it is possible to compare the rates of reorientation determined from the T_1 analysis with those found from sim-

Fig. 2. ^{13}C CPMAS powder spectrum of the acetone/TATM inclusion compound (spin rate = 5 kHz).

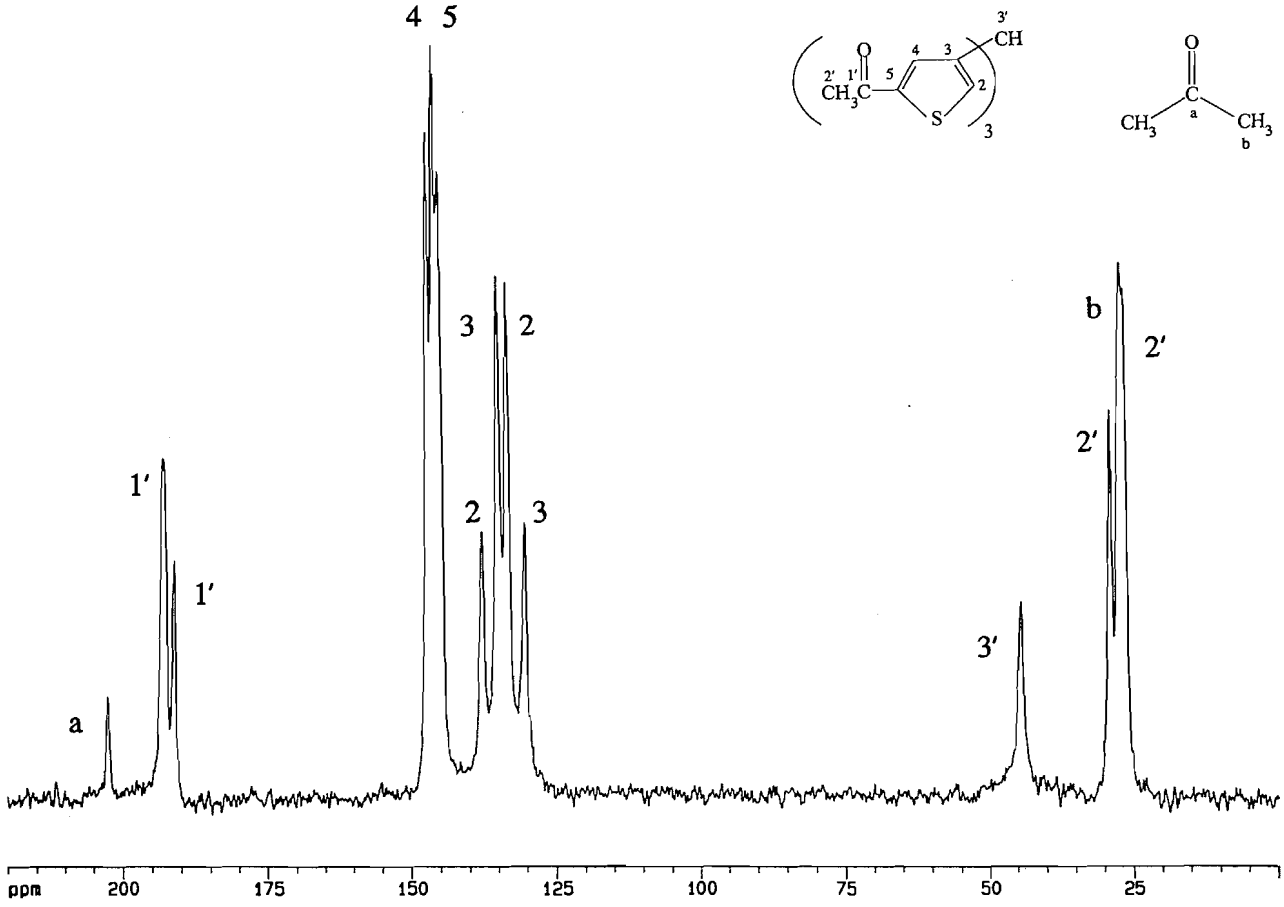

ulation of ^2H spectra. The two methods give the same results within experimental error. In addition, it can be seen that the two lowest temperature points in Fig. 5 fall below the fitted curve. This suggests the presence of a second T_1 minimum at much lower temperatures that can be associated with rotation of the methyl groups.

Analytical expressions for the deuterium spin-lattice relaxation time, for a two-site jump model, were derived from the following general equations (5):

$$[5] \qquad \frac{1}{T_1} = \frac{\chi^2}{3}[J_1(\omega_0) + 4J_2(2\omega_0)]$$

$$[6] \qquad \chi = \frac{6\pi e^2 qQ}{4h}$$

The quadrupolar coupling constant is defined as χ, with eq and eQ representing the electric field gradient of the surrounding charge distribution and the nuclear quadrupolar moment, respectively. The spectral density functions J_1 and J_2 are defined with respect to the direction of the applied field. For two-site jump motion about a z axis fixed in the crystal with the angle between the two sites being 2θ, the expression for T_1 is given by

$$[7] \qquad \frac{1}{T_1} = \frac{9}{160}\left(\frac{2\pi e^2 qQ}{h}\right)^2 \sin^2 2\theta[J_1'(\omega_0) + 4J_2'(2\omega_0)]$$

Now J_1' and J_2' are defined with respect to the crystal axis. Therefore, the constant K in eq. [3] is equal to

$$[8] \qquad K = \frac{9}{160}\chi^2 4\pi^2(\sin^2 2\theta)$$

In addition, the spin-lattice relaxation time minimum is determined to be:

$$[9] \qquad \frac{1}{T_{1\min}} = \frac{9}{160}\left(\frac{2\pi e^2 qQ}{h}\right)^2 \sin^2 2\theta\left(\frac{1.42}{\omega_0}\right)$$

From the value of K, determined from the T_1 fit (3.3×10^9 s^{-2}), and the angle 2θ (123°), found from simulations, we calculated the effective quadrupolar coupling constant to be approximately 46 (±1) kHz. This compares with an observed χ_{eff} of 45 (±1) kHz at 273 K (found from ^2H spectra). The T_1 minimum occurs at approximately 270 K. This quadrupolar coupling constant is averaged by methyl rotation and the librational motion, but not by the twofold flip.

The experimental value of the ^2H spin-lattice relaxation time at the T_1 minimum, for acetone-d_6 in TATM, is about 60 ms. From eq. [9], using χ_{eff} of 45 kHz at the T_1 minimum and a spectrometer frequency of 44.669 MHz, we calculate that the ^2H T_1 minimum should be approximately 62 ms. The agreement here is apparently very good. The same calculations are performed for acetone:CTV in the next section.

Can. J. Chem. Downloaded from www.nrcresearchpress.com by 46.23.64.124 on 09/08/12
For personal use only.

Fig. 3. Deuterium NMR spectra for acetone-d_6 in the TATM inclusion compound at various temperatures, along with best-fit simulated lineshapes and twofold dimethyl flipping rate.

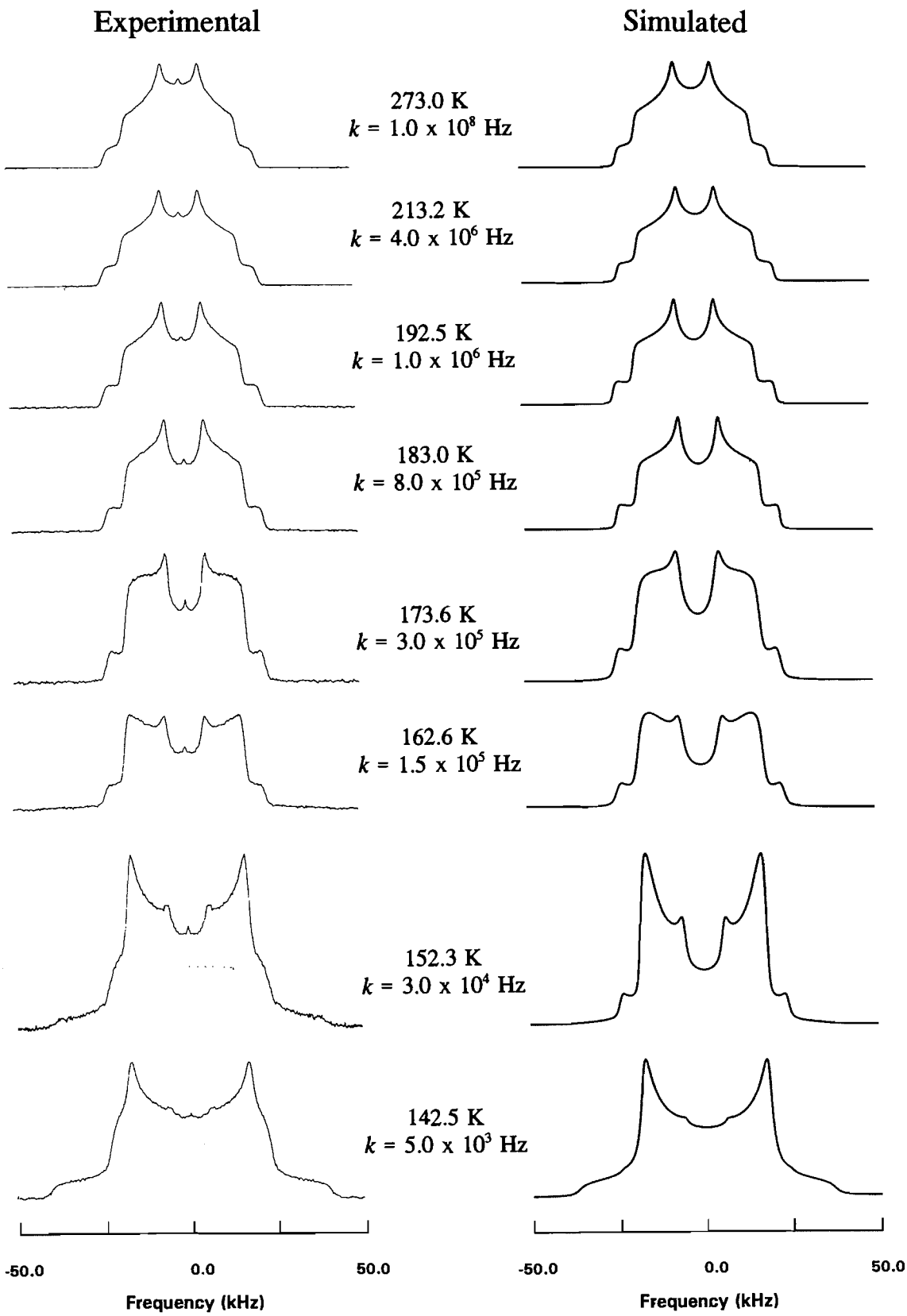

Can. J. Chem. Downloaded from www.nrcresearchpress.com by 46.23.64.124 on 09/08/12
For personal use only.

Can. J. Chem. Downloaded from www.nrcresearchpress.com by 46.23.64.124 on 09/08/12
For personal use only.

Fig. 4. Graph of ln k vs. $1000/T$ for the twofold flip of the acetone molecule in the TATM lattice. The solid line is a least-squares fit to the data. From the slope of the line, an activation energy of 20.8 kJ/mol was determined.

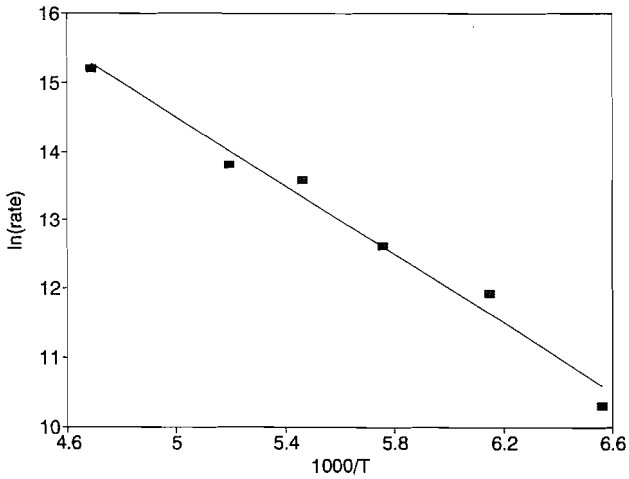

Fig. 5. Deuterium spin-lattice relaxation times, as a function of reciprocal temperature, for the acetone-d_6:TATM inclusion compound.

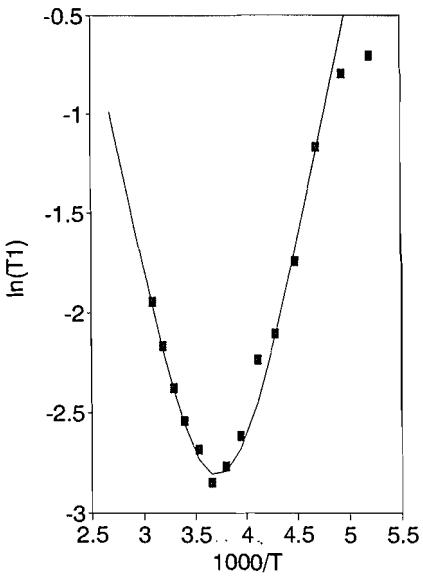

Finally, a third form of motion, precession on a cone, is present. This was deduced from the fact that the lineshapes were too narrow. The two previously described motional mechanisms cannot account for the observed spectral width. In the simulations, precession of the C_2 axis on a circular cone was assumed. However, since acetone is not an axially symmetric molecule, one would expect the precession to be much more asymmetric (i.e., elliptical). However, introducing elliptical precession in this case would overcomplicate the motional model. Elliptical precession might be considered because the spectrum at 142.5 K shows some asymmetry (i.e., $\eta > 0$). This is because precession of an elliptical nature introduces asymmetry into the spectrum, whereas circular precession does not. From the spectral simulation, the

Fig. 6. Deuterium powder spectrum of acetone-d_6:TATM, at 84 K, along with its simulation (below), as discussed in the text.

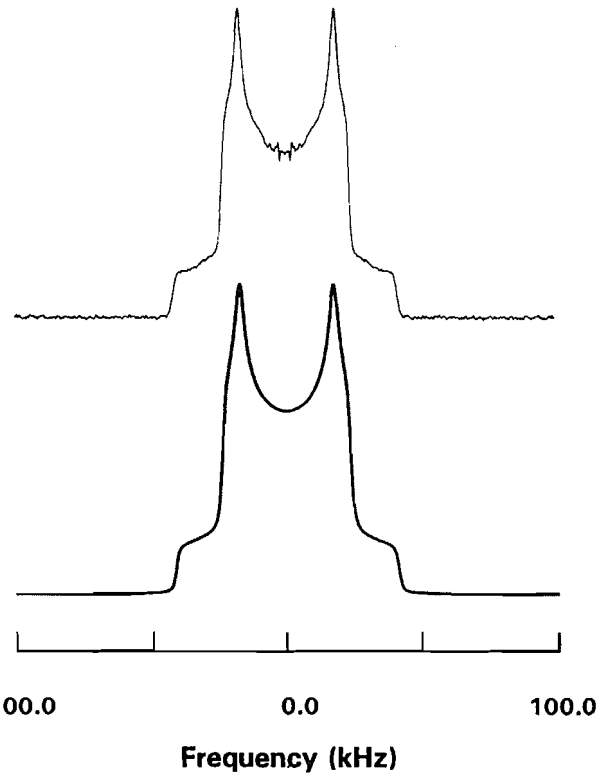

half angle of precession at this temperature is 16.9°. Facey et al. argue that their 77 K spectrum of acetone in tri-*ortho*-thymotide shows asymmetry because the three sites visited by the methyl deuterons are inequivalent, as they are adjacent to a carbonyl group (54). Possible explanations for this behaviour include a difference in the static quadrupole coupling constant for one of the three deuterons due to the perturbation of the electric field gradient by the electronegative carbonyl group (55), or a slight deviation in the projected angle of 120° between two of the deuterons (56). Facey's argument is valid, because the width of the 77 K spectrum is characteristic of no precession being present ($\chi = 57$ kHz). In our case, the conflict was resolved by obtaining a ^2H powder spectrum at 84 K. In Fig. 6, this spectrum is shown along with a simulation discussed below. The effective quadrupole coupling constant, averaged only by fast methyl rotation, was found to be 55.5 kHz at this temperature. Thus the corresponding static quadrupole coupling constant is approximately three times χ_{eff}, or 166.4 kHz. Since static quadrupole coupling constants of aliphatic deuterons are usually in the range 165–175 kHz, we would propose that there is very little motional averaging (i.e., wobble of the symmetry axis), other than methyl rotation, at this temperature. Yet the spectrum shows a considerable amount of asymmetry ($\eta = 0.14$). This implies that the asymmetry does not come from elliptical precession. Indeed, we were successfully able to simulate this spectrum (Fig. 6) by changing the projected angle between the two methyl deuterons, which are not parallel to the CO bond, from 120° to 124°. These calculations are outlined in more detail in ref. 56.

Can. J. Chem. Downloaded from www.nrcresearchpress.com by 46.23.64.124 on 09/08/12
For personal use only.

Fig. 7. ^{13}C CPMAS powder spectrum of the acetone:CTV inclusion compound (spin rate = 5 kHz).

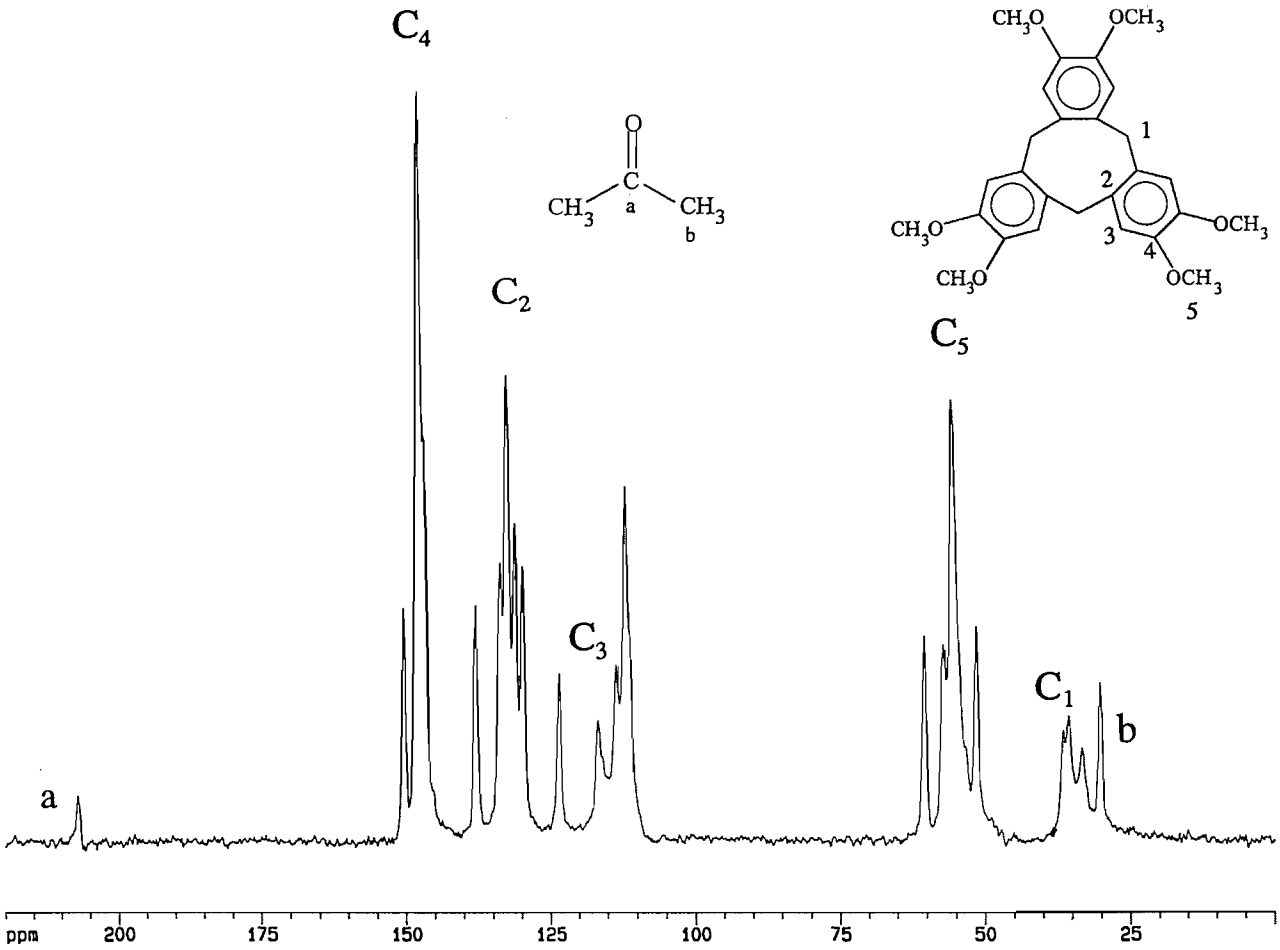

Acetone in cyclotriveratrylene

The ^{13}C CPMAS spectrum of the acetone:CTV inclusion compound is presented in Fig. 7. Again, the ^{13}C shifts were assigned using chemical shift correlation tables (48). Burlinson and Ripmeester characterized CTV inclusion compounds by means of solid state ^{13}C NMR in 1984 (40). They distinguished two ^{13}C spectra for the acetone:CTV clathrate, based on the method of preparation. Our spectrum most closely corresponds to the one that has a lower acetone content. Burlinson and Ripmeester concluded that, in this case, a clathrate with a significant number of vacancies in the channel could very well give a spectrum different in appearance from that for an inclusion compound with completely filled channels. This could very well be the reason why the ^{2}H spectra of acetone:CTV shows so much more line broadening than the same guest in TATM. Some acetone molecules might be surrounded by empty cavities, while other guests may interact primarily with neighboring filled cavities. Other possible origins of line broadening are discussed in the next paragraph. Note that the multiplicity of each signal is six. This implies, for example, that the six methoxy CH_3 carbons are all magnetically inequivalent in the solid; the same applies to the other four carbons. In solution, there are only five singlets in the ^{13}C spectrum, suggesting a high degree of symmetry that is lost in the solid. From ^{1}H solution spectra, we found a 1:1 host:guest ratio.

The deuterium NMR spectra of acetone-d_6 in CTV, along with their simulations, are presented in Fig. 8. Note the general similarity, apart from greater line broadening, with the spectra of acetone:TATM. Perhaps the greater line broadening is due to a distribution of rates for the two-site jump of the acetone molecule, or possibly the result of an increased dipolar interaction between the acetone guest and the protons of the CTV host (relative to TATM). The line broadening applied to the acetone:CTV simulations at the lowest temperatures was 5.0 kHz, whereas the corresponding line broadening for acetone:TATM was 1.5 kHz. The similarity in spectra indicate that the same general type of motion is occurring. Again, methyl C_3 rotation is proceeding at a rate greater than 10^8 Hz at all temperatures studied. The twofold flipping rate between methyl groups is in the intermediate exchange region. The rate of this motion, at each temperature, is labelled on each pair of spectra in Fig. 8. From the plot of ln k vs. $1000/T$ (Fig. 9), an activation energy of 25.0 (±3.2) kJ/mol for the methyl group exchange was determined. From the simulations, the CD_3-C-CD_3 angle was 120° (±2°).

The acetone:CTV ^{2}H spin-lattice relaxation data are presented in Fig. 10. From the best-fit curve, the activation en-

Fig. 8. Deuterium NMR spectra for acetone-d_6 in the CTV inclusion compound at various temperatures, along with best-fit simulated lineshapes and twofold dimethyl flipping rate.

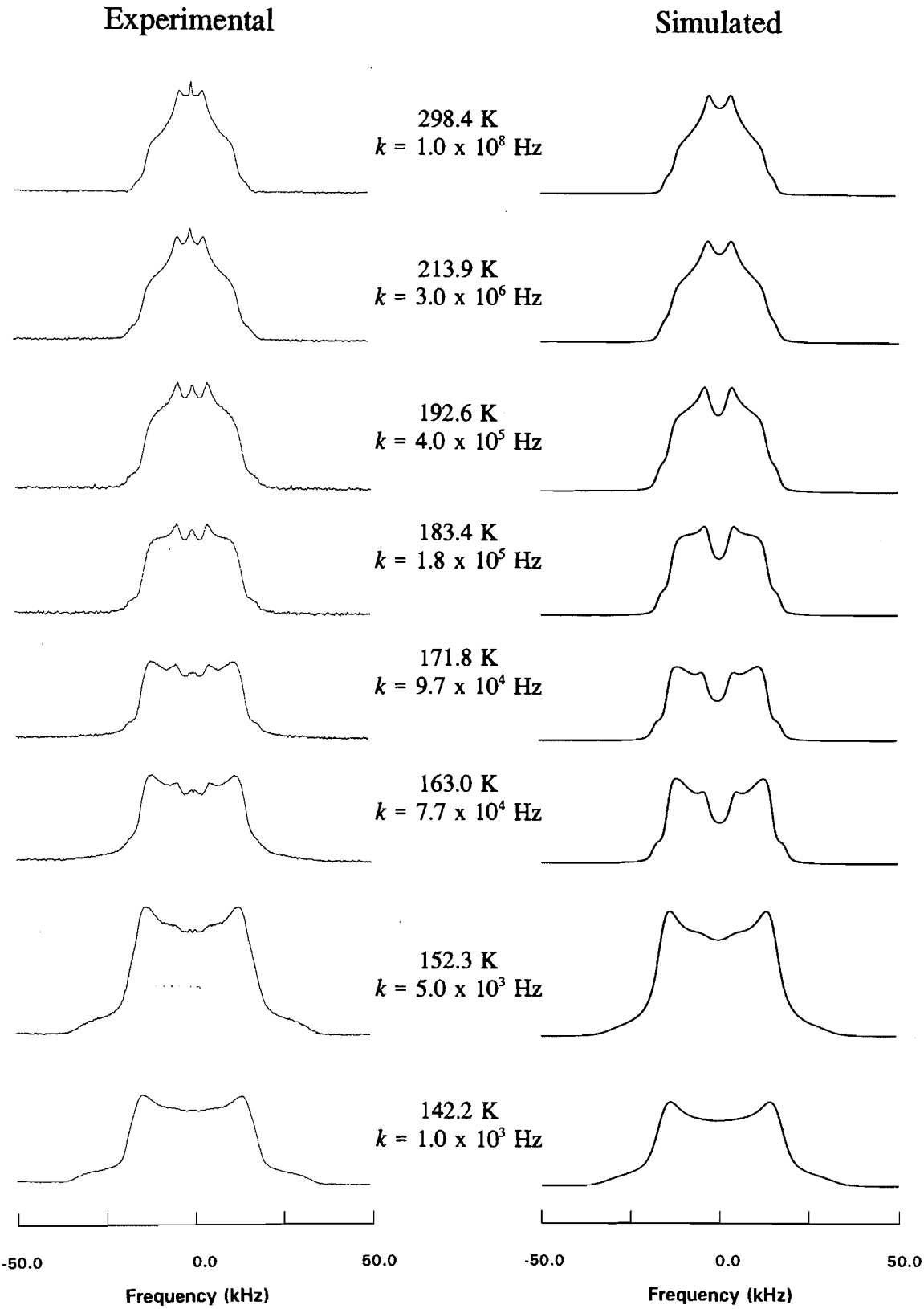

Can. J. Chem. Downloaded from www.nrcresearchpress.com by 46.23.64.124 on 09/08/12
For personal use only.

Can. J. Chem. Downloaded from www.nrcresearchpress.com by 46.23.64.124 on 09/08/12
For personal use only.

Fig. 9. Graph of ln k vs. 1000/T for the twofold flip of the acetone molecule in the CTV lattice. The solid line is a least-squares fit to the data. From the slope of the line, an activation energy of 24.1 kJ/mol was determined.

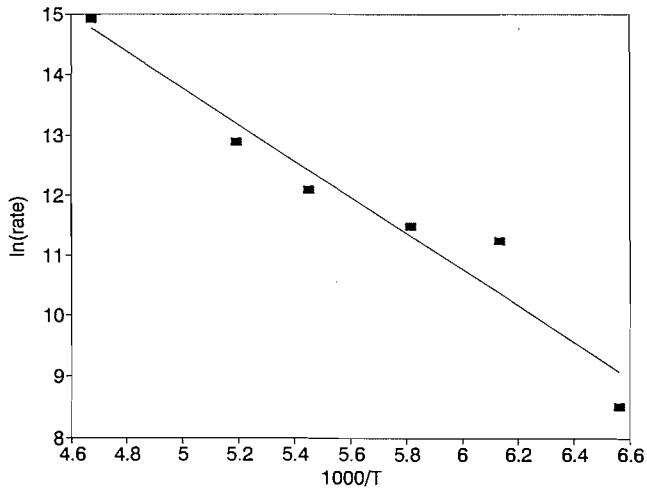

Fig. 10. Deuterium spin-lattice relaxation times, as a function of temperature, for the acetone-d_6:CTV inclusion compound.

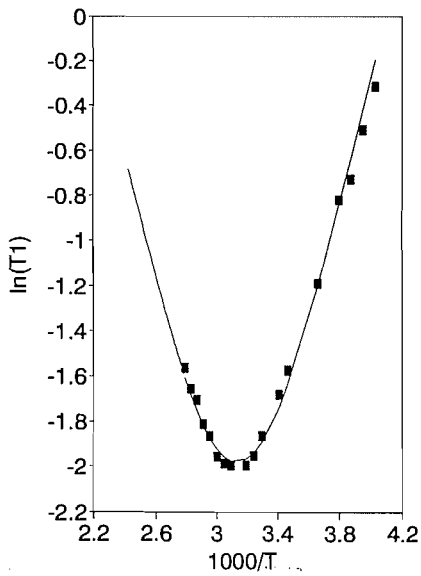

ergy for the methyl group exchange is 24.1 (±0.5) kJ/mol. The average activation energy (from the two determinations) is 24.5 kJ/mol. The constant K (see eq. [3]) was determined to be 1.4×10^9 s^{-2}. The correlation time at infinite temperature was found to be 2.49×10^{-13} s. Note that knowledge of the activation energy and τ_∞ allow the calculation of a motional rate at any temperature, according to eq. [4]. Such a comparison shows that the reorientational rates determined from the spectra and T_1 are the same within experimental error.

The same T_1 calculations performed on acetone:TATM can also be done in this case. The angle between the two deuterons is 120°, and $K = 1.4 \times 10^9$. This gives, from eq. [8], an effective quadrupolar coupling constant of 29 kHz. The experimentally determined value of χ_{eff}, at 298 K, is 33.6 kHz.

The value of T_1 at the spin-lattice relaxation time minimum is approximately 130 ms. Employing eq. [9], we calculate that the value of T_{1min} should be about 105 ms. Note that the value of T_{1min} for acetone:TATM (60 ms) is smaller than that for acetone:CTV. One might assume that if the same motion is occurring, then the values of T_1 at the relaxation minima should be approximately equal. Considering the difference in 2θ (3°), and the estimated error associated with each angle (±2°, see discussion below), the difference seems too small to reliably assign this to the disparity in T_{1min}. It is possible that the variation comes from a difference in the effective quadrupolar coupling constant. Indeed, as discussed below, acetone in CTV shows much more motional (wobbing) averaging than acetone in TATM; this manifests itself as a reduction in χ_{eff}, for the CTV guest compared to the TATM guest. As χ_{eff} is smaller for acetone:CTV, then from eq. [9] one would expect T_{1min} (acetone:CTV) to be larger than T_{1min} (acetone:TATM), which is exactly what is observed experimentally.

Considering the point just made about the difference between the two C-C-C bond angles, and the error associated with them, it may be instructive to briefly consider the origin of the estimated error in 2θ. The dependence of the asymmetry parameter, for the ^{2}H spectrum (in the fast rate limit), on the value of θ is fairly marked (43). However, we have not considered another possible contributing factor to the asymmetry parameter. It also depends on the anisotropy of the librational motion, which both acetone:TATM and acetone:CTV experience to some degree (see discussion below). As the fast rate limit spectrum of acetone in CTV ($\eta = 0.58$) shows more asymmetry than that corresponding to acetone in TATM ($\eta = 0.50$), this difference may indeed arise from the fact that acetone:CTV shows more anisotropy in its librational motion than acetone:TATM. However, distinguishing this possibility from the proposed difference in 2θ would be a problem more suited for an X-ray crystallographic study.

Regarding a basis for the difference between the proposed C-C-C bond angles of acetone in these two inclusion compounds with that reported in the gas phase (116°) (52, 53), it seems that a likely possibility may be the interaction between the atoms of the host molecule and the acetone guest. Rotational barriers in the gas phase are generally insignificant (joule per mole range) in comparison to the same in solids (approximately 100 to 1000 times greater). In the gas, the interactions are primarily intramolecular, while in these inclusion compounds and other solids, stronger intermolecular forces dominate, giving higher rotational activation energies. These differing interactions may also give rise to the slight difference in molecular geometry between the two phases.

Finally, as was the case in acetone:TATM, a precessional motion of the acetone molecule in the CTV lattice is present. The degree of this vibrational motion, for both acetone inclusion compounds, is presented in Fig. 11. By comparing the data obtained from simulations for each clathrate, it can be seen that the magnitude of the precession is much greater in acetone:CTV. This suggests that the guest–host interaction is greater in acetone:TATM than in acetone:CTV, possibly because the TATM cavity is smaller. Note that the spectrum at lowest temperature (142 K) shows only a small amount

Fig. 11. Graph of the half-angle precession, as a function of temperature, for the acetone:TATM (squares) and acetone:CTV (triangles) inclusion compounds.

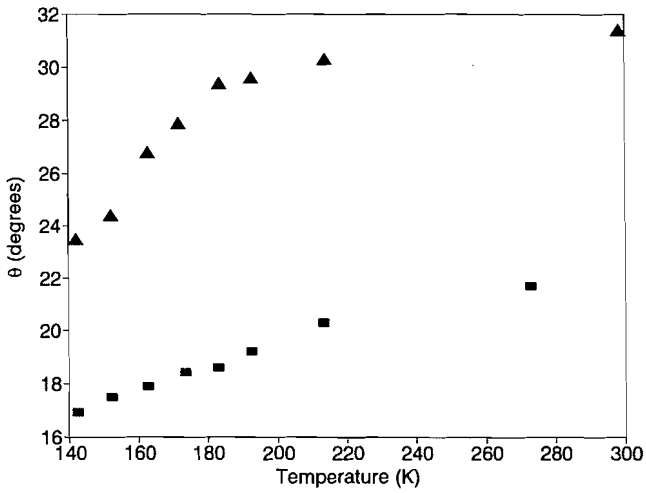

of asymmetry. This suggests that the precession on a cone is axially symmetric (circular), or that the three sites visited by the deuterons during methyl group rotation are equivalent. On the other hand, it may be that it is harder to recognize the asymmetry because the line broadening is greater than in acetone:TATM.

In their study of acetone:tri-*o*-thymotide (TOT), Facey et al. determined an activation energy of 13.6 kJ/mol, from spin-lattice relaxation data (54), for acetone's C_2 jump. This activation energy is significantly smaller than either of the values determined for the two current acetone inclusion compounds, suggesting that the cavity occupied by acetone in TOT is larger than those in acetone:TATM or acetone:CTV.

Another motional characteristic that can be used to provide information on the guest–host interaction is the averaging of the quadrupolar coupling constant. At 152.3 K, χ_{eff} for acetone:TATM is 49.0 kHz, for acetone:CTV it is 42.2 kHz, while for acetone:TOT, χ_{eff} is only 27.3 kHz at 156 K (54). This suggests that the strength of interaction between host and guest is strongest for acetone:TATM, intermediate for acetone:CTV, and weakest for acetone:TOT. This topic is pursued in the next paragraph.

It is interesting to compare the three hosts that enclathrate acetone (TATM, CTV, and TOT). Of the three, TATM is the most efficient at enclosing the guest molecule, because of the high activation energy for the twofold flip and the relatively small magnitude of precession (compared to CTV). It may be proposed that the TATM molecules have a high affinity for the guest molecules, based on the four crystal structures obtained for TATM inclusion compounds (26–29), and our experience with the same host. In contrast, from the crystal structures of CTV clathrates (38–42), it was observed that the cyclotriveratrylene host molecules preferred to associate with one another rather than with the guest molecules. This is also reflected in the fact that the precession of acetone in CTV is of greater magnitude than acetone in TATM. In comparison to tri-*o*-thymotide, which is a three-membered macrocycle of the same dimensions as CTV, it was seen that eight TOT molecules form a relatively large cavity in which the acetone guest resides (54). This is accompanied by an activation energy for the twofold jump that is almost half of that in TATM or CTV. Thus, it is possible to compare host molecule efficiency by studying a series of inclusion compounds with the same guest molecule.

Summary

In conclusion, it can be seen that deuterium NMR spectroscopy is a powerful technique for the investigation of guest molecule dynamics in solid inclusion compounds. Rather than the typical study of a series of guests in a particular host system, we have chosen to examine the dynamics of one guest in two quite different hosts and to compare these with a third, previously reported, acetone clathrate. Acetone requires similar activation energies for the two-site methyl group exchange in TATM and CTV (20.8 kJ/mol and 24.5 kJ/mol, respectively). These values are significantly larger than that for acetone:tri-*o*-thymotide (13.6 kJ/mol), which, along with the magnitude of the precessional motion, allows one to envisage the strength of interaction between host and guest.

Acknowledgements

We are very grateful to the Natural Sciences and Engineering Research Council of Canada (NSERC) for financial support. We would also like to thank Dr. Gordon Lange for providing a supply of veratrole to our laboratory.

References

1. H.W. Spiess. Adv. Polym. Sci. **66**, 23 (1985).
2. J.H. Davis. *In* Isotopes in the physical and biomedical sciences. Vol. 3. *Edited by* E. Buncel and J.R. Jones. Elsevier Science, Amsterdam. 1991.
3. R.G. Griffin. Methods Enzymol. **72**, 108 (1981).
4. R.J. Wittebort, E.T. Olejniczak, and R.G. Griffin. J. Chem. Phys. **86**, 5411 (1978).
5. D.A. Torchia and A. Szabo. J. Magn. Reson. **42**, 381 (1981).
6. J.H. Davis. Biochim. Biophys. Acta, **737**, 117 (1983).
7. K. Beshah, E.T. Olejniczak, and R.G. Griffin. J. Chem. Phys. **86**, 4730 (1987).
8. R.J. Wittebort, S.M. Oh, D.N. Hendrickson, D. Inniss, and C.E. Strouse. J. Am. Chem. Soc. **108**, 2938 (1986).
9. M.S. Greenfield, A.D. Ronemus, R.L. Vold, R.R. Vold, P.D. Ellis, and T.R. Raidy. J. Magn. Reson. **72**, 89 (1987).
10. L.J. Schwartz, E. Meirovitch, J.A. Ripmeester, and J.H. Freed. J. Phys. Chem. **87**, 4453 (1983).
11. P. Meier, E. Ohmes, G. Kothe, A. Blume, J. Weidrer, and H. Eibl. J. Phys. Chem. **87**, 4904 (1983).
12. J.H. Ok, R.R. Vold, and R.L. Vold. J. Phys. Chem. **93**, 7618 (1989).
13. A.F. Thomas. Deuterium labelling in organic chemistry. Meredith Corp., New York. 1971.
14. E. Meirovitch. J. Phys. Chem. **90**, 5825 (1986).
15. E. Meirovitch, T. Krant, and S.J. Vega. J. Phys. Chem. **87**, 1390 (1983).
16. E. Meirovitch and I. Belsky. J. Phys. Chem. **88**, 4308 (1984).
17. E. Meirovitch. J. Phys. Chem. **88**, 6411 (1984).
18. E. Meirovitch and I. Belsky. J. Phys. Chem. **88**, 6407 (1984).
19. R. Clement, M. Gourdji, and L. Guibe. Mol. Phys. **21**, 247 (1971).
20. R. Clement, J. Jegoudez, and C. Mazieres. J. Solid State Chem. **10**, 46 (1974).
21. H.U. Lenne. Acta. Crystallogr. **7**, 1 (1954).
22. H.U. Lenne. Z. Kristallogr. **118**, 454 (1963).

Can. J. Chem. Downloaded from www.nrcresearchpress.com by 46.23.64.124 on 09/08/12
For personal use only.

23. L. Bin Din and O. Meth Cohn. J. Chem. Soc. Chem. Commun. **21**, 741 (1977).
24. V. Caglioti, A.M. Liquori, N. Gallo, E. Giglio, and M. Scrocco. J. Inorg. Nucl. Chem. **8**, 572 (1958).
25. A.P. Yakubov, Yu K. Sudarushkin, L.I. Belenkii, and Ya L. Gold'farb. J. Org. Chem. (USSR), **9**, 1549 (1973).
26. P.H. Van Rooyen and H.M. Roos. Acta Crystallogr. Sect. C: Cryst. Struct. Commun. C**47**, 2468 (1991).
27. P.H. Van Rooyen and H.M. Roos. Acta Crystallogr. Sect. C: Cryst. Struct. Commun. C**47**, 2718 (1991).
28. H.M. Roos and J.L.M. Dillen. Acta Crystallogr. Sect. C: Cryst. Struct. Commun. **C48**, 1882 (1992).
29. J.L.M. Dillen and H.M. Roos. Acta Crystallogr. Sect. C: Cryst. Struct. Commun. **C48**, 2229 (1992).
30. R.E. Marsh. Acta Crystallogr. Sect. B: Struct. Sci. **B50**, 112 (1994).
31. G.M. Robinson. J. Chem. Soc. 267 (1915).
32. F. Bertinotti, V. Carelli, A.M. Liquori, and A.M. Nardi. Ric. Sci. (Suppl.), **22**, 65 (1952).
33. A.S. Lindsey. Chem. Ind. (London), 823 (1963).
34. A.S. Lindsey. J. Chem. Soc. 1685 (1965).
35. H. Erdtman, F. Haglid, and R. Ryhage. Acta Chem. Scand. **18**, 1249 (1964).
36. B. Miller and B.D. Gesner. Tetrahedron Lett. 3351 (1965).
37. V.K. Bhagwat, D.K. Moore, and F.L. Pyman. J. Chem. Soc. 443 (1931).
38. S. Cerrini, E. Giglio, F. Mazza, and N.V. Pavel. Acta. Crystallogr. Sect. B: Struct. Crystallogr. Cryst. Chem. **B35**, 2605 (1979).
39. G.I. Birnbaum, D.D. Klug, J.A. Ripmeester, and J.S. Tse. Can. J. Chem. **63**, 3258 (1985).
40. N.E. Burlinson and J.A. Ripmeester. J. Inclusion Phenom. **1**, 403 (1984).
41. H. Zhang and J.L. Atwood. J. Crystallogr. Spectrosc. Res. **20**, 465 (1990).
42. J.W. Steed, P.C. Junk, J.L. Atwood, M.J. Barnes, C.L. Raston, and R.S. Burkhalter. J. Am. Chem. Soc. **116**, 10346 (1994).
43. D.T. Amm, S.L. Segel, and K.R. Jeffrey. Can. J. Phys. **64**, 22 (1986).
44. S.J. Heyes and C.M. Dobson. Magn. Reson. Chem. **28**, S37 (1990).
45. A. Oliverio and C. Casinovi. Ann. Chim. (Rome), **42**, 168 (1952).
46. J.H. Davis, K.R. Jeffrey, M. Bloom, M.I. Valic, and T.P. Higgs. Chem. Phys. Lett. **42**, 390 (1976).
47. N. Bloembergen, E.M. Purcell, and R.V. Pound. Phys. Rev. **73**, 679 (1948).
48. D.H. Williams and I. Fleming. Spectroscopic methods in organic chemistry. 4th ed. McGraw–Hill Book Co. Ltd., London. 1987.
49. M.J. Potrzebowski. Magn. Reson. Chem. **29**, 35 (1991).
50. K. Borner, G. Diezemann, E. Rossler, and H.M. Vieth. Chem. Phys. Lett. **181**, 563 (1991).
51. A. Kintanar, T.M. Alam, W.C. Huang, D.C. Schindele, D.E. Wemmer, and G. Drobny. J. Am. Chem. Soc. **110**, 6367 (1988).
52. T. Iijima. Bull. Chem. Soc. Jpn. **45**, 3526 (1972).
53. J.D. Swalen and C.C. Costain. J. Chem. Phys. **31**, 1562 (1959).
54. G.A. Facey, C.I. Ratcliffe, R. Hynes, and J.A. Ripmeester. J. Phys. Org. Chem. **5**, 670 (1992).
55. R.G. Barnes. Adv. Nucl. Quadrupole Reson. **1**, 335 (1974).
56. M.H. Wann and G.S. Harbison. J. Chem. Phys. **101**, 231 (1994).

Can. J. Chem. Downloaded from www.nrcresearchpress.com by 46.23.64.124 on 09/08/12
For personal use only.

^{1}H nuclear magnetic resonance and molecular orbital studies of 2-formylstyrene. Three significant nonplanar conformers at 300 K

Ted Schaefer, Scott Kroeker, and David M. McKinnon

Abstract: The ^{1}H nuclear magnetic resonance spectra of 2-formylstyrene, from dilute solutions in CS_2–C_6D_{12} and acetone-d_6, are analyzed to yield precise chemical shifts and spin–spin coupling constants. The long-range coupling constants imply a conformational distribution in which the O-*trans* conformer is 55% abundant in both polar and nonpolar environments. They also imply that the vinyl group, on average, is twisted out of the aromatic plane to a much larger extent than in styrene. The 6-31G* basis set gives an ab initio potential for the torsion of the vinyl moiety with a relatively deep minimum at 38° out-of-plane, for the O-*cis* conformer. For the O-*trans* conformer, two minima are found, one at 45° and another at 129.6°. Essentially the same potential is obtained with the 6-31G** basis. The latter corresponds to a close approach of the hydrogen atom of the formyl group and π orbitals or the β-carbon atom of the olefinic side chain. This local minimum is interesting in terms of a hypothesis used to explain the photochemistry of the molecule. The long-range coupling constants are consistent with the conformational properties calculated for the free molecule; they also indicate no significant difference between the conformational behaviour of the molecule in the two solvents. A proximate coupling constant of −0.16 Hz exists between the formyl and methine (α) protons. The latter is strongly deshielded in the presence of the formyl group, so that it becomes even less shielded than some of the aromatic protons.

Key words: ^{1}H NMR, 2-formylstyrene (*o*-vinylbenzaldehyde); long-range spin–spin coupling constants, 2-formylstyrene; conformations, three nonplanar of 2-formylstyrene; molecular orbital calculations, conformations of 2-formylstyrene.

Résumé : Dans le but d'obtenir des déplacements chimiques et des constantes de couplage spin–spin précis, on a analysé les spectres RMN du ^{1}H de solutions diluées du 2-formylstyrène dans du CS_2–C_6D_{12} et de l'acétone-d_6. Les constantes de couplage à longue distance impliquent l'existence d'une distribution conformationnelle dans laquelle l'abondance du conformère O-*trans* est égale à 55% dans les environnements tant polaires que non polaires. Elles impliquent aussi que, en moyenne, le déplacement du groupe vinyle, par rapport au plan aromatique, est beaucoup plus prononcé que dans le styrène. Des calculs ab initio à l'aide d'un ensemble de base 6-31G* permettent d'évaluer le potentiel de torsion de la portion vinylique et d'établir que, pour le conformère O-*cis*, il existe un puits de potentiel relativement profond pour un décalage de 38° par rapport au plan aromatique. Pour le conformère O-*trans*, on a trouvé deux minima, un à 45° et l'autre à 129,6°. On obtient essentiellement le même potentiel avec un ensemble 6-31G**. Ce dernier correspond à un grand rapprochement de l'atome d'hydrogène du groupe formyle et des orbitales π de l'atome de carbone β de la chaîne latérale oléfinique. Ce minimum local est intéressant en termes d'une hypothèse utilisée pour expliquer la photochimie de la molécule. Les constantes de couplage à longue distance sont en accord avec les propriétés conformationnelles calculées pour la molécule libre; elles indiquent aussi qu'il n'y a pas de différences importantes entre le comportement conformationnel de la molécule dans les deux solvants. Il existe une constante de couplage à courte distance de −0,16 Hz, entre les protons du formyle et du méthine (α). Ce dernier est fortement déblindé en présence du groupe formyle; il devient donc encore moins blindé que certains protons aromatiques.

Mots clés : RMN du ^{1}H, 2-formylstyrène (*o*-vinylbenzaldéhyde); constantes de couplage à longue distance, 2-formylstyrène; trois conformations non planaires de 2-formylstyrène; calculs d'orbitales moléculaires, conformations de 2-formylstyrène.

[Traduit par la rédaction]

Received July 11, 1995.

T. Schaefer,[1] S. Kroeker, and D.M. McKinnon. Department of Chemistry, University of Manitoba, Winnipeg, MB R3T 2N2, Canada.

[1] Author to whom correspondence may be addressed. Telephone: (204) 474-9335. Fax: (204) 275-0905.

Can. J. Chem. Downloaded from www.nrcresearchpress.com by 46.23.64.124 on 09/08/12
For personal use only.

Table 1. The ^{1}H nmr chemical shifts and coupling constants within functional groups for 2-formylstyrene at 300 K.

Parameter	Solvent		Parameter	Solvent	
	CS_2–C_6D_{12}[a]	Acetone-d_6[b]		CS_2–C_6D_{12}[a]	Acetone-d_6[b]
ν_3	2308.103[c,d]	2361.030	$^3J_{34}$	7.712	7.739
ν_4	2201.117	2252.764	$^3J_{45}$	7.354	7.374
ν_5	2233.088	2290.355	$^3J_{56}$	7.822	7.858
ν_6	2245.712	2308.563	$^4J_{35}$	1.464	1.458
ν_7 (α)	2259.685	2302.246	$^4J_{46}$	1.206	1.191
ν_8 (*cis*)[e]	1686.709	1735.959	$^5J_{36}$	0.533	0.542
ν_9 (*trans*)	1620.604	1644.871	Transitions, calculated	1097	1097
ν (CHO)	3052.218	3094.369	Transitions, assigned	889	803
^2J_g	1.338	1.291	Peaks	590	549
^3J_c	10.965	11.045	Largest difference	0.015	0.009
^3J_t	17.353	17.453	Root-mean-square deviation	0.006	0.004

[a]As a 5.6 mol% solution in CS_2, containing also 10 mol% of C_6D_{12} and 0.5 mol% TMS.
[b]As a 4.4 mol% solution in acetone-d_6, containing also 0.25 mol% TMS.
[c]In Hz at 300.1351 MHz to high frequency of internal TMS.
[d]All standard deviations were less than 0.001 Hz.
[e]The olefinic proton *cis* to the aromatic ring.

Introduction

The title molecule, 2-formylstyrene (*o*-vinylbenzaldehyde), is of interest to photochemists because two chromophores are present in conjugation (1). Apparently (1), irradiation of an assumed O-*cis*-conformer, **A**, leads to the slow formation of a spiro triene, leading to further reaction, while the putative O-*trans* conformer, **B**, undergoes a fast 1,5-hydrogen shift under irradiation to produce a methyl group at the β-carbon atom (transfer of the formyl hydrogen atom).

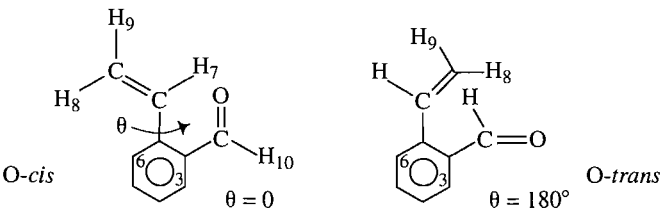

A **B**

The purpose of the present report is not to comment in detail on the photochemistry, but to describe a molecular orbital and ^{1}H nmr investigation of the conformational properties of 2-formylstyrene. Interatomic distances in the planar conformers, even for θ = 0, imply substantial steric strain and, therefore, that conformers characterized by θ > 0 are likely, the torsional barrier of the vinyl being much smaller than that of the formyl group. Many of the long-range coupling constants between vinyl or formyl protons and the aromatic protons depend on conformation and on torsion angles in known ways (2–5). Hence their measurement and interpretation in terms of O-*cis* and O-*trans* orientations, together with nonzero values of θ (see **A**), is informative. The molecular orbital calculations, which can approximately reproduce the torsional potential in styrene (6–11), are a valuable aid to such an interpretation. It turns out that computations predict nearly equal energies of the O-*cis* and O-*trans* conformations for the free molecule, together with three nonplanar minima in the torsion angle, θ, two of these belonging to the O-*trans* molecule. The long-range spin–spin coupling constants, derived for 2-formylstyrene in polar and nonpolar solvents, are consistent with the existence of three significant conformers at 300 K. One of these conformers has a close approach of the formyl hydrogen to the π orbitals of the vinyl substituent, possibly conducive to a fast (1) 1,5-hydrogen shift in the electronically excited state.

Experimental

2-Formylstyrene was prepared from *N*-2-phenethylformamide, as described (12). Dilute solutions in CS_2–C_6D_{12} and acetone-d_6 (see Table 1 for details) were filtered into 5 mm o.d. nmr samples tubes, which were then degassed by five cycles of the freeze–pump–thaw procedure and flame-sealed to produce reasonably symmetric tops.

The ^{1}H nmr spectra were obtained using a Bruker AM 300 spectrometer at a probe temperature of 300 K. Typically, the homogeneity of the external magnetic field was monitored and refined every eight scans by shimming on the free induction decay (FID) of internal tetramethylsilane. For high-resolution spectra, 32 FIDS were recorded, using acquisition times of 30 s for the CS_2–C_6D_{12} solution and 41 s for the acetone-d_6 solution. The resulting digital resolution is 0.017 and 0.012 Hz/point, respectively. After zero-filling to twice the original data set and multiplying FIDS by standard resolution enhancement functions, Fourier transformation produced frequency domain spectra with the linewidths less than 30 mHz for the acetone solution and about 40 mHz for the CS_2–C_6D_{12} solution.

Molecular orbital computations of the conformational behaviour of the side chains in 2-formylstyrene utilized the 6-31G* basis functions (13) and the computer program GAUSSIAN 92 (14). The energy of the molecule was calculated at intervals of 15° or less in the vinyl torsion angle, θ, for conformers **A** and **B**. During these optimizations, other bond lengths and angles were allowed to vary, with the constraint that the nuclei of the aromatic and formyl moieties were confined to a plane. For full geometry optimizations at local energy minima, and for θ values of 75° or greater in conformer

Can. J. Chem. Downloaded from www.nrcresearchpress.com by 46.23.64.124 on 09/08/12
For personal use only.

Table 2. Long-range coupling constants of the olefinic and formyl protons in 2-formylstyrene at 300 K.

	Solvent[a]			Solvent[a]	
Parameter	CS_2–C_6D_{12}	Acetone-d_6	Parameter	CS_2–C_6D_{12}	Acetone-d_6
$^4J_{67}$	−0.639[b]	−0.635	$^6J_{59}$	−0.017	−0.027
$^5J_{37}$	0.171	0.161	$^7J_{49}$	0.206	0.217
$^5J_{57}$	0.579	0.600	$^4J_{3,10}$	−0.251	−0.252
$^6J_{47}$	−0.353	−0.344	$^5J_{4,10}$	0.447	0.441
$^5J_{68}$[c]	−0.129	−0.136	$^5J_{6,10}$	0.362	0.364
$^6J_{38}$	−0.083	−0.086	$^6J_{5,10}$	−0.027	−0.020
$^6J_{58}$	−0.022	−0.026	$^5J_{7,10}$	−0.163	−0.163
$^7J_{48}$	0.180	0.184	$^6J_{8,10}$	0.039	0.030
$^5J_{69}$	0.049	0.045	$^6J_{9,10}$	0.038	0.025
$^6J_{39}$	0.051	0.053			

[a]Solvent conditions as in Table 1.

[b]Standard deviations are <0.001 Hz, except in two instances, where they are 0.001 Hz, viz., $^6J_{58}$ and $^6J_{59}$ in CS_2–C_6D_{12} solution.

[c]H-8 lies *cis* to the aromatic ring.

Can. J. Chem. Downloaded from www.nrcresearchpress.com by 46.23.64.124 on 09/08/12
For personal use only.

B, the twist angle of the formyl group was allowed to relax. Computations with the basis set 6-31G** gave potential energy profiles essentially equal to those obtained with the 6-31G* basis. INDO MO FPT (15, 16) calculations of some long-range proton–proton coupling constants employed the 6-31G* geometries.

Results and discussion

Spectral analyses

The ^{1}H nmr spectra were analyzed with the computer program NUMARIT (17), extensively altered by R. Sebastian. The chemical shifts and coupling constants are found in Tables 1 and 2.

Figure 1 displays a congested spectral region of the ^{1}H nmr spectrum of the acetone-d_6 solution. The spectral extent of ca. 19 Hz contains transitions from H-5 and H-7. The simulated spectrum assumes a linewidth of 0.025 Hz. While the congruence of the two spectra is imperfect, it is in our opinion sufficient to validate those spectral parameters pertinent to the conformational deductions described below. As one more example, Fig. 2 shows the spectrum of the formyl proton that, again imperfect, allows the conclusion that $^5J_{7,10}$ is negative.

The theoretical conformational properties

The 6-31G* energies for various torsion angles, θ, of the vinyl group (see structures **A** and **B**) are given in Table 3. The barrier to internal rotation in benzaldehyde is calculated as 37.5 kJ/mol with the 6-31G* basis (18), rather higher[2] than, for example, the free energy of activation of 32.2(6) kJ/mol in solution (19–21). In contrast, the 6-31G* barrier for styrene is only 12.0 kJ/mol (11) while, experimentally, the internal barrier height is 12.8(6) or 13.8(7) kJ/mol (twofold component) with a fourfold component of −3.3 kJ/mol (6, 7), yielding a very flat potential near θ = 0°. On the basis of these barriers, it is expected that steric strain will force the vinyl group out of the ring plane. The relative energies in Table 3 confirm these expectations, implying that the conformational properties of 2-formylstyrene can be discussed in terms of O-*cis* and O-*trans* conformers, each with potential for the out-of-plane excursion of the vinyl group. Figure 3 gives a plot of the energies as a function of θ.

The planar conformers (θ = 0 in Fig. 3) are stabilized by the π,π conjugational energies and are both destabilized by the energies due to repulsion between the *ortho* C—H and β-CH bonds. To a first approximation, therefore, the energy difference of 3.3 kJ/mol between the planar conformers corresponds to the difference in energy between the H,H and H,O repulsions of the α-CH bond of the vinyl group and the bonds in the formyl fragment. The H,O interaction must be repulsive because otherwise the planar form of **A** would be stable, as in styrene. The stable form of **A**, however, corresponds to a θ of 38°, representing a compromise between the loss of some π,π conjugation and a decrease in the two repulsions amounting to 4.0 kJ/mol (see Table 3). The twofold, conjugational, component of the 6-31G* barrier in sytrene is 12.0 kJ/mol. If the conjugational energy in 2-formylstyrene is very similar in magnitude, then about 4.5 kJ/mol of it would be lost at θ = 38°. Further analysis of the energies of **A** is not feasible, so it cannot be said whether an attractive H,O interaction exists at the twist angle of 38°. The H_α,O distance is somewhat less than 2.4 Å, very like the computed H,O distances[3] in the hydrogen-bonded complexes between water and some fluoromethanes (23). The high energy of **A** at θ = 90° is about 4.7 kJ/mol larger than that expected from the complete loss of π,π conjugation, very likely because of repulsion between the 2*p* orbital on C-α and the C=O bond

[2] There is a controversy concerning the internal barrier for the free molecule (22). However, it is agreed that the barrier in solution is not less than 27 kJ/mol, so that large out-of-plane deviations of the carbonyl group are not expected at 300 K except for θ values other than 90° in **B**. These conformers involve steric congestion in the sidechains.

[3] In 2-hydroxylbenzaldehyde, a molecule with a strong intramolecular hydrogen bond, perhaps as large as 29 kJ/mol (24, 25), the microwave spectrum of the vapor corresponds to a H,O distance of 1.76 ± 0.01 Å (26).

Can. J. Chem. Downloaded from www.nrcresearchpress.com by 46.23.64.124 on 09/08/12
For personal use only.

Fig. 1. A span of 18.7 Hz in the ^{1}H nmr spectrum of 2-formylstyrene is displayed for a 4.4 mol% solution in acetone-d_6 at 300 MHz and 300 K. The congestion arises because of overlap between the transitions of the α proton of the vinyl group, H-7, and of the ring proton, H-5. The simulated spectrum uses the spectral parameters found in Table 1.

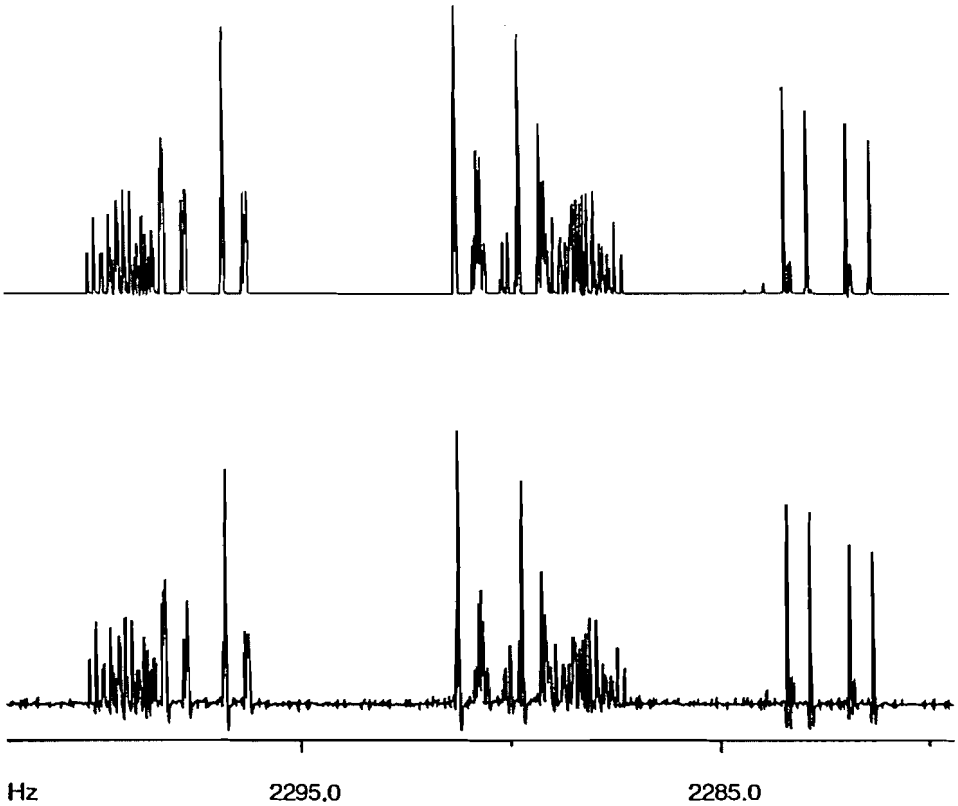

(reminiscent of the situation in 2-alkylthiobenzaldehydes (27), in which only the O-*trans* conformer occurs when the 3*p* orbital on sulfur is twisted into the molecular plane).

For conformer **B** the lowest energy occurs at θ = 45°, so that H,H repulsion between the α-CH and the formyl C—H bonds in the planar form is substantial. A local maximum at θ = 90° is 11.0 kJ/mol lower in energy than for **A**, and therefore about 6.3 kJ/mol lower than expected for complete loss of π conjugational energy, suggesting an incipient C—H···π hydrogen bond involving the formyl hydrogen and the π system of the vinyl group. As θ increases beyond 90°, the π conjugational energy again increases, contributing to a decrease in total energy. At θ = 129.6°, corresponding to the local minimum, the H,Cβ distance is 2.68 Å. Beyond θ = 129.6° repulsion between the β-CH and formyl C—H bonds becomes dominant. Consequently a local minimum near 129.6° occurs and may well be favorable for the fast 1,5-hydrogen shift from formyl to vinyl fragments, postulated (1) for the electronically excited state. The H_{10},H_8 distance is less than 2.6 Å at θ = 129.6°. Alternatively, the C—H bond of the formyl group is reasonably well placed to interact with the 2*p* orbitals of the double bond in the side chain: the hydrogen atom lies some 2.7 Å above the midpoint of the C=C bond and about 0.5 Å from the normal to the vinyl plane.

Given the potential energies in Table 3, it is of interest whether they are consistent with the long-range coupling constants in Table 2. Those involving the vinyl protons would sample the two energy profiles in Fig. 3 as given by a Boltzmann weighting. The long-range coupling constants over five bonds to the formyl proton are excellent measures of the proportions of **A** and **B** (25, 28, 29).

Long-range coupling constants

(a) The proportions of A and B

It has been established (25, 28, 29) that the ratio of ^5J(H-*m*, CHO), the coupling constant between the formyl proton and a ring proton placed *meta* to the formyl group, to the sum of the two such coupling constants in a benzaldehyde derivative is a good measure of the conformational bias of the formyl group. As applied to 2-formylstyrene, one has $^5J_{6,10}/(^5J_{4,10} + {}^5J_{6,10}) = 0.363/(0.363 + 0.444) = 0.45$ as the fractional population of conformer **A**. The values of the coupling constants in Table 2 are only slightly different in the polar and nonpolar solutions, so that their mean has been used above, implying also that these solvents do not alter the proportions of **A** and **B**.

It is interesting that the 6-31G* energies in Table 3 have **A** as 0.31 kJ/mol less stable than **B**. If this is also true at 300 K, then one has the theoretical fractional population of **A** as 0.47. Of course, this conclusion is only valid if corrections for zero-point energies, thermal energies, and entropies, as well as solvent effects, combine in such a way as to yield a free energy difference essentially unchanged from the energy difference in Table 3. The long-range coupling constants for the formyl proton indicate that such is indeed the case, and shall be assumed in further discussion.

Can. J. Chem. Downloaded from www.nrcresearchpress.com by 46.23.64.124 on 09/08/12
For personal use only.

Fig. 2. A span of 4.0 Hz from the ^{1}H nmr region in Fig. 1 is displayed in detail. The simulated spectrum has a linewidth at half-height of 0.03 Hz. The agreement between simulation and experiment, while not perfect, is sufficient for the purpose to which the underlying coupling constants are put in the text.

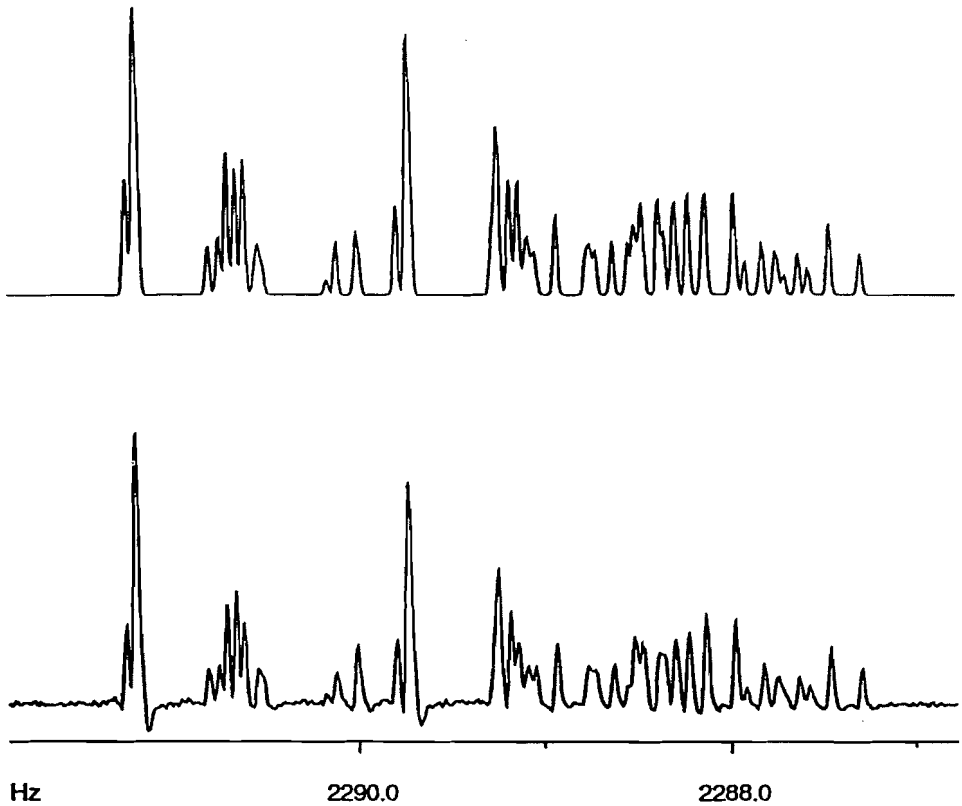

Fig. 3. The potential energy diagram for 2-formylstyrene, as given by 6-31G* molecular orbital computations, refers to the O-*cis* (**A**) and O-*trans* (**B**) conformers. The angle θ is zero if the α C—H bond of the vinyl group lies *cis* to the formyl group in the planar molecule. In the congested region, θ > 105° for **B**, the formyl group twists substantially away from the aromatic plane (see Table 3).

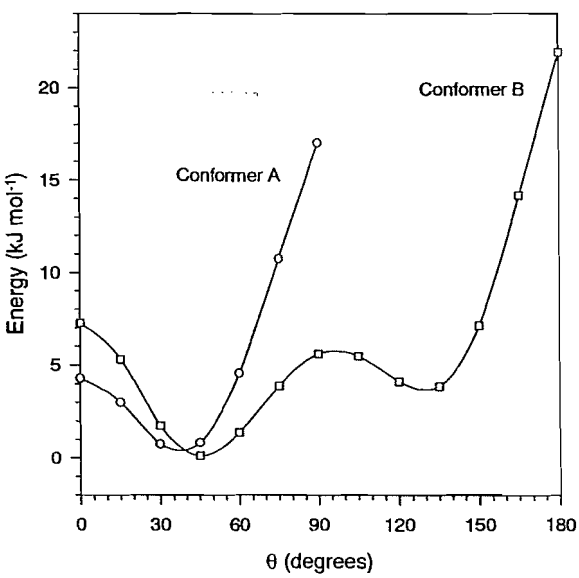

Furthermore, the potential energy curves in Fig. 3 imply various probabilities for the angles θ at a given temperature. The C—H bonds of the vinyl group sample various values of θ and, in so doing, cause the long-range coupling constants of their protons to vary because they are functions of θ. If the functionality is known, then the potential curves will predict the values of the coupling constants.

(b) Computation of $^6J_{47}$

Theoretically and experimentally (2–5), $^6J_{47}$ in styrene is a function of $\sin^2\theta$. We calculate the expectation value of $\sin^2\theta$ as

$$\langle \sin^2 \theta \rangle = \Sigma\, p_i \sin^2 \theta$$

where

$$p_i = \frac{\exp(-E_i/R)}{\Sigma \exp(-E_i/RT)}$$

The probability, p_i, at a given θ, is obtained from the energies, E_i at that θ, as found in Table 3. At 300 K, $\langle \sin^2\theta \rangle$ is then[4] 0.450.

[4] If a 3-site calculation is performed, using the three minima in Fig. 3, one finds $\langle \sin^2\theta \rangle$ as 0.456 at 300 K. This computation assumes the experimental populations of **A** and **B**; the theoretical populations of **A** and **B** entail a $\langle \sin^2\theta \rangle$ of 0.454.

Can. J. Chem. Downloaded from www.nrcresearchpress.com by 46.23.64.124 on 09/08/12
For personal use only.

Table 3. The relative 6-31G* energies in kJ/mol of the O-*cis* and O-*trans* conformers of 2-formylstyrene for various torsion angles of the vinyl fragment.

Conformer **A** (O-*cis*)		Conformer **B** (O-*trans*)	
θ/degrees[a]	Energy	θ/degrees[a]	Energy
0	3.98	0	7.25
5	3.81	15	5.30
10	3.35	30	1.74
15	2.66	45	0.10
20	1.86	45.1[c]	0.00[d]
25	1.07	60	1.36
30	0.44	75 (−1.4)[e]	3.88
38.0	0.00[b]	90 (0.9)	5.62
45	0.50	105 (4.5)	5.48
60	4.22	120 (10.0)	4.12
75	10.43	129.6 (14.2)	3.64
90	16.67	135 (16.5)	3.84
		150 (22.8)	7.12
		165 (27.5)	14.16

[a]A θ of zero corresponds to a conformation in which the vinyl group lies in the aromatic plane and the α C—H bond points towards the formyl group (see structure **A** in the text).

[b]The total energy is −420.310 715 a.u. The C=O bond of the formyl group twists out of plane by 0.1°.

[c]The total energy is −420.310 833 a.u. The angle of twist of the formyl group is 3°.

[d]This minimum in the energy for the O-*trans* conformer lies 0.31 kJ/mol below the minimum for the O-*cis* conformer.

[e]The numbers in parentheses give the torsion angle of the formyl group. A positive number means that the α and formyl C—H bonds both lie below the aromatic plane.

In studies of various styrene derivatives (3, 4) it was found[5] that $^6J_{47}$ could be written as $-0.149\cos^2\theta - 0.597\sin^2\theta$. This relationship then has $^6J_{47}$ as −0.351 Hz for 2-formylstyrene, to be compared with −0.349(6) Hz, the mean of the two values in Table 2. The mean is used because, in our opinion, the present model is hardly precise enough to corroborate the existence of different potentials in the two solvents. The approach used for $^6J_{47}$ is now applied to other coupling constants of the vinyl protons.

(c) Computation of $^5J_{37}$ and $^5J_{57}$

Odd though it appears, $^5J_{37}$ in styrene and some of its derivatives is reproduced by $A\langle\sin^2(\theta/2)\rangle$; where $\langle\sin^2(\theta/2)\rangle$ is 0.5 for an evenfold potential. Thus, for acetone-d_6 solutions of styrene (30) and 2,6-dichlorostyrene (measured in this laboratory) $^5J_{37} = {}^5J_{57}$ is 0.368(s) Hz and 0.391(1) Hz, respectively. The corresponding values of $^6J_{47}$ are −0.227(2) Hz and −0.540(2) Hz, implying that $\langle\sin^2\theta\rangle$ is very different for the two compounds. In 2-fluorostyrene, $^5J_{37} + {}^5J_{57}$ is 0.758(4) Hz, independent of the polarity of the solvents (4). From Table 2, this sum is 0.750(2) Hz in CS_2–C_6D_{12} and 0.761(2) Hz in acetone-d_6 for 2-formylstyrene. A final datum is the 0.372(1) Hz for $^5J_{3,7}$ in β,β-dibromo-2,6-dichlorostyrene, both in acetone-d_6 and in CD_2Cl_2–CCl_4 solutions at 296 K (5). It seems that a term in $\sin^2\theta$, due to a σ,π mechanism (2), is very small.

From these considerations, we can write $^5J_{37} = 0.755\sin^2(\theta/2)$. The energies in Table 3 yield $\langle\sin^2(\theta/2)\rangle$ as 0.214 and hence predict $^5J_{37}$ as 0.162 Hz and thus $^5J_{57}$ as 0.755 − 0.162 or 0.593 Hz. Of course, the ^5J numbers would also be consistent with two conformers having θ as zero; such a situation is contradicted by models, $^6J_{47}$, and, naturally, by the theoretical computations.

(d) Computation of $^4J_{67}$

$^4J_{67}$ has been assessed as $-0.476\cos^2\theta - 0.759\sin^2\theta$ in styrene and some methyl derivatives (3). This assessment predicts $^4J_{67}$ as −0.603 Hz in 2-formylstyrene, 5% lower in magnitude than the −0.637(2) Hz in Table 2. The term in $\cos^2\theta$ represents π electron spin correlation across the partial double bond.

(e) Coupling constants between ring and β protons, H-8 and H-9

It was postulated (3) that $^7J_{48}$ and $^7J_{49}$ follow $0.300\cos^2\theta + 0.065\sin^2\theta$, with perhaps a small additional term contributing as much as 0.04 Hz to $^7J_{49}$ (2, 3). A $\langle\sin^2\theta\rangle$ of 0.450 for 2-formylstyrene yields 0.194 Hz for $^4J_{48}$ and $^4J_{49}$, midway between the measurements of 0.182(2) Hz for $^7J_{48}$ and 0.211(7) Hz for $^7J_{49}$ in Table 2. In styrene (30), $^7J_{48}$ and $^7J_{49}$ are 0.237(3) and 0.281(3) Hz, respectively, reflecting the larger value of $\cos^2\theta$ in the parent compound (lower θ values).

In styrene, $^6J_{38}$ and $^6J_{39}$ are interesting because they are not detected (30). $^6J_{39}$ is calculated by INDO (2) as +0.12 Hz at θ = 0° ("all-*trans*") and as +0.07 Hz at θ = 90°. At θ = 180°, however, corresponding to $^6J_{59}$ in **A**, its value is −0.18 Hz. In styrene, of course, one measures the mean of $^6J_{39}$ and $^5J_{59}$, accounting for their absence. Write $^6J_{59}$ as $-0.10\cos^2\theta + 0.14\sin^2(\theta/2)$. The first term corresponds to the π electron component, which decreases in magnitude as spin correlation is lost with an increase in θ to 90°. The second term represents a rare (2, 4) positive σ electron contribution with a maximum in the all-*trans* arrangement of the intervening bonds. The discussion of the internal potential for styrene in solution (3) has $\langle\cos^2\theta\rangle$ as 0.825 and $\langle\sin^2(\theta/2)\rangle$ is 0.5 for an evenfold potential, so that this expression yields $^6J_{39} = {}^6J_{59}$ as −0.012 Hz, in satisfactory congruence with experiment. For 2-formylstyrene, $\langle\sin^2(\theta/2)\rangle$ is 0.786 for $^6J_{39}$ and 0.214 for $^6J_{59}$ (see above); also, $\langle\cos^2\theta\rangle$ is predicted as 0.550 from the computed potential. Hence $^6J_{39}$ is calculated as +0.055 Hz and $^6J_{59}$ as −0.025 Hz, again in reasonable agreement with the +0.052 and −0.022(6) Hz in Table 2. In 3-fluorostyrene, however, $^5J_{59}$ is +0.06 Hz (4). All methods agree that the *cis* conformer, which favors a positive $^6J_{59}$, is most abundant (4, 31–34). Yet $\langle\cos^2\theta\rangle$ is not smaller than in styrene (4), so that the expression above cannot reproduce $^6J_{59}$: the conformational dependence of $^6J_{39}$ or $^6J_{59}$ needs more study.

Turning to $^6J_{38}$ and $^6J_{58}$, they are calculated as -0.19_5 Hz in the planar form of styrene and −0.14 Hz in the perpendicular conformer by INDO MO FPT methods (2). These numbers imply a π electron part, proportional to $\cos^2\theta$, and a σ,π contribution in $\sin^2\theta$, increasing in magnitude as the π electron

[5] Another relationship (5), developed using data from β,β-dibromo-2,6-dichlorostyrene and 3,5-dichlorostyrene, is $-0.130\cos^2\theta - 0.800\sin^2\theta$. One then has $^6J_{47}$ in 2-formylstyrene as −0.440 Hz. The relationship used above (3, 4) was designed to reproduce spectral data for styrene itself.

Can. J. Chem. Downloaded from www.nrcresearchpress.com by 46.23.64.124 on 09/08/12
For personal use only.

component fades. The finite σ,π component is in line with the −0.1 Hz found in 2,6-dichlorostyrene (2). But, since $^6J_{38}$ is not detected in styrene, another, positive component presumably exists, neglected by the INDO parameterization, and active most prominently at small torsion angles, θ. A speculative mechanism invokes the through-space, or proximate, interaction between the β-CH and the *ortho* C—H bonds, postulated for styrene (2). In all known cases (2, 35–42) such an interaction leads to a negative coupling constant between the protons, as indicated in **C** by the parallel crossed arrows for H-6 and

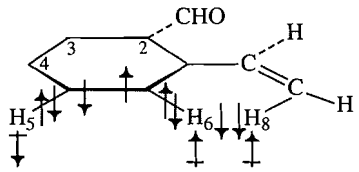

C

H-8. Schematically, the repulsive overlap of the 1*s* orbitals centered on these protons is consistent with a parallel-spin preference of the electrons in these orbitals. Given this situation, the spin correlation in the σ bonds of the aromatic ring, determined by the Pauli principle and Hund's rule, then leads to the spin state of the proton in H-5 as in **C** and hence a positive contribution to $^6J_{58}$ (see also **A**). At what θ value the proximate interaction is maximized is uncertain, it being very sensitive to interatomic distance and the mutual arrangement of the C—H bonds. In styrene, $^5J_{28} = {}^5J_{68}$ is not seen, presumably because the negative proximate component cancels the expected positive coupling components, σ and π, expected over five bonds. In 2-formylstyrene, $^5J_{68}$, not having a large σ contribution from a mainly *trans* pathway, is −0.132(5) Hz (Table 2), suggesting that the through-space mechanism also operates at substantial θ values corresponding to H_6,H_8 distances of 2.4–2.5 Å. The spin correlation proposed in **C** is consistent with the small magnitude of $^6J_{58}$ in 2-formylstyrene, acting to cancel the negative π and σ,π interactions. These are as large for $^6J_{38}$ as for $^6J_{58}$ and dominate the −0.084(3) Hz measured for $^6J_{38}$. Parenthetically, the present rationalization is consonant with the magnitudes (signs unknown) of $^6J_{58}$ and (or) $^6J_{38}$ in 2-fluoro- and 3-fluorostyrene (4).

The proximate nature of $^5J_{68}$ is mentioned above. As to $^5J_{69}$, one has $(^5J_{29} + {}^5J_{69})/2$ as 0.158(2) Hz in styrene (30), similar to the numbers for some *meta*- and *para*-substituted derivatives (2–4). The negative, proximate contribution to $^5J_{68} = {}^5J_{28}$ is not present in $^5J_{29} = {}^5J_{69}$. Valence-bond theory (2) suggests a π electron term, 0.59 $\cos^2\theta$, for $^5J_{69}$, while the INDO MO FPT procedure (2) has the coupling as 0.20 Hz at θ = 0° (see **A**) and 0.50 Hz at θ = 180°. These numbers imply a σ electron component of appreciable magnitude. However, INDO also calculates $^5J_{69}$ as 0.33 Hz at θ = 90°. In fact, $^5J_{69}$ is 0.047(3) Hz in 2-formylstyrene and, because $\langle\cos^2\theta\rangle$ is apparently equal to 0.550 and θ values nearer 180° are inappreciable, it appears that both methods strongly overestimate the π and σ electron components. In 2-fluorostyrene, $^5J_{69}$ is 0.084(2) Hz (4), corresponding to a larger $\langle\cos^2\theta\rangle$. A parameterization of the θ dependence of $^5J_{29}$ must await further experimental data.

(f) Coupling constants between olefinic protons and the formyl proton

$^5J_{7,10}$ is −0.163(1) Hz and is most likely a proximate coupling constant, similar in nature to the −0.38(1) Hz determined for the coupling constant between the formyl and methine protons in 2-formylisopropylbenzene (42). Such coupling constants are very sensitive to interatomic distance (43, 44). In the isopropylbenzene derivative, the experimental and theoretical evidence (42) is that the methine C—H bond is rather closely confined to the aromatic plane. In consequence, its hydrogen atom approaches that of the formyl C—H bond rather more closely on average than for the analogous interaction in 2-formylstyrene. The O-*trans* populations in the two compounds are almost equal.

CNDO/2 MO FPT computations of $^5J_{7,10}$ in 2-formylstyrene, employing the 6-31G* geometries, were used instead of the INDO formulation because both methods give very similar values for proximate contributions, while the latter strongly overestimates the σ electron component of a five-bond coupling constant in benzene derivatives. For planar **B**, in which H-7 and H-10 approach to within 1.95 Å in the 6-31G* geometry, $^5J_{7,10}$ is computed as −0.31 Hz, implying a negative proximate coupling, as expected. As θ increases (Fig. 3), the computed magnitude decreases. For **A**, $^5J_{7,10}$ is computed as small and positive, less than 0.1 Hz at θ = 0 and becoming negligible for θ = 60°. The potential energy curve in Fig. 3, applied as a weighting function to the computed values, yields $^5J_{7,10}$ as −0.08 Hz. In view of the high sensitivity of the proximate component to internuclear distance, this result may be considered as satisfactory in comparison with the experimental value of −0.16 Hz.

Intragroup coupling constants

The changes in ^2J_g, ^3J_c, and ^3J_t in 2-formylstyrene, caused by the polar solvent (Table 1), are parallel to those measured in 2-fluorostyrene (4). The same can be said for the coupling constants between ring protons in these two compounds and also for 2-formylisopropylbenzene (42). Such small changes, also measured for monosubstituted benzenes in this laboratory, follow patterns to a large extent independent of the nature of the substituent and are certainly not artifacts of the spectral analytical procedures.

The proton chemical shifts

Table 4 contains the δ values for the protons of benzaldehyde, styrene, and 2-formylstyrene dissolved in acetone-d_6. To within the uncertainties caused by differing concentrations, the ring proton shifts in 2-formylstyrene are nearly reproduced by an additive scheme. This result is reasonable in that the formyl group in 2-formylstyrene has almost the equal O-*cis* and O-*trans* populations experienced by the protons in benzaldehyde. Further, the computed potential suggests only small overall deviations from coplanarity of the formyl group, consistent with very similar conjugative shifts caused by this substituent in the parent compound and its derivatives and also with the ^6J(H-*para*, CHO) values in the two compounds. The perturbations of the proton chemical shifts in benzene by the vinyl group are relatively small (Table 4). At the *para* position an increased screening of 0.12(1) ppm occurs (π donor). If the *para* proton shift goes as $\cos^2\theta$ and $\langle\cos^2\theta\rangle$ is 0.825 for styrene (3) and 0.537 for 2-formylstyrene, then for the latter one expects a deviation of 0.04 ppm from additivity (larger δ value) at H-4; one measures 0.03(1) ppm. At H-5, the shift of which is dominated by the electron-withdrawing formyl

Table 4. Chemical shifts (δ values) of benzaldehyde, styrene, and 2-formylstyrene in acetone-d_6 solution.

			2-Formylstyrene	
Proton	Benzaldehyde[a]	Styrene[b]	Additivity[d]	Observed[c]
ν_3[e]	7.601	7.293	7.88	7.87
ν_4	7.698	7.220	7.48	7.51
ν_5	7.601	7.293	7.65	7.63
ν_6	7.928	7.417	7.68	7.69
ν (CHO)	10.054	—	—	10.310
ν_7	—	6.717	—	7.671
ν_8	—	5.764	—	5.784
ν_9	—	5.194	—	5.480

[a]For a 4.0 mol% solution in acetone-d_6, containing also 0.5 mol% TMS (45).

[b]For a 16 mol% solution in acetone-d_6 (30).

[c]For a 4.4 mol% solution in acetone-d_6 (Table 1).

[d]The δ values for C_6H_6 are 7.324 for a 16 mol% solution in acetone-d_6 and 7.349 for a 2.5 mol% solution (4). This column assumes the mean of the two numbers.

[e]In ppm (δ values) relative to internal TMS at 300 K; 298 K for styrene.

group, the deviation is negative by 0.02(1) ppm. It does appear that the ring proton chemical shifts in 2-formylstyrene are consistent with the conformational distribution assumed in the above discussion of the long-range coupling constants.

Perhaps the most striking chemical shift in Table 4 is that of H-7 in 2-formylstyrene. At 7.67 ppm, this proton is deshielded by 0.95 ppm in the presence of the formyl group. Because H-7 is characterized by larger θ values than in the parent compound, which would *decrease* its δ value arising from the diamagnetic anisotropy of the benzene ring, the 0.95 ppm must be due to perturbations by the proximate formyl group. A simple interpretation holds that repulsion by the C—H bond in **B**, and by the C=O bonds in **A**, of the α olefinic C—H bond, the main origin of the out-of-plane twist of the vinyl group, is also the concomitant cause of the descreening of H-7. Numerous examples (46–50) exist of significant deshielding of protons in steric proximity to other groups.[6] At the small interatomic distances applicable to the conformation of Fig. 3, it would be bootless to attempt a dissection of the 0.95 ppm into contributions such as those from the anisotropy of the carbonyl group or from the mean-square electric fields due to the lone-pair electrons on oxygen. It may be noted that in 2-fluorostyrene, for which there is no indication of nonplanarity of the vinyl group significantly larger than that in styrene (4), H-7 is deshielded by only 0.16 ppm relative to styrene. In summary, the large shift experienced by H-7 in 2-formylstyrene is consistent with the conformational distribution of the vinyl group in Fig. 3.

While the large chemical shift of H-7, induced by the presence of the formyl group, is reasonably attributed to proximity effects, the much smaller shifts induced at H-8 and H-9 likely include electric field and mesomeric shifts similar to those characterized for a series of 4-X-styrenes (52), as well as small changes in shielding due to a reduction in the descreening caused by the diamagnetic anisotropy of the benzene ring. Disentanglement of the various shift contributions could only proceed with data from a series of 2-X-styrenes. It is noteworthy that the δ values of H-8 and H-9 in 2-fluorostyrene are 5.88 and 5.39, not strikingly different from those for the title compound. Yet fluorine and the formyl group are characterized by contrasting mesomeric parameters.

The formyl proton is deshielded by 0.25 ppm by the vinyl moiety (Table 4), a minimum value for a proximity shift because in **B** the two local minima are such (Fig. 3) that, in sum, a shielding (49) should occur by the magnetic anisotropy of the C—C olefinic bond.

[6] For some current examples of descreening of protons caused by "proximity effects" see ref. 51.

Summary

The ^{1}H nmr spectral parameters of 2-formylstyrene show that the population of the O-*cis* and O-*trans* conformers are almost equal in both CS_2–C_6D_{12} and acetone-d_6 solutions; the formyl and phenyl groups are roughly coplanar. The theoretical torsional potential for the vinyl group has a minimum at a torsion angle of 38° for the O-*cis* conformer, whereas minima occur at 45° and at 129.6° in the O-*trans* conformer. The long-range coupling constants for the vinyl protons in both solutions are consistent with the theoretical potential. The existence is predicted of a conformer in which the hydrogen atom of the formyl group closely approaches the β-carbon centre of the vinyl group, thereby facilitating a 1,5-hydrogen shift postulated to occur under irradiation. Hydrogen atom transfers during irradiation can be very sensitive to interatomic distances (53).

Acknowledgments

We thank the Natural Sciences and Engineering Research Council of Canada for financial assistance. A referee is thanked for useful criticism.

References

1. S.V. Kessar and A.K.S. Mankotia. J. Chem. Soc. Chem. Commun. 1828 (1993), and references cited therein.
2. M. Barfield, C.J. MacDonald, I.R. Peat, and W.F. Reynolds. J. Am. Chem. Soc. **93**, 4195 (1971).
3. T. Schaefer, R. Sebastian, and G.H. Penner. Can. J. Chem. **66**, 584 (1988).
4. T. Schaefer and R. Sebastian. Can. J. Chem. **68**, 1383 (1990).
5. R. Laatikainen, E. Kolehmainen, T. Kuokkanen, and K. Tuppurainen. J. Magn. Reson. **78**, 9 (1988).
6. J.M. Hollas, H. Musa, T. Ridley, P.H. Turner, K.H. Weisenberger, and V. Fawcett. J. Mol. Spectrosc. **94**, 437 (1982).
7. W. Caminati, B. Vogelsanger, and A. Bauder. J. Mol. Spectrosc. **128**, 384 (1988).
8. R. Hargittai, P.G. Szalay, G. Pongor, and G. Forgarasi. J. Mol. Struct. (Theochem), **306**, 293 (1994).
9. T. Schaefer and G.H. Penner. Chem. Phys. Lett. **114**, 526 (1985).
10. C.W. Bock, M. Trachtman, and P. George. Chem. Phys. **93**, 431 (1985).
11. S. Tsuzuki, K. Tanabe, and E. Osawa. J. Phys. Chem. **94**, 6175 (1990).
12. W.J. Dale, L. Starr, and C.W. Strobel. J. Org. Chem. **26**, 2225 (1961).
13. P.C. Hariharan and J.A. Pople. Chem. Phys. Lett. **66**, 217 (1972.).
14. M.J. Frisch, G.W. Trucks, M. Head-Gordon, P.M.W. Gill, M.W. Wong, J.B. Foresman, B.G. Johnson, H.B. Schlegel, M.A.

Can. J. Chem. Downloaded from www.nrcresearchpress.com by 46.23.64.124 on 09/08/12
For personal use only.

Robb, E.S. Replogle, R. Gomperts, J.L. Andres, K. Raghavachari, J.S. Binkley, C. Gonzalez, R.L. Martin, D.J. Fox, D.J. Defrees, J. Baker, J.J.P. Stewart, and J.A. Pople. GAUSSIAN 92, Revision C. Gaussian, Inc. Pittsburg, Pa. 1992.
15. J.A. Pople, J.W. McIver, Jr., and N.S. Ostlund. J. Chem. Phys. **49**, 2960 (1968); **49**, 2965 (1968).
16. J.A. Pople and D.L. Beveridge. Approximate molecular orbital theory. McGraw Hill Book Co., New York. 1970.
17. A.R. Quirt and J.S. Martin. J. Magn. Reson. **5**, 318 (1971); J.S. Martin, A.R. Quirt, and K.E. Worvill. The NMR program library. Daresbury Laboratory, Daresbury, U.K.
18. T. Schaefer, R. Sebastian, and F.E. Hruska. J. Mol. Struct. (Theochem), **281**, 269 (1993).
19. F.A.L. Anet and M. Ahmad. J. Am. Chem. Soc. **86**, 119 (1964).
20. T. Drakenberg, R. Jost, and J.M. Sommer. J. Chem. Soc. Chem. Commun. 1011 (1974).
21. L. Lunazzi, D. Maccientelli, and A. Boicelli. Tetrahedron Lett. 1205 (1975).
22. T. Schaefer, C.S. Takeuchi, G.M. Bernard, and F.E. Hruska. Can. J. Chem. **73**, 106 (1995), and references therein.
23. I. Alkorta and S. Maluendes. J. Phys. Chem. **99**, 6457 (1995).
24. T. Schaefer. J. Phys. Chem. **79**, 1888 (1975).
25. T. Schaefer, R. Sebastian, D.M. McKinnon, P.W. Spevack, K.J. Cox, and C.S. Takeuchi. Can. J. Chem. **71**, 960 (1993).
26. H. Jones and R.F. Curl, Jr. J. Mol. Spectrosc. **42**, 65 (1972).
27. T. Schaefer, G.H. Penner, K.J. Davie, and R. Sebastian. Can. J. Chem. **63**, 777 (1985).
28. T. Schaefer and C.S. Takeuchi. Can. J. Chem. **68**, 339 (1990).
29. R. Laatikainen, K. Tuppurainen, Y. Hiltunen, and S. Lötjönen. Magn. Reson. Chem. **28**, 939 (1990).
30. H. Nies, H. Bauer, K. Roth, and D. Rewicki. J. Magn. Reson. **39**, 521 (1980).
31. J.M. Hollas and M.Z. bin Hussein. Chem. Phys. Lett. **154**, 228 (1989).
32. R.M. Villamañán and J.L. Alonso. Chem. Phys. Lett. **159**, 97 (1989).
33. T. Schaefer and R. Sebastian. Chem. Phys. Lett. **163**, 212 (1989).
34. J.J.C. Teixeira-Dias and P.J.A. Ribeiro-Claro. Struct. Chem. **3**, 95 (1992).
35. H.A. Gaur, J. Vriend, and W.G.B. Huysmans. Tetrahedron Lett. 1999 (1969).
36. T. Schaefer, H.D. Gesser, and J.B. Rowbotham. Can. J. Chem. **54**, 2235 (1976).
37. T. Schaefer and W.J.E. Parr. Can. J. Chem. **55**, 2835 (1977).
38. T. Schaefer, R. Sebastian, and S.R. Salman. Can. J. Chem. **62**, 113 (1984).
39. T. Schaefer, T.A. Wildman, and R. Sebastian. Can. J. Chem. **63**, 773 (1985).
40. T. Schaefer, J. Peeling, R. Sebastian, and J.D. Baleja. Can. J. Chem. **63**, 2217 (1985).
41. T. Schaefer, R. Sebastian, S.R. Salman, J.D. Baleja, G.H. Penner, and D.M. McKinnon. Can. J. Chem. **69**, 620 (1991).
42. T. Schaefer and K.J. Cox. Can. J. Chem. **69**, 919 (1991).
43. J. Hilton and L.H. Sutcliffe. Prog. NMR Spectrosc. **10**, 27 (1975).
44. R.H. Conteras and J.C. Facelli. Annu. Rep. NMR. Spectrosc. **27**, 255 (1993).
45. T. Schaefer and C.S. Takeuchi. Can. J. Chem. **67**, 827 (1989).
46. W.T. Raynes, A.D. Buckingham, and H.J. Bernstein. J. Chem. Phys. **36**, 348 (1962).
47. R.F. Zürcher. Prog. NMR Spectrosc. **2**, 205 (1967).
48. L.M. Jackman and S. Sternhell. Applications of NMR spectroscopy in organic chemistry. 2nd ed. Pergamon Press, Oxford. 1969. pp. 71, 72.
49. H. Günther. NMR spectroscopy. Wiley, New York. 1980. pp. 73–77.
50. R.K. Harris. NMR spectroscopy. Longman Scientific and Technical, Harlow, Essex. 1986. pp. 191–204.
51. R.J. Abraham, M. Edgar, L. Griffiths, and R.L. Powell. J. Chem. Soc. Perkin Trans. 2, 561 (1995).
52. G.K. Hamer, I.R. Peat, and W.F. Reynolds. Can. J. Chem. **51**, 897 (1973).
53. D. Gravel, R. Giasson, D. Blanchet, R.W. Yip, and D.K. Sharma. Can. J. Chem. **69**, 1193 (1991).

Can. J. Chem. Downloaded from www.nrcresearchpress.com by 46.23.64.124 on 09/08/12
For personal use only.

Cation binding and conformation of octafunctionalized calix[4]resorcinarenes

John R. Fransen and Philip J. Dutton

Can. J. Chem. Downloaded from www.nrcresearchpress.com by 46.23.64.124 on 09/08/12
For personal use only.

Abstract: The preparations of four calix[4]resorcinarene esters and two calix[4]resorcinarene amides are reported. The logarithms of association constants have been determined by the picrate extraction method for a variety of metal cations, including alkali metal, alkaline earth, lanthanum, and silver cations. Strong binding toward silver ion, and selectivity amongst the alkaline earth cations, was observed for the octa-α-(diethyl acetamide) **3***c*. Flattened cone conformations have been established for both *C*-undecylcalix[4]resorcinarene octa-α-(methyl acetate), **3***a*, and octa-α-(diethyl acetamide), **3***c*, in chloroform solutions at 200 K. Dynamic nuclear magnetic resonance was used to identify rapid conformational interconversions of both **3***a* and **3***c* corresponding to pseudorotation between flattened cone conformations. The silver complex of **3***c* also exhibits pseudorotation; however, the activation barrier was observed to increase from 42 kJ mol^{-1} in the free ligand to 49 kJ mol^{-1} in the complex. The NMR data indicate that the metal cation binding occurs in a symmetrical fashion using two pairs of binding sites that are disposed across the macrocyclic ring from one another. Considering these data it is concluded that four carbonyl functions are involved in the binding of a metal cation in a 1:1 complex with the ligand.

Key words: resorcinarene, picrate, association constant, dynamic NMR, pseudorotation.

Résumé : On a préparé quatre esters calix[4]résorcinarènes et deux amides calix[4]résorcinarènes. Faisant appel à la méthode d'extraction du picrate, on a déterminé les logarithmes des constantes d'association d'une variété de cations métalliques, y compris ceux de l'argent, des métaux alcalins et alcalino-terreux et de la série des lanthanides. Avec l'octa-α-(diéthyl acétamide), **3***c*, on a observé que les ions de l'argent sont fortement fixés et qu'il existe une grande sélectivité parmi les cations des alcalino-terreux. On a établi que, en solutions dans le chloroforme à 200 K, le *C*-undécylcalix[4]résorcinarène octa-α-(acétate de méthyle), **3***a*, ainsi que l'octa-α-(diéthyl acétamide), **3***c*, ont tous les deux des conformations coniques aplaties. On a utilisé la résonance magnétique nucléaire dynamique pour identifier les interconversions conformationnelles rapides des deux composés **3***a* et **3***c* qui correspondent à la pseudorotation entre des conformations coniques aplaties. Le complexe de l'argent avec le composé **3***c* présente aussi de la pseudorotation; toutefois, on a observé que la barrière d'activation augmente de 42 kJ mol^{-1} dans le coordinat libre à 49 kJ mol^{-1} dans le complexe. Le données de la RMN indiquent que le cation métallique se fixe d'une façon symétrique en utilisant deux paires de sites de fixation disposés l'un en face de l'autre de chaque côté du macrocycle. Sur la base de ces données, on en conclut que les quatre fonctions carbonyles sont impliquées dans la fixation d'un cation métallique dans un complexe 1 : 1 avec le coordinat.

Mots clés : résorcinarène, picrate, constante d'association, RMN dynamique, pseudorotation.

[Traduit par la rédaction]

Introduction

Calixarenes have been extensively studied and used in a variety of industrial and commercial processes and products (1). The closely related calix[4]resorcinarenes are the products of the acid-catalyzed condensation of resorcinol and various aldehydes, whose major structural feature is composed of four resorcinol units in a cyclic tetramer as shown in Scheme 1. This class of compounds has been used elegantly by Cram et al. in the development of the carcerands and hemicarcerands (2). Recently, Aoyama and co-workers have shown the extensive complexation properties that calix[4]resorcinarenes exhibit toward sugars and alcohols (3, 4).

There are many areas of calixresorcinarene chemistry that have not been explored. In this work, we report the synthesis and properties of octafunctionalized calix[4]resorcinarenes that have been used to extract a variety of cationic picrates from aqueous solutions.

Dynamic nuclear magnetic resonance (DNMR) experiments have been carried out on **3***a*, **3***c*, and **3***c*·Ag^+. In each case, a single conformation at the low-temperature limit was identified and the conformational energy barrier to pseudoro-

Received January 19, 1995.[1]

J.R. Fransen and P.J. Dutton.[2] Department of Chemistry and Biochemistry, University of Windsor, 401 Sunset, Windsor, ON N9B 3P4, Canada.

[1] Revision received September 25, 1995.

[2] Author to whom correspondence may be addressed. Telephone: (519) 253-4232, ext. 3549. Fax: (519) 973-7098. E-mail: dutton@uwindsor.ca

Scheme 1. Synthesis of octafunctionalized calix[4]resorcinarenes.

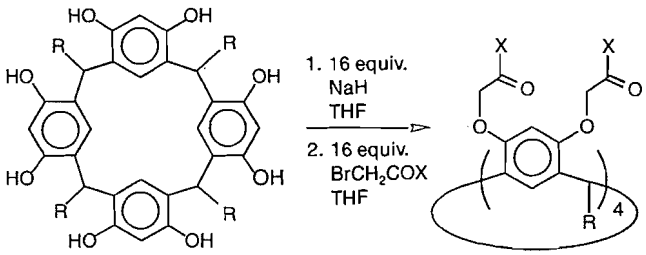

1 R = $C_{11}H_{23}$
2 R = C_7H_{15}

3*a-c* R = $C_{11}H_{23}$
4*a-c* R = C_7H_{15}

a X = OMe
b X = O-*t*-Bu
c X = NEt_2

tation was determined. The symmetry of the ligand and the characteristics of the DNMR spectra also allowed the determination of the mode of complexation of silver cation.

Experimental

Materials

Reagents were used as purchased except for tetrahydrofuran (THF), which was distilled from potassium and benzophenone under an N_2 atmosphere. *C*-Undecylcalix[4]resorcinarenes, **1** and **2** (4, 5) and 2-bromo-*N,N*-diethylacetamide (6) were prepared as previously described. Nuclear magnetic resonance spectra were run on a Bruker AC300 spectrometer at 300.1 MHz for ^1H, and at 75.5 MHz for ^{13}C and DEPT 135 pulse sequencing. DEPT experiments are noted by the multiplicity in brackets within the ^{13}C data. The AC300 was equipped with a Bruker VT1000 variable temperature unit. The chemical shifts are reported in parts per million with the solvent signal used as the standard relative to Me_4Si. Protons exchangeable with D_2O are noted as "D_2O ex." in the ^1H data. Fourier Transform infrared spectra were collected on a Nicolet 5DX spectrometer. Liquid samples were studied as neat films on potassium bromide plates and solid samples were run as potassium bromide pellets. The melting points were determined on a Fisher–Johns hot plate melting point apparatus and are not corrected. Elemental analysis determinations were performed by either M-H-W Laboratories, Phoenix, Arizona, or Galbraith Laboratories, Knoxville, Tennessee. Column chromatography was performed using Merck silica gel 60 (70–230 mesh) and thin-layer chromatography using Merck aluminum-backed 0.2 mm silica gel plates with 254 nm indicator.

Synthesis

C-Heptylcalix[4]resorcinarene, 2

C-Heptylcalix[4]resorcinarene was prepared following Aoyama's method (4). The product was obtained as a light tan powder after repeated recrystallizations from methanol and water (yield 83%); mp > 300°C. IR (cm^{-1}): 3294 br s, 3044 w, 2926 s, 2856 s, 1618 m, 1501 m, 1447 m, 1294 m, 1183 m. ^1H NMR (CD_3OD): 7.17 (s, 1H), 6.21 (s, 1H), 4.26 (t, 1H, 7.7 Hz), 2.16 (m, 2H), 1.31 (br s, 10H), 0.93 (t, 3H, 6.4 Hz). ^{13}C NMR (CD_2Cl_2): 150.5, 150.3, 124.8 (br), 123.8 (br) , 102.8 (br), 33.2, 33.15, 31.9, 29.6, 29.4, 28.1, 22.7, 14.1. ^{13}C NMR (CD_3OD): 152.9, 125.5, 124.6, 104.0, 35.0, 34.6, 33.1, 302.8, 30.5, 29.2, 23.8, 14.6.

General procedures for the functionalization of calix[4]resorcinarenes

Functionalization of the calix[4]resorcinarenes was carried out following the procedure of Ungaro and co-workers (7) except that the functionalization was carried out in 100% THF.

*C-Undecylcalix[4]resorcinarene octa-α-(methyl acetate), 3*a

The crude yellow solid (5.0 g) obtained from the reaction mixture was recrystallized from methanol to obtain a light yellow powder (1.26 g, 0.75 mmol, 68%, R_f = 0.26, 5:1 petroleum ether – ethyl acetate); mp 92–94°C. IR (cm^{-1}): 2922 s, 2852 m, 1762 s, 1732 m, 1616 m, 1587 m, 1505 s, 1306 m, 1228 m, 1202 m, 1166 m, 1124 m. ^1H NMR ($CDCl_3$): 6.58 (s, 1H), 6.19 (s, 1H), 4.56 (t, 1H, 7.2 Hz), 4.25 (s, 4H), 3.73 (s, 6H), 1.81 (br, 2H), 1.21 (br, 18H), 0.84 (t, 3H, 6.9 Hz). ^{13}C NMR ($CDCl_3$): 169.8 (s), 154.4 (s), 128.5 (s), 126.5 (d), 100.7 (s), 67.1 (t), 51.9 (q), 35.7 (d), 34.5 (t), 31.9 (t), 29.99 (t), 29.88 (t), 29.77 (t, CH_2), 29.70 (t), 29.4 (t), 28.1 (t), 22.7 (t), 14.1 (q). Anal. calcd. for $C_{96}H_{144}O_{24}$: C 68.55%, H 8.63%; found: C 68.60%, H 8.85%.

*C-Undecylcalix[4]resorcinarene octa-α-(*tert*-butyl acetate), 3*b

The crude oil (12.5 g) was chromatographed on silica gel (5:1 petroleum ether – ethyl acetate). A yellow solid (1.79 g, 0.89 mmol, 60%, R_f = 0.31, 5:1 petroleum ether – ethyl acetate) was obtained upon evaporation and evacuation; mp 50–53°C. IR (cm^{-1}): 2927 s, 1760 s, 1730 s, 1650 s, 1507 s, 1158 s. ^1H NMR ($CDCl_3$): 6.55 (s, 1H), 6.16 (s, 1H), 4.54 (t, 1H, 7.2 Hz), 4.12 (s, 4H), 1.79 (br, 2H), 1.43 (s, 18H), 1.20 (br s, 18H), 0.84 (t, 3H, 6.8 Hz). ^{13}C NMR ($CDCl_3$): 168.5, 154.5, 128.1, 126.4, 100.5, 81.5, 67.6, 35.7, 34.5, 31.9, 30.0, 29.9, 29.8 (2 × CH_2), 29.7, 29.4, 28.1 (CH_3 and CH_2 superimposed), 22.7, 14.1. Anal. calcd. for $C_{120}H_{192}O_{24}$: C 71.39%, H 9.59%; found: C 71.19%, H 9.53%.

*C-Undecylcalix[4]resorcinarene octa-α-(*N,N*-diethyl acetamide), 3*c

The crude oil (16.7 g) was chromatographed on silica gel (0–50% methanol in ethyl acetate). The product was evacuated for 24 h to obtain a white powder (1.71 g, 0.85 mmol, 85%, R_f = 0.23, ethyl acetate); mp 56–59°C. IR (cm^{-1}): 2972 s, 2928 s, 2858 m, 1640 vs, 1457 s, 1438 s, 1298 m, 1108 m. ^1H NMR ($CDCl_3$): 6.73 (s, 1H), 6.42 (s, 1H), 4.57 (t, 1H, 7.2 Hz), 4.42 (s, 4H), 3.30 (m, 8H), 1.77 (br, 2H), 1.21 (br, 18H), 1.06 (t, 6H, 6.9 Hz), 0.83 (t, 3H, 6.7 Hz). ^{13}C NMR ($CDCl_3$): 167.5 (s), 154.5 (s), 126.5 (s), 126.4 (d), 99.2 (d), 69.1 (t), 41.4 (t), 40.0 (t), 35.6 (d), 35.1 (t), 31.9 (t), 30.1 (t), 29.88 (t), 29.83 (t), 29.77 (t), 29.69 (t), 29.4 (t), 28.4 (t), 22.7 (t), 14.3 (q), 14.1 (q), 12.9(q). Anal. calcd. for $C_{120}H_{200}N_8O_{16}$: C 71.67%, H 10.03%, N 5.57%; found: C 71.55%, H 10.03%, N 5.69%.

*C-Heptylcalix[4]resorcinarene octa-α-(methyl acetate), 4*a

The crude solid (1.24 g) was recrystallized from methanol to obtain a light yellow powder (0.47 g, 0.32 mmol, 87%, R_f = 0.22, 5:1 petroleum ether – ethyl acetate); mp 101–102°C. IR

Can. J. Chem. Downloaded from www.nrcresearchpress.com by 46.23.64.124 on 09/08/12
For personal use only.

Table 1. Logarithm of association constants for hosts **3***a–c* and **4***a–c* with metal cation and ammonium picrates determined in $CDCl_3$ at 25°C. Standard deviation is given in parentheses.

	t-$BuNH_3^+$	NH_4^+	Na^+	K^+	Rb^+	Cs^+	Ag^+	Mg^{2+}	Ca^{2+}	Ba^{2+}	La^{3+}
3*a*	2.79	3.32	3.22	4.01	4.10	4.09	3.91	4.24	5.48	5.13	6.98
	(0.13)	(0.10)	(0.36)	(0.13)	(0.10)	(0.10)	(0.07)	(0.08)[a]	(0.04)[b]	(0.17)	(0.15)[a]
4*a*			3.50	4.12	4.07	4.04					
			(0.08)	(0.17)	(0.08)	(0.09)					
3*b*	3.38	3.86	4.24	4.65	4.65	4.53	4.60	4.28	5.57	5.34	6.98
	(0.27)	(0.70)	(0.23)	(0.07)	(0.05)	(0.07)	(0.12)	(0.05)[b]	(0.04)	(0.07)	(0.05)[b]
4*b*	3.27	4.24	3.74	4.60	4.57	4.63					
	()[c]	()[c]	(0.42)	(0.05)	(0.12)	(0.19)					
3*c*	4.51	5.76	5.25	5.73	5.56	5.50	7.63	5.73	7.74	8.75	11.11
	(0.13)	(0.06)	(0.06)[b]	(0.03)	(0.05)[a]	(0.19)	(0.07)	(0.27)	(0.31)	(0.28)	(0.03)
4*c*			5.26	5.76	5.64	5.43					
			(0.02)	(0.08)	(0.08)	(0.12)					

[a]Range from highest to lowest value, triplicate analysis.
[b]Range, duplicate analysis.
[c]Single determinations.

Can. J. Chem. Downloaded from www.nrcresearchpress.com by 46.23.64.124 on 09/08/12
For personal use only.

(cm^{-1}): 2952 m, 2926 s, 2854 m, 1763 vs, 1733 vs, 1611 m, 1589 m, 1507 s, 1438 s, 1307 s, 1193 s (with structure). ^1H NMR ($CDCl_3$): 6.58 (s, 1H), 6.18 (s, 1H), 4.55 (t, 1H, 7.2 Hz), 4.25 (s, 4H), 3.72 (s, 6H), 1.80 (br, 2H), 1.20 (br, 10H), 0.84 (t, 3H, 6.9 Hz). ^{13}C NMR ($CDCl_3$): 169.8 (s), 154.4 (s), 128.5 (s), 126.5 (d), 100.7 (d), 67.1 (t), 51.9 (q), 35.7 (d), 34.5 (t), 32.0 (t), 29.9 (t), 29.4 (t), 28.0 (t), 22.7 (t), 14.1 (q). Anal. calcd. for $C_{80}H_{112}O_{24}$: C 65.92%, H 7.74%; found: C 66.25%, H 7.74%.

C-*Heptylcalix[4]resorcinarene octa*-α-(tert-*butyl acetate), 4*b
The crude oil (8.72 g) was chromatographed on silica gel (5:1 petroleum ether – ethyl acetate). The product was evaporated under reduced pressure and dried in vacuo to obtain a yellow oil (2.72 g, 1.52 mmol, 69%, R_f = 0.29, 5:1 petroleum ether – ethyl acetate). IR (cm^{-1}): 2978 s, 2929 s, 2857 s, 1756 s, 1731 s, 1611 m, 1586 m, 1500 m, 1368 m, 1225 m, 1156 vs. ^1H NMR ($CDCl_3$): 6.57 (s, 1H), 6.16 (s, 1H), 4.55 (t, 1H, 7.2 Hz), 4.14 and 4.11 (ab, 4H, 12 Hz), 1.80 (br, 2H), 1.44 (m, 18H), 1.20 (m, 10H), 0.84 (t, 3H, 6.8 Hz). ^{13}C NMR ($CDCl_3$): 168.5 (s), 154.5 (s), 128.1 (s), 126.4 (d), 100.4 (d), 81.5 (s), 67.6 (t), 35.7 (d), 34.6 (t), 32.0 (t), 30.0 (t), 29.4 (t), 28.0 (q), 22.7 (t), 14.1 (q). Anal. calcd. for $C_{104}H_{160}O_{24}$: C 69.61%, H 8.99%; found: C 69.65%, H 8.89%.

C-*Heptylcalix[4]resorcinarene octa*-α-(N,N-*diethyl acetamide), 4*c
The crude oil (6.84 g) was chromatographed on silica gel (0–50% methanol in ethyl acetate). The product was evaporated under reduced pressure, and dried under vacuum to obtain a yellow oil (0.21 g, 0.12 mmol, 24%, R_f = 0.21, ethyl acetate). IR (cm^{-1}): 2961 m, 2928 s, 2855 m, 1652 vs, 1646 vs, 16385 vs, 1585 w, 1499 m, 1461 m, 1298 m, 1264 m, 1194 m, 1100 s. ^1H NMR ($CDCl_3$): 6.73 (s, 1H), 6.43 (s, 1H), 4.57 (t, 1H, 7.2 Hz), 4.43 (s, 4H), 3.31 (m, 8H), 1.79 (br, 2H), 1.21 and 1.07 (2 × m, 22H), 0.82 (t, 3H, 6.7 Hz). ^{13}C NMR ($CDCl_3$): 167.5, 154.6, 126.6, 126.4, 99.4, 69.1, 41.4, 40.1, 35.5, 35.1, 32.0, 30.0, 29.4, 28.3, 22.7, 14.3, 14.1, 12.9. Anal. calcd. for $C_{104}H_{168}N_8O_{16}$: C 69.92%, H 9.48%, N 6.27%; found: C 70.02%, H 9.44%, N 6.05%.

Determination of association constants

The association constants of **3***a–c* and **4***a–c* with ammonium and metal cations were determined using the picrate extraction method as described both by Cram and co-workers (8) and Chandler et al. (9). Picrate salts were prepared as previously described (10, 11) and the distribution constant of each picrate salt was determined by extraction of the salt from an aqueous solution (10.0 mL) to chloroform (25.0 mL) in a separatory funnel. The organic and aqueous phases were allowed to separate for 20 min and the chloroform layer was carefully separated. The residue after evaporation of the solvent was quantitatively transferred to a 1.00 mL volumetric flask and diluted with spectrophotometric grade acetonitrile. The extinction and distribution coefficients of the picrate salts were in agreement with literature values (8, 9). The distribution coefficient of the previously unreported lanthanum picrate was 0.126 dm^9 mol^{-3} and the extinction coefficient was 27 300 dm^3 mol^{-1} cm^{-1} based upon the concentration of $La(OC_6H_2(NO_2)_3)$. The concentrations of the picrate salts in the extraction experiments were determined by measurement of the absorbance at λ_{max} (380 nm).

During the extraction procedure 200 μL of host solution (approximately 7.00×10^{-2} M) in deuterated chloroform and 2.00 or 3.00 mL aliquots of picrate salt solution (approximately 1.00×10^{-2} M, or a water blank) were stirred vigorously for 24 h at 25.0 ± 0.1°C. An aliquot of the organic phase was diluted with spectral grade acetonitrile and the absorption of each acetonitrile solution was determined against a suitable blank at 380 nm to calculate the concentration of picrate salt in the organic phase.

The standard deviations in Table 1 were determined from at least four independent experiments. Initial experiments were repeated as many as 10 times to ensure sufficient control over experimental error. In later experiments, the determinations were performed in duplicate or triplicate. In those cases the range from highest to lowest value is reported.

General derivation of the K_a expression

Cram and co-workers (12) and Chandler (9) derived expres-

Can. J. Chem. Downloaded from www.nrcresearchpress.com by 46.23.64.124 on 09/08/12
For personal use only.

sions for the association constants of mono- and di-valent cations with host molecules in organic solvents. The expressions for K_a differ due to the change in the order of picrate concentration as a result of the requirement for electroneutrality of charge in the extraction. The general expression for the association constant of any metal ion in a two-phase extraction experiment is reported here in order to apply the equation to the extraction equilibria for the trivalent lanthanum cation. The reported expression holds for cases where the concentration of metal ion is determined by the extent that the counterion is coextracted.

The extraction equilibrium [1] is governed by the extraction constant K_e, eq. [2], and the distribution constant K_d, [3]. The host and the undissociated guest salt in equilibria are represented by (H) and (GX_n). The subscripts on the expressions indicate the solvents in which the species are dissolved. The terms for the dissociated guest ion and its counterion are given by (G^{n+}) and (X^-). The expressions for the concentration equilibrium constants, K_a, K_e, and K_d, are shown in eqs [4], [5], and [6], respectively. Concentrations of species are given in square brackets and subscripts refer to solvent as described above.

[1] $$(H)_{CDCl_3} + (GX_n)_{CDCl_3} \rightleftharpoons (H{\cdot}GX_n)_{CDCl_3} \qquad K_a$$

[2] $$(H)_{CDCl_3} + (G^{n+})_{H_2O} + n(X^-)_{H_2O} \rightleftharpoons (H{\cdot}GX_n)_{CDCl_3} \qquad K_e$$

[3] $$(G^{n+})_{H_2O} + n(X^-)_{H_2O} \rightleftharpoons (GX_n)_{CDCl_3} \qquad K_d$$

[4] $$K_a = \frac{[H{\cdot}GX_n]_{CDCl_3}}{[H]_{CDCl_3}[GX_n]_{CDCl_3}}$$

[5] $$K_e = \frac{[H{\cdot}GX_n]_{CDCl_3}}{[H]_{CDCl_3}[G^{n+}]_{H_2O}[X^-]^n_{H_2O}}$$

[6] $$K_d = \frac{[GX_n]_{CDCl_3}}{[G^{n+}]_{H_2O}[X^-]^n_{H_2O}}$$

Following the previous derivations (9, 12), the concentration of the picrate anion can be described in terms of the metal ion concentration, eq. [7]. The expression for K_e is therefore given by eq. [8].

[7] $$[X^-] = n[G^{n+}]_{H_2O}$$

[8] $$K_e = \frac{[H{\cdot}GX_n]_{CDCl_3}}{[H]_{CDCl_3}[G^{n+}]_{H_2O}(n[G^{n+}]_{H_2O})^n} = \frac{[H{\cdot}GX_n]_{CDCl_3}}{[H_i]_{CDCl_3}(n^n)([G^{n+}]_{H_2O})^{n+1}}$$

The fraction of host associated with metal cation, R, is given by eq. [9]. The concentration of host–guest complex in the organic phase can be expressed in terms of the initial concentrations of the host ($[H]_i$) and R. The concentration of guest remaining in the aqueous phase ($[G^{n+}]_{H_2O}$) can be expressed in terms of $[H]_i$ and the initial concentration of undissociated guest salt ($[GX_n]_{i,H_2O}$), eq. [10]. Therefore the general form of the expression for K_a is given by expression [11].

[9] $$R = \frac{[H{\cdot}GX_n]_{CDCl_3}}{[H]_{i,CDCl_3}}$$

[10] $$[G^{n+}] = [GX_{ni}]_{H_2O} - \left(\frac{V_{CDCl_3}}{V_{H_2O}}\right)R[H_i]_{CDCl_3}$$

[11] $$K_a = \frac{K_e}{K_d} = \frac{R[H_i]_{CDCl_3}}{n^n[H]_{i,CDCl_3}K_d\left([GX_{ni}]_{H_2O} - R\left(\frac{V_{CDCl_3}}{V_{H_2O}}\right)[H_i]_{CDCl_3}\right)^{n+1}}$$

Variable temperature NMR

Compounds **3***a* and **3***c* were examined by dynamic nuclear magnetic resonance techniques in deuterochloroform and deuterodichloromethane solutions. Spectra were collected at 10 K intervals from 300 K to just above the freezing point of the solutions.

Solutions of **3***c*·$AgNO_3$ in deuterochloroform or dichloromethane were prepared by extraction of silver ion from saturated aqueous solutions of $AgNO_3$. Variable temperature spectra were collected as described above.

Results and discussion

Synthesis

The parent calix[4]resorcinarenes, **1** and **2**, were prepared following Aoyama's procedure (4). A modification of Ungaro's procedure (7) was used to functionalize **1** and **2** to obtain the octa-α-(methyl acetates), **3***a* and **4***a*, octa-α-(*tert*-butyl acetates), **3***b* and **4***b*, and the octa-α-(diethyl acetamides), **3***c* and **4***c*. The etherification reaction was carried out in 100% THF rather than a THF–DMF mixture to simplify the purification. Yields of the long-chain calixresorcinarenes were unaffected by this change. The yields of the octasubstitution reactions compare favorably with the yields reported for tetrasubstitution of calix[4]arenes. Yields of esters reported in the literature range from 68 to 88% (7, 13, 14). The yield of octa-α-(diethyl amide) was found to be higher than the yield of the esters, which is also in agreement with the literature (15).

Complexation

The association of compounds **3***a–c* and **4***a–c* with metal cationic guests in $CHCl_3$ was studied using the picrate extraction method. Using the assumptions that Chandler et al. (9) and Cram and co-workers (8) identified for alkaline earth and alkali metal cations, respectively, a general expression for the association constant was derived in order to study the trivalent lanthanum cation. The expression that was derived specifically for the trivalent cation case fits the general form of the equation, as do the expressions of Cram and Chandler for the monovalent and divalent cations, respectively.

The logarithms of the association constants (log β) for the six calix[4]resorcinarenes with a variety of metal cations are given in Table 1. A comparison of the log β values for the undecyl calix[4]resorcinarenes **3***a–c* and the heptylcalix[4]resorcinarenes **4***a–c* reveals that the alkyl chain length has little effect on the alkali metal binding constants, as would be expected. Amongst compounds **4***a–c*, only **4***b* was exam-

Can. J. Chem. Downloaded from www.nrcresearchpress.com by 46.23.64.124 on 09/08/12
For personal use only.

ined for binding toward ammonium ions, and the log β's observed were within one standard deviation of the values observed for **3***b*. Subsequent studies of the binding of **4***a–c* toward cations other than the alkali metals and ammonium ions were not carried out since differences in cation binding between compounds **3** and **4** were not expected. The differences in chain length may cause changes in physical properties that would be observed in the formation of Langmuir or Langmuir–Blodgett films.

In comparing the resorcinarenes to the literature, the *R* value proves to be useful, since some literature data is reported as "extraction percent." The *R* values of the esters **3***a* and **3***b* were all <2%, indicating that these compounds exhibit low extractability toward all the cations studied. In contrast, the amide **3***c* exhibits much higher extractability. The *R* values for **3***c* with the metal cations in this study were as follows: Na^+, 7%; K^+, 22%; Rb^+, 13%; Cs^+, 11%; Ag^+, 75%; Mg^{2+}, 2%; Ca^{2+}, 25%; Ba^{2+}, 47%; and La^{3+}, 65%.

The strength of binding toward metal ions was observed to increase as the carbonyl functionality of the binding site was changed from methyl ester to *tert*-butyl ester to amide. The octaamide is the strongest complexing agent due to the nature of the amide carbonyl, which has the highest electron density on the carbonyl oxygen. The *tert*-butyl ester is intermediate in binding strength as a result of the greater electron donation from the *tert*-butyl group than that from the methyl group. Chang and Cho have reported similar results with calixarene derivatives (16). The calix[4]resorcinarenes behave more like the larger calix[6]- and calix[8]-arenes, but exhibit greater selectivity amongst the group IIa metal cations than do the calix[*n*]arene analogues. Compound **3***c* was selective across the group IIa cations whereas the calix[*n*]arenes were not. Calix[4]- and calix[6]-arene amides were not observed to differentiate between Ca^{2+} and Ba^{2+}, and the calix[8]arene did not differentiate between Mg^{2+} and Ca^{2+}(16, 17).

It was observed that **3***a–c* and **4***b* were able to interact with the hydrogen-bonding ammonium cations. Ammonium ion had a higher association constant with the hosts than the bulky *tert*-butyl ammonium ion due to the steric effect of the bulky alkyl group.

The size selectivity toward guest ions was evaluated using Shannon's definition (18) of cation radii rather than the standard Pauling definition. Pauling radii were defined using 6-coordinate systems based upon expandable donors in contrast to Shannon radii that were defined on the basis that O^{2-} in oxide crystals is clearly of a fixed size and that cation radii change with increasing coordination number. Since the actual coordination in solution is unknown, the discussion below is based upon hexacoordinate systems; however, the arguments hold for other coordinate systems.

No metal cation studied exhibited an *R* value greater than unity, which suggests that the assumption of a 1:1 cation–ligand complex was reasonable. If a 2:1 cation–ligand complex was possible, silver cation should show this stoichiometry as it was found to have the highest R value. Nuclear magnetic resonance experiments indicate that the stoichiometry of the **3***c*·Ag^+ complex is 1:1 and there was no reason to suspect that other metal cations would exhibit different behaviour.

The increase in log β with charge is linear over the series Na^+, Ca^{2+}, and La^{3+} (6-coordinate radii 1.02, 1.00, and 1.03 Å, respectively) (18) for **3***b* and **3***c*. The change in the log β with charge is greater in **3***c* than in **3***b* due to the greater relative electrostatic effects in the amide compared with the ester.

It was observed that amongst the alkali metal cations there is little selectivity exhibited by the hosts **3***a–c* and **4***a–c*. This behaviour, and the magnitude of the binding constants, is similar to that observed in the large-ring calix[*n*]arene esters and amides ($n > 4$). Ligands **3***a* and **3***b* show similar interactions with the singly charged silver cation as do the alkali metal cations; however, ligand **3***c* shows a high affinity for the soft silver ion with respect to the other singly charged ions. The magnitude of the binding constants of **3***c* toward sodium, potassium, and silver cations (1.02, 1.38, and 1.15 Å, respectively) (18) suggests that size selectivity was not of primary importance. The changes in the behaviour of the octaamide compared with the ester are attributed to a balance of hard and soft acid–base relationships with the guest cation. The Bu_4-C[4]A-$(OCH_2CONEt_2)_4$ host studied by Vicens (17) shows a similar binding constant toward silver as **3***c*; however, no selectivity between sodium ion and the silver cation was observed, indicating that size selectivity was of more importance in the calix[4]arene case. The selectivity of **3***c* toward the alkaline earth cations is not likely due to cation size since no size selectivity was observed among the alkali metal ions. The source of the selectivity is probably due to a combination of the large electrostatic interaction, as a result of cation charge, coupled with the hard/soft character of the metal cations. It is apparent that there is an electrostatic binding effect as a result of the change in surface charge on the cation.

Nuclear magnetic resonance

Variable temperature NMR studies were carried out on the free ligands 3*a* and 3*c* in $CDCl_3$ and CD_2Cl_2 to probe the conformations of the hosts. The spectra obtained from CD_2Cl_2 solutions are shown in Figs. 1 and 2. Complete separation of signals in $CDCl_3$ as the temperature was lowered was not observed due to the solvent freezing point limit. This problem was avoided in CD_2Cl_2 where the aromatic protons of 3*c* at 190 K were clearly separated into four signals. Based upon simple chemical shift calculations and shielding arguments, the signals were assigned as: $\delta H_l = 7.07$, $\delta H_{l'} = 5.84$, $\delta H_{u'} = 6.01$, and $\delta H_u = 5.91$ ppm, where H_l and $H_{l'}$ correspond to two different lower or small-rim protons and H_u and $H_{u'}$ correspond to two large or upper rim protons. Two coalescences were observed at 208 K and 224 K for the upper rim protons (H_u and $H_{u'}$) and the lower rim protons (H_l and $H_{l'}$), respectively.

In the cone or 1,3-alternate conformations,[3] only two aromatic proton signals would be expected, whereas the chair conformation would exhibit six aromatic signals. The NMR data clearly show that the free ligands are in flattened cone conformations in chloroform or dichloromethane solution.

Other areas of the spectrum are consistent with this conformational assignment and variable temperature effects were also observed. Using data from the $\mathbf{H_u}$, $\mathbf{H_l}$, OCH_2CO, NCH_2CH_3, and Ar_2CHCH_2R regions and determining $\Delta G^{\ddagger}$ from the coalescence temperatures (20), it was found

[3] Gutsche (ref. 1, p. 89) defines the nomenclature based on the [1.1.1.1]metacyclophane system. Alternative nomenclature (cone = crown; flattened cone = boat; 1,3-alternate = saddle; flattened partial cone = chair) has been suggested by Högberg (ref. 19).

Can. J. Chem. Downloaded from www.nrcresearchpress.com by 46.23.64.124 on 09/08/12
For personal use only.

Fig. 1. Variable temperature ^{1}H NMR study of **3***a*.

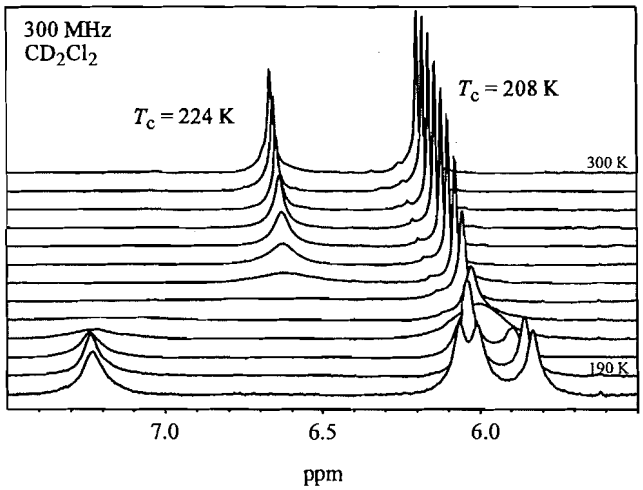

Fig. 2. Variable temperature ^{1}H NMR study of **3***c*.

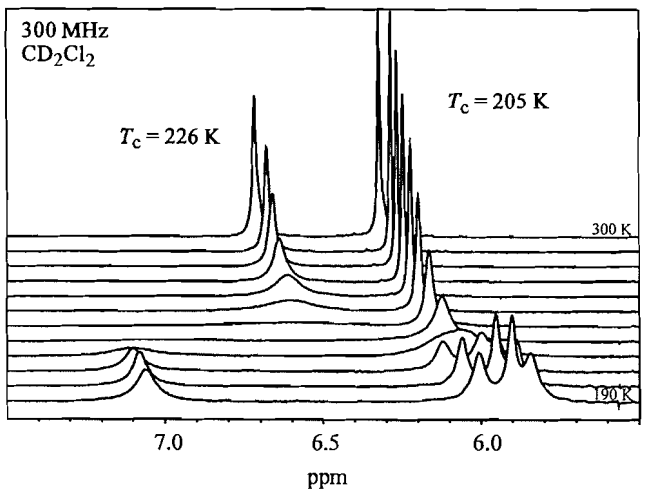

that the average barrier to pseudorotation in **3***c* was 42.3 kJ mol^{-1} (σ = 0.05). A similar analysis of **3***a* finds the average barrier to rotation to be 42.1 kJ mol^{-1} (σ = 0.11). The "exact" temperatures of coalescence reported in the figures were the nearest unit temperatures that resulted in calculated free energies of activation in agreement with all other regions of the spectrum. The data obtained in CD_2Cl_2 solution are in complete agreement with the data obtained in $CDCl_3$.

It is interesting to note that in the ^{13}C spectrum of *C*-heptylcalix[4]resorcinarene, **2**, dissolved in CD_2Cl_2, effects of the conformational interconversion were also observed. The lowest field aromatic signal was clearly split into two, while other aromatic signals were broadened. Variable temperature ^{13}C spectra were not collected for this compound; however, we have noted similar effects in other resorcinarenes and have found that the activation parameters determined from ^{13}C experiments agree well with the activation parameters obtained from ^{1}H NMR experiments. In CD_3OD as solvent, compound **2** was clearly in rapid exchange and only the averaged aromatic signals were observed.

The free energies of activation determined for **3***a* and **3***c* are 20 to 40 kJ mol^{-1} *lower* than those observed for esters of *C*-aryl- and *C*-methyl-calix[4]resorcinarenes, which range from

Fig. 3. Variable temperature ^{1}H NMR study of the **3***c*·$AgNO_3$ complex prepared by extraction of $AgNO_3$ from saturated aqueous solution to $CDCl_3$.

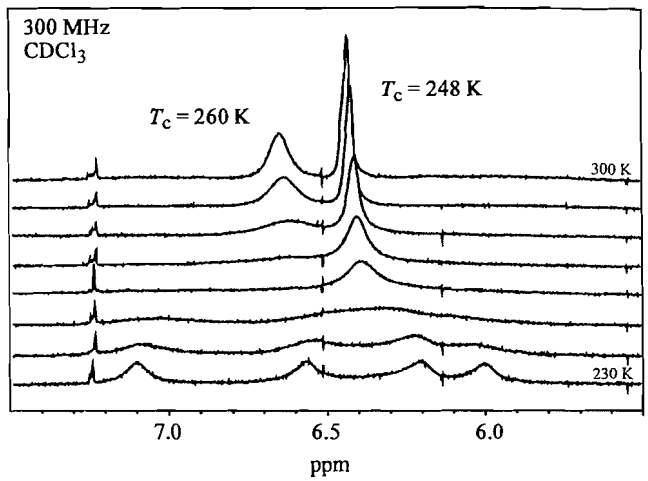

60 to 80 kJ mol^{-1} (19, 21). Two factors may be playing a role in apparent decrease of the activation barrier. The dipole–dipole interaction of the pendant carbonyl functions in the transition state must be different in **3***a* and **3***c* than in the acetate and propionate esters studied by Högberg, which could lower the activation barrier. This hypothesis is supported by preliminary data on Me_4-C[4]R-$(OCH_2CO_2Me)_8$, which has an activation barrier of 53 kJ mol^{-1} (P.J.D., unpublished) compared to 60.3 kJ mol^{-1} (21) for the octaacetate. An increase in the absolute free energy of the flattened cone conformation with respect to the cone conformation (transition state) would account for the missing 10–30 kJ mol^{-1}. The energy for this increase may be due to the "tail wagging the dog" in which thermal motion of the long alkyl tails transfers energy to the calixresorcinarene ring system.

Compound **3***c* was used to extract Ag^+ from an aqueous solution of silver nitrate into $CDCl_3$. The organic phase was examined by variable temperature ^{1}H NMR from 220 to 300 K. As with uncomplexed **3***a* and **3***c*, there are temperature-dependent changes in many areas of the spectrum. Figure 3 shows the aromatic regions of the spectra over the temperature range studied. Two coalescences are observed at 248 K (upper rim protons, H_u and $H_{u'}$, see Fig 4) and 260 K (lower rim protons, H_l and $H_{l'}$) and in the slow exchange regime the aromatic protons separate to four lines, indicating that the conformation of the ligand bound to silver ion is flattened cone. In addition, the symmetry of the proton NMR spectra at all temperatures clearly indicates that the silver ion is symmetrically bound by the ligand. The silver ion is therefore bound by the four carbonyl lone pairs from resorcinol units disposed *across* the calix[4]resorcinarene ring from one another. There is a possibility that the ether oxygens participate in binding but no specific evidence for this type of interaction was observed. No signals were observed due to the unbound host in the slow-exchange regime. Similar behaviour was observed for the **3***c*·Ag^+ complex in a CD_2Cl_2 solution. Considering the spectra, it is concluded that **3***c*·Ag^+ 1:1 complexes are present in both chloroform and dichloromethane solutions. These data support the assumption of a 1:1 complex made for the derivation of the K_a expression.

The free energies of activation determined from $\mathbf{H_l}$ and $\mathbf{H_u}$

Fig. 4. Conformation of the $3c \cdot Ag^+$ complex.

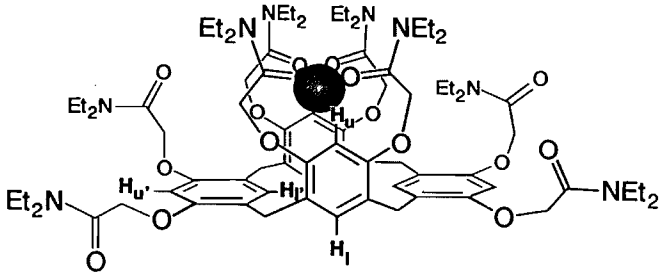

protons in $CDCl_3$ and CD_2Cl_2 were 49.1 and 49.2 kJ mol^{-1}, respectively. Other regions of the spectrum that showed variable temperature effects include the CH_2N and OCH_2CO protons. Using all coalescing signals, in both $CDCl_3$ and CD_2Cl_2 solutions, the free energy of activation for decomplexation of the silver complex of **3***c* was found to be 49.2 kJ mol^{-1} ($\sigma = 0.2$ kJ mol^{-1}).

Conclusion

It has been shown that the calix[4]resorcinarene ligands are capable of binding metal cations and that the octaamide **3***c* shows excellent potential as a selective ligand for soft polarizable cations such as Ag^+ and Ba^{2+}. The amide **3***c* exhibits extraction properties comparable with related calix[4]arenes but contrasting in selectivity. The flexibility of the ligands is apparent from both the DMR studies and from the ability of the ligands to bind both large and small metal cations. Ligands **3***a* and **3***c* were observed to be equilibrating rapidly at room temperature between the two possible flattened cone conformations with an activation barrier to the pseudorotation of 42 kJ mol^{-1} in both species. In the presence of the silver cation 1:1 complex, this barrier was increased due to the decomplexation of cation that was required before pseudorotation could occur. The activation barrier to decomplexation of silver cation from **3***c* was found to be 49 kJ mol^{-1}.

Acknowledgments

We would like to thank the University of Windsor and the Natural Science and Engineering Research Council of Canada for operating funds (P.J.D.) and the Ontario Graduate Scholarship Program (J.R.F.). We would also like to thank the Steacie Institute of the National Research Council of Canada for the donation of the UV–visible spectrophotometer.

References

1. C.D. Gutsche. Calixarenes. Royal Society of Chemistry, Cambridge. 1989.
2. D.J. Cram, L.M. Tunstad, and C.B. Knobler. J. Org. Chem. **57**, 528 (1992).
3. K. Kobayashi, Y. Asakawa, Y. Kikuchi, H. Toi, and Y. Aoyama. J. Am. Chem. Soc. **115**, 2648 (1993).
4. Y. Aoyama, Y. Tanaka, and S. Sugahara. J. Am. Chem. Soc. **111**, 5397 (1989).
5. W.C. Moreira, P.J. Dutton, and R. Aroca. Langmuir, **10**, 4148 (1994).
6. K.M. Kem, N.V. Nguyen, and D.J. Cross. J. Org. Chem. **46**, 5188 (1981).
7. A. Arduini, A. Pochini, S. Reverberi, R. Ungaro, G. D. Andreetti, and F. Ugozzoli. Tetrahedron, **42**, 2089 (1986).
8. S.S. Moore, T.L. Tarnowski, M. Newcomb, and D.J. Cram. J. Am. Chem. Soc. **99**, 6398 (1977).
9. C.J. Chandler, L.W. Deady, and J.A. Reiss. Aust. J. Chem. **41**, 1051 (1988).
10. M.A. Coplan and R.M. Fuoss. J. Phys. Chem. **68**, 1177 (1964).
11. Y. Inoue, M. Ouchi, and T. Hakushi. Bull. Chem. Soc. Jpn. **58**, 525 (1985).
12. J.M. Timko, S.S. Moore, D.M. Walba, P.C. Hiberty, and D.J. Cram. J. Am. Chem. Soc. **99**, 4207 (1977).
13. F. Arnaud-Neu, E.M. Collins, M. Deasy, G. Ferguson, S.J. Harris, B. Kaitner, A.J. Lough, M.A. McKervey, E. Marques, B.L. Ruhl, M.J. Shwing-Weill, and E.M. Seward. J. Am. Chem. Soc. **111**, 8681 (1989).
14. S.K. Chang and I. Cho. J. Chem. Soc. Perkin Trans. 1, 211 (1986).
15. B. Calestani, F. Ugozzoli, A. Arduini, E. Ghidini, and R. Ungaro. J. Chem. Soc. Chem. Commun. 344 (1987).
16. S.-K. Chang, S.-K. Kwon, and I. Cho. Chem. Lett. 947 (1987).
17. J. Vicens and V. Böhmer (*Editors*). Calixarenes: A versatile class of macrocyclic compounds. Kluwer, Dordrecht. 1991.
18. R.D. Shannon. Acta Crystallogr. Sect. A: Cryst. Phys. Diffr. Theor. Gen. Crystallogr. **A32**, 751 (1976).
19. A.G.S. Högberg. J. Am. Chem. Soc. **102**, 6046 (1980).
20. I.O. Sutherland. Annu. Rep. NMR. Spectrosc. **4**, 71 (1971).
21. A.G.S. Högberg. J. Org. Chem. **45**, 4498 (1980).

Can. J. Chem. Downloaded from www.nrcresearchpress.com by 46.23.64.124 on 09/08/12
For personal use only.

Synthesis, NMR and ultraviolet spectroscopy of [10](*N*6,9)-6-aminopurinophane; calculation of the chemical shifts in the [*n*](*N*6,9)-6-aminopurinophane series

Alfredo Capretta and Russell A. Bell

Abstract: [10](*N*6,9)-6-Aminopurinophane was prepared via a Mitsunobu reaction involving 6-chloropurine and 10-azido-1-decanol. Reduction of the azido moiety to an amine allowed for subsequent cyclization to the cyclophane. *N*6-Nonyladenine, 9-nonyladenine, and *N*6,9-dinonyladenine were also prepared using the established chemistry. Heating the [10](*N*6,9)-6-aminopurinophane to 90°C allowed for a complete assignment of the proton and carbon spectra, while cooling the sample to −77°C revealed additional isomers likely due to the *anti–syn* isomerization about the N6—C6 bond. A variable temperature proton NMR study revealed a $\Delta G_c^{\ddagger}$ of 59.4 ± 5.5 kJ mol^{-1} associated with the interchange between the two major conformers. The ultraviolet spectra of the [*n*](*N*6,9)-6-aminopurinophane series show a bathochromic shift and a hypochromic effect in the transitions as the methylene chain length decreases (i.e., n = 10 to 9 to 8). The aminopurinophanes are used to assess the relative merits of a semi-empirical model that allows for the calculation of the chemical shifts of the methylene bridge protons.

Key words: synthesis of heterocyclophanes, variable temperature NMR, cyclophane conformational analysis, ultraviolet spectroscopy, calculation of chemical shift.

Résumé : On a préparé le [10](*N*6,9)-6-aminopurinophane via une réaction de Mitsunobu impliquant la 6-chloropurine et le 10-azidodécan-1-ol. La réduction de la portion azido en amine a permis de réaliser la cyclisation subséquente en cyclophane. On a aussi préparé les *N*6-nonyladénine, 9-nonyladénine et *N*6,9-dinonyladénine utilisant des méthodes chimiques bien établies. Par chauffage du [10](*N*6,9)-6-aminopurinophane à 90°C, on a pu faire une attribution complète des spectres RMN du proton et du carbone alors que son refroidissement à −77°C a révélé la présence d'isomères additionnels qui sont probablement dus à une isomérisation *anti–syn* autour de la liaison N6—C6. Une étude des spectres RMN du proton à température variable a permis d'établir qu'un $\Delta G_c^{\ddagger}$ de 39,4 ± 5,5 kJ mol^{-1} est associé à l'interconversion entre les deux conformères principaux. Les spectres ultraviolets de la série des [*n*](*N*6,9)-6-aminopurinophanes montrent qu'une diminution de la chaîne méthylénique (lorsque n passe de 10, à 9 et à 8) est associée à un déplacement bathochrome et à un effet hypochrome dans les transitions. On a utilisé les aminopurinophanes pour évaluer les mérites relatifs d'un modèle semi-empirique qui permet de calculer les déplacements chimiques des protons des ponts méthylènes.

Mots clés : synthèse d'hétérocyclophanes, RMN à température variable, analyse conformationnelle des cyclophanes, spectroscopie ultraviolette, calcul des déplacements chimiques.

[Traduit par la rédaction]

Introduction

The shift to lower frequency of the heterobase protons in certain oligonucleotides is a well-documented phenomenon (1). Adjacent bases in a nucleotide strand are separated by as little as 3.4 Å and, at this proximity, can exert pronounced diamagnetic shielding on their neighbours. A detailed knowledge of the spatial distribution of the total diamagnetic shielding anisotropy about these purine and pyrimidine systems could aid in the assignment of the heterobase protons in the ^{1}H NMR spectra of large oligomers. Furthermore, this information could prove valuable in the study of the conformational properties of specific sequences.

[*n*]-Cyclophanes provide an unusual perspective of the diamagnetic shielding about aromatic systems. Unlike the methylene protons of an ordinary aliphatic chain (typically having chemical shifts around 1.3 ppm), the signals from the bridge protons of a cyclophane can assume a wide range of values (often between 3 and −1 ppm). For example, the chemical shifts of the bridge protons in [10]-paracyclophane ranged from 2.62 to 0.51 ppm (2). Work on other heteroaromatic sys-

Received June 12, 1995.

A. Capretta and R.A. Bell.[1] Department of Chemistry, McMaster University, Hamilton, ON L8S 4M1, Canada

[1] Author to whom correspondence may be addressed. Telephone: (905) 525-9140. Fax: (905) 522-2509.

Can. J. Chem. Downloaded from www.nrcresearchpress.com by 46.23.64.124 on 09/08/12
For personal use only.

Can. J. Chem. Downloaded from www.nrcresearchpress.com by 46.23.64.124 on 09/08/12
For personal use only.

Scheme 1.

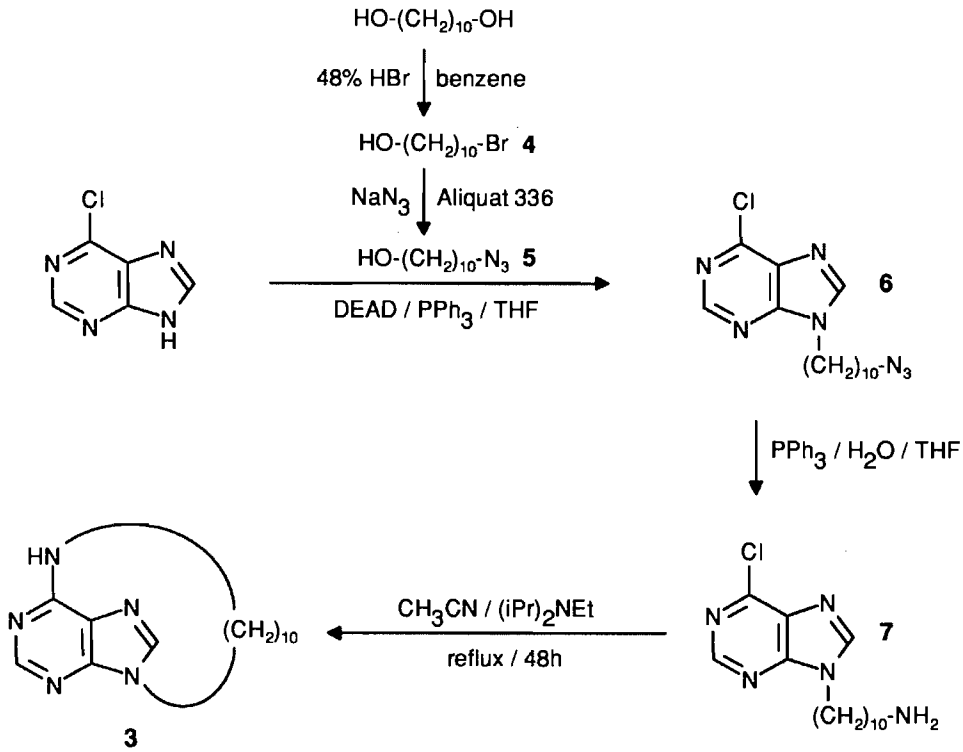

tems also shows similar dispersion of signals from the aliphatic chain protons (3).

Rather than dismiss these spectra as curiosities, they may be exploited in the study of magnetic anisotropy. Allowing an aliphatic chain to pass over the aromatic plane of a heterobase enables the methylene protons to act as "reporter" groups of the magnetic environment of the system. Ultimately, the proton chemical shifts can furnish values for the spatial definition of the diamagnetic susceptibility anisotropy around these aromatic systems and supply a viable means of appraising the theoretical calculations.

As part of a continuing effort to map the magnetic environment about adenine, the present work describes the synthesis of [10](*N*6,9)-6-aminopurinophane and a number of alkylated adenine derivatives. The NMR and UV spectra of these molecules are examined in order to provide some insight into the conformational and fluxional properties of these cyclophanes. Finally, the aminopurinophanes are used to assess the relative merits of a semi-empirical model that allows for the calculation of the chemical shifts of the methylene bridge protons.

Results and discussion

Synthesis

While many of the successful elements used in the syntheses of the octamethylene (4) and nonamethylene analogues (5), **1** and **2**, respectively, were implemented in the preparation of

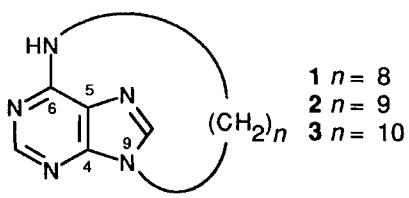

1 *n* = 8
2 *n* = 9
3 *n* = 10

[10](*N*6,9)-6-aminopurinophane **3**, a new preparation for the requisite azido-alcohol was developed. Although the method of Castro and co-workers in (6) for preparing azido-alcohols worked well in the synthesis of **2**, the price of hexamethylphosphorous triamide (HMPT) coupled with the diminished yields upon the "scaling-up" of the reaction prompted the search for a new preparative route to 10-azido-1-decanol (see Scheme 1, **5**). Kang, Kim, and Moon describe a simple method for the preparation of ω-bromo-alcohols from α,ω-diols (7). Refluxing a mixture of an aliphatic diol with an equivalent of aqueous hydrogen bromide (48%) in benzene using a Dean–Stark apparatus provided high yields of the monobromo-alcohol. Treating **4** with aqueous sodium azide in the presence of Aliquat 336 (primarily tricaprylmethylammonium chloride) then yielded the desired ω-azido-alcohol **5** (8). Ultimately, the implementation of this two-step procedure allowed for efficient access to large quantities of pure, low-cost azido-alcohols.

Attachment of the methylene bridge to the purine was then achieved using the protocol described previously (5). As shown in Scheme 1, a Mitsunobu reaction involving 6-chloropurine and 10-azido-1-decanol allows for alkylation at N9 to yield **6**. Following the reduction of the azide **6** to the amine **7**, nucleophilic attack at C6 resulted in the formation of the cyclophane **3**. As expected, the ^{1}H NMR spectrum of [10](*N*6,9)-6-aminopurinophane **3** was comparable to those of the other purine cyclophanes, although complicated to a greater extent by the presence of the additional methylene proton resonances and exchange processes (*vide infra*).

A number of alkylated adenines (to be used as standard compounds in the UV and NMR spectroscopy studies) were also prepared using much of the same chemistry as their cyclized counterparts (see Scheme 2). Dissolving 6-chloropurine in a solution of excess *n*-nonyl amine in acetonitrile readily provided *N*6-amininonyl-purine **8** in 83% yield. The

Scheme 2.

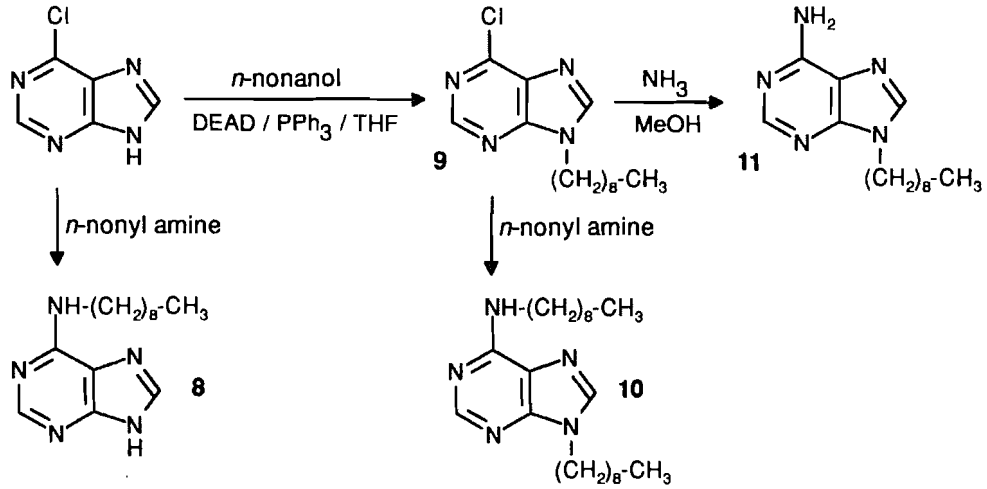

indispensable Mitsunobu reaction allowed for the synthesis of 6-chloro-9-nonyl purine **9**, which could then either be treated with *n*-nonyl amine to yield the *N*6,*N*9-dialkylated purine **10** or dissolved in methanolic ammonia to prepare 9-nonyladenine **11**.

NMR spectroscopy

The exceedingly cluttered ^{1}H NMR spectrum of [10](*N*6,9)-6-aminopurinophane at 25°C was further complicated by extensive broadening of resonances (Fig. 1, spectrum (*b*)). This was not unexpected since conformation flexibility of the aliphatic chain in the [*n*](*N*6,9)-6-aminopurinophanes should increase with each additional methylene. Within this exchange regime, attempts to assign the spectra using the regular 2D NMR experiments failed due to the lack of correlations. Note, for example, that one of the C1′ protons is not seen (highlighted by the arrow in Fig. 1, spectrum (*b*)) until the sample is warmed up to 90°C (see arrow in Fig. 1, spectrum (*a*)). At this elevated temperature, the spectrum showed a marked improvement with many of the signals sharpening and the appearance of some fine structure. Proton assignments were made possible through the application at 90°C of a 2D ^{13}C–^{1}H heteronuclear shift correlated spectrum and a 2D-COSY spectrum and appear in Table 1.

The NMR work carried out at lower temperatures revealed that [10](*N*6,9)-6-aminopurinophane could adopt a number of conformations; for example, at −77°C (Fig. 1, spectrum (*c*)), the multiple signals within the aromatic region revealed the presence of multiple conformations. The two major forms likely arise from the *anti–syn* isomerization about the N6—C6 bond and may be compared with those seen in the low temperature [9](*N*6,9)-6-aminopurinophane NMR spectrum (5). The *anti* conformer is preferred by approximately 4:1 over the *syn* orientation. Each of the *anti/syn* forms showed the presence of additional chain conformers, some with intensities comparable to the minor *syn* isomer, and their presence made it impractical to use simple intensity techniques to assign signals.

A variable temperature NMR study was undertaken to provide the activation parameters associated with the interchange between the major conformers. The low-field signals (H8) were the focus of the line shape analysis (9) and were monitored from −77°C to 30°C. Coalescence of the lines occurred at −20°C and the $\Delta G_c^{\ddagger}$ at this temperature was determined to be 59.4 ± 5.5 kJ mol^{-1}. With a number of minor conformers coalescing about the peaks of interest, the accurate matching of simulated spectra with the actual peaks became difficult and is reflected in the rather large error associated with the activation parameter.

Table 1. ^{1}H and ^{13}C NMR assignments of [10](*N*6,9)-6-aminopurinophane at 90°C (ppm).

	^{13}C	^{1}H	
C1′	42.2	3.79	4.43
C2′	31.5	1.54	1.73
C3′	29.6	1.24	1.41
C4′	29.0	0.96	1.32
C5′	28.1	0.61	0.77
C6′	28.9	1.11	1.18
C7′	28.9	0.30	0.59
C8′	25.8	1.12	1.21
C9′	29.1	1.64	2.04
C10′	44.7	3.96	4.57

Reitz et al. (10) have reported the barrier for rotation about the C6–N6 bond for a number of substituted adenine examples of about 54.0 kJ mol^{-1}, while [9](*N*6,9)-6-aminopurinophane showed a Gibbs' energy of activation of 50.2 kJ mol^{-1} (5). The higher $\Delta G_c^{\ddagger}$ for the decamethylene cyclophane is likely due to a combination of two effects. Unlike the H6-N6-C1′ fragment in the C9 homolog that is twisted about the C6—N6 bond, the longer chain length of the decamethylene cyclophane may allow this fragment to assume a more planar geometry. The barrier for rotation in [10](*N*6,9)-6-aminopurinophane, therefore, is likely to be more in keeping with the Reitz examples wherein the N6 nitrogens assume a more sp^2-like hybridization.

Ultraviolet spectroscopy

Conformational studies on the [10](*N*6,9)-6-aminopurinophane proved frustrating. Crystals suitable for X-ray analysis could not be obtained despite attempts to recrystallize from a variety of solvents. Crystals grown from toluene

Can. J. Chem. Downloaded from www.nrcresearchpress.com by 46.23.64.124 on 09/08/12
For personal use only.

Can. J. Chem. Downloaded from www.nrcresearchpress.com by 46.23.64.124 on 09/08/12
For personal use only.

Fig. 1. ^{1}H NMR spectra of [10](*N*6,9)-6-aminopurinophane, **3**, in deuterochloroform at (*a*) 90°C, (*b*) 25°C, and (*c*) −77°C.

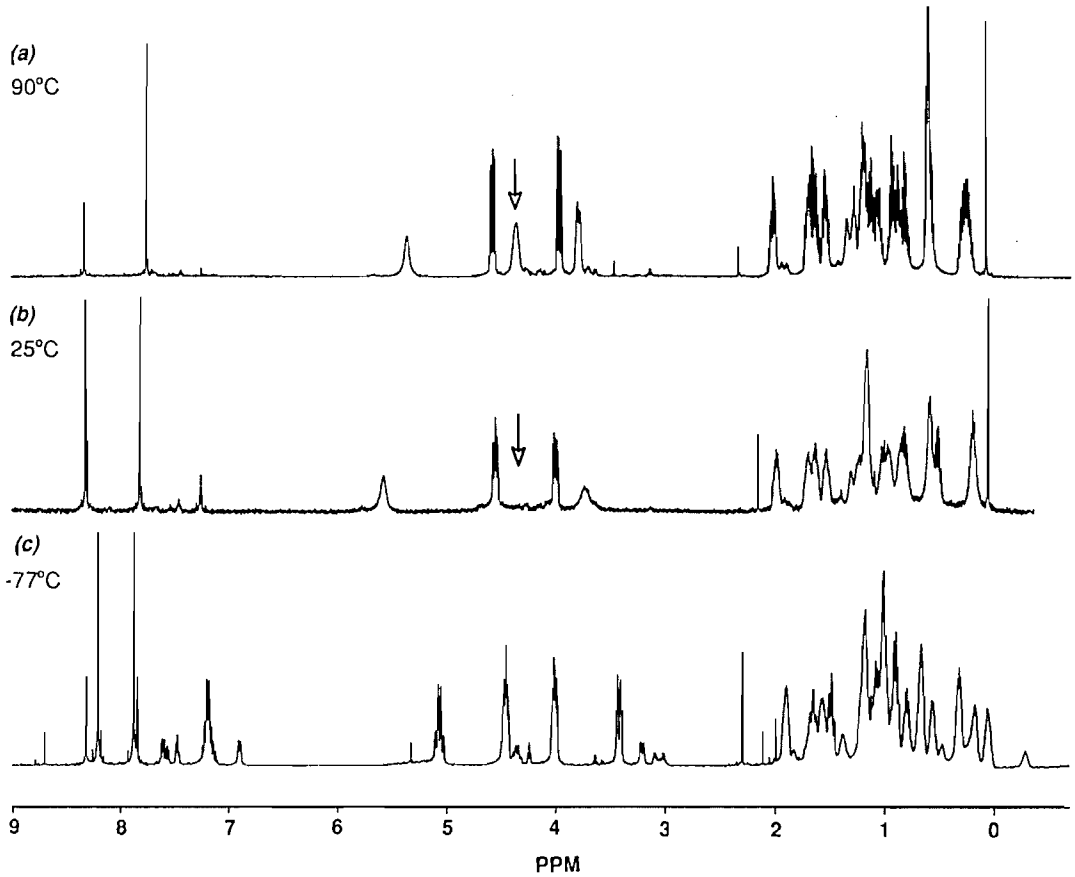

Table 2. Ultraviolet spectra of alkyl adenines and [*n*]-(*N*6,9)-6-aminopurinophanes.

Compound	λ_{max} (nm)	
Adenine	207	261
11	206	261
8	210	269
10	209	269
1	218 (ε 15 200)	278 (ε 13 100)
2	216 (ε 15 500)	276 (ε 13 500)
3	213 (ε 16 200)	273 (ε 13 800)

appeared normal but did not diffract. The computer modelling exercises undertaken were not as conclusive as in the octamethylene and nonamethylene cyclophane cases (5). The conformational freedom conferred by the additional methylene in [10](*N*6,9)-6-aminopurinophane allowed the chain to adopt a number of geometries very similar in energy and, as a result, many conformations were obtained with different structures but similar energies.

Ultraviolet spectroscopy performed on the purinophanes and the series of substituted adenines afforded some insight into the structural characteristics of these molecules. The spectra were recorded using absolute methanol as the solvent and the results are presented in Table 2. The spectra are characterized by two transitions. Alkylation at N9 in adenine seemed to have little effect on the appearance of the spectrum with the absorptions of N9-nonyladenine effectively unchanged from those of adenine. On the other hand, substitution at N6 seemed to have a major effect on the low-energy transition (269 nm in *N*6-nonyladenine compared to 261 nm in adenine) and a marginal effect on the high-energy transition. The low-energy transition, therefore, results from the excitation of an electron from the N6 lone pair in a nonbonding molecular orbital to an unoccupied π^* molecular orbital; while the high-energy transition was a result of a $\pi \rightarrow \pi^*$ excitation.

The cyclophane series of UV spectra were markedly different from that of the *N*6,*N*9-dinonyladenine standard. The bathochromic shift as the methylene chain length decreased had been observed previously in the UV spectroscopy of cyclophanes (11). The shift for the $\pi \rightarrow \pi^*$ transition in cyclophane spectra had been ascribed to the bending of the aromatic plane. The smaller the bridging chain, the greater the deformation of the purine π-system. This distortion raises the energy of the associated molecular orbital and reduces the energy difference between the π and the π^* states. The $n \rightarrow \pi^*$ transition is also a reflection of the cyclophane geometry. Studies have shown (12) that the highest energy absorption for N-substituted anilines occurs when the lone pair on the exocyclic nitrogen is conjugated with the aromatic ring (i.e., the C-NH_2 atoms all lie in the same plane). Twisting the lone pair out of this orientation results in a bathochromic shift. The situation is similar for the purinophanes. The maximum transition energy is required when the N6 lone pair is aligned with the aromatic purine system. Altering the electronic character of N6 by sub-

Can. J. Chem. Downloaded from www.nrcresearchpress.com by 46.23.64.124 on 09/08/12
For personal use only.

stitution or, more dramatically, by twisting the lone pair out of conjugation, as in the cyclophane series, raises the energy of the nonbonding molecular orbital. In essence, the greater the degree of bending and twisting, the less energy is required to induce a transition. These same structural features manifest themselves in a hyperchromic effect seen throughout the series as the chain length increases.

Some of the decamethylene cyclophane structural attributes can now be deduced. The relief of strain that the C-10 chain provides enables the purine ring to adopt a more planar geometry than in the C-8 and C-9 analogs as evidenced by the $\pi \rightarrow \pi^*$ transition. The UV spectra also imply that the degree twisting of N6 in [10]-purinophane is less severe than in the other cases. This lends further support to the statements made in the dynamic NMR study that implicated the relative planarity of the H6-N6-C1′ fragment as a major contributor to the activation energy.

Calculation of the chemical shifts in the [*n*]-(*N*6,9)-6-aminopurinophane series

Theoretical models aimed at determining the anisotropy of the molecular diamagnetic susceptibility of the purine system have been developed, adopting either a semi-empirical or quantum mechanical approach (13). The [*n*]-(*N*6,9)-6-aminopurinophane series can be used to assess these theoretical models in much the same way that the examination of the proton chemical shifts of [10]-paracyclophane provided a method of complimenting and assessing the calculated shielding anisotropy of benzene (2). In this previous work, calculated proton chemical shifts for the cyclophane were a composite of a standard methylene shift (14) and a contribution to the total shielding from ring currents and local atomic magnetic anisotropies. With the geometry of the cyclophane provided by a molecular model, estimates of the ring current effect were made using the "free electron" model of Waugh and Fessenden (15) while the local atomic contributions to the diamagnetic anisotropy were evaluated using the method developed by Barfield et al. (16). The same semi-empirical approach used successfully in the [10]-paracyclophane study has been applied to the purinophane system and its assessment appears below.[2] Preliminary work, which considered only ring current contributions to the total shielding, resulted in marginally acceptable values for the chemical shifts (17). It would seem necessary, therefore, to include local anisotropy contributions in the calculations.

While a discussion of the theories behind these calculations is beyond the scope of this present work (interested readers are directed towards references listed in the previous paragraph), some mention of the various components of the calculation is necessary. The standard chemical shift reference chosen was based on the work of Burke and Lauterbur who determined the typical value for the methylene shifts of large cycloalkanes averaged to 1.30 ppm (14). Any deviation from this value by a bridge methylene proton will be ascribed to ring current and local anisotropy effects.

Two ring currents were calculated: one resulting from each of the constituent five- and six-membered rings. Studies using CNDO/2 and MNDO methods to determine the ratio of π-electrons for each ring (18) showed that the pyrimidine and the imidazole rings should be allotted 5.275 and 4.881 electrons, respectively. However, varying the number of electrons circulating in each of the current loops resulted in the best chemical shift values when 6 electrons were used in the pyrimidine ring and 4 used for the imidazole moiety. Carbon atoms 4 and 5 are common to both the imidazole and pyrimidine rings and, as a result, two ring current contributions were calculated and an average was taken.

Our work has shown that introducing a loop separation into the ring current calculation results in very small changes in the chemical shift and does not improve the correlation between predicted and observed chemical shifts. Agarwal et al. (2) also found the best correlation was obtained without invoking a loop separation. As a result, a zero loop separation was used in the present calculation.

Implementation of the semi-empirical model required a knowledge of the purinophane's molecular structure as well as the principal values and directions of the magnetic shielding tensors (σ_{11}, σ_{22}, σ_{33}) of the constituent atoms of the aromatic system. The principal values of shielding tensors for each atom in the purine and pyrimidine bases have been determined computationally by Schindler (19). The conformational details required were provided by the crystal structure of [8]-(*N*6,9)-6-aminopurinophane (4) whose positional parameters were converted to orthogonal angstrom coordinates.[3]

It is worth pointing out that a number of approximations were introduced in an effort to simplify the calculations. The geometry of the adenine moiety was assumed to be planar for the ring current contribution to the chemical shift. In fact, the torsional angles C6-C5-C4-N9 (169.2°) and N7-C5-C4-N3 (176.3°) of [8]-(*N*6,9)-6-aminopurinophane, determined by diffraction studies, confirm the nonplanarity of the adenine moiety (4). The asymmetric nature of adenine also results in an irregular alignment of the shielding tensor values with respect to the molecular geometry (19), although these are not large differences. Forcing the σ_{11}, σ_{22}, and σ_{33} values to lie along more " convenient" molecular axes greatly simplifies the calculation of the local anisotropy contributions while introducing another source of error.

When the observed chemical shifts of the bridging methylene protons in [8]-(*N*6,9)-6-aminopurinophane (taken at 25°C)[4] are plotted against those predicted by the semi-empirical model, a good correlation is evident (Fig. 2). Inductively transmitted substituent effects from N6 and N9 are largely responsible for the deshielding of the protons on C1′ and C8′ and, therefore, for the purposes of comparison, these values have been omitted. It should be borne in mind that long-range inductive effects may after C2′ and C7′ proton resonances as well. If one looks at the differences in chemical shifts between the geminal protons on each methylene, the predicted values seem to follow the same general trend seen experimentally.

[2] The program used to calculate the chemical shifts in the [*n*](*N*6,9)-6-aminopurinophane series has been deposited as Supplementary Material, which can be purchased from: The Depository of Unpublished Data, Document Delivery, CISTI, National Research Council Canada, Ottawa, Canada K1A 0R6.

[3] The development of the model and the refinement of the calculations centered on the octamethylene purine cyclophane whose properties were most clearly defined.

[4] Inspection of the NMR spectra and structural data of [8](*N*6,9)-6-aminopurinophane have revealed an error in the labelling of the methylene bridge protons. The *pro-R* and *pro-S* designations for the geminal proton pairs at C3′, C5′, and C6′ have been switched.

Can. J. Chem. Downloaded from www.nrcresearchpress.com by 46.23.64.124 on 09/08/12
For personal use only.

Fig. 2. Plot of the predicted vs. observed chemical shifts for [8]-(*N*6,9)-6-aminopurinophane (from spectra at 25°C).

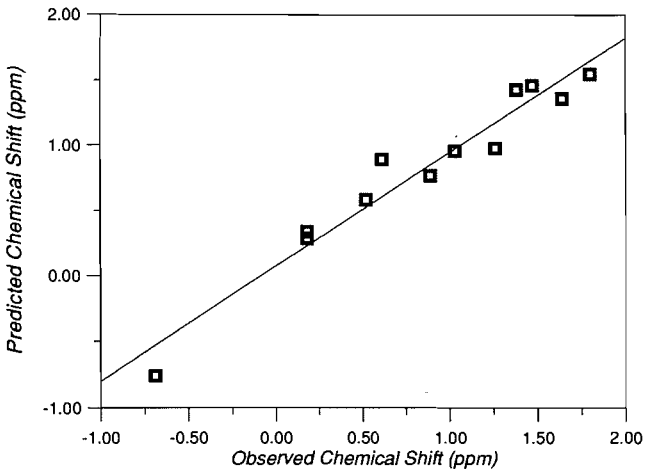

Fig. 3. Plot of the predicted vs. observed chemical shifts for *anti*-[9]-(*N*6,9)-6-aminopurinophane (from spectra at −59.5°C).

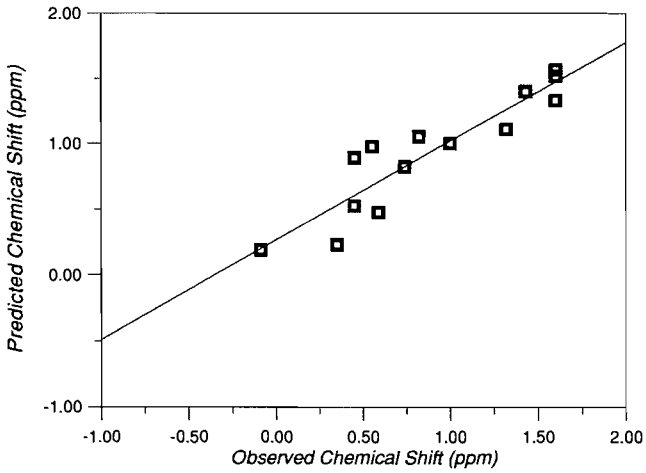

Linear regression analysis on the plot of observed chemical shifts against the predicted values, yields a least-squares correlation coefficient, *r*, of 0.9719.

The semi-empirical model was then modified so as to be utilized for the assignment of the nonamethylene homolog. Using the crystal structure geometry for the *anti* conformer and the computer generated molecular model (**9***b*, see ref. 5) for the *syn* conformation, the predicted chemical shifts were calculated and the values presented in a plot of the experimental (taken at −59.5°C) versus the calculated chemical shifts. For the *anti* case (see Fig. 3), omitting the protons on C1′ and C9′, a linear regression analysis of the data yielded a correlation coefficient of 0.9177. The data for the *syn* conformation of [9](*N*6,9)-6-aminopurinophane is a shown in Fig. 4 and linear regression analysis of this plot yields at least-squares correlation coefficient of 0.9715.

Overall, the chemical shift calculations of the purinophanes illustrate two important points. Firstly, in both the [8]- and [9]-(*N*6,9)-6-aminopurinophane cases, the results generated compare relatively well with the observed ^{1}H NMR resonances despite the approximations made to simplify the procedure.

Fig. 4. Plot of the predicted vs. observed chemical shifts for *syn*-[9]-(*N*6,9)-6-aminopurinophane (from spectra at −59.5°C).

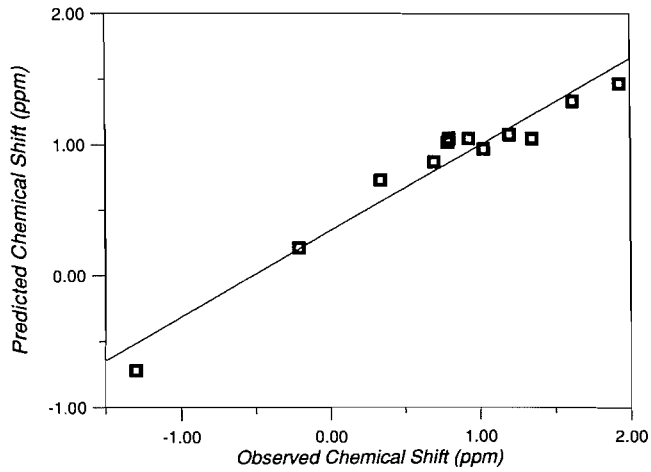

While its absolute predictive ability is limited, the calculations based on the semi-empirical model are relatively simple to set up and evaluate. Secondly, and perhaps more importantly, this exercise has demonstrated the usefulness of the aminopurinophanes in the assessment of a particular chemical shift calculation procedure. It is hoped that these cyclophanes may soon be applied to determine the relative merits of a more sophisticated, ab initio approach. The individual gauges for atoms in molecules (IGAIM) system being developed by Keith and Bader shows promise (20) and, although still in its formative stages, the purinophane series would be an ideal candidate for study using this new methodology.

Experimental methods

Melting points were recorded on a Gallenkamp capillary tube melting point apparatus and are uncorrected. Proton magnetic resonance (^{1}H NMR) spectra were recorded on a Bruker AC-200 or a Bruker AM-500 spectrometer with chloroform-*d* as the solvent unless otherwise noted. Unless specified, the internal references were tetramethylsilane (TMS) or chloroform. The abbreviations (s) = single, (d) = doublet, (t) = triplet, (q) = quartet, (m) = multiplet, and (br) = broad are used in the description of the spin–spin splitting pattern present in the spectra. The natural abundance carbon-13 magnetic resonance (^{13}C NMR) were recorded on a AM-500 (at 125.776 MHz) or AC-200 (at 50.324 MHz) instrument using chloroform-*d* as the solvent and internal reference unless otherwise noted. All ^{13}C spectra were broad-band decoupled. Low-resolution mass spectra (MS) and high-resolution mass spectra (HRMS) were obtained on either a VG Micromass 7070F or a VG ZAB-E mass spectrometer with samples being introduced through a direct inlet system. Ions were generated using electron impact (EI). Infrared spectra (IR) were recorded on a Perkin–Elmer 283 spectrometer. IR samples were run as neat liquids using NaCl windows or, if solid, as KBr pellets. The symbols (s) = strong and (br) broad were used in the recording of the IR data to indicate the intensity of the recorded bands. Ultraviolet (UV) spectra were recorded on a Perkin–Elmer Lambda 9 UV/VIS/NIR spectrophotometer.

Tetrahydrofuran (THF) was dried by refluxing and distilling from sodium and benzophenone under dry nitrogen. THF

Can. J. Chem. Downloaded from www.nrcresearchpress.com by 46.23.64.124 on 09/08/12
For personal use only.

was collected from the distillation apparatus as required. Acetonitrile was distilled from P_2O_5 followed by distillation from CaH_2, discarding the first 5% and the last 10%. The NMR solvent chloroform-*d* was stored over molecular sieves (4Å) prior to use.

Unless specified, column chromatography was performed by the "flash" method of Still, Kahn, and Mitra (21). The silica gel used for column chromatography (5.0% of 100 mesh up; 47.6% of 100–200 mesh and 47.4% of 200 mesh down) was purchased from Terochem. Silica gel 60 F_{254} (E. Merck Co.) plates of 0.2 mm thickness were used for analytical thin-layer chromatography (TLC). Visualization was achieved using a UV lamp at 254 nm or via treatment of the TLC with either a molybdic acid spray (20 g of molybdic acid and 15 g of ceric sulphate dissolved in 1 litre of 10% sulphuric acid) or a ninhydrin spray (0.2% ninhydrin in ethanol) followed by heating.

Synthesis of 10-bromo-1-decanol, 4

The procedure used was that of Kang, Kim and Moon (7). To a solution of 1,10-decanediol (17.4 g, 100 mmol) in benzene (200 mL) stirred in a 500 mL round bottom flask equipped with a Dean–Stark trap and a condenser was added hydrobromic acid (48%, 12.5 mL, 110 mmol). The reaction was left to stirr at reflux for 28 h during which time the water trapped was periodically drained. The mixture was washed with 6 N NaOH solution (100 mL), 10% HCl (100 mL), water (2 × 200 mL), and saturated NaCl solution (150 mL). The organic layer was dried with anhydrous magnesium sulphate, evaporated under reduced pressure, and the residue purified via distillation. The yield was 80% (18.9 g, 80 mmol). The compound showed bp 110°C/0.2 Torr (lit. (7) bp 125–127°C/3 Torr (1 Torr = 133.3 Pa)); ^{1}H NMR (200 MHz), δ: 1.23 (m, 12H, $(CH_2)_6$), 1.45 (m, 2H, CH_2-CH_2-OH), 1.78 (m, 2H, CH_2-CH_2-Br), 3.34 (t, 2H, *J* = 6.8 Hz, CH_2-Br), and 3.53 (t, 2H, *J* = 6.5 Hz, CH_2-OH); ^{13}C NMR (50 MHz), δ: 25.58, 27.98, 28.58, 29.21, 29.23, 29.33, 32.51, 32.64, 33.90 (CH_2-Br), 62.58 (CH_2-OH); MS[EI], *m/z* (RI%): 237 $[M + 1]^+$ (18), 221 (63), 190 (100), 177 (44); HRMS: Exact Mass calcd. for $C_{10}H_{22}BrO$ $[M + 1]^+$: 237.0854; found: 237.0863.

Synthesis of 10-azido-1-decanol, 5

The procedure was a modification of that used by Reeves and Bahr (8). 10-Bromo-1-decanol (10.0 g, 42.3 mmol) was added to a stirred solution of 25% aqueous sodium azide (10.25 g in 40 mL of water). Aliquat 336 (1.62 g, 4 mmol) was added the mixture heated to 100°C. After 30 h, the reaction was cooled and the phases separated. The 10-azidodecanol was purified via distillation. Yield 87% (7.3 g, 36.9 mmol). The compound showed bp 103°C/0.3 Torr; IR, ν_{max}: 3360 (br, OH), 2095 (s, N_3) cm^{-1}; ^{1}H NMR (200 MHz), δ: 1.24 (m, 12H, $(CH_2)_6$), 1.53 (m, 4H, CH_2-CH_2-OH and CH_2-CH_2-N_3), 3.19 (t, 2H, *J* = 6.8 Hz, CH_2-N_3), and 3.54 (t, 2H, *J* = 6.6 Hz, CH_2-OH); ^{13}C NMR (50 MHz), δ: 25.58, 26.52, 28.65, 28.96, 29.24, 29.33 (CH_2-CH_2-N_3), 32.56 (CH_2-CH_2-OH), 51.29 (CH_2-N_3), 62.62 (CH_2-OH).

Synthesis of 6-chloro-9-(10-azidodecyl)purine, 6

The procedure used was similar to that of Iwakawa et al. (22). To a mixture of 6-chloropurine (4.77 g, 30.86 mmol), triphenylphosphine (8.09 g, 30.84 mmol), and diethyl azidocarboxylate (6.64 g, 6 mL, 30.81 mmol) in 120 mL of dry THF was added a solution of 10-azidodecanol (6.00 g, 30.15 mmol) in 40 mL of THF. The solution was allowed to stir at room temperature for 48 h at which time the reaction mixture was concentrated under reduced pressure. The residue was chromatographed on silica gel using chloroform as the eluent, yielding a viscous yellow oil. TLC of the product with 5% methanol in chloroform gave R_f = 0.62. The yield was 32% (3.31 g, 9.88 mmol). The compound showed ^{1}H NMR (200 MHz), δ: 1.25 (m, 12H, $(CH_2)_6$), 1.57 (m, 2H, CH_2-CH_2-N_3), 1.94 (m, 2H, CH_2-CH_2-N9), 3.23 (t, 2H, *J* = 6.8 Hz, CH_2-N_3), 4.27 (t, 2H, *J* = 7.3 Hz, CH_2-N9), 8.14 (s, 1H, H2), 8.74 (s, 1H, H8); MS [EI], m/z (RI%): 336 $[M + 1]^+$ (100), 295 (6), 265 (10), 209 (18), 115 (23); HRMS: Exact Mass calcd. for $C_{15}H_{23}N_7Cl$ $[M + 1]^+$: 336.1703; found: 336.1714.

Synthesis of 6-chloro-9-(10-aminodecyl)purine, 7

The procedure used was similar to that of Vaultier and coworkers (23). To 6-chloro-9-(10-azidodecyl)purine (1.0 g, 2.99 mmol) in 3 mL of THF was added triphenylphosphine (783 mg, 2.99 mmol), water (80 μL, 4.50 mmol), and a boiling chip. The evolution of N_2 began immediately. The mixture was left standing at room temperature for 18 h. TLC of the reaction mixture showed the complete disappearance of the azide starting material and the appearance of a ninhydrin positive spot on the baseline. The solution was then concentrated, redissolved in 50 mL of chloroform, and extracted with three 20 mL portions of 0.01 M HCl. The combined aqueous solutions were adjusted to pH 8 with 1 M NaOH and extracted with three 30 mL portions of chloroform. These combined organic solutions were dried over anhydrous sodium sulphate and evaporated under reduced pressure. The product was subjected immediately to cyclization conditions.

Synthesis of [10](*N*6,9)-6-aminopurinophane, 3

6-Chloro-9-(10-aminodecyl)purine (700 mg, 2.27 mmol) was dissolved in 50 mL acetonitrile. Diisopropylethylamine (2 mL, 11.48 mmol) was added and the solution diluted with an additional 450 mL of acetonitrile. The reaction was left stirring at 60°C for 48 h at which time the solution was evaporated and the resultant residue was chromatographed on silica gel using 5% methanol in chloroform. TLC of the product in 10% in chloroform gave R_f = 0.50. The yield was 37% (229 mg, 0.84 mmol). The compound showed UV, λ_{max} (methanol): 273 nm (ε 13 800), 213 nm (ε 16 200); ^{1}H NMR (500 MHz at 90°C; sealed tube with $CDCl_3$), δ: 0.30 (m, 1H, C7′H), 0.59 (m, 1H, C7′H), 0.61 (m, 1H, C5′H), 0.77 (m, 1H, C5′H), 0.96 (m, 1H, C4′H), 1.11 (m, 1H, C6′H), 1.12 (m, 1H, C8′H), 1.18 (m, 1H, C6′H), 1.21 (m, 1H, C8′H), 1.24 (m, 1H, C3′H), 1.32 (m, 1H, C4′H), 1.41 (m, 1H, C3′H), 1.54 (m, 1H, C2′H), 1.64 (m, 1H, C9′H), 1.73 (m, 1H, C2′H), 2.04 (m, 1H, C9′H), 3.79 (m, 1H, C1′H), 3.96 (m, 1H, C10′H), 4.34 (m, 1H, C1′H), 4.57 (m, 1H, C10′H), 5.3 (br, 1H, NH), 7.8 (s, 1H, H2), and 8.2 (s, 1H, H8); ^{13}C NMR (125 MHz), δ: 25.8 (C8′), 28.1 (C5′), 28.9 (C7′), 28.9 (C6′), 29.0 (C4′), 29.1 (C9′), 29.6 (C3′), 31.5 (C2′), 42.2 (C1′), 44.7 (C10′), 124.1 (C5), 146.9 (C8), 155.3 (C2), 159.7 (C6); MS [EI], *m/z* (RI%): 273 $[M]^+$ (100), 244 (7), 230 (23), 216 (12), 176 (15), 148 (29), 120 (13), 84 (38); HRMS: Exact Mass calcd. for $C_{15}H_{23}N_5$: 273.1953; found: 273.1945.

Synthesis of *N*6-nonyladenine, 8

6-Chloropurine (1 g, 6.47 mmol) was dissolved in a solution of

Can. J. Chem. Downloaded from www.nrcresearchpress.com by 46.23.64.124 on 09/08/12
For personal use only.

1-nonylamine (2.78 g, 3.56 mL, 19.41 mmol) in 25 mL of acetonitrile and allowed to stir at room temperature for 48 h. The solution was concentrated under reduced pressure and chromatographed on silica gel using 5% methanol in chloroform as the eluent. The alkylated purine was recrystallized from toluene. TLC using 10% methanol in chloroform showed the desired product with R_f = 0.36. The yield was 83% (1.40 g, 5.37 mmol). The compound showed mp 162–164°C; UV, λ_{max} (methanol): 210 nm, 269 nm; ^{1}H NMR (500 MHz), δ: 0.86 (t, 3H, J = 6.7 Hz, CH_3), 1.25 (m, 8H, CH_3-(CH_2)$_4$), 1.34 (m, 2H, NH-(CH_2)$_3$-CH_2), 1.43 (m, 2H, NH-(CH_2)$_2$-CH_2), 1.71 (m, 2H, NH-CH_2-CH_2), 3.66 (br, 2H, NH-CH_2), 6.16 (br, 1H, NH), 7.97 (s, 1H, H2), 8.43 (s, 1H, H8); ^{13}C NMR (125 MHz), δ: 14.04 (CH_3), 22.61 (CH_2-CH_3), 26.91, 29.21, 29.33, 29.48, 29.68, 31.82, 40.85 (NH-CH_2), 137.94 (C8), 152.24 (C2); MS [EI], *m/z* (RI%): 261 [M]$^+$ (47), 246 (6), 232 (12), 218 (20), 204 (43), 190 (70), 176 (36), 162 (39), 149 (100), 135 (88), 108 (27), 94 (7), 67 (13), 55 (27); HRMS: Exact Mass calcd. for $C_{14}H_{23}N_5$: 261.1953; found: 261.1963.

Synthesis of 6-chloro-9-nonyl purine, 9

The procedure used was similar to that of Iwakawa et al. (22). To a mixture of 6-chloropurine (4.77 g, 30.86 mmol), triphenylphosphine (8.09 g, 30.84 mmol), and diethyl azidocarboxylate (6.64 g, 6 mL, 30.81 mmol) in 120 mL of dry THF was added a solution of 1-nonanol (4.35 g, 5.26 mL, 30.15 mmol) in 40 mL of THF. The solution was allowed to stir at room temperature for 48 h, at which time the reaction mixture was concentrated under reduced pressure. The residue was chromatographed on silica gel using chloroform as the eluent. TLC of the product with 5% methanol in chloroform gave R = 0.75. The yield was 80% (6.75 g, 24.12 mmol). The compound showed ^{1}H NMR (200 MHz(, δ: 0.85 (t, 3H, J = 6.7 Hz, CH_3), 1.23 (m, 12H, (CH_2)$_6$-CH_3), 1.90 (m, 2H, N9-CH_2-CH_2), 4.24 (t, 2H, J = 7.3 Hz, N9-CH_2), 8.12 (s, 1H, H2), 8.72 (s, 1H, H8).

Synthesis of *N*6, *N*9-Dinonyladenine, 10

6-Chloro-9-nonyl-purine (1 g, 3.57 mmol) was dissolved in a solution of 1-nonyl amine (1.53 g, 2 mL, 10.71 mmol) in 25 mL of acetonitrile and allowed to stir at room temperature for 48 h. The solution was concentrated under reduced pressure and chromatographed on silica gel using ethyl acetate as the eluent. TLC using ethyl acetate showed the desired product with R_f = 0.73. The yield was 62% (857 mg, 2.21 mmol). The compound showed UV, λ_{max} (methanol): 209 nm, 269 nm; ^{1}H NMR (500 MHz), δ: 0.76 (t, 6H, J = 6.8 Hz, 2 × CH_3), 1.14 (m, 16H), 1.21 (m, 4H), 1.29 (m, 2H), 1.56 (m, 2H), 1.78 (m, 2H), 3.54 (br, 2H, NH-CH_2), 4.07 (t, 2H, J = 7.3 Hz, N9-CH_2), 6.14 (s, 1H, NH), 7.63 (s, 1H, H2), 8.30 (s, 1H, H8); ^{13}C NMR (125 MHz), δ: 13.80, 22.41, 26.48, 26.77, 28.88, 28.96, 29.06, 29.12, 29.12, 29.33, 29.62, 29.95, 31.60, 31.66, 40.57, 43.66, 119.99 (C5), 139.25 (C8), 148.77 (C4), 152.97 (C2), 154.90 (C6); MS [EI], *m/z* (RI%): 387 [M]$^+$ (100), 371 (73), 358 (58), 344 (44), 330 (60), 316 (96), 302 (39), 288 (95); HRMS: Exact Mass calcd. for $C_{23}H_{41}N_5$: 387.3362; found: 387.3370.

Synthesis of 9-nonyladenine, 11

6-Chloro-9-nonyl-purine (1 g, 3.57 mmol) was dissolved in 50 mL of saturated methanolic ammonia and left to stir for 30 days. The solvent was removed under reduced pressure and the residue chromatographed on silica gel using 5% methanol in chloroform as the eluent. The alkylated purine was recrystallized from toluene. TLC using 10% methanol in chloroform showed the desired product having R_f = 0.44. The yield was 25% (232 mg, 0.89 mmol). The compound showed mp 121–126°C UV, λ_{max} (methanol): 206 nm, 261 nm. ^{1}H NMR (500 MHz), δ: 0.84 (t, 3H, J = 6.8 Hz, CH_3), 1.22 (m, 8H, CH_3-(CH_2)$_4$), 1.30 (m, 4H, N9-CH_2-CH_2-(CH_2)$_2$), 1.87 (m, 2H, N9-CH_2-CH_2), 4.16 (t, 2H, J = 7.3 Hz, N9-CH_2), 5.90 (s, 2H, NH_2), 7.77 (s, 1H, H2), 8.35 (s, 1H, H8); ^{13}C NMR (125 MHz), δ: 14.02 (CH_3), 22.58 (CH_3-CH_2), 26.58, 26.63, 29.01, 29.11, 29.33, 30.06, 31.75, 43.95 (N9-CH_2), 119.71 (C5), 140.43 (C8), 152.85 (C2), 155.47 (C6); MS [EI], *m/z* (RI%): 261 [M]$^+$ (10), 245 (6), 190 (10), 177 (10), 162 (26), 148 (100), 135 (82), 119 (19), 93 (8), 55 (11); HRMS: Exact Mass calcd. for $C_{14}H_{23}N_5$: 261.1953; found 261.1958.

Acknowledgements

The authors acknowledge with thanks the financial support of the Natural Sciences and Engineering Research Council of Canada, and the award of an NSERC post-graduate scholarship to A.C. The authors also wish to thank Professor M.J. McGlinchey for discussions dealing with the development of the chemical shift calculations.

References

1. F.S. Ezra, C.-H. Lee, N.S. Kondo, S.S. Danyluk, and R.H. Sarma. Biochemistry, **16**, 1977 (1977); R.A. Bell, J.R. Everett, D.W. Hughes, J.M. Coddington, D. Alkema, P.A. Hader, and T. Neilson. J. Biomol. Struct. Dyn. **2**, 693 (1985); P.O.P. Ts'O (*Editor*). Basic principles in nucleic acid chemistry. Vol. 1. Academic Press, New York. 1974. pp. 453–584.
2. A. Agarwal, J.A. Barnes, J.L. Fletcher, M.J. McGlinchey, and B.G. Sayer. Can. J. Chem. **55**, 2575 (1977).
3. H. Nozaki, T. Koyama, and T. Mori. Tetrahedron, **25**, 5357 (1969).
4. R.A. Bell and H.N. Hunter. Tetrahedron Lett. **28**, 147 (1987); and R.A. Bell, H.N. Hunter, C.J.L. Lock, and R. Fagiani. Can. J. Chem. **70**, 186 (1992).
5. A. Capretta, H.N. Hunter, C.S. Frampton, and R.A. Bell. Can. J. Chem. **71**, 96 (1993).
6. R. Boigegrain, B. Castro, and C. Selve. Tetrahedron Lett. 2529 (1975); B. Castro. Org. React. **29**, 1 (1983).
7. S.-K. Kang, W.-S. Kim, and B.-H. Moon. Synthesis, 1161 (1985).
8. W.P. Reeves and M.L. Bahr. Synthesis, 823 (1976).
9. D.A. Kleier and G. Binsch. DNMR3 Program 165. Quantum Chemistry Program Exchange, Indiana University, Bloomington, Ind. 1970.
10. A.B. Reitz, D.W. Graden, A.D. Jordan, Jr., and B.E. Maryanoff. J. Org. Chem. **55**, 5761 (1990).
11. N.L. Allinger, J.T. Sprague, and T. Liljefors. J. Am. Chem. Soc. **96**, 5100 (1974).
12. H.H. Jaffe and M. Orchin. Theory and application of ultraviolet spectroscopy. John Wiley and Sons, Inc., New York. 1962. p. 407.
13. C. Giessner-Prette, B. Pullman, P.N. Borer, L.-S. Kan, and P.O.P. Ts'o. Biolpolymers, **15**, 227 (1976); C. Giessner-Prettre and B. Pullman. Biochem. Biophys. Res. Commun. **70**, 578 (1976); C. Giessner-Prettre, B. Pullman, and J. Caillet. Nucleic Acids Res. **4**, 99 (1977); C. Giessner-Prettre and B. Pullman. Q. Rev. Biophys. **20**, 11 (1987).
14. J.J. Burke and P.C. Lauterbur. J. Am. Chem. Soc. **86**, 1870 (1964).

15. J.S. Waugh and R.W. Fessenden. J. Am. Chem. Soc. **79**, 846 (1957).
16. M. Barfield, D.M. Grant, and D. Ikenberry. J. Am. Chem. Soc. **97**, 6956 (1975).
17. H.N. Hunter. Ph.D. Thesis, McMaster University, 1988.
18. F. Jordan and H.D. Sostman. J. Am. Chem. Soc. **94**, 7898 (1972).
19. M. Schindler. J. Am. Chem. Soc. **110**, 6623 (1988).
20. T.A. Keith and R.F.W. Bader. Chem. Phys. Lett. **194**, 1 (1992).
21. W.C. Still, M. Kahn, and A.J. Mitra. J. Org. Chem. **43**, 2923 (1978).
22. M. Iwakawa, B.M. Pinto, and W.A. Szarek. Can. J. Chem. **56**, 326 (1978).
23. N. Knouzi, M. Vaultier, and R. Carrié. Bull. Soc. Chim. Fr. No. 5, 815 (1985); M. Vaultier, N. Knouzi, and R. Carrié. Tetrahedron Lett. **24**, 763 (1983).

Can. J. Chem. Downloaded from www.nrcresearchpress.com by 46.23.64.124 on 09/08/12
For personal use only.

Attachment of $C_5Me_4HSi(Me_2)NH$-*t*-C_4H_9 to yttrium via amine elimination. X-ray structure of [(η^5-C_5Me_4)$Si(Me_2)$-η^1-N-*t*-C_4H_9]$YN(SiMe_3)_2$

Ying Mu, Warren E. Piers, Mary-Anne MacDonald, and Michael J. Zaworotko

Abstract: Reaction of the homoleptic yttrium amido complex $Y[N(SiMe_3)_2]_3$ with $C_5Me_4HSiMe_2N(H)$-*t*-C_4H_9, Cp*HSiNHR, at 100°C resulted in elimination of 2 equivalents of $HN(SiMe_3)_2$ and attachment of the Cp-amido donor to yttrium. The product $(Cp^*SiNR)YN(SiMe_3)_2$, **1**, was isolated in 40% yield and was characterized crystallographically (triclinic, space group $P\bar{1}$, a = 8.9759(23) Å, b = 9.504(7) Å, c = 18.294(6) Å, V = 1423.4(12) Å^3, Z = 2, R = 0.061, R_w = 0.053). Metrical parameters associated with the $N(SiMe_3)_2$ ligand were suggestive of weak β-SiC agostic interactions that stabilize the electron-deficient yttrium center. Alkylation of **1** resulted in unstable alkyl derivatives that could not be isolated.

Key words: cyclopentadienyl-amido, amine elimination, yttrium complex.

Résumé : La réaction du complexe homoleptique amido yttrium, $Y[N(SiMe_3)_2]_3$ avec du $C_5Me_4HSiMe_2N(H)$-*t*-C_4H_9, Cp*HSiNHR, à 100°C, conduit à une élimination de 2 équivalents de $HN(SiMe_3)_2$ et à un attachement du donneur Cp-amido à l'yttrium. On a isolé le produit $(Cp^*SiNR)YN(SiMe_3)_2$, **1**, avec un rendement de 40% et on l'a cristallisé par cristallographie (triclinique, groupe d'espace $P\bar{1}$, a = 8,9759(23), b = 9,504(7) et c = 18,294(6) Å, V = 1423,4(12) Å^3, Z = 2, R = 0,061 et R_w = 0,053). Les paramètres métriques associés au coordinat $N(SiMe_3)_2$ suggèrent la présence d'interactions agostiques β-SiC faibles qui stabilisent le centre yttrium qui est électrodéficient. L'alkylation du composé **1** conduit à des dérivés alkyles instables qui n'ont pas pu être isolés.

Mots clés : cyclopentadiényl-amido, élimination d'amine, complexe d'yttrium.

[Traduit par la rédaction]

Introduction

The use of "constrained geometry" Cp-amido type ligand arrays in homogeneous Ziegler Natta olefin polymerization catalysts has allowed for production of polymers with different properties and applications than those produced from bis-cyclopentadienyl stabilized catalyst precursors (1). In the Cp-amido ligand family one of the cyclopentadienyl donors from the classical "bent" metallocene bis-cyclopentadienyl ligand arrangement is replaced by an amido donor that is linked to the other cyclopentadienyl ligand, usually by a dimethyl silyl bridge (2). In addition to having two fewer electrons than a bis-cyclopentadienyl array, the chelating nature of the Cp-amido ligands serves to constrain the ancillary ligand set, opening up the geometry about the reactive metal center.

Traditional protocols for attachment of Cp-amido type ligands ("CpSiNR") to early transition metals using dilithio salts of the ligands and the transition metal chlorides are often fraught with disadvantages. In some instances, the protonated ligands are prone to Si—N bond cleavage upon treatment with alkyllithium reagents, leading to low yields of the dilithium salts required for attachment to the transition metal. Yields of these salt elimination reactions can also be highly variable and sensitive to reaction conditions. Furthermore, and this is particularly applicable when M is a group-3 metal, purification of the resulting (CpSiNR)MCl complex can be tedious owing to the difficulty in complete removal of the eliminated salt or the coordinated THF ligands that solubilize the halide starting materials (2*b*).

To circumvent some of these problems Teuben and coworkers (3) drew upon some chemistry originally reported by Chandra and Lappert in the late 1960s (4) that involved amine elimination from metal amides as a means for attaching cyclopentadienyl donors to early transition metals. High-yielding

Received August 18, 1995.

Y. Mu and W.E. Piers.[1] Guelph-Waterloo Centre for Graduate Work in Chemistry, Guelph Campus, Department of Chemistry and Biochemistry, University of Guelph, Guelph, ON N1G 2W1, Canada.
M.-A. MacDonald and M.J. Zaworotko. Department of Chemistry, Saint Mary's University, Halifax, NS B3H 3C3, Canada.

[1] Author to whom correspondence may be addressed. Present address: Department of Chemistry, University of Calgary, 2500 University Drive N. W., Calgary, AB T2N 1N4. Telephone: (403) 220-5746. Fax: (403) 289-9488. E-mail: wpiers@chem.ucalgary.ca

Can. J. Chem. Downloaded from www.nrcresearchpress.com by 46.23.64.124 on 09/08/12
For personal use only.

Can. J. Chem. Downloaded from www.nrcresearchpress.com by 46.23.64.124 on 09/08/12
For personal use only.

Table 1. Summary of data collection and structure refinement details for (Cp*SiNR)YN($SiMe_3$)$_2$, **1**.

Parameter	Value	Parameter	Value
Empirical formula	$C_{21}H_{45}Si_3N_2Y$	$F(000)$	532
fw	498.76	d_{calc}, g cm^{-3}	1.164
Crystal system	Triclinic	μ, cm^{-1}	2.19
Space group	$P\bar{1}$	h, k, l ranges	−8, 9; 0, 10; −19, 19
Crystal dimensions, mm	0.02 × 0.50 × 0.50	No. unique reflections	3736
Temp, °C	21	No. observed reflections	1992
a, Å	8.9759(23)	($I > 3.0\sigma$)	
b, Å	9.504(7)	No. of parameters	244
c, Å	18.294(6)	k value	0.000050
α, °	85.66(5)	Min./max. transmission	0.545/0.995
β, °	76.675(25)	Max. residual density, e Å^{-3}	0.630
γ, °	69.61(4)	Min. residual density, e Å^{-3}	−0.460
V, Å^3	1423.4(12)	R, R_w	0.061, 0.053
Z	2	gof	2.49

aminolysis reactions between M(NMe_2)$_4$ (M = Zr, Hf) and the ligand $C_5H_5CH_2CH_2CH_2N(H)Me$ were observed (3), producing bis-dimethylamido complexes of this ligand that could be subsequently converted to dichlorides. The generality and utility of this amine elimination strategy for catalyst synthesis is still being mapped out but results so far are clearly promising. For example, Jordan and co-workers (5) have shown that Brintzinger type *ansa*-metallocenes are accessible via this methodology and work from our laboratories indicates that the method is a viable alternative in cases where dilithio salts of ligands are inaccessible and (or) unstable (6).

Some of the problems outlined above were certainly encountered in the reported synthesis of [(Cp*SiNR)ScCl]$_n$, a precursor for hydrocarbyl derivatives with intriguing olefin chemistry (2*b*). We were interested in synthesizing derivatives of yttrium containing ligands of this general type but anticipated that the problems associated with using traditional methods of ligand attachment would be exacerbated in the chemistry of the larger metal. We thus sought a THF and salt-free route and have explored Teuben methodology as a possible alternative. As the chemistry described herein demonstrates, the amine elimination reaction is an effective means of attaching Cp*HSiNHR to yttrium using readily available Y[$N(SiMe_3)_2$]$_3$ (7) as the yttrium starting material.

Results and discussion

The reaction of Y[$N(SiMe_3)_2$]$_3$ and Cp*HSiNHR (Cp* = C_5Me_4; R = *t*-C_4H_9) occurs smoothly at 110°C in toluene (eq. [1]), producing the complex (Cp*SiNR)YN($SiMe_3$)$_2$, **1**, in 40% isolated yield. Although the reaction is quite clean and

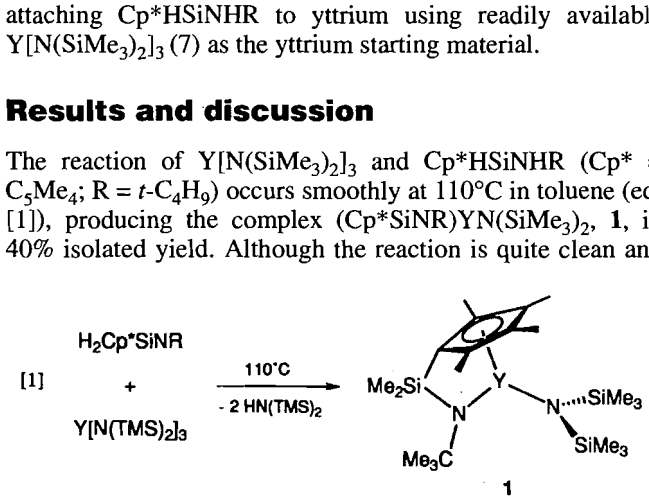

1

proceeds nearly quantitatively to **1**, the compound's high solubility in hexanes is responsible for the relatively poor isolated yield. To drive the reaction to completion, it was necessary to periodically remove the eliminated HN($SiMe_3$)$_2$ from the system by evacuating the vessel to dryness, reintroducing solvent, and continuing heating. Other homoleptic amides of yttrium (8) did not prove effective as starting materials for this reaction due primarily, we believe, to the oligomeric nature of such complexes containing smaller amide ligands, such as N(i-C_3H_7)$_2$. Thus, although a more volatile amine product HNR_2 may have been desirable, the N($SiMe_3$)$_2$ group proved to be the best compromise between volatility and steric bulk for this application.

Although the precise structure of Y[$N(SiMe_3)_2$]$_3$ has not been determined, closely related derivatives have been structurally characterized (9) and were found to deviate slightly from trigonal planarity. In all likelihood Y[$N(SiMe_3)_2$]$_3$ is isostructural. ^{1}H NMR experiments monitoring the reaction shown in eq. [1] suggested that it began at room temperature as evidenced by significant quantities of free HN($SiMe_3$)$_2$. Peaks attributable to **1** were not observed until heating commenced, driving the reaction forward. Thus a likely first step in the reaction of Y[$N(SiMe_3)_2$]$_3$ with Cp*HSiNHR involves approach of the sterically more accessible amine proton of the ligand along the more open vacant axial site towards the pyramidalized yttrium center. Amine–amine exchange anchors the Cp*SiNR ligand to the metal and aids in attachment of the cyclopentadienyl moiety to the metal via the chelate effect. That this reaction path is operative is supported by the observation that successful reaction between Cp*H and Y[$N(SiMe_3)_2$]$_3$ required a temperature of 120°C (10) before any reaction was observed.

Clear, white crystals of **1** suitable for X-ray analysis were grown from hexanes; an ORTEP diagram of the molecular structure of **1** is shown in Fig. 1. Crystal data are reported in Table 1, interatomic distances and angles are given in Table 2, and atomic parameters for the heavy atoms are given in Table 3.

The steric requirements of the ligand ensemble in **1** are sufficient to impose mononuclearity on the complex, which can be viewed as assuming a trigonal planar geometry at the yttrium center. The RMS deviation from the least-squares plane fitted to the Cp centroid (Cp_{cent}), Y, N(1), and N(2) is only 0.012 Å. The sum of the angles between yttrium and these vertices is 359.9° although each is necessarily distorted

Can. J. Chem. Downloaded from www.nrcresearchpress.com by 46.23.64.124 on 09/08/12
For personal use only.

Fig. 1. ORTEP diagram of (Cp*SiNR)YN($SiMe_3$)$_2$, **1**.

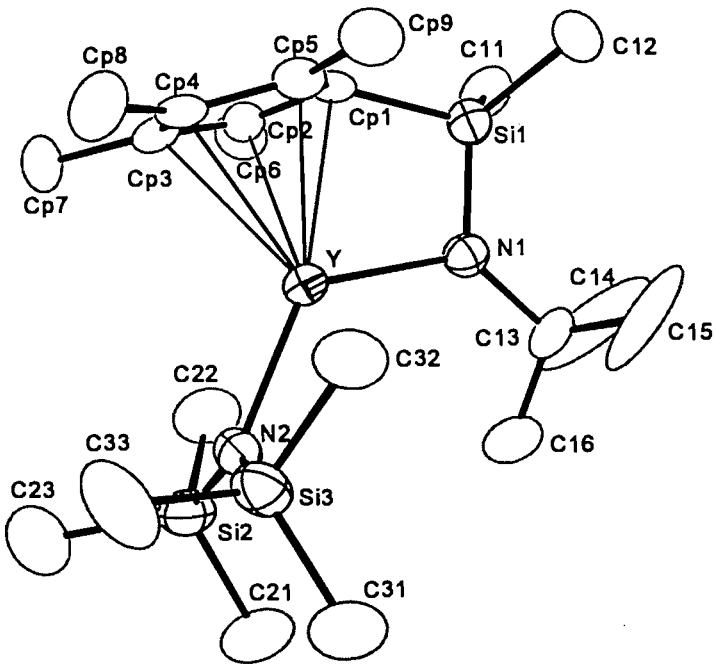

Table 2. Bond distances and angles for (Cp*SiNR)YN($SiMe_3$)$_2$, **1**.

Bond lengths (Å)					
Y—N1	2.184(7)	Si1—Cp1	1.872(10)	C13—C15	1.439(22)
Y—N2	2.255(8)	Si2—N2	1.678(8)	C13—C16	1.420(22)
Y—Cp1	2.535(9)	Si2—C21	1.869(12)	Cp1—Cp2	1.421(15)
Y—Cp2	2.575(10)	Si2—C22	1.900(13)	Cp1—Cp5	1.451(15)
Y—Cp3	2.661(10)	Si2—C23	1.876(13)	Cp2—Cp3	1.376(19)
Y—Cp4	2.665(10)	Si3—N2	1.670(8)	Cp2—Cp6	1.500(16)
Y—Cp5	2.570(10)	Si3—C31	1.846(12)	Cp3—Cp4	1.450(20)
Si1—N1	1.722(9)	Si3—C32	1.892(12)	Cp3—Cp7	1.541(15)
Si1—C11	1.880(10)	Si3—C33	1.857(13)	Cp4—Cp5	1.453(17)
Si1—C12	1.865(10)	N1—C13	1.484(14)	Cp4—Cp8	1.487(18)
C13—C14	1.416(22)	Cp5—Cp9	1.487(15)	Y—Cp_{cent}	2.300
Bond angles (deg)					
N1-Y-N2	125.6(3)	C21-Si2-C22	105.6(6)	C15-C13-C16	111.5(16)
N1-Y-Cp1	69.0(3)	C21-Si2-C23	109.3(6)	Y-Cp1-Si1	88.9(4)
N1-Y-Cp2	89.1(3)	C22-Si2-C23	107.4(6)	Si1-Cp1-Cp2	122.8(9)
N1-Y-Cp3	118.2(4)	N2-Si2-C31	114.1(5)	Si1-Cp1-Cp5	121.6(8)
N1-Y-Cp4	119.6(3)	N2-Si2-C32	106.0(4)	Cp2-Cp1-Cp5	106.9(9)
N1-Y-Cp5	88.4(3)	N2-Si2-C33	114.7(5)	Y-Cp2-Cp6	119.2(7)
N2-Y-Cp1	165.4(3)	C31-Si3-C32	108.5(5)	Cp1-Cp2-Cp3	108.8(11)
N2-Y-Cp2	138.6(3)	C31-Si3-C33	107.2(6)	Cp1-Cp2-Cp6	126.6(11)
N2-Y-Cp3	114.6(3)	C32-Si3-C33	105.8(6)	Cp3-Cp2-Cp6	124.4(10)
N2-Y-Cp4	112.0(3)	Y-N1-Si1	105.5(4)	Y-Cp3-Cp7	122.7(7)
N2-Y-Cp5	136.8(3)	Y-N1-C13	128.2(7)	Cp2-Cp3-Cp4	111.3(10)
N1-Si1-C11	117.8(5)	Si1-N1-C13	126.3(7)	Cp2-Cp3-Cp7	129.3(12)
N1-Si1-C12	116.3(4)	Y-N2-Si2	111.1(4)	Cp4-Cp3-Cp7	119.4(12)
N1-Si1-Cp1	96.6(4)	Y-N2-Si3	112.1(4)	Y-Cp4-Cp8	125.7(7)
C11-Si1-C12	101.3(5)	Si2-N2-Si3	136.7(5)	Cp3-Cp4-Cp5	104.1(10)
C11-Si1-Cp1	111.8(5)	N1-C13-C14	113.9(11)	Cp3-Cp4-Cp8	127.8(11)
C12-Si1-Cp1	113.7(5)	N1-C13-C15	111.6(11)	Cp5-Cp4-Cp8	127.7(12)
N2-Si2-C21	114.9(5)	N1-C13-C16	109.7(10)	Y-Cp5-Cp9	118.5(6)
N2-Si2-C22	106.1(4)	C14-C13-C15	102.9(17)	Cp1-Cp5-Cp4	108.9(10)
N2-Si2-C23	113.0(5)	C14-C13-C16	107.1(16)	Cp1-Cp5-Cp9	126.4(10)

Can. J. Chem. Downloaded from www.nrcresearchpress.com by 46.23.64.124 on 09/08/12
For personal use only.

Table 3. Atomic parameters x, y, z and B_{iso} for (Cp*SiNR)YN($SiMe_3$)$_2$, **1**.

Atom	x	y	z	B_{iso}[a]
Y	0.35022(13)	0.36164(13)	0.23158(6)	4.30(6)
Si1	0.2096(3)	0.6113(3)	0.12016(18)	4.67(19)
Si2	0.4671(4)	0.2976(4)	0.39059(19)	6.2(3)
Si3	0.2574(4)	0.1214(4)	0.35537(20)	5.99(23)
N1	0.1588(9)	0.5701(8)	0.2139(5)	4.1(5)
N2	0.3634(9)	0.2384(8)	0.3415(4)	4.7(5)
C11	0.2531(12)	0.7908(12)	0.0955(6)	6.6(7)
C12	0.0552(12)	0.6284(13)	0.0639(6)	7.5(8)
C13	0.0154(14)	0.6606(15)	0.2700(7)	6.0(8)
C14	−0.010(3)	0.8163(19)	0.2673(12)	21.5(18)
C15	−0.1341(19)	0.655(3)	0.2564(12)	22.2(20)
C16	0.0346(20)	0.6112(24)	0.3436(9)	19.9(15)
C21	0.3446(14)	0.3924(15)	0.4817(6)	9.3(10)
C22	0.5340(14)	0.4462(14)	0.3307(7)	8.6(9)
C23	0.6556(15)	0.1454(16)	0.4074(8)	10.7(11)
C31	0.0955(14)	0.1598(14)	0.4419(7)	8.8(9)
C32	0.1595(14)	0.1460(13)	0.2719(7)	6.9(7)
C33	0.3825(16)	−0.0806(14)	0.3562(8)	10.4(11)
Cp1	0.3979(12)	0.4424(12)	0.0954(5)	3.9(7)
Cp2	0.5446(13)	0.4259(15)	0.1177(6)	4.6(7)
Cp3	0.6256(13)	0.2757(17)	0.1272(6)	5.1(8)
Cp4	0.5332(15)	0.1850(15)	0.1146(5)	5.1(8)
Cp5	0.3896(13)	0.2930(12)	0.0935(5)	3.9(7)
Cp6	0.6096(12)	0.5486(12)	0.1249(6)	5.6(7)
Cp7	0.7936(12)	0.1982(13)	0.1465(6)	7.6(8)
Cp8	0.5843(14)	0.0184(14)	0.1132(7)	8.2(9)
Cp9	0.2600(13)	0.2535(12)	0.0711(6)	6.4(8)

[a] B_{iso} is the mean of the principal axes of the thermal ellipsoid.

from the ideal 120° due to the chelating nature of the Cp*SiNR ligand. Thus, the Cp_{cent}-Y-N(1) angle is 97.7°, while the bis-trimethylsilylamido ligand is placed so as to minimize steric repulsions between the $SiMe_3$ groups and the methyl groups of the Cp ring (Cp_{cent}-Y-N(2) = 136.6°) and the *tert*-butyl moiety (N(1)-Y-N(2) = 126.6(3)°).

The range of Cp carbon–Y distances of 2.535(9)–2.665(11) Å observed for **1** is on the short end of the "normal" range found in various other structurally characterized complexes of yttrium-containing cyclopentadienyl ligands (11, 12). The Y—N(1) distance of 2.184(7) Å in **1** is short in comparison to Y—N bond lengths in other yttrium silylamide complexes while the Y—N(2) length of 2.255(8) Å is closer to Y—N bond lengths in the two crystallographically distinct molecules in each of Cp*$_2$YN($SiMe_3$)$_2$ (11) (2.274(5) and 2.253(5) Å), and (R)-Me_2SiCp″[(−)-menthylCp]YN($SiMe_3$)$_2$ (12) (2.281(8) and 2.211(8) Å). The shortness of the Y—N bonds in these previously characterized complexes compared to predicted values of ≈2.36 Å (13) was rationalized on the basis of dative π-bonding between the nitrogen lone pair in the unhybridized p-orbital perpendicular to the plane bisecting the Cp donors and an empty orbital of b_1 symmetry that is slightly higher in energy than the in-plane trio of metallocene orbitals usually employed in ligand bonding (14). If one defines the Y–Cp_{cent} vector in **1** as the z-axis, strong π-bonding between Y and N(1) would be expected due to the availability of the metal-based d_{xy} orbital for interaction with the lone pair occupying the N p-orbital since the Cp_{cent}-Y–N(1) angle is only slightly greater than 90° (97.7°). Given the orientation of the N($SiMe_3$)$_2$ ligand with respect to the above-defined coordinate, the nature of the π interaction between Y and N(2) is more difficult to rationalize on a qualitative basis but is clearly significant, as evidenced by the Y—N(2) bond length and the trigonal planar geometry about N(2).

Formally **1** has a maximum electron count of 14 electrons, counting the two amido ligands as contributing four electrons each. The yttrium center should therefore be quite electron deficient. One mechanism by which complexes of this type alleviate electron deficiency is via β-SiC agostic interactions (15, 16). Usually, such interactions skew the N($SiMe_3$)$_2$ ligand in such a way as to bend one of the $SiMe_3$ groups toward the metal center, affording a Ln-N-βSi angle of between 105° and 109° and bringing one of the β-C atoms into close proximity of the metal center (typically 2.88–2.98 Å) (11, 12). As such, the symmetrical metrical parameters observed in the N($SiMe_3$)$_2$ ligand in **1** argue against the presence of any agostic interactions. On the other hand, the C_s symmetry of **1** makes possible a degenerate interaction between the electron-deficient yttrium center and *both* $SiMe_3$ groups. In support of this notion, the $SiMe_3$ groups on the N($SiMe_3$)$_2$ ligand in **1** are eclipsed such that both C(22) and C(32) come into close prox-

Can. J. Chem. Downloaded from www.nrcresearchpress.com by 46.23.64.124 on 09/08/12
For personal use only.

imity of the yttrium center (Y···C(22) = 3.03 Å; Y···C(32) = 3.05 Å). Also, the two Y-N(2)-Si angles of 111.1(4)°, for Si(2), and 112.1(4)°, for Si(3), are smaller than expected, while the Si(2)-N(2)-Si(3) angle is 136.7(5)°. These values are significantly different from corresponding data (118.4(6), 121.7(6), and 119.9(7)°, respectively) found in a more electron-rich yttrium silylamide containing a 4,13-diaza-18-crown-6 ligand (17) in which the $SiMe_3$ groups assume a more staggered geometry.

Alkylation of **1** with $LiCH_2SiMe_3$ proceeded with selective displacement of the $N(SiMe_3)_2$ ligand (as evidenced by the loss of $LiN(SiMe_3)_2$, ^1H NMR = 0.112 ppm in C_6D_6) but the alkyl complex presumed to be product was not isolable due to thermal instability (eq. [2]). The nature of the organometallic decomposition product(s) was not clear but the presence of ≈1

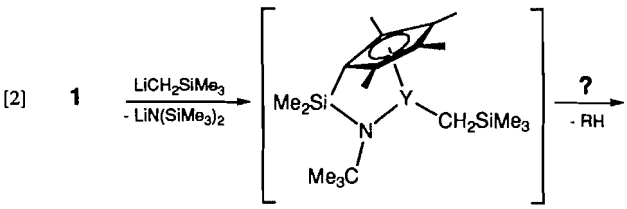

equivalent of RH in the product mixture was consistent with a product mixture resulting from σ-bond metathesis with ligand or solvent C—H(D) bonds. This is not entirely unexpected since the resulting alkyl complex would be a formally 12-electron complex and therefore extremely electron deficient and reactive. Previously reported scandium congeners were also highly reactive but could be stabilized by PMe_3 (2). This strategy was not successful in this chemistry; alkylation of **1** in the presence of excess PMe_3 led to an intractable mixture from which no well-defined products were isolated.

The amine elimination method is an effective means of attaching Cp-amido type ligands to yttrium. However, at least with the specific ligand employed here, the resulting amide complexes are less amenable to subsequent conversion to catalytically more important alkyl derivatives than their group-4 counterparts. This is, however, likely a function of the Cp*SiNR ligand employed, which does not appear to be sterically bulky enough to prevent facile σ-bond metathesis decomposition pathways in the desired alkyl complexes.

Experimental section

General

General laboratory procedures have been described in detail elsewhere (6). Materials were purchased from Aldrich and used as received. Cp*HSiNHR was prepared using the literature procedure (2*b*) while $Y[N(SiMe_3)_2]_3$ was synthesized by a slightly modified procedure as follows: 1.953 g of YCl_3 (10.0 mmol) and 5.030 g of $LiN(SiMe_3)_2$ (30.0 mmol) were combined with 50 mL of toluene at −78°C. The mixture was allowed to warm to room temperature first, then stirred at 90°C for 3 days. Toluene was removed and the residue was extracted with 50 mL of hexane. The extract was reduced in volume to about 10 mL and cooled to −78°C to let the product crystallize. The crystalline product was collected on a frit, washed with cold hexane, and dried under vacuum; 5.30 g of $Y[N(SiMe_3)_2]_3$ (9.30 mmol, 93.0%) was obtained. ^1H NMR (C_6D_6, ppm): 0.28.

Synthesis of (Cp*SiNR)YN(SiMe$_3$)$_2$, 1

Cp*HSiNHR (0.800 g, 3.18 mmol) was added to a solution of $Y[N(SiMe_3)_2]_3$ (1.600 g, 2.80 mmol) in 10 mL of toluene. The mixture was stirred at 110°C for 4 days. The reaction was pumped to dryness every 24 h to remove the free amine ($HN(SiMe_3)_2$) released from the reaction after which the residue was redissolved in toluene and heating was resumed. After the $Y[N(SiMe_3)_2]_3$ had been totally consumed, toluene was removed and the crude product purified by crystallization from hexane at −78°C; 0.555 g of pure product (1.11 mmol, 40%) was obtained. ^1H NMR (C_6D_6, ppm): 2.10 (6H, CpCH_3), 1.97 (6H, CpCH_3), 1.28 (9H, NC(CH_3)$_3$), 0.72 (6H, Si(CH_3)$_2$), 0.04 (18H, NSi(CH_3)$_3$); $^{13}C\{^1H\}$ NMR(C_6D_6, ppm): 128.4, 124.8 (*C*CH_3), 110.7 (Si-*C*), 53.2 (N*C*(CH_3)$_3$), 36.5 (NC(*C*H_3)$_3$), 14.1, 11.3 (C*C*H_3), 8.2 (Si(*C*H_3)$_2$), 3.0 (NSi(*C*H_3)$_3$)). Anal. calcd. for $C_{21}H_{45}N_2Si_3Y$: C 50.57, H 9.09, N 5.62; found: C 50.50, H 8.47, N 5.16.

Attempted alkylation of (Cp*SiNR)YN(SiMe$_3$)$_2$, 1

(Cp*SiNR)YN($SiMe_3$)$_2$ (100 mg, 0.201 mmol) and $LiCH_2SiMe_3$ (19 mg, 0.202 mmol) were placed in a 50 mL round-bottomed flask. Hexanes (≈20 mL) were condensed into the flask at −78°C. The mixture was allowed to warm to room temperature and stirred for 1 h. Solvent was removed under vacuum to leave a pale-yellow residue. ^1H NMR spectroscopy indicated the presence of $LiN(SiMe_3)_2$ and a complex set of signals for yttrium-containing products. When carried out in an NMR tube (20 mg **1**, 4 mg $LiCH_2SiMe_3$, C_6D_6) almost 1 equivalent of $SiMe_4$ was observed. When the preparative scale reaction described above was performed in the presence of an excess of PMe_3 (≈1 mL), similar results obtained.

X-ray structure of (Cp*SiNR)YN(SiMe$_3$)$_2$, 1

Single crystals were mounted in thin-walled glass capillaries and placed on an Enraf Nonius CAD-4 diffractometer. Unit-cell dimensions were determined via least-squares refinement of the setting angles of 24 high-angle reflections and intensity data were collected using the ω–2θ scan mode. Data were corrected for Lorentz, polarization, and absorption effects but not for extinction. Pertinent data collection and structure refinement parameters are presented in Table 1. The structure was solved using direct methods and all non-hydrogen atoms were refined with anisotropic thermal parameters. Hydrogen atoms were located via difference Fourier map inspection (D_{C-H} = 1.08 Å), given isotropic temperature factors based upon the atom to which they are bonded, and fixed during least-squares refinement. A weighting scheme based upon counting statistics was used with the weight modifier k in kF_o^2 being determined via evaluation of variation in the standard reflections that were collected during the course of data collection. Neutral atom scattering factors were taken from *International tables for X-ray crystallography* (18). Values of R and R_w are given by $R = (F_o - F_c)/EF_o$ and $R_w = [E(w(F_o - F_c))^2/E(wF_o^2)]^{1/2}$. All crystallographic calculations were conducted with the PC version of the NRCVAX program package (19) locally implemented on an IBM compatible 80486 computer. Anisotropic thermal param-

eters and hydrogen atom parameters are available as supplementary material.[2]

Acknowledgments

W.E.P. thanks the Institute for Chemical Science and Technology and the Research Partnerships Office (Industrially Oriented Research Program) of the Natural Sciences and Engineering Research Council of Canada for financial support of this work.

References

1. (*a*) J.C. Stevens, F.J. Timmers, D.R. Wilson, G.F. Schmidt, P.N. Nickias, R.K. Rosen, G.W. Knight, and S.Y. Lai. European Patent Application EP-416-815-A2, March 13, 1991 (Dow); (*b*) J.A. Canich. PCT Application WO 91/04257, April 4, 1991 (Exxon).
2. (*a*) P.J. Shapiro, E. Bunel, W.P. Schaefer, and J.E. Bercaw. Organometallics, **9**, 867 (1990); (*b*) P.J. Shapiro, W.D. Cotter, W.P. Schaefer, J.A. Labinger, and J.E. Bercaw. J. Am. Chem. Soc. **116**, 4623 (1994).
3. A.K. Hughes, A. Meetsma, and J.H. Teuben. Organometallics, **12**, 1936 (1993).
4. G. Chandra and M.F. Lappert. J. Chem. Soc. A, 1940 (1968).
5. G.M. Diamond, S. Rodewald, and R.F. Jordan. Organometallics, **14**, 5 (1995).
6. W.E Piers, Y. Mu, L.R. MacGillivray, and M.J. Zaworotko. Polyhedron, **14**, 1 (1995).
7. D.C. Bradley, J.G. Ghotra, and F.A. Hart. J. Chem. Soc. Dalton Trans. 1021 (1973).
8. M.F. Lappert, P.P. Power, A.R. Sanger, and R.C. Srivastava. Metal and metalloid amides. John Wiley and Sons, New York. 1980.
9. (*a*) M = Sc, Eu: J.S. Ghotra, M.B. Hursthouse, and A.J. Welch. J. Chem. Soc. Chem. Commun. 669 (1973); (*b*) M = Yb: P.G. Eller, D.C. Bradley, M.B. Hursthouse, and D.W. Meek. Coord. Chem. Rev. **24**, 1 (1977); (*c*) M = Nd: D.H. Templeton, R.A. Andersen, and A. Zalkin. Inorg. Chem. **17**, 2317 (1978).
10. M. Booij, N.H. Kiers, H.J. Heeres, and J.H. Teuben. J. Organomet. Chem. **364**, 79 (1989).
11. (*a*) K.H. den Haan, J.L. de Boer, J.H. Teuben, A.L. Spek, B. Kojić-Prodić, G.R. Hays, and R. Huis. Organometallics, **5**, 1726 (1986), and references therein.
12. M.A. Giardello, V.P. Conticello, L. Brard, M. Sabat, A.L. Rheingold, C.L. Stern, and T.J. Marks. J. Am. Chem. Soc. **116**, 10212 (1994).
13. R.D. Shannon. Acta Crystallogr. Sect. A: Cryst. Phys. Diffr. Theor. Gen. Crystallogr. **A32**, 751 (1976).
14. J.W. Lauher and R. Hoffmann. J. Am. Chem. Soc. **98**, 1729 (1976).
15. (*a*) K. Tatsumi and A. Nakamura. J. Am. Chem. Soc. **109**, 3195 (1987); (*b*) B.E. Bursten and A. Fang. Inorg. Chim. Acta, **110**, 153 (1985); (*c*) N. Koga and K. Morokuma. J. Am. Chem. Soc. **110**, 108 (1988).
16. (*a*) C.J. Schaverien. Adv. Organomet. Chem. **36**, 283 (1994); (*b*) C.J. Schaverien and G.J. Nesbitt. J. Chem. Soc. Dalton Trans. 157 (1992).
17. L. Lee, D.J. Berg, and G.W. Bushnell. Inorg. Chem. **33**, 5302 (1994).
18. International tables for X-ray crystallography. Vol. IV. Kynoch Press, Birmingham, England. 1974.
19. E.J. Gabe, Y. Le Page, J.-P. Charland, F.L. Lee, and P.S. White. J. Appl. Crystallogr. **22**, 384 (1989).

[2] Copies of the supplementary material may be purchased from: The Depository of Unpublished Data, Document Delivery, CISTI, National Research Council Canada, Ottawa, Canada K1A 0R6. The table of hydrogen atom parameters has also been deposited with the Cambridge Crystallographic Data Centre, and can be obtained on request from The Director, Cambridge Crystallographic Data Centre, University Chemical Laboratory, 12 Union Road, Cambridge, CB2 1EZ, U.K.

Can. J. Chem. Downloaded from www.nrcresearchpress.com by 46.23.64.124 on 09/08/12
For personal use only.

A cycloaddition approach to tricyclic taxoid skeletons

Yee-Fung Lu and Alex G. Fallis

Abstract: A cycloaddition approach to the functionalized tricyclo[9.3.1.$0^{3,8}$]pentadecene skeleton contained in Taxol® is described. The cyclohexenone **13** was converted as illustrated to the nitrile-aldehyde **24** to which the diene and acetylenic side chains were attached by sequential nucleophilic additions. Removal of the trimethylsilyl protecting group and Dess–Martin oxidation afforded the triene **35**. Microwave-assisted thermal cyclization stereoselectively generated the tricyclic ketone **36** whose structure was further established by conversion to the aromatic system **37** upon treatment with 2,3-dichloro-5,6-dicyano-1,4-benzoquinone (DDQ). An epoxidation sequence was developed to introduce the epimeric C13 alcohol **47** as required for this cycloaddition strategy. Alternatively, an allylic oxidation (CrO_3, 3,5-dimethylpyrazole) afforded the C13 ketone **49**.

Key words: Taxol®, Diels–Alder, synthesis, diterpene, alkaloid.

Résumé : On décrit une approche, impliquant une cycloaddition, au squelette du tricyclo[3.3.1.$0^{3,8}$]pentadécène fonctionnalisé contenu dans le Taxol®. Tel que représenté dans le diagramme 1, on transforme la cyclohexénone **13** en nitrile-aldéhyde **24** auquel on attache les chaînes latérales diénique et acétylénique par une séquence d'additions nucléophiles. Après enlèvement du groupe protecteur triméthylsilyle et oxydation de Dess–Martin, on a obtenu le triène **35**. Une cyclisation thermique sous l'effet de micro-ondes a fourni stéréosélectivement la cétone **36** dont la structure a été reconfirmée par conversion en système aromatique **37** par traitement avec de la 2,3-dichloro-5,6-dicyano-1,4-benzoquinone (DDQ). On a développé une séquence d'époxydations (diagramme 2) qui permet d'introduire l'alcool épimère en C_{13} (**47**) qui est requis par cette stratégie de cycloaddition. D'une manière alternative, une oxydation allylique (CrO_3, 3,5-diméthylpyrazole) a fourni la cétone en C_{13}, **49**.

Mots clés : Taxol®, Diels–Alder, synthèse, diterphène, alcaloïde.

[Traduit par la rédaction]

Introduction

The potent antitumor agent paclitaxel (Taxol,® **1**) was approved for the treatment of ovarian and breast cancer in 1993. This was more than 20 years after its structure was initially reported (1), and more than 30 years after its cytotoxicity was first detected. The medicinal potential for the taxoid family is further illustrated by the fact that a semi-synthetic analog, docetaxel (Taxotere,® **2**), is in final clinical trials and also

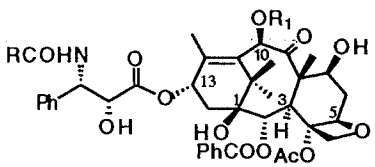

1 Taxol® R = Ph, R_1 = Ac
2 Taxotere® R = tBuO, R_1 = H

shows considerable therapeutic promise (2) (approved in Canada in September 1995). These compounds belong to a new class of antitumor drugs that interfere with the normal microtubule–tubulin cascade prior to cell division (3). This novel mode of action, plus the significant synthetic challenge presented by the sterically congested multicyclic structure, has stimulated worldwide interest in these molecules (4). Recently two groups reported total syntheses of taxol itself (5, 6). In spite of this success much remains to be investigated and over the next decade it is likely that simpler analogues with a better therapeutic profile will be synthesized and become useful pharmaceutical products. They will thus follow the path from natural products to medicine established earlier for penicillins, tetracyclines, etc., a path that depends upon improved knowledge of structure–activity relationships, the development of efficient synthetic and (or) semi-synthetic routes to the functionalized tricyclo[9.3.1.$0^{3,8}$]pentadecene nucleus, and the development of medicinally interesting analogs that possess a better therapeutic profile than paclitaxel itself.

Thus, synthetic interest int his area continues unabated and several recent reviews summarize the progress that is being achieved and the diversity of synthetic approaches that are under development (4). In this paper we describe an intramolecular Diels–Alder approach that proceeds in the left-to-right direction (ring A to BC). Commencing with a ring A cyclohexene building block, the sequence relies on a cycloaddition reaction to construct the B and C rings simultaneously. This strategy is hlghly convergent, and leads to the functionalized

Received June 5, 1995.

Y.-F. Lu and A.G. Fallis.[1] Ottawa–Carleton Chemistry Institute, Department of Chemistry, University of Ottawa, 10 Marie Curie, Ottawa, ON K1N 6N5, Canada.

[1] Author to whom correspondence may be addressed. Telephone: (613) 562-5728. Fax: (613) 562-5170. E-mail: afallis@oreo.chem.uottawa.ca

Can. J. Chem. Downloaded from www.nrcresearchpress.com by 46.23.64.124 on 09/08/12
For personal use only.

Can. J. Chem. Downloaded from www.nrcresearchpress.com by 46.23.64.124 on 09/08/12
For personal use only.

Scheme 1. Convergent ring C Diels–Alder approach.

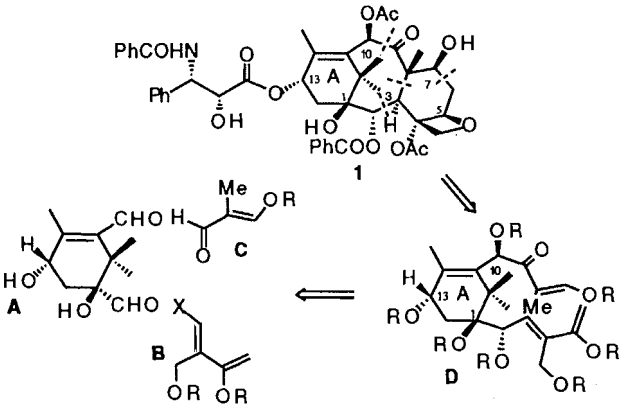

tricyclo[9.3.1.$0^{3,8}$]pentadecene skeleton in which the C2 epimer controls the adduct stereochemistry.

Synthetic strategy

In a retrosynthetic sense removal of the ring D oxetane followed by a double disconnection between C6—C7 and C3—C8 in ring C suggests a precursor related to the tetraene **D** (Scheme 1). In principle this intermediate could contain the majority of the Taxol® oxygen substituents, although in practice the use of less substituted systems may be more prudent. Construction of **D** may be envisaged in a direct manner from further disconnections between C2—C3 and C9—C10. In total, this leads to a highly convergent approach to the taxane nucleus from a suitably functionalized ring A synthon in the form of a masked dialdehyde synthon related to **A**, followed by attachment of the lower diene and upper dienophile units **B** and **C**, respectively. Subsequently, intramolecular Diels–Alder cycloaddition could afford the carbocyclic nucleus. However, several additional aspects must also be considered for this approach to have a reasonable chance of success.

Other research groups have also examined the potential utility of an intramolecular [4+2] cycloaddition to generate the tricyclic skeleton. In independent studies, Bonnert and Jenkins (7) as well as Shea and co-workers (8) generated the A ring with the bridgehead double bond in place, as illustrated in general terms in Scheme 2. Unfortunately, a recent study reported that the *gem* dimethyl bridge in the adduct does not have the correct orientation in a more highly functionalized example (i.e., epimeric at C1) (9), and a related bis-normethyl system behaved similarly (10). The C ring had been constructed previously from a bicyclo[2.2.2]octene precursor by Sakan and Craven (11). It was assumed that the rigid geometry imparted by this bicyclic framework was required to hold the diene in an axial orientation. This allows the close proximity of the reactive components in order to achieve the proper alignment for the cyclization transition state and overcome the entropic difficulties associated with a conformationally mobile ring system such as a cyclohexene. In addition, the formation of sterically congested cyclooctanes via [4+2] cycloadditions is known to be difficult (12). However, it was not clear whether the one-carbon bridge between the C13 center and the C17 methyl group is essential for a successful intramolecular cyclization in this series.

The conformer population in cyclohexenes is known to vary with the substitution pattern (13). Thus, the potential 1,3-diax-

Scheme 2. Other representative Diels–Alder approaches.

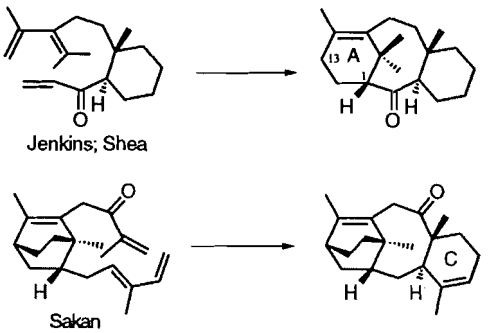

Scheme 3. Conformational considerations.

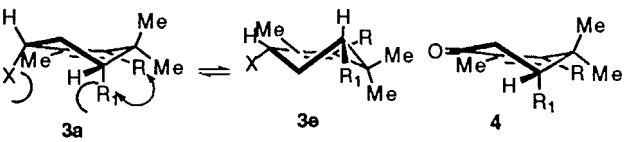

Scheme 4. Ring C construction with acetylenic dienophile.

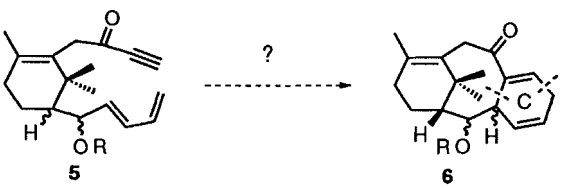

ial interaction (C—X versus C—R_1) in **3a** (Scheme 3) must be overcome if the reactive components represented by R and R_1 are to cyclize, since the equatorial conformer **3e** does not allow the two side chains to interact significantly. However, this limitation should not cause undue difficulty provided the reactive conformer makes up a reasonable percentage of the equilibrium mixture at the temperature selected. In addition, it will help if the cyclization step is sufficiently rapid that few collisions are required. When X = H the 1,3-interaction should be relatively minor and this will disappear entirely if a cyclohexenone such as **4** is employed. Nevertheless, there is a limitation to this approach for the total synthesis. The natural α orientation of the C13 ester side chain will increase the nonbonded interactions in the required conformer **3a** (X = OR). Thus for the Diels–Alder step to proceed, either the unnatural C13 epimer or the C13 ketone may have to be employed and the synthon **A** modified accordingly (Scheme 1). Consistent with this analysis, molecular mechanics calculations[2] indicated that 1,2,3,3,4-pentamethylcyclohexene preferred a conformation related to **3a** in which a slight twist minimized any 1,3-methyl-hydrogen interference. Therefore, additional ring constructions should not be required to access the transition state geometry for ring C directly when the diene and dienophile are attached to a cyclohexene. To further encourage the cycloaddition, the rotational parameters normally encountered with olefinic partners were minimized by selecting an acetylenic dienophile as illustrated in **5** (Scheme 4). Inherent in the transformation **5** to adduct **6** are several additional questions that require solution. These include the π-facial selectivity of

[2] Analysis by PCMODEL (Serena Software, Box 3076, Bloomington, IN 47402-3076, U.S.A.).

Can. J. Chem. Downloaded from www.nrcresearchpress.com by 46.23.64.124 on 09/08/12
For personal use only.

Chart 1. Synthetic sequence to **36** and **37**.

(a) DIBAL, C_6H_6, 0°C, 2 h, 21°C, 98%; (b) DDQ, dioxane, 25°C, 24 h, 92%; (c) TBSCI, imidazole, DMF, 24 h, 98%; (d) MeMgBr, CuI (cat), Et_2O, 0°C, 0.5 h; $CH(OMe)_3$, $BF_3{\cdot}OEt_2$, −78–0°C, 59%; (e) MeMgBr, CuI (cat), ether, Et_3N, TMSCl, 1 h 0°C, 4 h 21°C, 71%; (f) $(MeO)_3CH$, $TiCl_4$, CH_2Cl_2, −78–21°C, 1 h, 55%; (g) MeLi, Et_2O, 0°C, 0.5 h; or MeMgBr, toluene/Et_2O, 0–21°C, 30 min, 95%; (h) MeLi, Et_2O, HMPA, MeI, 0–21°C, 16 h, 94%; (i) $CH_2{=}CHCH_3$, TMSCl, NaI, CH_2Cl_2, 21°C, 5 min, CH_3ONa, CH_3OH, 65°C, 30 min, 70% or 15% aq. H_2SO_4, SiO_2, CH_2Cl_2, 2 min, 21°C, 96%; (j) $CH_2{=}CHCH_3$, TMSCl, NaI, CH_2Cl_2, 21°C, 5 min, CH_3ONa, CH_3OH, 65°C, 30 min, CH_3ONa, CH_3OH, 65°C, $NaBH_4$, $CeCl_3$, 21°C, 70%; (k) DIBAL, toluene, −78–21°C, 1.5 h, 21°C, 99%; (l) Ph_3PBr_2, Et_3N, CH_2Cl_2, −78°C, 1 h; then NaCN, methyl pyrrolidinone, 21°C, 1.5 h, 75%; (m) *n*-Bu_4NF, THF, 21°C, 4 h, 98%; (n) DMSO, $(COCl)_2$, Et_3N, CH_2Cl_2, −78–21°C, 94%; (o) *n*-BuLi, THF, −78°C, 0.5 h, 96%; (p) $(i\text{-}Pr)_2EtN$, MOMCl, CH_2Cl_2, 90%; (q) DIBAL, CH_2Cl_2, −78–0°C; 1–2 h, H_3O^+, 70–91%; (r) TBSCl, DMF, DMAP, 21°C, 3 d, 81%; (s) *n*-BuLi, thiophene, THF, −78°C, 15 min, **24**, THF, −78°C, 30 min, 69%; TBSCl, $AgClO_4$, pyridine, CH_3CN, 21°C, 16 h, 72%; (t) HCCTMS, *n*-BuLi, THF, −78°C, 1 h, 95%; (u) HCCTMS, *n*-BuLi, THF, −78°C, 1 h, 0°C, 1 h, 93%; $(COCl)_2$, DMSO, CH_2Cl_2, −78°C, 15 min, Et_3N, 21°C, 30 min, 38%; (v) KOH, MeOH, CH_2Cl_2, 21°C, 99%; (w) Dess–Martin periodinane, CH_2Cl_2, 21°C, 55%; (x) microwave oven, sealed tube, toluene, 10 h, 34%; (y) DDQ, benzene, 80°C, 2 h, 69%; (z) *n*-BuLi, 2-bromopropene, THF, −78–21°C, 30 min, 72%; $(COCl)_2$, DMSO, CH_2Cl_2, −78°C, 15 min, Et_3N, 21°C, 30 min, 88%.

Scheme 5. Transition states for C_2 epimers.

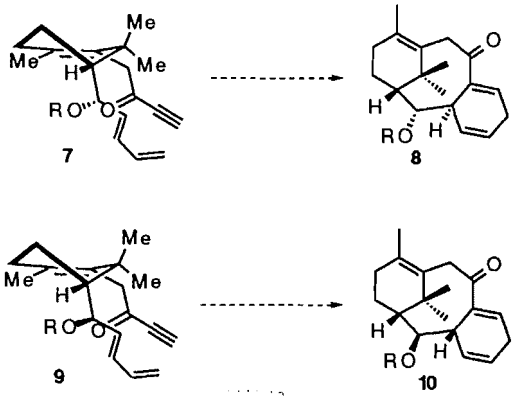

the cycloaddition and the influence of the C2 substituent on the transition states. These considerations are illustrated in Scheme 5 for the transition states of the C2 epimers **7** and **9**. This suggests that the orientation of this C2 group will determine the facial preference of the cycloaddition and hence the resultant stereochemistry of C3 in the adduct. The validity of these analyses have been demonstrated below by the synthesis of the tricyclic taxane nucleus **36** and the related aromatic system **37** (preliminary communication, ref. 14).

Results and discussion

To ascertain the practicality of this plan the carbonyl groups in Hagemann's ester (**11**) were reduced with DIBAL (diisobutylaluminum hydride) in benzene (Chart 1), the allylic alcohol oxidized with DDQ (2,3-dichloro-5,6-dicyano-1,4-benzoquinone), and the remaining primary alcohol protected as a *tert*-butyldimethylsilyl ether to afford the cyclohexenone **13** (15). Treatment of cyclohexenone **13** with methylmagnesium bromide in the presence of cuprous iodide, followed by the addition of methylorthoformate mediated by boron trifluoride etherate, afforded the keto-acetal **14** in 59% yield (Chart 1). Alternatively this compound was prepared in a two-step

Can. J. Chem. Downloaded from www.nrcresearchpress.com by 46.23.64.124 on 09/08/12
For personal use only.

Fig. 1. A view of 1-(2-thiophenyl)methyl-2-cyanomethyl-1,3,3-trimethylcyclohexene (**30**).

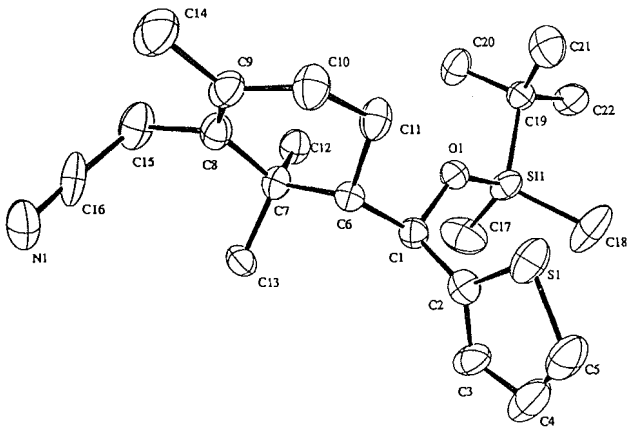

sequence via the intermediacy of the trimethylsilyl enol ether **17** and methylorthoformate in the presence of titanium tetrachloride. Addition of methyllithium to the carbonyl group in **14** allowed preparation of the tertiary alcohol **15**, or it could be alkylated directly in the presence of added HMPA (hexamethylphosphoramide) to give the trimethoxy ether **16**. Trimethylsilyliodide generated in situ (16) released the aldehyde function (i.e., **19**) so that direct treatment with base led to elimination of methoxide ion and the formation of the cyclohexene aldehyde **20** in 70% overall yield from **16**.

Reduction of aldehyde **20** ($NaBH_4$, $CeCl_3$, 70%) provided the alcohol **21** accompanied by a small amount of the less substituted endocyclic isomer (ratio 12:1). Alternatively, this alcohol could be prepared directly from **16** by sequential treatment with trimethylsilyl chloride, sodium iodide, sodium methoxide, and sodium borohydride – cerium trichloride. Chain extension to the nitrile **22** was accomplished by cyanide displacement (NaCN, methyl pyrrolidinone, 75%) of the primary bromide generated from the alcohol upon treatment with Ph_3PBr_2, Et_3N in CH_2Cl_2 at −78°C for 1 h. Removal of the silyl protecting group with fluoride ion (n-Bu_4NF, THF, 21°C, 3 h, 98%) followed by Swern oxidation (DMSO, $(COCl)_2$, Et_3N, CH_2Cl_2, −78°C, 94%) afforded the aldehyde **24**. The required nucleophilic diene unit was prepared by transmetallation of E-1,3-(1-tributylstannyl)butadiene (17) with n-BuLi and added to the aldehyde **24** (THF, −78°C, 0.5 h, 96%). From direct analysis of the resulting secondary alcohol (6:1 diastereomer ratio) it was not possible to determine which of the isomers corresponded to the Taxol® stereochemistry at C2. The stereochemistry was determined by condensation of 2-lithiothiophene with aldehyde **24**, followed by silylation with tert-butyldimethylsilyl chloride, to give the crystalline derivative **30**. X-ray determination showed the major isomer to have the opposite stereochemistry (C1—C2) to Taxol® as shown (Fig. 1). Alcohol **25** was assigned the same relative stereochemistry by analogy and comparison of spectral data and, as outlined, this isomer was used for subsequent experiments.

The secondary alcohol in **25** was protected as either a methoxymethyl ether (MOMCl, $(iPr)_2EtN$, CH_2Cl_2, 90%) or, alternatively a *tert*-butyldimethylsilyl ether to afford **26** and **27**, respectively. Diisobutylaluminum hydride reduction of the nitrile group in these compounds provided the corresponding aldehydes **28 and 29**. In a parallel, but independent, manner, these aldehydes were treated with lithium trimethylsilylacetylide (HCCTMS, n-BuLi, THF, −78°C, 95%) and then transformed into the desired ketones by oxidation either before or after removal of the trimethylsilyl group. These apparently straightforward operations were surprisingly challenging. Removal of the trimethylsilyl group from the acetylenic ketones proved very difficult in contrast to the ease with which this bond cleavage was affected on the acetylenic alcohol. Thus it was important to remove the trimethylsilyl group (KOH, MeOH, CH_2Cl_2, 21°C, 99%) at the alcohol stage on compound **33**. Only the Dass–Martin periodinane oxidation method (18), of several examined, generated the required ketone **35** in reasonable yield (55%). Attempted cycloadditions with ketones **31**, **32**, and the ketone derived from **33** all failed under the various conditions examined.

Fortunately, cyclization of ketone **35** could be affected by heating a 0.05 M toluene solution containing 1% mol-equiv. hydroquinone in a sealed glass tube in a modified microwave oven (19) for 10 h to afford the tricyclic system **36** stereoselectively in yields of 30–40%. This major adduct arose via the preferred transition state in which the nonbonded interactions were minimized due to the alignment of the dienophile under the triene remote from the MOM substituent as illustrated in **35**. This pattern of π-facial selectivity was consistent with related intermolecular cycloadditions involving acetylenes and acylic dienes (20) and implies that with the "natural" C2 stereochemistry the preferred geometry will resemble **7** and should provide the relative stereochemistry illustrated in **8** as required for Taxol® itself. The structural assignment of the adduct **36** was further established on the basis of its ^1H NMR spectrum, in which the C3 proton appeared at δ 2.95 as a doublet of doublets (J = 5.6, 9.6 Hz) due to coupling with the adjacent vinylic C4 and secondary C2 hydrogens.[3] Confirmation

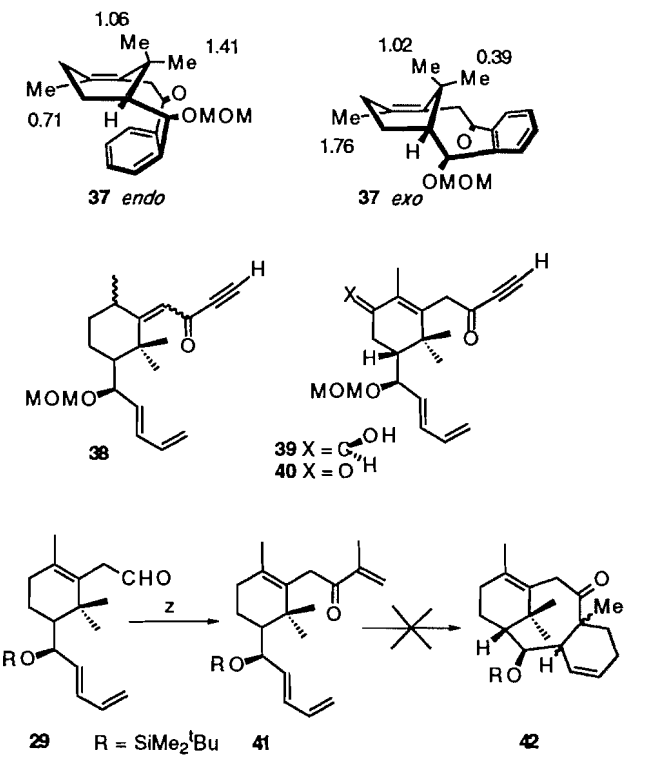

[3] In addition to adduct **36**, the minor adduct epimeric at C3 was also formed (5–7%). This arose from the approach of the addends from the opposite face.

Can. J. Chem. Downloaded from www.nrcresearchpress.com by 46.23.64.124 on 09/08/12
For personal use only.

of the tricyclo[9.3.1.$0^{3,8}$]pentadecatriene skeleton was provided by the conversion of **36**, upon treatment with DDQ in refluxing benzene, to the aromatic ketone **37**. In keeping with related literature examples, this material existed as a mixture of exo and endo isomers (~1:1) (21) in which the vinyl methyl signal appeared at 0.71 (endo) or 1.76 (exo) depending upon the orientation of the benzene ring.

Unfortunately, it was not possible to catalyze the cycloaddition with Lewis acids, due to the ease with which the cyclohexene double bond migrated into conjugation with the acetylenic ketone and afforded the complex mixture of isomers represented by **38**. These components accounted for some of the uncyclized material in the thermal reaction. It is anticipated that, with the C13 ketone in place as in ketone **43** (Taxol® numbering), the cyclohexenone will help suppress this tendency for bond migration, flatten the ring, and reduce the axial interaction, and should lead to improved yields. Alternatively, the epi-C13 alcohol **39** is a potential Diels–Alder precursor, and a route to a suitable ring A building block is described below.

The direct introduction of the C8-methyl was also examined. Thus vinyl anion addition to aldehyde **29**, followed by Swern oxidation, afforded **41**. Unfortunately, this material could not be induced to undergo an intramolecular cycloaddition. The failure of the attempted cyclizations with **32** and **41** appears to be a consequence of the large protecting group attached to the C2 alcohol. Thus nonbonded interactions between this substituent and the germinal methyls inhibit attainment of the requisite geometry for cycloaddition. It remains to be established whether adducts of type **42** can be generated if different protecting groups and stereochemical combinations are employed.

An important feature of taxol itself is the C13 oxygen side chain. The requisite oxygen may be installed directly by allylic oxidation as illustrated by the **22** to **49** conversion (Chart 2). It is of interest that in spite of modest yields the reaction is clean and yields are 65–70% based on the recovered starting material. In addition, no oxygen was introduced at the position corresponding to C10 in Taxol® (6, 22, 23). A suitable synthon for the epimeric C13 alcohol (**47**) was prepared from the acetal **15**. Dehydration of this material was affected with thionyl chloride and pyridine to provide **43** and the major isomer **44** with the endocyclic double bond (1:3). This is a consequence of the relative stereochemistry in **15** and the favorable trans diaxial elimination that arises from the preferred conformation **50**. Thus the axial proton adjacent to the germinal methyl groups (H_a) is in a sterically encumbered environment and elimination from the other side (H_b) or the methyl group is more facile. The major isomer **44** was treated with acid to hydrolyze the acetal to give **45**, and oxidation of **45** with dioxirane provided the epoxide **46**, with the oxirane trans to the bulky silyl ether. Treatment with sodium methoxide in refluxing methanol installed the double bond and generated the secondary alcohol **47**, which was characterized as the silyl derivative **48**. This provided a direct route to epi-C13 precursors as required, based on the stereochemical analysis in the introduction. Stork and co-workers (24) have developed a different preparation of epimeric C13 ring A alcohol intermediates.

In conclusion, a carefully designed [4+2] cycloaddition strategy with an acetylenic dienophile can be employed to generate the substituted taxane nucleus directly, with good stereochemical control, in a convergent manner from a functionalized

Chart 2. Oxygen introduction at C13.
(a) $SOCl_2$, pyridine, CH_2Cl_2, 0–21°C, 0.5 h, 80%; (b) $(HOOC)_2$, H_2O, HOAc (cat), 100°C, 2 h, 85%; (c) Me_2CO_2, $Me_2C{=}O$, −4–21°C, 1 h, 77%; (d) NaOMe, MeOH, 65°C, 3 h, 66%; (e) TBSCl, imidazole, 21°C, 16 h, 91%; (f) CrO_3, 3,5-dimethylpyrazole, CH_2Cl_2, −4–21°C, 16 h, 31%.
Legend: DIBAL = diisobutylaluminium hydride; DDQ = 2,3-dichloro-5,6-dicyanoquinone; DMF = dimethylformamide; TBSCl = *tert*-butyldimethylsilylchloride

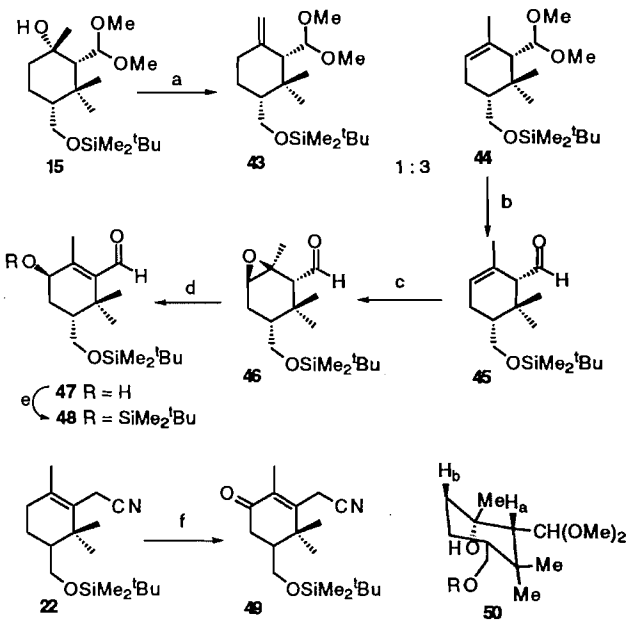

cyclohexene substrate. We are currently extending these results toward the total synthesis of Taxol® and the preparation of therapeutically promising analogs, using more highly oxygenated precursors, in which the C13 ketone and "natural" C2 epimer are expected to facilitate and control the cyclization.

Experimental section

Melting points were determined in capillary tubes with a Thomas–Hoover Unit-Melt apparatus and are uncorrected. Infrared (IR) spectra were recorded on a Perkin–Elmer 783 spectrometer or a Bomem MB 100 FTIR spectrometer. Proton magnetic resonance spectra (^{1}H NMR) were measured at 60 MHz with a Varian spectrometer or at 200 MHz with a Varian Gemini spectrometer or at 300 MHz with a Varian XL-300 spectrometer in deuterochloroform unless otherwise stated. Carbon magnetic resonance spectra (^{13}C NMR) were measured at 50 MHz (Varian Gemini) or at 75 MHz (Varian XL-300). Chemical shifts are reported in ppm downfield from tetramethylsilane (δ scale). The multiplicity, number of protons, and coupling constants are indicated in parentheses. Mass spectra (MS) were determined on a VG micromass 7070 HS instrument using an ionization energy of 70 eV. Gas chromatograph – mass spectral (GC–MS) analyses were determined on a Hewlett–Packard 5890 Series II gas chromatograph – 5971A Mass Selective Detector equipped with a 12.5 m capillary column (0.2 mm i.d.) coated with cross-linked dimethylsilicone (0.33 μm). Elemental analyses were conducted by M-H-W Laboratories, Phoenix, Ariz. Analytical thin-layer chromatography (TLC) employed commer-

Can. J. Chem. Downloaded from www.nrcresearchpress.com by 46.23.64.124 on 09/08/12
For personal use only.

cial aluminum sheets precoated (0.2 mm layer thickness) with silica gel 60 F_{254} (E. Merck). Flash column chromatography using E. Merck silica gel 60 (70–230 or 230–400 mesh) was employed for all column chromatography. The purity of all title compounds was judged to be >95% as determined by a combination of GC—MS, ^{1}H NMR, and ^{13}C NMR analyses.

Petroleum ether refers to a fraction with boiling range 30–60°C. Anhydrous diethyl ether (ether) and diisopropylamine were obtained by distillation from $LiAlH_4$ and anhydrous tetrahydrofuran (THF) from potassium–benzophenone. Absolute methanol and ethanol were dried by distillation from magnesium. Dry benzene, dimethylformamide (DMF), and carbon tetrachloride (CCl_4) were prepared by distillation from phosphorus pentoxide. Anhydrous hexamethylphosphoramide (HMPA) was obtained by distillation from calcium hydride, and acetone was dried by distillation from anhydrous K_2CO_3. Dioxane was distilled from $LiAlH_4$ and stored over Linde type 4A molecular sieves. CuI (99.99%, Aldrich) was purified by repeated Soxhlet extraction with THF and dried (80°C) under vacuum for 7 h. Solutions in organic solvents were dried over anhydrous magnesium sulfate or anhydrous sodium sulfate and stripped of solvents with a Büchi rotatory evaporator connected to a water aspirator. Unless otherwise stated, all reactions were conducted under at atmosphere of dry nitrogen in flame-dried flasks equipped with a magnetic stirring bar and rubber septa.

X-ray measurements were made on a Rigaku diffractometer with Mo Kα radiation at −158°C using the ω–2θ technique to a maximum 2θ value of 46.9. Cell constants and an orientation matrix for data collection were obtained from least-squares refinement using the setting angles of 25 reflections in the range $40 < 2\theta < 47$ corresponding to an orthorombic cell for compound **30** ($C_{22}H_{35}NOSSi$) with dimensions $a = 22.055$, $b = 9.031$, $c = 23.593$ Å. For $Z = 8$ and FW = 389.67, the calculated density is 1.102 g/cm^3. Based on the systematic absences, the space group was *Pbcn*. The data (3479 reflections) were collected for Lorentz and polarization effects (25). The structure was solved by direct methods all atoms refined except hydrogen. The hydrogen atoms were calculated by assuming a distance of 1.07 Å. The final cycle of full-matrix least-squares refinement was based on 1852 observed reflections ($I > 2.5\ \sigma(I)$) and 236 variable parameters using weights based on counting statistics. The maximum and minimum peaks on the final differences Fourier map were 0.55 and −0.47 e/Å^3, respectively. All calculations were performed using the NRCVAX crystallographic software package (26).[4]

4-Hydroxymethyl-3-methyl-2-cyclohexene-1-ol

Diisobutylaluminium hydride (1 M solution in toluene, Aldirch, 16.5 mL, 16.5 mmol) was added dropwise to a cold (0°C) solution of Hagemann's ester **11** (1.0 g, 5.5 mmol, Aldrich) in benzene (5 mL) and the mixture stirred at 0°C for 2 h, followed by a further hour at 21°C. The aluminum salts were decomposed at 0°C by dropwise addition of excess methanol (20 mL). The resulting white precipitate was removed by filtration and washed several times with hot methanol. The combined filtrate and washings were evaporated to give a thick oil plus a gel-like precipitate that was removed by a second filtration. The crude product was chromatographed (acetone/petroleum ether; 1:1) to afford the diol (770 mg, 98%). In subsequent experiments the initial product was used directly. IR (neat): 3350, 1660 cm^{-1}; ^{1}H NMR (200 MHz) δ: 5.65 (m, 1H), 4.16 (br s, 1H), 3.79 (m, 2H), 1.79 (s, 3H), 2.15 (m, 1H), 1.5–2 (m, 6H). ^{13}C NMR (50.3 MHz) δ: 136.8, 127.7, 65.3, 63.2, 41.4, 30.6, 29.3, 21.4. HRMS calcd. for $C_8H_{12}O$ ($M^+ - H_2O$): 124.0888; found: 124.0890.

4-Hydroxymethyl-3-methyl-2-cyclohexen-1-one (12)

The diol above (3.80 g, 26.8 mmol) was dissolved in dry dioxane (10 mL) and a dioxane solution of dichlorodicyanoquinone (7.92 g, 34.9 mmol, Aldrich) was added dropwise by syringe. The reaction was stirred at 21°C overnight (23 h, reaction complete by TLC). The reaction was concentrated, diluted with ether, filtered through Celite, and washed several times with ether until the washings were colourless. Concentration of the crude filtrate and chromatography (20% acetone – petroleum ether) on alumina (basic or neutral) gave the ketone **12** (3.5 g, 92%). IR (neat): 3300, 1665 cm^{-1}; ^{1}H NMR (200 MHz) δ: 5.92 (s, 1H), 3.79 (m, 2H), 1.98 (s, 3H); ^{13}C (50.3 MHz) δ: 199.5, 162.1, 128.5, 70.0, 42.1, 34.2, 24.9, 22.7. Anal. calcd. for $C_8H_{12}O_2$: C 68.54, H 8.62; found: C 67.91, H 8.70.

4-(*tert*-Butyldimethylsilyloxy)methyl-3-methyl-2-cyclohexen-1-one (13)

The alcohol **12** (0.97 g, 6.8 mmol) was dissolved in DMF (2 mL), imidazole (1.16 g, 17.0 mmol) and *tert*-butyldimethylsilyl chloride (1.23 g, 8.18 mmol, Aldrich) were added, and the mixture was stirred overnight (23 h) at 21°C. The reaction was diluted with ether and the combined organic extracts were washed with small portions of water (2 × 2 mL) and brine, dried, filtered, and concentrated. Chromatography (ethyl acetate/petroleum ether; 1:20) gave **13** (1.7 g, 98%). IR (neat): 1675 cm^{-1}; ^{1}H NMR (200 MHz) δ: 0.02 (s, 6H), 0.85 (s, 9H), 2.02 (m, 2H), 2.39 (m, 3H), 3.72 (d, 2H, $J = 5.5$ Hz), 5.87 (s, 1H); ^{13}C NMR (50.3 MHz) δ: −5,3 (2C), 17.8, 22.7, 25.1, 25.5 (3C), 34,3, 42.7, 63.3, 128.1, 162.5, 199.4. HRMS calcd. for $C_{10}H_{17}O_2Si$ ($M^+ - C_4H_9$): 197.0998; found: 197.1013. Anal. calcd. for $C_{14}H_{26}O_2Si$: C 66.08, H 10.3; found: C 65.91, H 9.51.

4-(*tert*-Butyldimethylsilyloxy)methyl-3,3-dimethyl-2-formyl(dimethylacetal)cyclohexanone (14)

A solution of methyl magnesium bromide (5.14 mL, 7.71 mmol, 1.5 M) in toluene – direthyl ether was added to a cold (0°C), stirred suspension of cuprous iodide (100 mg, 0.52 mmol) in dry diethyl ether (50 mL). After the reaction mixture had been stirred at 0°C for 10 min, a solution of the enone **13** (1.31 g, 5.14 mmol) in dry diethyl ether (2 mL) was added dropwise. The resulting light yellow mixture was stirred at 0°C for 30 min and then cooled to −78°C. Trimethyl orthoformate (5.62 mL, 51.4 mmol) and boron trifluoride etherate

[4] Tables of atomic parameters, anisotropic temperature factors, bond lengths and angles, and torsion angles have been deposited and can be purchased from: The Depository of Unpublished Data, Document Delivery, CISTI, National Research Council Canada, Ottawa, Canada K1A 0R6. The tables of atomic parameters and bond lengths and angles have also been deposited with the Cambridge Crystallographic Data Centre, and can be obtained on request from The Director, Cambridge Crystallographic Data Centre, University Chemical Laboratory, 12 Union Road, Cambridge, CB2 1EZ, U.K.

Can. J. Chem. Downloaded from www.nrcresearchpress.com by 46.23.64.124 on 09/08/12
For personal use only.

(3.16 mL, 25.7 mmol) were syringed sequentially into the cold reaction mixture. After stirring for 5 min at −78°C, the solution was warmed to 0°C for 2 h. Saturated ammonium chloride solution was added and the mixture was extracted with diethyl ether. The combined ether extracts were washed with brine, dried, and concentrated. The residual oil was chromatographed (petroleum ether/diethyl ether; 3:1) to afford 1.05 g (59%) of the ketal **14**. IR (neat): 2970, 1720, 1475, 1120, 880, 780 cm^{-1}; ^1H NMR (200 MHz) δ: 0.02 (s, 6H), 0.78 (s, 3H), 0.86 (s, 9H), 1.04 (s, 3H), 1.45–1.70 (m, 1H), 2.00–2.60 (m, 5H), 3.27 (s, 3H), 3.29 (s, 3H), 3.42 (t, 1H, J = 10 Hz), 3.85 (dd, 1H, J = 4, 10 Hz), 4.71 (d, 1H, J = 7 Hz); ^{13}C NMR (50.3 MHz) δ: −5.7 (2C), 17.9, 22.9, 25.6 (3C), 25.9, 26.0, 38.1, 40.0, 43.2, 52.6, 53.1, 63.3, 64.7, 101.9, 210.6; HRMS calcd. for $C_{14}H_{27}O_4Si$ ($M^+ - C_4H_9$): 287.1679; found: 287.1680. Anal. calcd. for $C_{18}H_{36}O_4Si$: C 62.75, H 10.53; found: C 62.83, H 10.43.

Minor products from this reaction were
*4-(*tert*-Butyldimethylsilyloxy)methyl-3,3-dimethylcyclohexanone*: IR (neat): 2960, 1720, 1475, 1260, 1105, 840, 780 cm^{-1}; ^1H NMR (200 MHz) δ: 0.03 (s, 6 H), 0.81 (s, 3H), 0.87 (s, 9H), 1.05 (s, 3H), 1.55–1.84 (m, 2H), 2.02–2.41 (m, 5H), 3.45 (dd, 1H. J = 7.8, 10 Hz), 3.82 (dd, 1H, J = 3.8, 10 Hz); ^{13}C NMR δ: 212.0, 63.3, 55.1, 47.0, 40.0, 37.2, 30.3, 25.6, 25.4, 22.0, 18.3, −5.7; HRMS calcd. for $C_{15}H_{30}O_2Si$ ($M^+ - C_4H_9$): 213.1310; found: 213.1266.
*4-(*tert*-Butyldimethylsilyloxy)methyl-1-(dimethoxy)oxy-3,3-dimethylcyclohex-1-ene* (**18**): IR (neat): 2960, 1600, 1480, 1100, 840, 780 cm^{-1}; ^1H NMR (200 MHx) δ: 0.03 (s, 6H), 0.82 (s, 3H), 0.88 (s, 9H), 1.06 (s, 3H), 1.35–1.50 (m, 2H), 1.80–1.95 (m, 1H), 2.05–2.15 (m, 2H), 3.34 (s and overlapping dd, 7H), 3.74 (dd, 1H, J = 4, 10 Hz), 4.62 (s, 1H), 5.35 (s, 1H).

Alternative preparation of 14 via 4-(*tert*-butyldimethylsilyloxy)methyl-3,3-dimethyl-1-trimethylsilyloxycyclohex-1-ene (17)

A solution of methyl magnesium bromide (0.48 mL, 0.072 mmol, 1.5 M) in toluene – diethyl ether was added to a cold (0°C), stirred suspension of cuprous iodide (0.01 g), in dry diethyl ether (4 mL). After stirring the reaction for 10 min at 0°C, a solution of enone **13** (0.122 g, 0.48 mmol) in dry diethyl ether (1 mL) was added dropwise. After 30 min at 0°C, triethyl amine (0.20 mL, 1.43 mmol) and trimethylsilyl chloride (0.12 mL, 0.95 mmol) were added sequentially. The reaction was stirred for 1 h at 0°C, warmed to 21°C, and stirring was continued for a further 4 h. A few drops of aqueous saturated ammonium chloride were added and the solution filtered through a short column of sand (1 g). The filtrate was concentrated, chromatographed on Florisil (petroleum ether/ether; 30:1), and the eluent concentrated to afford the enol silyl ether **17** (0.117 g, 71%). IR (neat): 2930, 1250 cm^{-1}; ^1H NMR (200 MHz) δ: 0.01 (s, 6H), 0.14 (s, 9H), 0.78 (s, 3H), 0.86 (s, 9H), 1.02 (s, 3H), 1.37–1.42 (m, 2H), 1.83–1.92 (m, 1H), 1.93–1.96 (m, 2H), 3.30 (dd, 1H, J = 8.7, 9.2 Hz), 3.72 (dd, 1H, J = 3.8, 9.9 Hz), 4.54 (br s, 1H); HRMS calcd. for $C_{18}H_{38}O_2Si_2$ (M^+ − Me): 327.2186; found: 327.2184.

Trimethyl orthoformate (0.78 mL, 7.10 mmol) and titanium tetrachloride (0.20 mL, 1.80 mmol) were syringed sequentially into a cold (−78°C), stirred solution of enolsilyl ether (0.229 g, 0.670 mmol) in dry dichloromethane (7 mL). The reaction mixture was stirred at 0°C for 1 h. Saturated ammonium chloride solution was added and the mixture was extracted thoroughly with diethyl ether. The combined ether extracts were washed (saturated $NaHCO_3$ solution, brine), dried, and concentrated. The residual oil was chromatographed (petroleum ether/diethyl ether; 3:1) to afford 0.126 g (55%) of the ketal **14**.

1-Hydroxy-2-formyl(dimethylacetal)1,3,3-trimethyl-4-*tert*-butyldimethylsilyloxycyclohexane (15)

A 1.5 M solution of methylmagnesium bromide (2.0 mL, 3.0 mmol) in toluene – diethyl ether was added dropwise to a cold (0°C), stirred solution of the ketone **14** (0.713 g, 2.07 mmol) in dry diethyl ether (10 mL). The resulting mixture was stirred at 0°C for 10 min and then warmed to 21°C for 30 min. Saturated aqueous ammonium chloride solution was added and the mixture was extracted thoroughly with diethyl ether. The combined ether extracts were washed with brine and dried. Removal of the solvent afforded 0.708 g (95%) of the alcohol **15**. IR (neat): 3560, 2960, 1090, 840, 780 cm^{-1}; ^1H NMR (200 MHz) δ: 0.01 (s, 6H), 0.86 (s, 9H), 1.00 (s, 3H), 1.15 (s, 3H), 1.29 (s, 3H), 1.30–1.65 (m, 4H), 1.90–2.10 (m, 2H), 3.34 (s, 3H), 3.47 (s, 3H), 3.55–3.75 (m, 2H), 3.98 (br s, 1H), 4.43 (s, 1H); ^{13}C NMR (50.3 MHz) δ: −5.8, −5.7, 17.9, 19.6, 25.7 (3C), 26.2, 28.4, 31.6, 34.6, 35.9, 47.4, 51.3, 55.8, 56.7, 62.2, 72.0, 109.6. Anal. calcd. for $C_{19}H_{40}O_4Si$: C 63.28, H 11.18; found: C 63.34, H 11.1.

1-Methoxy-2-formyl(dimethylacetal)-1,3,3-trimethyl-4-*tert*-butyldimethylsilyloxycyclohexane (16)

A solution of methyllithium (7.90 mL, 11.1 mmol, 1.4 M) in diethyl ether was added dropwise to a cold (0°C), stirred solution of the acetal **14** (2.50 g, 7.26 mmol) in dry diethyl ether (35 mL). After the reaction mixture has been stirred at 0°C for 30 min, hexamethylphosphoramide (2.52 mL, 14.5 mmol) and methyl iodide (1.80 mL, 28.9 mmol) were added sequentially. The resulting mixture was stirred at 0°C for 1 h and warmed to room temperature overnight (16 h). Water was added and the mixture was extracted thoroughly with diethyl ether. The combined ether extracts were washed (saturated sodium bicarbonate, water, and brine), dried, and concentrated. The residual oil was chromatographed (petroleum ether/diethyl ether; 9:1) to afford 2.07 g (76%) of the trimethoxy compound **16** and 0.418 g (16%) of the alcohol **15** (see below). IR (neat): 2950, 1470, 1260, 1200, 1080, 840, 780 cm^{-1}; ^1H NMR (200 MHz) δ: 0.00 (s, 6H), 0.85 (s, 9H), 1.00 (s, 3H), 1.18 (s, 3H), 1.19 (s, 3H), 1.30–1.80 (m, 6H), 3.10 (s, 3H), 3.32 (s, 3H), 3.36 (s, 3H), 3.54 (t, 1H, J = 10 Hz), 3.73 (dd, 1H, J = 10, 5 Hz), 4.65 (d, 1H, J = 4 Hz); ^{13}C NMR (50.3 MHz) δ: −5.7, −5.6, 18.0, 18.5, 25.0, 25.7 (3C), 26.4, 28.7, 28.9, 35.5, 47.8, 48.7, 54.7, 56.1, 61.2, 75.8, 108.4. Anal. calcd. for $C_{20}H_{42}O_4Si$: C 64.12, H 11.30; found: C 64.19, H 11.47.

Methyllithium (9.34 mL, 13.08 mmol) was added to a solution of **15** (3.0 g, 8.7 mmol) in ether (50 mL) at 0°C. HMPA (3.03 mL, 17.44 mmol) was added, followed by MeI (1.08 mL, 17.4 mmol), the reaction mixture was allowed to warm to 22°C, and stirring was continued overnight. The reaction was quenched with water and washed several times with saturated aqueous NH_4Cl solution, dried, and concentrated. Chromatography (5% Et_2O – petroleum ether) gave **16** in 94% yield.

Can. J. Chem. Downloaded from www.nrcresearchpress.com by 46.23.64.124 on 09/08/12
For personal use only.

2-Formyl-1,3,3-trimethyl-4-*tert*-butyldimethylsilyloxymethycyclohex-2-ene (20)

Method I

Propylene was bubbled through a solution of **16** (650 mg, 1.7 mmol) in CH_2Cl_2 (3 mL) at 21°C. NaI (279 mg, 1.86 mmol) was added, followed by trimethylsilyl chloride (0.24 mL, 1.86 mmol), and stirring was continued for 5 min. The reaction was quenched with water, and washed with water, aqueous 6% $Na_2S_2O_4$, and brine. The organic layer was concentrated to give the product **19**, which was directly dissolved in MeOH, and NaOMe (91.3 mg, 1.69 mmol) added. The reaction was heated under reflux for 30 min. The mixture was concentrated, ether added, the ether extracts washed with water, brine, and dried. Concentration followed by chromatography (5% Et_2O – petroleum ether) gave **20** (350 mg, 70% from **16**).

Method II

An aqueous 15% H_2SO_4 solution (1.2 mL) was added with continuous stirring to a suspension of silica gel (70–230 mesh, 12 g) in CH_2Cl_2 (15 mL). After 3 min, the aqueous phase disappeared, a solution of **16** (1.1 g, 2.9 mmol) in CH_2Cl_2 (2 mL) was added, and stirring continued at 21°C for 2 min during which time the reaction was completed. $NaHCO_3$ (0.1 g) was then added and stirring continued for 5 min, followed by filtration of the reaction mixture through a small plug of $MgSO_4$. Concentration gave the aldehyde **19**, which was used directly for the next step. NaOMe (140 mg, 2.6 mmol) was added to a solution of the aldehyde (876 mg, 2.6 mL) in MeOH (10 mL). The mixture was refluxed for 8 h, concentrated, ether added, and the ether extracts washed with water and brine, and dried. Concentration and chromatography (5% Et_2O – petroleum ether) gave the aldehyde **20** (846 mg) in 96% yield. IR (neat): 2921, 1698 cm^{-1}; ^1H NMR (200 MHz) δ: 0.01 (s, 6H), 0.85 (s, 9H), 1.01 (s, 3H), 1.30 (s, 3H), 1.36–1.20 (m, 2H), 1.84–1.87 (m, 1H), 2.02 (s, 3H), 2.10–2.20 (m, 2H), 3.33 (dd, 1H, J = 8.75, 10 Hz), 3.83 (dd, 1H, J = 3.65, 10 Hz), 10.62 (s, 1H); ^{13}C NMR δ: 192.3 (conjugated CHO), 156.3, 140.4, 62.9, 47.8, 35.3, 34.6, 26.3, 25.9, 21.4, 20.7, 19.4, 18.0, −5.3; HRMS calcd. for $C_{13}H_{23}O_2Si$ ($M^+ - C_4H_9$): 239.1467; found: 239.1466.

Method III

Hydrogen fluoride (1 mL, 50% solution) was added to a stirred solution of hydroxy-acetal **15** (0.40 g, 1.11 mmol) in acetonitrile (10 mL). The resulting mixture was refluxed for 15 min in a preheated oil bath. The solution was cooled and a saturated aqueous solution of sodium bicarbonate was added. Acetonitrile was removed under reduced pressure and the aqueous solution was extracted with dichloromethane. The combined organic extracts were washed (water, brine) and dried. Concentration afforded the aldehyde-alcohol. *tert*-Butyldimethylsilyl chloride (0.200 g, 1.33 mmol) was added to a stirred solution of the aldehyde-alcohol and imidazole (0.190 g, 2.79 mmol) in dry dichloromethane (10 mL). The resulting solution was stirred at 21°C for 16 h. Aqueous ammonium chloride solution (10%) was added and the mixture was extracted thoroughly with dichloromethane. The combined organic extracts were washed (water, brine), and dried, and concentrated. The residual oil was chromatographed (petroleum ether/diethyl ether; 9:1) to afford 0.15 g (45%) of the aldehyde **20**.

2-Hydroxymethyl-1,3,3-trimethyl-4-*tert*-butyldimethylsilyloxymethyclohex-1-ene (21)

Treatment of the acetal **16** (1.34 g, 3.56 mmol) as described in Method I above; dry dichloromethane (35 mL), trimethylsilyl chloride (0.68 mL, 5.35 mmol), sodium iodide (0.80 g, 5.33 mmol), followed by sodium methoxide (0.19 g, 3.52 mmol) and methanol (10 mL) afforded the crude aldehyde **20**. Cerium(III) chloride heptahydrate (1.33 g, 3.57 mmol) and sodium borohydride (0.135 g, 3.56 mmol) were added slowly and the mixture was stirred at 21°C for 1 h. Water was added and the methanol was removed from the mixture under reduced pressure. Diethyl ether and 5% hydrochloric acid were added and the resulting solution extracted with diethyl ether. The combined ether extracts were washed (water, brine), dried, and concentrated. This material consisted of two alcohols (12:1 ratio), which were separated by chromatography (petroleum ether/diethyl ether; 9:1) to afford 0.745 g (70%) of alcohol **21** as a white solid and 0.070 g (6.5%) of the positional isomer (data below), as a colorless oil. **21**plainc: mp 53.5–55°C; IR ($CHCl_3$): 3620, 2960, 1260, 1090, 840 cm^{-1}; ^1H NMR (200 MHz) δ: 0.01 (s, 6H), 0.84 (s, 3H), 0.86 (s, 9H), 1.11 (s, 3H), 1.20–1.55 (m, 3H), 1.73 (s, 3H), 1.75–1.90 (m, 1H), 1.95–2.05 (m, 2H), 3.33 (dd, 1H, J = 10, 8.5 Hz), 3.75 (dd, 1H, J = 10, 3.9 Hz), 4.05 (d, 1H, J = 12 Hz), 4.13 (d, 1H, J = 12 Hz); ^{13}C NMR (75 MHz) δ: −5.3 (2C), 18.3, 19.7, 21.5, 22.3, 25.9 (3C), 27.1, 31.6, 36.3, 47.0, 58.8, 63.8, 133.9, 137.8. Anal. calcd. for $C_{17}H_{34}O_2Si$: C 68.39, H 11.48; found: C 68.50, H 11.26.

Alternatively, diisobutylaluminum hydride (1 M solution in toluene, 53.6 μL, 0.08 mmol) was added to a solution of the aldehyde **20** (20 mg, 0.07 mmol) in toluene (1.5 mL) at −78°C and the mixture stirred for 1.5 h at −78°C. The reaction was warmed to 0°C and MeOH was added until a white precipitate formed. The crude product was filtered through Celite and washed free of remaining product with hot MeOH. Concentration gave **21** (20 mg, 99%).

*1,5,5-Trimethyl-4-*tert*-butyldimethylsiloxy)methyl-6-hydroxymethylcyclohexene*: IR (neat): 3382, 2917, 1086, 843, 776 cm^{-1}; ^1H NMR (200 MHz) δ: 0.00 (s, 6H), 0.79 (s, 3H), 0.85 (s, 9H), 1.00–1.05 (m, 1H), 1.04 (s, 3H), 1.15–1.25 (m, 1H), 1.50–1.60 (m, 1H), 1.70 (s, 3H), 1.75–2.00 (m, 1H), 2.10–2.28 (m, 1H), 3.30–3.55 (m, 2H), 3.65–3.80 (m, 2H), 5.50–5.65 (m, 1H); HRMS calcd. for $C_{13}H_{23}OSi$($M^+ - C_4H_9$): 224.1463; found: 224.1463.

2-Cyanomethyl-2,3,3-trimethyl-4-*tert*-butyldimethylsilyloxymethylcyclohexene (22)

Bromine (0.011 mL, 0.218 mmol) was added dropwise to a stirred solution of triphenylphosphine (0.57 g, 0.217 mmol) in dry methylene chloride (2 mL). Triethylamine (0.11 mL, 0.789 mmol) was added to the reaction mixture. After stirring at 21°C for 10 min, the resulting light yellow solution was cooled to −78°C. A solution of the alcohol **21** (59.3 mg, 0.198 mmol) in methylene chloride (1 mL) was added dropwise and the reaction mixture was allowed to stir for 1 h at −78°C. Petroleum ether was added and the precipitate was removed via filtration under reduced pressure. Concentration of the petroleum ether fractions precipitated additional triphenylphosphine oxide. Subsequent filtration and concentration provided a quantitative yield of the allylic bromide. IR (neat):

Can. J. Chem. Downloaded from www.nrcresearchpress.com by 46.23.64.124 on 09/08/12
For personal use only.

2917, 1466, 1253, 1093, 844, 776 cm^{-1}; ^1H NMR (200 MHz) δ: 0.02 (s, 6H), 0.85 (s, 9H), 0.91 (s, 3H), 1.19 (s, 3H), 1.19 (s, 3H), 1.30–1.50 (m, 2H), 1.73 (s, 3H), 1.75–1.85 (m, 1H), 2.00–2.10 (m, 2H), 3.33 (t, J = 8 Hz, 1H), 3.75 (dd, J = 8, 6 Hz, 1H), 4.01 (d, J = 10 Hz, 1H), 4.09 (d, J = 10 Hz, 1H). Sodium cyanide (19.0 mg, 0.397 mmol) was added to a solution of this allylic bromide in dry *N*-methyl pyrrolidinone (2 mL). The reaction mixture was stirred at 21°C for 1.5 h, pour into water, and extracted with diethyl ether. The combined ether extracts were washed (brine), dried, and concentrated. The crude product was chromatographed (petroleum ether/diethyl ether; 9:1) to afford 45.0 mg (75%) of the nitrile **22** IR (neat): 2960, 2260, 1550, 1260, 1100, 840, 780 cm^{-1}; ^1H NMR (200 MHz) δ: 0.02 (s, 6H), 0.84 (s, 3H), 0.86 (s, 9H), 1.12 (s, 3H), 1.30–1.50 (m, 2H), 1.70 (s, 3H), 1.71–1.85 (m, 1H), 1.95–2.05 (m, 2H), 2.94 (br s, 2H), 3.35 (dd, 1H, J = 10, 8.2 Hz), 3.73 (dd, 1H, J = 10, 4.2 Hz); ^{13}C NMR (50.3 MHz) δ: −5.6 (2C), 15.8, 18.0, 20.0, 21.2, 21.3, 25.7 (3C), 26.4, 31.5, 37.0, 46.5, 63.5, 119.2, 127.5, 134.0; HRMS calcd. for $C_{14}H_{24}ONSi$ ($M^+ - C_4H_9$): 250.1627; found: 250.1654.

2-Cyanomethyl-1,3,3-trimethyl-4-hydroxycyclohexene (23)

A solution of compound **22** (1.00 g, 3.25 mmol) in dry THF (20 mL) was cooled to 0°C and a 1 M solution of tetra-*n*-butyl ammonium fluoride (6.50 mL, 6.50 mmol) and added dropwise. The mixture was warmed to 21°C for 4 h. Water was added and the resultant mixture was extracted with diethyl ether. The combined ether extracts were washed (brine, water), dried, and concentrated. The residual oil was chromatographed (petroleum ether/diethyl ether; 3:1) to afford 0.620 g (98%) of the alcohol **23**. IR (neat): 3405, 2924, 2246, 1465, 1030 cm^{-1}; ^1H NMR (200 MHz) δ: 0.85 (s, 3H), 1.13 (s, 3H), 1.30–1.55 (m, 3H), 1.71 (s, 3H), 1.80–1.92 (m, 1H), 2.00–2.10 (m, 2H), 2.95 (s, 2H), 3.39 (dd, 1H, J = 11, 8 Hz), 3.83 (dd, 1H, J = 11, 4 Hz); addition of D_2) simplified multiplet at δ 1.30–1.55; ^{13}C NMR (50.3 MHz) δ: 15.8, 19.9, 21.2 (2C), 26.3, 31.4, 36.9, 46.8, 63.3, 119.1, 127.4, 134.0; HRMS calcd. for $C_{12}H_{19}ON$: 193.1467; found: 193.1466. Anal. calcd. for $C_{12}H_{19}ON$: C 74.57, H 9.91; found: C 74.16, H 9.71.

2-Cyanomethyl-4-formyl-1,3,3-trimethylcyclohexene (24)

Oxalyl chloride (0.310 mL, 3.55 mmol) was added to a cold (−78°C), stirred solution of dry dimethyl sulfoxide (0.250 mL, 3.52 mmol) in dry dichloromethane (25 mL). The reaction mixture was stirred at −78°C for 15 min, a solution of **23** (620 mg, 3.21 mmol) in dry dichloromethane (2 mL) was added dropwise, and the resulting mixture stirred for 15 min. Dry triethylamine (1.78 mL, 12.7 mmol) was added and the solution stirred at −78°C for a further 5 min and then at 21°C for 30 min. Saturated aqueous ammonium chloride solution was added and the mixture was extracted with dichloromethane. The combined organic extract were washed with brine, dried, and concentrated. The residual oil was chromatographed (petroleum ether/diethyl ether; 1:1) to afford 579 mg (94%) of the aldehyde **24**. IR (neat): 2934, 2734, 2244, 1718, 1464 cm^{-1}; ^1H NMR (200 MHz) δ: 1.05 (s, 3H), 1.28 (s, 3H), 1.73 (s, 3H), 1.60–2.00 (m, 2H), 2.04–2.14 (m, 2H), 2.23 (dt, 1H, J = 11, 3 Hz), 3.00 (AB, 2H, J = 19 Hz), 9.83 (d, 1H, J = 5 Hz); ^{13}C NMR (50.3 MHz) δ: 15.7, 19.1, 20.0, 22.5, 26.7, 30.8, 36.9, 56.7, 118.6, 126.9, 133.8, 204.7; HRMS calcd. for $C_{12}H_{17}ON$: 191.1310; found: 191.1313.

2-Cyanomethyl-1,3,3-trimethyl-4-(1-hydroxy-2,4-pentadienyl)cyclohexene (25)

A solution of *n*-butyllithium (0.40 mL, 1.00 mmol, 2.5 M) in hexane was added dropwise to a cold (−78°C), stirred solution of (E)-1-tri-*n*-butylstannyl-1,3-butadiene (373 mg, 1.08 mmol) in dry THF (9 mL). After the reaction mixture had been stirred at −78°C for 10 min, a solution of aldehyde **24** (173 mg, 0.90 mmol) in dry THF (1 mL) was added dropwise. The resulting mixture was stirred at −78°C for 30 min. Water was added and the mixture warmed to 21°C and extracted with diethyl ether. The combined ether extracts were washed with brine, dried, and concentrated. The residual oil was chromatographed (petroleum ether/diethyl ether; 1:1) to afford 213 mg (96%) of the alcohols as colorless oils (ratio 6:1). Further chromatography afforded the major isomer **25**. IR (neat): 3461, 2927, 2245, 1463, 1007 cm^{-1}; ^1H NMR (200 MHz) δ: 1.02 (s, 3H), 1.11 (s, 3H), 1.20–1.68 (m, 4H), 1.69 (s, 3H), 1.90–2.10 (m, 2H), 3.00 (AB, 2H, J = 19 Hz), 4.48 (t, 1H, J = 4 Hz), 5.06 (d, 1H, J = 8 Hz), 5.20 (d, 1H, J = 16 Hz), 5.74 (dd, 1H, J = 16, 4 Hz), 6.10–6.44 (m, 2H); ^{13}C NMR (50.3 MHz) δ: 16.1, 17.4, 19.9, 21.8, 26.3, 32.4, 38.3, 49.6, 70.4, 117.1, 119.1, 127.8, 130.1, 133.8, 136.3, 137.3; HRMS calcd. for $C_{16}H_{23}ON$: 245.1780; found: 245.1760.

2-Cyanomethyl-4-(1-methoxymethyloxy-2,4-pentadienyl)-1,3,3-trimethyl-2-cyanomethylcyclohexene (26)

Chloromethyl methyl ether (0.11 mL, 1.45 mmol) was added to a cold (0°C) solution of the alcohol **25** (301 mg, 1.23 mmol) and diisopropylethylamine (0.58 mL, 3.04 mmol) in dry dichloromethane (15 mL). The resulting solution was stirred at 0°C for 5 min and warmed to 21°C for 16 h. Aqueous ammonium chloride solution (10%) was added and the mixture was extracted with dichloromethane. The combined organic extracts were washed with brine, dried, and concentrated. The residual oil was chromatographed (petroleum ether/diethyl ether; 4:1) to afford 321 mg (90%) of the nitrile **26**, as a slightly reddish oil. IR (neat): 2924, 2245, 1602, 1028, 914, 733 cm^{-1}; ^1H NMR (200 MHz) δ: 1.00 (s, 3H), 1.12 (s, 3H), 1.70 (s, 3H), 1.30–1.80 (m, 3H), 1.95–2.05 (m, 2H), 2.95 (AB, 2H, J = 19 Hz), 3.34 (s, 3H), 4.24 (br d, 1H, J = 10 Hz), 4.46 (d, 1H, J = 8 Hz), 4.65 (d, 1H, J = 8 Hz), 5.10 (br d, 1H, J = 18 Hz), 5.17 (dd, 1H J = 18, 2 Hz), 5.63 (dd, 1H, J = 18, 10 Hz), 6.05–6.42 (m, 2H); ^{13}C NMR (75 MHz) δ: 16.4, 18.8, 20.1, 21.5, 26.6, 32.9, 38.5, 50.1, 56.4, 76.0, 94.4, 117.5, 119.1, 127.9, 132.3, 133.7, 134.0, 136.2; HRMS calcd. for $C_{18}H_{27}O_2N$: 289.2042; found: 289.2032. Anal. calcd. for $C_{18}H_{27}O_2N$: C 74.70, H 9.40, O 11.06; found: C 74.62, H 8.92, O 11.56.

2-Cyanomethyl-1,3,3-trimethyl-4-(1-*tert*-butyldimethylsilyloxy-2,4-pentadienyl)-cyclohexene (27)

To a solution of alcohol **25** (213 mg, 8.70 mmol) in dry DMF (5 mL) was added sequentially *tert*-butyldimethylchlorosilane (170 mg, 1.13 mmol, Aldrich) and 4-(N,N-dimethylamino)pyridine (270 mg, 2.21 mmol). The resulting solution was stirred at 21°C for 3 days. Water was added, the mixture was extracted with diethyl ether, and the combined extracts were washed with brine, dried, and concentrated. The residual oil was chromatographed (petroleum ether/diethyl ether; 19.1) to afford **27** (254 mg, 81%). IR (neat): 2925, 2245, 1603, 1114, 1068, 1006, 838, 774 cm^{-1}; ^1H NMR (200 MHz): δ −0.06 (s, 3H), 0.00 (s, 3H), 0.83 (s, 9H), 0.95 (s, 3H), 1.09 (s,

Can. J. Chem. Downloaded from www.nrcresearchpress.com by 46.23.64.124 on 09/08/12
For personal use only.

3H), 1.3–1.4 (m, 1H), 1.50–1.70 (m, 2H), 1.68 (s, 3H), 1.95–2.1 (m, 2H), 2.98 (AB, 2H, J = 19 Hz), 4.37 (d, 1H, J = 8 Hz), 5.07 (d, 1H, J = 10 Hz), 5.16 (d, 1H, J = 16 Hz), 5.75 (dd, 1H, J = 10, 16 Hz), 5.98–6.40 (m, 2H): ^{13}C NMR (75 MHz) δ: −4.8, −3.0, 16.3, 18.1, 18.7, 20.2, 22.2, 25.9 (3C), 26.6, 32.9, 38.5, 51.7, 72.6, 116.9, 119.2, 127.9, 129.9, 133.7, 136.5, 137.9; HRMS calcd. for $C_{18}H_{28}ONSi$ ($M^+ - C_4H_9$): 302.1940; found: 302.64. Anal. calcd. for $C_{22}H_{37}ONSi$: C 73.47, H 10.37, N 3.89; found: C 73.44, H 9.95, N 3.85.

2-Formylmethyl-1,3,3-trimethyl-4-(1-*tert*-methoxymethyloxy-2,4-pentadienyl)cyclohexene (28)

A solution of diisobutylaluminum hydride (1.5 M, 0.71 mL, 1.06 mmol) in toluene was added dropwise to a cold (−78°C), stirred solution of the nitrile **26** (207 mg, 0.715 mmol) in dry dichloromethane (10 mL). The resulting mixture was stirred at −78°C for 1 h and warmed to 0°C for another hour. Saturated ammonium chloride solution was added and the mixture was stirred at 21°C for 30 min. The resulting solution was extracted with dichloromethane. The combined organic extracts were washed with brine, dried ($MgSO_4$), and concentrated. The residual oil was chromatographed (petroleum ether/diethyl ether; 4:1) to afford 147 mg (70%) of the aldehyde **28**. IR (neat): 2915, 2717, 1721, 1029 cm^{-1}; ^{1}H NMR (200 MHz) δ: 0.97 (s, 3H), 1.00 (s, 3H), 1.54 (s, 3H), 1.40–1.85 (m, 3H), 1.90–2.10 (m, 2H), 3.07 (br s, 2H), 3.34 (s, 3H), 4.25 (br d, 1H, J = 8 Hz), 4.47 (d, 1H, J = 7 Hz), 4.65 (d, 1H, J = 7 Hz), 5.00–5.25 (m, 2H), 5.65 (dd, 1H, J = 14, 8 Hz), 6.00–6.44 (m, 2H), 9.48 (t, 1H, J = 2 Hz); ^{13}C NMR (75 MHz) δ: 18.9, 20.3, 21.7, 26.7, 33.0, 38.3, 43.8, 50.3, 56.4, 76.1, 94.4, 117.4, 129.1, 132.1, 132.5, 134.3, 136.2, 201.3; HRMS calcd. for $C_{18}H_{28}O_3$: 292.2038; found: 292.2052.

2-Formylmethyl-1,3,3-trimethyl-4-(1-*tert*-butyldimethylsilyloxy-2,4-pentadienyl)cyclohexene (29)

A solution of diisobutylaluminum hydride (1.0 M, 0.26 mL, 0.260 mmol) in toluene was added dropwise to a cold (−78°C), stirred solution of the nitrile **27** (72 mg, 0.201 mmol) in dry dichloromethane (5 mL). The reaction was stirred at −78°C for 2 h followed by 2 h at 0°C. Water was added and the mixture was stirred at 21°C for 30 min. The resulting solution was extracted with dichloromethane and the combined organic extracts were washed with brine, dried, and concentrated. The residual oil was chromatographed (petroleum ether/diethyl ether; 9:1) to give aldehyde **29** (66.3 mg, 91%). IR (neat): 2946, 2713, 1723, 1648, 1252, 1066, 1004, 838, 775 cm^{-1}; ^{1}H NMR (200 MHz) δ: −0.05 (s, 3H), 0.00 (s, 3H), 1.10–1.40 (m, 2H), 1.50)\(s, 3H), 1.60–1.75 (m, 1H), 1.80–2.10 (m, 3H), 3.08 (br s, 2H), 4.38 (d, 1H, J = 10 Hz), 5.05 (d, 1H, J = 10 Hz), 5.15 (d, 1H, J = 20 Hz), 5.78 (dd, 1H, J = 10, 20 Hz), 5.95–6.40 (m, 1H), 9.47 (t, 1H, J = 4 Hz); HRMS calcd. for $C_{18}H_{29}O_2Si$ ($M^+ - C_4H_9$): 305.1937; found: 305.1958.

1-(2-Thiophenyl)methyl-2-cyanomethyl-1,3,3-trimethylcyclohexene (30)

A solution of *n*-butyllithium (0.52 mL, 1.30 mmol, 2.5 M) in hexane was added dropwise to a cold (−78°C), stirred solution of thiophene (0.114 mL, 1.42 mmol) in of dry THF (10 mL). After the reaction mixture had been stirred at −78°C for 15 min, a solution of the aldehyde **24** (0.227 g, 1.19 mmol) in dry THF (1 mL) was added dropwise. The resulting orange mixture was stirred at −78°C for 30 min. Water was added and the mixture was extracted with diethyl ether. The combined ether extracts were washed with brine, dried, and concentrated. The residual oil was chromatographed using radial chromatography (petroleum ether/diethyl ether; 2:1.5). Concentration of the appropriate fractions afforded 0.226 g (69%) of the major isomer and 0.0464 g (14%) of the minor isomer. Minor isomer, IR (neat): 3450, 2929, 2247, 1425, 1038 cm^{-1}; ^{1}H NMR (200 MHz) δ: 1.06 (s, 3H), 1.07–1.37 (m, 2H), 1.39 (s, 3H), 1.69 (s, 3H), 1.6–2.10 (m, 4H), 2.99 (br s, 2H), 4.87 (br d, 1H, J = 9 Hz), 6.9–7.0 (m, 2H), 7.2–7.28 (m, 1H); ^{13}C NMR (50.3 MHz) δ: 16.2, 20.0, 20.2, 22.5, 27.5, 32.1, 38.9, 51.0, 72.7, 119.3, 125.2, 125.3, 126.4, 128.6, 133.5, 149.0; HRMS calcd. for $C_{1621}ONS$: 275.1319; found: 275.1316.

Major isomer, IR (neat): 3458, 2918, 2247, 1376, 1110, 1045, 706 cm^{-1}; ^{1}H NMR (200 MHz) δ: 1.10 (s, 3H), 1.20 (s, 3H), 1.71 (s, 3H), 1.5–1.7 (m, 2H), 1.88 (d, 1H, J = 5.5 Hz), 1.95–2.10 (m, 2H), 2.99 (AB, 2H, J = 19 Hz), 5.28 (d, 1H, J = 5.5 Hz), 6.88–7.0 (m, 2H), 7.15–7.25 (m, 1H); ^{13}C NMR (50.3 MHz) δ: 16.1, 17.3, 20.0, 21.8, 26.3, 32.4, 38.5, 52.3, 69.2, 119.1, 122.7, 123.9, 126.8, 127.6, 134.1, 150.3; HRMS calcd. for $C_{16}H_{19}NS$ ($M^+ - H_2O$): 257.1238; found: 257.1238.

tert-Butyldimethylsilyl chloride (0.130 g, 0.862 mmol) was added to a stirred solution of silver perchlorate (0.160 g, 0.772 mmol) in dry acetonitrile (5 mL). The resultant white suspension was stirred at 21°C for 15 min. Pyridine (0.23 mL, 2.84 mmol) and a solution of the major alcohol (0.154 g, 0.561 mmol) were added sequentially and the mixture was stirred overnight at 21°C. Diethyl ether was added and the solids were removed by filtration. The ether filtrate was washed (5% aqueous sodium bicarbonate solution, brine), dried, and concentrated. The residual oil was chromatographed (petroleum ether/diethyl ether; 9:1 initially followed by petroleum ether/diethyl ether; 3:1) to afford 0.157 g (72%) of the silyl ether **30** and also 0.0154 g (10%) of the starting alcohol. The product **30** was recrystallized from petroleum ether/diethyl ether (1.1) to give colourless needles, mp 113–114°C. IR (KBr): 2945, 2244, 1109, 1072, 831, 744 cm^{-1}; ^{1}H NMR (200 MHz) δ: −0.36 (s, 3H), 0.03 (s, 3H), 0.84 (s, 9H), 1.01 (s, 3H), 1.12 (s, 3H), 1.45–1.70 (m, 1H), 1.68 (s, 3H), 1.90–2.10 (m, 1H), 2.95 (AB, 2H, J = 18 Hz), 5.18 (br s, 1H), 6.8–6.9 (m, 2H), 7.1–7.18 (m, 1H); ^{13}C NMR (75 MHz) δ: −4.87, −4.23, 16.5, 18.5, 20.0, 21.8, 25.9 (3C), 26.6, 30.6, 32.9, 38.8, 54.2, 69.7, 119.0, 123.1, 123.6, 125.7, 127.5, 133.8, 150.4; HRMS calcd. for $C_{18}H_{26}ONSSi$ ($M^+ - C_4H_9$): 332.1504; found: 332.1496.

4-(1-*tert*-butyldimethylsilyloxy-2,4-pentadienyl)-1,3,3-trimethyl-2-(2-oxo-4-trimethylsilyl-3-butynyl)cyclohexene (31)

A solution of *n*-butyllithium (1.50 mL, 3.75 mmol, 2.5 M) in hexane was added dropwise to a cold (−78°C), stirred, solution of (trimethylsilyl)acetylene (0.53 mL, 3.75 mmol) in dry THF (30 mL). After stirring at −78°C for 10 min, a solution of the aldehyde **29** (0.450 g, 1.24 mmol) in dry THF (5 mL) was added dropwise. The resulting mixture was stirred at −78°C for 1 h and at 0°C for a further hour. Water was added and the mixture was warmed to 21°C and extracted with diethyl ether. The combined ether extracts were washed with brine and dried. Concentration of the organic material afforded 186 mg (93%) of the acetylenic alcohol, which was used directly.

Can. J. Chem. Downloaded from www.nrcresearchpress.com by 46.23.64.124 on 09/08/12
For personal use only.

Oxalyl chloride (0.017 mL, 0.194 mmol) was added to a cold (−78°C), stirred, solution of dry dimethyl sulfoxide (0.014 mL, 0.197 mmol) in dry dichloromethane (5 mL). After the reaction mixture had been stirred at −78°C for 15 min, a solution of the acetylenic alcohol (0.0766 g, 0.166 mmol) in dry dichloromethane (1 mL) was added dropwise and the resulting mixture was stirred for 15 min. Dry trimethylamine (0.10 mL, 0.717 mmol) was added, the solution was stirred at −78°C for 5 min, and at 21°C for 30 min. Water was added and the mixture was extracted with dichloromethane. The combined organic extracts were washed with brine, dried, and concentrated. The residual oil was chromatographed (petroleum ether/diethyl ether; 19:1) to afford 0.029 g (38%) of the ketone **31**. IR (neat): 2947, 2151, 1676, 1253, 1090, 851, 772 cm^{-1}; ^1H NMR (200 MHz) δ: −0.05 (s, 3H), 0.00 (s, 3H), 0.19 (s, 9H), 0.84 (s, 9H), 0.92 (s, 3H), 0.95 (s, 3H), 1.15 (s, 3H), 1–1.7 (m, 3H), 1.9–2.10 (m, 2H), 3.24 (br s, 2H), 4.37 (d, 1H, J = 7 Hz), 5.03 (br d, 1H, J = 8 Hz), 5.17 (br d, 1H, J = 18 Hz), 5.75 (dd, 1H, J = 10, 18 Hz), 6.03 (dd, 1H, J = 10, 18 Hz), 6.28 (dd, 1H, J = 10, 18 Hz); HRMS calcd. for $C_{23}H_{31}O_2Si_2$ ($M^+ - C_4H)_9$: 2332; found: 401.2340.

Alternative oxidation: pyridinium dichromate (0.080 g, 0.213 mmol) was added to a stirred solution of the acetylenic alcohol (0.036 g, 0.0793 mmol) in dry dichloromethane (5 mL). The resulting mixture was stirred at room temperature for 4 h. The solid was removed by filtration through a sintered glass funnel under aspirator pressure and was washed thoroughly with diethyl ether. The ether filtrates were concentrated to provided a tan oil. This residual oil was chromatographed (petroleum ether/diethyl ether; 40:1) to afford 0.010 g (26%) of the ketone **31**.

4-(1-*tert*-Butyldimethylsilyloxy-2,4-pentadienyl)-1,3,3-trimethyl-2-(2-oxo-3-butynyl)cyclohexene (32)

A solution of potassium hydroxide (0.200 g, 3.57 mmol) in methanol (5 mL) was added to a stirred solution of the acetylenic alcohol (0.531 mg, 1.15 mmol) (prepared as described above) in dichloromethane (5 mL). The resulting mixture was stirred for 3 h at 21°C. The organic solvent was removed under reduced pressure to provide yellow oil. A mixture of diethyl ether/water (1:1) was added and the solution was extracted thoroughly with diethyl ether. The combined ether extracts were washed with brine and dried. Concentration of the organic material afforded a quantitative yield of the deprotected acetylenic alcohol.

Dess–Martin periodinane (1.00 g, 1.71 mmol) was added to a solution of the deprotected acetylenic alcohol in dry dichloromethane (15 mL). The resulting bright yellow solution was stirred at 21°C for 2 h. Dilute aqueous sodium hydroxide solution (10 mL, 10%) was added and the mixture was stirred for a further 10 min. The solution was extracted with diethyl ether. The combined organic extracts were washed (10% sodium hydroxide solution, water, brine), dried, and concentrated. The residual oil was chromatographed (petroleum ether/diethyl ether; 9:1) to afford 0.133 g (30%) of the ketone **32**. IR (neat): 3266, 2918, 2091, 1684, 839, 775 cm^{-1}; ^1H NMR (200 MHz) δ: −0.05 (s, 3H), 0.01 (s, 3H), 0.85 (s, 9H), 0.99 (s, 3H), 1.01 (s, 3H), 1.34–1.46 (m, 1H), 1.51 (s, 3H), 1.55–1.75 (m, 2H), 1.90–2.25 (m, 3H), 3.21 (s, 1H), 3.30 (d, 1H, J = 16 Hz), 3.42 (d, 1H, J = 16 Hz), 4.36 (br s, 1H), 5.05 (d, 1H, J = 10 Hz), 5.17 (d, 1H, J = 16 Hz), 5.72 (dd, 1H, J = 16.6 Hz); HRMS calcd. for $C_{29}H_{38}O_2Si$: 382.2641; found: 386.2649.

2-(2-Hydroxy-4-trimethylsilyl-3-butynyl)-4-(1-methoxymethyloxy-2,4-pentadienyl)-1,3,3-trimethylcyclohexene (33)

Addition of lithium trimethylacetylide to the aldehyde **29** (147 mg, 0.5.04 mmol) was conducted as described above to afford 186 mg (95%) of the alcohol **33**. IR (neat): 3415, 2918, 2170, 1648, 1045, 871 cm^{-1}; ^1H NMR (200 MHz) δ: 0.13 (s, 9H), 1.03 (br s, 3H), 1.07 (br s, 3H), 1.67 (br s, 3H), 1.00–1.80 (m, 5H), 1.90–2.10 (m, 2H), 2.48–2.60 (m, 1H), 3.34 (br s, 3H), 4.20–4.32 (m, 1H), 4.40–4.52 (m, 2H), 4.60–4.70 (m, 1H), 5.06 (br d, 1H, J = 20 Hz), 5.18 (br d, 1H, J = 20 Hz), 5.55–5.75 (m, 1H), 6.05–6.45 (m, 2H); MS (CI): 329 ($MH^+ - C_2H_6O_2$).

2-(2-Hydroxy-3-butynyl)-4-(1-methoxymethyloxy-2,4-pentadienyl)-1,3,3-trimethylcyclohexene (34)

A solution of potassium hydroxide (250 mg, 4.46 mmol) in methanol (5 mL) was added to a stirred solution of the alcohol **33** (471 mg, 1.21 mmol) in dichloromethane (5 mL). The resulting mixture was stirred for 3 h at 21°C. The organic solvent was removed under reduced pressure to provide a yellow oil. A mixture of diethyl ether/water (1:1) was added and the solution was extracted with diethyl ether. The combined ether extracts were washed with brine and dried. Concentration afforded a quantitative yield of alcohols **34**. IR (neat): 3431, 3300, 2926, 2112, 1647, 1027 cm^{-1}; ^1H NMR (200 MHz) δ: 1.03 (s, 3H), 1.06 (br s, 3H), 1.68 (br s, 3H), 0.8–1.8 (m, 7H), 1.90–2.05 (m, 2H), 2.44 (dd, 1H, J = 8, 2 Hz), 2.50–2.60 (m, 1H), 3.33 (br s, 3H), 4.26 (br d, 1H, J = 10 Hz), 4.46 (br d, 1H, J = 8 Hz), 4.62 (br d, 1H, J = 8 Hz), 4.62 (br d, 1H, J = 8 Hz), 5.09 (br d, 1H, J = 20 Hz), 5.15 (br d, 1H, J = 20 Hz), 5.63 (dd, 1H, J = 16, 8 Hz), 5.95–6.45 (m, 1H); ^{13}C NMR (50.3 MHz): ~3:2 diastereoisomer mixture, major isomer, most signals doubled, δ: 18.7, 21.1, 22.7, 27.3, 32.8, 36.8, 38.3, 50.3, 56.2, 62.1, 72.5, 76.1, 85.4, 94.2, 117.2, 131.9, 132.9, 134.2, 134.3, 136.1; MS (CI): 257 ($MH^+ - C_2H_6O_2$).

4-(1-Methoxymethyloxy-2,4-pentadienyl)-1,3,3-trimethyl-2-(2-oxo-3-butynyl)cyclohexene (35)

Dess–Martin periodinane (997 mg, 1.71 mmol) was added to a solution of the alcohol **34** (384 mg, 1.21 mmol) in dry dichloromethane (10 mL). The resulting bright yellow solution was stirred at 21°C for 1 h. Diethyl ether (20 mL) and aqueous sodium hydroxide solution (10 mL, 10%) were added and the mixture was stirred for a further 10 min. The solution was extracted with diethyl ether. The combined organic extracts were washed (10% sodium hydroxide solution, water, brine), dried, and concentrated. The residual oil was chromatographed (petroleum ether/diethyl ether; 6:1) to afford 210 mg (55%) of the ketone **35**. IR (neat): 3252, 2918, 2089, 1681, 1074, 913 cm^{-1}; ^1H NMR (200 MHz) δ: 0.95 (s, 3H), 0.96 (s, 3H), 1.51 (s, 3H), 1.40–1.80 (m, 4H), 1.90–2.10 (m, 2H), 3.16 (s, 1H), 3.30 (br s, 2H), 3.34 (s, 3H), 4.23 (d, 1H, J = 8 Hz), 4.46 (d, 1H, J = 6.6 Hz), 4.64 (d, 1H, J = 6.6 Hz), 5.08 (d, 1H, J = 18 Hz), 5.15 (dd, 1H, J = 18, 2 Hz), 5.64 (dd, 1H, J = 15, 8 Hz), 6.05–6.40 (m, 1H); ^{13}C NMR (50.3 MHz) δ: 18.9, 20.8, 22.0, 26.6, 32.9, 38.2, 45.3, 50.1, 56.4, 76.2, 78.3, 81.7, 94.4, 117.3, 129.7, 132.8, 134.4, 136.3, 186.0; MS (CI): 317 (MH^+).

(1*R**,2*S**,3*S**)-2-Methoxymethyloxy-9-oxo-12,15,15-trimethyltricyclo[9.3.1.$0^{3,8}$]pentadeca-4,7,11-triene (36)

A solution of the acetylenic ketone **35** (0.121 g, 0.382 mmol)

Can. J. Chem. Downloaded from www.nrcresearchpress.com by 46.23.64.124 on 09/08/12
For personal use only.

in dry toluene (25 mL) containing hydroquinone (0.01 g, 0.09 mmol) was placed in a thick-walled Pyrex pressure tube equipped with a threaded plastic cap. The top of the tube extended through a small hole in the top of the microwave oven. Argon was bubbled through the solution for 10 min and the vessel sealed. The diameter of the even opening is less than 3 cm and is shielded to minimize microwave leakage. The base of the tube inside the microwave oven was surrounded by a beaker of damp (H_2O) vermiculite to facilitate heat transfer. A commercial oven was used (Toshiba model ERF-6630C (720 W) at a power setting of 500 W in which the magnetron was tuned to the water frequency (2450 MHz). The reaction was conducted behind a shield in a fume hood. The reaction was heated for 12 × 0.5 h intervals, after which the tube was allowed to return to room temperature between each session and fresh moist vermiculite added to the beaker. The tube was cooled, solvent evaporated, and the residual oil chromatographed (petroleum ether/diethyl ether; 3:1) to afford the adduct **36** (0.041 g, 34%). (Unfortunately, the minor adduct, epimeric at C3, could not be fully characterized.) IR (neat): 2920, 1694, 1148, 1033, 919 cm^{-1}; ^1H NMR (200 MHz) δ: 1.04 (s, 3H), 1.50–2.30 (m, 4H), 2.50–2.60 (m, 1H), 2.60–2.70 (m, 1H), 2.71–2.85 (m, 1H), 2.95 (dd, 1H, J = 9.6, 5.6 Hz), 3.30 (br s, 2H), 3.32 (br s, 3H), 3.4–3.70 (m, 1H), 4.53 (br s, 2H), 5.5–6.1 (m, 3H); HRMS calcd. for $C_{20}H_{28}O_3$: 316.2040; found: 316.2061.

(1*R,2*S**)-3,4-Benzo-2-methoxymethyloxy-9-oxo-12,15,15-trimethyltricyclo[9.31.0^{3,8}]pentadec-11-ene (37) (*endo/exo* mixture, ~1:1)**

Dichlorodicyanoquinone (0.049 g, 0.216 mmol) was added to the diene (0.034 g, 0.108 mmol) dissolved in dry benzene (5 mL). The stirred reaction was refluxed for 2 h. The mixture was then cooled to 21°C and the solvent removed under aspirator pressure. The residual oil was chromatographed (petroleum ether/diethyl ether; 3:1) to afford 0.023 g (69%) of the mixture of aromatic products **37**. IR (neat): 2919, 1695, 1452, 1031, 923 cm^{-1}; ^1H NMR (200 MHz) δ: 0.39 (s, 3H), 0.71 (s, 3H), 1.02 (s, 3H), 1.06 (s, 3H), 1.41 (s, 3H), 0.8–1.70 (m, 4H), 1.76 (s, 3H), 1.90–2.50 (m, 6H), 3.20 (br s, 3H), 3.35 (br s, 3H), 3.25–3.65 (m, 3H), 3.59 (d, 1H, J = 12 Hz), 4.02 (d, 1H, J = 9.6 Hz), 4.09 (d, 1H, J = 6 Hz), 4.27 (d, 1H, J = 6 Hz), 4.30 (d, 1H, J = 6 Hz), 4.40 (d, 1H, J = 6 Hz), 4.49 (d, 1H, J = 3 Hz), 7.00–7.60 (m, 8H); ^{13}C NMR (75 MHz) δ: 20.17, 20.58, 20.78, 21.58, 26.77, 27.78, 27.81, 28.81, 30.25, 30.47, 37.22, 38.72, 46.98, 47.45, 49.09, 53.78, 55.39, 56.46, 78.85, 86.32, 93.40, 95.02, 125.64, 126.18, 126.31, 127.29, 127.84, 127.92, 128.30, 129.24, 129.43, 129.58, 134.52, 135.85, 137.86, 138.50, 140.91, 143.38, 200.95, 209.43; HRMS calcd. for $C_{20}H_{26}O_3$: 314.1882; found: 314.1883.

4-(1-*tert*-Butyldimethylsilyloxy-2,4-pentadienyl)-1,3,3-trimethyl-2-(2-oxo-3-methyl-3-butenyl)cyclohexene (41)

A solution of *tert*-butyllithium (0.35 mL, 0.60 mmol, 1.7 M) in pentane was added dropwise to a cold (−78°C), stirred solution of 2-bromopropene (0.05 mL, 0.62 mmol) in of dry THF (2 mL). After the reaction was stirred at −78°C for 5 min, a solution of the aldehyde **29** (0.09 g, 0.25 mmol) in dry THF (1 mL) was added dropwise. The resulting mixture was stirred at −78°C for 30 min and warmed to 21°C. Ammonium chloride solution (saturated) was added and the mixture was extracted with diethyl ether. The combined ether extracts were washed (water, brine), dried, and concentrated. The residual oil was chromatographed (petroleum ether/diethyl ether; 9:1) to afford 0.072 g (72%) of the alcohol, which was used directly.

Oxalyl chloride (0.014 mL, 0.160 mmol) was added to a cold (−78°C), stirred solution of dry dimethyl sulfoxide (0.0136 mL, 0.192 mmol) in dry dichloromethane (3 mL). After the reaction was stirred at −78°C for 15 min, a solution of the above alcohol (0.0519 g, 0.128 mmol) in dry dichloromethane (1 mL) was added dropwise and the resulting mixture stirred for a further 15 min. Dry triethylamine (0.070 mL, 0.502 mmol) was added and the solution was stirred at −78°C for 5 min and at 21°C for a further 30 min. Saturated aqueous ammonium chloride solution was added and the mixture was extracted with dichloromethane. The combined organic extracts were washed (water, brine), dried, and concentrated. The residual oil was chromatographed (petroleum ether/diethyl ether; 15:1) to afford 0.045 g (88%) of the enone **41**. IR (neat): 2923, 1686, 1463, 1335, 1064, 1003, 837, 774 cm^{-1}; ^1H NMR (200 MHz) δ: −0.06 (s, 3H), −0.01 (s, 3H), 0.83 (s, 9H), 0.86 (s, 3H), 0.87 (s, 3H), 1–1.5 (m, 1H), 1.39 (s, 3H), 1.5–1.8 (m, 2H), 1.86 (s, 3H), 1.90–2.20 (m, 2H), 3.40 (AB, 2H, J = 20 Hz), 4.36 (d, 1H, J = 7.4 Hz), 5.02 (d, 1H, J = 10 Hz), 5.11 (d, 1H, J = 17 Hz), 5.71 (bs s, 1H), 5.99 (br s, 1H), 5.70–6.40 (m, 3H). HRMS calcd. for $C_{21}H_{33}O_2Si$ (M^+ − $C_4H)_9$: 345.2250; found: 345.2250.

5-(*tert*-Butyldimethylsilyloxy)methyl-3-formyl(dimethylacetal)-2,4,4-trimethylcyclohexene (44)

Thionyl chloride (0.070 mL, 0.960 mmol) was syringed into a cold (0°C), stirred solution of the alcohol **15** (0.174 g, 0.485 mmol) and dry pyridine (0.078 mL, 0.964 mmol) in dry dichloromethane (5 mL). The reaction was warmed to 0°C for 1 h and to 21°C for 30 min. Saturated sodium bicarbonate solution was added and the mixture was extracted with dichloromethane. The combined organic extracts were washed (water, brine), dried, and concentrated. The residual oil was chromatographed (petroleum ether/diethyl ether; 9:1) to afford 0.132 g (80%) of a 3:1 mixture of the olefin acetals **44** and **43**. Compound **44**: IR (neat): 2914, 1090, 842, 775 cm^{-1}; ^1H NMR (200 MHz) δ: 0.01 (s, 6H), 0.79 (s, 3H), 0.85 (s, 9H), 1.00 (s, 3H), 1.00–1.50 (m, 1H), 1.77 (d, 3H, J = 1 Hz), 1.50–2.00 (m, 2H), 2.05–2.30 (m, 1H) 3.34 (s, 3H), 3.37 (s, 3.20–3.40 (m, 1H), 3.71 (dd, 1H, J = 5, 10 Hz), 4.29 (d, 1H, J = 4 Hz), 5.44–5.52 (br s, 1H); ^{13}C NMR (50.3 MHz) δ: −5.3 (2C), 18.2, 23.4, 25.9 (3C), 26.3, 27.5, 33.6, 39.9, 55.0, 55.2, 56.7, 64.2, 108.2, 123.0, 131.8; HRMS calcd. for $C_{19}H_{38}O_3Si$ (M^+ − MeOH): 310.2328; found: 310.2307.

5-(*tert*-Butyldimethylsilyloxy)methyl-3-formyl-2,4,4-trimethylcyclohexene (45)

Saturated oxalic acid solution (2 mL) and a drop of glacial acetic acid were added to a solution of **44** (0.056 g, 0.164 mmol) in diethyl ether (2 mL). The reaction was refluxed for 2 h, then cooled to 21°C. Water was added and the mixture was extracted with diethyl ether. The organic extracts were washed (water, brine), dried, and concentrated. The residual oil was chromatographed (petroleum ether/diethyl ether; 9:1) to afford 0.0411 g (85%) of the aldehyde **45**. IR (neat): 2940, 1724, 1200, 1080, 840, 780 cm^{-1}; ^1H NMR (200 MHz) δ: 0.01 (s, 3H), 0.86 (s, 9H), 1.04 (s, 3H), 1.58 (s, 3H), 1.70–2.00 (m,

Can. J. Chem. Downloaded from www.nrcresearchpress.com by 46.23.64.124 on 09/08/12
For personal use only.

2H), 2.10–2.40 (m, 2H) 3.30–3.50 (m, 1H) 3.78 (dd, 1H, $J = 4$, 10 Hz), 5.73 (br s, 1H), 9.54 (d, 1H, $J = 4$ Hz). HRMS calcd. for $C_{13}H_{23}O_2Si$ ($M^+ - C_4H_9$): 239.1468; found: 239.1469.

5-(*tert*-Butyldimethylsilyloxy)methyl-1,2-epoxy-3-formyl-2,4,4-trimethylcyclohexane (46)

A solution of freshly prepared dimethyloxirane (excess) in acetone (25 mL) was added dropwise to a cold (−4°C), stirred solution of aldehyde **45** (0.184 g, 0.622 mmol) in acetone (5 mL). After stirring at −4°C for 1 h, the reaction mixture was warmed to 21°C. Concentration of the mixture provided a residual oil that was chromatographed (petroleum ether/diethyl ether; 9:1) to afford 0.150 g (77%) of the epoxide **46**. IR (neat): 2946, 2742, 1720, 1467, 1100, 842, 778 cm^{-1}; ^1H NMR (200 MHz) δ: −0.00 (s, 6H), 0.85 (s, 9H), 0.89 (s, 3H), 0.93 (s, 3H), 1.32 (s, 3H), 1.70–1.90 (m, 2H), 1.98 (d, 1H, $J = 4.6$ Hz), 2.06–2.28 (m, 1H), 3.12 (t, 1H, $J = 1.6$ Hz), 3.51 (dd, 1H, $J = 10.4$, 5.6 Hz), 3.63 (dd, 1H, $J = 10.4$, 4 Hz), 9.66 (d, 1H, $J = 4.6$ Hz); ^{13}C NMR (50.3 MHz) δ: −5.5 (2C), 18.2, 23.4, 24.7, 24.8, 25.7, 25.8 (3C), 32.8, 37.2, 57.4, 58.5, 62.0, 63.1, 203.3. HRMS calcd. for $C_{13}H_{23}O_3Si$ ($M^+ - C_4H_9$): 255.1416; found: 255.1424.

5-(*tert*-Butyldimethylsilyloxy)methyl-3-formyl-2,4,4-trimethylclohex-2-en-1-ol (47)

Sodium methoxide (0.031 g, 0.574 mmol) was added to the epoxide **46** (0.15 g, 0.481 mmol) and methanol (10 mL). The reaction mixture was stirred under reflux for 3 h, then cooled to 21°C. Water was added and the solvent was removed. The residual oil was chromatographed (petroleum ether/diethyl ether; 3:1, then the petroleum ether/diethyl ether; 1:1). Concentration of the appropriate fractions afforded 0.0989 g (66%) of the alcohol **47**. IR (neat): 3402, 2942, 2761, 1673, 1254, 1094, 842, 777 cm^{-1}; ^1H NMR (200 MHz) δ: 0.02 (s, 6H), 0.86 (s, 9H), 1.02 (s, 3H), 1.27 (s, 3H), 1.5–1.80 (m, 3H), 1.80–2.0 (m, 1H), 2.17 (s, 3H), 3.39 (dd, 1H, $J = 10$, 8 Hz), 3.78 (dd, 1H, $J = 10$, 4 Hz), 3.95–4.10 (m, 1H), 10.11 (s, 1H); ^{13}C NMR (75 MHz) δ: −5.5, −5.4, 16.9, 18.2, 20.3, 35.92 (3C), 26.4, 30.3, 36.0, 42.3, 62.9, 69.7, 141.9, 151.1, 194.0. HRMS calcd. for $C_{17}H_{32}O_3Si$: 312.2120; found: 312.2110.

1-(*tert*-Butyldimethylsilyloxy)-5-(*tert*-butyldimethylsilyloxy)methyl-3-formyl-2,4,4-trimethylcyclohex-2-ene (48)

tert-Butyldimethylsilyl chloride (0.057 g, 0.378 mmol) was added to a stirred solution of the alcohol **47** (0.099 g, 0.317 mmol) and imidazole (0.53 g, 0.778 mmol) in dry dichloromethane (10 mL). The resultant solution was stirred at 21°C for 16 h. Water was added and the mixture was extracted with dichloromethane. The combined organic extracts were washed with brine, dried, and concentrated. The residual oil was chromatographed (petroleum ether/diethyl ether; 19:1). Concentration of the appropriate fractions afforded 0.123 g (91%) of the silyl ether **48**. IR (neat): 2912, 2762, 1681, 1467, 1254, 1079, 841, 777 cm^{-1}; ^1H NMR (200 MHz) δ: 0.02 (s, 6H), 0.10 (s, 6H), 0.87 (s, 9H), 0.88 (s, 9H), 1.0 (s, 3H), 1.27 (s, 3H), 1.45–1.63 (m, 1H), 1.66–1.82 (m, 1H), 1.90 (dt, 1H, $J = 2$, 12 Hz), 2.08 (s, 3H), 3.33 (dd, 1H, $J = 10$, 12 Hz), 3.76 (dd, 1H, $J = 10$, 4 Hz), 4.02 (t, 1H, $J = 4$ Hz), 10.10 (s, 1H); ^1H NMR ($CDCl_3$, 50.3 MHz) δ: −5.39, −5.35, −4.67, −4.14, 16.82, 18.1, 18.4, 20.5, 25.8 (3C), 26.0 (3C), 26.5, 30.4, 35.7, 42.3, 63.1, 70.1, 141.0, 152.9, 194.1. HRMS calcd. for $C_{23}H_{46}O_3Si_2$: 426.2985; found: 426.2988.

5-(*tert*-Butyldimethylsilyloxy)methyl-2,4,4-trimethyl-3-cyanomethyl-2-cyclohexen-1-one (49)

3,5-Dimethylaminopyridine (0.33 g, 3.43 mmol) was added to a cold (−4°C) suspension of chromium trioxide (0.35 g, 3.50 mmol) in dry dichloromethane (4 mL). the reaction mixture was stirred at 0°C for 20 min and a solution of nitrile **22** (0.450 g, 0.146 mmol) was added. The resulting red-brown solution was stirred at −4°C for 1 h and warmed to 21°C for 16 h. Dilute sodium hydroxide (6 M, 1 mL) was added and the mixture was stirred at 21°C for 20 min. Water (5 mL) and dichloromethane (10 mL) were added and the resulting solution extracted thoroughly with dichloromethane. The combined organic extracts were washed (water, 10% HCl, and brine), dried, and concentrated. The residual oil was chromatographed (petroleum ether/diethyl ether; 1:1) to afford recovered **22** (40–50%) and 0.144 g (31%) of the enone **49**, mp 75–77°C. IR (neat): 2946, 2250, 1669, 1093, 846, 776 cm^{-1}; ^1H NMR (200 MHz) : 0.00 (s, 6H), 0.84 (s, 9H), 1.11 (s, 3H), 1.29 (s, 3H), 1.86 (s, 3H), 1.9–2.10 (m, 1H), 2.42 (dd, 1H, $J = 18$, 11 Hz), 2.65 (dd, 1H, $J = 18$, 5 Hz), 3.18 (br s, 2H), 3.57 (dd, 1H, $J = 10.2$, 6.4 Hz), 3.72 (dd, 1H, $J = 10.2$, 4.6 Hz); ^{13}C NMR (75 MHz) δ: −5.6, 11.8, 17.8, 18.2, 20.9, 25.8, 26.3, 37.1, 38.8, 45.8, 63.1, 116.4, 134.7, 150.6, 197.4. HRMS calcd. for $C_{17}H_{28}O_2Si$ (M^+ − Me): 306.1889; found: 306.1861.

Acknowledgment

We are grateful to Dr. C. Bensimon for the X-ray analysis, Dr. T. Wong for additional spectral data, and to the Natural Sciences and Engineering Research Council of Canada, Merck–Frosst Canada Ltd., Rhône-Poulenc Rorer, and the Canadian Breast Cancer Research Initiative for financial support of this research and to the referees for their helpful comments.

References

1. M.C. Wani, H.L. Taylor, M.E. Wall, P. Coggan, and A.T. McPhail. J. Am. Chem. Soc. **93**, 2325 (1971).
2. F. Lavelle, F. Guéritte-Voegelein, and D. Guénard. Bull. Cancer, **80**, 326 (1993).
3. M.L. Rothenberg. Curr. Opin. Invest. Drugs, **2**, 1269 (1993).
4. (*a*) A.N. Boa, P.R. Jenkins, and N.J. Lawrence. Contemp. Org. Synth. **1**, 47 (1994); (*b*) K.C. Nicolaou, W.-M. Dai, and R.K. Guy. Angew. Chem. Int. Ed. Engl. **33**, 15 (1994); (*c*) D.G.I. Kingston, A.A. Molinero, and J.M. Rimoldi. Prog. Chem. Org. Nat. Prod. **61**, 1 (1993); (*d*) C.S. Swindell. Org. Prep. Proced. Int. **23**, 465 (1991).
5. (*a*) R.A. Holton, C. Somoza, H.-B. Kim, F. Liang, R.J. Biediger, P.D. Boatman, M. Shindo, C.C. Smith, S. Kim, H. Nadizadeh, Y. Suzuki, C. Tao, P. Vu, S. Tang, P. Zhang, K.K. Murthi, L.N. Gentile, and J.H. Liu. J. Am. Chem. Soc. **116**, 1597 (1994); (*b*) R.A. Holton, H.-B. Kim, C. Somoza, F. Liang, R.J. Biediger, P.D. Boatmen, M. Shindo, C.C. Smith, S. Kim, H. Nadizadeh, Y. Suzudi, C. Tao, P. Vu, S. Tang, P. Zhang, K.K. Murthi, L.N. Gentile, and J.H. Liu. J. Am. Chem. Soc. **116**, 1599 (1994).
6. (*a*) K.C. Nicolaou, Z. Yang, J.J. Liu, H. Ueno, P.G. Nantermet, R.K. Guy, C.F. Claiborne, J. Renaud, E.A. Couladouros, K. Paulvannan, and E.J. Sorensen. Nature, **367**, 630 (1994); (*b*) K.C. Nicolaou, P.G. Nantermet, H. Ueno, R.K. Guy, E.A. Couladouros, and E.J. Sorensen. J. Am. Chem. Soc. **117**, 624 (1995); (*c*) K.C. Nicolaou, J.J. Liu, Z. Yang, H. Ueno, E.J. Sorensen, C.F. Claiborne, R.K. Guy, C.K. Hwang, M. Nakada, and P.G. Nantermet. J. Am. Chem. Soc. **117**, 634 (1995); (*d*) K.C. Nicolaou, Z. Yang, J.J. Liu, P.G. Nantermet, C.F.

Claiborne, J. Renaud, R.K. Guy, and K. Shibayama. J. Am. Chem. Soc. **117**, 645 (1995); (*e*) K.C. Nicolaou, H. Ueno, J.J. Liu, P.G. Nantermet, Z. Yang, J. Renaud, K. Paulvannan, and R. Chadha. J. Am. Chem. Soc. **117**, 653 (1995).
7. (*a*) R.V. Bonnert and P.R. Jenkins. J. Chem. Soc. Chem. Commun. 1540 (1987); (*b*) J. Chem. Soc. Chem. Soc. Perkin Trans. 1, 413 (1989).
8. R.W. Jackson, R.G. Highby, J.W. Gilman, and K.J. Shea. Tetrahedron, **48**, 7013 (1992).
9. R.W. Jackson and K.J. Shea. Tetrahedron Lett. **35**, 1317 (1994).
10. C.A. Alaimo, C.A. Coburn, and S.J. Danishefsky. Tetrahedron Lett. **35**, 6603 (1994).
11. (*a*) K. Sakan and B.M. Craven. J. Am. Chem. Soc. **105**, 3732 (1983); (*b*) K. Sakan, D.A. Smith, S.A. Babirad, F.R. Fronczek, and K.N. Houk. J. Org. Chem. **56**, 2311 (1991).
12. (*a*) A.G. Fallis. Can. J. Chem. **62**, 183 (1984); (*b*) E. Cignek. Org. React. **32**, 1 (1984); (*c*) D. Craig. Chem. Soc. Rev. **16**, 187 (1987).
13. (*a*) G.P. Kugatova-Shemyakina, G.M. Nikolaev, and V.M. Andreev. Tetrahedron, **23**, 2721 (1967); (*b*) N.M. Viktorova, S.P. Knyazen, N.S. Sefirov, Y.D. Gavrilov, G.M. Nilolaev, and V.F. Bystrov. Org. Magn. Reson. **6**, 236 (1974).
14. Y.-F. Lu and A.G. Fallis. Tetrahedron Lett. **34**, 3367 (1993).
15. M.T. Thomas and A.G. Fallis. J. Am. Chem. Soc. **98**, 1227 (1976).
16. (*a*) G.A. Olah, S.C. Narang, B.G.B. Gupta, and R. Malhotra. J. Org. Chem. **44**, 1247 (1979); (*b*) G.A. Olah, A. Husain, B.P. Singh, and A.K. Mehrotra. J. Org. Chem. **48**, 3667 (1983).
17. A.G. Angoh and D.L.J. Clive. Chem. Soc. Chem. Commun. 534 (1984).
18. D.B. Dess and J.C. Martin. J. Org. Chem. **48**, 4155 (1983).
19. (*a*) B. Lei and A.G. Fallis. J. Am. Chem. Soc. **112**, 4609 (1990); (*b*) Y.F. Lu, C.W. Harwig, and A.G. Fallis. J. Org. Chem. **58**, 4202 (1993).
20. A.G. Fallis and Y.-F. Lu. *In* Advances in cycloadditions. Vol. 3. *Edited by* D.P. Curran. JAI Press, Greenwich, Conn. 1993. pp. 1–66.
21. (*a*) K.J. Shea and J.W. Gilman. Tetrahedron Lett. **25**, 2451 (1984); (*b*) K.J. Shea, J.W. Gilman, C.D. Haffner, and T.K. Dougherty. J. Am. Chem. Soc. **108**, 4953 (1986).
22. A.S. Kende, S. Johnson, P. Sanfilippo, J.C. Hodges, and L.N. Jungheim. J. Am. Chem. Soc. **108**, 3512 (1986).
23. Y. Queneau, W.J. Krol, W.G. Bornmann, and A.S. Danishefshy. J. Org. Chem. **57**, 4043 (1992).
24. T. Doi, J. Robertson, G. Stork, and A. Yamashita. Tetrahedron Lett. **35**, 1481 (1994).
25. D.F. Grant and E.J. Gabe. J. Appl. Crystallogr. **11**, 114 (1978).
26. E.J. Gabe, F.L. Lee, and Y. Lepage. J. Appl. Crystallogr. **22**, 384 (1989).

Can. J. Chem. Downloaded from www.nrcresearchpress.com by 46.23.64.124 on 09/08/12
For personal use only.

Taxamycins: a new enediyne family with synthetic and biological potential

Yee-Fung Lu, Curtis W. Harwig, and Alex G. Fallis

Abstract: The Pd(0) based synthesis of two disilyl synthons (Z-1-trimethylsilyl-6-*tert*-butyldiphenylsilylhex-3-ene-1,5-diyne (**18**) and Z-1-trimethylsilyl-6-triisopropylsilylhex-3-ene-1,5-diyne (**19**)) and the selective removal of the trimethylsilyl group (K_2CO_3, MeOH) to afford **24** and **25** is described. These building blocks are employed in the construction of the taxamycin-12 compound **38** (16,17,18-trimethyl-2-methyloxymethoxy-9-hydroxybicyclo[9.3.1]pentadec-5-ene-3,7-diyne). The final ring closure to the 12-membered ring utilizes an intramolecular Cr–Ni mediated condensation of the iodoalkyne **37** (1,3,3-trimethyl-2-(2-oxoethyl)-4-(Z-1-methyloxymethoxy-7-iodohept-4-ene-2,6-diynyl)cyclohexene).

Key words: cancer, enediynes, synthesis, Pd(0) coupling.

Résumé : On décrit la synthèse, basée sur l'utilisation du Pd(0), de deux synthons disilyés (Z-1-triméthylsilyl-6-*tert*-butyldiphénylsilylhex-3-ène-1,5-diyne (**18**) et Z-1-triméthylsilyl-6-triisopropylsilylhex-3-ène-1,5-diyne (**19**)) et l'enlèvement sélectif du groupe triméthylsilyle (K_2CO_3, MeOH) pour conduire aux composés **24** et **25**. On a utilisé ces blocs pour la préparation du composé **38** (16,17,18-triméthyl-2-méthyloxyméthoxy-9-hydroxybicyclo[9.3.1]pentadéc-5-ène-3,5-diyne), un dérive de la taxamycine-12. La cyclisation finale du cycle à 12 chaînons fait appel à une condensation de l'iodoalcyne **37** (1,3,3-triméthyl-2-(2-oxoéthyl)-4-(Z-1-méthyloxyméthoxy-7-iodohept-4-ène-2,6-diynyl)cyclohexène) aidée par du Cr–Ni.

Mots clés : cancer, ènediynes, synthèse, couplage Pd(0).

[Traduit par la rédaction]

Introduction

Historically, medicinal leads have arisen from novel structures provided by nature. Frequently, it is not the natural products themselves that become drugs but modified forms of the original structure so that the actual therapeutic agents have improved biological activity. These changes minimize side effects, improve efficacy, and simplify the synthetic and manufacturing steps. The penicillins and tetracyclines provide well-known examples. In the antitumor cancer chemotherapy field, two quite different classes of natural products, the enediynes and taxoids, are receiving intense worldwide attention. The enediyne family forms an important new class of antitumor antibiotics that destroy cells by DNA cleavage. Compounds such as esperamicin A (**1**) (1) and calicheamicin γ_1 (**2**) (2) have generated widespread interest due to their novel mechanism of DNA cleavage (3) and the synthetic challenge these structures represent. Consequently, considerable effort is being devoted both to the synthesis of the natural products themselves (4) and a variety of structural analogues (5). (Esperamicin A_1 is currently in clinical trials in North America and Europe.)

Received June 5, 1995.

Y.-F. Lu, C.W. Harwig, and A.G. Fallis.[1] The Ottawa–Carleton Chemistry Institute, Department of Chemistry, University of Ottawa, Ottawa, ON K1N 6N5, Canada.

[1] Author to whom correspondence may be addressed. Telephone: (613) 562-5728. Fax: (613) 562-5170. E-mail: afallis@oreo.chem.uottawa.ca

In a similar manner, the potent antitumor agent paclitaxel (Taxol,® **1**) (6) and the related analog, docetaxel (Taxotere,® **2**) (7) have proven therapeutic utility as summarized in the preceding paper. These structures have also stimulated significant research interest due to their complex structure and novel mode of action with tubulin (8). The number of new biologically active analogues is growing rapidly and a better understanding of the key structure–activity relationships is slowly emerging (9). It has been established that in certain cases the paclitaxel side chain may be attached to modified nuclei with retention of respectable tubulin activity (10). Consequently, we have designed a new family of potentially biologically active agents called taxamycins and wish to report the synthesis of the parent nucleus **38** (preliminary communication, ref. 11).

Structures **5** and **6** are representative of the parent taxamycin-12 ring system (where the number represents the size of the ring containing the enediyne unit). Structure **7** summarizes some other members of this new family but many variations are possible depending upon the ring sizes and substitution patterns. It is anticipated that with suitable functionality in place these compounds will associate with tubulin in the cell. Equipped with an appropriate cycloaromatization trigger, they should aromatize and result in DNA or related damage by hydrogen abstraction. This will depend in part on the ring size, strain, and separation of the acetylenic termini.

The sequence by which DNA cleavage occurs in the esperamicin–calicheamicin duet involves nucleophilic attack on the trisulfide followed by conjugate addition. This reaction brings the two acetylene termini into bonding distance and

Can. J. Chem. Downloaded from www.nrcresearchpress.com by 46.23.64.124 on 09/08/12
For personal use only.

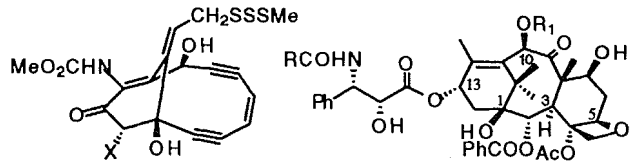

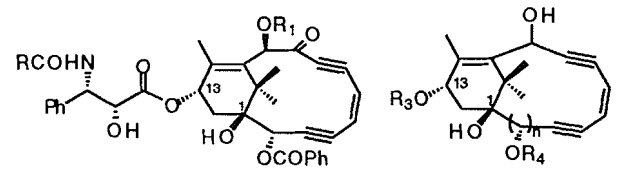

Bergman cyclization (12) ensues to form a *para*-benzyne intermediate. Preferential abstraction of the C5′ hydrogen from the deoxyribose followed by oxygenation and reduction generates a hemi-acetal, which collapses to the aldehyde causing the strand to break. Related analogs have been shown recently to exert similar effects and for some systems the aromatization sequence may be initiated by thiolate (13). These dynemicin models displayed considerable in vivo potency and activity. Similarly, a synthetic calicheamicin displayed good potency against several cancers including breast and ovarian cancers, areas where taxoids are also most effective (14). This emphasizes the medicinal potential of the molecules we intend to synthesize. They may be viewed as doubly armed warheads in the fight for control and destruction of cancerous cells.

The taxamycins are also of interest for their synthetic versatility both for the construction of aromatic systems in a direct fashion and for the capture of the *para*-benzyne intermediate to functionalize the benzenoid system under neutral conditions (15). This potential is summarized in Scheme 1 by the implicit conversion of **8** to **9**. In the cell, DNA damage should occur, while in the laboratory *para* functionalization may generate **10** for taxoid synthesis. Several approaches for the total synthesis of taxol utilize benzenoid intermediates for the preparation of the C ring (16) and some recent ring C aromatic systems have displayed interesting biological activity (10*c*). The synthesis of the taxamycin-12 **38** has been examined in order to investigate these various possibilities, including the synthetic utility of the Bergman cycloaromatization in these large rings and the factors responsible for biradical formation in this series.

Results and discussion

The initial synthetic approach envisaged the use of the protected diol acetylene **14**, which was prepared from the ring A synthon, aldehyde **11**, described in the preceding paper (Chart 1). This aldehyde **11** was condensed with the lithium trimethylsilylacetylide to afford **12** as a mixture of diastereomers (1:1). The trimethylsilyl group was removed with KOH at room temperature (21°C) and the secondary alcohol protected as its MOM ether. Unfortunately, under various conditions the

Scheme 1. Taxamycin-12 cyclization potential.

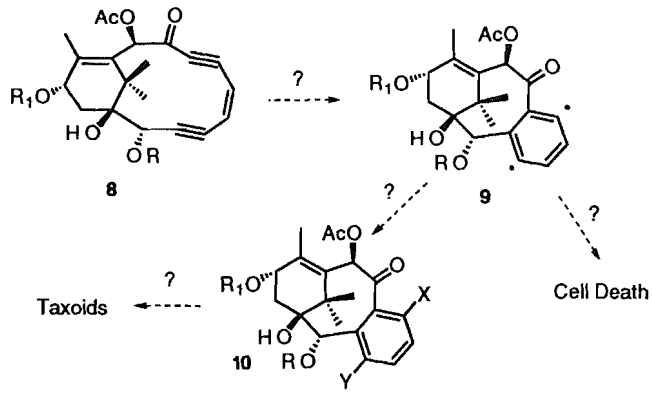

Chart 1. Initial clockwise approach to a taxamycin.

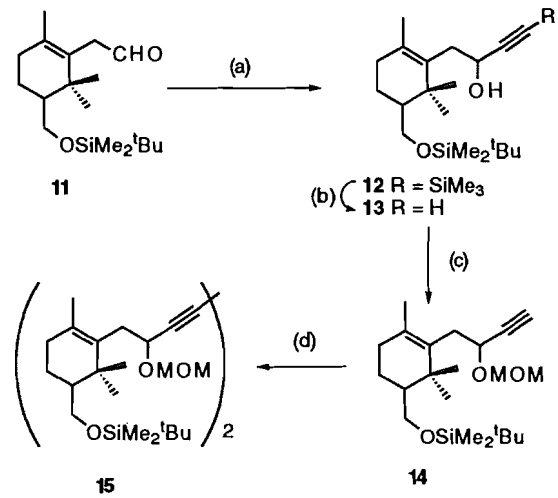

(a) HCCTMS, ^{n}BuLi, THF, −78–21°C, 1.5 h, 93%; (b) KOH, MeOH/CH_2Cl_2 (1:1), 21°C, 4 h, 90%; (c) MOMCl, $EtN^i(Pr)_2$, CH_2Cl_2, 21°C, 16 h, 70%; (d) ClCH=CHCCTMS, $Pd(Ph_3P)_4$, ^{n}BuNH$_2$, CuI, Et_2O, 21°C, 16 h, 95%.

Pd(0)–CuI mediated coupling failed to give the desired enediyne and afforded the dimer **15** (95%) instead. Competitive dimerizations have also interfered with other enediyne syntheses (17). To circumvent this problem a versatile approach based on preconstructed enediyne building blocks was selected. These compounds **17**–**19** should suffice for a variety of objectives.

The use of the dilithio salts derived from **16** to insert the enediyne chromophore was examined previously with variable results and requires the handling of a very volatile precursor (18). Our initial attempts to prepare systems such as **17** with different elements, for example silicon and tin, at the terminal acetylenes were disappointing. It is well established that

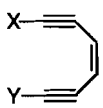

16 X = Y = H
17 X = Me_3Si, Y = Me_3Sn
18 X = Me_3Si, Y = ^{t}BuPh$_2$Si
19 X = Me_3Si, Y = ^{i}Pr$_3$Si

Can. J. Chem. Downloaded from www.nrcresearchpress.com by 46.23.64.124 on 09/08/12
For personal use only.

Chart 2. Synthesis of enediyne synthons.

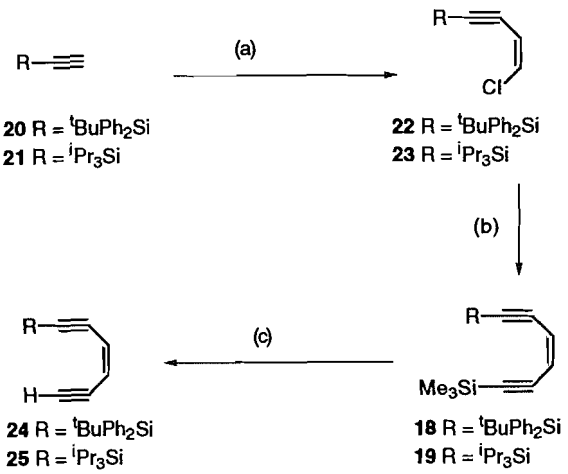

(a) ClCH=CHCl, $Pd(Ph_3P)_4$, $^nBuNH_2$, CuI, Et_2O, 21°C, 15 h, 83–95%; (b) HCCTMS, $Pd(Ph_3P)_4$, $^nBuNH_2$, CuI, Et_2O, 21°C, 16 h, 64–78%; (c) K_2CO_3, MeOH, C_6H_6, 21°C, 2 h, 90–95%.

the rates of base-induced cleavage of silylalkynes depend upon the relative steric bulk of the groups involved. (Relative rates: Et_3Si (1), Ph_3Si (12), $EtMe_2Si$ (49), Me_3Si (277) (ref. 19).) This should allow selective protection and release of the appropriate silyl group at the terminus of interest. Thus the synthesis of two suitable building blocks, Z-1-trimethylsilyl-6-*tert*-butyldiphenylsilyhex-3-ene-1,5-diyne (**18**) and Z-1-trimethylsilyl-6-triisopropylsilylhex-3-ene-1,5-diyne (**19**) was examined. As outlined in Chart 2, these compounds were prepared by repetitive Pd(0) based coupling followed by removal of the trimethylsilyl group in K_2CO_3–methanol. The triisopropyl system **25** has proven more useful than **24**. This is a consequence of the bulk and polarity of *tert*-butyldiphenylsilyl fluoride and the difficulty encountered upon chromatographic separation (silica gel) of this material from the enediyne-alcohol product in some cases. Schreiber and co-workers (20) have used a related compound, 1-*tert*-hexyldimethylsilylhex-1,5-diyne-3-ene, to introduce the enediyne unit.

For the synthesis of the model taxamycin system, the cyanoaldehyde **26** was prepared from Hagemann's ester as described in the preceding paper for the synthesis of the taxane nucleus by an intramolecular Diels–Alder approach (21). The lithium acetylide derived from **25** was condensed with **26** (Chart 3) to afford a 4:1 mixture of alcohol diastereomers. Protection of the secondary hydroxyl of the major diastereomer as its monomethyl ether proceeded slowly but smoothly to give **27** (98%). Diisobutylaluminum hydride reduction of the nitrile function in **27** could be terminated at the aldehyde stage to generate **29** directly or could be reduced further with additional reagent to generate the primary alcohol **34**. A variety of methods have been examined for the intramolecular ring closure of medium-sized cyclic enediynes, particularly for 10-membered rings that mimic calicheamicin and esperamicin. These include ring contraction of a cyclic ether by [2,3]-Wittig rearrangement (5*e*), Nicholas-type cyclization of η^2-dicobalthexacarbonyl complexed propargylic cations with Lewis acid (5*d*), direct condensation of the acetylenic anion with an aldehyde (18*a*, 22), fluoride-induced desilylation–condensation (17*a*, 23), and chromium(II)-mediated coupling of an iodoacetylene and an aldehyde (24).

Chart 3. Synthesis of the taxamycin-12 compound **40**.

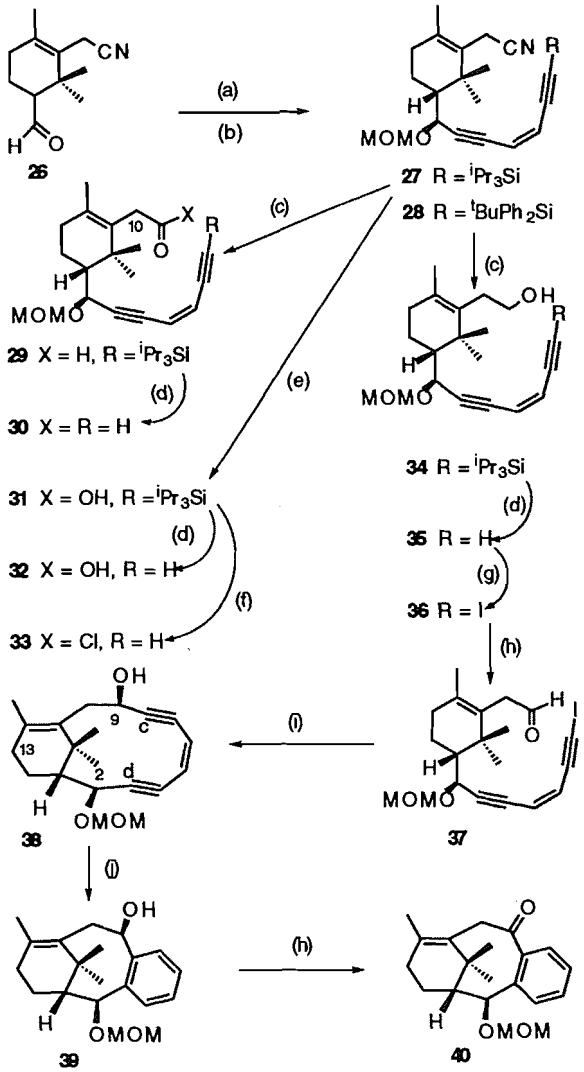

(a) **24** or **25**, ^{n}BuLI, THF, −78–0°C, 1 h, 94%; (b) MOMCl, $EtN^i(Pr)_2$, CH_2Cl_2, 21°C, 16 h, 98%; (c) DIBAL-H, CH_2Cl_2, −78–0°C, 2 h, 66%; (d) $^nBu_4NF$, THF, −78°C, 2 h, 86%; (e) DIBAL-H, CH_2Cl_2, −78°C, 1 h, aq NH_4Cl; ^{t}BuOH/CH_2Cl_2 (2:1), $NaClO_2$, NaH_2PO_4, 30% H_2O_2, 21°C, 16 h, 74%; (f) $(COCl_2)$, THF, 21°C, 2 h; (d); (g) morpholine, I_2, C_6H_6, 40°C, 2 h, 86%; (h) PDC, CH_2Cl_2, 21°C, 16 h, 82%; (i) $CrCl_2$, $NiCl_2$ (cat.), THF, 21°C, 4 h, 60%; (j) sealed tube, microwave, 4 h; (h) PDC, CH_2Cl_2, 21°C, 6 h.

In spite of the success of fluoride-mediated desilylation – intramolecular condensation of silyl acetylenes with aldehydes in other systems, this direct, concurrent desilylation–cyclization with **29** to **38** did not occur under a variety of conditions. Completely anhydrous fluoride sources such as tretrabutylammonium difluorotriphenylstannate (25) also suppressed desilylation. Thus it proved most efficient to prepare **30** directly with tetrabutylammonium fluoride CsF in THF. Similarly the direct anionic condensation was unsatisfactory,

Can. J. Chem. Downloaded from www.nrcresearchpress.com by 46.23.64.124 on 09/08/12
For personal use only.

Can. J. Chem. Downloaded from www.nrcresearchpress.com by 46.23.64.124 on 09/08/12
For personal use only.

including the use of $Sn(OTf)_2$ and 1,8-bis(dimethylamino)naphthalene (26). A complication in the present example is the fact that the ring size is larger (12-membered) than any of the reported cases. In addition, the C10 hydrogens (Taxol® numbering) are both allylic and adjacent to the aldehyde so their acidity is higher than that of the acetylene proton. In an attempt to overcome these difficulties the acid chloride **33** was prepared from the corresponding carboxylic acid **31**. This was obtained from the nitrile **27** by diisobutylaluminum hydride reduction followed by sodium chloride – hydrogen peroxide oxidation (27). Unfortunately, treatment of the acid chloride under various conditions, including Pd(0) or base, was unsuccessful. In the latter case it was anticipated that ketene formation would be competitive with acetylene anion formation and the corresponding flattening of the reactive components would bring them closer together to encourage addition. In simple systems we have developed a procedure to add lithium acetylides to dimethoxy acetals in the presence of zinc chloride and boron trifluoride etherate.[2] Unfortunately, except for model aldehydes, the yields with these silyl-substituted enediynes have been poor (10–15%). In the case of aldehyde **30** attempts to form the dimethoxy acetal with cerium trichloride or other catalysts failed.

In view of the success of the $CrCl_2$–$NiCl_2$ based coupling of iodoacetylenes with aldehydes to form smaller enediyne ring systems, this approach was examined next. Desilylation of **34** with tretrabutylammonium fluoride in THF and conversion of the resulting alkyne **35** into the alkynyliodide **36** was accomplished with morpholine and iodine (86%). The primary alcohol was oxidized to the aldehyde **37** with pyridinium dichromate (82%). The desired ring closure was effected smoothly with the nickel-catalyzed chromium-based procedure to provide the bicyclo[9.3.1]pentadecadienediyne system **38** in 60% isolated yield. Recent studies (28) have used THF as the solvent and found that the yields for 10-membered rings were almost as high in the absence of $NiCl_2$. A single diastereomer of **38** was formed. Based on molecular models, preferential attack from the bottom (si face) was anticipated and thus it seems likely the new secondary alcohol at C9 is *syn* relative to the C2 MOM group. This stereochemical result is consistent with related intramolecular cases in which the same stereochemical preference was observed for closure to 10-membered rings (22*c*).

The cycloaromatization of **38** was examined to ascertain the potential for direct entry to aromatic taxanes without triggering devices or saturation of the cyclohexene double bond. Thus **38** was heated for 4 h in a sealed tube in toluene in a microwave oven. The crude alcohol **39** was oxidized directly with pyridinium dichromate to provide the aromatic ketone **40** (5% from **38**) prepared previously by a Diels–Alder-aromatization route (preceding paper). Clearly this is not a viable synthetic route to aromatic taxanes at present. Molecular mechanics calculations indicated that the c–d distance in **41** is ~3.8 Å and thus this separation is significantly larger than the separation of ~3.1 Å required for spontaneous cyclization. This separation is less than the simplest enediyne system **43** (*cis*-3-hexene-1,5-diyne) with a separation of approximately 4.1 Å, which underwent cycloaromatization – ring opening above 200°C with low efficiency. Recent calculations have determined that this reaction is endothermic by 13 kcal/mol. In contrast, the related allene system **46**, with a c–d separation of ~3.4 Å in the most favorable conformation for cyclization, closes much more readily and is exothermic by 15 kcal/mol (29). Literature examples display this same relative ease of cyclization (17*b*). As summarized in Chart 4, the lower taxamycin homologues **44** and **45** reduce the c–d separation by approximately 0.1 Å. Isomerization of the double bond away from the bridgehead as in **42** results in a 0.5 Å improvement. These features suggest that synthetic modifications to this family will in the future yield useful synthons that cycloaromatize more easily.

Chart 4. Calculation summary of c–d separations.

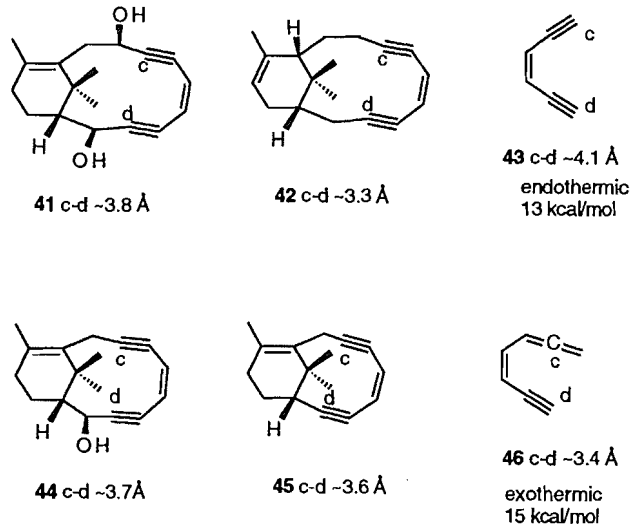

In conclusion, the directness of this approach to enediyne systems, using the disilyl-enediyne unit **19** followed by an intramolecular Ni–Cr mediated coupling, should prove beneficial for a variety of synthetic objectives. These include the cycloaromatization of more highly functionalized skeletons to aromatic taxoids and the synthesis of ring-contracted taxamycin-10 nuclei that should mimic their esperamicin and calicheamicin relatives.

2

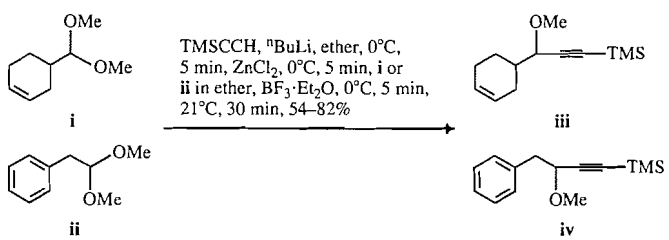

Experimental

For general experimental see preceding paper.

4-*tert*-Butyldimethylsilyloxymethyl-1,3,3-trimethyl-2-(2-hydroxy-4-trimethylsilyl-3-butynyl)cyclohexene (12)

A solution of *n*-butyllithium (0.27 mL, 0.675 mmol, 2.5 M) in hexane was added dropwise to a cold (−78°C), stirred, solution of trimethylsilylacetylene (0.095 mL, 0.672 mmol) in dry THF (5 mL). After 30 min at −78°C, a solution of the alde-

Can. J. Chem. Downloaded from www.nrcresearchpress.com by 46.23.64.124 on 09/08/12
For personal use only.

hyde **11** (140 mg, 0.451 mmol) in dry THF (2 mL) was added dropwise and the resulting mixture was stirred at −78°C for 1 h. Saturated aqueous ammonium chloride solution was added and the mixture was warmed to 21°C (room temperature) and extracted with diethyl ether. The combined ether extracts were washed with brine and dried. Concentration of the organic material afforded 171 mg (93%) of the alcohol **12** (1:1 ratio). IR (neat): 3384, 2921, 2171, 1462, 1253, 844 cm^{-1}; ^1H NMR (200 MHz) δ: 0.00 (br s, 6H), 0.15 (br s, 9H), 0.86 (br s, 12H), 1.08 (br s, 3H), 1.10–1.60 (m, 1H), 1.69 (br s, 3H), 1.70–1.89 (m, 2H), 1.90–2.05 (m, 2H), 2.52 (br d, 2H, J = 6 Hz), 3.34 (br s, 1H, J = 10 Hz), 3.75 (br dd, 1H, J = 10, 3 Hz), 4.40–4.55 (m, 1H); MS (CI): 409 (MH^+, $C_{23}H_{44}O_2Si_2$).

4-*tert*-Butyldimethylsilyloxymethyl-1,3,3-trimethyl-2-(2-hydroxy-3-butynyl)cyclohexene (13)

A solution of potassium hydroxide (200 mg, 3.57 mmol) in methanol (5 mL) was added to a stirred solution of the alcohol **12** (171 mg, 0.419 mmol) in dichloromethane (5 mL). The resulting mixture was stirred for 4 h at 21°C. The organic solvent was removed under reduced pressure to provide a yellow oil. A mixture of diethyl ether/water (1:1) was added and the solution was extracted with diethyl ether. The combined ether extracts were washed with brine and dried. Concentration afforded alcohol **13**, 126 mg (90%, 1:1 ratio). IR (neat): 3400, 3307, 2917, 1466, 1254, 1069, 843, 776 cm^{-1}; ^1H NMR (200 MHz) δ: 0.016 (br s, 12H), 0.86 (br s, 18H), 0.88 (br s, 6H), 1.07 (br s, 6H), 1.69 (br s, 6H), 0.9–2.0 (m, 13H), 2.4–2.6 (m, 4H), 3.34 (br t, 2H, J = 10 Hz), 3.69–3.80 (m, 2H), 4.49 (br t, 2H, J = 8 Hz); MS (CI): 337 (MH^+, $C_{20}H_{36}O_2Si$).

4-*tert*-Butyldimethylsilyloxymethyl-1,3,3-trimethyl-2-(2-methoxymethylether-3-butynyl)cyclohexene (14)

Chloromethyl methyl ether (0.043 mL, 0.566 mmol, Aldrich) was added to a cold (0°C) solution of the alcohol **13** (0.126 g, 0.376 mmol) and diisopropylethylamine (0.100 mL, 0.574 mmol) in dry dichloromethane (5 mL) and the solution stirred at 21°C for 16 h. Additional chloromethyl methyl ether (0.0285 mL, 0.376 mmol) and diisopropylethylamine (0.065 mL, 0.375 mmol) were added and the mixture was stirred for another 16 h. Water was added and the mixture was extracted thoroughly with dichloromethane. The combined organic extracts were washed with brine, dried, and concentrated. Chromatography of the residual oil (20:1; petroleum ether/diethyl ether) afforded 0.099 g (70%) of the ether **14** (1:1 ratio). IR (neat): 3301, 2925, 2113, 1465, 1090 cm^{-1}; ^1H NMR (200 MHz) δ: 0.02 (br s, 12H), 0.87 (br s, 18H), 1.07 (br s, 6H), 1.53 (br s, 6H), 1.67 (br s, 6H), 1.2–2.0 (m, 12H), 2.3–2.4 (m, 2H), 2.52 (br d, 4H, J = 8 Hz), 3.29 (s, 3H), 3.32 (s, 3H), 3.3–3.4 (m, 2H), 3.7–3.8 (m, 2H), 4.38–4.55 (m, 4H), 4.86 (d, 1H, J = 6 Hz), 4.89 (d, 1H, J = 6 Hz); MS (CI): 381 (MH^+, $C_{22}H_{40}O_3Si$). Anal. calcd. for $C_{22}H_{40}O_3Si$: C 69.42, H 10.59; found: C 69.48, H 10.59.

Bis-4-*tert*-butyldimethylsilyloxymethyl-1,3,3-trimethyl-2-(2-methoxymethylether-3-butynyl)cyclohexene (15)

An anhydrous ether solution (50 mL) containing the chloride **22** (0.082 g, 0.517 mmol), acetylene **14** (0.666 g, 0.174 mmol), *n*-butylamine (0.034 mL, 0.343 mmol), tetrakistriphenylphosphine palladium (0.010 g, 0.009 mmol, Aldrich), and cuprous iodide (0.002 g, 0.010 mmol) was stirred at 21°C for 16 h. Concentration followed by chromatography (9:1; petroleum ether/diethyl ether) afforded the dimer **15**, 0.061 g (69%, 1:1 ratio. IR (neat): 2919, 2157, 1467, 1253, 1095, 1028, 848 cm^{-1}; ^1H NMR (200 MHz) δ: 0.17 (br s, 24H), 0.20 (br s, 36H), 0.86 (br s, 24H), 1.05–1.98 (m, 8H), 1.53 (s, 24H), 2.52 (br d, 8H, J ~ 8 Hz), 3.28 (s, 12H), 3.31 (s, 12H), 3.41 (m, 4H), 3.75 (d m, 4H), 4.48 (m, 8H), 4.85 (m, 4H).

***Z*-1-Chloro-4-triisopropylsilylbutene-3-yne (23)**

An anhydrous diethyl ether solution (50 mL) containing triisopropyl acetylene (1.98 g, 10.8 mmol, Aldrich), 1,2-*cis*-dichloroethylene (1.63 mL, 21.0 mmol, Aldrich), *n*-butylamine (2.10 mL, 21.6 mmol), tetrakistriphenylphosphine palladium (0.376 g, 0.30 mmol, Aldrich), and cuprous iodide (0.061 g, 0.30 mmol) were stirred at 21°C for 15 h. The reaction mixture was concentrated and chromatographed (silica gel, petroleum ether) to provide the eneyne **23** (2.17 g, 83%). IR (neat): 2945, 2154, 1463, 882, 671 cm^{-1}; ^1H NMR (200 MHz) δ: 1.06 (s, 3H), 1.08 (s, 18H), 5.88 (d, 1H, J = 7.4 Hz), 6.37 (d, 1H, J = 7.4 Hz); ^{13}C NMR (50 MHz) δ: 11.2 (3C), 18.6 (6C), 100.1, 100.7, 112.3, 129.2; HRMS (EI) calcd. for $C_{13}H_{23}SiCl$: 242.1257; found: 242.1285.

***Z*-1-Trimethylsilyl-6-triisopropylsilylhex-3-ene-1,5-diyne (19)**

An anhydrous ether solution (50 mL), containing the chloride **23** (1.96 g, 8.07 mmol), trimethylsilyl acetylene (2.27 mL, 223 mmol), *n*-butylamine (1.60 mL, 16.2 mmol), tetrakistriphenylphosphine palladium (0.280 g, 0.242 mmol, Aldrich), and cuprous iodide (0.046 g, 0.241 mmol) was stirred at 21°C for 16 h. The brown residue obtained upon concentration under reduced pressure was chromatographed (petroleum ether) to afford enediyne **19** (1.91 g, 78%). IR (neat): 2948, 2153, 2121, 1250, 1069, 848 cm^{-1}; ^1H NMR (200 MHz) δ: 0.17 (s, 9H), 1.04–1.10 (br s, 21H), 5.83 (s, 2H); ^{13}C NMR δ: 0.22 (3C), 11.2 (3C), 18.7 (6C), 99.8, 101.9, 102.9, 103.8, 120.0, 120.4; HRMS (EI) calcd. for $C_{18}H_{32}Si_2$: 304.2042; found: 304.2032.

***Z*-1-Triisopropylsilylhex-3-ene-1,5-diyne (25)**

Potassium carbonate (0.11 g, 0.80 mmol) was added to a benzene/methanol solution (1:1, 10 mL) containing **19** (0.217 g, 0.713 mmol) and the resulting mixture stirred at 21°C for 2 h. The solvent was removed, water added, and the mixture extracted thoroughly with diethyl ether. The combined ether extracts were washed with brine, dried, filtered, and concentrated to give **25** (0.157 g, 95%). IR (neat): 3303, 2945, 2149, 1463, 1049, 882, 746 cm^{-1}; ^1H NMR (200 MHz) δ: 1.0–1.1 (br s, 21H), 3.29 (dd, 1H, J = 0.8, 2.2 Hz), 5.79 (dd, 1H, J = 2.2, 11 Hz), 5.93 (dd, 1H, J = 0.8, 11 Hz); ^{13}C NMR (50 MHz) δ: 11.2 (3C), 18.6 (3C), 80.8, 84.8, 100.1, 103.3, 119.3, 121.9; HRMS (EI) calcd. for $C_{15}H_{24}Si$: 189.1099; found: 189.1100.

***tert*-Butyldiphenylsilylacetylene (20)**

tert-Butyldiphenylsilyl chloride (1.45 mL, 5.57 mmol, Aldrich) was added to a cold (0°C), stirred solution of lithium acetylide – ethylene diamine complex (0.618 g, 6.70 mmol) in anhydrous THF (30 mL). The resultant solution was stirred at 0°C for 1 h and warmed to 21°C for 16 h. Water was added slowly and the mixture was extracted thoroughly with diethyl ether. The combined organic extracts were washed with brine,

Can. J. Chem. Downloaded from www.nrcresearchpress.com by 46.23.64.124 on 09/08/12
For personal use only.

dried ($MgSO_4$), and concentrated. The residual oil was recrystallized from petroleum ether/diethyl ether (1:1), to provide **20** (1.15 g, 65%): IR (KBr): 3266, 2943, 2034 cm^{-1}; ^1H NMR (200 MHz) δ: 1.08 (s, 9H), 2.69 (s, 1H), 7.30–7.40 (m, 6H), 7.70–7.80 (m, 4H); ^{13}C NMR δ: 18.4, 27.0 (3C), 85.4, 97.3, 127.8 (4C), 129.7 (2C), 132.7 (2C), 135.6 (4C); HRMS (EI) calcd. for $C_{18}H_{20}Si$: 264.1334; found: 264.1343.

Z-1-Trimethylsilyl-6-*tert*-butyldiphenylsilylhex-3-ene-1,5-diyne (18)

Copper(I) iodide (0.017 g, 0.089 mmol) was added to a stirred anhydrous diethyl ether solution (20 mL) containing the acetylene **20** (0.776 g, 2.94 mmol), *n*-butylamine (0.58 mL, 5.86 mmol), *cis*-1,2-dichloroethylene (0.44 mL, 5.83 mmol), and $Pd(Ph_3P)_4$ (0.10 g, 0.0865 mmol, Aldrich). The greenish reaction mixture was stirred at 21°C for 16 h and the resultant brownish mixture concentrated. The residual oil was chromatographed (3:1, petroleum ether/diethyl ether) to afford 0.871 g of the vinyl chloride **22** as a yellowish oil that was used directly in the next reaction. ^1H NMR (200 MHz) δ: 1.10 (s, 9H), 6.02 (d, 1H, J = 8 Hz), 6.50 (d, 1H, J = 8 Hz), 7.30–7.40 (m, 6H), 7.70–7.90 (m, 4H).

Copper(I) iodide (0.007 mmol) was added to a stirred, anhydrous, diethyl ether solution (20 mL) containing trimethylsilylacetylene (0.750 mL, 5.31 mmol), *n*-butylamine (0.53 mL, 5.36 mmol), $Pd(Ph_3P)_4$ (0.07 g, 0.060 mmol), and the vinyl chloride **22**. The reaction mixture was stirred at 21°C for 16 h and then concentrated. The black residual oil was chromatographed (petroleum ether) to afford 0.665 g (64%) of the enediyne **18**. IR (neat): 2948, 2154, 2122, 1428, 1109, 1070, 843, 700 cm^{-1}; ^1H NMR (200 MHz) δ: 0.13 (s, 9H), 1.10 (s, 9H), 5.94 (s, 2H) 7.30–7.40 (m, 6H), 7.70–7.80 (m, 4H); HRMS (EI) calcd. for $C_{21}H_{21}Si_2$ (M^+ − *tert*-butyl): 329.1181; found: 329.1163.

Z-1-*tert*-Butyldiphenylsilylhex-3-ene-1,5-diyne (24)

A benzene solution (5 mL) of **18** (0.662 g, 1.71 mmol) was added to a stirred solution of potassium bicarbonate (0.260 g, 1.88 mmol) in methanol (10 mL). The reaction mixture was stirred at 21°C for 3 h and then concentrated. Water was added and the mixture was extracted thoroughly with diethyl ether. The combined ether extracts were washed with brine, dried ($MgSO_4$), and concentrated to give 0.508 g (94%) of the enediyne **24**. IR (neat): 3293, 2944, 2152, 1428, 1187, 1051 cm^{-1}; ^1H NMR (200 MHz) δ: 1.10 (s, 9H), 3.38 (d, 1H, J = 4 Hz), 5.92 (dd, 1H, J = 4, 10 Hz), 6.05 (d, 1H, J = 10 Hz), 7.30–7.45 (m, 6H), 7.75–7.90 (m, 4H); HRMS (EI) calcd. for $C_{18}H_{13}Si$(M^+ − *tert*-butyl): 257.0787; found: 257.0792.

1,3,3-Trimethyl-2-cyanomethyl-4-(*Z*-1-methyloxymethoxy-7-triisopropylsilylhept-4-ene-2,6-diynyl)cyclohexene (27)

A solution of *n*-butyllithium (1.45 mL, 3.62 mmol, 2.5 M) in hexane was added dropwise to a cold (−78°C), stirred solution of the enediyne **25** (0.837 g, 3.61 mmol) in dry THF (30 mL). After stirring at −78°C for 15 min, a solution of (1,3,3-trimethyl-2-cyanomethyl-4-formyl)cyclohexene (**26**) (0.541 g, 2.83 mmol) in dry THF (5 mL) was added dropwise. The reaction was stirred at −78°C for further 1 h, warmed to 0°C for an additional hour, and water added. The mixture was warmed to room temperature and extracted thoroughly with diethyl ether. The combined ether extracts were washed with brine, dried ($MgSO_4$), and concentrated. The residual oil was chromatographed (5:1, petroleum ether/diethyl ether) to afford 1.13 g (94%) of the alcohol (4:1 epimeric ratio). Major diastereomer, IR (neat): 3450, 2914, 2247, 2140, 1462, 1018, 883, 669 cm^{-1}; ^1H NMR (300 MHz) δ: 1.02 (s, 3H), 1.06 (br s, 3H), 1.08 (br s, 18H), 1.15 (s, 3H), 1.59 (d, 1H, J = 4 Hz), 1.62–1.69 (m, 2H), 1.72 (s, 3H), 1.84–1.94 (m, 1H), 2.01–2.15 (m, 2H), 2.97 (AB, 2H, J = 12 Hz), 4.82 (br d, 1H, J = 4 Hz), 5.83 (br s, 2H); ^{13}C NMR (75 MHz) δ: 11.21 (3C), 16.25, 18.64 (3C), 18.83, 20.17, 21.17, 26.67, 32.42, 38.27, 50.89, 62.92, 82.19, 98.55, 99.70, 103.6, 118.9, 119.4, 120.0, 127.6, 133.8; HRMS (EI) calcd. for $C_{24}H_{34}ONSi$ (M^+ − isopropyl): 280.2410; found: 280.2424.

Chloromethyl methyl ether (0.23 mL, 3.03 mmol, Aldrich) was added to a cold (0°C) dichloromethane solution (25 mL) of the alcohol (0.863 g, 2.04 mmol) and diisopropylethylamine (0.71 mL, 4.07 mmol). The resultant solution was stirred at 0°C for 10 min and warmed to 21°C for 16 h. Water was added and the mixture was extracted thoroughly with diethyl ether. The combined organic extracts were washed sequentially with aqueous 10% HCl, water, brine, dried, filtered, and concentrated to provide the ether **27** (0.934 g, 98%). IR (neat): 2913, 2247, 2140, 1455, 1066, 883, 667 cm^{-1}; ^1H NMR (200 MHz) δ: 1.02 (s, 3H), 1.06 (s, 21H), 1.16 (s, 3H), 1.71 (s, 3H), 1.59 (d, 1H, J = 4 Hz), 1.60–1.80 (m, 2H), 1.85–2.00 (m, 1H), 2.00–2.15 (m, 2H), 2.96 (br s, 2H), 3.36 (s, 3H), 4.52 (d, 1H, J = 6.6 Hz), 4.73 (br s, 1H), 4.95 (d, 1H, J = 6.6 Hz), 5.83 (s, 2H); ^{13}C NMR (50 MHz) δ: 11.2 (3C), 16.3, 18.6 (6C), 19.8, 20.2, 22.1, 26.8, 32.7, 38.3, 50.3, 56.6, 66.7, 83.0, 94.7, 96.4, 99.5, 103.6, 119.0, 119.4, 119.6, 129.5, 133.8; HRMS (EI) calcd. for $C_{26}H_{38}O_2NSi$ (M^+ − isopropyl): 424.2671; found: 424.2655. Anal. calcd. for $C_{29}H_{45}O_2NSi$: C 74.46, H 9.70; found: C 74.43, H 9.88.

1,3,3-Trimethyl-2-cyanomethyl)-4-(*Z*-1-methyloxymethoxy-7-*tert*-butyldiphenylsilylhept-4-ene-2,6-diynyl)cyclohexene (28)

A solution of *n*-butyllithium (0.21 mL, 0.53 mmol, 2.5 M) in hexane was added dropwise to a cold (−78°C), stirred solution of the enediyne **24** (0.162 g, 0.517 mmol) in dry THF (8 mL). The black solution was stirred at −78°C for 15 min and a solution of (1,3,3-trimethy-2-cyanomethyl-4-formyl)cyclohexene (**26**) (0.090 g, 0.471 mmol) in dry THF (2 mL) was added dropwise. The reaction was stirred at −78°C for 1 h further, warmed to 0°C for an additional hour, and water added. The mixture was warmed to 21°C and extracted thoroughly with diethyl ether. The combined ether extracts were washed with brine, dried, and concentrated. The residual black oil was chromatographed (3:1, petroleum ether/diethyl ether) to afford 0.205 g (85%) of the alcohol (3:1 epimeric ratio). Major diastereomer, IR (neat): 3454, 2918, 2247, 2144, 1026 cm^{-1}; ^1H NMR (200 MHz) δ: 0.90 (s, 3H), 1.02 (s, 3H), 1.06 (s, 9H), 1.62 (s, 3H), 0.8–2.10 (m, 5H), 2.7–3.05 (m, 2H), 3.30 (s, 3H), 4.40 (d, 1H, J = 6.7 Hz), 4.75 (br d, 1H, J = 8 Hz), 4.93 (d, 1H, J = 6.7 Hz), 5.96 (br s, 2H), 7.3–7.4 (m, 6H), 7.7–7.85 (m, 4H).

Chloromethyl methyl ether (0.072 mL, 0.948 mmol, Aldrich) was added to a cold (0°C) dichloromethane solution (6 mL) of the alcohol (0.321 g, 0.636 mmol) and diisopropylethylamine (0.27 mL, 1.55 mmol). The resultant solution was

Can. J. Chem. Downloaded from www.nrcresearchpress.com by 46.23.64.124 on 09/08/12
For personal use only.

stirred at 0°C for 10 min and warmed to 21°C for 16 h. Water was added and the mixture was extracted thoroughly with dichloromethane. The combined organic extracts were washed sequentially with aqueous 10% HCl, water, brine, dried, filtered, concentrated, and chromatographed (3:1, petroleum ether/diethyl ether) to provide the ether **28** (0.271 g, 78%). IR (neat): 2913, 2247, 2140, 1455, 1066, 883, 667 cm^{-1}; ^1H NMR (200 MHz) δ: 0.95 (s, 3H), 1.07 (s, 3H), 1.08 (s, 9H), 1.54 (s, 3H), 1.5–1.9 (m, 5H), 2.89 (AB, 2H, $J \sim 18$ Hz), 3.30 (s, 3H), 4.40 (d, 1H, $J = 6.7$ Hz), 4.70 (br s, 1H), 4.91 (d, 1H, $J = 6.7$ Hz), 5.96 (br s, 2H), 7.3–7.42 (m, 6H), 7.75–7.82 (m, 4H); ^{13}C NMR (50 MHz) δ: 16.3, 18.7, 19.9, 20.2, 22.1, 26.8, 27.1 (3C), 32.5, 38.2, 50.2, 56.6, 66.7, 83.0, 94.7, 97.8, 97.9, 105.6, 119.0, 119.3, 120.6, 120.7, 127.3, 127.8 (4C), 129.6 (2C), 132.9, 133.8; HRMS (EI) calcd. for $C_{32}H_{34}O_2NSi$: 492.2358; found: 492.2349.

1,3,3-Trimethyl-2-(2-oxoethyl)-4-(*Z*-1-methyloxymethoxy-7-triisopropylsilylhept-4-ene-2,6-diynyl)cyclohexene (29)

A toluene solution of diisobutylaluminum hydride (1 M, 0.58 mL, 0.58 mmol, Aldrich) was added dropwise to a cold (−78°C), stirred solution of the nitrile **27** (0.136 g, 0.291 mmol) in dry dichloromethane (5 mL). The reaction was stirred at −78°C for 1 h and warmed to 0°C for an additional hour. Dilute HCl (aqueous 5%) was added, the mixture was stirred at 21°C for 30 min, and the solution was extracted thoroughly with diethyl ether. The combined organic extracts were washed with water, brine, dried, filtered, and concentrated and the residual oil was chromatographed (3:1, petroleum ether/diethyl ether) to afford 0.091 g (66%) of the aldehyde **29**. IR (neat): 2914, 2718, 2141, 1723, 1463, 1029, 883 cm^{-1}; ^1H NMR (200 MHz) δ: 0.98 (s, 3H), 1.06 (s, 24H), 1.55 (s, 3H), 1.60–1.84 (m, 2H), 1.85–2.00 (m, 1H), 2.00–2.20 (m, 2H), 3.07 (br s, 1H), 3.35 (br s, 1H), 3.36 (br s, 3H), 4.53 (d, 1H, $J =$ 8 Hz), 4.73 (br s, 1H), 4.95 (d, 1H, $J = 8$ Hz), 5.82 (br s, 2H), 9.47 (t, 1H, $J = 1.5$ Hz); ^{13}C NMR (75 MHz) δ: 11.3 (3C), 18.7 (6C), 20.1, 22.3, 27.1, 32.9, 43.8, 50.7, 56.6, 66.9, 82.8, 93.7, 94.7, 96.7, 99.4, 103.5, 119.4, 128.7, 132.5, 201.0; HRMS (EI) calcd. for $C_{27}H_{41}O_2Si$ (M^+ − isopropyl): 425.2876; found: 425.2877.

1,3,3-Trimethyl-2-(2-oxoethyl)-4-(*Z*-1-methyloxymethoxyhept-4-ene-2,6-diynyl)cyclohexene (30)

A dry THF solution (6 mL) of the silyl acetylene **29** (0.038 g, 0.107 mmol) was cooled to −78°C and then a 1 M solution of *n*-tetrabutyl ammonium fluoride (0.11 mL, 0.11 mmol) added dropwise. The reaction was stirred at −78°C for 2 h, water was added, and the resultant solution was extracted thoroughly with diethyl ether. The combined ether extracts were washed with brine, dried ($MgSO_4$), filtered, and concentrated and the residual oil was chromatographed (3:1, petroleum ether/diethyl ether) to give 0.027 g (86%) of the acetylene **30**. IR (neat): 3275, 2918, 2720, 2094, 1720, 1462, 1150, 1000 cm^{-1}; ^1H NMR (200 MHz) δ: 0.99 (s, 3H), 1.07 (s, 3H), 1.55 (s, 3H), 1.0–2.2 (m, 5H), 3.07 (br s, 2H), 3.28 (br s, 1H), 3.38 (s, 3H), 4.57 (d, 1H, $J = 6.5$ Hz), 4.73 (br s, 1H), 5.02 (d, 1H, $J = 6.5$ Hz), 5.76 (br d, 1H, $J = 10$ Hz), 5.90 (d, 1H, $J = 10$ Hz), 5.90 (d, 1H, $J = 10$ Hz), 9.49 (t, 1H, $J = 2$ Hz); HRMS (EI) calcd. for $C_{18}H_{21}I_2$ ($M^+ - CH_3OCH_2$): 269.1541; found: 269.1530.

1,3,3-Trimethyl-2-(2-carboxyethyl)-4-(*Z*-1-methyloxymethoxy-7-triisopropylsilylhept-4-ene-2,6-diynyl)cyclohexene (31)

Diisobutylaluminum hydride (0.350 mL, 0.525 mmol, 1 M in toluene) was added dropwise to a cold (−78°C), stirred solution of the nitrile **27** (0.171 g, 0.366 mmol) in dry dichloromethane (10 mL). The resulting mixture was stirred at −78°C for 1 h. Saturated aqueous ammonium chloride was added; the mixture was stirred at room temperature for 30 min and extracted thoroughly with dichloromethane. The combined organic extracts were washed (water, brine), dried, and concentrated. Sodium chlorite (0.060 g, 0.663 mmol) was added to a solution (2:1, *tert*-butanol/dichloromethane, 15 mL) of the aldehyde **29**, aqueous NaH_2PO_4 (0.10 g in 2 mL), and 30% H_2O_2 (0.12 mL, 1.06 mmol). The mixture was stirred at 21°C for 16 h and concentrated. 10% HCl was added and the resulting mixture was extracted thoroughly with diethyl ether. The combined ether extracts were washed (water, 6% sodium thiosulphate solution, and brine), dried, and concentrated. Flash chromatography (1:1, petroleum ether/diethyl ether; then 2:1, petroleum ether/diethyl ether) afforded 0.140 g (74%) of the acid **31**. IR (neat): 2924, 2703, 2141, 2103, 1711, 1463, 1028 cm^{-1}; ^1H NMR (200 MHz) δ: 1.01 (s, 3H), 1.06 (s, 3H), 1.07 (br s, 20H), 1.59 (s, 3H), 1.5–2.15 (m, 6H), 3.10 (s, 2H), 3.37 (s, 3H), 4.52 (d, 1H, $J = 6.7$ Hz), 4.78 (br s, 1H), 4.97 (d, 1H, $J = 6.7$ Hz), 5.83 (br s, 2H), 10.0 (br s, 1H); ^{13}C NMR (75 MHz) δ: 11.3 (3C), 18.5, 18.6 (6C), 19.9, 20.5, 22.6, 27.1, 32.4, 33.7, 37.9, 50.1, 56.7, 67.1, 83.2, 94.8, 96.5, 99.5, 103.6, 119.5, 119.5, 130.1, 132.9, 176.0.

1,3,3-Trimethyl-2-(2-carboxyethyl)-4-(*Z*-1-methyloxymethoxyhept-4-ene-2,6-diynyl)cyclohexene (32)

A solution of the silyl acetylene **27** (0.084 g, 0.162 mmol) in dry THF (5 mL) was cooled to −78°C and *n*-tetrabutyl ammonium fluoride (0.32 mL, 0.32 mmol, 1 M THF) was added dropwise. The mixture was stirred at −78°C for 5 h, quenched with water, and extracted thoroughly with diethyl ether. The combined ether extracts were washed (10% HCl, brine), dried, concentrated, and chromatographed (3:1 petroleum ether/diethyl ether, then 1:1 petroleum ether/diethyl ether) to provide **32**, 0.0410 g (77%). IR (neat): 3281, 2929, 2094, 1714, 1464, 1151, 1029 cm^{-1}; ^1H NMR (200 MHz) δ: 0.87 (s, 3H), 1.08 (s, 3H), 1.59 (s, 3H), 1.5–2.30 (m, 5H), 1.58 (s, 3H), 3.08 (br s, 2H), 3.28 (d, 1H, $J = 2.2$ Hz), 3.37 (s, 3H), 4.55 (d, 1H, $J = 6.7$ Hz), 4.74 (br s, 1H), 5.01 (d, 1H, $J = 6.7$ Hz), 5.76 (dd, 1H, $J = 10.9$, 2.2 Hz), 5.88 (d, 1H, $J = 10.9$ Hz), 10.50 (br s, 1H).

1,3,3-Trimethyl-2-(2-hydroxymethyl)-4-(*Z*-1-methyloxymethoxy-7-triisopropylsilylhept-4-ene-2,6-diynyl)cyclohexene (34)

A toluene solution of diisobutylaluminum hydride (1.5 M, 0.55 mL, 0.825 mmol, Aldrich) was added dropwise to a cold (−78°C), stirred solution of the nitrile **27** (0.351 g, 0.752 mmol) in dry dichloromethane (10 mL). The resulting mixture was stirred at −78°C for 1 h and warmed to 0°C for an additional hour. Dilute HCl (aqueous 5%) was added and the mixture was stirred at 21°C for 30 min. The solution was extracted thoroughly with dichloromethane. The combined organic

Can. J. Chem. Downloaded from www.nrcresearchpress.com by 46.23.64.124 on 09/08/12
For personal use only.

extracts were washed with water, brine, dried ($MgSO_4$), filtered, and concentrated and the residual oil was filtered through a short column of neutral alumina to afford the aldehyde **29**. This material was dissolved in dry dichloromethane (10 mL) and the reduction procedure repeated (diisobutylaluminum hydride, 1.5 M, 0.55 mL, 0.825 mmol). Chromatography (silica gel; 3:1, petroleum ether/diethyl ether) of the resulting oil provided the alcohol **34** (0.180 g, 51%). IR (neat): 3348, 2913, 2141, 1461, 1028 cm^{-1}; ^1H NMR (200 MHz) δ: 1.00 (s, 3H), 1.06 (br s, 24H), 1.1–1.4 (m, 2H), 1.62 (s, 3H), 1.5–2.1 (m, 4H), 2.32 (br t, 2H, J = 8 Hz), 3.36 (s, 3H), 3.58 (br q, 2H, J = 8 Hz), 4.52 (d, 1H, J = 6.6 Hz), 4.77 (br s, 1H), 4.94 (d, 1H, J = 6.6 Hz), 5.81 (br s, 2H); ^{13}C NMR (50 MHz) δ: 11.2 (3C), 18.6 (6C), 19.9, 20.3, 22.9, 27.3, 32.2, 32.6, 38.1, 50.8, 56.5, 62.4, 66.9, 82.7, 94.7, 97.0, 99.3, 103.6, 119.4, 119.5, 129.6, 132.8, 201.0; HRMS (EI) calcd. for $C_{29}H_{48}O_3Si$: 472.3373; found: 472.3426.

1,3,3-Trimethyl-2-(2-hydroxymethyl)-4-(*Z*-1-methyloxymethoxyhept-4-ene-2,6-diynyl)cyclohexene (35)

A dry THF solution (10 mL) of the silyl acetylenic alcohol **34** (0.130 g, 0.275 mmol) was cooled to −78°C and then a 1 M solution of *n*-tetrabutyl ammonium fluoride (0.55 mL, 0.540 mmol) was added dropwise. The reaction was stirred at −78°C for 1 h, warmed to 0°C, water was added, and the resultant solution was extracted thoroughly with diethyl ether. The combined ether extracts were washed with brine, dried ($MgSO_4$), filtered, and concentrated and the residual oil was chromatographed (1:1, petroleum ether/diethyl ether) to give 0.079 g (91%) of the acetylene **35**. IR (neat): 3366, 3286, 2921, 2094, 1459, 1150, 1029 cm^{-1}; ^1H NMR (200 MHz) δ: 0.99 (s, 3H), 1.09 (s, 3H), 1.60 (s, 3H), 1.5–2.0 (m, 6H), 2.30 (br t, 2H, J = 8 Hz), 3.27 (d, 1H, J = 1 Hz), 3.36 (s, 3H), 3.55 (t, 2H, J = 8 Hz), 4.54 (d, 1H, J = 6.8 Hz), 4.71 (br s, 1H), 4.99 (d, 1H, J = 6.8 Hz), 5.75 (dd, 1H, J = 11, 2.2 Hz), 5.88 (dt, 1H, J = 11. 0.5 Hz); HRMS (EI) calcd. for $C_{18}H_{21}O_2$ ($M^+ - CH_3OCH_2$): 269.1541; found: 269.1530.

1,3,3-Trimethyl-2-(2-hydroxymethyl)-4-(*Z*-1-methyloxymethoxy-7-iodohept-4-ene-2,6-diynyl)cyclohexene (36)

Freshly dried morpholine (0.29 g, 3.31 mmol) and iodine (0.11 g, 0.433 mmol) were added sequentially to the acetylene **35** (0.070 g, 0.222 mmol) dissolved in dry benzene (10 mL) in a round-bottom flask (25 mL) equipped with a condenser. The reaction mixture was heated and stirred at ~40°C for 3 h. The mixture was then cooled to 21°C and aqueous sodium thiosulphate solution (6%) added. The resulting mixture was extracted thoroughly with diethyl ether. The combined organic extracts were washed with brine, dried, filtered, concentrated, and chromatographed (1:1, petroleum ether/diethyl ether) to afford the iodoalcohol **36** (0.084 g, 86%). IR (neat): 3376, 2927, 2247, 2153, 1029, 914 cm^{-1}; ^1H NMR (200 MHz) δ: 1.02 (s, 3H), 1.13 (s, 3H), 1.1–2.1 (m, 6H), 1.63 (s, 3H), 2.34 (br t, 2H, J = 8 Hz), 3.38 (s, 3H), 3.60 (br t, 2H, J = 8 Hz), 4.58 (d, 1H, J = 6.3 Hz), 4.73 (br s, 1H), 5.00 (d, 1H, J = 6.3 Hz), 5.78 (dd, 1H, J = 10, 1 Hz), 5.89 (d, 1H, J = 10 Hz); ^{13}C NMR (50 MHz) δ: 20.2, 20.4, 22.8, 27.5, 32.3, 32.8, 38.2, 50.9, 56.6, 62.5, 67.0, 82.5, 91.7, 94.7, 97.4, 119.6, 119.8, 121.7, 129.7, 132.8.

1,3,3-Trimethyl-2-(2-oxoethyl)-4-(*Z*-1-methyloxymethoxy-7-iodohept-4-ene-3,6-diynyl)cyclohexene (37)

Pyridinium dichromate (0.136 g, 0.359 mmol) was added to a stirred solution of the alcohol **36** (0.080 g, 0.181 mmol) in dry dichloromethane (10 mL). The resulting mixture was stirred at 21°C for 16 h. The reaction mixture was filtered through a sintered glass funnel under aspirator pressure and the collected precipitate washed thoroughly with diethyl ether. The ether filtrates were concentrated to provide a brownish oil that was purified by chromatography (3:1, petroleum ether/diethyl ether) to afford the aldehyde **37** (0.065 g, 82%). IR (neat): 2924, 2721, 2251, 2154, 1718, 1042, 1021 cm^{-1}; ^1H NMR (200 MHz) δ: 1.00 (s, 3H), 1.08 (s, 3H), 1.0–2.2 (m, 5H), 1.55 (s, 3H), 3.08 (br s, 2H), 3.39 (s, 3H), 4.58 (d, 1H, J = 7 Hz), 4.73 (br s, 1H), 5.00 (d, 1H, J = 7 Hz), 5.77 (dd, 1H, J = 9, 1.5 Hz), 5.91 (d, 1H, J = 9 Hz), 9.48 (t, 1H, J = 2.3 Hz); ^{13}C NMR (50 MHz) δ: 20.4, 22.3, 27.1, 29.7, 33.0, 38.1, 43.8, 50.7, 56.6, 66.9, 82.7, 91.7, 94.7, 97.2, 119.9, 121.7, 128.8, 131.6, 132.7, 201.2; HRMS (EI) calcd. for $C_{18}H_{20}O_2$ ($M^+ - CH_3OCH_2$): 395.0467; found: 395.0501.

16,17,18-Trimethyl-2-methyloxymethoxy-9-hydroxybicyclo[9.3.1]pentadec-5-ene-3,7-diyne (38)

Nickel(II) chloride (0.012 g, 0.096 mmol) and chromium(II) chloride (0.170 g, 1.38 mmol) were added to a stirred solution of the aldehyde **37** (0.061 g, 0.138 mmol) in dry THF (20 mL). The resulting mixture was stirred at 21°C for 4 h, water was added, and the mixture was extracted thoroughly with diethyl ether. The combined organic extracts were washed with brine, dried ($MgSO_4$), filtered, concentrated, and chromatographed (3:1, petroleum ether/diethyl ether, then 1:1, petroleum ether/diethyl ether) to the cyclic enediyne **38** (0.026 g, 60%). IR (neat): 3380, 2924, 2204, 1029 cm^{-1}; ^1H NMR (200 MHz) δ: 1.10 (s, 3H), 1.29 (s, 3H), 1.5–2.1 (m, 5H), 1.64 (s, 3H), 2.3–2.7 (m, 3H), 3.35 (s, 3H), 4.50 (d, 1H, J = 6.8 Hz), 4.59 (br s, 1H), 4.89 (d, 1H, J = 6.8 Hz), 5.02–5.18 (m, 1H), 5.78 (br s, 2H); ^{13}C NMR (50 MHz) δ: 21.0, 25.1, 25.3, 29.4, 32.0, 36.7, 37.2, 49.1, 55.6, 63.5, 70.1, 82.8, 84.9, 93.3, 95.4, 98.4, 120.7, 121.2, 131.1, 132.5; HRMS (EI) calcd. for $C_{18}H_{21}O_2$ ($M^+ - CH_3OCH_2$): 269.1542; found: 269.1541.

3,4,5,6,7,8-Hexadehydro-2*a*-methoxymethyl-9-oxo-12,15,15-trimethyltricyclo[9.3.1.$0^{3,8}$]pentadec-11-ene (40)

The alcohol **38** (0.015 g, 0.05 mmol) in dry toluene (10 mL) containing 1,4-cyclohexadiene (0.5 mL) was placed in a thick-walled Pyrex pressure tube equipped with a threaded plastic cap. The top of the tube extended through a small hole in the tope of the microwave oven. Argon was bubbled through the solution for 10 min and the vessel sealed. The diameter of the oven opening is less than 3 cm and is shielded to minimize microwave leakage. The base of the tube inside the microwave oven was surrounded by a beaker of damp (H_2O) vermiculite to facilitate heat transfer. A commercial oven was used (Toshiba model ERF-6630C (720 W)) at a power setting of 500 W in which the magnetron was tuned to the water frequency (2450 MHz). The reaction was conducted behind a shield in a fume hood. The reaction was heated for eight 0.5 h intervals in which the tube was allowed to return to room temperature between each session and fresh moist vermiculite was

added to the beaker. The tube was cooled, solvent was evaporated, and the residual oil chromatographed (petroleum ether/diethyl ether, 3:1) to generate the alcohol, which was used directly. Alcohol **39** was dissolved in CH_2Cl_2, pyridinium dichromate (0.10 g) was added, and the reaction was stirred at 21°C for 6 h. After filtration through a sintered glass funnel under reduced pressure (water aspirator) the solution was concentrated and chromatographed (petroleum ether/diethyl ether, 3:1) to afford 0.001 g (6%) of ketone **40**. Identified by spectral comparison (NMR, IR, MS) with an authentic sample (preceding paper).

Acknowledgment

We are grateful to the Natural Sciences and Engineering Research Council of Canada, to Merck-Frosst Canada Ltd. and Rhône-Poulenc Rorer for financial support of this research, and to Torcan Chemical Ltd. for a gift of trimethylsilylacetylene. We thank the referees for their comments.

References

1. (*a*) J. Golik, J. Clardy, G. Dubay, G. Groenewold, H. Kawaguchi, M. Konishi, B. Krishnan, H. Ohkuma, K.I. Saitoh, and T.W. Doyle. J. Am. Chem. Soc. **109**, 3461 (1987); (*b*) J. Golik, G. Dubay, G. Groenewold, H. Kawaguchi, M. Konishi, B. Krishnan, H. Ohkuma, K.I. Saitoh, and T.W. Doyle. J. Am. Chem. Soc. **109**, 3462 (1987).
2. M.D. Lee, T.S. Dunne, M.M. Siegel, C.C. Chang, G.O. Morton, and D.B. Borders. J. Am. Chem. Soc. **109**, 3464 (1987); (*b*) M.D. Lee, T.S. Dunne, C.C. Chang, G.A. Ellestad, M.M. Siegel, G.O. Morton, W.J. McGahren, and D.B. Borders. J. Am. Chem. Soc. **109**, 3466 (1987).
3. (*a*) M.D. Lee, G.A. Ellestad, and D.B. Borders. Acc. Chem. Res. **24**, 235 (1991); (*b*) J.J. Hangeland, J.J.D. Voss, J.A. Health, C.A. Townsend, W.D. Ding, J. S. Ashcroft, and G.A. Ellestad. J. Am. Chem. Soc. **114**, 9200 (1992).
4. (*a*) K.C. Nicolaou, C.W. Hummel, E.N. Pitsinos, M. Nakada, A.L. Smith, K. Shibayama, and H. Saimo. J. Am. Chem. Soc. **114**, 10082 (1992); (*b*) R.D. Groneberg, T. Miyazaki, N.A. Stylianides, T.J. Schulze, W. Stahl, E.P. Schreiner, T. Suzuki, Y. Iwabuchi, A.L. Smith, and K.C. Nicolaou. J. Am. Chem. Soc. **115**, 7593 (1993); (*c*) A.L. Smith, E.N. Pitsinos, C.K. Hwang, Y. Mizuno, H. Saimoto, C.W. Hummel, M. Nakada, K. Shibayama, E.N. Pitsinos, H. Saimoto, Y. Mizuno, K.U. Baldenius, and A.L. Smith. J. Am. Chem. Soc. **115**, 7625 (1993); (*e*) R.L. Halcomb, S.H. Boyer, and S.J. Danishefsky. Angew. Chem. Int. Ed. Engl. **31**, 338 (1992); (*f*) S.A. Hitchcock, S.H. Boyer, M.Y. Chu-Moyer, S.H. Olson, and S.J. Danishefsky. Angew. Chem. Int. Ed. Engl. **33**, 858 (1994); (*g*) T. Skrydstrup, G. Ulibarri, H. Audrain, and D.S. Grierson. Recent Prog. Chem. Synth. Antibiot. Relat. Microb. Prod. **2**, 213 (1993).
5. (*a*) K.C. Nicolaou and W.-M. Dai. Angew Chem. Int. Ed. Engl. **30**, 1387 (1991); (*b*) K.C. Nicolaou, A.L. Smith, and E.W. Yue. Proc. Natl. Acad. Sci. U.S.A. **90**, 5881 (1993); (*c*) P. Magnus, P. Cartier, J. Elliott, R. Lewis, J. Harling, T. Pitterna, W.E. Bauta, and S. Fortt. J. Am. Chem. Soc. **114**, 2544 (1992); (*d*) P. Magnus. Tetrahedron, **50**, 1469 (1994); (*f*) M.E. Maier and T. Bandstetter. Liebigs Ann. Chem. **9**, 1009 (1993); (*g*) K. Toshima, K. Ohta, A. Ohashi, T. Nakamura, M. Nakata, and S. Matsumura. J. Chem. Soc. Chem. Commun. **19**, 1525 (1993); (*h*) D.L. Boger and J. Zhou. J. Org. Chem. **58**, 3018 (1993).
6. M.C. Wani, H.L. Taylor, M.E. Wall, P. Coggan, and A.T. McPhail. J. Am. Chem. Soc. **93**, 2325 (1971).
7. F. Lavelle, F. Guéritte-Voegelein, and D. Guénard. Bull. Cancer, **80**, 326 (1993).
8. (*a*) A.N. Boa, P.R. Jenkins, and N.J. Lawrence. Contemp. Org. Synth. **1**, 47 (1994); (*b*) K.C. Nicolaou, W.-M. Dai, and R.K. Guy. Angew. Chem. Int. Ed. Engl. **33**, 15 (1994); (*c*) D.G.I. Kingston, A.A. Molinero, and J.M. Rimoldi. Prog. Chem. Org. Nat. Prod. **61**, 1 (1993); (*d*) C.S. Swindell. Org. Prep. Proced. Int. **23**, 465 (1991).
9. M. Hepperle and G.I. Georg. Drugs Future, **19**, 573 (1994).
10. (*a*) S. Blechert and A. Kleine-Klausing. Angew. Chem. Int. Ed. Engl. **30**, 412 (1991); (*b*) G. Samaranayake, N.F. Magri, C. Jitrangsri, and D.G.I. Kingston. J. Org. Chem. **56**, 5114 (1991); (*c*) K.C. Nicolaou, C.F. Claiborne, P.G. Nantermet, E.A. Couladouros, and E.A. Sorensen. J. Am. Chem. Soc. **116**, 1591 (1994).
11. Y.F. Lu, C.W. Harwig, and A.G. Fallis. J. Org. Chem. **58**, 4202 (1993).
12. (*a*) R.G. Berman. Acc. Chem. Res. **6**, 25 (1973); (*b*) T.P. Lockhart, P.B. Comanita, and R.G. Bergman. J. Am. Chem. Soc. **103**, 4082 (1981); (*c*) T.P. Lockhart and R.G. Bergman. J. Am. Chem. Soc. **103**, 4091 (1981).
13. (*a*) P. Magnus, S.A. Eisenbeis, W.C. Ross, N. Zein, and W. Solomon. J. Am. Chem. Soc. **115**, 12627 (1993); (*b*) N. Zein, W. Solomon, A.M. Casazza, J.F. Kadow, B.S. Krishnan, M.M. Tun, D.M. Vyas, and T.W. Doyle. Bioorg. Med. Chem. Lett. **3**, 1351 (1993).
14. K.C. Nicolaou, T. Li, M. Nakada, C.W. Hummel, A. Hiatt, and W. Wrasidlo. Angew. Chem. Int. Ed. Engl. **33**, 183 (1994).
15. (*a*) J.W. Grissom, T.L. Calkins, and M. Egan. J. Am. Chem. Soc. **115**, 11744 (1993); (*b*) E. Kraka and D. Cremer. J. Am. Chem. Soc. **116**, 4929 (1994); (*c*) R. Lindh and B.J. Persson. J. Am. Chem. Soc. **116**, 4963 (1994).
16. (*a*) K.J. Shea, J.W. Gilman, C.D. Haffner, and T.K. Dougherty. J. Am. Chem. Soc. **108**, 4953 (1986); (*b*) K.J. Shea and S.T. Sakata. Tetrahedron Lett. **33**, 4261 (1992); (*c*) Y. Horiguchi, T. Furukawa, and I. Kuwajima. J. Am. Chem. Soc. **111**, 8277 (1989); (*d*) T. Furukawa, K. Morihira, Y. Horiguchi, and I. Kuwajima. **48**, 6975 (1992); K. Morihira, M. Seto, T. Furukawa, Y. Horiguchi, I. Kuwajima. Tetrahedron Lett. **34**, 345 (1993); (*f*) P.A. Wender and T.P. Mucciaro. J. Am. Chem. Soc. **114**, 5878 (1992).
17. (*a*) T. Nishikawa, A. Ino, and M. Isobe. Tetrahedron, **50**, 1449 (1994); (*b*) A.G. Myers, P.S. Dragovich, and E.Y. Kuo. J. Am. Chem. Soc. **114**, 9369 (1992).
18. (*a*) S.J. Danishefsky, N.V. Mantlo, and D.S. Yamashita. J. Am. Chem. Soc. **110**, 6890 (1988); (*b*) D.S. Yamashita, V.P. Rocco, and S.J. Danishefsky. Tetrahedron Lett. **32**, 6667 (1991).
19. W.T. Brady and T.C. Cheng. J. Org. Chem. **42**, 732 (1977).
20 D. Elbaum, T.B. Nguyen, W.L. Jorgensen, and S.L. Schreiber. Tetrahedron, **50**, 1503 (1994).
21. Y.-F. Lu and A.G. Fallis. Tetrahedron Lett. **34**, 3367 (1993).
22. (*a*) A.S. Kende and C.A. Smith. Tetrahedron Lett. **29**, 4217 (1988); (*b*) K.C. Nicolaou, A.L. Smith, C.-K. Hwang, E. Pitsinos, and G.R. Scarlato. J. Am. Chem. Soc. **114**, 3134 (1992); (*c*) J.F. Kadow, D.J. Cook, T.W. Doyle, D.R. Langley, K.M. Pham, D.M. Vyas, and M.D. Wittman. Tetrahedron, **50**, 1519 (1994).
23. (*a*) P.A. Wender, C.K. Zercher, S. Beckman, and E.-M. Haubold. J. Org. Chem. **58**, 5867 (1993); (*b*) T. Nishikawa, S. Shibuya, and M. Isobe. Synlett, 482 (1994).
24. (*a*) C. Crevisy and J.-M. Beau. Tetrahedron Lett. **32**, 3171 (1991); (*b*) K.C. Nicolaou, A. Liu, Z. Zeng, and S. McComb. J. Am. Chem. Soc. **114**, 9279 (1992); (*c*) M.E. Maier and T. Brandstetter. Tetrahedron Lett. **33**, 7511 (1992); (*d*) A.G. Meyers and N.S. Finney. J. Am. Chem. Soc. **114**, 10 982 (1992); (*e*) K. Takai, T. Kuroda, S. Nakatsukasa, K. Oshima, and H. Nozaki. Tetrahedron Lett. **26**, 5585 (1985); (*f*) H. Jin, J.

Can. J. Chem. Downloaded from www.nrcresearchpress.com by 46.23.64.124 on 09/08/12
For personal use only.

Uenishi, W.J. Christ, and Y. Kishi. J. Am. Chem. Soc. **108**, 5644 (1986); (*g*) K. Takai, M. Yagashira, T. Kuroda, K. Oshima, K. Uchimoto, and H. Nozaki. J. Am. Chem. Soc. **108**, 6048 (1986).
25. M. Gingras. Tetrahedron Lett. **32**, 7381 (1991).
26. M. Yamaguchi, A. Hayashi, and T. Minami. J. Org. Chem. **56**, 4091 (1991).
27. E. Dalcanale and F. Montanari. J. Org. Chem. **51**, 567 (1986).
28. T. Nishikawa, S. Shibuya, and S. Hosokawa. Synlett, 485 (1994).
29. P.G. Wenthold and R.R. Squires. J. Am. Chem. Soc. **116**, 6401 (1994).

Can. J. Chem. Downloaded from www.nrcresearchpress.com by 46.23.64.124 on 09/08/12
For personal use only.

Ion chemistry of second-row transition metals in hydrocarbon flames: cations and anions of Y, Zr, Nb, and Mo

Christine C.Y. Chow and John M. Goodings

Can. J. Chem. Downloaded from www.nrcresearchpress.com by 46.23.64.124 on 09/08/12
For personal use only.

Abstract: A pair of laminar, premixed, CH_4–O_2 flames above 2000 K at atmospheric pressure, one fuel-rich (FR) and the other fuel-lean (FL), were doped with $\sim 10^{-6}$ mol fraction of the second-row transition metals Y, Zr, Nb, and Mo. Since these hydrocarbon flames contain natural ionization, metallic ions were produced in the flames by the chemical ionization (CI) of metallic neutral species, primarily by H_3O^+ and OH^- as CI sources. Both positive and negative ions of the metals were observed as profiles of ion concentration versus distance along the flame axis by sampling the flames through a nozzle into a mass spectrometer. For yttrium, the observed ions include the $YO^+{\cdot}nH_2O$ (n = 0–3) series, and $Y(OH)_4^-$. With zirconium, they include the $ZrO(OH)^+{\cdot}nH_2O$ (n = 0–2) series, and $ZrO(OH)_3^-$. Those observed with niobium were the cations $Nb(OH)_3^+$ and $Nb(OH)_4^+$, and the single anion $NbO_2(OH)_2^-$. For molybdenum, they include the cations $MoO(OH)_2^+$ and $MoO(OH)_3^+$, and the anions MoO_3^- and $MoO_3(OH)^-$. Not every ion was observed in each flame; the FL flame tended to favour the ions in higher oxidation states. Also, flame ions in higher oxidation states were emphasized for these second-row transition metals compared with their first-row counterparts. Some ions written as members of hydrate series may have structures different from those of simple hydrates; e.g., $YO^+{\cdot}H_2O = Y(OH)_2^+$ and $ZrO(OH)^+{\cdot}H_2O = Zr(OH)_3^+$, etc. The ion chemistry for the production of these ions by CI in flames is discussed in detail.

Key words: transition metals, ions, flame, gas phase, negative ions.

Résumé : Une paire de flammes laminaires prémélangées de CH_4–O_2, l'une riche en carburant (FR) et l'autre déficiente en carburant (FL), ont été dopées par des métaux de transition de la deuxième période, Y, Zr, Nb et Mo (fraction molaire d'environ 10^{-6}), à des températures supérieures à 2000 K et à la pression atmosphérique. Puisque ces flammes d'hydrocarbures comportent des ionisations naturelles, les ions métalliques ont été produits dans les flammes par l'ionisation chimique (IC) des espèces métalliques neutres, principalement par des sources d'IC de H_3O^+ et OH^-. On a observé les ions tant positifs que négatifs des métaux sous la forme de profiles de la concentration ionique en fonction de la distance le long de l'axe de la flamme par le biais d'un échantillonnage des flammes à travers la tuyère dans un spectromètre de masse. Pour l'yttrium, les ions observés incluent ceux de la série $YO^+{\cdot}nH_2O$ (n = 0–3) et $Y(OH)_4^-$. Avec le zirconium, ils comportent ceux de la série $ZrO(OH)^+{\cdot}nH_2O$ (n = 0–2) et $ZrO(OH)_3^-$. Avec le niobium, on a observé les cations $Nb(OH)_3^+$ et $Nb(OH)_4^+$ ainsi qu'un seul anion, le $NbO_2(OH)_2^-$. Pour le molybdène, ils comportent les cations $MoO(OH)_2^+$ et $MoO(OH)_3^+$ ainsi que les anions MoO_3^- ainsi que $MoO_3(OH)^-$. Tous ces anions n'ont pas été observés dans toutes les flammes; avec les flammes FL, on observe principalement les ions des états d'oxydation les plus élevés. On a aussi observé que les états d'oxydation les plus élevés sont plus favorisés dans les flammes des métaux de transition de la deuxième période par rapport à leurs équivalents de la première période. Quelques-uns des ions pour lesquels des structures hydrates ont été proposées pourraient posséder des structures différentes, comme $YO^+{\cdot}H_2O = Y(OH)_2^+$ et $ZrO(OH)^+{\cdot}H_2O = Zr(OH)_3^+$. On discute en détail de la chimie ionique conduisant à la production de ces ions par IC dans des flammes.

Mots clés : métaux de transition, flammes, phase gazeuse, ions négatifs.

[Traduit par la rédaction]

Received July 19, 1995.

C.C.Y. Chow and J.M. Goodings.[1] Department of Chemistry, York University, 4700 Keele Street, North York, ON M3J 1P3, Canada.

[1] Author to whom correspondence may be addressed. Telephone: (416) 736–2100, ext. 33852. Fax: (416) 736–5936. E-mail: goodings@turing.sci.yorku.ca

Can. J. Chem. Downloaded from www.nrcresearchpress.com by 46.23.64.124 on 09/08/12
For personal use only.

Introduction

A few years ago, we studied the cation chemistry of the first row of 10 transition metals Sc–Zn in a premixed, fuel-rich, CH_4–O_2 flame (1, 2). The metals were introduced at a concentration of $\sim 10^{-6}$ mol fraction, and ions were produced by chemical ionization (CI) of metallic flame species by H_3O^+, which occurs naturally in any hydrocarbon flame. Metallic ions were observed by sampling the flame through a nozzle into a mass spectrometer. More recently, we observed the positive flame ionization of the group 3 metals Sc, Y, and La in H_2–O_2–Ar flames of both fuel-rich (FR) and fuel-lean (FL) composition that contain essentially no natural ionization (3). The CI of metallic species by H_3O^+ was also studied, where the H_3O^+ reagent was generated by adding 0.2 mol% of CH_4 to the hydrogen premixed flame gas. The objective of the present study was to extend this work to include further second-row transition metals Zr, Nb, and Mo as well as Y for comparison with the flame-ion chemistry of their first-row counterparts.

Much of the gas-phase organometallic ion chemistry that has been carried out at room temperature is not really applicable to flames because metal–carbon bond formation is not observed. Apart from atomic cations A^+, metallic flame ions exhibit metal–oxygen bonds almost exclusively, although AH^+ has been observed for Mn (2), Fe, Co, and Ni (1). For the second-row transition metals, Armentrout and co-workers (4, 5) have measured the bond dissociation energies $D(A^+ - H)$ to be 259±4 (Y), 230±13 (Zr), 226±13 (Nb), and 176±13 (Mo) kcal mol^{-1}. From gas-phase solvation studies with water, Wilson and Buckner (6) observed the ion series $YO^+ \cdot nH_2O$ ($n = 0$–3) in which the third solvent molecule attaches more rapidly than the second, i.e., to form $Y(OH)_2(H_2O)_2^+$ with $n = 3$. Similarly, Nb^+ with water follows the reaction sequence $Nb^+ \rightarrow NbO^+ \rightarrow NbO_2^+ \rightarrow NbO_2^+ \cdot nH_2O$ ($n = 0$–3) in which the second solvent molecule attaches more rapidly than the first; the ion can be interpreted as $ONb(OH)_2(H_2O)^+$ with $n = 2$. The negative molybdenum ions $HMoO_4^-$ and MoO_3^- were detected in H_2–O_2–N_2 flames seeded with potassium by Jensen and Miller (7), who determined approximate values for the corresponding electron affinities to be $EA(HMoO_4) = 410$ and $EA(MoO_3) = 249$ kJ mol^{-1}; a more recent value is $EA(MoO_3) = 277 \pm 19$ kJ mol^{-1} (8).

For the present study, a pair of CH_4–O_2 flames, one FR and the other FL (i.e., oxygen-rich), were doped with $\sim 10^{-6}$ mol fraction of Y, Zr, Nb, and Mo. Both metallic cations and anions, formed by CI of metallic flame neutrals reacting with natural flame ions (primarily H_3O^+ and OH^-), were observed as profiles of ion concentration versus distance along the flame axis by sampling the flame through a nozzle into a mass spectrometer. The addition of an FL flame for this work was intended to enhance anion formation for these heavier transition metals.

Experimental

These experiments employed small, conical, premixed, CH_4–O_2 flames ~4–5 mm high at atmospheric pressure whose bulk characteristics are given in Table 1. They were stabilized on a simple, tubular, quartz burner surrounded by a flowing argon shield to minimize the entrainment of atmospheric air. The transition metals Y, Zr, Nb, and Mo were introduced as an aerosol by spraying a 0.25 M (molar) aqueous solution of the metallic chloride using a pneumatic atomizer (9). The salts were obtained from the Aldrich Chemical Company (the stated purity is given in parentheses): $YCl_3 \cdot 6H_2O$ (99.9%); $ZrCl_5$ (99.5%); $NbCl_5$ (99%); and $MoCl_5$ (98%). The atomizer was operated by a flow rate of 1 standard cm^3 s^{-1} using part of the flame's oxygen supply, with one exception; with the molybdenum solution, part of the methane supply was employed instead to minimize the rapid oxidation of $MoCl_5$. This technique introduced nearly 1 ppm (9×10^{-7}, or $\sim 10^{-6}$ mol fraction) of metal into the burnt gas of the flame. The undoped flames had a bluish colour, which was more distinct in the FR than in the FL case. The addition of Y coloured the FR flame red but the colour was not noticeable in the FL flame. The addition of Nb gave the appearance of yellowish-orange streaks or lines in both flames. No change in colour was observed in either flame with the addition of Zr or Mo.

Table 1. Bulk characteristics of the CH_4–O_2 flames.

Parameter / flame	Fuel-rich	Fuel-lean
Equivalence ratio ϕ	2.25	0.219
Unburnt gas flow rate (cm^3 s^{-1})	16.43	17.35
CH_4/O_2	1.13/1	1/9.15
Adiabatic flame temperature (K)	2344	2254
Calculated equilibrium burnt-gas composition (mol fractions)		
H_2O	0.228 4419	0.189 9200
H_2	0.430 7200	0.000 3701
O_2	0.000 0022	0.696 8958
CO	0.303 5294	0.001 0201
CO_2	0.028 3011	0.097 0163
H	0.008 2495	0.000 1484
OH	0.000 7485	0.011 4172
O	0.000 0099	0.003 2108

The flame-ion mass spectrometer has been described in detail (10), and only a brief description will be given here. The burner is mounted on a motor-driven carriage, and the flame axis is accurately aligned with the mass spectrometer's sampling nozzle of diameter ca. 0.15 mm. Ions in the sampled flame gas are formed into a beam by an ion lens, and pass through two stages of differential pumping into a quadrupole mass filter. The mass-analyzed ions are detected with a parallel-plate Faraday collector connected to an electrometer having a grid-leak resistance of 10^{10} Ω. Ion signals in the figures below are given in volts, corresponding to the collected ion current passing through 10^{10} Ω. Positive or negative ions can be detected by reversing the polarity on all electrodes. In addition to individual ionic species, total positive ions (TPI) or total negative ions (TNI) are measured by removing the d.c. voltages applied to the quadrupole rods. Data are presented as profiles of ion signal versus distance z along the flame axis. A relatively sharp minimum in the pressure profile of the sampled gas provides a reproducible origin ($z = 0$) *in the flame* for the distance scale. It corresponds approximately to the downstream edge at the tip of the flame's bright luminous reaction zone. The pressure is measured with an ionization gauge mounted on the wall of the chamber housing the mass filter.

Some ion signals can be distorted during sampling by the

Can. J. Chem. Downloaded from www.nrcresearchpress.com by 46.23.64.124 on 09/08/12
For personal use only.

Fig 1. Total positive ion (TPI) profiles along the flame axis z of the fuel-rich (FR) and fuel-lean (FL) flames. The reaction zone is located upstream of $z = 0$ (negative z).

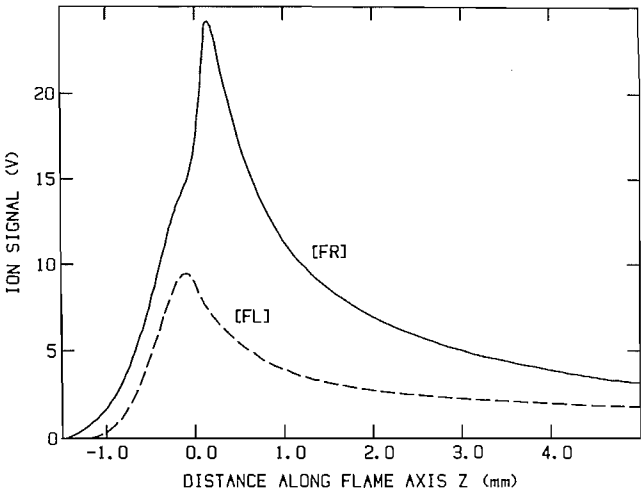

Fig 2. Total negative ion (TNI) profiles along the flame axis z of the fuel-rich (FR) and fuel-lean (FL) flames. The reaction zone is located upstream of $z = 0$ (negative z).

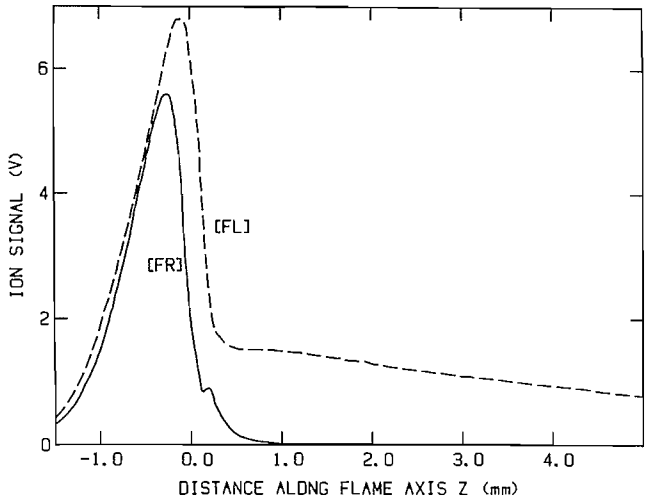

mass spectrometer. The flame gas cools in passing through the thermal boundary layer surrounding the sampling orifice (11), and during the expansion to supersonic velocity that occurs for a few orifice diameters downstream of the nozzle throat (12). A fast ionic equilibrium having a relaxation time comparable to the sampling time (~1 μs) can shift to enhance the product ion in the exothermic direction. A common example in flames is the enhanced formation of H_3O^+ hydrates. Thus, it should be remembered that the measured signal magnitudes can correspond to a temperature several hundred degrees cooler than the actual temperature of the flame.

Results and discussion

Reagent ions for chemical ionization (CI)

Any hydrocarbon flame contains natural ionization initiated by the chemi-ionization reaction (13, 14)

[1] $CH + O \rightarrow HCO^+ + e^-$

Although HCO^+ may undergo a variety of proton transfer reactions in the flame reaction zone, downstream in the burnt-gas region where water is the major product of relatively high proton affinity, the cation chemistry is dominated by H_3O^+ (15)

[2] $HCO^+ + H_2O \rightleftarrows H_3O^+ + CO$

which serves as the major positive reagent ion for CI of flame additives. Similarly, the natural anion chemistry stems from the free electrons e^- produced in reaction [1], initially by three-body attachment to O_2 oxidant molecules (16)

[3] $e^- + O_2 + M \rightleftarrows O_2^- + M$

where M is a third body. The O_2^- ions then charge transfer to other flame neutrals of higher electron affinity including the radicals OH and O

[4] $O_2^- + OH,O \rightleftarrows OH^-,O^- + O_2$

Although other anions are also formed, OH^- and O^- are major reagent anions for CI because they are strong bases, capable of abstracting protons from a variety of flame neutrals including additives; alternatively, these anions can undergo addition reactions with neutral flame species.

Concentration profiles of the total positive ions (TPI) versus distance z along the flame axis are shown in Fig. 1 for the FR and FL flames. The cations reach a maximum concentration near $z = 0$ on the flame axis, and are dominated by H_3O^+ downstream in the burnt gas where the signal decreases steadily by electron–ion recombination (17)

[5] $H_3O^+ + e^- \rightarrow H + H + OH$, or $H + H_2O$

In the FR flame, the peak concentration is approximately 10^{-8} mol fraction or 3×10^{10} ions cm^{-3}, and is about 1/3 that value or 1×10^{10} ions cm^{-3} in the FL flame (16). The total negative ions (TNI), whose profiles are shown in Fig. 2, maximize in the flame reaction zone upstream ($z < 0$). In the FR flame, the TNI signal disappears just downstream of $z = 0$, primarily by associative electron detachment reactions of any general anion X^- with H atoms (18)

[6] $X^- + H \rightleftarrows e^- + HX$

because [H] is large in the burnt gas of the FR flame. In contrast, the peak TNI signal in the FL flame decreases downstream of $z = 0$ but persists throughout the burnt gas where [H] is lower in the FL case. In summary, H_3O^+ is the major cation and OH^- (which exceeds O^-) the major anion to act as CI reagents for additives introduced into this pair of FR and FL methane–oxygen flames. The four metals Y, Zr, Nb, and Mo will be discussed in turn beginning with the cation chemistry, followed by the anion chemistry.

Yttrium ion chemistry

Since Y is a group 3 metal with electron configuration $5s^24d^1$, its chemistry should be dominated by the +3 oxidation state, leading to neutral compounds in flames such as the oxide hydroxide OYOH and the trihydroxide $Y(OH)_3$. However, the

Can. J. Chem. Downloaded from www.nrcresearchpress.com by 46.23.64.124 on 09/08/12
For personal use only.

Fig. 3. Axial profiles of yttrium positive ions observed in the fuel-rich (FR) flame.

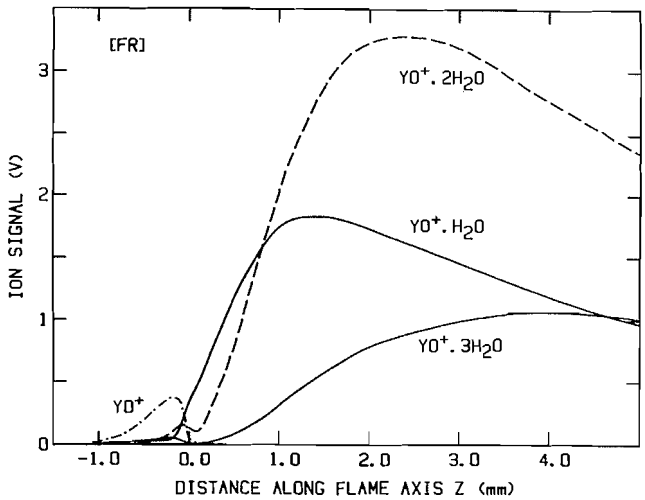

Fig. 4. Axial profiles of yttrium positive ions observed in the fuel-lean (FL) flame.

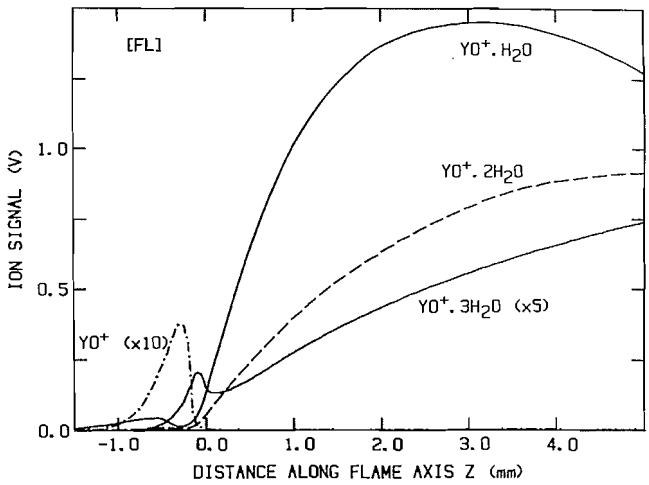

monoxide YO is known to have a very strong bond energy with D(YO) = 7.41 eV, and a rather low ionization energy IE(YO) = 5.85 eV because it is an odd-electron species (19). The YO and OYOH neutrals are expected to be linked in flames by the balanced reaction

[7] $YO + H_2O \rightleftarrows OYOH + H$

such that YO is dominant in FR flames where [H] is large; OYOH might have a comparable concentration in FL flames. In our previous study of group 3 metals in H_2–O_2–Ar flames that contain essentially no natural ionization, it was proposed that yttrium is ionized by the thermal (collisional) ionization of YO and (or) the chemi-ionization of OYOH reacting with H (3). In the present study, the emphasis is placed on CI processes that were considered previously (3), primarily for La, and will only be briefly summarized here for Y.

Figures 3 and 4 give profiles along the flame axis for all of the Y ions that were detected in the FR and FL flames, respectively. As for Sc and La (2, 3), the ions can be represented by a hydrated oxide ion series $YO^+{\cdot}nH_2O$ (n = 0–3) although the ion structures may not be simple hydrates; e.g., $YO^+{\cdot}H_2O$ is equivalent to $Y(OH)_2^+$, and $YO^+{\cdot}2H_2O$ to $Y(OH)_3H^+$ (the protonated trihydroxide), etc. Under normal operating conditions of the mass spectrometer, the YO^+ ion signal was small, and confined to the flame reaction zone ($z < 0$); the other ion signals were larger and persisted throughout the burnt gas. The largest signal was observed for n = 1 in the FL case, but for n = 2 in the FR flame although the latter has the higher temperature. The production of these ions by CI can be explained by proton transfer of H_3O^+ to the oxide hydroxide

[8] $H_3O^+ + OYOH \rightleftarrows H_2O + Y(OH)_2^+$ or $YO^+{\cdot}H_2O$

followed by hydration, or dehydration via the back reactions

[9] $YO^+{\cdot}nH_2O + H_2O + M \rightleftarrows YO^+{\cdot}(n+1)H_2O + M$; n = 0–2

Similarly, if the neutral trihydroxide were to exist in flames to any extent, proton transfer would lead directly to the dihydrate

[10] $H_3O^+ + Y(OH)_3 \rightleftarrows H_2O + Y(OH)_3H^+$ or $Y(OH)_2(H_2O)^+$ or $YO^+{\cdot}2H_2O$

with a planar trigonal structure. The third hydrate $YO^+{\cdot}3H_2O$ written as $Y(OH)_2(H_2O)_2^+$ with four ligands might have a tetrahedral structure with an electron octet around the central Y atom. In these and subsequent reactions, the double arrow denotes that the reaction proceeds in both directions. A balanced reaction indicative of true equilibrium at constant temperature would require that the ratio of the two ion currents remain constant. This situation is approached, for example, well downstream in Fig. 3 for the first two hydrate profiles, but the third hydrate grows as the first two decline. That could occur if the third hydrate is formed from the second in a slow three-body process. Alternatively, the growth would be favoured if the flame cools downstream, perhaps due to entrainment of the surrounding atmosphere, since the reactions [9] will be exothermic to the right.

The various electrodes of the ion lens were normally tuned to maximize the TPI signal. Under these conditions, the profile signal for the nude YO^+ ion was largely confined to the flame reaction zone. However, when the voltage on the single lens element immediately in front of the mass filter was increased, a considerable YO^+ signal was observed downstream as shown in Fig. 5 for the FL flame; the same behaviour is observed in the FR case. Presumably, acceleration of the ions by the high lens voltage promotes collision-induced dissociation (CID) of the higher hydrates with molecules of the background gas by the back reactions [−9] to enhance the YO^+ signal.

Only one anion corresponding to $Y(OH)_4^-$ at 157 u was observed in both the FR and FL flames as shown in Fig. 6. The major FR signal occurred in the reaction zone whereas the FL signal maximized downstream, in keeping with the notion that a major loss mechanism for these anions is associative detachment with H as in reaction [6]. Since $Y(OH)_4^-$ is equivalent to $YO(OH)_2^-{\cdot}H_2O = YO_2^-{\cdot}2H_2O$, the ion could be produced by proton abstraction from OYOH by OH^-

[11] $OH^- + OYOH \rightleftarrows YO_2^- + H_2O$

Can. J. Chem. Downloaded from www.nrcresearchpress.com by 46.23.64.124 on 09/08/12
For personal use only.

Fig. 5. Axial YO^+ profiles measured in the fuel-lean (FL) flame with the ion lens elements operating at normal voltages (solid line), and with a lens element at high voltage (broken line) to promote collision-induced dissociation (CID) of the YO^+ hydrates.

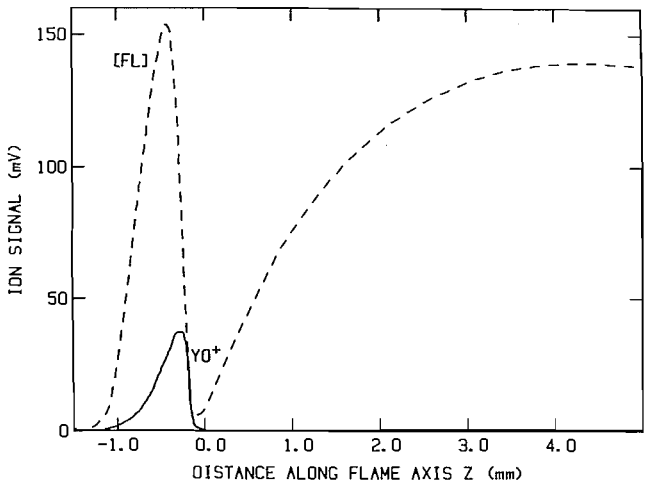

Fig. 6. Axial profiles of metallic negative ions of yttrium, zirconium, and niobium observed in both the fuel-rich (FR) and fuel-lean (FL) flames.

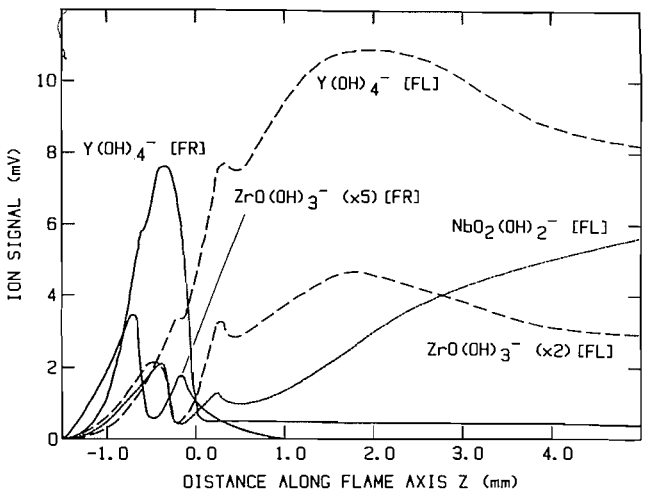

with subsequent hydration, or a one-step addition reaction of OH^- to the oxide hydroxide

[12] $OH^- + OYOH + M \rightleftarrows YO(OH)_2^- + M$

with one further hydration step to give $Y(OH)_4^-$. It is not clear whether reactions such as [12] proceed by a two-body mechanism, or involve a third body M.

Zirconium ion chemistry

The $5s^24d^2$ electron configuration of Zr might suggest a dominant +4 oxidation state although, like Ti, other oxidation states are known, including the +2 state. Generally, the higher oxidation states are more stable for the heavier transition metals (20). The +4 and +2 states would give rise to the neutral oxides ZrO_2 and ZrO, respectively. Neutral hydroxides such as $Zr(OH)_4$ and $Zr(OH)_2$, and a mixed oxide hydroxide $ZrO(OH)_2$, are also possible. Of the five natural isotopes of

Fig. 7. Axial profiles of zirconium positive ions observed in the fuel-rich (FR) flame.

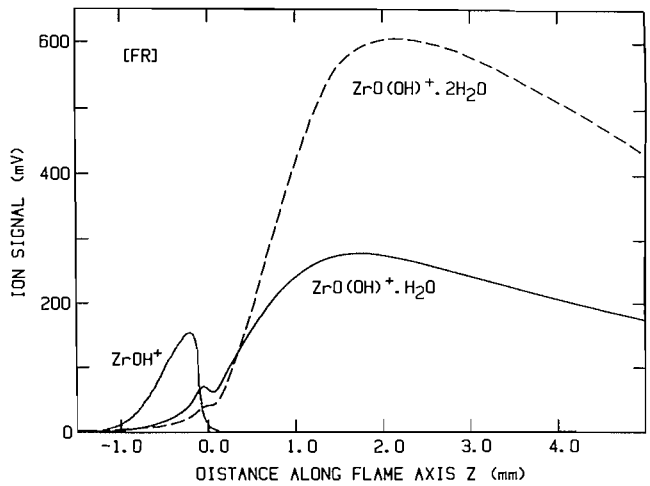

Fig. 8. Axial profiles of zirconium positive ions observed in the fuel-lean (FL) flame.

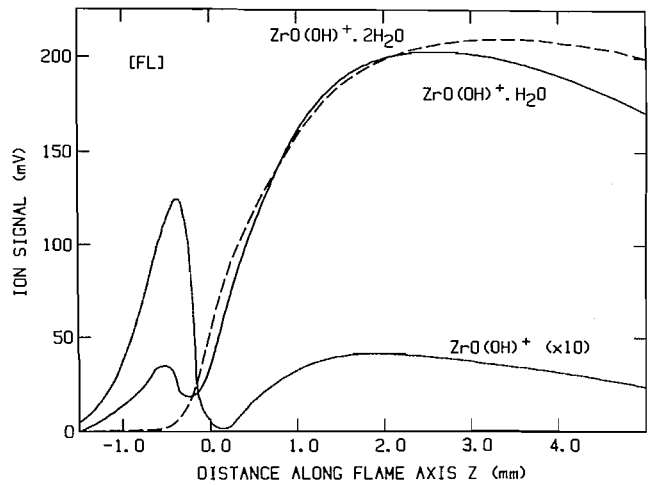

zirconium, ^{90}Zr has the lowest mass and the highest natural abundance of 51.9%; the mass spectral profiles were recorded for this single isotope.

Profiles for the detectable Zr cations are shown in Fig. 7 for the FR flame and in Fig. 8 for the FL flame. With one exception, the cations can be represented by members of a $ZrO(OH)^+ \cdot nH_2O$ series (n = 0–2) in both flames; the $ZrO(OH)^+$ ion signal with $n = 0$ in the FR flame was detected, but was too small to record as a profile. For all of these profiles, the peaks occurring upstream in the flame reaction zone ($z < 0$) are mainly due to natural $C_xH_yO_z^+$ ions at the same mass number; contributions from metallic ions, if present, are very small. The one exception was the detection of $ZrOH^+$ at 107 u in the reaction zone of the FR flame only.

The production of the cation series can occur by proton transfer to ZrO_2

[13] $H_3O^+ + ZrO_2 \rightleftarrows H_2O + ZrO(OH)^+$ or $OZrOH^+$

Can. J. Chem. Downloaded from www.nrcresearchpress.com by 46.23.64.124 on 09/08/12
For personal use only.

Fig. 9. Axial profiles of niobium positive ions observed in both the fuel-rich (FR) and fuel-lean (FL) flames.

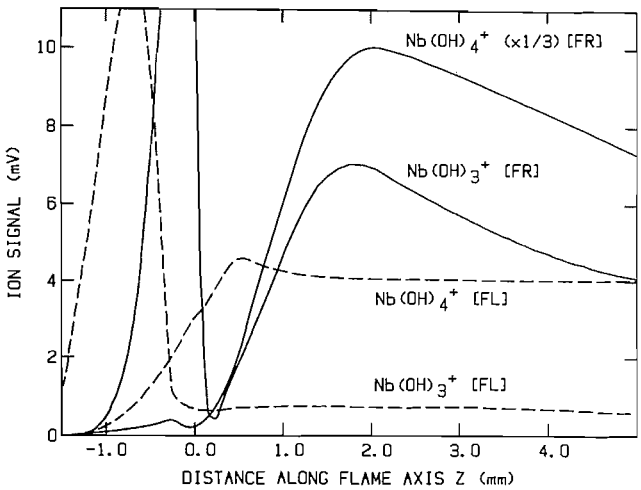

with subsequent hydration/dehydration equilibria

[14] $ZrO(OH)^+ \cdot nH_2O + H_2O + M \rightleftarrows ZrO(OH)^+ \cdot (n+1)H_2O + M;\ n = 0,1$

Note that the first hydrate with $n = 1$ is equivalent to $Zr(OH)_3^+$ with a possible planar trigonal structure. The second hydrate with $n = 2$ amounts to $Zr(OH)_3(H_2O)^+$, which might be tetrahedral with an electron octet around Zr; it could form directly by proton transfer to neutral $Zr(OH)_4$. Similarly, the $ZrOH^+$ ion, presumably in the +2 oxidation state ($OZrH^+$ in the +4 state is unlikely), can arise by proton transfer to the monoxide ZrO

[15] $H_3O^+ + ZrO \rightleftarrows ZrOH^+ + H_2O$

The ion was not detected in the FL flame; with excess oxygen present, [ZrO] will decrease in favour of increased $[ZrO_2]$.

With regard to the anion chemistry, the same $ZrO(OH)_3^-$ ion was detected in both flames, as shown in Fig. 6. The FR profile is confined to a region in and around the reaction zone, whereas the FL profile persists throughout the burnt gas. Logical production mechanisms include proton abstraction from the tetrahydroxide

[16] $OH^- + Zr(OH)_4 \rightleftarrows ZrO(OH)_3^- + H_2$

or OH^- addition to the mixed oxide dihydroxide

[17] $OH^- + ZrO(OH)_2 + M \rightleftarrows ZrO(OH)_3^- + M$

The disappearance of the anion downstream in the FR flame is probably not surprising; increased [H] will increase the loss rate by associative electron detachment

[18] $ZrO(OH)_3^- + H \rightleftarrows Zr(OH)_4 + e^-$

Reactions such as [18] reinforce the notion that the H atom is a very general and efficient "electron detacher."

Niobium ion chemistry

Niobium adds one more electron for a $5s^14d^4$ configuration with the possibility of a maximum +5 oxidation state that could give rise to such neutral compounds as $NbO_2(OH)$ or $NbO(OH)_3$. However, niobium shows little cationic behaviour in solution although multiple oxidation states are known, including +2, +3, +4, as well as +5 (20). Only the ^{93}Nb isotope occurs naturally with an abundance of 100%.

Small signals of the same two tetra- and trihydroxide cations were observed in both flames with $[Nb(OH)_4^+] > [Nb(OH)_3^+]$, and only in the downstream region. This is another example of the trend, for the heavier transition metals, towards a tendency for the higher oxidation state to be dominant (20). The profiles are shown in Fig. 9; the profile peaks in the reaction zone are due to natural $C_xH_yO_z^+$ ions at the same mass numbers, and not metallic cations. The $Nb(OH)_4^+$ ion could be formed directly by proton transfer to $NbO(OH)_3$

[19] $H_3O^+ + NbO(OH)_3 \rightleftarrows Nb(OH)_4^+ + H_2O$

However, $Nb(OH)_4^+$ is equivalent to the hydrates $NbO(OH)_2^+ \cdot H_2O = NbO_2^+ \cdot 2H_2O$. An alternative mechanism might be proton transfer

[20] $H_3O^+ + NbO_2(OH) \rightleftarrows NbO(OH)_2^+ + H_2O$

followed by hydration

[21] $NbO(OH)_2^+ + H_2O + M \rightleftarrows M + NbO(OH)_2^+ \cdot H_2O$ or $Nb(OH)_4^+$

Note that the +5 oxidation state is emphasized throughout. In a very similar manner, the trihydroxide ion can be produced starting with NbO_2

[22] $H_3O^+ + NbO_2 \rightleftarrows NbO(OH)^+ + H_2O$

[23] $NbO(OH)^+ + H_2O + M \rightleftarrows M + NbO(OH)^+ \cdot H_2O$ or $Nb(OH)_3^+$

In this case, the +4 oxidation state is emphasized throughout. The prominence of $Nb(OH)_3^+$ is somewhat surprising because it is a radical cation. A similar situation was encountered previously in flames with $V(OH)_3^+$ and also $Ti(H_2O)_3^+$, both radical cations (2). Perhaps the stability of these ions against chemical attack in the burnt-gas region is attributable to their high degree of symmetry, whether pyramidal or planar trigonal. It is conceivable that the reaction sequences [20] + [21] or [22] + [23] might take place in a single step. Also, the similar shapes of the pair of cation profiles in either flame suggest that the hydroxide ions might be linked by a balanced reaction such as

[24] $Nb(OH)_3^+ + H_2O \rightleftarrows Nb(OH)_4^+ + H$

Only one niobium anion $NbO_2(OH)_2^-$ was detected, and only in the FL flame in the downstream region as shown in Fig. 6. The same dichotomy exists for the production mechanism already encountered for both Y and Zr; namely, either proton transfer to OH^-

[25] $OH^- + NbO(OH)_3 \rightleftarrows NbO_2(OH)_2^- + H_2O$

Can. J. Chem. Downloaded from www.nrcresearchpress.com by 46.23.64.124 on 09/08/12
For personal use only.

Fig. 10. Axial profiles of molybdenum positive ions observed in both the fuel-rich (FR) and fuel-lean (FL) flames.

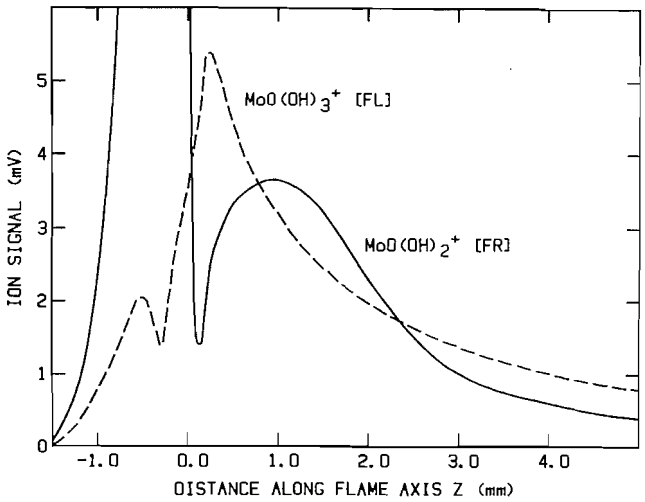

Fig. 11. Axial profiles of moybdenum negative ions observed in both the fuel-rich (FR) and fuel-lean (FL) flames.

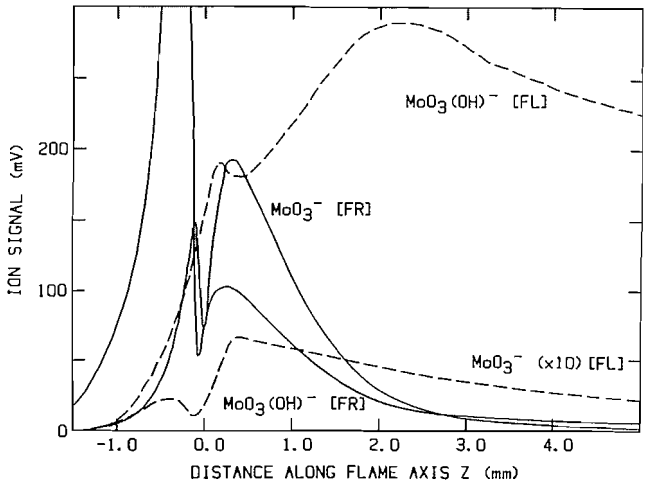

or OH^- addition

[26] $OH^- + NbO_2(OH) + M \rightleftarrows NbO_2(OH)_2^- + M$

The lack of detectable anions in the burnt-gas region of the FR flame is not surprising if the likely anions were to contain OH groups that are prime candidates for associative detachment with H atoms.

Molybdenum ion chemistry

Molybdenum has a $5s^14d^5$ electron configuration, and exhibits a wide variety of stereochemistries and oxidation states from +1 to +6 (20). It is inert to oxygen at ordinary temperatures, but at red heat it combines readily to give trioxides. If the higher oxidation states are favoured, some of the mixed oxide hydroxides such as $MoO_2(OH)_2$ and $MoO_2(OH)$ might be present in flames in addition to MoO_3. The element is difficult to work with mass-spectrometrically because it has seven isotopes with appreciable natural abundances (each >9.1%); flame ions were observed using the major ^{98}Mo isotope of abundance 24.1%.

Very small signals of just two cations were observed, whose axial concentration profiles are given in Fig. 10. They correspond to $MoO(OH)_2^+$ in the FR flame at 148 u in the +5 oxidation state, and $MoO(OH)_3^+$ in the FL flame at 165 u in the +6 state. In this case, it is convenient to discuss the cation production mechanism beginning with the FL flame in which neutral molybdenum is likely to be highly oxidized to the trioxide MoO_3. Proton transfer to MoO_3

[27] $H_3O^+ + MoO_3 \rightleftarrows H_2O + MoO_3H^+$ or $MoO_2(OH)^+$

followed by hydration

[28] $MoO_2(OH)^+ + H_2O + M \rightleftarrows M + MoO_2(OH)^+\cdot H_2O$ or $MoO(OH)_3^+$

yields the observed FL ion. In the presence of high [H] typical of the FR flame, a balanced reaction

[29] $MoO(OH)_3^+ + H \rightleftarrows H_2O + MoO(OH)_2^+$

would yield the observed FR ion $MoO(OH)_2^+$ when the equilibrium is far to the right. The dominance of this ion in the FR flame is somewhat surprising because it is a radical cation. Alternatively, proton transfer to $MoO_2(OH)$ in the +5 oxidation state

[30] $H_3O^+ + MoO_2(OH) \rightleftarrows H_2O + MoO(OH)_2^+$

yields the FR ion directly. In their study of *fuel-rich* H_2–O_2–N_2 flames seeded with potassium to which molybdenum compounds were added, Jensen and Miller (7) assume that the neutral reaction

[31] $MoO_3 + H_2O \rightleftarrows H_2MoO_4$ or $MoO_2(OH)_2$

is balanced. Proton transfer to this neutral product in the +6 oxidation state

[32] $H_3O^+ + MoO_2(OH)_2 \rightleftarrows H_2O + MoO(OH)_3^+$

yields our FL cation directly, but it was not observed in our FR flame. If molybdenum neutrals in the +5 oxidation state (which would be odd-electron species) do not exist in flames, our FR $MoO(OH)_2^+$ cation must be produced by hydroxyl extraction from $MoO(OH)_3^+$ via reaction [29] in which a change of oxidation number is involved.

The same two molybdenum anions $MoO_3(OH)^-$ and MoO_3^- found by Jensen and Miller (7) in their H_2–O_2–N_2 flames, all of them FR, were also observed in both of our FR and FL CH_4–O_2 flames; axial concentration profiles are given in Fig. 11. In our case, the Mo anion signals are much larger than those observed with Y, Zr, and Nb, suggesting that a different type of mechanism may be operative. Jensen and Miller postulated a production mechanism involving dissociative electron attachment

[33] $e^- + MoO_2(OH)_2 \rightleftarrows MoO_3(OH)^- + H$

Table 2. Peak values and properties of metallic positive and negative ions observed for the second-row transition metals Y, Zr, Nb, and Mo in both the fuel-rich (FR) and fuel-lean (FL) flames.

	Maximum or peak values (V)							
	Y		Zr[a]		Nb		Mo[a]	
Ions of metal A	FR	FL	FR	FL	FR	FL	FR	FL
(a) Positive ions								
AO^+	0.367[b]	0.038[b]						
$AO^+ \cdot H_2O$ or $A(OH)_2^+$	1.831	1.450						
$AO^+ \cdot 2H_2O$ or $A(OH)_2^+ \cdot H_2O$	3.282	0.915[c]						
$AO^+ \cdot 3H_2O$ or $A(OH)_2^+ \cdot 2H_2O$	1.061	0.148[c]						
AOH^+			0.297[b]					
$AO(OH)^+$			Trace	0.008				
$A(OH)_3^+$ or $AO(OH)^+ \cdot H_2O$			0.536	0.391	0.007	0.001		
$A(OH)_3^+ \cdot H_2O$ or $AO(OH)^+ \cdot 2H_2O$			1.174	0.404				
$AO(OH)_2^+$ or $AO_2^+ \cdot H_2O$							0.015	
$AO(OH)_3^+$ or $AO_2(OH)^+ \cdot H_2O$								0.022
$A(OH)_4^+$ or $AO_2^+ \cdot 2H_2O$					0.030	0.005		
(b) Negative ions								
$A(OH)_4^-$ or $AO(OH)_2^- \cdot H_2O$	0.008	0.011						
$AO(OH)_3^-$ or $AO_2(OH)^- \cdot H_2O$			0.001	0.004				
$AO_2(OH)_2^-$ or $AO_3^- \cdot H_2O$						0.006[c]		
AO_3^-							0.801	0.027
$AO_3(OH)^-$							0.426	1.200
(c) Oxidation numbers	3		2,4		4,5		5,6	
(d) Isotopic natural abundances (%)								
	^{89}Y	100.0	^{90}Zr	51.9	^{93}Nb	100.0	^{92}Mo	14.8
			^{91}Zr	11.2			^{94}Mo	9.3
			^{92}Zr	17.1			^{95}Mo	15.9
			^{94}Zr	17.5			^{96}Mo	16.7
			^{96}Zr	2.8			^{97}Mo	9.6
							^{98}Mo	24.1
							^{100}Mo	9.6

[a]The measured isotopic ion signals have been corrected to account for 100% natural abundance.
[b]The peak ion signal occurred upstream in the flame reaction zone ($z < 0$).
[c]The maximum ion signal occurred at $z = 5$ mm downstream.

followed by the balanced reaction

[34] $MoO_3(OH)^- + H \rightleftarrows MoO_3^- + H_2O$

This mechanism adequately explains the main features of the profiles shown in Fig. 9. In the FL flame, a low [H] value is consistent with higher anion signals overall from reaction [33]; also, a relatively large value of the ratio $[MoO_3(OH)^-]/[MoO_3^-] \propto [H_2O]/[H]$ is consistent with reaction [34]. From Table 1, the $[H_2O]/[H]$ ratio is 1280 in the FL flame, and 27.7 in the FR flame at equilibrium; i.e., a factor of 46.2 greater in the FL case. This agrees with the $[MoO_3(OH)^-]/[MoO_3^-]$ ratio measured in Fig. 9 at $z = 4$ mm downstream; the ratio is a factor of 47 greater in the FL flame than in the FR one. Coming out of the reaction zone of either flame and proceeding downstream ($z > 0$), the anion ratio increases; this is consistent with the realistic expectation that the $[H_2O]/[H]$ ratio increases downstream since $[H_2O]$ rises and [H] falls towards their equilibrium values. Of course, other production mechanisms are possible. For example, proton transfer to OH^- from neutral $MoO_2(OH)_2$ in the +6 oxidation state or from $MoO_2(OH)$ in the +5 state

[35] $OH^- + MoO_2(OH)_2 \rightleftarrows MoO_3(OH)^- + H_2O$

[36] $OH^- + MoO_2(OH) \rightleftarrows MoO_3^- + H_2O$

produces the corresponding anions in the +6 and +5 states, respectively. For both the cations and anions of molybdenum, it is noteworthy and consistent that the higher +6 oxidation state is emphasized for the more oxidizing atmosphere of the FL flame; the presence of the lower +5 state is more evident in the more reducing environment of the FR flame.

Can. J. Chem. Downloaded from www.nrcresearchpress.com by 46.23.64.124 on 09/08/12
For personal use only.

Can. J. Chem. Downloaded from www.nrcresearchpress.com by 46.23.64.124 on 09/08/12
For personal use only.

Summary and conclusions

A summary of all the cations and anions for each of the four second-row transition metals Y, Zr, Nb, and Mo observed in the pair of FR and FL CH_4–O_2 flames is given in Table 2, together with the oxidation numbers exhibited and the natural abundances of the metallic isotopes. Several general conclusions can be drawn from this work, particularly in regard to comparisons with the lighter first-row transition metals Sc, Ti, V, and Cr (2) from corresponding chemical groups; in the latter case, however, only cations were studied and only in the FR flame.

1. In general, the second-row metals tend to exhibit higher oxidation numbers, and the range of oxidation states is more restricted than with the first-row metals. The $AO^+ \cdot nH_2O$ cation series in the +3 state was dominant for both Sc and Y, although Sc also showed small signals of some $A^+ \cdot nH_2O$ ions in the +1 state. The Ti cations showed the full range of ion series (for brevity, the "$\cdot nH_2O$" hydrate series designation will be left out) including the A^+ series (+1 oxidation state), AOH^+ (+2), AO^+ (+3), and $AO(OH)^+$ (+4) series, with about 94% of the ion signals in the first two series; in contrast, nearly all the cations observed for Zr were $AO(OH)^+$ (+4) ions. A similar range of four cation series was observed for V with about 81% of the ions in the third AO^+ (+3) series, whereas the Nb cations were confined to the fourth $AO(OH)^+$ (+4) and a new AO_2^+ series (i.e., $A(OH)_4^+$ ions, +5 state). For Cr, about 99% of the cations were A^+ (+1) ions, compared with the observed pair of Mo cations $AO(OH)_2^+$ (+5) and $AO(OH)_3^+$ (+6). Thus, the trends towards higher and fewer oxidation states for second-row compared with first-row metallic cations is well established.

2. The second-row anions exhibit essentially the same oxidation numbers as the cations under similar flame conditions.

3. Ions in the higher oxidation state tend to be emphasized in the fuel-lean (FL) flame compared with the fuel-rich (FR) flame where, relatively, the lower oxidation state may be favoured. This trend is probably not surprising; the FL flame is a more oxidizing medium than the more reducing atmosphere of the FR flame.

4. At the relatively high temperatures of these flame studies, a large fraction of the observed ions appear to have four ligands around the central metal atom, suggestive of tetrahedral structures. The Y cations are exceptional, but the assumed $Y(OH)_4^-$ structure with four ligands for the anions is consistent.

5. It had been noted previously for the first-row transition metals (2) that radical cations seem to be stabilized by a high degree of structural symmetry; e.g., $Ti^+ \cdot 3H_2O$ and $V(OH)_3^+$. Further examples from the second-row metals include: $Nb(OH)_3^+$, the counterpart to vanadium; $MoO(OH)_2^+$, the only molybdenum cation observed in the FR flame, where the symmetry is less evident; and MoO_3^-, a radical anion that is dominant in the FR flame.

6. The formation mechanism for these ions by chemical ionization (CI) in CH_4–O_2 flames, which contain a high level of natural ionization, is dominated by proton transfer from H_3O^+ downstream in the case of the cations. For anion formation, the logical CI reagent is OH^-, capable of producing proton transfer in reaction with flame neutrals by proton abstraction because OH^- is a strong base. However, a dilemma exists for some of the anions because they could also be formed by addition reactions of OH^- to different neutral species.

7. Compared with similar studies of first-row transition metals (1, 2), the metallic ion signals obtained with the second-row transition metals using the same mass spectrometer under very similar conditions tend to be very small; the problem is exacerbated for Zr and Mo because the signal is spread out over a rather large number of isotopes. However, the detection of oxygenated anions provides a promising new dimension for possible exploitation in the future.

Acknowledgements

Support of this work by the Natural Sciences and Engineering Research Council of Canada, including partial student support for one of us (C.C.Y.C.), is gratefully acknowledged. We wish to thank Professor I.M. Walker for his encouragement and supply of chemicals in the early stages of the work.

References

1. Q. Tran, N.S. Karellas, and J.M. Goodings. Can. J. Chem. **66**, 2210 (1988).
2. J.M. Goodings, Q. Tran, and N.S. Karellas. Can. J. Chem. **66**, 2219 (1988).
3. P.M. Patterson and J.M. Goodings. Int. J. Mass Spectrom. Ion Processes, **148**, 55 (1995).
4. P.B. Armentrout. *In* Bonding energetics in organometallic compounds. *Edited by* T.J. Marks. ACS Symp. Ser. **428**, 18 (1990).
5. P.B. Armentrout and J.L. Beauchamp. Acc. Chem. Res. **22**, 315 (1989).
6. K.L. Wilson and S.W. Buckner. Rapid Commun. Mass Spectrom. **7**, 848 (1993).
7. D.E. Jensen and W.J. Miller. Symp. (Int.) Combust. [Proc.]. 13th. The Combustion Institute, Pittsburgh, Pa. 1971. p. 363.
8. E.B. Rudnyi, O.M. Vovk, E.A. Kaibicheva, and L.N. Sidorov. J. Chem. Thermodyn. **21**, 247 (1989).
9. J.M. Goodings, S.M. Graham, and W.J. Megaw. J. Aerosol Sci. **14**, 679 (1983).
10. J.M. Goodings, D.K. Bohme, and C.-W. Ng. Combust. Flame, **36**, 27 (1979).
11. N.A. Burdett and A.N. Hayhurst. J. Chem. Soc. Faraday Trans.1, **78**, 2997 (1982).
12. A.N. Hayhurst and N.R. Telford. Proc. R. Soc. London A, **322**, 483 (1971).
13. H.F. Calcote. Eighth Symp. (Int.) Combust. [Proc.]. 8th. Williams and Wilkins, Baltimore, Md. 1962. p. 184.
14. J.A. Green and T.M. Sugden. Ninth Symp. (Int.) Combust. [Proc.]. 9th. Academic Press, New York. 1963. p. 589.
15. J.M. Goodings, D.K. Bohme, and C.-W. Ng. Combust. Flame, **36**, 27 (1979).
16. J.M. Goodings, D.K. Bohme, and C.-W. Ng. Combust. Flame, **36**, 45 (1979).
17. A.N. Hayhurst and N.R. Telford. J. Chem. Soc. Faraday Trans. 1, **71**, 1999 (1974).
18. J.M. Goodings, N.S. Karellas, and C.S. Hassanali. Int. J. Mass Spectrom. Ion Processes, **89**, 205 (1989).
19. D.E. Clemmer, N.F. Daleska, and P.B. Armentrout. Chem. Phys. Lett. **190**, 259 (1992).
20. F.A. Cotton and G. Wilkinson. Advanced inorganic chemistry. 5th ed. John Wiley & Sons, Inc., New York. 1988.

Rhenium and technetium complexes from pentadentate (N_3O_2) and tetradentate (N_2O_2) Schiff base ligands

Hongyan Luo, Shuang Liu, Steven J. Rettig, and Chris Orvig

Abstract: The rhenium(V) and technetium(V) complexes: [ReO(apa)], [{ReO(epa)}$_2$O], and [TcOCl(epa)] have been prepared from a potentially pentadentate N_3O_2 ligand, *N,N'*-3-azapentane-1,5-diylbis(3-(1-iminoethyl)-6-methyl-2*H*-pyran-2,4(3*H*)-dione) (H_3apa), or a potentially tetradentate N_2O_2 ligand, *N,N'*-ethylene-diylbis(3-(1-iminoethyl)-6-methyl-2*H*-pyran-2,4(3*H*)-dione) (H_2epa). The N_2O_2 complexes were synthesized in low yields. There was also evidence indicating that H_2ppa, *N,N'*-propylene-diylbis(3-(1-iminoethyl)-6-methyl-2*H*-pyran-2,4(3*H*)-dione), hydrolyzed in the course of coordination, forms a rhenium complex of the bidentate monoprotic (O,O) dehydroacetate (dha$^-$), [Re(dha)Cl$_2$(OPPh$_3$)(PPh$_3$)]·EtOH. The structure of this complex was determined by X-ray crystallography. Crystals of [Re(dha)Cl$_2$(OPPh$_3$)(PPh$_3$)]·EtOH ($C_{44}H_{37}Cl_2O_5P_2Re \cdot C_2H_6O$) are monoclinic, a = 11.064(2), b = 24.167(2), c = 16.6687(8) Å, β = 98.779(7)°, Z = 4, space group $P2_1/c$. The structure was solved by the Patterson method and refined by full-matrix least-squares procedures to R = 0.030 and R_w = 0.025 for 6942 reflections with $I \geq 3\sigma(F^2)$.

Key words: dehydroacetic acetate based Schiff base ligands, rhenium, technetium, N_3O_2 Schiff base, N_2O_2 Schiff base, oxygen transfer.

Résumé : On a préparé les complexes du rhénium(V) et du technicium(V) : [ReO(apa)], [{ReO(epa)$_2$O] et [TcOCl(epa)] à partir d'un coordinat potentiellement pentadentate, N_3O_2, la *N,N'*-3-azapentane-1,5-diylbis(3-(1-iminoéthyle)-6-méthyl-2*H*-pyrane-2,4(3*H*)-dione) (H_3apa) ou d'un coordinat potentiellement tétradentate, N_2O_2, la *N,N'*-éthylènediylbis(3-(1-iminoéthyle)-6-méthyl-2*H*-pyrane-2,4(3*H*)-dione) (H_2epa). Les complexes du N_2O_2 ont été synthétisés avec des faibles rendements. On a obtenu des résultats qui suggèrent que le H_2ppa, la *N,N'*-propylènediylbis(3-(1-iminoéthyle)-6-méthyl-2*H*-pyrane-2,4(3*H*)-dione), s'hydrolyse au cours de la coordination et qu'il y a formation d'un complexe du rhénium du déhydroacétate (dha$^-$) monoprotique bidentate (O,O), [Re(dha)Cl$_2$(OPPh$_3$)(PPh$_3$)]·EtOH. On a déterminé la structure de ce complexe par diffraction des rayons X. Les cristaux du [Re(dha)Cl$_2$(OPPh$_3$)(PPh$_3$)]·EtOH ($C_{44}H_{37}Cl_2O_5P_2Re \cdot C_2H_6O$) sont monocliniques, groupe d'espace $P2_1/c$, avec a = 11,064(2), b = 24,167(2) et c = 16,6687(8) Å, β = 98,779(7)° et Z = 4. La structure a été résolue par la méthode de Patterson et elle a été affinée par la méthode des moindres carrés, matrice complète, jusqu'à des valeurs de R = 0,30 et R_w = 0,025 pour 6942 réflexions avec $I \geq 3\sigma(F^2)$.

Mots clés : coordinats formés de bases de Schiff dérivées de l'acétate déhydroacétique, rhénium, technicium, base de Schiff N_3O_2, base de Schiff N_2O_2, transfert d'oxygène.

[Traduit par la rédaction]

Introduction

In searching for new chelates from which to form stable Re/Tc complexes, in addition to the bidentate monoprotic ligands (1, 2), we have recently focussed on some pentadentate (3) and tetradentate Schiff base ligands. Coordination of these multidentate Schiff bases can result in the formation of numerous chelate rings, which may be useful in stabilizing Re/Tc complexes for use as radiopharmaceuticals.

Received July 15, 1995.

H. Luo, S. Liu, S.J. Rettig, and C. Orvig.[1] Department of Chemistry, University of British Columbia, 2036 Main Mall, Vancouver, BC V6T 1Z1, Canada.

[1] Author to whom correspondence may be addressed. Telephone: (604) 822-4449. Fax: (604) 822-2847. Internet: ORVIG@CHEM.UBC.CA

The ease of synthesis of multidentate Schiff base ligands has led to extensive investigation of their coordination chemistry with Tc (4) and with many other metal centers (5). Some Re/Tc complexes of tetradentate (6–9) and pentadentate (10, 11) Schiff base ligands have been studied. Most of the ligands are derived from salicylaldehyde; thus they have the disadvantage of producing lipophilic Tc complexes that tend to localize preferentially in the liver (4). To avoid this problem, we have prepared a dha (i.e., dehydroacetic acid, 3-acetyl-6-methyl-2*H*-pyran-2,4(3*H*)-dione)-based, potentially pentadentate (N_3O_2) ligand, H_3apa (3), that contains both lipophilic hydrocarbon chains and polar carbonyl groups (Scheme 1). With H_3apa, one neutral oxotechnetium(V) complex was synthesized in good yield (3); thus the feasibility of Tc(V) complexes of H_3apa has led us to further investigate Re/Tc coordination chemistry with this ligand and with other dha-based, N_2O_2 Schiff base ligands (H_2epa and H_2ppa, Scheme

Can. J. Chem. Downloaded from www.nrcresearchpress.com by 46.23.64.124 on 09/08/12
For personal use only.

Scheme 1. dha and dha-based Schiff base ligands.

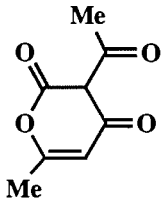

Dehydroacetic acid (dha)

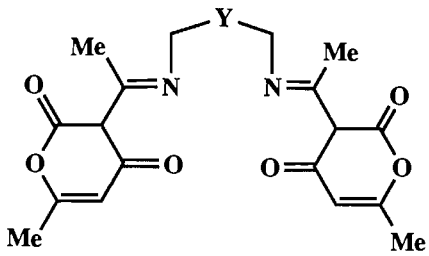

H_3apa = (dha)$_2$dien, Y = CH_2NHCH_2
H_2epa = (dha)$_2$en, Y = none
H_2ppa = (dha)$_2$pn, Y = CH_2

1). The N_3O_2 ligand H_3apa and the N_2O_2 ligands H_2epa and H_2ppa are derived from the condensation of 2 equivalents of dehydroacetic acid (dha) and 1 equivalent of diamine, i.e., diethylenetriamine (dien), ethylenediamine (en), or propylenediamine (pn), respectively. This paper summarizes the attempts to synthesize new Re/Tc complexes of the dha-based Schiff base ligands.

Experimental

Materials

$[NH_4][^{99}TcO_4]$ was obtained from the Du Pont Merck Pharmaceutical Company. Dehydroacetic acid, diethylenetriamine, ethylenediamine, and propylenediamine (all from Aldrich) were used without further purification. $[(n\text{-}Bu)_4N][TcOCl_4]$ (12) $[ReOCl_3(PPh_3)_2]$ (13), $[ReCl_4(PPh_3)_2]$ (14), and H_3apa (3) were prepared according to published procedures.

Caution! ^{99}Tc is a low-energy (0.292 MeV) β^- emitter with a half-life of 2.12×10^5 years. All manipulations of solutions and solids were performed in a laboratory approved for the handling of low-level radioisotopes, and normal safety procedures must be used at all times to prevent contamination.

Instrumentation

^{1}H NMR spectra were recorded on a Bruker AC-200E (^{1}H, ^{1}H–^{1}H COSY, 200 MHz), or a Bruker WH-400 (^{1}H–^{1}H COSY) spectrometer. Chemical shifts are reported as δ in ppm referenced to external TMS: δ (multiplicity, coupling constant, number of hydrogen nuclei, *assignment*). Mass spectra were obtained with either a Kratos MS 50 (electron impact ionization, EIMS) or a Kratos Concept II H32Q instrument (Cs^+-LSIMS with positive or negative ion detection). Infrared spectra were recorded as KBr pellets in the range 4000–400 cm^{-1} on a Perkin–Elmer PE 783 spectrophotometer previously calibrated against the spectrum of polystyrene. Analyses for C, H, N were performed by Mr. Peter Borda (for ligands and the Re complexes) in this department or by Canadian Microanalytical Services Ltd. (for the Tc compound).

N,N′-*Ethylene-diylbis(3-(1-iminoethyl)-6-methyl-2H-pyran-2,4(3H)-dione) (H_2epa)*

This was prepared from the condensation reaction of dha and en, via a similar procedure as that for H_3apa (3). IR (cm^{-1}, KBr disk): 3600–3300 ($\nu_{O\text{-}H}$); 3000–2800 ($\nu_{C\text{-}H}$); 1710, 1660, 1580 (all vs, mixed $\nu_{C=O}$ and $\nu_{C=C}$). ^{1}H NMR ($CDCl_3$): 14.6 (br s, 2H, O*H*), 5.60 (s, 2H, ring-*H*), 3.77 (d, 4H, imine-CH_2), 2.58 (s, 6H, imine-CH_3), 2.12 (s, 6H, ring-CH_3). EIMS; *m/z*: 360 (molecular ion $[C_{18}H_{20}N_2O_6]^+$). Anal. calcd. (found) for $C_{18}H_{20}N_2O_6$: C 59.97 (60.02), H 5.60 (5.70), N 7.78 (7.77).

N,N′-*Propylene-diylbis(3-(1-iminoethyl)-6-methyl-2H-pyran-2,4(3H)-dione) methanol hemisolvate (H_2ppa·0.5MeOH)*

This was prepared from the condensation reaction of dha and pn, via a similar procedure as that for H_3apa (3). IR (cm^{-1}, KBr disk): 3600–3300 ($\nu_{O\text{-}H}$); 3000–2800 ($\nu_{C\text{-}H}$); 1700, 1655, 1580 (all vs, mixed $\nu_{C=O}$ and $\nu_{C=C}$). ^{1}H NMR ($CDCl_3$): 14.4 (br s, 2H, O*H*), 5.60 (s, 2H, ring-*H*), 3.60 (q, 4H, imine-CH_2), 3.40 (s, ~1.5H, CH_3OH), 2.57 (s, 6H, imine-CH_3), 2.00 (m, 8H, central-CH_2 and ring-CH_3). EIMS; *m/z*: 374 (molecular ion $[C_{19}H_{22}N_2O_6]^+$). Anal. calcd. (found) for $C_{19.5}H_{24}N_2O_{6.5}$: C 59.99 (60.00), H 6.20 (6.16), N 7.18 (7.22).

[ReO(apa)]

Method A: To a mixture of $[ReOCl_3(PPh_3)_2]$ (167 mg, 0.200 mmol) and H_3apa (103 mg, 0.256 mmol) was added 6 mL of ethanol. A green solution resulted after boiling. Six drops of triethylamine were added, and the solution was refluxed for a further 30 min. The solution was kept overnight at −4°C, and the resulting brownish green precipitate was filtered off. The precipitate was recrystallized from acetone; brownish green crystals deposited as the solvent evaporated. These were collected by filtration, washed with diethyl ether, and dried in air to yield 85.8 mg (71% based on Re). The product is soluble in chloroform and dichloromethane, but insoluble in diethyl ether and water. IR (cm^{-1}, KBr disk): 1710, 1660, 1644, 1570, 1540 (all vs, mixed $\nu_{C=O}$ and $\nu_{C=C}$), 945 (s, $\nu_{Re=O}$). ^{1}H NMR (500 MHz, $CDCl_3$): 5.73 (d, ^4J = 0.9 Hz; 1H, ring-*H*), 5.05 (d, ^4J = 0.8 Hz; 1H, ring-*H*′),[2] 5.03 (dd, ^2J = 11.6, ^3J = 4.4 Hz, 1H, amido-$CH'_aH'_e$),[3] 4.77 (dd, ^2J = 12.8, ^3J = 6.0 Hz, 1H, amido-CH_aH_e), 4.33 (dd, ^2J = 12.5, ^3J = 6.9 Hz, 1H, amido-CH_eH_a), 4.09 (dd, ^2J = 12.2, ^3J = 5.8 Hz, 1H, amido-$CH'_eH'_a$), 4.07 (m, 1H, imino-CH_aH_e), 3.96 (dt, ^2J = 11.5, ^3J = 5.8 Hz, 1H, imino-$CH'_aH'_e$), 3.82 (dt, ^2J = 12.2, ^3J = 4.6 Hz, 1H, imino-$CH'_eH'_a$), 3.51 (m, 1H, imino-CH_eH_a), 3.04 (s, 3H, imino-CH_3), 2.91 (s, 3H, imino-CH'_3), 2.13 (d, ^4J = 0.8 Hz, 3H, ring-CH_3), 1.98 (d, J = 0.7 Hz, 3H, ring-CH'_3). LSIMS; *m/z*: 604 ([ReO(apa)+1]$^+$). Anal. calcd. (found) for $C_{20}H_{22}N_3O_7Re$: C 39.86 (39.91), H 3.68 (3.75), N 6.97 (6.77).

Method B: To $[ReCl_4(PPh_3)_2]$ (168 mg, 0.197 mmol) and H_3apa (86 mg, 0.21 mmol) was added 7 mL of ethanol. Fourteen drops of triethylamine were added, and the mixture was refluxed for 2.5 h. The dark brown solution was clarified by filtration and the solvent allowed to slowly evaporate at room temperature. Brown crystals were collected and found to be identical to the product obtained via Method A (yield 37 mg; 31% based on Re).

Can. J. Chem. Downloaded from www.nrcresearchpress.com by 46.23.64.124 on 09/08/12
For personal use only.

Can. J. Chem. Downloaded from www.nrcresearchpress.com by 46.23.64.124 on 09/08/12
For personal use only.

[{ReO(epa)}$_2$O]

To a mixture of [$ReOCl_3(PPh_3)_2$] (166 mg, 0.200 mmol), H_2epa (81.7 mg, 0.23 mmol), and Na_2CO_3 (70 mg, 0.66 mmol) was added 30 mL of ethanol. The mixture was refluxed for 3 h, resulting in a grey-green solution and white precipitate. A green precipitate was deposited on the white precipitate while filtering. The precipitate mixture was recrystallized from acetone–chloroform solution; green crystals and white crystals (dha, presumably from hydrolysis of H_2epa) deposited as the solvents evaporated. The green crystals (15 mg) were mechanically separated from the white crystals after being dried in air (13% based on Re). The product is soluble in chloroform and dichloromethane, but insoluble in diethyl ether and water. IR (cm^{-1}, KBr disk): 675 (s, $\nu_{Re\text{-}O}$). ^1H NMR ($CDCl_3$): 5.95 (s, 2H, ring-*H*), 4.14 (m, 2H, ethylene-*H*), 3.90 (m, 2H, ethylene-*H*), 2.72 (s, 6H, imino-CH_3), 2.28 (s, 6H, ring-CH_3). LSIMS; *m/z*: 561 ([ReO(epa) + 1]$^+$), 1137 ([{ReO(epa)}$_2$O] + 1]$^+$). Anal. calcd. (found) for $C_{36}H_{36}N_4O_{15}Re_2$: C 38.03 (38.10), H 3.19 (3.36), N 4.93 (4.75).

[TcOCl(epa)]·0.5H_2O

To a mixture of [$(n\text{-}Bu)_4N$][$TcOCl_4$] (49.7 mg, 0.10 mmol) and H_2epa (40.1 mg, 0.11 mmol) was added 25 mL ethanol. The suspension became clear after refluxing for 1 h. The solution was refluxed for an additional 2 h. The green-yellow solution was then kept at −4°C for several days. A brown precipitate was filtered out, washed with Et_2O, and dried in air to yield 12 mg (23% based on Tc). The product is slightly soluble in ethanol, chloroform, and dichloromethane, and insoluble in Et_2O and H_2O. IR (cm^{-1}, KBr disk): 960 (w, $\nu_{Tc=O}$). LSIMS; *m/z*: 473 ([TcO(epa)]$^+$). Anal. calcd. (found) for $C_{18}H_{19}ClN_2O_{7.5}Tc$: C 41.76 (41.89), H 3.70 (3.81), N 5.41 (5.58).

[Re(dha)Cl_2(OPPh$_3$)(PPh$_3$)]·EtOH

To a mixture of [$ReOCl_3(PPh_3)_2$] (84.5 mg, 0.10 mmol) and H_2ppa (39.1 mg, 0.10 mmol) was added 25 mL of ethanol. The suspension was refluxed overnight. The solution was clarified by filtration, then held at −4°C. Red crystals (X-ray quality) deposited from the solution. The supernatant solution was removed, then the crystals were washed with diethyl ether and dried in air. The product is soluble in chloroform and dichloromethane, and slightly soluble in diethyl ether. IR (cm^{-1}, KBr disk): 695 (s).

X-ray crystallographic analysis of [Re(dha)Cl_2(OPPh$_3$)(PPh$_3$)]·EtOH

Crystallographic data for [Re(dha)Cl_2(OPPh$_3$)(PPh$_3$)]·EtOH appear in Table 1. The final unit-cell parameters were obtained by least squares on the setting angles for 25 reflections with 2θ = 25.6°–30.0° (Rigaku AFC6S diffractometer). The intensities of three standard reflections, measured every hour of X-ray exposure time throughout the data collection, decayed linearly by 2.1%. The data were processed,[4] and corrected for Lorentz and polarization effects, decay, and absorption (empirical, based on azimuthal scans for three reflections).

Table 1. Crystallographic data.[a]

Compound	[Re(dha)Cl_2(OPPh$_3$)(PPh$_3$)]·EtOH
Formula	$C_{44}H_{37}Cl_2O_5P_2Re\cdot C_2H_6O$
fw	1010.90
Crystal system	Monoclinic
Space group	$P2_1/c$
a, Å	11.064(2)
b, Å	24.167(2)
c, Å	16.6687(8)
β, °	98.779(7)
V, Å^3	4405.0(6)
Z	4
ρ_{calc}, g/cm^3	1.524
F(000)	2024
T	21°C
λ (Å)	0.71 069
$2\theta_{max}$, deg	60
Total reflections	13 756
Total unique reflections	13 144
Reflections with $I \geq 3\sigma(F^2)$	6942
No. of variables	514
R	0.030
R_w	0.025
gof	1.42
Max Δ/σ (final cycle)	0.001
Residual density e/Å^3	−0.68 to 0.48 (both near Re)

[a] $R = \Sigma||F_o|-|F_c||/\Sigma|F_o|$, $R_w = (\Sigma w(|F_o|-|F_c|)^2/\Sigma w|F_o|^2)^{1/2}$, and gof = $[\Sigma w(|F_o|-|F_c|)^2/(m-n)]^{1/2}$. Values given for *R*, R_w, and gof are based on those reflections with $I \geq 3\sigma(F^2)$.

The structure was solved by the Patterson method, the coordinates of the Re atom being determined from the Patterson function and those of the remaining non-hydrogen atoms from subsequent difference Fourier syntheses. The asymmetric unit consists of one metal complex and one molecule of ethanol. Non-hydrogen atoms were refined with anisotropic thermal parameters and hydrogen atoms were fixed in calculated positions (orientations based on difference map peaks, C—H = 0.98 Å, O—H = 0.92 Å, $B_H = 1.2\ B_{bonded\ atom}$). No correction for secondary extinction was necessary. Neutral atom scattering factors for all atoms and anomalous dispersion corrections for the non-hydrogen atoms were taken from the International tables for X-ray crystallography (15). Final atomic coordinates and equivalent isotropic thermal parameters, selected bond lengths, and selected bond angles appear in Tables 2–4, respectively. The molecule is shown in Fig. 1. Hydrogen atom parameters, anisotropic thermal parameters, complete tables of bond lengths and angles, torsion angles, intermolecular

[2] Joined at the amido N atom, the two halves of the bound apa^{3-} are chemically nonequivalent with one enolic oxygen donor remaining in the equatorial plane and the other oxygen donor in the apical position (*trans* to Re=O). Thus, the corresponding half of the ligand is referred to as "equatorial" or "apical" (arbitrary), related to the Re=O unit, and the hydrogen nuclei are designated as *H* for that of the "equatorial" half, or as *H'* for that of the "apical" half. Please refer to the geometry of the complex [ReO(apa)] (Scheme 2).

[3] In the chelate ring, the methylene hydrogens are designated as H_e or H_a to refer its (pseudo)equatorial or (pseudo)axial position relative to the ring conformation. Please refer to the ring conformation (Fig. 2).

[4] *teXsan*: Crystal structure analysis package. Molecular Structure Corp. The Woodlands, Tex. 1985 and 1992.

Can. J. Chem. Downloaded from www.nrcresearchpress.com by 46.23.64.124 on 09/08/12
For personal use only.

Table 2. Final atomic coordinates (fractional) and B_{eq} (Å^2).[a]

Atom	x	y	z	B_{eq}
Re(1)	0.176321(14)	0.445436(7)	0.204979(9)	2.838(6)
Cl(1)	0.05838(11)	0.50580(5)	0.28021(6)	5.05(6)
Cl(2)	−0.00851(9)	0.40515(5)	0.14193(6)	4.06(5)
P(1)	0.29622(9)	0.39048(4)	0.12626(6)	2.82(4)
P(2)	0.21026(10)	0.36616(5)	0.38226(6)	3.40(5)
O(1)	0.3733(3)	0.64252(12)	0.1003(2)	5.2(2)
O(2)	0.4715(3)	0.63803(15)	0.2242(2)	7.1(2)
O(3)	0.1713(2)	0.50493(11)	0.12224(14)	3.0(1)
O(4)	0.3264(2)	0.48324(12)	0.26410(14)	3.5(1)
O(5)	0.1944(2)	0.38848(11)	0.29724(14)	3.8(1)
O(6)	0.2111(5)	0.6089(2)	0.3654(3)	12.0(3)
C(1)	0.3988(4)	0.6142(2)	0.1747(3)	4.8(2)
C(2)	0.3377(3)	0.5625(2)	0.1826(2)	3.4(2)
C(3)	0.2404(3)	0.5472(2)	0.1208(2)	3.0(2)
C(4)	0.2166(4)	0.5805(2)	0.0489(2)	3.7(2)
C(5)	0.2847(4)	0.6247(2)	0.0389(3)	4.3(2)
C(6)	0.3774(4)	0.5292(2)	0.2518(2)	3.7(2)
C(7)	0.4855(5)	0.5431(2)	0.3146(3)	6.0(3)
C(8)	0.2777(5)	0.6611(2)	−0.0344(3)	5.9(3)
C(9)	0.4554(3)	0.4123(2)	0.1475(2)	3.3(2)
C(10)	0.5046(4)	0.4502(2)	0.0983(2)	4.1(2)
C(11)	0.6205(5)	0.4712(2)	0.1204(3)	5.1(2)
C(12)	0.6912(4)	0.4544(2)	0.1902(3)	5.3(3)
C(13)	0.6451(4)	0.4169(2)	0.2400(3)	5.4(2)
C(14)	0.5267(4)	0.3965(2)	0.2192(3)	4.6(2)
C(15)	0.3009(4)	0.3159(2)	0.1453(2)	3.4(2)
C(16)	0.4028(4)	0.2837(2)	0.1384(3)	4.6(2)
C(17)	0.4005(5)	0.2269(2)	0.1502(3)	5.4(3)
C(18)	0.2985(6)	0.2017(2)	0.1674(3)	5.7(3)
C(19)	0.1951(5)	0.2327(2)	0.1751(3)	5.5(3)
C(20)	0.1959(4)	0.2898(2)	0.1627(2)	4.0(2)
C(21)	0.2563(3)	0.3942(2)	0.0155(2)	3.0(2)
C(22)	0.3250(4)	0.3649(2)	−0.0340(2)	4.0(2)
C(23)	0.2938(4)	0.3661(2)	−0.1172(3)	4.8(2)
C(24)	0.1927(4)	0.3963(2)	−0.1526(2)	4.7(2)
C(25)	0.1246(4)	0.4251(2)	−0.1047(2)	4.3(2)
C(26)	0.1554(4)	0.4238(2)	−0.0207(2)	3.5(2)
C(27)	0.1897(4)	0.4167(2)	0.4574(2)	4.0(2)
C(28)	0.2442(5)	0.4676(2)	0.4557(3)	5.7(3)
C(29)	0.2290(6)	0.5070(2)	0.5151(3)	7.3(3)
C(30)	0.1643(7)	0.4945(3)	0.5746(4)	7.9(4)
C(31)	0.1114(7)	0.4435(3)	0.5778(4)	9.2(4)
C(32)	0.1235(5)	0.4046(2)	0.5187(3)	6.6(3)
C(33)	0.3615(4)	0.3380(2)	0.4076(2)	3.5(2)
C(34)	0.4488(5)	0.3619(2)	0.4638(3)	5.4(2)
C(35)	0.5682(5)	0.3425(3)	0.4757(4)	7.0(3)
C(36)	0.5973(5)	0.2982(3)	0.4312(4)	6.5(3)
C(37)	0.5119(5)	0.2731(2)	0.3763(3)	5.8(3)
C(38)	0.3936(4)	0.2930(2)	0.3640(3)	4.5(2)
C(39)	0.1002(4)	0.3121(2)	0.3861(2)	4.0(2)
C(40)	0.1219(5)	0.2669(2)	0.4380(3)	5.3(2)
C(41)	0.0332(6)	0.2270(2)	0.4392(4)	6.9(3)
C(42)	−0.0755(6)	0.2324(3)	0.3900(4)	7.7(4)
C(43)	−0.0997(5)	0.2770(3)	0.3389(4)	8.2(4)
C(44)	−0.0117(4)	0.3174(2)	0.3366(3)	5.6(3)
C(45)	0.1569(9)	0.6527(3)	0.3224(5)	11.4(5)
C(46)	0.1619(10)	0.7003(4)	0.3630(7)	19.0(8)

[a] $B_{eq} = (8/3)\pi^2\Sigma\Sigma U_{ij}a_i^*a_j^*(\mathbf{a}_i\cdot\mathbf{a}_j)$

Table 3. Selected bond lengths (Å) for $[Re(dha)Cl_2(OPPh_3)(PPh_3)]\cdot EtOH$.

Re(1)—Cl(1)	2.430(1)	Re(1)—Cl(2)	2.362(1)
Re(1)—P(1)	2.404(1)	Re(1)—O(3)	1.987(2)
Re(1)—O(4)	2.061(3)	Re(1)—O(5)	2.051(2)
P(1)—C(9)	1.820(4)	P(1)—C(15)	1.831(4)
P(1)—C(21)	1.834(4)	P(2)—O(5)	1.502(3)
P(2)—C(27)	1.789(4)	P(2)—C(33)	1.796(4)
P(2)—C(39)	1.794(4)	O(1)—C(1)	1.407(5)
O(1)—C(5)	1.375(5)	O(2)—C(1)	1.207(5)
O(3)—C(3)	1.278(4)	O(4)—C(6)	1.276(5)
O(6)—C(45)	1.365(8)	C(1)—C(2)	1.437(6)
C(2)—C(3)	1.420(5)	C(2)—C(6)	1.421(6)
C(3)—C(4)	1.433(5)	C(4)—C(5)	1.334(6)
C(5)—C(8)	1.497(6)	C(6)—C(7)	1.503(6)
C(45)—C(46)	1.33(1)		

contacts, and least-squares planes have been deposited as supplementary material.[5]

Results and discussion

Ligands

The N_2O_2 Schiff base ligands, H_2epa and H_2ppa, were prepared in a manner similar to that for the N_3O_2 Schiff base ligand, H_3apa (3), i.e., the Schiff base condensation of ethylenediamine (en) or propylenediamine (pn), with 2 equivalents of dehydroacetic acid (dha). Each of these potentially tetradentate ligands contains an N_2O_2 donor set that may form three chelate rings. As in H_3apa, the infrared spectra of the free ligands show very broad O–H stretching vibrations at 3500 cm^{-1}, suggesting that the molecule probably exists mainly as the imine-enol form. This is also supported by the enol ^{1}H NMR signal, which lies downfield ($\delta > 14$ ppm, as a broad singlet) due to intramolecular hydrogen bonding (16*a*).

Synthesis of complexes

[TcO(apa)] was synthesized via both the ligand exchange route and the reduction–coordination route in moderate yields (49% and 54%, respectively) (3). [ReO(apa)] was prepared from the reaction of $[ReOCl_3(PPh_3)_2]$ or $[ReCl_4(PPh_3)_2]$ with H_3apa in ethanol in the presence of excess triethylamine. Scheme 2 describes the overall results of the synthetic studies. With an N_3O_2 Schiff base ligand H_3L, [MOL] was the only product (3, 10, 11). Upon coordination, the central amine group becomes more acidic due to the strongly electrophilic character of the $[M{=}O]^{3+}$ core, and is deprotonated to give a neutral metal(V) complex. The formation of a Re(V) product from the reaction of $[ReCl_4(PPh_3)_2]$ and H_3apa resulted from aerial oxidation. Oxotechnetium(V) complexes have been

[5] Supplementary material mentioned in the text may be purchased from: The Depository of Unpublished Data, Document Delivery, CISTI, National Research Council Canada, Ottawa, Canada K1A 0S2. Tables of hydrogen atom coordinates and bond lengths and angles involving hydrogen atoms have also been deposited with the Cambridge Crystallographic Data Centre and can be obtained on request from The Director, Cambridge Crystallographic Data Centre, University Chemical Laboratory, 12 Union Road, Cambridge CB2 1EZ, U.K.

Can. J. Chem. Downloaded from www.nrcresearchpress.com by 46.23.64.124 on 09/08/12
For personal use only.

Table 4. Selected bond angles (deg) for $[Re(dha)Cl_2(OPPh_3)(PPh_3)]\cdot EtOH$.

Cl(1)-Re(1)-Cl(2)	88.87(4)	Cl(1)-Re(1)-P(1)	176.59(4)
Cl(1)-Re(1)-O(3)	87.91(8)	Cl(1)-Re(1)-O(4)	86.72(8)
Cl(1)-Re(1)-O(5)	90.84(8)	Cl(2)-Re(1)-P(1)	92.40(4)
Cl(2)-Re(1)-O(3)	93.38(7)	Cl(2)-Re(1)-O(4)	175.58(8)
Cl(2)-Re(1)-O(5)	92.05(8)	P(1)-Re(1)-O(3)	88.86(7)
P(1)-Re(1)-O(4)	92.02(8)	P(1)-Re(1)-O(5)	92.28(8)
O(3)-Re(1)-O(4)	86.8(1)	O(3)-Re(1)-O(5)	174.4(1)
O(4)-Re(1)-O(5)	87.6(1)	Re(1)-P(1)-C(9)	109.4(1)
Re(1)-P(1)-C(15)	116.9(1)	Re(1)-P(1)-C(21)	117.0(1)
C(9)-P(1)-C(15)	104.5(2)	C(9)-P(1)-C(21)	105.0(2)
C(15)-P(1)-C(21)	102.6(2)	O(5)-P(2)-C(27)	114.0(2)
O(5)-P(2)-C(33)	109.2(2)	O(5)-P(2)-C(39)	108.2(2)
C(27)-P(2)-C(33)	107.9(2)	C(27)-P(2)-C(39)	108.3(2)
C(33)-P(2)-C(39)	109.2(2)	C(1)-O(1)-C(5)	121.9(3)
Re(1)-O(3)-C(3)	129.6(2)	Re(1)-O(4)-C(6)	131.9(3)
Re(1)-O(5)-P(2)	158.9(2)	O(1)-C(1)-O(2)	113.2(4)
O(1)-C(1)-C(2)	108.0(4)	O(2)-C(1)-C(2)	128.8(5)
C(1)-C(2)-C(3)	118.4(4)	C(1)-C(2)-C(6)	118.4(4)
C(3)-C(2)-C(6)	123.2(4)	O(3)-C(3)-C(2)	125.7(4)
O(3)-C(3)-C(4)	115.4(3)	C(2)-C(3)-C(4)	118.8(4)
C(3)-C(4)-C(5)	121.3(4)	O(1)-C(5)-C(4)	120.6(4)
O(1)-C(5)-C(8)	111.5(4)	C(4)-C(5)-C(8)	127.9(4)
O(4)-C(6)-C(2)	122.3(4)	O(4)-C(6)-C(7)	114.1(4)
C(2)-C(6)-C(7)	123.6(4)	O(6)-C(45)-C(46)	115.0(8)

Fig. 1. ORTEP drawing of $[Re(dha)Cl_2(OPPh_3)(PPh_3)]\cdot EtOH$; 33% probability ellipsoids are shown for the non-hydrogen atoms.

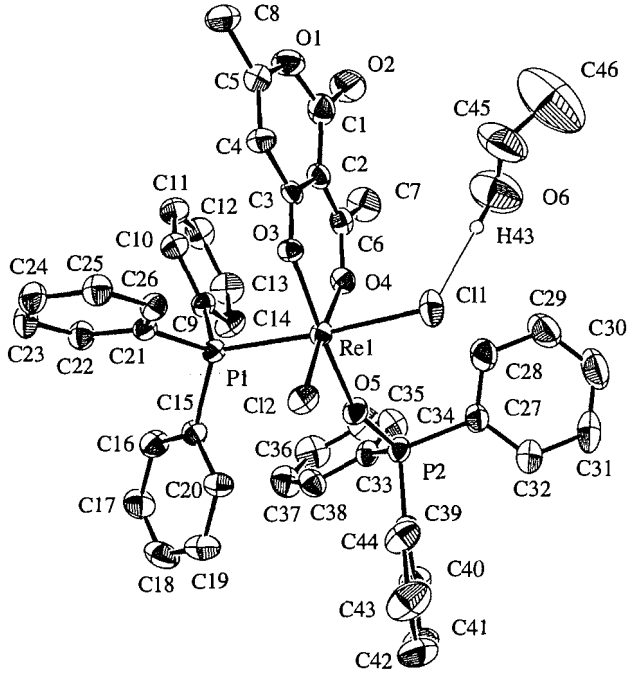

shown to form in a similar fashion from the reactions of $[TcCl_4(PPh_3)_2]$ and some N_2S_2 ligands (17).

In contrast to the N_3O_2 ligand H_3apa, the coordination of the N_2O_2 Schiff base ligands to Tc(V) and Re(V) metal centres was found to be much less favorable, and more complicated. The reaction of H_2epa with $[ReOCl_3(PPh_3)_2]$ produced the dinuclear complex $[\{ReO(epa)\}_2O]$ in low yield, and attempts to increase this yield failed. The reaction of H_2epa with $[TcOCl_4]^-$ gave the complex [TcOCl(epa)], also in low yield. It is common for the yields of tetradentate N_2O_2 Schiff base metal complexes to be low (7). The low yields in our reactions with H_2epa may be due to the diversity of the possible products (vide infra). In addition, the desired Schiff base complexes may be difficult to isolate due to reduction of the metal center (in the presence of PPh_3) and (or) hydrolysis of the Schiff base ligand during the reactions, as was seen for H_2ppa (vide infra).

Comparison of N_3O_2 and N_2O_2 ligands

It was reported that substitution reactions on to the TcO^{3+} core with N_2O_2 Schiff base ligands might lead to three types of complex, $[TcOX(N_2O_2)]$, $[\{TcO(N_2O_2)\}_2O]$, and $[TcO(OH_2)(N_2O_2)]^+$(7, 9), in addition to an isolable intermediate $[TcOCl_2(\underline{ON}\text{-}NO)]^-$ (7). Bandoli et al. assumed that all types of the complex are formed but that the isolated product is the most stable (7); this assumption is supported by other investigations wherein several bands were observed when the reaction mixture was loaded onto a column (9). Product purification is the crucial step in most of the N_2O_2 cases; chromatography is often required (8, 9). On the other hand, an N_2O_2 Schiff base ligand was found to form a $[MO(N_2O_2)]$ complex in the only mode for the five donor atoms to surround the M=O core, that in which the ligand is completely coordinated and there is only one complex (two enantiomers) that can be formed (3, 10, 11). This sole pathway in formation of the complex rationalizes the higher yield in synthesis for N_3O_2 vs. N_2O_2 ligands.

It should also be mentioned that all the donor atoms in the N_2O_2 Schiff base complexes were found in the equatorial (relative to M=O) plane, in contrast with the behavior of the bidentate NO Schiff base ligands in the oxo complexes (7). Two NO Schiff base molecules in $[MOX(NO)_2]$ are never found to be coplanar, i.e., one NO bidentate ligand chelates in the plane equatorial to, the other in the plane axial to, the M=O unit with the anionic donor atom *trans* to M=O. This non-coplanar configuration is thus considered thermodynamically more stable than a coplanar configuration (10, 11). Based on their observations and other results, Refosco et al. (11) and Tisato et al. (10) have concluded that tetradentate N_2O_2 Schiff base ligands could form a twisted configuration only when there are five or more atoms in the central chain between the two imine N donor atoms. The inability to adopt the thermodynamically more favored twisted configuration dictates the inherent instability of the N_2O_2 complexes, and therefore the low yield in the synthesis. Meanwhile, side reactions, such as reduction of the metal centers and (or) hydrolysis of the bound ligands, are enhanced, as observed. In the N_3O_2 complexes, such a twisted configuration is feasible, as is seen in all three solved structures (3, 10, 11); high bond strains have not been found in the constructed models of such a configuration (11).

The N_3O_2 Schiff base complexes result from the only coordination mode for the five donor atoms in surrounding the M=O core in a more stable configuration without high strain. In contrast, the N_2O_2 Schiff base complexes are a much less stable configuration with a significant *trans* influence, when

Can. J. Chem. Downloaded from www.nrcresearchpress.com by 46.23.64.124 on 09/08/12
For personal use only.

Scheme 2.

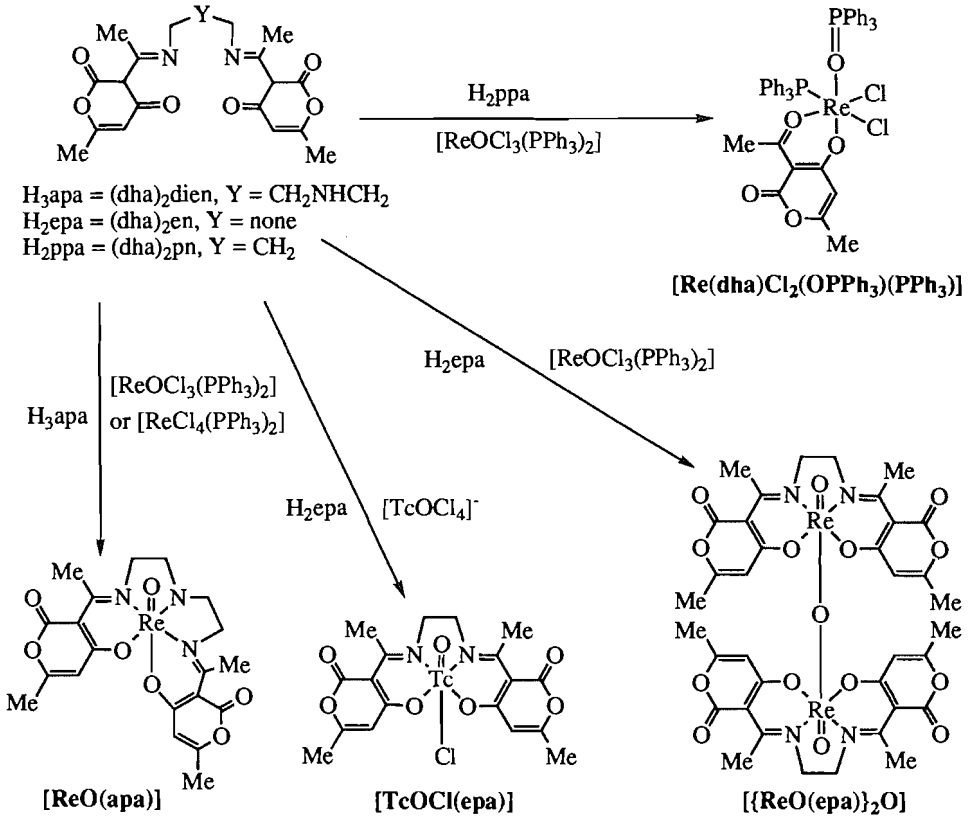

Scheme 3.

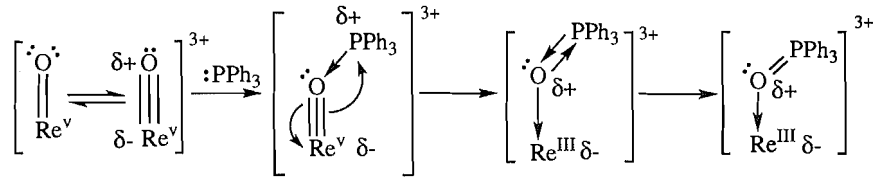

the four donor atoms of the ligand are bound to the metal in the equatorial plane and the oxo atom occupies the apical position. There are usually many anionic species competing for the sixth coordination site that is *trans* to, and labilized by, the M=O group (*trans* effect). Metal-enhanced hydrolysis of the N_2O_2 Schiff base ligands seriously hampers the synthesis of the complexes (vide infra).

Formation of $[Re(OPPh_3)(dha)(PPh_3)Cl_2]\cdot EtOH$

The trials with $[ReOCl_3(PPh_3)_2]$ and H_2ppa in ethanol resulted in an unexpected Re complex, with one PPh_3 migrating to the oxo oxygen, with the resultant vacant site filled, and with one chloro ligand being replaced by two oxygen donor atoms of dehydroacetate. The Re center is formally reduced to an oxidation state of three (Scheme 3). The $Re{=}O^{3+}$ core is known to react with phosphines and other oxygen acceptors, yielding Re(III) complexes and phosphine oxides (18*a*, 19, 20). In examining the $Re^{V}O + X = Re^{III} + XO$ transformation, Conry and Mayer observed that oxygen atoms were transferred to the substrate X when the X—O bond strength exceeded 127 kcal mol^{-1} (X = PMe_3 or PPh_3), and the reverse reaction proceeded when the bond strength fell below 110 kcal/mol (21). Thus, the fact that the isolated complex is intermediate between the extremes of the expected oxygen transfer indicates that the oxygen transfer is not only related to the O—X bond energy, but also to the ancillary ligands. Jurisson et al. observed that the reactions of acetylacetone-based Schiff base complexes $[TcO(N_2O_2)(H_2O)]^+$ and 3 equivalents of phosphines PR_3 yielded Tc(III) complexes $[Tc(PR_3)_2(N_2O_2)]$ with the N_2O_2 Schiff base intact (8).

The bound dha^- is obviously the hydrolyzed product of the original Schiff base. The ligated Schiff bases are known to be susceptible to metal-enhanced hydrolysis, as is known with some lanthanide complexes (22). The hydrolysis of Schiff bases coordinated to Tc(V) is important in the development of ^{99m}Tc radiopharmaceuticals. While this hydrolysis may be detrimental in many cases, it is postulated also to be advantageous in the design of ^{99m}Tc radiopharmaceuticals that would decompose under certain conditions in vivo (23). Thus it is necessary to characterize the decomposed products. The isola-

Can. J. Chem. Downloaded from www.nrcresearchpress.com by 46.23.64.124 on 09/08/12
For personal use only.

tion of this reduced and hydrolyzed Re species demonstrates one aspect of the decomposition.

Characterization

N_3O_2 complexes

The infrared spectrum of [ReO(apa)] exhibits an $\nu_{Re=O}$ vibration at 945, higher than the $\nu_{Tc=O}$ band at 915 in [TcO(apa)]; both are in the expected range for six-coordinated oxo complexes (18*b*). The $\nu_{Tc=O}$ absorption is usually found at lower frequencies than $\nu_{Re=O}$ in analogous oxometal complexes (18*b*). LSIMS of the complex showed a molecular ion peak at *m/z* 603, confirming that the complex is monomeric [ReO(apa)]. The stoichiometry of $[C_{20}H_{22}N_3O_7Re]$ for the complex was confirmed by elemental analysis and is consistent with the [TcO(apa)] complex, the structure of which has been determined by X-ray diffraction methods (3).

N_2O_2 complexes

The N_2O_2 donor set is found in the equatorial plane relative to the Tc=O group in all three possible types of complexes (vide supra) (7, 9). The infrared spectrum of $[\{ReO(epa)\}_2O]$ exhibits two ν_{Re-O} vibrations at 675 and 645 cm^{-1}, agreeing with the literature values of ν_{M-O} for other $[\{MO(N_2O_2)\}_2O]$ (M = Tc, Re) complexes (6, 7, 24, 25). No absorption bands could be assigned to $\nu_{Re=O}$; the two weak absorption bands at 950 and 910 cm^{-1} coincide with two moderate bands of the free ligands. A similar phenomenon was observed for other $[\{MO(N_2O_2)\}_2O]$ complexes, and was not rationalized: there was no absorption that could be attributed to $\nu_{Tc=O}$ in an N_2O_2 Schiff base complex (7) or an N_2O_2 amine phenol complex (25); the $\nu_{Re=O}$ bands were found in only moderate or weak intensity for two N_2O_2 amine phenol complexes (24). LSIMS shows $[ReO(epa)+1]^+$ and $[\{ReO(epa)_2O+1]^+$ at *m/z* 561 and 1037, respectively, suggesting that the complex is dinuclear with an oxygen atom bridging two ReO(epa) units. For [TcOCl(epa)], a weak IR absorption is present around 960 cm^{-1} and is tentatively assigned to the Tc=O stretching vibration, and the *m/z* values corresponding to $[TcO(epa)]^+$ and $[Tc(epa)]^+$ are shown in the LSIMS, indicating a mononuclear oxo complex. The absence of the molecular ion in the mass spectrum may be explained by a Tc—Cl bond weakened by the *trans* influence of the oxo group. In a similar complex, $[TcO\{(sal)_2en\}Cl]$, this *trans* influence was found to weaken the Tc—Cl bond significantly (9). The stoichiometry for $[\{ReO(epa)\}_2O]$ and $[TcOCl(epa)]\cdot 0.5H_2O$ was confirmed by elemental analyses.

^{1}H NMR studies

[ReO(apa)]

The resonances in the ^{1}H NMR spectrum (500 MHz) of [ReO(apa)] were assigned on the basis of the ^{1}H–^{1}H COSY (400 MHz, Fig. 2), and by comparison with the ^{1}H NMR spectra for H_3apa and [TcO(apa)] (3). [ReO(apa)] presented a spectrum similar to that of [TcO(apa)], except that resonances for the eight hydrogen nuclei of the two NCH_2CH_2N units were more distinguishable from one another. Thus it is possible to make a full assignment for the Re complex.

For the free ligand, the seven types of resonances were assignable to enol H (14.00 ppm), ring H (5.50 ppm), imine CH_2 (3.48 ppm), amine CH_2 (2.92 ppm), imine CH_3 (2.56 ppm), ring CH_3 (2.00 ppm), and amine NH (1.45 ppm), in order of increasing field (3). As in [TcO(apa)], upon coordination, the resonances corresponding to the enol H and amine NH disappeared due to deprotonation. Furthermore, the symmetry of the ligand is lost upon coordination; the two halves of the bound ligand, defined by the central nitrogen atom, became nonequivalent (as in [TcO(apa)]), as did the remaining hydrogens. The two halves were arbitrarily designated as "apical" and "equatorial", depending on the binding site of the enolate oxygen donor (Scheme 2, vide infra). Thus two sets of the ring H, imine CH_3, and ring CH_3 hydrogen nuclei were observed, and were assigned to the two arms based on the fact that the signals of nuclei (*H*) of the equatorial portion are more deshielded than those (*H'*) of the apical.[6] The ^{1}H–^{1}H COSY of this complex shows the correlation between the ring H and ring CH_3 of either the upfield or downfield set, or of the assumed equatorial or apical arm. The same two sets of signals were also observed in the ^{1}H NMR spectrum of [TcO(apa)], which is known to have two nonequivalent halves of the bound ligand. Obviously, a similar geometry to that of [TcO(apa)] holds true for [ReO(apa)].

The resonances for the two NCH_2CH_2N units fall almost into eight distinguishable multiplets when observed at 500 MHz, indicating the nonequivalence of the two units. These hydrogens were assigned based on ^{1}H–^{1}H COSY (Fig. 2) and on their similarity to the spectrum of [TcO(apa)]. The eight hydrogen signals were easily grouped into two sets corresponding to the two NCH_2CH_2N units. Two of the four H signals in each unit, each appearing as a doublet-of-doublets, were assigned to the pseudo-equatorial *H* nuclei (26), as only these two could define a dihedral angle of close to 90° (Fig. 2).[7] This assignment was supported by the fact that ring hydrogen atoms in pseudo-axial environments are usually more shielded than those in pseudo-equatorial environments (16*b*). The other two in each unit were more complicated, either doublets-of-triplets or multiplets, due to unequal coupling to three hydrogen nuclei. This assignment is consistent with that of [TcO(apa)], which was based on ^{1}H–^{1}H COSY, APT, and ^{1}H–^{13}C heteronuclear correlation spectra and those of the free ligand (3).

$[\{ReO(epa)\}_2O]$

The ^{1}H NMR spectrum was easily assigned by comparison to that of the free ligand. For the free ligand, the five types of resonances were assigned to enol H (14.6 ppm), ring H (5.60 ppm), imine CH_2 (3.77 ppm), imine CH_3 (2.58 ppm), ring CH_3 (2.12 ppm). As expected, upon coordination the resonance of the enol *H* disappeared while all other hydrogen resonances were shifted downfield from those of H_2epa. The ring H (5.95 ppm), imino CH_3 (2.72 ppm), and ring CH_3 (2.28 ppm) of the two halves of the ligands are indistinguishable, reflecting a symmetric molecule. The hydrogen resonances for the NCH_2CH_2N unit were split into two symmetrical multiplets, as an AA′BB′ system (Fig. 3). The ^{1}H NMR results suggest a

[6] As in $[MOXL_2]$, where the two bidentate L ligands are each bound equatorially and axially, the hydrogens in the equatorial ligand are usually more deshielded than those in the axial ligand (1, 2, 11).

[7] According to the Karplus Equation (27): $^3J = 4.2 - 0.5\cos\theta - 4.5\cos 2\theta$, a very small coupling constant (less than 1 Hz) is expected when θ is close to 90°.

Fig. 2. Ethylene hydrogen region of the ^1H–^1H COSY spectrum for [ReO(apa)].

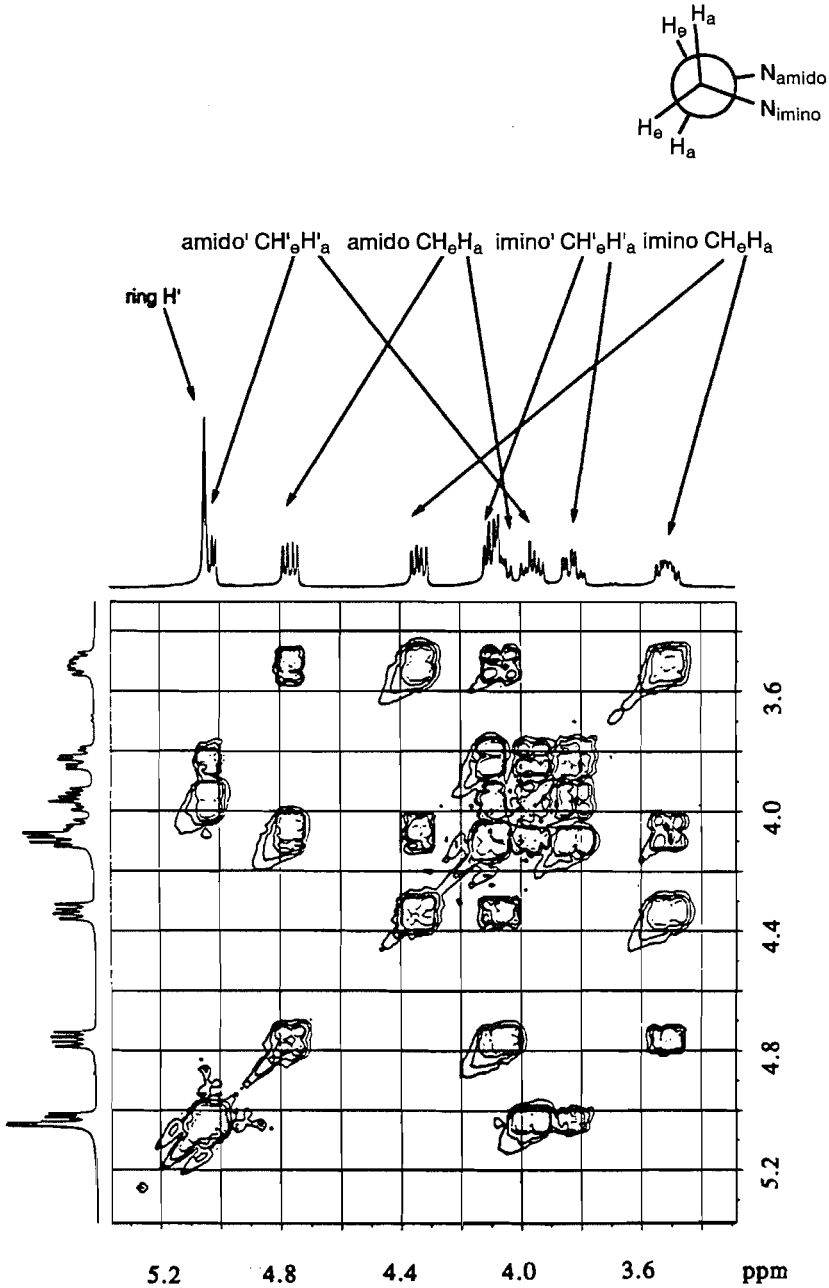

structure for the complex with coplanar coordinated ligands, consistent with a proposed dinuclear structure with C_i symmetry (known for other dinuclear Re(V) or Tc(V) complexes with two N_2O_2 ligands (6, 7, 24, 25)).

Structure of [Re(dha)Cl_2($OPPh_3$)(PPh_3)]·EtOH

The ORTEP drawing of the complex is illustrated in Fig. 1. The unit cell contains four discrete [Re(dha)Cl_2($OPPh_3$)-(PPh_3)]·EtOH molecules (two of each enantiomer), each of which has the Re(III) center coordinated by the two O donor atoms of the dha^- ligand, two Cl donor atoms, one triphenylphosphine P donor atom, and one triphenylphosphine oxide O donor atom. The coordination geometry is a distorted octahedron with the enolic oxygen of the dha^- located in the position *trans* to the Re-O=PPh_3 unit and the remaining donor atoms occupying equatorial sites relative to the O=PPh_3 group, such that the two chloro ligands are *cis* to each other. The distortion from an ideal octahedron is mainly caused by the variety of the donor atoms and their requirements (Table 3). In the absence of the sterically demanding oxo group, all the *cis* angles are close to 90°, within deviations of less than 4° (Table 4).

The Re—Cl(1) bond that is *trans* to the phosphine P is long (2.430(1) Å), while the Re—Cl(2) *cis* to the phosphine P is normal (2.362(1) Å) in comparison with the Re—Cl distances of 2.35 and 2.36 Å in *trans*-(P,P)-[$ReCl_3(PPh_3)_2(CH_3CN)$] (28), indicating that the phosphine P exerts a significant *trans* influence. The Re—P distance (2.404(1) Å) is short in com-

Can. J. Chem. Downloaded from www.nrcresearchpress.com by 46.23.64.124 on 09/08/12
For personal use only.

Can. J. Chem. Downloaded from www.nrcresearchpress.com by 46.23.64.124 on 09/08/12
For personal use only.

Fig. 3. Ethylene hydrogen region of the ^1H NMR spectrum (top) and a computer-simulated AA'BB' system ($\delta_A = 4.14$, $\delta_B = 3.90$; $J_{AB} = 13.2$, $J_{AB'} = 6.5$) for $[\{ReO(epa)\}_2O]$ (bottom). * = unidentified species; # = impurities.

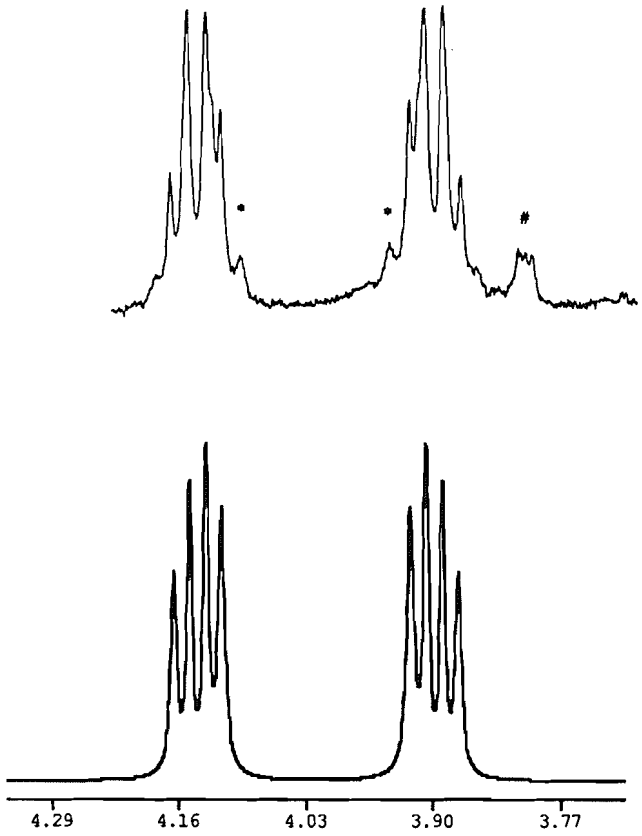

Scheme 4.

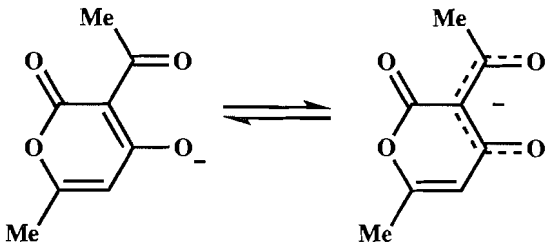

parison to the Re—P bonds of 2.47 and 2.48 Å in *trans*-(P,P)-$[ReCl_3(PPh_3)_2(CH_3CN)]$. This can be explained by the absence of a *trans* influence attributable to this PPh_3 group in $[Re(dha)Cl_2(OPPh_3)(PPh_3)]$. The two Re—O bonds are both close to the lengths found for other Re—O single bonds (29), with Re—O(3) = 1.987(2) Å, and Re—O(4) = 2.016(3) Å, indicating that the two oxygen donor atoms are involved in π-delocalization within the ligand (Scheme 4); in fact, an averaging of bond lengths is seen for this chelate ring (Table 3). The Re to phosphine oxide oxygen distance is longer (2.051(2) Å), but still comparable to the Re—O single bond (29). In contrast, the same oxygen is strongly bound to the phosphorus (O—P = 1.502(3) Å), only about 0.02 Å longer than the values found in the unligated $OPPh_3$ (O—P = 1.483(2) Å) (30), where the P—O is believed to be multiply bound (31). The maintenance of the multiple character of the P—O bond suggests that the O—Re is a coordinate bond (a typical P—O single bond is 1.60 Å (31)). Given the bonding features, it is analogous to a Re(III) complex of phosphine oxide.

In conclusion, the N_3O_2 dehydroacetic acid based Schiff base ligand precursor H_3apa has greater potential for use in radiopharmaceutical studies than its N_2O_2 Schiff base analogues, as stable oxotechnetium and oxorhenium complexes of H_3apa can be prepared in good yields. Complexes of N_2O_2 Schiff bases can be obtained ($[MO(N_2O_2)X]$, $[\{MO(N_2O_2)\}_2O]$, etc., Scheme 2); however, their formation is much less favorable, due to a variety of reaction pathways and a less stable coordination configuration. This severely limits the use of these tetradentate ligands in the design of radiopharmaceuticals.

Acknowledgments

We wish to thank the Natural Sciences and Engineering Research Council of Canada and the British Columbia Health Research Foundation for operating grants, the Du Pont Merck Pharmaceutical Company for support and NH_4TcO_4, Johnson Matthey, Inc. for NH_4ReO_4, and Professor J. Trotter for the very kind use of his crystallographic facilities.

References

1. H. Luo, I. Setyawati, S.J. Rettig, and C. Orvig. Inorg. Chem. **34**, 2287 (1995).
2. H. Luo, S.J. Rettig, and C. Orvig. Inorg. Chem. **32**, 4491 (1993).
3. S. Liu, S.J. Rettig, and C. Orvig. Inorg. Chem. **30**, 4915 (1991).
4. J.R. Dilworth. Transition Met. Chem. **15**, 411 (1990).
5. M. Calligaris and L. Randaccio. *In* Comprehensive coordination chemistry. Vol. 2. *Edited by* G. Wilkinson, R.D. Gillard, and J.A. McCleverty. Pergamon, Oxford. 1987. pp. 715–738.
6. F. Tisato, F. Refosco, U. Mazzi, G. Bandoli, and A. Dolmella. Inorg. Chim. Acta, **164**, 127 (1989).
7. G. Bandoli, M. Nicolini, U. Mazzi, and F. Refosco. J. Chem. Soc. Dalton Trans. 2505 (1984).
8. S. Jurisson, K.P. Dancey, M. McPartlin, P.A. Tasker, and E. Deutsch. Inorg. Chem. **23**, 4743 (1984).
9. S. Jurisson, L.F. Lindoy, K.P. Dancey, M. McPartlin, P.A. Tasker, D.K. Uppal, and E. Deutsch. Inorg. Chem. **23**, 227 (1984).
10. F. Tisato, F. Refosco, U. Mazzi, G. Bandoli, and M. Nicolini. Inorg. Chim. Acta, **189**, 97 (1991).
11. F. Refosco, F. Tisato, U. Mazzi, G. Bandoli, and M. Nicolini. J. Chem. Soc. Dalton Trans. 611 (1988).
12. A. Davison, H.S. Trop, B.V. Depamphilis, and A.G. Jones. Inorg. Synth. **21**, 160 (1982).
13. J. Chatt and G.A. Rowe. J. Chem. Soc. 4019 (1962).
14. G. Rouschias and G. Wilkinson. J. Chem. Soc. (Sect. A), 465 (1966).
15. (*a*) International tables for X-ray crystallography. Vol. IV. Kynoch Press, Birmingham, U.K. (present distributor Kluwer Academic Publishers, Boston, Mass. U.S.A.). 1974. pp. 99–102; (*b*) International tables for crystallography. Vol. C. Kluwer Academic Publishers, Boston, Mass. 1992. pp. 200–206.
16. R.M. Silverstein, G.C. Basser, and T.C. Morrill. *In* Spectrometric identification of organic compounds. 4th ed. John Wiley & Sons, New York. 1981; (*a*) pp. 194–197; (*b*) pp. 184–189.
17. A. Marchi, L. Marvelli, R. Rossi, L. Magon, V. Bertolasi, V. Ferretti, and P. Gilli. J. Chem. Soc. Dalton Trans. 1485 (1992).
18. W.A. Nugent and J.M. Mayer. *In* Metal–ligand multiple bonds. Wiley–Interscience, New York. 1988; (*a*) pp. 241–246; (*b*) pp. 115–118.

19. R.H. Holm and J.P. Donahue. Polyhedron, **12**, 571 (1993).
20. R.H. Holm. Chem. Rev. **87**, 1401 (1987).
21. R.R. Conry and J.M. Mayer. Inorg. Chem. **29**, 911 (1990).
22. S. Liu, L. Gelmini, S.J. Rettig, R.C. Thompson, and C. Orvig. J. Am. Chem. Soc. **114**, 6081 (1992), and references therein.
23. A. Duatti, A. Marchi, L. Magon, E. Deutsch, and V. Bertolasi. Inorg. Chem. **26**, 2182 (1987).
24. M.R.A. Pillai, C.L. Barnes, and E.O. Schlemper. Polyhedron, **13**, 701 (1994).
25. M.R.A. Pillai, C.S. John, E.O. Schlemper, and D.E. Troutner. Inorg. Chem. **29**, 1850 (1990).
26. E. Cole, R.C.B. Copley, J.A.K. Howard, D. Parker, G. Ferguson, J.F. Gallagher, B. Kaitner, A. Harrison, and L. Royle. J. Chem. Soc. Dalton Trans. 1619 (1994).
27. C.J. Creswell, O.A. Runquist, and M.M. Campbell. *In* Spectral analysis of organic compounds. Longman, New York. 1972. p. 141.
28. G.B. Drew, D.G. Tisley, and R.A. Walton. J. Chem. Soc. Chem. Commun. 600 (1970).
29. J.A. Conner and R.A. Walton. *In* Comprehensive coordination chemistry. Vol. 4. *Edited by* G. Wilkinson, R.D. Gillard, and J.A. McCleverty. Pergamon, Oxford. 1987. pp. 125–213, and references therein.
30. P.L. Goggin. *In* Comprehensive coordination chemistry. Vol. 2. *Edited by* G. Wilkinson, R.D. Gillard, and J.A. McCleverty. Pergamon, Oxford. 1987. pp. 487–503.
31. D.G. Gilheany. *In* The chemistry of organophosphorus compounds. Vol. 2. *Edited by* F.R. Heartly. John Wiley & Sons, Chichester. 1992. p. 1.

Can. J. Chem. Downloaded from www.nrcresearchpress.com by 46.23.64.124 on 09/08/12
For personal use only.